WELCOME MESSAGE

11TH INTERNATIONAL CONGRESS ON THE CHEMISTRY OF CEMENT

ICCC
2003
11th INTERNATIONAL CONGRESS ON THE CHEMISTRY OF CEMENT
DURBAN, SOUTH AFRICA
11 - 16 MAY

May 2003

A warm South African welcome is extended to all delegates at the 11th International Congress on the Chemistry of Cement, which, after a journey of 100 years, has at last reached the African continent and is this year, being held in Durban.

With more than 240 technical papers, a comprehensive exhibition running concurrently with the Congress, a choice of technical tours and a social programme that delegates will always remember, ICCC 2003 promises to provide members of the world cement industry a very stimulating and exciting 5 days.

The Congress has received the official endorsement of the South African Minister of Trade and Industry, Mr. Alec Irwin, MP, and he has urged visitors to our 'world in one country', to enjoy not only the scientific programme, but also the sights and sounds of Africa.

With the planning and preparation now behind us, it remains for me to welcome you all to the Congress and invite you to participate as actively as possible throughout the whole proceedings.

John Sheath
Chairman - ICCC 2003 Organising Committee

ORGANISATION STRUCTURE

11TH INTERNATIONAL CONGRESS ON THE CHEMISTRY OF CEMENT

CONGRESS PATRONS:

Alpha	Lafarge
http://www.alpha.co.za	http://www.lafarge.co.za
Natal Portland Cement	**Pretoria Portland Cement**
http://www.npc-eagle.co.za	http://www.ppc.co.za

CONGRESS ORGANISERS:

The Congress was organised under the auspices of:

Cement & Concrete Institute
P O Box 168
Halfway House, 1685
South Africa

Tel: +27 11 315 0300
Fax: +27 11 315 0584
E-mail: cnci@cnci.org.za
Web: http://www.cnci.org.za

With the professional assistance of:

Event Dynamics
P O Box 98009
Sloane Park, 2152
South Africa

Tel: +27 11 706 5010
Fax: +27 11 463 7195
E-mail: sandra@eventdynamics.co.za
Web: http://www.eventdynamics.co.za

ORGANISATION STRUCTURE

11TH INTERNATIONAL CONGRESS ON THE CHEMISTRY OF CEMENT

ORGANISING COMMITTEE

John Sheath (Chair)	johns@cnci.org.za
Leonie Barlow-Jones	lbarlow-jones@alpha.co.za
Ilse Boshoff	ilseb@lafarge.co.za
Craig Gallie	craigg@lafarge.co.za
Graham Grieve	graham@cnci.org.za
Jonathan Smith	jsmith@ash.co.za
Yvette Staples	yvettes@slagment.co.za
Peter Tiedt	peter.tiedt@npc-eagle.co.za
Lomaré van Wyk	lvanwyk@ppc.co.za

SCIENTIFIC COMMITTEE

Grieve, Dr G. (Chair)	graham@cnci.org.za
Alexander, Prof. M.	mark@eng.uct.ac.za
Amtsbüchler, Dr. R.	reinhold.amtsbuchler@lafarge.com
Asima, Mr E.	easima@ppc.co.zw
Ballim, Prof. Y.	ballim@civil.wits.ac.za
Barton, Mr R.E.	-
Brouard, Mr B.	brenton.brouard@aluminates.lafarge.com
Chatterjee, Dr A.K.	akchatterjee@acccement.com
Glasser, Prof. F.	f.p.glasser@abdn.ac.uk
Kearns, Mr M.J.	mkearns@ppc.co.za
Kereke, Mr K.	kkereke@circle.co.za
Kihara, Dr Y.	yushiro.kihara@abcp.org.br
Kruger, Dr. R.A.	rkruger@ash.co.za
Mullick, Dr A.K.	ajoy_mullick@rediffmail.com
Nagataki, Prof. S.	nagataki@eng.niigata.ac.jp
Roy, Prof. D.	dellaroy@psu.edu
Schutte, Mr R.	rolf.schutte@npc-eagle.co.za
Shayan, Dr A.	amads@arrb.com.au
Sheath, Mr J.	johns@cnci.org.za
Strydom, Prof. C.	cstrydom@scientia.up.ac.za
Tamas, Prof. F.D.	tamasf@almos.vein.hu
Venter, Mr G.	gventer@alpha.co.za

TECHNICAL REVIEWERS

The Organisers would also like to record their appreciation to the reviewers of the papers for their work and contributions.

Alexander, Prof. Mark G.	mark@eng.uct.ac.za
Amtsbüchler, Dr Reinhold	reinholda@lafarge.co.za
Asima, Mr Eggs	easima@ppc.co.zw
Ballim, Prof. Yunus	ballim@civil1.civil.wits.ac.za
Barton, Mr Roy E.	-
Blackbeard, Mr Vincent	vblackbeard@alpha.co.za
Brouard, Mr Brenton	brenton.brouard@aluminates.lafarge.com
Chatterjee, Dr A.K.	dr_akc@vsnl.net
Glasser, Prof. Fred	f.p.glasser@abdn.ac.uk
Graham, Mr Peter	peterg@civil.wits.ac.za
Grieve, Dr Graham	graham@cnci.org.za
Kearns, Mr Mike J.	mkearns@ppc.co.za
Kearsley, Prof. Elsabé	elsabe.kearsley@eng.up.ac.za
Kelly, Dr Ray	rayk@lafarge.co.za
Kereke, Mr Kennedy	kkereke@circle.co.zw
Krüger, Dr Japie	japiekruger@icon.co.za
Kruger, Mr Richard	rkruger@ash.co.za
Mullick, Dr Ajoy K.	ajoy_mullick@redifmail.com
Nagataki, Prof. Shigeyoshi	nagataki@eng.niigata-u.ac.jp
Oberholster, Dr Bertie	boberholster@ppc.co.za
Olorunsogo, Prof. Folarin	olorunsogof@nu.ac.za
Potgieter, Prof. Herman	hermanp@techpta.ac.za
Roy, Prof. Della	dellaroy@psu.edu
Schoonraad, Dr Johan	jschoonraad@alpha.co.za
Schutte, Mr Rolf	rolf.schutte@npc-eagle.co.za
Scott, Mr Dave	dscott@ppc.co.zw
Shayan, Dr Ahmad	ahmads@arrb.org.au
Smith, Mr Graeme	graemews@ash.co.za
Stevens, Mr Laurence	laurence.stevens@npc-eagle.co.za
Strydom, Prof. Christien	cstrydom@scientia.up.ac.za
Tait, Prof. Bob	btait@eng.uct.ac.za
Tamas, Prof. Ferenc D.	tam043@almos.vein.hu
Tembe, Mr Dumisane	dumisane.tembe@npc-eagle.co.za

ORGANISATION STRUCTURE

11TH INTERNATIONAL CONGRESS ON THE CHEMISTRY OF CEMENT

CONGRESS PATRONS:

Alpha	Lafarge
http://www.alpha.co.za	http://www.lafarge.co.za
Natal Portland Cement	**Pretoria Portland Cement**
http://www.npc-eagle.co.za	http://www.ppc.co.za

CONGRESS ORGANISERS:

The Congress was organised under the auspices of:

Cement & Concrete Institute
P O Box 168
Halfway House, 1685
South Africa

Tel: +27 11 315 0300
Fax: +27 11 315 0584
E-mail: cnci@cnci.org.za
Web: http://www.cnci.org.za

With the professional assistance of:

Event Dynamics
P O Box 98009
Sloane Park, 2152
South Africa

Tel: +27 11 706 5010
Fax: +27 11 463 7195
E-mail: sandra@eventdynamics.co.za
Web: http://www.eventdynamics.co.za

ORGANISATION STRUCTURE

11TH INTERNATIONAL CONGRESS ON THE CHEMISTRY OF CEMENT

ORGANISING COMMITTEE

John Sheath (Chair)	johns@cnci.org.za
Leonie Barlow-Jones	lbarlow-jones@alpha.co.za
Ilse Boshoff	ilseb@lafarge.co.za
Craig Gallie	craigg@lafarge.co.za
Graham Grieve	graham@cnci.org.za
Jonathan Smith	jsmith@ash.co.za
Yvette Staples	yvettes@slagment.co.za
Peter Tiedt	peter.tiedt@npc-eagle.co.za
Lomaré van Wyk	lvanwyk@ppc.co.za

SCIENTIFIC COMMITTEE

Grieve, Dr G. (Chair)	graham@cnci.org.za
Alexander, Prof. M.	mark@eng.uct.ac.za
Amtsbüchler, Dr. R.	reinhold.amtsbuchler@lafarge.com
Asima, Mr E.	easima@ppc.co.zw
Ballim, Prof. Y.	ballim@civil.wits.ac.za
Barton, Mr R.E.	-
Brouard, Mr B.	brenton.brouard@aluminates.lafarge.com
Chatterjee, Dr A.K.	akchatterjee@acccement.com
Glasser, Prof. F.	f.p.glasser@abdn.ac.uk
Kearns, Mr M.J.	mkearns@ppc.co.za
Kereke, Mr K.	kkereke@circle.co.za
Kihara, Dr Y.	yushiro.kihara@abcp.org.br
Kruger, Dr. R.A.	rkruger@ash.co.za
Mullick, Dr A.K.	ajoy_mullick@rediffmail.com
Nagataki, Prof. S.	nagataki@eng.niigata.ac.jp
Roy, Prof. D.	dellaroy@psu.edu
Schutte, Mr R.	rolf.schutte@npc-eagle.co.za
Shayan, Dr A.	amads@arrb.com.au
Sheath, Mr J.	johns@cnci.org.za
Strydom, Prof. C.	cstrydom@scientia.up.ac.za
Tamas, Prof. F.D.	tamasf@almos.vein.hu
Venter, Mr G.	gventer@alpha.co.za

TECHNICAL REVIEWERS

The Organisers would also like to record their appreciation to the reviewers of the papers for their work and contributions.

Alexander, Prof. Mark G.	mark@eng.uct.ac.za
Amtsbüchler, Dr Reinhold	reinholda@lafarge.co.za
Asima, Mr Eggs	easima@ppc.co.zw
Ballim, Prof. Yunus	ballim@civil1.civil.wits.ac.za
Barton, Mr Roy E.	-
Blackbeard, Mr Vincent	vblackbeard@alpha.co.za
Brouard, Mr Brenton	brenton.brouard@aluminates.lafarge.com
Chatterjee, Dr A.K.	dr_akc@vsnl.net
Glasser, Prof. Fred	f.p.glasser@abdn.ac.uk
Graham, Mr Peter	peterg@civil.wits.ac.za
Grieve, Dr Graham	graham@cnci.org.za
Kearns, Mr Mike J.	mkearns@ppc.co.za
Kearsley, Prof. Elsabé	elsabe.kearsley@eng.up.ac.za
Kelly, Dr Ray	rayk@lafarge.co.za
Kereke, Mr Kennedy	kkereke@circle.co.zw
Krüger, Dr Japie	japiekruger@icon.co.za
Kruger, Mr Richard	rkruger@ash.co.za
Mullick, Dr Ajoy K.	ajoy_mullick@redifmail.com
Nagataki, Prof. Shigeyoshi	nagataki@eng.niigata-u.ac.jp
Oberholster, Dr Bertie	boberholster@ppc.co.za
Olorunsogo, Prof. Folarin	olorunsogof@nu.ac.za
Potgieter, Prof. Herman	hermanp@techpta.ac.za
Roy, Prof. Della	dellaroy@psu.edu
Schoonraad, Dr Johan	jschoonraad@alpha.co.za
Schutte, Mr Rolf	rolf.schutte@npc-eagle.co.za
Scott, Mr Dave	dscott@ppc.co.zw
Shayan, Dr Ahmad	ahmads@arrb.org.au
Smith, Mr Graeme	graemews@ash.co.za
Stevens, Mr Laurence	laurence.stevens@npc-eagle.co.za
Strydom, Prof. Christien	cstrydom@scientia.up.ac.za
Tait, Prof. Bob	btait@eng.uct.ac.za
Tamas, Prof. Ferenc D.	tam043@almos.vein.hu
Tembe, Mr Dumisane	dumisane.tembe@npc-eagle.co.za

THE EFFECT OF COMPLEX ADMIXTURES ON STRENGTH OF ULTRA HIGH- STRENGTH CEMENT

Konstantin Sobolev and Svetlana Soboleva

Department of Civil Engineering, European University of Lefke, TRNC. E-mail: sobolev@lefke.edu.tr

ABSTRACT

Recent research has shown that a state-of-the-art process for high-performance (HP) cement adds a new dimension to "classical" cement technology. The key idea of the process involves the mechano-chemical activation of cement at the grinding stage. A silica-based complex admixture is used for the activation of the cement which imparts high strength and improved durability to mortars and concrete. This paper describes the effect of different complex admixtures on the strength of HP cement. According to the available results, mortars based on HP cement possess a compressive strength of up to 148 MPa. A comparison of alternative evaluation methods helps to recommend the test procedure for HP and high- strength cement.

1. INTRODUCTION

The latest developments in cement and concrete science show the following trends [1,2]:

- *Increasing Strength*: Major breakthroughs in knowledge have led to the design of cement based materials with greater strength; this has resulted in the development and application of super high-strength concretes with a compressive strength of up to 135-250 MPa, high flexural strength and improved ductility [3-12].
- *Application of Chemical Admixtures*: Added to the concrete mixture, relatively small amounts of chemical admixtures can alter the behavior of fresh or hardened concrete. Chemical admixtures can improve almost any problematic property of concrete: they are one of the essential components of modern concrete which help control strength and durability [13,14].
- *Utilization of industrial by-products and waste (IBPW)*: The use of IBPW as mineral additives has become an important part in cement and concrete technology. According to wide- ranging investigations [1,2,13-16], the performance of conventional concrete can be significantly improved by adding IBPW in specific quantities. Well-known mineral additives include granulated blast furnace slag, fly ash, and silica fume. These mineral additives not only yield a concrete which has better properties and is more cost effective, but they also reduce the environmental impact of construction activities [16].

Following these developments, the concept of high performance concrete (HPC) has been put forward and successfully applied worldwide. It is generally accepted that concrete with improved properties (workability, strength, permeability, durability, etc.) above the conventional benchmarks can be specified as HPC. According to Forster [17], HPC is "a concrete made with appropriate materials combined according to a selected mix design and properly mixed, transported, placed, consolidated, and cured so that the resulting concrete will give excellent performance in the structure in which it will be exposed, and with the loads to which it will be subjected for its design life".

Proceedings of the 11th International Congress on the Chemistry of Cement (ICCC)
'Cement's Contribution to the Development in the 21st Century'
Hosted by: The Cement and Concrete Institute of South Africa
CD-ROM produced by: Document Transformation Technologies
11 - 16 May 2003, Durban, South Africa
ISBN Number: 0-9584085-8-0
Editors: Dr G. Grieve and G. Owens
Congress Organised by: Event Dynamics

To realize the HPC concept, a range of chemical admixtures and mineral additives are required, and consequently, a modern concrete batching plant must use appropriate equipment for precise control, dispatching, dosing and batch processing [7-14]. This modernization of production facilities is an unavoidable cost for improved performance since variations in dosing or mixing the components of the concrete may affect the performance of the final product. The compatibility of the admixtures is yet another problem for the production and application of HPC [13,14].

However, an alternative method of controlling the concrete properties and design of HPC is the use of special cements possessing higher strength and better resistance to the deterioration caused by various physical, chemical, and mechanical factors [18-26]. These superior cements are often based on special clinkers or blended cements such as shrinkage compensating or expansive cements, high early strength cements, regulated-set and jet-cements [3]. The group of these cements also includes newly developed Ultimax cement, blended Pyrament and SF cements [20-24].

An advanced approach to improving cement performance arises from the application of chemical admixtures, which modify the cement grinding process [19]. Using this method, a number of chemical admixtures and cement products have been developed. Well- known examples include air-entraining, hydrophobic and plasticized cements, and also the family of cements which are manufactured using grinding aids. It has been suggested that the action of these modifiers is based on mechano-chemical activation [19].

The theory of mechano-chemical activation has been successfully applied to processing nanopowders, pigments, fillers, binders, ceramic and ferromagnetic materials. Using this method, an improvement of cement strength can also be achieved [19,20,23,26]. Low Water Demand Binder (LWDB) is produced by intergrinding cement and a dry modifier at a high energy [25]. In spite of a similar technique already suggested in [19,20], only the application of a specially selected admixture- modifier at a relatively high dosage (up to 4%) resulted in the manufacture of a cement with both reduced water demand and high strength.

The group of mineral-and-organic complex admixtures for application in cement technology was proposed [18]. Basically, these admixtures contain a reactive silica-based sorbent as a mineral constituent and a surfactant as its organic constituent plus some minor corrective admixtures (Figure 1, further details are provided in [18]). Supersilica, a reactive silica-based complex admixture was developed using this principle [16,18]. Although all the effects of Supersilica have not been completely investigated, it is hypothesized that, when added during the cement grinding process, Supersilica modifies the surface of cement particles and also promotes the formation of highly reactive amorphous structures and pre-hydrates [18]. Further, the reactive silica component also acts as a micro-filler and participates in a pozzolanic reaction. The mechano-chemical activation of cement with Supersilica at the grinding stage results in a high performance (HP) cement.

HP cement can be defined as a product manufactured by the mechano-chemical activation of certain proportions of clinker, gypsum, complex admixture and, optionally, a mineral additive of industrial (IBPW) or natural origin (Figure 1), which imparts high strength and extreme durability to the concrete or mortar made from such cement [18,26]. Such high strength can be used for the engineering of a cement with high volume mineral additives (HVMA). As a result, relatively large amounts (up to 70%) of portland cement clinker can be replaced with inexpensive locally available mineral additives. Natural pozzolanic materials, sand, limestone, granulated blast furnace slag, fly ash, glass cullet and ceramic waste, all can be used as mineral additives in HVMA cements [16].

There are two types of HP cement:

- Type A Basic HP cement;
- Type B Blended HP cement.

Basic Type A cement involves intergrinding the clinker, gypsum and a complex admixture. Blended Type B cement covers a wide range of HP cements with mineral additives. The content of a mineral additive in blended HP cement varies with the specified level of the properties and with the type of additive used. Preliminary research [16] demonstrated that Type B Blended HP cements with a mineral additive content within the standard limitations (25-50% as specified in EN 197-1, [27]) can be produced. Furthermore, the range of mineral additives can be extended for HVMA cement. New types of mineral additives (quartz sand, glass cullet and ceramic waste) can be used as components of the Blended HP or HVMA cements [16,18].

The application of granulated blast furnace slag (GBFS) in Blended HP cement in addition to high ultimate strength (more than 80 MPa), results in a product possessing high resistance to chemical attack and to elevated temperatures (up to 700 ^{o}C) [26].

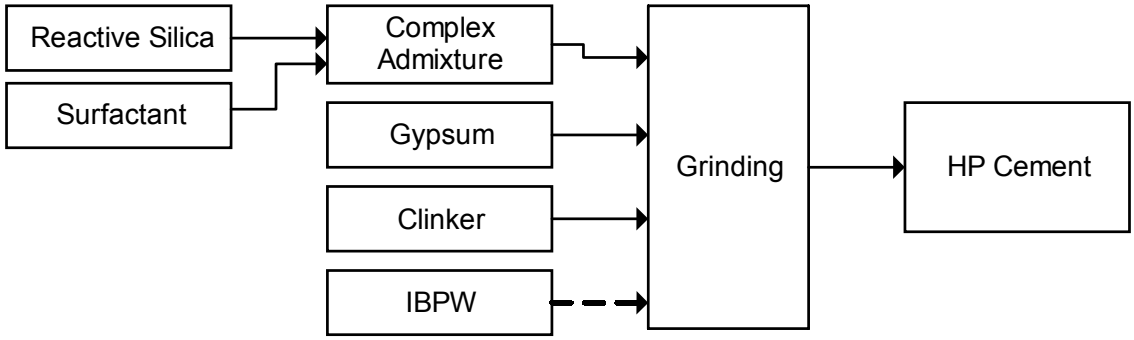

Figure 1. Flow Chart of HP Cement Technology

2. RESEARCH SIGNIFICANCE

The effect of silica fume on the behavior of cement- based materials has been extensively reported in the literature [1-14]. A number of published papers on HP cement deals with the application of a silica fume based complex admixture [16,26]. At the same time the use of other types of reactive silica products as a component of the complex admixture have been proposed [18]. Consequently, the evaluation of the effect of different reactive silica materials on the cement strength is important for the manufacture and practical application of HP cement based materials.

3. EXPERIMENTAL PROGRAM

3.1 Materials used

Three different reactive silica components were used in the complex admixture: silica fume (SF), natural microsilica (MS), and metakaolin (MK). The reference cements were: portland cement CEM-I 42.5 [27] (NPC-I, Type I according to ASTM C150 [28]) and low water demand binder (LWDB). The samples of optimized high-performance cement Type A (HPC-A) and Type B (HPC-BS containing 50% of GBFS and HPC-BL containing 35% of limestone, LS) were also tested for comparison [26]. The chemical composition of these materials is presented in Table 1. Standard Rilem Cembereau sand [29] was used in the preparation of the mortars.

Table 1. Chemical Analysis of Cementitious Materials

Composition	SF	MS	MK	NPC-I	BFS	LS	LWDB	HPC-A	HPC-BS	HPC-BL
SiO_2	90.00	84.60	86.80	19.42	37.43	-	19.77	28.47	34.28	20.87
Al_2O_3	0.40	5.14	5.17	5.27	10.91	-	5.15	4.18	7.83	4.74
Fe_2O_3	0.36	0.85	1.00	2.80	0.64	-	4.01	3.36	2.46	1.65
CaO	1.63	0.50	4.10	62.07	35.88	52.05	56.00	55.01	43.43	49.83
MgO	1.02	1.05	1.03	2.04	8.07	3.04	1.91	1.89	5.69	2.73
Na_2O	0.50	-	0.24	0.70	0.35	-	0.25	1.02	1.01	-
K_2O	2.28	-	0.46	1.00	1.17	-	0.42	0.38	0.19	-
SO_3	0.44	0.99	-	2.30	2.06	-	3.82	2.61	2.35	1.89
LOI	3.03	6.15	1.20	3.50	-	42.90	2.7	2.83	1.50	15.89

3.2 Research Program

The experimental program had two main components:

- The investigation of cement compressive strength at constant W/C according to EN 196 [30];
- The investigation of cement compressive strength at constant flow according to ASTM C109 [31-32].

3.3 Notations Used

The following notations were applied to distinguish the samples:

- NPC-# reference portland cement;
- LWDB-# reference low water demand binder;
- HPC-A-# reference high performance cement Type A;
- HPC-BS-# reference high performance cement Type B (50% of GBFS);
- HPC-BL-# reference high performance cement Type B (35% of LS);
- SFC-# high performance cement produced using SF admixture;
- MSC-# high performance cement produced using MS admixture;
- MKC-# high performance cement produced using MK admixture.

The additional letter after the main notation identifies of the test procedure as follows:

- I reference portland cement CEM-I 42.5 (without additional grinding);
- W for EN 196 mortars (constant W/C);
- F for ASTM C109 mortars (constant flow).

3.4 Mixture Proportioning

The strength properties of eight different cements were investigated. These included HP cements produced using different complex admixtures (SFC, MSC and MKC) and reference cements. Ten percent (by weight) of complex admixture was used to produce these cements. Quartz sand (S) was used in small amounts (5%) in the composition of the cements investigated in order to facilitate grinding in the ball mill. The composition of the cements investigated is given in Table 2.

Two sets of mortars were prepared: W according to EN 196 and F according to ASTM C109. For W mortars a constant W/C of 0.5 and a sand-to-cement ratio of 3.0 were used. F mortars were produced at W/C adjusted to constant flow (as described in ASTM C109). A sand-to-cement ratio (S/C) of 2.75 was applied for F mortars.

Table 2. Composition and Fineness of Cements Investigated

Cement Type	Cement Composition								Blaine Specific Surface, m^2/kg
	NPC-I	LWDB	LS	BFS	S	Complex Admixture			
						SF	MS	MK	
NPC	100	-	-	-	-	-	-	-	516
SFC	85	-	-	-	5	10	-	-	477
MSC	85	-	-	-	5	-	10	-	505
MKC	85	-	-	-	5	-	-	10	422
LWDB	-	100	-	-	-	-	-	-	409
HPC-A	85	-	-	-	5	10	-	-	570
HPC-BS	40	-	-	50	-	10	-	-	580
HPC-BL	50	-	35	-	5	-	-	10	416

3.5 Preparation of Specimens

Samples of high performance cement were obtained by grinding the mixtures specified in Table 2 in a laboratory ball mill. The sample batch weight was 5 kg and grinding media weight was 65 kg. Grinding time was 30 minutes. In order to eliminate the effect of the additional grinding on the properties of cements investigated, the reference portland cement NPC-I was also ground for an equivalent time. The resulting specific surface data of the investigated cements are summarized in Table 2.

Mortars based on these cements were prepared following EN 196 [30]. For F mortars the flow table was applied to obtain the standard flow of 105-115 mm. The mortars for the strength test were cast into three-gang (40x40x160 mm) prism molds, and compacted in accordance with EN 196 [30].

3.6 Curing of Specimens

After the compaction procedure, the molds were placed in a humidity cabinet for 24 hours (keeping a relative humidity of 95% and a temperature of 20°C). Following this period, the specimens were removed from the molds and kept in water until the testing age.

3.7 Tests Performed

Compressive strength tests were conducted using the portions of prisms broken in flexure [28]. The compressive strength results indicated are the average of the six values and flexural strength results are the average of the three values. Different age conditions reflecting the requirements of [25-27] were applied: W-mortars were tested at the age of 2, 7 and 28 days; and F-mortars tests were carried out at the age of 1, 3, 7 and 28 days.

4. TEST RESULTS

4.1 Compressive Strength of Mortars with Constant W/C

The test results of W- mortars (following EN 196) are presented in Table 3 and Figure 2. According to the obtained results the best 28-day compressive strength value of 62.1 MPa was obtained from the cement produced with metakaolin (MKC). This value is close to the strength demonstrated by an optimized sample of HPC-A (67.0 MPa). The silica fume (SFC) and natural microsilica (MSC) based cements reached 51.4 and 51.9 MPa, respectively, which is close to the 28-day compressive strength of HPC-BS (52.1 MPa). The reference sample of NPC demonstrated a compressive strength of 43.8 MPa (which meets the requirements for 42.5 Grade cement), while the strength of LWDB sample was only 26.6 MPa (outside the limits specified by EN 196 for a cement of the lowest Grade of 32.5). The strength of investigated HP cements at the 2-day age is almost the same for all investigated cements and lies in the range of 25.5-28.6 MPa, with the best value for MSC.

Table 3. Compressive Strength of W- Mortars (EN 196)

Mix Type	S/C	W/C	Compressive Strength, MPa at age, days		
			2	7	28
NPC-W	3.00	0.50	21.6	32.8	43.8
SFC-W	3.00	0.50	25.5	32.6	51.4
MSC-W	3.00	0.50	28.6	38.4	51.9
MKC-W	3.00	0.50	25.5	49.2	62.1
LWDB-W	3.00	0.50	14.3	22.6	26.6
HPC-A-W	3.00	0.50	31.5	45.6	67.0
HPC-BS-W	3.00	0.50	7.5	21.9	52.1
HPC-BL-W	3.00	0.50	13.3	25.4	33.0

At the 7 days MK- based cement demonstrated an even better strength value than optimized HPC-A, gaining 49.2 against 45.6 MPa. The intermediate level of 38.4 MPa was shown by MSC. In this group SFC was the least satisfactory, developing slightly lower strength compared with NPC : 32.6 and 32.8 MPa, respectively. The lowest 7-day strengths were obtained from HPC-BL, LWDB and HPC-BS with 25.4, 22.6 and 21.9 MPa, respectively.

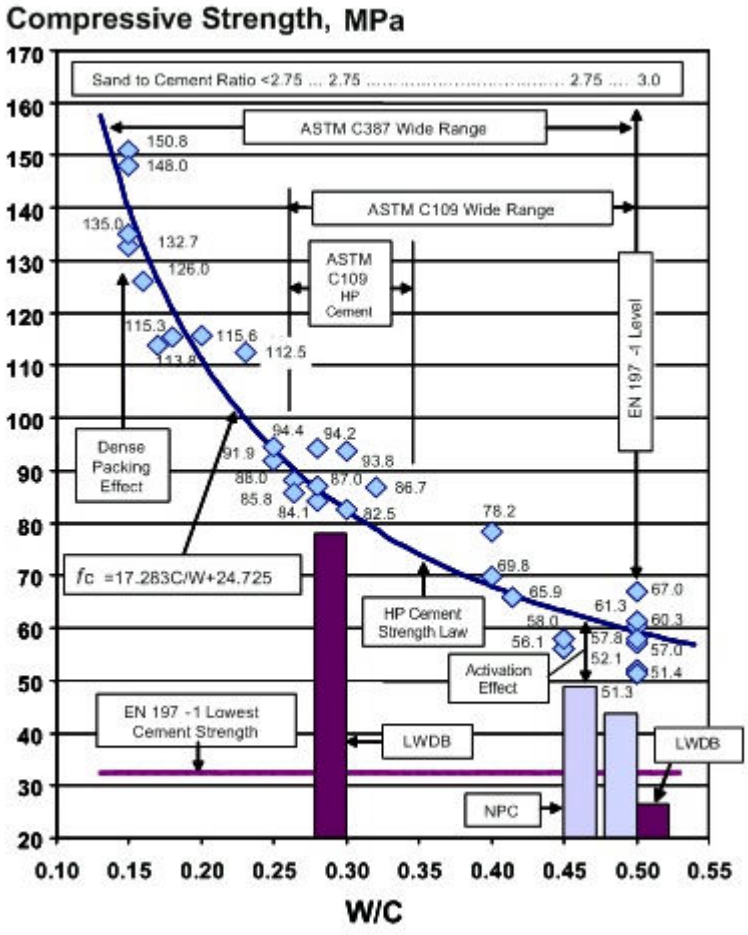

Figure 2. W/C Law for High Performance Cement

4.2 Compressive Strength of Mortars with Constant Flow

The test results of F- mortars (ASTM C109) are presented in Table 4 and Figure 2. Based on the flow test, a W/C ratio was selected for the mortars. It was found that all cements (except reference NPC) required a W/C in the range of 0.28-0.30 in order to obtain the standard flow of 105-115 mm. Due to its special design, the complex admixture overcomes the relatively high water absorption of

reactive silica component; yet, conversely, it also provides a strong water reducing effect, resulting in a cement with water demand comparable to or less than that of LWDB.

The results demonstrated that cement produced with a SF-based complex admixture (SFC) possessed the highest compressive strength of 84.1 MPa at 28 days. However, this value is lower than the strength of optimized samples of HPC-A and HPC-BS (94.4 and 92.7 MPa, respectively). The microsilica cement (MSC) demonstrated a strength value of 74.5 MPa, slightly lower than LWDB strength of 78.7 MPa. The lowest 28-day strength (66.8 MPa) was obtained for metakaolin cement (MKC), which is comparable to the strength of reference HPC-BL (66.7 MPa). The strength of NPC reference sample was only 48.9 MPa.

Table 4. Compressive Strength of F- Mortars (ASTM C109)

Mix Type	S/C	W/C	Compressive Strength, MPa at age, days			
			1	3	7	28
NPC-F	2.75	0.45	16.9	36.6	39.8	48.9
SFC-F	2.75	0.28	40.6	43.5	53.3	84.1
MSC-F	2.75	0.30	36.5	51.1	55.7	74.5
MKC-F	2.75	0.30	33.0	38.4	45.5	66.8
LWDB-F	2.75	0.30	35.1	59.2	69.0	78.7
HPC-A-F	2.75	0.28	44.3	62.2	74.1	94.4
HPC-BS-F	2.75	0.28	35.2	54.2	65.6	92.7
HPC-BL-F	2.75	0.28	21.6	40.7	54.8	66.7

The 1-day strength of all investigated HP cements was found to be very high: between 40.6 and 33.0 MPa, with the best value for SFC. Similar strength was also developed by HPC-BS. The strength of optimized HPC-A exceeded these values and reached 44.3 MPa. The strength of LWDB was found to be close to the strength of MSC and MKC. All these strength values are much higher than 16.9 MPa demonstrated by NPC.

The behavior of investigated cements at 3- and 7- days age was similar: microsilica- based HP cement (MSC) demonstrated the best strength 51.1 and 55.7 MPa, respectively. The NPC strength was lower than that of all tested cements.

5. DISCUSSION

5.1 Strength Development

The test results confirmed a similar effect of different reactive silica products on the strength properties of HP cement at a reduced W/C. The three different stages of cement strength development can be specified as follows:

- 1st Stage: Very rapid strength growth during first day of hardening;
- 2nd Stage: Latent period between 1 and 3 days characterized by a delay in hardening, especially noticeable for SFC and MKC;
- 3rd Stage: More intensive, strength development of SFC and MKC, comparing to HPC-A and MSC, at the age of 3- 28 days.

The strength development of investigated cements at a constant W/C of 0.50 has a clearly defined critical point at 2 days age (Table 3). According to the test results, MKC maintained a very high strength up to 7 days, giving remarkable strength values. The continuous strength growth up to 28 days was observed for HPC-BS. LWDB demonstrated very little increase in strength after 7 days.

5.2 HP Cement vs LWDB

The research has demonstrated the advantage of HP cement over LWDB for early and 28-day strength in the range of the investigated W/C. This advantage is even multiplied at high W/C, when HP cement showed 2- 2.5 times higher strength (Figure 2). It can be suggested that the criterion similar to the performance of plasticizers or superplasticizers in concrete [13], which allows only very small strength loss of modified concrete (being tested at the same W/C), must be applied in the case of new cements with low water demand. This procedure could provide a better understanding of the behavior of these cements and also, prevent an unexpected strength loss of the concrete at high W/C.

5.3 W/C Effect

The function of the HP cement compressive strength vs. W/C is presented in Figure 2. The 28-day compressive strength value for HP cement mortars can be estimated by the following equation:

$$f_{28} = \frac{17.283}{W/C} + 24.725$$

According to the empirical rule stated in [1,2], the pozzolanic effect of highly reactive silica dioxide materials (such as silica fume) is approximately equal to the strength of the cement used. In this case, the difference in strength between NPC and HP cement (or SF cement) at the same W/C can be explained by the contribution of mechano- chemical activation, which was also observed in [23]. The optimal composition of HP cement allows a significant reduction of the W/C ratio keeping a high workability level with consequent increase in strength due to super-dense packing.

5.4 The Comparison of EN 196 and ASTM C109 Test Procedures

The comparison of the test results demonstrated that the EN 196 procedure cannot be adopted for measuring the performance of newly developed high strength cements. Designed to compare portland cements of different manufacturers by its adjustment to a “common divider”, the compressive strength obtained at constant W/C is not sufficient to predict the performance of the different types of cement in concrete (for example, pozzolanic cements with high value of normal consistency). In the practical application of these types of cement the comparison of its performance in concrete may be required when the EN 196 test procedure is used. This test should consider not only the strength of concrete, but also cement effect on workability of concrete mixtures.

Since the constant flow procedure of ASTM C109 returns a compressive strength as an integrated value involving a workability parameter, it can be applied as a performance criterion to a wide range of cements. As a result, the ASTM strength can be directly used for the prediction of concrete strength based on different types cement. Therefore, the ASTM C109 procedure is suggested as the most appropriate strength test for high strength cements such as HP cement or LWDB.

6. CONCLUSIONS

1. Reactive silica additives like silica fume, natural microsilica, and metakaolin increase the early and ultimate strength of cement and concrete. These materials can be used as components of a complex admixture for consequent application in high performance cement. The test results demonstrated similar behaviors of different reactive silica additives in high performance cement.
2. Using the HP cement approach, cements with 28-day strength (according to ASTM C109) in the range of 66.8- 94.4 MPa were obtained.
3. The W/C ratio was recognized to be the most critical parameter in measuring the performance of high strength cement. The difference in strength according to different standards (EN 196 vs.

ASTM C109) was found to be in the range of 10-60% for different types of HP cement, and about 200% for LWDB. Based on completed research, the ASTM C109 is proposed as the most convenient procedure for testing high strength cements.

ACKNOWLEDGEMENTS

The authors would like to acknowledge the receipt of samples of metakaolin from PIERI-GRACE, natural microsilica from Microsilica NZ, HP cement from SCI Con Technologies, and LWDB from KOCA. The authors are grateful to the staff of Quality Control Laboratories of NIGBAS Precast Concrete, BEM and OYSA Cement for their help in conducting the tests. The suggestions of Dr. C. Podmore are highly appreciated.

REFERENCES

[1] Sobolev K. and Soboleva S. High- Performance Concrete Mix Proportioning. IV CANMET/ACI/JCI International Conference on Recent Advances in Concrete Technology, Tokushima, Japan, 1998.
[2] Sobolev K. High- Strength Concrete with Low Cement Factor, Ph.D. Dissertation, Chemical Admixtures Lab, Scientific and Research Institute of Concrete and Reinforced Concrete, Moscow, Russia, 1993, pp. 11-39. (in Russian)
[3] Neville A.M. Properties of Concrete, Pearson Education, Harlow, UK, 2000, pp. 71-75 and 674-687.
[4] Bache, H.H. Design for Ductility, Concrete Technology: New Trends, Industrial Applications, Proceedings of the International RILEM Workshop, E&FN Spon, London, UK, 1993, pp. 113-125.
[5] Dauriac C. and Dowd B. Reactive Powder Concrete, The Construction Specifier, No 12, USA, 1996, pp. 47-51.
[6] Russel H.G. High- Performance Concrete Applications in North America, High Performance High- Strength Concrete: Material properties, Structural Behavior and Field Application, Perth, Australia, 1998, pp. 213-226.
[7] Walraven J.C. High- Strength Concrete – Possibilities and Opportunities, Concrete Precasting Plant and Technology (BFT), No 11, Germany, 1994, pp. 37-44.
[8] Walraven J.C. High - Strength Concrete, Concrete Precasting Plant and Technology (BFT), No 6, Germany, 1991, pp. 45-52.
[9] Marikunte S., and Shah S.P. Engineering of Cement Based Composites, Concrete Technology: New Trends, Industrial Applications, Proceedings of the International RILEM Workshop, E & FN Spon, London, UK, 1993, pp. 83-102.
[10] Shah S.P. Recent Trends in the Science and Technology of Concrete, Concrete Technology: New Trends, Industrial Applications, Proceedings of the International RILEM Workshop, E & FN Spon, London, UK, 1993, pp. 1-18.
[11] Zia P., Ahmad S., and Leming M. High-Performance Concretes: A State-of-Art Report (1989-1994), USA, 1997. (FHWA-RD-97-030)
[12] Fidjestol P., and Knudsen K. High Performance Concrete for Durability – Using Microsilica, ERMCO-95, Proceedings of the XIth European Ready Mixed Concrete Congress, Istanbul, Turkey, 1995, pp. 379-389.
[13] Batrakov V.G. Modified Concrete, Stroyizdat, Moscow, Russia, 1990, pp. 6-37. (in Russian)
[14] Ramachandran, V.S. Concrete Admixtures Handbook, Noyes Publications, New Jersey, USA, 1995.
[15] Malhotra, V.M., High- Performance High- Volume Fly Ash Concrete, High Performance High- Strength Concrete: Material properties, Structural Behavior and Field Application, Perth, Australia, 1998, pp. 97-122.
[16] Sobolev K. and Arikan M. High Volume Mineral Additive ECO- Cement, American Ceramic Society Bulletin, Vol. 81, No 1, USA, 2002, pp. 39-43.
[17] Forster S.W. High- Performance Concrete - Stretching the Paradigm, Concrete International, Vol.16, No 10, USA, 1994, pp. 33-34.
[18] Sobolev K. and Soboleva S. Complex Admixture and Method of Cement Based Materials Production, International PCT Application PCT/TR98/00008, Vienna, Austria, 1998. (WIPO Publication No WO98/54108).
[19] Royak S.M. and Royak G.S. Special Cements, Stroyizdat, Moscow, Russia, 1983, pp.88-109. (in Russian)
[20] Skvara F., Kolar K., Novotny J., and Zadak Z. Cement Pastes and Mortars with Low Water-to-Cement Ratio - I, Cement and Concrete Research, Vol.10, No. 2, USA, 1980, pp. 253-262.
[21] Al-Manaseer A.A., Aquino E.B., and Kumbardi H. Properties of Concrete Containing Ultimax Rapid-Setting Hydraulic Cements, ACI Materials Journal, V.96, No. 5, USA, 1999.
[22] Muszynski L. C., Corrosion protection of reinforcing steel using pyrament blended cement concrete,International Conference on Blended Cements in Construction, Sheffield, UK; Ed. by R. N. Swamy; Elsevier Applied Science, London, 1991, pp 442-454.
[23] Ronin V., Jonasson J.-E., and Hedlund H. Advanced Modification Technologies of the Portland Cement Base Binders for Different High Performance Applications, 10th International Congress on the Chemistry of Cement, , Göteborg, Sweden, 1997. (Pub. No 2ii077).

[24] Jonasson J-E, Ronin V, Hedlund H, High Strength concretes with energetically modified cement and modelling of shrinkage caused by self-desiccation, Proceedings of 4th International Symposium on Utilazation of High Strength Concrete (BHP-96), Paris, 1996, pp. 245-254.
[25] Ioudovitch B.E., Dmitriev A.M., Zoubekhine S.A., Bashlykov N.F., Falikman V.R., and Serdyuk V.N. Low Water Requirement Binders as New Generation Cements, 10th International Congress on the Chemistry of Cement, Göteborg, Sweden, 1997. (Pub. No 3iii021).
[26] Sobolev K. and Soboleva S. High Performance Cement: Solution for Next Millennium, Materials Technology, Volume 14, No 4, UK, 1999, pp. 191-193.
[27] EN 197-1, European Standard Specification for Cement, European Standard, European Committee for Standardization, 1994.
[28] ASTM C150, Standard Specification for Portland Cement, Annual Book of ASTM Standards, Vol. 04.01, Philadelphia, USA, 1999, pp. 123-127.
[29] TS 819, Rilem - Cembureau Standard Sand, TSE, Ankara, Turkey, 1989.
[30] EN 196, Test Method for Determining Compressive Strength of Cement Mortar, European Standard, European Committee for Standardization, 1994.
[31] ASTM C109 Compressive Strength of Hydraulic Cement Mortars (Using 2-in or 50-mm Cube Specimens), Annual Book of ASTM Standards, Vol. 04.01, Philadelphia, USA, 1999, pp. 64-68.
[32] ASTM C349 Compressive Strength of Hydraulic Cement Mortars (Using Portions of Prisms Broken in Flexure), Annual Book of ASTM Standards, Vol. 04.01, Philadelphia, USA, 1999, pp. 214-217.

MECHANOCHEMISTRY SYNTHESIS OF NEW COMPOSITE BINDER FROM SECONDARY MINERAL RESOURCES

S.I. Pavlenko, Yu.M. Bazhenov, E.G. Avvakumov and A.V.Aksenov

ABSTRACT

The Siberian State University of Industry (SSUI) in association with the institutes of the Siberian Branch of the Russian Academy of Sciences has created a new composite binder consisting of high–calcium fly ash from the Abakan thermal power plant, waste molding sand mixture ("burnt sand") from foundry, Abakanvagonmash, and waste product from the Yurga abrasion plant. The fly ash contains up to 40 % SiO_2 and 35 % CaO including above 15 % free CaO. The waste sand mixture includes more than 90 % SiO_2, mostly in the amorphous state. The waste product of the abrasion production (high–alumina product) contains 80 % and more Al_2O_3.

The ash is a good binder, but the presence of free CaO destroys its binding properties during service. Grinding ash, sand and high–alumina product (HAP) together by means of mechano-chemical activation in planetary ball mills to the fineness of 750 m^2/kg and using thermal treatment produced a binder with a compressive strength above 50 MPa at 28 days.

It was found that during the process of mechano-chemical treatment, free CaO reacts with SiO_2 (chemistry of a solid), reduces its content in the mixture by 60 to 80 % and increases the strength by 1,5 to 2 times eliminating the process of concrete expansion.

The creation of a binder from industrial wastes and making good concretes with slag sand as an aggregate gives both economic (its cost is half that of Portland cement) and ecological benefits by eliminating landfills and reducing the CO_2 discharge into the atmosphere (the production of a ton of cement discharges above 0,5 ton CO_2).

Keywords: High–calcium Fly Ash, Burnt Sand, High–alumina Product, Amorphous Material, Mechanochemical Process, Planetary Mill, Reaction, Cementless Composite Binder.

1. INTRODUCTION

The department of civil engineering, SSUI, supported financially by the Ministry of Education of Russia, has created fine cementless ash – slag concrete from wastes of thermal power plants and ferroalloy plant (1). Concrete has been patented (patent № 2065420). A project for the construction of the binder and a silicate brick shop (2, 3) at the Abakan thermal power plant has been developed and approved. A technical certificate by the Government of Russia has been received. But as the Abakan thermal power plant is a part of the Abakanvagonmash with a large foundry which dumps used molding sand mixtures (1 ton of sand per 1 ton of founding), we thought of replacing silica fume with molding sand as a silica component of a new binder for concretes. Supported by the Federal INTEGRATION Program, the investigation was carried out in the laboratories of the SSUI, Associated Institute of Geology, Geophysics and Mineralogy (AIGGM) and the Institute of Chemistry of Solids and Mechanochemistry (ICSM), Siberian branch of the Russian Academy of Sciences (SBRAS).

As known, the following compounds are in composition of cement: $3CaO \cdot SiO_2$ (mass portion of 40 – 60 %); $2CaO \cdot SiO_2$ (15 – 35 %); $3CaO \cdot Al_2O_3$ (4 – 14 %); $3CaO \cdot Al_2O_3 \cdot Fe_2O_3$ (10 – 18 %) (4). The indicated compounds and also the initial components for their synthesis are in ashes from

coal combustion, in waste products of casting and abrasives production. Therefore these wastes are used for the production of cementless binding materials from them (5).

The quality of binding materials from wastes depends on the following factors:
1) selection of composition in order to correspond to a large extant to the composition of cement;
2) mixture of composition in order to have possibly the chemical interaction between them.

Thermal method in this case are less suitable for the reason of their high energy consumption, therefore the mechanical activation of mixture is used in grinding apparatuses (6 - 8).

However, the mechanochemical reaction with participation of waterless oxides is not so effective. Thermodynamically, the reactions with participation of hydrated oxides are more advantageous which are formed during addition to mixtures of waterless oxides to water. So, for reaction:

$$3CaO \cdot SiO_2 = CaSiO_3$$
$$Ca(OH)_2 + SiO_2 \cdot xH_2O = CaSiO_3 + xH_2O,$$

here Gibbs energy equals to 89.4 and 117.2 kJ/mole respectively. The experiment shows that the coherence of calcium in the second case proceeds more effectively in some cases than during the interaction of waterless oxides.

Roentgenamorphic hydrosilicates relating to the tobermorite group ($Ca(OH)_2 \cdot Si_6O_{16} \cdot 4H_2O$) are the products of mechanical activation in relation to components $Ca(OH)_2 : SiO_2 \cdot H_2O = 1 : 1$; during their scaling, pure wollastonite β-$CaSiO_2$ (9) is obtained.

It is possible to get dicalcium silicate by the indicated method. The work (10) the activation of calcium oxide and amorphous silica gel was being carried out in the presence of water, the quantity of which was larger than calculated on theoretical composition of $2CaO \cdot SiO_2 \cdot 2H_2O$. After activation over 14 hours in a vibration mill the roentgenamorphic product is obtained, in which the form of dicalcium silicate is obtained. After heating up to 550 ^{0}C, the peak appears belonging to β-$2CaO \cdot SiO_2$, but during heating to 1000 ^{0}C the product is already well crystallized.

By analogy during mechanical activation of calcium hydroxide mixtures and of aluminium the hydroaluminates of calcium $3CaO \cdot Al_2O_3 \cdot 6H_2O$ and $2CaO \cdot Al_2O_3 \cdot 4H_2O$ are formed, which are decomposed by heating to temperatures of 700 – 1000 ^{0}C with the formation of $12CaO \cdot 7Al_2O_3$ and $2CaO \cdot Al_2O_3$ having viscous properties (11 - 13).

In this work the use of mechanical activation for synthesizing of a composite binder from industrial waste containing the oxides of calcium, silicon and aluminium has been researched.

2. MATERIALS

2.1 Fly Ash

According to Ivanov (14), high – calcium fly ash from the electrostatic filters of the Abakan thermal plant is a coarse polydispersed ash with the surface area below 250 m^2/kg.It consists mostly of irregular agglomerated particles (Figure 1). The bulk density, absolute density and effective specific activity of the ash are 1120, 2680 kg/m^3 and 118,9 Bq/kg, respectively. Chemical analysis of the ash is given in Table 1.

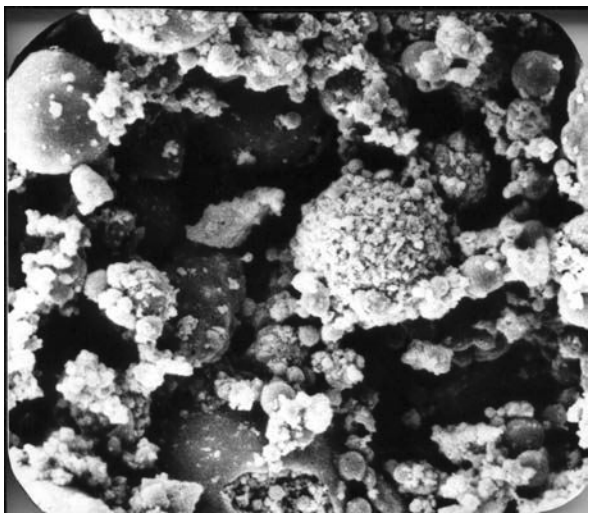

Figure 1. Structure of fly ash from the Abakan thermal power plant x 1000

Table 1. Chemical analysis of ash

Component	Compound, %								
	SiO_2	Cao total	Free CaO	MgO	Al_2O_3	Fe_2O_3	$Na_2O + K_2O$	TiO_2	LoI
Fly ash from Abakan TPP	40.47	34.94	15.75	7.28	4.87	10.32	1.1	0.80	1.02

As can be seen from the data, the ash has to be ground to break its agglomerated particles and expose free CaO, the presence of which would induce expansion and fracture of concrete. Furthermore, the method of Ovcharenko (15) showed that 58 % free CaO was in a glass phase which prevented it from hydration prior to strength gain.

2.2 Molding Sand Mixture

The molding sand mixture consists of 92 % quartz sand, 6 % bentonite and 2 % water glass. After its use in the foundry and after removing gritty scale from the material, it has a form of a black sand ("burnt" sand) with a fineness modulus of 1,91 (Figure 2). The bulk density, absolute density and the effective specific activity of the sand are 1450, 2380 kg/m^3 and 98 Bq/kg, respectively. Chemical analysis of the burnt sand is given in Table 2.

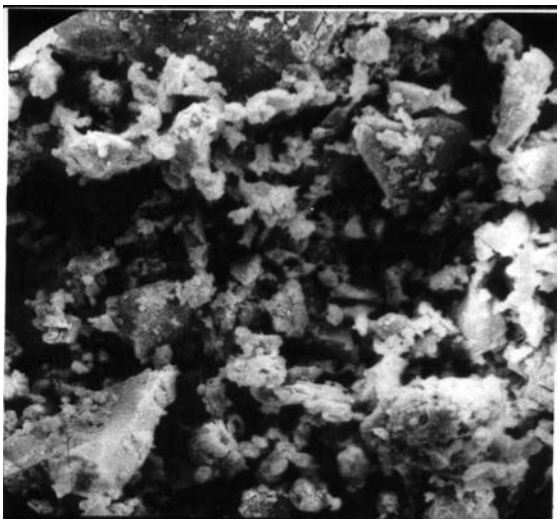

Figure 2. Structure of burnt sand x 1000

Table 2. Chemical analysis of burnt sand

Component	Compound, %						
	SiO_2	CaO	MgO	Al_2O_3	Fe_2O_3	$Na_2O + K_2O$	LoI
Burnt sand	92.28	1.80	0.2	2.71	2.38	1.02	-

The burnt sand has high content of silicon oxide in the amorphous state (thanks to a high – temperature treatment) which enhances the possibility of chemically binding free CaO in the ash into calcium silicates.

2.3 High – Alumina Product (HAP)

High – alumina product, the waste from the Yurga abrasion plant, is a grey powder (Figure 3). Its chemical analysis is shown in Table 3.

This powder is used to enhance strength and fire resistance in the binder and concrete.

Figure 3. Structure of HAP x 400

Table 3. Chemical analysis of HAP

Component	Compound, %							
	SiO_2	TiO_2	Al_2O_3	$FeO + Fe_2O_3$	MgO	CaO	$K_2O + Na_2O$	LoI
HAP	4.51	2.36	34.00	5.17	1.64	1.14	0.34	0.12

3. TESTING PROCEDURES

The following test series were undertaken.

3.1 Determining Optimum Mixture Proportions of a Binder

Correlation of the two components (fly ash and burnt sand) were determined. Fly ash was ground in a laboratory ball mill to the fineness of 400 m^2/kg, and the burnt sand was ground to a powder with the residue of 15 % on the sieve No 008. Strength and waterproofness of a binder versus fly – ash – to – burnt sand ratios are in Table 4.

Table 4. Compressive strength and waterproofness of a composite binder

Components, % by weight		Compressive strength, MPa		Coefficient of softening	Notes
sand	ash	R dry	R sat		
40	60	24.85	5.45	0.22	non-waterproof
30	70	34.4	6.70	0.13	non-waterproof
20	80	41.4	21.55	0.52	non-waterproof
10	90	21.2	31.75	1.5	higher waterproofness

The results of the initial investigation showed that a cementless binder can be produced from the above wastes of thermal power plant and foundry. The optimum components ratio as determined by a computerized analysis was 85 to 90 % fly ash and 10 to 15 % ground burnt sand. However, long – term testing in water and a chemical analysis of the binder showed that less than 50 % after free CaO interacted with SiO_2 with resulting cracks in specimens.

3.2 Mixture Activation

The preliminary researches were being carried out in a laboratory planetary mill AGO-2 (16) with samples of 10 gr. processed mixtures and in a large planetary mill AGO-3 (17) with total 1 kg mixture charge.

The power characteristics of the mills are close to each other. Mixtures made of chemically pure oxides of calcium, silicon and aluminium and also mixtures composed of wastes were activated in the mills. Roentgenphase analysis was carried out on device DRON-3 (radiation of CuKa). Determination of the content of calcium oxide was made by method described in work (15). The measurement of basic indices of binder and manufactured articles from it was made in accordance with State Standard 310 "Cement".

The influence of mechanical activation on interaction in mixture of oxides CaO, Al_2O_3, SiO_2 was investigated. Mixtures were activated for 10 minutes. Data of roentgenphase analysis of mixtures are presented in Figure 4.

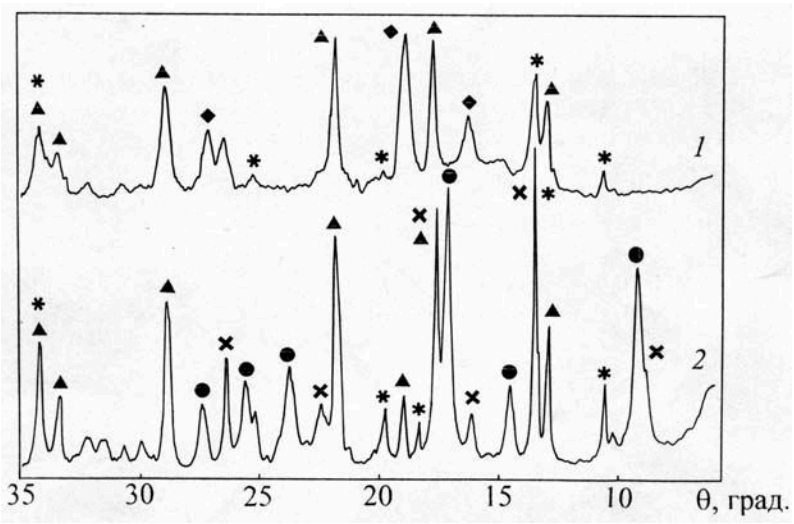

Figure 4. Diffractogrammes of activated mixtures CaO + Al_2O_3 + SiO_2 :
1 – waterless oxides; 2 – mixture contains 20 % H_2O

In the absence of water the chemical interaction, as seen from Figure 4, is practically absent (i.e. the dispersion and amorphisation of oxides are carried out). By adding water the responses of $Ca(OH)_2$

and also the responses corresponding to formation of calcium aluminate $3CaO \cdot Al_2O_3 \cdot 6H_2O$ appear. Thermodynamic calculations of hydrosilicates and hydroaluminates formation by reactions

$$5Ca(OH)_2 + 6SiO_2 = Ca(OH)_2 \cdot Si_6O_{16} \cdot 4H_2O$$
$$6Ca(OH)_2 + 2Al_2O_3 + 6H_2O = 2(3CaO \cdot Al_2O_3 \cdot 6H_2O)$$

show that the probabilities of forming the products mentioned above are approximately the same.

Gibbs energy for the first reaction equals to 303 kJ/mole (18) and for the second one it is equal to 303.2 kJ/mole (19). It means that hydrosilicates of calcium also may be present in product but, probably they are less crystallised and do not give a diffraction picture.

For obtaining the composite binder the high-calcium ash from Abakan TPS (Thermal Power Station), waste mould mixture (burnt sand) of casting production AO "Abakanwaggonmachine" and high-alumina product, i.e. the wastes from Yurginsk abbrasive production were taken.

For mechanical activation the mixture of 80 % ash and 20 % of burnt ground were selected and 5 % high-alumina product was added to it.

To enhance the activity of the binder components, a blend of 80 % fly ash, 10 % burnt sand and 10 % HAP was ground in a planetary activator mill AGO-3 (0,1 – 100 μm) designed by the ICSM, Siberian branch oh the RAS (Figure 5).

Figure 5. The laboratory activator mill AGO-3

The composition mentioned above was subject to different processing times in the mill AGO-3. It should be noted that water was not added to the mixture, but nevertheless one cannot consider that the process was carried out without water. One can believe that water adsorbed on the surface of initial products, the content of which, as it follows from data on LOI, is at the level of 2 %, will take part.

Grinding in this mill is performed in the field of three inertia forces (two centrifugal forces and the Koriolis force), due to which fact the electric tension of AGO-3 is 2 to 3 times higher than that of gravity ball mills (Figure 6). Mechanochemical activation of the components (chemistry of solids)

and partial interaction of the amorphous silica and CaO takes place during the process. The data on the free CaO content and the degree of the blend dispersity with respect to the duration of grinding in the planetary mill are shown in Table 5. In Figure 7 the structure of mixture after grinding is shown.

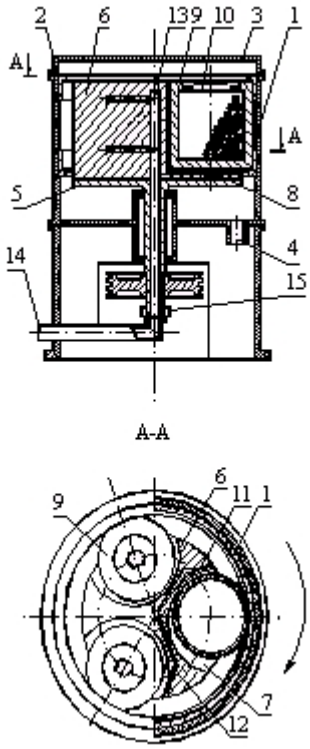

1. Body
2. Lug for a guided drum movement
3. Cover
4. Water outlet
5. Driver bottom
6. Driver
7. Recess for drum
8. Bearing
9. Drum
10. Drum cover
11. Water pocket
12. Water outlet
13. Water conduit
14. Branch pipe
15. Gland packing

Direction of the driver revolution

Figure 6. The scheme of activator mill AGO-3

Table 5. Free CaO content of the blend versus duration of treatment in AGO-3 mill

Mixture No	Duration of treatment, min	Dispersity, m^2/kg	Free CaO content, %
1	without treatment	200	12.60
2	1	400	6.33
3	3	500	4.82
4	6	600	3.92
5	10	750	2.80
6	15	1000	2.02

3.3 Casting and Testing of Specimens of a New Binder

2 – cms cubes of specimens were cast from the activated mixture at normal consistency. The test results are given in Table 6.

From the data shown in Table 6, it can be seen that the best results were obtained with the activator mill after 10 minutes (the dispersity of the blend was 750 m^2/kg). The binder exhibited high compressive strength and waterproofness. It was found that with further treatment (above 10 min, dispersity of 1000 m^2/kg), water demand and setting time of the mixture sharply increased, and a drop in the compressive strength was observed.

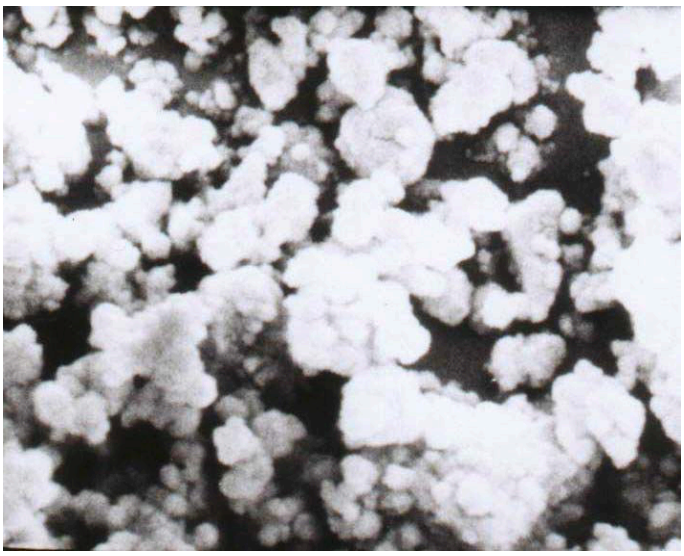

Figure 7. Structure of ground mixture of three wastes x 8000

Table 6. Strength and waterproofness of a composite binder

Mixture No	Compressive strength, MPa		Coefficient of Softening	Notes
	R dry	R sat		
1	27.82	6.36	0.49	non-waterproof
2	35.63	9.87	0.57	non-waterproof
3	41.35	25.73	0.88	non-waterproof
4	52.48	47.65	1.59	higher waterproofness
5	56.76	49.98	1.85	higher waterproofness
6	43.54	40.54	1.34	higher waterproofness

Tests for expansion (State Standard 310.3-76* Cements, Methods for Determining Normal Consistency, Setting Time and expansion) were carried out by boiling cakes in a bath and in an autoclave. Cakes made from the mixture No 1 had fractures and radial cracks while cakes from the mixture No 2 had smaller defects but with some warping. The remainder mixtures (nos 3 to 6) sustained both boiling and autoclave tests without cracks. The test results showed that the new binder was in accordance with the requirements of the State Standard 310 Cement.

4. PERSPECTIVE FOR PRODUCTION OF THE NEW COMPOSITE BINDER WITH THE HELP OF MECHANOCHEMICAL ACTIVATION

In practice the inter-grinding of the components of the new composite binder can be done in vibrating mills ICSM SBRAS (VCM-10G) shown in Figure 8 or in flowing mills made in Japan.

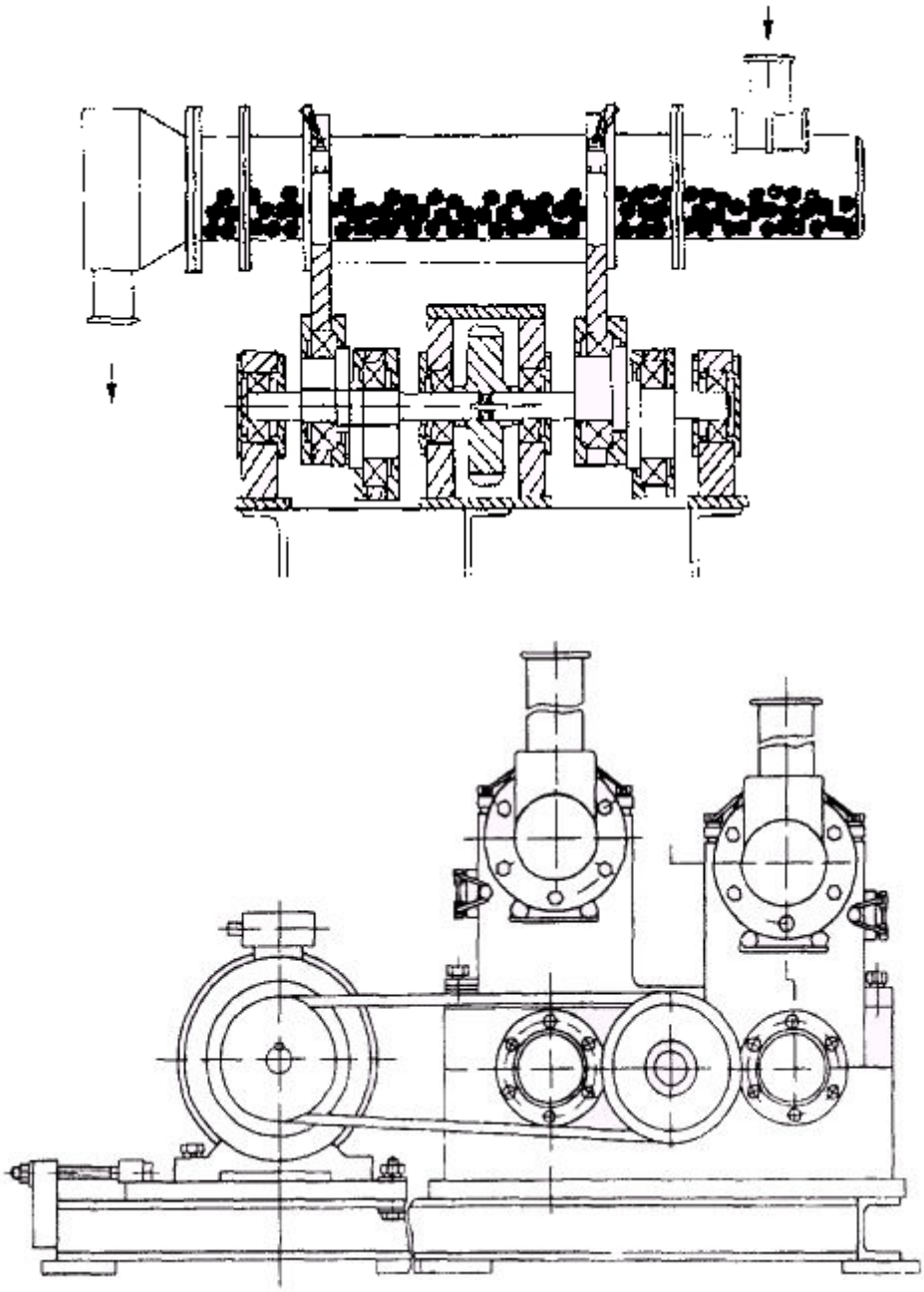

Figure 8. The scheme of mill VCM-10G

5. CONCLUSIONS

1. Previous investigation shows that wastes from thermal power plants burning brown coals of the KATPC in combination with silica by – products from other industries can be used for composite high – class binders (up to 60 MPa) and concretes on their basis which are equivalent to the traditional binders and concretes.
2. To bind free CaO in brown coal ashes, mechanochemical activation of the components has to be made through inter-grinding in planetary activator mills. This assists interaction of more than 50% CaO and SiO_2 and prevents destructive processes in concretes with a cementless binder.
3. Creation of binders from secondary mineral resources contributes much to environment protection and also helps towards the solving of economic and social problems (construction of dwellings from concretes with cementless binders).
4. Vibrating mills ICSM SBRAS or flowing mills made in Japan can be recommended for production of the worked out composite binder.

REFERENCES

[1] Pavlenko, S.I. Development of fine cementless concrete with high – calcium ash and slag from thermal power plants, Siberian State University of Industry, 1998, 82 pp.

[2] Pavlenko, S.I., Shishkanov, A.P., and Bazhenov, Yu. M., Technological complex for utilization of high – calcium ash and slag from the Abakan thermal power plant. Sixth CANMET / ACI International Conference on Fly Ash, Silica Fume, Slag and Natural Pozzolans in Concrete, Bangkok, Thailand, May 31 – June 5, 1998, Printed in ACI, SP 178-5.

[3] Pavlenko, S.I., and Shmelkov, M.A., Cementless binder and silica brick on its basis, 10 th International Congress on the Chemistry of Cement, Göteborg, Sweden, June 2 – 6, 1997.

[4] A Short Encyclopaedia of Chemistry. Ed by academician K.L. Knunyants. Moscow: Soviet Encyclopaedia, 1967, v. 5, 802 p.

[5] Pavlenko, S.I., Malyshkin, V.I., Bazhenov, Ju.M., Cementless Fine Grained Concrete from Secondary Mineral Resouces. Printed by Siberian Branch of the Russian Academy of Sciences, Novosibirsk, RUSSIA, 2000, 142 pp.

[6] Sulimenko, L.M., Journal "Cement", Moscow, 1994, No 2, p. 38.

[7] Sulimenko, L.M., Shalunenko, N.I., Urhanova, L.A., Journal "Proceedings of Universities. Construction", Novosibirsk, 1995, No 11, p. 63.

[8] Savinkina, M.A., Logvinenko, A.G., Ashes of Kansk-Achinsk coals, Novosibirsk, Publ. "Science", 1979, 287 pp.

[9] Kosova, N.V., Avvakumov, E.G., Siberian journal of chemistry, Novosibirsk, 1992, No 2, p.135.

[10] Sasaki, K., Masuda, T., Ishida, H., Mitsuda T., Journal "American Ceramic Society", 1996, No 80, p. 472.

[11] Kvitkovsky, A.K., Kosova, N.V., Avvakumov, E.G. et al. J. "Chemistry in interests of stable development". Printed by Siberian Branch of the Russian Academy of Sciences, Novosibirsk, Russian, 2000, № 8.

[12] Kano, I., Yamashito. H., Saito, F., et al., Journal "Powder Technology", 1998, № 98, p. 279.

[13] Temujin, I., Mackenzie, K.I.D., Iadambaa, T., et al., Journal "Materials of chemistry", 2000, No10, p. 1019.

[14] Ivanov, I.A., Lightweight concrete with ashes from thermal power plants, Book, 2 nd ed., Moscow, Stroyizdat, 1986, 136 pp.

[15] Ovcharenko, G.I., Plotnikova, L.P., Frantsen, V.B., Evaluation of the properties of ashes from the KATPC coals and their use in heavy concretes, Barnaul, AltGTU, 1997, 149 pp.

[16] Patent No 975068, RUSSIA, 1982.

[17] Patent No 1584203, RUSSIA, 1993.

[18] Mi, G., Saito, F., Hanada, M., Journal "Powder Technology", 1997, № 93, p. 77.

[19] Thermal constants of substances. Ed. by V.P. Glushko, VINITI, Moscow, 1979, issue 9.

DETERMINATION OF OPTIMUM GYPSUM CONTENT OF PORTLAND CEMENT USING THE HYDRATION CRITERION OF MAXIMUM ULTIMATE COMPRESSIVE STRENGTH

K. K. Sideris, P. Manita and K. Sideris

Laboratory of Building Materials, School of Engineering, Democritus University of Thrace, Xanthi, Greece.

ABSTRACT

In this study the determination of optimum SO_3 content of Portland cement was investigated. The optimum SO_3 content can be determined using as a criterion the maximum ultimate compressive strength, determined by the analysis of mortar' s compressive strength with the aid of the cement hydration equation. For this purpose the measured values of mortar compressive strength, taken from Lerch, were analyzed with the aid of the cement hydration equation. The SO_3 content significantly influences compressive strength of Portland cement III at early and later ages. The influence of SO_3 content is significant for cement type IV at later ages, especially at ultimate strength. This method can be used in any concrete laboratory without the aid of special equipment since only simple measurements are needed (mortar compressive strength).

1. INTRODUCTION

Gypsum is added during grinding of the clinker in order to regulate the setting time of Portland cement. However, it also affects some other properties, such as strength,[1] contraction,[1] size of pores in hydrated cement paste etc. at early and later ages. Lerch[1] investigated the way added gypsum controls the setting of cement in respect to protection against the abnormal expansion that might result from use of excess amount of gypsum. For this purpose the investigator measured the rate of hydration using conduction calorimetry on net cement pastes. Physical tests (compressive strength, expansion and contraction) were also performed on mortar prisms.

By the investigations of Lerch[1] and others,[2-3] the ultimate compressive strength was not taken in account because of the inability to comprehend the final hydration. This can be made now with the aid of the cement hydration equation,[4-5] which enables the determination of final hydration. Because of the validity of equal fractional rate of hydration of all components in the hardened paste of Portland cement,[6-7] the hydration products are the same at all stages of hydration, and therefore compressive strength could be considered as a measure for porosity and drying shrinkage. This is shown by the results of Lerch[1] concerning compressive strength and contraction, and by Sersale et al.[2] concerning strength and porosity. Consequently, it may be expected that porosity and drying shrinkage appear a minimum value when the maximum strength of a given mortar or concrete is achieved.

When the 1-day strength test (according to ASTM C 543-84) is used, it is not clear if the amounts needed to optimize strength, porosity, shrinkage and expansion are the same during the whole hydration period.[3] Hence, the determination of optimum gypsum content, which depends on aluminate and ferrite phases,[3] alkali content and on fineness of the cement,[1] has to be carefully watched. This was investigated in this study by using the measured values concerning mortar compressive strength, setting time, contraction and expansion of two Portland cements (type III and

Proceedings of the 11th International Congress on the Chemistry of Cement (ICCC) 11 - 16 May 2003, Durban, South Africa
'Cement's Contribution to the Development in the 21st Century' ISBN Number: 0-9584085-8-0
Hosted by: The Cement and Concrete Institute of South Africa Editors: Dr G. Grieve and G. Owens
CD-ROM produced by: Document Transformation Technologies Congress Organised by: Event Dynamics

IV according to ASTM specifications), taken from Lerch.[1] The measured values of mortar compressive strength were analyzed with the aid of the cement hydration equation[4-5] in order to determine the ultimate compressive strength as a function of SO_3 content (i.e. gypsum content) to determine its maximum ultimate strength, which gives the optimum gypsum content.

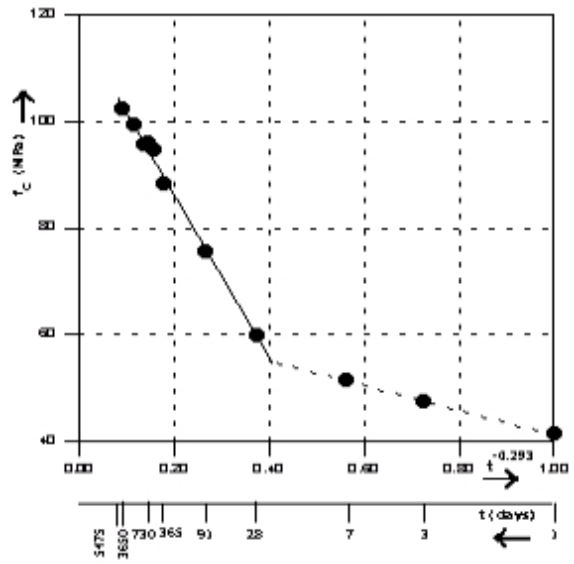

Figure 1. Compressive strength of concrete prepared with Portland cement as a function of hydration time. Portland cement 485 Kg/m^3. W/C = 0.27. Compressive strength of 100x200-mm cores taken from 2.0x1.2x1.35-m thick concrete blocks, cast, cured, and left exposed to elements in Toronto, Canada [measured values taken from Malhorta[8]]

1.1 Analyzing the data of Lerch concerning the measured values of mortar' s compressive strength of Portland cement type III and IV

According to the results given elsewhere,[4-5] the cement hydration equation is applicable to compressive strength. This is also shown by the example given in Figure 1 concerning the long-term compressive strength of concrete, where the first and second phase of hydration[4-5] are discernible. For this reason, the measured values of compressive strength obtained at different test ages constitute an established hydration criterion usable for analysis made with the aid of the cement hydration equation. In this case the cement hydration equation ($K = K_\infty \pm b*t^{-p}$),[4-5] takes the following form (Eqs. 1) by using the hydration criterion of mortar' s compressive strength (f_M).

$$f_M = f_{M\infty} - bt^{-p} \quad (1)$$

According to the results of previous studies[4-7] the paste hydration of Portland cement ends at the age of 15 years.

The measured values of compressive strength of cement type III and IV for different SO_3 content, taken from Lerch,[1] were analyzed with the aid of the cement hydration equation in Table 1 and 2, respectively. For this purpose, the hydration number (p) and the hydration equation (i.e. the compressive strength equations) of cement type III and IV examined (Tables 1-2) were determined according to the procedure given in previous studies[4-5]. The accurate values of compressive strength were further calculated (f_{Mcalc}) at different ages up to the final hydration at 5475 days (Tables 1-2) based on the defined hydration equations. The measured values of contraction and expansion of each cement used, taken from Lerch,[1] were also presented in Tables 1 and 2 in order to focus the discussion. The calculated values of cement III and IV mortar compressive strength (f_{Mcalc}) at the ages of 1, 3, 7, 28 and 5475 days were plotted in Figures 2 and 3 as a function of SO_3 content in order to localize the region of optimum SO_3 content. In the same figures the respective measured values were also plotted.

Table 1. Mortar' s compressive strength (f_M) prepared with Portland cement (type III, No 16823) with 1.0, 1.5, 1.9, 2.4, 3.0, 3.5 and 4.0 % SO_3. Curing temperature 70 F. [Measured values taken from Lerch[1]]

Hydration time (t) (days)	1	3	7	28	90	365	730	5475
Cement composition (%): C_3S = 70.0; C_2S = 8.0; C_3A = 12.5; C_4AF = 7.6; Fr. CaO = 0.21; MgO = 0.87; Na_2O = 0.05; K_2O = 0.25.								
1.0 % SO_3 content; Setting time (Vicat needle) hr.:min: Initial. 2:25; Final 9:50. Contraction at 1 yr.: 0.100; Expansion at 1 yr.: 0.007; Specific surface cm^2/g: 3280.								
F_{Mmeas} (Mpa)	3.94	30.65	47.80	59.33	60.74	58.42	-	-
Use of P/C program for the value pairs $f_{Mmeas} - t$	Hydration number p = 0.945 ; r = 0.99927; s = 0.653 (MPa) Hydration equation: $f_M = 62.4796 - 90.1377*t^{-0.0.945}$ (MPa), t≥3							
F_{Mcalc} (Mpa)	-	30.56	48.15	58.61	61.20	62.14	62.30	62.45
1.5 % SO_3 content ; Setting time (Vicat needle) hr.:min: Initial. 2:05; Final 6:00. Contraction at 1 yr.: 0.094; Expansion at 1 yr.: 0.006; Specific surface cm^2/g: 3440.								
f_{Mmeas} (Mpa)	12.30	39.09	53.57	64.25	67.35	65.73	-	-
Use of P/C program for the value pairs $f_{Mmeas} - t$	Hydration number p = 0.761 ; r = 0.99997; s = 0.114 (MPa) Hydration equation: $f_M = 69.7277 - 70.7328*t^{-0.0.761}$ (MPa), t≥3,							
f_{Mcalc} (MPa)	-	39.07	53.64	64.13	67.42	68.93	69.26	69.63
1.9 % SO_3 content; Setting time (Vicat needle) hr.:min: Initial. 2:00; Final 5:30 Contraction at 1 yr.: 0.081; Expansion at 1 yr.: 0.006; Specific surface cm^2/g: 3560.								
f_{Mmeas} (Mpa)	15.18	41.06	53.50	70.16	70.86	67.01	-	-
Use of P/C program for the value pairs $f_{Mmeas} - t$	Hydration number p = 0.617; r = 0.99025; s = 2.45 (MPa) Hydration equation: $f_M = 76.6946 - 71.2732*t^{-0.617}$ (MPa), t≥3							
f_{Mcalc} (MPa)	-	40.51	55.24	67.57	72.26	74.82	75.47	76.34
2.4 % SO_3 content; Setting time (Vicat needle) hr.:min: Initial. 2:40; Final 6:10 Contraction at 1 yr.: 0.078; Expansion at 1 yr.: 0.008; Specific surface cm^2/g: 3790.								
f_{Mmeas} (Mpa)	20.18	44.45	60.67	72.27	71.57	70.30	-	-
Use of P/C program for the value pairs $f_{Mmeas} - t$	Hydration number p = 0.767; r = 1.0; s = 0.006 (MPa) Hydration equation: $f_M = 78.3894 - 78.8229*t^{-0.767}$ (MPa), t≥3							
f_{Mcalc} (MPa)	-	44.45	60.67	72.27	75.89	77.53	77.89	78.28
3.0 % SO_3 content; Setting time (Vicat needle) hr.:min: Initial. 2:35; Final 6:25 Contraction at 1 yr.: 0.080; Expansion at 1 yr.: 0.004; Specific surface cm^2/g: 3970.								
F_{Mmeas} (Mpa)	23.13	45.41	61.72	68.82	71.28	70.51	-	-
Use of P/C program for the value pairs $f_{Mmeas} - t$	Hydration number p = 0.878; r = 1.0; s = 0.001 (MPa) Hydration equation: $f_M = 72.6544 - 71.481*t^{-0.0.878}$ (MPa), t≥3							
f_{Mcalc} (MPa)	-	45.41	59.71	68.82	71.27	72.25	72.44	72.62
3.5 % SO_3 content; Setting time (Vicat needle) hr.:min: Initial. 2:40; Final 6:40 Contraction at 1 yr.: 0.080; Expansion at 1 yr.: 0.007; Specific surface cm^2/g: 4160.								
F_{Mmeas} (Mpa)	22.85	44.99	56.17	68.75	65.52	70.02	-	-
Use of P/C program for the value pairs $f_{Mmeas} - t$	Hydration number p = 0.659; r = 1.0; s = 0.001 (MPa) Hydration equation: $f_M = 71.1238 - 53.9058*t^{-0.659}$ (MPa), t≥3							
f_{Mcalc} (MPa)	-	44.99	56.17	65.13	68.35	70.02	70.42	70.94
4.0 % SO_3 content; Setting time (Vicat needle) hr.:min: Initial. 3:00; Final 6:35 Contraction at 1 yr.: 0.081; Expansion at 1 yr.: 0.009; Specific surface cm^2/g: 4320.								
f_{Mmeas} (Mpa)	19.12	44.71	57.86	65.73	67.07	70.16	-	-
Use of P/C program for the value pairs $f_{Mmeas} - t$	Hydration number p = 0.994; r = 0.99985; s = 0.22 (MPa) Hydration equation: $f_M = 68.0226 - 69.5566*t^{-0.994}$ (MPa), t≥3							
f_{Mcalc} (MPa)	-	44.68	57.97	65.49	67.23	67.83	67.92	68.01

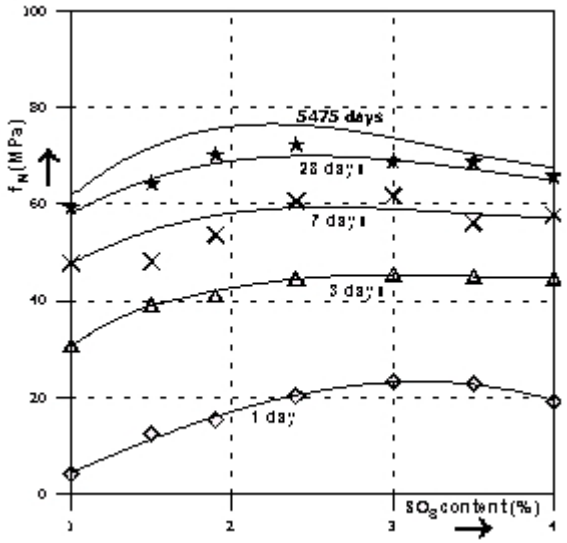

Figure 2. Mortar's compressive strength at 1, 3, 7, 28 and 5475 days as a function of SO_3 content [measured and calculated values taken from Table 1]

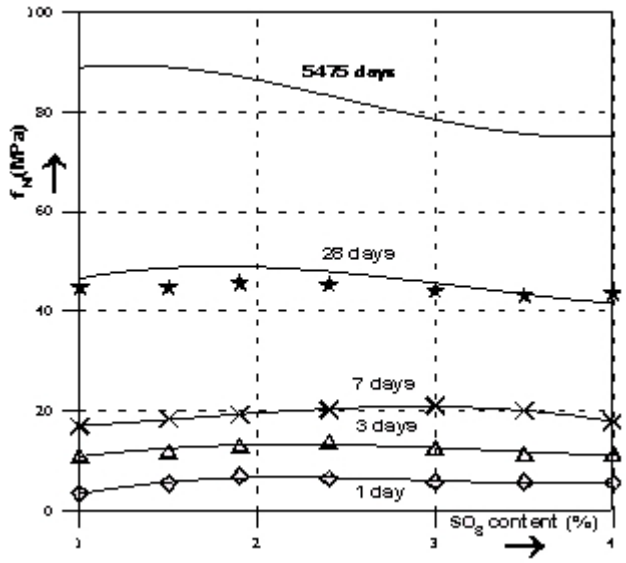

Figure 3. Mortar' s compressive strength at 1, 3, 7, 28 and 5475 days as a function of SO_3 content [measured and calculated values taken from Table 2]

Table 2. Mortar' s compressive strength (f_M) prepared with Portland cement (type IV, No 16890) with 1.0, 1.5, 1.9, 2.4, 3.0, 3.5 and 4.0 % SO_3. Curing temperature 70 F. [Measured values taken from Lerch[1]]

Hydration time (t) (days)	1	3	7	28	90	365	730	5475
Cement composition (%): C_3S = 28.0; C_2S = 53.5; C_3A = 5.1; C_4AF = 9.6; Fr. CaO = 0.44; MgO = 1.28; Na_2O = 0.32; K_2O = 0.02.								
1. 0 % SO_3 content; Setting time (Vicat needle) hr.:min: Initial. 3:40; Final 7:40 Contraction at 1 yr.: 0.110; Expansion at 1 yr.: 0.025; Specific surface cm^2/g: 2870.								
F_{Mmeas} (MPa)	3.37	11.04	16.94	44.71	67.0	75.08	-	-
Use of P/C program for the value pairs $f_{Mmeas} - t$	Hydration number p = 0.351 ; r = 0.9953; s = 3.077 (MPa) Hydration equation: $f_M = 104.8226 - 149.7846*t^{-0.351}$ (MPa), t≥7							
F_{Mcalc} (Mpa)	-	-	16.41	47.21	63.72	76.38	80.69	88.62
1.5 % SO_3 content; Setting time (Vicat needle) hr.:min: Initial. 3:50; Final 7:20 Contraction at 1 yr.: 0.100; Expansion at 1 yr.: 0.023; Specific surface cm^2/g: 3090.								
f_{Mmeas} (Mpa)	5.41	11.95	18.42	44.71	67.07	74.52	-	-
Use of P/C program for the value pairs $f_{Mmeas} - t$	Hydration number p = 0.343 ; r = 0.99408; s = 3.36 (MPa) Hydration equation: $f_M = 96.0874 - 152.5244*t^{-0.343}$ (MPa), t≥7							
f_{Mcalc} (MPa)	-	-	17.84	47.45	63.50	75.93	80.19	88.12
1.9 % SO_3 content; Setting time (Vicat needle) hr.:min: Initial. 3:40; Final 7:45 Contraction at 1 yr.: 0.093; Expansion at 1 yr.: 0.024; Specific surface cm^2/g: 3190.								
f_{Mmeas} (Mpa)	6.96	13.08	19.26	45.55	67.42	74.94	-	-
Use of P/C program for the value pairs $f_{Mmeas} - t$	Hydration number p = 0.346; r = 0.99458; s = 3.187 (MPa) Hydration equation: $f_M = 95.9474 - 151.4268*t^{-0.346}$ (MPa), t≥7							
f_{Mcalc} (MPa)	-	-	18.72	48.14	64.03	76.28	80.48	88.24
2.4 % SO_3 content; Setting time (Vicat needle) hr.:min: Initial. 2:40; Final 5:20 Contraction at 1 yr.: 0.094; Expansion at 1 yr.: 0.024; Specific surface cm^2/g: 3410.								
f_{Mmeas} (Mpa)	6.47	13.85	20.25	45.34	65.24	74.80	-	-
Use of P/C program for the value pairs $f_{Mmeas} - t$	Hydration number p = 0.459; r = 1.0; s = 0.005 (MPa) Hydration equation: $f_M = 85.4159 - 159.19*t^{-0.459}$ (MPa), t≥7							
f_{Mcalc} (MPa)	-	-	20.25	50.93	65.24	74.80	77.70	82.35
3.0 % SO_3 content; Setting time (Vicat needle) hr.:min: Initial. 3:30; Final 7:00 Contraction at 1 yr.: 0.097; Expansion at 1 yr.: 0.032; Specific surface cm^2/g: 3640.								
F_{Mmeas} (Mpa)	5.76	12.51	21.02	44.15	62.29	72.55	-	-
Use of P/C program for the value pairs $f_{Mmeas} - t$	Hydration number p = 0.592; r = 1.0; s = 0.0002 (MPa) Hydration equation: $f_M = 80.4996 - 261.3464*t^{-0.592}$ (MPa), t≥28							
f_{Mcalc} (MPa)	-	-	-	44.15	62.29	72.55	75.23	78.90
3.5 % SO_3 content; Setting time (Vicat needle) hr.:min: Initial. 3:30; Final 6:40 Contraction at 1 yr.: 0.107; Expansion at 1 yr.: 0.040; Specific surface cm^2/g: 3870.								
F_{Mmeas} (Mpa)	5.76	11.39	19.96	43.09	64.39	72.34	-	-
Use of P/C program for the value pairs $f_{Mmeas} - t$	Hydration number p = 0.925; r = 1.0; s = 0.007 (MPa) Hydration equation: $f_M = 75.3403 - 703.3154*t^{-0.925}$ (MPa), t≥28							
f_{Mcalc} (MPa)	-	-	-	43.09	64.39	72.34	73.76	75.10
4.0 % SO_3 content; Setting time (Vicat needle) hr.:min: Initial. 3:20; Final 6:50 Contraction at 1 yr.: 0.114; Expansion at 1 yr.: 0.045; Specific surface cm^2/g: 4060.								
f_{Mmeas} (Mpa)	5.48	11.25	17.86	43.52	63.97	72.90	-	-
Use of P/C program for the value pairs $f_{Mmeas} - t$	Hydration number p = 0.799; r = 1.0; s = 0.0002 (MPa) Hydration equation: $f_M = 77.2331 - 483.1456*t^{-0.799}$ (MPa), t≥28							
f_{Mcalc} (MPa)	-	-	-	43.52	63.97	72.90	74.74	76.74

2. DISCUSSION

1. From Tables 1-2 and Figures 2 and 3 it is shown that SO_3 content significantly influences the compressive strength of mortars prepared with cement type III. This finding is in agreement with the results given elsewhere.[5] The significant influence of SO_3 content appears at later ages when cement type IV was used. Hence, the optimum SO_3 content may be carefully monitored for each given cement and it strongly depends on its particular characteristics (i.e. composition, fineness etc.)

2. It is clearly shown from figures 2 and 3 that the SO_3 content needed to achieve the maximum compressive strength is not the same during the whole hydration period. This implies that the optimum SO_3 content determined according to ASTM C 543-84 (1-day strength) does not give the optimum SO_3 content needed to achieve the maximum ultimate strength at which ultimate porosity and shrinkage appear at their minimal values. In the same Figures is also shown that the region of the maximum ultimate strength appears between 1.9 and 2.4 % for cement III, and between 1.0 and 2.4 % SO_3 for cement IV. In these regions are also shown the values of contraction and expansion which are acceptable[1] (Tables 1-2). Consequently, the criterion of maximum ultimate compressive strength is preferable for determining the optimum SO_3 content, by using the cement hydration equation. The maximum ultimate strength can be determined with the aid of the cement hydration equation using compressive tests performed at several ages up to 28 days.[5] Better accuracy is obtained for the ultimate compressive strength, if more than 6 test ages belonging to the second phase of hydration[4-5] are used (e.g., for cement type I and III, the test ages of 3, 5, 8, 11, 14, 18, 22 and 28 days do belong to the second phase of hydration). For cement type II, IV and blended cement (with natural pozzolans, fly ash, silica fume, slags etc.), where the second phase of hydration (Figure 1) usually begins after 7 days, the test ages have to be extended after 28 days.

3. The method proposed for determining the optimum gypsum content of Portland cement leads to reliable results, and since only simple measurements are needed (mortar compressive strength), it can be used in any concrete laboratory without the aid of special equipment and special tests.

3. CONCLUSIONS

The SO_3 content significantly influences the compressive strength of Portland cement III at early and later ages. The influence of SO_3 content is significant for cement type IV at later ages, and especially, at ultimate strength.

The optimum SO_3 content can be determined using the criterion of the maximum ultimate compressive strength, analyzed with the aid of cement hydration equation. This method can be used in any concrete laboratory without the aid of special equipment and special tests since only simple measurements are needed (mortar compressive strength).

REFERENCES

[1] Lerch W. The influence of gypsum on the hydration and properties of Portland cement pastes, Proc. Am. Test. Mater., 46 1946, pp. 1252-1292.

[2] Sersale R., Cioffo R., Frigione G., Zenone F. Relationship between gypsum content, porosity and strength in cement, Cement and Concrete Research 21, No 1, 1991, pp. 120-126.

[3] Taylor H. F. W. Cement Chemistry, Thomas Telfold, London 1997, pp. 219.

[4] Sideris K. The cement hydration equation, Zement-Kalk-Gips, 12 (1993), Edition B, pp. E337- E344

[5] Sideris K., Sideris K. K. The Cement Hydration Equation and its Application to several Hydration Criteria according to the Literature, Proc. of the 10th Intern. Congress on the Chemistry of Cement, Göthenburg, Sweden, June 2-6, 1997, Volume 2, 2ii061.

[6] Sideris K. K. The stoichiometry in the paste hydration of C_3S, Alite and β-C_2S cured at 5, 25 and 50 °C. Journal of Advances in Cement Research, 2000, 12, No. 3, July, 113-120.

[7] Sideris K. K. Reliability of X-ray diffraction quantitative determination of the fraction unhydrated in the hardened paste of Portland cement, Journal of Advances in Cement Research, 2000, 12, No 3, July, 103-111.

[8] Malhotra V. M., Role of supplementary cementing materials in reducing greenhouse gas emissions. CANMET/Materials Technology Laboratory (1998), pp. 1-18.

DETERMINATION OF GYPSUM OPTIMUM CONTENT OF PORTLAND CEMENT USING THE HYDRATION CRITERION OF MAXIMUM ULTIMATE COMPRESSIVE STRENGTH

K. K. Sideris, P. Manita and K. Sideris

Laboratory of Building Materials, School of Engineering,
Democritus University of Thrace, Xanthi Greece.

K. K. Sideris

Dr. of Engineering, Laboratory of Building Materials, Civil Engineering Department
Democritus University of Thrace, P.O. Box 252 Xanthi, 671 00 GREECE
E-mail: kksider@civil.duth.gr

1. BIOGRAFICAL SCETCH

20-5-1969 : Born in Athens, Greece

1992 :	M.Sc. in Civil Engineering
1992 - 1994:	Military Service.
1992-1996 :	Ph. D. candidate of Democritus Univercity of Thrace
1997-1998:	Research assistant at the laboratory of building materials, Democritus University of Thrace
1998:	Lecturer at the lab. Of Building Materials, Democritus University of Thrace

2. PROFESSIONAL EXPERIENCE

I have worked in several construction offices in Athens as a consultant in terms of concrete technology and durability aspects. During my military service, I have worked in the construction of a military airport in Greece (buildings, motorways, shelters etc).

3. TEACHING AREA

Since 1997 I am teaching several lessons at the civil engineering department in the areas of Building Materials, Concrete Technology and Concrete Durability

4. RESEARCH INTERESTS

My research interests are in the area of cement hydration (empacized in the hydration of blended cements), concrete technology and concrete durability.

MICROSTRUCTURE AND THE DEVELOPMENT OF STRENGTH IN RPC CURED AT VARIOUS TEMPERATURES

Shin-ichi Igarashi[1], Akio Watanabe[1] and Mitsunori Kawamura[1]

[1] Department of Civil Engineering, Kanazawa University, Kanazawa, JAPAN.
E-mail: igarashi@t.kanazawa-u.ac.jp

ABSTRACT

Reactive Powder Concretes (RPCs) with common ingredients were produced by a simple processing method, in which a high pressure was not applied. Mechanical properties of the RPC cured at various temperatures were investigated with the emphasis on their relation to characteristic microstructure and hydration products. In spite of a relatively high value of 0.21 as a water/binder ratio for RPC, a high compressive strength of about 250MPa was attained by simple heating at 200°C in an oven under atmospheric pressure. However, elevating the curing temperature to 300°C remarkably decreased the strength. Crystalline products such as xonotlite and α-C_2SH were identified in the specimens autoclaved at 300°C. Curing at a high temperature decreased capillary porosity in the RPC mixtures. It was suggested that further reduction of the capillary porosity for coarse pores was necessary to obtain a higher strength when the RPC was cured under 200°C. The reduction in strength in the autoclaved RPC may result from the increase in porosity for much finer pores, which were due to the formation of the crystalline products with high density. The processing on post-setting heating must be optimised for obtaining an ultra high strength in RPC.

1. INTRODUCTION

RPC (Reactive Powder Concrete) is an ultra high strength concrete, of which mix proportions are quite different from those of ordinary high strength concretes. The ultra high strength has been attained on the basis of the principles of an extremely low water/binder ratio, homogenisation of microstructure, dense granular packing of particles and post-setting heating [1]. These principles are easily attained by several ingenious methods in selecting materials and processing for RPC. RPC also has the great advantage of being cast and cured at practical construction site conditions. Recently, the RPC has been widely available around the world [2] as a commercial product. RPC may be one of the most promising high performance concretes in the 21st century.

However, when a RPC is produced with local common materials, a suitable mix proportion and a processing method must be carefully designed to obtain an ultra high performance concrete. It is also necessary to rigorously choose appropriate ingredients available at the local sites. However, information available for mix proportions and suitable processing methods of RPC is limited. For example, it is pointed out that post-setting heating is necessary to obtain an ultra high strength greater than 200MPa. Such a thermal treatment for cementitious materials usually aims at growing hard crystalline products, which are considered to increase strength of the materials. This situation is very similar to the manufacture of synthesized silicate building materials. However, the process and reactions in the treatments are so complex that a universal optimum heating method to enhance the strength of the synthesized CSH systems has not been proposed. Performances of the hardened mixture depend on the types and quantity of reaction products of CSH. Many factors such as sizes of siliceous powder, the initial CaO/SiO_2 ratios and heating conditions sensitively affect mechanical properties of the mixture [3]. A specific mix proportion recommended for a RPC may not always

Proceedings of the 11th International Congress on the Chemistry of Cement (ICCC)
'Cement's Contribution to the Development in the 21st Century'
Hosted by: The Cement and Concrete Institute of South Africa
CD-ROM produced by: Document Transformation Technologies
11 - 16 May 2003, Durban, South Africa
ISBN Number: 0-9584085-8-0
Editors: Dr G. Grieve and G. Owens
Congress Organised by: Event Dynamics

result in the designed ultra high strength if ingredients with different qualities are used. Therefore, it is important to establish the way of designing mix proportions of RPC with desired performances, taking into account variable properties of each ingredient and curing conditions. Furthermore, it is also necessary to understand the sensitive dependence of properties of RPC on variation of ingredients.

The purpose of this study is to reveal effects of the amounts and types of siliceous materials used in RPC on the performance of the mixture. Effects of the addition of silica fume, fine quartz powder and silica sand on the microstructure of RPC were investigated in relation to the development of the compressive strength of RPC cured at different temperatures. Characteristics of microstructure in RPC at various curing temperatures were examined by the quantitative scanning electron microscopy-backscattered electron (SEM-BSE) image analysis for capillary porosity and X-ray diffraction (XRD) patterns for crystalline products. Roles of the siliceous materials such as silica fume and quartz powder in the formation of dense microstructure were discussed in relation to the types of CSH products and characteristic pore structures at various curing temperatures.

Table 1. Mix proportions of cement paste and RPC

	W/B	Silica Fume / Cement	Silica Fume＋Quartz Powder / Cement	Silica Sand+Quartz Powder / Binder	SP wt%Binder
Cement Paste	0.21	0.24	0.24	0	5
	0.21	0.325	0.325		5
	0.21	0.413	0.413		5
RPC-Qz	0.21	0.325	0.62	0.223	5
RPC-Qz/SS	0.21	0.325	0.62	1.3	5

Qz : Quartz powder, SS:Silica Sand, SP: Superplasticizer

Table 2. Curing regimens for cement pastes and RPC

Curing Temperature(°C)	**Age (Days)**						
	1	2	3	4	5	6	7
20	**Placed at room temperature**	**in water at 20°C**					
90		**in water at 20°C**		**in water at 90°C**			
200		**in water at 20°C**		**in oven at 200°C**			
300		**in water at 20°C**		**autoclaving at 300°C**			

2. EXPERIMENTAL

2.1 Materials and Mix Proportions of RPC

The cement used was ordinary Portland cement (C_3S=52, C_2S=24, C_3A=9, C_4AF=9%). A commercial silica fume (specific surface area=20m^2/g, Ig.Loss=1.85%, SiO_2=90.79%, density=2.2g/cm^3) was used with the combination of polycarboxylic acid type superplasticizer. The dosage of the superplasticizer was 5% by weight of binders. It was confirmed that no segregation was observed during mixing and subsequent setting periods. The size of silica sand used as a coarse sand ranged from 100 to 300μm. Crushed quartz with the mean size of 5.9μm was also used as a reactive siliceous powder (Ig.Loss=0.52%, SiO_2=79.6, Al_2O_3=11.28, Fe_2O_3=1.09, TiO_2=0.32, CaO=0.93, MgO=0.37, K_2O=3.31, Na_2O=2.00%).

The mix proportions of the RPC mixtures are presented in Table 1. The water/binder ratio of mixtures was 0.21. The ratio of silica fume to cement varied from 0.24 to 0.413. The ratio of the silica sand and the quartz powder to the binder (i.e. cement and silica fume) was 1.3. The ratio of silica fume and quartz powder to cement was 0.62. These three factors relation to silica and lime content are determinants for the density of granular packing and types of reaction products formed

at various temperatures. In this study, these ratios were established based on the pioneering works by Richard and Cheyrezy [1] and Bonneau et al[4].

2.2 Tests and Image Analysis

2.2.1 Compressive strength

Two types of cylinder specimens with 50mm diameter and 100mm height, and 20mm in diameter and 40mm in height were prepared. The smaller cylinder specimens were used in the autoclaving curing regimen at 300°C. In order to obtain workable mixtures, the total mixing time was changed about 20 minutes [4]. The specimens to be cured at 20, 90 and 300°C were demolded at 24 hours after casting, and then placed in water at 20°C for the subsequent 48 hours. For specimens to be cured at 200°C, in order to prevent them from drying at a high temperature under atmospheric pressure, the specimens with moulds were put in water directly for two days. After the initial water curing until the age of 3days, each specimen was stored under four different curing regimens. The curing regimens are summarized in Table 2. Compressive strength tests were conducted at the age of 3, 4 and 7days.

2.2.2 X-ray diffraction

Small portions of concrete were taken from RPC and cement paste specimens after the completion of compressive strength tests. They were finely ground with a mill. XRD patterns for the powders were obtained. The Cu-Kα radiation was used in the diffractometer.

2.2.3 Capillary porosity measurement by the quantitative SEM-BSE image analysis

The same cylinder specimens as the specimens for the compressive strength test were prepared. They were also cured under the same regimens as described previously. At prescribed ages, slices with about 10mm thickness were cut out from the middle portion of the specimens. They were immersed in ethanol, and then impregnated with epoxy resin. After the resin hardened at room temperature, the slices were polished with SiC papers and diamond slurry.

The polished surfaces were examined using the SEM equipped with a quadruple backscatter detector. BSE images were acquired at the magnification of ×500. Each image consists of 1148×1000 pixels. The size of one pixel is about 0.22×0.22μm. After the binary segmentation, the number of pixels corresponding to unhydrated cement particles and pores were tallied. Pore size distributions for coarse capillary pores were obtained by calculating equivalent diameters of pores

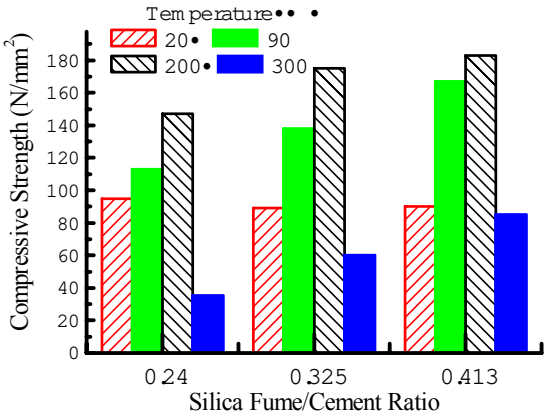

Figure 1. Compressive strength of cement pastes with various silica fume/cement ratios (Age=7days)

[5,6]. The measured size range of pores in the image analysis is much greater than that determined from mercury intrusion porosimetry (MIP). However, the image analysis technique can give

quantitative information of large capillary pores, which are not correctly resolved in the MIP method [6].

3. RESULTS

3.1 Compressive Strength

Figure 1 shows compressive strength of cement pastes with various silica fume/cement ratios. Silica fume contents did not substantially affect the compressive strength in pastes that were continuously cured in water at 20°C. However, if cement paste specimens were cured at 90°C, the higher the silica fume/cement ratio resulted in the greater compressive strength. The pozzolanic reaction of silica fume is dominant in the development of strength at 90°C. The paste specimens cured at 200°C exhibited greater strength than at 90°C. However, the rate of increase in compressive strength was dependent on the ratio of silica fume to cement. The compressive strength of the paste with the silica fume/cement ratio of 0.413 did not appreciably increase even when the curing temperature was elevated from 90 to 200°C.

The strength of cement paste cured at 200°C was greater than those cured at 90°C, as mentioned above. However, cement pastes cured at 300°C exhibited far lower compressive strength. The strength of some cement pastes cured at 300°C was even smaller than the pastes cured at 20°C. However, it should be noted that the reduction in strength by autoclaving was also dependent upon the silica fume content in cement pastes. Some cement pastes cured at 300°C exhibited almost the same strength as that at 20°C when they contained a greater amount of silica fume.

Comparisons in compressive strength between the cement pastes and RPC containing siliceous materials are shown in Figure 2. When the specimens are continuously cured in water at 20°C, there is little difference in compressive strength between cement pastes and RPC. Namely, quartz powder and silica sand did not play a role in increasing strength. However, when cured at 90 and 200°C, the RPCs exhibited greater strength than the corresponding cement pastes. Particularly, the higher the curing temperature except 300°C, the greater differences in the strength between pastes and RPC. The compressive strengths of RPC with the siliceous materials at 300°C were smaller than those at 90 and 200°C. However, the reduction in strength due to autoclaving in paste specimens was reduced in RPC to some degree. The strength of autoclaved RPCs was greater than the corresponding cement pastes. It is found from Figures 1 and 2 that the strength of cement pastes and

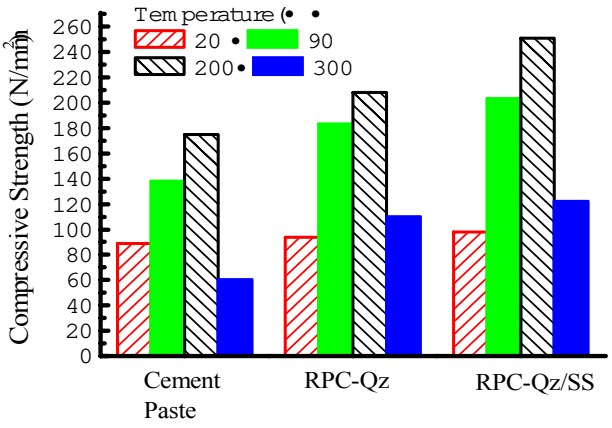

Figure 2. Comparison of compressive strength between cement pastes and RPCs (Age=7days)

RPCs was dependent on the content of silica, especially in the specimens cured at the high temperatures.

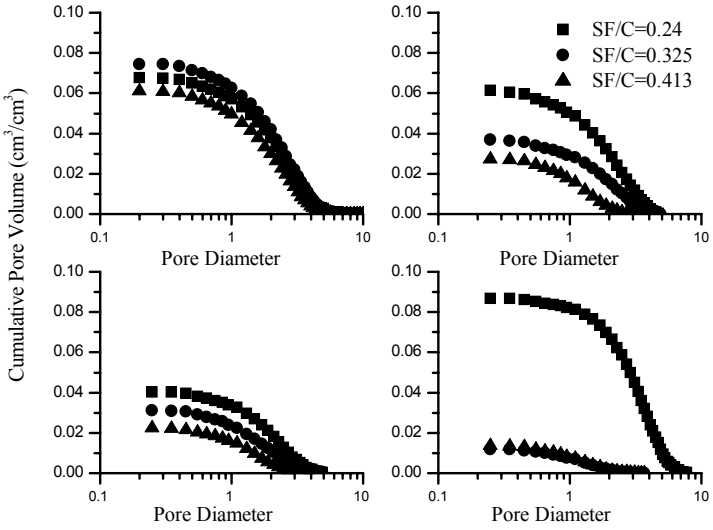

Figure 3. Pore size distributions of cement pastes cured at different temperatures (Age=7days)

3.2 Pore Size Distributions

Pore size distributions of cement pastes cured at various temperatures are shown in Figure 3. It should be noted that there were coarse capillary pores even in mature cement pastes with an extremely low water/binder ratio of 0.21. When cured at 20°C, the porosity of cement paste was not greatly influenced by silica fume content. Namely, the silica fume content did not affect the formation of coarse capillary pore structures. However, in the cement pastes cured at a high temperature of 90°C, the porosity of cement pastes decreased. Furthermore, the greater the silica fume content, the lower the porosity of coarse pores. At 200°C, the porosity was further decreased, but differences in porosity between different silica fume: cement ratios were found.

The pore structures formed by autoclaving at 300°C were considerably different from those formed

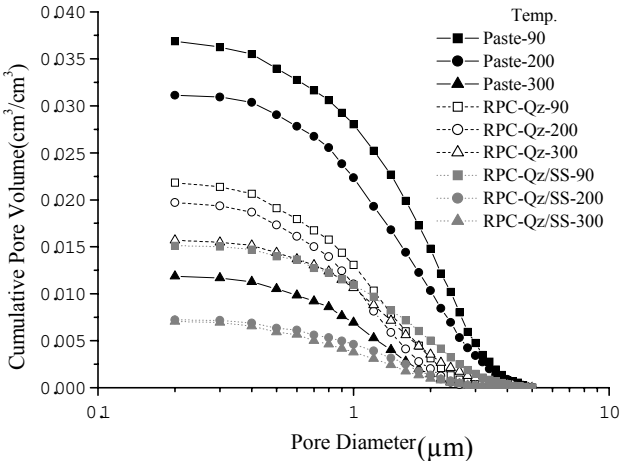

Figure 4. Comparison of pore size distributions between cement pastes and RPCs (Silica fume /Cement Ratio=0.325, Age=7days)

at lower temperatures. The cement pastes with high silica fume contents of 0.325 and 0.413 had little porosity for coarse pores. A threshold diameter of pores in the cement pastes was greatly decreased by heating at 300°C. Autoclaving is very effective to develop dense microstructure for these cement pastes. However, the cement paste with a silica fume content of 0.24 exhibited a

greater porosity than the one without any heating treatment. Such a heat treatment resulted in an increase in coarser pores in the cement paste with a less silica fume content. It is found that the effectiveness of autoclaving in the reduction in porosity was dependent on the content of silica fume in mixtures.

Pore size distributions for both RPCs and cement pastes are shown in Figure 4. From Figure 4, threshold diameters of pores are found to be reduced by the addition of quartz powder and silica sand. It is also found that the total porosity was decreased by the addition of siliceous materials in the specimens cured at 90 and 200°C. However, the porosity of RPC autoclaved at 300°C was almost the same as that of the cement paste. Figures 3 and 4 clearly show that heat treatments greatly changed porosities of RPC [7]. However, heat treatments should be carefully optimised for reducing porosity.

3.3 Identification of Reaction Products by XRD Patterns

XRD patterns for cement pastes are given in Figure 5. The diffraction patterns do not change with the ratio of silica fume to cement in the cement pastes cured at 90°C. Crystalline products such as calcium hydroxide are not present in the pastes. Addition of silica fume had no substantial effects on the types of hydration products as far as cured at 90°C. XRD patterns for cement pastes cured 200°C are almost the same as those at 90°C. However, slight peaks of 11Å tobermorite were detected in cement pastes cured at 200°C.

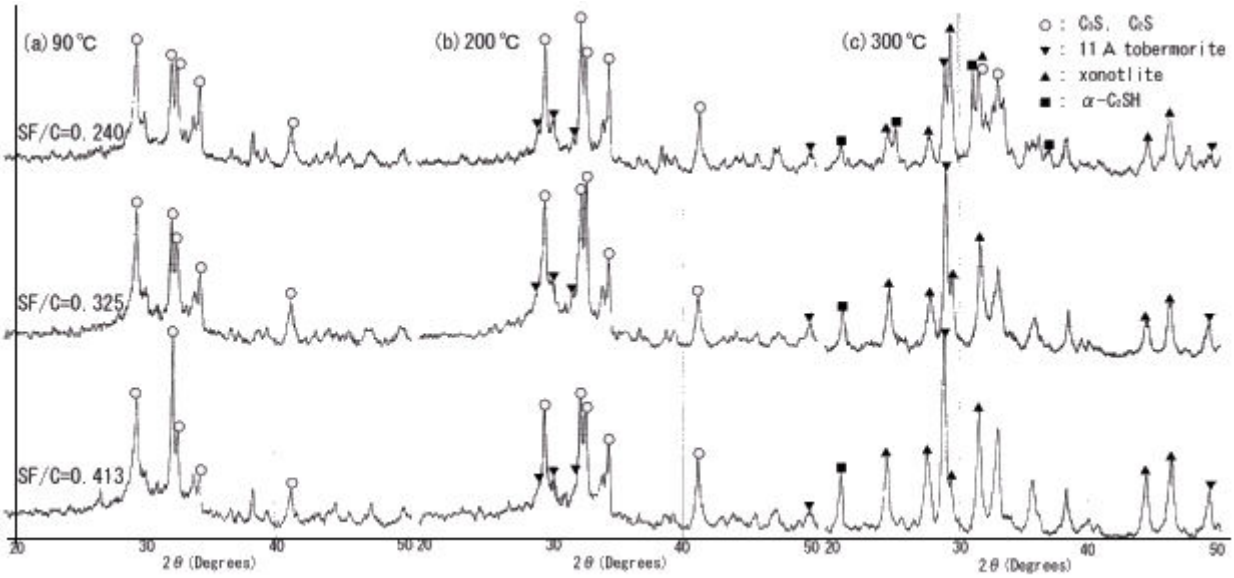

Figure 5. X-ray diffraction patterns of cement pastes at various curing temperatures (Age = 7 days)

When cement pastes were autoclaved at 300°C, the broad background around 2θ=30° was not so remarkable as cured at 90 and 200°C. This result suggests that parts of the amorphous CSH products transferred into crystalline ones. Actually, more peaks were present in the pastes cured at 300°C, compared with the pastes cured at 90 and 200°C. At a low silica fume to cement ratio of 0.24, xonotlite, α-C_2SH and tobermorite were identified in the autoclaved paste. Namely, these three crystalline CSH products with different Ca/Si ratios coexisted in the pastes. In the cement pastes with higher ratios of silica fume to cement, conspicuous xonotlite was found. This result implies the increase in the initial amount of amorphous silica such as silica fume led to the formation of xonotlite at 300°C. On the other hand, the increase in the initial amount of amorphous silica seems to reduce the intensity of peaks of α-C_2SH, as found in Figure 5(c). It is found from Figure 5 that differences in the initial content of silica fume results in different reaction products.

The addition of quartz powder and silica sand also affected the formation of crystalline products at high curing temperatures, as shown in Figure 6.

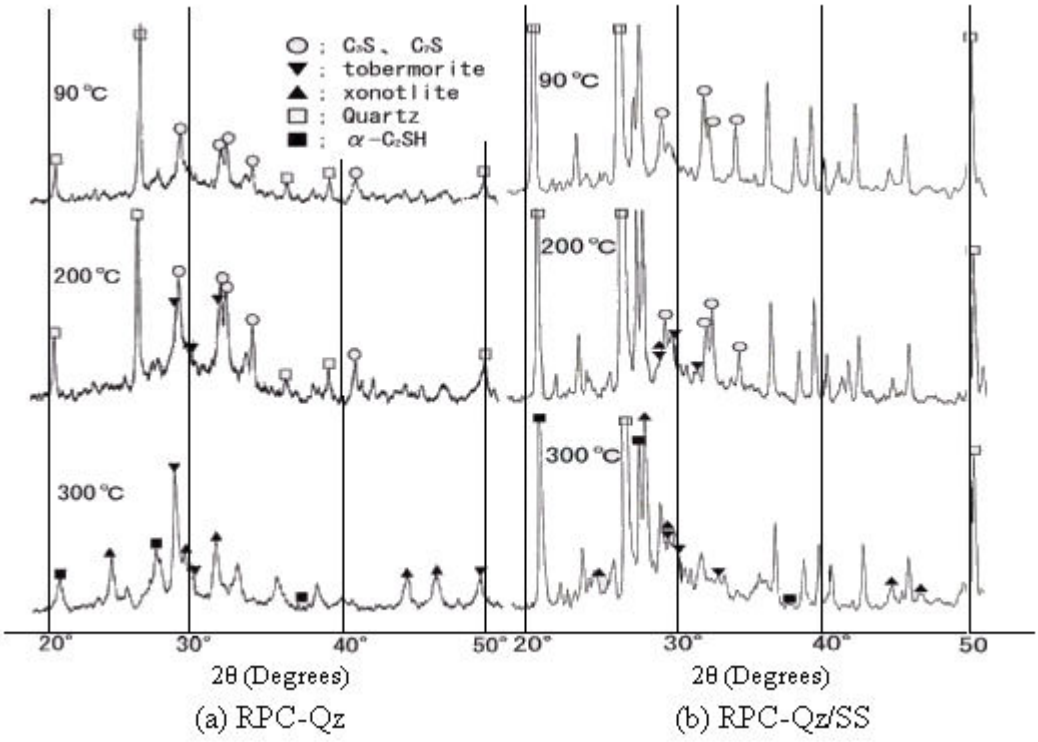

Figure 6. X-ray diffraction patterns of RPCs (Silica fume/cement ratio =0.325, Age=7days)

Those materials are expected to supply additional silica growing an optimum content of crystalline products. The intensity of tobermorite peaks in RPC with quartz powder cured at 200°C was not so conspicuous as in the corresponding cement paste cured at 200°C. At 300°C, all the X-ray diffraction peaks of quartz completely disappeared in the quartz powder-containing RPC. Quartz powder was fully consumed as a source of silica in the reaction with lime at a high temperature. This consumption of the silica from quartz, on the other hand, also contributes to the formation of amorphous CSH products judging from the fact that the background around 2θ=30° was slightly higher than in the paste cured at 300°C. Production of amorphous CSH products was also appreciable in RPC with quartz powder and silica sand. As shown in Figure 6, the background around 2θ=30° was raised further. It is found from Figures 5 and 6 that the addition of crystalline silica of quartz powder and silica sand promoted the growth of crystalline CSH products as well as amorphous CSH. Supply of so much silica from crystalline and amorphous original materials may result in different microstructures from the pastes without additional silica materials.

4. DISCUSSION

Post setting heating may be the most crucial treatment in enhancing strength at an extremely low water/binder ratio in RPC. The heating treatment is expected to reduce porosity of the system due to the formation of dense crystalline products.

Figure 7 shows the relationship between compressive strength and porosity obtained by the SEM-BSE image analysis in RPC with quartz powder and silica sand. A good correlation exists between both. It is found from Figure 7 that the strength of RPC with an extremely low water/binder ratio closely correlates with the porosity of large capillary pores, which were not occupied by reaction products. Therefore, in order to further increase the strength, it is necessary to remove those large pores from the system. However, it should be noted that the RPC cured at 300°C exhibited an extremely low strength whereas its porosity was quite low at 7days. Variation of porosity is closely

related not only to the degree of reaction but also to the types of reaction products. Therefore, such a dependence of compressive strength on the porosity should be also discussed from the viewpoint of effects of temperatures on the types of reaction products.

4.1 Strength Development of RPC Cured at 20°C and 90°C

The strength of RPC cured at 20°C is not so different from the strength of conventional high strength concrete. However, the mixture of RPC had an optimised granular packing. In other words, the homogeneity of constituent phases in RPC was also improved by granular packing without coarse aggregate. Nevertheless, the dense packing and homogeneity did not increase the strength in the RPC cured at 20°C. Therefore, it is realized that heating is the most important process to obtain an ultra high strength in RPC [7]. The homogenisation in terms of granular packing only had the secondary effect on the evolution of strength in RPC as far as cured at a room temperature.

Curing at 90°C in RPC increased strength, as shown in Figure 2. The increase in strength with curing temperature is found to be due to the lower porosity in RPC cured at 90°C when we compared it to the porosity of RPC cured at 20°C (Figure 3). Furthermore, as shown in Figures 5 and 6, X-ray diffraction peaks of calcium hydroxide crystals completely disappeared in the mixture cured at 90°C. Therefore, it is clearly found that the increase in compressive strength resulted from the acceleration of hydration of cement and pozzolanic reaction of silica fume [1]. The greater strength of RPC with quartz powder and silica sand than the paste is also derived from the reduction in porosity, as shown in Figure 4. However, quartz powder may be generally stable and inert at 90°C so that, probably, it does not take part in chemical reactions. Further research is necessary for the reduction in porosity when quartz powder is included in the system.

4.2 Strength Development of RPC Cured at 200 and 300°C

Curing at 200 and 300°C produced crystalline products in addition to the acceleration of chemical

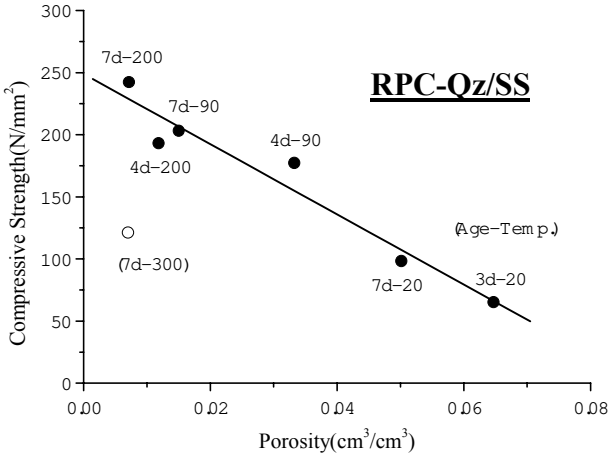

Figure 7. Compressive strength vs. capillary porosity determined by the SEM-BSE image analysis (Silica Fume/Cement =0.325)

reactions in the system. In CaO-SiO_2-H_2O systems, the amount and size of siliceous materials affect the process of the production of CSH. Namely, the final products of CSH depend on the reactivity and surface area of silica initially available for reactions. Generally, if the silica is crystalline, then tobermorite is easy to grow in the system at a high temperature of 200 and 300°C. When much amorphous silica is supplied to the reaction at hydrothermal conditions, the system prefers to transfer amorphous CSH gel into xonotlite as a final product [8]. Those products with different

CaO/SiO_2 ratios are also different in morphology and density. Therefore, the porosity of the system is influenced by the type of reaction products.

11Å tobermorite was identified as a main crystalline product in the cement paste cured at 200°C. This situation was not changed by the addition of fine quartz powder. Furthermore, the addition of quartz power and silica sand raised background around $2\theta=30^\circ$ in XRD patterns. This rising of the background may be due to the formation of amorphous CSH products. Taking account of the characteristics of hydration products and the pore size distributions obtained by the BSE image analysis, it may be concluded that the densification due to coexistence of the crystalline tobermorite with large amounts of CSH gel led to an ultra high strength of about 250MPa. A suitable mixture of well and poorly crystalline materials appears to lead to an ultra high strength in RPC cured at a high temperature of 200°C.

On the other hand, curing at 300°C reduced the strength significantly. The porosity for coarse pore was decreased remarkably in the RPCs with higher ratios of silica fume to cement. As found from XRD patterns of Figure 5, regardless of the ratio of silica fume to cement, X-ray diffraction peaks of α-C_2SH, 11Å tobermorite and xonotlite were detected in cement pastes. In particular, the peaks for xonotlite are conspicuous in the RPCs cured at 300°C. Even when fine quartz powder was incorporated into the RPCs, no remarkable differences in XRD patterns were found. Originally, the fine quartz powder is used to form reaction products with a low density at a high temperature. However, the addition of the quartz powder in the mixtures effectively failed to form crystalline materials, which contributed to the increase in strength. It is also pointed out that the addition of much silica is necessary so that α-C_2SH is not deposited in hydrothermal reactions of CaO-SiO_2 systems for producing a high strength cement system [9]. Feldman and Beaudoin [10] showed that formation of α-C_2SH with a high density resulted in the increase of porosity in the system. They also pointed out that poor bonding of the crystalline products resulted in low strength of the cement mixtures. Differences in the initial silica fume content in mixtures seem to relate to differences of amounts of silica available for reactions. In the RPC with insufficient silica fume in this study, so much α-C_2SH had been produced that the strength was decreased.

It should be also noted that the formation of xonotlite with a high density in the RPCs also increases the porosity of the paste. On the other hand, as shown in Figures 5 and 7, the RPCs cured at 300°C had a quite low porosity for coarse pores. Taking account of the low strength of the RPCs with a low porosity for coarse pores, the silica contents in the mixtures were not appropriate for increasing strength by autoclaving in this study. Such an improper combination of mix proportions with thermal treatments resulted in the formation of α-C_2SH with a high density so that porous pore structures were formed in the systems at a level of microscopic scale at least less than the resolution of image analysis of 0.22μm.

It is pointed out that the formation of crystalline products such as xonotlite contributes to an ultra high strength of RPC[1]. As reported by Richard and Cheyrezy [1], an ultra high strength of 800MPa was obtained for the RPC treated at high temperature of 250-400°C. Actually, the effectiveness of xonotlite has been also recognized in the synthesized CSH. Simple heating for RPC may make up hydrothermal conditions for producing xonotlite [1]. However, as mentioned above, the formation of xonotlite does not always increase the strength of RPC in this study. An excess formation of xonotlite should be avoided to obtain RPCs with an ultra high strength. It is necessary to establish appropriate curing regimen for a RPC, corresponding to its mix proportion and the property of ingredients.

5. CONCLUSIONS

- A RPC with an ultra high strength of 250MPa was obtained by heating at 200°C in a combination of relatively high water/binder ratio of 0.21 and common siliceous materials.
- A high strength of RPC at 90°C resulted from the reduction of porosity due to the acceleration of hydration and pozzolanic reaction. There were no crystalline products which contributed to the increase in strength.
- Heating at 200°C without applying a pressure led to the formation of a crystalline product of 11Å tobermorite. The coexistence of the crystalline materials with much CSH gel resulted in an ultra high strength.
- Autoclaving at 300°C drastically decreased the strength of RPC. Deposition of high density products of xonotlite and α-C_2SH may give rise to the formation of porous microstructures at a microscopic scale less than the resolution of the image analysis. Formation of much xonotlite should be avoided for producing RPCs with an ultra high strength.
- Large capillary pores still existed even in the mature RPC with an extremely low water/binder ratio. There was a good correlation between the strength of RPC and the porosity for large pores.
- Post-setting heating as a curing method is not always effective for increasing strength of RPC. The processing, especially heating temperature must be carefully optimised for obtaining an ultra high strength in RPC with variable ingredients.

ACKNOWLEDGMENT

This research project was partially supported by the Japan Society for the Promotion of Science, Grant-in-Aid for Scientific Research (C), #10650449, 1998-2001. The authors also gratefully acknowledge the financial support by the Japan Cement Association.

REFERENCES

[1] Richard, P. and Cheyrezy, M.: Composition of reactive powder concretes, Cement and Concrete Research, Vol.25, No.7, 1995, pp.1501-11.
[2] http://www.ductal.com/
[3] Taylor, H.F.W.: Cement Chemistry, Thomas Telford, London, 1997.
[4] Benneau, O. et al.: Mechanical properties and durability of two industrial reactive powder concrete, ACI Materials Journal, Vol.94, No.4, 1997, pp.286-290.
[5] Lange, D.L., Jennings, H.M. and Shah, S.P.: Image analysis techniques for characterization of pore structure of cement-based materials, Cement and Concrete Research, Vol.24, No.5, 1994, pp.841-853.
[6] Diamond, S. and Leeman, M.E.: Pore size distributions in hardened cement paste by SEM image analysis, Microstructure of Cement-Based Systems/Bonding and Interfaces in Cementitious Materials, MRS Symposium Proceedings, Vol.370, 1994, pp.217-226.
[7] Cheyrezy, M., Maret, V. and Frouin, L.: Microstructural analysis of RPC (Reactive Powder Concrete), Cement and Concrete Research, Vol.25, No.7, 1995, pp.1491-1500.
[8] Handbook of Hydrothermal Science, Gihodo, Tokyo, 1997 (in Japanese).
[9] Mindess, S.: Relationships between strength and microstructure for cement-based materials: An overview, Very High Strength Cement-based materials, MRS Symposium Proceedings, Vol.42, 1985, pp.53-68.
[10] Feldman, R.F. and Beaudoin, J.J.: Microstructure and strength of hydrated cement, Cement and Concrete Research, Vol.6, No.3, 1976, pp.389-400.

GRINDING AIDS:
A STUDY ON THEIR MECHANISM OF ACTION

Bravo Anna, Cerulli Tiziano, Giarnetti Mariagrazia and Magistri Matteo

Mapei S.p.A., via Cafiero 22, 20158 Milano, Italy. E-mail: dam_caf@mapei.it

ABSTRACT

Most of the recent works [1] on cement additives focused the attention on their effectiveness on cement performances in terms of mechanical and rheological properties. Our mission has been to monitor the interface between the components of cement additive and the cement grain surface, in the presence of small (cement grinding) and large (cement hydration) amount of water.

We assembled data concerning mill output, specific surface area, particle size analysis, electrophoretic mobility and particularly microstructures of hydrated cement products investigated by Environmental Scanning Electron Microscopy - Field Electron Gun (ESEM – FEG). Even if this work is still in progress, we can make a reliable hypothesis about the pre-hydration of clinker during grinding process, which is significantly influenced by the presence of the active components (alkanolamines and glycols) of cement additive, or better of Grinding Aids (GA).

1. INTRODUCTION

The introduction of GA, started more than 50 years ago, has as its ultimate task the prevention of cement particle re-agglomeration during and after the milling process [2]. What makes GA application even more desirable is their significant effects on mechanical properties of cement, whose particle size distribution narrows and shifts towards smaller diameters [3].

Their influence on cement chemico-physical behaviour has been attributed to the reduction of surface energy forces generated on cement grains during comminution. According to this thesis [4], GA are constituted of polar organic compounds such as alkanolamines, which arrange their dipoles so that they saturate the charges on the newly formed particle surface, reducing re-agglomeration. Nevertheless, this kind of additive is efficient even at very low dosage (< 500 ppm), which cannot give a complete cover on cement particle surfaces, that is for a complete screening of the free charges. Moreover, it cannot explain their effects on subsequent mechanical properties of cement paste.

Various research groups followed different approaches to go further in the interpretation of the GA action. Some authors [5] have been involved in the analysis of alkanolamines and glycols based GA, extracted from dry cement by different technics. Besides the intrinsic difficulty in the extraction of these polar compounds once they interact with cement, it has been hypothesized [5*(a)*] that either an irreversible physical adsorbtion or a chemical interaction with cement salts occurs, favoured by high temperatures (100-120°C) reached inside the mill during grinding.

Much more interest has been shown on the influence of these alkanolamines or glycols as admixtures on cement hydration and strength development. It is well known [6], for example, and well accepted that alkanolamines (especially TriIsoPropanolAmine - TIPA) interact preferentially

with iron based phases of cement [6*(b)*] . In the same way the effect of TriEthanolAmine (TEA) on cement setting time is still debated [1*(a)*,7].

Our approach to the study of the GA mechanism of action took advantage of our experience of cement behaviour during hydration and tried to focus the attention on the morphological effects of GA on cement.

2. EXPERIMENTAL

2.1 Materials

Beside the reference Portland clinker describe before, an OPC type I cement were used, whose chemical composition, expressed in element oxides, is reported in Table 3.

Table 3. Chemical Composition of the Reference Portland Clinker

SiO_2	Al_2O_3	Fe_2O_3	CaO	MgO	SO_3	Na_2O	K_2O
20.98	4.64	1.89	63.79	2.05	3.33	0.20	0.84

For Zeta potential measurements we also utilized other commercial cements: a Fondue, a white Portland cement and a ferric clinker.

Alkanolamines and glycols used in our experiments are commercial products which have been added by a sprinkler inside the mill or mixed with water before addition to cement in the concentrations indicated. The PolyCarboxylic Acid Esters (PCAE) superplasticizer is a laboratory test product (MW 50.000 D), while the poly-Naphtalene-Sulphonate (NS) comes from our production.

2.2 Chemical analysis (ICP-AES)

The sample is subjected to acid attack with concentrated HCl in a Parr bomb, using a microwave oven. The solution is filtered, diluted and analyzed by atomic emission spectroscopy on a Varian Liberty 220 ICP-AES.

2.3 Grinding process

For grinding experiments a laboratory mill type Bond for clinker grindability test has been used: rounds/minute = 70; grinding media = 32,5 kg (balls Ø = 17-40 mm). 2 kg of clinker is loaded after comminution to a grain diameter < 3 mm.

2.4 Blaine specific surface area measurements

After 30, 45 and 90 minutes a sample of 5 g of clinker is taken from the mill and its specific surface area is measured according to EN 196/6 (Blaine method).

2.5 BET surface area measurements

For the measurement of BET surface area of ground clinker powder a COULTER SA 3100 porosimeter has been utilized. Sample weight is 10 g and adsorbate gas is an He/N_2 mixture.

2.6 Alpine mechanical sieving

20 g of ground clinker is analyzed by an air-jet Alpine sieve 200 LS-N

2.7 Zeta potential measurements

For the measurement of Z potential of cement powder a COULTER DELSA 440 Multi-angle electrophoretic light scattering analyzer has been used. The sample powder has been dispersed in phosphate buffer pH 12 (12 mS).

2.8 ESEM-FEG analysis

The samples have been analyzed by scanning electron microscopy, without any previous treatment. We have used a Philips XL30 ESEM-FEG (Environmental Scanning Electron Microscope, equipped with a Field Emission Gun) in secondary electron mode. The instrumental configuration allows us to obtain a much higher brilliance of the electronic source than the one of an ordinary SEM, and to work in low vacuum conditions (6 Torr), with a voltage of 10kV, at a temperature of 5°C.

2.9 Temperature profile analysis.

The temperature variation during the first 24 hours of the hydration period is continuously recorded by a TESTO 781 digital thermometer, equipped with a TESTO DQF 826 probe (sensitivity: $^{1}/_{1000}$ °C). The probe is dept into the cement paste (500 g cement) immediately after mixing the cement with water. The system is kept in a thermostatic bath maintained at 20°C (reference temperature).

3. RESULTS AND DISCUSSION

We set up a grinding procedure utilizing a Bond type lab mill, in order to check the effectiveness of GA components we were going to study and to prepare all the samples we tested. Obviously our procedure has not much to do with the industrial process, since both particle size distribution and specific surface area are quite different in the two case. Nevertheless, we could easily verify its internal consistency.

We chose an Ordinary Portland clinker as a reference substrate, whose specific gravity is 3,11 g/cm^3 and chemical composition, expressed in element oxides, is shown in Table 1.

Table 1.Chemical Composition of the Reference Portland Clinker

SiO_2	Al_2O_3	Fe_2O_3	CaO	MgO	SO_3	Na_2O	K_2O
25,21	5,13	3,97	59,99	1,29	1,32	0,25	0,64

As a grindability parameter we used Blaine Specific Surface Area (BSS) development during the milling process. In Figure 1 we show BSS development utilizing some typical raw materials of GA at the dosage indicated.

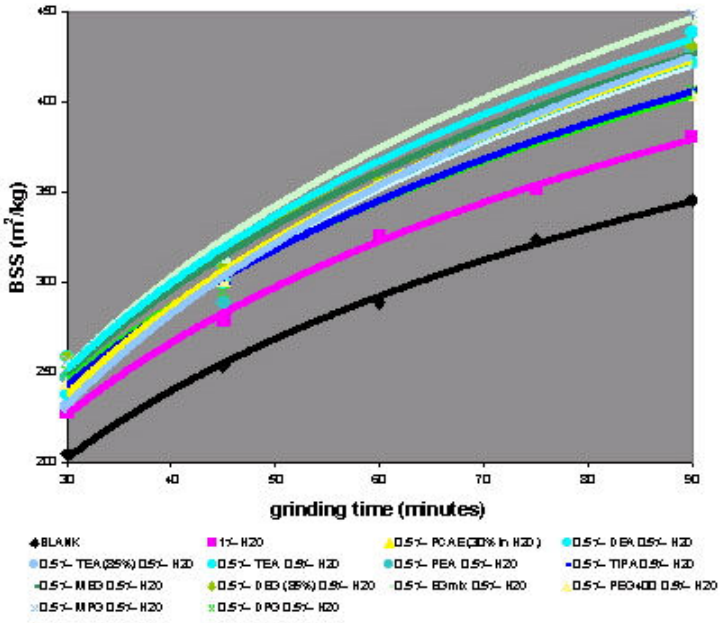

Figure 1. Blaine Specific Surface (BSS) area development of reference OP clinker ground in a lab mill Bond type.

These data clearly show that water is a decent GA, as is long known [4], but other components such as ethylene- and propylene-glycols or ethanol- and isopropyl-amines give a much larger contribution. Also PolyCarboxylic Acid Esters (PCAE), largely utilized as superplasticizers in concrete prove themselves to be as good GA. This lead us to hypothesize that also the further contribution by small organic molecules such as alkanolamines and glycols does not come necessarily and only from a further electrostatic screening, but also from steric or chemical interactions with cement particles. These BSS data has been confirmed by accurate adsorbtion/desorption isotherms measurements by BET calculation. Results are shown in Figure 2.

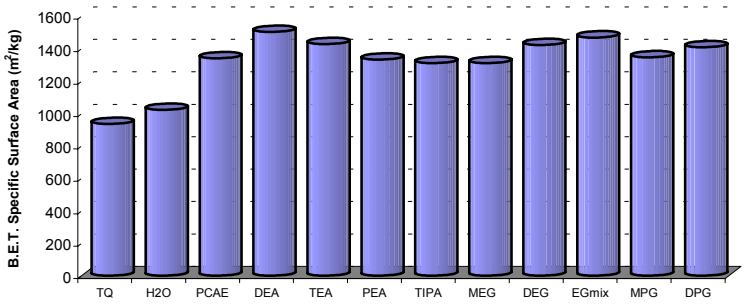

Figure 2. B.E.T. Specific Surface Area of reference clinker powder after 90 minutes' grinding

Also particle size analysis was performed using a mechanical Alpine sieve (Table 2): laser scattering of some of these samples give more or less the same trend.

Table 2. Sieve data with different grinding agents

Grinding Agents	Passing (%)		
	32 µm	40 µm	63 µm
Blank	77,0	83,9	94,8
1,0 ‰ H_2O	80,0	86,8	97,2
0,5 ‰ H_2O + 0,5 ‰ TEA	95,2	97,7	99,5
0,5 ‰ H_2O + 0,5 ‰ TIPA	96,4	98,1	99,5
0,5 ‰ H_2O + 0,5 ‰ DiEthyleneGlycol (DEG)	92,1	95,9	98,3
0,5 ‰ H_2O + 0,5 ‰ PolyEthyleneGlycol (PEG) 400	84,8	90,6	97,6
0,5 ‰ H_2O + 0,5 ‰ PCAE	74,8	83,6	92,0

Evident exceptions are PCAE and PEG, which do not give good results in term of granulometry. We hypothesized that sliding friction generates local heat, which makes polymers on grain surface sticky, preventing flowability of cement powder.

Z potential can give some indication of Ga influence on grain surface charge distribution, since in a suspension it is a function of the eletrophoretic mobility due to the electrostatic forces at the partlcle surfaces. Its values associated with cement particles suspended in an aqueous solution with fixed ionic strength and pH (see experimental) has been measured by multi-angle electrophoretic light scattering (ELS). The scattering angle of detection chosen was 17.1°, because it gives the highest resolution for particles with diameter less than 10 µm, the most significant for this kind of measurement. In Figure 3, the differences between Z potential values, obtained with and without admixtures, of particles from mineralogically different cements are reported. Since it is defined as the electric potential at the shared plane, this is the layer of water molecules which moves together with the particle, Z potential has negative absolute values. This means that the more positive difference value the higher the module of the negative potential and vice versa.

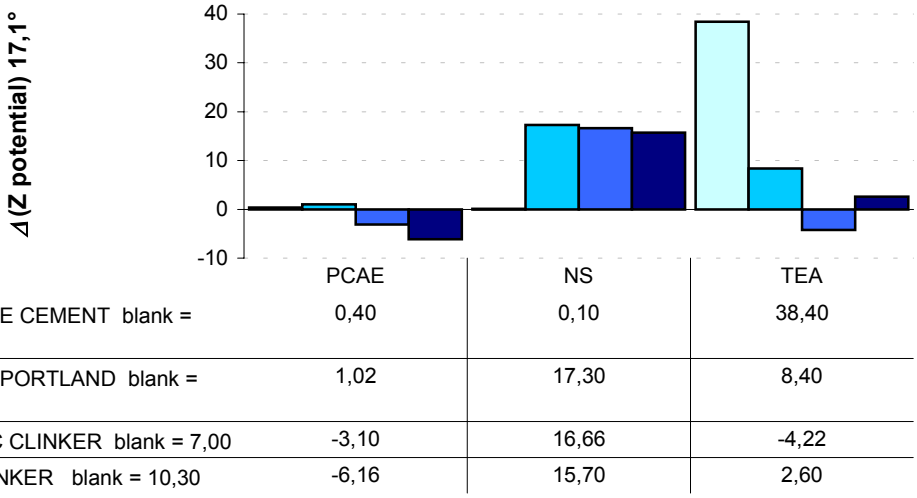

Figure 3. Z potential variation due to some admixture components

We compared TEA, a typical polar GA component, with two concrete superplasticizers admixtures such as PCAE and poly Naphthalene Sulphonate (NS), whose mechanism of action on cement paste is quite different. The former acts according to a steric mechanism coating cement grains, as is evident from the negligible, eventually negative, influence on Zeta potential of any kind of cement powder. The latter, instead, induce a strong electrostatic interaction between its sulphonate groups and positive charges on grain surfaces, which means a strong enhancement in Zeta potential values. TEA action is somehow in between the two situations. When C-A phases/C-Z-F phases > 1, TEA act as Zeta potential enhancer, while if C-A phases/C-A-F phases < 1, as in Portland cement clinker, its electrostatic effect is negligible. This can be explained by the well known chemical complex of TEA with the ferrite phase, whch gives higher importance to steric effect.

In order to make a definite breakthrough in we exploited the potential of the ESEM-FEG to explore the microstructure of cement (and clinker) paste in the early hydration period. We used an Environmental Scanning Electron Microscope equipped with a FEG source (ESEM-FEG), which allows to study the samples without any previous treatment, like gold or graphite sputtering, and in the presence of some residual water. We chose working parameters (pressure = 6 Torr; temperature = 5°C), in order to discriminate the kind of water present in the sample. Under these conditions, it is possible to see only the water saturated with salts or bound to gel-like structures, while free water has a sufficient vapor pressure to evaporate.

This powerful technique enabled us to observe directly the “supramolecular structures” forming on the surface of a cement grain, when it comes in contact with water, and to follow the details of the hydration process. We developed the following model mechanism of cement hydration, based also on our preceding observations [8].

When the cement comes in contact with water, we observe the almost immediate formation of a gel on the grain surface. This gel, based on complex sulfoaluminate hydrates, is rich in water and salts. It exerts a barrier effect and governs the mass flow between inner part of the grain and pore water, thus controlling the hydration of silicate phases.

This gel evolves with time, becoming “structured” and forming colloidal crystals that connect cement grains. All additives and admixtures that work on the plastic phase of cement paste interact with this gel and become part of it, modifying its structure in terms of quantity and quality. These modifications also depend on the chemical composition of the cement itself.

After an intermediate phase when the gel appears partially destructured, the first gel converts to a second one, from which calcium silicate hydrates (C-S-H) and ettringite form, not by precipitation but by mineralogical growth, probably influenced by free hydrated lime.

On one hand, the structures that arise from the second gel account for cement mechanical properties. On the other hand, timing and mode of the second gel "growth" strongly depend on the characteristics of the first gel in terms of thickness, chemical composition and stability. In the light of these considerations, we suppose that all kind of admixtures work on the first gel.

The hypothesis of a chemical composition based on sulfoaluminate hydrates comes from the fact that aluminate phases (C_3A and C_4AF) are the first to react with water, forming the corresponding aluminate hydrates, and that sulfate is present as a consequence of gypsum (or other forms of calcium sulfate) dissolution.

The delayed setting of cement is then caused by the formation of the gel, a form of colloidal ettringite, and not by precipitation of ettringite itself. Its distinct long hexagonal rods appear only after few hours from the beginning of the hydration, as a consequence of the sulfoaluminate gel transformation.

The relative amounts of Ca^{2+}, Al^{3+} and SO_4^{2-} changes with time, modifying the "permeability" of the gel and allowing the hydration of the silicate phases, that proceeds toward the inner part of the cement grain. This means that the C-S-H structures grow from and through the gel layer, rather than precipitate from the external pore water solution.

Since the gel forms within few seconds and covers cement grains completely, it actually represents the grain surface when water is present, and any substance added to the cement must interact with the gel.

This means, for example, that during industrial grinding process of clinker, carried out in presence of water and GA, we just have the conditions for a preliminary hydration of clinker: in fact the addition of aqueous additives, the high temperature (up to 150°C) and the presence of steam promote the hydration of clinker grain. For this reason in our investigation on the "mode" of action of alkanolamines based GA we focused our attention on morphological modifications of hydration products of clinker and cement. As a matter of fact, only small amounts of GA (3-5‰) are usually added into the mill, but they become significant, if we consider that only the 2-5% of clinker participates in the hydration process.

In this paper we describe only the effect of alkanolamines on morphological structures of calcium aluminate hydrates by ESEM-FEG analysis, also compared with PCAE used as a GA.

In order to emphasize the action of the additives, we used the clinker ground in the lab mill without gypsum in our experiments.

As shown in Figure 4, the dry clinker powder, ground with or without additives, does not show any particular morphological structure of hydrated products.

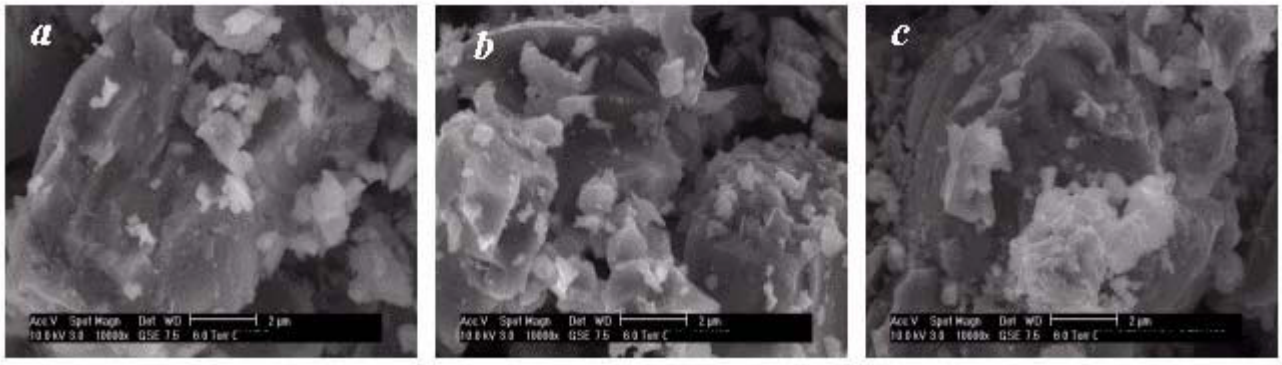

Figure 4. ESEM-FEG images of a Portland dry clinker grain ground with: a) no additive; b) 1,0 ‰ H_2O; c) 0.5 ‰ H_2O + 0.5 ‰ of TEA.

In our opinion, this is an effect due to a mechanical action of grinding media, which break the hydrates that, therefore, become too small to be seen by ESEM-FEG analysis. When we analyzed the morphological structures of a ground clinker paste with a water/clinker ratio of 0.4 (Figure 5), we noticed that the clinker grains still look well separated, but become covered with pseudo-regular gel-like structures, which cannot be observed in dry powder. It is evident that the gel formed by the paste of the clinker ground without GA (a) is less structured than that of the clinker ground with TEA (b).

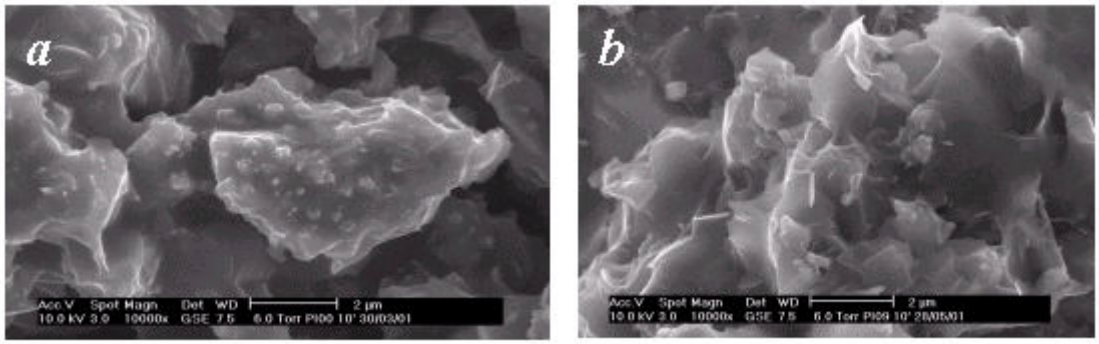

Figure 5. ESEM-FEG images of a Portland clinker paste (w/c = 0.40) ground with: a) no additive; b) 0.5 ‰ H_2O + 0.5 ‰ of TEA.

The chemical composition of this gel is based on aluminate hydrates: in fact the aluminate phases (C_3A and C_4AF) are the first to react with water, forming the corresponding aluminate hydrates which directly interact with TEA [7]. A great surprise comes from the morphological analysis of a clinker ground without GA and formed into paste with water and TEA (w/c = 0.4, TEA = 0.5% w/w on the clinker), shown in Figure 6.

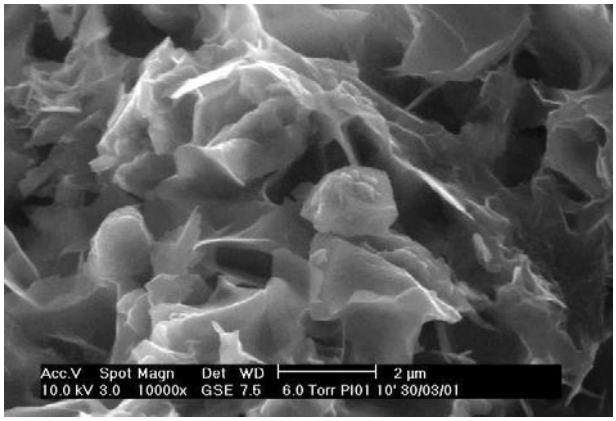

Figure 6. ESEM-FEG image of a clinker ground without GA and formed into paste with water and TEA (w/c = 0.4, TEA = 0.5% w/w on the clinker).

Comparing Figures 5*b* and 6, we can deduce that TEA produces the same kind of calcium aluminate hydrates added both into the mill and into the mixing water.

This observation suggests that the clinker maintains a "memory" of the manufacturing process. The shape of these hydrates looks like the hydration products of C_4AF, synthesized in our laboratory (Figure 7).

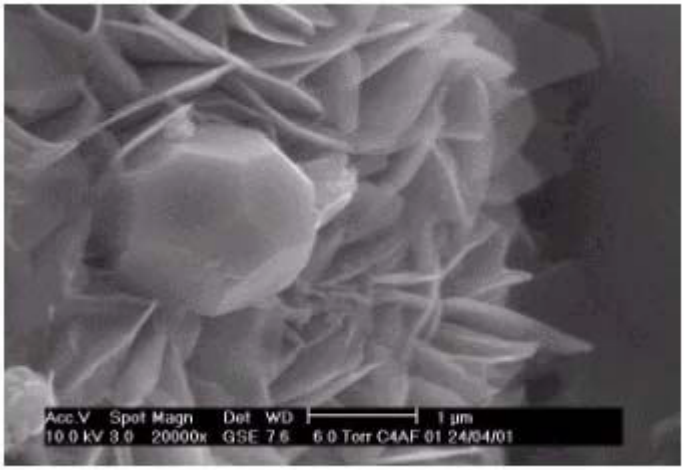

Figure 7. ESEM-FEG image of synthetic C_4AF paste (water/C_4AF = 0.4).

Figure 8 shows the gel formed during the hydration of a clinker ground with PCAE, with a water/clinker ratio of 0.4; as we can see, this gel does not show typical morphological changes on aluminate hydrates, even if the grinding process indicates the efficiency of this admixture as a GA.

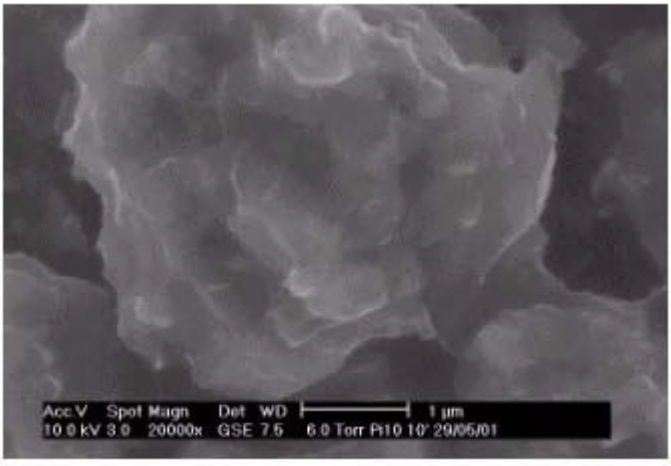

Figure 8. ESEM-FEG image of a clinker ground with 0.5‰ of PCAE + 0.5‰ of H_2O and pasted with water (w/c = 0.4).

Considering that, when PCAE is used as a superplasticizer, we observe a huge formation of structured gel (Figure 9), we can hypothesize that PCAE actually works on sulfoaluminate hydrates, that we can call colloidal-ettringite, rather than on aluminate hydrates.

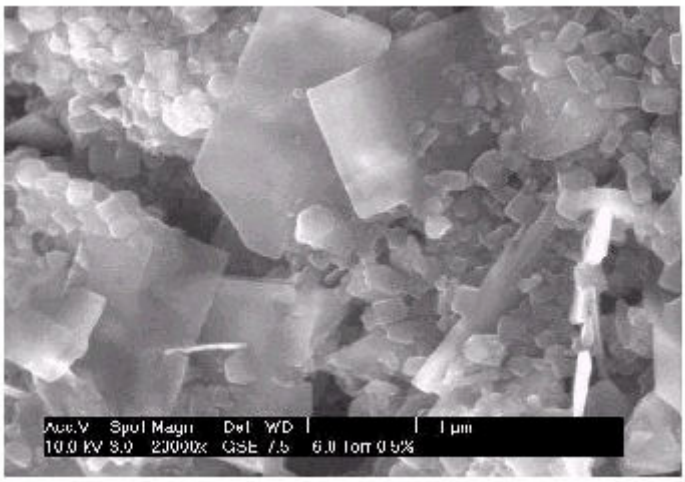

Figure 9. ESEM-FEG image of an OPC type I paste (w/c = 0.35), with the addition of 0.5% (w/w on the cement) of PCAE.

Since it is well known that TEA based GA also improve the cement performance, especially compressive strengths at 24 hours, we tested the effect of this component on the clinker mixed with gypsum (as in Portland cement) during hydration. This behavior is reflected in the temperature profile experiment. We recorded the temperature variation of two different “cementitious” pastes: one is a mixture of clinker ground with TEA and 5% of gypsum, the other a mixture of clinker ground without GA and 5% of gypsum. Both mixtures were hydrated with a water/cement ratio of 0.5. As shown in Figure 10, two distinct peaks are present: the first is very sharp and can be ascribed to the formation of hydrated sulfoaluminate phases, which is a quite exothermic reaction; the second peak is broad and is related to the formation of free lime and C-S-H, which develop the mechanical properties of cement.

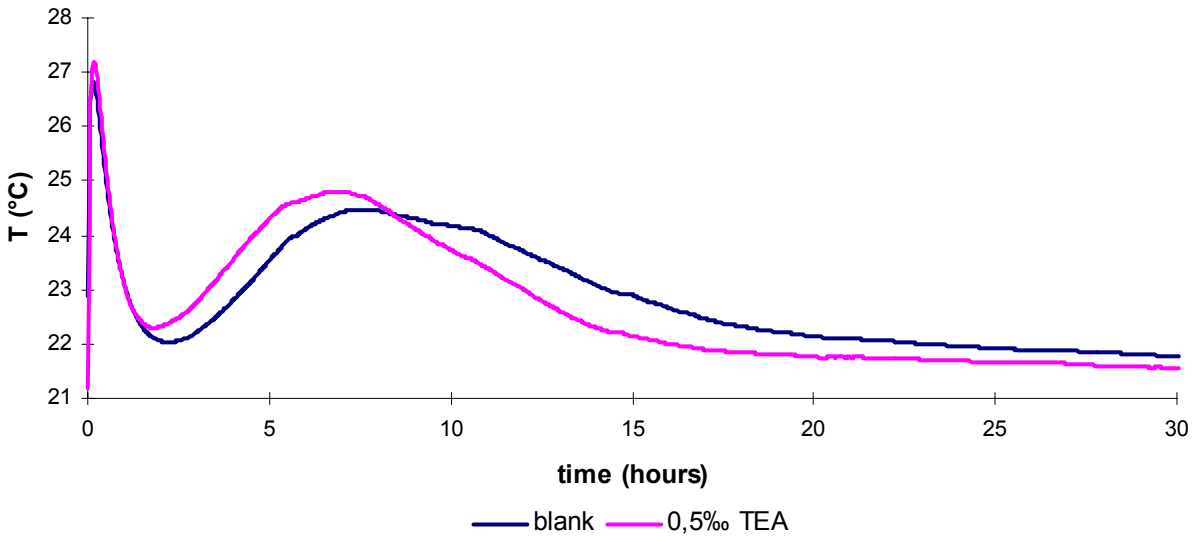

Figure 10. Temperature profile of clinker hydration with 5 % gypsum and w/c = 0,5.

From these analytical data it becomes apparent that TEA acts as an accelerator of C_3S hydration, then enhancing compressive strength of cement at the early ages. Morphological analysis of the two pastes reveals that the sulfoaluminate gel is the same in term of structures, which means that addition of gypsum hides any qualitative information. But, comparing structures at the same time of hydration, in the case of clinker ground with GA, C_3S hydration, and so the growth of C-S-H, is clearly faster and at 4 hours we already note the complete cross-linking of the grains by the structured gel.

With this work we have shown that alkanolamines interact with calcium aluminate hydrates, inducing morphological changes on the gel that covers clinker powder. In our opinion these structures could be the key point of clinker particles dispersion during grinding process and of their fluidizing effect. Therefore we can hypothesize both an electrostatic and a steric repulsive effect on the cement grain, probably related to the different chemical compositions of the gel.

4. CONCLUSIONS

According to these results GA, in particular alkanolamines, influence the early period of clinker and cement hydration and induce morphological changes in calcium aluminate (C_3A and C_4AF) hydrates. We can also remark that clinker undergoes a pre-hydration reaction when it is ground in the presence of water and GA, and that it somehow keeps memory of the effect of alkanolamines on the hydration products formed during the milling process. This study is part of a more general investigation, whose target is to evaluate the chemical composition of the gel and to clarify the "mechanism of action" of other classes of admixtures on the formation of the gel. At present time we are studying the characterization of the first gel. A direct chemical analysis (by ESEM-EDX or XRD) is not possible because the "structures" are too small (< 100 nm) and the gel layer is very thin (10-100 nm): in these condition the influence of the matrix (the cement grain) is too strong.

REFERENCES

[1] *(a)* Z. Heren, H. Ölmez, The influence of ethanolamines on the hydration and mechanical properties of Portland cement, Cement and Concrete Research, vol. 26 (5), 1996, p.701; *(b)* V.H. Dodson, Concrete Admixtures, Van Nostrand Reinhold Ed., 1990

[2] L. Sottili, D. Padovani, Einfluss von Mahlhilfsmitteln in der Zementindustrie, ZKG International, *(a)* Teil 1, vol. 53 (10), 2000, pp. 568-575; *(b)* Teil 2, vol. 54 (3), 2001, pp. 146-151

[3] J.S. Bathia, World Cement Technology, 1979

[4] F.J. Maurdulier, Rock Products, 1967

[5] *(a)* A.A. Jeknavorian, E.F. Barry, F. Serafin, Determination of grinding aids in Portland cement by pyrolysis gas chromatography-mass spectrometry, Cement and Concrete Research, vol. 28 (9), 1998, pp.1335-1345; *(b)* P. Cassat, J.F. Muller, A. Vichot, P. Colombet, Direct detection of grinding aids in a cement matrix, 10th international congress on cement chemistry, Goteborg, 1997, 3v014

[6] *(a)* M. Ichikawa, M. Kanaya, S. Sano, Effect of triisopropanolamine on hydration and strength development of cements with different character, 10th international congress on cement chemistry, Goteborg, 1997, 5iii003; *(b)* E. Gartner, D. Myers, Influence of tertiary Alkanolamines on Portland cement hydration, J. Am. Ceram. Soc., vol 76 (6), 1993, 1521-1530

[7] *(a)* M. Pauri, S. Monosi, G. Moriconi, M. Collepardi, Effect of triethanolamine on the tricalcium silicate hydration, 8th international congress on the chemistry of cement, Rio de Janeiro, 1986; *(b)* V. S. Ramachandran, Hydration of cement. Role of triethanolamine, Cem. Concr. Res., vol. 6, 1976, pp. 623-632; *(c)* V. S. Ramachandran, Action of triethanolamine on the hydration of tricalcium aluminate, Cem. Concr. Res., vol. 3, 1973, pp. 41-54

[8] F. Cella, T. Cerulli, D. Salvioni, S. Stella, Morphological variation of cement paste microstructure due to the use of admixtures, 23th international conference on cement microscopy, 2001.

GRINDING AIDS:
A STUDY ON THEIR MECHANISM OF ACTION

Bravo Anna, Cerulli Tiziano, Giarnetti Mariagrazia, Magistri Matteo

Mapei S.p.A., via Cafiero 22, 20158 Milano, Italy. E-mail: dam_caf@mapei.it

ANNA BRAVO

Place and Date of birth: Pordenone (PN), 25/05/1969

Home Address: via Cambiasi, 8 - 20131 - MILANO
work: tel. ++39-(02)37673713 - FAX ++39-(02)37673214
E-mail: anna.bravo@virgilio.it

1994 - GRADUATION IN CHEMISTRY - Università degli Studi di Milano (109/110)
discipline: BIO-ORAGNIC CHEMISTRY - Title of Thesis: *"Baker's Yeast Mediated Reduction of 2-Tetralones"* (*Tetrahedron*, 1995, *51*, 11531) - Supervisor: Prof. P. Manitto.

QUALIFICATIONS

1994 / 1997 PhD in INDUSTRIAL CHEMISTRY -curriculum ORGANIC CHEMISTRY
supervisor: Prof. Francesco Minisci - Dipartimento di Chimica del Politecnico di Milano.
Subject: *"Selective Oxidations and Homolitic Substitutions on Organic Compounds through Radical Processes"*.
Options included: *INDUSTRIAL ORGANIC CHEMISTRY and INDUSTRIAL CHEMISTRY*

1994 / 1996 SCHOOL IN CHEMICAL SYNTHESIS *"A. QUILICO" - Politecnico di Milano.*

1998 - course "QUALITY ASSURANCE – REGULATION ASPECTS ON SYSTEM, PRODUCT AND PROCESS CONTROL" - Associazione EURESIS - patrocinio di CERTICHIM Milano.

1999 - course "MANAGEMENT OF TECHNOLOGY"
Università degli Studi di Milano - patrocinio Pirelli S.p.A.

Approximately 17 publications and several meetings. (available on request)

DURABILITY OF BLAST FURNACE SLAG-BASED CEMENTING MATERIALS

Sersale R.[1] and Frigione G.[2]

[1] Department of Materials and Production Engineering, University of Naples. Piazzale Tecchio, I-80125 Naples, Italy.
[2] Department of Chemical Engineering and Materials, University of Calabria. I-87036 Arcavacata di Rende, (CS), Italy.
E-mail: g.frigione@unical.it

ABSTRACT

The influence of some activators (Portland clinker, gypsum, sodium silicate solution), just as found, or blended, on strength development and durability of cementitious materials, prepared with large amounts of granulated blast furnace slag, has been examined. It has been pointed out that small amounts of clinker and gypsum in the blends are determining factors for obtaining a binder with good compressive strength, resistant to carbonation, sulphate attack, freezing/thawing, and, most likely, to alkali-aggregate reaction, too.

Keywords: alkali-aggregate reaction, blast furnace slag, carbonation, compressive strength, durability, freezing/thawing, sulphate resistance.

1. INTRODUCTION

There is considerable interest [1] in utilising industrial by-products for preparing high-performance cementing materials, firstly for low production cost, energy saving and environmental protection through abatement of the greenhouse effect. Granulated blast furnace slag, ground to an appropriate fineness, appears to be well-suited for manufacturing through stimulation with a proper activator. High-performance cementing materials endowed with properties at least comparable, or sometimes better, than those of Portland cement [2] and therefore right for playing an important role in different construction fields, including waste storage. Among the various activators, - Portland clinker, gypsum, alkalis - sodium silicate solutions have shown many benefits in terms of upsurge of the latent hydraulic activity of the granulated slag and of the development of the strength of the related works.

Several aspects, however, are in need of further investigation, of which the first is the durability of the works. Considering that granulated blast furnace slag shows different properties, depending on nature and concentration of activators employed [3], we have thought worthwhile to assess the influence of some activators, just as found, or in blend, on the durability of cementing materials with high slag contents, against some agents, in order to optimise its composition in view of the performance expected.

2. EXPERIMENTAL

2.1 Materials

The select activators have been:
Portland clinker, gypsum ($CaSO_4.2H_2O$ 97%), sodium silicate solution (SiO_2/Na_2O) = 1.0), and some blends of the above mentioned activators.

The influence of the replacement of different amounts of Portland clinker and gypsum has been examined. As mixing liquid has been used not only water, but also sodium silicate solution, respectively. Terms of reference have been: plain granulated slag mixed with water and with sodium silicate solution, respectively, and a cement Type III/B (according to EN 197-1 Specification) containing 70% slag, 27% Portland clinker and 3% gypsum.

Fineness of clinker and slag has been 360 m^2/kg Blaine. Gypsum has been screened through a 63-micron sieve. The chemical compositions of the slag and Portland clinker used are summarised in Table 1.

Table 1. Composition of the Slag and Portland Clinker

Material	SiO_2	Al_2O_3	Fe_2O_3	CaO	MgO	loi	K_2O + Na_2O	C_3S	C_2S	C_3A	C_4AF
Granulated Slag	36.4	10.8	0.7	42.3	8.1	0.8	0.3				
Portland Clinker	21.2	4.9	3.3	66.2	1.8	0.1	0.9	56	18	7.3	10.0

The compositions of the blends, with the identification number quoted also in Figures are shown in Table 2.

Table 2. Composition of the Blends

Identification Number	Blends			Water as mixing liquid	Sodium silicate solution as mixing liquid
	% Slag	% Clinker	% Gypsum		
1	100			X	
2	95	5		X	
3	90	10		X	
4	95		5	X	
5	90	5	5	X	
6	85	10	5	X	
7	90		10	X	
8	85	5	10	X	
9	80	10	10	X	
10	100				X
11	95	5			X
12	90	10			X
13	95		5		X
14	90	5	5		X
15	85	10	5		X
16	90		10		X
17	85	5	10		X
18	80	10	10		X
19	70	27	3	X	

2.2 Test Procedures

Mortar prisms (40 x 40 x 160 mm) were produced from blends with standard aggregate, in accordance with EN 196-1 Specification, using, as mixing medium, water or sodium silicate solution, respectively. After 24 hours at 20°C and RH> 95%, the specimens were demoulded. All specimens were cured for 27 days in water before placement into its final environmental condition.

Triplet specimens of each blend was subjected to the following tests:

- compressive strength at 28 days age;
- compressive strength after storage of 365 days in water;
- compressive strength after storage of 365 days in air;
- depths of carbonation measured after 365 days on specimens stored at 20°C, RH 65% at normal CO_2 concentration (0.03% by volume). The prisms were split so that a fresh face was exposed for measuring the penetration of carbon dioxide. The face was sprayed with phenolphthalein so that the carbonation could be measured;
- resistance in magnesium sulphate solution: storage in a 5% $MgSO_4$ solution. After 365 days the specimens were visually inspected and characterised by a durability index;
- resistance in sodium sulphate solution: storage in a 2.1% Na_2SO_4 solution. After two years the specimens were visually inspected and characterised by a durability index;
- freezing/thawing resistance, through assessment of the specimen weight after every cycle of 20 hours in air at -18°C and 4 hours in a 5% sodium chloride solution or in water, respectively, at 20°C [4];
- resistance to alkali-aggregate reaction [6] according to ASTM C 227 Specification. Mortar bars were made with Pyrex glass.

3. RESULTS AND DISCUSSION

3.1 Compressive strength

Figure 1 shows the effects of storage conditions on compressive strength development.
It can be seen that using alkaline solution as mixing medium, after 27 days in water, specimens can achieve values higher than those using water. However, blends containing Portland clinker and gypsum, mixed with alkaline solution, give mortar specimens with lower strength values than those recorded for specimens prepared with slag alone. Blends containing 5% gypsum, mixed with water, achieve compressive strength values very near to those recorded for blends containing 25% clinker.

A subsequent one-year storage in water increases compressive strength both of specimens made with blends mixed with water and with alkaline solution, respectively. Alkaline solution however causes lower strength values than those recorded for specimens made with slag all by itself. Good results have been obtained by blends containing slag and gypsum, mixed with water and stored one year in water.

One-year storage in air of specimens produced with blends mixed with water causes a slight strength decrease, in comparison to values achieved after storage, for the same time, in water. The use of alkaline solution does not improve compressive strength values recorded after 28 days storage in water. Gypsum-free blends show a slight strength increase. There is therefore evidence that the use of an alkaline solution increases the compressive strength only for specimens produced with slag alone. On the contrary, the use of an alkaline solution as mixing medium of blends made with granulated slag and Portland clinker, or with slag and gypsum, respectively, does not prove to be effective.

Storage	BLENDS MIXED WITH WATER	BLENDS MIXED WITH SODIUM SILICATE SOLUTION
27 days in Water	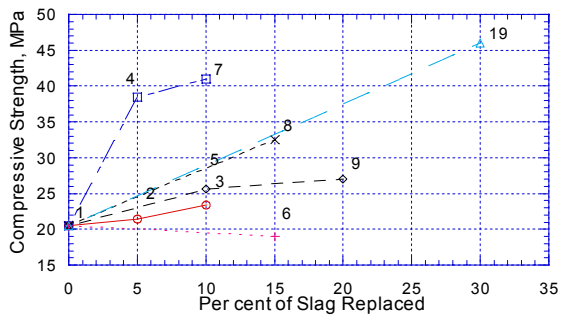	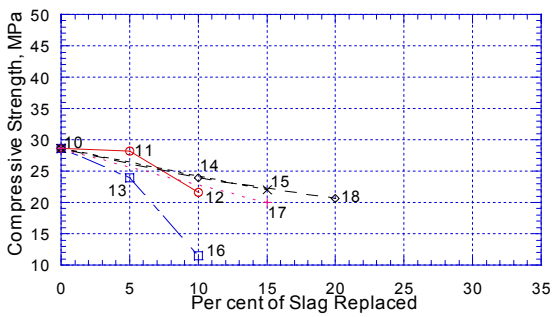
27 days in Water + 365 days in Water	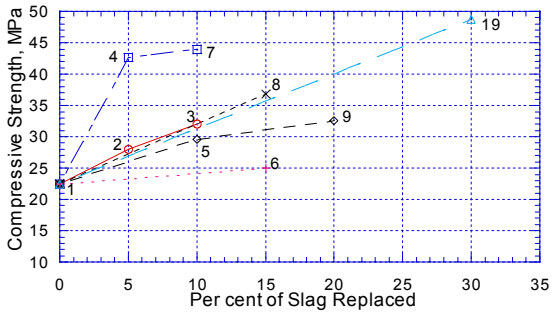	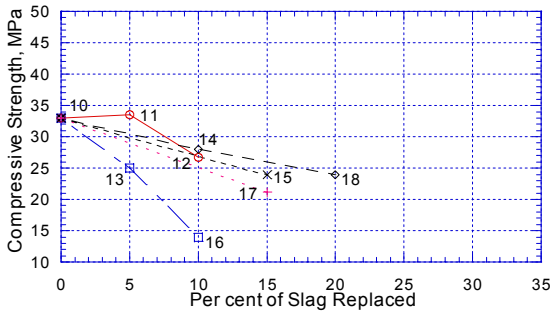
27 days in Water + 365 days in Air	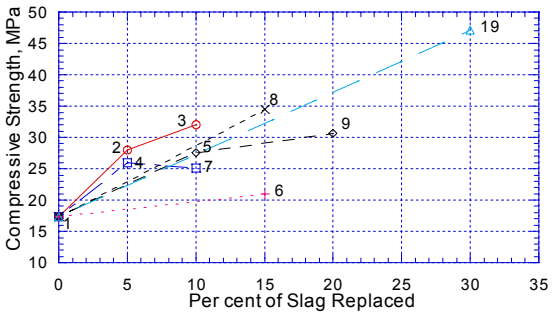	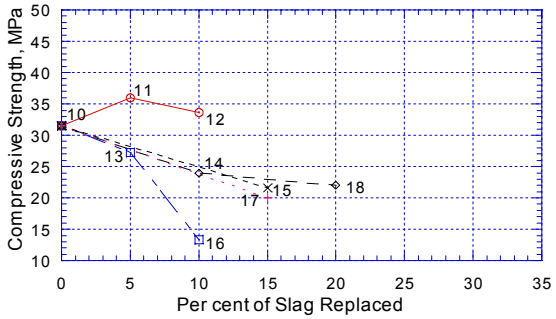

Figure 1. Compressive Strengths

	BLENDS MIXED WITH WATER	BLENDS MIXED WITH SODIUM SILICATE SOLUTION
Carbonation Depth	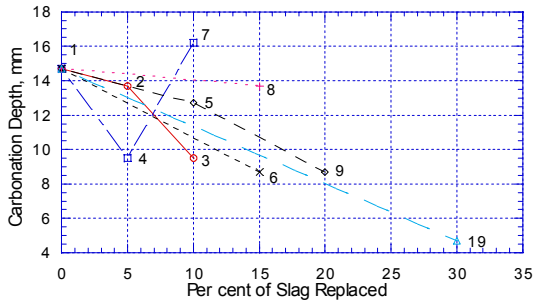	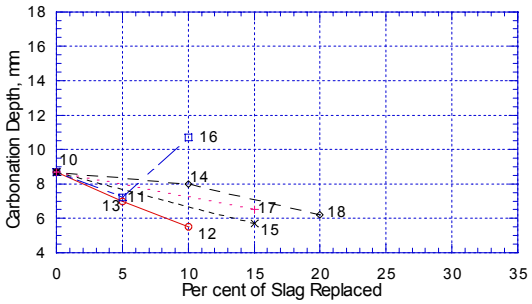
Durability Index in $MgSO_4$ Solution	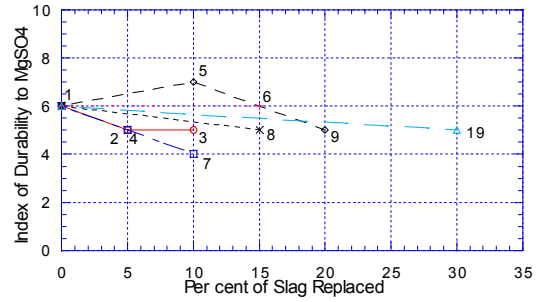	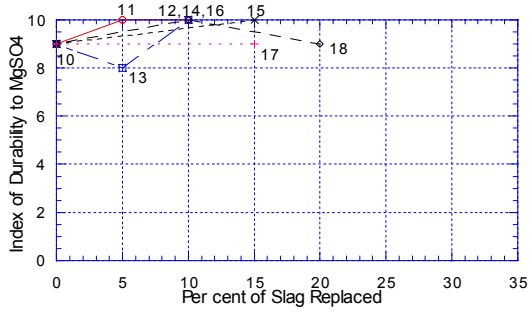
Freezing – Thawing Resistance Immersion in NaCl Solution	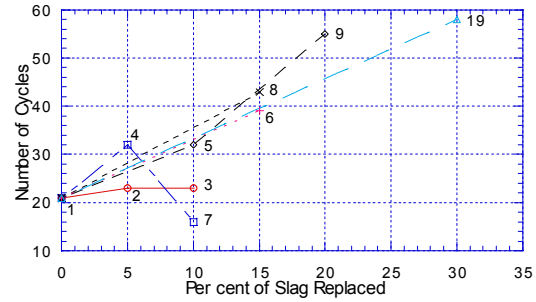	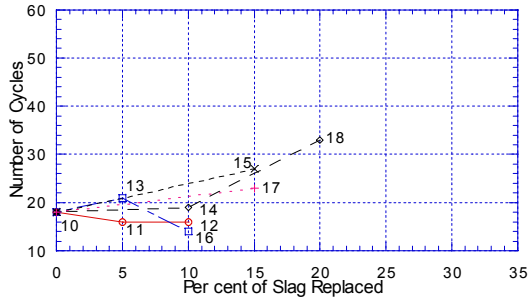
Freezing-Thawing Resistance Immersion in Water	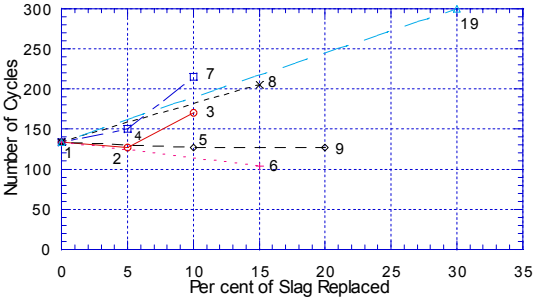	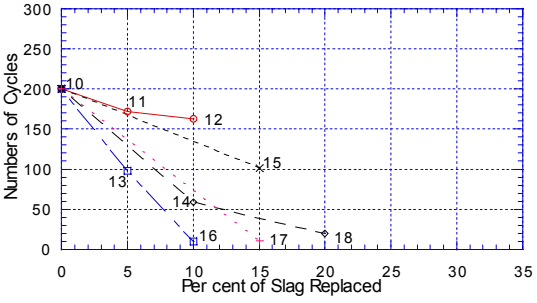

Figure 2. Durability Tests

3.2 Resistance to carbonation penetration.

Figure 2 shows carbonation behaviour. There is evidence of steady carbonation abatement for specimens mixed with sodium silicate solution, a benefit from the viewpoint of protection of reinforcement [7]. There is likewise evidence of a benefit attributable to increasing additions of Portland clinker and gypsum, within the limits, of course, of the compositions examined, both for specimens mixed with water and for those mixed with sodium silicate solution. Portland clinker-free specimens, prepared adding 5% gypsum to slag, have shown low carbonation depth. Carbonation increases with the increase in gypsum content in the blend.

3.3 Resistance to sulphate solution

Figure 2 shows durability assessment for specimens stored in a magnesium sulphate solution. A numerical index between 0 (specimen disrupted) and 10 (sound) has been adopted. There is evidence of a general benefit provided by using alkaline solution as mixing medium, with negligible fluctuations. All the blends, regardless of the nature of activator and mixing medium, stay completely sound after two years of immersion in the sodium sulphate solution.

3.4 Freezing/ thawing resistance through immersion in NaCl solution.

Figure 2 also shows the number of cycles required for a 30% weight loss of the specimens, as a function of blend composition. There is evidence of an adverse contribution of sodium silicate solution as mixing medium, whereas Portland clinker amount in a blends mixed with water exerts a favourable contribution. Anomalous, in this case, the action of the gypsum alone, even if it does not appear to exert a significant influence.

3.5 Freezing/ thawing resistance through immersion in water.

Finally, Figure 2 shows that the outlines of the curves are pretty similar to those, reported in the same figure, resulting from immersion of the specimens in chloride solution, both for blends mixed with water and with sodium silicate solution, respectively. With the exception of the slag alone, blends mixed with water show higher durability than those mixed with sodium silicate solution.

3.6 Resistance to alkali aggregate reaction.

The test has been performed using, of course, sodium silicate solution as mixing medium. Blend compositions examined are those reported in Table 2 with numbers 10, 11, 14 and 18. The first three blends revealed no expansion of the related mortars, after 56 days. Mortar prepared with blend no. 18, showed expansion. In the same case, the use of standard sand (EN 196-1) in the place of the reactive Pyrex glass indicated that the unsoundness is very likely due to high sulphate content present.

4. CONCLUSIONS

The test results described in this paper have confirmed the advantageous properties of blast furnace slag-based cementing materials, manufactured with the help of activation by means of moderate amounts of a mixture of Portland clinker/gypsum and sometimes with sodium silicate solution as mixing medium. The presence of 5 - 10% Portland clinker in the blends and that of small amounts of gypsum seem essential to produce the best properties of such a binder. It shows indeed good strength, resistance to carbonation penetration, to sulphate attack and to freezing/thawing. Alkali-aggregate reaction resistance was not well assessed during the short length of time of the test.

Thus, prefabricated components appear to be a suitable utilisation of such a binder.

REFERENCES

[1] Puertas, F. Martinez-Ramirez, S. Alonso, S. Vazquez, T. Alkali-activated fly ash/slag cement. Strength behaviour and hydration products. Cement Concr. Res. vol.30, (2000), pp.1625-1632.

[2] Roy, D.M. Alkali-activated cements. Opportunity and challenges. Cement Concr.Res., vol.29, (1999) pp.1249-1254.

[3] Fernandez-Jimenez, A. Puertas, F. Setting of alkali-activated slag cement. Influence of activator nature. Advances Cement Res., vol.13, (2001), pp.115-121.

[4] O' Farrel, M. Wild, S, Sabin, B.B. Resistance to chemical attack of ground brick-PC mortar. I. Sodium sulphate solution. Cement Concr. Res., vol.29, (1999), pp.1781-1790.

[5] Cheng-Ju, G. The effects of chloride salts on the volume changes and durability of cement pastes and concretes. Third Canmet/ACI Int. Conf. on Durability of Concrete. Supplementary Papers, Nice, (1994), pp. 403-430.

[6] Bakharev, T. Sanjayan, J.G. Cheng, Y.B. Resistance of alkali-activated slag concrete to alkali-aggregate reaction. Cement Concr. Res., vol.31,(2001) pp.331-334.

[7] Roy, D.M. Jiang, W. Silsbee, M.R. Chloride diffusion in ordinary, blended, and alkali-activated cement pastes and its relation to other properties. Cement Concr. Res., vol.30, (2000), pp.1879-1884.

SYNTHETIC ZEOLITES AS SUBSTITUTES OF SILICA FUME

Frigione G., Bonavita L., Katovic A. and Giordano G.

Department of Chemical and Materials Engineering, University of Calabria
I-87036 Arcavacata di Rende, (CS), Italy.
E-mail: g.frigione@unical.it

ABSTRACT

This paper presents the results of pozzolanic activity studies on synthetic high silica zeolites, their contribution to development of compressive strength of Portland-pozzolanic cements and the performance of high performance concretes (HPC) based on synthetic zeolites. Two types of zeolites (TON and MFI) in silica form and one (BEA) with a low aluminium content were prepared. Zeolites with sub-micronic particle sizes were also prepared.

The pozzolanic activity was determined in terms of zeolite's capacity for binding lime and the rate of the pozzolanic reaction. The contribution of synthetic zeolite to compressive strength development of Portland-pozzolanic cement was evaluated at 2, 7 and 28 days according to EN 196-1. The behaviour of HPC with synthetic zeolite was evaluated in terms of compressive strength and durability. The results were compared with those obtained by using silica fume.

From the experimental results the following observations were derived: the zeolite offering the best pozzolanic behaviour was TON; the zeolite producing in mortars and in concretes the higher mechanical properties was BEA; the general behaviour of zeolites was in any case superior to that obtained with silica fume.

Finally, the performance of HPC based on synthetic zeolites is in all cases similar or higher than that of concretes produced with silica fume.

Keywords: Pozzolanic activity, Silica fume, Synthetic zeolite, High Performance Concrete.

1. INTRODUCTION

The use of silica fume continues to increase despite its relatively high cost. The extensive utilization of silica fume in the concrete is due to its high degree of pozzolanic activity and its very high specific surface area. The pozzolanic and filler effects of silica fume reduce the porosity of the hydrated cement paste and the transition zone between the paste and aggregate. Therefore, the incorporation of silica fume in concrete increases the compressive strength and durability. However, the use of silica fume is limited to the geographic areas where its local supply is abundant [1]. In fact, its price is 2 to 20 times higher than the cement price, depending on the geographic area where it is used.

Pozzolanic activity includes two parameters, namely the maximum amount of lime that a pozzolan can combine and the rate at which such combination occurs. The high pozzolanic activity of silica fume derives from its chemical composition - very high silica content - and from the sub-micronic particle-size dimensions [2]. The small size of the particles speeds up the reaction with calcium hydroxide produced by the hydration of Portland cement [1].

The aim of this research was to study the production and utilization of a pozzolanic material that is suitable for use in the cement and concrete industries as a substitute for expensive silica fume.

Sersale and Frigione [3-7] have demonstrated that natural zeolites are excellent pozzolans and showed their use as constituents of blended cements and concrete. Katovic *et al*. [8-10] synthetized various zeolite types with very small particle sizes. So, the purpose was to transfer this knowledge to the cement and concrete field in order to find an effective substitute of silica fume.

For this purpose various zeolite-types having high specific surface areas were prepared. These synthetic zeolites were characterized on the basis of their pozzolanic activity, their contribution to the development of the mechanical resistance and the durability of the cement and concrete. The results were compared with those obtained by using silica fume.

2. MATERIALS AND EXPERIMENTAL PROGRAM

Three different synthetic zeolite types having small particle sizes were prepared [11]: BEA, TON,MFI (nomenclature according to the *Structure Commission of the International Zeolite Association* [12]):
- Silica fume (SF) "Force 10,000" by Grace;
- Cement CEM I 52,5R (EN 197/1): a commercial product. In Table 1 its characteristics are reported;
- Aggregate crushed limestone.
- Superplasticizer “Adva Flow” by Grace.

Table 1. Characteristics of the Portland Cement

s.s.a. Blaine, m^2/kg	Bogue Potential Compound Composition (%)				
	C_3S	C_2S	C_3A	C_4AF	$CaSO_4 \cdot 2\ H_2O$
390	55	19	7	11	5

2.1 Preparation of Zeolites

In this study the zeolites were prepared starting from the following initial reaction mixture:

$$x\ Na_2O - y\ ORG - z\ Al_2O_3 - SiO_2 - w\ H_2O$$

where:
x = 0.1; y = 0.1; z = 0.02; w = 20 for BEA;
x = 0.1; y = 0.08; z = 0.0; w = 20 for MFI;
x = 0.06; y = 15; z = 0.0; w = 10 for TON;
and ORG stays for the organic compound that is:
- tetraethylammonium hydroxide and bromide in the case of BEA type;
- tetrapropylammonium bromide in the case of MFI type and
- methanol for the TON type zeolite.

The synthesis procedure was the following: sodium aluminate was added to a sodium-hydroxide solution and after the homogenisation the organic compound and the silica source were added. For the synthesis of zeolites MFI and TON the procedure was identical but without the introduction of the aluminium source.

The zeolites BEA and MFI were prepared in Teflon lined autoclaves in static conditions under autogeneous pressure in a temperature range varying from 140 to 170 °C as a function of the zeolite type. The zeolite TON was prepared in a stainless steel autoclave under stirring (500 rpm) and

under autogeneous pressure at 140 °C. The products were cooled down to room temperature, washed and dried at 105 °C overnight. Further details on the synthesis procedures are reported in Katovic *et al* . [8-10].

The characterisation of the samples was performed by the following techniques: powder X-ray diffraction (Philips PW 1730/10, Cu $K\alpha_1$ radiation), atomic absorption spectrophotometry (GBC 932 AA), scanning electron microscopy equipped with an EDX facility (Stereoscan 360 Cambridge Instruments) and, finally, nitrogen adsorption-desorption isotherms at 25°C were recorded using an automatic porosimeter (Micromeritics Asap 2000).

The chemical characteristics of synthetic zeolites and silica fume are shown in Table 2. The shape and particle size of samples under investigation obtained by SEM and the values of specific surface area (BET) are also reported in Table 2.

Table 2. The Pozzolanic Material Characteristics

Material	Particle size (μm)	Shape	s.s.a. BET (m^2/g)	SiO_2 (%)	Na_2O (%)	Al_2O_3 (%)
TON	0.6 ÷ 1.0	needles	32	98.6	1.3	-
BEA	0.1 ÷ 0.3	spheres	70	93.0	2.0	4.9
MFI	0.3 ÷ 0.7	spheres	13	98.6	1.2	-
Silica Fume	0.1 ÷ 0.8	spheres	26	97.1	0.1	0.5

2.2 Materials Characterization

2.2.1 Pozzolanic Activity

The various synthetic zeolites were studied concerning the pozzolanic activity - in terms of both capacity of binding lime and rate of pozzolanic reaction. For this aim, the "pozzolanic test" following the European Standard (EN 196-5) was performed. The capacity of binding lime was determined by defining the minimum zeolite/fixed Portland cement (Z/PC) ratio that is necessary for complying with the test. The test is "positive" if the concentration of calcium hydroxide in the solution is lower than the concentration of saturation. The rate of pozzolanic reaction was determined from the time at which the lime combination occurs by defining a zeolite/Portland cement fixed ratio Z/PC = 15/85. The time needed to obtain a positive response to the pozzolanicity test was determined from data collected daily.

2.2.2 Consistency and Compressive Strength on Mortar

The contribution of synthetic zeolites as a partial substitute for Portland cement so as to produce pozzolanic cement (Type IV according to EN 197-1) to the development of compressive strength was evaluated on mortar after 2, 7 and 28 days according to EN 196-1. The cement mortar consistency was determined according to UNI 7044 [13]. For this purpose, mixtures with Portland cement CEM I class 52.5 substituting one part with one of the pozzolanic materials in quantities that made a sample positive after 8 days were prepared. The results were compared with those obtained by using silica fume.

2.2.3 Compressive Strength on Concretes

The contribution of synthetic zeolite addition to concrete at a high dosage and a low w/c ratio was evaluated after 2, 7 and 28 days in order to obtain high performance concretes (HPC). The concrete mixture proportions are given in Table 3. The concrete was mixed in a laboratory pan mixer. The compressive strength measurements were obtained on 100 mm cubes. These were fully compacted on a vibrating table, damp for 24 hours before demoulding, and then cured at 20°C and 95% RH until testing. Each reported strength measurement is the average of six cubes.

Table 3. Concrete Mixture Composition

Material	Kg/m^3
CEM I 52.5 R	500
Crashed limestone ø 12.5 – 8 mm	595
Crashed limestone ø 8 – 4 mm	265
Sand ø 4 – 0 mm	850
Superplasticizer	5.2
Water	165
Slump Test (UNI 9418) mm	50

2.2.4 Durability Measurements

The potential concrete durability may be inferred by measuring the resistance of the cover layer to transport mechanisms for different types of fluid [14, 15]. Three durability tests have been developed: oxygen permeability, capillary water absorption and chloride conductivity.

Oxygen permeability tests were performed for all mixtures (with 14 days curing 20°C and RH>95%) at the age of 56 days. Until testing the specimens were stored at 20°C and 70% RH. Details of curing and preparation of specimens can be found in [16]. Oxygen diffusion through concrete is strongly affected by moist curing. The moisture condition of the concrete under test also has a large influence because water in the pores significantly reduces the diffusion. However the purpose of our tests is not to determine absolute material characteristics but to produce reliable values to be used for comparative purposes. The test procedure is based on the Cembereau method; details of the equipment and test procedure are given in [17]. The test procedure applied for capillary water absorption can be found in [18]. The chloride penetration resistance of concrete was determined according to the AASHTO T 277 rapid test method [19]. The fresh concrete (w/c = 0.35) was cast into cylinders (Ø = 11 cm, h =22 cm) and 50 mm thick discs were sawed after one day of wet curing at 20°C. The specimens were stored at 20°C in 55% RH for 56 days before the chloride diffusivity measurements.

3. RESULTS AND DISCUSSION

The Ca^{2+} concentration values and the total alkalinity, expressed as hydroxide ion concentration (OH), that characterise the capacity and the rate of the pozzolanic reaction are reported in Table 4 and 5, respectively.

These data show that for complying with the pozzolanic test, the threshold amounts of zeolite in the mixture are, in the case of:

- TON type: 6 per cent;
- MFI type: 9 per cent;
- BEA type: 13 per cent;
- silica fume: 10 per cent.

From the results reported in Table 5, regarding the rate of the pozzolanic reaction, it can be seen that in the case of TON zeolite unsaturated solution in $Ca(OH)_2$ (positive test) appears just after 2 days. In the case of BEA zeolite the positive pozzolanic test is obtained after 3 days, while in the case of zeolite MFI and silica fume after 5 days.

In conclusion, for both capacity and rate of pozzolanic reaction, the best behaviour is showed by TON, with the pozzolanic activity greater than that of silica fume. The behaviour of BEA, MFI and silica fume is quite similar.

Table 4. Pozzolanic Capacity (after 8 days ageing)

Material	Conc. mmol/l	Pozzolanic Material/Cement					
		4/96	6/94	8/92	9/91	10/90	13/87
TON	Ca^{2+}	9.2	7.1				
	OH^-	59.4	53.1				
test		**negative**	**positive**				
BEA	Ca^{2+}					7.1	5.5
	OH^-					69.1	68.8
test						**negative**	**positive**
MFI	Ca^{2+}			7.9	7.5 p		
	OH^-			60.0	58.8		
test				**negative**	**positive**		
SF	Ca^{2+}		10.5	10.6	9.3	8.4	
	OH^-		57.2	54.3	54.0	51.6	
test			**negative**	**negative**	**negative**	**positive**	

Table 5. Rate of Pozzolanic Reaction (Pozzolanic material/Portland cement = 15/85)

Material	Conc. mmol/l	Days				
		1	2	3	4	5
TON	Ca^{2+}	13.6	7.5			
	OH^-	46.4	43.3			
test		**negative**	**positive**			
BEA	Ca^{2+}		8.6	6.5		
	OH^-		55.2	59.5		
test			**negative**	**positive**		
MFI	Ca^{2+}			11.3	8.0	
	OH^-			60.8	55.3	
test				**negative**	**positive**	
SF	Ca^{2+}				10.2	8.6
	OH^-				50.1	46.3
test					**negative**	**positive**

The compressive strength and the consistence of the standard mortars are given in Table 6. It can be seen that the compressive strength of the mortar incorporating silica fume and syntetic zeolites were approximately the same at 2 days as well as at 7 and 28 days, with values higher for the mixtures with BEA in both cases. As regards the workability, the behaviour of the zeolite TON is not satisfactory. The partial addition of the zeolitic material in the Portland cement does not reduce the early and final compressive strength. However, it can be observed that it is possible to produce pozzolanic cements (Type IV EN 197-1) that exhibit high resistance on compression also in the case of short curing.

Table 6. Consistency and Mechanical Strength of the Mortars

Cement	%	Pozzolanic material	%	2 days MPa	7 days MPa	28 days MPa	Consistency %
CEM I	100	-	-	36.4	47.7	56.2	68
CEM I	87	Zeolite BEA	13	37.1	49.2	64.3	57
CEM I	91	Zeolite MFI	9	37.0	46.1	56.0	72
CEM I	94	Zeolite TON	6	32.2	41.4	54.8	7
CEM I	90	Silica fume	10	34.9	44.8	58.9	52

Regarding the compressive strength of concretes, as seen in Table 7, the concrete made with addition of the zeolite BEA exhibits superior mechanical behaviour to those obtained with additions of silica fume.

Table 7. Concretes Compressive Strength

Concrete (made with)	w/c	compressive strength 2 days MPa	compressive strength 7 days MPa	compressive strength 28 days MPa
Zeolite BEA	0.35	78.5	89.3	102,7
Zeolite MFI	0.35	78.0	90.2	93,8
Zeolite TON	0.60	70.1	84.1	57,9
Silica fume	0.35	30.8	42.7	100,3

The concrete prepared with the addition of the zeolite MFI shows slightly inferior mechanical behaviour. In the case of the concretes prepared with the zeolite TON, it was necessary to operate at a w/c ratio equal to 0.60 in order to obtain a workability shown by other concretes. The obtained resistance values were, of course, substantially inferior to those shown by concretes with silica fume.
Regarding the durability, the results obtained are reported in Table 8.

Table 8. Durability test results

Concrete (made with)	Coefficient of Oxygen Permeability K (10^{-16} m^2)	Coefficient of absorption ($g/m^2/s^{0.5}$)	Chloride conductivity Coulombs
Zeolite BEA	0.049	9.5	111
Zeolite MFI	0.052	9.2	108
Silica fume	0.051	9.4	110

As seen from our aim, the tests on the concretes prepared with the zeolite TON were not made. From the results reported in Table 8, it can be seen that all the concretes tested have shown an excellent concrete performance.

4. CONCLUSIONS

Based on the studies of the pozzolanic behaviour, compressive strength and durability, the zeolites BEA and MFI exhibit a pozzolanic activity similar to that of silica fume and can be used as pozzolanic admixtures with high reactivity. The performances of concretes based on these synthetic

zeolites are in all cases similar or higher than those relative to cement and concretes produced with silica fume. The zeolite TON, even though it presented a high pozzolanic activity, is not suitable for the preparation of cements and high performance concrete (HPC) because the mixtures that contain it require a high w/c ratio.

In conclusion, zeolite materials obtained under particular conditions – high specific surface area – can favourably substitute silica fume either to obtain pozzolanic cements with high initial and final resistance or as an active addition to the HCP concrete.

REFERENCES

[1] Neville, A.M. Properties of Concrete, 4th ed. London, Publ. Longman, (1995), pp. 86-87 and pp. 666-667.

[2] Massazza, F. Pozzolana and Pozzolanic Cements, A Chapter of "Lea's Chemistry of Cement and Concrete. Fourth Edition, Ed.P.C.Hewlett, Publ. Arnold, London, (1995)pp. 487-488.

[3] Sersale, R. and Frigione, G. Italian Patent N° 49221 A 83, Milan, Italy, (1983).

[4] Sersale, R. and Frigione, G. Italian Patent N° 46061 A 84 Milan, Italy (1984).

[5] Sersale, R. and Frigione, G. Natural zeolites as constituents of blended cements, Chim Ind., Milan, Italy, vol.67 (1985), pp. 177-180.

[6] Sersale, R. and Frigione, G. Portland-zeolite-cement for minimizing alkali-aggregate expansion, Cem. Concr. Res., vol.17, (1987), pp. 404-410.

[7] Sersale, R. and Frigione, G. An effective utilization of natural zeolites, Rend. Acc. Sc. Fis. Mat. in Napoli, ed. Di Girolamo; Liguori, Naples. Special Issue, (1987), pp. 307-315.

[8] Katovic, A. Subotic, B. Smit, I. and Despotovic, Lj.A. Crystallization of Tetragonal (B_8) and Cubic (B_1) Modifications of Zeolite NaP from Freshly Prepared Gel, Part 2. Kinetics and Crystallization, Zeolite, vol.10, (1990), pp. 634-641.

[9] Katovic, A. Catanzaro, L. and Giordano, G. Synthesis of TON-Type Zeolite From Alcohol-Water Systems, in: Proceedings of AIZ-GIC 2000, Ravello, Italy, (2000), pp. 363-366.

[10] Cosentino, F. Katovic, A. Giordano, G. Lentz P. and Nagy, J. B. Preparation and Characterization of Ton Type Zeolite Catalysts, Stud. Surf. Sci. Catal., vol.125, (1999), pp. 109-116.

[11] Frigione, G.Bonavita, L., Katovic, A. and Giordano, G.; Italian Patent May 9th, (2002).

[12] Meier, W. M. Olson, D.H. and Baerlocher, Ch. Atlas of Zeolite Structure Type, Fourth Edition. ed. Elsevier, London, (1996).

[13] Italian Standards UNI 7044- Determination of consistency of cement mortars using a flow table.Milan, Italy. (1972).

[14] Alexander, M.G. Durability Performance of Concrete Containing Condensed Silica Fume, Cement Concrete Research vol. 29, (1999), pp. 917-922.

[15] Gjorv, O.E. Evaluation of concrete durability based on migration testing, Concrete Repair, Rehabilitation and Protection. Edited by RK Dhir and MR Jones. Publ. E & FN Spon, London, (1996), pp 205-215.

[16] Torrent, R.J. and Jornet, A., The Quality of the Covercrete of Low-, Medium- and High- Strength Concrete. Second Canmet /ACI. Int. Conf. On Durability of Concrete. SP 126-61, vol II, (1991), pp 1147-1161

[17] Kollek, J.J. The determination of the permeability of concrete to oxygen by the Cembureau Method – a Recommendation. Mater. & Struct. vol. 22, (1989), pp 225-230.

[18] Swiss Standards Association, SIA Norm 162/1: Betonbauten. Materialprüfung, Prüfung Nr 5: Wasserleitfähigkeit, (1989).

[19] Standard Method of Test for Rapid Determination of the Chloride Permeability of Concrete. AASHTO T 277-83. American Association of State Highway and Transportation Officials, Washington, D.C. ,(1983), pp 1229-1234.

USE OF FLUIDIZED BED COMBUSTION WASTES FOR THE SYNTHESIS OF LOW-ENERGY CEMENTS

Graziella Bernardo, Milena Marroccoli, Fabio Montagnaro and Gian Lorenzo Valenti

Dipartimento di Ingegneria e Fisica dell'Ambiente, Università degli Studi della Basilicata
Contrada Macchia Romana, 85100 Potenza (Italy), E-mail: valenti@unibas.it

ABSTRACT

Among the low-energy binders, calcium sulphoaluminate cements are worthy of consideration also because a wide range of industrial solid wastes can be utilized in their manufacture. In this paper, it has been proposed the use of mixtures composed of fluidized bed combustion wastes as raw materials for the synthesis of calcium sulphoaluminate cements. Several systems based on two fluidized bed combustion-derived wastes (a sulpho-calcic fly ash and a silico-aluminous fly ash), and a solid waste generated within a traditional coal-fired power plant, were heated in a laboratory electric oven for 2 hours at temperatures ranging from 1050°C to 1300°C. Calcium sulphoaluminate was often obtained and its formation was related to the waste nature and the burning temperature.

1. INTRODUCTION

In the last two decades much attention has been paid to low-energy cements which, compared to Ordinary Portland Cements (OPC), require lower synthesis temperatures or less grinding energy or inexpensive industrial wastes and by-products as raw materials [1-2].

All these features belong to calcium sulphoaluminate ($C_4A_3\bar{S}$)-based cements [3-9], inasmuch as they can be obtained at temperatures of 1300-1350 °C and the resulting clinkers are relatively friable. Furthermore, in the manufacture of Calcium Sulpho-Aluminate (CSA) cements a wide range of solid residues such as metallurgical slag, fly ash, chemical gypsum and other waste materials containing CaO, SiO_2, Al_2O_3 and SO_3 can be employed.

The aim of this work is to assess the suitability of Fluidized Bed Combustion (FBC) wastes as raw mix components for the CSA cements manufacture, and to investigate the influence of the thermal treatment on the synthesis process. This paper follows some preliminary investigations on residues generated in a FBC laboratory apparatus, whose results are reported elsewhere [10].

2. PROPERTIES AND USES OF CSA CEMENTS

The performance of sulphoaluminate cements is mainly due to the generation of ettringite, $C_6A\bar{S}_3H_{32}$, upon $C_4A_3\bar{S}$ hydration. Calcium sulphoaluminate can react with water in two ways: *i)* together with lime and calcium sulphate to give only ettringite, reaction (1); *ii)* combined with calcium sulphate alone to give ettringite and aluminium hydroxide, reaction (2):

$$C_4A_3\bar{S} + 6C + 8C\bar{S} + 96H \Rightarrow 3C_6A\bar{S}_3H_{32} \quad (1)$$

$$C_4A_3\bar{S} + 2C\bar{S} + 38H \Rightarrow C_6A\bar{S}_3H_{32} + 2AH_3 \quad (2)$$

Ettringite synthesized in the reaction (1) has expansive characteristics which can be exploited by special binders like shrinkage-resistant and self-stressing cements [11-12]. On the other hand, ettringite formed in the reaction (2) is not expansive and has the important property of giving high mechanical strength at early ages [13, 7].

Besides calcium sulphoaluminate, C_2S, C_4AF, $C_5S_2\bar{S}$, C_2AS, CA, $C_{12}A_7$ and C_3A can occur in CSA cements depending on the composition and proportioning of the raw materials employed for their manufacture. Among these compounds only C_2S, which reacts with water to produce calcium silicate hydrates like in OPC, is able to regulate strength and durability of the hydrated cements, especially at medium and long ages. The other above-mentioned phases have a poor hydraulic behaviour and provide a small contribution to the mechanical properties [14-15].

The commercially employed $C_4A_3\bar{S}$-based products are generally used in expansive binders for special applications. There are two types of these formulations: *i)* cements having a high $C_4A_3\bar{S}$ content acting as additives for OPC; *ii)* modified OPC containing $C_4A_3\bar{S}$ instead of C_3A. In both cases $Ca(OH)_2$, derived from hydration of C_3S and C_2S present in OPC, produces the desired expansive effect, due to its combination with $C_4A_3\bar{S}$ and $CaSO_4$.

Applications on industrial scale of CSA cements as structural and dimensionally stable materials have been made only in China. The first Chinese $C_4A_3\bar{S}$-based binders were manufactured about 30 years ago and the present production is about 1 million tons per year. The main features of these cements are, besides a high early strength, good impermeability and freezing-resistance, low dry-shrinkage and solution alkalinity, outstanding chemical corrosion resistance [8]. In other countries the synthesis of rapid-hardening CSA cements has been already performed at laboratory scale or in pilot plants and there is an increasing interest, especially in Europe, towards them [9].

3. CHARACTERISTICS OF FBC ASHES

The FBC technology is very effective in the burning of solid fuels ensuring also a low environmental impact. Among the main advantages of this technique there is the possibility of removing sulphur dioxide generated by coal combustion through the *in situ* injection of calcium-based sorbents (*e.g.* limestone). Under the common FBC operating conditions (850°C and 1atmosphere), a limestone-based sorbent is able to capture SO_2 by means of a two-step reaction mechanism:

$$CaCO_3 \Rightarrow CaO + CO_2 \quad (3)$$

$$CaO + SO_2 + \tfrac{1}{2}O_2 \Rightarrow CaSO_4 \quad (4)$$

Sorbent particles are subject to a rapid calcination, reaction (3), in which calcium carbonate fast decomposes into a porous CaO, further involved in a sulphation reaction (2) thus giving $CaSO_4$. Due to peculiar mechanistic aspects [16] the conversion of CaO into $CaSO_4$ is far from complete: exhausted sorbent particles are therefore composed of unconverted calcium oxide and reacted calcium sulphate. This is related to the onset of significant diffusional resistances as a sulphated shell, characterized by low porosity, builds up around a largely unconverted porous core [17].

One of the main obstacles to a definitive success of FBC technology is represented by the great quantity and the poor quality of solid residues, compared to those of the ashes coming from

traditional pulverized coal plants. Therefore FBC waste disposal and utilization is quite difficult, and the identification of suitable application fields for such residues is of critical importance [18, 10]. The high amounts of FBC residues (which mainly contain coal ash and exhausted sorbent) are due to the need of an overstoichiometric sorbent feed, because of the incomplete sorbent sulphation. In the United States, more than 50% of the electric power is produced within coal plants, thus leading to the formation of more than 100 million tons per year of coal combustion by-products. A remarkable contribution to the generation of such residues is given by FBC plants: about 100kg of waste per coal ton are produced during a combustion process with *in situ* desulphurization, namely ~40% more than that generated in a pulverized coal plant [19]. Moreover the scarcity of quality FBC wastes is related to their peculiar chemical and mineralogical characteristics, *i.e.* the high free calcium oxide concentration and the poor amorphous phase content (due to the relatively low combustion temperatures). CaO can interact in landfill with atmospheric agents giving rise to expansive phenomena, loss of stability and subsoil alteration [20-24], while the reduced formation of a glassy state in the ashes lowers their pozzolanic activity and compromises their re-use in traditional fields of utilization such as cement and concrete industries.

4. EXPERIMENTAL

As main characterization techniques, X-Ray Fluorescence (XRF) and X-Ray Diffraction (XRD) analyses were employed. XRD analysis was also used for quantitative determinations on burnt mixes, in order to study the reacting system behaviour in terms of conversion and selectivity towards $C_4A_3\bar{S}$ and other useful phases.

Two FBC wastes, ***A*** (a sulpho-calcic fly ash) and ***B*** (a silico-aluminous fly ash), coming from industrial plants, were utilized as raw mix components. Furthermore, a solid waste (***C***) generated within a traditional coal-fired power plant as well as AR-grade $CaCO_3$, Al_2O_3 and $CaSO_4 \cdot 2H_2O$ were usefully employed as raw mix ingredients. Several combinations of the above-mentioned materials were heated in a laboratory electric oven for 2 hours at temperatures ranging from 1050°C to 1300°C.

5. RESULTS AND DISCUSSION

5.1 Proportioning of Raw Mixes

Table 1 and Figure 1 show the XRF and XRD data on samples ***A***, ***B*** and ***C***, respectively. From the characterization results it can be argued that:
i) ***A*** shows a high amount of the sulpho-calcic fraction and a not negligible quantity of the silico-aluminous fraction. Traces of Fe_2O_3 (hematite) and $CaCO_3$ (calcite) were also detected by XRD analysis, according to the chemical composition data;
ii) ***B*** has a low calcium and sulphur content as well as a high concentration of the silico-aluminous fraction. Iron content and loss on ignition were mostly associated with Fe_3O_4 (magnetite) and calcite;
iii) ***C*** has the highest calcium content as well as sulpho-calcic and silico-aluminous fractions comprised between those contained in ***A*** and ***B*** samples. Traces of hematite and calcite were also detected by XRD analysis, according to the chemical composition data.

Three mixtures based on a single waste and two mixtures composed of a couple of wastes have been designed (Table 2). Mixtures ***1*** and ***2*** contain FBC fly ash ***A***, $CaCO_3$ and Al_2O_3; mixture ***3*** contains FBC fly ash ***B***, $CaCO_3$ and $CaSO_4 \cdot 2H_2O$; mixture ***4*** contains ***A*** and ***B***; mixture ***5*** contains ***B*** and ***C***. Compositions ***1*** and ***3*** were established with the purpose of converting all the sulphate into $C_4A_3\bar{S}$. Composition ***2*** was conceived for combining all the available sulphate and silica into $C_4A_3\bar{S}$ (as main component) and C_2S, respectively. Compositions ***4*** and ***5*** were aimed at obtaining

the maximum $C_4A_3\bar{S}$ concentration, allowing to avoid the use of external sources of lime, alumina and sulphate.

Table 1. Chemical composition of ***A***, ***B*** and ***C*** samples, wt%.

	A	***B***	***C***		***A***	***B***	***C***
CaO	48.39	3.86	54.46	TiO_2	0.20	0.92	0.28
MgO	1.57	3.11	1.50	Cr_2O_3	0.01	0.02	0.01
Al_2O_3	5.33	24.83	8.50	Mn_3O_4	0.06	0.12	0.06
SiO_2	11.81	48.57	18.23	Fe_2O_3	3.60	6.82	3.43
P_2O_5	0.70	/	0.50	Na_2O	0.05	0.32	0.06
SO_3	24.55	0.88	11.45	SrO	0.14	0.06	0.12
K_2O	0.39	4.52	1.02	l.o.i.*	3.05	6.11	0.65
				total	99.85	100.14	100.27

* loss on ignition at 975°C

Table 2. Raw mixes composition, wt%.

Mixture	***A***	***B***	***C***	AR-grade $CaCO_3$	AR-grade Al_2O_3	AR-grade $CaSO_4 \cdot 2H_2O$
1	44.47	/	/	16.19	39.34	/
2	37.85	/	/	28.67	33.48	/
3	/	76.53	/	14.22	/	9.25
4	24.40	75.60	/	/	/	/
5	/	62.10	37.90	/	/	/

5.2 Burning of Raw Mixes

5.2.1 Mixture 1

The most interesting results were obtained at 1250°C and 1300°C. No significant differences were observed between the samples heated at these temperatures. The principal observations are the following:

i) the main reactive oxides (CaO, SiO_2, Al_2O_3, SO_3) are completely consumed;

ii) the main product is $C_4A_3\bar{S}$;

iii) among the minor phases there are $C_5S_2\bar{S}$ (calcium sulphosilicate) and C_2AS (gehlenite).

Figure 2 shows the diffractogram for the sample heated at 1300°C.

5.2.2 Mixture 2

Again, the most interesting results were obtained at 1250°C and 1300°C. At both temperatures, the main products are, as planned, $C_4A_3\bar{S}$ and C_2S (larnite), respectively. Furthermore it can be noted (Figure 3) that the reagent oxides are fully converted, while $C_5S_2\bar{S}$ and C_2AS are present only in traces.

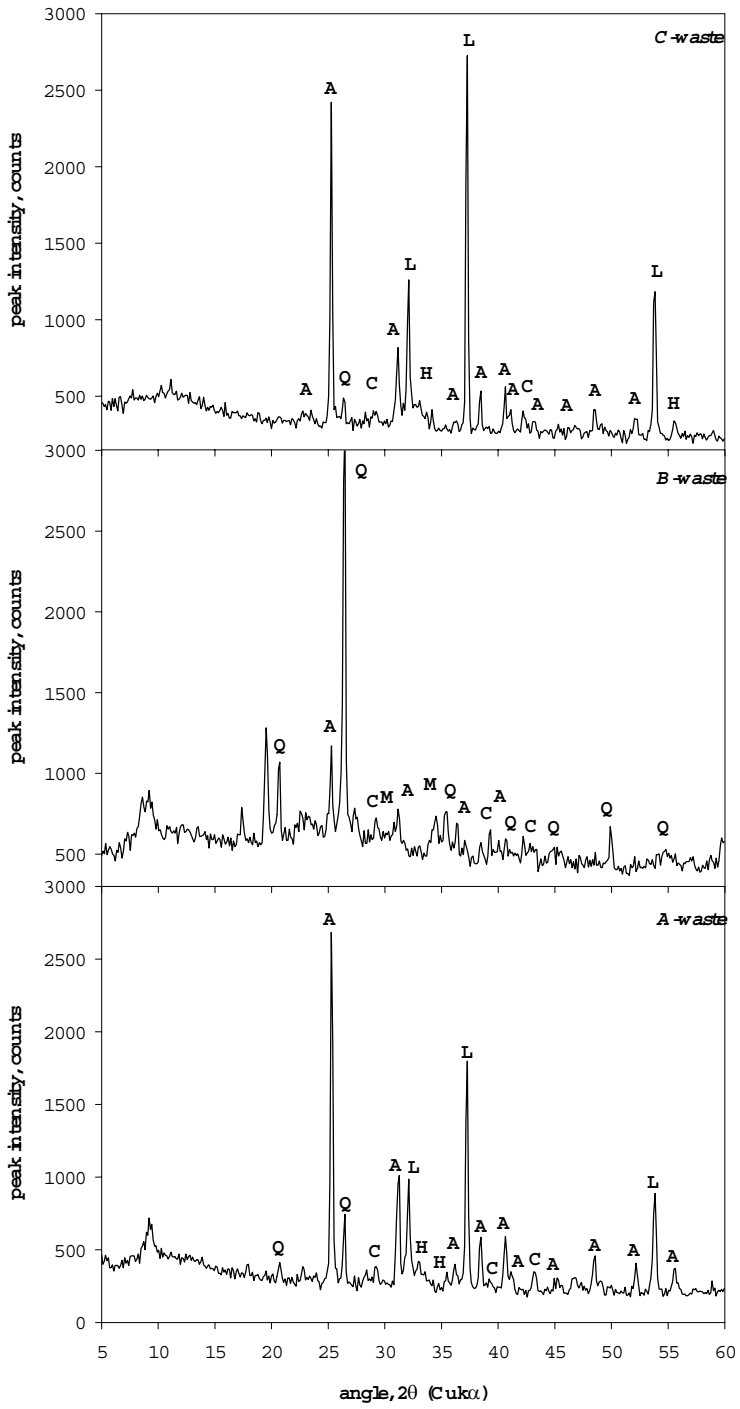

Figure 1. XRD analysis for ***A***, ***B*** and ***C*** samples. A=anhydrite ($CaSO_4$), C=calcite ($CaCO_3$), H=hematite (Fe_2O_3), L=lime (CaO), M=magnetite (Fe_3O_4), Q=quartz (SiO_2).

5.2.3 Mixture 3

At temperatures higher than 1100°C melting phenomena occurred. At the temperatures of 1050°C and 1100°C the most important results were the following:

i) CaO and Al_2O_3 are fully converted;

ii) SiO_2 and $CaSO_4$ are partially converted;

iii) the main products at 1050°C are $C_5S_2\bar{S}$-C_2AS and $C_4A_3\bar{S}$ (respectively);

iv) the main products at 1100°C are $C_4A_3\bar{S}$ and $C_5S_2\bar{S}$-C_2AS (respectively).

In Figure 4 are reported XRD analyses for the samples heated at 1050°C and 1100°C.

5.2.4 Mixture 4

At temperatures higher than 1150°C melting phenomena occurred. At 1100°C it was noted that:
i) CaO is fully converted;
ii) SiO_2, Al_2O_3 and $CaSO_4$ are partially converted;
iii) the main products are $C_5S_2\bar{S}$-C_2AS and $C_4A_3\bar{S}$ (respectively).

At 1150°C it was noted that:
i) CaO and $CaSO_4$ are fully converted;
ii) SiO_2 and Al_2O_3 are partially converted;
iii) the main products are $C_5S_2\bar{S}$-C_2AS, CAS_2 (anorthite) and $C_4A_3\bar{S}$ (respectively).
Figure 5 indicates the diffractogram for the sample burnt at 1150°C.

5.2.5 Mixture 5

At temperatures higher than 1150°C melting phenomena occurred. At 1100°C the principal findings are the following:
i) CaO, SiO_2, Al_2O_3 and SO_3 are partially converted;
ii) the main products are $C_5S_2\bar{S}$ and C_2AS;
iii) $C_4A_3\bar{S}$ is present only in traces.

At 1150°C it was observed that:
i) CaO, Al_2O_3 and $CaSO_4$ are fully converted;
ii) SiO_2 is partially converted;
iii) the main products are $C_5S_2\bar{S}$-C_2AS, CAS_2 and $C_4A_3\bar{S}$ (respectively).
Figure 6 reports XRD results for the sample heated at 1150°C.

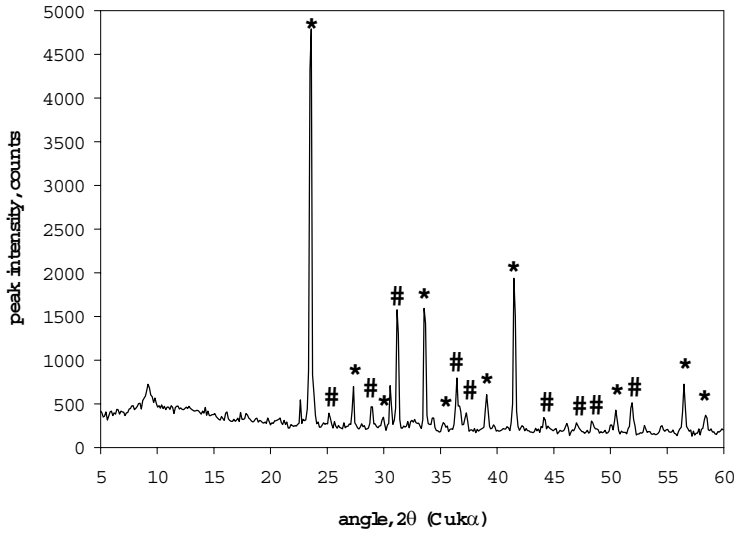

Figure 2. XRD analysis for mixture ***1*** burnt at 1300°C. *=calcium sulphoaluminate ($C_4A_3\bar{S}$), #=calcium sulphosilicate-gehlenite ($C_5S_2\bar{S}$-C_2AS, these phases can be present alone or together inasmuch as their strongest signals overlap).

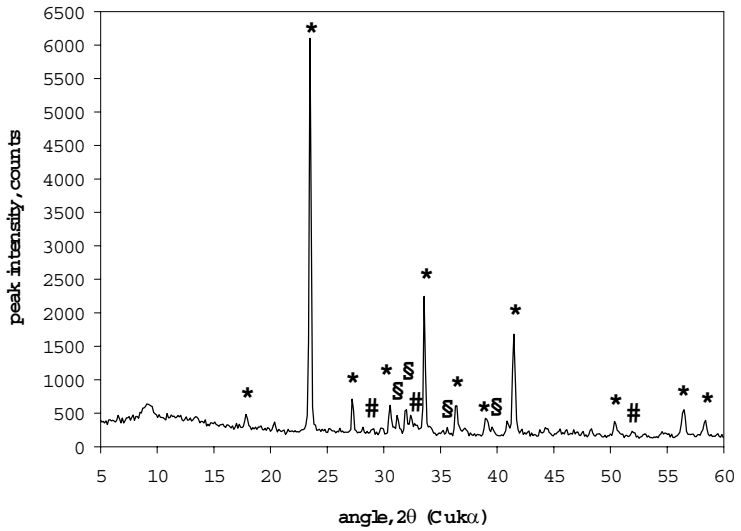

Figure 3. XRD analysis for mixture ***2*** burnt at 1300°C. *=calcium sulphoaluminate ($C_4A_3\bar{S}$), §=larnite (C_2S), #=calcium sulphosilicate-gehlenite ($C_5S_2\bar{S}$-C_2AS).

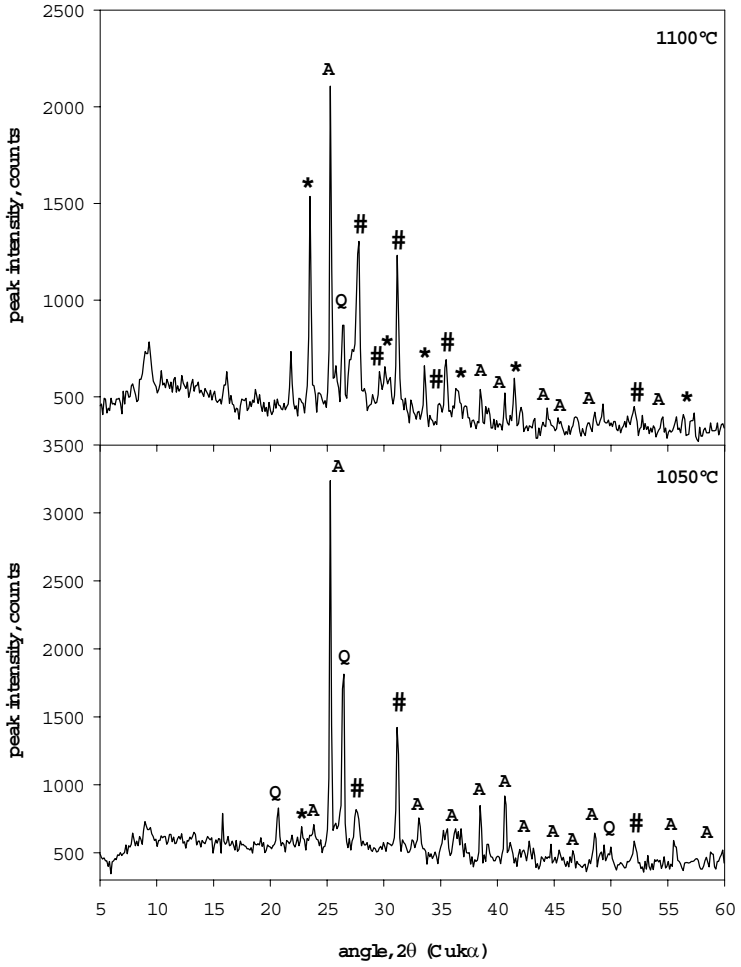

Figure 4. XRD analysis for mixture ***3*** burnt at 1050°C and 1100°C. A=anhydrite ($CaSO_4$), Q=quartz (SiO_2), *=calcium sulphoaluminate ($C_4A_3\bar{S}$), #=calcium sulphosilicate-gehlenite ($C_5S_2\bar{S}$-C_2AS).

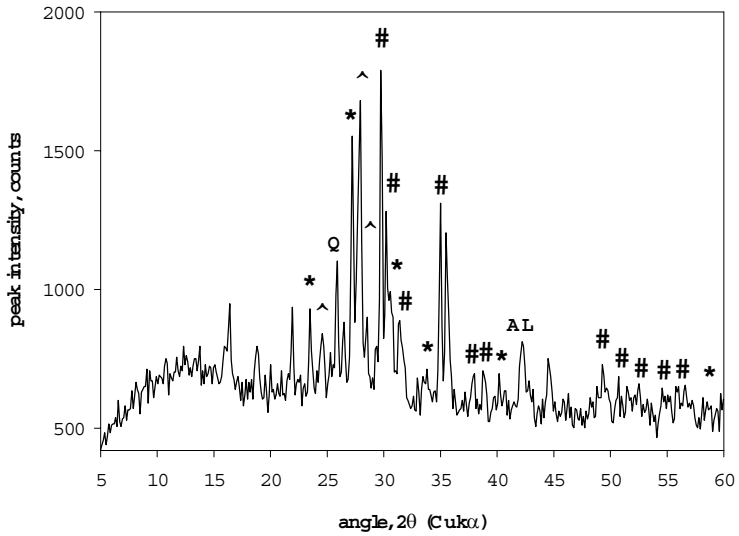

Figure 5. XRD analysis for mixture ***4*** burnt at 1150°C. AL=alumina (Al_2O_3), Q=quartz (SiO_2), *=calcium sulphoaluminate ($C_4A_3\bar{S}$), ^=anorthite (CAS_2), #=calcium sulphosilicate-gehlenite ($C_5S_2\bar{S}$-C_2AS).

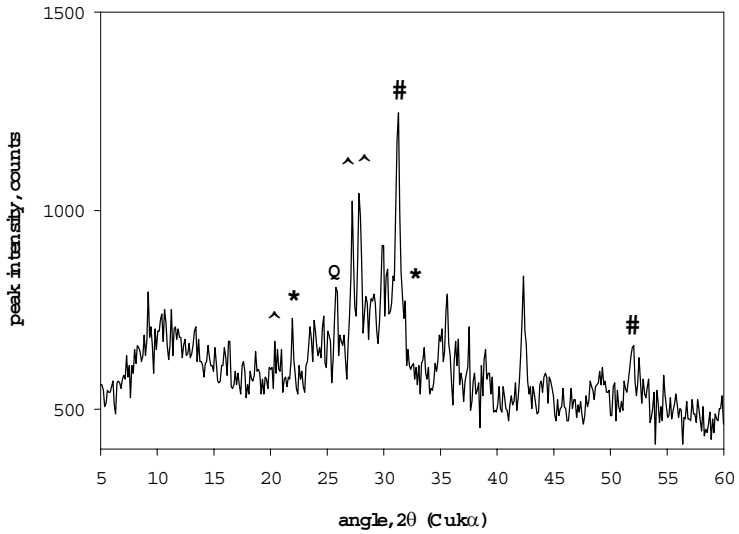

Figure 6. XRD analysis for mixture ***5*** burnt at 1150°C. Q=quartz (SiO_2), *=calcium sulphoaluminate ($C_4A_3\bar{S}$), ^=anorthite (CAS_2), #=calcium sulphosilicate-gehlenite ($C_5S_2\bar{S}$-C_2AS).

5.3 Principal Considerations

The above-mentioned results indicate that mixtures based on fluidized bed combustion wastes are able to generate phases of interest for calcium sulphoaluminate cements. This aptitude mainly depends on the nature of the wastes employed and on the synthesis temperature. The best results have been obtained at the highest temperatures (1250°C and 1300°C), whereas the poor performance of some systems has to be related to limitations on the maximum temperature which can be reached without the occurrence of melting phenomena.

It is unlikely that a single FBC waste can give the amounts of CaO, Al_2O_3, SO_3, and SiO_2 required by the formation of significant $C_4A_3\bar{S}$ and C_2S contents. It seems very interesting to rely on other industrial wastes and by-products, instead of commercial raw materials, as external sources of the

needed oxides. The results shown by mixtures in which a FBC waste or another industrial waste was added to a given FBC ash were unsatisfactory. Combinations of several FBC wastes and other industrial by-products will be experienced in order to obtain high conversion and selectivity degrees towards $C_4A_3\bar{S}$ and C_2S.

6. CONCLUSIONS

Fluidized bed combustion ashes are mainly composed by SiO_2, Al_2O_3, CaO and SO_3, have a poor pozzolanic behaviour and frequently contain high free lime amounts. Therefore, these wastes generally cannot be utilized in the manufacture of ordinary Portland and blended cements but may be of interest as raw materials for the synthesis of calcium sulphoaluminate-based cements.

It has been found that mixtures based on fluidized bed combustion ashes are able to generate $C_4A_3\bar{S}$ and C_2S, which are the main components of the calcium sulphoaluminate-belite cements. The nature of the employed wastes and the thermal treatment modalities can significantly affect the synthesis process.

In the near future the possibility of using different combinations of fluidized bed combustion ashes and other industrial wastes to achieve high conversion and degree of selectivity of $C_4A_3\bar{S}$ and C_2S will be explored.

REFERENCES

[1] Mehta, P.K. Investigations on energy-saving cements, World Cement Technology, May, p.166 (1980).

[2] Kouznetsova, T.V. Development of special cements, Proceedings of the 10th International Congress on the Chemistry of Cement (Goteborg), vol.1, p.i001 (1997).

[3] Beretka, J., Santoro, L., Sherman, N. and Valenti, G.L. Synthesis and properties of low energy cements based on $C_4A_3\bar{S}$, Proceedings of the 9th International Congress on the Chemistry of Cement (New Delhi), vol.3, p.195 (1992).

[4] Beretka, J., de Vito, B., Santoro, L. and Valenti, G.L. Utilization of industrial wastes and by-products for the synthesis of special cements, Resources, Conservation and Recycling, vol.9, p.179 (1993).

[5] Belz, G., Beretka, J., Marroccoli, M., Santoro, L., Sherman, N. and Valenti, G.L. Use of fly ash, blast furnace slag and chemical gypsum for the synthesis of calcium sulfoaluminate based cements, Fly ash, silica fume, slag and natural pozzolans in concrete (special publication n°153 of the American Concrete Institute), vol.1, p.513 (1995).

[6] Beretka, J., Cioffi, R., Marroccoli, M. and Valenti, G.L. Energy-saving cements obtained from chemical gypsum and other industrial wastes, Waste Management, vol.16, p.231 (1996).

[7] Beretka, J., Sherman, N., Marroccoli, M., Pompo, A. and Valenti, G.L. Effect of composition on the hydration properties of rapid-hardening sulfoaluminate cements, Proceedings of the 10th International Congress on the Chemistry of Cement (Goteborg), vol.2, p.2ii029 (1997).

[8] Su, M., Wang, Y., Zhang, L. and Li, D. Preliminary study on the durability of sulfo/ferro-aluminate cements, Proceedings of the 10th International Congress on the Chemistry of Cement (Goteborg), vol.4, p.4iv029 (1997).

[9] Glasser, F.P. and Zhang, L. High-performance cement matrices based on calcium sulfoaluminate-belite compositions, Cement and Concrete Research, vol.31, p.1881 (2001).

[10] Bernardo, G., Marroccoli, M., Montagnaro, F. and Valenti, G.L. Utilization of wastes derived from fluidized bed combustion and desulphurization of coals as sources of raw materials, Materials Engineering, vol.11, p.359 (2000).

[11] Mehta, P.K. Mechanism of expansion associated with ettringite formation, Cement and Concrete Research, vol.3, p.1 (1973).

[12] Mehta, P.K. and Polivka, M.S. Expansive cements, Proceedings of the 5th International Congress on the Chemistry of Cement (Moscow), p.3 (1974).

[13] Sudoh, G., Ohta, T. and Harada, H. High strength cement in the CaO-Al_2O_3-SiO_2-SO_3 system and its application, Proceedings of the 7th International Congress on the Chemistry of Cement (Paris), vol.3, p.152 (1980).

[14] Beretka, J., de Vito, B., Santoro, L., Sherman, N. and Valenti, G.L. Hydraulic behaviour of calcium sulfoaluminate-based cements derived from industrial process wastes, Cement and Concrete Research, vol.23, p.1205 (1993).

[15] Beretka, J., Santoro, L., Sherman, N. and Valenti, G.L. Long-term behaviour of hydraulic binders based on calcium sulfoaluminate and calcium sulfosilicate, Cement and Concrete Research, vol.25, p.113 (1995).
[16] Anthony, E.J. and Granatstein, D.L. Sulfation phenomena in fluidized bed combustion systems, Progress in Energy and Combustion Science, vol.27, p.215 (2001).
[17] Montagnaro, F., Scala, F. and Salatino, P. The influence of sorbent properties and reaction temperature on sorbent attrition, sulphur uptake and particle sulphation pattern during fluidized bed combustion, Proceedings of the 2nd Mediterranean Combustion Symposium (Sharm El-Sheikh), vol.2, p.827 (2002).
[18] Julien, S., Brereton, C.M.H., Lim, C.J., Grace, J.R., Chiu, J.H. and Skowyra, R.S. Spent sorbent reactivation using steam, Proceedings of the 13th International Conference on Fluidized Bed Combustion (Orlando), vol.2, p.841 (1995).
[19] Kim, A.G., Aljoe, W. and Renninger, S. Wastes from the combustion of fossil fuels: research perspective on the regulatory determination, Proceedings of the 16th International Conference on Fluidized Bed Combustion (Reno), cd-rom paper n°01-0156 (2001).
[20] Bland, A.E., Georgiou, D.N. and Anthony, E.J. Sea water conditioning of CFBC ash, Proceedings of the 12th International Conference on Fluidized Bed Combustion (San Diego), vol.2, p.835 (1993).
[21] Anthony, E.J., Iribarne, A.P. and Iribarne J.V. Study of hydration during curing of residues from coal combustion with limestone addition, Proceedings of the 13th International Conference on Fluidized Bed Combustion (Orlando), vol.2, p.1113 (1995).
[22] Anthony, E.J., Iribarne, A.P., Iribarne J.V. and Jia, L. Reuse of landfilled FBC residues, Fuel, vol.76, p.603 (1997).
[23] Bland, A.E. Effect of curing conditions on the geotechnical and geochemical properties of CFBC ashes, Proceedings of the 15th International Conference on Fluidized Bed Combustion (Savannah), cd-rom paper n°99-0148 (1999).
[24] Bulewicz, E.M., Dudek, K., Góra, D. and Taraszka, J. Possible causes of the variability of FBC ash behaviour, Combustion Science and Technology, vol.153, p.141 (2000).

USE OF FLUIDIZED BED COMBUSTION WASTES FOR THE SYNTHESIS OF LOW-ENERGY CEMENTS

Graziella Bernardo, Milena Marroccoli, Fabio Montagnaro and Gian Lorenzo Valenti

Dipartimento di Ingegneria e Fisica dell'Ambiente, Università degli Studi della Basilicata
Contrada Macchia Romana, 85100 Potenza (Italy), E-mail: valenti@unibas.it

Gian Lorenzo Valenti is Professor of Materials Science and Technology at the Department of Environmental Engineering and Physics, University of Basilicata (Potenza, Italy). He teaches also at Naples (University Federico II and Second University).

Since 1970, year of his Master Degree in Chemical Engineering, he has been engaged in researches concerning cement chemistry and technology as well as utilization of industrial wastes and by-products in the building materials industry.

He is the author or co-author of more than 100 papers published on scientific journals and proceedings of international conferences, among which the 7th, 8th, 9th and 10th International Congress on the Chemistry of Cement.

Prof. Gian Lorenzo Valenti
E-mail: valenti@unibas.it
Tel: +39 0971 205 224)
Department of Environmental Engineering and Physics
University of Basilicata
Contrada Macchia Romana
85100 Potenza (Italy)

SULFATE IN CEMENT AND CONCRETE - LET'S START AT THE BEGINNING

William G. Hime

Wiss, Janney, Elstner Associates, Inc., Northbrook, IL USA, E-mail: whime@wje.com

ABSTRACT

Until the end of the nineteenth century gypsum was not a deliberately introduced component of Portland cement. Then, from about 1900 to 1950, it was added at about 2% by weight as SO_3, and now, 50 years later, it is often nearly twice that level. However, the usual understanding of the chemistry of Portland cement and concrete has been based on the lower SO_3 levels.

Regarding distress due to sulfate intrusion into concrete, the development of sulfate resistant cements was based on the understanding that "sulfate attack" involved the production of ettringite. Now the term "sulfate attack" is also used when gypsum is the reaction product, and even for all those chemical and physical reactions that occur when substances such as sodium sulfate, magnesium sulfate, and hydrogen sulfate (sulfuric acid) intrude into concrete. As a consequence, the world literature has become so confused that the consequences of the reactions between sulfate-containing chemicals and concrete are erroneously reported in much of the literature. Further, changes in the sulfate content of the cement over the years have significantly increased the sulfate resistance of concrete.

This paper seeks to clarify the influence of sulfate on the properties of Portland cement concrete, in a historical context, and also considers the author's experiences with internal sulfate attack and delayed ettringite formation.

1. INTRODUCTION

Definitions of Portland cement often include the phrase: "and calcium sulfate as an interground addition." That phrase would not apply to Aspdin's invention or indeed to virtually any "Portland cement" produced during the nineteenth century.

Today's Portland cement often contains over 3% SO_3 by weight, and indeed an increasing number of manufacturers produce Type III cements with over 4% SO_3 – about the equivalent of 10% gypsum. The ramifications of this change have eluded most investigators, and are discussed herein.

2. HISTORY OF SULFATE IN PORTLAND CEMENT

2.1 The First 65 Years (1824-1889)

Impetus for the development of a hydraulic cement was provided by Smeaton in 1776 when he published his report showing that such a material required more than a lime system; siliceous or aluminous components, or both, were necessary [1].

Joseph Aspdin patented "Portland Cement" in 1824, but his son William said that his father had produced it as early as 1811. The patent failed to disclose either the raw material proportions or the need to heat the clinker to incipient fusion [2]. In fact, the historic evidence is that Aspdin's Portland cement was probably seldom similar to that which has been produced in the last eighty

years. Although Frost apparently was the first to make a plant for Portland cement production [3], Joseph and, independently, William Aspdin, both set up cement plants from 1826 to 1847 [4].

During this entire period there is no evidence that calcium sulfate, as plaster (hemihydrate) or gypsum, was intentionally added to the clinker. Aspdin and his sons James and William did add copper sulfate and other sulfates to the raw mix [5], very probably for no reason than as a subterfuge to confuse competitors. However, we have found copper slag in the fleur-de-lys at the top of the concrete wall around William Aspdin's home, Portland Hall, Gravesend, England [6], which is perhaps the oldest reinforced Portland cement concrete [7]. Some of the slag has the same fineness of the cement, and may have been a component of it rather than an admixture to the concrete.

William Aspdin did, at least at one plant, use thousands of tons of "alkali waste" as a patented raw material for Portland cement. This material contained calcium and alkali sulfates [8]. However, in attempts by others to use alkali wastes, "the amount of calcium sulfate present prevented the manufacture of a satisfactory cement" [9]. Indeed desulfurization processes were used to recover the sulfur, and to allow a "better chance of making a good cement" [10].

A question as to why the cement during this period of time did not set too quickly due to the rapid reaction of the tricalcium aluminate component with water has largely been unasked. One answer may be that the cement was ground too coarsely to expose much C_3A. Indeed, Portland cements of this period were far coarser than present-day cements that have 90-plus percent passing a 325 mesh screen. A fineness of 90% passing a 30 mesh screen was reported in 1879 [11].

A second possible answer to the setting question is that at that time vertical kilns were used to burn the raw materials. Thus sulfur oxides from the fuel circulated through the bed of raw materials. According to one report, "the atmosphere was always hot and sulpherous"[12]. Sulfate analyses during this period were apparently seldom made and were variously reported as "sulfuric acid"[13, 14], anhydrous sulfuric acid [15] "sulfuric anhydride"[16], "sulfate of lime"[17] and SO_3. Reported analyses for sulfur ranged from "a trace" as sulfuric acid for Aspdin's cement (but the same London chemist also found 45% calcium phosphate! [14]), to 1% as sulfuric anhydride (SO_3) for an 1849 sample [18]. Analyses of concrete in 1851 [19] found 0.31% sulfuric anhydride.

Eckel [20] presented analyses of Portland cements from 1849 to 1873. The SO_3 contents for English Portland cements were about 1%; however, for a 1873 cement from Austria the value was 2.1%. Analyses of English cements in the 1880s and 1890s disclosed 0.5% to about 2% "sulfuric acid" [21]. Cummings [22] detailed the analyses of 53 cements, some of which were decades old, but likely dated from the late 1890's. Only six were analyzed for "sulfate of lime," and seven of those ranged from 0.3 to 1.0% as SO_3. A "Gate of France Hydraulic Cement" contained 2% SO_3.

The production of Portland cement in the United States didn't start until late in the century. Saylor, in 1871 in the United States patented a "natural cement" that was "in every respect equal to the Portland cement made in England," and indeed may have been Portland cement. The Portland cement industry in the U.S. had apparently begun. [23].

2.2 The Next 30 years (1890-1920)

Beginning just before 1890, several events led to enormous changes in the composition and manufacturing process of Portland cement. Among the mechanical changes were the introduction of better grinding mills and the rotary kiln. The former made the cement (the ground clinker) much faster reacting. Over 95 percent of the cement particles now passed a No. 50 sieve [24]. The latter, as patented by Crampton in 1877 and Ransome in 1885 [25], substantially decreased the sulfur content of the clinker since the gases did not significantly pass through the charge. As a result, the

setting of cement generally changed from slow to rapid [26]. The rotary kiln did not "take firm hold" in the U.K. until 1903 [27].

Just how the discovery of the set-control properties of calcium sulfate came about has not been well established, but obviously the problem demanded urgent research. In the United States the deNavarro family led innovation in the industry in the 1880's and 1890's; they built the first rotary kiln (24 ft long!), established the Keystone Company (later the Atlas Cement Company) and performed "numerous experiments…(that) would fill a book" [28]. Fortuitously, the deNavarro's brought in a French chemist, P.I. Giron, who had learned in France that when making "cement sidewalks" the time of set of the mortar could be materially retarded by adding plaster into the mix water. As a result, carloads of plaster were brought into the plant to add to the clinker. To befuddle competitors, those carloads were billed as "returned cement"[29].

Although plaster was found to be more effective, on a weight comparison basis, than gypsum, someone realized the materials were the same after addition of water, and gypsum was a lot cheaper. By the early 1900's, most Portland cement manufacturers worldwide added gypsum to the ground clinker, or ground the kiln clinker with the gypsum.

The first ASTM and British specifications for Portland cement were issued in 1904. For ASTM the specification was designated C 9-04. The British specification limited the SO_3 content to 2.5% (changed to 2.75% in 1907) [30)], while the ASTM limit was 1.75% (increased to 2.0% in 1917).

This same period of time saw tremendous increases in production of Portland cement, in part because of the increased use of reinforced concrete. In 1890, the U.S. output was 335,000 barrels. This rose to one million barrels in 1895, $8\frac{1}{2}$ million in 1900, 35 million in 1905, and $76\frac{1}{2}$ million in 1910 [31]. European demand increased at a similar rate: Germany had three Portland cement works in 1854, 420 in 1882, and 1274 in 1894 [32].

2.3 The Next 30 years (1920-1950)

By 1920 Portland cement consisted of clinker interground with gypsum. In the same year, an ASTM Specification was adopted that represented an agreement "between all authorities in the United States" [33]. Interestingly ASTM C 9-21 as first published used a capital P for Portland. But as republished in 1924, the lower case was used, as it has been since then [34], and is so used herein. Further, the designation was changed from C 9 to C 150 in 1941 (C150-41). In 1941, due to increasing incidences of "sulfate attack," American specifications now covered five types of cement, with Types II and V having limits on both C_3A and SO_3, perhaps largely the result of studies by Tuthill [35]. Analyses by the Portland Cement Association [36], of several Portland cements from each of the five types, as reported by Bogue [37] and Eckel [38], disclosed that the SO_3 levels for each type of cement were generally less than 2%, and only Type III had an average level over 2%.

Interestingly, Anderegg in 1929 suggested that for the finer cements additional sulfate should be present to react with the aluminates and thus prevent the possibility of subsequent sulfate attack [39]. There is no evidence that subsequent increases in SO_3 content were made for that reason.

2.4 The Last 50 Years (1950-2000)

With greatly increased needs for low cost construction materials and for rapid procedures for building bigger and taller structures, the Portland cement industry began producing cements that provided substantially higher early strengths. To do this they increased the finenesses and the SO_3 contents of the cements, not only for Type III, but also for the other four types.

The most remarkable aspect of present-day Portland cements, at least for those produced in the U.S., is their SO_3 contents. In a survey by Gebhardt [40] of all of the Portland cements produced in this country during the mid-1990's, the average SO_3 contents of Types I, III and IV cements were above the numerical limits of the ASTM C 150 specification! (Gebhardt, however, had various classifications within each type) This interesting development occurred because the C 150 footnotes allow a cement to exceed the numerical limit if the cement passes a test to show that it will not cause deleterious expansion. Unfortunately, the test now used is unable to detect cements that can cause delayed ettringite formation.

3. THE EFFECTS OF SO_3 CONTENT CHANGES

3.1 Sulfate Minerals in Hydrated Cement

The literature is now in general agreement about the chemistry of sulfate in hydrated cement systems; ettringite ($C_3A{\cdot}3CaSO_4{\cdot}32H_2O$) is produced within minutes after addition of water. The calcium sulfate component reacts with tricalcium aluminate or its hydrates. When all the sulfate is combined as ettringite, then any excess C_3A will react with it to produce "monosulfate" (calcium monosulfoaluminate hydrate, $C_3A{\cdot}CaSO_4{\cdot}12H_2O$).

Investigators throughout the twentieth century have suggested that most or all of the ettringite is replaced by monosulfate in days, months, or years, apparently not realizing that SO_3/C_3A mortar ratios have increased over the century so that the ratio in many cements is now more than 1, meaning that some ettringite remains. And for some, the ratio is as high as 3, thus indicating that no monosulfate may ever be produced!

3.2 Sulfate Attack

Unfortunately, "sulfate attack" is now almost a meaningless phrase. Its meaning was simple back in the days when specifications began to recognize the need for sulfate-resistant cements, as created by limiting their C_3A contents. Sulfate from the environment reacted with monosulfate or calcium aluminate hydrates to destructively produce ettringite. No other sulfate-dependent chemistry was considered during most of the first half of the twentieth century.

From the discussion in the previous section, it is obvious that monosulfate and calcium aluminate hydrate levels in hydrated cement have been decreasing, and both may have reached 0% for some cements. Thus no "classical" sulfate attack is possible with many currently available cements (for simplicity, and because of conflicting literature, reactions of C_4AF are not considered herein).

During the twentieth century it gradually became popular for engineers to study sulfate attack by immersion of cylinders or prisms in sodium or magnesium sulfate solution. Studies by Miller and Manson [41] over several years, and by the Portland Cement Association (in Sacramento, California) over several decades [42, 43], investigated the effect of those sulfate solutions on concrete made with different types of cement, at various water-cement ratios, and with admixtures such as fly ash and slag. Virtually no chemical analyses or petrographic examinations of the deteriorating specimens were made.

During this period, and even back in the early 1900's, investigators found that sodium sulfate reacted with the calcium hydroxide product of cement hydration to produce gypsum. Some investigators reported that this reaction was destructive, and others reported that it was not. Some found that limiting the C_3S content was beneficial. Few, if any, called attention to the fact that if the intruding sulfate salt was gypsum, there was no reaction with calcium hydroxide. In fact, many papers discussed deleterious production of gypsum in concrete, loss of basicity, and decalcification of the calcium silicate hydrate phases, without considering that gypsum from the environment would cause none of these reactions.

It also was not until recently that Stark [44] reported that much or all of the above-ground distress to concrete prisms exposed to sodium sulfate solutions was due to "physical salt attack" or, as termed by this author and his colleagues [45], "salt hydration distress." No reaction of the sulfate ion is involved. The distress mechanism is now being debated. Among the more prominent theories are pressure due to crystallization of sodium sulfate hydrate from saturated solution or expansion due to conversion from anhydrous sodium sulfate (thenardite) to the decahydrate (mirabilite). Mirabilite occupies about four times the volume of thenardite.

Astonishingly, Stark [44] had found that below ground portions of the Sacramento prisms were generally unaffected by the exposure to sulfate. It is discouraging, if not frightening, to consider the monetary consequences of misidentification of a physical phenomenon as a chemical one.

Returning to the change of sulfate levels in Portland cement over time, it is obvious that classical sulfate attack was very likely in the 1800's, and then less and less likely as the cement sulfate levels increased. Although the destructive attack of sulfate on hydraulic cement systems was recognized as early as the 1700's by Smeaton [45], sulfate attack was not proven until Candlot [46] and LeChatelier [47] late in the 19th century identified ettringite in deteriorating concrete, and LeChatalier demonstrated the destructive development of ettringite. Indeed identification of ettringite led to the development of the sulfate-resistant cements, all based on lower amounts of tricalcium aluminate. Unfortunately, Miller and Manson and the Portland Cement Association failed to check for ettringite during their massive studies.

The beginning of the twenty-first century finds many reports of studies of attack by magnesium sulfate and even hydrogen sulfate (sulfuric acid), with the investigators failing to recognize that the cation, not the sulfate anion, may have caused most or all of the damage [48]. Further, it is often not recognized that low C_3A contents will do nothing to prevent alkali sulfates from reacting with calcium hydroxide, and that physical salt attack is neither prevented nor lessened by use of Types II or V cements, nor by decreasing calcium hydroxide production by limiting C_3S content.

4. DELAYED ETTRINGITE FORMATION

In the 1980's an internal sulfate attack phenomenon was reported by Heinz et al. [49]. Many other investigators soon reported studies of the phenomenon, the name of which has now been settled on as "delayed ettringite formation," or DEF. The phenomenon involves the late development of ettringite. The generally recognized explanation is that the ettringite normally formed in concrete is destroyed, or is prevented from forming, by temperatures above about 60°C, due to either deliberate heat curing or to heat development caused by the casting of massive structures, or by exposure to the sun in hot, dry environments. Subsequent formation of ettringite in the hardened concrete, such as caused by exposure to water, results in expansion of the paste system, with consequent loss of prestress or bond of reinforcement, and cracking.

Other conditions may be necessary for such DEF, including "proper" cement composition. Generally unrecognized is the fact that higher temperatures are required for ettringite decomposition if the vapor pressure is higher.

This author has found that cements with high clinker sulfate, especially as caused by burning high-sulfur fuels, may lead to DEF even when the concrete is not exposed to high temperatures. Others have argued against this on the basis that the sulfate in such cements is water-soluble and will produce ettringite normally. Such arguments fail to consider that SO_3 gases in the kiln must alter the chemistry of the cement. For example, $3CaO{\cdot}SiO_2+SO_3 \rightarrow 2CaO{\cdot}SiO_2+CaSO_4$, and the sulfate is thus found in the slowly reacting belite phase. Further, most structures undergoing DEF are made at low w/c, where complete solubility of anhydrite is unlikely.

Finally, it is noted that the ettringite formation in this distress mechanism is often evidenced as a gel [50], identical in appearance to alkali silica reaction (ASR). Thus prior occurrences of DEF may have been unrecognized. Indeed, Copeland reported this possibility to one of our clients in 1976 [51], but his findings were received with skepticism, and were not published.

5. INTERNAL SULFATE ATTACK

This subject may be divided into two classifications: (1) deliberate and beneficial, or (2) unanticipated and harmful. However, in the author's opinion, the word "unanticipated" may occasionally be replaced by "foolish" or even "reckless."

In the first classification is the use of ettringite development in those cement formulations designed to produce "shrinkage compensated" or "expansive" concrete. There are two mechanisms for this. In the first, the cement usually consists in part of "anhydrous ettringite" ($C_4A_3\overline{S}$) plus an additional sulfate component. The development of ettringite continues after hardening but ceases before expansion cracking occurs. Such cement permits large expanses of joint-free concrete when used in slab construction, provided that sufficient steel is present in the slab to restrain concrete expansion.

Also in the first classification are formulations where controlled excesses of gypsum are present, but again expansion is limited in time and amount by the component proportions and the design of the reinforced concrete.

In the second classification are mixtures consisting primarily of plaster of Paris (calcium sulfate hemihydrate) but with several percent Portland cement, or largely of Portland cement but with substantial amounts of plaster. For the former, Portland cement is added to give both alkalinity, and thus some steel passivation, and added strength. Unfortunately, failures of both systems when used as post hole fillers, etc., have been myriad. Many of such proprietary products are an effort to reproduce a successful product whose trade secret is use of a zero-C_3A Portland cement, which cannot produce ettringite. No sulfate reaction occurs. The other producers do not recognize the need for the zero-C_3A Portland cement.

6. SUMMARY

For almost all of the 1800's gypsum was not added to Portland cement clinker. As a consequence, SO_3 levels were generally well below 1%. For the first half of the 1900s, and longer, gypsum was interground with the clinker to bring SO_3 levels to just under 2%. Now, at least in the U.S., SO_3 levels are frequently 3 to 4, or even 5 percent.

The effects of the higher SO_3 levels have been scarcely, if at all, recognized. They include:

- the common presence of ettringite in aged Portland cement concrete
- significantly less chance of "classical" sulfate attack, since there are far less amounts of hydrated aluminates and monosulfate to develop ettringite upon sulfate intrusion into the concrete
- greater chance of significant delayed ettringite formation

As a consequence, misdiagnoses of sulfate distress mechanisms are now rampant.

7. AUTHOR'S NOTE

In doing the literature research for this paper, I was enormously impressed by the literary and historical research abilities of the nineteenth and early twentieth century authors. Cogent and amusing phrases abound. The extensive use of photographs in Stanley's *Highlights in the History of Concrete* made that book a joy to read. Henry Reid's *The Science and Art of the Manufacture of Portland Cement* not only detailed Portland cement manufacture from raw material selection to testing of the final product, but also included anecdotes having nothing to do with the subject but fascinating in their own light.

Perhaps the most interesting book is John Smeaton's "A Narrative of the Building and a Description of the Construction of the Eddystone Lighthouse with Stone," as published in 1793. This book also caused my hilarious "mistranslation" of phrases in old English print (f-like letter for some s's) such as "that we might be in poffeffion of all the beft materials for water building within ourfelves: and though I own I have not fucceeded with refpect to the latter, fo far as my ardent wifhes led me to hope [52]."

This literature made my paper a labor of love. That labor was aided in great measure by our librarian, Ms. Penny Sympson, by Ms. Connie Field and Mr. Paul Tennis of the Portland Cement Association, and by Ms. Ellie Barkley, Editor of ASTM. Unfortunately, my inabilities with regard to the French and German language largely restricted my subject to English and American history.

Finally, I note that the bibliography published in 1952 by Miller, Manson and Chen [53] was of significant value. That bibliography demonstrates that papers titled "alkali attack" actually usually refer to sulfate salts, and that many experiments with "sea water" were actually with sulfate salts. Any search using the word "sulfate" would fail to locate these papers.

REFERENCES

[1] Smeaton, J. A Narrative of the Building and a Description of the Construction of the Eddystone Lighthouse with Stone, London, 1793.
[2] Davis, A.C. A Hundred Years of Portland Cement, Concrete Publications Limited, London, 1924, p. 5.
[3] Reid, Henry The Science and Art of the Manufacture of Portland Cement, E.&F.N. Spain, London and New York, 1877, p. 29.
[4] Stanley, C.C. Highlights of the History of Concrete, Cement and Concrete Association, pp. 11, 14.
[5] Ref. [2], pp. 38, 49.
[6] Hime, W.G., Shotwell, B., and Marusin, S. A New Look at the Oldest Reinforced Concrete, in press.
[7] Figg, J. New light on the early history of reinforced concrete, Chemistry and Industry, 19 November 1984, pp. 793-795.
[8] Francis, A.J. The Cement Industry, 1796-1914: A History, David & Charles, London, 1977, pp. 122, 124.
[9] Ref. [8], pp. 243, 244.
[10] Ref. [3], p. 131.
[11] Ref. [8], p. 240.
[12] Ref. [8], p. 177.
[13] Lesley, R.W. History of the Portland Cement Industry in the United States, International Trade Press, Chicago, 1921, p. 44.
[14] Ref. [2], p. 53.
[15] Eckel, E.C. Cements, Limes and Plasters, John Wiley & Sons, London, 1922, p. 571.
[16] Ref. [2], p. 87.
[17] Cummings, U. American Cements, Boston, 1898, p. 35.
[18] Ref. [2], p. 87.
[19] Ref. [2], p. 87.
[20] Ref. [15], p. 520.
[21] Ref. 13, p. 45.
[22] Ref [17], pp. 35-37.
[23] Ref. [13], pp. 50, 51.
[24] Ref. [15], p. 555.

[25] Ref. [8], pp. 231-233.
[26] Ref. [15], pp. 474, 478.
[27] Ref. [4], p. 17.
[28] Ref. [13], p. 118.
[29] Hadley, E. J., The Magic Powder, G. P. Putnam's Sons, New York, 1945, p. 38.
[30] Ref. [2], pp. 198, 199.
[31] Ref. [15], p. 505.
[32] Ref. [8], p. 145.
[33] Ref. [13], p. 153.
[34] Gebhardt, R., Private communication.
[35] Tuthill, L.H. Resistance of Cement to the Corrosive Action of Sodium Sulfate Solutions, Proceedings, Journal of The American Concrete Institute. (33) Nov.-Dec. 1936, pp. 83-106.
[36] (PCA 26)
[37] Bogue, R.H. The Chemistry of Portland Cement, Reinhold Publishing Corporation, New York, 1947, p. 25.
[38] Ref. [15], pp. 521-523.
[39] Anderegg, F.O. Proceedings, American Concrete Institute, Vol. 25, Detroit, 1929, pp. 332-343.
[40] Gebhardt, R. F., Survey of North American Portland Cements; 1994, Cement, Concrete and Aggregates, Dec 1995, pp. 145-189.
[41] Miller, D. G. and, Manson, P. W., Long Time Tests of Concretes and Mortars Exposed to Sulfate Waters, Bulletin No. 194, University of Minnesota, May 1951.
[42] McMillan, F. R., Tyler, I. C. Hansen, W. C. Lerch, W. Ford, C. L. and Brown, L. S., Long-time Study of Cement Performance in Concrete, Bulletin 26, Portland Cement Association, Aug. 1948.
[43] Blanks, R. F., Ten-Year Report on the Long-term Study of Cement Performance in Concrete, Bulletin 43, Portland Cement Association, April 1952.
[44] Stark, D., Durability of Concrete in Sulfate-Rich Soils, Bulletin RD 09997.01T, Portland Cement Association 1989.
[45] Hime, W., Martinek, R. A., Backus, L. A., Marusin, S., Concrete International 23 (10) 2001, pp 43-50.
[46] Candlot, E., Bull, soc. encour. ind. natl, 1890, p. 682.
[47] LeChatelier, H., Compt. rend. 128, 1899, p.661.
[48] Hime, W. and Mather, B., Concrete International, in press.
[49] Heinz, D., Ludwig, V. an d Nasr, R., Model Experiments for Clarification of the Causes of Dam age to Heat Treated Pre-Fabricated Concrete Elements - Part 2 - Heat Treatment of Mortar and Porte Ettringite Formation, Tonind, ztg. 106, 1982, pp 178-183.
[50] Mielenz, R. C. Marusin, S. L, Hime, W. G. and Jugovic, Z. T., Investigation of Prestressed Concrete Railway Tie Distress, Concrete International, Dec. 1995, pp 62-68.
[51] Hime, W. , Dr. L. E. Copeland - Discoverer of D.E.F., Concrete International, in press.
[52] Ref. [1], p. 114
[53] Miller, D. G., Manson, P.W. and Chen, R.T.H., Bibliography On Sulfate Resistance of Portland Cements, Concretes and Mortars (annotated), University of Minnesota, Paper No. 708, April 1952.

SULFATE IN CEMENT AND CONCRETE - LET'S START AT THE BEGINNING

William G. Hime

Wiss, Janney, Elstner Associates, Inc., Northbrook, IL USA, E-mail: whime@wje.com

Biographical Data

William Hime graduated from Heidelberg College (Ohio) in 1948 with majors in chemistry and mathematics. He then attended Northwestern University, completing all non-research Ph.D requirements for a major in Analytical Chemistry. He joined the Portland Cement Associate as a Research Chemist in 1951, serving in various capacities for 20 years.

In 1971 he and colleague Bernard Erlin formed Erlin, Hime Associates, a company primarily serving clients having construction materials problems. In 1984 that company was obtained by Wiss, Janney, Elstner Associates, then primarily a firm investigating similar problems through engineering.

Mr. Hime has published over 50 papers on analyses of cement and concrete, corrosion, cement burns and related matters. He is a member of ASTM and an Honorary Member of Committees C1 and C9. He is a Fellow of the American Concrete Institute.

He is an avid (but not accomplished) golfer, and collects caps from courses he has played throughout the world.

THE PORE FLUID IN PORTLAND CEMENT: ITS COMPOSITION AND ROLE

F. P. Glasser

Department of Chemistry, University of Aberdeen
Meston Walk, Old Aberdeen, AB24 3UE Scotland

ABSTRACT

Pore fluid forms an essential component of Portland cement formulations. Its chemistry is discussed: the main pH control arises from dissolved alkali, Na and K, effectively present as hydroxide. This causes calcium solubility to diminish with the result that in many commercial cements, calcium solubilities in pore fluid are comparable with those of Aℓ and Si.

The redox potential (Eh) in cement pore fluids has been characterised: slag-rich blends have a low Eh. This is created and maintained by a vigorous sulfur chemistry: S^{2-},S_x^{2-},$S_2O_3^{2-}$ and SO_4^{2-} are present in the pore fluid.

Several models are described for the alkali distribution between aqueous and solid phases. The effectiveness of fly ash and silica fume in decreasing pore fluid alkalis is interpreted in terms of their impact on C-S-H composition.

It is suggested that pore fluid does not disappear even from low water: cement ratio "high performance" concretes: instead hydration ceases because of decreased water activity such that the critical humidity necessary to sustain hydration is no longer achieved.

1. INTRODUCTION

Portland cement is marketed and used as a fine powder typically having Blaine surface areas in the range 2500 – 5000 cm^2/g. The mineralogy of the powder is complex: it consists of mainly "clinker" with other mineral admixtures. Portland clinker is a sintered product chemically high in CaOH, *ca* 65 - 70 wt%, and consisting of four phases: Ca_3SiO_5, Ca_2SiO_4, $Ca_3A\ell_2O_6$ and $Ca_2(Fe,A\ell)_2O_5$ (idealised formulae): additionally a little, ca 1 – 2%, free lime may persist. This clinker is interground with other minerals: principally gypsum, $CaSO_4{\cdot}2H_2O$, which is used to control set times. In modern practise one or more supplementary cementing materials may be added. These include coal combustion fly ash, glassy iron blast furnace slag, natural or semi-synthetic pozzolanic materials, e.g., calcined clay, and limestone, $CaCO_3$.

The resulting mixed powder is used to bind coarser mineral aggregate; hydration is initiated by adding water. Traditionally pure or only slightly saline water is permitted although in certain applications, seawater has been allowed. However in modern practise, "water" may also include other soluble or dispersible substances added to achieve specific purposes: these include corrosion inhibitors, anti-freeze agents, chemicals to control bleed, foaming and air entrainment, accelerators, retarders and plasticisers. It follows that a range of inorganic and organic substances, the latter, often consisting of mixtures of substances, are added typically at levels up to 1 – 2% by weight.

Proceedings of the 11th International Congress on the Chemistry of Cement (ICCC) 11 - 16 May 2003, Durban, South Africa
'Cement's Contribution to the Development in the 21st Century' ISBN Number: 0-9584085-8-0
Hosted by: The Cement and Concrete Institute of South Africa Editors: Dr G. Grieve and G. Owens
CD-ROM produced by: Document Transformation Technologies Congress Organised by: Event Dynamics

The aqueous phase – which I will term 'water' despite its often complex constitution – serves two essential purposes. Upon mixing and for a few minutes or hours thereafter, it provides a freely-flowing semi-liquid mass which can be cast into formwork. Thereafter it continues to react with the cement powder forming a rigid mass. A complex series of reactions occur. Not surprisingly characterisation of these reactions, study of hydration mechanisms and of the resulting microstructures and of the relationship of these and mix formulation to engineering properties has provided an important stimulus to cement science as described in proceedings of previous Congresses. I make a number of points relevant to this presentation:

- Much of the added mix water becomes chemically bound into hydrates. While no absolute distinction between physically and chemically bound water is possible, all empirical and theoretical criteria agree that free water diminishes as hydration progresses. This water budget is important and will be discussed.
- As hydration progresses and solid paste hydrates self-assemble into an interconnected network, residual liquid water becomes increasingly confined to isolated pores: again no clear-cut distinction exists between mix water and pore water but final set, as determined by the Vicat test, may arbitrarily be taken as marking the transition between mix water and pore water.
- The free aqueous phase reacts with and dissolves cement components. Its physical and chemical properties: pH, Eh, ionic strength, conductivity, viscosity, etc., all undergo large changes as a consequence. These changes are continuous.
- Although concretes are normally formulated with more water than is required to hydrate the cement, thus leaving a permanent excess of pore water unless rigorously dried, modern "high performance" concretes are often formulated to low w/c ratios and, as a consequence, may undergo self desiccation. Self desiccation can still occur in the presence of pore fluid; this is discussed.

This review and discussion concentrates on internal chemistry; chemical fluxes such as diffusion of ions from the service environment into and out of cement paste have not been included. Nevertheless, many of the principles described here are applicable to service conditions, with appropriate modification in light of the development of concentration gradients within the aqueous phase and of accompanying mineralogical changes to the matrix.

The pore fluid of real cements was generally regarded as inaccessible to direct examination until Longuet and colleagues showed that pore fluid could be expressed from mature cement pastes using high hydrostatic pressure [1]. Since that time, numerous other investigators have expressed pore fluid: Taylor [2] references data from 212 superior analyses, defined as being accompanied by sufficient characterisation data for the cement and curing procedure. These data give new insights into the hydration process, many of which have yet to be incorporated into mainstream cement science. The purpose of this review is to highlight and correlate some of this work and discuss implications for concrete formulation and performance.

2. PORE FLUID CHARACTERISATION

2.1 Sampling

Most pore fluid collection has been done by uniaxial compression of a cylindrical sample. The yield of pore fluid is optimised if pressure is raised gradually and incrementally up to the maximum available pressure. Estimates of the efficiency of collection vary but it is unlikely that expression collects more than 50% of the total pore fluid. Doubts have been expressed that the compositions of the aqueous samples may be unrepresentative: that chemical potentials in thin films differ from those in bulk water. In support of this it has been claimed that systematic changes in pore fluid composition occur as a function of applied pressure although changes in concentration of some

substances, such as dissolved or dispersed superplaticisers, relate more directly to time, with selective removal of soluble low molecular weight fractions occurring [3]. However, the writer has not found significant pressure-related variation to occur. Instead, two other factors seem to be of greater importance: protection of pore fluid against reaction with air and the geometry of collection.

Pore fluid expression should if possible be done with a N_2 gas blanket atmosphere around the die and sample. Collection directly into a sealed drain coupled to a hypodermic syringe enables pore fluid to be removed by suction and free of contamination resulting from contact with air. The question of the impact of incremental pressure is much more complex than supposed. As is well known from industries requiring pressed products, e.g., tablets in the pharmaceutical industry, the pressure distribution in a uniaxial compression device is very unequal; friction between dies and along the sides generate high local pressures while the centre may remain at quite low pressure. Thus incremental increases in applied force do not necessarily achieve higher pressures in cement undergoing compression but instead to increase the volume fraction subject to sufficient pressure to express pore water.

Isostatic compression devices exist, for example multi-axial presses with tetrahedral or cubic geometry, but to the writer's knowledge have not been applied to pore fluid expression. Until this is done, the existence of compositional variations as a function of applied load must be regarded as not proven.

2.2 Chemical analysis

Analysis of expressed pore fluid can be made for pH, Eh and aqueous chemistry: Figure 1 shows the range of environments. As pore fluid is very atmosphere sensitive, the analytical emphasis is on rapid methods which minimise transfer and handling. The pH function is usually determined using a pH meter. Care should be taken to use an electrode that is insensitive to alkali and to calibrate the electrode. The Eh function is more difficult to determine; standard methods are only slow evolving. Ordinary Portland cements, are normally produced under oxidising conditions; they give a neutral to slightly oxidising redox potential (Eh), of +100 to +200mV at pH 12 – 13 relative to a standard hydrogen electrode. However, blast furnace slag cements blends, particularly if made with high (>40%) slag content can give very low Eh values, negative 250 to 400mV in the same pH range. Just as the application of pH concepts is unhelpful without specifying the nature and amount of pH buffering, if any, Eh measurements are most useful when the poising capacity – the equivalent of buffering - can also be defined. Portland cements lacks significant poising capacity, as a result of which its internal Eh is readily affected by electrochemically active additives, e.g., nitrites or other potential oxidising and reducing agents. Slag cements spontaneously develop an active internal chemistry involving sulfur. Slag hydration liberates sulfide, S^{2-}, ions, which in the alkaline cement environment react with sulfate from Portland cement, giving rise to species such as thisosulfate, $S_2O_3^{2-}$[4 - 10]. While the sulfur speciations are not yet completely understood, it seems likely that the source of the low Eh and the greater poising capacity of slag cement arises from electrochemically active couples involving sulfur.

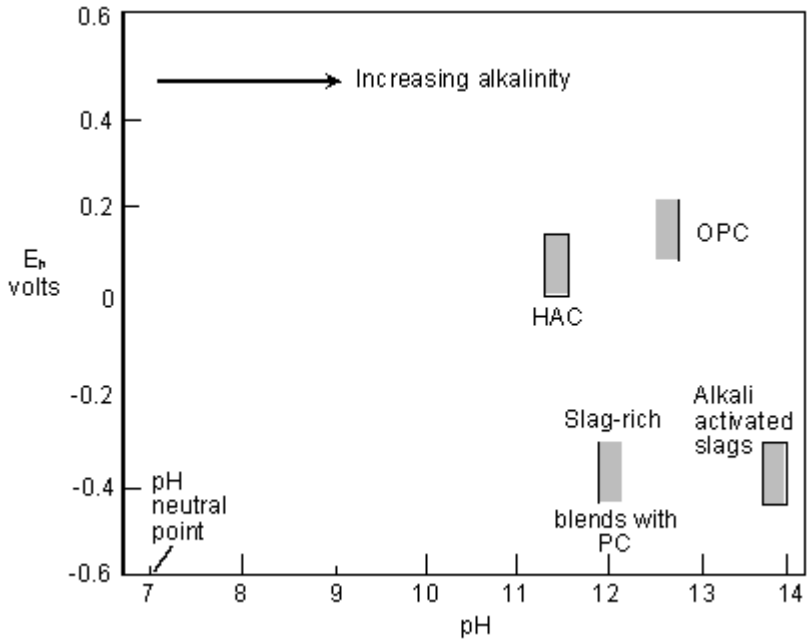

Figure 1. Range of Ph-Eh environments in alkaline cements. The units of Eh are volts, relative to a standard H_2 electrode, 1/2 H_2 0+ $H^+ + e^-$ at 25°C, pH = O and P_{H_2} = 1 bar.
HAC = high alumina cement.

Thus the internal environment of cements can be explored and characterised using inert electrodes with which to measure Eh; platinum appears to be a better choice of electrode than glassy carbon, silver, titanium or palladium [4, 6]. As noted, no standard method for determining poising capacity yet exists. Angus and Glasser [4] suggested titration against standard Cr (VI) solution; the method is frequently used and the writer is not aware of adverse comment but considers that the method still requires further investigation before it can be accepted as a standard.

The dissolved inorganic components of pore fluid can be analysed by a combination of flame photometry (Na, K), atomic absorption (Mg, Fe, Ca, Aℓ, Si) and ion chromatography (SO_4, Cℓ, etc). Figure 1 summarises the pH-Eh regime in a range of commercial and experimental cements. As can be seen, large numerical variations exist in Eh. The variations in pH scale, from 11 to 14, do not at first sight look large. However from the definition of pH, pH = $-\log_{10}[H^+]$, and rewriting this as pOH-$\log_{10}$[OH] as seems more appropriate for alkaline solutions, it can be seen from the form of the expression that a pH change of two units results in a hundred-fold change in hydroxide ion concentration. Organic constituents in pore fluid are best treated on the basis of molecular structure, choosing between mass spectroscopy, NMR, infrared, chromatography, fluorescence, perhaps with couplers, and classical C-H-N analysis; the latter requires selective recovery of the organics from the aqueous phase. Where high molecular weight organics occur, gel permeation chromatography, ultracentrifugation, light scattering and Raman spectroscopy may be applicable.

The labile nature of pore fluids has been mentioned. However, it is well known that pore fluids are liable to supersaturation: the same phenomena also occur in laboratory simulants. For example, if pore fluid is simulated using solid $Ca(OH)_2$, it is comparatively easy to prepare supersaturated solutions containing up to ~2g/ℓ $Ca(OH)_2$ at 20º - 25ºC. Such supersaturated solutions may appear clear but upon standing go cloudy and eventually precipitate $Ca(OH)_2$. Similarly, pore fluids removed by extraction from cement may appear clear when fresh but subsequently go cloudy. Several explanations are possible: supersaturation is only one. For example, the solution may contain colloidal particles that undergo ripening with time. A very real possibility, despite care being taken, is contamination by carbon dioxide resulting in precipitation of $CaCO_3$. It is often not certain which of these possibilities is applicable. In theory it should be possible to deal with the

presence of colloids by using ultrafiltration. Commercial filtration media are available which range in size to exclude even nm scale particles. However, these media may not be suitable for filtration of strongly alkaline solutions. Commercial filtration media down to ~0.4μm are reasonably certain not to interact with cement pore fluids but the finer media, intended to retain colloids, are designed for filtration of near-neutral biological material and may interact with alkaline cement pore fluids: results obtained from commercial ultrafiltration schemes cannot be accepted uncritically. Fortunately, the presence of supersaturated solutions, precursor to colloids, seems to be confined to the early stages of hydration, characteristic of the first few hours or days of reaction. The writer is unaware of any evidence of the persistence of colloids in pore fluids of matured pastes even in the presence of cellulose simulants such as sacharinic acid [11] and superplasticisers [12].

For many analytical purposes, pore fluids are best acidified with standard acid; the acidified solutions have better keeping power than the original alkaline solution. Of course dilution factors need to be taken into account in any subsequent analyses and, moreover, care should be taken that acidification does not precipitate amorphous silica which may interfere with subsequent analytical determinations.

3. IMPACT OF PORE FLUID ON CONCRETE PROPERTIES

3.1 pH and cement paste mineral stability

The range of OH concentrations in cement pastes has two impacts on mineral stability. Firstly, as the ionic strength of the pore fluid increases – and in this respect all ions present in solution have to be included – the activity of water is diminished. This results in stabilisation of lower hydrates. For example in the $CaSO_4$ - H_2O system, gypsum, the dihydrate, is stable across a broad range of temperatures. However, in solutions of high ionic strength as occur when soluble salts are added, hemihydrate and anhydrite are increasingly stabilised to lower temperatures. Secondly, as [OH] increases, 'amphoteric' ions such as aluminium are increasingly solubilised: the pattern of mineral stability, as established for hydrated Portland cement paste, is progressively altered. The high pH also affects calcium solubility, as will be discussed.

3.2 $Ca(OH)_2$ solubility

The solubility of $Ca(OH)_2$ is well known, ca 1.1 g/ℓ at 25ºC and is commonly regarded as controlling the high pH of pore fluid. A saturated solution of $Ca(OH)_2$ has a pH $\simeq$ 12.6 at 25ºC owing to ionisation of soluble $Ca(OH)_2$. This occurs in stages:

$$Ca(OH)_2 \rightarrow Ca(OH)^+ + OH^-$$
$$Ca(OH)^+ \rightarrow Ca^{2+} = OH^-$$

The ionisation goes virtually to completion in a saturated solution: $Ca(OH)^+$ has a negligible concentration. However, analysis of the pore solution compositions of real cements known to contain free portlandite, $Ca(OH)_2$, reveals a Ca solubility very much less, typically by more than an order of magnitude, than would be predicted from the known solubility of $Ca(OH)_2$. A simple and nearly quantitative explanation of these differences is as follows: Alkali (Na,K) dissolves in pore fluid and its positive charge requires to be balanced by a corresponding negative charge. Since anions other than OH^-, e.g., aluminate, silicate, and sulfate, are relatively insoluble in the cement environment, alkalis are effectively present dissolved in pore fluid as their hydroxides. These impact on $Ca(OH)_2$ solubility as follows. If we write a solubility product, sp, for $Ca(OH)_2$ it follows that at low concentrations:

$$Ksp = [Ca]\,[OH]^2$$

activities should be substituted for molar concentrations, but since this is a simplified treatment, the more familiar molar units will be used. The literature value for Ksp ($Ca(OH)_2$) is 4.21×10^{-5}; at

equilibrium a saturated solution is thus 2.19 x 10^{-2}M in Ca ions and 2 x 2.19 x 10^{-2} or 4.38 x 10^{-2}M in hydroxide. However, if hydroxide is furnished from some external source, most probably from alkali hydroxides, Ca solubility must decrease in order to maintain Ksp. The extent of the decrease can be calculated from the above equation but a more precise calculation, taking into account changes in activity coefficients and changing ionic potential of the solution, is shown in Table 1. The solubility of calcium in the presence of NaOH initially decreases rapidly to ~0.1M but thereafter less rapidly. At 0.5M, a reasonable average concentration for cement pore fluid, Ca solubility is diminished relative to its solubility in initially pure water by a factor exceeding 20.

These solubility trends have several important consequences to the hydration process. Firstly, as alkali continues to be released and concentrates in a diminishing volume of pore water, $Ca(OH)_2$ solubility continues to diminish. Secondly, the pH may rise above that of a saturated solution of $Ca(OH)_2$ as NaOH and KOH concentrate and alkalis increasingly control pH. A further and important consequence is that the solubilities of other species, particularly those in anionic speciations such as $A\ell(OH)_4$, increase with the result that solubilities of calcium, aluminium and silicon become more nearly equal. We are accustomed to thinking of calcium as the most soluble and most mobile species in hydrating cement. While this may be true of alkali-free simulants, it is not necessarily true for "real", i.e., alkali-containing cements where solubilities are more nearly comparable. The exception to this is magnesium: magnesium solubility as $Mg(OH)_2$ is orders of magnitude less than $Ca(OH)_2$ in pure water. However the common ion effect still operates with the result that, like $Ca(OH)_2$, its solubility diminishes even further in alkaline solution. Despite the small hydrated diameter of the Mg ion, its extremely low solubility renders it relatively immobile.

Table 1. Solubility of $Ca(OH)_2$ in NaOH, 25ºC*

NaOH mM	$Ca(OH)_2$ mM
0	21.91
10	18.60
20	15.72
40	11.26
60	8.32
80	6.42
100	5.16
200	2.49
300	1.63
400	1.20
500	0.95

* after Dow [13].

3.3 C-S-H Solubility

C-S-H refers to the principal bonding phase of Portland and blended Portland cement. The product, as encountered in cement and in certain laboratory preparations is nearly amorphous to X-ray powder diffraction and on that account, is termed "cement gel" or "C-S-H gel" although because of supposed similarities in structure to certain crystalline $CaO\text{-}SiO_2\text{-}H_2O$ minerals, it has also been termed "tobermorite gel" or "jennite gel". I will continue to use the designation C-S-H. The range of C-S-H compositions encompasses a range of molar Ca/Si ratios, although agreement is poor about numerical extent of the values, perhaps 2.0 to 0.8. Portland cements have high Ca/Si ratios often in the range 2.6 – 3.0: consequently the upper limit of C-S-H compositions is of greatest interest to Portland cement. In hydrated laboratory preparations made by hydrating mixtures of $Ca(OH)_2$ and silicic acid, my experience of combined electron microscopy with analysis and diffraction, coupled with X-ray diffraction and Franke extraction for free portlandite, is that the upper limit of homogeneity of C-S-H is in the range 1.7 to 1.8 at 25ºC (expressed as Ca/Si molar

ratio), decreasing to ~1.5 in the course of prolonged curing at 55º - 85ºC [14]. However, reports on hydrated Portland cement, reviewed by Taylor [15], claim higher ratio limits of 2.0. Whatever the 25ºC limits, the solubility properties of mixtures of $Ca(OH)_2$ and high ratio C-S-H are similar to those of $Ca(OH)_2$(silica excepted): Ca solubilities are in the order of 22mM and Si solubilities in the order of 1μm. Thus the ratio of Ca:Si in solutions coexisting with lime-rich C-S-H, or with mixtures of $Ca(OH)_2$ and C-S-H, is ~22 x 10^3. This ratio dominates the behavior of laboratory simulants for Portland cement. However, investigators frequently use silica sources containing soluble alkali and, as a consequence, laboratory simulations supposed to be of carefully controlled chemistry, frequently fail to achieve their intended purpose.

The impact of alkalis on Ca and Si solubilities is shown in Figure 2: KOH behaves in an essentially identical manner to NaOH. The impact of alkalis is generally to reduce the solubility of Ca while enhancing the solubility of silicon. Figure 3 illustrates these impacts. As can be seen, the combined effects of the common ion (hydroxyl) and increasing pH – not shown, but increasing to nearly 14 at 0.8M NaOH – are to decrease calcium solubility while at the same time increasing silica solubility, with the result that at high Ca/Si ratios, aqueous concentrations of Ca and Si become approximately equal at 0.8M NaOH. Thus the order-of-magnitude differences in Ca and Si solubilities, inferred from data on the $CaO\text{-}SiO_2\text{-}H_2O$ system, are greatly reduced or even reversed at typical pore fluid molarities, in the range 0.1 – 1.0M. This conclusion must inevitably affect how we think about hydration processes in fresh cements. The mobility of species is a function of several factors, concentration being one, but with the result that species generally regarded as immobile on the basis of laboratory simulants, e.g., Aℓ and Si, may be relatively mobile in pore waters whose alkalinity is conditioned by sodium and potassium.

Indeed, the solubility trends also affect how we model cement hydration processes. An often-used method to monitor hydration processes is the "chemical reactor" in which weighted amounts of cement or cement minerals are dispersed in water, typically at w/s ratios 5-50, while the stirred solution is monitored for pH, calcium and silicon contents, etc., as a function of time. The method works well for congruently-soluble substances although it may be less reliable for incongruently soluble substances. However, the seemingly good agreement obtained between, on the one hand, cement minerals, and on the other, real cements, results from the high dilution of alkalis which is achieved: real cement pastes formulated to much lower w/s ratios, *ca* 0.4 – 0.8, will behave quite differently than in the chemical reactor.

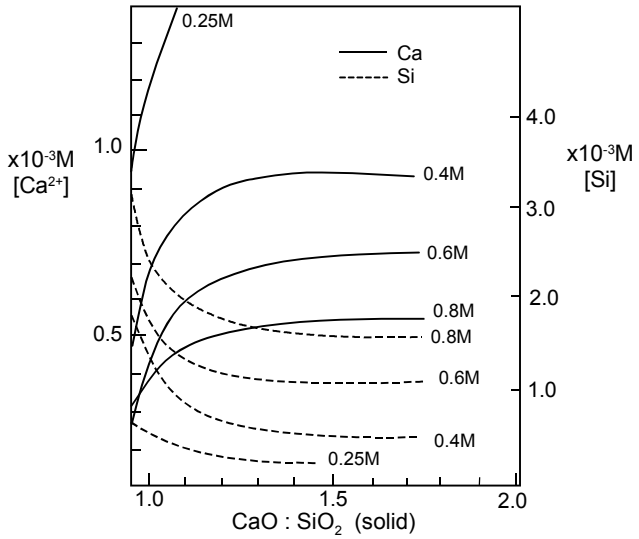

Figure 2. Relationship between solid $CaO:SiO_2$ ratio and aqueous composition: the vertical scale shows CaO concentrations (left-hand scale) and SiO_2 concentrations (right-hand scale) as a function of alkali (NaOH) molarity.

3.4 Solubility of Alkalis in Pore Fluid

Alkali releases into pore fluid are subject to a balance: some alkali remains sorbed in cement hydrates. Moreover, blending agents and aggregates are not totally inert and may (i) release alkali and (ii) by reacting with cement hydration products, alter their sorption characteristics. These factors jointly control the partition of alkali between solid and aqueous phases and require to be explored in light of recent knowledge. The rationale is, of course, to obtain a deeper understanding of the alkali-aggregate reaction (AAR). In AAR, susceptible siliceous aggregates are attacked by hydroxyl ions in the pore fluid. Their susceptibility increases rapidly as pH rises above the threshold conditioned by $Ca(OH)_2$. However, not all the alkali is available to elevate pH.

A partition of alkalis occurs between the aqueous phase and cement solids. Of these solids, alkalis are virtually insoluble in both portlandite $Ca(OH)_2$ and ettringite, leaving C-S-H and AFm phases as potential hosts. Of the potential hosts, C-S-H is much the most abundant in ordinary Portland cement where it comprises perhaps 70% by volume of the paste.

The general question of alkali partition between C-S-H and pore fluid has been approached in two ways. Taylor [19] collected pore fluid analysis from the literature, admitting data where cement alkalis were also reported. Sodium was treated separately from potassium. The results, after considerable recalculation and estimates of the total volume of residual pore fluid, were recast into semi-empirical equations which, starting from a cement analysis and w/c ratio, could be used to predict pore fluid alkali concentrations. Hong and Glasser [17, 18] took a somewhat different approach. Accepting that C-S-H was the principal sink for alkali, they prepared C-S-H gels of known C/S ratio and carefully homogenised the gels. A weighed amount of gel of known composition was mixed with a measured volume of aqueous solution having a known concentration of either NaOH or KOH. Aliquots of the aqueous phase were analysed periodically until a steady state was obtained: this generally required only a few days. The decrease in aqueous alkali concentration, coupled with other system parameters, enabled a distribution coefficient, Rd, to be calculated such that at constant temperature.

$$Rd = \frac{\text{Alkali in solid C-S-H, mM/g}}{\text{Alkali concentration in solution, mM/m}\ell}$$

Alkali-loaded gels were also used to determine desorption isotherms by dispersing the gel into initially pure water. It was concluded that sorption and desorption were not strictly reversible, although further tests of reversibility were recommended. But the ready release of alkali from "C-S-H" broadly supports the results of leach testing, which show sodium and potassium to be amongst the most weakly bound of the major components of cement. Concerning the sorption process, it was concluded that C-S-H and C-A-S-H gels were not alkali-saturated at (Na,K)OH aqueous concentrations in the range 0.2 – 0.3M: significant unused capacity remained. However, as pore fluid alkali concentrations exceeded about ~0.05 to 0.1M, sorption became less efficient as evidenced by a decrease in Rd. The introduction of Aℓ into C-S-H made only a slight difference to alkali uptake at high Ca/Si ratios. But as the Ca/Si ratio decreased, Aℓ had a progressively greater impact on increasing the numerical value of Rd: i.e., its introduction into C-S-H favoured alkali fractionation into the solid. This, it was suggested, helped explain the impact of fly ash on pore fluid alkalis concentrations and resolved the paradox, well recognised in the literature, that despite the often high (1 – 2wt%) alkali content of PFA's, their inclusion in a blended cement reduced pore fluid alkalis. The explanation is that not only was more C-S-H produced in blends, but the Ca/Si ratio of C-S-H was reduced. This, coupled with enhanced alumina substitution in low Ca/Si ratio C-S-H, increased the number of silanol, Si-OH, sites as well as their mean acidity. Thus increase in the number of silanol sites and the strength of binding at these sites more than overcame the impact of additional alkali liberated from the fly ash: the net result was to reduce pore fluid alkalinity.

Subsequent to the publication of these papers, Van Eijk and Brouwers [20] have incorporated the alkali partition function into an overall model of pore fluid composition, which they proceeded to test. They found that the empirical approach by Taylor for sodium agreed well with Hong and Glasser's model, but that the fit for potassium was markedly better for Hong and Glasser's data.

The foregoing presentation has concentrated on intrinsic alkali contents, i.e., alkali released by the hydration of cement and cement blending agents. Indeed, specifications on the selection of cements for use with aggregates susceptible to alkali-aggregate reaction (AAR) are often based on cement alkali contents typically defined as Kg Na_2O equivalent per m^3 of concrete. However, as Berube, *et al* have convincingly demonstrated, aggregates may also be a significant source of soluble alkali [21]. Berube, *et al* noted that some rock types, such as phonolites, were especially liable to alkali release but that even well-crystallised felspar, especially potassic felspars, as frequently occur in granitic rocks, could contribute as much or more alkali to pore fluid than commercial cements. Dow and Glasser [22] will also report that the impurity phases in semi-synthetic pozzolanic admixtures may release alkali. In this instance, the mica and felspar impurities in kaolin were activated in the course of heating, essential to convert kaolin to metakaolin.

In summary, therefore, the alkalis in pore fluid arise spontaneously in the course of hydration. The alkalis partition between pore fluid and the solid phases: in ordinary Portland cement, C-S-H is the principal alkali-binding solid. Its capacity to bind alkali is dependent on (i) C/S ratio and (ii) extent of Aℓ for Si substitution: both increase markedly the partition of alkali into the solid, other factors being equal. The kinetics of release from clinker are broadly understood. The cement itself contains alkali sulfates, which dissolve rapidly, as well as slower release sulfates, principally in the form of alkali in solid solution with clinker minerals, e.g., Na in tricalcium aluminate, potassium in belite. Depending on the balance between fast and slow release forms, alkali is liberated to pore fluid. The alkali is sorbed into C-S-H and, to a lesser extent, AFm. These phases equilibrate relatively rapidly with pore fluid, within hours or days, so pore fluid compositions change mainly in response to (i) changes in the volume of pore fluid, (ii) total alkali content and its fractional release rate and (iii) the alkali partition coefficient (Rd) into solid. The latter is of course composition dependent which helps explain the apparent paradox that coal combustion fly ash which, while often containing much more alkali than cement, nevertheless decreases pore fluid alkali contents: its contribution to increasing acidity of the C-S-H favours alkali partition into C-S-H and the effect is so marked as to outweigh the additional gain of alkali. However, not all fly ashes will necessarily achieve this favourable condition and there is a continuing need to refine and quantify the data. In this context, it should also be recalled that addition of alumina-rich phases, besides affecting C-S-H, also generates more AFm: preliminary indications are that AFm is also a strong sorber of alkali, especially potassium. Moreover the addition of reactive alumina-rich phases, besides affecting C-S-H, also generates more AFm.

4. WATER-DEFICIENT PASTES: "HIGH PERFORMANCE" CONCRETES

Much recent interest centres on high performance concretes. Formulations described in the literature have three characteristics: (i) they are formulated to low w/c ratio, usually <0.4, (ii) contain a high proportion of fines, e.g., specially ground, high surface area cement and other mineral admixtures and, (iii) they may need to be dosed with fairly high levels of superplasticisers to achieve workability. On account of the low w/c ratio, often less than that which is required completely to hydrate the clinker, even mature hardened pastes may contain much clinker: pores which are water filled in normal concretes either become empty, or fill with hydration product, or both. As a consequence the paste may self-desiccate with dimensional shrinkage. However, a special concern is the fate of dissolved components in pore fluid: as the aqueous phase depletes, concentrations of alkali presumably rise to levels not encountered in normal pastes: the internal

environment becomes hyperalkaline. We can at present only speculate on the consequences of developing hyperalkaline pore fluid in respect of initiating mineralogical reactions. Table 2 shows a tentative sequence of reactions. The effect of these reactions may vary in extent. For example, as sodium and potassium concentrate in residual pore fluid, its solubility for sulfate, aluminate and silicate increase. But because the volume of pore fluid is sharply diminished, the number of moles of sulfate, silicate and aluminate dissolved, relative to total moles in the solids, must be small. Thus the amount of a phase required to dissolve, e.g., of C-S-H to furnish sufficient silica to saturate the remaining aqueous phase, is small. Similarly, the total number of moles of sodium in pore fluid are unlikely to be sufficient to convert much of the AFm in the paste to U phase, probably $C_4A_{O.9}N_{0.5}S_{1.1}H_{16}$. However, dissolution of cement substance in residual pore water also lowers its activity and this may well exert the most important influence on late-stage hydration. It is well known that a critical humidity is needed to maintain cement hydration [15]. The reduced activity of "water" obtained by dissolution of cement substances is equivalent to reducing its relative humidity. Thus it is envisaged that water will not simply vanish in the course of hydration, but that hydration will effectively cease when the vapour pressure exerted by pore water - effectively converted to a concentrated salt solution - decreases to the minimum value necessary to sustain hydration. It is therefore opportune to revisit the Powers-Brownyard (P-B) model [33] of cement hydration to analise in more detail mineral balances, including the amount of residual aqueous phase, occurring in the transition between regimes, one of excess water and the other, of water deficiency. Figure 3 shows a reconstruction of the P-B model. Note that evaporable water was found to persist even at low total water content, providing support for the contention that pore water will persist even in the presence of unreacted clinker, and that the coexistence of unhydrated clinker and pore "water" may actually be consistent with a steady state. In this view, the continuous changes in the activity function of water permits a smooth curve to be drawn, without the inflection point assumed in the P-B interpretation. We would, however, predict (i) that the portion of the curve to the right of the inflection point, i.e., at high w/c ratios, would be relatively independent of cement alkali content but that (ii) the exact shape and disposition of the curve to the left (i.e. its prolongation to low w/c ratios), would depend on cement alkali contents and (iii) that blending agents, e.g. slag, fly ash, will displace the position of the curve, depending on fraction reacted and composition of the blending agent.

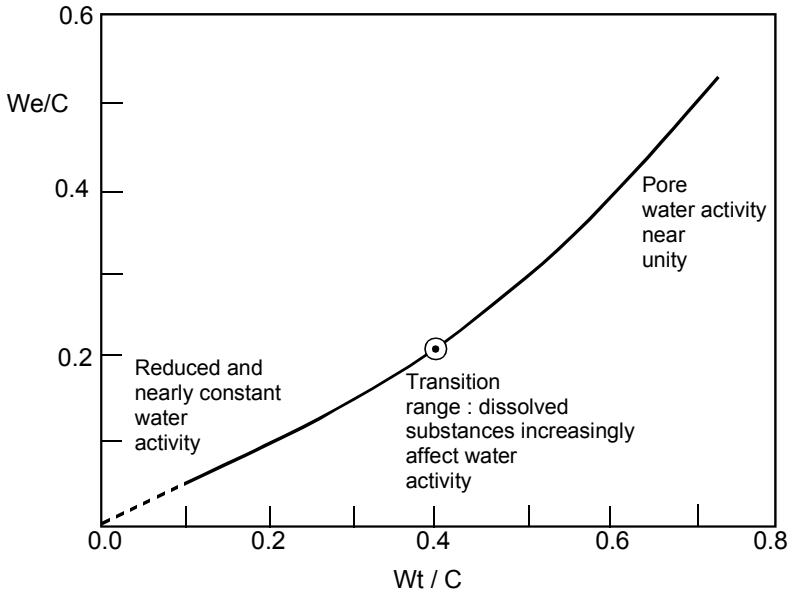

Figure 3. The graph of w/c (ratio of evaporable water to cement) and w/c (total water/cement ratio), assuming no bleed water. Data points from [22] are omitted but a reinterpretation is suggested. The dot marks the point at which in the original, an abrupt change of slope occurs but which in the present study is suggested to lie at an arbitrary point within a short region in which the physiochemical characteristics of "water" undergo accelerated change.

Table 2. Chemical and Mineralogical Changes in Cement Paste undergoing self-desiccation.

Reaction	Comment
Enhancement of alkali content in residual pore fluid.	Increase in sulfate, silicate and aluminate concentrations in residual fluid: conversion of AFm to "U phase".
Reduction of water content of hydrate phases.	Ettringite water decreases to $30H_2O$. Lower hydrates of AFm form. Self-desiccation of C-S-H occurs.
Precipitation	Direct precipitation of sodium aluminates, etc., as alkali concentrate and free water content approaches zero.

5. ADDITIONAL DISCUSSION AND CONCLUSIONS

The quantification of cement science has proved to be a slow process. Much work has been done in highlighting mineralogical changes in response to internal reactions (those initiated and conditioned by reaction with service environments are for the moment excluded). Yet the cement community, while freely using quantitative data and applying it to diverse problems such as heat treatment for accelerated curing, the selection of cements and aggregate to avoid alkali-aggregate reaction, and other important problems, has been reluctant to fund new initiatives, or even press a case for support to funding bodies such as national research councils, for basic science initiatives aimed at a fundamental understanding of the hydration process. Although some lines of research have reached a dead end, the new directions necessary to provide a scientific basis for improved cement properties are clear.

Quantification and modelling are seen as complementary: modelling is the tool whereby practical applications can be realised. While models are relatively well-developed, the weakness of their application is in the database: the wealth of validated data necessary to support and sustain calculations. By focussing on the internal chemistry, in this instance the aqueous phase, and relating to its practical examples, it is shown how many long-standing issues can be clarified, even if not resolved, at a stroke. For example, fractionation of alkalis between pore fluid and cement solids is conceptually presented as a series of partition functions, one for each pair of phases. The behaviour of a real cement pastes is the summation of the separate components multiplied by the mole fraction of each. Data are presently available only for C-S-H but, as it is the most abundant sorber of alkali, it enables a first generation model to be developed. To advance this model, additional data needs to be generated on the partition of alkali as a function of Aℓ content - possibly also of the sulfate content in C-S-H - and the resulting impact on distribution coefficients. Thus the way ahead is broadly clear, even if much important detail remains to be quantified. The outcome, a quantitative model for the alkalinity function of Portland and blended Portland cement, would enable a more scientific basis to be established in respect of aggregate selection, particularly for alkali-susceptible aggregates. Progress need not always rely on "frontier" methods: as shown in my reinterpretation of the Powers-Brownyard model, even the application of simple and assessable techniques will enable progress to be made.

Cement science is thus seen as being at the verge of a new era with respect to durability - and performance related improvements not necessarily entailing additional costs. The rate of progress towards these goals lies in the lands of producers, consumers and stakeholders.

REFERENCES

[1] Longuet, P., Burglen, L., and Zelwer, A. The Liquid Phase of Hydrated Cement (in Frehch). Rev. des Materiaux et Construction. No. 673, 35 - 41 (1973).

[2] Taylor, H. F. W. A Method for Predicting Alkali Ion Concentrations in Cement Pore Solutions. Advances in Cement Res. 1**,** 5 - 18 (1987).

[3] Bonen, D. And Sarkar, S.L. The Superplasticizer Absorption Capacity of Cement Pastes. Pore Solution Composition and Parameters Affecting Flow Loss. Cement and Concr. Res.1995, 25, 1423 - 1434.

[4] Angus, M. J. and Glasser, F. P. The Chemical Environment in Cement Matrices. "Scientific Basis for Nuclear Waste Management, 50, 546 - 556 Materials Res. Soc., Pittsburgh PA (1986).

[5] Luke, K and Glasser, F. P. Internal Evolution of the Constitution of Blended Cements, Cement and Concr. Res. 18, 495 - 502 (1988).

[6] Glasser, F. P., Luke, K. and Angus, M. J. Modification of Cement Pore Fluid Composition by Pozzolanic Additives. Cement Concr. Res. 18, 165 - 178 (1988).

[7] Macphee, D.E., Atkins, M. and Glasser, F. P. Phase Development and Pore Solution Chemistry in Agency Blast Furnace Slag - Portland Cement Blends in Proceedings Vol XII of "Scientific Basis for Nuclear Waste Management, 127, 475 - 480, (Materials Res. Soc., Pittsburgh, P.A. (1989).

[8] Glasser, F. P. Chemical, Mineralogical and Microstructural Changes Occurring in Hydrated Slag-Cement Blends in "Materials Science of Concrete II",. (Ed., J.S. Skalny). American Ceramic Soc., Westerville OH, 41 - 81 (1991).

[9] Macphee, D. E. and Glasser, F. P. Immobilisation Science of Cement Systems. Mater. Res. Soc. Bulletin Vol. XVIII, No. 3. 66 - 71 (1993).

[10] Lachowski, E. E., Kindness, A., Glasser, F. P. and Luke, K. Proceedings 10th Intl. Congress on the Chemistry of Cement (Gothenburg) Vol 3, Paper 3ii 091, pp 8 (1997).

[11] Ewart, F. T., Glasser, F. P., Groves, G., Jappy, T., McCrohon, T. R., Mosley, P. T., Roger, S. and Richardson, I. Mechanism of Sorption in the Near Field. Commission of the European Communities (Brussels and Luxemburg) EUR 13665 En pp 45 (1991).

[12] Yilmaz, V. T., Kindness, A. and Glasser, F. P. Determination of Sulphonated Napthalene Formaldehyde Superplasticizer in Cement: A New Spectrofluorimetric Method and Assessment of the UV Method. Cement Concr. Res., 27, 653 - 660 (1992).

[13] Dow, C. PhD Thesis, University of Aberdeen, 2000.

[14] Macphee, D. E., Luke, K., Glasser F. P., and Lachowski, E.E. Solubility and Ageing of Calcium Silicate Hydrates in Alkaline Solutions at 25°C. Jour. Amer. Ceram. Soc., 72, 645 - 654 (1989)

[15] Taylor, H. F. W. "Cement Chemistry" 2nd Ed., Thomas Telford, London (1997).

[16] Macphee, E. E., Luke, K., Glasser, F. P. and Lachowski, E.E. Solubility and Ageing of Calcium Silicate Hydrates in Alkaline Solution at 25°. Jour. Amer. Ceram. Soc. 72, 646 - 654 (1989).

[17] Hong, S.-Y. and Glasser, G. P. Alkali Binding in Cement Paste: Part I. The C-S-H Phases. Cement Concr. Res., 29, 1893 - 1903 (1999).

[18] Hong, S.-Y. and Glasser F. P. Alkali Sorption by C-S-H and C-A-S-H Gels. Part II. Role of Alumina. Cement and Concr. Res, 32, 1101 - 111 (2002).

[19] Taylor, H. F. W. A method for Predicting Alkali Ion Concentration in Cement Pore Solutions, Advances in Cement Res. 1, 5 - 16 (1987).

[20] Van Eigj, R. J. Brouwers, H. J. H. Prediction of Hydroxyl Concentrations in Cement Pore Water using a Numerical Cement Hydration Model. Cement and Concr. Res. 30, 1801 - 1806 (2000).

[21] Berube, M.-A., Duchesne, J. Dorion, J. F. and Riverst. MN. Laboratory Assessment of Alkali Contribution by Aggregates to Concrete and Application to Concrete Structures affected by Alkali-Aggregate Reactivity. Cement and Concr. Res. 32, 1215 - 1227 (200).

[22] Dow, C. and Glasser, F. P. Alkali Releases from Crushed Minerals and Thermally-Activated Constituents of Metakaolin (in preparation).

[23] Powers, T. C. and Brownyard, T. L. "Studies of the Physical Properties of Hardened Cement Paste". Portland Cement Association (US) Skokie, Il. Bulletin 22, (1948).

HYDRATION OF FLY ASH BLENDED PORTLAND CEMENT IN THE PRESENCE OF SUPERPLASTICIZERS AT DIFFERENT TEMPERATURES

N.B.Singh[1] , Shivani Chaturvedi[1] and Sarita Rai[2]

1-Department of Chemistry,DDU Gorakhpur University,Gorakhpur-23009,India
2-Department of Chemistry, IIT, Delhi, India. E-mail: dr_n_b_singh@rediffmail.com

ABSTRACT

Hydration of fly ash blended Portland cement was allowed to take place at 20 and 60^0C in the presence of sulphonated melamine formaldehyde condensate (SMF) and sulphonated naphthalene formaldehyde condensate (SNF) superplasticizers. Hydration properties varied considerably with temperature and superplasticizer. Compressive strength was highest in the presence of SMF at 60^0C.

1. INTRODUCTION

Many industrial materials considered essential for supporting a better quality of life consume large amounts of energy for their production. Ordinary Portland cement (OPC) is used widely as a building material and its manufacture consumes large quantities of energy. In India, the cost of energy accounts for >40% of the total cost of cement manufacture. The cost to manufacture cement is expected to increase because of increasing demands for energy. Scientists are attempting to prepare OPC and other binding materials at lower cost by using agricultural and industrial wastes during clinkerization and by making blended cements. These measures decrease the cost of production, conserve mineral resources and protect the environment by beneficial disposal of wastes. Blended cements are usually blends of Portland cement clinker with other finely ground materials (also known as mineral admixtures) that take part in the hydration reactions and thereby make a substantial contribution to the hydration products. A large number of blended cements using a variety of waste materials have been studied[1-7]. One of the most important blending components is fly ash that is obtained from thermal power plants using pulverized coal. Incorporation of fly ash in Portland cement concrete is common practice now, due to technological, economic and environmental benefits. It reduces the water requirement, rise in temperature and bleeding and improves the workability and strength development. These properties are further changed in presence of superplasticizers[8,9] and with temperatures[10]. In this paper hydration of OPC – Fly ash blended cement in presence of SMF and SNF at 20 and 60^0C has been studied.

2. EXPERIMENTAL

2.1 Materials

Ordinary Portland cement (Prism) was used for detailed hydration studies. The oxide and mineralogical compositions of the cement are given in Table 1 and 2 respectively. The Blaine surface area was 2.82 m^2 /g. The chemical composition of fly ash is given in table 3.

Sulphonated melamine formaldehyde condensate (SMF) and sulphonated naphthalene formaldehyde condensate (SNF) have been used as the superplasticizers.

Superplasticizers SMF and SNF of concentration 1.0 wt. % with reference to fly ash blended Portland cement was used for the hydration studies. The blended cement with 20 wt % fly ash is referred to as blended cement and all the experiments were done with this cement.

Table 1. Oxide composition of Portland cement

Oxide	SiO_2	Al_2O_3	Fe_2O_3	CaO	MgO	K_2O	Na_2O	TiO_2	PbO	ZnO	MnO	P_2O_5	SO_3
Composition wt%	19.75	4.84	3.26	62.66	4.19	0.54	0.06	0.44	0.77	0.09	0.15	0.03	2.13

Table 2. Mineralogical composition of Portland cement

Phase	**C_3S**	**C_2S**	**C_3A**	**C_4AF**
Composition wt%	67.8	5.51	7.31	9.92

Table 3. Oxide composition of Fly ash

Oxide	SiO_2	Al_2O_3	Fe_2O_3	TiO_2	P_2O_5	SO_3	CaO	MgO	Na_2O	K_2O
Composition wt%	59.06	24.34	7.59	1.40	0.97	0.43	1.42	1.85	1.79	1.15

2.2 Methods

2.2.1 Preparation of Blended Cements

OPC and FA were mixed in different proportions and homogenized. OPC was replaced by 5.0, 10.0, 15.0, 20.0, 25.0 and 30.0 wt. % FA and then stored in polythene bags.

2.2.2 Setting Time

Initial and final setting times were determined with the help of a vicat apparatus at room temperature.

2.2.3 Preparation of Hydrated Samples

Blended cement with 20 wt % FA was mixed with and without 1.0 wt % SMF and SNF separately with a W/S = 0.5 at 20 and 60 ^{0}C. Hydration was allowed to occur at different intervals of time and then stopped with the help of isopropyl alcohol and ether. The hydrated samples were then dried at 105 ^{0}C and stored in polythene bags for analysis.

2.2.4 Combined Water Content (Wn)

One gram of the hydrated blended cements was heated in ceramic crucibles at 1000^{0}C for one hour and from the weight loss the combined water contents were determined.

2.2.5 Free Calcium Hydroxide Content

One gram of the hydrated samples was refluxed for one hour in presence of 40 ml isopropyl alcohol: acetoacetic ester (20:3). The filtrate was then titrated against 0.1 N HCl in order to determine free calcium hydroxide content[11].

2.2.6 Electrical Conductivity Measurements

The electrical conductivities of the blended cement pastes in the absence and presence of 1.0 wt % SMF and SNF (W/S = 1.0) at 20 and 60^{0}C were determined with the help of a digital conductivity meter. In each experiment 10 g blended cement was taken. The measurements were made at 20 and 60^{0}C for about 3 hours.

2.3 Study of Adsorption of Superplasticizers

In order to study the adsorption of superplasticizers spectral studies were made. First the u.v. spectra of water solution (0.05 wt %) of SMF and SNF were recorded and the λ_{max} values were determined at 220 and 285 nm respectively. One gram of blended anhydrous blended cement and hydrated for 24 h in the absence of superplasticizer solution (0.05 wt %) was shaken for 5 minutes and then filtered. The optical density at λ_{max} was then determined. One gram of anhydrous blended cement was shaken with 10cc water for 5 minutes and then filtered. The optical density of this filtrate was determined at 220 and 285 nm. In order to determine the extent of adsorption these values were subtracted from the optical density values determined in the presence of superplasticizers. These experiments were carried out at 20 and 60 ^{0}C.

2.4 Compressive Strength Measurements

Blended cement was mixed with 1.0 wt % SMF and SNF (W/S = 0.32) and the pastes were filled in different moulds to form cubes (8 x 8 x 8 cm^3). These cubes were taken out of the moulds after 48 hours and submerged in clean water at 20 and 60 ^{0}C until taken out just prior to measurement. Compressive strengths were measured by breaking the cubes with the help of a compressive strength testing machine (AIMIL India. Each observation is an average of three observations.

2.5 Results and Discussion

Setting times of fly ash blended Portland cements of different composition in presence of 1.0 wt. % SMF and SNF were determined. It was found that both initial and final setting times increased with the increase of Fly ash but the increase was more pronounced when OPC was replaced by 20.0 wt. % Fly Ash. Thus this concentration of fly ash was considered as the optimum limit for making the blended cement.

The variations of combined water content (W_n) of the hydrated blended cement in the presence of superplasticizers at 20 and 60 ^{0}C are given in Figure 1. The values increased with hydration time and temperature indicating that the degree of hydration of the blended cement increased with time and the increase was more at higher temperatures. From the figure it is also clear that in the presence of SMF the extent of hydration is higher than in the presence of SNF.

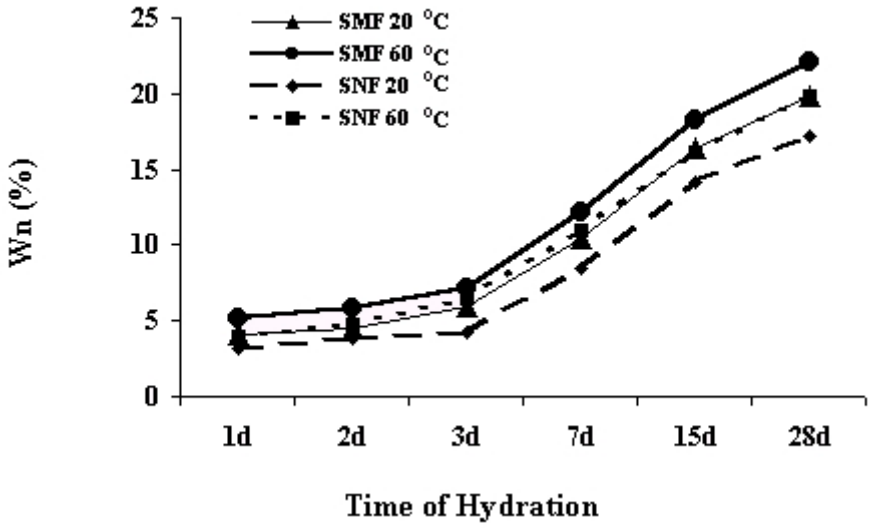

Figure 1. Variation of Combined Water Content (Wn %) in the presence of wt. % Superplasticizer at 20 and 60^0 C

The variation of free calcium hydroxide content with time is shown in Figure 2. The values increased up to 7 days of hydration at both the temperatures and then decreased. The results show that up to 7 days of hydration, free calcium hydroxide liberated either could not react or reacts very slowly with fly ash. But after this the pozzolanic reaction enhanced and the values decreased because of consumption of free calcium hydroxide. Both liberation and pozzolanic reaction of $Ca(OH)_2$ increased with the increase of temperature. The consumption of $Ca(OH)_2$ in the presence of SMF after 7 days is higher than in the presence of SNF indicating that at 60^0C, SMF enhances the pozzolanic reactions more than SNF.

The variation of electrical conductivities with time at a particular temperature was almost constant up to 3 hours (the time of measurement) in the presence of both SMF and SNF. However, the values were slightly higher at 60^0C as compared to those at 20^0C and also the values were slightly higher in the presence of SNF. It appears that the superplasticizers are adsorbed at the surface of cement and hinders the dissolution of ions in the solution responsible for conduction. Also SMF might be adsorbed more as compared to SNF.

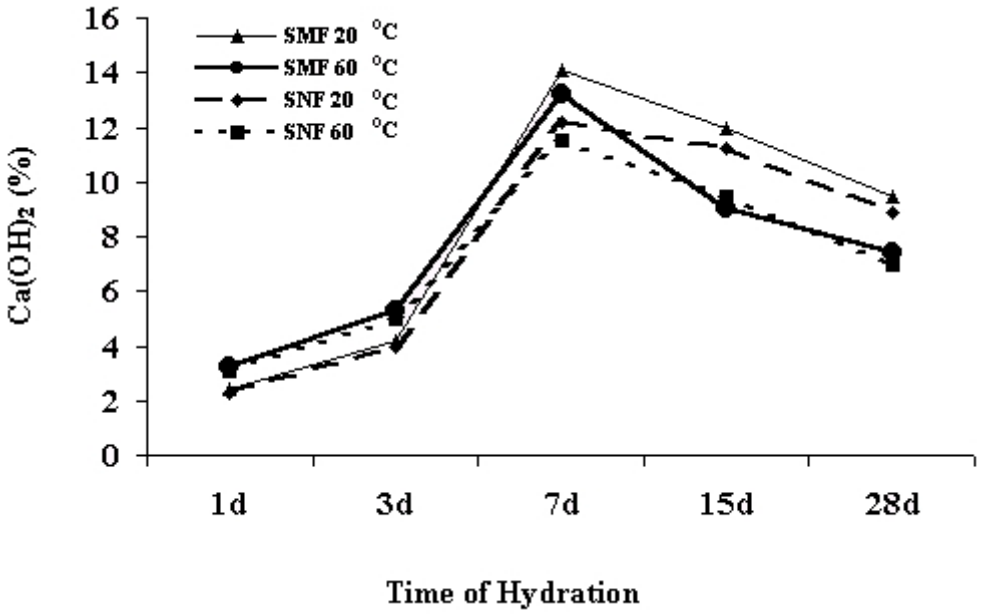

Figure 2. Variation of Free $Ca(OH)_2$ Content in the presence of 1.0 wt. % Superplasticizer at 20 and 60^0 C

The percent adsorptions of the superplasticizers on the surface of blended cement hydrated for 24 hours are given in Table 4. SMF is adsorbed more than SNF and the extent of adsorption is higher at lower temperatures.

Table 4. Extent of adsorption of SMF and SNF on the surface of blended cement hydrated for 24 h at 20 and 60^0C

Superplasticizers	Percent adsorption	
	20^0C	60^0C
SMF	45	38
SNF	41	36

The superplasticizers can affect the process of hydration by interacting at the surface of hydrated blended cement in a number of ways[12]. These include reduction of the surface tension of water, electrostatic repulsion between particles, lubricating film between cement particles, inhibition of surface hydration of cement, steric hindrance in particle-particle contact and change in the

morphology of hydration products. Both physical and chemical interactions may be involved, but it is difficult to differentiate. However, low adsorption at higher temperature is in favour of physical adsorption.

The variations of compressive strength with hydration time in the presence of SMF and SNF are shown in Figure. 3. The values increased with time and temperature. The compressive strength values are higher in the presence of SMF as compared to those in the presence of SNF. According to Mor and Mehta[13] the higher compressive strength is due to lower amounts of large capillary pores present in the presence of superplasticizer.

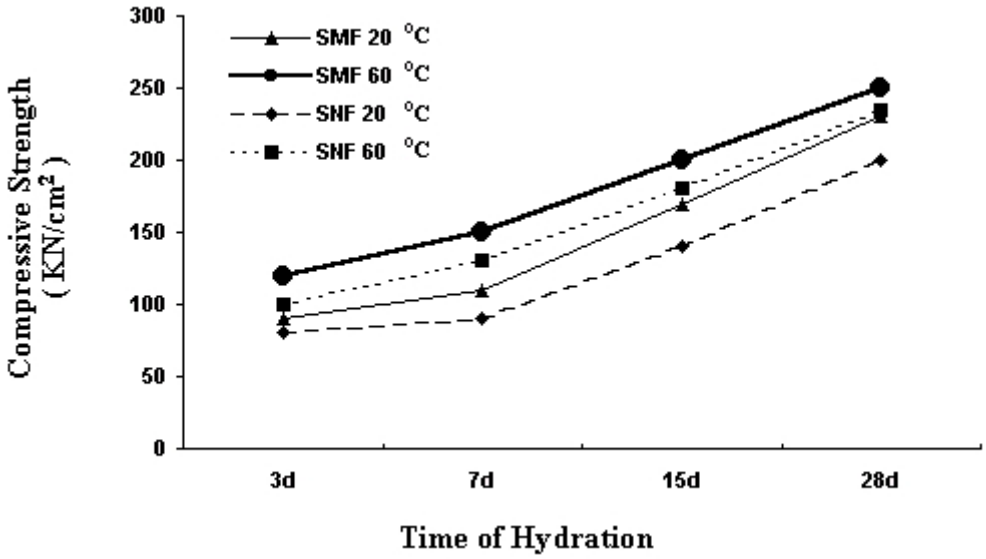

Figure 3. Variation of Compressive Strength in the presence of 1.0 wt. % Superplasticizer at 20 and 60^0 C

3. CONCLUSIONS

The results have shown that:

1. The hydration of fly ash blended Portland cement is more in the presence of SMF at 60^0C.
2. The adsorption of SMF on the surface of hydrated blended cement is more as compared to that of SNF and the extent of adsorption is higher at 20^0C.
3. SMF accelerates the pozzolanic reactivity of FA at 60^0C.
4. Compressive strength is highest in the presence of SMF at 60^0C.

It is concluded that SMF is a better superplasticizer as compared to SNF in accelerating the hydration of fly ash blended Portland cement especially at higher temperatures.

REFERENCES

[1] H.F.W. Taylor, "Cement chemistry" Academic Press Ltd. 277-344 (1990)
[2] H. Uchikawa "Effect blending components on hydraulic and structure formation", Proc. 8th Int. Cong. Chem. Cem. Rio. Brazil, Vol. I, 249-280 (1986)
[3] K.C. Narang, "Portland and Blended Cements" Proc. 9th Cong.Chem.Cem. New Delhi Vol. I, 213-257 (1992)
[4] R. Sersale, "Advances in Portland and blended cements" Proc. 9th Int. Cong.Chem.Cem., New Delhi Vol. I, 261-302 (1992)
[5] J.B. Udochkin, "Blended Cements" Proc. 9th Int. Cong.Chem.Cem. New Delhi Vol. I, 303-314 (1992)
[6] P.K. Mehta, "Mineral Admixtures for Concrete - An Overview of Recent Developments" Advances in Cement and Concrete", Proc. of an Engineering Foundation Conference, edited of M.W. Grutzeck and S.L. Sarkar, 243-256 (1994)

[7] F. Massaza “Blended Cements” special lecture of 4th NCB Int. Seminar on cement and building materials, New Delhi (1994)
[8] M. Collepardi, S. Monosi, M. Pauri, S. Biagini and I. Alvera, Proc. Int. RILEM Symp. Admixtures for concrete improvement of properties Barcelona, 1990, ed. E. Vasquez (Chapman and Hall, London) 1990.
[9] N. B. Singh, M.P. Dwivedi and N.P. Singh, Cem. Concr. Res. 22, 121 (1992).
[10] N. B. Singh, Reetika Sarvahi, N.P. Singh and A. K. Shukla, Thermochimica Acta, 247, 381 (1994).
[11] E. Pressler, S. Brunauer, D. L. Kantro and C. H. Weise, Anal. Chem., 33, 877 (1961).
[12] M. Collepardi and V. S. Ramachandran, Proc. 9th Int. Cong. Chem. Cem. , New Delhi 1, 529 (1992).
[13] Mor and P. K. Mehta, Cem. Concr. Res., 14, 754 (1984).

CHARACTERISATION OF PFA USING IMPEDANCE TECHNIQUES

G. Starrs[1], W. J. McCarter[1] and T. M. Chrisp[1]

[1]Department of Civil and Offshore Engineering, Heriot-Watt University, Edinburgh, UK.
E-mail: johnm@sbe.hw.ac.uk; E-mail: gstarrs@sbe.hw.ac.uk

ABSTRACT

This paper highlights the use of frequency domain electrical measurements for the investigation of PFA as a replacement material in OPC based mortar. Impedance data were acquired in the frequency range 1 Hz up to 10 MHz on mortar samples containing PFA from three different sources as well as plain OPC. The results corroborate and extend previous findings, confirming that the introduction of PFA produces a unique electrical signature when the data are viewed in complex-plane format. Analysis of the impedance and de-imbedded conductivity and dielectric constant show that this PFA-effect results from a polarisation mechanism operating largely between 1 kHz and 100 kHz, which is superimposed on the electrical response of the plain OPC. The exact characteristic of the PFA-effect is shown to be determined by the type of PFA present. These findings suggest that electrical measurements could provide the means for the detection and characterisation of PFA in cementitious materials for quality control purposes.

1. INTRODUCTION AND THEORY

The utilisation of replacement materials such as pulverised fuel ash (PFA[i]) has assumed an important role in the design of durable cementitious systems and extensive use continues to be made of these quality-enhancing by-products. However, design for, and prediction of, durability and performance are rendered irrelevant if quality is not monitored satisfactorily at all stages during production, and there is considerable on-going debate on the problem of non-compliance with product conformity standards. In the case of PFA the need for a simple-to-apply characterisation technique is of major importance, not merely because of its widespread use but because the amount and quality of PFA in the binder has a decisive effect on its performance. This paper highlights the use of the electrical response as the basis of a test method in this field and builds on previously reported work [1][2][3].

Impedance spectroscopy (IS[ii]) is now a developing technique in the characterisation of cementitious systems[iii]. IS involves monitoring the electrical response (usually current flow in amps) of a material as a function of the strength (in volts) and frequency (f, in hertz) of an applied sinusoidal electric field. The ratio of voltage to current, inclusive of the phase difference, is a frequency dependent complex parameter called impedance:

---

[i] PFA is also known as fly ash in European Standards and in many countries. Fly ash may also refer to non-coal ashes such as incinerator ash. These might have significantly different properties that don't offer the same advantages as PFA from coal.

[ii] sometimes known as IMMITTANCE spectroscopy, a catchall term covering a range of related electrical parameters such as impedance, admittance, relative permittivity, dielectric modulus, complex conductivity and complex resistivity.

[iii] see, for example, Advances in Cement Research, Vol. 10, No. 4, Oct 1998 – complete issue.

$$Z(\omega) = Z'(\omega) - jZ''(\omega) \quad \ldots(1)$$

where, Z' is the resistive component and Z'' the reactive component of impedance (both ohms), ω (=2∗π∗f) is the angular frequency (radian/sec) and j is the complex operator (≡√-1).

In aqueous, heterogeneous, non-magnetic materials such as cement paste, mortar or concrete the underlying mechanisms responsible for electrical behaviour are strongly correlated to the physical and chemical properties of the individual material components, and the way in which they are combined. This correlation is manifested in the frequency domain as dispersive behaviour characterised by frequencies of relaxation above which the *dielectric constant* ($\varepsilon'_r(\omega)$) falls, and the *conductivity* ($\sigma(\omega)$ Siemens/m) rises (the respective polarisation of bound charges and conduction of free charges within the material determine these intrinsic electrical parameters). The impedance is related to the dielectric constant and the conductivity in accordance with the expression:

$$Z(\omega) = \left(\left(\sigma + j\omega\varepsilon'_r\varepsilon_0\right)k\right)^{-1} \quad (2)$$

where, ε_0 is the permittivity of free space (=8.854×10^{-12} Farads/m), and k (m) is the cell constant, a factor determined by the sample holder and electrode system. Equation (2) is only valid at frequencies where the signal wavelength is significantly larger than the electrode dimensions.

Different materials, and different stages of material development, may therefore be identified using electrical measurements, provided these are obtained across a wide enough range of frequencies, making IS a potentially powerful diagnostic technique. Several other advantages may be afforded by the use of IS: the technique is non-destructive and non-invasive; samples need not be restricted to cement pastes as mortars and concretes can be easily studied; the acquisition of data is relatively simple, and continuous monitoring can be carried out under normal pressures and temperatures.

In this paper we report on the use of IS within the frequency range ≈1Hz-10MHz as a characterisation technique in the study of PFA binders, particularly in the early stages of hydration. IS is used to:

- investigate the complex immittance spectra of individual PFA's as a possible characterisation signature
- provide frequency spectra for the detection of PFA in concrete

2. EXPERIMENTAL WORK

2.1. Impedance Measurements

A Solartron 1260 frequency response analyser (FRA) was used to obtain electrical impedance data on mortar samples containing PFA. A 100 milli-volt energising signal was employed, and resultant current was monitored at 20 points per decade of frequency increase, giving a total of 141 points for the investigated 1Hz to 10 MHz range. Control of the FRA was by means of Solartron Z60 software run on a Hewlett Packard HP486/66 personal computer. Cuboid shaped samples were moulded in rigid Perspex cells of nominal internal dimensions 50×50×50 mm. Attached to two internal opposite faces were square (50×50 mm) 3 mm thick stainless steel electrodes. Electrical connection was facilitated by threaded stainless steel rods which were passed through the cell walls and welded to the back of the electrodes. Connection to the FRA was effected by individually screened coaxial cables of length 0.4 m.

At frequencies higher than ≈100 kHz the impedance of the leads can have a masking effect on the required impedance of the measurement cells. The acquired data was therefore subsequently processed to calibrate out this effect. The process involved the prior acquisition of data on three known impedances (a short circuit, an open circuit and a capacitor-resistor network containing precision components) at each frequency point [3]. The algorithm used to achieve this was developed in-house and run as a routine in Mathcad.

Impedance data thus acquired represent the electrical properties of the specific samples (including electrochemical interaction with the electrodes). In order to consider the *intrinsic* electrical properties of the materials under test, independently of sample dimensions, the parameters dielectric constant, ε_r', and conductivity, σ, were de-imbedded from the measured impedance in accordance with equation (2). The cell constant, k, for the parallel plate electrode system used is calculated from the area of the plates divided by the distance between them, or it can be obtained from measurements on materials of known electrical properties. For the present arrangement k has a value of 0.0565.

2.2. Materials, Samples and Curing

Ordinary portland cement (OPC) was used as the main binder in the mortar samples. PFA samples of part 1 quality [6] from several UK sources were investigated, and the results for three are presented here. These are Longannet Power Station in Scotland (PFAL), FerryBridge C Power Station in W. Yorkshire (PFAF), and Eggborough Power Station in E. Yorkshire (PFAE). The chemical analysis for each binder material is given in Table 1. PFA fineness is quoted as the percentage retained on a 45-micron sieve. Four mortars were fabricated, one using a pure OPC binder, and three others with OPC partially replaced by each PFA at a level of 33% by mass. The aggregate used for the mortars was a uniformly fine-grained Leyton-Buzzard sand. All four mortar samples had a sand:binder mass ratio of 3:1 and a water/binder ratio of 0.5.

Table 1. Chemical and physical properties of cementitious materials

	OPC	PFAL	PFAF	PFAE
Fineness (on 45 μm)	-	8%	9.5%	13.5%
Specific Gravity (g/ml)	3.15	2.09	2.1	2.1
% component				
SiO_2	20.68	51.0	50.5	44.3
Al_2O_3	4.83	34.7	24.7	24.7
Fe_2O_3	3.17	4.6	7.4	9.2
CaO	63.95	3.4	2.6	5.9
MgO	2.53	1.4	1.5	1.9
SO_3	2.80	0.7	0.8	0.69
TiO_2	-	1.6	1.0	1.4
K_2O	0.54	1.0	3.0	1.7
Na_2O	0.08	0.2	0.8	0.6
LOI	1.90	5.5	5.3	1.9

Prior to gauging all materials were thoroughly mixed by shaking together in a closed plastic storage bottle. Water was added to the dry blend in a ceramic bowl and hand mixed for about eight minutes. Samples were compacted in the measurement cells in layers using mild vibration and hand tamping. Following compaction, the tops of the measurement cells were covered with Perspex lids. In the case of the mortar samples the first swept frequency measurements were then taken (≈10 minutes) and the samples subsequently stored in the humid environment of a small plant propagator. The mortars were removed from the chamber prior to each subsequent measurement sweep (at 30 min, 60 min, 120 min, 240 min and 1-3 day).

3. RESULTS AND DISCUSSION

3.1. Impedance Measurements

Figure 1 displays impedance data obtained immediately after gauging (≈10 minutes) in complex plane format for the four mortar samples (plain OPC plus one each containing PFAF, PFAE and PFAL). Data are presented from ≈20 Hz up to 1 MHz. For freshly gauged material the impedance values (particularly the reactive component) are not measured reliably at frequencies higher than this. This appears to be due to the relatively high conductivity of the pore water, but the full reasons are not clear.

Indicated on the plot for plain OPC is the "cut-off" frequency (70 kHz). This is the point of convolution of the bulk material and electrode polarisation responses, above which the electrode effects become much less significant and below which the reactance of the sample material is considered to be less significant [4][5]. This feature has been previously noted by many workers and, because the reactance is at a minimum, is used to obtain an accurate approximation to the DC resistance of the sample (in this case 51.29 ohms at 70 kHz).

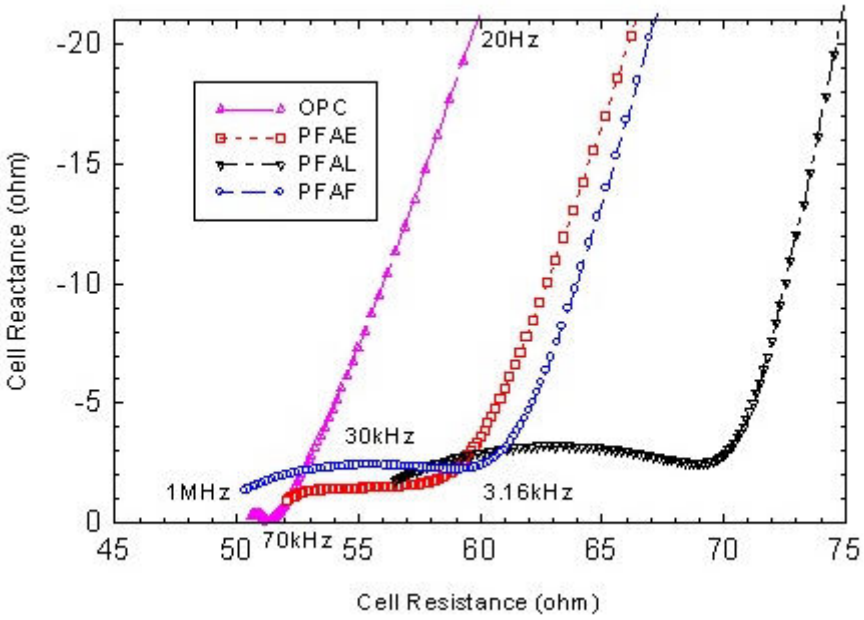

Figure 1. Impedance of Mortars at 10 min

It is clear from Figure 1 that each of the PFA mortars is quite distinct from the plain OPC case in that a plateau or shallow-arc region appears above the apparent cut-off frequency of the electrode effects. This confirms previous findings [3] (although these had been confined to PFA from Longannet power station) and suggests, together with results from other UK PFA samples (not presented here), that the "PFA-effect" is likely to be found in classified material from any similar coal burning power station. This general effect is *not* detected when other replacement materials (e.g. blast furnace slag, meta-kaolin, and micro-silica) are used [1][2]. There are, however, detectable differences between the three PFA samples. PFAL shows the most distinct arc-like plateau region and in this respect is closely followed by PFAF. PFAE lies closest to PFAF on the graph, indicating similar resistance, but the plateau region is not so prominent or obviously arc shaped.

The frequencies at which two of the key features of the PFA-effect occur are indicated on the plot for PFAF. The point at which the reactance reaches a minimum at the apparent upper end of the electrode arc occurs at 3.16 kHz, and the point at which the PFA-effect reactance is at a maximum is at 30 kHz.

Impedance plots for OPC and PFAF at approximately 3 days (73 hours) after gauging are displayed in Figure 2. This is the period during which the OPC component of the binders has begun hardening, but before the main reactions of the PFA have begun. These plots are presented to illustrate the persistence of the PFA-effect subsequent to the setting of the OPC. The data in this case are presented from 5 Hz up to 1 MHz. Again, the OPC cut-off and PFA-effect frequencies are indicated, with the addition of a second local reactance minimum at 126kHz on the PFAF plot.

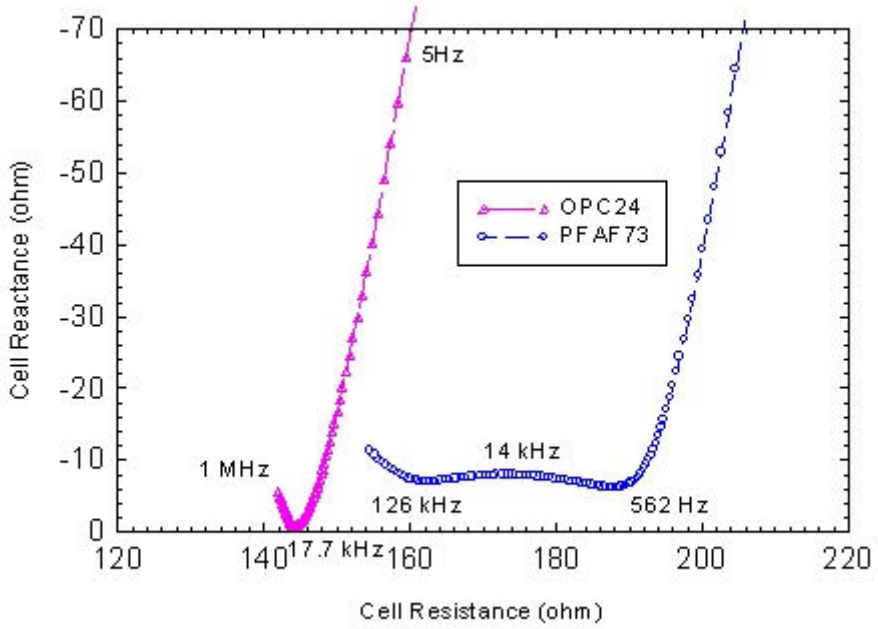

Figure 2. Impedance of Mortars at ≈3 Day

It can be seen in both Figure 1 and Figure 2 that the resistance of the PFAF mortar is about 10-20 percent higher than that of the OPC mortar. This is due to the partial replacement of the OPC, which is the major contributor of ions to the mix water. For an aqueous ionic conductor it is the ionic concentration which determines the level of electrochemical activity at the surface of the electrodes (electrode polarisation), and it can be generally observed that the higher the conductivity (i.e. ionic content) the higher the frequency to which such effects persist. The higher resistance of the PFA mortar can therefore be expected to promote a lowering of the cut-off frequency of the electrode polarisation, and it was previously assumed that the cut-off frequency for PFA binders was located at the extreme right hand end of the PFA-effect [3]. However, it is now thought that this point occurs at too low a frequency in comparison to those on the respective OPC plots. This suggests that the presence of the PFA is introducing a phenomenon that is significant at frequencies below and above the convolution point of the electrode and bulk material impedance arcs produced by a plain OPC binder. Obtaining an estimate for the DC resistance of the PFA mortars from their respective impedance plots is therefore not a simple matter as it is for plain OPC.

To explore this further, impedance data over the same frequency range were acquired from two modified “mortar” samples from which the OPC was removed. The first of these contained sand, PFAL, and sodium chloride solution at ≈0.1M concentration (6g/litre). The purpose of adding the salt to the mix water was to compensate for the loss of ionic conduction caused by the removal of the OPC. The mix proportions were 200 grams of sand to 33 grams of PFAL and 40 millilitres of salt solution. The second sample had identical mix proportions but the PFA was replaced by glass spheres of diameter 30-50 μm. The purpose of the glass spheres was to produce a material that was physically (i.e. morphologically) identical to the sample containing PFAL but which was essentially inert in regard to its polarisation properties, while at the same time having similar chemical and conductive properties. The results, from 7 Hz to 10 MHz, are presented in Figure 3.

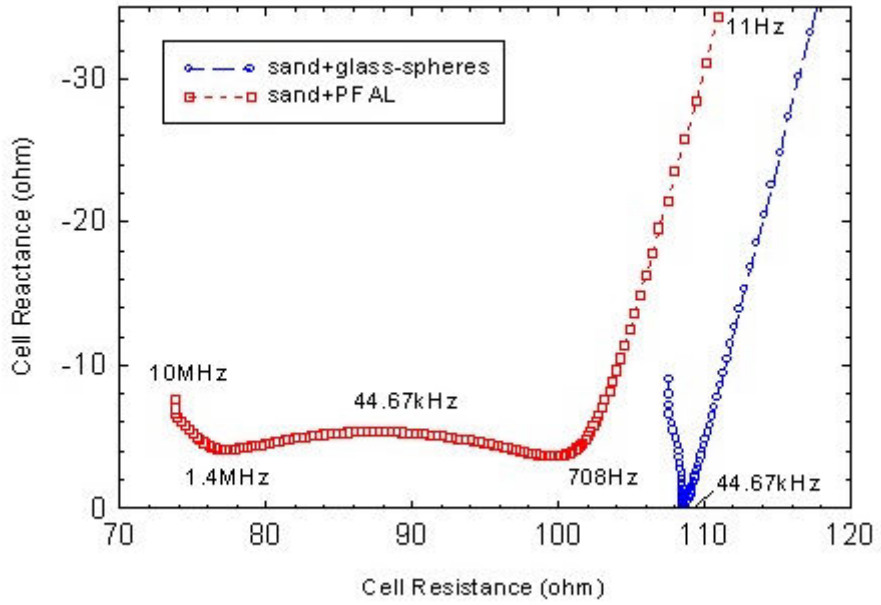

Figure 3. Synthesised PFA-Effect

The plot for the sample containing the sand and glass spheres can be seen to have a similar characteristic to that of the plain OPC with a sharply defined convolution point at 44.67 kHz. The sand and PFAL plot has a definite PFA-effect characteristic and has a slightly lower resistance. This is probably due to the low-level presence of ions dissolved from the PFA, but the lower density of the PFA might also be a determining factor. The frequency of the reactance minimum at the right hand side of the PFA-effect (708 Hz) is certainly too low to be the point of electrode polarisation cut-off. Interestingly, however, the frequency at which the shallow arc of the plateau region reaches its peak reactance (44.67 kHz) corresponds to the cut-off frequency of the plot for the glass spheres. Given that the materials are of comparable resistance and are morphologically very similar it seems reasonable to take this value as the cut-off frequency of the electrode polarisation effects. When this is applied to the plots for PFAF mortar in Figures 1 and 2, the electrode effect cut-off frequencies are 30 MHz and 14 kHz respectively, and these values accord well with those obtained from the associated plots for OPC mortar.

3.2. Conductivity and Dielectric Constant

Using equation 2, conductivity and dielectric constant data were de-imbedded from the impedance measurements obtained at 10 minutes after gauging (Figure 1). These data are presented in Figures 4 and 5, and they give a clearer view of the conductive-dispersive [7] behaviour of the mortars.

In Figure 4 the low frequency masking of the measurements caused by electrode polarisation is clearly seen, particularly below 100 Hz. At frequencies above 1 kHz the increased slope on the plots for the PFA mortars is evidence of the presence of dispersion due to dielectric relaxation. By contrast the OPC plot is levelling out towards the electrode effect cut-off frequency of 70 kHz. The dispersive effect is most pronounced in the case of PFAL, which, although having the lowest conductivity, also has the most distinctive impedance PFA-effect.

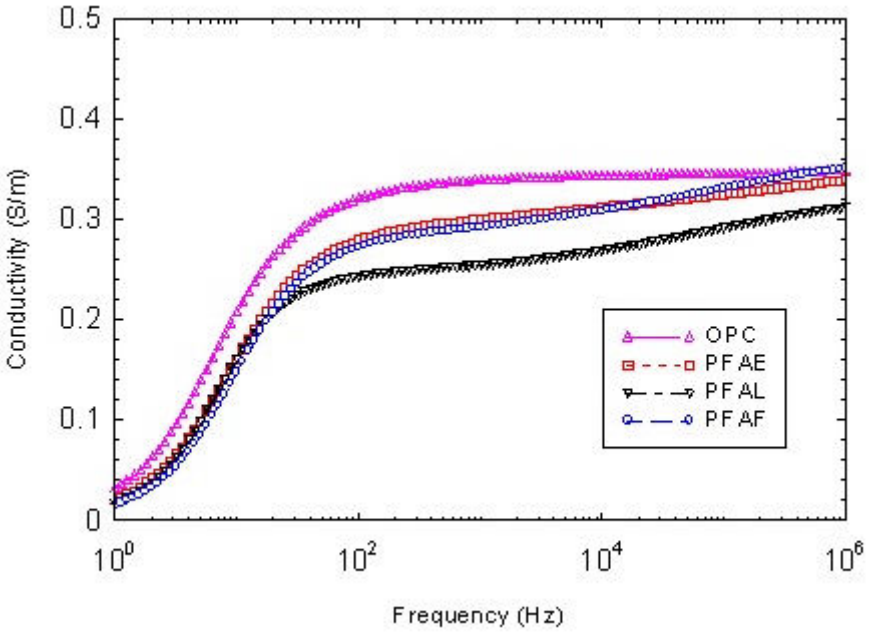

Figure 4. Conductivity of Mortars at 10 min

The PFAF mortar displays a similar dispersion characteristic to the PFAL and because it appears to have a higher DC conductivity the frequency dependent conductivity actually exceeds that of the OPC at 1 MHz. This is despite having a lower ionic concentration than the plain OPC. The PFAE mortar shows the least pronounced dispersion characteristic, which accords with its less distinct impedance PFA-effect.

In Figure 5 the large enhancement of the dielectric constant of the PFA mortars over that of the plain OPC is evident between 1 kHz and 1 MHz. It is clear from this graph that the mechanism responsible for this effect is operating above and below the cut-off frequency of the electrode polarisation effects, confirming what was surmised above from the impedance data. The principal relaxation frequency of the polarisation mechanism appears to lie in the range 10 to 100 kHz. Again, the relative differences between the PFA mortars are visible, with PFAL showing the most pronounced dielectric enhancement and PFAE the most dispersed.

3.3. Material and Electrical Properties

It can be seen in Table 1 that OPC and PFA have similar chemical composition but that the main oxides are present in very different amounts, and this is known to account for the major differences in mineralogy between the two. There is also a considerable difference in the morphology of OPC and PFA particles. Although the particles are of similar average dimensions, OPC has a greater spread of particle size and the grains themselves are jagged and non-uniform in shape. PFA particles, by contrast, tend to be more uniformly sized and mostly consist of smooth glassy spheres, some of which are hollow. We have previously hypothesised that the major difference in morphology between these two materials is what promotes the large enhancement of dielectric constant evident when OPC is partially replaced by PFA, the smooth glassy spheres of the PFA lending themselves to the setting up of a highly polarisable electrochemical double layer on the particle surfaces [3].

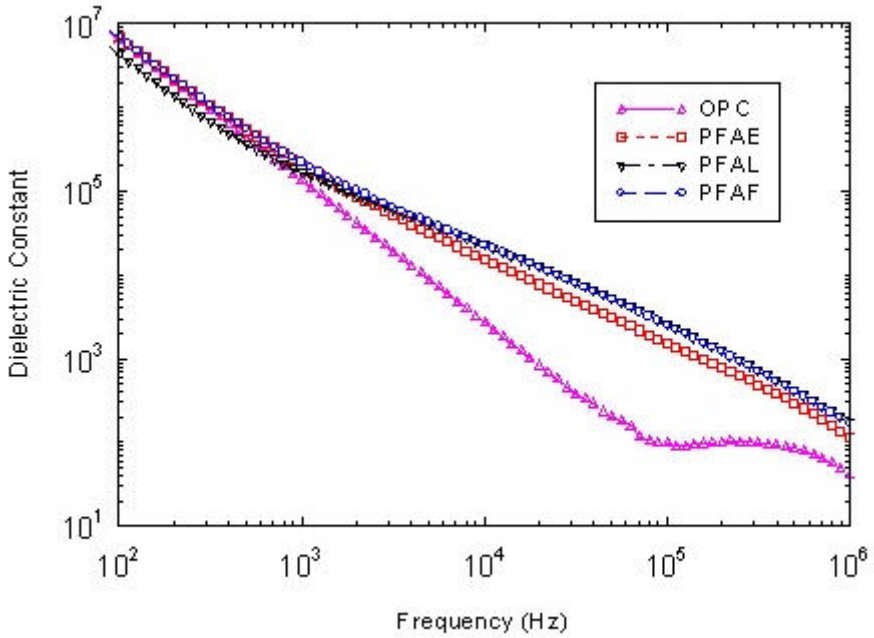

Figure 5. Dielectric Constant of Mortars at 10 min

The reasons for the differences observed between the electrical properties of the PFA samples are not yet clear but examination of Table 1 allows the following observations:

PFAL and PFAF, which show the most distinct PFA-effect, have:

- higher silica content than PFAE (51.0% and 50.5% compared to 44.3%)
- higher carbon content (LOI) than PFAE (5.5% and 5.3% compared to 1.9%)
- lower lime (CaO) content than PFAE (3.4% and 2.6% compared to 5.9%)
- lower fineness than PFAE (8% and 9.5% compared to 13.5%)

PFAF and PFAE, which are generally more conductive than PFAL, have:

- lower alumina content than PFAL (both 24.7% compared to 34.7%)
- higher potassium oxide (K_2O) content than PFAL (3.0% and 1.7% compared to 1.0%)
- higher sodium oxide (Na_2O) content than PFAL (0.8% and 0.6% compared to 0.2%)

With regard to the observation that the PFA-effect is less well defined in the case of PFAE (see Figure 1) it is possible that the CaO content plays a part in this. Previous measurements (unpublished) with unclassified high lime (type C) PFA from North America have shown no evidence of the PFA-effect, but the reasons for this are not yet fully known. Work is continuing to widen the range of PFA sources accessed and the types of PFA examined.

4. CONCLUSIONS

Impedance data over the frequency range 1 Hz to 1 MHz have been acquired on freshly mixed mortar samples containing a plain OPC binder and three blended binders where 33% of the OPC was replaced by PFA from three different UK sources. The results show that the presence of each of the PFA's alters the electrical signature of the mortars (from that of the plain OPC) and introduces a plateau region in the complex impedance plot, confirming previous findings that were limited to PFA from one source. This effect is shown to persist after the setting of the OPC.

The PFA-effect is shown to be caused by the presence of a frequency dependent polarisation mechanism that greatly enhances the dielectric constant and conductivity of the mortar in the range 1 kHz to 1 MHz. The exact characteristic of the PFA-effect is also shown to depend on the type of PFA used and its mineralogical composition.

While work is continuing on PFA from a wider range of sources, these preliminary findings demonstrate the feasibility of using electrical measurements for detecting the presence of PFA in cementitious material, and also the possibility of distinguishing between PFA from different sources.

ACKNOWLEDGEMENTS

The authors wish to acknowledge the financial support of the U.K. Engineering and Physical Sciences Research Council (grant GR/N16365). We are also grateful to Dr Lindon K. A. Sear of the U.K. Quality Ash Association for arranging the supply of PFA samples from a number of UK power stations, and to Mr Bill Armstrong of ScotAsh Limited for the supply of PFA from Longannet power station.

REFERENCES

Journal Papers

[1] McCarter, W. J. A parametric study of the impedance characteristics of cement-aggregate systems during early hydration, Cement and Concrete Research, Vol.24, No.6, 1994, pp.1097-1110

[2] McCarter, W. J. The a.c. impedance response of concrete during early hydration, Journal of Materials Science, Vol.31, 1996, pp.6285-6292

[3] Starrs, G. and McCarter, W. J. Immittance response of cementitious binders during early hydration, Advances in Cement Research, Vol.10, No.4, 1998, pp.179-186

[4] McCarter, W. J. and Brousseau, R. The a.c. response of hardened cement paste, Cement and Concrete Research, Vol.20, No.6, 1990, pp.891-900

[5] Christensen, B. J., Coverdale, R. T., Olsen, R. A., Ford, S. J., Garboczi, E. J., Jennings, H. M. and Mason, T. O., Impedance spectroscopy of hydrating cement-based materials: measurement, interpretation, and applications, Journal of the American Ceramics Society, Vol.77, No.11, 1994, pp.2789-2804.

Standards

[6] BS3892: Part 1. 1993, Specification for pulverised fuel ash for use in Portland cements, British Standards Institution, London, 1993

Books

[7] MacDonald, J. R. Analysis of immittance spectroscopy data: model comparisons, universality?, and estimation of distribution of activation energies, in Materials Research Society Symposium Proceedings, Vol.411, Electrically Based Microstructural Characterization, November 1995, Editors: Gerhardt,R. A., Taylor, S. R. and Garboczi, E. J. pp.71-83

CHARACTERISATION OF PFA USING IMPEDANCE TECHNIQUES

G. Starrs[1], W. J. McCarter[1], T. M. Chrisp[1]

[1]Department of Civil and Offshore Engineering, Heriot-Watt University, Edinburgh, UK.
E-mail: johnm@sbe.hw.ac.uk; E-mail: gstarrs@sbe.hw.ac.uk

W. J. McCarter was appointed to a personal Chair in Civil Engineering Materials in 1998. His main research area has been in the field of cement and concrete technology, with particular research interest in the application of a.c. impedance spectroscopy (ACIS) in the study of cementitious systems. He was one of the first workers to apply ACIS to such systems. The testing methodology is being exploited in a range of laboratory and field studies relating to corrosion monitoring; surface treatments for concrete; permeability and diffusion of blended cementitious binders; hydration of cementitious systems; performance monitoring of cover-zone concrete and in the study of pozzolanic materials.

MECHANICAL AND MICROSTRUCTURAL STUDY OF NEW ULTRA HIGH PERFORMANCE MATRICES

P. Fonollosa[1], P.C. Aïtcin[2], H. Zanni[3] and P. Gégout[4]

[1] Dept. of Civil Engineering, University of Sherbrooke, Sherbrooke, Canada.
E-mail: pfonol@hotmail.com
[2] Dept. of Civil Engineering, University of Sherbrooke, Sherbrooke, Canada.
E-mail: christine.couture@courrier.usherb.ca
[3] Laboratoire PMMH, ESPCI, Paris, France. E-mail: zanni@pmmh.espci.fr
[4] Ciments d'Obourg, Obourg, Belgium. E-mail: philippe.gegout@holcim.com

ABSTRACT

In Ultra High Performance Matrices (UHPM) mix design focuses on improving homogeneity, compactness, reactivity of the fine powders, and the microstructure of the cementitious matrix. Therefore, UHPM do not contain any coarse aggregate. Finely crushed quartz is also added to correct the granular distribution as well as to decrease the potential Ca/Si ratio of the C-S-H when the matrix is cured at high temperature.

The main purpose of this study was to see if UHPM could be made using less Portland cement and materials more reactive than crushed quartz such as fly ashes or blast-furnace slag. The consequences of these substitutions on the characteristics of fresh and hardened mortars were studied. Compressive strength was measured before and after hot-water curing at 90°C. For example, with slag, it was possible to reach a compressive strength of about 180 MPa with a replacement rate of 60 percent of Portland cement.

Slag matrices samples were also analysed using Nuclear Magnetic Resonance (NMR). ^{29}Si probe was used to identify and quantify all the phases produced during the hydration process. It was found that the Q_2/Q_1 ratio increased with the slag content, which means an increase of the average length of the C-S-H chain.

1. INTRODUCTION

Concrete is usually considered a low-tech commodity product despite the fact that many engineered concretes have been developed recently. The use of very efficient admixtures and silica fume, as well as the elaboration of new manufacturing processes, has resulted in an improvement of the mechanical properties of concrete. From the pioneering work of Brunauer and his colleagues [1] to the Reactive Powder Concrete (RPC) or Ductal© concept [2], very impressive compressive strengths have been achieved. These important mechanical and durability performances are mainly due to the high compactness and improved microstructure of this material made generally of sand, cement and silica fume. Designers could design lighter, more aesthetic structures, pushing back in this manner the frontiers of the imagination. In 1997, the first structure was built with an ultra high performance matrix in Sherbrooke [3].

One of the major difficulties when using UHPM concerns workability, which sometimes makes its casting difficult. Furthermore, because of the large amount of fine and ultrafine particles, high heat

Proceedings of the 11th International Congress on the Chemistry of Cement (ICCC)
'Cement's Contribution to the Development in the 21st Century'
Hosted by: The Cement and Concrete Institute of South Africa
CD-ROM produced by: Document Transformation Technologies
11 - 16 May 2003, Durban, South Africa
ISBN Number: 0-9584085-8-0
Editors: Dr G. Grieve and G. Owens
Congress Organised by: Event Dynamics

emission can be measured during hydration. Although many researchers have worked for years on UHPM, up to now studies have basically been concerned with the optimisation of superplasticizer dosage [4] and not the nature of the "raw" materials used. In this paper the influence of the nature of several supplementary cementitious materials such as blast-furnace slag or fly ashes on the properties of fresh and hardened matrices have been studied. ^{29}Si nuclear magnetic resonance (NMR) has been used to investigate the microstructure of UHPM and better understand its evolution with the slag content.

2. EXPERIMENTAL

2.1 Materials

The physical data and oxide composition of the different powders used for the design of UHPM are given in Tables 1 and 2.

Table 1. Physical data of the cementitious materials used

	Type 20M cement	Slag	Limestone filler	Siliceous filler	Fly ash	Silica fume
Specific gravity	3.33	3.03	2.82	2.75	2.46	2.42
Blaine surface (m^2/kg)	380	630	510	850	850	-
Surface BET (m^2/kg)	-	-	-	-	-	21 500

Table 2. Oxide composition of the cementitious materials

	Type 20M cement	Slag	Limestone filler	Siliceous filler	Fly ash	Silica fume
SiO_2	23.1	35.5	3.5	93.3	73.2	95.9
Al_2O_3	3.6	10.8	1.0	0.7	19.7	0.6
Fe_2O_3	4.7	1.4	0.6	0.3	1.1	0.2
CaO	61.5	41.4	51.6	4.4	2.9	0.1
Na_2O	0.1	0.2	0.1	0.1	0.1	0.1
K_2O	0.6	0.3	0.1	0.1	0.6	0.9
MgO	2.4	8.1	0.7	0.2	0.4	0.6
SO_3 total	2.3	2.2	-	-	-	0.3
Loss on ignition	0.95	0.7	42.0	0.6	0.7	1.4

A Type 20M cement was used for all the mechanical tests. This low-heat cement has a C_2S content higher than most of the cements available in North America and a low C_3A-content: consequently, it displays a very low reactivity and allows workability gains. European slag was also used which was essentially glassy but had a small amount of crystallized merwinite due to its high MgO content. The fly ash came from Australia. Its X-ray diffractogram showed the presence of quartz and mullite with some traces of haematite. The limestone and siliceous fillers were local.

2.2 Processing methods and NMR experiments

The matrices were designed from a reference made essentially of cement and silica fume for its hydraulic part with a W/C mass ratio of 0.19, a polysulphonate-based superplasticizer at a dosage of 1.65% and a sand volume content of 38%. Then the cement was progressively substituted with a supplementary cementitious material X, the substitution rate varying X/(X+C) from 10 to 80%.

At the end of mixing, flow was measured according to ASTM Standard C 230 [5]. Afterwards, 50-mm cubes were cast and placed immediately in lime-saturated water at a temperature of 20°C for 48 hours. The cubes were then submitted to hot-water curing at 90°C for 48 hours. Compressive strength tests were performed at 48 hours, 91 days and after hot water curing according to ASTM Standard C 109/C 109M [6] with a load rate of 1110 N/s.

^{29}Si NMR experiments were performed on samples made with a Type 20M cement which didn't come from the same lot as the one used for the mechanical tests. However, their oxide composition and specific gravity were similar. The hydration of all the matrices was stopped with the acetone-ether method before testing.

The Magic Angle Spinning (MAS) single pulse spectra were obtained on a 11.7-Tesla Bruker ASX500 spectrometer with a cross-polarization probe for 7-mm zirconium oxide rotors at 7 kHz. ^{29}Si chemicals shifts are given relative to tetramethylsilane (TMS) at 0 ppm.

3. RESULTS

3.1 Macroscopic properties of UHPM

3.1.1 Flow

Figure 1 shows the flow evolution as a function of the replacement rate of cement. It can be seen that the higher the content of slag or limestone filler, the higher the flow. A maximum flow of 110% was reached for a replacement rate of 60%. After this point, if more slag or limestone filler is added, the flow decreases.

The siliceous filler has an identical behaviour but the flow maximum is given for a content of only 30%. Afterwards, the matrix rheology worsens rapidly: the flow of a mix containing 80% of siliceous filler is half that of the reference.

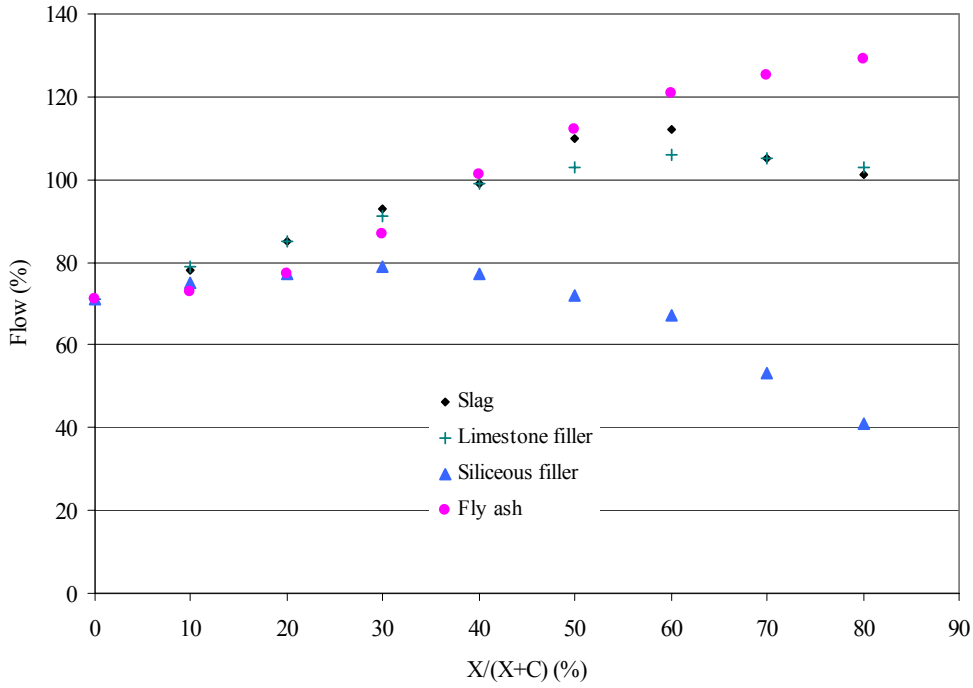

Figure 1. Flow evolution as a function of the supplementary cementitious materials content

As far as the fly ash is concerned, it induces a different rheological behaviour, and this in spite of its higher Blaine surface area. Indeed, the flow increases continuously with the fly ash content.

The supplementary cementitious materials used in this study have various surface states which explain the differences observed in the rheology of the fresh mortars [7]. In the case of the siliceous filler, cement is substituted by angular particles negatively charged, which are likely to absorb more superplasticizer or water molecules. Conversely, for the same Blaine surface area, the replacement of cement by fly ash, essentially made up of spherical particles of glassy material, results in an

improvement in the matrix rheology. In addition, the granular packing effect must be taken into account.

3.1.2 Compressive strength

The evolution of the compressive strength of UHPM at 48 hours, 91 days cured in lime saturated water at 20°C and after hot-water curing, is illustrated in Figures 2 and 3. Three 50-mm cubes were tested for each mix. Each experimental point is the average of three series of experiments done from three mixes prepared randomly.

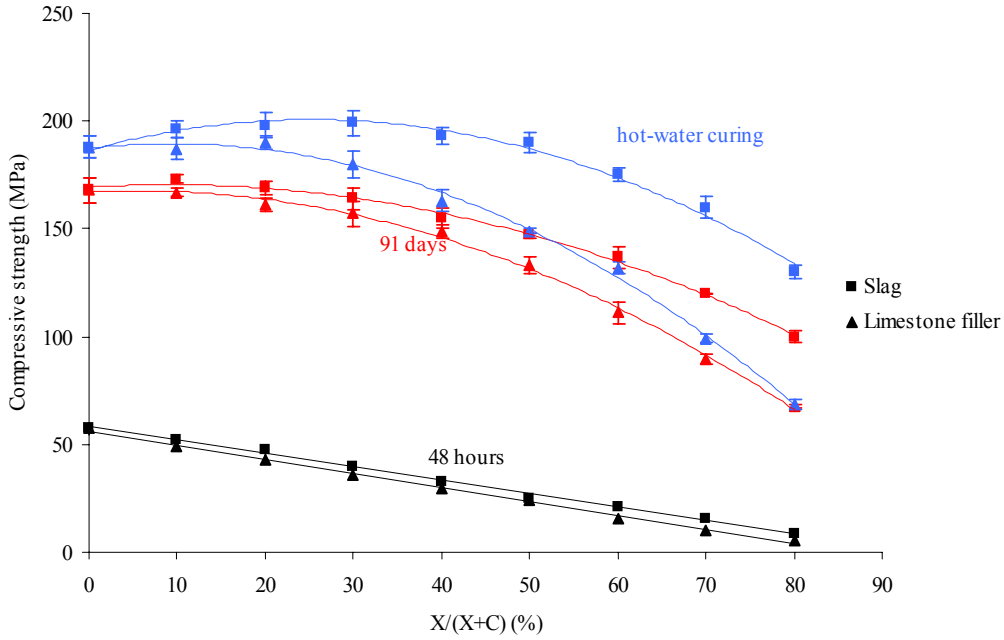

Figure 2. Compressive strength evolution as a function of the supplementary cementitious materials content

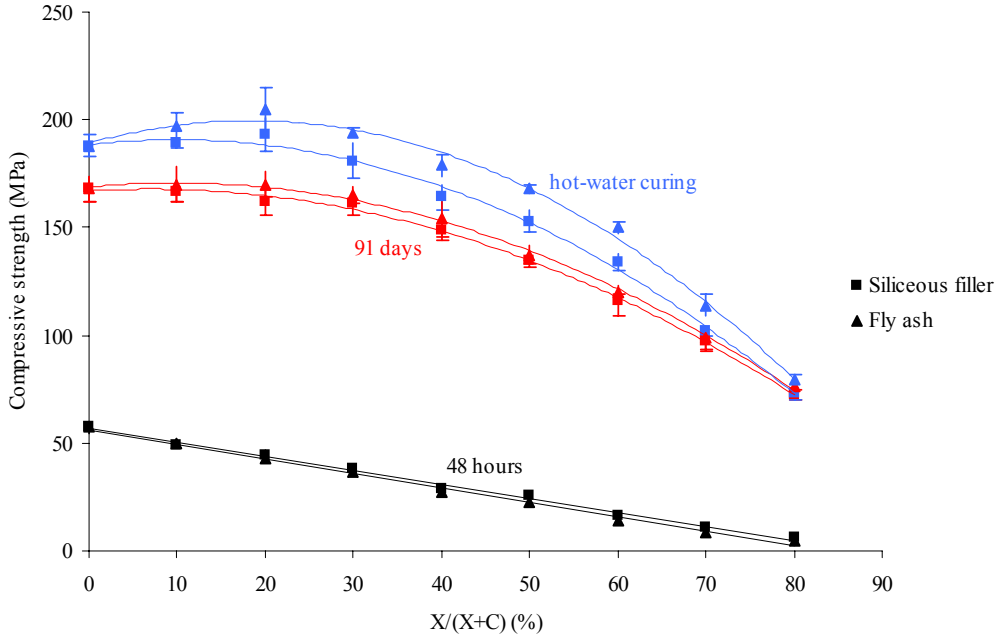

Figure 3. Compressive strength evolution as a function of the supplementary cementitious materials content

Whatever the supplementary cementitious material used, the compressive strength at 48 hours decreases linearly with the replacement rate of cement, the least important negative slope being measured for the slag matrix. This evolution could be explained by considerations of kinetics order. Indeed, in all the mixes studied, the hydration reaction developed during the first 48 hours depends mainly on cement. In that way, the slope can be seen as a measure of the physical (*filler effect*) and chemical activity of the supplementary cementitious material used, the origin ordinate being only characteristic of the initial mix {cement + silica fume}.

Each compressive strength curve at 91 days or after curing exhibits a maximum and can be expressed by second-order polynomials. Statistical considerations of variance lead us to consider that there is no significant difference for the mixes with a substitution rate between 0 and 30%. Except for slag, strength curves decrease linearly for higher replacement contents, which reflect the hydraulicity of the mineral additive.

Finally, the evolution of the compressive strength of the slag matrix differs from that of the other cementitious materials. Indeed, whereas for the filler or the fly ash the difference between the 91-day compressive strength and the one obtained after hot water curing tend to disappear with the substitution rate, it seems to remain in the case of slag.

Compressive strength can also be expressed as a function of the W/C ratio. This variable change is illustrated for example for slag in Figure 4.

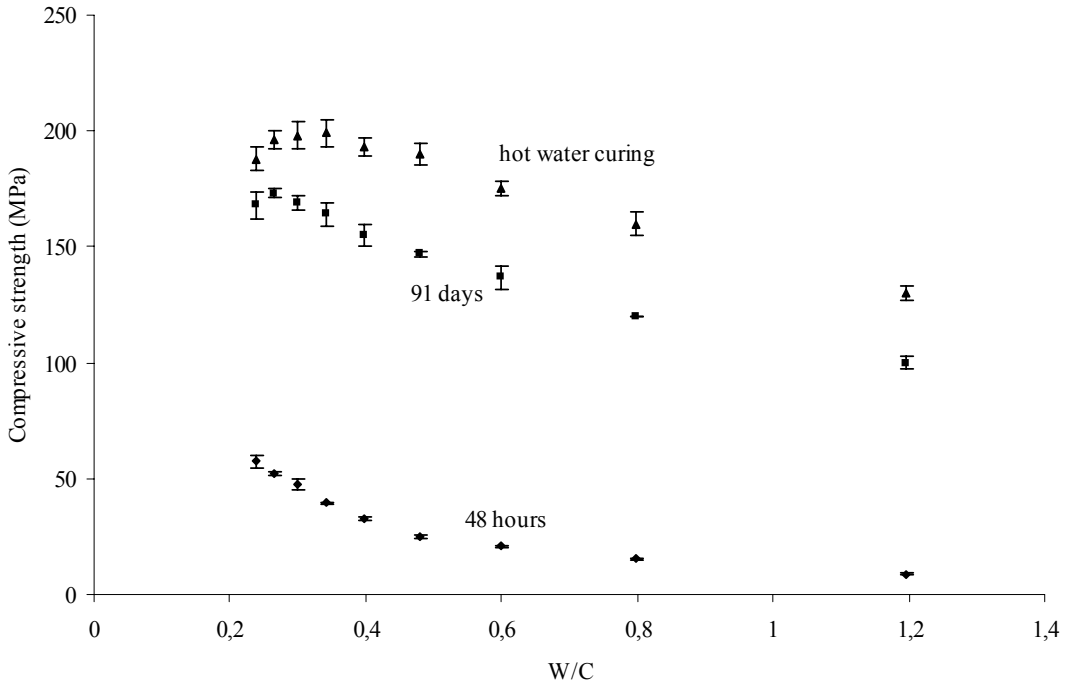

Figure 4. Compressive strength evolution as a function of the W/C ratio

It is possible to superimpose on the 48-hour compressive strength curves using the following equation:

$$y = A \times (x+1)^{v} \quad with \quad x = \rho_C \frac{W}{C} \tag{1}$$

Expression and regression coefficients are given in Table 3 for each type of substituting material.

Table 3. Equations of the fit curves for the 48-hour compressive strength

Complementary cementitious material	Curve fit	Regression coefficient (R^2)
Slag	$y=3.488(x+1)^{-5.148}$	0.9909
Limestone filler	$y=1.707(x+1)^{-6.469}$	0.9862
Siliceous filler	$y=2.101(x+1)^{-6.073}$	0.9891
Fly ash	$y=1.351(x+1)^{-6.912}$	0.9912

These expressions can be linked to the generalized Feret formula,

$$R = R^* \left(1+\frac{E}{C}\right)^{\upsilon} \quad (2)$$

where the coefficient R^* is a constant representing the compressive strength corrected by the initial porosity of the matrix. A hierarchical organization of the supplementary cementitious materials similar to the one previously obtained appears: the use of blast-furnace slag seems to give the matrix with the lowest porosity.
The exponent ν depends on the nature of the mix (cement paste, mortar or concrete). A previous study [8] indicates that it varies from 5 to 6 for cement pastes. In ours, the values of ν are between 5 and 7, which may indicate that the homogeneity of our matrices are close to the one made from a cement paste. This observation is consistent with the UHPM mix-design concept in which the choice and content of each powder aim to obtain the best homogeneity.

This model can hardly be applied to the 91-day compressive strength curves or those obtained after hot water curing because of the simultaneous reaction of the supplementary cementitious materials and the silica fume.

3.2 Microstructure of UHPM

^{29}Si NMR experiments were performed to follow the evolution of the C-S-H polymerization degree as a function of the slag content. This method allows a quantitative observation of the silicon chemical environment provided the relaxation of all silicate species, except the siliceous sand, is respected. The ^{29}Si spectra are displayed in Figures 5 to 7. Each peak corresponds to a given chemical environment of silicon nuclei according to the Engelhardt and Michel chemical shift table for silicates [9]. The cement presents Q_0 species at –71.0 ppm. In accordance with previous work on synthesized C-S-H [10] or similar materials [11], we could sort the C-S-H with Q_1 and Q_2 species at -80.2 and –85.0 ppm respectively. The silica fume and quartz sand present Q_4 species at –111.0 and –107.2 ppm respectively.

The emergence of a peak at –74.0 ppm was noticed, which corresponds to one of the slag phases. Therefore, in order to calculate the C-S-H Q_2/Q_1 ratio, very short (500 ms) pulses were also used for the high slag content mixes. In this way, the slag signal could be drastically diminished and it was possible to properly quantify the C-S-H phase. The results are displayed in Table 4.

Table 4. C-S-H Q_2/Q_1 ratio of UHPM for different slag content

		Slag content (wt%)				
		0	20	40	60	80
C-S-H Q_2/Q_1 ratio	48 hours	1.07	1.08	1.02	0.99	0.93
	91 days	1.43	1.47	1.32	1.17	1.02
	Hot curing	1.81	1.99	2.09	2.47	2.83

At 48 hours, the C-S-H Q_2/Q_1 ratio decreases insignificantly with the slag content. A similar tendency is observed for the 91-day matrices, the variation of the polymerization degree being linked with the slight activity of slag and silica fume. Hot-water curing has a different effect on the matrices, the C-S-H Q_2/Q_1 ratio increasing with the slag content, which may be linked to the higher substitution of silicon by aluminium as noticed in ^{27}Al NMR experiments [12].

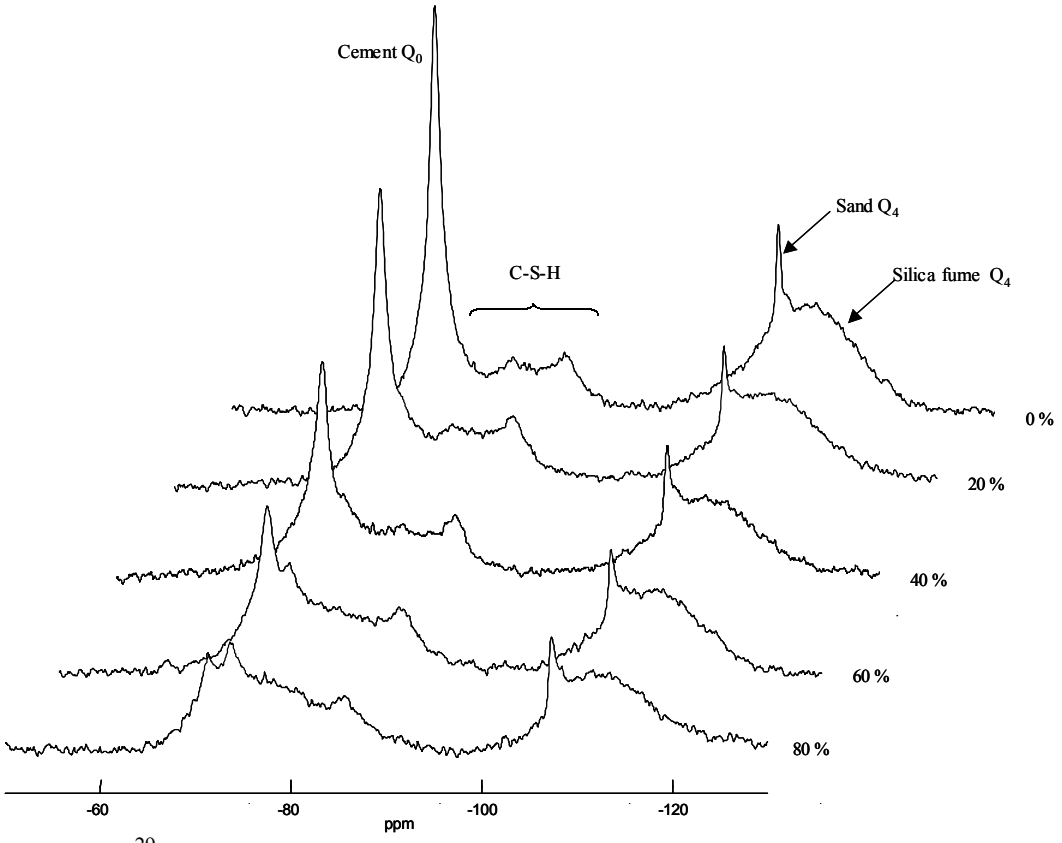

Figure 5. ^{29}Si NMR spectra of UHPM at 48 hours as a function of the slag content

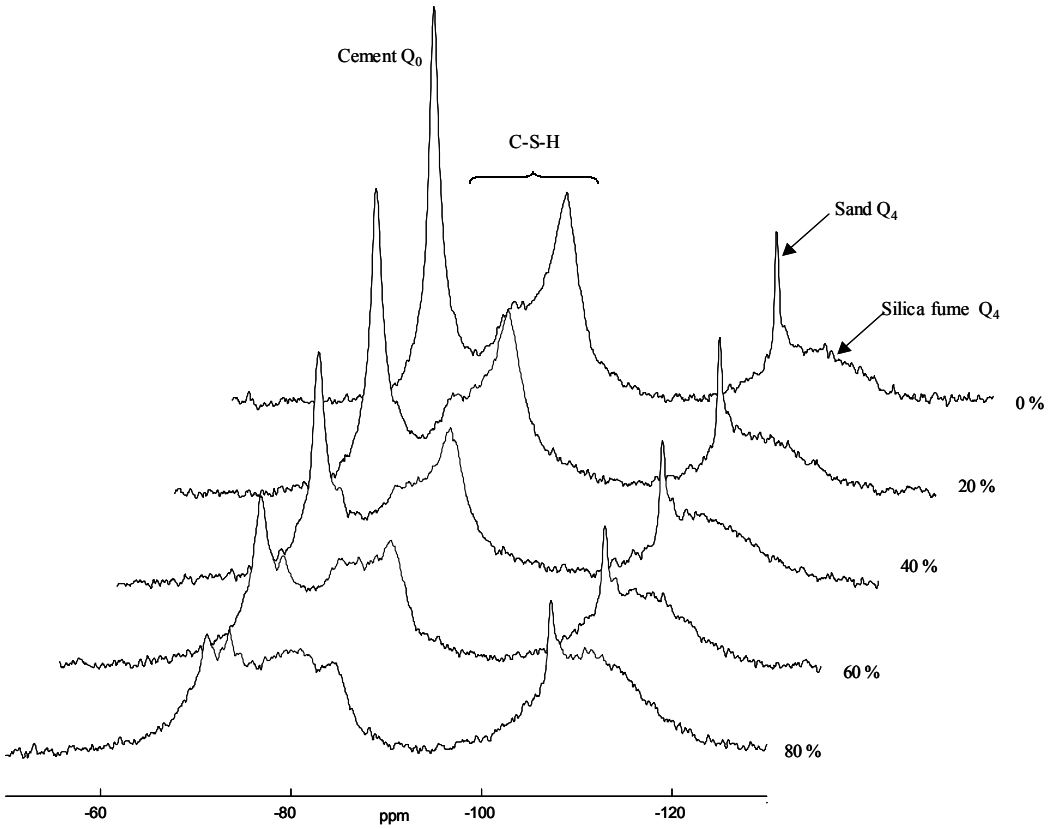

Figure 6. ^{29}Si NMR spectra of UHPM at 91 days as a function of the slag content

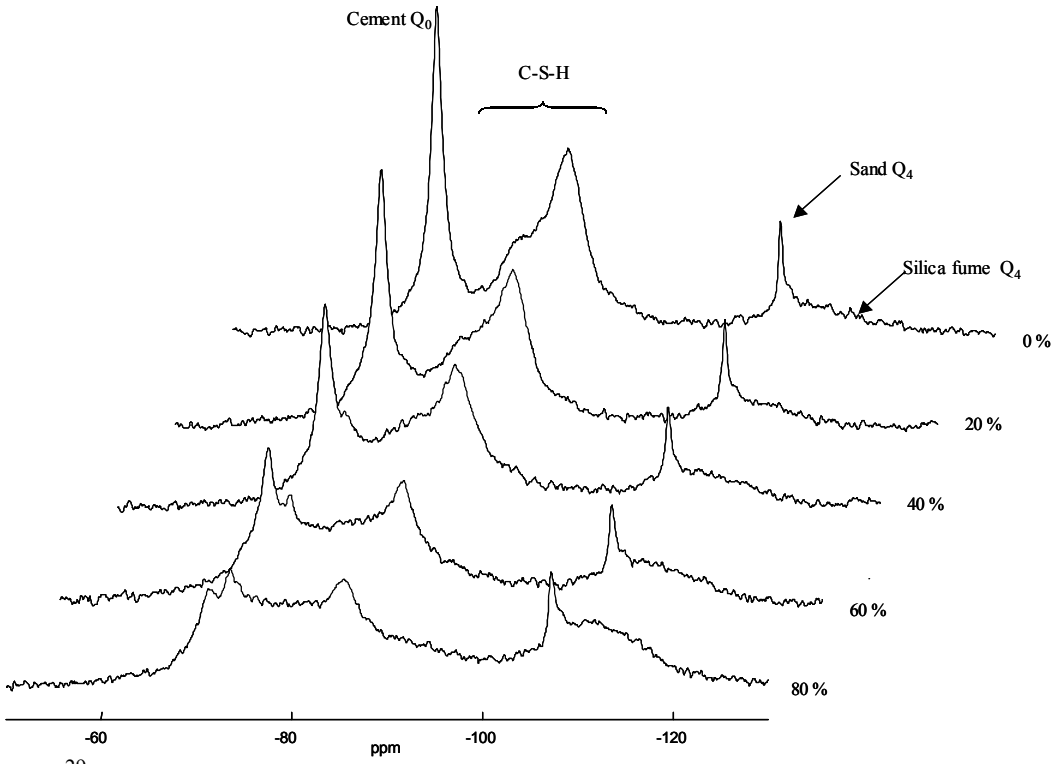

Figure 7. ^{29}Si NMR spectra of UHPM after hot-water curing as a function of the slag content

Table 5 allows us to compare the quantities of silica fume remaining in the paste.

Table 5. Relative amount of silica fume in UHPM for different slag content

		Slag content (wt%)				
		0	20	40	60	80
Relative amount of silica fume (%)	Initial	50.1	47.4	45.1	42.9	41.0
	48 hours	46.5	44.7	42.5	39.7	-
	91 days	22.5	26.5	27.6	30.8	40.2
	Hot curing	14.2	12.3	16.9	17.6	-

After 48 hours, the same amount of silica fume was used whatever the slag content, which is mainly due to its slow kinetics of hydration. If the values at 91 days are compared, it seems that the higher the slag content, the less the silica fume has reacted. As expected, at ambient temperature, the slag activation is preponderant on that of the silica fume. Silica fume is mainly consumed during the hot water curing, even for low-cement content. In that case, silica fume should react with the C-S-H resulting from the hydration of slag and cement in order to form secondary C-S-H of lower C/S ratio.

Hot water curing has another effect on the matrices. Indeed, the existence of a large peak around -90.3 ppm has been observed, which can be related to Q_3 species, and whose intensity increases with the slag content. This may reveal the presence of an aluminium and magnesium-rich silica gel [13].

4. CONCLUSION

This paper presents the impact of different types of cementitious materials on the properties of fresh and hardened ultra high performance matrices. Thus, except for the siliceous filler, the supplementary cementitious materials used improved the rheology of the mixes, which is mainly due to their surface state. As far as compressive strength is concerned, slag appears to be the most promising mineral additive. Aside from 48-hour compressive strength values higher than those obtained for the other supplementary materials, 175-MPa compressive strength can be reached after hot-water curing for a replacement rate of 60 percent of Portland cement. The difference between the long-term compressive strength and those obtained after hot-water curing indicates that the latter has more than a kinetic effect on the hydration of the matrices. Therefore, in addition to a refining of the capillary network, thermal curing modifies the nature of C-S-H.

Moreover, the microstructure of mortars containing different slag contents was investigated by ^{29}Si NMR experiments. It appears that cement substitution at 48 hours and 91 days results in a decrease of the polymerization degree of the C-S-H. Hot-water curing has the opposite effect: thus, the average chain length seems to increase with the slag content. This phenomenon, backed up by some ^{27}Al NMR experiments, is to be linked to a higher substitution of silicon by aluminium.

REFERENCES

[1] Yunderfreund, M., Odler, I. Brunauer, S. Hardened Portland cement pastes of low porosity – I. Materials and experimental methods, Cement and Concrete Research, vol.2, n. 3, 1972, pp.313-329.

[2] Richard, P. and Cheyrezy, M. Composition of Reactive Powder Concretes, Cement and Concrete Research, vol.25, n. 7, 1995, pp.1501-1511.

[3] Dallaire, E., Aïtcin, P.C., Lachemi, M. High Performance Powder, Civil Engineering, ASCE, vol. 68, n. 1, 1998, pp.48-51.

[4] Bonneau, O. Study of the physico-chemical effect of superplasticizers to optimise the rheological behaviour of ultra high performance concretes (in french), Ph.D. thesis, Université de Sherbrooke, 1997.

[5] ASTM C 230, Standard Specification for Flow Table for Use in Tests of Hydraulic Cement, West Conshohocken: American Standards for Testing Methods, 1998.
[6] ASTM C 109/C 109M, Standard Test Method for Compressive Strength of Hydraulic Cement Mortars, West Conshohocken: American Standards for Testing Methods, 1999.
[7] Neville, A.M. Properties of concrete, 4th and final ed. London: Longman, 1995, p.414.
[8] Granju, J.L. Modelisation of hardened cement pastes: characterization of the hydration state, compressive strength and Young modulus evolution (in french), Ph.D. thesis, Université Paul Sabatier, 1987.
[9] Engelhardt, G. and Michel, D High Resolution ^{29}Si NMR of Silicates and Zeolites, New York: Wiley, 1987, p.485.
[10] Klur, I., Pollet, B., Virlet, J, Nonat, A. C-S-H evolution with calcium content by multinuclear NMR, 2nd international conference on NMR spectroscopy of cement based materials, Bergamo, Italy, 1996, pp.119-141.
[11] Porteneuve, C. NMR Study of concretes: application to alteration by water (in french), Ph.D. thesis, Université Pierre et Marie Curie, 2001.
[12] Fonollosa, P. Mechanical and microstructural properties of new ultra high performance matrices (in french), Ph.D. thesis, Université de Sherbrooke, 2002.
[13] Richardson, I.G., Brough, A.R. Brydson, R., Groves, G.W., Dobson, C.M. Location of Aluminium in Substituted Calcium Silicate Hydrate (C-S-H) Gels as Determined by ^{29}Si and ^{27}Al NMR and EELS, Journal of the American Ceramic Society, vol.76, n. 9, 1993, pp.2285-2288.

HYDRATION OF TRICALCIUM SILICATE AT HIGH PRESSURE AND TEMPERATURE

F. Méducin[1], C. Noïk[2], A. Rivereau[2], G. Hamel[1], B. Bresson[3] and H. Zanni[4]

[1] Laboratoire de Physique des Milieux Condensés, UMR CNRS 7602, Université Pierre et Marie Curie, Boîte 77, 4, place Jussieu, 75252 PARIS Cedex 05, FRANCE. fm@pmc.jussieu.fr
[2] Institut Français du Pétrole, Boîte 311, 1 et 4, avenue de Bois-Préau, 92506 RUEIL-MALMAISON Cedex, FRANCE. christine.noïk@ifp.fr
[3] Laboratoire de Physique Quantique, SIEN FRE 2312, ESPCI, 10, rue Vauquelin, 75231 PARIS Cedex 05, FRANCE. bruno.bresson@espci.fr
[4] Laboratoire de Physique et Mécanique des Milieux Hétérogènes, UMR CNRS 7636, ESPCI, 10, rue Vauquelin, 75231 PARIS Cedex 05, FRANCE. zanni@pmmh.espci.fr

ABSTRACT

This study concerns the durability of *oil well cementing*. During this process, a cement slurry (water/cement ratio=0.44 usually) is pumped down the steel casing of the well up the annular space between the casing and the surrounding rock to support and to protect it. The setting conditions in terms of pressure and temperature in the well are therefore expected to be severe (up to 1 kbar and 250°C). Here we report the hydration of the main component of cement: synthetic tricalcium silicate Ca_3SiO_2, often called C_3S. Silicates hydrates are first elaborated in high temperature and pressure cell and then studied by various characterisation methods (^{29}Si- and ^{1}H-NMR, XRD, DTA-TG and SEM) to complete phase diagram (P,T) of the calcium silicate hydrates. To correlate macroscopic behaviour and physico-chemical properties of hydration products, mechanical tests are performed. C-S-H-phases are seen to disappear beyond 160°C and 0.4 kbar and to give crystalline phases such as α– and β–polymorphs of C_2SH, whose mechanical resistance is not so efficient.

1. INTRODUCTION

The aim of this study is to understand C_3S hydration under severe temperature and pressure conditions. Indeed, this hydration is well known at ambient temperature and pressure and leads to the formation of two phases: Portlandite and C-S-H. Portlandite is a crystalline phase with chemical formula $Ca(OH)_2$, also called CH in the conventional notation of the cement and concrete industry [1]. C-S-H are not stoechiometric and poorly crystallised phases, which bring its adhesion properties to cement. The question is to know if these poorly crystallised phases are still stable under high pressure and temperature setting conditions and if the phases formed under such severe conditions (T up to 250°C and P up to 1 kbar) are still efficient binders. From oil and gas companies point of view, the disappearance of mechanical resistance of cement at high pressures and temperature is critical: it can lead to a loss of integrity of cemented annular and consequently can induce hydrocarbons production stops.

Two types of high-pressure cell have been used during this study. The aim was to reveal different hydration kinetics. The structural results are presented for the oldest samples hydrated at different temperature and pressure with the high-pressure cell (hydration period of 28 days). Indeed, the pressure parameter is found to increase the hydration kinetics. A pseudo-equilibrium is assumed to be reached. Each sample (P, T hydrated) has been analysed by various methods. First, the

Proceedings of the 11th International Congress on the Chemistry of Cement (ICCC)
'Cement's Contribution to the Development in the 21st Century'
Hosted by: The Cement and Concrete Institute of South Africa
CD-ROM produced by: Document Transformation Technologies
11 - 16 May 2003, Durban, South Africa
ISBN Number: 0-9584085-8-0
Editors: Dr G. Grieve and G. Owens
Congress Organised by: Event Dynamics

crystalline phases have been detected by XRD. Then, a thermal analysis was performed in order to confirm the XRD results and quantify the different phases. In addition, (scanning electron microscopy) SEM was used to observe the morphology of the hydrated tricalcium silicate. At last, ^{29}Si then ^{1}H-NMR were used to confirm these results, to probe poorly crystallised phases, which may appear, and to achieve the quantification of the calcium silicate hydrates mixture. In order to correlate the macroscopic behavior and physico-chemical properties of the products, mechanical compression tests were performed.

2. EXPERIMENTAL

2.1 Sample elaboration

Synthetic C_3S (triclinic T1 structure) has been used for this study. Its quality has been verified by XRD, which showed a small amount of CaO (1,1%) and C_2S (less than 1 %, also revealed by NMR technique). In order to reproduce the conditions of a deep oil well (up to 1 kbar and 250°C), synthetic C_3S was mixed at room temperature with a water / cement (W/C) ratio of 0.44, which is a standard consistency requirement of class G cement. Distilled water was used.

In the first pressure cell (called LP - low pressure cell - in the following), a Teflon® pot filled up with this cement paste was placed in distilled water. Oil was the pressure transmitting fluid and the pressure was limited to 0.5 kbar. The pressure was increased before the extrernal heating was switched on. Stable pressure and temperature conditions were reached after three hours. Different periods of hydration, up to two months, have been performed in order to reach a pseudo-equilibrium for the products formed.

The second high-pressure cell could reach the desired temperature and pressure in only 30 minutes. This second cell (called HP in the following) has been built for this particular work and allowed to attain pressures up to 1 kbar, and to study different hydration kinetics than with the first cell (LP). The body of the cell is a steel cylinder of diameter 80 mm and length 205 mm. The cell is sealed by a « Bridgman unsupported seal ». During the experiments, the cell is oriented vertically. The pressure inlet is at the bottom of the cell. A thermocouple through the mushroom plug permits to measure and regulate the temperature. Here, a Teflon® pot filled up with this cement paste is also used and placed in the middle of the cell (figure 1). Argon gas was the pressure transmitting fluid. The low pressure (~200 bar) was first applied, then the heating was switched on, simultaneously regulating the pressure.

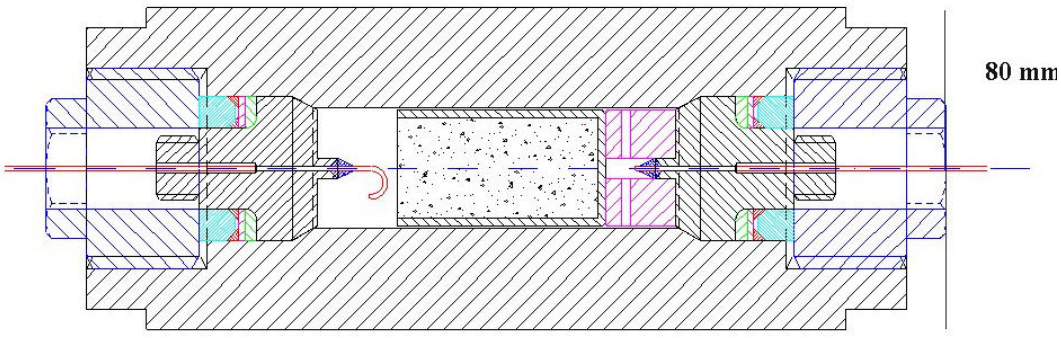

Figure 1. High-pressure cell (HP)

2.2 Structural analyses

After the hydration has been stopped by quenching and fast decreasing of pressure, the samples were crushed and analysed by various methods. First the crystalline phases were detected by powder XRD on a Philips PW 1820 diffractometer. The diffraction patterns were recorded from 2Θ= 10° to 80° with a step of 0.03° and 4 s accumulation time per step.

Then, the thermal analysis was performed, with a thermobalance TAG24 SETARAM, to confirm the XRD results and quantify Portlandite ($CaOH_2$). After being exactly weighed, the powdered sample was submitted to a increase in temperature ranging from 20°C up to 1050°C at a rate of 10°C/min. The weight loss was recorded simultaneously.

In addition, SEM and energy dispersive X-ray spectrometer (SEM-EDX), were used to observe the morphology of the hydrated tricalcium silicate. Secondary electron images of fractures and qualitative X-ray analyses were performed on a JEOL 6300F field emission electron microscope equipped with an IMIX PGT EDS spectrometer. The sample was covered by a thin metallic layer of platinum to increase the poor conductivity of the observed fracture. The observation was carried out in vacuum (4.10^{-6} Torr) and under 15kV acceleration voltage.

Finally, ^{29}Si and ^{1}H-NMR were used to confirm the previous results and to probe amorphous or poorly crystallized phases possibly present with a structure based on SiO_4 chains with variable length [2].

The sample with ^{29}Si isotopic natural abundance (4.7%) was investigated using an ASX 300 Bruker spectrometer at a resonance frequency of 59.6 MHz. The pulse sequences used - MAS Single Pulse and ^{1}H-^{29}Si CPMAS (Cross-Polarization at Magic Angle Spinning) - are well known in solid-state NMR studies [3,4]. The resolution is optimised with the signal of Q_8M_8 $[Si(CH_3)_3]_8Si_8O_{20}$, which was used as reference for the chemical shift measurement. The calibration gives the biggest peak at 11.6 ppm. MAS Single Pulse and CPMAS experiments were performed with the following parameters: a $\pi/2$ pulse length of 3.3 µs and spinning frequency of 5 kHz. A Single Pulse experiment was carried out with a recycle delay of 150 s and 500 scans of accumulation. The C-S-H relaxation - T_1=30 s - was respected, to allow for C-S-H [1] present in hydrated samples. A number of scans equal to 10000, a recycle delay of 5 s and a contact time ranging from 1 to 10 ms were used in the CPMAS experiments. With these CPMAS experiments the dynamics of polarization of each phase is clearly evidenced in agreement with previous work [5]. Therefore, CPMAS experiments are a valuable tool to distinguish hydrate phases in a mixture and are technically easier than 2D-NMR measurements. Moreover NMR experiments allow us to confirm the previous measurements by thermal analysis.

^{1}H NMR experiments were performed on an ASX 300 Bruker spectrometer at a resonance frequency of 300 MHz on a sample with ^{1}H isotopic natural abundance (~100%). The pulse sequence used - CRAMPS (Combined Rotation And Multi Pulse Spectroscopy) [6] - again well known in solid-state ^{1}H-NMR studies [7,8]. It permits screening of the homonuclear proton-proton dipolar interaction, which broadens the peaks in MAS ^{1}H-NMR experiments. Resolution and calibration are adjusted with the signal of adamantane $C_{10}H_{16}$, with a peak at 1.7 ppm.

Previous work has shown the efficiency of this method (using thermal analysis, XRD, SEM, ^{29}Si and ^{1}H-NMR) to determine the relative amount of each phase [9].

2.3 Macroscopic tests

The macroscopic tests consisted of the determination of the samples' compressive strength and Young's modulus E.

The samples' geometry was cylindrical with average height of 5 cm and diameter of 2.5 cm. Only for samples hydrated at the highest temperature and pressure (200°C and 0.6 kbar), compression tests were performed at the Institute Francais du Petrole. A preloading was applied then the loading was achieved with a 0.05 mm/min rate. The deformation of the sample was then recorded versus the loading intensity.

3. RESULTS

3.1 Structural analyses

3.1.1 High pressure and temperature silicate hydrates

C_3S hydration is well known at ambient temperature and pressure [1]. Two phases are formed: Portlandite $Ca(OH)_2$ and a poorly crystallised and not-stoechiometric phase: C-S-H. Previous works show that in addition to these two phases, other silicate hydrates (table 1) may appear under non-ambient temperature and pressure [1,10,11].

Name	Compound
Portlandite	$Ca(OH)_2$
C-S-H	$Ca_3(OH)_4H_4Si_2O_7$ (in the case Ca/Si=1.5)
Jaffeite (TSCH)	$Ca_6(Si_2O_7)(OH)_6$
Hillebrandite (β-C_2SH)	$Ca_2(SiO_3)(OH)_2$
α-C_2SH	$Ca_2(SiO_3)(OH)_2$

Table 1. P and T silicate hydrates

In order to characterise mixtures of different phases, ^{1}H and ^{29}Si-NMR experiments were performed on pure phases (Portlandite, C-S-H, α-C_2SH, β-C_2SH), elaborated by N. Lequeux at the ESPCI. Table 2 gives characterisation parameters for these phases.

Name	^{29}Si-NMR chemical shift (ppm)	^{1}H-NMR chemical shift (ppm)
Portlandite	-	1.4 ± 0.4
C-S-H	-79.5 and -85.8 ± 0.4	5.1 ± 0.5
Jaffeite (TSCH)	-82.9 ± 0.4	-0.2 ± 0.4
Hillebrandite (β-C_2SH)	-77.8 and -86.0 ± 0.4	0.7 and 2.0 ± 0.4
α-C_2SH	-72.3 ± 0.4	2.5 ± 0.4

Table 2. Silicate hydrates ^{29}Si- and ^{1}H-NMR chemical shifts (ppm)

With the chemical shifts determined on pure phases, NMR-spectra were easier to analyse even in the case of a phases mixture. Hydration with two different kinetics have been carried out to simulate the oil well conditions.

3.1.2 Hydration kinetics

Table 3 gives the description of the two pressure cells used to perform C_3S hydration **[9,12]**.

Name	P. max (kbar)	T. max (°C)	Internal vol. (cm^3)	increasing T period (h)	decreasing T period (h)
LP	0.5	350°C	800	5	6
HP	1	250°C	65	0.5	4

Table 4. Characteristics of the two high-pressure cells used in our experiments

During the oil well cementing, cement paste is rapidly (half an hour typically) in contact with a T and P tank, the conditions in cell HP are closer to those found in practice (excepted for off-shore cementing). Nevertheless, the use of both devices permits us to show the importance of the kinetics

in such non-equilibrium processes (for samples hydrated during short periods). As a comparison, figure 2 gives the amounts of hillebrandite (β-C_2SH) and jaffeite (TCSH) for two samples of C_3S hydrated during 15 days.

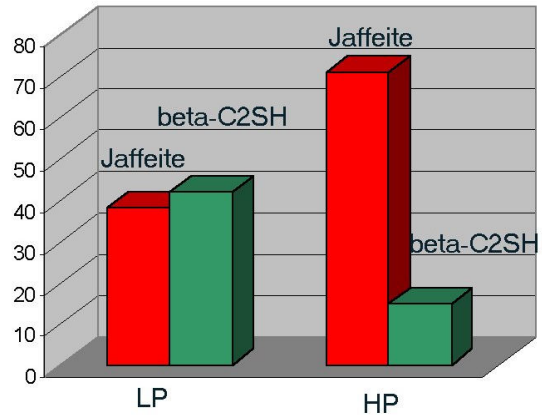

Figure 2. Amounts of hillebrandite (β-C_2SH) and jaffeite for two samples of C_3S hydrated 15 days

Jaffeite appears as the more stable phase, even if its activation barrier is higher than that of hillebrandite. It becomes obvious that the nucleation-growth process is highly dependent on the rate of temperature increase (slowly or fast). Furthermore, previous work has shown the acceleration role of pressure on silicates hydration **[5,13]**. For this reason, we have chosen to present hydration results for samples elaborated with cell HP for the longest hydration time (28 days).

3.1.3 Results

Different conditions of pressure and temperature were applied (table 5).

Temperature (°C)	120	160	160	200	200	200
Pressure (kbar)	0.4	0.07	0.4	0.07	0.4	0.6

Table 5. Temperature and pressure conditions of hydration (28 days)

In particular the quantitative results obtained by ^{29}Si- and ^{1}H-NMR will be presented and discussed for one sample: C_3S hydrated at 200°C under 600 bar for 28 days.

3.1.3a ^{29}Si- and ^{1}H-NMR

X-Ray powder diffraction allowed us to find the highly crystallized phases present in these samples, in agreement with the technical literature (JCPDS data). Thermal analysis confirms the trends observed by X-ray diffraction studies. The phases detected by these methods are the following: jaffeite mainly, hillebrandite, portlandite and α-C_2SH.

Finally, ^{29}Si and ^{1}H NMR experiments allow us to validate the previous results. The ^{29}Si and ^{1}H spectra are shown in figures 3 (^{29}Si) and 4 (^{1}H). In figure 3, a ^{29}Si Single Pulse spectra is represented. Three main peaks are observed at around –72.5 ± 0.4 ppm (Q^0 entities, signal reinforced by short contact times in CPMAS experiments), -83.0 ± 0.4 ppm (Q^2 entities) and -86.0 ± 0.4 ppm (Q^2 entities). The Q^n entities are SiO_4 tetrahedra linked to n other tetrahedra, according to Michel and Engelhardt's chemical shift table [2]. The second peak identifies jaffeite [5]. The other phases are hillebrandite (peak at -86.0 ± 0.4 ppm) and α–C_2SH (-72.5 ± 0.4 ppm). Chemical shifts for the three phases are in agreement with the literature [9,10].

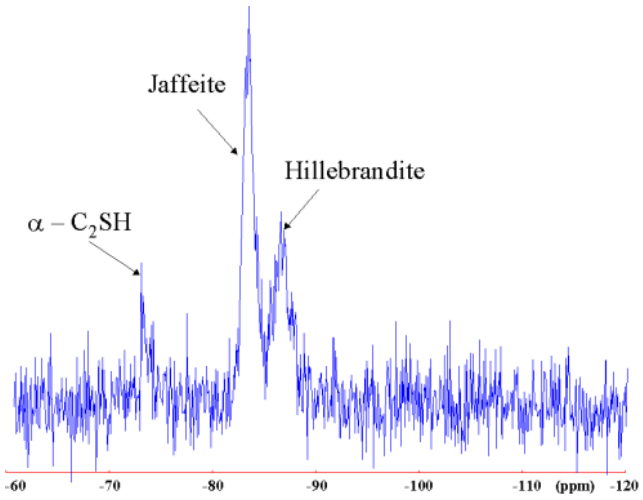

Figure 3. ^{29}Si Single Pulse spectra of C_3S hydrated 28 days at 200°C under 0.6 kbar.

Finally, ^{1}H-NMR experiments were performed to confirm the presence of these phases according to Heidemann's chemical shift table [8]. CRAMPS spectra (figure 4) can clearly be analyzed and is quantitative. Four peaks are found: at 4.9 ± 0.4 ppm (relative to free water in the sample due to porous volume water saturation), at 2.4 ppm ± 0.4 ppm (relative to α–C_2SH), at 1.6 ± 0.4 ppm (characteristic of hillebrandite), and at -0.2 ± 0.4 ppm (characteristic of jaffeite). We notice that the little amount of portlandite does not appear very clearly in CRAMPS spectra (certainly indistinguishable of the hillebrandite peak).

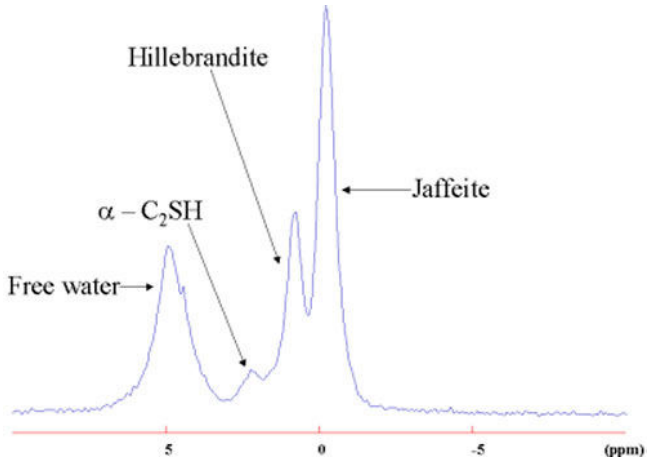

Figure 4. : ^{1}H-NMR CRAMPS spectra of C_3S hydrated 28 days at 200°C under 0.6 kbar.

All the methods used in this work are in good agreement and give following amounts of each phase: jaffeite mainly (68 ± 4 %), hillebrandite (11 ± 4 %), portlandite (10 ± 4 %), α–C_2SH (11 ± 4 %).

In comparison to results found at 200°C under 0.07 and 0.4 kbar, an equilibrium emerges between α– and β–polymorphs of C_2SH. The α– to β– C_2SH reaction seems to be enhanced at high temperature, which is consistent with Taylor's work [1], and the reverse reaction appears predominant at high pressure. The P/T-relation between α- and β-polymorphs of C_2SH has been pointed out, β-C_2SH formation will be considered more in details now, using SEM observations.

3.1.3b SEM observations

Previous work has shown the structural similarity between C-S-H and β-C_2SH [14]. Indeed, if we consider table 2, we can notice the extremely close chemical shift values for both phases by ^{29}Si-NMR, in particular for the tetrahedra at the middle of SiO_4 chains. Furthermore, this resemblance can be observed microscopically. A continuous phase (figure 5) is observed, which is most likely to be hillebrandite, in agreement with the electron dispersive X-ray analysis. This morphology is close to the C-S-H morphology, a sea-urchin with numerous disordered needles (figure 6).

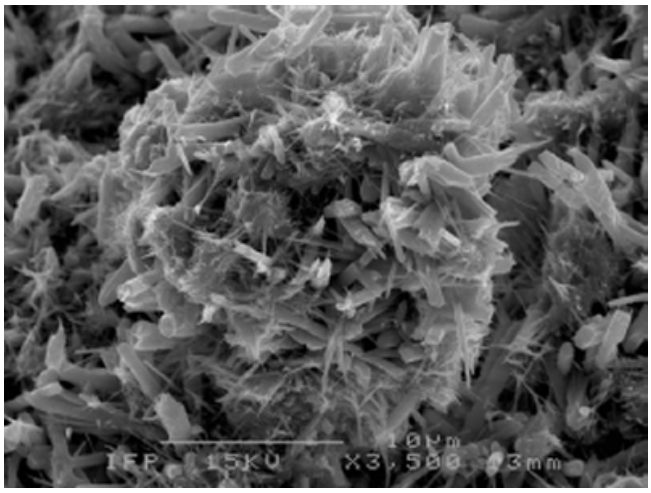

Figure 5. SEM image of secondary electrons (x 3500) of the C_3S hydrated sample (w/c=0.44) at 200°C under 0.6 bar during 28 days

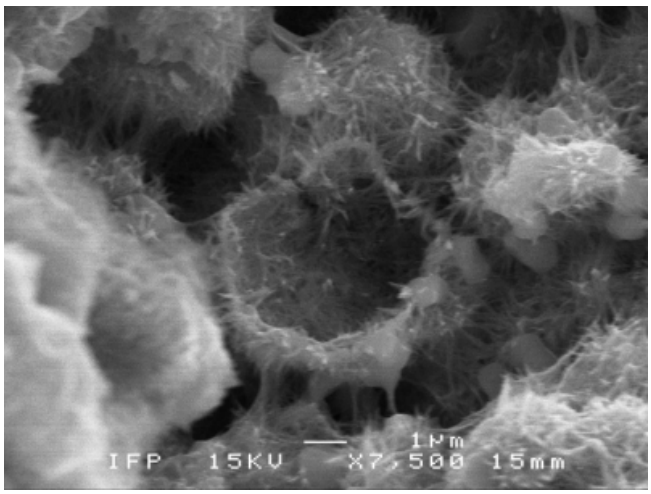

Figure 6. SEM image of secondary electrons (x 7500) of the C_3S hydrated sample (w/c=0.44) at 120°C under 0.4 bar during 7 days

This morphology likeness has already been reported [11] and in addition, the possibility to find C-S-H phases with a Ca/Si ratio about 1.7 (close to the Hillebrandite Ca/Si=2 ratio) at high temperature has been pointed out previously [1,11].

3.1.3c Quantitative results

Using the various techniques used, the quantitative evolution of each phase as a function of temperature and pressure has been determined.

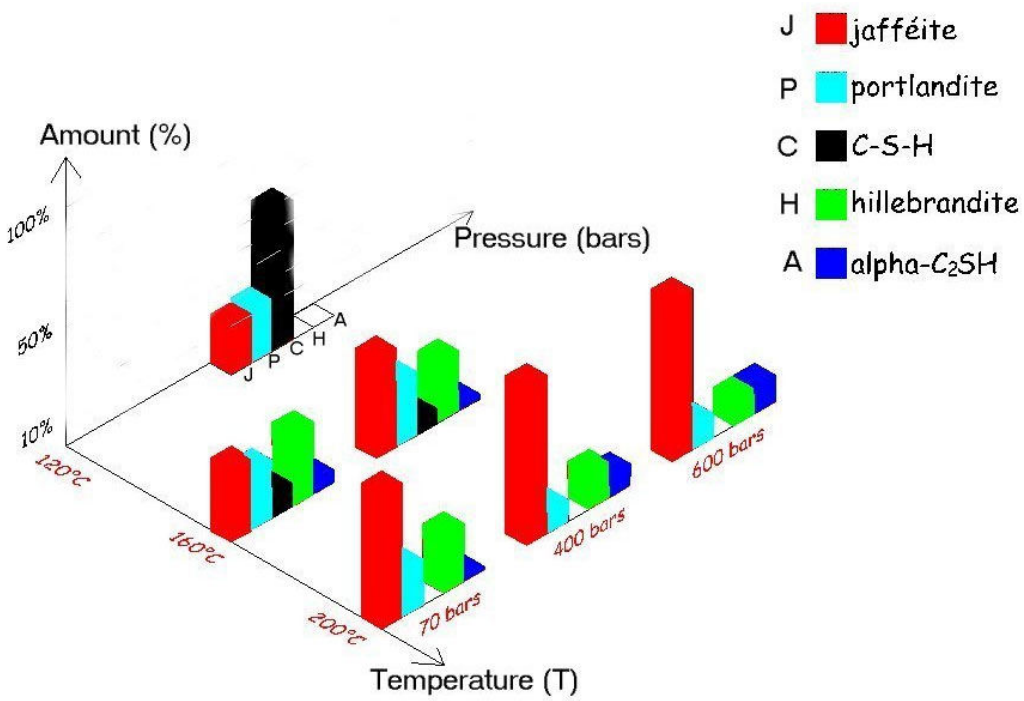

Figure 7. Phases fraction (%) formed during 28 days hydration of C_3S versus temperature and pressure

The C-S-H disappearing is revealed till 200°C and low pressure (0.07 kbar). This phase could react with portlandite and give β-C_2SH, as shown previously. Moreover, we noticed the competition between the thermodynamic (jaffeite) and kinetic (β-C_2SH) product of the high temperature and pressure C_3S hydration, which suggests the two following ways of jaffeite formation: CH and C-S-H or CH and β-C_2SH.

In addition the equilibrium between α- and β-C_2SH polymorphs has been pointed out in this work. The α–C_2SH seems to be enhanced at high pressure, and β–C_2SH seems predominant at high temperature.

3.2 Mechanical behaviour

The tested samples were hydrated at 200°C and 0.6 kbar during 2 to 28 days. The results are summarized in table 4.

Hydration duration (days)	Young's modulus (MPa)
2	7900 ± 3 %
4	7200 ± 4 %
6	4800 ± 4 %
14	6700 ± 2 %
28	10800 ± 6 %

Table 4. Young's moduli of Ca_3SiO_5 hydrated at 200°C and 0.6 kbar during 2 to 28 days

Measured Young's moduli are comparable to ones determined in a previous work on Ca_3SiO_5 studies with ultrasonic experiments [15]. But obviously the Young's Modulus continuously

decreases during the first 6 days and the hydrated Ca_3SiO_5 is then the more elastic. This hydration period corresponds to the highest α–C_2SH amount but these results have to be completed with porosity measurements. Rapidly the Young's modulus value increases and attains the same value as the modulus of Ca_3SiO_5 paste hydrated at room temperature and ambient pressure.

4. CONCLUSIONS

The NMR results are in fair agreement with the XRD, SEM and DTA data. Some methods are relevant to investigate crystalline phases (XRD, SEM and NMR) but NMR is very useful even in the case of poorly crystallized phases, such as C-S-H. Using chemical shift measurements on pure phases, NMR-spectra were easier to analyse even in the case of a phases mixture. This tool permits us to identify and to quantify hydrates of silicates by the use and comparison between various techniques. Two different hydration kinetics have been evidenced to simulate the oil well conditions. We have chosen to present hydration results for samples concentrated with the HP cell for the longest hydration period (28 days) because of the role of pressure in the activation on silicate hydration.

The existence of C-S-H was shown up to 200°C and low pressure (0.07 kbar). This phase may react with portlandite and give β-C_2SH (comparable morphology, structure and Ca/Si ratio). Jaffeite is the most stable phase at C/S=3 but β–C_2SH formation is faster. Moreover, the competition between the thermodynamic (jaffeite) and kinetic product (β-C_2SH) suggests two ways of jaffeite formation: CH and C-S-H or CH and β-C_2SH. In addition the equilibrium between α- and β-C_2SH polymorphs has been pointed out in this work. The α–C_2SH seems to be enhanced at high pressure, and β–C_2SH seems predominant at high temperature.

The Young's modulus of hydrated Ca_3SiO_5 at 200°C and 0.6 kbar for a period of between 2 and 28 days decreases during the first 6 days which corresponds to the highest α–C_2SH quantity. Nonetheless, correlation between these two observations cannot be made. Some work in this direction is under progress. In a second step, this Young's modulus value increases and becomes the same value as found in Ca_3SiO_5 paste hydrated at room temperature and ambient pressure.

There is the question whether the crystalline phases formed under the most severe conditions (200°C – 0.6 kbar) could play the role of a binder, because the usual glue C-S-H, formed during the first hours of setting, has disappeared and a phase with poor mechanical performance appears: the layered structure known as α–C_2SH.

ACKNOWLEDGMENTS

The authors want to thank the Institut Français du Pétrole for supporting this work. The authors are grateful to Ciments Français-Italcementi CTG for the tricalcium silicate synthesis, to Bernadette REBOURS for her help with the XRD-experiments, to Elisabeth ROSENBERG for the SEM-observations and to Nicolas LEQUEUX for access to the pure synthetic phases.

REFERENCES

[1] H. F. W. Taylor, Cement Chemistry, 2nd edition, Thomas Telford Edition, London, 1997.

[2] G. Engelhardt and D. Michel, High-resolution solid-state NMR of silicates and zeolites, Wiley, New York, 1989.

[3] E. Lippmaa, M. Mägi, M. Tarmak, W. Wieker, A. R. Grimmer, A High Resolution ^{29}Si NMR Study of the Hydration of Tricalcium Silicate, Cem. Concr. Res. 12 (1982), 597-602

[4] S. A. Rodger, G. W. Groves, N. J. Clayden, C. M. Dobson, Hydration of Tricalcium Silicate Followed by ^{29}Si NMR with Cross-Polarization, J Am Ceram Soc 71 (2) (1988), 91-96

[5] B. Bresson and H. Zanni, Pressure and temperature influence on tricalcium silicate hydration. A ^{1}H and a ^{29}Si NMR study, J. Chim. Phys 95 (1998), 327-331.

[6] B.C.Gerstein, CRAMPS, in: Encyclopedia of Nuclear Magnetic Resonance, Ed. D.M.Grant and R.K.Harris, Wiley, 1996, 3, pp. 1501-1509.

[7] B. Bresson, H. Zanni, S. Masse, C. Noïk, Contribution of ^{1}H combined rotation and multipulse spectroscopy nuclear magnetic resonance to the study of tricalcium silicate hydration. Journal of Materials Science, 1997, 32, 4633-4639.

[8] D.Heidemann and W.Wieker, Characterization of Protons in C-S-H Phases by Means of High-Speed ^{1}H MAS NMR investigations, in: P. Colombet, A.-R. Grimmer, H. Zanni, P. Sozzani (Eds), Nuclear Magnetic Resonance Spectroscopy of Cement-Based Materials, Springer-Verlag, Berlin Heidelberg, 1998, pp.169-180.

[9] F. Méducin, C. Noïk, A. Rivereau and H. Zanni, Complementary analyses of a tricalcium silicate hydrated at high pressure and temperature, Cem. Concr. Res., 32, (2002), 65-70.

[10] G.M.M. Bell, J. Bensted, F.P. Glasser, E.E. Lachowski, D.R. Roberts and M.J. Taylor, Study of calcium silicate hydrates by solid state high resolution ^{29}Si nuclear magnetic resonance. Advances in Cement Research, 1990, 3, 9, 23-37.

[11] E. Schlegel and R. Streinitz, Faserförmig kalziumsilikathydrate, Silikattechnik, 1990, 41, 8, 278-283.

[12] F. Méducin, C. Noïk, A. Rivereau, H. Zanni, « Oilwell cements: NMR contribution to establish the phase diagram pressure/temperature of the mixture H_2O / Ca_3SiO_5», C. R. Acad. Sci. Paris, Chimie / Chemistry 4, 2001, 801-804.

[13] B. Bresson, F. Méducin, H. Zanni and C. Noïk, Hydration of tricalcium silicate (C_3S) at high pressure and temperature, Journal of Materials Science, 37, (2002), 1-11.

[14] Y. Dai and J.E. Post, Crystal structure of hillebrandite:A natural analogue of calcium silicate hydrate (C-S-H) phases in Portland cement, American Mineralogist, 1995, 80, 841-844.

[15] Boumiz, A.; Vernet, C.; Cohen-Tenoudji, F. Mechanical properties of cement pastes and mortars at early ages, Adv. Cem. Based Mater. (1996), 3(3/4), 94-106.

HYDRATION OF TRICALCIUM SILICATE AT HIGH PRESSURE AND TEMPERATURE

Fabienne Méducin

Born 17th June 1974 (French)
Current workplace : Laboratoire de Physique des Milieux Condensés – T 13/23 – Boîte 77 - 4, Place Jussieu 75252 Paris cedex 05, France Tel: 33-(0)1.44.27.44.54 - Fax: 33-(0)1.44.27.44.69.
E-mail: fm@pmc.jussieu.fr

ACADEMIC BACKGROUND

1998 - 2001: Ph.D Thesis at the University Paris VI in collaboration with the French Petroleum Institute (IFP), the City of Paris Industrial Physics and Chemistry Higher Educational Institute (ESPCI) and the Physics of Condensed Matter Laboratory (PMC-Paris VI). Ph.D title: Structural study of cement silicate phases hydrated at high pressure and temperature. Thesis examination: 23 October 2001, Ph.D Supervisor H. Zanni (ESPCI) and C. Noïk (IFP). Referees K. Scrivener (Swiss Federal Institute of Technology Lausanne) and D. Petit (Polytechnic Engineer-Institution Palaiseau). Obtained with honours, my Ph.D thesis has been proposed for the IFP Ph-D reward.

1995-1998: Materials Science Degree ("DEA"), and "Licence" and "Maîtrise" degrees in physical chemistry (Paris VI). Obtained with honours.

EXPERIENCE

Since Sept. 2001: Full time assistant lecturer at PMC laboratory (192 hours teaching). Study of amorphous ice (HDA and LDA) in the group of Dr S. Klotz. During this year, I have observed structural HDA variation up to 3 GPa at 100 K, LDA-HDA transition (0,3 GPa) and crystal-amorphous transitions by neutron diffraction (ISIS neutron spallation source, Rutherford Appleton Laboratory, UK). In order to understand the role of phonons in the pressure-induced amorphisation of ice I_h (ordinary ice), I made the first measurements of the phonons dependence of TA modes by inelastic neutron scattering on single crystal at 130 K to 0.5 GPa (LLB, Saclay). This work, which will be completed by additional measurements later this year, will be presented at the IUCr meeting in Geneva. In parallel, I have determined elastic constants at $AgGaSe_2$ by ultrasonic method under pressure.

1998-2001: Ph.D thesis: Synthesis and hydration of the main component of cement (Ca_3SiO_5) under high pressure and temperature to simulate deep oil well conditions. During my Ph.D thesis, I have studied hydrated cement samples by various characterisation methods (^{29}Si- and ^{1}H-NMR, XRD, DTA-TG and SEM) to complete phase diagram (P,T) of the calcium silicate hydrates. I have established a systematic method (now in use at the IFP on the real oil well cements formulation) to characterise quantitatively silicate phases mixtures in comparison with studies on pure phases (characterised with the same techniques during my Ph.D thesis). To correlate macroscopic behaviour and physical-

chemistry properties of hydration products, mechanical tests and ultrasonic measurements have been performed too. Jaffeite has been found to be the most stable phase at these conditions. To simulate the hydration of real cement, hydration of C_3S with ground quartz with / without superplasticizers was performed. In those cases, new phases appear: mainly kilchoanite, and xonotlite. A large amount of □-C_2SH is also produced. Compression tests were done to correlate the macroscopic behavior and physico-chemical properties of the products. With superplasticizers, samples porosity was found to be lower and the 28-days aged samples recover the Young modulus they had at the early stage of hydration.

SOCIAL ACTIVITIES

Badminton (I have trained adult beginners from 1997 to 2001. And as a member of the association board, I am in charge of tournaments for three years)
Horse riding (3rd gallop), handball (3 years in a club)

NUCLEAR MAGNETIC RESONANCE SPECTROSCOPY AND SPIN RELAXATION ON CEMENT-BASED MATERIALS – A REVIEW

H. Zanni[1], Ph. Fonollosa[1], F. Méducin[1], C. Porteneuve[1], F. Barberon[2], J.-P. Korb[2] and D. Petit[2]

[1] Laboratoire PMMH, ESPCI, Paris, France. E-mail: zanni@pmmh.espci.fr
[2] Laboratoire PMC, Ecole Polytechnique, Palaiseau, France. E-mail: jpk@pmc.polytechnique.fr

ABSTRACT

Nuclear Magnetic Resonance (NMR) is a relevant technique for the investigation of disorganized or poorly crystallized systems. Indeed, in these materials where long-range crystalline order vanishes, traditional methods like X-ray diffraction are inefficient.

^{29}Si MAS NMR studies gave important structural and quantitative information about silicate and aluminate phases in anhydrous and hydrated cement. NMR strengthened many ideas concerning the hydration of the major component of clinker, tricalcium silicate (C_3S), and the C-S-H structure. Other studies were also realized to complete the phase diagram of C-S-H under high temperature and pressure.

Finally, NMR happened to be very useful to study high or ultra high performance concretes so that we could probe their microporosity. Being sensitive to water confined protons dynamics in pores, the measurement of their relaxation time allowed us to obtain an estimation of the average pore sizes. The results exhibited a fractal surface with an average dimension of 2.6, which confirmed previous works done by nitrogen adsorption-desorption isotherms.

1. INTRODUCTION

The techniques normally used, such as XRD, TDA or SEM, do not enable us to reach a sufficiently small scale to entirely understand the structure of cementing materials. Nuclear magnetic spectroscopy and spin relaxation have shown themselves to be particularly interesting techniques to reach nanoscopic scales and therefore understand the structure of various hydrates. Moreover, their non-invasive character allows us to monitor the evolution of hydration as well as the formation of the porous system.

2. FEW WORDS ON NMR PRINCIPLES

Atomic nucleii, as well as the fundamental particles that constitute them, possess a spin moment of their own, called **I**. If $\mathbf{I} \neq \mathbf{0}$, the result will be the simultaneous existence of a magnetic moment $\boldsymbol{\mu}$, co-linear with **I** and of the same direction. The orientation of nuclear spins is random except in the presence of an external magnetic field $\mathbf{B_0}$. They then tend to align either in a parallel or antiparallel fashion to this field following the Boltzmann statistic with a precession movement, known as the Larmor precession, at the following frequency:

$$\omega_0 = \frac{\gamma}{2\pi} B_0 \qquad (1)$$

where γ is the magnetogyric ratio which is characteristic of the nucleus under study. This spin arrangement results at the macroscopic scale in a magnetization **M** that must be measured (Fig. 1.1).

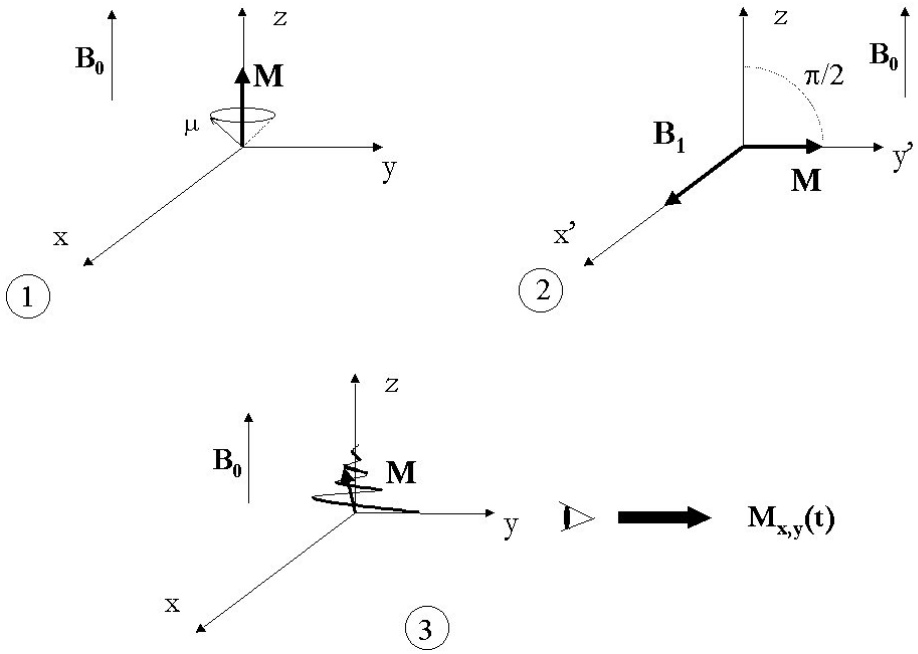

Figure 1. Single Pulse Experiment in NMR

NMR experiments consist of exciting the system using a transversal radiofrequency field $\mathbf{B_1}$. When its frequency ω_1 is close to that of the precession of all spins under consideration, the magnetization is reversed, which unbalances the system from a thermodynamic point of view. Practically, the $\mathbf{B_1}$ field is applied for a predetermined period to reverse magnetization on the transversal plane (Fig. 1.2). Once excitation stops, the spins, influenced only by the principal field, tend to return to the state of equilibrium with a free precession movement around the $\mathbf{B_0}$ axis, whose frequency ω depends on the interactions on the nucleus (Fig. 1.3). The signal obtained, after Fourier transform processing, produces a central peak at ω whose integrated intensity is proportional, under certain conditions, to the number of excited spins (Fig. 2).

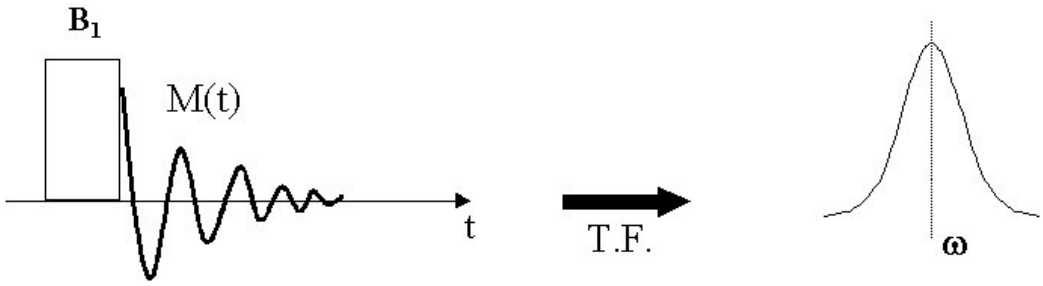

Figure 2. NMR spectrum produced by Fourier transform processing

Aside from the Zeeman effect resulting from the action of the principal magnetic field, the nuclear spins undergo various interactions through which the investigator can obtain information on the material. In the systems that interest us, there are mainly bipolar and quadripolar interactions, and especially, chemical displacement. This last interaction expresses the effect of the chemical environment around a nucleus on its frequency peak.

Silicates possess a structure based on the silicon tetrahedron SiO_4^{4-}, that can link itself with the help of oxygen atoms present at its peaks with one, two, three or four other tetrahedrons. The creation of

a bridging oxygen modifies the electronic environment as well as the magnetic field affecting the silicon nucleus, which results in a shift of its peak on the spectrum. Researchers such as Engelhardt have established a classification of these chemical shifts as a function of the degree of connectivity of silicon tetrahedron (Fig. 3) [1].

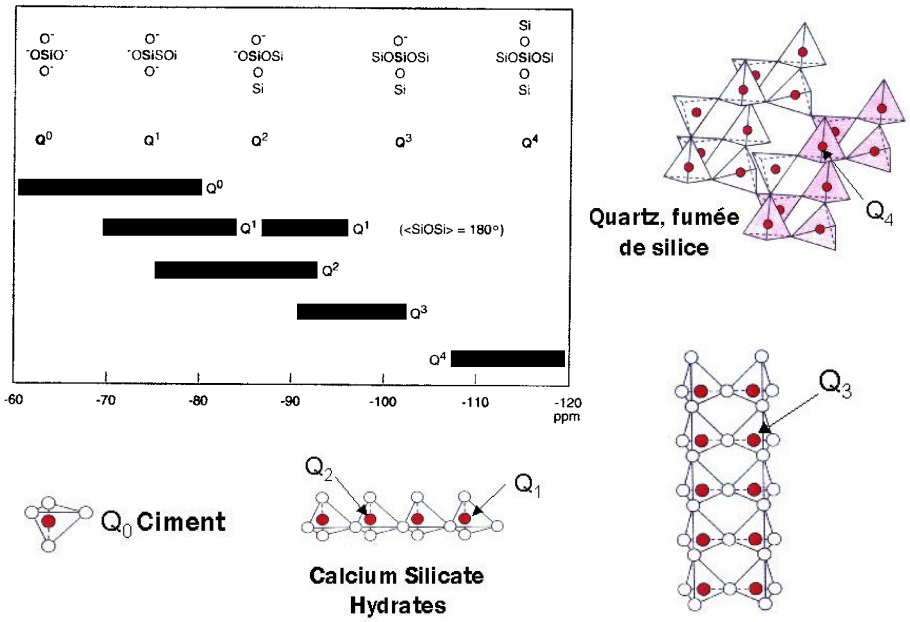

Figure 3. Chemical shift domains of ^{29}Si in solids and corresponding Q^n species connectivity [1]

The degree of sensitivity of NMR allows one to discriminate, on a given concrete spectrum, the peaks relative to cement from those of C-S-H or quartz sand and silica fume.

3. NMR OF ^{29}SI APPLIED TO SILICATES

Over twenty years ago, researchers initiated the study of cement hydration using NMR analysis of silicon and aluminium. Following in the footsteps of these pioneers, an ever increasing number of research teams are working on this research theme. This technique helped us to better understand the chemical species that develop within cementing materials, thus helping us to better understand phenomena such as the setting of cement.

3.1 Hydration kinetics and the stability of silicate phases

The study of the hydration reaction of cement and C_3S using NMR was initiated by Grimmer and Lippmaa [2, 3]. By following hydration using single pulse experiment with magic angle spinning, they brought out the appearance of Q^1 species after 6 hours of hydration, and then of Q^2 species after 14 hours of hydration.

These results were confirmed a few years later on samples obtained by hydrating C_3S enriched in ^{29}Si [4]. Their spectra, obtained by cross-polarization during and after the dormant period at room temperature, showed that the polymerisation process began within the first hour of hydration with the creation of Q_0H species, which correspond to a protonation of silicate ions at the surface of C_3S particles [5, 6]. These hydrated monomeric entities continue to be present as long as there is anhydrous C_3S (Fig. 5). In the same way, Q^1 and Q^2 species relative to C-S-H are created during the induction period. These appear long before oversaturation in calcium and the precipitation of portlandite, which is in agreement with the proposals concerning reaction mechanisms [7].

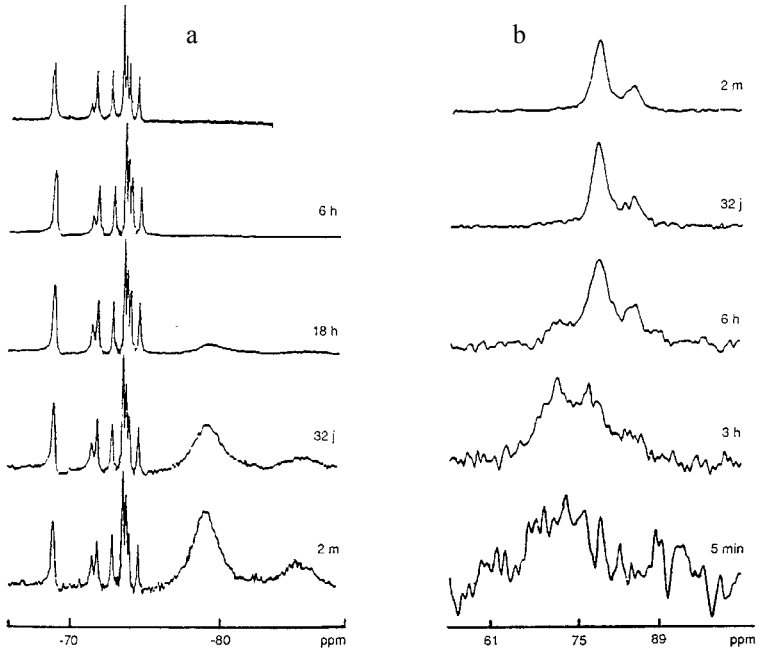

Figure 4. ^{29}Si NMR spectra of hydrated C_3S obtained by single-pulse experiment (a) and cross-polarisation (b) [6]

Some research has been done to identify and quantify the silicate phases resulting from the hydration of C_3S between 60 and 120°C [8]. Figure 5 shows the single pulse with magic angle spinning of samples at 14 days of age. The 60 °C spectra shows that the Q^1 peak at the end of the silicate chains is far superior to that of Q^2 from the middle of the chains, which shows that the silicate chains are still relatively short, as they would be at room temperature. On the other hand, for the sample hydrated at 120 °C, the Q^2 peak dominates which is related to the lengthning of the C-S-H. Moreover, the Q^0 peak, representing C_3S, has disappeared, which indicates that the hydration reaction is complete. Aside from accelerating the hydration reaction, an increase in temperature results in an increase of the mean length of silicate chains in C-S-H [9].

The literature tells us that such a lengthening of silicate chains occurs also during the carbonation of samples, the modification of the pH level of solutions during preparation of synthetic CSH and/or the addition of silica fume.

3.2 Pozzolanicity of silica fume

The addition of silica fume accelerates the process of hydration of clinker at room temperature, without necessarily affecting the induction period [10]. A study carried out during the first 24 hours on a mix of C_3S containing 20 % of finely ground silica fume showed the rapid evolution of Q^1 and Q^2 peaks relative to C-S-H [11]. According to its authors, the acceleration of C_3S hydration would depend mainly on the specific surface of microsilica. However, silica fume would have a tendency to delay the kinetics of cement in the long term, in particular for low water/binder ratios [12].
Moreover, silica fume increases the quantity of C-S-H through its reaction with portlandite. These also represent a high degree of polymerisation as shown in figure 6.

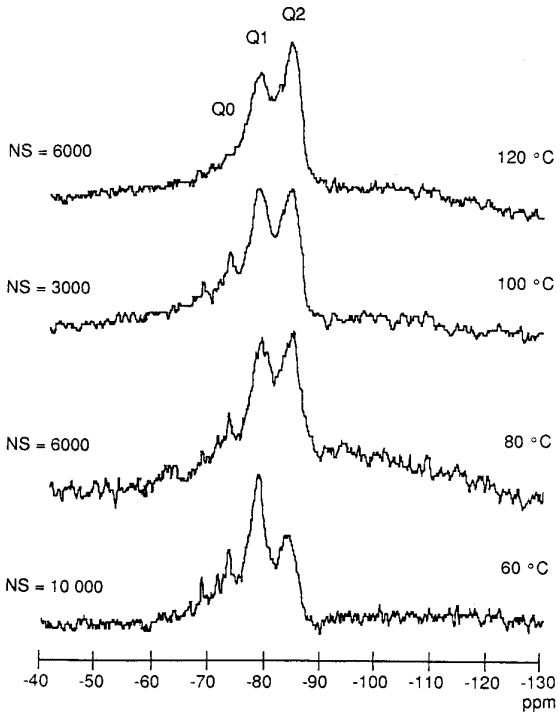

Figure 5. Evolution of the ^{29}Si NMR spectra of C-S-H as a function of the hydration temperature [8]

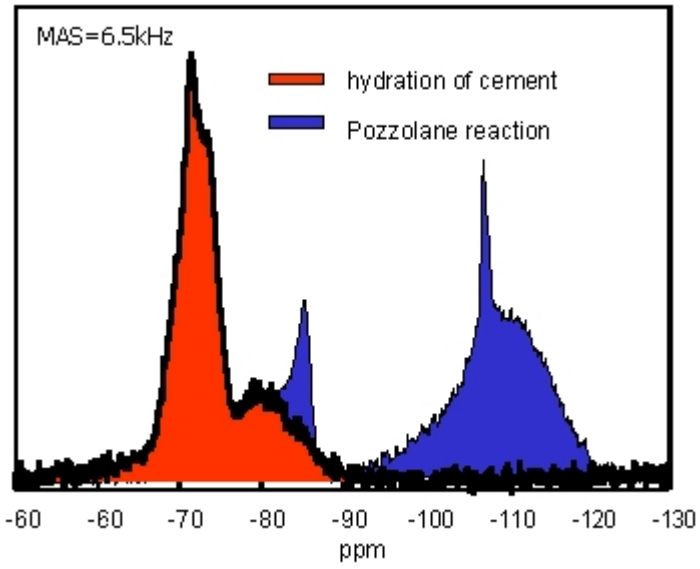

Figure 6. Contribution of the pozzolanic reaction to the C-S-H structure (according to Samuel Philippot's work).

4. PROTON RELAXATION AND POROSITY

The spin relaxation of protons offers a new alternative to the study of cement-based materials. Indeed, as hydration progresses, the confinement of water molecules in the cementitious matrix will modify relaxation rate. From several existing models, it is then possible to obtain a physical quantity such as the specific surface area or the microporosity of the material.

Measurements of relaxation rate $1/T_1$ as a function of frequency provide information on the dynamics of protons in pores. The relaxation model most often encountered in cement-based materials is the biphasic fast exchange model [13]. This model can separate contributions of bulk protons ($1/T_{1,bulk}$) from those of surface protons ($1/T_{1,surf}$). In this model, the longitudinal relaxation rate can be written, for a pore of S surface and V volume, as:

$$\frac{1}{T_1} = \frac{1}{T_{1,bulk}} + \frac{eS}{V}\frac{1}{T_{1,surf}} \qquad (2)$$

where e is the thickness of the surface layer. Recent experiments in relaxometry with variable magnetic fields on water confined in microporous silica glass containing paramagnetic impurities on the pore surface showed diffusive behaviour different from surface and bulk water molecules [14]. Similar phenomena have been observed in macroporous systems [15].

Previous studies [16] have shown that this model could be used in the case of discrete distribution of pore sizes. In that case, the relaxation process is no longer exponential, but exhibits three or four well-defined values for T_1. This was observed by Samuel Phillipot in his thesis on reactive powder concretes. He developed relaxation experiments to follow the evolution of more or less confined bulk water and water at the surface of particles. The first experiments correspond to measurements of T_1 carried out by inversion-recovery sequence on a Bruker ASX300 at 7,1 T (300 MHz). The second ones correspond to T_1 measurements to follow surface protons. Magnetization recovery curves were then analysed and fine-tuned using the least square method and the reverse Laplace transform. In both cases, this decomposition brings out many relaxation times corresponding to different pore sizes.

Figure 7 shows the evolution of T_1 distribution as a function of hydration time for a Ductal®-type concrete hydrated for 20 hours. At the beginning of this experiment, the first peak appears for high values of T_1 associated to weakly-confined water. As hydration progresses, this peak moves to lower values, which is characteristic of the confinement degree of water, and two more peaks appear. A more detailed study based on an extension of Eq. (2), has linked each peak to a pore size. The peak intensity representing the respective proportion of these pores in the overall distribution. For example, this results in the presence of protons between anhydrous grains and not within the C-S-H. On the contrary, as shown in figure 8, after several weeks, the $T_{1,i}$ distribution is reversed. This is normal for $T_{1\rho}$ measurements. $T_{1\rho}$ distribution characterizes the porosity refinement towards small-sized pores. This phenomenon is due to anhydrous grains that lead mainly to C-S-H whose porosity is caused first by dry granular stacking, followed by clogging of the porosity.

By considering the fast biphasic exchange model, the relaxation times of $T_{1,i}$ can be related to the pore size. Indeed, the longitudinal relaxation time $T_{1,i}$ is proportional to the corresponding pore mean radius $\langle R \rangle_i$ [17]

$$\langle R \rangle_i = \kappa T_{1,i} \qquad (3)$$

where the proportionality factor K depends on different known or measurable parameters (for example, paramagnetic spin density measurable by Electronic Paramagnetic Resonance). By using this relation, Korb *et al.* obtained four pore radii for a Ductal® of 8 months of age cured at 20°C :

$$\langle R \rangle_i = 0.7 \text{ nm} ; \langle R \rangle_i = 2.9 \text{ nm} ; \langle R \rangle_i = 8.9 \text{ nm} ; \langle R \rangle_i = 28.0 \text{ nm}.$$

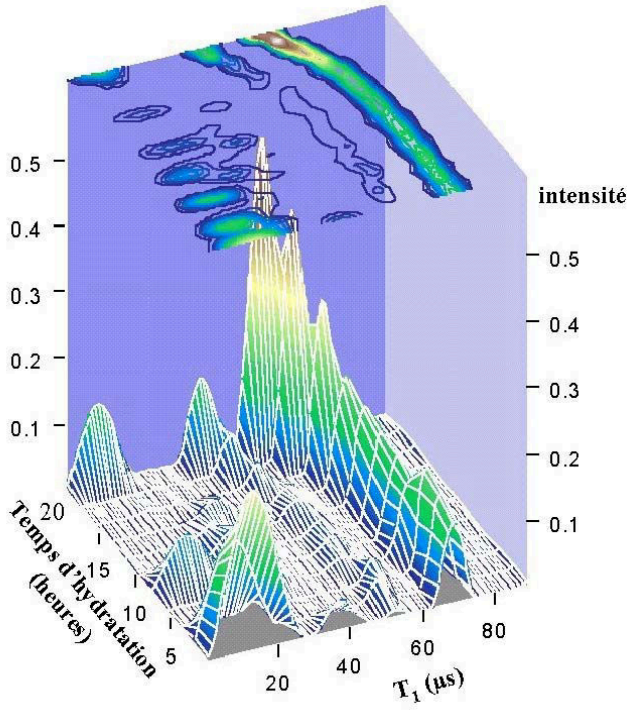

Figure 7. Evolution of T_1 distribution obtained with CONTIN (at 300 MHz) as a function of hydration time (according to Samuel Philippot's work)

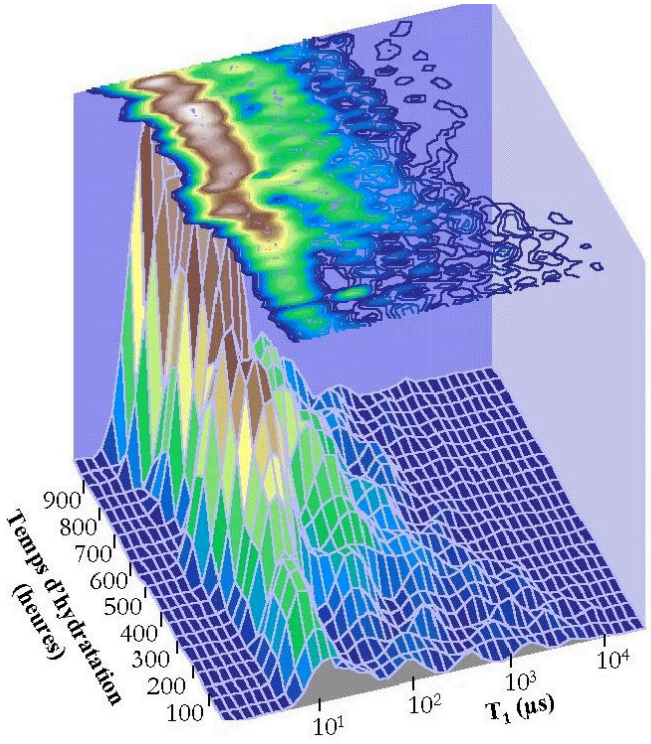

Figure 8. Evolution of $T_{1\rho}$ distribution obtained with CONTIN (à 17.8 kHz) as a function of hydration time (according to Samuel Philippot's research)

If the highest pore diameter values are in agreement with the dimensions of C-S-H crystallites [18] measured by other techniques, the smallest pores can be attributed to the C-S-H interlayer space. The limit of the resolution of other techniques cannot give a reliable measure of it. The other sizes obtained are related to the C-S-H inter-crystallite porosity, and stacking defects and gaps. It should

be noted, however, that there does not seem to be any well-defined border between these different porous modes.

The non-invasive character of NMR techniques benefits NMR as opposed to other techniques. As well, the relatively short length of experiments also allows an in-situ follow-up of concrete hydration at early ages. Finally, this method seems to be the only one giving information on the C-S-H inter-crystallite porosity.

This technique has been applied to other RPC in which the nature and content of silica fume varied. Figure 9 shows the $T_{1,i}$ distribution of protons in percentage (300 MHz) as a function of the $T_{1,i}$ for different UHPC mix-designs [19].

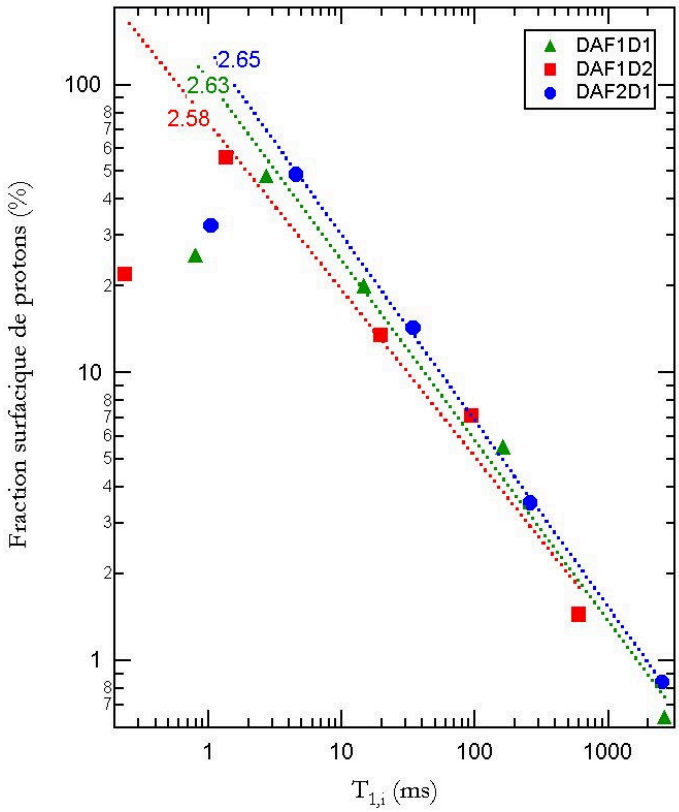

Figure 9. Logarithmic plot of the fraction of proton magnetization as a function of the relaxation time $T_{1,i}$ for UHPC designs. The dotted lines are the best fits obtained with a power law. (from [19])

The order of magnitude of 10 observed in the $T_{1,i}$ is due to frequency scale change. Indeed, the previous curves were obtained at 17.8 kHz while these were obtained at 300 MHz. In accordance to the results, five values are obtained for $T_{1,i}$ at similar ages. In fact, this figure represents the distribution of various "Contin" peaks *associated* with the various T_1. This evidence a power law of 3 to 4 orders of magnitude between the amount of surface protons and the average pore size. This phenomenon is to be related to the expression of total specific surface area $S_{total}(i)$ for each pore category $\langle R \rangle_i$ represented by:

$$S_{total}(i) \propto \langle R \rangle_i^{2-D_f} \qquad (4)$$

where D_f is the fractal dimension of the porous network surface ($2 \leq D_f \leq 3$). This parameter has a value of about 2.6 depending on the mix design, in agreement with those obtained by other techniques [20-23].

The fractal dimension increases significantly from 2.58 to 2.65 with the densification of the matrix by silica fume, a phenomenon which can be correlated to a higher specific surface area and so, potentially, to a higher quantity of hydrates. This observation was corroborated by ^{29}Si NMR experiments. The measurement of the fraction of proton magnetization as a function of T_1 gives us information about texture, i.e. the spatial organization of the material at middle scales, between the nano and mesoporosity [19].

5. CONCLUSION

Nuclear Magnetic Resonance (NMR) is particularly well-adapted to analyze amorphous or poorly crystallised systems. Therefore, it is of great use in the study of construction materials such as cement.

^{29}Si NMR has led to a better understanding of the kinetics of hydration of anhydrous silicates present in clinker. The presence of Q0H monomer species agrees with the reaction mechanisms commonly accepted today. It has also allowed us to better understand the architecture of C-S-H. The research conducted on synthetic C-S-H enriched with ^{29}Si and ^{43}Ca has emphasized the existence of two Q^2 species in C-S-H.

Also, measurements of the relaxation time of protons present in the pores of cementitious matrices provide information on their size distribution. These obey the scaling law on three or four orders of magnitude characteristic of a surface fractal. As well, NMR of protons allows the visualization of the distribution of water or voids in a porous material/system.
The application of magnetic imaging techniques (MRI), already used in porous systems, should bring a better understanding of the structuring mechanisms of cementitious materials during their hydration.

REFERENCES

[1] Engelhardt, G. and Michel, D. High Resolution ^{29}Si NMR of silicates and zeolites**,** New York: Wiley, 1987, p.487.

[2] Lippmaa, E., Mägi, M., Tarmak, M., Wieker, W., Grimmer, A.R. A High Resolution ^{29}Si NMR Study of the Hydration of Tricalciumsilicate, Cement and Concrete Research**,** vol.12, n. 5, 1982, pp.597-602.

[3] Mägi, M., Lippmaa, E., Samoson, A., Engelhardt, G., Grimmer, A.R. Solid-state High-Resolution Silicon-29 Chemical Shifts in Silicates, Journal of Physical Chemistry**,** vol.88, n. 8, 1984, pp.1518-1522.

[4] Rodger, S.A., Groves, G.W., Claydon, N.J., Dobson, C.M. Hydration of Tricalcium Silicate Followed by ^{29}Si NMR with Cross-polarization, Journal of the American Ceramic Society**,** vol.71, n. 2, 1988, pp.91-96.

[5] Rassem, R. NMR contribution to the study of the hydration mechanism of tricalcium silicate (in french), Ph.D. thesis, Université Pierre et Marie Curie, 1990.

[6] Rassem, R., Zanni-Théveneau, H., Schneid, I., Regourd, M. ^{29}Si high-resolution NMR study of tricalcium silicate hydration, Journal Chim. Phys., vol.86, 1989, pp.1253-1264.

[7] Barret, P. and Bertrandiet, D. Fundamental hydration kinetic features of the major cement constituents: tricalcium silicate (Ca_3SiO_5) and beta-dicalcium silicate (β-Ca_2SiO_4), Journal Chim. Phys., vol.83, 1986, pp.765-775.

[8] Masse, S., Zanni, H., Lecourtier, J., Roussel, J.-C. Rivereau, A. ^{29}Si Solid State NMR Study of Tricalcium Silicate and Cement hydration at High Temperature, Cement and Concrete Research, vol.23, n. 5, 1982, pp.1169-1177.

[9] Masse, S. Hydrothermal synthesis of tricalcium silicate hydrates, solid-state structural analysis (in french), Ph.D. thesis, Université Pierre et Marie Curie, 1993.

[10] Dobson, C.M., Goberdhan, D.G.C., Ramsey, J.D.F., Rodger, S.A. ^{29}Si MAS NMR study of the hydration of tricalcium silicate in the presence of finely divided silica, Journal of Materials Science, vol.23, n. 11, 1988, pp.4108-4114.

[11] Beedle, S.S., Groves, G.W., Rodger, S.A. The Effect of Fine Pozzolanic and Other Particles on the Hydration of C_3S, Advances in Cement Research**,** vol.2, n. 5, 1989, pp.3-8.
[12] Jutnes, H., Sellevold, E.J., Lundevall, G. High Strength Concrete Binders. Part A: Reactivity and Composition of Cement Pastes with and without Condensed Silica Fume, 4th CANMET/ACI international conference on the use of fly ash, silica fume, slag and natural pozzolans in concrete**,** Istanbul, Turkey, 1992, pp.873-889.
[13] Zimmermann, J.R. and Brittin, W.E. Nuclear Magnetic Resonance Studies in Multiple-Phase Systems: Lifetime of a Water Molecule in an Adsorbing Phase of Silica Gel, Journal of Physical Chemistry, vol.61, 1957, pp.1328-1333.
[14] Korb, J.-P., Whaley Hodges, M., Gobron, T., Bryant, R.G. Anomalous surface diffusion of water compared to aprotic liquids in nanopores, Physical Review E, vol.60, n. 3, 1999, pp.3097-3106.
[15] Godefroy, S., Korb, J.-P., Fleury, M., Bryant, R.G. Surface nuclear magnetic relaxation and dynamics of water and oil in macroporous media, Physical Review E, vol.64, 2001.
[16] Korb, J.-P., Petit, D., Philippot, S., Zanni, H., Maret, V., Cheyrezy, M. Nuclear relaxation of water confined in reactive powder concrete, 2nd international conference on NMR spectroscopy of cement based materials**,** Bergamo, Italy, 1996, pp.333-343.
[17] Philippot, S., Korb, J.-P., Petit, D., Zanni, H. Analysis of microporosity and Setting of Reactive Powder Concrete by Proton Nuclear Relaxation, Magnetic Resonance Imaging, vol.16, n. 5/6, 1998, pp.515-519.
[18] Vernet, C., Lukasik, J., Prat, E. Nanostructure, porosity, permeability and diffusivity of ultra high performance concretes, International Symposium on HPC and RPC**,** Sherbrooke, Canada, 1998, vol. 3, pp.17-35.
[19] Porteneuve, C. NMR Study of concretes: application to alteration by water (in french), Ph.D. thesis, Université Pierre et Marie Curie, 2001.
[20] Winslow, D.N. The Fractal Nature of the Science of Cement Paste, Cement and Concrete Research**,** vol.15, n. 5, 1985, pp. 817-824.
[21] Allen, A.J., Oberthur, R.C., Paerson, D., Schofield, P., Wilding, C.R. Development of the Fine Porosity and Gel Structure of Hydrating Cement Systems, Philosophical Magazine B, vol.56, n. 3, 1987, pp.263-288.
[22] Blinc, R.G., Lahajnar, G., Zumer, S., Pintar, M.M. NMR Study of the Time Evolution of the Fractal Geometry of Cement Gels, Physical Review B**,** vol.38, n. 4, 1988, pp. 2873-2875.
[23] Lange, D., Jennings, H.M., Shah, S.P. Image Analysis Techniques for Characterization of Pore Structure in Cement-Based Materials, Cement and Concrete Research**,** vol.24, n. 5, 1994, pp. 841-853.

NUCLEAR MAGNETIC RESONANCE SPECTROSCOPY AND SPIN RELAXATION ON CEMENT-BASED MATERIALS – A REVIEW

H. Zanni[1], Ph. Fonollosa[1], F. Méducin[1], C. Porteneuve[1], F. Barberon[2], J.-P. Korb[2] and D. Petit[2]

[1] Laboratoire PMMH, ESPCI, Paris, France. E-mail: zanni@pmmh.espci.fr
[2] Laboratoire PMC, Ecole Polytechnique, Palaiseau, France. E-mail: jpk@pmc.polytechnique.fr

Philippe Fonollosa graduated from the École Nationale des Travaux Publics de l'État (France). He holds a Ph.D. from the University of Sherbrooke (Canada) and the École Supérieure de Physique et de Chimie Industrielles (France), under the supervision of Prof. Aïtcin and Prof. Zanni, respectively.

DEVELOPMENT AND PRODUCTION OF CEMENTS FOR CONCRETE PRODUCTS

Wolfgang Dienemann, Manfred Tax, Gerd Bolte and Jürgen Halm

Managing Director, Heidelberg Cement Technology Center, Pleikartsfoerster Str. 99, 69124 Heidelberg, Germany. E-mail: wolfgang.dienemann@hzag.de
Cement Chemistry, Heidelberg Cement Technology Center, Rohrbacher Str. 95, 69181 Leimen, Germany. E-mail: manfred.tax@hzag.de
Cement Chemistry, Heidelberg Cement Technology Center, Rohrbacher Str. 95, 69181 Leimen, Germany. E-mail: gerd.bolte@hzag.de
Concrete Technology, Heidelberg Cement Technology Center, Oberklamweg 6, 69181 Leimen, Germany. E-mail: juergen.halm@hzag.de

ABSTRACT

In industrialized countries concrete products represent a significant market segment for cement. Requirements as to the characteristics of these products do not only refer to their strength and durability, but also to aesthetic aspects. In this sense, brown discolorations are a quality problem, the reasons for which Heidelberg Cement intensively examined by means of a research project.

The occurrence of brown discoloration, however, is connected to the existence of iron dissolved in the pore solution. Here, an essential contribution is made by clinker mineralization, the alkali content of the pore solution, the Fe (II)-content of cement and additives as well as by the grinding and concrete additives used.

The transport of this solution to the concrete surface is considerably influenced by concrete structure. Therefore, a dense structure must be striven for in order to effectively avoid brown discolorations. This can be achieved by the use of appropriate inter-grinding materials, such as slag, optimized particle-size composition and sufficient hydration of the concrete.

1. MARKET REQUIREMENTS AS TO CEMENTS USED FOR CONCRETE PRODUCTS

In Germany, 48 million tons of concrete products (paving units, pipes, etc.) are produced and sold every year. That means, with more than 15 % of cement used by this sector, the production of concrete products represents a considerable market segment for cement sales in Germany. Also in neighboring European and other developed countries, the share of cement used in this field of application is comparably high.

The specific production process involving highly automated processing of low-slump concrete together with product expectations of end users results thereby in a very specific requirement profile for the binders used. To enable optimized production with regard to economic and process-related aspects, the cement has to show appropriate processing characteristics. Hardening time must be sufficient for processing during standard operations, but also in the case of manufacturing-technical malfunctions. At the same time, the concrete must be sufficiently plastic enough to guarantee appropriate compaction during machine processing. For further treatment, that means piling and taping, a high early strength of the products is an absolute necessity. To achieve durable usage

Proceedings of the 11th International Congress on the Chemistry of Cement (ICCC) 11 - 16 May 2003, Durban, South Africa
'Cement's Contribution to the Development in the 21st Century' ISBN Number: 0-9584085-8-0
Hosted by: The Cement and Concrete Institute of South Africa Editors: Dr G. Grieve and G. Owens
CD-ROM produced by: Document Transformation Technologies Congress Organised by: Event Dynamics

properties, compliance with the corresponding standard requirements is necessary (for example DIN 18501 [1] and draft DIN EN 1338 [2]). That means that a corresponding final strength has to be achieved as well as sufficient resistance to abrasion and frost-thaw corrosion, for example.

Besides these production and usage characteristics, the aesthetic requirements of the end users as to pavement blocks, for example, are gaining more and more importance. The use of concrete products as design elements, for example in gardening and landscape architecture, results in the demand for high and even brilliance of color as well as high resistance to efflorescence and discoloration.

2. DISCOLORATION – CURRENT STATUS

While production and usage properties are reliably achieved by adjusting the corresponding processing and hardening characteristics of cements used for concrete products, sometimes problems arise with efflorescence and discoloration. One reason for complaints are brown discolorations, which can appear at different times after production. Due to the repair work necessary (for example re-installing), these complaints can cause considerable financial loss in addition to the associated loss of reputation.

Figure 1. Brown discoloration

In the literature soluble iron compounds are basically identified as major triggers of brown discoloration, among others in the “VDZ-Mitteilungen” No. 80 [3] and No. 98 [4] as well as in Engelbrechtsen [5] and Häring [6]. If these are dissolved and come to the surface together with the alkali- and calcium-hydroxide-rich pore solution, they oxidize into trivalent iron compounds in the carbonized lime layer and thus cause yellowish to brownish discoloration. Besides others the ferritic clinker phase C_4AF [6], elemental iron originating from grinding abrasion [3], [6], fly ash [5], [8], slag [3] or other concrete admixtures as well as iron-containing aggregates [5], [6] are identified as sources of the iron. Variables influencing the solubility of iron are on one hand represented by the share of bivalent iron, but above all by the alkalinity of the pore solution [6] as well as the grinding aids [4] and concrete admixtures [5] used.

Furthermore, various authors deal with the crystalline structure of concrete, which is responsible for an increased material circulation and thus an increased tendency towards brown discoloration. Correspondingly, according to a study conducted by the FMPA Baden-Württemberg [9], a high capillary porosity is of essential significance for the occurrence of these discolorations. This porosity can considerably be increased by a reduced hydration of cement, resulting from drying-out

too abruptly. A too low cement proportion in coincidence with a high proportion of fine inert materials can also cause an unfavorable shifting in pore size distribution (Häring [7]). The degree of carbonation is also named as a factor having an impact on the potential for discoloration [6].

In summary, it can be stated that relevant literature mentions a multitude of influencing variables without making it possible to derive an assessment of their importance.

3. VARIABLES INFLUENCING THE FORMATION OF BROWN DISCOLORATIONS

Against this background a project was set up in the Heidelberg Cement Technology Center. It was the objective of this project to find possibilities to limit the reasons for the formation of brown discolorations. Proceeding from the results obtained, the cement specific impacts should be eliminated as far as possible and user consulting services tailored to occurring problems should be offered.

The development of an appropriate lab test method for determination of the material potential for discoloration was the first basic step. For this test a porous special mortar is produced, which subsequently hardens in an airtight PE-bag. After hardening the PE-bag is cut several times. Through these openings the pore solution included in the mortar evaporates. Afterwards the dissolved salts remain as white to gray efflorescence at the cuts. Via chromatometry (LAB-system according to CIE) of the discolored as well as of the neighboring non-discolored areas of the cement mortar and subsequent subtraction of the values, the discoloration can be described quantitatively. Decisive for the degree of efflorescence is on one hand the difference of the brightness values ΔL^* as well as of the yellow value Δb^* of the (brown) discoloration.

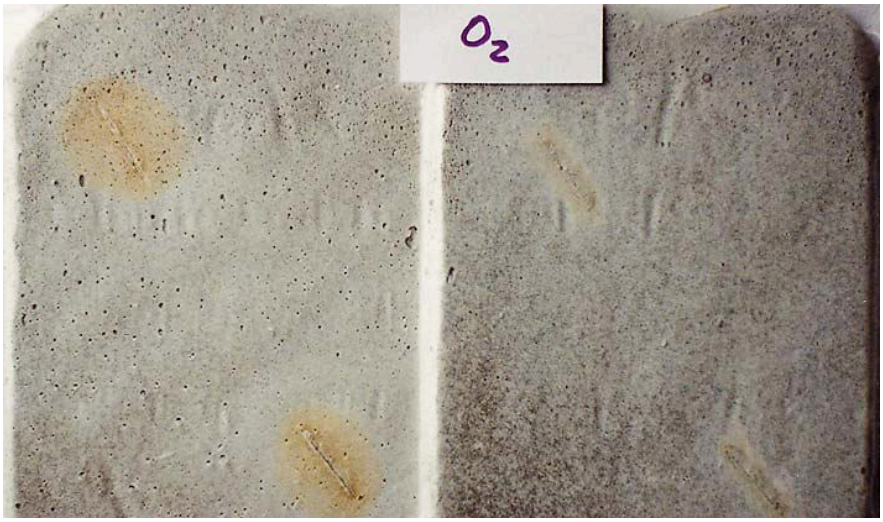

Figure 2. PE-bag test

The suitability of this test method was proven in numerous comparative tests on semi-industrially produced pavement blocks. There it was revealed that binding agents with Δb^* values below 0.3 show no discoloration potential. For Δb^* values between 0.3 and 0.6, slight discolorations can occasionally appear under extreme storing conditions, which result in low hydration levels. This tendency towards brown discoloration continues to increase with rising Δb^*, so that we can talk of a significant discoloration potential for values above approximately 1.0.

The simple test method enabled the analysis of hundreds of samples. Conditions of clinker production and origin, inter-grinding materials and additives, grinding aids and concrete admixtures varied in the course of the test series. In this test method examinations of 31 production clinker

types of one plant and thereof produced lab cements revealed besides others the following correlations as to the yellow value Δb*:

Parameter	SiO_2	Al_2O_3	Fe_2O_3	CaO	K_2O	Na_2O
Correlation coefficient	0.46	0.23	-0.11	-0.51	0.75	0.44

Parameter	CaO_{fr}	KSt	C_3S	C_2S	C_3A	C_4AF
Correlation coefficient	0.84	0.16	-0.81	0.79	0.18	-0.11

The example of this clinker shows the obvious dependence of discoloration tendency on the alkali content and above all on the included proportion of free lime (CaO_{fr}) as well as of alite (C_3S) and belite (C_2S). Supplementary tests with admixtures of quick lime disproved a significant impact of free lime. The latter is rather to be seen as indicator for sufficient mineralization of the clinker. In a similar way clinker and cement types from different plants, different inter-grinding materials and additives were examined. Thus, it could be proven that clinker containing increased amounts of bivalent iron (FeO ≥ 0.04 %) due to reducing burning conditions showed a noticeably higher tendency towards discoloration during the quick test. From the very low absolute FeO-contents in industrial clinker, which lie within traceable limits, mathematical correlations, however, cannot be derived.

From the multitude of individual data the following essential material variables influencing discoloration can be derived with sufficient statistical verification:

- composition of the pore solution regarding alkalinity and Fe^{2+} content
- clinker mineralization – a relatively low C_3S content increases the risk of discoloration
- content of soluble iron compounds in inter-grinding materials and additives
- grinding aids / concrete admixtures, which stimulate the solubility of iron

The material potential is of course not the only factor decisive for the development of brown discoloration. Circulation processes resulting from the pore structure have at least the same impact on their formation. The structure of the hardened cement paste (and of the whole concrete texture), determine the capillarity of the concrete, whereby especially the degree of hydration plays a major role. The impact of this variable was questioned in numerous semi-industrial tests on pavements followed by considerably differing storing conditions and additional tests via mercury intrusion porosimetry. In the course of this testing the substantial impact of curing and storing conditions on the tendency towards brown discolorations could be proven.

The more unfavorable hydration was due to quick drying-out or cold storing, the higher was the potential for discoloration. In contrast, when storing samples at 30°C, for example, and high air humidity they showed a significantly lower discoloration ratio. The semi-industrial block-making machine did not allow for sufficient variation of compression energy, so that influences resulting from that variable have remained unobserved up to now. Nevertheless, the results available allow conclusions to be drawn on how to minimize the danger of brown discolorations.

4. CEMENTS FOR CONCRETE PRODUCTS

Quality assurance in the production of cements for concrete products already starts with the burnout of clinker. A sufficient mineralization degree of the clinker must be taken care of and, at the same time, burning conditions leading to increased formation of bivalent iron are to be avoided.

During the examination, cements containing a high proportion of slag proved to be very favorable. By inter-grinding slag, alkalinity as well as the content of soluble iron is considerably reduced. The impact of the inter-grinding of different amounts of slag on the material's discoloration potential can be seen from figure 3.

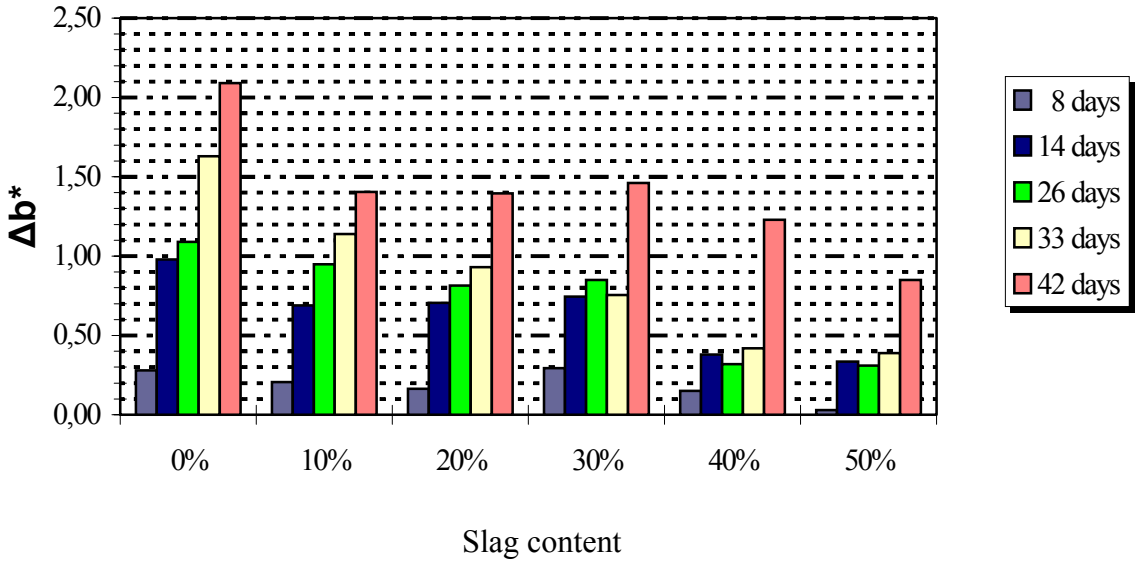

Figure 3. Diagram Δb*-value vs. slag content

The use of slag also results in a more dense structure, so that circulation processes are reduced. However, slag cannot be used unlimitedly due to the accompanying reduction of early strength. That means each plant has to find out individually the appropriate balance between required early strength on one hand and security against discoloration on the other hand. Additionally, grinding aids, which can cause increased solubility of iron, should be avoided.

Besides the traditional test methods included in the tight production control processes additional examinations (for example Fe(II)-content, test for brown discoloration) are useful to guarantee the desired product characteristics. By observing the above-mentioned principles, cement can be produced which is especially suitable for the production of concrete products.

Unfortunately, even such a type of cement does not completely exclude the risk of brown discoloration in case several unfavorable factors accumulate in the production process of concrete products. Therefore, the manufacturers are recommended to comply with some important principles. When selecting aggregates (especially fine additives and fillers) the content of (in alkaline medium) soluble iron must be observed. Thereby it must be considered that partly this solubility can substantially be increased by concrete admixtures [5]; in case of doubt corresponding examinations should be conducted.

Besides the selection of materials to be used in the production of concrete products, also the development of a dense concrete structure must be paid attention to in order to largely eliminate corresponding circulation processes. For this, a sufficient proportion of reactive cement is required in relation to the inert materials, which only contribute a little to developing a dense concrete. Above all, however, appropriate hydration of the cement must be assured, which means concrete products have to be protected against drying too rapidly.

By complying with the abovementioned parameters, the production of high-quality, durable and aesthetically satisfying concrete products is definitely possible.

Figure 4. Concrete pavement

REFERENCES

Standards

[1] DIN 18501, Pflastersteine aus Beton, 11/1982

[2] Draft DIN EN 1338, Pflastersteine aus Beton, 02/1994

Journal articles

[3] VDZ Mitteilungen 80, Braunverfärbungen an der Oberfläche, 09/1989, p. 10

[4] VDZ Mitteilungen 98, Braunverfärbung beschäftigt Forschung, 09/1995, p. 2

[5] J. Engelbrechsen, Flächenhafte braune Verfärbungen an grauen Betonwaren, Betonwerk + Fertigteiltechnik, vol. 2, 1996, p. 70 – 77

[6] Ch. Häring, Gelb-/Braunverfärbungen an Betonfertigteilen, Betonwerk + Fertigteiltechnik, vol. 1, 1997, p. 144 – 148

[7] Ch. Häring, Gelb-/Braunverfärbungen von Betonwaren bleiben aktuell, Betonwerk + Fertigteiltechnik, vol. 1, 2002, p. 66 - 68

Reports with a series number

[8] M. G. Miller, L. J. Powers, P. C. Taylor, Investigation of discoloration of concrete slabs, Portland Cement Association R&D Serial No. 22228, 1999

Unpublished report

[9] FMPA Baden-Württemberg, unpublished test report, 1989

STUDY OF THE INTERACTION BETWEEN THE HYDRATION OF CA AND OF C_3S AT ROOM TEMPERATURE

D. Damidot[1] and A. Rettel[2]

[1] Ecole Normale Supérieure de Cachan, Département de Génie Civil, 61 avenue du Président Wilson, 94235 Cachan Cedex, France. E-mail: damidot@lmt.ens-cachan.fr
[2] DARD Consulting, Dijon, France

ABSTRACT

There exists a strong interaction between the hydration of CA and of C_3S at room temperature. C_3S hydration is strongly delayed by the presence of aluminate ions issued from CA dissolution. On the other hand, CA hydration is progressively accelerated as calcium and hydroxide ions are released by C_3S dissolution. This leads to a complex CA hydration mechanism which displays two kinetic steps. The behavior of CA-C_3S mixtures is very similar to that of HAC-OPC mixtures due to a very close interaction mechanism which indicates that C_3S poisoning by aluminate ions persists even if different hydrates are found by the reaction of gypsum on calcium aluminates.

1. INTRODUCTION

Calcium aluminate cement (HAC) is often used as set accelerator for Portland cement (OPC). It is known that the setting time of calcium aluminate cement and Portland cement mixtures passes through a minimum for weight compositions between 20/80% and 50/50% [1-2]. As a consequence it is difficult to predict the exact composition that will induce the more rapid setting from a Portland cement to another one. The main reason is an imperfect understanding of the hydration behaviour of calcium aluminate cement and Portland cement mixtures. The purpose of this study is to provide new data by investigating well defined systems constituted by pure phases. The CA-C_3S system was first studied because it appears to be the simplest system relevant to HAC-OPC system as the setting time of pastes made by CA-C_3S mixtures also passes by a minimum (Figure 1).

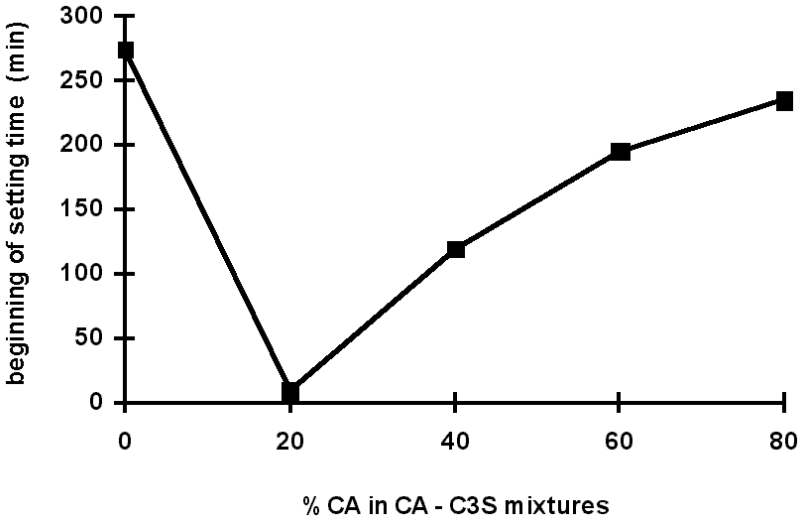

Figure 1: setting time of CA-C_3S mixtures (% in weight) obtained on pastes (W/C=0.4)

2. EXPERIMENTAL

Pure CA and C_3S were laboratory made and the purity was checked by XRD analysis. The mixtures were prepared by mixing the two powders several hours. The proportions in the mixtures are given in weight percent. The fineness was about for 350m^2/kg.

Hydration was followed by isothermal calorimetry on paste having a W/C ratio of 1. The heat flow (ϕ) is related to the rate (V) and the enthalpy (ΔH) of all reactions that occur simultaneously:

$$\Phi = \sum_j V_j \Delta H_j \quad (1)$$

Both the rate and the enthalpy are temperature dependant so the experiments were realized in isothermal condition at 20°C. The enthalpy of reaction is generally quite different between dissolution and precipitation; most of the heat generated during hydration of cement phases is due to the dissolution of the anhydrous phases whereas precipitation from the ions contained in the aqueous phase produced a small amount of heat or even can consume some heat (endothermic reaction).

Electrical conductimetry experiments were also performed on stirred suspensions in a thermoregulated vessel called a chemical reactor (W/C=10). During these experiments, it was possible to recover part of the suspension at different hydration times in order to analyze the aqueous phase composition by ICP-AES and the solids by XRD, DTA and SEM. The electrical conductivity of a solution (Λ) depends on the concentration and the ionic species. One can write in a general way:

$$\Lambda = \sum_i \lambda_i . \gamma_i . C_i \quad (2)$$

λ_i is the equivalent ionic conductivity of ion i and $\gamma_i.C_i$ corresponds to the activity of ion i. These values depend on temperature so the vessel is thermoregulated at 20°C but also stirred in order to reduce, as far as possible, concentration gradients between the surface of solids and the bulk of the solution. As a general rule, electrical conductivity increases with an increase of the ionic concentrations of the solution. Thus periods with an increase in the electrical conductivity correspond to periods where all or part of the ions generated by the dissolution of the solids are stocked in the aqueous phase: precipitation rate lower than dissolution rate and/or some ions are not used in the precipitated solid. On the contrary, a decrease of the electrical conductivity can be associated with a period of strong precipitation of solids. However, some variations of the electrical conductivity can also be induced by the replacement of an ion by another one: λ_i can vary strongly from an ion to the other one.

3. RESULTS AND DISCUSSION

The calorimetric and conductimetric results are presented in order to follow the evolution when an increasing content of C_3S is added to CA (Figures 2 to 4). As the experiments are made with different water to cement ratios, the time is not directly comparable between calorimetric and conductimetric experiments.

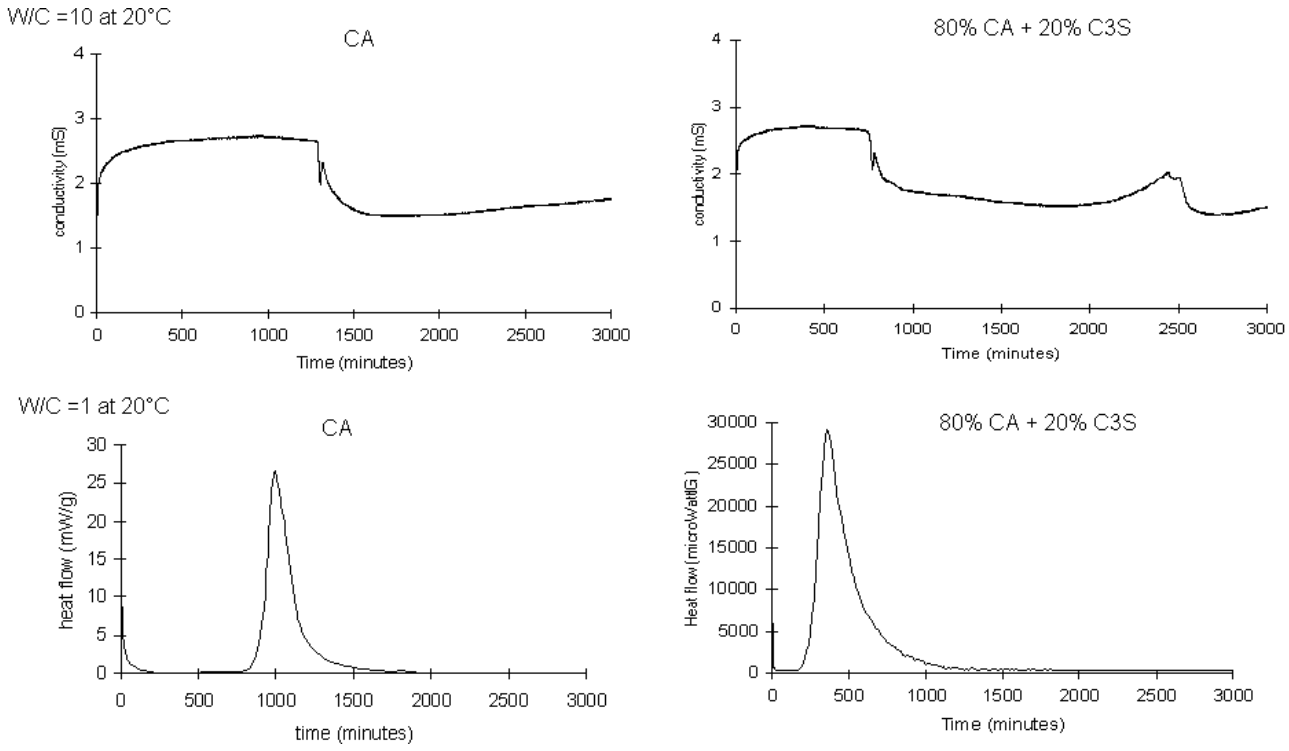

Figure 2: Plots of the rate of heat development and of the electrical conductivity versus hydration time for CA and a mixture containing 80%CA-20%C_3S

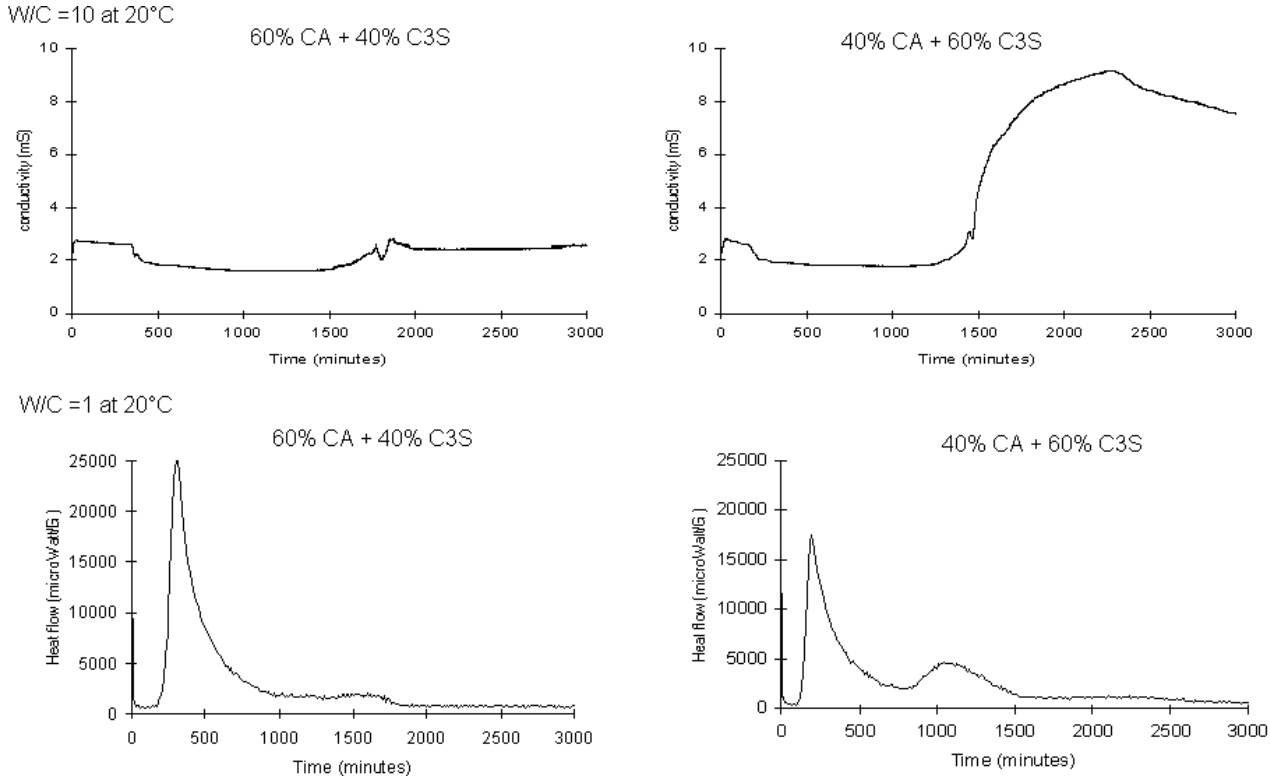

Figure 3: Plots of the rate of heat development and of the electrical conductivity versus hydration time for 60%CA-40%C_3S and 40%CA-60%C_3S

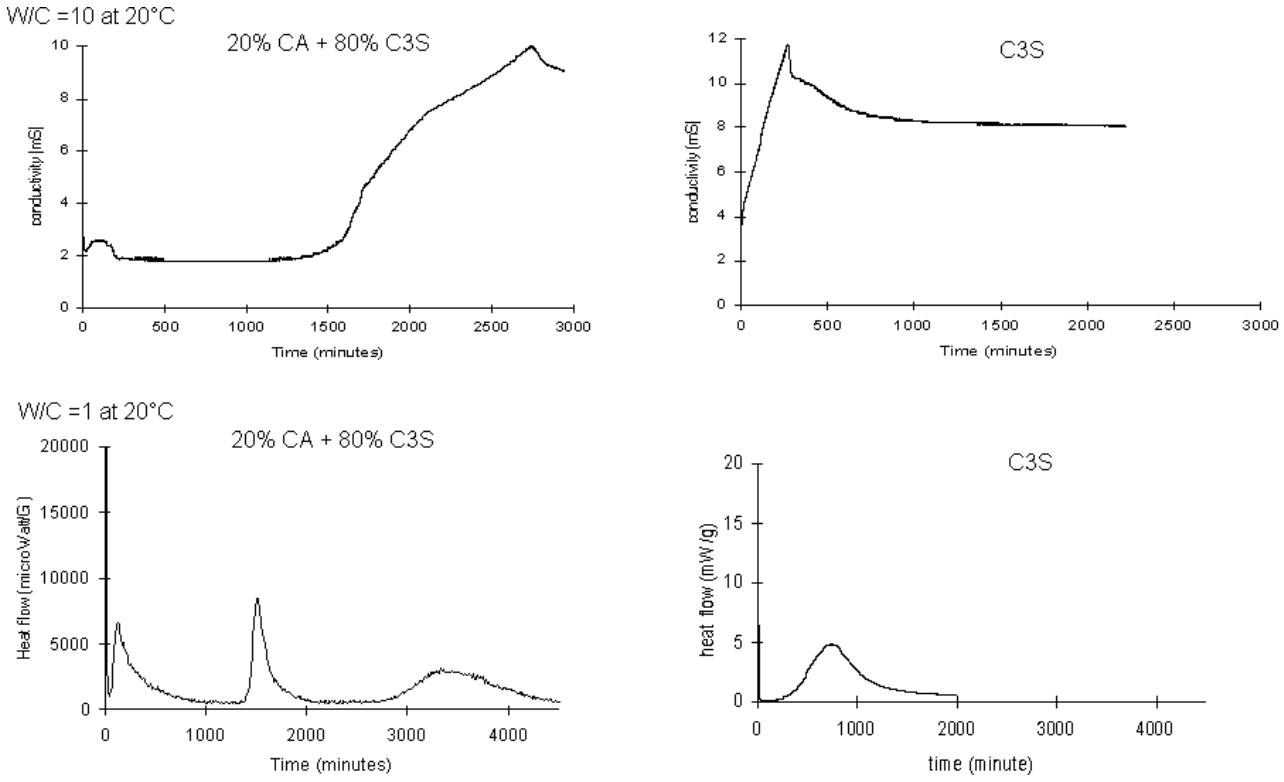

Figure 4: Plots of the rate of heat development and of the electrical conductivity versus hydration time for 20%CA-80%C_3S and C_3S

First of all, the mechanism of hydration of the two end members, CA and C_3S, has to be briefly described. CA hydration is composed of an initial period during which ions are accumulated in the aqueous phase (rise of electrical conductivity). This is associated with a short period of dissolution of CA (initial exothermic peak). Then an induction period is observed (very little heat flow and plateau of electrical conductivity). This period is due to the time needed to nucleate the first hydrates and especially AH_3 [3]. Once critical nuclei have been produced, growth occurs and a period of very rapid precipitation is observed (drop of electrical conductivity). This period is associated with a strong increase of the dissolution rate of CA (second exothermic peak). Then the reaction rate is reduced by the occurrence of several mechanisms such as the covering of CA grains by hydrates and the progressive return to the equilibrium state.

C_3S hydration contains similar periods but their length and time of occurrence are different [4]. The initial dissolution period (initial exothermic peak) is very short as C-S-H(β) is rapidly precipitated. Then a period of slow reaction rate is observed: period of low heat flow and of an increase in the electrical conductivity. This period corresponds to an induction time in order to nucleate C-S-H(γ) and CH. Once growth occurs (drop of electrical conductivity), a strong increase of C_3S dissolution is observed (second exothermic peak). Finally the reaction rate is reduced.

First it appears that the mechanism of hydration of CA-C_3S mixtures is more complex than the simple addition of CA and C_3S hydration: the heat flow curve can display three exothermic peaks in addition to the initial one (20%CA-80%C_3S) whereas only two exothermic peaks were expected.

When passing from pure CA to a mixture containing 80%CA and 20%C_3S (Figure 2), it appears that the period of induction observed during CA hydration, decreases. Only one exothermic peak is observed after the induction period whereas the electrical conductivity shows an additional increase then drop at longer time. For the 60%CA-40%C_3S mixture, the previous trends are amplified and a small second exothermic peak appears (Figure 3). This last exothermic is well observed in the 40%CA-60%C_3S mixture (Figure 3) which also displays a drastic change in the electrical conductivity: the late part of the curve resembles the curve obtained with C_3S (shape and value higher than 9 mS/cm). It can be also noticed that the previously observed rapid drop then increase of the electrical conductivity is still observed (t=1500 minutes) even if less intense. Moreover the plateau in the basal part of the second exothermic peak seems to indicate that a third exothermic peak is present. This last point is confirmed by the mixture 20%-80%C_3S (Figure 4).

From these experiments, it seems that after the initial exothermic peak, the first exothermic peak is associated with CA hydration: as a consequence the rate of CA hydration is accelerated whereas the rate of C_3S hydration is reduced. Complementary experiments have been carried out in order to attribute to C_3S or to CA, the second and the third exothermic peaks.

The analysis of the solids by XRD and of the composition of the aqueous phase, has been performed for mixtures 60%CA-40%C_3S and 40%CA-60%C_3S that delimit an important change in behavior as reported by the electrical conductivity. The evolution of the ([Ca], [Al]) concentration during the hydration, also called the kinetic path, is very similar for the two mixtures[1] (Figures 5 and 6). An initial increase of both [Ca] and [Al] is observed like for pure CA, then both concentrations decrease with a shape which is specific to the following of the maximum supersaturation curve with respect to C_2AH_8, also called curve I [5]. A similar kinetic path was observed previously with mixtures ranging from $C_{12}A_7$ to C_3A [6]. Here the lime enrichment of the aqueous phase due to the hydration of C_3S, has a similar effect to the increase of the C/A ratio in $C_{12}A_7$ or C_3A compared to CA. The higher C_3S contents of the 40%CA-60%C_3S mixture, enable it to reach higher final [Ca] concentration whereas [Al] remains very low: the aqueous phase can become supersaturated with respect to CH and typical features of C_3S hydration are then observed; values of electrical conductivity higher than 7 mS/cm.

As a consequence the hydration process passes progressively from a mechanism close to CA, then to $C_{12}A_7$ and finally to C_3A and C_3A-CH. This progressive change in the hydration process is at the basis of the minimum setting time when the initial hydration mechanism resembles C_3A (average amounts of C_3S) as C_3A rate of hydration is faster than C_3A-CH, $C_{12}A_7$ and than CA.

The important changes that are observed in the aqueous phase can be correlated with the evolution of the solids precipitated from the aqueous phase. During the first exothermic peak, both [Ca] and [Al] are high and the hydrates usually precipitated during CA and $C_{12}A_7$ hydration are found : CAH_{10}, C_2AH_8, AH_3 (amorphous and crystalline). If C-S-H is present, the amount is too low to be detected with our experimental techniques. Then once [Al] concentration remains lower than 1 mmol/l, C_3S hydration tends to accelerate. As a consequence [Ca] increases and all silicate ions liberated by C_3S dissolution are consumed as [Si] remains lower than 20 µmol/l. These changes in the composition of the aqueous phase, induce some modification of the previously formed hydrated which are no longer stable in these conditions. Globally C_2AH_8, CAH_{10} and AH_3 are dissolved and C_2ASH_8, hydrogarnet ($C_3AS_xH_{6-2x}$) and C-S-H are precipitated.

[1] [Si] concentration remains lower than 20µm/l and is not considered here in a first approach.

If [Ca] concentration is high enough, CH forms and C_2ASH_8 should disappear and be transformed into hydrogarnet in these conditions. When equilibrium is reached, the $CaO-Al_2O_3-SiO_2-H_2O$ phase diagram [7] indicates that the solids formed will evolve as a function of the amount of C_3S added between the following invariant points :

- AH_3-C_2ASH_8- C-S-H- aq. phase
- C-S-H -hydrogarnet-C_2ASH_8-aq. phase
- C-S-H -hydrogarnet-CH-aq. phase

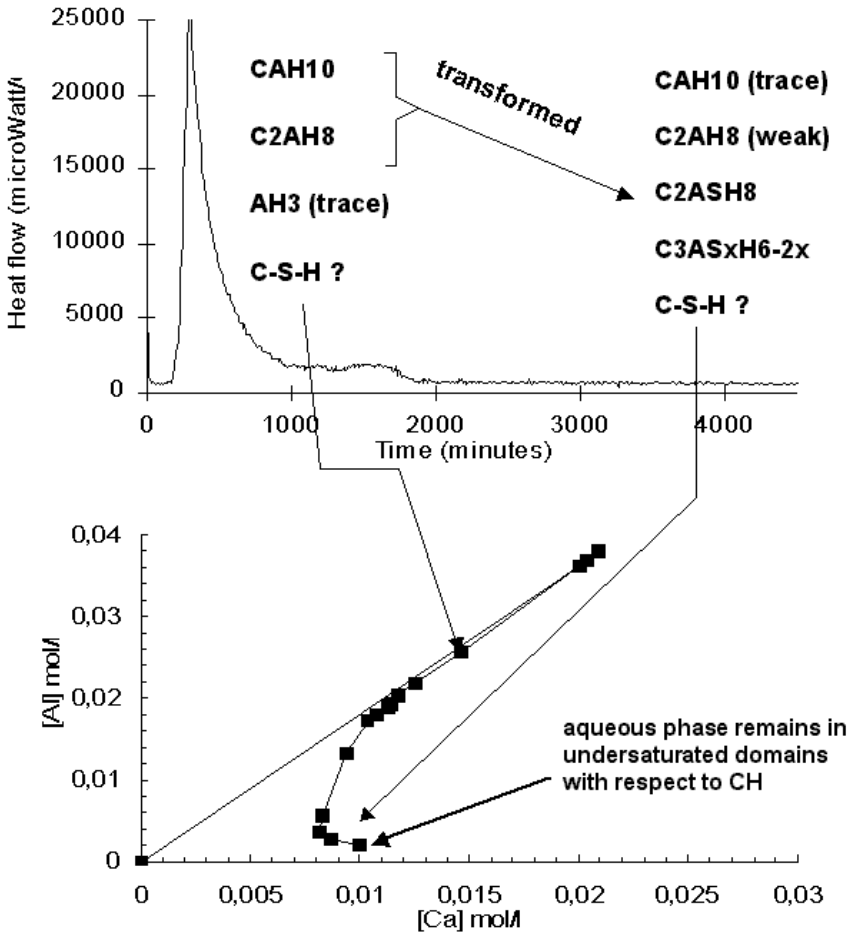

Figure 5: Plots of the rate of heat development versus hydration time for 60%CA-40%C_3S and of the kinetic path (evolution of the ([Ca],[Al]) concentrations during hydration)

C-S-H and CH are observed at the end of the hydration of 40%CA-60%C_3S mixture(Figure 6). Thus the third exothermic peak could be attributed to C_3S hydration. This is confirmed by the 20%CA-80%C_3S mixture (Figure 7); CA is completely consumed after the second exothermic peak while it remains about 80% of C_3S. Then in the presence of C_3S, CA hydration is composed of two exothermic peaks which indicate a more complex hydration mechanism ; CA hydration is firstly accelerated (first exothermic peak) and then delayed (second exothermic peak). Several hypotheses could be made to explain these two kinetic steps. The initial hydrates, C_2AH_8, CAH_{10}, AH_3, are covering the surface of CA particles. This could create a barrier layer and impede further CA hydration while C_3S hydration can become more efficient as the aluminate ion concentration is considerably reduced due to the slowing down of CA hydration. A part of the silicate ions released by C_3S dissolution is used in order to convert the primary hydrates into C_2ASH_8 and hydrogarnets. This may reduce the efficiency of the barrier layer and enable the restart of CA hydration. It can be also considered that an induction period is observed due to difficulties of nucleation of C_2ASH_8 and/or hydrogarnets. This last hypothesis is more flexible and more general. It also accounts for the known difficulties of forming C_3AH_6 or C_2ASH_8 directly from an aqueous phase at 20°C.

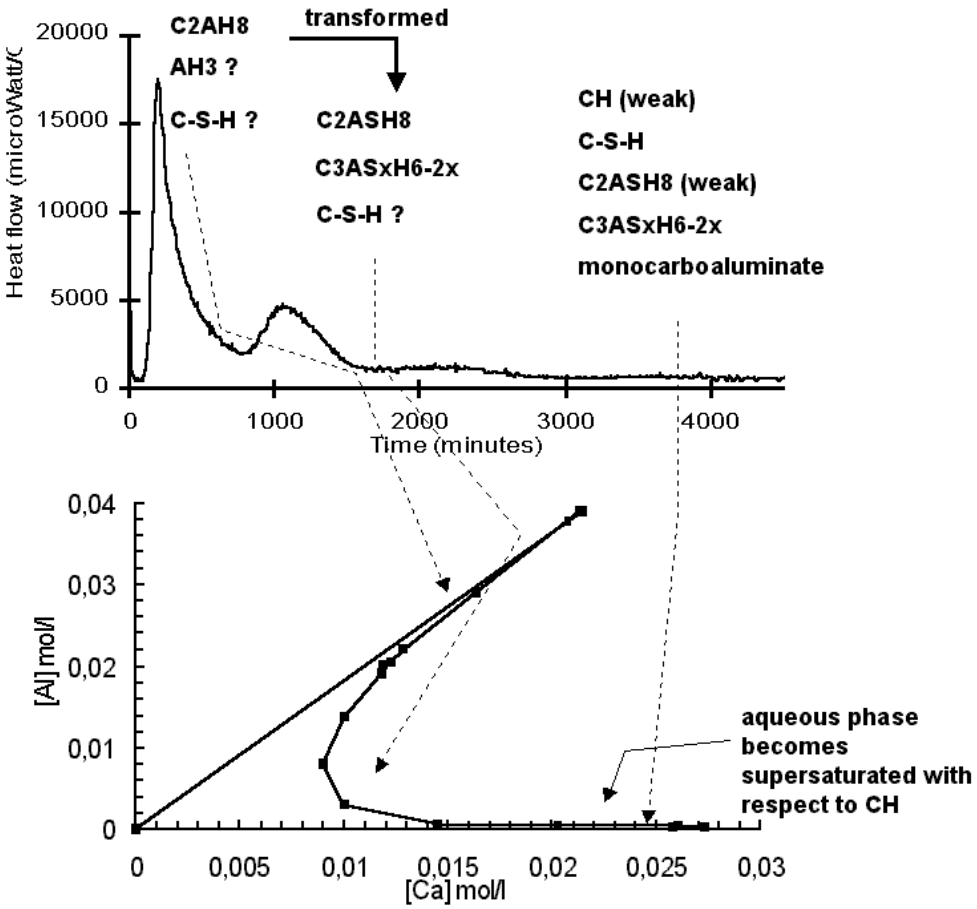

Figure 6: Plots of the rate of heat development versus hydration time for 60%CA-40%C_3S and of the kinetic path (evolution of the ([Ca],[Al]) concentrations during hydration)

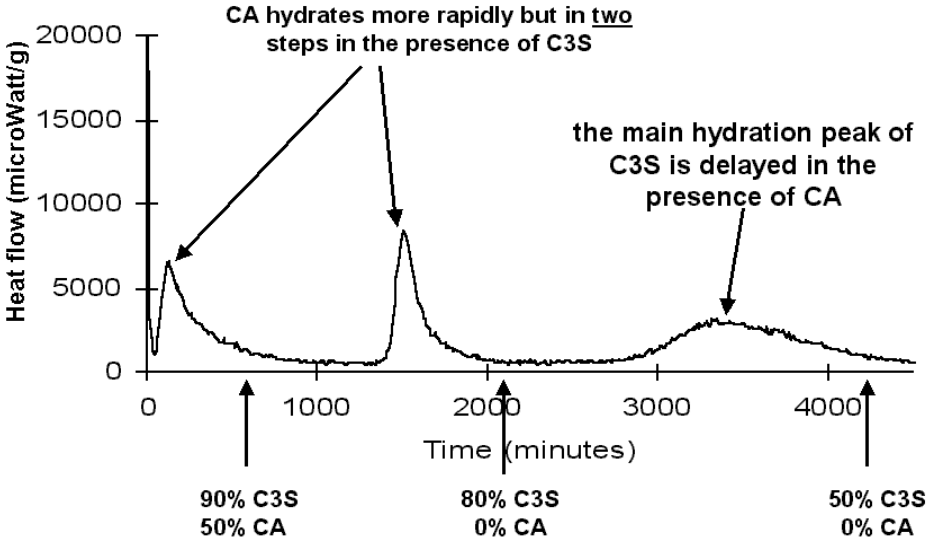

Figure 7: Plots of the rate of heat development versus hydration time for 20%CA-80%C_3S and of the relative percentage of CA and C_3S determined by XRD

Finally the fact that during CA hydration, the [Al] concentration can be much higher compared to C_3A hydration, is an indirect proof of the retardation of C_3S in the presence of aluminate ions. This was assumed by De Jong et al. [8] when these authors studied C_3A-C_3S mixtures and also by Cottin [9]. Aluminate ions retardation can be easily evidenced by hydrating C_3S in a aqueous phase saturated with respect to CA obtained by the filtration of a CA suspension hydrated about 5 hours: [Al] close to 37mmol/l (Figure 8). If the same aqueous phase is diluted by 2, the retardation is less important (Figure 8). The origin of the poisoning of C_3S by aluminate ions is still unclear, but from our experiments it seems that at the beginning of hydration C_3S is able to dissolve and that silicate ions are mostly incorporated in C_2ASH_8 and hydrogarnet. Thus the poisoning effect of aluminate ions would be more effective on C-S-H nuclei than on C_3S dissolution.

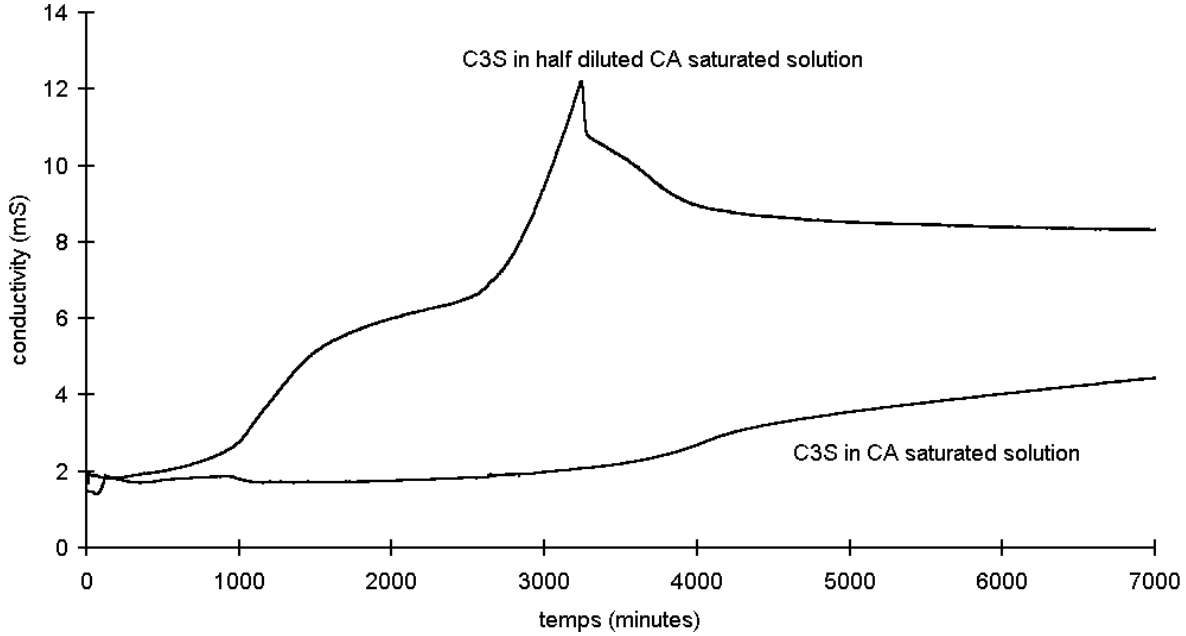

Figure 8: Electrical conductivity recorder during the hydration of C_3S (W/C=20) in saturated or half saturated solution with respect to CA

4. CONCLUSIONS

The hydration mechanism of CA-C_3S mixtures is initially governed by CA hydration : the reaction rate of C_3S is considerably reduced when the aluminate ion concentration in the aqueous phase exceeds 2 mmol/l during the early hydration. This can be associated with the poisoning of C-S-H nuclei by aluminate ions.

With an increasing quantity of C_3S added, CA behaves as $C_{12}A_7$, then as C_3A and finally as C_3A-CH due to greater amounts of calcium and hydroxide ions released by C_3S dissolution. The hydration of CA is accelerated by the presence of C_3S, which is in agreement with the hydration of HAC-OPC mixtures. However CA hydration is decomposed in two kinetic steps which are closely related to the consumption of CA depending on the nucleation and growth rates of the hydrates.

A comparable evolution of the rate of heat development versus hydration time was also previously observed in OPC/HAC mixtures. In this latter system, the main difference concerns the hydrates that are formed with aluminate ion: ettringite and calcium monosulfoaluminate instead of C_2AH_8, C_2ASH_8 and hydrogarnets in CA-C_3S system. But C_3S poisoning still exists as CA-gypsum mixtures can also lead to the accumulation of large quantities of aluminate ions at the beginning of hydration [10].

REFERENCES

[1] Lea, F.M., Desch, C.H., The chemistry of cement and concrete, Chapter XVI: Bulter and Tanner, 1956.

[2] Ping Gu, Yan Fu, Ping Xie and Beaudoin, J.J., Electrochemical behaviour of Portland-cement: high-alumina-cement systems at early hydration times, J. of Mat. Sc. Let., Vol. 12, 1993, pp. 1771.

[3] Damidot, D., Rettel, A. and Capmas, A., Action of admixtures on Fondu cement. I. Lithium salts compared to sodium salts, Advances in Cement Research, Vol.8(31), 1996, pp.111.

[4] Damidot, D. and Nonat, A., C_3S hydration in diluted and stirred suspension: (I) Study of the two kinetic steps, Advances in Cement Research, vol.6(21), 1994, pp.27-35.

[5] Damidot D., and Barret, P., Calculation of the maximum supersaturation curve of C2AH8 in the $CaO-Al_2O_3-H_2O$ system at 20°C, 10th Int. Symposium on the Chemistry of Cement, Goteborg, 1997, 2ii024, 8 pages.

[6] Damidot, D. and Sorrentino, F., Modification of the hydration process from $C_{12}A_7$ to C_3A at 20°C, 10th Int. Symposium on the Chemistry of Cement, Goteborg, 1997, 2ii025, 8 pages.

[7] Damidot, D. and Glasser F.PG., Investigation of the $CaO-Al_2O_3-SiO_2-H_2O$ system at 25°C by thermodynamic calculations, Cem. Conc. Res., vol.25(1), 1995, pp.22-28.

[8] De Jong, J. G. M., Stein, H. N. and Stevels, J. M., Mutual interaction of C_3A and C_3S during hydration, 5th Int. Symposium on the Chemistry of Cement, Tokyo, 1968, vol.2, pp.311.

[9] Cottin, B.F., Hydration of calcium silicates and aluminates mixes, 7th Int. Symposium on the Chemistry of Cement, Paris, 1980, vol.3, pp.V-113.

[10] Damidot, D. and Rettel, A. 'Effect of gypsum on CA and $C_{12}A_7$ hydration at room temperature' submitted to 11th Int. Symposium on the Chemistry of Cement, Durban, 2003.

STUDY OF THE INTERACTION BETWEEN THE HYDRATION OF CA AND OF C_3S AT ROOM TEMPERATURE

D. Damidot[1] and A. Rettel[2]

[1] Ecole Normale Supérieure de Cachan, Département de Génie Civil, 61 avenue du Président Wilson, 94235 Cachan Cedex, France. E-mail: damidot@lmt.ens-cachan.fr
[2] DARD Consulting, Dijon, France

Denis Damidot received his B.Sc., M.Sc., and PhD. in physico-chemistry from Burgundy University, France. His thesis research was based on the study of C_3S hydration. Then he obtained an European Community research grant and worked as a post doc fellow at the Department of Chemistry of the University of Aberdeen, Scotland, on the calculation of phase diagrams used to estimate the durability of cement based materials. He joined the Central Research Laboratory of Lafarge in 1993 and worked for 6 years on special cements and on durability. He is currently Professor in the Civil Engineering Department of Ecole Normale Supérieure, in Cachan (suburb of Paris), France. He carries out research on the relationships between the microstructure and the macroscopic properties and on durability of cement based materials.

EFFECT OF GYPSUM ON CA AND $C_{12}A_7$ HYDRATION AT ROOM TEMPERATURE

D. Damidot[1] and A. Rettel[2]

[1] Ecole Normale Supérieure de Cachan, Département de Génie Civil, 61 avenue du Président Wilson, 94235 Cachan Cedex, France. E-mail: damidot@lmt.ens-cachan.fr
[2] DARD Consulting, Dijon, France

ABSTRACT

Gypsum has a strong influence on CA hydration that is initially accelerated due to the rapid precipitation of ettringite. However it appears to remain an induction period governed by the rate of AH_3 nucleation, before a period of rapid reaction rate. As a consequence, admixtures usually used to accelerate or retard CA hydration, have similar effects in the presence of gypsum. During the last period, CA and gypsum can be completely consumed, but also calcium monosulfoaluminate can be formed in the place of ettringite, depending on the gypsum/CA molar ratio of the mixture studied. The effect of gypsum on $C_{12}A_7$ is similar to the one observed with CA.

1. INTRODUCTION

The effect of gypsum has been studied mostly on the hydration of C_3S and of C_3A due to its relevance to portland cement hydration [1-10]. The hydration of C_3A in the presence of gypsum, displays several periods and usually ettringite formed at the hydration beginning, is transformed into calcium monosulfoaluminate depending on the gypsum/C_3A molar ratio. However all the authors do not agree on the explanation of the mechanism involved in these periods. To the contrary, a systematic study of the effect of gypsum on CA and $C_{12}A_7$ hydration does not exist despite its importance in mixtures containing OPC and HAC. An initial study on mixtures of Ciment Fondu Lafarge and calcium sulphate [11] reported the formation of calcium monosulfoaluminate and/or ettringite depending on the amount of calcium sulphate, instead of the usual calcium aluminate hydrates. Thus some similarities with C_3A-gypsum hydration should exist even if the aqueous phase composition is richer in [Ca] and poorer in [Al] during C_3A hydration compared to the hydration of CA and of $C_{12}A_7$.

2. EXPERIMENTAL

Pure CA and $C_{12}A_7$ were laboratory made and the purity was checked by XRD analysis. Mixtures of different ratios of CA (or $C_{12}A_7$) and gypsum (given in weight percent) were prepared by mixing defined amounts of CA (or $C_{12}A_7$) and gypsum in order to have a lack (under-stoichiometric mixtures) then an excess (over-stoichiometric mixtures) of gypsum with regard to the following equations (Table 1) :

$$3\ CA + 3\ CaSO_4.2H_2O + 32\ H_2O \Rightarrow C_3A.3CaSO_4.32H_2O + 2\ AH_3 \quad (1)$$

$$C_{12}A_7 + 12\ CaSO_4.2H_2O + 113\ H_2O \Rightarrow 4\ C_3A.3CaSO_4.32H_2O + 3\ AH_3 \quad (2)$$

The hydration of these mixtures was followed by isothermal calorimetry at 20°C with a water to solid ratio (W/S) of 0.6 (paste). The hydration was also investigated in stirred and diluted suspensions (W/S=10) by recording the electrical conductivity at 20°C. During these experiments, it was possible to recover part of the suspension at different hydration times in order to analyze the aqueous phase composition by ICP-AES and the solids by XRD, DTA and SEM.

Table 1. Composition of the mixtures studied

Mixture Number	CA weight %	$C_{12}A_7$ weight %	Gypsum weight %	Gypsum / CA molar	Gypsum / $C_{12}A_7$ molar	Type of mixture
1	90		10	0,10		Under-stoichio.
2	80		20	0,23		Under-stoichio.
3	70		30	0,39		Under-stoichio.
4	50		50	0,92		Under-stoichio.
5	48		52	1,00		Stoechiometric
6	45		55	1,12		Over-stoichio.
7	42		58	1,27		Over-stoichio.
8		70	30		3,45	Under-stoichio.
9		30	70		18,80	Over-stoichio.

3. RESULTS

The calorimetric experiments indicate that the hydration of CA is markedly modified by the addition of gypsum (figure 1). Compared to CA, the initial exothermic peak is stronger but the main difference concerns the major heat release that always appears earlier and is composed of two peaks. However, there still exists a period of low heat flow between the initial exothermic peak and the major heat release but here, contrary to CA, the heat flow is not nil and indicates a moderate reaction rate. Globally the presence of gypsum accelerates CA hydration.

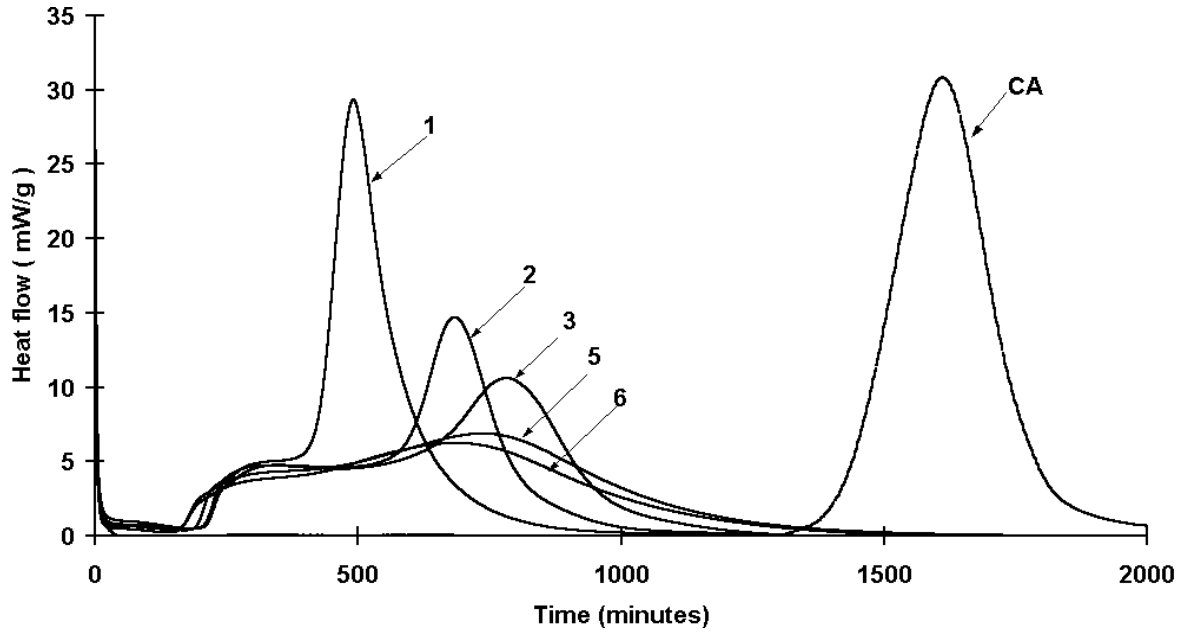

Figure 1. Plots of the rate of heat development versus hydration time for CA-gypsum pastes (W/C=0.6)

It is interesting to note that the heat flow curves are similar for all mixtures up to 400 minutes. Thus the hydration mechanism is similar up to that time. Then the second exothermic of the major heat release appears sooner and is more intense for the mixtures that are poorer in gypsum. However this peak is also observed for the over-stoichiometric mixture and thus it cannot be associated with changes in the hydration mechanism due to the total consumption of gypsum.

The analysis by XRD of the solids collected during the hydration of the stoichiometric mixture (N°5) indicates the following trends:

- a small quantity of ettringite is observed before the major heat release. Then the ettringite quantity is strongly increased during the two next exothermic peaks whereas both CA and gypsum amounts decrease markedly,
- the hydration is not completed at the end of the second exothermic peak.

For mixture N°1 (under-stoichiometric), gypsum is no longer detected by XRD at the end of the first exothermic peak during the major heat release. A decrease in the quantity of CA and of ettringite is observed during the second exothermic peak. A small quantity of calcium monosulfoaluminate is also detected at this time.

The evolution of electrical conductivity obtained on mixtures hydrated in diluted and stirred suspension brings additional information (figure 2).

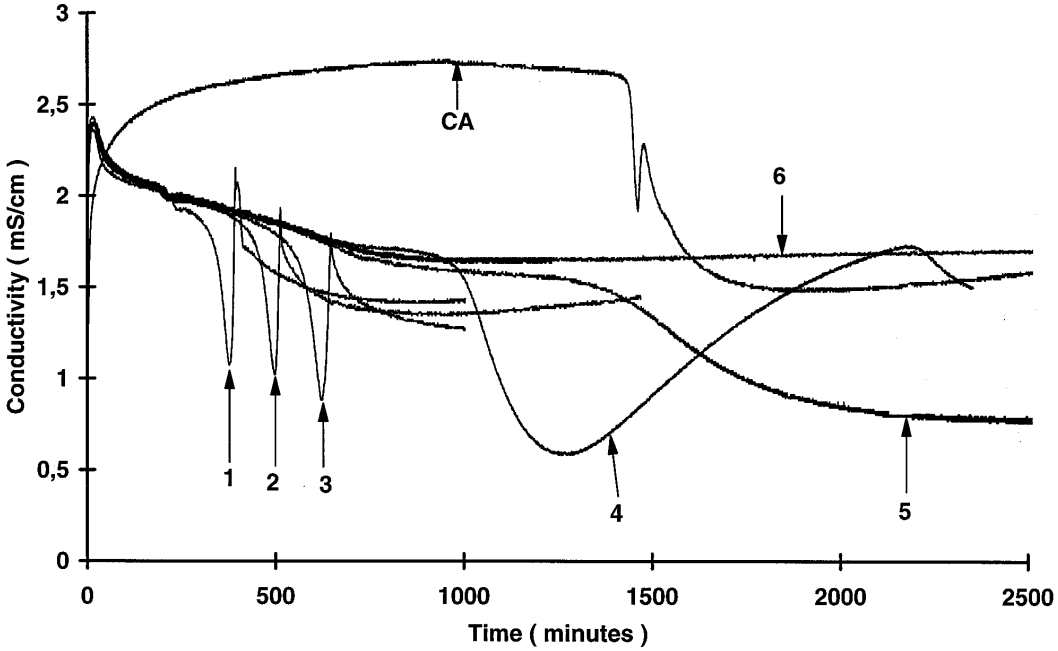

Figure 2. Plots of the electrical conductivity versus hydration time for CA-gypsum pastes (W/C=10)

There are three types of curves for the electrical conductivity which correspond to under-stoichiometric (N°1 to 4), stoichiometric (N° 5) and over-stoichiometric mixtures (N°6), respectively. All the mixtures produce the same conductimetric curve from the beginning of hydration until 220 minutes; a similar observation has been made on paste during calorimetric experiments, but over a different period of time due to the different W/C. The differentiation of the conductimetric curves indicates that the hydration mechanism evolves with an increasing amount of gypsum. Globally gypsum accelerates markedly the hydration of CA in diluted suspension as observed previously in paste by calorimetry.

At the beginning of hydration the conductivity increases more rapidly than during the hydration of CA: the rate of gypsum dissolution is then faster than the rate of CA dissolution. The period of increase of the electrical conductivity, is rapidly finished as the maximum conductivity is obtained after 15 minutes. Then the conductivity decreases and presents a small drop at about 220 minutes. During this period, the small decrease of the electrical conductivity is expected to be associated with a moderated precipitation of hydrates from the ions accumulated in the aqueous phase.

The shape of the electrical conductivity curve at the beginning of the hydration of CA in the presence of gypsum, is very similar to that observed for $C_{12}A_7$ hydrated in water (Figure 4.). This confirms the hypothesis of a rapid precipitation of hydrates in small quantities, followed by an induction period and then an acceleration of both dissolution and precipitation rates [12]. However this last period is more complex in the case of CA-gypsum mixtures. The electrical conductivity falls rapidly for under-stoichiometric mixtures (1,2 and 3), then increases quasi vertically and finally decreases again. This kind of pattern is common and indicates a strong competition between precipitation of the hydrates (decrease of electrical conductivity) and dissolution of the anhydrous solids (increase of conductivity). It is observed for CA hydrated in water (Figure 1) but its intensity is greater in the presence of gypsum. The last under-stoichiometric mixture (N°4) displays the same characteristics, but over a longer period of time indicating a slower kinetics. The stoichiometric mixture (N°5) does not present an increase of the electrical conductivity after the first drop, whereas the over-stoichiometric mixture (N°6) only shows a slight decrease of the electrical conductivity followed by a plateau.

Finally the electrical conductivity remains almost constant but at different values indicating different compositions of the aqueous phase. The analysis of the aqueous phase (Table 2) evidences the presence of:

- calcium and aluminate ions for under-stoichiometric mixtures whereas sulfate ions are under the limit of detection (25 µmol/l),
- calcium, aluminate, and sulfate ions for the stoichiometric mixture,
- calcium and sulfate ions for the over-stoichiometric mixture whereas aluminate ions are under the limit of detection (50 µmol/l). The concentrations of calcium and sulfate found, 15.63 and 15.6 mmol/l respectively, indicate that the aqueous phase is in equilibrium with the remaining gypsum.

Table 2. Composition of the aqueous phase at the end of the suspension experiments

Mixture number	[Ca] mml/l	[Al] mmol/l	[SO_4] mmol/l
1	6,52	9,14	< DL
2	5,96	7,50	< DL
3	5,71	8,32	< DL
4	4,88	3,62	< DL
5	9,50	3,62	4,69
6	15,63	< DL	15,60

The analysis of solids recovered with the analyzed aqueous phase, has been made by XRD. CA has been completely consumed and also gypsum except in the case of the over-stoichiometric mixture. Calcium monosulfoaluminate and ettringite are the main hydrates which are present. AH_3 is mainly in a not very well crystallized state and is better detected by DTA.

If we consider the composition of the aqueous phase and the identified solids, it appears that both under-stoichiometric and over-stoichiometric mixtures are not far from the equilibrium states even if those can be metastable. Indeed, if the aqueous phase in equilibrium with the hydrates found experimentally is calculated at 25°C, the compositions are comparable to those obtained experimentally :

- under-stoichiometric mixtures contain, $AH_{3\ (gel\ form)}$- calcium monosulphoaluminate - ettringite in equilibrium with the aqueous phase. The composition calculated at this invariant point is [Ca] = 5.06 mM/l, [Al] = 2.30 mM/l, [SO_4] = 0.006 mM /l and pH=11.81.
- over-stoichiometric mixtures contain, $AH_{3\ (gel\ form)}$ -ettringite - gypsum in equilibrium with the aqueous phase. The composition calculated at this invariant point is [Ca] = 15.3mM/l, [Al] = 0.03mM/l, [SO_4] = 15.2 mM/l and pH= 9.92.

The stoichiometric mixture that contains $AH_{3\ (gel\ form)}$ and ettringite, leads to aqueous phase compositions between these of the under and over-stoichiometric mixtures.

The semi-quantitative amounts of ettringite and calcium monosulfoaluminate produced at the end of the hydration of the different mixtures are presented in figure 3. Both calcium monosulfoaluminate and ettringite pass through a maximum but for different gypsum amounts. The maximum quantity of calcium monosulfoaluminate is observed for mixture having 20% by weight of gypsum whereas the maximum of ettringite is found for the stoichiometric mixture.

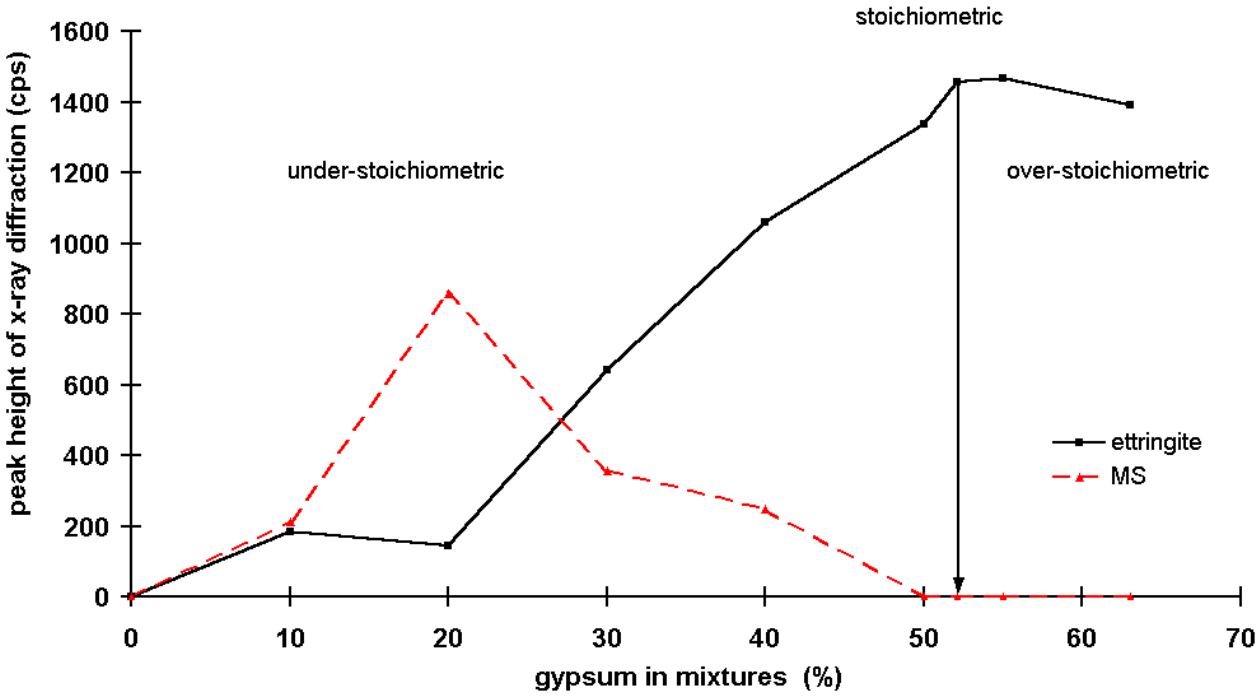

Figure 3. Semi quantitative amounts of ettringite and calcium monosulfoaluminate formed at the end of the conductimetric experiments

The main trends induced by the presence of gypsum on CA hydration are also found for $C_{12}A_7$ (figure 4). The hydration rate is increased at the hydration beginning as the electrical conductivity decreases rapidly till the beginning and all mixtures follow the same curve. Then under-stoichiometric mixtures present a period of very rapid drop and rise of the electrical conductivity, followed by a slower decrease, whereas over-stoichiometric mixtures just displays a slow decrease of the electrical conductivity.

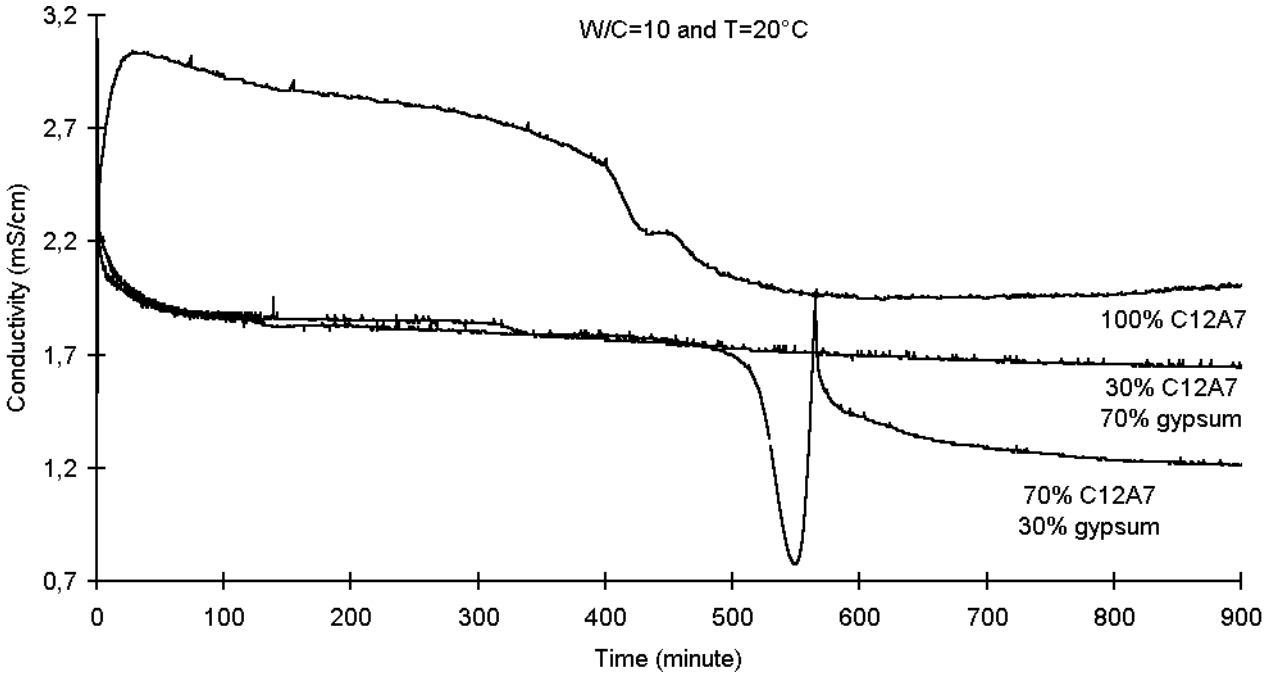

Figure 4. Plots of the electrical conductivity versus hydration time for $C_{12}A_7$-gypsum pastes (W/C=10)

4. DISCUSSION

The addition of gypsum to CA modifies strongly the hydration mechanism:

- ettringite and/or calcium monosulfoaluminate and AH_3 are formed,
- the overall kinetics is accelerated.

Globally the increase of the hydration rate is firstly due to a reduction of the induction period governed by the nucleation-growth of the hydrates. Contrary to CA, small amounts of ettringite and of AH_3 are precipitated till the beginning of this period. As a consequence, this period is shorter than during CA hydration where no hydrates are precipitated till the beginning of this period. With this respect, the beginning of the hydration of CA-gypsum mixtures resembles to $C_{12}A_7$ hydration in water. Consequently the addition of gypsum to $C_{12}A_7$, has a less intense effect on the beginning of $C_{12}A_7$ hydration ; ettringite is formed in place of C_2AH_8. However the quantity of AH_3 formed by the hydration of $C_{12}A_7$ in the presence of gypsum (eq. 2) is 3 times than that formed by $C_{12}A_7$ hydrated in water (eq. 3) :

$$C_{12}A_7 + 51\ H_2O \Rightarrow 6\ C_2AH_8 + AH_3 \qquad (3)$$

This explains the higher reaction rate during the induction period for $C_{12}A_7$ hydrated in the presence of gypsum compared to water hydration. Indeed, the reaction rate during the induction period is higher with higher amounts of AH_3 precipitated as these act as seeds.

In order to investigate further the control of the induction period by the rate of nucleation of AH_3, CA-gypsum mixtures have been hydrated in the presence of additives that are known to favor or reduce the nucleation rate of AH_3. First, lithium ions which accelerate AH_3 nucleation [13] have been added in the form of Li_2CO_3. As expected, the induction period observed at the beginning of CA-gypsum mixtures is all the more decreased with increasing Li_2CO_3 amounts (Figure 5); it even disappears if the amount of Li_2CO_3 is high enough (0,05 % by weight in our experiments). On the other hand, the duration of the major heat release is globally not modified even if the intensity of

the last peak is reduced with respect to the reference mix. As a consequence, it seems that lithium ions have no influence on the nucleation of both ettringite and calcium monosulfoaluminate.

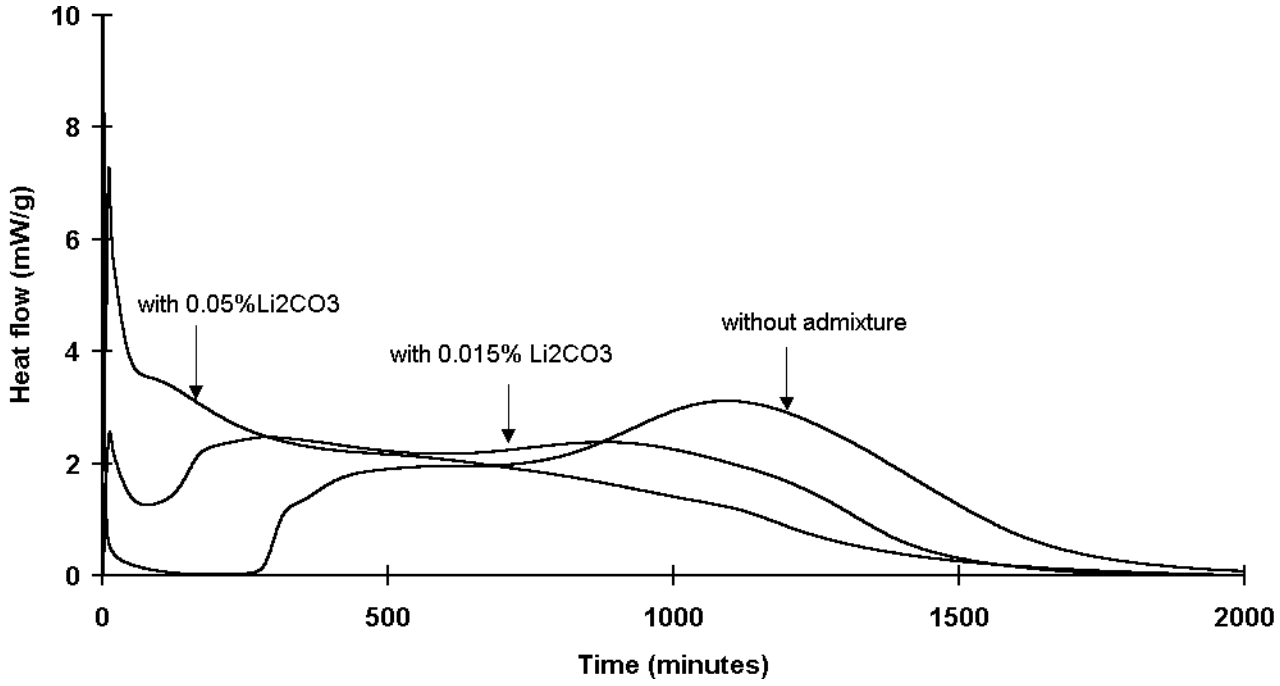

Figure 5. Plots of the rate of heat development versus hydration time for mixture N°7 hydrated in the presence of Li_2CO_3 (W/C=0.6)

Second, citrate ions that retard AH_3 nucleation [13], have been added in the form of trisodium citrate. The presence of citrate ions induces a longer induction period during the hydration of CA-gypsum mixture (Figure 6). Also it seems that citrate ions have an influence on the nucleation rate of the other hydrates as the major heat release appears over a longer period and is less intense.

Another important feature is the mechanism involved during the major heat release that contains two exothermic peaks. This indicates two periods of intense dissolution of CA and it appears that CA is more rapidly consumed when calcium monosulfaluminate forms. However these two periods are always observed even in the case of over-stoichiometric mixtures where only ettringite is formed in all periods. Thus it is not possible to just consider that;

- the reduction of the rate between the two exothermic peaks is due to the formation of an hydrate layer of ettringite,
- the starting up of the hydration is due to the partial or complete transformation of this hydrate layer.

The reaction rate is also governed by the consumption of CA which in this period mainly depends on the growth of the previously formed hydrate nuclei. During the first exothermic peak of the major heat release, nucleation and growth of both ettringite and AH_3 induce a strong consumption of CA.

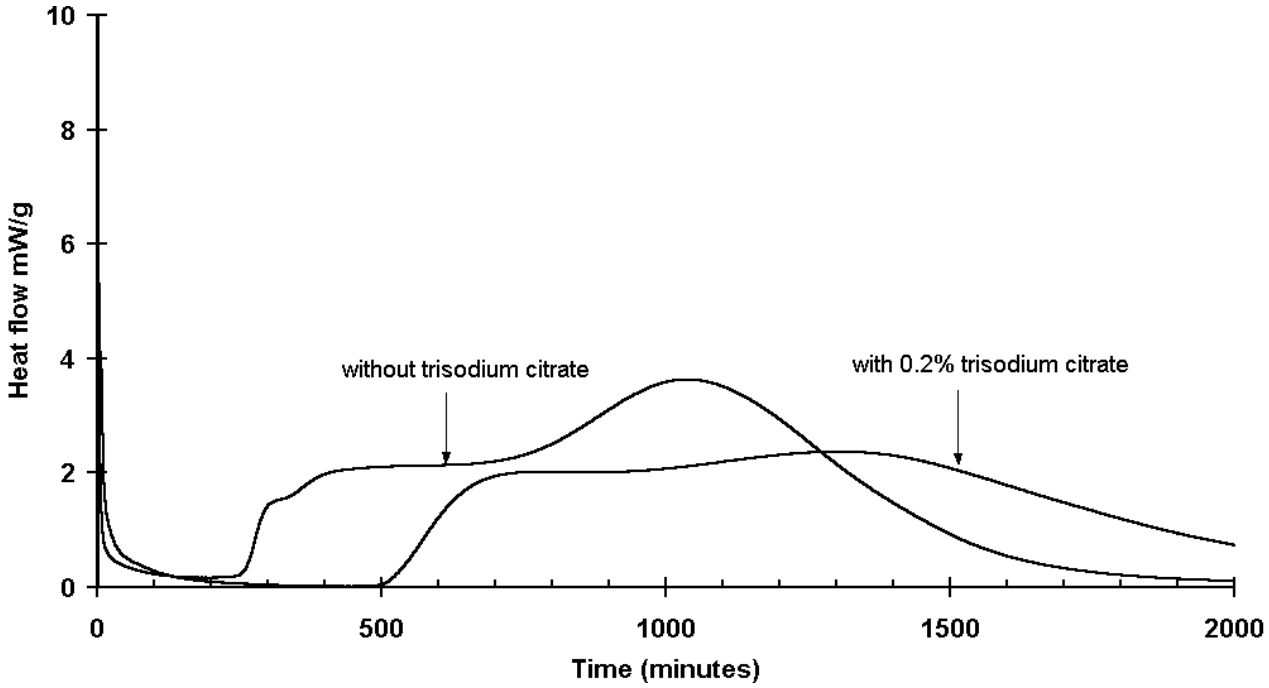

Figure 6. Plots of the rate of heat development versus hydration time for mixture N°7 hydrated in the presence of trisodium citrate (W/C=0.6)

Then depending on the gypsum content different mechanism can occur. For over-stoichiometric mixtures, the ettringite crystals are growing (no more nucleation) from an aqueous phase which has a low pH (about 10 close to the invariant point gypsum-ettringite-AH_3); in these conditions big ettringite crystals are grown (longer than 10 μm) from the ettringite nuclei and smaller crystals dissolve to form bigger one (Ostwald ripening). CA consumption rate is moderate so the second exothermic peak is large and averagely intense. For under-stoichiometric mixtures, the pH is higher (about 12 close to the invariant point calcium monosulfoaluminate-ettringite-gypsum). In these latter conditions, the average crystal size of ettringite is smaller and as a consequence the growth of ettringite crystal is less than in overstoichiometric mixtures but nuclei are more numerous. However an additional nucleation and growth process, that of calcium monosulfoaluminate, appears when the sulfate ions concentration is close to 10μmol/l. As a result, CA consumption is strongly increased in order to nucleate and growth calcium monosulfoaluminate crystals directly from sulfate ions contained in solution that may come from gypsum or ettringite dissolution. In this latter case, some supplementary AH_3 is produced (eq. 4) ;

$$6\ CA + C_3A.3CaSO_4.32H_2O + 16H_2O \Rightarrow 3\ C_3A.\ CaSO_4.12H_2O + 4\ AH_3 \qquad (4)$$

Thus the second exothermic peak lasts over a shorter period and is more intense for under-stoichiometric mixtures.

The presence of two exothermic peaks during the major heat release was also observed for C_3A - gypsum mixtures. Like CA-gypsum mixtures, the appearance of the second exothermic peak and its intensity vary with the content of gypsum; it appears sooner and is more intense with lower gypsum contents. In the same manner, ettringite is partly or completely transformed in calcium monosulfoaluminate for under-stoichiometric mixtures. It has been often hypothesized that the acceleration of the reaction rate during the second exothermic peak observed in C_3A-gypsum mixtures, corresponds to the destruction of an hydrate layer formed by ettringite during the early hydration thanks to the transformation of ettringite in calcium monosulfoaluminate. This may only be part of the answer, if we consider the previously reported experiments on CA-gypsum and the

similarities with $C_{12}A_7$-gypsum and C_3A-gypsum systems: it seems possible to consider the influence of nucleation and growth rates on CA, $C_{12}A_7$ or C_3A dissolution rate in order to explain the general mechanism involved during the hydration of these mixtures. The presence of CH added to C_3A-gypsum system in order to reach the high pH region of the $CaO-Al_2O_3-CaSO_4-H_2O$ phase diagram should not change markedly the hydration mechanism even if the variation of pH between under and over-stoichiometric mixtures is very weak (pH =12,52 at invariant point CH-ettringite-gypsum and 12,49 at invariant point CH-ettringite-monosulfoaluminate). This last point needs to be experimentally confirmed such as the action of C_3S and these systems, knowing that the release of aluminate ions by CA, $C_{12}A_7$ or C_3A hydration in the presence or not of gypsum will retard C_3S hydration as demonstrated in the study of CA-C_3S system [14].

5. CONCLUSIONS

The hydration mechanism of CA - gypsum mixtures can be described by three periods :

a) an initial period during which :
   - gypsum dissolves rapidly to reach the gypsum solubility,
   - CA dissolves moderately and small quantities of ettringite and AH_3 are formed

b) an induction period controlled by the nucleation and growth of AH_3 during which small amounts of ettringite and $AH_{3\ (gel\ form)}$ are precipitated. The duration of this period is independent on the quantity of gypsum in the mixtures.

c) a period of massive precipitation of the hydrates during which most of CA and gypsum are consumed in order to form :
   - calcium monosulfoaluminate, ettringite and AH_3 for under-stoichiometric mixtures,
   - ettringite and AH_3 for stoichiometric and over-stoichiometric mixtures.

   As in the hydration of C_3A-gypsum mixtures, the hydration rate in this last period, is divided in two exothermic peaks and is more rapid for under-stoichiometric mixtures for which ettringite is partially or completely transformed into calcium monosulfoaluminate. Thus, a hypothesis similar to that made for C_3A-gypsum mixtures, such as the formation and then the destruction of a protective layer, could be used to explain the appearance of these two peaks. From our point of view, it seems that an alternative explanation can be made by considering the consumption of CA that mainly depends on the nucleation and growth of the hydrates.

Finally it appears that the effect of gypsum on $C_{12}A_7$ is similar to the one observed with CA.

REFERENCES

[1] Tenoutasse, N. The hydration mechanism of C_3A and C_3S in presence of calcium chloride and calcium sulfate, 5th Int. Symposium on the Chemistry of Cement., Tokyo, 1968, vol.II, pp.372

[2] Tsuyuki, N., Hirota, N., Miyakawa, K. and Kasai J., The physical properties and the hydration mechanism of C_3A in the presence of $CaSO_4.2H_2O$ and $Ca(OH)_2$, 8th Int. Symposium on the Chemistry of Cement, Rio de Janeiro, 1986, vol.6, pp.400

[3] Kuzel H.J., Rietveld quantitative XRD analysis of Portland cement : Part I. Theory and application to the hydration of C_3A in the presence of gypsum, 18th Int. Conf. on Cement Microscopy, Houston , 1996, pp.87

[4] Bentur A, Effect of gypsum on the hydration and strength of C_3S pastes, J. Amer. Ceram. Soc., vol.59, 1976, pp.210-213

[5] Menetrier, D., Jawed, I. and Skalny, J., Effect of gypsum on C_3S hydration, Cem. Conc. Res., vol.10(5), 1980, pp.697-702

[6] Collepardi, M., Baldini, G., Pauri, M. and Corradi, M., Tricalcium aluminate hydration in the presence of lime, gypsum or sodium sulfate, Cem. Concr. Res., vol.8, 1978, pp.571

[7] Brown, P.W., Libermann, L.O. and Frohnsdorff, G, Kinetics of the early hydration of tricalcium aluminate in solutions containing calcium sulfate, J. Amer. Ceram. Soc., vol.67, 1984, pp.793-95

[8] RILEM 68 MMH, task group 3, The hydration of tricalcium aluminate and tetracalcium aluminoferrite in the presence of calcium sulphate, Materiaux et Construction, vol.19(110), 1984, pp.137-47

[9] Brown, P.W., The implications of phase equilibria on hydration in the tricalcium silicate-water and the tricalcium aluminate-gypsum-water systems, 8th Int. Symposium on the Chemistry of Cement, Rio de Janeiro, 1986, vol.3, pp 231

[10] Pommersheim, J. and Chang, J., Kinetics of hydration of tricalcium aluminate in the presence of gypsum, Cem. Conc. Res., vol.18(6), 1988, pp.911-22

[11] Bayoux, J.P., Bonin, A., Marcdagent, S. and Verschaeve, M., Study of the hydration properties of aluminous cement and calcium sulphate mixtures, Calcium Aluminate Cements Symp., Londres, 1990, pp320-334

[12] Damidot, D. and Sorrentino, F., Modification of the hydration process from $C_{12}A_7$ to C_3A at 20°C, 10th Int. Symposium on the Chemistry of Cement, Goteborg, 1997, 2ii025, 8 pages

[13] Damidot, D., Rettel, A. and Capmas, A., Action of admixtures on Fondu cement. I. Lithium salts compared to sodium salts, Advances in Cement Research, Vol.8(31), 1996, pp.111

[14] Damidot, D. and Rettel, A., Study of the interaction between the hydration of CA and of C_3S at room temperature, submitted to 11th Int. Symposium on the Chemistry of Cement, Durban, 2003

EFFECT OF GYPSUM ON CA AND $C_{12}A_7$ HYDRATION AT ROOM TEMPERATURE

D. Damidot[1] and A. Rettel[2]

[1] Ecole Normale Supérieure de Cachan, Département de Génie Civil, 61 avenue du Président Wilson, 94235 Cachan Cedex, France. E-mail: damidot@lmt.ens-cachan.fr
[2] DARD Consulting, Dijon, France

Denis Damidot received his B.Sc., M.Sc., and PhD. in physico-chemistry from Burgundy University, France. His thesis research was based on the study of C_3S hydration. Then he obtained an European Community research grant and worked as a post doc fellow at the Department of Chemistry of the University of Aberdeen, Scotland, on the calculation of phase diagrams used in order to estimate the durability of cement based materials. He joined the Central Research Laboratory of Lafarge in 1993 and worked for 6 years on special cements and on durability. He is currently Professor in the Civil Engineering Department of Ecole Normale Supérieure, in Cachan (suburb of Paris), France. He carries out research on the relationships between the microstructure and the macroscopic properties and on durability of cement based materials.

EFFECT OF SUPERPLASTICIZER TYPE ON THE FLUIDITY RETENTION OF PORTLAND CEMENT MORTARS AS A FUNCTION OF THE C_3A LEVEL AND THE NATURE OF ADDED CALCIUM SULFATES

E. M. Moulin[1] and V. Broyer[2]

[1]Centre Technique Inter-Unités, Lafarge, Saint Quentin Fallavier, France.
E-mail: eric.moulin@pole-technologique.lafarge.com
[2]Central Research Laboratory, Lafarge, Saint Quentin Fallavier, France
E-mail: veronique.broyer@pole-technologique.lafarge.com

ABSTRACT

Within the frame of concrete technology improvement, high performance properties such as high fluidity has been in great demand over the last few years.

Therefore, a number of new superplasticizers (SP) have been developed and among them, polycarboxylate-type superplasticizers (PCP) have become more widely used.

In this study, the effect of a common Polynaphtalene Sulfonate-type SP and of 2 PCP-type SP's as a function of the nature of the added calcium sulfates (gypsum, hemihydrate, anhydrite) and C_3A content (2 levels) in Portland cement has been compared through the fluidity behavior of mortars over a period of 90 minutes. Concurrently, SP adsorption rate has been monitored in the mortars over the same period of time. The mortars have been designed at a W/C of 0.5 and SP's have been introduced by a slight delayed addition. The results indicate that, for the high C_3A level, the initial fluidity increases as a function of calcium sulfates' solubility rate regardless of the type of SP. Concurrently, it is also observed that fluidity retention depends strongly on both calcium sulfates and SP type. In particular, the fluidity retention in the presence of PCP-type SP seems to be very sensitive to the nature of the added calcium sulfates. Those effects are less pronounced when the C_3A level is moderate.

1. INTRODUCTION

High performance properties such as high strength, high durability but also high fluidity and have been in great demand in the concrete technology over the last few years. Therefore, advanced superplasticizers (SP) have been developed to exhibit high dispersibility at small dosages and retention of dispersing effect for a long period of time. Among this new generation of SP's, the polycarboxylate-based superplasticizers (PCP) have recently become popular [1-4]. A characterisitic of this type of SP is that its chemical structure has the potential to be modified because its is composed of several components and it is a polymer. Electrical repulsion is the proposed mechanism of dispersion of polynaphtalene-sulfonate (PNS) and polymelamine-sulfonate (PMS) [1,2,5,6,7,8]. With PCP-based SP's, cement particles are supposed to be dispersed due to two factors: low electric repulsion caused by adsorption of negative ions of the carboxylic group in the chemical structure onto the surface of cement particles and more importantly, the steric effect by adsorption of the polymer [1,2,4,6].

SP's interact strongly with the various components of cements and influence cement hydration reactions. There are numerous studies on the interactions of common sulfonates-related SP with different cement types. A literature review [1,2,5-15] indicate that, in the presence of SP's such as PNS and PMS, the fluidity of concrete can be affected by the chemical nature of clinker (mainly C_3A and soluble alkalis content), the cement fineness, the amount and nature of added calcium sulfates, the SP dosage and its addition method, the chemical nature and molecular weight of the SP and the sulfonation degree of the SP. Initial dispersibility is related to SP adsorption capacity that appears to be governed by the initial ettringite formation that plays an important role on the rheological properties of cements [10-15]. Adsorption of the SP has been shown to modify the size, morphology and kinetics of ettringite formation [16-18].

The dispersibility retention appears to be strongly governed by the ionic strength of the pore solution and marginally by the ettringite formation [14,15].

It has been pointed out that the SP effectiveness depends also on the manner in which a SP is introduced to the system : either simultaneously in the mix water or by a delayed addition [2,19-21]. For instance, it has been described that a preliminary treatment of cement with even a small amount of water produces superplasticized concrete mixes that perform as well as the best concrete produced by delayed addition of PNS or PMS [2]. The effect would be related to the production of an ettringite coating on the surface of cement particles during the preliminary water treatment. The adsorption of PNS or PMS molecules on the prehydrated cement surface is reduced and more SP molecules are left in the pore solution for dispersion. That causes the subsequent dispersion action to be more effective than that recorded in the absence of preliminary treatment. It has been shown that the type of added sulfates and their difference in solubility rate could promote the early formation of some ettringite with the C_3A by providing Ca^{++} and $SO4^{=}$ ions and therefore contribute to reduce more or less the amount of adsorbed PNS-type SP [10, 12]. For the PCP-type SP's, it seems that adsorption does not depend so much on the method of addition, immediate or delayed [2]. Regarding the effect of added calcium sulfates in presence of the new generation of PCP-type SP's as a function of C_3A level, much less information is available and there are still unanswered questions regarding the effectiveness of specific cement / PCP-type SP combinations.

Therefore, in order to obtain more insights on the influence of PCP-type SP's as a function of the C_3A content and the nature of added sulfates on the fluidity retention of cement, a comparative study has been carried out .

The dispersing effect of a common PNS-type SP and of two PCP-type SP's as a function of the nature of added calcium sulfates (three types have been considered) and C_3A content of cement (two levels considered) have been evaluated over a period of 90 minutes on the rheological behavior of mortars prepared at a W/C of 0.5. During the mortar preparation, the cement has undergone a preliminary water treatment. In addition, the SP adsorption rate has also been monitored in the mortars. Results obtained are discussed in the frame of cement-SP interactions.

2. MATERIALS AND METHODS

2.1 The SP's selection

Three commercially available SP's in liquid form, one of the PNS type, having sodium as the counter-ion and two of the PCP-type based on metacrylate, having different solids content have been selected. A feature of the PCP-SP type is that the chemical structure has the potential to be modified because it is composed of several components. In this study, the chemical structure of SP's was not analysed but, due to their different dispersing properties, it is assumed that the two PCP-type SP's have been synthesized according to a different designed chemical structure. Table 1 gives details of the available manufacturers' specifications. Owing to the different SP dry content, the dosage of SP has been expressed as dry content % by weight of cement in the study.

2.2 Laboratory cements preparation

Two industrial clinkers having a high (clinker A) and moderate C_3A content (clinker B), according to Bogue calculations, have been selected for this study and their compositions are listed in Table 2.

Table 1. Manufacturers' specifications for the 3 SP's.

	PNS	PCP N°1	PCP N°2
Specific gravity (20°C)	1.21 (+- 0.02)	1.05 (+- 0.02)	1.1 (+- 0.02)
PH	8.1 (+- 0.1)	6.8 (+- 0.1)	6.8 (+- 01)
Total dry content in %	44.5 (+- 1)	20.2 (+- 1)	36.1 (+- 1)
Wt % free sulfate	1% (+- 0.05)		

Table 2. Industrial clinkers composition (oxyde wt % and Bogue % calculation)

	SiO_2	Al_2O_3	Fe_2O_3	CaO	MgO	K_2O	Na_2O	SO_3	TiO_2	P_2O_5	Free lime	L.O.I
Clinker A	22.58	4.99	1.63	68.22	0.45	0.13	0.02	1.0	0.31	0.13	0.5	0.26
Clinker B	21.96	4.75	2.25	67.55	0.76	0.19	0.19	1.2		0.1	0.3	0.69

	C_3S	C_2S	C_3A	C_4AF
Clinker A	66	15	11	4.9
Clinker B	71.4	9.9	7.8	5.7

Starting from each clinker, a series of 3 laboratory cements have been prepared by the addition of blends of calcium sulfates having different solubility rates. The nature and ratios of the added calcium sulfates have been as follows: 70% hemihydrate - 30% gypsum (H/G - high solubility rate), 70% gypsum - 30% hemihydrate (G/H - moderate solubility rate) and 70% anhydrite - 30% gypsum (A/G - low solubility rate). High purity (> 95%) laboratory grade gypsum and anhydrite have been provided for the study while hemihydrate has been prepared by dehydration of the laboratory grade gypsum. The calcium sulfates have been suitably added to the clinkers during the grinding in a laboratory planetary mill. Cements with a total calcium sulfate content of 3.5% and specific surface of 330 m^2/kg have been prepared from the clinker A, while cements with a total calcium sulfate content of 2.5% and specific surface of 300 m^2/kg have been prepared from the clinker B.

2.3 Mortars preparation and mixing

A fluid concrete formulation, with a W/C of 0.5 and providing at least 35 MPa compressive strength at 28 days in the laboratory, has been selected for reference and the recipe is shown in Table 3.

Table 3. Reference concrete formulation

Aggregates Fraction size (in mm)	0/0.315	0.315/1	1/4	4/8	8/12.5	12.5/20	**Cement**	**Water**
Content In Kg / M^3	284	246	260	190	350	480	**350**	**175**

The different mortar formulations have been designed with the same W/C as the reference laboratory concrete recipe. Since it was not possible to prepare cement pastes containing the various dosages of SP at such W/C without facing settling and bleeding problems, it has been decided, instead, to prepare mortars using a dry silica sand commercially available having a particle size

ranging from 0 to 315 microns. To prepare the mortars, it has been decided to keep the same ratio cement / "0-315 microns" sand as for the laboratory concrete.

Since the PNS-type SP's dispersing action is strongly dependent on the SP addition method (immediate or delayed) and, on the contrary, the PCP-type SP's are much less sensitive to the addition method [2], it has been decided to select a method of SP addition offering the best conditions for a comparison of SP efficiency, that is a method corresponding to a slight delayed addition of the SP. Some part of the water (38%) has been added to the dry sand prior to the cement addition. This step corresponds to the cement preliminary water treatment as mentioned earlier. Note that the 38% value would corresponds to the total water content originated from all the concrete aggregates. A typical water content of 6% for the fine aggregates (0-4 mm) and 1.5% for the coarse aggregates (4-20 mm) have been considered. Therefore, to prepare 500 ml of mortar, following composition has been used: 420 gr dry cement, 340 gr dry sand, 210 gr water (including 81 gr water to wet the sand) and the selected dosage of SP. Following procedure has been used to mix the mortar: weight the dry sand, add wetting water and stir gently for 1 minute; add cement to the mixture and stir gently for 1 minute; add the remaining mixing water (containing the SP dosage) and stir 30 seconds; pour the mortar mixture in a high speed laboratory propeller and mix for 1 minute at 3500 rpm. A high speed energy propeller has been indeed preferred for the mortars mixing, knowing the importance of laboratory mixing technique on the flow behavior [22].

2.4 Fluidity measurements

Fluidity has been measured as a function of the SP dosage over time. The fluidity measurements have been carried out by means of the mini-slump test. This method, extensively described elsewhere [7] consists in carrying out a slump test on a small amount of mortar. After the mixing stage, part of the mortar mixture is poured into a plexiglas cone with the same geometry as Abram's cone for common slump tests but with reduced size (namely: height of 60 mm, top inner diameter of 20 mm, bottom inner diameter of 40 mm). The minicone, standing on a glass board is lifted smoothly and quickly and the subsequent area of the mortar spread is measured and expressed in cm^2. Fluidity measurements have been performed after a period of 5, 15, 30, 60 and 90 minutes respectively. In the interval of time between the measurements, the mortars samples have been poured in a close-tight jar standing horizontally on rolling cylinders set at a speed of 5 rpm.

2.5 Measurement of SP adsorption on particles in mortar

When appropriate, after the same periods of time as for the fluidity measurements, the amount of SP adsorbed on mortars particules, has been evaluated by means of a total organic carbon (TOC) analyser, namely a TOC 5050A Shimadzu apparatus. The aqueous phase of mortar has been separated by filtration under suction (using a 4 microns Whatman® filter).The filtrate has been then suitably prepared for the TOC analysis. The reduction in the TOC value (at a period of time of 5, 15 and 90 minutes after mixing) compared to that of the mixing water with SP before contact with particles from the mortar, has been supposed to give the amount of SP adsorbed on mortar particles. Results have been expressed as the percentage of adsorbed SP relative to the total amount of SP.

3. RESULTS

3.1 Mortars rheological behavior

3.1.1 Comparison of the fluidity after a period of 5 minutes

Results of rheological measurements on the different laboratory cements as a function of the different SP's and as a function of the type of added calcium sulfates are illustrated in Figures 1 and 2. In Figure 1 the mortar spread results are represented as a function of the SP dosage for cements made from the clinker A (high C_3A content). Examination of this figure allows one to make the following comments: In the absence of SP, the fluidity of the cements with H/G or G/H is similar while the fluidity with A/G is lower. The evolution of the fluidity as a function of the SP dosage tends to follow an exponential law regardless of the nature of SP. The amount of PNS that is

required to obtain a given level of fluidity is much higher than the amount of PCP required to obtain the same given level of fluidity. Moreover, to obtain a given fluidity, the situation differs as a function of the type of added calcium sulfates. Regardless of the type of SP, dosage is always the highest with the cement containing A/G. Regarding the cements with other types of added sulfates (H/G and G/H), it can be seen that the trend is similar in presence of PNS and PCP N°2 : the necessary dosage of SP being the lowest with the H/P addition. The situation differs when the PCP N°1 is used: in this case, the cement with the G/H addition requires the lowest dosage. For a given dosage of SP, the PCP-type SP's effectiveness also seems to be more sensitive to the type of added calcium sulfates since the difference between the mortar spreads are more pronounced.

In Figure 2, the mortar spread results are represented as a function of the SP dosage for the cements prepared with the clinker B (moderate C_3A content). Examination of the figure allows to make the following comments. As for the cement with high C_3A content, in the absence of SP, the fluidity of the cements with H/G or G/H is similar while the fluidity with A/G is lower. The evolution of the fluidity as a function of the SP dosage tends to follow also an exponential law regardless of the nature of SP. For each type of SP, the overall dosage that is necessary to obtain a given fluidity is lower when compared with the cement with high C_3A content. Between SP's, the amount of PNS required to obtain a given fluidity is much higher than the dosage required when the PCP-type SP's are used. To obtain a given fluidity, regardless of the type of SP, the A/G cement is still the most difficult to disperse, while the SP dosage is roughly the same for the cements made with H/G or G/H.

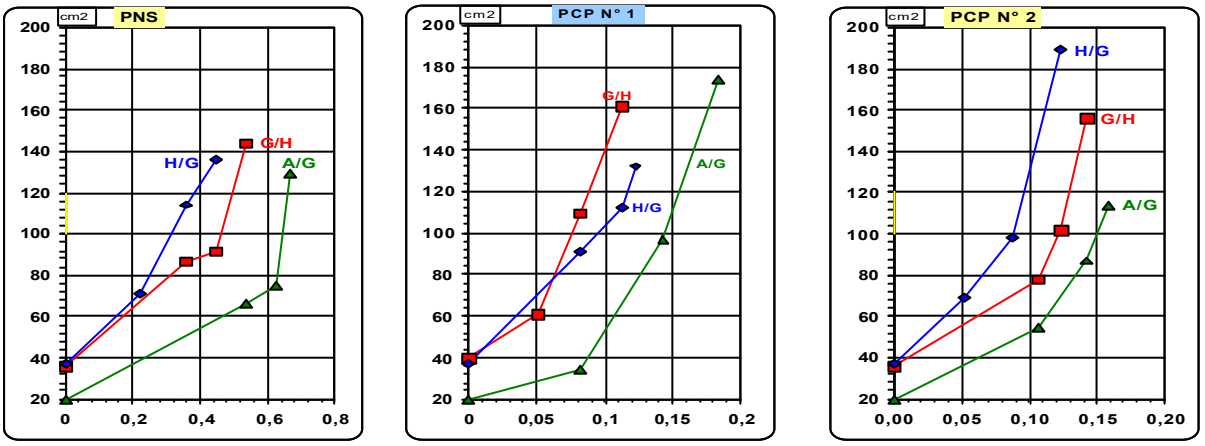

Figure 1. Mortar spreads (area in cm^2) as a function of SP dosage (% dry content) for the 3 types of added sulfates in cement with high C_3A content.

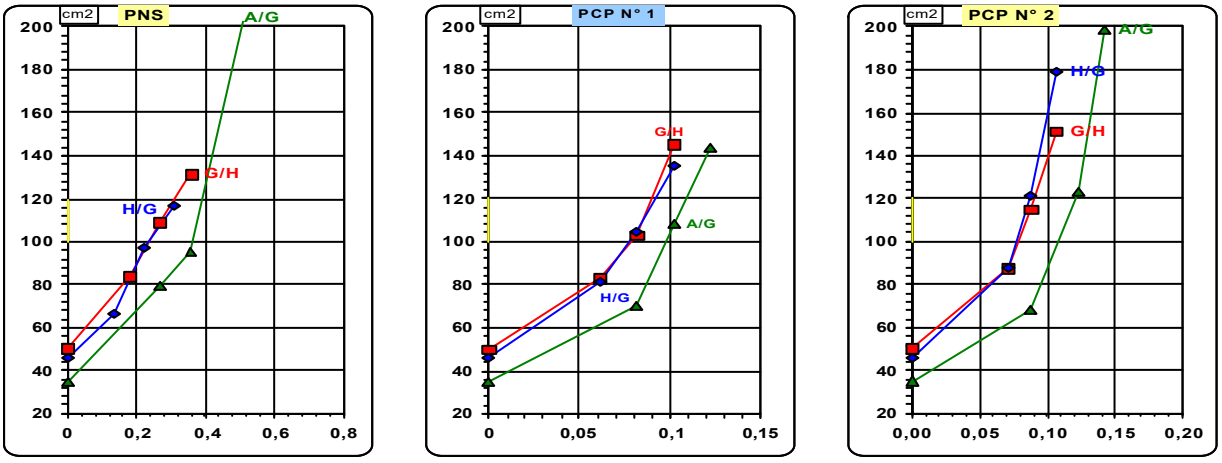

Figure 2. Mortar spreads (area in cm^2) as a function of SP dosage for the 3 types of added sulfates in cement with moderate C_3A content.

3.1.2 Comparison of the fluidity retention over a period of 90 minutes

In Figures 3 to 5 are shown the comparisons of fluidity retention in the cement with high C_3A for each type of added sulphates as a function of each SP dosage. The fluidity retention is always poor with the A/G sulfates when PCP –type SP's are used while a slightly better fluidity retention is obtained with PNS –type SP (see Figure 3). In this last case, one must remember that the SP dosage is much higher. For the other types of added sulfates systems, fluidity retention behaviour vary significantly as a function of SP's type and dosage. For the G/H system (see Figure 4), a good fluidity retention is observed with the 2 PCP-type SP's at different dosages. With high dosage of PNS-type SP, a sharp decrease is first observed at short term, followed by a period of relative stability in the fluidity retention. For the H/G system (see Figure 5), roughly the same behavior as for G/H is observed in the presence of PNS-type SP and PCP-type SP N°2 (but at lower dosage). Concurrently, the situation differs drastically in presence of the PCP-type SP N°1. Indeed, an optimum of fluidification is observed around a period of 30 minutes. It is also observed that the value of the optimum increases as a function of the SP dosage. This feature sheds light on the behavior observed at a period of 5 minutes as described in the previous paragraph. The H/G requires a higher PCP-type SP N°1 dosage at 5 minutes when compared to G/H, contrary to what is observed with the 2 other SP's. In the H/G system, a delay occurs before the maximum dispersion is obtained only after a period of 30 minutes.

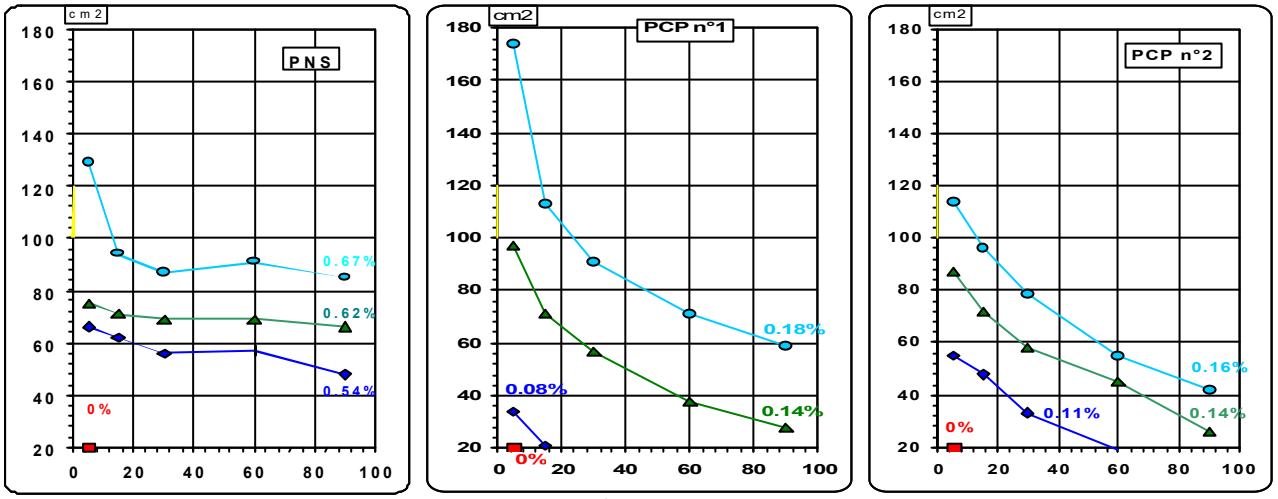

Figure 3. Mortar spread (area in cm^2) as a function of time and dosage of SP for the high C_3A cement containing A/G added calcium sulfates

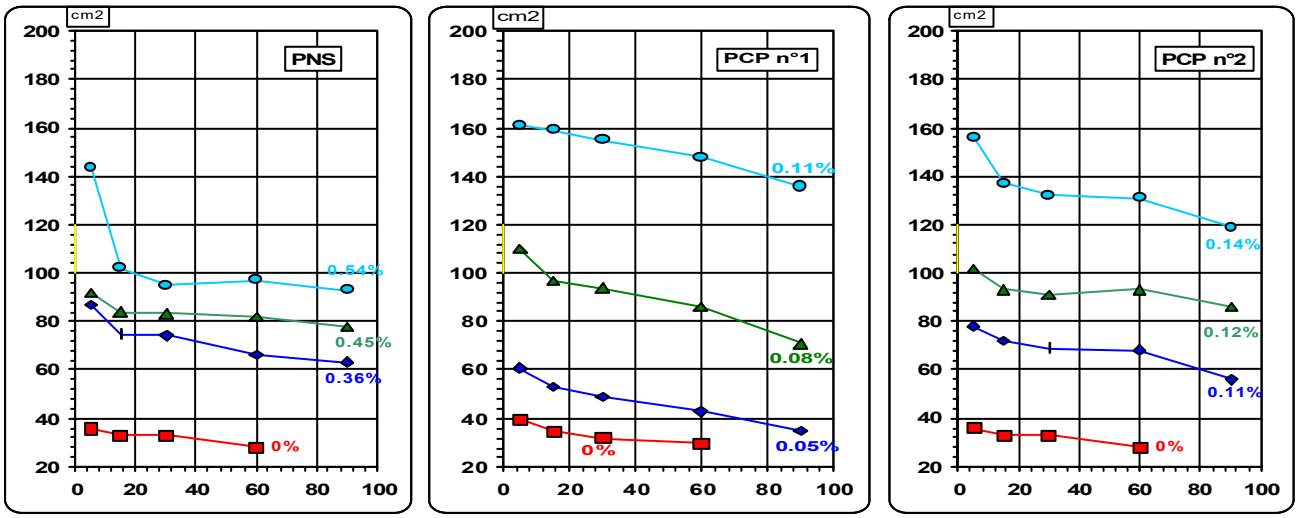

Figure 4. Mortar spread (area in cm^2) as a function of time and SP dosage for the high C_3A cement containing G/H added calcium sulfates

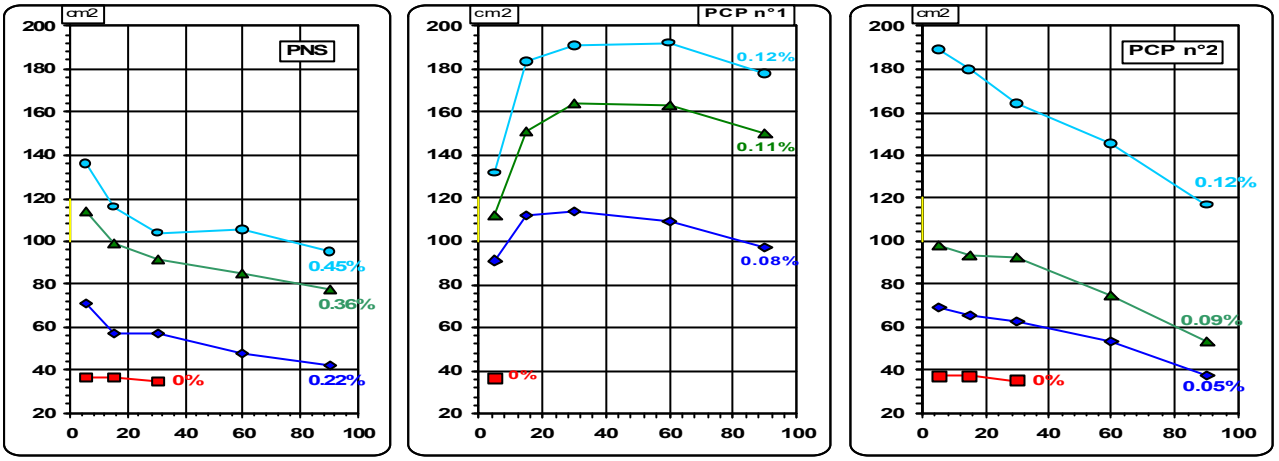

Figure 5. Mortar spread (area in cm^2) as a function of time and SP dosage for the high C_3A cement containing H/G added calcium sulfates.

In Figure 6 is shown the comparison of fluidity retention in the high C_3A cements for a given dosage of each SP as a function of 2 types of added sulfates, the H/G and G/H respectively. It can be observed that the shape of the fluidity retention is very sensitive to the type of added sulfates when PCP-type SP's are used. Same comparison is shown in Figure 7 for the cements containing moderate C_3A content (cements made with clinker B). In this case, the fluidity retention shape is much less sensitive to the nature of added calcium sulfates regardless of the SP type.

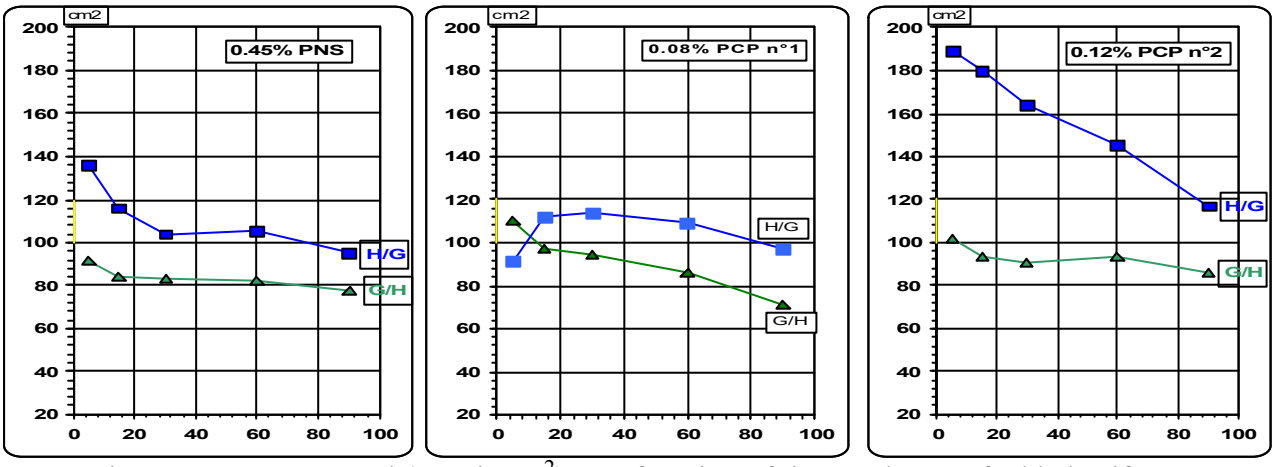

Figure 6. Mortar spread (area in cm^2) as a function of time and type of added sulfates for the high C_3A cement at given SP concentration

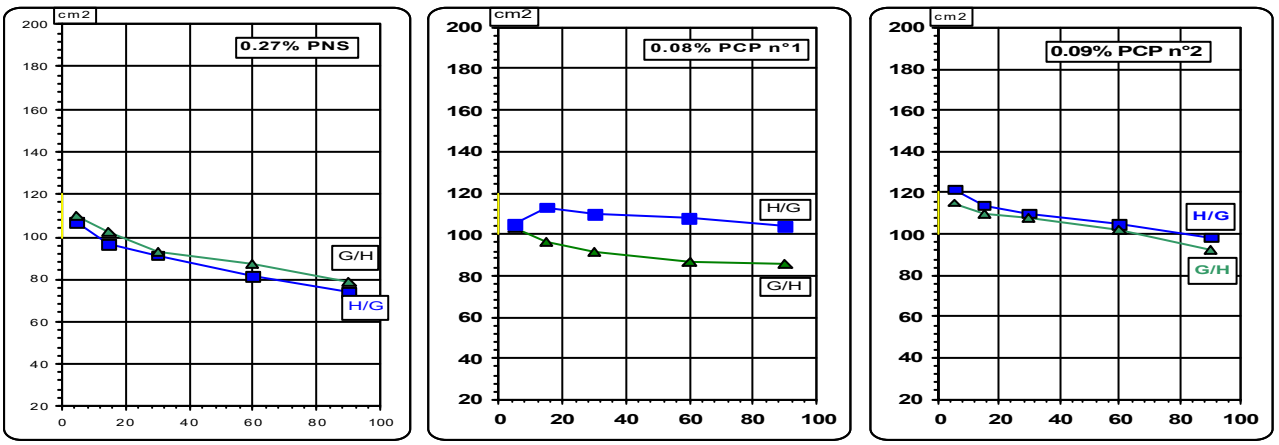

Figure 7. Mortar spread (area in cm^2) as a function of time and type of added sulfates for the moderate C_3A cement at given SP concentration.

3.2 SP adsorption in mortars over a period of 90 minutes

TOC measurements, as illustrated in Figure 8, have been performed on mortars prepared with the clinker with high C_3A content, calcium sulfates in the form of G/H and H/G and in presence of PNS or PCP N°2. The SP dosage selection and subsequent mortar early fluidity at 5 minutes are listed in Table 4.

Table 4. SP dosage and early fluidity on mortar selected for TOC measurement

SP % (dry content)	G/H cement	H/G cement
0.45 % PNS	95 cm^2	135 cm^2
0.12 % PCP 2	100 cm^2	190 cm^2

The results shown in Figure 8 indicate clearly that, apart from the fact that less dosage of PCP N°2 is needed to obtain a given fluidity when compared to the PNS-type SP, less amount of PCP N°2 has been adsorbed on the particles after a period of 5 minutes. Indeed, in presence of PNS-type SP, most of the adsorption has occurred in the first 5 minutes and furthermore, the adsorption does not evolve much beyond this initial period. On the contrary, adsorption is still important between the interval 5 and 15 minutes in presence of the PCP-type SP. For both SP's, less amount of SP is adsorbed in the H/G cement over the whole period of time. However, it is confirmed that the PCP-type SP efficiency seems to be more sensitive to the type of added calcium sulfates after a period of 5 minutes since the difference of adsorption between the cements made with H/G and G/H is more significant when compared to the PNS-type SP. Such results fully support the hypotheses that have been drawn from the fluidity results.

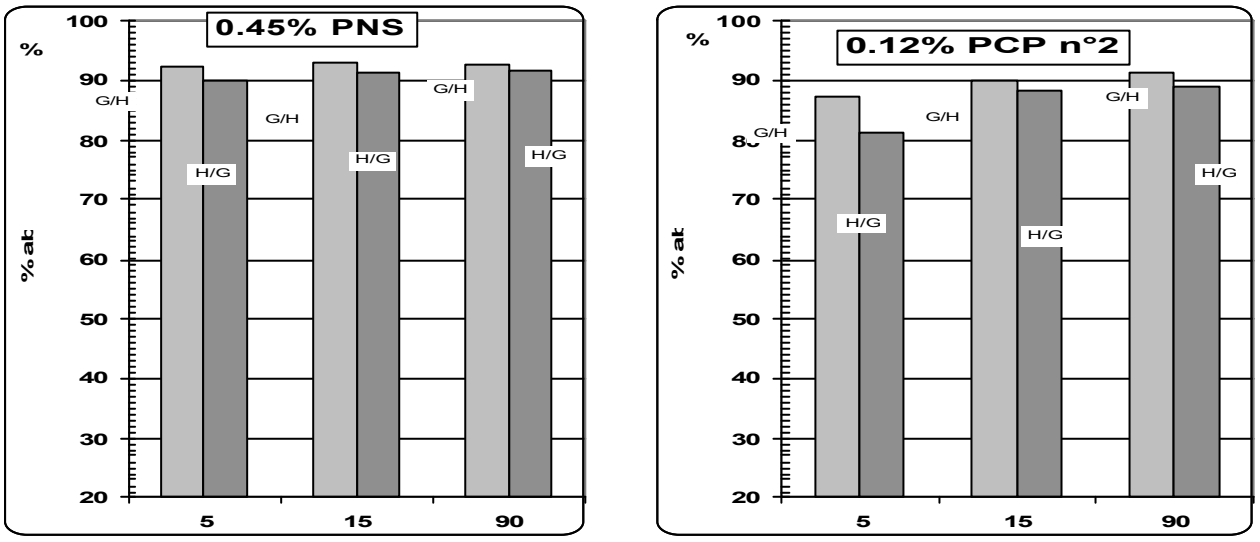

Figure 8. Adsorbed SP % in mortars in presence of PNS and PCP type SP for high C_3A cement containing H/G or G/H added sulfates at 5, 15 and 90 minutes

4. DISCUSSION

On the basis of these results, the difference of rheological behavior as a function of the nature of the added sulfates can be explained as follows. During the preliminary water treatment of the cement containing high C_3A, the added calcium sulfates will provide more or less Ca^{++} and $SO4^{=}$ ions to the pore solution as a function of their dissolution rate, the A/G system having the slowest rate and the H/G system having the fastest rate. Those ions, depending on their immediate availability, could promote the early formation of ettringite prior to SP addition by reacting with a C_3A content that is high. The faster the ettringite is promoted before the SP addition, the less the incorporation of the SP in the early hydration products and the better the efficiency. In the H/G system, ettringite can form quickly prior to the addition of SP and consequently, less SP will be incorporated after its

addition, leading to higher efficiency and therefore, such system requires the lowest SP dosage. In the G/H system, less ettringite can form prior to the SP addition and consequently, more SP will be incorporated after its addition and therefore, the system requires an intermediate SP dosage. This hypothesis seems to be valid in presence of PNS and PCP n°2 while the feature observed in presence of PCP N°1 is unclear. The delay in the maximum dispersion effectiveness seems to be related to a particular mechanism of action of the particular SP.

In the presence of A/G, much less ettringite can form prior to the SP addition and the early hydrates formation after the SP addition consumes a higher amount of SP and therefore, the system requires the highest SP dosage. This hypothesis seems to be valid for the 3 SP's.

Regarding the cement with a moderate C_3A content, the similar behavior observed for the H/G and G/H systems (same SP dosage necessary for a given fluidity) can be explained as follows. The systems H/G and G/H do not have the same dissolution rate, but in both cases, sufficient Ca^{++} and $SO4^{=}$ are provided to the pore solution prior to the SP addition for the production of a sufficient ettringite coating on the moderate amount of the C_3A. Consequently, for both systems, the efficiency of the SP is in the same range. This hypothesis seems to be valid for the 3 SP's.

For the A/G system, the same explanation as for the high C_3A cement can be proposed.

Considering the fluidity retention shape, it seems that the fluidity loss observed in some cases is linked to some subsequent higher consumption of the SP after the initial period of 5 minutes. It is likely that this consumption is due to a higher formation rate of hydrates between 5 and 90 minutes in such systems. However, the optimum of fluidization over the time observed with the PCP-type SP N°1 is unclear and requires further investigations.

5. CONCLUSIONS

In this study, the effect of different types of SP's on the fluidity retention of Portland cement mortars as a function of the nature of added calcium sulfates and C_3A content has been investigated.

After a preliminary water treatment of the cements, the results indicate that less dosage of PCP-type SP's is required to obtain a given initial fluidity when compared to PNS-type SP. Apart from the fact that the overall SP dosage is lower, the SP adsorption is also lower when compared to PNS-type SP's.

For a high C_3A level, cement dispersion is very sensitive to the nature of added calcium sulfates: the initial fluidity increases as a function of the calcium sulfates' solubility rate, regardless of the type of SP. It seems that the PCP-type SP's dosage is also more sensitive to the calcium sulfate nature.

For a moderate level of C_3A, the dosage of SP is reduced and the cement dispersion is less sensitive to the nature of added calcium sulfates, regardless of the type of SP.

Thus, the PCP-type SP's dosage, like the PNS-type SP's, depends also on C_3A content and the subsequent production of early hydrates. Like PNS-type SP's, the PCP-type SP's efficiency is also dependant on the type of added calcium sulfates.

Furthermore, the effectiveness of the fluidity retention in presence of PCP-type seems to be also very sensitive to the nature of added calcium sulfates when the cement C_3A content is high. This sensitivity is much less pronounced when the C_3A level is moderate.

ACKNOWLEDGEMENTS

Permission for publication of this paper is gratefully acknowledged to Lafarge management.

REFERENCES

[1] Tanaka, Y.O., Matsuo, S., Ohta A. and Veda, M. A new admixture for high performance concrete, Proceedings of the concrete in the service of Mankind, eds R.K. Dhir and M.J. McCarthy, 1996, pp. 291-300.

[2] Collepardi, M. Admixtures used to enhance placing characterisitics of concrete, Cement and Concrete Composites, vol. 20, 1998, pp. 103-112.

[3] Tsukada, K., Soeda, K., Hayashi, H.and Isomura, H. Performance of a new-developed powder polycarboxylic acid superplasticizer, 1st International Rilem Symposium on self compacting concrete, Stockholm, 1999, pp. 425-436.

[4] Ohta, A., Sugiyama, T.and Tanka, Y. Fluidizing Mechanism and applications of polycarboxylate based superplasticizers, 6th International Conference on Superplasticizers and other chemical admixtures in concrete, Nice, 2000, ACI, SP 173-19, pp. 359-369.

[5] Uchikawa, H., Hanehara, S., Shirasaka, T and Sawaki, D. Effect of admixture on hydration of cement, adsorptive behavior of admixture and fluidity and setting of fresh cement paste, Cement and Concrete Research, vol. 22, 1992, pp. 1115-1129.

[6] Jolicoeur, C and Simard, M.A. Chemical Admixture-cement interactions: phenomenology and physico-chemical concepts, Cement and Concrete Composites, vol. 20, 1998, pp. 87-101.

[7] Kim, B.G, Jiang, S., Jolicoeur, C.and Aïtcin, P.C. The adsorption behavior of PNS superplasticizer and its relation to fluidity of cement paste, Cement and Concrete Research, vol. 30, 2000, pp. 887-893.

[8] Mollah, M.Y.A., Adams, W.J., Schennach, R. and Cocke, D.L. A review of cement-superplasticizer interactions and their models, Advances in Cement Research, vol. 12 (4), 2000, pp. 153-161.

[9] Lahalih, S.M., Absi-Halabi, M. and Ali, A.M. Effect of polymerisation of sulfonated-melamine formadehyde superplasticizers on concrete, Cement and Concrete Research, vol.18, 1988, pp. 513- 531.

[10] Nawa, T. and Eguchi, H., Effect of sulfate on adsorption behavior of superplasticizer, 43 rd CAJ Proceedings of Cement and Concrete, 1989, pp. 90-95.

[11] Nawa, T., Eguchi, H.and Fukaya, Y. Effect of alkali sulfates on the rheological behavior of cement paste containing a superplasticizer, 3rd international conference on Superplasticizers, Ottawa, ACI, SP119-21, 1989, pp. 405-424.

[12] Dodson, V.H. and Hayden, T.H. Another look at the Portland cement/chemical admixture incompatibility problem, Cement, Concrete and Aggregates, CCAGPD, 1 (11), 1989, pp. 52-56.

[13] Nawa, T. and Eguchi, H. Effect of cement characteristics on the fluidity of cement paste containing an organic admixture, 9th International Congress on the Chemistry of Cement, vol. 4, 1992, pp. 597-603.

[14] Bonen, D and Sarkar, S.L. The superplasticizer adsorption capacity of cement paste, pore solution composition, and parameters affecting flow loss, Cement and Concrete Research, vol. 25 (7), 1995, pp. 1423-1434.

[15] Jiang, S.P; Kim, B.G and Aïtcin, P.C. Importance of adequate soluble alkali content to ensure cement/superplasticizer compatibility, Cement and Concrete Research, vol.29 (1), 1999, pp. 71-78.

[16] Massazza, F.and Costa, U., Effect of superplaticizers on the C_3A hydration, 7th Int. Congress on the Chemistry of Cement, Paris, vol. 4, 1981, pp. 529-534.

[17] Baussant, J.B., Vernet, C, Defosse, C. Growth of ettringite in diffusion controlled conditions, influence of additives on the crystal morphology, 11th Int. Conf. Cement Microscopy, New Orleans, 1989, pp. 186-197.

[18] Luke, K. and Aïtcin, P.C. Effect of Superplasticizer on ettringite formation, Ceramic Transactions, Am. Ceram. Soc. Westerville, vol; 16, 1991, pp. 147-166.

[19] Ramachadran, V.S., Feldman, R.F, Baudoin, J.J. Concrete Science, London, 1981, pp. 23-58.

[20] Uchikawa, H, Sawaki, D., Hanehara, S. Influence of kind and added timing of organic admixture on the composition , structure and property of fresh cement paste, Cement and Concrete Research, vol. 25 (2), 1995, pp. 353-364.

[21] Hsu, K.C., Chiu, J.J., Chen, S.D, Tseng, Y.C. Effect of addition time of a superplasticizer on cement adsorption and on concrete workability, Cement and Concrete Composites, vol. 21, 1999, pp. 425-430.

[22] Yang, M. and Jenning, H.M., "Influences of mixing methods on the microstructure and rheological behavior of cement paste", Advances in Cement Based. Materials., vol. 2, 1995, pp. 70-78.

CHEMICAL AND ENVIRONMENTAL ASPECTS OF HEAVY METALS IN CEMENT IN CONNECTION WITH THE USE OF WASTES

L. Opoczky [1], M. Fodor [1], D.F. Tamás[2] and J. Tritthart [3]

[1] Cement Research and Development Ltd, Budapest, Hungary. E-mail: cemkut@mail.datanet.hu
[2] University of Veszprém, Hungary. E-mail: tamasf@almos.vein.hu
[3] University of Graz, TVFA, Graz, Austria. E-mail: tritthart@tvfa.tu-graz.ac.at

ABSTRACT

The effect of Zn, Ni, Pb and Cr on the burnability of raw meals, clinker formation processes, properties of clinker and cement as well as their long term environmental effect in concrete was investigated. Zn, Ni and Pb do not influence clinker formation, or cement/concrete properties, and their use does not present any hazard during long-term behaviour. However Cr can be dangerous: in the atmosphere of cement burning the original Cr^{3+} is oxidized to Cr^{6+}, which negatively influences alite formation, and is soluble in water or weak acids, thus in long-term use it can be environmentally hazardous. By properly adjusting the sulfatization degree, the quantity of water-soluble chromates can be decreased. In certain cases, reducing agents are necessary to transform hexavalent Cr to a trivalent form.

1. INTRODUCTION

If wastes are used as alternative raw materials and/or fuels, the number and quantity of trace elements (esp. those of heavy metals) is increasing. Their amount may cause changes in the chemistry of cements and also their environmental influence must be known. During this research the effect of zinc (Zn), nickel (Ni), lead (Pb) and chromium (Cr) on the burnability of raw meals was investigated, jointly with their effect on clinker formation, clinker and cement properties. The distribution of heavy metals in various clinker phases, their characteristics were also studied. From an environmental point of view, tha fate of the heavy metals during the use of cement is of utmost importance; to investigate this, various leachibility tests were done.

1.1 Cement Chemistry

1.1.1 Methods

To investigate burnability, a “standard” raw material was preepared, made of high purity materials. Moduli of this standard: Lime saturation = 0,90, silica modulus = 2,2, alumina modulus = 1,7. Raw materials were mixed with various amounts of ZnO, NiO, PbO and Cr_2O_3 in quantities ranging 0,05 to 2,5 m/m%, ground to approx. 500 m^2/kg (Blaine), pressed to pellets and fired in an electric laboratory kiln (in air) at 1400 °C for 30 min. The free lime content was determined in these clinkers (ethylene glycol method) and investigated by XRD, optical microscopy (reflected light), SEM and EDAX. Selective dissolution methods were used for the investigation of heavy metals in various clinker phases.

To study the effect of heavy metals on physical and mechanical properties of cement, clinkers were ground to surface area approx. 320 m^2/kg (Blaine), with added gypsum (SO_3 = 3,5 m/m%).

In order to study the environmental effect of heavy metal-containing cements, leachability tests were also undertaken. The total heavy metals content was determined according to the Hungarian standard [1], by ICP-AES, from solutions after an attack by nitric acid / hydrogen peroxide.

Leachates were prepared as follows:

- leaching in de-ionised water, in order to study direct environmental hazard; this gives information on heavy metals which are released by the clinker when mixing with water, i.e. concrete manufacture;
- leaching in an ammonium acetate buffer of pH = 4.5; this gives information on heavy metals which are released during the working life of cement by the attack of weak acids;
- leaching in 2M nitric acid; this gives information on the "total quantity" of heavy metals. This gives information on the "potential" hazard of landfilling with demolished concrete.

The working life of cement in concrete can be investigated by analysing the heavy metal content of pore solutions. For these tests industrial clinkers were used: cements were made, after grinding in a lab mill and mixing with gypsum. Cylindrical samples were made of these cements using a 0.6 w/c ratio; demoulding was done at the age of 24 h, followed by storing in polythene bags. Pore solutions were expressed at ages of 28 and 120 days, by a pressing force of 600-650 kN.

2. RESULTS

2.1 Cement chemistry

Burnability results are tabulated in Table 1. It can be seern that by adding ZnO, NiO and PbO in increasing amounts, the free lime content was decreased, showing that these heavy metals improve clinker formation.

Table 1. Effect of Zn, Ni and Pb on the burnability (free CaO, in m/m%) of raw meal

Oxide content, m/m%						
0	0.05	0.10	0.25	0.50	1.0	2.0
ZnO						
1.20	1.05	0.85	0.75	0.73	0.68	0.55
NiO						
1.20	0.85	0.74	0.65	0.57	0.46	0.29
PbO						
1.20	0.98	0.87	0.72	0.65	0.60	0.50

On-hand SEM-micrographs and their EDAX spectra (Figure 1.), as well as results of selective dissolution (Table 2.) show that Zn is mainly concentrated in the alite- and aluminoferrite phase, while Ni and PbO in the aluminoferrite phase (although their presence can also be detected in the silicate phases).

Table 2. Distribution of heavy metals in clinker phases (m/m%)

Clinker phase	Zn	Ni	Pb
Silicate (alite, belite)	0.40	0.23	0.20
Aluminoferrite	0.72	1.82	2.00
Aluminate	0.15	0.18	0.12
Potential mineral composition of clinker (Bogue) C_3S = 59,5 m/m% C_2S = 19,8 m/m% C_3A = 9,2 m/m% C_4AF = 11,5 m/m%			
Metal oxide content in clinker: 0,5 m/m%			

XRD tests proved that these model clinkers contain monocline alite (M_I and M_{II}), as shown by the shape of the alite peak at $2\Theta = 51 - 53^{o}$.

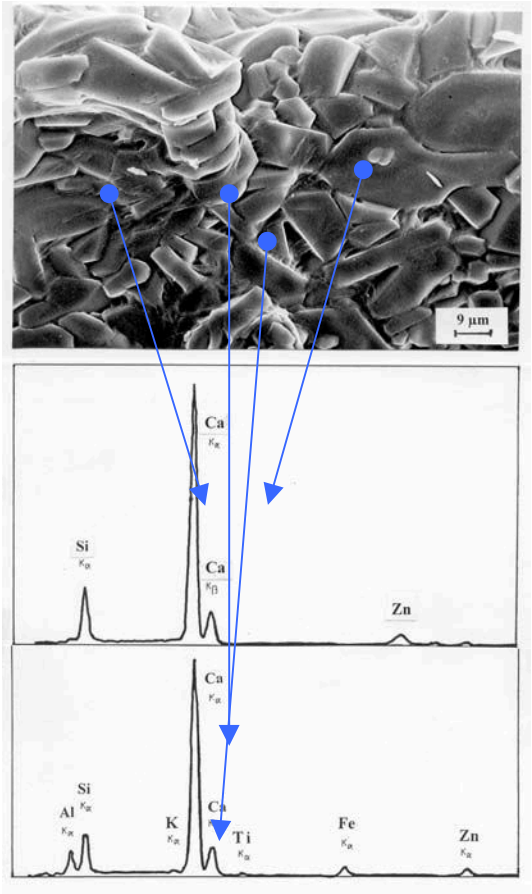

A. clinker containing zinc

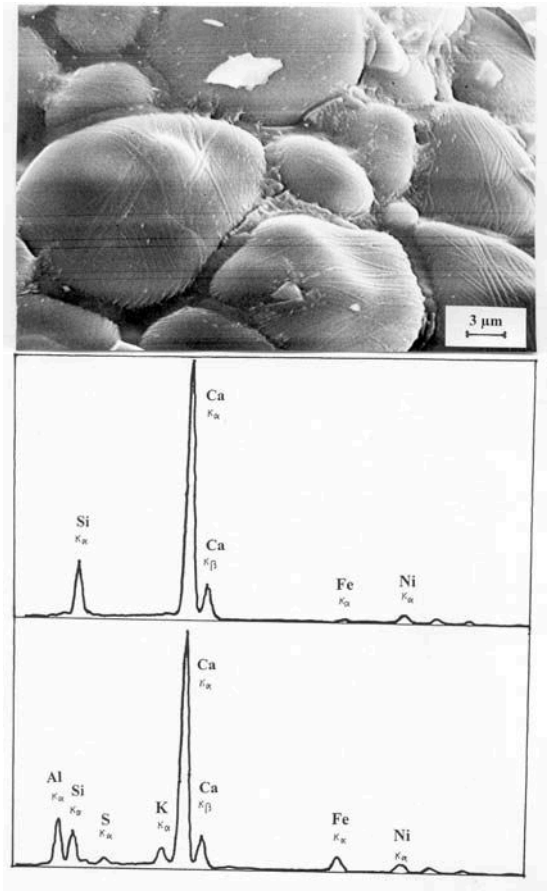

B. clinker containing nickel

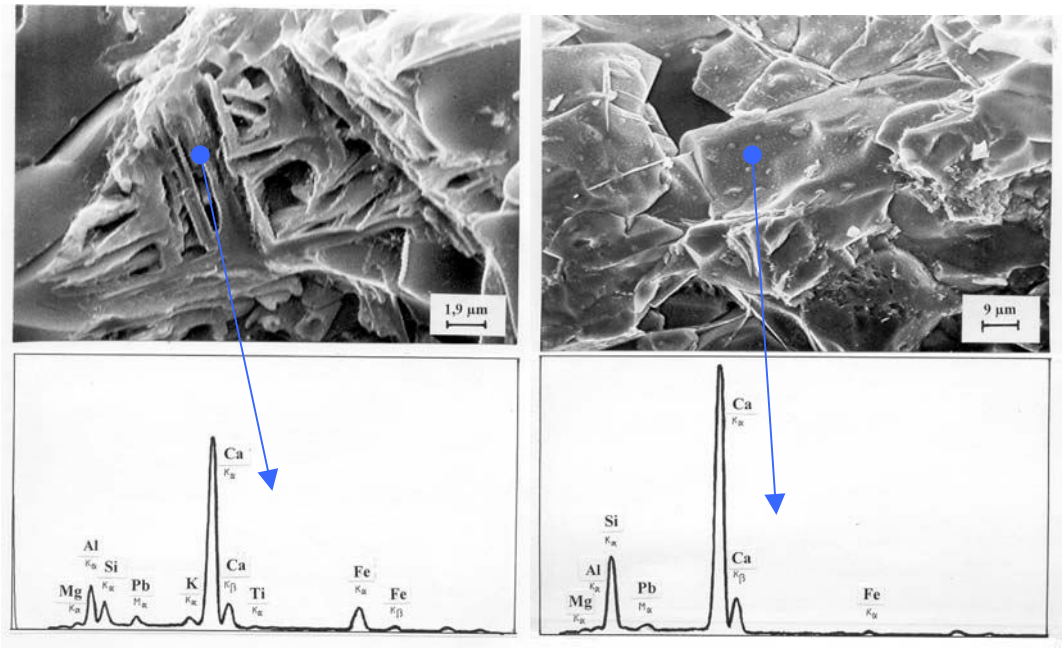

C. clinker containing lead

Figure 1. SEM micrographs and energy dispersive X-ray spectra of Zn- and Ni-containing clinkers

If the model clinkers contain < 0,1m/m% of metal oxide, the physical-mechanical properties of cement made of it do not differ from those made of no-heavy-metal clinker. This is illustrated by the cement containing ZnO (Table 3.)

Table 3. Comparison of physical-mechanical properties of cements made of standard (C_O) and 0.1 m/m% ZnO-containing (C_{Zn}) clinker

Property	C_O	C_{Zn}
Surface area (m^2/kg)	323	325
Setting data		
water to reach standard slump	27.0	27.5
initial set (h-min)	3-20	3-00
final set (h-min)	4-30	4-20
Soundness (Le Chatelier ring), mm	1.0	1.0
Compr. strength (MPa)		
2 days	15.8	15.0
7 days	26.2	25.8
28 days	34.8	35.2

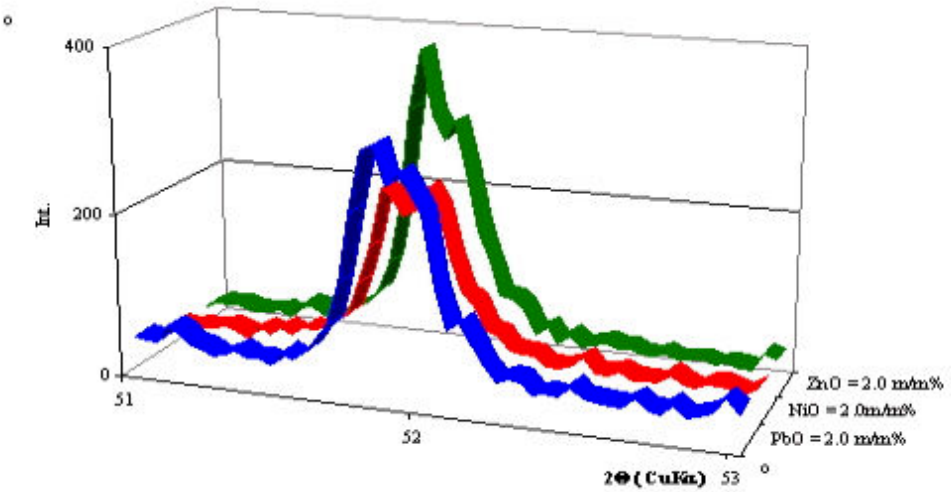

Figure 2. The 2Θ = 51 – 53° part of XRD patterns in ZnO-, NiO- and PbO-containing clinkers

The free CaO-, C_3S- and C_2S-content of clinkers, fired of raw meals containing various amounts of Cr_2O_3, is shown in Figures 3 and 4, respectively.

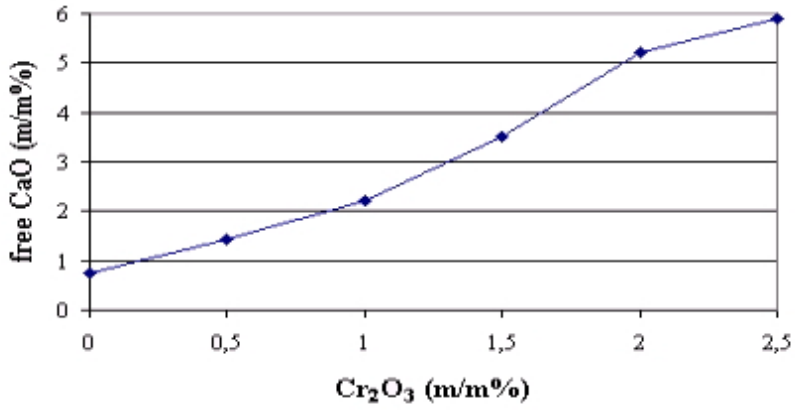

Figure 3. Free CaO-content of clinkers with various amounts of Cr_2O_3

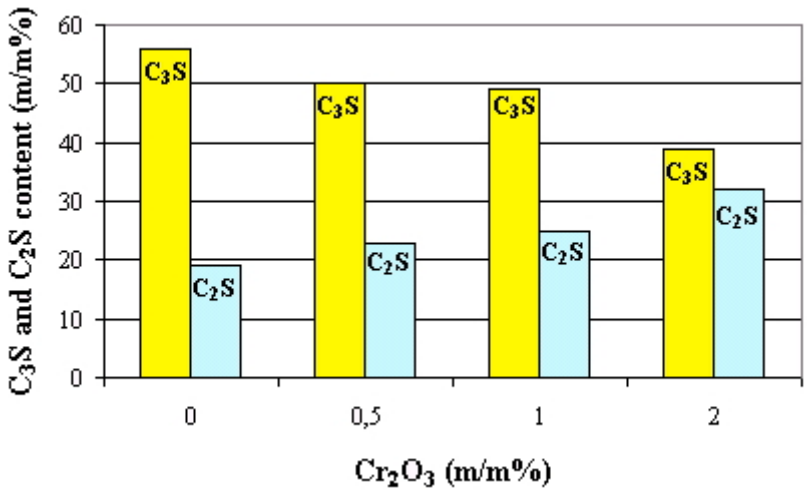

Figure 4. C_3S and C_2S content of clinkers with various amounts of Cr_2O_3

It is evident that by increasing the Cr_2O_3 –content, the free CaO-content is increased, showing that chromium is disadvantageous from the point of burnability. Jointly with the increasing of Cr_2O_3 and of free CaO, the C_3S and C_2S content of the clinker is decreasing, and increasing, respectively; in case of adding 2.5 m/m% of Cr_2O_3, the C_3S-content of the clinker is almost zero (Figure 5.). All this shows that the presence of Cr_2O_3 decreases the alite (C_3S) content, by the stabilization of β-C_2S.

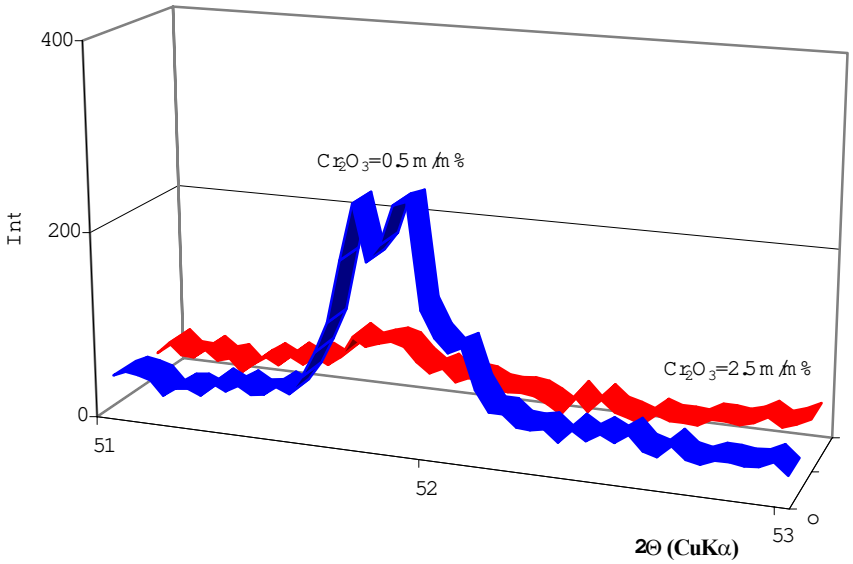

Figure 5. The $2\Theta = 51 - 53^{o}$ part of XRD patterns in Cr_2O_3-containing clinkers

SEM-micrographs and EDAX-spectra, jointly with selective dissolution show that chromium is mainly concentrated in the silicate (alite, belite) phases, although its presence in the aluminate-ferrite phase is also evident. (Figure 6A). A SEM-micrograph of a clinker, with maximum (2.5 m/m%) Cr_2O_3 addition shows decomposing alite, as well as belite and CaO crystals (Figure 6B).

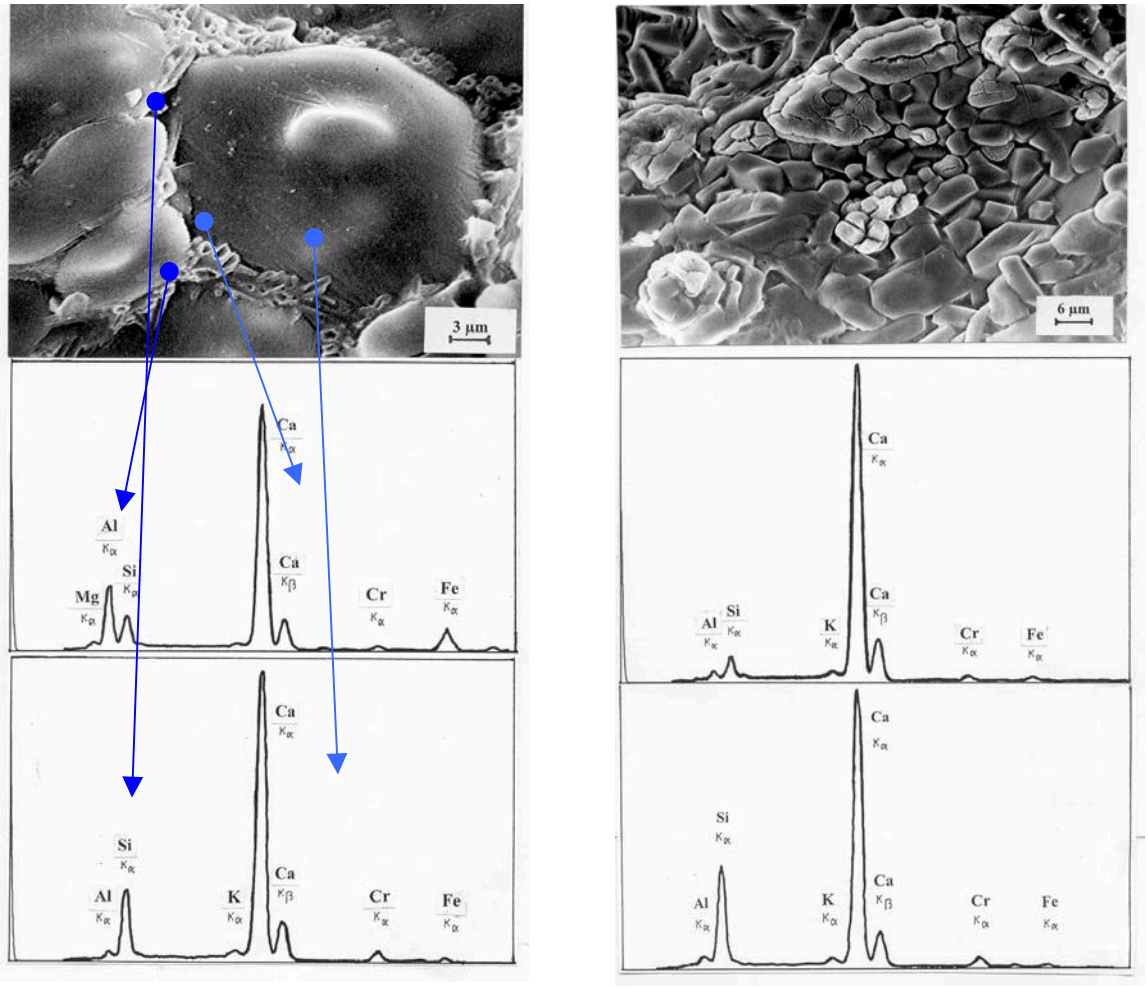

A. Cr_2O_3= 0.1 m/m%

B. Cr_2O_3= 2.5 m/m%

Figure 6. SEM micrographs and energy dispersive X-ray spectra of clinkers containing 0.1 and 2.5 m/m% Cr_2O_3

In the case of chromium-containing clinkers the micrograph shows large (>100 µm) "emerald" alite crystals, being strongly reflective. The green colour of alite is a consequence of chromium-incorporation (Cr^{3+} or Cr^{6+}). Chromium improves the grindability of clinker. If the chromium content in model clinkers is <0.1 m/m%, the cement has practically equal physical-mechanical properties as the no-Cr clinker.

2.2 Leachability

Results of leachability tests are summarized in Table 4.

Table 4. Heavy metal content and leachability of clinkers

Heavy metal content ppm (mg/kg)	**Model clinker***	**Industrial clinkers**	
		Clinker	**CEM I 42.5N**
z i n c			
total	793	66	93
leachability in water	<0.1	<0.1	<0.1
leachability in buffer**	<0.1	<0.1	<0.1
n i c ke l			
total	780	23	22
leachability in water	<0.1	<0.1	<0.1
leachability in buffer**	<0.1	<0.1	<0.1

l e a d			
total	890	27	33
leachability in water	<1	<1	<1
leachability in buffer**	<1	<1	<1
c h r o m i u m			
total	632	78	75
leachability in water	46.7	1.2	3.3
leachability in buffer**	48.0	1.5	3.6

* Metal oxide content: 0.1 m/m%
** Ammonium acetate, pH=4.5

Leachability of model clinkers shows that zinc, nickel and lead are bonded in clinker phases during burning very strongly: leachout was almost negligible in water and also in slightly acid media (pH = 4.5). However chromium-containing clinkers behave in a different way: the water leachate contains 46.7 ppm chromium as Cr^{6+} (of the 632 ppm total Cr-content model clinker), although Cr was added as Cr^{3+} (Cr_2O_3). Actually the oxidizing atmosphere of the kiln converts a part of Cr-content to a hexavalent state; this is partly bonded in clinker phases, but the rest is soluble in water or slightly acid media. These findings are supported by industrially produced clinkers and cements (20 and 55 samples, respectively).

The long-term leachability behaviour of cement (in concrete) can be studied by the pore fluid analysis of hardened cement paste. Results are tabulated in Table 5.

Table 5. Cr, Zn, Ni and Pb content of pore solutions, ppm (mg/kg)

Age	**Cement label**											
	C_1				**C_2**				**C_3**			
	Heavy metal content of pore solutions											
	Cr	Zn	Ni	Pb	Cr	Zn	Ni	Pb	Cr	Zn	Ni	Pb
28 days	1,1	<0,1	<0,1	<1	0,9	<0,1	<0,1	<1	2,1	<0,1	<0,1	<1
120 days	1,6	<0,1	<0,1	<1	1,5	<0,1	<0,1	<1	2,9	<0,1	<0,1	<1
	Heavy metal content of cements											
Total	75	177	27	13	107	88	26	24	147	70	35	20
Water soluble	12	<0,1	<0,1	<1	16	<0,1	<0,1	<1	17	<0,1	<0,1	<1

* Remark: pH of pore fluids was between 13.37 and 13.63

It is obvious that pore fluids do not contain Zn, Ni or Pb, and their Cr-content is much lower (at ages 28 or 120 days) than in aqueous leachates. This shows that during cement hydration, soluble Cr-content is bonded in hydrate phases.

3. SUMMARY

Heavy metal containing wastes are increasingly used in cement manufacture, although their effect is not fully known. This research is aimed at examining the effect of Zn, Ni, Pb and Cr on the burnability of raw meals, clinker formation processes as well as physical-technical properties of clinkers and cements. The long-term behaviour of cement in concrete was studied by analysing leachates (in water and weak acid, pH=4.5) and pore fluids (age: 28 and 120 days).

Results prove that ZnO, NiO and PbO, (from 0.05 to 2.00 m/m%) promote burnability and clinker formation. Zn is mainly incorporated in the alite and the ferrite phase, while Ni and Pb mainly in the ferrite, although it can be detected in the silicate phases too. Clinkers with 0.2 m/m% ZnO, NiO or PbO contain monoclinic alite. Clinker with ZnO addition shows well crystallized, hexagonal, prismatic and similar alite crystals of 10-50 μm size. Clinker with NiO contains well crystallized, but irregularly formed (rounded) alite of 15-20 μm size, while PbO causes prismatic, elongated alite crystals of 80 μm size and unusually high amounts of interstitial material. Leachates of cements in water and weak acid (pH = 4.5), as well as pore fluids of hardened cement contain practically nil (< than detection limit) of these heavy metals. These findings are also in accordance with the results of several industrially manufactured clinkers and cements.

The behaviour of chromium is different. In the range of 0.05 – 2.50 m/m% Cr_2O_3 content burnability and alite formation is deteriorated. This can be attributed to hexavalent chromium (Cr^{6+}), formed from the trivalent one in the oxidizing atmosphere of the burning. The presence of Cr^{6+} stabilizes β-C_2S; this is due to the replacement of $[SiO_4]^{4-}$ anion by $[CrO_4]^{2-}$ anion.. This stabilization causes dissolution of β-C_2S in the melt to be slowed down, thus deteriorating the formation of alite. The same replacement takes place in the lattice of alite too. Chromium can be not only in the form of $[CrO_4]^{2-}$ but also as Cr^{3+} in the lattice of C_3S and C_2S [2,3]. In the case of 2.5 m/m% Cr_2O_3, this replacement led to the decomposition of alite. Clinkers containing chromium show under the microscope large (> 100 μm) alite crystals of green "emerald" colour. Leachates and pore solutions of Cr-addition contain hexavalent (Cr^{6+}) chromium; however the Cr-content of pore fluids was much less than in leachates, showing that water-soluble chromates are bonded during cement hydration.

There are several sources of Cr in cement manufacture: besides wastes as alternative raw materials: it may come to the raw meal by the wear of grinding media, from refractories, by kiln dust recycling, etc. Although this Cr is usually trivalent, this is transformed into a hexavalent state in the oxidizing atmosphere of the kiln. A large part of this Cr^{6+} is bonded in clinker phases, but a part remains as soluble alkali chromates. Thus e.g. potassium chromate ($K_2Cr_2O_7$ or K_2CrO_4) was found in XRD patterns of high-chromium clinkers manufactured semi-industrially. Several factors determine oxidation, clinker formation and Cr-bonding in the kiln, e.g. burning temperature, oxygen level of the kiln, degree of sulfatization. The investigation of a number of industrial clinkers show that 1.5 – 11.0 % of the total the (Cr^{6+}) content becomes water soluble. Clinkers of almost identical total Cr-content contain more soluble (Cr^{6+}), where the sulfatization degree was not properly adjusted, i.e. those containing alkali surplus.

Cements made of model clinkers, containing 0.1 m/m% ZnO, NiO, PbO or Cr_2O_3 have physical-mechanical properties (water demand, setting time, soundness, strength at age 2, 7 or 28 days) similar to those without these oxides.

As a summary, it can be stated that clinker formation and properties of cements made by using alternative raw materials of usual Zn-, Ni- and Pb-content can be used without restriction; even the long-term behaviour is environmentally safe. Chromium, on the other hand, may dangerous, even if present in low quantities: it hinders alite formation. Still worse, a part of trivalent Cr is oxidized during burning to hexavalent Cr, which forms soluble chromates. This must be taken into consideration for the "working life" of concrete structures, as environmentally hazardous chromates might be released. If using Cr-containing wastes as raw materials, certain measures must be taken to decrease the soluble/insoluble ratio of chromium, e.g. adding reducing agent to prevent oxidation.

ACKNOWLEDGEMENTS

The support of OTKA (Hungarian National Foundation of Scientific Research) No. T029195 as well as the Intergovernmental Fund for Science and Technology Project No. A/8-2000 (covering exchange of scientists), is gratefully acknowledged.

REFERENCES

[1] MSZ 21978-9:1998. Investigation of hazardous wastes – Making of waste leachates for physical, chemical and ecotoxicological investigation. Hungarian Standard Institute in Budapest

[2] Boikova, A.: Solid solution of cement-minerals. Publisher: "Nauka", Leningrad 1974 (Russian) pp. 21-29

[3] Opoczky, L., Fodor, M., Révay Zs.: Cement chemistry and environmental effects of chromium introduced by waste materials. 14. Internationale Baustofftagunk (IBAUSIL), Weimar, 2000, Vol. 1. pp. 1-0061 – 1-0668

CHEMICAL AND ENVIRONMENTAL ASPECTS OF HEAVY METALS IN CEMENT IN CONNECTION WITH THE USE OF WASTES

L. Opoczky [1], M. Fodor [1], D.F. Tamás[2], and J. Tritthart [3]

[1] Cement Research and Development Ltd, Budapest, Hungary. E-mail: cemkut@mail.datanet.hu
[2] University of Veszprém, Hungary. E-mail: tamasf@almos.vein.hu
[3] University of Graz, TVFA, Graz, Austria. E-mail: tritthart@tvfa.tu-graz.ac.at

Martha Fodor

Received her M.Sc in Chemistry in 1968 (Eötvös Loránd University, Budapest)

Her first job was „chemical assistent", at the Spectroscopical Laboratory of the Hungarian Optical Works, to be followed by „analysis officer" from 1970.

From 1974 she became „scientific officer" at the Department of Silicate Chemistry, Central Institute of Research and Development for the Silicate Industries (SzIKKTI); later she became laboratory manager of the Research and Investigation Department.

Received her Ph.D. in chemistry in 1983, at the University of Chemical Engineering (Department of Silicate Chemistry).

In 1981-82 she spent 9 months at the University of Massachusetts, in the Spectroscopy Group of Prof. Ramon M. Barnes.

From 1995 she is CEO of the Cement Research and Development Co (CEMKUT); from 1998 CEO of the full organisation Hungarian Association of the Cement Industry.

Author, co-author or editor of >100 papers, books; author and organizer of numerous technical conferences, meetings.

Secretary-in-Chief of the Scientific Society of the Silicate Industry, member of several scientific committees and associations.

Speaks, reads, write in German, English and Russian.

IMPROVED SUPERPLASTICIZERS FOR HIGH PERFORMANCE CONCRETE

Annika Kauppi[1], Phil F.G. Banfill[2], Paul Bowen[3], Laurent Galmiche[4], Yves F. Houst[3], Françoise Lafuma[4], Urs Mäder[5], François Perche[3], Berit G. Petersen[6], Kåre Reknes[6], Irene Schober[5], Alain Siebold[3] and David Swift[2]

[1] Institute for Surface Chemistry, Stockholm, Sweden. E-mail: annika.kauppi@surfchem.kth.se
[2] Department of Building Engineering and Surveying, Heriot-Watt University, Edinburgh, UK. E-mail: p.f.g.banfill@hw.ac.uk, d.s.swift@hw.ac.uk
[3] Powder Technology Laboratory, Materials Science and Engineering Department, Swiss Federal Institute of Technology, Lausanne, Switzerland. E-mail: yves.houst@epfl.ch, paul.bowen@epfl.ch, françois.perche@epfl.ch, alain.siebold@epfl.ch
[4] Laboratoire de Physico-Chimie des Polymeres, Université Pierre et Marie Curie, Paris, France. E-mail: Laurent.galmiche@espci.fr, francoise.lafuma@espci.fr
[5] Sika AG, Zürich, Switzerland. E-mail: urs.maeder@ch.sika.com, irene.schober@ch.sika.com
[6] Borregaard Lignotech, Sarpsborg, Norway. E-mail: kare.Reknes@Borregaard.com, berit.gudding.petersen@borregaard.com

ABSTRACT

This paper describes preliminary results from a part of a current European Research Programme project addressing superplasticizers of improved properties for cement and concrete. In the project we are producing new superplasticizers and testing them in model systems and real concrete systems. The main goal of the project is to carefully study the mechanisms involved in the adsorption of polymers in concrete and the mechanisms with which they work. In this paper preliminary results are presented for one modified polycarboxylate polymer and one lignosulfonate polymer. Results are from rheological measurements, adsorption studies and AFM-colloidal probe measurements show the importance of the ionic concentration of the dispersing media both for model MgO powders and cement suspensions. The ionic medium composition (with or without Ca) influences in particular the polycarboxylate polymers. The ionic strength seems to control the relative contributions of the steric and electrostatic contributions to the repulsive interparticle forces, which manifests itself in a modification of the rheological behaviour.

1. INTRODUCTION

The performance demand on concrete is continuously increasing and this leads to the continuous development of new improved chemical admixtures used in concrete. Superplasticizers, one of the most important classes of chemical admixtures, are used for mainly three reasons, i) to produce highly workable concrete for easy placement ii) to produce concrete with a low water content for higher strength and durability or iii) to produce concrete with low cementitious and water contents for better economy. In this project we take a fundamental and systematic approach to analysing the plasticizing mechanisms of two classes of superplasticizers, modified polycarboxylates and lignosulfonates, in different cementitious systems. Our approach will be to carefully study the interaction between the polymer and the powder (cement or model system) to get more information on how the polymer is adsorbed on the surface and what the dominating dispersing mechanisms are. This approach demands that we use a model system for cement, since for example in the AFM-

colloidal probe measurements a reactive surface would not be possible to use. We have chosen to use dead burnt MgO as a model system. This has previously been used by Flatt *et. al.* with good results [1].

The results presented in this article are the first results in a larger project. The measurements have been performed in different labs and during slightly different conditions. This makes the interpretations a bit more difficult, but we think that the results are important and that they give information that is important for the understanding of the adsorption and the performance of superplasticizers in concrete.

2. EXPERIMENTAL

2.1 Materials

2.1.1 Polymers

The polymers used are experimental products specially produced for this project. The lignosulfonate polymer (LS) was produced by ultrafiltration of a sample of fermented, sugar reduced sodium LS. The ultrafiltration was carried out as a two-step ultrafiltration, starting with a small cut-off ultrafiltration membrane, followed by running the retentate through a high cut-off ultrafiltration membrane. The ultrafiltration was done to increase the molecular weight to a level above the molecular weight of current commercial available LS. Sugars and other "impurities" were also removed during the ultrafiltration. The overall MW for the LS polymer is about 157,000 g/mol.

The modified polycarboxylate polymer (PCP) is a branched polymer with methacrylic acid backbone and side chains of polyethylene glycol. The side chains are bound by ester linkages to the polymethacrylic backbone. The overall MW of the molecule is 45.000 g/mol.

2.1.2 MgO model powder

We used dead burnt MgO from Martin Marietta Magnesia (USA) of type MagChem P-98 in this work as non-reactive model powder for cement. This powder has a particle size distribution of D(v, 0.1)=2.88 μm, D(v, 0.5)=17.59 μm and D(v, 0.9)=54.65 μm with a span of 2.94 as measured by laser diffraction. To perform careful analysis on the interaction between the polymers and a powder it is absolutely necessary to use a model system for cement, since the errors would be too large with a reactive powder like cement. The reactivity of the powder has been tested by contacting the powder with 0.01M NaOH during 30 minutes, 1 hour and 24 hours, followed by filtering and drying at 110°C. The BET surface area was measured on the dry powders and the results indicate that there is a rapid hydration of the surface of the grains on contact with the solution, between 30 and 60 minutes no further change was observed. The powder is therefore regarded as a good "non-reactive" model powder for cement during this 30-minute period after an initial 30 minutes in contact with 0.01 M NaOH. The surface of the powder would then consist of $Mg(OH)_2$. The main characteristics and properties of this model powder are described in another article submitted to this congress [2].

2.2 Methods

2.2.1 Rheology

Previous experience in the evaluation of superplasticized grouts led to the development of a special rotor head for the Carri-Med CSL500[2] specifically for use with high solids content suspensions. Thus when considering the rheological evaluation of the model powder pastes containing the experimental superplasticizers, the Helix B test head was the best available tool, combining accuracy of determination with an ability to prevent settling of solids during the test.

The testing procedure was as follows. The powder and liquid were weighed separately and mixed together for 30 seconds by hand and then the paste was poured into the test cup and the test sequence initiated. The paste was subjected to 2 minutes of stirring at a shear rate of 50 s^{-1}, before

the initial test run was carried out. The shear stress was measured at 20 controlled shear rate points from 0-10 s^{-1}, and then another 20 controlled shear rate points from 10-200 s^{-1}. The paste was stirred for a further 5 minutes at a shear rate of 500 s^{-1}, which is designed to break down any existing structure in the paste. The test procedure was then run again. The total time for the whole procedure was approximately 25 minutes.

2.2.2 Adsorption

Adsorption isotherms of the PCP and LS polymers on MgO were measured by the depletion method. In this method, the amount of polymer is measured in a solution before and after contact with the powder. The reduction in polymer concentration in the aqueous phase before and after contact is assumed to be the adsorbed amount. The polymer solutions are analysed by High Performance Liquid Chromatography (HPLC) with a light scattering detector for PCP and by UV spectroscopy for the LS polymer. The samples were prepared by mixing 10 g MgO with 18 ml 0.01 M NaOH for 30 minutes when the polymer is added. After a further 30 minutes the supernatant was recovered by filtering through a 0.45 μm filter before the polymer concentration was measured.

The adsorption of the polymers onto MgO was also followed by acoustophoretic measurements using an AcoustoSizer II from Colloidal Dynamics. 53 g MgO powder was dispersed in 200 ml NaOH 0.01 M (gives a slurry of 21 wt%) under vigorous agitation and ultrasonic treatment for 15 minutes. The suspension was then allowed to cool down to 25 °C for another 15 minutes. Once the solution was loaded into the sample reservoir and pumped up through the measurement cell, polymer solution was then added as aqueous solution with a microburette. Between two additions, the suspension was allowed to equilibrate.

The AcoustoSizer II is only sensitive to particles that are smaller than 10 μm. Since our powder contains also larger particles the apparatus sees it as a dilution of the sample with large, invisible particles, and hence we detect a lower value than the real one. We have tested this interpretation by using an air-classified version of the MgO used in this project. This powder has only particles smaller than 10 μm and here we detect higher negative charge on polymer addition compared to the MgO powder with both small and bigger particles. Further work is being carried out to confirm that this is a quantitative approach. However, the trends that are found in our results for powders with particles >10 μm are good qualitative indications of the trends and very interesting to follow.

2.2.3 AFM colloidal probe

The atomic force microscope (AFM) was originally developed as a means of high resolution imaging of non-conducting samples. The AFM can be used not only as an imaging tool, but also as a powerful technique for surface force measurements [3]. The magnitude of the normal surface force between the tip and the sample can easily be evaluated by approaching and retracting the tip and registering the deflection as a function of the movement of the scanner in the Z direction. The raw data is transformed into a true force curve by a series of manipulations. The zero force level and the point where the surfaces are in "hard contact" are established from the raw data. The spring constant of the cantilever is used to transform the deflection data into force units, and a force curve as a function of surface separation is obtained [4]. Both attractive and repulsive forces can be measured, corresponding to negative and positive deflection respectively. By using a liquid cell, surface forces in organic or aqueous media can be studied.

Instead of using the tip as one surface in a surface force measurement, a customised probe can be attached at the apex of the cantilever. This is called the "colloidal probe technique" [5]. Although the probe can be made of any material it is preferable that it has a well-defined geometry *e.g.* a sphere shape, so that the data can be correctly interpreted.

The AFM liquid cell was mounted with a flat MgO substrate and a cantilever with a sphere of MgO. The cell was first flushed with 1 mM KCl, and then a first measurement was performed. After this the cell was flushed with a polymer solution containing 100 ppm polymer (pH 10). The adsorption of the polymer on the two surfaces was allowed to equilibrate for about 30 minutes before the polymer solution was flushed away with 1 mM KCl. After these procedures measurements were performed in different electrolytes. After each flushing with a new electrolyte the cell had to rest for about 15 minutes to allow all motions in the liquid and the cantilever to stop.

An AFM microscope has previously been used to measure the forces in cementitious systems in liquid by other groups [6-9], but this is believed to be the first time, that MgO has been used as a model system to study the forces between surfaces in liquid covered with superplasticizer.

2.3. Results

2.3.1 Rheology

Initial tests with the supplied MgO powder P98, showed that it was coarser than expected, *i.e.* than a typical OPC. It was possible to reduce the w/c ratio to 0.25 and still test the paste in the CSL. A check of the lowest tolerable w/c ratio of the three chosen OPCs gave a realistic lower w/c ratio limit of 0.375. Earlier work had indicated that the surface area of the powder under test has a marked influence on the observed rheology [10]. To verify this 1kg of the MgO powder was ground in a ceramic ball mill for one hour (MgO(B)), and a second 1kg was ground for 2 hours (MgO(C)). Comparison of the 25 µm residues revealed that for MgO(A) 55% passed a 25 micron sieve, for MgO(B) 74% and for MgO(C) 85%, indicating that MgO(C) was near to the specified OPC. A secondary influence was identified to be the electrolyte environment surrounding the cement particles. To simulate this a synthetic 'soup' was made up based on a chemical analysis of cement electrolyte solutions. The soup was made from 1 litre of water saturated with $Ca(OH)_2$ and in which 7 g Na_2SO_4, 6.5 g K_2SO_4 and 6 g KOH were dissolved. The results show that the slurry rheology is very sensitive to powder surface area, with MgO(C) giving a similar performance to the Cauldon OPC at shear rates up to 60 s^{-1} (Figure 1). It is also apparent that the slurries are more fluid when made with the soup compared to slurries made with water; the effect lessening with increasing 25 µm residue such that with MgO(A) the difference is minimal.

The PCP and LS polymers have been tested on MgO(C) pastes of 0.375 w/s ratio at a loading of 0.175 % (by weight of cement) for the PCP polymer and 1.0 % for the LS polymer (Figure 2). The PCP polymer shows a marked thickening of pastes made with soup compared to those made with water. In contrast, the LS polymer shows no such effect in pastes made with either water or soup. This indicates a different dispersion mechanism compared to the PCP polymer.

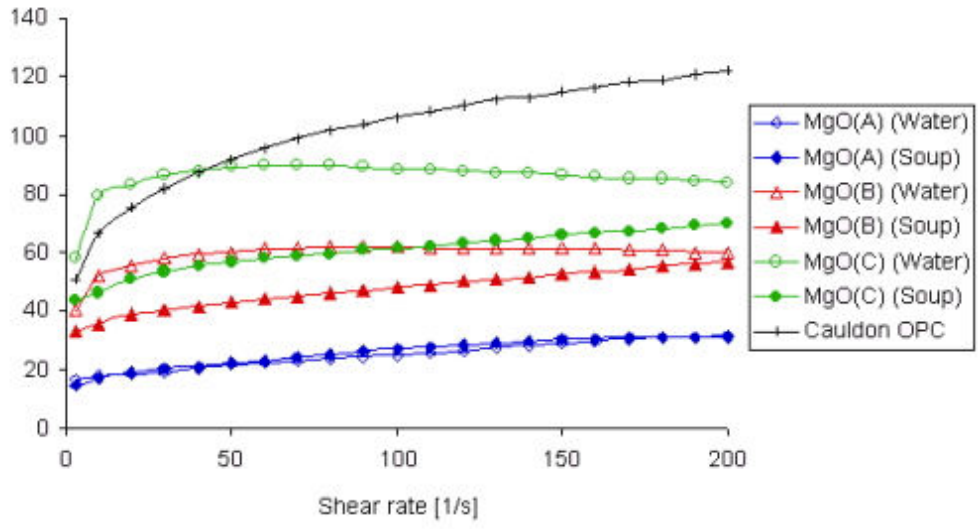

Figure 1. Rheology of MgO powders made from as-received (A) and milled (B,C) powders with soup and water compared to OPC w/c=0,375.

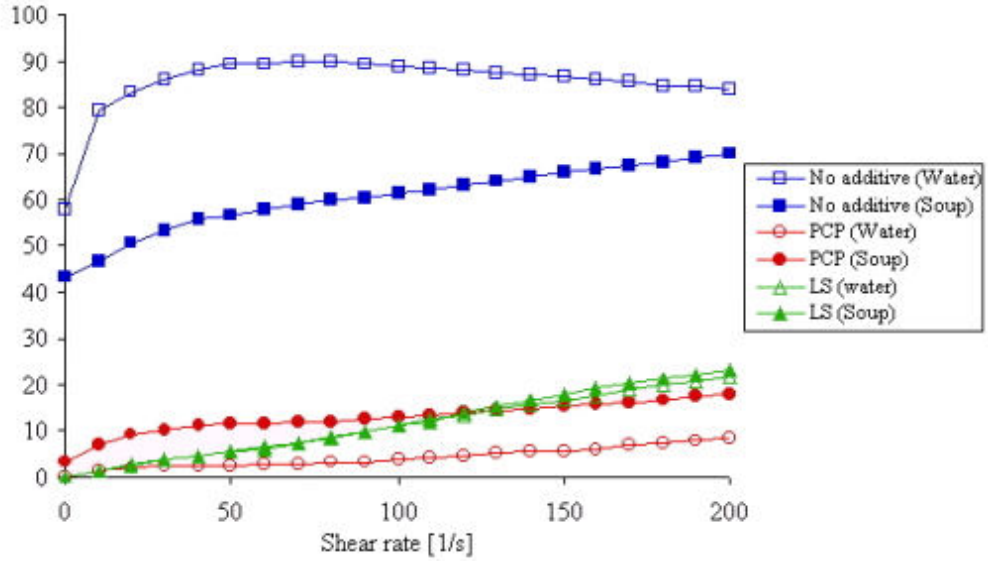

Figure 2. Rheology of MgO(C) with no additive, 0.175% PCP or 1% LS polymer in water and soup.

2.3.2. Adsorption

The adsorption measurements of PCP and LS presented in Figure 3 indicate that the adsorbed amount of polymer increases sharply for both polymers to a plateau value between 1 and 1.2 mg/g (milligram polymer per gram MgO). For PCP the plateau is reached at an initial polymer/powder ratio between 3 and 4 mg/g whereas for the LS polymer it is reached already at 2 mg/g. As can be seen in figure 3, the uncertainty in the measurements of the PCP polymer is rather large (about 20%). This is not very satisfactory, but still gives a good indication regarding the adsorption behaviour. The adsorption was also followed by acoustophoretic measurements. In Figure 4 the results of zeta potential as a function of polymer concentration are shown, and here we see that the powder has a positive charge without polymer, but that adsorption of either polymer gives the surface a negative charge. The LS polymer gives a slightly more negative charge compared to PCP. The same type of adsorption behaviour can be observed from the electroacoustics measurements as from the depletion measurements, with a sharp increase followed by a plateau, although the plateau is not as clear in the electroacoustics measurements as in the depletion measurements.

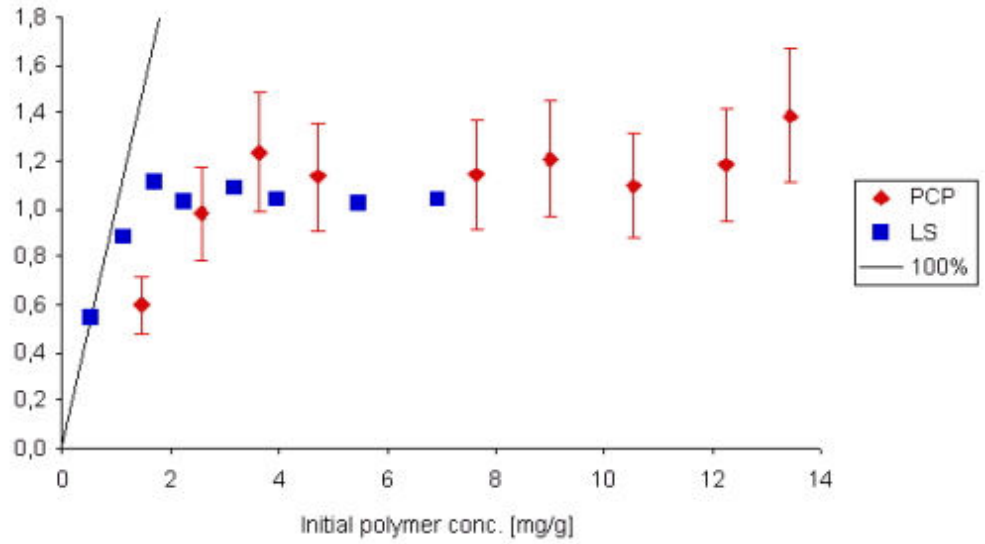

Figure 3. Adsorption Isotherms of PCP and LS on MgO measured by the depletion method.

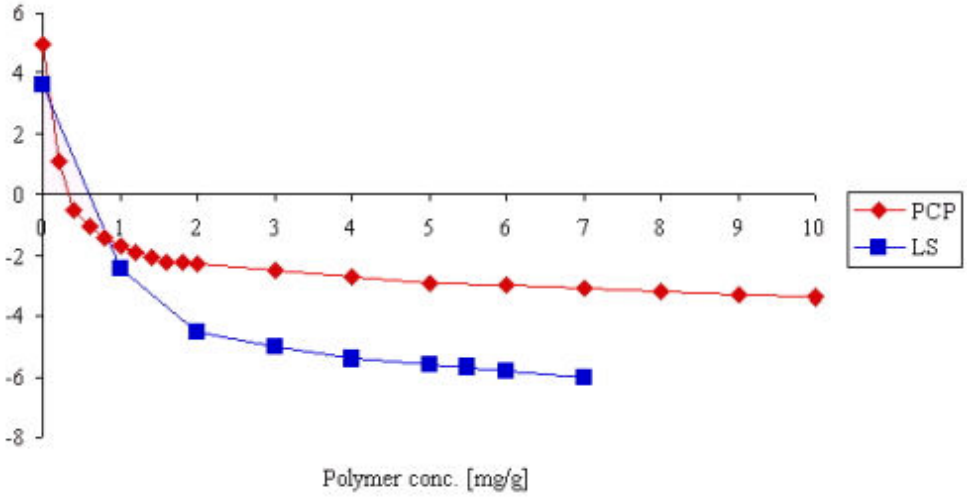

Figure 4. Variation of zeta potential as a function of added PCP or LS.

2.3.3 AFM colloidal probe measurements

The AFM colloidal probe measurements are performed to get an idea of how the polymer is adsorbed onto the MgO surface and what mechanisms are dominant in the dispersion of the powder. The two forces that are generally thought to be present when polymers are used to disperse a powder are electrostatic stabilisation, where surface charges induce a repulsion, and steric stabilisation that works through physical overlap of the polymer chains. The electrostatic effect is strongly affected by the ionic strength of the surrounding electrolyte since charges in the electrolyte screen the electrostatic force, therefore the electrostatic force acts over shorter distances for electrolytes with higher ionic strength. The steric forces, on the other hand, are not directly affected by the ionic strength of the solution, unless this has a strong effect on the conformation of the polymer. In figure 5 below the force/radius between a flat MgO surface and an MgO sphere covered with PCP and in KCl electrolytes of different ionic strength is shown together with EDL (Electric Double Layer) curves. The EDL curve is the expected slope that the force curve would have for different ionic solutions if only electrostatic forces were present in the system. The curves are not full DLVO calculations with boundary conditions but rather approximations according to the formula:

$$F/R = B * e^{-\kappa D} \tag{1}$$

where F is the force, R the radius of the sphere used, B a constant, D the distance between the flat surface and the sphere, and κ is the *Debye-Hückel parameter* given by:

$$\kappa = 3.288\sqrt{I} \tag{2}$$

at 25°C in a 1:1 electrolyte where I is the ionic strength of the solution [5, 11]. As can be seen in figure 5 the curves for 1, 10 and 100 mM KCl all match the slopes of the EDL lines very well for distances above about 4 nm, but for shorter distances they do not overlap at all with the EDL lines. Here on the other hand, the three curves overlap with each other. These results indicate that for distances longer that 4 nm between the two surfaces the electrostatic force is the dominant force for all electrolytes tested here, but for shorter distances steric forces are the dominant forces.

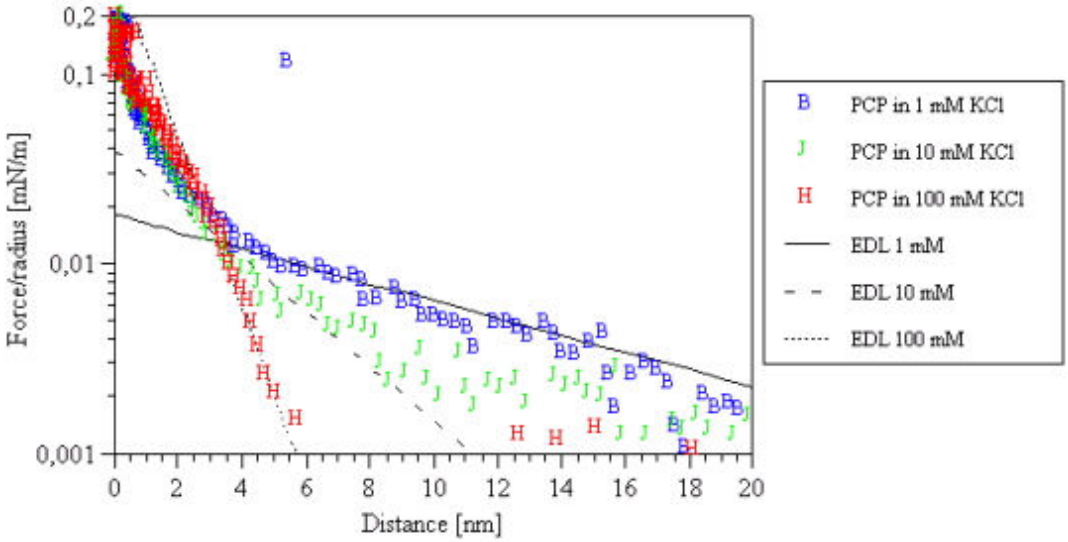

Figure 5. Force diagrams for two MgO surfaces covered with PCP in 1, 10 and 100 mM KCl, as measured with the AFM colloidal probe technique.

The results presented in Figure 5 are obtained with the PCP polymer adsorbed from a 10 mM solution of $CaCl_2$ at pH 10. We have also tried to adsorb the polymer from water and from a 100 mM KCl solution, and in both cases the polymer initially seems to adsorb onto the surfaces, but the adsorption does not seem to be very strong. When the measurements are performed the liquid cell containing the MgO surfaces are flushed with electrolytes of different ionic strength. When this was performed for the polymers adsorbed from water and KCl we observed a desorption of the polymer whereas this was not the case when the polymer was adsorbed from a $CaCl_2$ solution. We interpret this as being the effect of the Ca^{2+} ions on the adsorption of the polymer, making the adsorbing bond stronger by perhaps bridging the polymer-MgO interface.

3. DISCUSSION

From the rheological measurements in Figure 2 we could see that the effect of adding the "soup" compared to measuring in a water slurry was large both for the slurry without polymer and on addition of PCP but very small when LS was added. For the MgO slurry without polymer the flowability was increased on use of the soup compared to water, and this effect was largest for the powder with the finest particles (Figure 1). One explanation for this behaviour could be that the powders are agglomerated both in water and in soup, but that they are more highly aggregated in water. When the slurry is sheared, the agglomerates are broken, but it is much easier to break agglomerates between large particles compared to agglomerates between small particles. Therefore the aggregates in the MgO(A) slurries both with water and soup are broken rather easily, and we cannot detect any marked difference between them. For the slurries made with MgO(B) and MgO(C) more force is needed to break the agglomerates, and we detect a clear difference between the aggregated powder in soup and the strongly aggregated powder in water. As the shear rate is increased we see that the difference between soup and water get smaller and smaller, and this confirms this theory since more agglomerates are expected to be broken at a high shear rate. The experiments most relevant for cement slurries and concrete are probably those made with soup since the soup is an electrolyte that mimics cement water.

When PCP is present in the MgO slurry the flowability is decreased on use of the soup compared to water, *i.e.* the opposite behaviour compared to the pure MgO slurry, and when LS is used there is almost no difference in the flowability between water and soup. This indicates that the soup has a negative influence on the PCP polymer. One explanation could be that the polymer adsorbs more easily to the MgO powder in water, probably because the surface is positively charged (pH below

iso-electric point, (i.e.p.) and the PCP polymer is negatively charged, whereas when the soup is used the MgO particles have a negative charge (pH above i.e.p.), and there could also be a competitive adsorption from the ions in the soup. Another explanation could be that the PCP polymer conformation is affected by the ions in the soup giving a less favourable conformation. Even if there is a difference in the performance with water and soup the flowability is much higher in the presence of PCP than without. There could be several reasons why the LS polymer is not affected by the change from water to soup and this could be that it does not have any conformational changes on addition of soup, that the adsorption of the polymer is not affected by the soup or that it is added in such high amount that even if the adsorption is affected there is still enough polymer there to disperse the system. According to the adsorption measurements presented in Figure 3 the used PCP polymer concentration of 0.175 % is about half the concentration needed to reach the adsorption plateau whereas for the LS polymer the concentration 1 % is 5 times the concentration needed to reach the adsorption plateau. It would be interesting to see if the observed effects are concentration dependent.

Other authors have also recognised the importance of both cations and anions for the adsorption of polycarboxylate type polymers on different surfaces [12-14]. We conclude that since the ions seem to have such large importance for the adsorption of polymers, and also for the rheology of the system without polymer, it is very important to work with a relevant electrolyte when using a model system for cement and further detailed investigations are being carried out in this light. However we believe that the soup used in this work contain the essential ingredients for a model electrolyte and are confident that when used together with MgO it creates a relevant model system for cement slurries.

The measurement of the adsorption of the polymers was performed in two different ways in this work, a depletion technique and through acoustophoretic measurements. The results are rather similar but with the plateau reached at a slightly higher polymer concentration for the acoustophoretic measurements. The measurement procedure was rather different for the two methods. In the depletion measurements, the polymer concentration was measured in a solution that was filtered and fed into a machine, whereas in the acoustophoretic measurement the results were measured directly in the relevant slurry. Therefore we prefer the latter measurement technique that imposes less work in the laboratory and is more reliable at least for screening different polymers.

The AFM colloidal probe results presented in Figure 5 show that the PCP polymer gives steric repulsive forces between the two MgO surfaces up to 4 nm, indicating that the polymer layers are about 2 nm thick, since both surfaces are believed to be covered by polymer. This indicates that the PEG chains of the polymer have adopted a rather coiled conformation on the surface. The observation that the polymer desorbs more easily when the polymer has been adsorbed from water or a 100 mM KCl electrolyte compared to when the polymer is adsorbed from an electrolyte containing 10 mM $CaCl_2$ indicates that the Ca^{2+} ions make the interaction between the MgO surface and the polymer stronger. This might sound a bit contradictory to the statement above that the PCP polymer is adsorbed more readily from a slurry made from water than from one made with “soup”. However, the strength of the interaction and the adsorption amount does not have to follow the same trend. We also have to remember that the AFM measurements are performed at pH 10 independent of the other ingredients of the electrolyte, whereas for the rheological measurements in this work the pH is different between the slurry made with water and the one made with soup. The AFM liquid cell can unfortunately not cope with a pH higher than 10, since it is made from glass.

4. SUMMARY

Preliminary results using an MgO powder as a model for cement have shown interesting results for both effects of polycarboxylate and lignosulfonate superplasticizers. The lignosulfonates are more robust and the make up of the surrounding electrolyte has little effect on MgO suspension rheology. The lignosulfonates induces a small negative potential on the powder surface and is an effective dispersant. The polycarboxylate is also an effective dispersant for the MgO model powder but is more sensitive to the electrolyte composition. The results suggest an interaction between Ca^{2+} ions and the polycarboxylate-MgO interface, which has an important influence on the polymer adsorption strength. Further work on the electroacoustics method and adsorption isotherms should help clarify the nature of this interaction. The next steps in the project are to extend the work to other polycarboxylate and lignosulfonate systems and then move toward a move quantitative description of these systems

ACKNOWLEDGEMENTS

This work was funded by the 5th European Framework Programme (Contract G5RD-CT-2001-00435). It also received funding from Vinnova in Sweden and from the Swiss Federal Office for Education and Science (contract No 00.273-1).

REFERENCES

[1] Flatt, R.J., Houst, Y.F., Bowen, P., Hofmann, H., Widmer, J., Sulser, U., Mäder, U., Burge, T.A. Interaction of superplasticizers with model powders in a highly alkaline medium, Fifth CANMET/ACI international conference on Superplasticizers and other chemical admixtures in concrete, (Malhotra, V.M., Ed.) ACI, Farmington Hill, Mi, USA, 1997, SP-173, pp. 743-762.

[2] Flatt, R.J., Bowen, P., Siebold, A., Houst, Y.H. Cement model powders for superplasticizer properties studies, Submitted to the 11 the ICCC.

[3] Cappella, B., Dietler, G., Force-distance curves by atomic force microscopy, Surf. Sci. Rep., vol.34, 1999, pp.1-104.

[4] Cleveland, J. P., Manne, S., Bocek, D. and Hansma, P. K. A non-destructive method for determining the spring constant of cantilevers for scanning force microscopy, Rev. Sci. Instrum., vol.64, 1993, pp.403-405

[5] Ducker, W., Senden, T. J. and Pashley, R. M. Direct measurement of colloidal forces using an atomic force microscope, Nature, vol. 353, 1991, pp. 239-241.

[6] Uchikawa, H., Hanehara, S. and Sawaki, D. The role of steric repulsive forces in the dispersion of cement particles in fresh paste prepared with organic admixture, Cement and Concrete Research, vol.27(1), 1997, pp.37-50.

[7] Finot, E., Lesniewska, E., Mutin, J.-C. and Goudonnet, J.-P. Investigations of surface forces between gypsum crystals in electrolytic solutions using microcantilevers, Journal of chemical physics, vol.111(14), 1999, pp.6590-6598.

[8] Mansoutre, S., Colombet, P. and Van Damme, H. Mechanisms of action of a poly(naphthalene sulfonate) based superplasticizer on the rheology of paste of tricalcium silicate at very early ages, Sixth Canmet/ACI International Conference on Superplasticizers and other Chemical Admixtures in Concrete, Nice, 2000, Supplementary papers, pp.353-366.

[9] Lesko, S., Lesniewska, E., Nonat, A., Mutin, J.-C., Goudonnet, J.-P. Investigation by atomic force microscopy of forces at the origin of cement cohesion, Ultramicroscopy, vol.86, 2001, pp.11-21.

[10] Swift, D.S. Banfill, P.G.F., To be published.

[11] Israelachvili, J.N Intermolecular & Surface Forces, Academic Press, London, 1991.

[12] Yamada, K. and Hanehara, S. Interaction mechanism of cement and superplasticizers -The roles of polymer adsorption and ionic conditions of aqueous phase, Concrete Science and Engineering, vol.3, 2001, pp.135-145.

[13] Yamada, K., Ogawa, S. Hanehara, S. Controlling of the adsorption and dispersing force of polycarboxylate-type superplasticizer by sulfate ion concentration in aqueous phase, Cement and Concrete Research, vol.31, 2001, pp.375-383.

[14] Sun, J., Bergström, L., Gao, L. Effect of Magnesium ions on the adsorption of poly(acrylic acid) onto alumina, J. Am. Chem. Soc., vol.84(11), 2001, pp.2710-2712.

IMPROVED SUPERPLASTICIZERS FOR HIGH PERFORMANCE CONCRETE

Annika Kauppi[1], Phil F.G. Banfill[2], Paul Bowen[3], Laurent Galmiche[4], Yves F. Houst[3], Françoise Lafuma[4], Urs Mäder[5], François Perche[3], Berit G. Petersen[6], Kåre Reknes[6], Irene Schober[5], Alain Siebold[3] and David Swift[2]

[1] Institute for Surface Chemistry, Stockholm, Sweden. E-mail: annika.kauppi@surfchem.kth.se
[2] Department of Building Engineering and Surveying, Heriot-Watt University, Edinburgh, UK. E-mail: p.f.g.banfill@hw.ac.uk, d.s.swift@hw.ac.uk
[3] Powder Technology Laboratory, Materials Science and Engineering Department, Swiss Federal Institute of Technology, Lausanne, Switzerland. E-mail: yves.houst@epfl.ch, paul.bowen@epfl.ch, françois.perche@epfl.ch, alain.siebold@epfl.ch
[4] Laboratoire de Physico-Chimie des Polymeres, Université Pierre et Marie Curie, Paris, France. E-mail: Laurent.galmiche@espci.fr, francoise.lafuma@espci.fr
[5] Sika AG, Zürich, Switzerland. E-mail: urs.maeder@ch.sika.com, irene.schober@ch.sika.com
[6] Borregaard Lignotech, Sarpsborg, Norway. E-mail: kare.Reknes@Borregaard.com, berit.gudding.petersen@borregaard.com

Annika Kauppi

Dr Annika Kauppi is currently the area manager of concrete Admixtures at the Materials and Coatings Section at the Institutefor Surface Chemistry in Sweden. She has been working with surface chemistry related to cementitious materials for the past 5 years. Her background is basic academic training in chemistry followed by a PhD in Inorganic Chemistry at Uppsala University in Sweden.

THE EXPERIMENTAL LIME KILN: PRODUCTION AND CHARACTERISATION OF SUSTAINABLE LIME BINDERS

John J. Hughes[1], Phillip F.G. Banfill[2] and David S. Swift[2]

[1]Advanced Concrete and Masonry Centre, University of Paisley, High Street, Paisley, Scotland.
E-mail: john.hughes@paisley.ac.uk
[2]Dept. Building Engineering and Surveying, Heriot-Watt University, Edinburgh, Scotland.
E-mail: p.f.g.banfill@hw.ac.uk and d.s.swift@hw.ac.uk

ABSTRACT

In industrialised nations the technology of using lime binders was well established before the advent of cement, but has now been lost. However, much of the historic built environment predates modern cements and restoration and conservation projects on such buildings require binders which are compatible with the original limes. Contemporary industrial production of lime gives a product which is inappropriate in many ways and there is much interest in rediscovering the complexity of the original materials. In addition, lime is in many ways a more sustainable product than cement and offers advantages in situations where great strength or rapid hardening are not necessary.

An Experimental Lime Kiln (ELK) of 20 tonne capacity has been constructed and fully instrumented. It is a single shaft vertical kiln for use in a traditional batch process. Monitoring of the burning process includes recording of inlet air flow, temperature distribution and exit gas composition. It offers, for the first time, the integration of the properties of source limestone, fuel type and burning regime with the final properties and performance of traditionally produced lime based mortars and related materials. It will permit analogous studies of historic material and direct experimentation to unravel the complexity of historic production and working practices.

Details of the design and construction of the ELK are given and selected experimental results are presented to give insights into the relationship between raw material, product structure and properties and current research programmes outlined.

1. INTRODUCTION

The ELK is a facility for the production of fresh quicklime for the development of better building mortars, renders, grouts and plasters, primarily for use in the conservation of historic masonry structures, but also ultimately to produce better products for contemporary building works.

Awareness is increasing of the benefits of using appropriate, compatible materials, for the conservation and repair of historic masonry buildings. The use of inappropriate mortars, particularly those containing cementitious, hydraulic components where none were used originally has caused damage to historic fabric, including increased stone decay and the early loss and failure of the mortars, through spalling and leaching, for example.

In the study of the properties of historic mortars effort was initially directed toward the identification of composition, especially the ratio of binder to aggregate, and the hydraulic or non-hydraulic composition of the binder itself using wet chemical techniques [1, 2]. Increasingly,

Proceedings of the 11th International Congress on the Chemistry of Cement (ICCC)
'Cement's Contribution to the Development in the 21st Century'
Hosted by: The Cement and Concrete Institute of South Africa
CD-ROM produced by: Document Transformation Technologies
11 - 16 May 2003, Durban, South Africa
ISBN Number: 0-9584085-8-0
Editors: Dr G. Grieve and G. Owens
Congress Organised by: Event Dynamics

however, more information is sought on the detailed composition and texture of historic binders. For example, the identification of hydraulic components in 19th century mortars by Callebaut et al [3] recently began a debate about the possibility of the presence of hydraulic components such as C_3S in early natural hydraulic mortars and cements, and the technology employed in their manufacture.

Work by Hughes and Cuthbert on the petrography of historic mortars has partially clarified their complex component assemblages. Features that relate to the raw materials, the burning process and the post production hydration and use in mortars are becoming clear [4]. Comparisons with current commercially available limes, even when aged for up to ten years as mortar, reveals a world of difference from their historic counterparts [5]. This has raised the question of whether our current limes and restoration mortars are compatible with the historic mortars they interface with and with stone and brick. The selective preservation potential of historic buildings means that the mortar materials examined today are likely to be the successful, compatible ones, the ones we need to emulate. However, it is clear that the materials we use to replace them with are not the same texturally, to a lesser extent compositionally and differ in their means of production.

To investigate the problem of producing compatible lime-based mortar materials for the conservation and restoration of historic masonry we must experiment directly on the methods of production to understand how to make quicklimes and mortars in the ways used historically to construct the buildings we are now trying to repair. Experimentation to reproduce historic burning methods will also allow us to investigate the links between the features observed in historic mortars and burning regime parameters. Experimentation in a small laboratory furnace, though useful for careful characterisation of material reactions, is ultimately inadequate as it does not replicate the complex set of conditions to be found within a real kiln, or the complexities of fuel-stone interaction which affect the physical and compositional properties of the resultant quicklime. Hence the need to burn lime on a sub-industrial scale, to allow us to test the parameters of traditional burning methods. This is the reasoning behind the inception of the ELK.

2. LOCATION

The ELK is located in Charlestown (Figure 1) a village on the north shore of the Firth of Forth, in east central Scotland. Charlestown is one of the most significant industrial archaeological sites in Scotland. From 1776, Charlestown was Scotland's largest limeworks, with 9 operational kilns at its harbour (that survive to this day), supplied by waggonways linking the limestone quarries to the north of the village directly to the kilns [6]. The hinterland of the village comprises large-scale near-surface outcrops of Carboniferous age limestone, which was easily extracted for lime production. The lime produced until the 1950s was used widely throughout Scotland for building and other industrial uses.

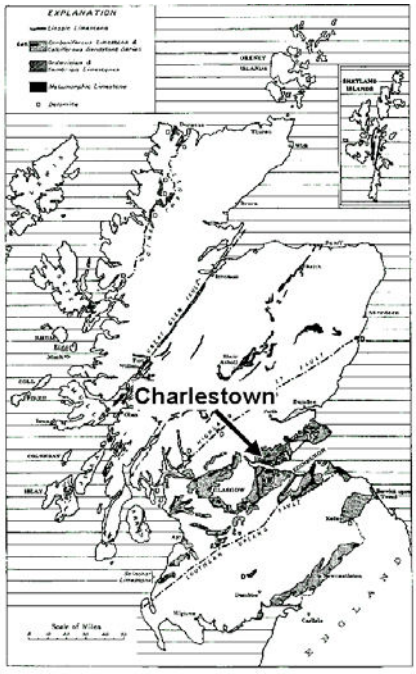

Figure 1. Location of the ELK at Charlestown, South East Fife. Map shows main outcrops of limestone in Scotland. From Robertson et al. (1949) [7].

3. DESIGN AND CONSTRUCTION

The ELK is a batch mode, single shaft vertical kiln. It has a capacity of up to 24 tonnes of combined fuel and stone. Full, computerised instrumentation is incorporated into the ELK, allowing the continuous monitoring of temperature, inlet air velocity and exhaust gas CO_2, CO and O_2 content. The ELK is a facility for fundamental, practical-based research into the

production of lime-based masonry binders using traditionally based methods of production.

The ELK site is located at the south west edge of the steeply banked rubble fill of the mid quarry site in Charlestown, where limestone for the production of lime was extracted for many years. The infill forms a steep bank against which the ELK was constructed. A reinforced concrete foundation slab was poured for the ELK itself, and to provide the basis for storage bays for stone and fuel. The concrete slab foundation is a minimum of 300 mm thick with 16 mm reinforcing bars at 200 mm spacing top and bottom, and with 40 mm minimum concrete cover.

Figure 2 shows cross sections through the ELK. An ash pit was constructed across the width of the kiln shaft and beneath a draw arch cast from Tri-Mor Hicast Super refractory concrete.

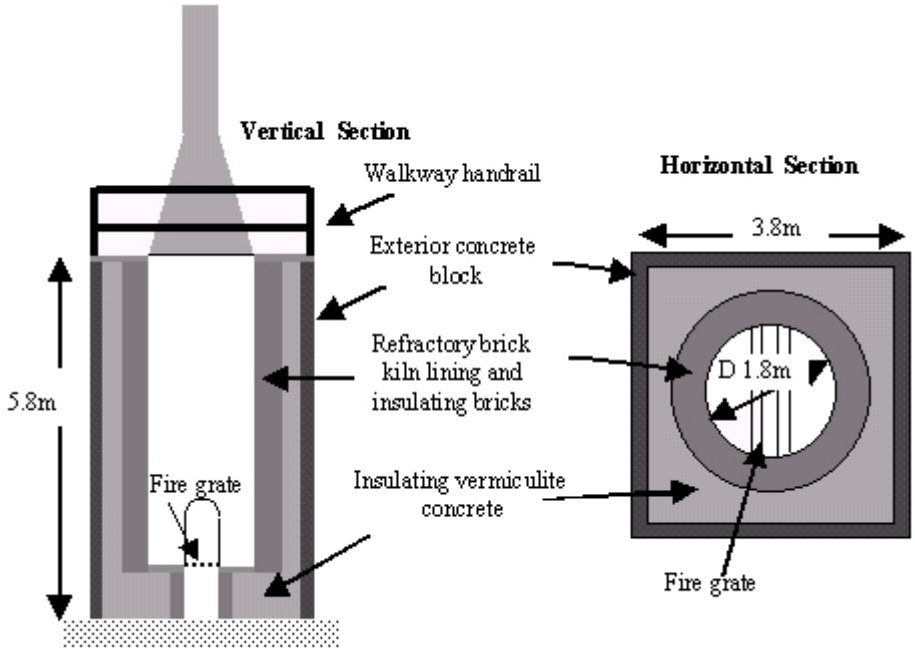

Figure 2. Vertical and horizontal cross sections through the ELK.

Figure 3. General side view, showing; mechanical hoist for top loading ELK, sloping front façade and restraining bars and end points of thermocouples arranged vertically on side next to hoist.

The circular shaft base was constructed from Burnaxe SP fireclay refractory bricks and finished at the level of the planned grate with a ring beam of refractory concrete. The ring beam was constructed with sufficient width to accommodate the double thickness brick shaft and the surrounding double thickness layer of Molar Supra insulating bricks (Figure 5). The brick kiln shaft then continued upwards to its full five metre height, construction being guided by a circular wooden former (Figure 4). The brick shaft was laid with 2 mm thick joints in fireclay, bentonite mortar. The surrounding insulating bricks were laid with bentonite clay and restrained by plastic strapping on every course.

Once the kiln shaft was complete the square concrete block skin was built up in a conventional brick bond using a 1:2 St Astier NHL 5 and topped out at the same level as the brick kiln shaft. The space between the block outer skin and the kiln shaft was then filled with a low strength insulating concrete of 1:2 St Astier NHL 3.5 : vermiculite. However, before the insulating concrete was poured, ducts for the monitoring sensors were inserted through the kiln shaft and the exterior concrete block skin (Figure 6). The holes for the sensor conduits were cored horizontally from the inside face of the kiln lining. The brick kiln shaft was also lined with paper before the concrete insulation was poured, to accommodate thermal movements between the shaft and the insulation during operation. Once the insulating concrete was in place the structure was closed off at the top by the pouring of a final refractory concrete slab, that provides a walking area for maintenance of the chimney and the control of kiln loading. The front elevation of concrete block skin extends laterally wider than the rear structure of the kiln and is on a slight 2 to 3 degree slope backwards (Figure 3). Metal restraining bars joined with tightened threaded ends and bolts wrap the kiln to counteract the thermal expansion and contraction forces that the kiln encounters during operation.

A steel firegrate runs along the length of the ash pit, and completely to the outside at the rear of the kiln. A steel frame fire door is fitted in two sections connected to the cast concrete door frame. The door itself is filled with refractory concrete. An interchangeable lower section is louvered to allow the airflow into the kiln beneath the grate to be controlled. It is on the inside of this section that an air velocity transmitter is fixed to measure the airflow. The welded steel chimney has in its lowest metre a double thickness steel cavity filled by an insulating blanket to reduce heat loss. The chimney has a welded door cut into its side, hinged to allow the loading of the kiln from above.

Temperature distributions around the interior surface of the kiln are continuously recorded using nine stainless steel K-type thermocouples placed through austenitic stainless steel (304) conduits inserted through the body of the kiln. The thermocouples rest 20 mm retracted from the interior surface of the kiln shaft brick lining. Temperatures are recorded by an ABB Instrumentation PR100 recorder linked to an Commander MR250 Chart Recorder. A hand-held thermocouple mounted on a 2 metre lance can be inserted through a further five vacant, normal steel conduits on the front and side of the kiln. These conduits can also be inserted into the centre of the kiln fill during loading. This permits the measurement of temperatures within the stone fuel mix while burning and the temperature in the wall of the kiln. A thermocouple is also inserted in the upper portion of the chimney, to record kiln exhaust gas temperature.

Gas compositions are monitored in a semi continuous fashion. CO, CO_2 and O_2 are measured by a Siemens Ultramat 23 gas analyser. Gas is collected at the vertical portion of the chimney and transferred by pipe to the analyser, via a simple moisture trap. Unfortunately, due to technical difficulties it was not possible in the burns completed to date to record the gas composition, so no data are presented here. Air flow into the kiln is recorded in the lower front door section using a Dwyer 640 Air Velocity transmitter. All the recording equipment are mounted on the outside of the kiln, protected from the weather in a wooden cabinet. Data from the monitoring is transferred through a permanent cable from there to a PC in nearby office accommodation, where it saves the data and allows it to be presented and interpreted on site.

Figure 4. Construction in progress, central circular kiln shaft rising from concrete base built around circular wooden former and with early stages of square outer concrete block skin.

Figure 5. Completed double thickness brick kiln lining with beginnings of double thickness block insulation, resting on refractory concrete ring.

Figure 6. Detail of one of 12 stainless steel conduits for thermocouple placement driven through outer concrete skin, insulating blocks and brick kiln lining, prior to pouring of insulating concrete.

4. OPERATION OF THE ELK.

Before loading the kiln with stone and solid fuel, a layer of wood pieces, coke and anthracite is first placed across the base of the kiln shaft and over the grate to establish the fire after lighting. Loading of the ELK is performed by the use of a hoist equipped with a bucket which is filled manually at ground level and then raised to the hatch on the chimney where it tips over and empties into the kiln shaft (see Figure 3). The hoist can hold approximately 80kg and loading in this fashion can take up to 3 days. The limestone and fuel are mixed together and are not layered. However, the overall distribution of fuel can be altered in order to control the pattern of burning. The fuel used to date is a mixture by mass of 1 part high volatility Pet-coke and 1 part low volatility anthracite. This was mixed in the initial firings in a concentration of 1 part fuel to 9 parts stone, by mass, mixed in the kiln. The fuel types were chosen for a clean burn and low ash content.

To light the kiln, a zinc plasterer's bath is filled with wood and paper kindling and set alight. This is then inserted into the kiln underneath the grate which is covered with more fuel. Early on in the burning cycle if the kiln burns a little slowly or does not seem dynamic enough to reach the temperatures required for calcination the draught can be assisted using an electric fan that can be attached to the door of the kiln below the grate. During operation the temperature is monitored continuously and changes made to draught conditions as seen necessary.

Figure 7 schematically depicts the locations of the thermocouples within the kiln and Figure 8 shows the temperature evolution during an actual firing of the ELK [8]. The evolution of a burn is not even throughout the kiln.

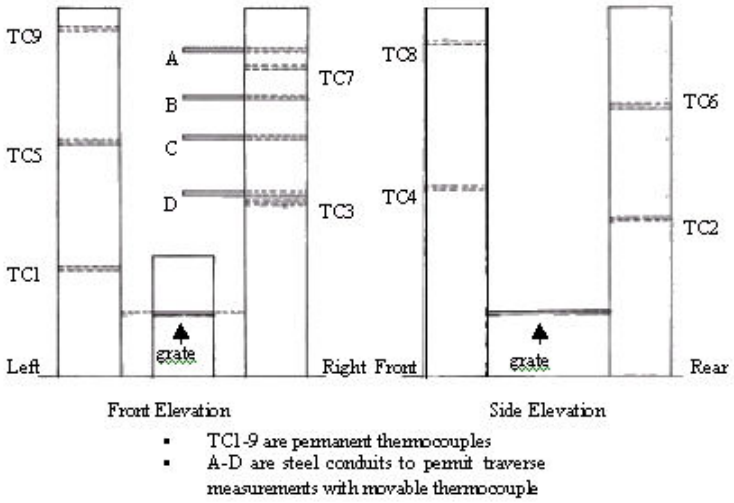

Figure 7. Schematic diagram of ELK showing locations of thermocouples.

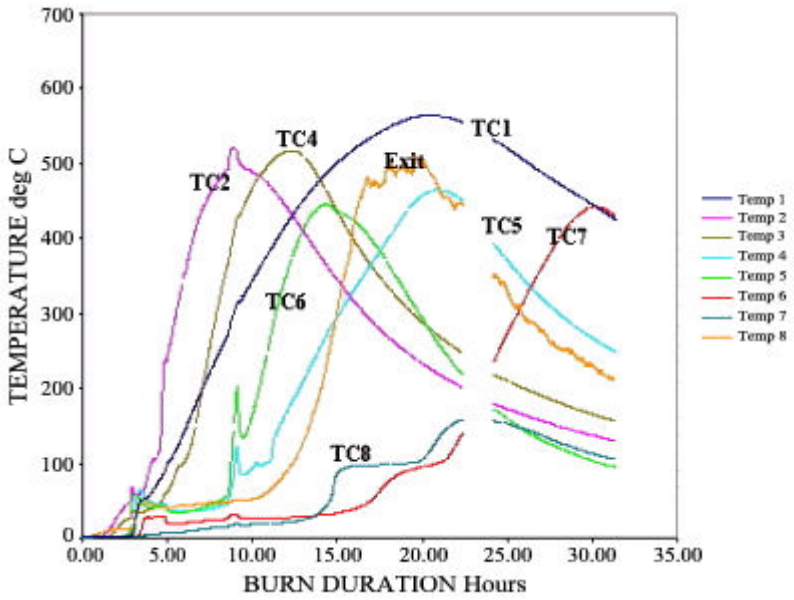

Figure 8. Temperature distributions during a firing of the ELK.
(See Figure 7 for locations of thermocouples.)

This is controlled by the origin of the draught, through the grate at the base of the shaft that runs in a rectangle form from front to back (Figure 2). This ensures that the temperature rises up the back and front initially. Differing calcination conditions occur in the kiln during operation. Also, the temperature of the exit gases during operation peak at just under 500°C. This is very hot, and represents one of the main thermal inefficiencies of the traditional method of lime production. Non continuous lime kilns will inevitably lose a considerable amount of energy through exhaust gasses which are not totally used to preheat stone above the burning front. Preheating of the stone higher up the kiln does take place, but the insulating layer of stone above the burning zone becomes thinner during burning. How to usefully recover this heat within a traditional process is a difficult question.

The full burning cycle takes approximately 36 hours and the kiln is cool enough to unload after approximately 72 hours. Unloading is done by hand, and takes up to three days to complete. The lime produced from the first burns was very reactive and had a degree of conversion of 75%. This figure is based on the loss of mass of similar volumes of quicklime and raw limestone, with knowledge of the LOI value for the limestone [9].

5. QUICKLIME CHARACTERISTICS.

In the initial firings of the kiln, high calcium, Carboniferous age Shap Limestone, from Cumbria, England, was used. This limestone is used for the large scale commercial production of lime, predominantly for the steel industry and other chemical uses, at a high temperature of 1200-1300°C, compared with temperatures encountered in the ELK of between 700-900°C. The limestone has a CaO content of 55.44% (from XRF analysis) and a Loss on Ignition value of 43.49%. Samples of the quicklime produced were subjected to a heat of hydration test based on EN 459-2 with samples prepared to ASTM C110. After crushing, ELK lump-lime was screened through a 3.35 mm aperture sieve. Figure 9 shows the result of this test for three sub-samples of the low-temperature quicklime produced in the second firing of the ELK, and compared with results from the commercially produced high-temperature quicklime. It clearly presents some considerable variation in character within the sampling from a single kiln firing with a time to 50°C of between 12 and 23 minutes, contrasting with the reactive commercial material which achieves 50°C in about 2.5 minutes.

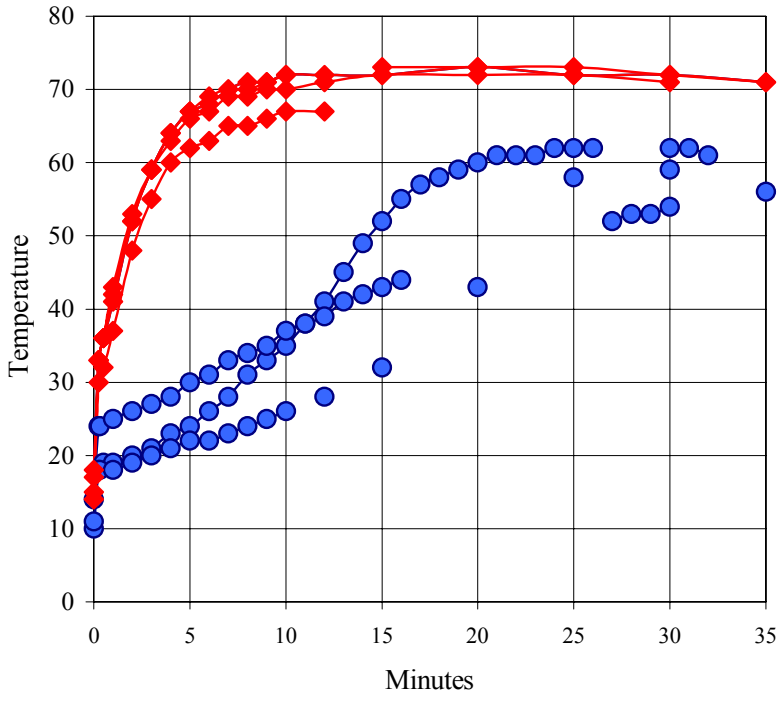

Figure 9. Heat of hydration of 3 samples of ELK Burn No. 2 of high calcium Shap quicklime (blue) compared with high-temperature, commercially produced quicklime of same limestone (red).

A Hitachi S4100 Cold Field Emission Scanning Electron Microscope was used to qualitatively compare the microstructures of the commercially produced quicklime, with those of the quicklime produced in the ELK.

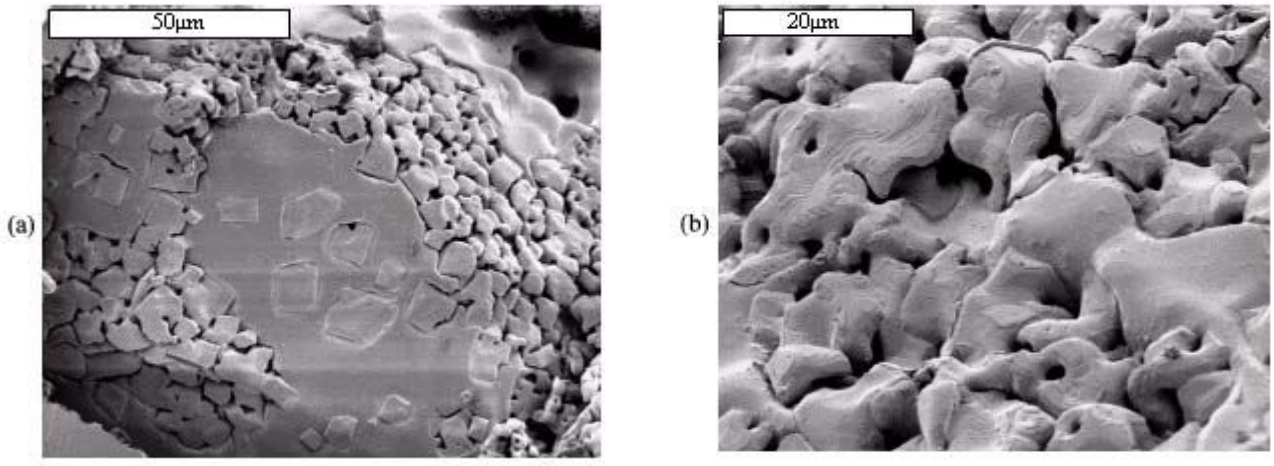

Figure 10. Commercially produced quicklime from Shap limestone, showing coalesced textures. Temperature approximately 1200-1300°C

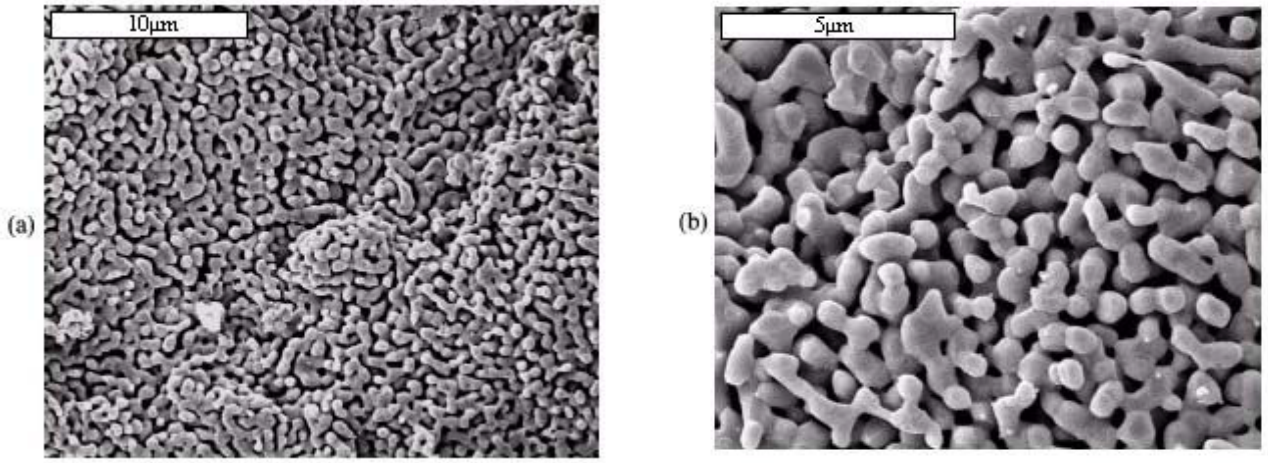

Figure 11. Quicklime produced from Shap limestone in the ELK, showing dimensions of CaO crystallites and porosity. Temperature approximately 700-900°C.

Figures 10a and 10b show examples of coalesced structures in the commercially produced high-temperature material. Figures 11a and 11b show typical microstructures of the low-temperature quicklime from the ELK. The textures in the low-temperature quicklime are very varied, however, but no examples of microstructure comparable to that seen in the high-temperature material were discovered. The low-temperature quicklime exhibits larger apparent surface area whereas the high-temperature material has a lower apparent surface area, but a larger volume of apparent porosity. This may account for the increased hydration reactivity of the high-temperature quicklime, as suggested by Boynton [10]. The form and size of the crystallites of CaO in the respective quicklime samples are related to temperature of calcination and to residence time [11]. This is an established relationship, through which it may be possible to calibrate microstructure in quicklime produced from a particular limestone to conditions within the kiln. Work has begun looking at the quantification of the microstructure of quicklime and its relationship to temperature and residence time as a possible guide to conditions within a traditional lime kiln. There is a clearly evident difference between the micrsotructure of quicklime produced traditionally in the ELK and that produced in a modern high temperature industrial process. It would be surprising if such a difference were not reflected in their performance as lime binders for masonry and conservation.

6. CONCLUSIONS

A fully instrumented ELK has been constructed, following traditional principles. The initial part of the project has clarified the operating parameters of the ELK, and demonstrated some simple performance characteristics of the quicklime produced using a traditional method. The recording of temperature in the ELK demonstrates that temperature evolution within a traditional type kiln is not even, and relates strongly to draft. In addition, the heat of hydration behaviour of the traditionally produced low temperature quicklime contrasts strongly with that of higher temperature commercially produced quicklime. Contrasts in apparent microstructure between traditional and commercial materials furnish a possible explanation of heat of hydration behaviour.

7. REFERENCES

[1] Jedrzejewska, H. Old mortars in Poland: a new method of investigation, Studies in Conservation, vol.5 (No. 4), (1960), pp.132-138.

[2] Cliver, E. B. Tests for the Analysis of Mortar Samples, Bulletin of the Association for Preservation Technology,vol.6 (No.1), (1974), pp.68-73.

[3] Callebaut K., Viaene W., Van Balen K., Ottenburgs R. Petrographical, mineralogical and chemical characterisation of lime mortars in the Saint Michael's church (Leuven, Belgium),Historic Mortars: Characteristics and Tests, Bartos P.J.M, Groot C.J.W.P & Hughes J.J. (eds.), RILEM, (2000), pp.115-126.

[4] Hughes, J.J., Cuthbert S.J., The petrography and microstructure of medieval lime mortars from the west of Scotland, Materials and Structures, vol. 33, (2000), pp.594-600.

[5] Leslie, A.B., Hughes J.J., Binder microstructure in historic lime mortars: Implications for the interpretation of mortar analysis results, Quarterly Journal of Engineering Geology and Hydrology, (2002), in press.

[6] Maxwell, I, Introduction to lime in Scotland, Proceedings of the Historic Scotland International Lime Conference, Dorrington Ward J. & Maxwell, I. (eds.), (1995), pp5-22.

[7] Robertson, T., Simpson J.B., Anderson, J.G.C., The Limestones of Scotland, Memoirs of the Geological Survey of Great Britain, (1949), 221pp

[8] Hughes, J.J., Swift, D.A., Bartos, P.J.M., Banfill, P.F.G., A traditional vertical batch lime kiln: thermal profile and quicklime characteristics, Masonry: Opportunities for the 21st Century, ASTM STP 1432, (2001)

[9] Mason K., The small-scale vertical shaft lime kiln, Intermediate Technology Publications, (1999)

[10] Boynton R.S., Chemistry and Technology of Lime and Limestone, Wiley–Interscience (1980)

[11] Eades, J. L., Sandberg P.A., Characterisation of the properties of commercial lime by surface area measurements and scanning electron microscopy, The Reaction Parameters of Lime, ASTM STP 472, (1970), pp. 3-24

THE EXPERIMENTAL LIME KILN: PRODUCTION AND CHARACTERISATION OF SUSTAINABLE LIME BINDERS

John J. Hughes[1], Phillip F.G. Banfill[2] and David S. Swift[2]

[1]Advanced Concrete and Masonry Centre, University of Paisley, High Street, Paisley, Scotland.
E-mail: john.hughes@paisley.ac.uk
[2]Dept. Building Engineering and Surveying, Heriot-Watt University, Edinburgh, Scotland.
E-mail: p.f.g.banfill@hw.ac.uk and d.s.swift@hw.ac.uk

P.F.G.Banfill

Phil Banfill studied chemistry at the University of Southampton and spent two years working in an industrial chemistry laboratory before returning to study for a PhD. He graduated in 1978 from the University of Liverpool with a thesis on waste materials in the construction industry, which initiated his interest in construction materials. He was lecturer and senior lecturer at the University of Liverpool from 1977 to 1994, before being appointed to the chair of construction materials at Heriot-Watt University, where he leads a research group with interests in rheology, chemistry, durability and conservation of cement, concrete and related materials. He has over 80 research publications, is a Fellow of the Royal Society of Chemistry and is active in education for professionals involved in conservation of historic buildings.

THE RHEOLOGY OF FRESH CEMENT AND CONCRETE – A REVIEW

P.F.G. Banfill

School of the Built Environment, Heriot-Watt University, Edinburgh, EH14 4AS, UK.
E-mail: P.F.G.Banfill@hw.ac.uk

ABSTRACT

The rheology of fresh cement, mortar and concrete is described and selected features of the behaviour of these materials are interpreted from a rheological perspective, making use of research results from the past 20 years.

1. INTRODUCTION

The hard, strong and durable cement-based product required by the user is only achieved following a period of plasticity but the attention paid to its fresh properties is small, despite the far-reaching effects of inadequate fresh performance. Pumping, spreading, moulding and compaction all depend on rheology and thanks to an increasingly scientific approach it is becoming possible to predict fresh properties, design and select materials and model processes to achieve the required performance. Rheology is now seriously considered by users, rather than being seen as an inconvenience and specialised branch of cement science.

This paper aims to review selected developments in our understanding of the rheology of cement-based materials since about 1980. During this period a comprehensive book [1], and proceedings of several conferences at which rheology of cement-based materials have played a major part [2,3,4,5] have appeared. In addition, papers on cement and concrete have been published in most of the rheology conferences -for example, the International Congress of Rheology and the conferences of the European Society of Rheology (both every 4 years)).

2. RHEOLOGY

Rheology is the science of the deformation and flow of matter, and the emphasis on flow means that it is concerned with the relationships between stress, strain, rate of strain, and time. Publication of accessible introductory texts [6,7] has helped to overcome perceptions of the difficulty of rheology with its often mathematically complex relationships. Flow is concerned with the relative movement of adjacent elements of liquid and in shear flows liquid elements flow over or past each other, while in extensional flow elements flow towards or away from each other. In a shear flow imaginary parallel layers of liquid move in response to a shear stress to produce a velocity gradient, which is referred to as the shear rate, equivalent to the rate of increase of shear strain. Elongational or stretching flows are rarely found in cement systems but there may be some elongation at the entry or exit of a pipe. They will not be considered further here. The rich variety of material behaviour can be characterised in various ways, of which the flow curve showing how shear stress and shear rate are related is very common, but equally data may be presented as the variation of viscosity (the ratio of shear stress to shear rate) with shear rate or time.

The Deborah number, defined as $De = t_r/t_o$, gives an indication of whether solid-like (elastic) or liquid-like (viscous) behaviour is likely for a particular material. When the relaxation time t_r is similar to a time characteristic of the experimental measurement t_o the material exhibits both types of behaviour and the material is said to be viscoelastic. Such behaviour is shown by dispersions of solids in water, since the interparticle forces resulting from surface charges and the electrical double layer (see Appendix) cause t_r to be in the range 10^{-4} to 10^4 seconds which is comfortably within the range of most laboratory instruments. Obviously long time-scale measurements are irrelevant for cement systems because they set before the measurement can be completed. In the flow and remoulding of cement-based materials the liquid-like behaviour is likely to be more important and can be measured in a variety of viscometers, both rotating and tubular. Established formulae enable shear stress and shear rate to be calculated from the torque and speed of rotation respectively in a rotational viscometer, or from pressure drop and flow rate in a tube.

Clearly there are also many situations where solid-like behaviour is important. Cement-based materials are able to stand unsupported without flowing under their own gravity and during setting they develop strength and stiffness. The simplest analysis involving solid-like behaviour is that of the Bingham model

$$\tau = \tau_o + \mu \dot{\gamma} \qquad (1)$$

where the material is an elastic solid at shear stress $\tau < \tau_o$, the yield stress, but flows at higher stresses, (μ is the plastic viscosity, $\dot{\gamma}$ the shear rate). The yield stress is a consequence of the interparticle forces, but these links are often broken irreversibly by shear and the measured shear stress is found to depend on time and previous shear history as well as on shear rate. An indication of yield stress can be obtained from controlled stress rheometers [8] where the shear stress to initiate flow is measured; from penetrometers [9] in which the force needed to insert a needle into the material is measured; from vanes [10] where the shear stress to overcome the internal structure and set the material in motion is measured; and the pulse shearometer [11] where the shear modulus can be determined from the velocity of propagation of a shear wave. Finally, oscillatory rotational and translational shear, enabling the elastic and viscous components of the material's response to be separated, and stress relaxation methods have all been used to a limited extent [12,13,14]. These have given information on the structure in the cement-water system.

In concentrated dispersions of solid in liquid, like cement systems, the proximity of particles gives rise to strong interactions, the strength of which depend on the shape of the particles, their size distribution, their concentration, their surface properties and the composition of the liquid. Commonly there is a net attraction which causes flocculation - the consequence of randomly moving particles coming together and sticking (see Appendix). The size and architecture of the flocs play a major role in the rheology of the dispersion, with vigorous shearing reducing the flocs to the primary particles accompanied by a reduced resistance to flow, often followed by reflocculation and thickening when the dispersion comes to rest. These shear-induced changes in microstructure take time and, if fully reversible are called thixotropy, but in cement systems it is better to refer to the two processes as structural breakdown and build-up. Their existence means that the rheology of cement systems is best studied in experiments where the shear rate is held constant until equilibrium is reached, but it will be shown below that progress can nevertheless be made from other approaches. Despite considerable advances in computational modelling of liquid rheology resulting from increases in computer power, it is not yet possible to model from first principles the flow of suspensions as complex as cement systems [15] but success can be anticipated in the next decade.

3. CEMENT-BASED MATERIALS - TESTING METHODS

There are well-established rules for the sizes of apparatus and sample to ensure that rheological measurements are reliable, chiefly that any gap must be 10 times the size of the largest particles and that the ratio of outer cylinder radius to inner must be less than 1.2. For coarse granular materials like concrete this means that a coaxial cylinders viscometer is impracticably large, requiring a sample volume of 2.5m^3 [1], whereas a specially designed one for mortar is feasible [16,17] and cement pastes are well within the capability of any of the wide range of laboratory instruments available commercially. These principles are equally applicable to other geometries and mean, for example, that the cone and plate viscometer cannot be used for suspensions because the gap is zero under the apex of the cone. This led to the development of the truncated and annular plate and cone geometries [8].

3.1 Solutions for fresh concrete

Because of the impracticability of using a coaxial cylinders viscometer of anything like ideal dimensions for fresh concrete, Tattersall and co-workers developed a highly successful and practical apparatus in which an interrupted helical impeller rotates in a cylindrical bowl of fresh concrete and the behaviour is analysed using the theory of mixing [1]. This has been developed further by Domone and Banfill [18] and the current computer assisted model of the Two-point apparatus is available commercially [19]. Following calibration it can deliver the yield stress and plastic viscosity of fresh concrete in fundamental units.

Other, broadly equivalent, approaches to the measurement of fresh concrete rheology have produced the IBB rheometer [20], the BML rheometer [21] and the BTRHEOM [22]. These instruments were developed in different countries and the question naturally arose as to whether the results can be compared. The first attempt to answer this was a programme of comparisons achieved by bringing all four instruments together at a single location with a fifth, the Cemagref-IMG [23], a large (0.5m^3) coaxial cylinders instrument used as a standard, all under the sponsorship of the American Concrete Institute [24]. While each instrument characterised fresh concrete as a Bingham material and the yield stresses and plastic viscosities measured on the 12 concretes tested remained in the same rank order, the results fell into two groups. The Cemagref-IMG and BTRHEOM agreed well, and the Two-point and BML agreed well, with the second group giving a generally lower yield stress. Pairwise correlations were highly significant and enable the result of one test to be predicted from another. Since the BTRHEOM uses parallel plates, the Cemagref-IMG uses coaxial cylinders, the Two-point uses an interrupted helix rotating in a cylinder and the BML uses coaxial cylinders this agreement is encouraging.

3.2 Solutions for mortar

Mortar can be considered to be fresh concrete without the coarse aggregate and its testing has attractions for the study of the effects of ingredients at small scale. A coaxial cylinders viscometer, while feasible, proved to be inconvenient and Banfill described the use of the Viskomat as a small calibrated mixer for mortar testing [25]. More recently Jin [26] used a scaled down interrupted helix (like the Two-point impeller) in an extensive study of the mortar fraction for design of self compacting concrete and demonstrated that its rheology could be predicted with a high degree of certainty from tests on the rheology of the mortar.

3.3 Progress with cement paste

Experimental challenges for testing cement pastes and slurries are the risks of slippage at the walls of the viscometer, sedimentation of the particles and plug flow. Depletion of particles at the viscometer surface can result in a thin (<1μm) layer of water which facilitates bulk flow of the sample, superimposed upon the shearing flow within the rest of the material. The result is an

underestimate of the stiffness of the sample [27]. The slip can be avoided using a roughened surface and Mannheimer [28] showed convincingly that slippage reduced measured yield stress by 85%. This is supported by comparisons between smooth coaxial cylinders and a vane-in-cup apparatus: slippage in the former reduced the measured yield stress by 50% but oscillatory measurements at lower stresses were indistinguishable [29]. However, proof that slippage does not occur with roughened surfaces above the yield stress has been elusive. At the high water contents representative of concrete, the particles in cement pastes may separate gravitationally and centrifugally and this can cause errors. When measurement geometries include devices to keep the paste homogeneous the results are much more satisfactory. These include angled blades to lift the particles [30], recirculating pumps [31], blades with interlocking fingers [32] and more conventional mixers [33]. The problem of plug flow, when the shear stress does not exceed the yield stress everywhere in the sample and some part of the sample does not shear, was first raised by Tattersall and Dimond [34] but has never been satisfactorily resolved. They found that hitherto irreconcilable anomalies in breakdown measurements were explained when filming the flow in the gap of a coaxial cylinders viscometer revealed that a solid plug of paste formed and was either stationary (rough cylinders) or slid round slowly (smooth cylinders). No satisfactory explanation has ever been offered for this anomalous plug flow but its existence casts doubt on all experimental data where full shearing flow has not been confirmed visually.

4. CEMENT-BASED MATERIALS - RHEOLOGICAL RESULTS

It might be expected that the rheology of the more complex material, concrete, containing a wider range of particle sizes, would be more complicated than that of one of its constituent materials, cement paste, but in fact fresh concrete has proved to be simpler. Considerable practical progress has been made with it and, more recently, with mortars.

4.1 Concretes

Much work has been done on the effects on the rheology of concrete of mix constituents and their relative proportions, cement properties and admixtures and cement blending agents [1,17,20,21,35]. Concrete conforms to the Bingham model and does not show structural breakdown over the range of shear rates used in the test. Yield stress and plastic viscosity vary in a complex fashion with composition and this makes rheology measurement a versatile way of controlling the quality of fresh concrete production: tests carried out on the fresh concrete can show up changes in the mix composition which may have implications for the concrete's hardened properties and performance in use [35]. With the recent advent of self-compacting concrete, characterised by a very low yield stress, it has been found that the thickeners used to prevent segregation in use by raising the viscosity of the water also change the flow curve from the normal Bingham behaviour to Herschel-Bulkeley type behaviour (see below) [26].

4.2 Mortars

Mortars undergo structural breakdown and measured data are sensitive to the previous shear history of the sample, but the equilibrium flow curve conforms to the Bingham model [25]. The effects of composition are similar to those observed in fresh concrete, and mortar tests can be used as small scale predictors of concrete rheology [26, also Banfill, unpublished].

4.3 Cement pastes

There are qualitative and quantitative disagreements between the results for cement paste reported by different research workers. The flow curve has been reported to fit several different mathematical forms, all of which indicate the existence of a yield stress:

Bingham [1] $$\tau = \tau_o + \mu \dot{\gamma} \qquad (1)$$

Herschel-Bulkley [7]	$\tau = \tau_o + A\dot{\gamma}^B$	(2)
Robertson-Stiff [6]	$\tau = A(\dot{\gamma} + B)^C$	(3)
Modified Bingham [36]	$\tau = \tau_o + \mu\dot{\gamma} + B\dot{\gamma}^2$	(4)
Casson [7]	$\sqrt{\tau} = \sqrt{\tau_o} + \sqrt{(\mu\dot{\gamma})}$	(5)
De Kee [36]	$\tau = \tau_o + \mu\dot{\gamma}e^{-A\dot{\gamma}}$	(6)
Yahia and Khayat [36]	$\tau = \tau_o + 2\sqrt{(\tau_o\mu\dot{\gamma}e^{-A\dot{\gamma}})}$	(7)

where A, B and C are constants.

Additionally the numerical values reported for the rheological parameters cover a very wide range, which cannot be wholly explained by variations in the materials used. It can only be accounted for by accepting that differences in experimental technique and apparatus of different workers have a much greater effect than has been generally realised. Differences in the shear history at the time of test, undetected plug flow and slippage at the smooth surfaces of a viscometer could all combine to give experimental variations as large as those reported. However, there is general agreement on two fundamental qualitative aspects of the behaviour of cement pastes.

First, the material breaks down during the test and hysteresis loops with the downcurve falling to lower stresses than the upcurve are obtained when the flow curve is determined over a short cycle time. The shape changes systematically with increasing cycle time through loops with a crossover point to loops showing structural build up [37], attributable to chemical reaction during the course of the test, but Hattori and Izumi [38] explained the effect in terms of the competition between coagulation and deflocculation processes. The apparent need to fit the range of models in equations 1-7 may be the result of not allowing for the possibility of structural breakdown during the test.

Second, the material has a yield stress which decreases, in line with reductions in the apparent viscosity indicated by the rest of the curve, as the total amount of shearing energy experienced by the paste increases. Thus, successive hysteresis loops fall to progressively lower values of torque in a coaxial cylinders viscometer [39], yield stress and plastic viscosity fall to an equilibrium value as the time of mechanical mixing is increased [40]. The effect can be quantified in terms of the total shear energy received by the sample prior to the test [41,42]. This structural breakdown has been amply confirmed by experiments carried out under both continuous steady shear rate and continuous steady stress. In the former the relationship between shear stress and time is affected by the shear rate in the experiment and was explained theoretically by Tattersall [39] using a linkage theory, in which the links between particles are broken by the work done in shearing the paste.

Space precludes description of the large amount of work carried out on the effect of experimental variables on the rheological parameters of cement pastes. It is sufficient to note that investigations have included paste concentration (water/cement ratio or % solids) cement composition (portland cements) and fineness, aluminous cement, oilwell cement, non-shrinking cement, flyash, silica fume, slags, chemical admixtures, polymer latexes, and effects of age and temperature [1,43].

4.4 Comparison of cement pastes, mortar and concrete

Table 1 shows that there is a trend in the rheological properties of cement-based materials, as quoted in the literature, which can be explained semiquantitatively by the presence of aggregate in the coarser grained materials. The flow properties of suspensions are governed by the interfaces

between solid and water and, in terms of the surface area of contact, the dominant contribution is due to the cement-water interface. This is progressively diluted by the presence of aggregate. Thus, for example in one comparison, two cements which gave pastes whose rheological parameters differed by a factor of two produced concretes of indistinguishable flow behaviour [1].

The yield stress and plastic viscosity increase as the maximum particle size increases. This is because in a typical concrete at least 50% by volume is in the form of aggregate which is capable of withstanding the applied stresses without deformation: consequently the yield stress is higher, a point confirmed by the increase with increasing aggregate content in concrete [1]. The increased plastic viscosity is partly due to the increased interparticle contact and surface interlocking, as demonstrated by the fact that for two concretes with the same yield stress containing rounded and angular coarse aggregates, the plastic viscosity of the latter is higher. It is also partly due to the inability of the aggregate to be sheared: when an overall shear rate $\dot{\gamma}$ is applied to an imaginary concrete consisting of aggregate and paste 50:50 per cent by volume, the shear rate within the solid aggregate particles is zero and that in the paste is $5\dot{\gamma}$. This higher shear rate results in a higher stress and resistance to flow in the paste which in turn accounts for the increase in measured plastic viscosity of the bulk material.

Table 1. Rheology of cement paste, mortar and concrete

Material	Cement paste, grout	Mortar	Flowing concrete	Self-compacting concrete	Concrete
Yield stress N/m^2	10-100	80-400	400	50-200	500-2000
Plastic viscosity Ns/m^2	0.01-1	1-3	20	20-100	50-100
Structural breakdown	Significant	Slight	None	None	None

In contrast, the yield stress and plastic viscosity of cement paste increase as the cement gets finer [44], which reflects the dominance of the water-cement interface in this system. Evidently the influence of particle size is a surface area effect in fine grained pastes and a simple volume effect in the coarser grained concretes. Perhaps further work on particles suspended in dispersions will suggest the particle size range where the change from one influence to the other occurs.[45]

The trend in structural breakdown behaviour may be explained qualitatively in a similar way. The work of shearing done on a material in unit time is proportional to the square of the shear rate. Structural breakdown experiments on cement paste show that the breakdown resulting from this work is rapid at first and complete in a few minutes and also that the rate of decay is proportional to the square of the shear rate. Thus, in the 50:50 concrete mentioned above the total shear work done on the paste by the end of a three minute mixing period at a mean shear rate of 10 sec^{-1} is equivalent to that done in a viscometer in 45 seconds at 100 sec^{-1} or 12 seconds at 200 sec^{-1}. This is enough to give almost complete breakdown and explains the absence of structural breakdown when concrete is tested: all the breakable structure has been broken down before the material leaves the mixer. Furthermore, the higher the aggregate content, the higher the shear rate in the paste and the more complete the breakdown at the end of mixing.

5. A STRUCTURAL MODEL

Any proposed structural model must be able to explain the irreversible breakdown which occurs on shearing cement-based systems, and which is different from thixotropic behaviour. Such a model is shown in Figure 1 [1,46], in which the yield stress can be accounted for by the usual Van der Waals

attraction (see Appendix) and electrical double layer repulsion effects. These result in links between particles reforming reversibly when the particles come to rest, but the irreversibly destroyed structure is much stronger than this. When dry cement powder first comes into contact with water the hydrated skin or membrane may form around pairs or groups of particles. When the skin is broken by the action of shear and the particles separate, that region of one particle that was in contact with other particles is exposed and hydrates to heal the broken skin. Because of this healing these links cannot then reform in the same way when the structure comes to rest, i.e. the breakdown of skin linkage is irreversible. This model is consistent with both the instantaneous formation of a protective layer on cement [47], and the notion of links between particles first proposed by Tattersall [39].

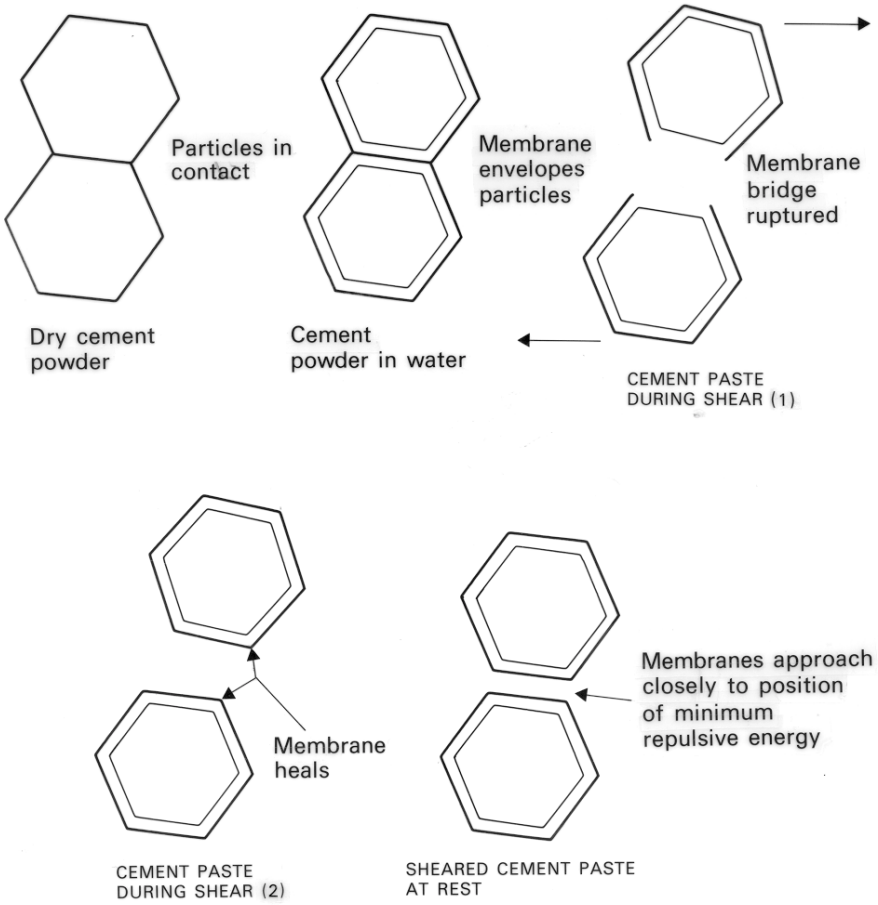

Figure 1. A structural model for the shear induced breakdown in cement systems.

6. MODELS FOR PARTICULAR SITUATIONS

6.1 Pumping

Transport of fresh concrete by pumping through pipes to the point of placement has been used since the 1930s, and is an obvious candidate for rheological studyto help select pumping equipment and conditions. Pipe flow of a Bingham material is well characterised and the variation of shear stress from a maximum value at the wall of the pipe to zero at the centre line means that a plug of solid unsheared material moves surrounded by a zone of shearing flow from which pressure-flow rate equations have been derived [1,7]. However, this assumes that the material is homogeneous, whereas pumped concrete actually forms a layer of paste that lubricates the wall and facilitates flow. Therefore, the pumpability of a concrete is mainly governed by its ability to form and maintain this layer under the pumping conditions and an acceptance test has been developed [48]. In

fact, practical problems with blockage of pipework have meant that most pumping trials have had to be done at full scale, which is both costly and inconvenient.

Kaplan found that the pressure loss-flow rate relationship is independent of pressure for saturated concretes and formulated the wall lubrication law as follows [49]

$$\tau_i = \tau_{oi} + \eta V \qquad (8)$$

where τ_i is the shear stress at the interface, τ_{oi} the interfacial yield stress, η the interfacial viscosity and V is the speed of the boundary layer. The full pressure loss-flow rate relationship with its zones of shearing and lubricated flow depends on these parameters and on the rheological constants for the material, which he measured by the BTRHEOM apparatus [22]. He determined the interfacial parameters in a modified version of the apparatus, using smooth cylinders to promote slippage (a so-called tribometer), and performed 36 full scale pumping tests in an experimental loop 150m long with pipe of 125mm diameter using a range of concretes (ordinary, high performance, self compacting and air-entrained). This innovative use of slippage measurements produced a model which was able to predict the pressure-flow relationship with a high degree of accuracy and therefore can be used for pumping system design.

A point of obvious interest is whether there is any relationship between the interfacial parameters and the bulk values: clearly there is no reason to expect one since the interfacial parameters depend on the ability of the concrete to establish and maintain a lubricating layer. In fact, Kaplan obtained excellent numerical agreement between the interfacial values from the tribometer and from the pumping tests, with τ_{oi} in the range 0-150 Pa and η 300-1200 Pa.s/m, the former being considerably lower than the corresponding bulk yield stresses of 300-2000 Pa. There was a broad positive correlation between τ_{oi} and τ_o for about half of the tested concretes but there were some extreme outliers in both directions, especially for some high yield stress concretes which had zero interfacial yield stress. There was no correlation between interfacial viscosity and the plastic viscosity of the concrete. These results confirm that while bulk rheology has a part to play in the flow of concrete in pumping the dominant lubricating effect is influenced by other properties of the concrete

6.2 Interactions at the surface of formwork

A related problem requiring a knowledge of friction at a concrete-wall interface is the pressure on formwork, which is lower than the equivalent hydrostatic pressure because of the yield stress within the material and the friction at the wall [50], but empirical predictions underestimate the actual pressures measured for modern highly fluid concretes. Friction between steel and fresh concrete was measured in a tribometer based upon moving a steel plate between opposed pressurised cylinders filled with concrete which exert a known stress normal to the surface [51,52,53]. Applying the coefficient of friction between steel and concrete determined in this apparatus enabled preliminary estimates of the formwork pressures exerted by fluid and self compacting concrete to be compared with those measured in full size formwork up to 12 metres high. This confirmed the complexity of the factors affecting formwork pressure and showed that it is about 25% less than hydrostatic for a self-compacting concrete, but the contribution of friction depends on surface roughness, concrete rheology and particle size distribution. Unfortunately, information on the rheology of the concrete used is not available (only slump and slump flow were measured) but Vanhove found that the friction stress (equivalent to τ_i in equation 8) is independent of velocity and roughly proportional to the normal stress, from which the coefficient of friction can be determined for use in pressure calculations. Vanhove's friction stress and Kaplan's τ_i can be compared only if Vanhove's data is extrapolated a long way to zero normal stress, an unreliable process. However, there is no doubt that this fundamental work on friction has the potential to contribute to the understanding of this important practical area.

6.3 Vibrational compaction

Vibration is the most popular means of compacting fresh concrete into formwork and around reinforcement and there is an extensive literature on the effects of such features as frequency, amplitude and acceleration, but several recent papers have significantly advanced understanding. Practically vibration removes the yield stress of fresh concrete which then flows under its own weight [54,55] and the important characteristic of the vibration is the peak velocity. The fluidity of vibrated concrete, defined as the reciprocal of its low shear rate viscosity, is proportional to peak vibrational velocity up to a critical value, above which it is constant, and the viscosity of the vibrated concrete is proportional to the plastic viscosity of the unvibrated concrete [56]. This work enabled the effect of vibration to be defined phenomenologically but a more rigorous investigation was recently completed by Teixeira et al [57].

They studied the propagation of vibration through analysing the effects of shear and compressive waveforms on the oscillatory flow of fresh concrete, and concluded that there is a liquid region near the vibrator where the flow is controlled by the shear waveform and in which hydrodynamic theory may be used in the calculations. Beyond this, there is a solid region where the motion is controlled by compressive waveforms and structural vibration theory is used in the predictions. The interface between the liquid and solid regions corresponds in practical terms to the radius of action of the vibrator. This wave propagation analysis was validated experimentally and was able to predict correctly the rapid decay of vibration near the source, a phenomenon that has previously been attributed to cavitation [58]. A software solution enabled the radius of action to be predicted from yield stress, plastic viscosity, density and the vibrational parameters and while experimental work on a range of concretes confirmed that the radius of action decreases linearly as yield stress increases, the measured and calculated values differ significantly for stiff concretes. These findings are encouraging and suggest that solution of the fresh concrete vibration problem may be near.

6.4 The action of superplasticisers

It has long been established that superplasticisers can have spectacular but sometimes unpredictable effects on the rheology of cement systems. The yield stress of cement and concrete are reduced to very low values by the dispersion of flocculated cement particles [1]. However, the progress of the hydration reaction causes stiffening (slump loss) and this can be a serious practical problem. Based on an extensive review of experimental data, Flatt and Houst proposed that there are three components of the behaviour of the superplasticiser added to the system [59].

The first part is consumed by intercalation, coprecipitation or micellization (see Appendix) within the hydrating cement minerals, forming an organo-mineral phase. These chemical reactions during the formation of AFt and C-S-H, mean the admixture is no longer available for dispersing flocs and are most important in the first minutes after addition, when the precipitation rate of AFt is highest, governed by the availability of sulphate. As a consequence, at the same addition level, a cement with a high degree of consumption will have less favourable rheology than an otherwise identical cement but with a low degree of consumption. Delayed addition can reduce this consumption, especially for long chain polyelectrolyte polymers, which are trapped in the organo-mineral phase, but has less effect on polymers with side chains extending through the surface hydration layers into the solution.

The second part is available for adsorption at the surface of cement particles and is effective in dispersing the flocs, but the adsorbed amount is not easily measured since current analytical methods are based on the amount removed from the solution and this cannot distinguish between admixture consumed in the first part (above) and adsorbed on surfaces. Consequently the dispersive power of superplasticisers and their effect on rheology can only be evaluated using model powders which do not react or under conditions of full surface coverage in cements.

The third part consists of the superplasticiser that remains dissolved in the aqueous phase and may play a part in dispersing cement particles [60], but has otherwise been ignored in experimental studies. They point out that too little attention has been paid to differentiating adsorption from consumption in the interpretation of data. Work on tailoring improved superplasticisers, based on these considerations, is currently in progress [61].

7. CONCLUSIONS AND FUTURE POSSIBILITIES

Rheology is important because of the scope it offers for characterising fresh cement paste, grout, mortar and concrete, and for understanding how they perform in practical applications. Without satisfactory fresh properties it is unlikely that the desirable properties of the hardened materials can be achieved. Their rheology is dominated by the structure that exists in the cement paste, but in mortar and concrete the structure has been partially or fully broken down during mixing. As a result they conform closely to the Bingham model and their behaviour during pumping, vibration and in formwork can be explained by reference to that model.

Reliable instruments for testing the coarser grained materials are available and experience in comparing the data is growing. In contrast there remain apparently conflicting results for cement pastes, which are probably due to the different experimental techniques used by different workers. The important effects of shear history, mixing energy and wall slippage on the results obtained in viscometers are only now being generally understood.

Building upon our current understanding of the rheology of fresh cement and concrete the future developments are likely to be incremental in the following areas:

- Steady increases in computing power and better algorithms will improve the modelling of more complex systems. A numerical model for the rheology of cement paste can be anticipated soon.
- The rheological modelling of practical situations will enable better tailoring of solutions in fields such as pumping, vibration, self-compacting flow, efficient grouting of voids and estimation of formwork pressures.
- There will always be a need for production quality control testing of rheology and inter-comparisons between the different instruments can be expected to enable a common basis of agreement to be established.
- Rheology will continue to be a product development tool as new materials become available and require objective and discriminating evaluation

REFERENCES

[1] Tattersall, G.H., Banfill, P.F.G. The rheology of fresh concrete, Pitman, (1983), 356pp.
[2] Banfill, P.F.G. (editor) The rheology of fresh cement and concrete, Spon, (1991), 373pp.
[3] Bartos, P.J.M, Marrs, D.L., Cleland, D.J. (editors) Production methods and workability of concrete, Spon, (1996), 541pp.
[4] Skarendahl, A., Petersson, O. (editors) First international RILEM symposium on self-compacting concrete, Spon, (1999), pp.786.
[5] Nonat, A. (editor) Why does cement set? An interdisciplinary approach, 2nd International RILEM workshop on hydration and setting, RILEM Publications Sarl, (1997), 419pp.
[6] Barnes, H.A., Hutton, J.F., Walters, K. An introduction to rheology, Elsevier, (1989), 199pp.
[7] Barnes, H.A. A handbook of elementary rheology, Institute of Non-Newtonian Fluid Mechanics, University of Wales, (2000), 200pp.
[8] Banfill P.F.G., Kitching, D.R.Use of a controlled stress rheometer to study the yield value of oilwell cement slurries, The rheology of fresh cement and concrete, Spon, (1991), pp125-136.
[9] Bombled, J.P. A rheograph for studying the rheology of stiff pastes: application to cement setting, Revue des Materiaux de Construction, no. 673, (1970), pp.256-277.
[10] Barnes, H.A., Carnali, J.O. The vane-in-cup as a novel rheometer geometry for shear-thinning and thixotropic materials, Journal of Rheology, vol.34. (1991), pp.841-866.

[11] Gregory, T. The measurement of early strength development in polymer modified cement pastes, 5th International congress on polymers in concrete, (1987), pp.205-208.
[12] O'Keefe, S.J. Rheological properties of polymer modified cement pastes, PhD thesis, Bristol Polytechnic, (1991), pp.232
[13] Banfill, P.F.G., Carter, R.E., Weaver, P. Simultaneous rheological and kinetic measurements on cement pastes, Cement and Concrete Research, vol.21, (1991), pp.1148-1151.
[14] Schultz, M.A., Struble, L.J. The use of oscillatory shear to study flow behaviour of fresh cement paste, Cement and Concrete Research, vol.23, (1993), pp.273-282.
[15] Keunings, R. A survey of computational rheology, 13th international congress on rheology, (2000), vol.1, pp.1.7-1.14.
[16] Banfill, P.F.G. Feasibility study of a coaxial cylinders viscometer for mortar, Cement and Concrete Research, vol.17, (1987), pp.329-33.
[17] Banfill, P.F.G. A coaxial cylinders viscometer for mortar: design and experimental validation, Rheology of Fresh Cement and Concrete, Spon, (1991), pp.217-226.
[18] Domone, P.L.J., Xu Yongmo, Banfill, P.F.G. Developments of the two-point workability test for high-performance concrete, Magazine of Concrete Research, vol.51, (1999), pp.171-180.
[19] Magna Projects and Instruments Ltd, http//www.magna-projects.com, (2002).
[20] Beaupre, D. Rheology of high performance shotcrete, PhD Thesis, University of British Columbia, (1994)
[21] Wallevik, O.H. The rheology of fresh concrete and its application on concrete with and without silica fume, Dr.ing. Thesis 1990:45, NTH Trondheim, (1990), pp.185.
[22] Hu, C., de Larrard, F.R. The rheology of fresh high-performance concrete, Cement and Concrete Research, vol.26, (1996), pp.283-294.
[23] Coussot, P. Rhéologie des boues et laves torrentielles - étude de dispersions et suspensions concentrées, Thése de doctorat de l'Institut National Polytechnique de Grenoble, série Montagne, No.5, (1993), pp.418.
[24] Ferraris C.F., Brower, L.E. (editors) Comparison of concrete rheometers: Inteernational tests at LCPC (Nantes, France) in October 2000, NISTIR 6819, (2001), pp.147.
[25] Banfill, P.F.G. Rheological methods for assessing the flow properties of mortar and related materials, Construction and Building Materials, vol.8, (1994), pp.43-50.
[26] Jin, J., Properties of mortar for self-compacting concrete, PhD Thesis, University of London, (2002), pp.398.
[27] Barnes, H.A. A review of the slip (wall depletion) of polymer solutions, emulsions and particle suspensions in viscometers: its cause, character and cure, Journal of Non-Newtonian Fluid Mechanics, vol.56, (1995), pp.221-251.
[28] Mannheimer, R.J. Effect of slip on flow properties of cement slurries can flaw resistance calculations, Oil and Gas Journal, December 5, (1983), pp.144-147.
[29] Saak, A.W., Jennings, H.M., Shah, S.P. The influence of wall slip on yield stress and viscoelastic measurements of cement paste, Cement and Concrete Research, vol.31, (2001), pp.205-212.
[30] Bhatty, J.I., Banfill, P.F.G. Sedimentation behaviour of cement pastes subject to continuous shear in rotational viscomenters, Cement and Concrete Research, vol.12, (1982), pp.69-78.
[31] Meeten, G.H. Rheometer, British Patent Application UK 9026294.0, (1990).
[32] Vlachou, V., Piau, J-M. A new tool for the rheometric study of oil well cement slurries and other settling suspensions, Cement and Concrete Research, vol.30, (2000), pp.1551-1557.
[33] Nachbaur,L., Mutin, J.C., Nonat, A., Choplin, L. Dynamic mode rheology of cement and tricalcium silicate pastes from mixing to setting, Cement and Concrete Research, vol.31, (2001), pp.183-192.
[34] Tattersall, G.H., Dimond, C.R. The use of the coaxial cylinders viscometer to measure the rheological properties of cement pastes, Hydraulic cement pastes: structure and properties, Cement and Concrete Association, 15.121, (1976), pp.118-133.
[35] Tattersall, G.H. Workability and quality control of concrete, Spon, (1991), pp.262.
[36] Yahia, A., Khayat, K.H. Analytical models for estimating yield stress of high performance pseudoplastic grout, Cement and Concrete Research, vol.31, (2001), pp.731-738.
[37] Banfill, P.F.G., Saunders, D.C. On the viscometric examination of cement pastes, Cement and Concrete Research, vol.11, (1981), pp.363-370
[38] Hattori, K. Izumi, K. A rheological expression of coagulation rate theory, Parts 1-3, Journal of Dispersion Science and Technology, vol.3, (1982), pp.129-145, pp.147-167, pp.169-193.
[39] Tattersall, G.H The rheology of portland cement pastes, British Journal of Applied Physics, vol.6, (1955), pp.165-167.
[40] Banfill, P.F.G. A viscometric study of cement pastes including a note on experimental techniques, Magazine of Concrete Research, vol.33, (1981), pp.37-47.
[41] Orban, J., Parcevaux ,P., Guillot, D. Influence of shear history on the rheological properties of oil well cement slurries, 8th International Congress on the Chemistry of Cement, vol. 6, (1986), pp.243-247.
[42] Hodne, H., Saasen, A., O'Hagan, A.B., Wick, S.O. Effects of time and shear energy on the rheological behaviour of oilwell cement slurries, Cement and Concrete Research, vol.30, (2000), pp.1759-1766.
[43] Banfill, P.F.G. Rheology of cement paste: progress since 1973, Properties of Fresh Concrete, edited by H.J. Wierig, Chapman & Hall, (1990), pp.3-9.

[44] Vom Berg, W.Influence of specific surface and concentration of solids upon the flow behaviour of cement pastes, Magazine of Concrete Research, vol.31, (1979), pp.211-216.
[45] Ancey, C., Jorrot, H. Yield stress for particle suspensions within a clay dispersion, Journal of Rheology, vol.45, (2001), pp.297-319.
[46] Banfill, P.F.G. The rheology of fresh mortar, Magazine of Concrete Research, vol.43, (1991), pp.13-21.
[47] Sujata, K., Jennings H.M. Formation of a protective layer during the hydration of cement, Journal of the American Ceramic Society, vol.75, (1992), pp.1669-1673.
[48] Browne, R.D., Bamforth, P. Tests to establish concrete pumpability, American Concrete Institute Journal, May, (1977), pp.193-203.
[49] Kaplan, D. Pompage des bétons, Thèse de doctorat de l'Ecole Nationale des Ponts et Chaussées, Paris, (2001).
[50] Gardner, N.J. Pressure of concrete on formwork, a review, Journal of the American Concrete Institute, vol.82, (1985), pp.744-753.
[51] Djelal, C. Designing and perfecting a tribometer for the study of friction of a concentrated clay-water mixture against a metallic surface, Materials and Structures, vol.34, no.34, (2000), pp.51-58.
[52] Vanhove, Y. Contribution à l'étude du frottement du béton autoplacant contre une surface metallique - application aux poussées contre les coffrages, Thèse de doctorat de l'Université d'Artois, Béthune, (2002), pp.162.
[53] Vanhove, Y., Djelal, C., Magnin,A. Influence of fresh concrete granular phase on the friction stress at the interface concrete/metallic wall, 13th International Congress on Rheology, (2000), vol.2, pp.418-420.
[54] Tattersall, G.H., Baker, P.H. The effect of vibration on the rheological properties of fresh concrete, Magazine of Concrete Research, vol.40, (1988), pp.79-89.
[55] Tattersall, G.H., Baker, P.H. An investigation into the effect of vibration on the workability of fresh concrete using a vertical pipe apparatus, Magazine of Concrete Research, vol.41, (1989), pp.3-9.
[56] Banfill, P.F.G., Xu Yongmo, Domone, P.L.J. Relationship between the rheology of unvibrated fresh concrete and its flow under vibration in a vertical pipe apparatus, Magazine of Concrete Research, vol.51, (1999), pp.181-190.
[57] Teixeira, M.A.O.M., Craik, R.J.M., Banfill, P.F.G. Vibrational processing of fresh concrete: predicting fluidification from rheological behaviour, 13th International Congress on Rheology, (2000), vol.4, pp.133-135.
[58] ACI Committee 309, Behaviour of fresh concrete during vibration, American Concrete Institute ACI 309.1R-93, Detroit, (May 1993).
[59] Flatt, R.J., Houst, Y.F. A simplified view on chemical effects perturbing the action of superplasticisers, Cement and Concrete Research, vol.31, (2001), pp.1169-1176.
[60] Lewis, J.A., Matsuyama, H., Kirby, G., Morissette, S., Young, J.F. Polyelectrolyte effects on the rheological properties of concentrated cement suspensions, Journal of the American Ceramic Society, vol.83, (2000), pp.1905-1913.
[61] Kauppi, A., Banfill, P.F.G., Bowen, P., Petersen, B.G., Houst, Y.F., Lafuma, F., Maeder, U., Reknes, K., Schober, I, Swift, D.S., Improved superplasticisers for high performance concrete, Submitted to this conference.

APPENDIX: GLOSSARY OF TERMS

Co-precipitation: The precipitation of one substance from solution, encouraged by the tiny solid nuclei which form during precipitation of another. Both substances precipitate together.

Electrical double layer: A model for the situation at a charged solid surface in solution where ions of opposite charge are attracted to the surface, but try to diffuse away to remain uniformly distributed in the solution, resulting in two plates of an electric condenser – the charged surface and a balancing charge in solution spread over a short distance from the surface.

Flocculation: The process by which particles in a suspension are mutually attracted by a combination of van der Waals and electrostatic forces, stick together to form agglomerates and either settle out of the suspension as flocs or form a three-dimensional network throughout the suspension.

Intercalation: The incorporation of molecules of one substance into the crystal lattice of a solid as it precipitates from solution.

Micellization: A process where polymer molecules with both hydrophobic and hydrophilic parts (such as detergents) group together in aqueous solution such that the hydrophobic parts associate to form regions from which water is excluded. The hydrophilic parts remain on the outer surface to maximise their interaction with the water. There is a critical concentration above which the dissolved polymer mostly exists as micelles and is therefore unavailable for active dispersion of the solid.

Van der Waals attraction: Weak forces of attraction between any pair of molecules due to oscillations in the charge distribution inside the individual atoms which produce electrostatic forces. When two solid surfaces are brought close together, all the atoms in the surface zones contribute to the forces of attraction, which are then large enough to be measurable.

THE RHEOLOGY OF FRESH CEMENT AND CONCRETE – A REVIEW

P.F.G. Banfill

School of the Built Environment, Heriot-Watt University, Edinburgh, EH14 4AS, UK.
E-mail: P.F.G.Banfill@hw.ac.uk

P F G Banfill

Phil Banfill studied chemistry at the University of Southampton and spent two years working in an industrial chemistry laboratory before returning to study for a PhD. He graduated in 1978 from the University of Liverpool with a thesis on waste materials in the construction industry, which initiated his interest in rheology and concrete. He was lecturer and senior lecturer at the University of Liverpool from 1977 to 1994, before being appointed to the chair of construction materials at Heriot-Watt University, where he leads a research group with interests in rheology, chemistry, durability and conservation of cement, concrete and related materials. He has over 80 publications from his research on rheology and cement-based materials and is Honorary Secretary of the British Society of Rheology, as well as a Fellow of the Royal Society of Chemistry.

COMPARATIVE STUDY TO EVALUATE THE REACTIVITY OF AGGREGATES

Ali Akbar Ramezanianpour

Civil Engineering Faculty, Amirkabir University of Technology, Tehran, Iran.
E-mail: aaramce@cic.aku.ac.ir

ABSTRACT

Alkali-aggregate reactivity in concrete is an undesirable chemical reaction that may occur between soluble alkalis in the pore fluid and certain types of aggregates. Alkali-aggregate reaction often develops as a slow progressively deteriorating process, with the first visible signs taking anywhere from a few months to many years to develop. AAR produces concrete expansion and can generally lead to a loss of strength, stiffness (cracking), and generates undesirable deformations and disturbances in the equilibrium of internal forces.

It is essential that the potential alkali-reactivity of aggregates be assessed prior to their utilization in concrete. This is usually carried out by a number of accelerated and long-term standard and proposed laboratory test methods. They have given satisfactory results for some aggregates, while in a number of cases and for aggregates in different parts of the world test results were unreliable. These contradictory results were observed in some of siliceous and carbonate aggregates, which were examined.

In this research program a comparative study of test results using three different methods is presented. The test methods are rock cylinder, accelerated mortar bar (NBRI-like test), and an accelerated concrete prism test. Aggregates obtained from various sources which were used or will be used in concrete mixtures of a number of dams. In order to control the alkali aggregate reaction of reactive aggregates several mixes containing silica fume were tested. The main test methods used to determine the reactivity level of the aggregates include the chemical method, accelerated mortar bar and concrete prism methods.

Results of the rock cylinder test show that almost all the aggregates investigated were non-reactive while in the accelerated concrete prism test some of the aggregates were found to be potentially reactive.Test results indicate that silica fume is highly effective in reducing expansion due to alkali silica reactions of some aggregates. The expansion reduction rate is related to the amount of silica fume used in the concrete mixtures.

Keywords: Alkali aggregate-reaction, carbonate rocks, accelerated tests, rock cylinder, mortar bar, concrete prism, silica fume, expansion

1. INTRODUCTION

Alkali aggregate reactions (AAR) are chemical reactions in concrete that can induce the premature distress and loss in serviceability of the concrete structures affected. The AAR related problems were first identified in California. Since then, AAR has been recognized in many countries around

the world. It is likely that the problems associated with AAR exist in almost all countries in the world but the severities are different.

Many test methods and guidelines for the prevention of alkali aggregate reaction in new concrete structures have been adopted by various national and international organizations around the world [1]. Most of these standards and guidelines are dealing with alkali-silica reaction and those related to carbonate rocks are really rare [2]. The tests are usually carried out by a number of accelerated and long term laboratory methods [3]. Prior to mortar bar and concrete prism tests, petrographic examination, chemical tests and rock cylinder tests are carried out. They have given satisfactory results for some aggregates, while in a number of cases and for aggregates in different parts of the world test results were not reliable [4]. The contradictory results were observed in most of the carbonate rocks which were assessed.

A few concrete dams and other concrete structures in Iran are suffering from deterioration induced by alkali-aggregate reaction that impairs the durability, serviceability, and also endangers the safety of the structures in future. Most of the aggregates used for the construction of these structures and those for dams to be constructed in the future are carbonate rocks [5].

The aim of this investigation is to study the reactivity of some carbonate aggregates from different sources which have been considered as concrete aggregates to be used for construction of dams. For comparison purposes and for evaluation of the validity of test methods, the rock cylinder test (ASTM C586-92)[6], the accelerated mortar bar test (NBRI-like test)[7], and an accelerated concrete prism test proposed for carbonate rocks were used throughout this investigation.

2. TEST PROGRAM

2.1 Materials

Portland cement - The physical properties and the chemical composition of the cement used is given in Table 1.

Aggregates - In this study four types of aggregate from four dam sites namely Rajai (R1), Maroon (M1), Karkheh (K1), and Ahar (A1) were selected for testing. The petrography and physical properties of the aggregates are given in Table 2. The grading of aggregates in the different test methods were selected in accordance with the specified grading curves in the different standards (Reference grading curves for fine aggregates in mortar bar tests and grading curves for coarse aggregates in concrete prism tests)[6,7].

2.1 Test methods

In this investigation three test methods were used. In the first test method (rock cylinder test), standard rock cylinders (9 mm diameter and 35 mm length) were immersed in a solution of sodium hydroxide at room temperature and the length changes were measured up to 8 weeks. Expansions in excess of 0.1 percent at 28 days are an indication of chemical reaction and additional tests are required. In the second test method (NBRI-like test) and similar to CAN/CSA A23.2-25A (Canadian Standard 1994), mortar bars (2.5 by 2.5 by 28.5 cm) were immersed in a 1 N sodium hydroxide at 80 C for 14 days and expansions were recorded. For some specimens measurement continued up to 56 days. In this test method expansions in excess of 0.1 percent for limestone aggregates are indicative of highly reactive aggregates. In the third test method i.e. concrete prism test [8], concrete prisms were prepared according to the proposed test method except that instead of using 310 Kg cement and addition of alkalis to 1.25 percent, 334 Kg cement with no addition of alkalis was used in all concrete mixes. This is believed to eliminate the increase of sulfate in the solution by the addition of sodium hydroxide [9]. The length changes of specimens are measured up to 180 days.

Table 1. Chemical and Physical Characteristics of the Cement

Chemical properties		Physical properties	
Chemical oxides	Percent		
SiO_2	20.65	Fineness :	2960 cm^2/gr
Al_2O_3	5.5	Initial setting :	85 min
Fe_2O_3	2.95	Final setting :	200 min
CaO	61.67		
MgO	3.68		
Na_2O	0.49		
K_2O	1.02		
SO_3	1.73		
L.O.I	3.03		

Compound compositions

C_3S 48.09(%)
C_2S 22.90(%)
C_3A 9.58(%)
C_4AF 8.98(%)
$Na_2O_{eq.}$ (%)= Na_2O(%)+ 0.658x K_2O(%)=1.16

Table 2. Petrography and Physical Properties of Aggregates

Aggregate	R1	M1	K1	A1
Type	Quarried carbonate Rock	Gravel glacial deposit	Carbonate rock	Carbonate rock
Rock Type	Limestone(more Calcite and less Dolomite)	Limestone(calcite dolomite quartz)	Siliceous limestone Quartz and feldspar calcite)	Siliceous limestone (calcite.quartz, feldspar)

3. TEST RESULTS AND DISCUSSIONS

The results of the rock cylinder tests (ASTM C586) for all aggregate types are shown in Table 3. For each aggregate three specimens were prepared and the length changes were measured. The average length changes presented as the expansion of rock cylinders for R1, A1, M1, and K1 aggregates are 0.031%, 0.022%, 0.038%, 0.043% respectively. It is clearly seen that the expansion of all specimens is well below 0.1 percent which is the expansion limit criterion in this method. Results show that these carbonate aggregates can be assessed as non-reactive.

Results of the expansion of mortar bar specimens containing various aggregates are illustrated in Figure 1 to Figure 4. The length changes of at least two specimens for each aggregate are shown in these figures. It can be seen that the expansion of mortar bars containing R1, M1 and K1 aggregates have exceeded 0.1 percent after 14 days while the expansion of specimens containing R1 aggregate is less than 0.1 percent. Thus, from the results of the mortar bar accelerated test, three aggregates were classified as highly reactive.

Table 3. Results of Expansion of Rock Cylinders

R1 Aggregate				A1 Aggregate			
Specimen No.	R1-1	R1-2	R1-3	Specimen No.	A1-1	A1-2	A1-3
Expansion (%)	0.029	0.040	0.026	Expansion (%)	0.024	0.018	0.024
Average (%)		0.031		Average (%)		0.022	
M1 Aggregate				K1 Aggregate			
Specimen No.	M1-1	M1-2	M1-3	Specimen No.	K1-1	K1-2	K1-3
Expansion (%)	0.036	0.041	0.038	Expansion (%)	0.044	0.055	0.030
Average (%)		0.038		Average (%)		0.043	

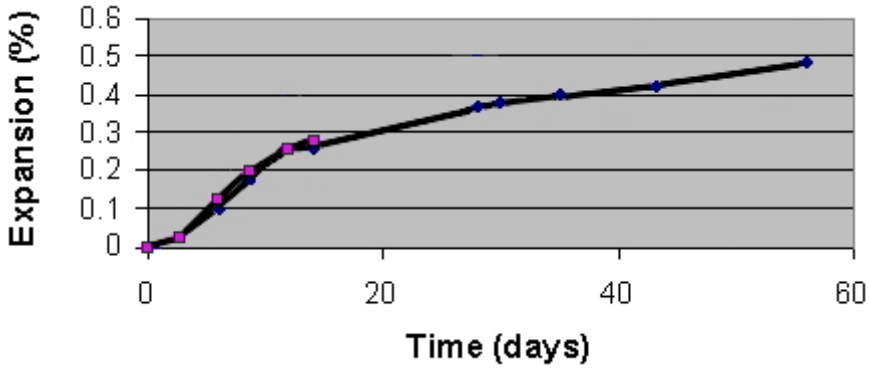

Figure 1. Expansion of mortar bars containing R1 aggregate

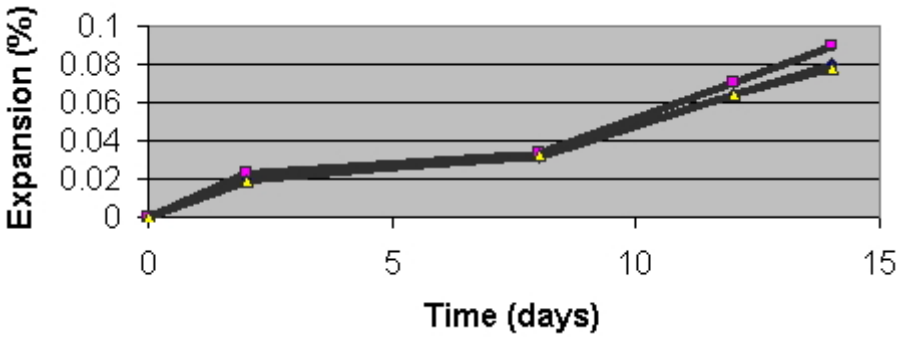

Figure 2. Expansion of mortar bars containing A1 aggregate

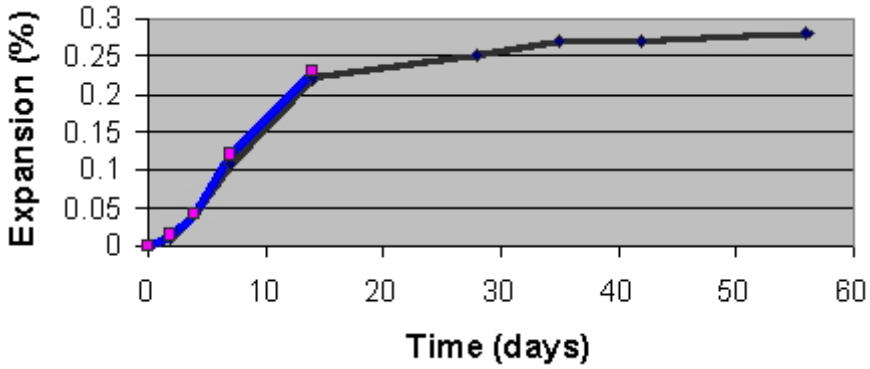

Figure 3. Expansion of mortar bars containing M1 aggregate

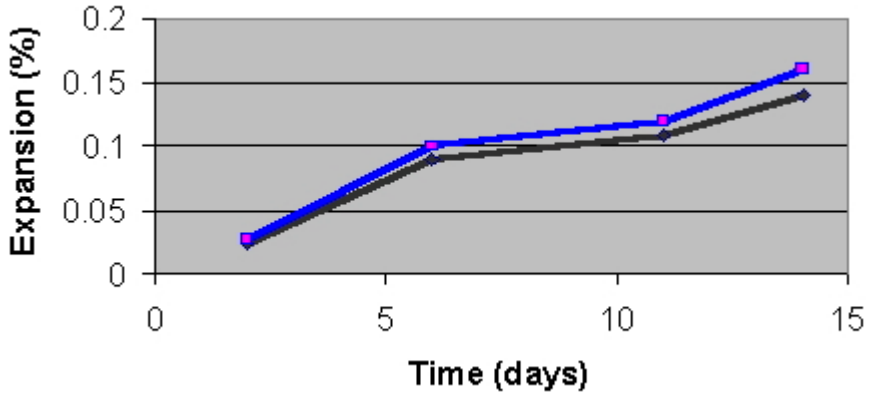

Figure 4. Expansion of mortar bars containing K1 aggregate

Results of expansion of concrete prisms incorporating aggregates from four different sources at various ages up to 180 days are depicted in Figure 5 to Figure 8. In these figures specimens containing R1, M1 and K1 aggregates have shown greater expansion when compared with the expansion of specimens containing A1 aggregate. These three aggregates can be evaluated as moderately reactive aggregates.

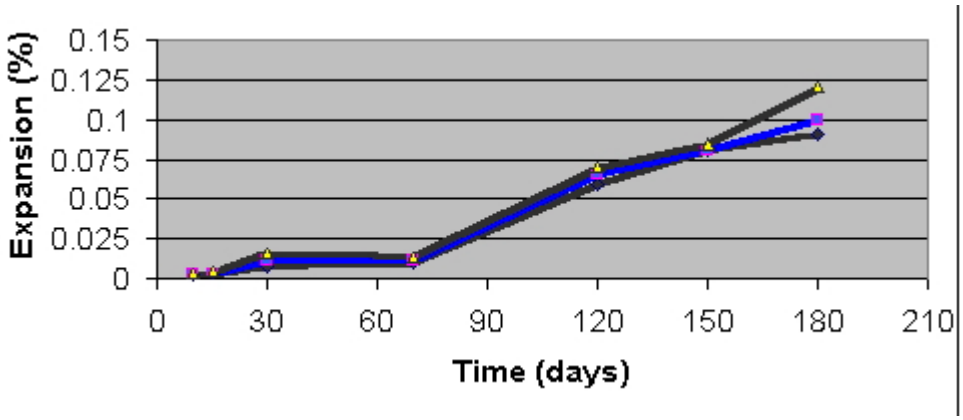

Figure 5. Expansion of concrete prisms containing R1 aggregate

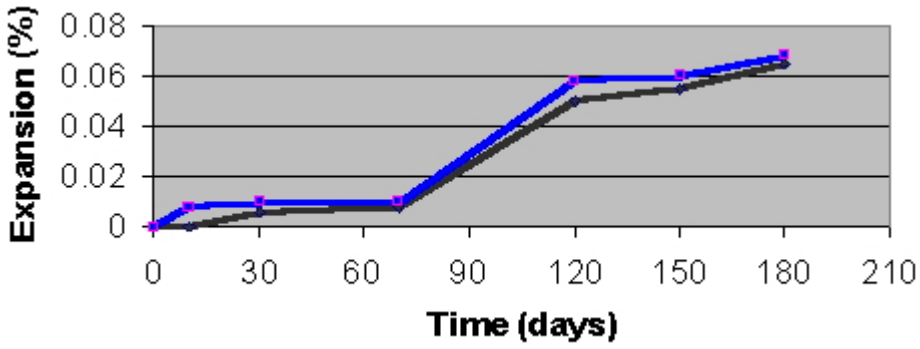

Figure 6. Expansion of concrete prisms containing A1 aggregate

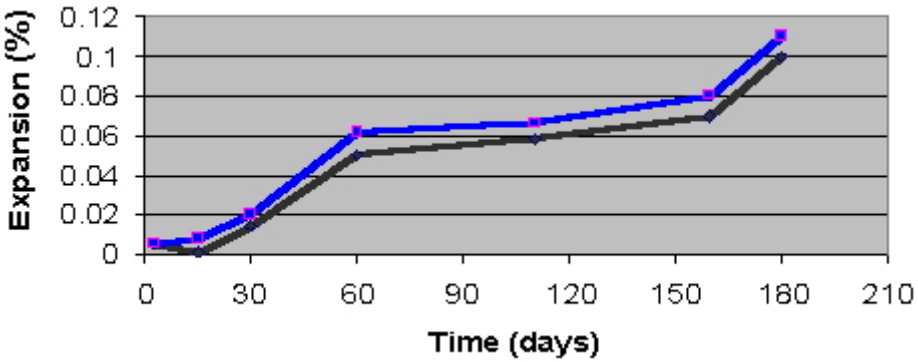

Figure 7. Expansion of concrete prisms containing M1 aggregate

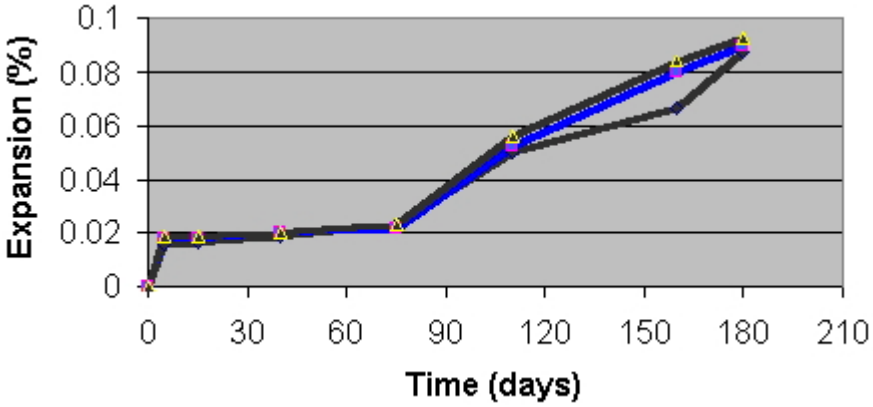

Figure 8. Expansion of concrete prisms containing K1 aggregate

Comparison of the results obtained from the three different test methods reveals that results of the mortar bar method coincide with the results of the concrete prism test. However, the reactive aggregates in these two test methods were evaluated as non-reactive aggregates by the rock cylinder test method (see Table 3). It seems that fine reactive particles will react with sodium hydroxide in the solution and create expansion of specimens in both mortar bar and concrete prism tests. This is not the case when rock cylinders are tested. It is seen that aggregates with different reactivities cannot be detected within 28 days by the rock cylinder test method. Comparison of results obtained with the rock cylinder test and mortar bar test shows that the mortar bar method can be a severe test for carbonate aggregates and aggregates rejected in this test should be checked using the other methods. Contradictory results of three different tests in this investigation support the fact that further alkali-carbonate reaction test methods applicable for particular areas are required.

4. CONCLUSIONS

From the test results obtained in this investigation, the following conclusion can be drawn:

- Contradictory results were obtained in evaluation of reactivity of various sources of carbonate rocks when tested by rock cylinder, accelerated mortar bar and concrete prism methods.
- Results obtained by the rock cylinder test method, show that aggregates with different reactivities can not be detected by this method. Further methods such as accelerated mortar bar and concrete prism tests are necessary for the final assessment of acceptance or rejection of carbonate aggregates.
- The concrete prism test method seems to be an appropriate test for evaluating the reactivity of carbonate aggregates.

5. RECOMMENDATIONS

Laboratory test methods for alkali-carbonate reactivity evaluation need further improvement in order to assess aggregates from various sources.

REFERENCES

[1] Berube, M.A. and Fournier, B. "Accelerated Test Methods for Alkali-Aggregate Reactivity. Advances in Concrete Technology, CANMET-Ottawa, Canada, 1992, pp. 583-627.

[2] William,D.A. and Rogers,C.A.,"Field Trip Guide to Alkali-Carbonate Reaction in Kingston,1991

[3] Ontario", Report MI-145, Ontario Ministry of Transportation, Engineering Materials Office, Downsview, Canada, 26 p.

[4] Hooton, R.D. and Rogers, C.A., "Evaluation of Test Methods for Detecting Alkali-Reactive Aggregates",Proceedings of the 8th International Conference on Alkali Aggregate Reaction in Concrete, Kyoto, Japan, 1989, pp. 439-444.

[5] Ramezanianpour, A.A. and Karimi, M., "Evaluation of Aggregates for AAR Using Accelerated Test Methods", 10th International Conference on Alkali Aggregate Reaction in Concrete, Melbourne, Australia, 1996, pp. 348-354.

[6] ASTM C 586-97. "Standard Test Method for Potential Alkali Reactivity of Carbonate Rocks for Concrete Aggregates (Rock Cylinder Method), Vol. 04.02(Concrete and Aggregates), PA, USA. 1992.

[7] CAN/CSA A23.2-25A. "Test Method for Detection of Alkali- Silica Reactive Aggregate by Accelerated Expansion of Mortar Bars", Canadian Standard., 1994.

[8] Alasali, M.M., Malhotra, V.M., Soles, A., "Performance of Various Test Methods for Assessing the Potential Reactivity of Some Canadian Aggregate", ACI Material Journal, 1992,V.22, No.6, pp.613-619

[9] Shayan, A., "Where is AAR Heading after 10th International Conference?", Cement and Concrete Composites, 1997, Vol.19,pp.481-490.

THE INTERACTION OF AROMATIC ORGANIC COMPOUNDS WITH CEMENTITIOUS MINERALS

Bernt O. Myrvold, Berit Gudding Petersen and Kåre Reknes

Borregaard LignoTech, P.O. Box 162, N-1701 Sarpsborg, Norway
E-mail: bernt.o.myrvold@borregaard.com

ABSTRACT

Lignosulphonates are an important group of plasticising additives for concrete. Different lignosulphonates have different effects on slump, slump loss and setting time. Lignosulphonates have a broad molecular weight distribution, and contain a number of different functional groups. We have investigated how the different functional groups influence the setting time by investigating the interactions between 18 different model compounds and both cement and a model system for cement. The functional groups include, carboxylic acids, sulphonic acids, phenols, catechols, metoxyls, guajacyls, esters, aldehydes and acetals.

We have also looked at the interactions between these model compounds and the cations commonly found in the pore water.

1. BACKGROUND

Lignosulphonates are an important group of plasticising additives for concrete. Different lignosulphonates have different effects on slump, slump loss and setting time. Lignosulphonates have a broad molecular weight distribution, and contain a number of different functional groups. The functional groups include, carboxylic acids, sulphonic acids, phenols, catechols, metoxyls, guajacyls, esters, aldehydes and acetals. There have been some attempts to correlate some of these structures with specific performance in concrete or mortar [1-4].

The model compounds in this study span all the most important functional groups in lignosulphonates and Kraft lignins, and also several combinations of these functional groups.

Usually, the effect of lignosulphonates on the properties of concrete has been discussed based on the adsorption of lignosulphonates to the surface of the cement particles. Cement is a reactive system. To avoid this complication we used magnesium oxide particles as a model for the cement minerals [5,6]. An additional benefit that became appearant during this investigation was that we also avoided colour changes due to the interactions between some of our model compounds and iron(III) ions.

2. EXPERIMENTAL

2.1. Model compounds used

The model compounds were either commercially available (Nos 4, 5, 6, 7, 8, 9, 11,15, 16, and 18) or synthesised in our laboratory, using simple, standard organic chemistry procedures (Nos 1, 2, 3, 10, 12, 13, 14, and 17).

Proceedings of the 11th International Congress on the Chemistry of Cement (ICCC)
'Cement's Contribution to the Development in the 21st Century'
Hosted by: The Cement and Concrete Institute of South Africa
CD-ROM produced by: Document Transformation Technologies
11 - 16 May 2003, Durban, South Africa
ISBN Number: 0-9584085-8-0
Editors: Dr G. Grieve and G. Owens
Congress Organised by: Event Dynamics

The structures of the compounds are shown in Figure 1.

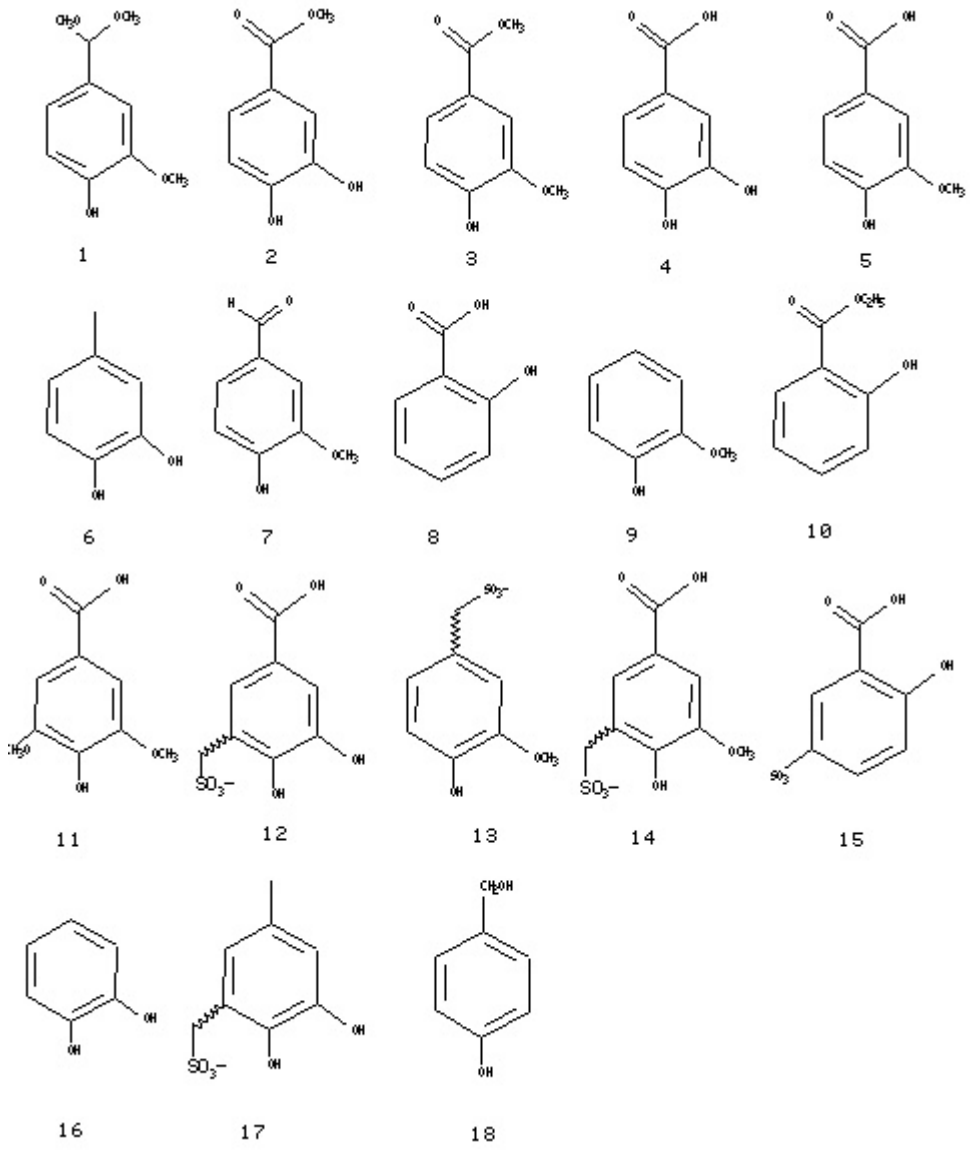

Figure 1. The compounds used in this study.

2.2. Isotherms

The model compound was dissolved in a solution adjusted to pH 12.8 with NaOH and saturated with $CaCl_2$. This is to approximate the pH and ionic strength of the water in cement pastes. Approximately 1% (10,000 ppm) solutions were made for most compounds. Some were only sparingly soluble and weaker stock solutions were made. The solution was further diluted with the solvent to the required strength.

1.0 gram of magnesium oxide was placed in a test tube. 10 ml of the solution with the model compound was added. The test tube was shaken vigorously to disperse the MgO and further shaken for 30 minutes on a Rock'n'Roller from Labinco. The MgO was removed by filtration through a 0.22 micron Millipore filter. The resulting solution was diluted with NaOH solution before UV measurement. The appropriate dilution was found for each compound. The adsorbance was measured for the longest wavelength peak in all cases, except vanillin where the peak at 248 nm was used. The amount of substance left was found from calibration curves. The difference between the amount left and the amount added was regarded as the amount adsorbed. The adsorbed amount was calculated as μmol/g substrate in all cases. As usual for adsorption isotherms the amount

adsorbed was plotted as a function of the equilibrium concentration in the solution. No tests were performed to check that the value after 30 minutes actually is an equilibrium concentration. 30 minutes were used to conform with the isotherms for cement and cement minerals.

Some of these model compounds, particularly the dihydroxy compounds, are unstable under the conditions used. The UV adsorbance would change over time. Fresh solutions were always used for the adsorption studies. It was also in all cases attempted as far as possible to use the same waiting times between dilutions and measurements. For catechol and dihydroxybenzoic acid methyl ester, the best isotherms were obtained by waiting for approximately 24 hours between the dilution of the samples and the UV measurements. During this time the dilute samples were fully oxidised and the UV spectra of the *ortho*-quinones were obtained instead.

Some of these compounds also change colour dramatically in the presence of ferric ions. All chemicals were of technical grade or purer to avoid contamination.

2.3 Setting times

The samples were dissolved in the mixing water for the cement paste at 0.20% sbwc dosage. The paste consisted of ordinary Portland cement at w/c-ratio of 0.30. The hydration was measured with a Vicat apparatus which automatically drops a needle into a sample of cement paste. In this way initial and final setting time is determined.

3. RESULTS

Table 1 shows a summary of all the results. A comparison between Table 1 and Figure 1 immediately shows the importance of the catechol group. All compounds with a catechol group and no sulphonic acid groups are strongly accelerating.

Table 1. Setting times for 0.20% addition of selected organics.

Sample	Initial setting/ min	Final setting/ min	Initial slope/ ml/g
1	171	220	0
2	~20	<30	167
3	167	212	0
4	~20	<30	50
5	158	221	0
6	~20	<30	118
7	166	240	0
8	182	244	4.2
9	190	223	0
10	208	276	4.2
11	153	221	0
12	207	272	8.0
13	173	219	5.7
14	137	191	0
15	251	320	1.8
16	~5	9	134
17	202	258	21
18	161	183	0
blank	137	205	n.a.

It was also noticed that several of the compounds tested gave strongly coloured cement paste samples. As phenols are known to give colour reactions with ferric ions we checked this further.

Table 2 shows the results. We see clearly that the accelerating compounds also give strong colour reactions with ferric ions. Several of the model compounds are sparingly soluble, and KOH was added to obtain solutions. In most cases this resulted in a white precipitate with Ca^{2+}, and often a reddish brown precipitate with Fe^{3+}.

Table 2. Interactions between the model compounds and different ions.

Com-pound	**+ Al^{3+}**	**+ Ca^{2+}**	**+ Fe^{3+}**	**+ Fe^{2+}**	**UV max for isotherms**
1	no change	no change	no change	greenish	249 nm
2	no change	white precipitate	**bluish violet**	**reddish violet**	302 nm
3	no change	white precipitate	reddish brown	no change	298 nm
4	no change	precipitate	**red**	no change	302 nm
5	no change	white precipitate	reddish brown	no change	298 nm
6	no change	no change	**green**	**green**	485 nm
7	dark yellow	white precipitate	reddish brown	no change	248 nm
8	no change	white precipitate	reddish brown	no change	296 nm
9	no change	white precipitate	reddish brown	light brown	289 nm
10	no change	white precipitate	reddish brown	light brown	296 nm
11	no change	white precipitate	reddish brown	reddish brown	303 nm
12	no change	dark yellow	**bluish violet**	**violet**	307 nm
13	no change	white precipitate	reddish brown	light brown	296 nm
14	no change	white precipitate	reddish brown	no change	298 nm
15	no change	no change	**violet**	**reddish violet**	298 nm
16	no change	**bluish violet**	**dark green**	**blue green**	296 & 311 nm
17	no change	no change	**violet then green**	**dark blue**	480 nm
18	no change	no change	brown precipitate	no change	290 nm

We then tested the adsorption of the different model compounds on to the magnesium oxide surface under conditions resembling cement.

Most compounds did not adsorb at all to the MgO surface. The ones that did adsorb all contained groups that can easily chelate metal ions. Either the catechol group (with two phenolic groups in ortho position) or the salicylic group (with a acid or ester and a phenolic group in ortho position). Molecules with sulphonic acid groups adsorb much less than those without.
We notice that fairly similar compounds give dramatically different results. The vanillic acid gives no adsorption but by removing one methoxyl group we obtain 3,4-dihydroxy-benzoic acid; this compound is more polar and we would expect it to be more water-soluble. Nevertheless, it shows a classical Langmuir isotherm. Sulphomethylating 3,4-dihydroxy-benzoic acid, the behaviour again changes and we obtain a linear relationship between the amount added and the amount left.

This compound seems to be more soluble and, we do not reach a plateau in the adsorption isotherm with the amounts used in this study.

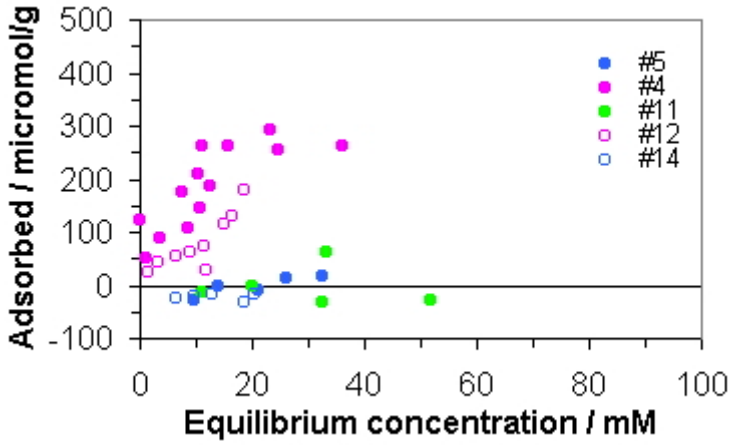

Figure 2. Adsorption isotherms for the compounds with a benzoic acid group.

The same trend is observed for the 4-methyl catechol, guajachol, sulphomethylated 4-methyl catechol triplet. Sulphomethyling the non-adsorbing guajachol also gives a product that does not adsorb, or only adsorbs to a very small degree. The 4-hydroxy-benzyl alcohol is also non-adsorbing.

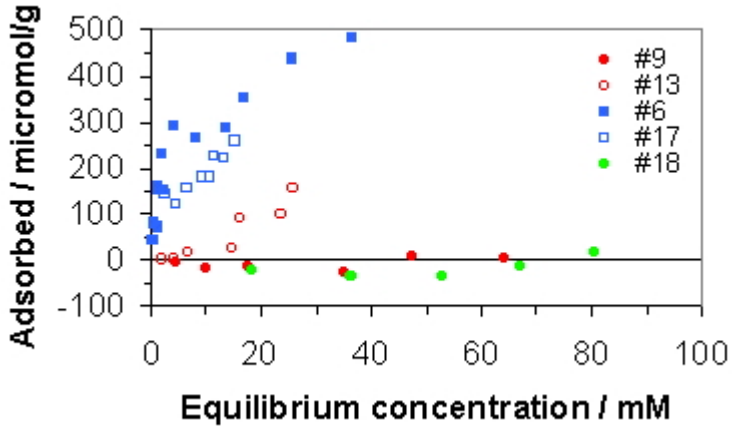

Figure 3. Adsorption isotherms for $C_7H_8O_2$ compounds, and their sulphomethylated versions

None of the three relatively non-polar vanillin derivatives, vanillin, vanillin dimethyl ketal, or vanillic acid methyl ester, adsorbs.

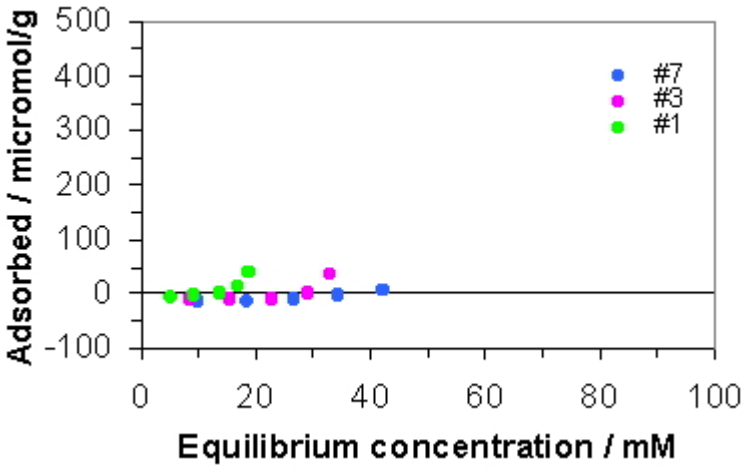

Figure 4. Adsorption isotherms for the vanillin derivatives.

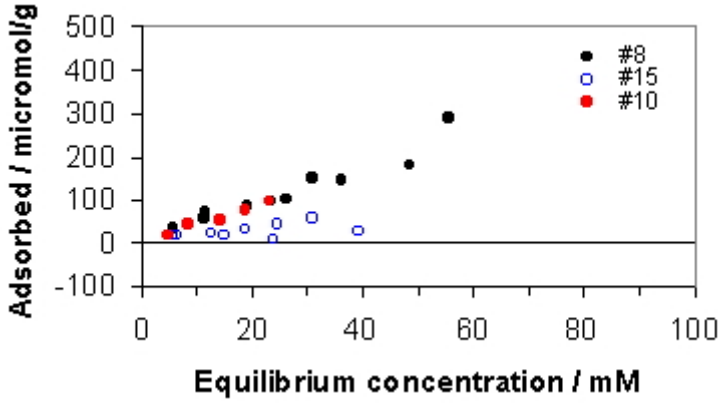

Figure 5. Adsorption isotherms for the salicylic acid derivatives.

Salicylic acid and salicylic acid ethyl ester shows the same adsorption while the more soluble 5-sulpho salicylic acid adsorbs much less.

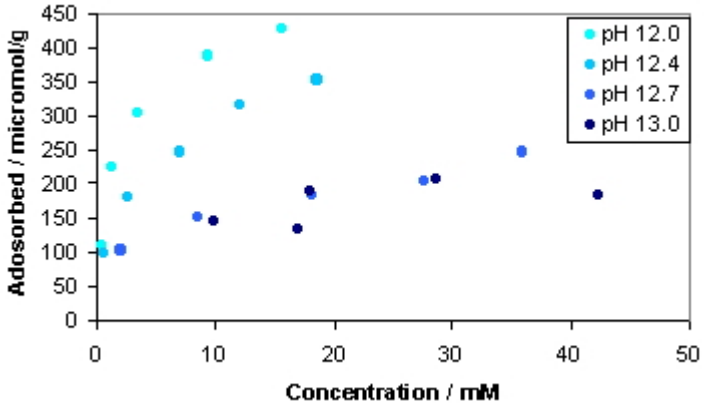

Figure 6. The pH dependence of the adsorption for catechol.

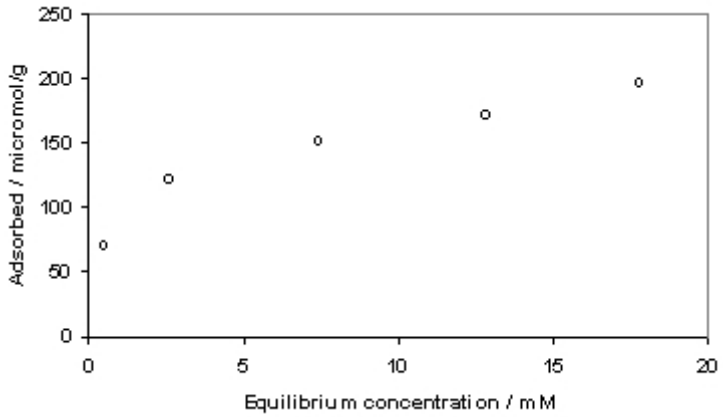

Figure 7. The adsorption of dihydroxybenzoic acid methyl ester.

All the catechols complexes with iron(III) ions. For 3,4-dihydroxy benzoic acid (#4) we also find increased amounts of iron and aluminium in the pore water. Compounds 6, 12 and 17 also give slightly increased amounts of aluminium in the pore water.

4. DISCUSSION

Other well-known complexing agents, like EDTA, also give acceleration. This implies that the formation of iron and/or aluminium complexes could be important. The catechol compounds 2, 4, 6 and 16 are all strongly accelerating. These four compounds also complex with iron(III) ions in solution, and adsorb strongly to the surface. Sulphomethylating the compounds give products which are non-accelerating. It is difficult to see why the sulphomethylation should destroy their complexing abilities. They also give the same type of coloured complexes with Fe^{3+}. In fact, for the salicylic acid it is only with the sulphonated compound that we observe coloured complexes.

If complex formation is important, just mixing lignin with the appropriate compounds should give acceleration. The mixing should not influence the formation constant for these complexes much. However, experiments show that a physical mixture has no such accelerating effect. The difference in behaviour must thus be due to their different adsorption characteristics.

We also see from Table 1 that the initial slope for the adsorption isotherms is closely related to the accelerating effect. A high slope (≥50 ml/g) gives a strong acceleration of the setting, while a low slope (<25 ml/g) shows no accelerating effect. The surface area of the cement used is 0.36 m^2/g and that of magnesium oxide 0.27 m^2/g. Within the accuracy of these determinations, they have about equal surface areas. We find at saturation coverage of 31-78 mg/g MgO. This corresponds to 115-290 mg/m^2. For benzoic acid, models show about that they occupy about 1.0 m^2/mg. The saturation coverage thus corresponds to many layers of organic material. However, the saturation coverage is of little relevance to the cement system. Only 0.2% organics on cement weight are added. This corresponds to 2 mg/g (or 5.6 mg/m^2). Moreover, not all the organics adsorb to the surface. The lowest slope among the compound that accelerate was found for #4. Here the saturation is reached at 10 mM concentration in the water phase. In the mortar used the w/c ratio is 0.3. This implies that 0.5 mg or one quarter of the organics is still in the water phase. This still gives a surface coverage of 4 mg/m^2, or enough to cover the entire surface. The non-accelerating compounds reach saturation at higher concentrations in the water phase, and there is not enough material to cover the entire surface.

The problem remains, though, why should something that adsorbs to the surface give a faster reaction?

The adsorbed species could form nucleation sites and thus promote reaction. Nucleation and growth usually requires a good match between the crystal structure of the "seed" and the growing crystal. It seems unlikely that the four different organics that are accelerating should all have crystal structures that match the growing phases of cement.

The organic materials that adsorb onto the surface are negatively charged, and will neutralise positive charges from the adsorbed metal ions at the surface. This will make it easier for other positively charged species to approach the surface.

In cement systems it is possible that the compounds will adsorb to some minerals and not to others. This could promote reaction at some sites and prevent reaction at other sites. The hardening demands contact between the different cement grains. Reaction at specific sites instead of all around the grains will promote the growth of needles instead of rounded particles. This will give a faster setting, as the needles are much more likely to contact each other, forming a network.

5. CONCLUSIONS

Although the mechanisms behind the effect are unresolved it is clear that catechol compounds that adsorb to the surfaces have a strong accelerating effect on the setting time of mortar samples.

REFERENCES

[1] Young, J.F. A review of the mechanisms of set retardation in portland cement pastes containing organic admixtures, Cement and Concrete Research, vol 2, 1972 pp 415-433.

[2] Hansen, W.C. Interactions of organic compounds in Portland cement pastes, J. Materials, vol 4, 1970, pp 842-855.

[3] Diamond S. Interactions between cement minerals and hydroxycarboxylic-acid retarders: I, apparent adsorption of salicylic acid on cement and hydrated cement compounds, J. Am. Ceramic. Soc., vol 54, 1971, pp 273-276.

[4] Singh, N.B., Singh, S.P. and Sarvehi, R. Effects of phenols on the hydration of Portland cement, Advances in Cement Research, vol 2, 1989, pp 43-48

THE INTERACTION OF AROMATIC ORGANIC COMPOUNDS WITH CEMENTITIOUS MINERALS

Bernt O. Myrvold, Berit Gudding Petersen and Kåre Reknes

Borregaard LignoTech, P.O. Box 162, N-1701 Sarpsborg, Norway.
E-mail: bernt.o.myrvold@borregaard.com

Bernt O. Myrvold

Master of Science in organic chemistry and Ph.D. in Physical Chemistry.

From 1985 to 1992 I worked in the R&D department of several smaller Norwegian and Swedish companies, as well as Manchester University, all in the field of liquid crystal displays. Most of the work was related to the understanding of the relationship between chemical structure and macroscopic properties. The work included both polymer synthesis and characterisation work.

February 1992 to September 1993 I worked as Visiting Researcher at Hitachi Research Laboratory in Japan. The work included polyimide synthesis, test device fabrication and optical measurements. All synthetic and fabrication work took place in a clean room environment. The result was a good understanding of the relationship between polymer structure and the effect on the liquid crystals, and of how chemical changes in the liquid crystals affect the interaction with the surface.

January 1994 – October 1995 I did Post Doc. research at the University of Oslo, department of Chemistry in the Colloid and Interphase group. I was mostly doing modifications of natural polymers for rheology control in oil wells.

November 1995 I joined Borregaard LignoTech. Here, I have worked on characterisation and chemical modifications of Kraft lignin and lignosulphonate polymers. I have brought new additives for starter batteries from the laboratory to successful production. I have also worked on new products for the oil industry, both gels for enhanced oil recovery, and emulsifiers for transport of heavy crude oils.

I have written 35 publications, 2 sports books and have 5 patents.

ADSORPTION STUDIES OF LIGNOSULPHONATES ON CEMENT AND CEMENT MODEL COMPOUNDS

Bernt O. Myrvold, Jonas Gustafsson and Kåre Reknes

Borregaard LignoTech, P.O. Box 162, N-1701 Sarpsborg, Norway
Telephone: (+47) 69 11 80 60, Fax: (+47) 69 11 87 85
E-mail: bernt.o.myrvold@borregaard.com

ABSTRACT

Lignosulphonates are important plasticizers for concrete. To learn more about their interactions with the cement adsorption isotherms were obtained for a high molecular weight lignosulphonate. The chemical reactivity of cement makes it impossible to obtain true isotherms. The different minerals present also have different adsorption characterstics. To overcome these problems several model systems, e.g., dicalcium/tricalcium silicate mixtures, tricalcium aluminate/tetracalcium aluminate ferrite, tricalcium aluminate, alumina, ferric oxide, magnesium oxide, calcium silicate, and kaolin were also investigated. In addition, Standard Portland Cement and White Aalborg Cement were used. All model systems were investigated at high pH, and moderate to high ionic strength to simulate the situation in pore water.

The lignosulphonates show adsorption isotherms that match the expected isotherms for polyions. The high molecular weight fraction of the lignosulphonates are preferably adsorbed. The di- and tri-valent cations present interact with the lignosulphonates and this interaction is important for the adsorption. The interaction with multivalent ions renders the lignosulphonate more hydrophobic.

1. BACKGROUND

Lignosulphonates are added to concrete to improve the flow of the fresh concrete. Exactly how they reduce the viscosity has been the subject of much speculation. Most workers assume that the first step is an adsorption of the lignosulphonate to the cement grains. A steric or electrostatic repulsion will then prevent the cement grains from approaching each other and impart colloidal stability to the system. The cement grains themselves are non-homogeneous and lignosulphonates will probably have a different preference for the different minerals. The mineral composition of the surface will also in most cases be different from the bulk. There might also be a difference in composition between grains of different sizes. It is thus clearly of interest to see how the lignosulphonates interact with the different minerals present.

There have been some studies of adsorption of lignosulphonates to cement [1-3] and cement model compounds. The model compounds studied are C_3S [4,5,6], β-C_2S [3,6] C_3A [3,6-8] , C_3AH_6 [8], $C_3A{\cdot}C\bar{S}{\cdot}H12$ [7], $CaSO_4$ [4] , C_4AF [4], C_2F [4] , $Ca(OH)_2$ [4,5] ,CH [5] H-C_3S [5]. Most of these studies are fairly old, and many of them use ill-characterised lignin samples.

2. EXPERIMENTAL

2.1 Adsorption isotherms

1.0 gram of the substrate was placed in a 25 ml tube. For the isotherms with salts present 10 ml of a salt solution with twice the required strength was added. 0 to 98 ml of water and 10 to 1 ml of the lignosulphonate solution was added. Always adding a total of 10 ml water and lignosulphonate solution. The tube was corked and shaken for 25-30 minutes.

For experiments with saturated salt solutions the lignosulphonate was dissolved in the salt solution. 1.0 gram of the substrate was placed in a 25 ml tube. 0 to 9 ml of the pure salt solution and 10 to 1 ml of the lignosulphonate solution was added. Always adding a total of 10 ml solution. The tube was corked and shaken for 25-30 minutes.

The solid substrate was removed by filtering through a 0.22 micron Millipore filter. At high pH there is no loss of lignosulphonates during the filtration step. Some fluid is trapped in the glass frit that supports the Millipore filter. The amount is small, and to reduce any dilution effects the series of solutions were either run from the strongest to the weakest, or from the weakest to the strongest. Repeated runs were performed in opposite directions if possible, but we could see no difference in calculated adsorption depending on the whether we started with the strongest or weakest solution.

The filtered solution was diluted with NaOH solution to the required strength for UV adsorbance measurements. The extinction constants of lignosulphonate are pH dependent and a high pH (>11) was thus used for all measurements. The content of lignosulphonate left in solution was calculated from the characteristic UV adsorbance band at 280-283 nm. A new standard curve from solutions of known strength was made for each set of measurements.

The adsorbed amount of lignosulphonate is calculated as the difference between the initially added amount and the amount left in the solution. The adsorbed amount is expressed as mg. pr. gram of substrate. In the isotherms the adsorbed amount is plotted against the equilibrium concentration, e.g. the concentration left in the solution.

For convenience we will use the term adsorbed, although consumed lignosulphonate will probably be more correct in many cases. As we will see, there is precipitation in many cases. In the more reactive systems, some of the lignosulphonate might also be buried in the reaction products.

To obtain reproducable isotherms gypsum had to be added to the C_3A/C_4AF phase, and also additional gypsum had to be added to the White Aalborg Cement.

2.2 Materials

The lignosulphonate used in this study is Ultrazine NA, an ultrafiltrated Norwegian Spruce soft wood lignosulphonate. The counter ion is sodium.
Characterics of the lignosulphonate used.

Mn	8.8 kDa
Mw	53 kDa
Organic Sulphur	5.1 %
Carboxylic Acids	4.5 %
Phenolic Hydroxyls	1.9 %
Methoxyl	10.9%

The substrates used were Standard Portland Cement from Embra and White Aalborg Cement from Aalborg Portland Cement were used. The C_3S/C_2S mixture (approximately 3.5:1) was obtained by extraction of the Embra standard portland cement with KOH/ sucrose solution. The C_3A/C_4AF mixture (~1:1) was obtained by extraction of the Embra standard portland cement with maleic acid in methanol. The rest of the substrates were commercially available in chemically pure form.
Alumina (Al_2O_3) from Fluka, lot no. 409370/1 32700
Ferric oxide (Fe_2O_3) from Fluka, lot no 411837/1 31101
Calcium silicate ($CaSiO_4$) from Alfa, lot no C04H03
Magnesium oxide (MgO) from Merck, lot no TA904765 129
Washed Kaolin from Prolabo, lot no 513G.

Salts of ferric chloride ($FeCl_3$), ferric sulphate ($Fe_2(SO_4)_3$), and aluminium chloride ($AlCl_3$), aluminium sulphate ($Al_2(SO_4)_3$), calcium chloride ($CaCl_2$), sodium chloride(NaCl), sodium sulphate(Na_2SO_4) and potassium sulphate(K_2SO_4) were added to some of the solutions.

2.3 Molecular weight determination

Molecular weights were determined on a Jordi Glucose DVB 10000 Å coloumn. The mobile phase consisted of 10% DMSO in water buffered to 10.5 with a sodium hydrogen phosphate buffer and 0.1% SDS added. A spectra System AS3500 sampler, P4000 pump, and UV2000 detector were used. The software allows the calculation of the different molecular weight averages (M_n, M_w, M_z and M_{z+1}) as well as polydispersity. The molecular weights are given relative to two in-house standards with M_w of 68,000 and 8,300 Da, respectively. The relative values of the different lignosulphonate fractions are accurate to +/-2000 Da, while the absolute values depend on the accuracy of the standards. For the purpose of this study, the absolute molecular weights are of less importance.

3. RESULTS

We found strong adsorption to Standard Portland Cement (containing 8 % C_4AF), White Aalborg Cement (containing 1% C_4AF), the C_3A/C_4AF phase and Fe_2O_3, while we could not detect any adsorption to the C_2S/C_3S phase, $CaSiO_4$, or Al_2O_3. This is in disagreement with the literature, which reports strong adsorption of calcium lignosulphonates also to the C_2S/C_3S phase [4,5]. We thus redid our experiment with this phase with Ultrazine CA, a product that has been ultra filtrated, but without any ion exchange. This product behaves as described in the literature. Adding calcium chloride to the solutions with Ultrazine NA also gave adsorption of the lignosulphonate.

Figure 1 shows the adsorption to alumina at three different pH levels. While Figure 2 shows the effect of adding Al^{3+} ions.

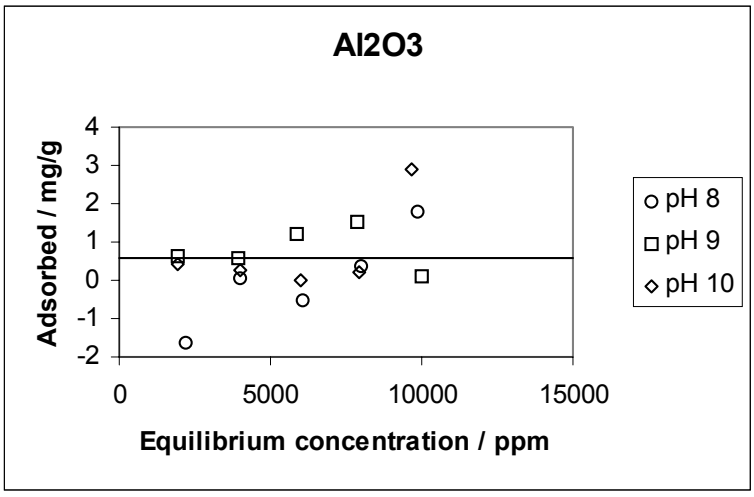

Figure 1. Adsorption of Ultrazine NA to alumina at three different pH values.

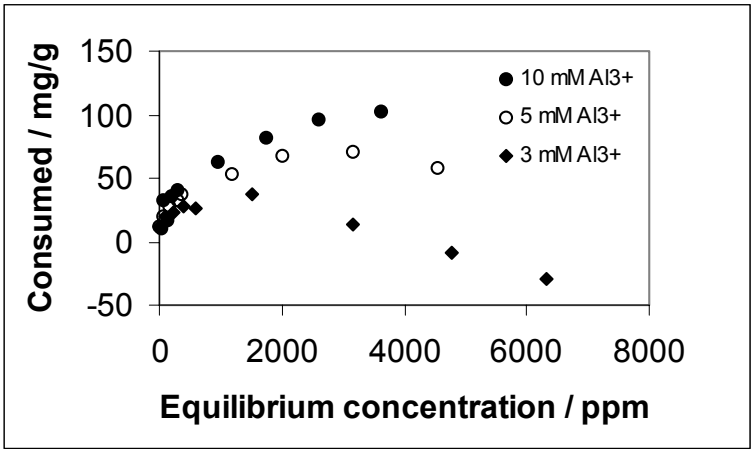

Figure 2. Adsorption of Ultrazine NA to alumina at different concentrations of Al^{3+}.

Figure 3 shows the "adsorption" of Ultrazine CA or Ultrazine Na in the presence of $CaCl_2$ to C_2S/C_3S. This looks more like a precipitation, where a constant portion of the lignosulphonate disappears.

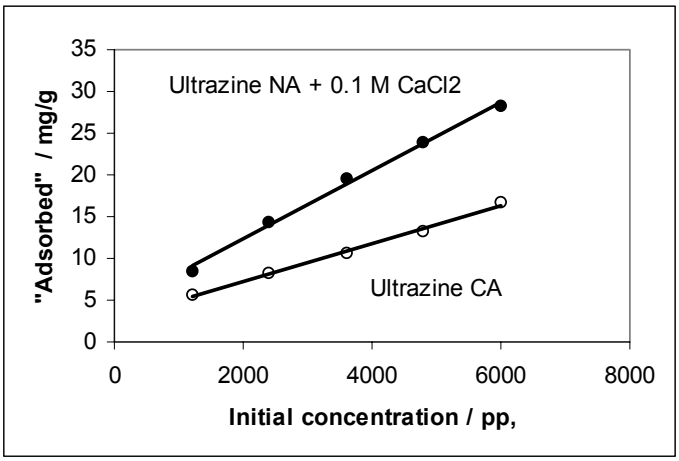

Figure 3. Adsorption of Ultrazine CA and Ultrazine NA with Ca^{2+} present.

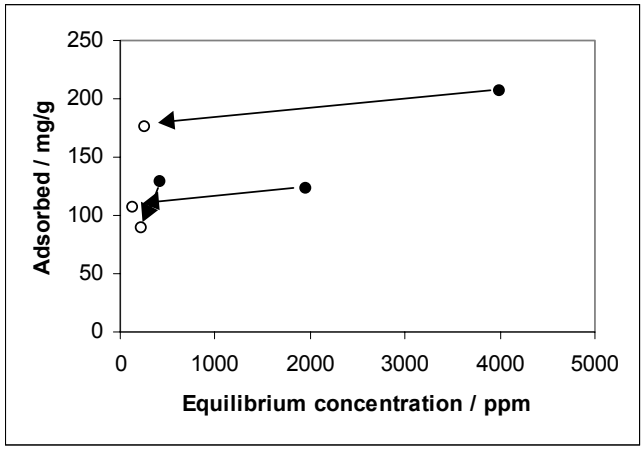

Figure 4. Desorption of Ultrazine NA in the presence of 10 mM Al^{3+}.

In the presence of Fe^{3+} Ultrazine NA will adsorb to C_2S/C_3S. This is shown in Figure 5.

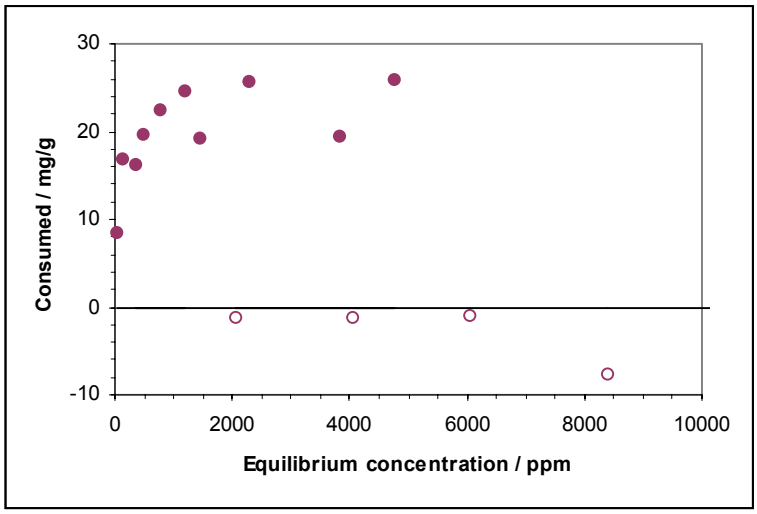

Figure 5. Adsorption of Ultrazine NA to C2S/C3S, in the absence (open circles), and presence (filled circles) of Fe^{3+}.

For the C_3A/C_4AF substrate the situation is more complex. As Figure 6 shows we obtain good isotherms except for one or two points. These two points correspond to the direct addition of lignosulphonate solution without any water first. It is clear that during the 30 to 60 seconds between the water being added and the lignosulphonate solution being added, the substrate changes enough to give different adsorption isotherms. As the particle size distribution of our substrates are unknown we are not comparing the absolute surface coverage. It is clear that both the C_3A/C_4AF and its hydration product adsorbs Ultrazine NA, and no further investigation of the difference between them was performed. The results are shown in Figure 6.

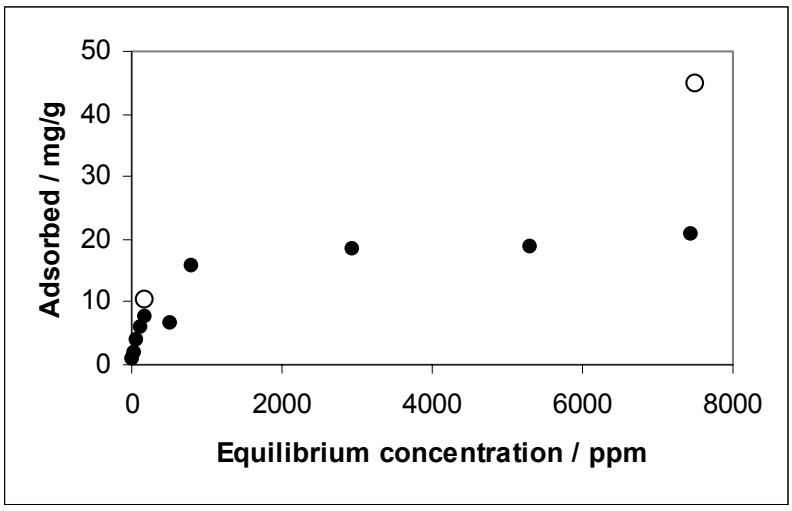

Figure 6. Adsorption isotherms for Ultrazine NA on C_3A/C_4AF. Open circles addition of lignosulphonate solution. Filled circles addition of water followed by lignosulphonate solution.

Figure 7 shows the adsorption to ferric oxide. We obtained a nice adsorption isotherm. In this case we probably underestimated the adsorption. Ferric ions interact with lignosulphonates to give a darker product. This ferric adduct also has a higher UV adsorption at 281 nm. Thus the UV method for determining the lignosulphonate content in solution will overestimate the amount of lignin left. When the amount left is overestimated the adsorbed amount consequently will be underestimated. As we are not concerned with the absolute coverage this problem is of no concern for our discussion.

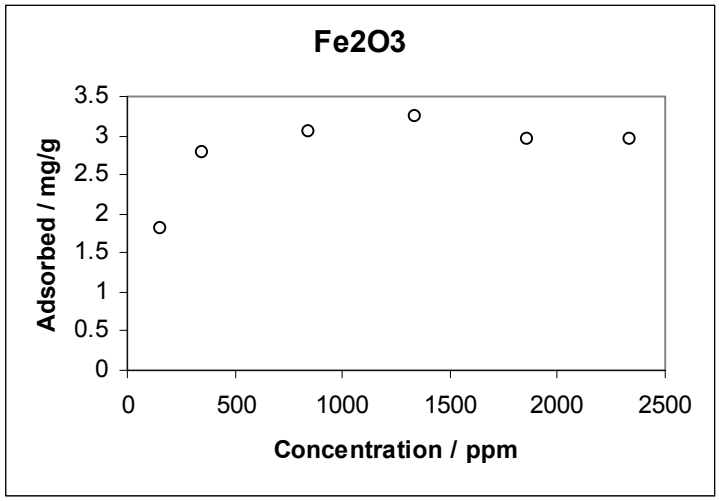

Figure 7. The adsorption isotherm for Ultrazine NA on ferric oxide.

All the substrates, to which Ultrazine NA adsorbs, contain ferric oxide. This means that there will be some soluble Fe^{3+} ions present. We saw in Figure 5 how the adsorption to C_2S/C_3S changed when 10 mM FeCl3 was added to the solution.

Some experiments were performed by keeping the amount of Ultrazine NA and varying the amount of iron(III) ions present. 5000 ppm Ultrazine NA was used for the MgO substrate and 1000 ppm for the kaolin substrate. The intention was to determine the optimum amount of ferric ions required.

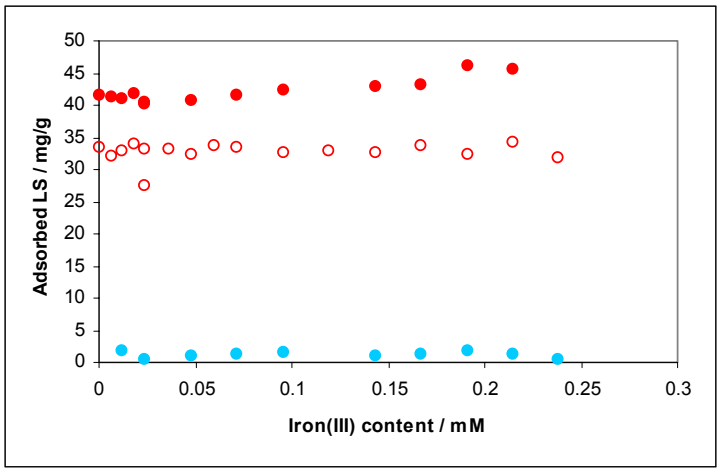

Figure 8. The effect of varying amounts of ferric ions on the adsorption to kaolin (blue) and magnesium oxide (red) at pH 10.1. Open symbols no additional salts, filled in 0.42 M NaCl.

The results in Figure 8 are in stark contrast to those in Figure 5. For these two substrates there seems to be no effect of the ferric ions.

We made a simulated pore water starting with a saturated solution of $Ca(OH)_2$ in de-ionized water and adding 7.0 gr/l Na_2SO_4, 6.0 gr/l KOH and 6.1 gr/l K_2SO_4. This solution was filtered through a 0.22 micron millipore filter and split in three. One part was left. 500 ml was added 62.5 mg $Al_2(SO_4)_3 \cdot 16H_2O$. (0.4 mM Al^{3+}), 500 ml was added 2.0 mg $Fe_2(SO_4)_3$ (0.04 mM Fe^{3+}), and the rest left unchanged. Ultrazine NA was dissolved in the three different solutions. We obtained adsorption isotherms with MgO and kaolin as substrates.

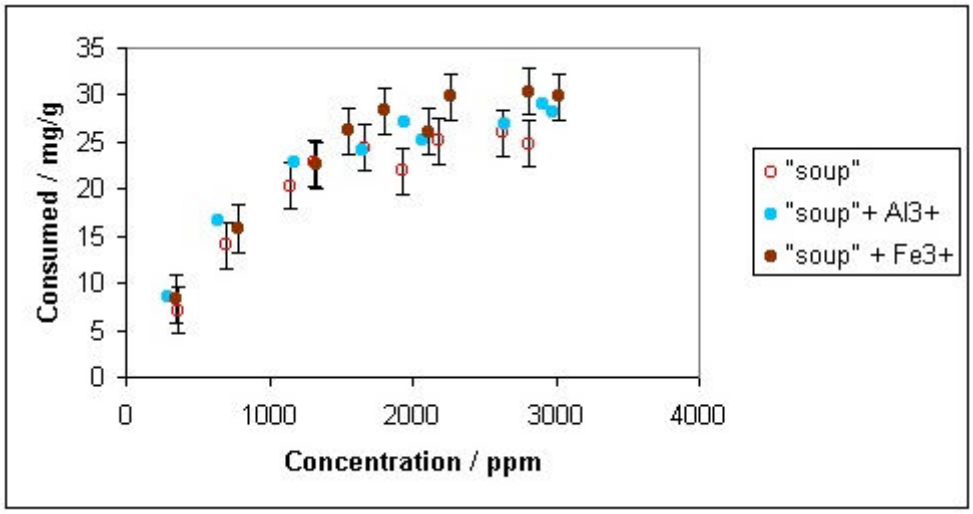

Figure 9. Adsorption to MgO in the presence of different salts. Error bars correspond to two standard deviations (for clarity they are omitted from Al^{3+}).

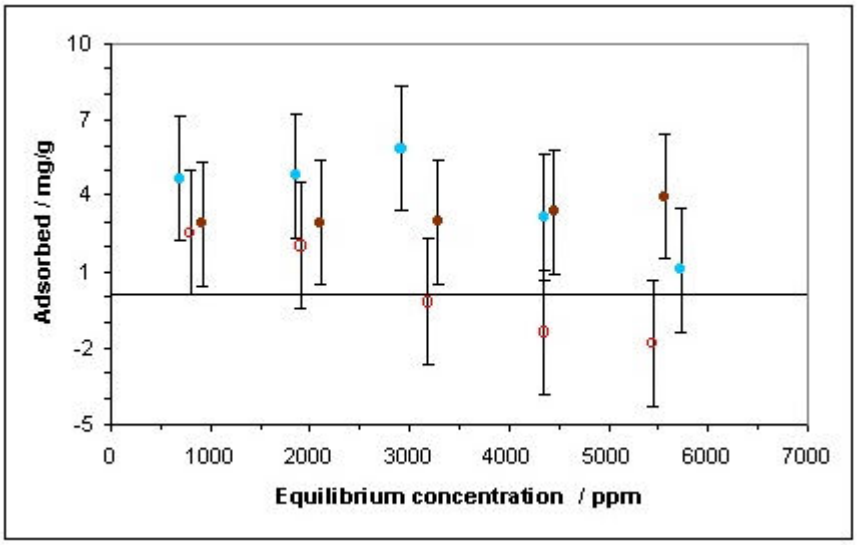

Figure 10. Adsorption to kaolin in the presence of different salts. Error bars correspond to two standard deviations. The symbols are as for Figure 8.

We see that both for the positively charged magnesium oxide and for the neutral (at this pH) kaolin the presence of trivalent ions there is a small and maybe insignificant increase in the adsorption.

The solutions shown in Figures 9 and 10 were further analysed with respect to the molecular weight of the remaining lignosulphonate. The results are given in Figures 11 and 12.

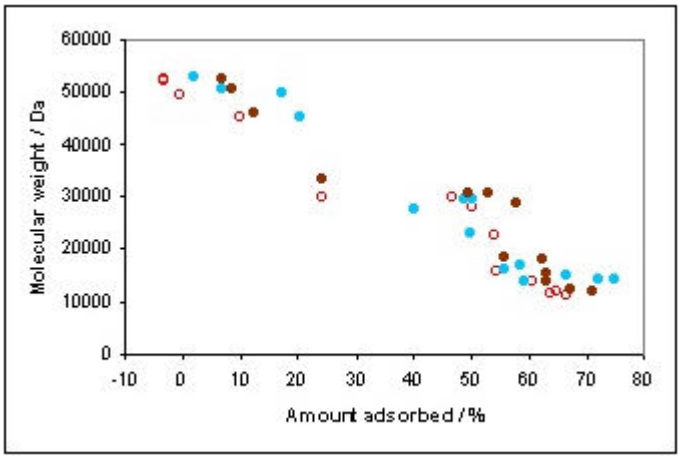

Figure 11. The molecular weight of the remaining lignosulphonates as a function of the fraction adsorbed.

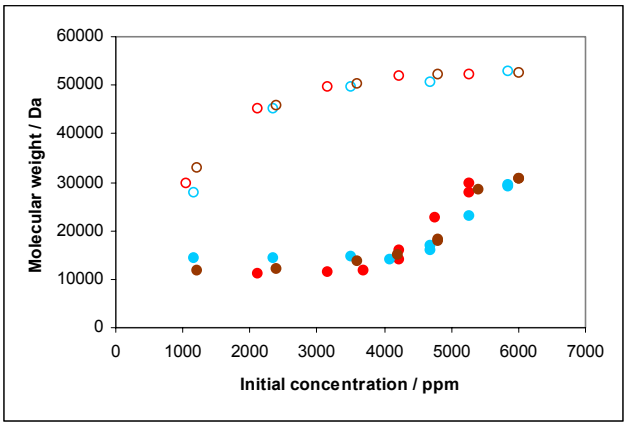

Figure 12. The molecular weight of the remaining lignosulphonate as a function of the amount initially added. Open symbols kaolin substrate (low adsorption), filled symbols MgO (high adsorption).

These figures clearly tell us that the highest molecular weight fraction is preferentially adsorbed. As more and more of the total amount of lignosulphonates are adsorbed to the substrates a lower and lower molecular weight fraction will be adsorbed. We also see that there seems to be a lower limit. At least some of the lignosulphonates with a molecular weight of less than 10000 are not adsorbed.

4. DISCUSSION

Adsorption of polyelectrolytes is a complex process. The charge of the surfaces and the polyelectrolyte will give rise to electrostatic attractions, or repulsions. These charges will be pH dependent. In addition the surfaces will be more or less hydrophobic, hydrophobic interactions can thus not be neglected, either. Complexing the lignosulphonates will also alter their hydrophobicity.

Ions in solution can also give insoluble salts with lignosulphonates. With the experimental procedure used here, and commonly used to obtain adsorption isotherms, it is impossible to distinguish directly between adsorption and precipitation.

Fe_2O_3 has a point of zero charge (pzc) at pH 4.8-8.6, Al_2O_3 at 9.0, and MgO at pH 12.0. Kaolin consists of platelets with large negative surfaces and edges with (pzc) at 7.3.

Silica has a pzc at pH 2 – 3.7. For most of the silicate minerals used in this study the pzc is unknown, but we would expect it to be between that of silica and kaolin due to the chemical similarities. This means that all the substrates – except MgO - are negatively charged under the experimental conditions used. This means that for electrostatic reasons the surfaces should repel the lignosulphonate and we should observe no adsorption. Although these values are found for pure, simple systems, they might not be relevant to the cement paste where dissolved ions will modify the surface charges. Most workers seem to agree that cement has a slightly positive surface charge.

All the substrates with ferric ions give adsorption irrespective of their charge. Some ferric ions are leached into the solution, which can be shown by colour tests with phenolic compounds. In the solution the ferric ions will interact with the lignosulphonate to give a more surface active species. The ferric ions could also conceivably interact with the different substrates to give a more positively charged surface, which would also react stronger with the lignosulphonate. However, the same effect of the ferric ions is also found in emulsions where there is no solid surface for the ferric ions to bind to [9,10]. The same effect of ions leaching from the substrate and rendering the lignosulphonate more surface active has also been invoked to explain the difference between cleaned lead surfaces and native lead surfaces [11]. For the more hydrophobic, and near neutral lignosulphonate-iron complex there will be no electrostatic barrier to the adsorption. This complex will adsorb to surfaces that are negatively charged as well. For MgO the surface is positively charged, under the conditions shown in Figure 8, the surface is saturated with lignosulphonate without iron present (we are on the plateau shown in Figure 9). The addition of ferric ions will not increase the adsorption. The apparent lack of increased adsorption to kaolin in the presence of ferric ions, might be an experimental artifact due to the small area of the edges where lignosulphonates normally adsorb. The hydrophobicity of the kaolin might also be so low that there is little driving force for adsorption. The ion exchange capacity of might also interfere and effectively remove the ferric ions from solution.

For the calcium and aluminium ions the effect seems to be more like a precipitation. The amount consumed is directly proportional to the amount added, and there is no clear plateau in the adsorption isotherms. Although for calcium, this plateau could be at higher lignosulphonate concentrations than the ones employed in this study. We also see that the "adsorption" to C_2S/C_3S in the presence of Al^{3+} is irreversible (Figure 4). Above 4 mM Al^{3+} in the solution we can clearly observe a precipitate forming with the lignosulphonate. For Fe^{3+} no precipitation is observed with up to 10 mM Fe^{3+} added.

We see in all cases that the highest molecular weight fraction is preferentially adsorbed. This is also previously found for cement [3], and other systems [11]. This is what we expect for polymer adsorption. In Figure 8 we also see a small salting out effect. The increased ionic strength of the solution gives a somewhat higher adsorption. This has also been described earlier for lignosulphonates [12].

5. CONCLUSIONS

Sodium lignosulphonates on their own will only adsorb to some of the minerals in cement grains. These are the minerals containing ferric ions. The leakage of small amounts of ferric ions from the Fe_2O_3 grains of the cement give rise to a lignosulphonate that is less hydrophilic and readily adsorbs to all the different mineral phases.

Aluminium or calcium ions give some of the same effects, but it seems more like a precipitation.

REFERENCES

[1] Ernsberger, F. M. and France, W. G. Portland cement dispersion by adsorption of calcium lignosulphonate, Industrial and Engineering Cehmistry, Vol.37, 1945, pp. 598-600

[2] Blank, B., Rossington, D. R., and Weinland, L.A., Adsorption of admixtures on portland cement, Journal of the American Ceramic Society, Vol.46, 1963, pp. 395-399

[3] Reknes, K, and Gustafsson, J., Effect of modifications of lignosulfonate on adsorpton on cement and fresh concrete properties, 6th CANMET/ACI International Conference, Nice, 2000, pp 127-142

[4] Kawada, N and Nishiyama, M., Action of calcium lignosulphonate upon portland cement clinker compounds, 14th General Meeting, Japan Cement Engineering Association, Tokyo, 1960, pp. 25-26

[5] Ramachandran, V. S., Interaction of calcium lignosulfonate with tricalcium silicate, hydrated tricalcium silicate, and calcium hydroxide, Cement and Concrete Research, Vol. 2, 1972, pp. 179-194

[6] Young, J. F., A review of the mechanisms of set-retardation in portland cement pastes containing organic admixtures, Cement and Concrete Research, Vol. 2, 1972, pp. 415-433

[7] Massazza, F., Costa, U., and Barrila, A., Adsorption of superplasticizers on calcium aluminate monosulfate hydrate, in Malhotra V. M. Development in the use of superplasticizers, Publication SP-68, American Concrete Institute, Detroit, 1981.

[8] Ramachandran, V. S., and Feldman, R. F., Adsorption of calcium lignosulfonate on tricalcium aluminate and its hydrates in a non-aqueous medium, Cement Technology, 1971, pp. 121-129

[9] Askvik, K. M., Complexation of lignosulfonates with multivaleet cations and cationic surfactants, and the impact on emulsion stability. Ph. D. Thesis University of Bergen, 2000

[10] Gundersen, S. A., Ese, M.-H. and Sjöblom, J., Langmuir surface and interface films of lignosulphonates and Kraft lignins in the presence of electrolyte and asphaltenes: Correlation to emulsion stability, Colloids and Surfaces, A., Vol. 182, 2001, 199-218

[11] Myrvold, B. O., Interactions between lignosulphonates and the components of the lead acid battery. Part 1. Adsorption isotherms, Physical Chemistry Chemical Physics, submitted.

[12] Heath, D. and Tadros, Th. F., Influence of molecular weight and electrolyte concentration on the adsorption of lignosulphonates on polystyrene latex particles and the stability of the dispersion, Colloid & Polymer Science, Vol. 261, 1983, 49-57

ADSORPTION STUDIES OF LIGNOSULPHONATES ON CEMENT AND CEMENT MODEL COMPOUNDS

Bernt O. Myrvold, Jonas Gustafsson and Kåre Reknes

Borregaard LignoTech, P.O. Box 162, N-1701 Sarpsborg, Norway
Telephone: (+47) 69 11 80 60, Fax: (+47) 69 11 87 85
E-mail:bernt.o.myrvold@borregaard.com

Bernt O. Myrvold

Master of Science in organic chemistry and Ph.D. in Physical Chemistry.

From 1985 to 1992 I worked in the R&D department of several smaller Norwegian and Swedish companies, as well as Manchester University, all in the field of liquid crystal displays. Most of the work was related to the understanding of the relationship between chemical structure and macroscopic properties. The work included both polymer synthesis and characterisation work.

February 1992 to September 1993 I worked as Visiting Researcher at Hitachi Research Laboratory in Japan. The work included polyimide synthesis, test device fabrication and optical measurements. All synthetic and fabrication work took place in a clean room environment. The result was a good understanding of the relationship between polymer structure and the effect on the liquid crystals, and of how chemical changes in the liquid crystals affect the interaction with the surface.

January 1994 – October 1995 I did Post Doc. research at the University of Oslo, department of Chemistry in the Colloid and Interphase group. I was mostly doing modifications of natural polymers for rheology control in oil wells.

November 1995 I joined Borregaard LignoTech. Here I have worked on characterisation and chemical modifications of Kraft lignin and lignosulphonate polymers. I have brought new additives for starter batteries from the laboratory to successful production. I have also worked on new products for the oil industry, both gels for enhanced oil recovery, and emulsifiers for transport of heavy crude oils.

I have written 35 publications, 5 patents, and 2 sports books.

CORRELATION OF PERFORMANCE AND CHEMICAL DATA FOR ADMIXTURES IN CEMENTITIOUS SYSTEMS BY MEANS OF CHEMOMETRIC METHODS

Berit G. Petersen[1] and Kåre Reknes[1]

[1] Borregaard LignoTech R&D, P.O. Box 162, N-1701 Sarpsborg, Norway.
E-mail: berit.gudding.petersen@borregaard.com

ABSTRACT

Chemometrics, i.e. multivariate data analysis, can be a very useful and cost-efficient tool for interpretation and comparison of experimental data.

The chemical composition of an admixture decides the admixture's impact on cementitious systems. This investigation uses chemometric methods to correlate the chemical composition of different lignosulphonates to their performance in mortar by means of principal component analysis (PCA).

Commercially available lignosulphonates and experimental modifications of these were tested in mortar using ordinary Portland cement with respect to air entrainment, heat evolution, density, flow and setting time. Chemical analyses were performed to find the amount of some of the most typical chemical groups.

This paper describes a decision-making process using multivariate data analysis in the simplest way. The decision-maker is not required to have any deep knowledge about statistics, but must have information on the experiments analysed. It is important for the user to trust his intuition, but be critical and use his contextual knowledge. The purpose of this paper was to show that multivariate data analysis is a useful tool for analysing the large amounts of experimental data generated during R&D work. Multivariate data analysis was used to pick the best overall samples and to set the direction for further research. This has reduced the number of trial-and-error-experiments.

1. INTRODUCTION

The chemical composition of an admixture decides the admixture's impact on cementitious systems. This investigation uses chemometric methods to correlate the chemical composition of different lignosulphonates to their performance by means of statistical models called principal component analysis (PCA). This is a form of multivariate data analysis.

In principal component analysis, the principal components (PC) are plotted, not the actual input variables. PCA is a bi-linear soft model (BLM) where the individual input variables are combined into a few principal components. Scores are the connection between the samples and the PCs, and loadings between the variables and the PCs. PCA gives a visual impression of how the components and the properties interact. Variables situated close to each other in the loadings-plot will increase as one of them increases. Accordingly a variable on the other side of the axis will be inversely correlated. This is not necessarily a direct relationship between the variables, but it shows a correlation. PCA is an easy way to interpret the results for someone with some knowledge on how

the variables will interact with the samples. It is not required to have any formal training in statistics. A layman's guide to multivariate data analysis is described by Martens [1].

Outliers are samples that are abnormal in some way. The software can automatically detect outliers or the user can spot them by visual inspection of the plots. An outlier brings extreme values to the group and therefore they affect the model strongly. The outliers should be removed to calculate a valid model for the data set in question.

2. EXPERIMENTAL METHODS

Commercially available lignosulphonates and experimental modifications of these were tested at dosages 0.20% and 0.40% solid by weight of cement in mortar using ordinary Portland cement (OPC, EN197-1 CEM I 42.5R), w/c = 0.50. The performance properties measured are given in Table 1. Chemical analyses of the admixtures were performed to find the amount of some of the most typical functional groups, see Table 2.

Table 1. The performance tests performed.

Performance property	**Short notation**
Flow	flow
Flow retention, 30 min.	flow loss
Air entrainment	air
Density	dens
Setting time by flow evolution.	ST

Table 2. The chemical analyses performed.

Chemical property	**Short notation**
Molecular weight	Mw
Reducing sugar	Sugar
Total amount of sulphur	S
Inorganic sulphur	inorgS
Organic sulphur	orgS
Methoxy groups	metoxyl
Phenolic OH	ph-OH
Weak acid groups	COOH
Sulphate	$-SO_4$
Sulphite	$-SO_3$

The multivariate data analysis was calculated using The Unscrambler 7.6.

3. RESULTS AND DISCUSSION

The entire data set consists of 33 samples and 24 variables. Outliers are excluded from all the plots shown here. Because the two first principal components explain more than 50% of the variations in all plots, i.e. PC1 and PC2 span the largest variation in the data set, only the graphs made up of PC1 and PC2 are shown.

3.1 First Sample

The data set was built upon a few samples that was collected from various projects at our R&D department. Scores and loadings from PCA of this set are shown in Figure 1.

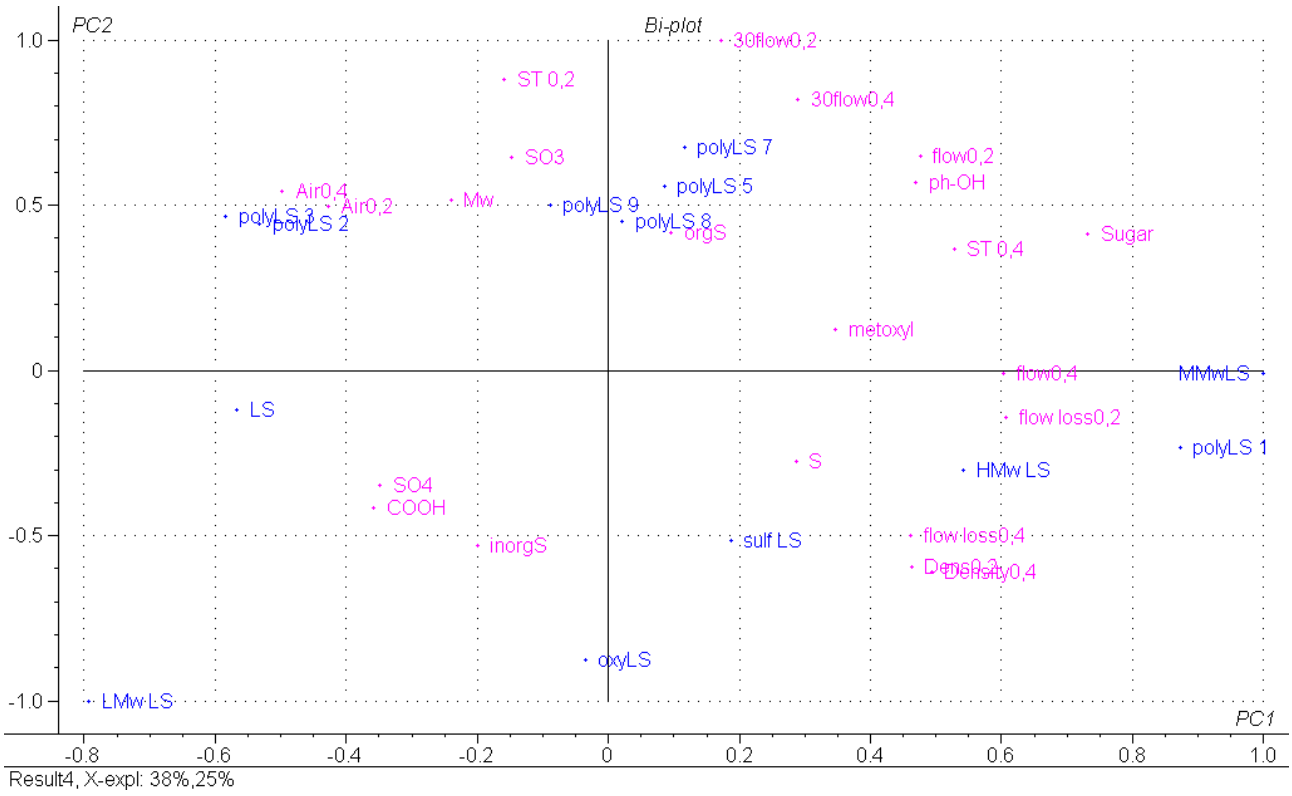

Figure 1. Scores (blue) and loadings (red) from the PCA for the first data set.

It can be seen that high molecular weight samples (HMwLS, MMwLS, polyLS1) are correlated to good initial flow, low air entrainment and low setting time. These samples are situated near the variables flow in the plot. It can therefore be assumed that performance tests of these samples give high values of the mentioned variables. The setting time at high dosage is situated near the variable Sugar because sugars retard setting time in cement. Thus, high dosage of an admixture that contains sugar will increase the setting time dramatically. Knowledge about the background of samples HMwLS, MMwLS and polyLS1 tells that they do not contain sugars, so the variable to compare with is ST0.2. This variable is inversely correlated in the plot, so these samples have low setting time. It can also be seen that these samples are at the opposite side from the variables describing the air entrainment. This is because these samples have a low air entrainment.

Attempting to improve the flow while lowering the setting time and air entrainment, it was decided to make a pure lignin sample with high molecular weight. The new sample was called DP684 and was included in the analysis in Figure 2.

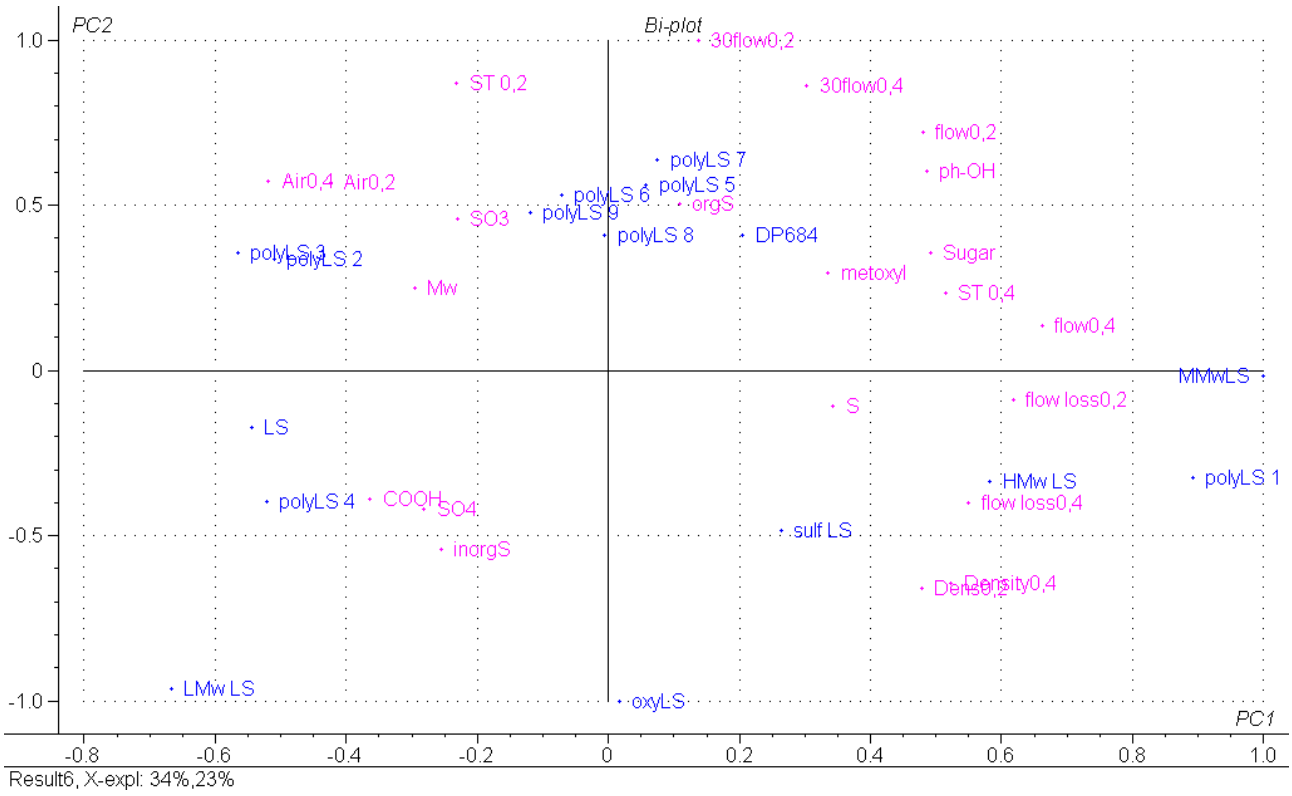

Figure 2. Scores (blue) and loadings (red) for the first two principal components from the PCA for the data set including the first sample.

3.2 Second Sample

Further, samples based on hardwood (HW1, HW2) and Kraft lignin (oxyLS) were added to the data set, Figure 3, to span the model to cover more of the lignosulphonate qualities.

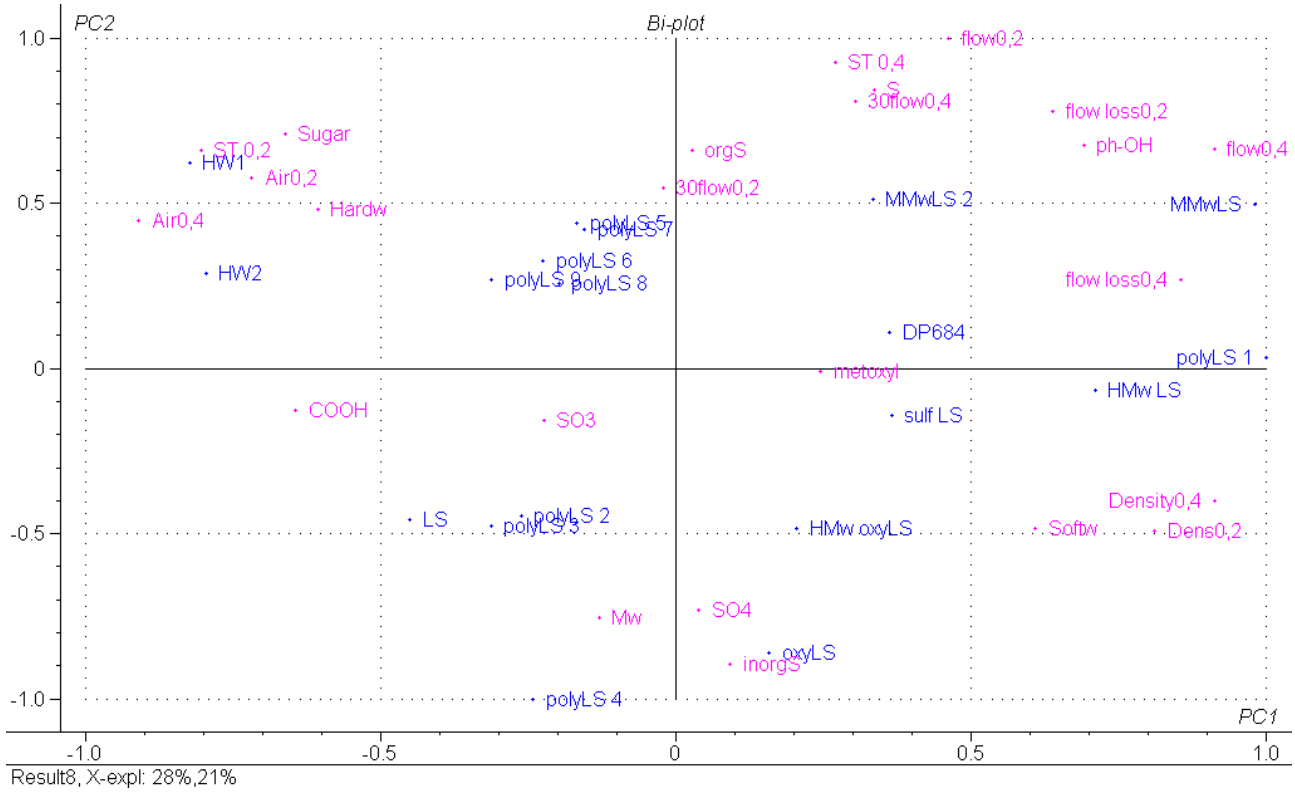

Figure 3. Scores (blue) and loadings (red) from the PCA when hardwood and Kraft lignin samples are included.

Phenolic-OH (ph-OH) groups seem to give good flow and low air entrainment. It was decided to make a desulphonated sample of lignosulphonate. Desulphonation increases the number of phenolic-OH groups and decreases the amount of combined sulphur. Organic sulphur (orgS) seems to increase the air entrainment and setting time and it was therefore desired to keep this amount as low as possible without losing the solubility.
Several desulphonation experiments were performed and the second sample, DP 702, was made based on the chemical analysis and Figure 4.

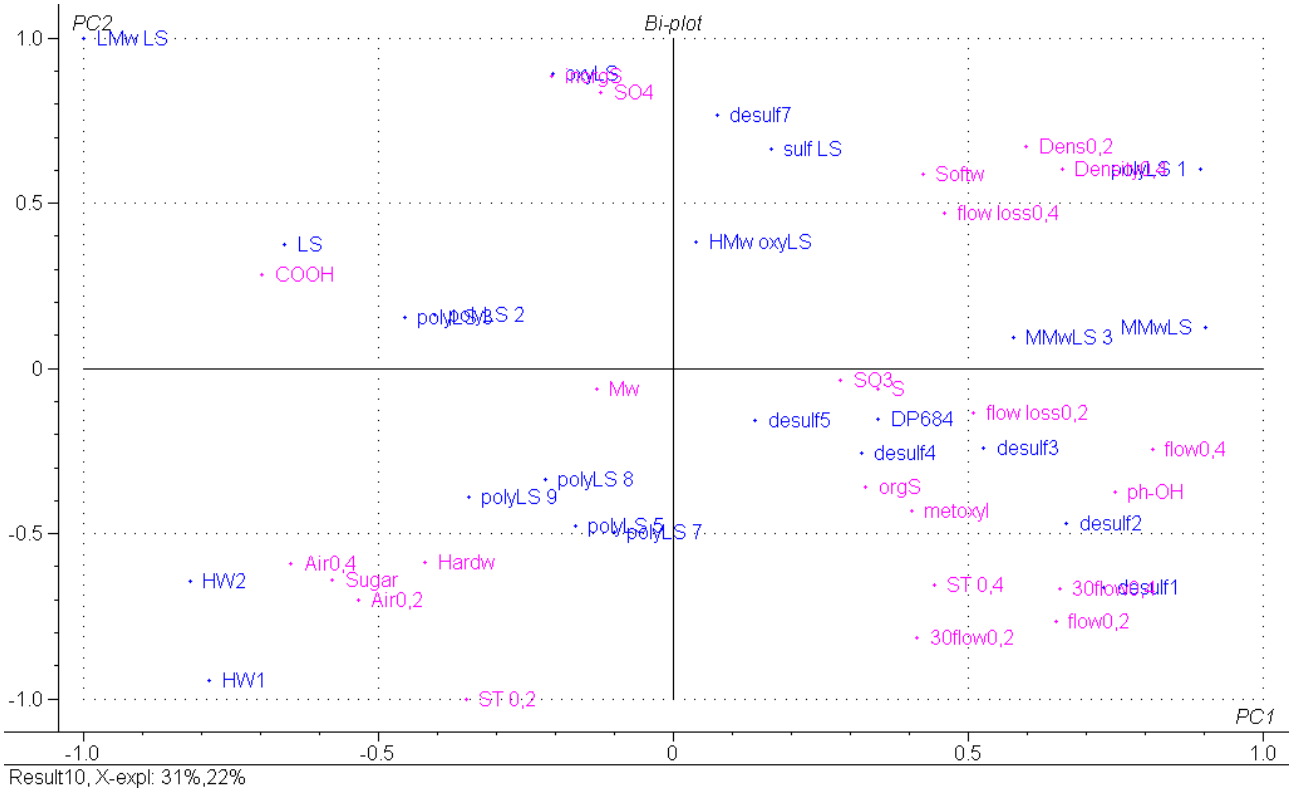

Figure 4. Scores (blue) and loadings (red) from the PCA including desulphonated samples.

3.3 Third sample

Figure 5 shows all samples until this point. To cover even more outskirts of the data set, it was decided to make a pure hardwood-based lignosulphonate sample, DP718.

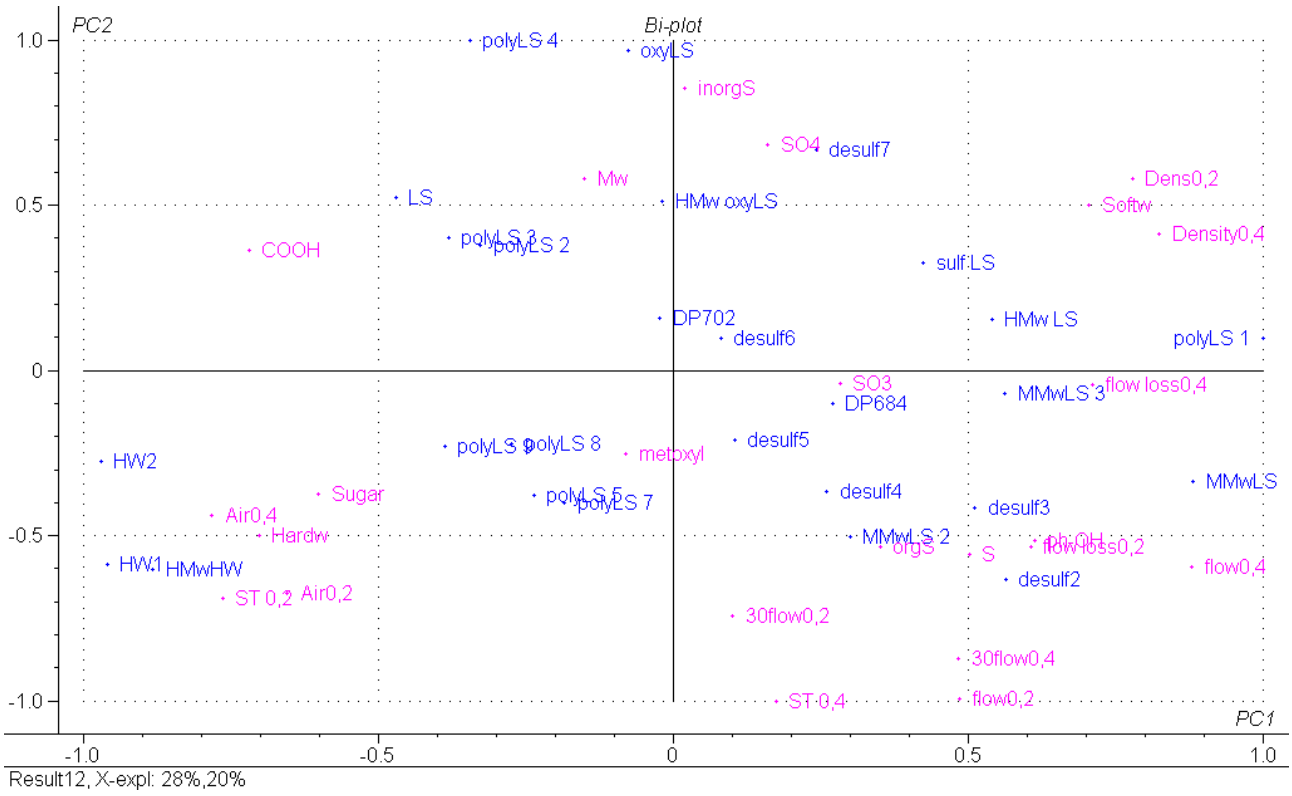

Figure 5. Scores (blue) and loadings (red) from the PCA of the data set until this point.

The variable hardwood (HW) has a great impact on the picture, and the PCA is recalculated without the hardwood and softwood (SW) variables to better see the effect of the chemical compounds, Figure 6, where the third sample, DP 718 also was included.

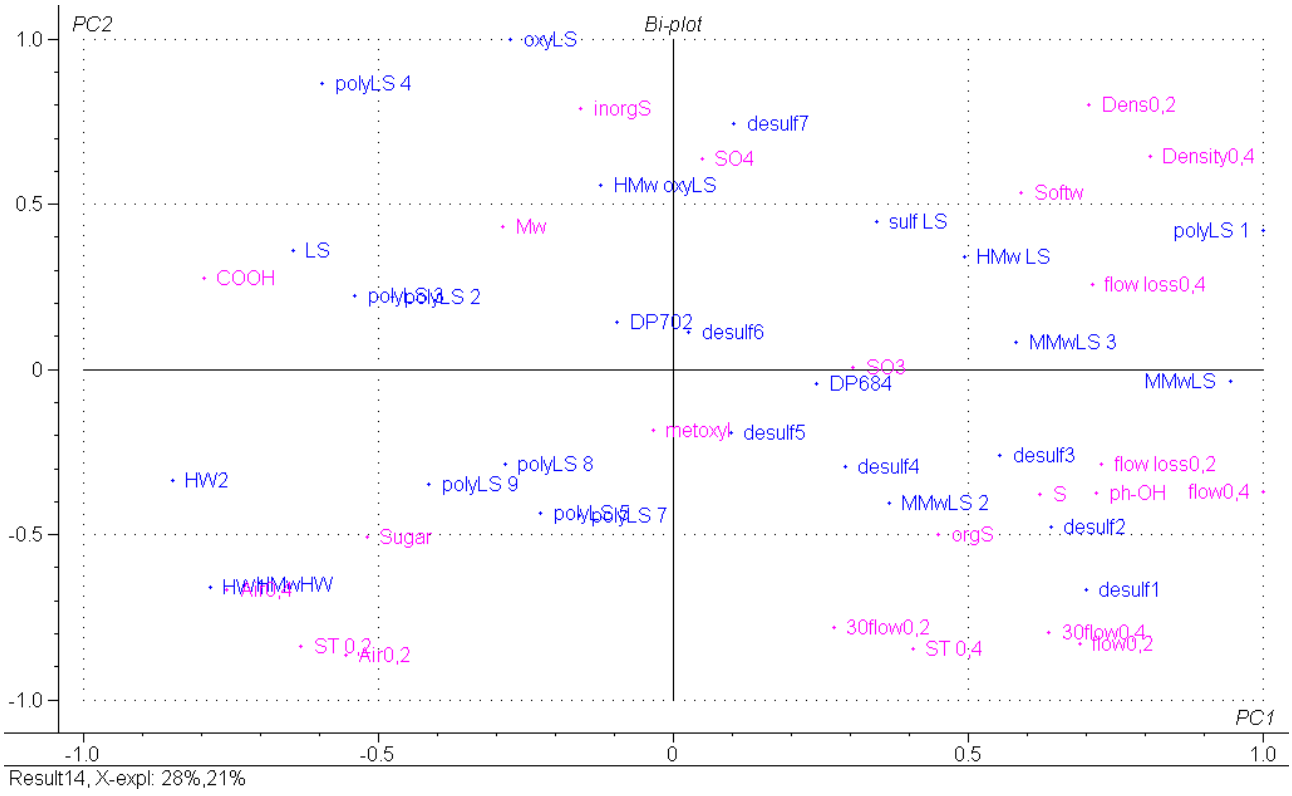

Figure 6. Scores (blue) and loadings (red) of the entire data set except hardwood/softwood variables.

3.4 General discussion

Lignosulphonate is a very polydisperse material. This causes the results of chemical analysis to provide average values covering the whole molecular weight range. The data discussed in this paper show some correlation between chemical data and mortar performance of the lignosulphonate. The different segments of the molecular weight range have different properties, as discussed by Gustafsson and Reknes [2 and 3]. The correlation is expected to be much stronger when narrower molecular weight fractions (less polydisperse) are studied.

4. SUMMARY AND CONCLUSION

Section 3 describes a decision-making process using multivariate data analysis in the simplest way. The decision-maker is not required to have any deep knowledge about statistics, but must have information on the experiments analysed. It is important for the user to trust his intuition, but be critical and use his contextual knowledge. The purpose of this paper was to show that multivariate data analysis is a useful tool for analysing the large amounts of experimental data generated during R&D work.

Multivariate data analysis was used to pick the best overall samples and to set the direction for further research. This has reduced the number of trial-and-error-experiments.

ACKNOWLEDGEMENTS

This work was supported by the EC-project Design and function of novel polymeric admixtures for more durable high performance concrete, SUPERPLAST.

Thanks go to our technicians who performed all our experiments in an excellent manner.

REFERENCES

[1] Martens, H., Martens, M., Multivariate analysis of quality. An introduction., Chichester, John Wiley and sons Ltd., 2001.

[2] Gustafsson, J., Reknes, K., Adsorption and dispersing properties of lignosulphonates in model suspensions and cement paste., Proceedings of the sixth CANMET/ACI international conference on superplasticizers and the chemical admixtures in concrete, Nice, 2000, pp. 181-193.

[3] Reknes, K., Gustafsson, J., Effect of modifications of lignosulphonate on adsorption on cement and fresh concrete properties., Proceedings of the sixth CANMET/ACI international conference on superplasticizers and the chemical admixtures in concrete, Nice, 2000, pp. 127-141.

CORRELATION OF PERFORMANCE AND CHEMICAL DATA FOR ADMIXTURES IN CEMENTITIOUS SYSTEMS BY MEANS OF CHEMOMETRIC METHODS

Berit G. Petersen[1] and Kåre Reknes[1]

[1] Borregaard LignoTech R&D, P.O. Box 162, N-1701 Sarpsborg, Norway.
Telephone: (+47) 69 11 80 73, Fax: (+47) 69 11 87 85,
E-mail: berit.gudding.petersen@borregaard.com

Berit Gudding Petersen

Master of Science in inorganic chemistry.

I have worked as a research scientist at Borregaard LignoTech, Reseach and development department, since May 2001. My work mainly concerns plasticizing admixtures for construction, i.e. cement and concrete. My previous employment was as a scientific assistant at The Department of Inorganic Chemistry, Norwegian University of Science and Technology (NTNU), where my work was related to teaching and cement chemistry.

I finished my Master Thesis entitled “Water reducing admixtures for Cement and Mortar based on Combinations of Lignosulphonates and Calcium Nitrate” in 1999 at NTNU.

In addition to my position at Borregaard LignoTech, I am persuing a doctoral degree on rheology of cement based binders.

HIGH PERFORMANCE SONIC IMPULSES – AN ALTERNATIVE METHOD FOR THE SELECTIVE CRUSHING OF CONCRETE

Dipl.-Ing. Elske Linß[1] and Prof. Dr.-Ing. habil. Anette Mueller[1]

[1] Bauhaus-University Weimar, Chair of Processing of Building Materials and Reuse
Weimar, Germany.
E-mail: elske.linsz@bauing.uni-weimar.de
E-mail: anette-m.mueller@bauing.uni-weimar.de

ABSTRACT

The high amount of concrete waste generated today requires the development of effective and sensitive crushing methods that allow the reuse of the material at a high level. In the paper a new method for crushing of concrete is presented. The stress needed for comminution is generated by high performance sonic impulses. Compared to the output of jaw and impact crushers, the crushed product of this method is of high quality. The coarse fractions have nearly no cement paste on the surface of the aggregates and provides an optimum size distribution. Thus it is possible to obtain high quality secondary aggregates and to reuse them in new concrete without any restrictions.

1. INTRODUCTION

Recycling of building materials becomes more and more important. In Germany about 77,100,000 Tons/a of Construction & Demolition Waste, i.e. 1 Ton/capita/a were generated in 1998 [1]. On the one hand in regions with a high population density the recycling of building materials can help to reduce the quantity of material that must be deposited. On the other hand in regions with a shortage of raw materials the recycling of building materials opens new sources.

In regard to concrete debris there are two main fields of application. Crushed concrete is often used as aggregate for stabilised or unstabilised sub-bases in road construction. In this case the processing with a jaw crusher or an impact crusher is well proven. The produced material almost meets the requirements with regard to the grading curve and the composition. The presence of old cement paste in these aggregates seems to be an advantage, because it causes a stabilising effect compared with inert material as sub-base material [2], [3]. If the concrete debris is to be reused as aggregate for new concrete, processing with crushers developed for natural rock is also possible but connected with some disadvantages. So the produced secondary aggregates are agglomerates of the old cement paste and the original aggregates. This causes a higher water adsorption and a lower strength of the grains. Moreover microcracks can occur between both components which are the result of initiated but not completed fracture processes. To overcome these problems the comminution by high performance sonic impulses for the processing of concrete debris was developed. This technology aims at the production of secondary coarse aggregates that can be used in new concrete without any restrictions.

The traditional crushing methods which are based on mechanical stresses are limited with regard to the quality of the produced material. They do not make possible a controlled effect of the stresses at the boundary layers of the concrete. The magnitude of the applied stresses results in an extensive destruction not only of the concrete, but also of the aggregates.

2. PRINCIPLE OF THE SELECTION BY HIGH PERFORMANCE SONIC IMPULSES

The tools of the new crushing method are high performance sonic impulses. The basic principle is the transformation of electrical energy (stored at a capacitor) into mechanical energy of sonic impulses. These impulses are generated under water by a disruptive electrical discharge. As a result pressure sonic waves are generated that propagate through the surrounding medium (in our case water). If they come across boundary layers of different densities, i.e. water and concrete or aggregates and cement paste, positive and negative interferences occur. As a result pressure and tensile stresses are generated directly at these boundary layers. The tensile stresses primarily destroy the bond between aggregates and matrix. Cracks mainly follow the boundaries between layers with different densities (Fig. 1).

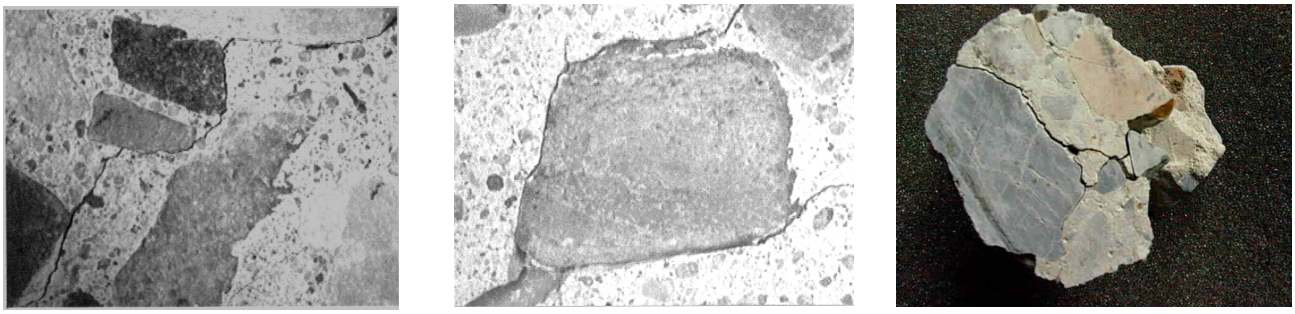

Figure 1. Progression of cracks between aggregates and matrix [4]

The energy feed happens over the total surface, because the sonic waves propagate in the water spherically. The stresses occur over the total surface, not homocentric like in the jaw or in the impact crusher. Moreover the stress can be dosed more precisely by the setting of the electrical parameters.

3. EXPERIMENTS

3.1 Targets of the Project

The target of the research project is to prove the performance of the new method. Especially the quality of the secondary aggregates as function of the technological parameters of the process and of the parameters of the processed material should be determined. It makes sense to develop a concept for the complete processing technology including fields of application for the fine fractions based on the quality of the material produced and the required energy.

In the project investigations about the following topics are in progress:

- Investigations of the influences of the electrical parameters and the electrical energy feed on the size reduction and the separation of the concrete constituents;
- Optimisation of the energy balance of the system and the process parameters;
- Investigations of the influences of concrete properties on the separation by high performance sonic impulses;
- Comparison of the crushed product with the products of traditional crushing methods.

In this paper will be reported about the dependence between the required power and the resulting size reduction effect as well as the separation effect. However the main topic is the dependence between the features of the input concrete and the properties of the output product. If such a dependence exists, then it is the question whether it can be explained by our knowledge about the material properties of concrete. Finally, the crushed product was compared with that of traditional crushing methods, like jaw and impact crusher, to characterise the advantages of the new method.

3.2 Test Device

A scheme of the device used for the experiments is shown in Figure 2. It consists of the electrical equipment, the water filled outer container and the inner, perforated container in which the concrete is treated. The pre-crushed concrete is put in the water filled container. After closing the container the treatment is started. During the treatment the fine material comes out of the inner container through the perforation. After the treatment the container is emptied and the crushed products are separated from the water by sieving and sedimentation.

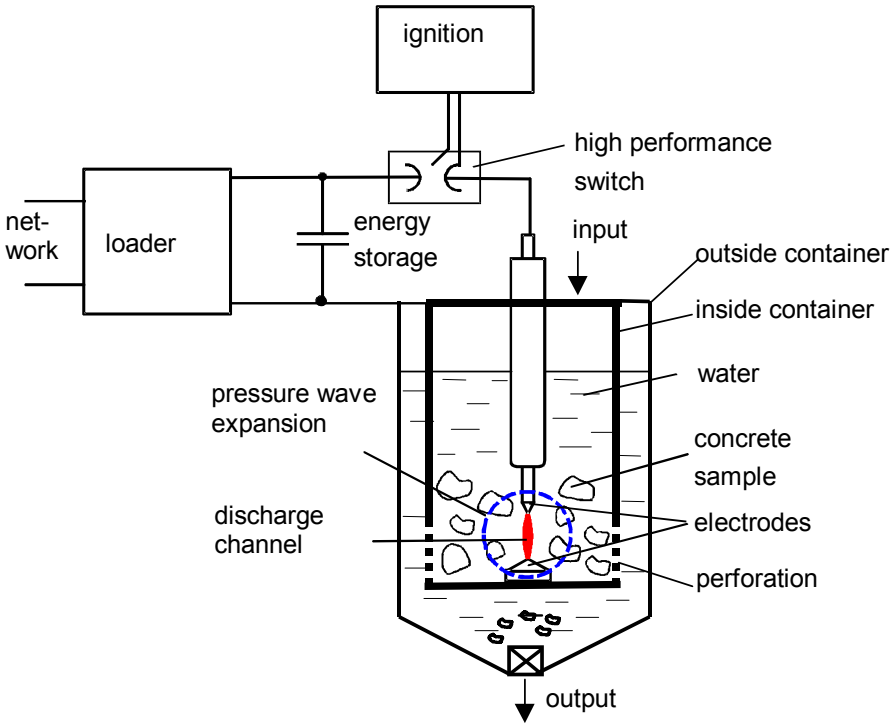

Figure 2. Scheme of the device for experiments [4]

The device is run with a capacity of capacitor C and a voltage of charge U_0 in the range of

- Capacity of capacitor C 6 ... 12 µF
- Voltage of charge U_0 20 ... 30 kV.

The electrical parameters and the operating parameters, like the distance between the electrodes and the number of the pulses, influence the properties of the crushed product. The experiments show that the particle sizes of the crushed product are mainly influenced by the number of impulses n, the voltage of charge U_0 and the interaction between them. An optimum is at a voltage of charge of 30 kV and a number of impulses of 30. Enhancing the number of impulses is more effective at a high level of voltage. The distance between the electrodes is less important for the mean particle size.

3.3 Parameters for the Evaluation of the Crushed Product

During the treatment of the concrete several things happen in dependence on the energy feed and the features of the material. The particle size is reduced as in a traditional crushing process. The separation between aggregate grains and cement paste occurs as an additional effect. If the treatment is too strong microcracks may be formed in the product. All three effects must be measured if the action of the sonic impulses as a crushing tool is to be be evaluated completely. The parameters used for evaluation are shown in Table 1. They give information about the following effects:

- The reduction of the particle sizes was checked to evaluate the effect of the sonic impulses as a crushing tool. The particle size distribution of the crushed product was compared with the distribution of the aggregates used in the original concrete.
- The separation between aggregate grains and cement paste was evaluated by three different parameters:
  - The whole content of cement paste in the fractions was analysed by the hydrochloric acid method according to the German Standard [5]. In the coarse fractions (> 2 mm) this content gives information about the average percentage of cement paste stuck on the surfaces of the aggregates. In the fine fractions this content is the sum of the free cement paste and the cement paste of agglomerates.
  - The purity of the product 2-16 mm gives information about the agglomerated aggregates remaining after the crushing process, and/or the destroyed aggregates. It can be calculated from the parameters of the particle size distribution and the content of cement paste of all sorted fractions.
  - The degree of liberation is the portion of aggregates without cement paste in the fractions > 2 mm. It was determined by counting the clean aggregates.
- The rate of damage of the aggregate grains was examined at two levels. The particle size reduction caused by the treatment is interpreted from the comparison of the particle size distributions of the original aggregates and the crushed concrete. The effects on the micro-structure of the coarse aggregate particles were examined in a first step by measurements of the water adsorption of the aggregates before the treatment and after. Because the water adsorption is influenced by the residues of cement paste on the surface of the aggregate grains, the grains must be cleaned by washing with hydrochloric acid before the measurement.

The methods of measurements of the parameters used for evaluation are shown in Table 1. In Table 2 the ranges of these parameters are summarised. Some important cases are discussed.

Table 1. Parameters for the evaluation of the crushed products

Evaluated effect	**Parameter**	**Method of measurement**
Particle size reduction of aggregates	Ratio of the mean particle sizes before and after crushing	Sieve analysis
Separation of cement paste and aggregates	Content of cement paste	Hydrochloric acid method
	Purity	Calculated from sieve analyses and hydrochloric acid method
	Degree of liberation	Counting
Effects on microstructure	Water absorption	24 h-Water absorption

Table 2. Discussion of the parameters for the evaluation of the different effects of the comminution by high performance sonic impulses

	Evaluated effect and used parameters	**Typical cases**	**Explanation/ Example**	
1	Particle size reduction of aggregates *Ratio of mean particle sizes r_m* $r_m = \frac{x_{m,crushing\,product}}{x_{m,original\,concrete}}$	$r_m = 1$	Ideal case, no destroyed aggregates (valid if the grains are cement paste free)	
		$r_m < 1$	Low effect on aggregate; agglomeration	
		$r_m > 1$	Intensive comminution; damage of aggregates	
2	Separation of cement paste and aggregate			
2.1	*Content of cement paste c in the fractions i* *c_i [%]* $c_i = 100 - (HCl\ Insolvabi)$	Perfect separation $c_i = 0$	Aggregate grains without any cement paste; ideal case (valid for grains > 2 mm)	
		Partly separation $0 < c_i < c_{concrete}$	Aggregate grains with a certain amount of cement paste (valid for grains > 2 mm)	
		No separation $c_i = c_{concrete}$	Aggregates form agglomerates with a composition that agrees with the composition of original concrete (valid for grains > 2 mm)	
2.2	*Purity P* *Quotient of the mass of aggregate in the product*	P = 100%	Only clean aggregates in the product, the total cement paste is enriched in the fine fraction	
	(fraction 2-16 mm) and the total mass of product	P > 100%	Too much aggregates in the product, because of the formation of agglomerates consisting of sand and cement paste	
	$P = \frac{m_{aggregate,crushing\,product}}{m_{crushing\,product}} \cdot 100$	P < 100%	Too little aggregates in the product, because of the destroying of aggregates into grains < 2 mm	
2.3	*Degree of liberation D_L* *Content of aggregates without cement paste per fraction*	*D_L = 100 %*	Ideal case; all aggregates are without cement paste on the surface	
3	Effects on microstructure *Water adsorption*	$w_{secondary\ aggregates} \approx w_{original\ aggregates}$	Ideal case	
		$w_{secondary\ aggregates} > w_{original\ aggregates}$	Damage of the structure	

3.4 Results

3.4.1 Influences of the electrical energy feed on the size reduction of concrete and the liberation of its components

The first step should be to find out the parameters for the best agreement of the particle size distribution of the crushed concrete with the particle size distribution of the original aggregates in the concrete. In Figure 3 some of the experimentally achieved particle size distributions after the

crushing by sonic impulses are shown. They will be compared with the particle size distribution of the original aggregates used in the concrete. The best agreement was found if the material was treated 50 times at a voltage level of 20 kV. Especially by variation of the number of the impulses the particle size distribution can be shifted in coarser or finer ranges.

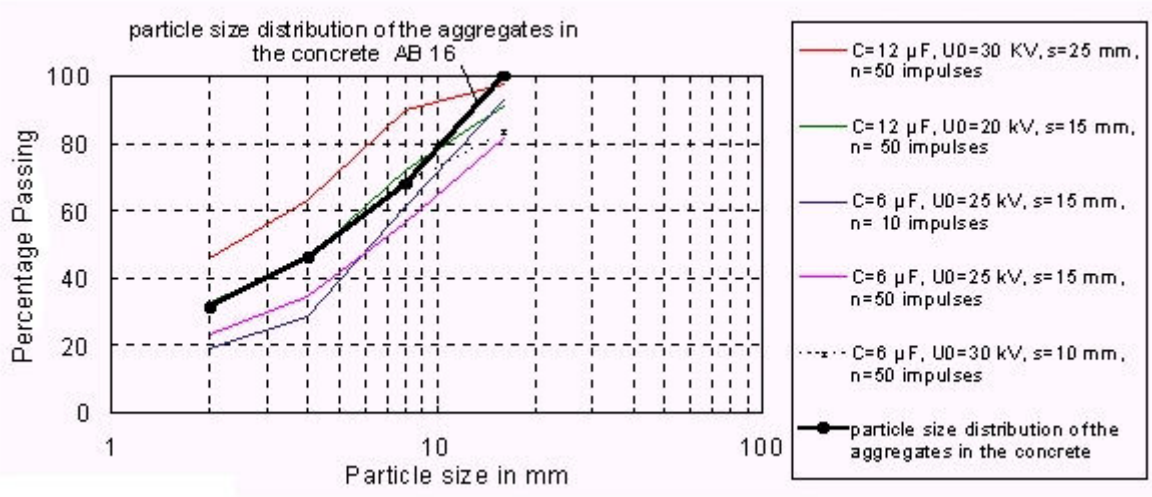

Figure 3. Examples for particle size distributions between 2 and 16 mm after crushing with sonic impulses at different levels of electrical parameters (material: concrete with a nominal strength of 25 N/mm^2)

The energy consumption for the treatment in the laboratory device results from the power that will be transformed in a very short time in the spark gap and the number of impulses that is necessary for a sufficient comminution. These parameters are summarised in the ratio $n \cdot W_{Fp}/t_{aPF}$ [4]. The term W_{Fp} means the power in the spark. The term t_{aPF} means the time in which the power rises (Fig. 4) and n means the number of the impulses. The terms W_{Fp} and t_{aPF} will be calculated during every test on the basis of measurements of electrical power and voltage.

Figure 5 shows the ratio of the mean particle sizes r_m of the crushed product and its purity P versus the parameter $n \cdot W_{Fp/taPF}$. From this figure it follows that the ratio r_m exponentially increases with increasing energy feed. The wanted ratio r_m=1 is achieved for an energy feed parameter of 10 kJ/µs. The purity increases with the energy feed also. The highest purity of the crushing product of 90 % is reached for a parameter of 13 kJ/µs.

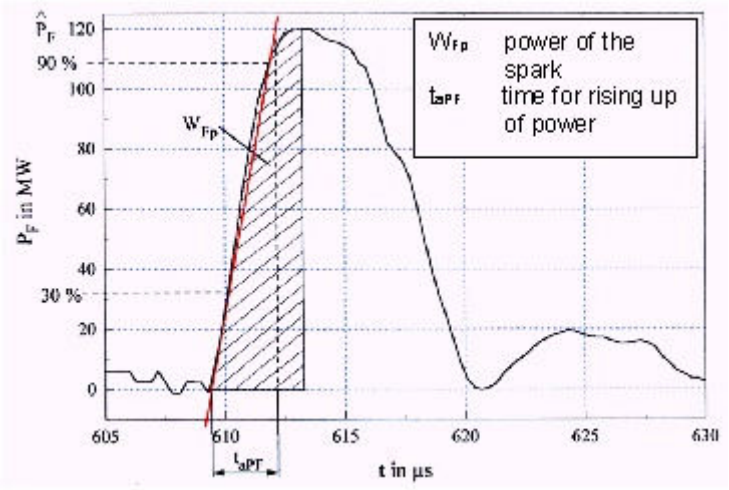

Figure 4. The definition of the parameter $n \cdot W_{Fp}/t_{aPF}$ which is used for the description of the transformation of energy in the spark gap [4]

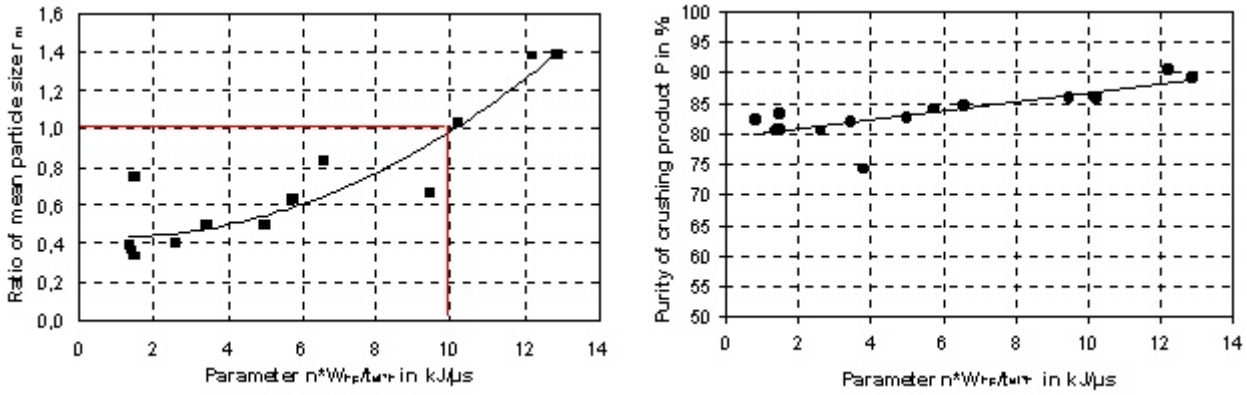

Figure 5. Ratio r_m (left) and purity P (right) versus parameter $n \cdot W_{Fp}/t_{aPF}$ for concrete with a Nominal strength of 25 N/mm^2

3.4.2 Characteristics of the crushed product

The crushed product is a composite material of cement paste and aggregate. But the cement paste is not distributed in all fractions consistently. As typical feature the content of cement paste increases at decreasing particle size (Fig. 6).

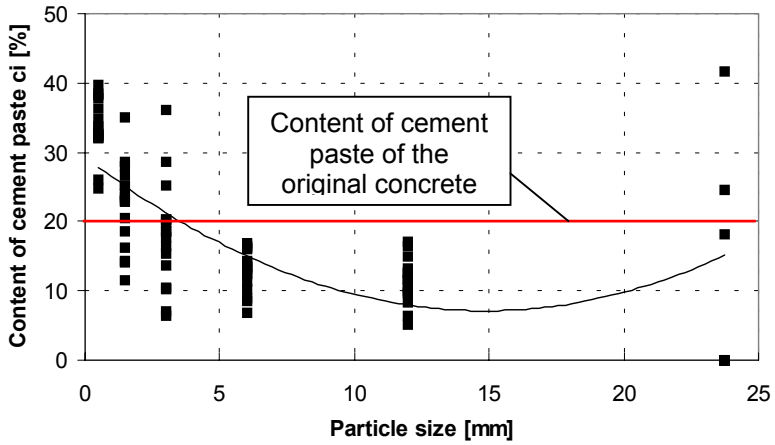

Figure 6. Typical feature: Dependence between the content of cement paste and the particle size

That means that in the fine fraction (< 2 mm) the cement paste is enriched by a factor two. The reason is the fact that the comminution takes place in this component of a composite material with the lower strength.

The water adsorption of the cleaned secondary aggregates (2,16 mass-% on the average) is systematically higher than the water adsorption of the aggregates for the original concrete (1,13 mass-% on the average) (Tab. 3). Because the statistical tests do not confirm this difference, there are still no clear statements about the occurrence of microcracks caused by the sonic impulses.

Table 3. Water adsorption of secondary aggregates and original aggregates

		Water adsorption in %		
	Fraction	**Mean**	**Maximum**	**Minimum**
Original aggregates	2/4 mm	1,07	1,31	0,82
	4/8 mm	1,09	1,54	0,64
	8/16 mm	1,23	1,43	1,03
Secondary aggregates	2/4 mm	2,66	3,82	1,76
	4/8 mm	2,16	2,97	1,07
	8/16 mm	1,68	2,57	0,80

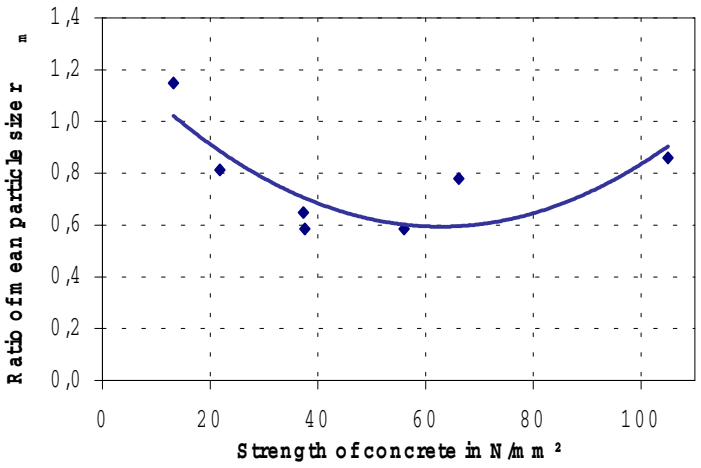

Figure 7. Ratio of mean particle sizes of crushed concrete with various compressive strength

The particle size reduction and the liberation of aggregates also depends on the properties of the material, especially its strength as shown in Figure 7, where the ratio of particle size reduction is plotted for concrete with systematically varied compressive strength but constant raw materials. Concrete with low strength can be crushed very easily. Concrete with high strength is very brittle. In both cases high values of the ratio r_m result. Concrete with medium average strength is most difficult to crush, because it is tough. The conclusion of these investigations is that the elastic behaviour, as well as the quality of the interfacial transition zone between aggregates and cement paste, is very important for the crushing process. This property will be investigated in later works in more detail.

3.4.3 Comparison of crushing method by high performance sonic impulses with traditional crushing methods

In Figure 8 the particle size distribution of a concrete which was crushed in an impact or in a jaw crusher was compared with that of the same concrete crushed by high performance sonic impulses. The secondary aggregates of the treatment by high performance sonic impulses are in the favourable range of aggregates (AB16) according to the standard. The particle size distributions of the traditional methods are coarser.

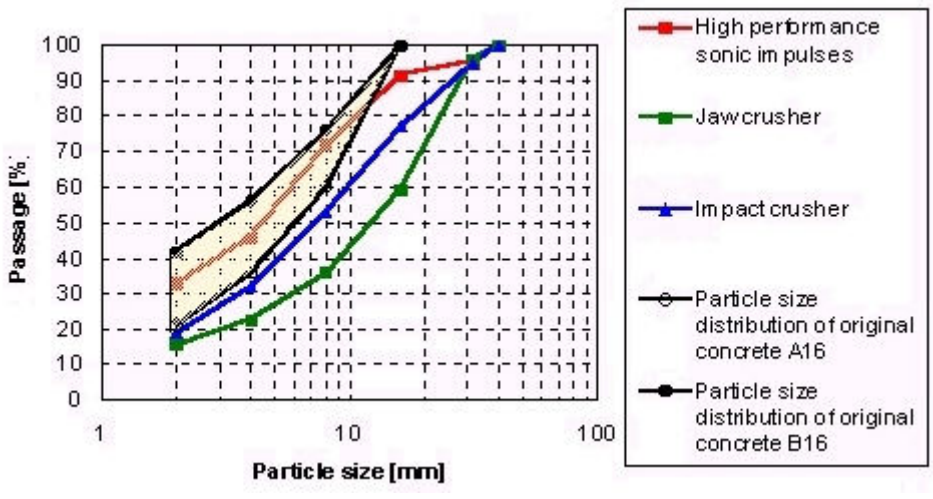

Figure 8. Comparison of the particle size distributions of concrete crushed by high performance sonic impulses and by traditional methods [6]

The comparison of the degree of liberation D_L of the aggregates according to Table 2 related to the particle size is really interesting. Here the advantage of the crushing with sonic impulses is most distinct. In Figure 9 is shown very clearly that the degree of liberation of the product crushed by high performance sonic impulses is higher compared with traditional crushed products in all analysed fractions. It increases with increasing particle size up to 70 %. For jaw crusher and impact crushers the content of aggregates without cement paste is considerable lower. It decreases with increasing particle size. Only about 10 % of grains free from cement paste will be achieved in the coarse fraction of the product of the impact crusher.

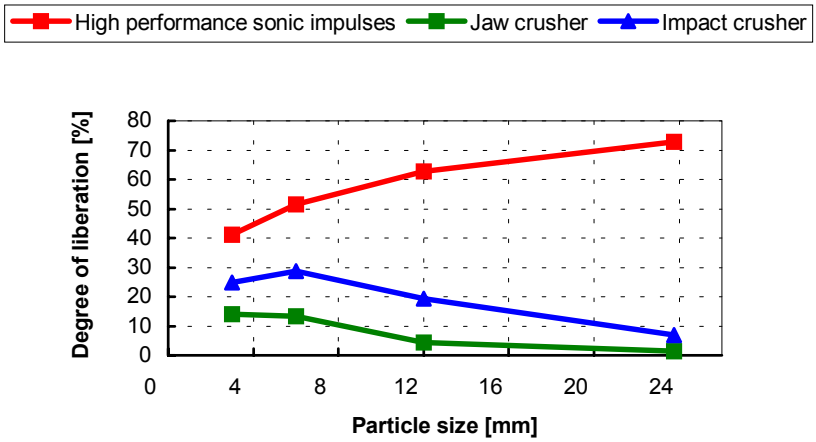

Figure 9. Comparison of the degree of liberation for secondary aggregates generated by jaw-, impact crusher and by high performance sonic impulses [6]

In agreement with the high degrees of liberation, the apparent density of the aggregates of high performance sonic pulses is only a little lower than that of the original aggregates and considerably higher than that of the traditional crushed aggregates. The fractions 16/32 mm and 8/16 mm have densities between 2.4 and 2.6 g/cm^3 if the concrete is crushed with high performance sonic pulses, and only 2.1 to 2.3 g/cm^3 if the concrete is crushed traditionally.

4. CONCLUSIONS

The results show that it is possible to use high performance sonic impulses as a tool for the crushing of concrete. The most important features of the method and the product are:

- The method bases on the forces of pressure sonic waves that act at boundaries of different densities in the concrete. The parameters of the method can be controlled in a wide range. The most important influences on the particle size reduction and the quality of the crushed product are the number of the impulses and the voltage of charge. For the examined concrete with a strength of 25 N/mm² an optimum treatment is possible with an energy feed of about 13 kJ/µs.
- Secondary aggregates obtained from the described method show significantly less content of cement paste in the coarse fractions than the secondary aggregates crushed in an impact or a jaw crusher. Up to 70 % of the grains > 2 mm are free of cement paste.

The new method is more sensitive than the traditional crushing methods. So the considerable enrichment of cement paste in the fine fraction is due to the effects that the comminution takes place at the boundaries of concrete as composite material and that the cement paste as its component with the lower strength is destroyed most. Moreover the influence of the quality of concrete is recognisable at the obtained ratio of particle size reduction.

Topics for further research will be the investigation of the process parameters, the optimisation of the energy balance and the influence of concrete properties on the separation. The development of a

prototype for a laboratory device as the next step will be the prerequisite for the production of secondary aggregates and to test them for concrete manufacturing. By the end of the project a concept for the whole process including proposals for the reuse of the fine fraction will be developed.

REFERENCES AND STANDARDS

[1] Selbstverplichtung erfüllt, Baustoff Recycling + Deponietechnik, No. 1—2 2002 ; pp 14-15

[2] Krass, K, Bautechnische und ökologische Aspekte des Betonrecyclings, Betonwerk+Fertigteil-Technik, No.1, 1994, pp 103-108

[3] NATAATMADJA, A, TAN, Y, L, The performance of recycled crushed concrete aggregates, Unbound Aggregates in Road Construction, A.A. Balkema/Rotterdam/Brookfield, 2000, pp 109-115

[4] Zange, R.: Anwendungsbezogenes Prozeßmodell der Wandlung elektrischer Energie in Energie des Leistungsschallimpulses. Dissertation Otto-von-Guericke-University of Magdeburg, 2000

[5] DIN 52179 T.1 - 4: Bestimmung der Zusammensetzung von erhärtetem Beton. February 1980

[6] Räß, S.: Vergleich zwischen den Zerkleinerungsprodukte des Verfahrens der Schallimpulszerkleinerung und konventionellen Zerkleinerungsverfahren für Altbeton. Student Research Projekt, Bauhaus-University Weimar, 2002

HIGH PERFORMANCE SONIC IMPULSES – AN ALTERNATIVE METHOD FOR THE SELECTIVE CRUSHING OF CONCRETE

Dipl.-Ing. Elske Linß[1], Prof. Dr.-Ing. habil. Anette Mueller[1]

[1] Bauhaus-University Weimar, Chair of Processing of Building Materials and Reuse
Weimar, Germany.
E-mail: elske.linsz@bauing.uni-weimar.de
E-mail: anette-m.mueller@bauing.uni-weimar.de

Dipl Ing Elske Linß

Elske Linß is a Junior Scientist at the chair of Processing of Building Materials and Reuse in the Civil Engineering Department of the Bauhaus-University in Weimar, Germany. Her interests are in the fields of processing technologies for construction and demolition waste. She has experience in the field of particle size analysis, quality control of processed materials and aspects of waste management.

Anette Mueller

Anette Mueller is Leader of the Chair of Processing of Building Materials and Reuse at the Bauhaus-University in Weimar, Germany. Her special research interests are the recycling of construction debris for new building materials, the influence of processing on bulk materials and the chemistry of cements.

CRYSTAL STRUCTURE OF THE SOLID SOLUTION $2CAO\text{-}SIO_2$ SYNTHESIZED AT LOW TEMPERATURE BY USING COMPOSITE MINERALIZER ($CUO + CAF_2$)

R. Sanjaasuren[1], D. Sangaa[2] and G. Batdemberel[3]

[1]Centre for Chemistry and Technology of New Materials, National University of Mongolia, P.O. Box 155, Ulaanbaatar-13, Mongolia.
[2]School of Physics and Electronics, National University of Mongolia, P.O. Box 659, Ulaanbaatar 210646, Mongolia.
[3]The team of Solid State Physics, School of Material Technology, Mongolian University of Science and Technology, P.O. Box 46/520, Ulaanbaatar, Mongolia.

ABSTRACT

The objective of our study is to obtain C_2S at low temperature in the presence of composite additives and to establish lattice parameters and constituent phase of C_2S and to determine the defect and it's type and concentration formed by additive atoms.

Numbers of studies have been conducted into the field of production of belite rich cement with high hydraulicity. For Instance, although there are many works on rapid cooling of belite rich cement clinker, it encounters difficulties in realizing this under real conditions. We have investigated ways of increasing the hydration reactivity of solid solution $2CaO\times SiO_2$, especially by physical and chemical methods which is one way of solving this problem.

In this paper we present the research results on our synthesis of solid solution $2CaO\times SiO_2$ (Ca_2SiO_4) in the presence of composite additions. The crystal structure of Ca_2SiO_4 was determined by Rietveld profile analysis using the GSAS program (sp.gr. $P2_1/n$, Z=4, a=5.05472 Å, c=9.32795 Å, $\beta=94.1667^0$, $R_{wp}=4.1\%$, $R_p=2.9\%$, $R_E=2.8\%$). The synthesized Ca_2SiO_4 was $\beta\text{-}C_2S$ with a monoclinic symmetry and some Ca atoms disordered and substituted with atoms of Fe and Cu. In this way, some O atoms replaced F atoms in the β-phase. After refinement of X-ray powder pattern by the Rietveld method, the chemical composition of solid solution $\beta\text{-}Ca_2SiO_4$ was defined with the following formula:

$$\beta\text{-}(Ca_{1.86}Fe_{0.07}Cu_{0.07})Si(O_{3.73}F_{0.27})$$

Results of our research have shown that temperature of forming $\beta\text{-}Ca_2SiO_4$ could be decreased to $1150\text{-}1200^0$C in the presence of composite mineralizers.

The solution of problems on the synthesis of C_3S and C_2S at low temperature will be helpful for production of cement clinker under low temperature conditions.

1. INTRODUCTION

Increasing numbers of studies have been undertaken on the production of belite rich cement with high hydraulicity [1,2,3,4]. It is observed from searching physical and physico-chemical research methods for increasing hydration reactivity that the rate of hydration of belite phase or the solid solution $2CaO\cdot SiO_2$ is slower than that of the alite phase. For instance, although there are many

works on rapid cooling of belite rich cement clinker, it encounters difficulties in realizing real condition [5].

Numerous publications have dealt with the synthesis of β-C_2S in the presence of some metal oxides. According to those study, defects formed such as substitution ($3Ca^{+2} \Leftrightarrow 2Me^{+3}$; $3Si^{+4} \Leftrightarrow 4Me^{+3}$) for Ca^{2+}, Si^{+4}. Interpretation depends on the metal ions radius therefore was changed cell parameters and stabilized modification β-C_2S and lowered by 100^0-150^0C temperature formation [6,7,8].

It is possible to obtain C_2S at low temperatures in the presence of a mineralizer whereas C_2S completely formed at 1400^0 – 1450^0 C in system of "2CaO + SiO_2" stabilized by Al_2O_3, Fe_2O_3. The solid solution formed spontaneously, because of increasing entrophy of the system and decreasing free energy in the presence of addition [6].

It was established that there is a vacant defect form in the crystal lattice of β-C_2S during stabilization of calcium orthosilicate with a composition of $Ca_2Me_xSi_{1-x}O_{4-x/2}$ (where: Me- Al, Fe, B; 0<x<1)[9]. Also M.Regourd defined lattice parameters a=5.506 Å, b=6.749 Å c=9.304 Å β=94.62^0 in the β-C_2S. But lattice parameters of numerous polymorph modifications of the solid solution C_2S changed interval in the lower [10].

Studies on the texture of solid solution C_2S in the presence of CuO are insufficiently conclusive, and M.Enculescu examined the solid solution structure of β-Ca_2SiO_4 with CuO as a $(Ca_{2-x}\,Cu_x)SiO_4$ [11].

M.Diamon [12] separated the constituents from the clinker and analyzed them from the crystallographic point of view. Especially the belite crystal structure is refined as determined by the Rietveld method and the texture can be observed with the optical microscope SEM and TEM. As a result the crystal structure of the β-phase was almost consistent with the results for single crystals, although there was some difference in the lattice parameters and Si-O bonding distances between them.

The objective of our study is to obtain C_2S at low temperature in the presence of a composite additive «CuO+CaF_2» and to establish lattice parameters and constituent phases of C_2S and to determine any defect, and their type and concentration formed by the additive atoms.

2. EXPERIMENTAL

In order to synthesize C_2S chemically pure $CaCO_3$ and SiO_2 have been blended in molecular radio 2:1 and were homogenized for 30 min with acetone in the ball mill, in the presence of (chemically pure) Al_2O_3, Fe_2O_3, H_3BO_3 stabilizers together with (chemically pure) CaF_2, CuO composite addition. The chemical composition of raw material is shown in Table 1.

Table 1. Chemical composition of the raw materials

	$CaCO_3$	SiO_2	Stabilizer			Composite addition	
			Al_2O_3	Fe_2O_3	H_3BO_3	CaF_2	CuO
Wt %	72.7	21.8	1.0	1.2	1.0	1.5	0.75

After mixing of the raw materials, pellets of ∅2.0 × 0.5 cm were pressed and dried at 105 ± 5^0C. The samples with a Pt cup were placed in a high temperature furnace, heated from room temperature to temperatures of 1000^0C, 1100^0C, 1150^0C and 1200^0C for 45 min. The heating-up rate is controlled at 20^0C/min and the burnt samples were rapidly cooled in air. The Free CaO of the samples was determined by titration with ethanol-glycerol [13]. The study of the solid solution structure of the synthesized C_2S was carried out with an X-ray powder diffractometer (Guinier diffractometer D-

83253, RIMSTING, Germany, λ = 1.540562 Å, the $2\theta_0$ - range $0\text{-}50^0$, stepsize 0.001^0, FWHM-0.035^0). The diffraction pattern was refined by Rietveld profile analysis using the GSAS program [14].

3. RESULTS

Comparative data of kinetics combining free CaO in the "$2CaO+SiO_2$" system are shown in Figure 1.

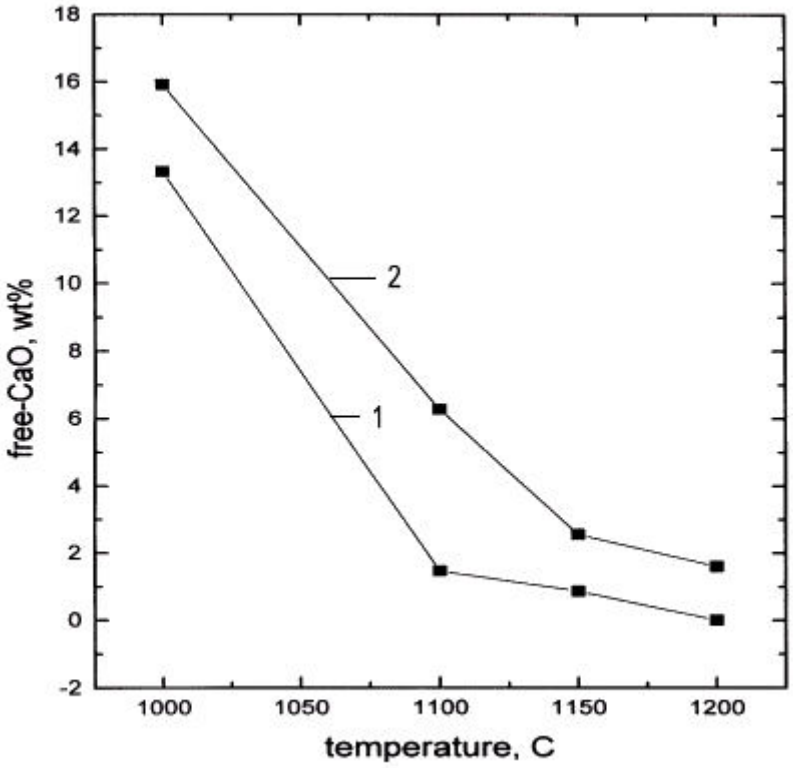

Figure 1. Kinetics of combining of free oxide CaO depending on the burning temperature in the "$2CaO+SiO_2$" system.
1- 1.5 wt% CaF_2, **2-** 1.5 wt% CaF_2 + 0.75 wt% CuO.

In Figure 1, it is clear that formation rate of C_2S solid solution is considerably increased and formation temperature is lowered to 1150^0C in the system of "$2CaO+SiO_2$" with CaF_2+CuO, addition used as shown in Table 1.

In the Figure 2, shows the x-ray powder diffraction pattern of C_2S with composite addition "CaF_2+CuO" at 1150^0C.

The observed intensities are shown by dots (+), and calculated ones by the solid line. The positions of the Bragg reflections showed by the small vertical lines below the pattern. The line at the bottom indicates the intensity difference between the experimental and the refined patterns.

X-ray powder diffraction studies confirmed that one phase (β-C_2S: sp.gr.$P2_1/n$, monoclinic) without additional diffraction peaks which expressed another phase at diffractogram. The diffractogram of β-Ca_2SiO_4 did not show any diffusion peaks in the angle intervals $2\theta=13\div80^0$. The experimental and calculation lines are shown in Figure 2. It is clear from Figure 2 that there is a good fit between measured and calculated values.

In the initial model for refinement we used lattice parameters of the structure β-Ca_2SiO_4 [12] and refined parameters of background, profile of diffraction peaks, constant of unit cell (a, b, c, β), occupancy (n) of atoms, isotropic temperature factors (B_{ij}), co-ordinates (x/a, y/b, z/c) of atoms. The results of the refinement β-Ca_2SiO_4 are listed in Tables 2 and 3.

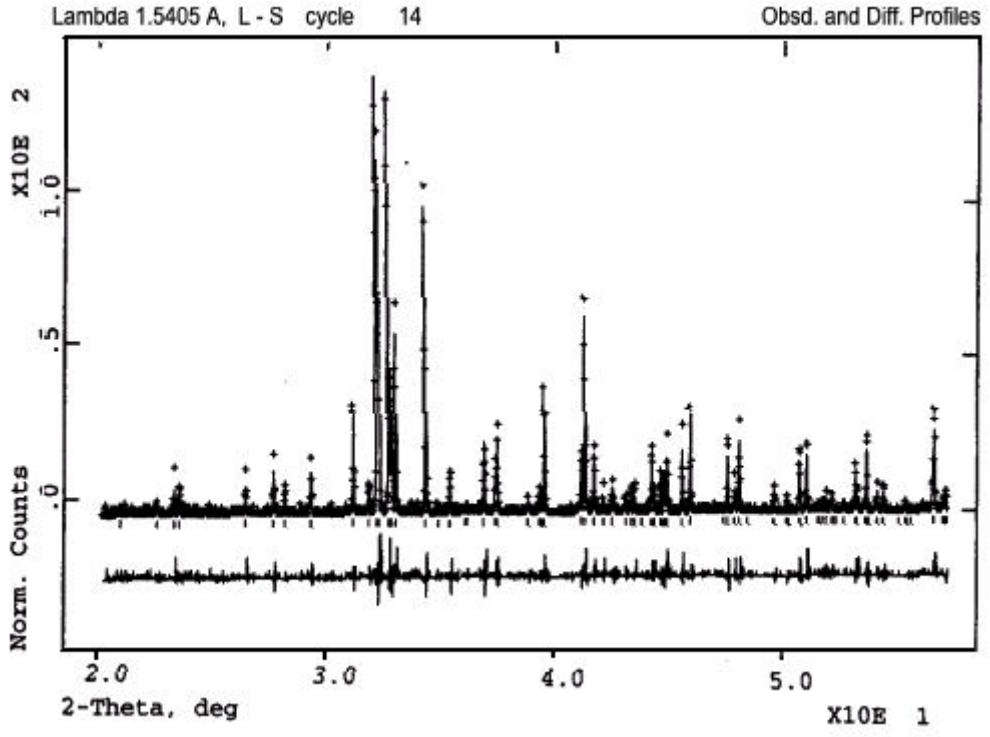

Figure 2. β-Ca_2SiO_4. Observed, calculated and difference X-ray powder diffraction pattern of crystal structure at 1150 ^{0}C (λ=1.540562 Å).

Table 2. Conditions measurement of the XRD pattern and lattice parameters β-Ca_2SiO_4

[1]	Parameters	
1.	Space group	P 2_1/n
2.	2θ ^{0} – range	20 ÷ 57
3.	Stepsize, 2θ^0	0.02
4.	I_{max}	1357
5.	Peak numbers	176
6.	Lattice parameters: a, Å b, Å c, Å V, Å^3 β Z	 5.50472 6.76212 9.32795 346.285 94.1667^0 4
7.	Agreement R-factors (%): R_{WP} R_p R_E	 4.1 2.9 2.8

Table 3. Atomic parameters of the solid solution β-Ca_2SiO_4

	Atoms	Atom coordinates			Therm. B_{ij}	Occup. (n)
		x/a	y/b	z/c		
1.	Ca(1)	0.230	0.342	0.431	0.025	**0.86**
2.	Fe	0.230	0.342	0.431	0.025	**0.07**
3.	Cu	0.230	0.342	0.431	0.025	**0.07**
4.	Ca(2)	0.228	-0.001	-0.294	0.107	1.00
5.	Si	0.270	-0.220	0.415	0.099	1.00
6.	O(1)	0.218	0.009	0.442	0.025	**0.73**
7.	F	0.218	0.009	0.442	0.025	**0.27**
8.	O(2)	0.029	-0.325	0.369	0.133	1.00
9.	O(3)	0.460	-0.260	0.316	0.125	1.00
10.	O(4)	0.325	-0.318	-0.422	0.115	1.00

After refinement, the diffractogram established the parameters of unit cell as follows: a=5.05472 Å, b=6.76212 Å, c=9.32795 Å, β=94.1667^0, V=346,285 Å^3. The conditions of the x-ray measurement and the constants of the unit cell are shown in Table 2.

During refinement of the diffraction spectrum, some atoms of Ca(1) were substituted by atoms Fe and Cu, and some atom of O(1) were replaced by atoms of F (Table 3: 0.86Ca + 0.07Fe +0.07Cu; 0.73O(1) + 0.27F). The R-factors improved appreciably in the first stage of the refinement structure with atoms Ca(1), O(1) being replaced by atoms Fe, Cu and F. The substitution of atoms was not noticeable in the change of parameters for the unit cell of β-Ca_2SiO_4. Obtaining positive means for isotropic temperature factors of atoms confirmed the selected structural model. The isotropic temperature factors chosen for substitution by other atoms provided the condition for stiochiometric substitution. In the first stage, calculation of diffraction spectrum R-factors were the following: R_{WP}=5.4%, R_p=3.2%, R_E=3.1%.

In this structure model, the R-factors for the profile of peaks for the substituting atoms Fe, Cu and F was as follows: R_{WP}=4.1%, R_p=2.9%, R_E=2.8%. In this selected model, the refined detail for isotropic temperature factors and atomic positions is shown in Table 2.

From the results obtained structural factors were used to calculate a Fourier map distribution density in the (110) phase of β-Ca_2SiO_4. The map distribution was calculated by using the GSAS program [14].

Figure 3 shows that the electron density is highest in the vicinity of Ca atoms, lower in the vicinity of Si atoma and lowest in the region where O atoms are present. The minimum electron density is ρ_{min}= -3.593e Å^{-3}, the maximum ρ_{max}= 11.492e Å^{-3} , $\Sigma\rho$ = 109.39e Å^{-3}

As we can see the corresponding symmetry is of monoclinic structure of β-Ca_2SiO_4 from the Fouriermap transformation of diffraction peaks. This calculation was consistent with research works [9, 12].

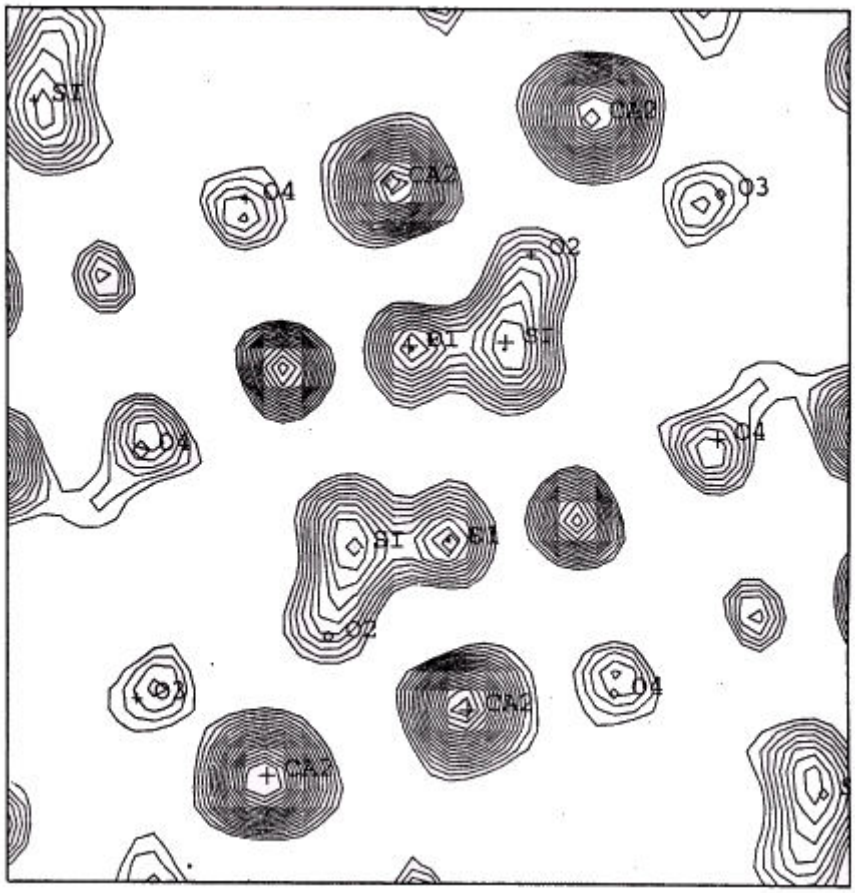

Figure 3. The distribution of density electron $\rho_{exp}(x,y,z)$ in the plane (110) of structure β- Ca_2SiO_4. Shown fragment 7×7Å with coordinates centre (1/2, 0, 1/2).
The number is indicated levels constant density electrons.

The isolated tetrahedrons $SiO_4^{-}4$ were connected to two types of Ca^{+2} ions. Four atoms from 8 atoms Ca(Ca(1)) situated above and below tetrahedrons SiO_4^{-4}, formed the chains or stations. These stations are connected among themselves to another four atoms Ca(2), which are located in the vacant structure between tetrahedrons.

The coordination Ca(1) is not regular and the distance between Ca and O in the polyhedral CaO_n (where n=6-9) varied from a 2.25 to 3.19 Å, in one case but in another case from, but in other kinds – from 2.98 to 3.86 Å. Similarly Ca(2) as well co-ordinated and the interatomic distance Ca-O varied between 2.39 ÷2.72 Å.

Our synthesized β-Ca_2SiO_4 is deficient in atoms of Fe, Cu, and F the positions of almost all atoms are displaced from ideal positions (Table 3). The atomic distance of β-Ca_2SiO_4 was consistent with [9, 12] research works. For the polyhedron our calculations indicate that Ca(1) was directly co-ordinated (bonded) to 9 oxygen atoms.

The Fouriermap transformation indicates a symmetric structure with the silicatetrahedra having Ca(2) atoms parallel to this plane.

It was be concluded that the substitution of the Ca(1) atoms by Fe and Cu mainly resulted in a disordered structure of β-Ca_2SiO_4.

Table 4. Interatomic distances and its interandles atoms β -Ca_2SiO_4

No	Type of bonds	length bonds, Å	Type of bonds	Interatomic angles, degree
1.	Ña1 – Ca1	3.621	Ca1-O2-Ca2	173.43
		3.808		88.82
	Ca1 – Ca2	3.459	Ca1- O2- Si	89.62
		3.540	Ca1- F-Fe	0.00
		3.583	Ca1-F-Ca2	94.26
		3.514		91.43
		3.730	Ca1-F-Si	162.58
	Ca1 – Si	2.975	Ca1-Ca2-O2	44.45
		3.254		137.67
		3.121	Ca1-Ca2-O3	54.69
	Ca1 – O1(F)	3.300	Ca1-Ca2-O4	101.89
		2.255	Ca1-Ca2-Cu	61.76
2.	2(Ca2 – Ca2)	3.484	Ca2-O1-Ca2	117.36
	Ca2 – Si	3.115	Ca2-O1-Si	98.04
		3.251	Ca2-F-Ca2	117.36
		3.406		93.78
	Ca2 – O1(F)	2.460	Ca2-O2-Ca2	85.04
		2.728	Ca2-O2-Si	96.95
	Ca2 - F	3.438		156.92
3.	Si – O1(F)	1.598	Si-Ca2-O1	30.52
	Si – O2	1.538	Si-Ca2-Si	91.73
	Si – O3	1.470	Si-Ca2-F	71.52
	Si – O4	1.666	Si-Ca2-O4	115.30
4.	O2– Ca1	2.556	O2-Ca2-O3	75.46
		2.432	O2-Ca2-O4	72.66
	O2 – Ca2	2.684	O2-Ca2-O2	105.53
		2.464	O2-Si-O3	112.24
	O2 – Si	1.538	O2-Ca1-O4	117.74
5.	O3 – Ca1	3.193	O3-Ca1-O4	75.76
		2.554	O3-Ca2-O4	82.84
		2.863	O3-Si-O4	114.19
	O3 – Ca2	2.482	O3-Si-O1	114.90
		2.462	O3-Si-Fe	114.907
	O3 – Si	1.469	O1-Si-O2	109.30
6.	O4 – Ca1	2.708	Ca1-O4-Cu	94.73
		3.054	Ca1-O4-Ca2	87.50
		2.462	Ca1-O4-Si	81.96
	O4 – Ca2	2.529	Cu-O4-Ca2	100.18
		2.400	Cu-O4-Si	96.32
	O4 – Si	1.666	Ca2-O4-Si	161.08
7.	Cu – F	2.535	Cu-O1-Ca2	94.26
			Cu-O1-Si	162.58
			Cu-F-Ca2	94.26
			Cu-F-Si	162.58
8.	Fe – F	2.535	Fe-F-Cu	0.00
			Fe-F-Ca2	94.26

Table 5. Interatomic distances of β - Ca_2SiO_4

1	Data of our determined	Data of Japanese [9]	Data of Russian [13]
	Ca(1)FeCuO$_9$polihedron Ca1-O1F 2.2538(Å) O2 2.5566 O3 2.5546 O4 3.0542 O2 2.4319 O3 2.8636 O4 2.4623 O3 3.1930 O4 2.7084	Ca(1)O$_{10}$ Ca1-O1 2.2581(Å) O2 2.5570 O3 2.5591 O4 3.0558 O2 2.4330 O3 2.8606 O4 2.4615 O2 3.3774 O3 3.1910 O4 2.7062	Ca1-O1 2.222(Å) O2 2.490 O3 2.540 O4 2.370 O2 2.880 O3 2.430 O4 2.640
	Ca(2)O$_8$ polihedron Ca2-O1F 2.4600(Å) O1 2.7278 O2 2.4644 O3 2.4621 O4 2.5296 O2 2.6844 O3 2.4815 O4 2.3976	Ca(2)O$_8$ Ca2-O1 2.4600(Å) O1 2.7258 O2 2.4690 O3 2.4599 O4 2.5268 O2 2.6821 O3 3.4806 O4 2.3976	Ca2- O1 2.430(Å) O1 2.640 O2 2.380 O3 2.390 O4 2.440 O2 2.390 O3 2.640 O4 2.620
	SiO$_4$tetrahedron Si–O1 1.5981(Å) O2 1.5378 O3 1.4699 O4 1.6659	SiO$_4$ Si–O1 1.5994(Å) O2 1.5359 O3 1.4697 O4 1.6701	Si–O1 1.610(Å) O2 1.630 O3 1.640 O4 1.650

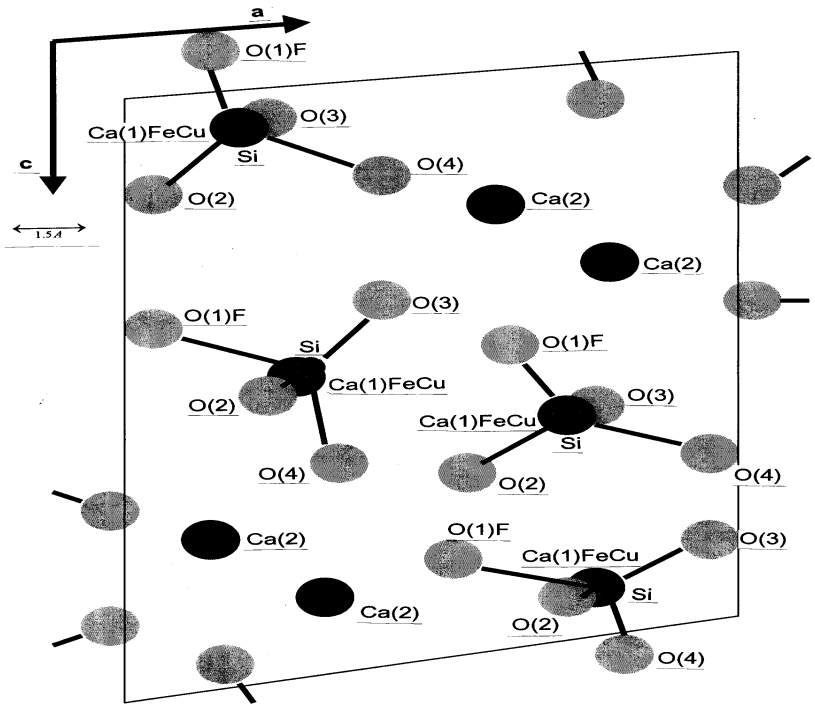

Figure 4. Atomic arrangement of structure β-Ca_2SiO_4.

4. CONCLUSIONS

The forming temperature of the β-Ca_2SiO_4 at low temperature was decreased to 1150^0C at synthesis of C_2S in the presence of composite addition.

Some Ca atoms were disordered and substituted by atoms of Fe and Cu, and some O atoms replaced F atoms in the β-Ca_2SiO_4 modification.

We are suggesting that the Ca(1)-O(2) 3.3774 Å bond is not contacted and defected in the crystal structure.

After refinement of the x-ray powder pattern by the Rietveld method, the chemical composition of solid solution β-Ca_2SiO_4 is defined by using composite addition. The final results show the following formula: β-$(Ca_{1.86}\ Fe_{0.07}\ Cu_{0.07})\ Si(O_{3.73}\ F_{0.27})$.

REFERENCES

[1] Gies.A, Knofel.D., "Influence of alkalies on the composition of belite-rich cement clinkers" Cement and concrete research.1986. Vol.16. pp.411-422

[2] Boldirov.A.E "The other cements (belite-rich cement) and its application", 7th Intern. Congress on the Chemistry of cement, Paris, France,1980 Vol.2, pp.318-334 (in Russian)

[3] Miekle.I,Muller.A, "Active belite cement" 9th Intern.Congress on the Chemistry of cement,New Delhi,India ,1992 Vol.2, pp.399-406

[4] Sanjaasuren.R, Rymyantsev.P.F "Synthesis of low temperature Portland cement clinker by using composite mineralizer" 10th Intern. Congress on the Chemistry of cement, Gothenburg, Sweden,1997 Vol.1 1037,10p

[5] Rajczyk.K, Nocuñ-Wczelik.W" Studies of belite cement from Barium containing by-product" 9th congress on the Chemistry of Cement, New Delhi, India, 1992 Vol.2.pp.250-255

[6] Timashev.V.V. "Synthesis and hydration of the binding materials" Moscow, 1986, pp.226-313 (in Russian)

[7] Aramastsev.H.I, "Influence of modified oxides in structure and hydration effect of silicate" Research letter of institute, Vol 90, Moscow1986, pp.29-46 (in Russian)

[8] Feng Xuyi, Long Shizong,: "Investigation of the effect of minor ions the stability of β-C_2S and the mechanism of stabilization"«Cement and Concrete research»,1986, Vol.16. pp.587-601

[9] Butt.Yu.M, Timashev.V.V, "Portland cement"1974, p.29 (in Russian)

[10] Regourd.M,Ginier.A, "The crystal chemistry of the constituents of Portland cement clinker" 6th Intern. Congress on the Chemistry of cement, Russia, Moscow, 1976, Vol.1 pp.25-5

[11] Enculescu.M, "Influence of oxides transitional elements on the properties of mineralogical components of clinkers " 6th Intern. Congress on the Chemistry of cement, Russia, Moscow, 1976, Vol.1 pp.104-110

[12] Daimon.M, Hirano.Y, "Crystal structure analysis of major constituent phases in ordinary portland cement" The 9th congress on the Chemistry of Cement,New Delhi, India, Vol.2,1992 pp.17-25

[13] Kurbatova I.I, "Methods of chemical analysis in the building materials", Moscow., 1972.p.128. (in Russian)

[14] Larson.A.C., Von Dreele R.B., "Generalized Crystal Structure Analyses System (GSAS)", LAUR 86-748. Los Alamos, 1988.p.150

CRYSTAL STRUCTURE OF THE SOLID SOLUTION $2CAO\text{-}SIO_2$ SYNTHESIZED AT LOW TEMPERATURE BY USING COMPOSITE MINERALIZER ($CUO + CAF_2$)

R.Sanjaasuren[1], D.Sangaa[2], G.Batdemberel[3]

[1]Centre for Chemistry and Technology of New Materials, National University of Mongolia, P.O.Box 155, Ulaanbaatar-13, Mongolia
[2] School of Physics and Electronics, National University of Mongolia, P.O.Box 659, Ulaanbaatar 210646, Mongolia
[3]The team of Solid State Physics, School of Material Technology, Mongolian University of Science and Technology, P.O.Box 46/520, Ulaanbaatar, Mongolia

Professor R.Sanjaasuren

Member of the Asia –Pacific Academy (APAM)
Member of Mongolia Academy of Natural Sciences.
E-mail: int_rel@num.edu.mn

EFFECT OF HYDRATION AND CARBONATION ON THE SILICATE ANION STRUCTURES OF PORTLAND BLAST-FURNACE SLAG CEMENT

Koshiro Koizumi and Naomitsu Tsuyuki

Department of Chemistry, College of Science and Technology, Nihon University,
7-24-1, Narashinodai, Funabashi, Chiba 274-8501, Japan.
E-mail: koizumi@chem.ge.cst.nihon-u.ac.jp, tsuyuki@chem.ge.cst.nihon-u.ac.jp

ABSTRACT

Granulated blast-furnace slag, BFS, exhibits a potential hydraulicity. Changes in the silicate anion structures during hydration of the BFS were studied with the trymethylsilylation method. A chain length development of the silicate anion during hydration was confirmed and an increase in relative abundance of trimer and pentamer was determined. Carbonation of the hydration products of BFS, ordinary portland cement and other binders resulted in shortening of the chain length of silicate anions. We concluded that the chain length distribution of silicate anion can reflect the degree of hydration as well as the degree of degradation of hardened body.

1. INTRODUCTION

Granulated blast-furnace slag, hereafter BFS, can be hydrated under an alkali stimulus exhibiting a potential hydraulicity. When BFS is added to ordinary portland cement, OPC, several new properties that can not be attained solely by the OPC are obtained. Thus BFS has been used as an admixture for concretes. Study of reactions during the hydration of these hydraulic binders and the resulting strength evolution of the hardened materials can be approached in terms of silicate structure. The silicate component in the hydraulic binders develops -O-Si-O- bonds during hydration forming polymeric silicate anions. The chain length development was determined by the trymethylsilylation, hereafter TMS, method in this study.[1]

We have studied the difference in surface structure of BFS with different Blaine surface areas by means of XPS, while in this study, effects of the Blaine surface area, type of alkali stimulus and age on the hydration of BFS powder were examined.[2] In addition, the chain length distribution of silicate anions during carbonation of BFS was also studied because the low resistance to carbonation, unlike to chloride attack, of the blast-furnace slag cement has been pointed out.[3]

2. EXPERIMENT

2.1 Materials used

The BFS powder specimen was a by-product of a factory and ground to a Blaine surface area of 4000, 6000, 8000, 11000 and 18000 cm^2/g. Chemical compositions were similar, as shown in Table 1, and ranging from 32.7 to 33.4 percent for SiO_2, 12.6 to 13.4 percent for Al_2O_3, 40.9 to 41.7 percent for CaO and 6.9 to 7.8 percent for MgO.[4] Table 2 shows some chemical properties of BFS. Degree of vitrification was more than 98 percent for all the specimen and it was difficult to distinguish the BFS powders by the factors such as chemical composition, degree of vitrification and basicity.

Proceedings of the 11th International Congress on the Chemistry of Cement (ICCC)
'Cement's Contribution to the Development in the 21st Century'
Hosted by: The Cement and Concrete Institute of South Africa
CD-ROM produced by: Document Transformation Technologies
11 - 16 May 2003, Durban, South Africa
ISBN Number: 0-9584085-8-0
Editors: Dr G. Grieve and G. Owens
Congress Organised by: Event Dynamics

Table 1. Chemical composition of blast-furnace slags

Blaine Surface Area (cm^2/g)	Composition (%)						
	MgO	Al_2O_3	SiO_2	CaO	TiO_2	S	T・Fe
4000	7.71	13.1	33.4	40.9	1.09	0.85	0.35
6000	7.63	12.7	33.1	41.7	1.10	0.85	0.26
8000	7.78	12.6	33.3	41.6	1.13	0.83	0.19
11000	6.9	13.4	32.7	41.6	---	0.3	0.5
18000							

Table 2. Chemical properties of blast-furnace slags

Blaine Surface Area (cm^2/g)	degree of vitrification	basicity
4000	98%	1.85
6000		1.87
8000		1.86
11000	---	1.89
18000		

2.2 Test Method

2.2.1 Hydration of BFS powder

Alkali stimulation of BFS powder was made using two types of alkali solutions: 0.1N-NaOH solution and $Ca(OH)_2$ saturated solution. 2.0 grams of BFS of each Blaine value was dispersed in 100 milliliters of the alkali solution and stirred thoroughly in an incubator. After being stimulated for a sufficient time, hydration of the BFS powder was interrupted by methanol and acetone and filtered under a reduced pressure to have the hydration products in a solid residue.

2.2.2 Carbonation of Hydrated Specimen

After hydration was interrupted, the suspension, a powder-water system, was subjected to an accelerated carbonation test. 3.0 grams of hydration product of OPC or BFS powder was dispersed in 300 milliliters of degassed water and stirred at a temperature of 20 ^{0}C, when a 100 percent carbon dioxide gas was introduced at a flow rate of 10 milliliters per minute for a specified time of 5, 10, 30 and 60 minutes. Subsequently, the suspension was filtered where hydration of the solid phase was again interrupted by methanol and acetone and subjected to silicate anion structure analysis.

2.2.3 Silicate Anion Structure Analysis by TMS Method

Derivatives of the hydration products of BFS were prepared according to the method improved for BFS trymethylsilylation by Suginohara and others[5],[6]. Trimethylchlorosilane (TMCS), hexamethyl-disiloxane (HMDS) and methanol were mixed at a volume ratio of 1:3:2. Resulting TMS agent of 18 milliliters was applied to 200 milligrams of specimen and stirred for 60 minutes at a temperature of 20 ºC. 20 milliliters of pure water was added to the reacted specimen and soluble components were removed from the organic solvent phase by the liquid-liquid extraction. 2 grams of nonionic ion-exchange resin, AMBERLYST 15 (Rohm and Haas), was added to the organic solvent phase to prevent isomerization, and after 24 hours, it was filtered and thickened to less than 1.0 milliliter under nitrogen gas and analyzed by gas chromatography (GLC). Conditions of the analysis are as follows, GLC:GC-14B, detector: FID (Shimazu), Column:Dexsil 400GC 2% on chromosorb w 60/80 AW, SUS column of 2 m x 3 mmϕ (GL Science) and column temperature: 80-340 ºC, 10 ºC per minute. Composition of silicate anion was determined by integrating the peak area of GLC.

3. RESULTS AND DISCUSSIONS

3.1 TMS Derivatives of Silicate Anion

A gas chromatogram of derivatives of trymethylsilylated unhydrated BFS powder is shown in Fig. 1. Silicate anions with a chain length from monomer to hexamer were able to be analyzed by the GLC. Silicate anion structure of BFS with various Blaine surface areas was also trymethylsilylated and analyzed, but no significant difference was found as shown in Fig.2.

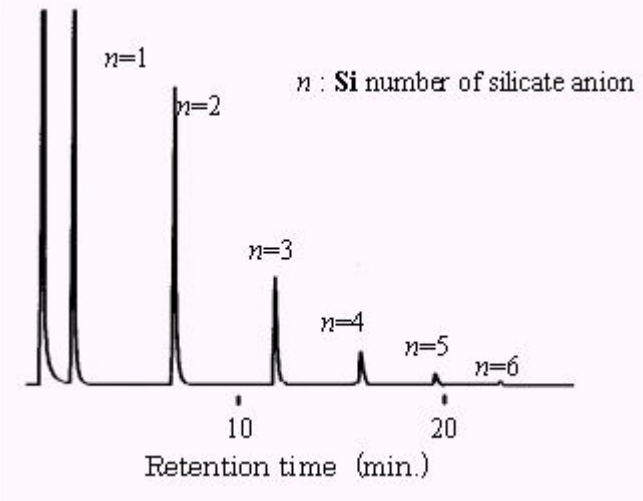

Figure 1. GLC chart of unhydrous BFS

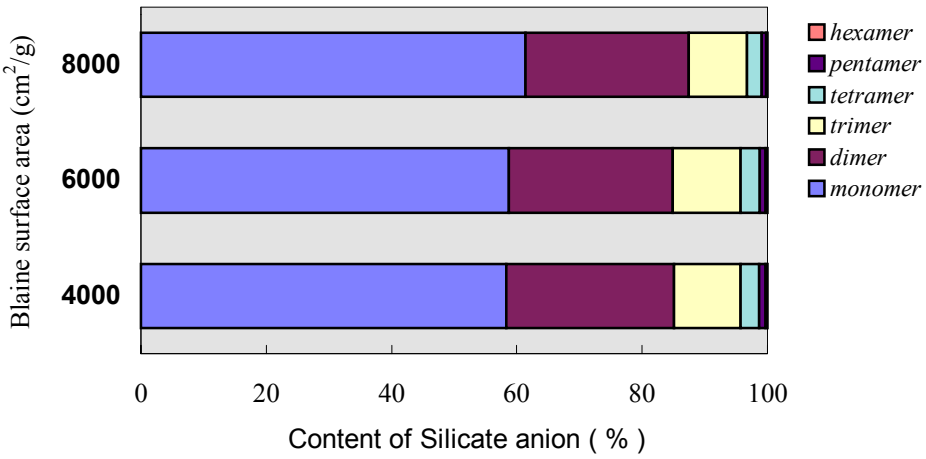

Figure 2. Distribution of silicate anion of unhydrous BFS

3.2 Influences of the Hydration Time of BFS

Polymerization of silicate anion was generally found when the hydration time became longer, where monomer decreased and dimer increased. Components with a chain length greater than trimer were also found exhibiting the general tendency that the chain length of silicate anion developed with the evolution of hydration. An example of this change is shown in Fig. 3. A close look at changes in a silicate anion structure with a chain length greater than trimer showed that pentamer increased to a greater extent with ages though the detectivity was low compared to that of dimer. In contrast to the inactive changes of tetramer and hexamer, prominence of the pentamer increase is very distinctive and can be regarded as a parameter representing the degree of polymerization of the silicate anion structure.

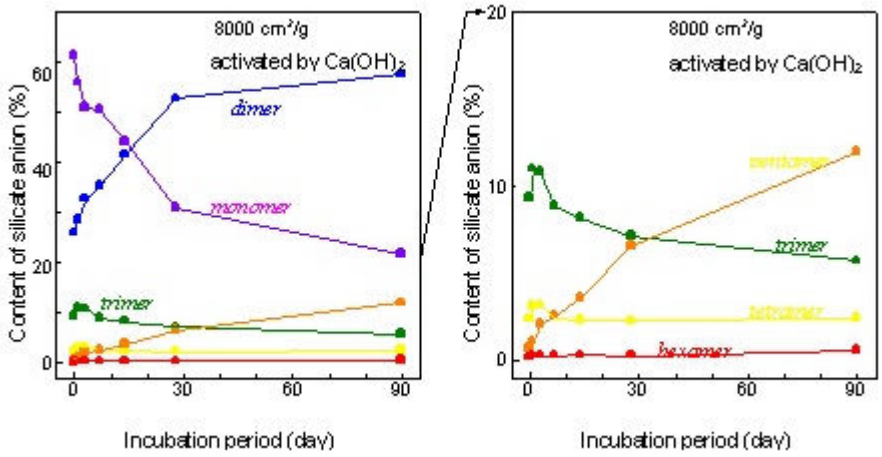

Figure 3. Time course of silicate anion structure of BFS on hydration by $Ca(OH)_2$

3.3 Influences of Alkali Stimulus

Changes in the distribution of monomer and dimer of silicate anions by the type of alkali stimulus are shown in Fig.4. When NaOH or $Ca(OH)_2$ was used as an alkali stimulus, the tendency described in the previous section was reproduced while the rate of polymerization was slightly quicker with $Ca(OH)_2$ than with NaOH.

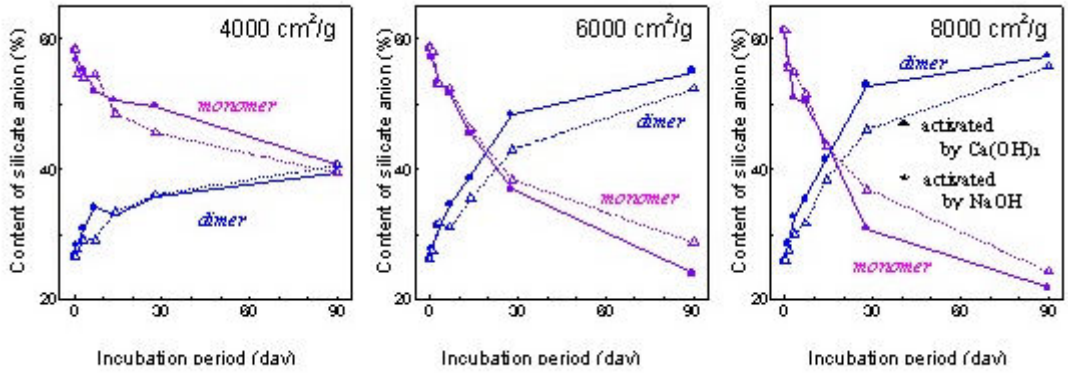

Figure 4. The comparison of alkali activator on hydration of BFS

3.4 Influences of the Blaine Surface Area

Comparison of changes with hydration time in the silicate anion structure of BFS powder with different Blaine surface areas is shown in Fig. 5. At an early stage of hydration, no significant difference in structure was found between BFS powders with different Blaine surface areas. However under a longer hydration time, the BFS powder with a higher Blaine surface area exhibited a greater degree of polymerization. Only a BFS powder with a Blaine surface area of 4000 cm^2/g showed nearly equal degree of polymerization without regard to alkali stimulus and age. As already proven by Tsuyuki and others [2], BFS powder with a different Blaine surface area exhibits several differences in the near-surface glassy phase. A BFS powder with a lower Blaine surface area has larger amount of Al_2O_3-SiO_2 glasses that shows lower reactivity than that of CaO-SiO_2 glass. Thus, when an alkali-stimulated hydration deposits C-S-H on the surfaces of BFS powder, considerable amounts of unreacted parts may be left inside of a BFS powder compared to those with a higher Blaine surface area. This accounted for the slow evolution in strength, at early ages, of a mortar partially substituted with BFS with a lower Blaine surface area. As a consequence from the viewpoint of silicate anion polymerization during BFS hydration, a considerable difference can be seen when the Blaine surface area of BFS, used as an admixture of OPC, exceeds 6000 cm^2/g.

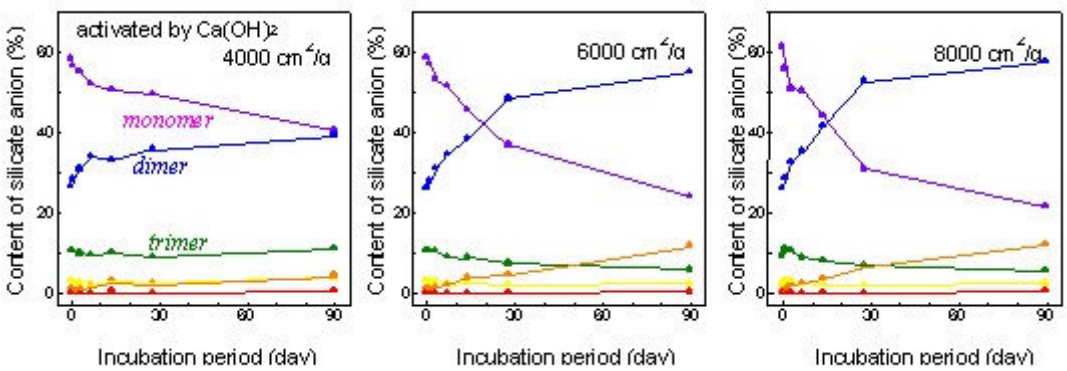

Figure 5. The difference in the hydration velocity by blaine surface area of BFS

3.5 Influences of Carbonation on the Chain Length Distribution of Silicate Anions

Chain length distributions of silicate anion in OPC and BFS (8000cm^2/g) treated in two different manners, hydrated for 28 days and then subjected to an accelerated carbonation, are compared in Fig. 6, Fig. 7, respectively. Similar to the case of OPC, silicate anion structure of hydrated BFS showed an increase in polymerization containing considerable trimers. When the hydrated BFS is subjected to accelerated carbonation, the chain length distribution tended to shift from longer to shorter and portion of monomer increased as the carbonation time increased. Thus the chain length distribution of silicate anion can reflect the degree of hydration as well as the degree of degradation of the hardened body.

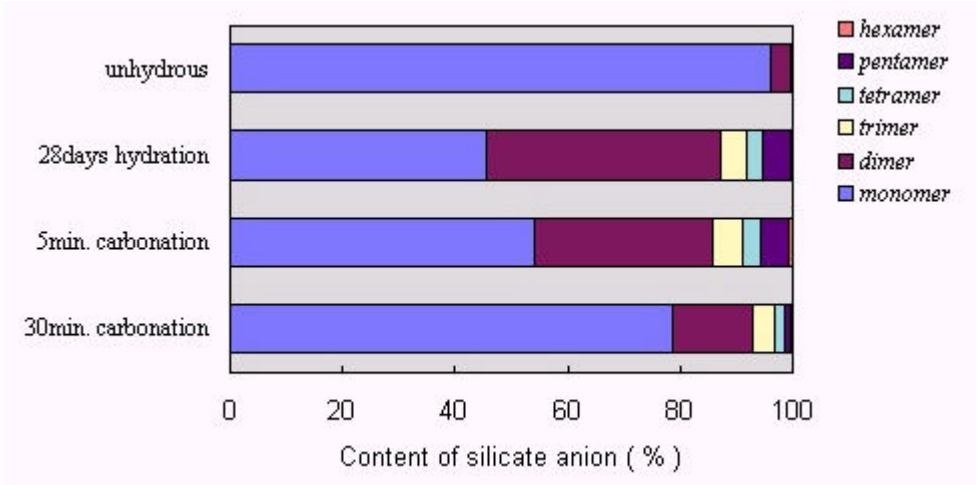

Figure 6. Chain length distribution of OPC under the condition of hydration or carbonation

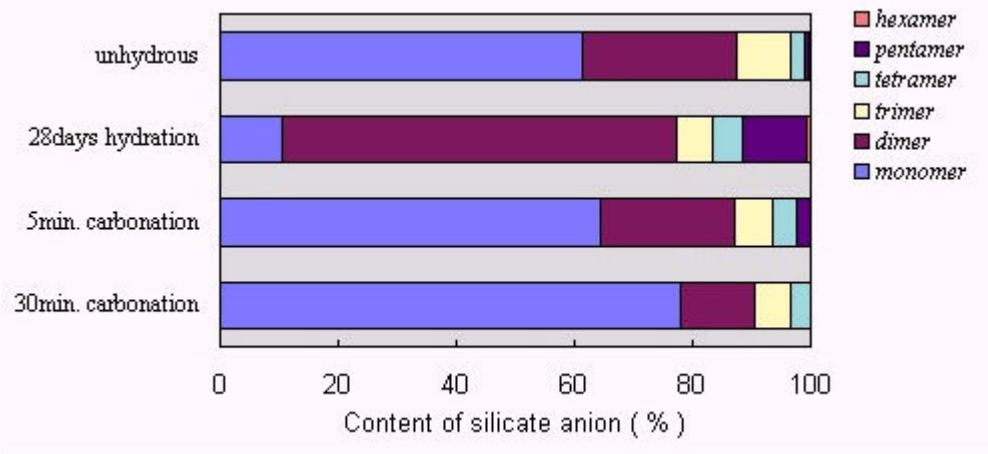

Figure 7. Chain length distribution of BFS under the condition of hydration or carbonation

4. CONCLUSIONS

Major findings in this study can be summarized as follows.

(1) Chain length of silicate anions in BFS, particularly dimer and pentamer, developed with the evolution of hydration.

(2) Hydration reactivity differed according to the Blaine surface area of BFS. Those with a larger Blaine surface area exhibited greater development in chain length during hydration, while those with a Blaine surface area less than 4000 cm^2/g were supposed to be less reactive due to an accumulation of C-S-H gels on the powder surfaces.

(3) When a hydraulic binder such as BFS or OPC is subjected to hydration or carbonation, the silicate anion structure, which is the main component of the reaction product, was altered greatly depending closely on the degree of hydration and carbonation.

REFERENCES

[1] Yasue, T. and Arai, Y., Analysis of silicate ions in silicate using trimethylsilylation method, Gypsum and Lime, vol.211, 1987, pp385-395 [in Japanese]

[2] Tsuyuki, N. and Koizumi, K., Granularity and surface structure of ground granulated blast-furnace slags, Journal of the American Ceramic Society, vol.82, 1999, pp2188-92

[3] Li, C., Yoda, A. and Yokomuro, T., Effect of ground granulated blast-furnace slag on pore structure and compressive strength of hardened cement pastes, J.Struct. Constr. Eng., vol.506, 1998, pp1-6 [in Japanese]

[4] Architectural institute of Japan (AIJ), State of the art report on concrete using ground granulated blast furnace slag, 1992, pp34-6 [in Japanese]

[5] Okusu, H., Masuda, G., Wakita, M. and Suginohara, Y., J. Japan Inst. Metals, vol.45, 1981, pp915-22 [in Japanese]

[6] Okusu, H., Takeshita, H., Mizuguchi, K. and Suginohara, Y., J. Japan Inst. Metals, vol.47, 1983, pp956-63 [in Japanese]

EFFECT OF HYDRATION AND CARBONATION ON THE SILICATE ANION STRUCTURES OF PORTLAND BLAST-FURNACE SLAG CEMENT

Koshiro Koizumi

Department of Chemistry, College of Science and Technology, Nihon University
E-mail: koizumi@chem.ge.cst.nihon-u.ac.jp
7-24-1, Narashinodai, Funabashi, Chiba 274-8501, Japan
Tel.& Fax: +81-47-469-5537

A short biography of the presenting author:

Koshiro Koizumi
Department of Chemistry, College of Science and Technology, Nihon University
E-mail : koizumi@chem.ge.cst.nihon-u.ac.jp
7-24-1, Narashinodai, Funabashi, Chiba 274-8501, Japan
Tel.& fax..: +81-47-469-5537

WORKING MECHANISM OF POLYCARYBOXYLATE SUPERPLASTICIZER CONSIDERING THE CHEMICAL STRUCTURE AND CEMENT CHARACTERISTICS

Kazuo Yamada and Shunsuke Hanehara

Research & Development Center, Taihieyo Cement Corp., Chiba, Japan.
E-mail: kazuo_yamada@taiheiyo-cement.co.jp and shunsuke_hanehara@taiheiyo-cement.co.jp

ABSTRACT

Polycarboxylate superplasticizer (PC) is the most advanced cement dispersant having a excellent performance of water reducing and a superior workability retention ability to other superplasticizers. The Fundamental dispersing mechanism of PC was presented at the previous ICCC. In order to estimate the behavior of fresh concrete containing PC, it is necessary to consider many other important factors affecting the performance of PC, *i.e.* the relationships of rheology among paste, mortar and concrete, the adsorption PC, adding effect of PC on the initial hydration of cement, the different adsorbing behaviors of PC on various cement hydrates, the adsorption equilibrium of PC, the competitive adsorption of PC with sulfate ions, and the molecular structure of PC. Considering these factors, based on the assumption that the performance of PC is proportional to the adsorbed amount of PC per surface area of solid phase (*Ad/SSA*), in this study, one model estimating the slump and its time change in concrete is proposed using only a few basic characteristics of cement and PC. In this model, PC is assumed to show a Langmuir type adsorption competitively with sulfate ions. This model is also applied to estimate the performance of several types of PC having different adsorbing abilities.

1. INTRODUCTION

In Japan, the studies of the working mechanisms of superplasticizer (PC) have been shifted from on beta-naphthalene sulfonate-type superplasticizer (BNS) during 1980s and early 1990s [1, 2, 3] to on polycarboxylate-type SP (PC) in this decade although the studies on BNS have been continued internationally [4, 5, 6, 7, 8, 9, 10]. Many developments were tried in order to improve the slump retention ability of BNS in Japan. However, the new PC with much superior performance to keep the fluidity constant up to several hours or more has been developed and the usage of BNS has been limited in precast concrete where the slump retention was not so important. This situation limited the study on the working mechanism of slump retaining behaviors of BNS. Instead of BNS, the slump retaining mechanism of PC has been studied intensely. Because the variety of chemical structure of polycarboxylate that can be modified, many functions can be adjusted and a high dispersing performance and a good slump retaining ability have been achieved by using new PC [11, 12, 13, 14, 15, 16].

After wide applications of PC for high-strength and high-fluidity concrete [17], it became clear that controlling workability uniformly was not always easy especially at low water-to-cement ratio (W/C). For example, the use of different types and different lots of cement and aggregate can cause unexpected fluctuation of the workability of concrete. Moreover, even if the same materials were used, the workability could be changed by mixing machines, procedures and environmental conditions. The mechanism of these unexpected fluctuations has not been clarified and these phenomena have been explained as incompatibility [18, 19].

Proceedings of the 11th International Congress on the Chemistry of Cement (ICCC)
'Cement's Contribution to the Development in the 21st Century'
Hosted by: The Cement and Concrete Institute of South Africa
CD-ROM produced by: Document Transformation Technologies
11 - 16 May 2003, Durban, South Africa
ISBN Number: 0-9584085-8-0
Editors: Dr G. Grieve and G. Owens
Congress Organised by: Event Dynamics

On the other hand, significant progress has been achieved in understanding the fundamental dispersing mechanism of SP. The electrostatic repulsive force and the steric hindrance effect have been shown to be fundamental dispersing mechanisms of BNS and PC, respectively [20]. In order to apply these fundamental mechanisms to control the workability of concrete and to prevent incompatibility phenomena, many researches have been carried out. Many of these studies were in simple forms of paste or mortar. It is very important to estimate the workability of concrete such as slump and it is meaningful to try to explain concrete slump.

Based on this background, in this study at first, the interaction mechanism of cement and PC is summarized based on many studies and the required factors and assumptions to be considered for the model used in the next step are discussed. After this, basic behaviors of PC are linked to concrete slump by a simple model using a Langmuir type adsorption equilibrium. Finally, this model is applied for the estimation of the slump retaining behavior of PC with different adsorption abilities when several kinds of cement are used.

2. CONSIDERING FACTORS

The fundamental dispersing mechanism of PC has been established by several studies [20, 21, 22]. The final goal of the study on the working mechanism is the estimation of the workability of concrete based on several material characteristics such as cement, aggregate, SP, mix proportion and mixing procedures by using this fundamental mechanism. In this chapter, in order to link the steric hindrance effect of PC with the workability of concrete, some factors necessary to be considered are shown with several assumptions.

A stratified image considered in this study is shown in Figure 1. By adsorbing PC, the inter-particle potential is determined by steric hindrance effect. For the adsorption, the solution chemistry, especially sulfate ions, play an important role. In order to convert the inter-particle potential to the paste rheology, the potential is assumed to be proportional to the adsorption amount of PC per surface area of solid phase of hydrated cement (*Ad/SSA*) and the *Ad/SSA* is assumed to be proportional to the paste flow as an index of the paste rheology. For the *SSA*, the initial hydration of cement affects. The initial hydration of cement is affected by the cement characteristics, PC addition, mixing procedure and others. Paste rheology determines mortar rheology. Clay minerals in the fine aggregate affect the performance of PC. The mortar rheology determines the concrete rheology subject to the effect of mix proportions.

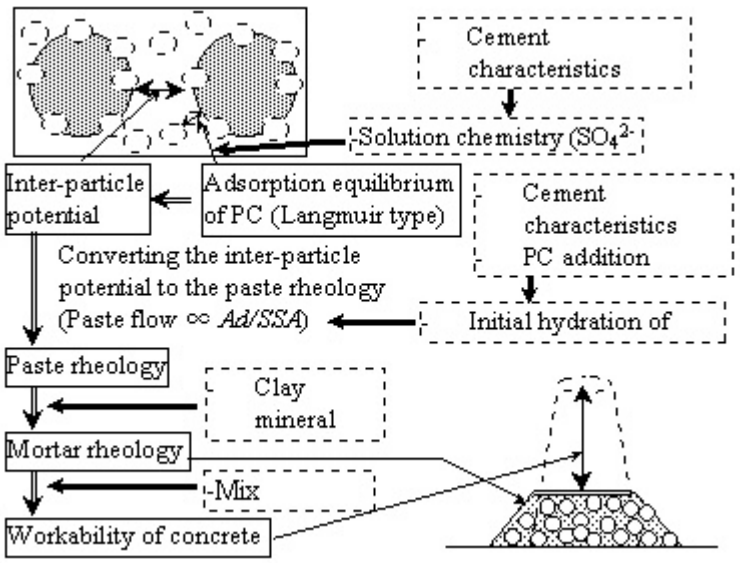

Figure 1. Conceptual diagram from the working mechanism of PC to the workability of concrete.

2.1 Inter-Particle Potential

2.1.1 Steric hindrance effect

It is assumed in general that the chemical structure of PC is a comb-type and the steric hindrance effect is attributed to the graft chains. However, it is quite difficult to analyze the actual structure of PC. As is the case for copolymers of maleic anhydrate and PEG-allylether, monomers are expected to be polymerized reciprocally to form a typical comb structure and show good performance even at very low W/C. As for copolymer of acrylic acid and acrylate-Mt-PEG ester, monomers are expected to be polymerized randomly and in some synthesizing conditions, the methoxy group is debonded at the end of the PEG chain, and from this portion another trunk chain can be grown to form an irregular shape [23]. Moreover, the conformation of the adsorption is also obscure. Although a computer simulation of the adsorption of PC shows the possibility of the adsorption may be initialized at the end of a trunk chain as shown in Figure 2 [24], the final conformation of the adsorption is not clear. This ambiguity may be important only at the very low W/C below 25% because superior dispersing effect is required in these conditions. A theoretical calculation indicates that the thickness of the adsorbed layer is required to be more than 10nm for particles of 1 μm radius. This thickness corresponds to the 20-30 repetitions of unit oxyethylene of PEG chain. The PEG concentration on the surface of solid phase is the critical point.

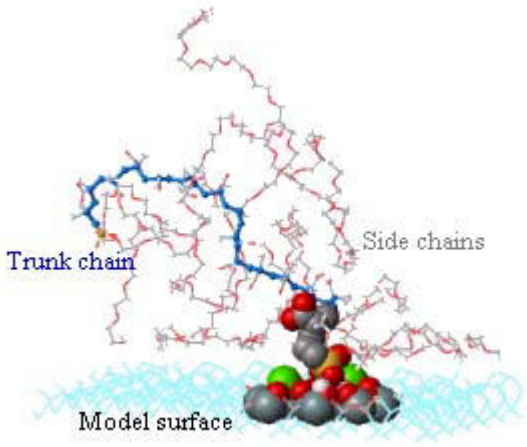

Figure 2. Simulation of the adsorption of PC

The first assumption is that the steric hindrance effect is proportional to the adsorption amount of PC in specific conditions. Required conditions of this assumption are the following: copolymers having carboxylic groups for the adsorption, W/C of paste higher than 30%, graft chain of PC longer than 20 repetitions of unit oxyethylene, and the adsorption amount is against the surface area of solid phase not against the mass of it.

2.1.2 Adsorption

There are two important factors that have not been recognized clearly for the adsorption of SP. One is the surface area of the solid phase and the other is the competitive adsorption equilibrium of SP with anions. The adsorption of PC on hydrated cement usually occurs in a Langmuir-type. However, hydrated cement is composed of multi phases. PC has been thought to be adsorbed on C_3A more than calcium silicates as well as BNS [3]. It is not the adsorption amount per mass of clinker minerals which is the important parameter but the adsorption amount per surface area of hydrates. C_3A cannot be an unhydrated phase in water but changes into some hydrates with larger surface area than originally. Besides, the adsorption of SP is not so strong. It was demonstrated the adsorption is reversible depending on the chemical composition of the aqueous phase [16]. Therefore, it is important to pay attention for the solution chemistry.

Considering these points, the adsorption isotherms of PC on typical hydrates were examined as shown in Figures 3 and 4 [25].

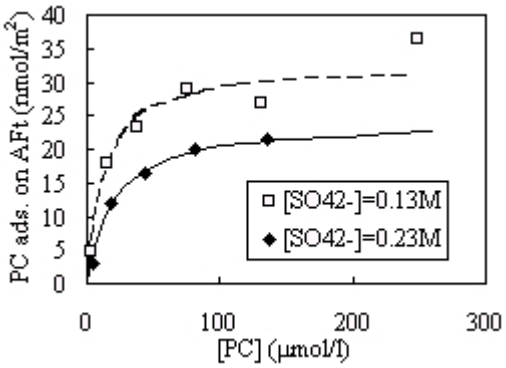

Figure 3. Adsorption isotherm of PC on AFt.

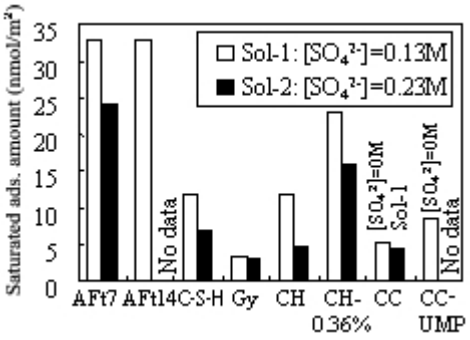

Figure 4. Saturated adsorption amount of PC [25].

As a result, the saturated adsorption amount per *SSA* of ettringite (AFt) is larger than those of other phases such as C-S-H, gypsum, portlandite, and calcite. This indicates that the initial hydrate of C_3A is important for the *Ad/SSA*. PC shows a Langmuir type adsorption isotherm for AFt, C-S-H, gypsum, and calcite. As for portlandite, PC shows a Freundrich type adsorption isotherm and when the dosage of PC is very high, *Ad/SSA* of portlandite will be close to that of AFt. It assumed the competitive adsorption between PC and SO_4^{2-}, *Ad/SSA* can be expressed by a function including parameters of PC concentration [*PC*] and SO_4^{2-} concentration [SO_4^{2-}] as shown in Equation (1).

$$N_{PC} = \frac{N_i \cdot K_{PC} \cdot [PC]}{1 + K_{PC} \cdot [PC] + K_{SO} \cdot [SO_4^{2-}]} \quad (1)$$

where N_{PC} is the number of adsorbed PC on the surface of solid *i*, N_i is the number of adsorption site on the surface of solid *i* corresponding to the saturated adsorption amount of PC, K_{PC} is the constant of adsorption equilibrium of PC, K_{SO} is the constant of adsorption equilibrium of sulfate ion.

In Equation (1), N_i is assumed as constant even when [SO_4^{2-}] is changed in this study. There is a possibility that N_i is dependant on [SO_4^{2-}]. The adsorption site of PC is Ca adsorbed on the hydrate and the Ca density is believed to be affected by [SO_4^{2-}] in a coexisting aqueous phase [26]. For the accurate discussion on this possibility, more data are needed. The second assumption is that *Ad/SSA* can be calculated by Equation (1).

2.1.3 Solution Chemistry

The steric hindrance effect by PEG is assumed not to be affected by ionic strength in aqueous phase and the electrostatic potential of BNS is assumed to be affected significantly in many cases. As for the later, besides the effect of ionic strength, the adsorption amount plays an important role. When NaCl is added to cement paste containing as much as 2M BNS, the adsorption amount is almost constant and the fluidity shows only a slight decrease. When Na_2SO_4 is added to cement paste with as much as 0.1M BNS, the adsorption amount and the fluidity decrease significantly [27].

In the case of PC, apart from the effect on the adsorption amount, there are two possibilities of the effect of solution chemistry; the shrinkage of PEG [28] and the shrinkage of trunk chain [12, 16]. A direct measurement of the steric size of PEG and PC in aqueous solutions by using a light scattering method shows that the size of PEG is independent of the ionic strength and that the size of trunk chain decreased in high ionic strength conditions [16]. The shrinkage of trunk chains may be caused by the reduction of electrostatic repulsive force among carboxylic groups in a trunk chain. This

result indicates that the dispersing performance of PC is almost constant as long as *Ad*/SSA is constant. However, a slight decrease of the performance of PC with the increase of ionic strength is observed experimentally even when the adsorption amount was constant [29]. This is thought to be the reduction of adsorbed area that one molecule of PC covers because the spread of trunk chain decreases.

The most important effect of solution chemistry is the behavior affecting the adsorption of PC. It has demonstrated that the adsorption of SP whether SP is PC or BNS, is in adsorption equilibrium. The adsorbing portion of PC is the carboxylic groups and they are adsorbed on calcium sites of cement hydrates competitively with anions showing affinity to calcium such as sulfate ion, carbonate ion, phosphate ion. The third assumption is the effect of solution chemistry only for the adsorption of PC.

2.2 Particle Dispersing Effect and Fluidity

2.2.1 Inter-Particle Potential and Paste Rheology

The main dispersing effects of particles by SP are electrostatic repulsive forces and steric hindrance effects. Presently, there is only one example that the inter-particle potential is converted to the paste rheology theoretically. That is HI theory estimating the plastic viscosity from the electrostatic potential [30]. In other cases, there is no theoretical method estimating the rheology of paste from the inter-particle potential. Therefore, in this study, the particle dispersing effect of SP is assumed to be proportional to *Ad/SSA* and *Ad/SSA* is proportional to the paste fluidity (the fourth assumption). Proportion constants are different for different kinds of SP or different mix proportions.

2.2.2 Specific Surface Area

Because cement shows hydration activity, *SSA* after the hydration and its time change should be considered. Moreover, SP affects the hydration of cement. Every SP shows affinity with Ca^{2+} and SP reduces Ca^{2+} concentration [Ca^{2+}]. The initial hydration of C_3A is restrained by the formation of Ca-S-Al-O-H hydrates. In this process, the supply of Ca^{2+} and SO_4^{2-} is very important. If the [Ca^{2+}] decreases, the hydration of C_3A is not restrained effectively and as a result more hydrates such as AFt will be formed and *SSA* increases. This effect is significant in the case of very low f-CaO in cement [31].

In the case of BNS, hydration processes of cement are completely different depending on the timing of addition [16]. By delayed addition, the increase of *SSA* is restricted and this seems to result in a good fluidity retention. In the case of PC, the number of carboxylic group per mass of PC is the critical point [23]. When a PC showing higher adsorbing ability that is not affected by SO_4^{2-} is used or the PC dosage is very high at very low W/C, more carboxylic groups reduce [Ca^{2+}] more and this results in the increase of *SSA*. From this evidence, the delayed addition of PC is very effective in the case of very low W/C conditions.

Moreover, aggregates affect the hydration of cement by the mixing effect [32]. The effect can be evaluated by the *SSA* of solid phase of the paste in mortar and concrete. Although clay minerals also affect the adsorption of PC [33], because the relationship between the PC adsorption by clay minerals and the fluidity is obscure, this effect is neglected in this study (the fifth assumption).

2.2.3 The mechanism of time change of paste flow

The time change of paste flow is assumed to be determined by the change of *Ad/SSA* (the sixth assumption). As shown in Figure 5, *Ad/SSA* can be changed by the change of *SSA* and [SO_4^{2-}]. *SSA* increases with the progress of cement hydration and reduces *Ad/SSA*. [SO_4^{2-}] decreases with the progress of cement hydration and raises *Ad/SSA*. By the balance of these two effects, the change of *Ad/SSA* with time is determined. *SSA* and [SO_4^{2-}] are regarded as given parameters for every experiment because the estimation of these parameters from basic characteristics of cement and mix

proportions are quite difficult (the seventh assumption).

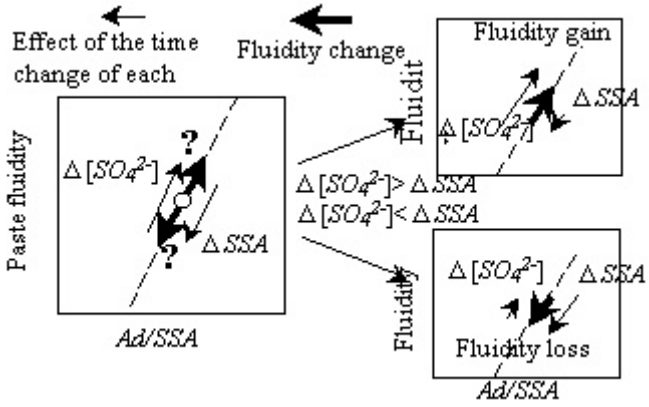

Figure 5. Fundamental concept of the working mechanism of the time change of paste fluidity containing PC.

2.3 The Workability of Concrete and the Fluidity of Paste

As an index of the workability of concrete, slump is considered in this study. By affecting the dispersion of cement particles, PC changes the paste flow. In order to explain the concrete slump by the working mechanism of PC, the required condition is that the concrete slump is governed by the paste flow (the eighth assumption). This condition is usually achieved in well-proportioned concrete. Of course, the characteristics of aggregate and mix proportion affect the relationship between the paste fluidity and the concrete slump. Proper proportioning of concrete is thought to be very important for the durability of concrete structures by eliminating by defects in the concrete placing process.

3. EXPLANATION OF CONCRETE SLUMP BY THE WORKING MECHANISM OF PC

Satisfying the eight assumptions mentioned above, concrete slump is determined by paste flow, paste flow is determined by *Ad/SSA*, *Ad/SSA* is determined by the adsorption isotherm of PC. In other words, by using several parameters describing the adsorption isotherm of PC, it is possible to estimate the concrete slump. Hereafter, a model estimating concrete slump is proposed. In this example, nine kinds of NPC from different plants satisfying the JIS standard were used. The difference of concrete slump by the difference of cement characteristics and the changes of slumps with time elapse are explained by the model. Finally, based on the model, the performances of several PC having different adsorbing abilities are estimated.

3.1 Experiments

In order to reproduce incompatibility phenomena, W/C was set as low as 37.5%. Maximum aggregate size was 20 mm, the unit cement content was 400kg/m^3, the air content was 4.5 1.0%, and the dosage of PC was 0.8 mass% of cement. PC used was commercial one and the solid concentration was 25.8%. The length of PEG was 23-repetition of oxyethylene.

Cement and aggregate for 30l of concrete were put in a pan-type mixer of 50l-capacity and mixed for 30s. Water containing PC was added and mixed for 90s. The mortar in the mixed concrete was extracted by wet screening with a sieve of 5mm opening. Cement paste was mixed for 3min with a Hobart mixer. The change of fluidity with time elapse was evaluated by the wet screened (WS) mortar.

Concrete slump was measured according to JIS A 1101. Mortar flow was measured according to JIS R 5201 without drops. The bottom radius of a cone was 10cm. Paste flow was measured according to JASS 15M103. A pipe of 50mm radius and 51mm height was used.

The analysis of paste was carried out as follows. Because *SSA* of concrete is mainly determined by the fine particles such as cement hydrate, the paste was separated by a sieve of 63 μm opening from the WS mortar from the concrete and the *SSA* was measured by one point BET method using N_2 gas adsorption. The aqueous phase was separated by a centrifugal separator from WS mortar. The adsorption amount of PC was estimated by comparing the PC concentration by a total carbon analyzer in the mixing water and in the extracted solution from paste of each age. The [SO_4^{2-}] was measured by an ion chromatograph.

3.2 Relationship between Concrete Slump - Mortar Flow - Paste Flow

The relationship between the concrete slump and the paste flow just after mixing is shown in Figure 6.

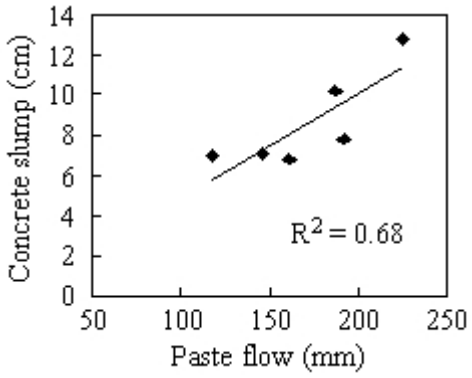

Figure 6. Concrete slump and paste flow.

The paste flow shows a good correlation with the concrete slump in this case and the concrete slump can be considered to be determined by the paste flow. The relationship between the concrete slump and wet screened (WS) mortar just after mixing and at one hour after mixing is shown in Figure 7. There is a good correlation between them. Hereafter, WS mortar flow is discussed. In Figure 8, the changes of WS mortar flow are shown. Initial flow is different from cement to cement. The flow decreases with time in all cement.

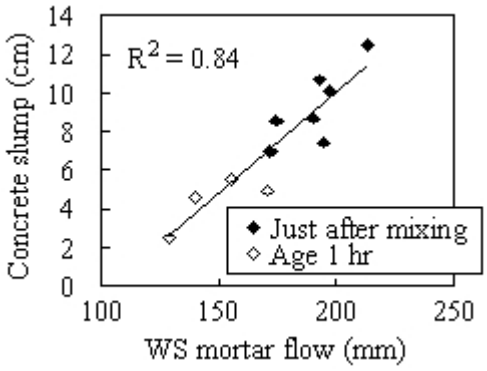

Figure 7. Concrete slump and WS mortar flow.

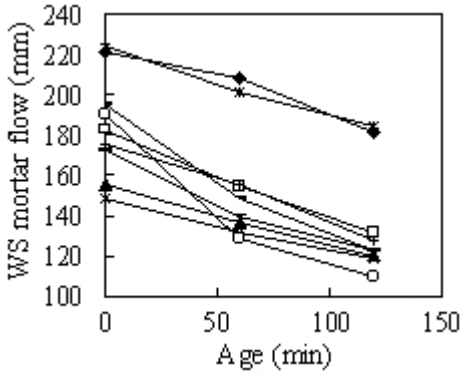

Figure 8. Change of WS mortar flow with time.

3.3 Analysis of WS Mortar Flow by the Working Mechanism of PC

Based on the working mechanism of PC, *Ad/SSA* is expected to show a correlation with WS mortar flow. The *SSA* just after mixing was in a range from 1.64 to 1.78m^2/g depending on the kinds of cement used. The SSA increased to a range from 1.81 to 2.01 m^2/g after 2 hours. PC adsorption ratio was in a range from 67 to 76% just after mixing and increased in a range from 74 to 83 %. [SO_4^{2-}] was in a range from 60 to 95 mM and decreased to a range from 44 to 76 mM. Based on these data, *Ad/SSA* was calculated and the relationship with the WS mortar flow is shown in

Figure 9. *Ad/SSA* is almost independent of time elapse and no clear relationship with MS mortar flow is obtained.

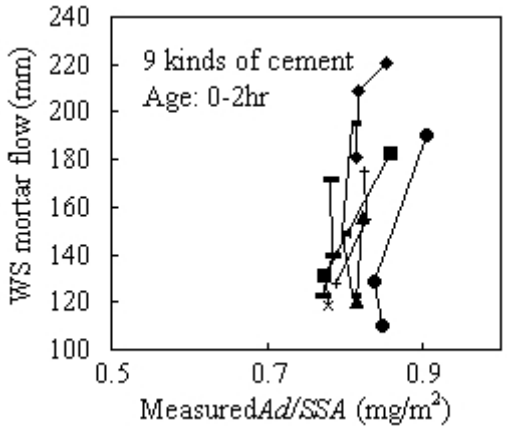

Figure 9. *Ad/SSA* and WS mortar flow.

Sugamata *et al*. [34] suggested a good relationship between the PC remained in the aqueous phase and the fluidity for a specific combination of PC and cement. The relationships in this study were examined and the result is shown in Figure 10. Although there are positive relationships for all kinds of cement, the relationships are different significantly from cement to cement.

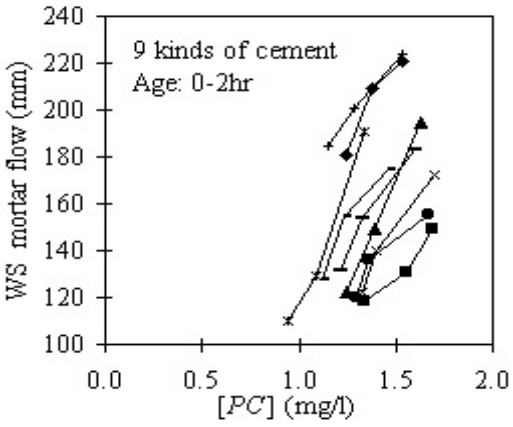

Figure 10. [*PC*] and WS mortar flow.

Why was no clear relationship observed between *Ad/SSA* and the WS mortar flow? One possible explanation is a wrong assumption. For the calculation of *Ad/SSA*, the values used of *SSA* were from the N_2 gas adsorption test. In this method, it is presumed that the PC adsorption is similar to the adsorption of N_2 gas. As described in the section 2.1.2, the adsorption amount of PC is different for each solid phase. AFt adsorbs PC three times more than C-S-H. This means that the *SSA* of each phase is important for the calculation of *Ad/SSA*. However, it is difficult to estimate the *SSA* of each phase in cement paste.

This problem can be avoided by using Equation (1) and the mass reservation equation for added PC, Equation (2).

$$Dos = [PC] \times W + N_{PC} \times N_i \tag{2}$$

where *Dos* is the added amount of PC and *W* is the water amount. N_{PC} and N_i correspond to *Ad/SSA* and *SSA* respectively. *Dos* can be separated to the amount of PC remaining in the aqueous phase: $[PC] \times W$ and the amount of PC adsorbed on the solid phase: $N_{PC} \times N_i$. By using Equation (2), an

unknown parameter N_i in Equation (1) can be eliminated. Finally, *Ad/SSA* can be calculated from only two parameters, [*PC*] and [SO_4^{2-}].

As for the K_{PC} and K_{SO}, both constants were calculated by a minimum least square method for the isotherm of AFt. In this calculation, because the significant hydrate phase for the PC adsorption is thought to be AFt, it is assumed that AFt is the only solid phase adsorbing PC. By using these constants and the experimental data of [*PC*] and [SO_4^{2-}], *Ad/SSA* was calculated from Eqs. (1) and (2). The relationship between the estimated *Ad/SSA* and the WS mortar flow is shown in Figure 11. Compared with Figure 9, each line becomes closer. Although there is some room to improve, the whole trend of MS mortar flow can be explained by this method.

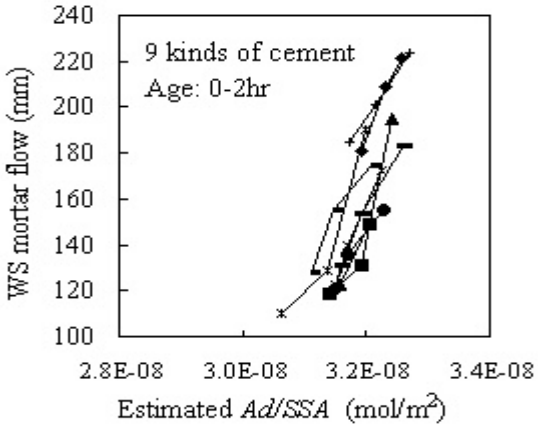

Figure 11. Estimated *Ad/SSA* and WS mortar flow.

4. AN APPLICATION OF THE MODEL FOR VARIOUS TYPES OF PC

By using the proposed model, the performances of various types of PC can be simulated. In this simulation, several types of PC with higher adsorbing ability and lower adsorbing ability are examined because one of the important characteristics of PC is the adsorbing ability [23]. As a standard PC, the PC used in the section 3.3 is used (PC1). PC with the higher adsorbing ability is relatively free from the effect of SO_4^{2-} and *vice versa*. On the other hand, PC with the higher adsorbing ability has poorer fluidity retaining ability and *vice versa*. PC with the higher adsorbing ability (PC2) and lower adsorbing ability (PC3) are simulated by changing K_{PC} five times higher and one-fifth lower, respectively, based on the experimental data [24]. Cements used are selected to have different content of alkaline sulfate. PC shows better initial fluidity but larger fluidity loss for cement with higher alkaline sulfate and *vice versa*.

From the results mentioned in 3.0, there are correlations between *Ad/SSA* and the WS mortar flow, and between the WS mortar flow and the slump of original concrete. Therefore, the concrete slump is expected to be estimated by *Ad/SSA*. In this estimation, three parameters, N_i, [*PC*], and [SO_4^{2-}] are used. In this case, by using Equation (2), [*PC*] is eliminated. From several kinds cement in the section 3, three kinds of cement showing different behaviors are selected. The dosage of each PC is adjusted to show the slump of 20cm for NPC3.

The slump retention of each combination of PC and cement is shown in Figure 12. The expected behaviors of PC are successfully demonstrated by this model. PC2 shows less variation of initial slumps and larger slump losses and PC3 shows larger variation of initial slumps and good slump retention behaviors.

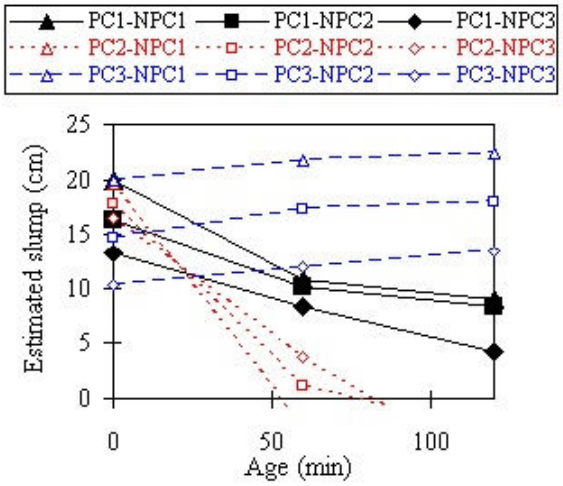

Figure 12. Estimated dispersing behaviors of various types of PC for different kinds of cement based on the working mechanism of PC.

5. SUBJECTS FOR THE FUTURE STUDY

In this study, the simulation of the performance of PC in concrete has been demonstrated by using several experimental data. It is ideal to estimate the workability of concrete or the slump from the characteristics of materials and mixing conditions. For this goal, the estimation of the time changes of *SSA* and $[SO_4^{2-}]$ of cement paste is inevitable. The contribution ratio of each of the mineral and gel phases to *SSA* and the PC adsorption is also important. These parameters are affected by many factors such as cement characteristics, mix proportion, types of SP, dosage of SP, adding method, mixing procedure and mixing temperature. Therefore, every effect of all factors is required for perfect estimation of the performance of PC. Although some of them have been clarified to some degree, much research is still necessary. As for BNS, a similar approach for the estimation of the performance of BNS is possible and it will be published in another report [34].

6. CONCLUSIONS

Based on the working mechanisms of PC clarified presently, a model using limited factors of cement paste have been proposed to explain the concrete slump with several assumptions. The model was also applied to estimate the behaviors of several kinds of PC with different adsorbing abilities.

- In order to link the most fundamental working mechanism of PC to the concrete slumps, several assumptions are necessary: 1) Proportional relationship between the steric hindrance effect and the adsorption amount of PC per surface area, *Ad/SSA*, 2) Expression of *Ad/SSA* by the Langmuir type equation including two parameters $[PC]$ and $[SO_4^{2-}]$, 3) Limited effect of solution chemistry on the adsorption equilibrium of PC, 4) Proportional relationship between *Ad/SSA* and paste flow, 5) No effect of clay minerals, 6) Obedience of the change of paste flow with time on the change of *Ad/SSA*, 7) Give data of $[PC]$ and $[SO_4^{2-}]$, and 8) Governance of concrete slump by the paste flow.
- On these assumptions, *Ad/SSA* is estimated from the measured $[PC]$ and $[SO_4^{2-}]$ in the aqueous phase of concrete with nine kinds of cement from different plants and a model using these parameters is poposed. The model successfully explains the WS mortar flows from concrete.
- The proposed model is applied to simulate the behaviors of various kinds of PC with different absorbing abilities by changing adsorption coefficients of PC five times higher or one-fifth lower than a commercial PC. The simulation estimates the typical behaviors of PC that the PC with higher adsorbing ability shows less fluctuation of slumps by the difference of cement characteristics just after mixing although it shows larger slump losses. Conversely, although the

PC with lower adsorbing ability shows more fluctuation of slumps just after mixing, it shows excellent slump retentions.

ACKNOWLEDGEMENTS

Concrete experiments were carried out by Mr. S. Shirokuni, Mr. K. Toriiminami and other members of the Concrete Laboratory of Kawara Taiheiyo Cement Corp. The chemical analyses were carried out by Mr. H. Ozu and Ms. M. Yano of Research & Development Center, Taiheiyo Cement Corp. The authors wish to express our gratitude for their cooperation.

REFERENCES

[1] Hattori, K., Okada., E. and Mizunuma, T., Characteristics of normal Portland cement and the dispersion by superplasticizer, JCA Proceedings of Cement & Concrete, vol. 38, 1984, pp. 122-125 (in Japanese).

[2] Nawa, T., Eguchi, H. and Hukaya, Y., Effect of alkali sulfate on the rheological behavior of cement paste containing a superplasticizer, Proceedings of the 3rd CANMET/ACI International Conference on Superplasticizers and Other Chemical Admixtures in Concrete, ACI, SP-119, 1989, pp. 405-424.

[3] Uchikawa, H., Hanehara, S., Shirasaka, T. and Sawaki, D., Effect of admixture on hydration of cement, adsorptive behavior of admixture and fluidity and setting of fresh cement paste, Cement and Concrete Research, vol. 22, 1992, pp. 1115-1129.

[4] Collepardi, M., Influence of polymerization of sulfonated naphthalene condensate and its interation with cement, Developments in the use of superplasticizers, SP68, ACI, 1981, pp. 485-498.

[5] Massazza, F. and Costa, U., Effect of superplasticizer on the C_3A hydration, Proceedings of 7th International Congress on the Chemistry of Cement, Paris, vol. IV, 1980, pp. 529-534.

[6] Anderson, P. J. and Roy, D. M., The effects of adsorption of superplasticizers on the surface on cement, Cement and Concrete Research, vol. 17, 1987, pp. 805-813.

[7] Bonen, D. and Sarkar, S. L., The superplasticizer adsorption capacity of cement pastes, pore solution composition, and parameters affecting flow loss, Cement and Concrete Research, vol. 25, 1995, pp. 1423-1434.

[8] Jolicoeur, C. and Simard, M. A., Chemical admixture-cement interactions: Phenomenology and physico-chemical concepts, Cement and Concrete Composites, vol. 20, 1998, pp. 87-101.

[9] Costa, U., Corazza, F., Colombet, P., Fernon, V. and Vichot, A., Mechanisms of cement-admixture interaction, 10th International Congress of the Chemistry of Cement, Gothenburg, vol. 3, 1997, p. 3 iii 003.

[10] Jiang, S., *et al*., Importance of adequate soluble alkali content to ensure cement/superplasticizer compatibility, Cement and Concrete Research, vol. 29, 1999, pp. 71-78.

[11] Kinoshita, M., Yamaguchi, S., Yamamoto ,T. and Tomosawa, F., Chemical structure and performance of new type high range water reducing AE agent. JCA Proceedings of Cement & Concrete, no. 44, 1990, pp. 222-227 (in Japansese).

[12] Ota, A., Sugiyama, T. and Tanaka, Y., Fluidizing mechanism and application of polycarboxylated-based superplasticizers, 5th CANMET/ACI International Conference on Superplasticizers and Other Chemical Admixture in Concrete, Rome, SP173, ACI, 1997, pp. 359-378.

[13] Hamada, D., Sato, T. Yamato, F. and Mizunuma, T., Development of new superplasticizer and its application to self-compacting concrete, 6th CANMET/ACI International Conference on Superplasticizers and Other Chemical Admixture in Concrete, Nice, SP, ACI, 2000, pp. 269-290.

[14] Popova, A., Geoffroy, G., Renou-Gonnord, M.F., Faucon, P. and Gartner, E., Interactions between Polymeric Dispersants and Calcium Silicate Hydrates, J. Am. Ceram. Soc., vol. 83, 2000, pp. 2556-2660.

[15] Jacknavorian, A.A., Roberts, L.R., Jardine, L., Koyata, H. and Darwin, D.C., Condensed polyacrylic acid-aminated polyether polymers as superplasticizers for concrete, 5th CANMET/ACI International Conference on Superplasticizers and Other Chemical Admixture in Concrete, Rome, SP173, ACI, 1997, pp. 55-81.

[16] Yamada, K. and Hanehara, S., Interaction mechanism of cement and superplasticizers – The roles of polymer adsorption and ionic conditions of aqueous phase, Concrete Science and Engineering, vol. 3, 2001, pp. 135-145.

[17] JCI, Special issue: Air entraining high-range water reducing agents, vo. 37, no. 6, 1999, Concrete Journal (in Japanese).

[18] Aictin, P.C., Jolicoeur, C. and MacGregor, J.G., Superplasticizers: How they work and why they occasionally don't, Concrete International, vol. 5, 1994, pp. 45-52.

[19] Hanehara, S. and Yamada, K., Interaction between cement and chemical admixture from the point of cement hydration, admixture adsorption and paste rheology, Cement and Concrete Research, vol. 29, 1999, pp.1159-1165.

[20] Uchikawa, H., Hanehara, S. and Sawaki, D., Effect of electrostatic and steric repulsive force of organic admixture on the dispersion of cement particles in fresh cement paste, 10th International Congress on the Chemistry of Cement, Gothenburg, vol. 3, 1997, p. 3 iii 001.

[21] Yoshioka, Y, Sakai, E., Daimon, M. and Kitahara, A., Role of steric hindrance in the performance of superplasticizers for concrete, J. Am. Ceram. Soc., vol. 80, 1997, pp. 2667-2671.
[22] Flatt, R.J., Houst, Y.F., Bowen, P. and Hofman, H., Electrosteric repulsive induced by superplasticizer between cement particles –An overlooked mechnism?, 6th CANMET/ACI International Conference on Superplasticizers and Other Chemical Admixture in Concrete, Nice, SP, ACI, 2000, pp. 29-42.
[23] Yamada, K, Okada, K. Ozu, H. and Yano, M., Polycarboxylate-type superplasticizer whose performance can be enhance by sulfate ion, Proceedings of JCI, vol. 23, 2001, pp. 27-34 (in Japanese).
[24] Yamada, K., Takahashi, T. Ogawa, S. and Hanehara, S., Molecular structure of the polycarboxylate-type superplasticizer having tolerance to the effect of sulfate ion, Cement Science and Concrete Technology, no. 54, 2000, pp. 76-83 (in Japanese).
[25] Yamada, K., Ozu, H. and Yano, M., The adsorbing behavior of polycarboxylate-type superplasticizer on cement hydrates and the effects of sulfate, Cement Science and Concrete Technology, no. 55, 2001, pp. 27-34 (in Japanese).
[26] Sakai, E., Akira Kawakami, Hiroaki Hamamoto, Susumu Honda, Akinori Itoh and Masaki Daimon., Effect of various types of inorganic salts on dispersion mechanisms of comb-type polymer containing grafted polyethylene oxides chains, J. Ceram. Soc. Japan, vol. 108, 2000, pp. 904-908 (in Japanese).
[27] Yamada, K., Study on working mechanism of polyether-type cement dispersant based on early cement hydration and composition variation of solution phase, Dissertation, Tokyo Institute of Technology, 2000, pp. 50-57.
[28] Kato, H. and Yoshioka, K., Effect of sulfate ion on the fluidity of cement paste with a superplasticizer, Cement Science and Concrete Technology, no. 52, 1998, pp. 144-151.
[29] Yamada, K., Hanehara, S. and Matsuhisa, M., Fluidizing mechanism of cement paste including polycarboxylate-type superplasticizer analyzed from the view point of adsorption behavior of superplasticizer, Proceedings of JCI, vol. 20, 1998, pp. 63-78 (in Japanese).
[30] Hattori, K. and Izumi, K., A rheological expression of coagulation rate theory, J. Dispersion Science and Technology, vol. 3, 1982, pp.129-145.
[31] Kang, J., Ohba, Y., Sakai, E. and Daimon, M., Influence of superplasticizers on the hydration in $Ca_3Al_2O_6$-$CaSO_4 \cdot 2H_2O$-CaO system, Cement Science and Concrete Technology, no. 54, 2000, pp. 22-27 (in Japanese).
[32] Ozu, H., Yamada, K. and Yano, M., Relationships of fluidities among paste, mortar and concrete with a polycarboxylate superplasticizer, Proceedings of JCI, vol. 24, 2002 (in print, in Japanese).
[33] Nakamura, H., Ogawa, S. and Asumi, K., Experimental study on disperse system, Cement Science and Concrete Technology, no. 53, 1999, pp. 455-461 (in Japanese).
[34] Sugamata, T., Hibino, M. Ouchi, M. and Okamura, H., Effects of the molecular structure of polycarboxylate polymers on the cement particle dispersibility, J. JSEC, no. 662/V-49, 2000, pp17-27 (in Japanese).
[35] Nakajima, Y., Goto, T. and K. Yamada, A fluidity model of BNS (in submission).

EQUILIBRIA IN THE SYSTEM CALCIUM HYDROXIDE-CALCIUM SULPHATE-ALKALI SULPHATE-WATER AT 5-30°C, AND THEIR RELEVANCE TO PORTLAND CEMENT HYDRATION IN THE PRESENCE OF SUPERPLASTICIZERS

Ellis M. Gartner[1], Serge Sabio[1] and Jean-Philippe Perez[2]

[1] Lafarge Laboratoire Central de Recherche, 38291 France; E-mail: ellis.gartner@lafarge.com
[2] LRSS, University de Bourgogne, Dijon, France; E-mail: jpperez@u-bourgogne.fr

ABSTRACT

We report new experimental data on the system calcium hydroxide-calcium sulphate-alkali sulphate–water over the temperature range 5° – 30°C. Experiments have been performed using either potassium or sodium as the alkali metal, and results for the pure system at 30°C are in very good accord with those of Hansen and Pressler (1947). The principal solid phases present are portlandite, gypsum and syngenite. Conductimetric measurements show that, in the "admixture-free" system, equilibrium is usually obtained within only a few tens of minutes. The solubility product of syngenite decreases with decreasing temperature, while those of portlandite and of gypsum increase, displacing the intersections between the solubility isotherms. In the presence of organic admixtures of the type generally used as "superplasticizers" (SP) in Portland cement concretes, some minor changes in apparent solubility products are observed that can be attributed to weak complexation of calcium ions and/or the neutralisation of hydroxide ions by the SP molecules.

1. INTRODUCTION

There is great interest in understanding the mechanisms by which high-range water-reducing admixtures, commonly known as superplasticizers (SP), are able to "improve concrete rheology" (i.e., to reduce the effective viscosity of fresh concrete at constant mix composition.) It is now well-established that SPs function by adsorption onto the surfaces of the particles in concrete, producing repulsive forces, which can be either electrostatic or steric in nature [1]. These repulsive forces can greatly reduce the tendency of cement grains and other fine particles in the concrete to flocculate, giving a suspension which is much better dispersed than the SP-free system. However, we still do not know exactly how typical SPs are adsorbed on the surfaces of cement grains, and how the performance of a given SP is related to its chemical composition. There are also important unanswered questions regarding the effectiveness of specific cement-SP combinations, since no two cements or SPs are identical: some couples work better than others for certain types of concrete.

In order to better understand cement-SP interactions, we must be able to model the chemistry of the aqueous phase in fresh concrete, or at least the equivalent liquid extracted from cement pastes or mortars which are believed to simulate the chemistry of fresh concrete. It has been known for many years that, in the admixture-free cement-water system, the aqueous phase contains principally alkali metal (potassium and sodium) ions, calcium ions, sulphate ions and hydroxide ions [2]. Other species, such as silicate, aluminate, iron compounds, etc., are present at much lower concentrations, except in very unusual circumstances. In many respects, the system can be regarded as a perturbed lime-gypsum solution, that is, it is close to equilibrium with crystalline portlandite and gypsum.

Proceedings of the 11th International Congress on the Chemistry of Cement (ICCC)
'Cement's Contribution to the Development in the 21st Century'
Hosted by: The Cement and Concrete Institute of South Africa
CD-ROM produced by: Document Transformation Technologies
11 - 16 May 2003, Durban, South Africa
ISBN Number: 0-9584085-8-0
Editors: Dr G. Grieve and G. Owens
Congress Organised by: Event Dynamics

In practice, it is usually slightly supersaturated relative to one or both of these phases [3]. The main independent variable is thus the amount of soluble alkali in the cement. Portland cement clinkers can contain alkali sulphates at levels of up to about 2% by mass, and these highly soluble salts dissolve very rapidly when the cement is mixed with water. Some additional alkali may also be released into solution at early ages (as hydroxide) by the hydration of the aluminate phases. The amount of soluble alkali, and its potassium/sodium ratio, is a characteristic of a particular cement.

In order to determine exactly how an organic additive, such as a SP, perturbs the composition of the aqueous phase in cement systems, it is not sufficient simply to run a control mix with no admixture. This is because such admixtures can influence both the equilibrium parameters and the kinetics of cement hydration; and, in studying fresh concrete, we are dealing with a reacting system far from equilibrium, in which many reactions occur simultaneously, several of which may be perturbed by the presence of the additive. Ideally, we should first study reference systems in which a true chemical equilibrium can be obtained, in order to obtain the influence of the additive on the equilibrium system, before studying the reacting system. We have chosen to do this by starting with the simple portlandite-gypsum system. The compositions of alkali solutions in equilibrium with portlandite and gypsum at 25°C and 30°C were established by Hansen and Pressler (H&P) over 55 years ago [4], but, as far as we are aware, no study has yet been made on how this system responds to perturbation by water-soluble organic polymers.

2. EXPERIMENTAL

In the present study, we chose to work at 30°C, 20°C and 5°C. 30°C was chosen so as to have data in common with those of H&P, 20°C was chosen because it is commonly used as a standard in lab experiments on cement and concrete, and 5°C was chosen a “practical” lower limit. We chose to use solid alkali sulphates as the source of alkalis, since they are easier to weigh in air than the hydroxides used by H&P; thus, we approached equilibrium from a different direction. We also chose a set of commercial superplasticizers that span the range of types commonly used in concrete.

For each equilibrium assemblage, we generally began by adding 6.75g of reagent-grade calcium hydroxide (portlandite) and 0.75g of reagent grade calcium sulphate dihydrate (gypsum) to 75ml of either de-ionised water or prepared solution in a 100ml Pyrex flask (which minimised the dead volume once the flask was sealed with a glass stopper). The prepared solutions contained dissolved superplasticizers, or alkali sulphates, or both, in order to give the desired initial concentrations of alkali metal ions and superplasticizers in the liquid phase. In no case did the amount of alkali sulphate or SP added approach the titration capacity of the 6.75 g of portlandite, thus ensuring that there was always some solid portlandite and gypsum present. [Note: since the alkali was provided as a sulphate, the ratio of solid portlandite/gypsum in the equilibrium mixtures decreased with increasing alkali concentration, but in cases where significant amounts of syngenite formed gypsum too was consumed, and in these cases more than 0.75g was used.] The sealed flasks were immersed in water baths controlled to within ± 0.1°C and agitated gently for at least 48 hours. In order to be able to follow the approach to equilibrium, the conductivities of the solutions were measured frequently, and were observed to approach steady-state values very rapidly (within a few minutes) in most cases, although some SPs appeared to retard this process slightly. Nevertheless, in order to be absolutely sure of equilibrium, we held all of the suspensions at the desired temperature for at least 48 hours before filtering and analysing any of the mixtures.

The suspensions were allowed to settle for a short period before samples of the supernatant were taken and filtered rapidly under an elevated pressure of nitrogen (to avoid carbonation). The resulting filtrate samples were weighed and immediately titrated with 0.1N HCl to pH 7.0, to stabilise them against carbonation and to obtain an estimate of the hydroxide concentration. The stabilised solutions were analysed for sodium and potassium by flame photometry, for calcium by

complexometry, and for sulphate by turbidimetric titration against a solution of $BaCl_2$. All three techniques were conducted following the procedures of EN 196, and the typical coefficients of variation (in-lab repeatability) were conservatively assumed to be 1.3% for the alkali metals, 1.2% for calcium and 2% for sulphate (by taking the higher of either the typical values quoted in the European norm or those obtained in our own calibrations). We also conservatively assumed a coefficient of variation of 5% for hydroxide. (Note: A second series of solutions, including those prepared at 5°C, was analysed slightly differently, and no hydroxide titrations were done on them.)

Four different commercial SPs were chosen for this study; one was of the MSFC class, (a modified melamine sulfonate formaldehyde condensate containing sulphanilic groups,) and the other three were members of the "PCP" class (comb polymers based on polycarboxylic acid polyoxyethylene esters.) The dosages used were based on the concentrations that were found to be necessary to give about the same initial slump in typical superplasticised concretes. In a few cases, the liquid phase was analysed for total SP by the total organic carbon method (TOC), conducted by an outside laboratory following the EN 1484 procedure, with a typical coefficient of variation of 2%.

3. RESULTS

3.1 Equilibrium in the absence of superplasticizers

All of the results obtained at 20°C are shown in Figure 1, and the results obtained at 5°C and 30°C are shown in Figure 2. The '2nd series' results in these figures were obtained by a different operator than the first series, but there is reasonably good agreement, as can be seen in the graphs. (Note that the results shown in figure 2 are all 2nd series except for those with Na at 30°C.)

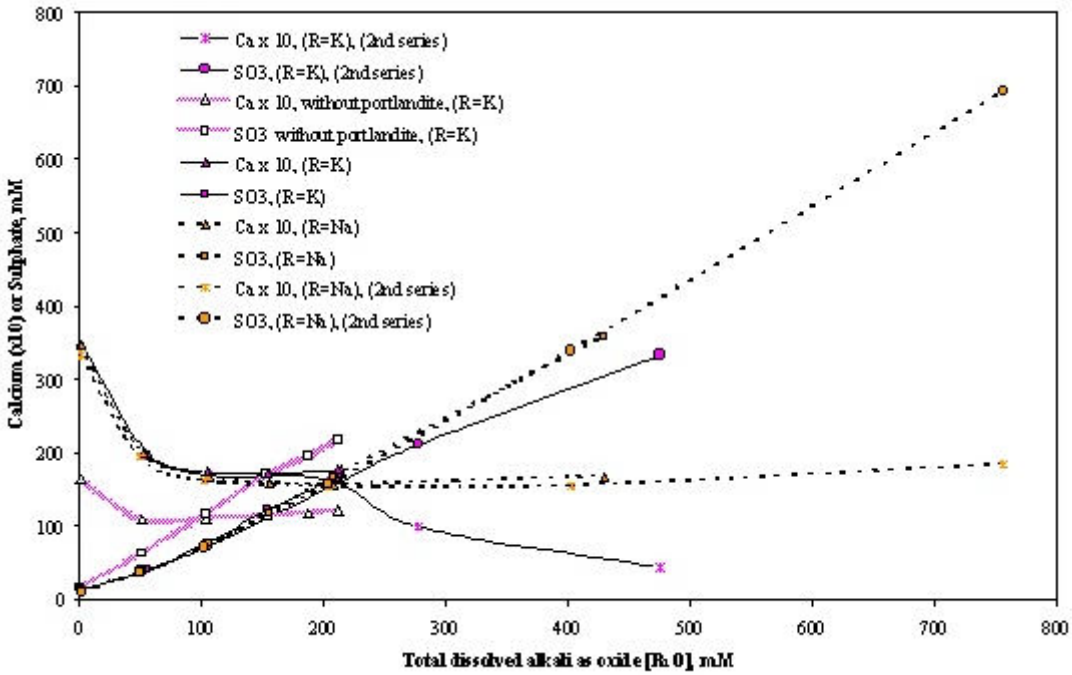

Figure 1. Results at 20°C

Also included in Figure 1 are a set of data obtained in the absence of portlandite, i.e. for the simple equilibrium between gypsum and potassium sulphate at 20°C. As expected, they show lower calcium concentrations and higher sulphate concentrations than the solutions in simultaneous equilibrium with portlandite at equivalent alkali concentrations.

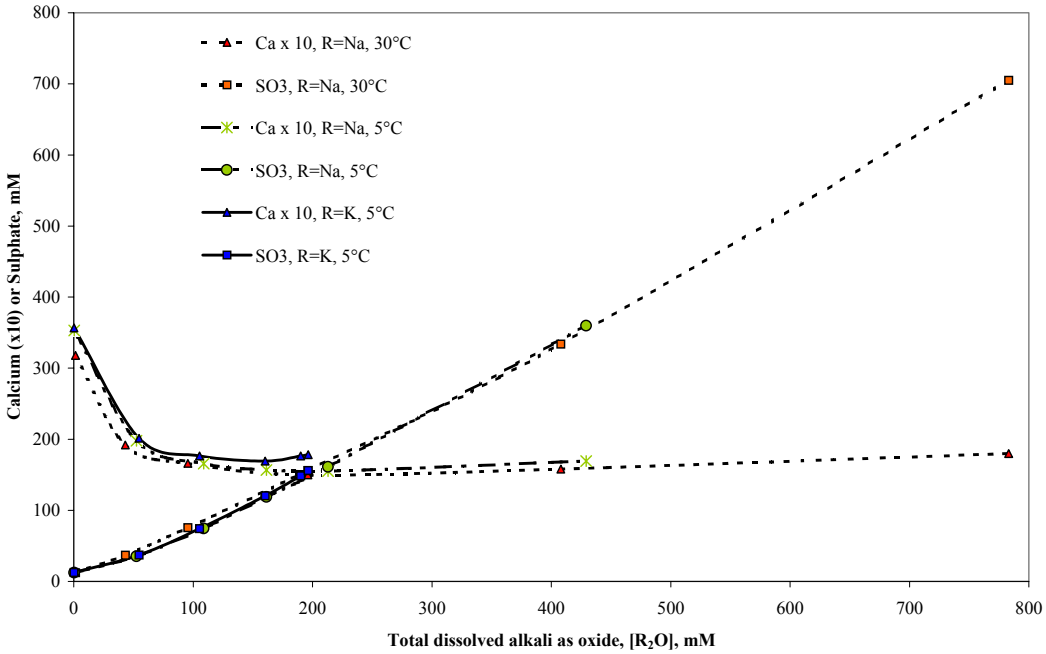

Figure 2. Results at 5° and 30° C

Table 1 gives the concentrations measured in the first series of experiments, without organic admixtures. (Note: In this case, Na^+ concentrations were not measured but rather assumed constant in the runs with added K_2SO_4, and vice-versa for K^+ in the runs with added Na_2SO_4.) The data at the highest sodium concentrations show a rather poor anion/cation balance, but are still within the probable range of error quoted for our analytical methods. Below $[R_2O]$ = 200mM, they generally show good agreement (at 30°C) with the data obtained by H&P [4], and there is also relatively little difference between our data obtained at 20°C and their data obtained at 25°C. However, at higher alkali concentrations there are some differences, which can be ascribed to two different effects:

(1) The formation of syngenite, (K_2SO_4-$CaSO_4$-H_2O), in the system with R=K. This was also observed in H&P's work. The onset of syngenite formation leads to decreases in potassium, calcium and sulphate concentrations below the portlandite-gypsum equilibrium curves, and this onset occurs at lower K_2O concentrations at 20°C than at 30°C. The effect of syngenite formation at 20°C can clearly be seen in Figure 1 for the second series of data with potassium. Similar results were obtained in the first series but we found that the amount of gypsum used in the initial mixtures had been set too low to compensate for syngenite formation, and it was increased in the 2nd series to ensure that there was always some residual gypsum at equilibrium. (Note: We also observed that the onset of syngenite formation occurred at lower alkali concentrations as the temperature decreased, but did not attempt to locate the invariant point precisely in the experiments reported here.)

(2) Anhydrite formation. There is also a divergence in the results at the highest sodium concentrations; H&P's final data point at 30°C and $[Na_2O]$ = 375 mM gives much lower concentrations of both calcium and sulphate ions than our data, and there is little reason to believe that any double salt (sodium-calcium-sulphate) forms at this sodium concentration.

This result supports the hypothesis of Gartner *et al* [6], who suggested that anhydrite may have formed in H&P's experiments at high sodium concentrations, because the alkali would decrease the activity of water in the system relative to the alkali-free system, and thus should lower the temperature of the gypsum-anhydrite equilibrium point, which is close to 40°C in the absence of other salts. There was no evidence for anhydrite formation (checked by IR analysis of the solid residue) in any of our experiments; however, the rates of nucleation, growth and dissolution of

anhydrite are known to be very slow relative to other calcium sulphates, and they may thus, under these conditions, be sensitive to the presence of anhydrite nuclei in some sources of gypsum [7].

Table 1. 'First Series' of results obtained at 20° and 30°C in the absence of admixtures

Initial concentration of Alkali sulfate used, mM	Analyses of equilibrated solutions (meq/L) Ca^{++}	Na^{+}	K^{+}	$SO_4^{=}$	OH^{-}	Sum
None added						
20°C	66.5	2.9	0	20.2	49.0	0
30°C	63.5	2.9	0	24.5	39.5	2
Na_2SO_4 @ 20°C						
49.4	39.0	98.2	0*	72.2	70.6	-6
98.4	32.4	204	0*	141	104	-9
203.9	30.7	409	0*	314	136	-10
404.7	31.0	804	0*	677	144	13
798.2	36.7	1512	0*	1385	160	4
K_2SO_4 @ 20°C						
49.6	39.2	2.9*	98.2	75.6	65.6	-1
100.0	33.8	2.9*	208	146	100	-1
202.1	32.5	2.9*	407	308	126	8
401.0	19.7	2.9*	552	421	157	-3
595.4	8.8	2.9*	948	666	283	11
Na_2SO_4 @ 30°C						
49.4	38.4	86.4	0*	73.6	61.8	-11
98.4	33.1	191	0*	151	81.6	-8
203.9	30.0	391	0*	311	109	2
404.7	31.6	816	0*	667	134	47
798.2	35.9	1566	0*	1410	147	45

The data for the SP-free solutions at 20°C were used to calculate simple ionic solubility products for the compositions $Ca(OH)_2$, $CaSO_4$ and $K_2Ca(SO_4)_2$, based on the simplifying assumption that the solutions contained only the simple ions K^{+}, Na^{+}, Ca^{++}, OH^{-} and $SO_4^{=}$. Results are shown in Figure 3. The first two of these three simple ionic solubility products represent the saturation values for portlandite and for gypsum, respectively, given that we had deliberately made sure that excess of these two solids was always present. The third solubility product represents the saturation values for syngenite, which is known to form at potassium sulphate concentrations of above about 165 mM at 20°C in the simple K_2SO_4-$CaSO_4$ system [5]. This product is only shown for the three solutions with values of [K_2O] well above 200mM, and formation of syngenite in these three mixes was confirmed by IR and DTA analyses of the filtered solids. Simple ionic products are, of course, not expected to be constant with varying ionic strength. All of the observed simple ionic solubility products increased with increasing alkali concentration, as would be expected, since the activity coefficients of all of the ions decreased with increasing ionic strength over the range of interest.

At first sight it seems surprising that the portlandite ionic product shows a smaller dependence than that of gypsum on alkali concentration. However, this is probably due to the two moles of water included in each mole of gypsum, because the activity of water decreases as alkali concentration increases, (which should then require an increase in the simple ionic solubility product to compensate). The syngenite solubility product shows by far the greatest alkali concentration dependence, which is not surprising since it is a quintuple ionic product, and the simple molecular formula of the solid phase also contains one molecule of water.

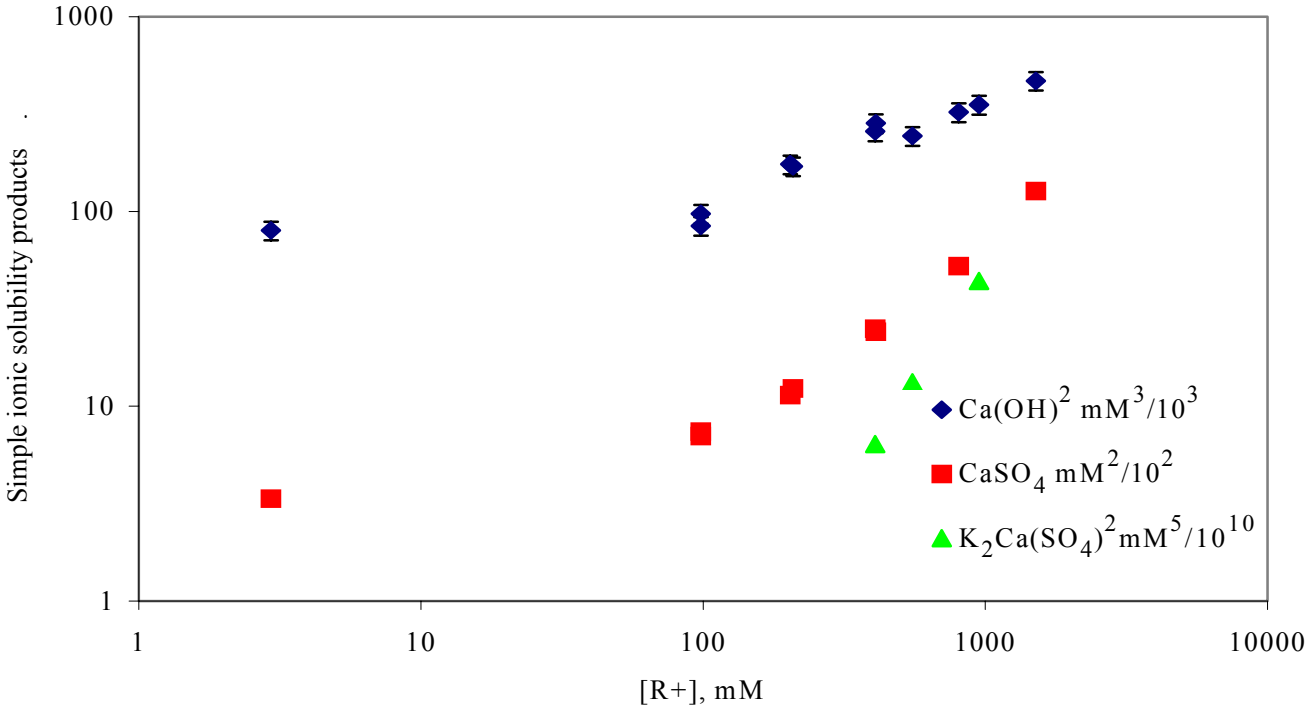

Figure 3. Simple ionic solubility products at 20°C as a function of alkali metal concentration.

3.2 Equilibrium in the presence of superplasticizers

The compositions of Na_2SO_4 solutions equilibrated with portlandite and gypsum in the presence of the four SPs are summarised in Table 2. Apart from the small increases in $[Na^+]$ observed with added SPs, due to the presence of sodium as the principal cation in all of the SPs, there is clearly relatively little change in the overall solution compositions due to the presence of SPs at the dosages used here. This result can be seen more clearly in the effects of SP addition on the simple ionic solubility products for portlandite and gypsum, shown in Figures 4 and 5, respectively. [Note: In the presence of SPs, hydroxide ion concentrations were estimated based on a calculation for electrical neutrality, deliberately neglecting the anionic nature of the SP. The results were generally close to those obtained by the titration of the solutions to pH 7 but presumably contains some error due to the influence of the SP on the charge balance. Estimated errors in the ionic products are shown on the graphs.]

Generally, we observed that all four SPs, at the dosages used here, increased the simple portlandite solubility product by about 30-50% over the whole range of alkali concentrations used, but increased the simple gypsum solubility product by only 20-30%. There are several possible explanations for such increases, the most likely ones being (a) the decrease in activity coefficients due to the ionic strength increase caused by the large polyanionic SP molecules, (b) the partial neutralisation of hydroxide ions by the SP, and (c) weak complexation of calcium ions by the polymers. If calcium ion complexation were the whole explanation, the portlandite and gypsum solubility products should both have been influenced in exactly the same proportions. However, the possible errors in estimation of hydroxide ion concentration make it impossible to say if this was or was not truly the case; partial neutralisation of hydroxide by organic admixture could lead to significant errors in the calculated ionic products. Very similar results to those given above were also obtained with Na_2SO_4 at 30°C, and also with K_2SO_4 at 20°C at concentrations below the syngenite precipitation point. Thus, it can be assumed that, under conditions typical of fresh Portland cement concrete, most common SPs have only a minor influence on the "effective solubility product" of gypsum and portlandite, and thus on the ionic equilibria in the liquid phase.

Table 2. Equilibrium concentrations at 20°C with and without superplasticizers
(* Note: SP concentration is expressed as grams of dry extract per litre of solution.)

Initial $[Na_2SO_4]$	Without SP	MSFC @7.39g/L	PCP1 @3.37g/L	PCP2 @3.22g/L	PCP3 @3.19g/L
		$[SO4^{=}]$, (mM)			
0	10.1	12.3	11.7	11.1	10.5
49.4	36.1	36.6	36.4	37.9	37.7
98.4	70.4	71.4	72.7	68.0	71.1
203.9	157.3	151.4	152.6	153.2	156.4
		$[Ca^{++}]$, (mM)			
0	33.3	34.9	35.0	36.7	35.1
49.4	19.5	22.6	21.2	21.9	21.4
98.4	16.2	18.8	18.2	18.4	20.3
203.9	15.4	16.6	16.3	16.4	15.9
		$[Na^{+}]$, (mM)			
0	2.9	9.6	5.9	3.8	3.2
49.4	98.1	119	111	112	107
98.4	203	221	222	210	212
203.9	409	419	429	425	429
		Total organic carbon, (mg/L)			
0	10	980	1020	1130	1260
49.4	0	1630	980	1140	1260
98.4	0	1570	1200	1220	1260
203.9	0	1690	1250	1260	1310
SP solution as introduced:		2910	1570	1720	1610

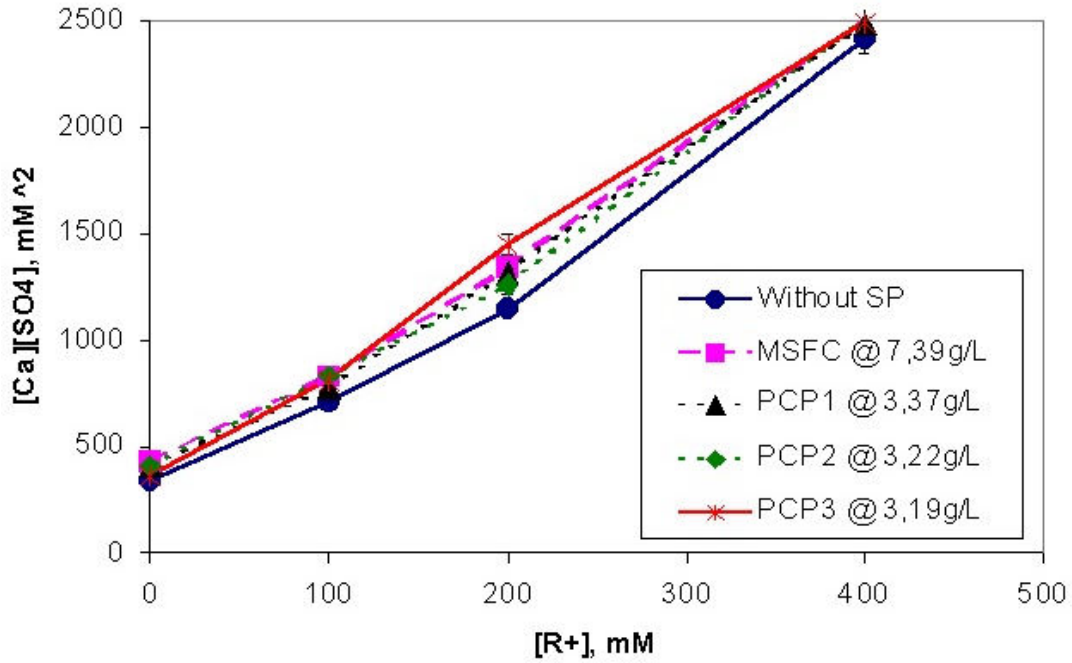

Figure 4. Gypsum ionic product as function of alkali concentration and SP additions

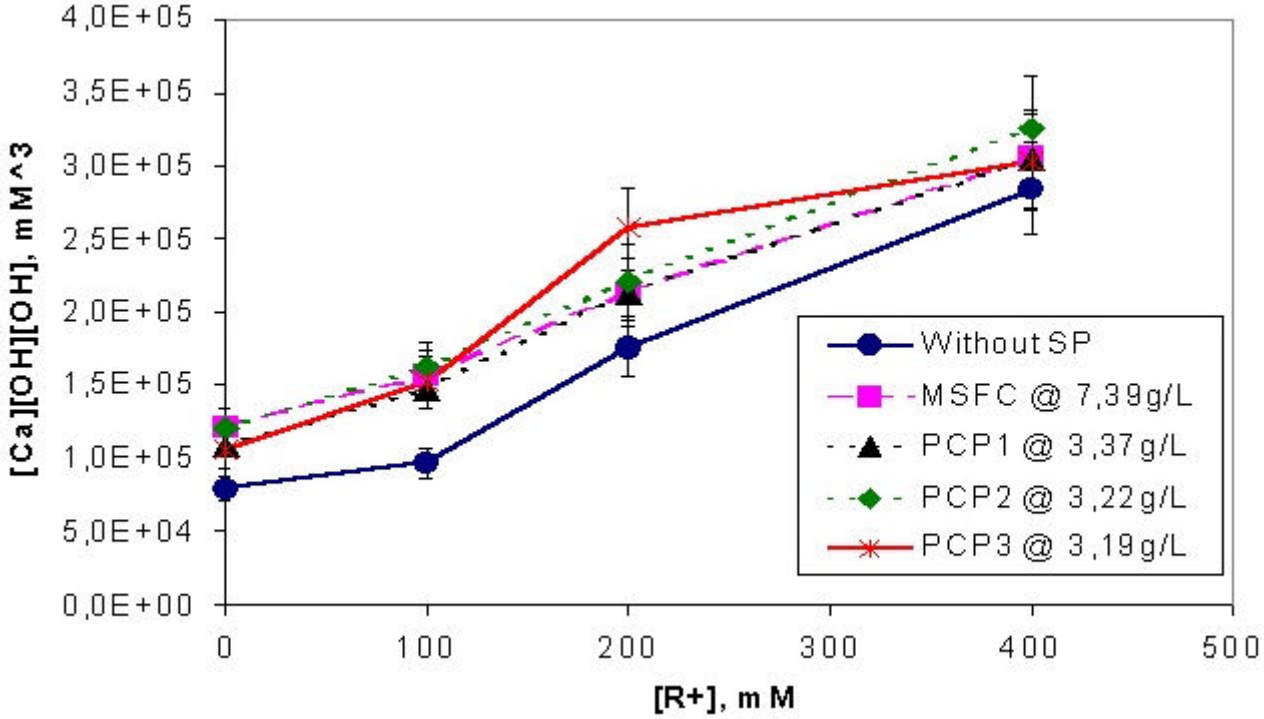

Figure 5. Portlandite ionic product as function of alkali concentration and SP additions

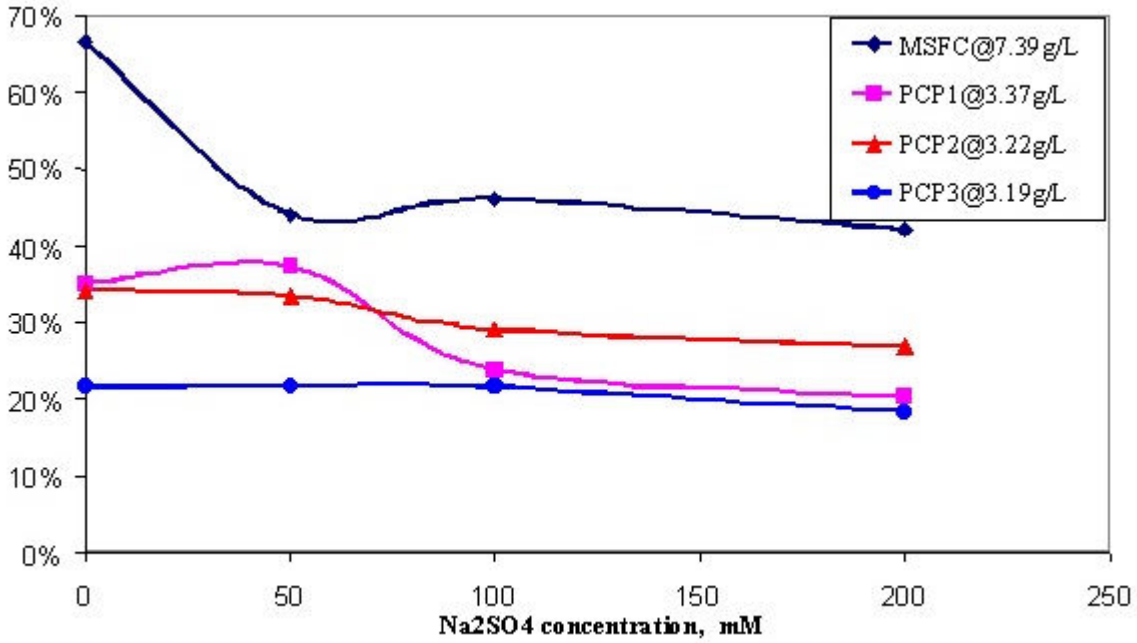

Figure 6. SP adsorption by portlandite-gypsum mix in Na_2SO_4 solutions at 20°C

The amounts of SP adsorbed by the residual solid phases at equilibrium were estimated from their reduced TOC concentrations, as given in Table 2. The degrees of adsorption were quite significant, as shown in Figure 6, despite the relatively high water/solids ratio used. It is notable that all of the SPs showed partial adsorption on the solids in the suspensions, with the strongest adsorption (66%) occurring for MSFC in the absence of additional alkali sulphate. This suggests that MSFC is probably adsorbed significantly by portlandite. The other three SPs showed weaker adsorption but a similar trend towards less adsorption with increasing sulphate concentration. [Note: it should be remembered that the proportion of gypsum in the residual solid phases also increased with increasing sulphate concentration due to the way that the solutions were prepared].

4. CONCLUSIONS

- We have extended the data of Hansen and Pressler [4] to 5° and 20°C, and obtained indirect evidence that anhydrite may have formed in their experiments with high sodium concentrations at 30°C. Our experimental techniques are also confirmed by good agreement with their results. There is indirect evidence that the invariant point syngenite-gypsum-portlandite occurs at a K_2O concentration of about 200 mM at 20°C and at lower K_2O concentrations as the temperature decreases, but we did not attempt to measure it precisely in these experiments.
- Both MSFC-type and PCP-type superplasticizers, at concentrations typical of those found in the aqueous phase of superplasticised Portland cement concretes, show only minor effects on the equilibrium solubility products of portlandite or gypsum in alkali solutions. The principal effect observed is a slight increase in the apparent solubility products of both solid phases, which can be interpreted as being due to either weak calcium ion chelation by the dissolved polymers, or to a decrease in ionic activity coefficients, or both.
- Weak adsorption on the residual solid phases (a portlandite-gypsum mixture) was observed for all of the SPs tested. This was especially notable at low sulphate concentrations, from which it is deduced that the adsorption probably occurs mainly onto the surface of portlandite, which was the preponderant solid phase in the residue after equilibrium in those cases. This adsorption was significantly stronger for MSFC-type than for PCP-type SP polymers. However, the adsorptions observed for all of the SPs tested were relatively small compared to those typically observed in Portland cement pastes at early ages, (when very little portlandite is present). This implies that portlandite is not the principal SP-adsorbing phase in hydrating Portland cements.

ACKNOWLEDGEMENTS

We would like to give special thanks to Thierry Rouillon for his contribution to the experimental work.

REFERENCES

[1] Uchikawa, H., Hanehara, S. and Sawaki, D. Effect of Electrostatic and Steric Repulsive Force of Organic Admixture in the Dispersion of Cement Particles in Fresh Cement Paste, 10th International Congress on the Chemistry of Cement, Gothenburg, 1997, vol. 3, paper 3iii001.

[2] Lawrence, C.D. Symposium on the Structure of Cement Pastes and Concrete, Highway Research Board Special Report No. 90, Washington DC, 1966, pp. 378-91

[3] Gartner, E. and Skalny, J. Computation of Solubility Relationships for Hydrating Cement Systems, 8th International Congress on the Chemistry of Cement, Rio de Janeiro, 1986, Vol. III, pp. 244-50

[4] Hansen, W.C. and Pressler, E.E. Solubility of $Ca(OH)_2$ and $CaSO_4$-$2H_2O$ in Dilute Alkali Solutions, Industrial and Engineering Chemistry vol. 39, 1947, pp.1280-82

[5] Hill, A.E. Ternary Systems. XIX. Calcium Sulfate, Potassium Sulfate and Water, Journal of the American Chemical Society, vol. 56, 1934, pp.1071-78

[6] Gartner, E.M., Tang, F.J. and Weiss, S.J. Saturation Factors for Calcium Hydroxide and Calcium Sulfates in Fresh Portland Cement Pastes, Journal of the American Ceramic Society, vol. 68, 1985, pp. 667-73

[7] Ridge, M.J. and Beretka, J. Calcium Sulphate Hemihydrate and Its Hydration, Reviews of Pure and Applied Chemistry, vol. 19, 1969, pp.17-44

EQUILIBRIA IN THE SYSTEM CALCIUM HYDROXIDE-CALCIUM SULPHATE-ALKALI SULPHATE-WATER AT 5-30°C, AND THEIR RELEVANCE TO PORTLAND CEMENT HYDRATION IN THE PRESENCE OF SUPERPLASTICIZERS

by Ellis M. Gartner[1], Serge Sabio[1] and Jean-Philippe Perez[2]

[1] Lafarge Laboratoire Central de Recherche, 38291 France.
E-mail: ellis.gartner@lafarge.com
[2] LRSS, University de Bourgogne, Dijon, France.
E-mail: jpperez@u-bourgogne.fr

E. M. Gartner

Directeur Adjoint, Pôle Composants Actifs,
Lafarge, Laboratoire Central de Recherche, 95 rue du Montmurier, 38291 St. Quentin Fallavier Cedex, France
Tel: (33)-474-82-1890; Fax: (33)-474-82-8011; E-mail: ellis.gartner@lafarge.com

42 rue Jean-Marc Bernard, 69003 Lyon, France
Tel/Fax: (33)-472-34-8719; E-mail: ellisgart@aol.com

Date of Birth: January 18, 1950, in Hampstead, (London,) England

University: Gonville & Caius College, Cambridge, (1968-74)
BA Natural Sciences (1971) (MA, 1974)
PhD, Physical Chemistry (1975) [Subject: "Infra-Red Emissions of Active Nitrogen"]

Work History:

1. UK Dept. Of the Environment, Building Research Establishment, Garston, Watford, Herts., UK
   - Higher Scientific Officer, Inorganic Materials Dept. (1974-77)

2. Portland Cement Association, Skokie, Illinois, USA
   a) Research Chemist, (1977-78)
   b) Senior Research Chemist, (1978-80)
   c) Manager, Basic Research, (1980-85)

3. W. R. Grace & Co., Washington Research Center, Columbia, Maryland, USA
   a) Senior Research Chemist, Construction Specialties Dept., (1985-89)
   b) Manager, Cement & Concrete Research, (1989-95)
   c) Research Associate, (1995-96)

4. Lafarge, Laboratoire Central de Recherche, (near Lyon,) France
   - Senior Scientist (1996-present)

STUDY ON HYDRATION MECHANISM AND MATERIAL DESIGN OF EXPANSIVE ADDITIVE

Minoru Morioka[1], Etsuo Sakai [2] and Masaki Daimon[2]

[1]Cement and Special Cement Additive Laboratory, Denki Kagaku Kogyo Co.Ltd.
Niigata, Japan. E-mail: minoru-morioka@denka.co.jp
[2]Graduate School of Science and Technology, Tokyo Institute of Technology, Tokyo, Japan.
E-mail: esakai@ceram.ac.jp and mdaimon@ceram.ac.jp

ABSTRACT

According to hydration reaction mechanism of conventional expansive additives, a material design for expansive additives with excellent expansive properties was proposed. In conventional CSA type expansive additives, by considering that expansion action of free-lime can be understood as an initial reaction of free-lime and then on gradual reaction of hauyne, and that more effective expansion action could be effected through the action of free-lime at a time showing its stronger plastic properties, a CSA type expansive additive containing excess free-lime (H-CSA) was proposed. By increasing free-lime content with high hydration activity the reaction of hauyne is accelerated, and H-CSA could more increase whole of reaction rate on the expansive additive than CSA. As a result of confirming the expansion characteristics using mortar, it was found that H-CSA showed larger expansion and better expansion characteristics on using blast furnace slag cement than those of conventional CSA. From the discussion on the role of hauyne in H-CSA based on the comparative study for the expansion properties obtained by free lime-anhydrite based expansive additives, it is showed that free lime solely contributes to its expansion in a system with free lime-anhydrite based expansive additive, but that ettringite generated from hauyne as a base material also contributes to the expansion mechanism for H-CSA.

1. INTRODUCTION

Crack prevention and bending capacity enhancement for reinforced concrete structures is important from the viewpoints of safety, durability and appearance of concrete structures, and further advancement in the technology of expansive additives, which can improve the problems mentioned above, is expected. In recent years, in order to enhance the performance of concrete, highly flowable concrete or high strength and highly durable concrete, which are not affected by construction workmanship and have superior durability, have been developed. For these kinds of concrete, it has been learned that in addition to the change in dimensions caused by drying, which was conventionally considered to be the cause of concrete cracking, autogenous shrinkage accompanied with hardening by hydration causes significantly large changes in the dimensions [1]. It is further pointed out that the effects of expansive additives was not fully realised due to a significantly low water to powder ratio made possible by various admixtures, and that the expansive force was decreased especially when ground granulated blast furnace slag was added [2][3]. At present, it is being considered whether the design method should be transferred to a performance-based design, and it is expected that even for evaluating the effect of cracking on the durability, performance-based design, which requires quantitative clearness, will be applied in the near future. In this case, the reduction of cracks would become an urgent issue even for ordinary concrete. In order to use expansive additives widely in general, concrete is necessary to achieve a smaller addition rate than the present one and accordingly to reduce its economic impact. Thus for achieving high performance of concrete and for responding to the new design method, development

Proceedings of the 11th International Congress on the Chemistry of Cement (ICCC)
'Cement's Contribution to the Development in the 21st Century'
Hosted by: The Cement and Concrete Institute of South Africa
CD-ROM produced by: Document Transformation Technologies
11 - 16 May 2003, Durban, South Africa
ISBN Number: 0-9584085-8-0
Editors: Dr G. Grieve and G. Owens
Congress Organised by: Event Dynamics

of a new expansive additive having superior expansive properties is highly needed. The authors have been investigating quantitatively the hydration of expansive additives used conventionally [4][5][6][7]. In this paper, based on this mechanism of hydration, the material design of a new expansive additive having superior expansive properties to conventional types is proposed.

2. HYDRATION MECHANISM OF CONVENTIONAL EXPANSIVE ADDITIVES[5],[6]

2.1 Reaction rate of compounds and changes in phase composition due to hydration

A calcium sulfo-aluminate based expansive additive (called CSA hereinafter) available on the market as a representative of the conventional expansive additives, was investigated through experiments. C_3A was synthetically produced from reagents, calcium carbonate and aluminum oxide. The gypsum used was that of the reagent grade chemical. CSA consists of free lime, hauyne, and anhydrite. The chemical composition of the CSA is shown in Table-1. The Mechanism of hydration is assumed for a case when 10 mass % of CSA is added to Portland cement containing 10 mass % of C_3A with addition of two thirds mole of gypsum to the C_3A amount. Therefore, the mixture proportion of C_3A, gypsum, and expansive additive is, 41.24 mass % of C_3A, 17.53 mass % of gypsum, and 41.24 mass % of expansive additive.

Table 1. Chemical Composition and Physical Properties of CSA

Expansive additive	Chemical composition (mass %)								Density (g/cm^3)	Baine (cm^2/g)
	Ig.loss	SiO_2	Fe_2O_3	Al_2O_3	CaO	MgO	SO_3	R_2O		
CSA	1.1	1.2	0.6	16.1	51.3	1.1	27.5	0.1	2.86	3010

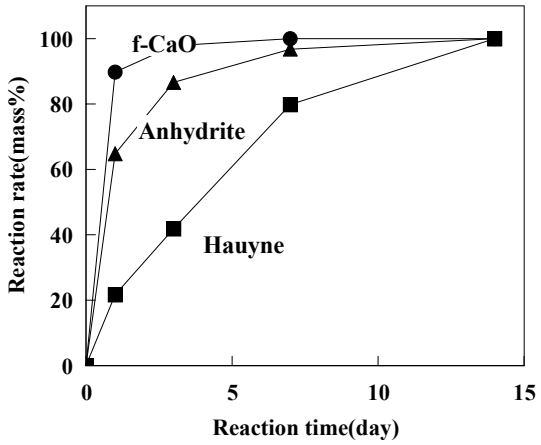

Figure 1. Reaction rate of compounds in CSA

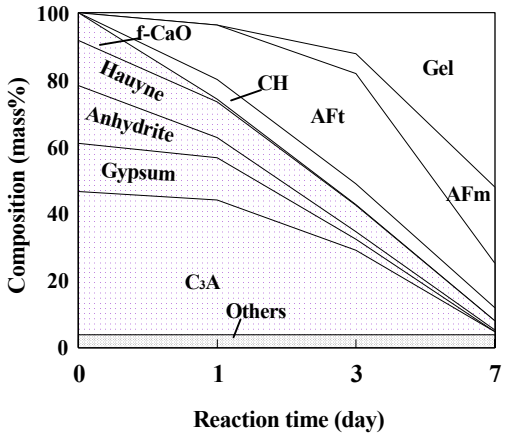

Figure 2. Composition change of C_3A-gypsum- CSA system due to hydration

Figure 1 shows the reaction rate of free lime, hauyne, and anhydrite in CSA. From the figure, free lime and anhydrite in CSA react at early stage, and hauyne reacts slowly at later ages. Changes in the phase composition accompanied by the hydration of C_3A-2/3 mole gypsum-CSA system are shown in Figure 2. The main hydration product is ettringite, but calcium hydroxide is also produced. The mole ratio between SO_3/Al_2O_3 is 1.1, and although it is close to the stoichiometric SO_3/Al_2O_3 mole ratio in mono-sulfate hydrate, a large amount of ettringite is produced. This is because the anhydrite in CSA rapidly reacts at initial hydration stages, which hinders the hydration of C_3A. Production of calcium hydroxide observed, is due to the fact that free lime rapidly reacts at early stages, and hauyne reacts subsequently. Therefore, it is true that the expansion mechanism of CSA-type expansive additive is mostly due to ettringite, however, the material design inevitably utilizes the expansion due to free lime.

3. MATERIAL DESIGN OF EXPANSIVE ADDITIVE WITH EXCELLENT EXPANSION PROPERTIES

3.1 Method of material design

The concept of an expansive additive having excellent expansive properties, properties such as exhibiting performance equivalent to that of a conventional expansive additive but at a lower addition rate, and its expansive properties not being inhibited by blast furnace slag, was already pointed out. It is then necessary to consider how to design the material of an expansive additive having these superior expansive properties. Relevant parameters shall be considered as follows. The first, two parameters are considered for material design of the expansive additive exhibiting performance equivalent to that of a conventional expansive at a lower addition rate, as follows.

3.1.1 Timing of expansion

In the relationship between the strength development of cement matrix and the time at which the expansive additive becomes effective, the moment at which the reaction of expansive additive commences for achieving the most effective expansion shall be considered.

3.1.2 The reaction rate shall be increased at the period when it can provide expansion effectively

If the period in which expansion can be provided effectively is known, the reaction rate of the expansive additive should be increased in this period.

Figure 3 schematically shows the strength development of cement matrix and timing of expansion. In the fresh state of the first period (plastic deformation can take place), effective expansion cannot be expected to occur, and on the other hand, in the fourth period when sufficient strength is developed and it starts to become brittle, expansion would lead to failure. Therefore the period in which effective expansion can be provided is considered to exist between these periods. This period is designated as the effective expansion period hereinafter. This effective expansion period is further divided into the second period in which the plastic property is dominant, and the third period in which solid properties increase.

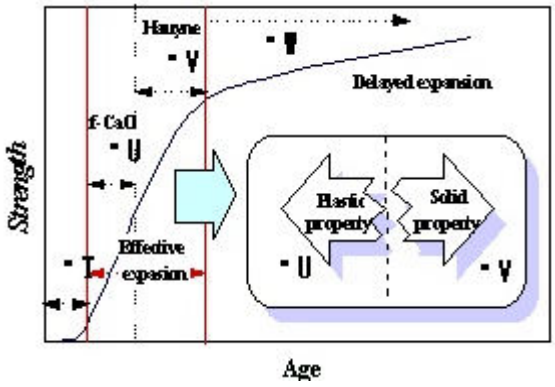

Figure 3. Strength development of cement matrix and timing of expansion

If the additive were designed to react in the second period showing rather plastic properties, even a small stress would generate large expansion. However, if it were designed to react in the third period showing more solid properties, a large stress would be required. Among CSA constituents, free lime and hauyne, which become the base materials for the expansive hydration products such as calcium hydroxide and ettringite, are taken into consideration together with their reactivity. The CSA hydration mechanism is such that free lime reacts at initial stages and hauyne reacts slowly at later stages, as mentioned before (Figure 1). Therefore it can be assumed that free lime reacts mainly in the second period, and that hauyne reacts mainly in the third period. In order to design an expansive additive having superior expansive properties, an effective means for material design is considered to be increasing the amount of free lime content as long as it does not cause an abnormal set. In this regard, the contents of hauyne and anhydrite shall also be reduced. However, as it is known that C_3A in cement also generates a large amount of ettrigite by reacting with anhydrite (refer to Figure 2), reducing the amount of hauyne in the material design is considered to be rather appropriate. By this, free lime itself can contribute to the expansion, and in addition, the content of free lime with high hydration activity becomes large, and thus the reaction of hauyne is accelerated,

and expansive properties are expected to be improved. Next, is considered how to avoid the negative effects of blast furnace slag. The reason why conventional CSA is significantly affected by blast furnace slag is considered as follows. Free lime, hauyne, and anhydrite, which are the compounds composing CSA, are all known as activators of blast furnace slag [8][9][10]. It is estimated that since these compounds are consumed by blast furnace slag, expansion originally due to CSA is not exhibited. In order to utilize an expansion mechanism due to ettringite, concentration of hydroxide ions and the SO_3/Al_2O_3 mole ratio have become extremely important parameters of the system [11]. However, in a system where blast furnace slag co-exists, the hydroxide ions become few, and as the blast furnace slag contains a large amount of Al_2O_3, the mole ratio SO_3/Al_2O_3 also becomes small. Therefore, it is considered that the expansion mechanism does not work normally. In order not to be affected easily by blast furnace slag, it is important to let the expansive additive react before the reaction of blast furnace slag, and an effective method shall be that most of the expansion is designed to be caused by free lime, which has high hydration activity and reacts at early ages. As shown above, a material design method to develop expansion equivalent to that of a conventional expansive additive at a lower addition rate, and a material design method that is not affected easily by blast furnace slag, are considered basically to be compatible.

3.2 Determination of composition and synthesizing expansive additive

Now that the principle of material design is fixed, the composition of a new CSA-based expansive additive can be determined. When determining the composition of compounds, a clinker of expansive material is synthesized by using the reagent of raw material, and the content of free lime is increased as much as possible without causing abnormal set or abrupt decrease in flowability, and then the amount of hauyne and gypsum anhydrite is conditioned to obtain the optimum composition.

Figure 4 shows the composition of the new expansive additive and those of conventional CSA-based expansive additives in a triangle phase diagram of CaO-Al_2O_3-SO_3. The first CSA-based expansive additive, recognized as the origin of the expansive additive, was developed by Poliet et chausson company in France in the 1930's [12]. This CSA-based expansive additive is estimated to be composed of approximately 70% hauyne and 30% anhydrite, and it had been used as an additive at about 20% to 30% to Portland cement. The CSA-based expansive additive developed by Klein in America in the 1960's [13], was actually composed of free lime and hauyne, and it had also been used as an additive of 20 to 30 mass % to Portland cement.

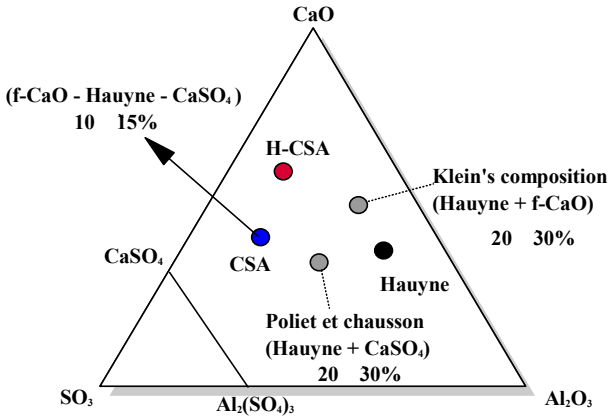

Figure 4. Composition of expansive additives in the triangle phase diagram of CaO-Al_2O_3-SO_3 system

Subsequently, based on an idea that expansion could be effectively provided if a unhydrous composition of ettringite were taken as an initial composition, a CSA-based expansive additive consisting of free lime, hauyne, and anhydrite was invented in Japan [14]. This CSA-based expansive additive has been used for over 30 years as an additive of 10 to 15 mass % to Portland cement. The new CSA-based expansive additive proposed by this research (abbreviated as H-CSA hereinafter) is regarded as one in which the CaO content was increased compared to the CSA composition currently used.

Next H-CSA was synthesized by using industrial raw material. The Raw material conditioned to a designated proportion was burned to synthesize in a rotary kiln at 1400°C. The chemical composition and physical properties of the H-CSA are shown in Table 2, and compounds and compositions of the H-CSA calculated based on the chemical composition compared to that of conventional CSA are shown in Figure 5. The amount of free lime in H-CSA is significantly larger compared to that of CSA, and its hauyne and anhydrite contents are smaller, and the amount of hauyne is especially small.

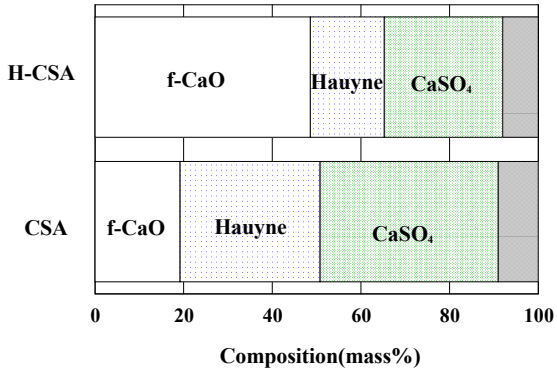

Figure 5. Compounds composition of H-CSA

Table 2. Chemical composition and physical properties of H-CSA

Expansive additive	Chemical composition (mass %)								Density (g/cm^3)	Brain (cm^2/g)
	Ig. loss	SiO_2	Fe_2O_3	Al_2O_3	CaO	MgO	SO_3	R_2O		
H-CSA	0.9	1.4	0.5	8.4	68.8	1.2	17.7	0.1	3.04	2970

4. HYDRATION AND EXPANSIVE PROPERTIES OF A NEW EXPANSIVE ADDITIVE

4.1 Hydration reaction

Figure 6 shows the reaction rate of hauyne and expansive additive. The rate of reaction for hauyne in H-CSA is accelerated compared to that in CSA. It is considered that by increasing significantly the content of free lime, which has a high hydration activity, the hydration of hauyne is accelerated. It is also revealed that the reaction rate of the expansive additive in total is accelerated for H-CSA compared to the case for CSA. This is because the free lime content of high hydration activity is significantly increased, and resultantly the reaction of hauyne is accelerated. In this manner, the reaction of the expansive additive in total was able to be accelerated by increasing the free lime content and decreasing the content of hauyne. As the reaction of the expansive additive is considered to be controlled at early stages, it is expected to exhibit superior expansion performance and not to be easily affected by blast furnace slag. Figure 7 shows changes in phase composition obtained by the quantitative research on the hydration of a C_3A-gypsum-H-CSA system by the same method as reported in the previous paper [5].

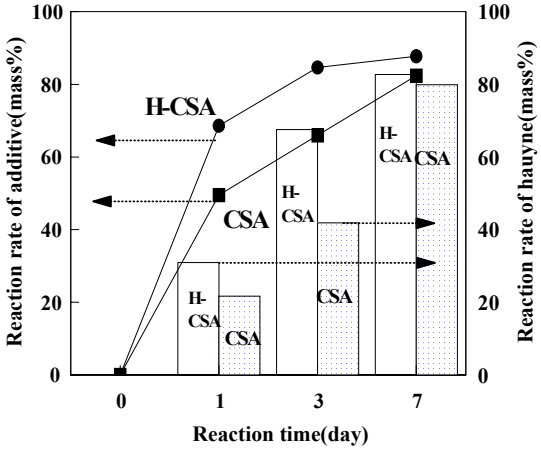

Figure 6. Reaction rate of hauyne and expansive additive

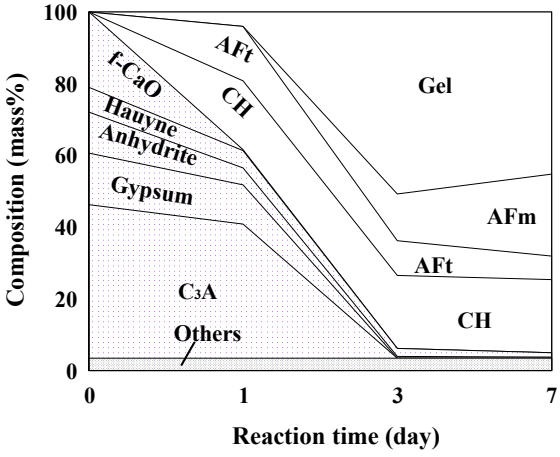

Figure 7. Composition change of C_3A-gypsum- H-CSA system by hydration

In the system added with H-CSA, a large amount of free lime produces a large amount of calcium hydroxide together with a significant amount of ettringite. In the hydration of the C_3A-gypsum-CSA system shown in Figure 2, most of the expansion was attributed to ettringite, whereas in the C_3A-gypsum-H-CSA system, free lime and ettringite equally contribute to the expansion.

4.2 Expansive properties

Performance evaluation of the expansive additive was carried out in a mortar. The mix proportion of the mortar was a water binder ratio of 50%, and the proportion of binder and sand was 1:3. The expansive additive was added by inner proportion to the binder consisting of cement and the expansive additive. The expansion rate measured was the expansion rate with uni-axial restraint in accordance with JIS A 6202. Specimens were demoulded at age one day, and cured in water at 20°C for 6 days until age 7 days. Measurement was carried out at days 1, 3 and 7. Figure 8 shows the relationship between the dosage of the expansive additive and the expansion rate at age 7 days. For all cases, the expansion rate increases with increasing dosage. For H-CSA, the required expansion rate is obtained with a smaller dosage than that for CSA. In the case that CSA is used for BB, the expansion rate did not become significantly large with increasing dosage. On the other hand, H-CSA exhibited about the same expansion rate in both cases of OPC and BB. Normally, when conventional CSA is used for OPC in order for compensation of drying shrinkage or introduction of some chemical prestress, the standard addition rate is about 10 mass %. However, when CSA is used for BB for the same purpose, an additional rate of about 14 mass % is required. Whereas for H-CSA, the required expansion rate can be achieved by adding 5 mass % of it to any type of cement, and it is capable of reducing the economical load significantly. This economical effect is considered to be a considerable difference for OPC, but it counts more significantly for BB. Figure 9 shows the period in which expansion developed due to expansive additives used for OPC. In the figure, the rate of expansion at a certain age is expressed as the ratio to the expansion rate (maximum expansion rate) at age 7 days (designated as Et/E7d hereinafter). However, as Et/E7d varies according to the dosage of expansive additives, it is shown by the average Et/E7d obtained for each dosage. The period in which expansion develops for H-CSA is shown to be earlier than that for CSA. It is closely related to the reaction rate of the expansive additive shown in Figure 6. As discussed in the previous chapter, expansion properties are largely affected by the period in which expansion develops, and it is confirmed that expansion performance can be enhanced by shifting the expansion period earlier. It is also confirmed that with early expansion this is not affected much by ground granulated blast furnace slag and expansion performance can be easily obtained even with blast furnace cement.

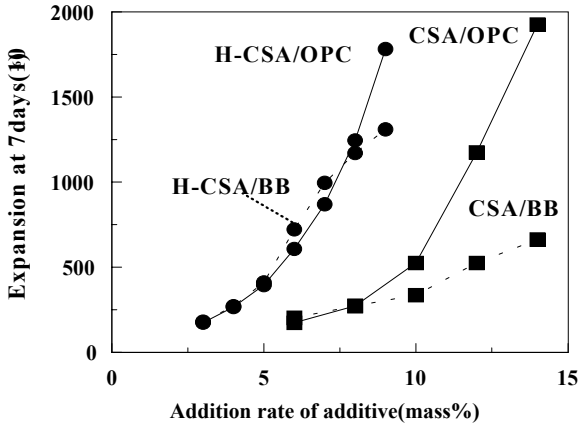

Figure 8. Relationship between addition rate of expansive additive and expansion at 7 days

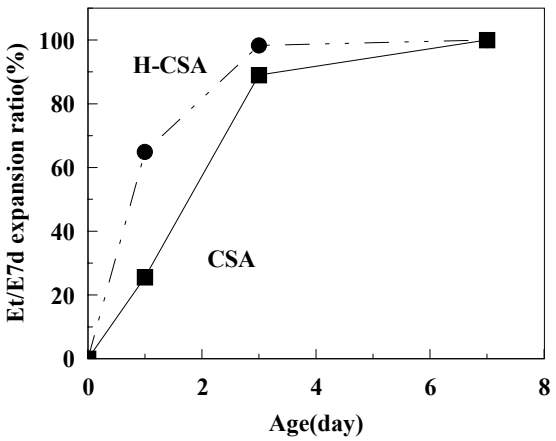

Figure 9. Et/E7d expansion ratio

4.3 Role of hauyne in H-CSA

H-CSA has a high free lime content, and its content is higher than that of the lime-based expansive additive available on the market. As a lower hauyne content is adopted, it is important to clarify the difference from the lime-based expansive additive, including that from the free lime-anhydrite based expansive additive proposed in the past [15][16]. This is done by focusing on the role of hauyne in H-CSA. Three types of free lime-anhydrite based expansive additives of which the contents of free lime and anhydrite vary, were prepared and these expansive performance were examined in comparison with H-CSA. Figure 10 shows the relationship between the free lime content for cement and the expansion rate.

It is confirmed that the expansive performance obtained by free lime-anhydrite based expansive additives was higher than that solely by free lime, which coincides with the conclusions of former studies. Even at various addition rates of free lime and anhydrite (30:70, 50:50, 70:30), it is known that a linear relationship appears when sorted by the addition rate of free lime to the mortar. On the other hand, the expansion rate for H-CSA is shown to be higher than that for free lime-anhydrite based expansive additives. It is because not only free lime contributes to the expansion for H-CSA, but ettringite generated from hauyne as base material also makes a contribution.

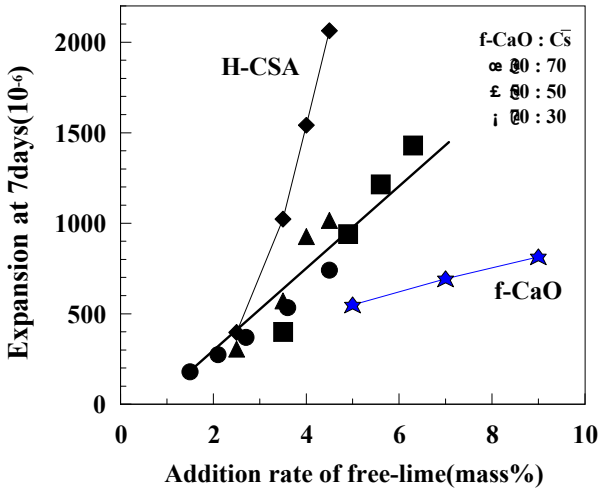

Figure 10. Relationship between addition rate of free-lime and expansion at 7 days

5. CONCLUSIONS

The following conclusions were drawn from the experimental results and discussions in this research.

Considering that expansion due to free lime can inevitably be counted based on the fact that free lime reacts initially and hauyne reacts slowly and later in a system with a CSA based expansive additive, and that expansion can be effectively provided by free lime which reacts in a period in which plastic properties are relatively dominant, a CSA based expansive additive containing a large amount of free lime (H-CSA) is proposed.

By increasing the free lime content of high hydration activity, and by the resultant accelerated reaction of hauyne, the reaction of a H-CSA expansive additive in total was able to take place earlier than that with CSA. In this expansive additive, free lime and ettringite evenly contribute to the expansion mechanism.

From the results of expansion performance examined with mortar, H-CSA exhibited a higher rate of expansion compared with conventional CSA, and also exhibited good expansive performance even with blast furnace slag cement.

From the discussion on the role of hauyne in H-CSA based on the comparative study for the expansion properties obtained by free lime-anhydrite based expansive additives, it is revealed that free lime solely contributes to its expansion in a system with free lime-anhydrite based expansive additive, but that ettringite generated from hauyne as a base material also contributes to the expansion mechanism for H-CSA.

REFERENCES

[1] Tazawa, E., Miyazawa, S. and Shigekawa, K. Macroscopic shrinkage of hardening cement paste due to hydration, CAJ Proceedings of Cement and Concrete, Vol.45, 1991, pp.122-127

[2] Tsuji, Y. and Kawamura, I. Expansive properties of expansive concrete added with blast furnace slag powder, Cement Science and Concrete Technology, Vol.33, 1979, pp.189-192

[3] Tsuji, Y. and Kobayashi, S. Expansive properties and compressive strength of expansive concrete using blast furnace slag powder, Proceedings of Japan Concrete Institute, Vol.6, 1984, pp.101-104

[4] Morioka, M., Hagiwara, H., Sakai, E. and Daimon, M. Hydration reaction of calcium sulpho-aluminate type expansive additive, Cement Science and Concrete Technology, Vol.52, 1998, pp.2-7

[5] Morioka, M., Hagiwara, H., Sakai, E. and Daimon, M. Effect of C_3A and gypsum on the hydration reaction of the calcium sulpho-aluminate type expansive additive, Cement Science and Concrete Technology, Vol.52, 1998, pp.8-15

[6] Morioka, M., Hagiwara, H., Sakai, E. and Daimon, M. Influence of expansive additives on hydration of C_3A, Cement Science and Concrete Technology, Vol.53, 1999, pp.23-29

[7] Morioka, M., Hagiwara, H., Kang, J.K., Ohba, Y., Sakai, E. and Daimon, M. Hydration reaction of calcium sulfo-aluminate type expansive additive - Alite system, Journal of the Ceramics Society of Japan, Vol.108, No.4, 2000, pp.392-396

[8] Song, C.T., Daimon, M. and Kondo R. Hydration reaction of high sulfated slag cement, Gypsum and Lime, No.163, 1979, pp.2-6

[9] Uchida, I., Nomi, K. and Minegishi, K. Activation effect of hauyne based clinker on hydration of high sulfated slag cement, CAJ Proceedings of Cement and Concrete, Vol.33, 1979, pp.67-69

[10] Sakai, E., Kim, S.K. and Daimon, M. Improvement of porous pore structures of carbonated blast furnace slag cements by addition of various types of mineral admixtures, CAJ Proceedings of Cement and Concrete, Vol.49, 1995, pp.714-719

[11] Schwiete, H.E., Ludwig, U. and Jager, P. Symposium on structure of Portland cement paste and concrete, Highway Research Board, 1966, pp.353-367

[12] French Patent No.813977, 1936

[13] U.S. Patent No.3155526, 1964

[14] Japanese Patent No.42-21840, 1967

[15] Sato, M., Ohkura, R., Sasaki, M., Miyazawa, Y. and Sato, S. Influence of anhydrite on expansive effect of “dead” free-lime, CAJ Proceedings of Cement and Concrete, Vol.29, 1975, pp.118-121

[16] Sato, M. and Saito, K. Influence of type Ⅱ-anhydrite on lime - calcium sulfate based expansive additive, CAJ Proceedings of Cement and Concrete, Vol.33, 1979, pp.126-130

STUDY ON HYDRATION MECHANISM AND MATERIAL DESIGN OF EXPANSIVE ADDITIVE

Minoru Morioka[1], Etsuo Sakai [2] and Masaki Daimon[2]

[1]Cement and Special Cement Additive Laboratory, DENKI KAGAKU KOGYO Co.Ltd., Niigata, Japan. E-mail: minoru-morioka@denka.co.jp
[2]Graduate School of Science and Technology, Tokyo Institute of Technology, Tokyo, Japan. E-mail: esakai@ceram.ac.jp and mdaimon@ceram.ac.jp

Minoru Morioka (Dr. Eng.)

DENKI KAGAKU KOGYO Co.Ltd., Oumi Plant, Cement and Special Cement Additive Laboratory, 2209 Oumi-cho, Nishikubikigun, Niigata, 949-0393, Japan.
E-mail: minoru-morioka@denka.co.jp

Minoru Morioka received degrees of Bachelor and Master of Engineering from Nihon University in 1989, 1991, respectively. He joined Cement and Special Cement Additive Laboratory of Denki Kagaku Kogyo in 1991 as a research engineer, and became group reader in 2002. From 1991 to present, he received degree of Doctor of Engineering from Tokyo Institute of Technology in 1999, and received award from Cement Association of Japan (CAJ) in 2001.

Etsuo Sakai (Dr. Eng.)
Tokyo Institute of Technology, Department of Metallurgy and Ceramics Science, Graduate School of Science and Technology, 2-12-1, Ookayama, Meguroku, Tokyo, 152-8552, Japan.
E-mail: esakai@ceram.ac.jp

Masaki Daimon (Dr. Eng.)
Tokyo Institute of Technology, Department of Metallurgy and Ceramics Science, Graduate School of Science and Technology, 2-12-1, Ookayama, Meguroku, Tokyo, 152-8552, Japan.
E-mail: mdaimon@ceram.ac.jp

RHEOLOGICAL AND SETTING PROPERTIES OF FGD-GYPSUM WHEN USED AS SETTING REGULATOR

Adriano Papo [1], Ludmilla Opoczky[2], László Sas[3] and Luciano Piani [1]

[1]DSTC, University of Udine, Italy; E-mail: Adriano.Papo@dstc.uniud.it
[2]Research and Development Co. Ltd. for Cement Industry, Budapest, Hungary
E-mail: cemkut@mail.datanet.hu
[3] DDC Ltd., Vác Factory, Vác, Hungary; E-mail: sasl@duna-drava.hu

ABSTRACT

FGD-gypsum cement pastes exhibit a thixotropic rheological behaviour; their flow curves derive from the down-curve of the second hysteresis cycle drawn after mixing according to the procedure proposed by the Authors, and are of shear-thinning type that may be very satisfactorily described by the Papo-Piani model, whose parameters for physical consistency have also been fully demonstrated. Cement slurries prepared with FGD-gypsum show lower viscosity values than the pastes made with an ordinary Portland cement with the same Blaine number. Finally, the tests performed in dynamic mode permitted the structure evolution of paste from mixing to the initial setting by using non-destructive measurements to be followed; in particular, the dynamic viscosity-time transient behaviour resembles that of apparent viscosity-time transient behaviour already noticed by the Authors for ordinary Portland cement pastes as well as for gypsum-free cement pastes.

1. INTRODUCTION

In recent years FGD-gypsum, resulting from the desulphurizing of flue gases of coal burning power stations using the limestone washing method, has been widely used in the cement industry as a cement setting regulator.

Our tests showed that the heat-affected loss of water processes, which take place partly also in production cement mills, and in relation to this the dissolving properties (solubility, rate of dissolving) of *calcium sulphate dehydrate* constituting the main component of FGD-gypsum differ somewhat from those of the natural limestone. This provided a justification to investigate in depth the rheological and setting properties of cement pastes made with FGD-gypsum addition.

Understanding cement paste rheological properties is of importance in order to develop a useful tool for controlling cement production, for collecting further information on the chemistry of cement, as well as in the preparation of cement suspensions for special applications, such as injections in loose soils. Moreover, a knowledge of fresh cement paste rheology may contribute to a better understanding of the flow behaviour of mortars and concrete.

Fresh cement pastes are highly concentrated suspensions; their rheological behaviour is generally very complex, it being dependent on several factors of different natures, such as physical factors (the water/cement ratio, the cement grain shape and size, etc.), chemical and mineralogical factors (the cement composition and its structural modifications due to hydration processes, etc.), mixing

conditions (the type and rate of stirrer, the stirring time, etc.), measurement conditions (the measuring instruments, the experimental procedures, etc.), presence of additives (water reducing agents).

A lot of work on cement rheology is available in the scientific literature; here mention is made of the most recent studies (1-5). The present paper is aimed at investigating the rheological and setting characteristics of fresh cement pastes prepared with FGD-gypsum addition; moreover, their rheological properties will be compared with those of an ordinary Portland cement paste with the same Blaine number and prepared at the same water/cement ratio as the FGD-gypsum cement investigated.

2. EXPERIMENTAL

Materials employed

A cement with a specific surface of ~340 m^2/kg (Blaine number) made in a production mill with FGD-gypsum addition was used as the testing material. FGD-gypsum was added into the mill in such a quantity that the SO_3 content of the cement produced should be ~3.5%. The $CaSO_4 \cdot 2H_2O$ content of the FGD-gypsum was 95.5%. Cement pastes were prepared with a vane stirrer (Ultra-Turrax T50, Janke & Kunkel, IKA-Labortechnik) according to ASTM C305); deionized water was used; water/cement ratio was in the range 0.34 to 0.42. Water/cement ratios lower than 0.32 were not taken into consideration owing to the very high viscosity of samples.

Apparatus and experimental procedure

Rheological measurements were carried out using the rate controlled coaxial cylinder viscometer Rotovisko-Haake 20, system M5-Osc., measuring device MV2P with serrated surfaces. The temperature was kept strictly constant at 25 ±0.1°C. The tests were accomplished under both continuous and oscillatory flow conditions. The following rheological procedures were applied:

1) Continuous flow conditions: Tests under variable shear rate (hysteresis cycles).A first hysteresis cycle was drawn immediately after mixing; changes in shear rate were made at the constant shear acceleration of 2.9 s^{-2}; the maximum shear rate reached was 352 s^{-1}. The same sample was subjected to a second hysteresis cycle 1 min after the previous one. The down curves of the second hysteresis loop have been utilized as flow curves for the cement pastes examined.

1) Oscillatory flow conditions:

A 0.1 to 1 Hz frequency sweep with 0.2 rad constant strain was applied, after determining the region of linear viscoelastic behaviour by means of a strain sweep at a 0.1 Hz constant frequency. A time sweep with a 0.1 Hz frequency was also applied in order to study the setting evolution of pastes.

3. RESULTS AND DISCUSSION

3.1 Continuous flow conditions

According to Procedure a) two hysteresis cycles were drawn after sample preparation. The first cycle shows a shape similar to that already described in a previous paper (6): the down-curve lies on the lower shear stress side than the upper one, i.e. structure breaks down during the test. The second hysteresis loop presents both up- and down-curves of a shear-thinning type and the rheological behaviour is strictly thixotropic. The thixotropic behaviour of FGD-gypsum cement pastes will be studied in depth in a further work.

Fig. 1 reports the shear stress vs. shear rate flow curves derived from the down-curve of the second hysteresis loop obtained for the cement pastes investigated in the present work. All the cement pastes tested exhibit a rheological behaviour of shear-thinning type; a yield stress is also evident. Among the rheological models which correlate shear stress with shear rate, the following equations,

which have already been applied both to cement pastes (7) and to ceramic powder suspensions (8), were tested:

The Casson model $\tau=\tau_o+\eta_\infty\gamma+2[\tau_o\,\eta_\infty]^{1/2}\gamma^{1/2}$ (1)

The Generalized Casson model $\tau^n=\tau_o^n+[\eta_\infty\gamma]^n$ (2)

The Herschel-Bulkley model $\tau=\tau_o+K\gamma^n$ (3)

The Papo-Piani model: $\tau=\tau_o+\eta_\infty\gamma+K\gamma^n$ (4)

All the models considered gave a distinct fit, as can be seen from an examination of both standard deviation estimates (STD) and determination coefficient values (COD), which are reported in Table 1, even if, from this point of view, a slightly superior fit was achieved by applying the Papo-Piani model, whose parameter values are shown in Fig. 2.

Table 1. Standard deviation estimates (STD) and determination coefficient values (COD) for the models inestigated.

		W/C				
		0.32	0.34	0.36	0.38	0.40
Eqn. 1	STD	2.59	2.99	3.08	2.12	1.91
	COD	0.998	0.997	0.996	0.998	0.998
Eqn. 2	STD	2.64	2.24	2.28	1.87	1.52
	COD	0.998	0.998	0.998	0.998	0.999
Eqn. 3	STD	2.71	2.41	2.39	1.95	1.63
	COD	0.998	0.998	0.998	0.998	0.999
Eqn. 4	STD	2.68	2.01	2.14	1.84	1.45
	COD	0.998	0.999	0.998	0.998	0.999

The physical consistency of the parameter values of Eqn. (4) may be evaluated by fitting the τ_o values with solid volume fraction by means of the following equation:

$$\tau_o=K[(\Phi-\Phi_o)/(\Phi_m-\Phi)]^m \quad (5)$$

where Φ_o is the volume fraction corresponding to transition from the newtonian or shear-thinning behaviour to the plastic one and Φ_m is the maximum volume fraction, i.e. that corresponding to the maximum particle packing in quiet conditions. A very satisfactory τ_o-Φcorrelation was found (see Figure 3); the fitting gave the following parameter values: K=50; Φ_o=0.44; Φ_m=0.53; m=0.5 (COD=0.997). Full agreement has been found between the Φ_m values calculated by means of Eqn. (5) and those determined experimentally by centrifugation (Φm,exp=0.54). Lower values of Φ_o with respect to the volume fraction of random particle packing Φ_{rp}, calculated equal to 0.64 in (9) for suspensions of monomodal non-interactive hard spheres, denote the presence of strong attractive forces among particles, i.e. the formation of flocs and/or clusters. The size distribution of the cement particles used being not monomodal, the Φ_{rp} should be slightly higher than 0.64. This means that the formation of a three-dimensional network may be expected at solid volume fractions considerably lower than Φ_{rp}=0.64.

Finally, from the comparison between the flow curve of the 0.32 w/c FGD-gypsum cement paste and that determined in a previous paper (10) for an ordinary Portland cement paste with the same Blaine specific surface (see Figure 1), the results show that the cement paste investigated in this work exhibits lower viscosity values than those presented by Portland cement; hence a higher workability may be expected from FGD-gypsum cement mixes.

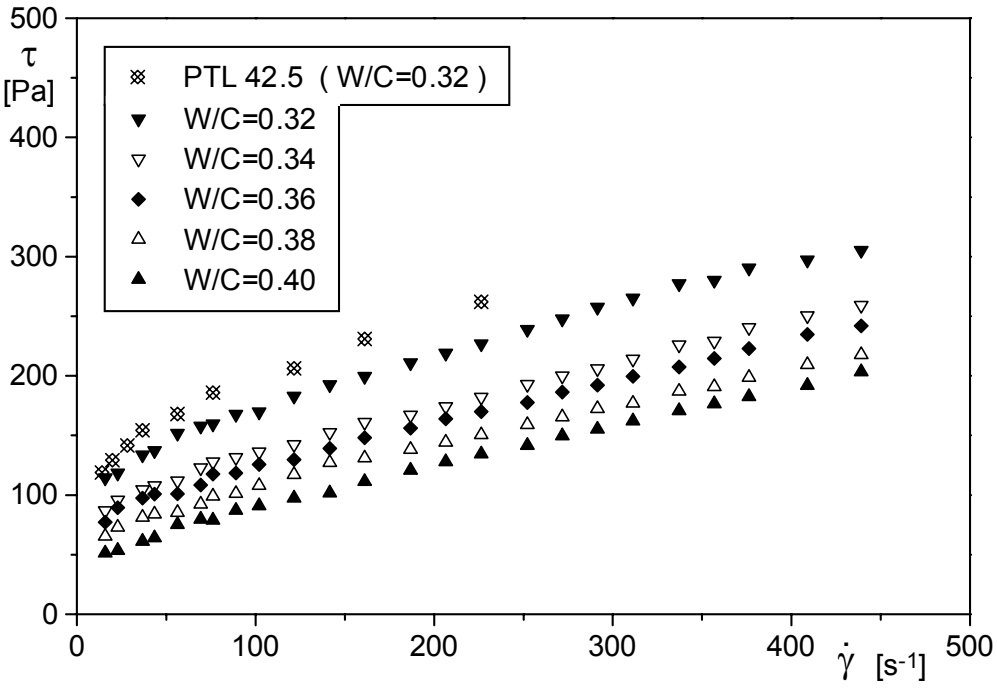

Figure 1. Shear stress (τ) vs. shear rate (γ) flow curves for the cement pastes investigated.

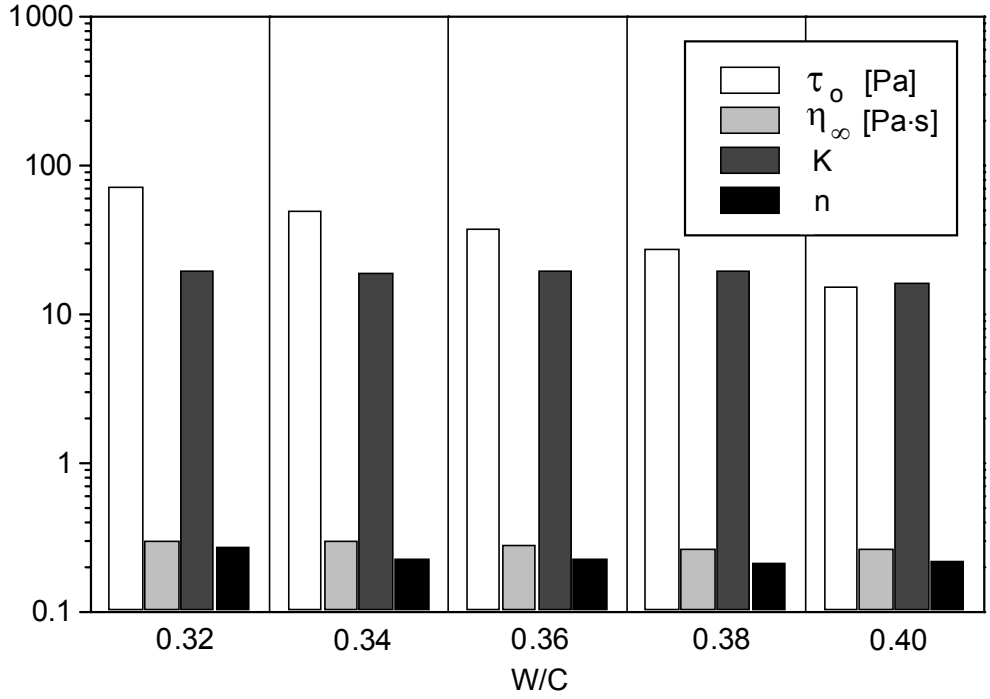

Figure 2. Variation of the parameter values of Eqn. (4) with water/cement ratio.

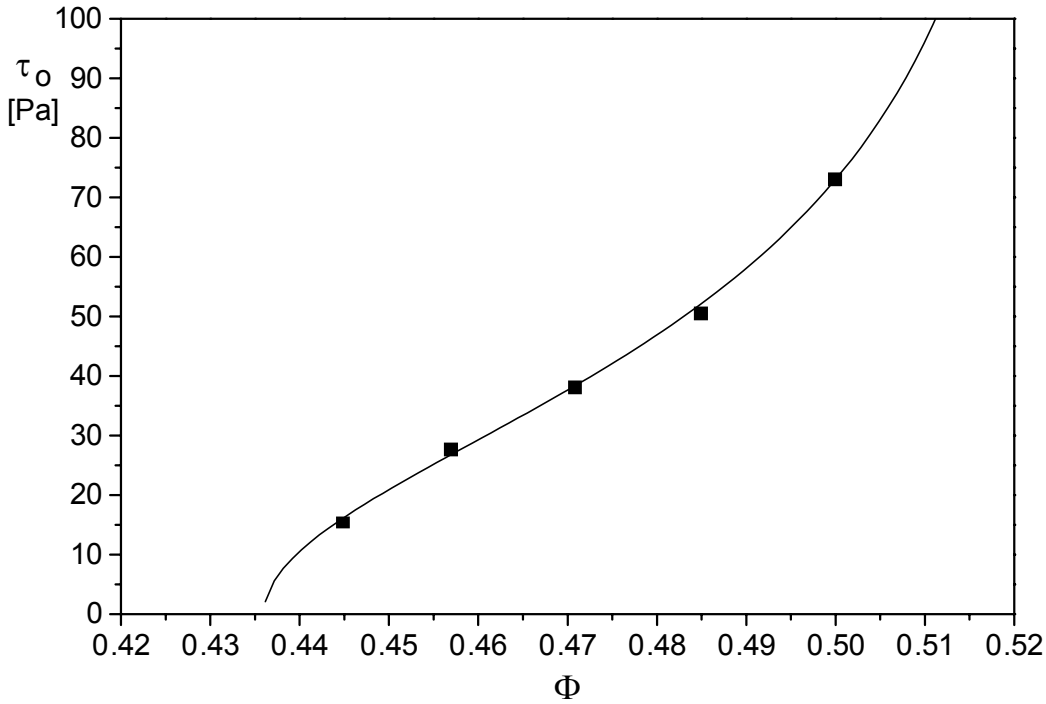

Figure 3. Yield stress (τ_o) vs. solid volume fraction (Φ): comparison between the data calculated with Eqn. (4) and those determined with Eqn. (5) [continuous line].

3.2 Oscillatory flow conditions

Dynamic flow tests were undertaken in order to add further information on the FGD-gypsum cement paste rheological behaviour as well as on the structure evolution of paste from mixing to the initial setting time by using non-destructive measurements (2,11). As far as the dynamic viscosity vs. angular velocity (frequency) flow curves are concerned, a monotonic decrease of dynamic viscosity with angular velocity is noticed, as can be expected, for all the cement pastes examined and for any water/cement ratios explored (see Figure 4).

As regards the mechanical spectra, i.e. the variation of both storage or elastic modulus G' and loss modulus G" with angular velocity, it can be noted that G' and G" moduli have parallel evolution vs. frequency; in particular G" is always higher than G' for all the cement pastes examined and for any water/cement ratios investigated (see Figure 5); this means that the viscous component of complex modulus G* always predominates over the elastic one; in addition, no transition from sol-like to gel-like behaviour is noticeable when decreasing the water/cement ratio: the paste always exhibits a liquid-like behaviour within the whole frequency range. This confirms that a satisfactory workability of the pastes formulated with FGD-gypsum may be expected also on the basis of the oscillatory flow tests results.

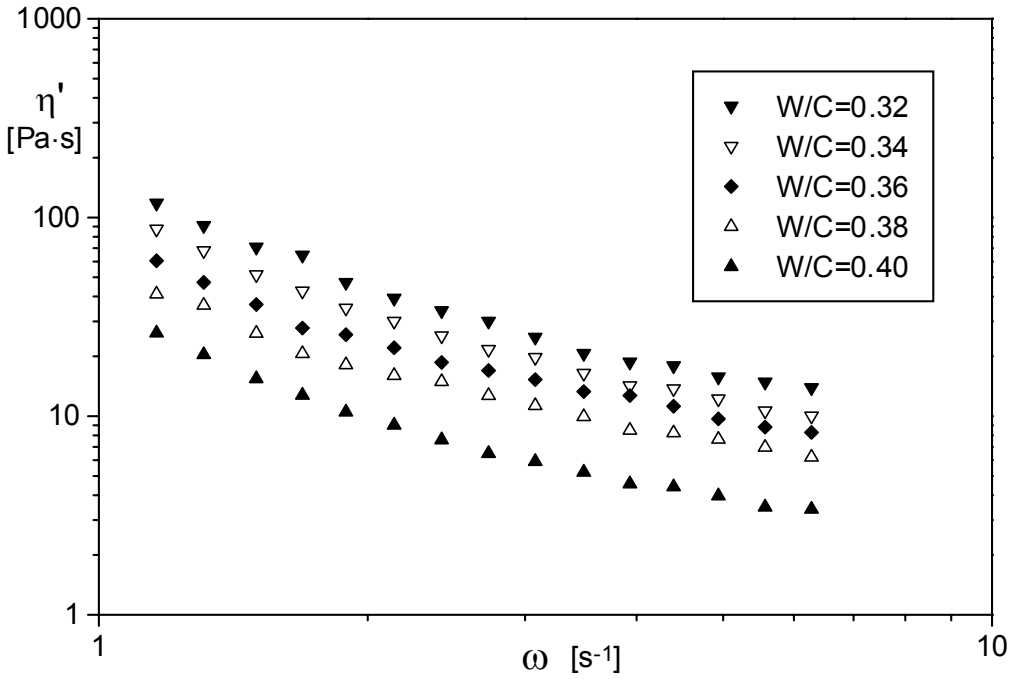

Figure 4. Dynamic viscosity (η') vs. angular velocity (ω) for the cement pastes investigated [0.2 rad of constant strain].

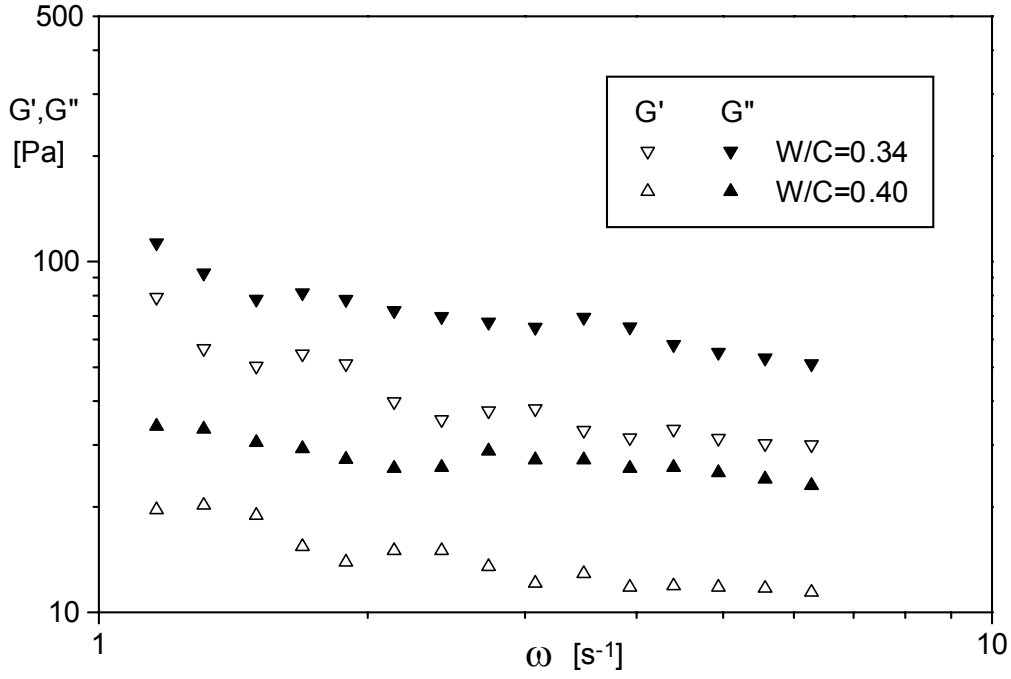

Figure 5. Storage (G') and loss (G") moduli variation with angular velocity (ω) for the 0.34 and 0.40 w/c cement pastes investigated [0.2 rad of constant strain].

The time sweep results are useful for describing the setting evolution of paste. Fig. 6 reports an example of dynamic viscosity-time transient behaviour. The dynamic viscosity-time trend resembles that of apparent viscosity with time already observed by the Authors for ordinary Portland cement pastes and also for gypsum-free cement pastes. (6, 11). It is evinced that FGD-gypsum cement pastes undergo a breakdown of their structure immediately after mixing, and also when subjected to dynamic tests at very low frequency: this is made evident by the initial η' decay with time down to a minimum value, that implies an equilibrium condition where floc aggregation and disaggregation balance; the lower the water/cement ratio, the greater is the amplitude of structure breakdown. After reaching the equilibrium condition, dynamic viscosity increases with time up to a maximum, sometimes nearly constant value; a further η' decay with time occurs and a second minimum is made evident. Then, dynamic viscosity rises again with time as the hydration reaction goes on. The same trend is observed for storage and loss moduli variation with time.

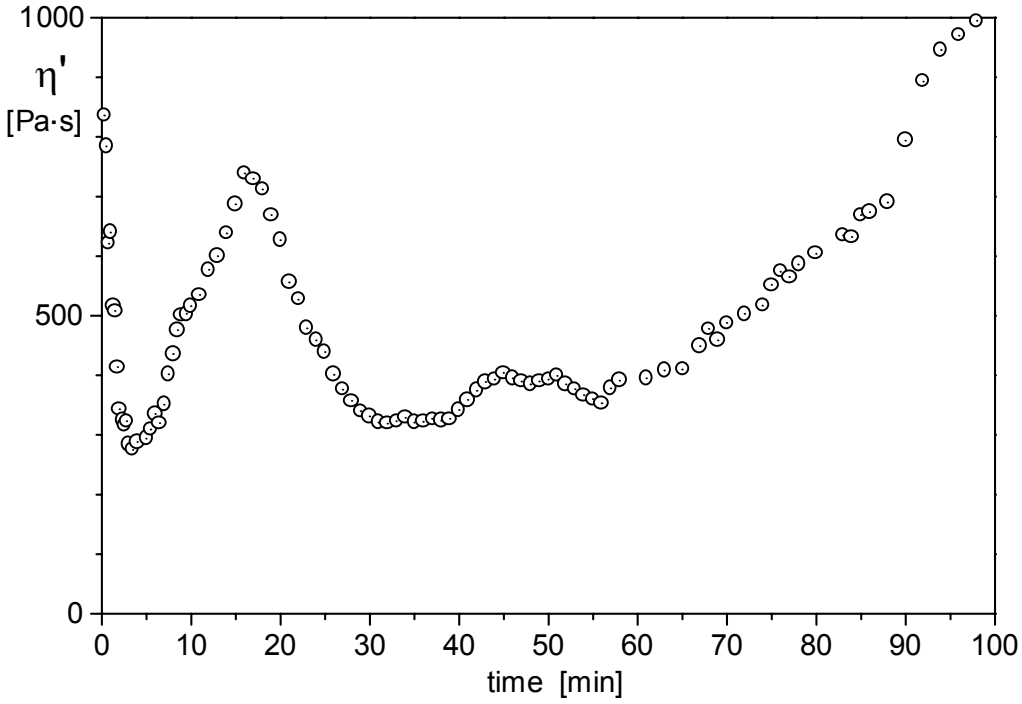

Figure 6. Dynamic viscosity (η') – time (t) transient behaviour for the 0.32 w/c cement paste investigated [0.2 rad of constant strain; 0.1 Hz of frequency].

4. CONCLUSIONS

FGD-gypsum cement pastes exhibit a thixotropic rheological behaviour; their flow curves, derived from the down-curve of the second hysteresis cycle drawn after mixing according to the procedure proposed by the Authors, are of shear-thinning type and may be very satisfactorily described by the Papo-Piani model, whose parameters for physical consistency have also been fully demonstrated. Cement slurries prepared with FGD-gypsum show lower viscosity values than the pastes made with an ordinary Portland cement with the same Blaine number. Finally, the tests performed in dynamic mode permitted the structure evolution of paste from mixing to the initial setting time to be followed by using non-destructive measurements; in particular, the dynamic viscosity-time transient behaviour resembles that of apparent viscosity-time transient behaviour already noticed by the Authors for ordinary Portland cement pastes and also for gypsum-free cement pastes.

REFERENCES

[1] G. Schmidt and E. Schlegel, Rheological characterization of C-S-H phases-water suspensions, “Cement and Concrete Reserach”, 32 (2002) 593-599.

[2] L. Nachbaur, J.C. Mutin, A. Nonat, and L. Choplin, Dynamic mode rheology of cement and tricalcium silicate pastes from mixing to setting, “Cement and Concrete Research”, 31 (2001), 183-192.

[3] C. Ferraris, K. Obla, and R. Hill, The influence of mineral admixtures on the rheology of cement paste and concrete, “Cement and Concrete Reserach”, 31 (2001), 245-255.

[4] M. Cyr, C. Legrand, and M. Mouret, Study of the shear thickening effect of superplasticizers on the rheological behaviour of cement pastes containing or not mineral additives, “Cement and Concrete Reserach”, 30 (2000) 1477-1483.

[5] H. Hodne, A. Saasen, A.B. O’Hagan, and S.O. Wick, Effects of time and shear energy on the rheological behaviour of oilwell cement slurries, “Cement and Concrete Research”, 30 (2000) 1759-1766.

[6] B. Caufin and A. Papo, Rheological behaviour of cement pastes, “Zement Kalk Gips”, 37 (1984) 656-661.

[7] A. Papo, Rheological models for cement pastes, “Materials and Structures”, 21 (1988) 41-46.

[8] A. Papo and L.Piani, Rheology of concentrated aqueous kaolin suspensions, “Silicates Industriels”, 65 (3-4) (2000) 27-32

[9] R.J. Pugh and L. Bergström (eds.), Rheology of concentrated suspensions, in Surfaces and colloid chemistry in advanced ceramics processing, “Surfactant Science Series”, Vol. 51, Marcel Dekker, New York, 1994, pp. 193-244.

[10] A. Papo and B. Caufin, A comparison of the rheological properties of cement pastes with different specific surfaces, “Hungarian J. of Ind. Chem.”, 16 (1988) 279-298.

[11] A. Papo and B. Caufin, A study o the hydration process of cement pastes by means of oscillatory rheological techniques, “Cement & Concrete Research”, 21 (1991) 1111-1117.

[12] L. Opoczky and A. Papo, Rheological and hydration properties of a high strength gypsum-free cement, in H. Justnes (ed.), Proceedings of the X International Congress on the Chemistry of Cement, Göteborg, June 2-6,1997, vol. 2: Cement Hydration, 2ii004.

RECENT ADVANCES ON THE FORMATION OF HYDRATED PHASES AND MICROPOROSITY IN METAKAOLIN-BLENDED PASTES CURED AT HIGH TEMPERATURE

M. Frías[1], M.I. Sánchez de Rojas[1] and J. Rivera[1]

[1] Institute of Science of the Construction Eduardo Torroja (CSIC), c) Serrano Galvache, s/n. 28033 Madrid, Spain. E-mail: mfrias@ietcc.csic.es

ABSTRACT

Due to its high pozzolanic activity, metakaolin (MK) is compared with silica fume. However, this material presents particularly important differences in its chemical composition as well as hydrated phases. Different factors can affect the reaction kinetics and the amounts of the hydrated phases produced during the pozzolanic reaction. Among them, curing temperature is the most important factor on the stability of phases and transformation process.

The current paper shows the results of an investigation focussing on the effect of MK on the reaction kinetics and microporosity of MK blended pastes. Pastes containing 0%, 10%, 20% and 25% of MK were prepared at a constant water/binder ratio of 0.55 and cured at 60ºC for hydration periods of 3, 9 and 34 days.

In the current research, the results show important differences compared with data previously reported by other researchers. In a MK/lime matrix cured at 60ºC, C_2ASH_8, C_4AH_{13} and hydrogarnet were the main hydrated phases, while in a MK-blended cement cured at the same conditions, the C_2ASH_8 (stratlingite) was the only hydrated phase from the pozzolanic reaction. From DTA and XRD, data also reveal an important fact, there is no evidence of the presence of hydrogarnet in MK- blended cement pastes.

The MK blended cement pastes demonstrated an important decrease of the partial porosity (in the interval 1-0,1 μm). At 3 days of curing, porosity values were reduced by between 75% and 86% with respect to the control paste. Therefore, the presence of MK in blended cement pastes was associated with neither a reduction of volume nor a considerable increase of its porosity, due to a possible instability of hydrated phases formed at high curing temperature.

1. INTRODUCTION

In recent decades, pozzolanic materials have been used in different aspects of construction, mainly for their influence on the microstructure and durability of blended cement concrete.

In most cases, mortars and concretes containing material with pozzolanic characteristics have porosity values equal to or superior to that of an OPC matrix [1]. This evolution of the porosity depends on the characteristics of pozzolanic materials, such as fineness, mineralogy, loss of ignition, chemical composition and water/binder ratio used. However, it is well known that the critical factor affecting the performance and durability of concrete structures is pore size distribution, rather than the total porosity.

Proceedings of the 11th International Congress on the Chemistry of Cement (ICCC)
'Cement's Contribution to the Development in the 21st Century'
Hosted by: The Cement and Concrete Institute of South Africa
CD-ROM produced by: Document Transformation Technologies
11 - 16 May 2003, Durban, South Africa
ISBN Number: 0-9584085-8-0
Editors: Dr G. Grieve and G. Owens
Congress Organised by: Event Dynamics

Nowadays, thermally activated kaolinite (metakaolin) is one of the most studied pozzolanic materials because it is very abundant in tropical and subtropical regions, and which do not require the energy necessary to manufacture clinker.

Due to its high pozzolanic activity, metakaolin is often compared with silica fume [2]. However, this material presents particularly important differences in its chemical composition as well as hydrated phases. Different factors can affect the reaction kinetics and the amounts of the hydrated phases produced during the pozzonalic reaction. Among them, curing temperature is the most important factor [2-4].

When MK reacts with calcium hydroxide, cementitious products are formed. It has been reported that CSH, C_2ASH_8 and C_4AH_{13} are the most important hydrated phases at 20ºC of curing temperature. In the literature, Khabit and Wild [5] and, Frías et al [6-7] reported a refinement of the pore structure and an increase of total intruded pore volume in MK-blended pastes cured at 20ºC.

Many previous researchers have showed the positive effect of MK in the incorporation of blended cement pastes (or mortars or concretes) [8-12]. BB. Sabir et al [13] reported that the MK alters the pore structure in cement paste, mortar and concrete and greatly improves the resistance to the transportation of water and diffusion of harmful ions which lead to degradation of the matrix.

In spite of excellent qualities shown by MK as pozzolanic material, its use is in part conditioned by a generalised idea about a possible conversion of some metastables hexagonal hydrates (C_2ASH_8 and C_4AH_{13}) to stable cubic phase (siliceous hydrogarnet with variable composition, $C_3AS_zH_{6-2z}$), when samples are submitted to high curing temperatures. [14].This phenomenon may lead to a negative influence on the performance of MK blended matrixes, mainly on durability.

In recent works Cabrera and M. Frías [3] and, Frías et al [15] reported that the hydrogarnet can be formed from a direct pozzolanic reaction in MK-lime systems at 60ºC and not from a conversion reaction.

Due to the importance that this fact can have on the durability of cementitious materials, as mentioned above, it is necessary to have a better knowledge of the evolution, development and stability phases, with special attention to the formation of a hydrogarnet phase in MK blended cement pastes.

The present paper forms part of an experimental study about the reaction kinetics in MK blended cement pastes cured at 60ºC. The results of this study show the latest advances in this field.

2. EXPERIMENTAL PART

2.1 Materials

A commercial metakaolin was used in the present work. MK has the $Si0_2$ + Al_20_3 content above 92%. It also presents as a product of low crystallinity. Quartz and mica (mainly muscovite) were identified as unique crystalline impurities present. A value of 15.5 m^2/g of specific surface and 130 Å of average pore diameter were obtained using BET techniques.

A commercial white Portland cement available in UK was also used for this study. The BET surface area of cement was 1.04 m^2/g. XRD patterns and chemical compositions for MK and white cement are given in Figure 1 and Table 1.

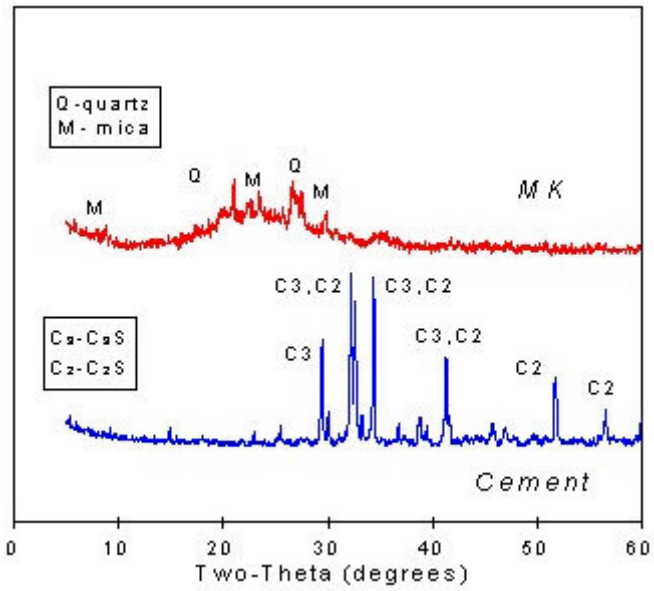

Figure 1. XRD patterns of MK and cement

Table 1. Chemical composition of cement and MK

Oxides (%)	Cement	Metakaolin
$Si0_2$	20.4	51.6
Al_20_3	5.02	41.3
Fe_20_3	2.92	4.64
Ca0	64.25	0.09
Mg0	2.83	0.16
$S0_3$	2.62	-
$Na_20 + K_20$	1.23	0.07
$Ti0_2$	0.21	0.08
L.O.I.	0.7	0.6

2.2 Preparation of specimens and curing

Four different pastes were prepared. White OPC was partially replaced with 0, 10, 20 and 25% of MK. The water/binder ratio was 0.55 by weight.

In all cases, mixtures were placed in plastic airtight containers and then left in a water bath at a temperature of 60ºC. Different hydration times were applied: 30 hours, 3 days, 9 days and 34 days for MK-blended cements. After the predetermined curing time, the hydration reaction was stopped using two different methods, depending on the parameter to be studied:

a) Vacuum oven method. The samples were left at 50^{o}C and 1 bar. After 3 days a constant mass was detected. This method was used for mercury porosity tests (MIP).
b) Microwave method. This procedure was good and quick to dry the samples. Further information can be found in a previous paper [3]. This method was used for DTA and TG tests.

Differential Thermal Analysis (DTA) and X-ray Diffraction (XRD) techniques were used to provide information about the effect of temperature on the pozzolanic reaction kinetics in different matrixes.

3. RESULTS AND DISCUSSION

The effect of temperature on the reaction kinetics in MK-blended cement pastes is clearly identified in Figure 2.

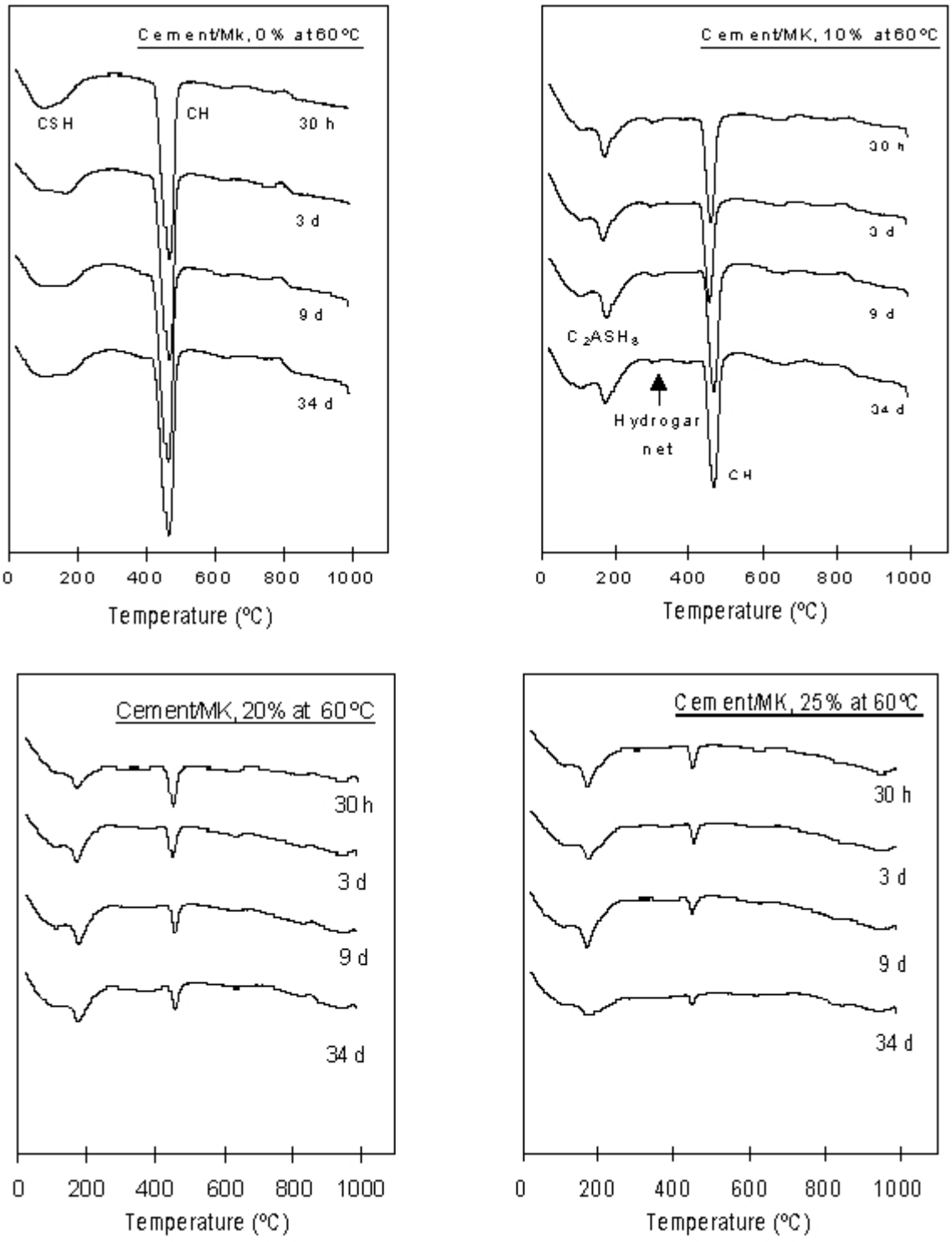

Figure 2. DTA thermograms for MK/cement pastes at 60ºC

Figure 2 shows the evolution of hydrated phases with the curing time for the cement pastes containing between 0 and 25% of MK. These DTA curves illustrate that the main hydrates in white cement were: CSH and CH (portlandite). However, in MK-blended cement pastes an endothermic

peak also appeared at about 170-175 ºC, which was attributed to the C_2ASH_8 phase [3]. The CH concentration decreases with the curing time and with the amount of MK incorporated.

An important aspect obtained from the DTA curves was the absence of compounds, such as: C_4AH_{13} and hydrogarnet, the main phases detected in MK/lime systems cured at 60ºC [15]. A detailed observation of MK blended cement pastes, mainly 10% of MK, showed the presence of a weak endothermic peak, which was situated at 300ºC. This peak might be assigned to the hydrogarnet phase. The intensity of this peak did not vary with the hydration time.

The XRD patterns for all mixtures with MK are very similar, showing that the crystalline compounds were C_3S, C_2S, CH and traces of calcium aluminium oxide carbonate hydrate (peaks at 10.9 and 21.8 2θ). The gehlenite hydrate does not appear as crystalline compound. Figure 3 shows the XRD patterns corresponding to the pastes with 20% of MK.

In this particular case, a weak crystalline peak is easy detected at 17.5 2θ. This fact confirms the presence of traces of hydrogarnet above 30 hours of hydration in blended cement pastes, mainly with 20% of MK. Hydrogarnet was not detected as crystalline phase in the rest of the blended pastes.

From these results, it is important to note that there is practically no hydrogarnet obtained from the pozzolanic reaction in MK blended cement pastes cured at high curing temperatures and in the conditions tested here. This means there is no conversion reaction from metastable hexagonal phases to the stable cubic phase.

The absence of the stable cubic phase (hydrogarnet) in MK blended cement pastes at 60ºC of curing temperature might be related to the different phenomena, which could be compatible at the same time: absence of conversion reaction, an insufficiency of calcium hydroxide to form hydrogarnet, presence of activators from cement, decrease of solubility of CH due to the presence of alkalis, etc.

This fact is a very important aspect from the engineering point of view since the incorporation of MK in the development of new blended matrices (mortars and/or concretes) does not have associated a conversion phenomenon and therefore, a loss of performances and durability.

These findings are totally in agreement with the results obtained from porosity data. Figure 4 shows the total and partial porosity for the four samples studied.

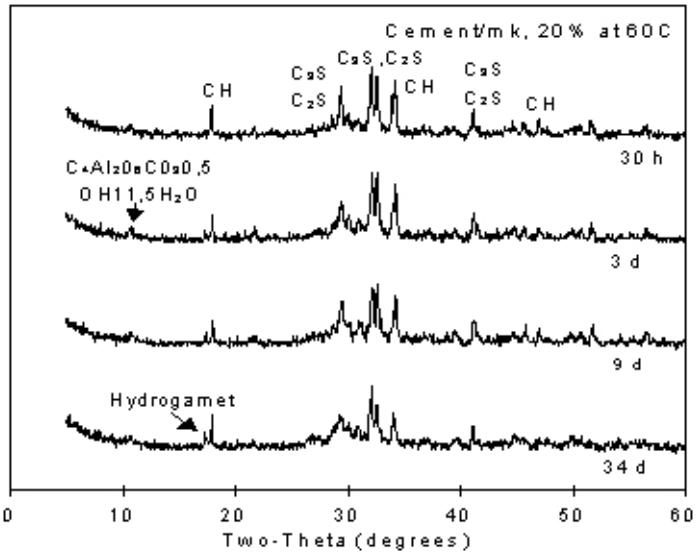

Figure 3. XRD patterns for MK cement pastes (20%) versus hydration time.

The total porosity values for the MK blended cement pastes were very similar to those obtained for the control pastes; except for the case of 10% of MK, a light decrease of total porosity is observed for all ages. The positive effect of the incorporation of MK in the development of blended pastes cured at 60ºC is clearly observed on the porous structure. Pore diameters between 1 and 0.1 μm showed an important decrease of the partial porosity. At 3 days of curing, a reduction was detected of porosity values between 75% and 86% with respect to the control paste.

New studies have been performed at longer curing times in order to confirm the non-formation of hydrogarnet in MK-blended cement pastes cured at high temperatures.

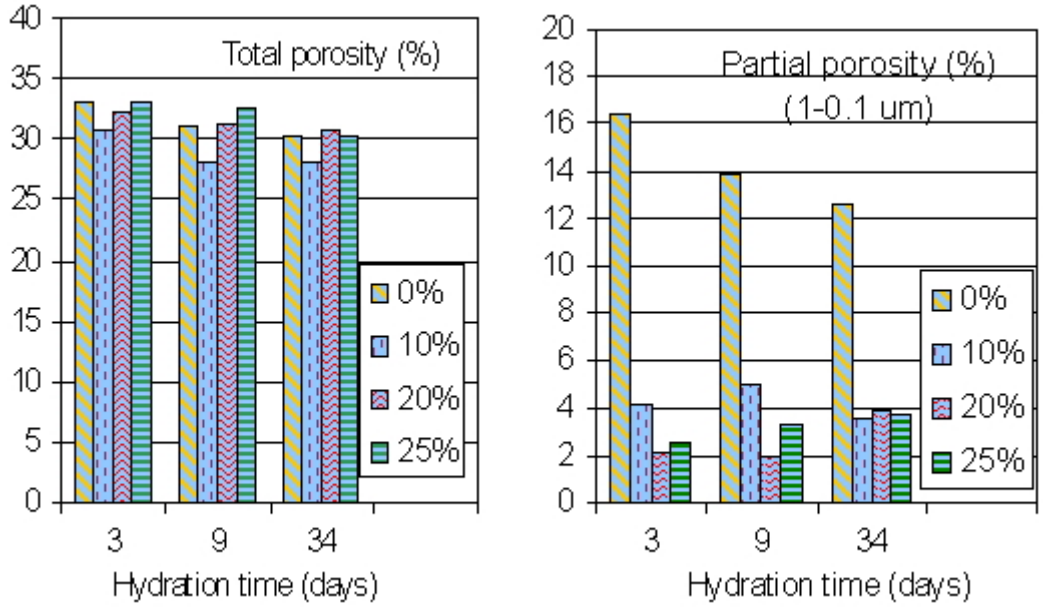

Figure 4. Evolution of porosity versus hydration time

4. CONCLUSIONS

The main conclusions derived from current study may be summarised as follows:

- The reaction kinetics of the pozzolanic reaction between MK and calcium hydroxide is closely related to the curing temperature. At 60ºC of curing, MK-blended cement pastes showed different kinetics to that obtained in MK-lime systems
- From STA and XRD data, the stratlingite (C_2ASH_8) was detected as unique non crystalline compound from pozzolanic reaction between MK and the lime liberated by cement in MK-blended cement pastes cured at 60ºC of curing temperature. There was no evidence of the formation of C_4AH_{13} and hydrogarnet (only traces in some cases).
- The absence of the hydrogarnet phase in MK blended cement pastes suggest that these blended cements will not experience a degradation process and therefore, a loss of performance and durability during its service life due to the conversion reaction.
- The incorporation of MK in the manufacture of blended cement pastes cured at 60º C had a positive effect on the porous structure. A very important pore refinement phenomenon was detected between 1 and 0,1 μm.

ACKNOWLEDGEMENT

The authors wish to thank the TMR Marie Curie grant (European Commission), which supported part of the present research.

REFERENCES

[1] Massazza, F. and Oberti, G. Durability of pozzolanic cements and Italian experience in mass concrete; in V.M. Malhotra (ED), 2nd Inter Conference on durability and Concrete, ACI, Montreal, Canada, 1991, vol.II, pp.1259-1283.

[2] Frías, M.; Sánchéz de Rojas, M.I. and Cabrera, J. The effect that the pozzolanic reaction of metakaolin has on the heat evolution in MK-cement mortars, Cement and Concrete Research, vol. 30, 2000, pp.209-206.

[3] Cabrera, J. and Frías, M. Mechanism of hydration of the MK-lime-water system, Cement Concrete Research, vol.31, 2001, pp.177-182.

[4] De Silva, P.S. and Glasser, F.P. Pozzolanic activation of MK, Advances Cement Research, vol.4,1992, pp. 167-178.

[5] Khabit, J.M and Wild, S. Pore size distribution of MK paste, Cement Concrete Research, vol.26,1996, pp. 1545-1553.

[6] Frías, M. and Cabrera, J. Pore size distribution and degree of hydration of MK cement paste, Cement Concrete Research, vol.30, 2000, pp. 561-569.

[7] Frías, M. and Sánchez de Rojas, M.I. Influence of the MK on pororus of matrixes based in MK/cement, Materiales de Construcción, vol. 50,2000, pp.57-67.

[8] Gruber, K.A.; Ramlochan, T., Boddy, A., Hooton,R.D. and Thomas, M.D.A. Increasing concrete durability with high reactivity MK, Cement and Concrete Composites, vol.23, 2002, pp.479-484.

[9] Dunster, A.M.; Parsonage, J.R. and Thomas, M.J.K. The pozzolanic reaction of MK and its effects on Portland cement hydration, Journal of Materials Science, vol. 28, 1993, pp. 1345-1350.

[10] Kostuch, J.A., Walters,V. And Jones, T.R. High performance concretes incorporating MK: a Review, Concrete 2000, Economic and Durable Construction through Excellence, Dundee, 1993, vol. 2, pp. 1799-1811.

[11] Pera, J.; Bonnin, E. And chabannet, M. Immobilitation of wastes by MK-blended cements, 6th CANMET/ACI International Conference on fly ash, silica fume, slag and natural pozzolans in concrete, Bangkok, 1998, vol. 2,pp. 997-1005.

[12] Cabrera, J.G. and Nwaubani, S.O. Strength and chloride permeability of concrete containing red tropical soils, Magazine of Concrete Research, vol. 45, 1993, pp.169-178.

[13] Sabir, S.S.; Wild, S. and Bai, J. Metakaolin and calcined clays as pozzolans for concrete: a review, Cement and Concrete Composites, vol. 23, 2001, pp.441-454.

[14] De Silva, P.S. and Glasser, F.P. Phase relations in the system Ca0-Al203-Si02-H20 relevant to MK -calcium hydroxide hydration, Cement Concrete Research, vol.23,1993, pp. 627-639.

[15] Frías, M.; Sánchez de Rojas, M.I. and Rivera, J. The effect of temperature on the formation of hydrogarnet in matrices made with MK/lime mixtures, 7th CANMET/ACI International Conference on fly ash, silica fume, slag and natural pozzolans in concrete, Michigan, 2001, vol. 2, pp. 757768.

A COMPARISON BETWEEN TRADITIONAL AND MICROWAVE DRYING METHODS OF CEMENT PASTE

Julian Rivera[1], Mº Isabel Sánchez de Rojas[2], and Moises Frías[3]

Instituto de Ciencias de la Construcción Eduardo Torroja, Madrid, España.
E-mail: [1]Julianrl@ietcc.csic.es, [2] mfrias@ietcc.csic.es and [3] srojas@ietcc.csic.es

ABSTRACT

The aim of this research is to study the viability of using the microwave oven technique as an alternative method to stop the hydration reaction of the cement paste.

In order to determine the effectiveness of this dried method, it has been compared and evaluated with other traditional dried methods (Propan-2-ol , 105ºC oven and 50º C vacuum-oven).

To determinate how the different drying methods stop the cement hydration reaction, the hydration degree of the cement paste is used, which is calculated by mean of the amount of $Ca(OH)_2$ (CH) and the amount of chemically combined water (CW) by Thermal-analysis Technique. Differential Thermal-Analysis (DTA) also is used since it gives very high quality information about the evolution of the compounds in the cement paste.

This research shows the microwave oven is a very effective technique capable of stopping the hydrated reaction of the cement paste quicker than other traditional methods without damaging the cement hydrated compounds.

1. INTRODUCTION

Cement hydration is a complex dissolution-precipitation process in which various hydration reactions proceed simultaneously at differing rates and influence each other. The dissolution of anhydrous phases enables the formation of compounds whose solubilities are lower than those of the anhydrous clinker minerals, thus leading to the precipitation of colloidal and crystalline hydrates that form the hardened paste [1].

A large number of studies about cement hydration or their constituent phases confirm the need to remove the free water from the sample after a specified curing time to stop the hydration reactions and to render the material less susceptible to carbonation, since it eliminates the water which dissolves the CO_2 [2].

The method used to dry the samples is very important. Insufficient drying may not effectively remove the physically bound water, but too severe a drying might dehydrate the chemically-bound water from the hydrated products.

Some papers don't give any specifications of the drying methods used, and the use of different drying methods can give different results. So, it is absolutely necessary to know the drying methods used in each research project.

Furthermore, considering the fact that both chemical and mechanical properties in the cement paste change the most during the earlier part of temporal evolution of the solid-liquid system (1 day), it is necessary to quickly find a drying method capable of eliminating the free water from the cement paste, in order to determine the exact time when the hydration reaction has been stopped.

This research studies how a microwave oven stops the cement hydration, and whether it produces any damage to the different hydrated components of the cement.

2. METHODOLOGY

2.1 Propan-2-ol method

Solvent exchange techniques have been used to preserve the existing structure of the cement paste by replacement of water with a liquid of lower surface tension, since hardened cement paste is extremely sensitive to heat drying methods.

The samples, in which the free water fraction was removed by grinding the material with acetone or alcohol, filtering it, washing it on the filter with additional acetone and ethyl-ether and finally drying in air [3] [4], in vacuum for 24h [5] or at 45ºC [6], are very gentle procedures employed to preserve the Aft and Afm phases, which are discomposed if more drastic water removed methods are employed.

On the other hand, soaking or grinding in polar organic liquids, such as methanol, propan-2-ol or acetone, should be used only in situations where it will not invalidate the subsequent test. Organic substances can be completely removed from C_3S pastes only by drastic procedures that seriously alter the material. Their presence is especially undesirable if any form of thermal analysis is to be carried out, since on heating they react with Calcium Silicate Hydrated (CSH) to give CO_2 [7].

Some workers consider that primary aliphatic alcohol alters structures of C_3S or cement pastes or of synthetic CSH preparations and it has also been claimed that methanol reacts with CH at ordinary temperatures, giving calcium methoxide [8].

For some procedures, such as XRD, the presence of organic material may not matter, but even here; the possibility of discomposing or altering hydrated aluminate phases must be considered [2].

Finally, Propan-2-ol was chosen for this work on the basis of previous studies [9] [10] [11]. Their studies have indicated minimal chemical and physical interference with the hydration products of cement during solvent replacement (methanol and acetone react with the products of hydration, in particular calcium hydroxide).

The samples were soaked in alcohol for 5 minutes and later were washed 3 times with more alcohol, finally they were placed into a vacuum-desiccator over silica gel. The filter used was one vacuum-filter. The samples were in contact with the alcohol for a short time to avoid all problems shown previously.

2.2 105ºC oven method

This method consists of heating the sample at 105ºC for 24h in a very low relative humidity atmosphere (<15%). All the samples are ground into 0.5cm diameter particles.

It is a drastic method, which can partially dehydrate the Calcium silicate hydrate (CSH) and, with cement pastes can also discompose crystalline hydrated calcium aluminates or aluminate sulfate phases.

2.3 50ºC vacuum oven method

This method is based in the elimination of the free water by heating the sample up to 50ºC for 3 days in a vacuum oven.

Although the temperature used is very low, this method can harm some cement compounds as the ettringite, which is decompounded over 60ºC or even at a lower temperature in very dry conditions.

2.4 Microwave oven method

A microwave is a kind of electromagnetic radiation with a wavelength range between 1mm-1m. In order words, it is an ultra high frequency radio, characterized by a fast heating rate, even dewatering and high-energy efficiency, stopping the cement hydration reaction at a determinate age. The equipment used was a 700 w conventional microwave.

To work with this non-traditional drying method, there was a need to prepare and develop an experimental method:

First of all, to avoid possible interference in the results, the sample weights were always the same (5g) and the particle sizes were lower than 0.5cm.

Secondly, the minimum time was calculated to completely dry the samples. To calculate this time several samples of cement paste (water/cement ratio = 0.4) and with different curing times (1h, 3h, 24h y 28 days), were dried for different times.

These samples were kept inside the microwave for 3, 5, 6, 7 and 8 minutes. The lost weight of the samples was calculated as a percentage, taking account of the 100% of the samples and the weight of the dried sample.

Finally, these results are compared with the results obtained by heating the samples up to 105ºC and 50ºC -Table 1.

Table 1. % free water obtained in a cement paste cured to different ages with different dry methods

Methods	**Microwave**					**105ºC**	**50ºC**
Curing (h)	**3 min**	**5 min**	**6 min**	**7min**	**8 min**	**24 h**	**72 h**
1	89,4	92,6	92,7	92,8	93	93	92,7
3	38	39	39,1	39,3	39,4	38,7	37,9
24	28	28,8	28,9	29	29	28,94	29
672	21	21,8	22,2	22,4	22,5	21,23	19,5

The minimum time needed to completely dry the samples was 5 minutes. The microwave oven temperature was checked with a digital thermometer, being 105ºC.

3. MATERIAL AND SAMPLES PREPARATION

The cement used was an ordinary Portland cement (OPC) CEM I 45.2 R supplied by Castle Cement (England). It complies with the requirement of UNE 80301:1996 [12].

The pastes were mixed at water/cement ratio of 0.4 by hand mixing for 2 minutes. Distilled water was used and the pastes made. They were cured in a fog room (RH 95%) kept at 20ºC until required for testing. At the age of testing (3, 6, 8, 10, 15, 20h and 1, 3, 7, 28 days) the samples were taken out of the curing room, ground to under 50mm and dried with the different methods.

The dried samples were sieved on a 0.75mm sieve and kept in sealed glass bottles and placed in a desiccator containing silica gel. At the convenient times they were taken from the desiccator and transferred to the test equipment.

4. EXPERIMENTAL

The hydration degree of the paste, which is calculated by a mean of the amount of $Ca(OH)_2$ (CH) and the amount of chemically combined water (CW) by the thermo-analysis technique, is used to determine how the microwave method stops the cement hydration reaction in comparison with the other methods.

Moreover, this research takes into account another technique, Differential Thermo-Analysis (DTA), which gives better quality information about the evolution of the compounds in the cement paste.

4.1 Thermogravimetry (TG)

The study of the TG curve is based in three specific areas:

1.- Lost weight from 400º-500ºC (aprox.) corresponding to the CH decomposition (table 2).
2.- Lost weight from 600º- 700ºC (aprox) corresponding to the $CaCO_3$ (table 2).
3.- Combined water is considered to the lost weight between 20ºC to 400ºC [14] [15] (table 3).

The Tables 2 and 3 also show the total percentage of CH in the samples, which has been calculated taking account of the correction of $CaCO_3$ formed [13], and the hydration degree of the paste. These values are calculated considering the amount of CH and CW as 100% of a hydrated paste, when the samples have been cured under 20ºC and HR 95% conditions for one year.

Table 2. Total amount of $Ca(OH)_2$ in the samples dried with different drying methods

	Lost weight (%) Ca(OH)2				Lost weight (%) CaCO3				Total lost weight (%)				Hydration degree			
Hours	Micro	105C	50C	alco	Micro	105C	50C	alco	Micro	105C	50C	alco	Micro	105C	50C	alco
3	0,02	0,31	0,24	0,02	0,11	0,35	0,31	0,14	0,27	1,93	1,59	0,36	0,96	6,81	5,61	1,25
6	0,28	0,70	0,59	0,25	0,28	0,58	0,47	0,32	1,67	4,00	3,33	1,65	5,88	14,09	11,73	5,81
8	0,81	1,10	1,13	0,70	0,33	0,54	0,29	0,24	3,96	5,56	5,20	3,33	13,94	19,57	18,29	11,74
10	1,24	1,79	1,66	1,50	0,38	0,78	0,60	0,32	5,84	8,86	7,98	6,79	20,54	31,19	28,09	23,88
15	2,37	2,42	2,49	2,19	0,57	0,90	0,79	0,61	10,83	11,68	11,76	10,18	38,13	41,11	41,41	35,85
20	2,98	2,96	2,98	2,85	1,04	0,81	1,05	0,73	14,22	13,74	14,26	13,11	50,07	48,37	50,20	46,14
24	3,11	3,10	3,14	3,00	0,88	1,14	1,21	0,86	14,47	14,91	15,21	13,98	50,95	52,47	53,53	49,20
72	4,24	4,10	4,09	4,16	1,21	1,17	1,25	1,27	19,75	19,10	19,22	19,53	69,53	67,21	67,65	68,73
168	4,71	4,84	4,69	4,55	1,72	1,73	1,70	1,69	22,65	23,19	22,52	21,94	79,71	81,64	79,28	77,22
672	5,37	5,28	5,16	5,12	1,51	1,79	1,79	1,76	24,95	25,14	24,64	24,40	87,83	88,48	86,72	85,90

Table 3. Combined water

	Lost weight (%)			Hydration degree		
Hours	Micro	105C	50C	Micro	105C	50C
3	0,77	1,29	1,19	6,12	10,31	9,47
6	1,50	2,10	1,94	11,98	16,74	15,42
8	2,47	2,35	2,65	19,69	18,73	21,10
10	3,35	3,38	3,37	26,66	26,95	26,88
15	4,53	4,19	4,77	36,08	33,43	37,99
20	5,84	5,37	5,74	46,52	42,83	45,75
24	6,11	5,69	6,44	48,66	45,36	51,28
72	7,90	7,58	8,40	62,92	60,38	66,96
168	9,28	9,20	9,80	73,98	73,31	78,11
672	10,59	10,02	11,77	84,38	79,85	93,80

The samples dried with alcohol are not absolutely dry, so that it is not possible to calculate the CW formed in these samples.

Finally, the hydration degree is shown in figures 1-3.

These results show that, up to 15h of curing, the samples dried in microwave oven and alcohol have a lower amount of CH than the other methods, but after 15 h curing all the dried methods show very similar hydration degree with a difference of 3 %.

The samples dried in 105ºC oven have the largest amount of CH at all the curing times, though the difference is very small. These differences are very clear at ages less than 10h, which can indicate that this method produces a little acceleration process in the cement hydration.

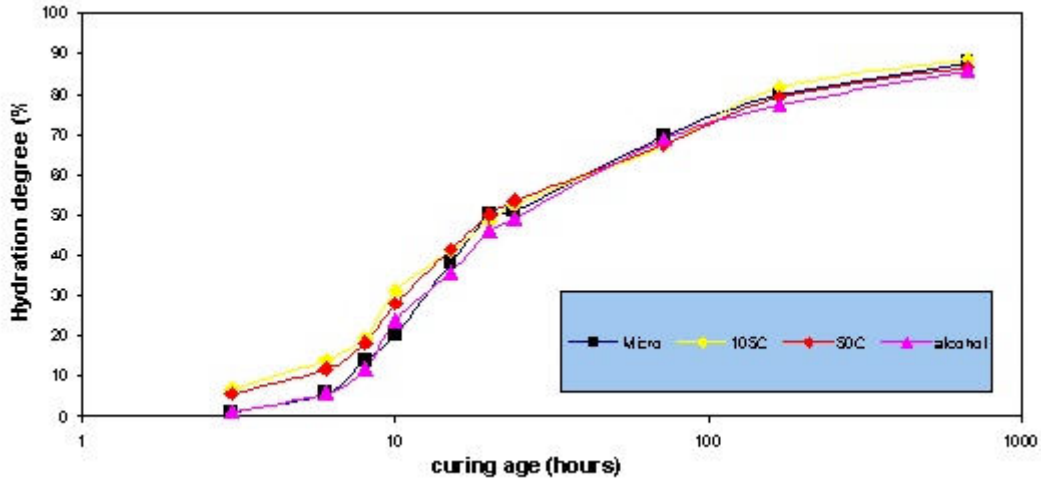

Figure 1. Hydration degree obtained by the calculated amount of $Ca(OH)_2$ in the samples dried with the different methods.

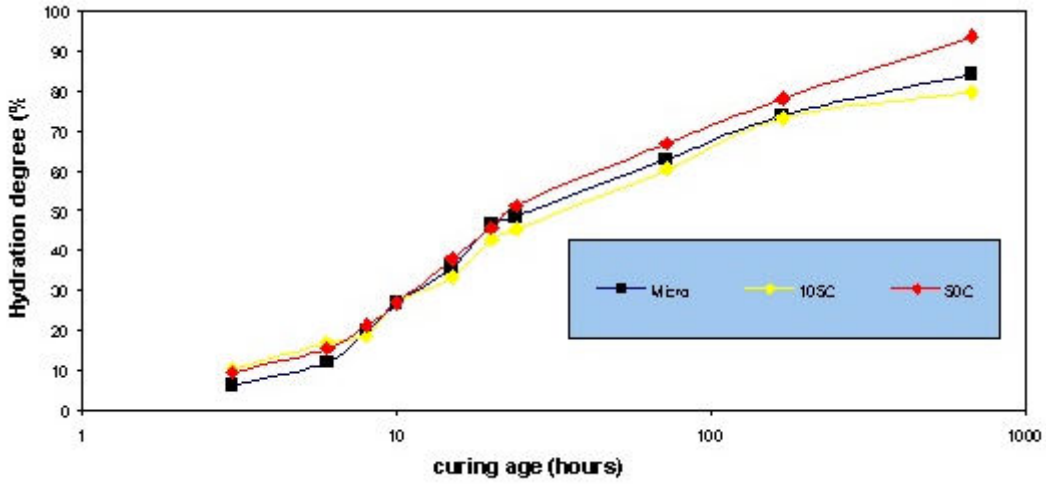

Figure 2. Hydration degree obtained by the calculated amount of CW in the samples dried with the different methods

When the hydration degrees of the same samples are studied taking account different hydrated compounds, the evolution of CW degree is very related to the degree of CH evolution, but in these cases this evolution shows small differences.

The CW microwave values obtained are lower than the 50ºC oven, at curing time less than 8 h, due to the microwave oven drying the samples quicker. But this difference starts to increase after 20h of curing, fact does not happen in the CH degree evolution, where these values are very similar.

Microwave results are lower than the samples dried to 105ºC at ages less than 8 hours, but afterwards the 105ºC samples have a lower amount of CW. This evolution is very different to CH degree evolution, where the 105ºC method shows the highest values.

This is due to the fact that the microwave and 105ºC oven are drying methods more drastic than the 50ºC. So, this different evolution between CH and CW degree evolution is due to microwave and 105ºC partially dehydrating the CW.

It only occurs after 24h curing, because at very early curing times the amount of free water in the samples is enough to avoid an extra heating of the samples, but when the curing time increases the amount of free water decreases, and the sample is more sensitive to the heat, the CW being the more sensitive compounds.

In both cases, it is observed that the microwave oven methods eliminate the water more quickly than the other studied methods

4.2 Differential Thermal Analysis (DTA)

The most representative of the DTA diagrams (figure 3 - 10) is:

a) At early ages (< 24h), the dried samples in 50ºC vacuum oven present a wide band situated in 120ºC, whereas in the dried samples in microwave and 105ºC oven, this band appears divided into two bands; one is situated at 100ºC and the second at 160ºC.

The dried samples in alcohol present a very sharp band in 89º-90ºC due to the free water non-evaporation in the samples. At later ages (>24h) the 160ºC band starts to be observed in the 50ºC dried samples, even in the alcohol dried samples where the free-water band almost hides it.

These bands are mainly due to the formation of CSH, which main bands are situated between 100º-230ºC [16] [17]. But this band can be also formed for other endothermic bands due to different cement compounds such as ettringite (120-145ºC), gypsum (145ºC-160ºC) and monosulphate (130º-190º), but their effects are very small, due to:

1. The amount of these compounds is very small in an Ordinary Cement Portland [18].
2. The only compound formed in the hydration cement that starts from the beginning of hydration and lasts and increases its amount until the hydration ends is the CSH gel.

b) Around *450ºC* there is a very sharp endothermic band due to lost water of the CH. This band increases its intensity and it shifts its position up to highest temperatures when the curing time increases too, due to the largest amount of CH.

The reasons for 105ºC and microwave oven dried samples showing two bands are due to these methods eliminating more combined water than the 50ºC method. The bands which intensity is reduced for these methods are situated under 120ºC (aprox), so that this water is due mainly to free water situated in pores between 10^{-4} - 10^{-5} m (100ºC) and 10^{-6} - 10^{-8} m (120ºC) and interlayer water of the silicates [19] [20].

This decrease of the band can also due to the ettringite decomposition. But this decrease cannot be easily related with the ettringite since all these methods (microwave, 105ºC and 50ºC) destroy the ettringite to a greater or lesser degree. These samples were studied by X-ray Diffraction (XRD), where there goes not appear to be any ettringite peak, except a very small peak in the sample dried with alcohol and by Infrared (IR), where the diagrams don't show any difference among the different samples (Julián Rivera, thesis), (21).

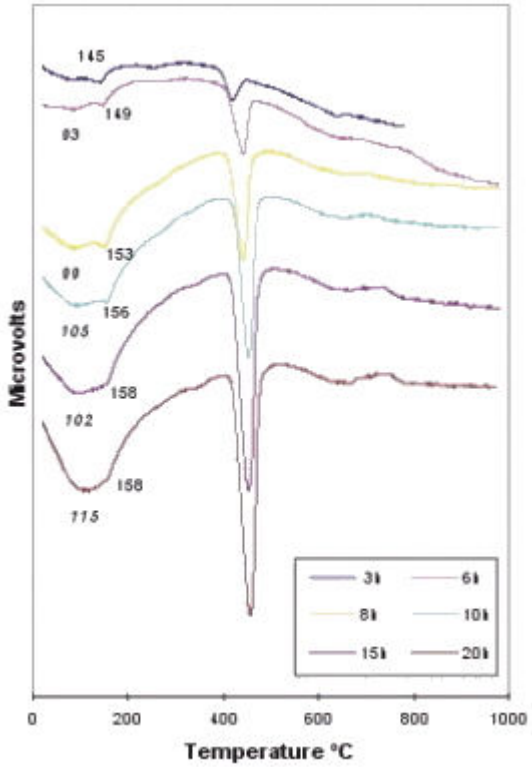

Figure 3. DTA curves,
microwave dried samples (3-20h)

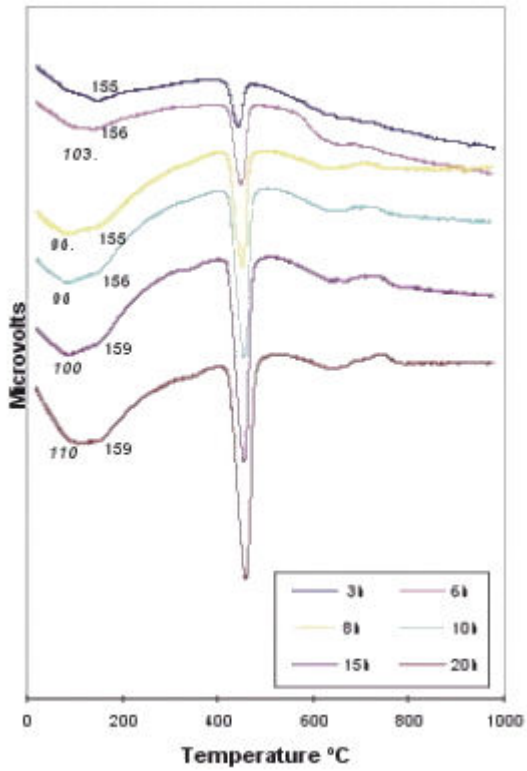

Figure 4. DTA curves,
105ºC dried samples (3-20h)

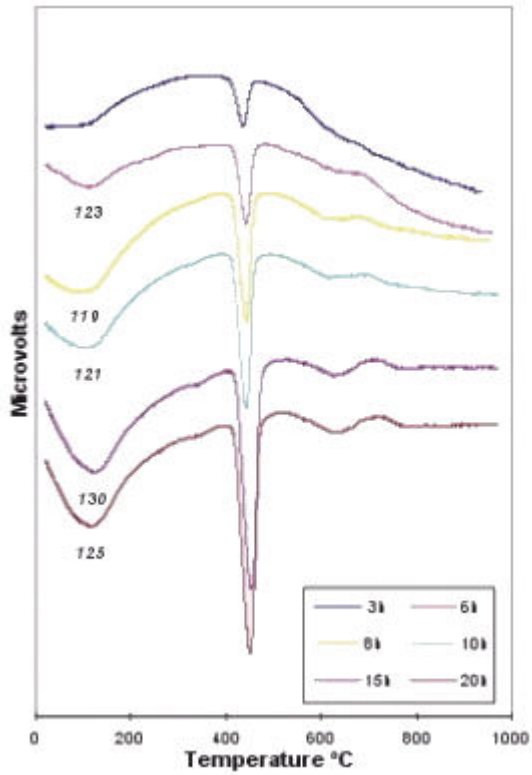

Figure 5. DTA curves,
50ºC dried samples (3-20h)

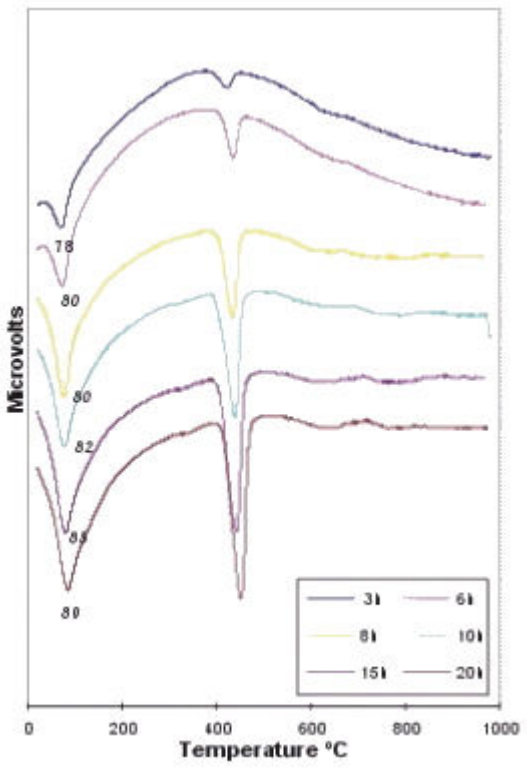

Figure 6. DTA curves,
alcohol dried samples (3-20h)

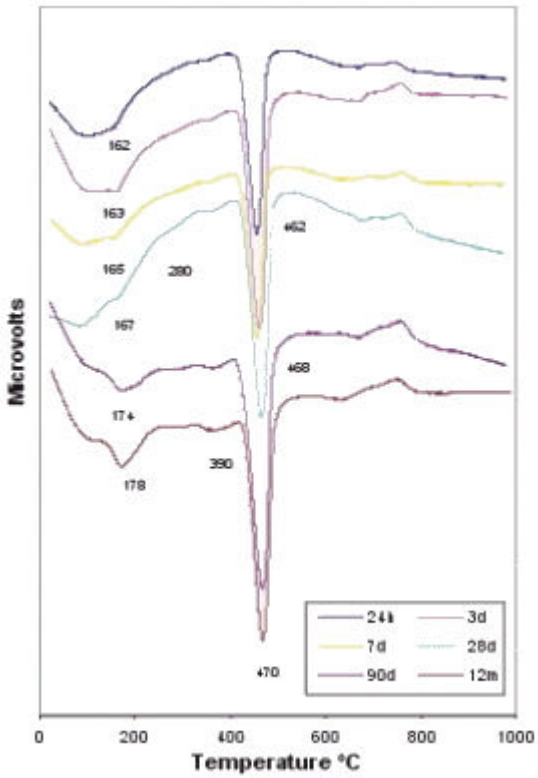

Figure 7. DTA curves,
microwave dried samples (1-365d)

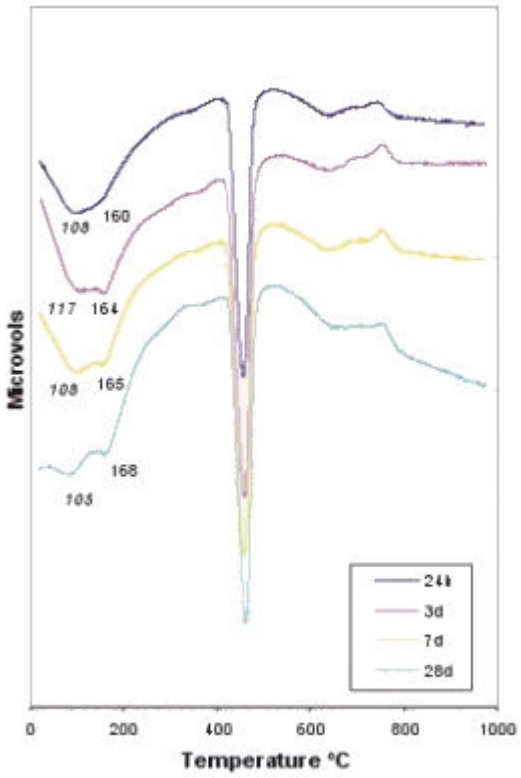

Figure 8. DTA curves,
105ºC dried samples (1-28d)

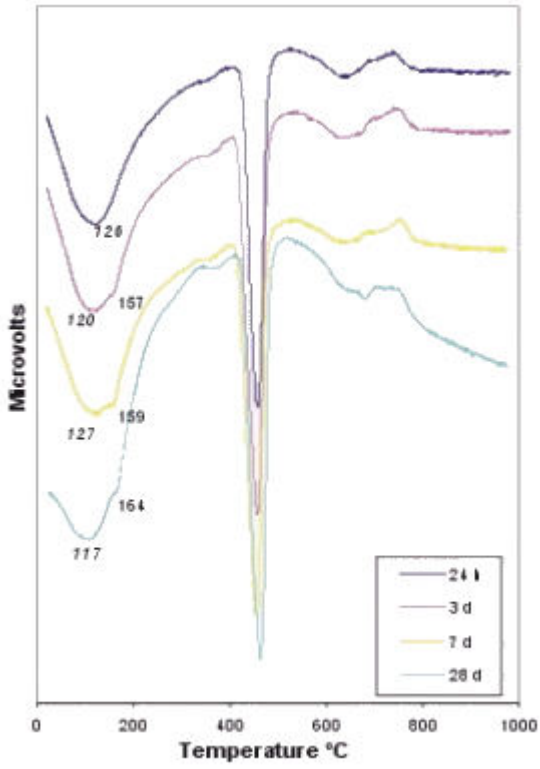

Figure 9. DTA curves,
50ºC dried samples (1-28d)

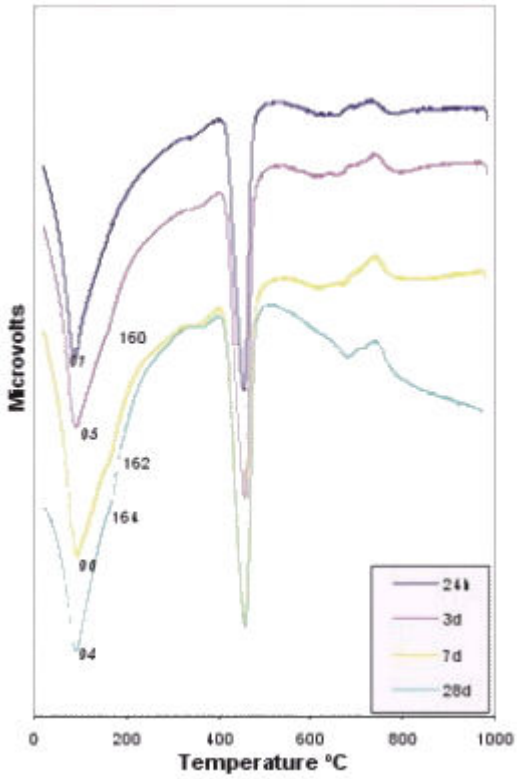

Figure 10. DTA curves,
alcohol dried samples (1-28d)

5. CONCLUSIONS

The microwave oven is a very fast drying method, which is indicated to dry the cement paste with more accurate timing than other methods. But this accuracy is only discernible at very early ages (< 24h) where the cement hydration reaction is more intensive.

The microwave and 105ºC methods are more drastic than the 50ºC and alcohol methods, producing at larger dehydration of the cement paste. Although, under these study conditions the microwave method is less aggressive than the 105ºC method.

This dehydration produced by the microwave method increases when the curing time increases, so it is very important to control the time and the temperature inside the microwave oven to avoid bigger dehydration.

The 105ºC method accelerates the cement hydration, giving different hydration degrees.

REFERENCES

[1] Jawed, I., Skalny. J., Young, J.F. Structure and performance of cements, Hydration of Portland Cement. Ed. Barnes, P. 1983 Chapter 6

[2] Taylor, H.F.W. Cement Chemistry, Academic press, London, UK 1997.

[3] Odler, I., Abdul-Maula, S. y Zhongya, L. Effect of hydration temperature on the cement paste structure, Materials Research Society. Microstructural Development During the Hydration of Cement, vol. 85, 1987, p. 140.

[4] Liang Tong y Nanru Yang. Hydration Products of calium alumino-ferrite in the presence of gypsum, Cement and Concrete Research, vol. 24, 1994, pp. 150-158.

[5] Ftikos Ch. y. Philippou Th. Preparation and hydration study of rich C_2S cements, Cement and Concrete Research, vol. 20, 1990. pp. 934-940.

[6] Sturmer S. Muller A. y Stark J. Hydration of C_3A and $C_2(A,F)$ – separated from sulphate-resisisting and white portland cement- under conditions of normal hardening and heat treatment, Cement and Concrete Research, vol. 24, 1994, pp. 503- 513.

[7] Harrison A.M., Winter N.B. y Taylor. Microstructure and Microchemistry of slag cement pastes, Materials Research Society, Microstructural Development During the Hydration of Cement. L.Struble, P.Brown, vol.85, 1987 p. 214.

[8] Taylor H.F. y Turner A.B. Reactions of Tricalcium silicate paste with organic liquids, Cement and Concrete Research, vol. 17, 1987, pp.613-623.

[9] Feldman R.F. Diffusion Measurements in Cement Paste by Water Replacement Using Propan-2-ol, Cement and Concrete Research, vol. 17, 1987, pp. 602-612.

[10] Robertson B. y Mills R.H. Influence of Sorbed Fluids on Compressive Strength of Cement Paste, Cement and Concrete Research, vol. 15, 1985. pp. 131-137.

[11] Thomas M.D.A. The suitability of solvent exchange techniques for studying the pore structure of hardened cement paste, Advance Cement Research, vol. 2, nº 5, 1987, pp. 29-34.

[12] Norma UNE 80.301:1996, Cementos. Cementos comunes. Composición, especificaciones y criterios de conformidad. Norma Española, 1996.

[13] Cabrera, J.G y Lynsdale, C.J. The effect of superplasticisers on the hydration of normal cement Portland, L´Industria Italiana del Cemento, nº 712, 1996.

[14] Hassan K.E.G,. Influence of surface treatments on the durability performance of concrete, Phd Thesis, University of Leeds. 1993.

[15] Hill, R y Daugherty, K. The iteration of calcium nitrate and a class C fly ash during hydration, Cement and Concrete Research, vol. 26, 1996, pp. 1131-1143.

[16] Saad, M., Hanna, B. y Kotkata, M.F. Effect of SF on the phase composition and microstructure of thermally treated concrete, Cement and Concrete Research, vol. 26, 1996, pp. 1479-1484.

[17] Ismail, M-R. y El-Hemaly, S. Hydration Kinetics of cement paste containg concrete admixture, Cement and Concrete Research, vol. 21, 1991, pp. 683-690.

[18] Gollop, R.S. y Taylor, H.F.W. Microstructural and microanalytical studies of sulphate attack. II. Sulphate-Resisting Portland cement: ferrite composition and hydration chemistry, Cement and Concrete Research, vol, 24, nº 7, 1994, pp. 1347-1358.

[19] Wang, S-D. y L.Scrivener, K. Hydration Products of alkali activated slag cement, Cement and Concrete Research, vol. 25, 1995, pp. 561-571.

[20] Teoreanu, I., Georgescu, M., Puri, A. Hydrated phases in slag-water-activator systems. 7th International Congress on the Chemistry of Cement, Paris, 1980, vol. 3, pp. 99- 104.
[21] Rivera Julian. Cement hydration with Industrial by-product and waste material. PhD Thesis, 2002 in study.

EXPLANATION OF LONG-TERM COMPRESSIVE STRENGTH OF CONCRETE CAUSED BY THE SET ACCELERATOR CALCIUM NITRATE

Harald Justnes

SINTEF Civil and Environmental Engineering, Cement and Concrete,
7465 Trondheim, Norway. E-mail: harald.justnes@civil.sintef.no

ABSTRACT

Calcium nitrate (CN) is used worldwide as an admixture for concrete, in particular for applications utilising its properties as set accelerator. However, CN also enhances the long-term compressive strength of concrete. This strength enhancing property should not be utilised before the reason for it is understood.

Concrete (low alkali portland cement, 4 % silica fume and w/(c+s) = 0.45) with additions of 2 % of the set accelerator calcium nitrate (CN) was shown to exhibit a long-term compressive strength increase relative to reference. The strength was also measured on equivalent paste cubes of 50 mm with and without 2% CN of cement weight. Thus, the strength increase could not be due to improvement of aggregate/binder interface alone. The paste was also subjected to detailed investigations by NMR, MIP, DTA/TG and SEM.

As an overall conclusion, the long-term strength increase of concrete caused by the addition of 2 % calcium nitrate to the fresh mix seems to be due to lower porosity of the binder only observable by gentle drying techniques (i.e. water replacement by ethanol followed by drying at 50°C).

1. INTRODUCTION

During the later years of research on calcium nitrate as a concrete admixture, particularly as a set accelerator, substantial long-term strength increase has been observed. The possible causes for this have recently been discussed [1, 2] based on non-systematic observations over several years. The present study, on the other hand, is the first attempt at a systematic study of the phenomenon, making concrete specimen and paste specimen of identical binder composition with and without 2% dry calcium nitrate of the cement weight. This dosage was chosen since previous data showed that there was no extra strength gain at even higher dosages for the low alkali type cement used.

2. EXPERIMENTAL

2.1 Components

Norwegian high strength Portland cement (ENV 197/1 CEM I 52.5 R-LA) produced by Norcem, Brevik, was used. The cement conformed to the requirements given in ENV 197/1 and had the following properties: Characteristic compressive strength in plastic mortar: $\sigma_{c,1}$ = 18.8 MPa, $\sigma_{c,7}$ = 44.6 MPa and $\sigma_{c,28}$ = 58.3 MPa. Specific surface according to Blaine was 366 m^2/kg. The cement showed no sign of false setting and the content of C_3A was 5.3 % according to Bogue calculations.

The silica fume was delivered by Fesil, Lillleby, Norway, and had specific surface 22.1 m^2/g a measured by BET and consisted of 94.7% SiO_2.

Limestone filler was delivered by Franzefoss, Norway, while Årdal aggregate was supplied by Norstone AS, Norway.

A granulated, technical quality calcium nitrate (CN) was used that may be expressed as $xNH_4NO_3 \cdot yCa(NO_3)_2 \cdot zH_2O$, with x = 0.092, y = 0.500 and z = 0.826. In other words it consisted of 19.00 % Ca^{2+}, 1.57 % NH_4^+, 64.68 % NO_3^- and 14.10 % H_2O. The manufacturer was Norsk Hydro, Porsgrunn, Norway.

2.2 Concrete

The concrete mixes with recipes as given in Table 1 were tested with respect to workability in terms of slump and spread, air content, fresh density and compressive cube strength at a number of ages (samples made and stored for up to 10 years). Experimental details are found in the next section. Furthermore, the concrete quality was characterised by a capillary suction technique as described in section 2.2.2 after 28 days curing at 90% RH and 20 °C. Cubes of 15 mm were also cut from the specimen and prepared for analysis by scanning electron microscopy (SEM) in order to spot possible differences in transition zones between aggregate and binder.

Table 1. Concrete recipes

Components	Mix 1 (reference)	Mix 2 (2% CN)
CEM I 52.5 R-LA	13,300 g	13,300 g
50% silica fume slurry (E8)	1,060 g	1,060 g
Årdal sand 0-8 mm	36,798 g	36,798 g
Årdal crushed gravel 8-11 mm	14,700 g	14,700 g
Årdal crushed gravel 11-16 mm	14,700 g	14,700 g
40 % SP (Mighty 150)	0.168 g	0.250 g
50 % dissolved CN	-	530 g
Deionised Water	4,696 g	4,432 g

The recipes in Table 1 translate into a composition of 4% dry silica fume of cement weight, w/c = 0.46 and w/(c+s) = 0.44.

2.2.1 Fresh concrete properties and compressive strength of hardened concrete

Measurements of slump, spread, apparent density and air content were performed according to methods given in the Norwegian Standards NS 3662 (ISO 4109), NS 3664 (ISO 9812), NS 3660 (ISO 6276) and NS 3659 (ISO 4848), respectively. Compressive strength was determined after storage at +20°C in air of 100 % relative humidity as a mean of 3 tests per mix and testing age. 100-mm cubes were used as test specimens. Moulding and testing were performed according to the specifications given in Norwegian Standards NS 3669 and NS 3668 (ISO 4012), respectively.

2.2.2 Capillary suction

Six 20 mm slices were cut from the middle of each of epoxy coated concrete ϕ100·200 mm cylinders. The method recommends 105°C drying before capillary suction measurements. After drying, the discs are placed on a grating 1 mm below the water surface in a covered box. The increase in weight as the specimen suck water is monitored for 4 days and plotted versus square root of time. The results from the capillary suction test can be expressed by means of linear regression analyses of two lines. The first line represents the value until the waterfront reaches the top of the specimen and the second, nearly horizontal, line the suction thereafter. The crossing between the two straight lines is calculated and expressed by the water absorption value (Q_{cap}) and time for exposure (t_{cap}). These values can be used to calculate the capillary coefficient, k, and the resistance coefficient, m [1]. The procedure consists of 6 important steps for the specimen:

1. Drying to constant weight.
2. Capillary suction for 4 days with weight monitoring.
3. Water saturation by submersion 3 days in water at 1 atm.
4. Pressure saturation by submersion 3 days in water at 80 atm.
5. The outer volume is recorded by differential weighing of the specimen under water and saturated surface dry in air according to the principle of Archimedes.
6. Drying the specimen to constant weight at 105°C.

From these 6 steps, one can calculate the initial moisture content, total porosity (ε_{tot}), the capillary porosity (ε_{cap}), the air volume (ε_{air}), the average density of the concrete solids (ρ_{sol}) and the dry density of the concrete (ρ_{dry}). A more detailed procedure with formulas is given elsewhere [1].

2.2.3 SEM/EDX

The samples for SEM/EDX were cut into slices with 15 mm diameter and thickness 3 mm and cast in epoxy after drying at 105°C, plane polished and coated with a carbon layer in vacuum in order to conduct electrons. The samples were inspected by SEM (Scanning Electron Microscopy) in the BEI (Backscattered Electron Images) modus. For some images, spot-analyses of chemical elements were recorded by EDX (Energy Dispersive Analyses of X-rays) in order to explain details.

2.3 Cement paste

The cement paste samples were subjected to detailed investigation by the following methods:

- MIP/HeP (Mercury Intrusion Porosimetry/Helium pychnometry)
- ^{29}Si MAS (Magic Angle Spinning) NMR (Nuclear Magnetic Resonance).
- DTA/TG (Differential thermal analysis/Thermogravimetry)
- SEM/EDX (Scanning Electron Microscopy/ Energy Dispersive analyses of X-rays)

2.3.1 MIP/HeP

The samples for MIP/HeP (Mercury Intrusion Porosimetry/Helium Pychnometry) were crushed into bits of about 5 mm and stored in excess ethanol for two months to exchange the free water with ethanol. The selected samples were dried at only 50°C to prevent distortion of the pore structure before the MIP experiments were carried out with the Carlo Erba Porosimeter (Model 2000). This porosimeter records the pore size (radii) distribution of the sample between 50 and 500,000 Å, assuming spherical pores. The density of solid material, ρ_s, was determined by Micrometrics AccuPyc 1330 He-pycnometer, while the particle density, ρ_p, was determined by Carlo Erba Macropores Unit 120. The accuracy of total porosity is within ±0.5 units and the density within ±0.01 units.

2.3.2 ^{29}Si MAS NMR

The samples intended for NMR (Nuclear Magnetic Resonance) were crushed and dried at 105°C. The solid-state ^{29}Si MAS (Magic Angle Spinning) NMR spectra were recorded on a Varian INOVA 300 Spectrometer at the Department of Chemistry, University of Aarhus, Denmark. The single pulse MAS NMR experiments employed high-power ^{1}H decoupling ($\gamma B_1/2\pi$ = 36 kHz) and an observed pulse width of 4.5 μs (45° flip angle). The spinning speed was about 7 kHz and the relaxation delay 60 s. Chemical shift values were calibrated prior to the experiments and given relative to TMS (trimethylsilane). Since the active silicon isotope ^{29}Si only has a natural abundance of 4.5 %, each spectrum shown under results is really an average of more than 1,000 scans to obtain satisfactory signal to noise ratio. The accuracy of the chemical shifts is ±0.1 ppm.

2.3.3 DTA/TG

The samples for DTA/TG (Differential Thermal Analysis/Thermo Gravimetry) were crushed to a fine powder and dried at 105°C (i.e. to remove adsorbed water). The DTA/TG experiments were carried out at a NETZSCH 409 STA with a heating rate of 10 °C/min until 1000°C and nitrogen as a carrier

gas. The sample (≈150 mg) was contained in an alumina crucible and alumina powder was used as a reference. The accuracy of the temperature determined for thermal decompositions was within ±2°C, while the accuracy of the mass losses was within ±0.3 mg.

3. RESULTS AND DISCUSSION

3.1 Concrete

3.1.1 Fresh properties and compressive strength

The fresh properties of the concrete are given in Table 2, while the compressive strength development is listed in Table 3. The reason for the higher dosage of SP (see Table 1) for concrete with CN, was to obtain roughly equal spread.

Table 2. Fresh properties of concrete with and without 2% CN

Fresh properties	0% CN	2% CN
Slump (mm)	170	160
Spread (mm)	443	438
Air (vol%)	1.5	1.6
Density (kg/m^3)	2420	2415

Table 3. Cube mass, m (g), and compressive strength, σ_c (MPa), for concrete without and with 2% CN. Average with standard deviation for 3 parallels.

	0 % CN		2 % CN	
Curing time	m (g)	σ_c (MPa)	m (g)	σ_c (MPa)
8 hours	2465±13	5.9±0.2	2439±8	7.5±0.1
1 day	2456±7	30.9±0.5	2437±11	28.4±0.6
28 days	2449±13	71.1±1.7	2446±5	81.4±1.5
90 days	2458±18	76.6±0.5	2448±9	86.0±1.6
365 days	2465±15	83.1±1.1	2454±6	91.4±0.7

3.1.2 Capillary suction test

The average capillary suction profiles for 6 parallel discs sawn from cylinders of concrete without and with 2% CN are compared in Figure 1, while the results derived from the test are listed in Table 4. As seen from Table 4, the total porosity for the concrete is not significantly different for the two mixes and can thus not explain the increase in compressive strength brought about by the 2% CN addition. However, the k and m values in Table 4 and the profiles of Figure 1 reveal that the concrete with CN absorb water with a slower rate (k) than the reference and that the time for the waterfront to reach the top (m) is somewhat longer.

Table 4. Concrete properties derived from the capillary suction test for concrete without and with 2 % CN. Average values with standard deviations for 6 parallel discs.

Properties	0% CN	2% CN
Air content, ε_{air} (vol%)	1.3±0.1	1.4±0.1
Capillary porosity, ε_{cap} (vol%)	13.0±0.7	12.8±1.0
Dry density, ρ_{dry} (kg/m^3)	2295±21	2299±26
Solid density, ρ_{sol} (kg/m^3)	2678±5	2679±6
k (g/m^2·√s)	18.2	15.5
m (10^6·s/m^2)	46.6	58.4

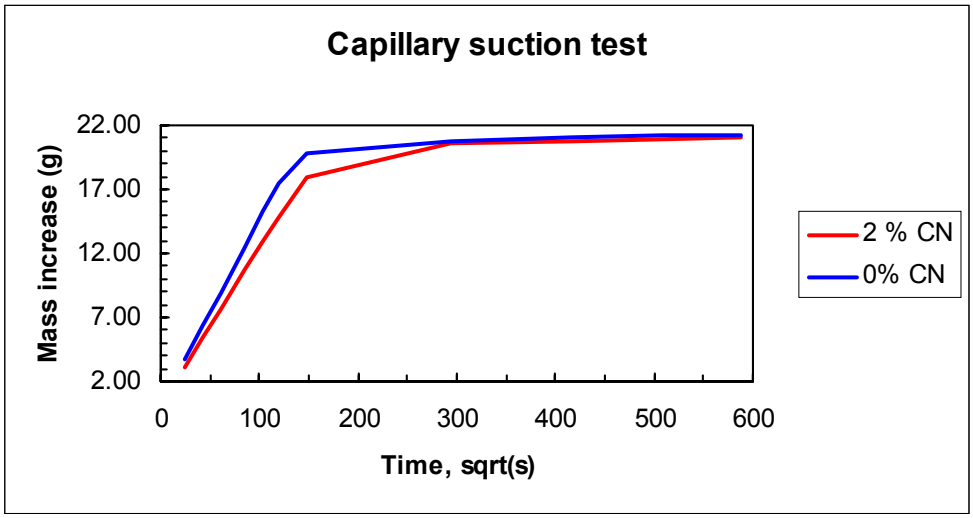

Figure 1. Average capillary suction profiles for concrete without and with 2% CN

Since 105°C may coarsen the porosity, prolonged drying at 50°C was tried out first followed by the normal procedure of 105°C drying used in a former study [1, 2]. However, both drying procedures gave about the same result, [1,2] and the concrete based on low alkali cement and 2% CN had actually marginally higher porosity than its reference.

3.1.3 SEM/EDX

An overview of concretes without CN and with 2 % CN are shown in the upper and lower part of Figure 2, respectively. The binder is the more porous part with black holes (i.e. "Hadley grains" = dissolved cement grain), while the aggregate appears smoother (less pores) even though it contains domains of different chemical composition appearing in different shades of grey.

There is no sign of different porosity in the transition zone between aggregate and binder in the two photos of Figure 2. The only marginal difference may be that there seems to be a slightly higher amount of "Hadley grains" in the concrete with 2% CN (right photo of Figure 2). The irregular, bright grains distributed throughout in both cases are unreacted cement grains and the amount seems to be about equal in both cases.

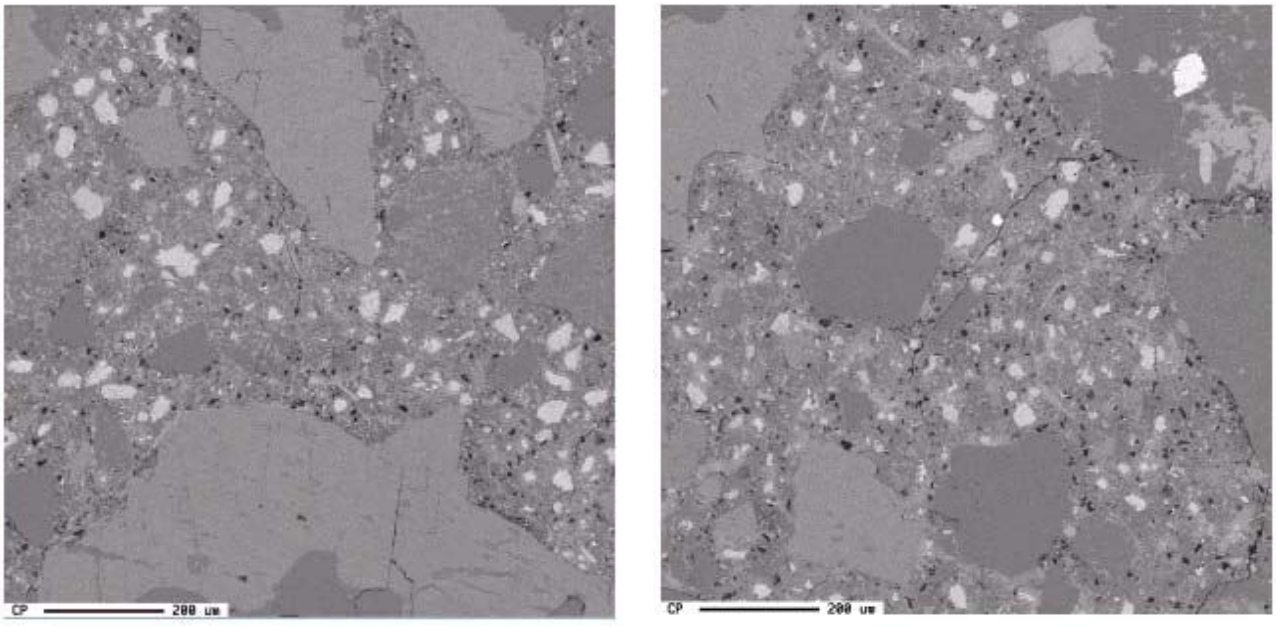

Figure 2. BEI overview of concrete without CN (left image) and with 2% CN (right image).

3.2 Paste

The results from the different investigations of the paste specimen (i.e. containing all the ingredients as for the concrete, except sand and gravel) are reported and discussed in the following sub-sections.

3.2.1 Compressive strength

Testing compressive strength of paste samples is difficult, since the chemical shrinkage of the binder is higher per volume unit than for concrete where the binder is "diluted" by aggregate and where the shrinkage also is restrained by aggregate. Paste samples are thus likely to show a too low strength since they may contain a number of microcracks. This tendency is limited by using smaller samples (often down to 20 mm), but in this case 50 mm cubic specimens were used. However, immediately after setting (i.e. stiffening) the moulds were submersed in water so that the empty contraction pores formed by the chemical shrinkage could be filled with water and less strain formed by water menisci in the pores.

First 4 series with 0 and 2% CN and without and with 20% limestone filler to dilute the cement were made. However, there were too few parallels so it was difficult to draw a conclusion even though the tendency was that samples with 2% CN had higher strength than the reference without. Therefore, new series of plain paste without and with 2% CN were made with 9 parallels and the compressive strength was 69±3 and 74±4 MPa, respectively. The increase in compressive strength both for paste and concrete when CN is added, indicates that it cannot be explained by improved interface between aggregate and binder, but rather by physical or chemical changes of the binder itself.

3.2.2 MIP/HeP

The 4 series with 0 and 2% CN and without and with 20% limestone filler were subjected to pore size distribution (MIP) and total porosity (HeP) studies. Since a recent study [3] has demonstrated that drying at 105°C may substantially alter the pore structure by coarsening the CSH-gel, a very gentle treatment was chosen. First the water in about 5 mm pieces of sample was exchanged with ethanol over a period of 2 months. The ethanol was in great excess and changed several times during the period. Finally, the sample pieces weighing about 1.5 g were dried only at 50°C rather than the usual 105°C prior to the MIP/HeP study. The specific surface; S_g (m^2/g), particle density; ρ_p (kg/m^3), solid density; ρ_s (kg/m^3), specific pore volume; V_g (m^3/kg), specific particle volume; V_p (m^3/kg), mercury accessible porosity; $\varepsilon_{Hg} = 100\% \cdot V_g/V_p$ (%), and helium accessible porosity; $\varepsilon_{He} = 100\% \cdot (1-\rho_p/\rho_s)$, are listed in Table 5 for the 4 paste mixes. The pore size distribution for neat pastes and pastes with 20% limestone filler are plotted in Figure 3.

The results in Table 5 show that the addition of 2 % CN leads to a substantial decrease of the total porosity. Since the difference in mercury and helium accessible porosity is about the same, the difference lies in pore sizes accessible to mercury. The pore size distributions plotted in Figure 3 show that the pore entry size for mercury is shifted from about 20 nm to10 nm when 2 % CN is included in the mix.

Note that the pore size distributions from MIP really represent pore entries. In the case of for instance coarse "Hadley grains" (irregular holes) embedded in a gel with small pores (as seen in Figure 2), the pores around such a hole will be misinterpreted as high in numbers since the mercury will flow through them and into the larger hole. This is a serious drawback to the MIP method and the effect is often nicknamed the "ink-bottle" effect.

Table 5. Results from porosity studies of pastes

CN	0 %	2 %	0 %	2 %
Limestone filler	0 %	0 %	20 %	20 %
m (g)	1.66	1.39	1.65	1.32
S_g (m^2/g)	26.46	28.57	22.58	21.83
ρ_p (kg/m^3)	1,648	1,674	1,726	1,787
ρ_s (kg/m^3)	2,127	2,067	2,196	2,142
V_g ($10^{-3}\cdot m^3/kg$)	0.1282	0.1029	0.1108	0.0768
V_p ($10^{-3}\cdot m^3/kg$)	0.6068	0.5974	0.5794	0.5596
ε_{Hg} (%)	21.1	17.2	19.1	13.7
ε_{He} (%)	22.5	19.0	21.4	16.6

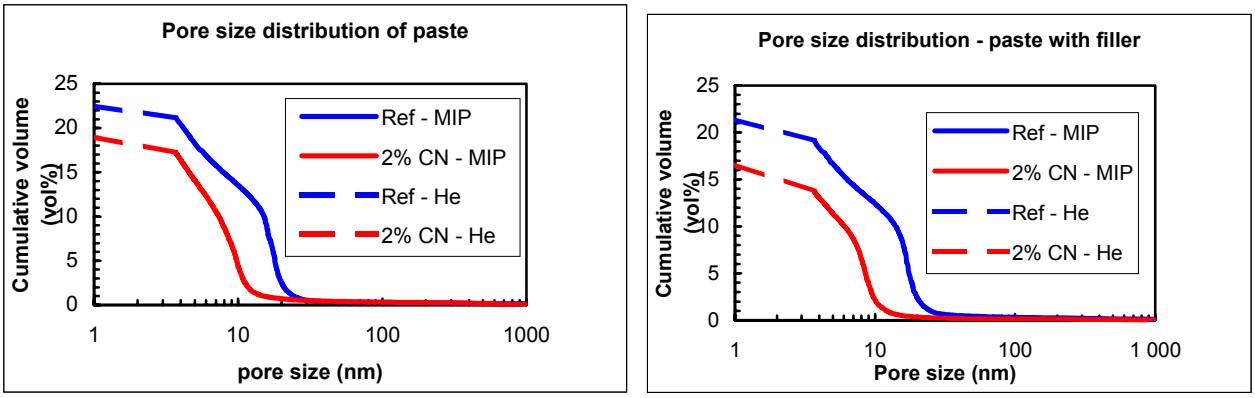

Figure 3. Pore size distribution of paste without and with 2% CN (left) and paste with 20% limestone filler and without and with 2% CN (right).

3.2.3 DTA/TG

The thermogravimetry curves of paste without and with 2 % CN showed only marginal differences between the two samples. The total weight loss at 105°C is somewhat higher for the reference (23.25 %) than for the mix with 2% CN (23.01 %). If chemically bound water is 25% for 100% hydration, the mass losses give a degree of hydration of 93.0 % for the reference and 92.0% for the mix with 2 % CN. However, if anything, this should contribute to an opposite effect on strength than observed.

A sharp mass loss in the range 470-520°C is due to the thermal decomposition of calcium hydroxide. The difference is negligible and the mass loss of water corresponds to a content of calcium hydroxide relative to the paste at 105°C of 11.5% for the reference and 12.0% for the paste with 2% CN. Properly hydrated cement paste without silica fume should have in the order of 25% calcium hydroxide, so about half the content is consumed in the pozzolanic reaction of the 4% silica fume added.

3.2.4 ^{29}Si MAS NMR

The interpretation of ^{29}Si NMR spectra is described in detail elsewhere [4]. The ^{29}Si MAS NMR spectra of cement paste without and with 2% CN are shown in Figure 4. Contributions from unreacted alite and belite are peaks at –67 and –76 ppm, respectively, and the relative intensity from this "doublet" Q^0 is 28.8 and 27.2 for paste without and with 2% CN, respectively, corresponding to the degree of hydration for the silicate minerals of 70.0 and 71.7 % (remembering the 4 % silica fume that has fully reacted). The end group of the silicate anion in the CSH gel (Q^1) at –80 ppm has relative intensity 37.6 and 43.5 % for paste without and with 2% CN, while the mid group (Q^2) at –85 ppm has intensity 30.4 and 26.3 %. There is also a signal from a mid-group in the silicate anion bridged to

an AlO_4-tetrahedron, $Q^2(1Al)$, at –82 ppm with respective intensities of 3.3 and 2.9 %. If the latter is included in the calculation of the average polysilicate anion length, values of 3.8 and 2.2 are obtained for the paste without and with 2% CN, respectively. This is in contradiction to Justnes and Nygaard [4] who observed a slight elongation of the average polysilicate anion when 5.26 % CN was added to paste of OPC (+17%) and SRPC (+5%). However, bot cement types and dosage were quite different.

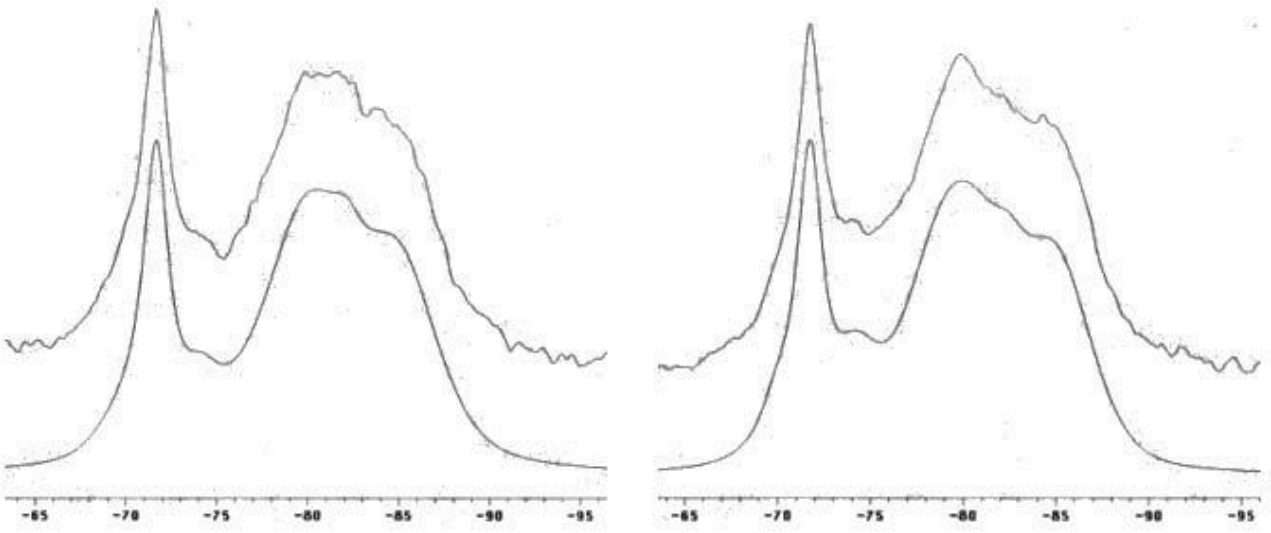

Figure 4. Experimental (upper) and deconvoluted (lower) ^{29}Si MAS NMR spectra of cement paste without (left) and with 2% CN (right).

3.2.5 SEM/EDX

An overview of cement paste without and with 2% CN is depicted in Figure 5, while enlarged images are reproduced in Figure 6. The bright grains evenly distributed in the images of Figure 5 are unreacted cement grains embedded in the dark grey amorphous CSH binder. The lighter grey, irregular areas are calcium hydroxide (CH). These should not be confused with rounded, non-dispersed silica fume agglomerates (some are marked with SF in the images as examples). The only difference between the two samples as seen from the images in Figures 5 and 6 is perhaps that calcium hydroxide seems to appear in somewhat larger cluster in the paste with 2% CN. This may be understood by slightly lower solubility of calcium hydroxide in the paste with CN due to the common ion effect (i.e. Ca^{2+}).

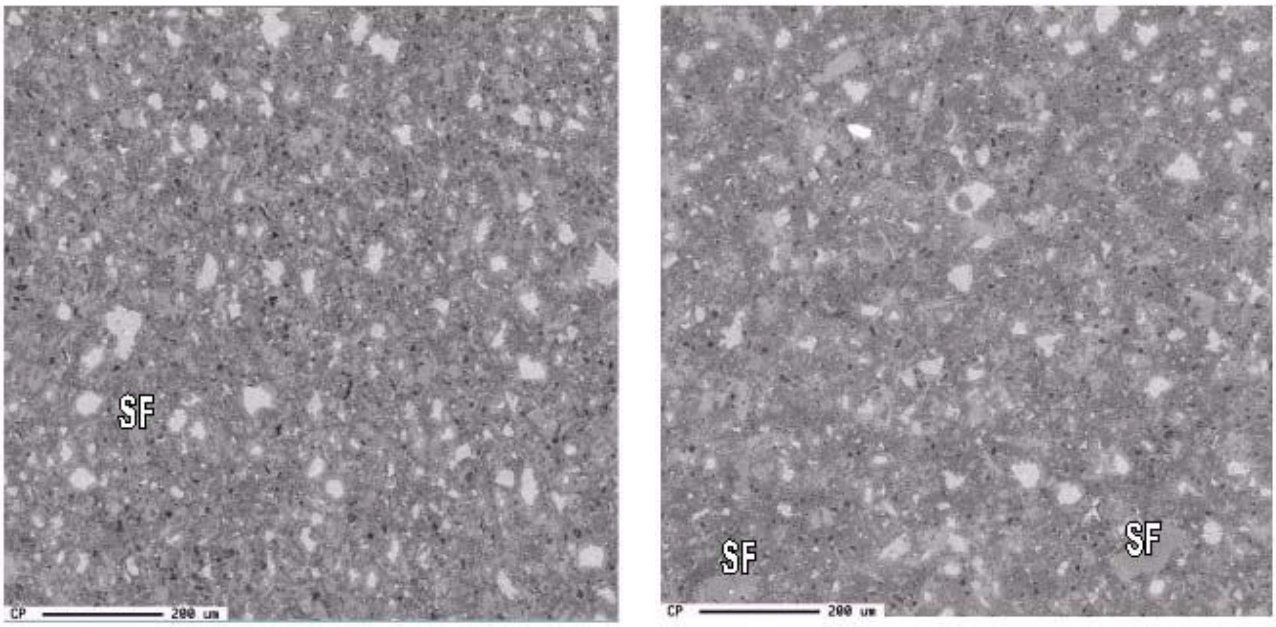

Figure 5. BEI overview of cement paste without (left image) and with 2 % CN (right image).

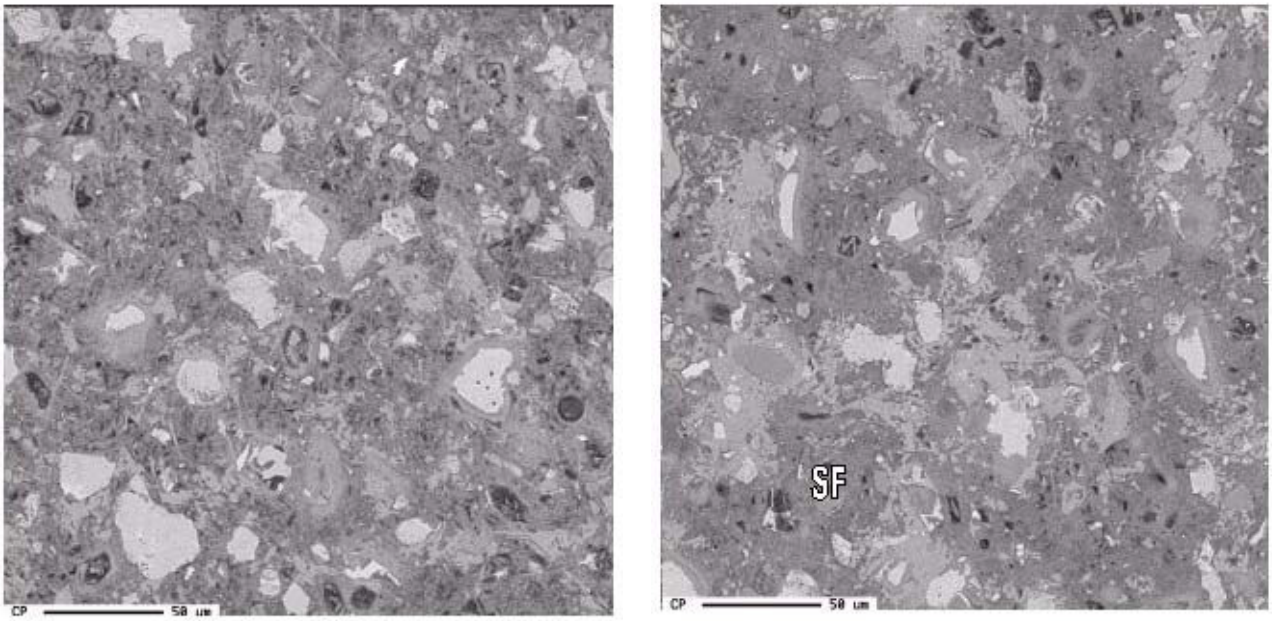

Figure 6. BEI of cement paste without (left image) and with 2 % CN (right image).

4. CONCLUSIONS

The compressive strength of concrete was about 10 MPa higher than the reference at both 28 and 90 days when 2 % calcium nitrate (CN) was added to the fresh mix. Extra specimens are stored at 20°C and 100% RH to see if the strength enhancement prevails for up to 10 years.

The capillary suction test showed that concrete without and with 2% CN had no significant difference in total porosity. However, the water suction rate was somewhat slower (-17%) and the time required for the water to reach the top of the specimen was somewhat longer (+25%) when 2 % CN was added. This could indicate finer capillaries or capillaries partly segmented to a higher degree. Note that specimens were dried at 105°C prior to the capillary suction test.

SEM/EDX of concrete did not reveal any striking differences. The aggregate/binder interface was about the same. There appeared to be marginally more “Hadley grains” (i.e. irregular holes) in the binder of the concrete with 2% CN.

The compressive strength of binder without aggregate (i.e. paste) was about 5 MPa higher than the reference when 2 % CN was included in the recipe. Although the standard deviation was high, it is significant and points to the fact that aggregate/binder interface improvement alone cannot explain the strength increase.

The paste specimens for porosity investigations were treated with a gentle ethanol/water exchange and drying at only 50°C. The total porosity was then significantly less (≈ 30 %) when 2 % CN was included, and the majority of the pore entry sizes was reduced from ≈ 20 nm to ≈ 10 nm.

No significant difference in chemically bound water, calcium hydroxide content or degree of hydration of paste without and with 2 % CN was observed by thermal analysis. ^{29}Si MAS NMR showed a significantly lower chain length of the linear polysilicate anions of the CSH gel when 2 % CN was included, which may be explained by a higher Ca/Si molar ratio of the CSH gel. SEM/EDX of the pastes indicates that calcium hydroxide may be in the form of larger clusters when CN is included, which may be understood by calcium hydroxide solubility suppression due to the common ion effect of Ca^{2+}.

As an overall conclusion, the long-term strength increase of concrete caused by the addition of 2 % calcium nitrate to the fresh mix seems to be due to lower porosity of the binder only observable by gentle drying techniques.

REFERENCES

[1] Justnes, H., Thys, A. and Vanparijs, F.: “Reasons for Long-Term Compressive Strength of Concrete by the Set Accelerator Calcium Nitrate”, Proceedings of Kurdowski Symposium “Science of Cement and Concrete”, Kraków, Poland, June 20-21, 2001, pp. 265-278.

[2] Justnes, H., Thys, A., Vanparijs, F. and Van Gemert, D.: ”Porosity and Diffusivity of Concrete with Long-term Compressive Strength Increase due to Additions of the Set Accelerator Calcium Nitrate”, Proceedings of the 9th International Conference on Durability of Building Materials and Components, Brisbane, Queensland, Australia, 17th-20th March, 2002.

[3] Gallé, C.: “Effect of Drying on Cement-based Materials Pore Structure as Identified by Mercury Intrusion Porosimetry. A Comparative Study between Oven-, Vacuum-, and Freeze-drying.”, Cement and Concrete Research, Vol. 31 (2001) pp. 1467-1477.

[4] Justnes, H., Meland, I., Bjørgum, J.O. and Krane, J.: "Nuclear Magnetic Resonance (NMR) -A Powerful Tool in Cement and Concrete Research." Advances in Cement Research, Vol.3 (1990) No. 11, pp. 105-110.

[5] Justnes, H. and Nygaard, E.C.: "Changes in Microstructure of Cement Paste and Concrete due to Calcium Nitrate Additions", Proceedings of 5th CANMET/ACI International Conference on Superplasticizers and Other Chemical Admixtures in Concrete, October 8-10, 1997, Venice, Italy, ACI SP-173, pp. 657-672

EXPLANATION OF LONG-TERM COMPRESSIVE STRENGTH OF CONCRETE CAUSED BY THE SET ACCELERATOR CALCIUM NITRATE

Harald Justnes

SINTEF Civil and Environmental Engineering, Cement and Concrete,
7465 Trondheim, Norway. E-mail: harald.justnes@civil.sintef.no

Dr. Harald Justnes is Chief Scientist at SINTEF Civil and Environmental Engineering, Cement and Concrete. He has been with the Foundation for Scientific and Industrial Research (SINTEF) since 1985. His field of interest covers the chemistry of cement, concrete, admixtures and additives (including polymers) from production, through reactivity, to durability. He was educated at the Institute of Inorganic Chemistry, Norwegian University of Science and Technology (NUST), and is now Adjunct Professor in "Cement and Concrete Chemistry" at the same institute.

WASTE PRODUCTS FROM PREFABRICATED CERAMIC MATERIALS AS POZZOLANIC ADDITION

M.I. Sánchez de Rojas[1], M. Frías[1], J. Rivera [1] and F.P. Marín [2]

[1]Institute of Science of the Construction Eduardo Torroja (CSIC), c) Serrano Galvache, s/n. 28033 Madrid, Spain. E-mail: srojas@ietcc.csic.es
[2]ITECE. Grupo Uralita

ABSTRACT

The recycling and re-valuation process of waste products involves studies leading to deep knowledge of them and finding applications for their intended use.

In this work, the utilisation of waste products from calcined clay as a pozzolanic material in cement manufacture is studied. One of the first materials used as pozzolan in history was thermal treated clays, material similar to the calcined clay precast elements, whose wastes are the base of this research. For this study, the materials selected are clay products, which have been rejected for various reasons: a low temperature inside the kiln, dimensional and mechanical failures and durability loss.

The kinetics of the pozzolanic reaction is investigated following chemical methods. The hydrated phases were studied by means of X-ray diffraction (XRD). Also, the mechanical properties and hydration heat are studied in the blended mortars.

The pozzolanic activity does not vary significantly for the different samples selected and, on the other hand, this activity is very similar to those products fabricated suitably. So, these ceramic materials with some anomalies due to the calcining temperature, and which are not suitable for commercialisation, can be recycled as pozzolanic materials in the manufacture of blended cements.

1. INTRODUCTION

The utilisation and revaluation of industrial by-products have to acquire greater priority in the future for various reasons: energy cost, cost of raw materials and manual labour, necessity of controlled sinks and mainly, environmental damage caused by the progressive increase of all types of wastes.

For this reason, different world-wide initiatives have appeared to control and regulate the management of industrial wastes and materials from demolition. In this way, the legal restrictions will become stricter to minimise and recycle these products. However, finding definite applications requires additional knowledge for the waste materials,.

In the European Union, the amount of construction and demolition waste varies from 720 Kg/person/year in Germany and Holland to 17 Kg/person/year in Ireland and Greece, giving an EU average of 480 Kg/person/year. Nowadays, the recycled construction and demolition waste average in the EU is between 25% and 30% of production and, the rest is deposited at dumps (1). Holland (90%), Belgium (87%), Denmark (81%) are the countries which recycle most residues in Europe, whereas Spain only recycles 5%. So, The Waste National Plan [1] identifies amongst its ecological objectives the reusing of, at least, 40% in 2005 and a 60% in 2006.

In spite of the improvements in manufacturing process, factories produce significant amounts of material considered not suitable for sale, i.e. waste material. Spain produced more than 21 million tons/year of ceramic material (bricks, tiles, blocks, etc). The amount of factory rejected products depended on the type of manufacture and product requirements.

The ceramic products come from natural materials, which contain a large percentage of clayey minerals. The activation of clay is achieved by means of the dehydration process, followed by the separation of amorphous and active alumina. Clayey minerals such as Kaolinite, mormorillonite or mixtures between them become pozzolanic materials by mean of a controlled calcination process (540ºC -980ºC). If the clays are illites or contain large amount of vermiculite, chlorite and micas, it will be necessary to use higher temperatures for activation [2-3].

This paper studies three waste materials coming from the ceramic sector, researching their applications as pozzolanic materials. The pozzolanic reaction kinetic are studied following a chemical method, X-ray diffraction as well as hydration heat and compressive strength of blended mortars.

2. EXPERIMENTAL, RESULTS AND DISCUSSION

2.1 Materials

This work has chosen 5 ground and milled samples from two different waste ceramic materials. These samples show different particle size distributions, since they were only controlled on the 45 microns residue. Their Blaine specific area was subsequently determined in the laboratory.

The different materials used and their finenesses are shown below:

Bricks: There are three samples of waste ceramic materials producted at different temperatures:
L1: Adequate firing temperature(Blaine 6000 cm^2/g u.). L2: Correct firing temperature (higher temperature) (Blaine 5500 cm^2/g u.). L3: Incorrect firing temperature (lower temperature) (Blaine 5000 cm^2/g u.)

Tiles: Waste materials with adequate firing temperature (one sample with two different fineness):
T1 (3500 cm^2/g u. Blaine) y T2 (3200 cm^2/g u. Blaine)

These materials have a chemical composition similar to other industrial by-products such as silica fume and fly ashes [4] (Table 1). All of them present a marked acid character with alumina and silica as main components and also iron oxide (about 70%); except for sample L3 which shows a high CaO content (48,11%).

Table 1. Chemical Compositions of the samples used in the study

Chemical Compositions (wt%)	L1	L2	L3	T1-T2
LOI	10,82	1,73	4,26	3,44
SiO_2	45,18	50,53	25,97	52,88
Al_2O_3	17,56	19,13	10,50	16,80
Fe_2O_3	5,05	6,62	4,14	5,29
CaO	15,00	14,39	48,13	12,41
MgO	3,35	3,56	3,21	3,64
SO_3	0,00	0,00	3,11	0,79
Na_2O	0,50	0,51	0,41	0,58
K_2O	2,63	3,13	1,20	3,10

The mineralogical composition of the samples were studied by mean of X ray Diffraction. The product L1, Figure 1, comprises quartz (Q), illite (I), calcite (C), hematite (H) and traces of montmorillonite (Mo). The product L2, Figure 2, is rich in feldspans as anorthite (An), piroxenes as augite (Au), quartz (Q) and hercynite (He). The sample L3, Figure 3, is mainly formed from calcium silicate Ca_3SiO_5 (CS) and calcium magnesium aluminum oxide silicate (CM). Samples T1 and T2 have the same composition and are very similar to the L1 sample, although T1 and T2 samples present some more crystalline compounds such as calcium aluminum oxide (CA) and augite (Au), Figure 4.

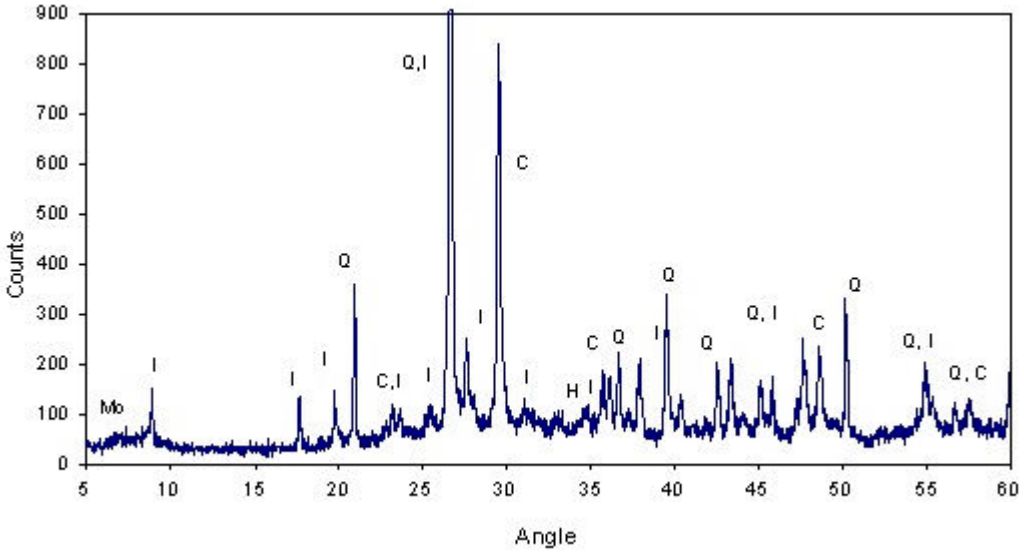

Figure 1. XRD pattern for sample L1

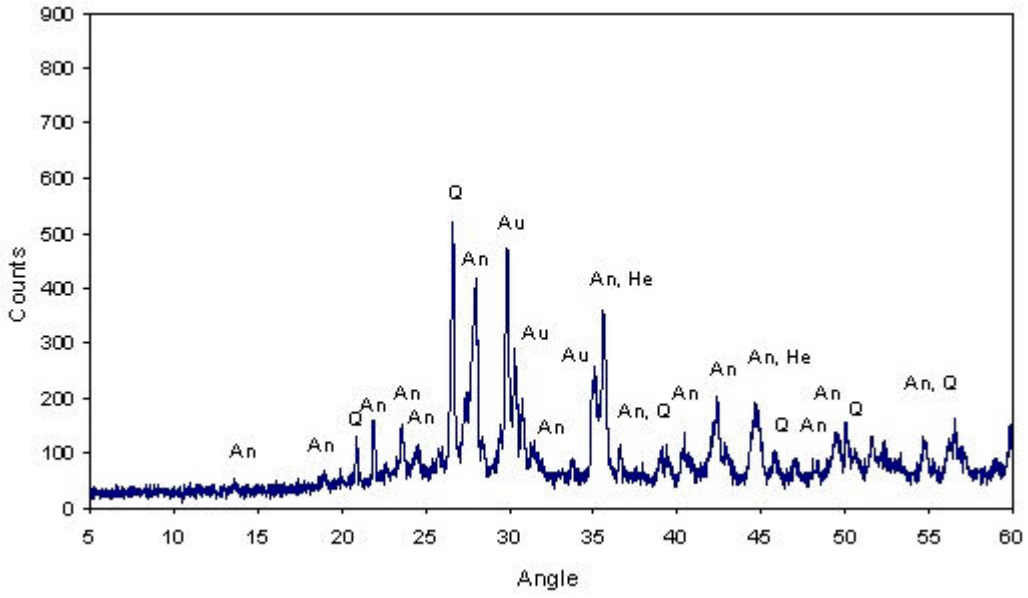

Figure 2. XRD pattern for sample L2

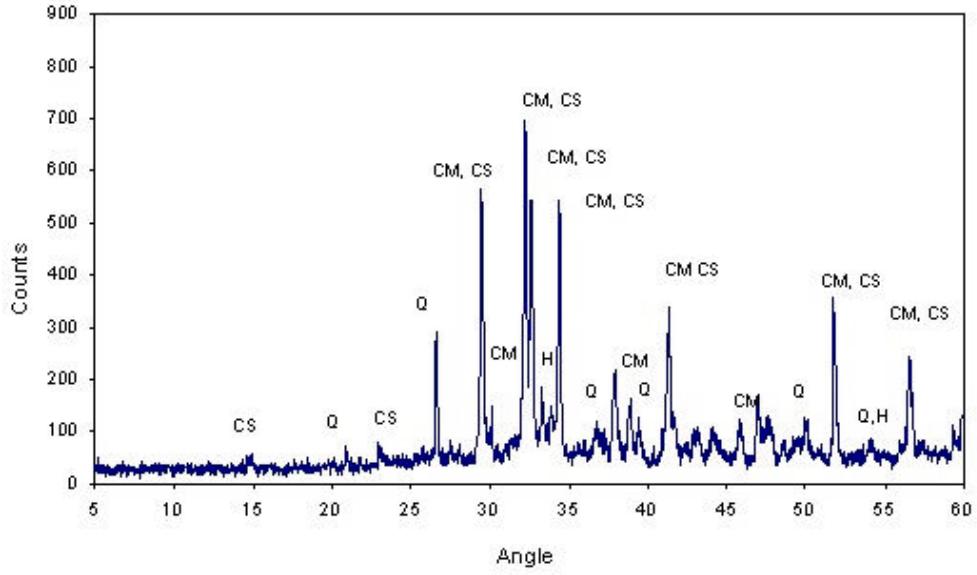

Figure 3. XRD pattern for sample L3

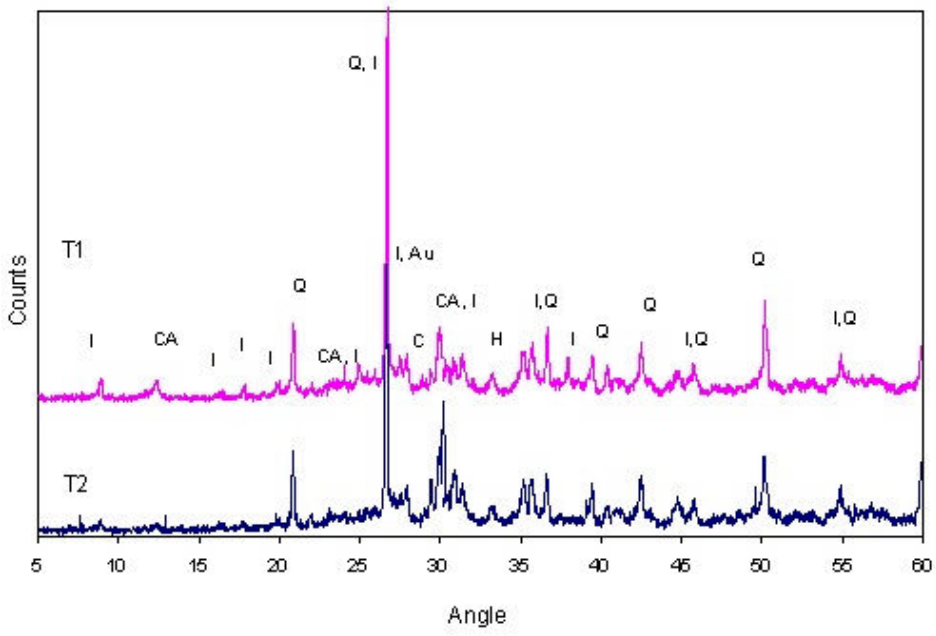

Figure 4. XRD pattern for samples T1 and T2

2.2 Pozzolanic Activity

In order to study the pozzolanic activity of these materials, an accelerated method was used, i.e. the material-lime reaction with time. The test consisted of putting the different pozzolanic materials in contact with a saturated lime solution at 40 ± 1 °C for 1 day, 3 days, 7 days, 28 days and 90 days. At the end of that time, the CaO concentration in the solution was established. The fixed lime (%) was obtained from the difference between the concentration in the saturated lime solution and the CaO found in the solution in contact with the sample, at the end of the given period.

The results (Figure 5) show that the brick residues have an acceptable pozzolanic activity, since at the age of 1 day, samples L1, L2 and L3 fixed 46%, 26% and 11% of lime, respectively. The mineralogical composition has a direct effect on the pozzolanic activity. However in this case, an increase of pozzolanic activity with increasing fineness is observed. This shows a very low activity due to its low fineness. Subsequently, all these samples fix about the same amount of lime, being about 50% at 3 days and 80% at 90 days, when the pozzolanic test finishes

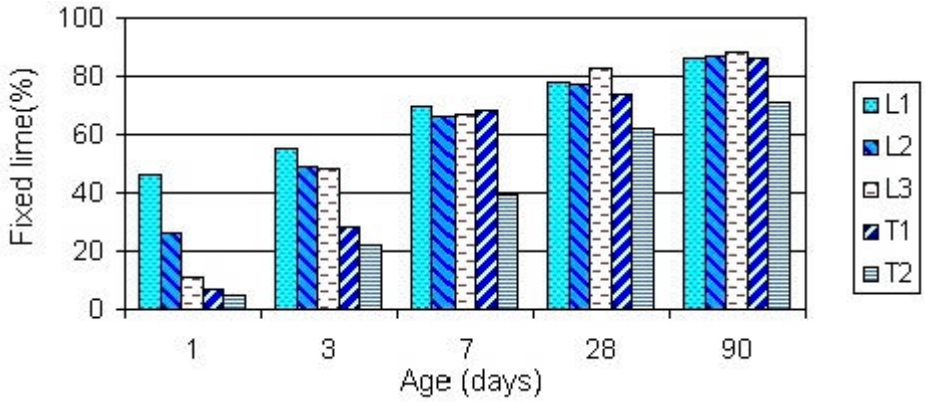

Figure 5. Pozzolanic activity

These results show that the calcining temperature of these ceramic materials (about 900ºC) is enough to activate the clays, giving pozzolanic properties.

The samples with ground ceramic tiles show similar results to the ceramic bricks, although the lower finenesses delay the beginning of the pozzolanic activity. At 7 days, the fixed lime for the T1 sample is 68%, and the low fixed lime of the T2 samples is due to the low specific surface area and is not due to the chemical and mineralogical composition, since both T1 and T2 are made with the same clay material and calcined at the same temperature.

2.3 Pozzolanic Reaction Products

The mineralogical composition of the samples, which have been submerged in lime saturated solution, for 1, 7, 28 and 90 days are studied by mean of X-ray difraction.

The original crystalline compounds in the L1 and L2 samples are maintained during all the ages, but in the L3 sample the CS and CM reacts partially. In this sample new crystalline compounds are formed due to the reaction with the calcium hydroxide, very similar results to those obtained with fly ash [5-6]. In the sample L1 (Figure 6) calcium aluminium hydrate and more specifically C_4AH_{13} (CAH) as well as carboaluminate C_4AcH_{11} (CAc) is formed, although at early ages (24h) is observed monosulfoaluminate (C_4AsH_{12}) (CAs) is observed.

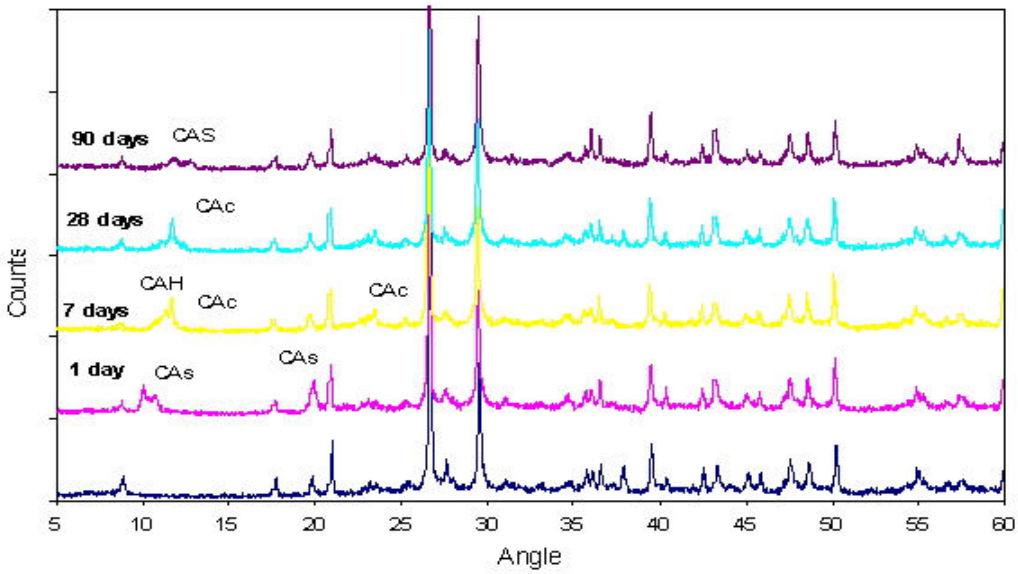

Figure 6. XRD pattern for sample L1 with lime over time

At 90 days ages, the composition progress up to formation of calcium aluminum silicate hydrate (CAS). In L2 and L3 samples (Figure 7) observe mainly the formation of C_4AcH_{11} (CAc), T1 and T2 the tendency is the same, although at 90 days the C_4AH_{13} (CAH) predominates, Figure 8.

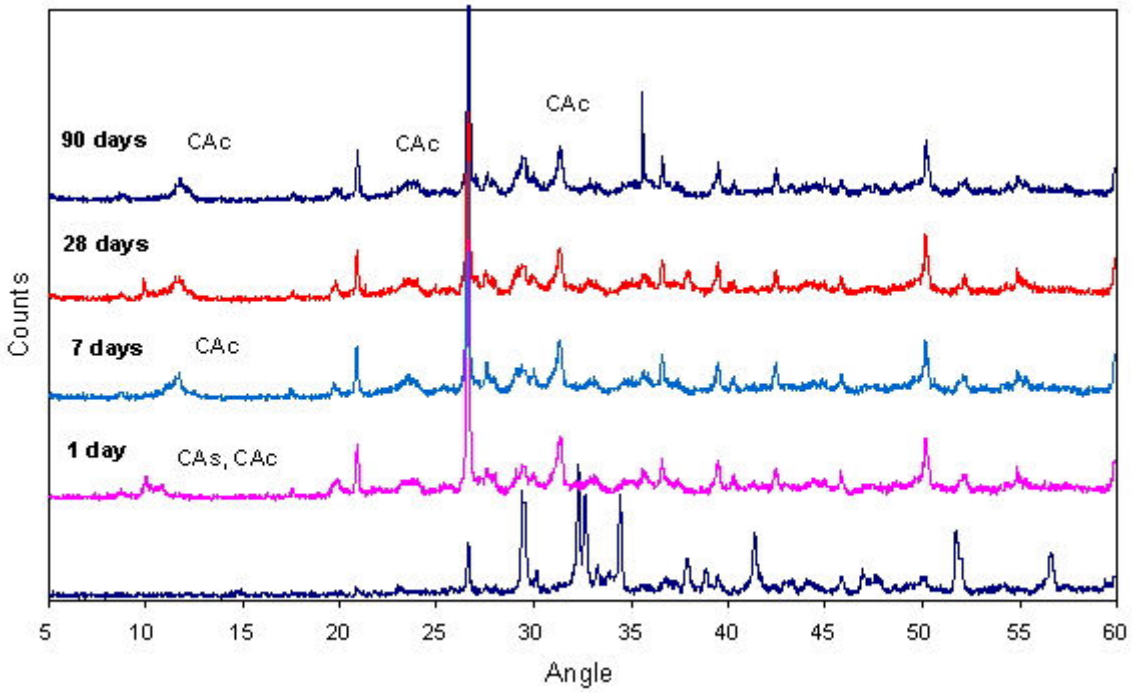

Figure 7. XRD pattern for sample L3 with lime over time

The presence of C-S-H, cannot be confirmed by the x-ray difractograms, because it is hidden by the main peak of calcite and other mineralogical components of the original samples.

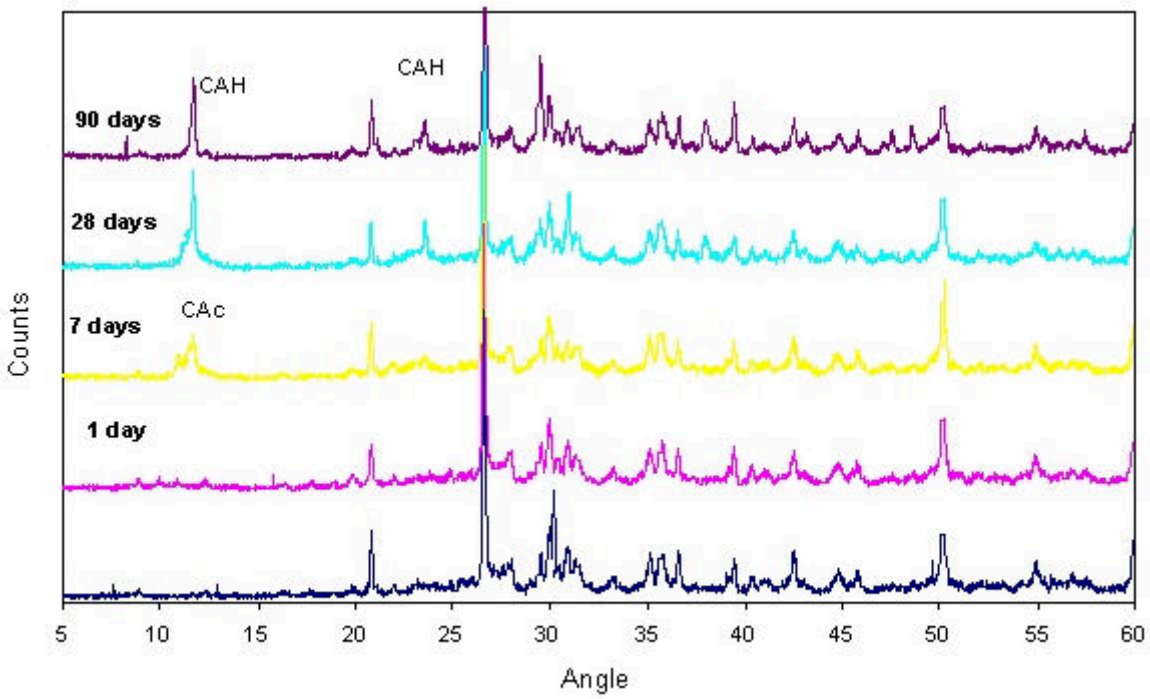

Figure 8. XRD pattern for sample T1 with lime over time

2.4 Mixed Mortar Study

2.4.1 Hydration heat

Waste material T1 was used as the pozzolanic material. The cement is a CEM I-42,5 N, according to UNE EN 197-1:2000 standard [7] and standard sand according to EN 196-1: 1994 standard [8], with a silica content upper to 98% and with a particle size less than 2 mm.

The method given for determining heat hydration in the Spanish standard [9] is based on the Langavant Calorimeter. This semi-adiabatic method consists in quantifying the heat generated during cement hydration using a Dewar flask, or, more exactly, a thermally isolated bottle. Since the exterior conditions are very influential, the test is carried out in a climatized room at 20°C ± 2°C.

The measurements were made over five days, as is required by the standard, since the heat increase is observed to be very low at later times, and also since the relative error of the measurement increases beyond that time.

Samples analysed are:
Reference Mortar: 100 % cement
Blended mortar: cement/ceramic material (T1): 80/20

These mixed cements were used to prepare mortars, whose sand/cement proportion was 3/1 and W/C was 0.5.

The calcined clay decreases the heat developed during hydration of the mixed cement (cement/clay material: 80/20), as shown in Figure 9 and, more clearly in Figure 10.

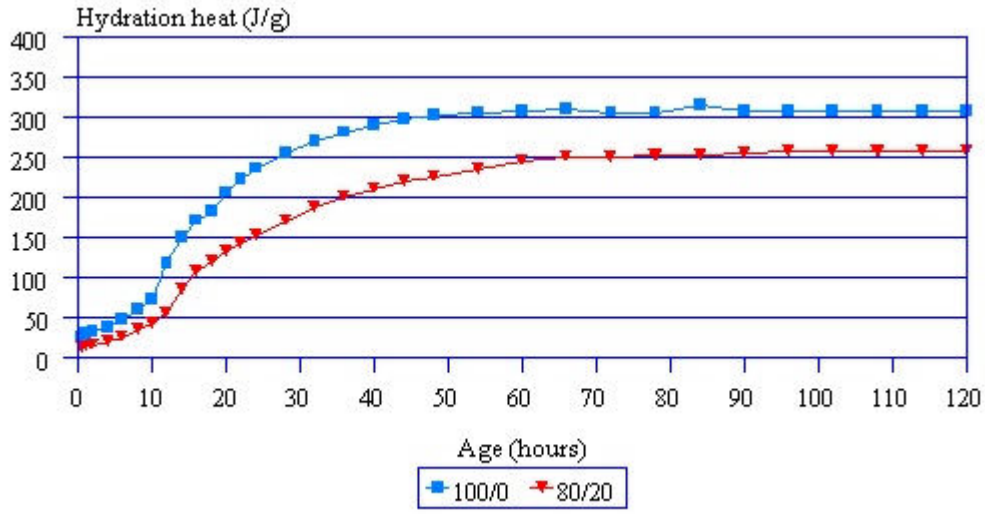

Figure 9. Evolution of the hydration heat

Figure 10 showed the heat increase, positive or negative, developed by the mixed cements with respect to the reference cements taken as zero. As observed, fly ash and clay material present negative values in the heat of hydration test. This is in contrast to that of silica fume with higher pozzolanic activity formerly studied [10] which provokes an increase in the heat of hydration with respect to the reference cement. This increase is due to the weakly exothermal pozzolan-lime reaction, that, in the case of silica fume is able to increase the heat released.

Thus, the calcined ceramic material presents a pozzolanic activity, but the heat developed in this reaction is not able to increase the heat released in the cement hydration, decreasing this heat in a percentage similar to that of the cement substitution by the clay in the mix. So, at 24 hours, the maximum heat for mortar 80/20 is 19% less than that of the reference mortar.

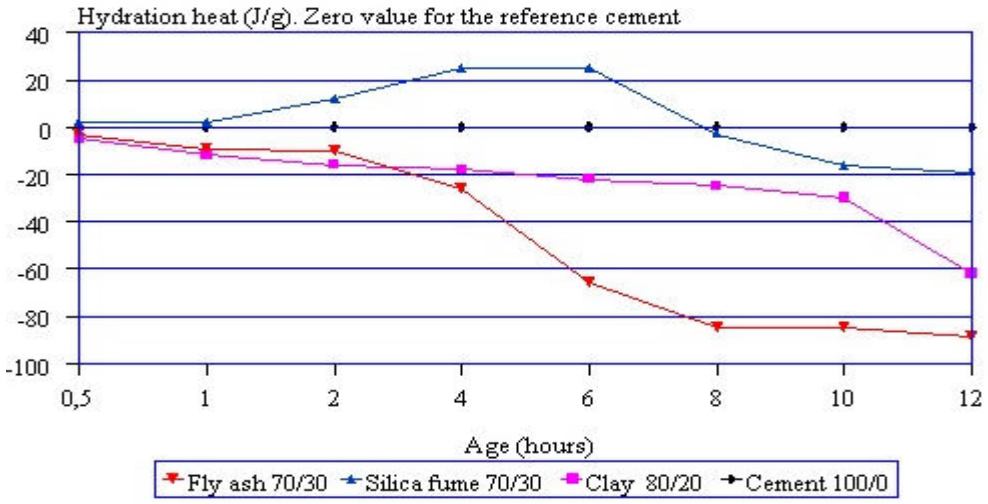

Figure 10. Increase of the hydration heat

2.4.2 Mortar mechanical strengths

The mortar proportioning and mixing is done according to the EN 196-1:1994 standard [8]. The mortar composition was 3/1: sand/cement and W/C was 0.5. The ceramic waste materials used replace a 15% of cement.

The mortar produced are:
M1: Reference Mortar (100% cement)
M2: Mortar with product L1, replacing 15% of cement
M3: Mortar with product L2, replacing 15% of cement
M4: Mortar with product L3, replacing 15% of cement

The results of the flexural and compressive strength tests of the 4x4x16 specimens at 24h and 28 days are shown in the Figure 11. The flexural strengths at 24 hours do not vary significantly. At 28 days of curing, the values obtained are slightly lower than the reference mortar in all cases.

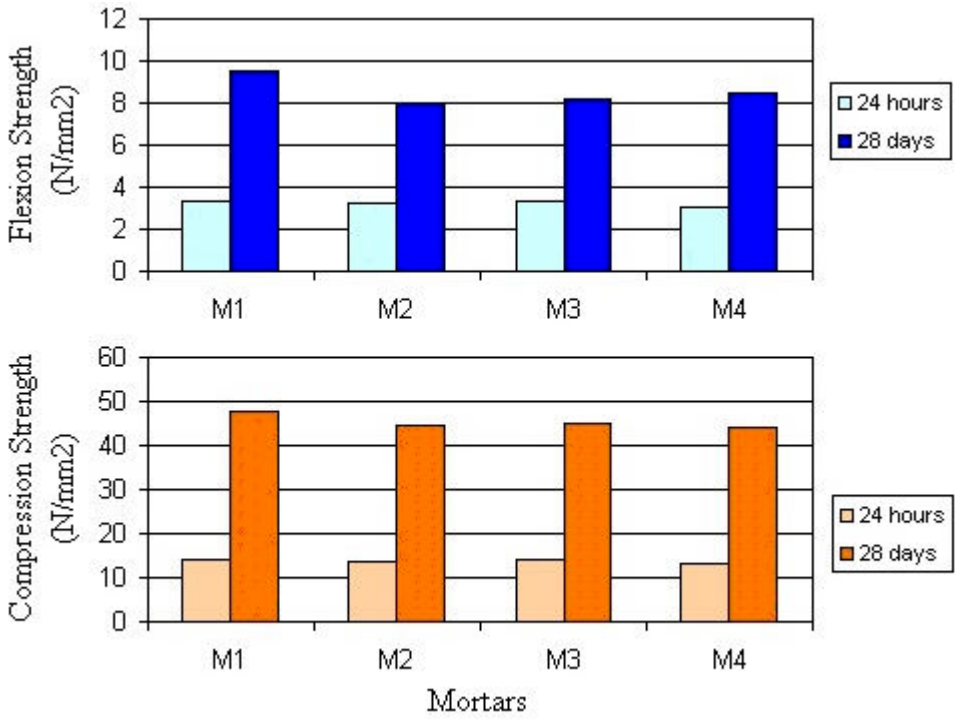

Figure 11. Mortar mechanic strengths

The compression strength results do not show important changes. For the mortars M2, M3, and M4 with a 15% of replacement, the compression strengths decrease slightly compared with the reference mortar, but those are less than the percentage of cement substitution, indicating that these materials act as pozzolanic material improving the compression strengths.

3. CONCLUSIONS

The studies carried out indicate the feasibility of using these waste materials from calcined clay as pozzolans. These results indicate that the firing temperature of these materials (around 900ºC) is enough to activate the clays, giving them pozzolanic properties. The hydration products are similar to those obtained from fly ashes [5].

Mortars that have pozzolanic material incorporated in them usually increase hydration heat, with respect to the reference mortar, during the first hours of the test, depending on the pozzolanic activity of the material, because the reactions taking place with the lime also give off heat [10]. The heat developed in the cement hydration with a 20% of calcined clay is lower than that of reference cement. This is because the percentage of cement substitution counteracts the heat from the pozzolanic reaction, and the substitution effect predominates over the effect of the pozzolanic activity the cement substitution effect is stronger than the pozzolanic activity of the material.

In the mortars with a 15% replacement, the compression strengths decrease slightly compared with the reference mortar, but those are less than the percentage of cement substitution, indicating that these materials act as pozzolanic material improving compression strengths.

ACKNOWLEDGEMENTS

These researches have been done under a Research Project (AMB 96-1095) supported by Technology and Science Interministerial Commission (CICYT), and the collaboration of the Tiles Division of the Uralita Group

REFERENCES

[1] Plan Nacional de Residuos de la Construcción y Demolición 2001-2006. Resolución de 14 de junio de 2001, de la Secretaría General de Medio Ambiente. BOE n.166, 25305-25313, 12 julio 2001.

[2] Calleja, J.: "Las puzolanas". Ión, Ns. 340, 341, 343 y 344, Noviembre y Diciembre, 1969, Febrero y Marzo, 1970. 623-638,700-713, 81-90, 154-160.

[3] Johansson, S; Andresen, P.J.: " Pozzolanic activity of calcined moler clay". Cement and Concrete Research, 1990. V.20, 447-452.

[4] Sánchez de Rojas, M.I., Frías, M. Rivera, J. Escorihuela, M.J., Marín, F.P.: " Investigaciones sobre la actividad puzolánica de materiales de desecho procedentes de arcilla cocida". Materiales de Construcción, 2001. 51, N.261, 45-52.

[5] Luxán, M.P.; Sánchez de Rojas, M.I.; Frías, M: "Investigations on the flyash - calcium hydroxide reactions". Cement and Concrete Research, 1989. 19, 69-80.

[6] Aitcin, P.C.; Autefage, F.; Carles-Gibergues, A.; Vaquier, A.: "Comparative study of the Cementitious properties of different fly ashes". Second CANMET/ACI Int. Conference Fly Ash, Silica Fume, Slag and Natural Pozzolans in Concrete. 1986, Vol. 1, 91-114. Madrid, Spain..

[7] Norma UNE EN 197-1/2000: "Cemento. Parte 1:Composición, especificaciones y criterios de conformidad de los cementos comunes".

[8] Norma UNE EN 196-1/1994: "Métodos de ensayo de cementos. Parte 1: Determinación de resistencias mecánicas".

[9] Norma UNE 80 118/1986: "Métodos de Ensayo de Cementos. Ensayos Físicos: Determinación del Calor de Hidratación por Calorimetría Semi-adiabática (Método del Calorímetro de Langavant)".

[10] Sánchez de Rojas, M.I., Frías, M."The influence of silica fume on the heat of hydration of portland cement". Fifth CANMET/ACI Int. Conference Fly Ash, Silica Fume, Slag and Natural Pozzolans in Concrete, 1995. Vol. 2, 829-843. Milwaukee, Wisconsin, USA.

HEAVY METALS EMISSION MEASUREMENT AND CONTROL

C. Gutierrez-Cañas., C. Urcelay., M. Larrion, E. Guede, E. Garcia, Y. Parra and J.A. Legarreta

Prof. Dr. Ing. C. G.-Cañas, Dpt. Ingeniería Química y del Medio Ambiente. Escuela Superior de Ingenieros. UPV. 48013. Bilbao. Spain. E-mail: iapgumac@bi.ehu.es
Ing. Ind. C.Urcelay, Cementos Lemona S.A., B. Arraibi s/n. 48040 LEMOA-Spain. E-mail: urcelay@lemona.com
Dr. Ing. Ind., Assoc Prof., M.Larrion, Dpt. Ingeniería Química y del Medio Ambiente. Escuela Superior de Ingenieros. UPV. 48013. Bilbao. Spain. E-mail: iaplarum@bi.ehu.es
E. Guede, Cementos Lemona S.A., B. Arraibi s/n. 48040 LEMOA-Spain. E-mail: e.guede@lemona.com
Ing. Quim., E. Garcia, Dpt. Ingeniería Química y del Medio Ambiente. Escuela Superior de Ingenieros. UPV. 48013. Bilbao. Spain. E-mail: iabgarue@bi.ehu.es
Ing. Ind. Parra Y., Dpt. Ingeniería Química y del Medio Ambiente. Escuela Superior de Ingenieros. UPV. 48013. Bilbao. Spain. E-mail: biapagoy@bi.ehu.es
Prof. Dr. Ing. J.A. Legarreta, Dpt. Ingeniería Química y del Medio Ambiente. Escuela Superior de Ingenieros. UPV. 48013. Bilbao. Spain. E-mail: iaplefej@bi.ehu.es

ABSTRACT

Clinker production presents substantial problems of atmospheric emissions, either of flow rates either for the presence of specific pollutants in the fine fraction (heavy metals and, to a lesser extent, organic compounds). The levels of particle size ranges (between 70% and 90% of particles in dry process kiln gas <10 10^{-6}m) imply that global efficiency values cannot be used to estimate either of fine particle emission values or of its variations, the likely direction for any evolution in emission limits. In the range of emission limits, global efficiency values leads to uncertain operation practices to control heavy metals emission and should be replaced by fractional efficiency criteria (concerning total mass loading or a metal of concern). In this work, cascade impactors, used normally to measure the size distribution of particulate matter, are to be employed as sample preseparators. Further analysis of target elements or compounds proceed in the laboratory.

The results lead to a combination of operation variables for emission control (measurement of in-stack size distribution and electrofilter fractional efficiency) with the knowledge acquired from the distribution of heavy metals along the size distribution of emitted dust, which include: Size distributions measured at the inlet and at the outlet of a clinker dust electrofilter, analysis and physicochemical characterization of impactor stages, using AAS, ICP/OES and ICP/MS) and microscopy. The operational result is a curve of fractional efficiency of the electrofilter.

Conclusions cover the observed separation of most relevant trace metals, its usefulness as criterium to specify the raw meal (secondary fuels or feeds), and the use of fractional efficiency as the main criterium to specify and to operate a dust separation unit. Also prospects for real-time monitoring will be discussed.

1. SCOPE

Clinker production presents substantial problems of atmospheric emissions, either of flow rates or for the presence of specific pollutants in the fine fraction (heavy metals and, to a lesser extent, organic compounds). Consideration of some basic data concerning size ranges, for raw gas is particularly important for dry clinker processes. The values of size ranges between 70% and 90% of particles in dry process kiln gas <10 10^{-6}m imply that global efficiency values cannot be used to estimate either fine particle emission values or their variations, the likely direction for any evolution in emission limits. In the range of emission limits, global efficiency values leads to uncertain operational practices to control heavy metal emissions and should be replaced by fractional efficiency criteria (concerning total mass loading or a metal of concern).

1.1 Limits of HM's

The Directive on the incineration of waste (which in conjunction with the Directive 1999/31/CE on landfill disposal and Directive 96/61/EC concerning integrated pollution and prevention control, defines the main legal framework) states emission limits for cement kilns as co-incineration plants with special provisions. Strictly, any variation in material or fuel pattern could be covered by these provisions . The permit shall include emission limit values for dust, SO_2, NO_x, VOC and metals. These limit values may be supplemented or replaced by other equivalent parameters or technical measures.

In the U.S.A., the emission limit values are established in the "40 CFR Part 63, Subpart EEE. NESHAPS: Final Standards for Hazardous Air Pollutants for Hazardous Waste Combustors. Final rule, 30 September in 1999." Table 1 summarizes the different emission limit values.

Table 1. Comparison between emission limit values

Pollutant	IPPC Directive[1]	Final Standards for Hazardous Air Pollutants for Hazardous Waste Combustors.[2]	
		Existing sources	New sources
Dust load[3]	30 mg/m^3	0.15 kg/Mg dry feed Estimates of ELV's: -Dry proc./ preheat./ precalc. 0.040 gr/dscf, (0.092 g/Nm^3) -Long kiln/dry process:0.037 gr/dscf, (0.085 g/Nm^3) -Dry process/ preheater:0.051 gr/dscf (0.12 g/Nm^3)	0.15 kg/Mg dry feed Estimates of ELV's: -Dry proc./ preheat./ precalc.: 0.040 gr/dscf, (0.092 g/Nm^3) -Long kiln/dry process: 0.037 gr/dscf (0.085 g/Nm^3) -Dry process/ preheater 0.051 gr/dscf (0.12 g/Nm^3)
Hg	0.05 mg/m^3	0.120 mg/m^3	0.56 mg/m^3
Cd + Tl	0.05 mg/m^3		
Sb+As+Pb+Cr+Co+Cu+Mn+Ni+V	0.5 mg/m^3		
Cd + Pb		0.240 mg/m^3	0.180 mg/m^3
As+Be+Cr		0.056 mg/m^3	0.54 mg/m^3

[1] Daily mean values. Unit: mg/m^3, referred to 273 K, 101,3 kPa, dry gas and 10% O_2.
[2] Values in dscm (dry standard cubic meter) are referred to standard conditions, 7% O_2 and dry gas.
[3] Under this control, MACT rules consider Co + Mn + Ni + Se + Sb.

The tendency of emission limits (ELV's) has taken cognisance of the experimental knowledge about fine fractions. National ELV'S (for the kiln stack) differ not only on target metals but also in measurement conditions, methods, time interval and frequency. So, there is not yet a common language concerning trace metals emissions, which could provide a common basis for the interpretation of several sampling, analysis, and result reporting approaches.

1.2 Secondary raw materials and fuel substitutes (including typical range of concentrations for the most relevant heavy metals)

Recently, the interest and role of wastes as fuels or secondary raw materials in the cement industry is rapidly growing. Large regional discrepancies are also reported, closely related to the structure of the local market, and policies. But secondary raw material consumption in clinker production should neither be considered merely as a waste treatment option, nor as a privileged co-incineration option; it constitutes a beneficial action over the process life-cycle from other industries and also a traditional practice that contributes to lessen the depletion of natural resources. The use of trace metals as a fingerprint of maximum feed ratio for a specific type of waste is yet to be reported on.

2. EXPERIMENTAL WORK

Data presented here have been collected in a cement plant with nominal production of 2000 t of Portland clinker/day, which uses marl and limestone, and occasionally lime mud and pool rolling, and petroleum coke and tyres as fuel. In spite of the fact that particle emissions are below limits (TSP about 30 mg/Nm^3), real uncertainties have been observed in the achievement of the limits in metal content. This makes it necessary to design a specific experimental program with the additional objective of correlating the dose and operational parameters with the metal emissions.

On-line methods for the measurement of aerosol chemical properties represents a serious gap in existing aerosol instrumentation. Consequently, the control of composition must be periodic and by extracting a representative sample. In this context, the continuous monitoring of PM10 as surrogate for heavy metal control has been proposed. The speciation (relevant to the environmental fate of such an emitted metal) is not generally determined. Continuous emission monitoring, most of the systems being spectroscopy-based, is so far unable to ensure plant monitoring, despite progress in this field. However, continuous emission monitoring could be considered as the up-to-date maximum achievable monitoring- technology.

In this work, cascade impactors, used normally to measure the size distribution of particulate matter, are to be employed as sample preseparators. Further analysis of target elements or compounds proceed in the laboratory. Using this kind of sampling instruments, measurements must meet two conflicting requirements. First, the isokinetic condition require a continuous adjustment of sampling velocity in the probe to match the local in-stack gas velocity. But in order to be able to obtain the particle size distribution, the cut points in each stage of the impactor must be constant over the measuring period, that is, the flow velocity through the impactor must be constant. The results here presented were obtained adjusting the flow at each point.

The size distribution of emitted particles was measured by means of the combination of a sampling train (Napp) and a cascade impactor placed in-stack. The preliminary tests to ensure isokinetic conditions were conducted following the EPA Reference Methods 1 to 5. Two cascade impactors were used in this campaign: a Dekati PM10 (3 stages and a back filter, with nominal cut diameters of 10, 2.5 and 1 μm) and a Pilat Mark III (seven stages and a backfilter), depending on the main goal of the measurement: size distribution and/or chemical analysis.

Sampling and analysis of heavy metals was conducted following the VDI3868, B. 1, 2EVDI 2268, B. 1- 4 standards, and VDZ analytical recommendations.

The size distribution (aerodynamic diameter) of particles in the gas exiting from the preheater and from the conditioning tower were measured using a Ströhlein apparatus for in-duct collection and further fractionation using a laboratory impactor. The sampling conditions (temperature and dust load) leads to unacceptable measuring errors in the case of stack sampling, and values obtained must be considered approximate.

The results lead to a combination of operation variables (measurement of in-stack size distribution and electrofilter fractional efficiency) with the knowledge acquired from the distribution of heavy metals along the size distribution of emitted dust.

3. RESULTS

Figure 1 shows the typical size distribution of particles in the raw gas. The effect of water spray in the conditioning tower is mainly concentrated in the coarse fraction. During the experimental program, only in a few cases were particles larger than 13 μm observed at the electrofilter inlet, and their presence was associated with high gas temperatures and, consequently, poor cooling efficiency by means of water addition. These approximate results are consistent with VDI (1985) figures about raw gas size distribution.

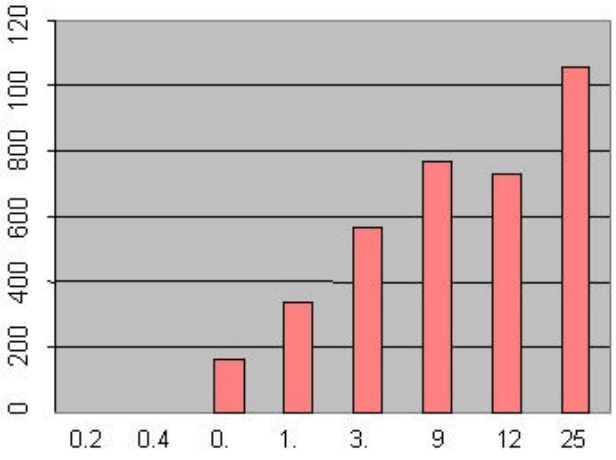

Figure 1. Particle size distribution in raw gas: dM/d(logD) versus aerodynamic diameter in μm

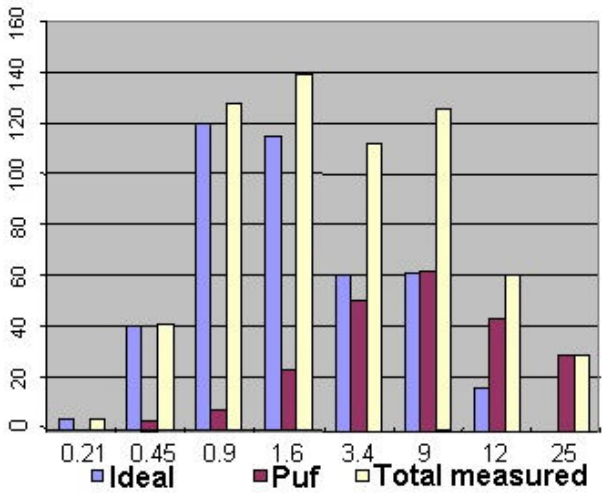

Figure 2. Emission size distribution (Mark III). dM/d(logD) versus aerodynamic diameter in μm

Figure 2 shows the typical size distribution measured at the clinker kiln stack in less favourable conditions, that is, when the crude mill gases are also emitted by this source. The size distribution of the puff due to the electrode and plate rapping was inferred as the difference between total or measured size distribution, and the ideal conditions (no rapping), and filled to a log-normal distribution with 6,0 10^{-6} m of median diameter with a deviation of 2,5, which is considered as a conservative hypothesis

Figure 3 shows the relative contributions of the feed and the fuels to the entry of heavy metals. The differential enrichment of the traces in the clinker kiln dust (CKD), recirculated from the hoppers of clinker kiln electrofilter are observed.

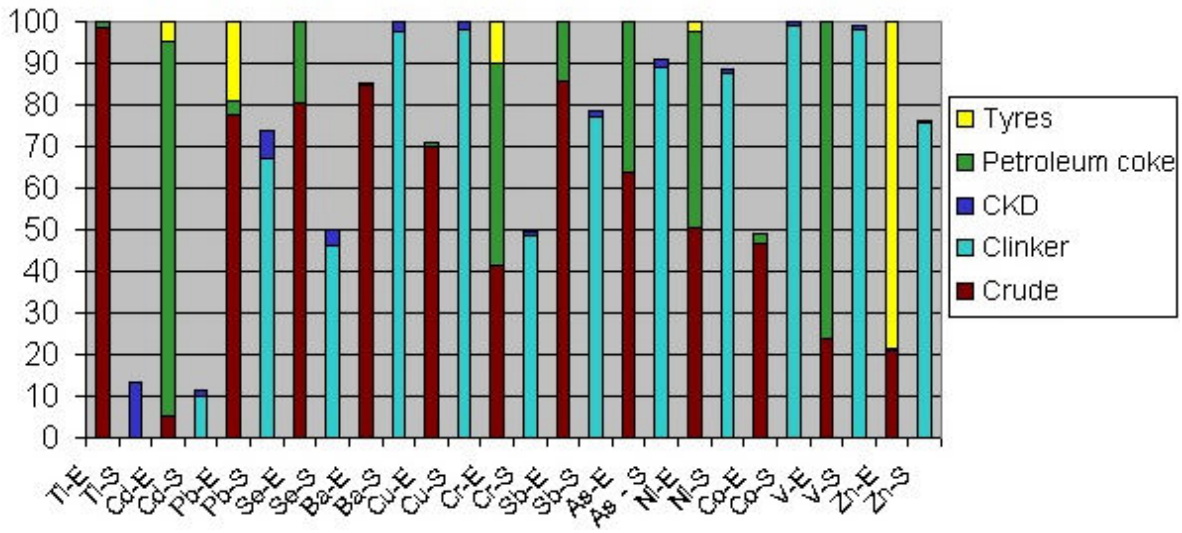

Figure 3. Relative contributions of the main streams
(crude feed, petroleum coke, tyres, recirculated CKD and clinker)

Figures 4a to 4d summarize the range of concentrations (minimum and maximum for each heavy metal) along the experimental campaign. These results have been obtained by AAS, following the recommendations and methods of VDZ In full scale processes, considerable difficulties arise in order to establish a uniform closure of mass balances due to the relative weighing precision and the mass flows of relevant trace metals, and also because of the variability along an entire operating campaign. These results lead to the identification of experimental mass balances methodology and the interpretation of individual measurements.

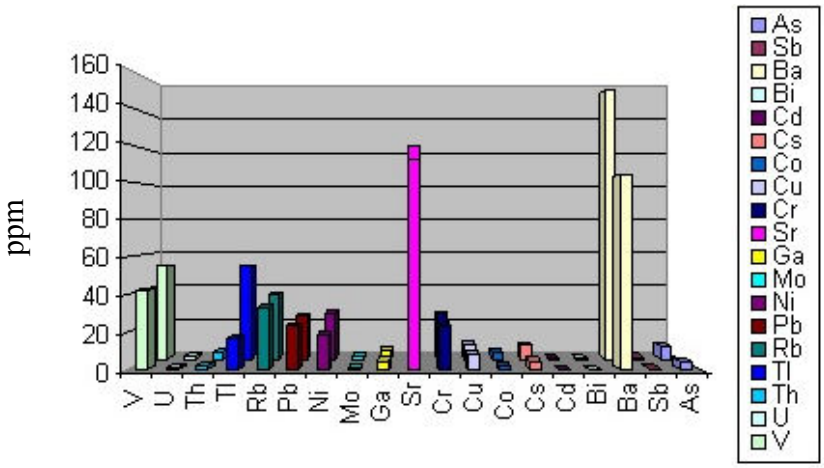

Figure 4a. Variability of trace metals concentration (ppm) in crude

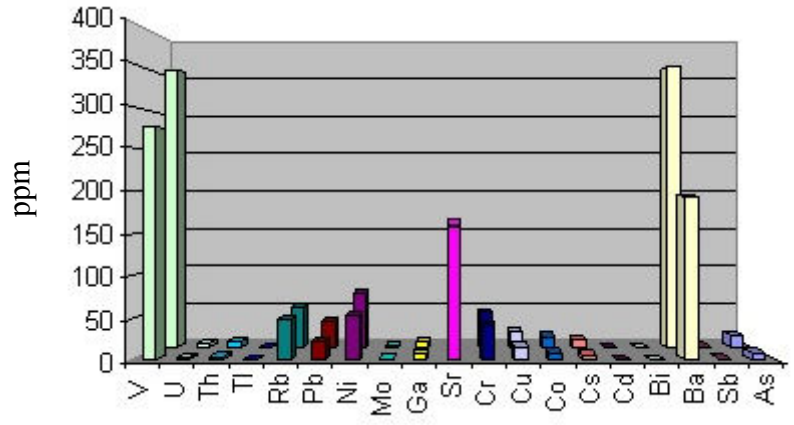

Figure 4b. Variability of trace metals concentration (ppm) in clinker

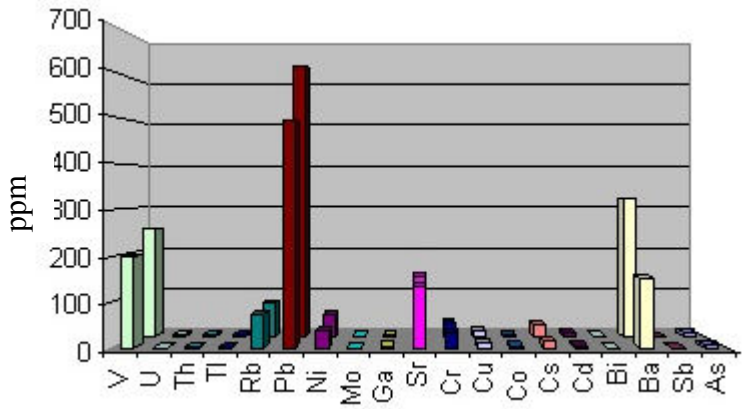

Figure 4c. Variability of trace metals concentration (ppm) in precalcinator

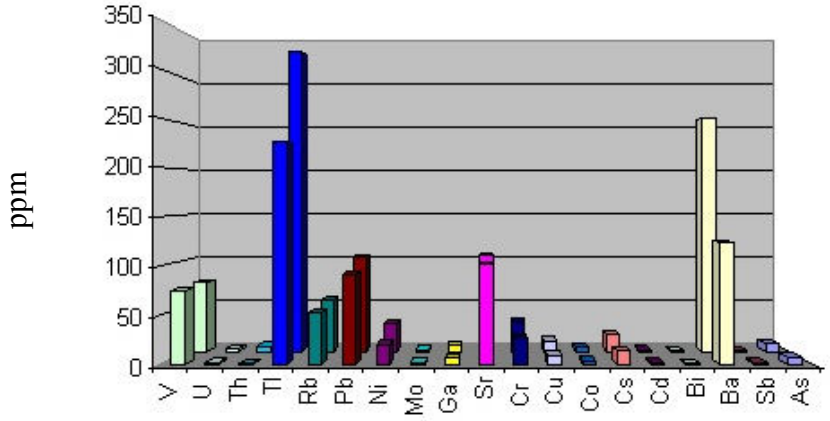

Figure 4d. Variability of trace metals concentration (ppm) in CKD (ppm)

An intensive analysis and physicochemical characterization of impactor stages, using AAS,ICP/AE,S ICP/MS and microscopy was carried out to determine the usefulness of elemental analysis as the main tool to understand the environmental fate of heavy metals, and also to ascertain the possibilities of emission control under operating conditions.

The collected dust in the PM2.5 stage of a Dekati PM10 impactor, Figure 5b, could correspond to a rather slow formation of fractal-like aggregates, whereas in Figure 5a, corresponding to the same sampling period, shows a condensate of nearly spherical geometry.

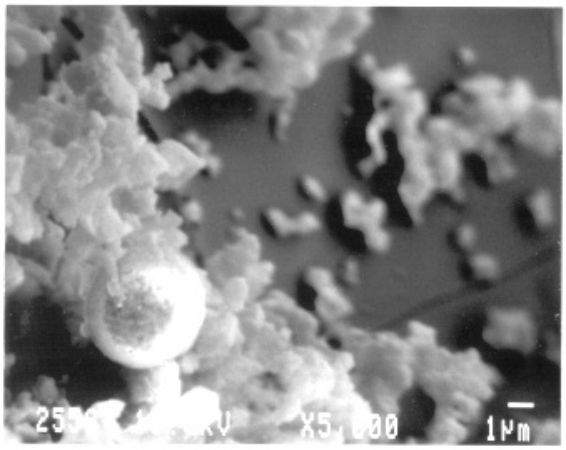

Figure 5a. SEM image of a DekatiPM10 cut corresponding to the nominal 1µm

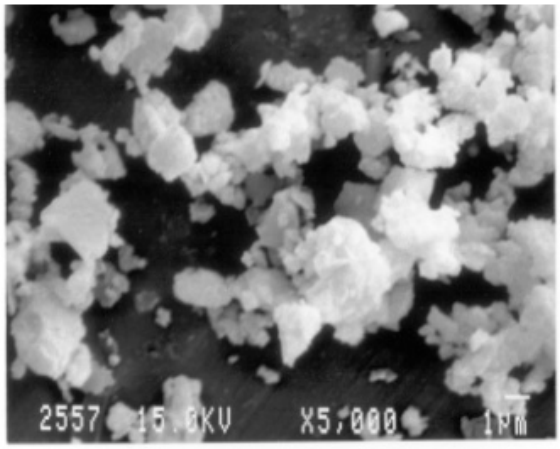

Figure 5b. SEM image of a DekatiPM10 cut corresponding to the nominal 2.5µm

In Figure 6, two fractions of fractionated CKD are shown. These images correspond to operating conditions for mixed clinker and crude mill dust. Figure 6a presents, as typical for these conditions, a very large range of physical diameters, whereas the aerodynamic diameters are approximately the same due to the chemical composition and origin of the two components. Figure 6b shows an extreme case of this situation, in which the condensation aerosol enriched in heavy metals and their compounds behaves aerodynamically in the same manner as the lighter components.

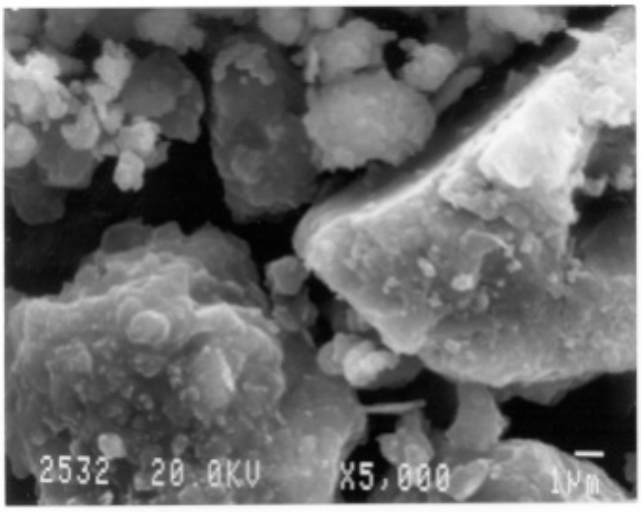

Figure 6a. SEM image of fractionated clinker kiln dust

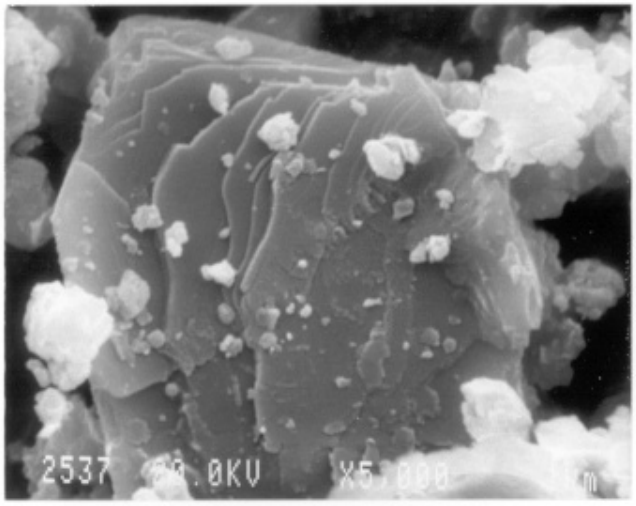

Figure 6b. SEM image of fractionated CKD

The fractionated CKD was also chemically analyzed after leaching with demineralized water. The analysis was for major (Ca, Al) and minor elements (S insoluble, alkalis, Mg, Fe) and for trace elements. As an example, in Figure 7 are presented the representative values for Pb and Tl (ppm on the basis of the total sample mass) in the soluble and insoluble fraction, analyzed by means of ICP/AES. The stage numbers correspond to the following intervals (calculated assuming a mean value of the relative bulk density, 1.5): 0.39-0.81, 0.81-1.67, 1.67-3.31, 3.31-6.64, 6.64-12.9, 12.9-26.45, 26.45-32 μm.

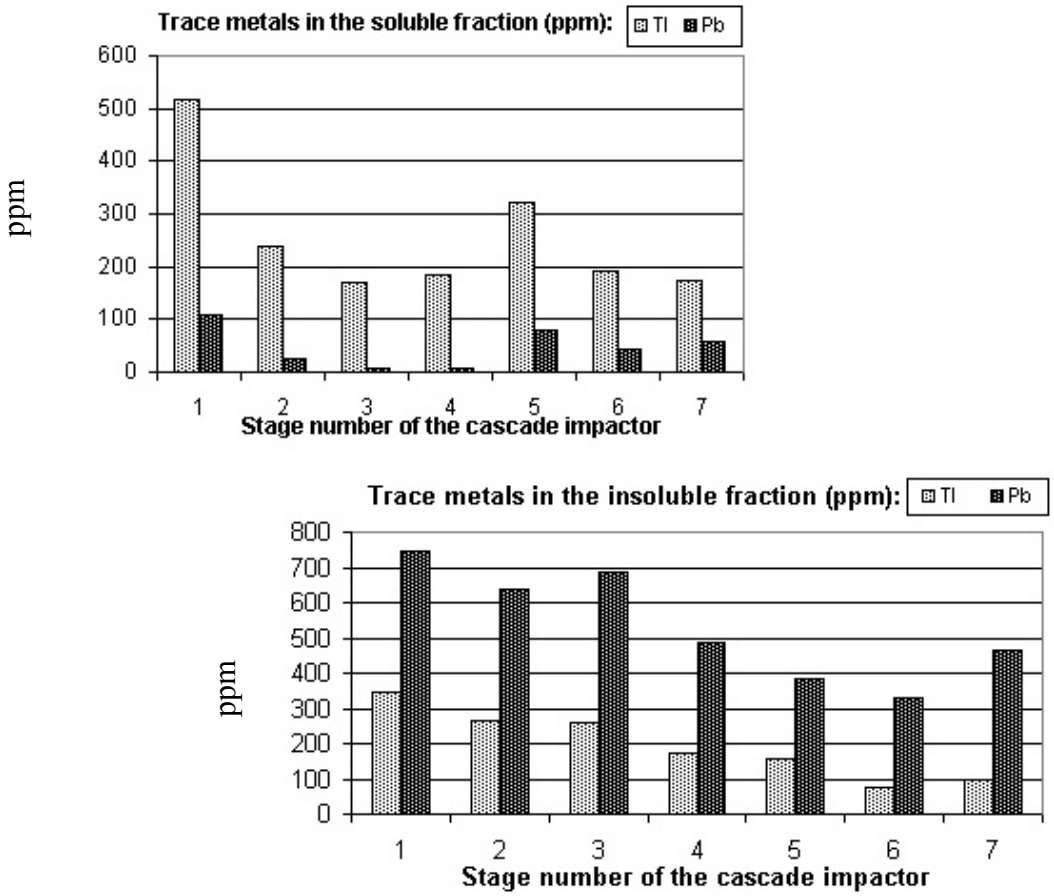

Figure 7. Behaviour against water leaching of Tl and Pb in the CKD.

In the soluble fraction, thallium exhibits a bimodal distribution with pronounced modes in stages 1 and 5. Lead in the soluble fraction appears to be less concentrated and presents maxima in stages 1 and 5. The insoluble fraction shows a very different pattern of size distributed elemental composition of Tl and Pb. Lead seems to be clearly enriched in this fraction, with maxima below stage number 3, and another local but less pronounced maximum in stage number 7. Thallium distributes rather uniformly below the stage number 4, and its less pronounced positive gradient in the stage 7 could be attributed to condensation on fractal-like structures.

Figure 8 shows the structure of control variables to maintain the emission of heavy metals under the set points fixed on administrative requirements, This nearly real-time information is used to regulate the flows in order to match with correlations obtained for each metal.

Figure 9 shows the experimentally obtained fractional efficiency curve for the electrofilter in the field campaign. There is a clear penetration window in the size range of enrichment in volatile heavy metals, due to the intrinsic operation of electrofilters. Whilst the advantages of this type of dedusting equipment are notorious in cement plants, they are not able to separate in the range about 1 μm with the necessary efficiency to ensure compliance with ELV's of certain metals. The set points for applied voltage, which is the unique reliable control variable, should rely on experimental evidence about the behaviour of metals, which in turn depends on the feed and fuels characteristics and trace contribution.

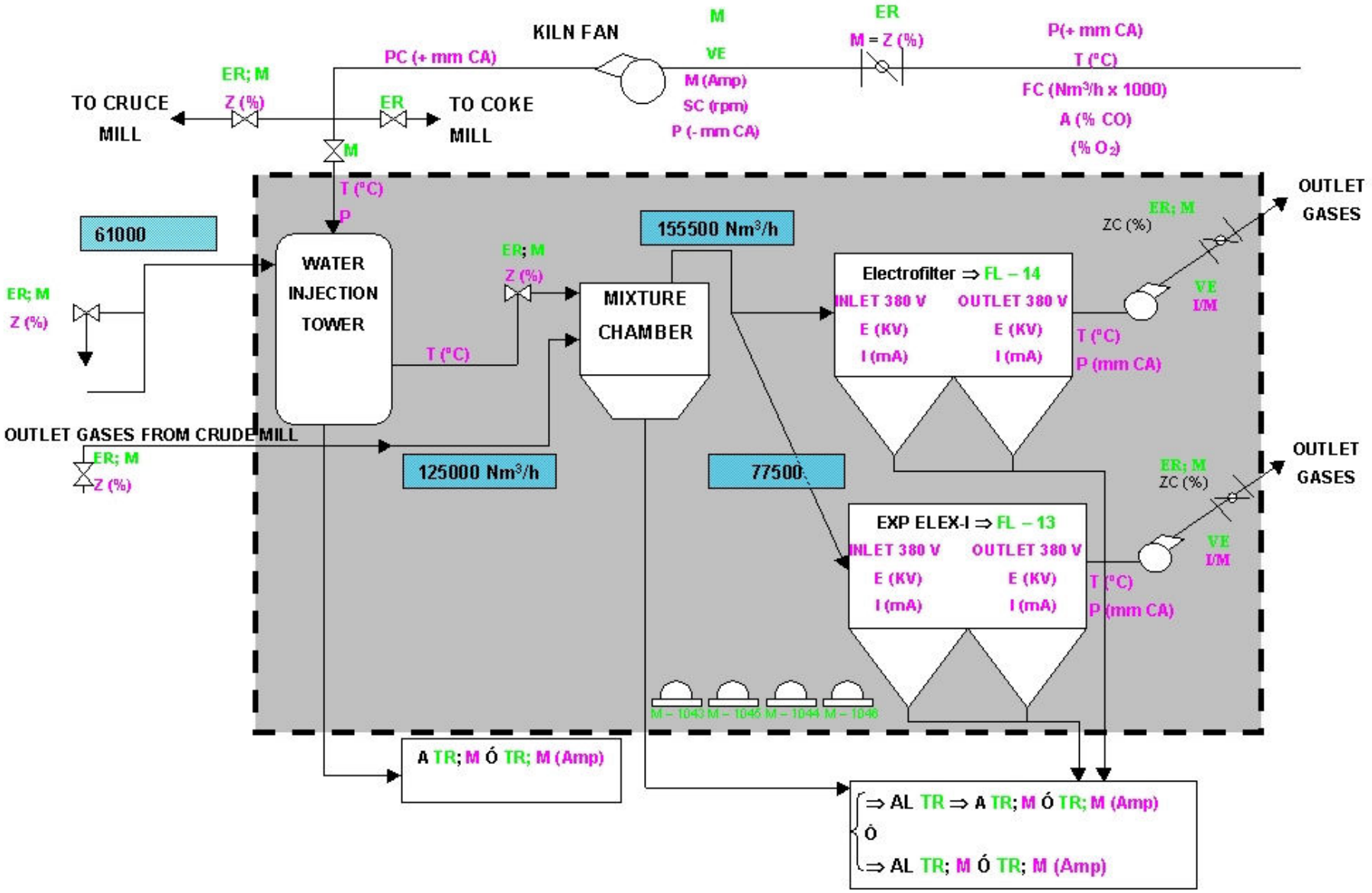

Figure 8. Operation variables for emission control

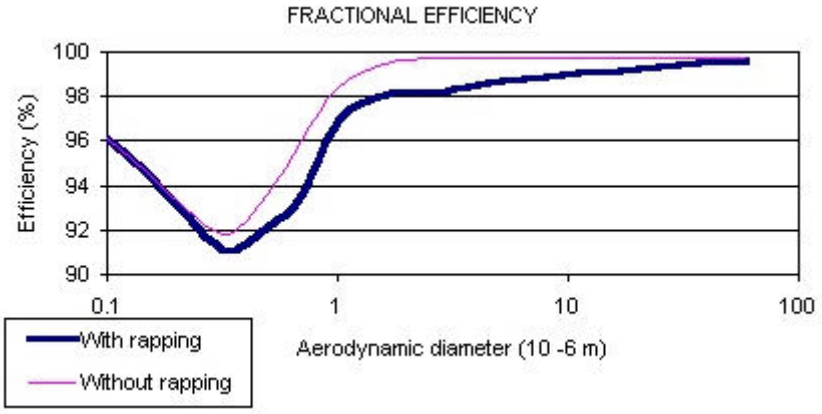

Figure 9. Fractional efficiency of electrofilter

4. CONCLUSIONS

The observed separation of most relevant trace metals requires further explanation on the basis of local analysis and speciation. The size of phases implies limitations for the application of several techniques (IMP/MS with laser ablation, and so on). Morphological and chemical information could be used together to gain insight about the nature of fine particulate fractions of emissions from clinker kilns generally, the metals are concentrated on finer fractions, either in water- soluble and insoluble fractions. Thallium is concentrated in soluble phases.

Although, its usefulness as a criterium to specify the raw meal (secondary fuels or feeds), the best practices observed for heavy metal emission control, and the use of fractional efficiency as the main criterium to specify and to operate a dust separation unit. Also prospects for real-time monitoring will be discussed.

The design, operation and maintenance practices for emission control and compliance must be based on fractional efficiency observed for the particular feed mixture and fuels used. This fractional efficiency should be established on the basis of experimental correlations with operating variables and conditions.

A very important fraction of emissions appears in a size range that does not modify substantially the overall efficiency. So, this parameter loses its quantitative significance for ESP performance quantification. Overall efficiency explains neither the basic geometry of the electrode configuration nor the rapping sequence, nor the performance for emission control purposes.

Prospects for real time monitoring depend on the accumulation of full-scale experimental evidence of heavy metals mass flows and trajectories, depending on operating practices. This is the previous step to develop thermodynamically-based approaches, which could use the measured temperatures to predict heavy metals, their species, and behaviour. It is confirmed that ESP is not a valid subrogated for heavy metals.

REFERENCES

[1] Krmac W., Untersuchungen über das Verhalten der Spurenelemente bei der Zementherstellung, Ph. D. Thesis, TH Karlsruhe (1991)

[2] Verein Deutscher Ingenieure, Emissionsminderung. Zementwerke. Richtlinie VDI 2094, 1985) VDZ, Spurenelemente

HEAVY METALS EMISSION MEASUREMENT AND CONTROL

C. Gutierrez-Cañas., C. Urcelay., M. Larrion, E. Guede, E. Garcia, Y. Parra and J.A. Legarreta

Prof. Dr. Ing. C. G.-Cañas, Dpt. Ingeniería Química y del Medio Ambiente. Escuela Superior de Ingenieros. UPV. 48013. Bilbao. Spain. E-mail: iapgumac@bi.ehu.es
Ing. Ind. C.Urcelay, Cementos Lemona S.A., B. Arraibi s/n. 48040 LEMOA-Spain. E-mail: urcelay@lemona.com
Dr. Ing. Ind., Assoc Prof., M.Larrion, Dpt. Ingeniería Química y del Medio Ambiente. Escuela Superior de Ingenieros. UPV. 48013. Bilbao. Spain. E-mail: iaplarum@bi.ehu.es
E. Guede, Cementos Lemona S.A., B. Arraibi s/n. 48040 LEMOA-Spain. E-mail: e.guede@lemona.com
Ing. Quim., E. Garcia, Dpt. Ingeniería Química y del Medio Ambiente. Escuela Superior de Ingenieros. UPV. 48013. Bilbao. Spain. E-mail: iabgarue@bi.ehu.es
Ing. Ind. Parra Y., Dpt. Ingeniería Química y del Medio Ambiente. Escuela Superior de Ingenieros. UPV. 48013. Bilbao. Spain. E-mail: biapagoy@bi.ehu.es
Prof. Dr. Ing. J.A. Legarreta, Dpt. Ingeniería Química y del Medio Ambiente. Escuela Superior de Ingenieros. UPV. 48013. Bilbao. Spain. E-mail: iaplefej@bi.ehu.es

Cristina G. Cañas (Prof. Dr. Ing.) works since 17 years ago in Air pollution control and full scales processes.

Main areas of interest:
Experimental mass balance of trace elements and compounds, modelling of desdusting equipment and engineering tools for environmentally integrated production.

She has developed specific products for a cement industry: waste dosification control, procedures of vigilance standard of metals, electrostatic precipitators operation control among other.

Research topic:
Deal with fine particulate measurement and control that is predictive thermodynamic models, aerosol measurements and characterization, intergrating advanced measuring techniques (aplication of ELPI), and CFD models for gas – solid flows.

USING SOFT X-RAY TRANSMISSION MICROSCOPY TO EXAMINE CEMENT HYDRATION IN THE PRESENCE OF RETARDERS

M.C. Garci Juenger[1], P.J.M. Monteiro[2], E.M. Gartner[3] and G.P. Denbeaux[4]

[1] Department of Civil Engineering, University of Texas, Austin, Texas 78712, USA.
E-mail: mjuenger@mail.utexas.edu
[2] Department of Civil and Environmental Engineering, University of California, Berkeley, California 94720, USA. E-mail: monteiro@ce.berkeley.edu
[3] Lafarge, Laboratoire Central de Recherche, 38291 St. Quentin Fallavier, France.
E-mail: ellis.gartner@lafarge.com
[4] Center for X-ray Optics, Lawrence Berkeley National Laboratory, Berkeley, California 94720 USA, E-mail: gpdenbeaux@lbl.gov

ABSTRACT

Recently, soft x-ray transmission microscopy has emerged as a useful technique for the examination of cement based materials. The unique advantage of this method is that it allows for high resolution (25 nm) observation of samples under wet conditions at atmospheric pressure. Thus, hydration of cementitious materials can be followed over several hours. For this study, Portland cement was hydrated in solutions saturated with calcium hydroxide and gypsum, with and without retarders (sucrose, calcium lignosulfonate, tetrasodium pyrophosphate and sodium gluconate). The delayed growth of hydration products on the surface of cement grains was documented.

1. INTRODUCTION

While there are many microscopy techniques available for the study of cement-based materials, they all have some drawbacks. There is usually a trade-off between resolution and artifacts introduced by sample preparation. The recently adopted soft x-ray transmission microscope does not transcend this problem, but it does offer the extremely valuable and unique ability to study cement hydration in situ. High-resolution (25 nm) images are obtained in real time of wet samples at atmospheric pressure. While the water-to-cement ratio (w/c) must be high and the cement particles small, the chemistry of the solution can be easily tailored, allowing observation of the effects of chemical admixtures on hydration.

Soft x-ray microscopy has been successfully applied to the study of alkali–silica gels and tricalcium silicate (C_3S) hydration [1-4]. Research on hydration of C_3S, ordinary Portland cement (OPC), calcium aluminate cements and pozzolans is ongoing. The work presented here examines OPC hydration in the presence of chemical retarders. There are many substances that retard hydration of OPC and its constituent phases, including sugars and many other water-soluble organic substances, as well as some inorganic species. The mechanisms of retardation are in most cases not well proven, but it is believed that most retarders form complexes on the surfaces of hydrating grains or hydration products thereby inhibiting hydration [5-7]. The retarders chosen for this study were the following: sucrose, one of the strongest and most widely-used retarders; calcium lignosulfonate, a water-reducing agent (dispersant) that also acts as a retarder; plus tetrasodium pyrophosphate and sodium gluconate, ingredients in some commercial concrete admixtures. OPC was mixed in dilute

Proceedings of the 11th International Congress on the Chemistry of Cement (ICCC)
'Cement's Contribution to the Development in the 21st Century'
Hosted by: The Cement and Concrete Institute of South Africa
CD-ROM produced by: Document Transformation Technologies
11 - 16 May 2003, Durban, South Africa
ISBN Number: 0-9584085-8-0
Editors: Dr G. Grieve and G. Owens
Congress Organised by: Event Dynamics

suspensions containing these retarders and the growth of hydration products was observed using a soft x-ray transmission microscope.

2. MATERIALS AND METHODS

The experiments described here were conducted using the soft x-ray transmission microscope (XM-1) located on beam line 6.1.2 of the Advanced Light Source (ALS) at the E.O. Lawrence Berkeley National Laboratory (LBNL) in Berkeley, California and operated by the Center for X-Ray Optics (CXRO). The synchrotron generates radiation with a wide spectrum of wavelengths. This radiation is filtered by a plane mirror and only that in the soft x-ray regime with wavelengths between 0.7 and 4 nm (300 to 1800 eV) is sent to a condenser zone plate, which then focuses the radiation onto the sample. X-rays transmitted through the sample are refocused with a micro zone plate onto an x-ray CCD camera (Figure 1). More detailed information on the microscope has been reported elsewhere [8,9].

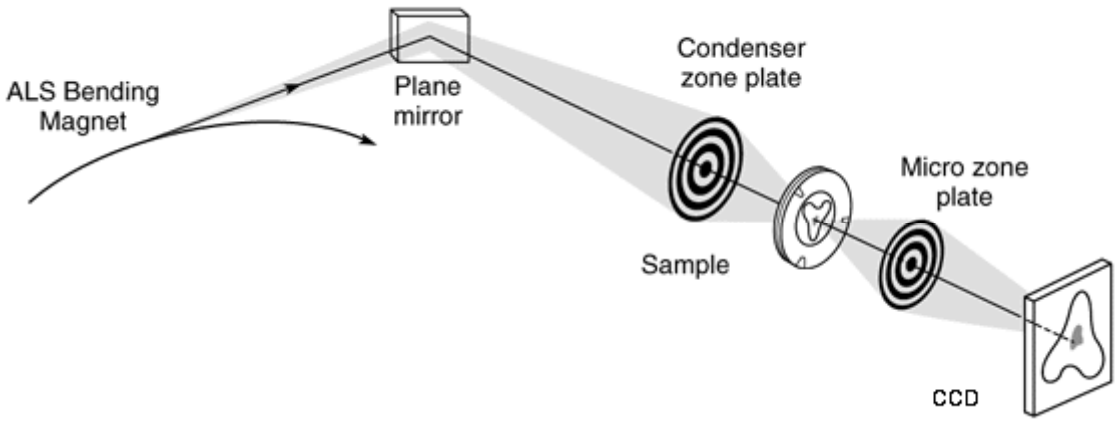

Figure 1. Soft x-ray transmission microscope

The use of soft x-rays, with wavelengths more than 100 times shorter than visible light, leads to a maximum resolution of 25 nm. In these experiments, a wavelength of 2.400 nm (516.6 eV) was used. The magnification of the images is between 1600 and 2400x and remains fixed during a given session. The images have a circular field of view of approximately 10 μm in diameter. If a larger field of view is desired, several images are taken across a grid and a composite image is created by montage alignment using a custom autocorrelation process [10]. All of the images presented in this paper have been processed in this manner.

Cementitious suspensions are placed between two silicon nitride membranes and sealed into a stainless steel mounting cell prior to examination. Rubber O-rings in the sample cell prevent water loss and carbonation. In order for sufficient x-rays to be transmitted, the total thickness of the sample must not exceed 10 μm, necessitating the use of dilute suspensions of small particles. There is some risk of carbonation during the mixing, centrifugation and transfer of the sample, although we did our best to minimize exposure of the suspensions to air.

A commercial Portland cement (Lafarge) was used with a density of 3110 kg/m^3, Blaine specific surface area of 387 m^2/kg, volume mean diameter of 12 μm and chemical composition shown in Table 1. Distilled water was boiled to remove dissolved carbon dioxide, and then cooled to room temperature. Retarders were dissolved in the prepared, room temperature water at a concentration of 1g/L. Determining an appropriate concentration of retarder was problematic because of the high water-to-cement ratio used for these studies; 1g/L enabled us to see retardation of the growth of hydration products, but may not be exactly equivalent to concentrations used in practice. The retarders used were sucrose (Fisher Scientific), an ultrafiltered calcium lignosulfonate ("Ultrazine

Ca," Børregaard Lignotech), tetrasodium pyrophosphate decahydrate (Aldrich Chemicals) and sodium gluconate (Sigma). All solutions were then saturated with respect to calcium hydroxide and gypsum by adding 3.5 g $Ca(OH)_2$ (Sigma) and 1 g $CaSO_4 \cdot 2H_2O$ (Sigma) per 100 mL at room temperature. The solutions were shaken vigorously in sealed, polyethylene bottles for one minute and allowed to settle overnight. On the day of testing, 14 mL of solution was pipetted from the top of the settled mixtures and placed in sealed, polystyrene containers for each sample to be studied. Care was taken not to disturb the solids at the bottom of the containers and minimize exposure of the solutions to air.

Saturation of the solutions with calcium hydroxide and gypsum was done in order to compensate for the diluteness of the final suspensions, and to ensure that the cement was hydrating in a liquid medium not too different from that typical of ordinary concrete applications. Without such an approach, we might have expected excessive dissolution of the anhydrous particles due to the high dilutions used. The pre-saturation with respect to calcium hydroxide was intended to prevent excessive dissolution of the silicate phases, and the pre-saturation with respect to gypsum was intended to prevent excessive dissolution of the aluminate phases. An excess of calcium hydroxide and gypsum were used in order to guarantee saturation because some chemical admixtures may change their solubility. Likewise, the presence of calcium hydroxide and gypsum may change the solubility of some admixtures so that the initial 1g/L concentration of the retarders listed above may not necessarily be accurate in the final solution.

Immediately before testing, 0.28 g of cement was added to 14 mL of solution (w/c = 50), and the mixture was shaken for approximately 15 seconds to ensure mixing. Aliquots of 2 mL were removed from these mixtures and then centrifuged briefly in order to isolate the smallest particles in the supernatant. One small drop of supernatant was then placed on the silicon nitride membrane and sealed in the sample cell for immediate observation. Mixing and imaging was always done at room temperature, 22 ± 2°C. All of the images shown in this paper were chosen for their quality and clarity out of several showing similar phenomena.

Table 1. Chemical composition of Portland cement

Oxide Composition (% by mass)	
CaO	64.8
SiO_2	20.7
Al_2O_3	4.5
Fe_2O_3	1.9
MgO	0.76
TiO_2	0.23
P_2O_5	0.15
K_2O	0.21
Na_2O	0.16
SO_3	3.35
LOI	2.81

3. RESULTS AND DISCUSSION

3.1 Neat Portland Cement

Images from OPC hydrated in a solution saturated with calcium hydroxide and gypsum are shown in Figure 2. On all samples there is layer of finely divided hydration products with a "sheaf-of-wheat" morphology. These are believed to be a form of calcium silicate hydrate (C-S-H) [1,11]. The density and thickness of the fibers differ between samples, but these products are always immediately present (images have been taken as early as 8 minutes after mixing), and look like the initial products formed around pure C_3S particles under similar conditions [unpublished work].

Once formed, these products do not change during the first several hours. In Figures 2c and 2d, angular crystals believed to be ettringite are growing (top center). Ettringite growth has been observed in some, but not all, early age OPC samples. Note that the shadow on the bottom left of Figure 2c is an artifact of the montage alignment and does not reflect a change in the nature or volume of hydration products.

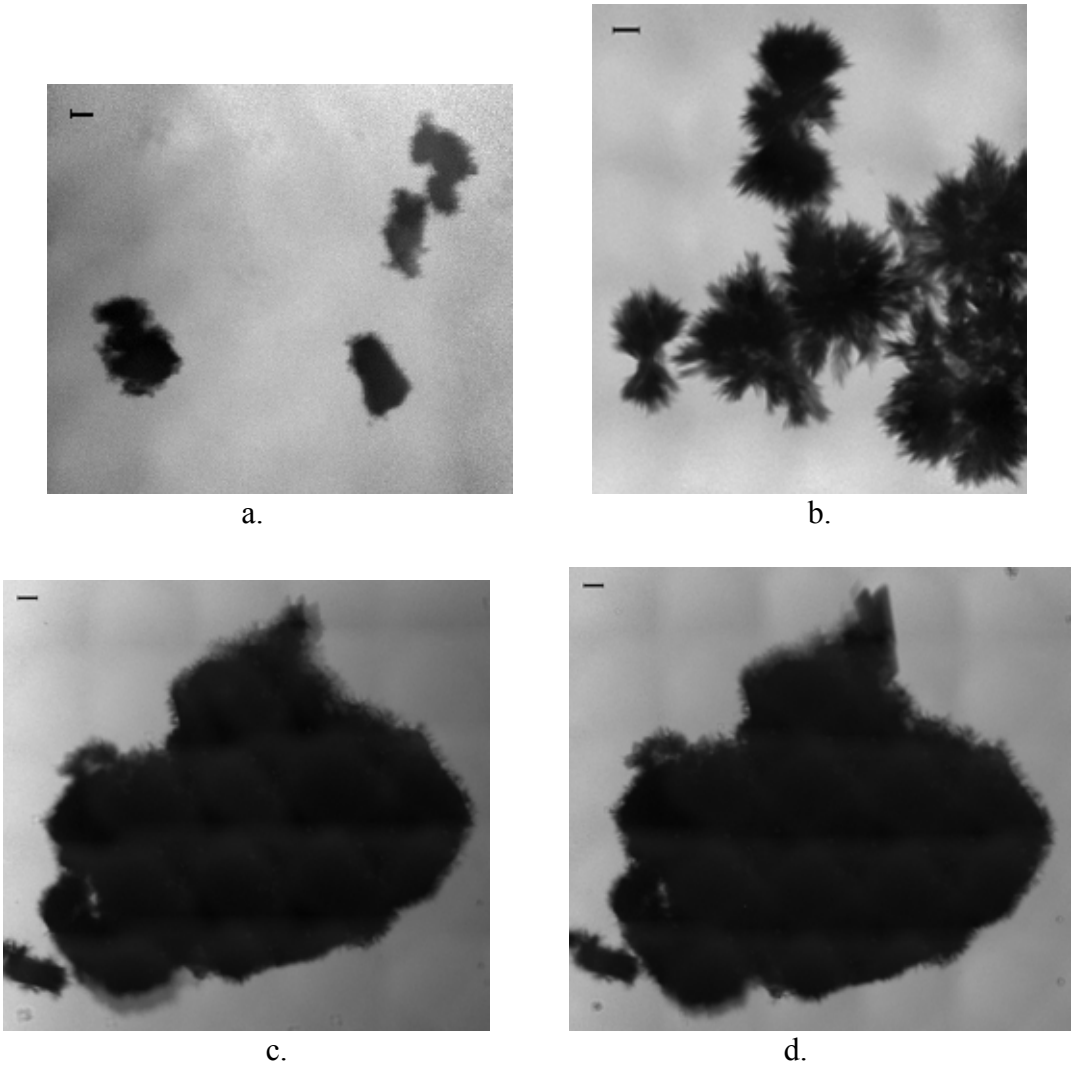

a. b. c. d.

Figure 2. Three different samples of OPC hydrated in a solution saturated with calcium hydroxide and gypsum, w/c = 50, a. 28 minutes, b. 49 minutes, c. 34 minutes, d. (same location as c) 72 minutes. Scalebars = 1 μm.

3.2 Sucrose

Sucrose is well-known as a very strong retarder of cement hydration. Figure 3 shows images taken of OPC in a solution containing sucrose (1g/L). It is difficult to see if there are hydration products on the cement grains in Figure 3a or if the surfaces of the grains are simply rough. The chains of small spheres in Figure 3a are unidentified products that have apparently dissolved or dispersed in the later images. They might be precipitated calcium carbonate formed during the transfer of the sample into the cell. Hydration products with a sheaf-of-wheat morphology form after one hour as seen in Figure 3b. Clearly, the sucrose has delayed the formation of this type of C-S-H. Unfortunately, the resolution of these images is too low to discern whether an initial layer of hydration products forms on the hydrating grains which is later poisoned, or if the cement grains themselves are poisoned by the sucrose.

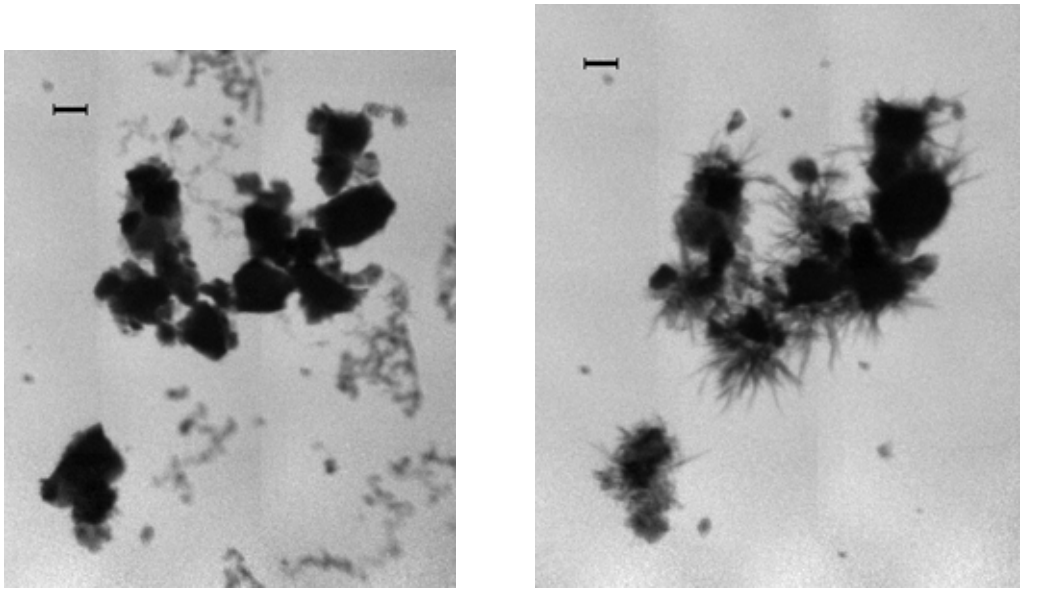

a. b.

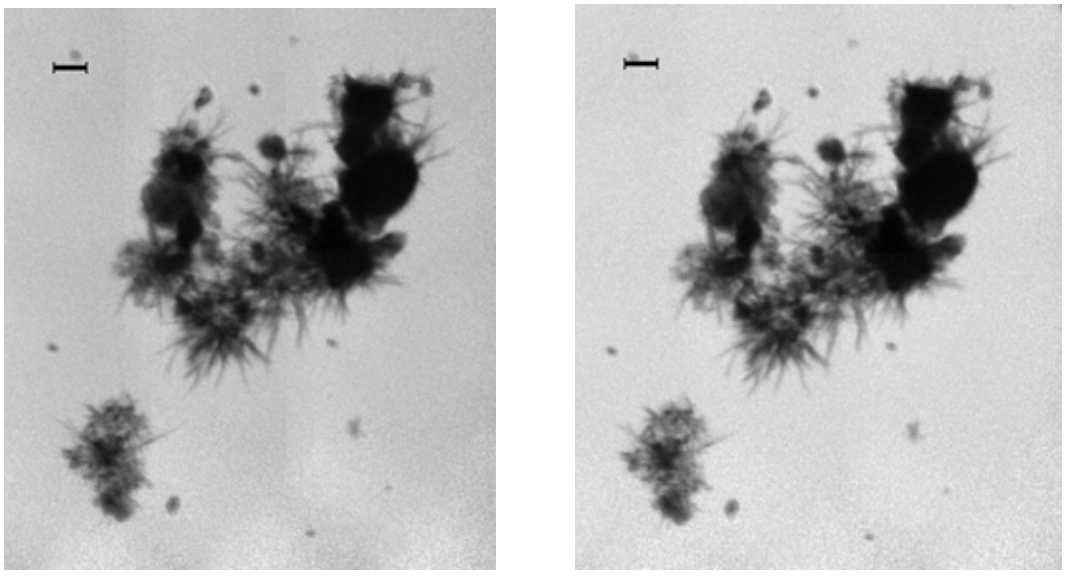

c. d.

Figure 3. OPC in solution saturated with calcium hydroxide and gypsum containing sucrose (1g/L), w/c = 50, a. 31 minutes, b. 68 minutes, c. 100 minutes, d. 130 minutes. Scalebars = 1 μm.

Evidence of further hydration appears in Figure 3c as some of the dark solid grains have been replaced by what we call an "inner product" C-S-H. It has either lost a lot of calcium relative to the anhydrous materials or has become thinner or less dense, thus increasing its transparency to x-rays. By 2 hours, hydration has slowed again as there are no significant differences between Figures 3c and 3d. Sucrose has often been referred to as a "delayed accelerator," meaning that after the retarding period is over, hydration proceeds more rapidly than usual [5,12]. The apparent rapid growth of this inner product as seen in Figure 3c has also been seen in samples that have been accelerated with calcium chloride [13].

As discussed in reference to accelerators [13], the "pseudomorphic" hydration that results in inner product C-S-H is essentially a leaching process, i.e. the inner product that forms is presumably calcium-poor relative to the anhydrous material. Given the high dilutions necessitated by the x-ray transmission microscopy technique, it is very possible that this leaching process is rather

exaggerated compared to what would in principle be observed in cement pastes made at the much lower water-to-cement ratios typical of concrete applications. Since it is known that calcium hydroxide is the main component that leaches out of the anhydrous grains during cement hydration, we did take the precaution of using a pre-saturated calcium hydroxide solution as the dilution medium, in order to minimize this type of artifact. Nevertheless, calcium hydroxide supersaturations of 2-3 generally occur at fairly early ages during OPC hydration [14] and we cannot preclude this possibility in our experiments, implying that the loss of calcium could still be much greater than would be expected in more concentrated suspensions. Moreover, any loss of calcium hydroxide due to carbonation, or complexation by the admixtures used, would tend to enhance the leaching effect.

3.3 Lignosulfonate

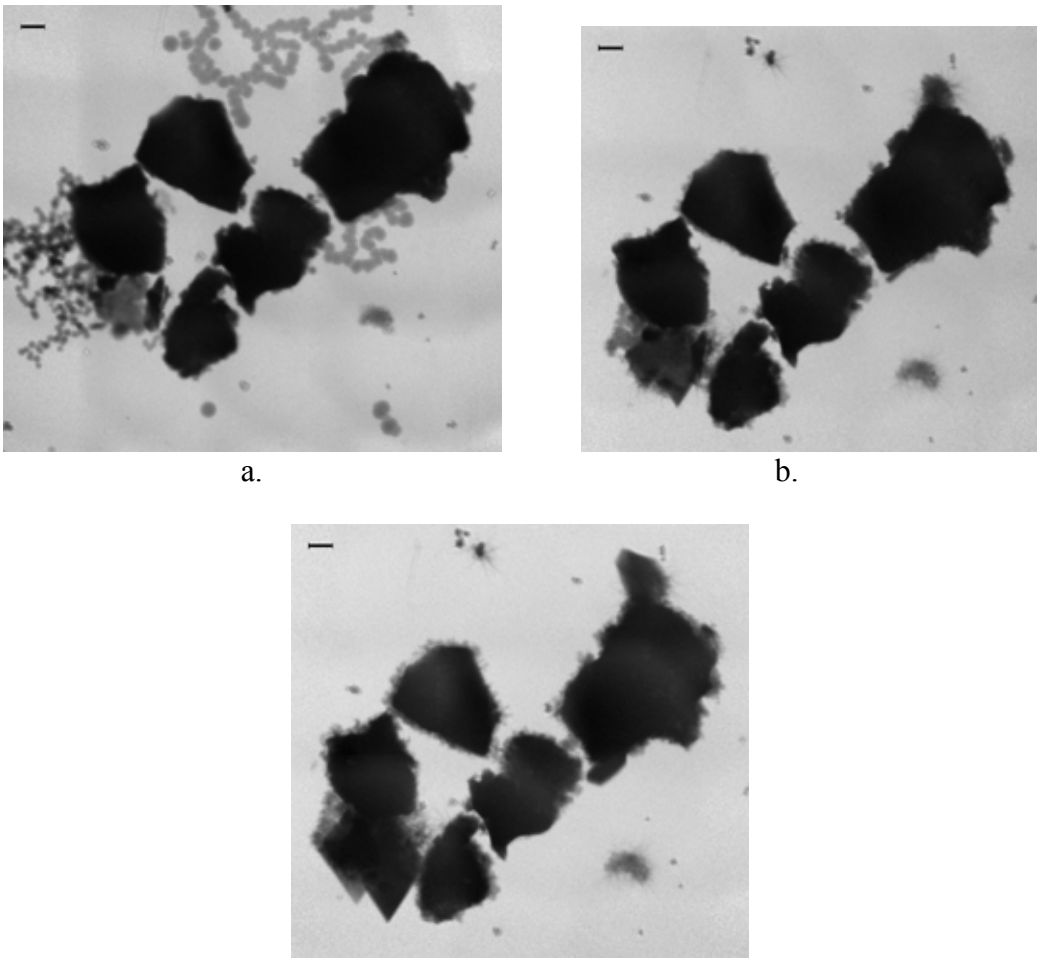

a. b. c.

Figure 4. OPC in solution saturated with calcium hydroxide and gypsum containing calcium lignosulfonate (1g/L), w/c = 50, a. 11 minutes, b. 88 minutes, c. 162 minutes. Scalebars = 1μm.

Calcium lignosulfonate is a much weaker retarder than sucrose, but lignosulfonates are important commercially as the principal ingredients in many concrete admixtures sold as "water-reducing agents." The retarding effects of lignosulfonates are often attributed to the presence of sugars in the commercial products, but even "pure" lignosulfonates have some retarding power [15]. Like sucrose, calcium lignosulfonate delays the growth of sheaf-of-wheat C-S-H; none is present in Figure 4a, but by 162 minutes (Figure 4c) the grains are almost completely covered with a thin layer of this type of product. The fibers are much smaller and finer than in the sucrose sample, but this may not be important since the morphology varies even in neat OPC samples (Figure 2). Ettringite

is also growing in this sample as seen clearly in Figure 4c. It is difficult to say whether ettringite formation has been delayed by calcium lignosulfonate as it does not appear in all samples nor does it form at a consistent time. Rapid growth of inner product C-S-H is not seen in these samples. This may be a result of the fact that lignosulfonates do not influence hydration as strongly as sucrose [15].

3.4 Phosphate

Phosphates are known to be good retarders [16] and can be used to control slump and setting times in concrete. They are weaker retarders than sucrose [15]. The results of a tetrasodium pyrophosphate addition are shown in Figure 5. Since the earliest picture was taken after 45 minutes of hydration, it is impossible to know whether the formation of sheaf-of-wheat C-S-H was delayed or if the image was simply taken too late. A similar experiment with C_3S instead of OPC showed very little sheaf-of-wheat product after 40 minutes and much more after 77 minutes, demonstrating the retarding power of phosphates (images not shown). The images in Figure 5 are similar to those with sucrose (Figure 3) in that inner product C-S-H is observed; the dark solid center of the grain visible in Figure 5a is replaced by hydration products in Figures 5b and 5c.

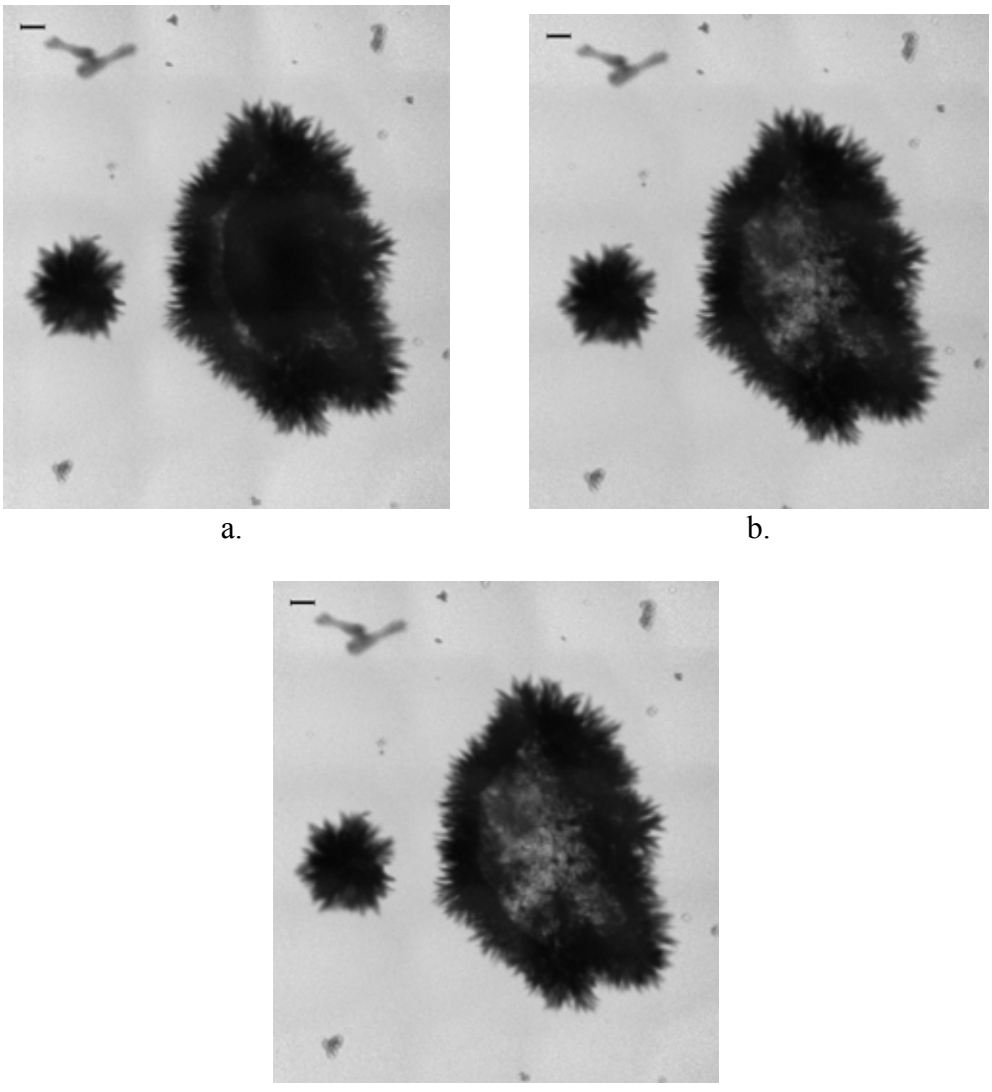

a. b. c.

Figure 5. OPC in solution saturated with calcium hydroxide and gypsum containing tetrasodium pyrophosphate (1g/L), w/c = 50, a. 45 minutes, b. 94 minutes, c. 143 minutes. Scalebars = 1 μm.

3.5 Gluconate

Gluconates are very strong retarders that are thought to delay hydration by poisoning the nuclei of some hydration products [17]. Sodium gluconate is known to strongly affect the nucleation and crystallization of gibbsite ($Al(OH)_3$) [18] and may affect the formation of cement hydration products as well. The difference between the images in Figure 6 in the presence of sodium gluconate and Figures 2-5 is striking. Sheaf-of-wheat hydration products are conspicuously absent. Instead, the hydration products are globular and appear to have precipitated "homogeneously" out of the solution rather than on the surfaces of the cement grains. The apparent volume of solids increases over time, as the globular products appear to increase in size. Perhaps sodium gluconate not only delays growth by poisoning cement hydration products, but also changes the nano-structure of C-S-H.

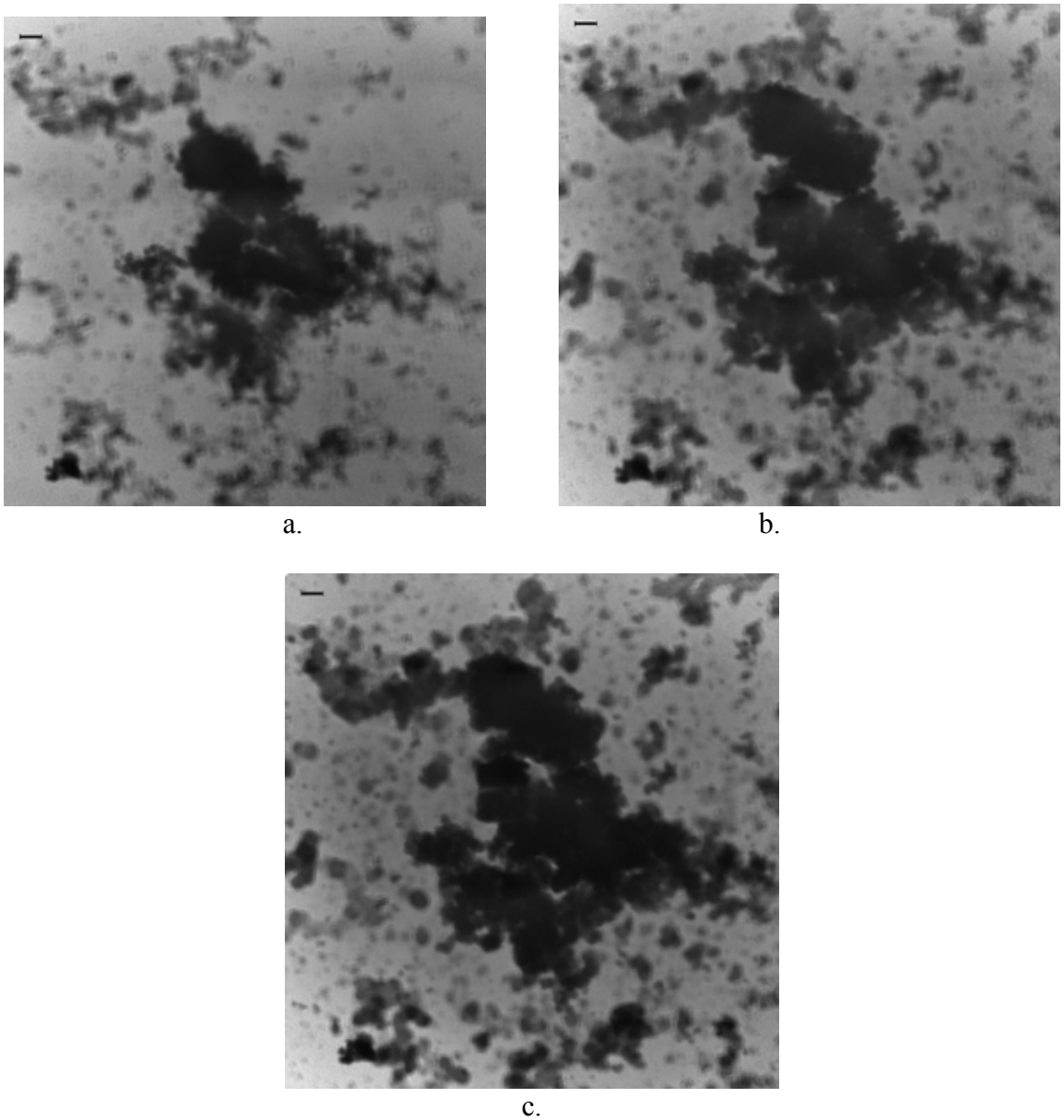

a. b. c.

Figure 6. OPC in solution saturated with calcium hydroxide and gypsum containing sodium gluconate (1g/L), w/c = 50, a. 24 minutes, b. 70 minutes, c. 120 minutes. Scalebars = 1 μm.

4. CONCLUSIONS

Soft x-ray transmission microscopy is an excellent technique for continuous monitoring of the hydration of cementitious materials at early ages in dilute suspensions. High magnification images are obtained of cement grains hydrating in solutions over time. The effects of admixtures are easily studied as the chemistry of the solutions can be varied as needed.

The early hydration products of Portland cement, as seen using a soft x-ray microscope, appear as bundles of fibers, often described with the term "sheaf-of-wheat." It is likely that these products are a form of calcium silicate hydrate. The addition of chemical retarders, including sucrose, calcium lignosulfonate, and tetrasodium pyrophosphate, delays the formation of these sheaf-of-wheat products, with the retardation time being dependent on the strength of the retarder. Sodium gluconate appears to be unique, among the retarders that we have tested, in that sheaf-of-wheat products do not form in its presence. Instead, globular products form in the solution surrounding the cement grain and grow with time.

Some retarders appear to act as "delayed accelerators" in the sense that, once the initial retardation is overcome, further "pseudomorphic" hydration apparently continues more rapidly than in the unretarded control specimens. This "pseudomorphic" hydration results in the decrease in x-ray transmission density of the material within the confines of the original anhydrous particle, leaving behind a material that we refer to as "inner product."

ACKNOWLEDGEMENTS

We would like to gratefully acknowledge guidance and financial support for this project from Lafarge. Research at XM-1 is supported by the United States Department of Energy, Office of Basic Energy Science under contract DE-AC 03-76SF00098. This work was facilitated by A.L. Pearson and the previous accomplishments of V.H.R. Lamour and K.E. Kurtis.

REFERENCES

[1] Gartner, E.M., Kurtis, K.E., and Monteiro, P.J.M. Proposed mechanism of C-S-H growth tested by soft x-ray microscopy, Cement and Concrete Research, vol.30, 2000, pp.817-822.

[2] Clark, S.M., Morrison, G.R., and Shi, W.D. The use of scanning transmission x-ray microscopy for the real-time study of cement hydration, Cement and Concrete Research, vol.29, 1999, pp.1099-1102.

[3] Kurtis K.E., Monteiro P.J.M., Brown J.T., and Meyer-Ilse W. High resolution transmission soft x-ray microscopy of deterioration products developed in large concrete dams, Journal of Microscopy, vol.196, 1999, pp.288-298.

[4] Kurtis K.E., Monteiro P.J.M., Brown J.T., and Meyer-Ilse W. Imaging of ASR gel by soft x-ray microscopy, Cement and Concrete Research, vol.28, 1998, pp.411-421.

[5] Young, J.F. A review of the mechanisms of set-retardation in Portland cement pastes containing organic admixtures, Cement and Concrete Research, vol.2, 1972, pp.415-433.

[6] Thomas, N.L, and Birchall, J.D. The retarding action of sugars on cement hydration, Cement and Concrete Research, vol.13, 1983, pp.830-842.

[7] Birchall, J.D., and Thomas, N.L. The mechanism of retardation of setting of OPC by sugars, British Ceramic Proceedings, vol.35, 1984, pp.305-315.

[8] Meyer-Ilse, W., Medecki, H., Jochum, L., Anderson, E., Attwood, D., Magowan, C., Balhorn, R., Moronne, M., Rudolph, D., and Schmahl, G. Synchrotron Radiation News, vol.8, 1995, pp.23-33.

[9] Denbeaux, G., Anderson, E., Chao, W., Eimuller, T., Johnson, L., Kohler, M., Larabell, C., Legros, M., Fischer, P., Pearson, A., Schuetz, G., Yager, D. and Attwood, D. Soft X-ray microscopy to 25 nm with applications to biology and magnetic materials, Nuclear Instruments & Methods in Physics Research, Section A – Accelerators, Spectrometers, Detectors and Associated Equipment, vol.467(2), 2001, pp.841-844.

[10] Loo, B.W., Meyer-Ilse, W. and Rothman, S.S. Automatic image acquisition, calibration and montage assembly for biological X-ray microscopy, Journal of Microscopy - Oxford, vol.197(2), 2000, pp.185-201.

[11] Williamson, R.B. Constitutional supersaturation in Portland cement solidified by hydration, Journal of Crystal Growth, vol.3, 1968, pp.787-794.

[12] Juenger, M.C.G., and Jennings, H.M. New insights into the effects of sugar on the hydration of Portland cement, Cement and Concrete Research, vol.31, 2002, pp.393-399.
[13] Juenger, M.C.G., Monteiro, P.J.M., Gartner, E.M., and Denbeaux, G.P. A soft x-ray microscope investigation into the effects of calcium chloride on tricalcium silicate hydration, unpublished manuscript.
[14] Gartner, E. M., Tang, F. J. and Weiss, S. J. Saturation factors for calcium hydroxide and calcium sulfates in fresh Portland cement pastes, Journal of the American Ceramic Society, vol.68, 1985, pp.667-673.
[15] Ramachandran, V.S. and Lowery, M.S. Conduction calorimetric investigation of the effect of retarders on the hydration of Portland cement, Thermochimica Acta, vol.195, 1992, pp.373-387.
[16] Ghosh, S.N. Advances in Cement Technology, Oxford, England: Pergamon, 1983.
[17] Singh, N.B. Effect of gluconates on the hydration of cement, Cement and Concrete Research, vol.6, 1976, pp.455-460.
[18] Watling, H., Loh, J. and Gatter, H. Gibbsite crystallization inhibition, 1. Effects of sodium gluconate on nucleation, agglomeration and growth, Hydrometallurgy, vol.55, 2000, pp.275-288.

USING SOFT X-RAY TRANSMISSION MICROSCOPY TO EXAMINE CEMENT HYDRATION IN THE PRESENCE OF RETARDERS

M.C. Garci Juenger[1], P.J.M. Monteiro[2], E.M. Gartner[3] and G.P. Denbeaux[4]

[1] Department of Civil Engineering, University of Texas, Austin, Texas 78712, USA.
E-mail: mjuenger@mail.utexas.edu
[2] Department of Civil and Environmental Engineering, University of California, Berkeley, California 94720, USA. E-mail: monteiro@ce.berkeley.edu
[3] Lafarge, Laboratoire Central de Recherche, 38291 St. Quentin Fallavier, France.
E-mail: ellis.gartner@lafarge.com
[4] Center for X-ray Optics, Lawrence Berkeley National Laboratory, Berkeley, California 94720 USA, E-mail: gpdenbeaux@lbl.gov

Maria Garci Juenger
Department of Civil and Environmental Engineering, University of California, Berkeley
721 Davis Hall. Berkeley, CA 94720. Tel: (510) 643-7647, E-mail: garci@ce.berkeley.edu

Date and Place of Birth
March 5, 1972 Gettysburg, Pennsylvania USA

Education

1994-1999	Northwestern University Ph.D., Materials Science and Engineering, Advisor: Hamlin Jennings
1990-1994	Duke University B.S., Chemistry; B.A., Spanish, with Distinction; Summa Cum Laude

Research Experience

2002	Assistant Professor, Department of Civil Engineering, University of Texas, Austin
1999- 2002	Postdoctoral Research, Department of Civil and Environmental Engineering, University of California, Berkeley *Investigating mechanisms of alkali silica reaction using synthetic aggregates; examining effects of admixtures on cement hydration and microstructure using soft x-ray microscopy*
1994- 1999	Ph.D. Thesis Research, Department of Materials Science and Engineering, Northwestern University *Developed quantitative relationships between processing, microstructure and properties of cement based materials*
1997- 1999	Independent Consulting, Dr. Hamlin Jennings *Assisted with projects involving drying shrinkage of cements and inorganic coatings for aluminum*
1993-1994	Undergraduate Thesis Research, Department of Chemistry, Duke University *Studied the time resolved response of liquid crystals to an applied electric field using step-scan FT-IR spectroscopy*
1993-1994	Undergraduate Thesis Research, Department of Romance Languages, Duke University *Compiled a literary concordance dictionary for La Celestina by Fernando de Rojas*

1992 N.S.F. Research Experiences for Undergraduates, Department of Chemistry, University of Arizona
Synthesized organic chromophores for use in non-linear optical materials

1991 Howard Hughes Fellowship in the Biological Sciences, Department of Pharmacology, Duke University
Investigated neurotransmitters and secondary receptors in rat cerebella for psychopharmacological purposes

Honors and Awards

1998 G.E. Faculty for the Future Internship, Northwestern University

1994-1997 National Science Foundation Graduate Fellowship

1994 National Physical Science Consortium Scholarship for Graduate Research, declined

1994 Cabell Fellowship, Northwestern University, declined

1994 Predmore Award for Most Outstanding Spanish Major, Duke University

1993 American Chemical Society Regional Scholarship for Undergraduate Research

1993-1994 Undergraduate Research Grant, Duke University

1993 Phi Beta Kappa

THERMAL STABILITY OF THE MINERAL $3CAO{\cdot}3AL_2O_3{\cdot}BASO_4$

Wensheng Zhang, Hongtao Zhang, Zhen Lin, Suihua Guo, Yimin Chen

China Building Materials Academy, Guanzhuang Beijing, 100024, P. R. of China.
E-mail: bjzhangwensheng@sohu.com

ABSTRACT

In this paper, the formation and decomposition of the mineral $3CaO{\cdot}3Al_2O_3{\cdot}BaSO_4$ have been researched comprehensively by using chemical reagents as the raw materials. The tested temperature range is from 900°C to 1450°C. Samples are tested by means of TG-DTA, EPMA and XRD. During the formation process of the mineral $3CaO{\cdot}3Al_2O_3{\cdot}BaSO_4$, aluminate minerals, such as $CaO{\cdot}Al_2O_3$ and $12CaO{\cdot}7Al_2O_3$, are the medium states. The formation of $BaO{\cdot}Al_2O_3$ results from the chemical reaction between BaO and Al_2O_3 and BaO forms from the decomposition of the $BaSO_4$ reagent. Results state that when the temperature is more than 1360°C, $3CaO{\cdot}3Al_2O_3{\cdot}BaSO_4$ decomposes and new minerals will form. The decomposition solid products of the mineral $3CaO{\cdot}3Al_2O_3{\cdot}BaSO_4$ include $12CaO{\cdot}7Al_2O_3$, $CaO{\cdot}Al_2O_3$ and $BaO{\cdot}Al_2O_3$ on condition that the temperature ≥1360°C. The chemical equation of the decomposition may be described as follows:
$3CaO{\cdot}3Al_2O_3{\cdot}BaSO_4 \rightarrow 12CaO{\cdot}7Al_2O_3 + CaO{\cdot}Al_2O_3 + BaO{\cdot}Al_2O_3 + SO_2\uparrow + O_2\uparrow$

Keywords: $3CaO{\cdot}3Al_2O_3{\cdot}BaSO_4$; Formation Process; Medium States; Formation Mechanism of $BaO{\cdot}Al_2O_3$; Decomposition Equation.

1. INTRODUCTION

Teoreanu I. reported the new mineral $3CaO{\cdot}3Al_2O_3{\cdot}BaSO_4$ in 1986 and researched the formation problem of the pure mineral $3CaO{\cdot}3Al_2O_3{\cdot}BaSO_4$. [1] And then Feng Xiuji et al studied comprehensively the crystal structure characteristics of the mineral $3CaO{\cdot}3Al_2O_3{\cdot}BaSO_4$ and its application, such as the new type of barium-containing sulphoaluminate cement. [2,3,4] The characteristic of the mineral $3CaO{\cdot}3Al_2O_3{\cdot}BaSO_4$ at high temperatures (>1300°C) has also been studied.[5] However, the results of the characteristics of the mineral $3CaO{\cdot}3Al_2O_3{\cdot}BaSO_4$ at high temperatures, such as the formation temperature and the decomposition temperature, are different. Meanwhile, there are many observations about the formation mechanism of the mineral $BaO{\cdot}Al_2O_3$ in the clinkering process of the mineral $3CaO{\cdot}3Al_2O_3{\cdot}BaSO_4$. In this paper, the formation process of the mineral $3CaO{\cdot}3Al_2O_3{\cdot}BaSO_4$ has been researched and the ideal burning temperature, which could produce the pure mineral $3CaO{\cdot}3Al_2O_3{\cdot}BaSO_4$, is decided. The stability of the mineral $3CaO{\cdot}3Al_2O_3{\cdot}BaSO_4$ at high temperature is researched through burning the pure mineral $3CaO{\cdot}3Al_2O_3{\cdot}BaSO_4$ at different temperatures (>1350°C). Meanwhile, the formation mechanism of the mineral $BaO{\cdot}Al_2O_3$ is discussed because of its importance for the research problem.

2. EXPERIMENT AND TEST

$CaCO_3$, Al_2O_3 and $BaSO_4$, which are used in the experiment, are the chemical reagents. The sieve residue of each raw material on the 80μm fine-mesh sieve is zero. According to the chemical composition of the mineral $3CaO\text{-}3Al_2O_3\text{-}BaSO_4$, the ratio of each raw material in the raw meal is calculated. The experimental raw meal is prepared after the mixed raw material is homogeneous.

The tested temperature range of the raw meal is between 900°C and 1450°C. The burned samples were tested by means of TG-DTA, EPMA and XRD.

3. RESULTS AND DISSCUSION

3.1 The Formation Process of the Mineral $3CaO\text{-}3Al_2O_3\text{-}BaSO_4$

The raw meal is respectively burned at the temperature 900°C, 1150°C, 1200°C, 1300°C and 1350°C and the burned sample is tested with the XRD. The test results of each sample are shown in the Figure 1.

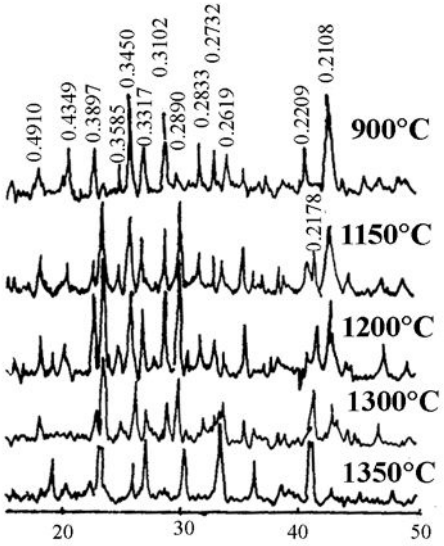

Figure 1. XRD patterns of the raw meal of $3CaO\text{-}3Al_2O_3\text{-}BaSO_4$ burned at different temperature

From Figure 1, it can be seen that $12CaO\text{-}7Al_2O_3$(d=0.2680nm, 0.4889nm, 0.3204nm), $BaO\text{-}Al_2O_3$ (d=0.3130nm, 0.2605nm) and $CaO\text{-}Al_2O_3$ (d=0.2971nm, 0.2514nm) exist in the burned sample. The mineral $3CaO\text{-}3Al_2O_3\text{-}BaSO_4$ has been formed at the temperature 900°C. At the temperature 1350°C there exists only the mineral $3CaO\text{-}3Al_2O_3\text{-}BaSO_4$ and the rest of the minerals disappear in the burned sample.

From the XRD results of the burned raw meal, it could be deduced that the formation velocity of the mineral $3CaO\text{-}3Al_2O_3\text{-}BaSO_4$ is lower than that of the aluminate minerals. The mineral $3CaO\text{-}3Al_2O_3\text{-}BaSO_4$ is formed from the chemical reaction of the aluminate mineral, such as $12CaO\text{-}7Al_2O_3$ and $CaO\text{-}Al_2O_3$, with the mineral $BaSO_4$. The mineral $12CaO\text{-}7Al_2O_3$ and $CaO\text{-}Al_2O_3$ are the median phases during the formation process of the mineral $3CaO\text{-}3Al_2O_3\text{-}BaSO_4$.

The formation mechanism of the mineral $BaO\text{-}Al_2O_3$ is important for the research of the mineral $3CaO\text{-}3Al_2O_3\text{-}BaSO_4$. It will be discussed separately in part 3.3.

3.2 The Stability of the Mineral $3CaO\text{-}3Al_2O_3\text{-}BaSO_4$ at the High Temperature

3.2.1 TG-DTA analysis

The thermal result of the pure mineral $3CaO\text{-}3Al_2O_3\text{-}BaSO_4$ between the ambient temperature and 1450°C are shown in Figure 2. The velocity of the temperature increase is 10°C /min during the test process.

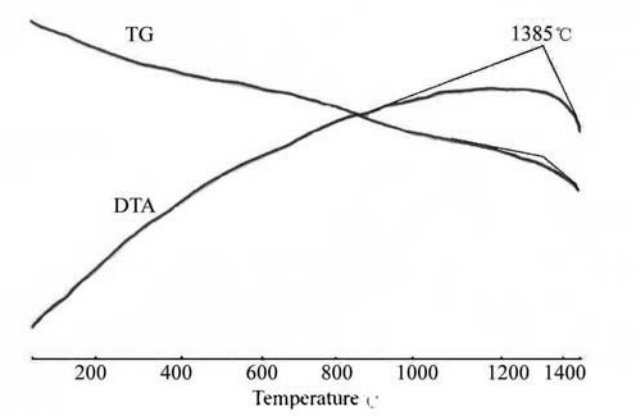

Figure 2. TG-DTA curves of the pure mineral $3CaO\text{-}3Al_2O_3\text{-}BaSO_4$ between ambient and 1450°C

On the DTA curve there is an endothermic peak, which begins from the temperature 1385°C. Correspondingly, there is a mass loss on the TG curve at the same temperature. This suggests that the mineral $3CaO\text{-}3Al_2O_3\text{-}BaSO_4$ is not stable when the temperature is more than 1385°C

3.2.2 EPMA Analysis

The pure mineral $3CaO\text{-}3Al_2O_3\text{-}BaSO_4$, clinkered at the temperature 1450°C for 300 minutes, is tested with the method of the EPMA. The content of the element S at the different planes and points of the clinkered sample is listed in Table 1. The micrograph of the plane distribution of the element S in the clinkered sample is shown in Figure 3.

Table 1. Mass fraction of the element SO_3 at the different planes and points of the burned sample

Position	**Planes**					**Points**				
No.	1	2	3	4	5	1	2	3	4	5
SO_3 (wt.%)	5.65	8.02	6.36	6.14	7.80	8.28	5.31	4.78	7.07	3.25

The content of the SO_3 in the clinkered sample is less than the theoretical content 11.31 wt.% (based on the chemical composition of the mineral $3CaO\text{-}3Al_2O_3\text{-}BaSO_4$). The distribution of the element S in the clinkered pure mineral $3CaO\text{-}3Al_2O_3\text{-}BaSO_4$ is not homogeneous according to Figure 3.

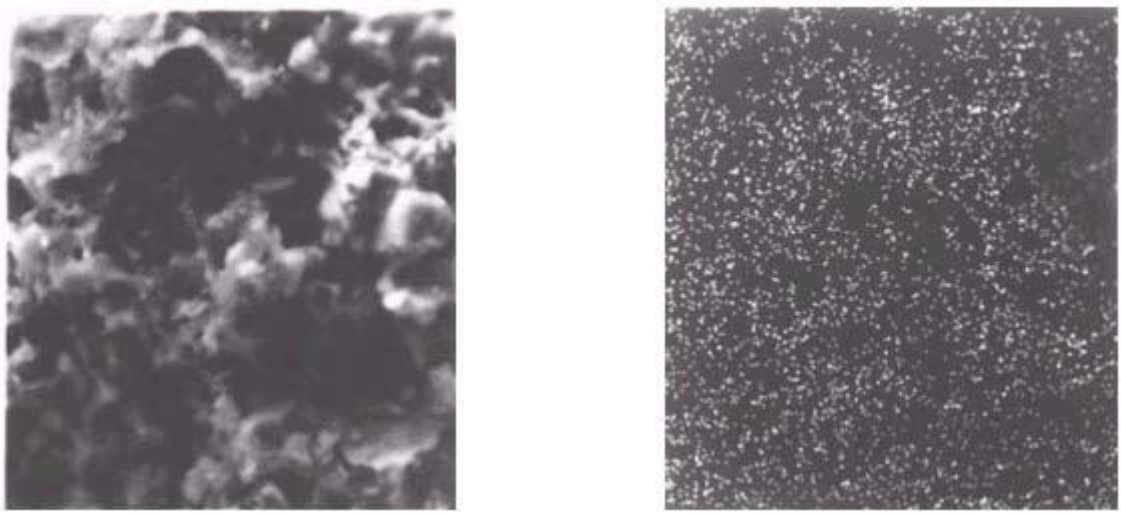

Figure 3. Micrographes of the mineral $3CaO\text{-}3Al_2O_3\text{-}BaSO_4$ burned at temperature 1450°C for 300 minutes and element distribution for S

The results of the EPMA test state that the decomposition of the mineral $3CaO\text{-}3Al_2O_3\text{-}BaSO_4$ will form the gas phase SO_2.

3.2.3 Burned experiment of the mineral $3CaO\text{-}3Al_2O_3\text{-}BaSO_4$

The mineral $3CaO\text{-}3Al_2O_3\text{-}BaSO_4$ is respectively burned at the temperature 1350°C, 1360°C, 1380°C, 1400°C and 1450°C for 300 minutes. The mass loss of the burned sample is tested with the analytical balance (the precision: 0.0001g). The results are shown in Table 2.

Table 2. Mass loss of the mineral $3CaO\text{-}3Al_2O_3\text{-}BaSO_4$ burned at the high temperature

Parameter	Temperature/°C				
	1350	1360	1380	1400	1450
Mass loss (%)	0	1.32	1.53	2.42	5.01

At the temperature 1360°C, the mass of the mineral $3CaO\text{-}3Al_2O_3\text{-}BaSO_4$ has decreased. It could be deduced that the pure mineral $3CaO\text{-}3Al_2O_3\text{-}BaSO_4$ clinkered at the temperature 1360°C has been decomposed and the gas phases SO_2 and O_2 have been formed. The decomposition temperature is lower than the test result of the TG-DTA because of the difference of the test condition.

3.2.4 XRD analysis

The XRD result of the pure mineral, which is made from the raw meal clinkered at the temperature 1350°C for 240 minutes, is shown in Figure 4. The free CaO content of the sample is zero with the alcohol-glycerol method. It is stated that the pure mineral $3CaO\text{-}3Al_2O_3\text{-}BaSO_4$ may be prepared on condition that the temperature is 1350°C for 240 minutes. In order to research the stability of the mineral $3CaO\text{-}3Al_2O_3\text{-}BaSO_4$, the pure mineral is clinkered at temperatures from 1350°C to 1450°C. The XRD results of the clinkered samples are shown in Figure 5.

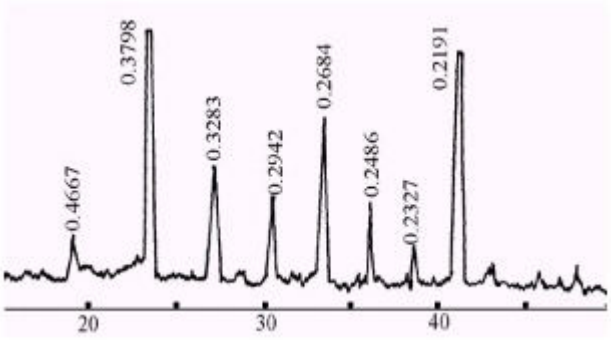

Figure 4. XRD pattern of the pure mineral $3CaO\text{-}3Al_2O_3\text{-}BaSO_4$

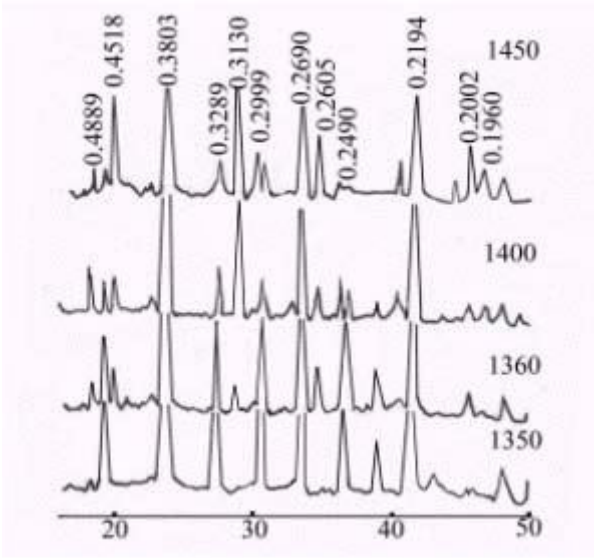

Figure 5. XRD partterns of $3CaO\text{-}3Al_2O_3\text{-}BaSO_4$ burned at the different temperature

There exist the minerals $12CaO\text{-}7Al_2O_3$(d=0.2680nm, 0.4889nm,0.3204nm), $BaO\text{-}Al_2O_3$ (d=0.3130nm,0.2605nm)and $CaO\text{-}Al_2O_3$(d=0.2971nm, 0.2514nm) in the clinkered pure mineral $3CaO\text{-}3Al_2O_3\text{-}BaSO_4$ at a temperature of 1360°C. The characteristic peak strength of the mineral $3CaO\text{-}3Al_2O_3\text{-}BaSO_4$ decreases as the clinkered temperature rises. However, the characteristic peak strength of the mineral $BaO\text{-}Al_2O_3$ increases with the increase of the temperature. When the clinkered temperature reaches to 1450°C the peak strength of two minerals is approximately equal.

It could be deduced that the mineral $3CaO\text{-}3Al_2O_3\text{-}BaSO_4$ has decomposed at the temperature 1360°C. The minerals $12CaO\text{-}7Al_2O_3$, $BaO\text{-}Al_2O_3$ and $CaO\text{-}Al_2O_3$ are formed because of its decomposition. Based on the analysis of the other test results, the decomposition equation of the mineral $3CaO\text{-}3Al_2O_3\text{-}BaSO_4$ may be described as follows:

$$3CaO\text{-}3Al_2O_3\text{-}BaSO_4 \rightarrow 12CaO\text{-}7Al_2O_3 + CaO\text{-}Al_2O_3 + BaO\text{-}Al_2O_3 + SO_2\uparrow + O_2\uparrow$$

It also states that the preparation condition of the pure mineral $3CaO\text{-}3Al_2O_3\text{-}BaSO_4$ in the reference [1] is not suitable.

3.3 The Formation Mechanism of the Mineral $BaO\text{-}Al_2O_3$

According to the thermodynamics data, the enthalpy of formation of $BaO\text{-}Al_2O_3$ through the reaction of $BaSO_4$ with Al_2O_3 is +27.33kJ/mol when the temperature is less than 1327°C. Why does the mineral $BaO\text{-}Al_2O_3$ exist in the burned sample (as shown in Figure 1) when the temperature is not more than 1300°C? Because the $BaSO_4$ reagent used in the experiment is not stable. In the ideal

state, $BaSO_4$ does not decompose at temperatures ≤1300°C. However, the $BaSO_4$ reagent (class: analytical reagent) decomposes at temperatures ≤1300°C [6] and the solid decomposition product is BaO. The reaction of Al_2O_3 with BaO forms the mineral $BaO\text{-}Al_2O_3$ when the temperature is less than 1300°C. The formation process of $BaO\text{-}Al_2O_3$ is described as follows:

$$BaSO_4 \text{ (analytical reagent)} \rightarrow BaO + SO_2\uparrow + O_2\uparrow$$
$$BaO + Al_2O_3 \rightarrow BaO\text{-}Al_2O_3$$

The former research results that show that the formation of the mineral $BaO\text{-}Al_2O_3$ results from the decomposition of $3CaO\text{-}3Al_2O_3\text{-}BaSO_4$ at temperatures ≤1300°C are not validated and acceptable.

The formation of $BaO\text{-}Al_2O_3$ results from the decomposition of the mineral $3CaO\text{-}3Al_2O_3\text{-}BaSO_4$ when the temperature is more than 1360°C according to the research result in the part 3.2 of the paper.

4. CONCLUSION

1. During the formation process of the mineral $3CaO\text{-}3Al_2O_3\text{-}BaSO_4$, $12CaO\text{-}7Al_2O_3$ and $CaO\text{-}Al_2O_3$ are the middle phases. The chemical reaction between $BaSO_4$ and aluminate minerals is the formation type for the mineral $3CaO\text{-}3Al_2O_3\text{-}BaSO_4$. The pure mineral $3CaO\text{-}3Al_2O_3\text{-}BaSO_4$ may be prepared on condition that the temperature is ≤1350°C.

2. The mineral $3CaO\text{-}3Al_2O_3\text{-}BaSO_4$ is stable when the temperature is not higher than 1350°C. However, when the temperature is higher than 1360°C, $3CaO\text{-}3Al_2O_3\text{-}BaSO_4$ is decomposed and new minerals are formed. The chemical equation of the decomposition may be described as follows:
$$3CaO\text{-}3Al_2O_3\text{-}BaSO_4 \rightarrow 12CaO\text{-}7Al_2O_3 + CaO\text{-}Al_2O_3 + BaO\text{-}Al_2O_3 + SO_2\uparrow + O_2\uparrow$$

3. $BaO\text{-}Al_2O_3$ forms from the chemical reaction of the raw materials at the temperature ≤ 1350°C. because of the decomposition of the chemical reagent $BaSO_4$. When the temperature is higher than 1360°C., $BaO\text{-}Al_2O_3$ is from the decomposition of the mineral $3CaO\text{-}3Al_2O_3\text{-}BaSO_4$.

REFERENCES

[1] Teoreanu, I. Muntean, M. and Dragnea, I. Type $3(CaO\text{-}Al_2O_3)\text{-}M_x(SO_4)_y$ compounds and compatibility relation in $CaO\text{-}Al_2O_3$-- $M_x(SO_4)_y$ systems. IL Cemento□1, 1986, pp. 39-46.

[2] Feng Xiuji, Liao Guanglin and Long Shizong. Investigation on the structure and the performance of $3CA{\cdot}SrSO_4$ and $3CA{\cdot}BaSO_4$, Proceedings of Second Symposium on Cement and Concrete, Beijing, 1989, vol. 1, pp. 222-229.

[3] Zhang Wensheng, Yu Qijun and Feng Xiuji. Study on the clinkering process of the barium-containing sulphoaluminate cement clinker. Journal of Building Materials, vol.1, 1998, pp. 185-198. (in Chinese)

[4] Feng Xiuji, Long Shizong and Liao Guanglin. Barium-containing sulphoaluminate cement. China Invention Paten, No.89100506.4, 1989. (in Chinese)

[5] Long Shizong, Liao Guanglin and Zhao Sanyin. Study on some clinkering problems of the mineral $3CaO\text{-}3Al_2O_3\text{-}BaSO_4$, China Building Materials Science and Technology, vol. 5, 1996, pp. 11-16.(in chinese)

[6] Duan Changqiang, Meng Qingfang, Zhang Su et al. Handbook of the Chemical Reagent, Beijing: Chemical Industry Press, 1986, p. 160.(in chinese)

THERMAL STABILITY OF THE MINERAL $3CAO{\cdot}3AL_2O_3{\cdot}BASO_4$

Wensheng Zhang, Hongtao Zhang, Zhen Lin, Suihua Guo and Yimin Chen

China Building Materials Academy, Guanzhuang Beijing, 100024, P. R. of China.
E-mail: bjzhangwensheng@sohu.com

WENSHENG ZHANG

Name: Wensheng Zhang

Affiliation: The Key Laboratory of Cement-based Materials Science of China Building Materials Academy

Mailing Add:

Key Laboratory of Cement-based Materials Science of China Building Materials Academy
Guangzhuang, Beijing, 100024,
P. R. of China

WORLD MAP OF CLINKERS - VISUALIZATION OF TRACE ELEMENT CONTENT OF CLINKERS BY SELF-ORGANIZING MAP

Ferenc D. Tamás and János Abonyi

[a] Dept. of Silicate- and Materials Engineering,
University of Veszprém, Hungary, H-8201 VESZPRÉM, P.O.B. 158 Tel. +36-88-422022/4354
Fax +36-88-423091; E-mail: tam043@almos.vein.hu
[b] Dept. of Process Engineering, University of Veszprém, Hungary, H-8201 VESZPRÉM, P.O.B. 158; Website: www.fmt.vein.hu/softcomp

ABSTRACT

The analysis of data taken from the measurements of trace elements in clinkers may lead to extremely valuable insights into the properties of raw materials and can be used to solve practical problems too: to determine the origin of the clinker (i.e. the manufacturing works). For this purpose, several hundred clinker sorts have been analysed by replicated quarterly samples, collected from factories of nine countries to determine their Mg, Sr, Ba, Mn, Ti, Zr, Zn and V content. This paper describes a soft-computing based approach where the Self-Organizing Map (SOM) is used for the extraction of knowledge from this database related to the trace element content of clinkers. The SOM is a vector quantization method which places prototype vectors (cluster centers) on a regular low-dimensional grid in an ordered fashion. Since SOM provides a compact representation of the data distribution, the typical clinkers are detected by the SOM via clustering of the data. As the typical trace element contents are arranged on a two-dimensional grid, efficient vizualization can then be performed in the two-dimensional projection of the concentration variables, hence the model can be effectively used to analyze the relationships between different factories and different trace elements

1. INTRODUCTION

The trace element content of clinkers is of high scientific interest, and can be used to solve practical problems too, e.g. to determine the origin of the clinker (i.e. the manufacturing works). The first paper of similar topics was published in 1993 by Goguel and StJohn, showing the Ba, Sr and Mn concentration of portland cements in New Zealand concretes. This first attempt suggests that advanced statistical methods, called “pattern recognition” or “fingerprinting” can help qualitative identification [1].

For the qualitative “fingerprinting” of clinkers, obviously a set of well defined clinker samples are necessary. To obtain such informative database, a Technical Committee “QIC” (Qualitative Identification of Clinkers and Cements) has been established in 1996 (TC 180/QIC). This project enabled collection of composite average samples from 9 countries (Austria, Hungary, Portugal, South Africa, Slovakia, Slovenia, Spain, Switzerland and United Kingdom). Over 200 samples have arrived to date, and analysed to determine their Mg, Sr, Ba, Mn, Ti, Zr, Zn and V content.

Among the wide range of advanced statistical and “pattern recognition” methods, in our previous papers the analytical data were transformed by principal component analysis into a two-dimensional space and dendograms were constructed for cluster formation. The visualisation of trace element content of clinker/cement is not an easy task. At the 10th International Congress on the Chemistry of

Cement, J.H. Potgieter [2] presented a method to construct “star plots”, where the visual impact of chemical differences are more striking. This “star plot” method has been further developed in our previous paper [3]; to facilitate the visualisation of the trace element content a new star plotting is presented where every clinker is compared to the proposed standard.

The term knowledge discovery in databases (KDD) refers to the overall process of discovering knowledge from data. KDD has evolved from the intersection of research fields such as machine learning, pattern recognition, databases, statistics, artificial intelligence, and more recently it gets new inspirations from soft computing. KDD methods have been successfully applied for the analysis of process systems, and the results have been used for process design, process improvement, operator training, and so on [4].

When we attempted to use standard data mining, KDD, and multivariate statistical tools for industrial problems, like extracting knowledge from large amounts of data, we realized that production systems are typically ill-defined systems, difficult to model and they have large-scale solution spaces. In these cases, precise models are impractical, too expensive, or non-existent. Furthermore, the relevant available information is usually in the form of empirical prior knowledge and input-output data representing instances of the system's behavior. Therefore, we need an approximate reasoning system capable of handling such imperfect information. Computational Intelligence (CI) and Soft Computing (SC) are recently coined terms describing the use of many emerging computing disciplines.

The aim of this paper is to show how SC can be used in finding useful patterns in data obtained by the measurement of trace element content of clinkers. Most of the SC based models can be effectively used in data mining and lend themselves to transformation into other traditional data mining or advanced SC-based model structures that allow information transfer between different models. For example, in [5] a decision tree was mapped into a feedforward neural network. A variation of this method is given in [6] where the decision tree was used for the input domains discretization only. Another example is that as radial basis functions (RBF) are functionally equivalent to fuzzy inference systems [7], tools developed for the identification of RBFs can also be used to design fuzzy models. The KDD process also includes the interpretation of the mined patterns. This step involves the visualization of the extracted patterns/models, or visualization of the data given the extracted models. Among the wide range of SC tools [8], the Self-Organizing Map (SOM) is the most applicable for this purpose [9]. The main objective of this paper is propose a SOM based methodology that can be effectively used for the analysis of operational process data and product quality.

The SOM algorithm performs a topology preserving mapping from high dimensional space onto a two dimensional grid of neurons so that the relative distances between data points are preserved. The net roughly approximates the probability density function of the data and, thus, serves as a clustering tool [9]. It also has the capability to generalize, i.e. the network can interpolate between previously encountered inputs. Since SOM is a special clustering tool that provides compact representation of the data distribution, it has been widely applied in the visualization of high-dimensional data. The SOM facilitates visual understanding of processes so that several variables and their interactions may be inspected simultaneously. For instance, Kassalin used the SOM to monitor the state of a power transformer and to indicate when the process was entering a non-desired state represented by a "forbidden" area on the map [10]. Tryba and Goser [11] applied the SOM in monitoring of a distillation process and discussed its use in chemical process control in general. Alander [12] and Harris [13] have used the SOM in fault detection. Since the model is trained using measurement vectors describing normal operation only, a faulty situation can be detected by monitoring the quantization error (distance between the input vector and the best matching unit (BMU)), as a large error indicates that the process is out of normal operation space.

Based on the above mentioned beneficial properties of the SOM, a new approach for the analysis and visualization of the trace element content of clinkers is proposed in this paper. The paper is organized as follows. In Section 2., the SOM is introduced. In Section 3., a detailed application study is presented. Conclusions are given in Section 4.

2. SELF-ORGANIZING MAP

Cluster analysis organizes data into groups according to similarities among them. In metric spaces, similarity is defined by means of distance based upon the length from a data vector to some prototypical object of the cluster. The prototypes are usually not known beforehand, and are sought by the clustering algorithm simultaneously with the partitioning of the data. In this paper, the clustering of the operational data is considered. Hence, the data are the measured input and output process variables, parameters of the operating conditions, and laboratory measurements of the product quality. Each observation consists of l measured variables (l measured trace element concentration in this case), grouped into an l-dimensional column vector $\mathbf{x}_i = [x_{i,1}, \ldots, x_{i,l}]^T$. A set of N observations is denoted by $\mathbf{X}$ and represented as a matrix $\mathbf{X} = [\mathbf{x}_1, \ldots, \mathbf{x}_N]^T$. In pattern recognition terminology, the columns of $\mathbf{X}$ are called patterns or objects, the rows are called the features or attributes, and $\mathbf{X}$ is called the pattern matrix. The objective of clustering is to divide the data set $\mathbf{X}$ into c clusters.

The SOM algorithm is a kind of clustering algorithm which a performs a topology preserving mapping from high dimensional space onto map units so that relative distances between data points are preserved. The map units, or neurons, form usually a two dimensional regular lattice. Each neuron, i, of the SOM is represented by an l-dimensional weight, or model vector $\mathbf{m}_i = [m_{i,1}, \ldots, m_{i,l}]^T$. These weigh vectors of the SOM form a codebook and can be considered as cluster prototypes. The neurons of the map are connected to adjacent neurons by a neighborhood relation, which dictates the topology of the map. The number of the neurons determines the granularity of the mapping, which affects the accuracy and the generalization capability of the SOM.

SOM is a vector quantizer, where the weights play the role of the codebook vectors. This means, each vector represents a local neighborhood of the space, also called Voronoi cell. The response of a SOM to an input $\mathbf{x}_k = [x_{k,1}, \ldots, x_{k,l}]^T$ is determined by the reference vector (weight) $\mathbf{m}_{i^0}$ which produces the best match of the input

$$i_k^0 = \arg\min_i \left\| \mathbf{m}_i - \mathbf{x}_k \right\|$$

where i_k^0 represents the index of the Best Matching Unit (BMU) of the k-th input.

During the iterative training of SOM, the SOM forms an elastic net that folds onto the "cloud" formed by the data. The net tends to approximate the probability density of the data: the codebook vectors tend to drift there where the data are dense, while there are only a few codebook vectors where the data are sparse.

The training of SOM can be accomplished generally with a competitive learning rule as

$$\mathbf{m}_i^{(t+1)} = \mathbf{m}_i^{(t)} + \eta \Lambda_{i_k^0, i} \left(\mathbf{x}_k - \mathbf{m}_i^{(t)} \right)$$

where $\Lambda_{i_k^0, i}$ is a spatial neighborhood function and η is the learning rate, and the *(t)* upper index denotes the iteration step. Usually, the neighborhood function is

$$\Lambda_{i_k^0,i} = \exp\left(-\frac{\left\| \mathbf{r}_i - \mathbf{r}_{i_k^0} \right\|^2}{2\sigma^{2,(t)}} \right)$$

where $\left\| \mathbf{r}_i - \mathbf{r}_{i_k^0} \right\|$ represents the Euclidean distance in the low dimensional output space between the *i*-th vector and the winner neuron (BMU), and $\sigma^{2,(t)}$ represents the time-variant with of the Gaussian function used for the representation of the neighborhood function.

There are two phases during learning. First, the algorithm should cover the full input data space and establish neighborhood relations that preserve the input data structure. This requires competition among the majority of the weights and a large learning rate such that the weights can orient themselves to preserve local relationships. Hence, in the first phase relatively large initial σ^2 is used. The second phase of learning is the convergence phase where the local detail of the input space is preserved. Hence the neighborhood function should cover just one unit and the learning rate should be also small. In order to achieve these properties, both the neighborhood function and the learning rate should be scheduled during learning [9].

3. APPLICATION TO THE FINGERPRINTING OF CLINKERS

A qualitative identification obviously requires a database, to compare the trace element content of unknown clinkers/cements with characteristic known samples. For the qualitative "fingerprinting" of clinkers, obviously a set of well defined clinker samples are necessary: composite average samples of a longer period of kiln operation. Such samples were collected quarterly, over a longer period (2-3 years) in all Hungarian cement factories. A nationwide sample collection has a limited value only; to obtain a higher area, a Technical Committee 180/QIC, (Qualitative Identification of Clinkers and Cements), was stablished in 1996 under the auspices of RILEM (Réunion Internationale des Laboratoires d'Essais et de Recherches sur les Matériaux et les Constructions) (TC 180/QIC). This enabled the collection of composite average samples from 8 further countries (Austria, Portugal, South Africa, Slovakia, Slovenia, Spain, Switzerland and United Kingdom). Over 200 samples have arrived to date, and been analysed. Detailed analytical data can be obtained from the author. At the request of the companies, factory and sampling data cannot be revealed, only the country and a codenumber. The details of the analytical experiments and the data are described in our previous papers [14, 15, 16,17].

In this paper the Self-Organizing Map (SOM) is applied to visualize the data collected from nine countries. SOM places the prototype vectors of typical clinkers on a regular two-dimensional grid in an ordered fashion. This makes it a powerful tool for the analysis of clinkers as it maps the 6-dimensional input vector (a clinker is defined by six trace element concentration) into a two dimensional space.

A SOM consists of neurons organized on a regular two-dimensional grid. Each neuron is a 6-dimensional weight vector (prototype vector, codebook vector).

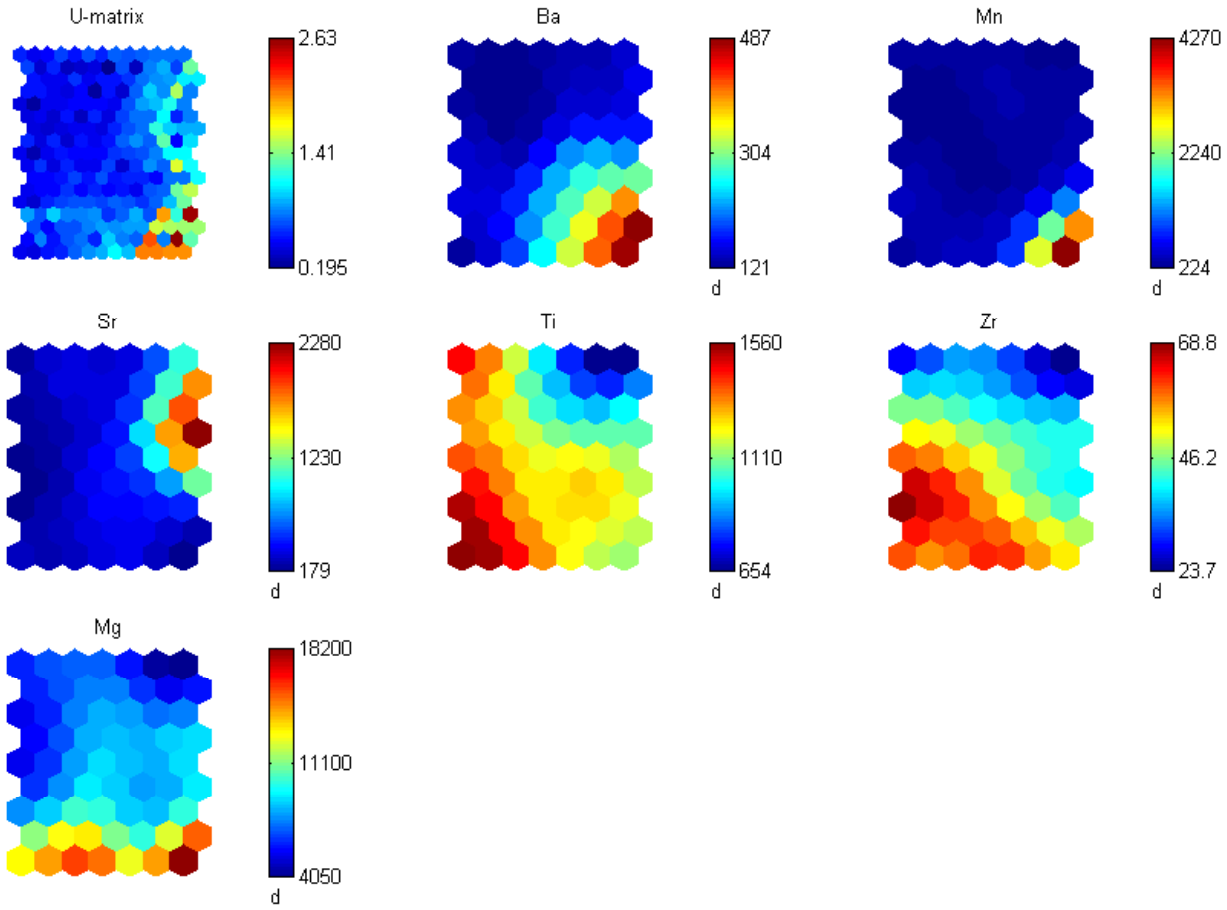

Figure 1. SOM map of trace elements of clinkers

Figure 1. represents the results of the application of SOM where a 7 times 8 grid has been used to represent the "world map" of trace elements. As the previous section showed, the neurons are connected to adjacent neurons by a neighborhood relation, which dictates the topology, or structure, of the map. Hence, the neighboring objects in the SOM have similar properties.

The trace element content of a cell in this grid can be easily seen in this figure. As can be observed, the Ba has a similar distribution to Mn and Ti is also similar to Zr. This fact is also reflected by the analysis of the correlation of the data, as the two highest correlation coefficients are the Ba-Mn (0.5769) and Ti-Zr (0.4312). Hence, SOM is an effective tool for "correlation hunting".

The main benefit of the proposed approach can be seen from Figure 2 where the countries and factories on the world map of clinkers are depicted.

This map can be easily used to classify a clinker and analyze the similarity of clinkers produced in different factories.

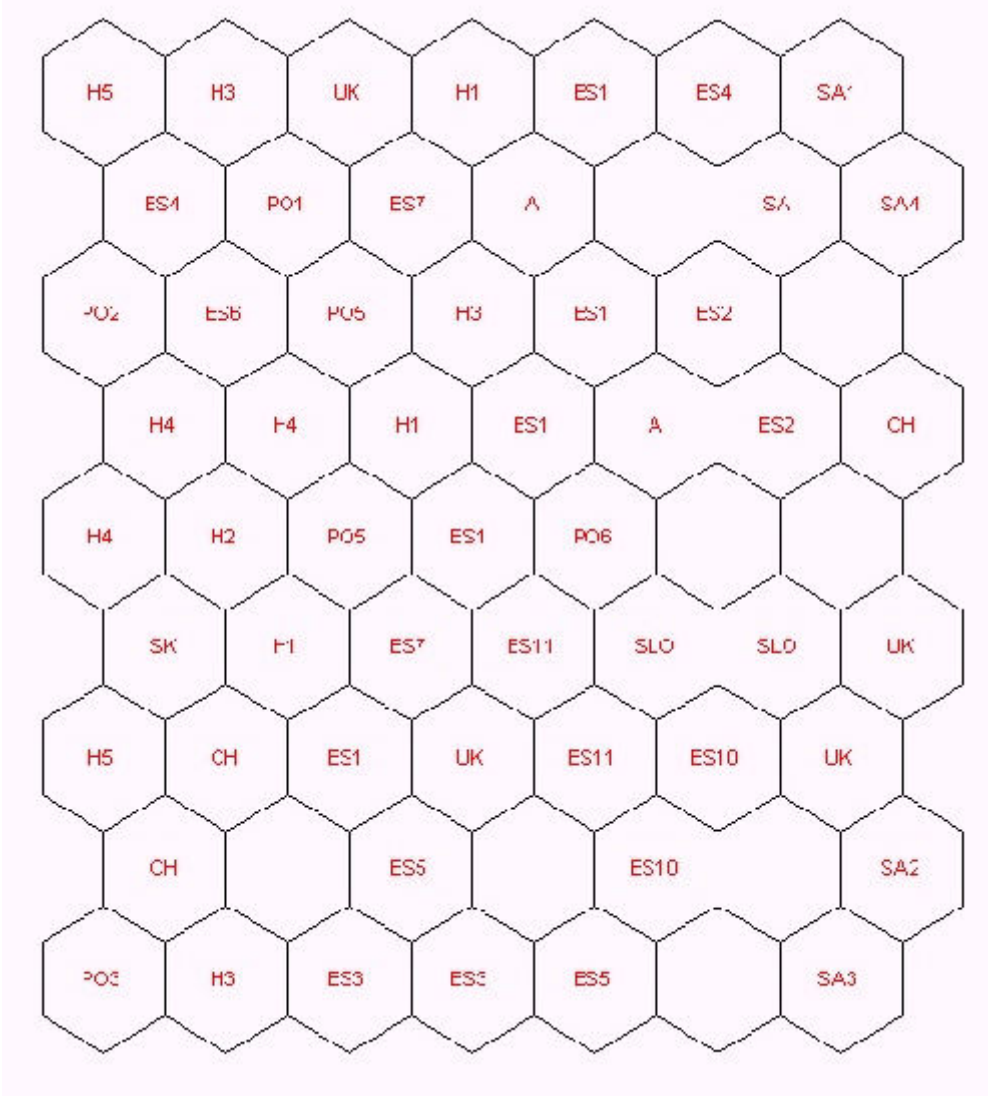

Figure 2. Countries and factories on the world map of clinkers.

4. CONCLUSIONS

Quarterly average samples from 9 countries were collected over a longer period and their trace element contents (Ba, Mn, Sr, Mg; Ti, Zr; Zn and V) determined. The trace element content of clinkers can be used for the qualitative identification. The paper presented the application of Self-Organizing Maps that have been found to be particularly useful in the qualitative analysis of the trace element content of these clinkers. The proposed approach can be used to solve practical problems: to determine the origin of the clinker (i.e. the manufacturing works), to provide visual impact of chemical differences of the materials, and to detect correlation among the trace elements.

A detailed description of the tools helps the construction of the algorithms; still easier, a computer program has been written (in MATLAB©) and it can be downloaded from www.fmt.vein.hu/softcomp.

ACKNOWLEDGEMENT

The financial support of OTKA (Hungarian National Research Foundation), No. T026307 and No. T037600 are gratefully acknowledged. Thanks are due to the laboratories of Hungarian cement factories as well as to members of the Technical Committee „180-QIC" (Qualitative Identification of Clinkers and Cements) of RILEM (Réunion Internationale des Laboratoires d'Essais et de Recherches sur les Matériaux et les Constructions) for collecting composite average clinker samples. Janos Abonyi is grateful for the Janos Bolyai Research Fellowship of the Hungarian Academy of Science.

REFERENCES

[1] R.L. Goguel, D.A. StJohn, Chemical identification of Portland cements in New Zealand concretes, Part I. Characteristic differences among New Zealand cements in minor and trace element chemistry. Cem Concr Res 23 (1) (1993) 59-68; Part II. The Ca-Sr-Mn plot in cement identification and the effect of aggregates. Cem Concr Res 23 (2) (1993) 283-293

[2] J.H. Potgieter, Fingerprinting S.A. cements by chemical analysis. In: H. Justnes (Ed.) Proceedings of the 10th International Congress on the Chemistry of Cement. (1997). Amarkai AB and Congrex Göteborg AB Paper No. 3v011 pp. 1-6.

[3] F.D. Tamás, J. Abonyi, Trace elements in clinkers – I. A graphical representation. *Cem. Concr. Res.* 32, (1319-1323)

[4] X.Z. Wang, Data Mining and Knowledge Discovery for Process Monitoring and Control, Springer, 1999)

[5] L.K.Sethi, Entropy Nets: From Decision Trees to Neural Networks *Proc. IEEE* 78 (1990) 1605--1613

[6] I.Ivanova and M. Kubat, Initialization of Neural Networks by Means of Decision Trees, *Knowledge-Based Systems* 8, (1995) 333--344

[7] J.-S.R. Jang and C.-T. Sun , Functional Equivalence Between Radial Basis Function Networks and Fuzzy Inference Systems, IEEE Transactions on Neural Networks, 4, (1993) 156--159

[8] N.R. Pal, Soft computing for feature analysis, *Fuzzy Sets and Systems*, 103 (1999) 201-221

[9] T. Kohonen The Self-Organizing Map, *Proceedings of the IEEE*, 78(9) (1990), 1464-1480

[10] M.Kassalin, J. Kangas, O. Simula, Process state monitoring using self-organizing maps, In *Artificial Neural Networks*, Vol. II, (1992) 1531-1534, North-Holland

[11] Tryba, K. Goser, Self - Organizing feature maps for process control in chemistry, In *Artificial Neural Networks*, (1991) 847-852, North-Holland

[12] J.T. Alander, M. Frisk, L. Holmström, A. Hämäläinen, J. Tuominen, Process error detection using self-organizing feature maps, In *Artificial Neural Networks*, Vol. II, (1991) 1229-1232, North-Holland

[13] T. Harris, A. Kohonen, S.O.M. based, machine health monitoring systems which enables diagnosis of faults not seen in the training set. In *Proc. of the Int. Conf. On Neural Networks (IJCNN`93), Nagoya, Japan*, Vol. I, (1993) 947-950

[14] F.D. Tamás, É. Kristóf-Makó, Chemical „fingerprints" in Portland cement clinkers in: A. Gerdes (Ed.), Advances in Building Materials Science – Festschrift Wittmann, Aedificatio Publishers, Freiburg – Unterengstringen, (1996), pp. 217-228

[15] F.D. Tamás, A. Tagnit-Hamou, J. Tritthart, Trace elements in clinker and their use as „fingerprints" to facilitate their qualitative identification. In: M. Cohen, S. Mindess, J. Skalny (Eds.), Materials Science of Concrete – The Sidney Diamond Symposium, Honolulu, HI, September (1998). American Ceramic Society, Westerville OH, pp. 57-69

[16] F.D. Tamas, Pattern recognition methods for the qualitative identification of Hungarian clinkers. World Cement / Res. & Development 27 (1996) 75-79

[17] F.D. Tamás, J. Abonyi, Trace elements in clinkers – II. Qualitative Identification by Fuzzy Clustering. Cem Concr Res, Accepted

WORLD MAP OF CLINKERS - VISUALIZATION OF TRACE ELEMENT CONTENT OF CLINKERS BY SELF-ORGANIZING MAP

Ferenc D. Tamás[a] and János Abonyi[b]

[a] Dept. of Silicate- and Materials Engineering,
University of Veszprém, Hungary, H-8201 VESZPRÉM, P.O.B. 158 Tel. +36-88-422022/4354
Fax +36-88-423091 E-mail: tam043@almos.vein.hu
[b] Dept. of Process Engineering, University of Veszprém, Hungary, H-8201 VESZPRÉM,
P.O.B. 158; Website: www.fmt.vein.hu/softcomp

Ferenc D. Tamás

A native of Hungary, F. D. Tamás was born in 1928. Received his M. Eng. in Chemical Engineering at Budapest Technical University in 1951; his D. Tech. In 1951 from Veszprém University; his Candidate of Chemical Science (equivalent of Ph.D) degree and Doctor of Chemical Science (D.Sc.) degree from the Hungarian Academy of Sciences in 1968 and 1978, resp.

After receiving his M.S. he worked at universities and research institutes in Hungary. At present he is Emeritus Professor at the University of Veszprém, Faculty of Engineering, Department of Silicate- and Materials Engineering.

His career is connected to the physical chemistry and technology of silicates; fields of interest include cement chemistry (esp. trace elements in clinker and cement), materials science, silicate mineralogy, phase equilibria, testing of engineering materials and recently cement/environment interactions (use of wastes as fuels or raw materials, cement based immobilization of hazardous wastes, etc.).

Dr.Tamás is author of over 100 publications in Hungary and abroad. He is author, co-author and/or editor of 16 technical books, the most important of which is the volume "Handbook f the Silicate Industries", published in 1982, where he acted as Editor-in-Chief. His books "Mullite: Formation, Properties and Significance" (1962) and "Phase Equilibria Spatial Diagrams" (1970) were published in English too. Was Scientific Committee chairman of the series of the international Conferences on Silicate Science and Technology, Budapest and editor of their Proceedings (1961, 1964, 1967, 1970, 1973, 1977, 1981, 1985 and 1989).

Dr. Tamás has supervised research of a high number of Ph.D. students (his former students workin Hungary and abroad (Canada, U.S., Denmark, Egypt, etc.), directed numerous research projects in Hungary and was co-principal investigator of several international research projects (U.S.A. - Hungary, Austria - Hungary. Acted as a visiting professor at several European, Israeli and American universities.

Dr. Tamás attended several international scientific meetings, gave plenary or contributory papers in practically all European countries, in the U.S.A, Canada, Australia, India and Brazil. Was invited overseas speaker at the Gordon Research Conference on "Solid/Liquid Interactions in Cement Hydration", Plymouth, NH, USA, 1996. Acted several times for the most important meeting of cement chemists, the International Cement Chemistry Congresses: was Rapporteur at the 6th, in Moscow–1974; 7th, Paris–1980; 8th, Rio de Janeiro–1986, was International Scientific Committee member and Panel coordinator of the 9th Congress, in New Delhi, India–1992. and of the 10th

Congress, in Gothenburg Sweden–1997. The next, 11th will be held in Durban, 2003; he serves as International Scientific Committee member of this congress too. Other former activities: was chairman of the waste destruction panel at the World Conference on Hazardous Wastes, Budapest,1987, keynote speaker at the „Waste Destruction Seminar" organized by the Environmental Protection Authority, Melbourne, Australia, 1993, invited overseas speaker at the Engineering Foundation Conference, Durham, NH, USA, 1994, at the Gordon Research Conference on Chemistry & Physics of Cement-based Materials, Plymouth, NH, USA, etc.

In 1989 he has been elected Academician, International Academy of Ceramics; holds memberships in several scientific committees, both in Hungary and abroad. He is Chairman of the RILEM Technical Committee "Qualitative Identification of Clinkers and Cements", President of of the Hungarian "lndustry for Environment" Foundation.

Dr.Tamás is editorial board member of four scientific journals: Cement and Concrete Research, USA; Journal of Materials in Civil Engineering, USA; InterCeram, Germany; and Épitöanyag (Building Materials), Hungary.

INFLUENCE OF HEAVY METALS ON THE PROPERTIES OF CEMENT AND CONCRETE - BINDING MECHANISMS AND FIXATION

D. Stephan[1], D. Knöfel[2] and R. Härdtl[3]

[1] Lehrstuhl für Bauchemie, Technische Universität München, München, Germany.
E-mail: dietmar.stephan@bauchemie-tum.de (former: HeidelbergCement)
[2] Institut für Bau- und Werkstoffchemie, Universität-Gesamthochschule Siegen, Siegen, Germany. E-mail: knoefel@chemie.uni-siegen.de
[3] HeidelbergCement Technology Center, Heidelberg, Germany.
E-mail: reiner.haerdtl@hzag.de

ABSTRACT

The chemical composition of Portland cement mainly depends on the composition of the natural raw materials that are used for the clinker production. Beside geological variations in the raw material, the use of secondary raw materials and fuels can also influence the concentration of some minor and trace elements. Results described the potential effects of some heavy metals on clinker properties and subsequent products.

The impact of the heavy metals can vary during the life cycle of cement from the clinker production to the recycling of the building material. Different aspects are presented about the influence of heavy metals on pure clinker phases and clinker produced in the laboratory. The binding of heavy metals in cement, mortar and concrete are additional environmental aspects.

The main focus in this work was on Cr, Ni and Zn. These metals were used in different concentrations, ranging from natural concentration up to 25 000 ppm. The presented results indicate that the heavy metals can influence both the manufacturing of pure clinker phases or clinker and the hydration activity of the binder. The most decisive fact is, that the phenomena described can only be detected at concentrations many times higher than the naturally occurring concentrations of these heavy metals. Generally, up to 1 000 ppm of Cr, Ni and Zn had no or only a negligible effect, and in many cases even 5 000 ppm had no influence on the properties of clinker and cement.

The leaching procedures showed that Ni and Zn are nearly completely fixed in the hydrated cement matrix, even if the heavy metal concentration is many times higher than normal. Cr is not fixed that strongly, and the concentration of Cr during the leaching rises in proportion to the total amount of Cr in the cement. The leaching test with concrete blocks produced with industrial cements showed that the concentration of leached heavy metals is much lower than the limits for drinking water.

1. INTRODUCTION

The main and minor components of Portland cements (CaO, SiO_2, Al_2O_3, Fe_2O_3, MgO, SO_3, K_2O etc.) are responsible for the basic properties of the cements. Cements also contain trace elements (mainly heavy metal oxides). With more frequent use of alternative fuels and due to geologically caused fluctuations of the concentration of trace elements in the raw material and fuels, increased concentrations of heavy metals can occur from time to time. The aim of this project was to investigate potential effects of Cr, Ni and Zn on clinker and its subsequent products, including environmental aspects.

The level in Portland cement clinker ranges from around 10 to 90 ppm for Cr, 10 to 50 ppm for Ni and 28 to 350 ppm for Zn [1], but also higher concentrations have been reported [2]. In order to measure underlying effects, the samples were doped with much higher concentrations of heavy metals than are normally present in industrial clinker.

1.1 Pure and doped C_3S, C_3A and C_4AF

Portland cement clinker is a multi-phase product. During the production different clinker phases are formed. There are several chemical reactions going on at the same time, which can influence each other. Such a complicated system is a difficult basis for fundamental research about the influence of heavy metals on the formation of clinker and the reaction of cement. Therefore the pure clinker phases were for fundamental research.

To pure clinker phases C_3A, C_4AF, C_3S and C_3S with 1 wt.-% of free lime, heavy metal oxides in concentrations of 200, 1 000, 5 000 and 25 000 ppm were added (in some cases up to 50 000 ppm, in each case relative to the heavy metal). The treated samples were fired several times. The production of pure phases and sample preparation is described in detail elsewhere [3, 4].

1.1.1 Unhydrated pure clinker phases

The influence of heavy metal oxides on the stability and modification of pure phases was investigated. In most samples the heavy metals were trapped almost quantitatively, only from the C_3S-samples about 25 % of Zn evaporated. The changes of free lime with the addition of heavy metals were monitored by the Franke wet chemical method. Fairly high changes in free lime content with heavy metal addition were only found with the clinker mineral C_3S shown in Figure 1. Even if there are no clear stochiometric correlations, the results indicate that Cr is incorporated into the lattice instead of Si, and Ni and Zn are incorporated instead of Ca. Very high intakes of Cr stabilize C_2S, hence C_3S decomposes to give C_2S with Cr and free lime. The findings confirm the results of other reports [5, 6, 7, 8, 9].

Data obtained by X-ray diffraction (XRD) revealed that different polymorphs of C_3S could be stabilized by the intake of heavy metal oxides. But only above 5 000 ppm could a clear change of the modification be registered. The results for very high intakes are shown in Figure 2. These results largely confirm earlier investigations [7, 8, 10, 11].

1.1.2 Hydration of pure clinker phases

The early hydration kinetics of samples that were ground to the same fineness was investigated by heat flow calorimetry. Detectable differences only occurred above addition levels of 5 000 ppm.

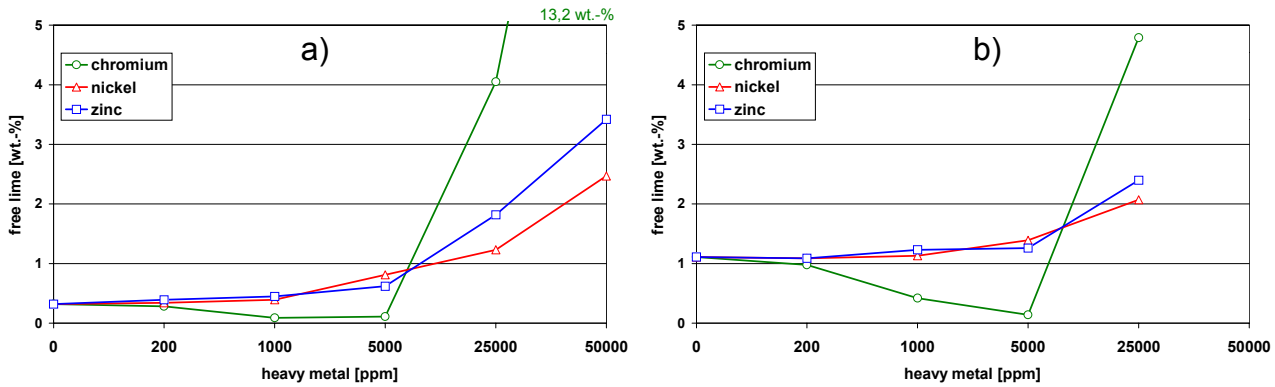

Examples for hydration curves of samples with very high intakes are illustrated in Figure 3.

Figure 1. Free lime in samples with and without heavy metals; a) made from C_3S with 0.3 wt.-% free lime, b) made from C_3S with 1.1 wt.-% free lime

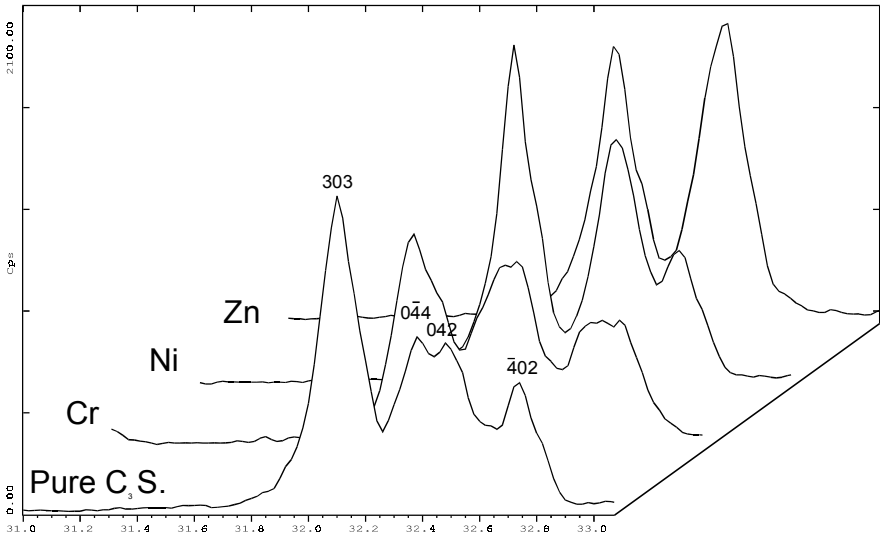

Figure 2. XRDs of pure C_3S and C_3S with 25 000 ppm of heavy metal; modification: pure C_3S→ T_1; Cr→ T_2+C_2S+CaO_{free}; Ni→ T_2; Zn→ M_2

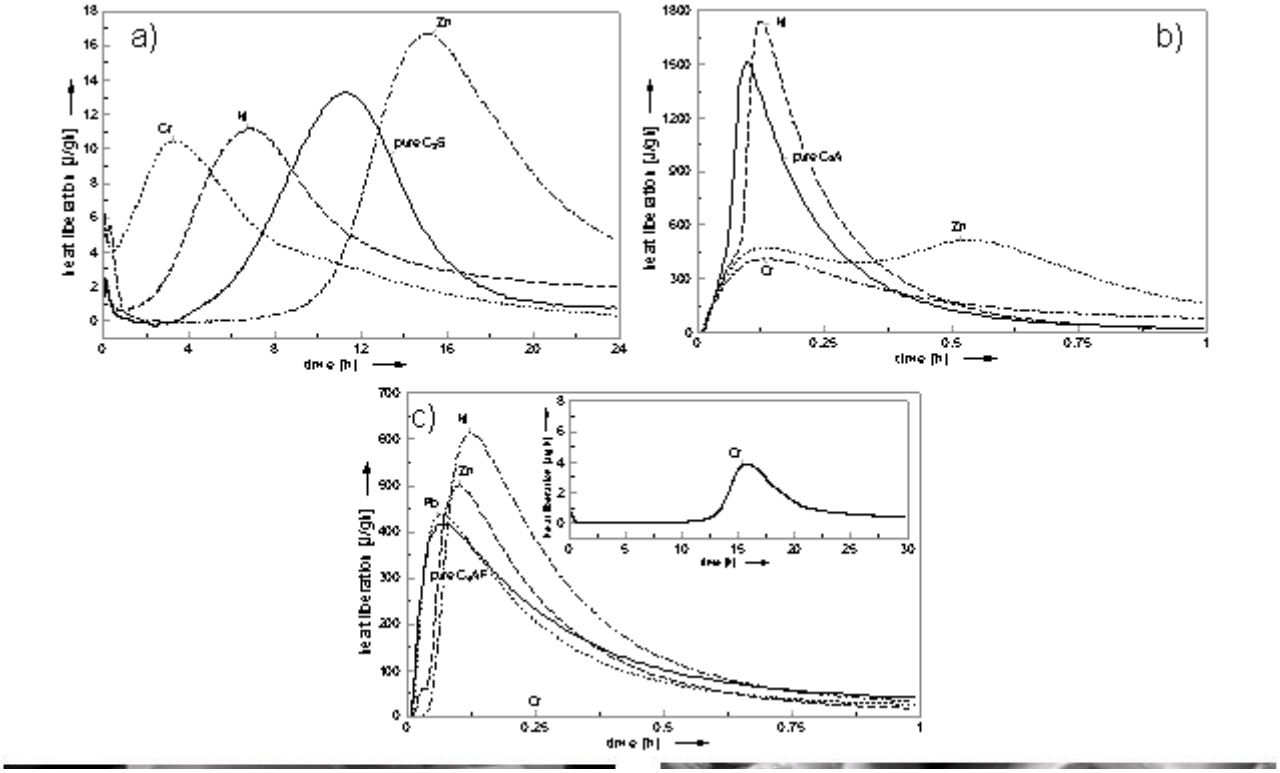

Figure 3. Heat flow calorimetry of control and samples with 25 000 ppm of heavy metals

Figure 4. Hydration products of a) pure C_3A and b) C_3A with 25 000 ppm Cr; plates with high Cr content, octahedron with low Cr content

The hydration products were analysed by XRD and scanning electron microscopy (SEM). Some pictures of the hydration products are given in Figure 4. The composition of different products could be detected by energy-dispersive X-ray fluorescence analysis (EDX).

From the hydration of pure phases and samples with heavy metals or higher concentrations of free lime it can be concluded that:

- Cr accelerates the hydration of C_3S.
- the acceleration of samples with Ni is because of higher concentrations of free lime.
- Zn retards the hydration of C_3S; in the hydration product $Ca[Zn(OH)_3]_2*2H_2O$ could be analysed [12, 13, 14].
- the heavy metals are enriched in C-S-H products, the concentration of heavy metals in portlandite is below the detection limit of EDX.
- well crystallized areas of portlandite and C-S-H are smaller in the samples with Ni or Cr than in the control and somewhat larger in the samples with Zn.
- C_3A is retarded by Cr and Zn, while Ni does not influence the hydration characteristic.
- the morphology of hydration products of C_3A are not changed by Ni and Zn, but Cr does sharply influence the morphology (Figure 4).
- Cr suppresses the hydration of C_4AF nearly completely at 25 000 ppm, but at lower concentrations this effect is greatly reduced; Ni and Zn have virtually no effect.

2. PURE AND DOPED CLINKER

The clinker phases have a mutual effect on one another during production and subsequent hydration. Thus the actual effect of the heavy metals on the product properties has to be examined in the clinker and cement. In order to measure the influence of heavy metals on real clinker and cement, three different raw materials where chosen. The composition of these raw materials is given in Table 1. The samples were taken from industrial raw meal for the production of clinker for ordinary Portland cement (PC), high sulphate resisting Portland cement (SRPC) and white Portland cement (WPC). Different amounts of heavy metal oxides were added to the raw material to give 200, 1 000, 5 000 and 25 000 ppm in the final clinker respectively (in each case relative to the heavy metal). The burning conditions for the three series of samples were chosen to give a content of free lime between 1.0 and 1.3 wt.% for the pure raw meal of PC, SRPC and WPC (Table 1).

Table 1. Composition of raw materials for clinker production and burning conditions

Material (wt.%)	PC	SRPC	WPC
SiO_2	14.1	13.0	14.4
Al_2O_3	3.5	2.5	2.7
Fe_2O_3	2.2	4.9	0.1
CaO	41.3	42.2	44.7
MgO	1.7	1.2	0.3
K_2O	1.1	0.4	0.2
SO_3	0.6	0.1	0.7
Cr (ppm)	51	46	12
Ni (ppm)	55	15	5
Zn (ppm)	88	111	48
Specific surface (m^2/cm^3)	1.71	2.06	3.19
Burning conditions			
Temperature (°C)	1400	1450	1550
Time (min)	60	70	180

2.1. Unhydrated clinker

The analysis of Cr, Ni and Zn in the clinker showed that the concentration did not differ much from the amount predicted by calculations based on concentrations in the raw material and the ignition loss. Only Zn evaporated from the samples in amounts of 15-25 %. The Zn losses in the clinker presumably occur because the heavy metal reacts with secondary constituents in the raw meal and forms compounds, which are more volatile.

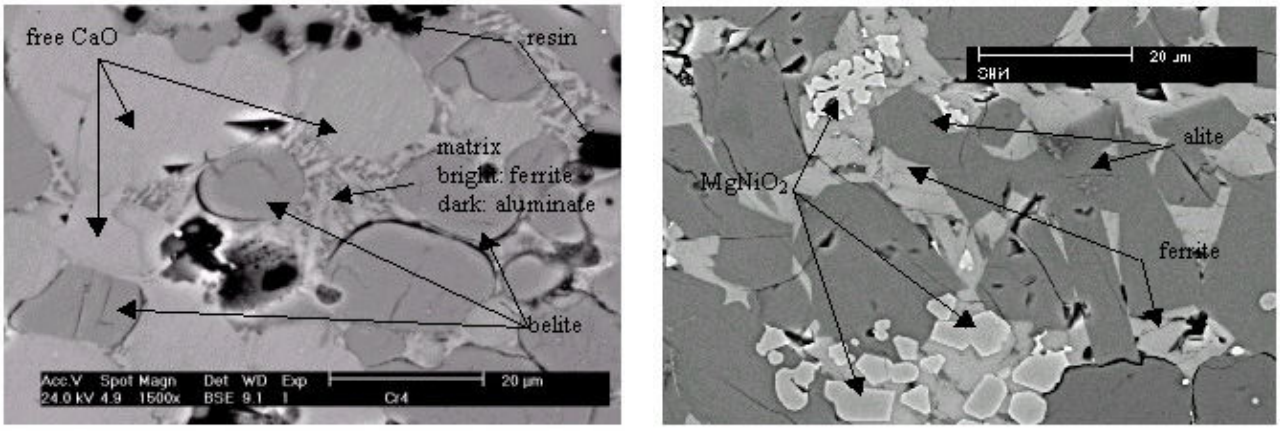

Figure 5. Left: PC clinker with 25 000 ppm of Cr; Right: PC clinker with 25 000 ppm of Ni

As predicted from results with pure clinker phases, no changes in the clinker could be detected up to 1 000 ppm of heavy metals and even 5 000 ppm had only a negligible influence. The clinker was analysed for free lime and polished clinker sections were analysed by light microscopy, SEM and EDX. Compared to the control the content of free lime is lower for all samples with added heavy metals in all concentrations, except for the samples with 25 000 ppm of Cr. This result confirms that

alite is destabilized by very high concentrations of Cr. On the other hand, low concentrations of all heavy metals react as mineralising agent. By means of SEM and EDX in the PC clinker with Cr, a new phase was found which had the approximate composition of $K_2Cr_2O_7$. In the two other clinkers with lower concentrations of K, this compound could not be detected. In all three clinkers the concentration of Cr was especially high in belite (up to 5.6 wt.-%) and very often CaO_{free} was found in direct contact with belite, which is not normal for a sufficiently well burned clinker (see Figure 5). In the PC and SRPC clinker with Ni, a new phase with the composition $MgNiO_2$ was formed, and is shown in Figure 5. Because of the lower content of Mg this compound could not be detected in the WPC clinker and the Ni was mainly incorporated into the interstitial phase. The formation of $MgNiO_2$ could be verified by the results of XRD. Recently the formation of this compound was also reported by Lopez [15]. In all three clinkers the highest concentrations of Zn were found in the interstitial phase.

2.2 Hydration of cements

Taking into consideration the sensitivity of measurement, a concentration of up to 1 000 ppm of heavy metals does not have any effect on the hydration of cement. This is the same result as in the investigation of pure clinker phases. Even at concentrations of 5 000 ppm of heavy metals, the early hydration is only slightly accelerated (Figure 6). This might be a result of a higher number of crystal defects in alite. A concentration of 25 000 ppm Cr accelerates the hydration, Ni has no effect and Zn gives a strong retardation, which is caused by a surface passivation of the hydration product of incorporated Zn. The compound $MgNiO_2$ was not attacked during the hydration process. An important result is the preferred incorporation of the heavy metals into the C-S-H phases and not into the portlandite, which could be proved by SEM combined with EDX. This causes a good fixation of the heavy metals in the hydration products.

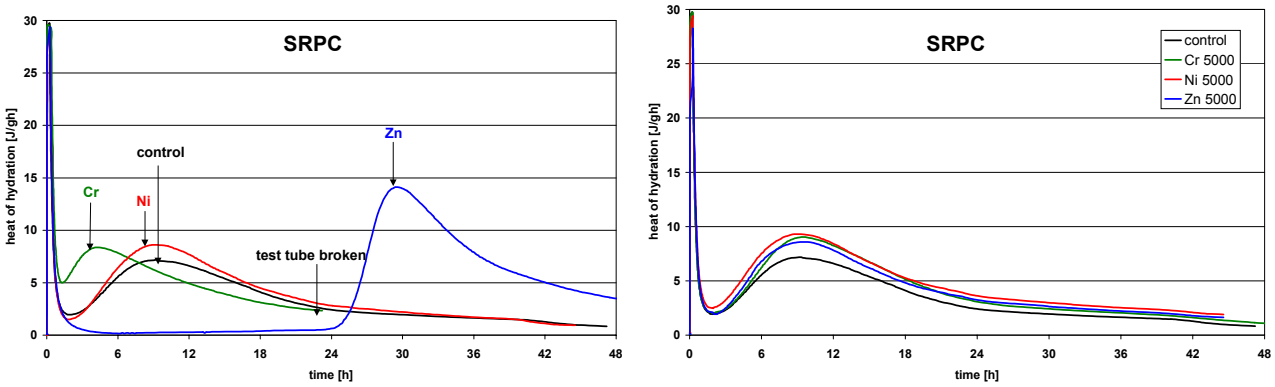

Figure 6. Hydration of SRPC with 25 000 ppm (left) and 5 000 ppm (right) of heavy metals

Results of the physical properties of the samples showed a good correspondence between flexural strength, compressive strength and dynamic modulus of elasticity. Concentrations of up to 1 000 ppm of heavy metals have no influence on the strength. Figure 7 shows the compressive strength of SRPC-mortar with 5 000 and 25 000 ppm of heavy metals after 1, 7 and 28 days. Except for the PC-sample with Cr, 5 000 ppm of heavy metals caused a slight increase in strength. An intake of 25 000 ppm Cr always results in a decrease of strength. This is due to the high content of free lime with corresponding expansion phenomena and the lower content of alite. The influence of Ni at this concentration is different. Zn induces an increased strength after 7 and 28 days apart from a lower strength in the early period of hydration. More details about the influence of heavy metals on the formation of clinker and hydration of cement are given elsewhere [16, 17].

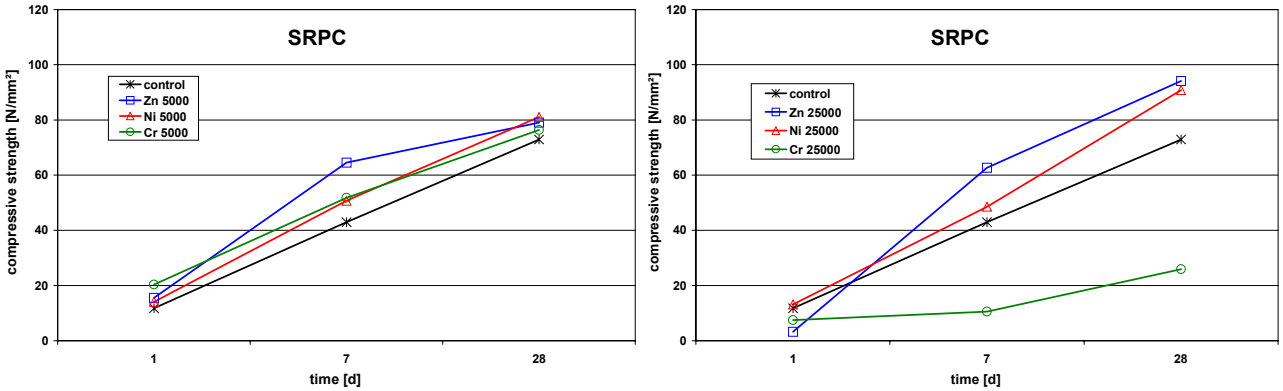

Figure 7. Compressive strength of control and samples with 5 000 and 25 000 ppm of heavy metals.

3. FIXATION OF HEAVY METALS

During the project the fixation of heavy metals in the building material cement and its following products was analysed by three different procedures. For that purpose cements were produced from three different industrial raw meals (PC, SRPC and WPC). Before burning the raw meals were doped with heavy metal oxides in different concentrations (aim: 200 – 5 000 ppm in the cement).

The investigation of the wash-out of cements showed, that even very high intakes of Ni and Zn did only result in metal concentrations in the leachates within the range of the detection limit. On the one hand this extreme low solubility is brought about by the high pH, which causes precipitation of heavy metal hydroxides of these metals. Additionally it is due to the high concentrations of different ions in the solution that lead to a more complete precipitation by reactions that are not yet known. Cr, however is washed-out from the cement very quickly and it remains in solution even at high pH [18]. The rate of the washed-out Cr compared to the absolute Cr depends on the type of cement and not on the absolute content of Cr in the cement. The rate of washed-out Cr was about 25 % for the PC-cement, 2 % for SRPC-cement and 1 % for WPC-cement (Table 2).

Table 2. Concentration of Cr in the cements and leachates from the wash-out procedure and the DEV-S4 procedure

	cement	wash-out of cements		leaching of mortars (DEV-S4)	
sample	[ppm]	leachate [ppm]	leaching [%]	leachate [ppm]	leaching [%]
PC control	81	3,7	18,3	0,033	1,77
PC all 200	216	10,8	20,1	0,107	2,19
PC all 500	460	37,4	32,5	0,293	2,80
PC all 1000	924	67,1	29,0	0,600	2,86
PC Cr 500	491	26,8	21,8	0,360	3,22
PC Cr 5000	5063	309,8	24,5	3,077	2,67
SRPC control	94	0,27	1,1	0,026	1,19
SRPC all 500	526	2,55	1,9	0,296	2,47
WPC control	41	0,10	1,0	0,012	1,32
WPC all 500	536	0,80	0,6	0,256	2,10

The tank leaching test for standard prisms (aggregate-cement-ratio= 3:1, water- cement-ratio= 0.5), that will probably become the basis for a planned European Standard was used to simulate the period of using the building material [19, 20]. After the storage of the mortar under water at a liquid-solid-ratio of 5, the concentration of Ni and Zn in the leachates was below detection limit. Even at 5 000 ppm of heavy metal in the cement the concentration of heavy metal in the leachate was insignificant. On the one hand this is brought about by high pH in the solution and it is also due to an incorporation of the metals in the C-S-H-phases. The analysis of Cr in the leachates again

shows that this element is much more soluble. In this project the diffusion control of the leaching was confirmed. Figure 8 shows exemplary graphs of the total amount of Cr that was leached from two cement mortars. The leaching of Cr from mortar is < 1 % after 56 days and it is nearly independent of the composition of the cement. If the leaching mechanism does not change in the cause of time, an extrapolation gives a leaching rate of < 3 % after 10 years (see Table 3).

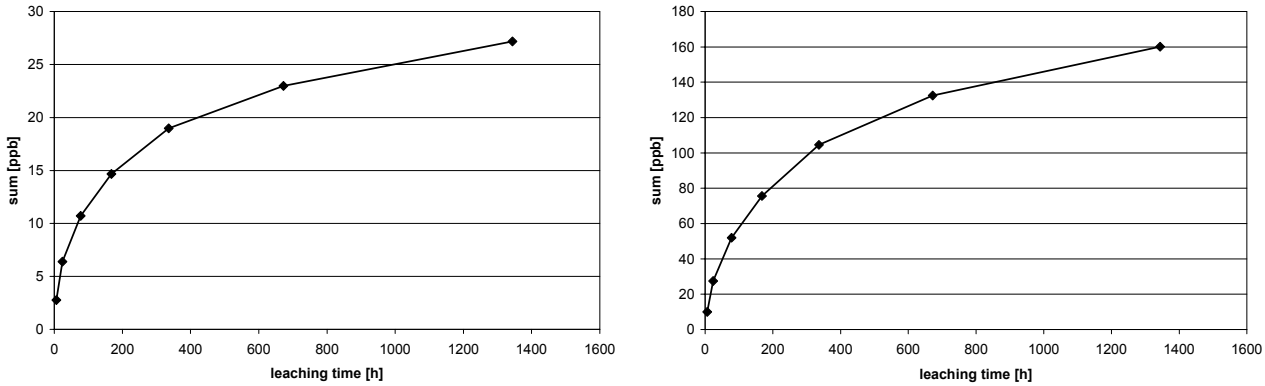

Figure 8. Sum of leached Cr in the leachates of tank leaching test in [ppb]; a) control PC (81 ppm Cr in the cement); b) PC Cr 500 (491 ppm Cr in the cement)

The leaching with the DEV-S4 procedure was done to simulate the period of demolition and recycling and in part as an availability test. In this test 100 g of the material is crushed <10 mm and shaken with 1l of water for 24 h. The concentrations of Ni and Zn in the leachates are again very low, even with very high intakes of heavy metals. The average leaching rate of Cr from PC-mortar was about 2.6 % and it was independent of the absolute content of Cr. The leaching rate from SRPC- and WPC-mortar was similar (see Table 2).

Table 3. Leaching with tank leaching test after 14 d and 56 d and some extrapolations

	Measured leaching rate [%]		extrapolated leaching rate [%]		
	14 d	56 d	6 month	1 year	10 years
PC control	0,52	0,74	1,13	1,29	1,88
PC all 200	0,46	0,68			
PC all 500	0,50	0,77	1,24	1,45	2,30
PC all 1000	0,44	0,69			
PC Cr 500	0,55	0,83			
PC Cr 5000	0,56	0,82	1,39	1,63	2,59
∅ *PC*	0,51	0,76			
SRPC control	0,35	0,43			
SRPC all 500	0,60	0,76			
WPC control	0,48	0,60			
WPC all 500	0,88	1,09			

4. CONCLUSION

The results of this study show that the heavy metals Cr, Ni and Zn can influence both, the manufacturing of pure clinker phases respectively clinker and the hydration activity of the binder. But the most decisive fact is that these influences can only be detected at concentrations many times higher than the naturally occurring concentrations of these heavy metals. The investigation of the binding mechanisms showed that the leaching of Ni and Zn under usual environmental conditions is insignificant, even if the heavy metal concentration is higher than normal. The leaching of Cr is much easier. The concentration of Cr in the leachates rises in proportion to the total amount of Cr in the cement.

REFERENCES

[1] Verein Deutscher Zementwerke e.V., Forschungsinstitut der Zementindustrie, Tätigkeitsbericht 1990-93, Düsseldorf: Beton-Verlag, 1993. (in German)

[2] Lawrence, C. D., The constitution and specification of Portland cements, In: Lea's Chemistry of cement and Concrete, by Hewlett, P. C., London: Arnold, 1998, pp.131-191.

[3] Stephan, D.; Maleki, H.; Knöfel, D.; Eber, B. and Härdtl, R. Influence of Cr, Ni, and Zn on the properties of pure clinker phases Part I. C_3S, Cement and Concrete Research, vol.29, 1999, pp.545-552.

[4] Stephan, D.; Maleki, H.; Knöfel, D.; Eber, B. and Härdtl, R. Influence of Cr, Ni, and Zn on the properties of pure clinker phases Part II. C_3A and C_4AF, Cement and Concrete Research, vol.29, 1999, pp.651-657.

[5] Fierens, P. and Verhaegen, J.-P. Structure and reactivity of chromium-doped tricalcium silicate, Journal of The American Ceramic Society, vol.55, 1972, pp.309-312.

[6] Sakurai, T.; Sato, T. and Yoshinaga, A. The effect of minor componets on the early hydraulic activity of the major phases of portland cement clinker, Proceedings of the 5th International Symposium on the Chemistry of Cement, 1969, S. 300-321.

[7] Woermann, E.; Hahn, Th. and Eysel, W. Chemische und strukturelle Untersuchungen der Mischkristallbildung von Tricalciumsilicat – 1. Bericht, Zement-Kalk-Gips, vol.16, 1963, pp.370-375. (in German)

[8] Odler, I. and Abdul-Maula, S. Polymorphism and hydration of tricalcium silicate doped with ZnO, Journal of The American Ceramic Society, vol.66, 1983, pp.1-4.

[9] Hahn, Th.; Eysel, W. and Woermann, E. Crystal chemistry of tricalcium silicate solid solutions, Proceedings of the 5th International Symposium on the Chemisty of Cement, 1969, pp.61-66.

[10] Mtschedlow-Petrossian, O. P.; Stschotkiana, T. J., Jerschow, L. D. and Starominskaja, P. A. Untersuchung der Rolle geringer Fremdoxidgehalte im Trikalziumsilikat, Silikattechnik, vol.25, 1974, pp.55-58. (in German)

[11] Bigaré, M; Guinier, A.; Maziéres, C.; Regourd, M.; Yannaquis, N.; Eysel, W.; Hahn, Th. and Woermann, E. Polymorphism of tricalcium silicate and its solid solutions, Journal of The American Ceramic Society, vol.50, 1967, pp.609-619.

[12] Jawed, I.; Skalny, J.; Young, J. F. Hydration of portland cement, In: Structure and Performance of Cements, (Editor) Barnes, P., Applied Science Publishers, Barking, 1983, pp237-317.

[13] Yousuf, M.; Mollah, A.; Vempati, R. K.; Lin, T.-C.; Cocke, D. L. The interfacial chemistry of solidification/stabilization of metals in cement and pozzolanic material systems, Waste Management, vol.15, 1995, pp.137-148.

[14] Lieber, W.; Gebauer, J. Einbau von Zink in Calciumsilicathydrate, Zement-Kalk-Gips, vol.22, 1969, pp.161-164. (in German)

[15] Lopez, P.; Bolio-Arceo, H., Effect of large intakes of Ni in the mineralogical composition of clinker, Proceedings of the 20th International Conference on Cement Microscopy, 1998, pp.8-17.

[16] Stephan, D.; Mallmann, R..; Knöfel, D. and Härdtl, R. High intakes of Cr, Ni, and Zn in clinker Part I:. Influence on burning process and formation of phases, Cement and Concrete Research, vol.29, 1999, pp.1949-1957.

[17] Stephan, D.; Mallmann, R..; Knöfel, D. and Härdtl, R. High intakes of Cr, Ni, and Zn in clinker Part II. Influence on the hydration properties, Cement and Concrete Research, vol.29, 1999, pp.1959-1967.

[18] Sprung, S., Rechenberg, W., Einbindung von Schwermetallen in Sekundärrohstoffe durch Verfestigen mit Zement, beton, 38, 1988, pp.193-198. (in German)

[19] de Groot, G. J.; Hohberg, I.; Lamers, F. J. M.; Van der Veen, A. M. H.; Wassing, W.; Quevauviller, Ph., Development of a leaching method for the determination of the environmental quality of concrete, bcr information, European Commission, EUR 17869 EN, Brüssel, 1997.

[20] Hohberg, I.; Müller, C.; Schießl, P.; Volland, G., Umweltverträglichkeit zementgebundener Baustoffe, Sachstandsbericht, Deutscher Ausschuß für Stahlbeton – Heft 458, Beuth Verlag, Berlin, 1996. (in German)

INFLUENCE OF HEAVY METALS ON THE PROPERTIES OF CEMENT AND CONCRETE - BINDING MECHANISMS AND FIXATION

D. Stephan[1], D. Knöfel[2] and R. Härdtl[3]

[1] Lehrstuhl für Bauchemie, Technische Universität München, München, Germany.
E-mail: dietmar.stephan@bauchemie-tum.de (former: HeidelbergCement)
[2] Institut für Bau- und Werkstoffchemie, Universität-Gesamthochschule Siegen, Siegen, Germany. E-mail: knoefel@chemie.uni-siegen.de
[3] HeidelbergCement Technology Center, Heidelberg, Germany.
E-mail: reiner.haerdtl@hzag.de

C u r r i c u l u m V i t a e

Surname	Stephan
First name	Dietmar
Birthday	29th of October 1968

Professional training

1985 - 1988	Apprenticeship as a chemical laboratory worker

University

1990 - 1996	Study of Chemistry at the University of Siegen Main focus: Building and materials chemistry Diploma thesis: Formulation of recipes for restoring of bricks with slurries and sandstone with repair mortar.
9/1994 - 4/1995	Study of Chemistry at the Bristol University (GB)

PhD-thesis

8/1996 - 10/1999	PhD-thesis in the group of Prof. Dr. D. Knöfel at the University of Siegen: Chromium, Nickel and Zinc in clinker and cement – incorporation, influence on properties and leaching-

Professional Career

11/1999 - 10/2000	Engineer-In-Training program at Heidelberg Cement
11/2000 - 12/2001	Senior Scientist Cement Chemistry at Heidelberg Cement Technology Center
Since 1/2002	Qualified as a university lecturer at the Technical University of Munich, Institute for Construction Chemicals Main focus: Interaction of inorganic binder with construction chemicals.

POZZOLANIC REACTION OF FLY ASH CEMENT SYSTEM

Makoto Kobayakawa[1], Shunsuke Hanehara[2], Kwangryul Hwang[3] and Fuminori Tomosawa[4]

[1]Research & Development Center, Taiheiyo Cement Corporation, Chiba, Japan.
E-mail: makoto_kobayakawa@taiheiyo-cement.co.jp
[2]Research & Development Center, Taiheiyo Cement Corporation, Chiba, Japan.
E-mail: shunsuke_hanehara@taiheiyo-cement.co.jp
[3]Department of Building Materials and Components, Building Research Institute, Ibaraki, Japan.
E-mail: hwang@kenken.go.jp
[4]Socio-environmental Engineering, Graduate School of Engineering, Hokkaido University, Hokkaido, Japan. E-mail: tomosawa@eng.hokudai.ac.jp

ABSTRACT

An increase of compressive strength and durability of concrete containing fly ash is well known as the effect of pozzolanic reaction. However, the specific mechanisms of pozzolanic reaction, which affect these properties of concrete, are not clearly understood.

The aim of this study is to determine the effect of the pozzolanic reaction of fly ash on properties of hardened paste; such as combined water, calcium hydroxide, pore distribution and BET specific surface area. In this study a quantitative investigation on the reaction ratio as a criterion of pozzolanic reaction is conducted. The reaction ratio of fly ash is important in this study. The reaction ratio of fly ash is calculated by determining the levels of insoluble residue in the specimen at several ages.

Firstly, the effects of the water/powder ratio, mixing ratio of fly ash and curing temperature on the pozzolanic reaction of fly ash in cement paste are investigated. Evidentially these conditions have an affect on the pozzolanic reaction speed of fly ash.
Secondly, the effects of the pozzolanic reaction on the microstructure in the cement paste are determined. There had been no study that has tried to clarify pozzolanic reaction with a quantitative approach.

As a result of this experiment, the effect of the pozzolanic reaction on many properties of the cement paste can be described as a function of the reaction ratio of fly ash.

1. INTRODUCTION

The progress of pozzolanic reactions in hardened cement mixtures containing fly ash is sometimes discussed in relation to the compressive strength [1]. Specifically, the reaction quantity is indirectly estimated from the quantity of calcium hydroxide formed in the hardened cement mixture [2], [3]. Although many studies on the effects of pozzolanic reaction on concrete have been done, the effects of absolute quantity of pozzolanic reaction are still unclear. The effect appears to vary in each experiment because the pozzolanic reaction is affected by the chemical composition of fly ash, mixture proportions of concrete and curing conditions. Furthermore evaluations of the durability of concrete in each study were carried out with different pozzolanic reaction ratios.

Proceedings of the 11th International Congress on the Chemistry of Cement (ICCC)
'Cement's Contribution to the Development in the 21st Century'
Hosted by: The Cement and Concrete Institute of South Africa
CD-ROM produced by: Document Transformation Technologies
11 - 16 May 2003, Durban, South Africa
ISBN Number: 0-9584085-8-0
Editors: Dr G. Grieve and G. Owens
Congress Organised by: Event Dynamics

As a result of our study [4], the pozzolanic reaction ratio of fly ash was determined to be influenced by the curing temperature, ratio of water to cementitious material, and the replacement dosage of fly ash. The pozzolanic reaction ratio of fly ash was calculated by determining the levels of insoluble residue in the acid. A simple constant pozzolanic reaction model can be derived for this reaction [5]. Mixtures of moderate heat cement containing fly ash were investigated using the same method. The microstructure of the paste was compared with concrete [6].

The purpose of this study is to clarify the effect of the pozzolanic reaction on properties of hardened paste; such as combined water, calcium hydroxide, pore distribution and BET specific surface area. Also the quantitative change of these properties of hardened paste accompanied with increasing pozzolanic reaction ratio of fly ash is evaluated. Quantitative study of the effects of pozzolanic reaction helps clarify the mechanism of pozzolanic reaction.

If the chemical function of pozzolanic reaction adjusting on curing condition, mixture proportion or age changes, it is expected that the correlation between pozzolanic reaction ratio and the quantitative effects of pozzolanic reaction on hardened paste will be weak. However, results from this experiment showed a strong correlation, whereby the function of pozzolanic reaction is almost constant. It was verified that the effect of condition differences were only observed as a pozzolanic reaction speed difference.

This information about the pozzolanic reaction mechanism contributes to the rational use of industrial by-products as a concrete material.

2. MATERIALS AND EXPERIMENTAL METHODS

2.1 Materials

As listed in Table 1, ordinary Portland cement and fly ash produced at the Hekinan Power Plant (Japan) were used. In addition, the paste of calcium hydroxide (CH) reagent containing fly ash at the same plant is also produced. The specific gravity and Blaine specific surface area of each material are shown in Table 1. The chemical composition of cement and fly ash are shown in Table 2. The glass phase of fly ash determined by XRD with internal standard is 65.8 %.

Table 1. Physical Properties of Materials

Materials	Specific gravity (g/cm^3)	Blaine specific surface area (cm^2/g)
Ordinary Portland cement	3.14	3370
Calcium hydroxide	2.23	–
Fly ash	2.33	4000

Table 2. Chemical Composition of Used Cement and Fly Ash

Materials	Chemical composition (% by mass)											L. O. I. (%)
	SiO_2	Al_2O_3	Fe_2O_3	CaO	FCaO	MgO	Na_2O	K_2O	TiO_2	SO_3	C	
Cement	20.8	4.7	2.9	64.7	-	1.7	0.4	0.4	0.3	2.0	-	1.7
Fly ash	54.4	31.1	4.6	4.4	0.1	0.8	0.6	0.8	1.4	0.4	1.3	1.4

2.2 Paste Specimens

The mixture proportions of cement paste containing fly ash are shown in Table 3. Two different W/P(water/powder) ratios of 30% and 50% are considered in the present study. Fly ash is substituted for cement by weight.

Table 3. Mixture Proportions of Cement Paste with Fly Ash

Curing temperature	W/P (%) P: powder	W/C (%)	Replacement dosage of Fly ash (% by mass)	Mixture proportions (% by mass)		
				Water	Cement	Fly ash
20°C 40°C	30	30.0	0	23.1	76.9	0
		33.3	10	23.1	69.2	7.7
		37.5	20	23.1	61.5	15.4
		50.0	40	23.1	46.2	30.8
		75.0	60	23.1	30.8	46.2
20°C 40°C 65°C (2 days) --> 20°C	50	50.0	0	33.3	66.7	0
		55.6	10	33.3	60.0	6.7
		62.5	20	33.3	53.3	13.3
		83.3	40	33.3	40.0	26.7
		125.0	60	33.3	26.7	40.0

The powder and water are mixed for 3 minutes at low speed using a Hobart mixer at 20°C room temperature. A test piece for each age is molded in a 100ml plastic bottle, which is then sealed. Specimens are cured at 3 different temperatures of 20°C, 40°C, and 65°C. The temperature of 65°C imitates the steam curing state. The specimens that are cured at 65°C are kept for 2 days before decreasing the temperature to 20°C.

The CH paste is prepared similarly. The mixture proportion is shown in Table 4.
Test specimens are prepared by cutting off a 7-mm cube out of each molded sample with a diamond cutter at a specified age. The hydration reaction is then stopped by dipping the cube samples in acetone and drying them by D-drying method under 5 x 10^{-4} mmHg vapor pressure. If necessary, test specimens are ground.

Table 4. Mixture Proportions of Calcium Hydroxide Paste with Fly Ash

Curing temperature	W/P (%)	Replacement dosage of Fly ash (% by mass)	Mixture proportions (% by mass)		
			Water	$Ca(OH)_2$	Fly ash
20°C, 40°C	50	60	33.3	26.7	40.0

2.3 Experimental Methods

2.3.1 Loss on ignition

The ignition loss and combined water of D-dried sample are determined at a temperature of 950°C.

2.3.2 Content of calcium hydroxide

CH amount in D-dried sample is determined by differential scanning calorimetry. In order to eliminate the variation of sample weight due to combined water with different age, the combined water content is compensated for with the ignition loss value. Content of CH percentage then is indexed to the weight of the specimen without combined water.

2.3.3 Pozzolanic Reaction Ratio of Fly Ash

The insoluble residue of D-dried sample is determined according to JIS R 5202 standard. The sample is in hydrochloric acid (1+1) and sodium carbonate solution, then neutralized using hydrochloric acid, and insoluble residue is filtrated. The residue is ignited and its mass is weighed. The pozzolanic reaction ratio of fly ash is calculated using equations (1) and (2).

$$b_d = (f_r * f_i - a_d) / (f_r * f_i / 100) \quad (1)$$

$$a_d = a_d' / (1 - IG_d / 100) \quad (2)$$

b_d: The pozzolanic reaction ratio per 1g of fly ash after d days that is determined from insoluble residue (%)
a_d: The insoluble residue that compensated for combined water of the hardened paste after d days (%)
a_d': The insoluble residue of the hardened paste after d days (%)
f_r: The replacement dosage of fly ash
(example: 0.4 for 40% of replacement dosage)
f_i: The insoluble residue of unhydrated fly ash (%)
IG_d: The ignition loss of the hardened paste after d days (%)

For example, the values needed for the calculation of the reaction ratio are shown in Table 5.
In the case of CH paste, an equation of (3) is used instead of the equation (1).

$$b_d = (f_r * f_i - k * a_d) / (f_r * f_i / 100) \quad (3)$$

$$k = (1 - 18 / 74 * (1 - f_r)) \quad (4)$$

k: Dehydrate of CH

Table 5. Example Values Needed for the Calculation of Pozzolanic Reaction ratios of Fly Ash (Curing temperature = 40°C, W/P= 50%, FA=40%, Age = 1 year)

	Insoluble residue (% by mass)	L.O.I. (% by mass)	Insoluble residue compensated for combined water (% by mass)
Unhydrated fly ash	$f_i = 83.9$	–	–
Hydrated sample (Age d days)	$a_{d'}$: $a_{365'} = 18.60$	IG_d : $IG_{365} = 17.09$	$a_d = a_{d'} / (1 - IG_d / 100)$: $a_{365} = 22.43$
Replacement dosage of fly ash : f_r (by mass)		f_r = FA / (Cement + FA) = 0.4	
Reacted ratio of fly ash : b_d (% by mass)		$b_{365} = (f_r * f_i - a_{365}) / (f_r * f_i / 100) = 33.2$	

2.3.4 BET specific surface area of hardened paste
D-dried cubic sample is crushed with a hammer into 1mm size grains. Approximately 1g of grains with size between 0.6mm and 1.0mm are sieved out to be used for determining BET specific surface area. Microstructure in the sample remains in each grain due to the coarse crush. BET specific surface area increases with the degree of crush. But the effect of crush is reduced with the selection of specific grain sizes.
BET specific surface area is then determined by 1point method with nitrogen gas.

2.3.5 Pore Structure of hardened paste
Pore structure of hardened paste is determined with mercury intrusion porosimetry. Approximately 6g of D-dried cubic samples are used for each measurement. Pore distribution of the diameter from 60 micrometer to 3nm in paste specimen is determined.

2.3.6 BEI and SEI observation
Secondary electron image (SEI) of hardened cement paste is observed by FE-SEM. The back scattered electron image (BEI) is observed by EPMA and applying the accelerating voltage of 15 kV.

3. EXPERIMENTAL RESULTS AND DISCUSSION

3.1 The Pozzolanic Reaction Ratio of Fly Ash

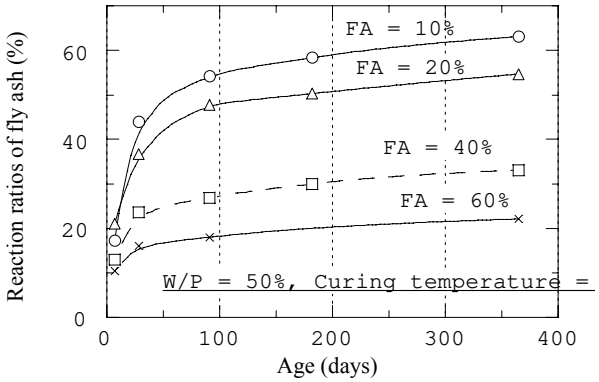

Figure 1. Effect of fly ash replacement dosage in cement paste on reaction ratio of fly ash determined from insoluble residue.

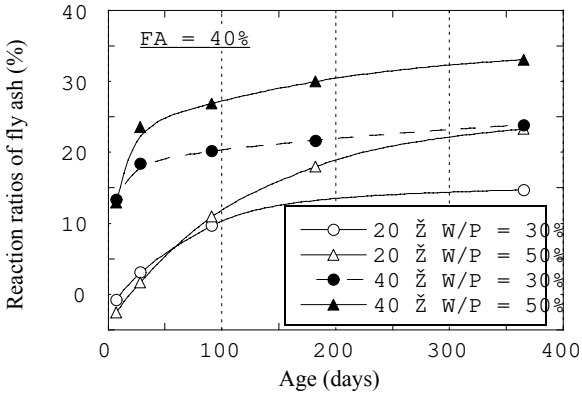

Figure 2. Effect of curing temperature and water powder ratio on pozzolanic reaction ratio of fly ash in cement paste.

The pozzolanic reaction ratio of fly ash determined from the insoluble residue of the hardened cement paste with different fly ash replacement dosages is shown on Figure 1. For 40°C curing temperature and 50% W/P, the reaction ratio per 1 g of fly ash reduces as the replacement dosage increases. The pozzolanic reaction is active until the age of 91 days. After this age, the reaction becomes slow. When fly ash dosage was 10%, the reaction ratio of fly ash at 1 year of age almost reached glass phase content of fly ash.

The pozzolanic reaction ratio of fly ash in cement paste with 40% fly ash is shown on Figure 2. The reaction ratios of fly ash at 7 days are 0 and 13% when samples are cured at 20 and 40°C, respectively. There is a big difference in the reaction ratio at early periods. The reaction ratio at 1 year increases with increasing curing temperature and W/P.

3.2 Combined Water of Pozzolanic Reaction

The relation between the reaction ratio of fly ash and combined water of hardened paste is investigated. Combined water due to fly ash is calculated with equation (5).

$$Wf_d = (Wr_d - W0_d * (1 - f_r)) / f_r$$

Wf_d: The difference of combined water result from 1g of fly ash at d days (%)

Wr_d: The combined water of hardened paste with fly ash replacement dosage f_r at d days (%)

$W0_d$: The combined water of hardened paste without fly ash of each W/P and curing condition at d days (%)

f_r: The replacement dosage of fly ash

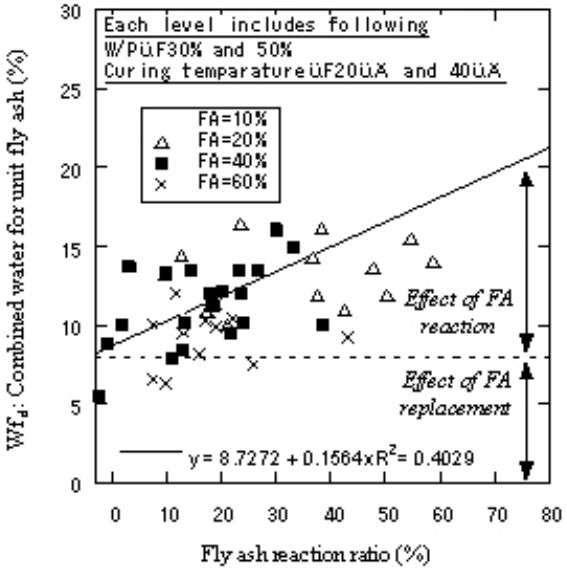

Figure 3. Effect of pozzolanic reaction of fly ash on combined water.

Effect of the pozzolanic reaction of fly ash on combined water is shown on Figure 3. Each legend includes 2 different curing temperatures, 2 different water/powder ratios at different ages. These conditions are shown in Table 3. Combined water of cement paste due to fly ash (Wf_d) increases along with the reaction ratio of fly ash increasing. Fly ash contributed to the acceleration of cement hydration when cement was only replaced with fly ash, which did not react. If 100g of fly ash reacts 100%, combined water increases 15.6g.

3.3 Consumption of Calcium Hydroxide due to Pozzolanic Reaction

The amount of CH consumed due to the pozzolanic reaction is shown in Figure 4. The relations between CH consumption and amount the reaction ratio of fly ash are shown in Figure 5. Value of various water/powder ratios, fly ash replacement dosages and ages are plotted in Figure 5. In addition, the values for CH paste of 5 ages at 2 different curing temperatures and 5 ages in CH paste are also plotted in Figure 5. The quantities of fly ash reacted and the reaction ratios in cement paste in Figure 1 and Figure 2 are different with given the mixture proportions and curing conditions. However, when these two conditions can be ignored in Figure 5, one can see that CH is consumed in proportion to the reaction ratio. The produced quantity of CH increases 0.051 g for every 1 g of fly ash substituted for cement in the cement paste. This is because the W/C is increased.

Regardless of the replacement dosage of fly ash, W/P, curing temperature, and test age, the CH is consumed at a rate of 8.04 mg per 1% of reaction ratio for each 1g of fly ash. This constant consumption of CH means that Ca/Si mole ratio in C-S-H formed by the pozzolanic reaction of fly ash is unchanged.

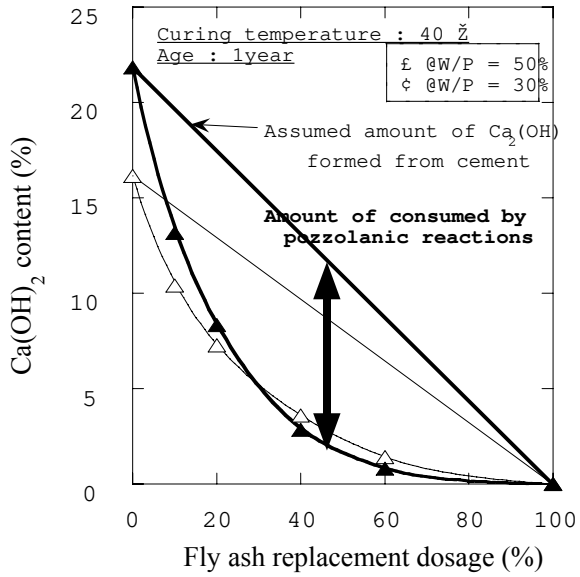

Figure 4. Relationship between fly ash replacement dosage and the amount of $Ca(OH)_2$ consumed by pozzolanic reactions.

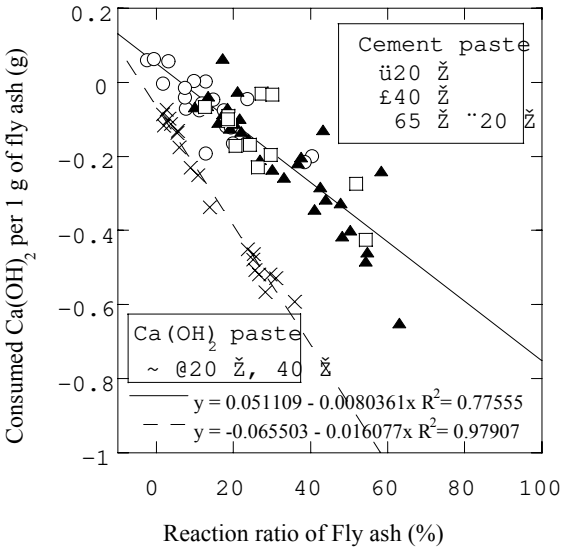

Figure 5. Effect of pozzolanic reaction of fly ash in cement paste and in $Ca(OH)_2$ paste on the amount of $Ca(OH)_2$ consumed, as determined through DSC thermal analysis.

The slope of the consumption line of CH paste on Figure 5 is different from the slope of the cement paste. In the case of CH paste, CH is more consumed than in the cement paste. This may be due to the difference of pH condition in the paste. The relationship between pH and C-S-H, which is produced by the pozzolanic reaction, is described in section 3.7.

3.4 Effect of Pozzolanic Reaction on BET Specific Surface Area of Hardened Paste

The pozzolanic reaction rate of fly ash is much slower than the hydration rate of cement. Therefore the formation of microstructure in the paste appears to proceed in two separate reactions.

Variation of BET specific surface area of hardened paste, which is different fly ash replacement dosage, with age is shown on Figure 6.

The relation between the reaction ratio of fly ash and BET specific surface area of hardened paste is investigated. BET specific surface area due to fly ash is calculated with equation (6).

$$Sf_d = (Sr_d - S0_d * (1 - f_r)) / f_r \quad (6)$$

Sf_d : The difference of BET specific surface area result from 1g of fly ash at d days (%)

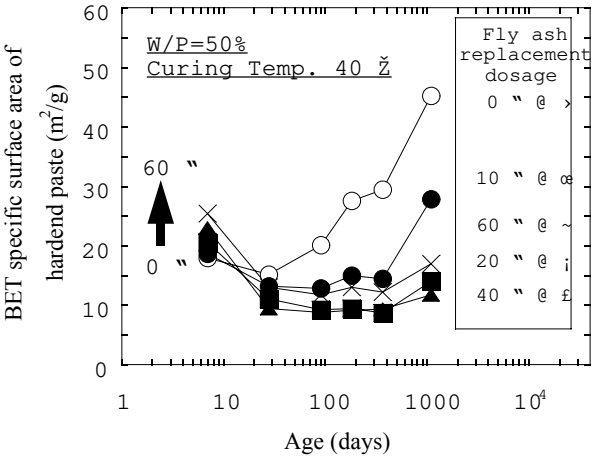

Figure 6. Variations of BET specific surface area of hardened paste with age.

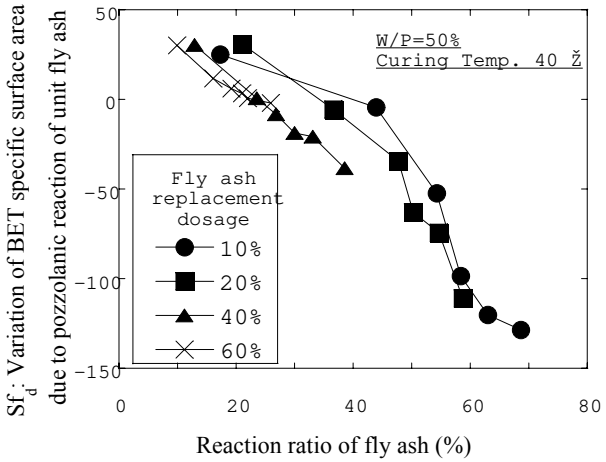

Figure 7. The effect of pozzolanic reaction of unit fly ash on BET specific surface area of hardened paste.

Sr_d : The BET specific surface area of hardened paste with fly ash replacement dosage f_r at d days (%)
$S0_d$: The BET specific surface area of hardened paste of fly ash 0% at d days (%)
f_r : The replacement dosage of fly ash

Effect of pozzolanic reaction of fly ash on BET specific surface area of hardened paste is shown in Figure 7. BET specific surface area due to fly ash (Sf_d) decreases as the reaction ratio of fly ash increases. Fly ash reduces permeability to nitrogen gas. On the assumption that BET specific surface area is related to the microstructure of C-S-H, we predict that the BET value increases as pozzolanic reaction continues. However the BET value almost constantly decreases with reaction ratio of fly ash.

3.5 Affect of Pozzolanic Reaction on Pore Distribution of Hardened Paste

Pore distribution of hardened paste is shown in Figure 8.
Pore diameter in partition of 3nm-6nm is related to the gel of C-S-H. Pore diameters 6nm-50nm are the capillary pores. These three partitions of pore diameters mostly cover pore volume in hardened paste.

Pore diameters of 50nm-10 micrometer are seldom seen in the hardened paste. It is normally observed in concrete and distributed transition zone between aggregate surface and paste matrix.
At 7 days, when cement was replaced with fly ash, pore diameters of 10nm-50nm initially increases but then decreases with age. Pores with diameters of 3nm-10nm increased with age. Total pore volume is constant with age at 60% of fly ash replacement dosage.

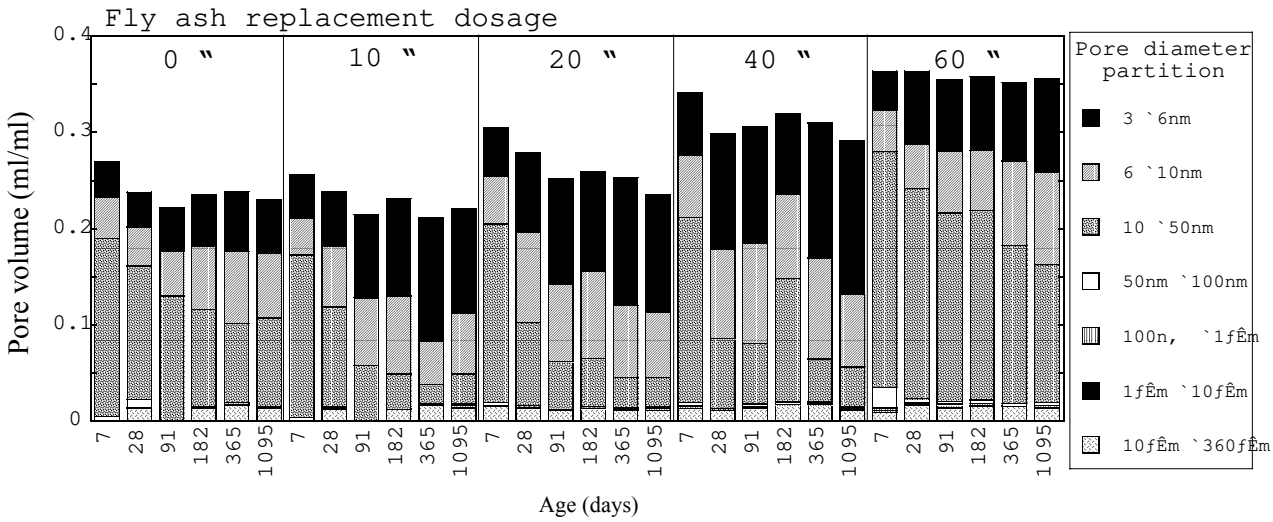

Figure 8. Pore distribution of hardened paste (W/P=50%, Curing Temperature 40°C).

The effect of pozzolanic reactions on pore distribution is investigated. Pore volumes due to fly ash were calculated with equation (7) as same as BET specific surface area.

$$Pf_d = (Pr_d - P0_d * (1 - f_r)) / f_r \quad (7)$$

Pf_d: The difference of pore volume result from 1g of fly ash at d days (%)
Pr_d: The pore volume of hardened paste with fly ash replacement dosage f_r at d days (%)
$P0_d$: The pore volume of hardened paste of fly ash 0% at d days (%)
f_r: The replacement dosage of fly ash

The relationship between the reaction ratio and variations of pore volume due to pozzolanic reaction of unit fly ash is shown in Figure 9. Pf of 3nm–10nm positively correlated with the reaction ratio of fly ash. This increase of Pf suggests C-S-H is constantly produced by the pozzolanic reaction. Pf of 10nm-50nm negatively correlated with the reaction ratio of fly ash. Pozzolanic reaction contributed to densify of paste by reducing capillary pore. When the reaction ratio of fly ash is 0%, Pf of 3nm-10nm is 0, therefore replacement of fly ash does not affect to C-S-H product of cement hydration. However Pf of 10nm-50nm increases when fly ash is replaced even though the reaction ratio is 0%. Therefore it suggests that fly ash affects capillary pores.

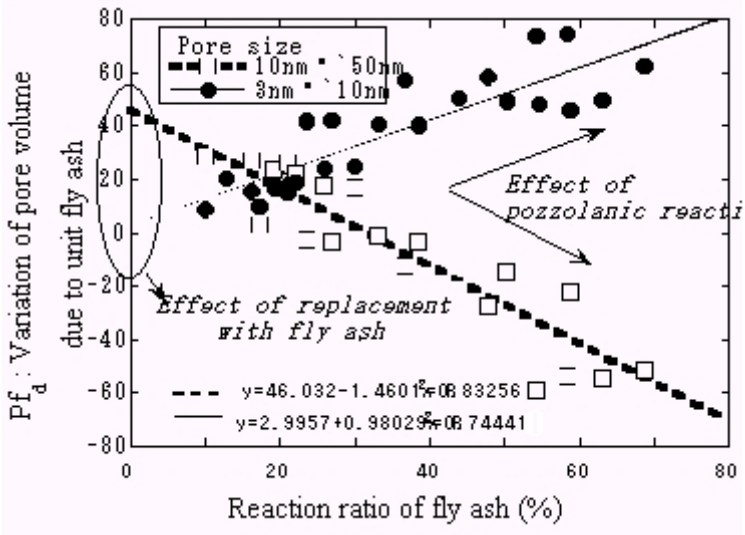

Figure 9. The effect of pozzolanic reaction of unit fly ash on microstructure of hardened paste.

3.6 Effect of Pozzolanic Reaction on Hardened Paste

Results of pozzolanic reaction on combined water, consumption of calcium hydroxide, BET specific surface area and pore distribution of hardened paste suggest that pozzolanic reaction of fly ash and cement hydration can be almost separate in these macro studies. Furthermore these phenomena quantitatively correlate with the reaction ratio of fly ash. This information on pozzolanic reaction of the fly ash contributes to elucidating the variation of properties and durability of concrete that includes all kinds of pozzolanic materials.

3.7 Ca/Si mole ratio of the hardened cement paste polished surface

EPMA is used to measure Ca/Si distribution on the polished surface of hardened cement paste. BEI of the measured areas and Ca/Si distributions are shown in Figure 10. Particles of C-S-H are smaller than the measurement beam diameter of 5 micrometer. Therefore the measured Ca/Si is the average of vicinity of the measuring point.

The appearance rate of Ca/Si for each measurement point is shown in Figure 11. By substituting the fly ash, the mode of Ca/Si lowers. In the case of the sample with 0% fly ash, frequency around -20 micrometer.

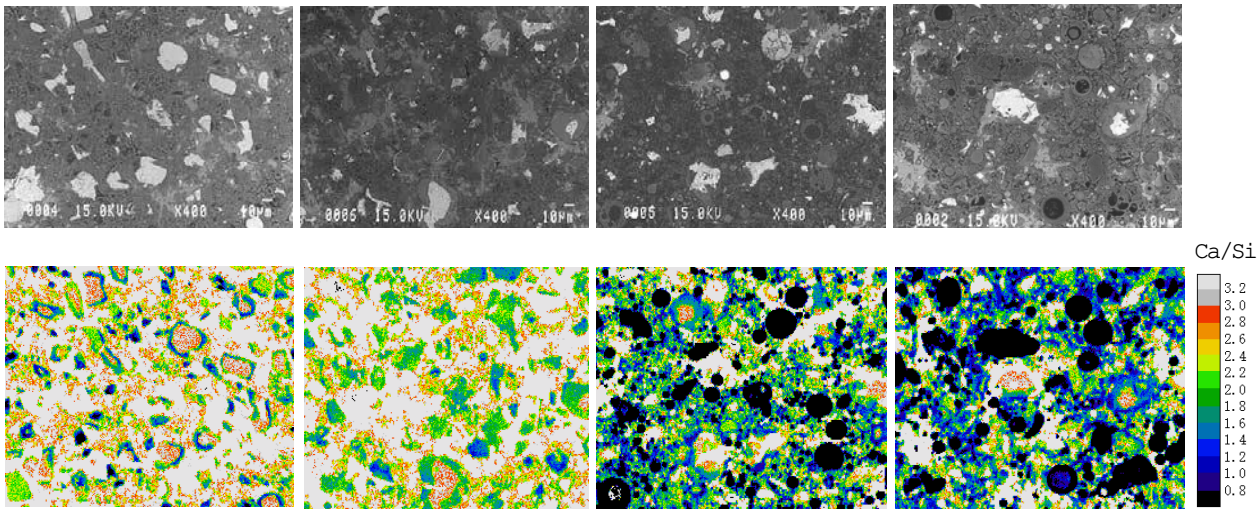

FA = 0% Age 7 days | FA = 0% Age 182 days | FA = 40% Age 7 days | FA = 40% Age 182 days

Figure 10. Back scattered electron images and Ca/Si atom ratios images on polished surfaces of hardened paste (W/P = 50%, Curing temperature = 40°C).

Ca/Si = 1.8 increased with age. Frequencies between Ca/Si of 1.0 to 1.5 are low. However fly ash dosages are 40%, there are high frequencies between Ca/Si of 1.0 to 1.5 even at 7 days. The range of Ca/Si below 1.5 increases with age.

3.8 Ca/Si of C-S-H Produced by Pozzolanic Reaction

The Ca/Si mole ratios of C-S-H produced by pozzolanic reaction in cement paste and in CH paste were 0.28 and 1.47 respectively [7]. The values of Ca/Si were calculated as follow functions (8, 9) from the consumption of CH due to pozzolanic reaction which was determined in Figure 5.

$$FA[0.907\ SiO_2,\ 0.305\ Al_2O_3,\ 0.079\ CaO] + 80.4/74\ Ca(OH)_2 + r\ H_2O \text{ ---> } p\ (CaO \cdot 1/xSiO_2 \cdot H_2O) + q\ (3CaO \cdot Al_2O_3 \cdot 6H_2O) \quad (8)$$

$$Si: 0.907 = P / X,\ Al: 0.305 = q,\ Ca: 0.079 + 1.086 = p + 3q,\ H_2O: 1.086 + r = p + 6q$$
$$p = 0.28mol,\ q = 0.305mol,\ r = 0.994mol,\ x = 0.276mol,\ 1/x = 3.62$$

$$100g\ FA + 80.4g\ Ca(OH)_2 + 17.9g\ H_2O \text{ ---> } 72.8g\ C\text{-}S_{3.62}\text{-}H + 115.3g\ C_3AH_6 \quad (9)$$

When the sample has 40% fly ash, the mode of Ca/Si in Figure11 becomes low with age. Because C-S-H with Ca/Si ratio of 0.28 is produced by pozzolanic reaction, it affects the mode of Ca/Si.

The relationship between Ca/Si of C-S-H and pH [8] is shown in Figure12. The pH value of calcium hydroxide paste is about 12.6. Whereas in cement paste, it is higher than 12.6 due to alkali metal. At early ages, cement paste is porous. This allows Ca ions and water to easily react with fly ash. After a long period, cement paste becomes denser. Ca ions and water supply to fly ash are then controlled by diffusion speed. As a result that pH value in close area of fly ash becomes low.

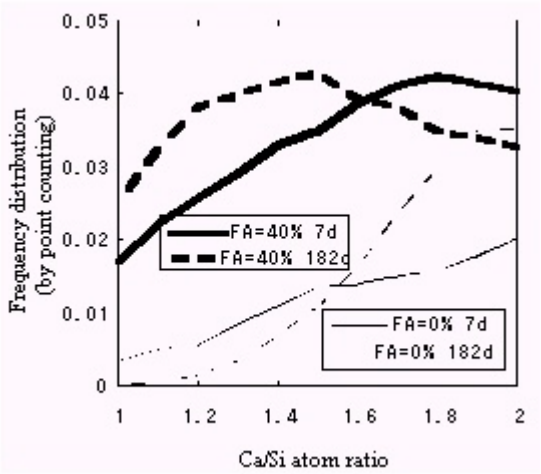

Figure 11. Ca/Si atom ratio measured by point counting in the area of Figure 10.

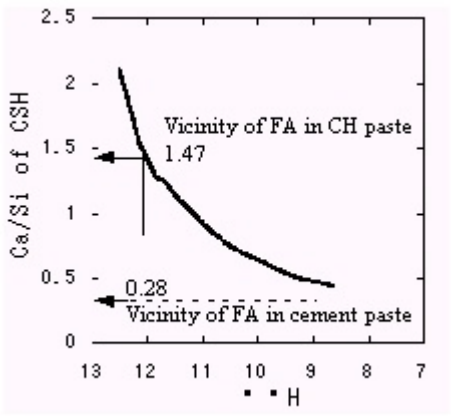

Figure 12. Calculated change in CSH composition with pH [8].

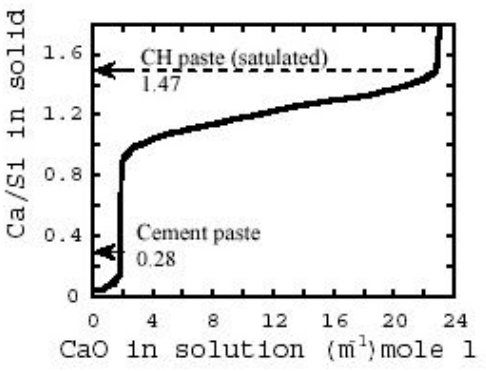

Figure 13. Metastable equilibrium curve relating the Ca/Si ratios of C-S-H [9].

CH paste is also porous even after a long period so the pH value of close vicinity to fly ash is almost 12.6. Concerning pH, there was good agreement on Ca/Si of C-S-H.

The typical metastable equilibrium curve relating the Ca/Si ratio of C-S-H with Ca ion concentration [9] is shown on Figure13.

It has been reported that Ca ion concentration in the pore solution of hardened cement paste is quite low, below 2 mmol/l [10], [11], [12]. In CH paste, Ca ion concentration is almost 20 mmol/l. These two figures support our results of Ca/ Si of C-S-H. This result shows that the pH value surrounding the fly ash in the paste is a key factor of the pozzolanic reaction.

4. CONCLUSION

The pozzolanic reaction of fly ash in cement pastes was investigated. Using paste specimens, which were prepared with various water cement ratios, fly ash replacement dosages and curing temperatures. The effect of the pozzolanic reaction on hardened paste was elucidated. The effects of the pozzolanic reaction can be regarded as quantitative phenomena. Details of these are described below.

(1) The pozzolanic reaction ratio of unit fly ash increases with decreasing replacement dosage of fly ash. Fly ash reaction ratio was calculated by determining the levels of insoluble residue of hardened paste.
(2) The pozzolanic reaction ratio of unit fly ash was increased with increasing water/powder ratio and increasing curing temperature.
(3) The pozzolanic reaction can be described as a constant chemical function in a macro model. Mixture proportion and curing conditions affect only the pozzolanic reaction speed of fly ash.
(4) Variations of combined water, consumption of calcium hydroxide, variations of BET specific surface area and variations of pore distribution in hardened paste due to the pozzolanic reaction proceeding can be separated from the results of cement hydration.
(5) The effect of pozzolanic reaction on cement paste, such as combined water, consumption of calcium hydroxide, BET specific surface area and pore distribution, could be described as a function of fly ash reaction ratio.
(6) The expected Ca/Si mole ratios of C-S-H in cement paste, which were calculated from experimental results, agreed with its observation values of EPMA. Furthermore, the expected values in the cement paste and in the calcium hydroxide paste corresponded to the equilibrium curve between C-S-H and pH, and the relationship between Ca ion concentration and metastable Ca/Si ratio in the solution.
(7) pH was a key factor of pozzolanic reaction, therefore these results seem to apply to different kinds of fly ash and pozzolans.

REFERENCES

[1] Malhotra V.M. and Ramezanianpour A.A., Fly Ash in Concrete, Second edition : CANMET, 1994
[2] Taylor, H.F.W. Cement chemistry, 2nd edition, London: Thomas Telford, 1997, pp.261-293.
[3] Uchikawa, H. Effect of Blending Components on Hydration and Structure Formation, 8th International Congress on the Chemistry of Cement, Rio de Janeiro, 1986, Vol. 1, pp.249-280.
[4] Hanehara, S., Tomosawa, F., Kobayakawa, M. and Hwang, K. Effects of Water/Powder Ratio, Mixing Ratio of Fly Ash, and Curing Temperature on Pozzolanic Reaction of Fly Ash in Cement Paste , Cement and Concrete Research, Vol. 31, 2001, pp.31-39.
[5] Kobayakawa, M., Hanehara, S. and Tomosawa, F. Pozzolanic Reaction of Fly Ash in Cement Paste –Influence of W/C, Cement Replacement, and Temperature, 7th CANMET/ACI International Conference Fly Ash, Silica Fume, Slag and Natural Pozzolans in Concrete, Chennai, 2001, Supplement papers, pp.443-457
[6] Kobayakawa, M., Ozu, H., Sathou, M. and Kagimoto, H., The Pozzolanic Reaction of Fly Ash in Hardened Mixture Made with Moderate Portland Cement, Cement Science and Concrete Technology, No.54, 2000, pp.153-160.
[7] Kobayakawa, M., Ozu, H., Hanehara, S., Hwang, K. and Tomosawa, F. The Influence of Mix Proportion and Curing Temperature on Pozzolanic Reaction Ratio of Fly Ash, Journal of Research of the Taiheiyo Cement Corporation, Vol. 139, 2000, pp.14-27.
[8] Reardon, E.J. An ion interaction model for the determination of chemical equilibra in cement/water systems, Cement and Concrete Research, 1990, 20, pp.175-192.
[9] Taylor, H.F.W. Cement chemistry, 2nd edition, London: Thomas Telford, 1997, p.145.
[10] Diamond S. Long-Term Status of Calcium Hydroxide Saturation of Pore Solutions in Hardened Cements, Cement and Concrete Research, 1975, Vol. 5. pp.607-626.
[11] Kobayakawa, M., Ozu, H., and Hanehara, S. The Change of Ion Concentration in the Pore Solution Extracted from Hardened Fly Ash-Cement Mortar with Curing Time, Cement Science and Concrete Technology, 1999, N0.53, pp.102-109.
[12] Kobayakawa, M. and Ozu H. The Review on Pore Solution Extracted from Hardened Cement Mixture, Journal of Research of the Taiheiyo Cement Corporation, Vol. 137, 1999, pp.47-60.

THE FORMATION AND PERFORMANCE OF HIGH BELITE CEMENT CLINKER WITH DIFFERENT INTERSTITIAL PHASE CONTENT

Sui-hua Guo, Hong-tao Zhang, Lin Zhen, Wen-sheng Zhang and Yi-min Chen

China Building Materials Academy, Beijing, P. R. China. E-mail: shguocbma@sohu.com

ABSTRACT

The paper studied the formation and burning process of high Belite cement (HBC) clinker when it had different interstitial phases' content. The results showed that the texture of Belite in HBC clinker would be remarkably different when the interstitial phases content in it was different. If the interstitial phases content in it was not higher than 10w%, the clinkering temperature required for HBC clinker would not be improved notably when interstitial phases content in it decreased. On the contrary, the clinkering temperature range of the clinker would be wider. The physical properties of the clinkers with different interstitial phases+ content would be notably different. The paste made of the cement prepared with the clinker with an interstitial phase content less than 15w% would have a fine workability and the 28-day strength of the mortar would also be high.

1. INTRODUCTION

High Belite cements (HBC) have been one of the highlights in the area of cement since the 1970's energy crisis. In the 1980's, it had become one of the high performance cements for preparing high performance concrete because the cement had such advantages as low heat of hydration, good resistance to chemical attack, and having a high strength and low shrinkage after a long hydration age [1].

For HBC clinker in which compositions lie in CaO-SiO_2-$A1_2O_3$-Fe_2O_3 system and Belite content in it is higher than 40%, the clinker would be easily dust during the quenching and the range of clinkering temperature of it would be generally sharp. Furthermore, the early strength of HBC is often very low and the quality of the cement would be not stable. One method to obtain high quality Portland cement (PC) and to simplify the burning process of the clinker is to control the mineral composition of it. However, there have been few studies published on HBC [2, 3]. It is well known that interstitial phases can influence the burning process of PC clinker notably and can also affect early hydration and performance of the cement. Because the guiding mineral of HBC is different from that of ordinary PC, the influences of interstitial phases on the burning process of HBC clinker or the performance of HBC would be also different. This paper studied the formation process and performance of Belite clinker when it had different interstitial phases' content.

2. EXPERIMENTAL

The raw materials used for the raw meals of HBC were limestone, clay and limonite, which were selected from some cement plants in China. Each raw material had first to be ground to a certain fineness and then mixed together to prepare the raw meal. The clinker samples were burned in an electric furnace and had been kept at the burning temperature for a certain time. To make samples for the burnability test, the time kept was 30min. To make samples for physical performance tests, they would be kept for 60 min. All clinker samples were quenched in air. Then chemical analysis,

XRD, optical examination and EDS would be carried out.

The cement samples were prepared with a SO_3 content of 3.5w% by mixing clinker with gypsum and then grinding them together to a specific surface area of about 325$m^2.kg^{-1}$. Physical performances of cement such as setting time of cement, fluidity and strength of mortar were tested according to such national standards as GB1346-89, GB/T2419-94 and GB177-85 in China.

3. RESULTS AND DISCUSSION

3.1 The compositions and formation process of Belite clinkers

The chemical compositions of clinkers made as above, are shown in Table 1. Based on the Bogue method [3], the mineral compositions of clinker samples can be calculated and ares listed in Table 1. The results indicated that the Belite in these samples were all higher than 65% and the difference of mineral compositions among them is the content of interstitial phases in the clinker.

The free calcium oxide contents of clinker samples are listed in Table 2, by which we can analyze the clinkering degree of the clinker when it is burned at different temperatures and can also analyze the clinkering temperature range of the clinker.

Table 1. Chemical composition and mineral compositions of clinker samples

No.	Chemical compositions /(w%)					KH	Mineral compositions /(w%)						Interstitial phases content /(w%)
	SiO_2	Al_2O_3	Fe_2O_3	CaO	MgO		C_3S	C_2S	C_3A	C_4AF	C_2F	f-SiO_2	
p-1	24.93	5.17	6.60	56.67	1.83	0.650	0	70.41	2.51	20.06	0	0.37	22.94
p-2	26.38	3.34	5.18	58.30	1.53	0.690	7.02	70.33	0.07	15.75	0	0	15.82
p-3	27.43	2.18	3.96	60.26	1.28	0.717	15.74	66.76	0	10.40	0.91	0	11.31
p-4	28.95	1.90	2.87	61.35	1.04	0.706	12.98	73.20	0.17	8.72	0	0	8.89
p-5	30.44	1.72	1.60	63.64	0.88	0.707	14.00	76.70	1.80	4.86	0	0	6.70

Table 2. Free CaO contents and the burning temperature range of clinker samples

No.	Interstitial phases content /(w%)	1250°C	1300°C	1350°C	1400°C	1450°C	1500°C	1550°C	Clinkering temperature range of the clinker
p-1	22.94	1.00	0.33	0*	0**	0	0	0	1250~1350°C
p-2	15.82	2.00	0.66	0*	0**	0	0	0	1250~1350°C
p-3	11.31	4.68	1.00	0.17	0	0*	0**	0	1300~1450°C
p-4	8.89	11.19	3.68	0.50	0.33	0.33	0.22	0*	1350~1550°C
p-5	6.70	20.05	7.51	3.01	1.51	1.34	1.00	0.50	1400~1600°C

* The clinker sample shran notably. **The clinker began to melt.

When the content of interstitial phases is higher than 15w%, the clinker can be burned at a low temperature, but the clinkering temperature range of it will be very sharp and can only vary in a range not larger than 100ºC. When the content of interstitial phases in clinker lies in the range of 10-15w%, the clinkering temperature required for the clinker will not be increased significantly and the clinker can be burned over a wide temperature range which can reach 150-200ºC. When the interstitial phases content in it is lower than 9w%, the clinker should be burned at a high temperature.

According to XRD, the dusting amount of the clinker can be reduced when it is burned in a high temperature or the interstitial phases in it is high. When the burning temperature of the clinker is lower than 1300ºC, the clinker will be dust easily, i.e. Belite of type β will be easy to transform to Belite of type γ during the quenching. When interstitial phases content in the clinker is lower than 10w% and the clinker is burned in a temperature not higher than 1300ºC, there will be a lot of γ-C_2S in the clinker as shown in Figure 1(b).

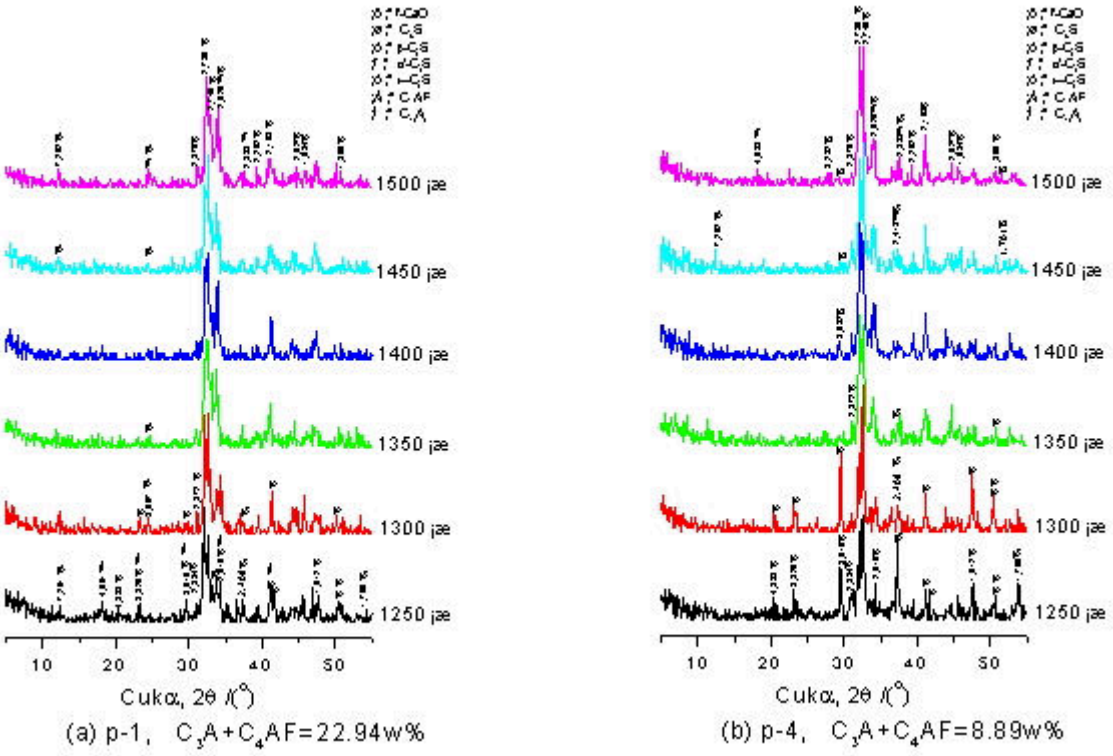

Figure 1. XRD patterns of HBC clinkers having different compositions which had been burned at different temperature conditions

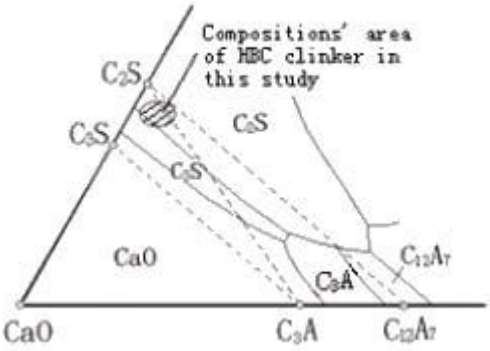

Figure 2. Compositions' area of HBC (having a low aluminate content) in the phase diagram [2] of CaO-C_2S-$C_{12}A_7$ system

When the burning temperature of the clinker was higher than 1400ºC, there would be some α′-C_2S formed in the clinker. This result was consistent with that of Fukuda [4, 5]. The result in the study had also indicated that the burning temperature required that α′-C_2S began to appear in the clinker would become lower when the interstitial phases content in the clinker was decreased. When the clinkers having different interstitial phases amount were burned in one given temperature, more α′-C_2S would form in the clinker having a low interstitial phases' content as shown in Figure 1.

When the interstitial phases content in the clinker is high, one of aluminates-$C_{12}A_7$ would be easily formed in the clinker. The main reason is that the composition of the clinker lies in the shadow area of Figure 2 and very close to the composition line of C_2S-C_3A. When the clinker compositions' point lies in the upper area of the line or the clinker is burned in a non-equilibrium state, the low-calcium aluminate mineral-$C_{12}A_7$ will be formed in the clinker.

3.2 Texture and compositions of Belite in the clinker

In HBC clinker of the same chemical compositions, the variation of burning temperature would not show a distinct influence on the texture of Belite. In contrast, the amount of interstitial phases in the clinker would have a great influence on the texture of Belite as shown in Figure 3.

When the interstitial phases content is higher than 10w%, Belite crystals formed in the clinker are rounded and normally striated. When the interstitial phases content decrease from 22.94w% to 11.31w%, the sizes of crystals will increase slightly but there will be more pores in the clinker. When the interstitial phases content in the clinker is lower than 10w%, Belite crystals will exhibit an irregular angular shape which may be even close to a hypidiomorphic texture.

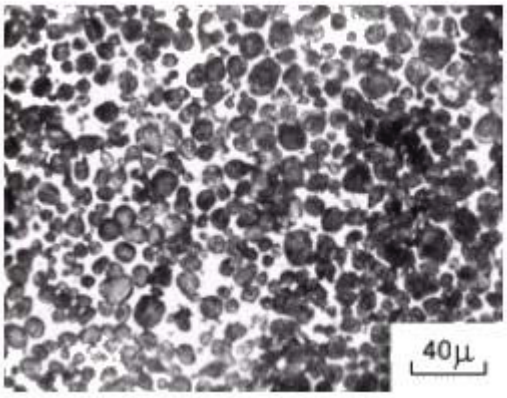

p-1，1350ºC, C_3A+C_4AF=22.94%

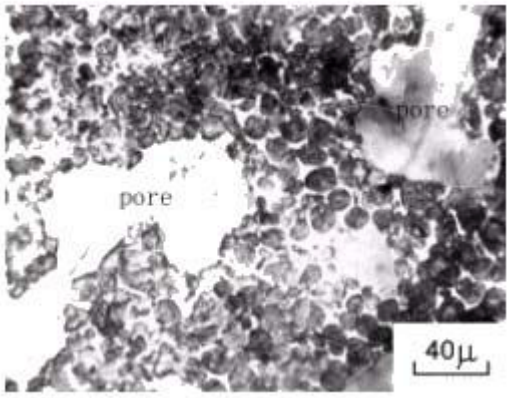

p-2，1380ºC, C_3A+C_4AF=11.31%

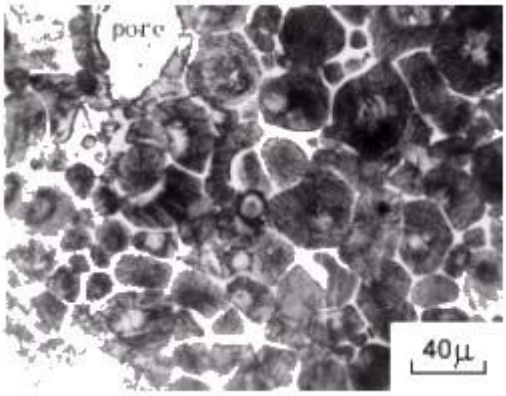

p-4,1450ºC, C_3A+C_4AF=8.89%

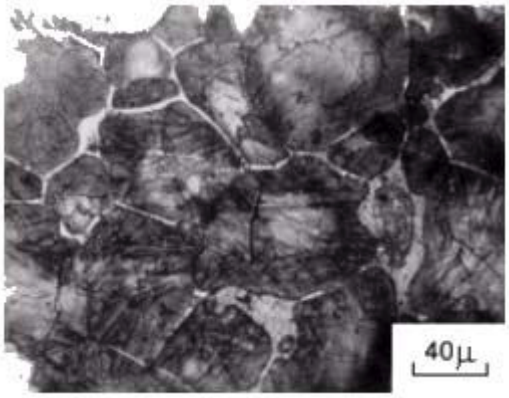

p-5, 1500ºC, C_3A+C_4AF=6.70%

Figure 3. Polished surface of Belite in clinkers having different interstitial phases' contents, etched with 1.0w% HNO_3 in alcohol

When the interstitial phases content in the clinker was different, the compositions of Belite (solid solution) would also be different. According to EDS analysis, we can see this variation of Belite's compositions as (Ca+Mg+K+Na)/(Si+Al+Fe) mole ratio which is shown in Figure 4. Belite in the clinker having a higher interstitial phase content would have a relatively higher n(Ca+Mg+K+Na)/n(Si+Al+Fe) ratio.

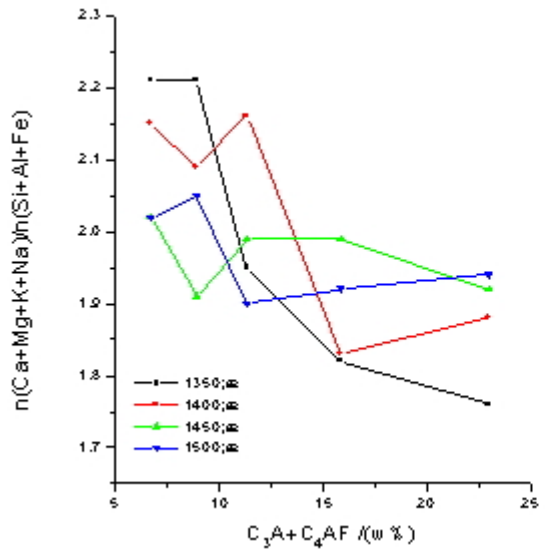

Figure 4. The n(Ca+Mg+K+Na)/n(Si+Al+Fe) ratio of Belite solid solution in the clinker having different interstitial phases content

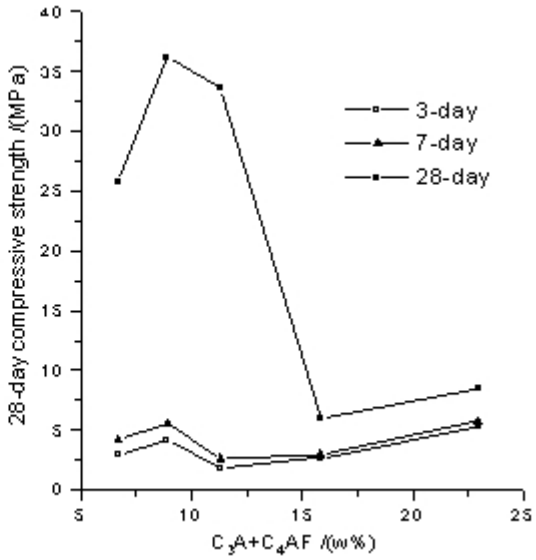

Figure 5. The relationship between interstitial phases amount and strength performance of HBC cement

3.3 Influence of interstitial phases on physical performance of HBC

All cement samples were prepared with the same gypsum content and the test results of their physical performance are listed in Table 3. It was found that the grindability of the clinker would be very bad when the content of interstitial phases in it was higher than 15%.

Table 3. Physical properties of HBC when the clinker had a different interstitial phases content

No.	Interstitial phases content /(w%)	Clinker		Fineness of cement /(w%)	Specific surface area of cement /($m^2.kg^{-1}$)	Setting time /(min)		Fluidity of mortar /(mm)	Bending strength /(MPa)			Compressive strength /(MPa)		
		Burning temperature	f-CaO /(w%)			Initial	Final		3d	7d	28d	3d	7d	28d
p-1	22.94	1350℃	0	13.6	329	6	9	102	1.48	1.85	2.19	5.21	5.74	8.53
p-2	15.82	1350℃	0.25	3.7	324	5	9	105	1.05	1.04	1.97	2.66	2.91	6.03
p-3	11.31	1380℃	0.33	0.8	327	109	225	131	0.90	1.16	4.98	1.85	2.62	33.6
p-4	8.89	1450℃	0.33	0.5	326	200	328	130	0.80	1.70	6.65	4.17	5.55	36.2
p-5	6.70	1550℃	0.50	0.3	322	234	281	133	0.60	1.18	5.51	2.96	4.17	25.7

The influence of interstitial phases content on strength performance of HBC is shown in Figure 5. The early strength of the mortar would be improved by the increase of interstitial phases content when this content in the clinker was higher than 15%, but the strength of all samples were low. The 28day strength performance of the cement in which the clinker had an interstitial phases content not more than 15% would be far higher than that of other cement made of the clinker having a high interstitial phases content. The compressive strength of the former would be 30MPa higher than that of the later. To the clinkers having a high interstitial phases content, the strength increase of the mortar between 7-day and 28-day hydration age would be very small. The 28-day compressive strength of them would be not higher than 10MPa, which indicated that the Belite in the clinker had a very low hydration activity. This may be caused by the variation of Belite's composition. Figure 6 indicates that when the n(Ca+Mg+K+Na)/n(Si+Al+Fe) ratio of Belite in the clinker was larger than 1.9, the 28-day compressive strength of the mortar would be far higher than that of the mortar in which the ratio of Belite in the clinker was lower than 1.9.

There may be another reason that the cement made of the clinker having a low content of interstitial phases had a higher strength performance. That is, there would be some α′-C_2S formed in the clinker as shown in Figure 7 or they had a higher C_3S content as in Table 1 than the clinkers having a higher interstitial phases content.

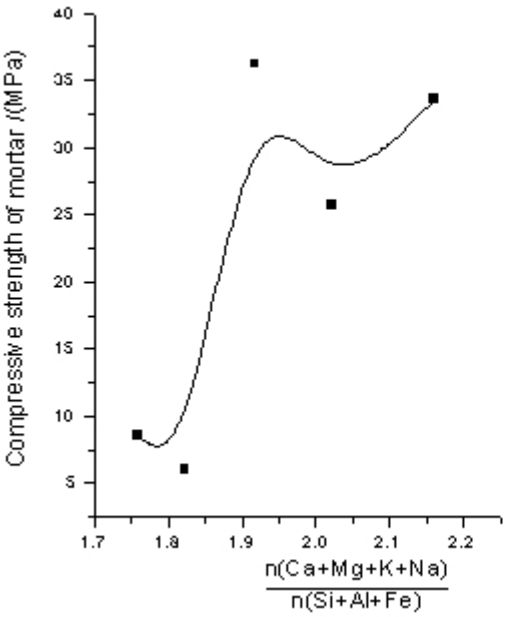

Figure 6. The relationship between n(Ca+ Mg+ K+ Na)/n(Si+ Al+ Fe) ratio and strength performance of the mortar

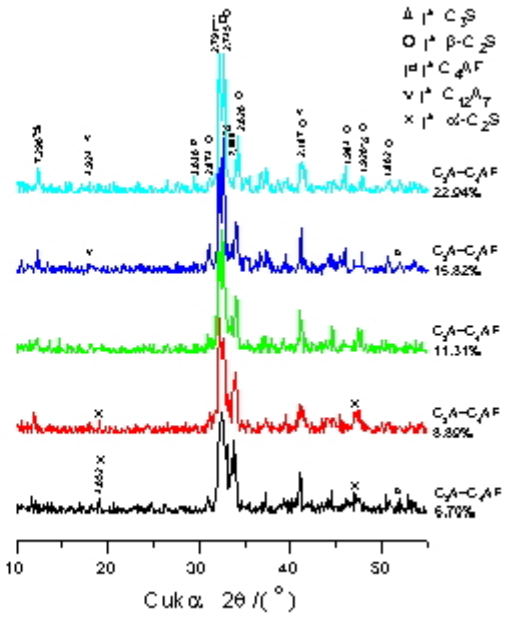

Figure 7. XRD pattern of HBC clinkers having different interstitial phases content

When the interstitial phases content in the clinker was higher than 15%, the cement will set rapidly and the mortar have a bad fluidity. This is because these samples have formed the low-calcium aluminate mineral $C_{12}A_7$ as in Figure 7.

4. CONCLUSIONS

(1) When the content of interstitial phases in clinker lies in the 10-15%range, the clinkering temperature required for the HBC clinker will not be increased significantly by the decrease of interstitial phases content and the clinker can be clinkered in a wide temperature range. When the interstitial phases content in it is lower than 9%, the clinker should be burned at a high temperature.

(2) The dusting amount of the clinker can be reduced by burning it at a high temperature or by improving the interstitial phases content in it.

(3) When the interstitial phases content is higher than 10%, Belite crystals are rounded and normally striated. When the interstitial phases content in the clinker is lower than 10%, Belite crystals formed in the clinker will exhibit an irregular angular shape which may be even close to a hypidiomorphic texture.

(4) The more interstitial phases in the clinker, the higher the n(Ca+Mg+K+Na)/n(Si+Al+Fe) ratio of Belite would be. The 28-day compressive strength of the mortar prepared with the clinker in which Belite had a ratio higher than 1.9 would be far higher than that of others.

(5) When the interstitial phases content in the clinker was very high, there would be some $C_{12}A_7$ formed in the clinker, the cement would set rapidly and the mortar would have a bad fluidity.

REFERENCE

[1] Chaterjee, A. K. High Belite Cement -present status and Future Technological Options, Cement and Concrete Research, vol.26, 1996, pp.1227-1237

[2] Shen, W. Huang, W. X. Min, P. R. Cement Technology (in Chinese), Wuhan: Wuhan University of Technology, 1991, pp16-24

[3] Guo, S. H. Zhang W. S. Mineral compositions of high performance low-calcium Portland cement, Cement (in Chinese), vol.25(2), 1999, pp31-35

[4] Fukuda, K. Maki, I. Toyoda, K. Kinetics of the α-to-α_H' Polymorphic Phase Transition of Ca_2SiO_4 Solid Solution. Journal of American Ceramic Society, vol.76, 1993, pp1821-1824

[5] Fukuda, K. Thermal hysteresis for the α_L'-β Transformations in Strontium Oxide-Doped di-calcium silicates. Journal of American Ceramic Society, vol.79, 1996, pp2969-2970

THE FORMATION AND PERFORMANCE OF HIGH BELITE CEMENT CLINKER WITH DIFFERENT INTERSTITIAL PHASE CONTENT

Sui-hua Guo, Hong-tao Zhang, Lin Zhen, Wen-sheng Zhang and Yi-min Chen

China Building Materials Academy, Beijing, P. R. China. E-mail: shguocbma@sohu.com

Guo Sui-hua is an engineer for China Building Materials Academy (CBMA), at Guanzhuang, Chaoyang District in Beijing, P. C. China. He is a member of Beijing Ceramic Society. His research expertise includes cement technology, special cement, cement chemistry and cement petrograhpy. His current researches involve in the areas of high Belite cement and high reactive Portland cement.

E-mail address: shguocbma@sohu.com
Mail address: Guo Sui-hua
Cement Institute
China Building Materials Academy
Guanzhuang, Chaoyang District
Beijing, 100024
P. R. China

THE RELATIONSHIP AMONG THE AGGLOMERATION, MICROSTRUCTURE OF CLINKER AND THE PERFORMANCE OF HIGH BELITE CEMENT

Sui-hua Guo, Hong-tao Zhang, Zhen Lin, Wen-sheng Zhang and Yi-min Chen

China Building Materials Academy, Beijing, P. R. China. E-mail: shguocbma@sohu.com

ABSTRACT

The relationship between the agglomeration, microstructure of clinker and the performance of high Belite cement (HBC) is discussed in the paper. The results showed that, for similar dense particles larger than 3mm, the smaller the size, the faster the cooling of the clinker and the more α′-C_2S formed in it. The microstructure of the clinker and the performance of HBC will also be better. The strength performance of HBC will be best when the sizes of clinker particles lie between 5-15mm and Belite crystals formed are characterized by the intersecting lamella texture in which there are many foreign ions. The C_3S content in loose clinker will be relatively lower than that in the dense one of similar size and there will be no α′-C_2S in it. The strength performance of the cement made with it will also be lower than that of the cement made of dense clinker.

1. INTRODUCTION

During the production and application of high Belite cement (HBC) in which C_2S content is higher than 40w%, some puzzles probably exist. For example the clinkering temperature range of the clinker will be relatively sharp, the clinker will be dust easily during cooling and the early strength of the cement will probably be very low [1, 2]. The previous research has shown that the quality and hydration activity of HBC could be improved by optimizing the composition of the clinker, for example by adjusting the content of fluxing minerals in clinker [3]. It is believed that there is a close relationship between the microstructure and the burning process of the clinker according to the petrography theory of cement [4]. Therefore by optical examination, the quality of the clinker can be controlled conveniently. The paper studied the relationship between the agglomeration, microstructure of clinker and the performance of high Belite cement.

2. EXPERIMENTAL

2.1 Clinker of high Belite Portland cement

The clinkers studied were burned in a rotary kiln of ϕ2.4/2.0/2.4×45m with a shaft preheater. The clinker samples were then classified according to their densities and agglomeration sizes. Their compositions are listed in Table 1.

2.2 Phase and microstructure analysis

Phases of clinkers were analyzed by X-Ray diffractometer (D/MAX-IIIA, CuKα) in a condition of 37kV, 40mA with a scanning speed of 2°/min. Before scanning, the samples were ground to a fineness less than 40μ. The microstructure of clinker was observed with a microscope of ORTHOLUX II POL-BK. The samples used in optical examination and EDS analysis were solidified with resin and etched first in a solution of 1% HNO_3 in alcohol.

2.3 Tests for physical performance of cement

The cement samples were prepared by grinding clinker and gypsum together with a SO_3 content of 3.2w%. The physical properties of cement such as setting time, fluidity and strength were tested according to GB1346-89, GB/T2419-94 and GB177-85 in China.

3. RESULTS AND DISCUSSION

3.1 Mineral compositions of clinker

The composition analysis showed that the larger the agglomeration sizes, the higher the C_3S content would be in the clinker. When particle sizes were similar, the C_3S content in loose clinker would be lower than that in the dense one as shown in Figure 1 and Table 1.

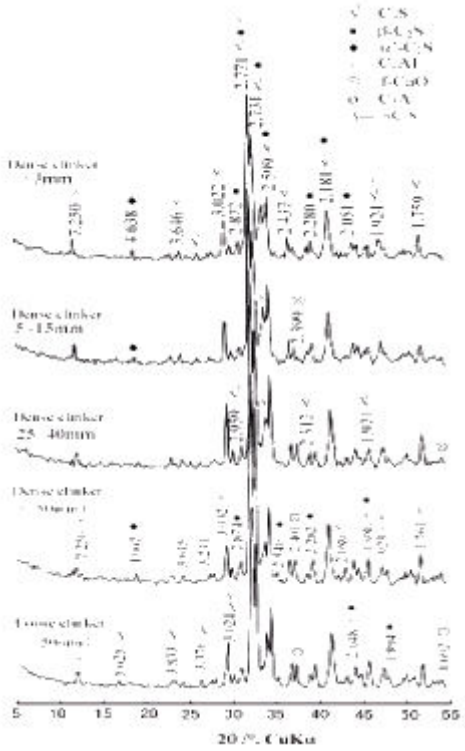

Figure 1. XRD patterns of clinker particles having different agglomeration sizes or different densification degrees

Table 1. Compositions of HBC clinker with different agglomerations

No.	Agglomeration sizes /mm	Chemical compositions /w%						Modulus			Mineral compositions /w%				
		SiO_2	Al_2O_3	Fe_2O_3	CaO	MgO	Σ	KH	SM	IM	C_3S	C_2S	C_3A	C_4AF	f-CaO
B6	<3，dense	24.93	4.42	5.18	62.10	1.25	97.88	0.759	2.60	0.85	26.3	51.6	3.0	15.8	0.39
B5	5~15，dense	24.95	4.00	4.94	62.53	1.42	97.84	0.765	2.79	0.81	28.0	50.4	2.3	15.0	0.45
B7	25~40，dense	24.52	3.95	4.77	62.17	1.68	97.09	0.786	2.81	0.83	33.4	45.1	2.4	14.5	0.62
B3	>50，dense	24.64	3.84	4.73	62.80	0.99	97.43	0.794	2.88	0.81	35.8	43.7	2.2	14.4	0.61
B4	>50，loose	24.95	4.23	4.79	62.30	1.21	97.76	0.768	2.77	0.88	28.8	49.8	3.1	14.6	0.48

When agglomeration sizes or densities of clinkers were different, there were also some other differences in mineral composition. With clinkers of similar density, the α′-C_2S formed in small particles would be more and the f-CaO content in it would be relatively lower than that in the larger clinker particles as shown in Figure 1 and Table 1. For the clinkers of different densities, the α′-C_2S content formed in the denser one would be higher than that in the loose clinker. When the clinker was very loose and particle sizes were very big, some γ-C_2S could be found in it. The f-CaO contents in clinkers of different densities were close to each other.

DTA showed that, when the clinker was very loose, there would be an endothermic peak emerging in DTA pattern near the temperature of 810°C. This endothermic peak was caused by the phase transition from γ-C_2S to α'_L-C_2S, which was consistent with the result of XRD.

3.2 Microstructures of clinkers having different agglomerations

The color of HBC clinker is lighter than that of the ordinary Portland clinker and the litre weight of it (1.30-1.50kg.L^{-1}) is also remarkably lower than that of the latter. When the burning temperature in the kiln was too high, the clinker would be very dense and a brown core would appear in it. The agglomeration sizes of clinker particles out of the kiln would be in two opposing extremes, i.e. there was not only too many large particles but also too many small particles of less than 3mm in the clinker. When the burning temperature was relatively low, the particles of clinker would very loose and the litre weight of it would be even less than 1.10kg.L^{-1}.

3.2.1 Microstructure of clinker particles with a size of 5-15mm

The microstructure of the clinker that had an agglomeration size of 5-15mm is shown in Figure 2. The interstitial phases consist of dendritic ferrite (light) in a matrix of aluminate (dark). Alite and Belite had grown well and their boundaries were very clear. Belite crystals were rounded and normally striated. There were also many small crystals of Belite as inclusions in Alite. The sizes of Alite crystals lay in 10-30μ range and the sizes of Belite in 10-25μ. The interstitial phases in the clinker were about 15-20w% of the clinker and distributed uniformly in the clinker, which was suitable for the clinker to have a high performance. The microstructure of the clinker showed that the burning temperature of the clinker was high, the cooling of it was quick and the clinker had been burned in an oxidation condition [4].

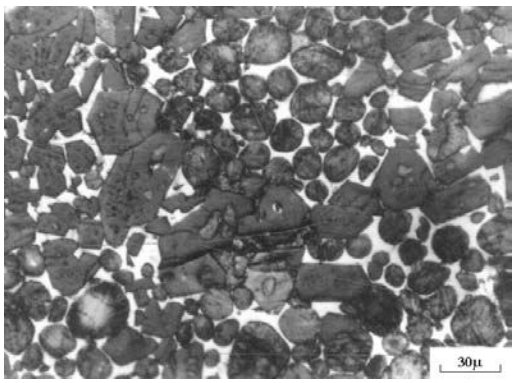

Figure 2. Polished surface of clinker particles with a size of 5-15mm

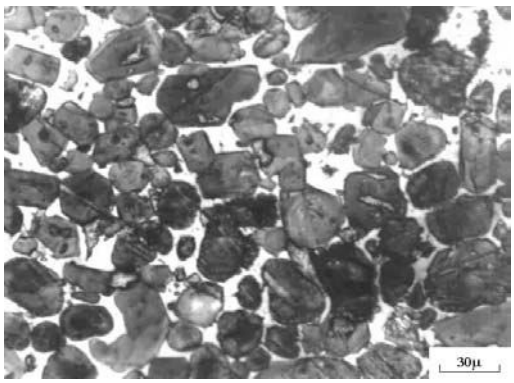

Figure 3. Alite and fingered Belite in the fine clinker particles

3.2.2 Microstructure of small-and-dense clinker particles

The polished surface texture of small-and-dense clinker particles (<3mm) is shown in Figure 3 and Figure 4. The crystals of C_3A represented a state of rectangle or line shape. Much of the Alite in it had been grown together and there had been many melting phenomena in their boundaries. A kind of girdle banded texture was also found in their boundaries. The configuration of Belite had some different categories among which the fingered shape was typical and there were intersecting coarse striae in their surfaces. Part of the Belite was also like that in the clinker particles of 5-15mm and a part of the Belite showed a kind of encephalon texture as in Figure 4. The sizes of Alite and Belite crystals in the clinker were not uniform and in a range of 5-50μ respectively. The distribution of various minerals in the clinker was also not uniform. In the field of crystal clusters of Belite, the amount of interstitial phases was few and in the field of Alite, there were more interstitial phases distributed.

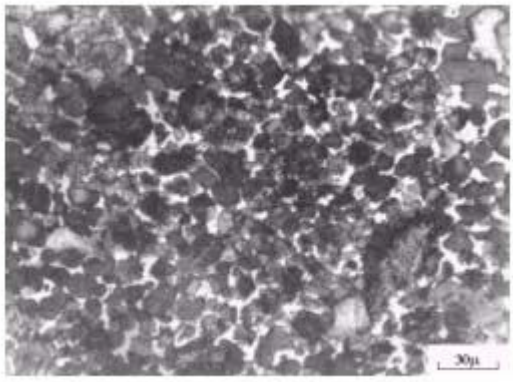

Figure 4. Crystal cluster composed of different Belite textures in fine-and-dense clinker

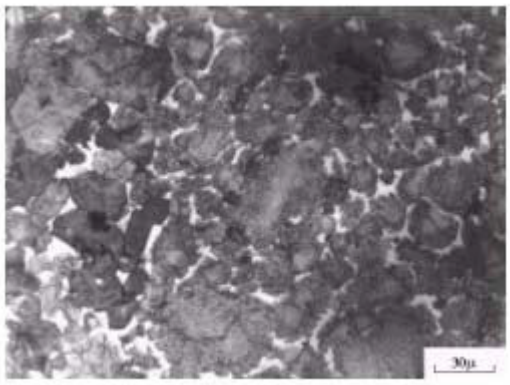

Figure 5. Polished surface of clinker with a particle size of 25-40mm

This kind of clinker usually emerged together with the large particles of dense clinker. The microstructure of the clinker showed that the clinker had been over burned and had been burned unevenly. The cooling of the clinker particles was also relatively slow.

3.2.3 Microstructure of large clinker particles with a size larger than 25mm

For the clinker particles of 25-40mm, the interstitial phases consist of dendritic ferrite in a matrix of aluminate. Alite had grown very well and their boundaries were very clear. But a part of Alite crystals emerged as a kind of striated texture. Belite in the clinker had grown as fingered shape with a multi-pock surface or exhibited as a kind of encephalon shape with crossed striae in their section plane. The microstructure of it indicated that the clinker had been burned in a reductive atmosphere and had not been cooled quickly.

The structure of Belite in dense clinker particles larger than 50mm was similar to that in the dense clinker of 25-40mm. But the crystal sizes were approximately 30μ and remarkably larger than the latter. Furthermore there were also little of Belite emerged as dendritic shape (Figure 6). Compared with the clinker particles of 25-40mm, the sizes of Alite crystals in it were relatively high which were about 50μ. The boundaries of Alite also had much melting phenomena, moreover part of the Alite had decomposed completely into secondary free CaO and secondary Belite, and formed a misleading phenomenon as an Alite configuration (Figure 7). The C_3A in the clinker showed as a state of sheet texture. The optical examination of the clinker showed that the clinker had been burned at a very high temperature in a heavy reductive air and had been cooled slowly.

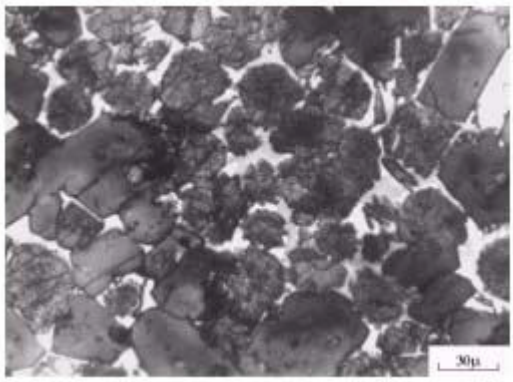

Figure 6. Microstructure of large particles of dense clinkers

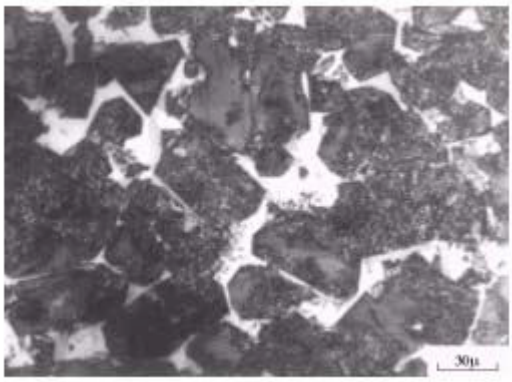

Figure 7. Pseudo-Alite in the large particles of dense clinkers

3.2.4 Difference between the microstructures of loose HBC and dense HBC clinker

The microstructure of loose HBC clinker particles with a size larger than 50mm is shown in Figure 8 and Figure 9. Compared with the dense clinker having the same sizes range, the crystals of Alite were remarkably smaller and had a size of 10-20μ. The texture of Belite was also different. Part of Belite emerged as a spindly shape and had a kind of parallel striae texture in their twins as in Figure 8. Other part of Belite showed as kidney shape with a multi-pock surface as in Figure 9. The C_3A in the clinker also showed as a kind of sheet texture, which showed that the clinker had been burned at a relatively low temperature and had been cooled very slowly.

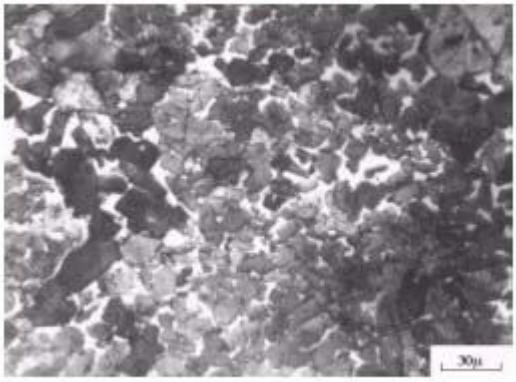

Figure 8. Spindle-shaped Belite in the large particles of dense clinker

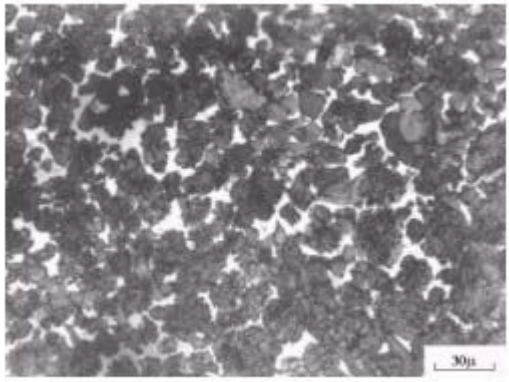

Figure 9. Pockmarked Belite like kidney shape in the large particles of loose clinker

3.3 Relationship between physical properties of HBC and clinker agglomerations

3.3.1 Particle density of clinker agglomeration

The physical properties of HBC having different clinker agglomerations are shown in Table 2. The test showed that the strength performance of HBC made of dense clinker would be higher than that of HBC made of loose clinker which had similar agglomeration sizes to the dense one. One reason would be that the C_3S content of dense clinker was higher than that of loose clinker.

Table 2. Physical properties of high Belite cement prepared with different agglomeration clinkers

No.	Agglomeration sizes /mm	Specific surface area /($m^2.kg^{-1}$)	Fineness /% (in mass)	Water demand of paste at normal consistency /%（in mass）	Setting time		Bending strength /MPa						Compressive strength /MPa					
					Initial	Final	1d	3d	7d	28d	60d	91d	1d	3d	7d	28d	60d	91d
B6	<3, dense	376	2.8	25.4	2:40	3:30	3.5	4.1	5.4	8.6	10.8	11.0	11.2	16.4	24.7	52.6	68.1	80.5
B5	5~15, dense	379	2.2	25.2	2:35	3:25	4.0	5.2	6.5	9.1	10.3	10.3	15.4	21.8	33.4	54.0	69.6	78.5
B7	25~40, dense	390	2.8	25.4	2:25	2:50	2.8	4.6	6.0	8.5	9.8	10.2	10.7	20.7	28.7	51.4	64.9	76.9
B3	>50, dense	412	2.6	25.2	2:05	2:25	3.2	5.2	5.8	8.1	8.8	8.8	12.5	22.8	30.3	47.8	61.5	68.6
B4	>50, loose	401	1.8	24.8	2:05	2:30	3.1	4.5	5.3	7.8	9.5	9.4	10.6	19.2	25.0	44.8	62.8	68.5

According to the optical examination, the burning temperature of loose clinker was lower than that of dense clinker, which showed that increasing the burning temperature would also improve the strength properties of HBC. Fukuda believed that [5, 6] the original Belite at low temperature would be type α′ and then could be as type α in high temperature conditions. When the two clinkers were cooled at the same speed, a transformation of $\alpha' \rightarrow \beta\text{-}C_2S+L$ for the Belite burned at low temperature and another transformation of $\alpha \rightarrow \alpha' \rightarrow \beta+L$ for the Belite burned at high temperature would take place respectively. Therefore, the $\alpha'\text{-}C_2S$ amount reserving in the twins of Belite burned in high temperature would be remarkably higher than that burned at low temperature as shown in Figure 2. The analysis of XRD showed that there would be some $\gamma\text{-}C_2S$ in the loose clinker particles.

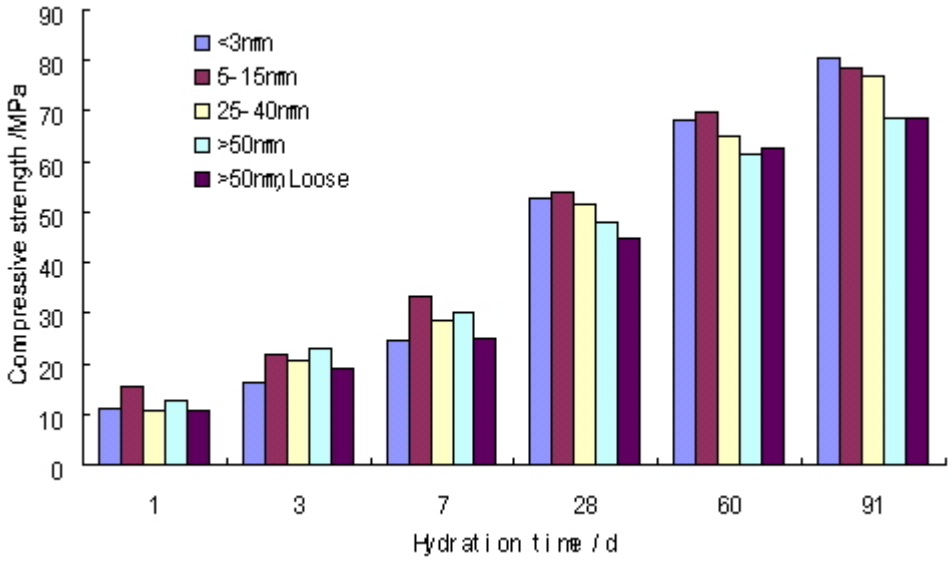

Figure 10. Strength properties of high Belite cement prepared with clinkers of different agglomeration sizes

3.3.2 Agglomeration sizes of clinker

The influence of clinker agglomeration on the strength properties of HBC was shown in Figure 10. The chemical analysis showed that the larger the agglomeration sizes of the clinker, the more C_3S would be in the clinker. But when the particle size of the clinker was larger than 3mm, the compressive strength of HBC, especially the strength performance after hydrating for 3 days would be decreased by the increase of the clinker particle sizes. This showed that the texture of Belite crystals had great influence on the performance of HBC. XRD analysis showed that the smaller the clinker particle was, the more α'-C_2S would be formed in the clinker. Moreover, the optical examination showed that the cooling speed of clinker would be decreased, the burning condition of clinker would become in a reductive air and the texture of Belite would not be very good when the particle size of clinker became larger in a similar particle density.

For the clinker having a particle size not larger than 3mm, the cooling of it was also not very good because it always come out of kiln along with the large and dense clinker particles. The texture of Belite in it would not be very good and the strength performance would also be relatively low.

The tests showed that the strength properties of HBC would be the best when particle sizes of the clinker were in the range of 5-15mm. This kind of clinker had been burned in a high temperature without reductive air and had been cooled rapidly. And there would be much more α'-C_2S formed in the clinker. According to the analysis of EDS, the foreign ions in the Belite would also be high.

Table 3. Ca/Si mole ratios and foreign ions content in Alite and Belite

No.	Agglomeration sizes	n(Ca)/ n(Si)		Foreign ion fraction /w%	
		Alite	Belite	Alite	Belite
B6	<3mm, dense	2.64	1.96	2.54	3.59
B5	5~15mm, dense	2.93	2.02	1.84	5.00
B7	25~40mm, dense	3.21	2.22	2.39	2.33
B3	>50mm, dense	2.73	2.05	3.04	3.90
B4	>50mm, loose	2.75	1.98	3.75	3.90

4. CONCLUSIONS

(1) The analysis showed that the larger the size of clinker particles, the more C_3S in it. When particles sizes are similar, the C_3S content in loose clinker would be lower that in the dense one.
(2) For dense clinker, the smaller the size of the agglomeration, the more α'-C_2S would be formed. No α'-C_2S would form in loose clinker and there would be even some γ-C_2S formed in it when particle sizes of it were very large. The strength performance of HBC made of dense clinker would be better than that of HBC made of the loose one.
(3) For similar dense clinker, the smaller the size of particles, the faster the cooling of the clinker and the higher the content of α'-C_2S formed when the particle sizes of clinker are larger than 3mm. The microstructure of the clinker and the performance of high Belite cement will be improved by the decreasing agglomeration size of the clinker.
(4) The strength properties of HBC will be the best when the size of clinker agglomerations was in the range of 5-15mm. This clinker had been burned in a condition of high temperature without reductive air and had been cooled rapidly. There would be much more α'-C_2S formed in the clinker and the foreign ions in the Belite will be high.

REFERENCES

[1] Shen, W. Huang, W. X. Min, P. R. Cement Technology (in Chinese), Wuhan: Wuhan University of Technology, 1991, pp16-24
[2] Guo, S. H. Zhang W. S. Mineral compositions of high performance low-calcium Portland cement, Cement (in Chinese), vol.25(2), 1999, pp31-35
[3] Guo, S. H. Zhang H. T. Li J. Z. Chen Y. M. The formation of Belite and the performance of clinker in different interstitial material content. Science and Technology of Cement-base Materials (in Chinese), Beijing:, 1999, pp37-40
[4] China Building Materials Academy. Cement Petrography (in Chinese), Beijing: Book Concern of China Building Technology, 1975, pp104-157
[5] Fukuda, K. Maki, I. Toyoda, K. Kinetics of the α-to-α_H' Polymorphic Phase Transition of Ca_2SiO_4 Solid Solution. Journal of American Ceramic Society, vol.76, 1993, pp1821-1824
[6] Fukuda, K. Maki, I. Ikeda, S. Ito, S. Microstructures Formed by the Remelting Reaction in Belite Crystals. Journal of American Ceramic Society, vol.76, 1993, pp2942-2944

THE RELATIONSHIP AMONG THE AGGLOMERATION, MICROSTRUCTURE OF CLINKER AND THE PERFORMANCE OF HIGH BELITE CEMENT

Sui-hua Guo, Hong-tao Zhang, Zhen Lin, Wen-sheng Zhang and Yi-min Chen

China Building Materials Academy, Beijing, P. R. China. E-mail: shguocbma@sohu.com

Guo Sui-hua is an engineer for China Building Materials Academy (CBMA), at Guanzhuang, Chaoyang District in Beijing, P. C. China. He is a member of Beijing Ceramic Society. His research expertise includes cement technology, special cement, cement chemistry and cement petrograhpy. His current researches involve in the areas of high Belite cement and high reactive Portland cement.

E-mail address: shguocbma@sohu.com
Mail address: Guo Sui-hua
Cement Institute
China Building Materials Academy
Guanzhuang, Chaoyang District
Beijing, 100024
P. R. China

PARTICULAR FEATURES OF BY-PASS DUST UTILIZATION IN SLAG CONTAINING BINDERS

J. Stark[1], I. Chartchenko[1], P. Krivenko[2], R. Runova[2], M. Kochevykh[2] and I. Rudenko[2]

[1] F.A. Finger-Institut für Baustoffkunde, Coudraystraße 11, D-99421 Weimar, Deutschland.
E-mail: johen.stark@bauing.uni-weimar.de
[2] State Scientific Research Institute on Binders and Materials, P.O. Box 161, Kiev 03037, Ukraine.
E-mail: sribm@mail.kar.net

ABSTRACT

The purpose of this study is to develop an effective way of utilization of the by-pass cement kiln dust (BP) in slag containing binders intended for general application in civil engineering. The study's results concluded that an alkaline activation of the slag by the salts contained in the BP is a problem because these are the salts of alkali of metals and strong acids, in particular, sulfates and chlorides. Moreover, the content of chlorides and sulfates is a main factor in determining the intensity of the development of corrosion of reinforcement in concrete, thus affecting its durability. The BP itself may be utilized as an alkaline component of the slag containing cements such as the slag alkaline binders (SAB), on condition that there is enough activity and degree of binding of the chlorides into new formations to use them in making durable reinforced concretes. A scheme of the process of how to lower concentration of free chlorine in the pore solution of the slag containing binders with the use of the BP has been of proposed and is discussed in detail. A range of compositions of the modified binder in the system "slag- BP" to be used for making both non-reinforced and reinforced concretes has been developed.

1. INTRODUCTION

One of the key problems of the cement industry related to environmental protection is how to provide full recovery of cement kiln dust, including BP and its rational utilization. Utilization of the BP within the cement and concrete compositions, which would possess high strength, durability, and resistance to chemicals including those chemicals that are aggressive with regard to reinforcement, is of first priority.

The BP contains alkali metal salts of strong acids (such as R_2SO_4, RCl), CaO, and clinker minerals. The BP aqueous leakage is characterised by high pH values varying between 13 and 14. Due to this, of interest is to use the BP for activation of blast furnace granulated slag in cement composition. The BP may be used not only as a complex activator of slag-containing cement, but as its structure-forming component. In this case, the slag containing cement may be classified as SAB that are known to contain ground granulated slag and alkaline component in a form of alkali metal compounds creating an alkaline medium. The composition of hydration products of the SABs is represented, predominantly, by low-basic calcium hydrosilicates and hydroaluminates as well as alkaline hydroaluminosilicates and these hydration products determine their high performance properties.

The purpose of this study is to develop an effective way of utilizing the BP in composite cement containing slag intended for general application in civil engineering.

2. OBJECTS AND METHODS

For the research presented the mineralogical and chemical composition BP and blast granulated slag used were representative of European materials. The mineralogical content of BP is represented by free calcium oxide (CaO), salts of alkali metals and strong acids such as potassium chloride (KCl), potassium sulphate (K_2SO_4) and complex salt of alkali metals ($K_3Na(SO_4)_2$). The chemical composition BP is represented in table 1.

The slag used belongs to a group of neutral slags with the value of a basicity Mo < 1 (table 1), that determines its low hydraulic activity. The specific surface of the slag is S = 3860 cm^2/g. The slag is represented by a glass-like phase which contains calcium aluminosilicates.

Portland cement (PC) was used as calcium-containing admixture. The chemical composition CEM I 42.5R (complying with EN 197) is represented in table 1. A mineralogical composition of PC, mass. %:C_3S-42.3, C_2S - 28.6, C_3A - 8.8, C_4AF - 7.6.

Table 1. Chemical composition of BP, slag and PC

	Content of oxides, mass. %										
	SiO_2	Al_2O_3	Fe_2O_3	CaO	CaO_{fr}	MgO	SO_3	Na_2O	K_2O	Cl	TiO_2
BP	9.1	2.8	1.7	27.1	10.1	0.9	12.0	1.3	24.9	14.3	-
Slag	36.4	12.0	1.1	39.9	-	7.3	0.4	0.3	0.6	0.0	0.47
PC	21.1	4.9	2.5	63.1	2.1	1.5	3.2	0.2	1.2	0.1	0.19

For involving of free chlorine in structure of hydrated products, hydrated calcium aluminate ($C_3A{\cdot}6H_2O$) was utilized as an admixture. This is a by-pass product of ettringite production. The chemical composition the calcium aluminate admixture (CAA) is tabulated in table 2.

Table 2. Chemical composition of CAA*, mass. %

Al_2O_3	CaO	SO_3	Cl
23.2%	44.4%	0.1%	0.007%

note: CAA contains 86.07 % $C_3A{\cdot}6H_2O$.

Preparation of the binders was undertaken in laboratory conditions by mechanical homogenization of dispersible dosed components. In the research presented the methods X-ray diffractometry (XRD), differential-calorimetric analysis (DCA), chemical analysis of pore solution of hydrated binders, and experimental-statistical simulation were applied.

3. RESULTS AND DISCUSSION

3.1 Activation of slag by BP

With the purpose to determine the influence of BP alkaline on structure formation processes during hydration of the binder and to define the rational composition limits of BP in this binder, the binders researched had a content of BP from 10 up to 100 % (remaining part of the binders was represented by the slag). The activity of the binders was taken as criterion to determine the rational content of BP in their composition.

The obtained results demonstrate (fig. 1), that with increase of hydration period leads to augmentation of BP amount that is involved in structure formation process. Thus the maximum activity of SAB can be achieved after 2 days of hydration at a content 10% of BP, and after 28 days of hydration at a content of near 30% of BP in SAB. These phenomena can be connected to the high density of silica-aluminium phase of slag, which causes a long period of interaction between

components of SAB and correspondingly – the involving of above quantity of BP. In this connection the role BP as an alkaline component SAB should be considered in view of a time factor.

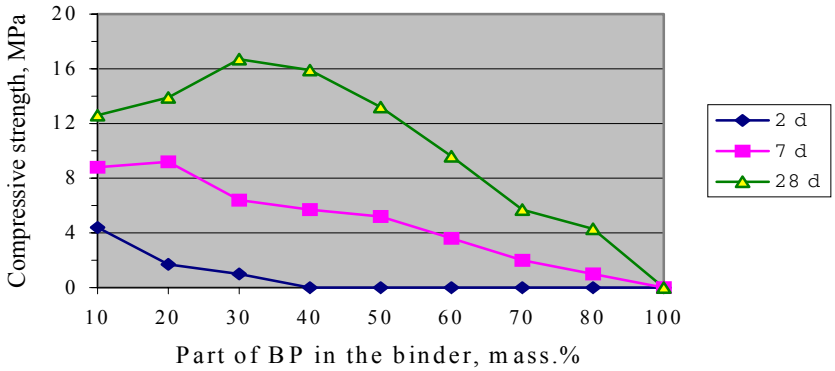

Figure 1. Dependence of activity of SAB* upon composition and period of hydration
* - In further under SAB the composition "slag - BP" was meant.

Basing on the results, it was concluded that BP can be utilized as an alkaline component SAB. The components ratio in a system «slag - BP» should meet the following requirement: the ratio between the content of potassium and sodium oxides ($K_2O + Na_2O$) in BP and the content of alumina (Al_2O_3) in slag should be equal

$$\frac{K2O + Na2O}{Al2O3} \geq 1.$$

However, from the shown data follows, that despite a significant amount of dissoluble R_2O present in the system "slag - BP", obtained SAB does not differ by high activity. This binder can not be attributed to any class on classification EN 197. The reasons of this fact can be connected as with weak hydration activity of slag with glass-like dense structure, so with the nature of anionic component of salts introduced in the binder with BP. The increase of SAB activity that is based on neutral slag can be achieved by utilization of portland cement clinker [1, 2, 3].

3.2 Activation of slag containing binder by PC

The three-component binding system "slag – BP - PC" was investigated. The carried out researches (figure 2) testify that in this binding system the optimal ratio between components is as follows: mass.%: slag -69.0, BP - 17.5, PC – 13.5.

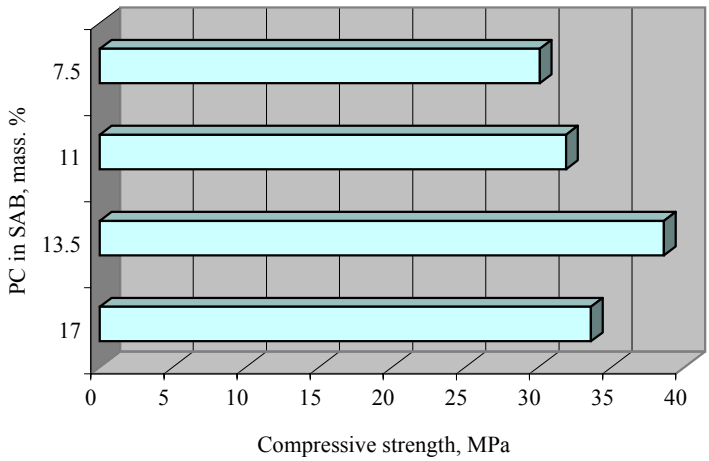

Figure 2. The dependence of SAB activity after 28 d of hardening upon the content of PC

The binder of such composition essentially is the modified SAB. This binder is characterized by the class on strength 32.5 according to EN 197. The increase of compressive strength of this binder from 2 to 28 days of hardening is approximately in 4 times (9.6 and 38.6 MPa respectively). This fact can be connected with formation of low calcium hydrosilicates. The formation of these products can be confirmed by increase of intensity of a diffuse hum on the XRD of the binder radiogram astringent in characteristic for identification of such hydration products reflection angles $2\Theta = 28\text{-}34^{o}$ (figure 3, curves 2 and 3).

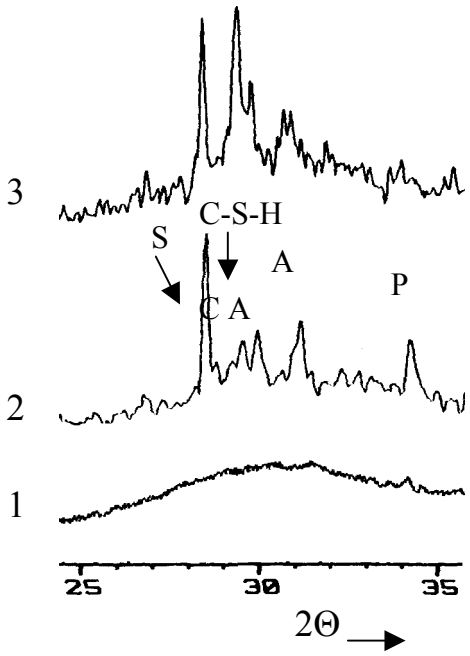

S – Sylvite (KCl)
C – Calcite ($CaCO_3$)
A – Arcanite (K_2SO_4)
P – Portlandite ($Ca(OH)_2$)

1 – slag in initial state,
2 – SAB after 2 d of hydration,
3 – SAB after 28 d of hydration

Figure 3. XRD of slag and modified SAB

It is known [4] that the main criterion for an estimation of aptitude of a binder for application in reinforced concretes alongside with activity, is the content of free chlorine in the pore solution. The high content of chlorine in a structure BP (as dissoluble salts) predetermines the necessity for the substantiation of BP usage in SAB, providing safety of steel reinforcement.

3.3 The regulation of conditions for passivation of steel reinforcement in medium of a binder

It's known that the most representative criterion for an estimation of probability of appearance of corrosion of the reinforcement in concrete is the ratio of ions Cl^-/OH^- [5]. It was shown that no conditions for depassivation of reinforcement can be observed at ratio Cl^-/OH^- in the pore solution not more than 0.6 [6].

The pore solution of SAB modified with PC is characterized by the molar relation Cl^-/OH^- equal to 9.83, i.e. by a value that exceeds the limit of 0.6. Therefore, it was necessary to solve the problem of this value reduction.

It is expedient to consider the process of free chlorine reduction in pore solution of SAB by its binding both chemically and adsorptive, including cases when the total content of chlorine exceeds the normative limits.

3.4 The hypothetical process of AFm-phases formation during hydration of SAB

In an initial stage of hydration up to crystallization of portlandite ($Ca(OH)_2$) the next reaction takes place:

$$2KCl + Ca^{2+} + 2OH^- \rightarrow CaCl_2 + 2K^+ + 2OH^- \quad (1)$$

The beginning of this process is determined by dissolution KCl of BP. The calcium chloride ($CaCl_2$) forms with portlandite the complex salt $Ca(OH)_2 \cdot CaCl_2 \cdot 2H_2O$, and the ions of alkali metal increase pH of pore solution. As hydration passes, the surface dissolution of $Ca(OH)_2.CaCl_2 \cdot 2H_2O$ take place. The reason of this process is determined by smaller dissolubility of portlandite in comparison with calcium chloride. The crystallization of portlandite and the migration of chlorine ions in the pore solution can be observed as a result.

It is known that chlorides of alkali metals can be bound in a slightly soluble AFm-phase known as Friedel's salt [7]. In view of the presence of potassium chloride in BP, the process of formation of Friedel's salt can take place according the following reaction [8]:

$$3CaO \cdot Al_2O_3 \cdot 6H_2O + 2KCl + Ca(OH)_2 + 4H_2O = 3CaO \cdot Al_2O_3 \cdot CaCl_2 \cdot 10H_2O + 2KOH \quad (2).$$

It suggests the possibility of modifying of the binder by one more additive – CAA. The role of CAA consists in accelerated formation of AFm-phases, which are presented by the system of complex salts $3CaO \cdot Al_2O_3 \cdot CaSO_4 \cdot nH_2O$- $3CaO \cdot Al_2O_3 \cdot CaCl_2 \cdot 10H_2O$ - $3CaO \cdot Al_2O_3 \cdot Ca(OH)_2 \cdot nH_2O$. These salts can be formed as thin pseudo-hexagonal slices only up to crystallization of portlandite. The crystals of these salts consist of brucite-like main layers $[Ca_2Al(OH)_6]^+$ and interlayer material $[1/2SO_4 \cdot 3H_2O]^-$, $[Cl \cdot 2H_2O]^-$ or $[OH \cdot 3H_2O]^-$ [9].

The nature of AFm-phases is that the anion can be freely changed. Thus the priority of involving of anions in a structure of AFm-phases varies in line: $SO_4^{2-} > Cl^- >> OH^-$ [9].

The presence in the system of ions SO_4^{2-} determines composition of interlayer substance as $[1/2SO_4 \cdot 3H_2O]^-$, that under known conditions will determine the formation of ettringite covers around grains of aluminate and thus will slow down its reactivity. However, at high concentrations of ions OH^- and SO_4^{2-} the formation of ettringite in SAB is absent. This fact is caused by the following reaction:

$$C_3A \cdot C \cdot S \cdot H_{12} + 2KCl \rightarrow C_3A \cdot CaCl_2 \cdot H_{12} + K_2SO_4 \quad (3)$$

Thus, the formation of a complex $C_3A \cdot C \cdot S \cdot H_{12}$ does not occur, as well as the formation of two-water calcium sulphate ($C \cdot S \cdot H_2$).

The sulphate-ions in solution do not directly cause depassivation of reiforcement, but determine the formation of sulphite hydrogen (H_2S), which is a catalyst of oxidation (carbonization) of hydrated products in SAB:

$$Ca(OH)_2 + H_2CO_3 \rightarrow CaCO_3 + 2H_2O \quad (4)$$

$$C\text{-}S\text{-}H + HCO_3^- \rightarrow CaCO_3 + SiO_{2(gel)} + H_2O \quad (5)$$

During carbonization the formation of solid solution of complex salts $3CaO \cdot Al_2O_3 \cdot CaCl_2 \cdot 10H_2O$ and $3CaO \cdot Al_2O_3 \cdot 0.5Ca(OH)_2 \cdot 0.5CaCO_3 \cdot 10H_2O$ is possible. Besides the anions $[Cl \cdot 2H_2O]^-$ can be replaced by $[OH \cdot 3H_2O]^-$ in already formed Friedel's salt [10].

As follows from above mentioned, prior to the beginning of portlandite crystallization the formation of Friedel's salt is marked predominantly among known AFm-phases . Thus the factors, which determine the composition of interlayer substance in the complex salt are: molar relation Cl/Al in the system, intensity of carbonization in the system.

The first factor determines the correlation between anions $[Cl \cdot 2H_2O]^-$ and $[OH \cdot 3H_2O]^-$, the second – the correlation between anions $[Cl \cdot 2H_2O]$- and $[0.5CO_3 \cdot OH \cdot 5.5H_2O]^{2-}$ in interlayer material of AFm-phases.

Utilization of BP as the alkaline component of SAB ensures values of pH not less than 11 and lack of corrosion of the reinforcement under intensive carbonization of the system at catalytic influencing of H_2S. At high pH values (more than 12.7) the period of formation and existence of Friedel's salt is determined only by intensity of portlandite crystallization and its further transformation in calcite ($CaCO_3$).

At modification of SAB by PC the replacement of anion $[Cl \cdot 2H_2O]^-$ in Friedel's can be indemnified by formation of a sufficient amount of gel-like or submicrocrystalline calcium hydrosilicates (see fig. 3). It is known that such hydrated products are capable to adsorb chlorine in their structure [11]. However the process of formation of calcium hydrosilicates is stretched in time, caused by low hydration activity of the slag. This suggests that the role of CAA in SAB consists in intensification of directional formation of Friedel's salt at the initial stage of hydration.

3.5 SAB modified with CAA

CAA has the much greater surface of molecules in comparison with one- or two-calcium aluminate. This fact caused a larger adsorption and, accordingly, larger degree of binding of chlorine in Friedel's salt according to equation (2).

Based on suggested process of Friedel's salt formation among other hydrated products of SAB, the rational value of a molar ratio Cl/Al was under investigations. The researches were conducted on the model system «BP - CAA», because BP determines main content of chlorine and CAA - main content of reactive (in the initial stage of hydration) aluminium in modified SAB.

In fig. 4 the results obtained for model systems after 7 days of hydration are represented. The results testify to optimal molar relation Cl/Al = 1, that corresponds to stoichiometry of Friedel's salt. Such relation between ions Cl and Al corresponds to 53.06 % BP and 46.94 % CAA in model system, that is caused by chemical composition of BP and CAA.

The proportional decrease in the degree of chlorine binding at lowered Cl/Al less than 1 is caused by replacement of anions $[Cl \cdot 2H_2O]^-$ by $[OH^- \cdot 3H_2O]^-$ in the interlayer substance of complex salts $3CaO \cdot Al_2O_3 \cdot CaCl_2 \cdot 10H_2O$ and $3CaO \cdot Al_2O_3 \cdot Ca(OH)_2 \cdot nH_2O$. It confirms the AFm-phase formation described above and is compatible with results [10].

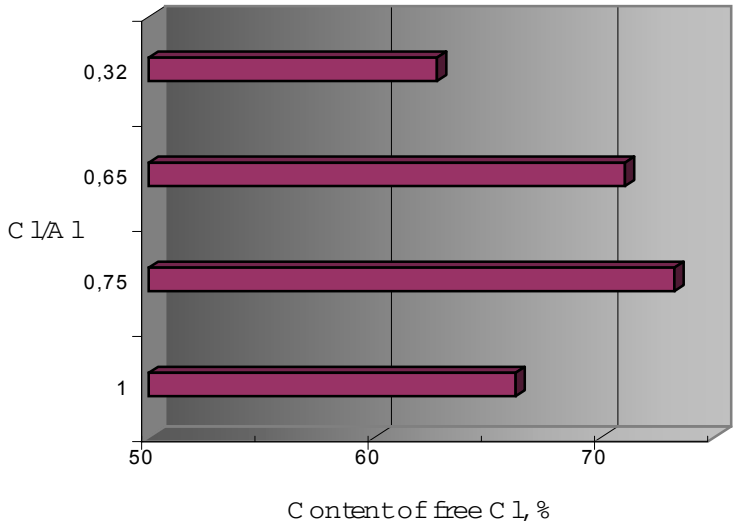

Figure 4. The dependence of degree of chlorine binding upon molar relation Cl/Al in model system «BP - CAA» during hydration

The low absolute degree of chlorine binding at sufficient C_3A content can be explained by different kinetics of portlandite and Friedel's salt crystallization. So, the curve of heat evolution of BP during hydration demonstrates completion of transformation of CaO in portlandite within the first 3 hours of hydration (fig. 5). The intensive formation of Friedel's salt passes during first 4-5 days of hydration [11]. It follows that in the system of complex salts $3CaO \cdot Al_2O_3 \cdot CaCl_2 \cdot 10H_2O$ and $3CaO \cdot Al_2O_3 \cdot Ca(OH)_2 \cdot nH_2O$ an equilibrium displaces in towards the last complex salt. The high concentration SO_4^{2-}-ions determines formation of H_2S and, as a corollary, high intensity of carbonization of the system. Such evolution of hydration explains the slow formation of Friedel's salt at known priority of ions Cl^- before ions OH^-.

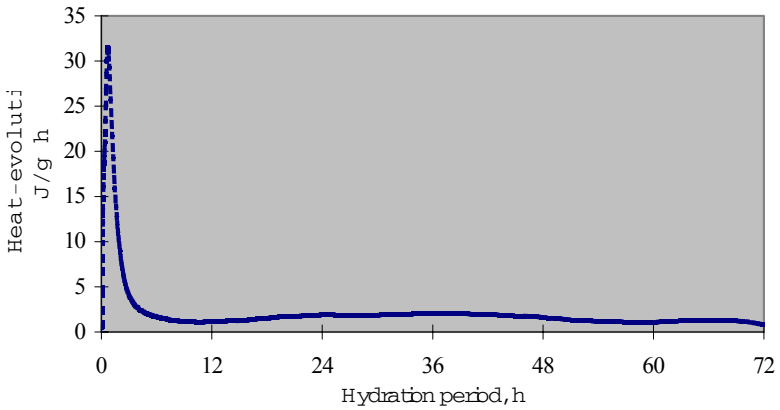

Figure 5. Integral heat-evolution during BP hydration

The results obtained are confirmed by XRD of the considered model system "BP - CAA". The analysis of kinetics of Friedel's salt formation in the system under the action carbonic acid and its lack is presented in fig. 6. So, let's accept the integral square of the defining reflex of Friedel's salt (area of the reflex angle 11^o) after 28 d of hydrations as 100 %. In this case the intensity of Friedel's salt formation will be arranged in time as follows. The greatest intensity of Friedel's salt formation is fixed during first 48 h of a hydration as at absence of carbonic acid (fig. 6a) as well as under its influence (fig. 6b). However, despite an identical salt content that was formed in different conditions within the first 48 hours of hydration, its mass part in relation to the common content is various and depends on influence of carbonic acid on the system. So the mass part of Friedel's salt, which was formed during first 48 hours, makes 32 % in a system without the influence of carbonic acid and 67 % - in analog. This fact can be explained by considerable deceleration of formation of Friedel's salt under the influence of carbonic acid and is determined by intensive carbonization of the system in the presence of H_2S as catalyst. Thus the augmentation of Friedel's salt content in the system-analog (under influence of carbonic acid) up to 28 days of hydration is determined by presence of portlandite among hydrated products.

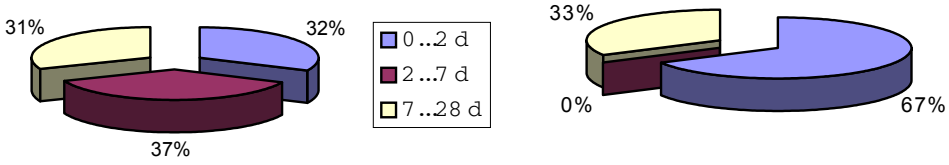

a) – without influence of carbonic acid

b) – under influence of carbonic acid

Figure 6. The Friedel's salt formation during 28 d of hydration in the model system «BP - CAA»

Thus, portlandite formation during the hydration of the model system «BP - CAA» and its transformation into calcite determines the intensity of Friedel's salt formation and the duration of the phase prior to the beginning its dissolution under the action of carbonic acid.

On the basis of the carried out research, the conclusion was made that the practical interest for usage as a binder for reinforced concretes has the system «BP - Slag - PC - CAA ». It was supposed that such a system could be characterized by a high degree of intense chemical binding of chlorine in Friedel's salt by pH-values (modifying function of CAA). And determine the absence of the corrosion process of reinforcement during carbonization – the function of alkalis that are formed from BP's salts according to equations (1) and (2) by high activity. (The combination of BP with modifier PC determines the mixed nature of activation of slag.)

3.6 Compounding decisions on BP's utilization in slag containing binders for reinforced concrete

By the method of experimental - statistical simulation of the dependence «composition - properties» the compositions of SABs (usable in reinforced concretes) was defined. This area is described by limits exhibited in tab. 3. The correspondence of SABs composition to indicated limits ensures its correspondence to the class on strength 42.5 (according to EN 197) and values Cl^-/OH^- in its pore solution in limits 0.6.

Table 3. The compounding of the binders for reinforced concretes

Components of the binder	Content, mass %
Slag	66 – 74
PC	26 – 34
BP	not more than 4.2
CAA	not more than 3.8

4. CONCLUSION

1. The investigation of slag-containing binders, which were projected as SABs, confirmed the complex activating influence of BP on hydration properties of blast granulated slag. It was established that slag-containing binders for both unreinforced and reinforced concretes can be obtained through BP usage as their component. The BP content in such binders is determined by degree of chlorine binding during hydration.

2. Slag containing-binders with high BP contents (17.5 %) and appropriate to the class on strength 32.5 (on EN 197) can be obtained if it is projected as SAB. The component ratio in this binder must meet the following requirement: the ratio between content of alkali metals oxides (K_2O + Na_2O) of BP and alumina content (Al_2O_3) of slag should correspond the inequality $\frac{K2O + Na2O}{Al2O3} \geq 1$.
   Degree of chlorine binding (by criterion Cl^-/OH^-) in this binder predetermines its usage in unreinforced concretes.

3. The particular feature of BP utilization in slag-containing binders for reinforced concretes is the necessity of chlorine steady binding during hydration. For this purpose it was theoretically proved and experimentally confirmed the process of chlorine binding in slightly soluble Friedel's salt among other hydrate products of slag and containing BP. The stoichiometric calculation of the reaction of Friedel's salt formation confirms the necessity to preserve the equality Cl/Al = 1 in the binder. Based on data analysis about hydration activity of slag taking into account their chemical and phase structure, stoichiometry of Friedel's salt, the

compounding decisions on BP's utilization (up to 4.2 mass %) in slag-containing binders for reinforced concrete (by criterion Cl^-/OH^-) were proposed.

4. The supposition, that the process of chlorine binding during hydration of the binder system «BP - slag» is carried out both on chemical (primary), and on adsorptive (secondary) processes, was proved. The chemical binding of chlorine is caused by Friedel's salt formation, the adsorptive binding – by gel-like or submicrocrystallin calcium hydrosilicates. It was shown, that for such processes the investigated binder system should be modified by the following combination of additives:
    - Calcium compounds (PC), which provide an increase in hydration activity of slag (as well as binding activity) due to calcium activation, as well as due to alkaline activation on the part of alkali which is formed by cation exchange between portlandite and alkali salts of BP;
    - Aluminate compounds (CAA), which provide intensive chlorine binding in Friedel's salt at the initial stage of hydration.

REFERENCES

[1] Глуховский, В.Д., Кривенко, П.В., Пушкарева, Е.К., Гелевера, А.Г. Особобыстротвердеющие шлакощелочные вяжущие, Цемент, 1984, No.11, pp. 13-14 (in Russian).

[2] Глуховский, В.Д., Кривенко, П.В., Румына, Г.В., Герасимчук, В.Л. Производство бетонов и конструкций на основе шлакощелочных вяжущих, Киев, Будивельник, 1988, pp. 144 (in Russian).

[3] Krivenko, P.V. Alkaline cements and concretes: problems of durability, 2nd inttrnational conference on alkaline cements and concretes, Ukraine, Kyiv, 1999, pp.3-43.

[4] Breit, W. Untersuchungen zum kritischen korrosionauslösenden Chloridgehalt für Stahl in Beton, Von der Fakultät für Bauingenieur- und Vermessungswesen der Rheinisch-Westfälischen Technischen Hochschule Aachen yur Erlangung des akadem. Grades eines Doktors der Ing., genehmigte Dissertation, 1997.

[5] Alonso, C., Andrade, C., Castellote, M. and Castro, P. Chloride threshold values to depassivate reinforcing bars embedded in a standardized OPC mortar, Cement and Concrete Research, vol.30, 2000, pp.1047-1055.

[6] Hausmann, D.A. Steel corrosion in concrete. How does it occur? J. Mater. Prot., 1967, pp. 19-23.

[7] Friedel, P.M. Sur un chloro-aluminate de calcium hydrate se maclant par compression, Bull Soc Franc Mineral 19, 1897, pp. 122-136.

[8] Lunk, P. Kapillares Eindringen von Wasser und Salzlцsungen in Beton, Building Materials Reports, No.8, AEDIFICATIO Verlag, 1997, pp. 208.

[9] Taylor, H.F.W. Cement Chemistry, Academic Press, London, 1990, pp. 173.

[10] Pöllmann, H., Kuzel, H.-J. Synthesis and polymorphic transformations of solid solutions in the system $3CaO{\cdot}Al_2O_3{\cdot}CaCl_2{\cdot}nH_2O$-$3CaO{\cdot}Al_2O_3{\cdot}Ca(OH)_2{\cdot}nH_2O$-$H_2O$, N. Jb. Miner. Mh., H.5, 1988, S.193-202.

[11] Corrosion of metals in concrete, Reported by ACI Committee 222, ACI 222R-96.

PHASE COMPOSITION OF 40% AL_2O_3 CALCIUM ALUMINATE CEMENTS

B. Touzo[1], A. Gloter[2], K. Scrivener[3], T. Füllmann[3] and G. Walenta[4]

[1] Lafarge Aluminates R&D, St Quentin F., France. E-mail: bruno.touzo@aluminates.lafarge.com
[2] Laboratoire de physique des solides, Université d'Orsay, Orsay, France.
E-mail: gloter@lps.u-psud.fr
[3] Laboratory of Building Materials, EPFL, Lausanne, Switzerland.
E-mail: karen.scrivener@epfl.ch and thomas.fuellmann@epfl.ch
[4] Lafarge, Laboratoire Central de Recherche, St Quentin F., France.
E-mail: Gunther.walenta@pole-technologique.lafarge.com

ABSTRACT

Calcium aluminate cements (CAC) are special cements that contain from about 40 to 80% alumina. Their wide range of composition and properties make them usable for a great number of applications. The most commonly used CAC's are those containing 40% Al_2O_3. They are manufactured from natural raw materials by fusion and have complex phase compositions. This is due to the presence of elements other than Ca and Al in the clinker. The main impurities are Fe_2O_3 and SiO_2. Smaller amounts of MgO and TiO_2 may also be found, depending on the raw materials used. Some of the iron is present as Fe^{2+}, as a result of a partially reducing atmosphere in the kiln. Recent applications of techniques such as X-ray quantification by the Rietveld method and TEM observations of the clinker have provided a better understanding of the mineralogy. This includes characterisation of a perovskite type phase, not previously identified because of its similarity (structure and composition) to brownmillerite. New SEM, TEM and Rietveld studies are presented in this paper. Comparisons of these analyses make it possible to obtain a new and coherent description of the mineralogical composition of this category calcium aluminate cements.

1. INTRODUCTION

Calcium aluminate cements (CAC) are a range of special cements. Their chemistry is quite different from Portland cements, in that the main reactive phases are calcium aluminates (CA, $C_{12}A_7$) rather than calcium silicates. For refractory concretes, they are produced with alumina contents ranging from 40 to 80%.

The principal applications of CACs are (a) in refractory concretes; (b) as a component, with Portland cement and other materials of mixed binder systems for special "building chemistry" mortars; and (c) to produce specialist CAC concretes with properties such as resistance to abrasion, chemical attack and rapid hardening.

The most commonly used CACs are those containing around 40% Al_2O_3. These are manufactured from natural ores as raw materials – primarily bauxite and limestone. These raw materials are melted in a reverbatory kiln in a continuous process. The melt pours leaves the furnace by a tuyere and is cooled down in ingots. The use of natural ores means that elements other than Ca and Al are also present, which leads to a clinker with a complex mineralogical composition. The most important minor elements are Fe_2O_3 and SiO_2. MgO and TiO_2 are also frequently found; their

Proceedings of the 11th International Congress on the Chemistry of Cement (ICCC)
'Cement's Contribution to the Development in the 21st Century'
Hosted by: The Cement and Concrete Institute of South Africa
CD-ROM produced by: Document Transformation Technologies
11 - 16 May 2003, Durban, South Africa
ISBN Number: 0-9584085-8-0
Editors: Dr G. Grieve and G. Owens
Congress Organised by: Event Dynamics

amount depends upon the raw materials used. Some of the iron may be reduced to Fe^{2+}, according to the oxygen partial pressure in the kiln.

In all CACs, the principal phase is monocalcium aluminate $CaAl_2O_4$ (CA). The other calcium aluminate phase, present in much smaller amounts, is $C_{12}A_7$. All the other phases present have very much lower reactivity. The silicates are mainly present in C_2S (belite) and /or C_2AS (gehlenite). The iron is mainly present as a ferrite solid solution, based on $C_2(A,F)$ and a perovskite solid solution. Small amounts of an iron rich spinel structure are usually present. Phases such as $C_{12}A_7$, pleochroite and wüstite can also be found in small amounts.

All these phases show solid solution, which makes it difficult to develop any simple relation between chemistry and phase composition such as the Bogue equations for Portland cement. Attempts in this field are based on the subsolidus phase assemblage of simplified oxide system [1], which give only a partial description of the phase composition.

In order to control the phase composition of the product, it is then necessary to develop a method to measure the proportion of each phase. Quantitative X-ray diffraction analyses using the Rietveld method is the most accurate and efficient method, but an accurate crystallographic knowledge of the structure and composition of all the phases is needed to obtain reliable results.

In this paper, recent analyses carried out on the identification and quantification of phases of standard grade CACs are reported. Microstructural studies and chemical microanalyses by secondary (SEM) and transmission (TEM) electron microscope of clinker are shown and quantification by Rietveld analysis discussed. The use of this combination of techniques allows a coherent description of the mineralogy of these cements. In particular, it is shown that the regions previously identified just as “ferrite” contains one or both of a brownmillerite type phase and a perovskite type phase.

2. EXPERIMENTAL

The analyses reported in this study were carried out on a single calcium aluminate cement clinker. Its overall chemical composition is given in Table 1. For SEM characterisation, the samples were embedded in resin, polished, and coated with carbon. The polished sections were observed in the BSE mode on a JEOL 5800LV equipped with a PGT energy dispersive X-ray spectrometer (EDS) for chemical microanalyses. Microanalyses were done at 15 kV with a 1 nA current. For study by TEM, the samples were dry ground by the tripod polishing method. Ion milling was then used to reach electron transparency. The thin foil obtained was carbon coated on one side. Observations were done with a TOPCON OO2B TEM (200 KeV) equipped with a LaB_6 gun. Chemical analyses were performed with a TRACOR EDS equipment attached to the microscope. These two techniques for chemical microanalyses allow quantification of the oxide composition with oxygen calculated by assuming that the valence of each element is known. The oxidation state of iron was investigated by electron energy loss spectrometry (EELS), also available on the TEM. The methodology developed for the EELS study is described in detail in refs. 2 and 3.

Table 1. Chemical composition of the clinker investigated (wt%)

SiO_2	Al_2O_3	Fe_2O_3	CaO	MgO	TiO_2	Mn_2O_3	Cr_2O_3	K_2O	Na_2O	Others	l.o.i.	Total
4.6	38.5	16.2	36.8	0.7	1.8	0.8	0.1	<0.02	0.04	0.46	0.2	100.2

For the XRD analysis of calcium aluminate cements, described here, a Siemens diffractometer (Kristalloflex D5000) was used. This machine operates according to the Bragg-Brentano principle and uses CuKα-radiation. The K_β-radiation was eliminated by a Ni filter. The samples were X-

rayed in a range between 10° to 60° 2θ with a step width of 0.02°-2θ. For quantification the Rietveld method was used [4,5,6]. The principal of the method is that the intensities calculated from the crystalline structures are fitted to the observed X-ray powder pattern by a least squares refinement. This is done by varying the parameters of the crystal structures and of the peak profiles to minimise the difference between observed and calculated powder patterns. Because the whole powder pattern is refined by the Rietveld method, problems of peak overlap are minimised and a very accurate quantitative analysis can be obtained. Quantitative Rietveld phase analysis of calcium aluminate cements is also described in ref. 7.

3. RESULTS

3.1 General description of the phase composition

A typical BSE SEM image of the CAC clinker is shown in Figure 1. The dark grey areas are CA (monocalcium aluminate). This is the first phase to crystallise from the melt and the areas are sections of dendritic crystals that are linked in three dimensions.

Between the CA regions, a number of other phases can be identified. In order of increasing brightness, these are: gehlenite, dicalcium silicate (belite), "ferrite" and spinel. The chemistry of these phases is discussed in the following sections. No distinct areas of $C_{12}A_7$ were observed in this sample by SEM. Although pleochroite was identified by X-ray diffraction, its low concentration and grey level close to CA made identification in the microstructure difficult, but it was observed in some areas. No other phases were identified, even at highest SEM magnification and the ferrite grains appear homogeneous.

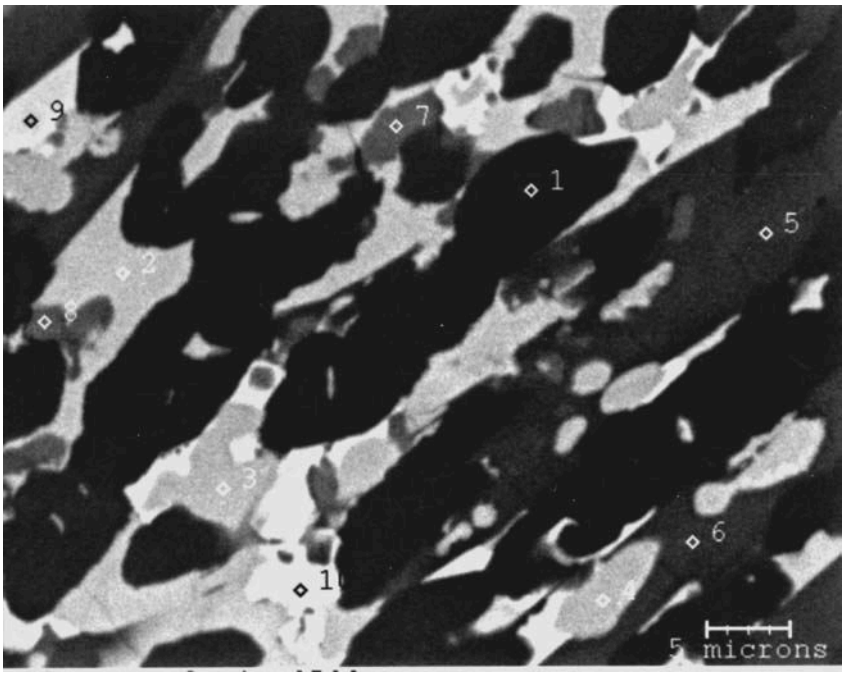

Figure 1. BSE micrograph of a polished section of CAC clinker. A: CA; B: Ferrite; C: gehlenite; D: C_2S; E: spinel. Pleochroite and $C_{12}A_7$ phases have too low concentration to be detected easily by SEM.

3.2 Calcium aluminates.

Fe^{3+} substitutes for Al^{3+} in monocalcium aluminate. The level of substitution measured by both TEM and SEM was 5 at%. This level of substitution does not change the crystal structure or lattice parameters, but does have an impact on the peak intensities in the diffraction pattern.

Detailed characterisation of $C_{12}A_7$ was not possible because of its small amount and crystal size. However, observations in the TEM indicated that both iron and to a lesser extent silicon, substitute for aluminium.

3.3 Ferrite phases

Until recently, the regions identified as ferrite were supposed to be monophasic, with the crystalline structure of brownmillerite Ca_2AlFeO_5 [7], which is a member of the solid solution $Ca_2(Fe_{1-x}Al_x)_2O_5$ where x ranges from 0 to about 0.7 [9,10]. This phase is known to contain impurities and some authors have suggested a correlated substitution of trivalent cations by Mg^{2+}–(Si^{4+}+Ti^{4+}) to ensure the charge balance of this phase in Portland cements [11,12]. In CACs fluctuation in the amount of these impurities had been observed but not explained. Jeanne [13] suggested the presence of two types of brownmillerite in CAC, with the composition of varying from grain to grain [14].

Studies using Rietveld analysis suggested the presence of a new phase not mentioned previously in CACs [15,16]. The structure of this phase was first proposed to be similar to that of merwinite C_3MS_2, but with a different composition. It was not observed previously by XRD because of its similarity (structure and composition) to brownmillerite. However, even with the help of selective dissolution [17], it was not possible to characterise this phase in terms of its chemical composition, its precise structure or of its location in the microstructure.

TEM examination has allowed the resolution of this problem. It reveals that the "ferrite" regions can contain two phases: one phase has the structure of brownmillerite. TEM diffraction patterns suggest that the second is a perovskite-type phase. The ferrite regions can be monophase regions of either the brownmillerite or the perovskite phase types or they can consist of fine lamellae of both phases as shown in Figure 2.

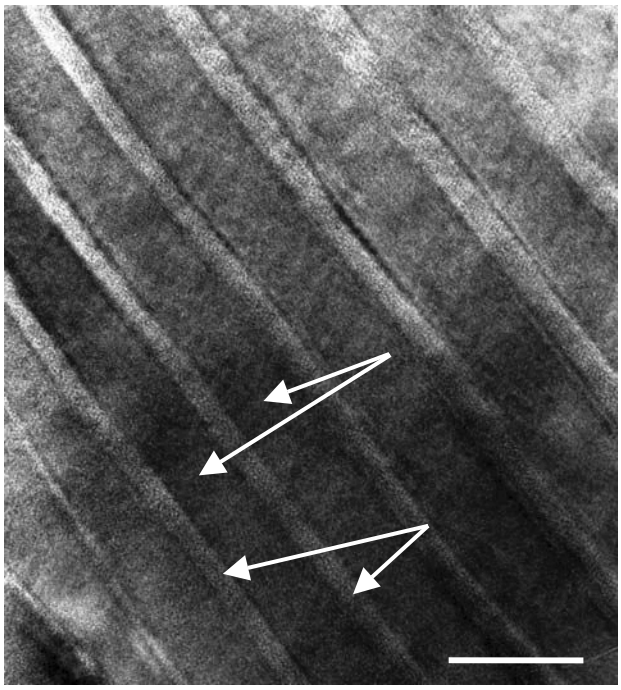

Figure 2. "Ferrite" observed by TEM. Area with lamellae,
Brownmillerite layers of 40 nm separate Perovskite layers with 10-nm thickness.

The ferrite domains were analysed by both SEM and TEM, the (Fe+Al) versus (Ti+Si) content of these analyses are shown in Figure 3. This indicates that there is good agreement between the two

sets of analyses, although it is not possible to differentiate between the three types of assemblage in the SEM.

With TEM it is possible to verify the crystal structure associated with different compositions. At low titanium content, only brownmillerite is present. For intermediate Ti levels, perovskite appears in lamellae. For the highest Ti contents only perovskite is present. The levels of Si substitution tend to vary in the same way, but less consistenly. This suggests that the presence of titanium, and maybe silicon, in solid solution stabilise the perovskite type phase.

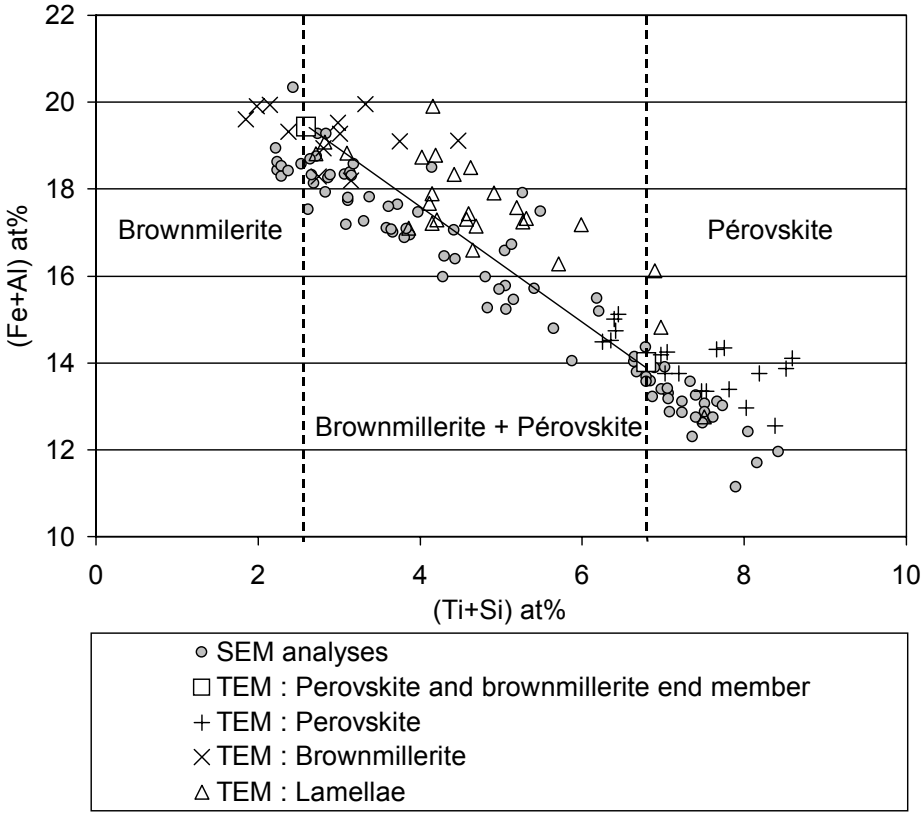

Figure 3. Composition of "ferrite" regions, by SEM and TEM.

Similar layered microstructures have been already reported in previous studies on brownmillerite/perovskite or TiO_2 systems [18,19]. Although more investigations would be needed to confirm the mechanism, this structure probably results from the decomposition of a single high temperature phase into the two phases as described in ref. 19 for a series of perovskite related structures. The crystal structures of perovskite and brownmillerite are closely related. In perovskite, of ideal composition ABO_3, layers of octahedra share corners. Brownmillerite, $ABO_{2.5}$ can be described on the basis of a perovskite structure where $1/6^{th}$ of the oxygen anion sites are vacant [19]. These vacancies are ordered in chains along the [101] direction of the perovskite lattice or [001] direction of the brownmillerite lattice. This leads to an arrangement made of successive layers of octahedra and tetrahedra (OTOT') along the [010] direction. Figure 4 shows this structural relationship in the plane of tetrahedra.

This transformation from the unique high temperature phase to the perovskite/brownmillerite lamellae mixture would in this hypothesis occur by an order/disorder transition of oxygen vacancies with an adjustment of their concentration. The latter would occur through solid state diffusion, which is possible only on a short scale, hence the fine lamellae. The presence of Ti^{4+} and Si^{4+} favour a lower content of oxygen vacancies and hence the perovskite type structure. It is also found that both phases are non-stoichiometric in oxygen; the perovskite having a deficit and the brownmillerite an excess.

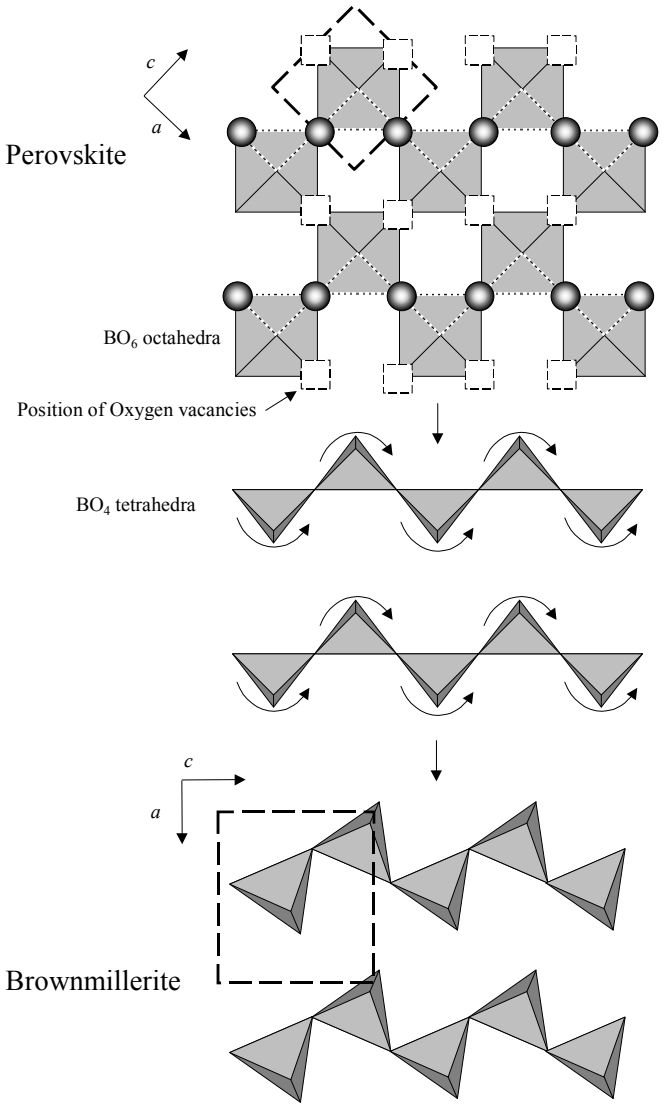

Figure 4. Illustration of the structural relation between perovskite and brownmillerite (simplified)

3.4 Silicates

TEM analyses of dicalcium silicate indicate a low level of substitution of silicon by aluminium and iron. No other impurities were detected in this phase. Analyses in the SEM indicate higher levels of Al and Fe. This difference results from a matrix effect for the SEM analyses, where the interaction volume of the electron beam is broader and the analyses include contributions from the adjacent phases.

Gehlenite and pleochroite are the two other silicates present in CAC. TEM studies on synthetic samples [20,21] indicate that these two phases show intergrowth on the nanometric scale (similar to the biphasic areas of brownmillerite and perovskite). This explains why it was difficult to identify these two phases unambiguously in the SEM microstructure. SEM microanalyses of gehlenite regions gave more trivalent cations than expected from the ideal composition ([A+F]/S ~ 1.5 instead of 1). This is consistent with previous studies [22,23], which suggested that the phase in CAC is actually a solid solution between C_2AS-CA_2–C_5A_3, with complex crystallographic site exchange. In this study, no detailed observations of gehlenite and pleochroite were made in the TEM.

Pleochroite (sometimes referred to as Q phase or fibres) is generally accepted to form when there is some reduction of the iron in the melt, from Fe^{3+} to Fe^{2+}. Its crystallographic structure is similar to the quaternary phase $Ca_{20}Al_{32-2n}Mg_nSi_nO_{68}$ [23]. The SEM measurements performed in this work give an average formula computed for 68 oxygen atoms of $Ca_{19.6}Al_{23.6}Fe_{4.0}Mg_{0.6}Si_{2.6}O_{68}$. This is close to the composition established by Sourie *et al*. [21], except for MgO that was absent in the composition studied by these authors. However, the MgO measured in the present investigation is lower than that reported in other studies [14]. This element does not appear as a major constituent of pleochroite. The substitution mechanism that leads to the chemical composition and structure of pleochroite in Fondu from the parent quaternary phase has not been completely solved.

3.5 Minor phases

The only other phase found in this clinker had a spinel structure, AB_2O_4. This phase contains most of the MgO present in the clinker as there is very low substitution of this oxide in pleochroite or in any of the other phases. The chemical analyses indicate a solid solution between two spinel type compositions: $MgAl_2O_4$ and (Ca, Fe^{2+})/$Fe^{3+}{}_2O_4$. The $Fe^{2+}/\Sigma Fe$ ratio of 0.3 estimated by EELS in the TEM is consistent with this interpretation. The Mg/Al and (Fe^{2+}+Ca^{2+})/Fe^{3+} ratios are close to the theoretical value 1/2. There is also a low level of manganese in the structure which could correspond to a third spinel: $Mn^{2+}Mn^{3+}{}_2O_4$. SEM Microanalyses (as well as TEM [2])carried out on the spinel grains show a strong correlation between (Mg+Al) and (Ca+Fe+Mn) content, which further strengthens the idea of a ternary solid solution.

No other phases were found in the clinker studied here. It has been suggested that magnesio-wüstite (Mg,Fe^{2+})O can occur in this type of cement. The iron-containing phases present will depend on the degree of reduction of Fe^{3+} to Fe^{2+}, which in turn depends on the clinkering atmosphere. In the pure iron - oxygen system, one moves from Fe_2O_3, through Fe_3O_4, FeO and finally Fe as the oxygen partial pressure is reduced. This is shown schematically in Figure 5. In the more complex system found in CAC clinker, this sequence is replaced by overlapping zones of brownmillerite, perovskite, pleochroite, spinel, Mg-wüstite. In extreme conditions even Fe-metal could be formed.

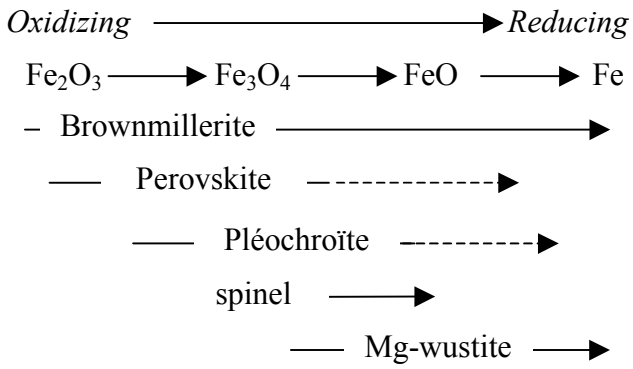

Figure 5. Sequences of Fe-compound as a function of the clinkering condition. Estimation of the stability domains of CAC iron containing phases with respect to the Fe-compounds.

3.6 Quantitative XRD-analysis

The clarification of the phases present in CAC and of their chemical composition makes it possible to further improve the phase quantification by Rietveld analysis. The suggested phase composition of the CAC clinker examined here is CA, $C_{12}A_7$, gehlenite, pleochroite, dicalcium silicate, spinel, brownmillerite and the perovskite type phase. The quantification of a cement of similar composition is shown in Figure 6.

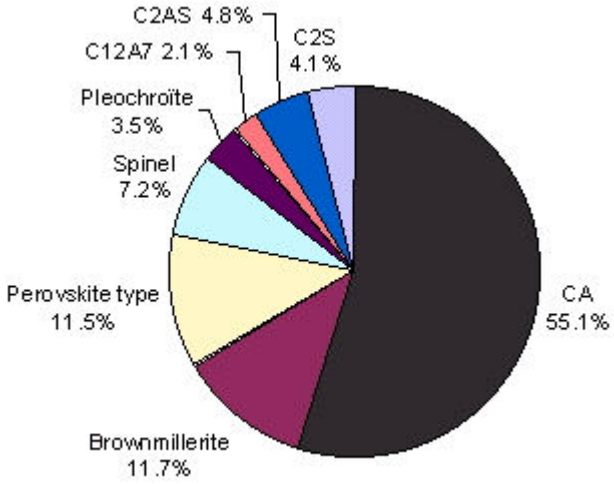

Figure 6. Quantitative Rietveld phase analysis of a standard grade CAC

To test the precision of the Rietveld method for such cement compositions, mixtures of defined amounts of synthetic produced phases $CA_{0.95}F_{0.05}$, $C_2A_{0.9}F_{0.1}S$, $C_4A_{0.5}F_{1.23}T_{0.54}$, CT, $MA_{0.15}F_{0.85}$, CaO, $C_{20}A_{13}M_3S_3O_{68}$, and $C_{12}A_7$.were made. This phase composition of the mixture was close to that of the cements. The samples were prepared and X-rayed ten times. The actual weight of the phases, calculated average amounts and the standard deviations are given in Table 2:

Table 2. Quantitative Rietveld phase analysis of a defined mixture of the synthetic phases $CA_{0.95}F_{0.05}$, $C_2A_{0.9}F_{0.1}S$, $C_4A_{0.5}F_{1.23}T_{0.54}$, CT, $MA_{0.15}F_{0.85}$, CaO, $C_{20}A_{13}M_3S_3O_{68}$, and $C_{12}A_7$. (wt.-%)

Phases	Weight in	Calculated composition (average)	Standard deviation
$CA_{0.95}F_{0.05}$	62.2	63.4	±0.3
$C_2A_{0.9}F_{0.1}S$	3.2	3.0	±0.2
$C_4A_{0.5}F_{1.23}T_{0.54}$	16.2	16.6	±0.3
$MA_{0.15}F_{0.85}$	4.8	3.9	±0.1
CaO	1.5	1.7	±0.2
CT	7.0	6.7	±0.2
$C_{20}A_{13}M_3S_3$	3.4	3.2	±0.1
$C_{12}A_7$	1.7	1.5	±0.1

A comparison of the oxide composition calculated from the Rietveld phase analysis with that measured directly by XRF for the same sample is shown in Figure 7. There is a generally good agreement between the results. XRD and Rietveld analysis can be done very quickly and is adaptable for routine use.

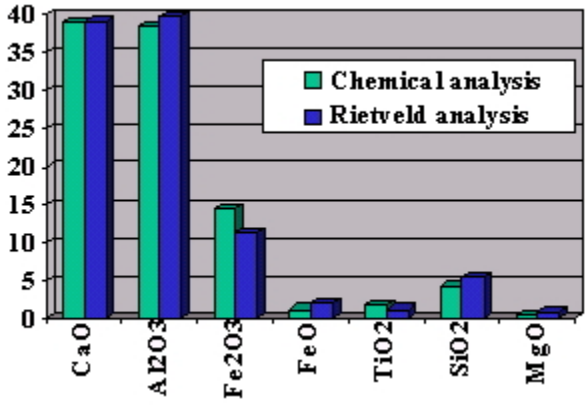

Figure 6. Comparison of the Rietveld analysis with chemical analysis

4. CONCLUSIONS

The low alumina CAC studied in this work contains eight phases. CA is the predominant compound. Its proportion, as measured by Rietveld, is around 55%. The other phases present in significant amounts (about 10%) are the two phases that are included in the domain previously assigned to ferrites. The first is the traditional brownmillerite, while the second could be called ferro-perovskite as it has a perovskite type crystalline structure and has a chemical composition close to the brownmillerite. Cross analyses by TEM and SEM observations, and X-ray diffraction have allowed identification of this latter phase. With the development of the Rietveld method for the analysis of clinkers, the detailed knowledge of this phase is of considerable importance.

This phase is unlikely to have an impact on the hydraulic activity of low alumina CAC clinkers. The iron-bearing phase shows negligible reactivity in these systems at early ages. Besides theses main phases, $C_{12}A_7$, gehlenite, pleochroite, dicalcium silicate and spinel have been characterised.
The improved knowledge of phase composition and element partition contributes to the understanding of the relationship between chemical composition and mineralogy and to the optimisation of CAC's of this type.

REFERENCES

[1] Calleja, J. Calculation of hypothetically possible potential compositions of high alumina cements, Proceedings of the 7th International Congress on Cement chemistry, Paris, Vol. 3, 1980, pp. 102-107.

[2] Gloter, A. Etude de l'état chimique du fer et de la structure à l'échelle nanométrique d'oxydes cimentiers par spectroscopie des pertes d'énergie d'électrons et microscopie électronique en transmission, PhD thesis, University of Paris-Sud, Centre d'Orsay, 2000.

[3] Gloter, A. Ingrin, J. Bouchet, D. Scrivener, K. L. Colliex, C. TEM evidence of perovskite–brownmillerite coexistence in the $Ca(AlxFe_{1-x})O_{2.5}$ system with minor amounts of titanium and silicon, Phys. Chem. Minerals vol.27, 2000, pp. 504-513.

[4] Rietveld, H. M. A profile refinement method for nuclear and magnetic structures. J. Appl. Cryst., vol.2, 1969, pp. 65-71.

[5] Malmros, G. Thomas J. D. Least squares structure refinement based on powder film intensity data. J. Appl. Cryst., vol.10, 1977, pp. 107-111

[6] Young, R. Mackie, D. B. von Dreele, R. B. Application of the patter-fitting structure refinement method to X-ray powder diffractometer patterns. J. Appl. Cryst., vol.14, 1977, pp. 262-269.

[7] Füllmann, T. , Walenta, G. Bier, T. Espinosa, B. Scrivener, K. L. Quantitative Rietveld phase analysis of calcium aluminate cements, World Cement, vol.6, 1999, pp. 91-96.

[8] Colville,, A.A. Geller, S. The crystal structure of Brownmillerite, Ca_2FeAlO_5, Acta Cryst., Vol.B27, 1971, pp. 2311-2315.

[9] Hansen, W.C. Brownmiller, L.T. Bogue, R.H. Studies on the system calcium oxide–alumina–ferric oxide, J. Am. Chem. Soc., vol.50, 1928, pp. 396-406.

[10] Guirado, F. Gali, S. Chinchon,S. "X-ray profile analysis of $Ca_2Fe_{2-x}Al_xO_5$ solid solutions", World Cement,vol.12, 1996, pp.73-76.

[11] Bergstrom, T.B. Hall, C. Scrivener, K.L. Interstitial material in oilwell cement: evidence from X-ray microanalysis, Adv. Cem. Res., vol.4, 1991, pp. 141-147.

[12] Richardson, I.G. Hall, C. Groves, G.W. TEM study of the composition of the interstitial phase in an oilwell cement clinker, Adv. Cem. Res., vol.5, 1993, pp. 15-21.

[13] Jeanne, M. Etude de ciments alumineux industriels à la microsonde électronique, Revue des Matériaux de Construction pour Travaux Publics, vol.629, 1968, pp. 53-58.

[14] Scrivener, K.L. Capmas, A. Calcium aluminate cements, in P.C. Hewlett (ed), Lea's Chemistry of Cement and concrete, 4th edition, Arnold, London, 1998, pp. 709-778.

[15] Walenta, G. Synthesen und Rietveld – Verfeinerungen der Einzelphasen von Tonerdezementen", PhD thesis, University of Erlangen, 1997.

[16] Füllmann, T. Quantitative Rietveld-Phasenanalyse von Tonerdezementen, PhD Thesis, University of Erlanger, 1997.

[17] Motzet, H. Poellmann, H. Quantitative phase analysis of high alumina cements, Proceedings of the International Conference on Cement Microscopy, Guadalajara, Mexico, 1998, pp. 187-206.

[18] Marinho, M.B. Glasser, F.P. Polymorphism and phase changes in the ferrite phase of cements induced by titanium substitution, Cem. Conc. Res., vol.14, 1984, pp. 360-368.

[19] Smyth, D.M. Defects and order in perovskite-related oxides, Ann. Rev. Mater. Sci., vol.15, 1985, pp. 329-357.

[20] Sourie, A. Mineralogy of aluminous cements and their reactivity, PhD Thesis, University of Aberdeen, 1991.
[21] Sourie, A. Glasser, F.P. Lachowski, E.E. Microstructural studies on pléochroïte, Br. Ceram. Trans., vol.93, 1994, pp. 41-48.
[22] Scrivener, K.L. Taylor, H.F.W. Microstructural development in pastes of a calcium aluminate cement, in Calcium aluminate cements, R.J. Mangabhai (Ed), E. & F. Spon, London, 1990, pp. 41-51.
[23] Sourie, A. Glasser, F.P. Composition of melilites crystallised from $CaO–Al_2O_3–Fe_2O_3–SiO_2$ melts, Br. Ceram. Trans., vol.92, 1992, pp. 152-154.
[24] Hanic, F. Handlovic, M. Kapralic, I. Studies of the $C_3A–CA–MS$ Section of the $CaO–MgO–Al_2O_3–SiO_2$ quaternary system, Acta Cryst., vol.36, 1980, pp. 2863-2869.

PROPERTIES OF WHITE CEMENT WITH REDUCED CONTENT OF TRICALCIUM ALUMINATE

L.I. Sycheva and O.V. Ostapchuk

Mendeleev University of Chemical Technology**,** Moscow, Heroev Panfilovtsev st., 20, Russia.
E-mail: sivkov@rctu.ru

ABSTRACT

White cements with reduced contents of tricalcium aluminate were obtained. The raw mixtures for obtaining of such cement had a high saturation factor and silica modulus, as well as a small content of a clay constituent, that made them to be difficultly sintered. For intensification of processes of mineral formation high-activity silica constituent was added to a raw mixture, that allowed to reduce temperature of a burning of white clinker. The content of tricalcium aluminate (C_3A) in experimental clinker was reduced to 3 - 9 %, against 13-15 % in ordinary white clinker.

The cements with the reduced content of C_3A had high hydration activity, stability to effects of aggressive media and good frost resistance.

1. INTRODUCTION

White Portland cement (WPC) is a material with high operation properties, based on which it is possible to obtain coloured cements and concretes simulating a natural rock as well [1]. Despite its high aesthetic and construction-technical properties, a white Portland cement has a low resistance to corrosion, that does not allow it to be utilized widely in building and reduces its potential market ability.

One of the factors determining a low corrosion resistance of white cement, is the higher content in it of tricalcium aluminate. At the hydration of Portland cement, the interaction of C_3A with water results in cement paste containing large quantities of metastable calcium hydroaluminates along with ettringite. Further they chemically react with anions of SO_4^{2-}, existing in corrosive media, with the formation of additional amounts of ettringite late in the hydration, that results in destruction of cement paste and decrease of its strength [2]. Thus, one way to increase the corrosion resistance of white Portland cement is to decrease the content of tri-calcium aluminate in it.

2. EXPERIMENTAL

For analysis of impact of the content of C_3A on properties of white Portland cement, clinkers were produced, having the following parameters: the values of lime saturation factor (L.S.R.) was varied from 0.90 up to 0.94, and the content of tricalcium aluminate from 3 up to 9 % (Table 1).

To obtain white Portland cement clinker the most pure raw materials were utilized with minimum amounts of painting oxides: white limestone, clay, sand. The content of the clay component in the raw mixture was reduced.

As the raw mixture for production of WPC is difficultly sintered because of high indexes of L.S.R., silica modulus (SR), alumina modulus (AR) and a small content of Fe_20_3, the temperature of a burning of white Portland cement clinker is usually 1500-1550 ^oC. For mineralization of a raw mixture and the decrease of temperature of a burning a part of sand was substituted by a waste of chemical production – silica gel.

Table 1. Modulus and mineralogical composition of studied clinkers

No	Modulus at L.S.R. = 0.92		Calculated mineral content, mass.,%				Factual* mineral content, mass., %			
	SM	AM	C_3S	C_2S	C_3A	C_4AF	C_3S	C_2S	C_3A	C_4AF
1	12.93	2.71	75.7	18.2	3.0	1.6	78.0	18.0	4.0	---
2	8.95	3.82	74.0	17.7	5.0	1.8	79.0	14.0	5.5	---
3	6.79	4.76	72.2	17.3	7.0	1.9	76.0	17.0	7.0	---
4	5.40	5.57	70.5	16.9	9.0	2.1	77.0	14.0	10	---

* Factual mineral content was determined by quantitative XRD

Silica gel represents an amorphous high dispersive silica, in which there are also impurities of alkaline and earth alkaline oxides and fluorides. The presence of impurities, amorphism of structure of silica gel make it a highly reactivity raw material having mineralization action. For intensification of a sintering process a highly reactivity additive of silica gel instead of a part of sand was injected into a raw mixture. The ratio of silica gel to sand (sg/s) was varied from 0 up to 1,0 in raw mixture. It was supposed, that the usage of silica gel would allow to decrease the viscosity of a clinker melt and intensify process of clinker formation.
Clinker were synthesized in a laboratory furnace at 1450 ^0C.

Temperature of decarbonization of $CaCO_3$ increased by 20-30 ^0C as the content of clay in a raw mixture decreased. On the other hand introducing of silica gel in a raw mixture resulted in a decrease of temperature of decarbonization of $CaCO_3$ and formation of C_2S and C_3S by 20-30 ^0C. The change of temperature of decarbonization was fixed by DTA of raw mixes.

The resultant fluid phase at sintering of white clinker is mainly represented by a highly aluminate melt. The increase of a clay component in a raw mixture leads to an increase of amount of a fluid phase when clinker burning and, as a consequence, an increase in its shrinkage. When silica gel is added, shrinkage of clinker increases by 2-4 % on the average (Table 2).

Table 2.Clinker shrinkage at sintering of raw mixture

Parameters of raw mixture C_3A-L.S.R. - sg/s	Shrinkage*, % Burning temperature, ^oC			Parameters of raw mixture C_3A-L.S.R. - sg/s	Shrinkage*, % Burning temperature, ^oC		
	1400	1450	1500		1400	1450	1500
3-0.9 0-0.0	6.3	7.1	7.9	9-0.90-0.00	11.5	13.0	13.6
3-0.90-0.25	6.5	8.2	8.3	9-0.90-0.25	12.6	14.6	14.9
3-0.90-0.50	8.7	9.0	9.3	9-0.90-0.50	13.6	15.5	15.7
3-0.92-0.00	6.6	9.3	9.9	9-0.92-0.00	14.5	17.0	17.8
3-0.92-0.25	7.1	10.8	11.3	9-0.92-0.25	17.1	18.8	19.3
3-0.92-0.50	9.3	11.8	12.3	9-0.92-0.50	18.8	21.0	23.1

* Shrinkage of samples was determined by the measuring of sample sizes before their sintering and after that. Then the results were calculated in %.

As amount of a clinker melt increases the processes of dissolution CaO and C_2S, defining a rate of alite formation, are speeded up. When a ratio of sg/s in a raw mixture was increased from 0 up to 0.5 content CaO_{free} was reduced from 7.2 up to 2.0 % in clinkers with 3 % C_3A and from 3.3 up to 1.2 % in clinkers consisted of 9 % C_3A. When L.S.R. of raw mixtures and amount of alitee in clinker was increased the role of the additive of silica gel raised (Figure 1).

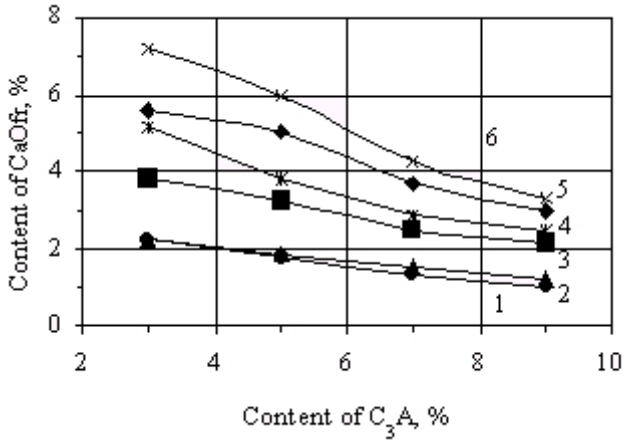

Figure 1. Content of CaO_{free} in clinkers ($T_{burning}$ = 1450 °C).
S.F. – sg/s: 1 - 0.90-0.5; 2 - 0.92-0.5; 3 - 0.90 - 0.25; 4 - 0.92-0.25; 5 - 0.90-0; 6 - 0.92-0.

Thus, in a raw mixture with the reduced content of a clay component, the addition of silica gel has led to more complete binding of lime. Such intensifying action of silica gel is associated with its high activity and presence in it of fluorine-containing compounds, which influence the properties of a clinker melt in turn, namely, reducing its viscosity, and decreasing temperature of decarbonization of limestone and alite formation.

The analysis of a microstructure of clinkers has shown that with increase of the ratio of silica gel to sand in a raw mixture structure sealing of clinker takes place. The porosity of clinker is reduced. The main clinker minerals have an indistinct crystallization, the amount of larger intergrown pieces of alite crystals (Figure 2) is raised.

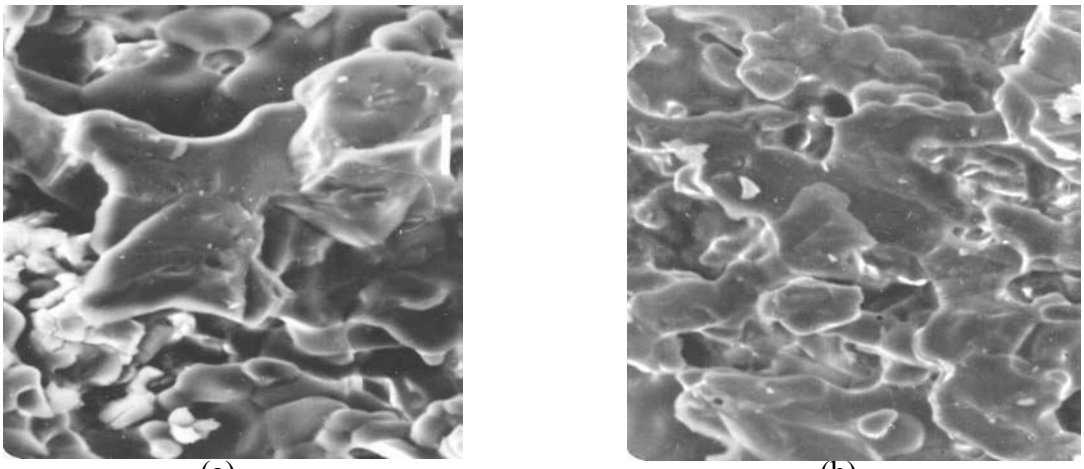

(a) (b)

Figure 2. The microstructure of white clinker obtained with the additive of silica gel . The content of C_3A is equal to 9 % (a) and 3 % (b). Magnification 1000^x.

Grindability of experimental clinker consisted of C_3A equal to 9 % and ordinary clinker which had a C_3A content of 13 % were determined. Grindability was assessed by the residue on an 80 μm

sieve and by specific surface area (s.s.a.). The experimental clinker with the smaller content of C_3A is more easily ground than the ordinary one. It is explained by the fact that at a burning of a raw mixture with the small content of a clay component an amount of a forming clinker melt is less than for burning of ordinary raw mixture. The experimental clinker contains a smaller amount of glass phase, which is more difficult to grind. Its structure is more porous and friable. Besides, the minerals of clinker obtained in the presence of fluorine-containing additive, have defect structure and is more easy to grind (Figure 3).

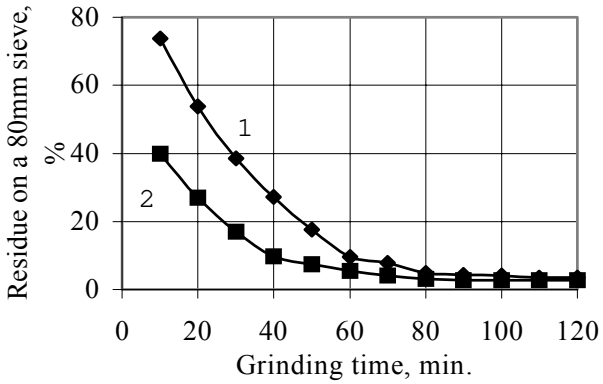

Figure 3. Grinding of white clinkers: ordinary one (1) and clinker with reduced content of C_3A (2).

The study of impact of C_3A on construction-technical properties of white cement was carried out on cements obtained by joint grinding of laboratory synthesized clinkers with the addition of gypsum (2 % by SO_3) up to specific surface area equal to 340-380 m^2/kg.

The various content of C_3A did not render appreciable impact on normal consistency and setting time of investigated cements. The normal consistency was varied in the range from 28 to 29 %, and setting time in the order: a beginning - 45 - 60 min., end – 1 h 45 min. – 2 h 10 min (Table 3).

Table 3. Construction-technical properties of cements

The content of C_3A, %	S.s.a., m^2/kg	W/C, %	Setting time, min		Compressive strength*, MPa			
			beginning	end	3 days	7 days	14 days	28 days
3	380	28	60	130	51	57	59	60
5	355	28	55	120	57	62	66	69
7	350	29	50	112	61	64	73	75
9	342	29	45	105	69	72	77	79
14 (ordinary cement)	340	29	35	90	48	51	57	67

* strength of cement paste samples (without sand)

It is well known that the rate of hydration of cements depends both on alite and tri-calcium aluminate contents. The introduction of the additive of silica gel in a raw mixture while obtaining of white clinker influenced its hydration activity as well. The extent of a hydration of cements with C_3A equal to 9 % obtained without the addition of silica gel and with the substitution of a part of sand by silica gel, for 3 days of hardening was increased from 40 up to 53 %, and for 28 days - from 63 up to 69 %, accordingly. It is caused by greater imperfection of the crystalline structure of clinker and its minerals obtained with the additive of silica gel. Under a decrease of the content of C_3A up to 3 % the extent of a hydration of cement was increased and has comprised 64 and 78 % at 3 and 28 days of hardening, respectively.

As the content of C_3A in white cement increased from 3 up to 9 % its strength increased by 25 % on the average. When further increase of the content of C_3A took place the strength of cement has decreased.

It is well known that one of the reasons for a low stability to corrosion of cements is the higher content of calcium aluminates in them. Stability of cements to aggressive media and frost resistance were instituted on samples from paste previously hardening during 14 days in aerial - wet conditions.

As aggressive media 1 - 5 % solutions of $MgSO_4$, Na_2SO_4 and seawater were chosen, as they render most strong corrosive attack on cement paste.

Strength of cement, stored in aggressive media, was reduced as concentration of solution and content of C_3A in cement increase. So for cement with the content of C_3A equal to 3 % the decrease of strength concerning the standard samples has comprised - 6 % after 60 days of hardening in seawater, in solution of Na_2SO_4 - 11 % and in solution of $MgSO_4$ - 18 %. The cements with the contents of C_3A equal to 9 % at storage in aggressive media have lowered strength by 10, 15 and 21 %, accordingly. The extent of affecting of aggressive media was increased for white cement in an orderly sequence: seawater - Na_2SO_4 - $MgSO_4$.

The white cements are more subject to corrosion in environment of $MgSO_4$, because under its effect a breaking down occurs of hydroaluminates and calcium hydrosilicates as well.

The frost resistance of white cements with the various contents of C_3A was determined. The trials were conducted in rigorously controlled conditions on samples based on cement paste without sealing. After 35 cycles of freeze-thawing samples of ordinary white cement (14 % C_3A) were completely destroyed. Samples with the content of C_3A equal to 3 and 9 % after 60 cycles of freeze-thawing did not change their strength in comparison with standard samples. The reason of low frost resistance of cements with higher contents C_3A is the additional ettrigite formation late in the hydration. Products of hydration of tricalcium aluminate are ettringite, monohydrosulphoaluminate and hydroaluminates of calcium. As composition of a fluid phase varies at hardening of cement ettrigite partially transfers in calcium monohydrosulphoaluminate of calcium. The gypsum formed at transferring of the trisulphate calcium hydrosulphoaluminate in the monosulphate form, interacts with hydroaluminates of calcium, resulting in destruction of cement paste.

Based on laboratory studies the batch of white cement (L.S.R. 0.91; C_3A 5 %) was produced in an industrial kiln. Production of white cement with lower content of C_3A has allowed to diminish the consumption of a clay component in 1,8-2,0 times. Despite of high silica modulus of a raw mixture the formed clinker was well sintered and had not the high content CaO_{free} (0,5-1,5 %). Consumption of fuel rate has decreased. The clinker was more easily ground, raising the output of the grinding mills. The activity of experimental clinker was by 2-4 MPa above.

The experimental white cement with reduced content of C_3A was tested in concretes. Based on the given cement it is possible to obtain vibrocompressed and heavy-weight concretes of classes B 30 - B 45, having the type of frost resistance no less than F 200.

3. CONCLUSION

By the reduction of the clay content and the use of the high dispersed silica component instead of part of the sand in raw mix, it is possible to produce a white highly active cement. Because its corrosion and frost resistance also increases, the potential areas of application for this cement becomes far wider.

REFERENCES

[1] Lea, F.M. The Chemistry of Cement and Concrete, New York: Chemical Publishing Company, Inc., 1971, 365 p.
[2] Taylor, Y.F.W. Cement Chemistry, London: Academic Press, 1990, 475.

SOME TECHNOLOGY FACTORS INFLUENCING THE QUALITIES OF HIGH SULFATE RESISTANT WELL CEMENT

Zinovi B. Entin[1], Serge P. Sivkov[2] and Alexandr P. Osokin[2]

[1] ZAO "Scientific & Research Center", Moscow, Russia.
[2] D. Mendeleev University of Chemical Technology of Russia, Moscow, Russia.
E-mail: sivkov@rctu.ru

ABSTRACT

As already determined, manufacture of high sulfate resistant well cement with stable plugging qualities will need cement clinker based on raw material containing appropriate quantities of crystal silicon dioxide SiO_2. Such raw mixtures have high reacting capacity in comparison with mixtures based on pure or high siliceous limestone and allow the production of high quality well cement.

1. INTRODUCTION

Manufacturing of high sulfate resistant well cement is complicated not only because of strict requirements regarding the chemical and mineralogical composition of the cement, but also because of the necessity to ensure that the compound exhibits of its physical and mechanical qualities – the so called plugging qualities.

According to API Spec 10A (ISO 10426-1) the content of C_3A in high sulfate resistant well cement should not exceed 3 mass. %, C_3S content should not be less than 48 and not more than 65 mass. % and the sum of minerals $2C_3A+C_4AF$ not more than 24 mass. %. Such cement can be produced only when limestone (used as raw material), has the desirable SiO_2 content or a special correcting component with a high level of silicon dioxide added. The difference in reacting capacity of raw materials composed of components of a different nature, influence the qualities of clinker greatly and thus the qualities of the oil well cement produced.

2. EXPERIMENTAL

To manufacture well cement clinker, three raw mixes were taken with close modulus characteristics: saturation coefficient 1.01, alumina ratio p 0.70 and silica ratio n 2.02-2.05.

The raw mix 1 has been prepared on the basis of pure limestone (SiO_2 content in the limestone 0.89 mass. %) and of large quantity (~ 9 %) of correcting component - siliceous schist with SiO_2 content of 86.54 mass. %. Raw mix 2 has been prepared on the basis of limestone with moderate SiO_2 content (4.28 mass. %) and small quantity (~ 2.6 %) of correcting component. Raw mix 3 has been fully composed on the basis of limestone with high SiO_2 content (12.47 mass. %).

All the raw mixes were ground under the same conditions, then burned at the temperature of 1420 C^0 for 5, 10, 15, 20 and 30 minutes. In the burned mixes measures were taken of the general level of calcium oxide assimilation α_1, as well as the level of CaO assimilation during the formation of calcium silicates C_2S+C_3S α_2 and separately the same of the mineral C_3S α_3. The computation was done using the formulas:

$$\alpha_1 = 1 - \frac{C_{free\,\tau}}{C_{total}} \quad (1)$$

$$\alpha_2 = 1 - \frac{C_{free\,\tau}}{C_{total} - (1{,}65A + 0{,}35F)} \quad (2)$$

$$\alpha_3 = 1 - \frac{C_{free\,\tau}}{C_{total} - (1{,}87S + 1{,}65A + 0{,}35F)} \quad (3)$$

where C_{total}, S, A and F - content of corresponding oxides in the composition of the raw mix (calculated as ignited matter), and $C_{free\,\tau}$ - content of free calcium oxide in the mix at the moment τ.

The computation of the clinker formation process was made following the Erofeev-Kolmogorov equation:

$$\alpha_i = 1 - exp(-k \cdot \tau^n) \quad (4)$$

where k - constant of chemical reaction rate, min $^{-1}$, τ - isothermal burning time, min, and n - the constant showing the stage limiting the process rate: when $n > 1$ the limiting stage is chemical reaction rate, when $n < 0{,}5$ - diffusion rate, and when $0{,}5 < n < 1$ the clinker formation process is going in the transition tract.

3. RESULTS AND DISCUSSION

The results of computation of k and n parameters of reaction kinetics equations are presented in Table 1.

Table 1. Kinetics process equation parameters

Process	Raw mix	k, min^{-1}	n
General reaction	1 2 3	0,407 0,525 0,472	0,530 0,536 0,530
C_2S+C_3S Formation	1 2 3	0,3165 0,4382 0,4012	0,562 0,577 0,550
C_3S Formation	1 2 3	0,00015 0,00329 0,00018	2,534 1,909 2,692

In accordance with the results obtained, the raw mixes can be ranged in the following order according to their reacting capacity:

Raw mix 2 > Raw mix 3 > Raw mix 1

The meaning of the n parameter shows that the general clinker formation process and the process of calcium silicate synthesis C_2S+C_3S are taking place in the transition area and the rate of the process of mineral C_3S synthesis is limited by the rate of the chemical reaction. At the same time the higher n_1 and n_3 meanings in comparison with the parameter n_2 point to the lower reacting capacity of the chemical reaction components, depending on the presence in the mixes 1 and 3 of considerable

amount of a crystalline silicon dioxide. This conclusion is confirmed by the results of X-ray and differential-thermal analysis, as well as by the results of particle size distribution of the initial raw mixes studies: the presence in the mixes 1 and 3 of high quantity particles measuring 180-240 micrometers, points to the presence of difficult to crush crystalline quartz particles.

The clinker produced by burning of raw mix 2 is characterized by more profoundly completed clinkergenerating process. Its content of C_3S mineral determined by X-ray quantity method corresponds to estimated values, though in the mixes 1 and 3 it is 2 - 3% lower than estimated.

There were marked visible differences in the microstructure of the clinkers. Crystallization of the principal clinker minerals in the clinker based on mix 2 is more distinct, though in the clinkers based on mixes 1 and 3 there are wide agglomerations of badly formed belite crystals and alite crystals often having defective forms.

To determine the influence of reacting capacity of the raw mix on the quality of clinker and well cements of G and H classes it was necessary to previously determine the meanings of the cement parameters - specific surface and SO_3 content, under which the requirements of technical specifications of API Spec 10A for these cements are met.

With this in mind, 25 cements manufactured with the above clinkers were ground in a laboratory mill to the specific surface of 270 - 410 m^2/kg and SO_3 quantity of 1.6-3,2 mass. %. For all cements thus manufactured, the set of plugging qualities has been determined with water contents of 44 % (class G cement) and 38 % (class H cement).

Using the results received from the binary diagram - specific surface / SO_3 content - there have been traced the lines of qualities corresponding to requirements specified by API Spec 10A - Figure 1(a) and 1(b):

- free fluid content - maximum 5.5 ml;
- consistency 15 - 30 minutes after stirring period - maximum 30 B_c (Bearden units consistency);
- thickening time to 100 B_c - minimum 90 and maximum 120 min.;
- compressive strength after 8 hours of hardening at 38 ^0C (R_{38}) - minimum 2.1 MPa and 60 ^0C (R_{60}) - minimum 10.3 MPa.

The areas where at least one of the specification requirements were not met have been colored gray. It is seen that for class G cement - Figure 1(a), to ensure free fluid capacity of less than 5.5 ml, the cement specific surface must be more than 330 - 360 m^2/kg depending on SO_3 content. The upper acceptable value of the cement specific surface is limited by starting thickening time, and the maximum acceptable SO_3 content - by starting consistency of the cement paste.

For class H cement, as shown in Figure 1(b), the area of acceptable values is limited by free fluid lines (shown in the lower left and the upper right parts of the diagram), the critical thickening time (shown in the lower left part), as well as the starting consistency (shown in the upper left part). With low cement specific surface, which limits the content of SO_3 for this cement, is the standard specification.

The clear part of the diagram shows the sphere of specific surface values and SO_3 content under which this clinker can be used to manufacture the cement corresponding to all the requirements specified by the standard. In the central part of the diagram the spheres of acceptable parameters are marked where the risk to break at least one of the specified requirements has been reduced to a minimum.

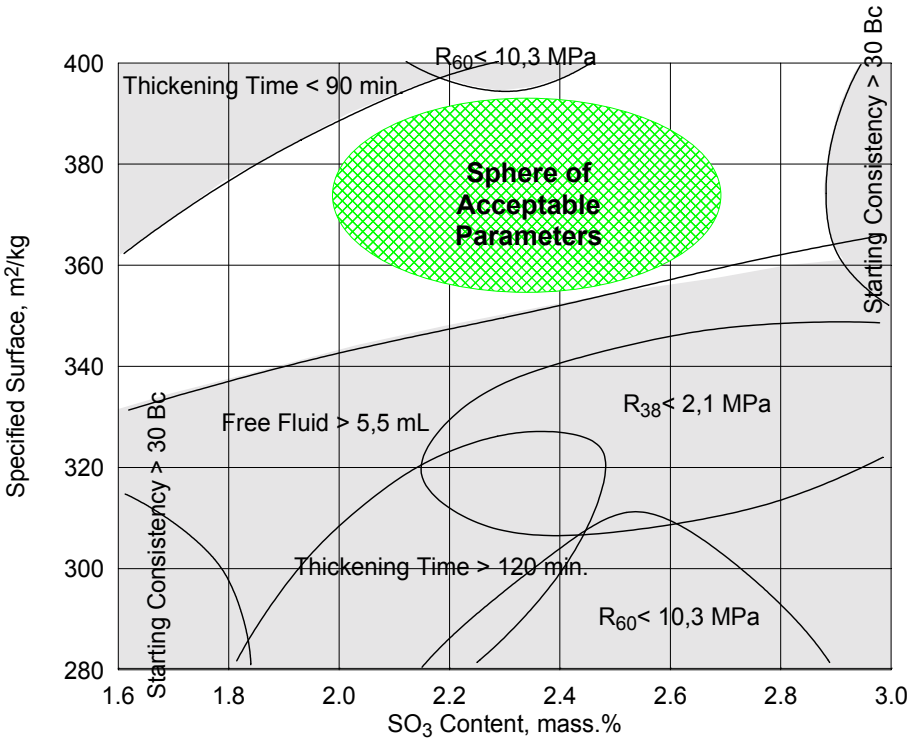

(a)

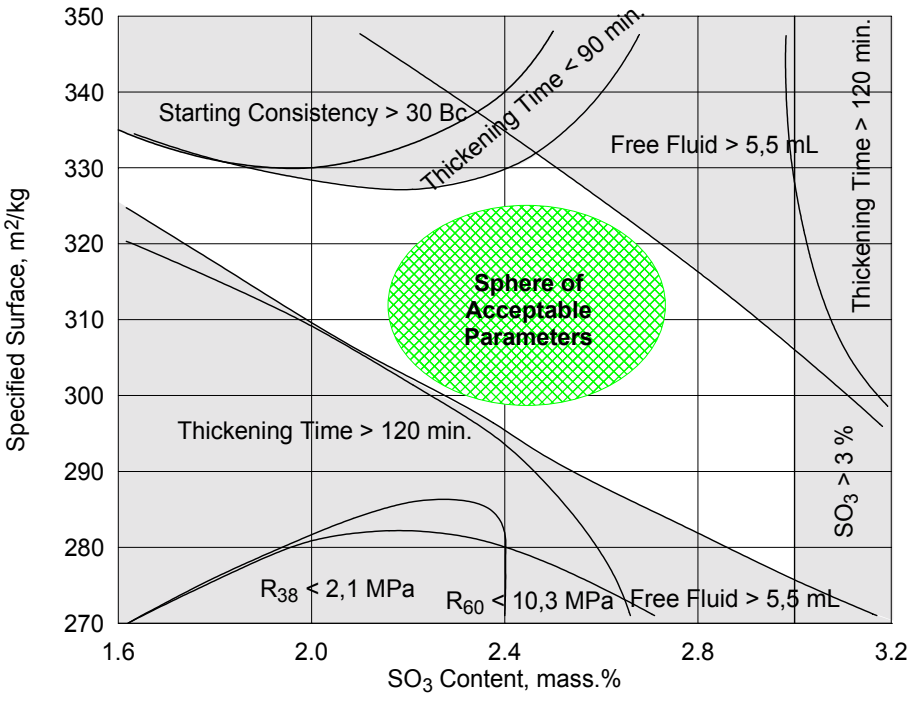

(b)

Figure 1. Areas of acceptable parameters corresponding to requirements specified by API Spec 10A for high sulfate-resistant well cements: (a) Class G; (b) Class H

For class G cements the center of the areas of acceptable parameters will have a specific surface value of 370 m^2/kg and SO_3 content 2.36 mass %. The same acceptable parameters for class H cements will have corresponding specific surface values of 310 m^2/kg and SO_3 2.55 mass %.

The limits obtained for cement dispersion and gypsum content have been used in further research on raw materials' reaction capacities to influence cement qualities.

The qualities of high sulfate resistant oil well cements of G and H classes according to API Spec 10A manufactured from clinkers based on raw mixtures 1, 2 and 3 are presented on Table 2.

Table 2. Cements plugging qualities

Clinker based on raw mix No	Specific surface, m^2/kg	SO_3, mass.%	Free fluid, ml.	Consistency after 15-30 min. stirring period, Bc	Time before consistency 100 Bc, min.	Compressive strength, MPa, 8 hours curing time	
						At 38 ^{0}C	At 60 ^{0}C
Well cement, Class G							
1	373	2,38	3,2	17	105	2,4	11,8
2	375	2,36	2,9	21	100	3,4	14,2
3	371	2,39	2,9	18	100	2,9	13,6
Well cement, Class H							
1	312	2,54	3,3	24	95	3,1	13,7
2	311	2,51	2,8	26	105	3,8	15,4
3	308	2,56	2,9	26	115	3,3	12,6

It is evident that, other things being equal, the cements manufactured from clinker based on raw mix 2 have the highest compressive strength after 8 hours of hardening under the fixed curing temperature. Further research showed that cements based on this raw mixture exhibit more stable plugging qualities that change little during 3 months of cement storage in appropriate packaging.

4. CONCLUSIONS

Raw mix components' reaction capacity influences not only the kinetics of the clinker generating process, but also the quality of manufactured cements. For the production of high sulfate resistant well cements showing stable plugging qualities, it is necessary to use the raw mixtures composed of the components which allow (within the fixed chemical composition), the content of crystalline silica in the raw mix to be minimized.

SOME TECHNOLOGY FACTORS INFLUENCING QUALITIES OF HIGH SULFATE RESISTANT WELL CEMENT

Zinovi B. Entin[1], Serge P. Sivkov[2], Alexandr P. Osokin[2]

[1] ZAO “Scientific & Research Center", Moscow, Russia.
[2] D. Mendeleev University of Chemical Technology of Russia, Moscow, Russia.
E-mail: sivkov@rctu.ru

Short biography of the presenting authors:

Professor Zinovi B. Entin, Vice-director of ZAO “Scientific & Research Center". His research interest is the chemistry and technology of special multi-component cements. He is the author of over 350 research publications.

Assistant Professor Serge P. Sivkov, Senior lecturer in D. Mendeleev University of Chemical Technology in Russia. His research work is concerned with the chemistry and technology of special cements. He is the author of over 85 research publications.

Professor Alexander Osokin is Head of Cement and Composite Material Department at Mendeleev Chemical Technology University in Russia. His research interests are in clinker formation and chemistry of Portland cements. He is the author of over 300 research publications and two books.

STABILITY OF ETTRINGITE UNDER CARBONATE CORROSION AT HYDRATION OF SULPHOALUMINATE CEMENT

Kouznetsova, T.V.[1], Ivaschenko, S.I.[2] Samchenko, S.V.[2]

[1]Mendeleev Chemical Technological University of Russia, Miusskaja sq., 9, Moscow, 125047, Russia, E-mail: sivkov@ rctu.ru
[2]Moscow Institute of Engineering, Srednaja Kalitnikovskaja st., 30, Moscow, 109807, Russia, E-mail: mikxis@cityline.ru

ABSTRACT

In this paper the results of the formation and stability of hydrated phases in the hardened sulphoaluminate cement (SAC) are presented.

The study of the influence of carbonation on the calcium hydrosulphoaluminates shows that AFt is stable in some aggressive mediums. AFm under carbonation is decomposed and ettringite is formed instead of calcium monosulphate.

Influence of carbonate and hydro carbonate ions on crystallization of AFt and AFm is investigated. It is established that at the first stage carbonate phases are crystallized. When all carbonate ions are bonded into hydro carbonate phases and carbonate ions are absent in the liquid phase, ettringite is formed. Similar processes take place in the case of prepared liquid phase to obtain AFm. Instead, ettringite is crystallized.

1. INTRODUCTION

The formation and stability of hydrated phases under the effect of CO_2 and hydro carbonate or carbonate ions in the pores is the actual problem. It is known that carbon dioxide in air or dissolved in water reacts with hydrated phases of cement [1,2]. $Ca(OH)_2$ is more exposed to carbonation than the other phases. According to thermodynamic calculation [3] the reaction of calcium hydroxide and carbon dioxide leads to the formation of $CaCO_3$ and the equilibrium pressure of CO_2 is lower than the partial pressure of CO_2 in air. To indicate a stability of AFt and AFm hydration of calcium sulphoaluminate in the presence of carbon dioxide and carbon ions was studied. Their influence on the formed crystals of AFt and AFm was also investigated.

2. MATERIALS

According to methods [4] $C_4A_3\bar{S}$, hydrated AFt and AFm were prepared for the study. Chemical compositions of the samples are presented in Table 1.

Table 1. Chemical composition of initial materials (%)

Sample	CaO	Al_2O_3	SO_3	Ig.loss
C_4A_3S	36.55	50.32	13.08	0.20
$C_3A3CSH31$ (AFt)	27.2	8.2	19.4	45.2
C_3ACSH_{12} (AFm)	36.1	16.1	12.9	34.9

To study hydration and carbonation, the following methods were used: XRD, IRS, SEM and chemical analysis.

3. EXPERIMENTS AND DISCUSSION

3.1 Thermodynamic analyses of reaction under carbonation

At the first stage of the investigation, the thermodynamic calculation of the probability of interaction of ettringite and calcium monosulphate with carbonate ions was undertaken. Calculations were carried out by the methods described by Babuschkin V.I., Matveev G.M., and Mtchedlov-Petrossian O.P. [3]. According to thermodynamic analysis, calcium monosulphate in the presence of HCO_3^- and CO_2 can be decomposed. In this case the hydrated products are formed as follow as: CAH_{10} , $CaSO_4$, $CaCO_3$, calcium hydrocarboaluminate (CHCA) and gibbsite $Al_2O_3.H_2O$ (Table 2).

Table 2. Results of thermodynamic calculation of the reaction of carbonation

№	Scheme of reaction	ΔG^0_{298}, kJ/mol
1	$C_3ACS_3H_{31} + CO_2 \rightarrow C_3ACaCO_3H_{11} + C_2AH_8 + CaSO_4{\cdot}2H_2O + Ca(OH)_2 + H_2O$	-23,3
2	$C_3ACS_3H_{31} + CO_2 \rightarrow CAH_{10} + CaSO_4{\cdot}2H_2O + CaCO_3 + Al(OH)_3$	+14,5
3	$C_3ACS_3H_{31} + HCO_3^- \rightarrow C_3ACaCO_3H_{11} + C_2AH_8 + CaSO_4{\cdot}2H_2O + Ca(OH)_2 + H_2O$	-15,8
4	$C_3ACS_3H_{31} + HCO_3^- \rightarrow CAH_{10} + CaSO_4{\cdot}2H_2O + CaCO_3 + Al(OH)_3$	-3,9
5	$C_3ACSH_{12} + CO_2 \rightarrow C_3ACaCO_3H_{11} + C_2AH_8 + CaSO_4{\cdot}2H_2O + Ca(OH)_2 + H_2O$	-140,47
6	$C_3ACSH_{12} + CO_2 \rightarrow CAH_{10} + CaSO_4{\cdot}2H_2O + CaCO_3 + Al(OH)_3$	-339,3
7	$C_3ACSH_{12} + HCO_3^- \rightarrow C_3ACaCO_3H_{11} + C_2AH_8 + CaSO_4{\cdot}2H_2O + Ca(OH)_2 + H_2O$	-412,17
8	$C_3ACSH_{12} + HCO_3^- \rightarrow CAH_{10} + CaSO_4{\cdot}2H_2O + CaCO_3 + Al(OH)_3$	-11,2

Table 2 data shows that AFt under carbonation is stable (reaction No.2 has ΔG = +14,5 kJ/mol) and there is thermodynamic probability of the decomposition of Afm (reaction No.6 has ΔG = 339,3 kJ/mol). Reaction takes place at the pressure of CO_2 lower the partial atmospheric pressure that it is need to the beginning of reaction. As thermodynamic calculation shows the probability of reaction only, therefore the experiments of carbonation influence on AFt and AFm were carried out.

3.2 Experimental data on the influence of carbonation on Aft and Afm phases

AFt and AFm were stored in the air for one year. The changes of hydrates were studied by IR-spectroscopy (IRS). Infrared absorption spectra of AFm show strong bands at 1420 and 1480 cm^{-1} due to CO_2 after 9 month of the storage of samples. But, AFt spectra are characterized by weak peaks in abovementioned regions only after one year storage (Figure1).

AFt under water consisting of hydrocarbonate and carbonate ions is stable for 6 months. At the further period crystal edges begin to alter due to the extraction of calcium and aluminium ions

into liquid phase. Up to 9 month the partial crystal destruction is observed. Colourless hexagonal plates with the refractive indices n_o =1.554 and n_e = 1.538 are appeared. After one year storage of AFt crystals in water saturated by carbon dioxide calcium carboaluminate $3CaO.Al_2O_3.CaCO_3.12H_2O$ and a small amount of gibbsite are fixed by XRD (Figure 2).

AFm – phase is less stable to the exposure of hydrocarbonate and carbonate ions. Even in one month of exposure the sample begins to disintegrate. This process is accompanied by the formation of calcium hydro carbonate, gibbsite, calcium aluminates and calcium sulphate. After 3 months of exposure, AFm is destroyed completely and ettringite is crystallized (Figure 3).

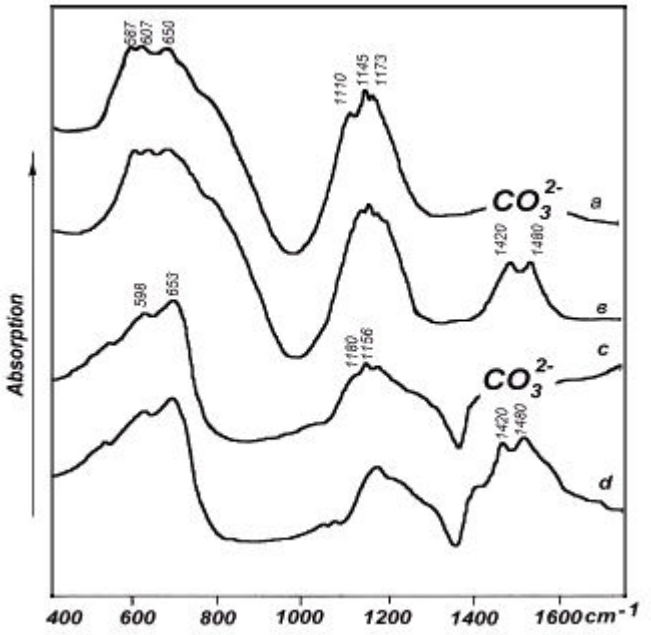

Figure 1. Infrared spectra of the prepared AFt (a), AFm(c) and after their storage during: AFt – 1 year (b), AFm – 9 month (d)

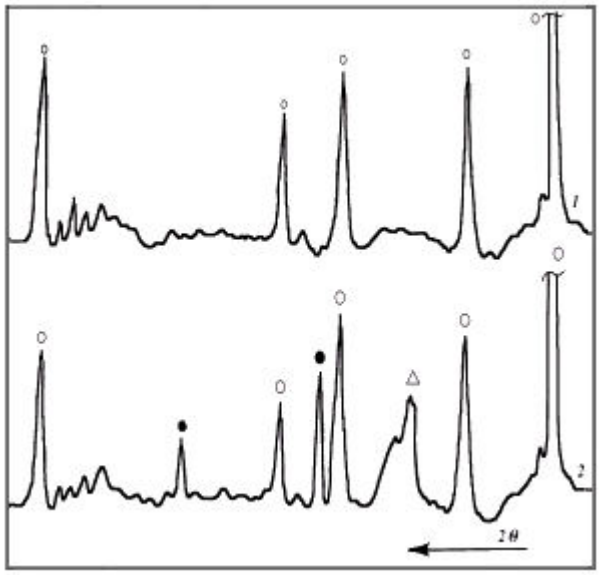

Figure 2. XRD powder diffraction (Cu Kα) of AFt before (1) and after carbonation (2)
Symbol: o – $3CaO.Al_2O_3.3CaSO_4.31H_2O$
Δ - $3CaO.Al_2O_3.CaCO_3.12H_2O$
• - $Al_2O_3.H_2O$

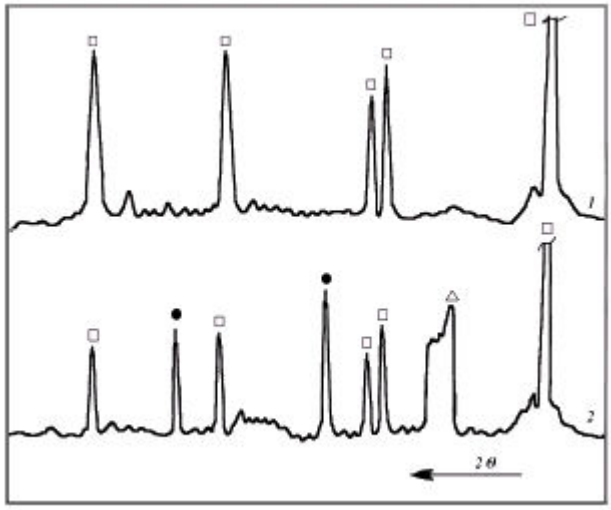

Figure 3. XRD powder diffraction (Cu Kα) of AFm before (1) and after carbonation (2)
Symbol: □ – $3CaO.Al_2O_3.3CaSO_4.31H_2O$
Δ - $3CaO.Al_2O_3.CaCO_3.12H_2O$
• - $Al_2O_3.H_2O$

Recrystallization of AFm into AFt leads to the destruction of the samples due to their difference in sizes and the morphology of crystals.

It was noticed that crystallization of AFt and AFm from a solution saturated by HCO_3-ions is difficult because Al-ions form gel of $Al(OH)_3$ and Ca-ions form $CaCO_3$. In the presence of hydrocarbonate the pH of liquid phase reduces from 12 to 10.9. As a result, there are calcium hydroaluminates and gypsum in the solid phase. When $CaCO_3$ precipitates from the solution completely, calcium hydroaluminates react with gypsum, producing ettringite. The same process takes place at the study of AFm – phase.

For the investigation of hydration of calcium sulphoaluminate (CSA) suspensions were prepared. Mineral \ water ratio was equal 1:50. Suspensions were mixed during 24 h. After that CO_2 was passed through part of suspensions, and the other part of suspensions was used as the control.

At the first stage calcium sulphoaluminate reacts with water and is dissolved. The concentration of SO_4^{2-} reduces rapidly in the liquid phase and after 24 h it equals 38 mg\l. The $CaO\backslash Al_2O_3$ ratio is equal to 1 and concentrations of Ca-ions and Al-ions reduce quickly (Figure 4). In the samples of suspensions consisting of CO_2 concentration of Ca-ions and Al-ions reduces rapidly and C\A=2.

Concentration of SO_4^{2-} is changed very little during 6 h (Figure 5). Gibbsite, calcium carbonate and calcium hydrocarboaluminate are fixed in solid phase.

In the presence of CO_2 hydration of calcium sulphoaluminate is reacting intensively. Ettringite is fixed by XR-analyses on peaks with d= 0.971, 0.557, 0.494, 0.254 nm (Figure). It is noted that ettringite peaks are more intensive in the control samples (Figure 7).

The reduction of amounts of Ca-ions in the liquid phase consisting of CO_2 during 6-18 h is the result of its ability to transform into $CaCO_3$ and $Ca(HCO_3)_2$ which are fixed by XRD on peaks with d= 0.303, 0.206, 0.187 nm ($CaCO_3$) and d= 0.433, 0.284, 0.248 nm ($Ca(HCO_3)_2$).

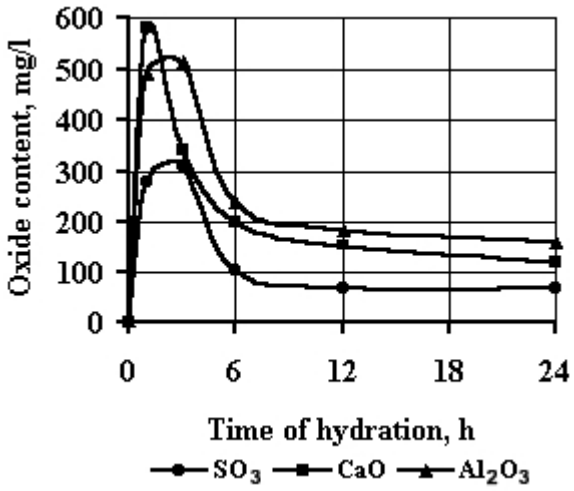

Figure 4. Chemical composition of liquid phase at hydration of calcium sulphoaluminate

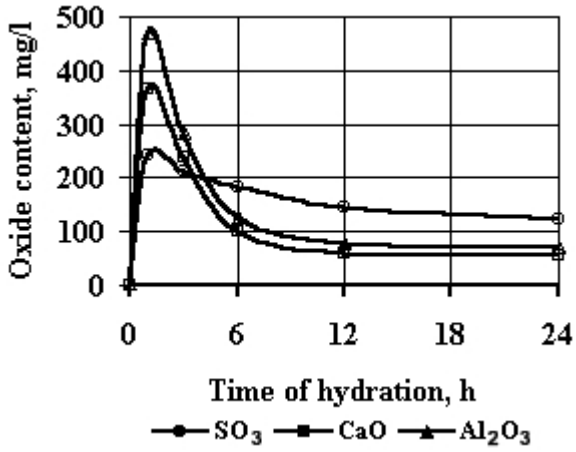

Figure 5. Chemical composition of liquid phase at hydration of calcium sulphoaluminate in the presence of CO_2

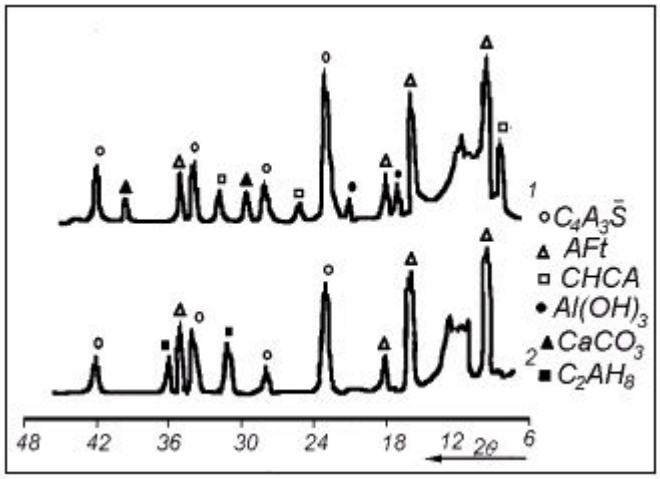

Figure 6. XRD powder diffraction (Cu Kα)$C_4A_3\bar{S}$ hydrated in CO_2 medium (1) and in water (2)

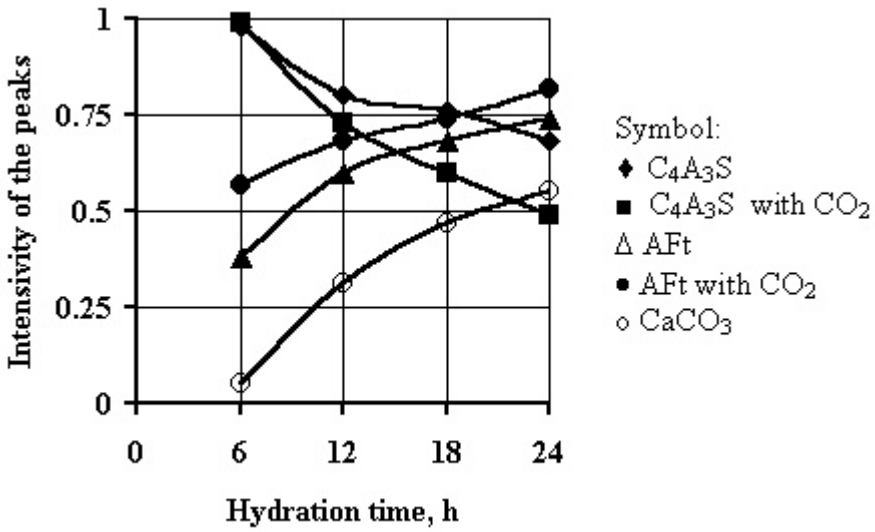

Figure 7. Change of intensity of peaks of calcium sulphoaluminate hydrated in O_2 medium and in water

Infrared spectra show the bands in regions 1420 and 1480 cm^{-1} due to CO_2 (Figure 8). Liquid phase at hydration of calcium sulphoaluminate in the presence of CO_2 has a small amount of Al-ions because calcium carboaluminates are formed. The final products are : carboaluminate, gibbsite and calcium carbonate. Calcium carbonate can react with sulphate-ions and form ettringite in the late period.

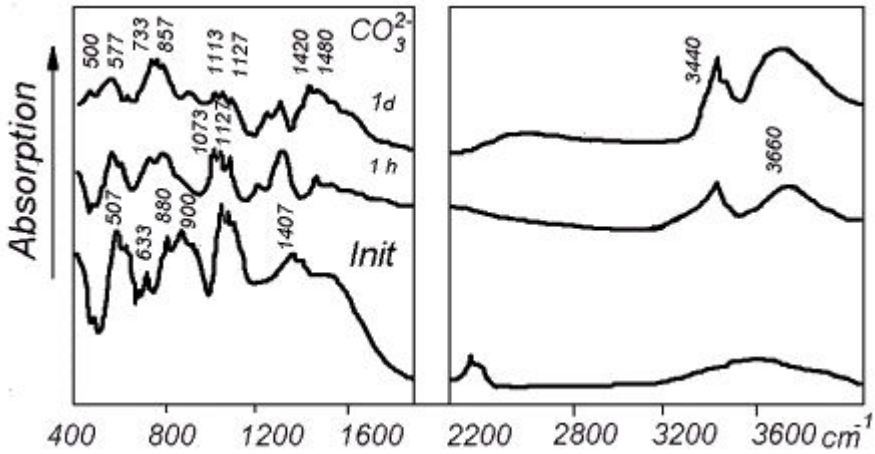

Figure 8. IR-spectra $C_4A_3\bar{S}$ hydrated in CO_2 medium

4. CONCLUSION

Exclusion of the influence of CO_2 at hydration of calcium sulphoaluminate leads to ettringite formation. In the presence of CO_2 the formation of calcium carboaluminate inhibits the growth of ettringite. After AFt phase formation hydrocarbonate and CO_2 do not influence the stability of ettringite.

REFERENCES

[1] Mehta P.K. and Gerwick B.C. Cracking-Corrosion Interaction in Concrete Exposed to Marine Enviroment, Concrete International, vol.4, № 10, 1982, pp.45-52.

[2] Roy D.M. Mechanisms of cement paste degradation due to chemical and physical factors, Proceedings of 9th International Congress on the Chemistry of Cement, Rio-de-Janeiro, 1986, vol. 1, pp.362-380.

[3] Babuschkin V.I., Matveev G.M., Mtchedlov-Petrossian O.P. Thermodynamics of silicates, Moscow: Strojizdat, 1979, p.361.

[4] Kouznetsova T.V. Alumina and sulphoalumina cements, Moscow, 1986, p.206.

STABILITY OF ETTRINGITE UNDER CARBONATE CORROSION AT HYDRATION OF SULPHOALUMINATE CEMENT

Kouznetsova, T.V.[1], Ivaschenko, S.I.[2], Samchenko, S.V.[2]

[1]Mendeleev Chemical Technological University of Russia, Miusskaja sq., 9, Moscow, 125047, Russia, E-mail: sivkov@ rctu.ru
[2]Moscow Institute of Engineering, Srednaja Kalitnikovskaja st., 30, Moscow, 109807, Russia, E-mail: mikxis@cityline.ru

Professor Tamara Kouznetsova is Head of Cement Department in the Mendeleev University of Chemical Technology and Corresponding Member in the International Engineering Academy, Moscow. She is author of over 300 articles and 12 books, had received numerous awards and was a member of the scientific committees of the 7th, 8th and 9th International Congresses on Chemistry of Cement

Professor Sergej Ivaschenko is Head of Chemistry Department in the Moscow Institute of Engineering. His research interests are the Chemistry of cement, he is the author of over 150 articles.

Professor-assistant Svetlana Samchenko is Senior Lecturer of Inorganic Chemistry in Moscow Institute of Engineering. Her research interests are the Chemistry of cementitous materials and physical-chemical methods of their study. She is the author of 125 publication.

INFLUENCE OF SUPERPLASTICISER AND ACCELARATOR ON ALUMINA CEMENT PROPERTIES

Kouznetsova,T.V[1]., Spizyn,V.V[2]., Dudoladova,T.G[2]., Krivoborodov,A.R.[2] and Lutikova, T.A[1].

[1]Mendeleev Chemical Technological University of Russia, Miusskaja sq.,9, Moscow, 125047, Russia. E-mail: sivkov@rctu.ru
[2] Company "Pashia Metallurgical Cement Plant", st. Pashia, Perm region, Russia.
Tel/Fax: +(34269)-21-124 or +(34269)-22-899

ABSTRACT

The use of plasticisers and accelerators with Portland Cement is now well established enabling the production of extremely workable mixes with significantly reduced water contents.

With reference to alumina cements, the use of such admixtures is seldom described. Previous studies on alumina cement with plasticisers have shown the tendency for unacceptable set retardation. It was noted that the use of accelators increases the water/ cement ratio that was responsible for the loss of strength of alumina cement mixes.

This paper describes the influence of superplasticisers and accelarators and their mixes on the hydration of alumina cements, their properties at usual temperatures, hardening and also as refractory cements.

1. INTRODUCTION

Calcium alumina cement was found to have excellent resistance to many forms of chemical attack and to set normally but to harden rapidly. Its strength at 24 h equals to that of Portland cement in 28 days. This cement is used in a wide range of general and specialized applications [1,2,3]. It is suitable for use at low temperatures for winter construction in cold climates or for repairs in cold stores. Calcium alumina cement is especially useful to make castables having applications in the steel and heat-using industries. However, the strength of this cement can be reduced due to conversion of $C_2AH_8 \rightarrow C_3AH_6$. Conversion and its practical implications have been widely studied but not always well-understood [4,5]. In our research we studied the influence of some admixtures on conversion and the properties of calcium alumina cement.

2. EXPERIMENTAL AND DISCUSSION

For the study the materials used were follows as:

- alumina cement with the bulk composition (weight %): Al_2O_3 =52.4, SiO_2= 7.5, CaO= 38.0, Fe_2O_3 = 0.4, R_2O = 0.2, TiO_2=1.0. The mineralogical composition of alumina cement was calcium monoaluminate (CA), gelenite (C_2AS) and small quantity of alumoferrite phase.
- accelarator - LiOH
- plasticiser - sulphonated naphtalene formaldehyde condensate

The first step of the study was the influence of LiOH on the properties of the cement. It was shown that it accelerated the setting and thus decreased the rate of hydration. When 0.2% LiOH was added to alumina cement, an exothermal effect was detected immediataly and cement paste became so thick, that it was not possible to mix cement with water. The optimal addition of LiOH to cement is 0.05 - 0.1 %. (This is shown in Table 1).

Table 1. Influence of LiOH on the properties of alumina cement

Quantity of LiOH,%	W/C	Setting time (minutes) initial	final	Compressive strength, MPa, after hardening during hours 2	6	24
0	0.35	55	120	–*	–*	25
0.05	0.35	23	50	3.2	25	38
0.1	0.35	12	20	4.5	30	40
0.5	0.35	8	10	5.5	23	30
1.0	0.35	2	5	5.0	12	20

"–*" means the samples had no strength.

In spite of high heat evolution of hydrated cement paste, the cubic form C_3AH_6 was not formed. Among the hydrated products CAH_{10}, C_2AH_8 and $Al(OH)_3$ were detected. X-ray pattern showed the peaks of 0.524, 0.349, 0.287 nm (C_2AH_8), and 0.141, 0.356, 0.255 nm (CAH_{10}). Besides them the diffraction peaks $LiH(Al0_2)_2.5H_20$ (0.534nm) were registered. In the authors' opinion this compound increases the hydration rate and hardening of alumina cement. In the presence of LiOH the strength of cement is high, even after 6 hours hardened cement paste reached 25-30 MPa. Alumina cement without the addition of LiOH has such strength only after 24 hours of hardening. But when LiOH was added to alumina cement in qualities of 0.5% and more, the strength of the cement paste became less than with the addition of 0.1% LiOH in the cement. It was explained by very high thickening process of cement paste with high qualities of LiOH. It was not possible to mix cement with water and the prepared samples had high porosity. That is why the rate of hydration of cement, samples showed low strength due to their porosity.

It is known that the addition of superplasticizers to Portland cement produces extremely workable mixes of cement with water. In our paper we tried to investigate the influence of superplasticizer (sulphonated naphthalene formaldehyde condensate).

It is fact, the addition of superplasticiser to alumina cement made setting time lower but improved flowability of cement paste but the setting time of cement paste decame longer in comparison the setting time of cement without superplasticizer. The duration of improved workability is dependent on temperature (Table 2).

Table 2. The influence of superplasticizer on setting time and compressive strengthof alumina cement paste

Quantity of superplasticizer, %	Final setting time (minutes) and hardened temperature, ^{0}C 20	30	40	Compressive strength, MPa, after 24 h hardening at 20^{0}C
0	120	65	30	25
0.3	140	85	50	24
0.6	220	135	100	15
1.0	300	175	135	8

The addition of LiOH and Plasticiser simultaneously allowed us to increase the water/cement ratio up to 0.3, to reach the high strength of cement paste at early ages as well as at 28 days of hardening without its decrease (Table 3).

Table 3. The properties of alumina cement as a function of quantity of complex additives

Additives,%		W/C	Porosity, cm^3/g	Setting time (min)		Compressive strength, MPa, after hardening for		
LiOH	Superplasticizer			initial	final	2 h	6h	28 days
–	–	0.35	0.0510	50	120	–	–	42.5
–	0.3	0.32	0.0480	70	140	–	–	46.0
–	0.5	0.30	0.0460	102	220	–	3.6	48.5
0.5	0.3	0.30	0.0024	20	45	10	20.5	52.8

The reason for this phenomenon is the formation of hexagonal hydrates of calcium aluminate that did not recrystallize into cubic C_3AH_6.

A very important property of alumina cement is its suitability for refractory applications. The study of cement paste after thermal heating at 200, 400, 600, 800, 100, 1200^0C showed that the addition of the above mentioned admixtures have improved all refractory properties of the cement paste: strength after heating, pore structure, microstructure of cement stone, heat resistance, contact zone formation.

3. CONCLUSION

It was established that the use of accelarators and plastisicizers as the admixtures with alumina cements is useful in both the ordinary applications and to make refractory castables.

REFERENCES

[1] Midgley H.G. High alumina cement in construction – a future based on experience, Calcium Aluminate, ed R.J.Mangabhai, London: E & F.N.Spon, 1990, pp. 1-15

[2] Taylor H.F.W. Cement Chemistry, London: Academic Press, 1990, 475 p.

[3] Kouznetsova T.V. , Talaber J. Alumina cement, Moscow: Strojizdat, 1989, 317 p.

[4] Midgley H. G. , Midgey A. Conversion of high alumina cement, Magazine of Concrete Research, 1975, № 27,pp.59-77

[5] Gill S.M., Banfill P.F.G. and El-Jazairi B. The effect of superplasticizers in the hydration of Aluminous cement, Proc.8th International Congress on Chemistry of Cement, Rio de Janeiro, 1986, vol. IV, pp. 322-327.

INFLUENCE OF SUPERPLASTICISER AND ACCELARATOR ON ALUMINA CEMENT PROPERTIES

Kouznetsova,T.V[1]., Spizyn,V.V[2]., Dudoladova,T.G[2]., Krivoborodov,A.R.[2] and Lutikova, T.A[1].

[1]Mendeleev Chemical Technological University of Russia, Miusskaja sq.,9, Moscow, 125047, Russia. E-mail: sivkov@rctu.ru
[2] Company " Pashia Metallurgical Cement Plant", st. Pashia, Perm region, Russia.
Tel/Fax: +(34269)-21-124 or +(34269)-22-899

Professor Tamara Kouznetsova is Head of Cement Department in the Mendeleev University of Chemical Technology and Corresponding Member in the International Engineering Academy, Moscow. She is author of over 300 articles and 12 books, had received numerous awards and was a member of the scientific committees of the 7th, 8th and 9th International Congresses on Chemistry of Cement.

Spizyn V.V. is the general director of Company " Pashia Metallergical Cement Plant". This plant produces metal and special cements as follow as: special oil well cements, alumina, expansive and selfstressing cements. He is the author of many research papers and patents.

Dudoladova T.G. is Head of laboratory of Company " Pashia Metallergical Cement Plant". This plant produces metal and special cements as follow as: special oil well cements, alumina, expansive and selfstressing cements. She is the author of many research papers and patents.

Candidate of Sci Krivoborodov A.R. is research woker of laboratory. His research interests are chemistry and technology of alumina and sulpoalumina cements, durability of high performance concrete. He is the author of over 100 papers and revivers.

Candidate of Sci Lutikova T.A. is researcher of Cement Department in Mendeleev Chemical Technological University of Russia. She is the author of 67 papers in the Chemistry of alumina Cement and concrete on its base.

EXPANSIVE AND NON-SHRINKAGE SULPHOMINERAL CEMENTS

A.P.Osokin [1], Y.R. Krivoborodov [1] and S.V. Samchenko[2]

[1]Mendeleev Chemical Technological University of Russia, Moscow. E-mail: sivkov@rctu.ru
[2]Moscow Institute of Engineering, Moscow.

ABSTRACT

Usually expansive cements are manufactured from sulphoaluminate clinker or mix aluminate clinker with calcium sulphates (gypsum, hemihydrate, anhydrate). For these cements ettringite is an important hydration product and reaction kinetics of this phase plays an important role in determining performance. The alternative aluminate phases may be ferrite-containing ones.

This paper deals with the composition and properties of solid solution calcium sulphoaluminate, sulphoferrite and sulphoaluminoferrite cements. The influence of calcium sulphate on structure and properties of calcium aluminate and ferrite phases, and their stability under high temperatures was studied. In addition, the properties of cements containing these phases were studied.

The investigation of hydration and properties of sulphomineral cements shows that ettringite and its analogies are formed thus providing expansion and compression of cement stone. The degree of expansion and self-stressing of cement stone depends not only on the composition of sulphated minerals but also on the ratio and types of clinkers. Higher expansion is achieved by the use of high alite containing Portland cement clinker together with sulphoaluminate or sulphoalumoferrite and lower expansion is found by addition of sulphoalumoferrite and sulphoferrite clinkers. These cements are classified as selfstressing, expansive or shrinkage-compensating cements depending on the degree of expansion after 28 days of curring.

1. INTRODUCTION

The chemistry of expansive cements was comprehensively discussed at the previous congresses and in many research publications [1,2,3,4,5]. The majority of practical expansive cements have depended on the modification of a Portland cement in such a way as to increase the formation of ettringite. Single expansive cement clinkers are made and they are blended or interground with a normal Portland cement or clinker. In widely used terminology, expansive cements based on Portland cement and calcium sulphate are categorized as types K, M or S, according to the source of additional Al_2O_3 that is required. Usually cement K is produced by intergrinding Portland cement clinker, gypsum and clinker consisting of $C_4A_3\overline{S}$. Type M cements contain Portland cement, a high alumina (CA) cement and additional calcium sulphate. Type S cements are Portland cements high in C_3A and with suitable contents of calcium sulphate.

The proportions of expansive clinker and of gypsum added to the Portland cement depend on composition of the expansive clinker and the degree of expansion required. Depending on the degree of expansion all these cements can be made as shrinkage-compensated, expansive [6] or self-stressing cements. It should be noted that there are some problems in production and

Proceedings of the 11th International Congress on the Chemistry of Cement (ICCC) 11 - 16 May 2003, Durban, South Africa
'Cement's Contribution to the Development in the 21st Century' ISBN Number: 0-9584085-8-0
Hosted by: The Cement and Concrete Institute of South Africa Editors: Dr G. Grieve and G. Owens
CD-ROM produced by: Document Transformation Technologies Congress Organised by: Event Dynamics

application of the above mentioned cements. For example, Type S cements have found little favour as they too difficult to control. To produce cement of Type M calcium aluminate cements are heeded, but it is too costly for wide application. The composition of expansive clinker can be varied considerably by the use of raw materials most economically available.

2. MATERIALS AND METHODS

Calcium sulphoaluminate (CSA) and calcium sulffoferrite (CSF) were sinthesized previously. To examine the solubility of ferric oxides in CSA ferric oxides an amount of 1 to 15 % by mass was added. The mix of CSA and ferrite oxide had been held for 20 minutes at 1350^0C and then the samples were analyzed by XRA and optical microscopy.

Minerals were blended to investigate the solid solutions of CSA and CSF. The ratio in all the experiments ranges from 25 to 75 %. The prepared mixes were pressured in the form of briquettes and fired at temperatures of 1050 - 1300^0C for 20 minutes each. The obtained cakes were subjected to XRA and optical microscopical analyses.

Calcium sulphoferrites were obtained by the burning of raw mixes intended for the production of calcium alumoferrates with composition of C_6AF_2, C_4AF, C_6A_2F with the addition of calcium sulphate and a blend of calcium alumoferrites having been synsthesized beforehand with anhydrite, as well as by the crystallization of sulphated alumoferrite melts.

The expansive clinkers obtained were used to produce expansive cements by intergrinding with Portland cement and gypsum. Cements were tested according to Standard methods.

3. RESULTS OF EXPERIMENTS

To study the solubility of ferrite oxides in CSA the samples were analyzed after sintering at 1350^0C. XR-analysis has revealed that the addition of Fe_2O_3 caused a shift in the major diffraction peaks of $C_4A_3\overline{S}$, this being more evident as Fe_2O_3 levels increase (Table 1). The IRE-spectra data show a shift and spreading of the band refering to the various oscillations of the SO_4^{2-} group in the original $C_4A_3\overline{S}$ (absorption bands 1093 and 1180 cm^{-1}) which is due to a change in the coordination environment of that group as a result of the incorporation of ferrite oxides whose presence is evidenced by the emergence of absorption bands in the region of 400 to 500 cm^{-1}.

Table 1. XRD of calcium sulphoaluminate with addition of Fe_2O_3

Sample	Position of the major diffraction peaks (hkl)		
	422	444	822
Without addition	3.750	2.650	2.166
1% Fe_2O_3	3.748	2.644	2.163
3% Fe_2O_3	3.745	2.641	2.161
5% Fe_2O_3	3.740	2.636	2.158
7% Fe_2O_3	3.733	2.630	2.156
9% Fe_2O_3	3.729	2.575	2.138

Such changes in spectra of calcium sulphoaluminate occur when up to 9% ferrite oxides are added, but when the iron content is greater than 9% the formation of aluminoferrite phase was observed. The structure of calcium sulphoaluminate can comprise up to 9% Fe_2O_3, the principal pattern of its crystall lattice remaining unchanged.

The study of the hydration of modified $C_4A_3\overline{S}$ in micropreparations has demonstrated that the oxides available in the calcium sulphoaluminate structure retards the hydration reaction. $C_4A_3\overline{S}$ reacts with water during the first minutes of being mixed with water, whereas the start of the hydration of modified $C_4A_3\overline{S}$ is shifted by one hour in proportion to the amount of Fe_2O_3 addition. By the end of the first day, however, the quantity of ettringite is equal to its amount at hydration of the initial calcium sulphoaluminate. The study of powders, consisting of preliminary synthesized minerals (C_4A_3S, C_2F and $CaSO_4$) shows that there is an exchange of aluminate and ferrite oxides between minerals and they are stable under heating up to 1350^0C. The following increase of temperature causes the decomposition of calcium sulphoaluminate find melt appearance which solves the formed earlier phases. During melt cooling calcium aluminoferrites with varying composition are formed. They consist of sulphates. It has been found that minerals burned together changed their colour, while XR-spectra feature a shift of major diffraction peaks of the minerals compared with their initial matrixes, i.e. an exchange of aluminium and iron ions takes place between the minerals.

XR-spectra microanalysis of the samples shows that calcium sulphoaluminate has Fe_2O_3 in its structure and calcium ferrite has aluminium oxide (Table 2).

Table 2. Composition of calcium sulphoaluminate and sulphoferrite

Compound	Content o f oxides, % y mass			
	CaO	Al_2O_3	Fe_2O_3	SO_3
$C_4A_3\overline{S}$	35.69	47.69	3.12	13.76
$C_4A_3\overline{S}$	34.26	46.28	5.24	12.20
$C_4A_3\overline{S}$	36.39	43.15	7.28	13.45
$C_2FC\overline{S}$	44.82	3.76	46.09	4.98
$C_2FC\overline{S}$	43.58	1.89	48.67	6.01
$C_2FC\overline{S}$	42.42	4.41	47.42	5.94

The results of burning calcium aluminoferrites C_6A_2F, C_4AF, C_6AF_2 together with calcium sulphate testify to the fact that there occurs a location of the latter with aluminoferrite, for the XRD analysis does not indicate the formation of the other compounds.

The general aspect of the radiographs of calcium aluminoferrites and sulphoferrites remains almost unchanged. It indicates the fact that the major pattern of the crystalline structure is preserved. In all cases, however, calcium sulphoaluminoferrites differ from calcium aluminoferrites in the intensity of the characteristic diffraction peaks and the shift of interplanar spacings is caused by a distortion of the crystal lattice of calcium aluminoferrites by calcium sulphates (Table 3).

The investigation of calcium sulphoalumoferrite crystallization from the melt shows that the composition of crystals emerging depends on the cooling rate. It has been established that in the case of a rapid cooling of the melt the crystals are enriched in aluminium to a greater extent than is the case for solidified melt. In the case of slow cooling the composition of the crystalising phase is indentical with that of the melt.

Calcium aluminoferrites modified by calcium sulphate differ both in the composition and hydraulic activity. It is to be noted that the degree of hydration increased with the increase of the A\F ratio in calcium sulphoaluminoferrite.

Using these data, three clinkers were produced at an experimental plant. Chemical composition of these clinkers is given in Table 4.

Backscattered electron (BE) imaging and X-ray microanalysis are very useful in examining the microstructure of polished clinker sections. Clinker phase identification from SEM images is made on the basis of phase brightness, grain morfology, and grain association via the BE image, and chemical composition by qualitative and quantitative EDS analysis.

Table 3.XRD characteristics of aluminoferrites and sulphoaluminoferrites

Compounds	Podition of peaks (hkl)		
	200	141	202
$6CaOAl_2O_32Fe_2O$	2.7914	2.6395	1.9285
$6.3CaOAl_2O_32Fe_2O_3\ 0.3SO_3$	2.7805	2.6485	1.9318
$4CaOAl_2O_3Fe_2O_3$	2.7830	2.6335	1.9212
$4.4CaOAl_2O_3Fe_2O_3\ 0.4SO_3$	2.7733	2.6401	1.9245
$6CaO2Al_2O_3Fe_2O_3$	2.7701	2.6230	1.9151
$6.5CaO2Al_2O_3Fe_2O_3\ 0.5SO_3$	2.7681	2.6395	1.9228

Table 4.Chemical composition of clinkers, in weight percent

Clinker Index	SiO_2	Al_2O_3	Fe_2O_3	CaO	MgO	SO_3	R_2O
CSF	11.14	3.93	32.64	41.70	2.08	7.53	0.13
CSAF	16.60	9.88	13.02	53.15	1.61	4.27	0.16
CSA	10.36	28.6	3.46	43.75	2.03	6.94	0.30

CSF is sulphoferrite clinker, CSAF - sulphoaluminoferrite clinker, CSA - sulphoaluminate clinker.

Clinker CSF exhibits a fine - grained microstructure composed of dicalcium silicate and a matrix of calcium ferrites. Two calcium ferrite phases appear in the BE images, the first is bright and massive and the second ferrite is calcium, iron and SO_3-rich and Al-poor (Fig.1a).

Clinker CSAF is a medium -grained clinker with subhedral alite, well-rounded belite, blocky ferrite matrix. Brightness of the ferrite phase varies within this clinker and the bright ferrite will be referred to as ferrite-1, and the darker designated sulphoaluminoferrite (ferrite-2). Ferrite-1 is higher in iron, and ferrite-2 higher in aluminum and SO_3 (Fig.1b).

Clinker CSA consists of belite and aluminate matrix. Spot EDS analyses indicate that parts of grain have aluminate, and others are aluminium and SO_3 in a similar manner to the clinker (Fig.1b).

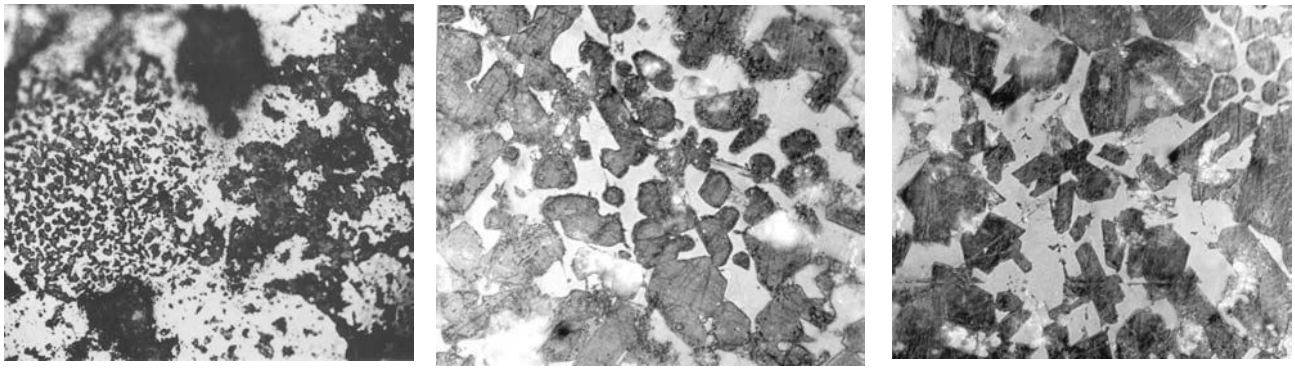

a b c

Figure 1. Microstructure of clinker CSF (a), CASF (b), CSA (c)

All clinkers were used as an addition to Portland cement clinker. All components were ground to a fineness of 4000 cm^2 /g.

The investigation of hydration and properties of sulphomineral cements shows that ettringite and its analogies are formed thus providing expansion and compression of cement stone. The degree of expansion and self-stressing of cement stone depends not only on the composition of sulphated minerals but on the ratio and types of clinkers. Higher expansion is achieved by using high-alite Portland cement clinker together with sulphoaluminate clinker (Table 5). Lower expansion is found with addition of sulphoalumoferrite and sulphoferrite clinkers. Thus cements are classified as expansive with expansion of 0.1 to 0.4% and strength of 57 to 62 MPa after 28 days of curring.

Table 5. Results of tests of expansive cements

Type of clinker as additive to OPC	Strength, MPa		Expansion, %		Self-stressing, Mpa	
	1 day	28 days	2 days	28 days	1 day	28 days
CSF	15	57	0.04	0.1	0.5	1.5
CASF	16.2	58	0.1	0.2	0.6	2.1
CSA	18	62	0.1	0.4	1.0	3.2

Corrosion resistance is of inverse relationship: sulphoferrite cements are more resistant to attack of aggressive media. These cements are suitable for obtaining waterproof, crack-resistant and corrosion-resistant concretes.

4. CONCLUSION

A new type of clinker was obtained consisting of sulphoferrite, sulphoaluminoferrite phases and dicalcium silicate. These clinkers are used for the production of expansive cements.

REFERENCES

[1] Kouznetsova, T.V. Expansive and selfstressing cements, Moscow, VNIIESM, 1980, 60 p.

[2] Kurdowski, W. and Sorrentino, F. Special cements, Structure and Performance of Cements, ed Barnes, London: Appl. Science, 1983, pp. 471-554.

[3] Osokin, A.P., Krivoborodov, Y.R. Sulphoferrite cements and their properties., Moscow, RCTU, 1983, v. 137, pp. 23-29.

[4] Krivoborodov, Y.R., Samchenko, S.V. Phase formation in alumoferrite systems in presence of calcium sulphate. 2 International symposium on cement and concrete. Beijing, China. 1989, v.4, pp.78-81.

[5] Taylor H.F.W. Cement Chemistry, London: Academic Press, 1990, p.475.

[6] Scrivener K.L., Butler S. Application of calcium aluminate and other special cements, Modern concrete materials: binders, additions and admixtures, London: Thomas Telford Limited, 1999, pp. 247-260.

EXPANSIVE AND NON-SHRINKAGE SULPHOMINERAL CEMENTS

A.P.Osokin [1], Y.R. Krivoborodov [1] and S.V. Samchenko [2]

[1]Mendeleev Chemical Technological University of Russia, Moscow. E-mail: sivkov@rctu.ru
[2]Moscow Institute of Engineering, Moscow.

Professor Alexander Osokin is Head of Cement and Composite Material Department at Mendeleev Chemical Technology University of Russia. His research interests are in clinker formation and Chemistry of Portland Cements. He is the author of over 300 research publication, 2 books.

Professor-assistant Yuri Krivoborodov is Senior Lecturer in Mendeleev Chemical Technology University of Russia. His research work is concerned with the Chemistry and Technology of Special Cements. He is the author of over 200 research publication.

Professor-assistant Svetlana Samchenko is Senior Lecturer of Inorganic Chemistry in Moscow Institute of Engineering. Her research interests are the Chemistry of cementitous materials and physical-chemical methods of their study. She is the author of 125 publication

INFLUENCE OF LIQUATION ON CLINKER FORMATION

Osokin A.[1] and Potapova E.[1]

[1]Mendeleev University of Chemical Technology, Moscow, Heroev Panfilovtsev st., 20, Russia.
E-mail: sivkov@rctu.ru

ABSTRACT

The formation of alite phase, micro- and macrostructure of clinker pellets runs at occurrence of a steady melt in system, the nature of these processes is instituted by quantity, composition and constitution of clinker fluid. The catalytic influence on the process of alite formation is affected by melts with lower viscosity and high surface energy. The formation of melts with high fluidity in clinker grain can be carried out at the expense of variation of the acid-base equal balance between the various coordination molding boxes of aluminum and iron in the direction of increasing of a part of a fraction of octahedral cations and by making halogen-containing regions of liquation, which activate dissolution of CaO. The all-up influence of elements, achieved by applying of various wastes, is more effective than operating of individual compounds. Optimization of structure of compositions allows to reach considerable catalyzed effect and to obtain alite clinkers at 1350ºC The inhibition sulphate-alcaline or activating of a halogen-containing liquation in clinker melt is one of the effective paths of optimization of clinker structure and improvement in quality of Portland cement.

1. INTRODUCTION

The formation of clinker pellets, their phase composition, micro- and macrostructure is a multiphase process including both aggregation at a stage of liquid-phase sintering and staircase reactions of clinker formation causing variation of morphology, modification, type and quantity of defects in the mineral structure. The mechanism and kinetics of these processes in many respects depend on composition and properties of a clinker melt.

In plant clinkers regions of nonuniform distribution of minerals and distinctions in their microstructure are practically always observed [1]. It is explained by chemical heterogeneity of an initial raw mixture. Regions of a crystallization of a C_2S solid phase, being in equilibrium with a fluid phase, are separated from fields of a CaO crystallization by regions containing alite in a melt. Immediately during a burning such factors, influencing on heterogeneity of composition and structure of clinker, as occurrence in an oxide melt of microbulks of sulphate-alcaline or halogen-containing composition can appear [2]. It is owing to recycling of material streams in a kiln, especially of dry method one, or due to fuel ash additive, agglomeration of particles of burnt material present in a melt [3], fluctuation of heat rate of a material and burning temperature [4,5].

Liquation phenomena are well enough studied in acidic silicate melts and glasses [6-14]. They are explained by the ability for cations to associate with the complex groups. Weakly polarizing cations (K^+, Na^+, etc.) are concentrated in the tetrahedrons $[AlO_4]$ and they form $[AlO_4]R^+$ or $[AlO_4]R^{2+}$. The stronger cations (Mg^{2+}) are close to oxygen ions of tetrahedrons $[SiO_4]^{4-}$. Moreover Al_2O_3 can form with SiO_2 heteropolyacids ($AlSiO_4^-$, $AlSi_2O_6^-$, $AlSi_3O_8$-) which associate with cations of the

strong bases thus promoting the association of less basicity cations with silica-oxygen anions [10,11].

At the liquation, the melt consists of two liquid phase: high silicate and high calcium melts which have different structure and properties. Aluminate complexes are dissolved in the high-calcium and strongly depolymerized phase thus increasing its polymerization and making its properties close to the high silicate one. As a result the mutual solubility of two phases increases but liquation temperature decreases. The solubility rises with the decrease of the bond force Al-O what is observed when field force of compensated cation in aluminate complexes $[AlO_4]R^+$ and $[AlO_4]R^{2+}$ increased [10].

The liquation region of the binary and the ternary silicate systems increases with the growth of the cation force field but the complex ability for the homogenization decreases as follows: $[AlO_4]K \rightarrow [AlO_4]Na \rightarrow [AlO_4]Ca \rightarrow [AlO_4]Mg$ [10]. Similarly the mean size of a disperse phase decreases at the expense of dominance of the entropic factor and the width of the region of a metastable liquation is narrowed. The addition of the third component (oxide) to binary liquation melts results in its distribution between coexisted phases. In the presence of oxide, containing a weaker cation, liquation phenomena are loosened in melts, having a stronger cation.

Anion solubility in silicate melts depends on the structure and basicity of the system. It decreases in number as follows [12]: $BO_4^{5-} \rightarrow PO_4^{3--} \rightarrow SO_4^{2--} \rightarrow F^{--} \rightarrow Cl^{--} \rightarrow OH^{--} \rightarrow CO_3^{2-}$. Tetrahedron groupings (BO_4, PO_4, SO_4) are characterized by higher solubility than trigonal ones. When the basicity of liquid phase increases the anion solubility rises.

The considered rules of liquation phenomena take place in clinker melts as well though their high basicity promotes the different anomalies. These data were obtained by our research.

2. EXPERIMENTAL

2.1 Materials and methods

To study the influence of microelements (alkaline- and halogen contained additives) on the properties of eutectic oxide melt forming in the burning row mixes at 1338^0C we prepared a raw mix, with composition as follows: CaO = 54,8%; SiO_2 = 6,0%; Al_2O_3 = 22,7%; Fe_2O_3= 16,5% . By heating the above mentioned mix to 1500^0C, we obtained "oxide melt".

"Oxide melt" is high basicity melt in system C-A-F-S. At 1338^0C it consists of (weight %): CaO = 54,8; SiO_2 = 6,0; Al_2O_3 =22,7; Fe_2O_3 = 16,5 . With further increase of temperature melt the saturated by calcium, silicon, aluminum, iron oxides and at 1450^0C, the melt consists of CaO=57%; SiO_2= 7,5%; Al_2O_3= 22,6%; Fe_2O_3= 12,9% . When salt agents are added into the melt, they dissolve in melt matrix. When concentrations of salt agents are more than their solubility in the melt matrix, salt melt is displaced from oxide melt matrix and oxide-salt melt is formed.

In our research "salt melts" were obtained by agitation of the above mentioned raw mix with eutectic salt mixes (CaF_2, $CaSO_4$, Na_2SO_4, K_2SO_4, $CaCl_2$, $BaCl_2$, , $MgCl_2$, $Ca_3(PO_4)_2$, etc.) or oxides (MgO, Mn_2O_3, R_2O, etc). All mixes were heated to 1500^0C and after homogenization they were quenched.

The Immiscibility of oxide and salt melts, and the formation of calcium silicates in oxide melt were studied by SEM, IRS, XRD, DTA and chemical analysis. Solubility of CaO, SiO_2, Al_2O_3 and Fe_2O_3 in salt melts was determined by the method of isothermic saturation of liquid phase with corresponding oxides.

Viscosity was determined by rotary electroviscosimeter EVI-70PM. The surface tension of the melt was determined by the gas-bubble technique, density was determined by hydrostatic weighing.

For the preparation of the model system CaO and β-C_2S were used. Their synthesis was made by two-multiple sintering at 1450^0C and 1800^0C over two hours.

3. DISCUSSION

In our study it was determined that depending on the nature and concentration of impurities in a clinker grain the oxide or oxide-salt melts are formed, the properties which one are instituted by a proportion of elements in local volume of a reshaped clinker pellet. The occurrence of a salt component conditions liquation phenomena, and the propensity to segregation of melts increases with growth of acidity of p-elements and with growth of basicity of s-elements. It correlates well with the value of their interphase surface energy.

The appearance of the salt liquation region melt was detected in the high basicity oxide under the combined influence of SO_4^{2-}, Na^+, K^+. When sulphate content is equal to 0.5-0.8%, mass., sulphates dissolve completely in oxide melt. When this melt quenched the fairly homogeneous glass phase is formed. Micro liquation is observed when the R_2SO_4 content is equal to 1% and more (Figure 1). It was determined that there is a correlation between width of a liquation region and the parameters of cations, from which it is possible to determine ionic potential, force of the field of the cation or its electronegativity. Potassium sulphate melt has a lower surface energy than a melt with Na^+. Thus at the expense of dominance of entropy from Na → K the mean size of particles will be decreased and the width of the field of a metastable liquation will be narrowed. If for a melt containing 1%, mass, of K_2SO_4, the size of liquation drops is equal (0.6-1.3) $\cdot 10^3$ A, to a melt containing 1%, mass., of Na_2SO_4, the mean size of drops comprises (1-3) $\cdot 10^3$ A. When the K_2SO_4 content increases up to 2% by weight it is observed that individual drops are merged and they form a net structure. When concentration of the salt phase exceeds 3% the matrix of the oxide salt melt is not able to hold large regions of salt melt together. They start to move towards the surface layer (micro liquation transfers to macro liquation) (Figure1 a,b).Taking into account, that in a sintering grain 25-30 %, mass. of a melt is formed, the micro liquation arises at the content of alkaline sulphates in clinker equal to 0.5-0.6 %, mass., and with growth of their quantity, macro liquation regions arise.

In terms of obtaining quality clinker (a good aggregation of a material in a sintering zone and a stable operation of a rotary kiln) macro liquation phenomena are undesirable for forming during phase separation melt drops, having sulphate-alkaline composition which are characterized by low values of a surface tension. It assists in the formation of dust-like clinker grains during aggregation of a sintering powder that leads to impairment of kiln operation and decrease of clinker activity.

Liquation phenomena may be considerably depressed by the introduction of a third component (MgO, for example) into liquating sulphate-alkaline melts. In this case it is distributed throughout coexisting phases. As a result of increasing surface energy of an oxide melt, solubility of alkaline sulphates rises. The structure and properties of clinker melt in the presence of both individual (MgO, Mn_2O_3) and complex (R_2O-MgO-SO_3 , Mn_2O_3-TiO_2-SO_3, R_2SO_4- MgO- Mn_2O_3, TiO_2-Fe_2SO_4-MgO) compounds were studied.

Liquation phenomena in halogen-containing melts are observed at a lower concentration of anions than in sulphate melts. It is attributable to the theory of screening, according to which degree of screening of cations increases with an increase of anion polarization. Since F^- ions have a lower value of polarization (0.96 A^3) than oxygen ions (2.74 A^3), it is completely displaced from a coordination sphere of complex formation (Si, Al, Fe) into a coordination sphere required to screen cations Ca^{2+} and especially Na^+ and K^+ that defines differentiation of a composition of a liquid

phase. At concentration of F^- up to 0.7%, mass., it is dissolved completely in an oxide melt. Subsequent increasing of its content, liquation regions occur with dimension $(2\text{-}3)\cdot10^3$ A in size (Figure 1 c). Cl^- ions are characterized by higher polarization than F^- ions. That is the reason that a degree of screening increases in their presence and a micro liquation occurs at higher concentration of Cl^- (2-3%, mass.). It is accompanied by formation of liquation regions of smaller dimension. In the presence of alkaline cations liquation is observed at a lower concentration (0.3-0.5%, mass.) of halogen ions in a melt.

At halogen inducing along with sulphates microliquation occurs at lower absolute concentration of p-elements with formation of regions with larger sizes (Figure 1 d). With substitution of $CaCl_2$ by $CaSO_4$ in fluorine-containing melt the size of liquation regions increases from $(0.5\text{-}1.0)\cdot10^3$ A up to $(6\text{-}12)\cdot10^3$ A. For halogen-containing melts, immiscibility phenomena are shown even in the absence of alkaline cations, and at a complex salt inducing their concentration reduces by about a factor of two. It results in the occurrence of salt melts. That is the reason that at the total content in a sintering clinker equal to 0.3-0.5%, mass., of compounds of fluorine, sulfur and chlorine in combination with R^+ microliquation regions should be expected in an oxide melt, which influences the mechanism and kinetics of alite formation.

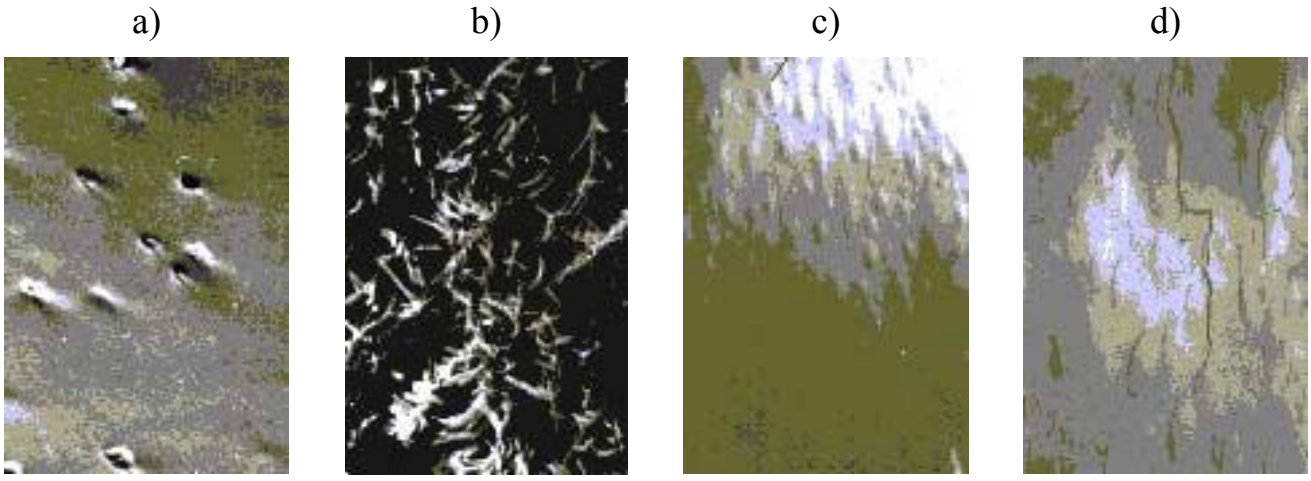

Figure 1**.** Microstructure of clinker glasses, modified by (%, mass):
a – 1.0 Na_2SO_4; b – 4.2 Na_2SO_4; c – 1.0 F^- ; d – 1.0 CaF_2 + $CaSO_4$
magnification of 6000 ^{x}

In systems of R_2O-$CaSO_4$-MgO, $CaCl_2$-$CaSO_4$, CaF_2-$CaSO_4$ the formed composite oxide-salt melts are characterized by 2-4 times (Table 1) the lower viscosity (η) and lower surface tension (σ) in than oxide melts formed in the C-A-F-S system. That is the reason that their function in a mineral formation cannot be ignored. So, for the combination of $CaCl_2$-CaO the salt melt viscosity decreases in the range $(2.5\text{-}5)\cdot10^{-3}$ Pa·s with the temperature rise in the range from 900 to 1100 ^{0}C, and the surface tension is not practically changed and it is equal to 0.14-0.15 N/m. The melt structure consists of Ca^{2+} and $CaCl^+$ cations, and $[Ca_{(4-x)}O_x]^{2-}$ anions. The volume of microspaces increases in 5-10 times in the salt melts in comparison with the oxide melts and therefore the viscosity mechanism changes. The fluidity of the salt melt and the fluidity of the structure formed ions increase.

The solubility of salt melts in the oxide one does not exceed 3-5% at 1450 ^{0}C, but at the bigger concentration micro-and macroliquation appears. When temperature falls dawn the solubility is reduced that promotes the separation of eutectic melt, containing below 1% of the salts, at slow cooling. The liquated salt melts dissolve 8-16 % of calcium oxide, below 3% of Al_2O_3, SiO_2 and Fe_2O_3. The solubility of oxides (especially CaO) is changed considerably depending on temperature as is the composition of the liquated phase. In the salt melts based on R_2SO_4 , 5.9-

5.95% of CaO , 1.3-1.4% of SiO_2, but Al_2O_3 and Fe_2O_3 are insoluble practically. In the melts based on Na_2SO_4 - K_2SO_4 - $MgSO_4$, $Na_2SO_4 \cdot 3\ MgSO_4$, $K_2SO_4 \cdot 2MgSO_4$, the concentration of CaO comprises 13.49 - 13.78%, the content of SiO_2 increases from 1.93 to 2.31 % , the solubility Al_2O_3 and Fe_2O_3 is in the range 0.19 -1.09%. So, if in salt melt of potassium sulphate there are 5.9% of Ca0; 1.30% of SiO_2; 0.08% of Al_2O_3; 1.09% of Fe_2O_3, then in the eutectic melt of $K_2SO_4 \cdot 2MgSO_4$ there are 13.98% of CaO; 2.28% of SiO_2; 0.98% of Al_2O_3; 1.09% of Fe_2O_3%. High solubility of CaO in sulphate - magnesium melts is caused by the formation of intermediate complexes of $K_2SO_4 \cdot CaSO_4$ - $MgSO_4$, $K_2SO_4 \cdot 2CaSO_4$.

Table 1. Properties of salt and oxide-salt melts

Addition	Salt melt					Oxide-salt melt				
	Tmel, ^{0}C	Properties at T=900^{0}C			% of addition**	Tfor, ^{0}C	Properties at T=1450^{0}C			
		η, Pa·s	σ, N/m	ρ, kg/m^3			η, Pa·s	σ, N/m	ρ, kg/m^3	r***, 10^{-7} m
-					-	1338	0.080	0.55	2800	-
$CaCl_2$	772	0.0020	0.142	2050	3	1310	0.036	0.34	2680	7.4
CaF_2- $CaCl_2$	651	0.0055	0.144	2140	1	1320	0.018	0.45	2730	8.3
CaF_2-$CaSO_4$*	951	0.0100	0.146	2520	1	1305	0.024	0.48	2780	4.3
$CaCl_2$-$CaSO_4$	708	0.0028	0.120	2090	3	1310	0.015	0.35	2680	7.6
$CaCl_2$-$BaSO_4$	592	0.0005	0.110	2550	5	1310	0.040	0.27	2720	12.7
$CaCl_2$-$BaCl_2$-$CaSO_4$	569	0.0048	0.095	2540	5	1295	0.037	0.25	2700	12.7
$CaCl_2$-$Ca_3(PO_4)_2$	769	0.0040	0.125	2040	3	1320	0.032	0.48	2660	8.8

* - the properties of a melt are gauged at T=950^{0}C;

** - quantity of the addition in an oxide melt resulting in a liquation;

*** - maximal size of drops of a salt melt at the given concentration of the additive.

In the range 950-1220 ^{0}C solubility of CaO in the composite salt melts based on CaF_2-$CaCl_2$, $CaSO_4$ -CaF_2 , $CaCl_2$ - $CaSO_4$ increases. The temperature coefficient is equal to 2.10^{-2} % by mass/degree. Maximum solubility of CaO (12-15%, mass.,) at 950-1300 ^{0}C is observed for the salt melt based on $CaCl_2$ - $CaSO_4$. Its value reduces when anions change in the following number $Cl^- \rightarrow F^- \rightarrow SO_4^{2-}$. However all studied melts were characterized by the rather high solubility of CaO at relatively low temperatures. If the dependencies are extrapolated up to 1450 ^{0}C then the top solubility of CaO will essentially exceed the value defined for alkaline-sulphate compositions. In the saturated composite salt melts SiO_2 dissolves up to 1.15 % (at 900 ^{0}C in the system CaF_2 - $CaCl_2$) and up to 0,58% of aluminum and iron oxides (Table 2).

The study of the salt melt properties showed that their viscosity is 1-2 times less ($1 \cdot 10^{-3}$ - $5 \cdot 10^{-3}$ Pa·s) and the surface tension is 2-3 times less (0.09-0.15 N/m) than the viscosity and the surface tension of the oxide melts (Table 1). When calcium silicon, aluminum and iron oxides are added to

the salt melts η of the liquid phase rises to (5-9)·10^{-3} Pa·s (at 900 ^{0}C) (Figure 2). In the presence of CaO viscosity of chlorine-contained melts increases due to the amalgamation of the viscous units and the strengthening of the interaction between the separate structure units of the melt. The increase of CaO in chlorine melts leads to the formation the larger complex groups $(CaCl_{4-x}\ O_x)^{(2-x)}$, which have the greater size and electric charge than these parameters of the structure unit of calcium chlorine melt ($CaCl_4$). This promotes the interaction between the melt groups and the increase of the system viscosity. In the fluorite- and sulphate-containing melts the formation of the complex double compounds of $CaO.xCaF_2$-type (where x = 1 or 2) is possible, which structuralize the system, decreasing the fluidity of the main structure formation ions.

Table 2. Equilibrium concentrations of silicon, aluminium and iron oxides in salt melts, saturated by calcium oxide

		Concentration of oxides, % by weight, at the temperature, ^{0}C				
Melt	Oxide	800	850	900	950	100
$CaCl_2$ + 10.7% CaO	SiO_2	0.15	0.19	0.22	0.26	0.32
	Al_2O_3	0.02	0.03	0.05	0.06	0.08
	Fe_2O_3	0.02	0.03	0.05	0.06	0.08
	CaO_{Free}	0.05	0.07	0.11	0.09	0.11
CaF_2 + $CaCl_2$ + 11.33% CaO	SiO_2	0.50	0.81	1.15	1.56	1.83
	Al_2O_3	0.04	0.05	0.08	0.11	0.15
	Fe_2O_3	0.41	0.45	0.50	0.51	0.55
	CaO_{Free}	0.04	0.05	0.05	0.07	0.09
$CaCl_2$ + $CaSO_4$ + 15.38% CaO	SiO_2	0.15	0.54	0.90	1.22	1.65
	Al_2O_3	0.02	0.03	0.05	0.08	0.10
	Fe_2O_3	0.44	0.55	0.63	0.75	0.85
	CaO_{Free}	0.08	0.10	0.15	0.28	0.35

The salt melt viscosity is changed exponentially as a function of temperature. Activation energy of the melt viscosity has low values (25-48 kJ/moll.) and increases as the quantity of the dissolved oxides increases. In the presence of calcium, silicon, aluminum, iron the salt melt surface tension increases slightly: from 0.005 to 0.002 N/m.

The density (ρ) of the salt eutectic melts is 2000 -2500 kg/m^3 (at 1500 ^{0}C) . When CaO, SiO_2 , Al_2O_3, Fe_2O_3 are dissolved in them it is observed the common trend is for the density to increase, although for the same compositions the relationship passes through the inflection point and the extremums, which characterize the definite interaction in the system. The density is a readily decreasing function of temperature. The low density and the surface tension of the salt melts confirms the low ability to aggregate of the liquating systems and the negative impact of macroliquation in the clinker oxide melt on the agglomeration and sintering processes.

In the salt melts with high fluidity CaO dissolves more readily and these melts carry out the function of the transport surroundings for calcium cations which diffuse into the local regions. These regions are enriched in silica-containing components. The alite formation and crystallization take place there. The low density and surface tension of the salt melts confirms the bad aggregate ability of the liquating systems and the negative influence macro liquation in the clinker oxide melt on the agglomeration and sintering processes. It has been found that liquating salt melts when saturated with calcium, aluminum, silicon and iron oxides, crystallize , the individual or complex melts and silicate phase, especially C_3S, are formed. In alkaline-sulphate melts 4-5% by weight of calcium silicates are formed. In eutectic halogen-containing salt melts, saturated with the oxides, C_3S and C_2S are crystallized up to 9% by weight.

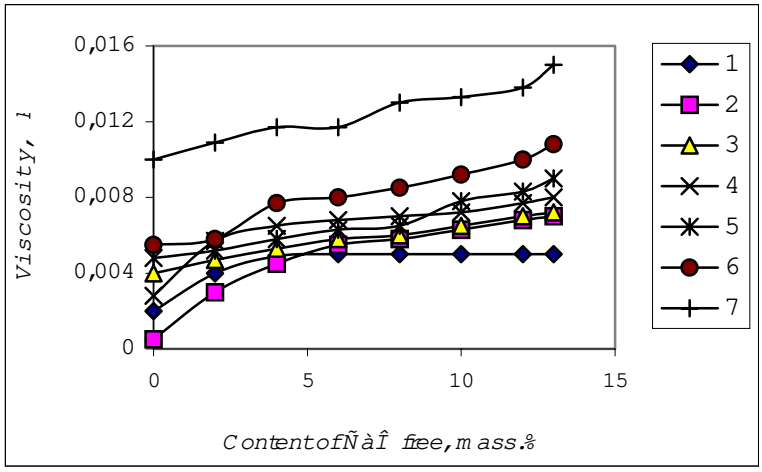

Figure 2. Change of viscosity of salt eutectic melts versus content of calcium oxide: 1 - $CaCl_2$;2 – $CaCl_2$ - $BaCl_2$; 3 - $CaCl_2$-$Ca_3(PO_4)_2$; 4 - $CaCl_2$- $CaSO_4$; 5 - $CaCl_2$- $BaCl_2$- $CaSO_4$; 6 - CaF_2- $CaCl_2$; 7 - CaF_2- $CaSO_4$. (1-6 T=900 ^{0}C; 7 – T=950 ^{0}C)

The process of the formation of alite phase in actual sintering clinkers proceeds at the start of equilibrium melt and at sufficient temperature in volume of pellets. By the time of the advent of melt topochemical reactions of mineral formation and in the system the grains of CaO and C_2S are present, relatively uniformly distributed in clinker melt, which quantity varies in the range from 25-35%, mass.

For modeling of alite formation, taking place in microvolumes of clinker grain, the system of CaO-C_2S-melt was used. Particles of CaO and C_2S were obtained by burning of briquettes at 1800^{0}C during 2 h in vacuum oven and subsequent grinding of cakes and extraction of fraction equal to 40-60 mcm. The density of particles comprises 3280 (C_2S) and 3370 (CaO) kg/m^3; the size of crystals varied in the range from 25 to 60 mcm. The structure of thus obtained grains consisted of one or two crystals that excluded dispergation in melt and allowed to study diffusion nature of the process. The ratio of CaO (14.83%), C_2S (55.17%) and a mix for obtaining a melt (M=30%) corresponded to clinker with L.S.F.=0.92.

In clinker melt involving Na_2SO_4 and K_2SO_4 liquating regions with sulphate-alkaline composition are formed. In these regions belite is corroded actively under the effect of surface-active cations of Na^+ and K^+. In this case the rate of dissolution (J) of C_2S exceeds J_{CaO} two or three times and alite formation is limited by the kinetics of interaction between calcium oxide and a melt.

As a result of fast dissolution of belite in a clinker liquid and slow diffusion of the silica-oxigen anions formed they enrich the melt in the immediate regions of dissolving grains of C_2S. The resulting concentration gradient is a motive force, which seeks equilibrium, that is uniform distribution of ions in a melt. However, a lower fluidity of silica-oxygen radicles as against such ions as Al^{3+}, Fe^{3+}, Ca^{2+}, Na^+, K^+, etc. and steadily going on process of dissolution of C_2S supports the higher concentration of complexes in these regions and provides formation of micro-ununiformities. Cations of Ca^{2+}, Mg^{2+}, Na^+, K^+, etc., surrounding these microvolumes, interact with complexes $[Si_nO_{3n+1}]^{(2n+2)}$ –type, that leads to their depolimerization and the formation of isolated tetrahedrons of $[SiO_4^{4-}]$. These tetrahedrons are bonded with Ca^{2+} ions thus forming the lattice of C_3S.

Liquating sulphate-alkaline melts marked by a low surface tension hamper the dispergation of CaO grains and diffusion dissolution of individual crystals. As a result alite formation is retarded, liquid phase is slowly saturated with Ca^{2+}, and due to diffusion, the progressive growth of formed alite

crystals takes place that defines a coarse-crystal structure of clinker. With slow dissolution of CaO crystals their capture by growing alite crystals is observed. In this case interlocked grains of calcium oxide do not enter into a reaction of alite formation. Their occurrence provides an increase of CaO_{free} content and decrease of alite content in clinker in comparison with calculated value (Figure 3).

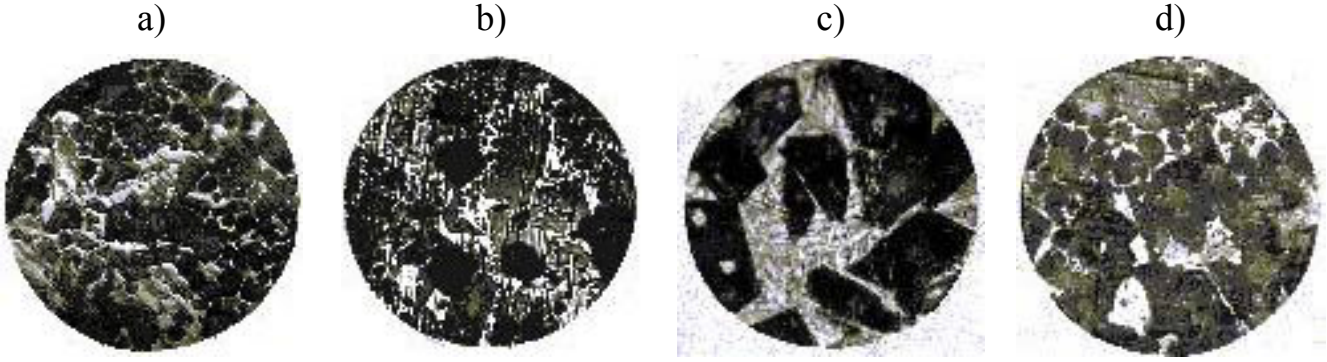

Figure 3. Crystallization of minerals in model systems at addition in a melt (%, mass.):
a) - 2.0 Na_2SO_4; b) – 2.0 $K_2SO_4 \cdot 2MgSO_4$; c) – 1.0 Cl^-; d) – 1.0 CaF_2 + $CaSO_4$
the photo was made by the optical microscopy, magnification of 400 ^{x}

With the suppression of liquation in the presence of Mg, (or at a low content of sulphate-alkaline melts) a fine-crystal clinker structure is formed with a clear mineral crystallization.

With the dissolution of CaO and C_2S in halogen-containing melts, alite forms immediately. Fine-crystal C_3S is indicative of fast supersaturation of liquid phase and a formation of a greater content of crystallization centers. It is significant that changes of crystal nature do not occur as F^- and Cl^- content in a melt increases. Needle-like crystals of C_3S bear witness to its crystallization from a melt. In the presence of F^- and Cl^- J_{CaO} is greater than $J_{C2S.}$

In the presence of all halogen-containing modified additions the following function is observed as a whole: with increase of liquation regions alite crystal sizes decrease. Their faces develop broad and indefinite appearance due to recrystallization taking place in salt melts. The rate of CaO dissolution exceeds J_{C2S} and this distinction increases with increase of the acidity of the interface layer with adsorption of ions of F^-, Cl^- and SO_4^{2-}. In the liquating salt melts $J_{CaO} \geq J_{C2S}$ and crystallization frequently occurs at the surface of C_2S. The most intensive alite formation occurs in the presence of combined salt melts and the rate of reaction increases as follows: $CaCl_2$- $CaSO_4 \rightarrow CaF_2$- $CaSO_4 \rightarrow CaF_2$- $CaCl_2$. Accordingly the size of C_3S crystals decreases.

The resulting liquid phase in burned material fills separate pores and capillaries thus forming films on particles. In [13, 14] it is shown that a melt is represented by continuous phase with grains of CaO, C_2S and C_3S Interaction between these minerals and melt takes place restrained conditions when diffusion of required ions for growth of C_3S crystals limits the progress of a reaction of synthesis. Between grains of CaO – C_2S, CaO – C_3S melt regions, enriched in Ca^{2+}, occurs. In these regions, crystals of C_3S are in prospect. Locally positioned melts, characterized by concentration gradients and different acid-basicity properties, exchange ions on interface on contact, tending to equilibrium. At large melt volumes convection is favorable to the averaging of melt composition. However, in thin capillaries and films material transfer executes due to diffusion only. The conservation of non-uniform melt volumes in clinker grains (metastable micro liquation), the availability of liquation regions leads to extraction of solid phases, which are in equilibrium with these fluids.

In the system CaO-C_2S-M liquid phase is formed at 1338^0 C, because of this at burning of mix without addition at 1300^0 C CaO and C_2S does not bind together. Initial content of calcium oxide (14.83%, mass.) is contained in cakes (Figure 4), that is confirmed by the absence of solid-phase interaction between CaO and C_2S under these conditions. In the presence of modifiers, temperature of the occurrence of melt decreases (up to 1240-1300^0 C) and at the occurrence of liquid phase absorption of CaO starts. The degree of completion increases with growth of content in melt (in the range from 1 to 5%, mass.) of all studied modifiers. The nature of influence of individual and complex modifiers is defined by both change of viscosity of oxide component and the occurrence of liquation regions of salt composition.

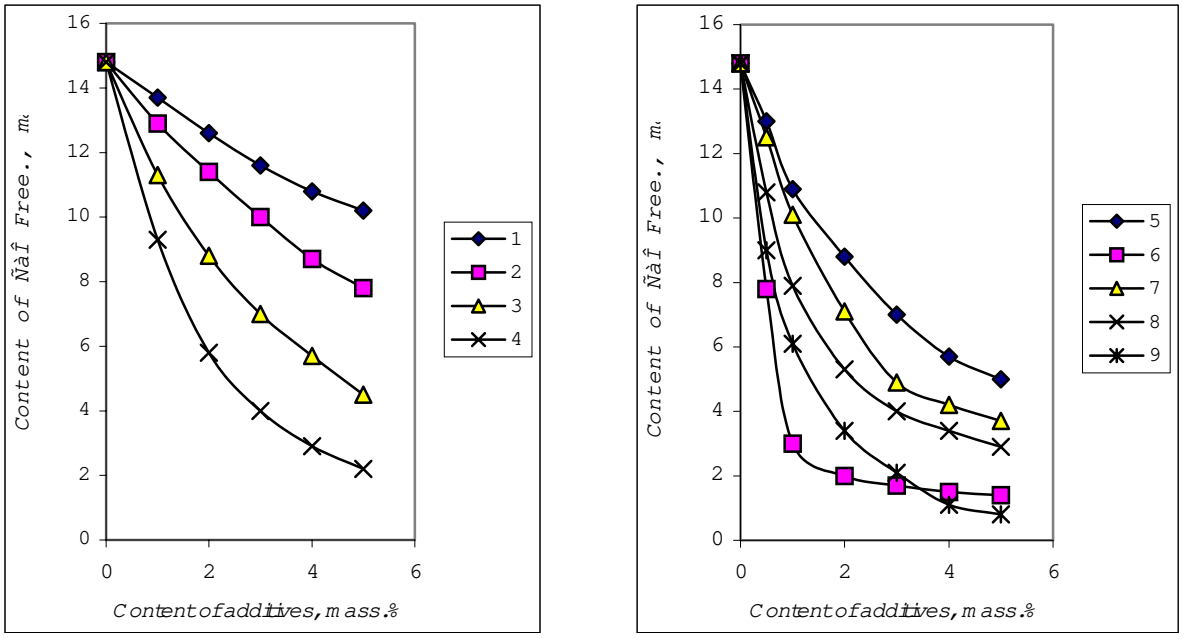

Figure 4. Impact of content of addition on binding of free calcium oxide in the presence:
1 - Na_2SO_4; 2 - $K_2SO_4 \cdot 2MgSO_4$; 3 – MgO; 4 – R_2O-MgO-SO_3; 5 - Cl^-; 6 – F^-;
7 – $CaCl_2 + CaSO_4$; 8 - $CaF_2 + CaSO_4$; $CaF_2 + CaCl_2$ ($T=1300^0$ C, τ=20 min)

With incorporation of alkaline sulphates, alite formation intensified mainly due to essential acceleration of C_2S solubility in the presence of R^+. The degree of transformation of CaO increases with decrease in melt viscosity, but this rule is violated by the occurrence of salt melt. At increase of the trend of melt to separation in the following order: R_2O-MgO-$SO_3 \rightarrow Na_2SO_4 \cdot 3MgSO_4 \rightarrow Na_2SO_4$ - K_2SO_4 - $MgSO_4 \rightarrow K_2SO_4 \cdot 2MgSO_4 \rightarrow Na_2SO_4$ slowing down of binding of calcium oxide is observed that corresponds with impact of cations Mg → Na → K on liquation. This rule is conditioned by the lower solubility and the rate of CaO dissolution in sulphate-alkaline melts. Suppression of liquation assists in activation of the process. So, for the system R_2O-MgO-SO_3, liquation is observed at the higher oxide content (over 3%,mass.) in comparison with other sulphate-alkaline compositions, as manifests by its catalyzing ability. As this takes place, before the start of liquation process occurs intensively while at the advent of salt melts it slows down at the concentration of complex more than 3%, mass.

For halogen-containing melts, liquation phenomena catalyze alite formation in the order $SO_4^{2-} \rightarrow Cl^- \rightarrow F^-$ that agrees with the sequence, typical for strengthening of liquation ability of clinker melt. F^- ion has the highest effectiveness, absolute concentration being the same. However, the injection of eutectic salt melts anion concentration changes to a lesser extent than with halogen injection. As this takes place, Cl^- (1.6-2.65%, mass.) combined with a small quantity of F^- (0.07-0.35%, mass.) considerably overcomes impact of single F^- in intensity. Substitution of F^- by SO_4^{2-} leads to

considerable slowing down of the reaction, concentrations being the same that agrees with comparison of their impact on viscosity of an oxide melt and an liquation ability of the system. That is, liquation phenomena in halogen-containing clinker melts catalyzes alite formation. The opposite type of impact of halogen-containing and sulphate-alkaline melts is explained in terms of the higher solubility of CaO in salt melts based on F^- and Cl^- and their lower values of viscosity as well.

4. CONCLUSIONS

In the presence of salts or their compositions and depending on ion concentration in clinker melt a separation of clinker melt is observed. A separation takes place into two coexisting fluids: an oxide one with disssolved ion salt and a salt fluid with oxide ions. The trend of the system to liquation increases with growth of acidity of induced anions in the order $SO_4^{2-} \rightarrow Cl^- \rightarrow F^-$ and with increase of basicity of s-elements $Mg^{2+} \rightarrow Na^+ \rightarrow K^+$ that agrees with change of surface tension of a melt and correlates with the rules determined for more acidic systems. Calcium oxide is dissolved in salt melts, having high fluidity, to the greatest extent. In so doing higher concentrations of CaO were observed in melts, containing Mg^{2+} and Ca^{2+} , and the lowest ones in fluids of sulphate-alkaline composition. It can be explained by the fact that dissolution of calcium oxide occurs by ion exchange $Mg^{2+} \rightarrow Ca^{2+}$ at the phase interface of CaO – salt melt. The proximity of energetic and geometric parameters of these cations just defines process of dissolution. For alkaline cations an exchange between Na^+, K^+ and Ca^{2+} is hampered due to distinction in their charges that reduces CaO concentration in melts of R_2SO_4 and RCl. Ions of silica, aluminium and iron have not isomorphous anions in salt melts, that is why their concentrations are small. At crystallization of salt melts, saturated with oxides of calcium, silica, aluminium and iron, 4-9%, mass., of calcium silicates are formed. It testifies that alite formation is possible in liquating liquid phases of salt composition. The decrease of viscosity of oxide melt due to transfer $[MeO_4] \rightarrow [MeO_6]$ and occurrence of liquation regions with high fluidity is called upon to support acceleration of mineral formation at synthesis of clinkers with different compositions. The change of kinetics and mechanism of clinker formation in accordance with composition of liquating melts was found. The control over composition and properties of melts allows intensifying clinker formation with optimization of a phase composition and clinker microstructure. Joint impact of elements, achieved by usage of various wastes, is more effective than action of individual compounds. The optimization of composition allows considerable catalyzed effect and to obtain alite clinkers at 1350 ^{0}C. The suppression of sulphate-alkaline or halogen-containing liquation in a clinker melt is one of the helpful means of optimization of clinker structure and improving Portland cement quality.

REFERENCES

[1] Johansen, V., Kouznetsova, T.V. Clinker formation and new processes, 9th International Conference on Chemistry of Cement , theme 1 “Chemistry, structure and properties of clinker”, New Dely, 1992, vol. 1, pp.67

[2] Osokin, A.P., Krivoborodov, Yu.R., Potapova, E.N. Modified Portland cement, Moscow: Strojizdat: 1993, p.322.

[3] Sulimenko, L.M., Albats, B.S. Agglomeration processes at production of building materials, Moscow: VNIESM: 1994, p.297.

[4] Maki, I. Relationship of processing parameters to clinker properties; influence of minor components, 8th International Conference on Chemistry of Cement , theme 1 “Clinker formation and properties”, Rio de Janeiro, 1986, pp.34-47.

[5] Albats, B.S., A.P., Krivoborodov, Yu.R., Rjazin, V.P. Formation of phase composition of Portland cement clinker and kinetics of alite formation, Moscow, 1993, Cement, N3, pp.14-16.

[6] Appen, A.A. Glass chemistry, Leningrad: 1974, Himija, p.351.

[7] Pavlushkin, N.M. The foundations of technology of glass ceramics, Moscow: Strojizdat, 1979, p.538.

[8] Andreev, V.N., Mazurin, O.V., Porai-Koshits, E.A. Liquation phenomena in glasses, Leningrad: Nauka, 1974, p.195.

[9] Anfilogov, V.N., Dimkin, A,M., Bobil, I.B. Phenomena of unmixing in magma melts, Sverdlovsk, 1981, pp.3-5.

[10] Varshal, B.G. Chemical aspects of liquation phenomena in silicate and alumosilicate melts, Sverdlovsk, 1981, pp.41-51.

[11] Lisenkov, A.A. The study of distribution of calcium and magnesium cations between silicate and alumosilicate anions, Leningrad, 1981, Glass physics and chemistry, vol. 7, N5, pp.584-594.
[12] Klein, I. Die Rolle der Anionen bei der Glassschmelze, 1975, Silikates Industrie, vol. 12, pp.373-380.
[13] Johansen, V., Model for reaction between CaO particles and portland cement clinker, 1973, J.Amer.Ceram.Soc., vol. 56, N9, pp.450-454.
[14] Kondo, R., Choy S. The reaction of portland cement clinker formation, 1970, Yogyo-Kyckai-Shi., vol. 78, N1, pp.8-13.

INVESTIGATION OF GRANULATED BLAST FURNACE SLAG (GBFS) REACTIVITY BY SNMS

A.Wolter[1], G.H.Frischat[1] and E.Olbrich[2]

[1] Inst. for Nonmetallic Materials, Clausthal Techn. University, Germany.
E-mail: a.wolter@tu-clausthal.de
[2] Saint Gobain ISOVER G+H AG, Ladenburg, Germany, eva. E-mail: olbrich@saint-gobain.com

ABSTRACT

The hydration mechanisms of granulated blast furnace (GBFS) slag sand can be described as a corrosion process. It was investigated by several sophisticated methods, i.e. SEM (Scanning Electron Microscopy), AFM (Atomic Force Microscopy) and SNMS (Secondary Neutral Mass Spectrometry) after being treated with water and $Ca(OH)_2$ -, KOH - and $CaSO_4$ -containing solutions. The layers of hydration products on the surface of the glassy slag particles could be analysed accurately against hydration time, accompanied by the parallel running analysis of the eluate composition. It was observed that at first the dissolution of mainly Ca and other ions occurs, leaving the solid surface enriched in the residual composition. The composition of those surface layers, however, undergoes significant alterations upon the kind of solution and during the time of hydration. The formation of initial and subsequently formed layers and their composition is illustrated and discussed.

1. INTRODUCTION

Slag cements have gained increasing market share during recent years due to their advantages in low heat development, high durability and resistance against sulphate and other chemical attack, their light colour, low production cost and high CO_2-savings potential. The major drawback, however, is the slow early strength development in relation to portland cement.

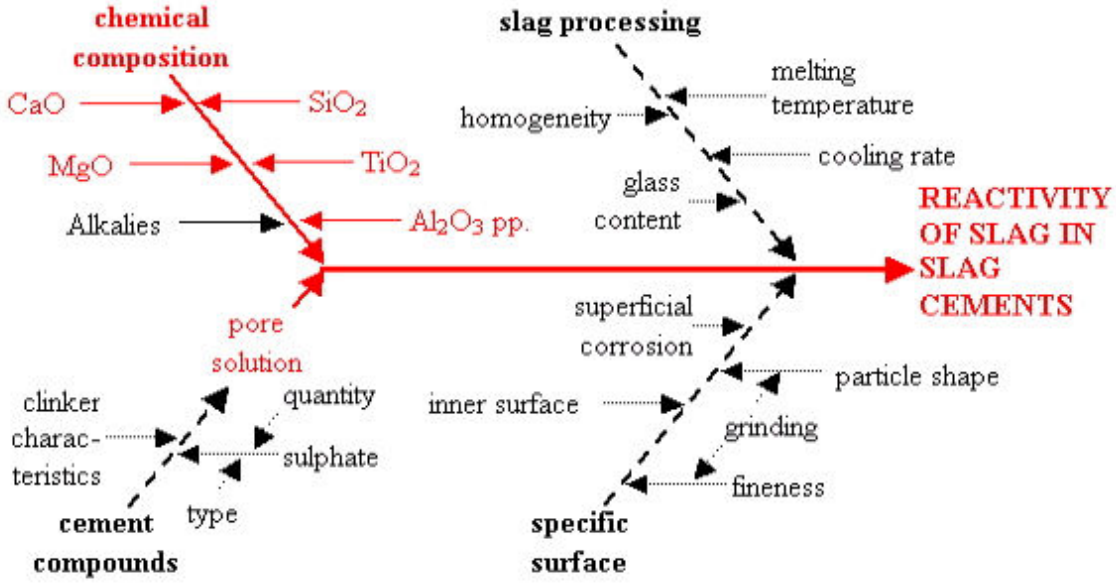

Figure 1. Systematics of influences on slag reactivity (red = considered in this contribution)

Slag cements have been produced for more than 100 years and repeatedly it has been reported that the strength performance is varying within a broad range and being subject to many influences as shown in Figure 1. Most recently a very comprehensive study on the optimization of slag cements has been published, which also contains a very detailed literature list on the subject. [1].

Since the influences on slag reactivity are rather complex, a detailed study was carried out to obtain more information about the relationship between the properties of the slag and the kind of aqueous solutions which attack the glass structure. Very advanced investigation methods like Electron Paramagnetic Resonance Spectrometry (EPR), Scanning Electron Microscopy with micro analyses (SEM-EDX), Atomic Force Microscopy (AFM) and the Secondary Neutral Mass Spectrometry (SNMS) were applied. All details of the materials, apparatus and procedures applied are given in [2] and [3].

2. MATERIALS

15 industrial and artificial slags and slag glasses were investigated which covered the common range of chemical compositions, but also the extremes like a very high alumina content, a highly increased titanium content or an increased C/S ratio. Some attention was given to the magnesium oxide content, as well. Out of that large quantity of data, only experiments with one material, "HSM/0", can be reported within this contribution in detail. The chemical composition of HSM/0 is given in table 1.

Table 1. Chemical composition of slags in mass-%

	CaO	SiO_2	MgO	Al_2O_3	TiO_2	MnO	Fe	S	Alk.	C/S
HSM-0	39	36	11,5	10,1	0,5	0,3	0,1	1,2	(0,5)	1,07

The corrosive solutions used were
pure water,
lime saturated water,
lime and sulphate saturated water,
aqueous potassium hydroxide solution and
pore solutions gained from industrial mortars after some hours of hydration by high pressure.

For all corrosion experiments the glass fraction 25-63µm was used at a water/solid ratio of 200. Such a high excess water amount was necessary for ensuring that slag grains hydrate independently and do not form a solidified microstructure. Otherwise the layer investigations by SNMS etc. could not be carried out in the way they are done here. The suspension was treated within air-sealed polyethylene bottles at 20 – 25 °C, which were agitated constantly. After the desired period, a part of the suspension was extracted and the hydration process was stopped by acetone.

3. REACTIVITY AND STRUCTURE

Slag sand <63µm was cooked for one hour in pure water. The total amount of diluted ions was determined with HCl by titration. This is called the hydrolytic reactivity which is in good relation to the value of non-bridging oxygens in (SiO_4-)tetraedra (NBO/T), see Figure 2. The NBO/T value was calculated according to [4]. Except for very high alumina slags the HCl-reactivity-value also corresponds quite well with the strength development in early and late ages (Figure 3). Therefore, we can suppose that the structural influences on the slag reactivity are mainly governed by those glass components, which are modifying the network towards higher NBO/T's, i.e. CaO, MgO, alkalis etc.

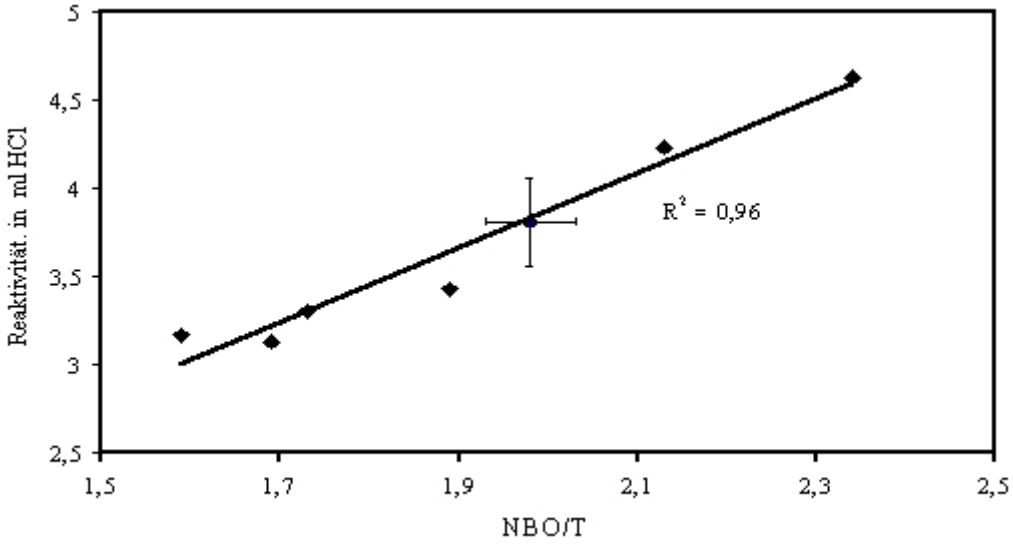

Figure 2. Correlation of hydrolytic reactivity and NBO/T values of GBFS

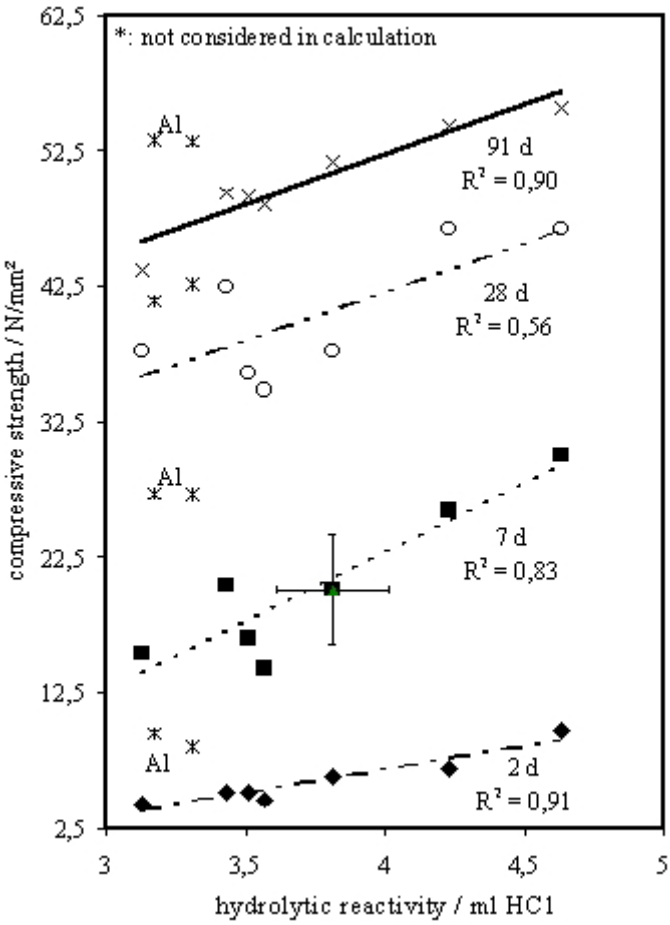

Figure 3. Correlation between hydrolytic GBFS reactivity and its compressive strength

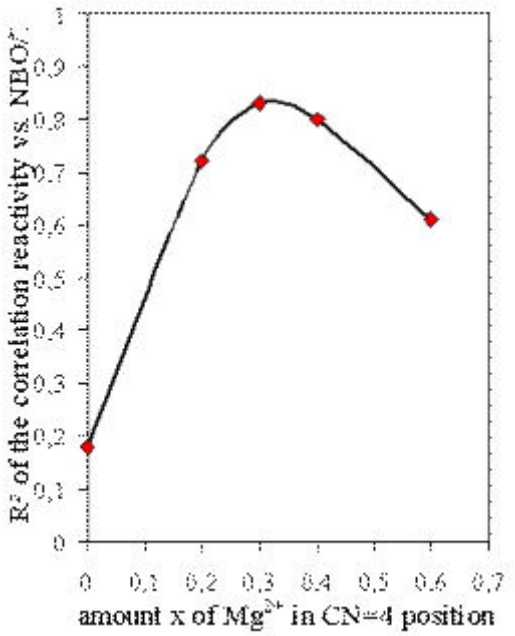

Figure 4. Fitting of reactivity vs. strength coefficient by coordination number variation of Mg

Magnesium oxide normally is considered as a 1/1 substitute of calcium oxide. However, magnesium can occur within tetrahedral oxygen co-ordination, which calcium in glassed never enters [5]. By fitting the correlation between reactivity and NBO/T values of all the slags, the best values were gained if between 25 and 35% of the magnesium was considered to be tetrahedrally co-ordinated (see Figure 4). Since manganese as Mn^{2+} follows exactly the positions of magnesium, it could be checked very accurately by EPR that around 30% of the Mn^{2+} - and Mg resp. - is network stabilizing and only 70% of it may be calculated as being equivalent to calcium in terms of slag reactivity. Furthermore titanium was investigated towards Ti^{4+}/Ti^{3+} distribution. It was found that both oxidation states occur simultaneously in GBFS, Ti^{4+} on Si^{4+} sites, whereas Ti^{3+} replaces Ca^{2+} preferably. The latter has a tightening effect on the network, thus explaining its liquifying effect on molten slag as well as its well known retarding influence on hydration.

4. CORROSION EXPERIMENTS

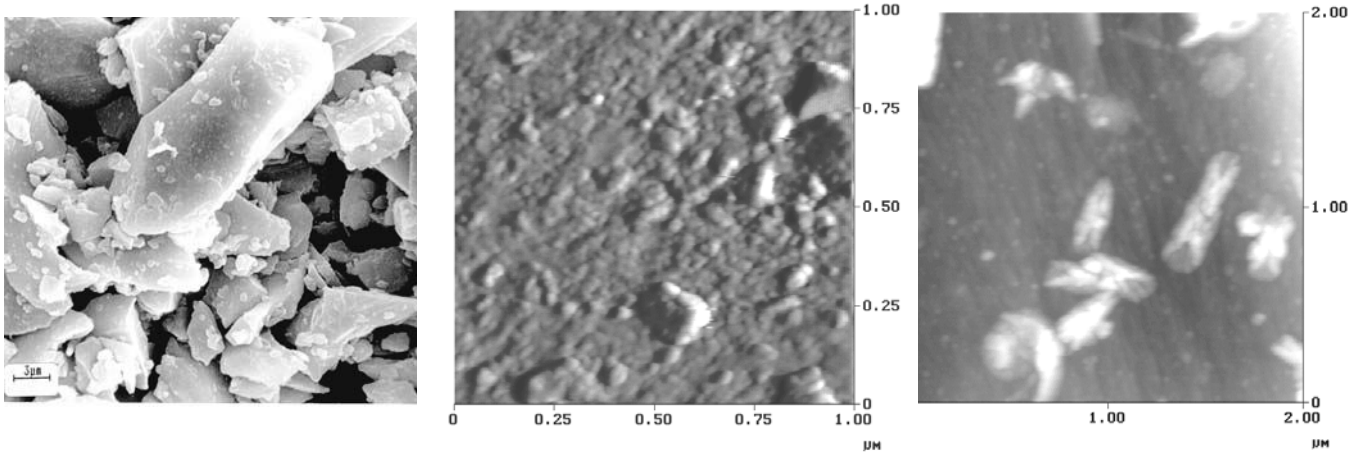

a) SEM b) AFM c) AFM (filtered)

Figure 5. Images of the untreated GBFS

Figure 5a shows a SEM image of a sharply edged morphology of normal slag sand HSM-0. Quite high resolution of the surface microstructure could be achieved with the AFM (Figure 5b). The surface of such "fresh" slag can be considered as gel-coated already. As far as the gel contains

calcium hydroxide, carbonation can proceed as shown in Figure 5c. This means that the corrosion process starts already during the wet or humid storage period before the slag is further processed.

The corrosion experiments also started with water treatment. Figure 6 shows in the upper part the development of the ionic concentration in the eluate. At the beginning, magnesium is leached out, but with increasing calcium and silicon content in the solution the magnesium precipitates almost completely. The alumina content in the solution is also very low.

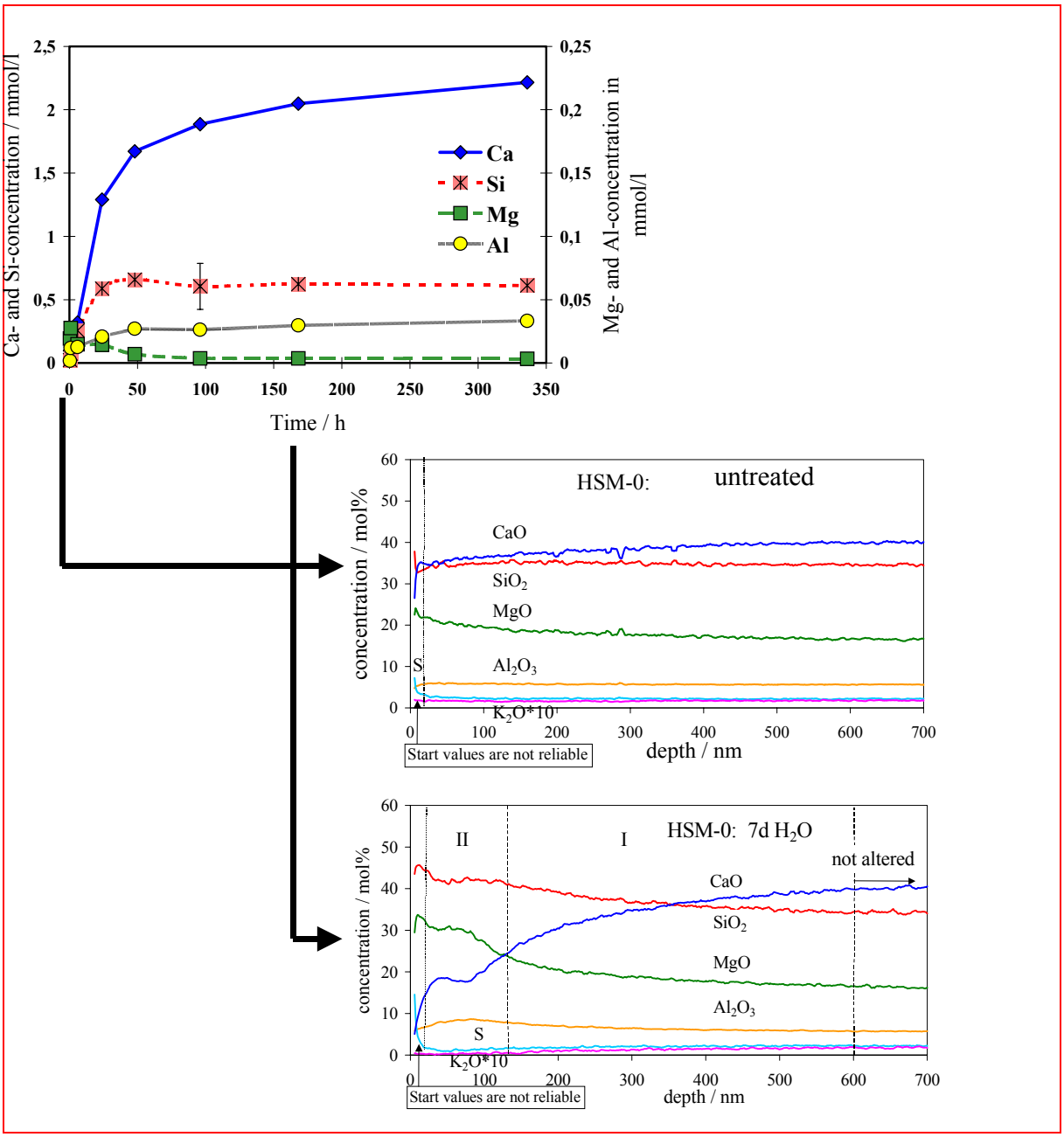

Figure 6. Eluate concentration and SNMS of corrosion layer composition: water treatment

From the fresh material and after seven days of water treatment a SMNS profile was taken (Figure 6, lower part). To obtain such composition profiles of fine grained materials, it had to be softly pressed into an indium foil before being sputtered. Comparing the fresh slag and the one after seven days of water treatment, it can be seen that the corrosion has already reached a depth of some hundred nm. It divides into at least two zones - an outer one being enriched in magnesium and silicon at a very low calcium content and an inner corrosion zone, where the calcium content slowly

comes up to its normal concentration. This corresponds very well to the eluate compositions, which show calcium dissolution quite dominantly.

If the corrosive solution is made more basic by calcium hydroxide, the alumina content in the solution is almost only half of that in water. In the beginning of the corrosion process silicon is leached out of the GBFS, which results in a reduced silicon level in zone I. Due to the low solubility of silicon in the Ca(OH)2 saturated solution, CSH and calcium hydroxide precipitate (see also Figure 8) which leads to a second zone II wich is characterized by high concentrations of silicon and calcium and low concentrations of magnesium (Figure 7, lower part). Right at the top surface silicon seems to be even more enriched, where calcium and magnesium are very low. Below that top layer magnesium goes up, but only at the beginning of the corrosion process inside to grains that seem to be somewhat increased. This finding is almost in accordance with [6], which investigated slag hydration in alkaline environments.

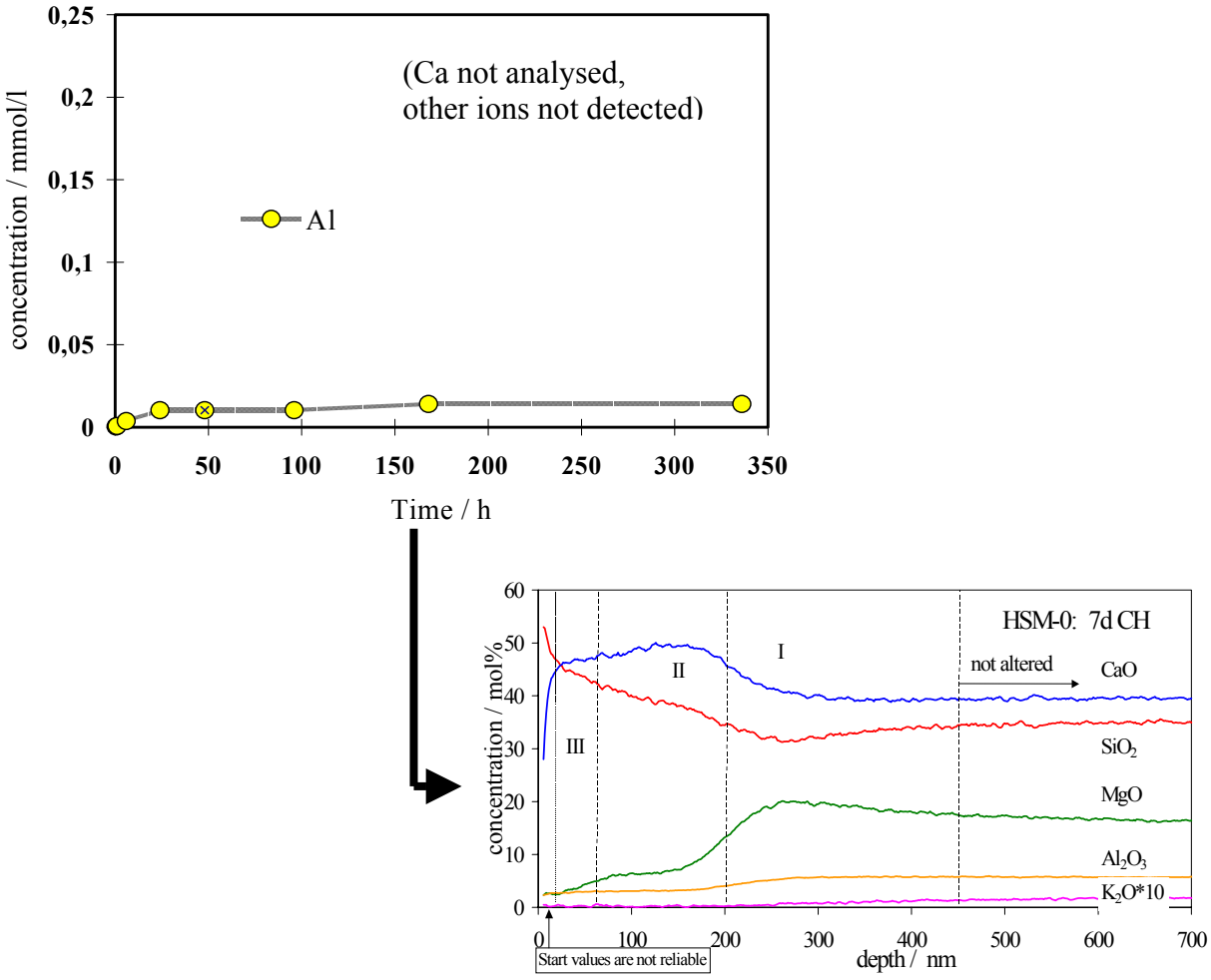

Figure 7. Eluate concentration and SNMS of corrosion layer composition: CH treatment

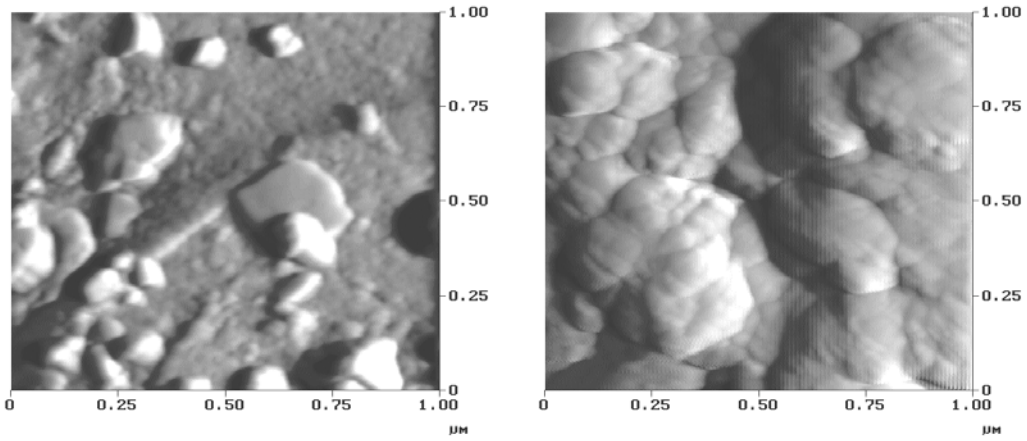

Figure 8. AFM images of CH and CSH on hydrated GBFS surface: 7 d CH treatment

Closest to the practical pore solution composition at the beginning of hydration should be one saturated by calcium hydroxide and calcium sulphate. Figure 10 shows a very slight but not significant increase in the magnesium content of the solution. The SNMS profiles however (Figure 10, lower part) show the CSH-layer formation at the surface accompanied by a decreased magnesium content. Also the sulphate seems to penetrate that corrosion layer to some extent. The calcium sulphate visible at the top surface in early ages, seems to be replaced later by a silicon rich cover layer.

The SEM and AFM images (Figure 9) show a mixture of CSH-phases and well crystallised AFt. If the tri-phases would consist only of ettringite, the alumina content in the surface layer should be significantly increased. This is definitely not the case. The explanation could be that already from the beginning silica is entering the AFt-phases to some extent. Regarding magnesium it can be stated that it does not easily enter the hydration products because in layer II its content is very low. However, the corrosion layer I of GBFS shows significantly less MgO related to water or CH treatment. This behaviour could be explained by the higher solubility of $MgSO_4$ in water compared to $Mg(OH)_2$, promoting thereby its leaching out of the GBFS.

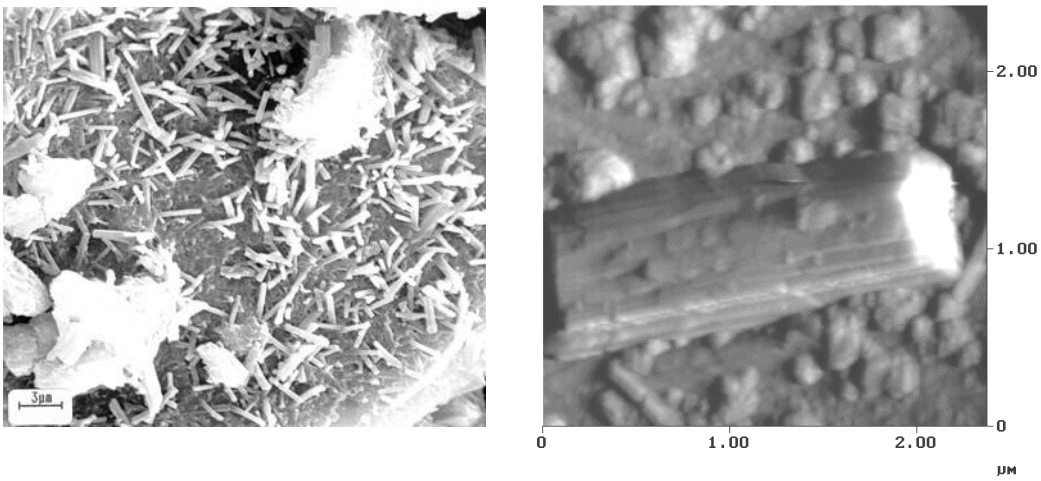

Figure 9. SEM and AFM images of GBFS surface corroded 7d by CH- and $CaSO_4$-solution

Finally, a 0,1-n-KOH solution was used as the corrosive medium. This is justified by the observation of [7,8] that, already after one day of hydration, the pore solution of mortar can contain almost only alkali hydroxides and almost no calcium and sulphate ions any longer. Figure 11 shows in the upper part an increased solubility of alumina whereas decreased silica and calcium, correspondingly.

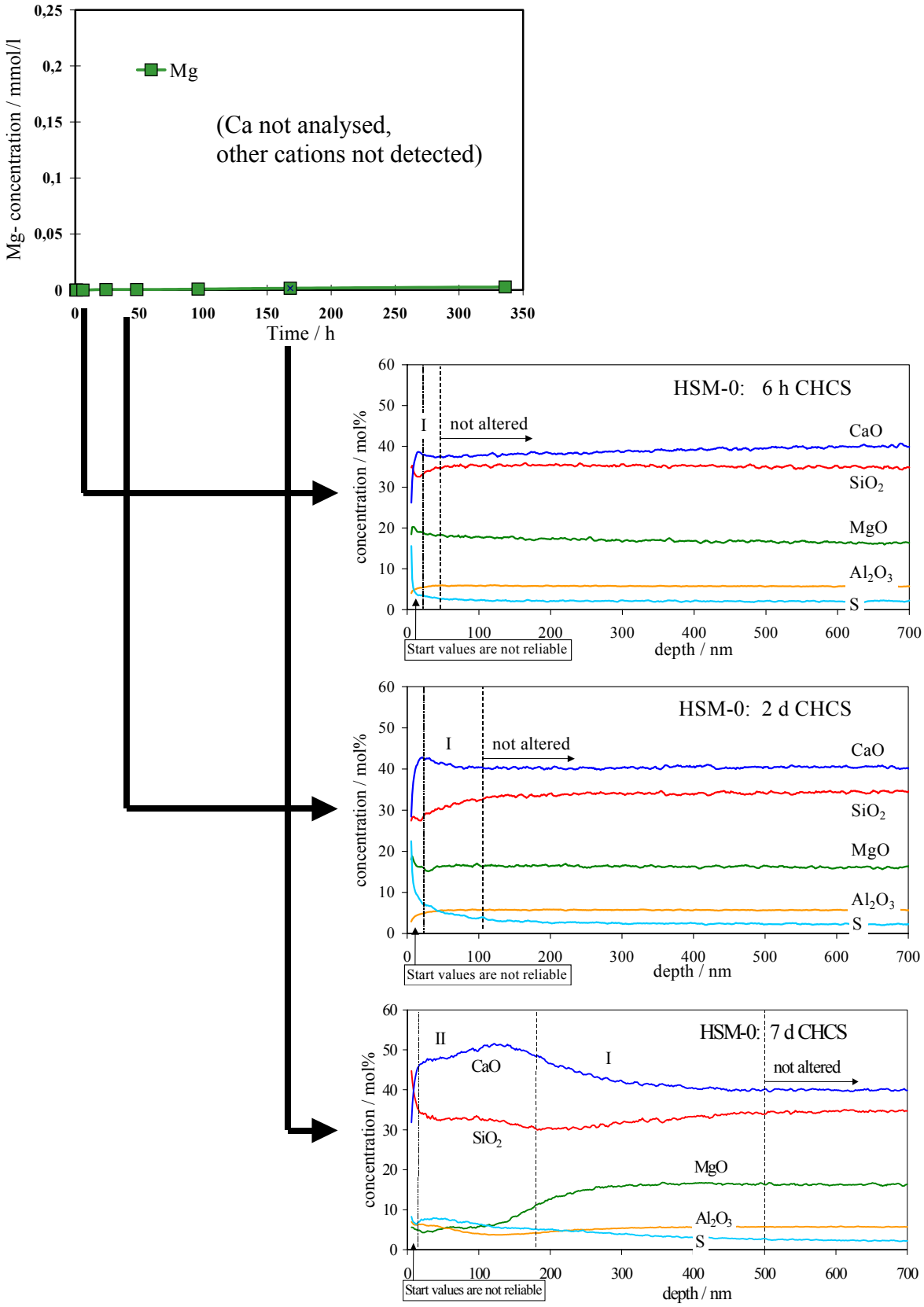

Figure 10. Eluate concentration and SNMS of corrosion layer composition: CH and $CaSO_4$

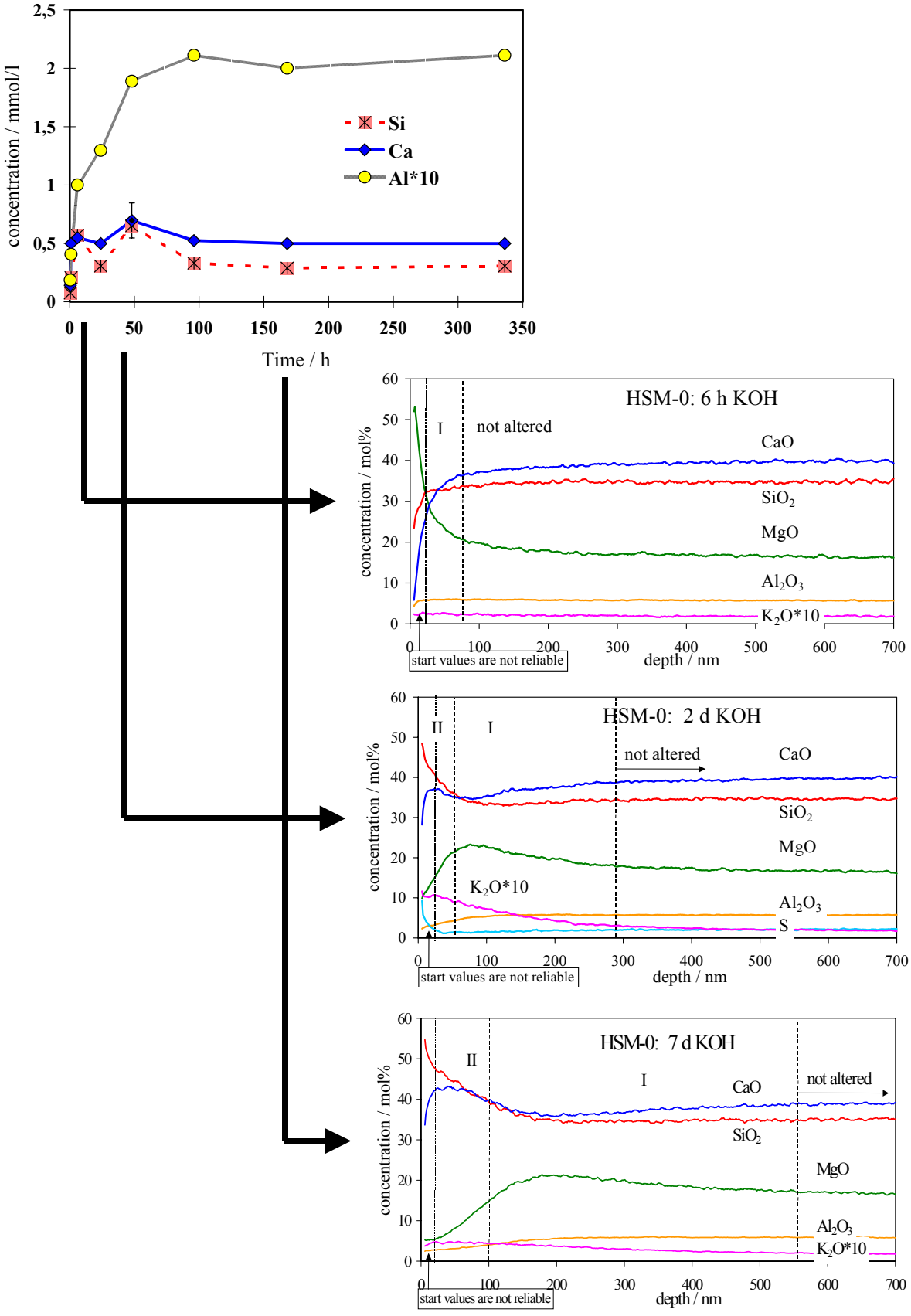

Figure 11. Eluate concentration and SNMS of corrosion layer composition: 7d KOH treatment

The outer hydration layer now contains even more silicon and some potassium is penetrating. Magnesium is sharply enriched at the outer surface at the beginning of hydration, but this effect should not be relevant in practice, because the presence of sulphate makes the magnesium more soluble. After seven days, it again seems that magnesium is reduced in the outer hydration layer but increased in the inner one.

Other experiments carried out with varying chemistry of the slag glass showed that in principle layer formation is always similar. A higher C/S-ratio significantly increases the depth of the hydration layer, whereas increased amounts of titanium act as a retarder.

The role of alumina during hydration has to be re-evaluated upon the above reported findings, because it seems that an increased alumina content only boosts the early hydration due to accelerated ettringite or AFt formation. At the later stage, if no sulphate is available any longer for reacting with the alumina, the latter seems to retard hydration and strength development.

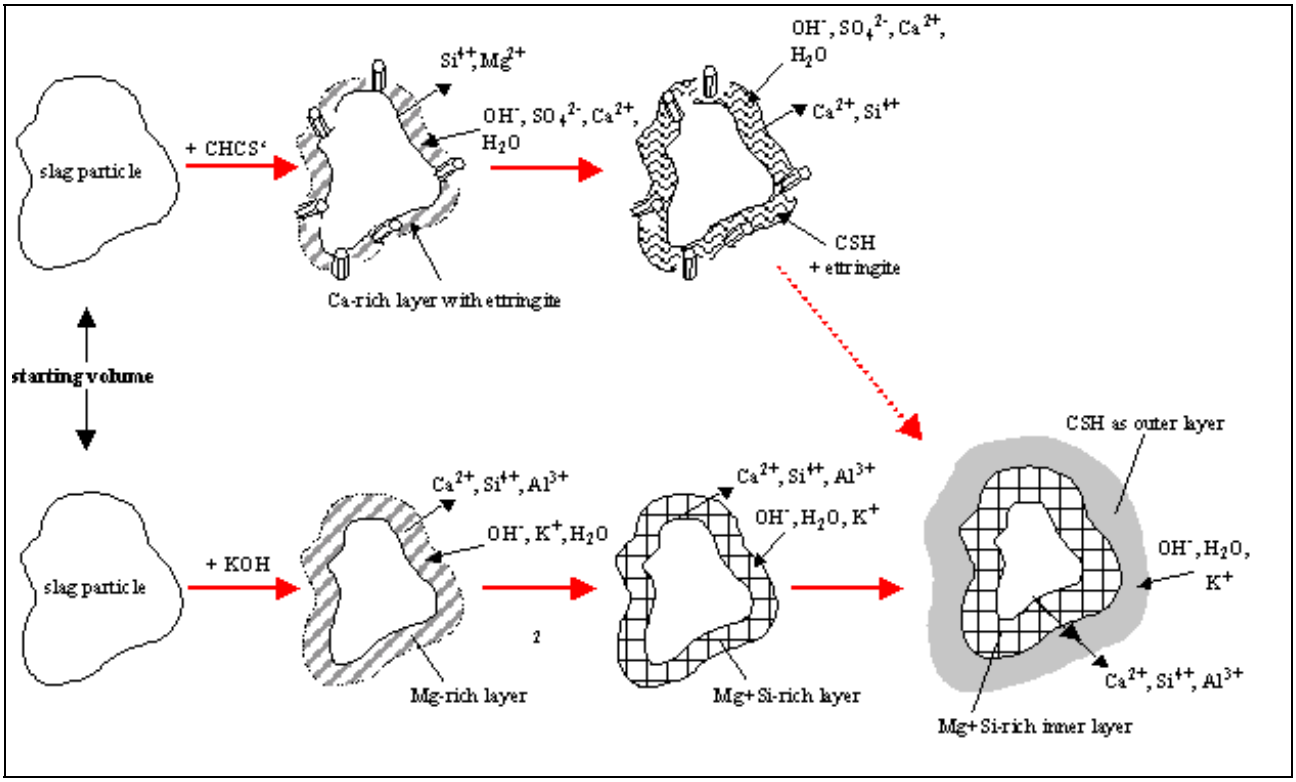

Figure 12. Layer formation model of GBFS corrosion under CH/$CaSO_4$ (upper series) and KOH treatment (lower series); the dotted red arrow indicates the transformation of the reactions following the pore solution alteration during hardening from $CaSO_4$- to KOH-dominated

5. CONCLUSIONS

The reactivity of glassy blast furnace slag is controlled by the corrosion process of the glass framework. The more the glass structure incorporates ions which produce non-bridging oxygens (NBO`s) at the SiO_4 tetrahedra, the faster the corrosion starts.

Primary acting according to this mechanism is calcium. Magnesium cannot simply be considered as a substitute for calcium, because around 20-35% of the magnesium is substituting silicon in tetrahedral oxygen co-ordination. Therefore magnesium is also partially stabilizing the glass framework.

Titanium stabilizes the glass framework, both as Ti^{4+} instead of Si^{4+} and as Ti^{3+} instead of Ca^{2+} in octahedral co-ordination. But, in contrast to calcium, titanium is tightening the framework in this position.

Also alumina is stabilising the glass framework because it is always tetrahedrally co-ordinated. This seems to be senseless because the alumina-rich slags are well known to be the most reactives. An explanation could be that only at the early hydration stages sulphate is present in the solution which makes the alumina react faster than silicon. Later on, however, if sulphate is missing the alumina is not released faster than the silicon out of the framework and the stabilizing effect of alumina limits the GBFS reactivity.

At later hydration stages when alkali hydroxide is the main constituent of the pore solution and calcium sulphate is no longer available, CSH-phases are formed predominantly at the outer part of the hydration layer. Magnesium is only a little increased deeper inside, where the corrosion starts. Taking into account the transient area of the layers, only minor differences in the corrosion depths after corrosion in the various basic solutions for seven days can be observed. Because of the continuous agitating of the suspensions in the laboratory and the high excess of water available, that might be different in practice.

The composition of the outer layer changes significantly if KOH is present because the OH^- is quasi catalytic promoting the corrosion process. It can be assumed that the concentrated KOH in pore solutions of aged mortars would act much faster than the 0,1-n-KOH applied here. Additional experiments were carried out with pore solutions pressed out of ordinary mortars after 6 and 16 hours - not discussed here - which in principle show a similar reaction scheme but deeper corrosion, faster precipitation and much higher Si concentration at the surface (at reduced solution/solid ratio of only 5).

The hydration mechanism observed here is principally divided into two steps (Figure 12)

1. a leaching of the glass structure and
2. the formation of surface layers by secondary phases occur.

Moreover, the significant difference between pore solution compositions of early stage ("CHCS") and later stages ("CH" … "KOH") must always be considered.

The reactivity of slags can never only be calculated from their chemical composition. The pore solution as well as many other factors have to be considered when modelling it.

ACKNOWLEDGMENTS

The investigations reported in this paper have been part of a research project of Readymix Cement, Germany, under the project management of Dr. Joachim Bruckmann and the supervisory of Dr.-Ing. Hans A. Brodersen. The project was supported by the German Ministry of Science, Research and Technology within its PIUS-Program, Project.-Nr. 01 RK 9651.

REFERENCES

[1] Ehrenberg, A. Optimizing of grain size distributions in slag cements (in German), Schriftenreihe der Forschungsgemeinschaft Eisenhüttenschlacken, Heft 10, Duisburg 2002.
[2] Olbrich, E. Structure and reactivity of glassy blast furnace slag (in German), Dissertation 1999, Technische Universität Clausthal.
[3] Olbrich, E. and Frischat, G. H. Corrosion of granulated glassy blast furnace slags in aqueous solutions, Glastech. Ber. Glass Sci. Technol., 74 (2001), No. 4, pp 86-96.
[4] Mills, K.C. Structure of liquid slags, Slag Atlas, Verlag Stahleisen, Düsseldorf 1995, pp. 2-8.
[5] Scholze, H. Glass – origin, structure and properties (in German), Springer Verlag Berlin etc. 1988

[6] Rajaokarivony-Andriambololona, Z., Baillif, P., Thomassin, J.H. and Touray, J.C. Hydration mechanisms of glass from granulated blast furnace slag in water and alcalic milieu (in French), Competes Rendus hebdomadaies des Séances de L'Academie des Sciences, Paris, Série II, 1988, **307**, pp. 347-354 (cited in Lea's 1998, p. 656)
[7] Lawrence, C.D. in Symposium on Structure of Portland Cement Paste and Concrete, Highway Research Board, Sp. Rpt. 90 (1966), p. 378, Washington DC (cited in H. F. W. Taylor 1997, p. 213)
[8] Locher, F.W. Cement – fundamentals of production and use (in German), Düsseldorf 2000, p. 205.

PERFORMANCE OF BLENDS OF POLYCARBOXYLATE POLYMERS IN DIFFERENT CEMENTS

U. Maeder and I. Schober

Research and Development, Sika Schweiz AG, Zürich, Switzerland.
E-mail: maeder.urs@ch.sika.com and schober.irene@ch.sika.com

ABSTRACT

The number of different cement types, aggregates and consequently concrete mixes is increasing. Incompatibilities of the different constituents with admixtures can therefore not be excluded, especially when low water/cement ratios are used.

Effects of polymers having a different number of polyoxyethlene (PEO) graft chains relative to the length of the backbone or having modified backbones were evaluated in cement paste by measuring adsorption and in mortar and concrete compositions. The effects of the polymers on the fluidity of the cementitious systems are significantly different. Whilst one polymer gives a very strong initial water reduction another one shows increasing flow with time. Different blends of the two polymers have been successfully used in RMC and self-compacting concrete mixes in different climate zones.

U. Maeder is Product Technology Director, Construction Chemicals and Mortars at Central R+D, Sika Schweiz AG, Zürich, Switzerland.

I. Schober is Head of the Polymer Development Lab at Central R+D, Sika Schweiz AG, Zürich, Switzerland.

Keywords: adsorption, polymer blends, cement, polycarboxylates, superplasticizers, workability, retention.

1. INTRODUCTION

In the last few years special concretes have become increasingly important in many parts of the world, but especially in Japan. There is a trend within the ready mixed concrete industry towards trademark concretes with specific performance characteristics.

These concretes can be used to improve appearance, construction efficiency and technical performance of concrete structures.

Apart from high strength, high durability or low density concrete the SCC (Self compacting concrete) is taking increasing market share. SCC is able to flow under its own weight through and around densely packed reinforcement without bleeding or segregation, forming a compact void free mass without the need for any vibration.

The benefits of this technique include reduced construction time, reduced noise, less manpower for placing and potential for increased automation (1).

To achieve this goal a new approach to concrete mix design is required. The volumes of paste and fines are increased while the coarse aggregate volume is reduced to minimize the risk of aggregate bridging. The low water content combined with the high paste volume leads to a cohesive mix with low tendency to segregate. The required flow and the flow retention is achieved by using special types of superplasticizers.

While concrete with normal requirements can be produced using traditional superplasticizers like Naphthalenesulfonate, Vinylcopolymers or Melamine sulfonate, the high requirements of special concretes and in particular SCC requires the use of special polymers (2, 3, 4). Among these special polymers the polycarboxylate-type superplasticizers have become the most widely used within the last few years.

The molecular structure of the new polymers differs completely from conventional ones (8, 9-11). The traditional polymers consist of long main chains carrying negatively charged side groups. These polymer adsorb strongly onto the surface of the cement grains and the ionic groups exert an electrostatic repulsion that prevents particles coming too close together.

The new polymers on the other hand typically feature short principal chains (backbone) containing ionic functions and very long polyether type side chains, that can separate particles by strong steric repulsion.

Considering the manifold properties of a polymer, like molecular weight of the whole polymer, backbone or side chains, ionic strength, chemical composition or production conditions, an extraordinary variety of special performing polymers is feasible.

Worldwide an increasing number of different cements, binders and aggregates are used for concrete production and different climates have to be considered. With a set of different polycarboxylatetype superplasticizers that can be blended, nearly all requirements to fit the various applications are covered. The blending of water reducing and slump-retaining polymers will be presented in this paper as well as case studies, which benefited from the principle.

2. EXPERIMENTAL

2.1 Polymers:

Five polymers of the polycarboxylate-polyglycolether type were tested in this study. Polymers P1 and P2 are based on polymethacrylic acid and polymer P3 is based on polyacrylic acid. Polymers P1 and P5 are specifically designed as water reducing polymers while polymers P2, P3 and P4 are designed as slump-retaining polymers. Molecular weight and sodium content of the polymers are listed in Table 1.

Table 1. Physical data

Polymer	M_w	Na^+ (%)
P1	24 000	5.8
P2	24 000	2.6
P3	20 000	1.1
P4	31 000	4.7
P5	22 000	3.8

2.2 Composition of the Mortar Mixtures

The two most widely used Swiss cements (C1, C2) and one Japanese cement (C3) were used for testing the polymers. The composition of the cements can be found in Table 2.

A rotary type laboratory mixer (Hobart X1 N) was used to manufacture all mortars employing the same standard procedure: The superplasticizer was dissolved in the water and the solution added to the previously dry mixed (1 minute) sand and cement. The mortar was then mixed for three minutes and The consistency was determined using the "flow table spread" according to DIN 18555, part 2.

The diameters of the spread mortar were measured in two directions and the average value was regarded as initial flow value. The measurement was repeated after 30 and 60 minutes with 30 seconds mixing of the mortar. The change of the flow value with time is a measure of the loss of fluidity of the mortar. The water cement ratio was fixed at 0,42. The cement used in the single tests is always indicated. A defoamer was added to all polymers prior to the tests.

In a second series of tests, the polymers P4 and P5 were tested in cement pastes with cements C1 and C3. This test was described by Nawa et. al. [6] and consists of placing a cement slurry with constant W/C ratio into a cylindrical cone of 50 mm diameter and 51 mm height. The cone is lifted and the width of flow of the slurry measured.

Table 2. Cement types

Cement	C1	C2	C3
C3S (%)	66.3	67.5	64.7
C2S (%)	10.8	5.7	13.9
C3A (%)	6.4	1.2	7.6
C4AF (%)	8.2	21.3	8.9

2.3 Adsorption measurements

Cement and water including the superplasticizer were mixed with a mechanical stirrer at a constant speed. The water cement ratio was fixed at 0,5. The dosage of the polymer was chosen as 1% of a 40% solution (400mg solids per 100 g PC). After a determined period of time the slurry was centrifuged and the supernatant separated and filtered. The remaining amount of polymer in solution was then determined by high performance liquid chromatography (HPLC). The difference of polymer concentration in solution before and after contact with cement was calculated as adsorbed polymer.

This procedure was feasible and accurate for P1, P2, P4 and P5 but not for P3. P3 contains side chains that are cleaved off in alkaline media resulting in a change of the polymer peak in HPLC detection. In this case the adsorption could not be measured.

The cements used in the adsorption measurements are listed in Table 2. The cement phases were determined according to Bogue's equation. The specific surface was of the same order for all three types (Blaine value 3500 cm2/g +/- 100)

3. DISCUSSION

3.1 Mode of action of Superplasticizers

Due to an optimised ratio of methacrylic acid to polyoxyethylene side chains, polymer P1 was designed as a water reducer for type I cements. The dispersing effect is due to ionic repulsion combined with sterical hindrance. The relatively high ionic strength leads to a fast adsorption on the cement grains during the mixing process and, thus, a strong initial plasticizing effect.

P2 is designed as a slump-retaining polymer due to a different ratio of methacrylic acid and polyoxyethylene side chains. The ionic content is much lower compared to P1 and thus adsorption

is slower and less giving a lower initial flow. The polymer remaining in the water phase of the cement paste can adsorb later on the growing surface of the hydrated cement particles.

Polymer 3 was also designed as a slump-retaining polymer. It is based on polyacrylic acid. The side chains are attached via ester bonds that are cleavable under the highly basic conditions we have in hydrating cement paste (pH 13.5). The very low ionic content of the polymer causes a very low initial flow, leading to the interpretation that only a small portion of the polymer adsorbs on the cement grain. However, as the cleaving of the side chains starts immediately after addition to the cement, the molecule gets a more ionic character and its adsorption potential increases with time. The result in mortar or concrete is an increased workability over the time (6, 8-9).

Polymer P4 is another slump-retaining polymer, which shows its best performance at moderate to low w/c ratios. It is based on polymethacrylic acid and has a similarly low ionic content to P3.

Polymer P5 is similar to P1 with about the same number of ionic groups but with a smaller molecular weight distribution.

3.2 Influence of cement quality

Superplastizicers (SP) are increasingly used for the production of quality concrete. The problem is that a SP might work well with one cement but not with another, or in one place but not the other. Some of the results from experimental work with Portland cement are presented in earlier papers (2, 3, 4).

Even in a small market like Switzerland (4 Million tons/year), cements of the same class (CEM I 42.5) from different suppliers sometimes produce concrete with a completely different performance with the same admixture and aggregates. With the help of adsorption measurements, we are able to reveal but not necessarily explain such differences in all cases.

3.3 Adsorption Tests

Adsorption of water reducing polymers on the cement is one key factor to obtaining a plasticizing effect. The influence of the C3A content on adsorption is understood today (4-7, 9-10). In Figure 1 the adsorption of Polymer P1 and P2 is shown on three different cements that are listed in Table 2.

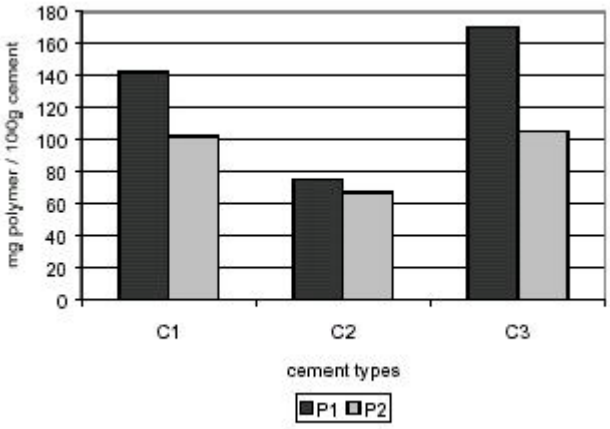

Figure 1. Adsorption of P1 and P2

Polymer P1 adsorbs on all cements in a higher amount compared to P2 due the higher ionic strength of P1. The amount of adsorbed polymer of P1 on C3 is much higher compared to C1 while the adsorption of P2 is of a similar order. Although C1 and C3 have nearly the same composition the adsorption of P1 on these cements is significantly different.

As the adsorption is closely related to water reduction (12) a different performance can be expected in mortar.

We found that P1 is more sensitive towards different cements in adsorption, and hence should also be more sensitive in water reduction.

Comparing adsorption of P4 and P5 on Swiss (C1) and Japanese cements (C3), we find a clearly higher amount of slump-retaining polymer P4 adsorbed on C3 whereas the adsorption of P5 is in the same range with both cements. The water-reducing polymer P5 is clearly more adsorbed than P4 in both cements.

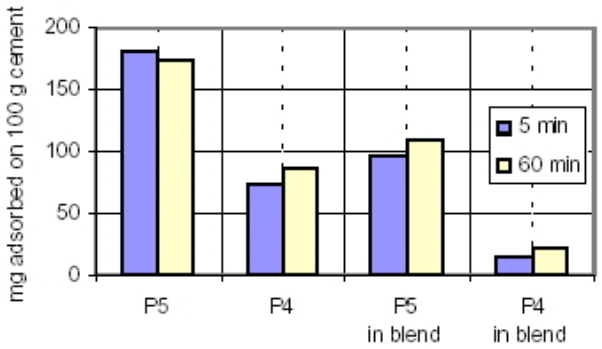

Figure 2. Adsorption of P4 and P5 on C1 (400 resp. 200/200 mg in blend per 100 g PC)

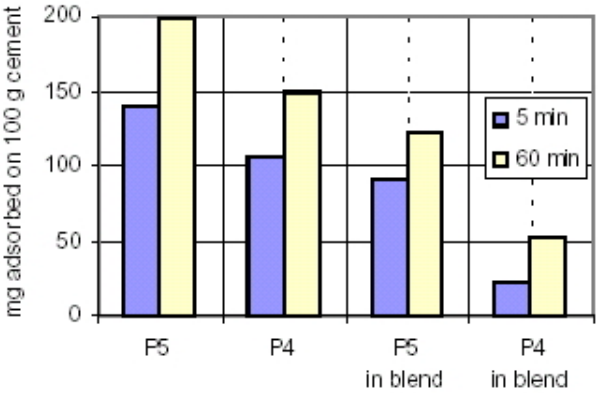

Figure 3. Adsorption of P4 and P5 on C3 (400 resp. 200/200 mg in blend per 100 g PC)

However, both polymers adsorb faster on C1 than on C3. In both cements the 1:1 blend of the polymers adsorbs less than the individual components and polymer P5 is preferentially adsorbed.

3.4 Results in Mortar

Mortar tests of a polymer 1 based SP with three different commercial cements (CEM I 42.4) and with one blend (C1-3) of the three are shown in Figure 4. The admixture shows the best performance in the cement blend. Significant differences were obtained with the single cements. A much higher flow and the best flow retaining effect was observed with C1 compared to mortars with C2 and C3. Hence, P1 is less useful as SP for C2 and C3 compared to C1. The synergistic effect of P1 in a blend of the three cements has often been observed and could be explained by the resulting broader grain size distribution of the blend.

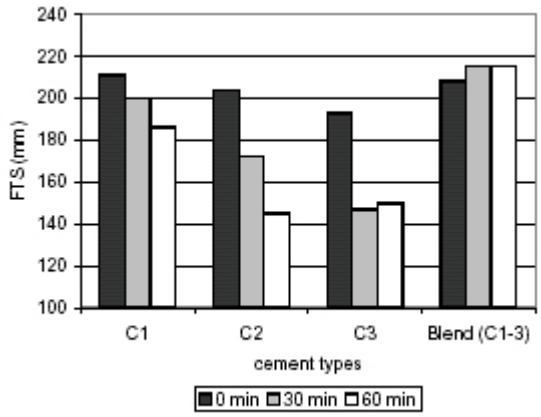

Figure 4. Mortar tests of P1 on different cement types

Both adsorption and mortar tests revealed that an admixture often has to cope with a large number of cements having different chemical and physical characteristics. Considering furthermore all different types of aggregates (spherical, crushed, volcanic) used to prepare concrete, or the different climates concrete is used in, the adaptation of polymers or admixtures to face this problem is essential. Blending of P1 with P2 or P3 is one possibility.

3.5 Performance of P5 and P4 in cement pastes

Comparing the flow results of polymers P4 and P5 in Swiss (C1) or Japanese (C3) cement pastes we see a higher water demand for C1 compared with C3. The flow with P5 alone is high and steady in both cements, but much lower with slump-retaining polymer P4 which showed increase of slump with time in C3. The 1:1 blend of the two polymers shows good effect in C3 with constant flow with time, whereas the effect of blending P5 with P4 in C1 is poor. We see a generally more sensitive behaviour towards different polymers of the Swiss cement compared to the Japanese one.

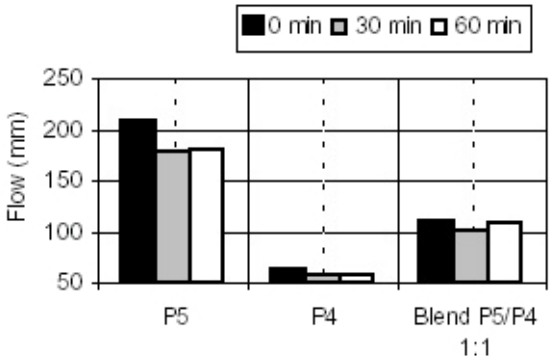

Figure 5. Cement paste flow with C1 (W/C = 0.30)

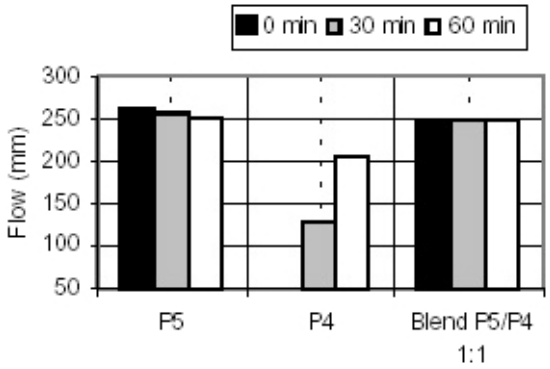

Figure 6. Cement paste flow with C3 (W/C = 0.23)

3.6 Performance of polymer blends in mortar

Blending polymer P1 with P2 or P3 has the main target to produce a SP with high initial flow and good flow retaining capabilities with time. Figure 7 shows mortar tests of admixtures based on P1 and P 2. For this tests cement C1 was used.

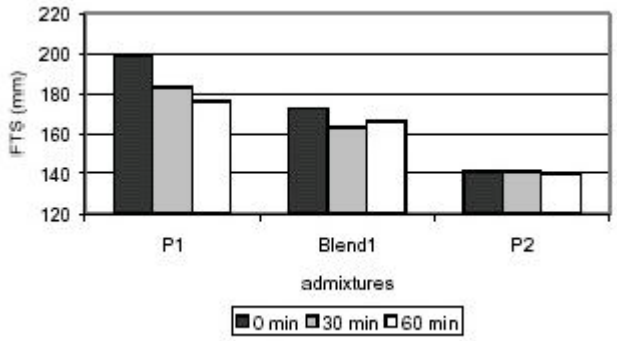

Figure 7. Mortar tests of Blend 1

P1 shows a high initial plasticizing effect followed by a loss of workability whereas P2 shows a constant but lower flow over time. Blend 1 is obtained by mixing P1 and P2 in a ratio of P1/P2 = 2/1. As a result the flow retaining capabilities are enhanced at lower flow level than with P1 alone.

However, the reduction of the initial flow is due to a reduced amount of P1. P1 adsorbs fast because of its higher ionic strength. P2 remains in the liquid phase of the cement paste and will adsorb when

the specific surface of the hydrated cement increases and the hydration products would lead to stiffening of the paste.

Figure 8 shows mortar tests of admixtures based on P1 and P3. For this tests cement C1 was used. The main characteristic of P3 is its increasing plasticizing effect over the time. Blend 2 is obtained by mixing P1 and P3 in a ratio 3.5/1. Compared to P1 a more constant flow retaining effect can be observed, however, some loss of initial flow has to be accepted. P1 adsorbs preferably and more rapidly, while most of P3 remains in the liquid of the cement paste. As soon as a certain number of side chains of P3 are cleaved, P3 will be able to absorb more readily as well and compensate for the fluidity loss of P1.

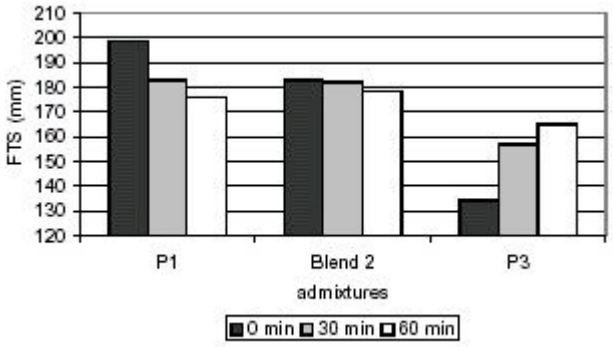

Figure 8. Mortar tests of Blend 2

Although the flow retaining capabilities of P2 and P3 are based on different modes of action, both can be used to compensate for loss of flow of a water reducing polymer like P1. The ratio of P2 and P3 to be used depends on cement type and water cement ratio. Hence, a tool to compensate for fluctuations in concrete mixes due to different cements, climates or aggregates is at hand.

In order to improve the flow retaining capabilities of a P1 based admixture, blend 3 (P1/P2 = 1.5/1) and Blend 4 (P1/P3 = 2.5/1) were tested. In both cases the desired property was improved and especially the performance of blend 4 was now comparable to the mortar made with cement C1 with polymer P1. (Figure 9) Hence, the blending of the polymers P1, P2 and P3 is a smart solution to overcome problems due to variations in cement.

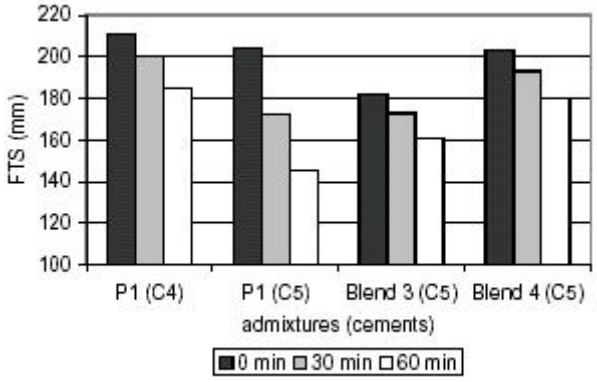

Figure 9. Mortar tests of Blends 3 and 4

4. CASE STUDIES

Two case studies demonstrate the successful application of this concept on construction sites with SCC applications. Having different cements, aggregates, and requirements for both job sites, the

same basic polymers were used by simply varying the polymer ratio. The concept has been successfully used in numerous applications in all parts of the world and in SCC, precast or ready mix concrete applications.

4.1 Protection shield of a railway tunnel

4.1.1 Problem

For protection of a railway tunnel a shield of several horizontal jacked concrete pipes was designed. The pipes had to be filled with concrete to increase their stability. Each pipe was 150 meters long with a diameter of 1.5 m. For this purpose 2000 m3 concrete had to be placed (Figure 10).

Figure 10. Railway tunnel

4.1.2 Solution

The pipes had to be filled completely in two stages of 75 meters each. A posterior injection was not necessary. SCC was proposed to be the concrete of choice for this difficult task. Blend 3 was chosen because of the best compatibility with the cement used for this job, regarding both slump retention and strength requirements. The mix design used is listed in Table 3.

Table 3. Mix Design

Aggregate	0 / 16 mm
Cement	380 kg/m^3, CEM II / A – L 32.5
Additive	50 kg/m^3 Flyash
Admixture	1.7 % admixture for SCC based on P1 and P3
Water	200 l/m^3
Slump flow	71 cm

4.1.3 Application

The concrete was pumped over a distance of 120 m and had to flow for an additional distance of 25 m. The quality of concrete did not suffer at all even after this long transportation distance. Quality checks before and after pumping gave comparable results regarding flowability. Furthermore, the early strength (7 days) before (35.2 N/mm2) and after pumping (37.9 N/mm2) as well as the final strength (28 days) before (47.2 N/mm2) and after pumping (44.6 N/mm2) gave

nearly the same values. This indicates the homogeneity achieved with the selected SCC mix after placing.

Compared to conventional concreting (207 working days), a time saving of 2500 working hours was achieved by the use of SCC. By using SCC the job was completed in 28 stages of 50m lengths, instead of 90 stages of 15m lengths using traditional concreting.

Additionally, the use of vibrators would make the operation difficult and time consuming, something which is unnecessary when SCC is used.

4.2 Reconstruction of a Hydro Power Station

4.2.1 Problem

For the reconstruction of a hydro power station, columns had to be filled with concrete. The height of each column was 9 meters. A special feature of these columns was their particularly dense reinforcement and their varying cross-sections. Hence, in this case the use of normal concrete with vibrating equipment was hardly possible. Figure 11 shows a picture of the columns.

Figure 11. Hydro Power Station

4.2.2 Solution

As a solution SCC concrete was proposed. The columns could be perfectly filled with a crane bucket only using a Tremie near to the bottom of the formwork. The mix design listed in Table 4 was used:

Table 4. Mix Design

Aggregate	0 / 16 mm
Cement	350 kg/m^3, CEM I 42.5
Additive	80 kg/m^3 Flyash
Admixture	1.4 % admixture for SCC based on P1 and P3
W/B	0.44
Water	190 l/m^3

4.2.3 Application

The filling could be done in one pour. The columns were completely filled without any bugholes. The hardened concrete achieved a compressive strength of 59 N/mm2 after 28 days as planned. The constructor was able to reduce his costs due to time and labour saving during the placing of the concrete.

5. CONCLUSIONS

It is well known and it was shown in this paper that different cements often interact in a different way with a particular superplasticizer.

There are many ways to overcome cement/superplasticizer incompatibilities, which can be expressed as a rapid loss of fluidity with time. One way is to formulate the superplasticizer with flow enhancing admixtures or, what was shown in this paper, to combine water reducing and flow retaining polymers.

The new developments in concrete technology like HPC or SCC require a new generation of polymers with their extremely high water reduction and /or flow retaining properties. Polycarboxylate polymers can be designed to show different adsorption properties on specific cements. The different adsorption properties can be correlated with high initial flow in cement paste or mortar and with retarded action of the molecules, giving flow-retaining properties.

The numerous successful applications of this blending concept, which have been completed worldwide, confirm the findings made in this lab study.

REFERENCES

[1] Skarendal, A., Petersson, O., Self-Compacting Concrete, Proceedings of the First International Symposium, Stockholm, September, 1999, RILEM Proceedings 7, 1999

[2] Flatt, R.J., Houst, Y.F., Bowen, P., Hofmann, H., Widmer, J., Sulser, U., Mäder, U. and Bürge, T.A.: Optimization of superplasticizers: from research to application', Proceedings of the international RILEM Symposium, Monterrey, Mexico, March 1999, RILEM Publications s.a.r.l., Cachan Cedex, 1999

[3] Flatt, R.J., Houst, Y.F., Bowen, P., Hofmann, H., Widmer, J., Sulser, U., Mäder, U. and Bürge, T.A.: 'Interaction of superplasticizers with model powders in a highly alkaline medium', Proceedings of the 5th CANMET/ACI International Conference on Superplasticizers and other Chemical Admixtures in Concrete, (ACI Institute, Detroit, SP-173, 1997)

[4] Mäder, U., Kusterle, W. and Grass, G.: 'The rheological behaviour of cementitious materials with chemically different superplasticizers', Proceedings of the international RILEM Symposium, Monterrey, Mexico, March 1999, RILEM Publications s.a.r.l., Cachan Cedex 1999

[5] Yamada, Takahashi, Hanehara, Matsuhisa, Effects of the chemical structure on the properties of polycarboxylate-type superplasticizer, Cement and Concrete Research 30 (2000), 197 – 207

[6] Nawa, T., Ichiboji, H., Kinoshita, M.: Influence of Temperature on Fluidity of Cement Paste Containing Superplasticizer with Polyethylene Oxide Graft chains, 6th CANMET/ACI 2000, SP 195-13

[7] Ohta, A., Sugiyama, T., Uomoto, T.: Study of Dispersing Effects of Polycarboxylate-based Dispersant on Fine Particles, , 6th CANMET/ACI 2000, SP 195-14, pp 211-227

[8] Hamada, D., Sato, T., Yamato, F., Mizunuma, T.: Development of New Superplasticizer and Its Application to Self-Compacting Concrete, 6th CANMET/ACI 2000, SP 195-17, pp 269-290

[9] Ferrari, G., Cerulli, T., Clemente, P., Dragoni, M., Gamba, M., Surico, F.: Influence of Carboxylic Acid-Carboxylic Ester Ratio of Carboxylic Acid Ester Superplasticizer on Characteristics of Cement Mixtures, 6th CANMET/ACI 2000, SP 195-31, pp 505-519

[10] Uchikawa, Functions of Organic Admixture Supporting High Performance Concrete, Rilem Proceedings 5, pp. 69 – 95

[11] Yoshioka et. al., Role of Steric Hindrance Effects of Superplasticizer on the Dispersibility of Cement Particles, Proceedings of the Japan Concrete Institute, Vol. 19, No. 1. pp 335-340 (1997)

[12] Yamada, K., Ogawa, S., Hanehara, S.: Working Mechanism of Poly-Beta-Naphthalene Sulfonate and Polycarboxylate Superplasticizer Types from Point of Cement Paste Characteristics; 6th CANMET/ACI International Conference on Superplasticizers and other Chemical Admixtures in Concrete, SP 195-23, 2000, pp.367-382

THE EFFICIENCY IMPROVEMENT IN CEMENT PRODUCTION BY KILN PRODUCTION UPGRADES, MODERNIZATION AND THUS OPTIMIZING PRODUCTIVITY - A STEP BY STEP APPROACH

Tapash Mukherjee

Works General Manager, Fujairah Cement Industries, U.A.E.

ABSTRACT

Often the plant manager of cement plant with comparatively old and obsolete technology faces the problem of maintaining stable operation of the plant and thus optimizing the cost of production. Such plants are often prone to breakdowns, and have higher cost of production due to old technologies with high cost of maintenance and manpower requirements. Here in most of the cases, the plant manager would like to modernize his facilities and at the same time upgrade the production to the maximum extent possible and completely modernize the plant. Such decisions can be considered only when the market is moving upward and permits some investment. However, the huge investment that might be required for complete upgrading and modernization may not be available and it always become difficult to get approval from higher authorities/Board of Directors. The best course in this case, as per the experience of the author, is to take a step by step approach so that each time the investment cost is maintained within tolerable limits and achieving at the same time considerable improvement. Thus the additional money made by such steps can be further utilized for taking further steps for achieving the final goal of optimum production and upgrading. This was tried in Fujairah Cement Industries (FCI Plant) located at a small town called Dibba in Emirates of Fujairah in United Arab Emirates. This was one of the smallest plants in the whole of the Emirates. Voest Alpine of Austria originally supplied the plant. The kiln was manufactured by Sket of then East Germany, having diameter of 4.6 M and 69 M long with Sket design 5-Stage shaft type preheater having one of the lowest thermal efficiencies. The plant capacity was under utilized with annual production remaining between 450-465,000 tons of clinker per annum.

It was decided to upgrade and modernize the plant facilities and this was done step by step keeping always the investment as small as possible with maximum benefit. The projects were formulated so that they could be executed in the shortest possible time to take advantage of upbeat market. Thus, with the benefit achieved in each step, the next step was taken easily with the additional revenue generated. The present paper describes these step by step approaches taken by Fujairah Cement Industries starting with stabilizing the existing plant and then upgrading and modernizing the plant facility. Thus, making today a plant having largest clinker production facility from a single kiln and one of the most modern plants in the whole of the Emirates.

1. DETAILS OF STEP BY STEP APPROACH ADAPTED FOR STABILIZATION, UPGRADING AND MODERNIZATION OF FUJAIRAH CEMENT PLANT.

As noted in the abstract, Fujairah Cement Industries commissioned in 1992, the following stepwise approach to reach the ultimate goal of increased production with optimum productivity by optimizing the cost of production.

Proceedings of the 11th International Congress on the Chemistry of Cement (ICCC)
'Cement's Contribution to the Development in the 21st Century'
Hosted by: The Cement and Concrete Institute of South Africa
CD-ROM produced by: Document Transformation Technologies

11 - 16 May 2003, Durban, South Africa
ISBN Number: 0-9584085-8-0
Editors: Dr G. Grieve and G. Owens
Congress Organised by: Event Dynamics

The first step taken was to stabilize and optimize the operation of the existing plant with minor investment solving the existing bottlenecks. The emphasis was given on stable and continuous operation lowering breakdowns or plant stoppages as far as possible. This in itself increased the production by around 10-15% excess of the rated capacity and thus reducing the cost of production as well. From this point onwards, the plant started turning around.

Seeing the boom in the cement market starting around 1993, Fujairah Cement Industries embarked on an ambitious project of expansion and modernization of their kiln line. However, this upgrading was only partial, keeping the capital cost as low as possible. The production was targeted to be increased by 50% at the same time lowering the heat consumption by more than 25-30%. This was done by replacing the shaft preheater with a six-stage cyclone type preheater and incorporating an air through in-line precalciner system. Also, the existing control system through PLC was replaced by Distributed Control System (DCS).

After commissioning the new facilities, production reached around 10% beyond rated capacity. The maximum production reached was around 860,000 tons clinker per year in place of guaranteed 750,000 tons clinker per year. The specific heat consumption came down from average 900-950 k.cal/kg. to around 700-725 k.cal/kg.

The market for cement at this point still continued to be good and Fujairah Cement Industries decided on second step of plant upgrading to take the capacity to One Million tonnes per year. This was done by replacing the air through precalciner system by air separate precalcining system with tertiary air ducts. The first grate of the cooler was modified with a stationery step grate and a third cooling grate was added.

Again this project was completed in record time of just over one year, and after initial teething troubles, the production was stabilized at around 3500 tons per day against a guaranteed production of 3300 tons per day.

At this stage, complete process measurements were made and it was found that pressure drop from the preheater last stage to ID fan was too high. Also ID fan was under utilized. At this time, the oil price also started going up from end of 2000/beginning 2001 and cement price also started dropping due to excess supply in the market and the Far East crisis. At this stage, FCI decided and implemented a dual firing system with provision for firing coal/petrocoke or other solid fuel as a substitute for oil, keeping the oil firing intact. Together with this, the ducting, from stage 6 to ID fan, diameter was increased to reduce the pressure drop. After completing this project in May-June 2001, today FCI is kiln is the only one in Gulf, even probably in the Middle East, being operated with 100% coal firing. Together with this, the daily average daily output has been taken to 4100-4150 tpd.

FCI has not stopped here and is already planning to take further cost saving measures in the future and if possible further increase in the production at a future opportune moment when again the market starts going up.

2. STABILIZATION OF THE EXISTING PLANT

The initial plant commissioned in 1982 was found to have mostly 3 main problems, namely, increasing vibration of ID fan due to build-up, build-up in the inlet of the shaft preheater due to high alkali and continuous snow man formation in the cooler. These problems were solved by strengthening the ID fan foundation, putting selective air blasters in the preheater to avoid build-up and also by putting air blasters in cooler to break/avoid snow man formation. By this, production could be optimized and 1990 onwards production reached around 540-560,000 tons of clinker per

year. With a single cement-grinding mill, it was difficult to cope with the market requirement and thus the cement-grinding mill was modified by replacing the old Sturtevant separator with a high efficiency separator.

3. FIRST UPGRADING PROJECT

Seeing the boom in the market the first project of upgrading was commenced at end 1993/beginning 1994 and executed over one year to complete the project in middle of 1995 in record time. Only five weeks shutdown was taken to connect the new facilities to the existing plant. The emphasis on this project was to increase production and at the same time reduce the cost of production by lowering heat consumption with the introduction of more modern technology. With this project, the kiln capacity was designed to be increased by 50% from the existing 1600 tpd to 2500 tpd at the same time to reduce the heat consumption by more than 25-30% from level of 900-950 kcal/kg of clinker in the past to around 700 kcal/kg of clinker guaranteed. Krupp Polysius was selected for detail engineering as well as supplying the main machinery. UB Engineers of India was selected for fabricating steel structures and normal steel items and for erection of the plant.

Krupp Polysius supplied the following:

- Kiln feed system with new AEROPOL for feeding kiln at the higher output.
- 6 stage DOPOL-90 Preheater with PREPOL AT in place of the existing Sket shaft preheater.
- New I.D. fan with new exhaust gas duct. ID fan was driven by a VFD in place of old D.C. motor.
- Oil fired Precalciner burners.
- Enlarged kiln inlet section to reduce the velocity at inlet.
- Increase Kiln speed increase 2 to 2.7 rpm by putting a new gear box and girth gear and pinion.
- Modification of the existing clinker cooler with larger throat, jet ring plates and different cooling air fans.

A vertical roller mill with 80 tph capacity was added to meet the additional demand of raw meal keeping the existing ball mill operating as it is.

The kiln was back on stream after a short shutdown of five weeks in May 1999. This was a unique achievement with 6 stage preheater of 135 m height, which is one of the tallest industrial structures in the whole of United Arab Emirates and was built in record time of just one year. Within a short period, the kiln reached its rated capacity and in fact it exceeded its design output by more than 10% using the built-in provision kept in the design.

Stage I Operating Results:

	Guaranteed	Achieved
Throughput:	2500 tpd of clinker	2925 tpd of clinker
Heat consumption:	721 kcal/kg clinker	723 kcal/kg clinker
Power consumption:	16 kWh/t	14.28 kWh/t
Clinker temperature:	90 Deg. C above ambient	132 Deg. C above ambient.

The increased clinker outlet temperature has to be seen in connection with the very high clinker throughput. The electrical system was supplied by ABB of Dubai and old PLC with Procontic computer was replaced by a Distributed Control System with kiln and mill operation controlled through colour monitors and an operating station recording and logging all the parameters and giving commands for plant operation through a keyboard and mouse.

A baghouse was introduced in the kiln and raw mill exhaust system parallel to the existing electrostatic precipitator to take care of increased exhaust gas and the conditioning tower was modified for improved ESP efficiency.

4. UPGRADING AND MODERNIZATION

Seeing the continued upbeat market, it was decided to further upgrade production to one million tonne clinker per annum at the same time emphasizing further cost reduction and introducing greater environment or pollution control. The latest electrostatic precipitator was provided for dedusting of the cooler exhaust air and a further baghouse unit was added for dedusting of the kiln and mill system.

The project design for the kiln line was to incorporate the following:

- New larger kiln feed system with AEROPOL.
- New larger dedusting cyclones on top of preheater.
- New larger I.D. fan.
- Tertiary air duct.
- New Precalciner burners to increase the proportion of oil firing in the calciner from40-60%.
- Increased Kiln speed increase to 2.7 to 4 rpm.
- New static grate at existing clinker cooler.
- Additional 3rd clinker cooler grate.

To meet the additional demand of raw meal, a new ball mill of 2500 KW was added with combiflex drive having 4.2m in dia. x 9 m long working in tandem with the first ball mill to increase the ball mill output from 110-130 tph to around 210 tph. The actual achieved output was 240-250 tph by changing the grinding media pattern and replacing the old mill liner to have only crushing at this stage and grinding being taken care of in second mill. This tandem operation was done in conjunction with a sepol separator with provision for reject going to both the ball mills.

After a stoppage of around seven weeks, for the tie-in works, as well as changing the kiln roller bearing system, the kiln line went back on stream on March the 15th, 1999. Initial teething trouble was faced by way of a blockage in the riser duct after the calciner and in the first stage preheater cyclone as well as buildup in the tertiary duct at the inlet to the venturi. These were solved by selectively putting blasters in the venturi as well as tertiary air duct and 6 stage cyclone inlet. As the pressure drop across the cyclone was found to be comparatively higher a guide vane was put to reduce the pressure drop. After this, the production became stable and kiln output reached around 3500 tons per day.

Stage II Operating Results:

	Guaranteed	Achieved
Throughput:	3300 tpd of clinker	3500 tpd of clinker
Heat consumption:	700 kcal/kg clinker	742 kcal/kg clinker
Power consumption:	18 kWh/t	16 kWh/t
Clinker temperature:	135 Deg. C above ambient.	145 Deg. C above ambient.

Together with the above project, the second phase of the project also included increasing the clinker grinding capacity by 110 t/h with a Polysius ball mill with Combiflex drive 4.2m dia. x 15.2m length.

5. ADDITIONAL CEMENT-GRINDING UNIT

To take care of additional grinding requirements with the increased clinker output, together with the above second stage kiln upgrading project, another project was undertaken to add a second grinding unit again supplied by Krupp Polysius. The ball mill was of 4.2m dia. and 15.2 m long driven through a combiflex drive. The mill was also equipped with a sepol separator. The output reached was 110-120 tph against guaranteed output of 110 tph. This plant was also commissioned immediately after restarting of the kiln. A Polcid NT DCS system was used this time for controlling the old as well as the new cement-grinding mills.

As mentioned above, Krupp Polysius was the supplier and engineering contractor for both the plants whereas Petron Emirates LLC., based at Dubai was used in second phase expansion for local fabrication of structure and equipment as well as erection. During both the phases, East Coast Contracting based at Fujairah was used for civil construction.

6. CONVERSION TO SOLID FUEL FIRING AND FURTHER OPTIMIZING THE PLANT OUTPUT

After completing the stage II upgrading project in 1999, in the next year, i.e. year 2000, all-time record production figures were achieved which were as follows:

FCI'S RECORD PRODUCTION/SALES
YEAR 2000

CLINKER PROD. (TONNES)	CEMENT GRINDING (TONNES)	CEMENT SALES (TONNES)
1,103,705.00	1,112,740.00	1,093,456.50

After enjoying a good market for a period of 7-8 years starting 1991-92, the UAE cement industry, as a whole started sliding down mainly due to over supply of cement in the market and a steep hike in the oil price. At this stage FCI, which was totally dependent on oil firing contributing higher percentage in operating costs decided to make provision for coal/petrocoke firing thus reducing the cost. For this, a coal/petrocoke crushing and grinding mill was added with two Poldos for firing coal or petrocoke to the front burner and calciner. Two solid fuel burners were added in the calciner and the main burner was replaced by a dual fuel burner capable of using, both oil as well as coal or mixture thereof. The calciner loop was extended to ensure complete combustion in case of petrocoke firing. Taking advantage of this project, the ducting from stage 6 preheater to ID fan diameter was increased to reduce the pressure drop and the impellor of dopol fan was changed to take care of the additional gas flow from the preheater. This project was again executed in less then one year and complete coal firing was started from 27.06.2001. Polcid NT was included for coal grinding and coal firing system. During this phase of the project, ETA Electric Co. based in Dubai was used for local fabrication of structures and equipment as well as erection including installation of electrical and instrumentation equipment. Once again for civil construction, East Coast Contracting based at Fujairah were awarded the job.

7. CONCLUSION

Thus FCI went on taking step by step movements forward and has not stopped yet. It has always believed in taking the right decision at the right moment to take the best of the market condition at the same time lowering the cost of production so that it can survive even in bad market conditions.

Further studies are in the pipeline for future projects including upgrading the pollution control system, further production upgrade, improving cooler efficiency to reduce heat consumption and considering other alternative fuels, including waste, in the future.

View Of Fujairah Cement Plant As It Was In 1982-1995.
(Clinker Production Capacity 500,000 Tons Per Annum)

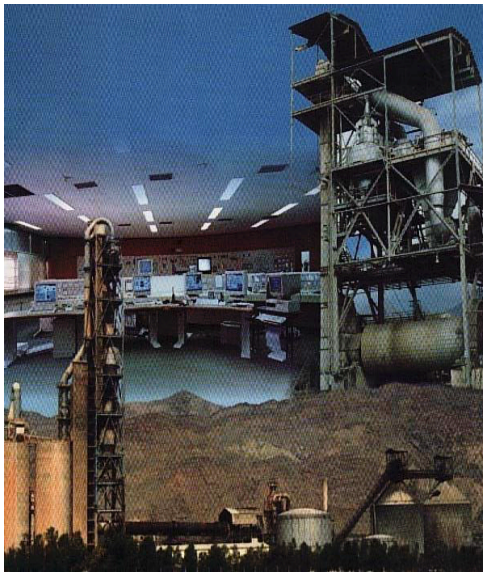

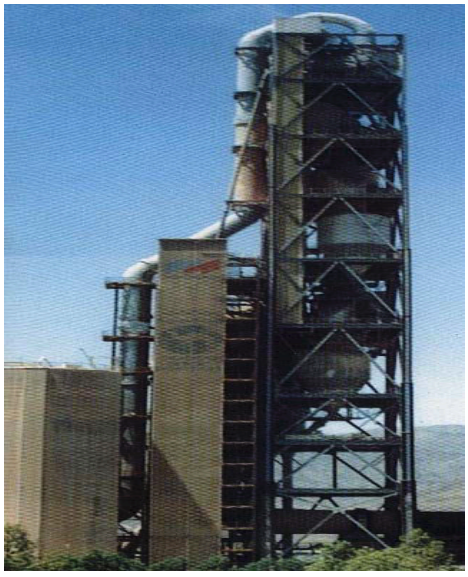

View Of Fujairah Cement Plant After 1st Phase Of Modernization And Upgrading In 1995.
(Clinker Production Capacity 750,000 Per Annum)

View Of Fujairah Cement Plant After 2nd Phase Of Modernization And Upgrading In 1998.
(Clinker Production Capacity Over One Million Tonnes)

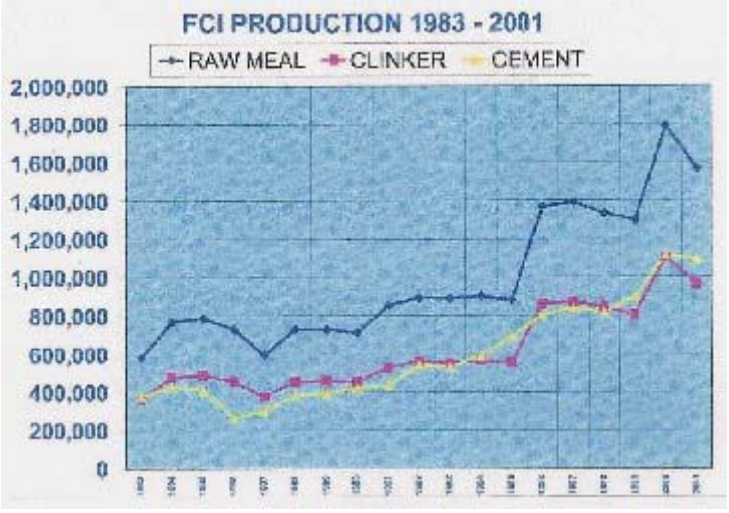

FUJAIRAH CEMENT IND.

Leistungssteigerung von 1600 auf 2500 tato

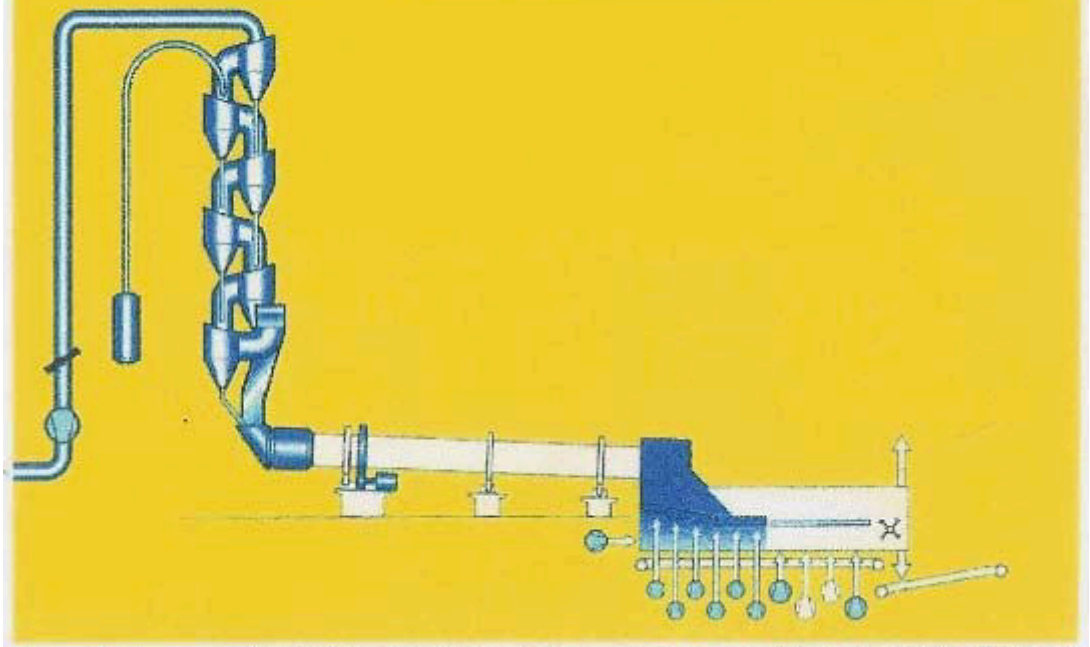

Capacity increase from 1600 to 2500 tpd/Aumento de capacidad de 1600 a 2500 t/d

FUJAIRAH CEMENT IND.

Leistungssteigerung von 2500 auf 3300 tato

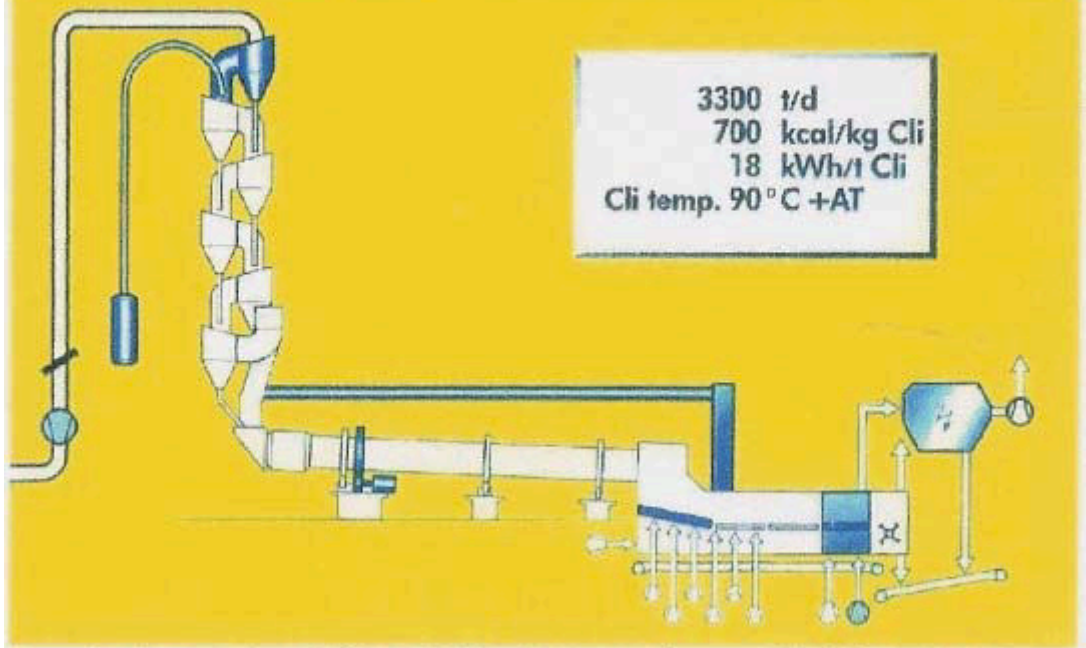

Capacity increase from 2500 to 3300 tpd/Aumento de capacidad de 2500 a 3300 t/d

COMPOSITE CEMENTS FOR A THIN LAYER TECHNOLOGY

Runova R.F.[1] and Nosovsky Y.L.[2]

[1]Kiev National University of Construction and Architecture, P.O. Box 161, Kiev 03037, Ukraine.
E-mail: runova@i.com.ua
[2]Henkel Bautechnik (Ukraine), P.O. Osvity 4, Kiev 03037, Ukraine.
E-mail: nosovsky@henkel.com.ua

ABSTRACT

The purpose of this paper – to investigate the composite cement, which provides high early strength (40 MPa after 24 hours) with a small amount of high alumina cement (HAC) in comparison with well known binder compositions. The cement with such properties is required for use in thin layer applications for finishing and special building work. The composition meeting such high requirements was made using blast-furnace slag (20-25 %) and Al_2O_3 as an additive. It was shown the effectiveness of using such materials in dry building admixtures for self-leveling floor.

1. INTRODUCTION

It is known that the thin layer technology of using Portland cement includes such special building works, as surfacing interiors and exteriors, tiling, joint filling, and smoothing horizontal and vertical surfaces [1]. This technology makes demands of Portland cement, which are different from ordinary uses of Portland cement in concrete. The common requirement is high water retention in the hardening thin layer due to intensive water adsorption by the sub-floor and evaporation in to the air [2].

Modern technology of using Portland cement solves this problem by using additives of cellulose ether and plasticizers, but the problems of a high early strength, control of deformation and an economic effectiveness are unsolved [3]. It should be noted, that cement compositions for thin layer applications have a high price due to the inclusion of special cements. The combination of those components in one binder system permits it to be classified as “Composite cement” due to its content of one or two inorganic materials, which take part in hydration with the formation of new phases besides Portland cement [4]. Definitely, this classification generally implies the use of mineral active additives, but doesn’t exclude using such mineral binders, as Portland cement. HAC and gypsum. Such compositions are very complicated for their high hydration activity and the recipe is very sensitive to deviation from the optimal proportions. Such compositions allow obtaining properties which are needed for the self-leveling compounds in floor preparations. A good example of using composite cements is in dry building admixtures, which are produced by «Henkel Bautechnik (Ukraine)» which distinguishes itself by its high quality from those of other producers [5].

This work researched the effective additives for substitution of HAC in composite cements with the same performances for thin layer applications.

2. OBJECTS AND METHODS

The chemical composition of the binders tested are shown in Table 1. Their properties are shown in Table 2. The composite cements were made by grinding the ingredients to a fineness of 350-420 m^2/kg. The cement activity was determined by testing 4x4x16 cm specimens made according to EN 196 with water/cement ratio 0,5. The tests were carried out after 1 and 28 days of curing at laboratory conditions at temperature 20^0C and relative humidity of 60 %. The deformation was measured to within 0,001 mm/m from the moment of stripping up to 28 days. When analyzing the structure formation processes X-ray phase and differential thermal methods were applied. Mathematic methods were applied to analyzed with obtained data.

Table 1. Chemical composition of binders

Binder		Al_2O_3	CaO	SiO_2	Fe_2O_3	MgO	TiO_2
Portland cement 500		8,5	63,4	24,0	4,6	0,9	0,5
HAC	Gorkal 40	39,4	40,5	4,5	15,4	-	-
	Lafarge 40	37,5	39,0	5,0	18,0	-	-
	Istra 40	41,0	39,0	25,0	16,0	1,1	-
Mariupol blast-furnace slag		9,4	45,2	38,8	2,3	3,6	-

Table 2. Properties of ingredients

Binder		Water demand, %	Setting time, h		Strength, MPa Rf/Rc at			
			initial	final	1 day	2 days	7 days	28 days
Portland cement 500		24,2	1-50	3-00	-	3,5 / 18,0	5,5 / 30,0	6,9 / 53,5
High alumina Cement	Gorkal 40	25,0	4-20	4-48	4,5 / 50,7	-	5,6 / 53,9	7,5 / 69,3
	Lafarge 40	26,0	6-10	6-35	4,9 / 59,4	-	6,3 / 64,2	6,5 / 66,0
	Istra 40	27,0	7-00	7-25	7,0 / 68,1	-	6,4 / 70,0	6,3 / 68,5
Gypsum G5		63,0	0-15	0-21	2,8 / 6,5	-	-	-

3. RESULTS AND DISCUSSIONS

The compositions investigated consisted of the following components: Portland cement M 500 (30 to 60 %), High alumina cement M 400 (30 to 50 %) and Gypsum M 5 (10 to 25%). The results of strength tests shows existing large strength variations for such systems even for small changes of composition, as shown in Figure 1. Unfortunately, these data can't fully describe the principles in these 3-components system.

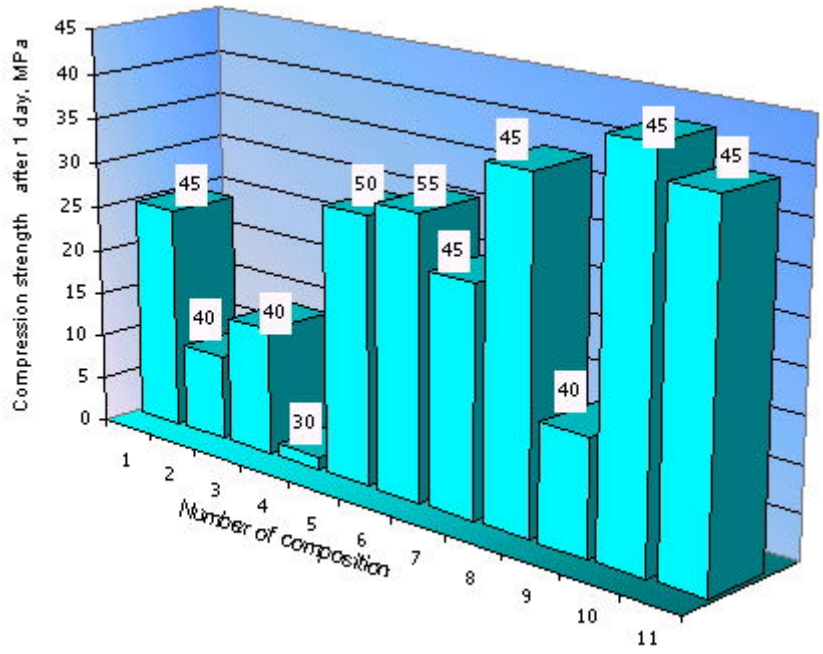

Figure 1. Analyses of 3-component cements (above the bars are shown the content of HAC)

The mathematical analysis of the data obtained was used for the determination of the principles and properties. This method required 10 experiments according to the following plan for 3-component systems (Table 3).

Table 3. The plan of 3-component experiments

Test No	Component PC500	Component HAC	Component GGBS	Rc, 1 day
1	0,000	0,333	0,667	15,8
2	0,667	0,333	0,000	24,3
3	0,333	0,333	0,333	10,1
4	0,333	0,000	0,667	4,2
5	0,000	0,667	0,333	58,3
6	0,000	1,000	0,000	54,1
7	0,333	0,667	0,000	45,8
8	0,000	0,000	1,000	5,4
9	1,000	0,000	0,000	10,3
10	0,667	0,000	0,333	9,2

After processing the early strength results, the following graphics model depicts the response surface for the 3-components composition.. Figure 2 shows the strength fields of the investigated systems.

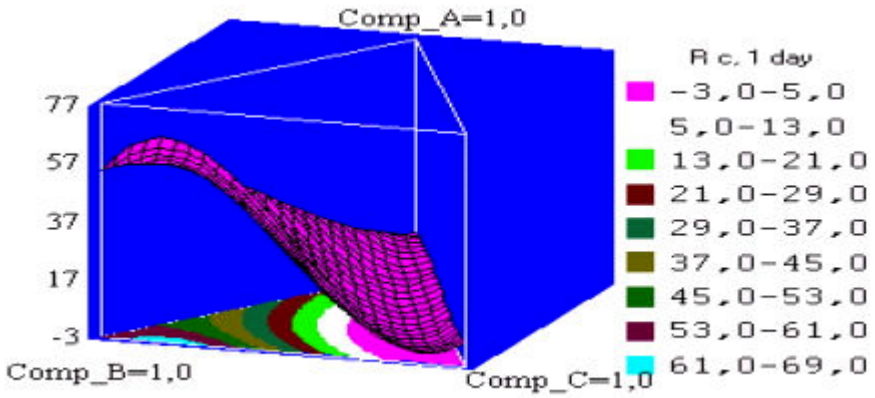

Figure 2. The response surface # 1

This surface is described by the next regression equation, which was obtained after analyzing the data from Table 3.

Rc, 1 day = 9,8*Comp_A + 58,9*Comp_B + 1,2*Comp_C + 3,3*Comp_A*Comp_B + 5,6*Comp_A*Comp_C + 31,7*Comp_B*Comp_C - 477,1*Com_A*Com_B*Com_C

The observed relationship shows that the compression strength after 1 day depends on amount of component B (High Alumina Cement) and common action of components B (HAC) and C (Gypsum). Their estimated coefficients are accordingly 58,9 and 31,7. The estimated coefficient for common influence of the three components is negative and has very high value. This indicates weak interaction of those components for the compressive strength after 24 h. This fact is confirmed by the absence of peaks on the response surface in Figure 2, which has hollow behavior in the central area.

Improvement of the system reliability was obtained by combining all 21 recipes' results: the sum of the first 11 samples from Figure 1 and the other 10 from Table 3 (Figure 3). The new response surface has some differences from first one and the new regression equation is more complicated.

Rc, 1 day = 11,9*Comp_A + 53,5*Comp_B + 4,8*Comp_C -13,6*Comp_A*Comp_B - 11,4*Comp_A*Comp_C + 43,0*Comp_B*Comp_C -287,1*Comp_A*Comp_B*Comp_C - 133,9*Comp_A*Comp_B*(Comp_A-Comp_B) - 23,4*Comp_A*Comp_C*(Comp_A - Comp_C) + 196,4*Comp_B*Comp_C*(Comp_B - Comp_C)

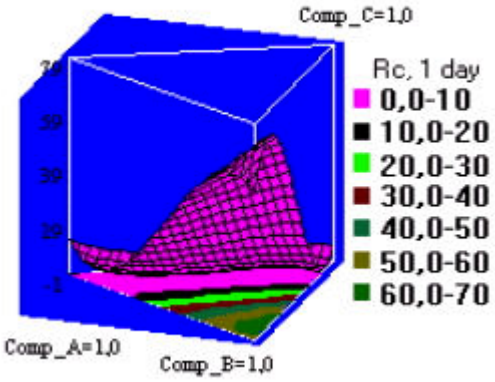

Figure 3. The response surface # 2

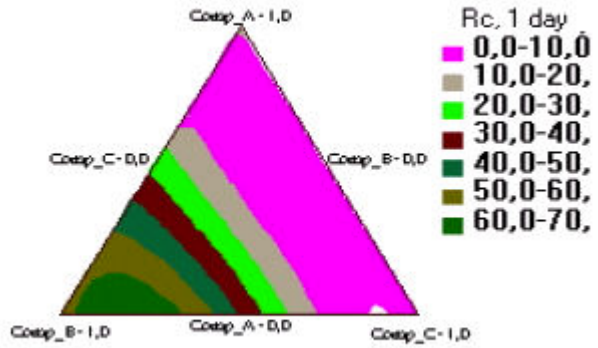

Figure 4. The cantors of response surface # 2

The main activity in the investigated system belongs to component B (HAC) and compatible influence of components B and C (Gypsum). The estimated coefficients are accordingly 53,5 and 43,0. It should be noted that the compatible influence was increased by 25 %.

The obtained results were used as a base for continuance of researching new additives for reduction of the amount of HAC in the composite cement, but with the same early strength.

It is known that milled blast-furnace slag has a positive influence on the time-constant properties of HAC /6/. But thin layer applications demand information about the influence of slag on early strength development. The following results can give an answer on this question (Table 4).

Table 4. Properties of HAC-Slag admixtures

HAC, %	Slag, %	Water demand, %	Initial setting time, h-min	Final setting time, h-min	Compressive strength, MPa		
					1 day	7 days	28 days
100	-	25,20	3-40	3-45	49,7	58,8	68,7
95	5	25,10	3-50	3-55	48,1	56,4	67,2
90	10	24,45	3-50	4-00	49,6	55,2	64,7
80	20	24,01	4-10	4-20	52,4	57,1	65,6
75	25	23,75	4-10	4-25	50,2	56,0	62,3
70	30	23,10	4-15	4-30	48,2	50,1	54,6

These data show that adding of 20-25 % blast-furnace slag to HAC provides the optimum result: the strength of this cement with additive is 5-6 % higher than the pure cement. The setting time is a little elongated but with the same short term between initial and final setting time [6]. Together with this the influence of 30 % slag on the time-constant strength level is not confirmed. Probably, it could be explained by difference in raw materials.

Aluminium oxide Al_2O_3 was used as a chemical additive based on its strong impact on Portland cement. The recommend gel ratio is 1,0 - 1,5 % by the weight of Portland cement. As it follows from Tables 5 and Figure 5, the optimal amount of Al_2O_3 to HAC is 0.5; meanwhile with 0,25 % Al_2O_3 the result is similar

Table 5. The influence of Al_2O_3 on Alumina cement

High Alumina Cement, %	Al_2O_3	Compression strength, MPa After 1 day
100	-	49,7
99,95	0,05%	57,4
99,9	0,10%	61,8
99,75	0,25%	66,7
99,5	0,50%	67,8
99,25	0,75%	61,5
99,0	1%	59,4
98,0	2%	56,7
97,0	3%	55,8
95,0	5%	23,6

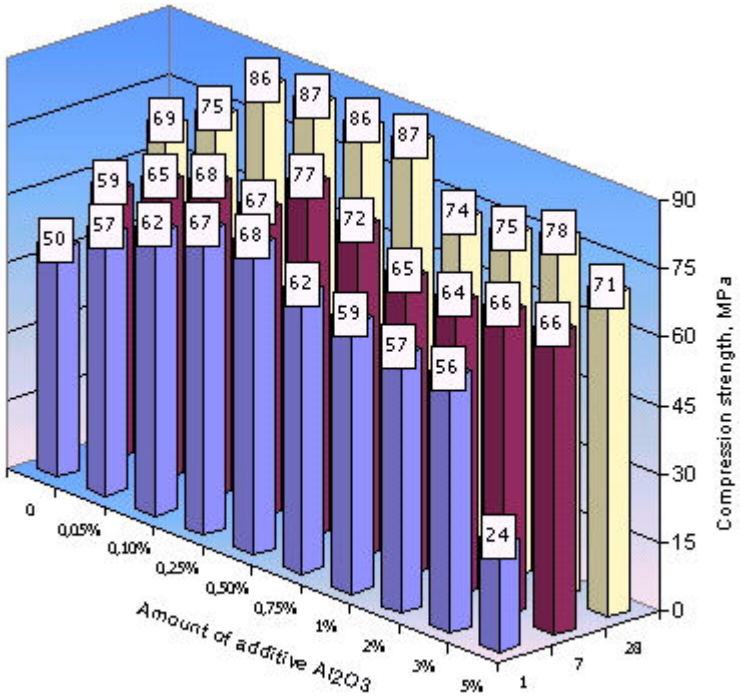

Figure 5. The influence of Al_2O_3 on Alumina cement

It could be expected that the combination of slag additives + Al_2O_3 reduces the quantity of HAC in composite cement. But, as it follows from table 5 the addition of Al_2O_3 increases the strength of alumina cement by 5-6 % more, and together with additive of 20 % slag the strength is reduce dramatically, even less then pure alumina cement.

The X-ray and differential thermal researches have shown that the slag retards the hydration of High alumina cement. This fact confirmed by significant quantity permanent CA (d=0,471; 0,297; 0,242 nm) and CA_2 (d=0,307; 0,279; 0,206 nm) after 24 h hardening at 20 ± 2^0C. But in the composite system «Portland cement-High Alumina Cement-Slag-Gypsum» the slag function is more constructive, especially during the formation of $Ca(OH)_2$. So, in the system «Portland cement-High alumina cement-Gypsum» is observed the formation of C_3AH_6 (d=0,776; 0,568; 0,390 nm), which is known for its negative influence on binder composition. Meanwhile, the phase C_2AH_8 is forming (d=0,350; 0,288; 0,269; 0,256 nm) and the phase C_3AH_6 is not identified. Probably, the formation of C_2ASH_8 and of $Al(OH)_3$ cause this positive effect. This way of hydration is confirmed by capture of heat on DTA: three-steps endothermic effect at 140^0C, 175^0C and 280^0C. This effect ended at the high temperature of $380\text{-}400^0$C.

It was roughly difficult to identify the products of hydration in the system «Portland cement-High alumina cement-Gypsum» with additive Al_2O_3. But generally it is obvious that the hydration goes in the same way due to its developed specific surface. The phase C_2AH_8 is the most common in the products of hydration.

So, it could be two types of recipes with using the low amount of high alumina cement.
1. using 20-25 % of milled blast-furnace slag
2. using 0,25-0,5 of Al_2O_3

Figure 6 shows the hardening development of these binders. So, the most effective is using the chemical additive of Al_2O_3 from the technical and technological aspects. However, the binder with milled blast-furnace slag is cheaper and has acceptable strength.

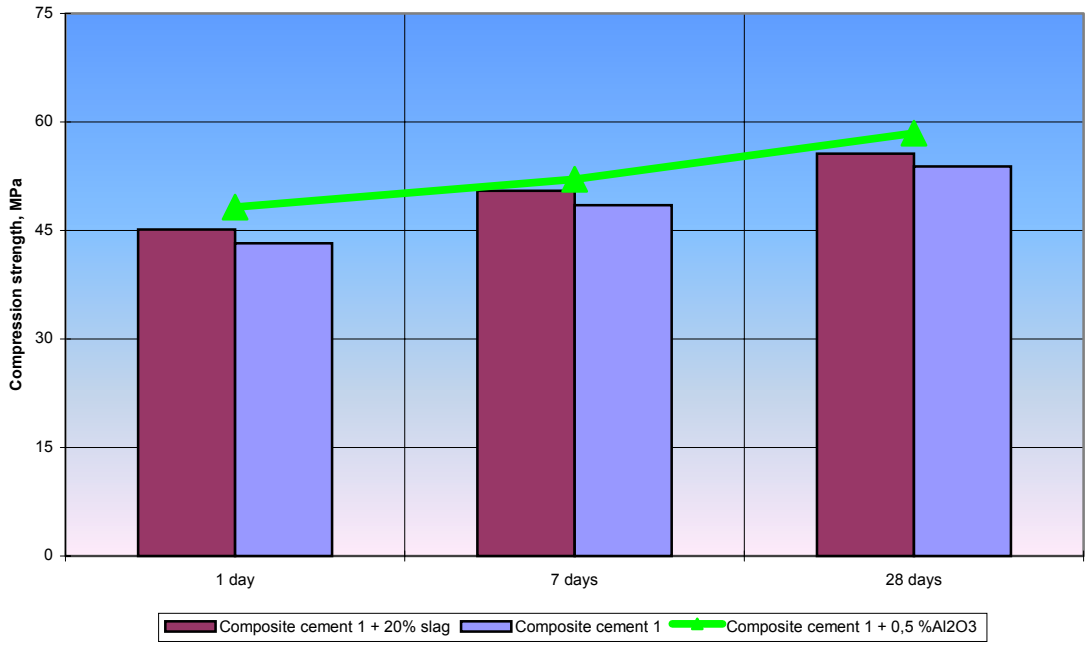

Figure 6. The strength development of investigated composite cements

The deformation processes in this system have similar behaviors and their values are reasonable. Investigated composite cements were used in thin bed mortars for leveling compounds, which consisted of sieved fillers and organic additives.

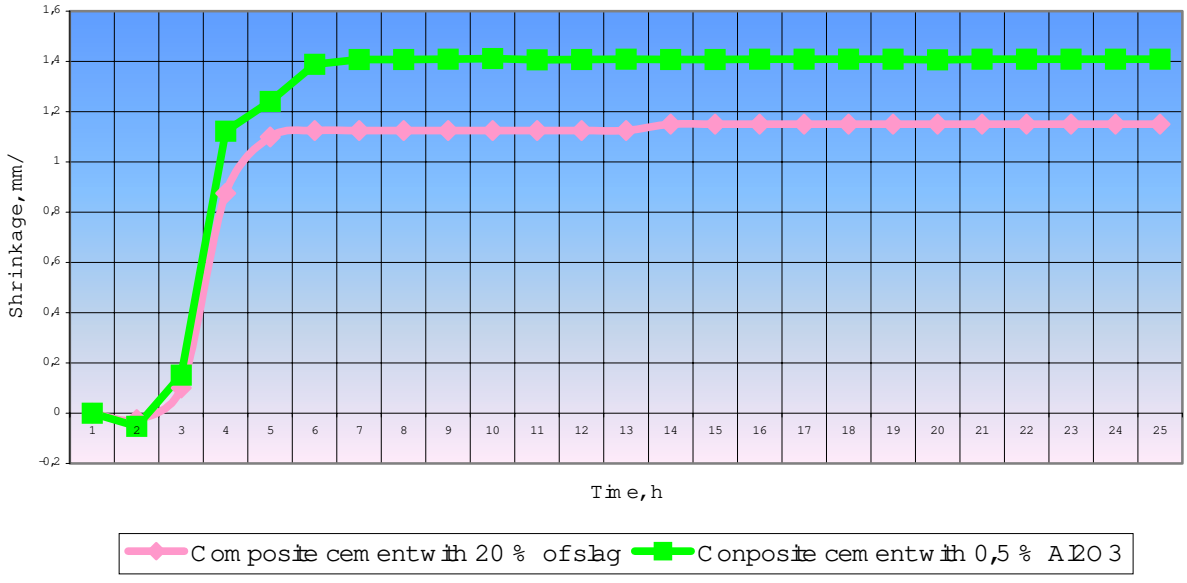

Figure 7. The shrinkage development of investigated composite cements

Based on this investigation of composite cements the leveling compounds were prepared and tested. The properties of leveling compounds with the developed composite cements are given in Table 6.

Table 6. The properties of leveling compounds

Properties	The leveling compounds					
	M0	M1	M2	M3	L1	L2
Amount of slag, %	0	10	20	25	-	-
Amount of Al_2O_3, %	-	-	-	-	0,25	0,5
Flow properties, cm after 10 min	26,5	26,0	25,0	25,0	26,0	26,0
Working time, min	35	30	30	30	30	30
Initial setting time, min	54	62	65	66	52	50
Final setting time, min	62	70	72	75	58	55
Compression strength, MPa after 1 day	17,5	16,5	16,3	13,4	16,5	16,8
3 days	20,4	18,2	17,9	14,9	18,9	20,1
7 days	26,2	24,2	23,2	15,5	23,8	23,5
28 days	33,1	29,2	32,0	31,6	32,1	33,1

4. CONCLUSIONS

- Composite cement with Portland cements, High alumina cement and gypsum provide high early strength during hardening, when the optimal proportion of components is well adjusted.
- Beside the well known stabilizing influence of slag on HAC, it was shown that 20-25 % of lime-base milled blast-furnace slag has a beneficial effect on strength development of Alumina cement after 1 day. It permits reductions of the amount of expensive Alumina cement in composite cement without early strength reduction.
- It was determined that the influence of 0,5 % Al_2O_3 on the structure formation of HAC, is more effective than its influence on PC.
- The observed compounds are effective for using in thin layer applications in dry mixtures for leveling floors.

REFERENCES

[1] Wohrmeyer, T. Bier, L. Amathieu, P. Chassaing. The benefits of calcium aluminate cemetn in selfleveller and tile works. “MixBUILD” St.Petersburg, 2000, h. 59-63.

[2] G.Luts, P. Meshkov, Polymer binders in products of building chemistry. “Construction of Ukraine” 1996, #5, p.32-35 (in Russian).

[3] E. Uretskaja, B. Smirnov, N. Gukova, Z. Filipchik. The modification of dry building admixtures by disperse powders and cellulose ether. “MixBUILD”, St. Petersburg, 2000, p. 28-35 (in Russian).

[4] H.F.W.Taylor. Cement Chemistry. 1990, p. 560.

[5] Runova R.F., Nosovsky Y.L. The deformation processes in the multi-component mineral binder. IBAUSIL 2000, p. 2-0485.

[6] Marcdargent, M Testud, J P Bayoux, A Mathieu. Hydration and strength of composition “HAC-Silica-fume” and hydrates stability. ICCC, Göteburg, 1997, p. 243-254

ABOUT THE BEHAVIOUR OF GLASS POWDER IN PASTES AND MORTARS WITH CEMENT

W. Remarque [1], L. Urbonas, [1] and D. Heinz[2]

[1]Institute of Mineral Engineering, University of Aachen, Mauerstr. 5, D-52064 Aachen, Germany.
E-mail: remarque@ghi.rwth-aachen.de
[2]TU München, Germany.

ABSTRACT

In the present study the pozzolanic behaviour of glass powder was investigated. Coloured container glass was crushed and milled in to two finesses. Mortars or pastes containing lime or cement and glass or fly ash were made. The structure of the pastes and mortars were analysed by SEM and the compressive strength of mortars was measured. Comparable investigations were made with a fly ash (PFA). At early ages CSH phases were detected on the surface of the glass particles. With similar particle size distribution the compressive strength from mortars with glass powder is lower than that of mortars with fly ash. To reach comparable compressive strength, glass powder must be ground very fine (> 500 m²/kg).

1. INTRODUCTION

Glass can be recycled many times to produce new glass. For this reason, in many countries used glass containers are collected and returned back to the glass producer. There are two cases in which waste glass can't be sent back to the glass producer: Firstly when there is a high content of impurities like ceramics in the recycled glass, secondly when there is a surplus of mixed coloured glass.

These cullet usually go to landfill or can be used as road material. Furthermore there are the possibilities for using waste glass in building materials for example as aggregate in concrete, cast stones or tiles. With glass as aggregate, special coloured effects can be obtained at the surface of the concrete or the tiles. However, by using glass as aggregate in concrete or cast stones often alkali-aggregate-reactions were observed [1], [2], [3].

Another way is the use of ground waste glass as pozzolanic addition for cements. Pozzolans (natural or industrial) are high in (reactive) SiO_2 and often also Al_2O_3. Mixtures with water and CaO produce C-S-H at ordinary temperatures [4]. Well known and mostly used in the concrete production as pozzolan is fly ash (PFA). Until today, glass powder as pozzolan is only used on laboratory scale. In accordance to ASTM C 618, the chemical composition of glass meets the basic requirements ($SiO_2 + Al_2O_3 + Fe_2O_3 \geq 70$ %). Because of the high content (≥ 10 %) of Na_2O it does not conform to the optional requirements.

Sugita et al. [5] produced mortars with OPC and glass powder addition up to 20 %. The final setting was prolonged and the strength after 28 days decreased. The addition of glass powder with a higher specific surface and 0.5 % NaOH caused a better strength and the average pore radius was lower. Sugita deduced that the glass cannot be activated under normal alkalinity of Portland cement hydration. Archibald et al. [6] used fine ground container glass as a partial pozzolanic replacement for normal Portland cement in various types of back fill. After 224 days slurry backfill materials

with ground glass showed equivalent or even better backfill strength characteristics. Dyer [7] determined that glass undergoes a pozzolanic reaction when combined with cement and the expansion caused by ASR can be reduced by using glass powder. Shao [8] also used fine ground glass as addition for concrete. The used glass was from fluorescent lamps and contained 1 % B_2O_5. The glass was sieved in three size classes and the pozzolanic activity tested in accordance to ASTM C 593. Only the glass that was smaller than 38 µm satisfied the requirements in compressive strength. The expansion by ASR was reduced by all glass fractions. By using fine ground glass and glass as aggregate in concrete, there was a strong expansion by ASR [1], [3]. Meland tested the long time durability above water in a closed container and Warianka at 40°C/100 % humidity, while Dyer and Shao used the short time test according to ASTM C 1260 without glass as aggregate.

In the present study the pozzolanic behaviour of glass powder was investigated. Glass cullet from coloured container glass were crushed and milled into different finenesses. Investigations concerning the lime-pozzolan-reaction were made in accordance to the ASTM C 593 and to the German standard DIN 51043. Pastes from cement and glass powder were stored under water and analysed by SEM at different times. Key objective was the observation of the contact zone cement-glass and the condition from glass particles. Furthermore the strength development from mortars according to the German standard DIN EN 196 with a cement replacement up to 50 % by glass powder or fly ash and fine ground quartz as reference was investigated. Because of the small particle size of the glass powder a damaging alkali-silica-reaction must not be expected [9].

2. PHYSICAL AND CHEMICAL PROPERTIES

The physical and chemical properties of cement, glass powders, fly ash and quartz powder are shown in Table 1 and Table 2.

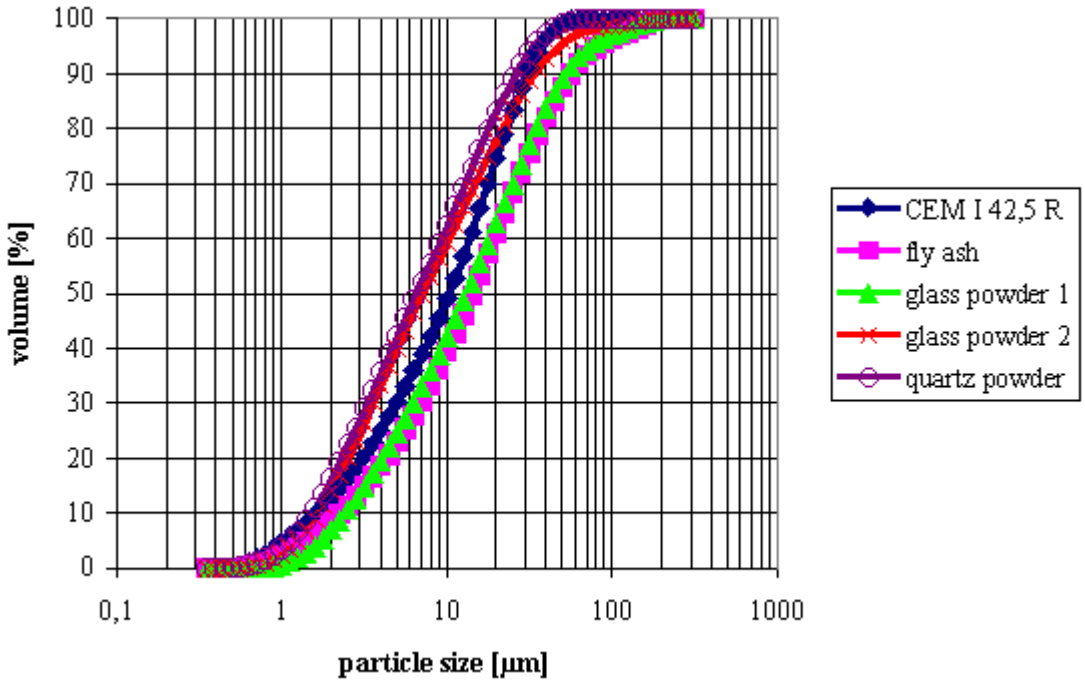

Figure 1. Particle size distribution

According to Blaine, glass powder 1 and fly ash have nearly the same particle size distribution and specific surface. The specific surface for fly ash according to BET is nearly four times higher than that of glass powder 1 and three times higher than that of glass powder 2.

Table 1. Physical properties

	Density	Specific surface		Average particle size
		Blaine	BET	
	[kg/m³]	[m²/kg]		[µm]
CEM I 42,5 R	3160	430	n.d.	10,8
Glass powder 1	2560	300	500	13,2
Glass powder 2	2560	540	700	7,1
Fly ash	2210*	310	1900	14,3
Quartz powder	2620	520	n.d.	6,6

*) Grain density n.d.: not determined

Table 2. Chemical composition

	CEM I	Fly ash	Glass	Quartz
	Mass- %			
SiO_2	21,21	52,29	70,21	96,80
Al_2O_3	5,65	28,91	1,77	1,06
Fe_2O_3	2,90	6,18	0,41	0,35
$SiO_2+Al_2O_3+Fe_2O_3$		87,38	72,39	98,21
CaO	64,43	3,36	10,16	0,27
MgO	1,25	2,25	1,97	0,14
K_2O	0,84	3,24	0,77	0,51
Na_2O	0,11	0,82	12,74	0,19
SO_3	3,27	0,61	0,03	<0,01
Cl^-	n.d.	n.d.	0,03	n.d.
Loss on ignition	2,75	4,02	0,54	0,55
SiO_2 reactive	n.d.	36,70	70,21	n.d.

3. EXPERIMENTS

3.1 Glass-Lime-Reaction

Mortars containing lime and glass powder or fly ash were made according to German standard DIN 51043. The mortars were stored 4 days at 20°C and 95 % humidity and after demoulding they were cured for 24 days in water of 20°C. The strength was measured after 24 days under water. Mortars with fly ash and lime disintegrated within the first hour. Investigations about the structure of the mortars were made with SEM. The results are presented in Table 3 and in Figures 2 to 6.

Table 3. Compressive strength from glass-lime-mortars according to German standard DIN 51043

mixture	flexural strength	compressive strength
	[N/pa²]	
lime/fly ash	-	-
lime/glass powder 1	1,7	4,6
lime/glass powder 2	3,3	9,3

After 28 days the mortars must reach a minimum compressive strength of 5 N/pa. Mortars with glass powder reach 4.6 N/pa² and 9.3 N/pa². According to the German standard 51043 only glass powder 2 meets the requirements.

Also mortars containing lime (180 g), glass or fly ash (360 g) and German standard sand with a water-cement-ratio of 0.28 were made and cured according to ASTM C 593. Mortars with fly ash reached the highest values in compressive strength after 7 days storage at 54°C. The results are given in Table 4.

Table 4. Flexural and compressive strength from lime-glass-mortars after 7 days at 54°C

mixture	flexural strength	compressive strength
	[N/pa²]	
lime/glass powder 1	1,6	6,7
lime/glass powder 2	2,3	9,2
lime/fly ash	3,1	11,3

Figures 2 and 3 show mortars with lime and glass or fly ash after the setting on air at 20°C and 95 % humidity. On the surface of the glass particles first CSH phases can be seen. On the surfaces of the spherical fly ash particles there are less or no CSH phases.

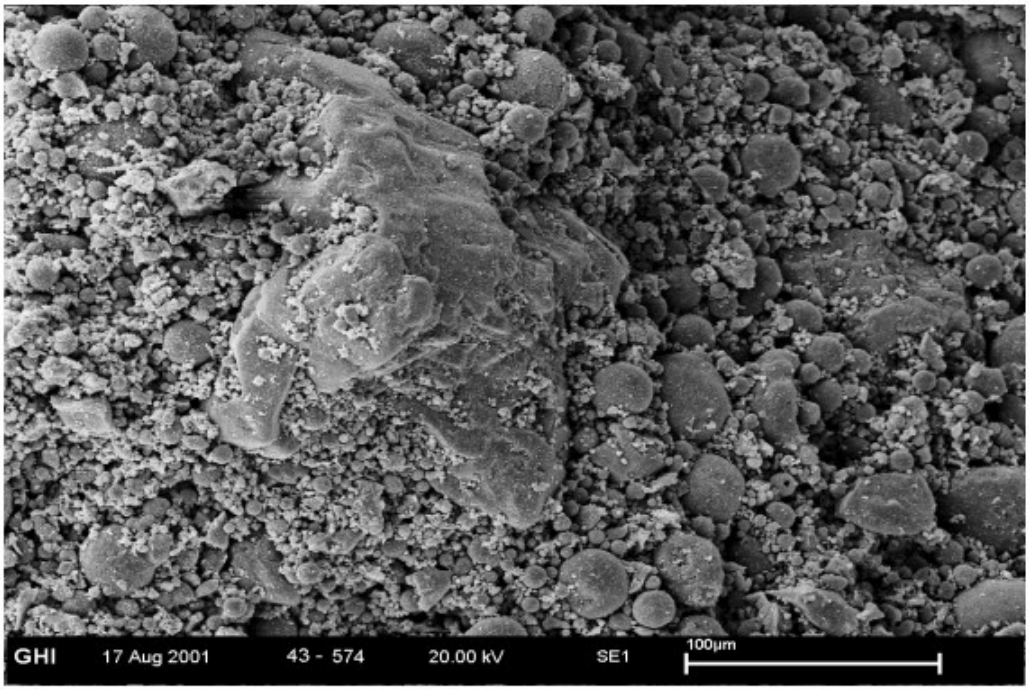

Figure 2. Mortar with lime and fly ash after 4 days at 20°C/95 % humidity

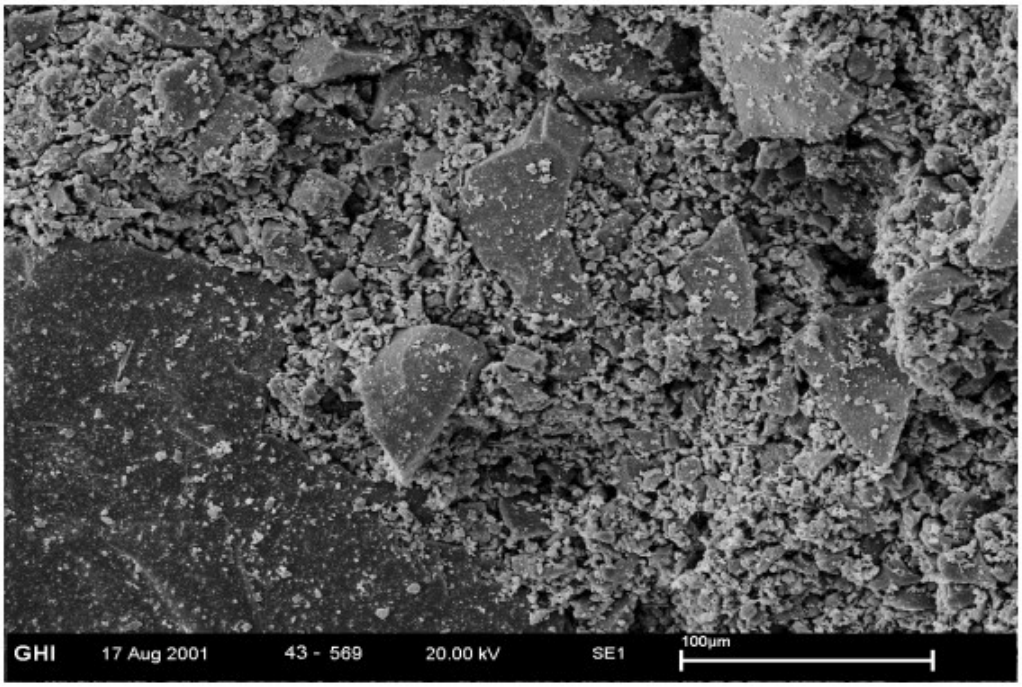

Figure 3. Mortar with lime and glass powder 1 after 4 days at 20°C/95 % humidity

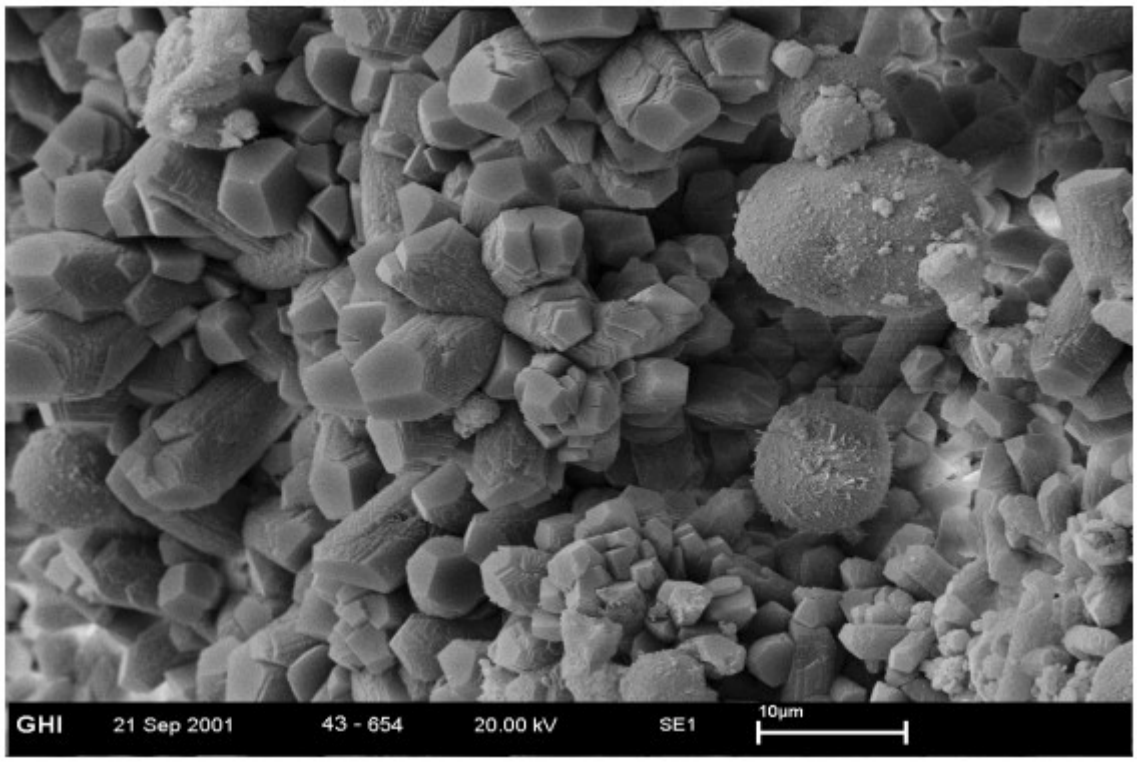

Figure 4. Mortar with lime and fly ash after 4 d at 20°C/95 % humidity and 24 days under water

Figure 4 shows the reason for the decomposition of the lime/fly ash mortar. In some places there are no contact-zones between the lime and the fly ash. There is nearly no corrosion on the surfaces of the fly ash particles. The lime is carbonated and there are no CSH phases between lime and fly ash.

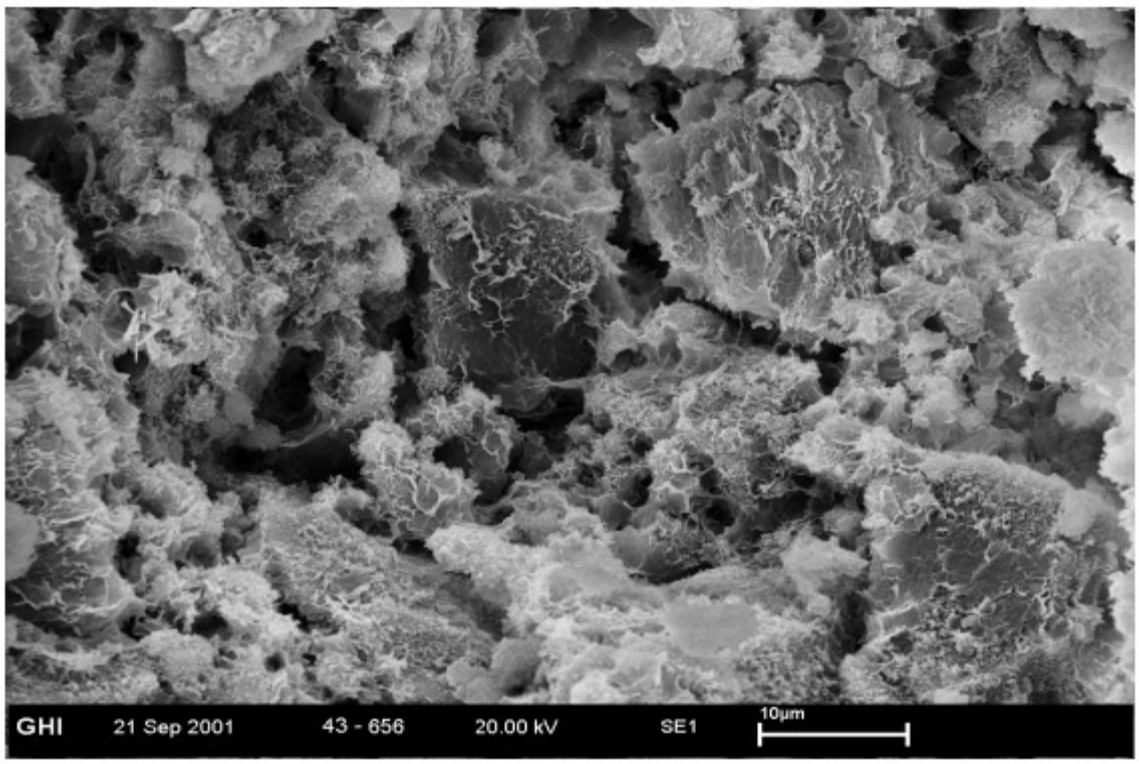

Figure 5. Mortar with lime and glass powder 1 after 4 days at 20°C /95 % humidity and 24 days under water

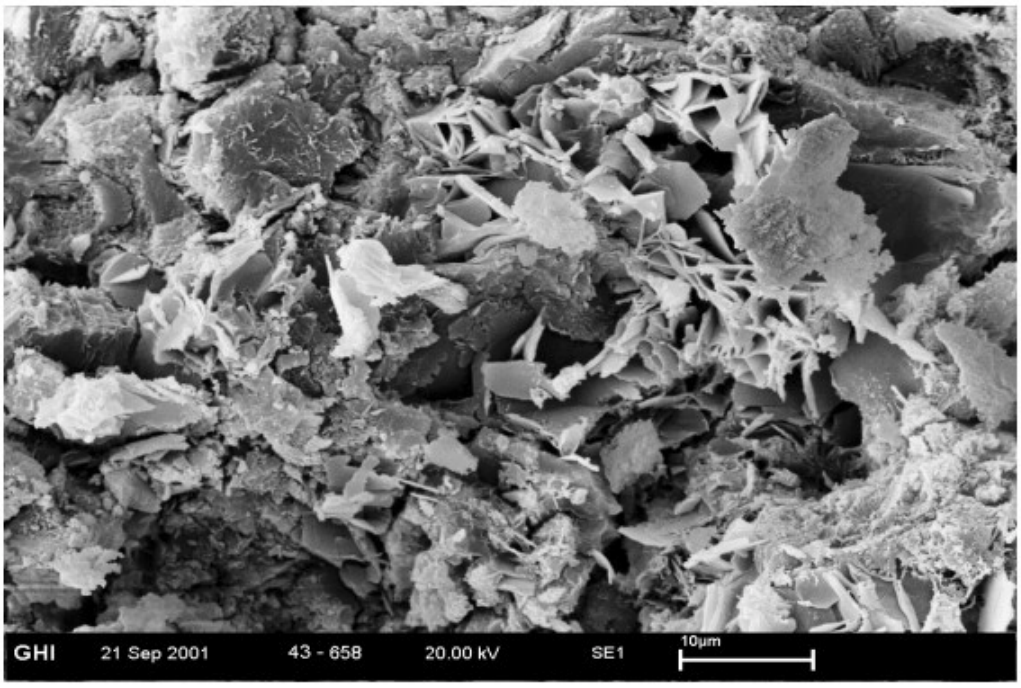

Figure 6. Mortar with lime and glass powder 2 after 4 days at 20°C /95 % humidity and 24 days under water

Figure 5 and 6 show mortars with lime and glass after 24 days under water. The surface of the glass particles is corroded and there are CSH phases on the surface or between the glass particles.

3.2 Glass-Cement-Reaction

Pastes of cement with 25 % replacement of cement by glass with a particle size from 90 to 125 µm were made. The particle size of the glass was selected to find easily the glass particles by SEM in the cement paste. The water-cement-ratio was 0.28. The pastes were stored one day at 20°C/95 % humidity. After demoulding they were stored under water. At different times a sample was dried and examined by SEM. The results are presented in the Figures 7-11.

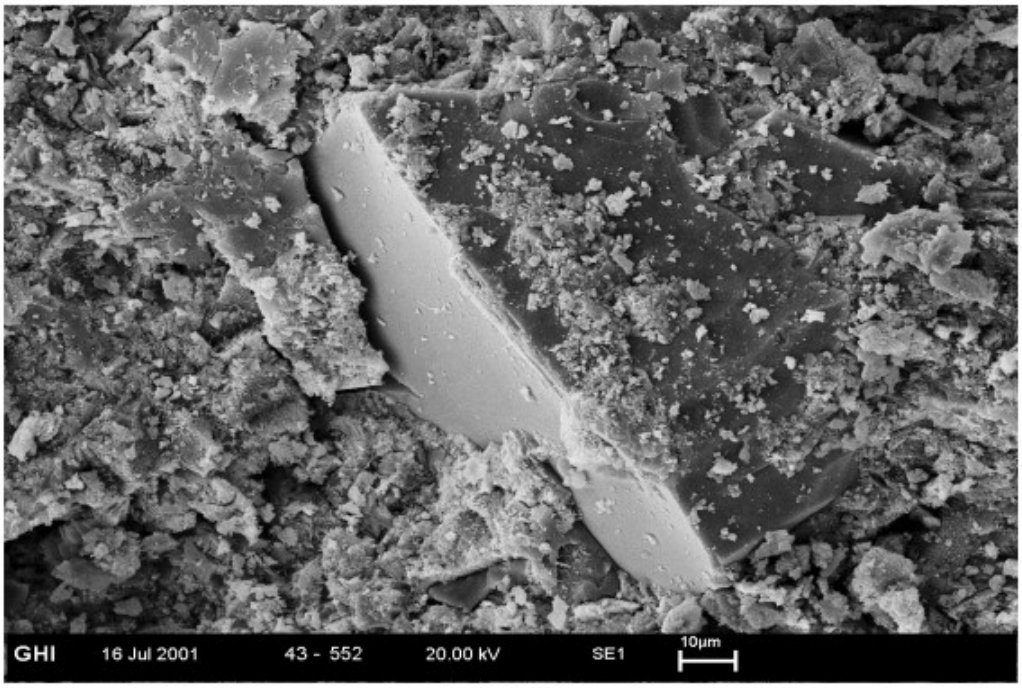

Figure 7. Glass-cement-paste, 2 days

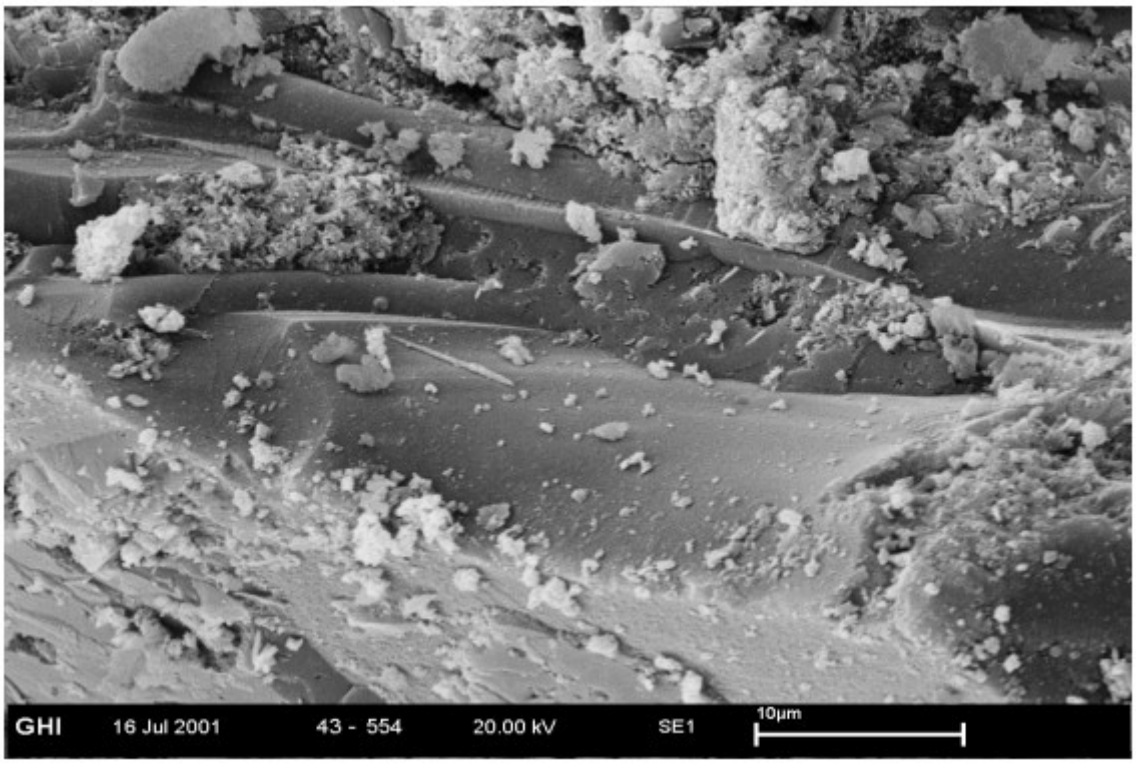

Figure 8. Glass-cement-paste, 2 days

At the age of 2 days there are a few CSH phases on the surface of the glass particles. The edges of the glass particles are sharp. Particular at rough edges accumulations of CSH phases can be found. At the age of 28 days there are more CSH phases on the surface of the glass particles. The surface of the glass particles is more corroded. The edges are lacerated.

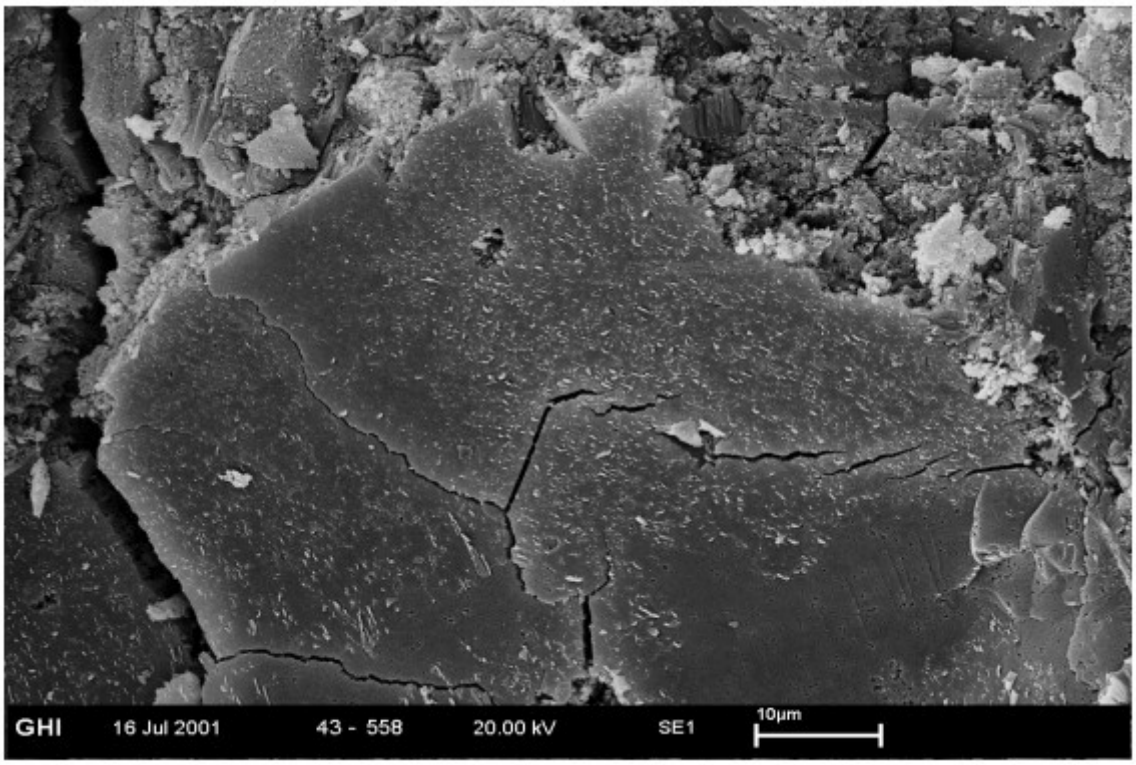

Figure 9. Glass-cement-paste, 28 days

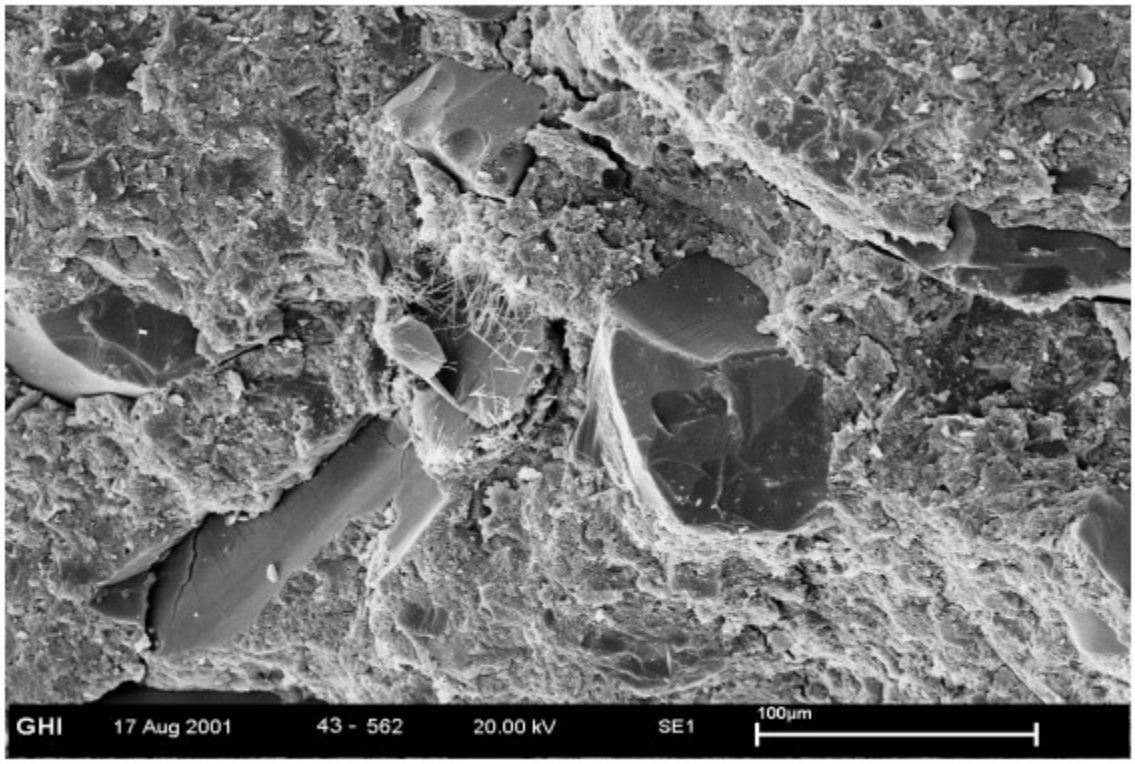

Figure 10. Glass-cement-paste, 91 days

At later ages often cracks between the glass and CSH phases are detected. Partially the cracks go through the glass particles. On the surface of the glass particles CSH phases can be detected, Figure 11 (1 = glass, 2 = CSH).

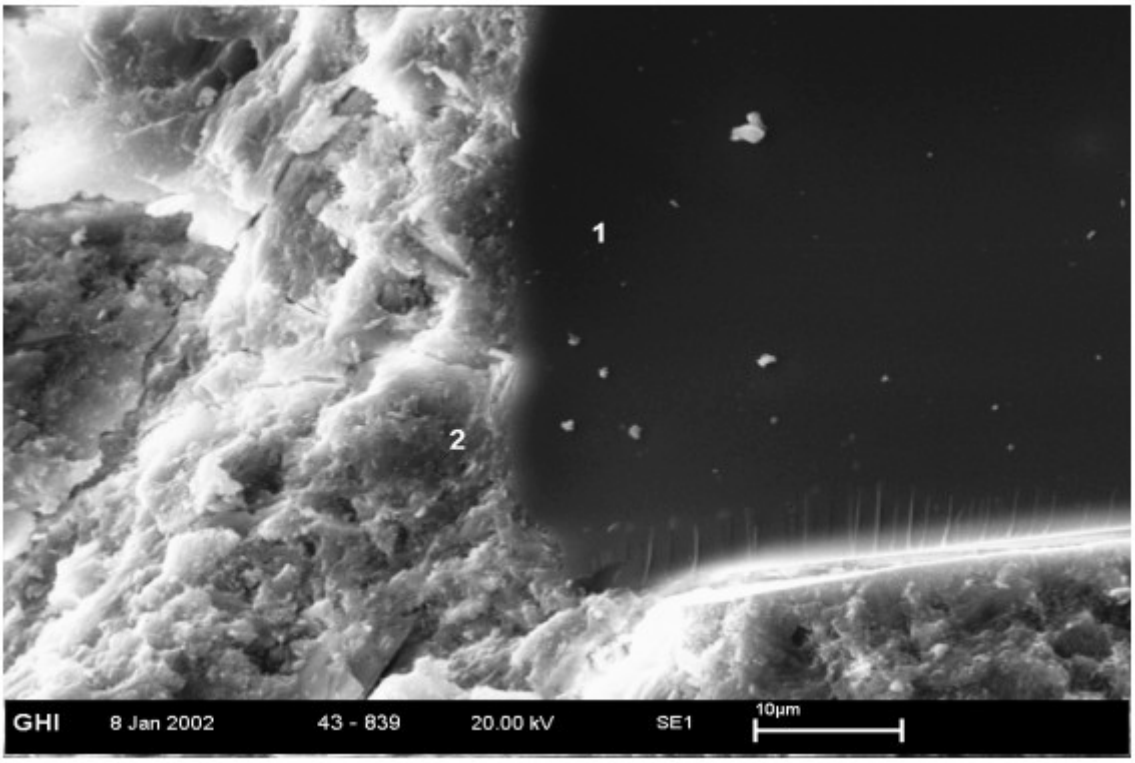

Figure 11. Glass-cement-paste, 182 days

3.3 Glass-Cement-Mortars

Mortar prisms according to DIN EN 196 part 1, were made with CEM I 42.5 and up to 50 mass-% cement replacement by glass powder or fly ash. After one day the specimens were demoulded. The specimens were cured under water. The compressive strength was measured up to the age of 365 days.

Water demand and setting time were measured according to DIN EN 196. The values for pastes with 25 mass-% cement replacement by glass powder or fly ash are given in Table 4. The water demand of the cements with the additions is not significantly different to that of the pure cements. The setting time is, as expected, higher for the cements with the additons. The final setting time of all binders was shorter than 12 hours.

Cement replacement by 25 % fly ash and glass powder 1 cause none or only a small increase of the mortar spread. Cement replacement by glass powder 2 gives a marked increase of 1 to 1.5 cm.

Table 5. Water demand, setting time and mortar spread of mortars with 25 mass-% cement replacement by glass powder or fly ash

	Water demand	Setting time	Mortar spread
	[%]	[min]	[cm]
CEM I	28,3	135	17,4
CEM I + fly ash	28,7	180	17,8
CEM I + glass powder 1	28,1	150	17,8
CEM I + glass powder 2	28,3	165	18,6

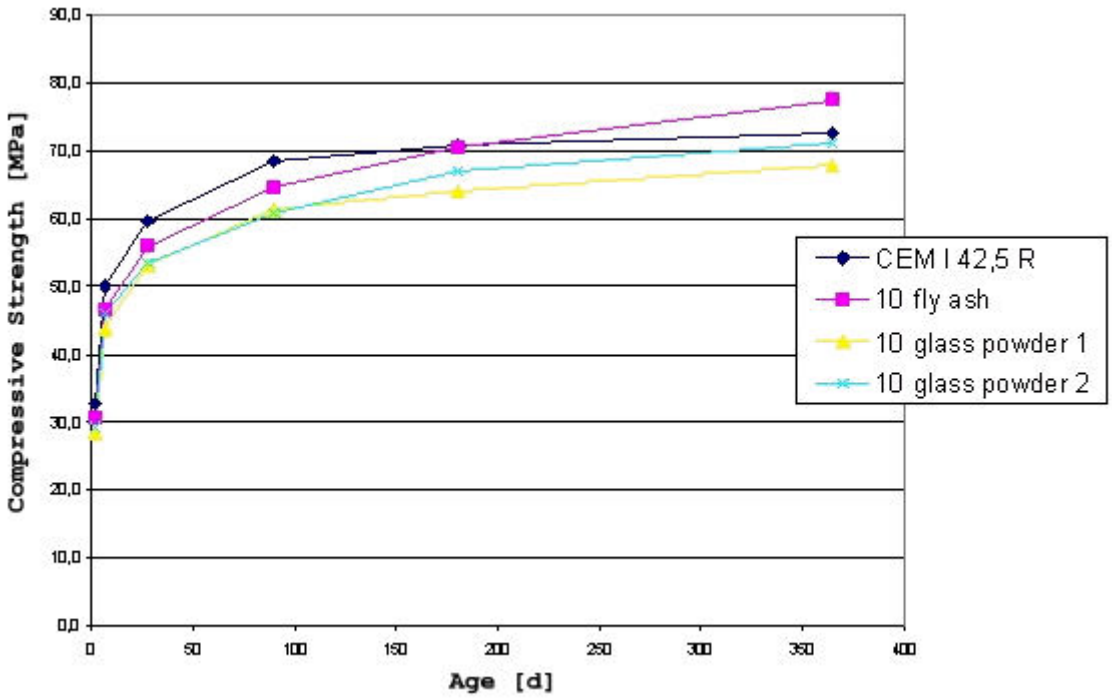

Figure 12. Compressive strength from mortars with 10 mass-% cement replacement by glass or fly ash

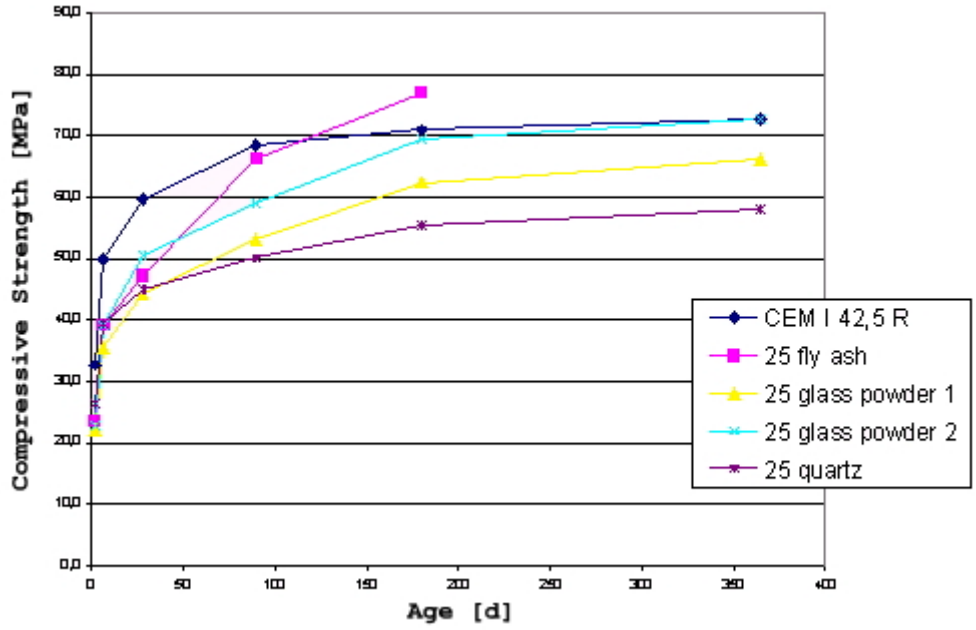

Figure 13. Compressive strength from mortars with 25 mass-% cement replacement by glass or fly ash

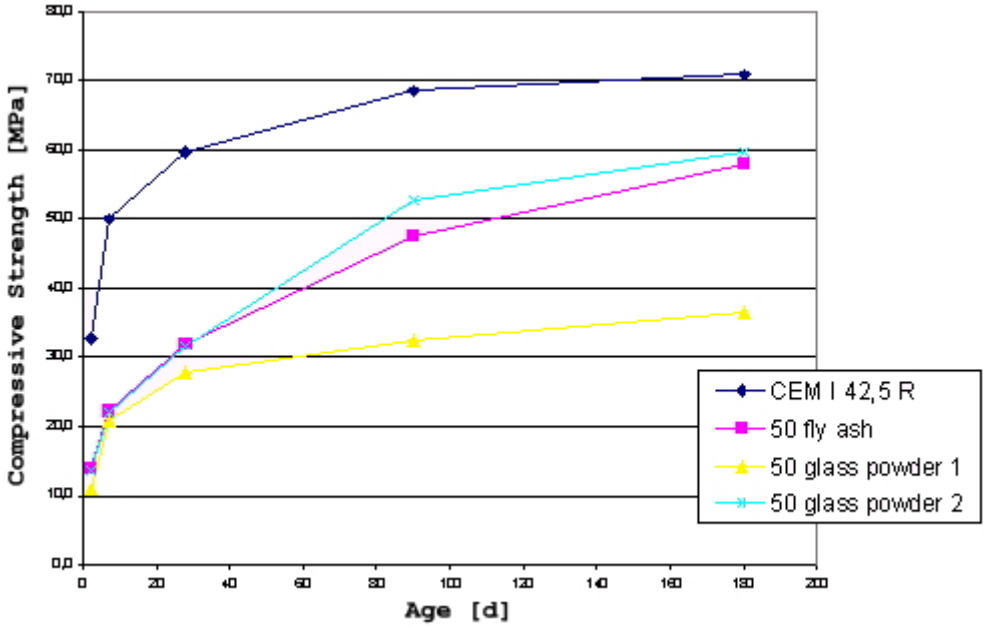

Figure 14. Compressive strength from mortars with 50 mass-% cement replacement by glass or fly ash

First of all the replacements of cement by fly ash or glass powder reduces the compressive strength. Up to the age of 90 days, mortars without cement replacement reach the highest values. At higher ages, mortars with 10 and 25 mass-% cement replacement by fly ash and glass powder 2 reach nearly the same or even better compressive strengths as mortars without cement replacement. Glass powder 1 reacts very slowly. After 180 days mortars with glass powder 1 reach about 90 % compressive strength of the mortar without replacement.

The compressive strength from mortars with 50 mass-% cement replacement is, up to 90 days, very low. After 180 days mortars with 50 mass-% glass powder 1 reaches 37 N/pa². Mortars with glass powder 2 and fly ash show nearly the same values (58 and 60 N/pa²) for the compressive strength.

However in contrast to mortars with 10 or 25 mass-% replacements, the mortar with glass powder 2 reaches higher values.

4. CONCLUSIONS

Fine ground container glass reacts as a pozzolan when combined with lime or cement. At early ages there are still reactions between the glass powder and the cement and lime respectively. CSH phases can be found on the surface and especially at rough edges of the glass particles. At later ages cracks are often found between the glass particles and CSH phases and particularly through the glass particles. A similar phenomenon was described by Pickel [10]. He used glass as aggregate for cast stones. These cast stones were damaged by ASR and loss of the bond between the glass particles and the cement as a result of corrosion of the glass was also detected. In the present case there is no damaging of the samples. So, it can be said that the shrinking during the drying period at 50°C probably causes the cracks.

Both, the reactivity and the strength depend on the particle size of the glass. To reach comparable compressive strength to mortars with fly ash, the glass powder must be ground very fine (> 500 m²/kg). Mortars with glass powder 1, which has a comparable particle size distribution to fly ash, reaches lower, but satisfactory compressive strengths at all ages. A reason can be the higher BET-surface of the fly ash and the higher amount of hydraulic components.

When mixed with lime, glass reacts pozzolanic at normal conditions. After four days storage at 20°C/95 % humidity glass-lime-mortars can be cured under water and are stable. The compressive strength depends on the particle size of the glass powder. With a heat treatment the compressive strength of glass-lime-mortars with coarse glass was improved.

The investigations show, that glass can be used as a pozzolanic material for concrete or lime mortars. At the present there are still some open questions concerning the influence of fine ground glass on ASR and chemical resistance on mortars or concrete. These questions are part of the current investigations.

REFERENCES

[1] Design von Baustoffen am Beispiel eines Putzes und eines Betons mit Glaszuschlag, Diss. Universität-Gesamthochschule Siegen, 2000.

[2] Heeß, S., Mutke, S. Gefahr beim Einsatz von Glas, www.dyckerhoff-weiss.de.

[3] Meland,I., Dahl, P.A. Recycling glass cullet as concrete aggregates, applicability and durability, Recycling and reuse of Glass Cullet, Proceedings of the International Symposium, Dundee, 2001.

[4] H.F.W. Taylor: Cement Chemistry, 2nd Edition, Thomas Telford, London.

[5] Sugita, S., Yu, Q., Shoya, M., Tsukinaga, Y., Isojima, Y. The effect of waste glass powder on the properties and pore structure of ordinary Portland cement hydrates, Proceedings of the 10th International Congress on the Chemistry of Cement, Volume 3, 1997, pp.3ii119.

[6] Archibald, J.F., Chew, J.L., Lausch, P. Use of ground waste glass and normal Portland cement mixtures for improving slurry and paste backfill support performance, CIM Bulletin Volume 92, pp 74-80.

[7] Dyer, T.D., Dhir, R.K. Use of Glass cullet as a cement component in concrete, Recycling and reuse of Glass Cullet, Proceedings of the International Symposium, Dundee, 2001.

[8] Shao, Y., Lehoux, P. Feasibility of using ground waste glass as a cementitious material, Recycling and reuse of Glass Cullet, Proceedings of the International Symposium, Dundee, 2001.

[9] Locher, F.W., Sprung, S. Ursache und Wirkungsweise der Alkalireaktion, Betontechnische Berichte 1973, Düsseldorf: Betonverlag 1974.

[10] Pickel, U. Glaseinstreuung in Betonwerkstein, Betonwerk- und Fertigteil- Technik, 58, Nr. 5 S. 56-58, 1992.

ABOUT THE BEHAVIOUR OF GLASS POWDER IN PASTES AND MORTARS WITH CEMENT

W. Remarque[1], L. Urbonas[1] and D. Heinz[2]

[1]Institute of Mineral Engineering, University of Aachen, Mauerstr. 5, D-52064 Aachen, Germany.
E-mail: remarque@ghi.rwth-aachen.de
[2]TU München, Germany.

W. Remarque

Dipl.-Ing. Werner Remarque
University of Aachen
Institute of Mineral Engineering
Mauerstr. 5
D- 52064 Aachen
Germany

Tel: 0049 (0)241 80 94969
E-Mail: remarque@ghi.rwth-aachen.de

PARTICLE SIZE DISTRIBUTION OF CEMENTS AND MINERAL ADMIXTURES – STANDARD AND SOPHISTICATED MEASUREMENTS

Ursula Stark[1] and. Anette Mueller[1]

[1]Bauhaus-University Weimar, Chair of Processing of Building Materials and Reuse
Weimar, Germany.
E-mail: ursula.stark@bauing.uni-weimar.de and anette-m.mueller@bauing.uni-weimar.de

ABSTRACT

This paper reports different aspects of the measurements of particle sizes of fine dispersed materials, like cement or mineral admixtures. The most important prerequisites for correct measurements of particle size distributions of these materials are the sampling and the complete dispersing. In the example of a fly ash, the specific features of the sampling of powders with very broad particle size distributions are explained. Because the mass of the sample is limited by the measuring technique the problem arises that the sample is not representative with regard to the coarse particles. To overcome this problem and to get a representative result, it is only possible if a lot of separate runs with an new sample is carried out. So the analysed quantity of sample is increased indirectly.

With regard to materials in the submicron range, the deagglomeration is the most important prerequisite for correct measurements. By a treatment with ultrasonic waves the agglomerates in the sample must be destroyed, thus to analyse the primary particles. The necessary duration of the treatment is reached if no further changes of the particle size are detectable. In the example of silica fume, the results of particle analyses based on light scattering agree with that of ESEM-analyses. With this example, it is shown that a complete deagglomeration can be achieved even for very fine powders which tend to the formation of agglomerates, provided that the sample is stressed by a suitable treatment.

Particle size analyses are also suitable to detect interactions in suspensions of different materials:

- In mixtures without interactions the measured particle size distributions must agree with those distributions calculated from the basic materials and the portions in the mixture.
- In mixtures where interactions occur, there is no agreement between measurement and calculation.

Furthermore, the changes of the particle size due to the reaction between water and cement in the early period of hydration can be observed in situ. Although not all measured effects are clear, a change of the particle size distribution and an increase of the mean particle size was found to be in agreement with the fact that the size of the hydration products is larger than the size of the original cement particles.

1. INTRODUCTION

The particle size distribution of cements and mineral admixtures is an important factor for the controlling of the properties of cement and concrete. Thus, the workability and the strength development can be influenced. Furthermore, a wide range of binders for different fields of application can be manufactured by the modification of the fineness.

Proceedings of the 11th International Congress on the Chemistry of Cement (ICCC)
'Cement's Contribution to the Development in the 21st Century'
Hosted by: The Cement and Concrete Institute of South Africa
CD-ROM produced by: Document Transformation Technologies
11 - 16 May 2003, Durban, South Africa
ISBN Number: 0-9584085-8-0
Editors: Dr G. Grieve and G. Owens
Congress Organised by: Event Dynamics

The most usual method to describe the fineness of a cement is the measurement of the specific surface area. This surface area is an integral parameter and gives no information about details of the size distribution. That's why nowadays the particle sizes are characterised with complete distributions analysed with laser light diffraction or laser light scattering. Reliable results can be achieved if the influences of the sampling and the preparation of the sample are taken into consideration as shown in the first part of this paper.

The standard measurements do not exhaust the potential of the measuring technique. In the second part examples for sophisticated measurements are described. So it is possible to obtain changes of the particle size as a result of an interaction between components of a mixture or to observe the change of the size of the cement particles during the first stage of the hydration in situ.

2. EXPERIMENTAL PROCEDURES OF PARTICLE SIZE ANALYSES

2.1 Method of Analysis

The presented results of this paper were measured with the instrument COULTER® LS 230. This instrument analyses a range of particle sizes from 0,04 to 2000 µm without the need to make changes in the optical bench or the lens system. In the range above 0.4 µm the theoretical basis of the measurement is the Fraunhofer-theory of laser diffraction. In the range of particle sizes smaller than 0.4 µm the Mie-theory of light scattering is used (Figure 1). Altogether 116 size channels are available for the complete analysis with 151 detectors. The measurement is carried out in a liquid. This means that the sample must be dispersed in a suitable liquid before it is analysed.

Despite the continuously increasing automation of the particle size analyses it is possible to get different results in dependence of the preparation of the specimen. For coarse–grained materials the sampling and the splitting of the sample are the most important steps during the sample preparation. For fine-dispersed materials the process of disintegration of agglomerates is the key factor for reliable and reproducible results.

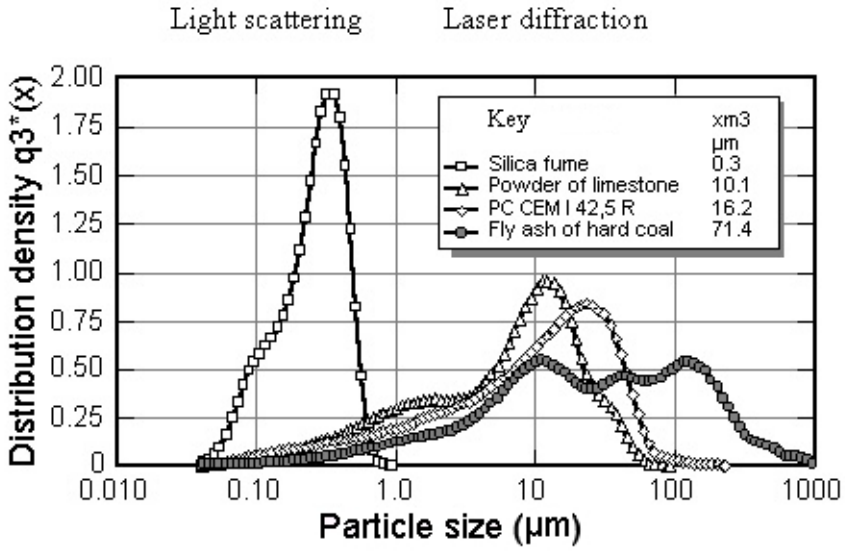

Figure 1. Standard measurement - particle size distribution of cement and different mineral admixtures

2.2 Sample preparation

The sample mass that is needed for the measurement of particle size distributions in general depends on the maximum particle size and the measuring method that is used or that is realised in the used instrument used. In the case of the measuring of broad distributions with the method of laser diffraction both effects have contrary tendencies. Broad distributions require a sufficient

quantity of sample, to ensure that coarse grains are also present in the sample in a representative manner. In contrast, the method of laser diffraction requires a very small sample, since it should reduce the total intensity of the laser light only slightly. Only so, it is possible to determine properly the signals at the various channels that correspond to the particle size. In the following example these influences are demonstrated and a strategy of minimising errors is explained.

In Figure 2, the particle size distribution of a fly ash of lignite is shown. The mass of the sample was about 50 mg. The sampling was done with the so-called “shovel method” since such a small sample cannot be obtained with sample dividers. The reason for the small mass of the sample follows from the high portion of fine material in this sample that causes a considerable reduction of the total light intensity. Therefore it is possible that the few coarse particles are not contained in the sample representatively.

This is the reason for the considerable deviations in the range above 400 µm between the single measurements with a new sample as shown in Figure 3. The differences depend on the random number of coarse particles in the sample. To overcome this effect and to obtain a representative result, it is only possible if a large number of separate runs with a new sample is carried out. So the analysed sample mass is increased indirectly.

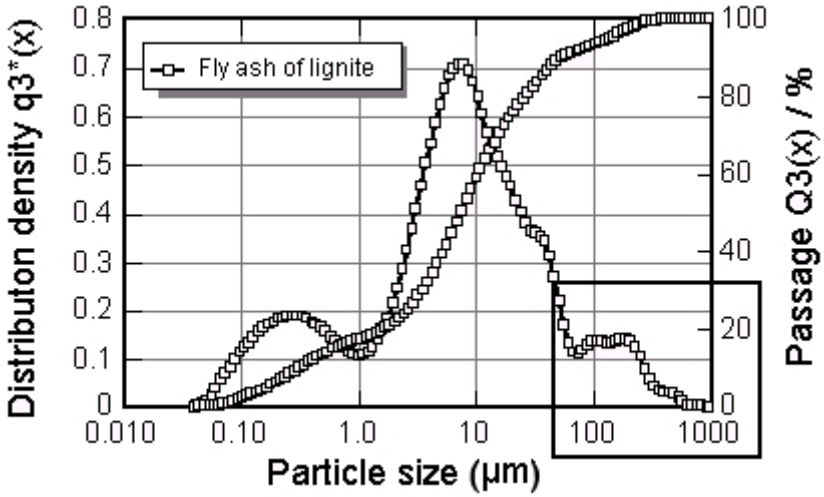

Figure 2. Particle size distribution of a fly ash from lignite

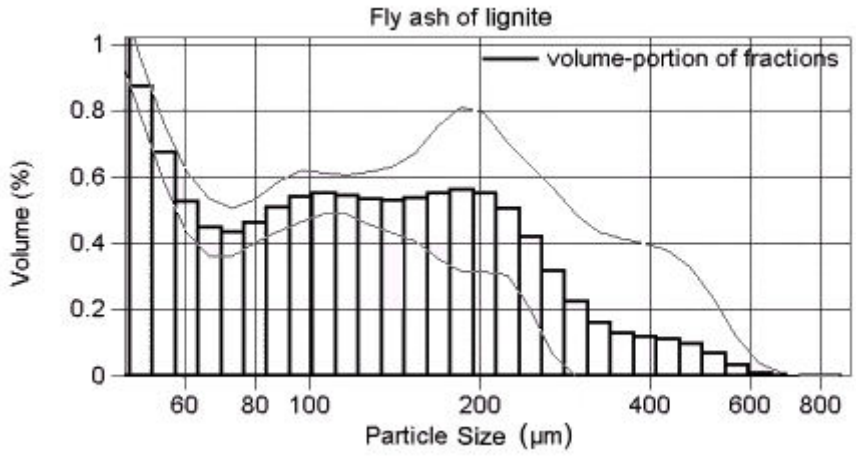

Figure 3. Detail of particle size distribution - maximum and minimum deviations of the measurements from the mean value

For the measurement of the particle size distribution of fly ash in Figure 2, nine separate runs were done. The single results are the basis of summarized result calculated as an average. In addition, a sieve analysis was carried out in the particle range > 400 µm. This should always be done as confirmation of the results.

2.3 Dispersing of the sample

For fine-dispersed materials it is most important to deagglomerate them sufficiently. This means that the forces of attraction that act between the small particles and increase with decreasing particle size have to be overcome. Therefore a regime for the sample treatment with ultrasonic waves must be created for each material. Thus the particle size distribution of primary particles is obtained and a good reproducibility of the results is achieved.

For most of the fine bulk materials a treatment for 2 to 4 minutes with a disintegrator driven by ultrasonic waves is enough. For silica fume as the finest material with particle sizes below 1 µm that is used in the construction industry no distribution of the primary particles can normally be achieved. From extensive experiments with altogether 15 different samples of silica fume it was found that the silica fume has to be treated for 9 minutes with ultrasonic waves.

The deagglomeration of a sample volume of about 20 cm^3 was done with a power of about 42 W in intervals of 3 minutes. Thus a too large heat development could be avoided. The influence of the time of treatment on the different characteristic particle sizes x_{10}, x_{90} and the mean particle size x_m is shown in Figure 40 at the example of one sample of silica fume.

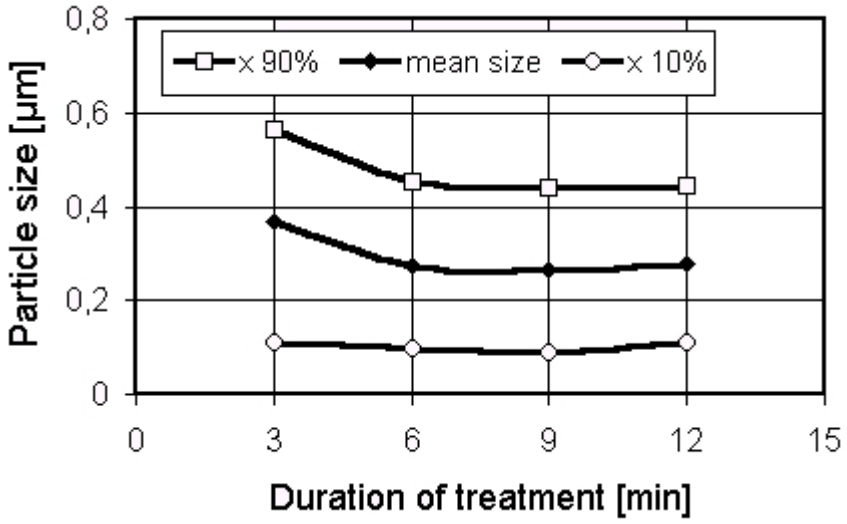

Figure 4. Influence of the time of ultrasonic treatment on the particle size distribution of silica fume

From this graph follows that the smallest particle sizes are measured after a treatment of 9 minutes. Then the particle size is unchanged also by the further input of power, i.e. the deagglomeration seems to be finished. In Figure 4, each point drawn is the mean of 3 separate runs for getting a sufficient statistical reliability.

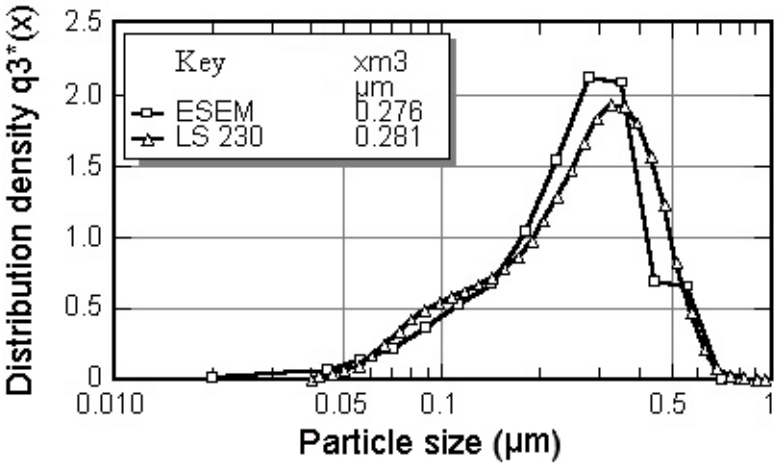

Figure 5. Particle size distribution of silica fume measured by Laser light scattering and ESEM-images [3]

A comparison of two distributions is shown in Figure 5, on the one hand measured on the basis of the Mie-theory with laser light scattering, and on the other hand calculated on basis of ESEM-images by a particle count. The prerequisite for such a direct comparison is that the compared particles are spherical which is true for silica fume. From Figure 5, it follows that a complete deagglomeration can be achieved even for very fine powders, which tend to the formation of agglomerates, provided that the sample is stressed by a suitable treatment. Then the distribution of the real primary particles is measured.

3. STANDARD MEASUREMENTS OF PARTICLE SIZE DISTRIBUTIONS OF CEMENTS AND MINERAL ADMIXTURES

The properties of cements can be controlled by their fineness. Since this tool is most practicable in the cement manufacturing process, a considerable number of different cements is offered nowadays which mainly differs in the particle size distribution. In Figure 6, a selection of cements with different fineness is shown, and from the evaluation of a large number of further measurements, the ranges of particle size that are typical for different types of cements can be summarised below.

The mean particle sizes of cements are in the following ranges:

- for Ordinary Portland Cements 18 to 26 µm (CEM I+II 32,5R)
- for High-early-strength Cements 12 to 18 µm (CEM I 42,5R)
- for Very high-early-strength Cements 9 to 10 µm (CEM I 52,5R)
- for Special highly fine Cements, i.e. Microcem. 2.5; 3.1; 5.2; 8.0 µm

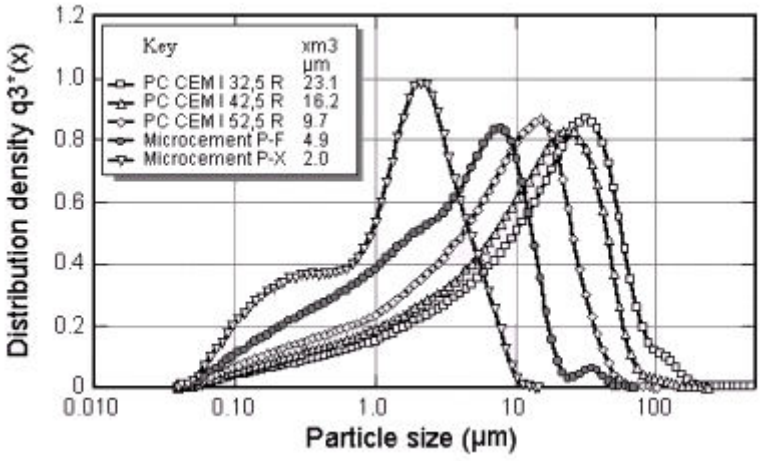

Figure 6. Particle size distributions of different cements [5]

As another possibility for the influencing of the properties of cement, the addition of blending materials or mineral admixtures must be named. The most important admixtures are industrial by-products that result in powders. These materials have particle sizes in the following ranges:

- Fly ash is characterized by particle sizes between 0.1 and 1000 µm, the mean particle size is between 23 and 67 µm.
- Silica fume is characterized by particle sizes between 0.02 and 1 µm; the mean particle size is about 0.3 µm.

Limestone will be also interground or added as powder to the concrete. Added powders are characterized by particle sizes between 0,05 and 200 µm, the mean particle size is between 6 and 23 µm.

4. SOPHISTICATED MEASUREMENTS

4.1 Measurement of interactions between components of mixtures

In addition to standard measurements the measuring technique of particle sizes can be used also to check if interactions between components of mixtures take place.

If there are no interactions, then the measured particle size distribution must be the same as that which is calculated by mixing the distributions of the components. This is demonstrated by the example of a mixture from natural plaster plus REA-gypsum in Figure 7.

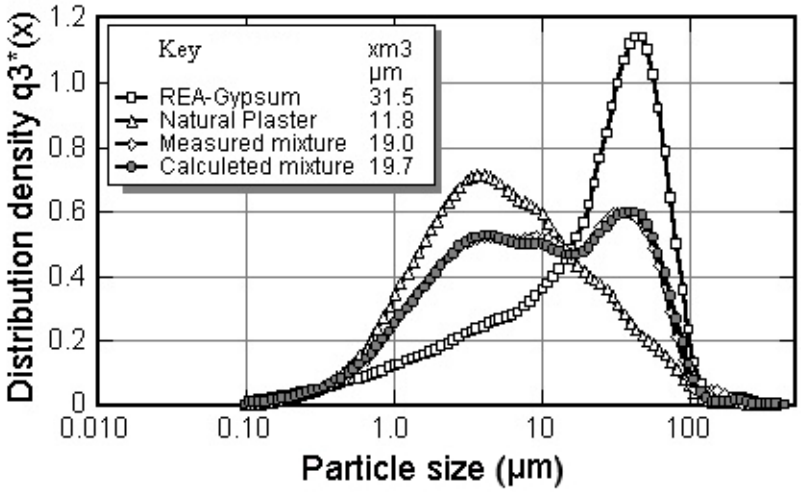

Figure 7. Particle size distribution of natural plaster and REA-Gypsum and a mixture of both with a ratio of natural plaster to REA-Gypsum of 1:1,5

If interactions between components take place, or reactions occur then the measured distribution does not agree with the calculated one. The example of a polymer-modified cement shows such considerable deviations between measured and calculated distributions as a result of an interaction. The particle size distributions of the separate components of polymer and cement are shown in Figure 8.

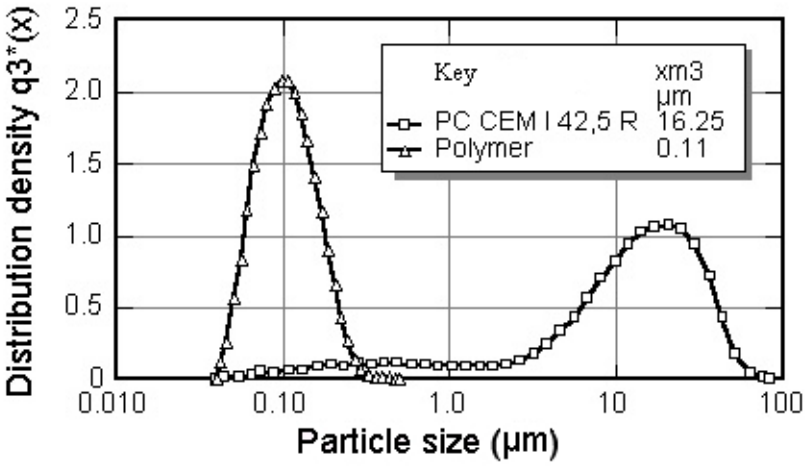

Figure 8. Particle size distribution of cement and polymer

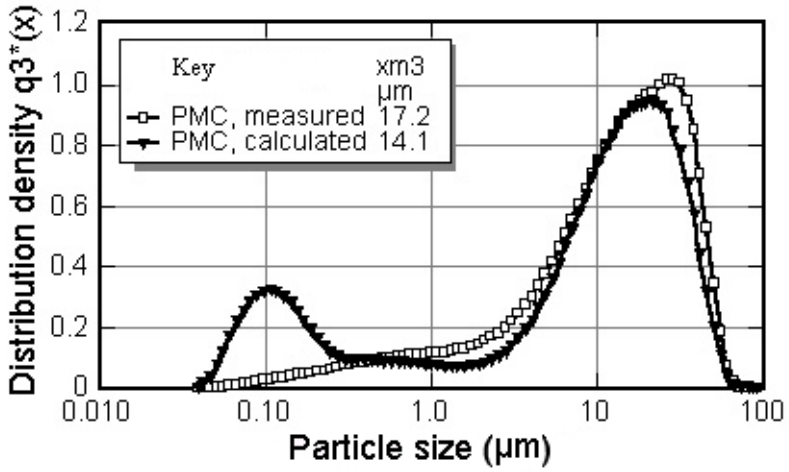

Figure 9. Particle size distributions of polymer–modified cement - comparison of measurement and calculation [4]

The components were measured under the same conditions as the mixtures. The distribution of the mixture differs widely from the calculated distribution (Figure 9). A considerable coarsening takes place compared with the theoretically calculated mixture. Especially the first peak at 0,1 µm of the calculated distribution that is caused by the polymer does not appear in the measured distribution. It must be assumed that the polymer is fixed on the surface of the cement particle somehow.

4.2 Hydration of cement

The changes of the particle size distribution in the early period of hydration of cement can be observed in situ if the measuring regime is fitted to this special question. The most important difference compared with the standard measurements is the use of water instead of isopropanol as measuring liquid because the cement particles will react with the water in contrast to the standard measurements where such a reaction is not desired. Two different kinds of preparation methods were applied. For the one method a suspension with a water-cement ratio of 8 was used. Then the hydration could be observed for about 480 minutes. The other method was carried out with a paste with w/c = 1. Then the changes of the particle sizes due to the hydration could be measured for about 60 minutes, before the setting process began. The particle size of the Portland Cement at the starting point (time zero) was analysed in isopropanol in order to exclude reactions.

With the dynamic particle size measurements the following influences were examined:
fineness of cement:

- temperature of cement-suspension,
- water-cement ratio.

Figure 10 shows the changes of the mean particle size in dependence of the time of hydration of Portland Cements with different fineness and a water-cement ratio of 8 The first contact of the cement with the water results in an increase of the particle size. A period follows, while the particle size decreases. This period is finished after approximately 200 minutes. Then the mean particle size increases again.

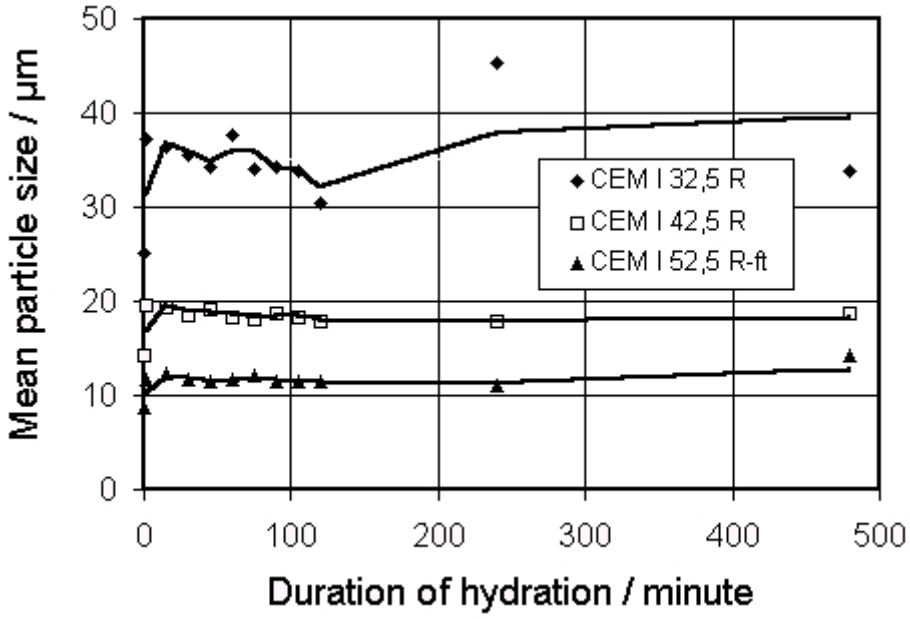

Figure 10. Changes of the mean particle size of cement with different fineness during the early period of hydration, suspension with w/c = 8

If a finer or coarser cement is analysed, the shape of the plot “particle size versus time of hydration” is very similar. Only the height of the maximums is shifted.

The results of the particle size measurements can be explained with the theories of hydration known from the literature. A decrease of the particle size can be attributed to the through-solution mechanism assumed by Le CHATELIER. An increase may be caused by a topochemical reaction according to the hypothesis of MICHAELIS.

The observed influence of temperature on the growth of the particles can be noted in Figure 11. The acceleration of the process by increasing temperatures is no surprising effect. These results show that the method is able to make visible small differences.

In Figure 12, the results of the suspension measurements and the paste measurements are compared for three cements with different fineness. It follows that the paste measurements have systematically smaller mean particles than the suspension measurements. This difference increases with decreasing fineness. This effect statistically ensured by repeated runs can not be explained till now.

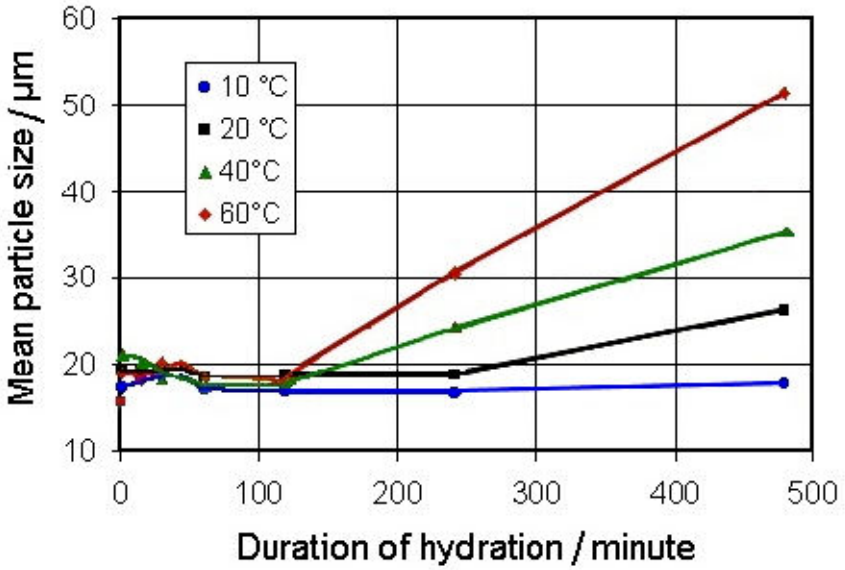

Figure 11. Changes of particle size in dependence of different temperature, PC CEM I 42,5 R, w/c = 8

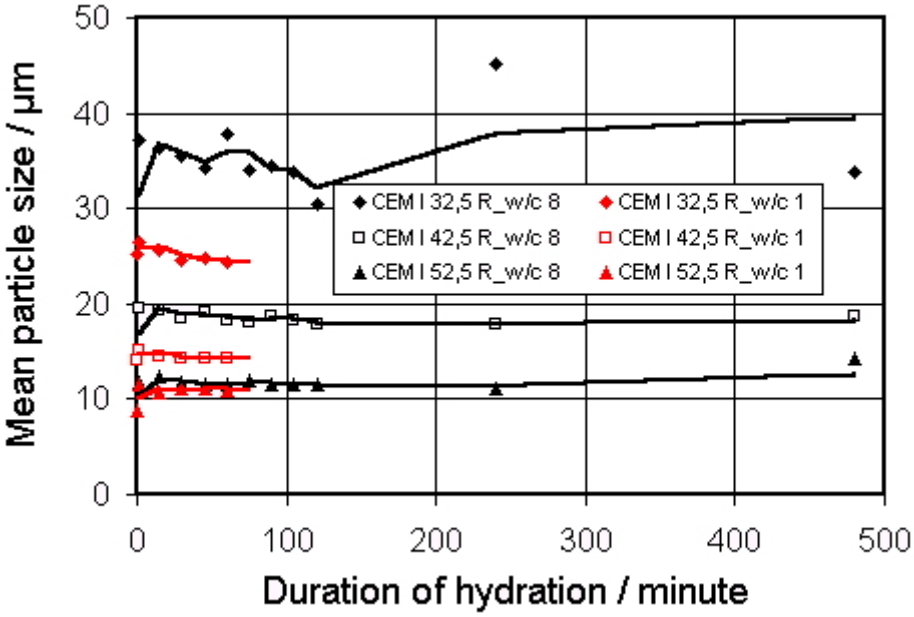

Figure 12. Influence of different w/c – ratios to the hydration behaviour

5. CONCLUSIONS

In the first topic of the paper the performance of laser based measurements of the particle size distributions of fine-dispersed materials could be shown. If certain prerequisites of the sample preparation are fulfilled then reliable results are obtained even for problematic materials like powders with a very broad distribution or materials with very small particle sizes.

In the second topic new ideas were introduced for the application of particle size measurements and demonstrated by some examples. Obvious conclusions about interactions between the components of a mixture follow from the particle size distributions, measured in the separate components on the one hand and in the mixtures on the other hand.

The in situ measurements of cement suspensions or cement pastes point to a new possibility for the quantitative determination of changes of particle sizes in the early stage of hydration. In this field further investigations are necessary to improve the procedures of sample preparation, to prolong the period in which measurements are possible even in pastes, and to explain some of the measured effects. Furthermore a new method of evaluation must be figured out since the mean particle size as unit of the progress of the hydration is not expressive enough.

REFERENCES

[1] Stark, U.: Granulometrische Charakterisierung feindisperser Schüttgüter des Bauwesens; Fallstudienreihe, Heft Mikrosilica; Herausgeber Coulter Electronics GmbH Krefeld

[2] Stark, U.; Müller, A.: Granulometrische Charakterisierung von Sekundärrohstoffen in der Bau- und Baustoffindustrie; Vortrag zum 49. Berg- und Hüttenmännischen Tag 1998 in Freiberg; Freiberger Forschungshefte A 841 Grundstoff-Verfahrenstechnik 1998, Technische Universität Bergakademie Freiberg; S. 26-40

[3] Maiwald, Y.: Granulometrische Charakterisierung von Mikrosilica; Studienarbeit, 2000, Bauhaus-Universität Weimar, Fakultät Bauingenieurwesen, Professur Aufbereitung von Baustoffen und Wiederverwertung; Betreuer: Stark, U. / Möser, B.

[4] Müller, S.: Untersuchungen zu den Wechselwirkungen von Zement und Polymeren im frühen Stadium der Erhärtung von PCC; Studienarbeit, 1999, Bauhaus-Universität Weimar, Fakultät Bauingenieurwesen, Finger-Institut für Baustoffkunde; Betreuer: Stark, U. / Dimmig, A.

[5] Jung, M.: Datenatlas für feindisperse Baustoffe; Diplomarbeit, 1999, Bauhaus-Universität Weimar, Fakultät Bauingenieurwesen, Professur Aufbereitung von Baustoffen und Wiederverwertung; Betreuer: Stark, U.

[6] Radtke, N.: In-Situ-Messungen zu Korngrößenveränderungen während der Zement hydratation; Studienarbeit, 2000, Bauhaus-Universität Weimar, Fakultät Bauingenieurwesen, Professur Aufbereitung von Baustoffen und Wiederverwertung; Betreuer: Stark, U.

[7] Radtke, N.: Untersuchungen zu Korngrößenveränderungen während der Zementhydrytation; Diplomarbeit, 2001, Bauhaus-Universität Weimar, Fakultät Bauingenieurwesen, Professur Aufbereitung von Baustoffen und Wiederverwertung; Betreuer: Stark, U.

PARTICLE SIZE DISTRIBUTION OF CEMENTS AND MINERAL ADMIXTURES – STANDARD AND SOPHISTICATED MEASUREMENTS

Ursula Stark[1] and. Anette Mueller[1]

[1]Bauhaus-University Weimar, Chair of Processing of Building Materials and Reuse
Weimar, Germany.
E-mail: ursula.stark@bauing.uni-weimar.de and anette-m.mueller@bauing.uni-weimar.de

Dr Ing Ursula Stark is Scientific Assistant at the chair of Processing of Building Materials and Reuse of the Department of Civil Engineering at the Bauhaus-University in Weimar, Germany. Her interests are in the fields of building materials, processing technologies for minerals, industrial by-products and construction and demolition waste. She has broad experience in the field of particle sizes analysis.

Prof Dr Ing habil Anette Mueller is Leader of the Chair of Processing of Building Materials and Reuse at the Bauhaus-University in Weimar, Germany. Her special research interests are the recycling of construction debris for new building materials, the influence of processing on bulk materials and the chemistry of cements.

USE OF TYRE RUBBER PARTICLES IN SLAG-MODIFIED CEMENT MORTARS

Nádia Segre[1], Alexandre D. Galves[2], José A. Rodrigues[2], Paulo J. M. Monteiro[3] and Inés Joekes[1]

[1] Chemistry Institute, University of Campinas, Campinas-SP, Brazil.
E-mail: nadia@iqm.unicamp.br
[2] Department of Materials Engineering, Federal University of São Carlos, São Carlos-SP, Brazil.
E-mail: josear@power.ufscar.br
[3] Department of Civil and Environmental Engineering, University of California, Berkeley, USA.
E-mail: monteiro@ce.berkeley.edu

ABSTRACT

Mortar specimens were prepared using slag-modified Portland cement and 10% (by weight of mortar) of NaOH-treated rubber particles, smaller than 300 μm, from truck tyres (mainly SBR rubber). Water sorption by capillarity and by immersion, resistance to acid attack, surface of fracture analysis by scanning electron microscopy and flexural strength experiments were performed. Flexural strength was reduced with the addition of the rubber (3.6 ± 0.5 MPa for the specimens with rubber, 6.5 ± 0.8 MPa for the control). On the other hand, advantageous effects of the addition of the rubber were observed on the transport properties of mortar. Sorptivity coefficient was reduced from 0.29 (control) to 0.06 mm/min$^{1/2}$. By immersion, the amount of water absorbed by the specimens with rubber was reduced in 16 %. A significant decrease in the rate of weight loss by acid attack was observed for specimens with rubber. SEM micrographs showed the presence of microcracks in the specimens and closed pores in the specimens with rubber. These results show that small rubber particles can improve some mortar properties even when used in a high proportion.

1. INTRODUCTION

The ever-increasing volume of rubber waste in landfills from the disposal of used tyres has grown into a serious environmental problem. Because rubber waste does not biodegrade readily, even after long periods of landfill treatment, there is renewed interest in developing alternatives to disposal. One possible solution for this problem is to incorporate rubber particles into cement-based materials. Unfortunately, most research on using untreated tyre rubber in cement-based materials shows that the degree of adhesion is poor, i.e., the rubber-cement interface is weak, leading to poor mechanical properties. [1-7]

In a previous research, we studied ordinary Portland cement pastes with 10% of powdered tyre rubber (35 mesh maximum size). This rubber, a mixture of SBR, natural rubber, polybutadiene, oils, curatives, antioxidants, carbon black, among others, was used untreated and after surface–treatment with NaOH saturated aqueous solution. Mechanical properties such as flexural strength and fracture energy were improved with the addition of these rubber particles, and the decrease in the compressive strength observed was significantly lower than that described in the literature. The rubber-matrix adhesion was improved with the NaOH treatment as observed in the SEM

Proceedings of the 11th International Congress on the Chemistry of Cement (ICCC)
'Cement's Contribution to the Development in the 21st Century'
Hosted by: The Cement and Concrete Institute of South Africa
CD-ROM produced by: Document Transformation Technologies
11 - 16 May 2003, Durban, South Africa
ISBN Number: 0-9584085-8-0
Editors: Dr G. Grieve and G. Owens
Congress Organised by: Event Dynamics

micrographs, rendering abrasion resistance and water absorption results significantly better than in pastes with the untreated rubber particles. [8]

Extending this work, the surface modification of tyre rubber after the treatment was investigated by HATR infrared analysis, potentiometric titration and contact angle measurements. Infrared analysis of the powdered treated rubber showed a decrease in absorption at 1540, 1450 and 1395 cm^{-1}. This decrease is attributed to the removal of zinc stearate, an additive present in tyre formulations that often migrates and diffuses to the surface, resulting in poor adhesion between the rubber and other materials. The potentiometric titration of the suspension of powdered rubber in 0.1M NaCl showed that more hydrochloric acid was consumed by the untreated rubber, most likely a result of the presence of basic groups on its surface due to the interaction between the zinc salt and the rubber. The contact angle of tyre pieces remained unchanged until 24 hours of exposure to NaOH. The decrease of the zinc stearate on the treated rubber surface can explain the improvement in the adhesion of this material to the cement matrix. [9]

The overall results of these works showed that the use of powdered rubber in cement composites is suitable for engineering purposes. Since cement paste is not commonly used in civil engineering and since ordinary Portland cement is unusual in Brazil, mortar was now prepared with the addition of NaOH-treated rubber to slag-modified Portland cement.

The use of tyre rubber as addition to cement paste (10% in weight of paste) showed satisfactory results in mechanical properties in our previous research [8]. In this work, 10% (in weight of mortar) of NaOH-treated tyre rubber was incorporated into the mortar, which represents roughly 35% of the cement content. This was the maximum amount of rubber that could be added to obtain a reasonable workability with a 0.6 w/c ratio, which is the maximum water amount for a mortar with reasonable mechanical properties. In other words, these mortars should be considered a case of ultimate powdered rubber addition.

2. EXPERIMENTAL

Powdered tyre rubber, supplied by Borcol Industria de Borracha Ltda, Sorocaba-SP, Brazil, 50 mesh maximum size (300μm), was surface-treated with saturated NaOH aqueous solutions for 20-30 min, at room temperature, under stirring. The mixture was filtered and the rubber was rinsed with water until neutral pH and allowed to dry at room temperature.

Mortar test specimens were prepared with Brazilian slag-modified Portland cement (which contains 6 to 34% of blast-furnace slag), washed natural sand with 2.6 fineness modulus and water. The mixture composition was water/cement ratio = 0.6, sand/cement ratio = 2. For specimens with NaOH-treated rubber, 10% (by mass of mortar) was added to the mixture. The specimens were cured for 28 days at room temperature (25°C) and 100% relative humidity.

Water sorption by capillarity was followed gravimetrically. Cured cylindrical specimens measuring 100 x 60mm were dried at 50°C in an oven until constant weight and placed on a support grating in a dish supplied with a water leveler at room temperature. The water level was sufficient to wet only the lower surface of the test specimens, not more than 5mm or so above the base of the specimen. The lower parts of the sides of the specimens adjoining the inflow face were sealed with an adhesive to prevent absorption into the surface pores. Mass data of each specimen was obtained after several periods of time, until constant weight. Triplicate specimens were used.

Water sorption by immersion was measured using 45 x 30mm cured cylindrical specimens. The specimens were dried at 50°C until constant weight, and then immersed in water at room

temperature. Mass data of each specimen was obtained after several periods of time, until constant weight. Quintuplicate specimens were used.

For resistance to acid attack, cured cylindrical specimens measuring 45 x 30mm were dried at 50°C until constant weight and then immersed in HCl 5% (1.4M). Mass data of each specimen was obtained after several periods of time, until constant weight. The HCl solution was replaced once a day. Quintuplicate specimens were used.

For flexural strength experiments, prismatic test specimens measuring 150 x 25 x 25mm were used. A three-point bend test was performed. These measurements were performed in a MTS model 810 testing machine. A displacement rate of 10mm/min was used. A set of 46 control specimens and a set of 47 specimens with rubber were used.

Scanning electron microscopy (SEM) was used to characterize the bulk region of the mortar specimens prepared. Fractures were obtained from specimen fragments and the samples were sputtered with gold. The SEM micrographs were obtained in a Jeol JSM 840A microscope.

3. RESULTS AND DISCUSSION

The failure of cement materials is governed by a process of microcracking, mainly associated with the interfacial region between the cement and the aggregate particles. These internal cracks can arise, for example, from processing defects such as pores. The uniaxial strength in compression is commonly accepted as a general index of cement material strength. Nevertheless, the flexural test is usually preferred for quality control of pavements, where the cement material is loaded in bending rather than in axial tension.

Figure 1 shows the results of flexural strength for control and specimens containing NaOH-treated rubber. A set of at least 46 specimens was tested in order to calculate the Weibull modulus, the cumulative probability that a specimen fails during stressing in uniform tension (not shown in this work). A reduction of c.a. 45% in flexural strength was observed for specimens with rubber.

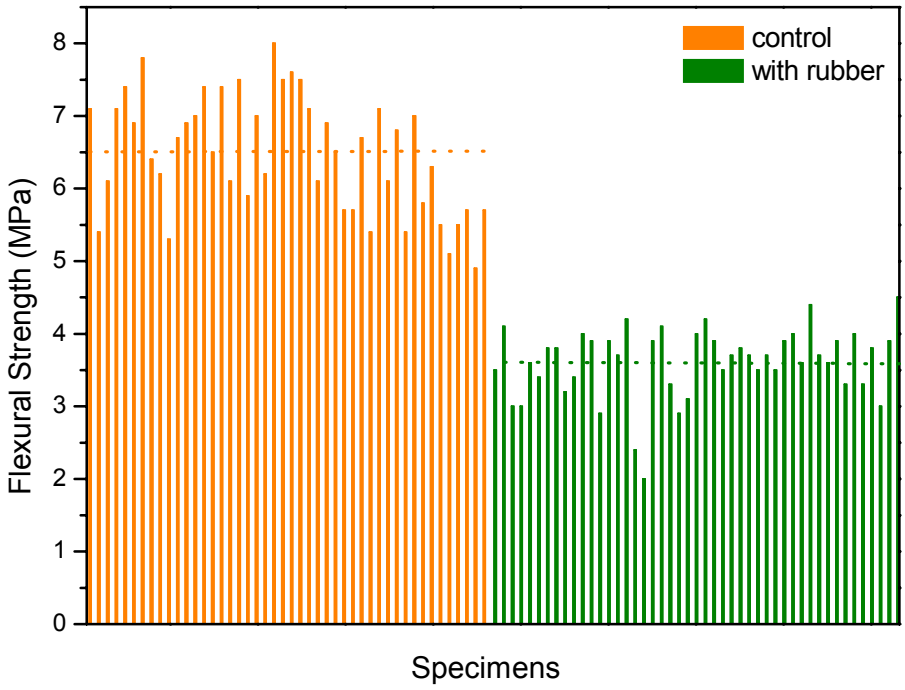

Figure 1. Flexural strength for mortar test specimens. In orange: control specimens, in green: specimens with 10% (by mass of mortar) of NaOH-treated tyre rubber particles. Dashed lines indicate the averages.

The high variability in strength shown is probably caused by the presence of a distribution of cracks and other flaws, both in size and position. In direct tension tests the entire volume of the specimen is under applied stress, whereas in the bending test only a small volume of the specimen near the bottom is subjected to high stresses. Figure 2 shows fracture surfaces of the specimens submitted to bending stress, after failure. It is interesting to note that control specimens with different bulk characteristics (a and b) showed the same strength value (5.5 MPa). For specimens with rubber a better value of flexural strength (4.1 MPa) was obtained for a specimen with more defects (c) when compared with the value 3.5 MPa obtained for a more homogeneous specimen (d).

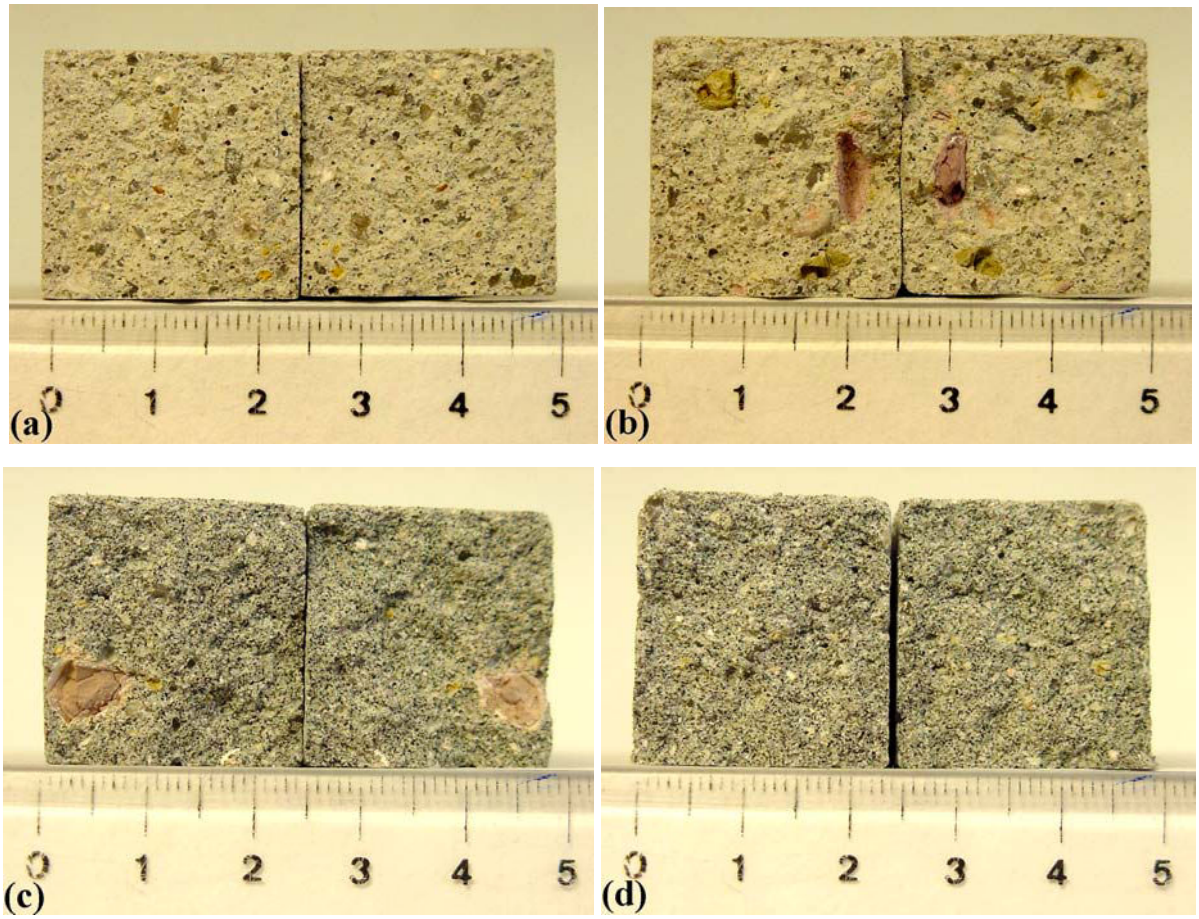

Figure 2. Fracture surfaces of specimens submitted to bending stress, after failure. (a) and (b): control specimen; (c) and (d) specimen with NaOH-treated rubber particles.

In cement technology, strength is the commonly specified property. However, the strength of a hardened cement material is by no means its only important characteristic. Properties such as elastic modulus, impermeability, and resistance to weathering agents including aggressive waters, are directly related to durability.

The amount of water absorbed is related to the porosity of the test specimens and gives a picture of the internal microstructure. An understanding of moisture transport in concrete and mortar is important to estimate their application as a building material and to improve their quality. The primary transport mechanisms by which aggressive substances enter cement materials are diffusion and capillary action, but capillary transport is the dominant entry mechanism. In this sense, the smaller the capillarity, the higher the durability. Figure 3 shows that the addition of rubber particles lowers radically the amount of water absorbed.

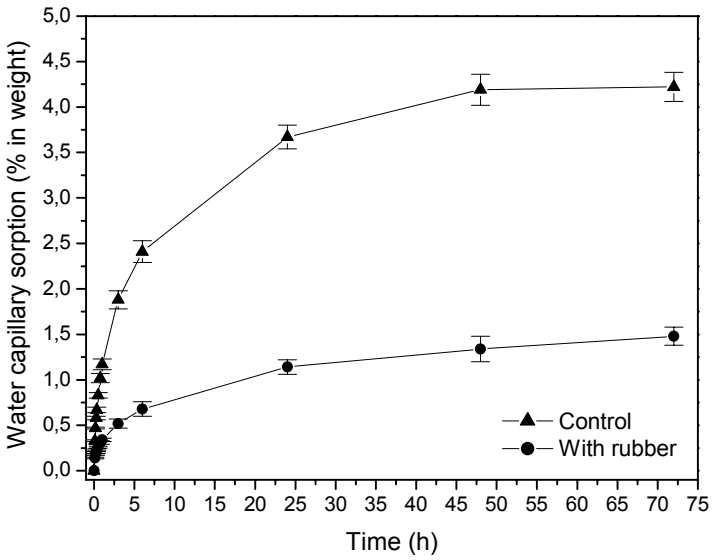

Figure 3. Water sorption by capillarity as a function of time, for mortar test specimens with 10% (by mass of mortar) of NaOH-treated tyre rubber particles. Control: mortar only. Room temperature. Results of triplicate specimens.

The sorptivity coefficient (S) characterizes the tendency of a porous material to absorb and carry water by capillarity, and can be obtained by considering the application of Equation 1, where Δw is the increase in weight, A is the cross-sectional area, ρ is the density of water and t is the time. A finite (generally small, positive) intercept, b, is usually found. The origin of this arises from the filling of open surface porosity on the inflow surface and along the sides of adjacent faces. [10, 11]

$$\frac{\Delta w}{A.\rho} = St^{1/2} + b \qquad (1)$$

Figure 4 shows the water sorption per unit area of inflow surface as a function of the square root of the time, as obtained from Figure 3. For the control specimens, a sorptivity coefficient of 0.29mm/min$^{1/2}$ was calculated, and for the specimens with the rubber particles, 0.06mm/min$^{1/2}$.

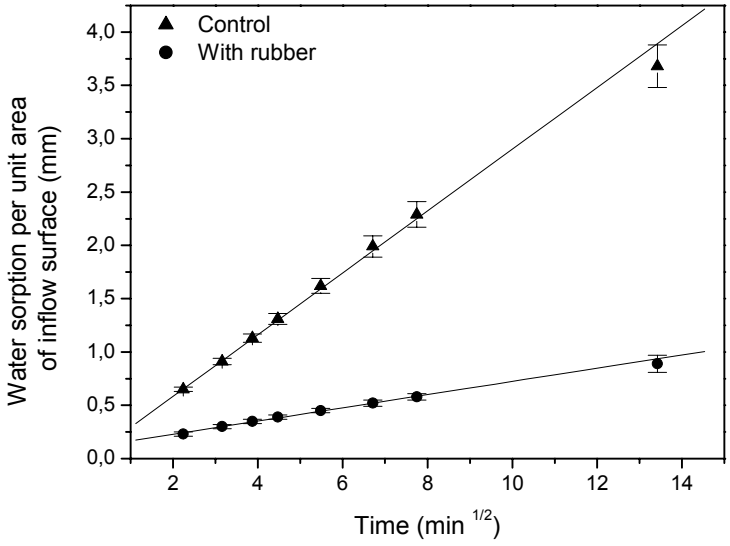

Figure 4. Water sorption per unit area of inflow surface as a function of time for mortar test specimens with 10% (by mass of mortar) of NaOH-treated tyre rubber particles. Control: mortar only. Results of triplicate specimens.

This behavior arises from the hydrophobicity of the rubber particles. In channels in which a rubber particle is exposed, a hydrophobic barrier arises, which can even stop capillary ascension, increasing the local interface tension between water and the channel surface. The probability that a rubber particle is in the surface of a channel is roughly the same as that of a sand particle (regarding the mass ratio) since the particle fineness is inside the sand fineness.

Figure 5 shows the results of the sorption of water by immersion, which is also related to the open porosity of the specimens tested. However, water sorption by immersion is always higher than by capillarity, since capillary ascension takes place only in open pores of relatively small diameter. A 17 % reduction in the amount of water absorbed is found for the rubber-containing specimens, meaning that they have fewer pores or that fewer pores are reachable by the water (closed pores or very narrow capillaries). Since the hydrophobic effect is not expected to be prominent in this case, and since the microstructure of both, with or without rubber, mortar specimens shows detachments at interfaces, this effect arises probably from occluded pores.

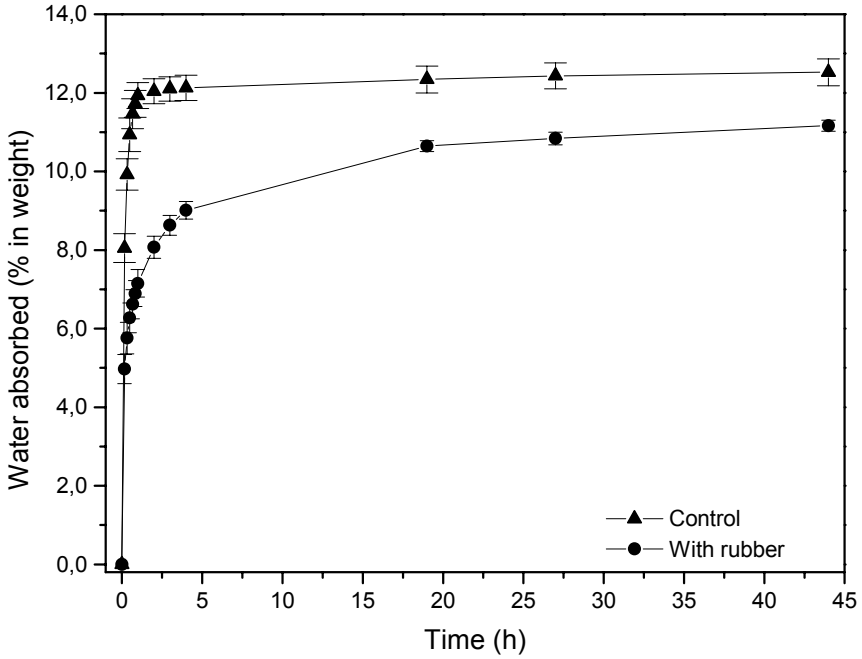

Figure 5. Water sorption by immersion, at room temperature, as a function of time for mortar test specimens with 10% (by mass of mortar) of NaOH-treated tyre rubber particles. Control: mortar only. Results of quintuplicate specimens.

Figure 6 show micrographs of a typical fracture surface bulk region of a control test specimen (a) and specimens with rubber (b and c). Microcracks are observed in the rubber or sand -matrix interface (transition zone). During early hydration periods, the transition zone is weak and vulnerable to cracking due to differential strains between the cement paste and the aggregate induced generally by drying shrinkage, thermal shrinkage, and externally applied load. [12] Supporting our hypothesis, the presence of closed pores is observed in the specimens with rubber.

The durability of a cement-based material relates to its service life under given environmental conditions. The hydrated cement paste is alkaline and, therefore, acidic waters are expected to be particularly harmful to these materials. Deleterious chemical effects of this acidic attack include leaching of the calcium hydroxide. Acidic fluids will also increase the porosity, thus making the material more vulnerable. Under these conditions, impermeability becomes a primary factor in determining durability.

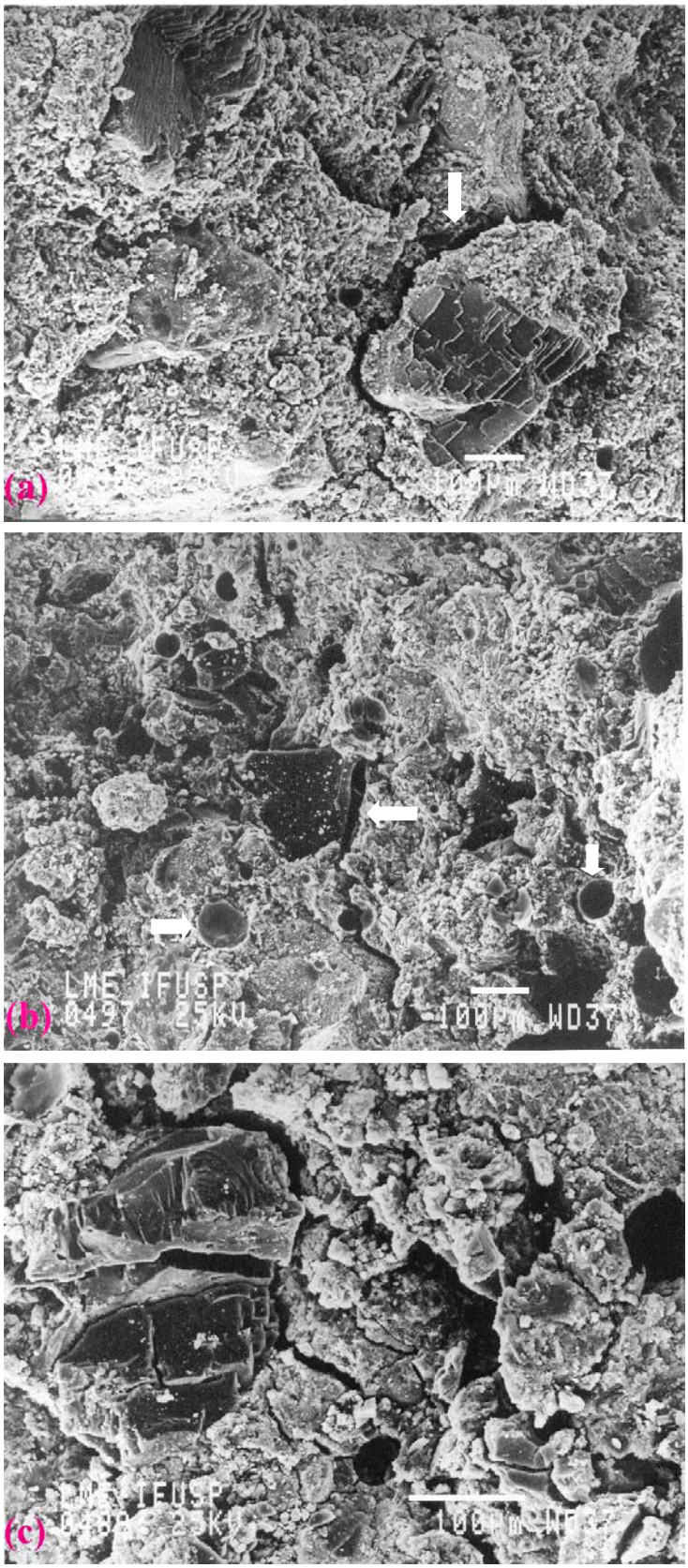

Figure 6. SEM images of fracture surface of mortar test specimens. (a) Control: mortar only; (b) and (c) with 10% (in weight of mortar) of NaOH-treated rubber particles. Bars: 100 μm. A: sand particle. B: rubber particles. Arrows: detachments or closed pores.

The effect of the addition of rubber on the acid resistance was investigated. Results displayed in Figure 7 show that the rubber particles have a positive effect on the acid resistance. A faster surface

leaching was observed for the specimens without rubber. In this case, the rubber particles act by shielding the mortar inner parts from the incoming acid.

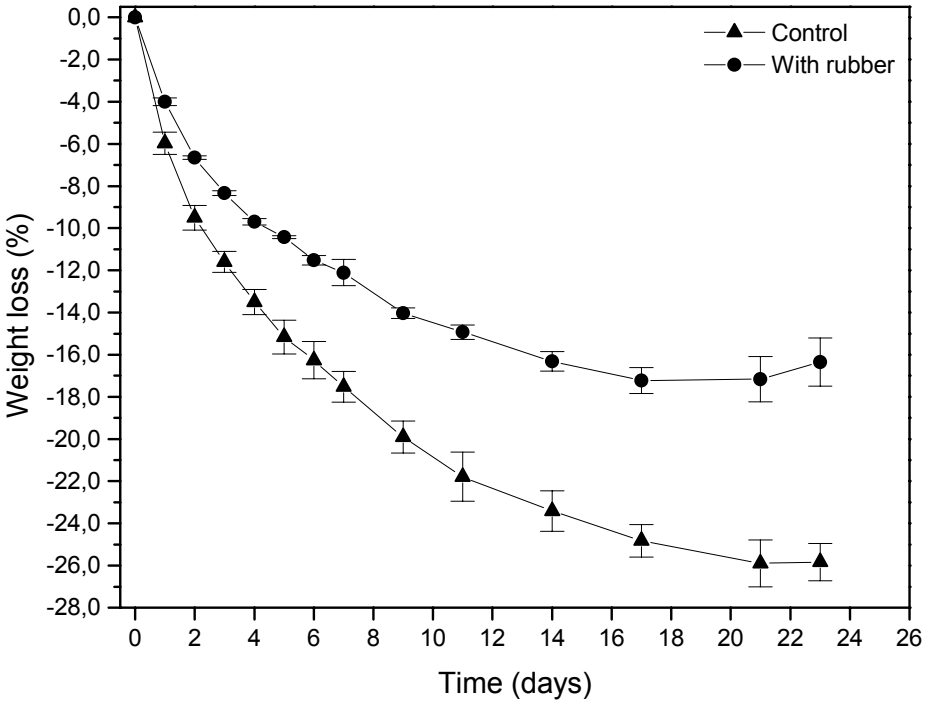

Figure 7. Acid resistance, as a function of time, for mortar test specimens with 10% (by mass of mortar) of NaOH-treated tyre rubber particles. Control: mortar only. Results of quintuplicate specimens.

4. CONCLUSIONS

Very few papers describe the properties of mortars with small rubber particles. In every case, only mechanical properties are measured, which worsens [2,7]. We have shown that the addition of 10% (by weight of mortar) of NaOH-treated tyre rubber particles in mortar reduced the sorptivity significantly, and enhanced the resistance to acid attack, demonstrating the favorable effects of the rubber on the transport properties despite the reduction in flexural strength observed in the specimens.

ACKNOWLEDGMENTS

N. Segre and A.D. Galves wish to thank the Fundação de Amparo à Pesquisa do Estado de São Paulo - FAPESP for the support (Processes 01/04929-7 and 02/00328-1). J.A. Rodrigues wishes to thank the Conselho Nacional de Desenvolvimento Científico e Tecnológico - CNPq. Laboratório de Microscopia Eletrônica - IF/USP and Dr. Flávia Cassiola are gratefully acknowledged for the SEM micrographs.

REFERENCES

[1] Lee, B.I.; Burnett, L.; Miller, T.; Postage, B. and Cuneo, J. Tyre rubber/cement matrix composites, Journal of Materials Science Letters, vol. 12, 1993, pp. 967-968.

[2] Eldin, N.N. and Senouci, A.B. Observations on rubberized concrete behavior, Cement, Concrete and Aggregates, vol. 15, 1993, pp. 74-84.

[3] Toutanji, H.A. The use of rubber tyre particles in concrete to replace mineral aggregates, Cement & Concrete Composites, vol. 18, 1996, pp. 135-139.

[4] Raghavan, D.; Huynh, H. and Ferraris, C. F. Workability, mechanical properties and chemical stability of a recycled tyre rubber-filled cementitious composite, Journal of Materials Science, vol. 33, 1998, pp. 1745-1752.
[5] Li, Z.; Li, F. and Li, J. S. L. Properties of concrete incorporating rubber tyre particles, Magazine of Concrete Research, vol. 50, 1998, pp. 297-304.
[6] Bignozzi, M.C.; Saccani, A.and Sandrolini, F. New polymer mortars containing polymeric wastes. Part 1. Microstructure and mechanical properties, Composites – Part A, vol. 31, 2000, pp. 97-107.
[7] Raghavan, D. Study of rubber-filled cementitious composites, Journal of Applied Polymer Science, vol. 77, 2000, pp. 934-942.
[8] Segre, N. and Joekes, I. Use of tyre rubber particles as addition to cement paste, Cement and Concrete Research, vol. 30, 2000, pp.1421-1425.
[9] Segre, N.; Monteiro, P.J.M. and Sposito, G. Surface characterization of recycled tyre rubber to be used in cement paste matrix, Journal of Colloid and Interface Science, vol. 248, 2002, pp.521-523.
[10] Hall, C. Water sorptivity of mortars and concrete: a review, Magazine of Concrete Research, vol. 41, 1989, pp. 51- 61.
[11] Martys, N.S. and Ferraris C.F. Capillary transport in mortars and concrete, Cement and Concrete Research, vol. 27, 1997, pp.747-760.
[12] Mehta, P.K. and Monteiro, P.J.M. Concrete: Structure, Properties and Materials, 2nd ed. Englewood Cliffs: Prentice-Hall, 1993.

DURABILITY OF SURFACE-COATED CONCRETE

Haimoon Cheong[1], Sang-Heul Choi[2], Hwan-Gu Yu[1] and Tae-Song Ahn[1]

[1]Highway Research Center, Korea Highway Corporation, Kyunggi-do, KOREA.
E-mail: haimoon@freeway.co.kr
[2]Department of Ceramic Engineering, Hanyang University, Seoul, KOREA

ABSTRACT

Chloride penetration into concrete is the main cause of the corrosion of steel in concrete structures exposed to chloride-rich environments. Protective surface coatings are increasingly being applied to concrete structures to reduce chloride penetration. In this study, the performance of various surface coatings was evaluated. Most coatings showed good results for the various tests of the performance evaluation. Surface coatings can effectively delay deterioration such as chloride-induced reinforcing bar corrosion.

1. INTRODUCTION

Large-scale concrete structures directly exposed to seawater such as SeoHae Grand Bridge are increasingly being constructed along the coast in Korea. Chloride ingress into concrete followed by reinforcement corrosion and deterioration of concrete is a major problem for many structures under chloride attack. Previous experience emphasized the need for high quality concrete for the assurance of long-term durability[1]. In the case of high quality concrete structures, the typical protection methods against chloride attacks consist of thickening the cover thickness of concrete, using cathodic protection, applying a coating layer on the surface of concrete to reduce the penetration of chloride ions, and using non-corrosive materials, such as epoxy coated re-bars, FRP, corrosion inhibitors etc.

Currently, various types of protective surface coatings are increasingly introduced to reduce chloride penetration into concrete. In applying these materials, however, we have few reasonable standardized programs of tests for evaluating them. Therefore, in this study, the performance of surface coatings for protecting chloride ingress was evaluated, and proper test methods were investigated.

2. EXPERIMENTAL PROGRAM

2.1 Coating Materials

As shown in Table 1, five kinds of surface coating materials have been prepared to investigate the performance of coating materials effectively. Free films and surface-coated specimens were prepared. Free films were prepared by painting only with intermediate and top coating without substrate, and surface-coated specimens were prepared by painting on the substrate. Their painting methods were based on the manufacturer's recommendation. The specimens were cured in open air in the laboratory at room temperature for 28 days (standard condition). For investigation of the performance after accelerated deterioration, the specimens were exposed to the QUV accelerated weathering for 250 hours, seawater(3% NaCl) for 15 days and alkaline solution (saturated $Ca(OH)_2$) for 15 days.

Proceedings of the 11th International Congress on the Chemistry of Cement (ICCC)
'Cement's Contribution to the Development in the 21st Century'
Hosted by: The Cement and Concrete Institute of South Africa
CD-ROM produced by: Document Transformation Technologies
11 - 16 May 2003, Durban, South Africa
ISBN Number: 0-9584085-8-0
Editors: Dr G. Grieve and G. Owens
Congress Organised by: Event Dynamics

Table 1. Type of Coating Materials

Speci-men	Chemical Component of Coating System				Thickness (㎛)**
	Primer	Putty	Intermediate Coat	Top Coat	
AS	epoxy	epoxy	acrylic silicone	acrylic silicone	50
EP	epoxy	epoxy	epoxy	epoxy	250
UR	polyurethane	PCM*	polyurethane	polyurethane	125
AC	acrylic	PCM*	acrylic	acrylic	400
AU	acrylic urethane	acrylic urethane	acrylic urethane	acrylic urethane	100

*Portland Cement Mortar **Intermediate coat + Top coat

2.2 Experimental methods

Various tests employed in this study are summarized in Table 2.

2.2.1 Water penetration test

The water penetration test for surface-coated specimens was performed according to JIS A 1404. $3kg_f/cm^2$ of water compressive force was applied.

2.2.2 Vapor penetration test

The vapor penetration test for free films was carried out according to ASTM D 1653. Desiccant used was calcium chloride. The specimens were put in the test chamber of 23 0.6℃, and 50 2%R.H., and the weight of specimen was measured every 24 hours for 3 weeks until it became constant.

2.2.3 Chloride penetration test

70 70mm of free films were fixed on diffusion cells. 3% NaCl solution was filled in the one side of the cell and distilled water was also filled in the other side of the cell. The test set-up was kept for 30 days at 20℃ in laboratory. After 30 days, chloride ion concentration was analyzed in the distilled water.

2.2.4 Bond strength test

The bond strength test of coatings with concrete was performed in accordance with ASTM D 4541. Bond strength tests under wet conditions were also performed to evaluate the effect of water contained on the concrete surface. The specimens were stored in water for 10 days and then cured for 48 hours in a dry condition before testing.

Table 2. The Tests Used in This Study

Test Method	Specimen Type	Condition*	Remarks
Water Penetration	Surface-coated Concrete	S, AW, N, A	$\sigma_{28}=24N/mm^2$
Vapor Penetration	Film	S, AW, N, A	
Chloride Penetration	Film	S, AW, N, A	
Bond Strength	Surface-coated Concrete	S, AW, W, N, A	$\sigma_{28}=45N/mm^2$
Crack-Bridging	Surface-coated Mortar	S, N, A	W/C=0.5
Accelerated Cl^- Ion Diffusion	Surface-coated Concrete	S	$\sigma_{28}=24N/mm^2$
Freezing-Thawing	Surface-coated Concrete	S	
Carbonation	Surface-coated Concrete	S	

*S : Standard, AW : QUV Accelerated Weathering for 250 hours, W : Wet Condition(JIS A 6909 5.8.3)
N : Seawater(3%NaCl) Immersion for 15 days
A : Alkaline Solution(Saturated $Ca(OH)_2$) Immersion for 15 days

2.2.5 Crack-bridging test

The crack-bridging test for surface-coated specimens was conducted using Japan Highway's method. The specimens used were one face-coated mortar prisms. The specimens were extended at a speed of 5mm/min. The test was carried out at 20℃.

2.2.6 Accelerated chloride diffusion test by applying electrical potential

To determine the chloride diffusion coefficient of surface-coated concrete specimens, the rapid test method proposed experimentally by Tang & Nilsson[2] was employed. The effective chloride diffusion coefficient was calculated using equation (1) proposed experimentally as follows:

$$D_{eff} = \frac{RTL}{ZFU}\frac{X_d - \alpha\sqrt{X_d}}{t} \quad (1)$$

D_{eff} : effective chloride diffusion coefficient determined by non-steady state migration test
Z : absolute value of ion valence F : Faraday constant t : test duration
U : absolute value of potential difference R : gas constant T : temperature
L : thickness of the specimen X_d : chloride penetration depth

2.2.7 Freezing-thawing test and accelerated carbonation test

The freezing-thawing test for surface-coated concrete specimens was conducted according to ASTM C 666. Accelerated carbonation tests for surface-coated concrete specimens were carried out at 40℃, 60% R.H., 10% CO_2 concentration for 4 weeks.

3. RESULTS AND DISCUSSIONS

3.1 Water penetration and vapor penetration

Most coating materials except acrylics had no water penetration. Also, water penetration was not shown after accelerated deteriorating tests such as QUV accelerated weathering (AW), seawater immersion(N) and alkaline solution immersion(A). Acrylic coating materials showed 0.17～0.83ml of water penetration after accelerated deteriorating test (Figure 1).

Figure 2 showed the vapor penetrations of surface coating membranes. The vapor penetration of acrylic coating membrane was much greater than that of the other types. And the results showed larger penetration after accelerated deterioration tests.

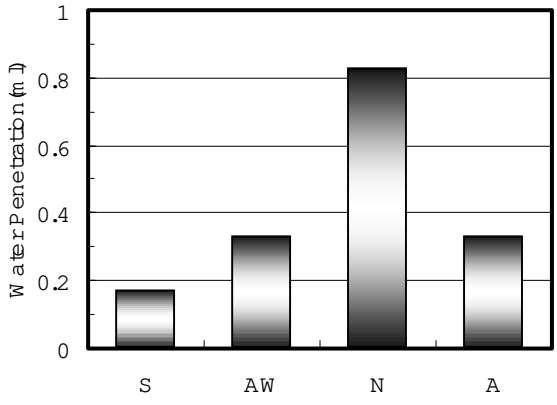

Figure 1. Water penetration of acrylics after accelerated deteriorating tests

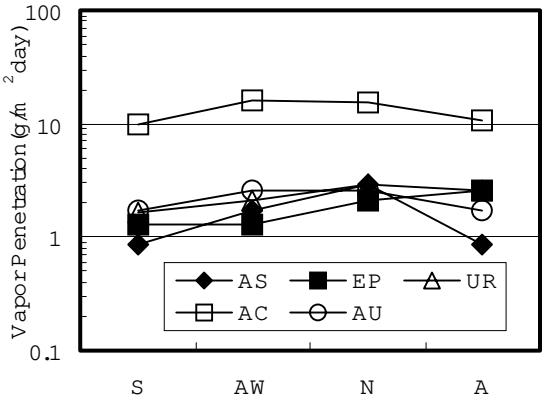

Figure 2. Vapor penetration of coatings after accelerated deteriorating tests

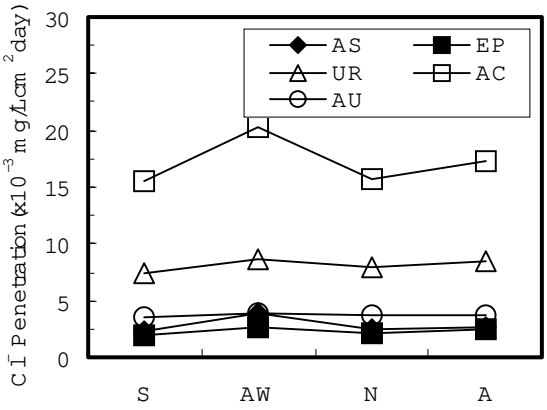

Figure 3. Cl^- ion penetration of various coatings after accelerated deterioration tests

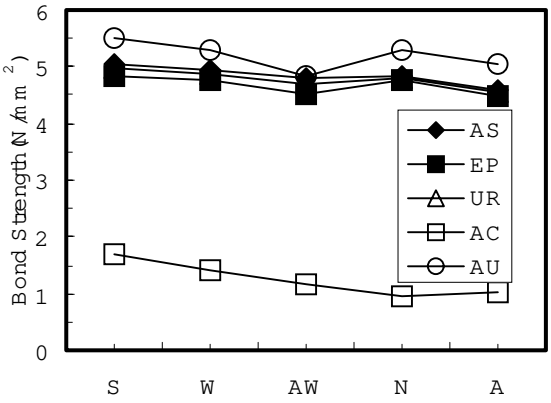

Figure 4. Bond strength of coatings with concrete

3.2 Chloride ion penetration

The results of the chloride penetration test is given in Figure 3. As can be seen, chloride ion penetration increased in accelerated deterioration tests. Especially, the effect of accelerated weathering and alkaline solution immersion was remarkable.

3.3 Bond strength

Figure 4 shows the bond strength of the coatings with concrete. Except for acrylics, most coatings showed over 4N/mm^2 of bond strength. The results of bond strength tests were similar to those of the water, vapor and chloride penetration tests. Acrylic coatings exhibited much lower bond strength, and the reduction rate after accelerated deterioration tests was more than the other types of materials. The results from accelerated weathering and alkaline solution immersion had a tendency to show less bond strength than those of seawater immersion.

3.4 Crack-bridging test

Figure 5 showed the results of crack-bridging test for various surface-coated specimens. The test results showed that the polyurethane type of coating exhibited much greater tensile strength than any other types, and elongation was much larger for the acrylic type although its tensile strength was very low. The reduction of tensile strength and elongation after seawater and alkaline solution immersion were not so great.

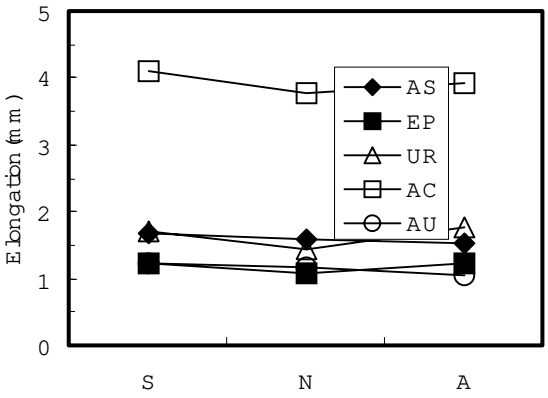

Figure 5. Elongation of coatings after accelerated deterioration tests

3.5 Accelerated chloride diffusion test by applying electrical potential

Figure 6 illustrates the effective diffusion coefficients which took into account the combined effect of coating materials and concrete specimens. Surface-coated specimens showed 10～20 times lower diffusion coefficients than plain specimen without surface coating treatment.

3.6 Freezing-thawing test and accelerated carbonation test

Figures 7 and 8 show the results of freezing-thawing and accelerated carbonation tests for surface-coated concrete specimens, respectively. The surface-coated concrete specimens were found to have good resistance to freezing-thawing and carbonation. The carbonation depth, especially, decreased greatly for surface-coated concrete specimens.

3.7 Discussion

Most coatings showed good results for the various performance evaluation tests. Their performance depended upon the types of coating materials[3]. In this study, acrylics showed poor performance in various accelerated penetration tests. Although the film thickness of acrylics was larger than the other coatings, the results of various accelerated penetration tests were poorer. It seemed that the penetration properties of coatings were affected much more by material characteristics than coating thickness. Figure 9 shows the relationship between chloride penetration and vapor penetration. Good relationship between protecting performances such as chloride penetration and vapor penetration for coating materials was given in this study(R^2=0.83).

However, acrylic coatings revealed lower bond strength with concrete and protection performance, but larger elongation. It was regarded to be a typical result for elastic material such as acrylics[4]. Protection properties of the films from various harmful factors showed the reverse to the crack-bridging property. Therefore, it is necessary to do further studies to obtain reasonable standardized values for protection and crack bridging properties.

The performance of surface coatings was reduced after accelerated deterioration tests. Figure 9 shows that 250-hours accelerated weathering influenced the penetration performances of coatings very greatly in this study. However, the field test results for coating materials were limited, the ranking of coating materials according to the results from this study cannot be supported. For correlations with field testing, the field test for surface coating materials were conducted in a marine environment.

4. CONCLUSIONS

(1) Most coatings showed good results for the various performance evaluation tests. The degree of performance depended upon the types of coating materials.

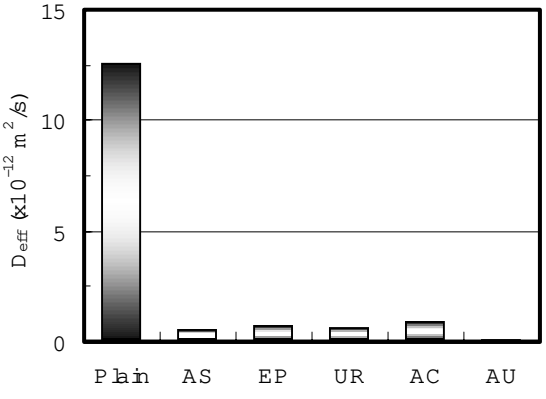

Figure 6. Effective diffusion coefficient of surface-coated concrete specimens

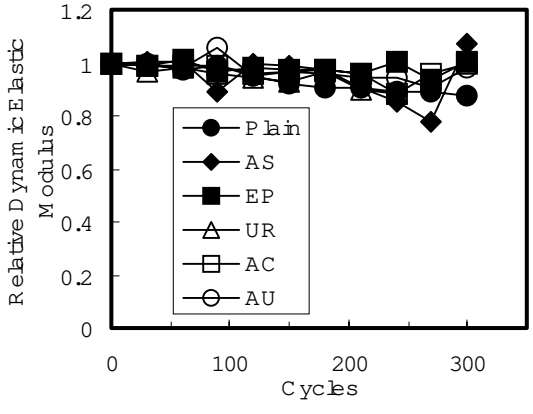

Figure 7. Relative dynamic elastic modulus of surface-coated concrete specimens

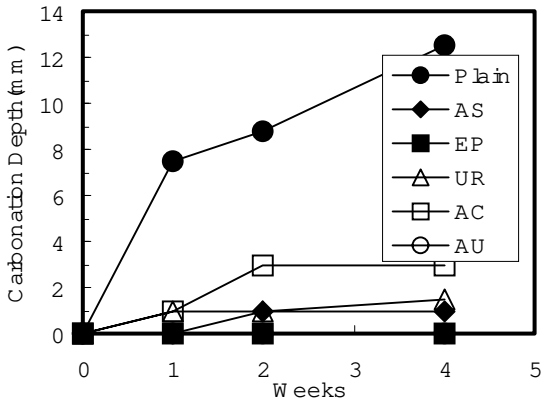

Figure 8. Accelerated carbonation depth of surface-coated concrete specimens

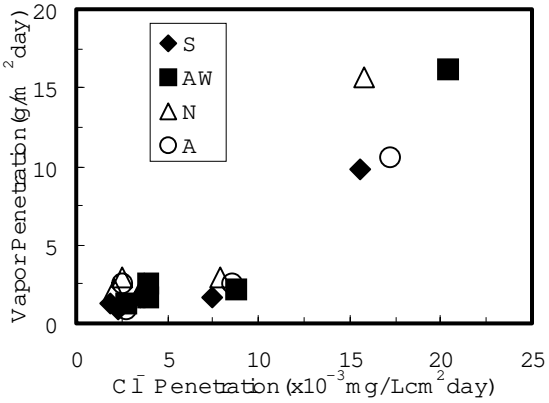

Figure 9. Relationship between Cl^- penetration and vapor penetration

(2) Surface-coated specimens showed 10～20 times lower chloride diffusion coefficients than plain specimen without surface coating treatment. Surface coatings can effectively delay deterioration such as chloride-induced reinforcing bar corrosion effectively.

(3) Acrylics showed poor performance in various accelerated penetration tests. It seemed that the penetration properties of coatings were affected much more by material characteristics than by coating thickness.

(4) The performance of most surface coatings was reduced after accelerated deterioration tests. However, the field test results for coating materials were limited, the ranking of coating materials according to the results from this study cannot be supported. It is necessary to study further for correlating accelerated testing with field testing.

REFERENCES

[1] ACI222R, Corrosion of Metals in Concrete, ACI Manual of Concrete Practice, American Concrete Institute, 1999.

[2] Tang,L. and Nilsson,L.O., Rapid Determination of the Chloride Diffusivity in Concrete by Applying Electrical Field, ACI Materials Journal, Vol.89, No.1, 1992, pp.49～53.

[3] NCHRP Synthesis 209, Sealers for Portland Cement Concrete Highway Facilities, Transportation Research Board, National Academy Press, 1994.

[4] Concrete Research Committee, Concrete Engineering Series, No.26, pp.217-218, Japan Society of Civil Engineers, 1997.

DURABILITY OF SURFACE-COATED CONCRETE

Haimoon Cheong[1], Sang-Heul Choi[2], Hwan-Gu Yu[1] and Tae-Song Ahn[1]

[1]Highway Research Center, Korea Highway Corporation, Kyunggi-do, Korea.
E-mail: haimoon@freeway.co.kr
[2]Department of Ceramic Engineering, Hanyang University, Seoul, KOREA

Haimoon Cheong

Affiliation:
Materials and Environmental Research Group
Highway Research Center
Korea Highway Corporation

E-mail: haimoon@freeway.co.kr

Address :
293-1 Keumto-dong, Sujong-ku, Sungnam-shi,
Kyunggi-do, KOREA

Telephone: 82-2-2230-4859
Fax: 82-2-2230-4187

SORPTION OF CRO_4^{2-} FOR CEMENT HYDRATES AND THE LEACHING FROM CEMENT HYDRATES AFTER SORPTION

Shigeru Takahashi[1], Masaki Daimon[2] and Etuo Sakai[2]

[1]Research & Development Laboratory, Japan Cement Association, Tokyo, Japan.
E-mail: shigeru-takahashi@jcassoc.or.jp
[2]Department of Metallurgy and Ceramics Science, Graduate School of Science and Technology, Tokyo Institute of Technology, Tokyo, Japan.
E-mail: mdaimon@ceram.titech.ac.jp and esakai@ceram.titech.ac.jp

ABSTRACT

This study was undertaken to investigate the immobilization of Cr(VI) by cement hydrates, the behavior of the sorption of CrO_4^{2-} for cement hydrates and the leaching from cement hydrates after sorption. The hydrates were ettringite, monosulfate hydrate and the mixture of C-S-H and $Ca(OH)_2$. The solutions for sorption were prepared to use $CaCrO_4 \cdot nH_2O$ and the pH of solutions were adjusted with $Ca(OH)_2$ to the equilibrium pH of each hydrate in water. The leaching of CrO_4^{2-} from the hydrate after sorption was also determined.

The relation between equilibrium concentration of Cr and amount of sorption of Cr for CH and CSH was analysed using Freundlich's adsorption isotherm. Test results agreed well with the relation of Freundlich's adsorption isotherm. On leaching, this relationship was found. The CrO_4^{2-} is only slightly adsorbed on ettringite. The amount of Cr sorption on monosulfate hydrate was very large and CrO_4^{2-} was incorporated into monosulfate hydrate.

1. INTRODUCTION

The heavy metals in industrial waste have been immobilized by hardened cement, and a lot of studies on this subject have been carried out. In recent years, the leaching of trace elements from mortar or concrete was studied from environmental standpoint [1].

In trace elements, hexavalent chromium is easy to be leached from cement [2]. CrO_4^{2-} is fixed as a solid solution of ettringites containing CrO^4_{2-} during the hydration of C_3A [3]. But, the sorption of CrO_4^{2-} for cement hydrates has been studied sufficiently.

For the purpose of investigating the mechanism and the influence of various ions on immobilizing and leaching of CrO_4^{2-}, the fundamental behavior on the sorption of CrO_4^{2-} for cement hydrates was examined in this study.

2. EXPERIMENTAL

2.1 Hydrates

The hydrate(ETT) corresponding to ettringite(AFt) and the hydrate(MSH) corresponding to monosulfate hydrate(AFm) were synthesised by the hydration of C_3A and gypsum. The mixture(CSH-CH) of C-S-H and $Ca(OH)_2$ as obtained through the full hydration of C_3S. After each hydrate was placed in acetone, it was dried in an aspirator at room temperature. And each hydrate was ground to pass 150 m.

Proceedings of the 11th International Congress on the Chemistry of Cement (ICCC)
'Cement's Contribution to the Development in the 21st Century'
Hosted by: The Cement and Concrete Institute of South Africa
CD-ROM produced by: Document Transformation Technologies
11 - 16 May 2003, Durban, South Africa
ISBN Number: 0-9584085-8-0
Editors: Dr G. Grieve and G. Owens
Congress Organised by: Event Dynamics

2.2 Measurement of equilibrium pH of each hydrate in water

After 0.5g of each hydrate was stirred in 50ml of fresh distilled water at 25°C for 1 hour, the hydrate was filtered through a 0.45 m membrane filter. The pH of the filtrate was measured.

2.3 Solutions for sorption

The solutions for sorption were prepared by dissolving $CaCrO_4 \cdot nH_2O$ in fresh distilled and deionized water. The amount of Cr was about 1/10, 1/100 and 1/1000 mol for each hydrate. And, the pH of the solutions were adjusted with $Ca(OH)_2$ to the equilibrium pH of each hydrate in water at 25°C

2.4 Measurement of amount of sorption

The method of sorption and leaching is shown in Figure 1. After 0.5g of the hydrates was stirred in 50ml of solution for sorption at 25°C for 1, 2 and 4 days, the hydrates were filtered through a 0.45 m membrane filter. The concentration of Cr solution for sorption is shown in Table 1. The amount of Cr in the filtrate was determined by ICP-AES.

Table 1. The concentration of Cr of solution for sorption

Hydrate	Solution (mg/l)		
	I	II	III
CH	183.5	18.35	1.835
CSH-CH	183.5	18.35	1.835
MSH	76.7	7.67	0.767
ETT	36.8	3.68	-

2.5 Measurement of amount of leaching from hydrates after sorption

After the 0.4g of hydrates after sorption was stirred in 40ml of fresh distilled and deionized water which were adjusted with $Ca(OH)_2$ to the equilibrium pH of each hydrate in water at 25°C for 1day, the hydrates were filtered through a 0.45 m membrane filter. The amount of Cr in filtrate was determined by ICP-AES.

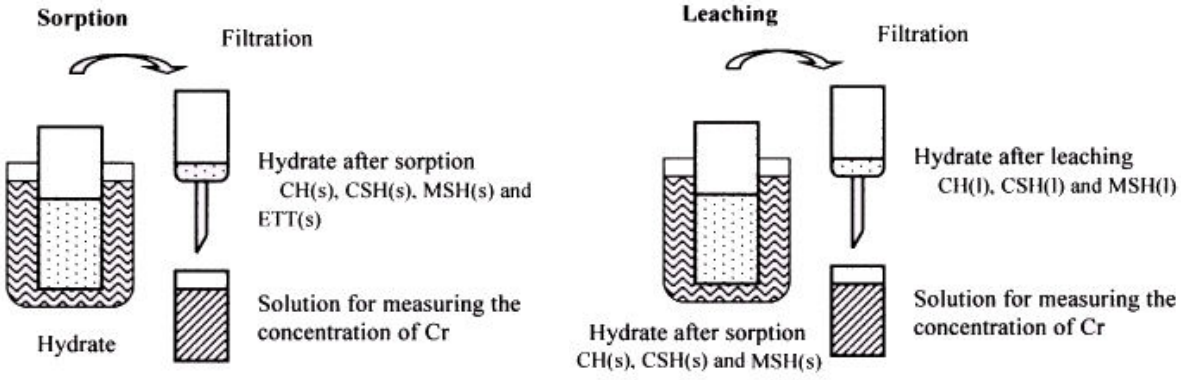

Figure 1. The method of sorption and leaching

3. RESULTS AND DISCUSSION

3.1 Hydrates and equilibrium pH of each hydrate in water

The compositions and the equilibrium pH of hydrates are shown in Table 2. The amount of CSH in CSH-CH was calculated by the content of SiO_2. The amount of CH in CSH-CH was determined by thermal analysis (TG). MSH contained a small amount AFt, and ETT contained 0.288(mmol/g) of gypsum.

Table 2. Compositions and equilibrium pH of hydrates

Hydrate	Compositions (mmol/g)					equilibrium pH
	CH	CSH	AFm(*)	AFt(**)	$CaSO_4 \cdot 2H_2O$	
CH	13.5	–	–	–	–	12.5
CSH-CH	3.14	3.58	–	–	–	12.5
MSH	–	–	1.35	0.05	–	11.8
ETT	–	–	–	0.713	0.288	10.8

(*) $C_3A \cdot CaSO_4 \cdot 12H_2O$

(**) $C_3A \cdot 3CaSO_4 \cdot 32H_2O$

3.2 Concentration of Cr in solution at various pH

Solutions(Cr:305mg/l) were adjusted with $Ca(OH)_2$ at various pH, and they were stirred for 1 day at 25°C. The concentration of Cr in solution after stirring is shown in Figure 2. This figure shows that CrO_4^{2-} does not precipitate at high pH.

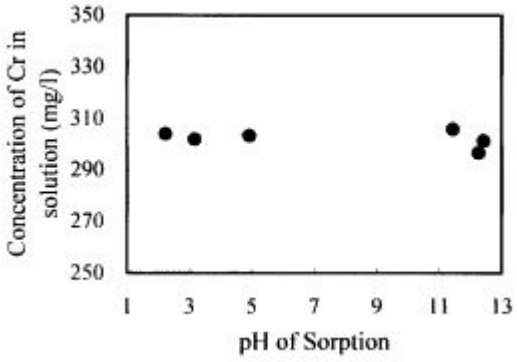

Figure 2. The influence of pH of solution to the concentration of Cr

3.3 Sorption of CrO_4^{2-} for CH and leaching

The concentration of Cr in solution after sorption for CH is shown in Figure 3 and the amount of sorption of Cr for CH is shown in Figure 4. The sorption of Cr for CH reached the equilibrium at 1day. The amount of sorption of Cr for CH depends on the initial concentration of Cr in solution.

The relationship between the equilibrium concentration of Cr and amount of sorption of Cr for CH was analysed with Freundlich's adsorption isotherm [Equation (1)]. The result is shown in Figure 5 and it agreed well with the relation of Freundlich's adsorption isotherm. The correlation equation is Equation(2).

$$v = aP^{1/n}$$

$$\ln(v) = \ln(a) + (1/n)\ln(P) \quad (1)$$

where, v : amount of adsorption

P: equilibrium concentration

$$\ln(v) = 1.394 + 0.572\ln(P) \quad (2)$$

On the leaching of Cr from CH(s), the relationship between the equilibrium concentration of Cr and amount of sorption of Cr for CH(l) agrees with the relation of Freundlich's adsorption isotherm also (see Figure 5). These results show that CrO_4^{2-} is absorbed on CH with Freundlich's adsorption isotherm.

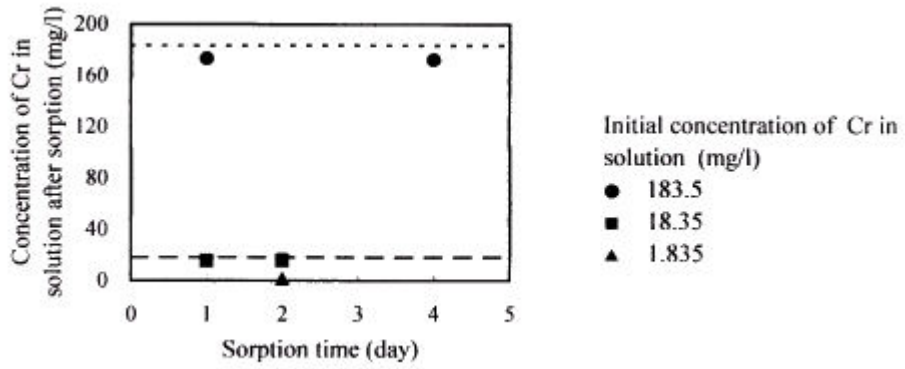

Figure 3. The concentration of Cr in solution after sorption for CH

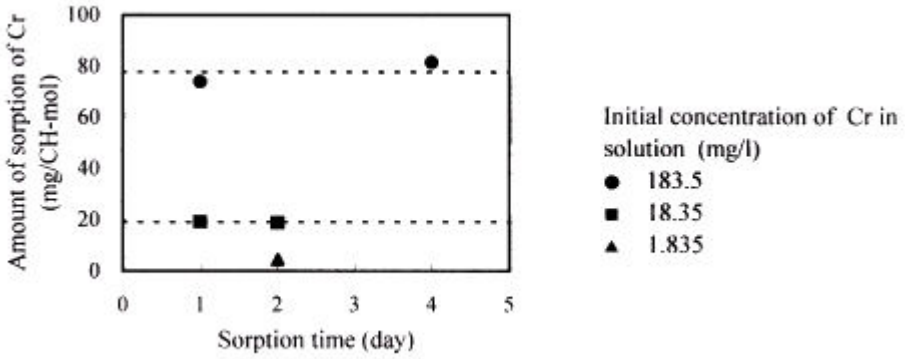

Figure 4. The amount of sorption of Cr for CH

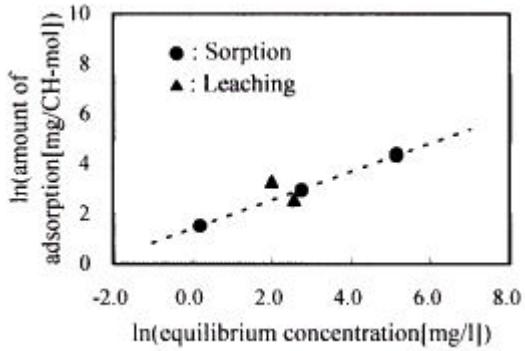

Figure 5. The relation between equilibrium and Cr and amount of sorption of Cr for CH

3.4 Sorption of CrO_4^{2-} for CSH and leaching

In the calculation of the amount of sorption of Cr for CSH, the amount of sorption of Cr for CH was corrected.

[amount of sorption for CSH]=
amount of sorption for CSH-CH] - [amount of sorption for CH] (3)
where, [amount of sorption for CSH-CH]:measured
[amount of sorption for CH]:calculated with equation (2)

The amount of sorption of Cr for CSH is shown in Figure 6. The sorption of Cr for CSH reached the equilibrium at about 2days. And, the amount of sorption of Cr for CSH depends on the initial concentration of Cr in solution, too. The relation between equilibrium concentration of Cr and amount of sorption of Cr for CSH was analysed with Freundlich's adsorption isotherm. The result is

shown in Figure 7 and it agreed well with the relation of Freundlich's adsorption isotherm. The correlation equation is Equation(4).

$$\ln(v) = 3.303 + 0.717\ln(P) \quad (4)$$

On the leaching of Cr from CSH(s), the amount of sorption of Cr for CH was corrected with equation (2). The relation between equilibrium concentration of Cr and amount of sorption of Cr for CSH(l) was agreed with the relation of Freundlich's adsorption isotherm (see Figure 7).

These results show that CrO_4^{2-} is absorbed on CSH with Freundlich's adsorption isotherm similarly to CH, and the $CrO_4^{2-}$is not incorporated into CSH.

In comparison with equation (2) and (4), the amount of adsorption of Cr for CSH is about 20 times as large as CH.

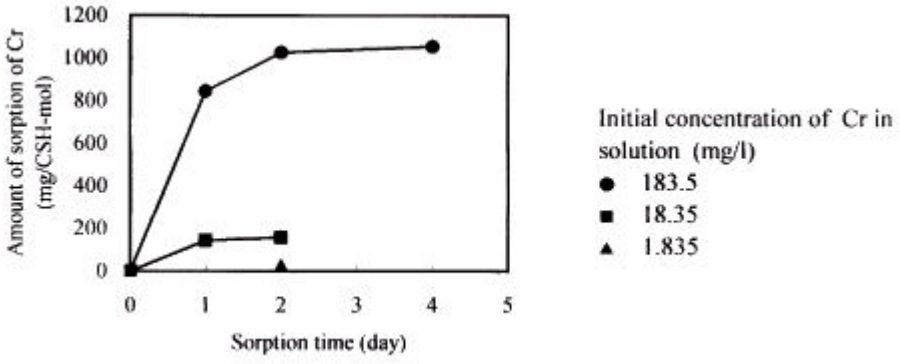

Figure 6. The amount of sorption of Cr for CSH

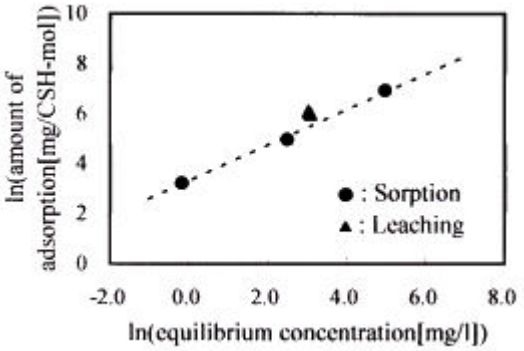

Figure 7. The relation between equilibrium of Cr and amount of sorption of Cr for CSH

3.5 Sorption of CrO_4^{2-} for ETT

The concentration of Cr in solution after sorption for ETT is same as initial concentration. From this result, it is considered that the CrO_4^{2-} is hardly adsorbed on ettringite. Isozaki *et al.* found that the Cr^{3+} was incorporated into ettringite, but Cr^{6+} was not incorporated into ettringite [4]. But, this ETT contained considerable gypsum, and it is necessary to discuss the influence of SO_4^{2-}.

3.6 Sorption of CrO_4^{2-} for AFm and leaching

As mentioned in 3.1 and 3.5, the content of AFt in MSH is small and CrO_4^{2-} is hardly adsorbed on AFt. So, it is considered that all sorption of Cr is the sorption for AFm. The amount of sorption of Cr for AFm is shown in Figure 8. The sorption of Cr for AFm reached the equilibrium at 1day, and the ratios of sorption were 98.0 – 99.5% regardless of initial concentration. In the leaching of Cr from MSH(s) on condition that the initial concentration of Cr was 76.7mg/l and the sorption time was 4 days, the amount of leaching of Cr is 0.8%. These results show that CrO_4^{2-} is hardly adsorbed

on AFm, but CrO_4^{2-} is incorporated into AFm. The XRD patterns of MSH and MSH(s) are shown in Figure 9. In comparison with MSH, the intensity of AFt of MSH(s) is larger and the intensity of AFm is less. From this result, it is considered that the SO_4^{2-} in AFm is replaced by CrO_4^{2-} in solution, and the reaction of the released SO_4^{2-} and AFm formed AFt. The illustration of these reactions is shown in Figure 9. The sorption capacity of CrO_4^{2-} for AFm is very large, and AFm fixes CrO_4^{2-} strongly.

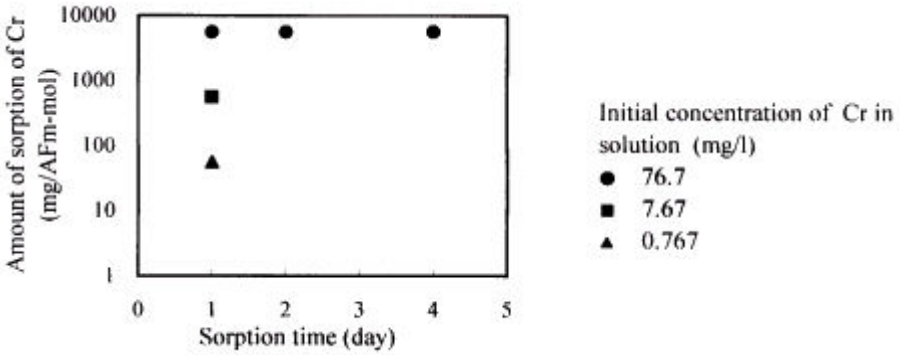

Figure 8. The amount of sorption of Cr for AFm

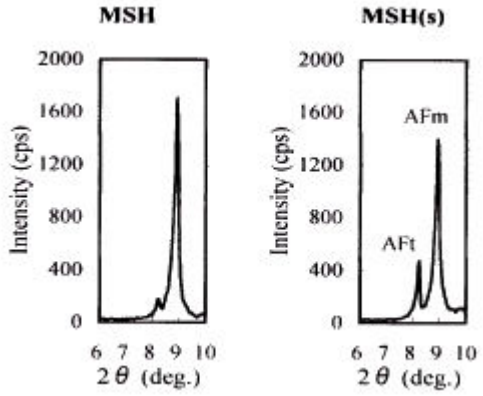

Figure 9. The XRD patterns of MSH and MSH(s)
(X-ray : CuK ß)

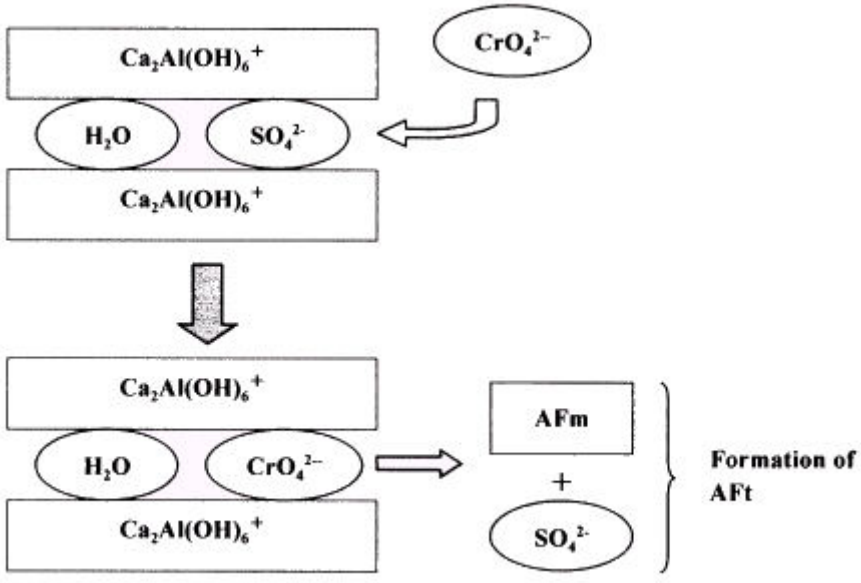

Figure 10. The illustration of sorption of CrO_4^{2-} for AFm

4. CONCLUSIONS

The results in the present study are summarised as follows:

(1) The $Ca(OH)_2$ and CSH adsorbed CrO_4^{2-} according to Freundlich's adsorption isotherm. CrO_4^{2-} is not replaced in the structure of C-S-H. The amount of adsorption of CrO_4^{2-} for CSH is about 20 times as large as CH.

(2) Ettringite hardly adsorbed CrO_4^{2-} in solution. This result shows that the CrO_4^{2-} can be fixed in ettringite during the hydration process.

(3) The sorption of Cr for monosulfate hydrate reached the equilibrium within 1day, and the ratios of sorption were 98.0 – 99.5% regardless of initial concentration. The amount of leaching is small. SO_4^{2-} in monosulfate hydrate is replaced by CrO_4^{2-}, and CrO_4^{2-} is not leached into water.

REFERENCES

[1] Sloot, H.A.Comparison of the characteristic leaching behavior of cements using standard (EN 196-1) cement mortar and an assessment of their long-term environmental behavior in construction products during service life and recycling, Cement and Concrete Research, vol.30, 2000, pp.1079-1096.

[2] Poellman, H., Auer, St. and Kuzel, H.-J. Solid solution of Ettrigites Part II, Cement and Concrete Research, vol.23, 1993, pp.422-430.

[3] Takahashi, S. The effects of the trace elements in cement on the environment, Cement & Concrete, No.640, 2000, pp.20-29, (in Japanese).

[4] Isozaki, A., Nakamura, T. and Okutani, T. Determination and separation chromium(III) and chromium(VI) with Ettringite by ICP-AES, BUNSEKI KAGAKU, vol.44, No.2, 1995, pp.111-115, (in Japanese)

SORPTION OF CRO_4^{2-} FOR CEMENT HYDRATES AND THE LEACHING FROM CEMENT HYDRATES AFTER SORPTION

Shigeru Takahashi[1], Masaki Daimon[2] and Etuo Sakai[2]

[1]Research & Development Laboratory, Japan Cement Association, Tokyo, Japan.
E-mail: shigeru-takahashi@jcassoc.or.jp
[2]Department of Metallurgy and Ceramics Science, Graduate School of Science and Technology, Tokyo Institute of Technology, Tokyo, Japan.
E-mail: mdaimon@ceram.titech.ac.jp and esakai@ceram.titech.ac.jp

Shigeru Takahashi

Position: Leader, Basic Research on Cement/Environment Group, R & D Laboratory, Japan Cement Association
4-17-33, Tosima, Kita-ku, Tokyo, JAPAN
Date of birth: August 18, 1954

Career
Entered the department of science and engineering, Saitama University, April, 1974
Entered Japan Cement Association, April, 1978
Entered the doctoral course of Department of Metallurgy and Ceramics Science, Graduate School of Science and Technology, Tokyo Institute of Technology, April, 2000

Subjects of study or work

(1) The mechanism and the influence of various ions on immobilizing and leaching of trace elements (cooperated with Prof. Daimon and assistant Prof. Sakai)
(2) The development of method of analysis of trace elements
(3) The preparation of drafts of Japanese Industrial Standard in relation to cement
(4) The chemical research of various properties of hardened cement and concrete (adiabatic temperature rise, hydration rate, pore structure, etc.)

Hobbies: Fishing, travels and walk
Marital Status: Married, two children (two girls, aged 18 and 14) and a dog

PHASE ASSEMBLAGES RELEVANT TO CALCIUM ALUMINATE CEMENTS IN THE MULTICOMPONENT PHASE DIAGRAM, $CaO-Al_2O_3-SiO_2-Fe_2O_3-MgO-TiO_2$

Sorrentino, F.P. and Castanet R.

Lafarge , Laboratoire Central de Recherche, 95 rue de Montmurier 38291 St Quentin Fallavier Cedex , France; E-mail: francois.sorrentino@lafarge.com

ABSTRACT

The increase of minor elements, such as MgO and TiO_2 in the raw materials of calcium aluminate cements leads to the crystallisation in large quantities of phases such as $Ca_{20}Al_{32-2n}Mg_nSi_nO_{68}$ and calcium ferro-titanate. To account for the presence of these phases, the results for phase assemblages found in the system $CaO-Al_2O_3-SiO_2-Fe_2O_3$ have been extended to the multi-component systems containing MgO and TiO_2. Experimental data obtained at the laboratory scale allows a description of the compatibility between the phases $CaAl_2O_4$, $Ca_2Al_2SiO_7$, $Ca_{20}Al_{32-2n}Mg_nSi_nO_{68}$, Ca_2SiO_4, $Ca_4Al_2Fe_2O_{10}$ and calcium ferro-titanate. Ti re- places Fe in the calcium alumino-ferrite and when the amount increases, calcium ferro-titanate is formed. Monocalcium aluminate crystallises in significant quantity (up to 20%) in most of the samples containing $Ca_2Al_2SiO_7$, $Ca_{20}Al_{32-2n}Mg_nSi_nO_{68}$, Ca_2SiO_4, $Ca_4Al_2Fe_2O_{10}$ and calcium ferro-titanate.

1. INTRODUCTION

Control of the cement manufacturing process firstly requires knowledge of the chemistry and the mineralogy of the clinker (i.e. the identity and the percentage of individual phases).

To achieve the optimum mineralogy of a clinker, it is then necessary to calculate the proportion of raw materials. This calculation uses predictive methods that correlate the chemistry with the mineralogy, with assumptions for the process conditions.

The analytical methods for the phase determination are similar for Portland cement and high alumina cement. The methods used are X-ray diffraction [1,2], microscopical point counting (ASTM C 1356), selective dissolution [3], or scanning electron microscopy coupled with EDS analyses [4]. In the case of high alumina cement (HAC), the presence of crystal intergrowths between certain phases results in a major analytical problem for phase identification. This is the case for the phases $Ca_{20}Al_{32-2n}Mg_nSi_nO_{68}$ with C_2AS [5,6] and for calcium ferro-titanate with calcium alumino- ferrite [7].

Concerning Portland cement (OPC = Ordinary Portland Cement), the predictive method is essentially the well known "Bogue calculation" based on the knowledge of the phase diagram $CaO-Al_2O_3-SiO_2-Fe_2O_3$ with the assumption of equilibrium conditions and very limited solid solutions (ASTM C 150).

The prediction of the phase percentage is more complicated in the case of HAC, which is produced by melting due to the following reasons: i) the range of compositions for HAC is wider than that for OPC clinker; ii) a wide range of solid solutions exists; iii) the equilibrium conditions are not reached; iv) the presence of minor elements, such as TiO_2 and MgO have a major effect. These reasons render the tentative phase calculation difficult for applications at the industrial scale [8].

A few years ago, we studied the area in the phase diagram $CaO-Al_2O_3-SiO_2$ and Fe_2O_3 that is relevant to HAC, [9,10]. From these results, it was possible to define different phase assemblages and to calculate the mineralogical composition of HAC. The assumption of equilibrium and the restrictive hypothesis of specific combination of MgO however limited this model of calculation [11]. The non-equilibrium conditions are mainly due to the melting temperature and the rate of cooling, which leads to the presence of variable quantities of glass in the final solid. These conditions have been assessed by theoretical studies and applied industrially [12,13].

The following step is to take into account the influence of minor elements such as MgO and TiO_2. It is known that Mg is an essential constituent of $Ca_{20}Al_{32-2n}Mg_nSi_nO_{68}$ (called Q phase) [14]. It must be noted that 1% of MgO (which is common in a HAC) forms 25 % of the Q phase. In addition, the isomorphous replacement of MgO by FeO also contributes to the increased amount of the Q phase.

Titanium (as Ti^{4+}) substitutes Fe^{3+} in calcium alumino ferrite [15,16] and, at higher concentrations, calcium ferro-titanate can form. An average chemical composition of HAC cement made by melting is (as weight %): Al_2O_3 =38.9%, CaO=38.4%, SiO_2=3.8%, Fe_2O_3=12.2%, FeO=3.7%, TiO_2=2%, MgO=1%, represented by a mineralogical composition of CA=44%, $C_{12}A_7$=3%, C_2AS=1%, C_2S=5%, Q=2%, glass=8%, calcium ferrite =37%. Therefore, the percentage of TiO_2, which can be expected in the ferrite phase, is between 5 and 6%

The objective of this paper is to obtain experimental data to describe the compatibility between the phases, $Ca_2Al_2SiO_5$ (C_2AS), $Ca_4Al_2Fe_2O_{10}$, (C_4AF), $CaTiO_3$ (CT) and $Ca_{20}Al_{32-2n}Mg_nSi_nO_{68}$ (Q) at the solidus temperature. Figure 1 shows the volume (regions of the phase diagram) that has been studied ;

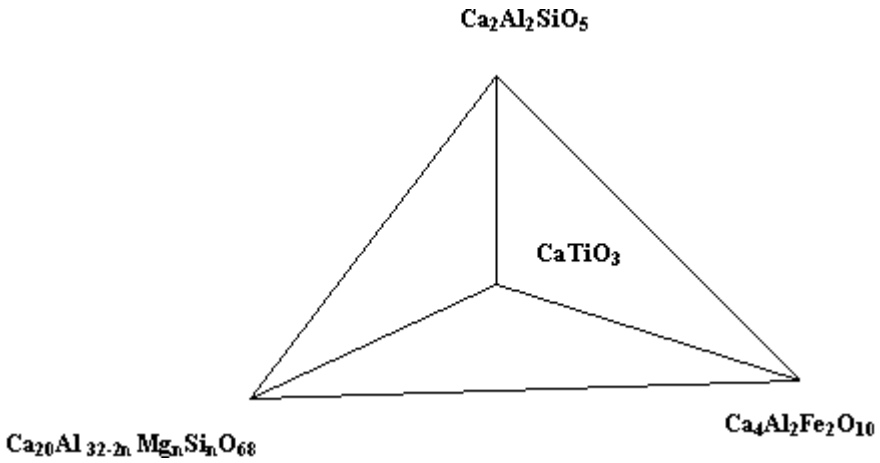

Figure 1. Regions of the phase diagram explored in this study

2. EXPERIMENTAL PROCEDURE

Mixtures have been chosen to cover the phase combinations of the phases shown in Figure 1, i.e assemblages of two phases (CT/Q, C_2AS/Q, C_2AS /CT, C_2AS /C_4AF, C_4AF /CT, C_4AF /Q), assemblages of three phases C_2AS/CT/Q, C_4AF/CT/Q, C_4AF/C_2AS /CT, C_4AF/C_2AS / CT), assemblages of four phases C_2AS, C_4AF, CT,Q.

The mixtures were prepared by two methods:

1) The first method synthesises the phases C_2AS, C_4AF, CT, Q from pure oxides (Merck reagent Fe_2O_3 or Prolabo Al_2O_3, SiO_2, light MgO and rutile) and 'Analar' calcium carbonate respectively at 1500°C, 1350°C, 1300°C and 1250°C (the phase Q, $Ca_{20}Al_{32-2n}Mg_nSi_nO_{68}$ was prepared with n = 3).
   After checking the purity of the phases by X-ray diffraction, the phases are mixed by cogrinding in ethanol (mixtures prepared by this method are named by a single letter in Table 1, ex A, B, C).
2) The second method uses the pure oxides, Al_2O_3, SiO_2, Fe_2O_3, MgO, TiO_2 and calcium carbonate as starting material; they are mixed by cogrinding in water for the first mixing and in ethanol for the successive further grinding. (mixtures prepared by this method are named by a double letter eg.AA, BB, CC, .. etc in Table 1)

The prepared mixtures are pressed into pellets and burned in a muffle kiln for 12 hours at the temperatures shown in Table 1. The temperatures are chosen to prevent the formation of liquid but nevertheless to have a kinetic, which enables reasonably fast combination (few hours). After the heat treatment the samples are examined by X-ray diffraction. If the results obtained by the two methods (pure phases or oxides) are different, the mixtures are reground and the procedure is reapplied (pellets/ heat). If the results obtained by X ray diffraction are the same, an examination of polished sections is undertaken using SEM associated with EDS analysis. With the analysis of each phase and the bulk composition, it is then possible to calculate the phase percentages.

Table 1: Chemical and mineralogical composition of the samples

	Chemical composition						Starting material	
	A	S	F	T	M	C		T°
A	22.5	3	2.1	29.4	2.2	40.8	CT/Q	1320
AA	22.5	3	2.1	29.4	2.2	40.8	Oxides	
B	41.1	14.0	2.1	0	2.2	40.6	C_2AS/Q (50/50)	1350
BB	41.1	14.0	2.1	0	2.2	40.6	Oxides	
C	18.6	11.0	0	29.4	0	41.1	C_2AS /CT (50/50)	1420
CC	18.6	11.0	0	29.4	0	41.1	Oxides	
D	29.1	11.0	16.4	0	0	43.6	C_2AS /C_4AF (50/50)	1280/1320
DD	29.1	11.0	16.4	0	0	43.6	Oxides	
E	10.5	0	16.4	29.4	0	43.8	C_4AF /CT (50/50)	1300
EE	10.5	0	16.4	29.4	0	43.8	Oxides	
F	33	3	18.5	0	2.2	43.3	C_4AF /Q (50/50)	1270/1290
FF	33	3	18.5	0	2.2	43.3	Oxides	
G	27.4	9.3	1.4	19.6	1.4	40.8	C_2AS /CT/Q (33/33/33)	1350
GG	27.4	9.3	1.4	19.6	1.4	40.8	Oxides	
H	22.0	2	12.3	19.6	1.4	42.6	C_4AF /CT/Q (33/33/33)	1300
HH	22.0	2	12.3	19.6	1.4	42.6	Oxides	
I	19.4	7.3	10.9	19.6	0	42.8	C_4AF / C_2AS /CT (33/33/33)	1300
II	19.4	7.3	10.9	19.6	0	42.8	Oxides	
J	34.4	9.3	12.3	0	1.4	42.5	C_4AF / C_2AS /Q (33/33/33)	1280
JJ	34.4	9.3	12.3	0	1.4	42.5	Oxides	
K	25.8	7	9.2	14.7	1.1	42.2	C_4AF / C_2AS /CT/Q (25/25/25/25)	1285/1320
KK	25.8	7	9.2	14.7	1.1	42.2	Oxides	

3. RESULTS

The results are presented in Table 2 and discussed as follows: (Note: the stoechiometry of the phases is related to one mole of CaO)

Assemblage A, AA: (CT/Q)
At 1285°C and 1320°C, the same result is obtained for A and AA. By XRD and SEM , the major phases found are CT and the Q phase in quantity of 54% and 37%. There is a small amount of CA (5%), C_2S (3%) and C_2AS (1%). The phase percentage is calculated from the mass balance between the chemical composition of the bulk (X-ray fluorescence analysis) and the individual phases analyses by EDS (SEM).
Assemblage B,BB: C_2AS /Q
At 1350°C, the same result is found for B and BB. By XRD and SEM, the major phases found are C_2AS and the Q phase but a small quantity of CA is also detected. The lack of accuracy of the chemical analyses of the C_2AS and Q crystals due to their intergrowth prevents their percentage calculation. As it has been already noted [5], such intergrowths vary in thickness from a few nanometers to a few micrometers. It is thus not possible to have a reliable analysis for these individual phases by SEM/EDS techniques.
Assemblage C/CC: C_2AS /CT
At 1420°C, the results are the same for C and CC. Two phases C_2AS (51%) and CT (49%) are found. The proportion is modified from the starting material (50%/50%) due to the atomic exchange between Ti which enters C_2AS and for Al and Si which substitute the perovskite.
Assemblage D/DD: C_2AS / C_4AF
At 1280°C and 1320°C, the same result is found for D and DD. C_2AS (50%), and C_4AF (43%) are detected as major phases, accompanied by C_2S (2%) and CA (3%). Iron oxide enters the gehlenite (C_2AS) as a probable substitution for alumina, while silica is detected in the calcium ferrite.
Assemblage E/EE: C_4AF /CT
At 1300°C E and EE give the same results. By SEM techniques, only one phase is detected, corresponding to the bulk reaction :
$0.103\ C_4AF + 0.368\ CT \rightarrow C_{0.78}A_{0.103}F_{0.103}T_{0.368}$.
By SEM technique, it was not possible to separate the different phases and thus not possible to know if there is a real solid solution of titanium with the calcium ferrite or an intergrowth of several phases as described in [7].
By XRD, the main peaks of the ferrite phase C_4AF disappear [17] and an additional calcium titane phase is detected : $Ca_3\ Ti\ (Fe\ Al)_2O_{13}$ (20%) in combination with CT (80%). Traces of $CaFe(Ti_2O_6)$ are also detected. The solid solution of Ti in ferrite C_4AF gives a series of complex changes that have been previously studied and published [16]. The authors found an extensive range of 14Å body centred solid solutions which become more disordered at higher Ti contents and lead to a formula close to that of $Ca_5Fe_4TiO_{13}$. The present results are in agreement with these findings although our composition is higher in TiO_2 than that published. Conversely we do not find an increase in free lime for TiO_2 contents higher than 18% as it is claimed [18].
Assemblage F/FF: C_4AF / Q
At 1270°C and 1290°C, by XRD and SEM, C_4AF (43%) and Q (55%) are the phases found in the samples F and FF. The difference in the composition between the starting proportion of 50/50 compared to 43/55 after the heat treatment is due to the modification of the solid solution composition from the starting composition. For example, the decrease from 3% to 2% of the percentage of MgO measured in the Q phase leads to an increase in the % of the Q phase formed.
During the burning period, the molar ratio MgO/SiO_2 of the Q phase varies from 1 to 0.9
Assemblage G/GG: C_2AS /CT/Q
At 1350°, G and GG give the same results . XRD detects the following phases Q (15%), C_2AS (35%), CT (37%) and CA (13%) . SEM techniques do not however detect the Q phase. This is

probably due to the intimate intergrowth between C_2AS and the Q phase that prevents the separation of these phases by SEM. To calculate the % of phases, we have used the composition of the Q phase given by its stoechiometry for n=3. The occurrence of CA in these samples is consistent with the results obtained in the sample B (C_2AS /Q) and A (Q/CT).

Table 2: Results of the mineralogical determination by XRD and SEM/EDS techniques

	Phases detected by X Ray diffraction	Phases detected by SEM
Binary : A/AA (Q/CT)	CT, Q and CA, C_2S, C_2AS as minor phases	$C A_{0.01} F_{0.004} S_{0.013} M_{0.026} T_{1.05}$ (CT) $C A_{0.62} F_{0.02} S_{0.19} M_{0.075}$ (Q) $CA_{0.95} F_{0.02} S_{0.01}$ (CA) $C A_{0.01} S_{0.51,}$ (C_2S) $C A_{0.48} F_{0.02} S_{0.51,}$ (C_2AS)
Binary : B/BB (C_2AS /Q)	C_2AS, Q ,CA	$CA_{0.47} F_{0.01} S_{0.49}$ (C_2AS) $C A_{0.62} F_{0.02} S_{0.19} M_{0.075}$ (Q) $CA_{0.95} F_{0.02} S_{0.01}$ (CA)
Binary : C/CC (C_2AS /CT)	C_2AS, CT	$C A_{0.48} T_{0.04} S_{0.50}$ (C_2AS) $C A_{0.02} T_{1,0}$ (CT)
Binary : D/DD (C_2AS / C_4AF)	C_2AS, C_4AF, CA, C_2S	$C A_{0.01} S_{0.51,}$ (C_2S) $C A_{0.48} F_{0.02} S_{0.51}$ (C_2AS) $C A_{0.23} F_{0.21} S_{0.04}$ (C_4AF) $CA_{0.95} F_{0.051}$ (CA)
Binary : E/EE (C_4AF /CT)	CaTiO3 , $Ca_3TiFe_2O_8$, CaFe Ti 2 O6	$C A_{0.14} F_{0.14} T_{0.53}$ (FT)
Binary : F/FF (C_4AF /Q)	C_4AF , Q	$C A_{0.26} F_{0.38} S_{0.02} M_{0.04}$ (C_4AF) $C A_{0.65} F_{0.04} S_{0.11} M_{0.1}$ (Q)
Ternary : G/GG (C_2AS /CT/Q)	C_2AS,CA, Q, CT	$C A_{0.44} F_{0.01} S_{0.48} M_{0.03}$ (C_2AS) $C A_{0.96} F_{0.12} S_{0.11} M_{0.03} T_{0.02}$ (CA) $C A_{0.01} F_{0.004} S_{0.013} M_{0.026} T_{1.05}$ (CT)
Ternary : H/HH (C_4AF /CT/Q)	Q,CA, C_4AF, $Ca_3TiFe_2O_8$	$C A_{0.64} F_{0.04} S_{0.09} M_{0.09} T_{0.01}$ (Q) $C A_{0.93} F_{0.03} M_{0.01}$ (CA) $C A_{0.18} F_{0.13} T_{0.38}$ (FT)
Ternary : I/II (C_4AF / C_2AS /CT)	C_2AS,CA, $Ca_3TiFe_2O_8$	$C A_{0.47} F_{0.02} S_{0.48} T_{0.01}$ (C_2AS) $C A_{0.91} F_{0.04} S_{0.01} T_{0.01}$ (CA) $C A_{0.13} F_{0.11} S_{0.09} T_{0.46}$ (FT)
Ternary : J/JJ (C_4AF /C_2AS/Q)	C_2AS, Q, C_4AF	$C A_{0.48} F_{0.002} S_{0.50}$ (C_2AS) , $C A_{0.64} F_{0.05} S_{0.12} M_{0.06}$ (Q) $C A_{0.23} F_{0.25}$ (C_4AF) $C A_{0.02} F_{0.002} S_{0.53}$ (C_2S)
Quaternary K/KK (C_2AS / C_4AF /CT/Q)	C_2AS,C_2S,CA,Q, $Ca_3TiFe_2O_8$	$C A_{0.49} S_{0.51}$ (C_2AS) $C A_{0.62} F_{0.03} S_{0.11} M_{0.08}$ (Q) $C A_{0.96} F_{0.043}$(CA) $C A_{0.12} F_{0.09} S_{0.04} M_{0.02} T_{0.54}$ (FT)

Assemblage H/HH: C_4AF /CT/Q

At 1300°C, by SEM, three main phases are detected in H and HH ; Q phase (16%), calcium ferro-titanate (54%), CA (23%), and small quantity of C_2S (4%) . By XRD, it is possible to separate the calcium ferrite (24%) from calcium ferro-titanate (31%). In this case the crystals of calcium ferrite and ferro-titanates are probably intergrown with a thickness lower than the detection limit of the SEM as previously described in [7].

Assemblage I/II: C_4AF / C_2AS /CT.
At 1300°C, the same result is obtained for I and II ; three phases are detected by SEM , C_2AS (23%) CA (7%) and calcium ferro-titanate (70%). By XRD, the peaks of calcium ferrite disappear, meaning that there is a transformation of the calcium ferrite and not an intergrowth of two separated phases.
Assemblage J/JJ: C4AF/ C_2AS /Q.
At 1280°C, 4 phases are detected by SEM techniques i.e Q (55%), C_2AS (14%), C_4AF (26%) and C_2S (4%) in J and JJ. XRD does not confirm the presence of C_2S.

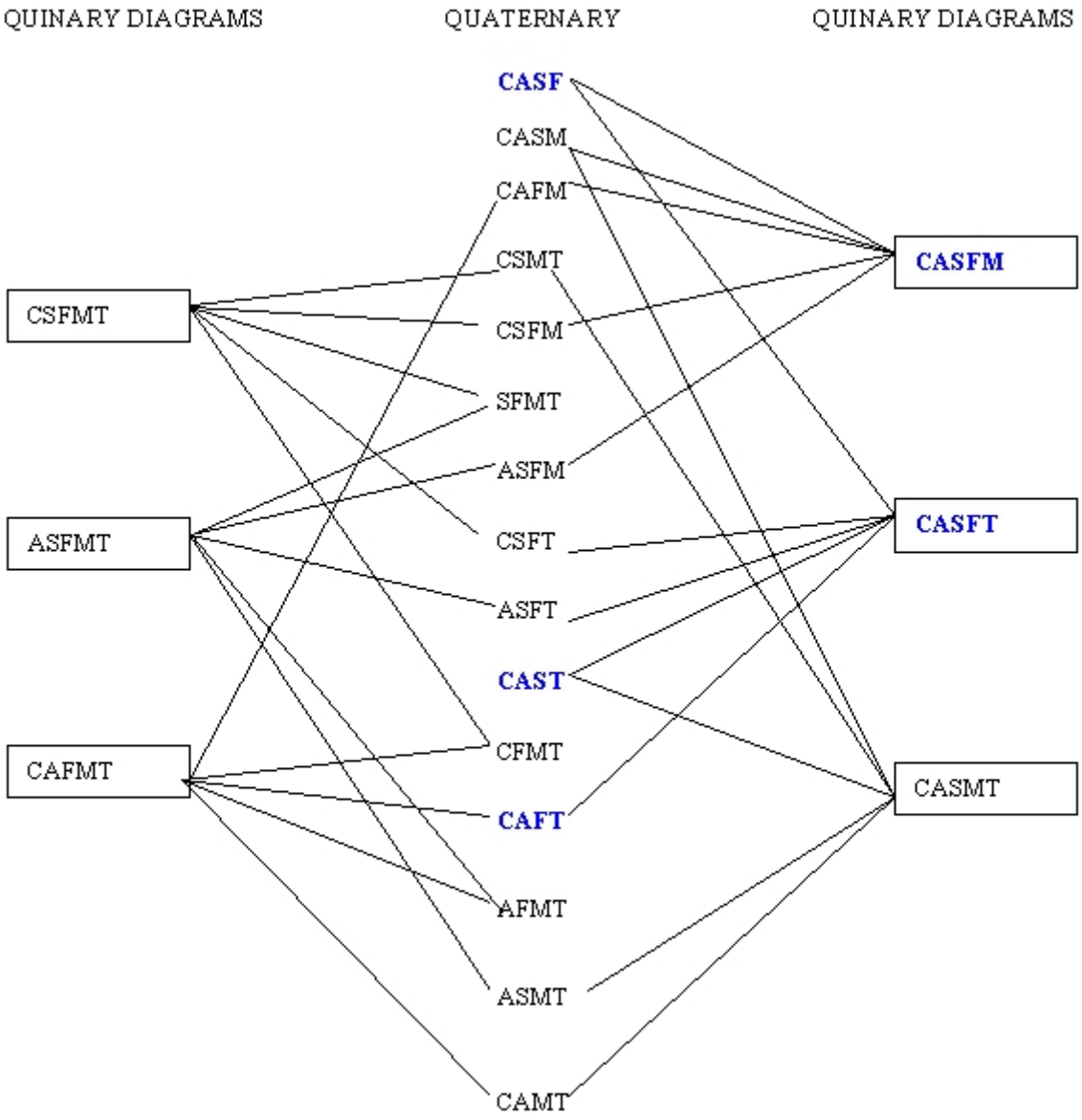

Figure 2. Connection between the mono and divariant assemblages in the diagram CASFMT

Assemblage K/KK: C_4AF / C_2AS /CT/Q .
At 1285°C and 1320°C SEM shows the presence of Q (25%), C_2AS (16%), calcium ferro-titanate (48%) and the occurrence of CA (8%) and traces of C_2S (2%). XRD confirms the presence of these phases and the almost total disappearance of the calcium ferrite phase.

In the phase diagram $CaO\text{-}Al_2O_3\text{-}SiO_2\text{-}Fe_2O_3\text{-}MgO\text{-}TiO_2$, (CASFMT), a maximum of six phases can be found together at a given temperature. This senary phase diagram is formed itself by 6

quinary diagrams, CASFM, CASFT,CASMT, CSFMT, ASFMT and CAFMT, issued from 15 quaternary diagrams . The connection is shown in Figure 2.
The starting phase assemblages, which have been studied here fall into the quinary and quaternary shown in the colour blue: quinary diagram CASFM for the samples B, F, J , CASFT for the samples I, CASF for the samples D, CAST for the samples C, CAFT for the samples E, The samples A, G, H and K fall into the senary diagram CASFMT.
The phase assemblages found in this study are summarised in Figure 3 as follows (in bold)

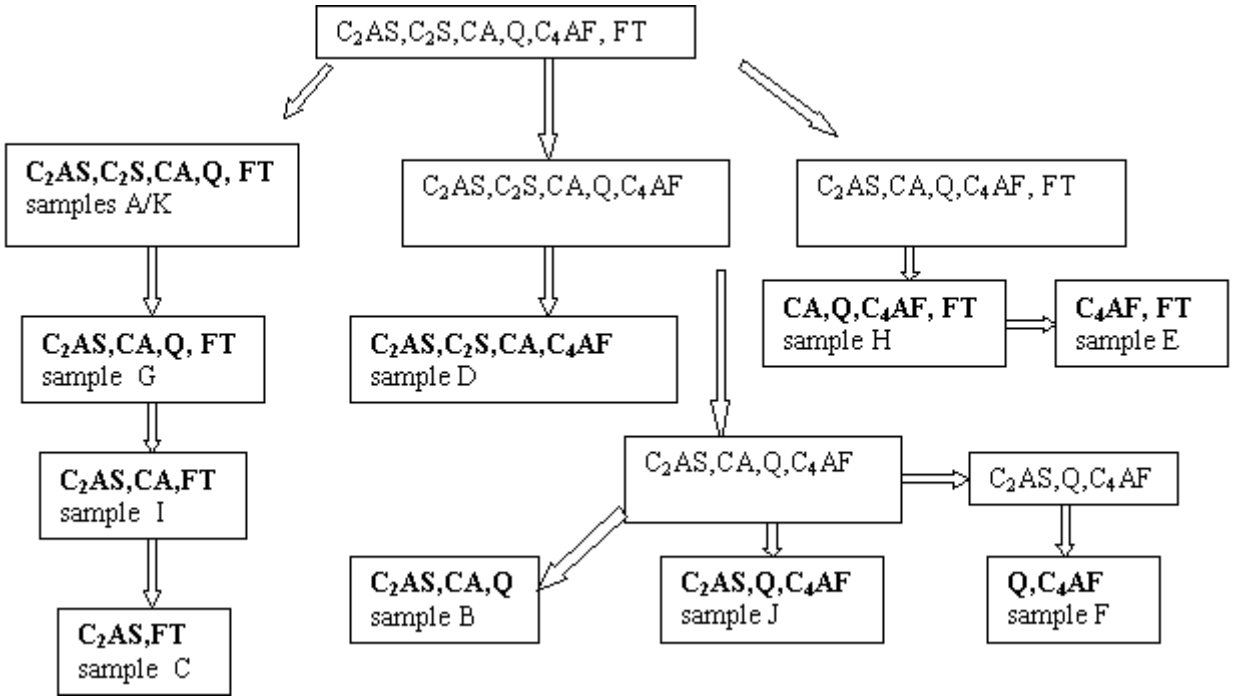

Figure 3. Assemblage found experimentally (bolt, FT= calcium ferro-titanate)

4. CONCLUSIONS

- The simultaneous use of XRD and SEM techniques in combination with calculations from the mass balance overcomes the difficulties in identifying C_2AS and Q phase or calcium ferro-titanate and calcium ferrite due to the intergrowth of these phases.
- The starting phase assemblage C_2AS, C_4AF, CT and Q phases, is modified in the following way:
  - i) diminishing and disappearance of the ferrite phase when the % of titanium increases
  - ii) appearance of calcium ferro-titanate
  - iii) decrease of the amount of the Q phase
  - iv) occurrence of CA and C_2S
  - v) modification of the solid solution composition and the percentage of the phases
- When the amount of titanium increases, the phase assemblage C_2AS, C_2S, Q, CA and calcium ferrite becomes C_2AS, C_2S, Q, CA , solid solution of calcium ferrite with titanium, and finally C_2AS, C_2S, Q, CA and calcium ferro-titanate.

REFERENCES

[1] Walenta, G.: Synthesen und Rietveld-Verfeinerung der Einzelphasen von Tonerdezementen- Dissertation, Erlangen, 1997.
[2] Füllmann. T.: Quantitative Rietveld-Phasenanalyse von Tonerdezementen. – Dissertation, Erlangen, 1997.
[3] Motzet H., Pöllman H. : Quantitative phase analysis of high alumina cement, Proceedings of the international microscopy Guadalajara Mexico, 1998, pp187-206

[4] Sorrentino F.P.: Comparison of Methods for Quantitative Determination of Phases in High Alumina Cement Clinkers. lnt. Symp. on Calcium Aluminate Cements, additionaly paper, non included in the proceedings, London, 1990.
[5] Sourie A., Glasser F.P., Lachowski E.E. : Microstructural studies on pleochroite, 1994 93, 2, pp 41-48.
[6] Sourie A., Glasser F.P. Composition of melilites crystallised from $CaO-Al_2O_3$ Fe_2O_3- SiO_2 melts, British. Ceramic. Transaction. Journal 1992, 92, 4, pp 152-154
[7] Gloter A. Etude de l'état chimique du fer à l'échelle nanométrique d'oxydes cimentiers par spectroscopie des pertes d'énergie d'électrons et microscopie électronique à transmission, Ph. D thesis University of Paris sud , Orsay 2000.
[8] Calleja, J.: Calculation of hypothetically Possible Potential Compositions of High Alumina Cements, Proceedings. of the 7th International.. Congress. on the Chemistry of Cement, Paris, 1980 Volume III, pp. 102-107.
[9] Sorrentino F.P.: Study in the system $CaO-Al_2O_3$ -SiO_2-Fe oxide, Ph.D. thesis Aberdeen 1974
[10] Sorrentino F.P., Glasser F.P.:The system $CaO-Al_2O_3$ - SiO_2-Fe oxide , British. Ceramic Transaction Journal Part 1 the pseudo ternary section C_2F/C_2AS: 1975, 74, pp 253-256; Part 2 the system C/A/F/S: 1976,76, pp 95-103.
[11] Sorrentino F.P. , Glasser F.P. : The phase composition of high alumina cement clinkers, Seminaire international 1982, pp14-43, Turin
[12] Sourie, A., Glasser, F.P.: Studies on the Mineralogy of High Alumina Cements,. - British. Ceramic Transaction. Journal., 1991,Vol. 90 . pp. 71-76
[13] Sourie A, : Mineralogy of aluminous cement and their reactivity, Ph D thesis University of Aberdeen 1991
[14] Kapralic I., Hanic F. : Studies of the system $CaO-Al_2O_3-MgO-SiO_2$ in relation to the quaternary phase Q, British. Ceramic. Transaction. Journal., 1980,79, pp 128-133,
[15] Kimura S., Muan A. Phase relations in the system CaO-Iron oxide –TiO_2 in air, American Mineralogist , 1971, 56, pp1332-1346
[16] Marinho M.B. Glasser F.P. Polymorphism and phase change in the ferrite phase of cements induced by titanium substitution, Cement Concrete Research 1984, vol 14, pp 360-368,
[17] Guirado, F. Gali P., Chinchon S. : " X ray profile analysis of Ca_2Fe_{2-x} Al_x O_5 solid solution, World cement 12, 1996, pp 73-76
[18] Knofel D. : Der Einbau von TiO2 indie phasen des Portlandzementklinkers, Zement . Kalk. Gips, 1979, 1, pp35-40

PHASE ASSEMBLAGES RELEVANT TO CALCIUM ALUMINATE CEMENTS IN THE MULTICOMPONENT PHASE DIAGRAM, $CaO-Al_2O_3-SiO_2-Fe_2O_3-MgO-TiO_2$

François P. Sorrentino

Lafarge , Laboratoire Central de Recherche, 95 rue de Montmurier 38291 St Quentin Fallavier Cedex , France; E-mail: francois.sorrentino@lafarge.com

7 Garnier street 69330 Meyzieu (FRANCE)

Chemical Engineer (Grenoble 1964) D.Sc Material science (Grenoble 1969) Ph.D; Thermodynamic (Aberdeen 1972)

Scientific backround : thermochemistry, thermodynamic, high temperature chemistry

Technical background : analytical method (SEM, TEM, thermal analysis, XRD, XRF ....)

Professional experience : Material science (cement, ceramics, glass, metallurgy) author of more than 100 refered papers , 4 chapters , 10 international patents.

Actual Position : Senior scientist (Lafarge) , member of the scientific council of University Lyon 1 (France)

MINERALOGY OF MODIFIED STEEL SLAGS

François Sorrentino and Michel Gimenez

Lafarge Laboratoire Central BP 15 38291 St Quentin Fallavier France,
E-mail: francois.sorrentino@lafarge.com, michel.gimenez@lafarge.com

ABSTRACT

Among the residues and by-products waiting for a sustainable valorisation, steel slags present the most interesting potential because of their chemical and mineralogical composition. In spite of that, the degree to which steel slag is used remains limited because of the quantity of free lime contained in this type of slag. Many processes have been tried to solve this problem but their economic balance has been limited by the quality of the final product and has prevented industrialization. Two processes, however, have a significant potential for indus- trial application. These involve treatments under oxidising or reducing conditions and a modification of the chemistry and the mineralogy by a mineral addition (addition of silica or alumina) between the converter and the slag discharge process step ('Upstream' process modification).

With such modifications, it is possible to eliminate the free lime and to obtain sound aggregates or a product with cementitious properties similar to or better than a blast furnace slag. In this study, we compare the mineralogy of the final "modified slags" obtained by these processes and its impact on the reactivity. The best results are obtained by the addition of alumina and lime under oxidising conditions. The iron rich cement produced has a similar reactivity to that of a Portland cement with potential advantages in terms of durability thanks to the absence of alkalis.

1. INTRODUCTION

The steel industry produces several types of by-products (slags, dusts, slurry, scraps etc...), generated during the successive stages of the process that starts with the iron ore going through to the final steel. The steel manufacturing process consists mainly of three stages; reduction, steel making and secondary metallurgy stage. Pig iron and blast furnace slag (B.F. slag) result from the reducing stage. From the transformation of pig iron into steel, result the steel and the basic oxygen process slag (BOP slag, or LD slag) and the electric arc furnace slag (EAF slag) and finally from the secondary metallurgy processes result the "SMP" slag. BF slag is air cooled, granulated or pelletised. BOP, EAF, SMP slags are air-cooled. Most of the slag that is produced is either BF slag or BOP steel slag.

The BF slag is widely used as aggregate when it is crystallised and crushed or as cementitious additive when it is glassy and finely ground. The steel slags have not found a real valorising destination, mainly because of their high level of free lime content but also because they contain undesirable elements such as Mn, Ti or Cr in the case of stainless steel.

Steel slags are produced during the refining of iron to obtain steel. The transformation occurs by blowing oxygen into the molten pig iron and lime, limestone or dolomite is added to entrap the impurities. During this process, the current practice is to add more lime than the stoechiometry would require in order to improve the efficiency of the refining. Hence a large amount of free lime

Proceedings of the 11th International Congress on the Chemistry of Cement (ICCC)
'Cement's Contribution to the Development in the 21st Century'
Hosted by: The Cement and Concrete Institute of South Africa
CD-ROM produced by: Document Transformation Technologies
11 - 16 May 2003, Durban, South Africa
ISBN Number: 0-9584085-8-0
Editors: Dr G. Grieve and G. Owens
Congress Organised by: Event Dynamics

is found in the final slag, with the consequence of expansion when these types of products are used as aggregates or cement or concrete additives.

The increasing cost of landfill, due to environmental constraints generates research to find ways of valorising steel slags [1,2,3] and old studies, that a few years ago were abandoned because of lack of economic advantages are arousing new interest [4,5]. Nevertheless, when looking at the methods for valorising by-products, attention must be paid to the process and to its evolution.

In the past, the steel slag was the by-product of the transformation of high-phosphorus basic Bessemer pig iron and it could be used as a fertiliser (Thomas type phosphate slag). Today low phosphorus pig iron is almost exclusively produced and the use of slag as fertiliser is reduced.

The different ways of using steel slags can be deduced from the process itself, which can be summarised in three steps:

Input material: Pig Iron, Oxygen, Lime

STAGE 1	CONVERTER
Operation	separation by density
Output material	Steel, Steel slag

STAGE 2	TRANSFER VESSEL
Operation	deferrisation
Output material	recovered steel, deferrised steel slag

STAGE 3	DUMPING
Operation	classification, beneficiation
Output material	sieved , treated steel slag

Any utilisation or treatment of slag can be carried out during one of these three stages.

The treatment during stage 3 is certainly the easiest as the slag is already cold and the treatment does not interfere with the steelmaking process. On the other hand, the levers of these treatments are limited and the cost probably high. The steel slags are mainly used as aggregates for the civil (road, railway ballast) and water construction [6,7]. Physical strengths, resistance to frost and constant volume are the principal qualities required for these products .The presence of large quantities of free lime in the steel slag is the main limitation when using these slags as aggregates for roads or concrete [8]. Also due to the quantity of free lime, the addition of ground steel slags to clinker is not allowed (same practice as for BF slag). Classification of the different sizes of the slag according to their free lime content and the use of the lowest lime content slag is a solution.

Another solution is to water or to carbonate the slag in order to transform the free lime into $Ca(OH)_2$ and $CaCO_3$, which are innocuous.

The addition to the raw material in the manufacture of cement is an interesting option, although limited because of the high iron content of the slag. The steel slag provides lime and iron oxide and acts as a mineralizer in the clinkering process [9].

The most promising processes are based on the modification of the chemistry and the mineralogy of the slag, mainly by the addition of silica to neutralise the free lime. The slag can be treated during the first or second stage of steel manufacture.

During stage 1, it is possible to modify the thermodynamic path of the slag composition to prevent the formation of dicalcium silicate shell around the lump of lime and to decrease the quantity of free lime. The study of the primary crystallisation fields of CaO, C_3S, and C_2S in the system CaO-iron oxide-SiO_2 in air shows that the slags that are saturated with CaO at 1650°C will be in equilibrium with CaO when the SiO_2/iron oxide is less than 21/79. In the system CaO-iron oxide-SiO_2 in equilibrium with metallic iron, the ratio becomes 24/76 [10,11]. The question of how far the range over which the saturated slag coexists with lime can be extended at steelmaking temperature has been solved by the use of oxide addition such as bauxite or calcium aluminate [12,13,14].

During stage 2, the liquid slag can be treated in different ways. By reduction of the steel slag, it is possible to recover iron as metal and to obtain a slag of a defined composition, provided that the raw material composition is adjusted [15]. This process requires an external energy, supplied as electricity. During the treatment, iron (Fe^{2+} and Fe^{3+}) are reduced to iron metal and are separated from the slag. (Other oxides are also reduced, depending on the efficiency of the reducing agent and the conditions of treatment). If there is no mineral addition during the treatment, the final product will contain a high amount of lime, its melting point will be too high for it to become a liquid at the furnace temperature (1500°C), and thus the process will stop. If silica is added, the chemical composition can be adjusted to obtain a liquid phase at the furnace temperature. The final product contains very little iron oxide and its chemical composition is similar to that of a BF slag. As for a BF slag, this can be used crystallised or it can be quenched to increase its reactivity when it is used as cementitious addition. This treatment, difficult to achieve on a laboratory scale, has been studied at pilot plants and is now being tested on an industrial scale.

By oxidation (injection of oxygen) and addition of silica, it is possible to obtain a sound aggregate [16]. During oxidation, divalent iron oxide (wüstite, or magnesiowüstite), and iron metal oxidise to give Fe_2O_3. This exothermic reaction produces sufficient energy for the dissolution of minerals such as silica.

The added silica combines with the free lime to produce calcium silicates and finally, calcium silicates and calcium ferrite crystallise. In this case, the final product contains the same elements as the starting material, plus the mineral additions. It contains the iron in its maximum oxidation state.

In this paper, we propose a new treatment in which the slag is oxidised but instead of adding silica, we add alumina or an alumina containing compound [17]. The slag displays a new type of mineralogy and interesting hydraulic properties described below.

Figure 1 shows the different compositions of modified slags, which can be obtained by adding silica (path 1), or alumina (path 2)

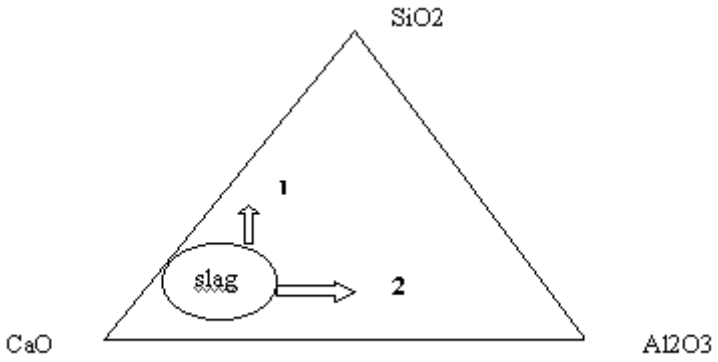

Figure 1. Chemical modification of steel slag

2. EXPERIMENTAL PROCEDURE

In this study, we have used an industrial steel slag as the raw material (chemical composition given table 1) which has been submitted to different treatments in the laboratory:

1) Oxidation at 1500°C,
2) Reduction at 1500°C,
3) Mixing with silica and oxidation
4) Mixing with silica and reduction
5) Mixing with alumina and lime and oxidation

The quantity of silica added is calculated in order to obtain a liquid slag at 1500°C with a minimum of residual free lime (respectively 5% and 15 % in the treatment by oxidation and reduction). The addition of alumina and lime is calculated to obtain a potential phase assemblage that is able to generate hydraulic properties and that is compatible with the constraints of the process (30% alumina 15 % lime).

Pilot plant tests have been performed in a similar way to the oxidation process with the addition of silica but with additional quenching of the final product [15].
Free lime was analysed after the different treatment processes.

Table 1. Chemical composition of the industrial steel slag

SiO2	Al2O3	Fe2O3	CaO	MgO	TiO2	MnO	P2O5	FeO	Free lime
15.22	1.68	11.06	50.03	6.59	0.7	2.38	2.06	11.61	10.40

Polished sections have been studied by SEM techniques associated with EDS measurements and the crystallography controlled by X ray diffraction.

A comparison of the reactivity has also been performed for samples produced under oxidising conditions in the laboratory and for those produced in reducing conditions in pilot trials. The reduction process and the addition of silica gave a product whose composition is similar to a BF slag. It is known that the reactivity of slag is increased when the degree of vitrification (% of glass) is high. The degree of vitrification required is obtained by a quenching system, which is possible on an industrial but not on a laboratory scale. This is not the case with oxidising conditions where the quenching can be carried out on a laboratory scale. In terms of reactivity, the most reactive products available at present have been compared.

Experiments 3 and 4 corresponding to silica additions have been described in more detail elsewhere (18) and are therefore only summarised in this paper.

3. RESULTS AND DISCUSSION

The experimental results obtained by SEM associated with the X Ray diffractograms are compared with the phases composition calculated from the chemical composition, and a mass balance which assumes an assemblage of probable phases that exist.

Figure 2 shows the micrograph obtained on a polished section of the industrial steel slag before the treatment (SEM, backscattered electrons mode). The phases detected are: solid solution of dicalcium silicates, magnesio wüstite, calcium ferrite, and free lime. The experimental and calculated results are consistent and in good agreement with the published studies [19, 20]. The entire indexation of the X-Ray diffractogram of the steel slag represented Figure 4 is well known and has been published [18]. We show here only the main peaks in order to highlight the evolution of the phases during the transformation

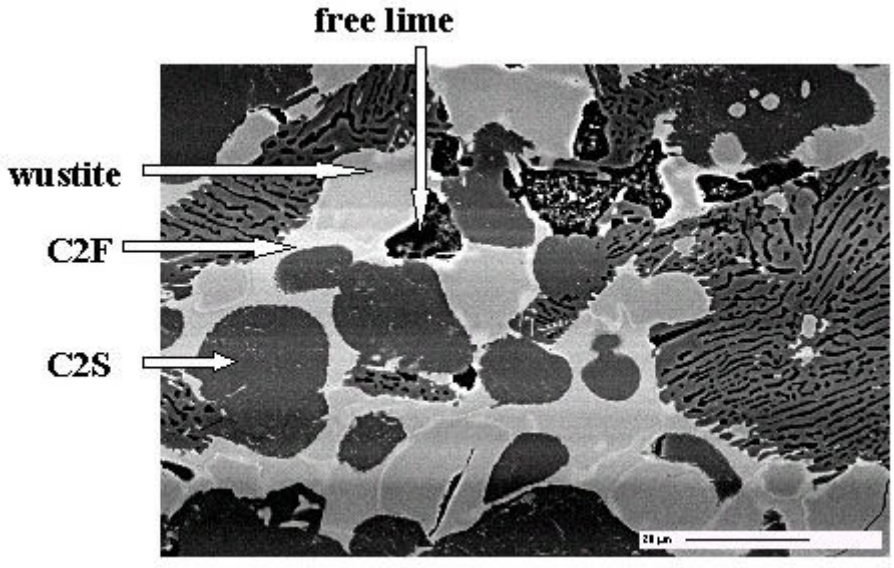

Figure 2. Micrograph of industrial steel slag (polished section, BEI)

After oxidation, magnesio-wüstite disappears (oxidation of divalent iron) and the magnesium oxide precipitates as periclase. The main phases are then solid solutions of dicalcium ferrite (containing Mn, Al, etc.), dicalcium silicate solid solution (containing large amounts of phosphate) and periclase. The occurrence of periclase, the disappearance of lime and wüstite and the increase of calcium ferrite are clearly shown by X-ray diffraction.

After reduction and silica addition, bright particles of iron metal and tricalcium silicate are found by SEM in large quantities. Small particles of free lime have also been detected. After this treatment, the sample is sintered due to its chemical composition

After oxidation and with silica addition, the main crystallised phase is dicalcium silicate surrounded by a phase containing iron oxide and eutectoid precipitation that is difficult to identify by SEM (particles less than 1 µm). Even by theoretical consideration, it is not easy to identify the interstitial phase. An X-Ray diffractogram shows the presence of merwinite and akermanite and traces of enstatite and perovskite.

With the addition of 15% silica under reducing conditions, the calculated phase assem- blage (system CaO-SiO_2-MgO with a very small amount of Al_2O_3) indicates the presence of merwinite (C_3MS_2), dicalcium silicate, and wollastonite. The results from SEM micrographs and the XRD indicate the presence of dicalcium silicate, periclase and iron metal.

The results of the free lime analysis and phase assemblage are shown in Table 2.

Table 2. Comparison of the experimental and predicted phase assemblage

		Phases
Steel Slag Untreated	theoretical	magnesio wüstite (24%), calcium ferrite (23%), dicalcium silicate (43%)
	experimental	dicalcium silicate, magnesio wüstite, calcium ferrite, free lime (10%)
Oxidised	theoretical	Dicalcium silicate (46%), calcium ferrite (46%), periclase (6%)
	experimental	tricalcium and dicalcium silicate, iron, periclase free lime (1%)
Oxidised + Alumina + lime	theoretical	monocalcium aluminate (20%), dicalcium silicate (25%), calcium ferrite (43%)
	experimental	monocalcium aluminate,dicalcium silicates, calcium ferrite, Q phase, free lime (< 0,5%)

In the case of the slag oxidised with alumina and lime addition, the micrograph (Figure 3) shows the presence of monocalcium aluminate (CA), dicalcium silicate, (C_2S), calcium ferrite (C_4AF), gehlenite (C_2AS) and the phase $C_{20}A_{16-x}(Mf)_xS_x$ also called Q phase [21]. This finding is in good agreement with the calculated mineralogical composition. The presence of Q phase is explained by the presence of MgO.

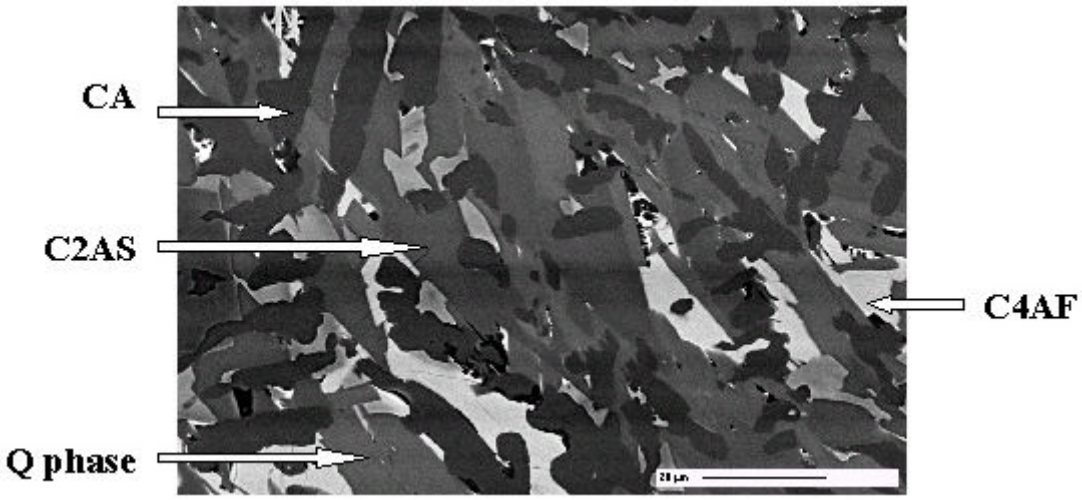

Figure 3. Micrograph of industrial steel slag (polished section, BEI) treated with oxygen, alumina and lime - slow cooling

The results obtained by SEM are confirmed by X-ray diffraction in Figure 4 where the evolution of the mineralogy, due to the oxidation and the addition of alumina is evidenced (only the major peaks are quoted).

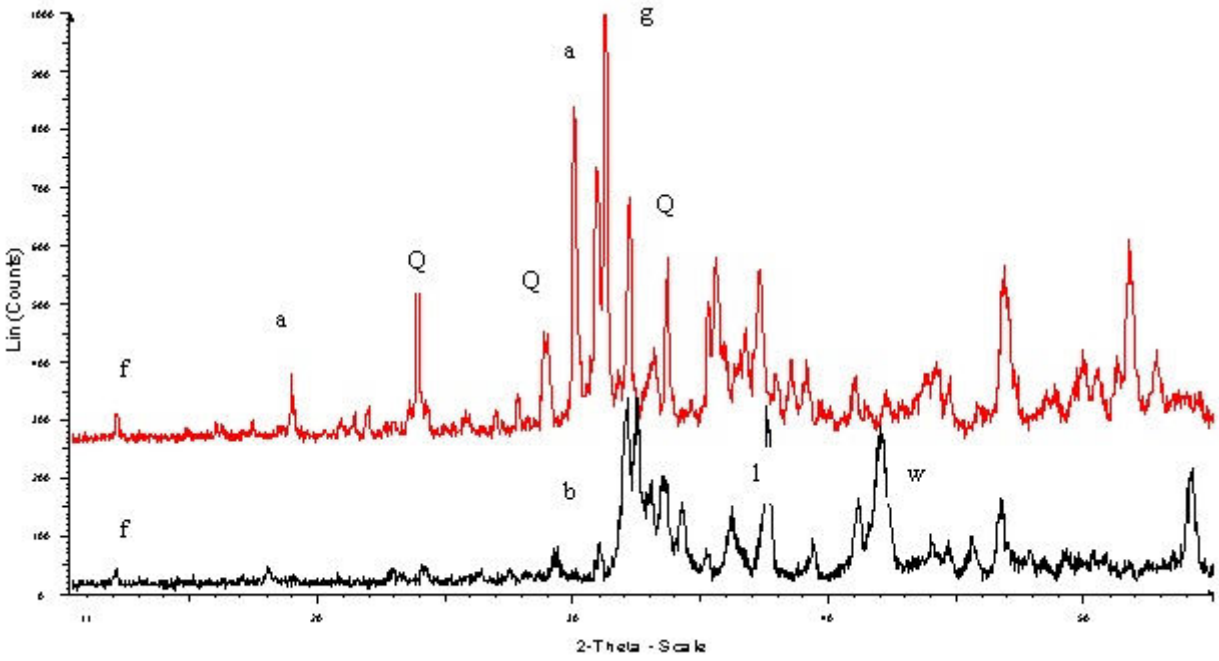

Figure 4. X ray diffractogram of the industrial steel slag (bottom) and steel slag modified by oxidation and alumina and lime addition (above) l (lime), w (wustite) , (b) C2S, (f) calcium ferrite , (a)calcium aluminate, (g) gehlenite (C2AS) ,(Q), Q phase

The reactivity of the cementitious additive is based on the measurement of the reactivity index (RI), standardised by ASTM C 989 978b. The reactivity index is the ratio of the compressive strengths obtained with a mixture of 50% slag 50% cement to the compresssive strengths obtained with 100% cement.

Four slags have been used for the test:

N°1 An industrial BF slag, ground at 400 m^2/g

N°2 The slag produced under oxidising conditions and with addition of 5% SiO_2. This slag has been produced on a laboratory scale and it is crystallised.

N°3 The slag produced under reducing conditions and with addition of 15% SiO_2. It has been produced at the pilot plant scale, in order to have a glassy product.

N°4 The crystallised slag produced on a laboratory scale by addition of alumina and lime

Figure 5 shows the evolution of the reactivity index versus time for these slags.

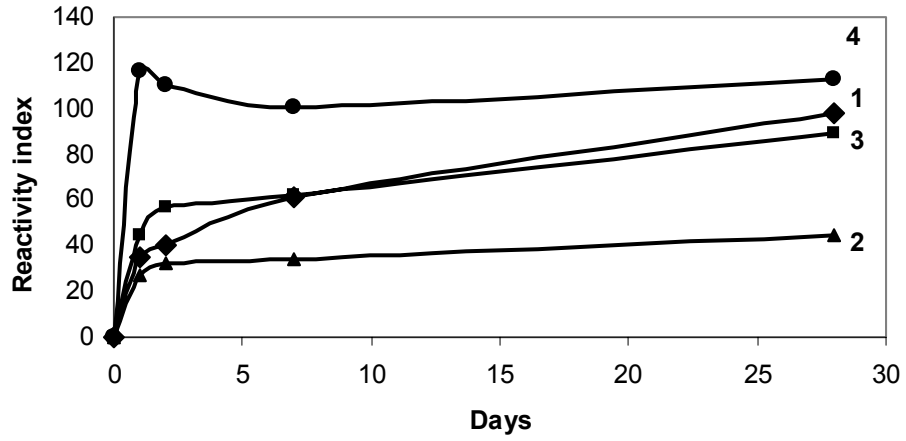

Figure 5. Reactivity index versus time

These results show that the slag N°2 (Figure 5), produced under oxidising conditions and with silica addition is less reactive than the industrial BF slag N°1 (Figure 5). The slag produced under reducing conditions N°3 (Figure 5) behaves like an industrial BF slag. The addition of alumina and lime, under oxidising conditions gives the best results (N°4 Figure 5) and with 50% substitution, the same performance as a pure cement (RI=100%) or even better (early strength) is obtained. Nevertheless, the reactivity of the slag is only one factor determining the choice between these processes and the final decision must take into account other parameters such as the presence of toxic elements in the slag (different in both processes) and the thermal balance. The economic balance also involves the cost of the energy and the mineral additions.

4. CONCLUSIONS

- The "upstream" process modification to the chemistry and mineralogy of the steel slag is a viable solution that can be used to transform this by-product into a valuable product.
- Each process (oxidising or reducing conditions) gives products with a mineralogical composition favourable for use as an addition to OPC clinker.
- These processes are technically feasible (the oxidising process is under develop- ment) and the reducing process has been tried at a pilot plant.
- The reactivity of the slag produced under reducing conditions is similar to that of BF slag, while the reactivity of the slag produced under oxidising conditions and with the addition of silica is lower.
- The best results, especially at an early age are obtained in oxidising conditions and addition of alumina.
- The reactivity, expressed as a reactivity index is only one criterium determining the choice of process and some other technical aspects (trace of heavy metals, heat of hydration, grinding energy, etc.) and economic aspects (transport, cost of landfill,) must be kept in mind.

REFERENCES

[1] George C..M., Sorrentino F.P.Valorisation des scories d'acièrie LD " 7th International Congress on Cement chemistry Paris,1980, III, pp 140-144.

[2] J. Geiseler J. Steelmaking slags; properties and uses. Information day on utilisation of blast furnace and steelmaking slags January 27, 1988, Liège Commission of the European communities, Bruxelle 1988.

[3] Piret J. Valorisation de la scorie LD, aspects généraux du problème et réalisation dans le domaine de la construction routière, Revue de métallurgie, 1978, pp 321-328.

[4] Conjeaud M., George C.M. Sorrentino F.P. A new steel slag for cement manufacture: mineralogy and hydraulicity, Cement and Concrete Research , 1981, 11, pp 85-102

[5] Sorrentino F.P., George C.M. New concrete based on oxygen steel slag containing alumina, Silicates industriels, 1982, 44, 3, pp 77-83.

[6] Krass K., Fix W. . LD Schlacken ein neuer Mineralstoff im Strassenbau, Strassen und Autobahn, 1977, 28, 8, pp 326-334.

[7] Emery J. Steel slag application in high way construction, Silicates industriels, 1977, 4/5, pp 209-218.

[8] Kawamura M., Torii, Hasaba S. Applicability of basic oxygen furnace slag as a concrete aggregate, Montebello, ACI SP-79, 1983, 2, pp1123-1141.

[9] J. White Processes for steel making by oxygen refining of iron, US patent N° 4010027, 1977.

[10] White J. Slag control in basic steelmaking processes: an examination of the possibility of eliminating fluorspar, Iron and steelmaking, 1974, 2, pp115-117.

[11] Sorrentino F.P.,George C.M., Vershaeve M. Procédé de fabrication d'une scorie de désulfuration, Brevet Francais N° 83 02666 , 18/02/1983.

[12] Sorrentino F.P.,George C.M. Nouvelle méthode de valoriation des scories d'affinage BOP, Colloque international sur la valorisation des sous produits et déchets dans le génie civil Paris,1978.

[13] Grosjean J.C., Hamman M., Pazdej R., Sorrentino F.P, George C.M.. Etude du traitement des scories d'acièrie en vue de leur utilisation dans l'industrie du ciment, Energy; conference industrielle Dusseldorf, 1984, 3, pp 256-269.

[14] Texas Industry. Method and apparatus for using steel slag in cement clinker pro- duction US Patent 5421880, 1995.

[15] J. Piret J. Total transformation of steel slags and other solid by products into value added mineral and metallic phases: the IPBM (in plant by product melting). Process project N°9621 part 2. Evaluation of the product,1998.

[16] Kühn M., Drissen P. , Geiseler J., Schrey H. . A new BOF slag treatment technology Proceedings. 2d European Oxygen Steelmaking Congress, AIM Milano, 1997, pp 445-453.

[17] Sorrentino F.P., Chaperon G. ,Bayoux J.P. Method for oxidising treatment of steel Works slag and resulting LD Slag, Patent WO 01/90019, 2001.

[18] Sorrentino F.P., Gimenez M., and Crumbie A.. Mineralogy of modified steel slag, International conference of cement microscopy San Diego (USA), 2002, pp 32-41.

[19] Wang, Yu Ji Xie, Gong Xin. Research on the main mineral phase and its cementitious properties of oxygen converter slag. 7 th International conference on cement chemistry., Paris, 1980, 2, pp 19-24.

[20] Chavepeyer G., Dumortier C., Gohy C., Levert J.M., Riquier Y. Etude de la composition minéralogique des scories LD" Silicates industriels, 1979, pp 21-233.

[21] Kapralic I., Hanic F. Studies of the system CaO-Al2O3-MgO-SiO2 in relation to the quaternary phase Q, Transaction British Ceramic Society Journal, 1980,79, pp128-133.

MINERALOGY OF MODIFIED STEEL SLAGS

François Sorrentino, Michel Gimenez

Lafarge Laboratoire Central BP 15 38291 St Quentin Fallavier FRANCE ,
E-mail: francois.sorrentino@lafarge.com, michel.gimenez@lafarge.com

François Sorrentino:

Address : 7 Garnier street 69330 Meyzieu (FRANCE)
Degree: Chemist engineer (Grenoble 1964) D.Sc Material science (Grenoble 1969) Ph.D; Thermodynamic (Aberdeen 1972)
Scientific backround : thermochemistry, thermodynamic, high temperature chemistry
Technical background : analytical method (SEM, TEM, thermal analysis, XRD, XRF ....)
Professional experience : Material science (cement, ceramics, glass, metallurgy) author of more than 100 refered papers , 4 chapters , 10 international patents.
Actual Position : Senior scientist (Lafarge) , member of the scientific council of University Lyon 1 (France)

Michel Gimenez:

is a chemical engineer and has followed his PhD studies in Physical Chemistry in Brussels dealing with non-linear phenomena in various chemical and physical systems.

He then joined the plastics & cement industries where he occupied positions in Research, Process, Quality and Production management. He is currently in charge of R&D for Cementitious materials within the Lafarge organisation.

CHARACTERISATION OF INTERSTITIAL TRANSITION ZONE (ITZ) OF HIGH PERFORMANCE CEMENT BY NANOINDENTATION TECHNIQUE

Denis Damidot[1], Karine Velez [2] and François Sorrentino[3]

[1] Ecole des Mines de Douai, Département de Génie Civil, 941 rue Charles Bourseul BP 838, 59508 Douai cedex France. E-mail: damidot@ensm-douai.fr
[2] Institut National des Sciences Appliquées (INSA), Lyon , France.
[3] Lafarge, Laboratoire Central de Recherche, St Quentin Fallavier, France.
E-mail: francois.sorrentino@lafarge.com

ABSTRACT

The evolution of the performance of concrete achieved during the past years is mainly due to the improvement of our understanding of the microstructure of the cement paste and especially of the interstitial transition zone (ITZ). The ITZ of very high performance concrete only extends to a few microns from the inclusions (anhydrous cement, aggregates, fibers, silica fume) and required the development of new techniques of investigations such as nanoindentation.

With this technique it is possible to measure, in a composite material, the mechanical properties (elastic modulus, hardness) of particles having a size of a few cubic micrometers. This technique is based on the record of the load versus displacement curve at a very low load (less than 50mN). In a first step, the mechanical properties (elastic modulus) of the pure components of the clinker ($C_3S/C_2S/C_4AF/C_3A$) and of the cement paste (CH, C-S-H) have been studied. Then nanoindentation was applied to the high performance concretes.

The results show that the values of the elastic modulus obtained for the different constituents in the concrete are in agreement with those for the same constituents taken independently at constant porosity. In this study, the creep behaviour of the C-S-H is also highlighted. Associated to classical SEM and EDS analysis, the nanoindentation technique can be used as a "micro-mechanical probe" to scan the surface of hardened cement paste.

1. INTRODUCTION

The quality of hardened concrete (mechanical strengths, dimensional variations, resistance to the aggressive conditions, …) depends on the concrete mix design (proportion, type of cement, quality of the aggregates, etc.), on the processing and curing. Because the microstructure of hardened concrete depends also on the same parameters, it can be assumed that there is a correlation between the microstructure and the bulk properties of concrete.

Based on this concept, researches have been undertaken to describe the microstructure of the concrete. The results of these researches have been at the origin of the improvement achieved during the last decade moving from ordinary concrete to high performance concrete (HPC), to very high performance concrete (VHPC), reactive powder concrete (RPC) and the new concrete *Ductal*® [1,2,3].

In the final state, the microstructure of the hardened concrete is determined by the characteristics of the different constituents, the residual clinker, the cement paste, the aggregates, the fibers and their bond (Interstitial Transition Zone). According to many researchers, the interstitial zone appears to be the weakest part of the concrete (reviewed in [4]). In ordinary concrete, the thickness of the ITZ is about 40-50µm. The pore distribution, the chemistry and mineralogy of the ITZ differ from the bulk of the cement paste. The influence of the ITZ on the mechanical properties of the concrete has been investigated according to two approaches. In the first approach, the bulk elastic modulus of concrete is measured and compared to a calculation based on the data of the elastic modulus of each constituent linked by different models [5, 6, 7]. The second approach is based on the measurement of the mechanical properties (elastic modulus, hardness) of the interfacial zone by microhardness testing (nanoindentation techniques) [8, 9,10, 11,12]. After the description of the microstructure, it is necessary to use a model to link the data obtained at different scales.

The techniques of indentation have been developed to allow a measurement of mechanical characteristics at the micro-scale. These techniques, well known in the polymer industry, in metallurgy, electronic and ceramics, [13,14,15] are based on forcing an indenter into the surface of the mate- rial by a dynamic or static loading and determining the response of depth of penetration or size of indentation.

They are many techniques of indentation, classified according to the load applied to the sample: i) macrohardness when the load is higher than 10 Newtons (N), ii) microhardness when the load is between 0.05 and 10N, iii) nanohardness, also called nanoindentation or deep sensing micro-indentation, when the load is around 50mN. The microhardness technique is standardized [16, 17] and has been widely used in the cement field [8,9,10,11,18,19], but it has many disadvantages:

a) it cannot be applied to study the ITZ of high performance concrete, because the thickness of the ITZ is the same as the size of the indent (10µm) and consequently, it is necessary to have a smaller indent (1µm).
b) the load is too high to keep the stress/strain curve in the elastic part, and to measure the fine layer of compound in a heterogeneous matrix.
c) optical measurement of the trace of the indents is necessary, inducing an important standard deviation of the measurement.
d) The size and shape of the indenter (most often Vickers type) are not always adapted to the problem and cannot be easily modified.

The main difference between the microhardness technique and the nanoindentation technique comes from the measurement of the displacement. In the microhardness, the size of the print of the indenter in the cement paste must be measured, but in that case, because of the intensity of the load, this print is visible through an optical microscope or in SEM. In nanoindentation, the size of the print of the indenter is no longer useful to determine the displacement, but it is necessary to identify which phase has been measured, in the case of a heterogeneous material such as a cement paste. Because of the low intensity of the load (few mN), the print of the indenter is hardly visible. The technique to locate the trace of the indents in cement paste has been used successfully in experiments and reported in published works. [19, 20].

In this work, we first measured the elastic modulus of the clinker phases and of the main hydrates i.e. CH and C-S-H of different ratio C/S. In the second step, we measured the elastic modulus of a heterogeneous sample such as a high performance concrete.

EXPERIMENTAL PROCEDURES

2.1 Description of the equipment

The experiments at microscopic scale by nanoindentation were performed using a nano indenter TM II shown schematically in figure 1. The complete description of the equipment can be found elsewhere [19] and is summarised below. The instrument continuously monitors the displacement of the indenture by a capacitance gauge as a load is applied. The load and displacement resolution of the apparatus are respectively 75 nN and 0.04 nm. The measu- rements of elastic modulus were obtained using a Berkovich indenter, i.e. three-sided pyramid diamond, with the same nominal area to depth relationships as the standard Vickers pyramid.

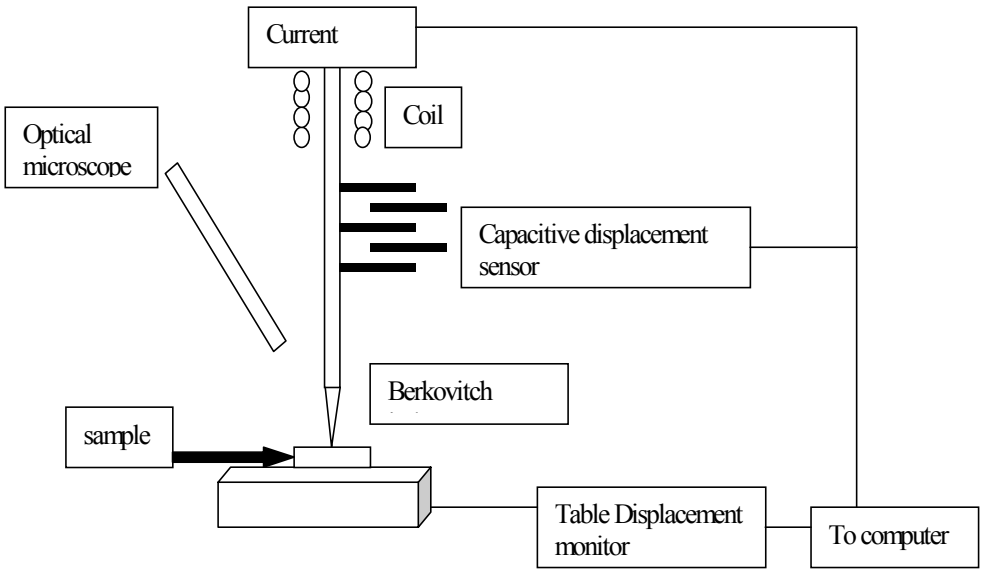

Figure 1. A schematic representation of experimental equipment used to perform the indentation experiments.

Experiments were performed using a load-time sequence that is shown in figure 2. The indenter was first loaded and then unloaded three times at a constant rate of loading. In order to insure that the contact was maintained between the specimen and the indenter, the load reached at the end of unloading is 10 % of the maximum load (i.e if the maximum load is 40 mN, the minimum is 4 mN, see figure 2). The multiple loadings and unloadings are necessary to check the reversibility of the deformation and thereby to make sure that the unloading data used for analysis purpose are mainly elastic. Every three unloading, the load was held constant for a period of 100 seconds ("hold" period) at 10 % of the peak value while the displacement was carefully monitored to establish the ratio of displacement produced by thermal expansion in the system.

The system is thermally regulated from its surrounding and from the room within which it is housed. The room is temperature controlled within 1°C. Following the "hold " period, the specimen was loaded for a fourth and final time, with another 50 second "hold " period during the peak load, to avoid plastic effects, and finally the specimen was fully unloaded.

The simultaneous measurement of the load and the displacement during the indentation allows a direct measurement of the elastic modulus and the hardness without direct imaging of the indentation using the method described by Oliver and Pharr [21, 22] and developed by Boudouka for ceramics [15].

The formula used to obtain the effective indentation modulus E_r, from the measured data is:

$$S=\frac{dP}{dh}=\beta\frac{2}{\sqrt{\pi}}\sqrt{A}E_r \quad (1)$$

Where S is the contact stiffness, P is the peak load, h is the displacement, A is contact area, and β is a correction factor (approximately equal to 1.034 for the Berkovich indenter [21]). For the indentation data studied in this paper, 90% of the unloading curve was fitted to the relation described by Oliver and Pharr [21, 22] used to determine the contact stiffness S.

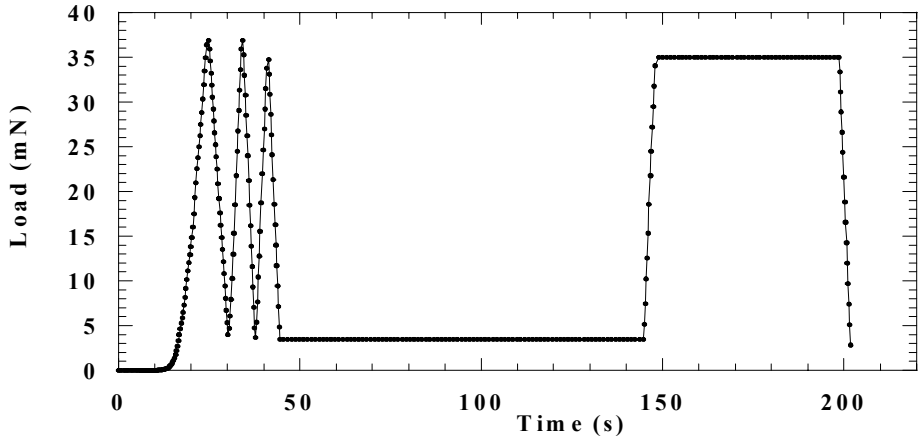

Figure 2. Typical load-time sequence

The equation (1), which follows an analytical solution derived by Sneddon [23], for the penetration of an elastic half space by an axisymmetric indenter of arbitrary smooth profile, relates the experimental stiffness and the contact area to the effective elastic modulus.
From the measurement of the effective modulus, Er, the elastic modulus of the material, E, is obtained using the equation:

$$\frac{1}{E_r}=\frac{1-\nu^2}{E}+\frac{1-\nu_i^2}{E_i} \quad (2)$$

where ν_i and E_i are the Poisson coefficient and the elastic properties of the diamond indenter and ν is the Poisson coefficient of the measured phase.

The methods used to compute the effective indentation modulus E_r, from the measured data, are published elsewhere [23].

2.2 Sample preparation

2.2.1 Pure Phase

The preparation of pure phase of Portland cement [tricalcium silicate (C_3S), dicalcium silicate (C_2S), tricalcium aluminate (C_3A), calcium aluminoferrite (C_4AF), C-S-H, or CH can be found in [24, 25]. The structure and the purity of the synthesised phases were checked by X-Ray diffraction.

The samples for the nanoindentation tests are pressed. The pellets are embedded in a low viscosity epoxy resin and polished by using, at first, abrasive papers of 400, 600 and 1200 grade and then diamond suspensions (6, 3, 1 and 0.25 μm). The quality of the surface of the sample (flatness, cracks and scratches) is an important parameter to insure the reproducibility of the small penetration of the indenter. The chemical homogeneity is checked by SEM/EDS (after carbon coating of the polished section). The pressure is used to densify the particles in order to obtain a polished section to check the chemical homogeneity and to minimise the standard deviation of the results of E (elastic modulus). It is more difficult to carry out these experiments on powders. The volume of

matter which is concerned for the nanoindentation test is about 5µm^3 (the order of magnitude of the volume analysed by the electron beam in SEM). In this case it is not necessary to have a large pellet of high bulk density but dense particles of a few millimetres are recommended.

2.2.2 Heterogeneous matrix. (cement paste and concrete)

This experimental technique is described in detail elsewhere [19] and summarised here ;

1) A mortar containing 33 % OPC type I, 10% ground sand, 10 % silica fume, 47 % of sand (< 1mm) is prepared at W/C = 0.2 and 1.4 % of polyphosphonate admixture is added to insure a good workability.
1) After 28 days, the samples are embedded in a low viscosity epoxy resin and polished as described previously.
2) A copper grid is pasted on the polished surface (this grid is commonly used as sample holder in transmission electron microscopy). The sample is coated with gold or gold palladium (same technique as for SEM preparation).
3) The grid is removed leaving its trace on the sample.
4) The quality of the sample is checked by SEM.
5) The nanoindentation is started by 2 indents separated by 50 to150 µm(depending on the sample). These indents correspond to a relatively important load, in order to leave a print, visible by optical microscopy SEM. These two indents are necessary to identify the area where the measurements are carried out, but the figures found for these 2 indents are not taken into account. We called them "locating indents".
6) Between these "locating indents", a few indents are carried out corresponding to a given distance (5 to 15 µm).
7) The sample is removed from the nanoindenter and the identification of the phases which have been indented, as well as their chemical analysis are carried out by SEM (EDS).

The grid helps to identify the right zone to be explored. The presence of the "locating indent" helps to locate the phases where the indents have been printed and allows their chemical analysis

2. RESULTS

3.1 Elastic modulus of the clinker phases

The elastic modulus of C_3S, alite, C_2S, belite, C_3A, C_4AF, are measured by nanoindentation at penetration depths of about 300 nm and 500 nm. Figure 3 presents the typical load-displacement curves at applied penetration of 500 nm for C_3S. For this penetration depth, corresponding to applied forces ranging between 40 mN and 50mN, this phase exhibits first an elastoplastic behaviour during the first loading, and then during the successive cycles an hysteresis loop occurs. No creep phenomenon is observed at constant force. The hysteresis behaviour corresponds to energy dissipation (damping phenomenon) probably due to a viscoelastic behaviour appearing after plastic deformation.

However, this effect can be neglected in order to calculate the elastic modulus (the elastic modulus is measured by using the last unloading curve). Table 1 shows the elastic moduli of the phases of Portland cement, measured at two depths of penetration. These values are an average of ten to twenty experiments and are calculated using an approximate Poisson's ratio of 0.3 for all constituents.

We checked that the samples were homogeneous as the elastic moduli values do not vary with the penetration depth. The elastic moduli are similar to each other in the range of 125 GPa to 145 GPa. The comparison of moduli between a pure C_3S phase and alite shows clearly that the influence of minor element included as solid solution in C_3S is not significant. The same conclusion stands for the pure C_2S and belite.The standard deviation of the measurement is about 10 %, except for C_2S and C_4AF. In the first case, this greater scatter can be explained by the polymorphic transformation

during the cooling generating microcracks in the matrix and in the second case by the presence of microcracks generated by the indenter during the first loadings.

Table 1. Elastic modulus of the clinker phases

	C_3S	alite	C_2S	belite	C_3A	C_4AF
Elastic modulus (GPa)	135	125	130	143	145	125
Standard deviation	7	7	20	10	10	25

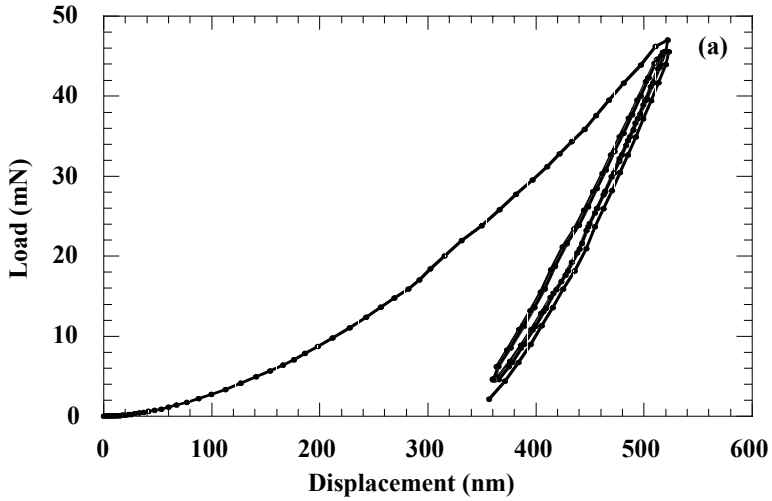

Figure 3. Load versus Displacement curve for C_3S

3.2 Case of calcium silicate hydrates

Figure 4 shows (as example) the load displacement curve for a C-S-H of C/S=1. In this case, creep occurs. The elastic moduli of C-S-H (C/S from 0.5 to 1.76) and CH are given in the Table 2.

Table 2. Elastic modulus as function as C/S for CSH

	CH	C-S-H C/S=0.5	C-S-H C/S=0.6	C-S-H C/S=0.7	C-S-H C/S=0.8	C-S-H C/S=1	C-S-H C/S=1.13	C-S-H C/S=1.2	C-S-H C/S=1.76
Elastic modulus (GPa)	34	22	19	24	24	28	34	29	28
Standard deviation	2	2	3	4	3	2	4	2	2

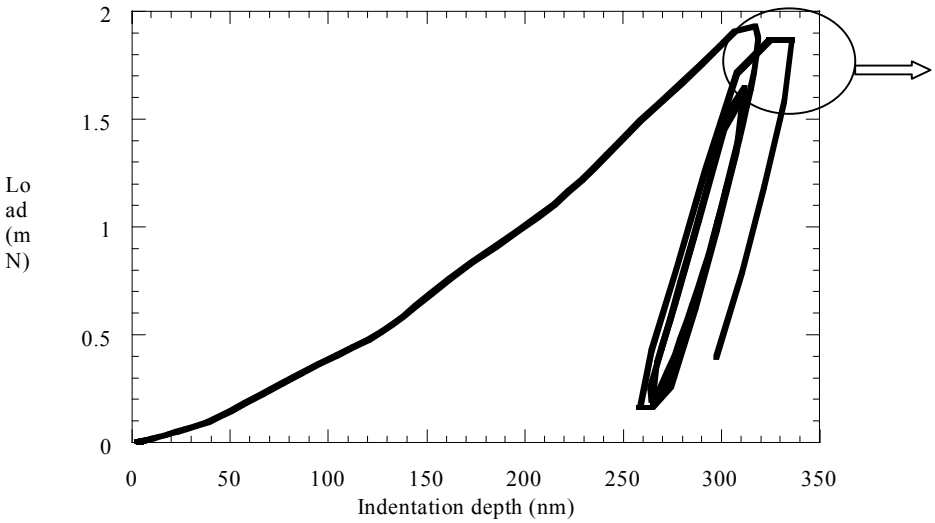

Figure 4. Load versus displacement curve for CSH of C/S=1

3.3 Case of heterogeneous sample, cement pastes

The micrograph (Figure 5) shows a polished section of a powder reactive concrete (PRC) sample (SEM, back scattered electrons). Particles of quartz aggregates, residual clinker, and cement paste are easily recognized.

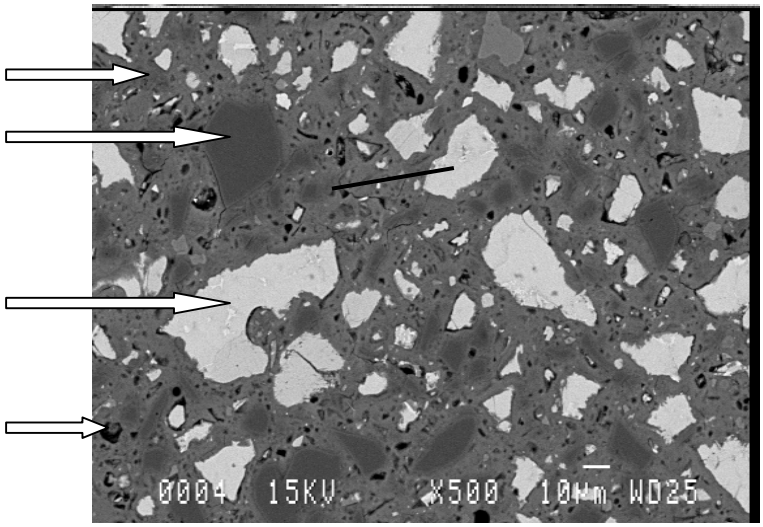

Figure 5. Powder reactive concrete (polished section, Backscattered electrons)
The straight line shows the explored area

The distance between two particles (quartz/residual clinker, quartz/ quartz or clinker/clinker) rarely exceeds 20 µm and consequently, the number of measurements in the paste is limited to 2 to 3. Table 3 shows, as an example, the results of the elastic moduli and the analysis by SEM (EDS) of the corresponding area.

Table 3. EDS analysis and Elastic modulus determination

Point	1	2	3	4	5	6	7
C/S ratio	2.45	2.2	0.85	1.50	1.34	0	0
Elastic modulus (GPa)	135	120	40	47	45	75	80

The points 1 and 2 correspond to the clinker, the points 6 and 7 correspond to the quartz. The points 3, 4, 5 correspond to the cement paste. Many linescans of this type have been carried out and can be summarized in table 4

Table 4. Elastic modulus in concrete , average

	Residual clinker	Cement Paste	Quartz aggregates
Elastic modulus (GPa)	100 to 140	30 to 45	70 to 90

3. DISCUSSION

It is difficult to find reliable figures for the elastic moduli of the constituents of cement (anhydrous or hydrate phases) in the literature

Granju [26] measured the elastic moduli of clinker on polished blocks. He found an elastic modulus for the clinker ranging between 60 and 300 GPa. The scatter of the results was due to the cracks introduced during the preparation of the sample.
Boumiz [27] measured the elastic modulus of compacted powder of C_3S by the acoustic method. He prepared cylindrical samples with a density of the same order as the density of C_3S grains (3.14g

/cm_2). He found that the elastic modulus of C_3S was equal to 117 GPa. that is consistent with the values obtained in the present work. There is also a good agreement between the values obtained by nanoindentation and those obtained at the macroscopic scale by other techniques such as resonance techniques [23]

The elastic modulus of Portlandite has been measured by Monteiro [28] and Wittman [29] and Beaudouin [30]. The figures obtained range from 35,2 to 48 against 34 GPa for nanoindentation measurement. The discrepancy could come from the porosity of the sample

In the case of concrete (table 3), there are together, quartz grains, residual clinker, cement paste, and some other constituents such as silica fume or fibers. Elastic moduli of pure C_3S, SiO_2, CH, C-S-H, are respectively 135GPa, 78GPa, 34GPa and between 22 and 34GPa depending on the C/S ratio of C-S-H. These values stand for a non-porous material and a decrease could be expected when the porosity increases.

In a cement paste (or C_3S paste) the range of the porosity extends from a few Angströms (for the gel pores) to a few microns for the capillary porosity. Consequently, in the volume concerned by the nanoindentation test (a few microns), it is possible to have some capillary pores. This could explain the low value of the elastic modulus obtained for some constituents.

The results obtained at the microscopic scale come from the measurement of the elastic properties of small particles (a few μm^3). At this scale and being given the method of the preparation of the sample, it is easy to check that the porosity of the particles can be taken at zero (the density of the particles close to the theoretical mass density of the compound). If the porosity was different from particle to particle, the standard deviation of the measurement would be very high.

The elastic modulus varies from 22 to 34 GPa for the CSH with a ratio C/S varying from 0.5 to 1.76 (Table 2) . The figure of 34 GPa is in agreement with the findings of Beaudoin et al [31] who did not highlight the variation of the elastic modulus with the ratio C/S of the CSH. This discrepancy is due to the lack of accuracy of the method of measurement (extrapolation to zero porosity of a result obtained by a static method)

In the case of concrete (table 3), the high moduli represent the location of the indent in quartz aggregate or in clinker. The low moduli represent the measurement in the cement paste. The elastic modulus is constant for the sample with a C/S varying from 0.8 to 1.9 (corresponding to inner or outer C-S-H, or a mixture of C-S-H and Portlandite) and higher than those obtained for pure C-S-H. Probably this phenomenon is due to the presence of fine silica intimately mixed with
C-S-H.

From these measurements, it is difficult to see a difference of elastic modulus versus the distance from an aggregate or a particle of clinker, and thus to evidence the presence of ITZ in this type of concrete.

4. CONCLUSIONS

The results found at the microscopic scale by nanoindentation show that:

1. The elastic moduli of C_3S, C_2S, C_3A, C_4AF, are similar and range between 125 GPa to 145 GPa. These results obtained at the microscopic scale by nanoindentation are in good agreement with those obtained at the macroscopic scale by frequency resonance technique.
2. The elastic modulus of C-S-H varies as a function of the ratio C/S from 22 to 34 GPa. The creep behavior of C-S-H has been shown.

The technique used to locate the indents in heterogeneous material allows us the identification of the area which has been indented and consequently, the nanoinentation can be applied to cementitious material to study in situ the mechanical properties of the cement or concrete matrix.

The results obtained by the nanoindentation technique with a sample of a hardened cement paste, show that the elastic moduli of the different constituents in the paste are in agreement with those obtained for the same constituents independently, provided the porosity of the particles is taken into account.

There is no significant difference of the elastic modulus between inner and outer C-S-H.
No evidence of a difference of the elastic modulus has been found close to the particles, and consequently the ITZ, if it exists in this case is less than 1 to 5 μm (for this type of material)

Associated to SEM and EDS analysis, the nanoindentation technique can be used as a "micro-mechanical probe" to scan the surface of hardened cement paste and to obtain information on i) the microstructure and mineralogy of such concrete. ii) the elastic modulus of the constituents of the cement "in situ", iii) the elastoplastic behavior and the occurrence of creep phenomenon iiii) the mechanical properties of the cement paste in UHPC and *Ductal*®.

REFERENCES

[1] P. Richard, M. Cheyrezy, Composition of reactive powder concretes, Cement and Concrete Research, 1992, 25, pp1501-1511

[2] M. Cheyrezy, V. Maret, L. Frouin, Microstructural analysis of RPC (reactive powder concrete), Cement and Concrete Research, 1995, 25, pp1491-1500

[3] Metal fibre concrete, cementitious matrix and premixes for preparing matrix and concrete, Patent WO 99/28267 (27 Nov 1998).

[4] S. Diamond, S. Mindness, F.P. Glasser, L.R. Roberts, J.P. Skalny, L.D. Wakeley (eds), Microstructure of cement-based system. Bonding and interfaces in cementitious materials", Proceedings Material Research Society Symposium, Boston,1994, vol 370,

[5] G. Prokopski, J. Halbiniak, Interfacial zone in cementitious materials, Cement and Concrete Research, 2000, 30, pp 579-583.

[6] M.D. Cohen, T-F. Lee, A. Goldman, A method for estimating the dynamic moduli of cement Paste Aggregate Interfacial zones in mortar, Proceedings Material Research Society Symposium, Boston,1994, vol 370, pp 407-412

[7] C.C. Yang, Effect of the transition zone on the elastic moduli mortar, Cement and Concrete. Research,1988, 289, 5, pp 727-736

[8] S. Igarashi , A. Bentur, S. Mindness,Characterization of the microstructure and strength of cement paste by microhardness testing, Advances in Cement Research, 1996, 8, 30, pp 87-92

[9] S. Igarashi, A. Bentur, S. Mindness, Microhardness testing of cementitious materials, Advanced Cement Based material, 1996, 4, pp 48-57 .

[10] P. Trtik, J.M. Bartos, Micromechanical properties of cementitious composites, Materials and structures, 1999, 32, pp 388-395.

[11] V.V. Deshmukh, V.H. Hargrave, Rapid prediction of early strength of OPC by micro hardness of clinker phases, Indian cement review, 1989, 36, pp 35-39

[12] P.Trtik, P.Bartos, Nanotechnology and concrete : what can we utilise from the upcoming technologies, Cement and Concrete, Trends and Challenge edt by J. Boyd , S. Mindness, J. Skalny pbd by the American Ceramic Society, 2002, pp 109-120

[13] M.R.VanLandingham, J.S.Villarubia, W.F.Guthrie, G.F.Meyers, Nanoindentation of polymers : an overview, Macromolecular Symposia, Wiley-VCH Verlag GmbH, Tsukruk, V.V. and Spencer N.D., Editors, 2001, pp 15-43.

[14] M. Tazaki, M. Nishibori, K. Kinosita, Ultra-microhardness of vacuum deposited films, results for silver, gold, copper, MgF2, LiF and ZnS, Thin solid films, 1978, 51, pp 13-21

[15] L.Boudoukha, Etude par nanoindentation de l'effet de l'implantation ionique sur le comportement mécanique de céramiques, Ph.D. Thesis, INSA-Lyon 1, 1996

[16] ASTM E 92 Standard test method for Vickers Hardness of metallic compounds.

[17] ASTM E 384 Standard tests method for microhardness of materials

[18] W. Zhu, P.J.M. Bartos, Application of depth-sensing microindentation testing to study of interfacial transition zone in reinforced concrete, Cement Concrete Research, 2000, 30, pp1299-1304

[19] K. Velez, F.Sorrentino, Nanoindentation: a complementary technique for microscopy to study the microstructure of concrete, International conference on cement microscopy, Albuquerque (May 2001).pp 272-286
[20] K. Velez, F. Sorrentino, Characterization of cementitious materials by nanoindentation, Kurdowski symposium, Science of cement and concrete , Krakow, 2001, pp 67-78
[21] W.C. Oliver, G.M. Pharr, An improved technique for determining hardness and elastic modulus using load and displacement sensing indentation experiments, Journal of Material Research, 1992, 7, pp1564-1583
[22] W.C. Oliver, G.M. Pharr, On the generality of the relationship among contact stiffness, contact area and elastic modulus during indentation, Journal of Material Research, 1992, 7, pp 613-617
[23] I.N. Sneddon, The relation between load and penetration in the axisymmetric Boussinesq problem for a punch of arbitrary profile, International Journal Engineering Science, 1967, 3 , pp 47-57
[24] K.Velez, S. Maximilien, D.Damidot, G. Fantozzi, F.Sorrentino, Determination of elastic modulus and hardness of pure constituents of Portland cement clinker, Cement Concrete Research, 2001, 31, pp 555-561.
[25] K. Velez, S. Maximilien, D. Damidot, G. Fantozzi, F. Sorrentino, Determination of elastic modulus and hardness of pure constituents of Portland cement, Cement and Concrete Research To be published (2002).
[26] J.L. Granju, Modélisation des pâtes de ciments durcies: caractérisation de l'état d'hydratation, lois d'évolution de la résistance en compression et du module de déformation longitudinale, PhD. thesis, Université Paul Sabatier de Toulouse, France (1987).
[27] A.Boumiz, Etude comparée des évolutions chimiques et mécaniques des pâtes de ciment et mortiers à très jeune âge, PhD. thesis, Université Denis Diderot – Paris 7, France,1995
[28] P.J.M. Monteiro, C.T. Chang, The elastic moduli of calcium hydroxide, Cement and Concrete Research, 1995, 25, 8, pp 1605-1609
[29] F.H. Wittmann, Estimation of the modulus of elasticity of calcium hydroxide, Cement and Concrete Research, 1986, pp 971-972
[30] J.J.Beaudouin, Comparison of mechanical properties of compacted calcium hydroxide and Portland cement pastes systems, Cement Concrete research, 1983, 13, pp 319-324
[31] J.J.Beaudouin, R.F. Feldman, J.Baron, M. Conjeaud , Dependence of degree of silica polymerization and intrinsic mechanical properties on C/S ratio, 8th International Congress on the Chemistry of cement, Rio de Janeiro, 1986, theme 2, vol III, pp 337-342

APPLICATION OF NEW FINE PARTICLE CHARACTERIZATION TECHNIQUES TO CONCRETE DURABILITY

R.I. Malek

Director, Particle Characterization Laboratory, Materials Research Institute, The Pennsylvania State University, 109 MRL Building, University Park, PA 16802, USA. E.mail: rqm@psu.edu

ABSTRACT

Concrete durability as well as its failure is directly related to the physical nature of the fine particle fraction. Concrete technology has become so sophisticated that the simple techniques are no longer suitable for cement particle characterization. The problem becomes more complicated with blended cement where a variety of particles with diverse properties are mixed together. The unique particle characterization laboratory at Penn State University compiles a variety of state-of-the-art instruments for complete particle characterization. It includes atomic force microscope, zeta potential analyzers (Zeta PALS and DELSA), particle size distribution (Micron Air Jet sieve, centrifugal, wet and dry laser diffraction and ultra fine particle size analyzers), BET and mercury intrusion porosimetery, rheometery, thermal analysis (DSC, DTA, TGA and TMA). The application of these techniques to cement and concrete has led to better understanding of the physical properties of cementitious particles. The purpose of this paper is to present the state-of-the-art capabilities in fine particle characterization techniques and their applications to solve durability problems.

1. INTRODUCTION

Particulate material in concrete plays a significant role in defining its durability. Concrete durability as well as its failure is directly related to the physical nature of the fine particle fraction. The current techniques of cement particle characterization are no longer appropriate for the modern performance of concrete. Concrete technology has become so sophisticated that the simple techniques are no longer suitable for cement particles characterization. The problem becomes more complicated with blended cement where a variety of particles with diverse properties are mixed together. The unique particle characterization laboratory at Penn State University compiles a variety of state-of-the-art instruments for complete particle characterization. The application of these techniques to cement and concrete has led to better understanding of the physical properties of cementitious particles.

2. THE PARTICLE CHARACTERIZATION LABORATORY FOR CEMENT AND CONCRETE APPLICATIONS

The Particle Characterization Laboratory at Penn State University is a core facility for physical characterization of fine particles. It includes:

- Digital Instruments multimode atomic force microscope.
- Brookhaven Zeta PALS zeta potential analyzer by electrophoretic light scattering.
- Coulter DELSA 440SX zeta potential analyzer.
- Electroacaustophoresis zeta potential analyzer.
- Horiba CAPA 700 centrifugal sedimentation particle size analyzer.
- Malvern Mastersizer S-wet and dry laser diffraction

- MicroTrac UPA 150 ultra fine particle size analyzer.
- Hosokawa Micron Air Jet sieve.
- Micromeritics GIMINI 2375 surface area analyzer.
- Micromeritics Autopycnometer 1320
- Pascal 140, and 440 Mercury Intrusion Porosimeter.
- CSL TA Instruments Rheometer
- TA Instruments Thermal Analysis system.
    - Differential Scanning Calorimetery (DSC)
    - Differential Thermal Analysis (DTA).
    - Thermogravimetric Analysis (TGA)
    - Simultaneous DSC/TGA – DTA/TGA (SDT).

2.1 The Atomic Force Microscope

The atomic force microscope (AFM) is operated in such a way that a thin tip (mounted on a cantilever) scans the surface of a sample. The attractive and repulsive forces between the tip and the surface move the cantilever vertically for a distance proportional to these forces, and in turn, on surface structure. This movement is recorded through the deflection of a laser beam (centred on the tip of the cantilever) on a mirror and piezoelectric elements. An image of the surface structure of the sample can be obtained by the signals sent from the piezoelectric elements. AFM can be used to investigate the fabric of cement and clinker surfaces.

The AFM was used to investigate the degree of coverage of a curing compound on the surface of cement particles. The contact mode of Scanning Probe Microscope (SPM), a new development in the AFM technology was used [1, 2]. Fresh cement particles were spread on a freshly cleaved mica surface. The mica disc was then placed together with the AFM scanning head inside a glove box flooded with nitrogen gas to prevent the effect of moisture. The curing compound was sprayed over the cement particles and the mica disc was placed on the scanning head of the microscope. The microscope was operated over an area of 25 μm x 25 μm. The image, shown in Figure 1, was obtained for the surface of a single particle. The colour hue of the image was arbitrarily chosen to reflect a better contrast. It is noticed that the curing compound is concentrated in certain areas. That this preferential distribution is related to the heterogeneous surface composition is the subject of an ongoing investigation.

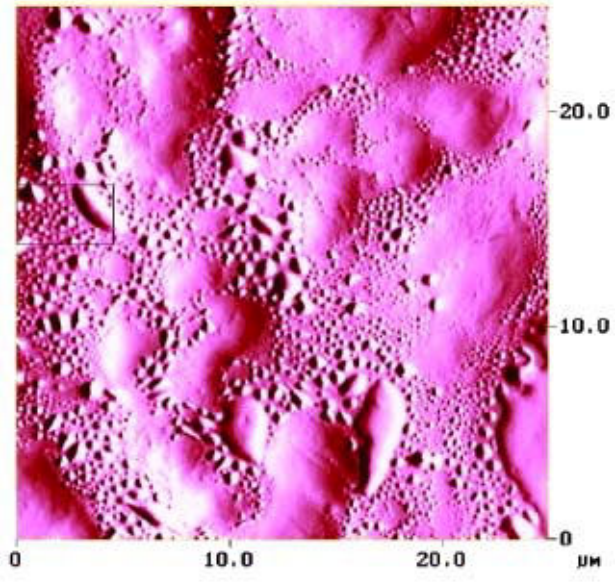

Figure 1. AFM image of curing compound over the surface of a single cement particle.

2.2 Zeta PALS Zeta Potential Analyzer

Modern instruments for the determination of zeta potentials by Electrophoretic Light Scattering (ELS) are very easy to use and much more accurate than traditional microelectrophoresis. They have achieved a widespread use in many research and applied fields. Their ultimate use is for materials with very low mobility such as cementitious materials. The low mobility of cementitious material is due to the compression of Stern double layer as a result of high ionic strength of th4e medium. The Brookhaven Zeta PALS is used. The Zeta PALS determines zeta potential using Phase Analysis Light Scattering: a technique that is up to 1,000 times more sensitive than traditional light scattering methods. The Zeta PALS utilizes phase analysis light scattering to determine the electrophoretic mobility of charged, colloidal suspensions. Unlike its cousin, Laser Doppler Velocimetry (LDV) (sometimes called Laser Doppler Electrophoresis (LDE)); the PALS technique does not require the application of large fields which may result in thermal problems because in the measurement of phase shift, the particles need only to move a fraction of their own diameter to yield good results. In this technique, an alternating current is applied and the amplitude of oscillation of particles is measured, which is related to the composition of the double layer and zeta potential. In salt concentrations up to 3 molar and with electric fields as small as 1 or 2 V/cm enough movement is induced to get excellent results. In addition, the Autotracking feature compensates for thermal drift. The excellent agreement of the three runs in experiments involving cementitious materials is an evidence of excellent reproducibility.

The Zeta PALS was used to study the stabilization of expansive clays. Expansive soils cause annual damage to manmade structures resulting in an estimated $9 billion in losses. Lime and Portland cement were used as stabilisers in the mid-1930’ and expanded with many applications in World War II. Use of cement as a treatment of expansive clay soils continues on a limited basis today. Lime treatment was first used for this purpose by the Texas Highway Department in the mid-1940’s. Soil stabilisation products are available on the market today. Some of them work on the principle of substitution of a cationic species in the clay lattice for a sodium ion. The cationic species is generally selected such that its radius of hydration is less than that of the sodium ion, hence resulting in less swelling when the clay comes in contact with a foreign fluid. More recently, polymers containing 400 to 7500 cationic sites are used. In order for the polymer to “desorb” from the clay, all of these cationic sites must simultaneously be displaced. The probability of this occurring is negligible, hence stabilising the soil. The disadvantage of these stabilisers is due to the physical size of the molecule preventing its migration through the formation pores. It is crucial that the surface charge of the soil be adjusted for maximum interactions with the stabilisers. The Zeta PALS was used to determine the isoelectric point (point of zero charge) of stabilised clay (Figure 2).

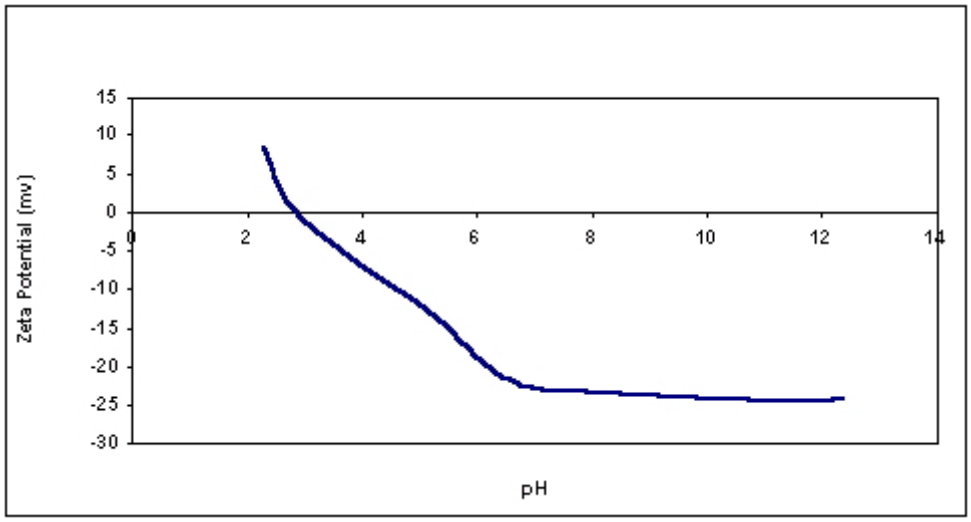

Figure 2. The change in zeta potential as a function of pH of stabilized clay.

2.3 Coulter DELSA 440SX Zeta Potential Analyzer

The DELSA (Doppler Electrophoretic Light Scattering Analyzer) analyzes data from 4 angles (7.5°, 15°, 22.5°, and 30°). The simultaneous multi-angle analysis simplifies data interpretation by giving information similar to that obtained with consecutive measurements made at different electric field strengths on a single angle instrument. It also distinguishes between particle charge heterogeneity and diffusion effects over a wide range of particle sizes. The instrument is automated and provides a simple analysis which can detect small charges. It also measures particle size distribution. The DELSA zeta analyzer is particularly useful in studying the changes that take place during the hydration of blended cements.

2.4 Electroacoustophoresis Zeta Potential Analyzer

Electroacoustic effects are defined as the generation of electric fields by sound waves or conversely, the generation of sound waves by electric fields. An alternating electric field is applied at a single frequency of about 1MHz. The generated electroacoustic signals are received by means of a dip-type probe placed in direct contact with the sample. It has been demonstrated that the electroacoustic signals are related to both the zeta potential and the size of particles of the colloidal suspension. The major advantage of the electroacoustics over the electrokinetic and particle sizing methods is that the technique does not involve the passage of light through the sample. The use of sound waves instead of light means that optical clarity of the sample is not required, hence concentrated suspensions (such as cement slurries) may be studied in their original formulations i.e. without dilution. One other advantage is the ability to analyze very large particles that may otherwise cause opacity in light scattering techniques.

The electroacoustic technique was used to study the variation of surface charge of silica fume particles as a function of hydration time. Paste containing 35% by volume of silica fume in saturated lime was prepared. The paste was left to hydrate in the electroacoustic sample holder. At designated times, the sample holder was placed in the electroacoustic device and an alternating electric field is applied at a single frequency of about 1MHz. The generated electroacoustic signals are received by means of a dip-type probe placed in direct contact with the sample. The zeta potential of silica fumes particles (before mixing) was found to be –24mv. The zeta potential of the mixture shows a sharp change to more positive potentials during the first few minutes of reaction due to adsorption of Ca++ ions on the surface particles (Figure 3). Then a slight decrease toward less positive potentials at 1 hour is noticed, due to the chemisorption of OH^- ions and the start of hydrolysis process. This is followed by a gradual increase to reach a plateau at 3 hours.

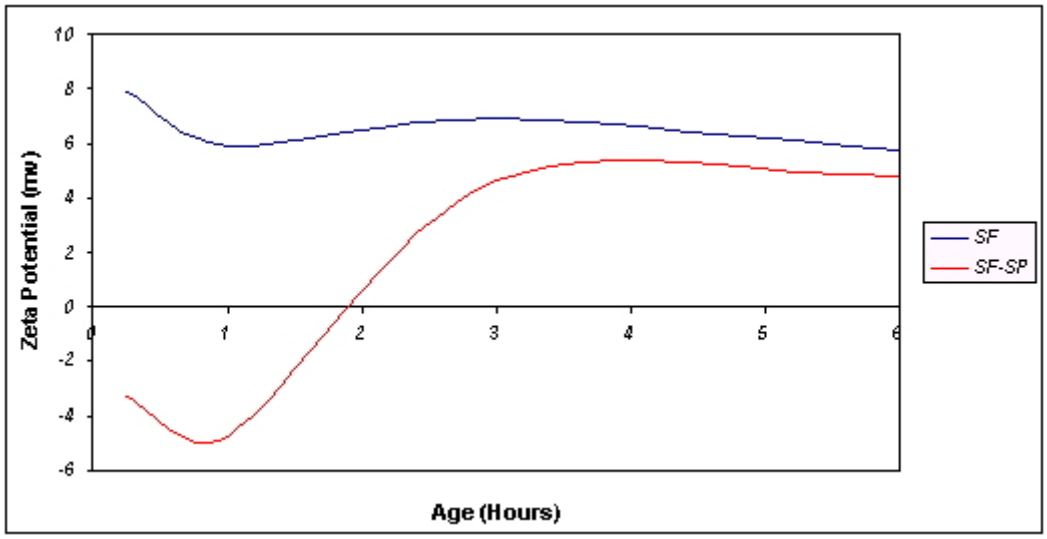

Figure 3. Electroacoustic Zeta potential of silica fume/lime mixture with and without superplasticizer.

The zeta potential and electrophoretic mobility of the superplasticized mixture (sulfonated naphthalene-formaldehyde condensate) show that the surfaces of superplasticized particles acquire an initial charge (Figure 3). This is attributed to the adsorption of superplasticizer molecules on the surface of particles. The sulfonated naphthalene-formaldehyde condensate molecule has a strong electrophilic sulfonate group which allow the hydrophobic organic chain to adhere to the particle's surfaces with $SO3^-$ group projecting outwards. This leads to an increase in the negative charge of the particles. The negative zeta potential (and mobility) of the superplasticized silica mixtures decreases gradually then converts to a positive charge and resumes the normal course of change as the pastes without superplasticizer. The conversion to positive charge is due to the hydrolysis of superplasticizer molecules under the effect of the strong alkaline medium and continuous conversion to CSH gel.

2.5 Particle Size Distribution

Over the past two decades, the development of miniaturized computers and monochromatic laser light sources has prompted particle size distribution analysis to a sophisticated level involving mathematical modelling and statistical analysis. The equipment design has made the analysis rapid and routine provided that the material being analyzed adheres to certain assumptions regarding particle morphology and optical characteristics. The particle size distribution techniques are divided into two categories: the light scattering methods and the sedimentation method. Almost all the zeta potential analyzers that use light scattering can also be used for particle size distribution. In addition, other light scattering equipment is specifically dedicated for particle size distribution. These include:

(1) Malvern Mastersizer S- wet and dry laser diffraction particle size analyzer

The mastersizer has the advantage of analyzing dry powders which have the ability of fast agglomeration when placed in contact with liquid medium. It analyses particle sizes up to 900mm.

(2) MicroTrac UPA 150 ultra fine particle size analyzer

The MicroTrack has the advantage of analyzing very fine particles in the nanometer range.

(3) Horiba CAPA 700 centrifugal sedimentation particle size analyzer

The method is based on the sedimentation of particles (under the influence of centrifugal force) in a liquid medium, optical transmission and application of Stokes law. The method assumes spherical morphology of the particles.

Cement particles have a lognormal distribution curve and acquire a non spherical shape. The shape factor can be derived by comparing the average particle diameter from the two techniques, light scattering and sedimentation. The principle is to determine the divergence of the particle shape from the sphericity assumed by the sedimentation technique. Therefore, a shape factor can be derived from the ratio of average diameter from the light scattering to that from the sedimentation (1). The shape factor is 1 for a sphere and increases from this value with increasing divergence from sphericity.

2.6 Particle Classification and Analysis

Separation of fine particles into size fractions is an important aspect of research and development in cement and concrete. We utilized the Hosokawa Micron Air Jet sieve in which the particles are separated into size fractions down to 5 μm fraction. These studies help understand the grindability of different components of the clinker. Particle surface area is determined with the 5-point BET nitrogen adsorption with surface area analyzer. The true density of particles, as determined by helium pycnometer, help to understand the internal porosity of cementitious particles and its effect of hydration and performance. The internal porosity and pore size distribution of cementitious particles are determined with Pascal 140, and 440 Mercury Intrusion Porosimeter. In this technique the intrusion data from the low pressure stage (140 MPa) and high pressure stage (440 MPa) are

combined. The packing density of particles is used to calculate the internal porosity of particles. In addition, rheometer is used to assess the rheological properties of pastes.

2.7 Thermal Analysis

Thermal analysis instruments are very useful in obtaining quantitative data on components of the hardened pastes. An example is obtaining quantitative data on gypsum, hemihydrate and ettringite using DSC. The difficulty arises from the fact that their endothermic peaks are superimposed. We can omit the ettringite peak by methanol treatment (Figure 4) and we can use hermetic sample pan to separate the hemihydrate from the dehydrate peaks (Figure 5).

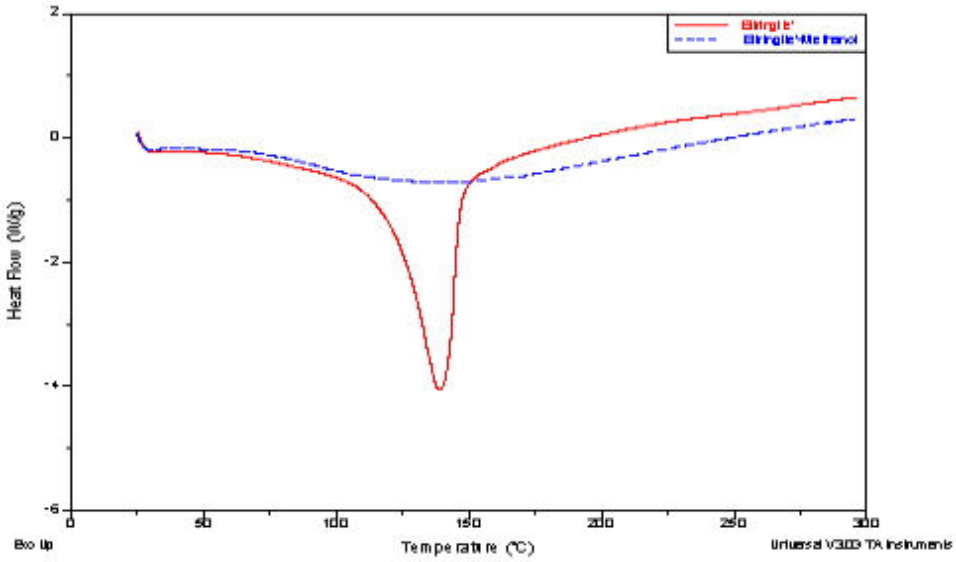

Figure 4. An example of removing ettringite peak using methanol treatment.

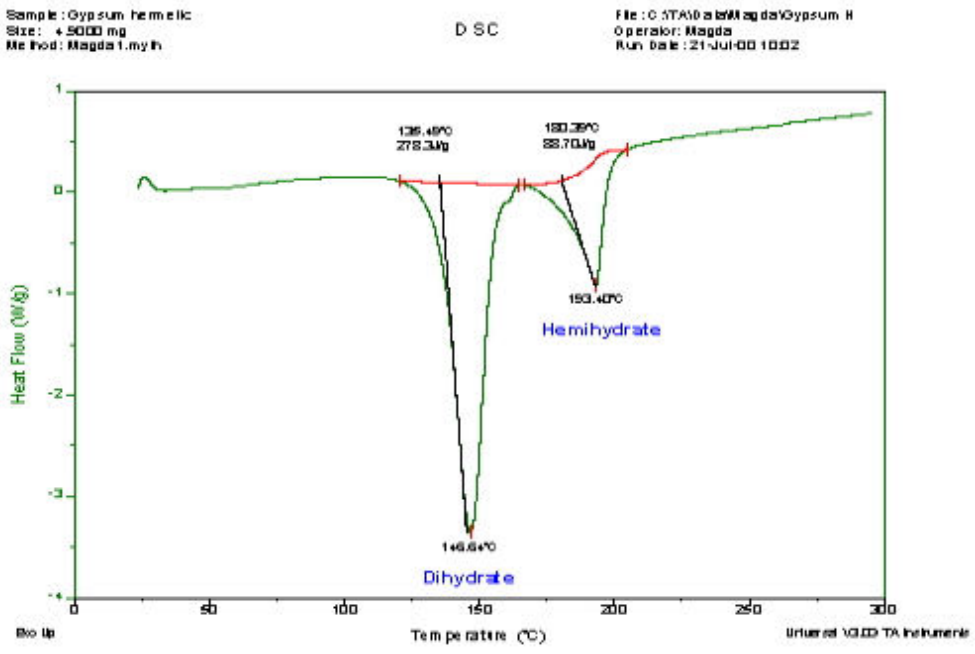

Figure 5. High resolution DSC using hermetic pan.

3. CONCLUSIONS

New particle characterization techniques offer a unique opportunity in the area of cement and concrete applications. They include: atomic force microscope, zeta potential analyzers (Zeta PALS and DELSA), particle size analyzers (Micron Air Jet sieve, centrifugal, wet and dry laser diffraction

and ultra fine particle size analyzers), BET and mercury intrusion porosimeters, theometers, and thermal analysis instruments (DSC, DTA, TGA and TMA). The application of these techniques to cement and concrete can lead to a better understanding of the physical properties of cementitious particles. The information gained from such analyses is a significant step towards joining the research community in exploring fine particle characteristics, which will be crucial in cement and concrete technology.

REFERENCES

[1] Hemunghaus, S., A. Fery and D. Reim, Ultramicroscopy, 69, p.211 (1997).

[2] Xu, L., A. Lio, J. Hu, D.F. Ogletree, and M. Ssalmeron, J. Phys. Chem. B, p. 102 (1998).

[3] (Allen, T., “Particle Size Measurement,” Chapman and Hall, London (1990).

ELECTROACOUSTOPHORESIS OF CEMENT AND FLY ASH PASTES

R.I. Malek[1] and M.N. Salama[2]

Materials Research Institute, The Pennsylvania State University, 109 MRL Building, University Park, PA 16802, USA. E-mail: rqm@psu.edu, and mns3@psu.edu.

ABSTRACT

The purpose of this paper is to report on the application of a new technique that studies the changes in surface charge of cement and fly ash particles during hydration. The new technique is superior to other techniques in that concentrated suspensions (such as cement slurries) may be studied in their original formulations i.e. without dilution. The mechanism of hydration was monitored by x-ray diffraction at various ages. Solid state ^{29}Si magic angle spinning nuclear magnetic resonance spectroscopy (MAS NMR) was used to characterize the detailed structure of hydration products after 28 days. The new technique represents a step towards exploring the actual changes in surface charge during hydration.

1. ELECTROACOUSTICS

Electroacoustic effects are defined as the generation of electric fields by sound waves or conversely, the generation of sound waves by electric fields [1]. The former effect is termed the Ultrasonic Vibration Potential (UVP), while the latter is known as the Electronic Sonic Amplitude (ESA). The UVP was first investigated in 1933 by Debye [2] in an attempt to determine the hydration number of ions in electrolyte solution. Only in 1985 was the ESA was discovered [3]. It is based on the principal that when an alternating electric field is applied to a suspension, the particles move backwards and forwards between the electrodes because of their surface charge. This motion generates pressure changes which propagate in the medium as a sound wave. The UVP and ESA effects have been shown theoretically by Obrien [1, 4, and 5] to be linked by the reciprocal relation:

$$ESA = QK^{*}UVP \tag{1}$$

where the ESA is in Pascals per unit field strength (Vm^{-1}), the UVP is in volts per unit pressure gradient ($Pa.m^{-1}$), Q is an instrument constant, and K* is the complex conductivity of the suspension. By the late 1980's, and early 1990's, Obrien et al demonstrated that the electroacustic signals are related to both zeta potential and the size of the particles [6]. By 1995, a new instrument has been commercialized which enabled the estimation, simultaneously, of the zeta potential and size distribution of suspended particles [6]. The major advantage of the electroacoustics over the electrokinetic and particle sizing methods is that the technique does not involve the passage of light through the sample. The use of sound waves instead of light means that optical clarity of the sample is not required, hence concentrated suspensions (such as cement slurries) may be studied in their original formulations i.e. without dilution. One other advantage is the ability to analyze very large particles that may otherwise cause opacity in light scattering techniques.

Several investigators have determined the zeta potential of cementitious materials by the traditional microelectrophoresis [7, 8, 9, and 10] or the more advanced light scattering techniques [11]. These

techniques require infinitely diluted suspensions. Infinite dilution of cementitious materials reduces the ionic strength and expands the double layer giving rise to interfacial properties that are totally different from the real situation in pastes. The electroacoustic technique is applied on highly concentrated suspensions where the interfacial properties of particles are not different from the real situation in pastes.

2. EXPERIMENTAL

Type-I cement (Keystone cement, Pennsylvania, USA), silica fume, and class-F fly ash (Pennsylvania Power and Light Co., USA) are used in this study. Pastes containing 35% by volume of cement in water, silica fume in saturated lime and fly ash in saturated lime were prepared. The pastes were left to hydrate in the electroacoustic sample holder. At designated times, the sample holder was placed in the electroacoustic device and an alternating electric field is applied at a single frequency of about 1MHz. The generated electroacoustic signals are received by means of a dip-type probe placed in direct contact with the sample. The technique has been used to study the changes in surface charge, as a function of hydration time, of concentrated cement, silica fume/lime, and fly ash/lime slurries. A diagram of the electroacoustic device is presented in Figure 1.

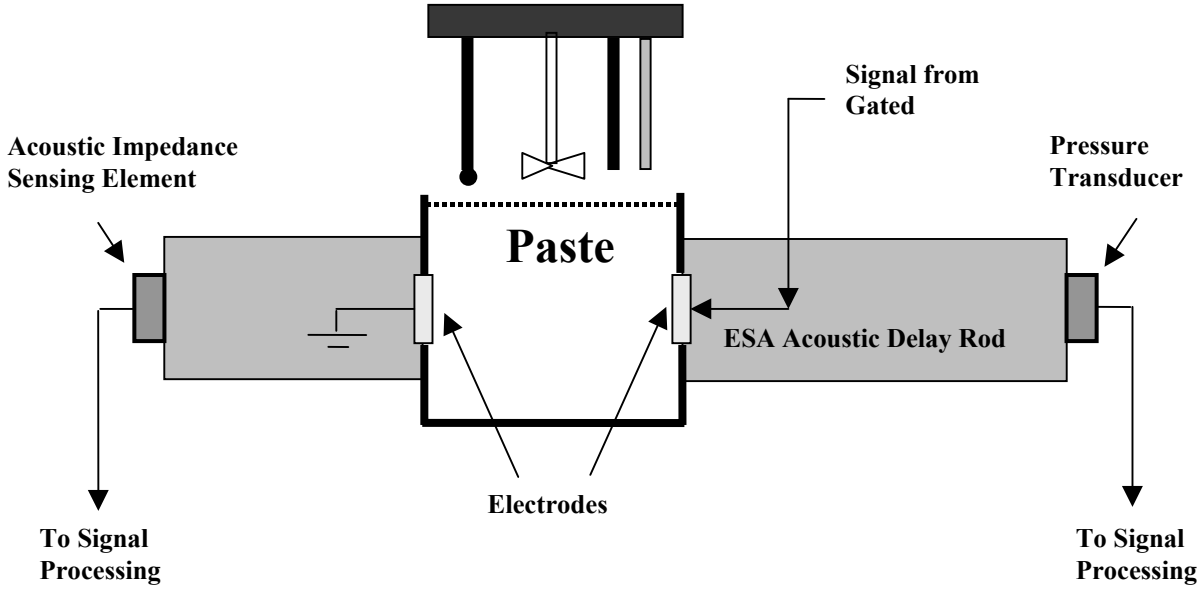

Figure 1. Electroacoustic device

X-ray diffraction was used to monitor the phase changes in hydration products as a function of time. A computerized search/match program was used to identify the nature and quantity of each hydration product. The solid state ^{29}Si magic angle spinning nuclear magnetic resonance spectroscopy (MAS NMR) was used to characterize the detailed structure of hydration products after 28 days. The NMR spectra were referenced to tetramethylsilane (TMS). The signals due to ^{1}H were decoupled so that the signals due to Si-O-Si and Si-O-Al connectivities are not affected by the proton signals.

3. RESULTS AND DISCUSSION

The zeta-potential of cement, silica fumes and fly ash particles (before mixing) were found to be: -10mv, -24mv and -27mv, respectively. The zeta-potential of the cement/water, silica fume/lime, and fly ash/lime mixtures show a sharp change to more positive potentials during the first few minutes of reaction due to adsorption of Ca^{++} ions on the surface particles (Figures 2, 3 and 4). The mixtures containing cement/water and silica fume/lime show a slight decrease toward less positive

potentials, at 24 hours and 1 hour, respectively, due to the chemisorption of OH^- ions and the start of hydrolysis process. This is followed by a gradual increase to reach a plateau at 72 hours and 3 hours for cement and silica fume, respectively. The mobility and zeta potential show minor changes afterwards.

The x-ray patterns of the solid reaction products of cement after 7 days and silica fume after 6 hours show the presence of portlandite crystals and CSH as evidenced by the broad peaks at 3.04 Å, 2.97 Å, and 1.83 Å.

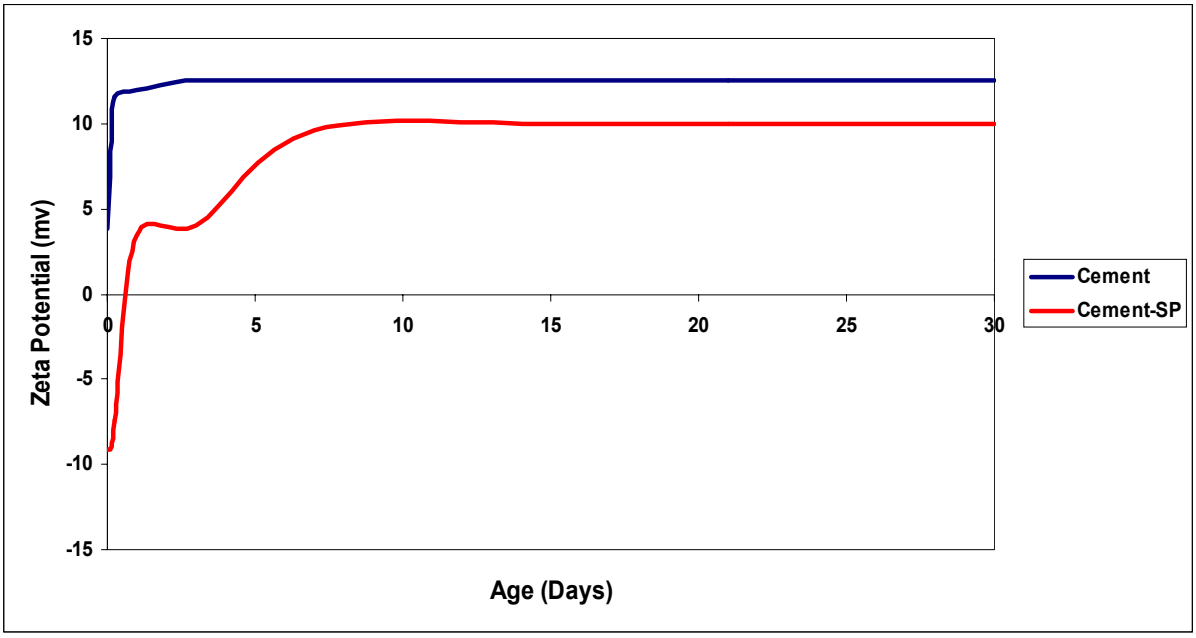

Figure 2. Electroacoustic zeta potential of cement with and without superplasticizer.

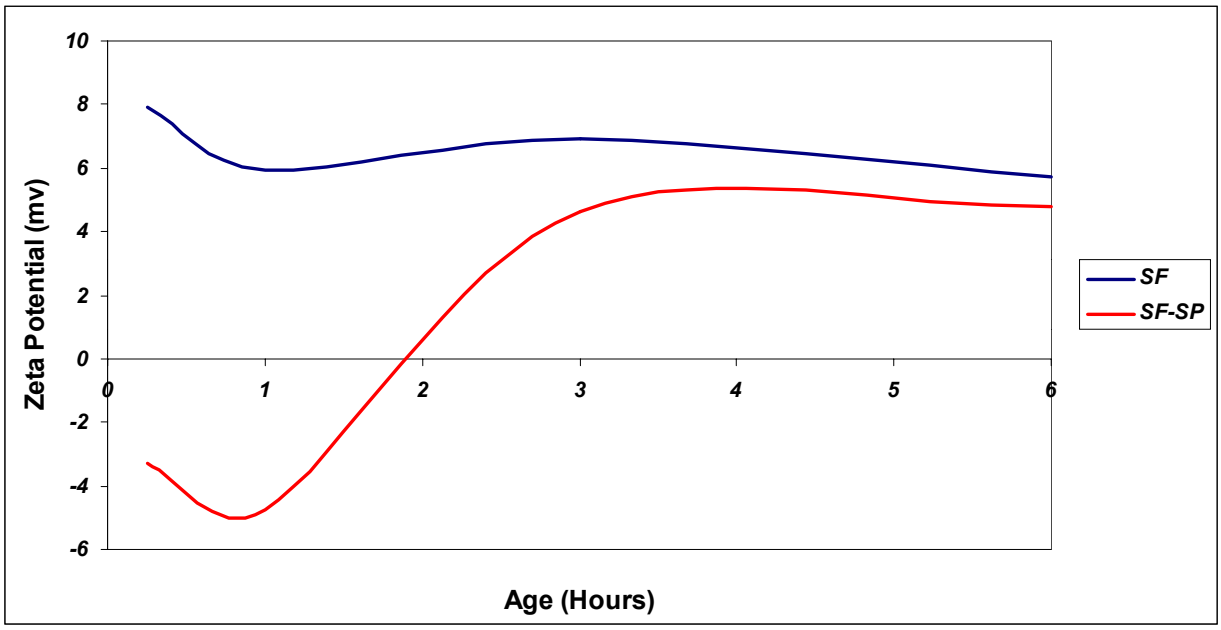

Figure 3. Electroacoustic zeta potential of silica fume/lime mixture with and without superplasticizer.

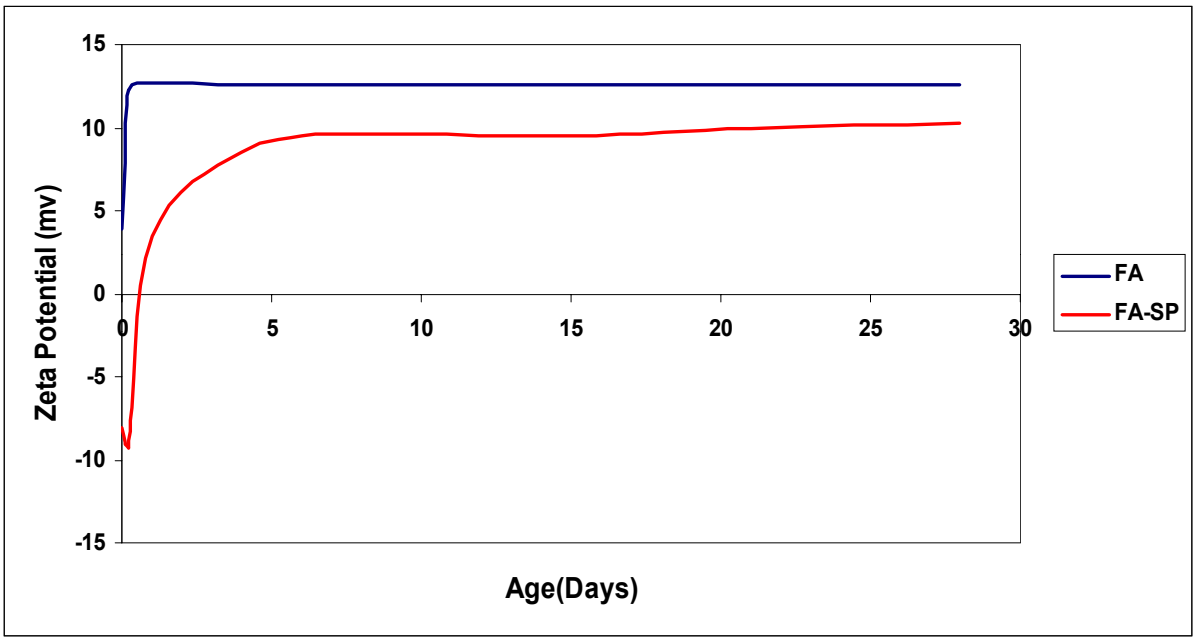

Figure 4. Electroacoustic zeta potential of class F fly ash/lime mixture with and without superplasticizer.

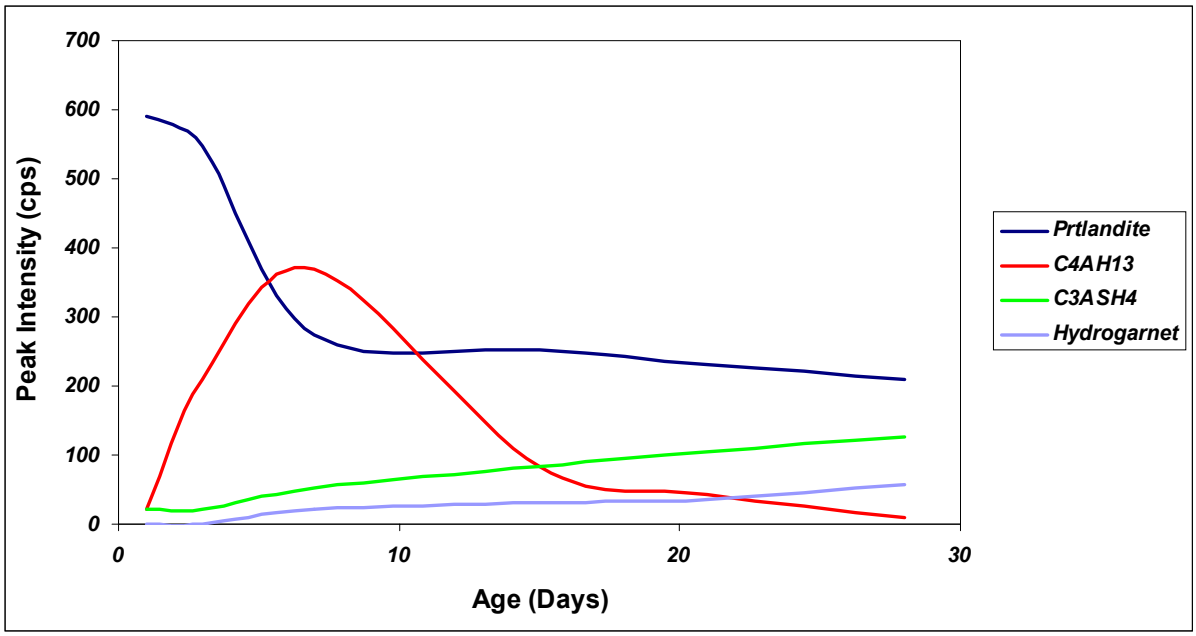

Figure 5. Variation of x-ray peak intensity vs. time of class F fly ash/lime mixture.

The zeta potential of the fly ash/lime mixtures show the initial sharp change to more a positive potential during the first few minutes due to adsorption of Ca^{++} ions on the surface particles (Figure 4). It does not, however, show the subsequent decrease toward less positive potentials, and the change in zeta potential reaches a plateau which continues unchanged afterwards.

The zeta-potential and electrophoretic mobility of the superplasticized mixtures (sulfonated naphthalene-formaldehyde condensate) show that the surfaces of superplasticized particles acquire an initial negative charge (Figures 2, 3, and 4). This is attributed to the adsorption of superplasticizer molecules on the surface of particles. The sulfonated naphthalene-formaldehyde

condensate molecule has a strong electrophilic sulfonate group which allow the hydrophobic organic chain to adhere to the particle's surfaces with SO_3^- group projecting outwards. This leads to an increase in the negative charge of the particles. The negative zeta-potential (and mobility) of the superplasticized silica mixtures decrease gradually then convert to a positive charge and resume the normal course of change as the pastes without superplasticizer. The conversion to positive charge is due to the hydrolysis of superplasticizer molecules under the effect of the strong alkaline medium and continuous conversion to CSH gel.

The x-ray analysis of Fly ash/lime mixture (Figure 5), show that Portlandite continues to diminish with time. C_4AH_{13} forms within the first few days of hydration and continues to increase up to 7 days then it converts to the more stable phases, hydrogarnet and C_3ASH_4 (an AFm phase). CSH is detected at 3 days and continues to increase in intensity. The mechanism of hydration can be explained as follows. The first step is the adsorption of Ca^{++} ions from solution on the surface of the negatively charged fly ash particles. This is immediately followed by an attack on the Al_2O_3-SiO_2 framework in the glassy phase of the fly ash by the OH^- ions resulting in the breakdown of the Al-O and Si-O bonds. The breakdown of the aluminosilicate frame work will release alkali ions (K^+ and Na^+) into solution. The immediate product is likely to be an amorphous material with K^+ and Na^+ as the dominant cations. The abundant supply of Ca^{++} and the lower solubility of CSH are an indication that the CSH gel is the first intermediate product formed. Afterwards, due to the removal of Ca^{++} and depression of solubility of lime under the effect of increasing alkali concentration in solution a low Ca/Si ratio CSH is expected to form. The addition of Al ions in solution will promote the formation of C_4AH_{13}. This is an intermediate metastable compound which later converts to hydrogarnet and AFm phase (C_3ASH_4). Sersale [14] argues that there exists a strong dependency of the breaking down of the glass phase on the alkalinity of solution which becomes significant only after few days which may explain the early incubation period in fly ash hydration. This incubation period is decreased with temperature due to increased solubility of the glass. In addition, the reactivity of fly ash/lime mixtures increases by optimization of the fine particle range, due to two factors: enlargement of the reaction surface area and the enrichment of chemically active constituents. The relative concentrations of CaO, SiO_2 and Al_2O_3 define the nature of hydration products formed. Therefore, low concentrations of CaO and high concentrations of SiO_2 and Al_2O_3 favours stratlingite formation whereas high concentrations of CaO, SiO2 and low concentration of Al_2O_3 favours the formation of C_4AH_{13} [14]. The later compound converts with age to more stable AFm phases Hydrogarnet and C_3ASH_4.

The solid state ^{29}Si magic angle spinning nuclear magnetic resonance spectroscopy (MAS NMR) of the dried mixtures after 28 days of hydration were obtained. The signals due to ^1H have been decoupled so that the signals due to Si-O-Si and Si-O-Al connectivities are not affected by the proton signals. It should be noticed that, Q^0, Q^1, Q^2, Q^3, Q^4 correspond to a SiO_4 tetrahedron connected to 0, 1, 2, 3, and 4 SiO_4 tetrahedra, respectively, whereas, Q^n(0 Al), Q^n(1 Al), Q^n(2 Al), Q^n(3 Al), Q^n(4 Al), correspond to Si tetrahedron connected to 0, 1, 2, 3, and 4 Al tetrahedra, respectively. The solid state ^{29}Si MAS NMR spectrum of cement showed the presence of Q^0 doublet, at ~ – 71.5 ppm characteristic of the unreacted C_3S. On the other hand, the spectrum of silica fume/lime mixture showed the presence of Q^4 peak at ~ – 111.5 ppm, characteristic of unreacted silica fume. The two spectra contain Q^1 and Q^2 peaks, at ~ – 79 ppm and at ~ – 85 ppm, respectively, characteristic of CSH, with various C/S ratios. The deconvoluted peak areas were calculated and the average chain lengths were calculated from the formula (Richardson, et al, 1999 [12]).

$$\text{Av. Chain Length} = \frac{1/2\ Q^1\ (0\ Al)}{Q^1\ (0\ Al) + Q^2\ (0\ Al) + Q^2\ (1\ Al)} \quad (2)$$

It was found that the average chain length of the CSH is 3.5 and 4 for cement and silica fume, respectively.

The NMR pattern of fly ash/lime mixture shows a small peak at -107 ppm which is assigned to the unreacted fly ash. In addition, peaks at ~ – 79 ppm and ~ – 85 ppm are attributed to Q^1 (0 Al) and Q^2 (0 Al) species, respectively. That is terminal and middle (unbranched) silicon tretrahedra, respectively. An additional peak at ~ – 81 ppm is assigned to Q^2 (1 Al). The deconvoluted peak areas are used to calculate average Al/Si from the formula [12 and 13].

$$\text{Al/Si} = \frac{1/2\ Q^2\ (1\ Al)}{Q^1\ (0\ Al) + Q^2\ (0\ Al) + Q^2\ (1\ Al)} \quad (3)$$

The Al/Si ratio was found to be 0.24. The average chain length is 10 units. The presence of Al as ~ one fifth of the Si in a chain length of 10 units suggests that Al tetrahedra may be present in bridging positions.

4. CONCLUSIONS

A new technique that studies the changes in surface charge of particles in pastes has been used. An alternating electric field was applied at a single frequency of about 1MHz, on each paste, which generated an electroacoustic signals that are received by means of a dip-type probe placed in direct contact with the paste. The electroacoustic signals are used to calculate the zeta potential of particles in the paste. The technique has been used to study the changes in surface charge, as a function of hydration time, of concentrated cement, silica fume/lime, and fly ash/lime slurries. The new technique is superior to other techniques in that concentrated suspensions (such as cement slurries) may be studied in their original formulations i.e. without dilution. The mechanism of hydration monitored the changes in phase composition by x-ray diffraction at various ages. Solid state ^{29}Si magic angle spinning nuclear magnetic resonance spectroscopy (MAS NMR) was used to characterize the detailed structure of hydration products after 28 days. The new technique represents a step towards exploring the actual changes in surface charge during hydration.

REFERENCES

[1] O'Brien, R.W., J. Fluid Mech., 190, 1988, 71.
[2] Debye, P., J. Chem. Phys., 1, 1933, 13.
[3] Oja, T., Pwterson, G.L., Cannon, D.W., US. Ptent No.4 497 208, 1985.
[4] O'Brien, R.W., Midmore, B.R., Lamb, A., Hunter, R.J., Faraday Disc. Chem. Soc., 90, 1990, 301.
[5] O'Brien, R.W., Cannon, D.W., Rowlands, W.N., Langmuir. 10, 1994, 931.
[6] O'Brien, R.W., Midmore, B.R., Lamb, A., Hunter, R.J., J. Colloid Interface Sci., 173, 1995, 406.
[7] Nagele, E., Cem. Concr. Res., 16, 1985, pp. 453-462.
[8] Nagele, E., Cem. Concr. Res., 16, 1986, pp. 853-863.
[9] Nagele, E., Cem. Concr. Res., 17, 1987, pp. 573-580.
[10] Nagele, E., Cem. Concr. Res., 19, 1989, pp. 978-986.
[11] Malek, R.I. Application of New Fine Particle Characterization Techniques to Concrete Durability, This Proceeding, 2003.
[12] Richardson, I.G, "The Nature of CSH in Hardened Cements," Cem. Concr. Res., 29, (1999), 1131-1147.
[13] Brough, A.R. and I.G. Richardson, "^{29}Si Enrichment and Selective Enrichment for Study of the Hydration of Model Cements and Blended Cements," 10th ICCC, 3v001, Sweden (1997).
[14] Sersale, R. "Advances in Portland and Blended Cements," 9th ICCC, Vol.1, p261 Sersale, R. "Advances in Portland and Blended Cements," 9th ICCC, Vol.1, (1994), p 261.

BEHAVIOR OF CHLORIDE IONS IN HARDENED ECO-CEMENT: A NEW TYPE PORTLAND CEMENT MADE FROM MUNICIPAL WASTE INCINERATOR ASH

Hiroshi Hirao [1] and Shigeru Yokoyama [2]

[1] Taiheiyo Cement Corporation, Japan;
E-mail: hiroshi_hirao@taiheiyo-cement.co.jp
[2] Taiheiyo Cement Corporation, Japan;
E-mail: shigeru_yokoyama@taiheiyo-cement.co.jp

ABSTRACT

Eco-cement is made from municipal waste incinerator ash, which contains large amounts of Al_2O_3 and Cl^-. Consequently, Eco-cement contains greater quantities of calcium aluminate and ferrite phases and Cl^- than OPC. Although 20 to 40 mass% of Cl^- in Eco-cement dissolved into free water within 3 hours of the start of hydration, Cl^- concentration decreased rapidly after that. When Cl^- content in cement was adjusted to 0.1 mass% (added as NaCl), almost all of Cl^- in free water was bound as Friedel's salt in mortars made with Eco-cement, OPC and Blast furnace Slag Cement. The value of [Cl^-/OH^-] molar ratio of free water in each mortar was under 0.6 at 28 days, so steel corrosion is not likely to occur. When Cl^- content was increased to 1.0 mass%, Eco-cement bound more Cl^- than other cements by producing a large amount of Friedel's salt. The Remaining Cl^- in free water, which was not bound as Friedel's salt, was sorbed in hydrates such as C-S-H.

1. INTRODUCTION

Municipal waste, the main waste product of domestic life, reaches 50 million tons a year in Japan. Most of it is usually reduced in volume (to about 1/10 of the original volume) by incineration and disposed in landfill sites without being recycled. Therefore, treatment and disposal of waste materials are becoming a serious social problem. The cement industry in Japan has accepted many kinds of waste materials from other industries and uses 2,800 million tons of them as raw materials or fuels every year. Based on this information, it is expected that the cement industry will become a solution provider to waste problems, in addition to being a provider of basic construction materials as it has been [1]. Eco-cement has been developed in response to this trend [2][3][4][5].

Eco-cement is a new type of Portland cement made from municipal waste incinerator ash as main raw material. Incinerator ash generally includes much larger amounts of Cl^- and Al_2O_3 than natural raw materials such as clay. Therefore, using incinerator ash at about 50% of raw materials leads to an increase Cl^- and calcium aluminate and ferrite phases in cement. Taking this into consideration, two types of Eco-cement are produced [4][6]: (1) normal type that contains 500 ppm Cl^-, and (2) rapid-hardening type that contains about 1 mass% Cl^-.

The behavior of Cl^- in concrete has been investigated by many researchers because it has a potential to accelerate steel bar corrosion. However, there are few papers on behavior of Cl^-, incorporated into cement clinker, in concrete. Cl^- in concrete is classified into free Cl^- in free water (pore solution) and bound Cl^- by cement hydrates [7][8]. It is thought that the former directly associates with the steel corrosion. Since Eco-cement has a different mineral composition and Cl^- content from Portland cements, the concentration of free Cl^- in free water is probably different from that in Portland

Proceedings of the 11th International Congress on the Chemistry of Cement (ICCC)
'Cement's Contribution to the Development in the 21st Century'
Hosted by: The Cement and Concrete Institute of South Africa
CD-ROM produced by: Document Transformation Technologies
11 - 16 May 2003, Durban, South Africa
ISBN Number: 0-9584085-8-0
Editors: Dr G. Grieve and G. Owens
Congress Organised by: Event Dynamics

cements.

In this study, the dissolution of Cl^- incorporated into cement clinker is investigated by using Eco-cement that contains much greater quantities of Cl^- and calcium aluminate and ferrite phases than Portland cement. Also, the Cl^- binding mechanisms and Cl^- binding capacity of Eco-cement are investigated as compared with ordinary Portland cement and blastfurnace slag cement.

2. EXPERIMENT

2.1 Materials used

Normal Eco-cement (EC), rapid hardening Eco-cement (ECR), ordinary Portland cement (OPC) and blastfurnace slag cement (BB) were used for experiment. Their chemical compositions, mineral compositions, densities and Blaine specific surface areas are listed in Table 1. For mineral composition, EC contains much greater quantities of calcium aluminate and ferrite phases (15 mass% C_3A and 12 mass% C_4AF) than OPC. ECR contains 16 mass% calcium chloro-aluminate ($C_{11}A_7$•$CaCl_2$), due to its higher content of Cl^- (8,900ppm). BB contains more Al_2O_3 (8.4 mass %), originated from blastfurnace slag, and less Fe_2O_3 (2.1 mass%) than OPC.

Table 1. Chemical composition, mineral composition, density and specific surface area of cement used

Cement	Chemical composition (mass%)												f.CaO	Mineral composition (mass%)					Density	Blaine*2
	ig.loss	SiO_2	Al_2O_3	Fe_2O_3	CaO	MgO	SO_3	Na_2O	K_2O	P_2O_5	Cl^-	Total	(%)	C_3S	C_2S	C_3A	C_4AF	C_{11}*1	(g/cm^3)	(cm^2/g)
EC	1.5	17.0	8.1	3.9	61.0	1.9	3.7	0.23	0.02	1.22	0.066	98.61	0.4	48	12	15	12		3.18	4500
ECR	0.8	15.7	9.4	2.2	58.7	2.0	8.5	0.44	0.05	1.01	0.890	99.69	0.1	52	6		7	16	3.13	5710
OPC	1.7	21.1	5.1	2.9	64.2	1.4	2.0	0.30	0.44	0.10	0.005	99.36	0.6	53	22	9	9		3.16	3470
BB	1.0	25.8	8.4	2.1	56.5	2.9	1.9	0.27	0.38	0.08	0.003	99.25	0.2						3.05	3710

*1. Calculated by Bogue's Equation (for ECR, calculated according to TR R 0002), C_{11}: $C_{11}A_7$-$CaCl_2$
*2. Blaine specific surface area

2.2 Experimental methods

2.2.1 Sample preparation

Cement pastes were prepared at w/c of 0.5, 20°C. Free water in cement paste was expressed by centrifugal separator at 30 min, 1, 3, 6 hours. The free water (pore solution) in ECR paste was expressed by a pore expression device [9] at all ages.

The total Cl^- content (added as NaCl) in cement used for mortar was adjusted to 0.1, 1.0, 3.0 and 5.0 mass% (by mass of cement). Mortar specimens were prepared at w/c of 0.5, s/c of 1.0 and 20 °C. Toyoura sand was used as fine aggregate. The Mortar was cast into 5cm diameter, 20cm height cylindrical molds that were tightly sealed. The free water in mortar was expressed by a centrifugal separator at 0.5, 1, 3, 6 and 12 hours, and by a pore expression device at 1, 3, 7, 28 days. Free water in mortar with ECR was expressed by a pore expression device at all ages.

At the same age as expression of free water from mortar, hardened mortar was cut into approximately 5mm cubes. These cubes were immersed in acetone to terminate the hydration and dried by D-drying or in the atmosphere with the RH of 11%. They were used for hydration analysis.

2.2.2 Analysis

The concentration of Cl^- in free water was determined with ion chromatography. The concentration of OH^- was determined by titration against standard NaOH of 0.01N using phenolphthalein as indicator. Amount of Friedel's salt (C_3A•$CaCl_2$•$10H_2O$) was determined according to Shirasaka et.al. [10] in such way that it is determined by using heat absorption peak around 330 °C measured by DSC. Non-evaporable water of D-dried hardened mortar was determined by ignition loss according to JIS R 5202. Specific surface area was determined by BET.

3. RESULT AND DISCUSSION

3.1 Dissolution of Cl^- from clinker

Dissolutions of Cl^- into free water in cement paste were determined by ion chromatography. As shown in Figure 1, the concentration of Cl^- in free water in EC paste reached a maximum of 300 mg/l at 3 hours. If it is assumed that free water to cement ratio was 0.5 at 3 hours, this result means that about 23 % of Cl^- in EC was detected in free water. The concentration of Cl^- in EC paste decreased gradually after 3 hours and became almost equal to OPC paste at 12 hours.

The concentration of Cl^- in free water in ECR paste was highest of all pastes. Although, about 40 % of Cl^- in ECR paste was detected in free water at 3 hours at the maximum, the concentration of Cl^- in ECR paste decreased gradually after 3 hours as same as EC paste. These results indicate that the amount of Cl^- bound by cement hydrates of EC and ECR exceeded that dissolved from them after 3 hours.

3.2 Cl^- binding capacity

As mentioned above, Cl^- in hardened cement is classified into free Cl^- in free water and Cl^- bound by cement hydrates. It is considered that the latter one doesn't participate in the steel corrosion process as far as cement hydrates that bind Cl^- do not decompose by carbonation or other degradation mechanisms. Some techniques are proposed for determination of free Cl^-: extraction free Cl^- with water or ethyl alcohol (Leaching technique), press out pore water by pore expression device, etc. Trithart [11] reported that a pore expression device is suitable for expression of free water to determine the amount of free Cl^- and leaching technique is likely lead overestimation of free Cl^-. From consideration of this, the concentration of Cl^- in free water was determined by using expressed pore water in this experiment. Cl^- in free water is called "free Cl^-", and other Cl^- is called "bound Cl^-".

The Cl^- binding capacity of cement depends on the mineral composition and the type of blending materials used in the mixture. For example, cements with high calcium aluminate and ferrite phases or blast furnace slag are able to bind large amounts of Cl^- [7][12]. For cement hydrates, it is thought that Friedel's salt that binds Cl^- chemically and C-S-H that has high specific surface area are closely related to binding capacity of Cl^-. It is expected that the Cl^- binding capacities of EC and ECR are higher than OPC because of higher content of calcium aluminate and ferrite phases. In this section, Cl^- in cements were adjusted to 0.1-5.0 mass% by NaCl for comparison of the Cl^- binding capacity between cements.

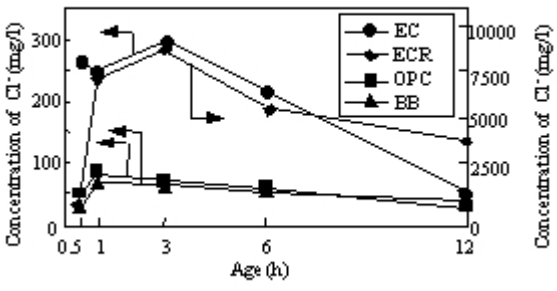

Figure 1. Concentration of Cl^- in free water in cement paste

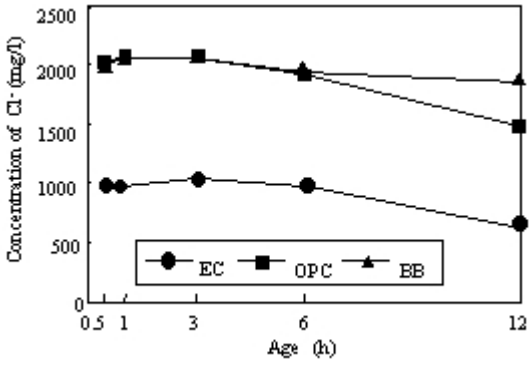

Figure 2. Concentration of Cl^- in mortar with cement with 0.1 mass% Cl^-

3.2.1 Cement with 0.1 mass% Cl^-

(1) Concentration of Cl^- and SO_4^{2-} in free water

The concentrations of free Cl^- and SO_4^{2-} in free water in mortars with 0.1 mass% Cl^- from 30 min to 12 hours are shown in Figure 2 and Figure 3. At 30 min, the concentration of free Cl^- in OPC, BB and EC mortar were 2,050, 2,030 and 960 mg/l, respectively. The amounts of free Cl^- at this age were almost equal to the total sum of Cl^- dissolved from cement (as shown in Figure 1) and those added as NaCl. The concentration of free Cl^- in each mortar increased slightly from 1 to 3 hours. After that, it started decreasing gradually. This result indicates that the amount of Cl^- bound by cement hydrates exceeded the amount of Cl^- dissolved from cement in each mortar after 3 hours.

At 30 min, the concentrations of SO_4^{2-} in free water in OPC, BB and EC mortar were 5,900, 5,430 and 1,700 mg/l, respectively. That in EC mortar was lower than those in OPC and BB because of the lower content of alkali sulfate in EC. The concentration of SO_4^{2-} in EC and OPC mortar decreased earlier than that in BB because they contain high amounts of calcium aluminate and ferrite phases that react with SO_4^{2-} at early age. The concentration of free Cl^- in EC and OPC mortar decreased rapidly with decreasing concentration of SO_4^{2-} after 6 hours. This result suggests that Friedel's salt is related to binding amount of Cl^- at early age.

The concentrations of free Cl^- in free water in mortars are shown in Figure 4. The concentration of free Cl^- in BB mortar was higher than others at 12 hours. It decreased rapidly from 12 hours to 1 day and became 40 mg/l at 7 days. The concentration of free Cl^- in OPC mortar decreased slowly after 12 hours. It decreased to 80 mg/l at 28 days. The concentration of free Cl^- in EC mortar decreased earlier than others. It decreased to 30 mg/l at 3 days and hadn't increased at 28 days.

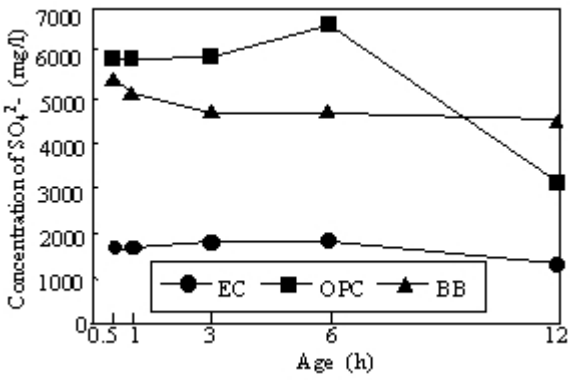

Figure 3. Concentration of SO_4^{2-} in mortar with cement with 0.1 mass% Cl^-

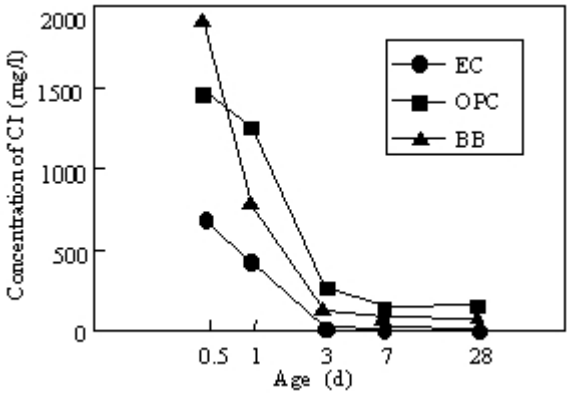

Figure 4. Concentration of Cl^- in mortar with cement with 0.1 mass% Cl^-

(2) Proportion of bound Cl^- to total Cl^-

It is assumed that water in mortar, except for non-evaporable water shown in Figure 5, is free water. In that case, the amount of free water (FW) in mortar is calculated by using Equation (1). The amount of bound Cl^- (BCL) is calculated by using Equation (2). The proportions of bound Cl^- to total Cl^- (BCLR), calculated by using Equation (3), are shown in Figure 6. The proportions of bound Cl^- in each mortar increased rapidly from 6 hours to 3 days. At 3 days, almost all the free Cl^- in each mortar was bound. The proportions of bound Cl^- in EC, OPC and BB at 28 days were 99, 91 and 95 mass%, respectively.

$$FW = W - C * BW / 100 \quad (1)$$

$$BCL = TCL - FCL * FW / C \quad (2)$$

$$BCLR = (BCL / TCL) * 100 \quad (3)$$

where FW: Unit amount of free water (g/cm^3), W: Unit amount of water (g/cm^3), C: Unit amount of cement (g/cm^3), BW: Non-evaporable water (mass% to cement), BCL: Amount of bound Cl^- (ppm to

cement), TCL: Total amount of Cl^- (ppm to cement), FCL: Concentration of free Cl^- in free water (mg/l), BCLR: Proportion of bound Cl^- (mass% to total Cl^-)

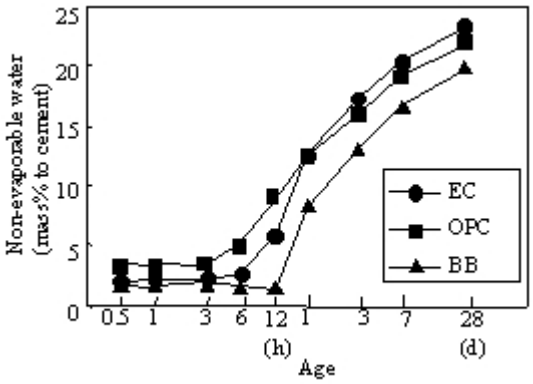

Figure 5. Non-evaporable water in mortar with cement with 0.1 mass% Cl^-

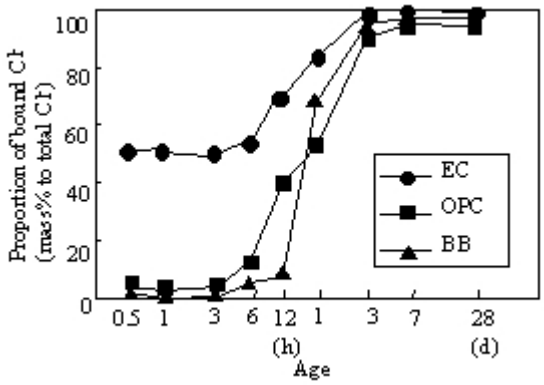

Figure 6. Proportion of bound Cl^- in mortar with cement with 0.1 mass% Cl^-

3.2.2 Cement with 1.0 mass% Cl^-

(1) Concentration of free Cl^- in free water

When Cl^- content in cement was 0.1 mass%, the concentration of free Cl^- in free water in EC mortar decreased earlier than OPC and BB as described in section *3.2.1*. However, there was not a significant difference between the proportions of bound Cl^- to total Cl^- of 3 mortars at 3 days. In this section, the same examination as in section *3.2.1* was done by using cement with 1.0 mass% Cl^- for investigation of the Cl^- binding capacity of each cement. The concentrations of free Cl^- in free water in mortar are shown in Figure 7. For EC, OPC and BB, concentration of free Cl^- at 1 day was about 20,000 mg/l. This result means that only a little amount of free Cl^- was bound by sorption into hydrates. From 1 to 3 days, the concentration of free Cl^- in each mortar decreased rapidly. The Cl^- concentration in EC mortar decreased earlier than that of OPC and BB. At 28 days, that of EC, BB and OPC mortar was 4,130, 6,600 and 12,500 mg/l, respectively. That of ECR mortar was much lower than the other mortars from an early age. This result is attributed to the un-hydrated $C_{11}A_7$•$CaCl_2$ still remaining in ECR mortar and to the higher binding capacity of ECR due its higher content of calcium aluminate and ferrite phases.

(2) Proportion of bound Cl^- to total Cl^-

The proportions of bound Cl^- to total Cl^- in mortars with 1% Cl^- (by mass of cement) are shown in Figure 9. These results were calculated by using Equation (1) to (3), and the results of Cl^- concentration and non-evaporable water are shown in Figure 7 and Figure 8, respectively. The proportions of bound Cl^- to total Cl^- increased rapidly from 1 to 3 days. At 3 days, the proportions of bound Cl^- to total Cl^- of EC, ECR and OPC were 81, 92 and 52 mass%, respectively. The proportion of bound Cl^- in each mortar decreased with increasing total amount of Cl^-. The proportion of bound Cl^- in ECR mortar was much higher from an early age. At 28 days, that became almost the same value as EC mortar.

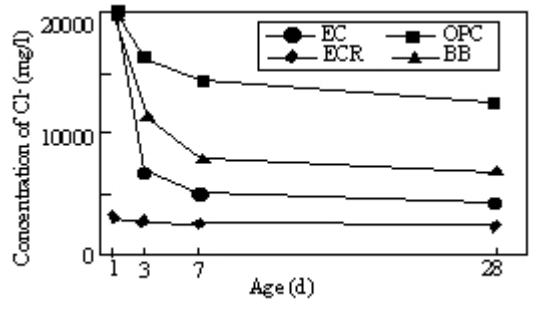

Figure 7. Concentration of Cl^- in mortar with cement with 1.0 mass% Cl^-

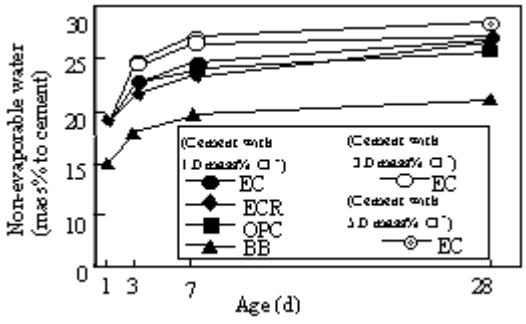

Figure 8. Amount of non-evaporable water in mortar with cement with 1.0 – 5.0 mass% Cl^-

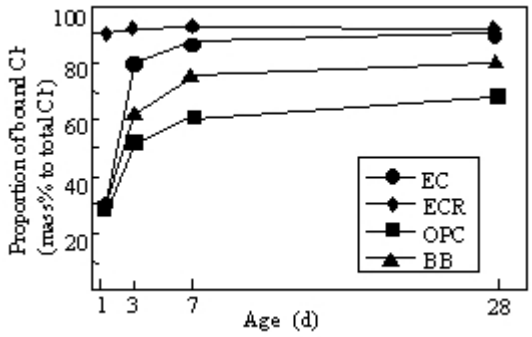

Figure 9. Proportion of bound Cl^- in mortar with cement 1.0 mass of Cl^-

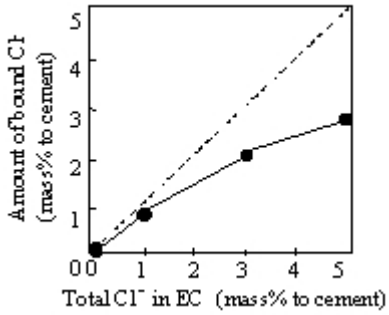

Figure 10. Relationship between Cl^- content in EC and amount Cl^- (28d)

3.2.3 Cement with 3.0 to 5.0 mass% Cl^-

As mentioned above, when Cl^- content in cement was adjusted to 0.1 to 1.0 mass%, EC has a higher Cl^- binding capacity than OPC and BB. In this section, Cl^- in EC was adjusted to 3.0 and 5.0 mass% by NaCl and concentrations of Cl^- in mortar with the cement at 28 days were measured to investigate the Cl^- binding capacity of EC. Figure 10 shows that the amount of bound Cl^- calculated by using Equation (1) and (2), and non-evaporable water is shown in Figure 8. Proportion of bound Cl^- to total Cl^- of EC decreased with increasing total Cl^- in cement. When Cl^- content in EC was adjusted to 5.0 mass%, about 2.8 mass% of Cl^- bound in cement hydrates. According to the results of Someya et.al. [12], when Cl^- content in OPC was adjusted to 3.0 mass%, the amount of bound Cl^- in OPC mortar at w/c of 0.5 and 28 days was 1.2 mass%. In the same condition, EC bound 2.1 mass% of Cl^- is shown in Figure10. Therefore, it is considered that the Cl^- binding capacity of EC is much higher than that of OPC. This is attributed to the fact that the amount of calcium aluminate and ferrite phases in EC is much higher than that in OPC.

3.3 Cement hydrates

The relationship between the proportion of bound Cl^- to total Cl^- and the amount of Friedel's salt was investigated. The amount of Freidel's salt was expressed as mass% to cement revised by using loss of ignition.

3.3.1 Cement with 0.1 mass% Cl^-

The amounts of Friedel's salt from 6 hours to 3 days are shown in Figure 11. In general, after SO_4^{2-} in free water decreases with proceeding of hydration, monosulfate hydrate is produced. When Cl^- is in free water, Friedel's salt is produced instead of monosulfate hydrate. For OPC in this study, Friedel's salt was detected after 12 hours and 0.7 mass% at 3 days. For BB that contains relatively smaller amounts of calcium aluminate and ferrite phases, Friedel's salt was detected after 1 day and 0.8 mass% at 3 days. This result means that blastfurnace slag that contains large amounts of Al_2O_3 reacted after 1 day. EC produced much greater amounts of Friedel's salt than OPC at 12 hours. Friedel's salt in EC was 0.8 mass% as same as OPC at 3 days. This is attributed to the much higher content of calcium aluminate and ferrite phases (27 mass%) in EC. It can be noticed in Figures 6 and 11 that the increase of the proportion of bound Cl^- and the increase in the amount of Friedel's salt occurred at the same period, suggesting a correlation between the two.

3.3.2 Cement with 1.0 to 5.0 mass% Cl^-

The amounts of Friedel's salt in mortar are shown in Figure 12. Friedel's salt in OPC increased gradually from 1 to 7 days. At 28 days, it was 2.9 mass%. Amount of Friedel's salt in BB mortar was more than OPC at 3 days and 5.3 mass% at 28 days. For ECR which indicates the high proportion of bound Cl^- to total Cl^-, the amount of Friedel's salt was more than the other cement types and it was 5.1 mass% at 28 days. Similar to the case of cement with 0.1 Cl^- the proportion of bound Cl^- to total Cl^- and the amount of Friedel's salt increased at the same period as shown in Figures 9 and 12.

As shown in Figure 12, the amount of Friedel's salt at 28 days increased up to 3.0 mass% of total Cl. Therefore, it is considered that for this range of Cl^- content in cement, Cl^- was mainly bound by Friedel's salt. For the range of 3.0 mass% or more of Cl^- in cement, however, the amount of Friedel's salt didn't increase with increasing total Cl^- in cement. This result indicates that the amount of bound Cl^- by hydrates except Friedel's salt increased when Cl^- content in cement was 3.0 mass% or more. Maybe this is because the amount of un-hydrated calcium aluminate and ferrite phases was not enough to produce more Friedel's salt and OH^- was saturated in free water. That is, when Friedel's salt is produced according to Equation (4), OH^- in $Ca(OH)_2$ substitutes for Cl^- in free water and OH^- saturated in free water. In this case, further production of Friedel's salt will be prevented [13].

$$C_3A + 2NaCl + Ca(OH)_2 + 10H_2O \rightarrow C_3A{\bullet}CaCl_2{\bullet}10H_2O + 2Na^+ + 2(OH)^- \quad (4)$$

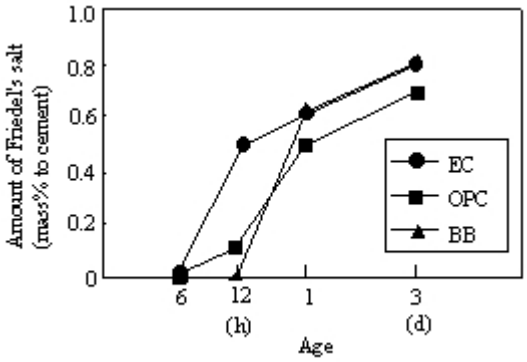

Figure 11. Amount of Friedel's salt in mortar with cement with 1.0 mass% Cl^-

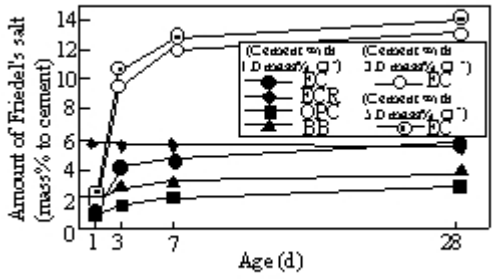

Figure 12. Amount of Friedel's salt in mortar with cement with 1.0 – 5.0 mass% Cl^-

3.4 Cl^- binding mechanisms

From these results, it is considered that the Cl^- binding capacity is closely related to the production of Friedel's salt. In this section, Cl^- binding mechanisms were considered.

3.4.1 Cl^- in Friedel's salt

When Cl^- content in cement was adjusted to 0.1 mass%, 91 to 99 mass% of Cl^- was bound to cement hydrates at 3 days. At same age, Cl^- bound as Friedel's salt was 780 to 910 ppm. These results mean that most of Cl^- (1,000 ppm) in cement was bound as Friedel's salt in mortar. It is reported that C-S-H, which is main cement hydrate, also binds Cl^- by sorption [14]. When Cl^- content in cement was less than 0.1 mass%, however, Cl^- was bound by mainly Friedel's salt until 3 days [10].

When Cl^- content in cement was 1.0 mass%, the proportions of bound Cl^- to total Cl^- were 52 to 92 mass% at 28 days. This result means that much of the Cl^- remained in free water. Cl^- in hardened mortar at 28 days is classified into free Cl^- and bound Cl^- as shown in Figure 13. Bound Cl^- is classified again into Cl^- in Friedel's salt and Cl^- in other cement hydrates. Bound Cl^- was determined in the same way as in *3.2.2*. The amount of Cl^- in Friedel's salt was determined by using stoichiometric calculations from values in Figure 12. When Cl^- content in cement was 1.0 mass%, 0.38 mass% of Cl^- was bound into Friedel's salt in OPC. This value agrees with the result obtained by Richartz [7]. EC and ECR bound more Cl^- (about 0.7 mass%) as Friedel's salt than OPC. Therefore, it is considered that the amount of calcium aluminate and ferrite phases is closely related to the amount of Friedel's salt. For BB, the amount of Cl^- bound in Friedel's salt was 0.43 mass%, a little more than OPC. This result is attributed to the contribution of Al_2O_3 in blastfurnace slag to produce Friedel's salt. On the other hand, the amount of Cl^- bound into other cement hydrates in OPC was higher than others. This result tends to suggest that Cl^- sorbed into other cement hydrates increases with decreasing amount of Cl^- bound in Friedel's salt.

For EC with 3.0 to 5.0 mass% Cl^-, amounts of free and bound Cl^- obtained in same manner as in Figure 13 are shown in Figure 14. The amount of bound Cl^- and Cl^- in Friedel's salt increased with increasing total Cl^-. When Cl^- content in cement was 3.0 mass% or more, however, the amount of Cl^- in Friedel's salt was little increased with increasing total Cl^-. That is, in this range of Cl^-, the proportion of Cl^- in other cement hydrates to total Cl^- increased with increasing total Cl^-.

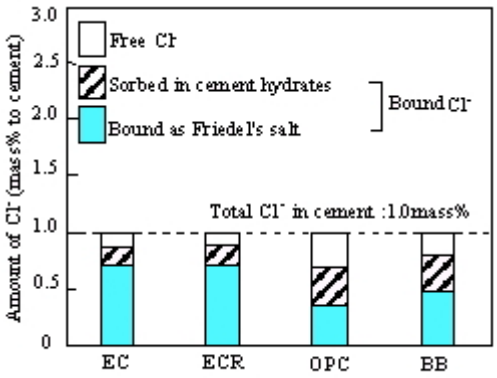

Figure 13. Free Cl^- and bound Cl^- in mortar with cement with 1.0 mass% Cl^- (28 days)

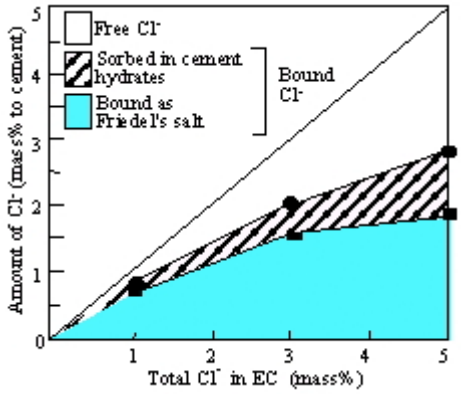

Figure 14. Free Cl^- and bound Cl^- in mortar with cement with 0.1 – 5.0 (28 days)

3.4.2 Cl^- binding mechanisms

When Cl^- content in cement was 0.1 mass%, Cl^- was mainly bound as Friedel's salt. This result was true for all tested cements. When Cl^- content in cement was 1.0 mass%, however, there were significant differences in the proportion of bound Cl^- to total Cl^- among the different types of cements. It tended to increase with an increasing amount of Friedel's salt. These results suggest that Cl^- binding mechanisms vary with the types of cements and the total Cl^- content.

The amount of Cl^- bound as Friedel's salt depends on the amount of calcium aluminate and ferrite phases and gypsum, and their reaction ratio [15]. Cl^- in other cement hydrates is bound by sorption. Therefore, it is considered that the amount of Cl^- in other cement hydrates depends on the concentration of Cl^- in free water. Figure 15 shows that the relationship between the concentration of Cl^- in free water (shown in Figure 7) and the amount of Cl^- sorbed in other hydrates per surface area of mortar. The amount of Cl^- sorbed in other cement hydrates per surface area is calculated by using the amount of Cl^- sorbed in cement hydrates (shown in Figure 13 and Figure 14) and the value of BET specific surface area. With increasing the concentration of Cl^- in free water, the amount of Cl^- sorption per surface area increased regardless the types of cement and the amount of total Cl^-.

From these results, the Cl^- binding process is considered as follows: although Cl^- sorption starts just after mixing with water, the amount of Cl^- sorption at early age is a little because of the smaller amount of cement hydrates. On the other hand, Friedel's salt is produced vigorously from 6 hours to 7 days and binds Cl^-. Sorption of Cl^- has a relationship to the concentration of Cl^- in free water as shown in Figure 15. Therefore, it is considered that the sorption of Cl^- increases with increasing free Cl^- in free water, which isn't bound as Friedel's salt. When Cl^- content in cement is 0.1 mass% or less, each cement contains enough calcium aluminate and ferrite phases to produce Friedel's salt. Therefore, the amounts of Friedel's salt and bound Cl^- in all cements were almost equal. However, when Cl^- content in cement was 1.0 mass% or more, the amount of calcium aluminate and ferrite phases is not enough to bind all Cl^- as Friedel's salt. Therefore, EC, which contains large quantities of calcium aluminate and ferrite phases, produces much more Friedel's salt. Consequently, the concentration of Cl^- in free water in EC mortar decreases from an early age.

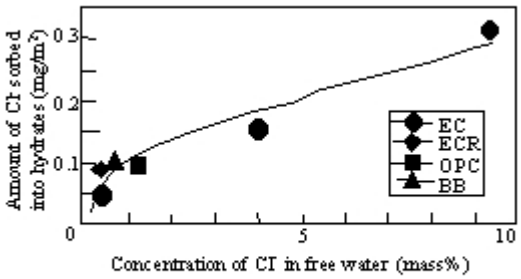

Figure 15. Relationship between the concentration of Cl^- in free water and the amount of Cl^- sorbed into hydrates in mortar with cement with 0.1 – 5.0 mass% Cl^-

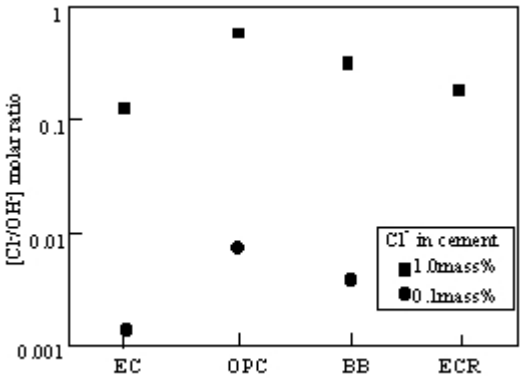

Figure 16. $[Cl^-/OH^-]$ molar ratio in free water in mortar with cement 0.1 – 1.0 mass% Cl^- (28 days)

3.5 Molar ratio of $[Cl^-/OH^-]$ in free water

The most serious problem of Cl^- in concrete is the initiation and propagation of steel corrosion. Generally, the steel bar in concrete is protected by the high alkaline environment. However, when Cl^- exist in concrete and $[Cl^-/OH^-]$ molar ratio in free water excess 0.6, the oxidized layer on steel bar becomes unstable [16]. Kawai et.al. [17] investigated the relationship between $[Cl^-/OH^-]$ molar ratio and corrosion speed of steel bar and reported that the corrosion speed of steel bar depends on $[Cl^-/OH^-]$ molar ratio, rather than the concentration of Cl^- in free water. And in water with $[Cl^-/OH^-]$ molar ratio of 0.01 or less, the steel corrosion didn't occur [17].

$[Cl^-/OH^-]$ molar ratios in free water in mortar with cement with Cl^- of 0.1 and 1.0 mass% are shown in Figure 16. When Cl^- content in cement was 0.1 mass%, $[Cl^-/OH^-]$ molar ratio in OPC was highest in all cements. However, $[Cl^-/OH^-]$ molar ratio in OPC was under 0.01 and much lower than 0.6 of the threshold of corrosion. In consideration of the result of Kawai et.al. [17], the steel corrosion in each cements are not likely to occur. When Cl^- content in cement was 1.0 mass%, $[Cl^-/OH^-]$ molar ratio of EC and ECR, which bound much more Cl^-, was lower than those of OPC and BB. $[Cl^-/OH^-]$ molar ratio of OPC a little exceeded 0.6. These results mean that $[Cl^-/OH^-]$ molar ratios are different from the mineral composition of cement even if total Cl^- in cements is constant.

4. CONCLUSIONS

Eco-cement, made from municipal waste incinerator ash as main raw material, contains greater quantities of calcium aluminate and ferrite phases and Cl^- than OPC. Eco-cement is classified into normal type (EC) that contains about 500 ppm Cl^- and rapid hardening type (ECR) that contains 1.0 mass% Cl^-. In this study, the dissolution of Cl^- from EC and ECR were investigated. The Cl^- binding capacity of EC and ECR was also investigated as compared with OPC and BB by adjusting Cl^- in cement by NaCl. The results obtained are as follows:

(1) The concentration of Cl^- in free water in EC and ECR paste was highest at 3 hours. At that age, the proportion of Cl^- detected in free water in EC and ECR paste were about 20 and 40 mass% of total Cl^- content, respectively. The Cl^- concentrations decreased rapidly after that.
(2) When Cl^- content in cement was adjusted to 0.1 mass%, the concentration of Cl^- in free water in EC mortar decreased earlier than others. At 3 days, almost all the Cl^- in each mortar was bound mainly by Friedel's salt. $[Cl^-/OH^-]$ molar ratio in free water in each mortar was much lower than the corrosion threshold of steel.
(3) When Cl^- content in cement was adjusted to 1.0 mass%, EC and ECR bound much more amount

of Cl^- than OPC and BB. Hence, the concentrations of Cl^- in free water in EC and ECR mortar decreased earlier than OPC and BB mortar.

(4) When Cl^- content in cement was adjusted to 3.0 mass%, EC mortar bound about twice the Cl^- of OPC. The Cl^- binding capacity of EC is considered to be higher than OPC.

(5) At early ages, Cl^- in free water is mainly bound as Friedel's salt produced by hydration of calcium aluminate and ferrite phases. The remaining Cl^- that isn't bound as Friedel's salt, is sorbed by other cement hydrates. The amount of Cl^- sorption increased with increasing concentration of Cl^- in free water.

REFERENCES

[1] Shimoda,T., Jour. of Res. of the Taiheiyo Cement Corp., No.138, 2000, pp.1-4.
[2] Clean Japan Center, Production Technology of Eco-cement, 1999.
[3] Uchikawa,H. and Obana,H., World Cement, Vol.26, No.11, 1995, pp.33-40
[4] Shimoda,T., Yokoyama,S. and Hirao,H., Jour. of Res. of the Taiheiyo Cement Corp., No.138, 2000, pp.5-15.
[5] Japanese Industrial Standards Committee, Technical Report, TR R 0002, 2000
[6] Takuma,Y., Tsuchida,Y. and Uchida,S., 10ICCC, 1997, pp.3iill8.
[7] Richartz,R., Z-K-G, Vol.22, 1969, pp.447-456.
[8] Page,C.L. and Treadaway,K.W.J., Nature, vol.297, 1982, pp.109-115.
[9] Kobayakawa,M., Ozu,H. and Hanehara,S., Cement Science and Concrete Technology, No.53, 2000, pp.102-109.
[10] Shirasaka,T, Irino,S. and Goto,T., Proc. Japan Cement Association, vol.53, 1999, pp.22-23.
[11] Tritthart,J., Cement and Concrete Research, vol.19, No.4, 1989, pp.586-594.
[12] Someya,K., Otsuki,N., Tiong-Huan Wee and Nagataki,S., Proc. Japan Concrete Institute, Vol.11, No.2, 1989, pp.603-608.
[13] Kobayashi,K., Funato,M., Shiraki,R., Uno,Y. and Kawai,K., Jour. of the Institute of Industrial Science, University of Tokyo, vol.41, No.12, 1989, pp.42-44.
[14] Nakamura,A., Sakai,E., Nishizawa,K., Oba,Y. and Daimon,M., Jour. of the Chemical Society of Japan, No.6, 1999, pp.415-420.
[15] Hirao,H., Kume,M. and Hanehara,S., Cement Science and Concrete Technology, vol.52, 1998, pp.74-81.
[16] Hausmann,D.A., Materials Protection, 1967, pp.19-23.
[17] Kawai,K., Tazawa,E., Tanaka,S. and Yokoyama,S., THIRD CANMET/ACI International Symposium, SP-202, 2001, pp.285-298.

BEHAVIOR OF CHLORIDE IONS IN HARDENED ECO-CEMENT: A NEW TYPE PORTLAND CEMENT MADE FROM MUNICIPAL WASTE INCINERATOR ASH

Hiroshi Hirao [1] and Shigeru Yokoyama [2]

[1] Taiheiyo Cement Corporation, Japan,
E-mail: hiroshi_hirao@taiheiyo-cement.co.jp
[2] Taiheiyo Cement Corporation, Japan,
E-mail: shigeru_yokoyama@taiheiyo-cement.co.jp

Mr Hiroshi Hirao is a Research Chemist of Cement Chemistry Group, Taiheiyo Cement Corporation, Japan.

QUALITATIVE AND QUANTITATIVE ANALYSIS OF SELECTED ORGANIC ADDITIVES IN HARDENED CONCRETE BY THERMAL ANALYSIS AND INFRARED SPECTROSCOPY

R. Kriegel[1], R. Hellrung[2] and A. Dimmig[3]

[1, 2] Bauhaus-Universität, 99421 Weimar, Germany.
[1] Professur Bauchemie, E-mail: ralf.kriegel@bauing.uni-weimar.de
[2] F.A. Finger-Institut für Baustoffkunde, E-mail: ralf.hellrung@bauing.uni-weimar.de
and andrea.dimmig@bauing.uni-weimar.de

1. INTRODUCTION

According to German technical specification a PCC is a cement mortar or a concrete with a maximum particle size of 8 mm which is modified with polymer additives. Usually, mortars made with Portland cement are used for PCC's. The function of the polymer additive depends on its type and amount, e.g. it could be serve as a plasticiser, a bonding aid or a binding material. If polymers are added to conventional mortars, one expects that such an additive improves the properties of fresh mortar (e.g. consistency, water retention capacity) and/or the properties of the hardened one (e.g. tensile bending strength, modulus of elasticity, adhesive power) in a special way and to a larger degree than common additives [1, 2]. The main component of such modifier is a thermoplastic polymer or a polymer mixture usual in the trade as a dispersion, as redispersible powder or a thermosetting system. Because of the easier handling of the former, dispersions are widely used, whereas thermosetting epoxy resins are designed for special applications according to its higher inherent stability and its temperature resistance. The quality control of these materials requires the identification and quantification of the polymer additives in dry mortar mixtures just as much as in hardened mortars or concrete. Therefore, four different polymer additives were investigated as a raw additive and also as a component of hardened mortars using FTIR spectroscopy and simultaneous thermal analysis.

2. EXPERIMENTAL

All investigated mortar samples were prepared using the same Portland cement (CEM I 42,5R) and standardised aggregate in constant amounts, but with different polymer : cement ratios, water : cement ratios and storage conditions because of the adjustment of the workability and of its use for further investigations [2]. Sample markings, preparation and storage conditions are summarised in Table 1. The samples aged for a half year were manually crushed, edge areas were removed and the remaining pieces were milled for 10 seconds at 1400 r.p.m. in a disk vibration mill.

Vinyl acetate-versatic acid vinylester-copolymers (PA), styrene-acrylate-copolymers (SA) and thermosetting epoxy resins (EP) are the most frequently used polymer additives for PCC's in Germany [3]. According to this, four commercial products based on these systems were used in this work, two of them as redispersible powders (RP) and the others as an aqueous dispersion (DI) or thermosetting emulsion (CU). One redispersible powder (SA-RP) and one dispersion (SA-DI) based on the same main component, a styrene-acrylate-copolymer.

The real polymer content within the hardened mortars deviates from the values resulting from the

Proceedings of the 11th International Congress on the Chemistry of Cement (ICCC)
'Cement's Contribution to the Development in the 21st Century'
Hosted by: The Cement and Concrete Institute of South Africa
CD-ROM produced by: Document Transformation Technologies
11 - 16 May 2003, Durban, South Africa
ISBN Number: 0-9584085-8-0
Editors: Dr G. Grieve and G. Owens
Congress Organised by: Event Dynamics

amounts of the single components, because of the moisture exchange with the environment and the carbonation. Therefore, the polymer contents were corrected using the total mass change of the concrete up to 1000 °C according to equation 1.

$$w_{pol} = \frac{m_{pol}}{m_{cement} + m_{aggregate}} \cdot (1 + \Delta m_{total}) \quad (1)$$

The as-corrected polymer contents are also listed in Table 1.

Table 1. Preparation conditions and polymer contents for PCC samples

sample marking	polymer	m_{cement} [c] [g]	$m_{polymer}$ [h] [g]	$m_{aggregate}$ [i] [g]	m_{water} [g]	w/c [l]	p/c [m]	Δm_{total} [n] [w.-%]	w_{pol} [o] [w.-%]
CC-0[a]	-	450	0	1350	225	0.50	0		0
PCC1-5[a]	EP-CU[d]	450	22.5	1350	157.5[k]	0.35	0.05	-6.884	1.16
PCC2-5[a]	SA-RP[e]	450	22.5	1350	157.5	0.35	0.05	-6.924	1.16
PCC3-5[a]	PA-RP[f]	450	22.5	1350	157.5	0.35	0.05	-6.740	1.17
PCC4-5[a]	SA-DI[g]	450	22.5	1350	157.5[k]	0.35	0.05	-5.888	1.18
PCC1-15[b]	EP-CU[d]	450	67.6	1350	180[k]	0.40	0.15	-9.729	3.39
PCC2-15[b]	SA-RP[e]	450	67.6	1350	180	0.40	0.15	-8.780	3.43
PCC3-15[b]	PA-RP[f]	450	67.6	1350	180	0.40	0.15	-9.462	3.40
PCC4-15[b]	SA-DI[g]	450	67.6	1350	180[k]	0.40	0.15	-8.677	3.43

[a] 1 day in mould, until to the 28. day at 20 °C and 65 % r.h.; [b] as[a], but additionally 6 days in water after form remove; [c] CEM I 42,5R; [d] emulsion of an epoxy resin, curing agent polyamine; [e] redispersible powder of a Styrene-acrylate-copolymer; [f] redispersible powder of a vinyl acetate-versatic acid vinylester-copolymer; [g] dispersion of a styrene-acrylate-copolymer; [h] corresponds to the solid polymer content; [i] standardized sand (Normsand I); [k] includes the water amount of the dipersion/emulsion; [l] water/cement ratio; [m] polymer/cement ratio; [n] total mass loss (thermogravimetric) of the hardened concrete up to 1000 °C; [o] polymer content in hardened concrete calculated by cement and aggregate amounts and by the total mass loss[n]

The infrared transmission measurements were carried out on a Fourier transform spectrometer BioRad FTS 175C within a wavenumber range of 4000 cm^{-1} to 400 cm^{-1} with a resolution of 2 cm^{-1}. The hardened polymers and the PCC's were milled with a surplus of KBr (x 130) and pressed to cylinders in a conventional manner. Polymer solutions were dropped on quadratic pieces of a Silicon wafer, so that the solvent evaporates within some seconds. Each Silicon piece was measured for background correction before the polymers were deposited.

A reliable identification of small polymer contents nearly or below 1 w.-% is complicated because of the mortar peaks covering weak polymer infrared peaks. Therefore, polymer additives were enriched by reflow extraction using a Soxhlet extractor related to EN ISO 6427 standard [4]. The extractions were carried out with 20 g PCC and 100 ml Acetone, a full extraction cycle took place within 2 or 3 minutes. Approximately a third of the total polymer content was typically extracted within 8 hours.

A simultaneous thermal analyser Setsys 16/18 by Seteram SA was used for the thermal analysis. The measurements were carried out with a heating rate of 10 K/min in a flowing atmosphere (appr. 1 l/min) of purified air or Argon. The sample mass varied from 8 to 25 mg, open corundum crucibles with a volume of 100 µl were used. All measurements were corrected for buoyancy.

Because of the significant differences of the expected and the experimental mass changes caused by polymer decomposition, mixtures of a cement paste with hardened polymer additives SA-RP and

PA-RP were prepared. The cement paste (CS) was made from a CEM I 42,5R, hardened and stored in a closed vessel for one year. The cement paste and all mixtures were prepared and milled for 30 seconds in a vertical vibration ball mill just before measurement. The total handling time in air was comparable for all these samples to prevent different carbonation.

3. RESULTS AND DISCUSSION

3.1 Infrared measurements

The IR spectra of the reference mortar CC-0 and of the hardened polymers are depicted in Figure 1. The polymer-free mortar shows wide valence vibrations of the inorganic groups $[SiO_4]^{4-}$ and $[CO_3]^{2-}$ at 993 cm^{-1} and 1486 cm^{-1}, respectively. The sharp peak at 3645 cm^{-1} corresponds to a free O-H valence vibration, the wide peak at 3442 cm^{-1} is assigned to associated OH groups.

Plain hints for organic additives in cement mortars should be given by the presence of ν-C-H vibrations in the range from 2840 to 3110 cm^{-1}. Surprisingly, two small peaks below 3000 cm^{-1} (at 2922 and 2852 cm^{-1}) point to organic impurities in the polymer-free mortar, just as in the Portland cement (not shown) itself which was used for the mortars. We assume that these organic impurities came from a milling agent usually used in the cement production process.

Nevertheless, the called range is very meaningful for the identification of the additives. All additives excepting PA-PR show peaks between 3020 and 3120 cm^{-1} which were assigned to ν-C-H vibrations of aromatic compounds. Correspondingly, the sole polymer without aromatic components should be the vinyl acetate-versatic acid vinylester-copolymer built up of aliphatic monomers only.

Another important range for the identification of polymer additives in cement mortars is enclosed

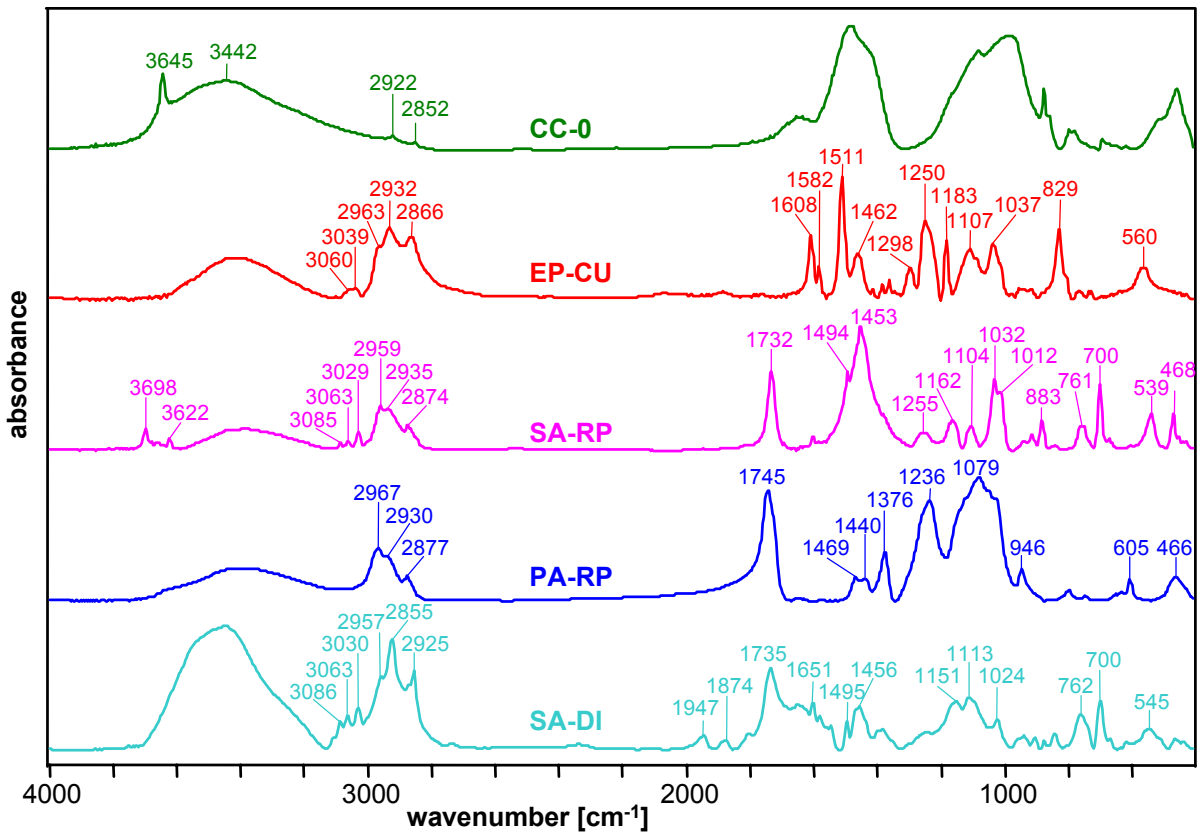

Figure 1. IR spectra of the CC-0 reference and the hardened polymer additives

by the wavenumbers 1700 up to 2000 cm^{-1}. The absence of the strong ν-C=O vibration at 1720 - 1750 cm^{-1} excludes ester groups, this is valid for the EP-CU epoxy system in the present work. Moreover, the accurate wavenumber of the ν-C=O vibration peak top makes it possible to distinguish between the vinyl acetate-versatic acid vinylester-copolymer PA-RP with 1745 cm^{-1} and the styrene-acrylate-copolymer (SA-RP, SA-DI) with 1732 cm^{-1}. Additional weak peaks were observed for SA-DI above the ν-C=O vibration. These peaks were assigned to C-C combination vibrations of the aromatic core.

The comparison of the IR spectra in Figure 1 shows clearly that a lot of polymer peaks of PCC's should be overlapped by vibrations typical for cement mortars. In fact, the polymer peaks in the IR spectra of PCC's are mostly covered for wavenumbers below 1700 cm^{-1}. Besides, small polymer contents nearly or below 1 w.-% results in very weak polymer peaks preventing a reliable polymer identification.

Therefore, polymer additives were removed from the PCC's and enriched by reflow extraction and deposited on silicon wafer pieces as described above. The IR transmission spectra on polymer films deposited from polymer solutions in acetone are compared in Figure 2 for PA-RP and the related PCC3. No significant differences between the absorption peak positions were observed for this example or for the other polymer additives. According to that, the reflow extraction makes possible a reliable identification of hardened polymer additives. A reactive conversion of the polymers can be excluded for the described storage conditions.

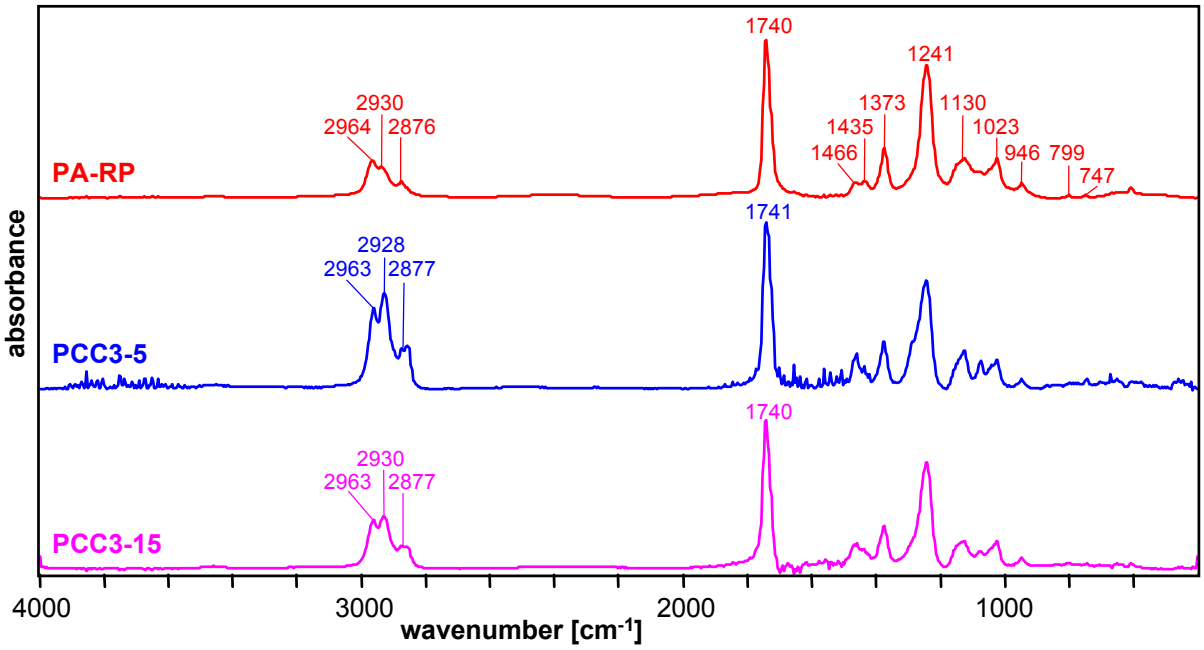

Figure 2. IR spectra on films deposited from PA-RP solution and from PCC3 extracts

3.2 Thermal analysis

3.2.1 Characterisation of polymers and PCC's

Thermoanalytic measurements were carried out in atmospheres of purified air and argon, respectively. Corresponding measurements on PCC4-15 are shown in Figure 3 for example. The thermogravimetric curve (TG) and its first derivative (DTG) were used for characterisations, the heat flow was removed for clarity. As expected for a cement mortar the sample mass changes slowly up to 900 °C according to the dehydration of the cement paste. The extended mass loss is superimposed by the portlandite dehydration and by the calcite decomposition. The measurement in

air shows an additional mass change caused by the polymer decomposition. Obviously, the use of an inert argon atmosphere shifts the polymer decomposition in the range of the portlandite dehydration so that these two mass steps can not be distinguished.

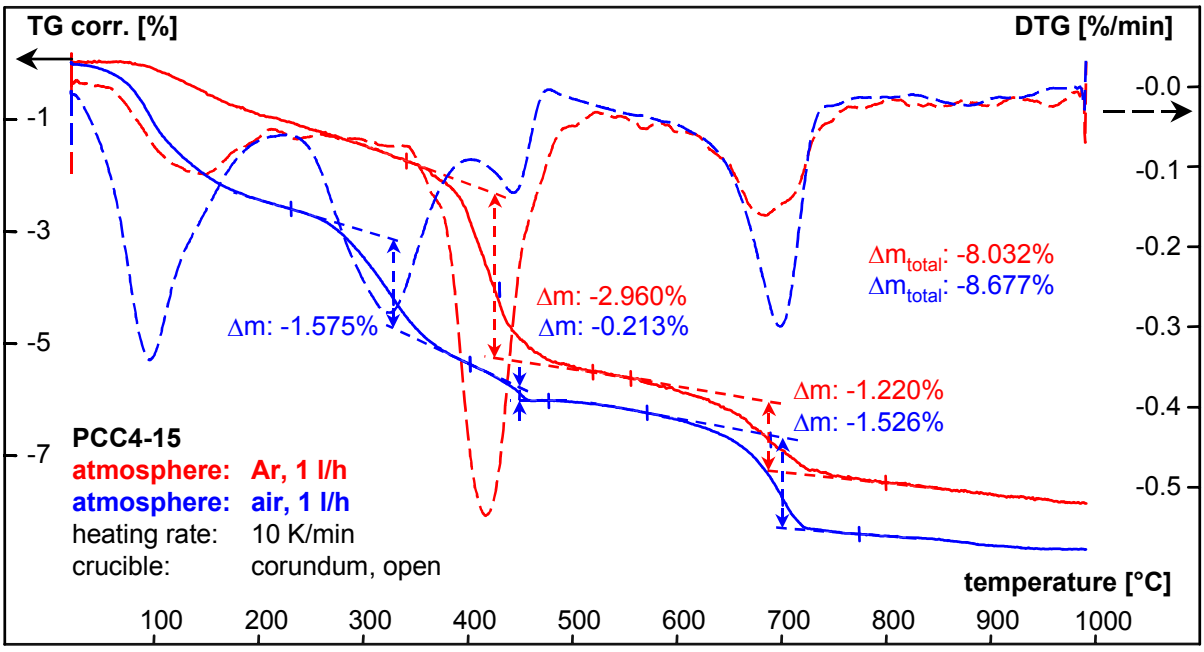

Figure 3. Thermogravimetric measurements on PCC4-15 in different atmospheres

A quantitative analysis of the mass changes by the sole use of the TG curve is difficult since the decomposition reactions superimpose each other. Therefore, the limits for mass changes were consequently selected using the DTG curve maximums near the relevant mass changes. The mass changes were determined using a tangential baseline correction in contrast to the usual evaluation with horizontal baselines. In that way the superimposed cement stone dehydration was eliminated from the other mass steps. The tangential evaluation method was verified on synthetic mixtures of cement paste (CS) with $CaCO_3$. According to [5] the tangential evaluation gave results close to the true $CaCO_3$ content in contrast to the horizontal evaluation [6] resulting in values much too high.

The DTG curves of the PCC's in air are depicted in Figure 4, the DTG peak top temperatures of the polymer decomposition of pure hardened polymers and of PCC's are summarized in Table 2. Although the peak temperatures of PCC's are shifted compared to the pure polymers possibly caused by the homogeneous distribution in PCC's, the polymer additives in PCC's can be clearly distinguished using the DTG peak top temperatures.

Table 2. DTG peak top temperatures of polymers and PCC samples in air

PCC	base peak		polymer	base peak	further polymer peaks				Δm_{total}
	-5[a] [°C]	-15[a] [°C]		[°C]	[°C]	[°C]	[°C]	[°C]	[w.-%]
PCC1	353	353	EP-CU	350	620				-98.525
PCC2	340	337	SA-RP	374	275	485	560	708	-82.182
PCC3	313	317	PA-RP	334	440	551			-87.582
PCC4	332	340	SA-DI	388	503				-99.571

[a] last number in the sample mark, e.g. 15 in PCC1-15

In contrast to the measurements in air, an inert argon atmosphere sometimes causes a peak shift to higher temperatures, especially for the styrene-acrylate-copolymer. A separate determination of the polymer decomposition and the portlandite dehydration was not possible for the samples SA-RP and SA-DI in an argon atmosphere.

3.2.1 Characterisation of synthetic mixtures of cement paste and hardened polymers

The measurements on PCC4 in different atmospheres depicted in Figure 3 shows different mass steps for the calcite decomposition. This observation was made for all PCC's, but not for the reference mortar CC-0. It is clear that the CO_2 content within the sample should not be influenced by a change of the atmosphere. Besides, the experimental mass changes for the polymer decomposition of PCC's amount less than 50 % of the expected values. For example, the mass loss of SA-DI amounts nearly 100 % (Table 2), the content in PCC4-15 is 3.43 % (Table 1) and the polymer decomposition results only in a mass loss of 1.58 %.

Where does the additional carbon dioxide come from? It suggests that it is generated by the oxidation of the polymer, but why is it released at such elevated temperatures? The most simple explanation is the assumption that a considerable part of the CO_2 produced by the polymer reacts immediately with free $Ca(OH)_2$ or CaO contained in the sample. For this reason, an increasing polymer content in a PCC should be accompanied by mass changes decreasing for the $Ca(OH)_2$ and increasing for the $CaCO_3$ decomposition. This hypothesis cannot be checked using the PCC samples since the polymer content perhaps influences the hydration or the carbonation of the mortars. Therefore, synthetic mixtures of an aged cement paste with hardened polymers SA-RP and PA-RP were prepared and characterised with thermal analysis. Figure 5 shows measurements on pure cement paste and on mixtures of the same cement paste with hardened SA-RP. The experimental mass changes vary with the polymer content corresponding to the behaviour predicted here.

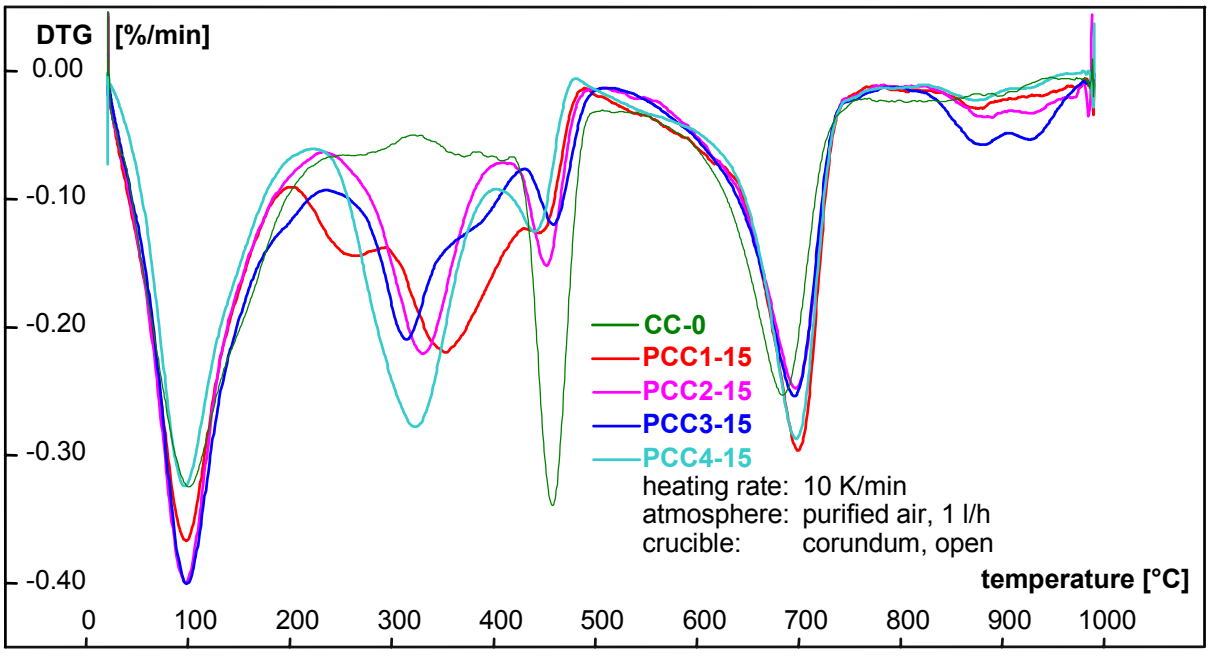

Figure 4. Differential thermogravimetric measurements on PCC

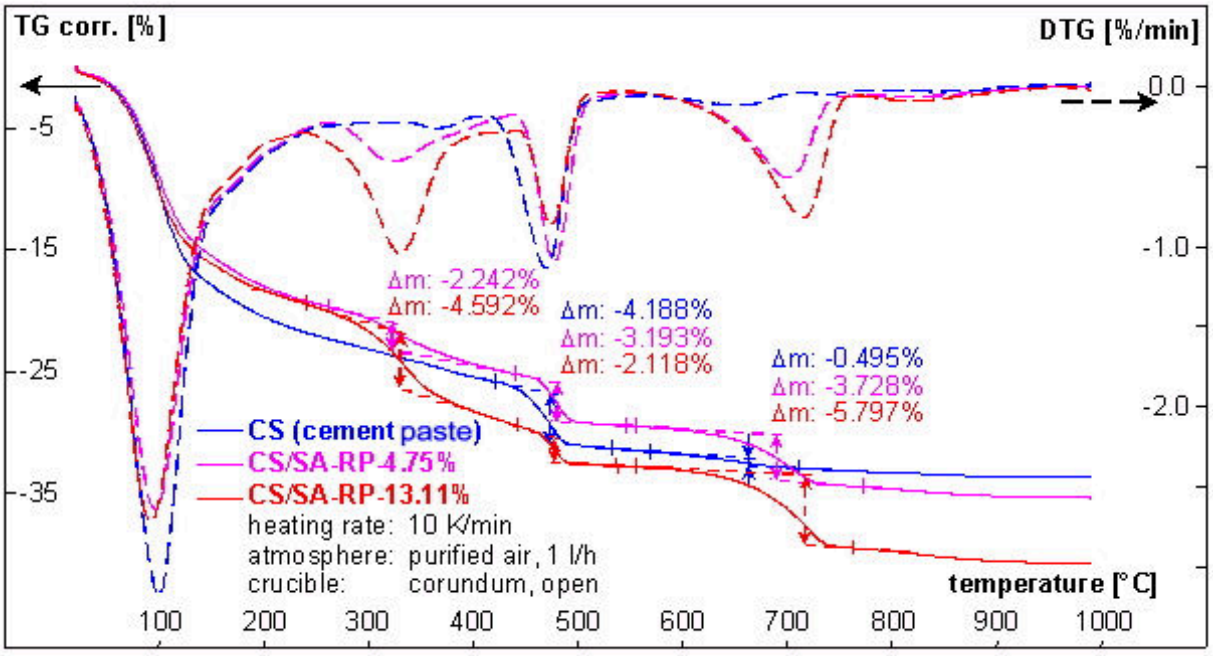

Figure 5. Thermogravimetric measurements on mixtures of cement paste with SA-RP

The theoretical mass changes for the synthetic mixtures $\Delta m_{th.,\,mi}$ can be calculated using the experimental mass changes of the pure cement paste $\Delta m_{exp.,\,CS}$ and the polymer content w_{pol} according to Equation 2.

$$\Delta m_{th.,\,mi} = \Delta m_{exp.,\,CS} \cdot (1 - w_{pol}) \tag{2}$$

This equation is valid if no reactive interaction exists between the components of the mixture. For this case an increasing polymer content should only generate a slight decrease of the mass changes generated by the cement paste. In contrast to that, the observed distinct differences $\Delta\Delta m_{pol.}$ between the theoretical $\Delta m_{th,\,mi}$ and the experimental mass changes $\Delta m_{exp.,\,mi}$ of the $Ca(OH)_2$ and $CaCO_3$ decomposition should be assigned to the influence of reactive CO_2 coming from the polymer.

$$\Delta\Delta m_{pol.} = \Delta m_{exp.,\,mi} - \Delta m_{th.,\,mi} \tag{3}$$

The values $\Delta\Delta m_{pol.}$ were used to calculate the additional CO_2 amounts $m_{pol.}$-CO_2 which decreases the $Ca(OH)_2$ and increases the $CaCO_3$ mass change.

$$\underset{m_{pol.}\text{-}CO_2}{\overset{44{,}008\ g/mol}{Ca(OH)_2\ (CS) + CO_2\ (pol)}} \rightarrow \underset{\Delta\Delta m_{pol.}\text{-}Ca(OH)_2}{\overset{18{,}015\ g/mol}{CaCO_3\ (pol) + H_2O\ (CS)}} \tag{4}$$

The simple stoichiometric calculation according Equation 4 shows that the CO_2 amount consumed by $Ca(OH)_2$ is significantly smaller than the polymer-generated CO_2 amount found by the $CaCO_3$ decomposition. Therefore it was concluded that free CaO existing above the portlandite decomposition temperature also consumes polymer-generated CO_2. This conclusion is supported by the measurements in Figure 5 since the TG curves above the portlandite decomposition show more horizontal slopes for the mixtures compared to the cement paste. Surprisingly, a recently published work [7] even describes a distinct mass gain after or above the portlandite dehydration in a nitrogen atmosphere for a concrete modified by ethylene/vinyl acetate. This fact was explained by a reaction of an intermediate formed organic carboxylate with hydroxyl ions released by cement hydrate phases. However, a sample mass gain during thermoanalytic measurement requires absolutely the take up of a gaseous component. Therefore, the described mass increase has to be assigned to the

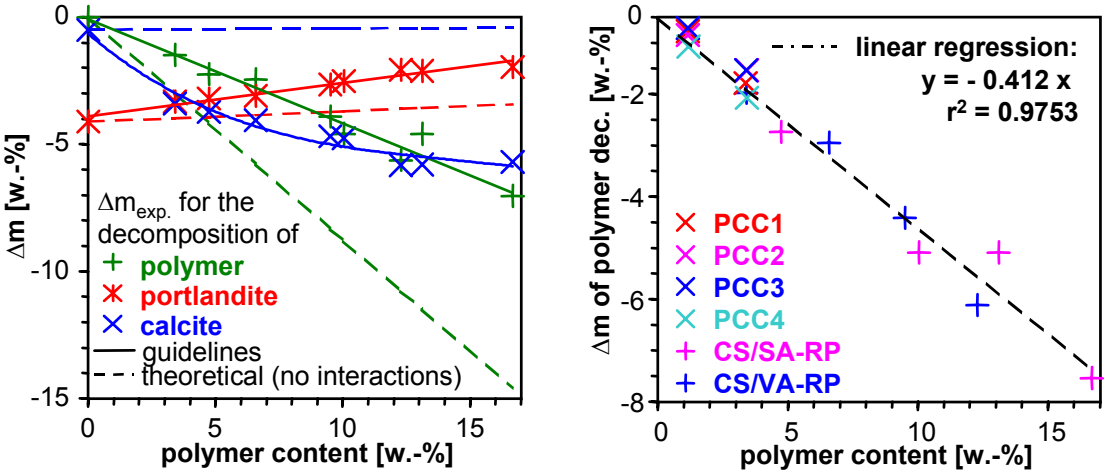

Figure 6. (a) Thermoanalytic mass changes of mixtures of cement stone with hardened polymers (b) Mass changes of the polymer decomposition of synthetic mixtures and PCC's

oxidation of organic components caused by oxygen impurities of the atmosphere instantaneously followed by the take up by the sample. Besides, the content of hydroxyl groups is comparatively low at temperatures above the portlandite dehydration.

The relevant mass changes determined for all synthetic mixtures are shown in Figure 6a dependent on the polymer content. The opposite behaviour of the experimental and the theoretical mass changes demonstrates the strongly reactive interaction of the polymer-generated CO_2 with $Ca(OH)_2$ and CaO. Unfortunately, a thermal analysis in an inert atmosphere is also not suited to fully suppress the reactions corresponding to the data of other works [7].

Fortunately, the mass change of the polymer decomposition in air shows a linear dependence on the polymer content and is obviously independent on the kind of polymer. This is supported by Figure 6b containing the mass changes of the polymer decomposition for PCC's and for the synthetic mixtures together. A linear regression using the whole data set results in a well-defined functional dependence with a satisfactory quadratic correlation coefficient.

4. CONCLUSIONS

It was shown that the polymer additives can be identified with IR spectroscopy and by thermal analysis. On principle, IR spectroscopy makes it possible to identify the basic polymer system of an additive without a reference sample. Nevertheless, a reliable identification of additives in concrete mortars requires the reflow extraction of the polymer component, since the vibrations of a typical mortar covers the majority of polymer peaks below 1700 cm^{-1}. A differentiation between some basic polymer systems can be made by some peaks within the wavenumber ranges from 1700 cm^{-1} to 2000 cm^{-1} and from 2840 to 3110 cm^{-1}, but a reliable assignment requires the measurement of reference samples to get "finger print" spectra. The main reason for this limitation is the unknown composition of commercial products consisting of a multitude of components. For example, small amounts of surfactants are able to change the properties of a polymer dispersion significantly, but these small amounts were normally not noticed in IR spectra.

The extraction of nearly 30 % of the polymer additives from hardened PCC's within 8 hours with an ordinary non-toxic solvent such as acetone was a real surprise, especially for the thermosetting epoxy resins. Because of the high molecular mass of the copolymers used it is understandable that an extraction of the whole polymer was not possible within such a short time, but the opinion that the extraction of polymers from hardened concrete is not possible [8] should be given up.

The IR spectra on the polymer films deposited from the extracts show no significant differences compared to those deposited from polymer solutions. In other words, no significant variations of the spectrum caused by the mortar hardening and no hints for a reactive conversion of the hardened polymer additives were observed in contrast to references [9, 10, 11].

The identification of polymer additives in PCC's with thermal analysis always requires the measurement of reference products, because the characteristic decomposition temperatures do not only depend on the measurement conditions as heating rate or atmosphere, but also on the special conditions of the thermal analyser used such as crucible shape and material, thermocouple, thermal contact, sample mass, gas flow etc. Nevertheless, the thermal analysis is well-suited for the quantification of the additives because of the high reproducibility of the mass changes. Although the experimental mass changes of the polymer decomposition amounted to only 40 % of the theoretical ones, the well-defined functional dependence on the real polymer content can be used for the quantitative determination of all polymers tested. In contrast to previous works [6, 7] the thermal analysis should be carried out in an oxidising atmosphere since, for some polymers, a shifting of the polymer decomposition step into the $Ca(OH)_2$ dehydration step was observed.

The most surprisingly result of this work is the evidence that a considerable part of the polymer-generated CO_2 reacts with $Ca(OH)_2$ and CaO during the thermoanalytic measurement. According to our previous comments, a quantitative thermal analysis of the portlandite and calcite content of a polymer containing concrete is accompanied by systematic errors at every time. Looked from this point of view, the opinions on the influence of the polymer content or more general of organic additives on the carbonation of concrete should be reconsidered if thermal analysis was used for the quantification [6, 7, 12, 13].

ACKNOWLEDGEMENT

This work results from a co-operation within the SFB 524 supported by the Deutsche Forschungsgemeinschaft DFG.

REFERENCES

[1] Ettel, W.-P. Kunstharze und Dispersionen für Mörtel und Betone. Struktur der Polymere, Planung, Bemessung, Prüfung, Düsseldorf, Beton-Verlag GmbH, 1998

[2] Dimmig, A. Einflüsse von Polymeren auf die Mikrostruktur und die Dauerhaftigkeit kunststofffmodifier Mörtel (PCC), PhD thesis, Weimar, 2002

[3] Kwasny, R., Roosen, A., Maultzsch, M. Comparative investigations on repair mortars (PCC). Betonwerk u. Fertigteil-Technik, vol.52, 1986 (12), pp.797-803

[4] EN ISO 6427, Bestimmung der extrahierbaren Bestandteile durch organische Lösungsmittel, European Standard, 1992

[5] Huppertz, F., Wiens, U. and Rankers, R. Methoden zur Bestimmung der Reaktivität von Zementen und Puzzolanen, GIT Labor-Fachzeitschrift, 1999 (6), pp.655-659

[6] Maultzsch, M. Die thermogravimetrische Analyse (TGA) in der Materialprüfung kunststoffmodifizierter Zementmörtel, Materialprüfung, vol.30, 1988 (5), pp.157-161

[7] Silva, D.A., Roman, H.R. and Gleize, P.J.P. Evidences of chemical interaction between EVA and hydrating Portland cement. Cement and Concrete Research vol.2079, 2002, pp.1-8

[8] Tubbesing, K. Mikrostruktur von PCC – Gefügeuntersuchungen an polymermodifizierten Zementsteinen, PhD thesis, TU Hamburg-Harburg, 1993

[9] Gierloff, M. Beeinflussung von Betoneigenschaften durch Zusatz von Kunststoffdispersionen, Forschungsbericht 104, Berlin, Bundesanstalt für Materialprüfung, 1984

[10] Pera, J. and Ambroise, J. Influence of Different Polymers on the Properties of Cementitious Matrices. 10. Intern. Congr. on polymers in Concrete and ICPIC/ICRI International Concrete Repair Workshop, Hawai, 2001, in press

[11] Atkins, K.M., Edmonds, R.N. and Majumdar, A.J. The hydration of Portland and aluminous cements with added polymer dispersions, Journal of Material Science, vol.26, 1991, pp.2372-2378

[12] Agarwal, S.K., Assod, I. and Malhotra, S.K. Compatibility of superplasticizers with concrete, Constr. and buliding Materials, vol.14, 2000, pp.253-259
[13] Dollimore, D, Gupta, J.D., Lerdkanchanaporn, S. and Nippani, S. A thermal analysis study of recycled portland cement concrete (RPCC) aggregates, Thermochimica Acta, vol.357-358, 2000, pp.31-40

EXPERIMENTAL STUDY AND NUMERICAL SIMULATION OF CEMENT HYDRATION AND THE DEVELOPMENT OF MICROSTRUCTURE IN CEMENTITIOUS MATERIALS

Ye Guang[1], K. van Breugel[1] and A.L.A. Fraaij[1]

[1]Faculty of Civil Engineering and Geosciences, Delft University of Technology, Delft, the Netherlands; E-mail: ye.guang@ct.tudelft.nl, k.v.Breugel@ct.tudelft.nl

ABSTRACT

A better understanding of the evolution of cement hydration and of the development of microstructural formation of cementitious materials at early age is a very important requirement for developing a numerical simulation method. Experimental studies and numerical modelling become increasingly significant for understanding the microstructural properties during cement hydration. In this study, a multifunctional experiment combining ultrasonic pulse velocity measurements and dielectric conductivity measurements was performed both on cement paste and on concrete mixtures with water/cement ratio 0.4, 0.45, and 0.55 and with different amounts of aggregate. The samples were cured isothermally at 20°C, 30°C and 40°C. The measurements were conducted up to an age of 3 days for the cement paste and 7 days for concrete.

The initial setting of cement paste was found at the time when a sudden increase in the ultrasonic pulse velocity occurred and a notable drop in the electric conductivity was observed. These sudden changes were also detected with the cement hydration simulation model HYMOSTRUC, in which a percolation threshold of the solid phase corresponded with the initial setting time. As expected, the lower water/cement ratio and the higher curing temperature exhibited a quick increase in ultrasonic pulse velocity and a remarkable decrease in conductivity. At a certain point of hydration, the pulse velocity showed a slow increase whereas at the same moment a full connectivity of solid phases was found with the simulation model. From this study, the validity of the HYMOSTRUC model was proved by comparison with the ultrasonic pulse velocity measurements and dielectric measurements. This multifunctional experimental setup also shows the potential for monitoring the evolution of cement hydration and the development of microstructure in hardening cement-based materials in a non-destructive way.

1. INTRODUCTION

It is well known that cement hydration is a complicated process of physical and chemical reactions between cement particles and water, in which a wide variety of factors, such as water/cement ratio and curing temperature, are involved. In the engineering practices, the presence of aggregates, further aggravates this already complex process of microstructure evolution.

Enormous attempts were dedicated to a better and comprehensive understanding and quantitative description of the microstructure development of cement paste and concrete, with particular emphasis to the duration of cement setting. However, many techniques are suffering from all kinds of limitations and deficiencies. For example, the application of scanning electron microscopy image and small angle X-ray scattering is restricted due to the demanding process of sample preparation [1, 2]. The interpretation of mercury intrusion porosimetry experiments is very difficult because of

Proceedings of the 11th International Congress on the Chemistry of Cement (ICCC)
'Cement's Contribution to the Development in the 21st Century'
Hosted by: The Cement and Concrete Institute of South Africa
CD-ROM produced by: Document Transformation Technologies

11 - 16 May 2003, Durban, South Africa
ISBN Number: 0-9584085-8-0
Editors: Dr G. Grieve and G. Owens
Congress Organised by: Event Dynamics

the so-called inkbottle effect and damages to the capillary pore structure [3]. Recently, non-destructive techniques have attracted increasing attention for monitoring the early-age behaviour of cementitious materials [4-8]. Among them, the ultrasonic technique seems to be a valuable tool for following the setting and hardening progress of cement and concrete because of its high sensitivity to the evolution of solid phases and especially to the solid phase percolation [4, 9]. In parallel, the electrical properties were found to be very useful in the investigation of properties and topology of aqueous phase [10]. It should be noted that ultrasonic pulse velocity (UPV) measurements and dielectric property measurements have the advantages of accuracy, simple test procedures, and applicability at early age of cement hydration.

A non-destructive multifunctional setup [11,12], consisting of a dielectric sensor and high-frequency ultrasonic transducers, was adopted in this research work to measure the electric conductivity and UPV of Portland cement pastes and concretes. Three important technical parameters, namely water/cement ratio, curing temperature and volume of aggregate, were taken into account. The experimental results were compared with the calculations performed with the cement hydration computer model HYMOSTRUC [13]. The detailed modelling concepts of this program will be given in section 2.

The purpose of this research work was to provide more accurate information about the microstructure development of cement and concrete and, on the other hand, to compare the numerical simulation of this evolution process with the experimental study in order to improve the reliability and applicability of HYMOSTRUC. Meanwhile, the technique employed in this study enables accurate monitoring of the setting and hardening process of concrete at the construction site, which is important for the time of removal of formwork and of applying the prestress.

2. MODELLING OF HYDRATION AND MICROSTRUCTURE DEVELOPMENT

For the simulation of reactions between water and cement and of the formation of microstructure in cement-based materials, a numerical simulation model called HYMOSTRUC was developed at Delft [13]. HYMOSTRUC stands for **HY**dration, **MO**rphology and **STRUC**tural development. A scheme of the model concepts and a simulated cement paste is shown in Figure 1.

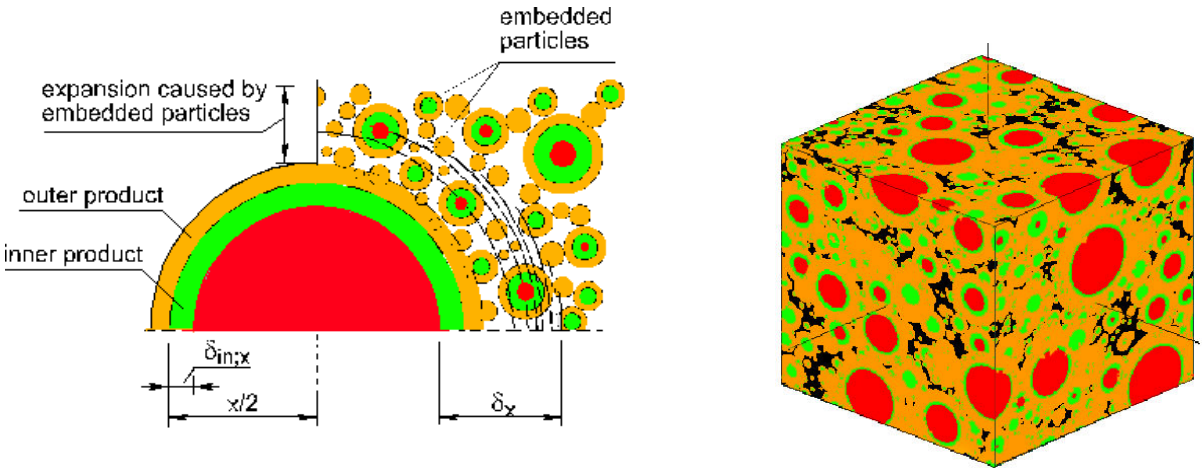

a) Cement particles interaction mechanism.

b) Simulated cement paste ($100 \times 100 \times 100$ μm^3), black color denotes capillary pore.

Figure 1. Formation of a microstructure in hardening cement paste, simulated with HYMOSTRUC model [13, 18].

In this model, the rate of hydration is modelled as a function of the particle size distribution and the chemical composition of the cement, the water cement ratio and the reaction temperature. Moreover, the effect of physical interactions between hydrating cement particles on the rate of hydration of individual cement particles is modelled explicitly. The cement particles are modelled as digitised spheres randomly distributed in a three-dimensional cement-water system and the hydrating cement grains are simulated as growing spheres. As cement hydrates, the cement grains gradually dissolve and a porous shell of hydration products is formed around the grain in the porous space. This results in an outward growth or "expansion" of the particles. The hydrates around the cement grains first cause the formation of small isolated clusters. Big clusters are formed when small cement particles become embedded in the outer shell of other particles, which promotes the outward growth of these particles. As hydration progresses, the growing particles become more and more connected and the material changes from the state of a suspension to the state of porous elastic solid.

3. EXPERIMENTAL PROCEDURES

3.1 Theoretical background

As discussed before, cement hydration is an evolution process from a suspension state of cement in water to a solid heterogeneous network of hydration products and unhydrated cement particles. The theoretical background of UPV and dielectric measurements lies in the fact that the electric conductivity is mainly sensitive to changes in the liquid phase, whereas the ultrasonic pulse velocity corresponding to changes in the solid phase [5-7,9,14,15].

A basic principle of physics says that the motion of any wave will be affected by the medium through which it travels [16], because the wave velocity is determined by the stiffness and density of the material. In the process of cement hydration, cement matrix acquires and accumulates stiffness as a result of the microstructural evolution. This allows us to correlate the change of UPV through cement paste with the microstructural development of cement matrix at early age. In concrete mixtures, during the fluid period, the ultrasonic velocity is not sensitive to structure formation in the paste [7], while the water/air phase plays a dominant role in ultrasonic pulse propagation [7,17]. As cement particles gradually dissolve and nucleate, a percolating solid network will be developed as a result of increasing connection between small clusters of particles. At this moment, the ultrasonic pulse propagation path switches from the liquid phase to the solid phase.

The permittivity is correlated to the electrical polarization of a material and gives insight into the density of energy stored in the material that is subjected to an electric field. The electrical conductivity instead, is correlated to the amount of dissipated energy due to the ohmic flow of charge carriers or to the orientational movement of dipoles under the applied field. In cement paste, the pore space is partly filled with a conductive water solution that is the main path for the flow of current.

3.2 Experimental setup

A multifunctional experimental setup [11,12] was designed, incorporating an ultrasonic and a dielectric measurement device with a temperature controlling system. The ultrasonic transducers, dielectric sensor and temperature probe were integrated in a 150×150×200 mm^3 steel mould. Figure 2 provides a detailed description of the experimental setup.

A 20 MHz dielectric sensor called CONSENSOR was used to perform the permittivity and conductivity measurements. At this frequency, it was realistic to simulate the cementitious material as a capacitor and a resistor, where the capacitor was correlated to the permittivity and the resistor to the conductivity. The sensor is made of two stainless steel rods 3 cm long, 1 cm diameter and

spaced 2 cm, which are attached to a circular disc. The circular disc was fixed onto the inner surface of the mould so that the electrodes penetrated into the concrete.

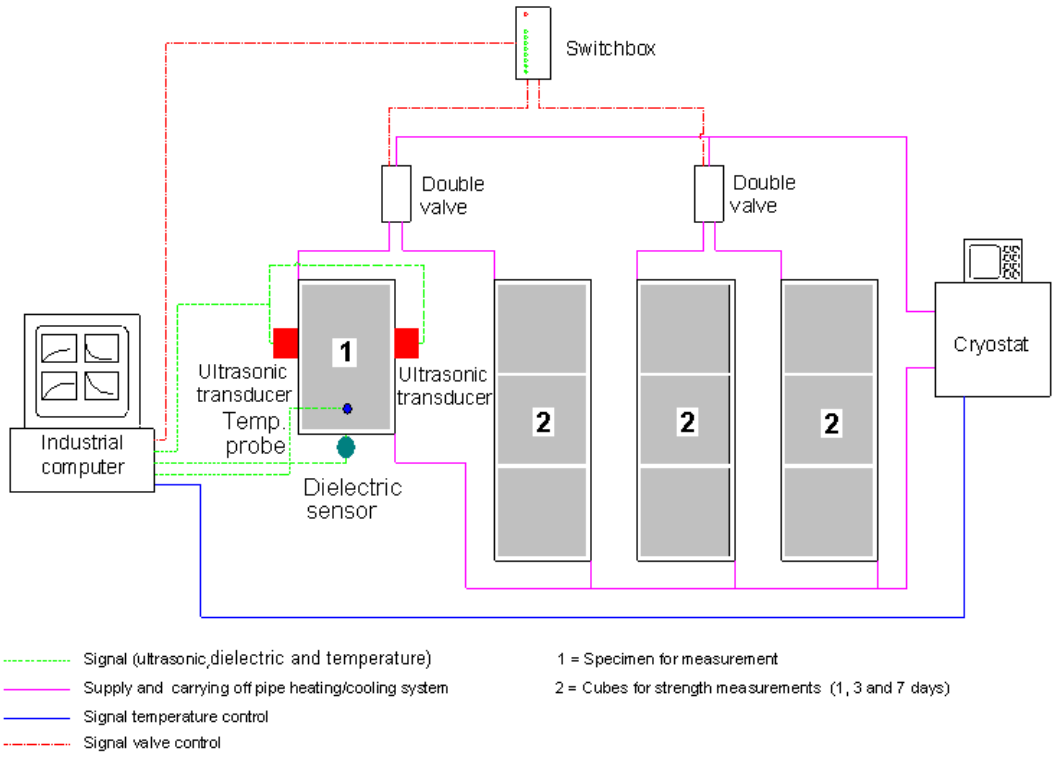

Figure 2. Experimental setup for monitoring UPV and dielectric conductivity.

The ultrasonic measurement was conducted with a PUNDIT plus equipment with a 54 kHz transducer. In order to avoid the influence of the wall of the steel mould on the ultrasound propagation, two holes with a 54 mm diameter were made in the wall. The transducers were fixed by a PVC ring and coupled directly through a piece of plastic membrane glued on the inner wall of the mould; four springs were used to adjust the transducer's contact pressure to guarantee good contact with the specimen. In this way, the attenuation of ultrasound waves that may be caused by the wall of the steel mould was completely avoided.

The temperature of the whole system was controlled by a cooling system with an accuracy of ΔT = 0.1°C. One Pt 100 probe was used for the thermal control. All control units were connected with a industrial computer. The hydration time, permittivity, conductivity, ultrasonic pulse velocity, and temperature were automatically recorded every 10 minutes.

3.3 Materials

A series of tests is performed on two groups of cement and concrete with water/cement ratio of 0.40, 0.45, and 0.55, and isothermally cured at 20, 30, and 40 °C. For the concrete samples, the amount of aggregates is given in Table 1. Measurements started 15 minutes after mixing. The specimens were subjected to vibration in order to remove the extra air bubbles. The compressive strength tests on cubes, 150×150×150 mm^3 are performed at an age of 1, 3 and 7 days.

Table 1. Mixture proportions of concrete

Specimen No.		Cement type	Cement content [kg/m^3]	Aggregate content [kg/m^3]	w/c [-]	Temperature [°C]	Curing age [days]
Concrete	PCA16350-40	CEM I/32.5	350	1942	0.40	20, 30,40	7
	PCA16350-45	CEM I/32.5	350	1884	0.45	20, 30,40	7
	PCA16350-55	CEM I/32.5	350	1792	0.55	20, 30,40	7
Cement paste	PCP-40	CEM I/32.5	350	0	0.40	20, 30,40	3
	PCP-45	CEM I/32.5	350	0	0.45	20, 30,40	3
	PCP-55	CEM I/32.5	350	0	0.55	20, 30,40	3

4. RESULTS AND DISCUSSIONS

4.1 Profile of UPV and conductivity with progressive hydration

UPV and conductivity were measured for all cement and concrete specimens with the evolution of cement hydration. The results were plotted versus hydration time. (see Figure 3). The profile of UPV indicated a very low value within the first few hours (corresponding to the fluid state) and then exhibited a sharp increase between 10 and 40 hours, which was followed by a plateau without significant changes. The quick and obvious increase in UPV revealed a concurrent increase in the connectivity of the solid phase. In fact, only connected solids are able to transmit high-velocity mechanical waves.

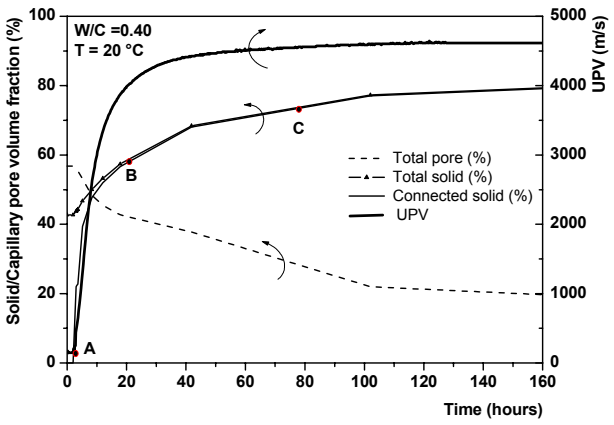

Figure 3. Correlation between UPV and microstructure development

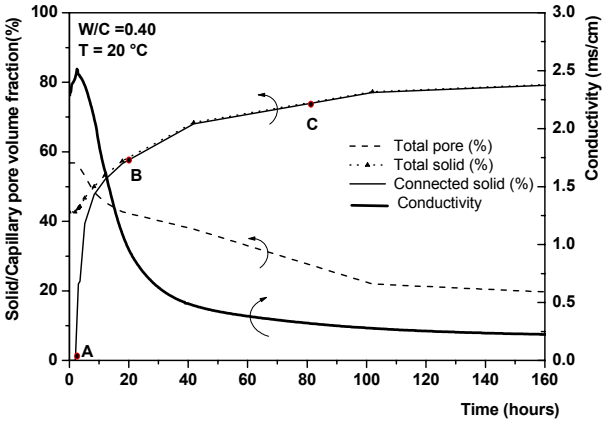

Figure 4. Correlation between conductivity and microstructure development

The curve of conductivity evolution (see Figure 4) presented a different picture, with a slight increase in the very early stage just after mixing. This could be explained by the ion dissolution and correlated effects. However, a subsequent large decrease of conductivity could be attributed to the continuous reduction of the amount of water in the capillary pores. Similar to UPV profile, after 80 hours hydration of cement, the dielectric properties did not exhibit pronounced changes.

From the above discussion, the evolution of UPV and conductivity can be simplified to four typical characteristic stages, as shown in Figure 5. This profile of four stages was general for all test specimens. The duration of each stage depended on the technical parameters including water/cement ratio and curing temperature. The influence of these parameters will be discussed in the following section.

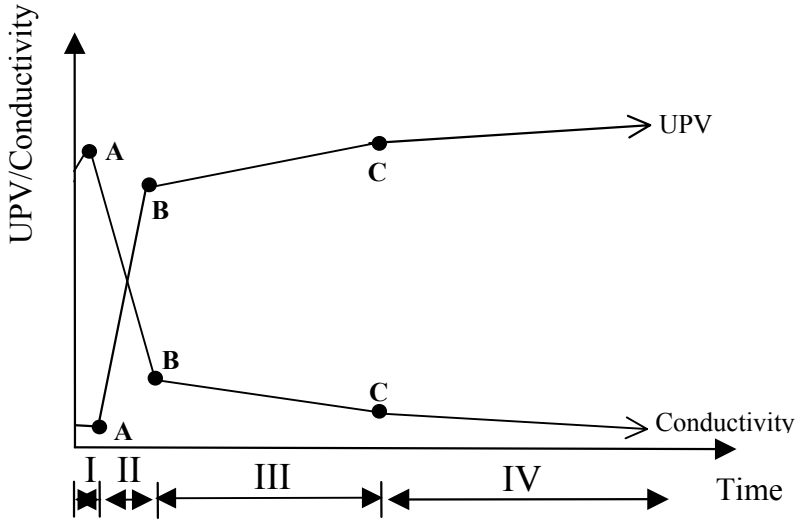

Figure 5. Simplification of the evolution of UPV/conductivity in four characteristic stages.

4.2 Correlation between UPV and dielectric properties with the microstructural evolution

With the progress of cement hydration, hydration products and unhydrated cement particles become interconnected, resulting in a porous network. The volume fraction of solid and pore phase will change and, as a consequence, the UPV and the dielectric properties will also change.

It was observed that the UPV value at the initial stage was lower than the UPV in water (1430m/s) and even lower than in air (340m/s). According to Keating and Sayers [6,7], this phenomenon was caused by air entrapped in the paste. Both the air bubbles in the mixing water and the tiny air bubbles that were entrapped into the paste during mixing contributed to the existence of air bubbles in fresh mixture. During this initial period, hydrates were formed in a very low amount and therefore, the entrapped air bubbles played a dominant role in the evolution of UPV [17]. The pronounced increase in the second stage could be accounted for by the following facts: (1) The entrapped air bubbles migrated to the surface of the concrete due to bleeding. Hence, the amount of entrapped air was reduced; (2) After the dormant period, the amount of solid phases became enough to interconnect the solid particles. At this moment, the material changed from a suspension system to the state of a porous elastic solid. Very slight increase in the pulse velocity was found when UPV had reached a plateau.

The HYMOSTRUC3D [18] model was utilized to study the quantitative relation between volume fraction of the solid/pore phase and the ultrasonic/dielectric properties. It was shown in Figure 3 that the percolation threshold of the solid phase (i.e. point A, when the solid phase became interconnected), calculated from HYMOSTRUC3D, was found to correspond exactly with the starting point of the sudden increase of the UPV. The percolation threshold of the solid phase is identified as the end of the dormant stage of cement hydration. When this threshold (about 3~4 hours of hydration in this research) was reached, a solid percolation path is formed in the hydrating paste. It was calculated from HYMOSTRUC3D that for a cement specimen with water/cement ratio of 0.45 and curing temperature at 20 °C, a percolation threshold was reached at a hydration degree of 2.7% [9]. At that moment, the volume fraction of the total solid was 52% and the volume fraction of connected solid was 30% of the cement paste. After this critical point, the UPV revealed a significant increase (A⟶B) because the stiffness of the cement paste largely depended on the connectivity of the solid phase. This period was accompanied by a similarly fast increase in volume fraction of connected solid from 30% to 60% (when degree of hydration is about 25%). However, after almost all the solid phases become connected (point C in Figure 5), the UPV showed a

plateau. The percolation threshold of the solid phase, point A in Figure 5, can be considered as the initial setting of the cement paste, whereas the point B, the end of the acceleration period, can be considered as the final setting of cement particles. Point C, in which most of the interparticle contacts are formed, is the significant moment for the removal of formwork and for applying the prestress.

While the UPV was sensitive to the connectivity of the solids, the electric properties were sensitive to the modifications of the aqueous phase. This could be proved by the good correspondence between the profile of conductivity and changes in the capillary pore phase. Therefore, the electric conductivity is a good parameter to monitor de-percolation of the capillary porosity [11, 12].

4.3 Influence of technical parameters

In this section, the influence of technical parameters on UPV and conductivity of cementitious material will be discussed.

4.3.1 Water/cement ratio

Results of UPV and conductivity measurements for cement and concrete of three different water/cement ratios revealed similar shapes and trends of the curves. A quicker increase in pulse velocity was observed in concrete than in cement paste with the same water/cement ratio. For example, the profile of UPV and conductivity for concrete cured at 20 °C is shown in Figure 6. Mixtures with a higher water/cement ratio showed lower values of the pulse velocity and higher conductivity. The pulse velocity was almost 8~10% higher in concrete with w/c ratio of 0.45 than in w/c ratio 0.55. This is expected because the higher the water/cement ratio, the lower the density of the microstructure of the cement paste.

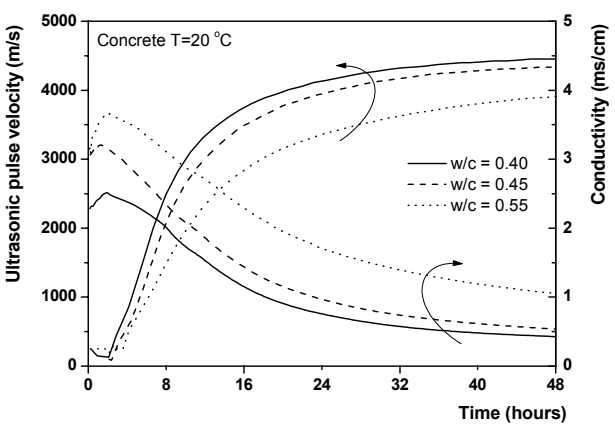

Figure 6. Influence of water/cement ratio on UPV and conductivity of early age concrete

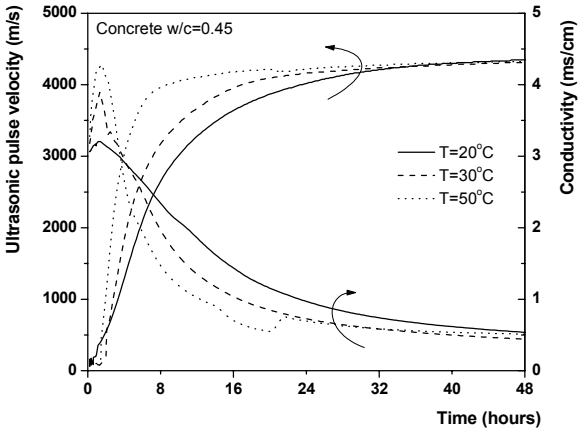

Figure 7. Influence of curing temperature on UPV and conductivity of early age concrete

4.3.2 Curing temperature

Due to the fact that the evolution of the UPV and conductivity were similar, results for a representative group of concrete with water/cement ratio 0.45 cured at different temperatures shown in Figure 7. It could be concluded that, the higher the isothermal curing temperature, the quicker the increase in pulse velocity during the second stage. In other words, the UPV reached a plateau within a shorter period if the specimen was cured at higher temperatures. As for the conductivity measurement, specimens with higher curing temperature also revealed a sharper decrease during the

second stage of profile evolution. After the plateau was reached, the temperature showed a less pronounced influence on both the pulse velocity and the conductivity.

4.3.3 Amount of aggregates

The influence of amount of aggregates was studied in the case of w/c ratio 0.37 and the aggregate volumetric fraction varied from zero (plain paste) up to 75% (concentrate concrete). The aggregate is composed of sand (lower than 4 mm) and crushed aggregate (between 4 and 16 mm). A constant weight ratio between the two components was kept. Additives were 5% silica fume on binder base (in slurry form), a lignosulphonate-based plasticizer and a naphthalene-sulphonate-based superplasticizer (see Table2). Tests were done till an age of 7 days. The temperature was kept at 10, 20 and 40°C. Figure 8 shows the effect of aggregate on the conductivity (left) and UPV (right). With increasing amount of aggregate, the UPV curve shifted upwards, this because the presence of aggregate contributed to the amount of connected solid phase in the concrete. It was well defined in [19], that the evolution of UPV in concrete is a function of the volume fraction of each phase (concrete was considered as a two phase system composed of paste and aggregate in this study). The calculation results of the evolution of UPV in concrete were proved to be in perfect agreement with the experimental results. In contrast, the number of charge carriers in the system decreased with increasing amount of aggregates so a gradual and continuous decrease was observed in the conductivity curves.

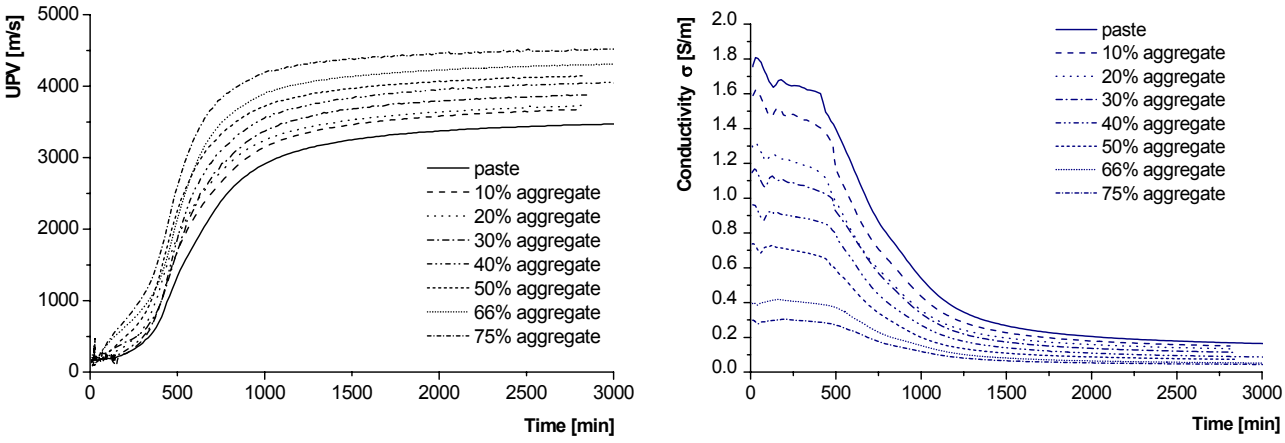

Figure 8. Evolution in time of conductivity (left) and UPV (right) of concretes having different aggregate concentrations at a temperature of 20°C [20].

5. CONCLUSIONS

A multifunctional experimental setup was designed and adopted in the measurements of dielectric and ultrasonic evolution versus hydration time for cement and concrete with different technical parameters. The validity of the computer based hydration model HYMOSTRUC was proved by the experimental results. The experimental results indicated that the profile of both dielectric and UPV evolution could be divided into four stages. At a certain hydration time, a threshold was found in the ultrasonic response, and at the same time a peak was observed in the conductivity curves. This critical point coincided exactly with the percolation threshold of solid phases calculated with the numerical simulation model HYMOSTRUC. Afterwards, in correspondence to the acceleration period simulated by the model, a sharp increase of UPV and a concurrent quick decrease of electric conductivity were recorded. This allows the determination of the setting and hardening process of cementitious materials at early-age hydration. On the other hand, non-destructive ultrasonic and dielectric measurements have the advantage of high accuracy and simple experimental procedures. They were demonstrated to be convenient and useful in monitoring the hydration

process of early-age cementitious materials. The comparison between experiments and numerical simulation revealed that the HYMOSTRUC model was able to provide an accurate and realistic quantitative description of the microstructural evolution of cementitious materials.

ACKNOWLEDGEMENTS

The authors wish to thank Mr. E.M. Horeweg for his expert assistance in conducting the experiments. Dielectric tests were performed in close cooperation with Dr. Principallo from Pisa University. His fruitful cooperation and discussions were greatly acknowledged. The research was financially supported by the Dutch Technology Foundation (STW), which is gratefully acknowledged.

REFERENCES

[1] Willis, L., Abell, A.B. and Lange, D.A. Image-based characterization of cement pore structure using wood's metal intrusion, Cement and Concrete Research, vol.28 (12), 1998, p.695-1705.

[2] Kriechbaum, M., Degovics, G., Laggner and P. and Tritthart, J. Investigation on cement pastes by small-angle X-ray scattering and BET: the relevance of fractal geometry, Advanced in Cement Research, vol.6 (23), 1994, p.93-101.

[3] Diamond, S. Mercury porosimetry. An inappropriate method for the measurement of pore size distributions in cement-based materials, Cement and Concrete Research, vol.30 (10), 2000, p.1517-1525.

[4] Boumiz, B., Vernet, C. and Cohen, F.T. Mechanical properties of cement pastes and mortars, Advanced Cement Based Materials, vol.3, 1996, p.94-106.

[5] Reinhardt, H.W. and Grosse, C.U. and Herb, A.T. Ultrasonic monitoring of setting and hardening of cement mortar - A new device. Materials and structures/Materiaux et Constructures 33, RILEM, November 2000, p.581-583.

[6] Keating, J. and Hannant, D.J. Correlation between cube strength, ultrasonic pulse velocity and volume change for oil well cement slurries, Cement and Concrete Research, vol.19, 1989, p.715-726.

[7] Sayer, C.M and Dahlin, A. Propagation of ultrasound through hydrating cement parts at early times, Advanced Cement Based Materials, vol.1, 1993, p.12-21.

[8] Gimet, N., Frageot, D., Gaillard, J.M., Smith, A. C. and Gault, J.P. Ultrasonic assessment of Portland cement at the early stages of hydration, Journal of Material Science Letter, vol.18, 1999, p.1335-1337.

[9] Ye, G., Lura, P., van Breugel, K. and Fraaij, A.L.A. Study on the development of the microstructure in cement-based materials by means of numerical simulation and ultrasonic pulse velocity measurement, Submitted to Cement and Concrete Composites, special issue on "Early Age Concrete – Properties and Performance", 2002.

[10] Principallo, A., Levita, G., Marchetti, A., Gallone, G. and Guerrini, G.L. Advancements In Modelling The Developement Of Microstructure In Cement Pastes, 7th European Conference on Advanced Materials and Processes (Rimini, 10-14 June 2001)

[11] Ye, G., Principallo, A., van Breugel, K and Fraaij, A.L.A. Non-destructive Monitoring of Setting and Hardening of Concrete Based on the Dielectric and Ultrasonic Properties, submit to 5th International Symposium on Cement and Concrete, Shanghai, China, 2002.

[12] Ye, G., van Breugel, K. and Fraaij, A.L.A. Experimental study on ultrasonic pulse velocity evaluation of the microstructure of cementitious material at early age, accept for publication in HERON, 2002.

[13] van Breugel, K. Simulation of Hydration and Formation of Structure in Hardening Cement-Based Materials, PhD thesis, Delft University of Technology, 1991.

[14] Pincigallo, A. Proprietà elettriche e dielettriche di leganti idraulici e applicazioni delle microonde nella maturazione accelerate di materiali cementizi, Doctorate Thesis, Politecnic of Milan, 2001.

[15] van Beek, A. Dielectric Properties of Young Concrete, Non-destructive Dielectric Sensors for Monitoring the Strength Development of Young Concrete, PhD thesis, Delft University of Technology, 1991.

[16] Krautkramer, J and Krautkramer, H. Ultrasonic Testing of Materials, 4th, Springer-Verlag, Berlin, 1990.

[17] Povey, M.J.W. Ultrasonic Techniques for Fluids Characterization, Academic Press, San Diego, 1997.

[18] Ye, G., van Breugel, K. and Fraaij, A.L.A. Three-dimensional microstructure analysis of numerically simulated cementitious materials. Accepted for publication in Cement and Concrete Research, 2002.

[19] Ye, G., van Breugel, K. and Fraaij, A.L.A. Non-destructive testing of microstructural development in hardening concrete by ultrasonic pulse velocity measurement, accept for publication in International Congress - Challenges of Concrete construction, Dundee, 5-11 September 2002.

[20] Principallo, A., Ye, G., Levita, G. andvan Breugel, K. Eletrical and ultrasonic properties of Portland cement mixs at early age of hydration, submitted to the International Conference on Performance of construction Materials, Cairo, Feb, 2003.

EXPERIMENTAL STUDY AND NUMERICAL SIUMLATION OF CEMENT HYDRATION AND THE DEVELOPMENT OF MICROSTRUCTURE IN CEMENTITIOUS MATERIALS

Ye Guang[1], K. van Breugel[1] and A.L.A. Fraaij[1]

[1]Faculty of Civil Engineering and Geosciences, Delft University of Technology, Delft, the Netherlands; E-mail: ye.guang@ct.tudelft.nl, k.v.Breugel@ct.tudelft.nl

Ye Guang is a researcher at the Delft University of Technology. His research topic is numerical simulation of the microstructure, porosity and permeability of cement-based materials, in particular non-destructive test at early age.

NUMERICALLY SIMULATED PORE STRUCTURE AND TRANSPORT PROPERTIES OF CEMENTITIOUS MATERIALS

Guang YE [1]; K. van Breugel[1] and A.L.A. Fraaij[1]

[1]Faculty of Civil Engineering and Geosciences, Delft University of Technology, Delft, the Netherlands. E-mail: ye.guang@ct.tudelft.nl, k.v.Breugel@ct.tudelft.nl.

ABSTRACT

In this paper, the features of different computer-based cement hydration models are discussed. Simulations of cement paste hydration and formation of 3D microstructure were carried out on the basis of a simulation model, called HYMOSTRUC. The simulated pore structures were visualised and analysed explicitly by applying a serial algorithm associated with an overlapping criterion. The internal surface area, the hydraulic radius, the characteristic pore size distribution and the total capillary porosity were evaluated. The shape of the pore size distribution curve was similar to the experimental results obtained by BSEM image. The capillary pore connectivity in terms of connected pore fraction was calculated and the capillary pore network was derived. The influence of the digital resolution on the connectivity of the capillary channel was discussed and compared with previous work. The generated information on the pore structure was used in the prediction of the absolute permeability, in which the Carman-Kozeny model was utilized.

1. INTRODUCTION

The structure of the capillary pore system strongly influences transport properties of concrete. In particular, the ingress of water and aggressive agents into concrete (structures) is largely related to the microscopic properties of the pore network. To access the pore structure, the available experimental techniques are not completely adequate for describing the topological and geometrical properties of the pore network structure. For example, the application of 2D scanning electron microscopy image and small angle X-ray scattering microtomography only supply 2D information. Mercury intrusion porosimetry measurements, on the other hand, usually damage and change the pore structure [1]. However, with the rapid development of computer technology, a number of experimental complications can be circumvented by using computer-based simulation models. With these models it is possible to simulate the evolution of the microstructure, especially a pore structure, in hardening cementitious materials. This led to a new subject in the last 20 years, computational material science of concrete [2]. With the progress of this technology a better understanding of transport phenomena and associated degradation mechanisms is to be expected.

A computer-based model is required to numerically represent the amount and spatial distribution of the different phases of the materials being studied. To further qualify as a model, the computer-based model must have the power to predict, directly from the numerical representation of microstructure properties that can be checked against experimental measurements [3]. Based on this concept, during the last two decades a few fundamental pore structure models [4-7] have been developed that can be used successfully for predicting the transport properties of cement-based materials. These models are based on numerical simulation techniques and on a digital-image processing approach. Pioneering work in this field dates back to Jennings and Johnson [4], who first

Proceedings of the 11th International Congress on the Chemistry of Cement (ICCC)
'Cement's Contribution to the Development in the 21st Century'
Hosted by: The Cement and Concrete Institute of South Africa
CD-ROM produced by: Document Transformation Technologies
11 - 16 May 2003, Durban, South Africa
ISBN Number: 0-9584085-8-0
Editors: Dr G. Grieve and G. Owens
Congress Organised by: Event Dynamics

proposed a cement hydration model. In their model, the cement particles were modelled as growing spheres. Another advanced model has been accomplished with the digital-image-based microstructure, which was developed by Bentz and Garboczi [5]. Their model allows the direct representation of multiphase and non-spherical cement particles. Based on the same principle of Jennings's model, van Breugel's model HYMOSTRUC [6], had the advantage of considering the individual particles interaction and reaction kinetics. These models vary widely in concept, accuracy, required computation time and "degree of reality". It is still very difficult for the present generation models to mimic the pore structure over the whole range of pore sizes satisfactorily.

In the present paper, the features of the cement hydration model HYMOSTRUC and reproduced microstructure are described. Four cement paste samples with different water/cement ratios, i.e. 0.3 to 0.6, have been simulated with HYMOSTRUC. The simulated microstructures are visualized. An integrated procedure for the characterization of the simulated microstructure structure (especially the pore structure) is presented and discussed. These include the extraction of the graph of the pore space, capillary network and the characterization of the pore size distribution curve. The geometrical characterizations of the pore structure will be used for the estimation of the absolute permeability of the cement paste, in which the Carman-Kozeny equation will be utilized.

2. 3D MICROSTRUCTURE SIMULATION AND ANALYSIS

2.1 Simulation of the degree of hydration of cementitious material

In the HYMOSTRUC model [6, 8], the degree of hydration is simulated as a function of the particle size distribution and the chemical composition of the cement grains, of the water/cement ratio and of the reaction temperature. The model starts from cement grains that are randomly distributed in a 3D body of cement paste. The cement particles are modelled as spheres. The three Cartesian coordinates of the centre and the radius of each particle are stored. The cement grains start to hydrate after mixing with water and the hydration processes are controlled by different mechanisms. Based on an expansion and interaction mechanism, the cement hydrates become part of gradually growing spheres. By taking into account the interaction kinetics, the growing particles become more and more connected; in this way, a simulated porous microstructure is formed (Figure 1a). In comparison to other models, HYMOSTRUC takes the embedded particles and overlap part into account explicitly.

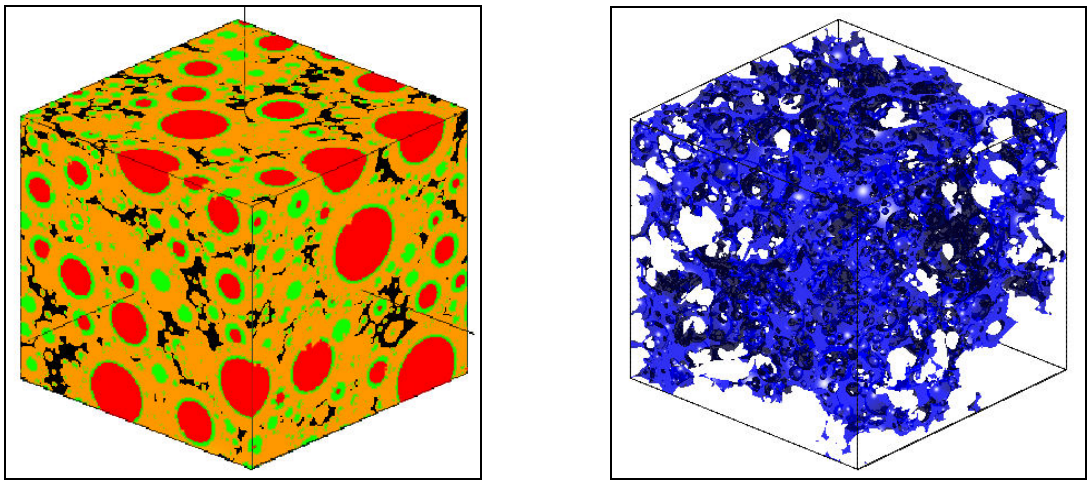

a) Cement paste b) Pore structure

Figure 1. The simulated cement paste and its pore structure (w/c=0.3, α=0.75)

2.2 3D microstructure visualization

It is important to visualize the simulated microstructure, since this can help us to understand how the pore structure looks like and help us also to develop a better permeability model. In the HYMOSTRUC model, the characterization of the cement particles distributed in a box and presented by its three Cartesian coordinates of the centre and the particle radius enables us to use a constructive solid geometry algorithm [9], using union and difference operators, to visualise the pore structure. Figure 2 shows a simulated cement paste and its pore structure. The simulated cement paste has been visualised by applying the union operator between all cement particles and the box, whereas the pore structure was displayed by using the difference operator between a box and the merged result of the individual particle components. It was interesting to compare the simulated pore structure with a "realistic" pore structure. For example, a cylindrical pore shape is commonly assumed in order to quantify the pore size distribution of cement paste when a mercury intrusion porosimetry is interpreted. However, the simulated pore structure illustrated in Figure 2b will not obey this assumption as it shows a very irregular shape.

2.3 Pore topology

A quantitative description of geometrical and topological properties of the simulated pore microstructure plays an important role in predicting the transport properties. As shown in Figure 1, the simulated pore structure is very irregular. An important issue is describing this complex simulated pore structure. A program called HYMOSTRUC3D [10] was developed for this purpose. In this program, a serial section algorithm with overlap criteria was utilized. The serial sectioning method starts with scanning the simulated 3D microstructure layer by layer (Figure 2). The program first determines the features of all points in a 2D section by checking whether an arbitrary point belongs either to the subset of the solid phase or to the subset of the capillary pore phase. Secondly, checking around of this point to determine whether its neighbor point has the same feature, renumber each set with the same features points as an individual object (pore or solid). The information of each object including coordinate, area, and perimeter are stored.

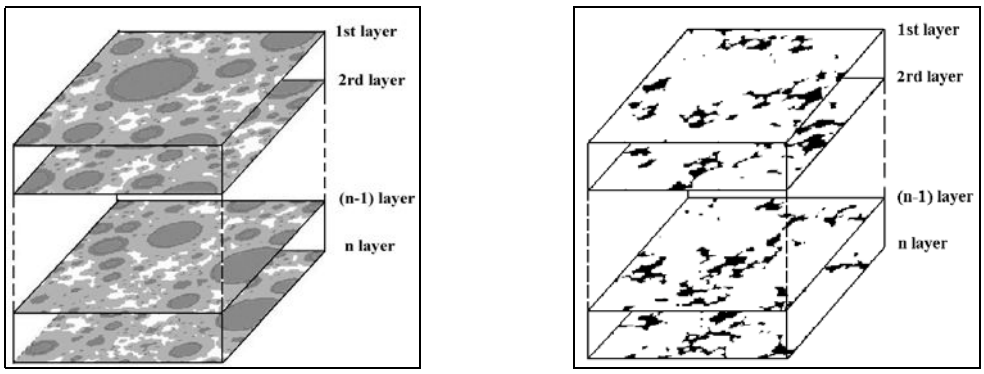

a) Solid phase b) Porous phase

Figure 2. Determination of pore topology by using serial sectioning method

The connectivity of the object between neighbor layers was determined by applying an "overlap criterion" (Figure 3). The overlap criterion checked each one of the objects on its up-layer and down-layer and examined whether this object was connected with its neighbors with the same feature. This procedure was repeated until the final layer of the body. A linked list network structure was built up to determine the interconnectedness of the structure. The hydraulic radius was calculated by taking the ratio of the total capillary pore volume to the total free surfaces of the hydration products. The volume fractions of the connected solid phase or capillary pore phase and the total internal surface area were derived. By applying these algorithms, the dead-end pores and isolated pores were distinguished. These pores will not be taken into account in the permeability prediction.

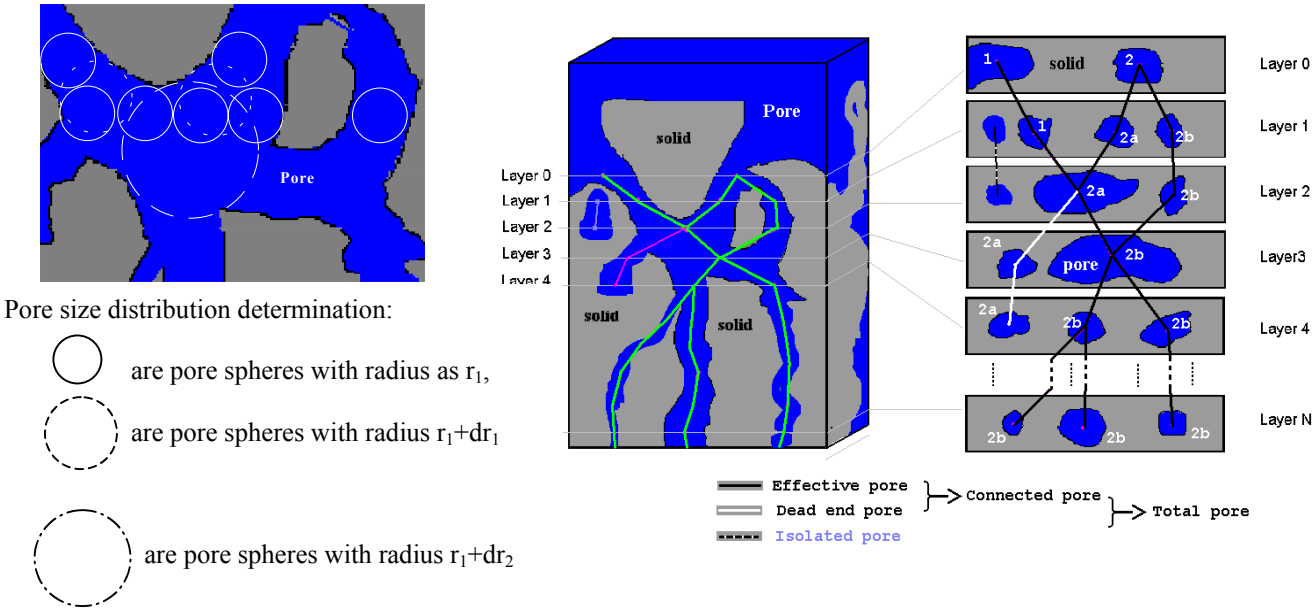

Figure 3. The pore network structure was determined by using an overlapping criterion. The effective pores, dead-end pores and isolated pores were distiguished. The pore size distribution was deterimined by calculting the pores which could be covered by fictitious spheres of radius r.

It is noticed that the connectivity of the pores is strongly influenced by the digital resolution and the layer depth in the image-based calculation. To accurately define the digital resolution, one has to consider the computational time needed and the reliability of the calculation result. If one applies this calculated pore structure to predict the transport properties, the validity of this calculated result will directly influence the reliability of capillary water permeability. For example, previous work [11] showed that the percolation threshold of capillary porosity changed from 30%, 12% to 0% when the digital resolution increased from 10μm/pixel, 5μm/pixel to 2μm/pixel for a cement paste with water/cement ratio 0.4. In the NIST pixel-based simulation model [12], the percolation threshold of the capillary porosity changed from 24%, 18% and 12% while the digital resolution shifted from 1μm to 0.5 μm and 0.25μm in a cement paste with 0.3 w/c. This can be explained because smaller pores can be resolved at the greater resolutions, and the pathway that would seem to be closed off at low resolution is seen to be narrowly open at higher resolutions. Further details of the effect of digital resolution were discussed in [10-12,].

2.4 Pore size distribution

The principle algorithms for the determination of the characteristic pore size distribution spectra of a simulated 3D binary image described by Bekri et. al [13], can be employed for our spherical-based 3D pore structure. In principle, the simulated pore structure is the inverse free space between the expanding cement grains. The characteristic pore size distribution curve can be determined in the following way. Consider the sub-volumes of the system that are accessible for spheres of different radii. Let $\rho_{(r)}$ be the volume fraction of the pore space "coverable" by spheres of radius r (Figure 3). We call these spheres pore spheres. $\rho_{(r)}$ is a monotonically decreasing function of r and can easily be compared with the "cumulative pore volume" curves measured by mercury intrusion porosimetry. The derivative $-d\rho_{(r)}/dr$ is the fraction of volume coverable by pore spheres of radius r but not by spheres of radius $r+dr$ and is a direct definition of the pore size distribution. The $\rho_{(r)}$ of the pore spheres with radius r can be computed by densely packing pore spheres in the free space.

3. CALCULATION OF PERMEABILITY

In general, permeability is a measure of the ease with which a fluid passes through a porous body [14]. Researches [15-16] have shown that the permeability of a porous medium is strongly influenced by the properties of liquids, by the hydraulic gradient and above all, by the geometrical properties. The most common expression used to describe the permeability, k, is Darcy's law:

$$k = -\upsilon \frac{Q}{A\delta g} \Delta P \tag{1}$$

where Q is the volume of fluid discharged per unit time through the cross sectional area A, ν is the viscosity of the fluid, δ is the density of the fluid, g is the acceleration of gravity, and Δp is the hydraulic gradient.

A frequently used absolute permeability model is the Carman-Kozeny model. This model considers some aspects of the geometrical properties of the porous medium. It relates the permeability to the total porosity and the specific surface area of the pores. The Carman-Kozeny model ca be calculated as:

$$k = -\frac{\rho \ (V_p / S)^2}{2\beta} \tag{2}$$

where ρ, Vp and S denote respectively the porosity, the volume and the internal surface area of the pore space. β is the tortuosity of the conducting channels.

4. RESULTS AND DISCUSSIONS

4.1 Parameters for simulation

Four Portland cement pastes were simulated. The chemical compositions of the cement listed in Table 1, are the same for all samples. The curing temperature was 20°C.

Table 1. Chemical composition of cement particles

Max heat(KJ/g)	C_3S(%)	C_2S(%)	C_3A(%)	C_4AF(%)
530	63.0	13.0	8.43	9.0

Table 2 shows the physical parameters for the simulations. The main variable is the water/cement ratio, i.e. 0.3 to 0.6. The particle size distribution curves are shown in Figure 4. A continuous particle size distribution, between minimum size 2 μm and maximum size 45 μm was used for all samples; the Blaine fineness of the particles was 420 m^2/kg. Figure 4 shows the consistency for all specimens. The physical size of the sample was a cube of 100μm side, while the resolution was 0.25 μm/pixel.

Table 2. Input parameter for the numerical experiments

w/c ratio [-]	Sample size [μm]	Particle size [μm]	Number of particles involved	Image size [Pixel]	Pixel resolution [μm/pixel]	Number of layers
0.3	100	2~50	8968	400	0.25	400
0.4	100	2~50	8168	400	0.25	400
0.5	100	2~50	6716	400	0.25	400
0.6	100	2~50	5898	400	0.25	400

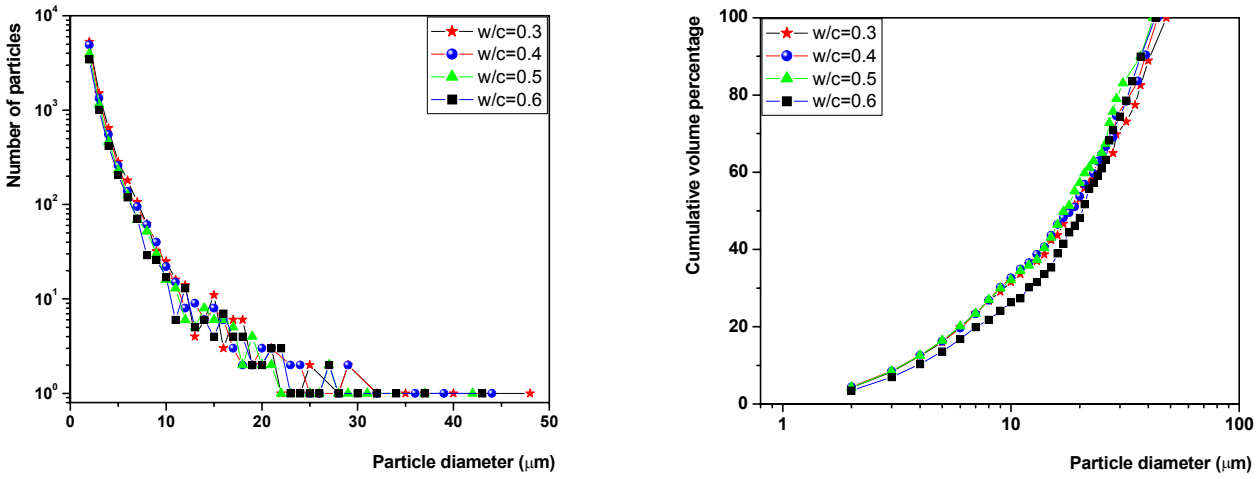

a) Particle size distribution b) Cumulative particle size distribution

Figure 4. Particle size distribution in the four simulated cement paste.

4.2 The geometry of the capillary porosity

The simulated pore structures are illustrated in Figure 5 for the sample with w/c ratio 0.3, 0.4 and 0.5, at a degree of hydration of 0.75. It is obvious that at the same degree of hydration, the sample with the lower water/cement ratio shows less porosity than the sample with a higher water/cement ratio. The calculated result revealed a capillary porosity of 6%, 19%, 28% for w/c 0.3, 0.4 and 0.5 respectively.

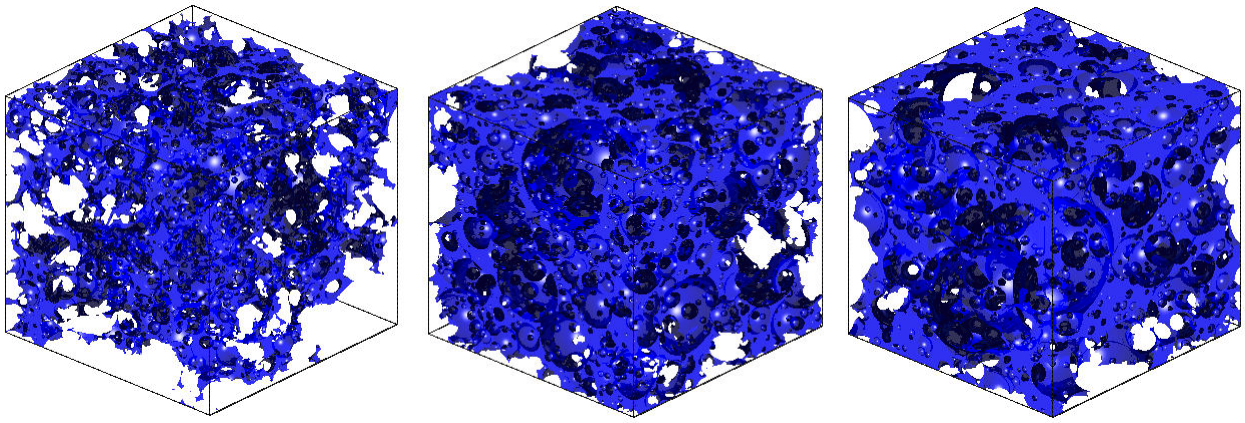

a) w/c= 0.3 b) w/c = 0.4 c) w/c = 0.5

Figure 5. Simulated pore structure for the sample with a) w/c ratio 0.3, ρ=6%, b) w/c ratio 0.4, ρ=19% and c) w/c ratio 0.5, ρ=28%, at degree of hydration 0.75.

The degree of hydration simulated by HYMOSTRUC is shown in Figure 6. For each sample at a different hydration stage, the internal surface area, the hydraulic radius, the total porosity and the connectivity of the porosity were calculated and shown in Figure 7~Figure 9. Because of the huge computational time, the characteristic pore size distribution curves were computed only at the degree of hydration 0.64.

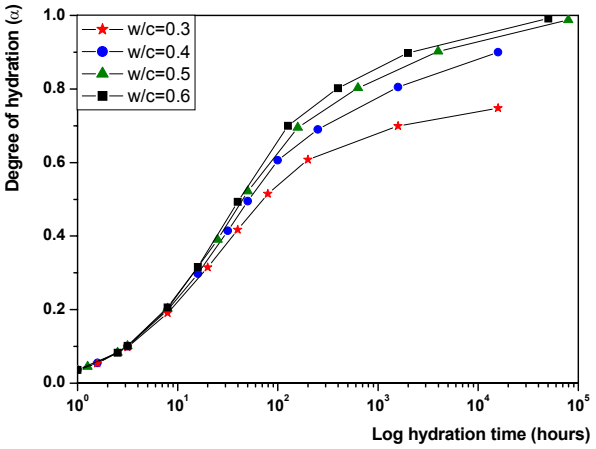

Figure 6. Degree of hydration of cement paste as function of hydration time.

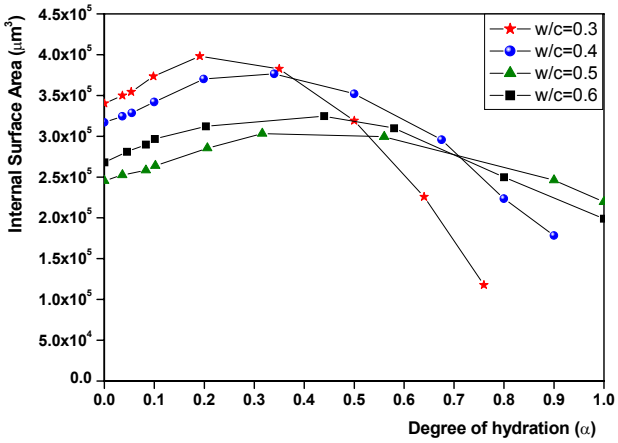

Figure 7. Internal surface area of cement paste as function of degree of hydration

As shown in Figure 7, the samples with the lowest w/c ratio displayed the highest internal pore surface area at early age. However, after a certain degree of hydration, the surface area of the lower w/c ratio sample decreases more rapidly. If we look back to Table 2 and Figure 4, the samples with lower w/c ratio have a higher solid fraction, i.e. greater number of cement particles. This implies that per unit volume of paste more cement surface is contact with water. However, in the later stage, since there is less initial water in the lower w/c sample and most of it has reacted and converted into hydration products, only little capillary pores remain. This explains why both the hydraulic radius and capillary porosity decrease with a reduction in w/c ratio and with an increase in the degree of hydration, as shown in Figure 8 and Figure 9. This was also shown by the visualized pore structure illustrated in Figure 5.

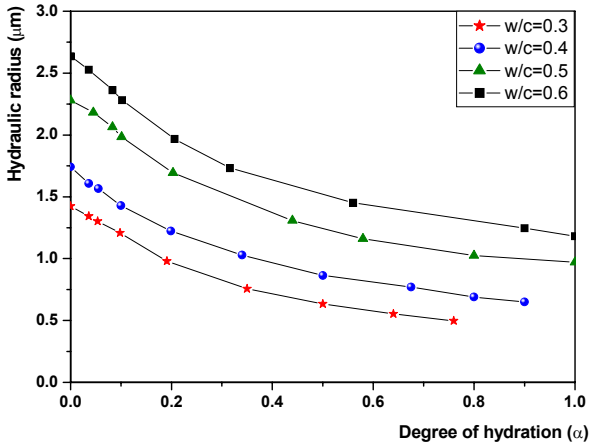

Figure 8. Simulated hydraulic radius in cement paste as function of degree of hydration

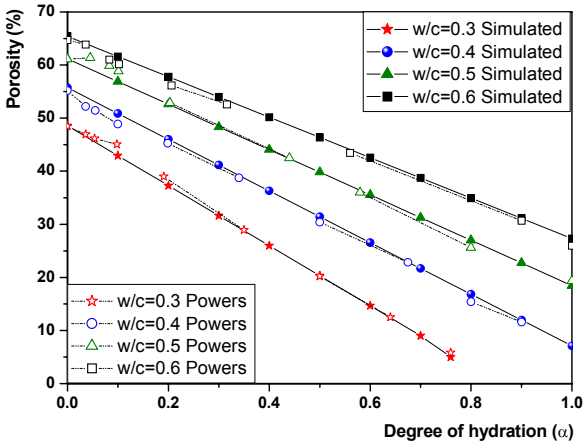

Figure 9. Simulated porosity of cement paste as function of degree of hydration compared with Powers' model

The hydraulic radius obtained in the present simulation decreases from 0.75 μm to 0.60 μm for a cement paste with w/c 0.3 with a degree of hydration from 0.3 to 0.8. The present results are two orders higher than experimental results observed by Jiang et al [17]. The total porosity compared with Powers' model as a function of the degree of hydration for different w/c ratio is plotted in Figure 9. The simulation results are consistent with Powers' model.

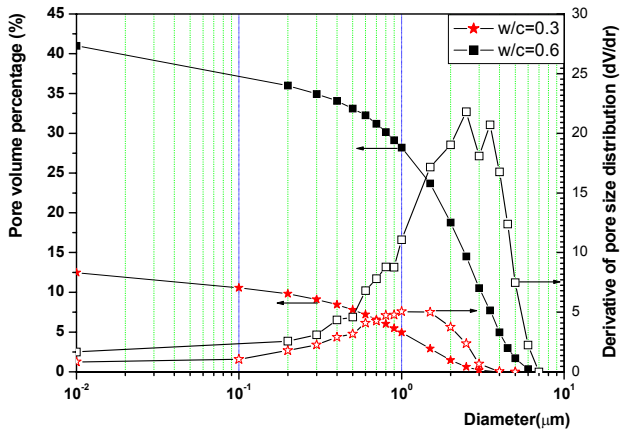

Figure 10. Pore size distribution of simulated cement pastes with w/c ratio 0.3 and 0.6 at degree of hydration 0.64.

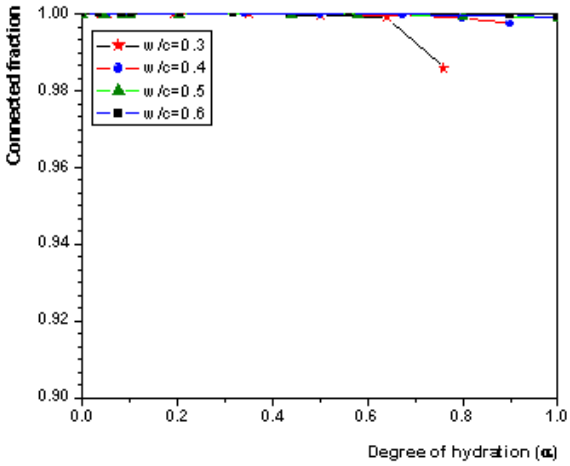

Figure 11. The connectivity of the porosity as function of degree of hydration.

The characteristic pore size distribution curve is plotted in the Figure 10 for the samples with w/c 0.3 and 0.6 at a degree of hydration 0.64. The sample with higher w/c ratio displays a wide range of pore sizes around 1~5 μm and the sample with lower w/c ratio exhibits a narrow range of pore size around 0.9 ~2 μm. The pore size is one order of magnitude above compared to experimental MIP data [18] and the total porosity is much higher. By applying Backscatter SEM or ESEM techniques, researches [1, 18] have proved that MIP measurements systematically underestimate the size of the capillary pores because of the so-called inkbottle effect. On the other hand, the numerical simulation agrees with SEM image reveals more realistic pore structures in cementitious materials.

4.3 Connectivity of the capillary porosity

The connectivity of capillary pores, in terms of connected porosity fraction is illustrated in Figure 11, as function of degree of hydration. It is noticed that, for all samples the capillary pores are almost always connected with each other even at ultimate hydration. No de-percolation of capillary porosity can be found. These results are quite different from the result of the NIST model [12], where a de-percolation threshold of the capillary porosity of 12% was found in cement paste with w/c ratio 0.4. On the other hand, the present results are quite similar to the results previously calculated by Navi [11]: when a resolution of 2μm/pixel was used, their results revealed that almost all pores were connected with each other. Why are so pronounced in different models? To answer this question, several aspects have to be considered. First, as discussed previously, the percolation threshold of the capillary porosity is largely dependent on the digital resolution. In the present simulation, the digital resolution was 0.25 μm/pixel; at this high digital resolution, even very small capillary pores pathways were detected, leading to a very low percolation threshold of the capillary porosity or no threshold at all. Another important factor, which influences the connectivity of the capillary porosity, is the fundamental principle of the different numerical models. As discussed earlier [12], the NIST model is a pixel-based model, where the different cement components are simulated as different sets of digital pixels and no shape constraint exist. In other models, such as HYMOSTRUC or Navi's model, the cement particles and hydration products are simulated as spheres. The growing spheres are overlapping when cement hydration take place. The pore space percolation threshold of the spherical based models has been numerically found always around a few percent porosity [19]. However, theoretically, in the cement pastes with w/c ratio from 0.3 to 0.6, even at the ultimate hydration stage, the capillary porosity will not be less than 5% (see Figure 9). This explains why no de-percolation of porosity can be found in a spherical based cement hydration model.

4.4 Transport properties

The simulated pore structure was used as bases for predicting the permeability. The absolute permeability of each system was computed using the Carman-Kozeny model. Figure 12 shows the computed water permeability curves as a function of degree of hydration, whereas Figure 13 shows its dependence on porosity.

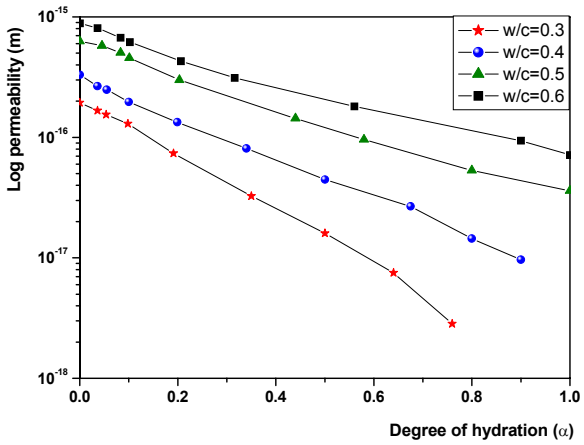

Figure 12. Permeability as a function of degree of hydration for four different pastes.

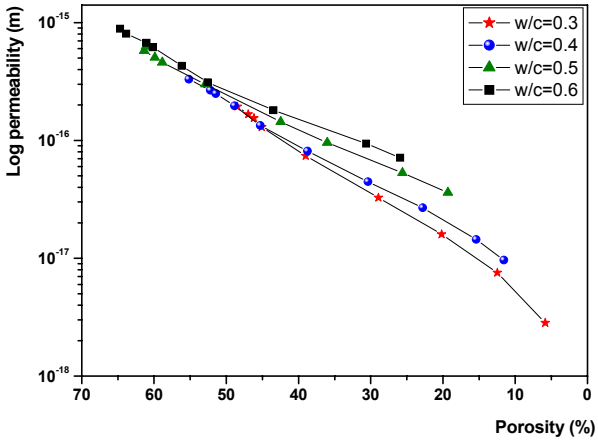

Figure 13. The relationship between porosity and permeability for four different pastes.

The permeabilities calculated by the Carman-Kozeny model are one order of magnitude higher than the results proposed by the NIST model [12], where a lattice Boltzmann model was applied. Another advanced permeability model, based on a network model is under development. This network permeability model will consider the water penetration channel. The simulation result is expected to be more precise and close to the experimental results.

5. CONCLUSIONS

The simulation of cement paste hydration and of the formation of a 3D microstructure, especially the pore structure, were carried out with the HYMOSTRUC model. The simulated pore structures were visualised and analysed explicitly by applying a serial algorithm associated with an overlapping criterion. The internal surface area, the hydraulic radius and the total capillary porosity were calculated and evaluated. The characteristic pore size distribution was computed successfully by densely packing pore spheres in the free space. It was found that the pore size was one order of magnitude above compared to MIP results, while the shape of the pore size distribution curve was quite similar to obtained by SEM processing. The capillary pore connectivity was calculated as well. It was found that the connectivity is strongly influenced by the digital resolution used in the calculation. In the present study, no de-percolation threshold was found in all samples when a higher digital resolution of 0.25 um/pixel was used. This is in line if compared with the work presented by Elam et al. [19] and Navi et al. [11]. The simulated pore structures were used for the prediction of permeability. For that purpose the Carman-Kozeny model was used. In a further work, an improved network permeability model will be studied and validated by comparing the numerical results with mercury intrusion porosimetry measurements and permeability measurement.

ACKNOWLEDGEMENTS

The authors wish to thank Mr. F.P.J. Schilperoort for his advice in programming and Mr. P. Lura for the useful discussion. The research was financially supported by the Dutch Technology Foundation (STW), which is gratefully acknowledged.

REFERENCES

[1] Olson, R.A., Neubauer, C.M. and Jennings, H.M. Damage to the pore structure of hardened Portland cement paste by mercury intrusion, Journal of American Ceramic Society, vol.80 [9], 1997, p.2454-2458.

[2] Garboczi, E.J., Bentz, D.P. and Frohnsdroff, G.J. The paste, present, and future of the computational materials science of concrete. Materials Science of Concrete Workshop, Lake Shelbyville, IL, April 27-29, 2000.

[3] Garboczi, E.J. and Bentz, D.P. Computer-based models of the microstructure and properties of cement-based materials, 9th International Congress on the Chemistry of Cement, New Delhi, India, 1992, vol.5, p.3-15.

[4] Jennings, H.M. and Johnson, S.K. Simulation of microstructure development during the hydration of a cement compound, Journal of American Ceramic Society, vol.69, 1986, p.790-795.

[5] Bentz, D.P. and Garboczi, E.J. A digitised simulation model for microstructural development, Advances in Cementitious Materials, edited by S. Mindess. Westerville, Ohio, USA, American Ceramic Society, 1989, p.211-226.

[6] van Breugel, K. Simulation of Hydration and Formation of Structure in Hardening Cement-based Materials, PhD thesis, Delft University of Technology, 1991.

[7] Navi, P. and Pignat, C. Three-dimensional characterization of the pore structure of a simulated cement paste, Cement and Concrete Research, vol.29 (4), 1999, p.507-514.

[8] Koenders, E.A.B. Simulation of Volume Changes in Hardening Cement-based Materials; Ph.D thesis, Delft University of Technology, 1997.

[9] M. Laszlo, Computational Geometry and Computer Graphics in C++, Prentice Hall, 1995.

[10] Ye, G., van Breugel, K. and Fraaij, A.L.A. Three-dimensional microstructure analysis of numerically simulated cementitious materials. Accepted for publication in Cement and Concrete Research, 2002.

[11] Navi, P. and Pignat, C. Simulation of cement hydration and the connectivity of the capillary pore space, Advanced Cement Based Material, vol.4, 1996, p.58-67.

[12] Garboczi, E.J. and Bentz, D.P. The effect of statistical fluctuation, finite size error, and digital resolution on the phase percolation and transport properties of the NIST cement hydration model, Cement and Concrete Research, vol. 31, 2001, p.1501-1514.

[13] Bekri, S., Xu, K., Yousefian, F., Adler, P.M., Thovert, J.-F., Muller, J., Iden, K., Psyllos, A., Stubos, A.K.and Ioannidis, M. A. Pore geometry and transport properties in north sea chalk, Journal of Petroleum Science and Engineering, vol. 25, 2000, p.107-134.

[14] Davis, S. Porosity and permeability of natural materials, Flow Through Porous Media. Academic press, New York, 1969.

[15] Dullien, F.A.L. Porous Media, Fluid Transport and Pore Structure, 2rd Edition, Academic press, San Diego, 1992.

[16] Seeburger, D.A. and Nur, J. A pore space model for rock permeability and bulk modulus, Geophysical Research. vol. 89, 1981, p.527-536.

[17] Jiang, S.P. Detriche, Ch. and Grandet, J. Relationships between mechanical properties of mortars and the hydraulic radius of their pores, 9th International Congress on the Chemistry of Cement , New Delhi, India, 1992, vol.5, p.191-195.

[18] Diamond, S. Mercury porosimetry an inappropriate method for the measurement of pore size distributions in cement-based materials, Cement and Concrete Research, vol. 30, 2000, p.1517-1525.

[19] Elam, W.T. Kerstein, A.R. and Rehr, J.J. Critical properties of the void percolation problem for spheres, Physical Reviewer Letters, vol.52, 1984, p.1516-1519.

GEOTHERMAL WASTE AS AN ADMIXTURE IN PORTLAND CEMENT, POZZOLANIC CHARACTERISTICS

Lauren Y. Gómez-Zamorano, José I. Escalante-García, Guillermo Mendoza-Suárez, and Alexandre V. Gorokhovski

Centre for Research and Advanced Studies IPN (Cinvestav) Saltillo Unit
Carretera Saltillo-Monterrey, km. 13, Saltillo, México
E–mail: jieg@saltillo.cinvestav.mx

ABSTRACT

This paper reports the results of the utilization of a silica waste from a geothermal power generation plant as replacement material of Portland cement. Pastes of OPC substituted with 0, 10, 15 and 20% of geothermal waste and water/solids ratio of 0.50 were cured at 20 and 40°C for up to six months. The pastes were characterised by thermogravimetry, compressive strength, non-evaporable water, and scanning electron microscopy. The results show that the presence of the silica enhances the compressive strength, which was also favoured by higher temperatures in the short term; however, at silica loads above 15% an anomalous strength reduction was noted; fracture microstructures under scanning electron microscopy showed the presence of Aft needle clusters. The geothermal silica shows pozzolanic character according to CH measurements and it also influenced the cement hydration in agreement with non-evaporable water results. The microstructures were more compact in the presence of geothermal silica.

Keywords: geothermal silica waste, pozzolanic reaction, blended cement, temperature, ettringite

1. INTRODUCTION

Using replacement materials for Portland cement is a practice that has increased considerably due to the advantages brought about not only in savings in natural resources and energy, but also in improvements in the properties of the cement. That is why it is important to search for new potential wastes or by products as replacements or additives to Portland cement. One potential waste is that obtained in the geothermal plants, as part of the process of energy production by means of steam extraction from the underground.

The geothermal waste is obtained from the mixture of geothermal brine and steam (naturally pressurized) that passes through the different stages of heat extraction. As the temperature is reduced (initially about 200°C) the silica precipitates from the mixture, which consists generally of amorphous silica and sodium and potassium chlorides. These precipitates produce serious problems, as they deposit in the ducts, forming a scale that grows several inches per month. In addition to these incrustations, a fraction of the remaining brine is reinjected to the underground and the rest is deposited in evaporation ponds that occupy large spaces containing thousands of tons of this geothermal sludge. The silica waste was obtained from the geothermal Cerro Prieto plant in Baja California, Mexico, which generates up to 50 thousand tons of it yearly. Preliminary characterisation of the geothermal silica has shown that it has properties that make it a good replacement material for Portland cement, such as: chemical composition rich in SiO_2; particle size of about 0.2 μm and highly amorphous [1].

Guttridge and Dalziel [2,3] reported the effect of replacement materials on the hydration of cement paste, they noted that the presence of a secondary component enhanced the hydration of Portland cement in the presence of PFA and slag, for which the finer the particle size the greater the improvement. The effect of temperature on the mechanical properties of mortars was reported by Verbeck and Helmuth [4], at short hydration times (14 days) the higher the curing temperature, the higher the compressive strength, but after 28 days, this effect was inverted in that at lower temperatures higher strengths were reached. They suggested that curing at higher temperatures resulted in a non uniform distribution of the hydration products building up around hydrating grains and retarding the posterior hydration, while at low temperatures, the products have sufficient time to diffuse and precipitate relatively more uniformly in the cement matrix.

Many reports about the effects of silica fume as a replacement of Portland cement in pastes, mortars and concretes pointed important effects of the silica fume, such as improved resistance to chemical attack [5] and improved strength [6] (especially on mortars and concretes) by means of its microfiller effect and its strong pozzolanic character [7,8]. There is very little information about investigation of the use of geothermal waste in Portland cement and in view of the similarities with silica fume, it was expected that the former would show pozzolanic behaviour and improve the properties of Portland cement pastes. As part of a more extensive study, this paper presents some results about the effects of silica waste on the chemistry of Portland cement hydration and the mechanical strength of Portland cement pastes under different hydration conditions.

2. EXPERIMENTAL PROCEDURE

2.1 Materials

One ordinary Portland cement (OPC) produced by Cementos Apasco (Planta Ramos Arizpe, Mexico) with calcite additions, a geothermal waste (GW) from Comision Federal de Electricidad (Planta Cerro Prieto, Mexico), and Rheobuild 1000 superplastizicer (SP) were used. The phase composition of OPC was (wt%): 66.9% alite, 7.3% belite, 2.4% C_3A, 7.2% C_4AF, 8.2% calcite, 2.7% gypsum and 4.8% quartz. The GW had to be treated in order to eliminate the chlorides present; washing with water at 80°C, as described by Diaz, resulted adequate for this purpose [9]. The chemical composition of the geothermal waste (GW) is shown in table 1, along with the phase and chemical composition of OPC. The average particle size of GW, by laser diffraction measurements, was of 7 μm; however further ultrasonic dispersion in HCl and methanol the particle size was of 100-200nm as noted by scanning electron microscopy.

Table 1. Chemical and phases composition of the silica waste and Portland cement

OXIDE	CaO	SiO_2	Al_2O_3	Fe_2O_3	MgO	Na_2O	K_2O	TiO_2	MnO	SO_3	**Total**
GW	1.72	94.67	1.04	--	0.53	0.66	0.53	0.84	--	--	**100**
OPC	67.53	18.16	3.5	2.52	1.89	0.89	0.57	--	0.14	4.05	**99.23**

2.2 Paste preparation and hydration

Cement pastes with water/solids ratios of 0.50 were prepared with replacement levels of 0, 10 and 15% GW, additional pastes with 20% were prepared for compression strength measurements only. The SP added was at 1, 1.25 and 1.5% for 10, 15 and 20% of GW, respectively. Cubes of 5 cm were cast and maintained for 24 hours at constant temperatures of 20 and 40ºC and relative humidity of 90%. The cubes were then demolded and submerged in water, in plastic containers, at the same temperatures for curing for up to six months.

2.3 Characterisation

The pastes were characterised by means of: compressive strength (CS), non-evaporable water (NEW), thermogravimetic analysis (TGA) and scanning electron microscopy (SEM).

After the curing periods of 3, 7, 14, 28, 90 and 180 days the compressive strength was estimated from the average of four cubes. Fragments of the cubes were dried in a vacuum oven at 105°C during 24 hours. A fraction of these fragments were used for SEM, samples were cold mounted in resin, ground and polished down to ¼ μm using diamond pastes. The specimens were then carbon coated. The images in SEM were obtained by backscattered electrons (BEI) and secondary electrons (SEI), the accelerating voltage was of 20kV. Additional fragments were further ground in agate containers in a planetary ball mill to pass a 106μm mesh. The powders were used for loss on ignition to estimate NEW and for TGA to estimate CH. The NEW was calculated by heating the hydrated samples at 130°C for one hour and then ignited at 950°C for one hour, the weight difference was referred to the ignited weight. The calcium hydroxide was graphically estimated by TGA from the weight loss step between 425-550°C, simultaneous decomposition of the C-S-H was considered by graphical correction.

3. RESULTS

3.1 Compressive strength

Figure 1 presents the results of compressive strength vs. time for all the studied mixes cured at both temperatures. The same colour and symbol codes were used for the subsequent figures. The effects of replacement level and temperature are analysed in all results.

3.1.1 Replacement level effect.

At 20ºC, the addition of 10 and 15% GW resulted in progressively increased compressive strength; for 20% GW the compressive strengths were lower than those obtained for 15%; however, in all cases the addition of GW resulted favourable relative to the neat OPC. Nonetheless, while all specimens cured at 20°C continued gaining strength after 28 days those cured at 40°C with 15 and 20% GW registered strength reductions from 48 to 29 and from 40 to 23 MPa, respectively.

3.1.2 Temperature effect

For the neat cement pastes the compressive strength was slightly increased with the increment of the temperature; however, for all times considered the strength difference between the two temperatures was only about 10%. For the 10% of silica load the effect of temperature is noticeable in the first 14 days of hydration, however for the coming times the difference was as for the neat cement. In the presence of 15 and 20% GW the temperature effect was similar to that described for the 10% of silica; except for the strength loss mentioned.

The effect of the temperature on strength development in cements cured at relatively high temperatures is that the strength gain is reduced after a given time and ascribed to the phenomena described by Verbeck and Helmuth [4]. In this case a clear drop of strength was noted at 15 and 20% GW load when cured at 40°C; for such specimens extensive cracking was observed in the cubes. SEM characterisation was performed to search for a possible origin of this problem, the results presented are a microstructure of a fracture zone with EDS analysis from it and also EDS results from a polished sample, as shown in Figure 2. Localised zones rich in clusters of needles (pointed in the photo) were noted throughout the fracture surface, the chemical composition indicated the presence of ettringite in such hydration products.

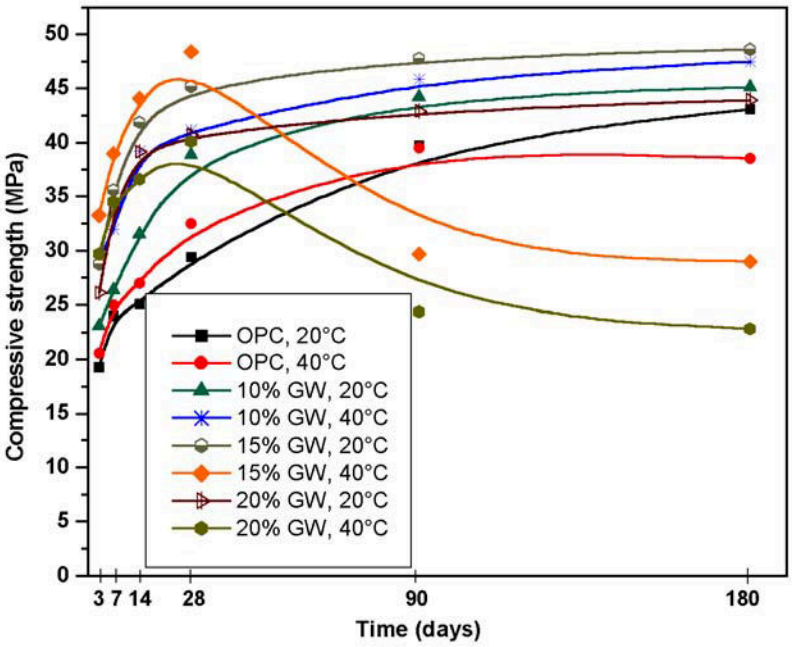

Figure 1. Compressive strength vs. time for the neat and blended cements

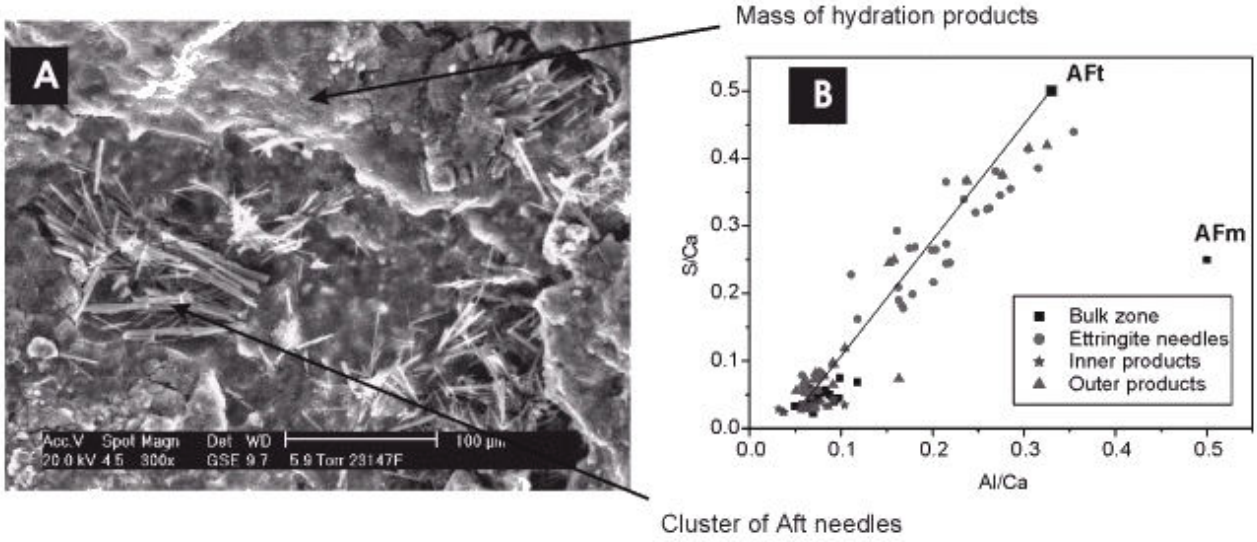

Figure 2. (A) MEB SEI fracture surfaces of non dried samples (environmental mode) OPC-20%GW cured at 40°C, (B) EDS analysis of sample (A) in atomic ratios. Inner and outer products in (B) from polished samples

3.2 Thermogravimetric analysis

Figure 3A shows the results of % calcium hydroxide vs. time for all cements. The data were normalised for an equivalent of 85% of cement. For the neat cement the CH values increased as time advanced and with the higher temperature. For both blended cements the CH amounts were lower compared to the neat cement; the values increased for the first 7 to 14 days and then the CH concentration was depleted. This provided evidence of the pozzolanic behaviour of the silica waste since the first days of hydration. The CH consumption was greater as the silica load and the hydration temperature increased. The trend towards lower CH concentrations indicates that the pozzolanic reaction is still in progress. The behaviour of the dependence of the pozzolanic reaction (with the temperature and the replacement level) is similar to that found in cement pastes with silica fume [7,8] and other replacement materials [10].

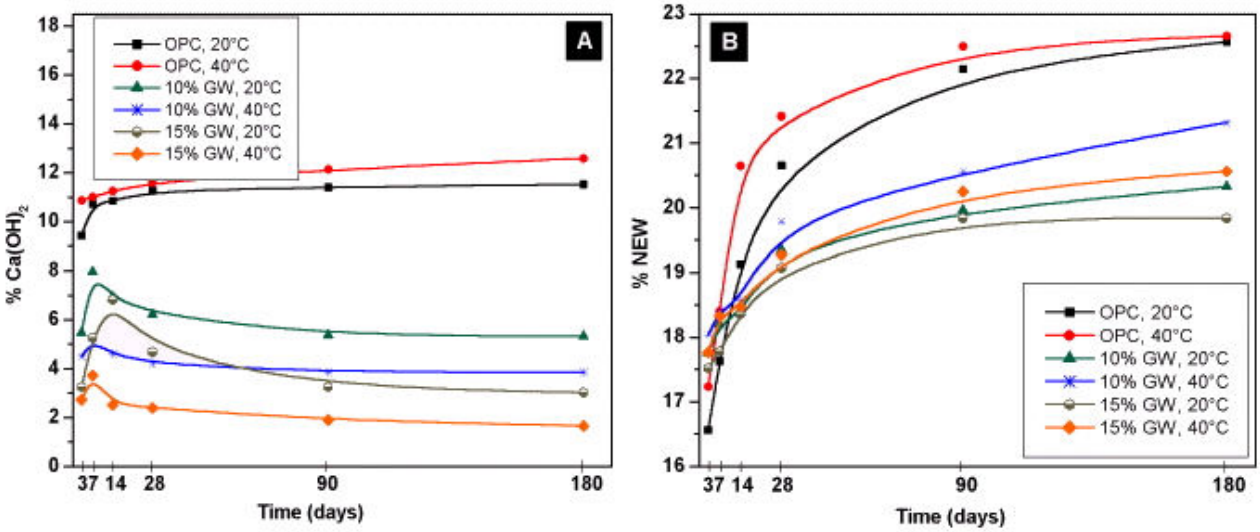

Figure 3. (A)% Calcium hydroxide vs. time for the neat and blended cements.
(B) % Non-Evaporable Water vs. time for the neat and blended cements

3.3 Non-evaporable water (NEW)

Figure 3B shows the results of non-evaporable water vs. time for neat and blended cements cured at both temperatures. The NEW results for the first three days with silica load of 10 and 15%, were higher than those of the neat cement, which suggest an actual increase of the cement hydration. After 14 days onwards the NEW values of the blended cements were lower. After 90 days curing, the NEW values were lower, for higher silica contents for a given temperature.

Several authors [7,8,11,12] have described the silica fume effect on the non-evaporable water produced by Portland cement with replacement levels from 5 to 30%, and various w/s ratios. They found that the amounts of NEW for neat cements were higher than those in blended cements for a given w/s ratio, especially at long periods of hydration. Moreover, the greater the silica load, the lower the NEW relative to the neat cement values. This phenomenon was reported with evidence of pozzolanic behaviour of the silica fume.

The reduced NEW values noted were explained in the literature in several ways. One is that described by Zhang and Gjorv [12], due to the increased average chain length of polysilicates in the C-S-H gel, with both silica fume content and time, which was believed to result in water release, hence lower NEW values. Attlasi [11] concluded that the water from CH involved in the pozzolanic reaction is released as evaporable water, lowering the total amount of NEW per hydrated cement content in silica fume blends. Yogendran et. al. [8], pointed that since the pozzolanic reaction reduces the CH amounts in OPC blended with silica fume, and the cement fraction is lower, the NEW values are reduced and it is not possible to directly compare NEW values of a neat and the blended cement; they suggested a direct comparison between NEW values that excluded CH water losses. In this way the latter authors found that the NEW values from the pozzolanic reaction and the accelerating effect on the cement hydration were greater than the NEW reduction due to a lower neat cement fraction.

Figure 4A presents modified NEW values (NEWH), in which the CH water losses were extracted. In the presence of the geothermal waste the NEWH higher values than those of the neat cement for the first 28 days hydration. This suggests that the silica accelerated the cement hydration, probably acting as nucleation sites [2,3] for deposition of the hydration products and also promoting the formation of calcium silicates hydrates by the removal of CH by the pozzolanic reaction, which favour further progress of the calcium silicates hydration. After 90 days, it can be noted that the

NEWH values for the neat and blended pastes at 20°C were similar; however, at 40°C the NEWH values were higher in both blended cements, indicating that the cement hydration and the pozzolanic reaction are favoured by increased temperatures. Figure 4B presents a plot of NEW vs NEWH, it can be noted that for a fixed NEW value, the corresponding NEWH are higher for the blended cements; the latter are higher for increased silica waste content and higher temperature (which corresponds to the CH depletion trends plotted in figure 2). This could suggest that the pozzolanic reaction consumes water, although is not clear whether is only that present in the CH, and the excess of NEWH relative to NEW is due to a mixed effect of the additional C-S-H formed by the pozzolanic reaction and the cement hydration acceleration.

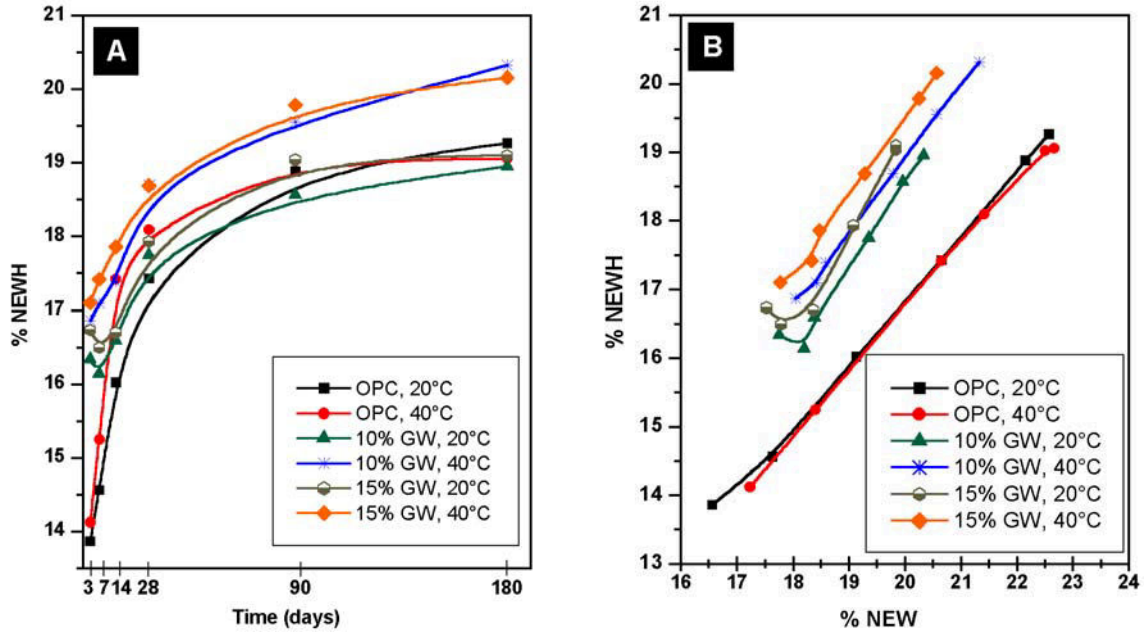

Figure 4. A) Non-evaporable water in hydrates vs. time, B) Non-evaporable water in hydrates vs. total non-evaporable water

These results indicate that the consumption of CH has a strong influence in the values of NEW obtained from blends of cement with pozzolanic materials. From the above comparison it seems that to analyse the effect of silica in the hydration of the cement is preferable compare the data of NEWH, however, the effect of the NEW reduction could be associated to the pozzolanic behaviour of the silica but the effect of a real cement fraction reduction must be taken into account.

3.4 Scanning electron microscopy

Figures 5 A and B show the microstructures of neat cements hydrated for 180 days at 20°C and 40°C respectively. The main features are those commonly observed in cement pastes with water/solids ratio of 0.50. In both cases a fraction of the cement was still unreacted, with calcium hydroxide crystals and porosity dispersed throughout the microstructure. There were no marked differences between the microstructures at both temperatures.

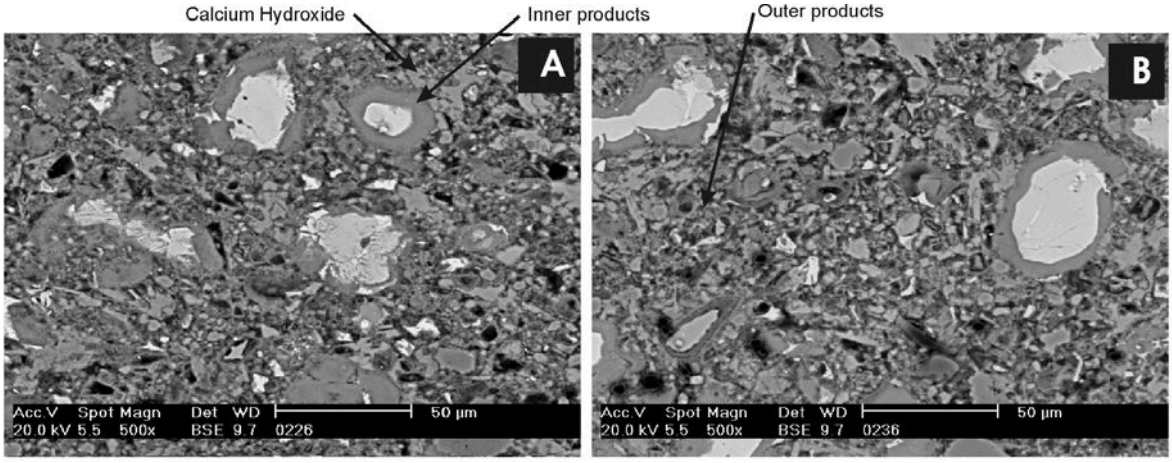

Figure 5. SEM-BEI of the microstructure of OPC after 180 days of hydration a)20°C and B)40°C.

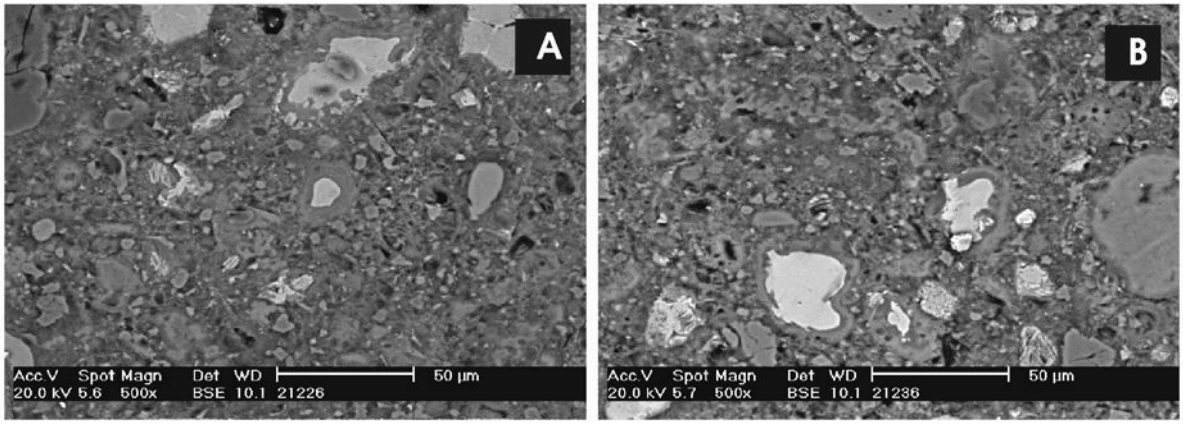

Figure 6. SEM-BEI of the microstructure of OPC-10%GW after 180 days of hydration a)20°C and B)40°C.

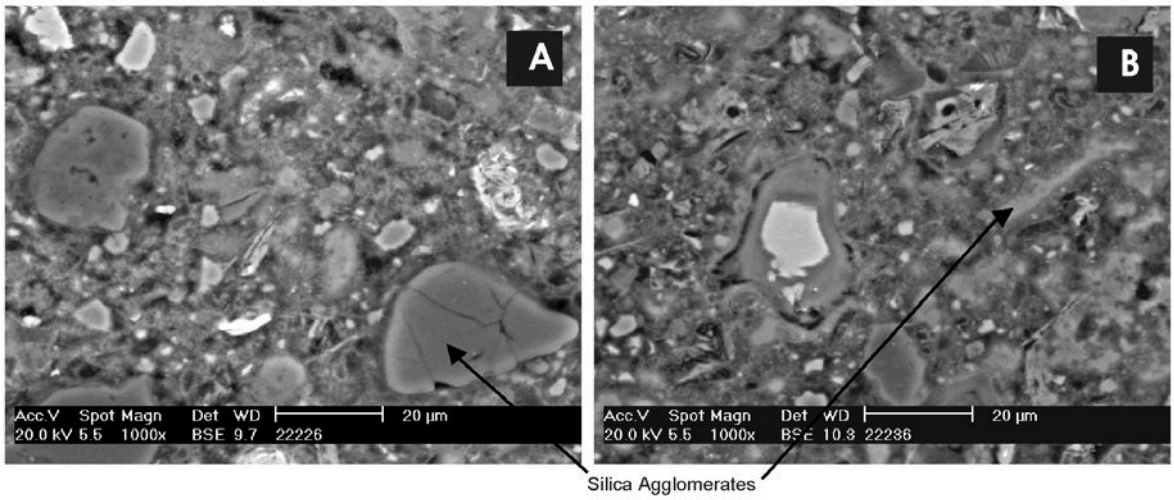

Figure 7. SEM-BEI of the microstructure of OPC-15%GW after 180 days of hydration a)20°C and B)40°C.

Figures 6 and 7 present the microstructures, after 180 days for both temperatures, of blended cements with 10 and 15% GW, respectively. For the two replacement levels was observed that the amount of calcium hydroxide crystals was drastically reduced. Also the silica waste was relatively well dispersed in the matrix, and occasionally some silica agglomerates were noted (Figure 7). Moreover, the apparent porosity was reduced in both replacement levels in comparison with the neat cement.

4. DISCUSSION

From the general analysis of the results it was observed that the presence of silica waste increased the compressive strength, this can be associated to several factors, which were evidenced by the results here presented. Increased reactivity of the cement was indicated by NEWH results. The formation of additional C-S-H was pointed by the CH consumption in the presence of the silica waste. These two factors led to an enhanced C-S-H formation which, together with a microfiller effect that was observed from the microstructures, resulted in a more compact matrix of hydration products.

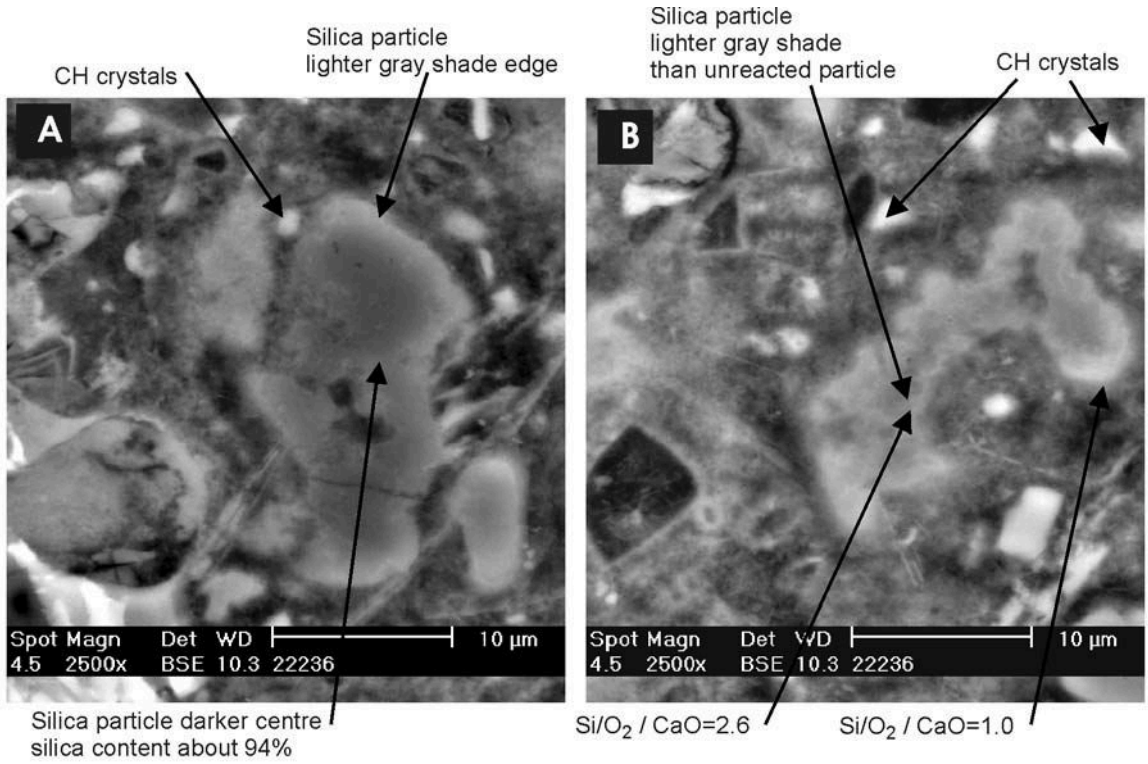

Figure 8. Microstructure of OPC-15%GW after 180 days of hydration at: A) 20°C and B) 40°C. Backscattered electron images

Evidence of the pozzolanic activity was indirectly obtained from thermal analysis. Careful observation of some relatively large silica particles, by backscattered electron images in Figure 8, allowed to note that the edges of such particles showed a lighter gray shade than the centre. Considering that the differences in chemical composition are reflected in the gray shades, lighter gray shades are expected from areas of higher average atomic number. On this basis, EDS analyses of various zones around and within some of the silica particles were taken. As the spot was moved from the edge towards the centre of some of the particles, it was noted that the SiO_2/CaO ratio increased from about 1 (lighter gray zones) to very high values (darker zones). This would provide an indication that there is a surface chemical interaction between the silica and the CH, with the absorption of Ca locally increasing the average atomic number. In figures 8 A and B small areas of CH crystals, what could be relics of larger crystals, were noted around the silica particles.

The circumstances under which ettringite appears are not yet fully explained. Collepardi [13] determined the preconditions of delayed ettringite formation (DEF): microcracks, relase of sulfate in later period and sufficient water supply; DEF damage would result provided all factors are present. Nevertheless, Yang et.al.[14] pointed out that the microcracks are induced by DEF. Taylor [15] established that there is no supporting evidence from laboratory studies of the existence of DEF without steam curing conditions; however, Diamond [16] found that DEF is to be expected in both steam and not steam cured concrete and that the microstructural features appear to be identical. Stark et. al.[17], presented a hypothesis on the possible causes of accumulation of ettrigite in hardened concrete: additional formation of ettringite by internal sulfate release and mobilization of existing ettringite, their transport and recrystallization; could be attributed to factors such as: heat treatement (above mentioned), freeze thaw attack, carbonation, chemical composition of the clinker, alternating moisture conditions and marginal conditions which promote damage like ASR and chemical shrinkage or self desiccation.

Localized zones rich in ettringite clusters were noted in fracture surfaces for 20% GW cured at 40ºC in the long term. Microanalysis (EDS) suggested that the extensive cracking observed was due to the formation of ettringite. The cracked samples were not submitted to any of the above mentioned conditions for DEF. The potential effect of the OPC composition for DEF could be disregarded since the cracking occurred only with 15 and 20% and not with 0 and 10% GW. The absence of sulphur in the GW composition brings additional questions as to whether the GW favour DEF with sulphur supply. In spite that some authors have been found that agglomerates of silica fume can cause ASR problems as pre-conditions for DEF, for the pastes analysed here no ASR evidence was observed. There is uncertainty whether the GW can participate in creating some kind of predamage that could favour DEF in the cement paste, which was clear is that the relatively higher temperature favoured DEF, nonetheless 40ºC is much lower than the temperature of about 70ºC reported for thermal treatment by some authors. Additional work is required to elucidate the causes DEF in the presence of GW.

5. CONCLUSIONS

- The silica presence in cement pastes increased the compressive strength, which was associated with the reduction of porosity in the microstructures.
- The cement hydration was accelerated by the presence of silica waste, in agreement with the results of non-evaporable water.
- The silica waste presented pozzolanic activity, depleting the CH concentration, which was strongly influenced by the curing temperature and the replacement level.
- Overall, the pozzolanic activity and the cement hydration enhancement increased the amounts of C-S-H, which together with the microfiller effect resulted in more compact hydration product matrix.
- The pastes with 15 and 20% of silica waste at 40°C presented extensive cracking, attributed to the formation of ettringite.

AKNOWLEDGMENTS

Research funded by CONACYT project J28273U. The operation of the scanning electron microscope by Martha Rivas is acknowledged.

REFERENCES

[1] Escalante, J. I., Mendoza, G., Mancha, H., López, J., Vargas, G., Pozzolanic properties of a geothermal waste material, Cement and Concrete Research, vol. 29, 1999, pp. 623-625

[2] Gutteridge, W. A., Dalziel, J. A., The effect of a secondary component on the hydration of Portland cement, Part I, A fine non hydraulic filler, Cement and Concrete Research, vol. 20, 1990, 778-782

[3] Gutteridge, W. A., Dalziel, J. A., The effect of a secondary component on the hydration of Portland cement, Part I, Fine hydraulic binders, Cement and Concrete Research, vol. 20, 1990, 853-861

[4] Verbeck G J, Helmuth R H, Structures And Physical Properties Of Cement Paste, Proceedings of the 5th Intnl. Symposium on the Chemistry of Cement in Tokyo, 1968, pp. 1-32

[5] Swamy, R. N., Laiw, J. C., Effectiveness of supplementary cementing materials in controlling chloride penetration into concrete, SP pp. 657-674

[6] Toutanji, H. A., El-Korchi, T., The influence of silica fume on the compressive strength of cement paste and mortar, Cement and Concrete Research, Vol. 25, 1995, pp. 1591-1602

[7] Cheng-Yi, H; Feldman, R. F.; Hydration Reactions in Portland Cement – Silica Fume Blends, Cement and Concrete Research, Vol. 15, 1985, pp. 582-592

[8] Yogendran, V., Langan B. W., Ward, M. A., Hydration of cement and silica fume paste, Cement and Concrete Research, vol. 21, 1991, p. 691-708

[9] Díaz, C.; Ph.D. thesis: Caracterización y purificación del residuo de sílice de la central Geotérmica de Cerro Prieto, Universidad Autónoma de Madrid, 1994

[10] Escalante, J. I., Gomez, L. Y., Johal, K., Mendoza, G., Mancha, H., Mendez, J., Reactivity of blast-furnace slag in Portland cement blends hydrated under different conditions, Cement and Concrete Research, vol. 3, 2001, pp. 1403-1409

[11] Attlasi, E. H., Non-evaporable water and degree of cement hydration in silica fime-cement systems, CANMET-ACI, Proceedings of Fifth International Conference, USA, 1995, pp. 703-717

[12] Zhang, M., Gjørv, O. E., Effect of silica fume on cement hydration in low porosity cement pastes, Cement and Concrete Research, vol. 21 1991, pp. 800-808

[13] Collepardi, M., A holistic approach to concrete damage induced by delayed ettringite formation, Proceedings of Mario Collepardi Symposium on Advances in Concrete Science and Technology, 1997, pp. 373-396

[14] Yang, R., Lawrence, C.D., Sharp, J.H., Delayed ettringite formation in 4-year old cement pastes, Cement and Concrete Research, vol. 26, 1996, pp. 161-170

[15] Taylor, H.W.F., Famy, C., Scrivener, K.L., Review: Delayed ettringite formation, Cement and Concrete Research, vol. 31, 2001, pp. 683-693

[16] Diamond S., Delayed ettringite formation – processes and problems, Cement and Concrete Composites, vol. 18, 1996, pp. 205-215

[17] Stark, J., Bollmann, K., Delayed ettringite formation in concrete, Nordic Concrete Research (on line publication), 1998, p. 1-25

[18] Diamond, S., Alkali-silica reaction – some paradoxes, Cement and Concrete Composites, vol. 19, 1997, pp. 391-401

[19] Lagerblad, B., Utkin, P., Undispersed granulated silica fume in concrete – chemical system and durability problems, Proceedings Materials Research Society Symposium: Microstructure of Cement-Based systems / Bonding and Interfaces in Cementitiuos Materials, vol 370, 1994, pp. 89-97

INTERNAL AND SURFACE DAMAGE OF CONCRETE DURING FREEZING AND THAWING LOADS

V.E. Penttala[1] and V.J. Räsänen[1]

[1]Laboratory of Building Materials Technology, Helsinki University of Technology, Finland.
E-mail: vesa.penttala@hut.fi and vesa.rasanen@hut.fi

ABSTRACT

The internal and surface damages during freezing and thawing tests of 45 different concretes were assessed by slab test and CIF-test procedures. Tests were performed with deionized water as the freezing liquid in which no additional salts were dissolved. The test concretes were produced so that a large range of compressive strengths, air contents, curing measures, and binder amounts were covered. In the slab and CIF-tests surface deterioration was measured by weighing the deterioration of the surface layer after 56 freezing and thawing cycles in which temperature varied between +20 and –20 °C. The internal damage in the test slabs was studied by measuring the change in ultrasonic pulse velocity of the test slabs.

The most significant variables affecting the freezing and thawing durability of concrete were calculated statistically and contours of estimated response surface were produced. Water-cement ratio and air content of the concretes were the most dominant variables affecting the internal and surface damage caused by the freezing and thawing loads. Water curing improved the R-squared values of the test population in the surface damage tests. In the internal damage tests the curing measures did not improve the statistical relevancy of the estimated response surfaces.

1. INTRODUCTION

Almost one third of the concrete volume cast in the Nordic countries must possess adequate freezing and thawing durability. Majority of concrete durability research and test methods concentrate on the degradation of concrete surface due to the freezing and thawing loads while only during the last decennium the internal damage of the frost action has gained increasing attention. It has been noticed that internal damage has been the dimensioning criterium in concretes produced by a low water-binder ratio.

2. LITERATURE REVIEW

The two classical freezing and thawing theories of concrete are based on the research work by T. C. Powers and his coworkers [1]-[5]. The theory of hydraulic pressure is not considered valid nowadays and even Powers replaced it by the theory of osmotic pressure. In these theories the direction of the pore water movements are opposite. In the theory of hydraulic pressure the pore water is considered to move from those parts of the capillary space in which ice is first generated towards other parts of the concrete matrix. However, test results and also theoretical considerations have shown that the direction of water movement during freezing is opposite. The unfrozen pore water in the nearby smaller pore spaces is drawn to those parts of the pore system in which ice is first induced. In the theory of osmotic pressure Powers deduced that the pore water is moving in this direction due to the osmotic pressure caused by the dissolved salts (mainly K_2O and Na_2O) which

are not incorporated to the formed ice structure. This increases the salt concentration so that the surrounding unfrozen pore water moves towards the frozen pore in the pursuit to dilute the larger salt concentration. In normal pore water into which no additional salts are introduced there are only few millimols of dissolved substances and, therefore, the osmotic pressures induced into the concrete matrix do not seem to be large enough to cause the large contraction noticed in concrete during the freezing phase.

In the 1970's G. Fagerlund [6] developed the concept of critical degree of saturation in freezing concrete. According to his findings there is in porous materials a critical degree of saturation which causes deterioration or cracks into the material if the material is frozen even once. The theory was first developed according to the theory of hydraulic pressure but because of the universal nature of the concept it is applicable also to other freezing theories. However, in order to give reasonable results the freezing and thawing cycles by which the critical degree of saturation is achieved ought to take place according to the freezing and thawing loads in real structures.

According to G. G. Litvan [7]-[10] water in the capillary pores cannot freeze in situ but the freezing takes place in the vicinity of the outer surface of the structure. The supercooled water causes water movements and drying in the porous body which can cause freezing and thawing deterioration. M. Setzer [11] took in his freezing theory into account the surface forces of the pores and revised Litvan's theory. He was also the first to propose the micro-ice lens theory [12] which explained the water suction from the environment during freezing and thawing cycles. V. Penttala [13],[14] derived a theory based on thermodynamics by which the pressures in pore water can be derived from temperature and relative humidity data measured in concrete during the freezing and thawing cycle. If the pore water amount is known the pressures in the concrete structures can be calculated. In the theory, the pore size distribution data is not needed. According to the theory based on thermodynamics the main reason for the pore water movements towards the ice bodies that are first induced is the difference in chemical potential between ice and the unfrozen pore water in the smaller pores surrounding ice and the osmotic pressures play only a minor role.

In the previously mentioned theories the need for air-entrainment, adequate pore size distribution or spacing cannot be calculated with the exception of the theory of hydraulic pressure. However, this theory is not considered valid in the modeling of freezing and thawing durability of concrete.

There exists a large number of test methods by which the internal damage and surface scaling of concrete can be evaluated. The critical dilation test ASTM C 671 [15] and rapid freezing and thawing test ASTM C 666 [16] are typical tests by which the internal damage of the concrete specimen can be assessed. Salt scaling test ASTM C 672 [17] measures the scaling of the specimen surface in the presence of de-icer salts. There are numerous national freezing and thawing tests that resemble these three which are so called direct tests performed by using actual freezing and thawing loads. In this paper two recently developed freezing and thawing tests will be applied. In the CIF test [18] and the slab test [19] both internal damage and surface scaling can be determined by the same specimen and test simultaneously.

3. MATERIALS AND TEST ARRANGEMENTS

All test specimens were cast by using the same cement type CEM IIA 42,5R of local origin produced by Finnsementti Oy. No other additional binders were used. The petrographic composition of the aggregates was mainly granite and the maximum aggregate diameter was 16 mm except for 4 batches in which it was 10 mm or 32 mm. The total amount of the different test concretes was 45.

The water cement ratio of the test concretes was varied so that the test population comprised of concretes having water cement ratios of 0.30, 0.40, 0.54, 0.65, 0.76, 0.94, and 1.12. The cement content of the test concretes varied from 170 to 634 kg/m^3. The air content of the test concretes varied from 0.6 to 10.5%. The water curing times ranged from 0 to 13 days after the stripping of the moulds at the concrete age of 24 hours. Thereafter, the test specimens were stored in a climate cabin in the temperature of 20±2 ^{o}C and relative humidity of 65±5%. The amount of the fine aggregates (<0.6 mm) varied from 34 to 384 kg/m^3.

The CIF test specimens had dimensions of 150x110x75 mm and at the age of 25 days a bituminous aluminium sheet was glued on the edge faces of the specimens according to the RILEM recommendation [18]. The dimensions of the test specimens of the slab test were 150x150x50 mm. As an exception to the Swedish standard [19] the freezing surface of the test specimens was the mould surface and not the sawn surface inside the the test cube so that the freezing surfaces of both tests were comparable to each other. At the age of 25 days a rubber sheet was glued on the other faces of the test specimens except the freezing surface of the slab test specimens according to the standard [19]. The tests of these two freezing and thawing test methods were performed otherwise according to the respective references [18], [19]. Both freezing and thawing tests started at the concrete age of 35 days. The freezing liquid was deionized water having electrical conductivity less than 3 μS/cm. Figure 1 shows the test layout for the CIF test and Figure 2 shows the layout for the slab test.

The test specimens of the CIF tests were weighed for scaling deterioration and the ultrasound measurements were performed after 6, 14, 20, 28, 34, 42, 48, and 56 cycles. Similar tests for the slab test specimens were done after 7, 14, 28, 42, and 56 freezing and thawing cycles. Both tests ended after 56 cycles. The test concretes were also tested by 100-mm^3 cubes in a salt freezing test according to Finnish standard SFS 5449 [20] but the results are not presented in this paper. The compression strength of the concretes was measured by loading six 100-mm cubes at the age of 28 days.

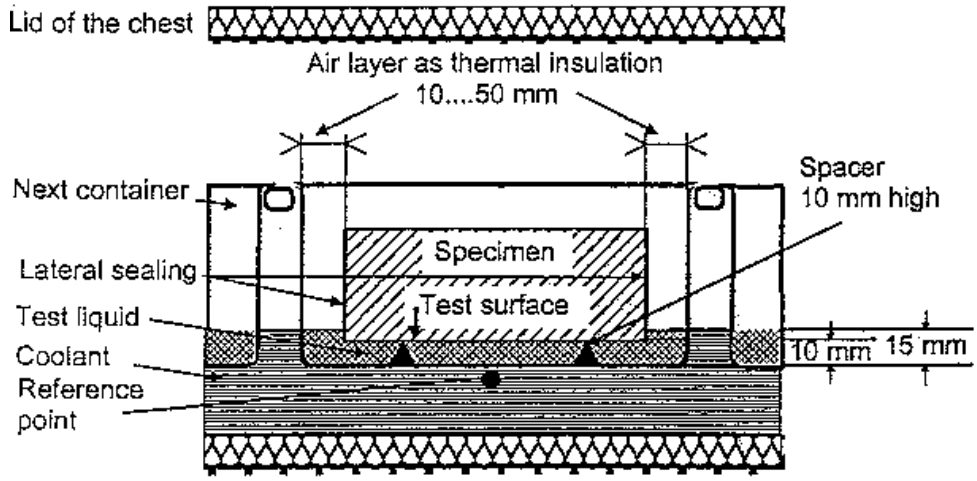

Figure 1. The test arrangement of the CIF test [18].

4. TEST RESULTS

The internal damage and surface scaling test results of the concretes have been analyzed statistically in two parts. Using the Statgraphics computer program the validity of the most relevant variables was first calculated by simple linear regression. Thereafter, the models for these variables were construed by nonlinear regression.

According to the results obtained from the linear regression calculations the most relevant variables to model the scaling results were cement content, water content, water cement ratio, air content, and curing time. In the internal damage modelling the same variables were the most relevant with the exception of curing time which did not increase the R-squared statistcs of the test population. The best nonlinear regression model of the scaling results was formulated as

$$D = a + b \cdot \left[(W/C)^c / A^d / B^e \right] \quad (1)$$

in which W is water content [kg/m^3]
C is cement content [kg/m^3]
A is air content [%]
B is curing time [d]
D is deterioration, if surface scaling [g/m^2] or if internal damage [decrease of ultra sound penetration time in %]
a,b,c,d,e are coefficients

The most suitable model of the internal damage is

$$D = a + b \cdot \left[(W/C)^c / A^d \right] \quad (2)$$

The coefficients of the models and the respective R-squared values are presented in Tables 1 and 2.

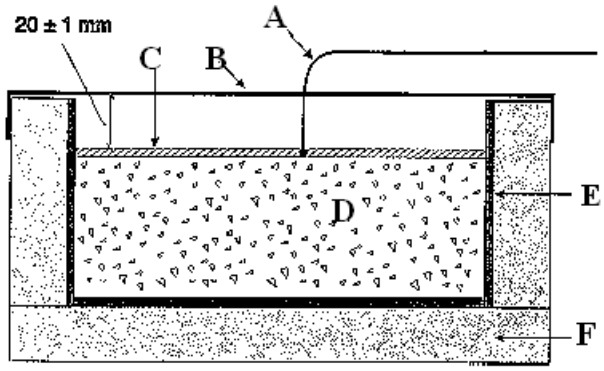

Figure 2. The test arrangement of the slab test [19]. In the picture A denotes a thermo-element, B is a evaporation protection, C is the freezing liquid, D is the concrete test specimen, E denotes a rubber cover, and F is thermal insulation.

Table 1. The model coefficients of Equation (1) and the R-squared values of the 45 test concretes.

Test/damage type	a	b	c	d	e	R^2 [%]
CIF/scaling	175.229	7574.63	6.96392	1.18921	0.637267	82.8
Slab test/scaling	-70.2615	8656.28	3.32138	0.48781	0.210174	89.1
CIF/internal damage	198.374	-121.202	-0.385581	-0.130708	0.0059914	71.7
Slab test/internal damage	-128.69	227.804	0.452682	0.142734	-0.004007	79.9

Table 2. The model coefficients of Equation (2) and the R-squared values of the 45 test concretes.

Test/damage type	a	b	c	d	R^2 [%]
CIF/scaling	173.998	2321.26	6.46967	1.0597	80.4
Slab test/scaling	-78.9908	5760.49	3.20856	0.475537	87.6
CIF/internal damage	-149.021	232.705	0.329404	0.121914	74.9
Slab test/internal damage	-130.691	231.776	0.450739	0.140754	79.9

The R-squared statistics indicates that the model explains the percentage of the variability in the test in question. The Durbin-Watson statistics of the residuals indicated that there may be some serial correlation in several of the different models. The contours of the estimated response surface of the different tests are presented in Figures 3 to 10 by using Equation (2). Two examples of the surface scaling of a CIF and slab test specimen are presented in Figures 11 and 12.

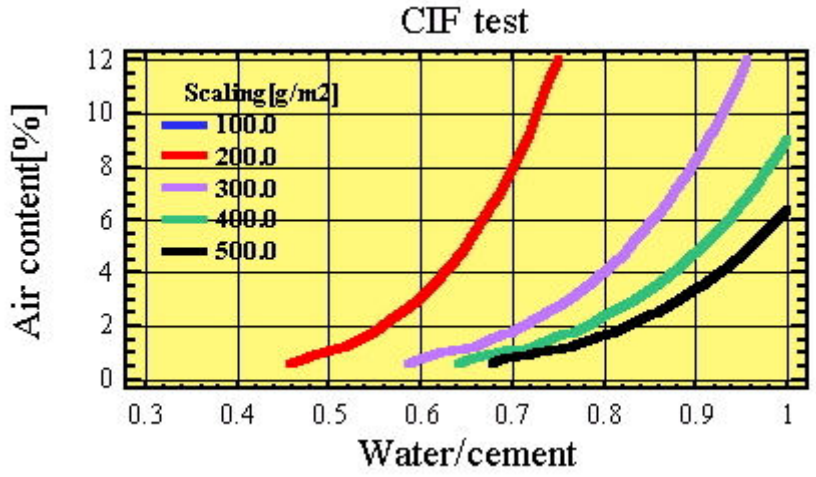

Figure 3. Curves of the estimated response surface of the surface scaling in the CIF test.

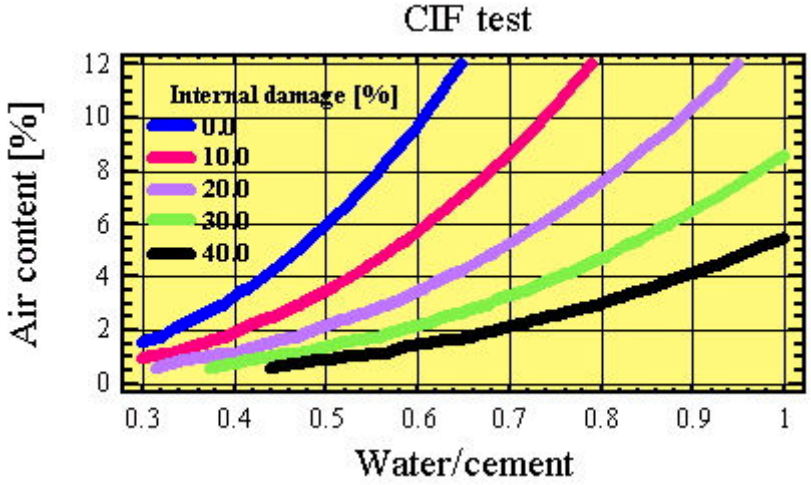

Figure 4. Curves of the estimated response surface of the internal damage in the CIF test.

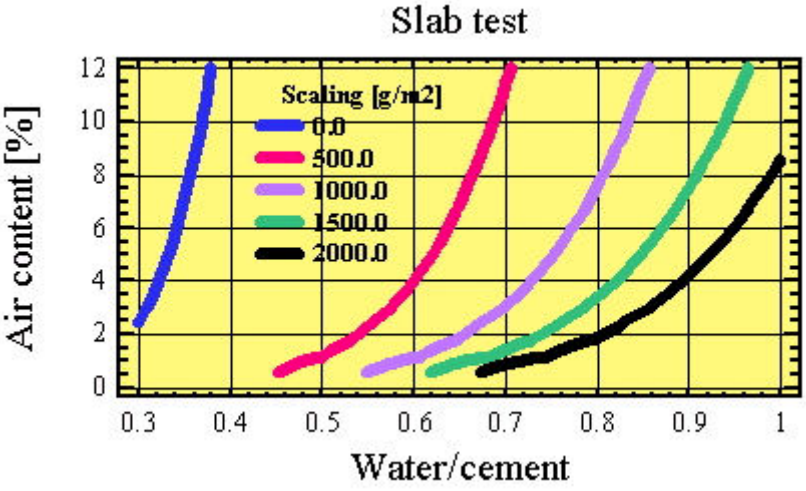

Figure 5. Curves of the estimated response surface of the surface scaling in the slab test.

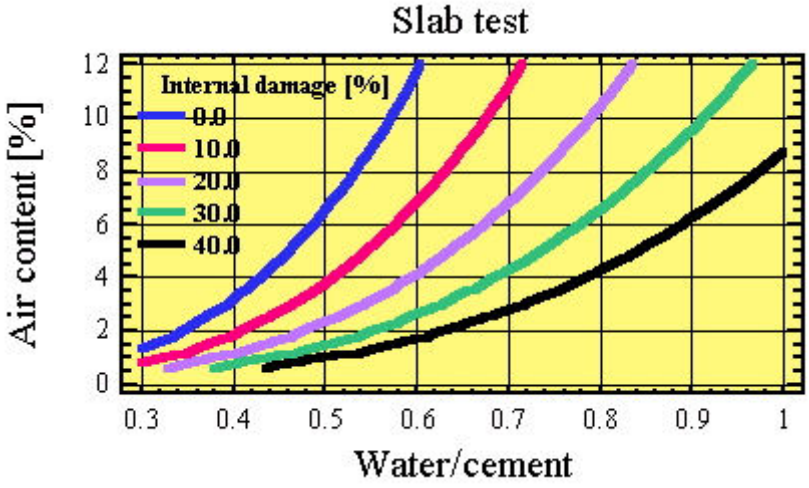

Figure 6. Curves of the estimated response surface of the internal damage in the slab test.

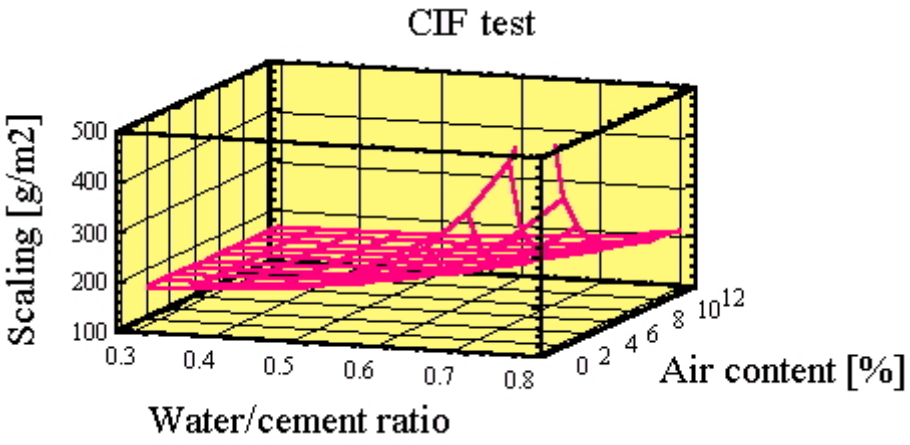

Figure 7. Contours of the estimated response surface of the surface scaling in the CIF test.

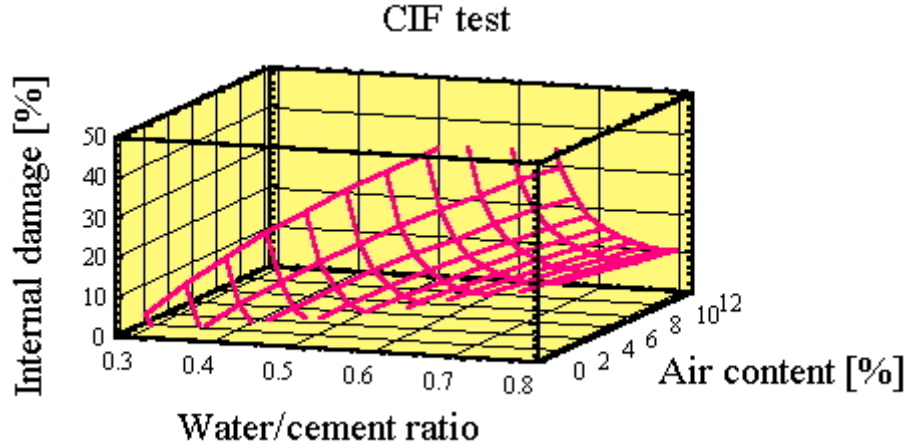

Figure 8. Contours of the estimated response surface of the internal damage in the CIF test.

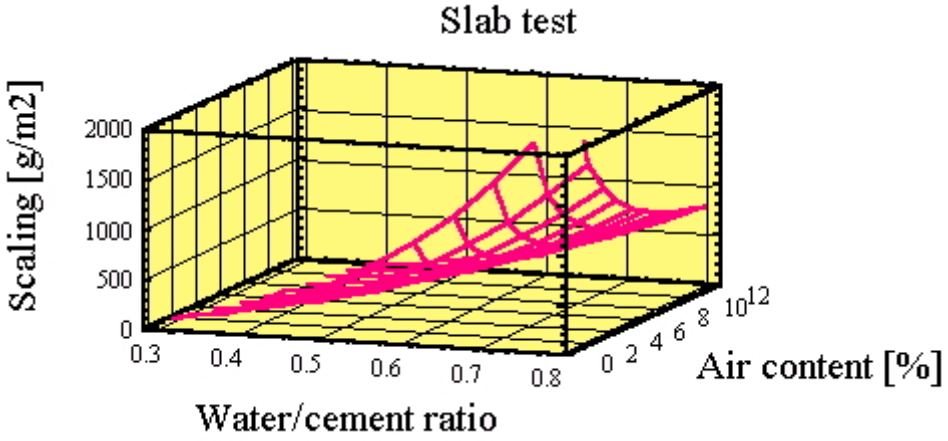

Figure 9. Contours of the estimated response surface of the surface scaling in the slab test.

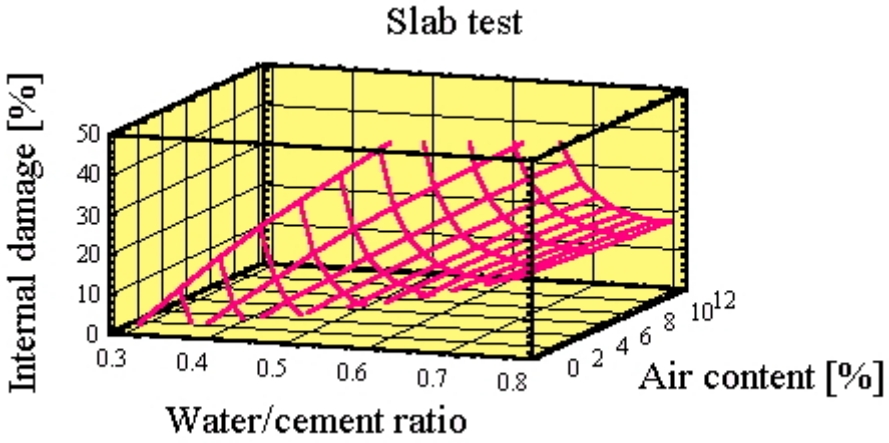

Figure 10. Contours of the estimated response surface of the internal damage in the slab test.

5. DISCUSSION

The R-squared results presented in Tables 1 and 2 show that if the curing measures are included in the model this increases the R^2-values of surface scaling damage and decreases the internal damage validity of the model. Similarly, as the exponent e of curing time B in Table 1 is a very small number in the internal damage situation, curing measures have very little effect on the internal damage of concrete. This seems quite obvious because curing enhances the quality of the surface layer of concrete, and hence improves the freezing and thawing durability of the surface. Curing increases the hydration degree inside the test slab only marginally especially in concretes which are produced by using a low water cement ratio, and therefore, curing does not effect the internal damage caused by freeze-thaw loads very much. The proposed deterioration models give to the slab test a somewhat higher R-squared values compared to the CIF test. The difference is over 6 percent-units in the scaling mode and from 5 to 8 percent-units in the internal damage mode.

Comparing the slab and CIF test results in Figures 3 to 10 one can notice that the slab test is a more severe test than the CIF test. This seems to be reasonable because in the slab test the freezing solution is situated on the top surface of the test slab, and therefore, gravity draws it towards the inside of the specimen. In the CIF test water is in contact to the lower surface of the test slab and it is drawn inside the test specimen only by capillary suction and due to the thermodynamic pumping action caused by the cyclic freezing and thawing load. This difference in the severity of the frost action is apparent both in the surface scaling results and also in the internal damage results. These

two freezing and thawing durability tests will be presumably approved as the official frost durability tests in the European concrete standardization, and therefore, the approval criteria must be different for these tests as can be seen in comparing the results of Figures 13 and 14.

When the contours of the estimated response surfaces of the CIF and the slab tests are compared with each other in Figures 7 and 9 it can be noticed that the scaling values in the CIF surface seem to level off to a constant value of 160 g/m^2 when water/cement ratio is diminishing. In Figure 9 the surface in the slab test cuts the plane where the scaling damage is zero. This gives a possibility to select the water/cement ratio and the air content so that no scaling takes place in the slab test. The internal damage surfaces of Figures 8 and 10 are quite similar for both test types even though the slab test surface is somewhat higher.

Figure 11. Surface scaling of 200 g/m^2 of a CIF test specimen after 56 freeze-thaw cycles.

Figure 12. Surface scaling of 550 g/m^2 of a slab test specimen after 56 freeze-thaw cycles.

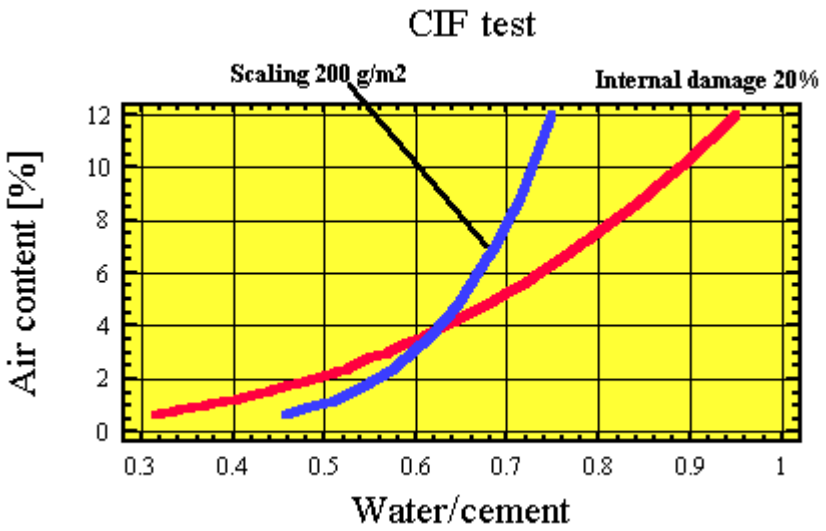

Figure 13. Two curves of the estimated response surfaces of the surface scaling and the internal damage results in the CIF test.

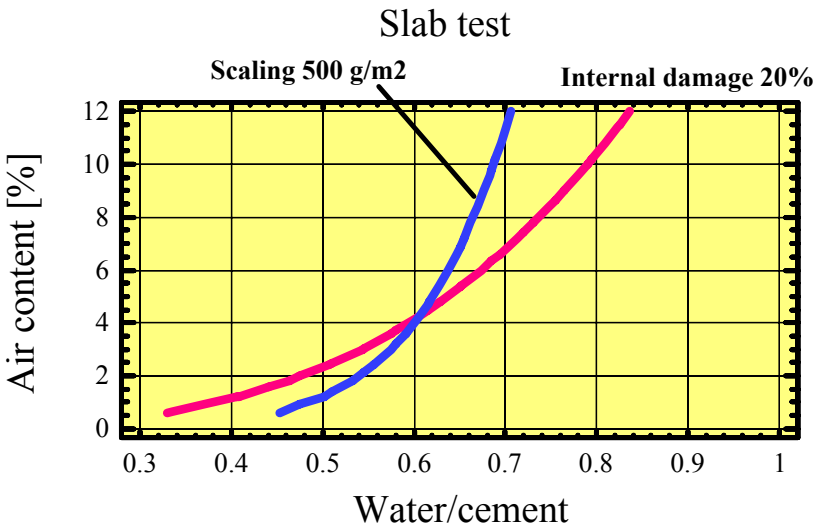

Figure 14. Two curves of the estimated response surfaces of the surface scaling and the internal damage results in the slab test.

In Figures 13 and 14 it can be seen that when the water/cement ratio of concrete increases the need of air entrainment increases due to surface scaling damage much faster compared to the need of air entrainment in the internal damage failure mode. On the other hand, in concretes possessing low water/cement ratios the dimensioning criteria for the air content comes from the internal damage curves in these figures. Comparing the curves of 200 and 500 g/m^2 surface scaling in these figures it becomes apparent how much more severe the slab test is compared to the CIF test. Similarly, also the internal damage loading is more severe in the slab test compared to the CIF test. However, the difference is not as pronounced as in the scaling deterioration.

The effect of water curing is compared in Figures 15 and 16 in the CIF-test and the slab test. The curing time has an remarkable effect on the required air content or water/cement ratio. In the internal damage situation the effect of curing is negligible taking into consideration the accuracy of the statistical method.

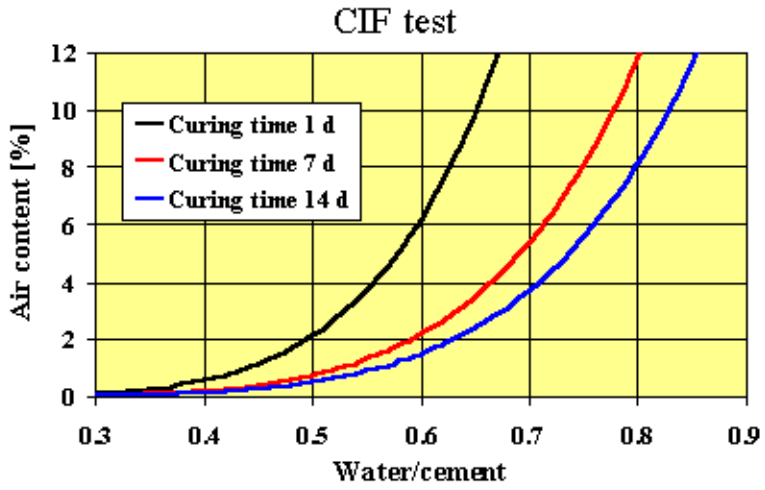

Figure 15. Comparison of the effect of water curing on the surface scaling of 200 g/m^2 in the CIF-test by using Equation (1).

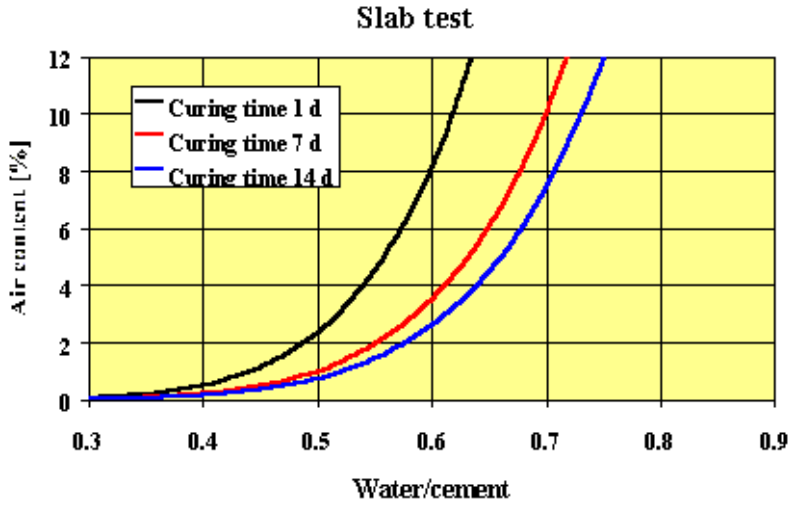

Figure 16. Comparison of the effect of water curing on the surface scaling of 500 g/m^2 in the slab test by using Equation (1).

6. CONCLUSIONS

One of the biggest merits of the CIF and slab tests is that both the surface scaling and the internal damage can be assessed from the same test specimen in a single test so that the two deterioration mechanisms do not interfere with each others test result in the same extent as in the other contemporary freezing and thawing tests. Similarly, the thermodynamic pumping effect is taken into consideration in these tests and the freezing action is taking place only in one direction. The test results give a good basis to estimate the serviceability life prediction of concrete structures.

REFERENCES

[1] Powers, T.C. A working hypothesis for further studies of frost resistance of concrete, Journal of the American Concrete Society, vol.16, 1945, pp. 245-271.

[2] Powers, T.C. The air requirements of frost-resistant concrete, Proceedings of the Highway Research Board, Portland Cement Association, Bulletin 33, 1949, pp. 1-28.

[3] Powers, T.C. and Brownyard, T.L. Studies of the physical properties of hardened Portland cement paste, Journal of the American Concrete Institute, vol. 18, 1947, pp. 549-602.
[4] Powers, T.C. and Brownyard, T.L. Studies of the physical properties of hardened Portland cement paste, Journal of the American Concrete Institute, vol. 18, 1947, pp. 933-969.
[5] Powers, T.C. and Helmuth, R.A. Theory of volume changes in hardened Portland-cement paste during freezing, Proceedings of the Highway Research Board, vol, 32, 1953, pp. 285-297.
[6] Fagerlund, G. The critical degree of saturation method of assessing the freeze/thaw resistance of concrete, Materials and Structures, vol. 58, 1977, pp. 217-229.
[7] Litvan, C.G. Phase transitions of adsorbates III: Heat effects and dimensional changes in nonequilibrium temperature cycles, Journal of Colloid and Interface Science, vol. 38, 1972, pp. 75-83.
[8] Sidebottom, E.W. and Litvan, C.G. Phase transitions of adsorbates – Vapour pressure and extension isotherms of the porous-glass+water system below 0^{o} C, Transactions of the Faraday Society, N:o 585, vol. 67, 1971, pp.2726-2736.
[9] Litvan, C.G. Phase transitions of adsorbates: IV, Mechanism of frost action in hardened cement paste, Journal of The American Ceramic Society, vol. 55, 1971, pp. 38-42.
[10] Litvan, C.G. Phase transition of adsorbates: V. Aqueous sodium chloride solutions adsorbed on porous silica glass, Journal of Colloid and Interface Science, vol. 45, 1973, pp. 154-169.
[11] Setzer, M. J. Einfluß des Wassergehalts auf die Eigenschaften des erhärteten Betons, Deutscher Ausschuss für Stahlbeton, Heft 280, 1977, pp. 43-117.
[12] Setzer, M. J. Basis of testing the freeze-thaw resistance: surface and internal deterioration. Proceedings of the International RILEM Workshop on Resistance of Concrete to Freezing and Thawing With or Without De-icing Chemicals, Proceedings 34, 1997, pp. 157-173.
[13] Penttala, V. Freezing-induced strains and pressures in wet porous materials and especially in concrete mortar, Advanced Cement Based Materials, vol.7, 1998, pp. 8-19.
[14] Penttala, V. Strains and pressures induced by freezing mortars exposed in sodium chloride solution. Concrete Science and Engineering, vol. 1, 1999, pp. 2-14.
[15] ASTM Standard C 671-86, Standard Test Method for Critical Dilation of Concrete Specimens Subjected to Freezing, Philadelphia: American Society for Testing and Materials, 1991.
[16] ASTM Standard C 666-90, Standard Test Method for Resistance of Concrete to Rapid Freezing and Thawing, Philadelphia: American Society for Testing and Materials, 1991.
[17] ASTM Standard C 672-91, Standard Test Method Scaling Resistrance of Concrete Surfaces Exposed to Deicing Chemicals, Philadelphia: American Society for Testing and Materials, 1991.
[18] Recommendations of RILEM TC 176-IDC: Test methods of frost resistance of concrete. CIF-Test- Capillary suction, Internal damage and Freeze thaw Test, Reference method and alternative methods A and B, Materials and Structures, vol. 34, 2001, pp. 515-525.
[19] Swedish standard SS13 72 44:1988, Betongprovning- hårdnad betong- frost. Stockholm, 1988.
[20] Finnish standard SFS 5449, Concrete, Durability, Frost-salt resistance. Helsinki, 1988.

IMPROVING CEMENT-SUPERPLASTICIZER COMPATIBILITY BY USING SOLUBLE ALKALIS AS A CHEMICAL ADDITIVE IN CONCRETE

G. Li[1], A. Tagnit-Hamou[2] and P.C. Aïtcin[2]

[1] Lafarge, Laboratoire Central de Recherche, 38291 St. Quentin Fallavier, France.
E-mail: guanshu.li@pole-technologique.lafarge.com
[2] Department of Civil Engineering, University of Sherbrooke, J1K 2R1 Canada.
E-mail: atagnit@andrew.sca.usherb.ca

ABSTRACT

To understand the effects of alkalis on the rheology, set and strength of superplasticized concrete, tests were carried out on four selected cements which did or did not present an incompatibility phenomenon and having high and low levels of C_3A and alkalis. The results obtained on cement pastes with addition of different salts of sodium and potassium show a great improvement in the slump loss for the cements presenting initially a problem of incompatibility. It has been shown the existence of an optimal amount of soluble alkalis varying as a function of the superplasticizer dosage. In contrast, the normal cements having a relatively high alkali content show a similar or even slightly deteriorated rheological behavior when the chemical additives are used. The results obtained on concrete confirm the improvement of rheological behavior by addition of the chemical additives. Moreover, they show the impact of added alkalis on the setting time and the improvement of the one day strength by up to 30% for the slump-improved concrete. The same effects were also observed when the lithium salts were used instead of the salts of sodium and potassium.

1. INTRODUCTION

The phenomenon of cement-superplasticizer incompatibility, increasing drastically in high performance concretes having a low W/C ratio and using superplasticizers, has been giving rise to the strong desire of researchers and attracting the attention of cement, concrete and admixture industries.

The phenomenon of cement-superplasticizer incompatibility, characterized generally by the rapid slump loss, is usually attributed to the lack of SO_4^{2-} ions in solution and the reaction of the SO^{3-} sites of the polysulfonated superplasticizer with C_3A [1, 2, 3, 4, 5, 6]. In this case, there is no longer enough polysulfonated superplasticizer molecules remaining in solution to plasticize the concrete. Therefore the compatibility of a particular cement and a particular superplasticizer depends on the balance between the amount and the reactivity of C_3A and the amount of SO_4^{2-} ions present in the mixing water as hydration is developing. The parameters controlling this balance in the presence of polysulfonated superplasticizer are first related to the characteristics of cement: finesse, content of the interstitial phase, crystalline form of C_3A, nature and amount of calcium sulfate added in the cement etc. It is also known that the characteristics of the superplasticizer should be optimized to produce a maximum of efficiency: sulfonation degree, percentage of beta sulfonated sites, chain length, nature of the counter-ion etc.

Proceedings of the 11th International Congress on the Chemistry of Cement (ICCC)
'Cement's Contribution to the Development in the 21st Century'
Hosted by: The Cement and Concrete Institute of South Africa
CD-ROM produced by: Document Transformation Technologies
11 - 16 May 2003, Durban, South Africa
ISBN Number: 0-9584085-8-0
Editors: Dr G. Grieve and G. Owens
Congress Organised by: Event Dynamics

The two practical solutions used to solve the problem of incompatibility based on this approach are the double introduction method and the use of a small amount of retarder [7, 8]. The first one consists of adding the superplasticizer in two steps: at the beginning of the mixing to neutralize the reactive sites of C_3A and then at the end of the mixing or just before placing the concrete to produce the fluidification effect. This solution presents often some technical complications and has a limited efficiency. The later one consists in using a retarder with the superplasticizer to slow down the reactivity of C_3A, but causes often, as a consequence, the early strength loss.

Within the framework of the research and development project on the phenomenon of cement-superplasticizer incompatibility conducted in the university of Sherbrooke in Canada between 1996 and 1998, one of the topics based on the chemical approach consists of studying some chemical factors inclined to affect at the same time the reactivity of the cement phases and the cement-superplasticizer interactions. This work aims the influence of the nature and the amount of the alkalis on the rheology, the set and the strength of superplasticized concretes.

2. MATERIALS AND METHODS

Four North-American commercial cements, named H, C, L and Q were selected according to their C_3A and alkali content. Their chemical composition and Bogue composition are indicated in Table 1. The cement H is characterized by its relatively low content of C_3A and low content of alkali. The cement C is characterized by its high content of C_3A but low content of alkali. The cements L and Q have a high content of alkali, but do not have the same C_3A content. It is to be noted the high SO_3% in the clinkers corresponding to the cements L and Q.

The superplasticizer used in this study is a pure sodium salt of polynaphthalene sulfonate (PNS) enhanced in an aqueous solution at 41% solids with the pH near 8 and specific gravity of 1.21.

The additives used are sodium, potassium and lithium salts.

Table 1. Chemical and phase composition of the cements

% by mass	L – type 10*	Q – type 10*	H – type I	C – type I
CaO	62.80	62.00	65.45	64.60
SiO_2	20.50	19.60	20.66	21.00
Al_2O_3	4.10	5.40	4.73	5.36
Fe_2O_3	3.00	2.30	3.69	2.00
MgO	2.60	2.60	1.25	3.00
SO_3	3.20	2.90	2.46	2.40
(SO_3 clinker)	1.60	1.50	0.34	0.22
Na_2Oeq	0.80	0.90	0.20	0.28
C_3S	59	56	65	58
C_2S	14	14	10	17
C_3A	6	10	6	11
C_4AF	9	7	11	6

* According to Canadian CSA standard. It's basically an ASTM type I with a maximum of 5% filler

The tests conducted on grout are the two simplified methods: the mini-slump and the Marsh cone methods. The mini-slump method consists of using the slump cone ϕ19 x ϕ38 x h57mm described by Kanto [9], allowing a quick comparison of the fluidity of various cement-superplasticizer mixtures on a small amount of grout. The paste was prepared with 200 g of cement, adequate amount of water, superplasticizer and chemical additive if necessary. The mixing was done by hand with a spatula for the first one minute and then with an electronic mixer at high speed for two

minutes. The paste was remixed by hand with a spatula for 30 sec just before measuring the spreading diameter at a given time.

The Marsh cone method consists of measuring the time required for 1 liter of grout contained in the Marsh cone to flow through a funnel having a diameter of 5 mm [10], allowing the characterization of the rheological behavior of the grout in more "dynamic" condition. The mixture was prepared in a mixer for mortar with appropriate amounts of cement, water and PNS to prepare 1.2 l of grout. Usually the test was done at a water/cement of 0.35 and around 1.8kg of cement is needed. The mixing time was generally 1 min 30 sec for introducing progressively the cement and 60 sec for final mixing. After introducing the grout (1.2 liter) in the Marsh cone, it was measured the time necessary to fill the 1 liter graduate placed under the cone. To keep the homogeneity of the grout and to simulate concrete transportation, the grout was put in a plastic bottle and then placed on two rollers.

The optimized cement-superplasticizer couples by using the mini-slump and Marsh cone methods were then tested on concrete with typical composition indicated in Table 2. The slump, the setting time and the compressive strength were measured according ASTM C143-90a, C403-95 and C39-94. The mixing procedure is described as follows:

- Introducing the sand in the mixer,
- Introducing the aggregate and then a half of the mixing water.
- Adding the chemical additives and then the superplasticizer in the remaining mixing water
- Introducing the total cement, starting the chronometer and mixing for 1 minute 30 seconds.
- Introducing the remaining water with superplasticizer and continuing the mixing for 1 minute 30 seconds.
- Stopping the mixing for 2 minutes.
- Restarting the mixing for 3 minutes and then stopping the mixing.
- One minute before a given time, mixing the concrete for 1 minute. After the measure, the used concrete used is then removed in the mixer and mixed for 30 seconds.

Table 2. Concrete composition at saturated surface state

	kg/m^3	Type and characteristics
Water	151	W/C=0.33
Cement	462	cements L, Q, H and C
Sand	733	natural siliceous, fineness modulus of 2.70, absorption of 1.2%
Coarse aggregate	1112	dolimitic limestone, 14 mm, absorption of 0.4%
Superplasticizer		PNS, generally at 0.6%, except indication
Alkali additives		Na_2SO_4, $Na_2SiO_3.9H_2O$ and Li_2SO_4, expressed as Na_2Oeq%

3. RESULTS AND DISCUSSION

3.1 Saturation point of superplasticizer – Marsh cone test

The saturation point of a superplasticizer for a given cement is defined as the optimal dosage after which any supplementary addition of superplasticizer does not significantly improve the rheology of the grout. According to the study [10], the flow time at 5 and 60 min. of a superplasticized grout with a Marsh cone may give reliable indications of the degree of cement-superplasticizer compatibility. Typically, four cases may be produced for a given cement-superplasticizer. The first case corresponds to a compatible combination for which the slump at 5 min and the loss of slump 5-60 min can be fully controlled. The second case corresponds to a poor compatibility for which a high dosage of superplasticizer is required to obtain a given slump at 5 min and the slump loss

increases rapidly with the time despite this high dosage. The two others cases correspond to intermediate situations: the initial slump can be easily obtained but the slump loss is high, or the initial slump is always difficult to obtain but the slump loss stays at a low level.

For four selected cements and the PNS used in this study, the flow times with Marsh cone are shown in Figure 1. The cement L presents a full compatibility with PNS with a saturation point situated between 0.6 and 0.8%. Even at a lower dosage, the grout still presents a reasonable fluidity at 60 min. A preliminary study shows that cement Q behaves in the same way as cement L despite the high C_3A content. With cement H, the saturation point is higher, between 1.0 and 1.2%, but when a lower dosage was used, the slump loss was so high that the flow time could not be recorded. Therefore cement H presents a partial compatibility with PNS. Concerning cement C, the saturation point is very high (>1.8%). The initial fluidity was more difficult and decreases rapidly when the dosage of PNS is lower than this saturation point. Therefore cement C presents a poor compatibility with PNS.

In a preliminary study, the use of a gluconate based retarder (0.1%) allows to improve the compatibility in the case of cement H when the superplasticizer is lower than the saturation point. In the case of cement C, the use of the retarder at a dosage as high as 0.2% can improve the initial fluidity, but not at all the slump loss. Moreover, the tests on concrete made with these cements showed that the early strength was strongly affected even with a dosage of retarder as low as 0.1%, for cement C as well as for cement H.

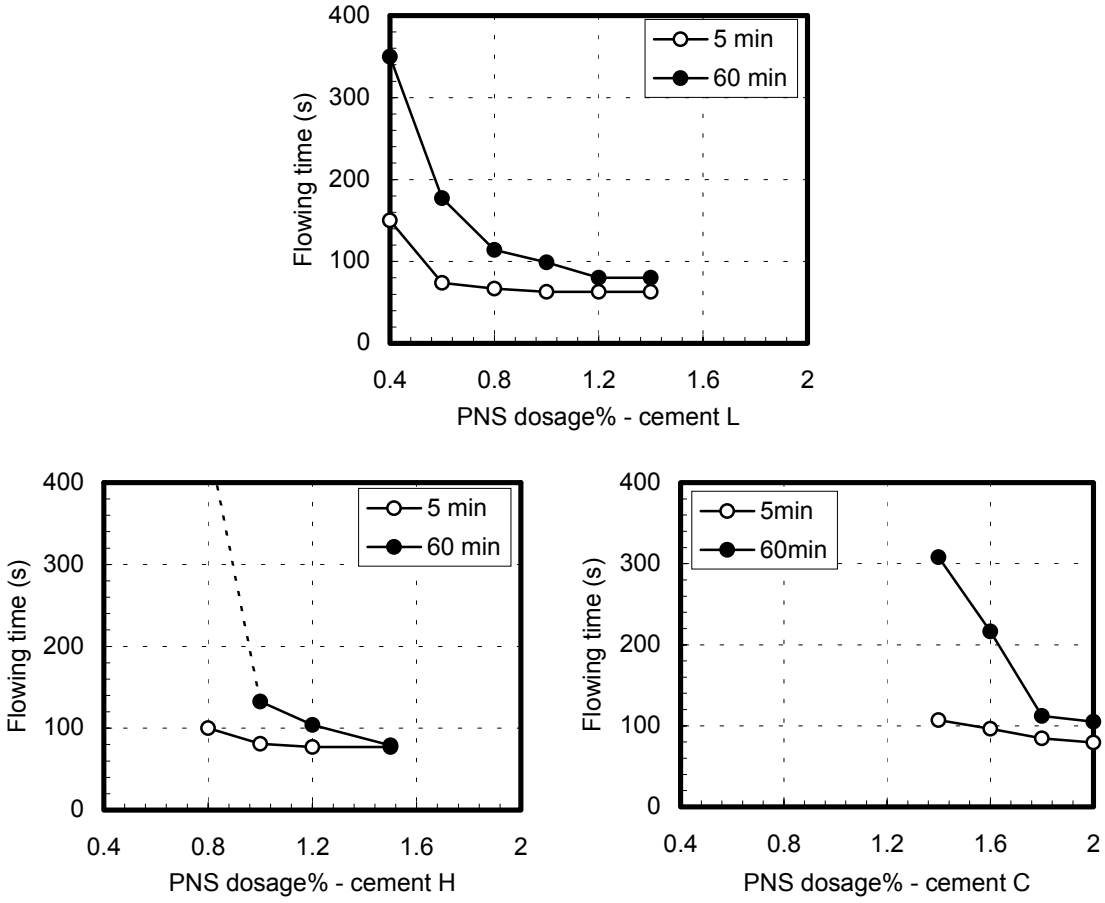

Figure 1. Marsh cone flowing time as function of superplasticizer dosage. E/C=0.35

3.2 Effect of soluble alkalis on the rheology – Mini-slump test

To observe the effect of alkalis on the rheology, the mini-slump test was carried out on pastes with PNS dosage lower than the saturation point previously determined by Marsh cone. Figure 2 shows the spreading area change vs time of pastes prepared with cement H. The different salts, with a

equivalent amount of 0.2% Na_2O, were added in the mixing water. The results indicate that the slump retention is greatly improved by adding sodium, potassium or lithium salts, except Na_2CO_3, $NaHCO_3$ and NaF. Among the tested salts, the highest improvement of the slump retention is given by Li_2SO_4, then followed by $Na_2SiO_3.9H_2O$. The potassium salts show a similar effect than the sodium salts. The same results were also observed with cement C presenting a poor compatibility.

With high-alkali cement, the added soluble alkalis have no effect or even a small negative effect on the initial slump as well as the slump retention, as shown in Figure 3.

To understand the influence of the amount of soluble alkalis in the case of cements H and C, different quantities of Na_2SO_4, expressed as Na_2Oeq were added. The results are shown in Figure 4. For cement H, the initial slump at 5 min is high and it is not affected by the added alkali content, but the slump loss at 60 or 90 min is reduced with the increased alkali content until an optimum of 0.2%Na_2Oeq is reached.

For cement C, the initial slump is very low, but the slump loss is small. The addition of soluble alkalis improves efficiently the initial slump, but the slump loss remains unaffected. The optimum content of soluble alkalis, determined from the initial slump for this cement, is around 0.12% Na_2Oeq when 1.0% PNS is used. This optimum content increases to around 0.25% when PNS dosage is cut to 0.8%PNS, to around 0.4% when PNS is cut to 0.6% PNS. The slump loss seems to increase with the decrease of PNS dosage, particularly in the case of an added alkali content lower than the optimum value.

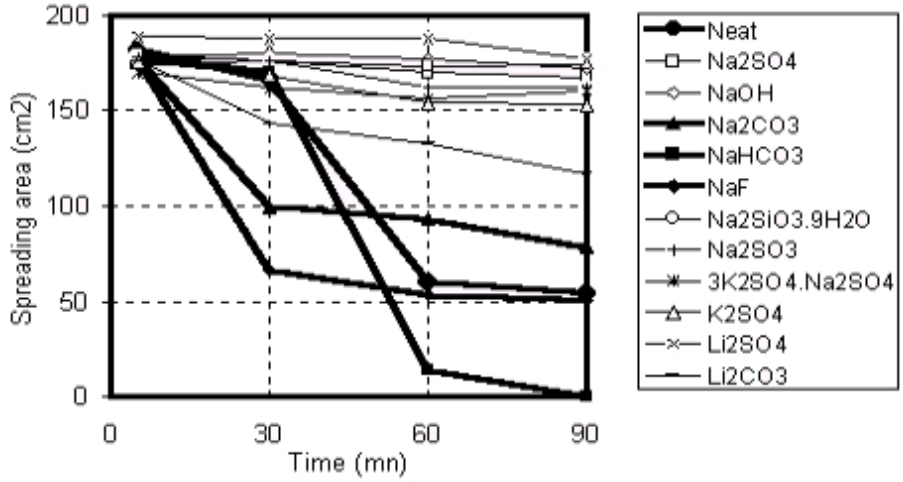

Figure 2. Effect of added alkali salts. Cement H with E/C=0.35, 0.6%PNS Na_2Oeq=0.2%

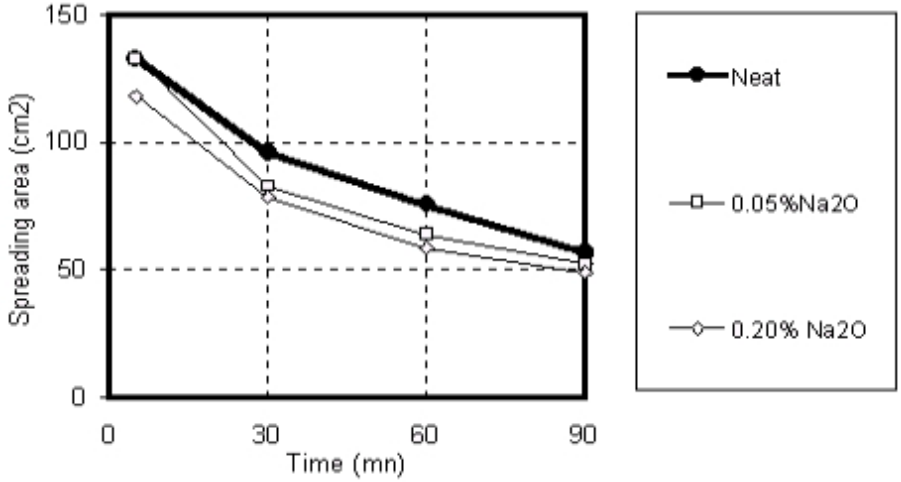

Figure 3. Effect of added Na_2SO_4 expressed as Na_2Oeq. Cement L with E/C=0.35, 0.6%PNS

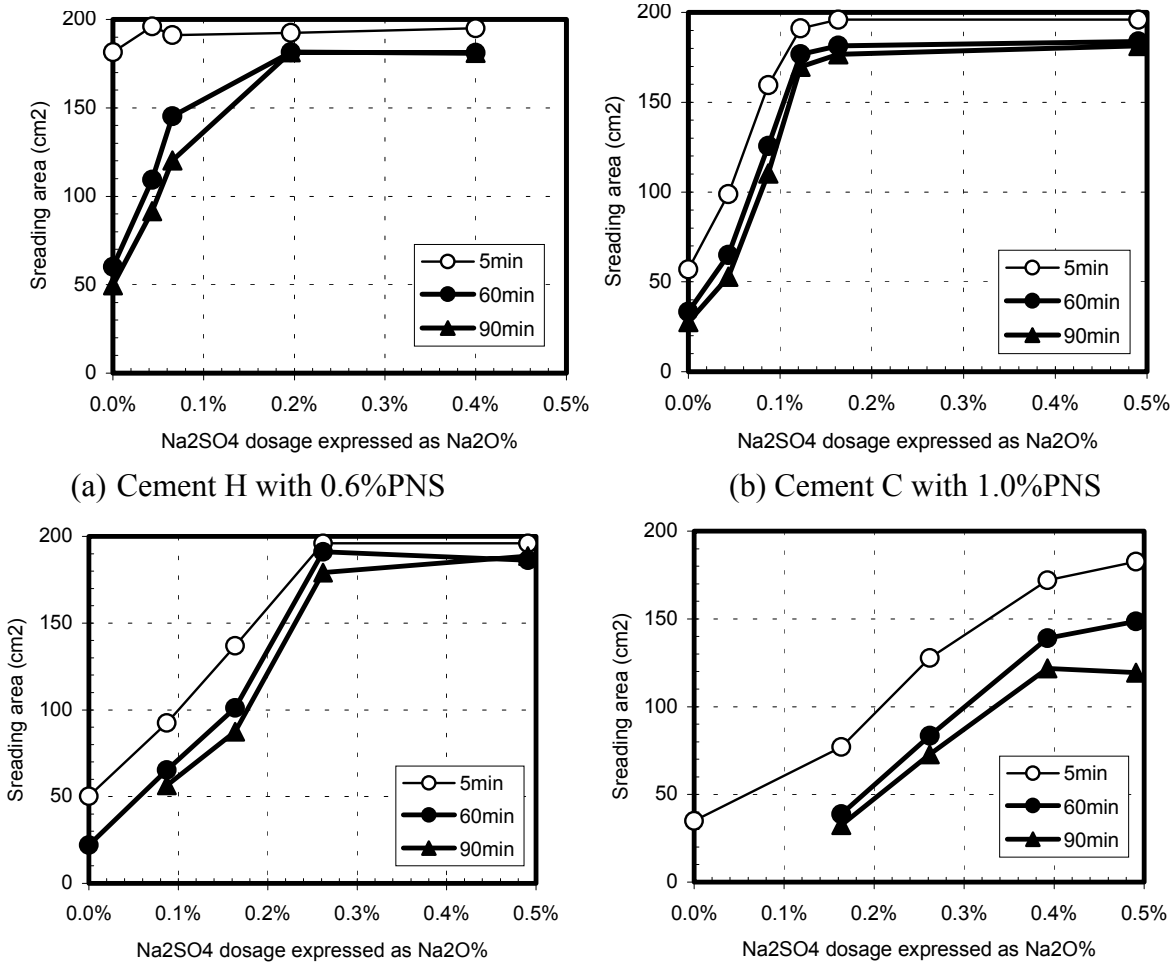

Figure 4. Rheology change as function of the amount of Na_2O. Cement H (a), cement C (b, c, d)

3.3 Effect of soluble alkalis on the hydration kinetics of the cement H in presence of PNS

The effect of added alkalis was also investigated using adiabatic calorimetry. The alkalis were introduced by Na_2SO_4, NaOH and $Na_2SiO_3.9H_2O$ added in mixing water. The calorimetric curves are shown in Figure 5. It can be observed that the alkalis brought by Na_2SO_4 or NaOH accelerate hydration. The sodium metasilicate presents a retarding effect on the initial hydration, but after this initial stage the hydration rate is accelerated. These results indicate that the addition of alkalis does not seem to have a negative effect on the one day strength.

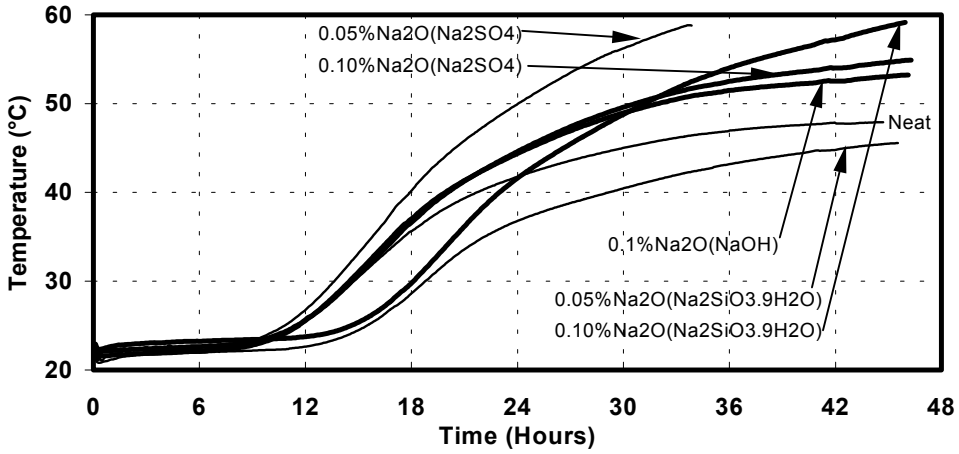

Figure 5. Effect of Na_2O on the heat evolution of hydration. Cement H with E/C=0.35, 0.6%PNS

3.4 Effect of soluble alkalis on the properties of concrete

The slump evolution is presented in Figure 6. For high alkali cements L and Q without a particular compatibility problem, the slump of the concrete without additive presents a normal evolution with time. Any addition of alkalis causes a lower initial slump and/or rapid slump loss. The more difficult rheology of cement Q may be attributed to its high C_3A content.

For low alkali cements H and C that present a partial or poor compatibility with PNS, the slump of the concrete without additive dropped quickly with time, from 24 cm at 10 min to only 5 cm at 30 min. The addition of alkalis in the form of Na_2SO_4, $Na_2SiO_3.9H_2O$ and Li_2SO_4 allowed to reduce greatly or even inhibit totally the slump loss. It is to be noted that when the alkalis were added at 0.2%Na_2Oeq, the concrete made of cements H and C presented systematically a pronounced bleeding phenomenon, therefore it was necessary to cut the PNS dosage from 0.6% to 0.5% or 0.4%. Even with a lower PNS dosage, the addition of alkalis still allowed the achievement of the same initial slump and the reduction of the slump loss as compared to the one found in the reference concrete with a higher PNS dosage.

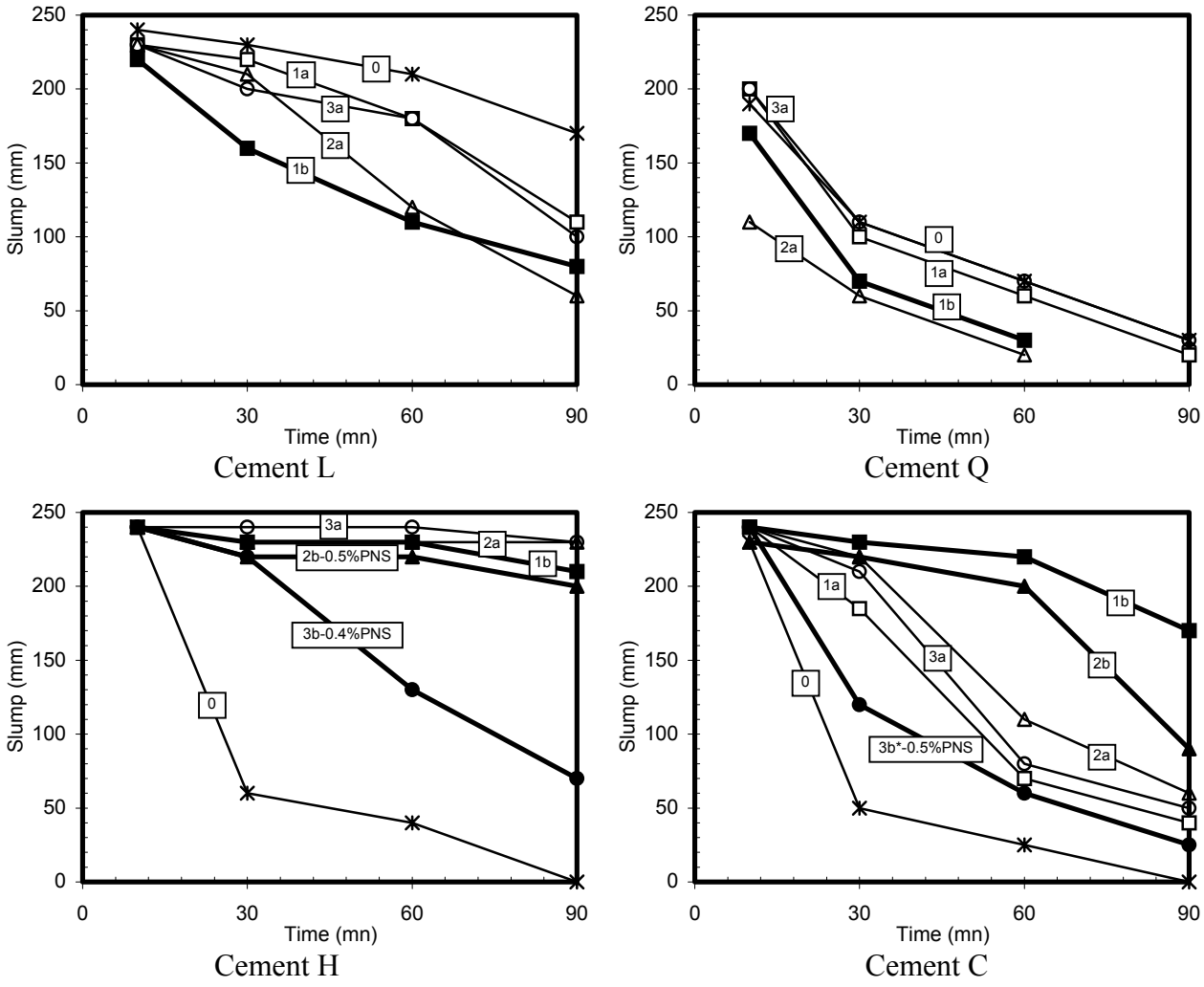

0 – Ref (no PNS)
1a – 0.1% Na_2Oeq (Na_2SO_4)
1b – 0.2% Na_2Oeq (Na_2SO_4)
2a – 0.1% Na_2Oeq ($Na_2SiO_3.9H_2O$)
2b – 0.2% Na_2Oeq ($Na_2SiO_3.9H_2O$)
3a – 0.1% Na_2Oeq (Li_2SO_4)
3b – 0.2% Na_2Oeq (Li_2SO_4) (*0.15%)

Figure 6. Effect of Na_2O on the slump of concrete with 0.6%PNS (except indication)

The setting time is presented in Figure 7. For high alkali cements L and Q, the setting time decreased with addition of alkalis, higher the added amount, shorter is the setting time. $Na_2SiO_3.9H_2O$ seems to have a more pronounced effect.

For low alkali cement H that presents a partial compatibility with PNS, the setting time increased significantly with added alkalis, the difference may reach as high as 2 hours for $Na_2SiO_3.9H_2O$ or Li_2SO_4 added at 0.1% Na_2Oeq. It can be hoped that this difference should be bigger for $Na_2SiO_3.9H_2O$ or Li_2SO_4 added at 0.2% Na_2Oeq if the PNS dosage was not cut to a lower level.

For low alkali cement C that presents a poor compatibility with PNS, the setting time increased or decreased slightly as function of the nature of alkali salts used and the added alkali amount. The difference does not exceed 0.5 hour.

It is interesting to point out that the alkalis are generally considered as accelerators for OPC as can be observed on cements L and Q. However, in the case of cements H and C that present a incompatibility phenomenon, the effect of alkalis is completely different.

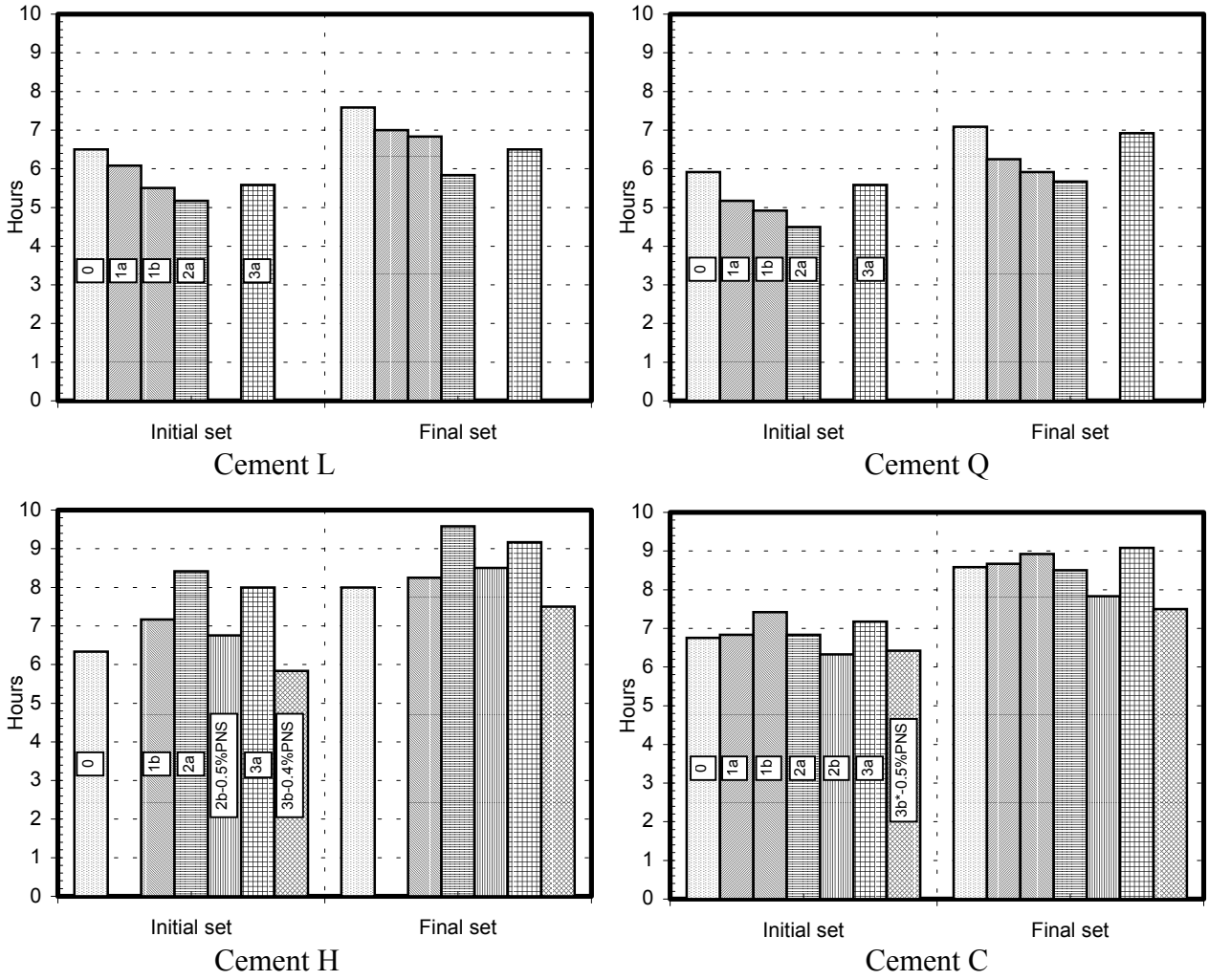

0 – Ref (no PNS)
1a – 0.1% Na_2Oeq (Na_2SO_4)
1b – 0.2% Na_2Oeq (Na_2SO_4)
2a – 0.1% Na_2Oeq ($Na_2SiO_3.9H_2O$)
2b – 0.2% Na_2Oeq ($Na_2SiO_3.9H_2O$)
3a – 0.1% Na_2Oeq (Li_2SO_4)
3b – 0.2% Na_2Oeq (Li_2SO_4) (*0.15%)

Figure 7. Effect of Na_2O on the setting time of concrete with 0.6%PNS (except indication)

The compressive strength measured at 1, 3 and 28 days is presented in Figure 8. For high alkali cements L and Q, the one day strength is not affected. The initial strength is high, but the later strength development is relatively slow, from about 40 MPa at 1 day to about 60 MPa at 28 days.

The concretes made with low alkali cements H and C showed a big difference if soluble alkali salts were added or not. Generally, the addition of soluble alkali salts in these cements increased the one day strength. The increasing rates, varying from 6% to up to 30%, depend on the nature of the salts, but especially on the amount of soluble alkalis. Li_2SO_4 shows an interesting performance for two cements H and C. It is to be noted that the initial strength is relatively low for these two cements, even with addition of alkalis, but the later strength development is high.

The impact of added alkalis on the 28 day strength is neglected. Anyway, a tendency of slight drop of 28 day strength could be observed on the concretes made with cements L, Q and C, compared to the reference concrete without any addition of alkalis.

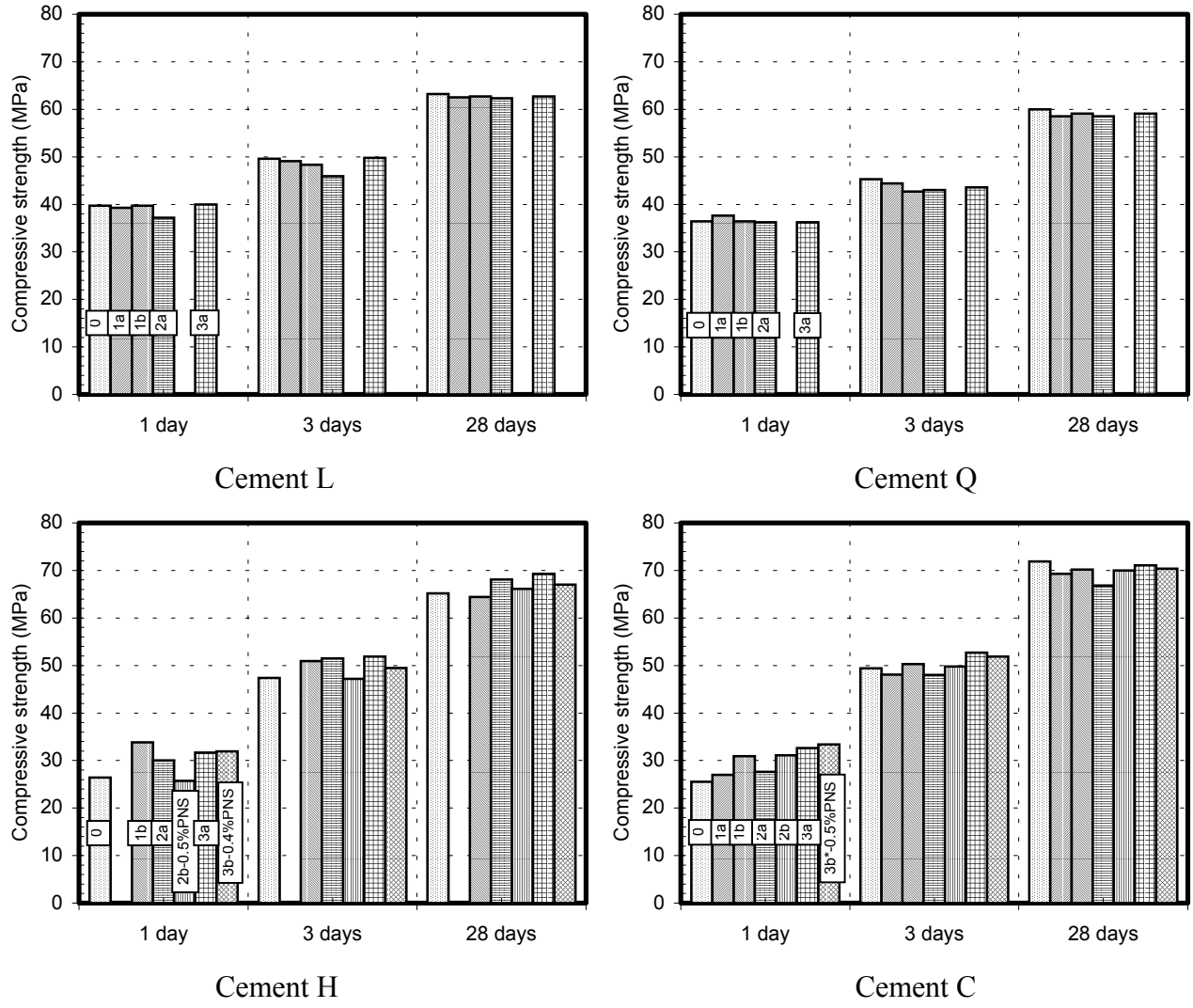

0 – Ref (no PNS)

1a – 0.1% Na_2Oeq (Na_2SO_4)

1b – 0.2% Na_2Oeq (Na_2SO_4)

2a – 0.1% Na_2Oeq ($Na_2SiO_3.9H_2O$)

2b – 0.2% Na_2Oeq ($Na_2SiO_3.9H_2O$)

3a – 0.1% Na_2Oeq (Li_2SO_4)

3b – 0.2% Na_2Oeq (Li_2SO_4) (*0.15%)

Figure 8. Effect of Na_2O on the strength of concrete with 0.6%PNS (except indication)

3.5 Discussions

The previous results show the different behavior of cements L (low C_3A, high alkali), Q (high C_3A, high alkali), H (low C_3A, low alkali) and C (high C_3A, low alkali), in the presence of PNS. The cements L and Q are totally compatible with PNS, the cement H is partially compatible with PNS and the cement C is poorly compatible with PNS. It can be concluded that the cement – superplasticizer compatibility depends not only on the C_3A content, but also on the availability of soluble alkalis. In fact, the alkali content, as well as SO_3%, is high in the clinkers corresponding to cements L and Q. These alkalis are most probably combined with SO_3 to form soluble alkali sulfates. In contrast, no soluble alkali sulfates are expected to present in cement H and C because of the very low alkali content and very low SO_3% in the original clinkers.

The problem of compatibility can be readily solved by adding an adequate amount of soluble alkalis. The working mechanisms [11, 12] are related to the rapid increase of the pH in the interstitial solution which controls the adsorption of the PNS on the cement particle, especially C_3A. Another possibility is the increase of the solubility of calcium sulfates in the presence of alkalis. The higher SO_4^{2-} reduces the amount of PNS adsorbed on the positive surface, such as C_3A and C_4AF.

However, adding sodium and potassium salts in concrete made a potentially reactive aggregate is not an acceptable solution due to the risk of AAR, even when the total Na_2Oeq is lower than 0.6%, accepted as a maximum limit. The previous results show that lithium salts perform in the same way or even better in improving the cement-PNS compatibility. Moreover, lithium salts do not cause any AAR or even can be used to fight AAR [13, 14]. It seems that lithium ions react preferentially and rapidly with reactive silica without forming an expanding gel.

4. CONCLUSIONS

The problem of cement-superplasticizer incompatibility is not only related to the C_3A content, but also to the availability of soluble alkalis in cements.

In the cements that have low alkali content and present a problem of incompatibility, soluble alkali salts can be used to reduce greatly or inhibit totally the slump loss. Meantime, the use of soluble alkalis in these cements improves significantly the one day strength and the 28 days is not affected. Among the chosen soluble alkali salts, metasilicate and sulfates are the most efficient additive to improve the cement-superplasticizer compatibility. It has been shown the existence of an optimum content of alkalis as a function of the superplasticizer dosage for a given W/C.

Lithium salts have shown the same or better performance than sodium or potassium salts. If the addition of sodium or potassium salts can be perceived as detrimental from ARR point of view, the addition of lithium salts as alternative is totally safe and even beneficial.

On the contrary, normal cements having a relatively high alkalis content show a similar or even slightly deteriorated rheological behavior when soluble alkalis are used. The setting time is systematically reduced by addition of alkalis, but the strength is not affected.

ACKNOWLEDGEMENTS

The authors would like to thank Natural Science and Engineering Research Council of Canada, Handy Chemicals Company and Hydro-Quebec Company for their financial support.

REFERENCES

[1] Paillère, A.M., Algère, R., Ranc, R. and Buil, M, Interaction entre les reducteurs d'eau – plastifiants et les ciments, Bulletin de Liaison du Laboratoire des Ponts et Chaussées, n°136, 1985, pp.105-108.

[2] Dodson, V.H., Hayden, T., Another look at the Portland cement/chemical admixture incompatibility problem, Cement, Concrete, and Aggregates, vol.11, n°1, 1989, pp.52-56.

[3] Ranc, R., Interaction entre les réducteurs d'eau-plastifiants et les ciments, Ciments, Bétons, Plâtres et Chaux, n° 782-1/1990, pp.19-21

[4] Aïtcin, P.C. and Neville, A., High-performance concrete demystified, Concrete International, vol.15, 1993, n°1, pp.21-26.

[5] Tagnit-Hamou, A., Aïtcin, P.C., Cement and superplasticizer compatibility, World Cement, august/1993, pp.38-42.

[6] Huynh, H.T., La compatibilté ciment-superplastifiant dans les bétons à haute performances – synthèse bibliographique Bulletin de Liaison du Laboratoire des Ponts et Chaussées, n°206, 1996, pp.63-73.

[7] Chiocchio, G. and Paolini, A.E., Optimum time for adding superplasticizer to Portland cement pastes, Cement and Concrete Research, vol.15, 1985, pp.901-908.

[8] Ramachandran, V.S., Effect of retarders/water reducers on slump loss in superplasticized concrete, Development in the use of superplasticizers, publication ACI SP-68, Detroit, 1981, pp.393-407.

[9] Kantro, D.L., Influence of water reducing admixtures on properties of cement pastes – A miniature slump test, Cement, Concrete, and Aggregates, vol.2, 1980, pp.95-102.

[10] Aïtcin, P.C., Jolicoeur, C., and MacGregor, J.G., Superplasticizers: How they work and why they occasionally don't, Concrete International, vol.16, n°15, 1994, pp.45-52.

[11] Nawa, T., Eguchi, H. and Fukaya, Y., Effect of alkali sulfate on the rheological behavior of cement paste containing a superplasticizer, Proceedings of the 3rd CANMET/ACI International Conference on Superplasticizers and Other Chemical Admixtures in Concrete, Ottawa, 1989, pp.405-424.

[12] Kim, B.G., Jiang, S.P. and Aïtcin P.C., Slump improvement mechanism of alkalis in PNS superplasticized cement pastes, Materials and Structures, vol.33, 2000, pp.363-369.

[13] Gajda, J., Development of a lithium bearing cement to inhibit alkali silica reactivity in hardened concrete, World Cement, vol.8, 1996, pp.58-62.

[14] Lumley, J.S., ASR suppression by lithium compounds, Cement and Concrete Research, vol.27, n°2, 1997, pp.235-244.

IMPROVING CEMENT-SUPERPLASTICIZER COMPATIBILITY BY USING SOLUBLE ALKALIS AS A CHEMICAL ADDITIVE IN CONCRETE

G. Li[1], A. Tagnit-Hamou[2] and P.C. Aïtcin[2]

[1] Lafarge, Laboratoire Central de Recherche, 38291 St. Quentin Fallavier, France.
E-mail: guanshu.li@pole-technologique.lafarge.com
[2] Department of Civil Engineering, University of Sherbrooke, J1K 2R1 Canada.
E-mail: atagnit@andrew.sca.usherb.ca

Guanshu Li

Guanshu Li is a research engineer in the Central Research Laboratory of Lafarge Company, located in France. His research interests include the cement-admixtures interactions, the durability relative to the ettringite formation and the development of special cements based on sulfoaluminate.

EFFECT OF CURING TEMPERATURE ON AUTOGENOUS DEFORMATIONS OF CEMENT PASTE AND HIGH PERFORMANCE CONCRETE FOR DIFFERENT CEMENT TYPES

P. Lura[1] and K. van Breugel[2]

[1]Delft University of Technology, Delft, The Netherlands. E-mail: P.Lura@citg.tudelft.nl
[2]Delft University of Technology, Delft, The Netherlands. E-mail: K.v.Breugel@citg.tudelft.nl

ABSTRACT

In High Performance Concrete (HPC) mixtures, a low water/binder ratio and addition of silica fume cause a significant drop of the relative humidity in the cement paste during hydration. As a consequence of self-desiccation, the cement paste undergoes shrinkage. In the case where shrinkage is restrained, micro- or macrocracking may occur, which impairs the concrete quality.

In research on autogenous shrinkage, emphasis has been on Portland cement mixtures cured isothermally at 20°C. In this paper, the results are presented of an experimental study on the influence of the curing temperature and the type of cement on the autogenous deformations of concrete mixtures. Three mixtures were tested with w/b ratio 0.35 and 5% silica fume, differing for the kind of cement, i.e. Portland cement, Blast-Furnace Slag cement and a blend of the two. The development of compressive strength, modulus of elasticity and linear free deformations in the first six days after casting for curing temperatures 10, 20, 30 and 40°C were measured. The evolution of the hydration process and the changes of the relative humidity at early ages were measured as well. It was found that higher temperatures do not lead to higher final deformations, but generally cause a higher shrinkage rate in the first hours. The mixtures with Blast Furnace Slag cement showed higher shrinkage in the first days than mixtures made with Portland cement. The potential of numerical simulation models for quantifying autogenous deformations is also addressed.

1. INTRODUCTION

In High Performance Concrete (HPC) mixtures, a low water/binder ratio and addition of silica fume cause a significant drop of the relative humidity during hydration. As a consequence of self-desiccation, the cement paste undergoes shrinkage. The shrinkage of the cement paste is restrained by the aggregates: this results in tensile stresses within the cement paste and in bulk deformation of the concrete itself. Both these phenomena should be limited since they could induce micro- or macrocracking and jeopardize the quality and durability of the concrete [1].

In the last two decades much experimental research on autogenous deformations has been performed. In most of this research the focus was on mixtures made with Portland cement cured at 20°C. Since autogenous shrinkage is related to the self-desiccation process and self-desiccation is strongly related to the hydration process, autogenous shrinkage should be a function of the degree of hydration. According to Koenders [2] and Hedlund [3] autogenous shrinkage strongly correlate to the degree of hydration. Hedlund [4] successfully used the maturity concept for quantification of the effect of temperature on the autognous shrinkage. In a number of other studies, however, a very unsystematic effect of temperature on the autogenous deformations has been found [5,6]. Moreover, besides autogenous shrinkage also autogenous swelling of some concretes, i.e. some cement types,

Proceedings of the 11th International Congress on the Chemistry of Cement (ICCC) 11 - 16 May 2003, Durban, South Africa
'Cement's Contribution to the Development in the 21st Century' ISBN Number: 0-9584085-8-0
Hosted by: The Cement and Concrete Institute of South Africa Editors: Dr G. Grieve and G. Owens
CD-ROM produced by: Document Transformation Technologies Congress Organised by: Event Dynamics

has been observed [7]. Since in practice non-isothermal curing regimes are more likely than isothermal temperatures and cement types other than Portland cement are often used, an extensive study was conducted in which both the type of cement and the curing temperature were varied.

2. EXPERIMENTAL STUDIES

2.1 Description of experiments

The experimental program on autogenous deformations included the determination of the compressive strength, the modulus of elasticity and the autogenous deformations of 3 different types of concrete, made with 2 different types of cement and cured isothermally at 4 different temperatures. The reaction kinetics and the evolution of the relative humidity in cement pastes were measured as well.

2.1.1 Isothermal heat evolution

Cement pastes made with Portland cement and blast furnace slag cement were examined using the isothermal calorimeter TAM Air from Thermometric AB, Sweden. The cement paste specimens weighed about 10 grams. The paste composition was identical to the pastes used in the concrete mixtures used for studying the autogenous deformations (see paragraphs 2.2).

2.1.2 Relative humidity

Measurements of the relative humidity were carried out in cooperation with Aalborg University in Denmark [8]. The measurements were performed on fresh cement paste, about 10 grams per sample. The samples were cast in the measuring chamber of two Rotronic hygroscopic DT stations equipped with WA-14TH and WA-40TH measuring cells. The RH stations were placed in a thermostatically controlled room at 20±0.1°C. The development of the RH in the samples and the temperature were measured every 15 minutes for a period of about one week after water addition. Before and after the measurements, calibration of the stations was carried out with four saturated salt solutions in the range of 75-100% RH. In this way a measuring accuracy of ±1% RH could be achieved.

2.1.3 Autogenous deformation

Measurements of the free deformations were performed with an Autogenous Deformation Testing Machine (ADTM) (Figure 1). The concrete was cast in a prismatic mould, 150×150×1000 mm, made with thin steel plates provided with an external insulating material. The mould could be cooled or heated by a system of tubes located between the plates and the insulating material. Temperature differences inside the concrete could be kept as low as 1.5° K. Length changes of the hardening concrete were measured with two external quartz rods provided with linear variable differential transducers at both ends. The quartz rods were connected to steel bars cast in the concrete and measured displacements over a length of 750 mm. The rods could be fixed to the cast-in bars when the concrete had reached sufficient strength to support them (see Figure 1, right). After casting, the top surface of the concrete was covered with a tight cover in order to avoid moisture loss to the environment. The autogenous deformation up to six days after casting was recorded.

2.1.4 Strength and modulus of elasticity

Compressive strength was measured on cubes, 150×150×150 mm, whereas the modulus of elasticity was determined on prisms, 100×100×400 mm. The concrete was cast in temperature-controlled steel moulds. During the first six days after casting the concrete was kept in the moulds. In this period curing took place under sealed conditions at temperatures exactly the same as that of the specimens used for determination of the autogenous deformation. In this way the curing regime of the concrete for the different types of tests was always the same at the moment of testing. The specimens tested at later ages were removed from the moulds after six days, sealed and stored at constant temperature until the moment of testing.

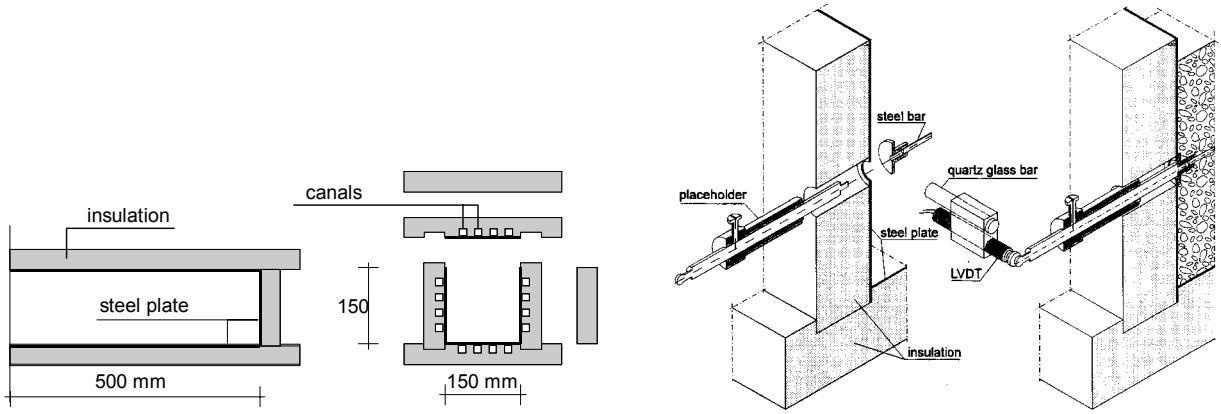

Figure 1. Mould (left) and details (right) of measurement device for determination of autogenous deformation of concrete.

2.2 Materials

Cements used were a Portland cement, CEM I 52.5 R, and a blast furnace slag cement, CEM III/B 42.5 LH HS. The Portland cement had Blaine fineness of 530 m^2/kg and calculated Bogue composition of C_3S 53.6%, C_2S 20.1%, C_3A 8.2%, and C_4AF 9.1%. The BFS cement contained 76% slag and had Blaine fineness of 390 m^2/kg.

For the measurement of the changes of the relative humidity with progress of the hydration process two cement pastes were studied, one with Portland cement and one with BFS cement. The w/b ratio of the pastes was 0.35. Silica fume with a BET surface area of 19 m^2/g was added in slurry form, 5% by cement weight. A lignosulphonate-based plasticizer (0.2%) and a naphthalene-sulphonate-based superplasticizer (1.7%) were also added to the mix.

The measurements for the strength, modulus of elasticity and autogenous deformations were performed on three concrete mixtures. Portland cement (CEM I 52.5 R) was used in mixture A, BFS cement (CEM III/B 42.5 LH HS) in mixture B and a blend of the two in mixture C. In all the mixtures a water/binder ratio 0.35 and 5% silica fume were used (see Table 1). Data about the performance of mixture C at 20°C were obtained in a previous research study [9]. For that particular mix and curing conditions, the Young's modulus was not measured.

Table 1. Mixture compositions of concrete with w/b 0.35.

Mixture composition	Unit	A	B	C
CEM I 52.5 R (Portland cement)	kg/m^3	475.0	---	238.0
CEM III/B 42.5 LH HS (BFS cement)	kg/m^3	---	475.0	237.0
Water (including water in admixtures)	kg/m^3	175.8	175.8	175.8
Crushed aggregate (4-16 mm)	kg/m^3	944.2	944.2	944.2
Sand 0-4 mm	kg/m^3	772.5	772.5	772.5
Lignosulphonate	kg/m^3	0.9	0.9	0.9
Naphtalene sulphonate	kg/m^3	8.1	7.1	7.6
Silica fume slurry (50% powder, 50% water)	kg/m^3	50.0	50.0	50.0

2.3 Experimental series – Curing regimes

For the determination of the strength, modulus of elasticity and autogenous deformation tests were carried out at isothermal temperatures, viz. 10, 20, 30 and 40°C. In all these tests curing took place under sealed conditions.

3. RESULTS

3.1 Isothermal heat evolution and relative humidity

Figure 2 shows the rate of heat liberation at 20°C of the two cement pastes in the first two days of hydration. The cement pastes were placed into the calorimeter after mixing; therefore, only a part of the first reaction peak, happening immediately after water addition, was recorded. Hydration of the Portland cement paste took place in the first hours at a very fast rate, also due to its very high fineness, 530 m^2/kg. In the case of the BFS cement paste, hydration of the Portland cement fraction, 24% by weight, was postponed. This is possibly due to a higher w/c ratio if related only to the Portland cement clinker in the mixture. The peak was correspondingly lower than in the Portland cement paste, about 1/4. Just after the first peak, the pozzolanic reaction of the slag with calcium hydroxide, formed by the Portland cement hydration, started [10]. This reaction peaked at about 30 hours after water addition.

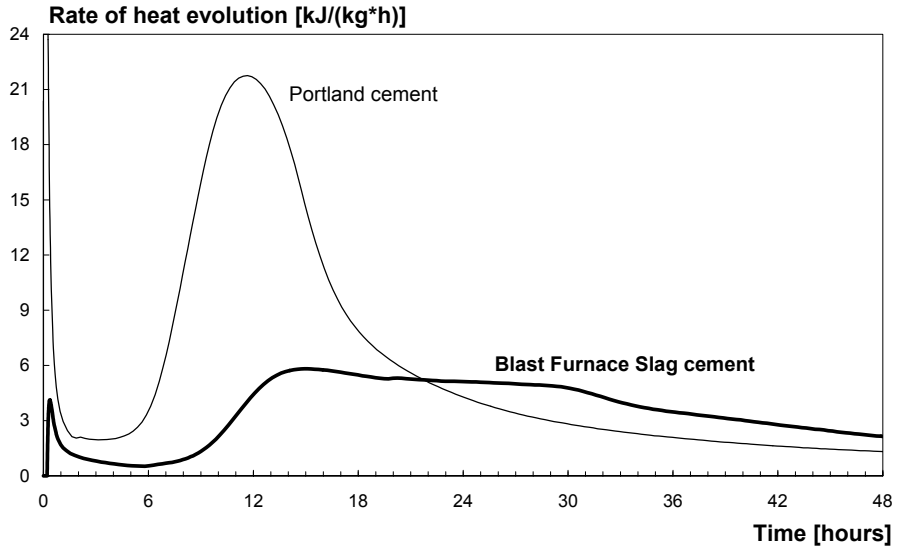

Figure 2. Rate of heat evolution in cement pastes, w/b = 0.35.

The evolution of the relative humidity in the cement pastes was measured in twofold over a period of at least 6 days. Results are shown in Figure 3. After casting and before starting the RH measurements, the BFS paste was rotated in order to avoid bleeding. Rotation started about 50 min after water addition and lasted for 4 hours. After an initial equilibrium of the sensors was achieved, the RH decreased with hydration time. The start of the RH drop coincided with the decrease in the rate of the reaction shown in Fig. 2.

It is emphasized that the RH measurements are very sensitive to the temperature [11]. It has been calculated that near saturation at 20ºC a temperature difference of 1ºC may lead to an error of about 6% RH [12]. The BFS cement paste develops less and slower heat of hydration than the Portland cement paste; therefore the temperature, also due to the small dimensions of the sample, is closer to isothermal and the measured RH should be more reliable. In fact, the temperature measured inside the Rotronic stations was always less than 21ºC in the case of the Portland cement paste, while for the BFS cement paste the temperature remained practically constant.

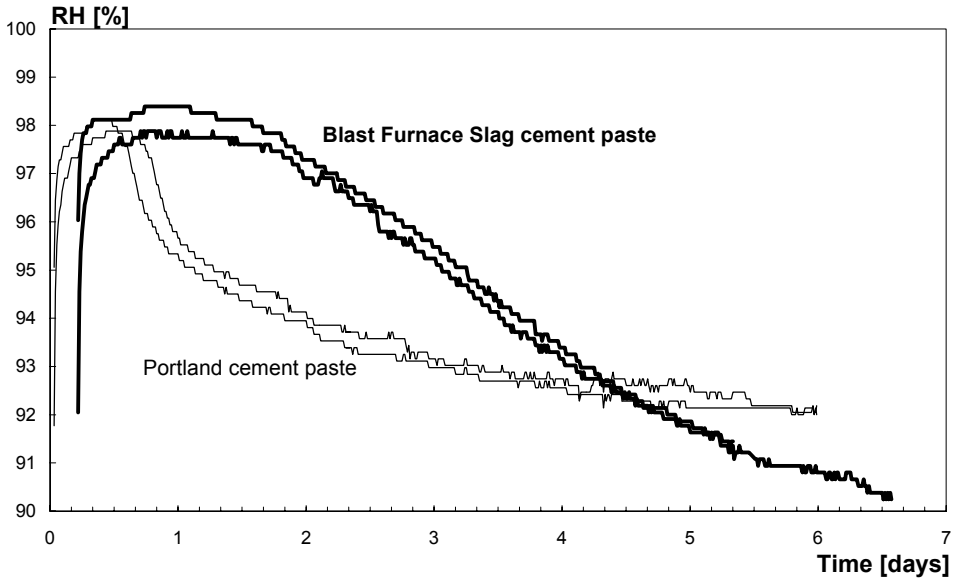

Figure 3. Internal relative humidity vs. time for the two cement pastes.

3.2 Compressive strength

The evolution of the cube compressive strength of the concrete is presented in Table 2. It is noticed that at later ages the strength achieved by the specimens cured at elevated temperatures is lower than the strength at lower temperatures. Similar effects were found for the modulus of elasticity.

Table 2. Cube compressive strength of concretes A, B and C (Table 1). Sealed curing at different isothermal temperatures.

		Mean cube compressive strength [MPa]						
Mixture	Temperature	1day	2 days	3 days	7 days	14 days	28 days	56 days
A	10°C	---	57.2	65.8	81.7	91.7	97.7	---
	20°C	53.2	65.1	---	85.9	94.0	99.5	---
	30°C	55.4	68.5	78.6	92.3	100.1	---	---
	40°C	66.5	74.2	86.6	92.5[1)]	97.0	---	---
B	10°C	---	5.2[2)]	13.1[3)]	34.5	51.8	58.9	---
	20°C	4.9	20.4	32.7	53.8	---	65.9	---
	30°C	23.6	44.6	50.6	59.6	64.8	---	---
	40°C	31.8	47.7	53.6	59.4[1)]	---	---	69.7
C	10°C	---	31.1[2)]	38.1[3)]	57.4	72.2	82.8	---
	20°C	42	52	58	70	---	82	---
	30°C	40.7	54.5	63.9	---	84.8	---	---
	40°C	44.9	65.1	71.4	78.8 [1)]	79.2	---	---

[1]) Tested 8 days after casting; [2)] Tested 1.5 days after casting; [3)] Tested 2.5 days after casting

3.3 Autogenous deformation

In Figures 4 to 6 the autogenous deformations of the mixtures A, B and C are plotted. The autogenous deformations were zeroed at the time when the deformations became stress inducing. This moment was determined in a Temperature Stress Testing Machine (TSTM), a test rig in which the concrete was cured under the same conditions as the concrete in the ADTM and in which the autogenous deformations were completely restrained [13]. Thus, only the stress-inducing deformations are shown. For mixtures A and C this means only shrinkage, since only tensile stresses were measured in the stress-rig. For mixture B, at some curing temperatures, swelling preceded shrinkage, resulting in a low compressive stress in the TSTM (<0.3 MPa). The stress-inducing deformations were preceded by a phase, lasting for some hours, where the concrete deformed plastically without generating any stress in the TSTM. In this plastic phase, all the concrete mixtures expanded shortly after the beginning of the measurements, with swelling up to 50 10^{-6}.

The autogenous deformations of mixture A are shown in Figure 4. The stress-inducing shrinkage developed rather unsystematically with temperature. Specimen cured at 40ºC showed a faster shrinkage in the first hours, but then slowed down. After one day the total shrinkage was less than for 20ºC curing. Shrinkage after six days varied between 130 10^{-6} and 170 10^{-6} for the four curing temperatures.

In Figure 5 the autogenous deformation of mixture B, made with BFS cement, is shown. Also in this case, the influence of the curing temperature on the autogenous deformation seems unsystematic.

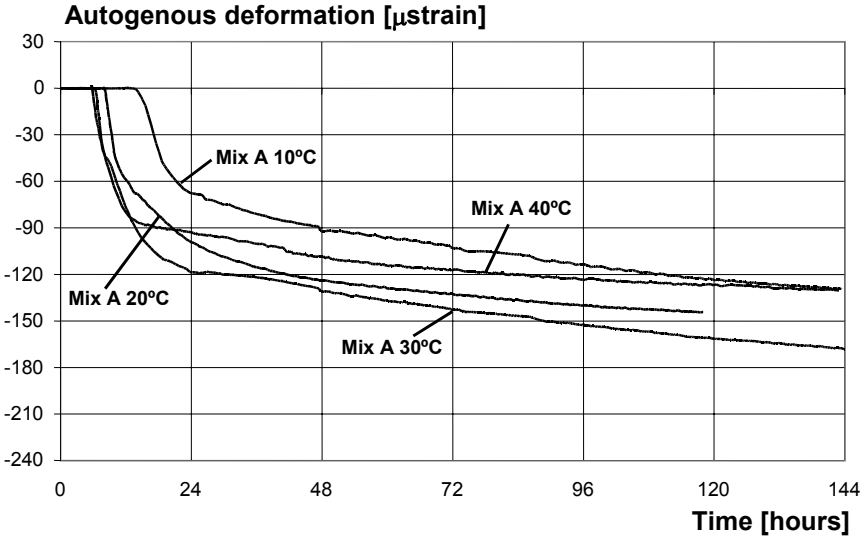

Figure 4. Autogenous deformation of mixture A (see Table 1). Isothermal sealed curing at 10, 20, 30 and 40ºC. Shrinkage is plotted as negative.

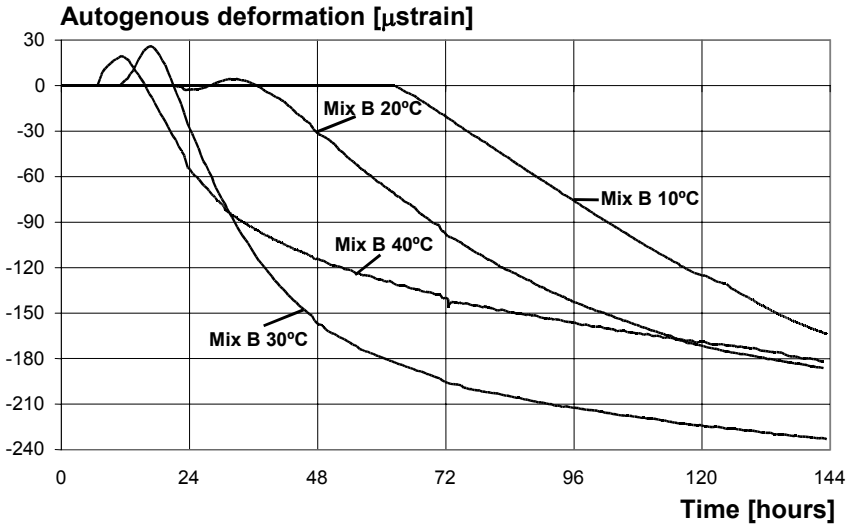

Figure 5. Autogenous deformation of mixture B (see Table 1). Isothermal sealed curing at different 10, 20, 30 and 40ºC. Shrinkage is plotted as negative.

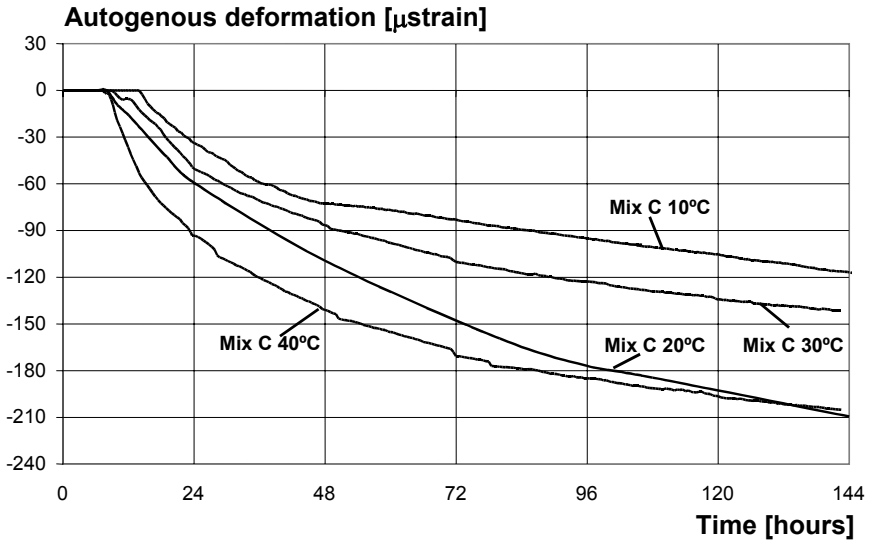

Figure 6. Autogenous deformation of mixture C (see Table 1). Isothermal sealed curing at 10, 20, 30 and 40˚C. Shrinkage is plotted as negative.

The initial swelling was followed by shrinkage, which occurred earlier for the specimen cured at 40ºC. However, 30 hours after casting the shrinkage of the specimen cured at 30ºC became higher. Shrinkage of the specimen cured at 10ºC developed slowly, but at the end of the test it was about the same as in the case of 40ºC curing. Shrinkage values after six days were about 170-180 10^{-6} for curing at 10, 20 or 40ºC, and about 230 10^{-6} for curing at 30ºC. These values are noticeably higher than those found for Portland cement mixtures (see Figure 4).

Results of tests on mixture C, made with blended cement, are shown in Figure 6. Shrinkage was lowest for 10ºC and highest for 40ºC curing. The specimen cured at 20ºC showed a faster rate of shrinkage than the one cured at 30ºC. It should be recalled, however, that the data at 20ºC curing had been obtained in a previous research [9]. The materials used might have been slightly different. Shrinkage values after 6 days were 120 10^{-6} for 10ºC curing, 140 10^{-6} for 30ºC and 210 10^{-6} for 20 or 40ºC. These values lay between the ones found for mixtures A and B.

4. DISCUSSION AND CONCLUSIONS

From the figures 4 to 6 it is clear that the effect of temperature on the autogenous deformation of concrete is unsystematic. The fact that also the type of cement gives rise to different autogenous deformation curves is clearly illustrated in Figure 7, showing the autogenous strain in the first 48 hours obtained at 40°C for the mixtures A, B and C.

The unsystematic effect of temperature on the autogenous deformations makes it difficult to apply the Arrhenius function to the curves obtained at different temperatures. On the other hand, it is noticed that for the mixtures A, B and C the Arrhenius function turned out to be applicable indeed for quantifying the effect of temperature on the strength. Figures 8 and 9, left, show the compressive strength at 5 days of age as a function of the degree of hydration (α) at the moment of testing. In the figures 8 and 9, right, the corresponding stress-inducing autogenous deformations are shown. The degree of hydration after 5 days for the different curing temperatures was calculated with the numerical simulation program HYMOSTRUC [14]. In this program the effect of temperature on the rate of hydration is accounted for with the Arrhenius function, here with a constant value of the apparent activation energy. The figures clearly demonstrate an almost linear relationship between compressive strength and degree of hydration.

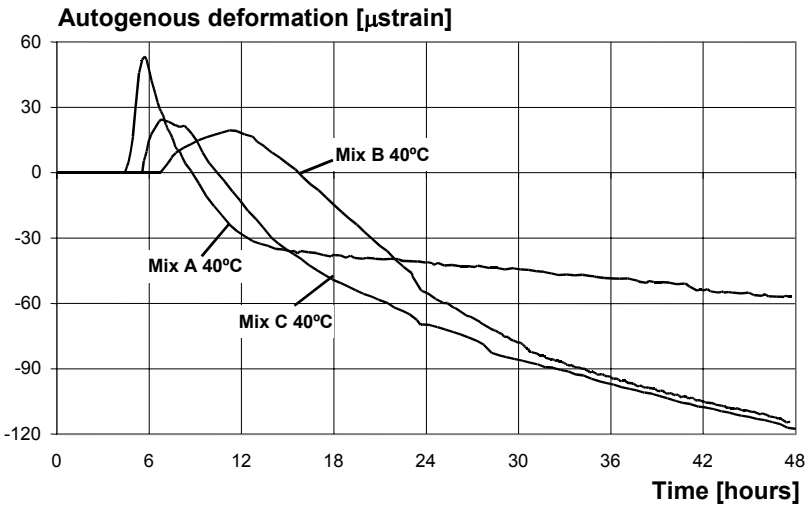

Figure 7. Autogenous deformations of mixtures A, B and C in the first 48 hours after casting, cured at 40º. The measurements include the non stress-inducing strains in the early stage of hydration.

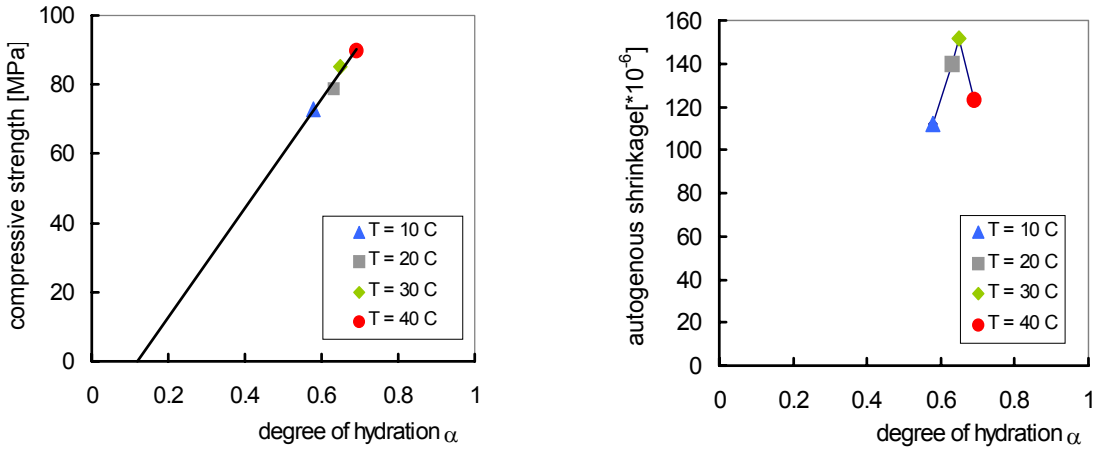

Figure 8. Compressive strength and stress-inducing autogenous shrinkage of a Portland cement based mixture (A) at t = 5 days.

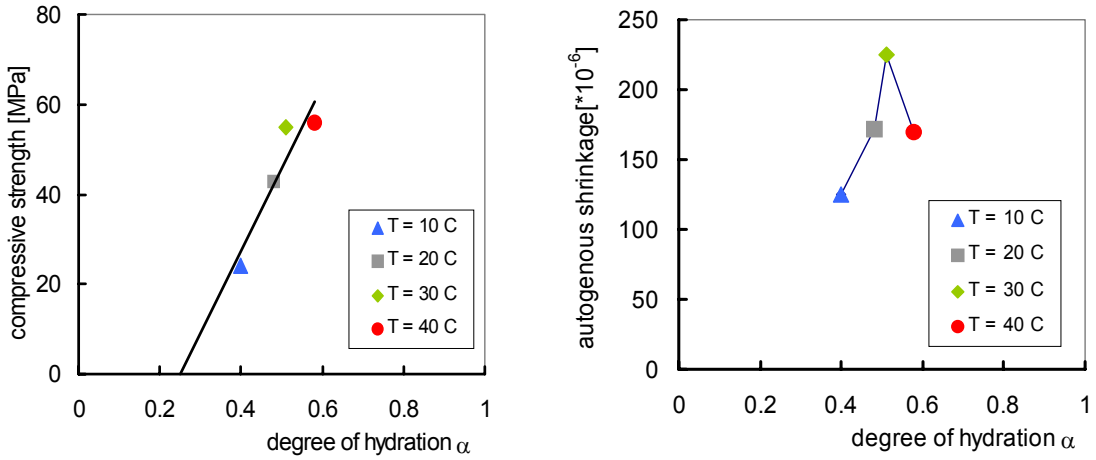

Figure 9. Compressive strength and stress-inducing autogenous shrinkage of mixture B, based on blast furnace slag cement at t = 5 days.

Such a linear relationship, however, did not hold for the autogenous deformations. This illustrates that the dependence of the autogenous deformations on the degree of hydration at different curing temperature is more complex. In this case, a simple Arrhenius function cannot be used for quantifying the effect of temperature.

It is widely accepted that autogenous shrinkage originates form the changes in the relative humidity in the pore systems and the associated changes in the capillary pressure in the pore water. In fact the degree of hydration is too crude a parameter to inform us about these microstructural phenomena in detail. From the figures 2 and 3 it can be deduced that both the rate of hydration and the evolution of the relative humidity in the paste develop quite differently for the Portland cement paste and the BFSC paste. The rapid heat evolution of the PC pastes is accompanied with a steep decrease of the RH between 16 and 28 hours. The slower reacting BFSC exhibits a RH-plateau until about 48 hours after casting. From that moment on the RH gradually decreases and reaches values substantially lower than in the PC pastes (see Fig. 3).

It is well known that pastes made with slag cement are very dense and have a fine capillary pore structure. Portland cement pastes have a coarser pore structure. The coarseness of the pore system also depends on the curing temperature: at elevated temperatures the capillary pore structures is coarser than in case of hydration at room temperature [15]. The characteristics of the pore structure, the water distribution and the relative humidity in the pore system are related to each other on a thermodynamic basis. This relationship can be described with the Kelvin's equation, which can be written like:

$$r = -\frac{2\gamma \cdot M}{\ln RH \cdot \rho \cdot RT} \tag{1}$$

where γ is the surface tension of water (0.073 N/m in pure water), M the molar weight of water (0.01802 kg/mol), ρ the density of water (approx. 1000 kg/m^3), r the radius of the meniscus, R the ideal gas constant (8.314 J/mol K), T the absolute temperature and RH the relative humidity. From equation (1) it can be seen that a low relative humidity means small values of the meniscus r. Small radii of the meniscus are accompanied with high values of the pore fluid pressure:

$$\sigma_{cap} = \frac{2\gamma}{r} \tag{2}$$

in which with σ_{cap} is the pore fluid pressure. These capillary forces put the solid skeleton of hydrated paste under compression, resulting in shrinkage. The fact that both the type of cement and temperature affect the capillary pore structure explains why a simple maturity law does not apply for evaluating the effect of temperature on autogenous deformations comprehensively. Autogenous deformations of hydrating pastes should be considered as the response of a complex and continuously changing system on changes in the pore fluid pressure. A quantitative evaluation of autogenous phenomena requires a description of the relevant phenomena active on a microstructural level, including the effects of temperature and type of cement. Against the background of the equations (1) and (2) it is conceivable that specimens made with blast furnace slag cement, because the slag results in a finer pore structure, exhibit a higher autogenous deformation, and the curing at elevated temperatures, because of a coarser pore structure of the paste, results in relatively low autogeneous shrinkage. This was in fact confirmed by the experimental data presented in this paper.

From the qualitative explanation of the effect of temperature and type of cement on autogneous deformation it can be concluded that further quantitative modeling of autogenous should focus on the modeling of the pore structure. Meanwhile promising results have been achieved in this field [16,17]. It believed that advanced microstructural models can support the design of modified and new cement-based materials with reduced hydration-induced volume changes and hence a lower susceptibility to micro- and macrocracking of hardening concrete and enhanced durability.

REFERENCES

[1] Paillere, A.M., Buil, M. and Serrano, J.J. Effect of fiber addition on the autogenous shrinkage of silica fume concrete, ACI Materials Journal, . vol. 86, no. 2, 1989, pp 139-144.

[2] Koenders, E.A.B. Simulation of volume changes in hardening cement-based materials, Delft University of Technology. PhD, Delft, 1997, p. 171.

[3] Hedlund, H. Hardening concrete – Measurements and evaluation of non-elastic deformation and associated restraint stresses. PhD, Lulea, 2000, p. 394.

[4] Hedlund, H. and Jonasson, J.-E. Effect on stress development of restrained thermal and moisture deformation, Proc. Shrinkage 2000 – Int. RILEM Workshop on Shrinkage of Concrete, Paris, 2000, pp. 355-375.

[5] Tazawa, E., Matsuoka. Y., Miyazawa, S. and Okamoto, S. Effect of autogenous shrinkage on self-stress in hardening concrete, Proc. Int. RILEM Symp. Thermal Cracking in Concrete at early Ages, Munich, 1995, pp. 221-228.

[6] Bjøntegaard, Ø. Thermal dilation and autogenous deformation as driving forces to self-induced stresses in high performance concrete, Doctoral thesis, NTNU Division of Structural Engineering, 1999, p. 256.

[7] Tazawa, E. et al. Autogenous shrinkage caused by self-desiccation in cementitious material. Proc. 9th Int. Congress on the Chemistry of Cement, vol. IV, 1992, pp. 712-718

[8] Lura, P., Jensen, O.M., van Breugel, K. (2002) Autogenous shrinkage in high-performance cement paste: An evaluation of basic mechanisms". Submitted to Cement and Concrete Research. 2002.

[9] Breugel, K. van, Vries, J. de, Mixture optimization of HPC in view of autogenous shrinkage, Proc. 5th Int. Symp. on Utilization of High Strength/High Performance Concrete, Sandefjord, 1999, pp. 1041-1050.

[10] Roy, D.M., Indron, G.M. Hydration, Structure and properties of blast furnace slag cement, Mortars and Concrete. J. American Ceramic Society, vol. 84, no. 1, 2001, pp.129-135.

[11] Nilsson, L.O., Temperature Effects in Relative Humidity Measurements on Concrete – Some Preliminary Studies. The Moisture Group. Report 1987:1. BFR. 1987, p. 84.

[12] Jensen, O. M. and Hansen, P. F. Influence of temperature on autogenous deformation and relative humidity change in hardening cement paste, Cement and Concrete Research,. vol.29, no. 4, 1999, 567-575.

[13] Lokhorst. S.J. Deformational behaviour of concrete influenced by hydration related changes in the microstructure. TU Delft, Research Report 25.5-99-05, 2001, p. 167.

[14] Breugel, K. van. Simulation of hydration and formation of structure in hardening cement-based materials, PhD thesis, Technical University Delft, 2nd edition, 1997, 305 p.

[15] Kjellsen, K.O., Detwiler, R.J., Gjørv, O.E. Development of microstructures in plain cement pastes hydrated at different temperatures. Cement and Concrete Research, vol. 21, 1991, p. 179-189.

[16] Bentz, D. P. Modeling Cement Microstructure: Pixels, Particles and Property Prediction, Materials and Structures, vol. 32, 1998, pp. 187-195.

[17] Ye G., Breugel, K. van, Fraaij, A.L.A. Numerical simulated pore structure and transport properties of cementitious materials. 11th Int. Congress on the Chemistry of Cement, Durban, 2003.

EFFECT OF CURING TEMPERATURE ON AUTOGENOUS DEFORMATIONS OF CEMENT PASTE AND HIGH PERFORANCE CONCRETE FOR DIFFERENT CEMENT TYPES

Pietro Lura[1] and Klaas van Breugel[2]

[1] Delft University of Technology, Delft, The Netherlands. E-mail: P.Lura@citg.tudelft.nl
[2] Delft University of Technology, Delft, The Netherlands. E-mail: K.v.Breugel@citg.tudelft.nl

Klaas van Breugel

Klaas van Breugel, (1952) is full professor at Delft University of Technology in the Division of Concrete Structures. He graduated at this university in 1979. After his graduation he became employed at the faculty of Civil Engineering of Delft University of Technology. His mean research and lecturing topics are structural design of concrete protective structures, structural response under extreme load conditions, design of reservoirs and tightness and self-healing of cracks. In 1991 he got his PhD at TU Delft on numerical modeling of hydration and microstructural development in hardening cement-based systems. Since that time young concrete and durability issues are among his main research topics.

ALKALI-ACTIVATED BINDERS AND POZZOLAN CEMENT BINDERS – COMPETE BINDER REACTION OR TWO SIDES OF THE SAME STORY?

A. Buchwald [1], Ch. Kaps [2] and M. Hohmann [3]

Bauhaus-Universität Weimar, Professur Bauchemie, Weimar, Germany.
E-mail: [1]anja.buchwald@bauning.uni-weimar.de, [2]christian.kaps@bauing.uni-weimar.de and [3]marc.hohmann@bauing.uni-weimar.de

ABSTRACT

Increasingly attention has been paid in recent years to alkali-activated binders such as alkali-activated fly ash and slag. Related binders are known as geopolymers which are at least alkali-activated metakaolin binders. In all cases the activation of the solid is made with different alkaline solutions containing alkali hydroxides, alkali silicates and/or alkali carbonates. It has be shown by other authors [1, 2] and the author's own investigations [3, 4] that other alumosilicate minerals and thermal activated clays also react into stable solids after alkali-activation. All these materials – fly ash, slag, metakaolin, thermal activated clays – are also well known as pozzolanic or latent-hydraulic components in cements.

Are these different binder reactions or not? It will be discussed the common and the different aspects of both binder systems based on literature and our own investigation. Results are presented for solubility tests and strength performance of different alkali-activated binders made from fly ash, slag, metakaolin, thermal activated clay and brick powder.

1. BINDER REACTION STEPS

1.1 Alkali-activated binder systems

A reactable material in the light of alkali-activated binders has to consist of a certain amount of highly active phases like a glassy phase (fly ash, slag). Clays can be transformed into a reactive material by a thermal activation process in which the dehydroxylation of the clay mineral leads to a highly active, unstable and nearly amorphous state of the solid. The reaction mechanism of alkali-activated materials can be described in two steps,

1) The generation of reactable species (alkaline activation)
   Alkali hydroxide disintegrates the solid network to produce small reactable silicate and aluminate species.

2) The real setting reaction
   Pure alumosilicate materials like metakaolin and some types of fly ash set under a condensation reaction which leads to the formation of alumosilicate polymers [5]. As could be shown by several authors, the setting of alkali-activated slag and calcium containing materials can be characterised by both a condensation reaction and a more or less hydration reaction forming CSH- (or Al-substituted CSH-) and CAH-phases depending on the calcium content and the alkalinity [6-9].

A detailed characterisation of the reaction products seems to be quite difficult because of the low crystallinity of the reaction products. Depending on curing temperature and alkalinity, the alumosilicate polymer changes into a zeolithic phase detectable by XRD.

1.2 Pozzolan cements and slag cements

The reaction of pozzolans and slag with OPC is usually described by the following two definitions. The pozzolan forms additional CSH-phases with the $Ca(OH)_2$ from cement hydration. The latent-hydraulic material needs an activation to form CSH-phases.

The different performance of pozzolanic cements has been shown in many reports, especially the loss of strength if the pozzolan content reaches high values or if using slag cements in combination with fly ash. A high pH-value in the pore solution is undoubtedly necessary to get a good pozzolanic performance of the cement [10, 11]. Obviously the alkali hydroxide is necessary to disintegrate the glassy or amorphous phases to produce reactable silicate and aluminate units. This units react with calcium hydroxide to CSH- and CAH-phases [12].

1.3 Similarity of the binder reactions

As one can see the two binder systems are more similar than different. The pozzolan cement looks like a special case of alkaline activated systems. The alkaline activation is guaranteed by the OPC pore solution. Therefore a certain amount of OPC is necessary for a good performance. But the first reaction step is the alkaline activation of the reactive solid to produce reactable monomers which can afterwards react with calcium ions.

2. EXPERIMENTAL INVESTIGATIONS

2.1 Solubility of SiO_4- and AlO_4-monomers by alkaline solutions

How alkali hydroxide disintegrates the reactive phases of the solid material can by seen directly in the solubility tests. The usefulness of such tests to determine the reactivity of different raw materials has been described by several authors [2, 13, 14] and has been widely used in our own investigations.

Several test regimes have been used to determine the release of silicate and aluminate monomers in alkaline solution:

Regime 1: The solubility of the solid in 10% NaOH-solution has been measured for a long-term period investigation up to 90 days. The mass ratio solution to solid of 400 was used.

Regime 2: The same conditions as in regime 1 (40g of 10% NaOH-solution) with a contact time of 20 h but under variation of the mass of the solid (mass ratio solution to solid between 8 and 400, resp. between 2 and 139 mg solid per ml solution).

Regime 3: The influence of concentration and kind of alkaline solution has been investigated with the following test parameters:

- alkaline solution: KOH, NaOH, LiOH
- concentration of the solutions: 0.01, 0.03, 0.06, 0.1, 0.3, 0.6, 1 and 2.8 mol/l
- solid-to-solution of 2,5 mg/ml
- duration of test: 20 h

The concentration of silicate and aluminate monomers are determined by measuring the element concentration of Si and Al using Optical Emission Spectroscopy. It has been proven that the silicate species are really monomeric units under these conditions. Therefore the small reactive species will be designated as monomers henceforth.

2.2 Binder preparation and strength measurements

Pure binder specimens were prepared by mixing the solid material with the defined amount of solution containing water and solved sodium hydroxide. The amount of water has been levelled on the same workability of the paste. No aggregates are added.

The flexural strength (centre point loading) has been measured on specimen with an geometry of 10×10×60 mm^3, the compressive strength on the broken samples with an compression area of 10×20 mm^2. Before testing all samples were cured for one day at 35°C without drying and the following days at room temperature under 60% relative humidity.

3. CHARACTERIZATION OF THE RAW MATERIALS

Five different materials were used in our investigation: a commercial metakaolin, a slag, a fly ash, the brick powder and the thermal activated clay base on the raw material which contained the main phases of quartz, illite and kaolinite beside some feldspar and carbonate. Both are heated up to 850°C, the brick under reduced oxygen, water enriched atmosphere and the clay in a normal laboratory oven under normal air. The chemical composition of these materials are shown in Figure 1.

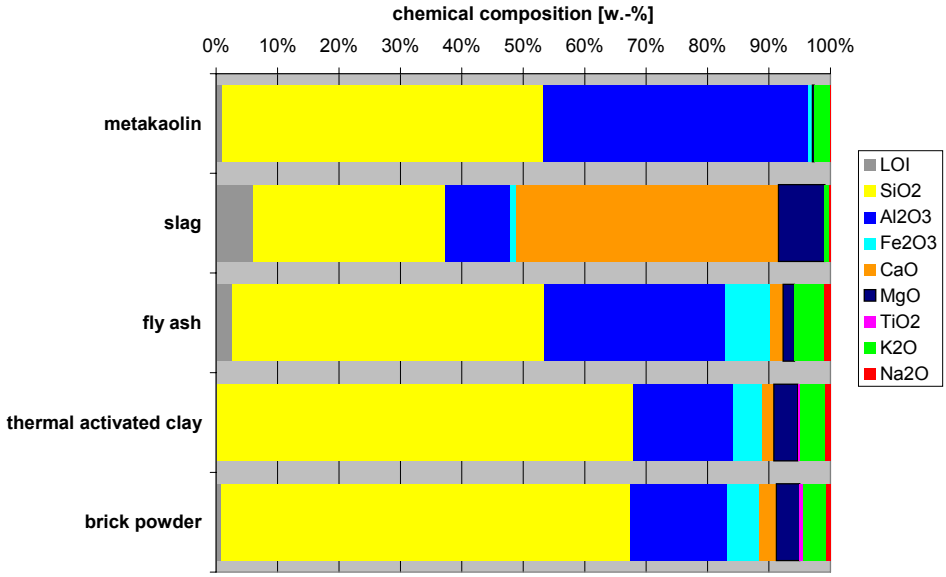

Figure 1. Chemical composition of the investigated materials

4. RESULTS AND DISCUSSION

4.1 Influence of the contact time of the reactive solid with NaOH solution on the release of silicate and aluminate monomers and strength performance of the binder

Figure 2 presents the results obtained by measuring the release of silicate and aluminate monomers in a 10% sodium hydroxide solution after different contact time with the solid material (test regime 1). As one can see the metakaolin shows the highest release per weight of both silicate and aluminate even after few hours. It is followed by the fly ash, but this material needs some time before a certain amount of monomers are detectable in the solution. This is clear because of the smaller surface of the particles and the higher stability of the glassy phase compared to the metakaolinite phase. The amount of released aluminate monomers is lower according to the lower amount of aluminate in the material.

The thermal activated clay and the brick powder reach almost the same amount of silicate and aluminate in the solution which is understandable because of the almost identical chemical and phase composition. The differences in the light of the release kinetics are due to the different surfaces of the materials.

The results of the slag material depart from those of the other materials. The measured amount of silicate and aluminate are quite low and do not change over the contact time. The available calcium ions seem to react with the released silicate and aluminate monomers to insoluble CSH- and CAH-phases as precipitate. CAH-phases and partly carbonated CAH-phases could be detected in the elution residue by XRD. The amount of crystalline C_2S and C_3S-Phases were decreasing as well.

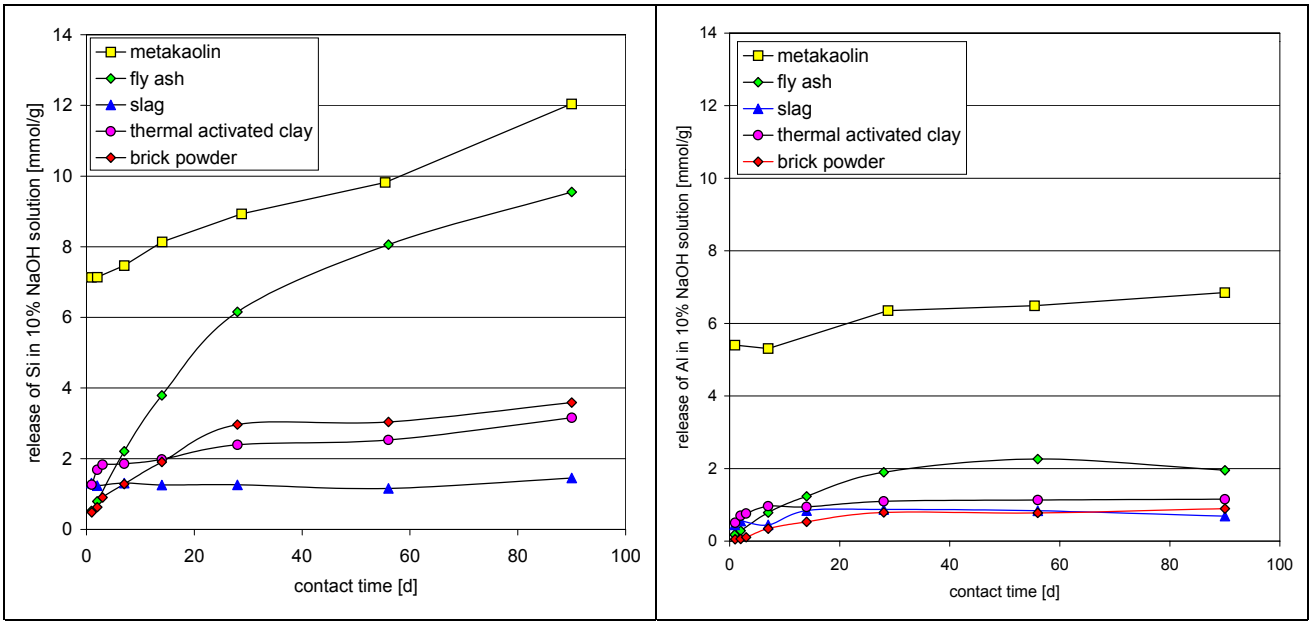

Figure 2. Influence of contact time on the release of silicate (left side) and aluminate (right side) monomers, measured after regime 1

Will the release behaviour be found again in the strength performance? The results of the compressive strength measured after the same curing time steps are presented in Figure 3. Looking only at the progress of the compressive strength one is forced to correlate the results of both investigations. But the trends are not significant and the distribution of the strength values is quite high. Apart from this it is noticeable that the only “latent hydraulic material” – the slag – performs at best as was to be expected. The different strength levels can not be compared directly as will be discussed later.

Should one expect to find the same progress of both the release of monomers in the solubility test and the strength performance? If looking at the parameters used in the solubility test of regime 1, there has been set ideal conditions for analysis and discussion of the reactivity. In contrast to the solubility test, the solid-to-solution-ratio of real binder systems easily reaches values over 1 g/ml pore solution. That’s why we used test regime 2 to measure the influence of solid-to-solution-ratio on the silicate and aluminate monomer concentration released from metakaolin by keeping the NaOH concentration constantly. The results are presented at Figure 4.

It can be seen that the concentration of silicate and aluminate monomers reaches a maximum around a ratio of 20 mg/ml. Either the solution process arrives an equilibrium or released monomers condensate already to insoluble alumosilicate which will remain in the elution residue.

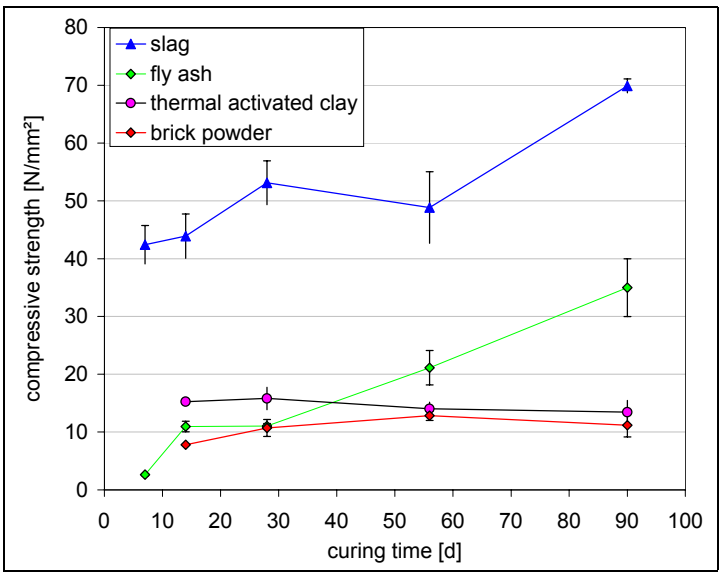

Figure 3. Influence of curing time on the strength development of some alkali-activated binders (compositions of the same ratio NaOH to solid material are compared)

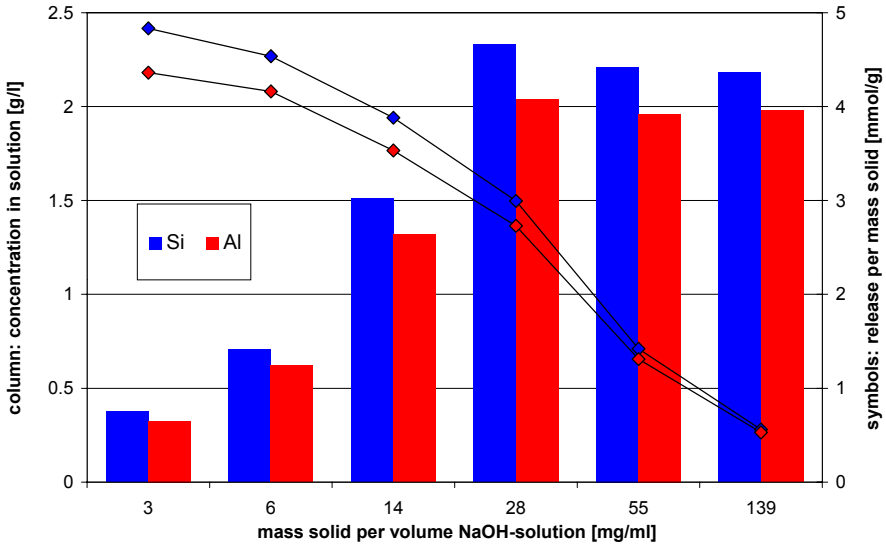

Figure 4. Influence of the ratio solid to solution on the release of silicate and aluminate monomers from metakaolin (test regime 2)

4.2 Influence of the concentration of sodium hydroxide on the release of silicate and aluminate monomers and strength performance of the binders

The concentration of the alkaline solution plays an important role for the reaction step 1 (disintegration of the solid material). The silicate and aluminate monomers released from metakaolin using different concentrations of sodium hydroxide are presented in Figure 5. The lower the pH-value of the solution, the lower the monomer concentration will be. There is no selectivity between silicate and aluminate.

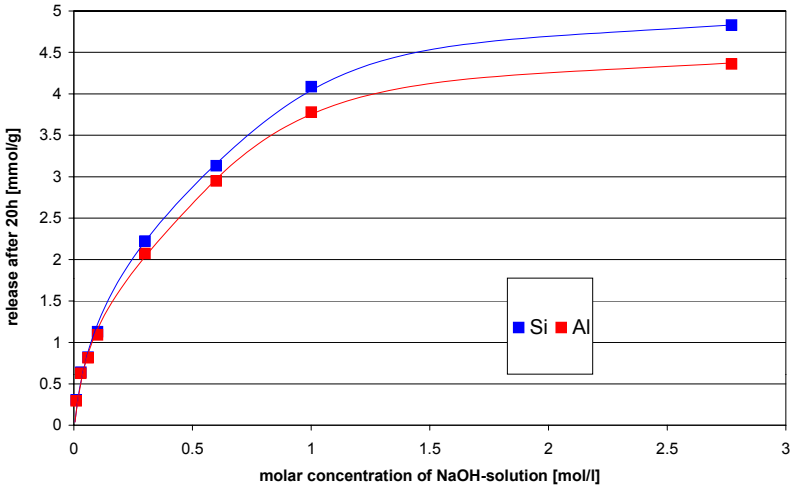

Figure 5. Influence of the NaOH concentration on the release of silicate and aluminate monomers from metakaolin (test regime 3)

The strength performance of binders prepared with different NaOH amounts per solid material are presented in Figure 6. In general the strength increases by an increasing content of sodium hydroxide.

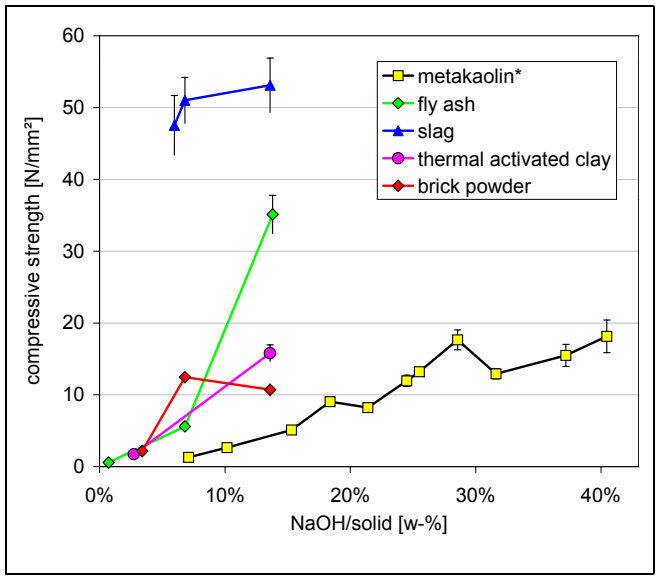

Figure 6. Influence of the NaOH content on the compressive strength of the alkali-activated binders after 28 days (*14 days)

Because of the different water contents used to obtain a certain workability, the concentration of the pore solution will be different for two binders even with the same NaOH amount per solid material. Therefore the strength values are presented again in dependence of the NaOH concentration in the initial pore solution (Figure 7). The compressive strength shows almost the same dependence from the NaOH concentration for all materials apart from the slag. However in every binder the pore volume which has to be filled by the reaction products is very different. Metakaolin needs many more reactable monomers than fly ash because of its higher surface area. On the other hand the reactivity of the materials by means of releasable amounts of monomers is also quite different (see results in 4.1). A different setting behaviour shows again for the slag material. The building of CSH- and CAH-phases leads to good strength performance even at low alkalinity.

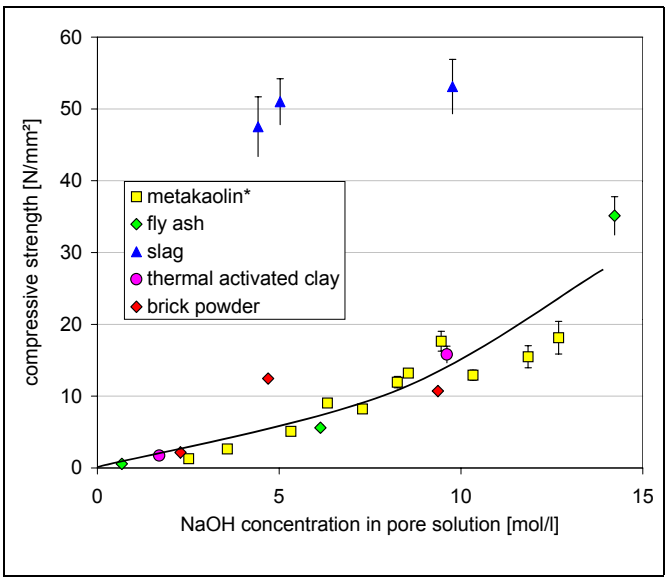

Figure 7. Influence of the NaOH concentration in the pore solution on the compressive strength of the alkali-activated binders after 28 days (*14 days)

4.3 Influence of the kind of alkaline hydroxide on the release of silicate and aluminate monomers from metakaolin

The pH-values of the single alkaline solutions varying in concentration and kind of alkali ion are shown in Figure 8. If one replaces the sodium ions by other alkaline ions in the solubility test one would expect an order of released monomers correlated to the hydroxide activity. That means we would expect a higher solubility performed by KOH than by NaOH because of the higher alkalinity.

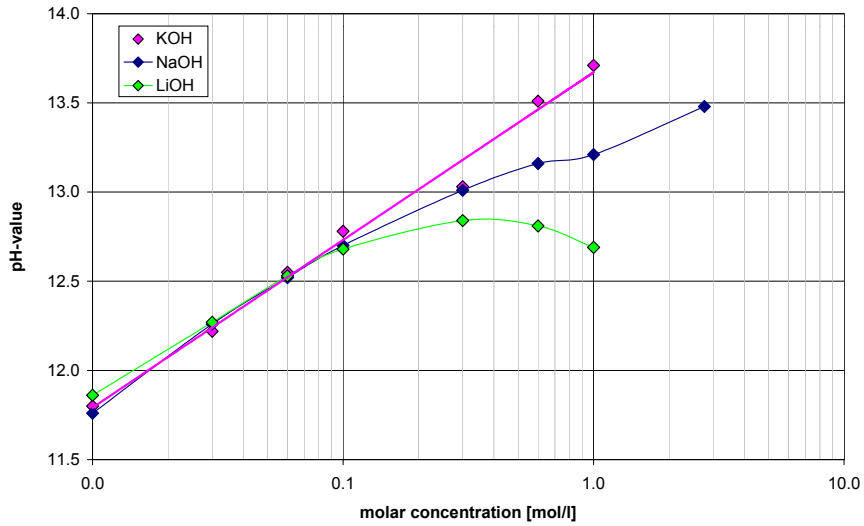

Figure 8. Influence of the concentration and kind of the alkaline solution on the pH-value (an electrode with a low alkaline error was used for measurements)

The results using test regime 3 to determine the influence on the kind of alkaline solution are shown in Figure 9. The diagram shows only the release of silicate from metakaolin. Similar to Figure 5 there is no selectivity between silicate and aluminate. The order of monomer releasing followed our expectations only as regards NaOH and LiOH. The KOH which has a much higher hydroxide activity doesn't show a higher monomer releasing. FRAAY [13] got similar results if eluting fly ash with KOH and NaOH solution. Obviously this effect can't be described thermodynamically alone. Maybe there are kinetic effects due to the different ion sizes (diffusion rate in the reaction zone) playing an important role by the disintegration of glassy and dehydroxylated solid phases.

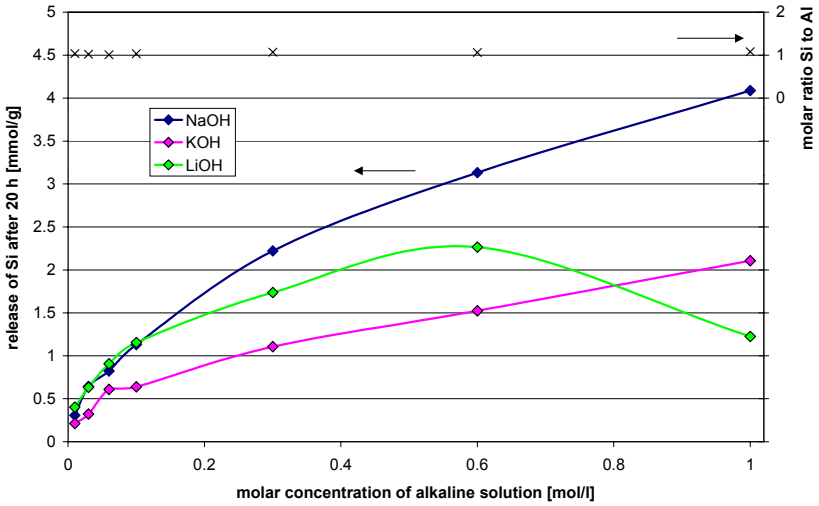

Figure 9. Influence of the concentration and kind of alkaline-solution on the on the release of silicate monomers from metakaolin (test regime 3)

5. CONCLUSIONS

The disintegration of glassy and dehydroxylated phases could be shown by the presented results of the solubility tests. The chosen test parameters were optimised for ideal measurement conditions and therefore they are not identical with those in the real process in the pore solution. Nevertheless one can extract the following conclusions:

1) Glassy and dehydroxylated alumosilicate phases will be disintegrated by alkaline solutions into silicate and aluminate monomers.

2) The amount of released silicate and aluminate monomers depends on the content of the reactive phase and the kind and concentration of the alkaline solution.

3) The kinetics of disintegration depend on the contact surface and the kind of the reactive phase and also on the degree of disorder.

4) The maximum of released monomers will not be reached in real binder systems because of the lower amount of alkaline solution. The layer which has been precipitated during alkaline activation can limit the process of further disintegration. The remaining solid grains will then work as aggregates.

5) If calcium ions are present in the solution as well the building of insoluble CSH- and CAH-phases will be preferred.

These points confirm the assertion that alkali-activated binders and pozzolanic cement binders are two sides of the same story. In pozzolanic cement binders two connected reaction types exist, ordinary cement hydration and alkali-activation of the pozzolanic material by the alkaline pore solution. As reaction products one can find primary CSH and CAH-phases (from the OPC), secondary CSH- and CAH-phases (from the reaction of $Ca(OH)_2$ with the released silicate and aluminate monomers) and maybe alumosilicate polymers. Alkali-activated binders which will be activated by alkali hydroxide lead to alumosilicate polymers partly detectable as crystalline zeolitic phases or to CSH and CAH-phases if calcium ions are present in the solution [9].

REFERENCES

[1] Davidovits, J.; Buzzi, L.; Rocher, P.; Gimeno, D.; Marini, C.; Tocco, S.: Geopolymeric cement based on low cost geological materials. Results from the European research project GEOCISTEM, 2nd international conference of geopolymere, 1999, pp.83-96.

[2] Xu, H. and van Deventer, J.S.J.: The geopolymerisation of alumino-silicate minerals. Int. J. Miner. Process, vol.59, 2000, pp.247-266.

[3] Kaps, Ch. and Hohmann, M.: Mineralische Polymerbinder aus hydrothermal gebranntem Ton, 4th Ibausil, Weimar, 2000, vol.1, pp.415-424.

[4] Kaps, Ch.; Hohmann, M. and Hohmann, H.: Ein mineralisch gebundener Leichtbau-Werkstoff, Materials Science and Restoration, MRS V; Esslingen, 1999, pp.1593-1602.

[5] Davidovits, J.: Geopolymers:inorganic polymeric new materials, Journal of Thermal Analysis, vol.37, 1991, pp.1633-1656.

[6] Brough, A.R.; Katz, A.; Bakharev, T.; Sun, G.-K.; Kirkpatrick, R.J.; Struble, L.J.; Young, J.F.: Microstructural Aspects of zeolite formation in alkali activated cements containing high levels of fly ash, Materials Research Society Symposium Proceeding, vol.370, 1995, pp.199-208.

[7] Brough, A. R. and Atkinson, A.: Sodium silicate-based, alkali-activated slag mortars. Part I. Strenght, hydration and microstructure, Cement and concrete research, vol.32, 2002, pp.865-879.

[8] Alonso, S. and Palomo, A.: Calorimetric study of alkaline activation of calcium hydroxide + metakaolin solid mixtures, Cement and Concrete Research, vol.31, 2001, pp.25-30.

[9] Granizo, M.L.; Alonso, S.; Blanco-Valera, M.T.; Palomo, A.: Alkaline activation of metakaolin: Effect of calcium hydroxide in the products of reaction, Journal of American Ceramic Society, vol.85, 2002, pp.225-231.

[10] Fraay, A.L.A.; Bijen, J.M .; de Haan, Y.M.; Larbi, J.M.: The reaction of fly ash in concrete – A critical examination. Fly ash, silica fume, slag an natural pozzolans in concrete, supplementary papers of CANMET/ACI Int. Conference, 1989, pp.33-48.

[11] ACI commitee (ed.) Use of fly ash in concrete. ACI 232.2R-96

[12] Hübert, C.; Wieker, W.; Heidemann, D.: Investigation of hydration products in high volume fly ash binders, Fly ash, silica fume, slag an natural pozzolans in concrete, 7th CANMET/ACI Int. Conference, Chennai, vol.1, 2001, pp.83-98.

[13] Fraay, A.L.A.: Fly ash a pozzolan in concrete, PhD-Thesis at University Delft, 1990.

[14] He, C.; Osbæck, B.; Makovicky, E.: Pozzolanic reaktions of six principal clay minerals: Activation, reactivity assessments and technological effects, Cement and Concrete Research, vol.25, 1995, pp.1691-1702.

ALKALI-ACTIVATED BINDERS AND POZZOLAN CEMENT BINDERS – COMPETE BINDER REACTION OR TWO SIDES OF THE SAME STORY?

A. Buchwald [1], Ch. Kaps [2] and M. Hohmann [3]

Bauhaus-Universität Weimar, Professur Bauchemie, Weimar, Germany.
E-mail: [1]anja.buchwald@bauning.uni-weimar.de, [2]christian.kaps@bauing.uni-weimar.de and [3]marc.hohmann@bauing.uni-weimar.de

Christian Kaps

Prof. Dr. rer. nat. habil. Christian Kaps, graduated in Chemistry in 1971 at the Friedrich-Schiller-Universität Jena in Germany. From 1973 working as Research Assistant in Solid State Chemistry, he was involved in projects for Electronic and Glass Industry. In 1978 he obtained his doctorate in chemistry of thin amorphous films. The thesis for habilitation were dealing with ion exchange reactions in oxide glass 1989. From 1992 he was teaching as a Professor of Inorganic and Glass chemistry at Fachhochschule Jena. In 1998 he has been nominated as professor and head of the chair of Building Chemistry at the Bauhaus-Universität Weimar.

Contact Details:
Mail: Prof. Dr. Christian Kaps
Bauhaus-Uiversität Weimar, Professur Bauchemie
Coudraystr. 13C
99421 Weimar
Germany

Tel: +49 3643 584793
Fax: +49 3643 584790
E-mail: christian.kaps@bauing.uni-weimar.de
Web: www.uni-weimar.de/bauchemie

INFLUENCE OF THE MOLECULAR WEIGHT OF POLYCARBOXYLATE ETHER SUPERPLASTICIZERS ON THE RHEOLOGICAL PROPERTIES OF FRESH CEMENT PASTES, MORTAR AND CONCRETE

R. Magarotto, I. Torresan and N. Zeminian

MAC S.P.A. – Degussa, Treviso, Italy; E-mail: mactv@mac-mbt.com

ABSTRACT

This paper highlights the influence of the molecular weight on the performances of polycarboxylate ether (CE) superplasticizers.

A polymer was separated into different fractions on a laboratory scale by means of ultrafiltration membranes. The weight average molecular weight ($\overline{M}w$) and the molecular weight distribution of such fractions were determined through gel permeation chromatography and their performances were investigated in fresh cement pastes and in mortar mixes and compared to those of the original unfractioned polymer. The data collected indicate that the performances of the polymer are considerably affected by its molecular weight, the best effect being obtained with the highest molecular weight fractions (>30K and >50K Dalton). The lowest fraction (< 30K) performs far less well than the original unfractionated polymer.

The higher molecular weight fractions are adsorbed in a greater amount and more increasingly over time, while the smaller are adsorbed weakly and more constantly over the time.

It can be concluded that there is an ideal molecular weight for the best performance of the superplasticizer investigated. This could be taken into account for optimisation of the product.

Keywords: Admixture, Superplasticizer, Polycarboxylate, Adsorption, Rheological Properties, Mortar, Minislump, Concrete

1. INTRODUCTION

In the last decades, the technology of concrete has evolved and nowadays the market increasingly demands concrete with properties such as higher flowability, higher early mechanical strengths and increased durability. The use of high range water reducing admixtures (HRWRA) has represented a fundamental step in this direction. Since the introduction of salts of sulfonated naphthalene formaldehyde condensate (NS) invented in Japan, and salts of sulfonated melamine formaldehyde condensate (MS), which appeared on the German market in the '60s, a new generation of admixtures, based on polycarboxylate ether polymers (CE) has been recently developed. The widespread diffusion of such compounds has stimulated research aimed at understanding the mechanism of action and to find out if a correlation exists between their structure and their performances, in order to optimise them.

Among the most important parameters of a polymer are its molecular weight and polydispersion (1,2). The weight average molecular weight $\overline{M}w$ is expressed by formula **i)**:

$$\overline{M}w = \frac{\sum_i w_i \cdot M_i}{\sum_i w_i} = \frac{\sum_i n_i \cdot M_i^2}{\sum_i n_i M_i} \qquad \textbf{i)}$$

and the numerical average molecular weight $\overline{M}n$, expressed by formula **ii)**:

$$\overline{M}n = \frac{weight\ of\ polymer}{moles\ of\ macromolecules} = \frac{\sum_i n_i \cdot M_i}{\sum_i n_i} \qquad \textbf{ii)}$$

where M_i = molecular weight of the i-species
w_i = weight of the i-species
n_i = moles of the i-species,

The polydispersion, defined as the ratio between $\overline{M}w$ and $\overline{M}n$, represents the width of the curve of the molecular weight distribution.

Previous studies were carried out on the effect of molecular weight on the performances of traditional superplasticizers, based on ligninsulfonate and β-naphthalenesulfonate polymers (3-8) but similar studies on polycarboxylate ether admixtures have not yet been reported in the literature.

The present study is therefore aimed at investigating of the effect of molecular weight on the performances of sodium salts of a polycarboxylate ether based superplasticizer (CE).

2. EXPERIMENTAL

2.1 Materials employed

Table 1 shows the chemical composition, determined according to the methods reported in UNI ENV 196/2, of the two cements (A and B) employed in the present work. The polymer fractioned was a polycarboxylate ether with total solid content 40.0%, density 1.05 g/cm^3 and pH 7.

The gel permeation chromatography analyses were performed using a GPC system from Shimadzu, with UV detector SPD10A (Shimadzu) and RI detector 10A (Shimadzu).

The instrument calibration was performed by means of narrow MWD standards of polyethylene oxides. They represent the closest commercially available approximation to CE polymers but their molecular structure is still distinct from that of polycarboxylate ethers; therefore the $\overline{M}w$ values given by GPC are meant as relative molecular weights.

Table 1. Chemical analyses of cements employed

	Cement A (type II A/L 42.5)	**Cement B (type I 52.5)**
free CaO	1.0	0.84
R.I.	3.0	0.04
LOI	3.9	1.1
SiO_2	21.1	20.1
Al_2O_3	6.2	4.8
Fe_2O_3	2.7	5.5
CaO	61.0	63.8
MgO	1.4	1.4
SO_3	2.9	2.7
Na_2O	0.4	0.3
K_2O	0.7	0.9
Blaine (cm^2/g)	3327	3940

2.2 Ultrafiltration

Prior to ultrafiltration the polymer, diluted with tap water to a 10% concentration, was submitted to dialysis through cellulose dialysis tubes by SIGMA CHEMICAL. The tubings employed have a 49 mm diameter and retain, according to SIGMA specifications, molecules with molecular weights 12,000 or greater. They are designed more specifically for protein dialysis.

The polymer was put into closed tubes made with the cellulose membranes and left for 72h under running water. The dialyzed product was concentrated through evaporation at the roto-evaporator.
After dialysis, the polymer was submitted to ultrafiltration through stirred cell devices with a membrane of polyethersulfone (low release), encapsulated within the cell, with a filtering area of 23.2 cm^2 and a capacity of 150 ml. The polymer sample, diluted again to a 10% dry concentration, was placed within the cell; nitrogen gas at 50 psi pressure was used as the driving force for filtration, together with a magnetic stir plate which, moving the stir bar, created a gentle turbulence at the membrane surface. This caused macromolecules to be swept off the membrane surface, minimising the phenomenon called "concentration polymerization"; the build-up of a dense macromolecular layer at the membrane surface precluding filtration. Two molecular weight cut-off (MWCO) membranes were used: 30K and 50K Dalton.

After completing the filtration through one membrane, the filtrate was reprocessed in the same membrane for two more times in order to obtain a cleaner fraction. Previous GPC investigations have in fact shown the usefulness of this procedure.

Figure 1 shows the molecular weight distribution, as obtained by GPC, of the starting polymer and of all the fractions gained from it.

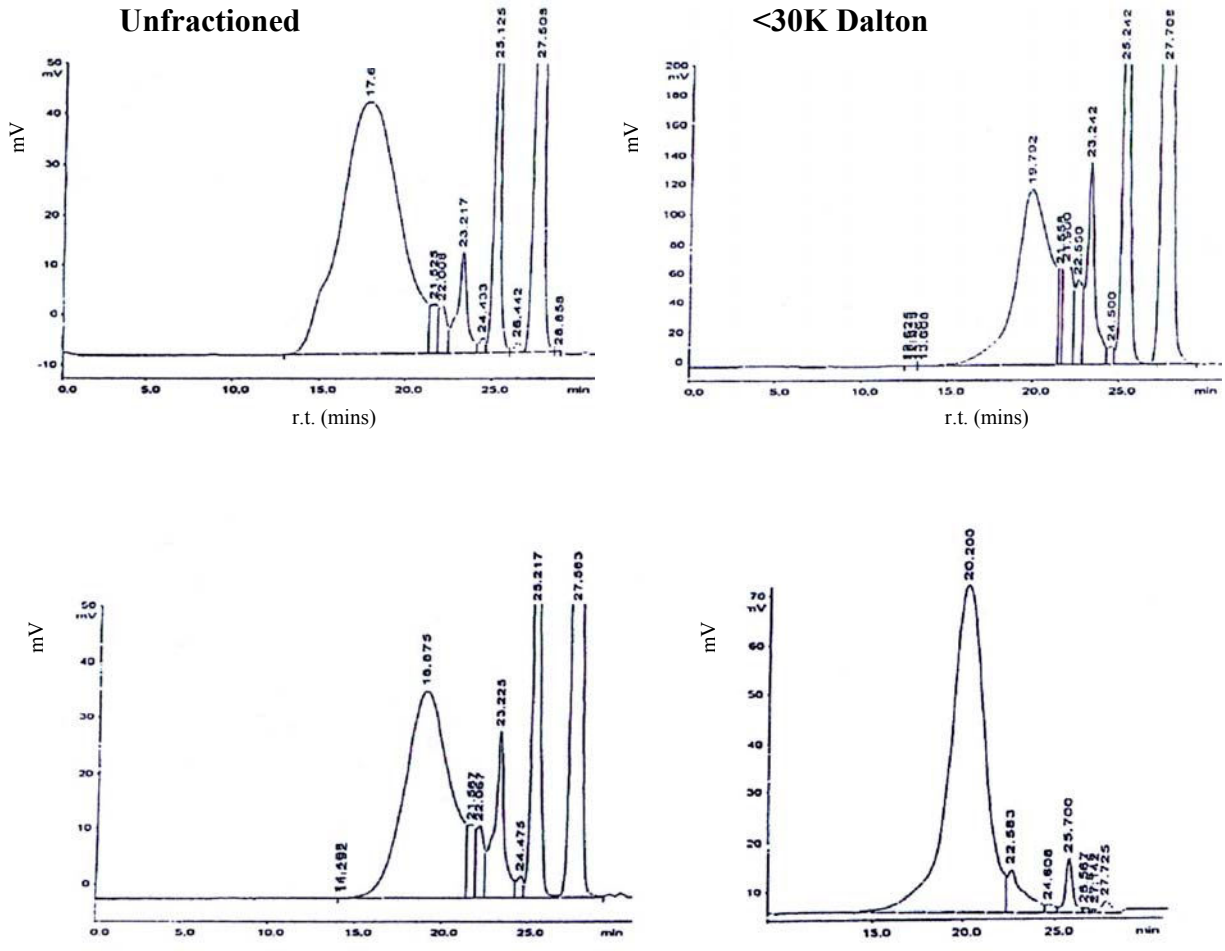

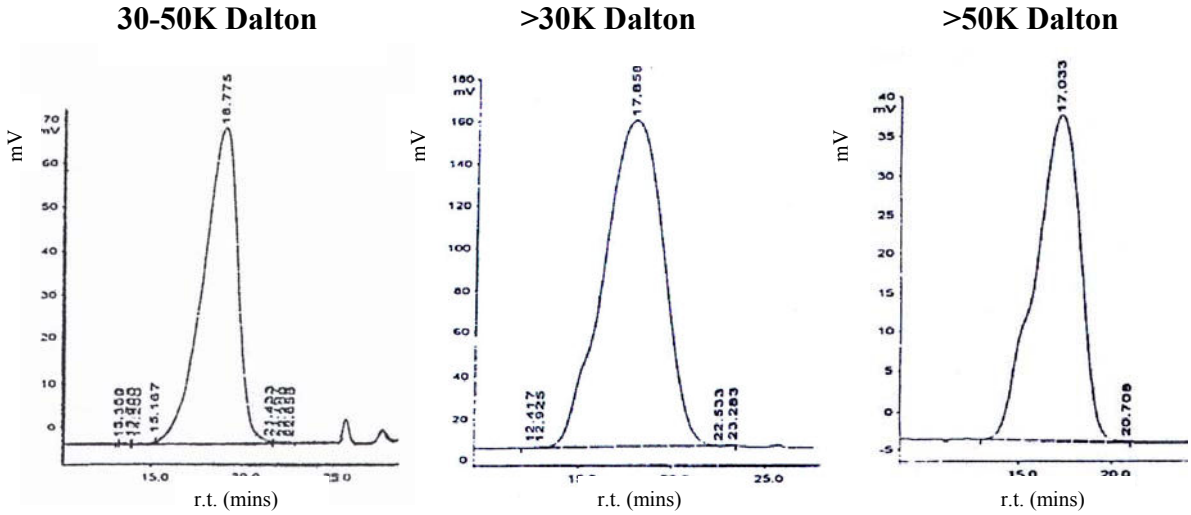

Figure 1. Molecular weight distribution of the polymer fractions from GPC analyses

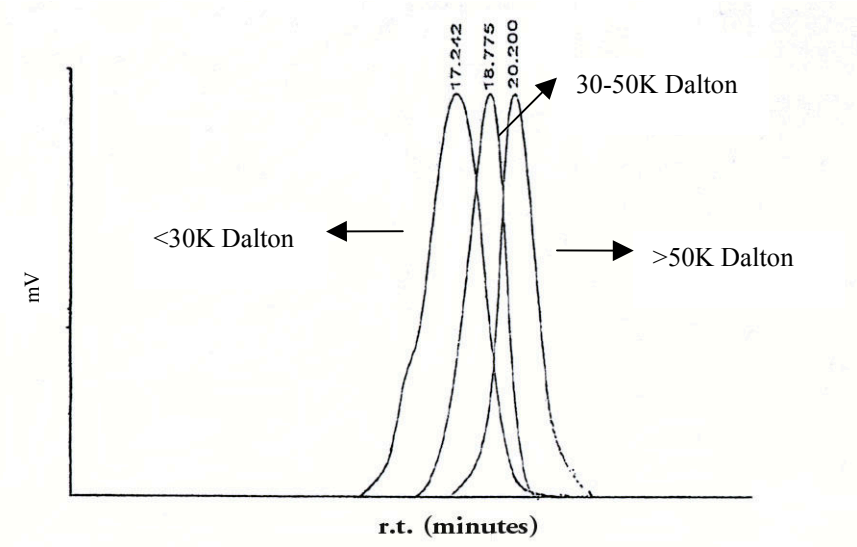

Figure 2. Superimposition of GPC analyses from <30K Dalton, 30-50K Dalton and > 50K Dalton fractions of the GPC analyses.

Table 2 shows some data regarding the initial polymer and its fractions. The percentage of the initial polymer represented by each fraction was determined as the ratio between the dry matter of the two. Besides the other data ($\overline{Mw}$, polydispersion, retention time), Table 2 reports the molar ratio between carboxylate groups and ether chains in the polymer molecule of each fraction as determined through TCAV (Total Carboxylic Acid Value) analysis, with respect to that of the whole polymer.

Table 2. Polymer fractions features

	Whole polymer	<30K Dalton	30-50K Dalton	>50K Dalton
% in the unfractioned polymer	100	18	28	54
WAMw as determined by GPC analyses	22 900	5 400	11 400	31 100
r.t. (mins)	17.7	20.2	18.8	17.1
Polydispersion (D)	3.37	2.11	1.65	1.8
Molar Ratio variations (from TCAV determinations)		no variation	no variation	no variation

2.3 Rheological evaluations on cement pastes - minislump tests

The rheology of cement pastes treated with the different fractions of superplasticizer or with the whole polymer at the dosage of 0.25% dry material by weight of cement (bwc), was investigated by means of the minislump test: the cement/water paste was poured, after mixing, into a metallic truncated cone mould standing on a flat Plexiglas surface; the cone was then lifted and the diameter of the collapsed paste measured. Both cements A and B were employed for these tests. Results are reported in Figures 3 and 4.

2.4 Rheological evaluations on mortars

Mortars were prepared according to the norm EN 196/1 with normalized sand and the two cements. The unfractioned CE polymer and all the fractions obtained from it were used as admixtures. The flow was evaluated for each mortar according to the norm EN 413-2.

The dosage of admixtures was 0.20% active by weight of cement (act. bwc.) in the case of cement A (type II A/L 42,5) and 0.28% act. bwc. for cement B (type I 52,5). These dosage rates have been chosen in order to represent the two situations found in the Italian ready-mix concrete and precast concrete industries.

Since ultrafiltration was carried out on a laboratory scale, the amounts of each fraction obtained were insufficient to test them directly in concrete. In order to better simulate concrete practice, where the performances of a superplasticizer are expressed in terms of slump according to EN 12350-2, one more parameter was considered and evaluated in the mortar tests, which will be referred to as “static” flow: it is the flow measured on the drop table after lifting the truncated cone (EN 413-2). The flow measured according to the Norm EN 413-2 after the 15 drops will be called “dynamic” flow in order to distinguish it from the previous one.

Two series of mortar tests were carried out with cement A, the first keeping constant the W/C ratio and the other at constant initial flow. Specimens for compressive strength evaluation were also prepared (EN 196/1); results are reported in Tables 3a and 3b. In this case each fraction was formulated with a little antifoam agent, in order to bring the air entrained to what is considered an an upper limit for a superplasticizer (about 5% in mortar).

Two series of mortars, both at the same initial flow, were made with cement B: in the first the samples were previously formulated with antifoam while in the second they were used as obtained, in order to evaluate their natural air entrainment; furthermore the “static” flow was measured over time in order to predict the flowability maintenance of concrete. All the results regarding mortar tests on cement B are reported in Tables 4a, 4b.1 and 4b.2.

2.5 Adsorption analyses

T.O.C. (Total Organic Carbon) analyses were carried out with a Shimadzu 5000A T.O.C. analyser in order to evaluate the adsorption of the different polymer fractions by cement/water pastes.

Both Cement A and B were used, and the superplasticizer fractions were dosed at 0.25% dry content bwc. The water/cement ratio was kept constantly at 0.50.

The samples were prepared according to the following procedure: cement and water, the latter containing the superplasticizer, were stirred for the defined time and then filtered in a büchner with a vacuum pump. The amount of polymer adsorbed was determined by difference between the organic carbon originally contained in the polymer solution and the amount left in the solution filtered from the paste. The results are expressed as percentage of polymer adsorbed (Tables 5, 6 and Figures 8 and 9).

3. RESULTS

3.1 Polymer fractionation

As Figures 1 and 2 show, dialysis and ultrafiltration were quite effective in fractionating the polymer. Figure 2 is a superimposition of the main fractions obtained from ultrafiltration, namely <30K, 30-50K and >50K Dalton. It can be observed from Table 2 that the >50K fraction represents more than 50% by weight of the total polymer, while the lowest molecular weight, <30K, represents only 18%. The fraction taken out by dialysis is therefore less than 18%, but a more precise determination was not possible.

Figure 1 shows the differences between the two fractions with $\overline{Mw}$ lower than 30K Dalton, in the dialysised and the non-dialysised sample. Basically, the effect of dialysis consists of removing monomers and residues from the polymerization process. The dyalisised sample is therefore “cleaner”, in terms of polymer, than the non dialysised one.

3.2 Minislump rheological tests

As shown in Figures 3 and 4, the minislump diameter and therefore the flowability of cement pastes after 1 minute mixing increases with increasing polymer molecular weight.

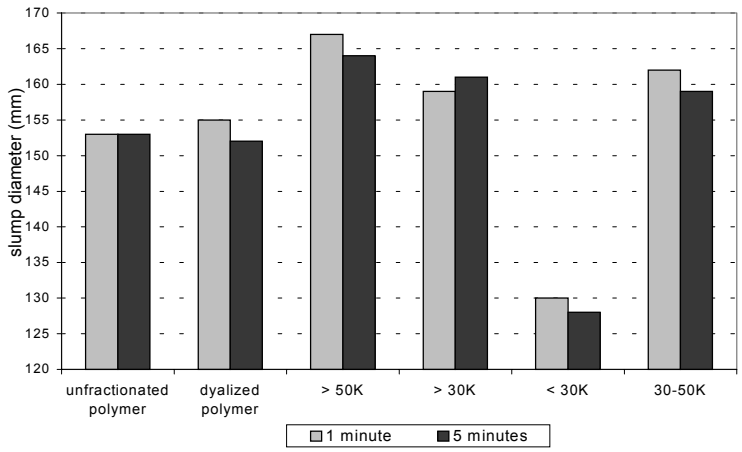

Figure 3. Minislump results – cem. A (II A/L 42.5)

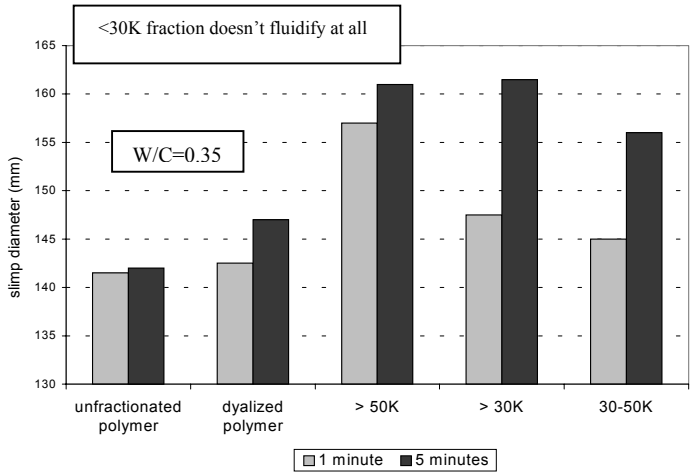

Figure 4. Minislump results – cem. B (I 52.5)

The fraction <30K does not perform well in both cases; with cement B (type I 52.5) the paste was so stiff that it was not even possible to lift the cone. With both cements, the >50K Dalton fraction has a much greater flow than the >30K.

Considering the minislump values obtained after 5 minutes (abbreviated) mixing, it may be noted that:

- in the case of cement A, there are no significant difference between 1' and 5' mixing; there is a good workability retention;
- in the case of cement B, there are greater differences between 1' and 5'mixing; the flowability is higher at 5' for each fraction, >30K and 30-50K fractions being those with the highest increment: >30K, at 5' becomes even more flowable than >50K.

It is possible to conclude from the minislump evaluations that the higher $\overline{Mw}$ fractions perform better; at 1' >50K gives the greatest diameter, but >30K seems better at 5', at least with cement B.

3.3 Mortar tests

Table 3a. Mortar tests with cement A (II A/L 42.5) – W/C ratio constant – admixture dosage: 0.20% active by weight of cement.

Sample	W/C	Initial "static flow" (%)	Flow (%)				Compressive Strength 20°C (MPa)		
			0'	15'	30'	60'	24h	7 days	28 days
Unfractioned Polymer	0.49	28	121	109	95	88	17.7	40.4	46.4
Fraction <30K	0.49	12	89	85	82	76	17.8	41.6	49.2
30-50K	0.49	46	118*	115	110	99	15.5	42.6	50.3
> 30K	0.49	75	146*	134	132	130	17.7^{++}	38.0^{++}	41.9^{++}
> 50K	0.49	47	126*	124	124	110	13.9^{++}	32.6^{++}	35.6^{++}

*= bleeding ++= values not reliable because of bleeding

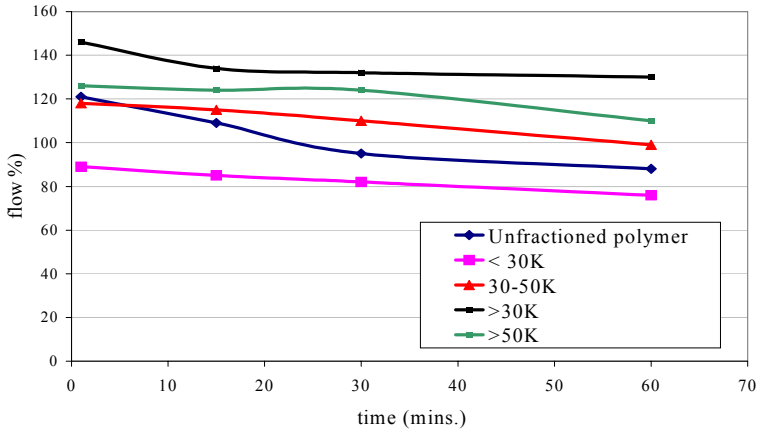

Figure 5a. Mortar tests – cement A – W/C constant (0.49)

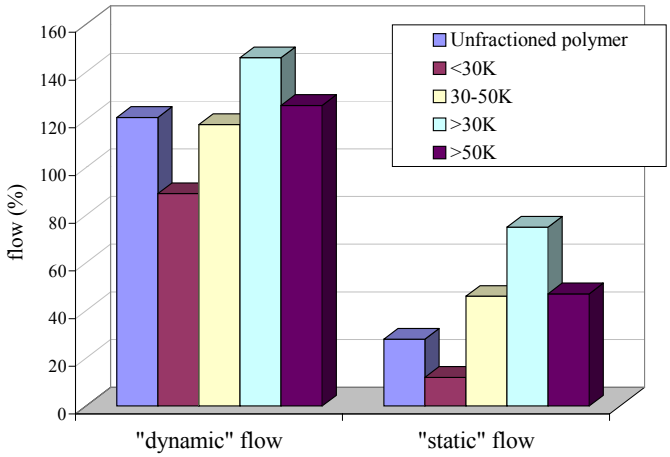

Figure 5b. Mortar tests – cement A – comparison between “static” and “dynamic” flow

Considering cement A first, the following observations can be made:

- in the mortars at the same W/C ratio (Table 3a, Figures 5a and 5b), the fractions giving the highest initial flow are >30K and >50K Dalton; the first works better than the second.
- The <30K fraction gives very low fluidifying effect.
- The 30-50K fraction gives intermediate performance, only slightly better than the unfractionated polymer.
- Concerning the flow retention over the time, as shown by the slope of curves in Figure 5a, the fractions 30-50K and >50K perform better than the unfractioned polymer and the >30K Dalton fraction;
- The initial “static” flow values confirm that >30K has the best performance.
- There is a good correspondence between “static” and “dynamic” flow for the three heaviest fractions, while their differences with respect to the unfractioned polymer and the <30K fraction are more accentuated in the “static” flow than the “dynamic” one. We can therefore expect that the differences in performances among the fractions will eventually be more evident in concrete than they appear in the mortar.
- The compressive strength values from the mortar tests of the first series are not so reliable because of bleeding.

Table 3b. Mortar tests - cement A (II A/L 42.5) – different W/C ratio
admixture dosage: 0.20% active by weight of cement.

Sample	W/C	Initial "static" flow (%)	Flow (%)				Compressive Strength (MPa) 20°C		
			0'	15'	30'	60'	24 h	7 days	28 days
Unfractioned polymer	0.49	20	108	90	76	-	16.5	30.0	44.6
> 50K	0.44	25	118	110	104	96	17.3	36.3	43.2
30-50K	0.48	30	104	94	83	-	17.8	33.4	46.6
>30K	0.42	46	122	90	80	-	21.2	44.2	46.2

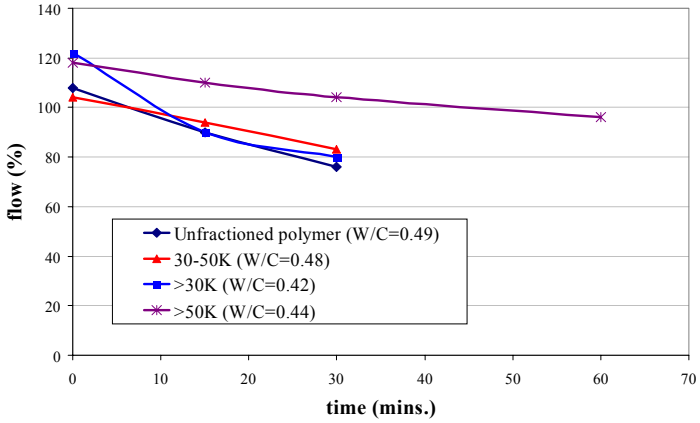

Figure 6a. Mortar tests – cement A – "dynamic" flow

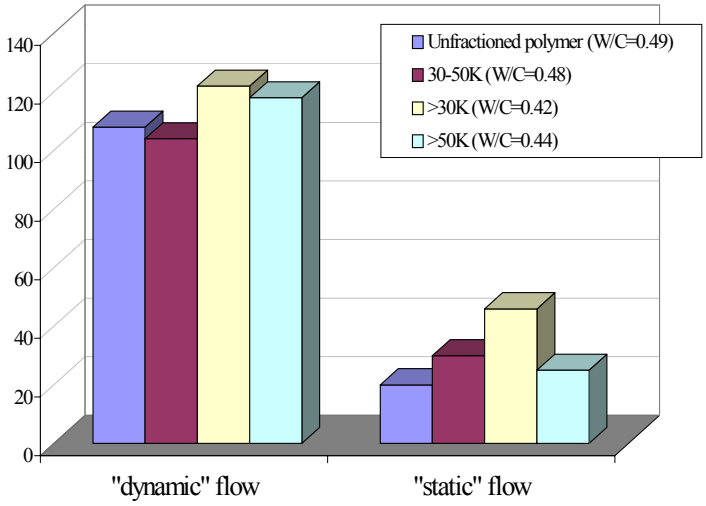

Figure 6b. Mortar tests – cement A comparison between "static" and "dynamic" flow

- Mortars, at the same initial flow: >30K reduces the water demand, with respect to the unfractioned polymer, by a 14%, and >50K fraction by a 10%. The medium fraction, 30-50K Dalton, does not give any improvement (Table 3b and Figures 6a and 6b).
- Again the >50K fraction offers a better flow retention than >30K.
- The "static" flow values are more differentiated than the "dynamic" flow values. The greatest difference is shown by the >30K fraction, which has a static flow much higher than all the others, even at the lowest W/C ratio.
- Looking at compressive strengths values, >30K fraction seems to give the highest early strengths, but the results are similar at 28 days.

Considering cement B, the following results are found (see Tabs. 4a, 4b.1 and 4b.2):

Table 4a. Mortar tests - cement B (I 52.5) – different W/C ratio
Admixture dosage: 0.28% active by weight of cement.

Sample	W/C	Initial "static" flow (%)	Air entrainment (%)*	Flow (%)		Compressive strength (MPa) 20°C		
				0'	15'	24h	7days	28days
Unfractioned Polymer	0.43	39	5.4%	122	70	40.9	74.5	88.2
Fraction >50K	0.41	32	5.4%	117	75	42.5	78.2	94.8
30-50K	0.44	15	5.2%	104	75	36.1	68.5	84.8
<30K	0.46	-	4.8%	63	-	34.3	60.8	74.8
>30K	0.41	25	5.2%	114	65	40.4	74.8	87.\7

Table 4b.1. Mortar tests - cement B (I 52.5) – different W/C ratio – "dynamic flow"

Sample	Dosage	W/C	Air entrainment (%)		Flow (%)			
			0'	30'	0'	15'	30'	60'
Unfractioned Polymer	0.28% act.	0.42	23%	22%	120	110	110	-
Fraction >50K	0.28% act.	0.41	20%	20%	127	115	113	110
30-50K	0.28% act.	0.44	19%	21%	119	101	101	97
<30K	0.28% act.	0.47	13%		96	85	-	-
<50K	0.28% act.	0.47	18%	17%	121	108	105	101

Table 4b.2. Mortar test – cement B (I 52.5) – different W/C ratio – "static" flow

Sample	Dosage	W/C	Static Flow (%)			
			0'	15'	30'	60'
Unfractioned polymer	0.28% act.	0.42	62	55	55	-
>50K	0.28% act.	0.41	85	75	65	60
30-50K	0.28% act.	0.44	62	45	45	42
<30K	0.28% act.	0.47	10	-	-	-
<50K	0.28% act.	0.47	60	33	30	30

- the >50K and >30K fractions are the best performing. They both bring about a reduction of 5% in the water/cement ratio.
- The >50K fraction, gives better flow retention;
- the <30K fraction requires more water than the unfractioned polymer (ca 7%.);
- both early and long term strengths are much higher for the >50K fraction compared to others.
- As regards the air-entrainment, there are no substantial differences among the samples: the <30K Dalton fraction entrains a smaller amount of air both with and without antifoam (Tables 4 and 4b.1), and the >50K one entrains a little bit less than the unfractioned polymer (20% versus 23%) in the absence of antifoam.
- Comparing the values of "static" and "dynamic" flow for cement B, (Figs. 7a and 7b) it is confirmed that the "static"exalts the differences among the fractions.

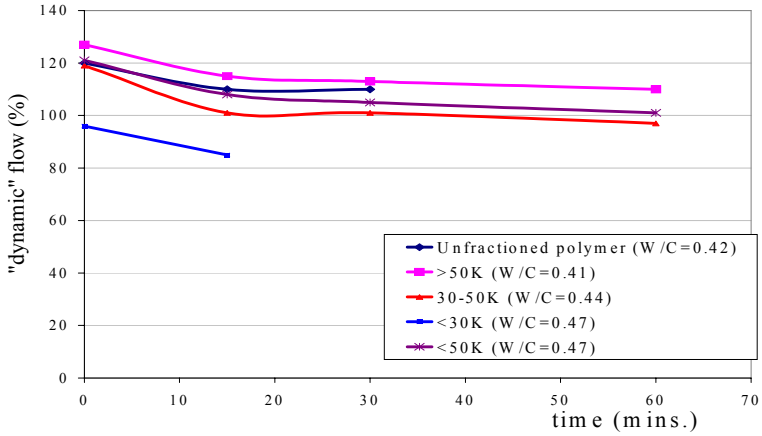

Figure 7a. Mortar tests – cement B – "dynamic" flow

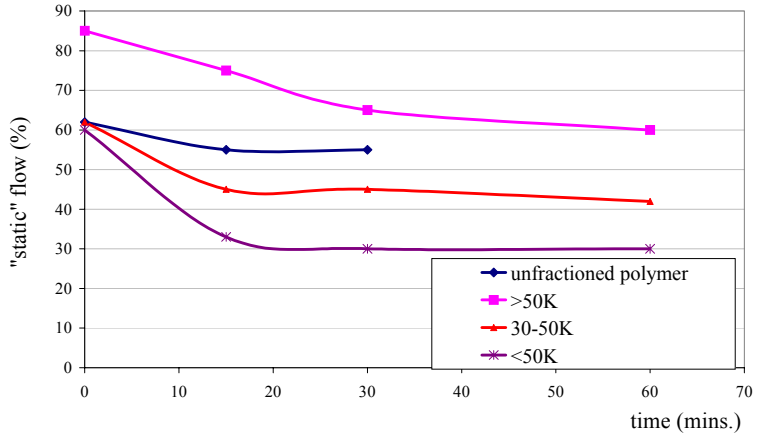

Figure 7b. Mortar tests – cement B – "static" flow

3.4 Adsorption analyses

As shown in Table 5 and Figure 8, in the case of cement A (type II A/L 42,5) the percentage of polymer adsorbed by cement pastes varies from 40 to 63%. The highest molecular weight fraction, >50K Dalton, is adsorbed in higher amount, in the range 55,4-63% within 30 minutes. The fraction lower than 30K Dalton is far less adsorbed (40-42% within the 30 minutes). The adsorption of the unfractioned polymer is exactly in the middle between those of the high and low molecular weight fractions.

For cement B (type I 52,5), adsorption values of the polymer are generally much lower than the previous ones, about half the amount. The lowest molecular weight fractions, which is <30K dialysised and not dialysised, in particular, are only 15% adsorbed, reaching 20% within 30 minutes.

Table 5. Adsorption tests - cement A

	Polymer adsorpted (%)				
Time (mins.)	**all polymer**	**>30K**	**>50K**	**<30K**	**<50K**
1	52.4	54	55.4	39.7	44.1
5	52.9	54.3	57.6	41.2	46.8
10	54.6	57.3	60.8	43.2	46.6
30	56.2	60	63	42.3	47.3

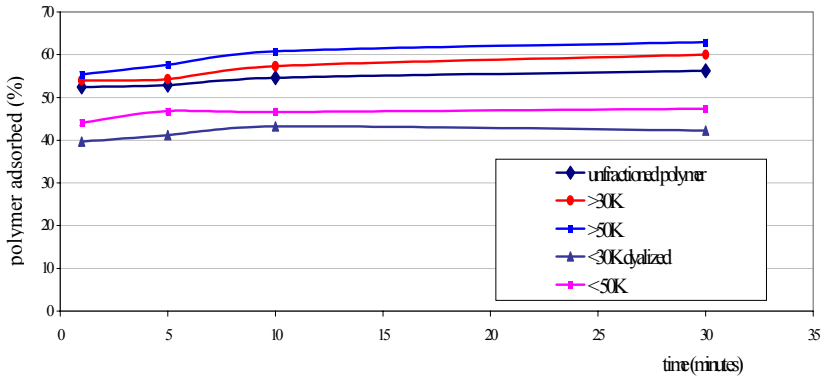

Figure 8. Adsorption values of the different polymer fractions onto cement A (type II A/L 42.5)

Table 6. Adsorption tests - cement B

	Polymer adsorpted (%)				
Time (min.)	**all polymer**	**<30K n.d.**	**<30K D.**	**30-50K**	**>50K**
1	26.7	15.3	14.7	19.6	28.2
5	29.2	19.4	19	26.1	30.9
10	33	19.3	17	27.8	34
30	34.7	19.5	18.9	29.4	41.5

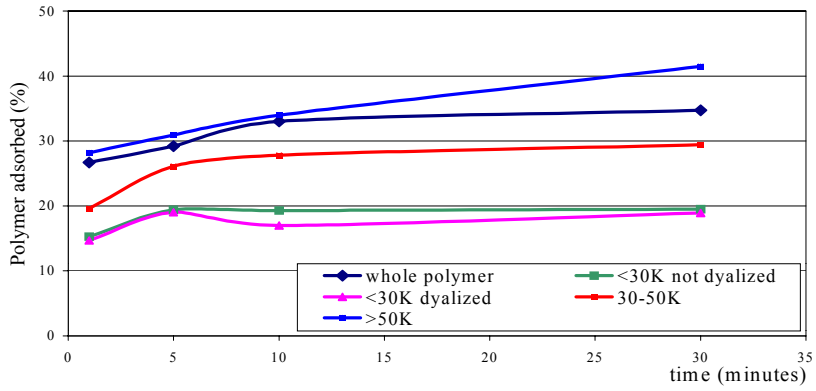

Figure 9. Adsorption values of the different polymer fractions onto cement B (type I 52.5)

In the case of cement B, the differences among the fractions are bigger than for cement A: both initial and final adsorption of the highest fraction are double the amount of the lowest molecular weight fraction. There seems to be a good correspondence, in the sense that the fractions that are adsorbed more, also perform better.

The reason for the much higher adsorption of polymer shown by cement A is not associated with higher surface area: as Table 1 shows, the Blaine value is higher for cement B. The explanation presumably lies in the nature of limestone present in the type II A/L 42,5 cement. Previous studies, performed by our research group (9), revealed how some kinds of limestone, because of their porosity, can bring about a high adsorption of admixture, which is entrapped inside these pores and in this way subtracted from the clinker phases.

4. CONCLUDING REMARKS

The data obtained can be used for an optimisation of polycarboxylate ether admixtures. A displacement towards higher molecular weights and a reduction of low-molecular weight material could, for instance, improve the performances of investigated admixtures. Also elimination of the residue of the polymerization process and of the monomers seems to have a positive effect.

The “static flow” measurement can presumably be applied while conducting mortar tests, to predict admixture behaviour in concrete.

REFERENCES

[1] Rabek, J.F., Experimental methods in polymer chemistry, Wiley & Sons edition, 1980.

[2] Ezrin, M., Polymer Molecular Weight Methods, Advances in Chemistry series, The American Chemical Society, number 125, 1973.

[3] Zhor, J., Bremner, T.W., Influence of ligninsulphonate molecular weight fractions on the properties of fresh cement paste, Industria Italiana del Cemento, n.6/98, pp. 554-565.

[4] Ferrari, G., Basile, F., Dal Bò, A., Mantoni, A., The influence of the molecular weight of beta-naphthalensulfonate based polymers on the rheological properties of cement mixes, Il Cemento, vol. 83, Ott.-Dic. 1986.

[5] Stránel, O., Sebök, T., Relationships between the properties of ligninsulphonates and parameters of modified samples with cement binders, Part. I, Characterizing ligninsulphonates and studying their sorption properties, Cement and Concrete Research, vol. 27, 1997, pp.185-191.

[6] Stránel, O., Sebök, T., Relationships between the properties of ligninsulphonates and parameters of modified samples with cement binders, Part. II, Study of relationships between molar parameters of ligninsulphonates and characteristics of the samples tested, Cement and Concrete Research, vol. 29, 1999, pp. 591-594.

[7] Stránel, O., Sebök, T., Relationships between the properties of ligninsulphonates and parameters of modified samples with cement binders, Part. III, Determination of sulphonated compounds content, characteristic of sulphonation, sorption studies, Cement and Concrete Research, vol. 29, 1999, pp. 1769-1772.

[8] Stránel, O., Sebök, T., Relationships between the properties of ligninsulphonates and parameters of modified samples with cement binders, Part. IV, Influence of sulphonated compounds and sulphonation characteristics on the properties of mortar samples, Cement and Concrete Research, vol. 30, 2000,pp. 511-515.

[9] Torresan, I, Magarotto, R., Zeminian, N., Interaction Between Superplasticizers and Limestone Blended Cements-Rheological Study, Sixth CANMET/ACI, Nice, October 2000.

INFLUENCE OF THE MOLECULAR WEIGHT OF POLYCARBOXYLATE ETHER SUPERPLASTICIZERS ON THE RHEOLOGICAL PROPERTIES OF FRESH CEMENT PASTES, MORTAR AND CONCRETE

R. Magarotto, I. Torresan and N. Zeminian

MAC S.P.A. – Degussa, Treviso, Italy. E-mail: mactv@mac-mbt.com

Ivana Torresan, graduated in Industrial Chemistry at Venice University, Italy, 1988. Since 1988 has worked in the field of concrete admixtures, focusing on the development of new polymeric superplasticizers. Head of the R&D Dept., since 2001, at present Technology Marketing Manager for the Business Line Admixture Systems (Degussa Construction Chemicals) MAC, Modern Advanced Concrete in Treviso (Italy).

Roberta Magarotto, graduated in Industrial Chemistry, Venice University, Italy, 1993. She has been working in the field of concrete admixtures, focusing on the development of new polymeric superplasticizers. At present she is Development Head for the Business Line Admixture Systems (Degussa Construction Chemicals) MAC, Modern Advanced Concrete in Treviso (Italy).

Nicoletta Zeminian, graduated in Industrial Chemistry, Padua University, Italy,1997. Since 1998 she has been working by the Admixture Department for the Business Line Admixture Systems (Degussa Construction Chemicals) MAC, Modern Advanced Concrete in Treviso (Italy), focusing on the development on new formulative admixtures and on the investigation of incompatibility problems between superplasticizers and binders.

EFFECT OF ALKALINE SULPHATES ON THE PERFORMANCE OF SUPERPLASTICIZERS

R. Magarotto, I. Torresan and N. Zeminian

MAC s.p.a. - Degussa, Treviso; E-mail: mactv@mac-mbt.com

ABSTRACT

Polycarboxylate-based superplasticizers (CE) are acquiring increasing importance in the production of concrete since they allow the production of high workability concrete with lower water/cement and reduced slump loss as compared to the old generation superplasticizers like β–naphthalene sulphonate formaldehyde condensate (NS) and melamine formaldehyde condensate. Extensive study is therefore necessary to better understand the mechanism of action of these new types of admixtures and how the composition of cement affects their performance.

In the present study, the effect of alkali sulphates on the interaction between cement and superplasticizer is investigated by means of minislump tests, mortars and adsorption tests, with special reference to an admixture of this new generation.

The data collected reveal that the CE superplasticizer performs in any case better than NS. An increased amount of sodium sulphate leads altogether to a lower adsorption of the CE superplasticizer, together with a reduced performance in terms of water reduction. When it is employed in the presence of added sodium sulphate, the performances of a CE superplasticizer become closer to those of NS.

No effect is observed on the maintenance of workability.

The performance of an NS type admixture is almost independent from the alkali sulphate addition, at least up to 1% sodium sulphate.

Keywords: superplasticizer, high performance concrete, alkali sulphates, mortar, adsorption

1. INTRODUCTION

The performance of superplasticizers depends to a great extent on the cement they act on. It is important to identify which variables in a cement composition affect more the interaction with the admixture (1). Previous investigations pointed to the C_3A content, calcium sulphate amount and its nature (anhydrite, emihydrate, bihydrate). Each of these factors contributes presumably to the performance of the superplasticizer. Among the others, soluble sulphates, i.e. alkaline sulphates contained in cement have been found to be very important and will be investigated in this paper.

Alkali sulphates, which form during Portland cement production in the clinkerization phase, are the most soluble of the sulphates contained in cement; together with calcium sulphate, added as a set regulator, they provide the sulphate ions necessary for the reaction with C_3A in the early stages of cement hydration.

The standard specification for cement EN 197/1, states that total sulphates, expressed as SO_3, must not exceed 3,5% for a type II A/L cement and 4.0% for a type I; however, no explicit mention is made of the acceptable amount of soluble alkali.

ASTM C 150-94, on the other hand, suggests, among additional requirements for cement, an equivalent alkali content not exceeding 0.6% but such indication has no mandatory value.

Analyses undertaken in the present study show that a wide range of variability exists among different cements regarding the content of sodium and potassium sulphates.

The nature and concentration of soluble species in cement, which dissolve soon after coming into contact with water containing the superplasticizer, is particularly important because they determine the environment in which the first stages of cement hydration occur (3a, 3b). They influence the rate of reaction and the morphology of the products formed and thus the properties of concrete.

Soluble sulphates can react with C_3A to form different products. According to Aïtcin (2), it is not the total amount of SO_3 in cement that is important, but rather the availability, or the rate of dissolution of SO_4^{2-} ions.

Some previous studies have focused on the effect of alkali sulphates on the interaction between cement and an NS admixture. Nawa (4) states that the viscosity reduction performed by the NS superplasticizer is due to its adsorption on C_2S and C_3S phases, although it tends to be easily adsorbed on C_3A and C_4AF. An increase in alkali sulphates reduces viscosity of cement pastes because they reduce the adsorption on C_3A and C_4AF and increase the one on C_2S and C_3S phases. A too high increase in soluble sulphates produces a negative result, since it brings about a compression in the electrical double lawyer, increasing viscosity. There is, therefore, an optimum amount of such compounds in cement.

Jiang (5), while investigating incompatibility between sodium β–naphtalene sulfonate polymers and cement, states that the ideal amount of soluble alkali is 0,4-0,5% (expressed as equivalent sodium), both for initial flowability and for slump retention.

The effect of alkali sulphates is presumably associated with polymer adsorption and desorption phenomena: an increase of alkali, simulated by means of KOH additions as in Diamond's work (6) produces as effect the partial desorption of NS polymer, associated with a total dissolution of anhydrite.

Most of the previous works have focused on β–naphtalene sulfonate based polymers. A work has recently been published (7), regarding the effect of sulphates on the fluidity of cement pastes added with polycarboxylic acid type superplasticizer: the authors have found that the viscosity of paste is increased and the amount of adsorbed admixture is decreased by addition of sodium sulphate.

In the present study, the effect produced by sodium sulphate additions on the rheological properties of mortars, in the presence of a superplasticizer, is investigated.

The aim of the work on the new superplasticizers, based on polycarboxylate polymers, is to undertake an investigation similar to that previously conducted on NS polymers, in order to clarify whether the alkali sulphate contents are responsible for the unexpected behaviour that is sometimes experienced with certain cement-plasticizer combinations, despite the fact that both components satisfy their respective acceptable requirements.

Two superplasticizers were examined: a traditional one, i.e. a β-naphtalene sulfonate formaldehyde condensed (NS) and a new generation one (CE), based on a polycarboxylate ether polymers.

2. EXPERIMENTAL

2.1 Materials employed

Nine different Italian commercial cements were investigated (A to I); five type II A/L 42.5 (A to E) and four type I 52.5 (F to I) cements (EN 197/1).

The cements were chemically analysed with respect to their total sulphate and total alkali content, by means of a flame photometer, according to EN 196/2. Soluble sulphates and soluble alkalis were also determined, by means of ionic chromatography.

The results are reported in Tables 1 and 2.

Four of the previous cements, the one with the highest and the one with the lowest alkali sulphate contents, both among the type I 52.5 and among the type II A/L 42.5 cements, have been intensively investigated. Their complete chemical analysis has been carried out according to the methods reported in EN 196/2 and is reported in Table 3.

Table 1. Alkali and sulphates (total and soluble) content of the cements employed

	total sulphates (% SO_3)	**soluble sulphates (% SO_3)**	**Na_2O eq.tot.**	**$Na_2O_{eq.sol.}$**
Type II A/L 42.5 cements				
Cement A	2.73	2.28	0.94	0.69
Cement B	2.42	1.91	0.87	0.57
Cement C	2.50	2.17	0.65	0.43
Cement D	2.21	1.90	0.68	0.26
Cement E	2.94	2.08	0.84	0.61
Type I 52.5 cements				
Cement F	3.62	3.13	0.97	0.82
Cement G	3.14	1.86	0.81	0.58
Cement H	2.64	1.96	0.68	0.44
Cement I	2.89	2.58	1.00	0.65

Table 2. Sodium and potassium (total and soluble) content of the cements employed

	Total Na_2O (%)	**total K_2O (%)**	**soluble Na_2O (%)**	**Soluble K_2O (%)**
Type II A/L 42.5 cements				
Cement A	0.28	1.01	0.11	0.88
Cement B	0.38	0.73	0.16	0.63
Cement C	0.19	0.70	0.05	0.58
Cement D	0.38	0.46	0.09	0.25
Cement E	0.28	0.85	0.13	0.72
Type I 52.5 cements				
Cement F	0.31	1.13	0.13	1.05
Cement G	0.26	0.83	0.10	0.73
Cement H	0.20	0.73	0.05	0.59
Cement I	0.47	0.81	0.19	0.70

2.2 Test procedures

Mortars were prepared with all the nine cements studied, according to EN 196/1, in the presence either of NS or of CE superplasticizers. CE was dosed at 0.25% active bwc., NS 0.40% active bwc., which are the dosages usually applied in practice in concrete production.

These mortar tests were made in the attempt to see if a correlation exists between the alkali sulphate content of these cements and their interaction with the admixtures. Results are reported in Figs.1a, 1b for the CE admixture and Figures.2a and 2b for NS.

Four cements mentioned before, namely cement A, D, F and H, were selected for rheological evaluation in cement pastes. Samples A and F represent cements that are very rich in alkali sulphates, type II A/L 42.5 and I 52.5 respectively, while D and H have the lowest amount of such components.

The rheological evaluations of cement pastes were undertaken through the empirical minislump test: the paste was poured, after mixing, into a metallic truncated cone mould standing on a flat plexiglass surface. The cone was then lifted and the diameter of the collapsed paste measured.

Both with CE and with NS superplasticizer (0.25% and 0.40% active dosage bwc. respectively), the minislump tests were made first without addition and then adding sodium sulphate in amounts varying from 0.5 to 2.0% bwc.

Results of the minislump tests are reported in Figures 3a, 3b, 3c and 3d.

The four cements selected were later used for the preparation of mortars with NS and CE admixtures, in which a percentage of cement of 0.5 % was substituted with an equal amount of sodium sulphate of pure reagent degree. Flow values of such mortars, determined in accordance with UNI 7044/72, are reported in Figures 4a and 4b.

The degree of adsorption onto cement of the polycarbolylate-based (CE) admixture and of the β-naphtalensulphonate-based (NS) one was determined in cement pastes by T.O.C. analyses performed with a Shimadzu 5000-A. Both the superplasticizers were dosed at 0.25% dry content by cement weight. The water/cement ratio was kept constant at 0.50.

The samples were prepared according to the following procedure: the cement and the water containing the superplasticizer were stirred for the defined time and then filtered in a büchner with a vacuum pump. The amount of polymer adsorbed was determined by the difference between the organic carbon originally contained in the polymer solution and the amount left in the solution filtered from the paste.

Such evaluations were undertaken on cement pastes with and without the addition of sodium sulphate (0,5% bwc.). Cements A, D, F and H were employed also for T.O.C. analyses.

The results of such evaluations, expressed as percentage of polymer adsorbed, are reported in Tables 4a and 4b.

Table 3. Chemical analysis of cements

	Cement A	Cement D	Cement F	Cement H
free CaO	1.0	0.7	0.7	0.74
I.R.	3.0	2.0	0.6	0.7
L.O.I.	3.9	6.7	1.2	3.0
SiO_2	21.1	19.7	19.6	20.9
Al_2O_3	6.2	4.4	6.3	4.6
Fe_2O_3	2.7	2.7	2.1	2.2
CaO	61.0	62.1	63.3	64.8
MgO	1.4	1.1	0.85	1.58
SO_3	2.7	2.2	3.6	2.6
Na_2O	0.28	0.38	0.31	0.20
K_2O	1.0	0.46	1.1	0.73

3. RESULTS

3.1 Analysis

The values reported in Tables 1 and 2 show that the nine cements examined, contain different amounts of soluble alkali sulphates. Actually, all the cements exceed the 0.6% content of alkali suggested by ASTM C 150-94. Among the type II A/L 42.5 cements (A to E), cement D contains the lowest percentage and A and E the highest amount of alkali sulphates; a comparison between the last two deserves a note: E contains more total sulphates, but A has more soluble sulphates, i.e. alkali sulphates.

Among type I 52.5 cements, the differences between the four samples considered are even higher: cement H has very low alkali sulphates content and cement F a very high content.

3.2 Mortar tests of all the nine cements

Figures 1a and 1b show the flow values of mortars made with 9 cements and CE superplasticizers at 30-minutes intervals. Comparison of data reported in Tables 1a, 1b, 2a and 2b suggests that a kind of correlation exists between the rheological behaviour and the alkali sulphate contents. The initial flow seems lower in cements with higher alkali sulphate (i.e. soluble sulphates and soluble alkali). This trend is shown both by the type II A/L 42.5 cements (Figure1a) and by the I 52.5 cements (Figure 1b).

Variations in alkali sulphates, which are more soluble, are presumably more important than total sulphates in determining the flowability. This is suggested by the better performance of cement E with respect to cement A.

The results reported in Figures 2a and 2b with NS superplasticizer don't show any correspondence between alkali sulphate contents and flowability.

In order to confirm that a reduction of the performance of a CE admixture can be brought about by an excess of alkali sulphates, further investigations were performed on the cements A, D, F and H, both in cement pastes (minislump tests) and in mortar.

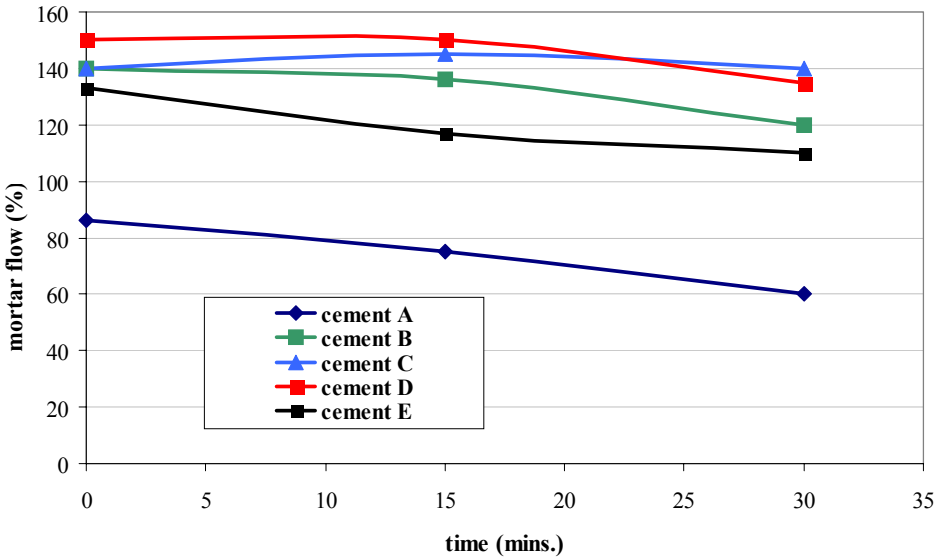

Figure 1a. Mortar flow results- cements type II A/L 42.5 – CE admixture (W/C=0.43)

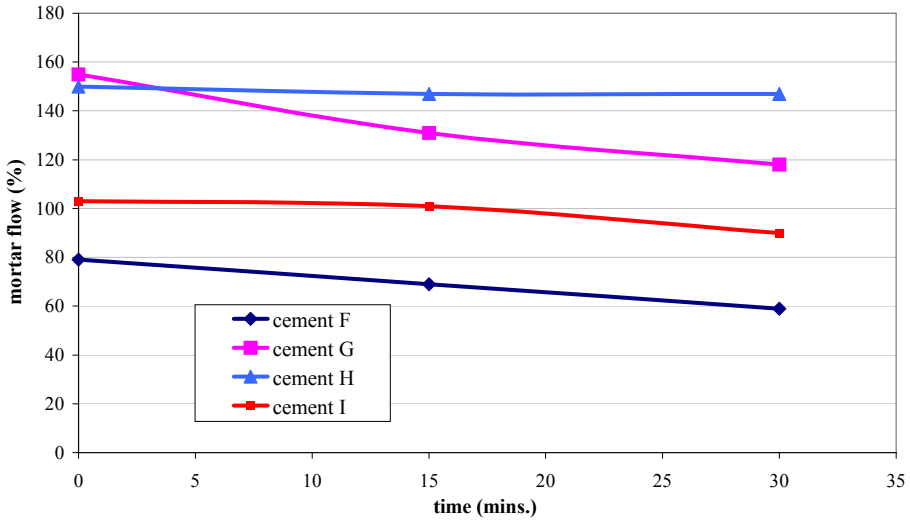

Figure 1b. Mortar flow results – cements type I 52.5 – CE admixture (W/C=0.40)

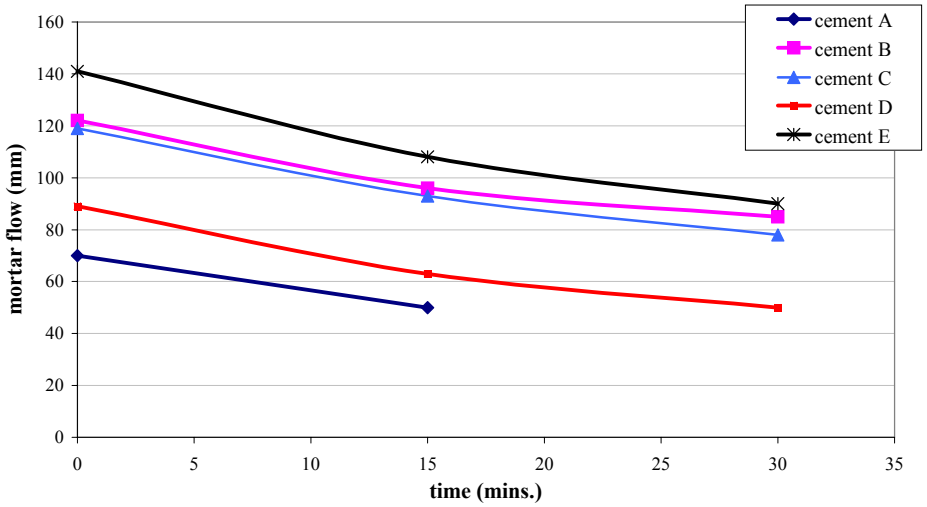

Figure 2a. Mortar flow results – cements type II A/L 42.5 – NS admixture (W/C=0.47)

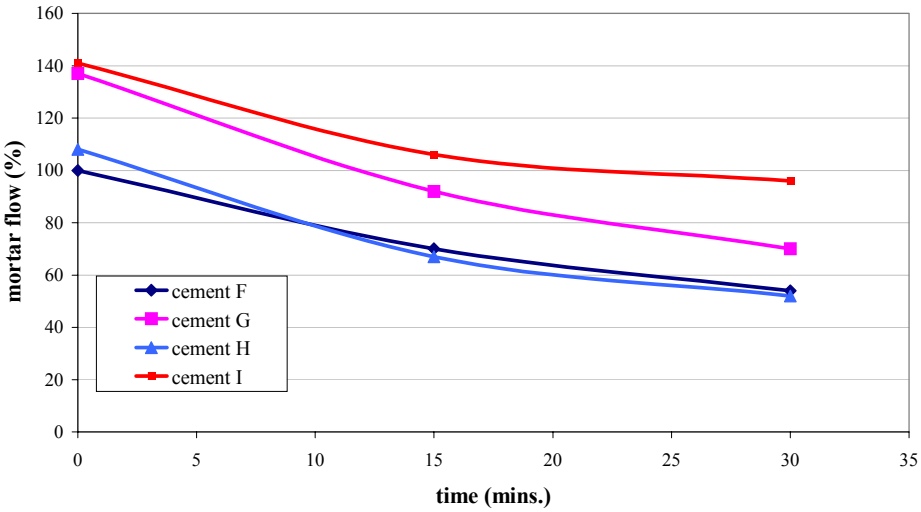

Figure 2b. Mortar flow results – type I 52.5 cements – NS admixture (W/C=0.47)

3.3 Minislump tests

Figures. 3a, 3b, 3c and 3d show the results of the minislump tests carried out on cements A, D, F, and H. Cement A, which is very rich in soluble sulphates shows a considerable reduction of the minislump with CE superplasticizers as a consequence of addition of sodium sulphate, 14% reduction by 0,5% addition and 33% reduction by 2% Na_2SO_4 addition. When NS is employed, no variation of minislump diameter is detected up to 1% addition, and 14% reduction is observed with a 2% addition. Since the W/C ratio was a little different with the two admixtures, a trial was made for cement A and F to change the dosage of NS or CE in order to get the same W/C ratio for the two. No change was detected in the result.

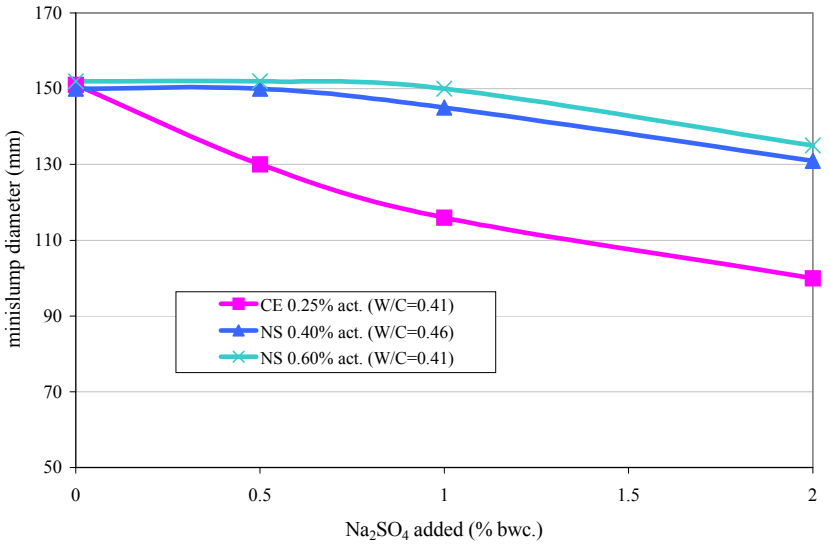

Figure 3a. Results of minislump rheological tests – cement A

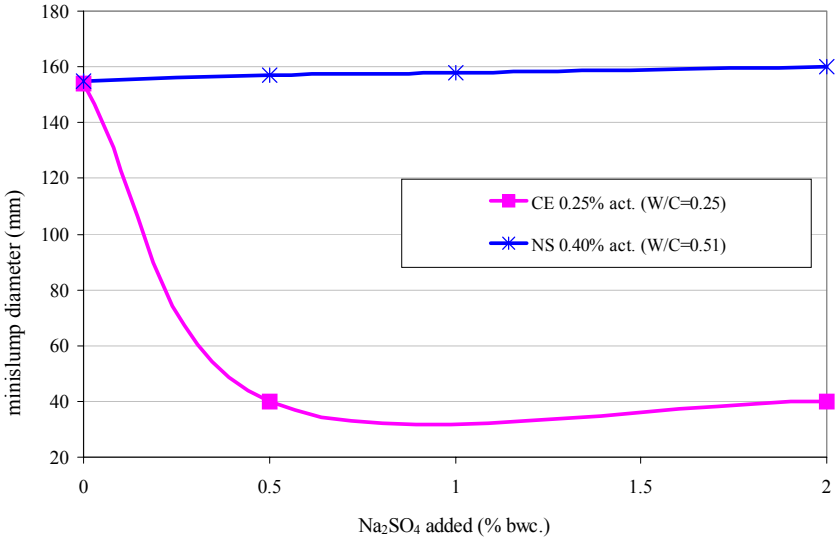

Figure 3b. Results of minislump rheological tests – cement D

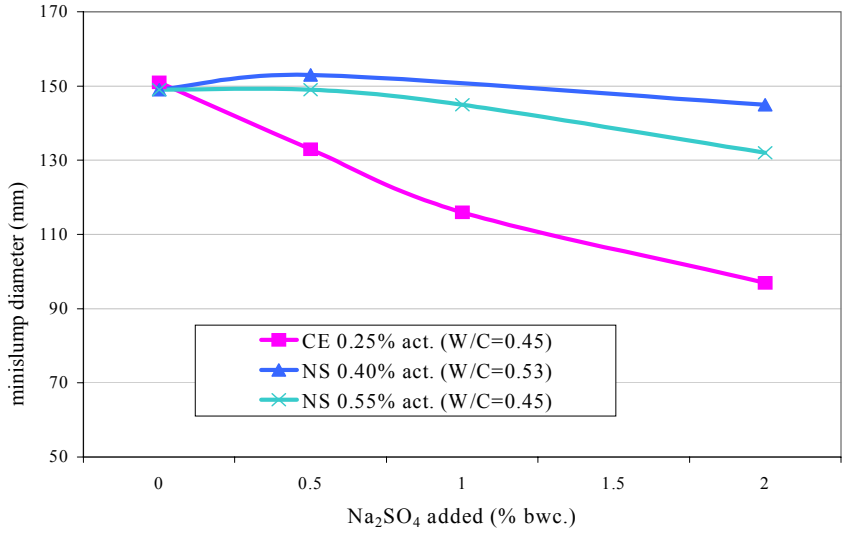

Figure 3c. Results of minislump rheological tests – cement F

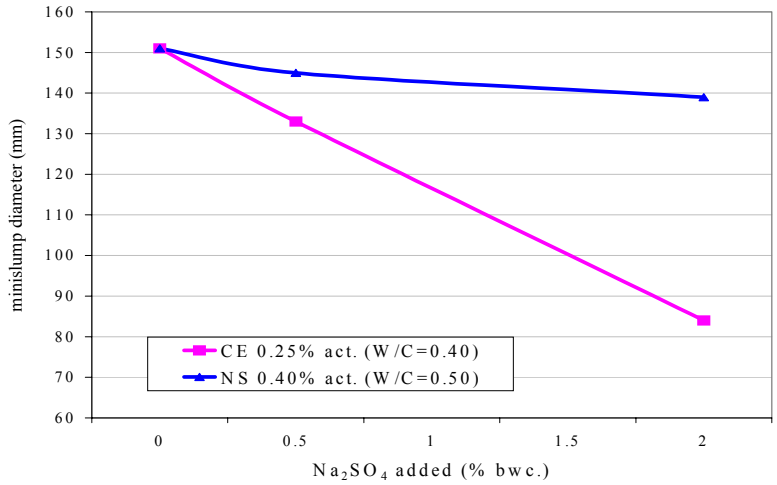

Figure 3d. Results of minislump rheological tests – cement H

3.4 Mortar tests on cements A, D, F and H with sodium sulphate addition

Mortar tests give a lot of information on the rheological effect of alkali sulphates, and the situation they depict is practically closer to the real one in concrete with a plasticizer.

Figures 4a and 4b confirm that a reduction of the performance of a CE admixture can be brought about by an excess of alkali sulphates. The addition of sodium sulphates in percentage of 0.5 % causes little or no variation in the initial flow when a NS admixture is used while in the case of a CE admixture the negative effect is particularly high.

It's worth noting that the addition of 0.5% sodium sulphate corresponds to a variation of alkali sulphates in the cement of 0.21%, if expressed as sodium equivalent content (Table 1), which is well the difference between some of the cements, for example G and I.

The negative influence of an increase in soluble alkali sulphates is not observed in the workability retention: the loss of workability is basically the same in all the tests undertaken.

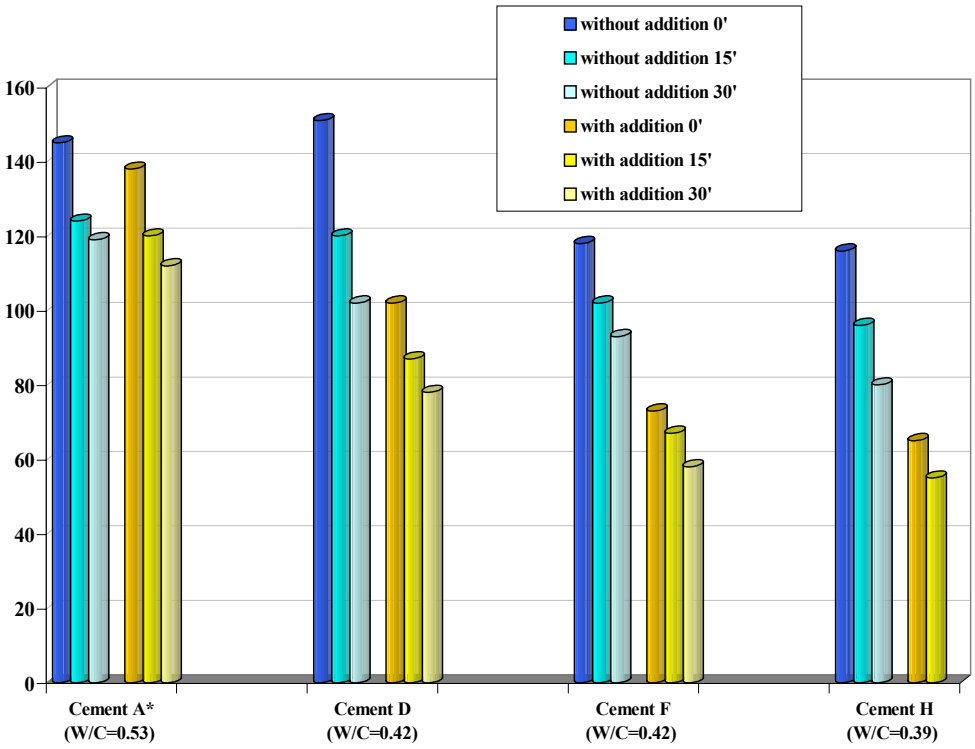

*= presence of some bleeding - not reliable test

Figure 4a. Mortar flow results (%) – CE admixture

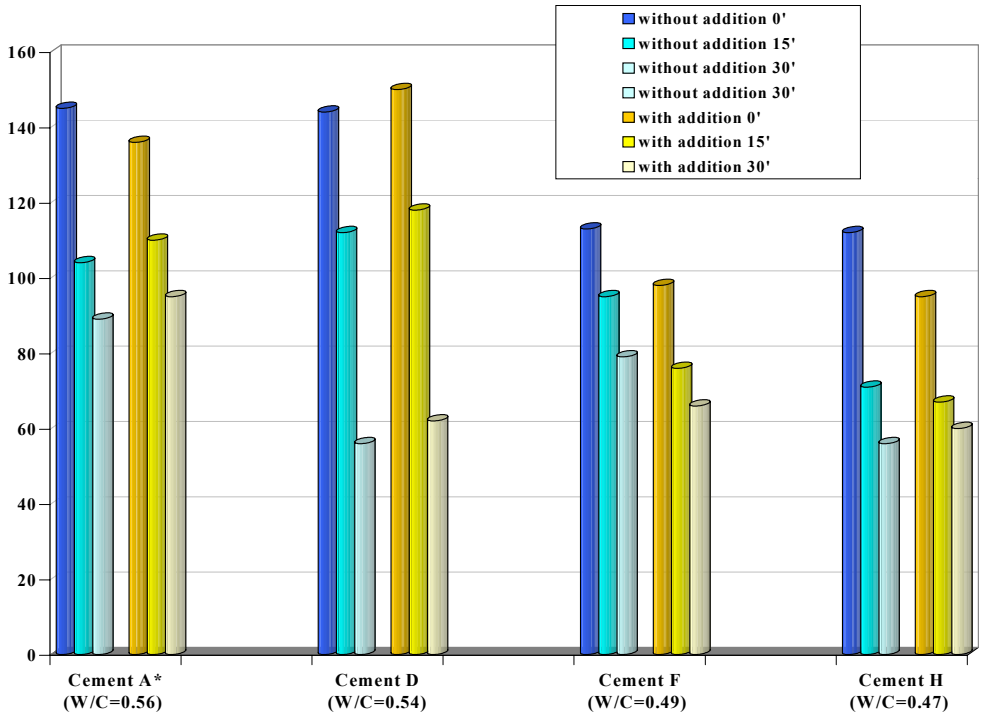

*= presence of some bleeding

Figure 4b. Mortar flow results (%) – NS admixture

3.5 Adsorption measures

Adsorption tests (Figure 3) illustrate how the addition of sodium sulphate brings about a reduction in the sorption capability of cement towards CE admixture. The lower adsorption of plasticizer evidently reflects a reduced interaction between the cement particles and the admixture, and, therefore, a diminished plasticizing effectiveness.

It may be concluded that sodium and potassium sulphate contents can have a strong negative effect on the performance of a superplasticizer, specially a CE type, with reference to water reduction.

Such values should therefore be checked, whenever incompatibility phenomena between cement and the plasticizer occur.

Table 4a. Polymer adsorption onto cement – CE admixture
dos.: 0.25% act. bwc.; W/C=0.50

	Polymer adsorbed (%)						**% reduction of adsorbtion due to sulphate addition**		
	without addition			**with 0.5% bwc. Na_2SO_4 added**					
	1'	**15'**	**30'**	**1'**	**15'**	**30'**	**1'**	**15'**	**30'**
cement A	48.0	51.9	52.3	38.0	40.9	43.3	21	21	17
cement D	57.5	62.5	61.7	46.9	54.8	51.7	18	12	16
cement F	35.7	40.6	41.4	27.6	37.5	39.8	23	8	4
cement H	36.8	42.6	44.1	28.2	28.5	28.4	23	33	36

Table 4b. Polymer adsorption onto cement – NS admixture
dos.: 0.40% act. bwc.; W/C=0.50

	Polymer adsorbed (%)						% reduction of adsorbtion due to sulphate addition		
	without addition			with 0.5% bwc. Na_2SO_4 added					
	1'	15'	30'	1'	15'	30'	1'	15'	30'
cement A	61.1	68.6	67.4	56.2	64	64	8	7	5
cement D	85.7	90.7	90.9	74.9	83.8	84.9	13	8	7
cement F	68.8	75.2	78.1	58.3	66.5	69.4	15	11	11
cement H	77.3	85.8	88.1	70.3	77.5	79.9	9	10	9

4. CONCLUDING REMARKS

From the above experimental results, the following conclusions can be drawn:

1. Commercial cements available on the Italian market, both for type I and for Type II A/L cements, show a wide range of variability in the amount of alkali sulphates.
2. A traditional β–naphtalene sulfonate admixture does not seem to be significantly influenced by an increase in the alkali sulphate content up to a 1.0% addition. A CE admixture is strongly affected by the increase of alkali sulphates dissolved. Reduced performances in terms of water demand are shown both in cement pastes and in mortars.
3. No effect of the sodium sulphate amount on workability retention is observed with NS or with CE admixture.
4. There seems to be an ideal alkali sulphate content of cements for their interaction with this new, high performance, generation of superplasticizers.
5. In the case of cements rich in alkali sulphates, the early stages of hydration occur in a solution that is, presumably, not balanced for what concerns dissolved sulphates when a CE superplasticizer is used. The amount of alkali sulphates in a cement seems to be a potential source of incompatibility between cement and polycarboxylate-based superplasticizers.

REFERENCES

[1] Tagnit-Hamou, A., Aïtcin, P.C., Cement and superplasticizer campatibility, World Cement, August 1993, pp.38-42.

[2] P.C. Aïtcin, C. Jolicoeur and J. G. MacGregor, Superplasticizers: How They Work and Why They Occasionally Don't, Concrete International, May 1994, pp. 45-52.

[3] (3a) Inam Jawed and Jan Skalny, Alkalies in cement: a review. II: Effects of Alkalies on hydration and Performance of Portland Cement, Cement and Concrete Research, Vol. 8, 1978, pp. 37-52.

[3] (3b) Inam Jawed and Jan Skalny, Alkalies in cement: a review. I: Forms of Alkalies and their effect on clinker formation, Cement and Concrete Research, Vol. 7, 1977, pp. 719-730.

[4] T. Nawa, H. Eguchi and Y. Fukaya, Effect of Alkali Sulphate on the rheological Behavior of Cement Paste Containing a Superplasticizer, Ottawa Conference, 1989, ACI SP- 119-21, pp. 405-424.

[5] Shiping Jiang, Byung-Gi Kim, Pierre-Claude Aïtcin, Importance of adequate soluble alkali content to ensure cement/superplasticizer compatibility, Cement and Concrete Research, Vol. 29, 1999, pp. 71-78.

[6] Sidney Diamond and Keisuke Matsukawa, Unexpected Release and Re-Sorption of Superplasticizer, Mario Collepardi Symposium on Advances in Concrete Science and Technology, Editor Mehta, 1997, pp. 315-329.

[7] Akira Ohno and Takanori Yamamoto, Fluidity of various cement pastes added polycarboxylic acid type admixture, JCA Proceedings of cement & concrete, N°. 51, 1997.

EFFECT OF ALKALINE SULPHATES ON THE PERFORMANCE OF SUPERPLASTICIZERS

R. Magarotto, I. Torresan and N. Zeminian

MAC s.p.a. - Degussa, Treviso; E-mail: mactv@mac-mbt.com

Ivana Torresan, graduated in Industrial Chemistry at Venice University, Italy, 1988. Since 1988 has worked in the field of concrete admixtures, focusing on the development of new polymeric superplasticizers. Head of the R&D Dept., since 2001, at present Technology Marketing Manager for the Business Line Admixture Systems (Degussa Construction Chemicals) MAC, Modern Advanced Concrete in Treviso (Italy).

Roberta Magarotto, graduated in Industrial Chemistry, Venice University, Italy, 1993. She has been working in the field of concrete admixtures, focusing on the development of new polymeric superplasticizers. At present she is Development Head for the Business Line Admixture Systems (Degussa Construction Chemicals) MAC, Modern Advanced Concrete in Treviso (Italy).

Nicoletta Zeminian, graduated in Industrial Chemistry, Padua University, Italy, 1997. Since 1998 she has been working by the Admixture Department for the Business Line Admixture Systems (Degussa Construction Chemicals) MAC, Modern Advanced Concrete in Treviso (Italy), focusing on the development on new formulative admixtures and on the investigation of incompatibility problems between superplasticizers and binders.

THE INFLUENCE OF HIGH VOLUMES OF PFA ON THE WORKABILITY OF PASTES

Jan H C Pretorius[1] and Elsabe P Kearsley[2]

[1] Duraset Mining Products, Westonaria, South Africa.
E-mail: janpreto@postino.up.ac.za
[2] Department of Biosystems and Civil Engineering, University of Pretoria, Pretoria, South Africa.
E-mail: elsabe.kearsley@eng.up.ac.za

1. INTRODUCTION

In this study five different types of Pulverized Fuel Ash (PFA) from the same source were assessed and their influence on concrete properties investigated. The properties of the PFA-types were first determined to quantify their differences. Thereafter they were incorporated into concrete mixtures and their effects tested in terms of workability and compressive strength. To study the effect of PFA-type on mortar properties, tests were also conducted on pastes containing only PFA and cement. The effect of the PFA was enhanced by replacing up to 67% of the cement with PFA.

2. BACKGROUND

PFA is a byproduct of coal combustion and has been used as a cement-replacement material for a number of years. Partial replacement of cement in concrete by PFA is believed to influence the properties of the wet slurry as well as the hardened concrete mortar. Researchers have shown that the workability as well as later strength and durability of concrete can be improved by this partial replacement [1].

Figure 1 shows a schematic diagram of five different fractions of PFA marketed by Ash Resources and produced at the Lethabo power station, which is situated near Sasolburg, South Africa and produces around 5.3 million tons of PFA annually [2]. For the purpose of this paper, the different PFA-types are numbered A to E as indicated in Figure 1.

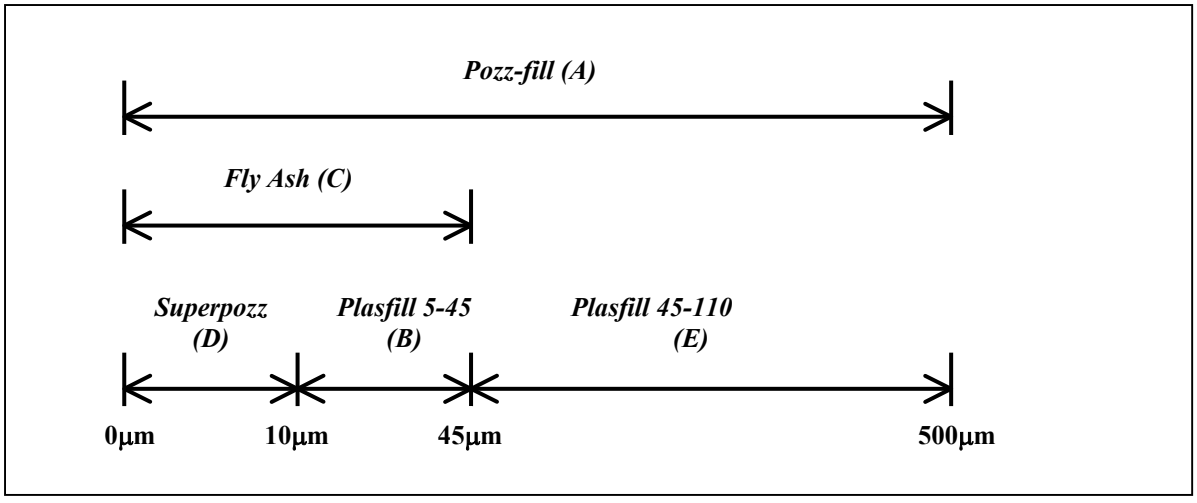

Figure 1. Five different types of PFA from Lethabo power station.

Proceedings of the 11th International Congress on the Chemistry of Cement (ICCC)
'Cement's Contribution to the Development in the 21st Century'
Hosted by: The Cement and Concrete Institute of South Africa
CD-ROM produced by: Document Transformation Technologies
11 - 16 May 2003, Durban, South Africa
ISBN Number: 0-9584085-8-0
Editors: Dr G. Grieve and G. Owens
Congress Organised by: Event Dynamics

3. MATERIAL PROPERTIES

The PFA fractions were obtained from the Lethabo power station and were collected from different stages in the classification process. Particle size distribution curves are shown in Figure 2 as determined using a Malvern apparatus. Chemical analyses were performed by means of X-ray fluorescence. Results are shown in table 1 and indicate no major differences in chemical composition between PFA-types. The effect of variation in chemical composition was thus minimized in this investigation.

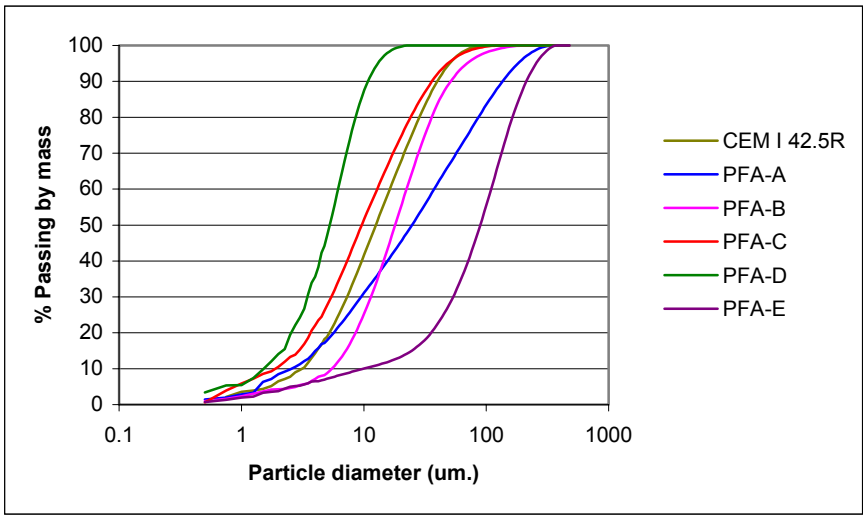

Figure 2. Particle size distribution curves of cement and PFA.

Table 1. Chemical analyses of cement and PFA samples.

%	CEM I 42.5R	PFA-A	PFA-B	PFA-C	PFA-D	PFA-E
SiO_2	21.3	54.9	55.9	54.1	51.0	55.6
TiO_2	0.29	1.55	1.54	1.6	1.74	1.47
Al_2O_3	4.07	31.5	31.1	32.4	34.2	29.9
Fe_2O_3	1.96	3.34	3.07	3.13	3.11	4.00
MnO	0.21	0.03	0.03	0.03	0.03	0.03
MgO	1.82	1.16	1.06	1.18	1.39	1.17
CaO	65.2	4.69	4.20	4.52	4.88	5.33
Na_2O	0.27	0.24	0.27	0.26	0.25	0.22
K_2O	0.42	0.63	0.65	0.68	0.72	0.60
P_2O_5	0.05	0.37	0.30	0.43	0.68	0.31
Cr_2O_3	<0.01	0.03	0.04	0.04	0.04	0.03
NiO	<0.01	<0.01	<0.01	<0.01	<0.01	<0.01
V_2O_5	<0.01	0.03	0.02	0.03	0.03	0.02
ZrO_2	<0.01	0.05	0.05	0.06	0.05	0.05
LOI	2.57	0.21	-0.22	0.10	0.24	0.22
TOTAL	98.1	98.8	98.1	98.5	98.4	99.0

Relative densities of the PFA-types were determined [3] and it was found that values differed significantly and that these differences may be related to particle size as shown in Figure 3.

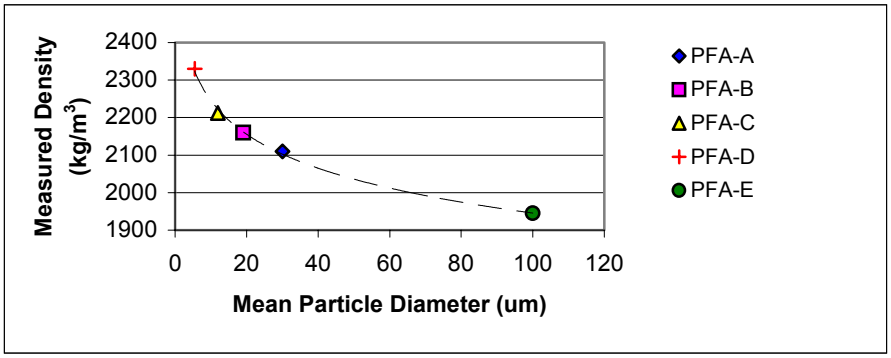

Figure 3. Density as a function of mean particle diameter for the different PFA-types.

In this investigation the PFA was blended with a CEM I 42.5R with a particle size distribution and chemical composition as indicated in Figure 2 and table 1 respectively. Oven dried crushed dolomite was used as aggregate in concrete tests.

4. CONCRETE TESTS

Three sets of mixtures with compositions as indicated in table 2 were cast. The first mixture was a standard containing cement, sand, stone and water. In the second mixture 30% cement was replaced with PFA and in the third 15% of cement was replaced and the cementitious content was further extended by 15%. By replacing and extending it was assumed that 50% of the PFA would act as binder and the other 50% as inert filler. The water content was kept constant for all mixtures. The mixtures containing PFA were cast using each of the five different types of PFA (A to E).

Table 2. Mix proportions (kg/m^3).

Mix no.	Cement (kg)	Pfa (kg)	Sand (kg)	Stone (kg)	Water (L)	Water/binder ratio	Water/cement ratio
1	300	0	1080	790	225	0.75	0.75
2	210	90	1047	790	225	0.75	1.07
3	256	90	1033	790	225	0.75	0.88

Workability was measured by means of the slump test [4]. Compressive strength measurements [5] were performed on sets of three 150mm cubes at 28 days after curing samples in water at 25°C. The test results obtained from these mixtures can be seen in Figure 4.

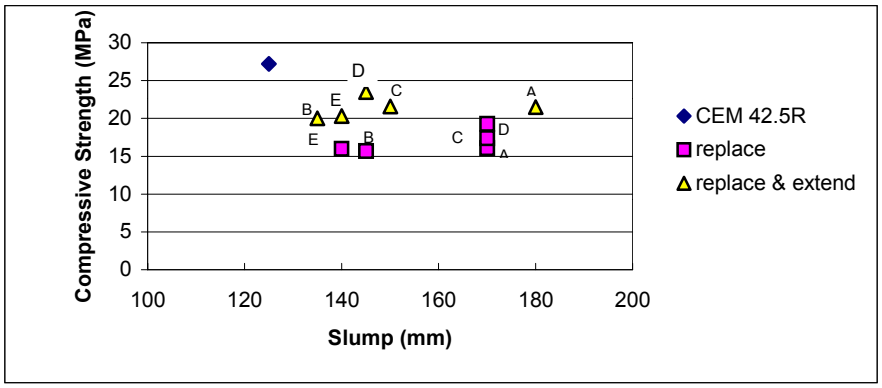

Figure 4. Test results for concrete mixtures.

Although the water content of all mixtures was kept constant the workability of the mixtures (as measured by slump) varied from 125mm for the reference mixture containing no PFA to 180mm for mixture 3 with type A-PFA (replacement and extending). It can thus be concluded that the PFA has a significant influence on workability.

As expected, mixtures containing no PFA had the highest 28-day strength. At later ages the strength difference should reduce or even disappear. It is a well-documented fact that high PFA contents reduce early age strengths, for up to 3 months [1]. Mixtures where 30% of cement was replaced showed slightly lower strengths than mixtures where 15% was replaced. The type of PFA used did not significantly influence the compressive strength of the concrete. It can thus be concluded that the type of PFA used does not affect the strength of the concrete significantly. The strength of the concrete will however be affected if constant workability is required.

5. PASTE TESTS

To establish why the workability of the concrete is affected by the type of PFA used it was decided to concentrate on the properties of the paste used in the concrete. For the rest of the project slurries containing only cement and PFA were compared. To emphasize the effect of the PFA up to 67% of cement was replaced.

Slurries were made containing cement and PFA on their own as well and in blends of 33% cement and 67% PFA. This time the water content was varied for each mix to obtain constant workability. Various researchers have concluded that one-point tests like the slump test are not suitable for measuring workability of mixtures with high PFA contents [6; 7]. Two-point workability tests considered include shear mixers [6], modified slump tests [7] and j-tube tests [8]. The workability test used was the j-tube test, which is used in Japan as a standard test for prestressed concrete grouts [9].

When gravity forces concrete to flow in a vertical tube, the velocity of the concrete in the center of the tube is higher than that for the concrete on the sides. The concrete can be seen as cylinders sliding over one another with radii ranging from r=0 at the center to $r=R_{tube}$ at the inside surface of the tube. The velocity of these cylinders increases quadratically from zero at the sides of the tube to maximum in the center, thus creating intra laminar shear stress between these cylinders. The magnitude of the difference in velocity between the center and the sides of the tube will thus be governed by the intra laminar shear resistance of these cylinders, and this relates back to the viscosity of the concrete.

The test set-up is shown in Figure 5. A tube was mounted onto a load cell connected to a signal amplifier and computer. By using software, it was possible to log the mass loss of the slurry-filled j-tube at time-intervals of 0.1 seconds as the flow proceeded. A shallow bin was put under the lower mouth of the tube to catch the out-flowing slurry. The mouth of the j-tube was cut at an angle of 30° to prevent accumulation of slurry (drag-before-drip effect) before it falls over into the bin as this would result in a step-like flow curve.

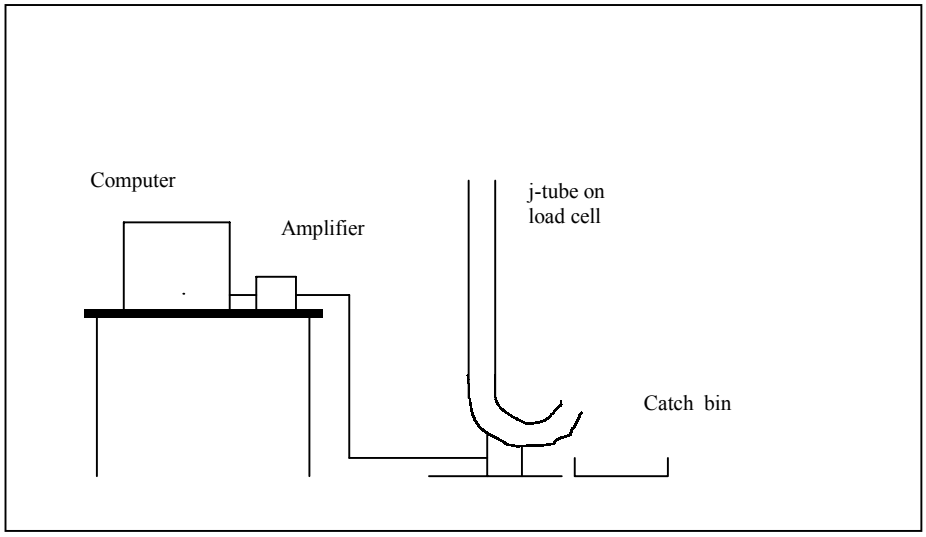

Figure 5. The j-tube apparatus set-up.

A typical flow curve is shown in Figure 6. The results in this graph are for mixtures that differed only in water/binder ratio. As the water/binder ratio of the mixtures is increased, their flow rate also increases resulting in a steeper slope for the mass/time-graph. This relates to a decrease in viscosity. The end height of the slurry in the tube when flow seizes relates to the yield stress of the slurry. The higher the end height the higher the yield stress.

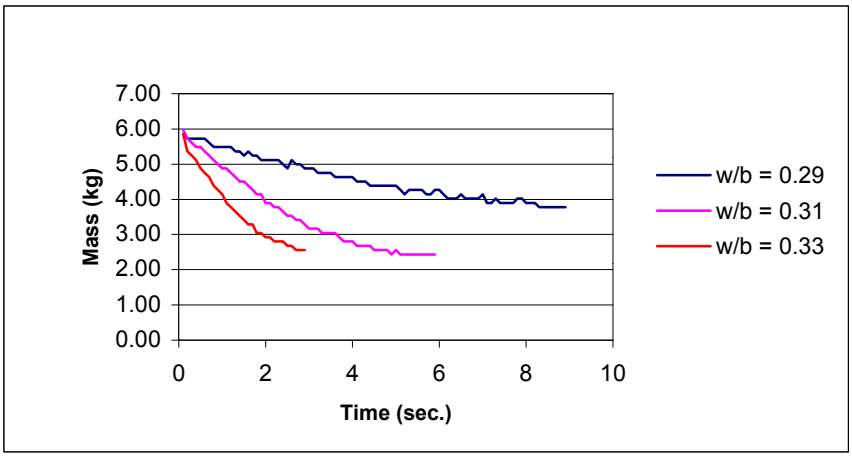

Figure 6. Typical flow curves for the j-tube test.

Shear stress and shear rate values for each time interval were calculated as for capillary viscometers [8; 10]. The average fluid velocity (V) was calculated using the following equation:

$$V = \frac{4Q}{\pi D^2} \tag{1}$$

Where: V = Average fluid velocity (cm/s)
Q = Volumetric flow rate (cm^3/s)
D = Inside diameter of tube (cm)

The shear stress at the tube wall was calculated using the following equation:

$$\tau_w = \frac{D\Delta P}{4L} \tag{2}$$

Where: τ_w = Shear stress (g/cm.s^2)
L = Effective length of tube (cm)
ΔP = Pressure drop due to elevation (g/cm.s^2)

The rate of shear at the tube wall was calculated from the following equations:

$$S = \frac{1+3n}{4n} \times \frac{8V}{D} \tag{3}$$

Where S = Rate of shear (1/s) and;

$$n = \frac{\partial \ln \frac{D\Delta P}{4L}}{\partial \ln \frac{8V}{D}} \tag{4}$$

Concrete is believed to be a Bingham fluid, thus the τ_w versus S plot should be linear with the τ_w-axes intercept value being the yield stress and the slope of the plot the viscosity. Shear stress and shear rate values were calculated and plotted. Figure 7 shows the shear stress versus shear rate plot for the same mixtures shown in Figure 6.

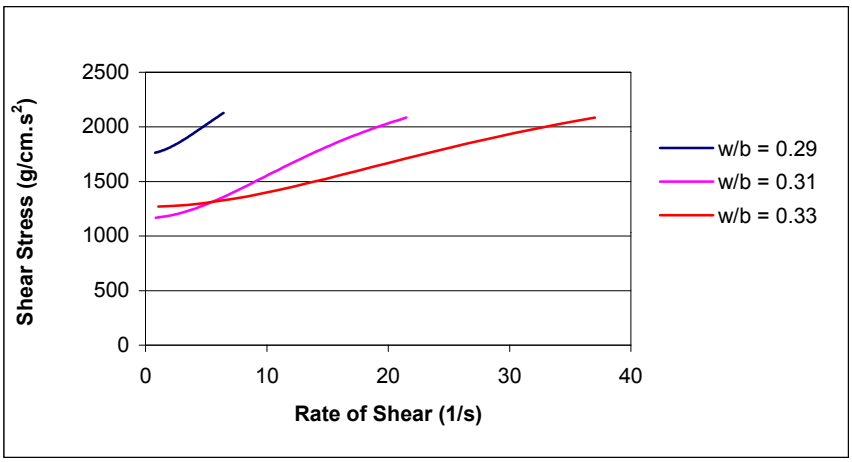

Figure 7. Shear stress versus rate of shear graph.

The workability range for which the test can be used is relatively small. The lower range limit is set by initiation of flow and the upper by maximum shear velocity for transition from laminar to turbulent flow, as the test is only valid for laminar shear flow. The water demand required for each PFA-blend to fall within this workability range differed, thus different water contents were used. For comparative purposes, flow table tests were also performed. Workability results and 28-day compressive strength values are shown in table 3.

Table 3. Results of binder tests.

Mix	Binder type	Water-binder ratio	Flow radius (mm)	Yield stress ($g/cm.s^2$)	Viscosity (cp)	Compressive strength (MPa)
1	PFA A	0.19	-	1195	79	-
2	PFA A	0.21	-	870	49	-
3	PFA A	0.23	-	819	14	-
4	PFA A & Cem I 42.5R	0.27	87	1835	79	40
5	PFA A & Cem I 42.5R	0.28	92	1269	78	39
6	PFA A & Cem I 42.5R	0.29	97	1077	54	35
7	PFA B	0.29	-	1682	67	-
8	PFA B	0.31	-	1072	48	-
9	PFA B	0.33	-	1179	25	-
10	PFA B & Cem I 42.5R	0.30	92	2100	*	30
11	PFA B & Cem I 42.5R	0.31	97	1581	72	29
12	PFA B & Cem I 42.5R	0.33	104	1155	46	25
13	PFA C	0.22	-	1164	86	-
14	PFA C	0.24	-	1029	43	-
15	PFA C	0.27	-	405	13	-
16	PFA C & Cem I 42.5R	0.28	96	1955	134	35
17	PFA C & Cem I 42.5R	0.29	101	1598	100	34
18	PFA C & Cem I 42.5R	0.31	107	1406	72	29
19	PFA D	0.23	-	1505	82	-
20	PFA D	0.25	-	1449	74	-
21	PFA D	0.29	-	1208	6.5	-
22	PFA D & Cem I 42.5R	0.34	100	1909	118	27
23	PFA D & Cem I 42.5R	0.36	106	1407	68	18
24	PFA D & Cem I 42.5R	0.38	107	1314	52	17
25	PFA E	0.28	-	1286	86	-
26	PFA E	0.30	-	876	48	-
27	PFA E	0.33	-	336	18	-
28	PFA E& Cem I 42.5R	0.28	95	1189	56	33
29	PFA E & Cem I 42.5R	0.29	97	916	48	27
30	PFA E & Cem I 42.5R	0.30	110	1098	25	29
31	CEM I 42.5R	0.31	90	2043	61	69
32	CEM I 42.5R	0.32	86	2121	51	69
33	CEM I 42.5R	0.33	93	1670	42	63

* The viscosity of this slurry was too high to determine

In Figure 8 compressive strength results for all mixtures are plotted as a function of water/binder ratio. These results confirm our earlier finding that the strength of mixtures containing high volumes of PFA is influenced by the water/binder ratio and not by the PFA type. If the workability of the mortar is kept constant the water/binder ratio and thus the strength will be influenced.

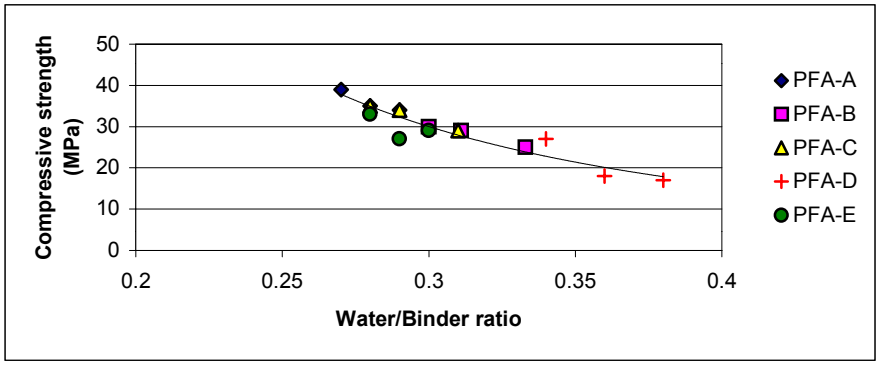

Figure 8. Compressive strength values of cement/pfa mortars.

The effect of water/binder ratio on the flow (as tested by the flow table test) of different types of PFA can be seen in Figure 9. The measured flow radius values for all the mortars varied between 88mm and 110mm. From this graph it can be seen that the water/binder ratio to produce a flow radius of between 100 and 110mm can vary from 0.28 to 0.38 depending on the type of PFA used. The flow characteristics for PFA-types A, C and E are similar, while B has a higher water demand and PFA-D has the highest water demand for a given flow.

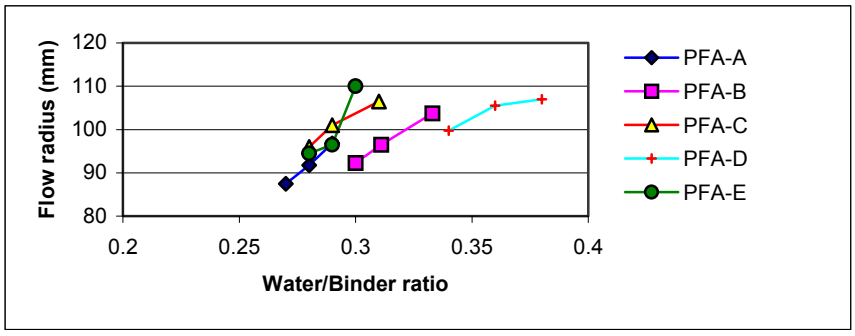

Figure 9. Flow table test results.

The effect of water/binder ratio on viscosity and yield stress of cement/PFA-blend slurries can be seen in Figure 10.

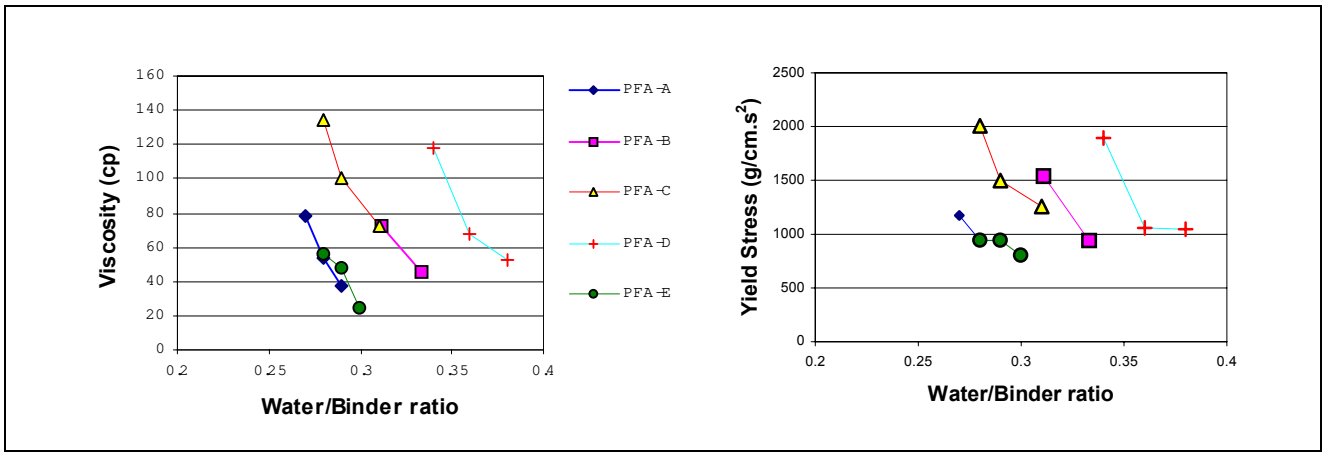

Figure 10. Viscosity and yield stress values for cement/PFA slurries

Figure 10 indicates that the viscosity and yield stress is not only a function of the water/binder ratio but also of the PFA-type used. For a given water/binder ratio the viscosities of PFA-A and E are similar as are the viscosities of PFA-B and C at a higher water/binder ratio. PFA-D requires significantly more water than any of the other PFA-types to produce the same viscosity and yield stress. As there are no significant differences in chemical composition of the five PFA samples the workability must be affected by physical differences.

To establish the effect of particle size on workability, the water/binder ratio needed to produce a viscosity of approximately 50cp was calculated for each of the PFA-types. The effect of PFA-particle size on this calculated water/binder ratio can be seen in Figure 11. The particle size distribution of the PFA-types as shown in Figure 2 was used to determine D50 and D90 values. These values are the particle sizes where 50% and 90% respectively of the particles (per mass) are smaller than the given value.

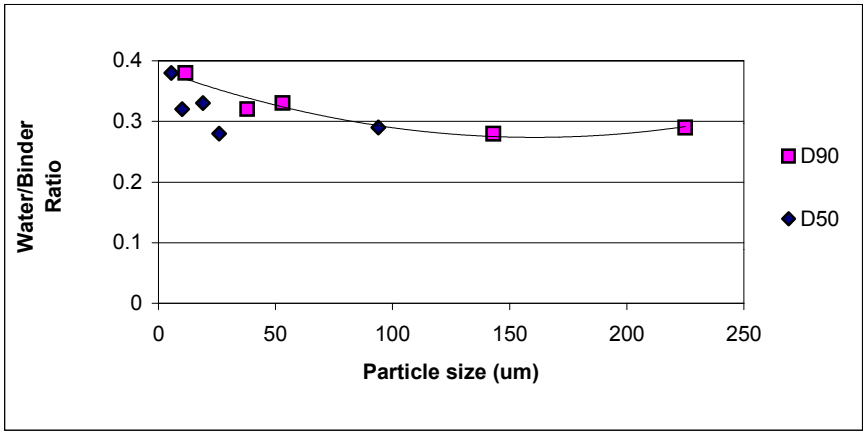

Figure 11. Effect of D50 and D90 on water demand

From Figure 11 it can be seen that there is an optimum water/binder ratio for a D90 value in the region of 150µm. For this cement-type and PFA replacement level the highest compressive strength (for constant workability) will be obtained for PFA where 90% of the particles are smaller than 150µm. These results indicate that for a specific mixture an optimal PFA particle size exists.

6. CONCLUSIONS

The properties of five different PFA-types from the same source were found to differ significantly in terms of particle size and distribution. It was found that their relative densities varied with average particle size from 1.94 for the coarsest fraction to 2.33 for the finest.

Concrete mixtures were made at constant water content. It was found that concrete strength did not differ significantly for PFA-types with only expected variations due to cement replacement and extension. However, a significant variation in workability for different PFA-types was observed.

Further tests on slurries containing high volumes of PFA were also performed. The j-tube test proved to be rather sensitive and differences in workability at very small water/binder ratio increments could be observed. Different water contents had to be used for different PFA-types to fit into the workability range of the test method. It was again found that water/binder ratio was the main contributing parameter to compressive strength.

The physical properties of PFA have an influence on concrete workability. This influence will also reflect on strength when constant workability is desired due to water demand. For a given cement and PFA-replacement an optimal particle size distribution could exist, which would result in maximum workability and therefore minimum water/binder ratio and optimum strength. For each type of cement and PFA an optimum percentage cement replacement should exist which should result in an optimum combined particle size distribution and thus optimum workability and strength.

Currently tests are under way on all physical aspects of the different PFA-types including effects on particle packing. Attempts are made to quantify particle size distribution parameters. Success will hopefully explain the influence of PFA on concrete workability conclusively.

REFERENCES

[1] Neville AM. And Brooks, J. J. Concrete Technology, Updated. London: Longman, 1987, p. 33.

[2] Kruger, J. E. Origin, history and properties of South African fly ash and Portland fly ash cements, Guide 2, South African Coal Ash Association, March 1999, p. 2.

[3] SABS Method 747, Density of cement (Metric units), Pretoria: South African Bureau of Standards, 1971.

[4] SABS method 862-1, Concrete tests – Consistence of freshly mixed concrete – Slump test, Pretoria: South African Bureau of Standards, 1994.

[5] SABS method 863, Concrete tests – Compressive strength of hardened concrete, Pretoria: South African Bureau of Standards, 1994.

[6] Tattersall G. H. and Banfill P. G. H. The Rheology of Fresh Concrete. Pitman, London, 1983, p. 76.

[7] Ferraris, C. F. and de Larrard, F., Modified Slump Test to Measure Rheological Parameters of Fresh Concrete, Cement, Concrete and Aggregates, CCAGDP, Vol. 20, No. 2, Dec. 1998, pp 241-247.

[8] Homma A., Yamamoto, Y. and Kitsutaka, Y. Testing Method of the Rheological Characteristics of High Fluid Concrete, Concrete under severe conditions 2: Environment and Loading. Proceedings of the Second International Conference on Concrete under Severe Conditions, Tramso, Norway, 1998, pp. 1864+.

[9] Japanese Society of Civil Engineers. Standard Concrete Specification (work edition). JSCE, Tokyo, 1992, pp. 259-262.

[10] Govier G. W. The Flow of Complex Mixtures in Pipes, Florida: Robert. E Kriegler Publishing Company; 1972, p. 58.

THE INFLUENCE OF HIGH VOLUMES OF PFA ON THE WORKABILITY OF PASTES

Jan H C Pretorius[1], Elsabe P Kearsley[2]

[1] Duraset Mining Products, Westonaria, South Africa.
E-mail: janpreto@postino.up.ac.za
[2] Department of Biosystems and Civil Engineering, University of Pretoria, Pretoria, South Africa.
E-mail: elsabe.kearsley@eng.up.ac.za

Jan H. C. Pretorius

Duraset Mining Products, Westonaria, South Africa

E-mail: janpreto@postino.up.ac.za

Department of Civil Engineering, University of Pretoria University, Pretoria, South Africa
Tel: +27 (12) 420 4129 Fax: +27 (12) 420 4129 Cell: +27 82 879 3311

INVESTIGATION ON THE PRODUCTION AND USE OF METAKAOLIN, ORIGINATED FROM POOR GREEK KAOLINS, AS CEMENT EXTENDER

S. Tsivilis[1*], E. Badogiannis[1], G. Kakali[1], E. Chaniotakis[2] and V. Papadakis[3]

[1] National Technical University of Athens, School of Chemical Engineering, Labs of Inorganic and Analytical Chemistry, Athens, Greece. E-mail: stsiv@central.ntua.gr
[2] Titan Cement Company S.A., Research and Quality Dept., Kamari Plant, Elefsina, Attica, Greece. E-mail: haniotakise@titan.gr
3 University of Patras, Chemical Engineering Department, Patras, Greece. E-mail: vgp@pat.forthnet.gr

ABSTRACT

In this paper the production and use – as a cement and concrete constituent - of metakaolin, originated from poor Greek kaolins, is investigated. The kaolin was thermally treated at optimized conditions and the produced metakaolin was ground superfine. In addition, a commercial metakaolin of high purity was used. Four mixture proportions were used to produce blended cements and high performance concrete. The mechanical and physical properties of the blended cements were measured. Furthermore, the properties of the fresh concrete, the strength development and some properties concerning the concrete durability - chloride permeability, air permeability, sorptivity and porosity – were studied. It is concluded that kaolinite is completely converted to metakaolinite after 3 hours at 650°C and at these conditions the metakaolin exhibits higher pozzolanic reactivity. The produced metakaolin as well as the commercial one indicate a similar behavior concerning cement strength development and concrete strength development and durability and lead to the production of cement and concrete with an excellent performance. Metakaolin has a very positive effect on concrete strength after 2 days and particularly at 28 days and 90 days. Metakaolin concrete exhibits significantly lower chloride permeability, gas permeability, sorptivity and pore size compared with OPC concrete. Metakaolin, originated from poor Greek kaolins, can be efficiently used as a cement and concrete constituent.

1. INTRODUCTION

The most common cementitious materials that are used as concrete constituents are fly ash, ggbs and silica fume. They save energy, conserve resources and have many technical benefits [1]. Metakaolin, produced by controlled thermal treatment of kaolin, can also be used as a concrete constituent, since it has pozzolanic properties [2-3].

According to the literature, the research work on metakaolin is focused on two main areas. The first one is the effect of the kaolin structure on the kaolinite to metakaolinite conversion and the use of thermoanalytical methods for the investigation of kaolin thermal treatment [4-12], while the second one concerns the pozzolanic behaviour of metakaolin and its effect on concrete properties [2-3, 13-26]. Although there is a disagreement on specific issues, the knowledge level is satisfactory and continuously extended.

* Corresponding author: 9, Heroon Polytechniou St., 15773 Athens, Greece; Tel.: +30-1-7723262; Fax: +30-1-7723188

Concrete performance depends mainly on the environmental conditions, the microstructure and the chemistry of the concrete. The two latter factors are strongly affected by the concrete components. It is obvious that the metakaolin addition affects the concrete performance. The present work deals with the study of the kaolin to metakaolin conversion as well as the investigation on the effect of metakaolin on cement and concrete properties and behaviour. This work belongs to a research project aimed at the exploitation of Greek kaolins in concrete technology.

2. EXPERIMENTAL

2.1 Materials

A poor Greek kaolin (K), originated from Milos Island, was used. In addition, a commercial metakaolin (MKC) of high purity was also used as a reference material. The chemical analysis of the materials is given in Table 1 and their mineralogical analysis in Table 2. Concerning the commercial metakaolin, for comparison reasons, the characteristics of the commercial kaolin (KC), instead of MKC, are given.

Table 1. Chemical analysis of kaolins (%)

	SiO_2	Al_2O_3	CaO	MgO	Fe_2O_3	L.O.I.	SO_3
KC	47.85	38.20	0.03	0.04	1.29	12.30	-
K	65.92	22.56	0.36	0.02	0.90	8.60	2.00

Table 2. Mineralogical analysis of kaolins (%)

	Kaolinite	Alunite	Quartz*	Illite
KC	96	-	-	3
K	52	5	41	-

*: Quartz (mainly) + cristobalite

Ordinary Portland Cement (OPC: I/55) of industrial origin was used for the production of the mixtures. The chemical analysis of OPC and the characteristics of clinker are given in Table 3.

Table 3. Chemical analysis of OPC and characteristics of clinker

Cement		Clinker	
Chemical analysis (%)		Mineralogical composition (%)	
SiO_2	21.54	C_3S	57.8
Al_2O_3	4.83	C_2S	18.1
Fe_2O_3	3.89	C_3A	6.2
CaO	65.67	C_4AF	11.8
MgO	1.71	Moduli	
K_2O	0.60	LSF	0.949
Na_2O	0.07	SR	2.47
SO_3	2.74	AR	1.24
Cl^-	0.00	HM	2.17

2.2 Thermal treatment of kaolin

The thermal treatment of the kaolins was carried out in a laboratory programmable furnace under controlled conditions and the optimum conditions of thermal treatment were determined. Thermogravimetric analysis (TGA) was applied in order to measure the weight loss during the thermal treatment of the samples. Mineralogical analyses in the raw and thermally treated samples were carried out by means of X-ray diffraction (XRD). The pozzolanic activity of thermally treated samples was measured according to the Chapelle test [12, 27-28].

In order to define the optimum temperature, the sample K was thermally treated (m=140g) at varying temperature (T: 550°C-950°C) for constant time t=3h. The temperature was raised at a constant rate (10°C·min $^{-1}$) from ambient to the desired temperature. In order to define the optimum heating time, the sample K was thermally treated at the previously defined temperature for varying time (t:1-8h).

The definition of the optimum thermal treatment conditions was based on the determination of the unconverted kaolinite in the burnt samples. Each sample of calcined kaolin is subjected to thermogravimetric analysis (TGA) using a Mettler Toledo TGA/SDTA 851 instrument. The samples (~50mg) were heated over the range 20°C to 950°C at a constant rate of 20°C/min in an atmosphere of air. The weight loss of the calcined samples indicate mainly the amount of kaolinite that has not been converted to metakaolinite during the thermal treatment. Mineralogical analysis in the thermally treated samples was carried out by X-ray diffraction (Siemens D5000 diffractometer - Cu Kα radiation - Ni Filter), in order to certify the disappearance of kaolinite peaks.

The pozzolanic activity of the samples MK and MKC was measured according to Chapelle test. 1g of metakaolinite is mixed with 1 g of $Ca(OH)_2$ and 100 ml of water. The suspension is boiled for 16 hours and the free $Ca(OH)_2$ is determined by means of sucrose extraction and titration with a HCl solution.

2.3 Metakaolin production

The Greek kaolin was thermally treated in a pro-pilot plant furnace at the experimentally defined conditions (T=650°C, t=3h) and the produced metakaolin (MK) was ground superfine, using the AJ100 Aerojet Mill Minisplit Classifier of British Rema. The fineness characteristics of the ground metakaolin (MK) as well as the MKC are given in Table 4.

Table 4. Metakolin fineness characteristics

	d_{20} (μm)	d_{50}(μm)	d_{80}(μm)
MKC	10.3	5.1	1.9
MK	13.6	7.5	3.4

2.4 Cement properties

Blended cements were produced by replacing OPC with 10% w/w MK, 20% w/w MK, 10% w/w MKC and 20% w/w MKC. The compressive strength of the samples (EN 196-1) as well as the setting time (EN 196-3) was determined.

2.5 Concrete properties

The concrete production was carried out in a mixer of 50 l capacity. The mixture proportions of all concrete specimens are summarized in Table 5. Normal graded calcareous aggregates with maximum size 31.5 mm were used. A common superplasticizer was used at appropriate percentages in order to retain the slump of the fresh concrete between 50-90 mm (class S2 of EN 206). The dry materials were mixed for 2 min. Then the water, containing the plasticizer was added, and the mixing was continued for 2 min.

The slump (ASTM C 143-90a), the density (BS 1881-103/1993) and the air content (ASTM C 138-92) of the fresh concrete were tested. Concerning the hardened concrete, the compressive strength after 2, 7, 28 and 90 days (ASTM C 39) was measured.

The specimens for the durability tests were cast in steel cylinders of 100 mm diameter and 200 mm height. The molds were stripped after 24 h and the specimens placed under lime-saturated water at 20°C for 90 days. This long-term curing period under water ensures an advanced degree of both Portland cement hydration and pozzolanic activity.

Table 5. Concrete mix proportions

Sample	Content (Kg/m^3)					Superpl.	W/C	W/B
	C	MKC	MK	Aggregates	W	(%)		
OPC	350	-	-			0.057	0.50	
MKC-10	315	35	-	Fine: 720		0.140	0.56	
MKC-20	280	70	-	Medium: 400	175	0.170	0.63	0.50
MK-10	315	-	35	Coarse: 800		0.181	0.56	
MK-20	280	-	70			0.400	0.63	

The AASHTO T277 rapid test method was followed to rank the chloride penetration resistance of concrete by applying a potential of 60 V DC and measuring the charge passed through the specimen. The tested concrete cores were slices 51 mm thick, cut from the middle of the initially 200 mm specimens and coated with watertight tape on the cylindrical surface.

The air permeability tests were applied to a concrete cylinder of 100mm diameter and height varied between 45mm and 50mm. The samples were oven-dried at 105^{o}C, until a weight change of less than 0.1% over 24h was observed [29]. The drying period of these specimens was 4-6 days. A modified commercial triaxial cell for 100mm diameter samples, operating to maximum cell pressure of 1.7 N/mm^2, was used for the determination of the gas (N_2) permeability of the specimens. The equipment used as well as the detailed procedure is described in a previous work [30].

The sorptivity test was applied to a concrete cylinder of 100mm diameter and 125mm height, oven-dried at 105^{o}C for 24h. The equipment used as well as the detailed procedure is described in a previous work [30].

The concrete pore structure was studied using mercury intrusion porosimetry. More specifically, the porosity of the specimen as well as its pore size distribution were measured with a Carlo Erba 2000 Hg porosimeter.

3. RESULTS AND DISCUSSION

3.1 Thermal treatment of kaolin

Kaolin K was thermally treated at 550, 650, 750, 850 and 950^{o}C for 3 hours. Table 6 shows the weight loss (TGA) of calcined samples. The untreated kaolin loses 8.60% weight in the range 20-950^{o}C, which is mostly due to removal of the water combined in the structure of the kaolinite mineral. The weight loss of calcined samples indicates that the kaolinite to metakaolinite conversion is almost completed at 650^{o}C. The XRD patterns of K, treated at various temperatures for 3 hours, showed that the characteristic peaks of kaolinite disappear in samples calcined over 650^{o}C. Incomplete metakaolinization was found only in the sample burnt at 550^{o}C.

Table 6. Weight loss of calcined kaolin K, treated at different temperatures for 3h

Temperature (^{o}C)	Untreated	550	650	750	850	950
Weight loss (%)	8.60	1.35	0.71	0.35	0.23	0.00

In order to define the optimum duration of the thermal treatment, kaolin K was calcined at 650^{o}C for 1-8h. The weight loss (TGA) of the calcined samples is given in Table 7. As is shown, the samples, treated for 2, 3, 4, 6 and 8h, have negligible differences. The XRD patterns of K, treated at 650^{o}C for 1-8h, showed that the characteristic peaks of kaolinite disappear in samples calcined over 3h.

Table 7. Weight loss of calcined kaolin K, treated at 650°C for 1-8h

Time (h)	1	2	3	4	6	8
Weight loss (%)	1.49	0.77	0.75	0.78	0.61	0.75

Table 8 presents the results of the Chapelle test for the commercial metakaolin MKC and the MK, after thermal treatment at 550, 650 and 750°C. The pozzolanic reactivity is evaluated on the basis of the amount of $Ca(OH)_2$ consumed per gram of metakaolin during the pozzolanic reaction. The higher reactivity of the sample treated at 650°C, confirms the previous results. The lower reactivity of metakaolin at higher temperatures is attributed to the re-crystallization of amorphous minerals. As was expected, the commercial product MKC is the most reactive sample, since it has a considerably higher kaolinite content, compared with the MK. However, the reactivity of MK is higher than was expected, based on the metakaolinite content (MKC: 95% w/w, MK: 49% w/w). As is established elsewhere, kaolinite in kaolin K is less-ordered than kaolinite in KC and this has a positive effect on MK reactivity [12].

Table 8. Chapelle test - Reacted $Ca(OH)_2$ per gram of metakaolin

Sample	$Ca(OH)_2$ (g/g of metakaolin)			
	550 °C	650 °C	750 °C	-
MK	0.741	0.815	0.741	
MKC				0.926

3.2 Cement properties

Table 9 presents the compressive strength of the tested samples. It is observed that the addition of metakaolin does not significantly alter the 1-day strength, but it has a very positive effect on the strength after 2 days and specifically at 28 days. As far as the metakaolin type is concerned, it is concluded that MK and MKC have a similar contribution to strength development. OPC with 10% MK showed the best results.

The main factors that affect the contribution of a pozzolanic material to strength are: a) the filler effect, b) the (clinker) dilution effect and c) the pozzolanic reaction with CH. Due to metakaolin high reactivity and high fineness, the pozzolanic reaction of metakaolin is completed between 7 and 28 days [31, 32]. Thus, after 28 days the strength development of metakaolin cements is retarded, due to the dilution effect.

Table 9 presents the water demand of cement paste and the setting time of the tested samples. The "water demand" is the quantity of water that is required to prepare a cement paste of standard consistency as specified in EN 196-3. The blended cements demand significantly more water than the relatively pure cement and this phenomenon is mainly attributed to the high fineness of metakaolin. The increase of the metakaolin content causes a significant increase in the water demand. OPC with 10% MKC showed the lowest water demand, compared with the other blended cements. The initial and final setting time of metakaolin cements is higher than the setting time of pure cement.

Table 9. Mechanical and physical properties of blended cements with metakaolin

Sample	Composition (%)			Compressive strength (N/mm^2)					Water demand	Setting time (min)	
	OPC	MKC	MK	1 d	2 d	7 d	28 d	180 d	(%)	Initial	Final
OPC	100	-	-	17.6	29.4	44.5	57.5	70.3	27.5	105	140
MKC-10	90	10	-	20.2	32.4	52.7	71.3	75.0	31.0	95	130
MKC-20	80	20	-	18.8	29.1	50.4	69.7	75.8	37.5	140	170
MK-10	90	-	10	20.0	32.0	50.7	68.1	79.6	32.5	155	180
MK-20	80	-	20	18.0	28.5	50.0	65.3	77.1	41.0	205	230

3.3 Concrete properties

Table 10 presents the properties of the fresh concrete. The slump of the mixes was in the range 50-95 mm (class S2 of EN 206) with the appropriate use of superplasticizers (Table 5). The density of the fresh concrete varies from 2427 to 2453 kg/m^3. The concrete is well compacted as is shown from the air content values.

Table 10. Properties of fresh concrete

Sample	Slump (mm)	Unit weight (Kg/m^3)	Air content (%)
OPC	70	2453	1.4
MKC-10	95	2434	1.5
MKC-20	60	2440	1.0
MK-10	50	2433	1.5
MK-20	75	2427	1.0

Figure 1 presents the compressive strength of the tested samples (Table 5). It is generally observed that when metakaolin substitutes cement, higher strengths than the OPC concrete are achieved. More specifically, it is seen that the metakaolin concrete shows lower 2 day strength (with the exception of MK-10), but it has a very positive effect on the strength after 2 days and specifically at 28 days and 90 days. As far as the metakaolin type is concerned, it is observed that MK has a more substantial effect on strength development than MKC. Concrete with 10% MK showed the best results.

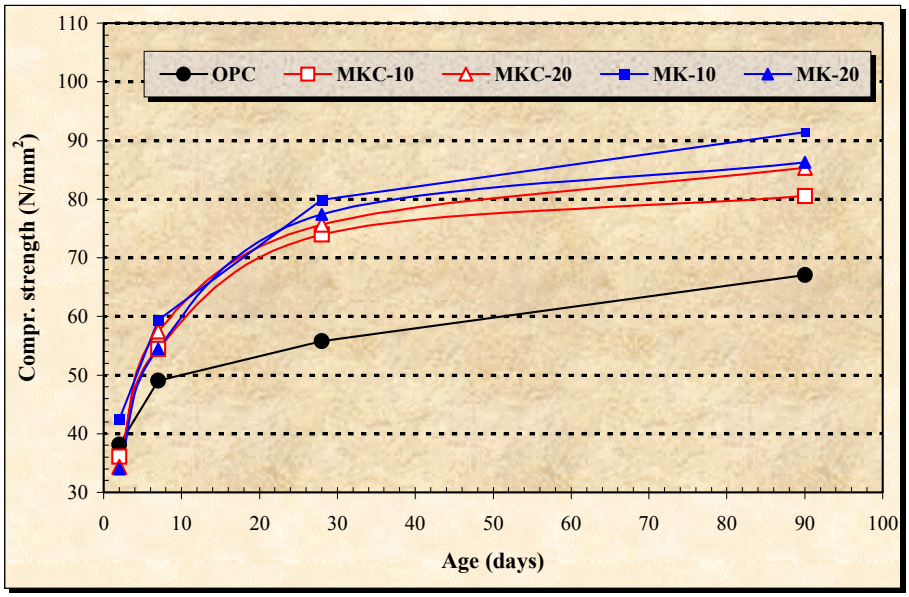

Figure 1. Compressive strength development of metakaolin concrete

Table 11 presents the chloride permeability, the gas permeability, the sorptivity and the mean pore size of the tested specimens. The results given in Table 11 are the average values of three different specimens.

The addition of metakaolin causes a significant decrease of concrete chloride permeability. The chloride permeability of metakaolin concrete varies from 240 to 760 C (Coulomb), while the OPC concrete presents a chloride permeability of 2460 C. The concrete with 20% MKC has the lower chloride permeability.

Table 11. Chloride permeability, gas permeability, sorptivity and mean pore size of metakaolin concrete

Sample	Chloride permeability (C)	Gas permeability (m^2 x 10^{-16})	Sorptivity (mm x $min^{0.5}$)	Mean pore size (nm)
OPC	2460	2.94	0.114	96
MKC-10	730	1.68	0.097	70
MKC-20	240	1.45	0.089	55
MK-10	690	1.35	0.080	74
MK-20	760	1.60	0.067	62

Concrete with metakaolin exhibits lower gas permeability values compared with the OPC concrete. The gas permeability of the metakaolin concrete varies from 1.35 to $1.68 \cdot 10^{-16}$ m^2, while the OPC concrete presents a gas permeability of $2.94 \cdot 10^{-16}$ m^2. The concrete with 10% MK shows the lower gas permeability.

The addition of metakaolin causes a relative decrease of concrete sorptivity. The sorptivity varies from 0.067 to 0.097 mm/$min^{0.5}$, while the OPC concrete presents a sorptivity of 0.114 mm/$min^{0.5}$. The concrete with 20% MKC has the lower sorptivity.

Concrete with metakaolin exhibits lower pore size compared with the OPC concrete. The mean pore size of the metakaolin concrete varies from 55 to 74 nm, while the OPC concrete has a mean pore size of 96 nm. The concrete with 20% MKC shows the lower mean pore size.

The enhanced properties of metakaolin concrete are attributed to the high reactivity and high fineness of metakaolin. It is generally accepted that the use of metakaolin leads to concrete with performance characteristics comparable to those of silica fume concrete [33].

In order to indicate more clearly the contribution of the metakaolin to the concrete durability the ratio (p/p_0) has been used, where p is the value of a specific property of metakaolin concrete and p_0 is the value of the same property in OPC concrete. Therefore, (p/p_0) values less than 1 indicate that metakaolin favors the concrete properties and improves the concrete performance. The (p/p_0) values presented in figure 2, show that the metakaolin addition has a positive effect on all the studied concrete properties. It is also concluded that metakaolin affects especially the chloride permeability and the gas permeability of the concrete.

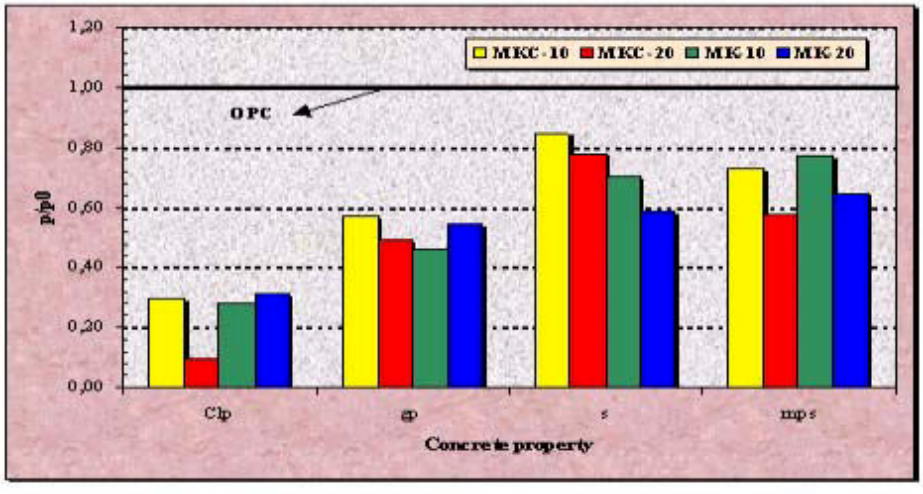

Figure 2. The effect of metakaolin on concrete durability (p: value of a specific property of metakaolin concrete, p_0: value of the same property in OPC concrete, Clp: chloride permeability, gp: gas permeability, S: sorptivity, mps: mean pore size)

4. CONCLUSIONS

The following conclusions can be drawn from the present study:

- Kaolinite is completely converted to metakaolinite after 3 hours at 650^0C. At these conditions the metakaolin exhibits the higher pozzolanic reactivity.
- Metakaolin has a very positive effect on the concrete strength after 2 days and specifically at 28 days and 90 days. Metakaolin concrete exhibits significantly lower chloride permeability, gas permeability, sorptivity and pore size compared with OPC concrete.
- The produced metakaolin as well as the commercial one indicate a similar behavior concerning cement strength development and the concrete strength development and durability and lead to production of cement and concrete with an excellent performance.
- Metakaolin, originated from poor Greek kaolins, can be efficiently used as a cement and concrete constituent.

REFERENCES

[1] Neville, A.M. Properties of concrete, 4th and final edition: Addison Wesley Longman Limited, England, 1996, p.844.

[2] Changling, H., Makavicky, E. and Osback, B. Thermal stability and pozzolanic activity of calcined kaolin, Applied Clay Science, vol.9, 1994, pp.165-187.

[3] Dunster, A.M., Parsonage, J.R. and Thomas, M.J.K. Journal of Materials Science, vol.28, 1993, pp.1345-1351.

[4] Dubois, J., Murat, M., Amroune, A., Carbonneau, X. and Garbon, R. Applied Clay Science, vol.10, 1995, pp.187-192.

[5] Kristof, E., Juhasz, AZ. and Vassanyi, I. The effect of mechanical treatment on the crystal structure and thermal behavior of kaolinite, Clays and Clay Minerals, vol.41, 1993, pp.608-612.

[6] Mitra, G.B. and Bhattacherjee, S. X-Ray Diffraction studies on the transformation of kaolinite into metakaolin: I Variability of interlayer spacings, The American Mineralogist, Vol.54, 1969, pp.1409-1418.

[7] Piga, L. Thermogravimetry of a kaolinite-alunite ore, Thermochimica Acta, vol.265, 1995, pp.177-187.

[8] Foldvari, M. Kaolinite-genetic and thermoanalytical parameters, Journal of Thermal Analysis and Calorimetry, vol.48, 1997, pp.107-119.

[9] Balec, V., and Murat, M. The emanation thermal analysis of kaolinite clay minerals, Thermochimica Acta, vol.282, 1996, pp.385-397.

[10] Sha, W. and Pereira, B. Differential scanning calorimetry study of ordinary Portland cement paste containing metakaolin and theoretical approach of metakaolin activity, Cement and Concrete Composites, vol.23, 2001, pp.455-461.

[11] Kaloumenou, M., Badogiannis, E., Tsivilis, S. and Kakali, G. Effect of the kaolin particle size on the pozzolanic behaviour of the metakaolinite produced, Journal of Thermal Analysis and Calorimetry, vol.56, 1999, pp.901-907.

[12] Kakali, G., Perraki, T., Tsivilis, S. and Badogiannis, E. Thermal treatment of kaolin: the effect of mineralogy on the pozzolanic activity, Applied Clay Science, vol.20, 2001, pp.73-80.

[13] Skanly, J.P. Materials science of concrete I, The American Ceramic Society Inc, Westerville, OH, 1989, pp.127-128, pp.163-179.

[14] Roumain, J.C. and Sarkar, S.L. Cements of the 21st Century, 2nd Int. Symposium on Cement and concrete technology in the 2000 s, Istanbul, 2000, vol. 1, pp.29-42.

[15] Mehta P.K., Durability of Concrete-Fifty Years of Progress, 2nd International Conference, Montreal, SP 126-1, 1991, pp 1-31.

[16] Collepardi, M. A holistic aproach to concrete durability-role of superplasticizers, in: R. N. Swamy (ed.), Infrastructure Regeneration and Rehabilation Improving the Quality of Life Through Better Construction - A Vision for the Next Millenium, Sheffield Academic Press, Sheffield, UK, 1999, pp.15-25.

[17] Khatib, J.M. and Wild, S. Pore size distribution of metakaolin paste, Cement and Concrete Research, vol.26, 1996, pp.1545-1553.

[18] Coleman, N.J. and Page C.L. Aspects of the pore solution chemistry of hydrated cement pastes containing metakaolin, Cement and Concrete Research, vol.27, 1997, pp.147-154.

[19] Khatib, J.M. and Wild, S. Sulphate Resistance of Metakaolin Mortar, Cement and Concrete Research, vol.28, 1998, pp.83-92.

[20] Ramlochan, T., Thomas, M. and Gruber K.A. The effect of metakaolin on alkali-silica reaction in concrete, Cement and Concrete Research, vol.30, 2000, pp.339-344.

[21] Gallias, J.L., Kara-Ali, R. and Bigas J.P. The effect of fine mineral admixtures on water requirement of cement pastes, Cement and Concrete Research, vol.30, 2000, pp.1543-1549.
[22] Brooks J.J., Megat Johari, M.A. and Mazloom, M. Effect of admixtures on the setting times of high strength concrete, Cement and Concrete Composites, vol.22, 2000, pp.293-301.
[23] Sabir, B.B., Wild, S. and Bai, J. Metakaolin and calcined clays as pozzolans for concrete: a review, Cement and Concrete Composites, vol.23, 2001, pp.441-454.
[24] Moulin, E., Blanc, P. and Sorrentino, D. Influence of key cement chemical parameters on the properties of metakaolin blended cements, Cement and Concrete Composites, vol.23, 2001, pp.463-469.
[25] Vu, D.D., Stroeven, P. and Bui, V.B. Strength and durability aspects of calcined kaolin-blended Portland cement mortar and concrete, Cement and Concrete Composites, vol.23, 2001, pp.471-478.
[26] Gruber, K.A., Ramlochan, T., Boddy, A., Hooton, R.D. and Thomas, M.D.A. Increasing concrete durability with high-reactivity metakaolin, Cement and Concrete Composites, vol.23, 2001, pp.479-484
[27] Kostuch, J. A., Walters, V. and Jones, T.R. High performance concretes incorporating metakaolin: a review. In: R. K. Dhir, M. R. Jones (Editors), Concrete 2000: economic and durable construction through excellence, E&FN SPON, London, 1996, pp.1799-1811.
[28] Largent, R. Estimation de l' activite pouzzolanique, Bull., Liasons Lab. Pont Chausees, 93, 1978, pp.61-65.
[29] Dhir, R., Hewlett, P. and Chan, Y. Near surface characteristics of concrete: intrinsic permeability, Magazine of Concrete Research, vol.41, 1989, pp.87-96.
[30] Tsivilis, S., Chaniotakis, E., Batis, G., Meletiou, C., Kasselouri, V., Kakali, G., Sakellatiou, A., Paulakis, G. and Pseimidas, C. The effect of clinker and limestone quality on the gas permeability, water absorption and pore structure of limestone cement concrete, Cement and Concrete Composites, vol.21, 1999, pp.139-146.
[31] Wild, S., Khatib, J.M., Jones, A. Relative strength, pozzolanic activity and cement hydration in superplasticized metakaolin concrete, Cement and Concrete Research, vol.26, 1996, pp.1537-1544.
[32] Badogiannis, E., Kakali, G., Dimopoulou, G., Chaniotakis E., Tsivilis, S. Metakaolin as a main cement constituent. Exploitation of poor Greek kaolins, Cement and Concrete Composites, submitted for publication, 2002.
[33] Nawy, E. Fundamentals of high strength high performance concrete, 1st edition: Longman Group Limited, England, 1996, p.340.

HYDRATION PROCESSES OF CEMENTS BLENDED WITH LIMESTONE POWDER: EXPERIMETAL STUDY AND NUMERICAL SIMULATION

Xiangjun Xiong and Klaas van Breugel

Faculty of Civil Engineering and Geosciences, Delft University of Technology,
Delft, The Netherlands. E-mail: x.xiong k.v.breugel@ct.tudelft.nl

ABSTRACT

Although limestone powder or crushed limestone has been used in the manufacture of composite cement since the 1980s, there were only a few researches focusing on the reaction mechanism of the cement blended with limestone powder. This paper focuses on the influence of limestone powder on the kinetics of the hydration processes of Portland cement in the early ages using isothermal Calorimetry. The temperature of isothermal calorimeter study was 20, 30 and 40 ºC. The weight percentage of limestone in the binder was 14% and 22% and water-solid ratio was 0.43 and 0.53. In order to facilitate the comparison, experiments are also done with blast furnace slag cement blended with the same limestone powder percentage levels with a water-solid ratio of 0.53.

Apparent activation energy for the cements blended with limestone powder was also determined based on experimental results and used in a numerical simulation program for cement hydration. Comparison between numerical simulation results and that of the experiments suggests a good correlation between the numerical hydration model and the experiments.

1. INTRODUCTION

Limestone is a very important material for the manufacture of cement. It was also reported by several authors that the addition of limestone might improve the properties of cement paste such as water demand, workability and strength. Of course, the use of limestone as replacement filler in concrete will reduce the cost and bring along significant environmental benefits because the manufacturing of cement produces huge amounts of CO_2. Actually, as a replacement of clinker, limestone has been used in Europe for about 25 years [4] and half of the French composite Portland cement is limestone filler cement [14]. There are mainly two types of Portland limestone cement specified in the European Standard prEN 197-1: type II/A-L containing 6-20% limestone and type II/B-L containing 21-35% limestone [3].

Finely ground limestone powder has a physical filler effect in the hydration process of ordinary Portland cement [3, 4, 5, 6, 8]. Due to its fine size, limestone powder particles will 1) improve the grain packing of the cements [11], 2) act as the nuclei and facilitate the nucleation and growth of hydration products such as calcium hydroxide crystals at early ages of hydration [12]. However, limestone would react with calcium aluminate to form calcium aluminate carbonates, which is more stable due to its lower solubility [9, 10]. This actually increases the rate of the hydration of C_3A.

In a system containing C_3A and $CaCO_3$, a high carbonate form of carboaluminate $C_3A \cdot 3CaCO_3 \cdot 32H_2O$ and a low carboaluminate form $C_3A \cdot 3CaCO_3 \cdot 12H_2O$ could be formed [7]. These resemble the high sulphate form Ettringite and the low sulphate form monosulfoaluminate, which are formed as a reaction product of C_3A and gypsum. In a blended system with C_3A, gypsum

and $CaCO_3$, there could be competition between the CO_3^{2-} and SO_4^{2-} ions for the C_3A. Mixed Ettringite like materials with CO_3^{2-} substitution for SO_4^{2-} was also observed [13] and in the presence of carbonate, the conversion of ettringite to monosulfoaluminate is delayed [3]. In addition, limestone powder was found to accelerate the hydration of C_3S and modify the Ca/Si ratio of C-S-H gel [5]. Vernet [19] suggested that the carbonate participates in the hydration quite actively.

This paper focuses on the influence of limestone powder on the hydration processes of ordinary Portland cement under different temperatures. In order to make a comparison and understand the behavior of paste with blast furnace slag cement and limestone powder, experiments were also done with blast furnace slag cement blended with the same limestone powder percentage levels using isothermal calorimetry.

Apparent activation energy for the cement blended with limestone is then calculated based on the heat released during the hydration processes and used in the numerical simulation program HYMOSTRUC [1] model developed in Delft University of Technology. Good correlations are found between numerical simulations and that of the experiments.

2. DESCRIPTION OF EXPERIMENT

2.1 Experimental Instruments

The isothermal Calorimetry study was carried out with a 3114/3236 TAM Air isothermal calorimeter, manufactured by Thermometric AB, Sweden. It is an eight-channel calorimeter operating in the milliwatt region. The capacity chosen in this research was 600 mW per sample with a precision of ±0.01 mW. It can operate in the temperature range from 5 to 60ºC with a fluctuation of the isothermal temperature ±0.02ºC.

The calorimeter was located in a room where temperature was set to 20ºC and RH 65%. At measurement temperatures higher than the environmental temperature, in order to prevent thermal shock to the calorimeter due to the temperature difference between the sample and calorimeter, both cement and water were kept in the oven for 24 hours at the desired mixing temperature before mixing and isothermal measurements. An industrial computer was used to record the heat release and the measurement was done over the first 7 days of the hydration.

2.2 Materials

The cements used are ordinary Portland cement (later referred to as OPC) and blast furnace slag cement (later referred to as BFSC). Both the cements and the limestone powder are produced by ENCI B.V., The Netherlands. The oxide composition of the cements and the limestone powder was measured using XRF analysis using a Philips X-Ray spectrometer (PW 2400) and the oxide contents were calculated using Uniquant software. The measured oxide contents are shown in Table 1. The mineral composition of the clinker in the OPC was calculated using the modified Bogue method [20] as C_3S 59.3%, C_2S 11.0%, C_3A 7.2% and C_4AF 10.4% and Q_{pot}, the total amount of heat that will be liberated at complete hydration, is 433 kJ/kg. The clinker content in the BFSC is 28% and the slag percentage is 68%. According to the European standard, the $CaCO_3$ content in limestone must be greater than 75% for using in the blended cement. The CaO content in the limestone used in this study is about 54.5 percent, which is quite close to the theoretical content (56%) and therefore, the $CaCO_3$ content is around 97%.

The particle size distribution of the two cements and limestone powder were measured using laser diffraction. The equipment used was a Coulter LS 230 and the results are shown in Figure 1. It can be seen from the figure that limestone powder has a much finer particle size distribution and the volume percentage has a plateau of about 2% volume percentage within the range of 2 to 40 micron.

Table 1. Chemical Composition of the Cements and Limestone Powder

Oxide Analysis (wt%)	Ordinary Portland Cement	Blast Furnace Slag Cement	Limestone Powder
CaO	62.86	45.27	54.47
SiO_2	19.63	30.79	0.225
Al_2O_3	5.02	9.88	0.074
Fe_2O_3	3.31	1.40	0.062
K_2O	1.23	1.17	0.304
Na_2O	0.30	0.22	-
SO_3	3.01	3.01	-
MgO	2.28	6.59	0.614
TiO_2	0.36	0.48	-
MnO	0.12	0.22	-
P_2O_5	0.45	0.14	0.008
Ignition Loss	1.06	0.76	44.10*)

*) The high value of ignition loss is due to the release of CO_2

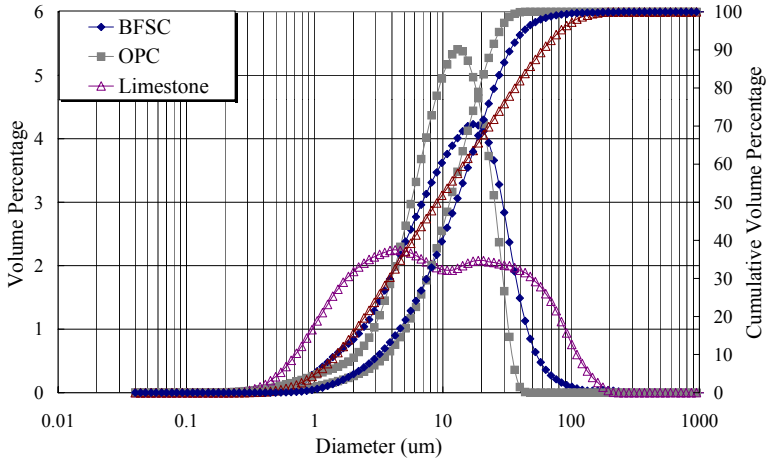

Figure 1. Particle size distribution of the cements and limestone powder

2.3 Mixture Composition

The mixture composition can be found in Table 2 and 10 gram cement paste was needed for the isothermal calorimetry measurement. Two weight percentage levels of limestone were used, namely 14% and 22%. The water-solid ratio was 0.43 and 0.53 for ordinary Portland cement blended with limestone.

Another mixture of blast furnace slag cement blended with limestone powder with the same level of limestone percentage was also prepared in order to make comparisons. The water-solid ratio used was 0.53. Isothermal calorimeter measurement was done for each mixture at three temperature levels, viz.: 20, 30 and 40 ºC.

3. EXPERIMENTAL RESULTS

Because the rate of heat release decreases quite significantly after 1 day, only the results in the beginning 30 hours are shown in the figures for a clear view. The rate of hydration or the thermal power is calculated based on the total weight of binder in the pastes.

Table 2. Mixture Composition for the Isothermal Calorimetry Study

Water-solid ratio	Cement	Limestone Powder	Note
0.53	6.54 g	0 g	Reference paste (100% OPC)
	5.62 g	0.92 g	86% OPC+14% LM
	5.10 g	1.44 g	78% OPC+22% LM
0.43	6.99 g	0 g	Reference paste (100% OPC)
	6.01 g	0.98 g	86% OPC+14% LM
	5.45 g	1.54 g	78% OPC+22% LM
0.53	6.54 g	0 g	Reference paste (100% BFSC)
	5.62 g	0.92 g	86% BFSC+14% LM
	5.10 g	1.44 g	78% BFSC+22% LM

3.1 Thermal Power

It can be seen in Figure 2 that at T=20ºC, the rate of hydration of blended cement pastes with both water/solid ratios are higher than that of reference paste in the first few hours. In the case of w/s ratio 0.43, cement paste containing 14% limestone powder shows a moderate acceleration of the hydration while higher content of limestone increased the hydration quite significantly and it also increased the value of the first peak. When the paste is older than 12 hours, the hydration of both blended pastes progresses slower than the reference paste. At a higher w/s ratio 0.53, paste with 14% limestone hydrates slower than the reference paste up to 5 hours. But it speeds up quite noticeably thereafter. Paste with 22% limestone shows a faster rate of hydration but it slows down quite significantly after 7 hours. After the first peak, blended paste exhibits an increasingly obvious shoulder or second peak with the increase of the limestone content.

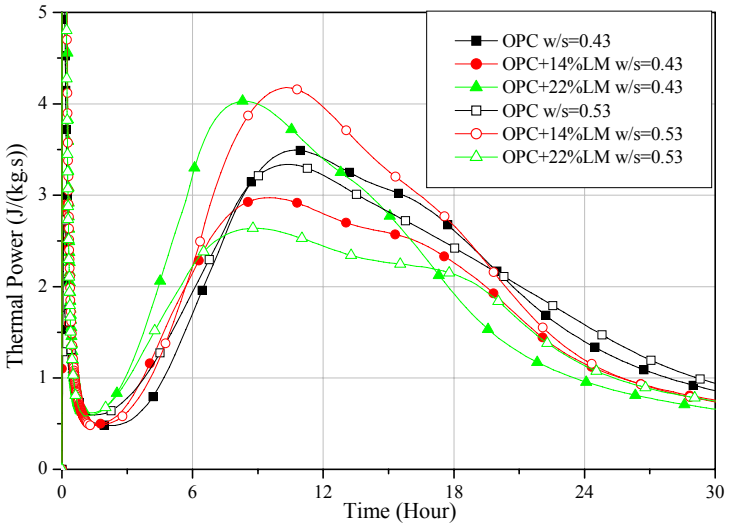

Figure 2. Rate of heat release of the pastes, T=20˚C

At T=30ºC (Figure 3), the reactions have been accelerated and the value of the first peak increases for all the samples. Paste with 22% limestone hydrates and w/s ratio 0.53 quite fast in the beginning and exhibits an obvious second peak, whose value is even larger the first peak. Paste with 14% limestone powder and w/s ratio 0.43 also shows the same behaviour. However, hydration of both of them is slower than the reference paste after 5 hours of hydration. Again, paste with 14% limestone powder and w/s ratio 0.53 has the highest value of the first peak, followed by paste with 22% limestone powder and w/s ratio 0.43. A more obvious shoulder or second peak is found again in all the blended pastes.

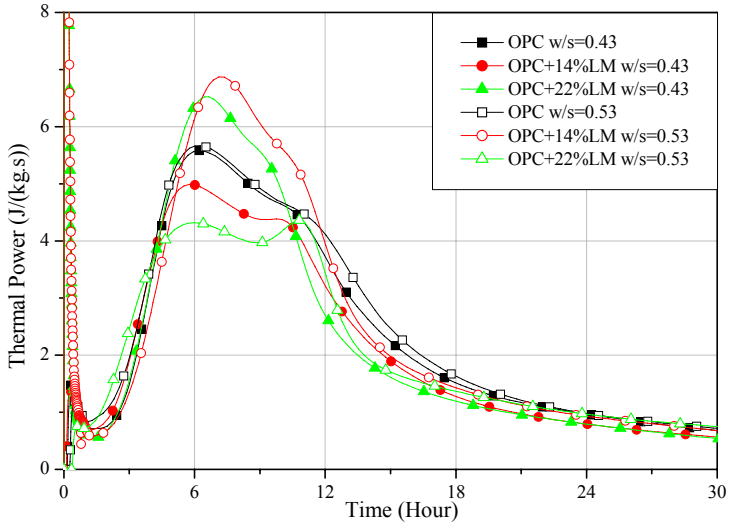

Figure 3. Rate of heat release of the pastes, T=30˚C

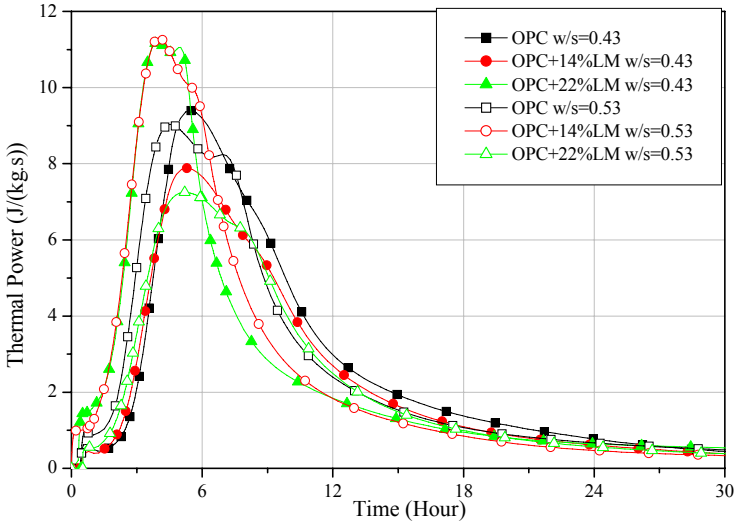

Figure 4. Rate of heat release of the pastes, T=40˚C

When the experiment temperature goes to 40ºC (Figure 4), hydration of paste with 14% limestone and w/s ratio 0.53 exhibits the highest value of first peak and that of paste with 22% limestone and w/s ratio 0.43 second. Both of the pastes show a much more obvious second peak than the lower degree cases, especially for paste with 22% limestone and w/s ratio 0.43. Similar to 30ºC, hydration of these two pastes slows down quite noticeably after the second peak.

3.2 BFSC blended with limestone

Figure 5 shows the thermal power of blast furnace slag cement blended with limestone powder. At T=20 ºC, the reference paste has the second peak at about 27 hours after the first peak. The addition of limestone powder has shortened the time interval of the first peak and the second peak by about 6 hours. When the temperature is 30 ºC, the speed of hydration is increased and paste with 14% limestone has a much higher second peak while the paste with 22% limestone shows a plateau at around 1.7 mW/g. At T=40 ºC, the heat release of paste with 14% limestone shows a very high peak immediately after the first peak, which makes the first peak into a small plateau.

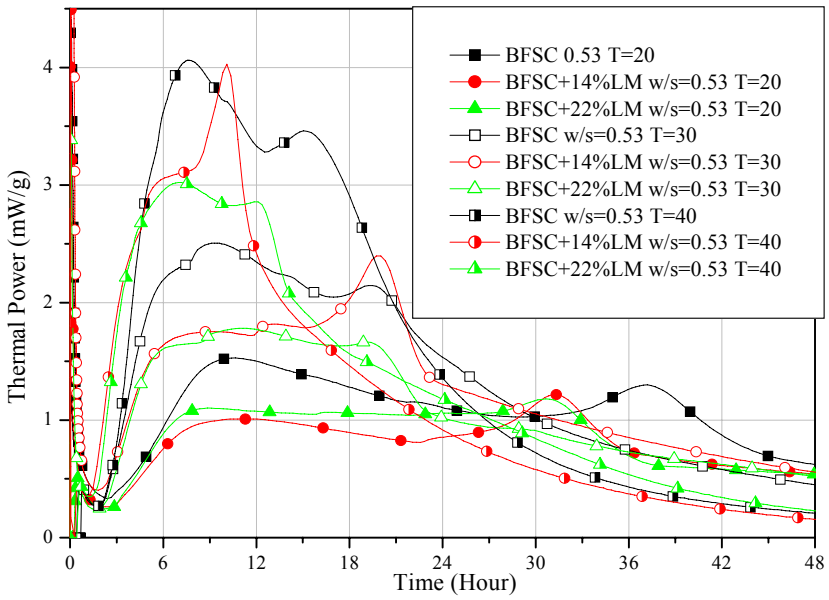

Figure 5. Rate of heat release of blended paste with blast furnace slag cement and limestone

The time interval between the two peaks is also shorter. It is worthwhile to point out that paste with 14% limestone with water/solid ratio 0.53 again shows significant change of the processes of the hydration. In comparison with the blended cement using Portland cement, the change is on the value of the second peak in this case.

4. DISCUSSIONS AND EVALUATION

4.1 Effect of limestone

Several authors, among others, Kakalis et al [3], Poitevin [4] and Pera et al. [5], suggest that limestone exhibits chemical activity during the hydration processes of Portland cement blended with limestone. Kakalis et al. [3] made a comparative study of the chemical activity of limestone and its effect on the hydration of C_3S, C_3A and Portland cement using XRD and TGA. They found that "the ettringite transformation to monosulphate is delayed and calcium mono-carboaluminate is preferably formed instead of monosulphate even at early ages". Moreover, they also found an increase of CH content in cement pastes with limestone powder and this is clearly an indication of the acceleration of the calcium silicate hydration.

Since the focus is on the reactions where C_3A is directly or indirectly concerned, it is necessary to point out that in the hydration of C_3A in OPC paste, anions like CO_3^{2-}, SO_4^{2-} and OH^- can all occupy the interlayer positions of the solid solution formed as a reaction product of monosulphate, C_3A and CH. In the case of paste with limestone, the ion interaction theory of physical chemistry suggests that the formation of the less soluble calcium mono-carboaluminate hydrates will significantly increase the solubility of $CaCO_3$ and consequently further reaction will also be promoted.

The shoulder or the second peak of Portland cement hydration is generally believed to be the conversion of Ettringite to mono-sulphoaluminate. A higher second peak observed in the blended paste using Portland cement might be explained by the difference in the heat released in the reaction forming calcium mono-carboaluminate and that forming mono-sulphoaluminate. The former has a heat release of 328 kJ/mole, while the latter is only 238 kJ/mole.

In [18], the amount of bound water in cement blended with limestone powder was measured until the paste was 3 months old. Experiment results show that with the increases of the percentage of limestone powder in the mixture, the amount of chemically bound water is also increased at 20 and 30 ºC. This also suggests that limestone powder could have participated in the reaction because it is generally believed that the nucleation and growth phase happens in the beginning hours of hydration of ordinary Portland cement hydration. Therefore, the physical "filler" effect of limestone powder as nucleation site for hydration products could only influence the early hours of the hydration.

4.2 Apparent Activation Energy

The isothermal calorimeter records the rate of the heat release or the thermal power. By integrating the thermal power with time, we can obtain the evolution of heat of hydration. Thereafter, the degree of hydration at time *t* can be defined as the heat released at time *t* divided by the potential heat that can be released at complete hydration, viz.:

$$\alpha = Q(t) / Q_{pot} \tag{1}$$

In order to describe the kinetics of the hydration processes of the blended cement, especially the temperature dependence of the hydration processes, Arrhenius equation is used, viz.

$$K(T) = A * \exp(-\frac{E_a}{RT}) \tag{2}$$

Where A is the collision number constant, R is the ideal gas constant, 8.314 J/mol·K and E_a is the activation energy. Because cement hydration is composed of several simultaneous chemical reactions and physical processes, apparent activation energy is used here instead. Obviously, apparent activation energy (E_a) is an experimentally obtained value from its definition.

From Equations (1) and (2), taking the rates of hydration K_1 and K_2 at two temperatures of isothermal curing T_1 and T_2 ($T_1>T_2$, absolute temperature), apparent activation energy can be calculated using the formula below:

$$E_a(T, Q) = -\frac{R * T_1 * T_2}{T_2 - T_1} * \ln(\frac{K_1}{K_2}) \tag{3}$$

The calculated E_a is shown in Figure 6. In order to use the obtained E_a in numerical simulations, we use the following expression for the estimation of E_a:

$$E_a(\alpha, t, T) = (44.92 - 0.043 * T) * \exp(\gamma_{LM} \times \frac{f_{LM}}{1 - f_{LM}}) * \exp(-\alpha(t)) \tag{4}$$

Where f_{LM} is the weight percentage of the limestone in the binder, $\alpha(t)$ is the degree of hydration of cement at time *t* , T is temperature (K). We define γ_{LM} as an activity factor of limestone, which considers the influence of the limestone to the hydration kinetics. It was found that γ_{LM} is not an constant and it is dependent on the temperature and water-solid ratio.

From Equation (4), we notice that the apparent activation energy becomes temperature dependent and it also changes along with hydration. For the complex heterogeneous reaction like that of cement hydration, van Breugel [1] calculated the values of the activation energy based on isothermal Calorimetry data on Portland cement carried out by Lerch and Ford and he suggested that E_a is a function of temperature, degree of hydration and the content of C_3S. D'Aloia [2] also confirmed that E_a shows dependency on the degree of hydration and the temperature.

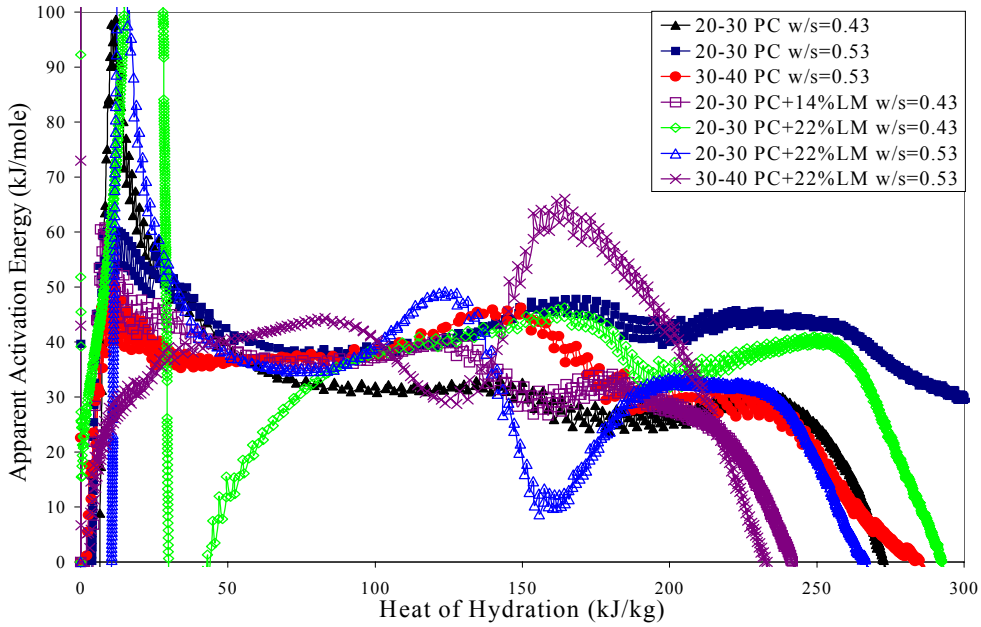

Figure 6. Calculated apparent activation energy for cements blended with limestone powder

5. NUMERICAL SIMULATION

5.1 Hymostruc

In the HYMOSTRUC model, the hydration can be described as the continuous growth of particles and the hydration product is divided into inner product and outer product. The embedment of smaller particles in the growing shell of bigger particles is also considered in the model. The microstructure is formed by the development of contacts between expanding particles.

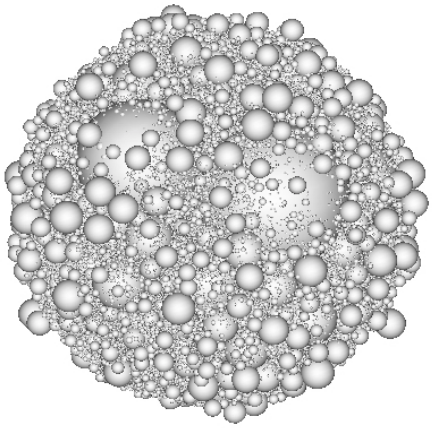

Figure 7. Simulated Initial 3D Random Distribution of Particles

5.2 Numerical Simulations

5.2.1 Numerical simulation result

Numerical simulations are performed for a mixture with 14% limestone powder and water-solid ratio 0.33. The isothermal curing temperature was 20 and 40 ºC respectively [18]. Based on the measured particle size distribution, a 3D random distribution of both the cement and limestone particles is first made to form the initial state of the hydration (see Figure 7). The particles are assumed to be spheres and they follow the Rosin-Rammler particle size distribution. The value of the activity factor of limestone, γ_{LM}, is taken as 0.34. This is only a small extension to the HYMOSTRUC model because the interaction between the limestone particles and cement particles is not simulated explicitly. However, we think that for engineering purposes, such a treatment can deal with the practical problems concerning concrete using cement blended with limestone powder.

In addition, a numerical simulation is also performed using the original implementation of apparent activation energy to facilitate the comparisons, where simulation using HYMOSTRUC with Equation (4) is denoted as "New Ea" and simulation using HYMOSTRUC with the original implementation in HYMOSTRUC as "Old Ea". The "Old Ea" in HYMOSTRUC is defined as

$$E_a(\alpha, T, C_3S) = 76 \times \alpha \times \exp(-2.52 \times 10^{-11} \times (C_3S)^{6.15} + 0.025 \times T^{1.5}) + 0.33 \times (C_3S) + 30 \quad (5)$$

Where C_3S stands for the weight percentage of C_3S.

It can be seen from Figure 8 that in the first few hours, the deviation between the calculated degree of hydration using Equation (4) and that of the experiment results is almost negligible.

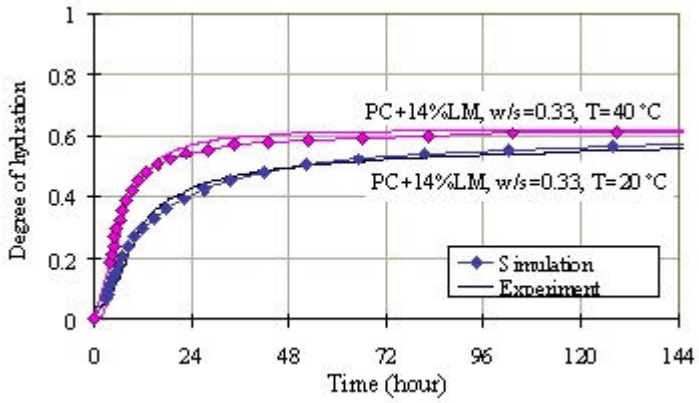

Figure 8. Comparison between numerical simulation results and experimental measurement of blended cement paste with 14% limestone and w/s ratio of 0.33

6. CONCLUSIONS

It is found that the addition of limestone to Portland cement increases the hydration at early age and the author suggest that effect of limestone is both physical and chemical. The appearance of a larger second peak could be explained by the replacement of the reaction of Ettringite to mono-sulfoaluminate by the reaction between C_3A and carbonate forming calcium mono-carboaluminate.

Pastes with 14% limestone and water/solid ratio 0.53 produce a significant change of the hydration processes for both the blended cement using Portland cement and blast furnace slag cement. But the effects of limestone are different in the two cases. For blended cement using Portland cement, the value of the first peak is increased while for the blast furnace slag cement case, the value of the second peak is increased.

Based on the isothermal calorimeter measurement, apparent activation energy for the blended cement with limestone is calculated and the limestone activity factor γ_{LM} is dependent on the temperature and water/solid ratio. The relationship between apparent activation energy and temperature, degree of hydration and limestone content is also found and utilized in the HYMOSTRUC model. Numerical simulation exhibits a good agreement with the experimental results at the early ages. This is quite important for the calculation of thermal stress, control of thermal cracks and durability.

ACKNOWLEDGEMENTS

The financial support from The Netherlands Science and Technology Fund (STW) is gratefully appreciated. The authors would also like to thank Mr. E. Horeweg in the Stevin Lab II of Delft University of Technology for the kind assistance in the experimental work.

REFERENCES

[1] Breugel K van, Simulation of hydration and formation of structure in hardening cement-based materials, Delft University Press, 2nd Edition, 1997

[2] D'Aloia L., Determination of the apparent activation energy of concrete using the equivalent age method: mechanical, calorimetric experiments and numerical simulations, Ph.D thesis, L'Ecole Nationale des Travaux Publics de l'Etat, 1998, 278 pp. (in French)

[3] Kakalis G et al, Hydration products of C_3A, C_3S and Portland cement in the presence of $CaCO_3$, Cem. Con. Res., 30 (2000) 1073-1077

[4] Poitevin P, Limestone aggregate concrete, usefulness and durability, Cem. Con. Comp., 21 (1999) 89-97

[5] Pera J et al, Influence of finely ground limestone on cement hydration, Cem. Con. Comp., 21 (1999) 99-105

[6] Vuk T et al. The effects of limestone addition, clinker type and fineness on properties of Portland cement, Cem. Con. Res., 31 (2001) 135-139

[7] Ingram, K., et al, Limestone Additions to Portland Cement: Uptake, Chemistry and Effects, 9th ICCC, India, Vol. III, pp 180-186, India

[8] Ranc R et al, Durability of cements with fillers, SP 126-66, 2nd International Conference, Durability of Concrete, ACI, Montreal, 1991

[9] Cochet G. et al, Limestone filled cements: Properties and uses, in : S.L. Sarkar, S.N. Ghosh (Eds), Mineral Admixtures in Cement and Concrete, vol.4 ABI Books, New Delhi, 1993, pp 266-295

[10] Tsivilis S et al, A study on the parameters affecting the properties of Portland limestone cements, Cem. Con. Comp., 21 (1999) 107-116

[11] Ellerbrock HG et al, Particle size distribution and properties of cements: Part III. Influence of grinding process, Zem-Kalk-Gips 43 (1990) 13-19

[12] Soroka I. Et al, The effect of fillers on strength of cement mortars, Cem. Con. Res. 7 (1977) 449-456

[13] Verent C. Sequences cinetiques des reactions d'hydratation de l'aluminate tricalcique en presence de gypse, de chaux et de fillers calcaires. Proceedings of the 8th International Congress on the Chemistry of Cement, Rio de Janeiro, 1986, III. pp 70-74

[14] Regourd M. Ciments specisaux et ciments avec additions, caracteristiques et activation des produits d'additions, Volume III , Theme 1, Proc. 8th ICCC, Rio de Janeiro, 1986

[15] LaMer VK, Dinegar RH, Journal of American Chemistry Society, 72 (1950), p.4847

[16] Hu, R.Z., et al, Thermal analysis kinetics, Science Press, 2001

[17] [Min, NB, The physical foundation of crystal growth, Shanghai Science & Technology Press, 1982

[18] Xiong, X., van Breugel, K., Hydration processes of cements blended with limestone powder, 5th International Symposium on Cement and Concrete, Shanghai, Oct 28-Nov 1, 2002 (accepted)

[19] Vernet, C., Mechanisms of the limestone Fillers reactions in the system {C3A-CSH2-CH-CC-H}: competition between calcium monocarbo- and monosulfo-aluminate hydrates formation, 9th ICCC, India, Vol. III, pp 430-436, India.

[20] Taylor, H.F.W. Modification of the Bogue calculation, Adv. Cem. Res. 2 (89) pp 73-77

HYGIENIC, HEALTH AND ENVIRONMENTAL COMPATIBILITY OF CEMENTITIOUS CONSTRUCTION PRODUCTS

M. Schneider and G. Spanka

Research Institute of the Cement Industry, German Cement Works Association, Düsseldorf, Germany. E-mail: Sch@vdz-online.de

ABSTRACT

Construction projects are essential to satisfy the requirements of the modern industrial society. However, each building activity is associated with an interference with the nature. The protection of the immediate environment of structural works belongs to the six essential requirements of the European Construction Products Directive (CPD). The German cement industry has dealt for many years with the environmental compatibility of cement and cementitious building materials in all phases of the product life. Mortar and concrete may contain small amounts of trace elements as well as organic substances deriving from, e. g. additives and admixtures. All investigations have shown that the hardened cement paste is a good binding and encapsulating matrix for these components and that their leaching rates are on a very low level. While for trace elements the leaching behaviour is important to be understood, for organic substances used in cementitious building materials also the release of volatile components must be taken into account. Investigations carried out so far have shown that cementitious materials, even when produced with organic additives or admixtures, cause only very slight emissions. Cement and cementitious construction products satisfy the fundamental requirements of the European Construction Products Directive and the corresponding national regulations.

1. INTRODUCTION

The modern Society relies to a great extent on houses, industrial installations, drinking water supply, transportation systems etc. Among many other building materials concrete plays by far the most important role in providing such reliable and durable infrastructure. The European Construction Products Directive (CPD) [1] allows construction products to be placed on the European common market if these products are fit for their intended use. Fitness for intended use must be assumed, if the construction products incorporated in the works satisfy – if properly installed – six essential requirements. In addition to the traditional essential requirements, e. g. mechanical resistance, the CPD directly addresses hygiene, health and the environment.

Cement and cementitious construction products satisfy the fundamental requirements of the CPD and the corresponding national regulations. Therefore, the European cement standard EN 197 [2] in general does not cover separate requirements in view of hygiene, health and environmental protection. In Germany further regulations are laid down in special cases where it appears necessary for constructive applications that require a particular protection of the water, soil and air. For new building materials to be approved the German Institute for Building Technology (DIBt) established a code of practice for the evaluation of the effects of construction products on the soil and ground water [3]. The DIBt was also involved in drafting a code regarding health-relevant evaluation criteria for interior-relevant construction products [4]. The German Gas and Water Association (DVGW) established the worksheet W 347 “Hygienic requirements for cement-bound materials for

Proceedings of the 11th International Congress on the Chemistry of Cement (ICCC)
‘Cement’s Contribution to the Development in the 21st Century’
Hosted by: The Cement and Concrete Institute of South Africa
CD-ROM produced by: Document Transformation Technologies
11 - 16 May 2003, Durban, South Africa
ISBN Number: 0-9584085-8-0
Editors: Dr G. Grieve and G. Owens
Congress Organised by: Event Dynamics

drinking water supply – tests and evaluation" for cementitious materials in contact with drinking water [5]. These three regulations are to be classed together in one DIN technical report as a basis for further European standardisation work.

The German cement industry has dealt for many years with the environmental compatibility of cementitious building materials in all phases of the product life, covering the production of cement, the concrete processing, the use in constructions or buildings as well as recycling and final disposal. At the beginning the research was focussed on the behaviour of trace elements in the clinker burning process, emissions from the kilns and their impact to the environment. Later, the behaviour of trace elements in the clinker, cement and concrete was examined at full length allowing cementitious materials to be used as an encapsulating and binding matrix for wastes. With increasing use of secondary materials for clinker production the attention has been concentrating on the initial materials required in cement manufacture and on the cement. Today, the behaviour of trace elements is well understood throughout the life cycle of cement and concrete. All investigations have shown that the hardened cement paste is a very good encapsulating and binding matrix for trace elements and that the leaching rates of trace elements from cementitious materials are on a very low level [6-8].

Mortar and concrete may also contain small amounts of organic substances deriving from additives and admixtures as well as from recycled materials, e. g. bituminous or tar-containing road construction materials. Extensive investigations have shown that the hardened cement paste is also an encapsulating and binding matrix for organic substances [9, 10]. While for trace elements the leaching behaviour from cementitious materials is important to understand, for organic substances the release of volatile components to the surrounding must also be taken into account. Investigations carried out so far have shown that cementitious materials, even when produced with typical amounts of organic concrete additives or admixtures, cause only very slight emissions of volatile organic substances [11, 12].

2. EUROPEAN REGULATIONS

2.1 Construction Products Directive

The Construction Products Directive required that construction works must be designed and built in such a way that they will not be a threat to the hygiene or health of the occupants or neighbours. In a corresponding Guidance Paper of the European Union (EU) [13] the CPD limits its requirements to the direct environment of the works during use. Hence regional or global environmental aspects as well as aspects of workers health are outside the scope of the Directive.

According to the European Economic Treaty, EU Member States remain responsible for ensuring that buildings and civil engineering works in their territory are designed and completed in a way that does not endanger the safety of persons, domestic animals and properties. Therefore, national provisions laid down by law, regulations or administrative actions are supplementary to the European Construction Products Directive. These legal instruments ensure the works built with the construction products admitted onto the European common market fulfil the regulations valid in the place of use. To cope with different requirements, national provisions and harmonised technical specifications should express the relevant product characteristics in terms of levels and classes.

2.2 Chemicals legislation on Dangerous Substances

The Directive on Dangerous Substances [14], with its corresponding amendments, specified the approximation of laws, regulations and administrative provisions relating to the classification, packaging and labelling of dangerous substances in the European Union. Currently there are 15 classes of danger in the Directive, e. g. "very toxic", "carcinogenic" or "dangerous for the environment". This Directive forms the basis for chemicals management in the EU and provides a

legal foundation for future EU-legislation on dangerous substances in construction products. At present, the legislation on dangerous Substances in construction products in force in the individual

Member States have been compiled in a database with more than 100 substances, which are either totally banned or limited [15]. Due to the differences in geographical and climatic conditions or in way of life as well as in the levels of protection that may prevail at national level, the Member States provisions to protect the direct environment of buildings vary significantly. Currently European provisions to protect the direct environment of works or buildings do not exist. Therefore, the first generation of harmonized product standards refer with respect to dangerous substances to national laws, regulations and administrative provisions, which must be complied with, when and where they apply.

2.3 European Acceptance Scheme for Construction Products in contact with Drinking Water

Construction products in contact with drinking water, which are referred to in national regulations, fall within the scope of the Construction Products Directive (CPD) [1] and are mentioned in the European Drinking Water Directive (DWD) [16]. In 1999 the Regulators Group for Construction Products in contact with Drinking Water (RG-CPDW) was established, as a working group of both the Standing Committee on Construction (SCC) and the Standing Committee on Drinking Water (SCDW), to work out an European Acceptance Scheme (EAS) for Construction Products in contact with Drinking Water (CPDW). In the meantime the RG-CPDW has prepared an interim report "EAS on Paper" [17] and a corresponding mandate to CEN, for the preparation of the necessary test methods to be included in the EAS and for harmonized European product standards (hENs) to cover the CPDW as far as possible. The main principles of the draft EAS are:

- The EAS will offer a high level of consumer protection that does not compromise the existing protection levels of the national Acceptance Schemes.
- The EAS will provide a level playing field for all materials and products, in particular using the same basis for consumer protection.
- All stages of the EAS-process will be transparent.
- The EAS will enable the satisfaction of the requirements of the DWD and the CPD.

The ranges of assessments to be carried out to ensure that the drinking water after contact with a product poses no significant risk to health and is acceptable to the consumer are:

- Organoleptic assessments.
- General hygiene assessments.
- Toxicological assessment of substances.
- Enhancement of microbial growth.

However, not all of the assessments and conditions apply to all products. Considering existing experience it seems not to be relevant to control the main constituents of cementitious materials, i.e. cement, water, sand and gravel. However, other constituents of cementitious products, e. g. admixtures, additions or fibres, especially those of an organic nature will be controlled, possibly by a positive list approach. Final acceptance will be based on the assessment of the finished product. However, for cementitious materials an alternative proceeding has been proposed by the cement and concrete industry to replace the direct acceptance by an indirect acceptance based on corresponding positive lists of the constituent materials. This alternative proceeding is indispensable in particular for site mixed mortar and concrete but may also be of advantage for prefabricated products.

3. GERMAN REGULATIONS

3.1 Evaluation of effects of construction products on soil and groundwater

For new construction products which need a general technical approval, a task force of the German Institute for Building Technology (DIBt) has established an interdisciplinary concept on possible dangers to soil and groundwater, which resulted from intensive deliberations between water, soil and building authorities and industry [3]. Standardised and already technically approved construction products are not included in the scope of this concept, which distinguishes between buildings in direct contact with the ground water and buildings installed above the groundwater level. In the first case the contact water between the building and the groundwater is relevant for evaluation, and in the second case the percolating water when it enters the groundwater. The evaluation is made in two subsequent phases (Figure 1).

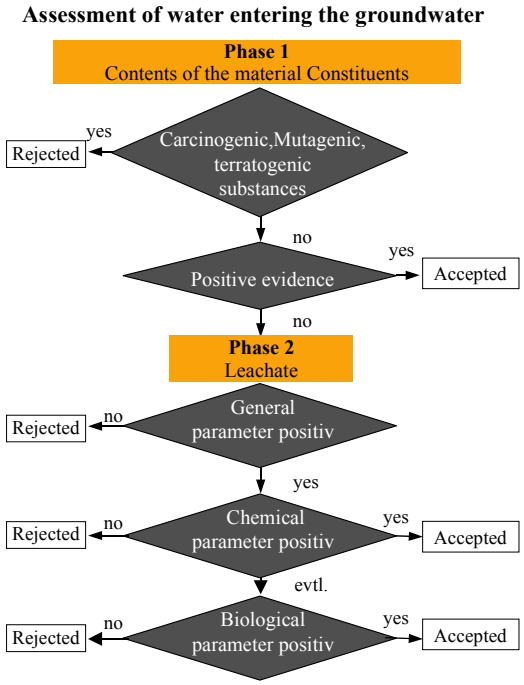

Figure 1. Assessment of water entering the groundwater

Phase 1 evaluates the material constituents of the construction product. Materials in which carcinogenic, mutagenic or terratogenic substances are actively used will be rejected. For materials for which undisputed positive evidence is given a generic acceptance without further testing will be possible in phase 1.

Table1. “No-Adverse-Effect-Levels” for inorganic parameters [3]

Inorganic Parameter	No-Adverse-Effect-Level [µg/L]	Inorganic Parameter	No-Adverse-Effect-Level [µg/L]
Antimony (Sb)	10	Nickel (Ni)	50
Arsenic (As)	10	Mercury (Hg)	1
Lead (Pb)	25	Selenium (Se)	10
Cadmium (Cd)	5	Zinc (Zn)	500
Chromium, total, (Cr)	50	Tin (Sn)	40
Chromate (Cr VI)	8	Cyanide, total (CN^-)	50
Cobalt (Co)	50	Cyanide, volatile (CN^-)	10
Copper (Cu)	50	Fluoride (F^-)	750
Molybdenum (Mo)	50		

Phase 2 evaluates those substances which are leached from construction products in standardised leaching tests. The leachates are to be analysed for general parameters, e. g. odour, colour and pH-value, for chemical parameters, e. g. trace elements and organic constituents, and if relevant for biological parameters. The chemical parameters in the leachates are transformed into values relevant for the water entering the groundwater on the basis of standardised calculation procedures, and are then evaluated against so called "No-Adverse-Effect-Levels" which have been fixed by the German Soil Authorities. Table 1 shows, as example, the "No-Adverse-Effect-Levels" for inorganic parameters [3].

3.2 Evaluation of effects of indoor pollution on human health

There is increasing discussion in public and among experts about the release of pollutants from building materials into the indoor air of residential accommodation. This has come about because, among other things, increasingly impermeable building claddings with less ventilation are being erected to save energy. Therefore, harmful substances released can build up as a result of the deficient air replacement. German Health Authorities have prepared a draft concept for the evaluation of volatile organic compounds (VOC) as basis for an approval scheme for construction products [4]. The scheme is based on a two phase evaluation similar to Figure 1.

In phase 1 the emissions, measured in a standardised testing arrangement, are controlled in view of carcinogenic, mutagenic or cytotoxic substances. In phase 2 the Total Volatile Organic Compounds (TVOC), determined after 3 days of exposure are evaluated. In order to assess the long term behaviour an additional TVOC-measurement is taken after 28 days. In addition to the TVOC also the Semi Volatile Organic Compounds (SVOC) are determined after 28 days. Since the toxic relevance of any individual VOC cannot be evaluated on the basis of TVOC and SVOC, it is proposed that any VOC with concentrations above a given level should be evaluated against an acceptable limiting value (Lowest Concentration of Interest LCI). The draft evaluation concept leaves many questions open and requires further intensive discussions. In particular the scientific background for the definition of the LCI for individual VOCs must be further analysed.

3.3 Hygienic requirements for cement-bound materials for drinking water supply

Due to the great importance of drinking water being supplied in perfect condition, all materials that come into direct contact with the drinking water are subject to strict drinking water hygienic specifications. According to § 31 of the German Foodstuff and Consumer Articles Act (LMBG) materials from which substances can be transferred into the water must not come into contact with drinking water. Exceptions are only proportions that are harmless to health and do not alter odour, taste etc., provided that they are technically unavoidable. For cementitious materials that have proven their worth in all sectors of the drinking water supply for decades, in 1999 the German Gas and Water Association (DVGW) established the worksheet W 347 "Hygienic requirements for cement-bound materials for drinking water supply – tests and evaluation" [5]. The worksheet is divided into four areas of application (see Table 2).

Table 2. Areas of application for cementitious materials in the drinking water sector

Area of application	Materials and structural elements
I	Cement mortar linings for cast-iron and steel pipes
II	Concrete pipes, concrete tanks, mortars for tank linings
III	Tile adhesives, jointing mortars, mortar linings for pipe fittings, repair mortars, e. g. for weld seams
IV	Concrete structural elements in drinking water protection zones

It specifies that all standardized or approved cements can be used, this also applies to standardized aggregates or additions. Also, concrete additions and admixtures contained in a “positive list” can be used if they have also passed the drinking water hygiene tests described in Table 3. The positive list covers all the currently in Germany used raw materials for concrete additions and admixtures. However, as the use of organic concrete additions or admixtures is viewed critically by drinking water hygiene specialists, such substances should only be used if they are necessary for achieving important mortar or concrete properties. Table 3 shows the tests to be performed for cementitious materials in the drinking water section in relation to the intended area of application. The 6-month-long microbiological test is only required if organic substances enter the cementitious material via concrete additions or admixtures. The tests are carried out on test pieces, e. g. standard mortar prisms, or on finished products, e. g. sections of pipes, after a prior storage and pretreatment appropriate for drinking water applications, e. g. rinsing with drinking water for 14 days.

Table 3. Scope of testing for cementitious materials in the drinking water sector

Tests to be performed	Drinking water supply	Raw water supply and constructions in drinking water protection zone I	Constructions in drinking water protection zones II + III
Migration tests			
Organoleptic tests	+	+	+
TOC release rate	+	+	-
Arsenic release rate[1)]	+	+	+
Lead release rate	+	+	+
Chromium release rate	+	+	+
Microbiological test			
DVGW Worksheet W 270[2)]	+	+	-[3)]

1) Testing only required if fly ash from bituminous coal is used
2) Testing only required if organic additions, admixtures or indirect materials are used
3) Testing only required for mortar encasement of pipes, microbiological growth is allowed

4. CONTENT OF TRACE ELEMENTS AND ORGANIC SUBSTANCES IN CEMENT AND CEMENTITIOUS MATERIALS

Even with exclusive use of primary raw materials and fossil fuels, trace elements are introduced into the clinker burning process. The trace elements are bound in the clinker more or less to the same extent as introduced into the process, and no residual materials will remain. Therefore, the concentrations of trace elements in the clinker mainly originate from the natural element distribution in the starting materials, which can differ markedly from each other depending on the deposit. If secondary raw materials and/or secondary fuels are used in the clinker burning process under today’s regular conditions – which are determined by the demands on product quality, suitability in terms of process engineering, as well as economic efficiency – the resulting concentrations of the respective trace elements may be increased negligibly, but also reduced. However, in most cases these changes are overlain by the natural concentration variations in the primary feed materials. In 1999 the Research Institute of the German Cement Industry investigated all Portland, Portland composite and blast furnace cements manufactured in Germany as defined in DIN 1164 for 17 trace elements [18]. Table 4 lists the bandwidths of the trace element contents of the German cements. These concentrations correspond to the concentration variations of trace elements found in natural rock, soil and clay.

On account of the high temperature of the clinker burning process with gas temperatures up to 2000 °C and the oxidizing kiln atmosphere, which prevails for reasons of product quality, organic substances are practically undetectable in Portland cement clinker.

Table 4. Bandwidths of trace element contents in German standard cements

Element	Content g/t (ppm)	Element	Content g/t (ppm)
Arsenic (AS)	< 1 – 55	Lead (Pb)	2 – 200
Beryllium (Be)	< 0.2 – 2.5	Antimony (Sb)	< 1 – 35
Cadmium (Cd)	< 0.1 – 8	Selenium (Se)	< 1 – 2.5
Cobalt (Co)	1 – 30	Tellurium (Te)	< 0.5
Chromium (Cr)	12 – 105	Thallium (Tl)	< 0.5 – 2
Copper (Cu)	5 – 280	Vanadium (V)	15 – 200
Mercury (Hg)	< 0.02 – 0.35	Zinc (Zn)	20 – 450
Manganese (Mn)	90 – 4200	Tin (Sn)	< 1 – 22
Nickel (Ni)	5.5 – 80		

During cement manufacturing grinding aids like glycols or triethanolamine are often added in concentrations less than 0.05 wt.%, e. g. to improve the utilization of energy. Higher amounts of organic substances may be introduced into concrete via additives or admixtures. Whereas organic additives play only a minor role for the production of concrete, modern concrete technology is to a great extent orientated towards the use of concrete admixtures. Today 80 to 90 % of all concrete is produced with admixtures in Germany, the majority being plasticizers and superplasticizers. However, in terms of quantity admixtures play only a minor role in the multi-component system concrete.

5. LEACHING BEHAVIOUR OF TRACE ELEMENTS AND ORGANIC SUBSTANCES

Numerous studies confirm that the chemical composition – i. e. the trace element content – of cement has no direct relation to the leaching characteristic of cementitious materials. They have also shown that the release of constituents, such as trace elements or organic substances, from cementitious materials in contact with water is mainly diffusion-controlled and affected by various chemical and physical retention mechanisms [6-8]. The transport in the fluid filled pores of the hardened cement paste is caused by diffusion of the dissolved substances in the fluid. Driving force for the diffusion is the difference in concentration of the substance in the pore solution and outside the porous solid. The concentration of trace elements and organic substances in the pore solution can be decreased to a great extend due to its

- incorporation in the crystal lattice of the hydrate phases,
- chemical binding to the surface of the hydrate phases,
- sorption onto the surface of the hydrate phases and
- formation of insoluble salts.

The transport speed is governed by the diffusion characteristic of the transported substances and the pore size distribution of the cementitious material. Therefore, for practical purpose the most important engineering tool to increase the resistance against leaching from concrete is to reduce the amount of connected capillary pores, in which transport processes can take place. For properly manufactured concrete the diffusion speed of the corresponding substances may be reduced by a factor up to 5000 compared with the free diffusion in water [7].

To investigate more closely the principal release mechanism of trace elements from hardened mortar and concrete, a special clinker was burnt from raw meal with artificially increased trace element contents in a pilot-scale rotary kiln. The cements manufactured from this clinker demonstrated element contents of up to 340 ppm for Arsenic, 1400 ppm for Chromium, 200 ppm for Molybdenum and 2000 ppm for Zinc. The leaching tests performed demonstrate similar leaching characteristics as cementitious materials made from ordinary Portland cements. For “regular” metals, such as Zinc, no significant increase in the eluted proportion occurs at pH values

that correspond to standard concrete applications (pH > 8). Also for Arsenic the increased contents in cements only lead to a slight rise in the eluted quantities. However, for Chromium and Molybdenum increased leaching occurs in line with higher concentrations in the cement [6]. Using the leaching of Chromium from uncrushed mortar prisms according to a trough method (64-day-test), Figure 2 shows that for the mortars investigated here a linear relationship exists between the Chromium content in the cements and the integral leached Chromium quantities. However, a deciding factor for the evaluation of these results is, that the leachable quantities are on a low level overall, and that the leaching rates decline considerably with progressing elution time. In summary these investigations confirm the large binding capacity of the hardened cement paste for trace elements. They further show that the release of trace elements from cementitious materials, even at clearly increased concentrations in the cement, is not environmentally relevant under normal application conditions, in which the natural alkalinity of the cementitious matrix is decisive for the leaching behaviour.

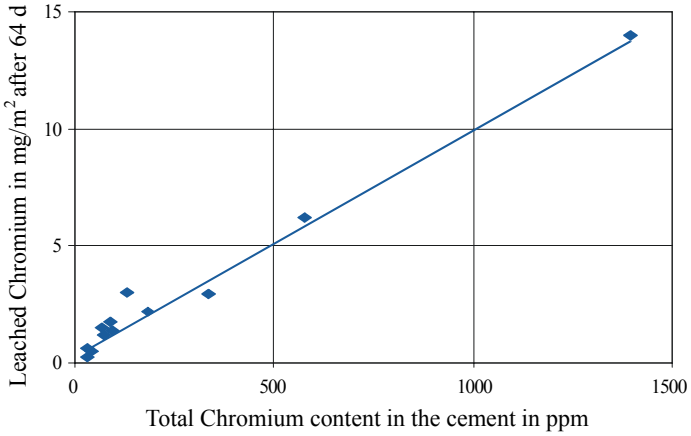

Figure 2. Relation between total Chromium contents in cement and the leached quantities after 64-day trough method test [6]

Intensive investigations into the behaviour of concrete admixtures have shown that these substances also are, to a great extent, rapidly adsorbed on the cement or precipitated in the pore solution [9, 10]. Further investigations on naphthalene sulphonates have shown that only monomeric sulphonates are eluted. Oligomers and polymers which form the major part of these plasticizing admixtures are immobilized in the hardened cement paste [9]. Figure 3 shows the results of trough leaching tests on hardened cement paste cylinders for test periods up to 3 days.

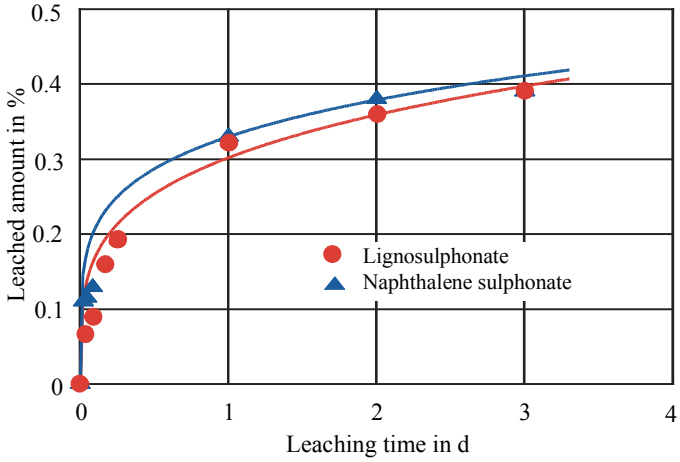

Figure 3. Dependence of the quantity of lignosulphonate and naphthalene sulphonate leached from hardened cement paste cylinders on time [10]

From the decrease of the release by time, it follows that with the quantities of plasticizing admixtures normally used in concrete - as a rule less than 1 wt.% as dry mass relative to the cement weight – only small quantities can be leached from impermeable concrete under practical leaching conditions.

6. EMISSION OF VOLATILE ORGANIC SUBSTANCES

Air borne emissions may be a threat to the hygiene and health of occupants in the indoor environment. Constructions made of traditional, proven building materials which are purely inorganic in nature, such as mortar, stucco, concrete, steel and glass, generally release insignificant amounts of harmful substances or none at all after installation [19]. However, today many cementitious materials are manufactured with organic additions or admixtures which may contain volatile substances, e. g. preservatives like formaldehyde, in small quantities. Figure 4 shows the cumulative amounts of formaldehyde released from cement pastes with five superplasticizers with different free formaldehyde contents.

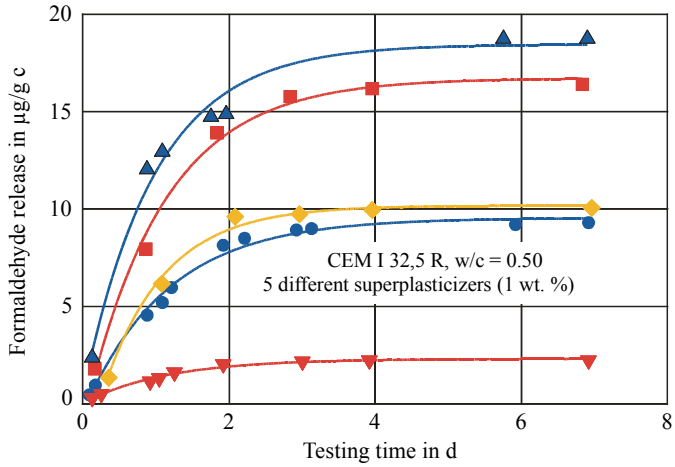

Figure 4. Formaldehyde release of cement pastes with five superplasticizers with different free formaldehyde contents [12]

It is clear from the figure that the initially rapid release slows down considerably after one or two days and from then only extremely small quantities are released, which after seven days result in concentrations which are no longer detectable. From the course of the curves it can concluded that there is no risk of any danger from the release of formaldehyde from cementitious building products made with concrete admixtures during the use of a building. Only under unfavourable conditions it is possible for the “maximum workplace concentration (MAK)” to be exceeded for short periods during production, e. g. in a concrete plant. However, workplace-specific measurements confirm that the formaldehyde concentration during concrete work is well within the “MAK” limit [20].

7. CONCLUSIONS

The leaching behaviour of trace elements and organic substances from cementitious materials is controlled by the degree of binding of these substances to the hardened cement paste and the pore size distribution of the cementitious matrix. The long-term leaching behaviour of substances from cementitious materials follows diffusion-controlled transport mechanism with low diffusion rates. This is especially the case for properly manufactured concrete. Therefore the most important engineering tool to minimize leaching from cementitious materials is to reduce the capillary porosity of the hardened cement paste matrix. For typical applications of organic additives or admixtures in concrete buildings the release of volatile organic substances is on a low level, and it

can be concluded that there is no risk of a nuisance or threat to the user. Cement and cementitious construction products satisfy the fundamental requirements of the European Construction Products Directive CPD and the corresponding national regulations.

REFERENCES

[1] Council Directive 89/106/EEC: 1988, Regulations and administrative provisions of the Member States relating to construction products, Brussels: Official journal of the European Communities L, vol. 40, 1989, p.12 ff.

[2] EN 197-1: 2000, Cement – Part 1: Composition, specifications and conformity criteria for common cements, Brussels: European Committee for Standardization, 2000.

[3] Schriften des Deutschen Instituts für Bautechnik, Reihe M: 2000, Merkblatt, Bewertung der Auswirkungen von Bauprodukten auf Boden und Grundwasser, Berlin: Deutsches Institut für Bautechnik (DIBt), 2000.

[4] AgBB, draft: 2001, Vorgehensweise bei der gesundheitlichen Bewertung der Emissionen von flüchtigen organischen Verbindungen (VOC) aus Bauprodukten, Berlin: Ausschuss zur gesundheitlichen Bewertung von Bauprodukten (AgBB), DIBt-Mitteilungen, 2001, pp.3-12.

[5] DVGW Regelwerk, Arbeitsblatt W 347: 1999, Hygienische Anforderungen an zementgebundene Werkstoffe im Trinkwasserbereich – Prüfung und Bewertung, Bonn: Deutscher Verein des Gas- und Wasserfaches (DVGW), 1999.

[6] Sloot van der, H.A., et al. Environmental criteria for cement based products (ECRICEM) – Phase I: Ordinary Portland Cements, Petten, Energy research Centre of the Netherlands, ECN, 2001. (ECN Report ECN-C-01-069).

[7] Hohberg, I., Müller, Ch., Schießl, P. and Volland, G. Umweltverträglichkeit zementgebundener Baustoffe, Sachstandsbericht, Deutscher Ausschuß für Stahlbeton (DAfStb), Berlin, Köln: Beuth Verlag GmbH,1996.

[8] Sprung, S., Rechenberg, W. and Bachmann, G. Umweltverträglichkeit von Zement, Zement Kalk Gips, vol. 47, 1994, pp.456-461.

[9] Herb, H., Köster, R. and Höll, W.H. Elution von sulfonathaltigen Betonzusatzmitteln aus Zementstein, Vom Wasser, vol. 95, 2000, pp.205-214.

[10] Spanka, G. and Thielen, G. Untersuchungen zum Nachweis von verflüssigenden Betonzusatzmitteln und zu deren Sorptions- und Elutionsverhalten, Beton, vol. 45, 1995, pp.320-327.

[11] Breuer, K. and Mayer, E. Kann man die Gesundheitsverträglichkeit von Bauprodukten ermitteln ?, Bauphysik, vol. 20, 1998, pp.226-232.

[12] Spanka, G. and Thielen, G. Freisetzung flüchtiger Substanzen aus zementgebundenen Bauprodukten, Beton, vol. 49, 1999, pp.111-114 and pp.173-177.

[13] Guidance paper H: 2001, A harmonised approach relating to dangerous substances under the Construction Products Directive, Brussels: EU, Enterprise Directorate-General, 2001.

[14] Council Directive 67/548/EEC: 1967, Approximation of laws, regulations and administrative provisions relating to the classification, packaging and labelling of dangerous substances, Brussels: Official journal of the European Communities, vol. 196, 1967, p.1 ff.

[15] Guidance paper H: 2001, A harmonised approach relating to dangerous substances under the Construction Products Directive, annex 2, dangerous substances in construction products ordered by country, Brussels: EU, Enterprise Directorate-General, 2001.

[16] Council Directive 98/83/EEC:1998, on the quality of water intended for human consumption, Brussels: Official journal of the European Communities L, vol. 330,1998, p.32 ff.

[17] Interims report: 2001, The European Acceptance Scheme for construction products in contact with drinking water, Brussels: EU, Enterprise Directorate-General, 2001.

[18] Verein Deutscher Zementwerke: 2000, Umweltdaten der deutschen Zementindustrie, Düsseldorf: Verlag Bau + Technik GmbH, 2000.

[19] Rühl, R. Prävention durch die Wahl schadstoffarmer Baustoffe, Kommission zur Reinhaltung der Luft im VDI und DIN, Schriftenreihe, vol. 19,1992, pp.53-60.

[20] Sachstandsbericht: 1999, Betonzusatzmittel und Umwelt, Frankfurt: Deutsche Bauchemie e. V., 1999.

HYGIENIC, HEALTH AND ENVIRONMENTAL COMPATIBILITY OF CEMENTITIOUS CONSTRUCTION PRODUCTS

M. Schneider and G. Spanka

Research Institute of the Cement Industry, German Cement Works Association, Düsseldorf, Germany. E-mail: Sch@vdz-online.de

Dr. rer. nat. Martin Schneider

German Cement Works Association, Duesseldorf, Germany.
E-mail: sch@vdz-online.de

Dr. rer. nat. Martin Schneider studied physics in Mainz and Bonn, Germany. After 4 years of scientific work both in Bonn and in the USA, he joined the Research Institute of the Cement Industry, where he was in charge of the “Environment Protection” and “cement chemistry” sections. In 1998 he was appointed Managing Director of the German Cement Works Association, since January 2000 he is Chief Executive of the VDZ and Head of the Research Institute.

SULFATE-RESISTING PROPERTIES OF CEMENTS AND CEMENT/FLY ASH MIXTURES

M. Schneider, S. Puntke, H.-M. Sylla and K. Lipus

German Cement Works Association, Research Institute of the Cement Industry,
Düsseldorf, Germany; E-mail: pk@vdz-online.de

ABSTRACT

High-sulfate-resisting cements include low-aluminate Portland cements and *slag-rich* blastfurnace cements. Some countries also permit the use of cements containing fly ash and pozzolana as well as mixtures of cement and fly ash for producing sulfate-resisting mortar and concrete. Sulfate attack usually occurs in the soil at ambient temperatures around 9°C (average value). The investigations reported have shown that the classical sulfate-resisting cements also exhibit a high sulfate resistance at these low temperatures. However, mixtures of cement and fly ash proved to be significantly less favourable than at 20°C and did not provide high sulfate-resisting properties under such test conditions. At temperatures of less than about 15°C the damage mechanism due to a sulfate attack changes because thaumasite can form under suitable conditions. This can result in a loss in strength of the microstructure that in extreme cases leads to a complete destruction. This thaumasite formation itself is in contrast to the classical expansion reactions due to ettringite and gypsum not necessarily accompanied by expansion of the concrete, but an exclusive thaumasite formation was not observed. However, the importance of the presented laboratory tests for practical building work has not yet been adequately investigated.

1. INTRODUCTION

A high chemical resistance of the hardened binder matrix is one essential requirement for the durability of concrete. The safety concept in case of sulfate exposure which is implemented in the European concrete standard EN 206 [1] and is based on long-term practical experiences stipulates the utilisation of cement with high sulfate-resisting properties (SR criterion) and furthermore a dense concrete with a high resistance to diffusion. According to German standard DIN 1164 SR-cements are Portland cements (CEM I) with a maximum C_3A content of 3.0 % by mass and a maximum Al_2O_3 content of 5.0 % by mass as well as blastfurnace cements of type CEM III/B and CEM III/C. According to the German concrete standard DIN 1045-2 mixtures of cement and fly ash can be used as an alternative to high sulfate-resisting cements in Germany to produce concrete to resist a sulfate attack of up to 1500 mg sulfate/l in the attacking water [2]. In these cases at least 20 % by mass fly ash according to EN 450 must be added to the concrete when using Portland cement, Portland-limestone cement or Portland-slag cement, and at least 10 % by mass fly ash must be added when using Portland-burnt shale cement and blastfurnace cement of type CEM III/A. The water/binder ratio [w/(c+0.4f)] must be ≤ 0.50. The measures to produce sulfate-resisting concrete in Germany are summarised in (Table 1). In Germany, due to the implementation of these measures, damage caused by sulfate attack are nowadays practically unknown.

Proceedings of the 11th International Congress on the Chemistry of Cement (ICCC)
'Cement's Contribution to the Development in the 21st Century'
Hosted by: The Cement and Concrete Institute of South Africa
CD-ROM produced by: Document Transformation Technologies
11 - 16 May 2003, Durban, South Africa
ISBN Number: 0-9584085-8-0
Editors: Dr G. Grieve and G. Owens
Congress Organised by: Event Dynamics

Table 1. Measures required in Germany to produce concrete with high sulfate resistance according to DIN EN 206-1/DIN 1045- 2

Exposure class [mg SO_4^{2-}/l]	Degree of attack	Measures
< 200	not attacking	none
XA1 200 – 600	weak	water/cement ratio ≤ 0.60; minimum compressive strength C25/30
XA2 600 - 1500	moderate	water/cement ratio ≤ 0.50; minimum compressive strength C35/40; SR-cement or mixture of CEM II/A-T, CEM II/B-T, CEM III/A and minimum 10 % by mass fly ash or CEM I, CEM II/A-S, CEM II/B-S, CEM II/A-LL and minimum 20 % by mass fly ash
XA2 1500 - 3000	moderate	water/cement ratio ≤ 0.50; SR-cement; minimum compressive strength C35/40
XA3 > 3000	strong	water/cement ratio ≤ 0.45; SR-cement; minimum compressive strength C35/40; sealing

Within the framework of quality control it is not practicable to test the sulfate-resisting properties of cements by testing mortar and concrete pieces under realistic conditions. Such tests would take too much time. Tests that provide representative guide values are therefore required so that the desired information can be obtained rapidly from “accelerated” laboratory tests. To test the sulfate resistance against an external sulfate attack, usually expansions of defined mortar specimens are measured. Such test methods have to cover the “chemical resistance” of the cement to the chemical reaction with sulfate ions, i.e. the “internal sulfate resistance” and the “physical resistance” of the mortar to the penetration of sulfate ions into the sample, i.e. the “external sulfate resistance” [3,4].

In Germany the Wittekindt method [5] and the so-called SVA method, adopted by the committee of experts at the German Institute for Construction Technology (SVA) [6], are the common methods to test sulfate-resisting properties of cements. A CEN method, named after the CEN TC51 Technical Committee [7], is the preferred performance test in many other European countries. Results of several investigations showed that the test results of all three performance tests often differ because of the great scatter of the measured values. One target of the recent investigations of the FIZ (Research Institute of the Cement Industry) of the VDZ (German Cement Works Association) was to compare these three test methods using different types of cement and cement/fly ash mixtures.

Concrete is usually exposed to sulfate attack when it comes into contact with groundwater containing sulfate. The temperature of the soil is about 9°C on average and therefore quite different from the temperature of 20°C regularly used in the laboratory tests. Another aim of the investigations was therefore to clarify the influence of the test temperature on the test results of mortars with cements and cement/fly ash mixtures.

A special form of sulfate attack has been identified in over 80 cases in Great Britain during the last 15 years. In these cases harmful thaumasite had been formed under wet and cold conditions and in the presence of carbonate [8]. Investigations at the VDZ had the further task to understand the causes and mechanisms of this harmful thaumasite formation, depending on the different cement and cement/fly ash mixtures used.

2. EXPERIMENTAL WORK

2.1 Test methods to determine the sulfate-resisting properties of cements

In Germany, the Wittekindt, the SVA and the CEN method are accelerated test methods that have been used for investigations in different research projects as well as comparative test programmes at the VDZ over the past years.

The Wittekindt method has the longest tradition and has been used for many years in a slightly modified form at the VDZ. Flat mortar bars of 1 x 4 x 16 cm³ are produced with standard sand in accordance with the German cement standard DIN 1164 of 1958 with a water/cement ratio of 0.60. The SVA method is quite similar to the Wittekindt method. The flat mortar bars are produced in accordance with European cement standard EN 196-1 with a water/cement ratio of 0.50. The CEN method is derived from the work of CEN TC 51 over the last 10 years with the target to be adopted in a common European standard. For this method 2 x 2 x 16 cm³ mortar bars are produced in accordance with EN 196-1 with a water/cement ratio of 0.50. Further details of the three test methods are shown in Table 2.

Table 2. Comparison of sulfate resistance tests: Wittekindt, SVA and CEN method

Test conditions	**Method**		
	Wittekindt	**SVA**	**CEN**
Specimen [cm^3]	1 x 4 x 16	1 x 4 x 16	2 x 2 x 16
Mortar acc. to	DIN 1164 (1958) former German Standard	EN 196-1	EN 196-1
Standard sand	I and II	I,II and III	I, II and III
w/c	0.60	0.50	0.50
Compaction	vibration table	vibration table	jolting table
In mould [d]	1	2	1
Preliminary storage [d]	13 days in H_2O	12 days in $Ca(OH)_2$	27 days in H_2O
Sulfate storage [% Na_2SO_4]	4.4	4.4	2.4
Test period/storage time [d]	56 days	91 days	not fixed
SR-criterion (expansion) [mm/m]	≤ 0.5	≤ 0.5	not fixed

In recent years, the sulfate-resisting properties of approximately 100 cements and cement/fly ash mixtures were assessed according to the test methods described.

The criterion for high sulfate-resisting properties of a cement is the relative change in length of the mortar bars, taken by the difference in the change of length between sulfate storage and water/calcium hydroxide storage after a certain storage period.

The accelerated test procedures must usually take place at a constant temperature of 20°C. Practical experience shows that sometimes construction parts are affected by sulfate attack, if they are located within the soil. There, sulfate-enriched ground water can come into contact with concrete structures. The average ground temperature in central European countries is about 9°C, which is different from the 20°C used in the test methods. Furthermore, due to thermodynamic calculations the known expansive minerals ettringite, gypsum and thaumasite are more stable at low than at higher temperatures. Therefore many of the reported investigations were also performed at 8°C.

2.2 Microstructural investigation

Besides the expansion measurements also the microstructure of the mortar specimens has been examined. By means of optical microscopy, scanning electron microscopy (SEM) combined with energy dispersive microanalysis (EDS), and X-ray diffraction (XRD), the mineralogical and chemical composition of the reaction products inside the deteriorated structures of the test pieces were analysed. From these results information could be obtained about the deterioration mechanisms of the sulfate attack for different cements and binder systems.

3. RESULTS

3.1 Comparison of the test methods

To compare the three test methods mentioned, samples of different cements and binder mixes were prepared. Therefore high sulfate-resisting cements (CEM I-SR and CEM III/B-SR), ordinary Portland cements and mixtures made of ordinary Portland cements combined with fly ashes (from melting and from dry chamber firing systems), blastfurnace slag, limestone meal and burnt oil-shale were used. The measurements showed that the specimens tested according to the Wittekindt and the SVA methods led to comparable results (Table 3), taking into account the different storage period.

Table 3. Expansion of test pieces made of ordinary Portland cement/granulated blastfurnace slag mixtures according to different test methods; cements: PC 1 with 7.7 % by mass C_3A, PC 2 with 14.3 % by mass C_3A; slags: ggbs1 with 12 % by mass C_3A, ggbs 2 with 17 % by mass C_3A

Binder mix	Expansion in mm/m		
	Wittekindt (56 d)	SVA (91 d)	CEN (140 d)
PC 1	0.61	0.54	0.18
PC 1 + 20% ggbs 1	0.50	0.65	0.23
PC 1 + 20% ggbs 2	0.68	0.68	0.29
PC 1 + 55% ggbs 2	0.45	0.48	0.18
PC 2	0.85	0.82	0.18
PC 2 + 20% ggbs 1	0.67	0.69	0.16
PC 2 + 20% ggbs 2	0.78	0.80	0.27
PC 2 + 55% ggbs 2	0.13	0.23	0.14

However, the Wittekindt method showed a larger spread and thus a clearer differentiation of the behaviour of the individual binder types. This can be explained by the higher w/c ratio. The test pieces made in accordance to the SVA method were denser because of the lower w/c ratio and took up less sulfate ions per time. As a consequence, it takes longer for mortar bars under the SVA method to come to the same expansion as under the Wittekindt method. The CEN method was proved to be the least suitable test for the assessment of binders with an accelerated time scale test. As compared with the other methods, fewer sulfate ions were taken up by the test specimens,

because they were as dense as the SVA pieces but had a smaller surface/volume ratio, were hydrated longer before the onset of sulfate exposure, and were stored at an SO_4 concentration in the test solution which was almost 50% lower.

Severe scattering of the expansion values was found in inter-laboratory tests using the three methods, even after the test instructions were precisely specified to ensure compatible test conditions. The CEN working group came to a comparable result for the CEN test method.

Because of the inadequate differentiation between individual cements and the inadequate comparability of the test results from different laboratories it has not yet been possible to recommend any test method for standardization. This will require further basic physical and chemical investigations into the sulfate resistance of mortar and concrete.

3.2 Sulfate resistance against conventional sulfate attack

3.2.1 Sulfate-resisting properties of standardized cements

Figure 1 shows the expansion values of test pieces of five different cements stored, according to the Wittekindt method, but at 8°C. The samples of both SR-cements expanded only insignificantly during 56 days and fulfilled the assessment criterion as expected. Based on that assessment even the samples of the cement with 8 % by mass C_3A show a high sulfate-resisting behaviour.

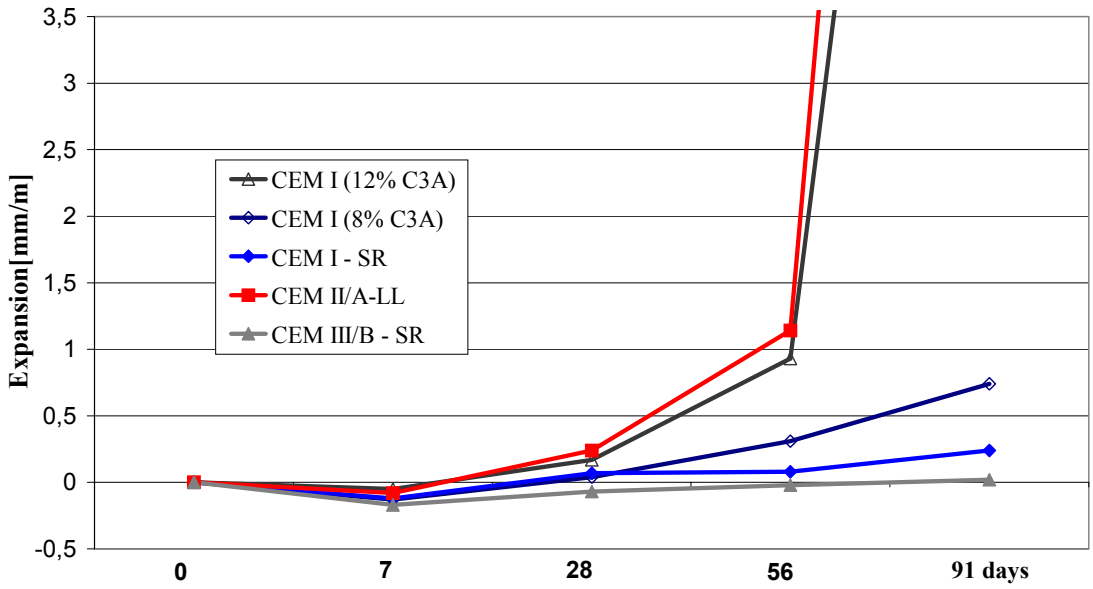

Figure 1. Expansion of 1 x 4 x 16 cm³ mortar prisms made from different cements; Wittekindt-test conditions at 8°C

Table 4 shows the expansion values of flat mortar samples made from different cements tested at 8°C and 20°C. The ordinary Portland cements and the Portland limestone cement did not fulfil the requirements for high sulfate resistance, neither at 20°C nor at 8°C. The differences between the values of the 8°C and 20°C measurement are small and within the range of the uncertainty of the measurement [9,10].

Table 4. Expansion of different cements tested according to the Wittekindt method

	Expansion after 56 d storage at 8°C [mm/m]	Expansion after 56 d storage at 20°C [mm/m]
CEM I 7,7% C_3A	0.54	0.61
CEM I 14,3% C_3A	0.93	0.85
CEM I 12% C_3A	0.95	0,88
CEM I - SR	0.11	0.13
CEM II/A-LL	1.1	0.91
CEM III/B - SR	0.04	0.07

3.2.2 Composite cements and cement/fly ash mixtures with high sulfate-resisting properties
Investigations on Portland cement/fly ash mixtures have shown that dry chamber firing ash with fairly low content of glass and Al_2O_3 tends to exhibit a more favourable behaviour than fly ash from melting chamber firing systems with higher levels of glass and Al_2O_3 (Figure 2).

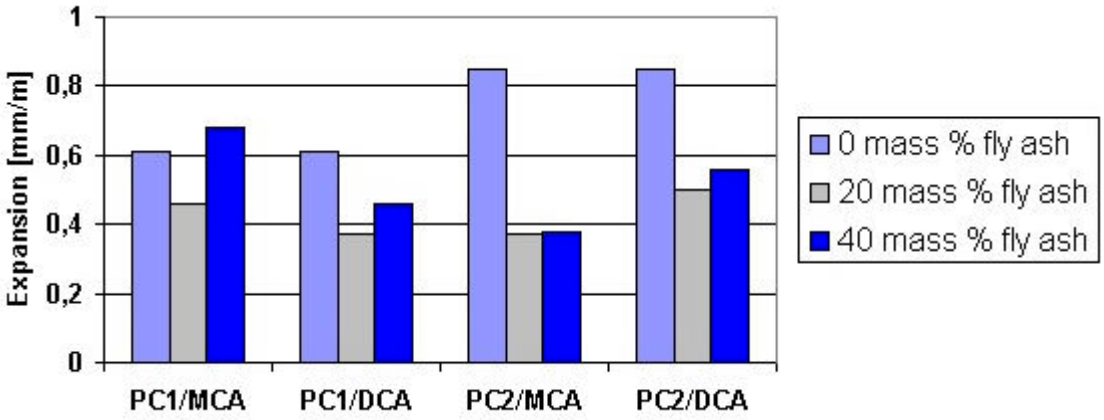

Figure 2. Expansion of test pieces made with mixtures of Portland cement and fly ash (tested by Wittekindt method, 56 days storage at 20°C in 29.800 mg sulfate/l; Portland cements: PC1 und PC2; fly ashes: MCA from melting chamber firing, DCA from dry chamber firing)

Mortar specimens made from mixtures of cement and fly ash exhibited significantly higher expansions at 8°C than at 20°C under the various test methods. Ordinary Portland cements, Portland-limestone cements and blastfurnace cements behaved therefore differently. The test criterion of the Wittekindt test could not be fulfilled by cement/fly ash mixtures at 8°C (Figure 3).

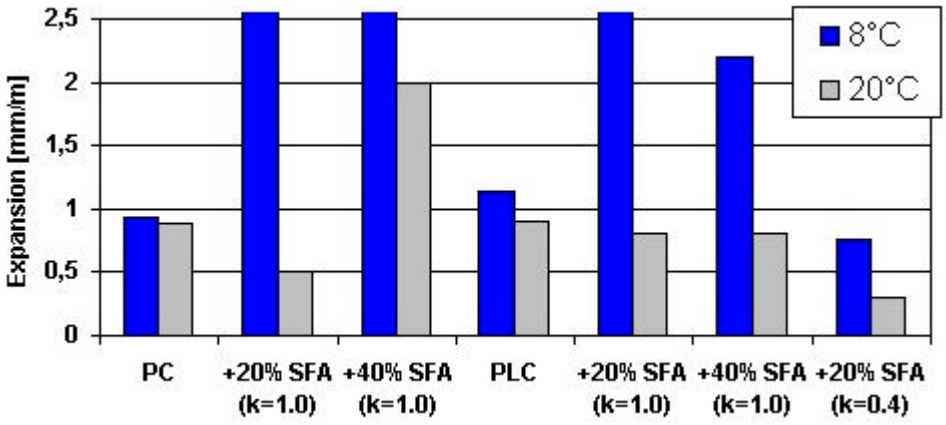

Figure 3. Expansion of flat mortar prisms made of mixtures from cement and fly ash (SFA) (tested according to Wittekindt method, 56 days' storage in 29800 mg sulfate/l, varying storage temperature)

These results are not affected by the k-factors, which was for these experiments k = 1.0 and k = 0.4, respectively

Additional investigations were also carried out at 1500 mg sulfate/l to conform with the use of fly ash permitted in the German standard, i.e. at significantly lower sulfate concentrations than in the usual laboratory tests. The behaviour of the cement/fly ash mixtures in such low concentrated sulfate solutions was different from that at higher concentrations. Mixtures with at least 20 % by mass fly ash showed here significantly higher sulfate-resisting properties than the pure cement. In particular, the test pieces made of mixtures with 40 % by mass fly ash exhibited only slight expansion and deterioration even after one year's sulfate storage.

3.3 Sulfate resistance against the thaumasite form of sulfate attack (TSA)

A research project to investigate the principles and mechanisms of thaumasite formation has been carried out at the VDZ [11]. The behaviour of various cements was examined with focus on limestone-containing cements and cement/fly ash mixtures on the one hand. On the other hand concrete samples made of carbonate-free cements and limestone-containing aggregates were investigated. Some results are shown in Table 5.

Table 5. Expansions of different cements and cement-limestone mixtures after 56 days storage in sulfate solution at 8°C (Wittekindt method), limestone 1 containing 92% $CaCO_3$, limestone 2 containing 84% $CaCO_3$

Cement	Expansion [mm/m]	Cement	Expansion [mm/m]
CEM I (12 % C_3A)	0.93	CEM I - SR	0.08
+ 5 % $CaCO_3$	1.4	+ 5 % limestone 1	0.22
+ 15 % $CaCO_3$	2.0	+ 15 % limestone 1	0.16
+ 5 % limestone 1	0.45		
+ 15 % limestone 1	1.5	CEM III/B - SR	-0.02
+ 5 % limestone 2	0.34	+ 5 % limestone 1	-0.01
+ 15 % limestone 2	1.7	+ 15 % limestone 1	-0.02

Both SR-cements, CEM I and CEM III/B showed the same small expansion behaviour with or without an addition of limestone meal. The ordinary Portland cement (non-sulfate-resisting) behaved differently. An addition of 15 % by mass limestone meal increased the expansion clearly. An addition of only 5 % by mass limestone had no significant effect on the expansion.

To investigate the reaction mechanisms of the sulfate attack the mortar bars had been stored in sulfate solution longer than necessary for the assessment test. After 56 days the specimens were only partly affected or showed no deterioration. However, within 180 days, and even more after 360 days, some samples were totally decomposed (Table 6).

In addition to the tests with high sulfate concentration also tests with lower concentration were performed. Table 6 also shows that within a year even at low sulfate concentration tests specimens were severely deteriorated. Over this long test period only the two SR-cements showed sulfate-resisting behaviour.

Table 6. Degree of Damage of mortar bars made with different cements and mixtures of cement and limestone meal after storage in sodium sulfate solution at 8°C

Binder mix	Degree of damage after storage in sulfate solution			
	29800 mg SO_4/l			1500 mg SO_4/l
	56 days' storage	180 days' storage	360 days' storage	360 days' storage
CEM I (12 % by mass C_3A)	partial	total	total	severe
CEM I + 15% mass limestone	partial	total	total	very severe
CEM I (8 % by mass C_3A)	none	partial	total	very slight
CEM I + 15 % by mass limestone	none	partial	total	severe
CEM I-SR	none	none	none	none
CEM I-SR+ 15 % by mass limestone	none	none	partial	none
CEM II/A-LL	partial	total	total	severe
CEM II/A-LL + 20 % by mass fly ash	partial	total	total	partial
CEM II/A-LL + 30 % by mass fly ash	partial	total	total	slight
CEM II/A-LL + 40 % by mass fly ash	partial	total	total	very slight
CEM III/B-SR	none	none	none	none
CEM III/B-SR + 15 % by mass limestone	none	none	none	none

Expansion examinations did not allow to decide if a test piece was deteriorated due to ettringite, gypsum or thaumasite formation. Only by microscopic investigations of the structure, aligned with microanalytical and diffractometric techniques a characterisation of the secondary reaction products was possible. The observation of the deterioration process on test pieces made of Portland-limestone cements showed that after an initial expansion and formation of first cracks, due to secondary ettringite and gypsum, the specimens decomposed faster into fine components at 8°C than at 20°C. By using scanning electron microscopic analysis thaumasite was found besides ettringite in such samples (Figure 4). However, the mortar investigations did not show significant amounts of thaumasite, when high sulfate-resisting cements were used.

4. CONCLUSIONS

Many countries have had regulations in force for many years for the production of sulfate-resistant mortars and concretes and for the requirements of sulfate-resisting cements. Various test methods for the high sulfate-resisting properties of cements are based primarely on expansion measurements.

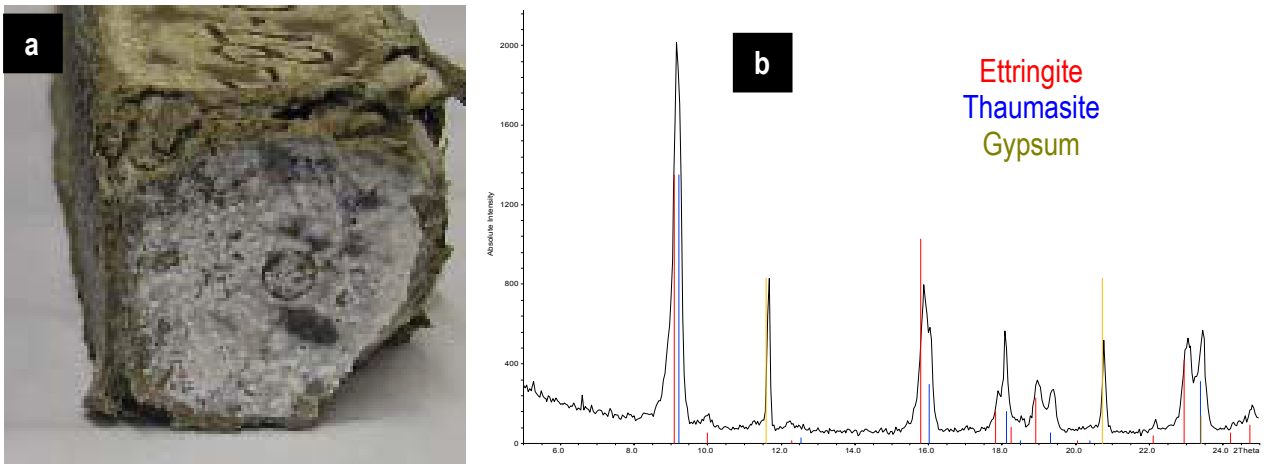

Continued…

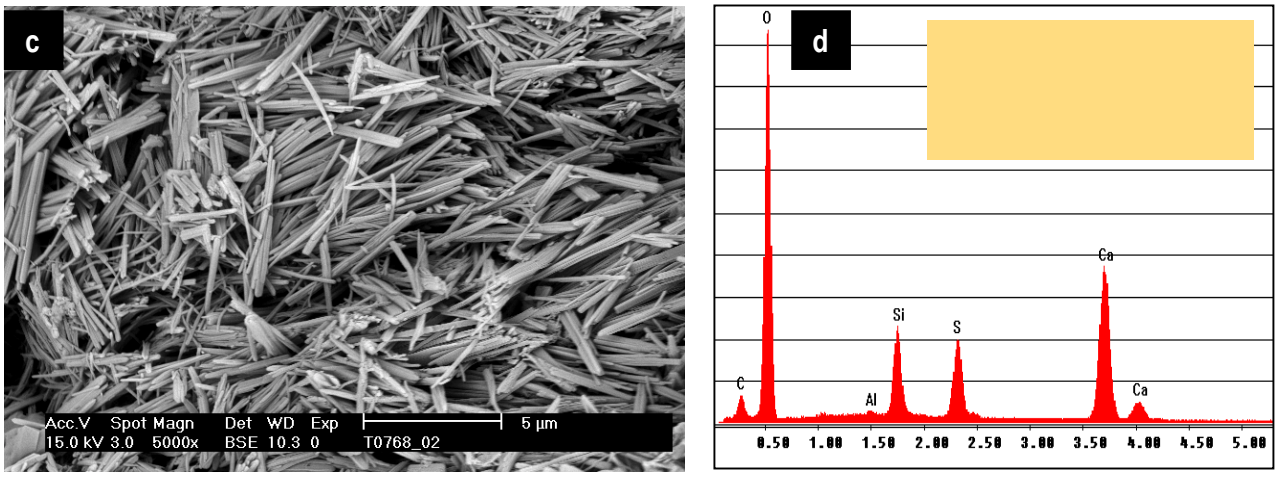

Figure 4. Deteriorated 4 x 4 x 16 cm³ prism (a); powder x-ray diffraction pattern of the deteriorated material (b); scanning electron micrograph of thaumasite crystals inside a deteriorated region (c) and energy dispersive x-ray spectrum of this area (d); sample after 400 days storage at 8°C in sodium sulfate solution of 29800 mg SO_4/l.

In the accelerated test methods examined recently by the VDZ, mortar prisms were stored at 20°C in solutions containing sulfate and then tested at some defined time. The test results reported exhibit good repeatability within a laboratory, but the comparability between different laboratories is not satisfactory because of the great scatter of the measured values. For this reason it has so far not been possible to standardise any of the methods under discussion.

The SR-cements tested, i.e. Portland cements with low C_3A content and blastfurnace cements which contain at least 66 % by mass blastfurnace slag,fulfil the performance test criterion of the accelerated Wittekindt and SVA method at 20°C as well as at lower temperature (8°C). These cements are therefore also suitable for structures which are exposed to a possible sulfate attack of exposure classes XA1 to XA3 as defined in EN 206-1 at low temperatures. Mixtures of cement and fly ash, which according to German DIN 1045-2 can be used for a sulfate attack up to 1500 mg/l, fulfil the performance test criterion of the Wittekindt and SVA method at 20°C generally. However, at 8°C these mixtures showed substantially higher expansions and missed the criterion. Only at low sulfate concentration, mixtures of cement and fly ash showed better sulfate-resisting properties than the pure cement also at low temperature. The importance of these laboratory investigations for building practice has not yet been sufficiently investigated.

Because a number of cases of thaumasite damage were found at the end of the 90s in Great Britain the basic material requirements for possible thaumasite formation were investigated systematically in a VDZ research programme. The required carbonate was provided as a cement constituent in the form of limestone meal. Not only secondary ettringite but also thaumasite was formed in many test pieces regardless of the limestone used. *This removed all the* strength from the damaged parts. Even the use of at least 20 % by mass fly ash led to no increase in sulfate resistance in these cases. However, the mortar investigations did not show significant amounts of thaumasite, when high sulfate-resisting cements were used for the mortar bar production.

Clarification of the basic relationships of the sulfate-resisting properties of cements and cement/fly ash mixtures, at low temperatures, including in the presence of carbonate, will form the subject of more extensive investigations.

REFERENCES

[1] European standard EN 206-1: 2001, Concrete, Brussel: European Committee for Standardization, 2001

[2] DIN-Fachbericht 100, Beton - Zusammenstellung von DIN EN 206-1 und DIN 1045-2, Berlin: Deutsches Institut für Normung e.V., 2001

[3] Mielke, I., Stark, J., Stürmer, S. Sulfatwiderstandsfähige Injektionsmörtel; Tagungsbericht 13. Int. Baustofftagung ibausil, Weimar 1997, vol. 2, pp. 2/1069-2/1082

[4] Locher, F.W. The sulphate resistance of cement and its testing; ZKG INTERNATIONAL, vol.51, 1998, no. 7, pp. 388-398

[5] Wittekindt, W. Sulfatbeständige Zemente und ihre Prüfung; Zement-Kalk-Gips, vol.13, 1960, no. 12, pp. 565-572

[6] Deutscher Ausschuss für Stahlbeton (DAfStb): DAfStb-Richtlinie „Verwendung von Flugasche nach DIN EN 450 im Betonbau“, (1996).

[7] European pre-standard prENV 196-X: Performance test for cement – Part X: Determination of the sulfate- or seawater resistance of cements; (1995).

[8] Report of the Thaumasite Expert Group: The thaumasite form of sulfate attack: Risks, diagnosis, remedial works and guidance on new constructions; Department of the Environment, Transport and the regions, London, 1999

[9] Activity Report 1996-1999, VDZ (German Cement Works Association), Düsseldorf, Germany, 1999, pp. 69-73

[10] Activity Report 1999-2001, VDZ (German Cement Works Association), Düsseldorf, Germany, 2001, pp. 62-64

[11] Lipus, K., Sylla, H.-M. Investigations in Germany of the Thaumasite form of sulfate attack, First International Conference of Thaumasite in Cementitious Materials , Watford, UK, 2002

USE AND REACTIVITY OF CEMENT MAIN CONSTITUENTS IN GERMANY

Martin Schneider, Stefan Puntke, Christian Schneider and Christoph Müller

Research Institute of the Cement Industry, German Cement Works Association, Düsseldorf, Germany. E-mail: Germany; E-mail: pk@vdz-online.de, sch@vdz-online.de

ABSTRACT

In Germany, more than 93 % of the blended cements are produced by using granulated blastfurnace slag or limestone as cement main constituents, while natural pozzolana and burnt shale are still of minor or local importance. Beyond the traditional main constituents, the new European cement standard opens the possibility to use other main constituents such as calcareous fly ash, limestone with higher TOC content, artificial pozzolana and silica fume. Since the introduction of the European standard EN 197-1 in the year 2000, a total of 27 cement types are described and defined concerning composition, specification and conformity criteria.

Major research activities have been initiated by the German Cement Works Association to deepen the understanding of the role of cement main constituents during hydration reactions and their influence on the properties of cement. Selected results are presented, referring to the application of granulated blastfurnace slag, calcareous fly ash and limestone.

1. INTRODUCTION

Traditionally, Portland cements are the most used cement types in Germany. In the past years an increasing amount of other main constituents besides clinker have been used for cement production. As a consequence, the amount of Portland Cement in proportion to the total cement production decreased from over 75 % in the year 1995 to some 62 % in 2000. In Germany the most frequently used constituents are granulated blastfurnace slag and limestone with natural pozzolana and burnt shale being used less often. According to the EN 197-1 an extended range of materials that has not yet been established in Germany can be used for cement production. The European cement standard covers a range of 27 different cement types. However, not all of them are of local importance for reasons of availability.

Specifications concerning the composition of cement main constituents, as well as other criteria are described in the EN 197. These specifications are proven to be sufficient for cement production of constant quality, fulfilling the demands of the European cement and concrete standards. The knowledge of further physical, chemical and mineralogical parameters can help to evaluate the quality of the cement constituents to a higher degree and with a greater accuracy. This understanding allows an effective improvement of the material properties by selection of specific processing methods.

2. GENERAL REQUIREMENTS FOR CEMENT MAIN CONSTITUENTS

The majority of specifications according to the EN 197-1 are related to material properties and correspond to the description concept [1]. Only a few exceptions can be classified as real

Proceedings of the 11th International Congress on the Chemistry of Cement (ICCC)
'Cement's Contribution to the Development in the 21st Century'
Hosted by: The Cement and Concrete Institute of South Africa
CD-ROM produced by: Document Transformation Technologies
11 - 16 May 2003, Durban, South Africa
ISBN Number: 0-9584085-8-0
Editors: Dr G. Grieve and G. Owens
Congress Organised by: Event Dynamics

performance criteria. Basic properties as well as the requirements of the EN 197-1 are described below for the use of granulated blastfurnace slag (GBS), calcareous fly ash (CFA), and limestone, respectively.

2.1 Granulated blastfurnace slag

In the year 2000, more than 66 % out of 7,53 Mio t blastfurnace slag were granulated and almost completely used as cementitious materials in Germany [2]. Middle European granulated blastfurnace slags usually consist of more than 95 % glassy particles. The EN 197-1 requires a glassy slag content of at least two-thirds by mass. Chemically, the slag has to consist of at least two-thirds of CaO, MgO and SiO_2, while the ratio of $(CaO + MgO)/(SiO_2)$ should exceed 1,0. The fulfilment of these requirements is seen to be the prerequisite for the slag to possess latent hydraulic properties and so be suitable for cement production.

Additional chemical parameters have been established in practice as hydraulic activity indexes to describe slag properties. The application experience reveals that a simple consideration of the CaO, MgO and SiO_2 content is not always sufficient. High amounts of Al_2O_3 can enhance the reactivity of slag, whereas high TiO_2 and MnO contents can reduce its hydraulic properties. Moreover, the glass content of GBS plays a key role in view of the reactivity. Evidently, not only the absolute glass content but also the glass structure, which can be influenced by the chemistry as well as by the quenching conditions during granulation, are of importance.

2.2 Calcareous fly ash

Due to their chemical composition, German lignite fly ashes basically correspond to the category of calcareous fly ash according to EN 197-1. They may be utilized as cement main constituents, if they contain at least 10,0 wt-% reactive CaO. If the proportion of reactive CaO does not exceed 15,0 wt-%, the ash has to contain at least 25,0 wt-% reactive SiO_2. Calcareous fly ash containing more than 15,0 wt-% reactive CaO has to achieve a compressive strength of 10,0 MPa according to EN 196-1. For this test the fly ash has to be adequately ground and must replace the cement in the mortar by 100 %. The soundness of calcareous fly ash shall not exceed 10 mm when tested in accordance with EN 196-3 using a mixture of 30 wt-% of fly ash and 70 wt-% of a CEM I cement.

In Germany 8 Mio t calcareous fly ash per year are produced, which are predominantly used to recultivate the exploited coal mining fields and mines. About 10 % of the ashes are available for alternative uses. Actually, German lignite fly ashes play only a minor role as cement main constituents, although developments of cementitious binders containing CFA have been in progress during the past five decades in Germany. In 1972 fly ash was established as a cement component by the standards of Eastern Germany [3, 4]. For the past 4 years, selected calcareous fly ashes have been certified as concrete additions [5].

2.3 Limestone

In Germany Portland-limestone cements with a limestone content up to 20 wt-% were developed by the cement manufacturers during the 1980's and were established then as cements with technical approval. After practical experience of more than 10 years in building construction and structural engineering they were included in the national standard DIN 1164-1:1994 as CEM II/A-L. Limestone used in these cements meets the following requirements according to EN 197-1:2000:

- The calcium carbonate ($CaCO_3$) content calculated from the calcium oxide content shall be at least 75 % by mass.
- The clay content, determined by the methylene blue test in accordance with EN 933-9, shall not exceed 1,20 g/100 g. For this test the limestone shall be ground to a fineness of approximately 5000 cm^2/g determined as specific surface in accordance with EN 196-3 (Blaine).

- The total organic carbon (TOC) content shall not exceed 0,20 wt-%. This type of limestone is marked with the letter „LL“ according to EN 197-1:2000. Therefore these Portland-limestone cements are now called CEM II/A-LL.
- The performance of concrete manufactured from Portland-limestone cement CEM II/A-LL, in terms of fresh and hardened concrete properties and durability, has been verified by extensive laboratory investigations and practical experience. In particular the freeze-thaw resistance of concretes, which fulfil the minimum requirements of the exposure class XF4 (freeze/thaw attack on concrete with high water saturation with de-icing salt or sea water) according to the German concrete standard DIN 1045-2, is generally high and can be compared to that of Portland cement concrete. In road construction Portland-limestone cement CEM II/A-LL may be used for the same applications as Portland cement. This was taken into account accordingly in drafting the supplementary technical terms of contract and guidelines for structural engineering (ZTV-ING). In general the strength development of concretes using Portland-limestone cement CEM II/A-LL is comparable to concretes with Portland cement CEM I of otherwise identical composition [6].

With the introduction of EN 197-1 further Portland-limestone cements have been standardized in addition to the CEM II/A-LL cements. Now it is possible to use limestone contents of up to 35 wt-% (CEM II/B-LL) as well as limestone with TOC contents of up to 0,50 wt-%. Portland-limestone cement with increased TOC contents in the limestone is labelled with the letter “L”.

Building practice experience with Portland-limestone cements of up to 35 wt-% is not available in Germany. Currently they may not yet be used for concrete with high resistance to freeze thaw or freeze thaw with de-icing salt.

3. ENHANCEMENT OF APPLICATION POTENTIAL

3.1 Granulated blastfurnace slag

With the aim to gain information about the glass structure of GBS and its influence on hydraulic activity, a number of industrial blastfurnace slags were examined in their as-received condition, after a subsequent laboratory granulation treatment, and after dotation with selected oxides. The samples were examined by differential thermal analysis, high-temperature X-ray diffraction, as well as optical and electron microscopy with cathodoluminescence devices.

The thermoanalytical results reveal characteristic differences even between slags of similar chemical composition (Figure 1). The curves exhibit up to 3 more or less overlapping endothermic signals caused by devitrification reactions in the range between 800 and 1000 °C.

High-temperature X-ray diffraction offers the opportunity to assign the devitrification peaks to the formation of crystalline products (Figure 3). Melilite, $Ca_2(Mg,Al)(Al,Si)_2O_7$, is the final main product of each of the examined slags. In some GBS, merwinite, $Ca_3MgSi_2O_8$, is formed as an intermediate product. In some cases merwinite stays stable until the devitrification is completed, while in other cases it is diminished with increasing temperature to the benefit of the formation of other phases as transition products.

Merwinite can also occur in industrial granulated blastfurnace slags without any further thermal treatment. These primarily formed merwinite crystals usually appear as segregation structures within the glassy particles and can be easily detected by their cathodoluminescence (Figure 2).

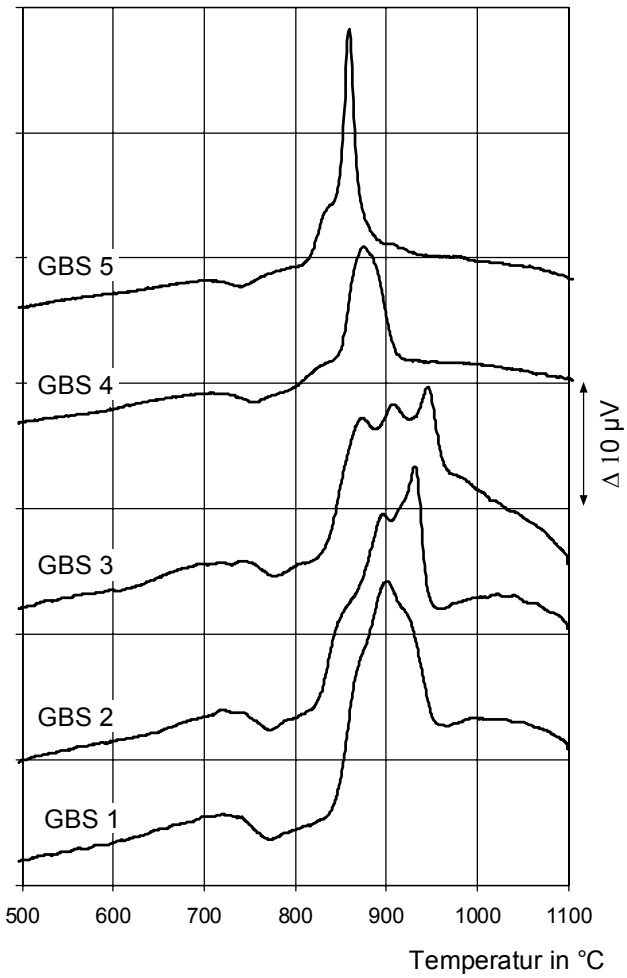

Figure 1. Devitrification peaks of different granulated blastfurnace slags measured by differential thermal analysis

A reasonably positive influence can be deduced from the tendency of a GBS to form merwinite [7]. Two reasons are considered to be crucial for this effect. One is the increase of the alumina content of the glass in the immediate vicinity of the merwinitic areas, as can be detected by EDX-analysis in the SEM. The other is a change of density by the formation of merwinite ($\rho = 3{,}3$ g/cm³) in comparison with the glass ($\rho = 2{,}9$ g/cm³). As a consequence, a microporosity with a locally increased surface area occurs and enhances the slag reactivity.

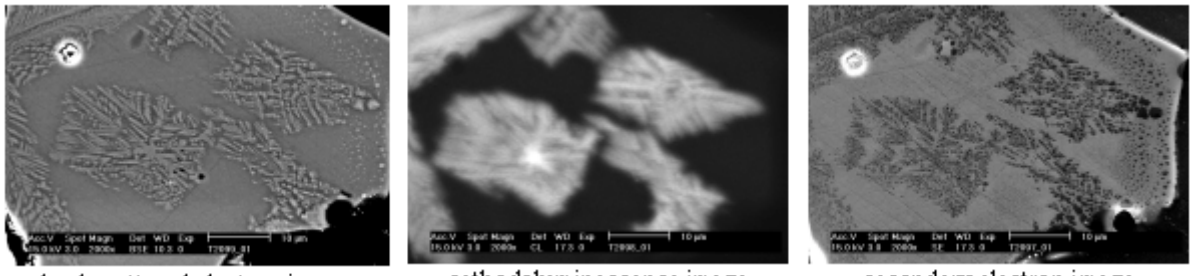

Figure 2. scanning electron microscopic pictures of merwinitic domains within GBS 3

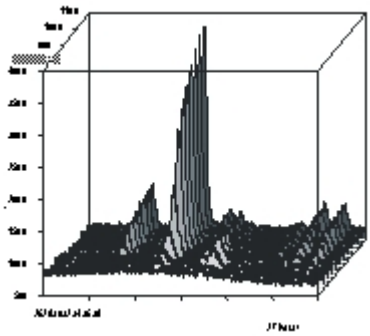

GBS 3, 3-dimensional plot

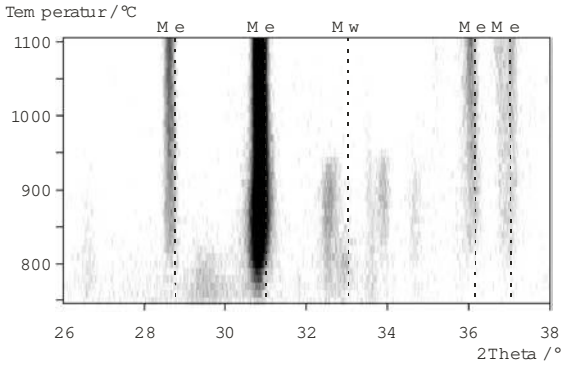

GBS 1, 2-dimensional top view

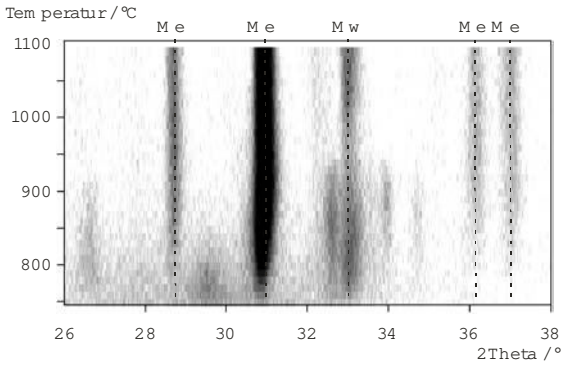

GBS 2, 2-dimensional top view

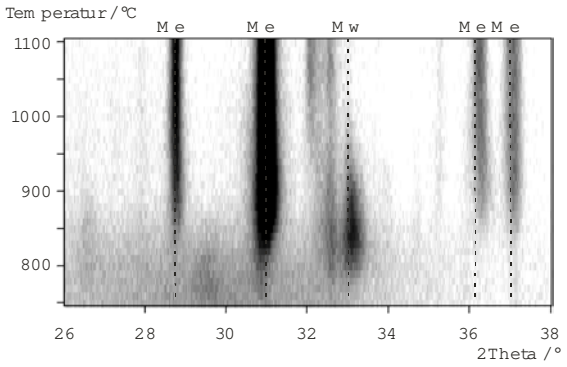

GBS 3, 2-dimensional top view

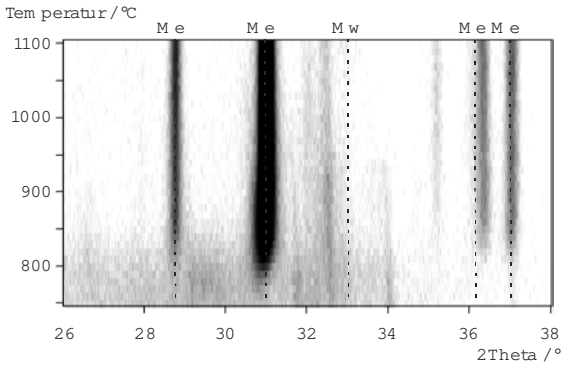

GBS 4, 2-dimensional top view

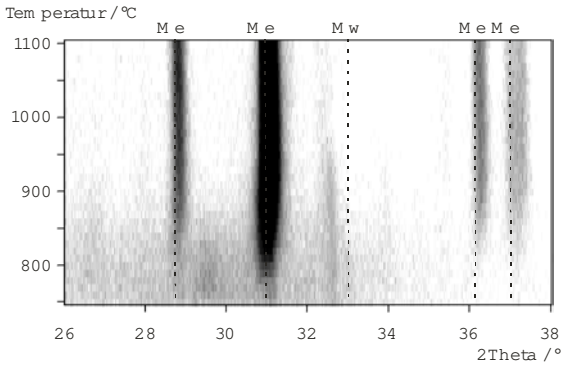

GBS 5, 2-dimensional top view

Figure 3. Devitrification peaks of different granulated blastfurnace slags measured by high-temperature X-ray diffraction

3.2 Calcareous fly ash

German lignite coal deposits are located mainly in three major areas called the Rhenish, the Lusatian and the Middle German area. Although the composition of the fly ashes derived from the corresponding power plants is dependent on the geological conditions of the coal deposits, large chemical variations can be found even within single locations. For the current research activities one fly ash from the Rhenish area and one from the Lusatian area were chosen out of a larger set of ashes. Their chemical and mineralogical compositions can be considered as representative for the respective regions (Table 1).

Each of the examined lignite fly ashes contains less than 25 wt-% reactive SiO_2. However the content of reactive CaO usually exceeds 15,0 wt-%. Compressive strength tests of hydrated mortars containing 100 % CFA show that 10 MPa after 28 days, which the EN 197-1 requires, are not achieved by all fly ashes.

Table 1. Chemical composition of the representative CFAs from the Rhenish and the Lusatian area chosen for the examinations (values in wt-%)

	BFA R1	BFA L1
SiO_2	34,80	38,84
Al_2O_3	3,80	8,41
TiO_2	0,39	0,73
P_2O_5	0,02	0,03
Fe_2O_3	11,89	22,79
Mn_2O_3	0,31	0,29
CaO	31,65	18,76
MgO	8,52	6,53
SO_3	7,04	2,70
K_2O	0,35	0,72
Na_2O	1,21	0,17
loss on ignition	1,76	0,66
reactive CaO	26,99	17,29
reactive SiO_2	7,79	12,79
free lime	8,85	0,34

Particularly the Rhenish fly ash contains higher amounts of free lime. Also free magnesia (periclase) can be detected by X-ray diffraction. To consider the influence of expansive components entirely, several soundness tests on cements containing up to 30 % CFA were applied (figure 4).

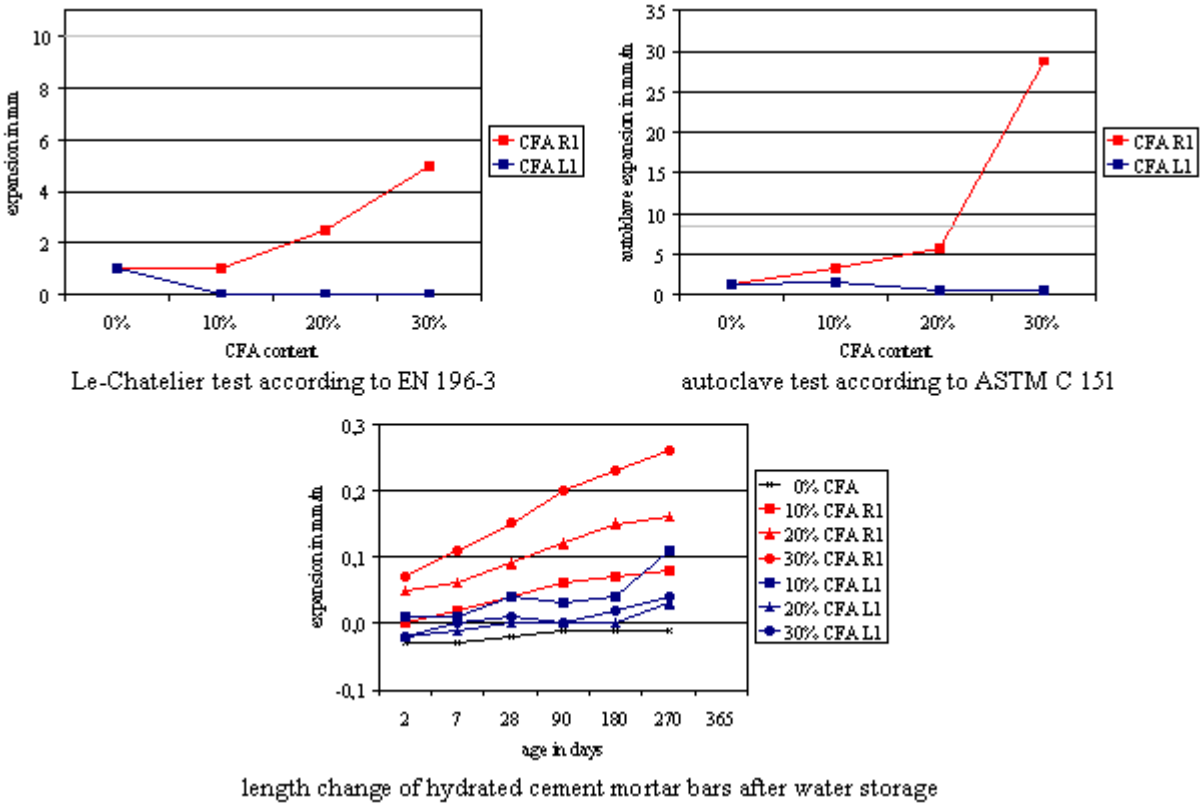

Le-Chatelier test according to EN 196-3

autoclave test according to ASTM C 151

length change of hydrated cement mortar bars after water storage

Figure 4. Results of different soundness tests on cements containing CFA

All cements show expansions lower than 10 mm when tested according to the Le Chatelier method. The limit of 8 mm/m under autoclave test conditions is exceeded by the cement containing 30 % Rhenish lignite fly ash. After long term water storage conditions cement mortar bars exhibited an

increase of expansion, with the increase of CFA content. The addition of 30 % Rhenish CFA resulted in an expansion of 0,26 mm/m after 270 days compared with 0,04 mm/m for 30 % Lusatian CFA and –0,01 mm/m for the plain Portland cement.

The examination of the development of compressive strength, according to EN 196-1, showed that the replacement of Portland cement clinker by CFA caused strength reductions that were partially compensated during progress of hydration. The strength level of the reference Portland cement after 28 days could only be reached if not more than 10 % of the cement was substituted by CFA.

It is known that the contribution of fly ash to the strength development of hydraulic binders can be increased by mechanical treatment [8 – 13]. As the specific energy consumption during grinding proved to be low for lignite fly ashes compared with clinker, the ashes were ground to fineness levels of 3500 cm²/g and > 6000 cm²/g, respectively. The mortar strength development of cements containing 20 % of unground and ground CFA is shown in figure 5. Again, the ashes caused strength losses after 2 days of hydration in a range of 8 to 13 %. The use of Lusatian CFA initially proved to cause greater strength reductions than the use of Rhenish fly ashes. In contrast an increase of relative compressive strength occurred already after 7 days for the cements containing ground and unground Lusatian CFA, whereas a significant positive strength contribution of Rhenish fly ash could be detected after hydration times longer than 28 days. An enhancing effect of grinding on the strength contribution was found to be more distinct for the Rhenish fly ash than for the Lusatian fly ash.

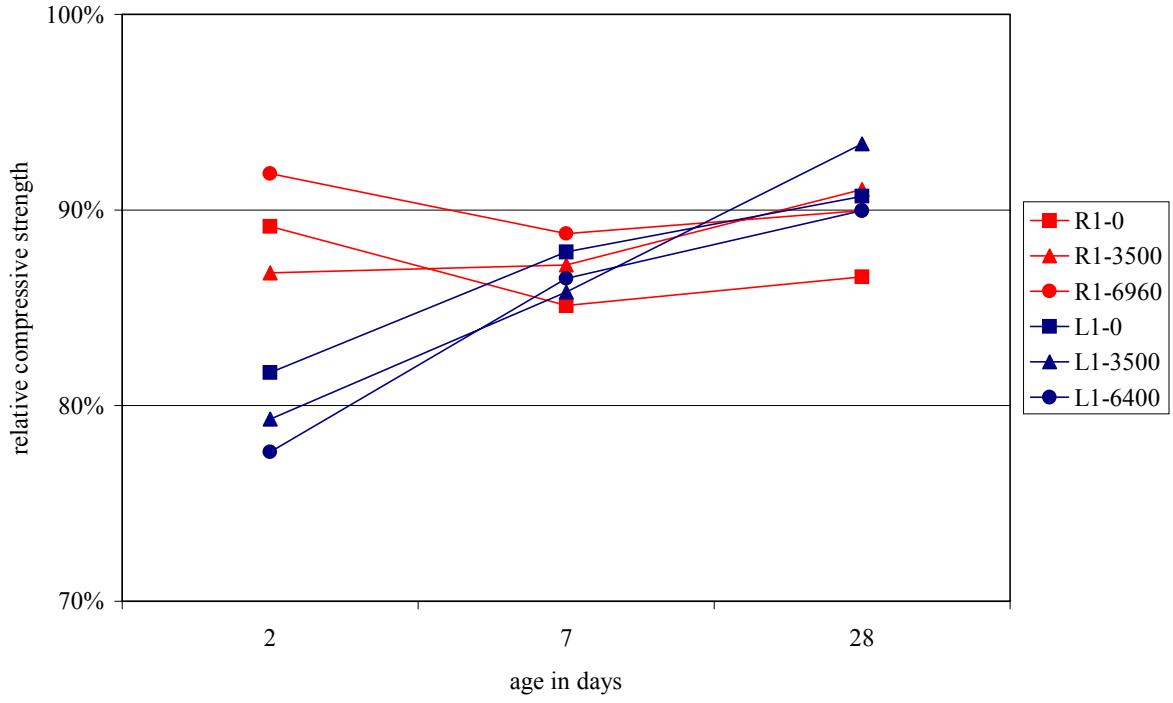

Figure 5. Relative compressive strength development of cement mortars containing 20 % Rhenish (R1) and Lusatian (L1) CFA in comparison with the Portland cement. The ashes were used in the as-received condition and ground to different values of fineness

3.3 Limestone

To reach the same compressive strength of concrete using CEM II-LL, in comparison to concrete with Portland cement CEM I, and of otherwise identical composition, the fineness of the clinker has to be increased. Increasing the fineness of the limestone without also increasing the clinker fineness has no significant influence on the compressive strength (figure 6).

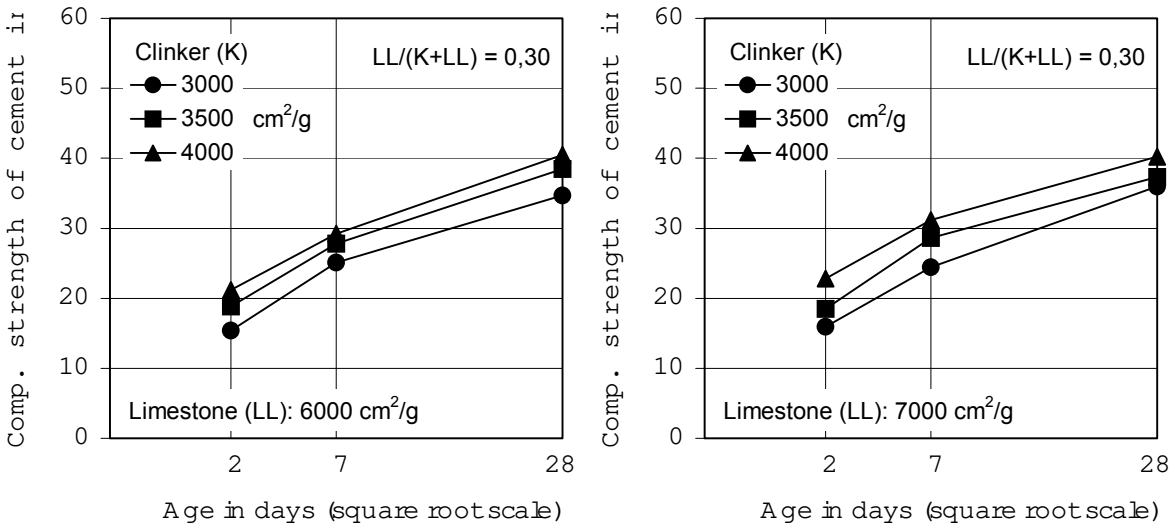

Figure 6. Compressive strength of Portland-limestone cements CEM II/B-LL with limestone contents of 30 wt-% depending on the fineness of clinker and limestone (values in cm^2/g in accordance with EN 196-6 (Blaine))

Using separate grinding and subsequent blending of clinker and limestone, the mechanical requirements of EN 197-1 for cements of the strength classes 32,5 N (compressive strength: 7 d ≥ 16,0 MPa; 28 d ≥ 32,5 MPa) and 32,5 R (compressive strength: 2 d ≥ 10,0 MPa; 28 d ≥ 32,5 MPa) have been reached using clinker with a fineness between 3000 and 4000 cm^2/g and a specific surface of the limestone of 6000 cm^2/g and 7000 cm^2/g respectively. The specific surfaces of the Portland-limestone cements including calcium sulfate vary between 4080 and 5100 cm^2/g. It can be seen in figure 7 as well that increasing the fineness of the limestone only leads to a slight increase of the early strength, but shows no significant increase of the compressive strength after 28 d.

The results of investigations on the freeze-thaw resistance of concrete from laboratory-made Portland-limestone cements with limestone contents of 20 and 30 wt-%, respectively, are shown in figure 7. The concretes demonstrated only minor scaling during the freeze-thaw test and thereby demonstrated a high freeze thaw resistance. The scaling of the concretes with 30 wt-% of limestone as a cement main constituent was higher than in Portland-limestone cements with up to 20 wt-% of limestone. However, it must be noted that the strength of these concretes was approximately 15 % lower than that of the reference concretes with Portland cements. In these investigations limestone with TOC ≤ 0,20 wt-%, 0,20 wt-% < TOC ≤ 0,50 wt-% and TOC > 0,50 wt-% have been used as a cement main constituent. Until now, no significant correlation between TOC and the scaling of concrete in laboratory investigations was established, but concretes using Portland-limestone cements with TOC ≤ 0,20 wt-% always showed high frost resistance.

Apart from this, other investigations have shown that the use of up to 25 wt-% of limestone, as a cement main constituent, shows no significant negative influence on the resistance of concrete against the penetration of chlorides [14]. Slightly increased depth of carbonation has to be expected.

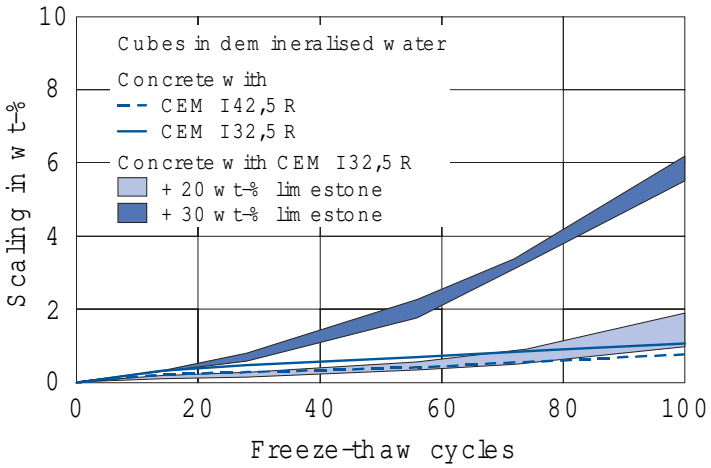

Figure 7. Freeze-thaw resistance of concretes made with Portland cement and Portland-limestone cement containing 20 and 30 wt-% limestone as a cement main constituent

4. CONCLUSIONS AND SUMMARY

A major aim of the activities in the Research Institute is to verify and to improve the usability of cement main constituents based on the extended range of standardized cements according to EN 197-1. For reasons of availability of materials the investigations are focused on granulated blastfurnace slag, calcareous fly ash and limestone.

The use of GBS as a cement main component has been well established over the past decades. However, a reliable prediction of the slag reactivity can only be accomplished if further properties exceeding the requirements of the EN 197-1 are taken into account. Besides the chemical composition and the glass content, the glass structure can act as a supplementary criterion to describe GBS properties. The morphology, as well as the glass composition, can be modified by the nucleation of crystalline segregations as merwinite. The tendency to form merwinite has been proven to be an indicator for enhanced slag reactivity.

The replacement of clinker by calcareous fly ash, derived from different German power plants, was found to decrease the compressive strength of cement especially after short hydration times. Continuous hydration leads to a compensation of the strength loss as latent hydraulic or pozzolanic particles within the ashes contribute to the cement strength development. An additional reduction of the initial strength loss can be achieved by grinding the ash to increased fineness. Sufficient soundness properties of cement are given for CFA contents up to 20 wt-%.

Recent investigations on Portland-limestone cements with more than 20 wt-% limestone showed that the performance of comparable Portland cements can be maintained if the cement fineness is increased. Apparently the fineness of the clinker is of more significant influence on the compressive strength development than the fineness of the limestone. Although building practical experience with these cements is not yet available in Germany, it can be presumed that Portland-limestone cements (CEM II/B-LL) and Portland-composite cements (CEM II/B-M (S-LL)) will be suitable for usual external components and structures of building construction, under the environmental exposure conditions given in Germany. Durability criteria such as resistance against frost and chloride diffusion are considered to be fulfilled by concretes made with Portland-limestone cements containing up to 30 wt-% limestone. High TOC-contents of up to 0,50 wt-% in the limestone do not seem to have a deteriorating influence on frost resistance. The Research Institute is conducting several research projects to confirm these presumptions.

Further investigations are planned to optimize the granulometric properties of cement main constituents. It is known that the strength development, as well as other properties of concrete, can be improved if the most dense grain structure is achieved by taking into account the grain fineness, grading and grain shape [15, 16]. A matrix optimization by adjusting the grain size distribution in consideration of the grain shapes promises further improvements in application of cementitious main constituents.

REFERENCES

[1] Wischers, G. „Leistungsfähigkeit“ als Kriterium für die Normung von Zement und Beton, Betonwerk und Fertigteil-Technik, vol.56, 1990, H.3, pp.51-60.

[2] Verein Deutscher Eisenhüttenleute (VDEh), Jahrbuch Stahl 2000, Düsseldorf: Verlag Stahleisen, 2001.

[3] TGL 190-72/03, Berlin: Amt für Standardisierung, 1972.

[4] TGL 28101, Zemente, Berlin: Amt für Standardisierung, 1989.

[5] Kahl, D. and Piper, K. Braunkohlenflugasche als Betonzusatzstoff nach DIN 1045, VGB/BVK-Fachtagung “Flugasche im Beton”, Düsseldorf, 1998.

[6] VDZ-Arbeitskreis „CEM II-Zemente“ Verwendung von CEM II-Zementen im Betonbau, Forschungsinstitut der Zementindustrie, Düsseldorf: 1999.

[7] Schneider, C. and Meng, B. Bedeutung der Glasstruktur von Hüttensanden für ihre Reaktivität. 14. ibausil, Weimar, 2000, vol.1, pp.455-463.

[8] Piazza, J.L. Untersuchungen über die Reaktivität von Steinkohle- und Braunkohleflugaschen in Mörtel und Zementpasten, PhD thesis, Clausthal, 1994.

[9] Richartz, W. Zusammensetzung und Eigenschaften von Flugaschen, Zement-Kalk-Gips, vol.37, 1984, H.2, pp.62-71.

[10] Payá, J., Monzó, J., Borrachero, M.V. and Peris-Mora, E. Mechanical Treatment of Fly Ashes, Part 1: physico-chemical Characterization of ground Fly Ashes, Cement and Concrete Research, vol.25, 1995, H.7, pp.1469-1479.

[11] Payá, J., Monzó, J., Borrachero, M.V., Peris-Mora, E. and González-López, E. Mechanical Treatment of Fly Ashes, Part II: Particle Morphologies in ground Fly Ashes (GFA) and Workability of GFA-Cement Mortars, Cement and Concrete Research, vol.26, 1996, H.2, pp.225-235.

[12] Payá, J., Monzó, J., Borrachero, M.V., Peris, E. and González-López, E. Mechanical Treatment of Fly Ashes, Part III: Studies on Strength Development of ground Fly Ashes (GFA) - Cement Mortars, Cement and Concrete Research, vol.27, 1997, H.9, pp.1365-1377.

[13] Wolf, R., Schulte, P. and Meyer, B. Veränderung der Oberflächeneigenschaften von Braunkohleaschen aus Wirbelschichtfeuerungen durch mechanische Aktivierung, Aufbereitungs-Technik, vol.39, 1998, H.2, pp.71-82.

[14] Matthews, J.D. Performance of limestone filler cement concrete, Euro-Cements: Impact of ENV 197 on Concrete Construction. Edited by R.K. Dihr and M.R. Jones – London: 1994, pp.113-147.

[15] Puntke, W. Grundlagen für die Matrixoptimierung und Ausführung in der Praxis, Technische Akademie Esslingen, Ostfildern, 1991.

[16] Puntke, W. Mix design considerations for granulometric optimisation of the matrix of high performance concrete. Radical Concrete Technology, Proceedings of the International Conference held at the University of Dundee, Scotland, UK un 27 – 28 June 1996, London: E & FN Spon/Chapmann & Hall, 1996.

USE AND REACTIVITY OF CEMENT MAIN CONSTITUENTS IN GERMANY

Martin Schneider, Stefan Puntke, Christian Schneider and Christoph Müller

German Cement Works Association, Research Institute of the Cement Industry, Düsseldorf, Germany; E-mail: pk@vdz-online.de, sch@vdz-online.de

Dr. rer. nat. Martin Schneider

Dr. rer. nat. Martin Schneider studied physics in Mainz and Bonn, Germany. After 4 years of scientific work both in Bonn and in the USA, he joined the Research Institute of the Cement Industry, where he was in charge of the "Environment Protection" and "Cement Chemistry" sections. In 1998 he was appointed Managing Director of the German Cement Works Association, since January 2000 he is Chief Executive of the VDZ and Head of the Research Institute.

Dipl.-Ing. Stefan Puntke

Dipl.-Ing. Stefan Puntke studied mineralogy and material science in Darmstadt, Germany and Orléans, France. After 7 years of work in the cement industry both in Germany and in France, he joined in January 2000 the Research Institute of the Cement Industry, where he is the head of the Cement Chemistry department.

CHEMICAL REACTION OF FLY ASH

H.J.H. Brouwers and R.J. Van Eijk

Department of Civil Engineering, University of Twente, P.O. Box 217, 7500 AE Enschede, The Netherlands. E-mail: h.j.h.brouwers@ctw.utwente.nl

ABSTRACT

In a previous paper, Brouwers and Van Eijk [1] presented a theoretical study on the dissolution (reaction) of pulverised powder coal fly ash. This fly ash was modelled as hollow spheres, and a shrinking core model was derived for these hollow spheres that contain two regions (an outer hull and an inner region). The obtained analytical equations were applied to the dissolution experiments by Pietersen [2, 3], yielding reaction rates at various temperatures and pH for two class F fly ashes. Based on the observed trends, in the present paper a reaction mechanism is proposed for the glass phase which accounts for the oxide composition of the fly ash (and that is applicable to slags as well). Finally, using the reaction product, the following thermodynamic properties of the studied fly ashes are derived: the free energy, enthalpy and entropy of reaction. The values obtained are in line with those of known substances: silica and an aluminosilicate ($2SiO_2.Al_2O_3$).

1. INTRODUCTION

The ability of fly ash and ground granulated blast furnace slag to react depends strongly on the alkali content and temperature of the ambient solution (Fraay et al. [4], Xu and Sarkar [5], Taylor [6], Hewlett [7], Song and Jennings [8], Song et al. [9]). To investigate the reactivity of fly ash, Pietersen [2, 3] performed dissolution experiments with two pulverised coal fly ashes. They were dissolved in sodium hydroxide (NaOH) solutions of pOH 0.3, 0.6 and 1, and at various temperatures. The two fly ashes originate from two different power plants and have broad and mutually different particle size distributions. One power plant was a "wet-bottom" type plant that operates at 1800 ^oC ("EFA"); the other FA originates from a low NO_x furnace plant ("LM"). For the dissolution experiments the particles were separated into a fraction of low density ("cenospheres") with a density smaller than 1400 kg/m^3 and in a fraction of high density ("solid spheres") with a density of 2300-2600 kg/m^3. SEM images of polished sections of these fractions revealed that the cenospheres were hollow thin-walled spheres. The dissolution experiments were executed with the hollow cenospheres and the solid spheres, which differ in density about a factor of two.

All dissolution experiments where executed with a sieved part of the fly ashes, the diameter lying between 38 μm and 50 μm. The fly ashes have also been ultrasonically vibrated to prevent agglomeration of small particles to large ones. As expected, dissolution rates (and related reaction rates as well) increased significantly with decreasing pOH (increasing pH) and temperature. The experiments revealed that for EFA and LM, Si, Al and K all congruently dissolve, implying bulk dissolution. Accordingly, the dissolution of one component, Si, represents an adequate measure for the dissolution of the entire glass mass.

Proceedings of the 11th International Congress on the Chemistry of Cement (ICCC)
'Cement's Contribution to the Development in the 21st Century'
Hosted by: The Cement and Concrete Institute of South Africa
CD-ROM produced by: Document Transformation Technologies
11 - 16 May 2003, Durban, South Africa
ISBN Number: 0-9584085-8-0
Editors: Dr G. Grieve and G. Owens
Congress Organised by: Event Dynamics

In a previous paper [1], the fly ash particles were considered to be spherical, and a shrinking core model was derived and applied to aforesaid experiments of Pietersen [2, 3]. Based on this application, the dependence of the reactivity on the hydroxide content of the solution was obtained, indicating a dissolution rate proportional to $[OH^-]^{0.9\text{-}1}$ for the outer region and to $[OH^-]^{1.4}$ in the inner region of the fly ash particle. Furthermore, it seemed that the outer region (outer hull) of solid spheres and cenospheres are having the same thickness, about 2 μm.
In this paper a chemical reaction equation for the fly ash is put forward that accounts for the silica, aluminium oxide, alkali, alkaline earth, iron oxide and titanium oxide contents. From this application and proposed reaction mechanism, the solubility of the fly ashes as a function of pH is obtained. Finally, thermodynamic properties (such as the equilibrium constant and free energy of reaction) are determined of the considered fly ashes, and compared with similar substances.

2. CHEMICAL REACTION MECHANISM

In Table 1 the mass fraction of all glass phases in the studied fly ashes are listed, based on the data of Brouwers and Van Eijk [1]. A part of the fly ash is crystalline (quartz and mullite) which is non-reactive. Assuming the same mass density for glass and crystalline phase, the volume fraction of crystalline material corresponds to 1- ϕ (ϕ is the glass volume fraction, i.e. the porosity of the leached shell). The vitreous SiO_2 and Al_2O_3 follow from the total mass fraction of each substance minus the crystalline SiO_2 (in quartz and in mullite) and crystalline Al_2O_3 (in mullite only), see Brouwers and Van Eijk [1], respectively. Using the mass fractions of all oxides in the glass, the mean mole fraction of all components in the glass can be computed using the molecular mass of each component, which are included in Table 1 for the EFA and LM solid spheres only (between the brackets). From the composition of the fly ashes as presented in Table 1 it is clear that the glass phases of both fly ashes consist of SiO_2, as well as the network formers Al_2O_3, Fe_2O_3, TiO_2 and P_2O_5, and the network modifiers CaO, MgO, Na_2O and K_2O (Hemmings and Berry [10]).

Table 1. Mass and mole fraction (between brackets) of the glass phases in LM and EFA solid and ceno spheres. Mass fraction is based on total fly ash mass, mole fraction is based on glass phase only.

	EFA		**LM**		**M**
	solid ($\bar{x}$)	ceno	solid ($\bar{x}$)	ceno	(g/mole)
crystalline					
$SiO_2 + Al_2O_3$ (= 1 - ϕ)	5.1%	8.4%	33.3%	37.8%	
glass					
SiO_2 (S)	51.96% (0.648)	47.05%	38.79% (0.695)	40.41%	60
Al_2O_3 (A)	25.89% (0.190)	28.06%	16.48% (0.174)	13.54%	102
Fe_2O_3 (F)	4.65% (0.022)	2.96%	3.50% (0.024)	2.02%	160
P_2O_5 (P)	n.d.	n.d.	0.54% (0.004)	n.d.	142
TiO_2 (T)	1.20% (0.011)	0.91%	1.90% (0.026)	1.43%	80
CaO (C)	2.83% (0.038)	0.80%	2.75% (0.053)	1.15%	56
MgO (M)	1.82% (0.034)	1.41%	0.28% (0.008)	0.24%	40
Na_2O (N)	1.84% (0.022)	1.94%	0.37% (0.006)	0.38%	62
K_2O (K)	4.40% (0.035)	5.68%	1.00% (0.011)	1.02%	94
$\alpha = x_A/x_S$	0.293		0.250		
$\beta = (x_A + x_C)/x_S$	0.111		0.087		
$\gamma = (x_N + x_K)/x_S$	0.088		0.026		
$\delta = x_F/x_S$	0.034		0.034		
$\varepsilon = x_T/x_S$	0.017		0.037		
a (eq. (10))	1.022		1.208		
$\bar{M}$	71		72		

In Pourbaix [11] the prevailing equilibria of the various substances can be found for pH > 12 and an electric potential ranging from –0.3 to 0.2 V, values that are found in ordinary Portland and slag cement systems (MacPhee and Glasser [12]). Paul [13, 14] also presented hydration reactions for vitreous SiO_2, Al_2O_3, Na_2O and K_2O. Accordingly, from all this literature it follows that for pH > 12 vitreous silica is hydrated as

$$SiO_2 + 2OH^- \Leftrightarrow SiO_3^{2-} + H_2O \quad (1)$$

and that Al_2O_3 is hydrated according to

$$Al_2O_3 + 2OH^- \Leftrightarrow 2AlO_2^- + H_2O \quad (2)$$

that CaO (and MgO) reacts as follows

$$CaO + H_2O \Leftrightarrow Ca^{2+} + 2OH^- \quad (3)$$

that Na_2O (and K_2O) reacts as follows

$$Na_2O + H_2O \Leftrightarrow 2Na^+ + 2OH^- \quad (4)$$

that Fe_2O_3 reacts as follows

$$Fe_2O_3 + 3H_2O \Leftrightarrow 2Fe^{3+} + 6OH^- \quad (5)$$

and that TiO_2 hydrates as follows

$$TiO_2 + OH^- \Leftrightarrow HTiO_3^- \quad (6)$$

Accordingly, the following reaction of the fly ash glass is proposed as

$$\begin{aligned} &SiO_2.\alpha Al_2O_3.\beta CaO.\gamma Na_2O.\delta Fe_2O_3.\varepsilon TiO_2 + (\beta+\gamma+3\delta)\, H_2O + (2+2\alpha+\varepsilon)\, OH^- \Leftrightarrow \\ &SiO_3^{2-} + 2\alpha AlO_2^- + \beta Ca^{2+} + 2\gamma Na^+ + 2\delta Fe^{3+} + \varepsilon HTiO_3^- + (1+\alpha)\, H_2O + 2(\beta+\gamma+3\delta)\, OH^- \end{aligned} \quad (7)$$

Note that silica, aluminium oxide and titanium oxide consume hydroxides, whereas the earth alkalis (CaO, MgO), alkalis (Na_2O, K_2O) and iron oxide produce them. As slag contain the same components as fly ashes, it is believed that the model might be applicable to the dissolution of this material as well. In case a fly ash or a slag also contains MnO and SO_3, the former reacts as CaO/MgO (to Mn^{2+}), and the latter likewise SiO_2 (to SO_4^{2-}).
As the activity of pure liquids and solids are unity, the equilibrium constant is defined as

$$K = \frac{[AlO_2^-]^{2\alpha}[Ca^{2+}]^{\beta}[Na^+]^{2\gamma}[Fe^{3+}]^{2\delta}[HTiO_3^-]^{\varepsilon}[SiO_3^{2-}]}{[OH^-]^{2+2\alpha-2\beta-2\gamma-6\delta+\varepsilon}} \quad (8)$$

Invoking $[AlO_2^-] = 2\alpha\,[SiO_3^{2-}]$, $[Ca^{2+}] = \beta\,[SiO_3^{2-}]$, $[Na^+] = 2\gamma\,[SiO_3^{2-}]$, $[Fe^{3+}] = 2\delta\,[SiO_3^{2-}]$ and $[HTiO_3^-] = \varepsilon\,[SiO_3^{2-}]$ yields

$$[SiO_3^{2-}] = \left(\frac{K}{(2\alpha)^{2\alpha}\,\beta^{\beta}\,(2\gamma)^{2\gamma}\,(2\delta)^{2\delta}\,\varepsilon^{\varepsilon}}\right)^{\frac{1}{1+2\alpha+\beta+2\gamma+2\delta+\varepsilon}} [OH^-]^a \quad (9)$$

with

$$a = \frac{2 + 2\alpha - 2\beta - 2\gamma - 6\delta + \varepsilon}{1 + 2\alpha + \beta + 2\gamma + 2\delta + \varepsilon} \tag{10}$$

Note that the powers appearing in the denominator of the first factor of equation (9), $(2\alpha)^{2\alpha}$ etc., are of order unity. The function x^x namely attains a value of 1 at x = 0 and x = 1, and has a minimum of $(1/e)^{(1/e)}$ (≈ 0.69) at $x = e^{-1}$. From Table 1 it can be seen that the values of α etc. are such that 2α etc. all fall in the range 0 to 1, so that $(2\alpha)^{2\alpha}$ etc. all have a value between 0.69 and 1. Furthermore, it will be demonstrated that K is (much) smaller than unity. So, with increasing α etc. (i.e. less silica) the power of the first factor decreases, and hence, the factor increases. Accordingly, when the silica content diminishes, the solubility (reactivity) is enhanced. This trend is also supported by the second factor on the right-hand side of equation (9). The power a decreases with increasing α, β etc., see equation (10). For β, γ and δ this effect is obvious. But this trend also holds for α and ε: the function (2+x)/(1+x) attains a value of 2 at x = 0, and monotonically decreases towards the asymptotic value of 1 for large x. Considering that $[OH^-]$ is usually smaller than 1 mole/l, increasing α, β etc. imply a smaller a and also a larger second factor in equation (9), i.e. the same trend as the first factor.

Considering the equilibrium product it follows that the hydration of pure silica is quadratically dependent on $[OH^-]$ (α = β = γ = δ = ε = 0). In case of a pure aluminosilicate glass (β = γ = δ = ε = 0), the power a is located between unity and 2, but depending weakly on changes in α. E.g., for α ranging from ¼ to 1, this power ranges from 1.66 to 1.33 (it equals 1.5 for α = 0.5). For alkali silicate glasses (α = β = δ = ε = 0), it follows from equation (10) that the power a is smaller than unity when γ > 0.25.

With the mole fractions listed in Table 1, subsequently the mean α, β, γ, δ and ε and a can be computed for solid EFA and LM, which are included in this table as well. For this calculation it is assumed MgO to react as CaO and K_2O as Na_2O. P_2O_5 can be neglected, as its presence is minor (Table 1).
One can readily see that the power a takes a value of 1.022 (EFA) and 1.208 (LM), which is reasonably in line with the power obtained by Brouwers and Van Eijk [1]: 1.4 in LM inner region, 0.9 and 1 in EFA and LM outer region, respectively. This deviation can probably be attributed to the inhomogeneity of the fly ash. Inner and outer region may have different composition, which would result in each region having its own value for a. Experiments by Dudas and Warren [15] confirm that the glass components K_2O, Na_2O, CaO, MgO, and Fe_2O_3 are concentrated in the exterior (outer) hull. Smith [16] found a similar enrichment in the outer layer, and explained this inhomogeneity by the fact that the boiling point of silica and aluminiumoxide are practically the same (2950 ^oC and 2980 ^oC, respectively), and higher than the boiling points of all other components. This will result in a concentration of more volatile components (i.e. the other oxides) in the outer layer. Considering equation (10), one can see indeed that the power a is smaller/larger for larger/smaller values of β, γ etc. This confirms the hypothesis of K_2O, Na_2O, CaO, MgO, and Fe_2O_3 concentrated in the outer region.

3. THERMODYNAMIC ANALYSIS

On the basis of the reaction times determined by Brouwers and Van Eijk [1] and the proposed reaction mechanism in the previous section, thermodynamic data for the fly ash can be determined. The first step in this analysis is the determination of $[SiO_3^{2-}]$ that appears in equations (8) and (9). This property follows from the scaled reaction time that reads:

$$\tau = \frac{x_S \rho_g R^2}{6\phi D_S C_{Sc}} \qquad (11)$$

The values of τ for EFA and LM followed from the application (fitting) of a shrinking core model to the experiments of Pietersen [2 ,3] by Brouwers and Van Eijk [1]. In equation (11) ρ_g is the molar density of the glass, x_S the mole fraction of silica in the glass, D_S the bulk diffusion coefficient of the SiO_3^{2-} ion, R the outer radius of the fly ash particle, and C_{Sc} the SiO_3^{2-} concentration at the glass core (i.e. on the reacting surface) and ϕ the glass volume fraction (porosity of leached shell).

It is expected that the dissolution process will be governed by the ion that diffuses the slowest through the leached shell. Here, only the diffusion coefficients of $[AlO_2^-]$ and $[SiO_3^{2-}]$ are compared, which are not both directly available. Accordingly, D_A^0 was estimated using the diffusion coefficients of the similar ions NO_2^- ($1.912\ 10^{-9}$ m^2/s) and ClO_2^- ($1.385\ 10^{-9}$ m^2/s), yielding $D_A^0 = 1.7\ 10^{-9}$ m^2/s at T = 298 K (Lide [17]). Similarly, D_S^0 was estimated using the diffusion coefficients of CO_3^{2-} ($0.912\ 10^{-9}$ m^2/s) and SO_3^{2-} ($1.064\ 10^{-9}$ m^2/s), yielding $D_S^0 = 1.0\ 10^{-9}$ m^2/s at T = 298 K (Lide [17]). Note that the molecular mass of aluminium lies between the molecular masses of nitrogen and chloride, and silicon between carbon and sulphur, so that the estimation is expected to a yield reasonable result. As D_A (but also the diffusion coefficients of Ca^{2+}, Na^+, K^+ and Fe^{3+} [17]) is larger than D_S, it is believed henceforth that the process is governed by the diffusion of SiO_3^{2-} and hence, $D_S C_{Sc}$ appearing in equation (11) to correspond to $D_S\,[SiO_3^{2-}]$. For deviating temperatures, D_S is determined via

$$D_S = \frac{T}{298K} D_S^0 \qquad (12)$$

whereby T is in Kelvin. Combining equations (11), (9) and (12) yields

$$K = (2\alpha)^{\alpha}(\beta)^{\beta}(2\gamma)^{2\gamma}(2\delta)^{2\delta}(\varepsilon)^{\varepsilon}\left[\frac{x_S \rho_g R^2}{6\phi D_S^0 \tau}\frac{298K}{T}\right]^{1+2\alpha+\beta+2\gamma+2\delta+\varepsilon}[OH^-]^{-2-2\alpha+2\beta+2\gamma+6\delta-\varepsilon} \qquad (13)$$

The physical properties that appear in this equation are known: R (22 μm), ϕ (Table 1), while ρ_g follows from the mass density of the glass (about 2450 kg/m^3) divided by the mean molar mass. The mean molar mass of the glass follows from the sum of the molar fraction of each constituent times its molar mass ($\overline{M} = \sum x_k M_k$), which are included in Table 1 as well.

Table 2. Reaction time τ for EFA solid spheres for various temperatures (pOH = 0.3).

T (K)	τ_o (days)	τ_i (days)	$t_{i\text{-}o}(1-\tau_i/\tau_o)$ (days)	K_o (l/mole)	ΔG_o (J/mole)
293	8000			$4.46\ 10^{-17}$	$9.1717\ 10^4$
303	3000			$2.84\ 10^{-16}$	$9.0179\ 10^4$
313	750	275	1.6	$4.02\ 10^{-15}$	$8.6264\ 10^4$
ΔH (J/mole)					$1.80\ 10^5$
ΔS (J/moleK)					298
ΔG_{298} (J/mole)					$9.120\ 10^4$

The τ at various temperature have been determined by Brouwers and Van Eijk [1] and are listed in Tables 2 and 3, as well as $[OH^-]$ and the temperature. The reaction time has been determined both for inner and outer region (denoted by τ_i and τ_o, respectively).

Using the data of Tables 2 and 3, the K of EFA and LM solid spheres, respectively, are computed using equation (13) and the result is included in both tables as well. For inner and outer region, K is denoted by K_i and K_o, respectively. For these computations the mean values α, β etc. and x_S have been used. Note that t_{i-o} is that the time when the outer region has fully reacted and the inner region starts to react (the outer region starts to react at t = 0 s. [1]).

Table 3. Reaction time τ for LM solid spheres for various temperatures (pOH = 0.3)

T (K)	τ_o (days)	τ_i (days)	$t_{i-o}(1-\tau_i/\tau_o)$ (days)	K_o (l/mole)	ΔG_o (J/mole)	K_i (l/mole)	ΔG_i (J/mole)
293	2000			$8.99\ 10^{-14}$	$7.3181\ 10^4$		
303	1500	900	1.0	$1.40\ 10^{-13}$	$7.4563\ 10^4$	$3.41\ 10^{-13}$	$7.2322\ 10^4$
313	700	190	1.0	$4.99\ 10^{-13}$	$7.3716\ 10^4$	$4.84\ 10^{-12}$	$6.7805\ 10^4$
ΔH (J/mole)					$8.00\ 10^4$		$1.90\ 10^5$
ΔS (J/moleK)					19		390
ΔG_{298} (J/mole)					$7.434\ 10^4$		$7.378\ 10^4$

The two tables indicate that K increases with temperature, implying improved dissolution/reaction with increasing temperature. Furthermore, the values of K and equation (9) confirm that $[SiO^{2-}]$ is much smaller than $[OH^-]$ indeed, so that the assumption that the process is governed by the diffusion of the SiO_3^{2-} ion is correct (Brouwers and Van Eijk [1]).
With these K one can determine the standard free energy of reaction ΔG by

$$K = e^{\frac{-\Delta G}{RT}} \tag{14}$$

ΔG is the sum of free energies of formation of the products in their standard states minus the free energies of formation of the reactants in their standard states (Paul [13, 14], Babushkin et al. [18]). In Tables 2 and 3 the resulting ΔG are included using R = 8.31439 J/moleK.

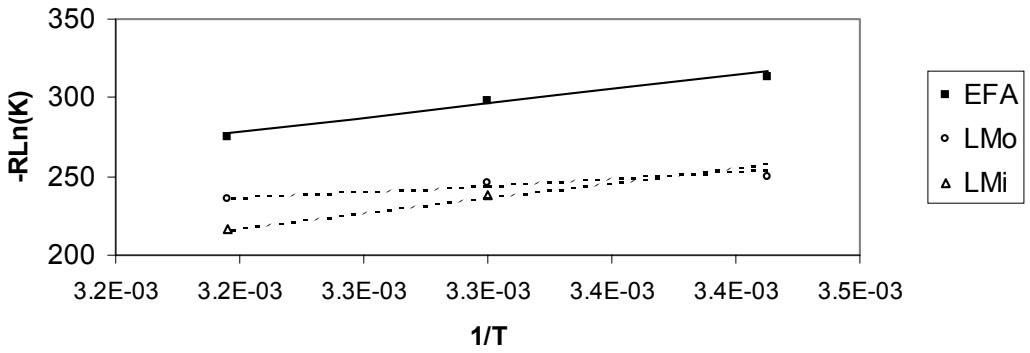

Figure 1. R Ln K versus 1/T for LM (inner and outer region) and EFA (outer region only) solid fly ash.

The connection of ΔG with enthalpy and entropy of reaction is

$$\Delta G = \Delta H - T\Delta S \qquad (15)$$

in which ΔH and ΔS are the sum of standard heats of formation and of the standard entropies, respectively, where each sum is constituted by the sum of the products minus the sum of the reactants. In order to specify ΔH and ΔS, –R Ln (K) has been set out against 1/T for LM and EFA in Figure 1, taking the values of Tables 2 and 3. A straight line has been fitted through the experimental values, whereby

$$-\text{R Ln (K)} = \frac{\Delta H}{T} - \Delta S \qquad (16)$$

see equations (14) and (15). The fitted values of ΔH and ΔS have been included in Tables 2 and 3.

Next, with the standard free energy of reaction ΔG, one is in a position to determine the free energy, enthalpy and entropy of formation of LM and EFA glass phase. In Table 4, the free energy, enthalpy and entropy of formation (ΔG^0, ΔH^0 and S^0, respectively) of some substances are listed (T = 298 K), taken from Paul [13] and Babushkin et al. [18], employing 1 cal = 4.184 J.

Table 4. Thermodynamic properties, taken from Babushkin et al. [18] (with exception of $HTiO_3^-$, which is taken from Paul [13]), and computed values.

	ΔH^0 (J/mole)	S^0 (J/moleK)	ΔG^0 (J/mole)
literature			
H^+	0	0	0
OH^-	- 229,999	- 10.753	- 157,277
AlO_2^-	- 918,806	- 20.92	- 823,411
SiO_3^{2-}	-	-	- 939,726
Ca^{2+}	542,665	- 55.23	- 552,706
Mg^{2+}	- 461.746	- 119.66	- 455,261
Na^+	- 240,454	- 58.99	- 262,211
K^+	- 252,295	- 102.17	- 282,671
Fe^{3+}	- 50,752	- 279.07	- 17,866
$HTiO_3^-$	-	-	- 467,353
H_2O	- 285,830	69.915	- 237,178
SiO_2 (gl)	- 901,568	46.861	- 848,641
SiO_2 (β-quartz)	- 911,066	41.840	- 856,674
$2SiO_2.Al_2O_3$ (cr)	- 3,378,412	124.18	- 3,173,397
computed			
EFA outer region (gl)			- 1,547,777
LM outer region (gl)			- 1,419,672
LM inner region (gl)			- 1,419,112

Unfortunately, from SiO_3^{2-} and $HTiO_3^-$ only ΔG^0 is available, so that it is only possible to determine ΔG^0 of the fly ash (and not ΔH^0 nor S^0).

Firstly, ΔG of the EFA and LM reaction is computed at 298K using equation (15) and the fitted values of ΔH and ΔS as listed in Tables 2 and 3. The resulting ΔG_{298} is being included in these tables as well. Considering reaction (7), ΔG^0 of EFA and LM glass now follow from:

$$\Delta G^0 = -\Delta G_{298} - (2+2\alpha-2\beta-2\gamma-6\delta+\varepsilon)\,\Delta G^0_{OH^-} + \Delta G^0_{SiO_3^{2-}} + 2\alpha\ \Delta G^0_{AlO_2^-} +$$
$$\beta\left(\frac{x_C}{x_C+x_M}\ \Delta G^0_{Ca^{2+}} + \frac{x_M}{x_C+x_M}\ \Delta G^0_{Mg^{2+}}\right) + 2\gamma\left(\frac{x_N}{x_N+x_K}\ \Delta G^0_{Na^+} + \frac{x_K}{x_N+x_K}\ \Delta G^0_{K^+}\right) \qquad (17)$$
$$+ 2\delta\ \Delta G^0_{Fe^{3+}} + \varepsilon\ \Delta G^0_{HTiO_3^-} + (1+\alpha-\beta-\gamma-3\delta)\ \Delta G^0_{H_2O}$$

Taking x_C, x_M, x_N, x_K, α, β, γ, δ, and ε from Table 1, the value of ΔG_{298} listed in Tables 2 and 3, and taking the free energies of formation from Table 4, ΔG^0 of EFA and LM is computed using equation (17) and included in this latter table as well.

Note that in reaction equation (7), β and γ and represent the total molar content of earth alkalis and alkalis to molar content of silica, respectively. But to compute ΔG^0, the actual contents of MgO, CaO, Na_2O and K_2O have to be accounted of. For that reason, the molar ratios $x_C/(x_M + x_C)$ etc. are appearing in equation (17).

From Table 4 one can conclude that with increasing α (i.e. A/S molar ratio) $-\Delta G^0$ increases. For EFA, α takes a value of about 0.29 and for LM about 0.25, and indeed, $-\Delta G^0$ of EFA is larger. Furthermore, one can see that for LM the values pertaining to inner and outer are very close. From this information it can be concluded that $-\Delta G^0$ is mainly governed by α.

In order relate the computed values of $-\Delta G^0$ with values reported in literature, values of $-\Delta G^0$ of silica (quartz and vitreous, α = 0) and of $2SiO_2.Al_2O_3$ (α = 0.5) are also included in Table 4. One can see that $-\Delta G^0$ of LM and EFA are located between the values of silica and of $2SiO_2.Al_2O_3$. Moreover, they are in line with the trend that for larger α, $-\Delta G^0$ also increases, confirming the reliability of the computed values of $-\Delta G^0$.

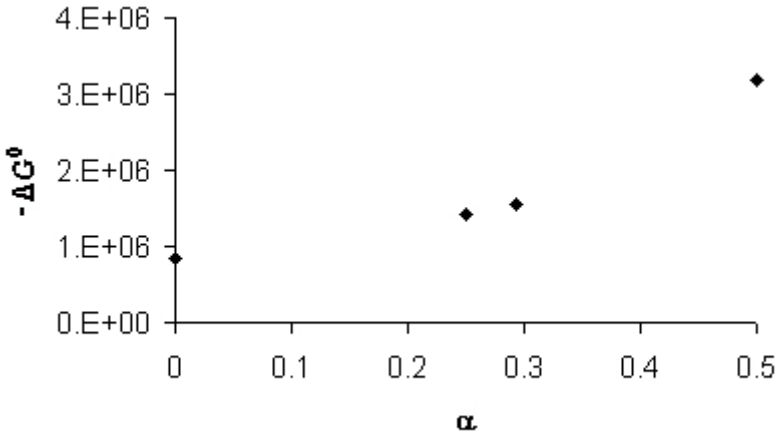

Figure 2. $-\Delta G^0$ versus α (A/S molar ratio).

In Figure 2, $-\Delta G^0$ is set out graphically against α, whereby the value of $-\Delta G^0$ is taken from vitreous silica (α = 0) and from EFA and LM outer regions.

For most fly ashes, α lies in the range 0.25-0.29. For these fly ashes a tentative value of $-\Delta G^0$ can be obtained from the values of LM and EFA determined here, e.g. by interpolation. For values in the range 0-0.25 and 0.29 to 0.5, interpolation between silica and LM and between EFA and $2SiO_2.Al_2O_3$, respectively, is recommended. The latter range generally holds for slags. A direct measurement (e.g. by dissolution experiments, applying a shrinking core model, the chemical reaction mechanism and the thermodynamic analysis) of $-\Delta G^0$ would be more accurate, but also more elaborate. Interpolation as proposed here will readily provide a value that can be useful for tentative reactivity computations.

4. CONCLUSIONS

Pietersen [2, 3] has carefully executed and reported dissolution experiments of several types of pulverised powder coal (class F) fly ashes (Table 1). To this end, the silica release in time was measured for various pOH and temperatures. In order to understand the dissolution and reaction behaviour of these fly ashes, in particular the EFA and LM fly ash, Brouwers and Van Eijk [1] derived a shrinking core model. They have applied the model to said experiments, yielding values of the reactivity time τ (eq. (11)) for both inner and outer region (τ_i and τ_o), which are summarised in Tables 2 and 3. Furthermore, it was found that the dissolution rate is proportional to $[OH^-]^{0.9\text{-}1}$ for the outer region (EFA and LM), and to $[OH^-]^{1.4}$ in inner region (information available about LM only).

Here, a reaction mechanism for the glass phase of the fly ash glass is put forward that accounts for its oxide composition (silica, aluminium oxide, iron oxide, titanium oxide, alkali and earth alkali content) and which also could be useful for slags.). From the proposed reaction mechanism and equilibrium constant, it follows that the solubility of the fly ashes is as a function of $[OH^-]^a$. The parameter a solely depends on the oxide composition of the glass phase. Using the average composition of EFA and LM fly ash, the power a takes a value of 1.022 (EFA) and 1.208 (LM). This result suggests that the outer layer is poorer in silica and aluminiumoxide, i.e. that K_2O, Na_2O, CaO, MgO, and Fe_2O_3 are concentrated in the exterior hull, which is in line with findings in previous publications.

Combining the equilibrium constant and the experimental data at various temperatures, also the free energy, enthalpy and entropy of reaction are computed of EFA and LM glass phase. Finally, these data are used to compute the free energy of formation ΔG^0 of both glasses. It follows that the free energy of formation is mainly governed by the molar ratio (α) of the major constituents SiO_2 and Al_2O_3. The values obtained are in line with those of known substances, silica (α = 0) and $2SiO_2.Al_2O_3$ (α = 0.5). With this information one can assess ΔG^0 of (fly ash and slag) glass phases with deviating A/S molar ratio, and subsequently, to assess their reactivity in a cement environment.

REFERENCES

[1] Brouwers, H.J.H. and Van Eijk, R.J. Reactivity of fly ash: extension and application of a shrinking core model, Concrete Sci. and Eng., vol 14, 2002, pp. 106-113.

[2] Pietersen, H.S. Reactivity of fly ash at high pH, Mat. Res. Soc. Symp. Proc., vol. 178, 1990, pp. 139-157.

[3] Pietersen, H.S. Reactivity of fly ash and slag in cement, Ph.D. Thesis, Delft University of Technology, The Netherlands, 1993.

[4] Fraay, A.L.A., Bijen, J.M. and De Haan, Y.M. The reaction of fly ash in concrete, a critical examination, Cement and Concrete Res., vol. 19, 1989, pp. 235-246.
[5] Xu, A. and Sarkar, S.L. Microstructural development in high-volume fly-ash cement system, J. of Mat. in Civil Eng., vol. 6, 1994, pp. 117-136.
[6] Taylor, H.F.W. Cement chemistry, 2nd ed. London: Thomas Telford, 1997.
[7] Hewlett, P.C. Lea's chemistry of cement and concrete, 4th ed. London: Arnold, 1998.
[8] Song, S. and Jennings, H.M. Pore solution chemistry of alkali-activated ground granulated blast-furnace slag, Cement and Concrete Res., vol. 29, 1999, pp. 159-170.
[9] Song, S., Sohn, D., Jennings, H.M. and Mason, T.O. Hydration of alkali-activated ground granulated blast furnace slag, J. of Mat. Sci., vol. 35, 2000, pp. 249-257.
[10] Hemmings, R.T. and Berry, E.E. On the glass in coal fly ashes: recent advances, Mat. Res. Soc. Symp. Proc., vol. 113, 1988, pp. 3- 28.
[11] Pourbaix, M. Atlas of electrochemical equilibria in aqueous solutions, Oxford: Pergamon, 1966.
[12] MacPhee, D.E. and Glasser, F.P. Immobilization science of cement systems, MRS Bulletin, vol. 18 No. 3, 1993, pp. 66-71.
[13] Paul, A. Chemical durability of glasses; a thermodynamic approach, J. of Mat. Sci., vol. 12, 1977, pp. 2246-2268.
[14] Paul, A. Chemistry of Glass, 2nd ed. London: Chapman, 1990.
[15] Dudas, M.J. and Warren, C.J. Submicroscopic model of fly ash particles, Geoderma, vol. 40, 1987, pp. 101-114.
[16] Smith, R.D. The trace element chemistry of coal during combustion and the emissions from coal-fired plants, Prog. Energy Combust. Sci., vol. 6, 1980, pp. 53-119.
[17] Lide, D.R.L. CRC Handbook of chemistry and physics, 76th ed. Boca Raton: CRC Press, 1995.
[18] Babushkin, V.I., Matveyev, G.M. and Mchedlov-Petrossyan, O.P. Thermodynamics of Silicates, Berlin: Springer, 1985.

INFLUENCE OF TEMPERATURE AND ALKALI CONCENTRATION ON THERMODYNAMICAL STABILITY OF SULPHOALUMINATE PHASES

Valérie Michaud-Poupardin[1] and Danielle Sorrentino[1]

[1] Lafarge Laboratoire Central de Recherche, 95 Rue du Montmurier BP 15, 38291 Saint Quentin-Fallavier Cedex, France;
E-mail: valerie.poupardin@lafarge.com, daniele.sorrentino@lafarge.com

ABSTRACT

Temperature plays a major role on the domains of thermodynamical stability of hydrates. However, controversy still exists concerning some of them. This is the case with the sulphoaluminate phases. It has recently been alleged that ettringite is not stable at temperatures above 60 – 70°C while monosulphoaluminate would be. However, other experiments have indicated the presence of ettringite at a temperature of 90°C and thermodynamical calculations also support the fact that ettringite is a stable phase at 85°C.

Besides, the impact of alkali concentration on the domains of stability of the sulphoaluminate phases at elevated temperature is not well understood.

The most comprehensive analysis regarding this combined effect of alkali concentration - temperature on the domains of stability of sulphoaluminate phases has been carried out by Damidot and Glasser using thermodynamical calculations. They showed a very strong impact of the temperature and alkali concentration on the domains of stability of the sulfoaluminate phases. However, these data have not been validated experimentally.

Results of this present study, carried out on pure phases, validate the thermodynamical calculations. This study also discusses the impact of the alkali ions (sodium or potassium) on the solid phase assemblages and aqueous phase compositions and the influence of the alkali concentration and temperature on the domain of stability of the sulfoaluminate phases.

Keywords: thermodynamical stability, solubility, sulphoaluminate phases, ettringite, calcium monosulfoaluminate, alkali concentration, temperature.

1. INTRODUCTION

Temperature plays a major role on the domains of thermodynamical stability of hydrates. Various studies have been carried out in order to determine the influence of temperature and alkali concentration on the stability of the hydrated calcium sulfoaluminate phases, and mainly on the ettringite stability. However, there is a lot of controversy regarding the results. It has been alleged that ettringite is not stable at temperatures above 60 – 70°C, while monosulphoaluminate would be. However, other experiments have indicated the presence of ettringite at a temperature of 90°C.

For instance, Abo-El-Enein et al. [1], Kalousek [2], Brown and Bothe [3] and Mori and al. [4] showed the presence of ettringite up to a curing temperature of 80 – 90°C, even when the alkali concentration of the solution was very high, equal to 2 mol/l [3].

However, in the studies of Ghorab and Kishar [5, 6], and Berger et al. [7], ettringite was stirred in NaOH solutions and was no longer detected after 24 hours at 60°C when NaOH concentration was higher than 0.2 mol/l [5, 6] and one hour at 85°C when the NaOH concentration of the solution was higher than 0,87 mol/l [7].

The most comprehensive analysis regarding the combined effect of alkali concentration - temperature on the domains of stability of sulphoaluminate phases has been carried out by Damidot and Glasser [8, 9, 10] using thermodynamical calculations. They determined the influence of temperature on the phase diagram in the system "CaO-Al_2O_3-SO_3-H_2O" for different sodium concentrations varying from 0 to 1 mol/l and temperatures (25°C, 50°C and 85°C). They found that some ranges of solution compositions stable under which ettringite is in the whole range of temperature and alkali concentration investigated (even at 85°C in the presence of a very high alkali concentration of 1 mol/l). Calculations also show that at temperatures above 45°C, monosulfoaluminate becomes increasingly stable at the expense of ettringite. The higher the temperature, the more the domain of solution composition is reduced under which ettringite is stable, and the more the one under which monosulfoaluminate is stable it is widened. However, these data have not been validated experimentally.

The present study aims at validating experimentally these thermodynamical data to enable its use when cement hydration occurs at elevated temperatures. Even if the system is dynamic (not at the equilibrium), as occurs at the beginning of hydration, these thermodynamical data can be used to draw the kinetic path of the reaction, so as to determine if the solution is supersaturated or undersaturated with respect to stable hydrates and predict the hydrates which may potentially precipitate with time. Besides, after a relatively short period, local equilibrium tend to assert itself and the concentrations tend towards the values predicted from a stable diagram.

The concentrations at various invariant points of the phase diagram « CaO-Al_2O_3-SO_3-K_2O-H_2O » including $Ca(OH)_2$ have been determined experimentally at 70°C and 90°C for 2 concentrations in alkali (0,42 and 1,05 mol/l), and at 25°C for an alkali concentration of 0,42 mol/l. Experiments have been limited to the invariant points including Ca(OH)2, since these are involved during the cement hydration.

In this paper, the impact of the alkali ions (sodium or potassium) on solid phase assemblages and aqueous phase compositions has also been discussed. In the last part of this paper, the influence of the alkali concentration and temperature on the domain of stability of the sulfoaluminate phases is examined.

2. EXPERIMENTAL

This study has been carried out using pure phase materials. $Ca(OH)_2$, C_3A (SSB = 450 m2/kg) and gypsum (high grade quality) were mixed in diluted suspension with KOH solutions. The specimens were prepared in diluted suspension in order to quicker reach the thermodynamic equilibrium.

Two KOH concentrations were used: 0.42 and 1.05 mol/l. The amount of C_3A and $Ca(OH)_2$ were kept constant for all the specimens, equal respectively to 0.07 and 0.05 moles per liter. $Ca(OH)_2$ was introduced in order to determine experimentally the compositions of the invariant points including $Ca(OH)_2$. Various amounts of gypsum have been used in order to cover the whole range of stability of the various sulfoaluminate phases. They are reported in the Table 1.

Table 1. Amount of gypsum introduced initially in the various mixtures investigated (moles per liter)

25°C	70°C		90°C	
[KOH]= 0.42 mol/l	[KOH]= 0.42 mol/l	[KOH]= 1.05 mol/l	[KOH]= 0.42 mol/l	[KOH]= 1.05 mol/l
0.445	0.445	0.71	0.445	0.71
0.365	0.26	0.46	0.295	0.565
0.31	0.16	0.32	0.19	0.42
0.26	0.13	0.27	0.16	0.32
0.21	0.065	0.175	0.085	0.225
0.14	0.02	0.07	0.04	0.15

The solids were stirred with the KOH solution in polypropylene flasks. Solid / liquid ratios between 40 and 7 were used depending on the initial amount of gypsum. The flasks were immersed in a thermostated bath and kept at constant temperature of 25°C, 70°C and 90°C during the whole experiment. At 70°C and 90°C, silicon oil was used to limit the evaporation.
The flasks were hermetically closed to avoid any carbonation and introduction of oil during the experiment.

Once the systems had reached their thermodynamic equilibrium (28 days at 25°C and 6 days at 70 and 90°C), the solid and liquid phases were separated by filtering. The solid phases, after being dried with acetone itself removed by ether, were analyzed by XRD. The solution concentrations were measured by ICP for calcium, sulfur (present here as sulphate only), aluminate and alkali ions, and by titration with a 0,05 N HCl solution in the presence of helianthine indicator for the hydroxide ions.

3. RESULTS

XRD analysis show that the C_3A had fully reacted after 6 days at 70 and 90°C, but not after 28 days at 25°C. In this last case, a significant amount of residual C_3A was still present for the systems containing high initial amounts of gypsym (0.445, 0.365 and 0.31 mole per liter). A trace of residual C_3A was also present for the systems containing 0.26 mole per liter.

The compositions of the filtrates and the solid phases in the mixtures are reported in the Table 2 for a potassium concentration of 0.42 mol/l and in the Table 3 for a potassium concentration of about 1 mol/l.

From now, the following abbreviations are used:

- Gyp. = Gypsum ($CaSO_4.2H_2O$) ,
- AFt = Ettringite ($C_3A.3CaSO_4.32H_20$),
- AFm = calcium monosulfoaluminate ($C_3A.CaSO_4.12H_20$),
- Syng. = Syngenite ($CaSO_4.K_2SO_4.H_2O$),
- Gorg. = Gorgeyte $(CaSO_4)_5.K_2SO_4.H_2O$),
- CH = calcium hydroxide ($Ca(OH)_2$).

Table 2. Composition of the liquid and solid phases for [KOH] = 0,42 mol/l

T (°C)	Initial amount Of gypsum (mmoles per liter)	Initial gypsum/C_3A mol. ratio	$[K^+]$ (mmol/l)	$[SO_4^{2-}]$ (mmol/l)	$[OH^-]$ (mmol/l)	$[Ca^{2+}]$ (mmol/l)	$[Al(OH)_4^-]$ (mmol/l)	Solid phases
25	445 (I)	6.3	403	166	102	16.6***	< 0.3*	Syng., Gyp., AFt, CH
	365 (I)	5.2	431	178	108	16.8***	< 0.3*	Gyp., AFt, CH
	310 (I)	4.4	412	171	100	15.8***	< 0.3*	AFt, CH
	260 (II)	3.7	419	90	240	2.8***	< 0.3*	AFt, CH
	210	3	428	3.0**	380	1.2***	0.3**	AFt, CH
	140	2	422	2.3**	380	1.2***	0.4**	AFt, AFm, CH
70	445	6.3	431	195	75	17.3***	< 0.3*	Syng., Gyp., AFt, CH
	260	3.7	434	109	217	2.4***	< 0.3*	AFt, AFm, CH
	160	2.3	422	93	240	1.9***	0.4**	AFm, CH
	130	1.86	425	63	305	1.5***	0.8***	AFm, CH
	65	0.93	425	3.8***	425	1.2***	6.7	AFm, C_4AH_{13}, CH
	20	0.29	425	3.8***	423	1.2***	6.7	AFm, C_4AH_{13}, C_3AH_6, CH
90	445	6.4	397	174	87	9.7***	< 0.3*	Syng., Gorg., AFt, CH
	295	4.2	422	172	111	6.4***	< 0.3*	AFt, AFm, CH
	190	2.7	422	129	187	2.5***	0.7***	AFm, CH
	160	2.3	419	97	244	1.6***	1.3	AFm, CH
	85	1.2	425	25	383	0.8***	7.6	AFm, C_4AH_{13}, CH
	40	0.6	443	15	426	0.7***	13.4	AFm, C_4AH_{13}, C_3AH_6, CH

The precision of the concentrations is +/- 2 % except for those annotated by *, ** or ***:

* below the detection limit

** very low precision (> 5 %)

*** precision = 5%

(I) significant amount of residual C_3A, (II) trace of residual C_3A

Table 3. Composition of the liquid and solid phases for [KOH] ≈ 1 mol/l

T (°C)	Initial amount of gypsum (mmoles per liter)	Initial gypsum/C_3A mol. ratio	$[K^+]$ (mmol/l)	$[SO_4^{2-}]$ (mmol/l)	$[OH^-]$ (mmol/l)	$[Ca^{2+}]$ (mmol/l)	$[Al(OH)_4^-]$ (mmol/l)	Solid phases
70	710	10.1	902	408	140	9.6***	< 0.7*	Syng., AFt, CH
	460	6.6	1024	382	313	2.8***	< 0.7*	AFt, AFm, CH
	320	4.6	1001	254	540	1.5***	1.9***	AFm, CH
	270	3.9	1008	206	640	1.4***	2.9	AFm, CH
	175	2.5	1008	116	825	1.0**	7	AFm, C_4AH_{13}, CH
	70	1	1001	37	970	1.1**	19.6	AFm, C_4AH_{13}, C_3AH_6, CH
90	710	10.1	1024	460	110	10.2***	< 0.7*	Syng., AFt, CH
	565	8.1	1077	482	120	10.8***	< 0.7*	AFt, AFm, CH
	420	6	1069	355	345	2.0***	1.9**	AFm, CH
	320	4.6	1069	258	545	1.3***	5.7	AFm, CH
	225	3.2	1084	174	730	1.0**	13.1	AFm, C_4AH_{13}, C_3AH_6, CH
	150	2.1	1077	125	830	0.9**	22.4	AFm, C_4AH_{13}, C_3AH_6, CH

4. DISCUSSION

Firstly, the compositions of the solutions, at the various invariant points determined experimentally, will be compared with those calculated by Damidot and Glasser. Then, the compositions of the various invariant points of the present study will be summarized. Finally, the impact of temperature and alkali concentration on the stability of AFt and AFm will be discussed.

The following notation have been used for the invariant points:

- A = Gyp., AFt, CH,
- B = Syng., AFt, CH
- C = Syng., Gyp., AFt, CH
- D = Syng., Gorg., AFt, CH
- E = AFt, C_3AH_6, CH
- F = AFt, AFm, CH
- G = AFm, hydrated calcium aluminate, CH

4.1 Comparison of the experimental and calculated values.

As experimental data were obtained using potassium and calculations using sodium (at 25°C potassium was also used), a preliminary discussion will be introduced on the impact of the nature of the alkali ions.

Then, the experimental and calculated values will be compared at 25, 70 and 90°C. Since the compositions of the invariant points predicted by calculation at temperature higher than 25°C are only reported in the literature for sodium concentrations of 0, 250, 500 and 1000 mmol/l and temperatures of 25, 50 and 85°C, the compositions for the alkali concentration and temperature investigated in the present study have been extrapolated using a polynomial extrapolation.

4.1.1 Difference between potassium and sodium

At 25°C, calculations showed that the system "$CaO\text{-}Al_2O_3\text{-}SO_3\text{-}H_2O$" behaves similarly in the presence of sodium or potassium as long as the alkali concentration is lower than 0.43 mol/l. The invariant points have similar compositions with both cations. This results from the fact that potassium and sodium affect the ionic strength identically. However, the system in the presence of K_2O is more complex due to the appearance of a new phase when the alkali concentration is higher than 0.43 mol/l, the Syng. which has no sodium counterparts. Thermodynamical calculations show that at a potassium concentration higher than 0.43, the phase diagram is similar to the one in the presence of sodium with Gyp. being replaced by Syng., and that the composition of the point B at 25°C is similar to the point A calculated for sodium and the same alkali concentration (table 4, line a).

Similarly, the composition of the point C is closed to the point A calculated for sodium and the same alkali concentration (Table 4, line b).

Table 4. Comparison of the experimental and calculated compositions at the points B - A (line a) and C - A (line b) at 25°

	$[K^+$ or $Na^+]$ (mmol/l)	$[SO_4^{2-}]$ (mmol/l)		$[Ca^{2+}]$ (mmol/l)		$[Al(OH)_4^-]$ (mmol/l)	
		with K^+	with Na^+	with K^+	with Na^+	with K^+	with Na^+
a	500	190	197	8.9	11.2	$1.06*10^{-6}$	10^{-6}
b	431	171	166	11.7	10.4	$5.6*10^{-7}$	$5.6*10^{-6}$

Therefore, at 25°C and beyond 0.43 mol/l, the compositions for either sodium and potassium remain similar whatever the alkali concentration, and the compositions of the points B and C can be compared to the point A calculated in the presence of sodium for the same alkali concentration.

At elevated temperature, the experimental data obtained using potassium and calculations using sodium are expected to remain comparable, since both cations are expected to affect the ionic strength identically similarly to room temperature. When Syng. will be present, the compositions of the points B or C will be compared to the point A calculated for sodium and the same alkali concentration.

4.1.2 Comparison of invariant point concentrations at 25°C

The experimental and calculated compositions for the points C and F are compared in the Table 5 (lines a and b respectively) and show similar compositions. Only differences have been noticed for the calcium concentration; calculation predicts lower concentration than experiments.

Since thermodynamic calculations do not predict AFm but C_3AH_6 to be the phase thermodynamically stable in the presence of AFt and CH at room temperature, in the Table 5 the experimental point F has been compared to the calculated point E. The presence of AFm in conjunction with AFt and CH in these experiments may be due to the fact that the system did not totally reach the equilibrium.

Table 5. Comparison of the experimental and calculated compositions at the points C (line a) and F (line b) at 25°C

	$[K^+]$ (mmol/l)		$[SO_4^{2-}]$ (mmol/l)		$[Ca^{2+}]$ (mmol/l)		$[Al(OH)_4^-]$ (mmol/l)	
	measured	calculated	measured	calculated	measured	calculated	measured	calculated
a	403	431	161	171	16.6	11.7	< 0.3	$5.6*10^{-7}$
b	420		2.3	2.2	1.2	1.0	0.36	0.07

4.1.3 Comparison of invariant points concentrations at 70°C

Similarly to room temperature, most of the compositions of the invariant points determined experimentally are in good agreement with those predicted by calculation (see Table 6). This is the case for the invariant points C (line a), B (line b) and F (lines c and d).

In Table 6, the compositions of the invariant points B and C have been compared to A for sodium and similar alkali concentration. Therefore, as assumed previously and similarly to room temperature, the compositions of the invariant points B and C are similar to A.

Besides, similarly to room temperature, predicted calcium concentrations are lower than experimental ones.

Table 6. Comparison of the experimental and calculated compositions at the points C (line a), B (line b) and F (lines c and d), G (lines e and f) at 70°C

	$[K^+]$ or $[Na^+]$ (mmol/l)	$[SO_4^{2-}]$ (mmol/l)		$[Ca^{2+}]$ (mmol/l)		$[Al(OH)_4^-]$ (mmol/l)	
	measured /calculated	measured	calculated	measured	calculated	measured	calculated
a	431	195	185	17.3	10.8	< 0.3	0.09
b	902	408	395	9.6	7.9	< 0.7	0.4
c	434	109	100	2.4	1.6	< 0.3	0.23
d	1024	382	361	2.8	1.1	< 0.7	0.3
e	425	3.8	27	1.2	0.6	6.7	2.5
f	1008 - 1001	116- 37	152	1.1	0.25	7 – 19.6	3.8

Disparities between experiments and calculations have only been observed for the invariant point G (Table 6, lines e and f). The sulfate concentrations measured were lower than those calculated. However, the accurate compositions of this invariant point have not been successfully determined probably due to the fact that the equilibrium was not totally reached. Indeed, thermodynamic predicts C_3AH_6 to be the most stable phase, but experiments always show the presence of C_4AH_{13} in conjunction with AFm and CH, and C_3AH_6 in addition to the others only in few cases. Besides, for most of the couples alkali / temperature investigated, AFm, hydrated calcium aluminate and CH have been observed in conjunction with two solutions of similar potassium concentration but different compositions, whereas thermodynamics predicts a sole composition. The different compositions are reported in the Table 6.

4.1.4 Comparison of invariant points concentrations at 90°C:

Similarly to 25°C and 70°C, most of the compositions of the invariant points determined experimentally are in good agreement with those predicted (see Table 7). This is the case for the invariant points D (line a), and F (lines c and d).

At 90°C, syng., AFt and CH have not been observed in conjunction with Gyp. (point C) but with Gorgeyite (Gorg.) (point D), indicating that this phase is probably more stable than Gyp. at this temperature. Therefore, the composition of the solution at the invariant point D determined experimentally has been compared to the composition of the predicted invariant point A.

The presence of Gorg. is consistent with the preliminary study performed by Damidot and Glasser in the presence of potassium and the work of Hill [11], which show the appearance of this phase in addition to Syng. and predict this phase to becomes stable at or above 40°C.

Table 7. Comparison of the experimental and calculated compositions at the points D (line a), B (line b), F (lines c and d), G (line e and f) at 90°C

	$[K^+]$ or $[Na^+]$ (mmol/l)	$[SO_4^{2-}]$ (mmol/l)		$[Ca^{2+}]$ (mmol/l)		$[Al(OH)_4^-]$ (mmol/l)	
	measured /calculated	measured	calculated	measured	calculated	measured	calculated
a	397	174	180	9.7	9	< 0.3	0.17
b	1024	460	351	10.2	6.2	< 0.7	1
c	422	172	164	6.4	2.2	< 0.3	0.33
d	1077	482	460	10.8	1.7	< 0.7	0.4
e	425 - 443	25 - 15	45	0.8 – 0.7	0.4	7.6 – 13.4	4.6
f	1080	174 - 125	224	0.9 – 1.0	0.2	13 – 22.4	7

However, a deviation between predictions and experiments have been observed for the point B when the alkali concentration is high (1000 mmol/l) (Table 7, line b), probably due to the high ionic strength reducing the accuracy of the calculation of the activity coefficient. The predicted sulfate concentration is lower than the experimental one. Therefore, for very high alkali concentration, thermodynamic calculations are not able any more to predict accurately the composition of the solution at the invariant point B at 90°C.

At 90°C, differences between experiments and calculations have also been observed for the invariant point G (Table 7, line e and f). The sulfate concentrations measured are lower than those calculated. However, similarly to 70°C, the accurate values of the compositions at this invariant point have also not been successfully determined since AFm, hydrated calcium aluminate and CH have been observed in conjunction with two solutions of different compositions for the both alkali concentrations investigated. The different compositions are reported in the Table 7 (lines e and f).

4.2 Summary of the invariant points determined in this study

The invariant points determined in this study are reported in the Tables 8 and 9 for potassium concentrations of 0.42 and 1 mol/l respectively.

Table 8. Summary of the invariant points for [K+] ≈ 0.42 mol/l

Point	T (°C)	$[K^+]$ (mmol/l)	$[SO_4^{2-}]$ (mmol/l)	$[OH^-]$ (mmol/l)	$[Ca^{2+}]$ (mmol/l)	$[Al(OH)_4^-]$ (mmol/l)	Solid phases detected
C (25, 70°C) or D (90°C)	25	403	166	102	16.6	< 0.3	Syng., Gyp.,AFt, CH
	70	431	195	75	17.3	< 0.3	Syng., Gyp.,AFt, CH
	90	397	174	87	9.7	< 0.3	Syng., Gorg.,AFt, CH
F	25	422	2.3	380	1.2	0.36	AFt, AFm, CH
	70	434	109	217	2.4	< 0.3	AFt, AFm, CH
	90	422	172	111	6.4	< 0.3	AFt, AFm, CH
G	70	425	3.8***	424	1.2***	6.7	AFm, C_3AH_6, C_4AH_{13}, CH
	90	425	25	383	0.82***	7.6	AFm, C_4AH_{13}, CH
		443	15	426	0.74***	13.4	AFm, C_3AH_6, C_4AH_{13}, CH

Table 9. Summary of the invariant points for [K+] ≈ 1 mol/l

Point	T (°C)	$[K^+]$ (mmol/l)	$[SO_4^{2-}]$ (mmol/l)	$[OH^-]$ (mmol/l)	$[Ca^{2+}]$ (mmol/l)	$[Al(OH)_4^-]$ (mmol/l)	Solid phases detected
B	70	902	408	140	9.6	< 0.7	Syng., AFt, CH
	90	1024	460	110	10.2	< 0.7	Syng., AFt, CH
F	70	1024	382	313	2.8	< 0.7	AFt, AFm, CH
	90	1077	482	120	10.8	< 0.7	AFt, AFm, CH
G	70	1008	116	825	1.0***	7	AFm, C_4AH_{13}, CH
		1001	37	970	1.1***	19.6	AFm, C_3AH_6, C_4AH_{13}, CH
	90	1084	174	730	1.02***	13.1	AFm, C_3AH_6, C_4AH_{13}, CH
		1077	125	830	0.89***	22.42	AFm, C_3AH_6, C_4AH_{13}, CH

4.3 Influence of temperature and alkali concentration on the domain of stability of AFt and AFm.

The present study shows that there exists some domains of solution composition under which ettringite is thermodynamically stable, whatever the temperature and alkali concentration in the whole range investigated, therefore even in the presence of a very high alkali concentration (1 mol/l) and for very high temperature (90°C). However, ettringite is not stable (i.e. is not the hydrate with the lowest solubility) whatever the composition of the solution. Therefore, this phase can disappear from a selected composition for instance, but it does not imply that it is unstable in the absolute thermodynamic sense, otherwise it must disappear from all compositions. This can explain at least partly why there are controversies regarding the influence of temperature and alkali concentration on the stability of ettringite.

The influence of temperature and alkali concentration will be examined respectively using a few thermodynamical rules which will be discussed first.

4.3.1 Few thermodynamical rules

In the present study, all the invariant points determined experimentally include CH, and one or two other phases. In the first case, the equilibrium conditions are represented by a curve. Therefore, if the sulfate concentration is fixed, the composition of the aqueous phase is fixed and is defined by the equilibrium between CH, and the hydrate which is stable in the presence of CH and has the lowest solubility. In the second case, only one composition of the aqueous phase describes the equilibrium.

4.3.2 Influence of temperature

At 25°C and according to the Tables 8 and 9, when the sulfate concentration is higher than the one at the point F (2.3 mmol/l for a potassium concentration of 422 mmol/l), the hydrate stable in the presence of CH and with the lowest solubility is ettringite (the equilibrium curve of ettringite is displaced to lower solubility than monosulfoaluminate and hydrated calcium aluminates). This hydrate is the one with the lowest solubility on a very wide domain of sulfate concentration varying from 2.3 mmol/l (point F) to 166 mol/l (point C) for a potassium concentration of 0.4 – 0.42 mol/l.

At 70 and 90°C, ettringite remains the hydrate which is stable in the presence of CH and the one with the lowest solubility when the sulfate concentration is higher than the one at the point F. This indicates that the equilibrium curve of ettringite starts to be displaced to lower solubility than monosulfoaluminate and hydrated calcium aluminates beyond this sulfate concentration. However, the sulfate concentration at point F drastically increases with the temperature (2.3 mmol/l at 25°C, 109 mmol/l at 70°C and 172 mmol/l at 90°C, for a potassium concentration of 420 - 430 mmol/l).

Besides, the points A, B, C or D mark the highest sulfate concentration at which ettringite is stable with the solution in the presence of CH. Table 8 and 9 show that the compositions of the solutions at these invariant points are very slightly influenced by the temperature from 25 to 90°C. Therefore, the domain of sulfate under which ettringite is stable in the presence of CH drastically reduces as the temperature increases. The influence of temperature on this domain is illustrated in the figure 1.

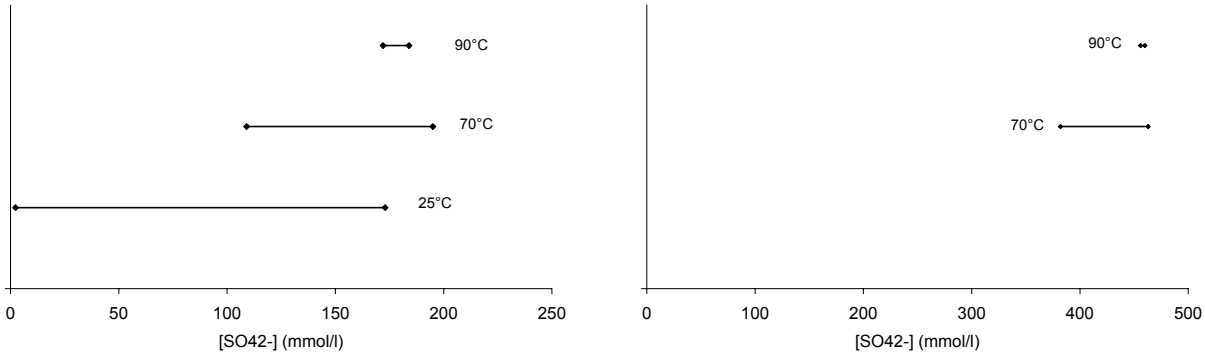

$[K^+]$ = 420 mol/l $[K^+]$ = 1020 mol/l

Figure 1. Influence of temperature on the range of sulfate concentration under which AFt and CH are stable.

Below the sulfate concentration corresponding to the invariant point F and above the one corresponding to G, ettringite and the hydrated calcium sulfoaluminate are metastable with respect to monosulfoaluminate, and the equilibrium solution is defined by the equilibrium between this latter phase and CH. The influence of temperature on the domain of sulfate concentration under which monosulfoaluminate is stable in the presence of CH is illustrated in the figure 2. It drastically increases with the temperature and is very wide at elevated temperature. Besides, this figure shows that monosulfoaluminate is stable in the presence of high sulfate concentrations at elevated temperature contrary to room temperature. This maximum sulfate concentration under which monosulfoaluminate and CH are stable increases with the temperature.

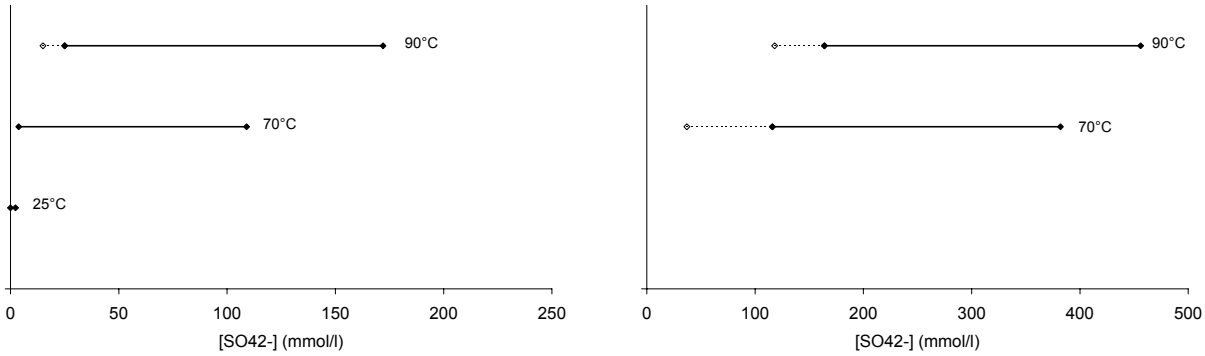

$[K^+]$ = 420 mol/l $[K^+]$ = 1020 mol/l

Figure 2. Influence of temperature on the range of sulfate concentration under which monosulfoaluminate and $Ca(OH)_2$ are stable.

Below the sulfate concentration corresponding to the point G, both ettringite and monosufoaluminate are metastable with respect to the hydrated calcium aluminates and mainly C_3AH_6. Therefore, the equilibrium solution is defined by the equilibrium between C_3AH_6 which is the phase with the lowest solubility and CH. The tables 8 and 9 show that, when the temperature increases, the domain of sulfate concentration under the hydrated calcium aluminate are stable in the presence of CH increases.

4.3.3 Influence of the alkali concentration

Figure 1 shows that the higher the alkali concentration, the higher is the sulfate concentration beyond which ettringite is stable in the presence of CH, whatever the temperature. Besides, at 90°C, the domain of sulfate concentration under which ettringite is stable is small, and even more reduced as the alkali concentration is high.

The higher the alkali concentration, the higher is also the minimum and maximum sulfate concentration over which monosulfoaluminate is stable in the presence of CH (see Figure 2 at 70 and 90°C). Therefore, at elevated temperature, the monosulfoaluminate is stable in the presence of CH when the sulfate concentration is high and even more so if the alkali concentration is high.

The displacement of the equilibrium curves with the alkali concentrations is due to a modification of the ionic strength which induced a modification of the activity coefficient.

5. CONCLUSIONS

The compositions of the invariant points determined experimentally are very consistent with those predicted by calculation, except for the invariant point B (AFt, AFm, CH) at 90°C when the alkali concentration is very high (1 mol/l). Under such conditions, there is a deviation between experiment and the composition predicted by thermodynamic calculations, probably because of the high ionic strength. Differences between experiments and predictions have also been observed for the invariant point G (AFm, hydrated calcium aluminate, CH) at 70 and 90°C whatever the alkali concentration. However, experimental difficulties were faced in this last case and the experimental data are not accurate.

The results also show that the system "CaO-Al_2O_3-SO_3-H_2O" behaves quite similarly in the presence of sodium or potassium. As long as the alkali concentration is lower than 0.40 - 0.43 mol/l, the invariant points are the same and have similar compositions with both cations. This results from the fact that potassium and sodium affect the ionic strength identically. The only

difference between sodium and potassium is the appearance of additional phases in the presence of potassium: the syngenite when the potassium concentration is higher than 0.4 – 0.43 mol/l whatever the temperature (from 25 to 90°C), and the gorgeyite more stable than gypsum at 90°C. However, the study shows that the compositions of the invariant points B (Syng., AFt, CH) , C (Syng., Gyp., AFt, CH for T≤ 70°C), or D (Syng., Gorg., AFt, CH for T = 90°C) are similar to A (Gyp., AFt, CH), calculated in the presence of sodium and the same alkali concentration, whatever the temperature (from 25 to 90°C).

This study also shows that there exists solution compositions under which ettringite is stable even in the presence of a very high temperature (90°C) and alkali concentration (1 mol/l). However, the minimum sulfate concentration above which this phase is stable drastically increases with the temperature, and for a given temperature with the alkali concentration.

Besides, at room temperature, monosulfoaluminate can be observed only in the presence of a low sulfate concentration even when the alkali concentration is high. On the opposite, at elevated temperature, this phase is stable for sulfate concentration varying from relatively low to very high sulfate concentrations. The maximum sulfate concentration under which monosulfoaluminate is stable strongly increases with the temperature, and for a given temperature with the alkali concentration.

REFERENCES

[1] Abo-El-Enein S.A., Salem T.M. and Hekal E.E., "Thermal and Physico Chemical Studies on Ettringite: I - Hydration Kinetics and Microstructure", Il Cemento, 1, 47-58 (1988)

[2] Kalousek G.L. and Adams M., "Hydration products formed in cement pastes at 25 to 175°C", J. Amer. Concr. Inst., 23,. 77-90 (1951)

[3] Brown P.W. and Bothe J.V. Jr, "The stability of ettringite", Advances in Cement Research, 18 (5), 47-63 (1993)

[4] Mori H. and Minegishi K., «Effect of the Temperature on the Early Hydration of the System 3CaO.Al2O3-CaSO4.2H2O-Ca(OH)2-H2O», V International Congress on the Chemistry of Cement (Tokyo),349-361 (1968)

[5] Ghorab H.Y. and Kishar E.A., "Studies on the Stability of the Calcium Sulfoaluminate Hydrates. Part I: Effect of Temperature on the Stability of Ettringite in Pure Water", CCR, 15,.93-99 (1985)

[6] Ghorab H.Y. and Kishar E.A., "The stability of the Calcium Sulfoaluminate Hydrates in Aqueous Solutions", VIII International Congress on the Chemistry of Cement (Rio de Janeiro), vol. 5 Theme 4, 104-109 (1986)

[7] Berger A.S. et al., "On Metastable Equilibrium of Calcium Hydroaluminates in Solutions of Hydroxides of Alkali Metals", VI International Congress on the Chemistry of Cement (Moscow), 3 III-4,.1-12 (1974)

[8] Damidot D. and Glasser F.P., «Thermodynamic Investigation of the CaO-Al2O3-CaSO4-H2O» system at 50°C and 85°C », Cem Concr. Res., 22, 1179-1191 (1992)

[9] Glasser F.P., Damidot D. and Atkins M., « Phase development in cement in relation to the secondary ettringite problem », Advances in Cement Research, 7, 26, 57-68 (1995)

[10] Glasser F.P., « The role of sulfate mineralogy and cure temperature in delayed Ettringite formation », Cement & Concrete Composites, 18, 187-193 (1996)

[11] Hill A.E., J. Amer. Chem. Soc., 56, 1071-78 (1934)

APPLICATION OF A THERMODYNAMIC ANALYSIS OF THE "CaO-Al_2O_3-$CaSO_4$-alkali-H_2O" SYSTEM TO REAL OPC MORTARS AT 90°C

V. Michaud-Poupardin and D. Sorrentino

Lafarge Laboratoire Central de Recherche, 95 Rue du Montmurier. BP 15, 38291 Saint Quentin-Fallavier Cedex, France. E-mail: valerie.poupardin@lafarge.com and daniele.sorrentino@lafarge.com

ABSTRACT

The influence of temperature on the thermodynamic stability of calcium sulfoaluminate phases has been investigated either by using calculation or experimentally on pure phases. However, it has never been established whether the composition of the liquid and solid phases present in mortar specimens directly after heating are consistent with these thermodynamic predictions. The present results show that this is the case.

Thermodynamics has also been used to determine the effect of cooling on the stability of hydrates formed at high temperatures. In agreement with the thermodynamic data at high temperatures, ettringite has only been observed in the presence of a very high sulfate concentration directly after heating at 90°C and remains stable under similar conditions at 25°C. In contrast, calcium monosulfoaluminate is stable in a wide range of sulfate concentrations at 90°C, but is not stable when the sulfate concentration is high at 25°C. Therefore, when the sulfate concentration in the solution directly after heating is high, calcium monosulfoaluminate is far from stabile at room temperature and converts to ettringite which is the stable phase in these conditions. This has been confirmed experimentally.

The composition of the solution and the calcium sulfoaluminate phases formed with time during hydration at elevated temperatures have also been predicted using thermodynamics and have been confirmed experimentally on real OPC systems. In specimens treated at 90°C, ettringite forms first and converts later to calcium monosulfoaluminate even if the alkali concentration is high (1 mol/l). However, the lower the cement SO_3 content, the earlier this conversion occurs. Therefore, when the cement SO_3 content is relatively low, ettringite is not present directly after heating since it has already been converted to calcium monosulfoaluminate. Ettringite is still present at the end of the heat treatment only in cements with very high SO_3 contents (7% SO_3 in the present study).

Keywords: thermodynamic stability, calcium sulfoaluminate phases, ettringite, calcium monosulfoaluminate, stability, temperature, mortar, durability.

1. INTRODUCTION

The influence of temperature on the thermodynamic stability of calcium sulfoaluminate phases has been investigated by calculation by Damidot and Glasser [1, 2]. The calculations were in agreement with experimental data obtained by Michaud – Poupardin and Sorrentino [3] on pure phases.
This paper aims at confirming that the composition of the liquid and solid phases present in mortars directly after heating is consistent with the thermodynamic data.

The nature of the calcium sulfoaluminate phases formed during curing at elevated temperature will be discussed based on the thermodynamic and experimental data of the present study.

Finally, the effect of cooling on the stability of the calcium sulfoaluminate phases formed during the heat treatment is examined.

This study has been carried out in the presence of pore solutions very concentrated in alkali ions to clarify whether ettringite can be present in such conditions in heat treated mortars directly after heating at 90°C. It has been reported [4] that the formation of ettringite is suppressed when temperature and alkali concentrations increase. Besides, ettringite is usually absent directly after heating when industrial cements are used and heat treated at 80°C or above [5 - 9]. However, Heinz and Ludwig [10] detected the presence of ettringite after a heat treatment of 12 h at 90°C for a cement SO_3 content of 8.6 %, and Kalousek [11] observed this phase in a cement paste hydrated in an autoclave at 90°C for 24 hours when the cement SO_3 content was higher than 5.5%.

2. EXPERIMENTAL

This study has been carried out on Portland cements with different SO_3 contents ranging from 2.5 to 16%.

These cements have been prepared from a clinker with a low alkali content of 0.3 % Na_2Oeq. The clinker alkali sulfate content has been increased by adding K_2SO_4 to the mixing solution. The amount of K_2SO_4 added increased the clinker Na_2O eq. by 0.8% and the clinker SO_3 by 1%. The cement SO_3 contents reported in this paper are the total SO_3 contents of the cements included the SO_3 contributed by the alkali sulfate.

The cements containing up to 6% SO_3 were produced in the laboratory by intergrinding clinker with a mix of 50% gypsum / 50% hemi-hydrate in a ball mill to a fineness of 330 m^2/kg. Higher SO_3 contents were reached by blending the 6% SO_3 cement with gypsum.

EN 196-1 Standard mortars were produced from these cements and 4*4*16 cm specimens were cast.

The heat treatments of these specimens were monitored in a climatic chamber regulated in hygrometry and temperature. The hygrometry targeted during the heat treatment was the highest one which can be reached at 90°C (determined by the Rosée curves), in order to limit the desiccation of the specimens.

The thermal profile used was 4 hours at 20°C, a heating rate of 20°C/h, then 12 hours at 90°C, and finally a cooling rate of 10°C/h.

2.1 Analysis of the liquid phases

The pore solution was extracted directly after heating using a high pressure apparatus. The solution was analysed by inductively coupled plasma atomic emission spectrometry (ICP - AES). The extraction was performed by applying a pressure slowly on the specimens (0.5 MPa/min up to 5 MPa, 10 min at 5 MPa, 0.5 MPa/min up to 6.3 MPa, plateau at 6.3 MPa). Solution was collected at the plateau at 6.3 MPa only, and the amount was small (2 – 3 ml).

This solution is likely to be the one contained in the macropores. The high pressure exerted on the specimens may affect the stability and / or the solubility of the hydrates. Such modifications will be discussed further.

2.2 Analysis of the solid phases

The hydration was stopped directly after heating (28 hours) and after 7 and 28 days of storage using ethanol. The hydrated phases were identified by X-ray diffraction (XRD), X-ray microanalysis (EDS) in a scanning electron microscope (SEM) on polished sections [12]. Some samples were also analysed with ^{27}Al nuclear magnetic resonance (NMR). The ^{27}Al NMR and SEM/EDS techniques have been used since they are more sensitive for detecting calcium monosulfoaluminate which is often undetectable by XRD directly after heating [12]. The XRD results presented here are consistent with this observation.

3. RESULTS

In this text, tables and figures, the following abbreviations have been used:

- AFt = ettringite ($C_3A.3CaSO_4.32H_2O$),
- AFm = calcium monosulfoaluminate ($C_3A.CaSO_4.12H_2O$),
- HG = hydrogarnet type phase,
- CH = calcium hydroxide ($Ca(OH)_2$).

3.1 Composition of the pore solutions and the solid phases directly after heating at 90°C

These are reported in Table 1. The nature of the solid phases has been determined combining XRD (Figure 1), EDS analysis, and ^{27}Al NMR for the cements containing 2.5, 6 and 9 % SO_3.

Table 1. Composition of the liquid and solid phases directly after heating at 90°C

Cement SO_3 (%)	$[K^+]$ (mmol/l)	$[Na^+]$ (mmol/l)	$[K^+ + Na^+]$ (mmol/l)	$[SO_4^{2-}]$ (mmol/l)	$[Ca^{2+}]$ (mmol/l)	$[Al(OH)_4^-]$* (mmol/l)	Solid phases present
2.5	792	116	908	178	2.4 – 6.6**	< 0.25*	C-S-H, AFm, HG, CH
4	880	120	1000	263	5.9**	< 0.25*	C-S-H, AFm., HG (ε), CH
6	888	128	1016	378	9.8**	< 0.25*	C-S-H, AFm., CH
7	871	126	997	366	5.5**	< 0.25*	C-S-H, AFm., AFt, CH
9	865	126	991	370	2.5**	< 0.25*	C-S-H, AFm., AFt, CH
16 (I)							C-S-H, AFt, Gypsum, CH

The precision of the concentrations is +/- 2 % except for those annotated by * or **:
* below the detection limit
** precision = 5%
(I): the pore solution has not been extracted
ε : low amount

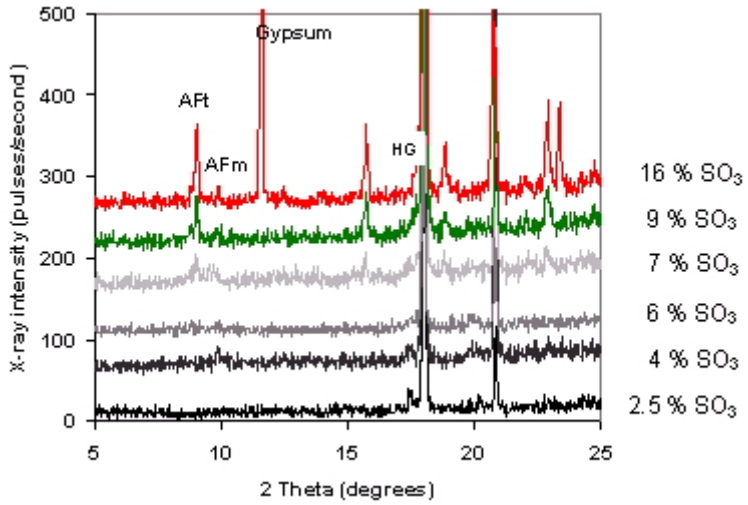

Figure 1. XRD patterns of the 1-day old cured mortars at different SO_3 cement contents

At low SO_3 contents (2,5 and 4 wt %), AFm and HG are present directly after heating. For the samples with a SO_3 content of 6%, only AFm was present. AFt is present beyond this value. At high SO_3 contents (7% and 9%), AFt is present together with AFm. If the SO_3 content increases to 16%, gypsum and AFt are detected.

3.2 Comparison between the solid / liquid systems extracted directly after heating and the thermodynamic prediction at elevated temperature

The Table 2 shows that the sulfate concentrations of the solutions extracted directly after heating in the mortars containing 2.5 % SO_3 is in good agreement with one of the invariant points "AFm, HG, CH" predicted by thermodynamic calculations [1, 2].

Table 2. Comparison of the concentrations directly after heating for the cement containing 2.5 % SO_3 to the thermodynamic predictions (mmol/l)

	$[K^+] + [Na^+]$	$[SO_4^{2-}]$	$[Ca^{2+}]$	$[Al(OH)_4^-]$
Conc. measured after heating. (present study)	908	178	2.4 – 6.6	< 0.25
Conc. at the invariant point "monosulf., HG, CH" at 90°C determined by calculation	908	175	0.2	7

The concentration of the solutions extracted directly after heating the mortars made with the cements at 7 and 9 % SO_3 are also in good agreement with the composition at the invariant points "AFt, AFm, CH" determined experimentally on pure phases [3] and by calculation [1, 2] (Table 3). However, the sulfate concentration given by thermodynamics is always higher than that determined in the mortars.

Table 3. Comparison of the concentrations directly after heating for the cement containing 7 or 9 % SO_3 to the thermodynamic predictions (mmol/l)

	$[K^+] + [Na^+]$	$[SO_4^{2-}]$	$[Ca^{2+}]$	$[Al(OH)_4^-]$
Conc. measured after heating for 7% SO_3 cement (present study)	997	366	5.5	< 0.25
Conc. measured after heating for 9% SO_3 cement (present study)	991	370	2.55	< 0.25
Conc. at the invariant point "AFt., AFm, CH" at 90°C determined experimentally	1000*	445*	10.3*	< 0.7*
Conc. at the invariant "AFt., AFm, CH" at 90°C determined by calculation	1000	439	1.9	0.4

* The concentrations at the invariant points "AFm, HG, CH" at 90°C have been determined experimentally from pure phases only at alkali concentrations of 420 and 1080 mmol/l and have been extrapolated to an alkali concentration of 1000 mmol (linear extrapolation).

The sulfate concentrations and calcium sulfoaluminate phases detected directly after heating, and the calcium sulfoaluminate phases predicted to be stable by thermodynamics at 90°C for the same sulfate concentrations are reported in Figure 2.

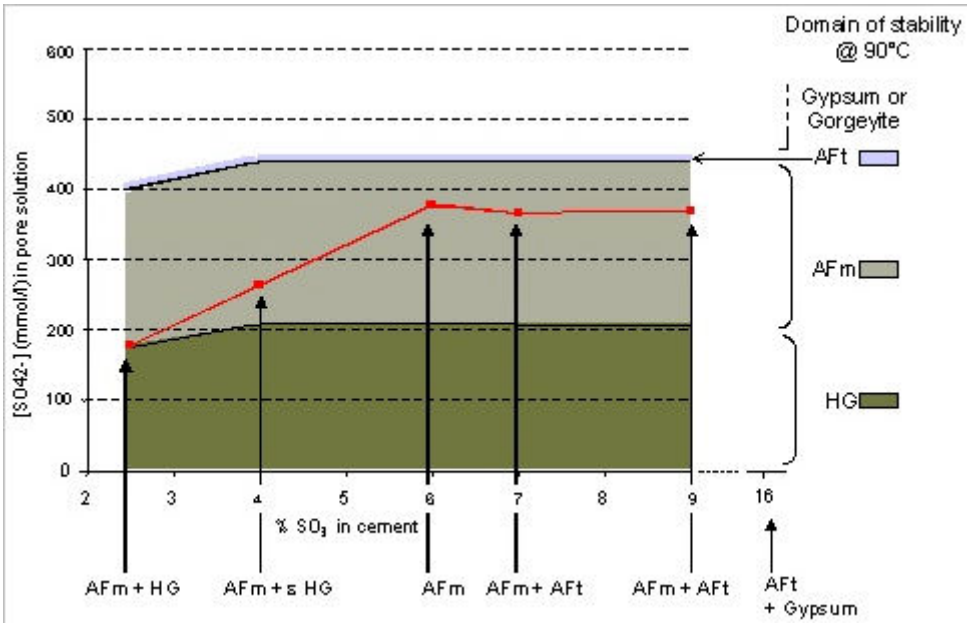

Figure 2. Comparison between the calcium sulfoaluminate phases present directly after heating at 90°C (red experimental points and corresponding solid phases under arrows) and the thermodynamic predictions (in the presence of CH).

Figure 2 shows that the sulfate concentration and solid phases directly after heating are consistent with the thermodynamic prediction. AFt has only been observed in the presence of a very high sulfate concentration (370 - 380 mmol/l at an alkali concentration of 1000 mmol/l) and AFm on a wide range of sulfate concentrations (180 to 370 mol/l at an alkali concentration of 910 – 1000 mmol/l). HG has also been observed in addition to AFm in the mortar with 2.5% SO_3. The presence of HG in the mortar at 4% SO_3 is likely to be due to the fact that the specimen may not have been exactly at equilibrium during the heat treatment. As mentioned previously, AFt has been detected at a sulfate concentration of 370 – 380 mmol/l and an alkali concentration of 1000 mmol/l whereas thermodynamics predicts this phase to become stable at a higher sulfate concentration (≈ 440 mol/l, see Table 2).

To conclude, the composition of the liquid and solid phases present in mortars directly after heating are generally consistent with those predicted by thermodynamics. This also indicates that the pressure exerted on the samples to extract the pore solution does probably not modify significantly the concentrations of the pore solution.

The reason why AFt is detected for a lower sulfate concentration than the one predicted by thermodynamics may have different origins:

- It may result from the fact that the heat treated mortar specimens are not exactly the equilibrium during the heat treatment as indicated by the presence of HG in addition to AFm for the cement containing 4% SO_3.
- It may also result from the fact that the concentrations are different locally in the structure whereas the concentrations measured after extraction correspond to a global and average composition.
- Thermodynamic data [1, 2, 3] do not take into account the presence of C-S-H. The presence of this hydrate may also slightly modify the composition of the invariant points.
- Sulfate ions have been shown to sorb on the C-S-H [12, 13].
- The high pressure exerted on the specimens may slightly affect the solubility of the hydrates.

3.3 Use of thermodynamic data to determine the kinetic path during cement hydration at elevated temperature

At the beginning of hydration, since the system is dynamic, the accurate determination of the composition of the solution and the hydrates requires the knowledge of the supersaturation curves of the different hydrates. However, since they have not been determined, thermodynamic data in the system "CaO-Al_2O_3-alkali- SO_3-H_2O" have been used. They allow a first estimation of the kinetic path of the reaction and prediction of the composition of the solution and calcium sulfoaluminate phases with time at elevated temperatures since thermodynamics is the driving force of hydration.

The hydration of the simplified system: gypsum + C_3A + CH at 85°C in water will be discussed first. The hydration on the real OPC system at 90°C will then be discussed:

As soon as gypsum and CH are in the presence of water, they dissolve until reaching their surface of solubility. The kinetic path followed during this period is illustrated by the line (1) in Figure 3. Simultaneously, C_3A dissolves. Once the solution becomes supersaturated with respect to AFt, this phase precipitates and consumes calcium, sulfate and aluminate ions from the solution. As long as gypsum is present, it continuously dissolves and brings calcium and sulfate ions into the solution in order to maintain the solution saturated with respect to this phase. Therefore, the concentrations in the solution remain constant with time until the gypsum is totally depleted. From that time, the sulfate concentration decreases and the kinetic path followed is given by the line (2) in Figure 3. Beyond a certain time, AFm starts becoming stable. AFt dissolves and AFm precipitates. Once all the AFt has been converted to AFm, the sulfate concentration decreases (kinetic path illustrated by the line (3)). AFm remains stable until the sulfate concentration becomes too low. From this time, HG starts becoming stable.

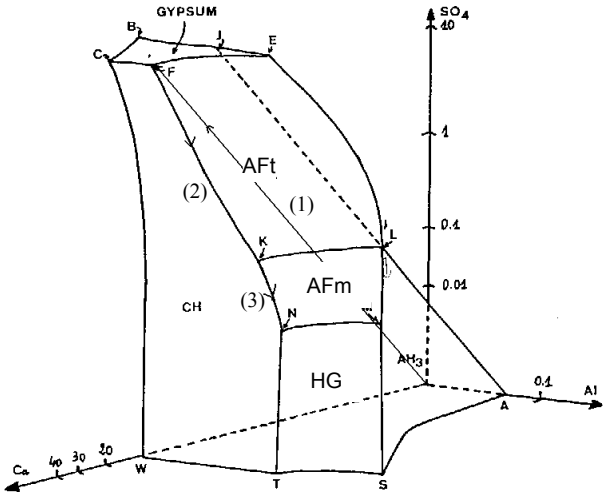

Figure 3. Phase diagram in the system « CaO-$CaSO_4$-Al_2O_3-H_2O » at 85°C, in the absence of alkalis [1] and kinetic path followed during the hydration of gypsum and C_3A in the presence of CH in water.

Using the same approach as previously and the thermodynamic data obtained at 90°C, the sulfate concentration and calcium sulfoaluminate phases formed with time have been predicted at alkali concentration of a solution close to the one extracted directly after heating (1000 mmol/l). A schematic representation is given in Figure 4.

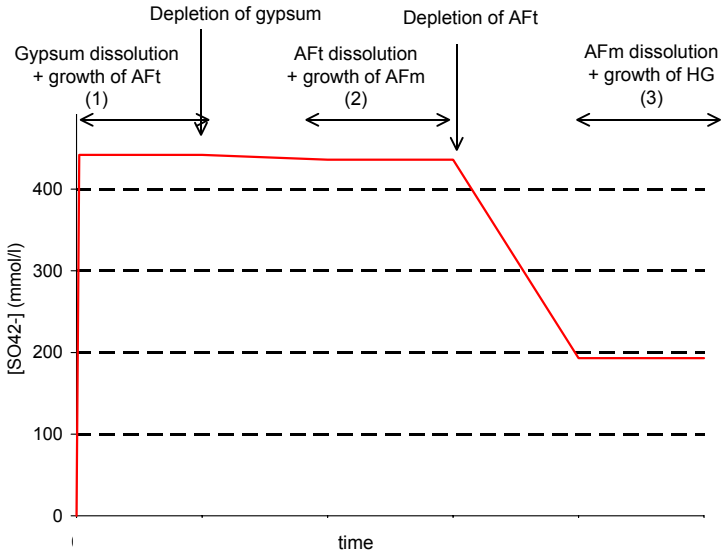

Figure 4.Thermodynamically predicted calcium sulfoaluminate phases and sulfate concentration at 90°C with time (alkali concentration = 1000 mol/l).

In 90°C-treated specimens, when alkali concentration of the pore solution is very high (1000 mmol/l), thermodynamics predicts that AFt forms first and converts later to AFm. AFm starts forming while the sulfate concentration is still very high. The sulfate concentration starts decreasing significantly only when all the AFt is totally depleted. Similarly at room temperature, the lower the cement SO_3 content, the earlier is the conversion of AFt to AFm, therefore, the earlier the depletion of AFt is expected to occur. As a consequence, the sulfate concentration decreases earlier.

The experimental results are consistent with this statement. For cement SO_3 contents varying from 2.5 to 6 %, AFt was totally converted to AFm directly after heating. Residual AFt is only observed after heating when the cement SO_3 content is very high (7% or higher). The sulfate concentration directly after heating decreases when the cement SO_3 content decreases from 6 to 2.5%. At 2.5% cement SO_3 content, the sulfate concentration directly after heating is so low that HG starts becoming stable. At that time, the invariant point "AFm – HG – CH" is reached.

The stage reached directly after heating by the mortars containing different cement SO_3 contents is illustrated in Figure 5.

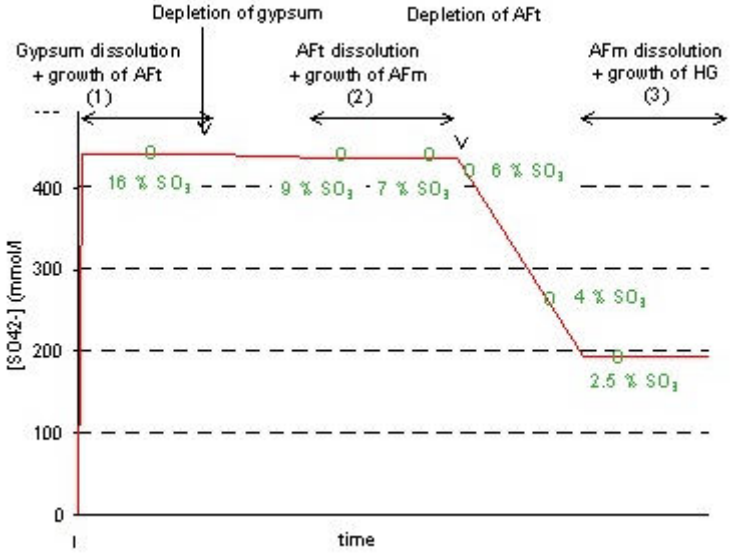

Figure 5. Stage reached by the six different mortars directly after heating

For instance, directly after heating, the mortar containing 16 % SO3 has reached stage (1) in which gypsum dissolves and AFt grows. On the other hand, the mortar containing 9 and 7 % SO3 are in the stage (2) in which AFt dissolves and AFm grows.

3.4 Effect of cooling on the stability of calcium sulfoaluminate phases in the 28-hour mortars

The domain of stability under which AFm is stable depends on temperature [1, 2, 3]. At elevated temperatures, AFm is stable in the presence of CH for a large range of sulfate concentrations. In the present study, this phase has been detected for sulfate concentrations varying from 180 mmol/l (in the 2.5% cement SO_3 content) to 370 mmol/l (in the 6 % , 7 % and 9 % cement SO_3 contents) at an alkali concentration of 910 – 1000 mmol/l.

However, this phase is not stable anymore in such conditions at room temperature. Thermodynamics indicates that this phase is never stable below 45°C [1]. Even if AFm forms at room temperature because the system is metastable, this phase can only be present in conjunction with a very low sulfate concentration, irrespective of the alkali concentration. According to thermodynamic calculations, AFt is stable at a sulfate concentration higher than 11 mmol/l if the alkali concentration is of 1000 mmol/l at 25°C. The sulfate concentration and calcium sulfoaluminate phases detected directly after heating and the nature of the calcium sulfoaluminate phases predicted by thermodynamics to be stable at 25°C are reported in Figure 6.

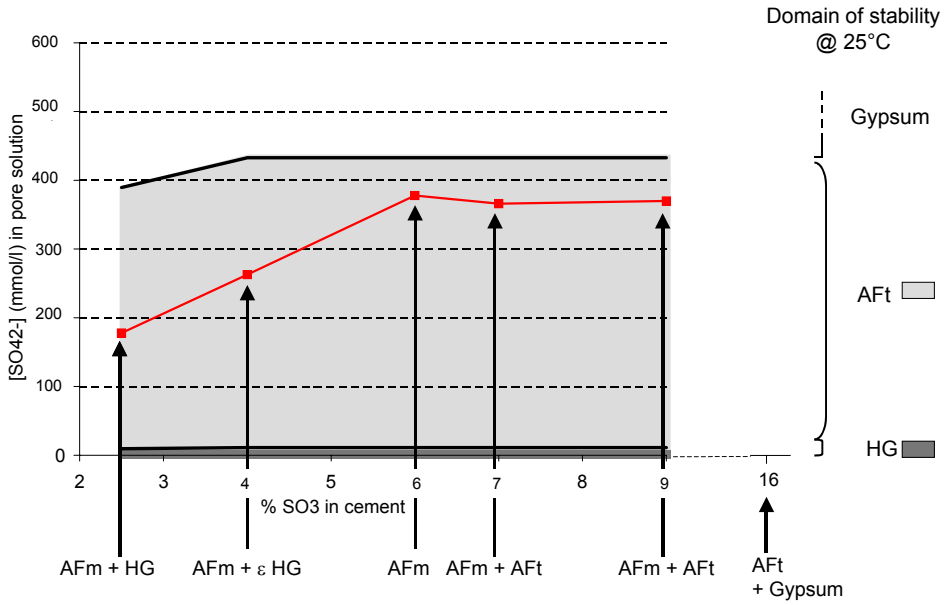

Figure 6. Prediction of the stability of the calcium sulfoaluminate phases present directly after heating once the specimens have been cooled to 25°C

Irrespective of the cement SO_3 content, AFt is stable once the specimens have been cooled to 25°C. If AFm is present directly after heating, it is no longer stable after cooling to room temperature and tends to convert to AFt. The XRD analysis of the hydrated phases present after 28 days of water storage at 25°C for the 4 and 6 % SO_3 cements confirms this result (Figure 7). The higher the sulfate concentration of the solution, the farther is the AFm from stability at room temperature (i.e. the solubility curve of AFm is very far from the one of AFt at 25°C) and the more rapidly the AFm tends to convert to AFt. This is the case for the 6% SO_3 cement.

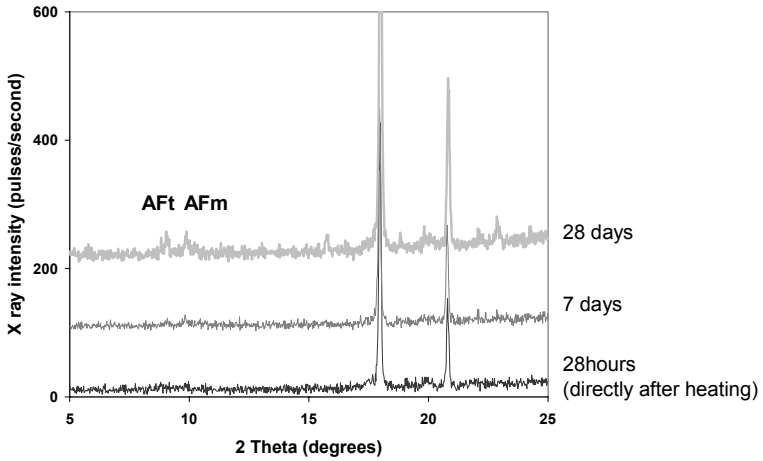

Figure 7. XRD patterns with time for the mortar containing 6% SO_3.

On the other hand, if AFt is present directly after heating, the sulfate concentration is always high. AFt remains stable under such conditions at 25°C and does not convert to an other phase as illustrated in Figure 8 for the mortar made with the 9% SO_3 cement.

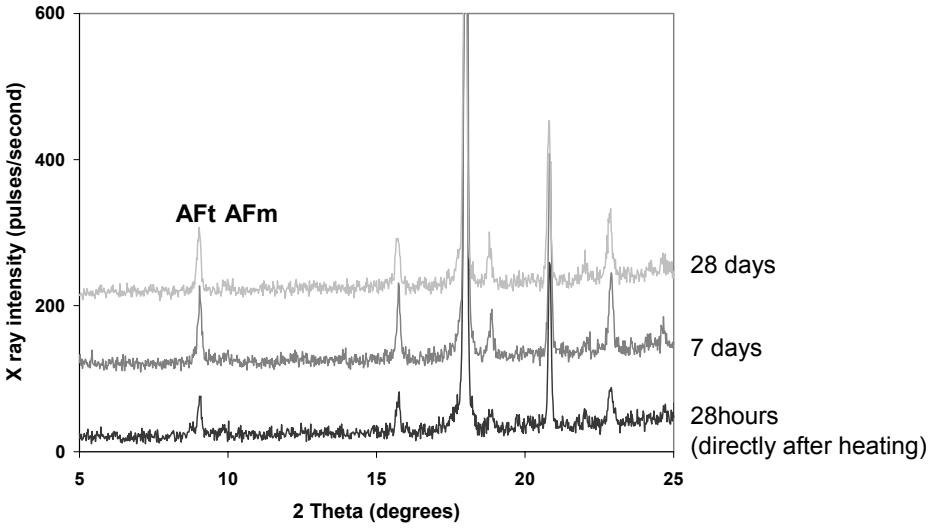

Figure 8. XRD patterns with time for the mortar containing 9% SO_3.

4. CONCLUSIONS

- This study shows that the composition of the liquid and solid phases in mortar specimens directly after heating are consistent with those predicted by thermodynamics at elevated temperatures.
- The pressure exerted on samples to extract the pore solution does not significantly modify the compositions of the solutions.
- Thermodynamics has been used to predict the kinetic path during hydration at elevated temperatures. In specimens treated at 90°C, thermodynamics predicts that ettringite forms first and converts later to calcium monosulfoaluminate even if the alkali concentration is high (1000 mmol/l). The results of the present study are consistent with this and show that the lower the cement SO_3 content, the earlier this conversion occurs.

Below a certain cement SO_3 content, ettringite is not present directly after heating since it has already converted to calcium monosulfoaluminate. However, ettringite is still present at the end of the heat treatment when the cement SO_3 content is elevated (in agreement with Heinz et al. [10] and Kalousek et al. [11]).

- Thermodynamics has also been used to determine the effect of cooling on the stability of the hydrates formed at elevated temperatures. In agreement with the thermodynamic data at elevated temperatures, ettringite has only been observed in the presence of a very high sulfate concentration after heat treatment at 90°C (370 mol/l at an alkali concentration of 1000 mmol/l). It remains stable under similar conditions at room temperature. On the other hand, calcium monosulfoaluminate is stable for a wide range of sulfate concentrations (180 to 370 mmol/l at an alkali concentration of 910 – 1000 mmol/) at 90°C, but is no longer stable when the sulfate concentration is high at room temperature. It can only be present in conjunction with a very low sulfate concentration, even when the alkali concentration is high. Therefore, when the sulfate concentration directly after heating is high, calcium monosulfoaluminate is far from stable at room temperature and converts to ettringite which is the stable phase in these conditions. This has been confirmed experimentally.

REFERENCES

[1] Damidot D. and Glasser F.P., "Thermodynamic Investigation of the CaO-Al2O3-CaSO4-H2O» system at 50oC and 85°C", Cem Concr. Res., 22, 1179-1191 (1992)

[2] Glasser F.P., "The role of sulfate mineralogy and cure Temperature in delayed Ettringite formation", Cement & Concrete Composites, 18, 187-193 (1996)

[3] Michaud Poupardin V. and Sorrentino D., "Influence of Temperature and Alkali Concentration on Thermodynamical Stability of Sulfoaluminate Phases", 11th International Congress on the Chemistry of Cement., Durban, South Africa, May 2003

[4] Ghorab H.Y. and Kishar E.A., "The stability of the Calcium Sulfoaluminate Hydrates in Aqueous Solutions", VIII International Congress on the Chemistry of cement (Rio de Janeiro), vol. 5 Theme 4, 104-109 (1986)

[5] Sylla H.M., "Reactions in Cementstone due to Heat Treatment", Beton, 28, 449-454 (1988)

[6] Lach V. and Bures J., "The Phase Composition and Microstructure of cement Pastes Hydrated at Elevated Temperatures", VI International Congress on the Chemistry of cement (Moscow), 1-13 (1974)

[7] Lach V., "The Effet of Temperature on the Cement Paste Hydration » in Hydraulic Cement Pastes: Their Structures and Properties", Proc. of a Conference held at the University of Sheffield, 82-86 (1976)

[8] Wieker W. and Herr R., "Some problems concerning the Chemistry of Portland cement", Zeitschrift fur Chemie, September, 29, 9, 321-327 (1989)

[9] Stadelmann C., Herr R. and Kurzawski I., "Determination of Ettringite in hardened cement pastes", Silicat technik, 39, 4, 120-122 (1988)

[10] Heinz and Ludwig, "Mechanism of Secondary Ettringite Formation in Mortars and Concretes Subjected to Heat Treatment", in Concrete Durability, Proc. K. and B. Mather, International Conf., ed. J.M. Scanton, ACI SP-100, 2059-71 (1987)

[11] Kalousek G.L. and Adams M., "Hydration products formed in cement pastes at 25 to 175°C", J. Amer. Concr. Inst., 23,. 77-90 (1951)

[12] Famy C., Scrivener K.L. and Taylor H.F.W. "Delayed Ettringite Formation", Chapter ten, Structure and Performance of cements, 2nd Edition. Edited by Bensted J. and Barnes P. (2001)

[13] Kalousek G.L., "Analysing SO3-bearing phases in hydrated cement", Mat. Res. & Std., 6, 292-304 (1965)

COUNTER-DIFFUSION AS AN INDICATOR OF DURABILITY

Paul D. Tennis[1], Raymond J. Krizek[2] and Hamlin M. Jennings[3]

[1] Portland Cement Association, Skokie, Illinois, USA; E-mail: ptennis@portcement.org
[2] Department of Civil Engineering, Northwestern University, Evanston, Illinois, USA; E-mail: rjkrizek@northwestern.edu
[3] Departments of Civil Engineering and Materials Science and Engineering, Northwestern University, Evanston, Illinois, USA; E-mail: h-jennings@northwestern.edu

ABSTRACT

Counter-diffusion of miscible fluids has been evaluated as a technique for characterizing the pore structure of cementitious materials. A water-saturated specimen is placed in a large excess of a water-miscible fluid and a counter-diffusion process is observed by monitoring the mass change of the specimen over time. Values for porosity and apparent diffusivity of the porous medium are obtained. However, wider acceptance of the method by cement and concrete researchers has been slow. One reason for this lack of acceptance has been that analysis of the data collected, measurements of mass as a function of elapsed time, is complicated by the three-dimensional nature of the specimens. A detailed analysis has been developed, and is presented here, to address this limitation. Data are provided for cement paste specimens of varying water:cement ratios and degrees of hydration.

1. INTRODUCTION

Mass transport through porous materials is important in the study of cement-based materials. Advantages of concrete as a construction material include its durability, cost, energy efficiency (on a life-cycle basis), and formability. It is also fire resistant and made out of materials that form a large proportion of the earth's crust and are, therefore, widely available. The durability problems that concrete encounters depend in large part on its transport properties. In concrete, damage from freeze/thaw cycles, sulfate ion attack, alkali-aggregate reactions (AAR), deicer salt scaling, and chloride-induced corrosion of reinforcing steel are potential problems that are strongly influenced by the mass transport properties. Therefore, a simple technique for characterizing the transport properties of cementitious systems would be a beneficial tool to researchers and field engineers for use in evaluating concrete materials. The counter-diffusion technique holds promise as a method to be that tool. More details can be found in reference [1].

1.1 Overview of technique

The driving force for flow in the counter-diffusion technique is a concentration gradient. A porous specimen saturated with one fluid is immersed in a large volume of another fluid with which it is miscible. The concentration gradient arises from the high concentration of the external fluid outside of the specimen and the low concentration of that fluid internally (and vice-versa for the internal fluid). The rate and extent of the fluid flow caused by this concentration gradient can be evaluated by periodically determining a mass of the specimen during the counter-diffusion process. There are several requirements for the procedure to be effective: 1) a difference in density of the two fluids, 2) a sufficient volume of connected porosity for the mass difference to be detected, 3) a diffusivity low enough so that the mass changes can be measured on a practical time scale, and 4) a lack of

Proceedings of the 11th International Congress on the Chemistry of Cement (ICCC)
'Cement's Contribution to the Development in the 21st Century'
Hosted by: The Cement and Concrete Institute of South Africa
CD-ROM produced by: Document Transformation Technologies
11 - 16 May 2003, Durban, South Africa
ISBN Number: 0-9584085-8-0
Editors: Dr G. Grieve and G. Owens
Congress Organised by: Event Dynamics

chemical interaction of the penetrating fluid with the solid. An advantage of the counter-diffusion technique is the relative ease of measurement, requiring only an analytical balance and a timer.

1.2 Review of literature

Although several authors have used counter-diffusion techniques to examine the pore structures in cementitious systems [2]-[12], only Feldman [6-7] and Gran and Hansen [8] have attempted to estimate diffusion coefficients from the data. In Feldman's research, the analysis used is not derived, but is stated [7] to be "a form of Fick's Law:"

$$\frac{M_t}{M_f} = 1.127\sqrt{\frac{Dt}{L^2}} \qquad (1)$$

where M_t is the mass of the specimen at time t, and M_f is the final mass, L is the half-thickness of the specimen, and D is the diffusivity. The equation appears to simplify the analysis of counter-diffusion to only account for diffusion across the faces of the disk, which may be reasonable, given the dimensions of the disks used (1.14 mm thick × 30 mm diameter).

Gran and Hansen (1998) used an approximation for their specimens that only accounted for radial diffusion. Their specimens were cylinders with a much higher length-to-diameter ratio (20 mm long × 5.5 mm diameter), so the approximation is also likely to be valid. However in the work partially presented here [1], specimens of different sizes and shapes were evaluated. Therefore, a slightly more complex analysis, taking into account diffusion on all faces, has been developed.

Because a plot of mass change as a function of time is non-linear, one method to characterize the data has been the time required for half of the exchange to take place [4], which has been given the symbol ${}_e\tau_{½}$. It has been suggested that this is related to the diffusivity of the specimen. This is not necessarily the case. As shown schematically in Figure 1, which contains three idealized curves for counter-diffusion data, this parameter is related to both the diffusivity and the volume of pores. Curves *a* and *b* compare data for specimens with the same porosity; however specimen *a* has a smaller value of ${}_e\tau_{½}$. Thus the pores in specimen *a* may be smaller or connected by smaller pores. Curves *b* and *c* compare specimens with similar rates of diffusion, but have different values of ${}_e\tau_{½}$ due to a smaller volume of porosity in specimen *c*. Comparing the curves for specimens *a* and *c* illustrates that differences for ${}_e\tau_{½}$ can also be due to differences both in diffusivity and porosity. Thus the meaning of the value of ${}_e\tau_{½}$ is complicated and best used for comparison of specimens with similar volumes of porosity. (In this discussion, it is assumed that the specimen dimensions have been accounted for and the counter-diffusing fluids are the same.)

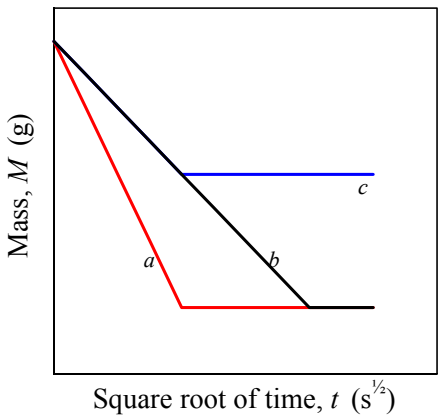

Figure 1. Diagram showing idealized counter-diffusion curves with different values of ${}_e\tau_{½}$. Changes in ${}_e\tau_{½}$ can be due to differences in porosity or diffusivity. See text for discussion of curves.

2. EXAMPLE ANALYSIS

2.1 Typical experiment and results

Details regarding specimen preparation are reported elsewhere [1]. After a saturated specimen is obtained, the specimen is then suspended in a thin wire mesh basket, and its mass determined while suspended in a large excess (on the order of 50:1 by volume of pores) of the replacing fluid. Its mass is measured periodically until the mass loss is less than 0.001 g in 24 hours (and generally several times thereafter to confirm that equilibrium has been reached). The counter-diffusion data reported here are based on suspended masses, rather than saturated, surface-dry masses, as suspended mass determinations are made more reliably.

In Figure 2, example mass data for a counter-diffusion experiment are plotted as a function of square root of time. When the data are plotted against the square root of time, it is possible to observe an initial portion of the curve that approximates a straight line, followed by an asymptotic approach to a constant mass. This is a characteristic of diffusion-controlled processes. The slope of the initial portion is indicative of the diffusivity of the specimen, but is also dependent on the size and shape of the specimen. If specimens of similar size and shape are compared, those with lower diffusivity will have a slope that is less negative. Because of this linear portion of the curve, the preferred method of plotting the counter-diffusion data in this paper is as mass change vs. square root of time.

Both methanol and isopropanol proved non-volatile enough to provide accurate masses. However the use of methanol was avoided as it appears to chemically react with calcium hydroxide in cementitious systems [12-13] and produce measurable dimensional changes [7], and enlarging the threshold pore diameter as measured by MIP [14]. As the extent of these interactions, and more importantly, their effects on the mass and volume of the specimen, could not be quantified, isopropanol was used as the replacing fluid in all the work reported here. Isopropanol has been shown to exchange with pore solution and not produce dimensional changes in Portland cement paste specimens [7]. Further, it is believed [15-16] that isopropanol accesses primarily the capillary porosity in cementitious systems, which are the pores usually expected to dominate the transport properties.

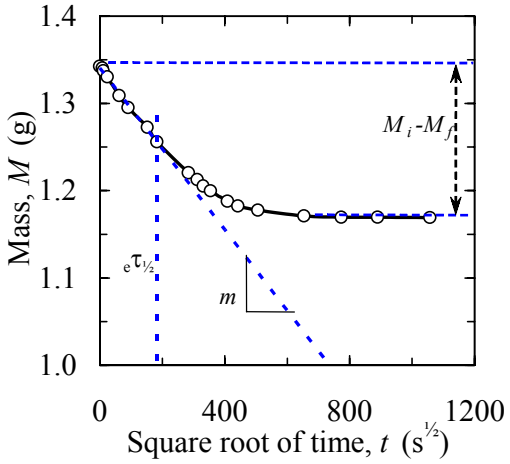

Figure 2. Example counter-diffusion data. Mass of a Portland cement paste specimen during counter-diffusion experiment is plotted against square root of time: ${}_e\tau_{½}$ is the time to half the mass change, m is the slope of the initial portion of the curve, M_i-M_f is the total mass change and is related to the porosity. Disk-shaped specimen of Portland cement paste, 3 mm thick, 26 mm in diameter, water:cement ratio of 0.70, after 28 days of hydration.

2.2 Apparent diffusivity

The approach used to estimate the diffusion coefficient from counter-diffusion data is based on solutions to Fick's second law. Analytical solutions to Fick's second law in one dimension for ideal cases (infinite slab, infinite cylinder) can be combined to provide closed-form solutions for more practical (three-dimensional) shapes (prisms, disks) by application of the superposition principle. This approach is discussed in a number of texts on diffusion [17-20], with a variety of solutions for common geometries. Figure 3 is an illustration for a finite cylinder formed from the intersection of an infinite cylinder and an infinite slab: a combination of the solutions for the two simple cases is used to provide a solution for the finite cylinder.

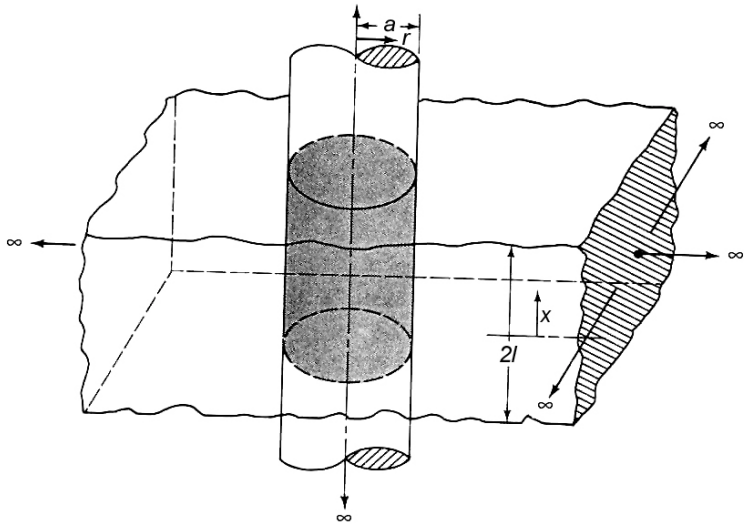

Figure3. Finite cylinder formed from the intersection of an infinite cylinder and an infinite slab. After [19].

A specimen with initial concentration, C_o, throughout is placed in solution of different concentration, C. Counter-diffusion over time acts to bring the specimen back to an equilibrium condition. In the case of a large excess of solution, the equilibrium concentration in the specimen is essentially C.

Consider a finite cylinder of diameter $2a$, and height $2H$ as shown in Figure 4. In this case diffusion can take place both radially and through the ends. The concentration at point r (x, a) and time t (t>0) in the cylinder is (see Figure 3) [18-19]:

$$C_{disk} = C_{slab} C_{cyl} \tag{2}$$

or

$$C_{disk} = \frac{8C_o}{\pi a} \sum_{m=0}^{\infty} \sum_{n=1}^{\infty} \frac{(-1)^m J_0(r\alpha_n)}{(2m+1)\,\alpha_n J_1(a\alpha_n)} \cos\frac{(2m+1)\pi x}{2H} e^{-Dt\left(\alpha_n^2 + \frac{(2m+1)^2\pi^2}{4H^2}\right)} \tag{3}$$

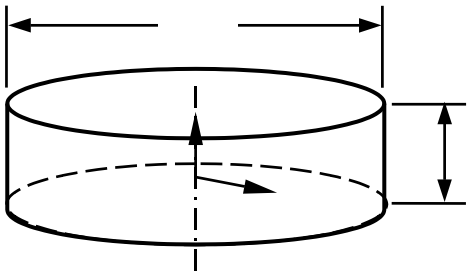

Figure 4. Disk (finite cylinder) showing definition of variables in Equations 4 and 5.

The average concentration in the cylinder is obtained by integrating over, and normalizing by, the volume of the disk:

$$C_{disk\ avg} = \frac{32C_o}{(\pi a)^2}\sum_{n=0}^{\infty}\sum_{m=1}^{\infty}\frac{1}{\alpha_m^2(2n+1)^2}e^{-Dt\left[\alpha_m^2+\frac{(2n+1)^2\pi^2}{4H^2}\right]} \tag{4}$$

where α_m are the roots of a zeroth order Bessel function [21], and other variables are as previously defined.

The diffusivity of porous specimens is determined by optimizing the fit between curves predicted for average concentration as a function of time to data measured for suspended mass as a function of time during counter-diffusion experiments, by varying the diffusivity, *D*. Equations for average concentrations during counter-diffusion are converted to a mass basis using Equation 5:

$$M_t = (M_i - M_f)\frac{C}{C_o} + M_f \tag{5}$$

where M_t is the mass at time, t, M_i is the initial suspended mass of the specimen, M_f is the final suspended mass of the specimen, and C is the average concentration in the specimen, and C_o is the initial concentration. C/C_o is taken as 100% at $t = 0$, and approaches 0 for large values of time. The optimum value of D is determined by the best fit between theoretical values and experimental results.

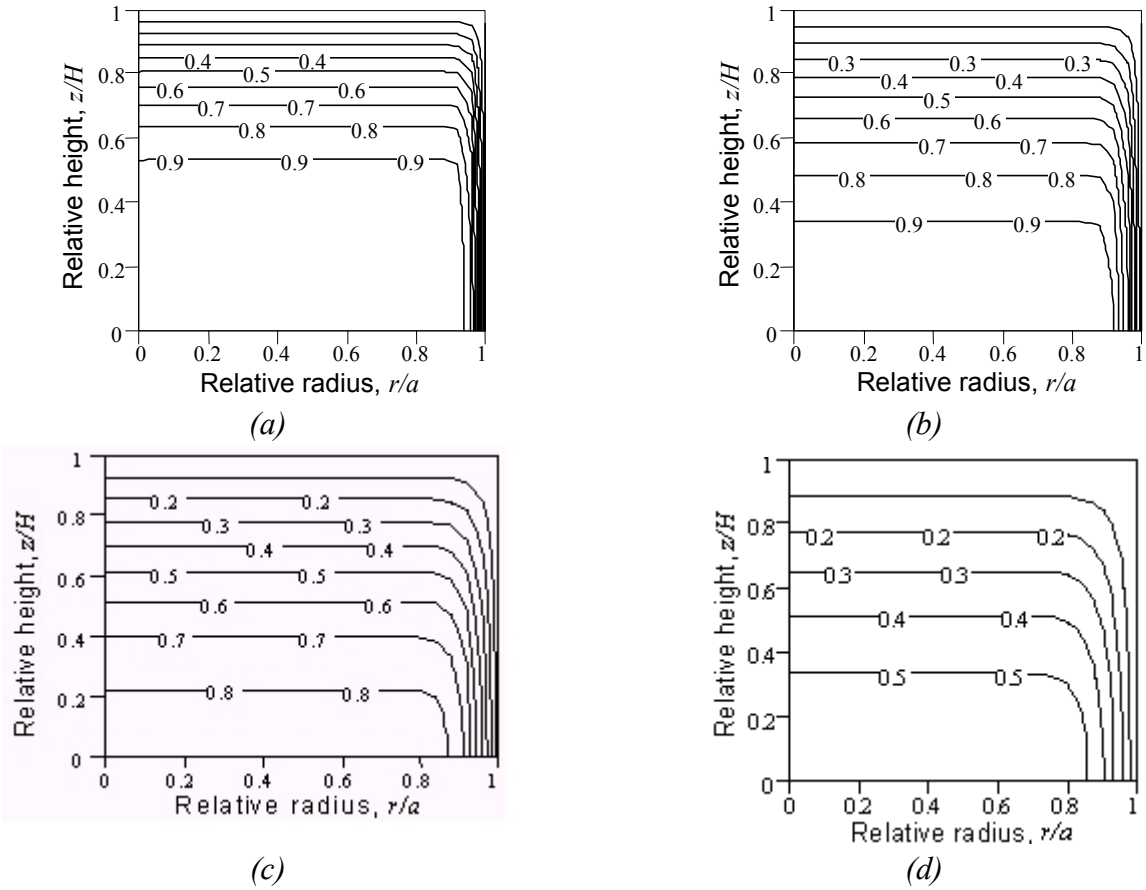

Figure 5. Concentration profiles for a quarter cross-section of a finite cylinder given by Equation 3. Case of $a = 9H$ (see Figure 4), as for cement paste specimens in this research. The origin of each plot represents the center of the disk. $D = 5 \times 10^{-11}$, time parameter ($D\ t/H^2$) of: (*a*) 0.04, (*b*) 0.08, (*c*) 0.16, and (*d*) 0.32, representing 26%, 37%, 50% and 68% fluid replacement respectively.

Figure 5 shows time series plots of the normalized isoconcentration lines as a function of location in the cylinder (r/a), and the dimensionless time parameter, $D\,t\,/a^2$, for a specimen with a width a=9H, resulting from Equation 3. Figure 6 illustrates the average concentration in the slab as a function of the dimensionless time, using Equation 4.

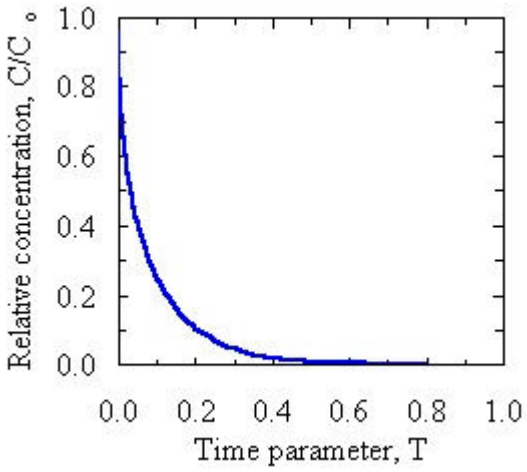

Figure 6. Average concentration in a finite cylinder given by Equation 4.

Figure 7 illustrates the variation of the predicted counter-diffusion curves for various values of D.

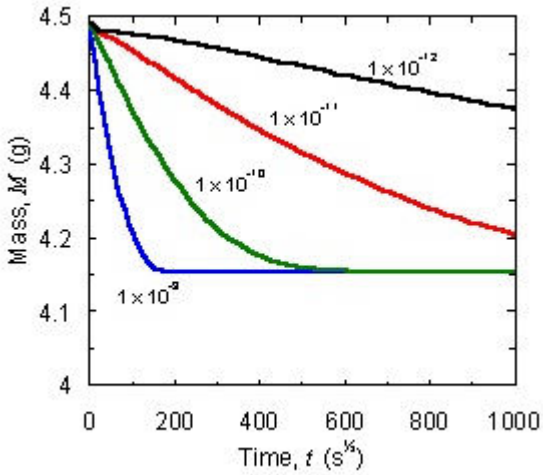

Figure 7. Plot of results of Equation 4 with values of D indicated.

3. RESULTS FOR CEMENT PASTES

3.1 Water to cement ratio and degree of hydration

Table 1 provides the mean values determined for the apparent diffusivity: the initial slope of the mass loss vs. time curve, and the porosity. The values stated are averages of four disks, with the standard deviation in parentheses. Figure 8 shows an example of the suspended mass data plotted against square root of time for the specimens cast at a water:cement ratio of 0.60 by mass. The initial slope was determined from the equation of the best-fit line using a minimum of five points. In all cases the correlation coefficient, r, was greater than 0.99.

Table 1. Apparent Diffusivity of Neat Cement Paste Specimens determined using Counter-Diffusion: mean value (standard deviation).

Water: cement ratio, mass basis	Age, days	Degree of reaction*, (%)	Diffusivity, D (10^{-12} m^2/s)
0.35	28	70	4.6 (0.93)
	259	76	5.6 (0.39)
	420	nd	5.7 (1.40)
0.40	28	70	5.4 (0.06)
	425	81	4.2 (0.26)
0.50	28	76	11.4 (1.91)
	320	90	8.7 (1.05)
	566	91	8.1 (0.59)
0.60	28	75	29.4 (1.25)
	280	92	6.7 (0.42)
	420	nd	8.0 (0.29)

nd: not determined.
*Degree of reaction determined based on loss of ignition tests assuming a non-evaporable water content of 0.24 g/g cement [22].

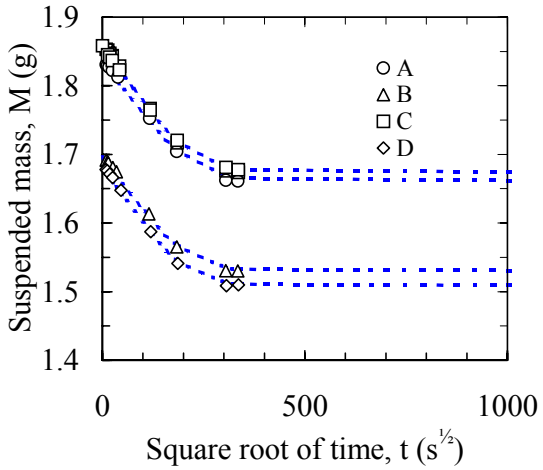

Figure 8. Mass loss as a function of time during counter-diffusion of 2-propanol into saturated Portland cement paste specimens A, B, C, and D. Dashed lines determined using Equations 4 and 5. Portland cement pastes cast at a water:cement ratio of 0.60, hydrated 28 days.

The trends for apparent diffusivity are that values decrease with age and increase with water:cement ratio. However, for the pastes with the two lowest water:cement ratios, the apparent diffusivity is low and relatively constant, while a larger decrease with age is noted for the pastes with higher water:cement ratios. This is likely to be related to the interconnectedness of the capillary pore structure. For example [23], the pores in a paste with a water:cement ratio of 0.35 will become disconnected when the cement is only about 55% reacted, while a paste with a water cement ratio of 0.60 will require almost complete hydration. Above a water:cement ratio of 0.70, the capillary pores do not become disconnected. By these estimates, at 28 days the pastes with water:cement ratios of 0.35 and 0.40 have a disconnected capillary pore structure. Increased hydration beyond 28 days does not substantially reduce the apparent diffusivity, because the capillary pore structure is already disconnected. For the specimens with a water:cement ratio of 0.60, the capillary pore structure is still connected at 28 days and the apparent diffusivity is high. At the later ages, the pore structures have become disconnected, leading to the observed substantial reduction in diffusivity.

3.2 Sensitivity

Figure 9 provides qualitative information on the sensitivity of the technique. The figure shows trial values of D plotted as a function of the degree of fit [25] between the experimentally determined values and those calculated using the procedures outlined in this work. The example shown in typical and represents Portland cement paste specimens cast at a water:cement ratio of 0.60 and hydrated 28 days. The data follows a relatively steep and symmetric curve, suggesting that the value of *D* is well-defined by the procedures developed.

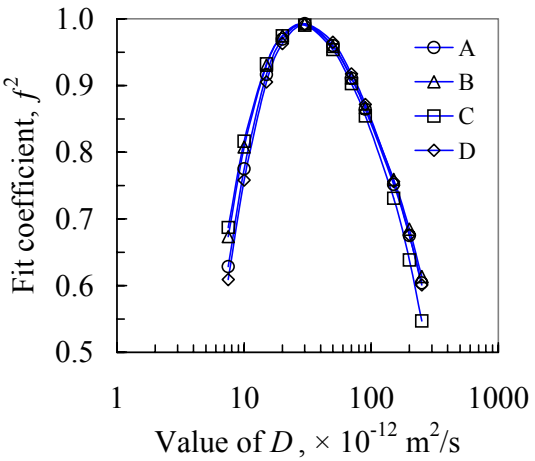

Figure 9. Sensitivity of counter-diffusion derived values of apparent diffusivity: fit coefficient plotted against trial values for *D* for Portland cement paste specimens A, B, C, and D (see Figure 8) mixed at water:cement ratio of 0.60.

3.3 Comparison of results to prior data

Values for diffusion coefficients determined through the counter-diffusion technique would be more beneficial if they could be related to diffusion coefficients of species important to the durability of concrete. Chloride ions are one such species as they destroy the passivation layer that develops around reinforcing steel in concrete, thereby allowing corrosion to proceed. Figure 10 shows a comparison of the results of chloride ion diffusivity measurements on neat Portland cement pastes at 25 °C [24] and those determined for specimens at the same water:cement ratios using the counter-diffusion technique in this work. Although the amount of data is limited, and differences in cement chemistry and age of specimens at test (60 days for the chloride ion data, 28 days for the isopropanol counter-diffusion data), the results show a high linear correlation (r^2=0.996). The high correlation lends support to the idea that the counter-diffusion technique could be used to relatively quickly provide a quantitative characteristic important to the durability of cement-based materials.

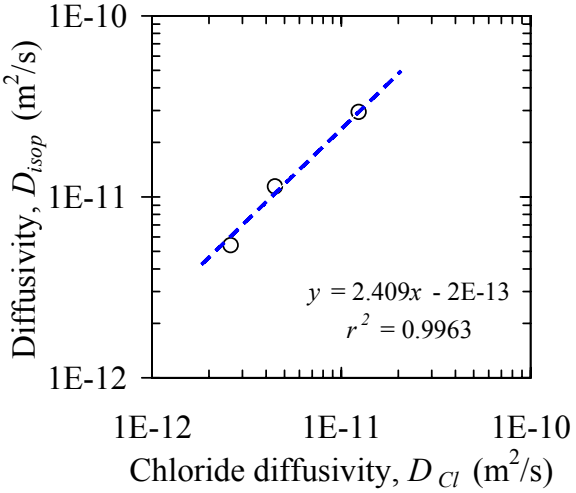

Figure 10. Comparison of diffusion coefficients for neat Portland cement pastes determined using chloride ions, D_{Cl} [24], and the counter-diffusion method, D_{isop},for specimens with identical water:cement ratios. Dashed line is the best fit (regression equation indicated).

4. CONCLUSIONS

An analysis method for apparent diffusivity has been developed that takes into account specimens of different shapes and sizes, including disks (finite cylinders). A suite of Portland cement pastes, with a range of water:cement ratios of between 0.35 and 0.60, was tested. For these specimens values of D on the order of 10^{-12} m^2/s were determined. Qualitative examination of the sensitivity of the approach indicates that the analysis provides well-defined values. Furthermore the technique is simple and provides parameters that are important to the study of durability of cement-based materials, namely, the transport properties. Correlations between diffusion coefficients determined using this technique appear to be linearly related to those determined using other techniques.

REFERENCES

[1] Tennis, P. D. Mass Transport Characteristics of Low-Permeability Materials Using Counter-Diffusion, Ph.D. Dissertation, Northwestern University, Evanston, Illinois, USA, 2001, 192 pages.

[2] Parrott, L. J. Effect of drying history upon the exchange of pore water with methanol and upon subsequent methanol sorption behavior in hydrated alite paste, Cement and Concrete Research, vol. 11, 1981, pp. 651-658.

[3] Parrott, L. J. Thermogravimetric and sorption studies of methanol exchange in an alite paste, Cement and Concrete Research, vol. 13, 1983, pp. 18-22.

[4] Parrott, L. J. An examination of two methods for studying diffusion kinetics in hydrated cements, Materials and Structures, vol. 17, 1984, pp. 131-136.

[5] Parrott, L. J., R. G. Patel, D. C. Killoh, and H. M. Jennings. Effect of age on diffusion in hydrated alite cement, Journal of the American Ceramic Society, vol. 67, 1984, pp. 233-238.

[6] Feldman, R. F. Diffusion measurements in cement paste by water replacement using propan-2-ol, Cement and Concrete Research, vol. 17, 1987, pp. 602-612.

[7] Feldman, R. F. Pore structure, permeability and diffusivity as related to durability, 8th International Congress on the Chemistry of Cement, Rio de Janeiro, Brasil, 1986, vol. 1, pp. 336-356.

[8] Gran, H. C., and E. W. Hansen. Exchange rates of ethanol with water in water-saturated cement pastes probed by NMR, Advanced Cement-Based Materials, vol. 8, 1998, pp. 108-117.

[9] Hughes, D. C. Pore structure and permeability of hardened cement paste, Magazine of Concrete Research, vol. 37, 1985, pp. 227-233.

[10] Hughes, D. C. The use of solvent exchange to monitor diffusion characteristics of cement pastes containing silica fume, Cement and Concrete Research, vol. 18, 1988, pp. 321-324.

[11] Hughes, D. C., and Crossley, N. L. Pore structure characterization of GGBS/OPC grouts using solvent techniques. Cement and Concrete Research, vol. 24, 1994, pp. 1255-1266.

[12] Beaudoin, J. J., P. Gu, J. Marchand, B. Tamtsia, R.E. Myers, and Z. Liu. Solvent replacement studies of hydrated Portland cement systems: The role of calcium hydroxide. Advanced Cement-Based Materials, vol. 8, 1998, pp. 56-65.

[13] Taylor, H. F. W., and A. B. Turner. Reactions of tricalcium silicate paste with organic liquids. Cement and Concrete Research, vol. 17, 1987, pp. 613-623.

[14] Feldman, R. F., and J. J. Beaudoin. Pretreatment of hardened hydrated cement pastes for mercury intrusion measurements. *Cement and Concrete Research*, vol. 21, 1991, pp. 297-308.

[15] Moss, G. M., B. J. Christensen, T. O. Mason, and H. M. Jennings. Microstructural analysis of young cement pastes using impedance spectroscopy during pore solution exchange. Advanced Cement-Based Materials, vol. 4, 1996, pp. 68-75.

[16] Jennings, H. M., and P. D. Tennis. Model for the developing microstructure in Portland cement pastes. Journal of the American Ceramic Society, vol. 77, 1994, pp. 3161–3172. See also Journal of the American Ceramic Society vol. 78, 1995, p.2575.

[17] Crank, J. The mathematics of diffusion. 2d ed. London: Oxford University Press, 1956.

[18] Carslaw, H. S., and J. C. Jaeger. Conduction of heat in solids. 2d ed. London: Oxford University Press, 1959.

[19] Chapman, A. J. Fundamentals of heat transfer. New York: Macmillan Publishing Company. 1987.

[20] Cussler, E. L. Diffusion mass transfer in fluid systems. 2d ed. Cambridge: Cambridge University Press, 1997.

[21] Abramowitz, M., and Stegun, I. A. Handbook of mathematical functions with formulas, graphs, and mathematical tables. National Bureau of Standards Applied Mathematics Series 55, Washington.: Government Printing Office, 1965.

[22] Powers, T. C. The physical structure and engineering properties of concrete, Skokie, Illinois, Portland Cement Association, 1958. (Research and Development Bulletin 90).

[23] Bentz, D. P., and E. J. Garboczi. Percolation of phases in a three-dimensional cement paste microstructural model. Cement and Concrete Research, vol. 21, 1991, pp. 325-344.

[24] Page, C. L., N. R. Short, and A. El Tarras. Diffusion of chloride ions in hardened cement pastes. Cement and Concrete Research, vol. 11, 1981, pp. 395-406.
[25] Popovics, S. A method for evaluating how well observed data fit the line Y = X. Materials Research and Standards, vol. 7, no. 5, 1967, pp. 195-202.

INCORPORATION OF MINOR ELEMENTS IN CLINKER: THEIR EFFECT ON THE REACTIVITY OF THE RAW MIX AND THE MICROSTRUCTURE OF CLINKER

G. Kakali[1], K. Kolovos and S. Tsivilis

[1]National Technical University of Athens, School of Chemical Engineering,Labs of Inorganic and Analytical Chemistry, 9 Heroon Polytechniou St., 15773 Athens, Greece.
Tel: +30-10-7723270; Fax: +30-10-7723188; E-mail: kakali@central.ntua.gr

ABSTRACT

The subject of this paper is the effect of foreign elements on the reactivity and the structure of clinker. One reference mixture and twenty two modified mixtures, prepared by mixing the reference sample with 1% w/w of chemical grade MnO_2, CuO, V_2O_5, PbO, CdO, ZrO_2, Li_2O, MoO_3, Co_2O_3, NiO, WO_3, ZnO, Nb_2O_5, CrO_3, Ta_2O_5, TiO_2, BaO_2, SnO_2, SrO, CaF_2, $CaCl_2$ and CaS were studied. The effect on the reactivity was evaluated on the basis of the free lime content in samples sintered at 1200°C and 1450°C. XRD was used for the identification of clinker phases, while SEM was used in order to examine the texture of the sintered samples. Selected clinkers were interground with gypsum and the setting time and the compressive strength of the prepared cements were measured. It was found that, the addition of certain elements in the raw mix is an efficient way to control the reactivity of the mixture. At 1200°C, the reactivity of the raw mix is increased in the presence of Sn, Cu, Li, S and Cl compounds. At the final stage of sintering, F, S, W, Ta, Sn and Cu compounds show the most positive effect, while Cr and Sr compounds have a negative effect on clinker burnability. The effect on the reactivity of the cement raw mix, at high temperature, is directly related to the electronic configuration of the added elements. Elements that show a positive effect are preferentially incorporated in the liquid phase. These elements do not considerably affect the strength development and the setting time of the cement.

1. INTRODUCTION

There is an increasing move towards the use of a variety of alternative raw materials and fuel in cement manufacturing aiming to obvious benefits. The main concern in these cases is the incorporation of the foreign elements in the clinker and their effect on the burning of the raw mix and the performance of the cement. It has been found that small amount of inorganic additives can considerably affect the sintering process, the structure and the properties of clinker and that is why their effect was successfully described as a catalitic one [1-5]. The role of minor components and their influence on clinkering is summarized, in general terms, from published reports as fluxing and mineralizing actions. Such compounds may lower the temperature of the first liquid phase formation and/or increase the amount of the melt (fluxes), accelerate the rate of the reactions occurring in the solid state, within the liquid phase, or at the liquid-solid interface (mineralizers), alter the viscosity and surface tension of the melt and affect both crystal growth and morphology. The technological consequences are evident: changes of the reactivity and burnability of the raw materials, formation of new phases in altered amounts, differentiation on hydraulic activity and properties of produced cements, chance of energy conservation and saving as well as alterations-precautions during clinker manufacture due to the high volatility of some compounds. The effect of foreign elements on the melt properties is well established in the literature [6]. In our previous work, it was shown that the well known effect of certain cations on the formation and the properties of the melt can be reflected on the overall reactivity of the cement raw mix [7,8].

Proceedings of the 11th International Congress on the Chemistry of Cement (ICCC) 11 - 16 May 2003, Durban, South Africa
'Cement's Contribution to the Development in the 21st Century' ISBN Number: 0-9584085-8-0
Hosted by: The Cement and Concrete Institute of South Africa Editors: Dr G. Grieve and G. Owens
CD-ROM produced by: Document Transformation Technologies Congress Organised by: Event Dynamics

When heavy elements are present in cement, the early hydration reactions are prohibited, probably through the formation of amorphous compounds that cover the unreacted cement grains. The hydration reactions start again after the crystallization and sedimentation of these compounds, which takes place when the Ca^{2+} and OH^- concentration becomes high enough [9-11]. The hydration process, however, of clinkers containing these compounds is expected to be different, since their incorporation in the clinker phases modifies their dissolution rate during hydration.

In this the paper, the effect of twenty-two elements (anions and cations) on the reactivity of the cement raw mix is evaluated and correlated with their electronic configuration. The modified clinkers were examined under SEM in an attempt to elucidate the way these elements affect the sintering process and examine their distribution in the clinker compounds. In addition, the effect of certain mineralizing elements on the cement properties is discussed.

2. EXPERIMENTAL

One reference mixture, composed of chemical grade $CaCO_3$, SiO_2, Al_2O_3 and Fe_2O_3 and having a composition very close to that of a typical cement raw meal, was prepared. Quartz and aluminum oxide were ground to a particle size less than 90μm and then were intensively mixed with Fe_2O_3 and precipitated $CaCO_3$ in a laboratory swing mill for 1 hour. Homogeneity was ascertained by measuring the loss on ignition (L.O.I.) in three individual samples of the mixture. The results indicated that L.O.I. values were very close to the estimated one (34.99%), certifying a good homogeneity of the raw mix. Table 1 shows the chemical and mineral composition (according to Bogue) of the reference mixture, after it was sintered at 1450°C.

Table 1. Chemical and mineral composition of the reference mixture after thermal treatment at 1450°C

Clinker chemical composition		Clinker mineral composition (according to Bogue)	
Oxide	wt (%)	Mineralogical constituent	wt (%)
CaO	68.08	C_3S	65.0
SiO_2	22.81	C_2S	15.0
Al_2O_3	5.84	C_3A	10.0
Fe_2O_3	3.27	C_4AF	10.0

Twenty two modified mixtures were prepared by mixing the reference sample with 1% w/w of chemical grade MnO_2, CuO, V_2O_5, PbO, CdO, ZrO_2, Li_2O, MoO_3, Co_2O_3, NiO, WO_3, ZnO, Nb_2O_5, CrO_3, Ta_2O_5, TiO_2, BaO_2, SnO_2, SrO, CaF_2, $CaCl_2$ and CaS. All the cations were introduced in the form of oxides, in order to avoid the effect of foreign anions on the reactivity of the mixture. In the case of Cl^-, F^- and S^{2-}, calcium salts were used in order to avoid the effect of foreign cations. When necessary, the added compounds were ground in order to have, approximately, the same fineness with the reference sample. Very fine compounds (e.g. ZnO), were sieved, prior to mixing, in order to avoid agglomeration. The homogeneity was ascertained by dosing the added element, in some indicative samples.

All the samples were pressed to form pellets, then sintered at 1200 °C and 1450 °C for 30 min in an electrical furnace and cooled rapidly in air. The sintered pellets were ground and analyzed by the ethylene glycol method in order to estimate the free CaO (fCaO) content.

The samples were, also, examined using a Siemens D-5000 X-ray diffractometer, with nickel-filtered Cu $K\alpha_1$ radiation (λ=1.5405 Å), for the identification of the mineralogical phases formed during sintering. Scanning Electron Microscopy was applied in order to examine the fracture

surface of the obtained clinkers. A JEOL JSM-5600 Scanning Electron Microscope, interfaced to an OXFORD LINK ISIS 300 Energy dispersive X-ray spectrometer (EDS) was used.

The reference clinker and the clinkers containing CuO, ZnO, MoO_3 and WO_3 were interground with 5% w/w gypsum in a pro-pilot plant ball mill of 5 kg capacity. The gypsum was of industrial origin (98% w/w $CaSO_4 \cdot 2H_2O$). The fineness of all the produced cements was found to be in the range between 3500 and 3700 cm^2/g (Blaine). The compressive strength of the samples (EN 196-1) and the setting time (EN 196-3) was determined.

3. RESULTS AND DISCUSSION

3.1 Reactivity of cement raw mix

The free lime content in all samples was measured after thermal treatment at 1200°C and 1450°C, in order to evaluate the effect of the additives on the solid state reactions and on the reactions in the presence of the melt, respectively. Figures 1 and 2 show the free lime content in the samples, at these temperatures, in relation to the added compound.

As it was expected, most of the added compounds have only marginal effect on the reactivity of the raw mix, at 1200°C. However, the addition of CuO, Li_2O and CaS causes a remarkable decrease of the fCaO (Figure 1).

The addition of 1% CuO in the raw meal caused a decrease of fCaO by approximately 60%, showing the best result among the other doping agents. In fact, CuO was reported to be an efficient mineralizer and flux, its action beginning already at 1100°C [12]. The mineralizing action of CuO and SnO_2 seems to be related to their incorporation in solid solutions with calcium oxide and/or the acceleration of the reactions among the four main oxides. The dark color of these samples, even at 1100 °C, indicates a high degree of combination of the main constituents and especially of Fe_2O_3. This color change is observed above 1300°C, in the other samples.

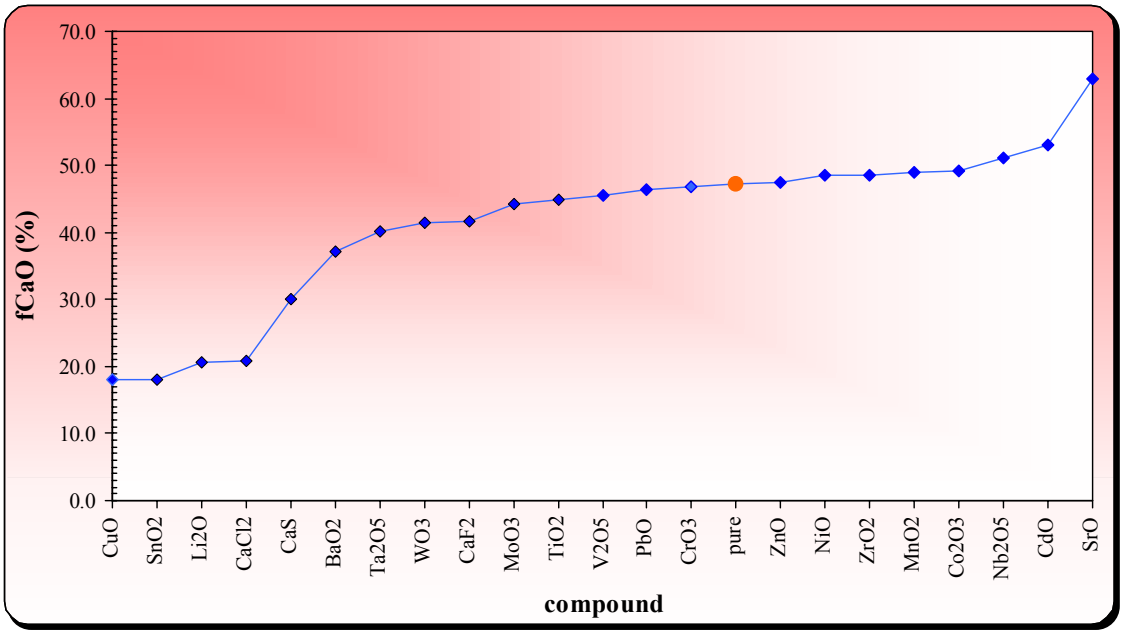

Figure 1. fCaO content in samples at 1200°C, in relation to the added compound

The TGA measurements showed that, in the presence of $CaCl_2$ and Li_2O the decomposition of calcium carbonate starts at much lower temperature (50°C and 70°C lower than in the reference sample, respectively). Saraswat et al have also observed the same effect, as well as an accelerated formation of belite in samples containing Li_2CO_3 and they have attributed these effects to the

formation of higher reactive CaO [13]. XRD measurements showed, also, some indications for the formation of Ca-Al-Cl-O solid solutions at 1200°C, in the sample containing $CaCl_2$. Cl compounds were also reported to favor the formation of spurrite, but we were unable to detect any spurrite in this sample [2]. Therefore, the increased rate of fCaO combination at 1200°C, can be attributed to the accelerated decomposition of calcium carbonate and the incorporation of CaO in new Cl containing phases.

Based on their effect at 1450°C, the added elements can be divided into three groups (Figure 2). F, S, W, Ta, Sn, Cu, Ti and Mo show the most positive effect, decreasing the fCaO content by 30-83%, compared with the pure sample. Cr and Sr cause an increase of fCaO content, while the rest of the elements exhibit a marginal positive effect.

In the case of clinkers containing Cr and Sr oxides, the XRD and SEM studies confirmed a high content of belite and free lime in these samples. It seems that either alite is decomposed in the presence of Cr and Sr, or belite is stabilized in a way that further reaction with lime is inhibited.

Most of the foreign ions, present in the raw mix, are dissolved in the melt and affect its properties. In previous works, quaternary mixtures, having the typical composition of the liquid phase, were studied and the correlation between the electronic configuration of the added ions (atomic radius, electronegativity, field intensity) and their effect on the properties of the melt was well established [1, 4]. However, it is not clear whether any changes of the melt properties can be reflected on the overall reactivity of the $CaO-SiO_2-Al_2O_3-Fe_2O_3$ mixture.

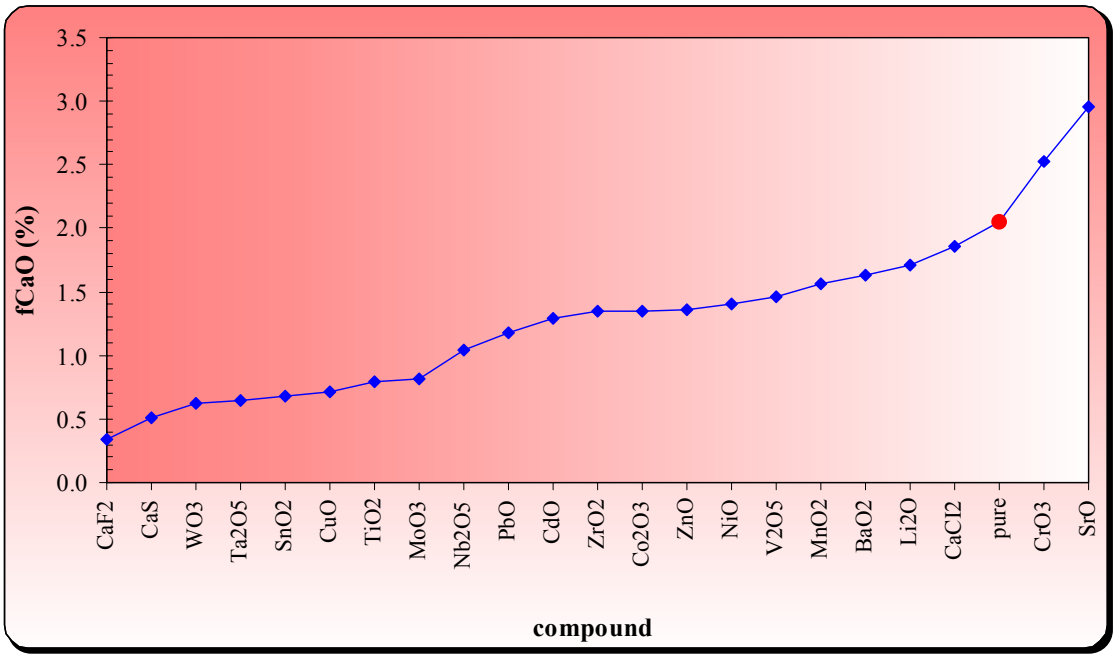

Figure 2. fCaO content in samples at 1450°C, in relation to the added compound

The effect of the added ions to the reactivity of the mixture, at 1450 °C, was evaluated on the basis of their electronic configuration. Figure 3 presents the fCaO ratio (ratio of fCaO content in modified samples to the fCaO content in the reference sample) and the atomic radii of the added elements, in relation to their atomic number.

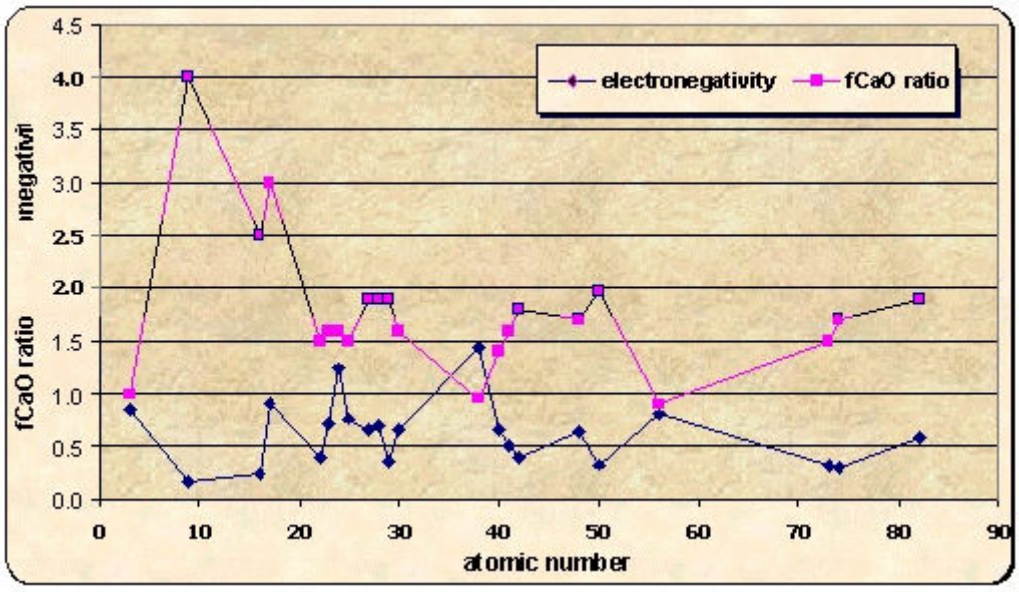

Figure 3. fCaO ratio at 1450 ^{0}C and atomic radii of the added elements, in relation to their atomic number.

Figure 4 presents the fCaO ratio and the electronegativity (according to Pauling) of the added elements, in relation to their atomic number. As it is shown, the changes of the free lime content closely follow the periodicity of the atomic radii and the electronegativity of the added elements. The presence of ions, having decreased size or increased electronegativity, favors the combination of the free lime and therefore improves the reactivity of the mixture. Our work confirms that the overall reactivity of the mixture can be correlated with the electron configuration of the added ions, in the same way as the properties of the melt. The addition of small amount of selected compounds can alter extensively the properties of the melt and these modifications of the melt properties are reflected on the reactivity and burnability of the raw mix, which is very important in the case of the cement production. The only deviation of this simple rule concerns two groups of elements: i) Cu and Sn and ii) Cr and V. The elements in the first group showed a positive effect on the reactivity, although they were expected to have a negative one. However these elements were proved to be efficient mineralizers even at low temperature and their action is probably irrelevant with their effect on the properties of the melt. The elements in the second group are preferentially concentrated in belite and they are not expected to affect the properties of the melt extensively.

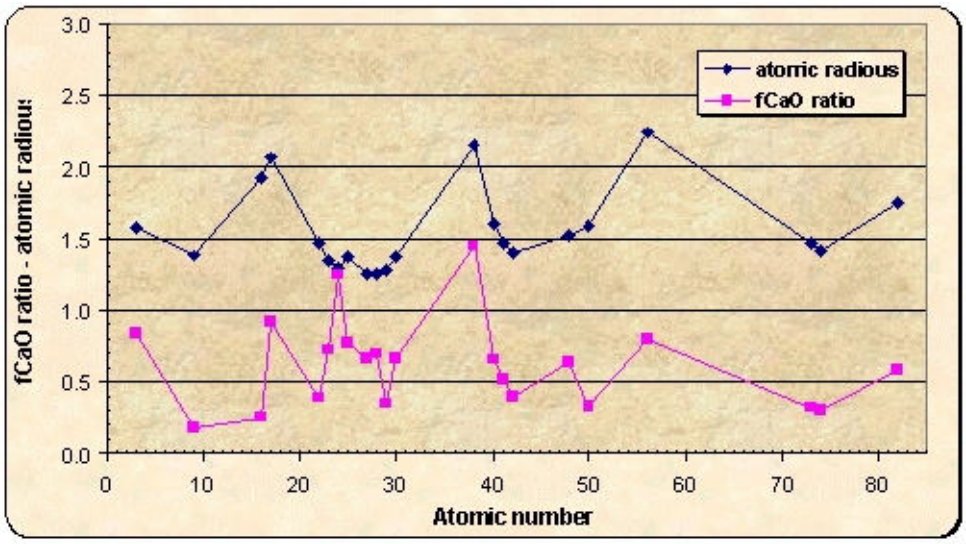

Figure 4. fCaO ratio at 1450^{0}C and electronegativity (according to Pauling) of the added elements, in relation to their atomic number.

Our measurements, concerning the volatility of the added elements showed that these elements can be divided into three groups:

High volatile elements: Cd, Pb, S, Cl (less than 20% remained in sample)
Moderate volatile elements: Cr, Co, Ni, Mn, F
Low volatile elements: Ti, Cu, Mo, W, V, Zn, Zr, Ba, Nb, Ta, Li (almost 100% remained in sample).

As it is obvious, the content of the added elements is not constant in all burnt samples, since each element has a different volatility. However, we have chosen to have a constant percentage of added oxides in the raw meal for two reasons: i) it is more convenient to control the composition of the raw mix than the composition of the clinker and ii) even the elements with increased volatility and small retention in clinker may considerably affect the reactions that take place before their removal from the mixture.

3.2 Structure of modified clinkers

Some of the modified clinkers were examined under SEM. Photos of the pure clinker, as well as the clinkers containing W, Ta, Sn, Cu and Sr oxide are presented in Figure 5. The photos were selected to be representative as far as the distribution, size and form of alite and belite crystals are concerned. With the spot analysis of EDS, the composition of the principal phases was analyzed at five to eight points.

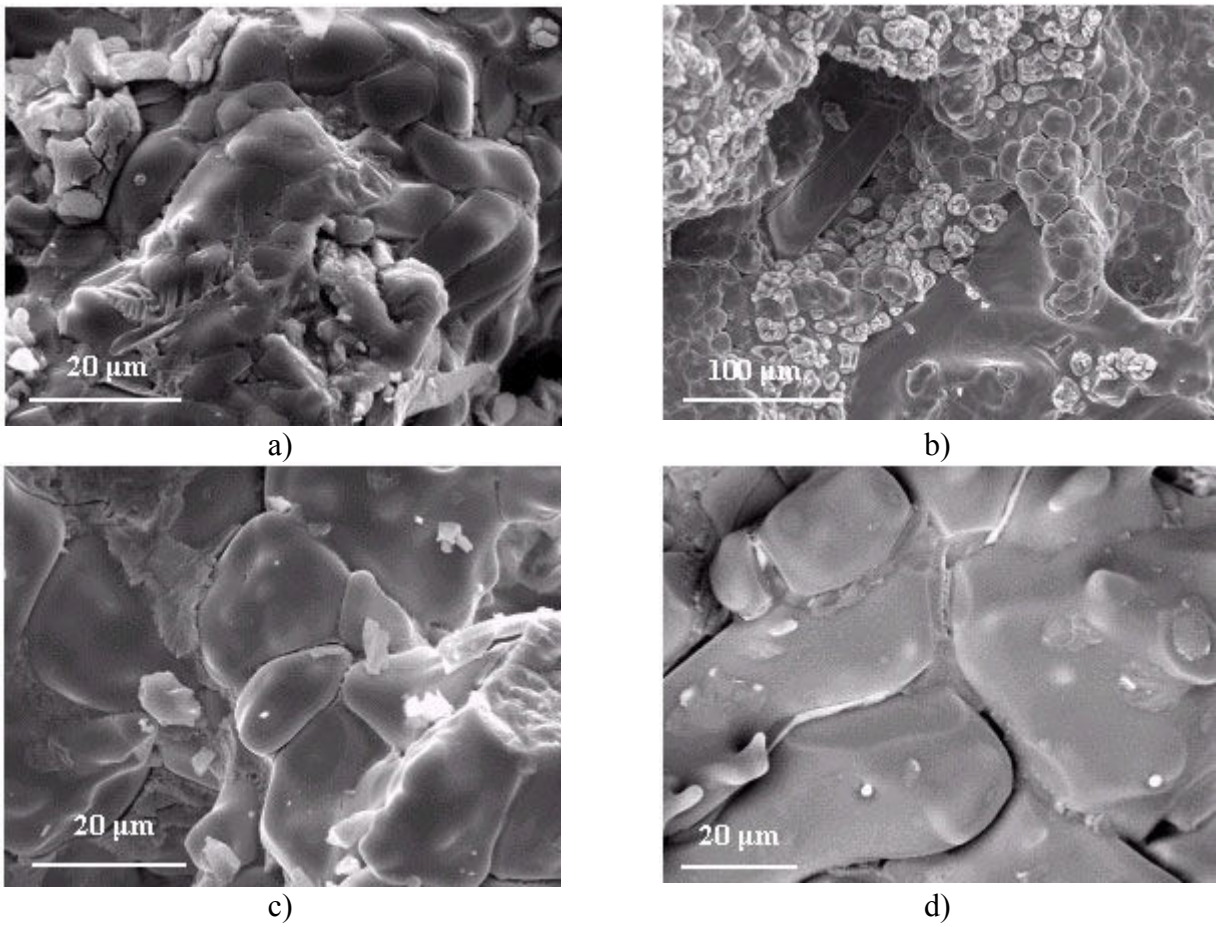

Figure 5. SEM photos of clinker
a. Reference, b. SrO, c. WO_3, d. CuO

In reference sample (Figure 5a) belite grains were uniformly distributed as small roundish grains, having a size of approximately 10-20µm. Alite crystals dominated the sample's texture, with particle size ranging from 20 to 30µm. Alite appeared as compact basal prismatic crystals of

slightly rounded hexagonal outline. The interstitial material had a fine-crystalline structure and it was generally adequate.

Clinkers containing Sr and Cr oxides (Figure 5b) present a similar texture that can be correlated with the similar behaviour during sintering. Belite, in both samples, forms clusters of rather rounded grains uniformly distributed in the sample. Free CaO grains are also evident as light white spherical crystals having a leaflet configuration. The coexistence of free lime with belite crystals indicates the decomposition of alite into belite and free lime. The XRD studies and the chemical test confirmed a high content of belite and free lime in these samples. EDS analysis resulted that Sr and Cr are preferentially incorporated in belite.

The elements that had a positive effect on the burnability of clinker during the final stage of sintering, had also a common effect on the texture of clinker (Figure 5c, 5d). These elements were mainly distributed in the liquid phase and they seem to favor the formation of big rounded alite crystals.

3.3 Cement properties

It is known that the presence of heavy metal compounds in cement causes a remarkable delay as far as the setting is concerned. The hydration process, however, of clinkers containing these compounds is expected to be different since the elements are incorporated in the clinker phases.

Figure 6 presents the strength development of the cements containing Cu, Zn, Mo and W oxides. The initial strength (2 days) fluctuated from 13.2 to 18.3 N/mm^2. After 28 days, the samples with CuO and ZnO presented slightly higher strength while the samples with WO_3 and MoO_3 had slightly lower strength than pure cement.

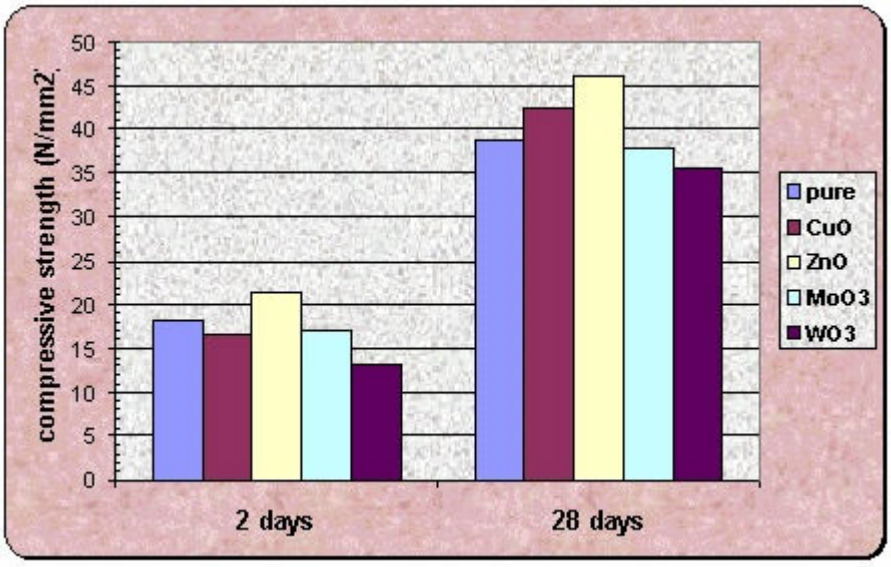

Figure 6. Compressive strength of cements in relation to the added oxides

Figure 7 presents the setting time of the produced cements. The sample containing ZnO showed the greater delay especially as far as the final setting is concerned (170 minutes). However, it must be noted that, according to our measurements, the addition of free ZnO in cement (0.5% w/w) delays the setting by 12-15 hours. When heavy elements are present in cement, the early hydration reactions are prohibited, probably through the formation of amorphous compounds that cover the unreacted cement grains. The hydration reactions start again after the crystallization and sedimentation of these compounds, which takes place when the Ca^{2+} and OH^- concentration becomes high enough [6-8]. ZnO, which greatly inhibits hydration when added in cement, does not have the same effect when added in cement raw mix. This must be associated with the different

dissolution rate of Zn^{2+}. The incorporation of Zn in the crystal lattice of clinker minerals delays the dissolution of Zn^{2+}. If Ca^{2+} concentration is high enough when Zn enters the solution, crystalline hydrated zincate salts are formed rather than amorphous zinc hydroxide and the retarding effect is decreased.

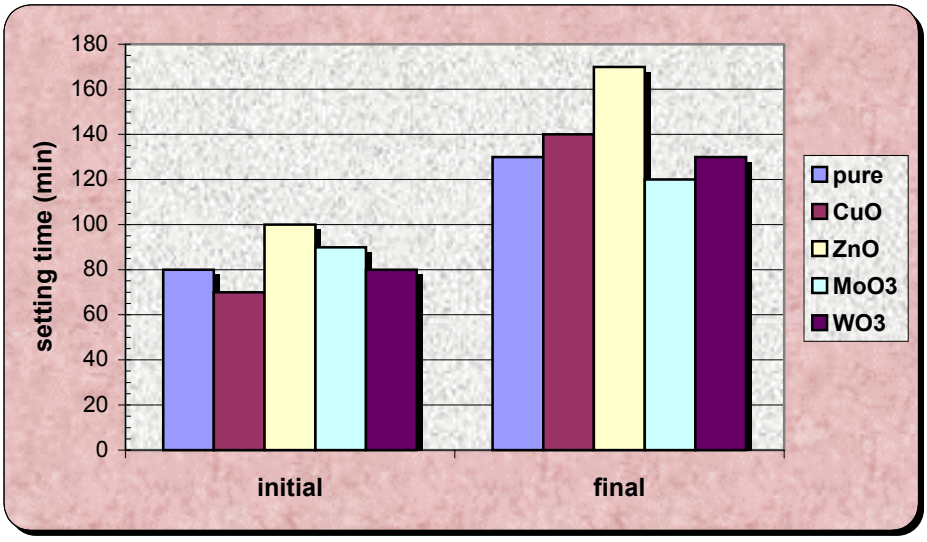

Figure 7. Setting time of cements in relation to the added oxides

4. CONCLUSIONS

From the present study the following conclusions can be drawn:

- ✓ The addition of selected elements in the raw mix is an efficient way to control the reactivity of the mixture. The effect on the reactivity of the $CaO\text{-}SiO_2\text{-}Al_2O_3\text{-}Fe_2O_3$ system, at high temperature, is directly related to the electronic configuration of these elements.

- ✓ At 1200°C, the reactivity of the raw mix is increased in the presence of Cu, Li, S and Cl compounds. At the final stage of sintering at 145°C, F, S, W, Ta, Sn and Cu show the most positive effect, while Cr and Sr compounds have a negative effect on clinker burnability.

- ✓ The incorporation of foreign elements in the clinker compounds eliminates their retarding effect on the hydration rate of the cement.

REFERENCES

[1] Bucchi, R. Features on the role of minor compounds in cement clinker. Part I, World Cement Technology, vol.12(6), 1981, pp. 210-231.

[2] Bucchi, R. Features on the role of minor compounds in cement clinker – Part 2, World Cement Technology, vol.12, 1981, pp. 258-273.

[3] Moir, G.K., Glasser, F.P. Mineralisers, modifiers and activators in the clinkering process, 9th International Congress on the Chemistry of Cement, Delhi, 1992, vol.1, pp.125-152.

[4] Bhatty, J.I. Role of minor elements in cement manufacture and use, Portland Cement Association, Skokie, Illinois, U.S.A., 1995.

[5] Shirasaka, T., Hanehara, S., Uchikawa, H. Influence of six minor and trace elements in raw material on the composition and structure of clinker, World Cement, vol. 27(3), 1996, pp.102-115.

[6] Timashev, V.V. The kinetics of clinker formation. The structure and composition of clinker and its phases, 7th International Congress on the Chemistry of Cement, Paris, 1980, vol.1, pp. I-3/1–I-3/20.

[7] Kolovos, K., Tsivilis, S., Kakali, G. The Effect of Foreign Ions on the Reactivity of the $CaO\text{-}SiO_2\text{-}Al_2O_3\text{-}Fe_2O_3$ system. Part II: Cations, Cement and Concrete Research , vol. 32(3), 2002, pp.463-469.

[8] Kolovos, K., Loutsi, P., Tsivilis, S., Kakali, G. The Effect of Foreign Ions on the Reactivity of the $CaO-SiO_2-Al_2O_3-Fe_2O_3$ System. Part I: Anions, Cement and Concrete research, vol. 31, 2001, pp. 425-429.

[9] Arligue, G., Grandet, J. Influence de la composition d' un ciment Portland sur son hydration en presence de zinc, Cement and Concrete Research, vol. 20(4), 1990, pp. 517-524.

[10] Tashiro, C., Takahashi, H., Kanaya, M., Hirakada, I., Yoshiba, R. Hardening properties of cement, mortar, adding heavy metal compounds and solubility of heavy metals from hardened mortar, Cement and Concrete Research, vol. 7(3), 1977, pp. 283-290.

[11] Uchikawa, H., Hanehara, S., Himi, H. Behaviour of heavy metal elements in the hardening of cement paste, 10th International Congress on the Chemistry of Cement, Gothenburg, 1997, vol. 2, pp.7.

[12] Kakali, G., Parissakis, G., Bouras, D. A study on the burnability and the phase formation of PC clinker containing Cu oxide, Cement and Concrete Research, vol. 26 (10), 1996, pp. 1473-1478.

[13] Saraswat, P., Mathur, V.K., Ahluwallia, S.C. Thermal Studies of the $CaCO_3:SiO_2$ (2:1) system containing Lithium as Dopant, Thermochimica Acta, vol. 97, 1986, pp. 313-320.

STRUCTURAL AND DURABILITY PERFORMANCE OF CONCRETE CONTAINING SALDANHA SLAG

J.R. Mackechnie [1], M.G. Alexander [2] and H. Jaufeerally [2]

[1] Dept. of Civil Engineering, University of Canterbury, Christchurch, NZ,
E-mail:j.mackechnie@civil.canterbury.ac.nz
[2] Dept. of Civil Engineering, University of Cape Town, Rondebosch, RSA,
E-mail: mark@eng.uct.ac.za

ABSTRACT

A new cementitious material has recently become available in the Western Cape region of South Africa. The product is a ground slag produced by the Corex process at the new Saldanha steel mill in South Africa. Detailed characterization of the new material was essential given the unique Corex process and the extensive optimisation of composition and grinding processes that was undertaken. Modern technology was able to produce a material with high performance characteristics not commonly found in ground slags. Detailed analysis of the raw material as well as analysis of the final concrete properties was therefore undertaken. Results from the laboratory research found that Corex slag not only enhances concrete durability properties but also produces good early strength and improves other structural properties. The emergence of this new slag source in the Western Cape has made a major impact on the durability and economy of concrete construction in the region. The high performance nature of the material has allowed durable concrete to be produced without compromising structural properties and at no additional cost.

1. INTRODUCTION

Slag is a by-product of iron manufacturing and has been used as a cementitious product in concrete for more than a century. The new Saldanha plant produces steel from Corex liquid iron and direct reduced iron thereby replacing the need for coke ovens and a blastfurnace. This change in technology has an influence on the chemistry and morphology of the slag that is produced at the end of the process. It was therefore important that Corex slag was fully characterized and compared to blastfurnace slag that has been successfully used in South Africa for several decades. This paper presents some of the results of an extensive investigation carried out during 2000 and 2001 at the University of Cape Town [1].

2. INTRINSIC CHARACTERISTICS

Corex slag from Saldanha (CS) was compared with blastfurnace slag from Vanderbijlpark (BS), which has a good track record as a cementitious material. Chemical and physical properties of the unreacted dry powders were analysed to predict the hydraulic activity of the two slag types. Portland cement (PC) of type CEM I 42.5 from Riebeek West cement works was used in this testing program and was also characterized where appropriate.

2.1 Chemical Composition

The hydraulic reactivity of slag powders is influenced by the chemical composition of the material. Compounds that increase reactivity include CaO, MgO and Al_2O_3 while SiO_2 reduces slag

hydraulicity. Oxide analysis was done by standard XRF techniques and results are compared in Table 1. Analysis showed that CS had higher CaO, Al_2O_3 and MgO concentrations than BS, and lower levels of SiO_2. These differences in composition indicate that CS should have higher hydraulic activity than BS of equivalent fineness, when compared with most accepted hydraulic activity formulas [2].

Table 1. Oxide analysis of binders (% by XRF analysis)

Oxides	PC	BS	CS
CaO	67.2	34.0	37.2
SiO_2	22.3	35.5	30.8
Al_2O_3	4.4	15.4	16.0
MgO	1.01	9.40	13.7
TiO_2	0.22	1.20	0.51
Fe_2O_3	3.4	0.98	0.87
MnO	0.08	0.88	0.09
K_2O	0.56	0.87	0.35
Na_2O	0.21	0.16	0.12
SO_3	0.58	2.49	3.19

2.2 Physical Properties

The reactivity of slag powders in cementitious systems is proportional to fineness (e.g. finer materials will have higher reactivity). The surface area of binders was determined by Blaine and BET fineness techniques. BET fineness results are significantly higher than Blaine values because adsorption also occurs on internal surfaces and microcracks. CS was found to be consistently finer than BS when measured by either BET or Blaine fineness tests (shown in Table 2). Particle size distribution of the two powders was also undertaken and showed that CS had a higher proportion of ultra fine particles in the range 1-10 microns. The increased fineness of CS should promote more rapid reaction than is commonly found with slag materials.

Table 2. Physical properties of Portland cement and slag powders

Method	PC	BS	CS
BET fineness (m^2/g)	-	991	1145
Blaine fineness (m^2/g)	310	390	467
% passing 1 micron	-	6	7
% passing 10 micron	-	45	51

Dry powder samples were examined using an analytical scanning electron microscope at magnifications of 2500 and 10000 times. Both types of slag were found to have angular particles with conchoidal marked faces as is typical for the material. CS grains were however slightly more chunky shaped and had a higher proportion of ultra fine particles compared to BS.

The extra fineness of CS was found to slightly decrease the workability of concrete compared with similar BS concrete. Greater fineness was also probably responsible for slightly shorter final setting times of CS pastes compared with BS pastes and lower bleed rates of concrete. Nevertheless some allowance needs to be made for the slower development of slag concretes within the first few days compared with PC concrete.

3. HARDENED CONCRETE PROPERTIES

A range of concrete mixes was cast using siliceous dune sand (fineness modulus of 2.5) and crushed 19 mm greywacke stone (Malmesbury shale). Concrete was proportioned using the Cement and Concrete Institute method except the stone content was fixed at 1100 kg/m^3. Binders used were PC, CS and BS material with a range of replacement levels, however only 0 and 50 % replacement levels with slag are reported in this paper. Water/binder ratios (w/b) were varied between 0.4 and 0.8 to obtain a range of concrete strengths. All concrete was cast with a slump in the region of 50 to 100 mm using a constant water demand of 180 L/m^3.

Reported results are average values taken from three samples for compressive strength and elastic modulus tests, two samples for creep and shrinkage tests and four samples for durability tests.

3.1 Compressive Strength

Concrete was tested for compressive strength in accordance with SABS 863 using 100 mm cube specimens [3]. Strength development was measured between 3 and 56 days and is shown in Figure 1. CS concrete was found to have rapid strength development between 3 and 14 days compared to BS and PC concrete and slower strength development between 14 and 56 days. Compressive strength of CS concrete was therefore 6 – 12 MPa higher than similar PC concrete. BS concrete in contrast showed slower early strength development but had better longer-term strength increase (i.e. between 14 and 56 days).

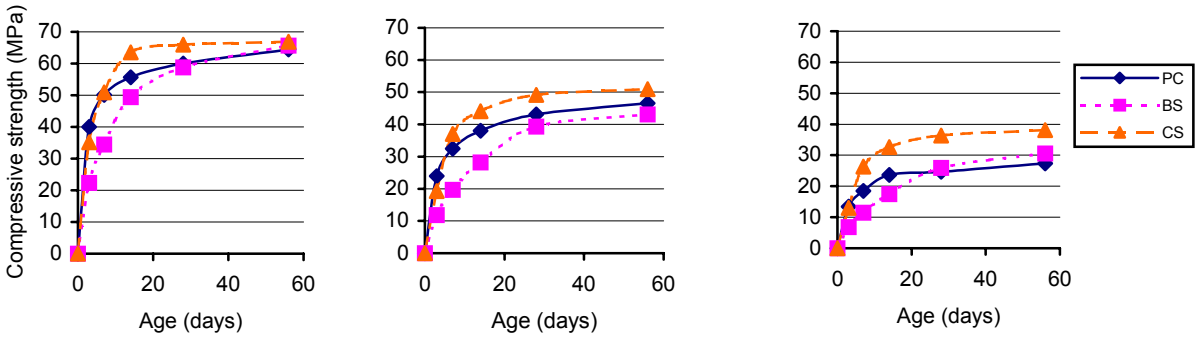

Figure 1. Compressive strength development of concrete
(for varying w/b ratios of concrete)

The more rapid maturity of CS concrete results in higher 28-day compressive strength than either PC or BS concrete. Design charts for predicting 28-day cube strengths using Western Cape materials are shown in Figure 2.

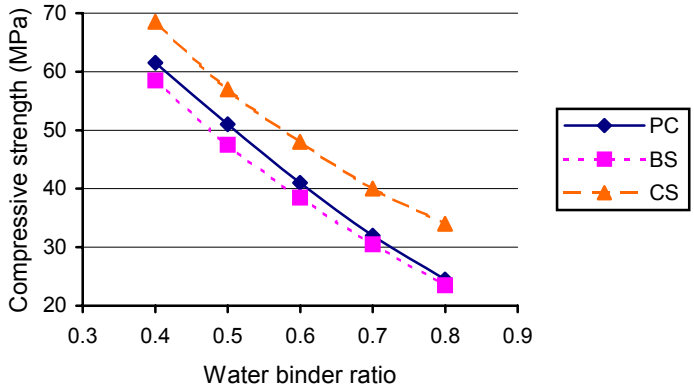

Figure 2. 28-day compressive strength design chart

3.2 Elastic Modulus

Earlier research done by Addis in South Africa found that there was almost no difference in modulus of elasticity between slag and Portland cement concrete [4]. Static elastic modulus was determined on fully wet cured concrete at 28 days using a mechanical compressometer attached to 200x100x100 mm concrete prisms [5]. Elastic modulus results showed a consistent trend with changing compressive strength (shown in Figure 3). Since the aggregate types and proportions were similar for all concretes, no major differences in concrete stiffness were expected. PC concrete results were found to be less sensitive to changes in compressive strength but this trend appears to be slightly anomalous and untypical of its normal elastic behaviour.

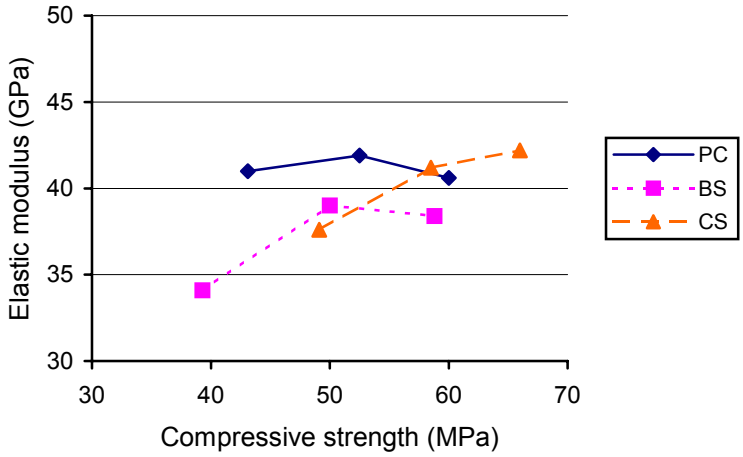

Figure 3. Elastic modulus versus compressive strength at 28 days

3.3 Creep of Concrete

Comparing research findings on creep of slag concrete, total creep strains are generally higher than PC controls while basic creep is consistently lower [1]. The lower basic creep of slag concretes may be partly due to these materials having greater increase in strength under load compared with PC concretes, which effectively decreases the stress to strength ratio.

Concrete cylinders of 105 mm diameter and 300 mm long were used in creep experiments conducted at 22 ^{0}C and 65 % R.H. Specimens were loaded at seven days with the stress to strength ratio being in the range of 18 – 34%. Sealed concrete cylinders used in the basic creep testing were coated with a bitumen emulsion and wrapped in heavy-duty aluminium foil. Specific creep

measurements for total and basic creep of concrete with w/b ratios of 0.5 are shown in Figure 4 (stress to strength ratios were 0.20, 0.27 and 0.18 for PC, BS and CS concrete respectively).

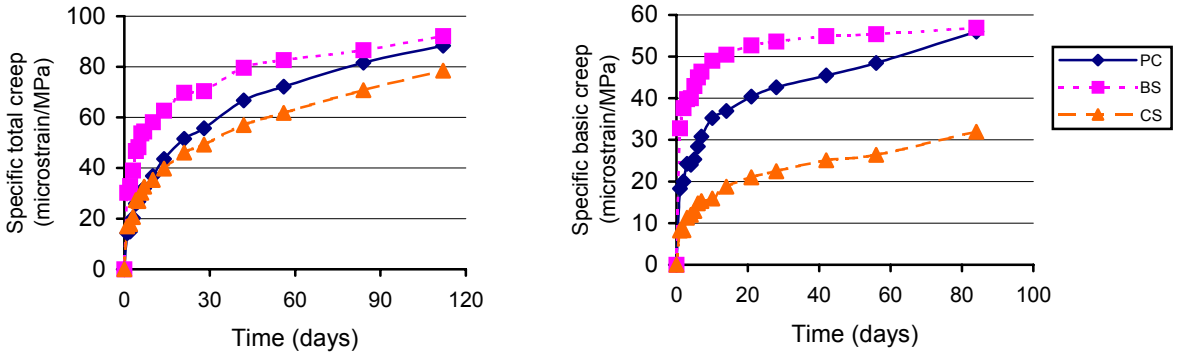

Figure 4. Specific creep measurements for concrete with w/b = 0.5

Total specific creep strains were found to be similar for all three concrete types after 112 days of loading. CS concrete had slower initial creep strains whilst BS concrete had higher strains during the first month of loading. This may be ascribed to the varying rates of strength development and therefore restraint inherent in these different materials. Specific basic creep of CS concrete was much lower than either PC or BS concretes (note basic creep measurements were terminated early after 84 days). This has major implications for the structural performance of large concrete elements where the effects of drying are less critical than the mechanism of basic creep.

3.4 Drying Shrinkage

Olorunsogo observed that drying shrinkage of slag concretes increased with an increase in slag fineness, which may be ascribed to the higher hydration rate leading to a higher degree of hydration [6]. Drying shrinkage is influenced by the amount of hydrate since moisture loss from gel pores is primarily responsible for contraction forces causing shrinkage.

Drying shrinkage testing was performed on 100x100x200 mm prisms after initial wet curing of 14 days. Samples were exposed to a constant drying environment of 22 ^{0}C and 65 % R.H. for a period of four months. Generally the drying shrinkage of concretes was similar with no significant bias based on binder type. This is shown in Figure 5 below.

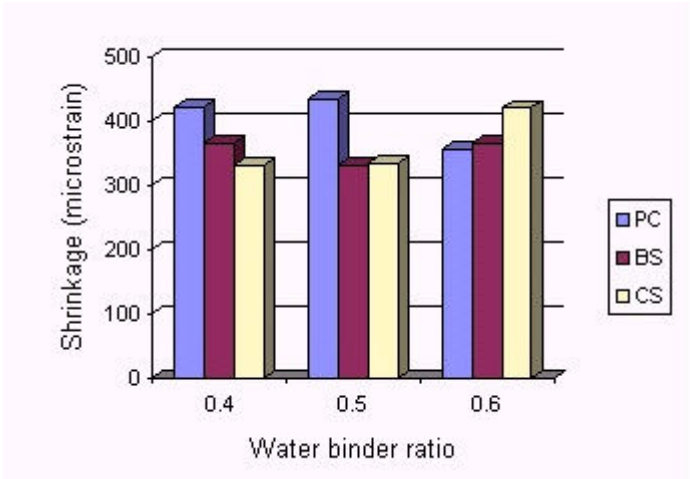

Figure 5. Drying shrinkage strain after 112 days drying

Slag concrete with a w/b ratio of 0.4 and 0.5 had lower drying shrinkage than PC concrete (typical results are shown in Figure 6). At higher w/b ratios, slag concrete had higher drying shrinkage than PC concrete. This reversal of the general trend may be due to the effect of early drying on slag cementing reactions in concrete with an open microstructure.

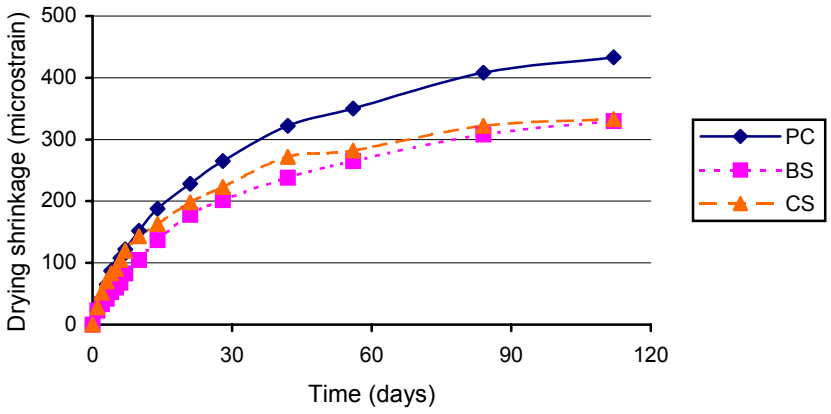

Figure 6. Drying shrinkage measurements for concrete with w/b = 0.5

3.5 Durability Index Tests

The use of slag in concrete should improve the microstructure due to improved packing efficiency, less bleeding and continued cementing reactions. Nevertheless slag concrete has often been found to have higher permeability than similar PC controls, even when fully wet cured. In contrast, slag concrete has been found to have excellent chloride resistance that may be largely ascribed to chloride binding of aluminate phases.

The potential durability of concrete was characterized at 28 days using a number of durability index tests [7]. Oxygen permeability testing uses a falling-head permeameter to assess the permeability of oven-dried concrete to oxygen. In order to avoid unwieldy exponential numbers, the oxygen permeability index (OPI) is defined as the negative logarithm of the Darcy coefficient of permeability. Values of OPI above 10.0 represent excellent quality in terms of impermeability, while values below 9.0 represent very poor quality. Figure 7a shows OPI values measured at 28 days for concrete with w/b ratios of 0.5. Slag concrete was found to have higher permeability than PC concrete, particularly when poorly cured. It is interesting to note that BS concrete improves consistently as duration of curing increases whereas CS concrete shows no improvement after 3 days of moist curing.

Chloride conductivity testing is able to quantify the potential chloride resistance of concrete using a rapid conduction technique. Oven-dried concrete samples are vacuum-saturated in a concentrated sodium chloride solution before being testing in a two-cell conduction rig. Chloride conductivity values below 0.75 mS/cm are recommended for high chloride resistance, such as marine structures. PC concrete with a w/b ratio of 0.5 only achieved chloride conductivity values of 1.5 mS/cm (see Figure 7b). In contrast, slag concretes that had received at least 3 days moist curing all achieved chloride conductivity values below 0.80 mS/cm.

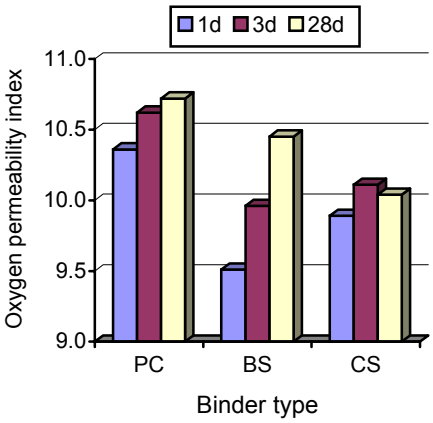

Figure 7a. Oxygen permeability results for concrete with w/b = 0.5 (different periods of wet curing)

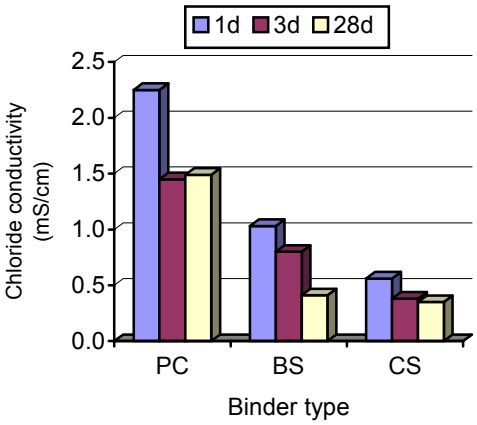

Figure 7b. Chloride conductivity results for concrete with w/b = 0.5 (different periods of wet curing)

3.6 Corrosion Protection

Slag concrete often has higher carbonation depths than similar PC concretes, particularly when poorly cured. This phenomenon has been blamed on inherently higher permeability of the material, sensitivity to curing and lower levels of carbonatable material in slag concretes. The use of slag in marine concretes has been promoted since slag concretes have been found to have excellent chloride resistance when exposed to seawater [8].

Longer-term durability performance of concrete was assessed by exposure to accelerated carbonation and actual marine environments. Accelerated carbonation of concrete was produced by limited exposure of concrete cubes in a controlled chamber at 30 ^{0}C, 85% R.H. and 10% carbon dioxide (with one week being equivalent to more than six months atmospheric exposure). Samples used for this testing were 100 mm cubes that had been wet cured for 28 days before exposure in the chamber. At intervals the cubes were split and the depth of carbonation measured using phenolphthalein indicator solution. Carbonation depths recorded after 20 weeks exposure in the chamber are shown in Figure 8a for concrete with a w/b ratio of 0.5 (note the good performance of CS concrete). Although CS concrete had poorer OPI values than either PC or BS concrete, carbonation depths of CS concrete were found to be lower than other concrete types.

Concrete blocks of size 200x250x300mm were placed in the tidal zone at Simonstown harbour with sheltered conditions and little wave action. Concrete used for this field exposure testing were cured in water for 28 days before being placed in the marine tidal zone. After eight months of wetting and drying in the sea, the blocks were removed and 45 mm diameter cores were drilled and cut into slices to assess the depth of chloride penetration (total acid-soluble chloride analysis) [9]. From the chloride profiles obtained, diffusion coefficients and surface concentrations were determined from the standard solution of Fick's second law of diffusion. The critical chloride depth (i.e. that depth at which the nominal chloride corrosion threshold level of 0.4% chloride by mass of binder had been achieved) was then calculated for each concrete and is shown in Figure 8b for concrete with w/b ratios of 0.4, 0.5 and 0.6. Whilst chloride penetration into PC and slag concrete appears fairly similar after eight months exposure, long-term differences are far more significant. Estimated time for corrosion activation of steel cast-in concrete with w/b ratio of 0.5, reasonable moist curing and cover to reinforcement of 50 mm could be less than 10 years for PC concrete but in excess of 100 years for slag concretes [8].

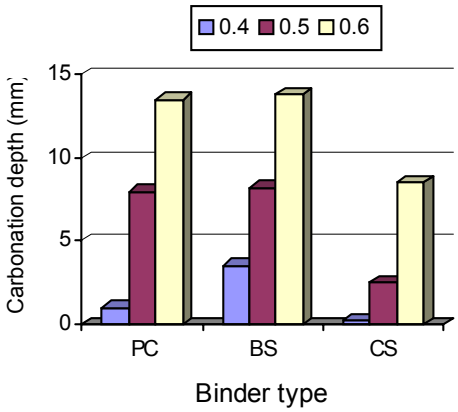

Figure 8a. Carbonation depths after 20 weeks accelerated exposure (different w/b ratios of concrete)

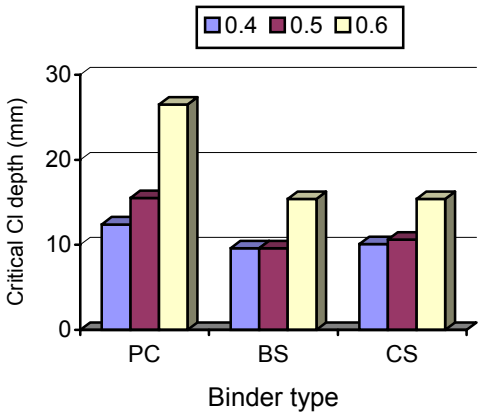

Figure 8b. Critical chloride depths after 8 months tidal marine exposure (different w/b ratios of concrete)

3.7 Alkali Silica Reaction (ASR)

The use of blastfurnace slag is widely accepted as a means of reducing the risk of ASR expansion. Research suggests that a minimum of 50% slag is required to prevent excessive expansion in the presence of sufficient alkalis and reactive aggregates [10].

Alkali-silica reaction testing was determined in accordance with SABS 1245 (accelerated mortar prism test) [11]. Malmesbury shale aggregate, noted for its ASR reactivity was used in the mortar. Total alkali contents (Na_2O_e) were 0.60, 0.90 and 0.50 % respectively for PC, BS and CS material. Active alkali components were 85, 42 and 45 % for PC, BS and CS powders.

Testing showed that PC mortar had considerably more expansion than any of the slag mortar mixes (Figure 9). When comparing equivalent replacement levels, BS was found to have better capacity to ameliorate ASR expansion than CS material. Replacement levels of 50% slag are generally required to guarantee negligibly low levels of expansion when using reactive aggregates such as Malmesbury shale (greywacke).

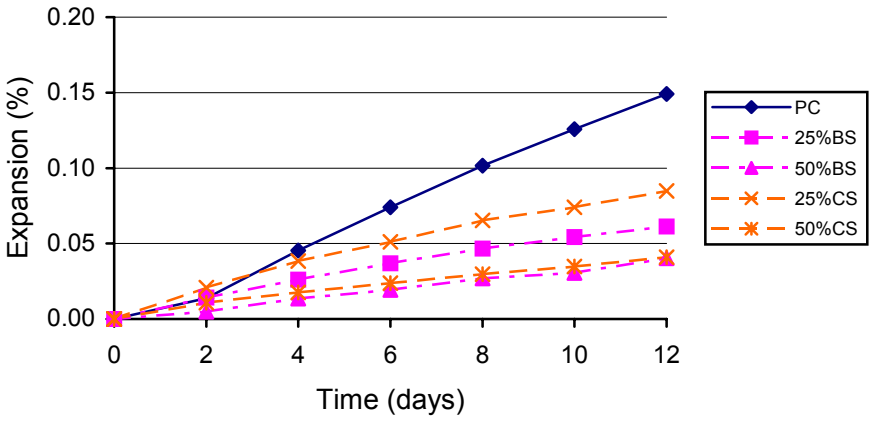

Figure 9. Alkali silica reaction expansion measurements of mortar bars

4. CONCLUSIONS

Extensive testing of Corex slag concrete found that the material displays all of the technical advantages expected from slag concretes. The improved fineness and chemical composition of the material produced rapid strength development and made the concrete less vulnerable to poor curing. Benchmarking of Corex slag with blastfurnace slag indicated that this new cementitious material performed within the expected norms of slag concretes. Given the evidence from this extensive laboratory testing, Corex slag concrete should perform excellently both in the shorter- and longer-term.

Corex slag has already had a major impact on the concrete market in the Western Cape province of South Africa. The product has been widely accepted because of economic, technical and environmental imperatives. Unlike some cement extender materials, Corex slag may be used without requiring much special attention during the construction process.

ACKNOWLEDGEMENTS

The authors wish to thank PPC South Africa for financial and technical assistance with this research project. They are particularly grateful for the expertise and valuable guidance provided by Steve Crosswell of PPC Western Cape.

REFERENCES

[1] Jaufeerally, H. Performance and properties of structural concrete made with Corex slag, Cape Town, UCT, 2002. (Masters degree thesis), p.156.
[2] Mantel, D.G. Investigation into the hydraulic activity of fine granulated blastfurnace slags with eight different Portland cements, Proceedings American Concrete Institute - Materials Journal, Vol. 91, 1994, pp. 471-477.
[3] SABS Method 863:1994, Concrete tests – compressive strength of hardened concrete, Pretoria, South African Bureau of Standards, 1994.
[4] Addis, B.J. The effect on properties of hardened concrete of substituting milled granulated blastfurnace slag, fly ash or silica fume for part of the portland cement, Midrand, Portland Cement Institute, 1987, p. 66.
[5] BS 1881 Part 121:1983, Testing concrete – method for determination of static modulus of elasticity in compression, British Standards Institute, 1983.
[6] Olorunsogo, F.T. Properties of slag cement mortar incorporating GGBS of different fineness, Proceedings Concrete Beton, No. 83, 1997, pp. 10-18.
[7] Alexander, M.G, Mackechnie, J.R and Ballim, Y. Guide to the use of durability indexes for achieving durability in concrete structures, Cape Town, 2001. (Research Monograph No. 2), p 35.
[8] Mackechnie, J.R. and Alexander, M.G. Durability predictions using early-age durability index testing, 9th international conference on durability of building materials and components, Brisbane, 2002, p. 11.
[9] BS 1881 Part 124:1988, Testing concrete – method for chloride content determination for concrete, British Standards Institute, 1988.
[10] Thomas, M.D.A. and Innes, F.A. Effect of slag on expansion due to alkali-aggregate reaction in concrete, Proceedings American Concrete Institute - Materials Journal, Vol. 95, 1998, pp. 716-724.
[11] SABS Method 1245:1994, Potential reactivity of aggregates with alkalis (accelerated mortar prism method), South Africa Bureau of Standards, 1994.

HYDRATION BEHAVIOR OF β-Ca_2SiO_4 AND RELATED CEMENTS: A SPECTROSCOPIC STUDY

Lucilene Betega de Paiva and Flávio Aparecido Rodrigues

Universidade de Mogi das Cruzes – Centro Interdisciplinar de I. Bioquímica (CIIB)
Av. Dr. Cândido Xavier de Almeida Souza, 200 – Mogi das Cruzes - SP – Brazil – CEP: 08780-911
E-mail: flaviorodrigues@yahoo.com

ABSTRACT

This work describes the use of FTIR/ATR Spectroscopy (Fourier Transform Infrared/ Attenuated Total Reflectance) to the study of early-hydration of β-Ca_2SiO_4. Here we present the influence of sodium chloride on the rate and hydration mechanism of this cement. Several NaCl concentrations were investigated (from 1 to 5%) and compared to the control (paste without addition). The hydration of normal paste is divided in two steps: in the first one, the hydration is faster (initial hydrolysis); the second step is much slower and proceeds indefinitely. The addition of sodium chloride makes the overall process even slower. These conclusions are based on the variation of the band areas of Si-O stretching (cement) and 1645 cm^{-1} (HOH bending).

1. INTRODUCTION

The study of cement hydration has long been a concern to researchers and technologists in this field. Although the term hydration, from the chemical viewpoint, may be related only to chemical reactions between water and the many components of cement, it is clear that this designation is generally understood as an overall process, relating to chemical, physical and mechanical aspects.

There are many techniques and methods currently used to investigate hydration or its effects. Among the methods applied to estimate hydration rate we can cite calorimetric methods [1], determination of calcium hydroxide released and chemically-bonded water [2], spectroscopic methods [3,4], diffraction and scattering [5,6]. Of course, this is not an extensive list. On the other hand, the effects of hydration are usually studied by physical and mechanical methods. For example there are many tests such as the Vicat test, slump loss and others, applied to fresh paste or concrete, in order to estimate their rheology.

This work describes the use of FTIR/ATR (Fourier Transform Infrared/ attenuated total reflectance) spectroscopy to study the initial hydration of cement. Although spectroscopic methods are usually restricted to structural information, this technique also provides some information about the hydration mechanisms.

1.1 Principles

In infrared spectroscopy most of the measurements are made by transmission, *i.e.* the infrared beam passes through the sample, interacts with it, and reaches the detector. Usually, a KBr disc is used to study solid samples. Liquid samples may be analysed using windows to support it. The most popular windows are made of KBr and NaCl and CaF_2. Although CaF_2 is more expansive, it has the advantage of being water insoluble.

The study of initial cement hydration by infrared is quite limited. This is because the fresh paste can not be sampled using windows since the scattering of the beam is too high rendering none or very small signals. In order to study the fresh paste as a solid, it must be dried. This procedure certainly will change the state of the sample. These experimental problems hinder infrared transmission measurements.

The recent development in computational and instrumental resources made possible the development of several accessories in infrared spectroscopy at accessible costs. Here we will briefly describe reflectance measurements.

There are three possible ways for measurements to be carried out by reflectance infrared spectroscopy: the external (specular), internal and diffuse reflectance. Süetaka [7] and Coates [8] provide excellent information about specular and diffuse reflectance.

Infrared Attenuated total reflection (FTIR/ATR) is based on the fact that a beam may undergo a total reflection inside a medium under certain conditions. As example, one may consider two different media, 1 and 2, with refraction indices, n_1 and n_2 and that $n_1>n_2$. In conventional refraction phenomenon the Snell's Law (Eq. 1) states:

$$n_1 sin\theta_1 = n_2 sin\theta_2 \quad (1)$$

For the particular case when the sine of the incident angle equals n_{21} ($n_{21}=n_2/n_1$), we have the so-called critical angle, θ_c. Beyond the critical angle, the incident beam does not pass through the interface between the medium 1 and 2; this is the case of a total reflection.

In FTIR/ATR spectroscopy the infrared beam interacts with the sample through the internal reflection element (IRE). The most usual experimental arrangement for the IRE is the trapezoidal plate, presented in Figure 1. As can be seen, the incident beam reaches the IRE at some defined angle and is reflected several times inside the IRE. Also, the IRE must be transparent to the infrared beam and should present a high refractive index. Table I presents some materials used as IRE in ATR/FTIR spectroscopy and some of its major characteristics.

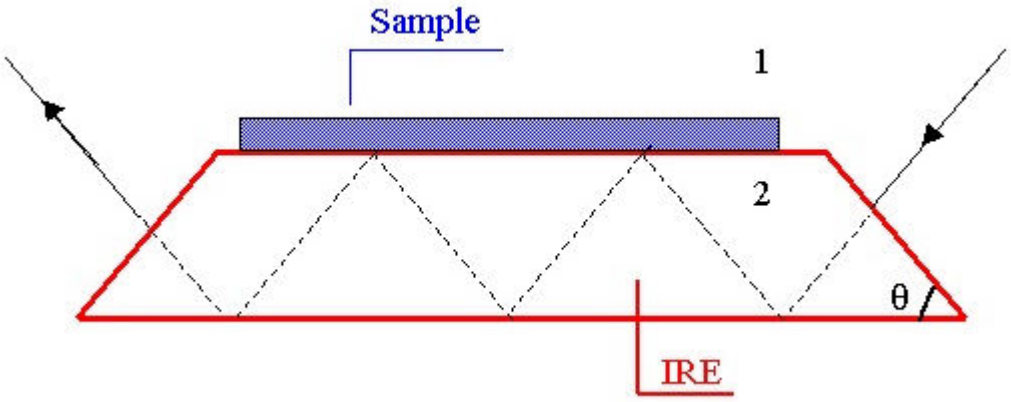

Figure 1. Internal Reflection Elements (IRE) used in ATR/FTIR spectroscopy. Indices 1 and 2 refer to the different media; θ is the incidence angle.

The interaction between the infrared beam and the sample occurs on the surface of the IRE. The analysis is possible due to an evanescent wave that interacts with the sample near to the IRE surface.

The amplitude of the evanescent wave falls off with the distance from the interface according to equation (2):

$$E = E_0 \exp(-z / d_p) \tag{2}$$

where d_p is the penetration depth. The penetration depth is described by equation (3):

$$d_p = \frac{\lambda l}{2\pi(sin^2\theta - n_{21}^2)^{1/2}} \tag{3}$$

The penetration depth is defined as the beam penetration when the energy of the beam, E, decays to a value of E_o exp[-1].

The penetration depth has a pivotal role in spectroscopic analysis. In order to achieve good spectral analysis, the sample must be in close contact with the IRE. In the case of cement paste, the presence of water helps to create a good contact. Also, in much of the commercial equipment, it is possible to apply an external pressure on the sample in order to improve the contact. . Under the same experimental conditions, the penetration depth is variable, and is higher to higher wavelength. In the presence of strong absorbers, such as water, it may cause "distortions" in relation to transmission spectra. However, since this phenomenon is well understood, it may be easily corrected. Commercial IR equipment usually provides an automatic correction for this effect.

Table 1. Major Internal Reflections Elements used in ATR/FTIR Spectroscopy

Materials	Refractive Index	Characteristics
ZnSe	2.24	Soluble in acids
KRS-5	2.35	Slightly soluble in water
Si	3.24	Chemically stable
Ge	4.0	Chemically stable

2. EXPERIMENTAL

The synthesis of β-Ca_2SiO_4 has been presented before [9,10]. FTIR/ATR measurements were done using a FTIR (Spectrum One) and the ATR accessory (ZnSe, incidence angle of 45° and flat surface). Water was added to one gram of cement in order to produce a paste with w/c ratio = 0.40. NaCl was added to the cement or previously dissolved in water, to attain a final concentration of 1, 2 and 5% (in relation to the cement mass). The experiments were conducted at 20°C and relative humidity of 54%. The spectra were recorded using 32 accumulations.

3. RESULTS AND DISCUSSION

Figures 2 and 3 show spectra recorded for the control (paste without additions) and with addition of sodium chloride 5%, respectively. An important experimental issue is that the paste is not manipulated once put in contact with the IRE. All spectral variations are due to the hydration process. It implies that many experimental conditions can be easily varied, such as temperature, humidity, additions, etc.

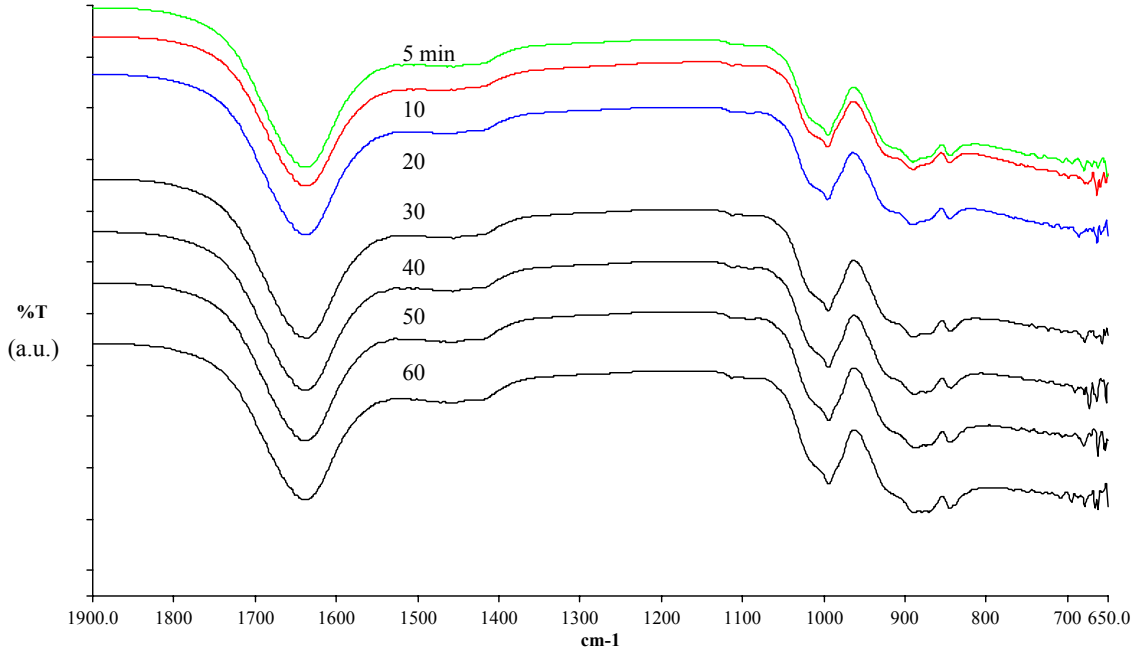

Figure 2. FTIR/ATR spectra for the control recorded as function of time.

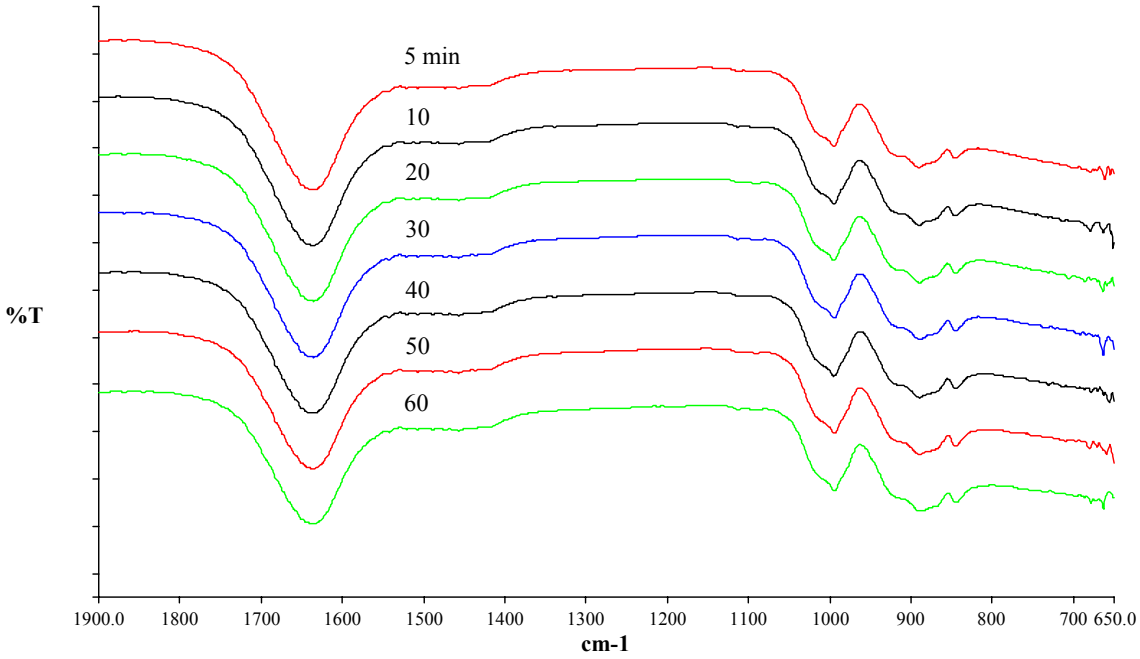

Figure 3. FTIR/ATR spectra for the fresh paste containing 5% NaCl recorded as function of time.

The major bands corresponding to water absorption are 3280 cm^{-1} (OH stretching), 2125 cm^{-1} (water association) and 1645 cm^{-1} (HOH bending). The major peak of unhydrated cement is located at 1000 cm^{-1} (Si-O asymmetric stretching). The analysis is conducted measuring the variation of the band located at 1645 cm^{-1} (water) and 1000 cm^{-1} (cement).

Figure 4 shows the variation of the peaks located at 1645 cm^{-1} for the control and the sample with 5% of NaCl. Previous results indicate that hydration proceeds in two distinct steps: initial hydrolysis (chemically controlled) and by water diffusion into cement grains (physically controlled). When we observe figure 4 the two steps are well defined, by a sharp fall in the band associated to water. For the control the second step starts at about 60 minutes while for the sample

with 5% of NaCl this step starts much later, around 130 minutes. This is a considerable delay, showing that NaCl retards the hydration of cement.

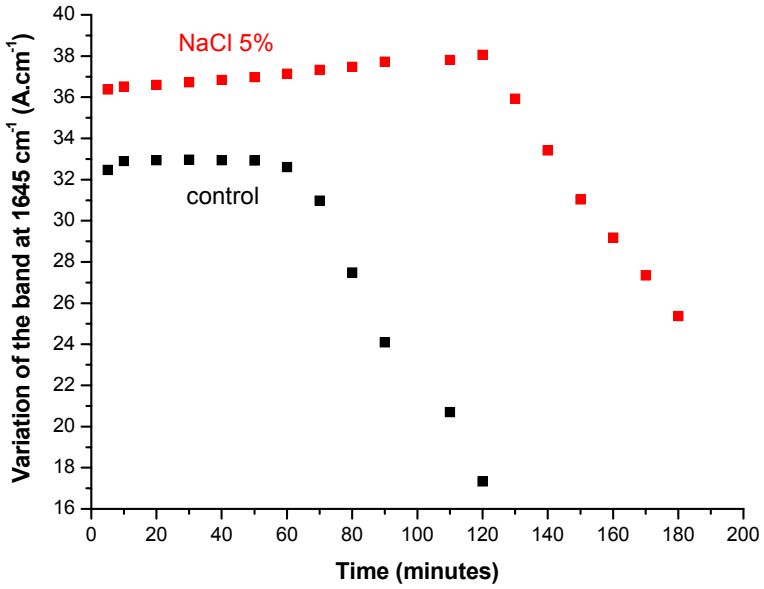

Figure 4. Variation of the area of the band located at 1645 cm^{-1} for control and sample containing 5% of NaCl, as a function of time.

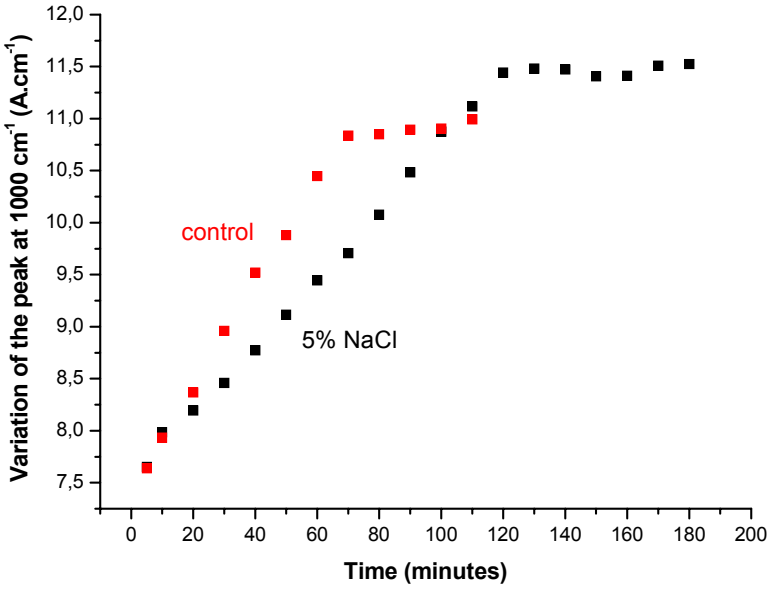

Figure 5. Variation of the area of the peak located at 1000 cm^{-1} for control and sample containing 5% of NaCl, as a function of time.

Figure 5 shows the variation of the peak area of cement as hydration proceeds. The initial slope for each curve confirms that hydration is faster in the absence of sodium chloride. An important point is that after about 60 minutes the peak area for control is almost constant, with a small increase over time. This is probably the result of water migration into cement grains, lowering the relative intensity of the peak at 1000 cm^{-1}.

4. CONCLUSIONS

This paper describes some applications of ATR/FTIR spectroscopy applied to hydration of β-Ca_2SiO_4 cement. The technique is very useful in the initial hydration process, allowing the distinction between two processes, already known: 1- initial hydrolysis, which is controlled by chemical aspects, such as cement composition and the presence of admixtures, and 2- diffusion control, when water starts to migrate into cement grains. The distinction between these processes is very clear when the area variation of the peaks located at 1000 cm^{-1} (Si-O stretching) and 1645 cm^{-1} (H-O-H bending) is plotted against time.

ACKNOWLEDGEMENTS

The first-named author is thankful to FAPESP (Fundação de Amparo à Pesquisa do Estado de São Paulo) for financial support (grant 98/09644-6).

REFERENCES

[1] Brandster, J., Polcer, J., Krátky, J., Holesinsky, R. and Havlica, J., Possibilities of the use of isoperibolic calorimetry for assessing the hydration behaviour of cementitious systems, Cement and Concrete Research, vol. 31, 2001, pp. 941-947.

[2] Asavapisit, S., Fowler, G. and Cheeseman, C. R., Solution Chemistry during cement hydration in the presence of metal hydroxide wastes, Cement and Concrete Research, vol. 27, 1997, pp. 1249-1260.

[3] Masse, S. and Zanni, H. ^{29}Si solid state NMR study of tricalcium silicate and cement hydration at high temperatures, Cement and Concrete Research, vol. 23, 1993, pp. 1169-1177.

[4] Long, S., Liu, C. and Wu, Y., ESCA study on the early C_3S hydration in NaOH solution and pure water, Cement and Concrete Research, vol. 28, 1998, pp. 245-249.

[5] Escalante-García, J. I. and Sharp, J. H., Effect of temperature on the hydration of the main clinker phases in Portland cements: Part I, neat cements, Cement and Concrete Research, vol. 28, 1998, pp. 1245-1257.

[6] Berliner, R., Popovici, M., Herwig, K. W., Berliner, M., Jennings, H. M. and Thomas, J. J., Quasielastic neutron scattering study of the effect of water-to-cement ratio on the hydration kinetics of tricalcium silicate, Cement and Concrete Research, vol. 28, 1998, pp. 231-243.

[7] Suëtaka, W., Surface Infrared and Raman Spectroscopy: Methods and Applications, Plenum Press, (1995) New York.

[8] Coates, J., Vibrational spectroscopy: instrumentation for infrared and Raman spectroscopy, Applied Spectroscopy Reviews, vol. 33, 1998, pp. 267-425.

[9] Rodrigues, F. A., Synthesis of Cements from Rice Hull, Symposia Papers Presented Before the Division of Environmental Chemistry, American Chemical Society, New Orleans, 39 (2) (1999) 30-31.

[10] Rodrigues, F. A. Low-Temperature Synthesis of Cements from Rice Hull Ash, accepted to publication in Cem. Concr. Res.

PROPERTIES, APPLICATIONS AND PRACTICALITIES OF SPECIAL CEMENTS

Karen L. Scrivener

Swiss Federal Institute of Technology Lausanne, Switzerland, E-mail: karen.scrivener@epfl.ch

ABSTRACT

Special cements must offer something that Portland cement cannot. Due to the widely distributed raw materials and advances in production technology, Portland cements can be produced cheaply and efficiently all over the world. It is argued that cheaper or more environmentally friendly cements are unlikely to come from new clinkers, but from blending Portland clinker with other by-product materials.

The opportunities for special cements are in providing different properties, which overcome some of the limitations of Portland cement. Good examples of this are calcium aluminate cements, which have a wide range of applications.

1. INTRODUCTION

Portland cement, in the form of concrete is the most widely used material in the world. There are many reasons behind this success:

- The raw materials are widely available and easily extracted.
- It is cheap to produce, with low energy input, compared to alternatives such as steel and masonry.
- With the simple addition of water it sets and hardens at room temperature, with minimal volume change.
- It is highly durable and resistant to water penetration (if well made).

The major weakness of concrete, lack of tensile strength is dealt with through the use of steel reinforcement and many decades of experience have led to the establishment of codes of practice ensuring an exceptional degree of safety of concrete structures. In the light of this, *special* cements must indeed offer something *special* in order to be competitive in certain applications.

There are two areas where it may be imaginable to produce *new clinkers* to give cements with an advantage over Portland cements:

- Lower environmental impact or cost.
- Special properties, which overcome the limitations of Portland cement.

In fact, as will be argued here, only the latter is really feasible and even in this case the possibilities are severely limited by the comparative availability of raw materials. Successful special cements are still essentially based in the CaO-SiO_2-Al_2O_3 system. Despite these limitations the opportunities that exist in this system are far from being fully exploited at the present time.

This paper considers present and possible future applications for special cements. The properties of Portland and special cements are discussed in terms of their microstructural development, which gives new insights into how cementitious materials with specially designed properties might be

developed from mixtures of cements currently available. As an example of successful special cement, the microstructural development and properties of calcium aluminate cements are discussed in detail.

2. LOWERING ENVIROMENTAL IMPACT

Sustainable development is rightly a major concern in the world today. Cement is NOT intrinsically a high-energy material. Comparisons are difficult, but on an equivalent performance basis concrete solutions have typically 4 to 6 times less energy requirement than alternatives, such as masonry, steel or plastic.

Nevertheless, the huge quantities of cement consumed, mean that overall cement production has a significant impact on energy consumption and CO_2 emissions and that worthwhile reductions can result from even small improvements.

In terms of special cements the potential advantage of lower firing temperatures is frequently cited as a means of reducing energy consumption, but the savings from such reductions in temperature are vastly overrated and more than cancelled out by other factors, for example:

- Availability and need for transportation of raw and finished materials.
- Efficiencies of heat recuperation and scale.
- Output of pollutants

2.1 Raw Materials and Transport

The major raw material for cement production, i.e. the calcareous component, is quarried within a few kilometres of the kiln; this allows direct transportation by a conveyor system, often enclosed, which minimises dust and noise. For the finished product, transport of cement by road is only economical within a radius of a few hundred kilometres. The energy required for transportation should thus be included in the calculation of energy consumption. Only raw materials that are widely available can be used for cement production, without significantly increasing energy consumption.

It is no coincidence that the five most important chemical elements in cement – oxygen, silicon, aluminium, iron and calcium are also the five most abundant elements in the earth's crust, together making up 91.2%. If the more important minor elements in cement are added – sodium, potassium, magnesium, titanium, and sulfur – 99.3% of the earth's crust is accounted for.

It is notable that most special cements currently produced stay within the CaO-SiO_2-Al_2O_3-Fe_2O_3-SO_3 system. The most important of which contain either CA (monocalcium aluminate, the basis of calcium aluminate cements, CACs) or $C_4A_3\$$[*] (Klein's compound, the basis of calcium sulfoaluminate cements CSAs) as the major ingredient. Even though aluminium is the third most abundant element, usable deposits of aluminium containing minerals (e.g. bauxites) are much rarer and less evenly distributed geographically, than the silico-aluminate minerals used in Portland cement production. This contributes to the higher cost of both calcium aluminate and calcium sulfo aluminate cements.

2.2 Efficiencies of Heat Recuperation and Scale

Since the 1960s, huge reductions in the unit energy consumption of cement production have been made through moves from the wet to dry process and through the installation of efficient heat exchange systems. By such methods, the heat consumption per tonne of clinker can be reduced by more than a factor of four. If heat recuperation is efficient the maximum temperature in the burning

[*] $\$ = SO_3$, otherwise conventional cement chemistry notation is used.

zone has little impact on overall energy consumption, as the heat input in this zone is recovered further back in the process.

Larger scale kilns are more efficient, with reduced heat losses and more stable operating conditions producing more regular products. Using waste materials as fuel has allows the effective energy consumption to be further reduced. Materials ranging from waste oils to industrial off-cuts of flammable materials (upholstery foam, packaging materials, wood, etc) have been successfully used in cement production. The temperatures occurring in the flame of a cement kiln (~2000°C) are much higher than those in incineration, destroying potentially dangerous organic materials.

Special cements are produced in much smaller quantities than Portland cements; this leads to enormous problems of producing them in large, efficient Portland kilns. For a major change in raw meal chemistry it may take several days to stabilise the production and only another few days to produce enough material for a year's consumption of a special clinker. This gives a very high ratio of poor quality to good quality material, which must be dealt with either through high wastage or more variable products.

2.3 Output of pollutants

As well as energy consumption and the related CO_2 emissions, attention must be paid to the emission of other volatile components. One of the most important elements in this respect is sulfur. Sulfur emissions from fossil-fuel fired power stations have been responsible for acid rain, although this problem is now being dealt with through flue gas desulfurisation (FGD). One of the most common forms of FGD is to inject calcite into the gas stream – this leads to the production of gypsum and the emission of CO_2. Cement plants already pay close attention to limiting sulfur emissions arising from the fuels used.

Special cements containing $C_4A_3\$$ require the presence of significant quantities of anhydrite or gypsum in the raw meal. Such increases in the sulfur content in the raw meal lead to higher emissions. The need to fit desulfurisation equipment would more than negate any marginal gains made by lowering firing temperatures in the production of calcium sulfo aluminate cements.

2.4 Impracticality of lower energy clinkers

For the reasons discussed above it is clear that novel low energy *clinkers* are not the way to produce lower energy cements. A much more realistic strategy is the one already being widely pursued, of mixing or intergrinding Portland clinker with the by-product materials of other industries, such as fly ash, slag and silica fume.

3. SPECIAL PROPERTIES – OVERCOMING THE LIMITATIONS OF PORTLAND CEMENTS

In terms of properties, the limitations to Portland cement arise from the way in which the microstructure forms during hydration. The major hydration product, C-S-H, is deposited as a layer around the reacting cement grains. This has three important consequences:

- **As soon as the reaction starts it retards further reaction**, this means that one needs to wait a considerable time for the service strength to be developed – at one day a typical concrete has only 25% of the strength it will have at 28 days. This is highly inefficient for the construction process and frequently results in concretes of higher than necessary strength being used in order to have adequate strength at early ages. This leads to higher than necessary cost and energy consumption. Such concrete with low water to cement ratio may also be more sensitive to early age cracking.

- **It is difficult to fill large pores**; these remain points of vulnerability to the ingress of substances that degrade the concrete. The only way to limit the presence of large pores is through the addition of finer materials such as silica fume. While bringing many advantages to concrete, such materials increase cost and complexity and may also have adverse effects on properties such as workability and shrinkage.
- **A significant amount of cement remains unhydrated**. Although this is wasteful of raw materials, the unhydrated material nevertheless has the advantage of acting as a hard filler material, which can improve mechanical properties.

The most advantageous properties of special cements are those that overcome these limitations of Portland cement:

- Rapid strength development after setting
- Infilling of porosity to improved resistance to chemical and mechanical attack

Another property often sought is:

- Compensation of shrinkage to avoid cracking.

However, this is very difficult to achieve reproducibly over practical temperature and humidity ranges, due to the different chemical and physical mechanisms involved.

4. PROPERTIES OF CALCIUM ALUMINATE CEMENT – AN EXAMPLE OF A SUCCESSFUL SPECIAL CEMENT

One of the first non-Portland cements to be developed was calcium aluminate cement. Many researchers developed versions towards the end of the 19th century, culminating in a viable means of industrial production patented by Bied in 1908. These cements have a radically different chemistry to Portland cements as shown in Figure 1.

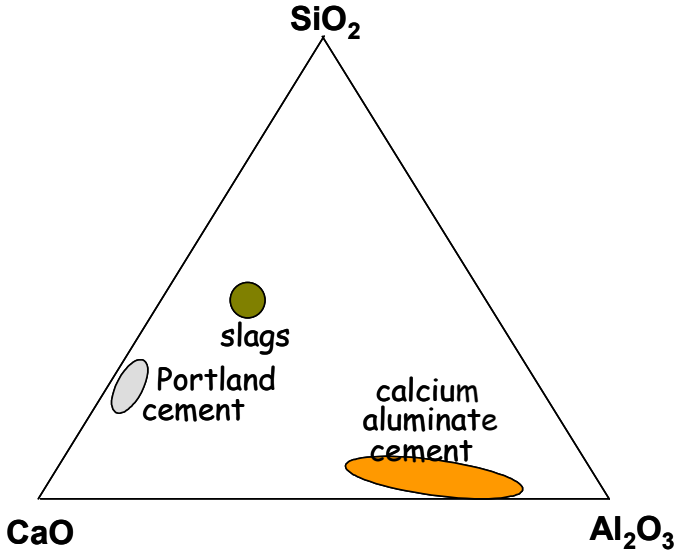

Figure 1. Composition ranges of Portland and Calcium Aluminate cements

There are three main areas of use of calcium aluminate cements today:

- Refractory concrete[†]
- As the main binder phase of special concretes
- As a component of formulated mixed binder systems with special properties.

[†] The field of refractory concretes is not discussed further here, as it is not related to application of special cements in construction.

This range of applications bears witness to the tremendous flexibility of calcium aluminate cements that, in different combinations with other materials, provide a wide range of properties. This flexibility is one of the critical factors for success as the sum of the materials used in the different applications provides a critical mass that can support the extra costs associated with small-scale production and need for specialist technical support.

In construction related applications, calcium aluminate cement produces radical changes in microstructure, which are responsible for many of the special properties discussed below:

- Rapid hardening of both pure and mixed binder systems
- Resistance to mechanical and chemical attack.

In addition mixed binder systems can be formulated to give shrinkage compensation.

4.1 Microstructural Development of Calcium Aluminate Cements and Rapid Hardening

The microstructural development of calcium aluminate cement is characterised by the deposition of the hydration products throughout the water filled space rather than around the reacting grains, Figure 1. It has been possible to observe this widespread nucleation directly in the X-ray microscope [1]. As hydration products do not block the surfaces of the reacting grains, the cement can continue to hydrate rapidly and it is possible to develop strengths of 20 MPa in 6 hours or less at a w/c of around 0.4.

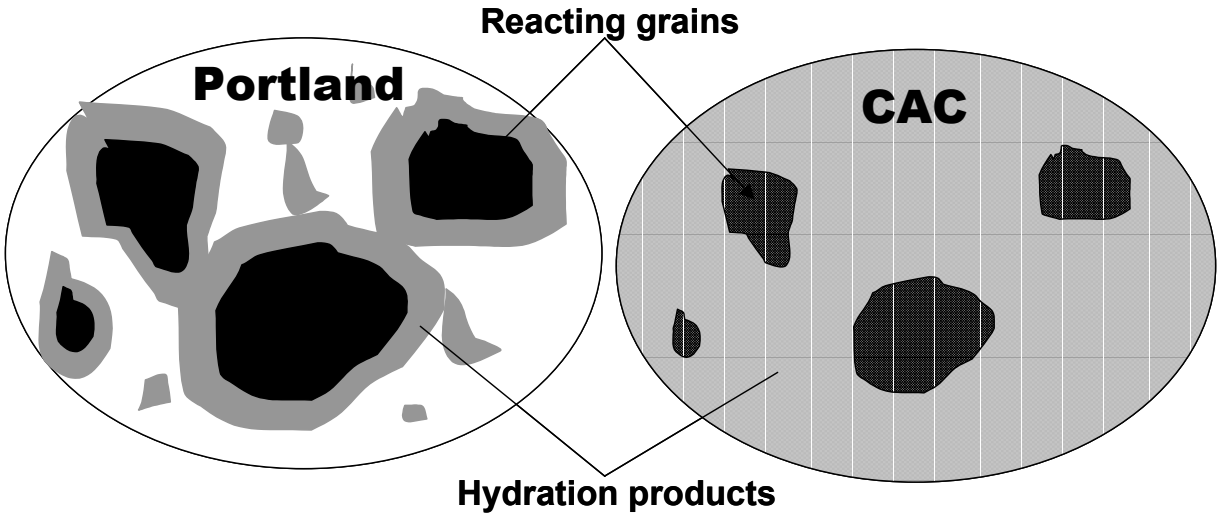

Figure 2. Schematic representation of the deposition of hydration products for the hydration of Portland and calcium aluminate cement.

In terms of strength development, the phenomenon of conversion must be taken into account. The hydrates that form initially at ambient temperature are meta-stable and transform over time to the stable hydrates – C_3AH_6 and AH_3. As the stable hydrates have a higher solid density, they occupy less space, so there is a lower volume of solid at the same degree of hydration. This results in a higher porosity and lower, but stable, strength. This stable long-term strength is slightly lower than that of Portland cement at the same water to cement ratio.

If the temperature of the concrete is maintained at or below 20°C during curing, then conversion may take several years to occur. However, for sections of any significant size, the heat generated during curing will be sufficient for temperatures of over 50°C to be generated in the concrete, which means that conversion occurs very rapidly (within the first day or so) and the strength development is essentially continually increasing (Figure 3).

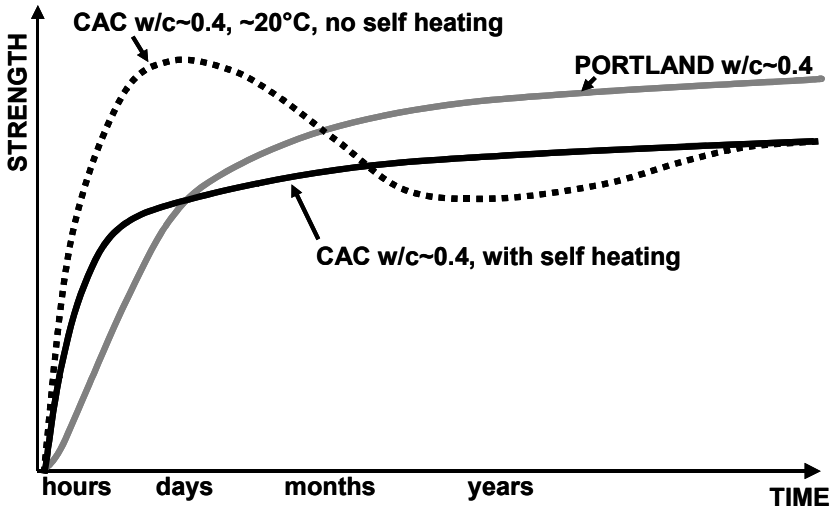

Figure 3. Schematic strength development of calcium aluminate cement concrete, with and without self-heating. With no self-heating the initial, very high strength, decreases on conversion to a lower, stable strength. In the more usual case, where self-heating occurs, no reversion of strength occurs after initial curing.

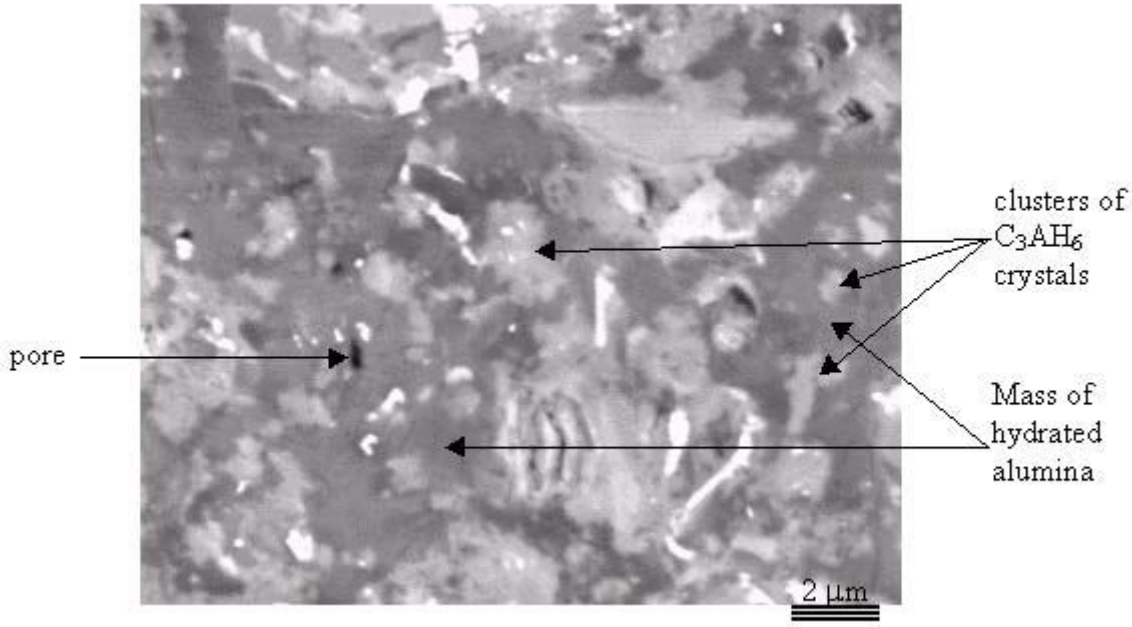

Figure 4. Microstructure of 30-year-old CAC concrete from structure (w/c ~0.4) - fully converted. A fine dispersion of C_3AH_6 (light grey) in a darker mass of hydrated alumina. There are very few, small isolated pores. The bright areas are unreacted iron rich anhydrous phases.

Even after conversion the impact of the mode of product deposition on the microstructure is apparent. Figure 4 shows the microstructure 30-year-old concrete. There is a low capillary porosity and these pores are small and isolated.

4.2 Other Special Properties of CACs as the Main Binder Phase in Concretes

In addition to rapid hardening, CAC concretes also have a number of other special properties which justify their use under certain conditions despite their high cost [2]. These include:

- High resistance to mechanical abrasion
- High resistance to chemical attack, particularly acidic conditions produced by bacteria
- High resistance to temperature extremes and thermal shock.

The abrasion resistance of CAC concrete is also related to their unique microstructure. The deposition of hydrates throughout space leads to a dense interfacial transition zone (ITZ) between cement paste and aggregate. Thus at the same strength, CAC concretes have 2 to 3 times the abrasion resistance of Portland concretes [3]. This leads to their use in dam spillways, motorway toll booths and industrial floors [4].

The use of CAC concrete for the lining of sewage networks is well established [4,5]. Here the action of the CAC is threefold:

- Down to pH4, resistance of alumina hydroxide to dissolution. This combined with the dense microstructure blocks penetration of the acid into the concrete.
- Below pH4, high neutralisation capacity of the alumina, which slows attack for a given amount of acid.
- Suppression of the activity of acid producing bacteria, which limits the pH produced on the surface of the concrete to just below 4, rather than 1 or less which occurs for Portland concretes.

In a field trial carried out in South Africa [6] sections made from Portland cement concrete with both siliceous and calcareous aggregates were so badly eroded after 12 years as to make the sewer unsafe. The section with Portland / siliceous aggregate had completed corroded through the 60 mm pipe thickness in places, while the section with Portland / calcareous aggregate had corroded to the level of the reinforcement. In contrast, the section made from CAC and siliceous aggregate showed only localised erosion to a depth of 10-15 mm, Figure 5.

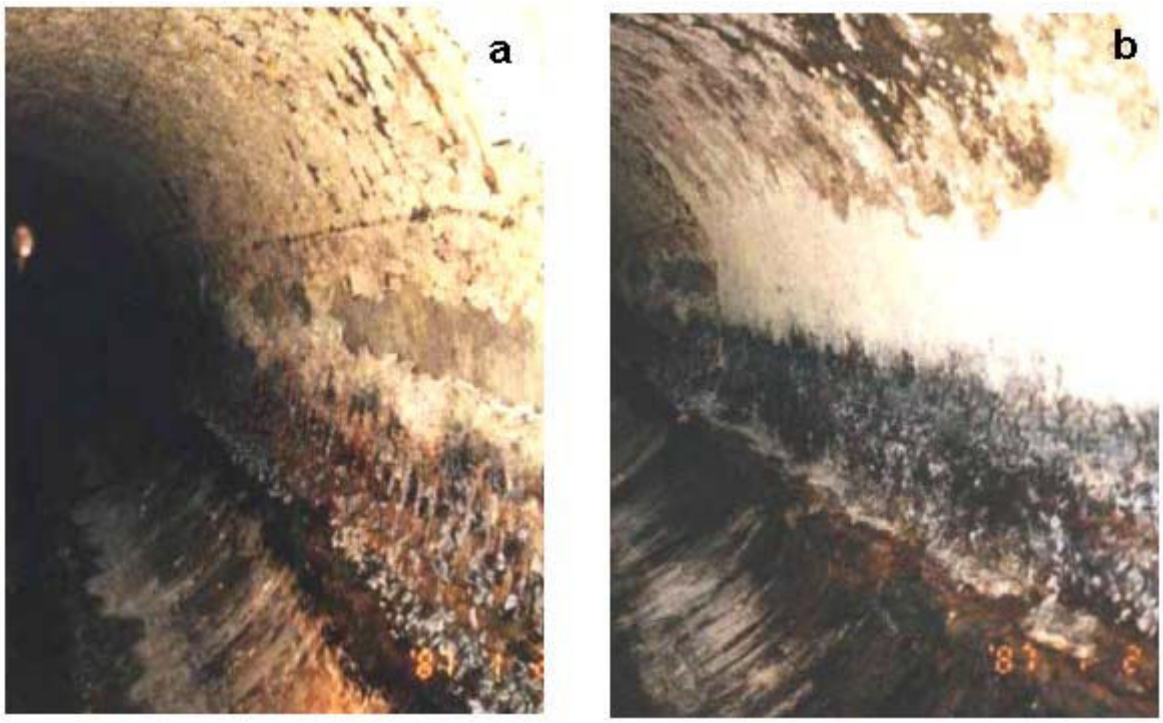

Figure 5. Sewage pipes after 12 year in a field trial in South Africa. The Portland/siliceous aggregate section (a) has completely eroded through its 60mm thickness in places. The CAC/siliceous aggregate section shows maximum erosion of 10-15 mm only at the water line.

The resistance of CAC concretes to temperature extremes and thermal shock is related to the nature of the hydrate phase, particularly the absence of calcium hydroxide. This feature leads to applications in foundry floor, cryogenic facilities and fire training buildings.

5. RAPID HARDENING AND EXPANSION IN ETTRINGITE FORMING SYSTEMS

Apart from uses of CAC as the sole binder phase in concretes, special cements with rapid hardening properties are mainly based on the formation of ettringite at early ages. Mixtures of CACs with Portland cement and calcium sulfate can also be made, which have such properties (Figure 6). Such cements can also be designed to expand during curing, to compensate drying shrinkage or give self-stressing.

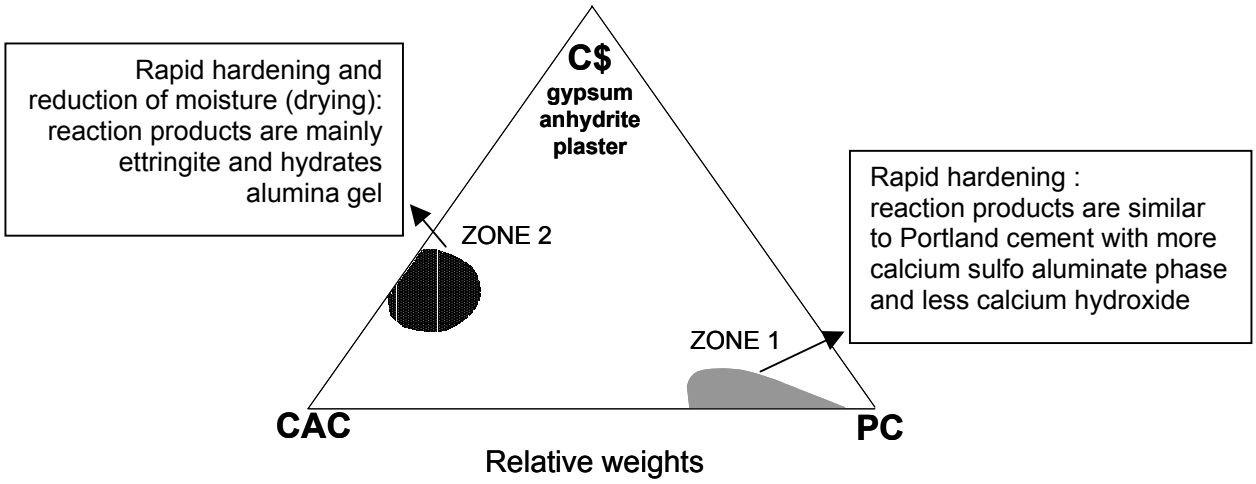

Figure 6. Formulation zones for mixtures of CAC, PC and calcium sulfate

As indicated by its characteristic morphology of hexagonal needles, ettringite is formed through solution:

$$6Ca^{2+} + 2Al(OH)_4^- + 3SO_4^{2-} + 4OH^- + 26H_2O \Rightarrow 3CaOAl_2O_3.3CaSO_4.32H_2O$$

ettringite, calcium trisulfoaluminate

Various different starting phases may provide the calcium, aluminate and sulfate ions to solution. The relative solubility and reactivity of these will control the rate, morphology and distribution of ettringite formation, which in turn determines the rate of setting and hardening, and whether expansion occurs

The usual sources of aluminate are either CA, from calcium aluminate cement or $C_4A_3\$$ from calcium sulfo aluminate cement (CSA). In both cases calcium sulfate, in the form of gypsum, anhydrite or hemi-hydrate (plaster of Paris), must be added. Although $C_4A_3\$$ also contains sulfate, the ratio of sulfate to aluminate ($\$/A = 0.33$) is very much lower than that in ettringite ($\$/A = 3$) and only transitory ettringite formation is seen in CSA cements without additions of calcium sulfate. Extra lime may come from added free or hydrated lime, or from the hydration of alite.

If the system is correctly formulated, ettringite forms throughout the water filled space, bridging the spaces between the hydrating cement gains and leading to rapid strength development. The large number of species involved in the reaction to form ettringite means that it is possible to adjust these to formulate systems with the desired properties in terms of setting and hardening. Similarly if the system is formulated so that ettringite formation continues once the paste has set and hardened, expansion and shrinkage compensation can be produced. The precise chemistry and physics of the various types of reaction are extremely complex and not well understood. At present, rapid setting and hardening, and expansive systems are designed empirically. Because of this it is important to have regular starting materials

6. CALCIUM SULFO-ALUMINATE CEMENT

Studies in the USA by Klein, in the 1950s, led to the development of Type K, or shrinkage compensating cements. The key compound in these cements is $C_4A_3\$$, also known as Klein's compound, present in amounts up to about 20%. Shrinkage compensating cements have been used successfully in concrete for a number of projects. However, due to their higher cost and the need to ensure wet curing over at least 7 days, they are now very little used. By adjusting the content of $C_4A_3\$$, free lime, added sulfate; related cements are now being sold as rapid setting (and hardening) cements. Due to the small quantities produced and the short setting times, it is difficult to produce such cements with consistent behaviour.

A different type of CSA is produced in China. Locally available, silicate rich bauxites, which are unsuitable for aluminium production, are fired with limestone and anhydrite to give cements essentially composed of $C_4A_3\$$ (60-70%) and belite (C_2S). According to the amount of gypsum, which is inter-ground, rapid hardening, shrinkage compensating and self stressing cements may be produced.

As described above the special properties of such cements arise from the formation of ettringite at early ages. Due to the many parameters that influence ettringite formation it is possible to obtain a range of properties by adjusting the exact formulation of the cement.

7. OTHER CONSIDERATIONS FOR SPECIAL CEMENTS

The practical use of special cements involves many other aspects of their performance, for example elastic modulus, creep, and toughness. Studies on CAC concretes [7] have indicated that these properties are correlated with compressive strength in a very similar manner to Portland cement concrete. This suggests that porosity is the primary factor controlling mechanical properties and the precise nature of the hydrate phases is of secondary importance. Nevertheless lack of data on the properties and performance of concrete made with special cements is another barrier to their use.

Experience with special cements shows that, like Portland cements, the control of water to cement ratio is the key to good performance. Rheological properties are important and the interactions of special cements with admixtures must be considered.

8. CO_2 EMISSIONS

Due to the high volumes produced, the manufacture of cement makes a significant contribution to CO_2 emissions. For every tonne of cement, roughly 1 tonne of CO_2 is emitted. About half of this comes from the fuel used and the other half from the decomposition of the calcareous part of the raw meal. Thus the quantity of CO_2 emitted is directly related to the CaO content of the clinker.

The CaO content of Portland type cements is around 60-65% and on a molar basis CaO constitutes ¾ of the main reactive phase C_3S. In CAC or CSA cements the reactive phases contain only ½ in their reactive phases (CA or $C_4A_3\$$) is CaO. So the overall CaO content of the clinkers is lower – in the range 40 – 60 %. This gives the potential to reduce the chemical decomposition part of CO_2 emissions by up to 30%. Although this reduction is significant, the overall reduction would be reduced, by lower efficiency, higher fuel consumption and transport. Larger reductions in CO_2 are possible through the incorporation of supplementary cementitious materials into cement, reducing its clinker content.

9. CONCLUSIONS

- The viability of special cements lies in their ability to provide properties not obtainable with Portland cement. For example:
  - Accelerated hardening;
  - Increased resistance to degradation in aggressive conditions.
- Given the constraints of raw material location and the current level of optimisation of Portland production in terms of heat recovery and scale; it is not plausible to imagine that new clinkers can provide cements with lower energy consumption. This objective must be obtained through further advances in blending Portland cement clinker with by-product materials.
- Calcium aluminate cements are one of the most successful special cements, due their particular properties that allow a wide range of applications.

REFERENCES

[1] Lamour, V.H.R., Monteiro, P.J.M., Scrivener, K.L. and Fryda, H., Microscopic studies of the early hydration of Calcium Aluminate Cements, pp199-213 in Proc. 2nd Int. Conf. of Calcium Aluminate Cements, ed. R.J. Mangabhai, Edinburgh 2001

[2] Scrivener, K.L. and Capmas, A. Calcium Aluminate Cements, pp 709-778 in "F.M. Leas's Chemistry of Cement and Concrete", 4th ed. ed. P.J. Hewlett, Arnold, London, 1998

[3] Saucier, F., Scrivener, K.L., Hélard, L., Gaudry, L. Calcium Aluminates Cement based Concretes for Hydraulic Structures: Resistance to Erosion, Abrasion & Cavitation, in Proc. 3rd Int. Conf. Concrete in Severe Conditions: Environment and Loading, CONSEC'01 Vancouver, Canada, June 2001, Vol II pp1562-1569

[4] Scrivener, K.L., Cabiron, J-L. and Letourneaux, R. High Performance Concrete based on Calcium Aluminate Cements Cem. Concr. Res., 29, 1999, 1215-1223,

[5] Letourneux, R. and Scrivener, K.L. : The Resistance of Calcium Aluminate Cements to Acid Corrosion in Wastwater Applications, in Dhir R.K. and Dyer, T.D. (eds) *Modern Concrete Materials: binders additions and admixtures,* Thomas Telford, London, 1999 pp275-283

[6] Goyns, A.. Calcium Aluminate Limings for Cost-Effective Sewers, in Mangabhai, R.J. and Glasser, F.P. (eds) *Calcium Aluminate Cements 2001*, IOM communications 2001, London pp617-631

[7] Lamour, V.H.R., Monteiro, P.J.M. Scrivener, K.L. and Fryda, H. : Mechanical properties of Calcium Aluminate Cement concretes, in Mangabhai, R.J. and Glasser, F.P. (eds) *Calcium Aluminate Cements 2001*, IOM communications 2001, London 199-213

PREDICTION OF MICROSTRUCTURE AND PROPERTIES OF PORTLAND CEMENT FROM PRODUCTION CONDITION IN CEMENT MILL
PART I: EVALUATION OF THE PREDICTION MODELS

K. Svinning[1] and K. A. Datu[2]

[1]NORCEM A/S, R&D Department, Brevik, Norway. E-mail: Ketil.svinning@norcem.no
[2] Mule, Porsgrunn, Norway.

ABSTRACT

The influence of production conditions in a cement mill on the microstructure and properties of rapid hardening Portland cement has been statistically investigated. In addition, the influence of the microstructure on the properties has been investigated. Properties being examined were water content required to achieving standard consistency, setting time and compressive strength at one day. Except for particle size distribution of cement, partial least square regression gave maximum explained variance in the cement properties and superficial microstructures of cement from 54 to 73 %. As low as 27 % explained variance in particle size distribution will make the prediction from the characteristics of this part of the microstructure too inaccurate.

1. INTRODUCTION

Since 1991 a general investigation of microstructure of clinker and cement has been carried out as part of several successive projects at the cement producer Norcem A/S.

More recently, the investigations have been organised in the three following subprojects:
1. Influences of the production conditions in the kiln and the cement mill on the microstructure of clinker and cement
2. Influences of the microstructure of clinker and cement on the cement properties
3. Establishment of models describing the influences of the production conditions in the kiln and the cement mill on the cement properties

Results from the previous investigations are presented by Svinning *et al.* [1] and [2], Svinning and Bremseth [3] and Svinning and Justnes [4].

In this paper the investigation on the influence of production condition in cement mill on the microstructure and properties of the Portland rapid cement is presented. In addition, the influence of the microstructure on the properties has been examined.

Properties being examined are as follows:
1. Water content required to achieve standard consistency.
2. Setting time.
3. Compressive strength at one day.

The properties: Setting time and compressive strength form together with fineness and soundness the basis of all specifications for cement. Therefore, a large number of papers on investigations of

correlation between the characteristics of cement and these two properties have been published. Some characteristics variables, which were reported by Lea [5] to have major impacts on setting time and which indicate the production conditions in a cement mill, are fineness, amount of di- and hemihydrate of $CaSO_4$ and aeration of cement. Assuming the amounts and structures of the clinker to be rather constant, the clinker quality is described by its component composition only. However, the pronounced influence of free lime on setting time as earlier reported in [3] and [4], makes it appropriate to include the amount of free lime as a variable in the investigations. The determination of setting time is affected to a marked degree by the quantity of water used in gauging. This water is required to be that necessary to bring the cement paste to a defined consistency. The variable: Water content required to achieving standard consistency (SC) is defined to be a response variable in this work but at the same time could be regarded as an input x-variable in the investigation of the y-variable: Setting time. SC indicates the flow behaviour of cement pastes. According to Mork [6], the more hemihydrate the better are the rheological properties over time, except initially, where the highest gypsum content gives the best rheological properties. In this connection the degree of dehydration of gypsum during grinding will be focused on and, likewise, how process conditions influence the degree of dehydration.

In this work the microstructure is defined to be particle size distribution and superficial microstructure describing the degree of prehydration of the clinker minerals and the degree of dehydration of gypsum. The superficial microstructure is characterised by thermogravimetric analysis (TGA). The correlations between the groups of variables describing production condition, microstructure and properties, respectively, were determined by application of partial least square regression (PLS).

The presentation of this work will be divided into the two following parts: Part I: Evaluation of the prediction model, and Part II: Prediction and sensitivity analysis [7]. The major part of the discussion of the results will be in Part II.

2. METHODS

2.1 Characterisation of superficial microstructure

As mentioned above, the superficial microstructure is characterized by thermogravimetric analysis (TGA). The apparatus used was a Netzsch STA – Apparatur 409 V/3/C®. A dynamic mode of thermogravimetry is used, in which the sample is heated in an environment whose temperature is changing in a predetermined manner, preferably at a linear rate. 4,2g of sample were analysed and the heating rate was 2°K/min. Limited space in the furnace due to the large amounts of samples restricted the measurement of temperature to that of the sample only. A more correct temperature measurement, to which the various mass losses are referred, should be that of an inert reference placed right beside the sample in the furnace. Due to the large volume of sample being analysed, the reaction involving mass loss of larger quantities of H_2O and CO_2 is partly diffusion controlled. The position [ºC] of a respective DTGA (the differentiate form of TGA) –peak will be at a higher temperature with an increase in the amount of the compound being dehydrated or decarbonised. The position of the peak could also depend on the fineness of the compound. Figure 1 shows two examples of thermograms from DTGA of neat cement and cement with limestone used as filler, respectively. The thermograms are interpreted with respect to the most common reactions occurring during the heating.

The information on the superficial microstructure is included as x- or y-variables in PLS in the form of mass loss per 4°C in the temperature range 20 - 330°C and mass loss per 8°C in the range 330 - 940°C. No further interpretation of results from TGA, or to be more correct, from DTGA prior to PLS was done. Qualitative interpretation of the thermograms will, however, be an important part of the discussion of the results in Part II of this work.

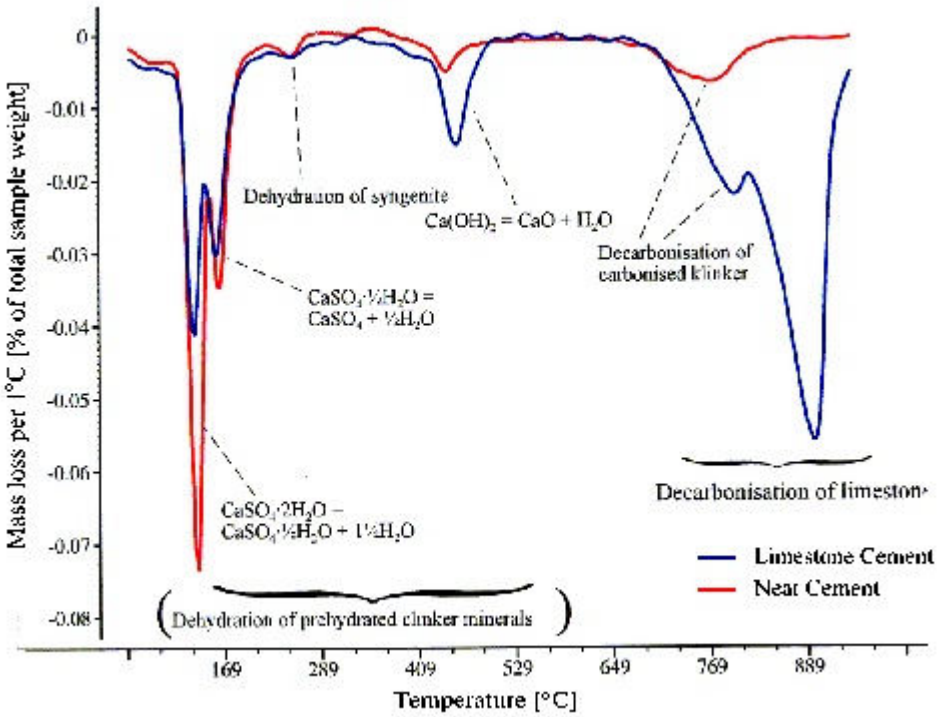

Figure 1. Two examples of thermograms from DTGA of neat cement (red line) and cement with limestone filler (blue line), respectively.

2.2 Statistical modelling

In the case of a large number of variables relative to number of observations or objects, data compression by expressing the original x - variables by fewer latent variables or factors could be necessary. Partial least square regression (PLS) does calculations and optimisation of a number of factors for maximum explanation of variance in the y-variables. In addition, model parameters are calculated for prediction of y for new values of the x-variables. In this work PLS of several y-variables together expressed as a vector of several y-variables, are performed. The models which relate the PLS model terms, are then given by the two expressions in the equations below:

$$\mathbf{X} = \mathbf{T}\mathbf{P}^T + \mathbf{E} \tag{1}$$

$$\mathbf{Y} = \mathbf{U}\mathbf{Q}^T + \mathbf{F} \tag{2}$$

T and **U** are factor scores, **P** and **Q** are x and y variables loadings and **E** and **F** are the residuals in **X** and **Y**, respectively. Alternatively, equation 1 could be expressed in the form:

$$\mathbf{X} = \mathbf{t}_1\mathbf{p}_1^T + \mathbf{t}_2\mathbf{p}_2^T + .. + \mathbf{t}_k\mathbf{p}_k^T + .. + \mathbf{t}_l\mathbf{p}_l^T + \mathbf{E}$$

Where l is equal to maximum number of latent variables for maximum explanation of variance in **Y**. In case of only one y-variable to be modelled (equation 2) could be replaced by the following equation:

$$\mathbf{y} = \mathbf{T}\mathbf{q}^T + \mathbf{f}$$

PLS with respectively one and several y-variables are denoted PLS1 and PLS2.

By scaling the variables, unreasonable dominance of variables with dominating standard deviations, s(x), on the model can be avoided. The centring and scaling of $x_{i,j}$ is performed according to the following formula:

$$x_{ij,\,centred\ and\ scaled} = \frac{x_{ij} - \bar{x}_j}{s(x_j)} \tag{3}$$

The iterative algorithms for calibration, validation and prediction are described in detail in Martens and Næs [8]. The software applied for PLS was UNSCRAMBLER ®, version 7.5.

3. DESCRIPTION OF THE CEMENT MILL

The location of the cement mill being examined is Dalen Plant, Norcem A/S in Brevik, Norway. The cement mill is of the two-chambers Combidan ball mill type. The mill system with a classifier, dust filter and the silos and feeding system is shown in Figure 2. The classifier is an FLS-SEPAX® separator type 400-2s. The finished product leaves the separator at the top and is deposited in a set of four cyclones. During the production it is possible to intergrind iron(II)sulphate for dechromatising or reduction of Cr^{6+} in clinker, and limestone as a supply of filler, in addition to clinker and gypsum. The limestone filler being fed into the mill had a sieve residue of approximately 14 % at 90 µm. Internal water sprays can be used at both the inlet and outlet ends of the mill. The location of sampling of the cement is right after the cement cooler. The grinding aid used was of the type Technochem TC-84 N, which contains aliphatic amine acetate diluted in water (21 % conc.).

4. EXPERIMENTAL

The experiments were carried out in two stages. In the first stage experiments with 2^3 factorial designs with three variables and two levels were performed. Actual variables chosen were Blaine, amount of limestone, temperature of cement leaving the mill (TC), amount of gypsum, amount of water sprayed into the mill at the inlet (AW) and amount of grinding aid. Performing 3 experiments with 2^3 factorial designs give 24 observations. Each observation contains the value of each of the 24 process variables, averaged over one hour, and results of the characterisation and tests of the sample of the cement of 10 kg being sampled during the last 15 minutes of this hour. The following three variation of the respective three variables (abbreviation as explained above): determinations were undertaken to investigate

1. Blaine, amount of limestone, temperature of the cement (TC)
2. Blaine, amount of gypsum, amount of water into the mill (AW)
3. Blaine, amount of limestone, amount of grinding aid.

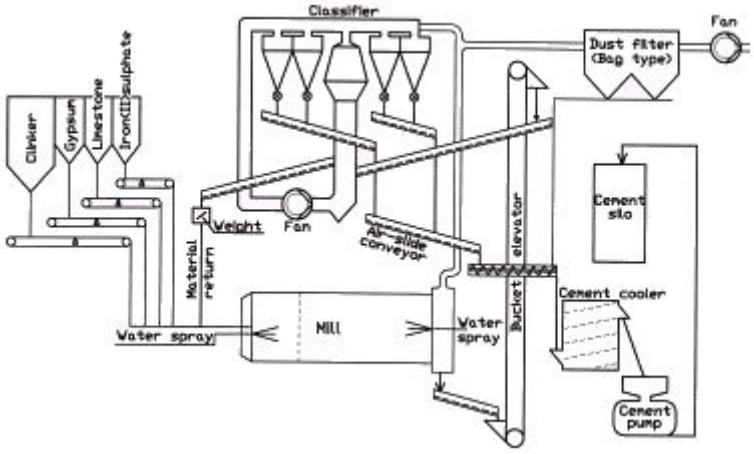

Figure 2. A schematic figure of the cement mill

There are at least two purposes for testing using factorial design. The first one is the possibility of calculation of the impact or effect of the respective variables being varied, and additional interactive effects on the response variable as cement properties and microstructure. The calculation of effects is described by Box *et al.* [9] among others. The second and a more significant reason for this type experiment is an achievement of a better span of the observed **X**-space. The calculations of effects after each factorially designed experiment were skipped to the benefit of PLS at the end with all the relevant variables and available observations included.

In the second stage more occasional observations with respect to process condition were collected, this to increase the total number of observations to be included in PLS.

5. RESULTS AND DISCUSSION

5.1 General

In the following chapters results from three independent PLS analyses are presented:

1. PLS1 (one y-variable at a time) of cement properties as a function of process conditions in the cement mill
2. PLS1 of cement properties as a function of microstructure of cement.
3. PLS2 (several y-variables together) of microstructure of cement as a function of process conditions in the cement mill

5.2 PLS of cement properties as a function of production conditions in the cement mill

The maximum explained variance from PLS of the respective y- variables and the number of PLS-components included for maximum explanation are presented in Table 1. The mean values and standard deviation of the production x-variables included in the PLS for prediction of water content required to achieve standard consistency, setting time and compressive strength at one day are presented in Table 2. The number of observations included was 50.

Table 1. Results from PLS of cement properties as functions of production conditions in the cement mill.

Response variable, y	Maximum explained variance [%]	The number of PLS-components or latent variables
water content required to achieving standard consistency	66	2
Setting time	66	4
compressive strength at one day	54	3

The regression coefficients $\mathbf{b}_w$: $b_{w1}, b_{w2}, \cdots, b_{wn}$ applied in model $y = b_{w1}x_1 + b_{w2}x_2 + \cdots + b_{wn}x_n$ from PLS with centred and scaled data for the three variables are presented in Table 2. The elements in $\mathbf{b}_w$, contrary to respective elements in **b** used for prediction from the x-variables in their original forms, *i. e.* neither centred nor scaled, give the information about by how much each x-variables influences the y-variable.

Table 2. Variables included in PLS, mean values and standard deviations. Regression coefficients, $\mathbf{b}_w$, from PLS of setting time (ST), water content to achieve standard consistency (SC) and compressive strength at one day (CS) with weighted data.

Variables	Mean value	Standard deviation	Regression coefficients, $\mathbf{b}_w$		
			ST	SC	CS
x-variables					
1. Feed of clinker [tonnes/h]	14.3	1.6	0.153	-0.066	-0.133
2. Feed of gypsum [tonnes/h]	0.62	0.13	0.010	0.010	0.253
3. Feed of iron(II)sulphate [tonnes/h]	0.045	0.014	0.111	-0.106	-0.089
4. Feed of limestone [tonnes/h]	0.26	0.31	0.120	-0.011	-0.036
5. Total feed [tonnes/h]	65.8	2.4	0.138	0.096	-0.061
6. Amount of water sprayed into the first chamber [l/h]	223	239	0.112	-0.201	-0.137
7. Amount of water sprayed into the second chamber [l/h]	649	230	-0.196	0.143	-0.029
8. Pressure at inlet of the mill [mbar]	-0.26	0.10	-0.051	-0.002	-0.099
9. Pressure at outlet of the mill [mbar]	-5.06	0.73	0.012	0.068	-0.043
10. Temperature of cement out of the mill [°C]	113.4	4.4	0.067	0.060	0.163
11. Rotor speed, classifier [rev./min]	379	15	-0.054	0.105	0.116
12. Effect for driving the rotor [kW]	51.2	6.4	-0.037	0.074	-0.042
13. Material return from classifier [tonnes/h]	50.43	3.08	0.022	0.092	0.042
14. Ampere, fan for closed-circuit transportation of air through the classifier [A]	182.1	13.1	0.012	-0.061	-0.069
15. Pressure of air before passing the dust filter [mbar]	-5.72	0.97	0.223	0.079	0.018
16. Pressure of air after the dust filter [mbar]	-14.9	1.8	0.195	0.019	0.040
17. Ampere, fan after the dust filter [A]	49.6	1.1	0.014	-0.051	0.086
18. Temperature, cement after the dust filter [°C]	84.58	4.21	-0.138	0.055	0.078
19. Temperature, cement before the cement cooler [°C]	79.3	4.6	-0.069	0.050	-0.074
20. Temperature, cement after the cement cooler [°C]	78.0	10.8	0.067	0.015	-0.096
21. Feed of grinding aid [ml/min]	488	110	0.414	-0.010	-0.022
22. Pressure [mbar] for regulating the ratio: Amount of air through the classifier : - through the dust filter	-2.96	0.10	0.131	-0.025	-0.025
23. Ampere, elevator [A]	45.2	1.6	0.011	0.156	-0.154
24. Effect, motor for driving the ball mill [kW]	1038	15	0.033	-0.047	-0.199
25. Effect, all the other motor in the mill system [kW]	153	35	-0.196	-0.019	0.040
26. Total effect, electrical consumption [MW]	1.846	0.208	-0.319	-0.051	-0.211
27. Total production [tonnes/h]	15.28	1.69	-0.192	-0.031	-0.073
28.The degree of material load [%]	52.10	20.41	-0.050	-0.094	0.040
29.SO3 [%]	3.37	0.35	0.094	0.075	0.348
30.Carbon [%]	0.19	0.19	0.168	0.001	0.010
31.Free CaO [%]	1.43	0.27	-0.304	-0.050	-0.061
32.Loss on ignition [%]	1.65	0.48	0.184	-0.069	-0.009
33.SiO2 [%]	19.60	0.28	-0.085	0.005	0.001
34.Al2O3 [%]	4.85	0.13	0.085	0.085	-0.099
35.Fe2O3 [%]	3.25	0.08	0.033	-0.065	0.003
36.CaO [%]	61.93	0.64	-0.050	-0.018	0.147
37.MgO [%]	2.74	0.07	-0.043	0.031	-0.244
38.K2O [%]	1.21	0.07	-0.049	0.038	-0.054
39.Na2O [%]	0.35	0.07	-0.087	0.056	0.043
40.Temperature, clinker [°C]	85.2	18.2	-0.183	-0.010	-0.126
y-variables:					
1. Setting time [min]	101	16			
2. Water content required to achieving standard consistency [%]	31.5	0.8			
3. Compressive strength at 1 day [MPa]	33.3	2.6			

5.3 PLS of cement properties as a function of microstructure of cement.

The following data describe or indicate microstructure:

- Mass losses per 4 ºC from DTGA in the region 85 – 217 ºC
- Particle size distribution, volume fraction, 32 size classes between 103 and 0.7 μm

- Mass losses per 8 ˚C from DTGA in the region 324 - 524ºC.
- Mass losses per 8 ˚C from DTGA in the region 604 – 946ºC

The total number of x-variables included in the PLS was 141. As mentioned in the introduction the clinker quality is included in PLS as variables representing the chemical bulk composition and free lime. The maximum explained variance from PLS of the respective y- variables and the number of PLS-components included for maximum explanation are presented in Table 3. Figure 3 shows the structure of the PLS-modelling; the variation in the respective group of variables presented in the list above. Figure 4 shows regression coefficients of the PLS for prediction of the three cement properties. Table 4 contains regression coefficients for the variables describing the chemical composition included in the same PLS-models.

Results from PLS confirms the results in Section 5.2 about the large influence of free lime on setting time and the compressive strength being more influenced by the chemical composition than the production conditions in the cement mill.

Table 3. Results from PLS of cement properties as function of the microstructure of cement

Response variable, y	Maximum explained variance [%]	The number of PLS-components or latent variables
Water content required to achieving standard consistency	54	3
Setting time	61	4
Compressive strength at one day	64	10

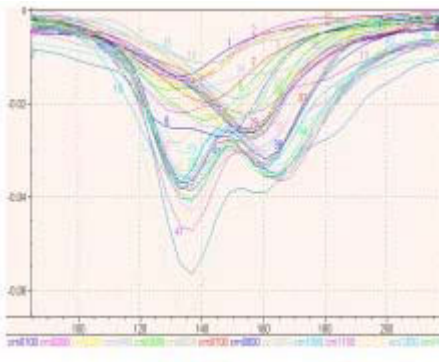

I. Mass losses per 4 ºC from TGA in the region 85 – 217 º

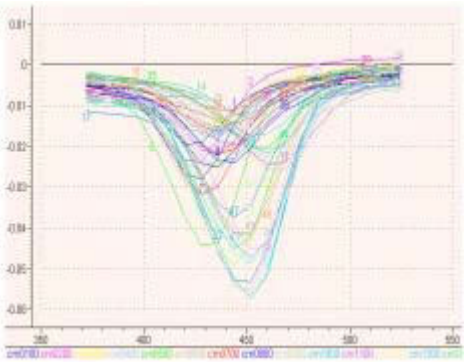

III. Mass losses per 8ºC from TGA in the region 324 - 524ºC.

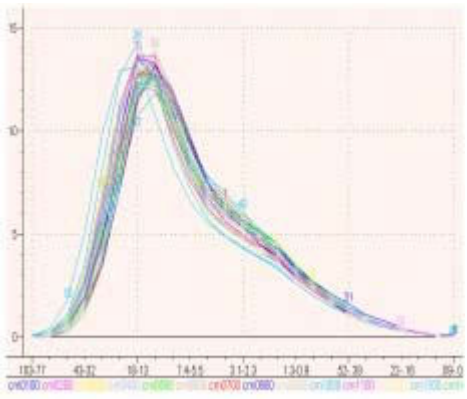

II. Volume fractions of cement in 32 size classes between 103 and 0.7 µm

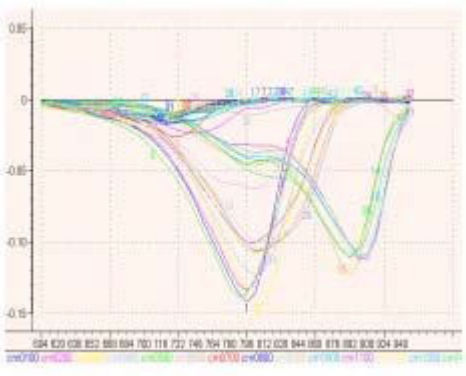

IV. Mass losses per 8ºC from TGA in the region 604 – 946ºC

Figure 3. The structure of the PLS-modelling of Cement properties as a function of microstructure of cement; variation in the x-variables describing the microstructure, regression coefficients, $\mathbf{b}_w$, for prediction of setting time.

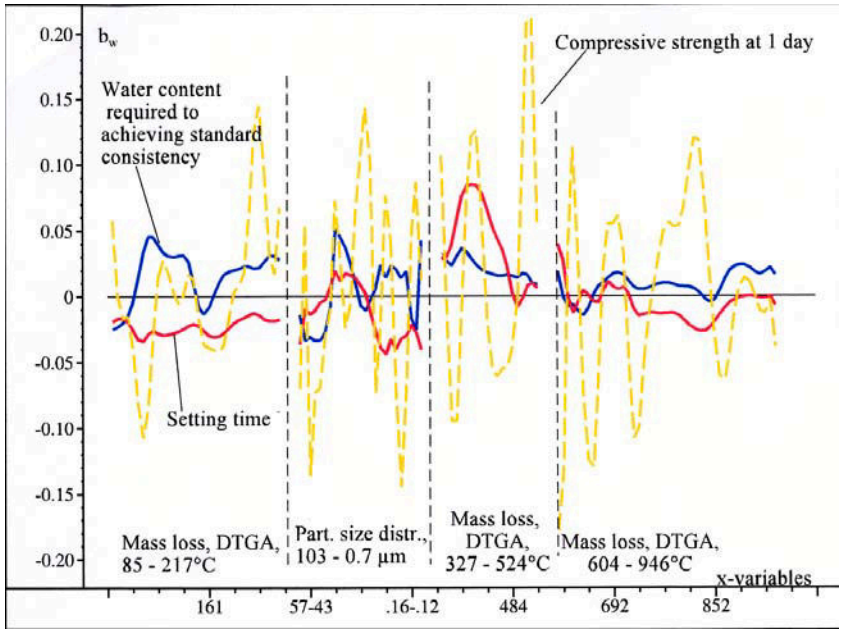

Figure 4. Regression coefficients, $\mathbf{b}_w$, for prediction of water content required to achieve standard consistency, setting time and compressive strength at one day from microstructure of cement.

Table 4. Regression coefficients, $\mathbf{b}_w$, for the variables representing the chemical composition part of the microstructure for prediction of setting time (ST), water content to achieve standard or normal consistency (NC) and compressive strength at one day (CS).

Variables	Mean value	Standard deviation	Regression coefficients, $\mathbf{b}_w$		
			ST	SC	CS
x-variables					
29.SO3 [%]	3.37	0.35	0.024	0.075	0.520
30.Carbon [%]	0.19	0.19	0.021	0.001	0.028
31.Free CaO [%]	1.43	0.27	-0.668	-0.050	-0.017
32.Loss on ignition [%]	1.65	0.48	0.103	-0.069	-0.002
33.SiO2 [%]	19.60	0.28	0.030	0.005	-0.042
34.Al2O3 [%]	4.85	0.13	0.002	0.085	-0.120
35.Fe2O3 [%]	3.25	0.08	-0.008	-0.065	0.003
36.CaO [%]	61.93	0.64	-0.008	-0.018	0.216
37.MgO [%]	2.74	0.07	-0.006	0.031	-0.293
38.K2O [%]	1.21	0.07	-0.014	0.038	-0.100
39.Na2O [%]	0.35	0.07	0.016	0.056	0.151
y-variables:					
1. Setting time [min]	101	16			
2. Water content required to achieve standard consistency [%]	31.5	0.8			
3. Compressive strength at 1 day [MPa]	33.3	2.6			

5.4 PLS of microstructure as a function of production conditions in the cement mill

The parts of microstructure, **y**, being modelled are presented in section 5.3 and the variations in Figure 3. The production x-variables included in PLS are presented in Table 2. The maximum explained variance from PLS of the respective groups of y-variables and the number of PLS-components included for maximum explanations are presented in Table 5.

Table 5. Results from PLS of microstructure of cement as functions of production condition in the cement mill.

Group of response variable, **y**	Maximum explained variance [%]	The number of PLS-components or latent variables
Mass losses per 4 ºC from DTGA in the region 85 – 217 ºC	73	6
Volume fractions of cement in 32 size classes between 103 and 0.7 μm	27	5
Mass losses per 8ºC from DTGA in the region 324 - 524ºC.	63	6
Mass losses per 8ºC from DTGA in the region 604 – 946ºC	59	3

The large number of regression coefficients from PLS2 (regression of several y-variables together) makes a simple presentation of the coefficients in Part I of this work difficult. Therefore, parts of regression matrices $\mathbf{B}_w$ will be presented in Part II: Prediction and sensitivity analysis. The low maximum explained variance in the particle size distribution of only 27 % does not justify further attention being given to the PLS-model on this issue in Part II. The explained variance in particle size distribution makes the prediction of this part of the microstructure too inaccurate.

6. CONCLUSION

Except for particle size distribution of cement partial least square regression gave maximum explained variance in the cement properties and superficial microstructures of cement from 54 to 73 %.

REFERENCE

[1] Svinning, K., Justnes, H., Viggh, E., Bremseth, S. K. and Johansson, S.-E. Examination of clinkers from four Scandinavian Plants with respect to microstructure and cement properties, 22nd international conference on cement microscopy, Montreal 2000, pp. 137-153

[2] Svinning, K., Bremseth, S. K. and Justnes, H., X-ray diffraction studies on variations in microstructure of Portland clinker correlated with variations in production conditions in the kiln, World Cement, 1996, pp. 80-86

[3] Svinning, K. and Bremseth, S. K., The influence of microstructure of clinker and cement on setting time and strength development until 28 days, 18th international conference on cement microscopy, Houston 1996, pp. 514-513.

[4] Svinning, K. and Justnes, H., Application of partial least square regression analysis in examination of correlations between production conditions, microstructure of clinker and cement and cement properties, 10th international congress on the chemistry of cement, Gothenburg 1997, li038, 8 pp

[5] Lea F. M., The chemistry of cement and concrete, 3rd edition, Surrey: Edvard Arnold Ltd. 1970, pp 297-298

[6] Mork, J. H., Effekt av sementens forhold mellom gips og hemihydrat på den ferske betongens reologi, Doktor ingeniøravhandling 1994:4, NTH, Institutt for bygningsmateriallære, Trondheim

[7] Svinning, K., Datu, K. A., Prediction of microstructure and properties of Portland Cement from production condition in cement mill. Part II: Prediction and sensitivity analysis, 11th international congress on the chemistry of cement, Durban 2003, (to be submitted?!)

[8] Martens, H., Næs, T., Multivariate calibration, 2nd edition, Chichester: Wiley 1989

[9] Box, G. E. P., Hunter, W. G., Hunter, J. S., An introduction to design, data analysis, and model building, New York: Wiley 1978

PREDICTION OF MICROSTRUCTURE AND PROPERTIES OF PORTLAND CEMENT FROM PRODUCTION CONDITION IN CEMENT MILL
PART II: PREDICTION AND SENSITIVITY ANALYSIS

K. Svinning[1] and K. A. Datu[2]

[1]NORCEM A/S, R&D Department, Brevik, Norway. E-mail: Ketil.svinning@norcem.no
[2]Mule, Porsgrunn, Norway.

ABSTRACT

The influence of production conditions in a cement mill on the microstructure and properties of rapid hardening Portland cement has been statistically investigated by application of partial least square analysis. In addition, the influence of the microstructure on the properties has been investigated. Properties being examined were water content required to achieving standard consistency, setting time and compressive strength at one day. Sensitivity analysis by predictions from simulated variation of single x-variables and latent variables has been performed. Special attention has been paid to the influence of water sprayed into the first and second chamber, respectively, of the cement mill on the dehydration of gypsum and prehydration of clinker minerals and further the influence on the cement properties. The influence of grinding aid on the fineness of limestone filler was also examined.

1. INTRODUCTION

To enable statistical investigations of the influence of production conditions in a cement mill on the microstructure and properties of rapid hardening Portland cement prediction models have been evaluated. The models are presented in Part I of this work [1]. In more details, partial least square regression (PLS) -models for prediction of dependant y- or group of y-variables from the following x-variables have been evaluated:

Cement properties:

- Water content required to achieving standard consistency predicted from
- Setting time
- Compressive strength

  All the three properties predicted from:
  - Production condition in the cement mill
  - Microstructure of cement

Microstructure of cement:

- Superficial microstructure from DTGA (85 – 217 °C), describing mainly the degree of dehydration of gypsum but also prehydration of clinker minerals
- Particle size distribution of cement
- Superficial microstructure from DTGA (324 – 524 °C), describing mainly the degree of prehydration of free lime
- Superficial microstructure from DTGA (604 – 946 °C), describing the degree of carbonation of clinker and the amount of limestone used as filler

  All the four parts of the microstructure predicted from:
  - Production condition in the cement mill

The location of the cement mill being examined with respect to how production conditions influence properties and microstructure, is Dalen Plant, Norcem A/S in Brevik, Norway. The cement mill is of the two-chambers Combidan ball type mill.

Except for particle size distribution of cement, partial least square regression gave maximum explained variance in the cement properties and superficial microstructures of cement from 54 to 73 %. Prediction from this part of the microstructure as low as 27 % explained variance in particle size distribution will make the too inaccurate.

The objective with sensitivity analysis is interpretation of a complex statistical model as for example PLS with respect to how much and in what direction a x- variable or selection of x-variables influences y. The type of sensitivity analysis applied is the same as used by Svinning *et al.* [2]. Here the sensitivity analysis is defined as examination of the predicted effect of an x-variable or a latent variable on the response y-variable relative to a defined confidence range of the predicted y. In addition, uncertainty testing on the regression coefficient can be performed. Martens *et al.* [3] have developed an improved method for uncertainty testing based on cross validation, Jack-knifing and stability plot. The method is included as an application in the Unscrambler® software, version 7.5.

2. METHODS

2.1 Sensitivity analysis of PLS models

Based on PLS-models as for example those given in [1], the influence of x-variables on the y-variable(s) may be evaluated in different ways [2]:

- Comparison of the regression coefficients of the different variables from PLS with centred and scaled data. Significance testing on the coefficients by application of Jack-knifing [3] with confidence interval of 0.95. Examples are shown in Figure 1.
- Prediction of variation in y including confidence intervals equal to $\hat{y} \pm s(y)$, from variation of one or several collinear x-variables while the others are kept constant and equal to their respective mean values. The region of variation in this work was limited to $\bar{\bar{x}}_j \pm 1.5 s(x_j)$. Examples are shown in Figures 2 and 3.
- Prediction of variation in y or $\mathbf{y}$ as a result of variation in one latent variable at a time from one 'observed' extreme to the other. By varying the k'th latent variable $\Delta t\, \mathbf{p}_k$ the variation in Δx_j in its original form, i.e. not scaled, will be calculated in the following way:

$$\Delta x_j = (\Delta t\ p_{jk})\, s(x_j)$$

An example is shown in Figure 4 where calculation of Δx_j's is demonstrated. Calculation of x_j, neither centred nor scaled, will then be as follows:

$$x_j = (t\ p_{jk})\, s(x_j) + \bar{x}_j$$

In the two latter ways of sensitivity analysis presented above, artificial observation X-matrices were constructed prior to the prediction. In the first case the variable to be examined with respect to influence were varied in five equal steps giving six observations within a given range of variation while all the other variables are kept constant. In the case of variation of a latent variable all the variables were varied in five equal steps. As a third alternative an artificial observation X-matrix could contain a selection of x-variables which could be varied in equal steps while the others are kept constant and equal to their mean values. The pattern of variation could be determined by the

principal component or latent variables from the principal component analysis (PCA) of these variables.

An influence of an x-variable or several on a y-variable in this work is defined to be significant if there is no overlap of confidence regions of $\hat{y} \pm 1std.$ of the predicted maximum and minimum y, respectively. Evaluation of the significance of the influence of a variable x_i from Jack knifing the influence could be defined as significant if the uncertainty level is less than $2|b_{wi}|$.

3. RESULTS AND DISCUSSION

3.1 Prediction of cement properties from the production conditions in the cement mill

Figure 1 shows how each production variables, x_i included in the PLS, influences the three cement properties by watching the size, direction (pos. or neg. influence) and the uncertainties of the respective b_{iw}. All the variables presented in the figure are listed in Table 2 in Part I [1] of this work. Examples of prediction of variation in cement properties from variations of one x-variable while all the others are kept constant and equal to their mean value, are shown in Figures 2 and 3. As an example of the influence of a latent variable on a y-variable, Figure 4 shows prediction of variation in water content required to achieve standard consistency from variation of latent variable no. 1.

From Figure 1, some of the variables which have major and significant influence on each of the cement properties are presented below (negative or positive influence is marked with – or +, respectively):

Water content required to achieving standard consistency:

- Feed of iron(II)sulphate (-)
- Amount of water sprayed into the mill at the inlet (-)
- Amount of water sprayed into the mill at the outlet (+)
- Rotor speed, classifier (+)
- Material return (+)

Setting time:

- Amount of water sprayed into the mill at the inlet (+)
- Amount, of water sprayed into the mill at the outlet (-)
- Amount of grinding aid (+)
- Total effect, electrical consumption (-)
- Carbonate (+)
- Free lime (-)
- Temperature of clinker entering the cement mill (-)

a)

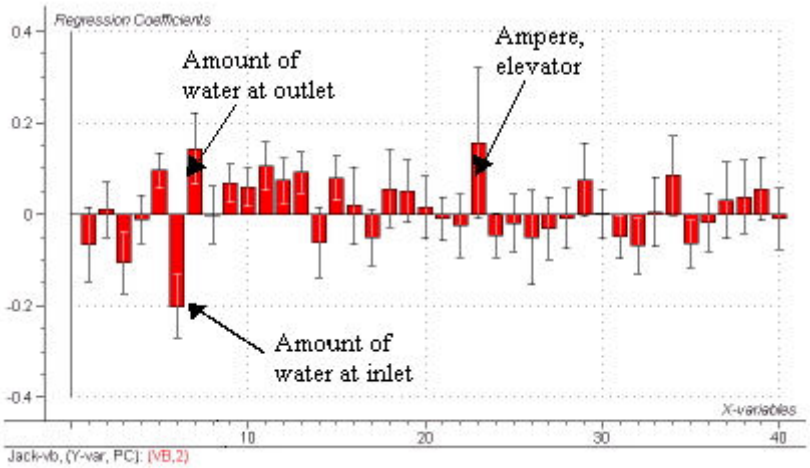

b)

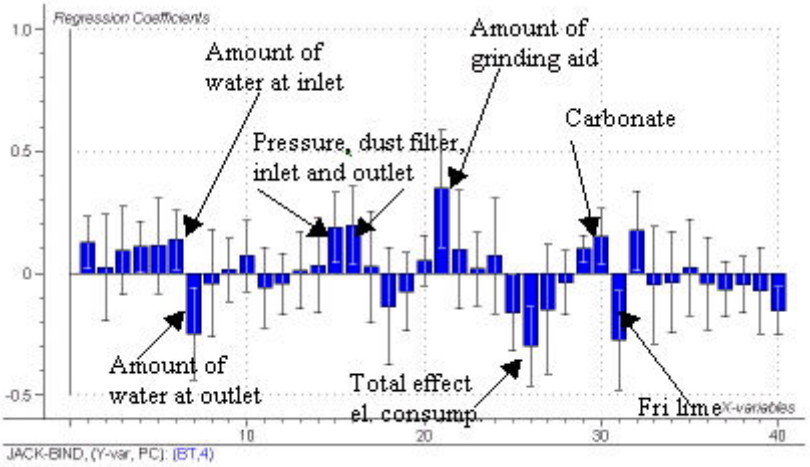

c)

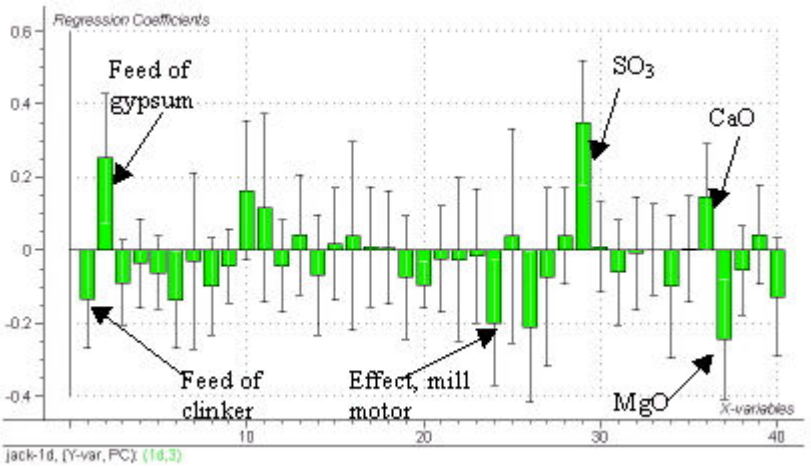

Figure 1. Regression coefficient (vertical axis) for prediction of cement properties from variables (horizontal axis) describing production conditions in the cement mill: a) Water content required to achieve standard consistency, b) Setting time, c) Compressive strength at one day. The numbers on the x-axis refer to the list of variables in Table 2 in Part I of this work [1].

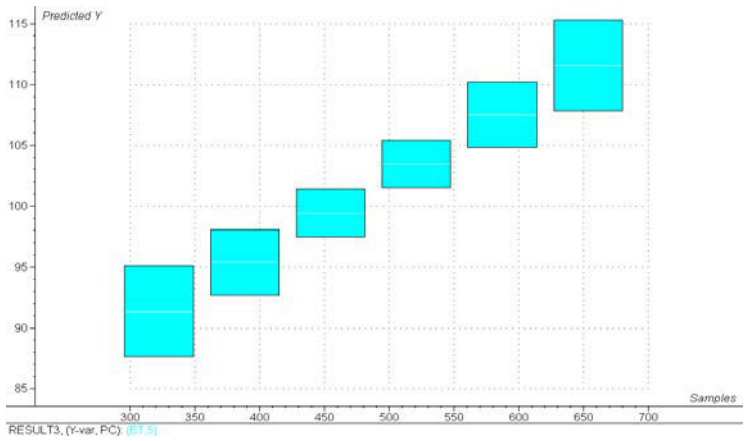

Figure 2. Predicted changes in setting time [min] (vertical axis) from changes in the amount of grinding aid [ml/min] (horizontal axis)

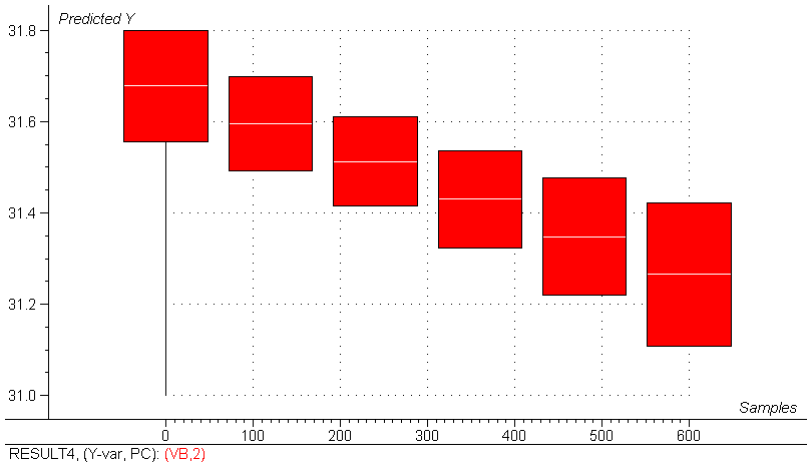

Figure 3. Predicted changes in water content required to achieve standard consistency [%] (vertical axis) from changes in the amount of water sprayed into the mill at the inlet [l/h].

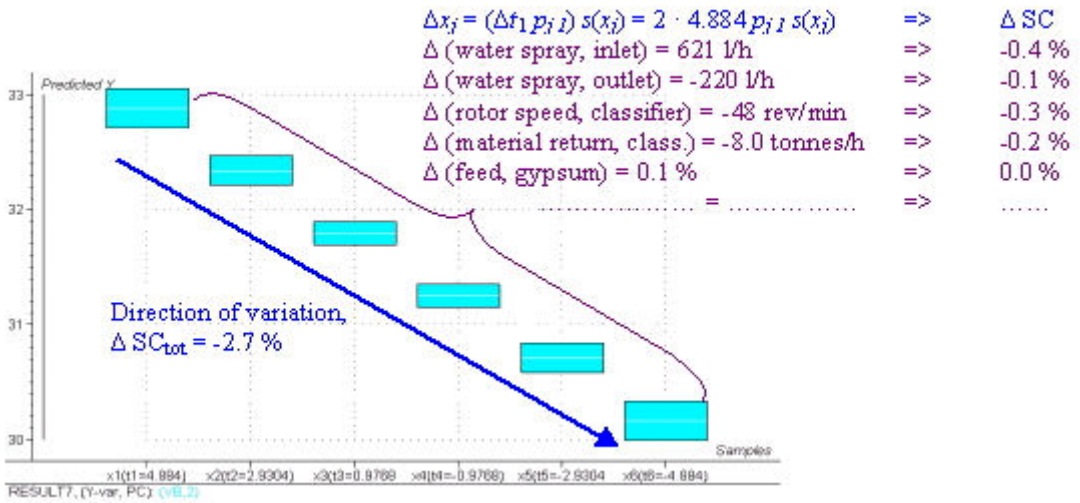

Figure 4. Predicted changes in water content required to achieve standard consistency (SC) [%] (vertical axis) from changes in latent variable (PLS-comp. no 1) (scores, $4.884 > t > -4.884$, on the horizontal axis). Contributions of some of the x-variables are calculated.

Compressive strength at one day:

- Feed of clinker (-)
- Feed of gypsum (+)
- Effect mill motor (-)
- SO_3 (+)
- CaO (+)

As reported by Lea [4], the compressive strength at one day increases significantly with the increase in SO_3. The fact that the strength also increase significantly with the increase in feed of gypsum could indicate the significant influence of SO_3 is independent of whether form, as gypsum or as SO_3 in clinker, it is supplied. The lack of influence of gypsum on setting time could, according to Lea [4] and as indicated by Figure 3 in Part I [1] of this work, be due to variation in the degree of dehydration of gypsum.

Figure 2 shows a significant increase in setting time with an increase in the amount of grinding aid. Possible reason for this will be discussed further in the next chapter.

According to Figure 1, the two process variables: Amount of water sprayed into the mill at inlet and outlet, respectively influence both setting time and the amount of water required to achieve standard consistency (SC). It is a little confusing that setting time decreases with the increase with the latter process variable. The opposite was expected from earlier experiences [5] that water wherever sprayed into the mill would prehydrate the clinker minerals. The significance as indicated by Figure 3 of the influence of water sprayed into the mill at the inlet on SC is smaller than indicated by Figure 1.

Simulation of more realistic variations in **x** should be based on variations of latent variables. Figure 4 shows that varying the latent variable no.1 gives a significant decrease in SC, gives an increase in the amount of water and a decrease in the amount of water at outlet, simultaneously. The presence of almost autocorrelation between the two variables, especially when defining only one PLS-component needed for obtaining maximum explained variance, could be explained by how the process is controlled and how the experiment is designed. In the experiments, by varying the amount of water sprayed into the first chamber the set point of the temperature of cement leaving the mill was kept constant. This is according to the usual procedure of the process control at this plant.

Both material return and the degree of material load in the mill while the clinker feed is almost constant varies the latent variable no.1 in the direction of negative Δ SC. This indicates that water sprayed into the first chamber eases the grinding and separation process in the classifier probably due to the tendency of less agglomeration. A shorter retention time in the mill combined with probably lower maximum temperature in the mill and higher partial pressure of H_2O could result in less dehydration of gypsum. According to Mork [6] a conversion of gypsum to $CaSO_2 \cdot ½H_2O$ will give poorer initial rheological properties and the water content required to achieve standard consistency will probably increase. This could be verified by TGA studies on cement.

Comparing Figures 3 and 4, it can be seen that the confidence intervals in the case of predicting the variation in y from the variation in a latent variable is much smaller than in the case of predicting from the variation of only one x-variable. The usability of PLS is connected to the existence of principal directions of variations in the observation X-matrix. The variation of a latent variable is within the space R^n where for this model n = 2. Limits of variation of a single x-variable, x_j, of $\bar{x}_j \pm 1.5 s(x_j)$ are most likely outside R^2 and the simulated variation should therefore be considered as being less realistic. Svinning *et al.* [7] have developed a method of optimisation based on variations constrained by R^n.

3.2 Prediction of cement properties from the production conditions with focus on microstructure of the cement

In the studies of correlation between the cement properties and the production condition with focus on microstructure of cement two-steps predictions will be performed. In the first step variation in a part of the microstructure will be predicted from the variation of a single latent variable of the production observation X-matrix or a combination of several. In the next step variation in one or several of the cement properties will be predicted from the predicted variation in the selected part of the microstructure.

As indicated in chapter 3.1 the degree of dehydration of gypsum will be highlighted with respect to change in water content required to achieve standard consistency (SC) and setting time (ST). To extract the effect of the degree of dehydration of gypsum only a combination of latent variables no. 1 and 2, which gives Δ(feed of gypsum) ≈ 0 was chosen. Figure 5 shows changes in the superficial microstructure described by mass loss per 4°C from TGA in the region 85 – 217°C, predicted from the changes in the latent variable $t\mathbf{p} = t(0.61\mathbf{p}_1 + 0.38\mathbf{p}_2)$. However, in this temperature region mass losses from dehydration of prehydrated clinker minerals are also recorded. An increase in mass losses in the temperature region about 217°C could indicate a moderate increase in prehydration with the increase in the amount of water sprayed into the first chamber.

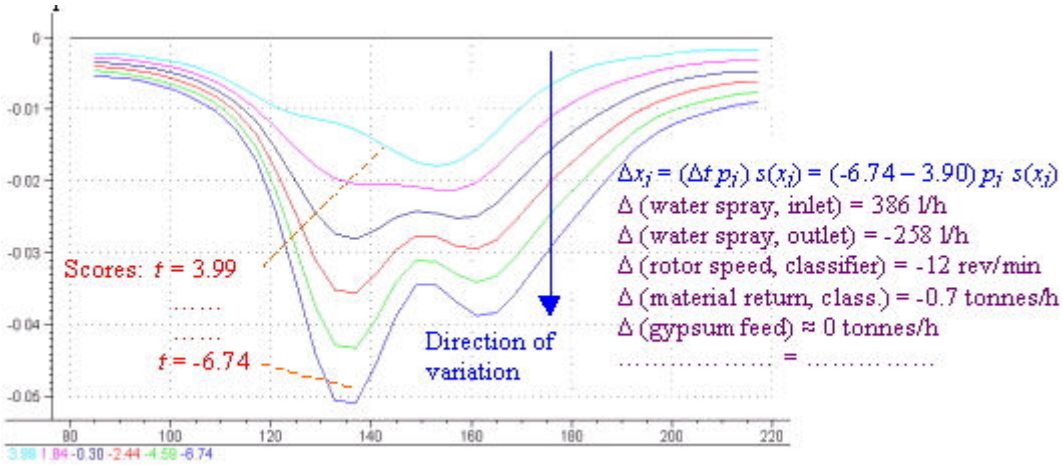

Figure 5. Predicted changes in the superficial microstructure described by mass losses [% of the total sample weight] per 4°C from TGA (vertical axis) in the region 85 – 217°C (horizontal axis), from changes in the latent variable $t\mathbf{p} = t(0.61\mathbf{p}_1 + 0.38\mathbf{p}_2)$ of the production observation X-matrix.

Comparing this latent variable with the latent variable presented in Figure 4 by comparing the change in the separate x-variable, it is easily seen that they are not quite identical. In spite of this lack of similarity the results as displayed in Figure 5 verify, as suggested in chapter 3.1, the correlation between the production conditions and the degree of dehydration of gypsum. An increase in the amount of water sprayed into the first chamber of the mill and a simultaneous decrease in the amount of water sprayed in the last chamber give a decrease in the conversion of gypsum to $CaSO_2 \cdot ½H_2O$. Further according to Figure 6, this will give a significant decrease in SC. The significant increase in setting time, as shown in Figure 7, could be partly due the moderate prehydration of the clinker minerals.

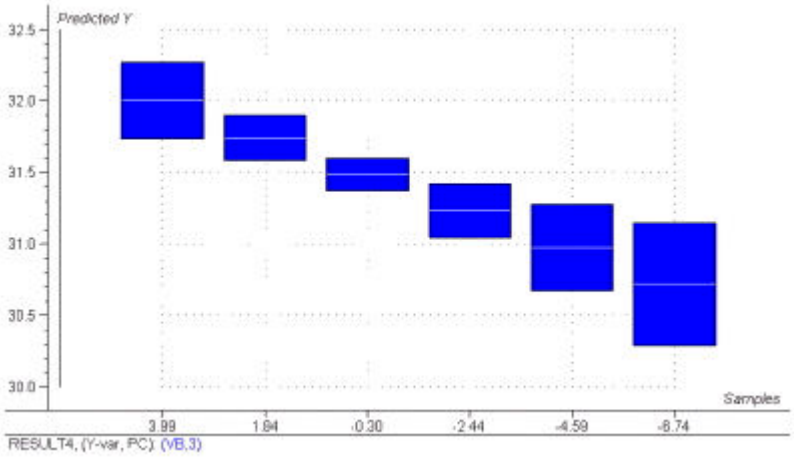

Figure 6. Predicted changes in water content required to achieve standard consistency [%] (vertical axis) from changes in the superficial microstructure described by the DTGA-curves in figure 5 (scores, *t*, on the horizontal axis).

Studying the variation in the DTGA-curve in the temperature region 604 – 946°C in Figure 3 in Part I of this work [1], the occurrence of a pronounced variation in the position of the peak, designated for decarbonisation of the limestone filler, is easily seen. The reason for this variation could be changes in the fineness of limestone filler. Even before being fed into the mill the limestone is rather finely ground and is after the grinding in the mill expected to be finer than the clinker part of the cement. Considering the decarbonisation reaction during TGA to be a heterogeneous and diffusion-controlled reaction, the temperature of the maximum rate of the reaction will probably increase with the decrease in the fineness of the filler part of the cement.

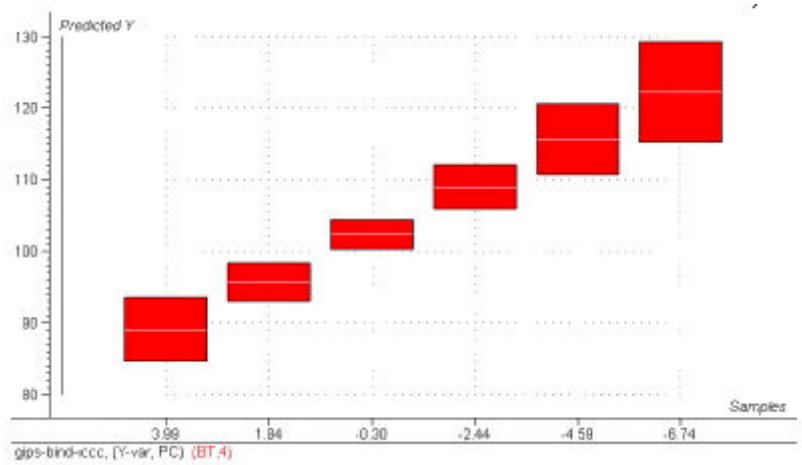

Figure 7. Predicted changes in setting time [min] (vertical axis) from changes in the superficial microstructure described by the DTGA-curves in figure 5 (scores, *t*, on the horizontal axis).

In the search of probable causes of an eventual change in the fineness of the limestone filler the regression coefficients of the PLS-model of DTGA-curve of the actual temperature region as a function of the production variables were studied. The regression coefficients of some of the variables, which have major influences on the curve or the thermogram, are presented in Figure 8. The "coefficient" curves indicate that a change in the amount of grinding aid will give a change in the peak position while by changing the feed of limestone filler, the change in the area of the peak will dominate.

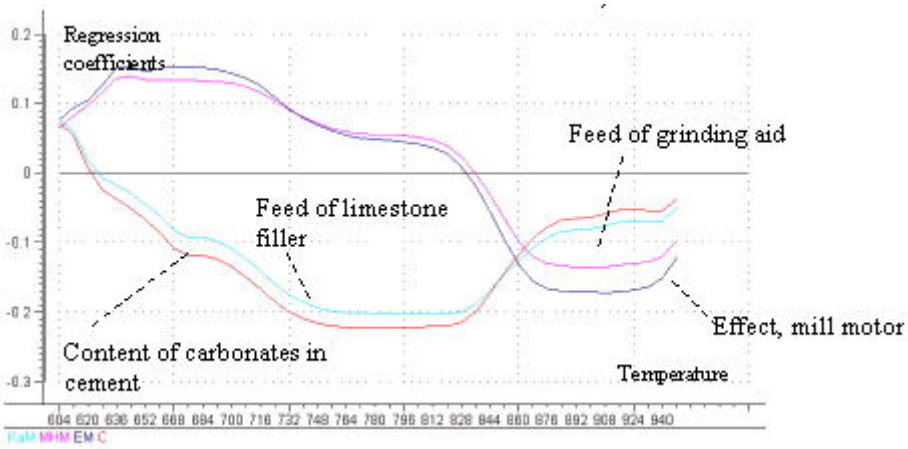

Figure 8. Regression coefficients of four production variables, a part of $\mathbf{B}_w$, from PLS of the superficial microstructure described by mass losses per 8°C from TGA in the region 604 – 946°C on the variables describing the production condition in the cement mill.

A realistic simulation of variation of the production conditions inclusive of the amount of grinding aid but keeping the feed of limestone filler constant, can be done by varying the latent variable no. 2, $t\mathbf{p}_2$. The predicted changes in the DTGA-curves from changes in the latent variable are exhibited in Figure 9. The change in the peak position with the change in the feed of grinding aid is pronounced. Coarser limestone filler in the final product could be explained by the tendency of lower agglomeration in the cement mill.

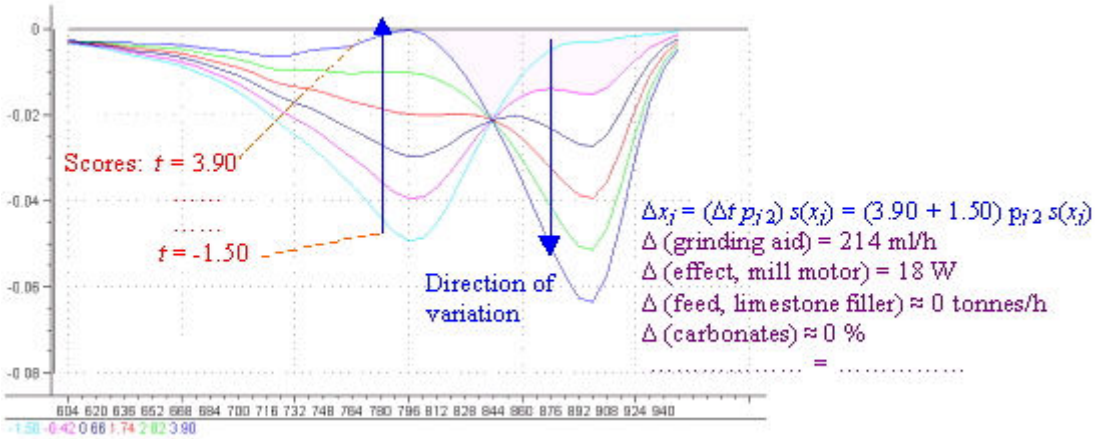

Figure 9. Predicted changes in the superficial microstructure described by mass losses [% of the total sample weight] per 8°C from TGA (vertical axis) in the region 604 – 946°C (horizontal axis), from changes in the latent variable $t\mathbf{p}_2$ of the production observation X-matrix.

Changes in setting time predicted from the changes in the superficial microstructure described in Figure 9 are shown in Figure 10. The influence is not significant at all. Further work could be studied on other parts of the microstructure to explain why the grinding aid has a significant influence on the setting time.

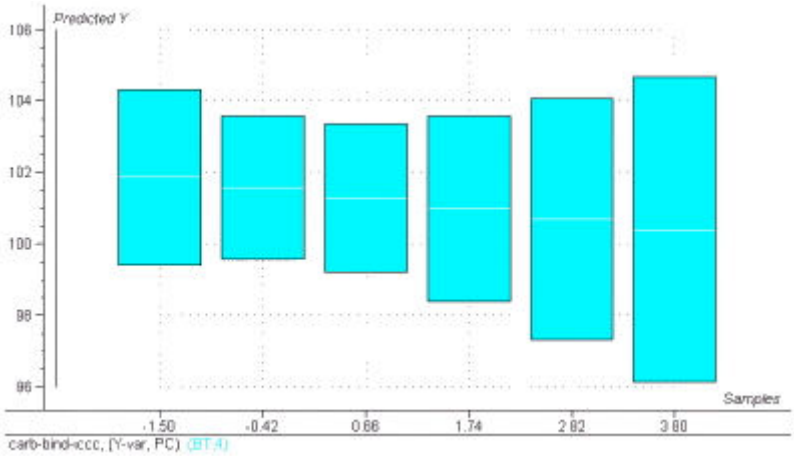

Figure 10. Predicted changes in setting time [min] (vertical axis) from changes in the superficial microstructure described by the DTGA-curves in figure 9 (scores, *t*, on the horizontal axis).

4. CONCLUSION

From the sensitivity analyses by prediction of cement properties and microstructure of cement from production conditions in the cement mill the following results should be mentioned:

- There were significant correlations between water sprayed into the first and second chamber, respectively, of the mill, and the degree of dehydration of gypsum and further the two properties: Water content required to achieving standard consistency and setting time
- The grinding aid influenced significantly the fineness of the limestone filler
- The significant change in setting time with the change in the amount of grinding aid cannot be explained as being due to the change in the fineness of the limestone filler

ACKNOWLEDGEMENTS

The authors wish to thank the supervisor Erik Stoltenberg-Hansson, Norcem R&D, Brevik, Norway, for his support and advice during this work.

REFERENCES

[1] Svinning, K., Datu, K. A., Prediction of microstructure and properties of Portland Cement from production condition in cement mill. Part I: Evaluation of prediction models, 11th international congress on the chemistry of cement, Durban 2003.

[2] Svinning, K., Tokheim, L.-A., Bjerketvedt, D., Statistical analysis of the correlation between Nox emissions and production conditions in a cement kiln applying staged combustion, World cement, vol. 29, 1998, pp.68-75

[3] Martens, H., Martens, M., Modified Jack-knife estimation of parameter unceriainty in bilinear modelling (PLSR), Food quality and preference, 1999

[4] Lea F. M., The chemistry of cement and concrete, 3rd edition, Surrey: Edvard Arnold Ltd. 1970, pp 297-298

[5] Svinning, K. and Bremseth, S. K., The influence of microstructure of clinker and cement on setting time and strength development until 28 days, 18th international conference on cement microscopy, Houston 1996, pp. 514-513.

[6] Mork, J. H., Effekt av sementens forhold mellom gips og hemihydrat på den ferske betongens reologi, Doktor ingeniøravhandling 1994:4, NTH, Institutt for bygningsmateriallære, Trondheim

[7] Svinning, K., Ingerøyen, Ø., Dalsveen, K., Optimization of a response variable y constrained by principal directions of variations in the observation X-matrix, J. Chemometrics, vol.14, 2000, pp.699-709

NEW APPROACHES TO CEMENT HYDRATION IN THE EARLY HARDENING STAGE

Stark J., Möser B. and Bellmann F.

F.A. Finger-Institute for Building Material Science, Bauhaus-Universität Weimar.
E-mail: bernd.moeser@bauing.uni-weimar.de and jochen.stark@bauing.uni-weimar.de

ABSTRACT

The visualization of structures resulting from processes taking place in a few nanometers is immensely important when studying the properties of concrete and mortar. Electron microscopy is in principle capable to getting images of structural constituents in this size. Unfortunately, studies using conventional electron microscopes are subject to serious limitations. For these reasons an Environmental Scanning Electron Microscope with Field Emission Gun (ESEM-FEG) in different operating modes has been used to investigate wet materials in their native state. These methods provide deep insights into the moist micro and nano world. It even makes it possible to carry out sophisticated observations of hydration processes in complicated multi-phase systems, such as Portland cement. The article describes the investigations of the phase development during the hydration of OPC from the induction to the final period. The results are summarized in a scheme for a new model of ordinary Portland cement hydration. ESEM investigations were supported by the calculation of saturation factors from ion concentration in the pore fluid. To broaden the view on the influence of temperature on the formation of hydration products, ESEM investigations on cement paste hydrated at different temperatures were correlated with thermodynamic calculations.

1. INTRODUCTION

The model of cement hydration developed by Powers and his colleagues [1953] is now considered as the first pioneering draft scheme. The hydration products of Portland cement were initially described as spherical [1]. With the first electron microscope micrographs the concept of spheres was replaced by the model of groups of randomly orientated and layered units (cement gel). The cement gel was described as a solid substance with an average pore diameter of approximately 1.8 nm [2]. On this basis Powers developed a model for the creep and shrinkage of the hardened cement paste. Feldmann and Sereda (1968) investigated the different types of water bonding to hydration products. C-S-H phases - the main hydration products - were described as corrugated platelets [3]. Kondo and Daimon (1974) presented a model which conformed to the two above-mentioned models [4]. As early as 1965 Richartz and Locher [5] introduced two different types of C-S-H phases (type I and II). In the C-S-H (I) the C/S ratio was said to be approximately 0.8 to 1.5 and in the C-S-H (II) it should be between 1.0 to 2.0. According to this model the crystallinity of the phases decreases with increasing C/S ratio. C-S-H (I) is shown in electron micrographs as flakes, while C-S-H (II) forms fibers. In this model the fibers corresponded to rolled platelets with layered inclusions of CH (Figure 1).

According to Locher, Richartz and Sprung as well as Sylla and Rechenberg [6-9] the observed C-S-H phases grow initially as long fibers and later as short fibers.

To clarify the interaction of the hardened cement paste with water, Setzer [1977] described by means of a model the maxima in the pore radius distribution of hardened cement paste to be around

Proceedings of the 11th International Congress on the Chemistry of Cement (ICCC)
'Cement's Contribution to the Development in the 21st Century'
Hosted by: The Cement and Concrete Institute of South Africa
CD-ROM produced by: Document Transformation Technologies
11 - 16 May 2003, Durban, South Africa
ISBN Number: 0-9584085-8-0
Editors: Dr G. Grieve and G. Owens
Congress Organised by: Event Dynamics

2.5 and 7.0 nm [10]. In the same year Wittmann introduced the hydration products of Portland cement as xerogels in which each particle is linked to its surroundings by different bonding forces [11]. Taylor [1992] designated the crystal structure of the hydration products, the C-S-H phases, as "similar to tobermorite"[12]. According to sheet silicates tobermorite consists of calcium layers located between silicate chains. Taylor also compares C-S-H phases with the mineral jennite, which has a higher C/S than tobermorite and is said to consist of distorted layers of CaO.

As a result of very intense evaluation of the literature Massazza and Daimon [1992] have pointed out five different morphologies of C-S-H phases, which grow during the hydration process [13]. There are descriptions of gel-like, needle-like and sword-shaped C-S-H phases as well as of flake-shaped phases. The morphological changes of the C-S-H phases during the hydration of C_3S were shown for the first time in detail by Meredith et al. [1995] on the basis of investigation with an Environmental Scanning Electron Microscope (ESEM) [14].

Jennings [2000] proposed a new model for the microstructure of calcium silicate hydrates in cement paste [15]. He referred to the "tobermorite-jennite model" by Taylor and proposed two types of C-S-H: LD C-S-H (low-density) which crystallize in the large capillary pore space during the main hydration period, and HD C-S-H (high density) which is formed in the significantly more restricted voids around the C_3S particles.

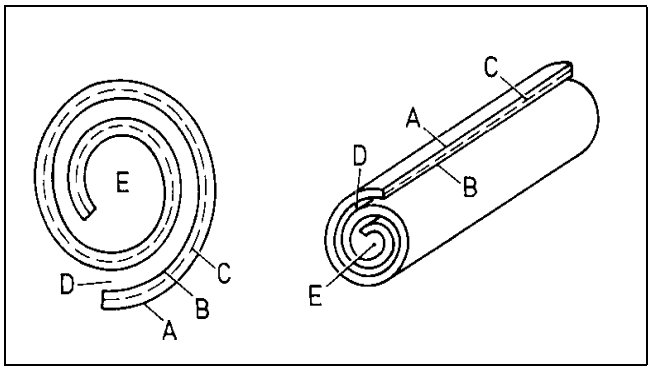

Figure 1. Rolled C-S-H (II) platelets: A and B C-S-H layers; C: interlayer region; D: space between the rolled leaves; E: internal space in the roll according to Richartz and Locher [5].

It can be concluded, that the existing theories on the morphology and structure of C-S-H phases arise from different kinds of investigation methods (mainly electron microscopy and NMR studies). Often these results are difficult to compare because of the lack of a unified classification of the hydration products and because of the artifacts produced during sample preparation for electron microscopy.

2. MATERIALS AND METHODS

Fortunately, the preparation of the specimens to be studied with the ESEM is uncomplicated, unlike that for conventional scanning electron microscopy, where drying and coating of the specimens is essential. In most cases with the ESEM it is unnecessary to stop the hydration process. The educts used for our investigations are synthetic C_3S, ß-C_2S, and ordinary Portland cement (OPC). All pastes were prepared with a water-cement ratio of 0.3. This value has proven to be favorable for most types of cement. Higher water-cement ratios result in sedimenting out and bleeding structures and thus initiate a thinning effect: readily soluble salts – like K_2SO_4, Na_2SO_4 - are dissolved in the excess fluid and settled on top of the specimen, i.e. they are not accessible for the hydration reactions. The hydration of the cement and the synthetic clinker minerals have been performed outside the microscope in airtight sealed containers at room temperature. While the paste is still plastic, a roughly pea-sized specimen was taken at preset times and applied to the sample holder on

a Peltier cooling stage of the ESEM. After setting the parameters inside the microscope chamber to the adequate pressure and temperature (to reach the desired humidity of 80-95%), the specimen is fractured with the aid of a micromanipulator. This fracturing is very important, because during the microscope adjustment to the relative humidity of 80-95% a skin consisting of alkali salts and presumably also carbonates is formed on the specimen surface. After the first setting of the paste fracture surfaces produced outside the microscope have been used for the examination.

The ESEM-FEG has been used in different operating modes: wet-[ESEM], low- as well as high-vacuum and low- and high-voltage mode. To identify the chemical composition of singular hydration phases we applied Energy Dispersive X-Ray Spectrometry (EDX) combined with the ESEM.

In addition to the ESEM investigations the concentration of important ions in the pore solution was analyzed. For this purpose pastes from the cement with a high K_2SO_4 (arcanite) content were prepared with a water-cement ratio of 0.4 and cured in sealed plastic containers at room temperature. At the times specified in Table 2 pore solution was obtained by filter suction (10 min – 90 min) or squeezed out from cement paste specimen (3 hours and later). Except for hydroxide, that was measured by titration with HCl after dilution, ICP was employed for analysis.

To monitor the hydration progress continuously, time resolved we measured the time resolved and evolved reaction heat with Differential Calorimetric Analysis (DCA). Powder-X-Ray-Diffraction (XRD) was applied to confirm the EDX-Analysis of the minerals.

3. RESULTS AND DISCUSSION

3.1 Hydration of C_3S (alite)

Calcium silicate hydrates (C-S-H phases) of variable chemical composition, as well as portlandite (CH), are formed during the hydration of C_3S. The hydration reaction can be divided into 5 time periods on the basis of the DCA (Figure 2). According to this five periods changes in the microstructure have been investigated with the ESEM. Systematic ESEM observations show typical morphological changes for each hydration period, these have been summarized in Table 1.

Table 1. Stages of C_3S hydration (adopted from Mindess and Young [16])

	period	time	reaction kinetics	chemical processes	phase description
1	induction period / initial hydro-lysis	first minutes after mixing	chemically controlled rapid reaction	start of hydrolysis, ions go into solution	formation of a smooth reaction layer around the grains
2	dormant period	approx. 20 min to 2h	core and diffusion controlled, slow reaction	very small chemical activity	first heterogeneous nucleation
3	acceler-ation period	2h to 11 h	Chemically controlled, rapid reaction	start of the formation of hydration products	µm-large, thin laminated portlandite crystals as well as short needle-like C-S-H fibers
4	Deceler-ation period	11 h to 26 h	chemically and diffusion controlled, reaction	continuous formation of hydration products	one-dimensional growth of the C-S-H fibers, aggregation of this fibers, stronger interlocking of the particles; intergrowth of the platy CH crystals
5	final period	after approx. 26 h	diffusion controlled reaction	slow formation of hydration products	further growth in length of the C-S-H fibers, interlocking

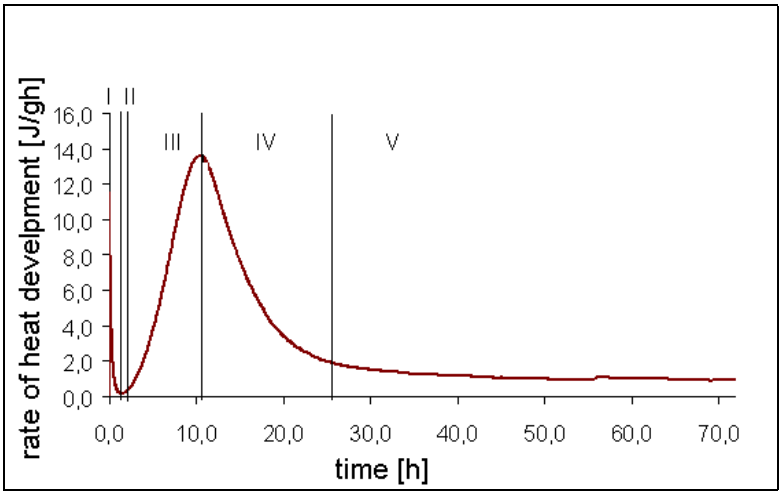

Figure 2. Heat rate shown in hydration periods (Table 1) of C_3S (DCA measurement).

It can be assumed that at the beginning of the acceleration period all C-S-H phases grow in the form of fibers. These fibers grow in length during the hydration process (Figure 3) with hardly any change in thickness. In compacted concrete the C-S-H fibers appear to grow together. They also interlock. This minimizes the pore space between the fibers. In fact, the pore diameter of these fibres must be in the range of the size of gel pores. Changes in reaction conditions have an extreme effect on the C_3S hydration: A drop in temperature from 22°C to 5 °C, for example, results in a retardation of the hydration reaction by several hours.

Conventional Scanning Electron Microscope (SEM) imaging requires samples which are stable in high vacuum and are electrically conductive. The necessary preparation steps (drying, coating or sputtering, etc.), prevent noninvasive observation of the C-S-H structures (Figures 4 and 5). The morphology of the C-S-H phases is changed drastically by the thermal stress during the coating process and by the vapour-deposited layer itself. Furthermore, we doubt that the chemical compositions given for C-S-H (I) and C-S-H (II) determined with EDX can be very precise. The C-S-H phases are nanometer scaled needle-shaped crystals (crystal thickness of a few nanometers). The excitation volume of electrons with an accelerating voltage of 15 kV is about a few cubic micrometers. Monte Carlo simulation calculations for a beam voltage of, for example, 15 kV give an excitation depth of approximately 2.5 µm, if the density of C-S-H phases - about 2.2 g/cm^3 - is applied. In comparison the low energy operation of 2.5 keV yields a high spatial resolution for the X-ray microanalysis between 50 – 100 nm, which is related to the approximate thickness of a single C-S-H phase (see Figures 4 – 8).

Thus we have to admit that the former measurements made with the conventional SEM/EDX give only a rough orientation on the C/S ratio of the small C-S-H phases. Analysis of uncoated and non-conducting specimens on the nanometer scale can only be obtained by working in the range of low accelerating voltage (low voltage SEM with field emitters) in combination with a sensitive, high resolution X-ray spectrometer. The use of a standard SEM equipped with a tungsten filament is not advisable to produce high resolution images at these voltages and magnification levels. Further prospective methods are ultra high resolution EDX analysis or Electron Energy Loss Spectroscopy (EELS) in the Transmission Electron Microscope (TEM).

Although many classical investigations on the formation and composition of cement hydrates have been correct in their time with the available methods, now they cannot stand a critical examination. It is now clear and widely accepted that C-S-H phases are nanoscale fibers but not rolled platelets or flakes. The frequently used designation C-S-H “gel” is quite correct from a physical point of view as a gel implies a particle size. From the point of view of cement chemistry_and mineralogy,

however, the C-S-H phases involved are definitely not gels (term derived from colloid chemistry) but are more probably highly disordered nano-crystalline minerals due to their large surface areas. This assumption is further supported by XRD measurements, where only very weak interferences occur. The term “amorphous to X-rays” is a very appropriate expression in the case of C-S-H phases.The formation of the C-S-H phases as long fibers initially and later as short fibers is also not sustainable [6]. In fact the C-S-H phases tend to start as short fibers and grow to a length of approximately 1.5 µm as the hydration progresses (Figure 3).

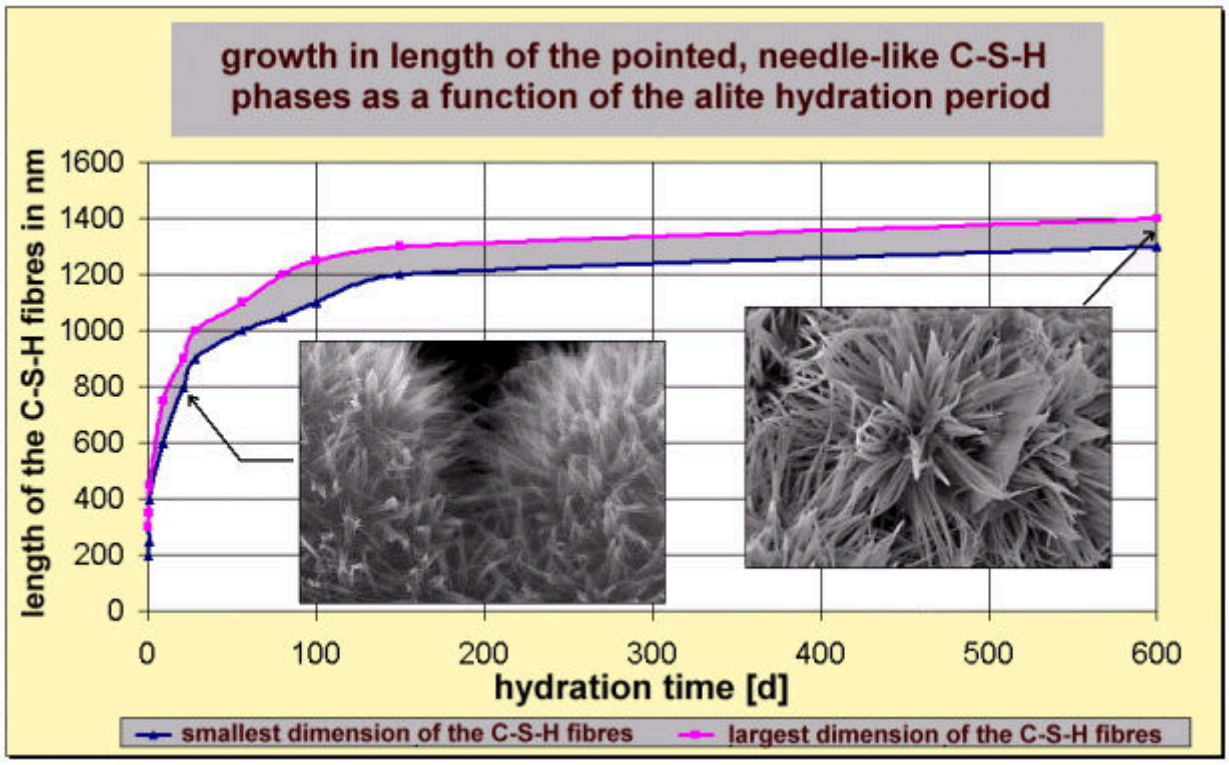

Figure 3. Longitudinal growth of C-S-H fibers during the C_3S hydration process.

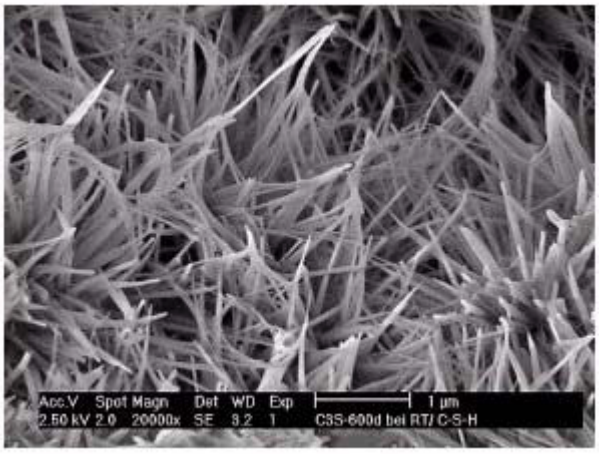

Figure 4. Formation of needle-like C-S-H phases during the hydration of C_3S. After 600 days hydration time the fibers grow up to a length of 1.5 µm and the needle tips have a diameter of only approx. 5 nm.

Figure 5. The same sample as in Figure 4, but with an approximately 30 nm thick layer of carbon for imaging in conventional SEM. The morphology of the C-S-H phases are changed drastically by the thermal stressing during the coating process and by the vapour-deposited layer.

The ESEM images in Figures 6 and 7 show the formation of the microstructure at selected times during the hydration process at room temperature.

In a time period of 21 days the C-S-H phases grow continuously to a length of 900 nm, the needle tips have only a diameter of approximately 5 nm. The longitudinal growth starts from the surface of the clinker grain. As a result of this merely one dimensional growth, C-S-H phases develop a tight interlocking due to their extremely tipped, needle like shapes (Figure 7). In very dense structures we assume an intergrowth between the fibers as well as interlocking of the fibers with one another.

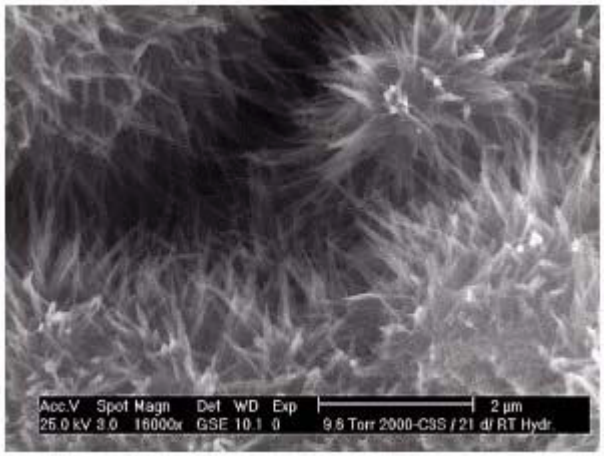

Figure 6. C_3S hydrated for 21 days: tipped, needle-like C-S-H phases (length up to 900 nm).

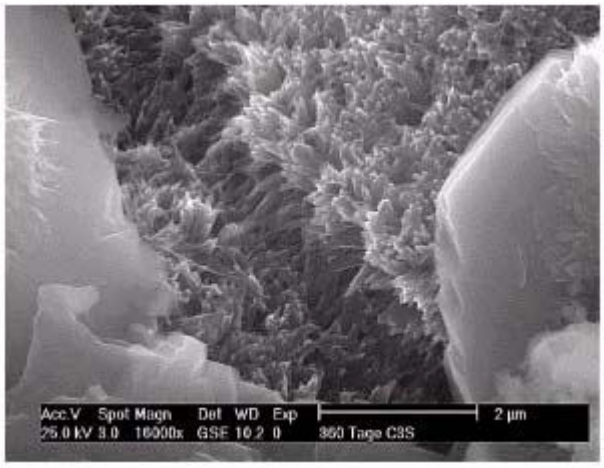

Figure 7. C_3S hydrated for 360 days: interlocking of the C-S-H phases (length up to 1200 nm) right and left portlandite.

3.2 Hydration of ß-C_2S (belite)

The same fiber-shaped hydration products as formed during the C_3S hydration are observed for the hydration of ß-C_2S. However, as already often reported by others, this hydration occurs significantly more slowly than that of the C_3S. After a hydration time of about one year, the fiber size in hydrated C_3S and ß-C_2S are equal. Extremely long C-S-H fibers (up to 2.5 µm) were imaged in an investigation of ß-C_2S which hydrated for 3 years (Figure 8). This length growth is expected to be a contribution to the secondary hardening.

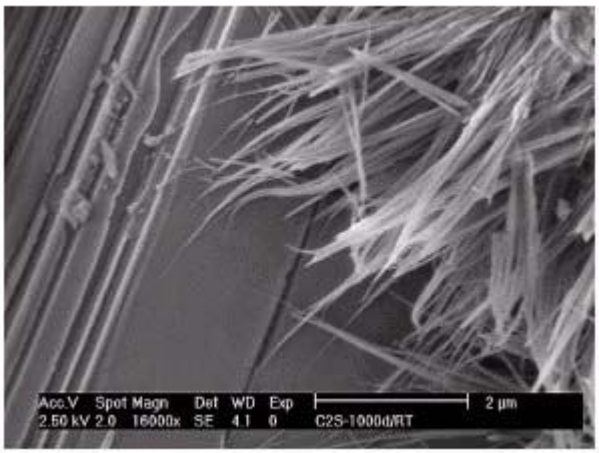

Figure 8. ß-C_2S hydrated for 3 years: formation of extremely long (up to 2500 nm) C-S-H fibers – here in front of a portlandite crystal . Note: the strength contribution made by huge portlandite crystal, is likely to be small or portlandite even can act as a slip plane under load.

3.3 Hydration of Ordinary Portland Cement (OPC)

Investigations of the phase development during the hydration of OPC from the induction period to the final period (Table 1) are summarized in Figure 16. This scheme for the normal hardening process of OPC at room temperature was derived from investigations of Stark, Möser, Eckart [17] and Hader [18]. Here we would like to give only a short overview about the hydration behavior of OPC with a low alkali content (sodium equivalent 0.49 % with 0.33 % water soluble potassium oxide - ESEM-images: -a) and a high alkali content (sodium equivalent 1.2 % with 1.09 % water soluble potassium oxide [mainly arcanite – potassium sulfate] - ESEM-images: -b). The hydration of industrial ordinary Portland cement differs significantly from the hydration of individual clinker phases. A different chemical equilibrium is set up in the aqueous phase as a result of the interaction between the hydration reactions of several adjacent phases, and this has a significant effect on the formation and sometimes on the morphology of the hydration products.

The behavior with time of OPC hydration can, like C_3S hydration, be divided into 5 time periods:

Induction period: Immediately after mixing with water very small ettringite crystals were formed. Ettringite is the first product formed shortly after mixing. The small prismatic ettringite crystals have a length of between 300 to 500 nm and a thickness between 50 to 250 nm (see Figures 9a and 9b). If a high quantity of potassium sulfate (mainly arcanite) is available, calcium-potassium sulfate double salts, like syngenite [K_2SO_4 $CaSO_4$ H_2O] crystallize. Syngenite forms long (up to 10 µm) lath-shaped crystals and can stiffen the cement paste (Figure 9b).

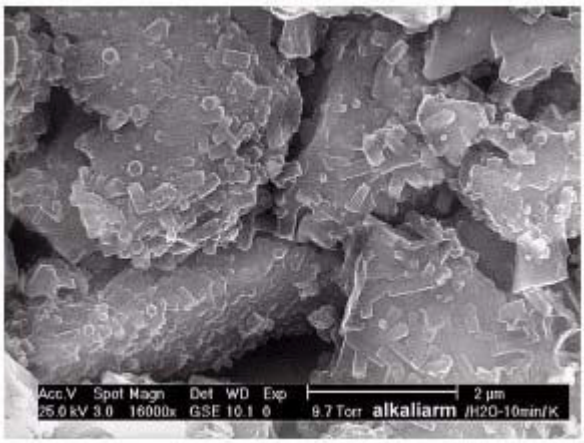

Figure 9a. Microstructure after 10 min hydration time [low potassium content]: Only small hexagonal ettringite crystals were formed on the surface of the clinker grains, the distribution is inhomogeneous.

Figure 9b. Microstructure after 10 min hydration time [high potassium content]: Ettringite with the same morphology as cement with low arcanite content. Formation of syngenite (lath-shaped crystals).

Dormant period (low chemical activity): Syngenite formation was also observed in cements with a very low potassium content but at a later hydration stage (after about 30 minutes). Figure 10a shows the microstructure of this low potassium cement after 2 h hydration time: bent syngenite crystal aggregates and ettringite with the same morphology as after 10 minutes are observable. The microstructure of cements with high potassium content (2 h) show ettringite and syngenite with the same morphology as after ten minutes (compare Figures 9b and 10b).

Acceleration period (high chemical activity): At the beginning of the acceleration period the C-S-H phases grow topochemical on the C_3S clinker surfaces. In the case of cements with low potassium content small (< 200 nm long), isolated and strongly inhomogeneous distributed C-S-H clusters can

be observed after 3 h hydration time. Ettringite has nearly the same morphology as after ten minutes. After 5 h the microstructure shows formations of small C-S-H phases with a length of up to 300 nm arranged in clusters (Figure 11a). Individual clusters of fibers are formed.

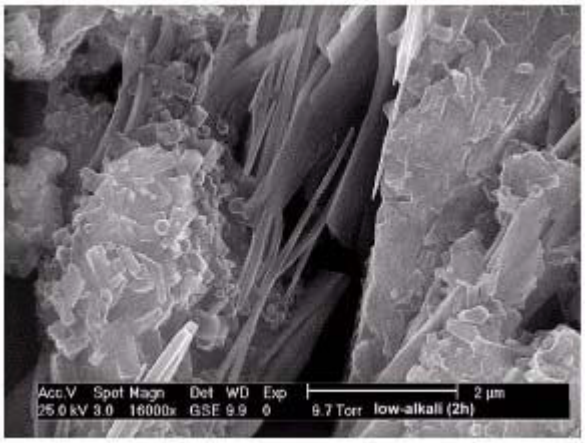

Figure 10a. Microstructure after 2 hours hydration time [low potassium content]: Ettringite with the same morphology after 10 minutes, increased syngenite formation.

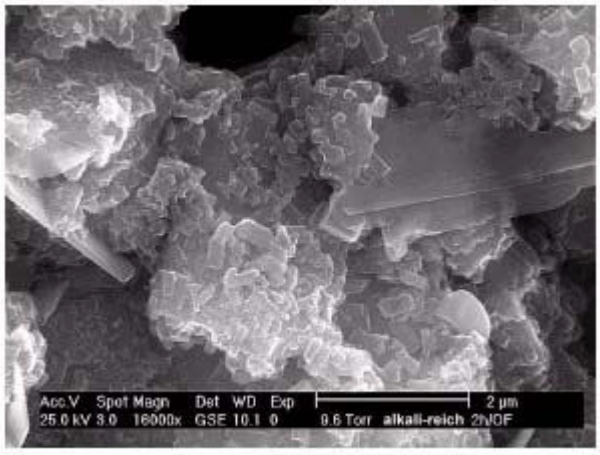

Figure 10b. Microstructure after 2 hours hydration time [high potassium content]: Ettringite and syngenite with the same morphology after 10 minutes.

Figure 11a. Microstructure after 5 hours hydration time [low potassium content]: Formation of small C-S-H phases (length up to 300 nm) arranged in clusters).

Figure 11b. Microstructure after 6 hours hydration time [high potassium content]: syngenite is starting to dissolve with formation of secondary gypsum (left).

As the hydration continues further, the tipped needle like C-S-H phases grow longitudinally (one-dimensionally – up to 600 nm long in 10 hours). Due to this one-dimensional growth, tight interlocking of the nanoscale C-S-H crystals occurs. The C-S-H phases formed in the hydration process of ordinary Portland cement during the first 24 hours exhibit a significantly faster growth than during the hydration of the pure C_3S clinker mineral. Up to 10 hours, the morphology of primary ettringite remains virtually unchanged. After a hydration period of 10 hours syngenite is no longer visible in the microstructure, but partial secondary gypsum is (Figure 12a).

In cement with high potassium content after 3 hours we observe many straight syngenite crystals in the form of stripes and plates and small but many C-S-H clusters. Ettringite has nearly the same morphology as after 10 minutes. Furthermore, first portlandite crystals are visible. After a hydration period of 5 hours the lath shaped syngenite crystals start to dissolve and formation of secondary

gypsum, potassium hydroxide and potassium sulfate (Figure 11b) is observed. After a hydration period of 10 hours only a few syngenite crystals are visible in a matrix of C-S-H and ettringite (Figure 12 b).

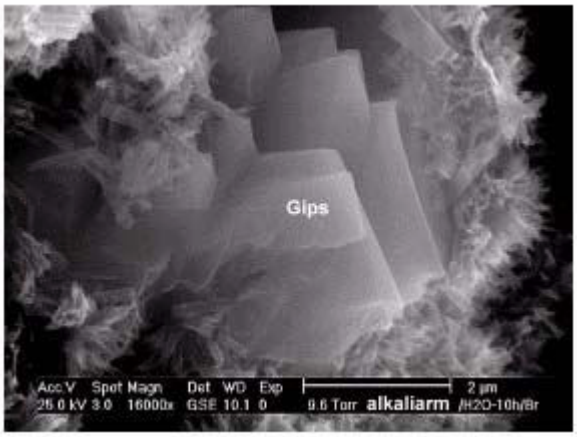

Figure 12a. Microstructure after 10 hours hydration time [low potassium content]: partial secondary gypsum, C-S-H (length up to 500 nm) and ettringite (length up to 600 nm).

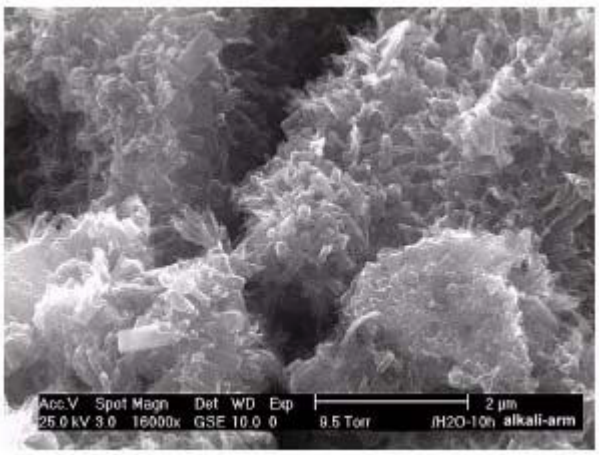

Figure 12b. Microstructure after 10 hours hydration time [high potassium content]: sporadic syngenite, C-S-H (length up to 500 nm) and ettringite (length up to 600 nm).

Deceleration period: Cement with low potassium content: The gap between the C-S-H reaction rim (about 600 nm thickness) and the hydrated clinker grain becomes even bigger (distance between 0.6 and 1 µm – Figure 13a). As the reaction process continues the space is filled initially by ettringite and later also with C-S-H phases from adjacent clinker grains (Figure 14a). The main growth phase of ettringite is between 12 and 24 hours. The length of the crystals is then up to 2.5 µm and they keep their thickness all the time.

Cement with high potassium content: We also observe gaps between the hydration rim and the hydrated clinker grain. Ettringite crystals growing along their c-axis penetrate the gaps between the clinker grains and the hydration products (Figure 13b). The longitudinal growth of ettringite can possibly be attributed to the newly released sulfate (dissolution of syngenite and formation of secondary gypsum). Further reason for the growth of ettringite is the release of C_3A through the progres- sive C_3S hydration.

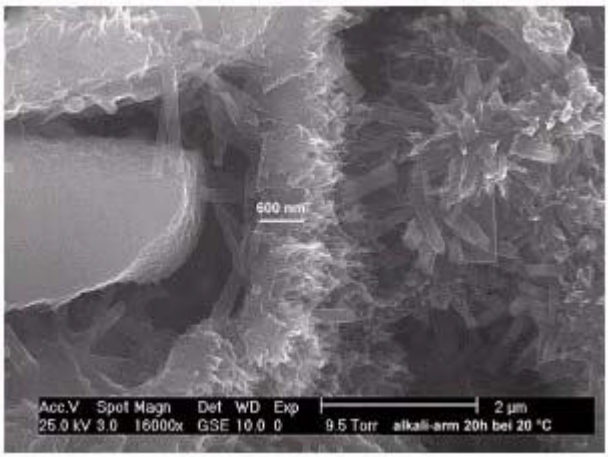

Figure 13a. Microstructure after 20 hours hydration time [low potassium content]: ettringite crystal penetrate the space between the clinker grain and new formations of C-S-H.

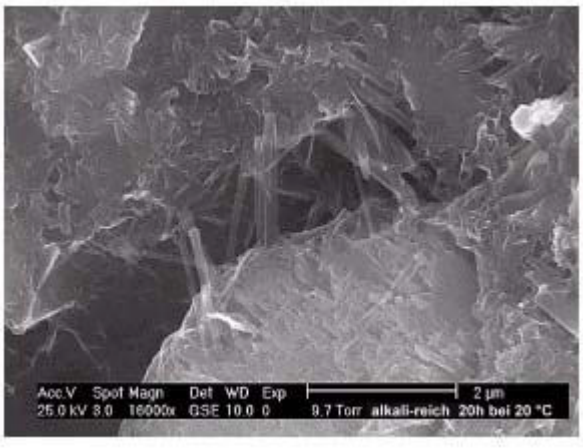

Figure 13b. Microstructure after 20 hours hydration time [high potassium content]: C-S-H phases on the surface of an incompletely hydrated clinker grain (gap).

Calculations as well as measurements have shown that in the first hours only 10 % of the C_3A content can react. Sporadic thin hexagonal-plate tetracalciumsulfoaluminate-hydrate clusters are visible. Tetracalciumsulfoaluminatehydrate is a solid solution of monosulfate and calcium-aluminate-hydrate. The voids and gaps were filled with C-S-H nanocrystals and ettringite (Figure 14b).

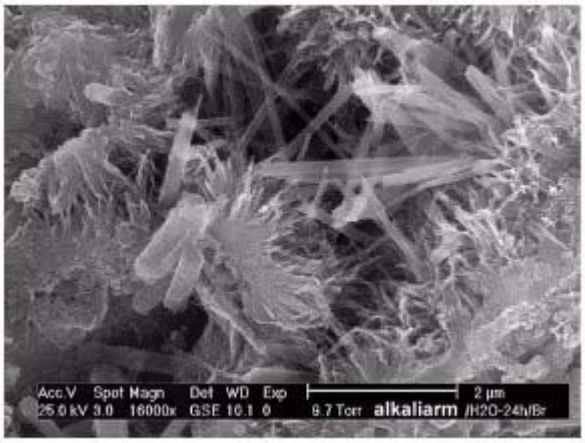

Figure 14a. Microstructure after 24 hours hydration time [low potassium content]: long prismatic ettringite (up to 2.5 µm), C-S-H (length approx. 600 nm).

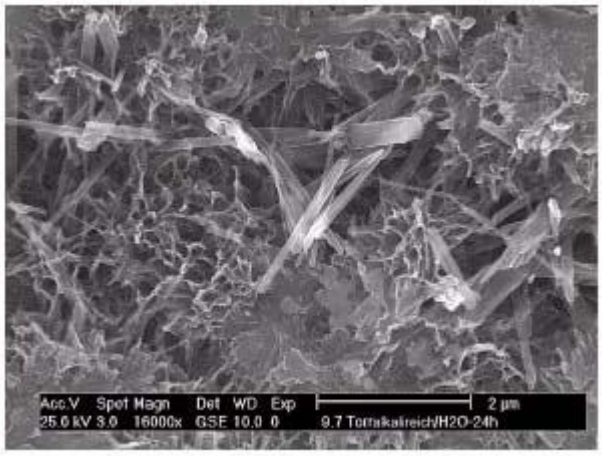

Figure 14b. Microstructure after 24 hours hydration time [high potassium content]: voids in the microstructure are filled by C-S-H (length up to 600 nm) and ettringite.

Final period: During the final period there is further slow growth of the C-S-H phases. Further basic consolidation of the microstructure occurs during this process, to which the slow reaction of the ß-C_2S also contributes.

After a hydration time of 7 days C-S-H reaction layers of about 900 nm thickness are visible. Figures 15a and 15b show typical occurrence of C-S-H reaction rims: Figure 15a shows direct growth on the clinker grain, Figure 15b shows the C-S-H reaction rim around a completely dissolved clinker grain. Long prismatic ettringite (up to 2.5 µm) and thin hexagonal-plate tetracalciumsulfoaluminatehydrate crystals are observable within the void of the clinker mineral (Figure 15b). These completely hydrated clinker grains exist mainly in cements with a high soluble potassium sulfate content.

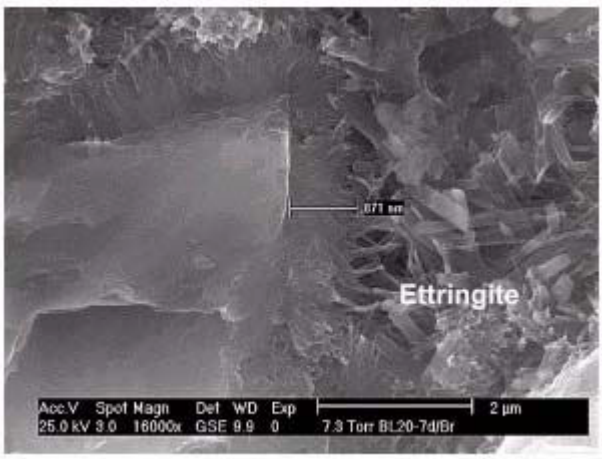

Figure 15a. Microstructure after 7 days hydration time [low potassium content]: long prismatic ettringite (up to 2.5 µm), and C-S-H (length approx. 900 nm).

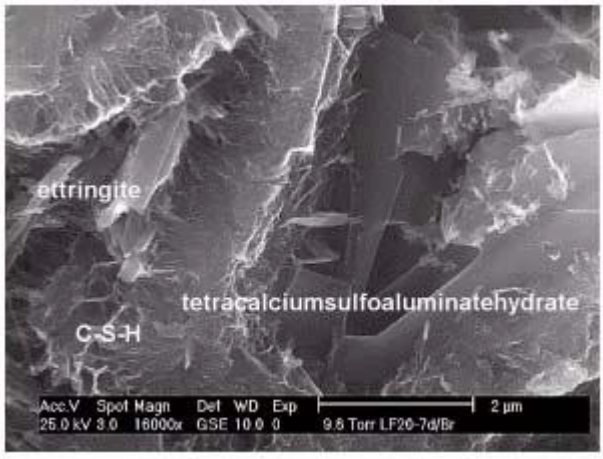

Figure 15b. Microstructure after 10 minutes hydration time [high potassium content]: voids of completely hydrated grains are filled mainly with a solid solution of monosulfate and calcium-aluminate-hydrate (tetracalcium-sulfoaluminatehydrate.

Scheme for ordinary Portland cement hydration:
A scheme for hydration of OPC can be concluded from the above described observations. DCA and XRD measurements confirm this scheme. Figure 16 was derived to give a time resolved summary on the occurrence of hydration products.

In the first hours temporary syngenite formation is observed. The time of formation and the amount of the syngenite growth depends on the contents of soluble potassium sulfate (mainly arcanite). After a hydration period of about 5 hours the lath-shaped syngenite crystals dissolve and are replaced by secondary gypsum and potassium sulfate. Ettringite is the first hydration product shortly after mixing. The small prismatic ettringite crystals have a length of approximately 500 nm and a thickness of up to 250 nm. During the first hours the morphology of primary ettringite remains virtually unchanged. Minimal crystal growth is observed. The main longitudinal growth of these phase occurs between 12 and 24 h. The length of the crystals is then up to 2.5 µm and they keep their thickness all the time. Contrary to previous hydration models ettringite does not become unstable and does not gradually convert into monosulfate or tetracalciumsulfoaluminatehydrate. Both ettringite and tetracalciumsulfoaluminatehydrate are the final products of hydration of OPC in our investigations.

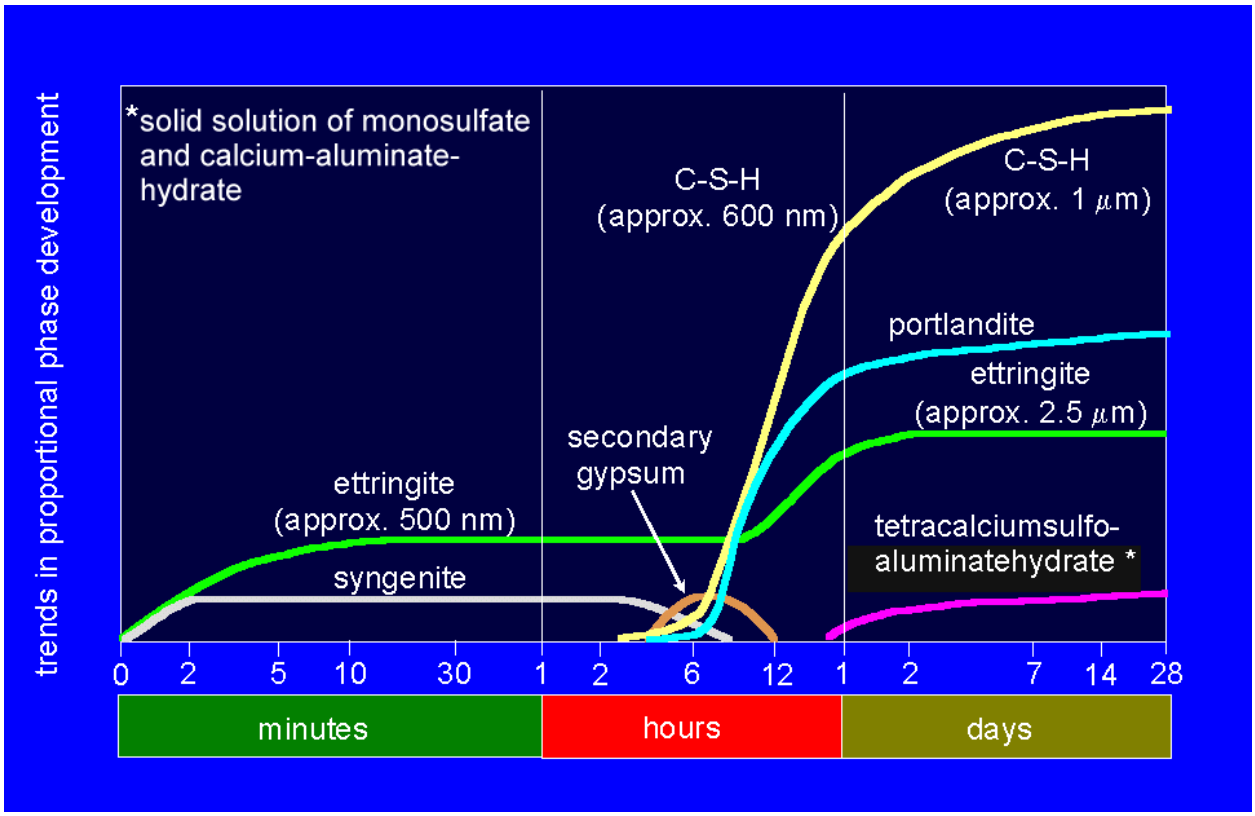

Figure 16. Scheme for ordinary Portland cement hydration at room temperature – derived from investigations by means of ESEM-FEG.

Tetracalciumsulfoaluminatehydrate is formed after approximately 24 hours in dependence of the content of the water soluble potassium sulfate. Thin hexagonal-plate crystals are formed. At room temperature these crystals are solid solutions of monosulfate and calciumaluminatehydrate.

C-S-H phases form on the C_3S clinker phase at the beginning of the acceleration period. Small (about 200 nm long), isolated and strongly inhomogeneous distributed clusters of C-S-H phases are observed. Within 24 hours the C-S-H phases grow continuously to a length of 600 nm, the needle tips have only a diameter of approximately 5 nm. The longitudinal growth takes place from surface

of the clinker grain outwards. The result is a strong interlocking of the microstructure due to the extremely tipped, needle-like shapes.

The structure of µm-scaled portlandite crystal aggregates is determined by stacks of crystals with a thickness between 20 and 200 nm. This leads to large $Ca(OH)_2$ aggregates with a strongly inhomogeneous distribution.

3.4 Pore solution and phase development

To support the ESEM investigations the concentrations of important ions in the pore solution of the OPC with high potassium content were analyzed. From the measurements of concentrations and the subsequent calculation of activities, ionic products and saturation factors, the formation of phases in the microstructure can be traced. The results of the analyses are given in Table 2. Electrochemical balance showed some deficit in negative charges at all times. Activities reflected are by a simple thermodynamic convention that part of the concentration contributes to the formation of phases. They were calculated from the concentrations using the Pitzer approach for high ionic strength [19]. Interaction parameters given by Reardon [20] were applied to the mathematical framework to describe the behavior of the ions in pore solution. From the obtained activities, ionic products according to equations 1-3 were calculated for gypsum, syngenite and portlandite at the reaction times specified in Table 2.

Table 2. Analysis of the pore solution from the paste made from the OPC with high potassium content at w/c=0.4 [mmol/l]

time	SO_4^{2-}	K^+	Na^+	Ca^{2+}	OH^-
10 min	205	463	50	14,9	74
30 min	208	471	52	16,6	81
60 min	205	476	54	19,0	89
90 min	205	460	53	19,8	96
3 hours	188	425	51	17,0	112
6 hours	191	432	55	17,8	118
24 hours	59	655	97	2,4	497

$$IP_{Gypsum}=\{Ca^{2+}\} \cdot \{SO_4^{2-}\} \quad (1)$$

$$IP_{Syngenite}=\{K^+\}^2 \cdot \{Ca^{2+}\} \cdot \{SO_4^{2-}\}^2 \quad (2)$$

$$IP_{Portlandite}=\{Ca^{2+}\} \cdot \{OH^-\}^2 \quad (3)$$

$$\Omega = \text{ionic product/solubility product} \quad (4)$$

In Figure 17, the calculated ionic products are compared with relevant solubility products by calculation of saturation factors according to equation 4. Saturation factors greater then 1.0 are indicating formation of a phase, whereas from values below 1.0 dissolution or absence of the phase can be derived. Solubility data from Greenberg & Møller [21] were used for syngenite ($3.37 \cdot 10^{-8}$ at 20°C) while thermophysical data from Babuskin et al. [22] were used to calculate the solubility products for portlandite ($5.54 \cdot 10^{-6}$) and gypsum ($2.14 \cdot 10^{-5}$).

In Figure 17, it can clearly seen, that there is a strong supersaturation for syngenite (Ω=1.3-1.9) from the beginning of the hydration until up to 6 hours, whereby precipitation of gypsum is also indicated (Ω=1.3-1.7). After 24 hours there is an overwhelming undersaturation for both phases (Ω<0.04), showing them to be absent from the microstructure. Saturation factors for portlandite are

below Ω=1.0 in the first hour of hydration and then constantly rise. So, formation of portlandite is not likely to take place in the first hour of the hydration of the investigated cement paste, but is strongly proceeding later on. All these conclusions are in good agreement with ESEM observations.

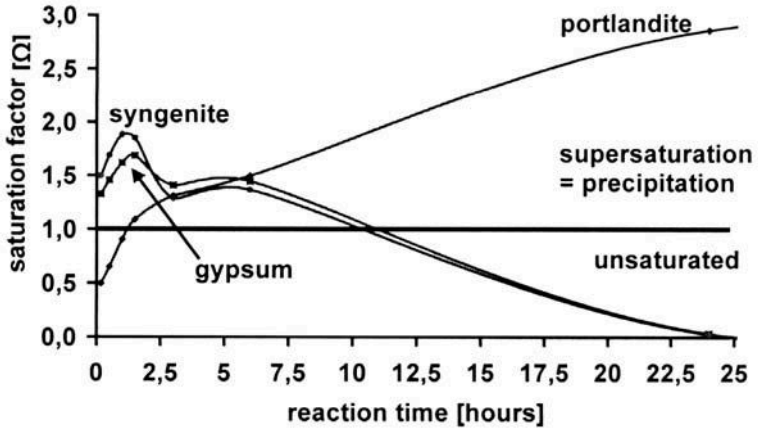

Figure 17. Indicated presence of relevant phases over reaction time calculated from pore solution concentrations.

3.5 Hydration of OPC at other temperatures

The investigations in hydration of OPC were mainly performed at room temperature. The phases found after 2 days were, as indicated in Figure 16, C-S-H phases (length up to 1 µm), ettringite (length up to 2.5 µm), portlandite and a tetracalciumsulfoaluminatehydrate. EDX-analyses of the latter phase showed a deficit in SO_3-content, when compared to monosulfate ($C_3A{\cdot}CaSO_4{\cdot}12H_2O$), indicating the formation of a solid solution between monosulfate and $C_3A{\cdot}Ca(OH)_2{\cdot}xH_2O$, with x ranging between 13 and 19 [23]. However, the phase detected in the investigations described here is likely to change with temperature.

To quantify the influence of temperature, ESEM investigations were performed and correlated with thermodynamic calculations based on the data given by Babuskin et al. [22] using the Gibbs-Helmholtz approach (Eq. 5). For these calculations it was assumed that C-S-H, portlandite and ettringite are formed over the whole range of temperatures from 5°C to 65°C during the early part of hydration. After consumption of the sulfate from the set regulator (gypsum, anhydrite) and from the clinker surface (alkalisulfate) with water and C_3A to ettringite, further reaction of C_3A can lead to formation of monosulfate or C_4AH_x. The formal expressions considered for the further reaction of C_3A are given in equations 6 and 7. The dependence of the formation of $C_3A{\cdot}CaSO_4{\cdot}12H_2O$ or C_4AH_{19} on temperature as obtained from thermodynamic calculations is given in Figure 18.

$$\Delta G_{T,P} = \Delta H - T \cdot \Delta S \qquad (5)$$

$$C_3A{\cdot}3CaSO_4{\cdot}32H_2O + 2\ C_3A + 4\ H_2O \rightarrow 3\ C_3A{\cdot}CaSO_4{\cdot}12H_2O \qquad (6)$$

$$2\ C_3A + 2\ Ca(OH)_2 + 36\ H_2O \rightarrow 2\ C_4AH_{19} \qquad (7)$$

Only a reaction according to equation 6 leads to a decrease in the primary formed ettringite and formation of monosulfate, as it is assumed in many textbooks on cement hydration. A reaction following equation 7 would yield a hydration of C_3A to a sulfate-free tetracalciumaluminatehydrate, so that there would be no reduction in the amount of the primary formed ettringite. As can be seen from Figure 18, the formation of monosulfate is not likely at room temperature, but becomes favourable with increasing temperature. At room temperature and below, C_4AH_{19} is the product to be formed as indicated by calculation.

Formation of C_3AH_6 and a solid solution between monosulfate and C_4AH_x was not considered in the calculations as there is a internal inconsistency in the data given by Babuskin et al. (C_3AH_6) or there are no thermodynamic data available (solid solution members).

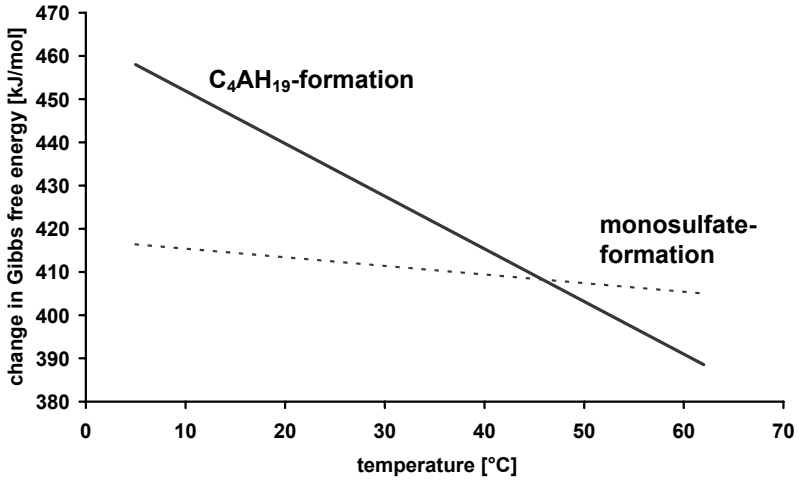

Figure 18. Change in Gibbs free energy during reaction of C_3A to C_4AH_{19} or monosulfate in dependence of temperature.

Experimental investigations were carried out on a sample of OPC paste hydrated for 21 days at 5°C and for 3 days at 62°C.

Hydration of OPC at 5°C (Figures 19a and 19b): The observed ettringite crystals have a length of up to 4 µm, a much greater value as compared with room temperature. Monosulfate or tetracalciumsulfo-aluminatehydrate could not be detected. Only pure C_4AH_x is formed (Figure 19b), which is in agreement with thermodynamic calculations (Figure 18).

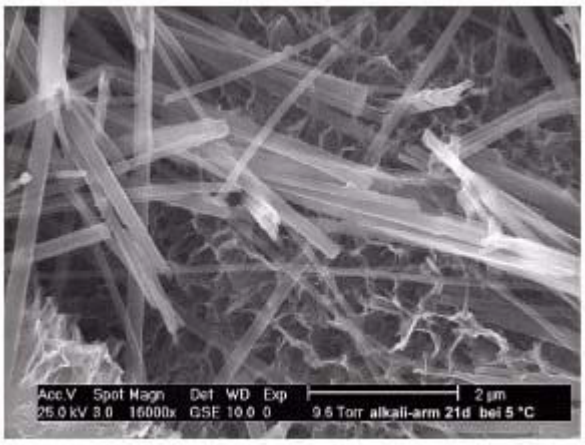

Figure 19a. Microstructure after 21 days hydration time at the temperature of 5 °C: very long prismatic ettringite (up to 4 µm).

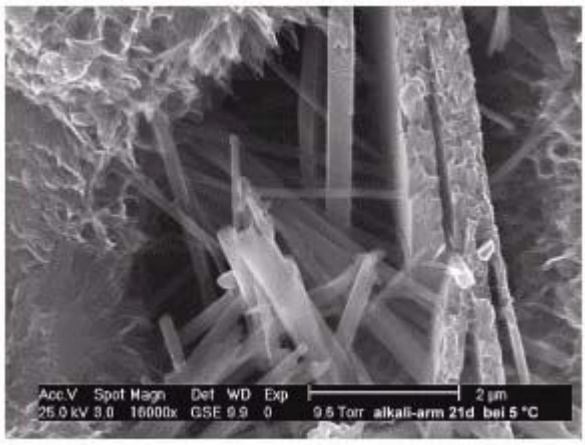

Figure 19b. Microstructure after 21 days hydration time at the temperature of 5 °C: hexagonal calciumaluminatehydrate.

Hydration of OPC at 62°C (Figures 20a and 20b): At this temperature ettringite, monosulfate, C-S-H, portlandite, hydrogarnet and hydrotalcite were observed. Ettringite formed at 62°C has a similar length to that crystallized at room temperature. As indicated by calculations, monosulfate becomes a stable phase, detectable by ESEM, whereas no sulfate-free C_4AH_x could be analyzed by EDX. In the areas of completely dissolved clinker grains, formation of hydrotalcite $Mg_6Al_2[CO_3(OH)_{16}]4H_2O$ (thin plates with a thickness of approximately 25 nm) and hydrogarnet

were observed. Hydrogarnet is a series of solid solutions of C_3AH_6, C_3AS_3, C_3FH_6 and C_3FS_3 that crystallize in a cubic shape.

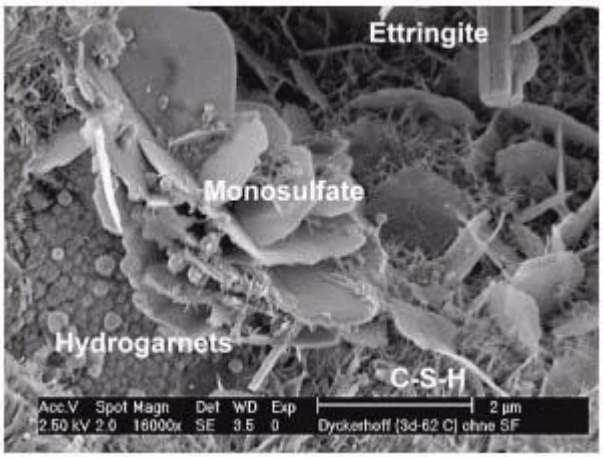

Figure 20a. OPC after 3 days at 62 °C: area of a completely hydrated clinker grain; hydrogarnet: solid solution of C_3AH_6, C_3AS_3, C_3FH_6 and C_3FS_3.

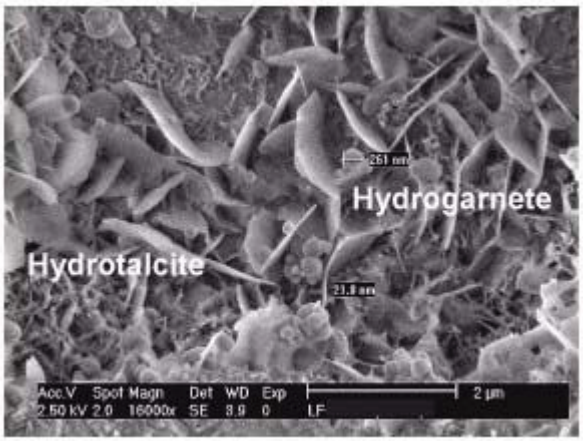

Figure 20b. OPC after 3 days at 62 °C: area of a completely hydrated clinker grain: hydrogarnet and hydrotalcite $Mg_6Al_2[CO_3(OH)_{16}]4H_2O$.

At room temperature, monosulfate is metastable with respect to ettringite and calciumaluminate-hydrate. This can be illustrated by the following experiment: monosulfate and water were stored at 22 °C in a glove box. After a relatively short period of time, monosulfate dissolves and the formation of hexagonal-plate calciumaluminatehydrates as well as ettringite is visible (Figures 21a and 21b).

Figure 21a. Storage of monosulfate in water at 22 °C: dissolution of monosulfate and formation of ettringite and calciumaluminatehydrate.

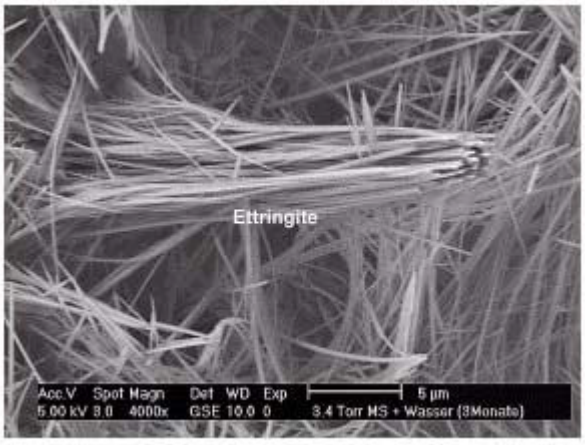

Figure 21b. Storage of monosulfate in water at 22 °C: formation of aggregates of parallel-grown ettringite crystals.

4. CONCLUSIONS

It has been shown that the Environmental Scanning Electron Microscope offers distinct benefits over a conventional SEM on the observation of hydrate phases. The hydration process can be traced realistically and the structures can be reproducibly imaged. It is possible to observe images of the temperature-and vacuum-sensitive and only several nanometer–thick hydration products of OPC. More especially, new insights for the early hydration state can be obtained. Sample preparation artifacts are very limited.

Comparative studies using the ESEM-FEG in different operating modes, for example, wet- (ESEM mode) and high vacuum- (conventional SEM) mode have been carried out. It can be shown that with the traditional methods, (drying, coating, beam damage) changes in the morphology of the C-S-H phases are dramatic.

Furthermore, the article describes the investigations of the phase development during the hydration of OPC from induction to the final period. The results are summarised in a scheme for the normal hardening process and can be correlated with phase development derived from ion concentrations in the pore solution. The formation of syngenite during the early part of hydration, derived by means of ESEM, was confirmed by these calculations, as there is a strong supersaturation for syngenite indicated.

The comparison of the ESEM investigations with the DC analyses reveals that the two typical maxims in these DCA-curves give a good correlation to the microstructure development. The second maximum of the DCA-curves (acceleration period) corresponds mainly to the first appearance of C-S-H phases.

REFERENCES

[1] Powers, T.C.,Helmuth, R.A. (1953) Theory of Volume Changes in Hardened Pordland Cement Paste during Freezing , Proc. Highway Research Board 32, 285

[2] Powers, T.C. (1960) Pysical Properties of Cement Paste, Proc. 4. Int. Symposium on the Chemistries of Cement, Washington, Vol. II, S.577

[3] Feldmann, R.F., Sereda, P.J. A Model for Hydrated Portland Cement Paste as deduced from Sorption length Change and mechanical Properties (1968), Materials and Structures 1, 509

[4] Kondo, R., Daimon, M. Phase Composition of hardenet Cement Paste (1974), auf dem VI Int. Congress on the Chemistry of Cement in Moskau

[5] Richartz, W., Locher, F.W. Ein Beitrag zur Morphologie und Wasserbindung von Calciumsilicathydraten und zum Gefüge des Zementsteins (1965), Zement Kalk Gips 18, S. 449 – 459

[6] Locher, F.W.; Richartz, W.; Sprung, S. Erstarren von Zement Teil 1: Reaktion und Gefügeentwicklung (1976), Zement Kalk Gips 29, S. 435 - 442

[7] Locher, F.W.; Richartz, W.; Sprung, S. Erstarren von Zement Teil 2: Einfluß des Calciumsulfatzusatzes (1980), Zement Kalk Gips 33, S. 271 - 277

[8] Locher, F.W.; Richartz, W.; Sprung, S.; Sylla, H.-M. Erstarren von Zement Teil 3: Einfluß der Klinkerherstellung (1982), Zement Kalk Gips 35, S. 669 - 676

[9] Locher, F.W.; Richartz, W.; Sprung, S.; Rechenberg, W. Erstarren von Zement Teil 4: Einfluß der Lösungszusammensetzung (1983), Zement Kalk Gips 36, S. 224 - 231

[10] Setzer, M.J. Einfluß des Wassergehalts auf die Eigenschaften des erhärteten Betons (1977), Dt. Ausschuß für Stahlbeton Heft 280

[11] Wittmann, F.H. Grundlagen eines Modells zur Beschreibung charakteristischer Eigenschaften von Beton (1977), Dt. Ausschuß für Stahlbeton Heft 290

[12] Taylor, H.F.W. Cement Chemistry (1992) Academic Press Limited San Diego, Second Printing

[13] Massazza, F., Daimon, M. Chemistry of Hydration of Cements and Cementitous Systems (1992) IX Int. Congress on the Chemistry of Cement in New Dehli, Congress Reports- Vol.1 S. 383 – 448

[14] Meredith, P., Donald, A., Luke, K. Pre-induction and Induction Hydration of Tricalcium Silicate: An Environmental Scanning Electron Microscopy Study (1995) Journal of Material Science 30, Cambridge , S.1921 – 1930

[15] Jennings, H.M. A Model for the mocrostructure of calcium silicate hydrate in cement paste (2000) Cement and Concrete Research 30, S. 101 - 116

[16] Mindess, S., Young, J. F. Concrete (1981) Prentice-Hall, New Jersey

[17] Stark, J., Möser, B., Eckart, A. New approaches to cement hydration (2001) ZKG International 54, S. 52 – 60 and 114 – 119

[18] Hader, K. Untersuchung der Zement-hydratation im frühen Erhärtungsstadium mittels ESEM-FEG, Diplomarbeit 2000 an der Bauhaus-Universität Weimar

[19] Pitzer, K. S. (1991) Activity coefficients in electrolyte solutions.- 2.th edition.- Boca Raton: CRC-Press

[20] Reardon, E. J. (1990) An ion interaction model for the determination of chemical equilibria in cement/water systems. In: Cement and Concrete Research, Vol. 20, pp. 175-190

[21] Greenberg, J. P.; Møller, N. (1989) The prediction of mineral solubilities in natural waters: A chemical equilibrium model for the Na-K-Ca-Cl-SO_4-H_2O system to high concentration from 0 to 250°C. In: Geochimica et Cosmochimica Acta, Vol. 53, pp. 2503-2518

[22] Babuskin, V. I.; Matveev, G. M.; Mcedlov-Petrosjan, O. P. (1986) Termodinamika silikatov.- 4th edition-Moskow: Strojizdat

[23] Glasser, F. P.; Kindness, A.; Stronach, S. A. (1999) Stability and solubility relationships in AFm phases Part I. Chloride, sulfate and hydroxide. In: Cement and Concrete Research, Vol. 29, pp. 861-866

NEW APPROACHES TO CEMENT HYDRATION IN THE EARLY HARDENING STAGE

Möser B. and Stark J.

F.A. Finger-Institute for Building Material Science, Bauhaus-Universität Weimar,
E-mail: bernd.moeser@bauing.uni-weimar.de and jochen.stark@bauing.uni-weimar.de

Bernd Möser

Humboldtstrasse 31
99423 Weimar / Germany

Date of birth:	March 27, 1953
Nationalty:	German

EMPLOYMENT

1985 - present	Bauhaus-University Weimar F.A. Finger-Institut for Building Material Science Member of scientific staff and head of the electron microscopic laboratory
1979 - 1985	Member of scientific staff of the HAB-University Weimar

ACADEMIC CAREER

1985	Final work for PhD: “Investigations on High Alumina Ceramics Doped with Transition Metal Oxides of the Fourth Period by means of Quantitative Electron Probe Microanalysis and Valance Band Spectroscopy”
1974 - 1979	Studies of physics at Martin-Luther University Halle Topic final work: “Investigations on the Real Structure of Cu-Ni, Fe-Al, Al-Zn and Al-Mg Alloys by means of Positron Annihilation”

HIGH RESOLUTION IMAGING OF WET BUILDING MATERIAL SAMPLES IN THEIR NATURAL STATE USING ENVIRONMENTAL SCANNING ELECTRON MICROSCOPE

Möser B. and Stark J.

F.A. Finger-Institute for Building Material Science, Bauhaus-Universität Weimar;
E-mail: bernd.moeser@bauing.uni-weimar.de and jochen.stark@bauing.uni-weimar.de

ABSTRACT

ESEM technology used in conjunction with a high resolution scanning electron microscope with Schottky type field emission gun promises a decisive expansion in the investigation capabilities in the field of building material research. With this instrument sensitive water-containing constituents of the microstructure can be observed electron-optically in their original state down to a range of a few nanometers. Artifacts caused by the sample preparation and the effects of high vacuum in the sample chamber, which are typical of conventional standard high-vacuum SEM, can be eliminated. The capability of ESEM-FEG to work in different operating modes (wet, low-vacuum-, high-vacuum- and low-voltage mode) were also used to explain changes in the nano- and microstructure which occur during the preparation and examination of some characteristic building material samples. By direct comparison of the same sample area using the different operating modes it was found that in the investigation of samples with different types of water-bonding, the original state can fundamentally by changed both morphologically and chemically. C-S-H phases which are the main binding phases in all Portland cement-based systems are thermally very unstable phases which can be destroyed by necessary preparation methods and by electron bombardment.

1. INTRODUCTION

The visualisation of structures resulting from processes that take place at the scale of a few nanometers is important when studying the properties of concrete and mortars. Electron microscopy is in principle capable of acquiring images of structural constituents at this size. Unfortunately, studies using standard conventional high-vacuum electron microscopes (conventional SEM) are subjected above all to serious limitations:

- The specimens must be solid.
- The specimens must be high-vacuum stable (essentially nonvolatile in nature) or correspondingly prepared.
- The specimens must in general be electrically conductive or be made conductive by a coating or sputtering of the surface.
- The specimens must be stable due to the electron-specimen interaction under high vacuum.

Therefore, the previous investigations carried out with conventional SEM have been based on special, multi-stage sample preparation methods. These methods (critical point drying, freeze drying, cryo preparation and so on) are extremely expensive both in terms of time and apparatus. In addition one has to take into account that the individual sample preparation stages take place without control of possible sample changes so that during the investigation of the samples there is no certainty whether or not, after a series of preparative stages, the “true” specimen structures are being observed and analysed or which specimen changes (artifacts) are caused by the preparation. In principle, it is also impossible by means of the conventional SEM to follow in-situ the dynamics

of dissolving, crystallisation, re-arrangement and re-organisation processes in which fluid media are involved. In-situ investigations also require uncoated samples.

Since the development of Environmental Scanning Electron Microscope with Schottky type Field Emission Gun (ESEM-FEG) we do not see these limitations anymore. The following important investigative capabilities are available with the ESEM-FEG:

- coating with a conductive film is not necessary
- all samples can, in principle, be investigated in the state in which they were found
- the behaviour of liquids can be observed in-situ
- it is also possible to investigate samples which contain oil or generate large quantities of gas
- it is possible to carry out wetting experiments with water from the supersaturated water vapour phase, since the pressure in the sample chamber can be raised to 1330 Pa [10 Torr]
- performing dynamic in-situ experiments within the microscope chamber (heating/freezing-, (de)hydration- and stress testing experiments)
- the production of quality images at low accelerating voltages < 5 kV (wet and low-vacuum mode) on samples with low mean atomic numbers and low density
- no sample coating and X-ray absorption interference in the Energy Dispersive X-ray analysis (EDX)
- less sample contamination caused by beam irradiation influences the high resolution image and the EDX analysis

The ESEM-FEG can be operated in different modes (ESEM, low-vacuum SEM, high-vacuum SEM and in the low-voltage mode). By using the different operating modes it was found that in the investigation of samples with different types of water-bonding the original state can be fundamentally changed both morphologically and chemically [1 - 3].

Investigations of frequently analysed building material samples show how the morphology and chemical composition of the sample is affected namely through high vacuum, contamination, temperature impact (application of an electrically conductive coating), and due to the electron beam of the SEM, as well as the coating film itself.

When using the previous traditional methods of electron microscopy the operator faces the difficult task of evaluating and interpreting the microstructure and the EDX analysis. One has to assess the influence of the high vacuum in the specimen chamber as well as the influence of the necessary preparation steps on the microstructure and the individual phases.

In the past it was not possible to provide a clear answer to these questions. So these factors were often ignored, assumptions as to possible effects were expressed [4, 5] but often interpreted incorrectly. Only through the use of ESEM technology with the capability of direct comparison between the original and the prepared states has it become possible to provide clear information.

The advantage of using the ESEM for the investigation of early hydration stages of a multi-component system as ordinary Portland cement (OPC) is explained in [6 – 9].

2. METHODS

Investigations were carried out using a high resolution ESEM with the high-brightness FEG source (FEI XL30 ESEM-FEG) which guarantees a resolution better than 2 nm at 30 kV at both 7 Torr and high vacuum conditions. This microscope is combined with an EDX for chemical analysis. A special Gaseous Secondary Electron Detector (GSED) is used in the water vapour atmosphere of the

ESEM to permit secondary electron imaging in a gaseous environment. During the investigation the sample can be cooled or heated between –10 and +60 °C. It is also possible to change the sample surface mechanically in the microscope chamber with a micromanipulator or to bring it into contact with liquids using the microinjector.

Microanalytical investigation of the chemical composition of the hydrated phases in their native state by EDX analysis is only partially possible due to small size (for example: C-S-H phases are nanometer scaled needle-shaped crystals), the surface roughness, the water content and because of the "beam skirt" in the ESEM mode. The gas pressure in the sample chamber causes significant scattering of the primary electron beam and results in the formation of a "skirt" of electrons. The diameter of this skirt can be many tens of microns wide [10 - 12]. Furthermore it comes to an interaction of the emitted X-rays with the gas molecules in the specimen chamber. By this, the X-rays are absorbed on their way to the EDX-detector. The absorption of characteristic X-rays and of the X-ray continuum in the atmosphere of the sample chamber leads furthermore to a fluorescence excitation of the gas molecules [13]. All these effects can be weakened down by reducing the gas path length and the sample pressure.

In order to assess how the sample preparation and high vacuum affect the material and morphological nature of the water-containing samples it is helpful to observe the same sample area under the following conditions:

2.1 ESEM-wet mode: (original state)
Some selected sample areas are observed, stored and analysed at different magnifications in a water vapour atmosphere using different relative humidities. The corresponding stage positions (x, y, z) of the selected sample areas are also stored.

2.2 Low-voltage mode (high-vacuum)
The effect of the high vacuum on the samples observed in ESEM-wet mode is shown when the sample chamber is evacuated down to the level which is normal for conventional SEM (about 4 x 10^{-4} Pa or 3 x 10^{-6} Torr, the water vapour pressure is then approximately 2 x 10^{-4} Pa). Since only non-conductive and non-coated samples were investigated here in order to observe the influence of high vacuum it was necessary to work with low accelerating voltages of the primary electrons of less than 2.5 kV. The stored stage positions are recalled and the sample areas are compared with the stored ESEM-wet images.

In order to improve the resolution, especially at very low accelerating voltages of 1 kV, a Sirion XL30 S FEG form FEI, and a new in-lens cold cathode field emission SEM S-5200 from Hitachi (FESEM: resolution 1.8 nm at 1 kV) were used.

2.3 Standard high-vacuum SEM (HV-SEM: high-vacuum, coating or sputtering)
A comparison with the preparation methods normally used for conventional SEM is carried out by removing the sample together with the sample holder from the microscope chamber after previously marking the position of the sample holder. The sample is then coated with a conductive film to avoid electrical charges at higher accelerating voltages (> 2.5 kV). This is realised either in a high vacuum by resistance vaporisation of carbon, or by sputtering with silver. For rough samples a layer thickness between 5 and 30 nm, depending on the coating material, is necessary for an adequate coherent coating on all sides. After coating with a conductive film, the sample is put back to the stage of the ESEM again, and the stored sample areas are examined.

By direct comparison of the same sample areas it is now possible to detect the changes in the water-containing samples being a result of the stressing by thermal radiation (carbon coating) and the effect of the carbon film or the sputtered layer, such as the inherent structure of the layer itself, the

covering of phases in the range of a few nanometers (masking), structuring through shadowing, etc. (vaporisation artifacts).

Possible artifacts which, for example, can occur during in-situ hydration experiments in the ESEM-wet mode, occur in the form of thin gel films on the sample surface and can easily be removed by the micromanipulator under direct electron-optical observation (in-situ preparation). During hydration experiments which are not carried out inside the sample chamber of the ESEM and during the storing of the hydration samples it should be borne in mind that these must take place in a CO_2-free atmosphere (glove box).

The Electron Backscatter Diffraction (EBSD) is a new and different application to obtain more crystallographic information at sub-micron resolution. It allows the linking between morphology (ESEM, SEM), chemistry (EDX and/or WDX) and crystallography for example for the phase identification of crystals with the same chemical composition (vaterite, aragonite and calcite).

3. RESULTS AND DISCUSSION

3.1 The structure of cement-based materials – comparative investigations

In principle investigations with a conventional SEM on samples in the early hardening stage seem to make little sense, even when much time and a very sophisticated apparatus is used in the preparation process. Investigations have shown that such structures (see Figure 1) - even when prepared very cautiously (dehydration through freeze-drying, critical point drying and others) are changed significantly through extraction, de-mixing, recrystallisation, emission of chemically and physically bonded water.

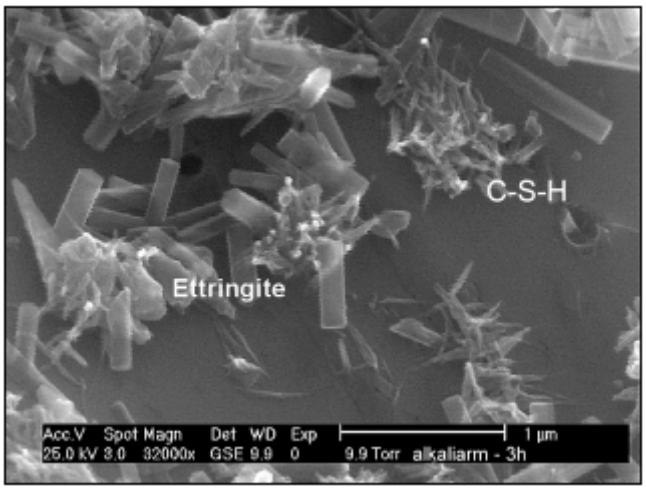

Figure 1. Microstructure of a OPC with low potassium content after 3 h hydration time. Individual clusters of C-S-H fibres (approx. 200 nm) and ettringite

Furthermore, mobile phases are enriched on the surface very often which are capable of disguising other phases completely. In Figure 3 for example one can recognise the sodium- and potassium containing salts (pore solution) efflorescing on the surface of the sample of a hydrated Portland cement due to drying, which cannot be observed in ESEM-WET mode at 95 % r. H. (Figure 2).

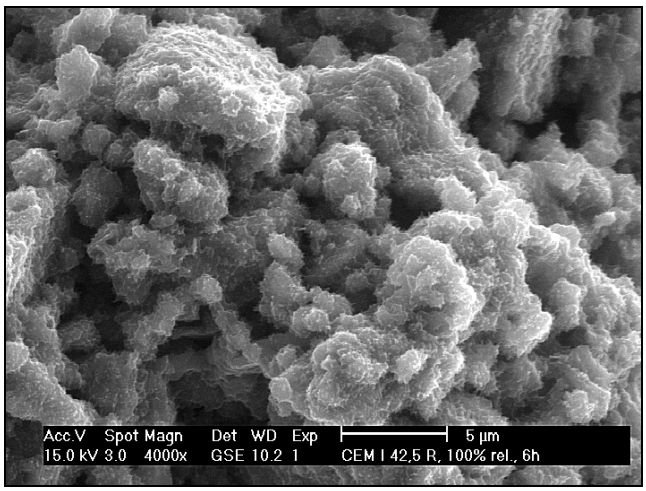

Figure 2. Early hydration of OPC after 6 h in ESEM-wet mode at 95 % r. H.

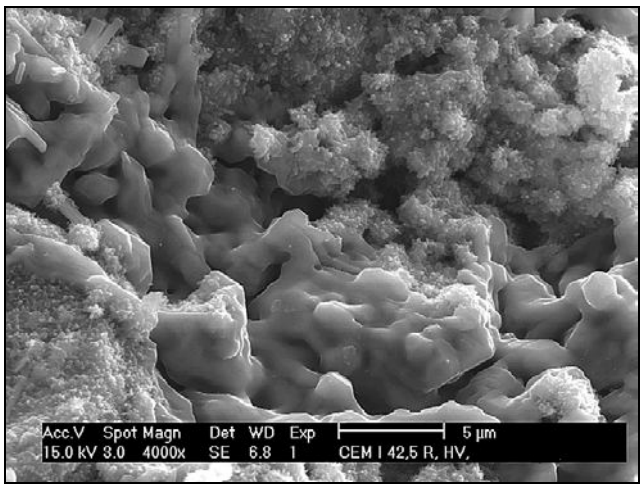

Figure 3. Same sample as in Figure 2 in standard HV-SEM: efflorescence of alkali salts on the sample surface during vacuum drying

Even samples in a hardened condition are in danger of forming artifacts and that even then when the magnification factor is small. It has been shown that a significant share of the cracks in the hardened cement paste matrix and in the contact zone to the aggregates become bigger (see Figure 4 and 5), or they are created in the first place during the drying of the samples in the high vacuum of the coating device and/or the HV-SEM.

Furthermore, it can be shown that even relatively stable crystal-water-containing crystals like gypsum give up some of their chemically bound water simply because of the high vacuum in the sample chamber of the SEM (see Figures 6 and 7). The relatively smooth surface of the gypsum crystals is textured and through the micro crack formation the different crystal orientations become clearly visible.

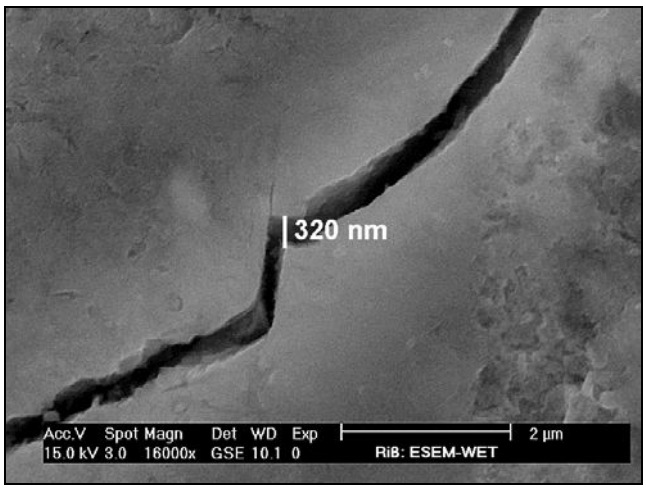

Figure 4. microstructure of hardened cement paste with crack (width: 320 nm) in ESEM-wet mode at 50 % r. H.

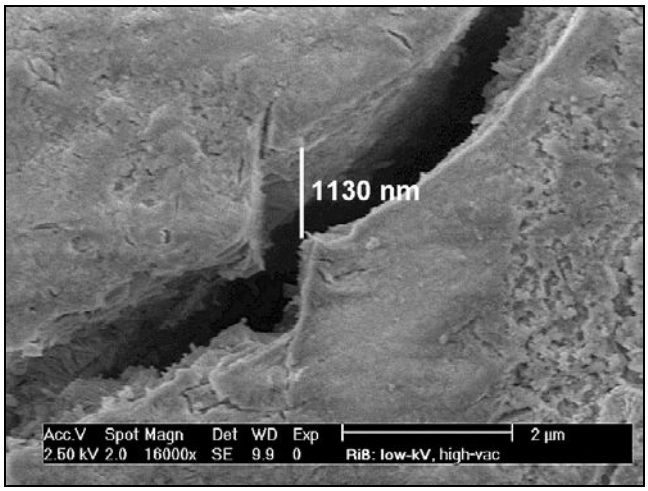

Figure 5. Same sample area as in Figure 4 in low voltage mode: the original crack width has increased to 1130 nm due to high vacuum stressing in sample chamber

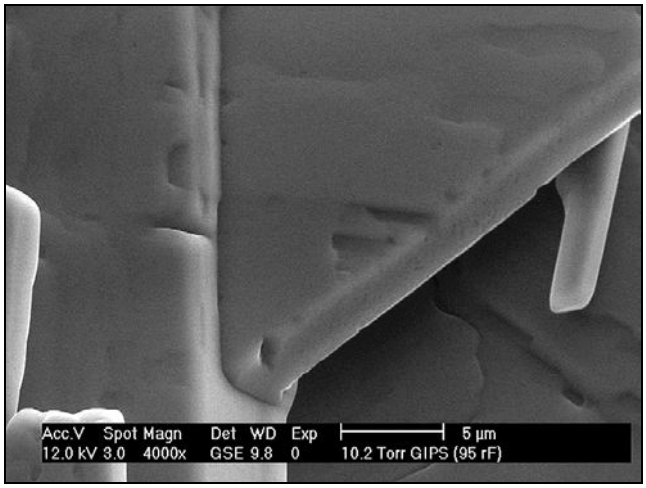

Figure 6. Gypsum crystals with relatively smooth crystal surface in ESEM-wet mode at 95 % r. H.

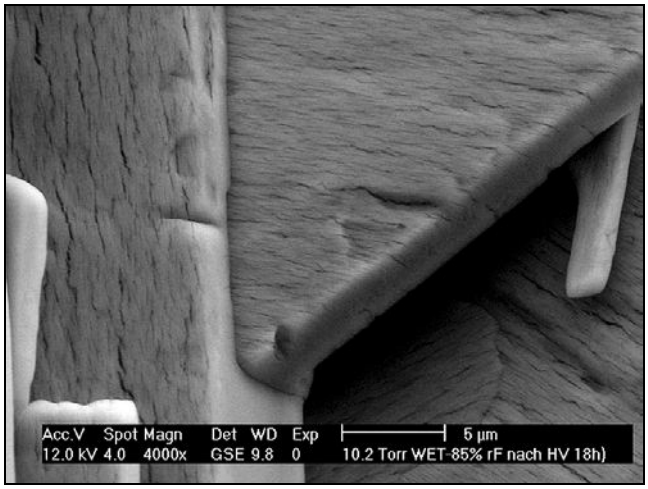

Figure 7. Same sample area as in Figure 6 after high vacuum stressing. Structuring of the surface through dehydration. (escape of crystal water)

The calcium silicate hydrate phases (C-S-H phases) being formed in the process of cement hardening show a very different picture when they are observed by means of conventional electron microscopy. The phases which are formed in the normal hardening process of cement are often described as gel-like, amorphous, tube-like, nap-like, blunt needle-like, and micro- or semi-crystalline with variable composition. Often blunt needle-like or nap-like C-S-H phases with a diameter of 100...130 nm can be observed as far as carbon coated samples are concerned. In contrast to this, the C-S-H phases observed by means of ESEM-wet mode or at a low stress in low-voltage mode appear in a long spiky form with the hydration time advancing.

The hydration progress can be seen mainly in the one-dimensional growth in which the C-S-H phases that are formed during the hydration of the clinker phase alite can reach a length of up to 1.5 µm at a constant diameter of 40 – 60 nm. A growing together of individual phases to form crystal aggregates can often be observed. The needle tips have a diameter of 5 nm and react extremely sensitively to thermal stress under high vacuum conditions. Through million fold interleaving of the nanocrystalline spiky C-S-H phases a solid structure is created.

To explain the observed discrepancy between the ESEM and the HV-SEM images, the influence of the coating and sputtering on the morphology was studied. For carbon coating a high vacuum vaporisation device according to Bredlay was used. The material was 1.13 nm tobermorite. Tobermorite is a calcium silicate hydrate phase which is formed during the autoclaved hardening of sand-lime brick. Tobermorite keeps its structure even under high vacuum conditions; this has been proven by comparative investigations with ESEM-wet. For this reason, changes of the preparation through thermal stress because of heat radiation during the coating process or because of the vaporisation layer itself (vaporisation artifacts) can be followed easily.

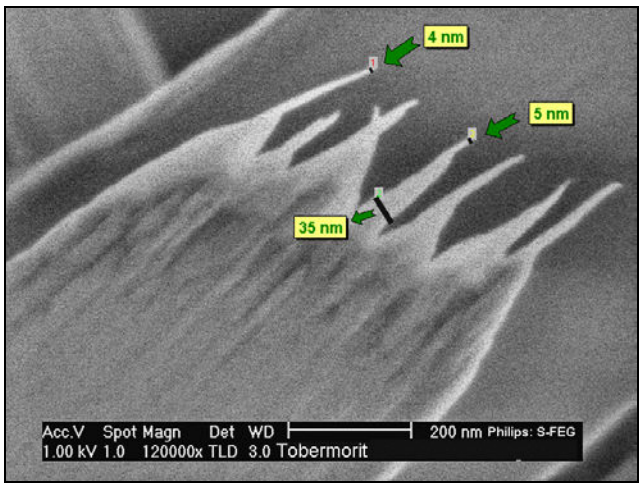

Figure 8. Tobermorite aggregate depicted by means of FE-SEM Sirion at ultra high resolution and very low accelerating voltage of 1 kV

The fine structure that is to be seen on uncoated preparations in low voltage mode at ultra high resolution is created by the directed aggregation of individual sword-like tobermorite crystals during the growth period.

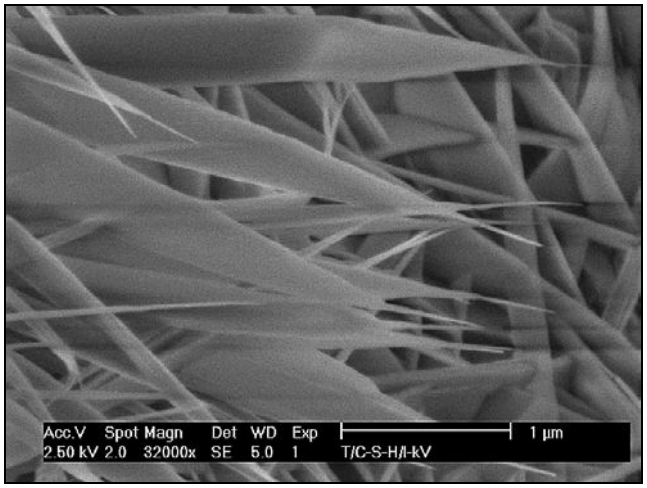

Figure 9. Detail of tips of the „sword-like“ tobermorite crystals in low voltage mode at 2.5 kV

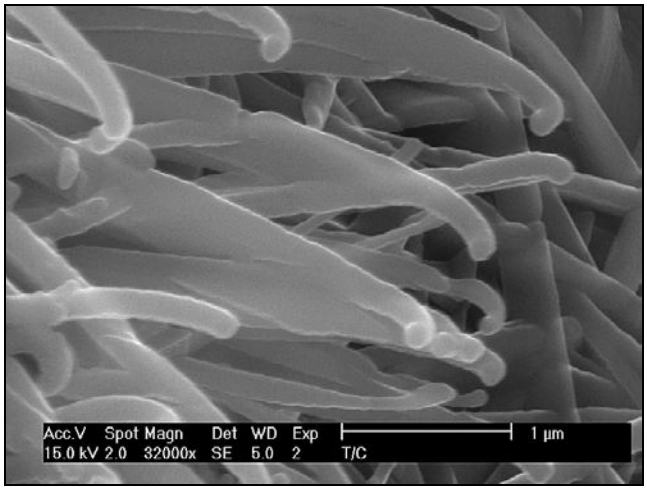

Figure 10. Same sample area as in Figure 9: deformed crystals coated with an approximately 30 nm carbon layer for the investigation in the HV-SEM (no structural stability)

This structurisation is to be seen very clearly 200 nm underneath the crystal tips, which are 5 nm thick, at the “comb-like” end. (Figure 8)

The influence of the resistance vaporisation with a carbon coating on the morphology of tobermorite which is stable under high vacuum can be seen by comparing Figures 9 and 10 directly. Both figures show the same sample area. The thermal stress of the crystals which occurs under high vacuum during vaporisation leads to a melting and vaporing off of the crystal tips, which are only a few nm thick, or ball-like particles with a diameter of 60 nm are formed.

Through the evaporated carbon layer, which is approx. 30 nm thick, the crystal tips now appear as spheroides with a diameter of approx. 130 nm. Figure 9 also shows that the “gel-like” structure of the carbon coating is depicted and not the surface structure of the sample.

Through shading effects on the strongly structured sample we have different layer thicknesses of the evaporated carbon film. The observed bending of the approx. 20 nm thick crystals occurs because of water extraction as a consequence of heat radiation and because of the surface tension coming about through the cooling off of the carbon layer. When the sample is sputtered with a 10 nm thick Ag-layer instead, we can see in principle the same effects. However, the sputter-layer tends to form clusters interferes with high resolution.

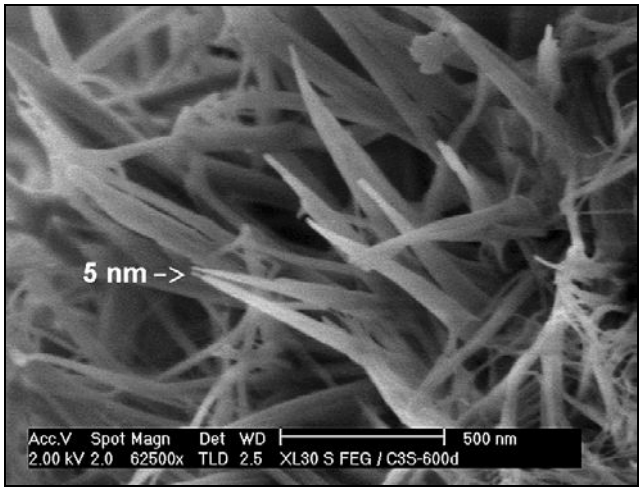

Figure 11. C-S-H phases (C_3S-hydration) with needle-like structure before radiation damage by electron bombardment in high vacuum

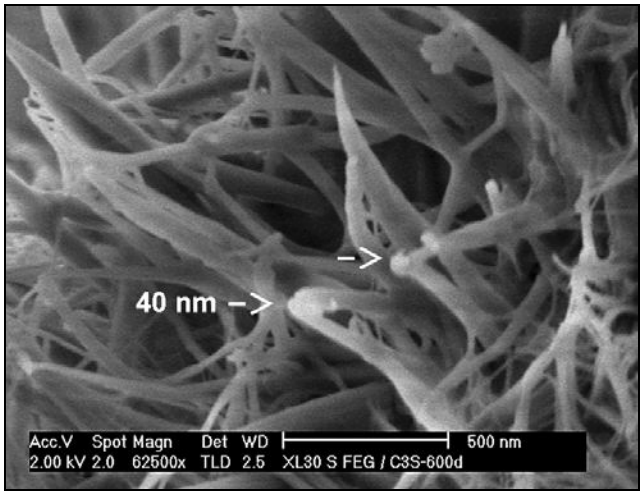

Figure 12. Same sample area as in Figure 11: damaged C-S-H phases: vaporized and shrunk fibre tips in high vacuum

When you compare Figures 11 and 12 which were made with the FE-SEM Sirion, you can see that the C-S-H phases formed during the Portland cement hydration from alite and belite are damaged at much lower beam current at 10 pA in comparison with tobermorite in high vacuum. The excitation processes cause a melting and vaporisation of the fibre tips. This can be explained by the higher sensitivity of the phases to thermal stress, but mainly this is because of the much lower heat conductivity under high vacuum and because of the very unfavourable relation between length and diameter. Under direct electron-optical observation it is possible here to comprehend the process that takes place during the coating in high vacuum.

3.2. Electron Probe Microanalysis and Imaging at Low Beam Voltage and Current

Usually the analysis of most samples is performed at 15 – 20 kV. The X-ray and resolution will be reduced because of electron scattering. The electron scattering is dependent of the electron energy, the density of the sample, and the deviation from the normal incidence of the electron beam. To achieve a better resolution, a lower voltage should be used. This causes a reduced interactive volume within the sample compared to higher accelerating voltages. Figure 13 illustrates the stimulant single scattering volume of the electron beam as determined by Monte Carlo calculations of 4000 electron trajectories at 15 and 2.5 kV electron energy for a calcium silicate hydrate (1.13 nm tobermorite).

As we can see very clearly, the conventional microanalysis at high voltages means an excitation volume of the electrons of some µm^3. Thus, not only one phase is analysed but a number of different ones. This applies especially for phases of low density (C-S-H phases have a density of approximately 2.2 g/cm^3) and a size of much less than 1 µm. By comparison the low-voltage mode of 2.5 kV produces a high spatial resolution (between 50 and 100 nm) for X-ray microanalysis, which relates to the approximate thickness of an individual C-S-H phase (see Figure 13).

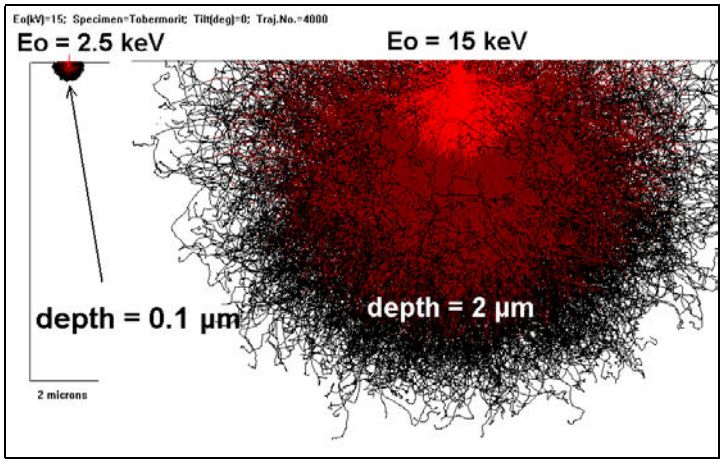

Figure 13. Monte Carlo calculations of 4000 electron trajectories at 15 kV (right) and 2.5 kV (left – the same scale) for a 1.13 nm tobermorite crystal

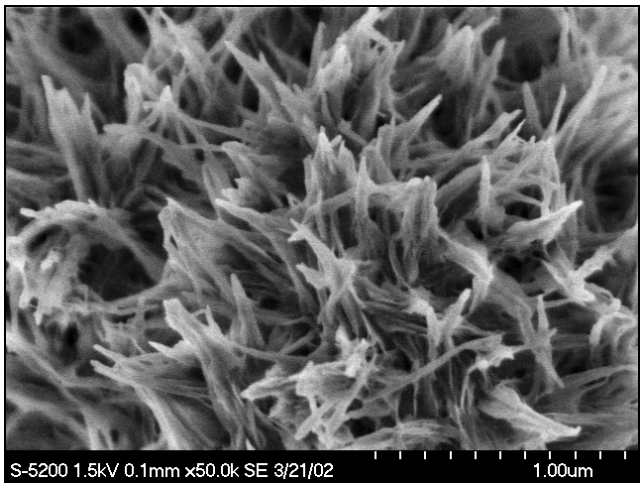

Figure 14. high resolution image at low accelerating voltage using the Hitachi FE-SEM S-5200 of C_3S, hydrated destilled water

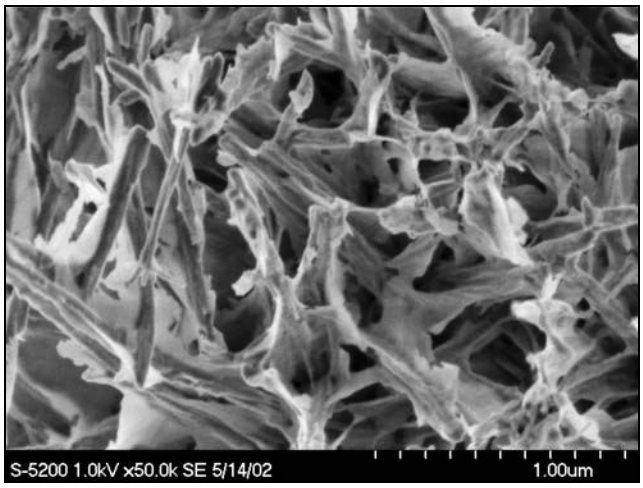

Figure 15. the same sample as in Figure 14 but C_3S hydrated with pore solution pressed out of OPC with a high potassium content

An analysis of uncoated and non-conducting specimens at the nanometer scale can only be obtained when you work in a range of low accelerating voltages in combination with a sensitive, high resolution X-ray spectrometer.

There are further problems as to the microanalysis of cement-based material because we have water-containing nanophases and pore solution in the microstructure.

If one compares the images of the structure of uncoated C_3S in Figures 14 and 15 made by the Hitachi FE-SEM S-5200 at 1 – 1.5 kV, one can clearly see that the C-S-H phases are covered with pore solution (mainly with KOH). The dried pore solution sets up very thin films (thickness < 10 nm) around the C-S-H phases. An increasing of the accelerating voltage to > 2 kV leads to the loss of the surface information that is to be seen in the previous images. The thin films are then beamed so strongly that they are not visible anymore. It has also been shown that this fine structure can only be imaged by means of an FE-SEM with a cold field emission gun and not by means of a Schottky emitter as an electron source. The higher gun brightness of the Schottky emitter leads to damage of the sensitive phases due to electron beam (melting and thermal decomposition – see also Figure 12).

But micrometer-size, water-containing crystals like monosulfate or ettringite, can also be damaged in the uncoated state under high vacuum conditions, see Figures 16 and 17 (low thermal conductivity). The damage through the electron beam caused by the temperature rise at the point of impact of the beam leads to the loss of the chemically bound water. This loss of water expresses itself in a bubble formation on the otherwise relatively even crystal surface. This phenomenon will be even stronger when the beam scans over a small area for micro- or point-analysis.

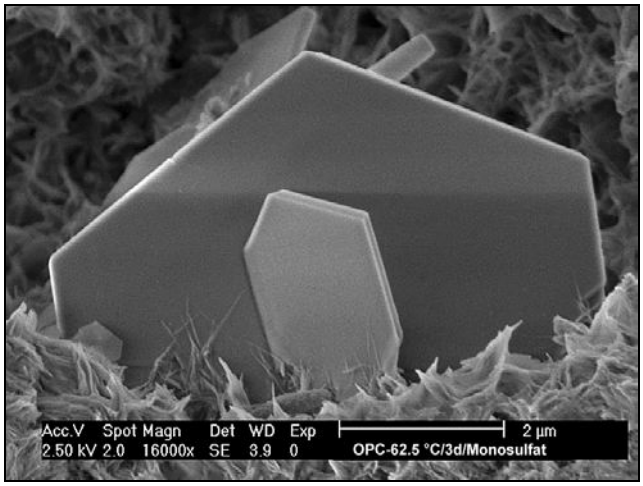

Figure 16. uncoated monosulfate crystals before microanalysis at 5 kV beam energy

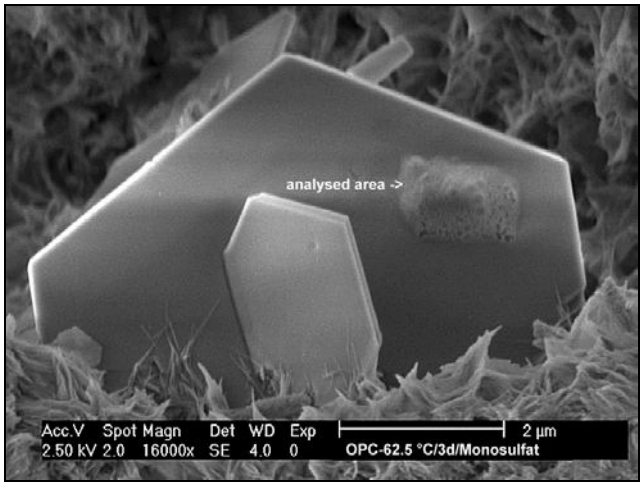

Figure 17. Same sample area as in Figure 16: analysed area exposed to 100 pA beam current (defects due to dehydration – bubbles)

3.3 Phase identification in nanometer range

To obtain further information by microbeam techniques the Electron Backscatter Diffraction (EBSD) can be deployed. EBSD is an accepted and important technique to obtain crystallographic information in the SEM or ESEM at sub-micron resolutions. EBSD is a powerful analytical tool which allows the rapid and accurate measurement of individual crystal orientations, with an accuracy of better than 1 %. It allows the interlinking between crystallography, morphology and chemistry at the same sample area.

Deploying an EBSD-system makes sense especially when you want to investigate crystals which have the same chemical composition but exist in various modifications. This is the case with the often occurring calcium carbonate with its three crystalline polymorphous modifications which are formed for example in the process of carbonation of the hydrated phases of lime mortar, on concrete surfaces or in the structure of deteriorated concrete. The modification change between them can very often not be followed morphologically since calcite is the richest mineral of all in form and surface.

Figures 18 – 21 show the phase identification of calcium carbonate ($CaCO_3$) by means of EBSD-pattern. Calcium carbonate always has the same chemical composition but various modifications (non-crystalline $CaCO_3$, vaterite, aragonite, calcite). Although the patterns shown here were produced by means of HV-SEM which means that they are not optimal because of contamination and charging effects, you can nevertheless clearly distinguish the individual calcium carbonate modifications aragonite and calcite.

Another wide field of deploying an EBSD-system would be the distinction of phases which are chemically very similar but show clear distinctions as to their crystal lattice. (e. g. gypsum and semi-hydrate).

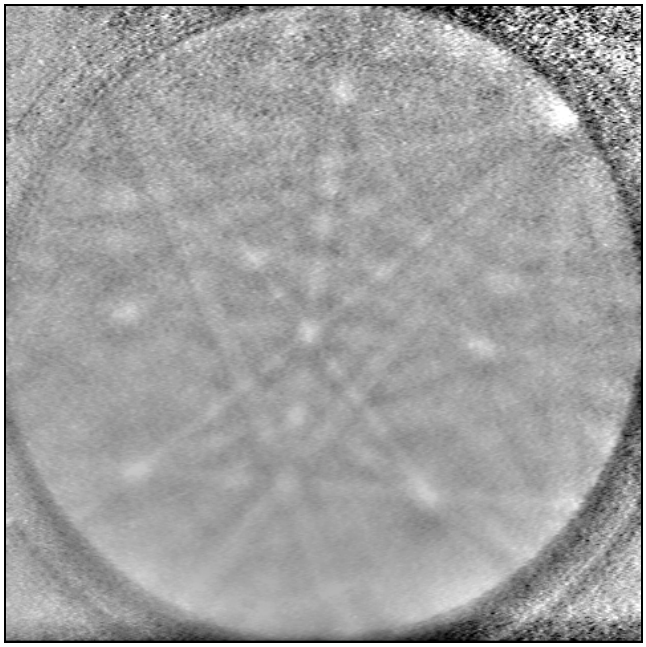

Figure 18. EBSD pattern of aragonite [$CaCO_3$]; taken in the TexSEM-Laboratories, Inc. USA of TSL with the DELPHY System

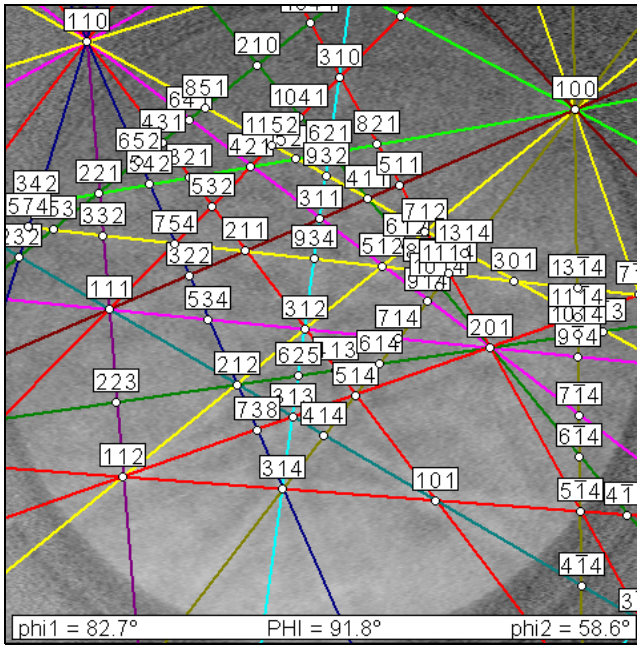

Figure 19. Indexed EBSD pattern of aragonite $CaCO_3$, crystal lattice: rhombic

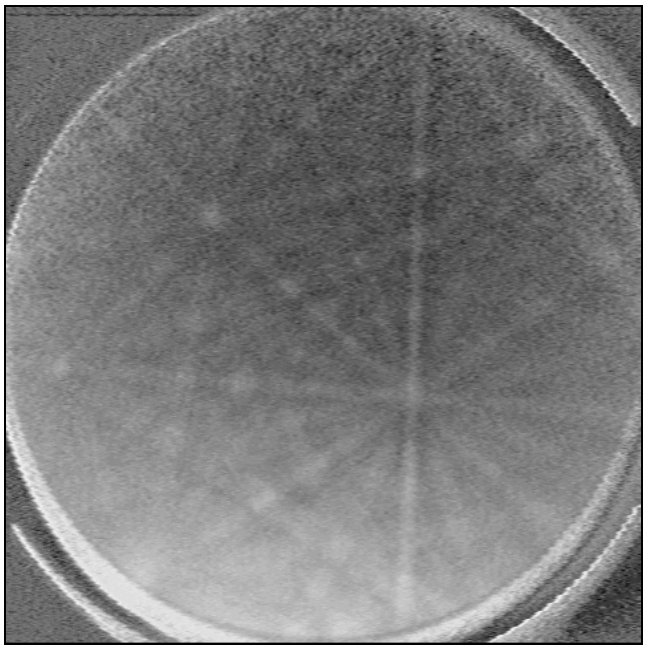

Figure 20. EBSD pattern of calcite [$CaCO_3$]; taken in the TexSEM-Laboratories, Inc. USA of TSL with the DELPHY System

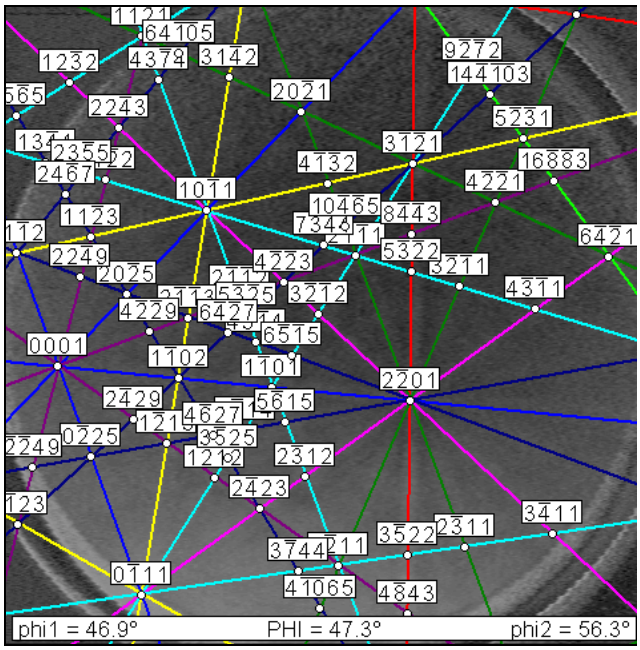

Figure 21. Indexed EBSD pattern of calcite $CaCO_3$, crystal lattice: trigonal

It should be possible, too, with the EBSD-system to identify phases on crystals which are only a few nm big, since the signal comes from a depth of 100 atom layers maximum. It woulds be interesting to see whether or not one gets pattern of the calcium silicate hydrate phases (C-S-H), which are formed during normal cement hydration respectively during the hydration of alite and belite, and if so, to which crystal structure they belong. These phases are generally seen as “ amorphous to X-rays ” because of their small crystal size and/or a strongly disturbed lattice, so they cannot be determined by means of XRD.

4. CONCLUSIONS

This article shows that it is possible by means of ESEM-FEG to carry out high resolution scanning electron optical and micro beam analysis investigations on sensitive water-containing building material samples in their original and unaltered state. The formation of the extremely sensitive hydrate phases which are only a few nanometers in size as well as the influence of concrete admixtures in the early hardening stage can only be followed close to reality by means of ESEM-FEG at present. The preparation time is also greatly reduced. Stopping the hydration process, drying and coating/sputtering of the surfaces are no longer necessary. This eliminates many potential artifact sources that in the past - by using the traditional high-vacuum electron microscopy (HV-SEM) - led to uncertainty in the evaluation of micro- and nanostructures and in some cases to incorrect interpretations.

By means of HV-SEM one reaches high resolution as to temperature- and vacuum-stable samples. But through the formation of a contamination layer in high-vacuum, fine object details may be covered and this decreases the resolution. Furthermore, insulating or poorly conductive specimens being charged on the surface by the electron beam in high-vacuum need a conductive coating/sputtering which covers the real structure, too. Both effects also influence the microanalysis negatively.

In ESEM mode, in contrast, the presence of positive ions in the irradiated gas in the sample chamber prevents the specimen from charging and reduces the contamination effect.
Since the ESEM-FEG can be used in different modes, i.e. ESEM, low- and high vacuum mode as well as low-voltage imaging mode, it is possible to investigate the same sample area under various modes chemically as well as optically. These capabilities were used to clarify object changes (artifacts) which occur when investigating and preparing some characteristic structure constituents by means of conventional methods.

Comparative investigations clearly showed that e.g. C-S-H phases which are formed in the normal hardening process of ordinary Portland cement, and which are often described as “gel-like” not only give up part of their water content in the high vacuum of the HV-SEM but they are severely damaged due to the temperature stress through heat- and electron radiation under vacuum conditions. Only the ESEM made it possible to illustrate the world of the C-S-H phases far more realistically.

The energy dispersive X-ray-spectroscopy offers advantages and capabilities compared with analysis by means of HV-SEM. For example the chemical determination of hydration-, dehydration-, carbonation-, and oxidation processes. The disadvantage of the ESEM mode, however, is the interaction between primary electrons and the emitted X-ray with the gas molecules. These effects can have influences as to the qualitative as well as the quantitative analysis.

By means of ESEM it could be shown that many decisive processes take place in a space of a few nanometers and that the formed phases themselves are only a few nanometers in size in some cases. Therefore, further investigations are important to get even deeper into the “nano-world”. This applies mainly for the capabilities of the chemical analysis and the phase identification. The latter can be carried out by means of Electron Backscatter Diffraction Pattern in the ESEM.

For the X-ray microanalysis of individual phases in the nanometer scale as well as for images of higher contrast, investigations must be carried out in the low-voltage mode. The reduction of the accelerating voltage means a small interactive volume. When an FE-SEM with cold cathode field emission is used it becomes possible to reduce the beam current in such a way that even sensitive phases, like C-S-H phases, are not damaged.

REFERENCES

[1] Neubauer, C.M. Jennings, H. M. (1996) The role of the Environmental Scanning Electron Microscope in the Investigation of Cement-Based Materials, Scanning Vol. 18, 515-521

[2] Bisschop, J; van Mier, J, G, M.:: ESEM as Tool to Study Microcracks in Cement-Based Materials. Internet: http://www.mechanics.citg.tudelf.nl/microlab/

[3] Möser, B. (1999) ESEM-FEG: Ein neues Rasterelektronenmikroskop in der Baustoff-Forschung, ZKG International Vol.52, 212 -221

[4] Möser, B. (1996) REM- und EDX-Untersuchungen an Beton, Wiss. Z. der Bauhaus-Univ. Weimar 42 No. 4/5, pp. 61-74

[5] Shayan, A., Quick, G. W., Lancucki, C. J. (1993) Morphological, mineralogical and chemical features of steam-cured concretes containing densified silica fume and various alkali levels, Adv. Cem. Res. 5 No. 20, pp. 151-162.

[6] Stark, J., Möser, B., Eckart, A. (2001) New Approaches to Cement Hydration, ZKG International Vol.54, Part 1: pp. 52-60 and Part 2: pp. 114-119

[7] Stark, J., Möser, B., Bellmann, F. (2003) New Approaches to Ordinary Portland Cement Hydration in the Early Hardening Stage, 11th ICCC, Durban, South Africa

[8] Möser, B. (2000) Cement hydration in the early hardening stage and the effect of concrete admixtures – imaged in the ESEM-FEG, ESEM application Note, FEI Company, Eindhoven, Netherlands

[9] Langenfeld, M. (1998) Der Einfluss von Verzögerern auf die frühe Hydratation von Portlandzementklinkerphasen – dargestellt in einem ESEM-FEG, Thesis-Wiss. Z. der Bauhaus-Univ. Weimar, Heft 1/2 , pp. 82-90

[10] Mansfield, J.F. (1999) X-ray Microanalysis in the Environmental SEM: A Challenge or a Contradiction ?, EMAS 6th European Workshop, pp. 69-84

[11] Bilde-Sörensen, B, J; Appel, C, C. (1999) Improvement of the Spatial Resolution of XEDS in the Environmental SEM. EUTREM 1996 – 11th European Congress on EM, Dublin, published by EUREM 96 on CD-ROM

[12] Doehne, E. A (1997) New Correction Method for High Resolution Energy-Dispersive X-Ray Analysis in the Environmental Scanning Electron Microscope, Scanning Vol. 19, 75-78

[13] Möser, B. (1999) Grundlagen und Anwendung der Rasterelektronenmikroskopie und Elektronenstrahlmikroanalyse. Baustoffpraktikum des F. A. Finger-Instituts für Baustoffkunde, Part 1 S. 85 - 115

HIGH RESOLUTION IMAGING OF WET BUILDING MATERIAL SAMPLES IN THEIR NATURAL STATE USING ENVIRONMENTAL SCANNING ELECTRON MICROSCOPE

Möser B. and Stark J.

F.A. Finger-Institute for Building Material Science, Bauhaus-Universität Weimar;
E-mail: bernd.moeser@bauing.uni-weimar.de and jochen.stark@bauing.uni-weimar.de

Bernd Möser

Dr. rer. nat.
Humboldtstrasse 31
99423 Weimar / Germany

Date of birth:	March 27, 1953
Nationalty:	German

EMPLOYMENT

1985 - present	Bauhaus-University Weimar F.A. Finger-Institut for Building Material Science Member of scientific staff and head of the electron microscopic laboratory
1979 - 1985	Member of scientific staff of the HAB-University Weimar

ACADEMIC CAREER

	Final work for PhD: “Investigations on High Alumina Ceramics Doped with Transition Metal Oxides of the Fourth Period by means of Quantitative Electron Probe Microanalysis and Valance Band Spectroscopy”
1974 - 1979	Studies of physics at Martin-Luther University Halle Topic final work: “Investigations on the Real Structure of Cu-Ni, Fe-Al, Al-Zn and Al-Mg Alloys by means of Positron Annihilation”

SOLIDIFICATION OF CARBON DIOXIDE WITH CALCIUM SILICATES

Seishi Goto[1], Koji Ioku[1], Hirotaka Fujimori[1], Minoru Fukuhara[2], Keiji Watanabe[3] and Tatsuhito Takahashi[3]

[1]Graduate School of Medicine, Yamaguchi University, Yamaguchi, Japan.
Tokiwadai 2-16-1, Ube, Yamaguchi, Japan. E-mail:sgoto@po.cc.yamaguchi-u.ac.jp,
[2]Okayama University of Science, Okayama, Japan.
[3]NKK Corporation, Fukuyama Works, Hiroshima, Japan.

ABSTRACT

The way to reduce the amount of exhaust CO_2, a green house gas and how to use steelmaking slag, has been examined. Both of them are waste materials or by-products. We can solidify CO_2 gas by using the carbonation reaction of steelmaking slag, and we can easily obtain useful materials which have a compressive strength of several 10's of MPa. Here we discuss the reaction process between steelmaking slag and CO_2 gas, the benefits of this reaction and the properties of the hardened materials.

1. INTRODUCTION

The emission of carbon dioxide is a matter of worldwide concern because of the green house effect. According to the protocol of the Third Convention of Parties on Climate Change at Kyoto in 1997, Japan has a target of 6% reduction in CO_2 and other green house gas emissions. On the other hand, about 10 million tons of steelmaking slag is produced each year in Japan. Because the composition of the slag varies depending on the characteristics of steels being produced, they have not been used extensively except as gravel for roadbeds, and have otherwise been treated as industrial waste materials. Therefore, it is necessary to develop new techniques to use these slags. Fortunately, they contain much $2CaO \cdot SiO_2 (C_2S)$ and $3CaO \cdot SiO_2 (C_3S)$ and also free lime in some cases. These calcium silicates can react with carbon dioxide to make hardened materials [1, 2]. So, the slag has the potential to make useful materials by solidifying CO_2 gas.

In this study, the mechanism and the process of the carbonation reaction of steelmaking slag will be discussed. The effects of water content, temperature and CO_2 content of the reaction gas were assessed by measuring heat liberation, strength development, texture formation and so on.

Carbonation bricks have been manufactured from blast furnace slag in Germany as early as the 1900's [3] and LD slag has been used to make high strength materials by carbonation in Japan[4, 5]. The distinguish feature of this process is the reuse or recycling of waste materials such as steel making slag and exhaust CO_2 gas and the low energy consumption during the reuse or recycling of waste materials. The carbonation reaction is an exothermic reaction, so no energy is required for the reaction except for handling, grinding and/or transportation of materials. The carbonation products of calcium silicates are very stable in air or marine environments.

We will report the application of this process to make a large-scale block such as one cubic meter, porous blocks and also to make very small particles such as artificial sand. If one third of

Proceedings of the 11th International Congress on the Chemistry of Cement (ICCC)
'Cement's Contribution to the Development in the 21st Century'
Hosted by: The Cement and Concrete Institute of South Africa
CD-ROM produced by: Document Transformation Technologies
11 - 16 May 2003, Durban, South Africa
ISBN Number: 0-9584085-8-0
Editors: Dr G. Grieve and G. Owens
Congress Organised by: Event Dynamics

steelmaking slag were used for this process in Japan, more than one million tons of carbon dioxide emission into the atmosphere would be saved every year.

Here we will report results obtained from several years' co-operative research between Yamaguchi University, Okayama University of Science and NKK Corporation.

2. PROBLEMS IN THE RECYCLING MATERIALS

Usually, we obtain many resources from the earth and we refine them, sometimes adding minor components to obtain highly functional materials. It means that we use pure materials which results in the production of contaminants. At the end of their life, they become waste materials, and are collected together with many contaminants, and then some are recycled as resources. There are 4 problems in material recycling. 1st, a useful material has been diluted as mentioned above. 2nd, sufficient amounts of material will not be supplied as resources, because waste material should not be generated to meet demand. 3rd, when the waste materials are used in existing processes many require high handling charges. The last problem is that more energy is required in the recycling process than that used with virgin materials. The recycling of materials saves resources, but it must be noted that every process uses energy, even the process of recycling.

The process proposed here has a very distinguishing feature – it products low emissions of CO_2 gas with especially low energy consumption except for handling, grinding and transportation of materials.

3. CHANGES IN THE CARBONATION PROCESS

3.1. Volume change

Many studies on the carbonation of calcium silicates have been done on the neutralization of concrete or concrete products, concerning with the durability of concrete. The solidification of slag by carbonation, proposed here, is also the same reaction, but it is used to make beneficial materials from waste materials. It does not need the texture formation by hydration reaction as does concrete. Consequently, through carbonation, calcium silicate will become calcium carbonate and silica gel, whether through hydration or not. At that time, the solid volume increases and fills the pore space to develop strength. The reaction equation is ;

$$\gamma\text{-}, \beta\text{-}C_2S + 2CO_2 \Rightarrow 2CaCO_3 + SiO_2 \text{ gel} \quad (1)$$

$$C_3S + 3CO_2 \Rightarrow 3CaCO_3 + SiO_2 \text{ gel} \quad (2)$$

When we assume the density of C_3S, β -, γ -C_2S, $CaCO_3$ and SiO_2 gel as 3.19, 3.28, 2.97, 2.71 and 2.22, respectively, the volume of carbonated C_3S, β -, and γ -C_2S will be 1.9 times, 1.9 times and 1.7 times, respectively. These increased volumes fill the pore space and combine the particles and develop the strength of the powder compacts.

3.2 Texture Formation

A small amount of water layer is important for the carbonation reaction, as it is the case for the carbonation of concrete. Under the condition of too little water, carbonation does not proceed because of the lack or very small space to react Ca^{2+} and CO_3^{2-}, and also in the case of too much water, the reaction does not proceed, because the reaction proceeds only at the surface of the liquid, as shown in Figure 1. It is desirable that the water exists to make a meniscus between particles. Both Ca^{2+} and CO_2 gas must dissolve into the water layer. Then they meet to react and to produce calcium carbonate. When there is too much water, the precipitates will produce a film at the surface of water, far from the particle. These films do not work to bond the particles. When there is an appropriate water layer, calcium carbonate is produced between the particles and binds them to develop the strength. When the products fill up the space between the particles, there is no water

space, so the reaction stops and no expansion occurs through the carbonation reaction. In contrast, in the carbonation of concrete (hydrated cement body), sometimes shrinkage occurs. This should be due to the effect of silica gel.

Figure 2 shows cross sectional images of carbonated compacts of C_3S and γ-C_2S. Both of compacts initially have same porosity of ca 50%. C_3S gains almost same volume of solids by the carbonation reaction, so the surface of about 10 μm thickness is changed to a very dense carbonated layer after 10 days' carbonation and no further reaction occurred. On the other hand, in the case of γ-C_2S, the reaction proceeded more than 100μm deep after 10 days' carbonation, because γ-C_2S compacts with 50% porosity had not filled the pore space completely by the carbonation reaction. These compacts gained very high compressive strengths of more than 200 MPa [6].

In Figure 3, another cross sectional images of carbonated steelmaking slag compact with high porosity are shown. In these porous compacts, carbonated products existed homogeneously at the surface and interior of compacts. It is clearly observed that the carbonation products of $CaCO_3$ formed like a film, covering and connecting each particle of slag. Especially in the case using coarse powder, there was much unreacted material in the core of the particles. When these materials were autoclaved at 180℃ for 64 h, no further hydration occurred [6]. The product layer is so dense that even water molecules cannot diffuse through the layer.

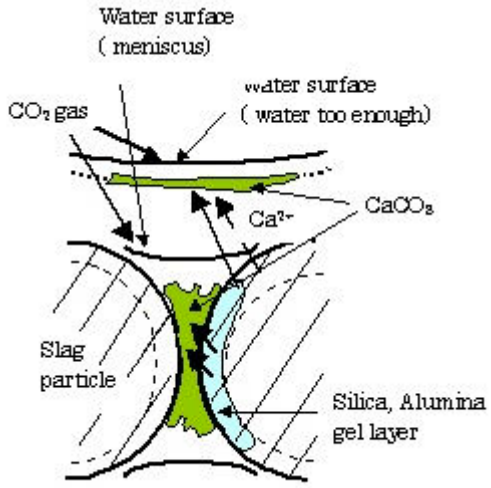

Figure 1. Illustration of carbonation process in the water layer.

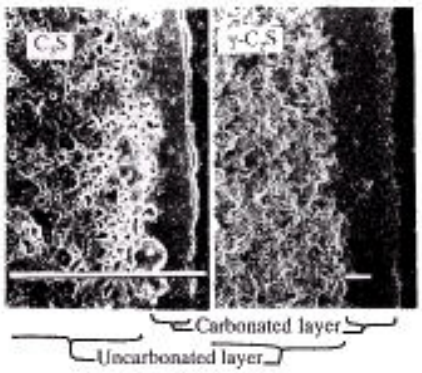

Figure 2. SEM of the fractured surface of carbonated compacts of C_3S and γ-C_2S, both of which have an initial porosity of ca 50 vol%.

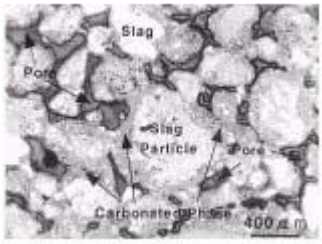

Figure 3. The cross sectional images of carbonated steelmaking slag compact.

3.3 Heat Evolution

The carbonation reaction mentioned as equation (1) and (2) is a neutralization reaction, so significant heat evolves. Here the enthalpy for the formation of γ-C_2S, CO_2(g), $CaCO_3$ and SiO_2 (glass) (here we substitute silica glass for silica gel) is -551.73、-94.05、-288.45 and -215.48 kcal·g^{-1},

$$C_2S+2CO_2 = 2CaCO_3 + SiO_2\,(glass) \qquad (3)$$

The heat of reaction of equation (3) is -52.54 kcal·mol^{-1} -C_2S. When we use a slag with a composition of CaO;39.0, SiO_2;12.4, Al_2O_3;3.46, FeO;13.5, total-Fe;20.4 and MgO;8.7 mass %, whose mineral composition is assumed as C_2S, C_2F, FeO and free CaO, the C_2S content was calculated as ca 35.5 mass%. When we assume that a mass of C_2S, which corresponds to 20% of total CaO, is carbonated, heat of reaction will liberate 3.66 kcal per 100 g of slag. This heat is able to increase the temperature up to 183 ℃ with an assumption of heat capacity of 0.2 cal·g^{-1}·K^{-1}, when it proceeds under adiabatic conditions. (100 g of slag with 5 g of water will be combined with 6.1 g of CO_2.)

Figure 4 shows the temperature change during carbonation of the steel making slag bed. Where 10kg slag powder with ca 500g water were put into a column 50 cm high and 10 cm in diameter, and then pure CO_2 gas was introduced at a pressure of 0.2 MPa and a flow rate of 180 ml·min^{-1} at room temperature. 5 thermocouples were set at the point of 5 cm, 15 cm, 25 cm, 35 cm and 45 cm from the bottom of the bed (each position is expressed as 1 - 5 in Figure 4). This figure means that the reaction proceeded in laminar fashion from bottom to upper position. The lower part increased the temperature in a short time, then after the reaction proceeded at the next position. The lower part reached the higher temperature of ca 35℃ more than the upper part.

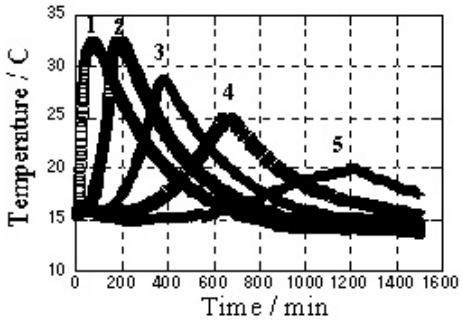

Figure 4. The temperature change during carbonation of steelmaking slag bed.

3.4 Development of Strength

In figure 5, the development of compressive strength for compacts of C_3S, and β-, γ-C_2S with carbonation time [6] are shown. The compacts had a dimension of 11 mm high and 8 mm in diameter contained 5 mass % of water and had initially 50 vol % porosity. They reacted with water vapor saturated with 5 % CO_2 gas. In the case of γ-C_2S, the compressive strength developed linearly with time to about 100 MPa at 96 h. In the case of C_3S, and β-C_2S, especially in C_3S, strength

developed faster than γ-C_2S in the early stages but did not reach as high a strength after a long time of reaction, giving 50-60 MPa at 96 h. This is owing to the formation of a dense layer at the surface of compacts as shown in Figure 2 and further reaction was hindered or stopped. The reaction should proceed faster with higher temperatures, but at more than 100℃ it requires an autoclave because the reaction needs a liquid water layer.

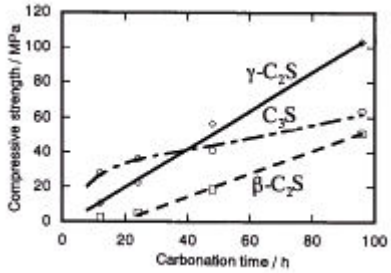

Figure 5. Changes in compressive strength with carbonation time.

The changes in compressive strength with carbonation ratio for compacts of many kinds of slag carbonated at temperatures of 25℃and 50℃ [6] are shown in Figure 6. There was not very much difference in the relationship between compressive strength and carbonation ratio for the samples carbonated at different temperatures. The strength of compacts reacted at 50℃ were twice as strong as those reacted at 25 ℃ for the same reaction period.

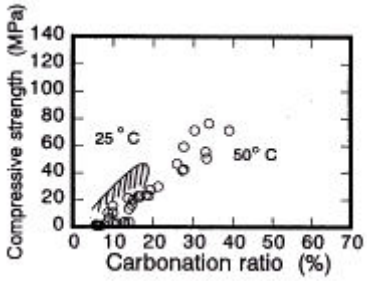

Figure 6. The changes in compressive strength at temperatures of 25℃(hatched area) and 50℃(open circles).

The relationship between compressive strength and porosity can be expressed using the Ryshkewitch equation [4, 6], in which the logarithmic strength is linearly related to porosity. The results of compressive strength and porosity for carbonated slag compacts are shown in Figure 7. The compacts with porosity of about 20 % had strength of about 100 MPa. In the region of porosity of more than 40 %, strength decreased largely with porosity. In the figure, the relationship for hydrated materials is also presented as a dotted line. The dependency on porosity for carbonated materials is greater than that of hydrated materials. The strength of a carbonated matrix is lower than that of a hydrated one in the region with greater than 10 % porosity, but in the region lower than 10 %, the strength for the carbonated matrix is greater than that of the hydrated one. It will be expected as 350 MPa at porosity of zero.

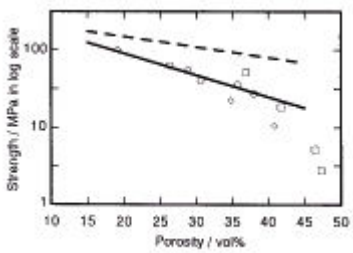

Figure 7. The relationship between compressive strength and porosity.

3.5 Alkalinity and an Application

The alkalinity of carbonated compacts was in the range of pH 9 to 10, because most of the CaO or $Ca(OH)_2$ converted to $CaCO_3$. When glass fiber is used for reinforcement of these compacts as GRC, the durability of glass should be superior to cement hydrated compacts [7]. Here we show the results of durability tests of soda-lime glass in cement hydrated compact and carbonated cement compact. Belite clinker (clinker for belite rich and alite poor cement, as low heat cement) obtained from Ube Industries Co.Ltd., was used as cement. Plates of soda-lime glass were put into the compacts of 20 x 40 x 5 mm and they were carbonated or hydrated. Fibers of E-glass were also put into the paste. Then they were autoclaved at 180℃ for up to 64 h. The surfaces of the glass plates were examined for Vickers hardness and observed by SEM. Changes in diameter of glass fiber by the reaction with alkali was also measured using SEM.

The results are shown in Figures 8, 9, and 10. Figure 8 shows the SEM images of the surfaces of soda-lime glass. Figure 9 shows the changes in hardness of the surfaces. Figure 10 shows the changes in the corroded thickness of the E-glass fiber. It was observed that a low degree of corrosion of glass occurred in carbonated matrix but very high in the hydrated matrix. When the E-glass was in hydrated matrix, it corroded 4 times faster than that of the carbonated matrix, as shown in Figure 10.

Glass fiber reinforced concrete is superior in tensile strength, anti-shock strength and toughness, but inferior in the durability of reinforced fiber. Many researchers have focusing on the upgrading of the fiber, for example, the improvement of its chemical composition and/or coating materials. Here we show another way to improve GFRC durability by changing the pH of the matrix, even when we use cheaper glass fiber.

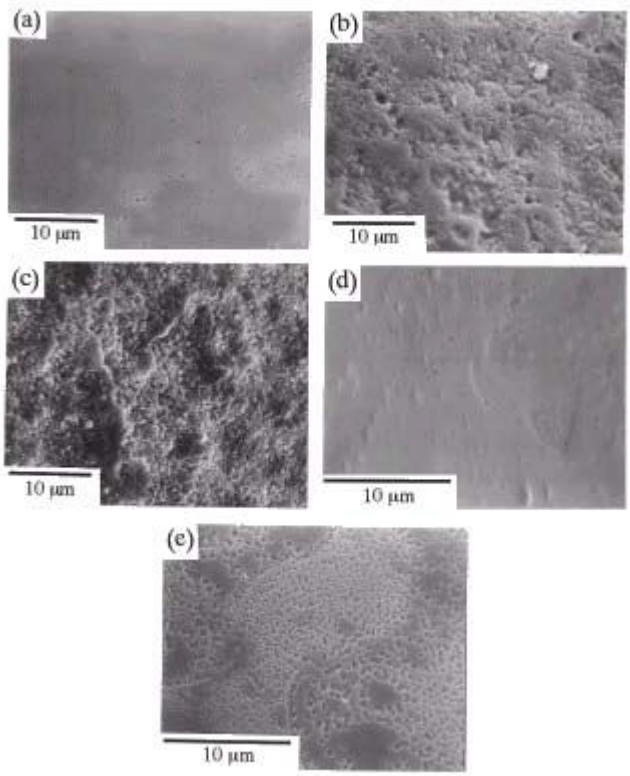

Figure 8. SEM images of corroded surface of E-glass with hydrated slag and carbonated slag. a) the surface with carbonated matrix treated at 60℃ for 1 week, b)that with hydrated matrix at 60℃ for 1 week, c) autoclaved at 180℃ for 1 h with hydrated matrix, d) autoclaved at 60℃ for 64 h with carbonated matrix, and e) locally observed image for that autoclaved at 180℃ for 16 h.

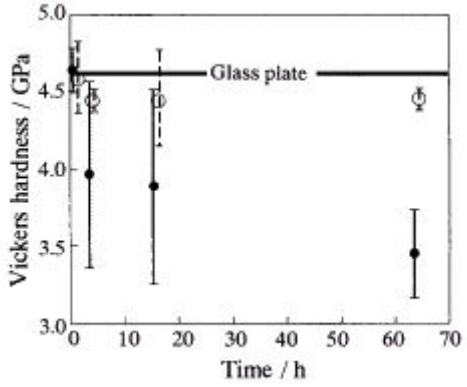

Figure 9. Changes in Vickers hardness of the surface corroded in the hydrated slag or carbonated slag. Open circles are for carbonated matrix, and dots are for hydrated matrix.

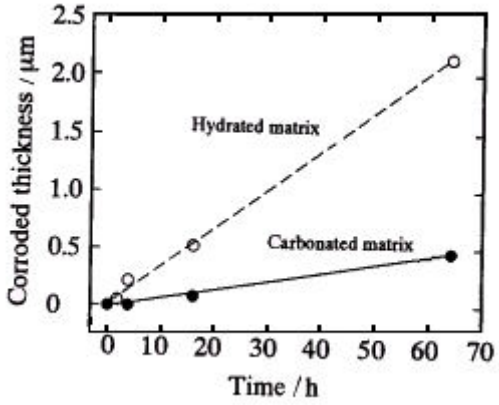

Figure 10. Changes in corroded thickness of the E-glass fiber with hydrated slag or carbonated slag.

3.6 Other Applications

3.6.1 Small Particles as artificial aggregate

Artificial aggregate can be manufactured from steelmaking slag powder by pelletizing and carbonation [8]. In Figure 11, the particles of carbonated slag aggregates, which was granulated by pan type pelletized are shown. Most were spherical particles. In Figure 12, the tensile strength by compaction, water absorption ratio and porosity for aggregates, whose carbonation time was 96 h, are compared between pelletizing times of 30 min and 1 h. Aggregates with 18 MPa and water absorption ratio of 7 % were obtained. The tensile strength by compaction was calculated with an equation proposed by Hiramatsu et al [9],

$$S_t=0.9\ F_0/d^2 \qquad (4)$$

where S_t is tensile strength by compaction, F_0 is compressive stress for fracture of spherical particles and d is diameter of the sphere.

3.6.2 Large Scale Blocks

Large scale blocks with size of 1m x 1m x 1m were made successfully by Takahashi et al [5]. Slag was compacted in a mold after mixing with 5.3 mass% water. The porosity of

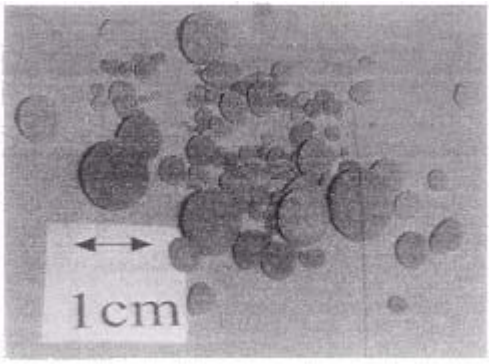

Figure 11. The particles of carbonated slag aggregates.

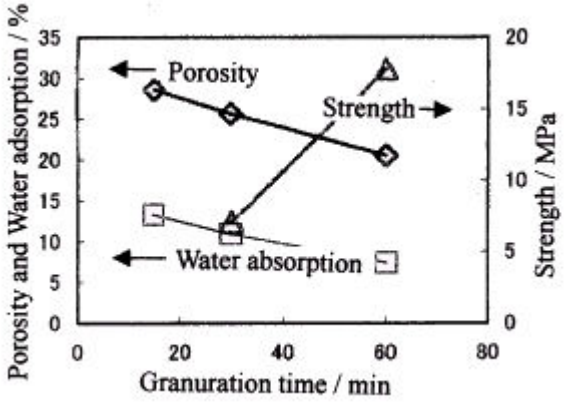

Figure 12. The tensile strength for carbonated slag aggregates by means of compaction.

the compacts was 28 %, and water saturated CO_2 was forcibly introduced into the mold at a pressure of 1.002 atm. through holes in the bottom. These blocks are using for seaweed beds and/or space for fish living, as shown in Figure 13. Blocks submerged in the sea have shown good durability for more than 4 years. No cracks or damage was observed. And surface floral changes by seaweeds like green algae are also observed.

Figure 13. Blocks with size of 1 m x 1m x 0.5 m made by carbonation of slag.

4. CONCLUSIONS

By a trial calculation, nearly 200 kt of exhaust CO_2 can be beneficially utilised with this process, if it is assumed that 10 % of steel making slag produced is used and the 20% of CaO in the slag will be carbonated.

The process of producing functional materials from slag and carbon dioxide has many advantages. Firstly, we can make useful materials from steel making slag which is an unavoidable byproduct of the steel industry and CO_2 gas which is considered as an important factor for green house effect.

Secondly, in the recycling technology, it may be the lowest energy consumption technology where almost no energy is need for the process except for grinding and transportation. The CO_2 does not need to be generated as it is available from industrial exhausts. This process will be expected in near future, with taking care of the behavior of minor components.

REFERENCES

[1] J. F. young, R. L. Berger, and J. Beese, J. Am. Ceram. Soc., 57, 394-397(1974)
[2] S. Goto, K. Ioku and T. Kado, PacRim2, 15-17 July 1996, Cairns, Australia, Symp.18A, 17-24 (Published in 1999 as CD ROM)
[3] T. Isoo, T. Takahashi, N. Okamoto and M. Fukuhara, Advances in Cement Research, 12, No.3, 97-101(2000)
[4] R. Kondo and Y. Aso, Gypsum and Lime, No.147, 61-65(1977)
[5] T. Takahashi, Concrete J., Japan Concrete Institute, 38, No.2, 3-9(2000)
[6] S. Goto, A. Nakamura and K. Ioku, J. Soc. Inorg. Mater., Japan, 5, Jan., 22-27(1998)
[7] S. Goto, M. Togawa, H. Fujimori and K. Ioku, J. Soc. Inorg. Mater., Japan, **7**, 178-184 (2000)
[8] S. Goto, Report for Regional Science Promoter Program in Yamaguchi, (2001.03)
[9] Y. Hiramatu, Y. Oka and H. Kiyama,J. Soc. Mineral Industry, Japan, Vol.81**,** No.932, 1024-1030(1965)

MODELLING INTERPARTICLE FORCES AND YIELD STRESS OF CEMENT SUSPENSIONS

Robert J. Flatt*, Paul Bowen, Yves F. Houst and Heinrich Hofmann

École polytechnique fédérale de Lausanne (EPFL), Laboratoire de technologie des poudres, MXD, CH 1015 Lausanne, Switzerland. E-mail: Paul.Bowen@epfl.ch, Yves.Houst@epfl.ch , Heinrich.Hofmann@epfl.ch
* Present address: SIKA A.G., Corporate Research and Analytics, P.O. Box 1300, CH 8048 Zürich, Switzerland. E-mail: flatt.robert@ch.sika.com

ABSTRACT

Cement particles in suspension are agglomerated and form a three-dimension network. The water trapped between particles has no more lubricating action. Superplasticizers, which disperse agglomerates, free the entrapped water and thus improve the fluidity. It is shown how theories of interparticle forces developed for ceramic materials can be adapted to the more complex case of cement suspensions. In particular, how this allows the (semi-)quantitative evaluation of the yield stress of cement suspensions. The particle size distribution and the activity of ions of the pore solution are taken into account. The total interaction force allowing agglomeration of cement particles take into consideration the sum of dispersion, electrostatic and steric forces. The model is dependent on input parameters, like polymer adsorption, the plane of origin for the calculation of the electrostatic force, the Hamaker constant of cementitious phases, which need to be treated in more detail.

1. INTRODUCTION

Dispersion of agglomerated cement particles is a key point to improve the workability of concrete or to reduce the amount of mixing water. This is the role of superplasticizers or high range water reducers (HRWR). The development of new products, more efficient and tailored for specific applications, should be based on the knowledge of the mechanisms of their interaction with the cement.

Dispersion or *London dispersion forces* play an important role in the properties of numerous materials and in particular in cement suspensions. The Lifshitz's theory was a major advance and founded our current understanding of these forces [1, 2]. In the last fifty years, it was successfully applied to various practical problems [2]. The dispersion forces are essentially attractive in suspensions of one type of particle (i.e. the same phase).

The balance between these dispersion forces and repulsive forces from surface charge or adsorbed species governs the behaviour of particulate suspensions [3]. The DLVO theory takes into consideration the sum of these interparticle forces, and can be used to understand and predict suspension stability and rheology. This theory has been used to describe cementitious systems [4-6] despite the fact that cement suspensions are not really in the colloidal domain. These approaches have proven to be very useful in trying to understand the complex systems of cement suspensions with polymeric additives. However, the full complexity of such systems was generally not taken fully into consideration perhaps undermining some of the conclusions that may have been drawn from the approach. In more recent years attempts have been made to take into account the

Proceedings of the 11th International Congress on the Chemistry of Cement (ICCC) 11 - 16 May 2003, Durban, South Africa
'Cement's Contribution to the Development in the 21st Century' ISBN Number: 0-9584085-8-0
Hosted by: The Cement and Concrete Institute of South Africa Editors: Dr G. Grieve and G. Owens
CD-ROM produced by: Document Transformation Technologies Congress Organised by: Event Dynamics

complexity of the ionic medium of cement suspensions, the effects of their broad particle size distributions and their interaction with superplasticizers [5, 6]. Steric repulsion, which plays a key role in superplasticizers of the latest generation, can be taken into account. The key parameters, which govern the steric repulsion, i.e. the adsorption layer thickness and its conformation at the solid liquid interface are often difficult to quantify.

2. INTERPARTICLE FORCES

3.1 Dispersion forces

In the following developments, particles are spheres with un-equal diameters a_k and a_l.
The dispersion force can be written as the derivative of the interaction potential, Φ, with respect to the interparticle distance, h, (surface to surface):

$$F \cong \frac{d\Phi}{dh} = -A_{(h)} \frac{dH_{(a_k,a_l,h)}}{dh} \tag{1}$$

where A is the Hamaker constant and H a geometric factor [2]:

$$H_{(a_k,a_l,h)} = \frac{1}{6}\left(\frac{2a_k a_l}{2(a_k+a_l)h+h^2} + \frac{2a_k a_l}{4a_k a_l + 2(a_k+a_l)h+h^2} + \ln\left(\frac{2(a_k+a_l)h+h^2}{4a_k a_l + 2(a_k+a_l)h+h^2} \right) \right) \tag{2}$$

Also in the particle size range of interest for cement suspensions (0.4 μm to 50 μm) a >>h which reduces (2) to:

$$F_{(a_k,a_l,h)} = -\frac{A_{(h)}}{6}\left(\frac{-\bar{a}}{2h^2} + \frac{-1}{2\bar{a}} + \frac{1}{h} \right) \tag{3}$$

With $\bar{a} = \dfrac{2a_k a_l}{a_k + a_l}$

Further for small separations, this simplifies to :

$$F_{(a_k,a_l,h)} \cong -A_{(h)} \frac{\bar{a}}{12h^2} \tag{4}$$

Flatt [5] showed that the final approximation of equation 4 gives precision better than 20% if the maximum interparticle force is found at separation distances less than 45 nm.

Reliable Hamaker constants are essential if interparticle potentials are going to help us predict the yield stress or rheological behaviour of cement dispersions. The Hamaker constant used needs to be corrected for screening and retardation because of the high ionic concentration generally found in cement suspensions. Reliable dielectric data for cement components are not yet available although Sakai and Daimon [7] give a value of a non-retarded, non-screened Hamaker constant for tricalcium silicate, C_3S, a major component of Portland cements of 4.55 x 10^{-6} J/mol. This value was not obtained using recent dielectric data of water. In several studies on the evaluation of superplasticizer adsorption and dispersion, Flatt et al [8-10] have shown that MgO is a good model non-reactive substitute for Portland cement suspensions. Using the same dielectric data for water as Sakai and Daimon [7], they calculate for MgO a non-retarded and non-screened Hamaker constant of 4.2 x 10^{-6} J/mol. Since the values for MgO and C_3S are so close, MgO seems to be an acceptable model for calculating the retarded and screened dispersion forces. An effective Hamaker constant, which takes into consideration these effects, has been estimated by Flatt [5] and has been used in this work for Portland cement dispersions.

3.2 Electrostatic forces

The relative importance of the electrostatic contribution to cement dispersion is currently under much debate. One aspect of this topic recently explored by Flatt and Bowen [11] is how the non-ideal electrolyte found in cement suspensions affects the simplified Debye-Hückel approximation for evaluation of electrostatic repulsion. They show that the non-ideality of the cement pore solution can be taken into account based on solubility equilibria of the possible ionic species present in typical cement suspensions. By replacing the normally assumed symmetric electrolyte (1:1, 2:2, or 3:3) with a non-integer symmetric electrolyte, the simple Debye-Hückel approach has been shown to remain valid for negative potentials up to around –30 mV. The repulsive electrostatic force between spheres maintaining an identical and constant potential upon approach can therefore be written as:

$$F_{ES} \cong -2\pi\varepsilon\varepsilon_0\bar{a}\psi^2\frac{\kappa e^{-\kappa h}}{\left(1+e^{-\kappa h}\right)} \tag{5}$$

With ε the relative dielectric constant for water, ε_0 the permittivity of vacuum, and κ^{-1} the Debye length, given by:

$$\kappa^{-1} = \sqrt{\frac{\varepsilon\varepsilon_0 k_B T}{2e^2 z_+^{\,2} n_+^b}} \tag{6}$$

Where n_+^b is the concentration of species k in the bulk, z_+ the charge of the equivalent symmetric electrolyte, e the electronic charge, k_B is the Boltzmann constant and T the temperature in Kelvin.

One of the problems in calculating this force is the evaluation of the surface potential ψ. This is the potential at the outer boundary of the Stern layer, which is the layer in which ions are linked to the surface and not influenced by Brownian motion. Often, one uses the experimentally determined zeta potential, which is the potential at a shear plane. This plane is situated somewhat farther from the surface than the Stern plane. So, it leads to an under-evaluation of the electrostatic force. In this study, the charge is induced by adsorption of ionic polymers. Zeta potential measurements are based on relative motion between particles and the surrounding fluid. This motion may compress the layer of adsorbed polymers, thus modifying the distance at which the potential might be measured. De Gennes [12] states that the hydrodynamic layer thickness scales in the same way as the adsorbed layer thickness. He mentions that this is confirmed by experimental data, though in some cases the hydrodynamic layer might be even larger.

This results because only a couple protruding polymer chains suffice to strongly alter the hydrodynamic behaviour around the particle, but have much less impact on the average layer thickness that matters most as far as interparticle forces are concerned. Nevertheless, we will consider that during zeta potential measurements, hydrodynamic forces are not sufficient to significantly compress the adsorbed layer and the plane of origin of electrostatic forces can be placed at the surface of the adsorbed layer. The electrostatic force can then be represented by equation 7, integrating the adsorbed layer thickness L:

$$F_{ES} = -2\pi\varepsilon\varepsilon_0\bar{a}\psi^2\frac{\kappa e^{-\kappa(h-2L)}}{\left(1+e^{-\kappa(h-2L)}\right)} \tag{7}$$

3.3 Steric force

The adsorption of superplacticizer at the cement particle-water interface not only induces a surface charge but gives an adsorbed polymer layer with a certain configuration, density and thickness. As particles in suspension approach one another a steric repulsive force acts as soon as the adsorbed layers begin to overlap. As the layers overlap they can be compressed and the repulsive force increases strongly and reaches infinity as the maximum compression is reached. The functionality of this increase is highly dependent on the adsorption conformation of the polymer. The adsorption configurations can be many and complex, but three modes useful for the evaluation of interparticle forces can be described as flat (pancake), intermediate (mushroom) and end-on (brush) [12]. Portland cements usually have a weakly positive surface charge whereas the superplasticizers used are negatively charged at the high pHs found in cement suspensions. Also the molar mass, Mw, are relatively high at around 25-40,000 g/mol it is unlikely that the molecules will adsorb in either the totally flat pancake or end-on brush-like mode. We consider that our suspensions will lead to a mushroom-type conformation. For such adsorption modes, the scaling theory developed by de Gennes [12] can be used to calculate the steric force [13] as follows:

$$F_{Ste} = \bar{a}\frac{6\pi k_B T}{5s^2}\left[\left(\frac{2L}{h}\right)^{5/3} - 1\right] \tag{8}$$

Where s is the distance between the centres of two neighbouring mushrooms. L is the maximum length extending into the solvent.

3.4 Total interaction

The equations above indicate that at small separations, dispersion, electrostatic and steric forces are all proportional to the interaction radius $\bar{a}$ for two dissimilar spheres. This can be written:

$$G = \frac{F}{\bar{a}} = \frac{F_{VdW} + F_{ES} + F_{Ste}}{\bar{a}} = -\frac{A_{eff(h)}}{12h^2} + 2\pi\varepsilon\varepsilon_0\kappa\psi^2\frac{\kappa e^{-\kappa(h-2\lambda)}}{\left(1+e^{-\kappa(h-2\lambda)}\right)} + \frac{6\pi k_B T}{5s^2}\left[\left(\frac{2L}{h}\right)^{5/3} - 1\right] \tag{9}$$

This is illustrated in Figure 1 and 2 for a model MgO powder with the key parameters being the adsorbed layer thickness and induced surface charge linked to the superplasticiser adsorption. The non-ideality of the pore solution is taken into account by the equivalent symmetric electrolyte. The positive values indicate repulsion and negative values attraction. In absence of electrostatic repulsion this maximum is reached for separations of about twice the maximum length of the layer extending from the surface into the solvent. When electrostatic effects come into play, the point of maximum repulsion is beyond this distance. There is a clear steric effect which can be significantly complemented by electrostatic repulsion, provided one can place the potential at the outer bound of the adsorbed layer [6].

The large sizes of cement particles (1 to 100 μm) means that shear forces largely dominate over Brownian motion, even at low shear rates. We therefore need to calculate the maximum attractive force between two particles in order to decide whether shear is capable of separating them.

4. YIELD STRESS EVALUATION

The evaluation of rheological properties with respect to interparticles forces of various ceramic systems shows, in general, only good qualitative agreement [4, 14]. This is partly because interparticle forces are a function of particle size and particle distribution. Most calculations are

limited to using some average diameter [4, 15]. The maximum solid loading of stable ceramic suspensions can approach the maximum packing fraction (65 % volume solids) while remaining a fluid suspension. Attractive non-flowing networks can be formed with cement pastes at much lower volume fractions, around 48 % solid loading (w/c = 0.35). It is why cement suspensions behave in general like a Bingham's fluid, i.e. with a yield stress. With superplasticizers, it is possible to suppress totally this yield stress and the paste behaves like a Newtonian fluid [16]. This is due to the fact that a fraction of water is trapped between agglomerated cement particles. So, a cement suspension is in fact like a cluster of agglomerates which have a higher effective volume than the real solid volume present in order to allow the cement suspension to flow. This effective volume has to be decreased by breaking apart a certain fraction of this attractive network.

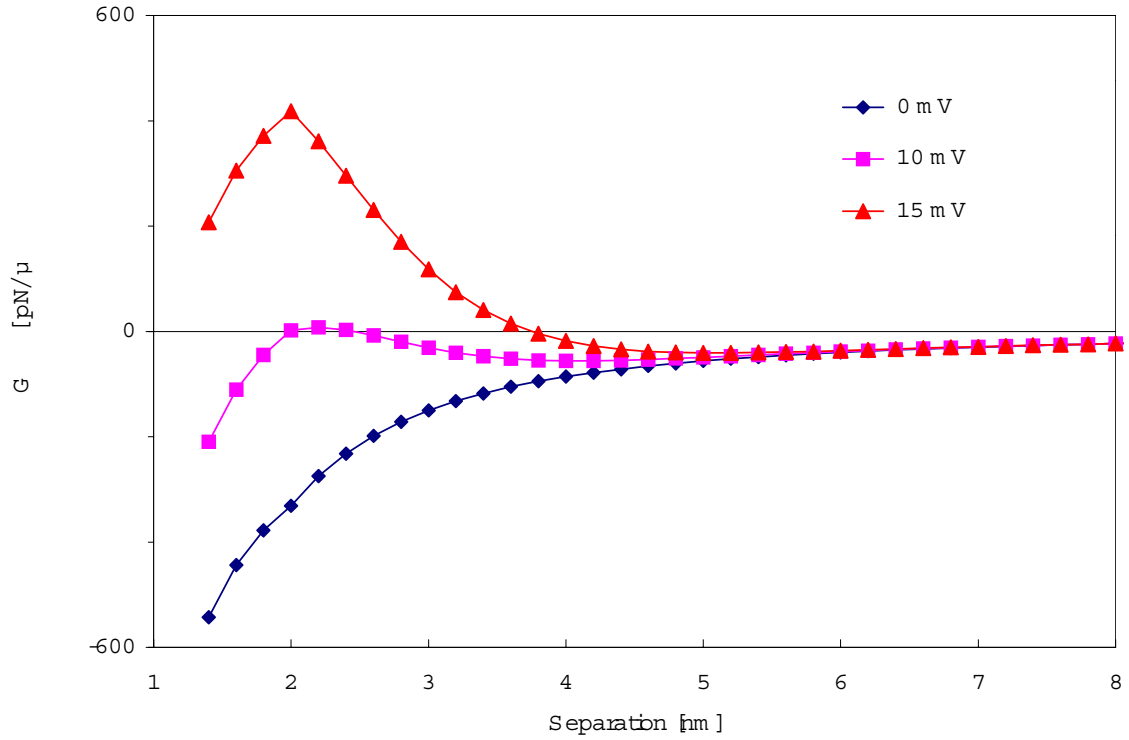

Figure 1. Normalised interparticle force G as a function of separation for three different potentials and an adsorbed layer thickness of 1 nm. Positive values indicate repulsion and negative value attraction.

A strategy has been developed to evaluate what decrease in effective volume fraction of solids would be needed so that the attractive cement particle network begins to flow. It is based on considering all the interacting particles by pairs. Each pair is considered to contribute to an increase in effective volume fraction of solids in suspension, in a way that is directly related to the size of the interacting particles. At a specified shear only some of those pairs can be moved or broken apart and this again depends on the size of the particles. In fact for each class of sizes of interacting particles we calculate in the following section the probability of bond breaking.

The problem we face is to define what exactly is the increase in effective volume fraction that each interaction causes. We have chosen to use a truncated cone tangent to both spherical particles as indicated in Figure 3(a). The additional volume is denoted $\Delta V_{k,l}$. The dispersion of doublets with different individual particle sizes will not have the same effect on the rheology, as each individual pair will have different effective to real volumes (Figure 3(b)).

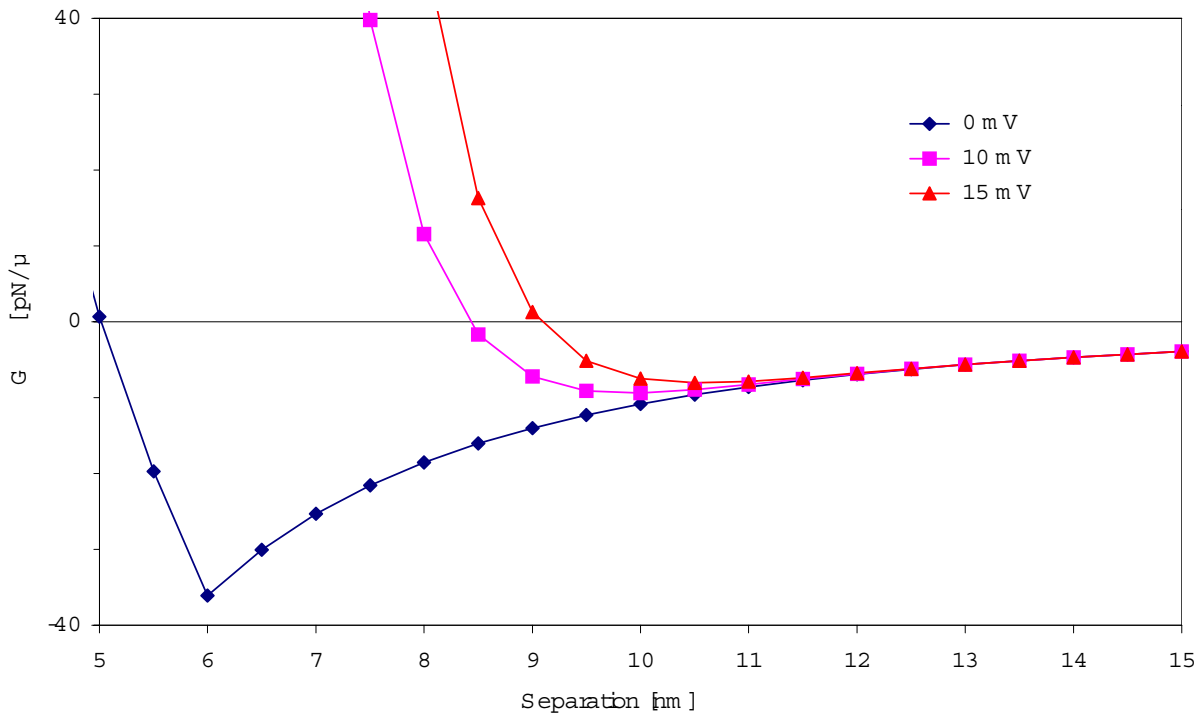

Figure 2. Normalised interparticle force G as a function of separation for three different potentials and an adsorbed layer thickness of 3 nm. Positive values indicate repulsion and negative value attraction.

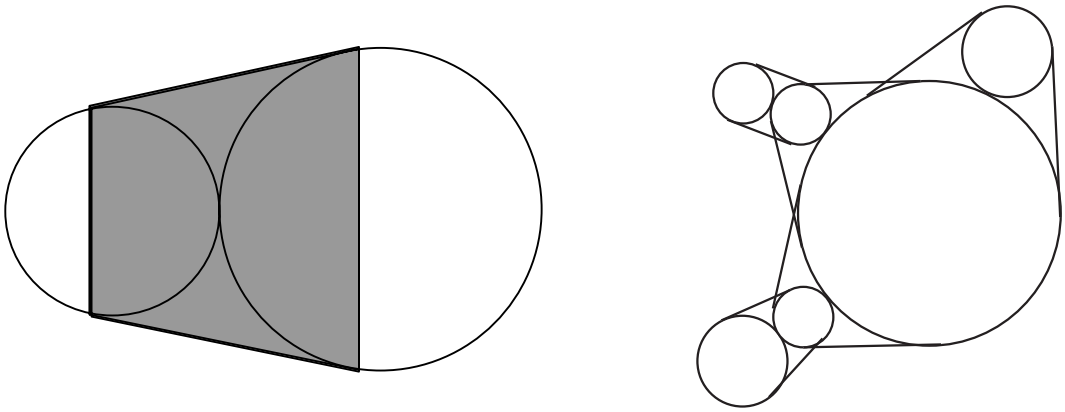

(a) (b)

Figure 3. (a) Truncated cone used to determine the effective volume change due to a doublet(b) different pairs of doublets illustrating the different effective volumes for different pairs.

This volume is given for two unequal spheres by:

$$\Delta V_{k,\,l} = \frac{2\pi}{3}\hat{a}^2\left(4\hat{a} - \bar{a}\right) \tag{10}$$

The interparticle forces can be used with the effective volume freed on agglomerate disruption to predict a yield stress for the attractive network. A simple method would be to take the average coordination number, the average interparticle interaction force, using the mean harmonic diameter

$\langle \bar{a} \rangle$, then use the number of interactions per unit volume to calculate the force necessary to break the network, similarly to the approach proposed by Kapur et al [17]. This has been done for a gamma alumina suspension [18] and the average coordination number resulting from a numerical particle packing model using measured PSDs [19] gave very coherent results. Similar coordination numbers to those from the models of Goto, and Iwata & Homma, cited by Kapur et al [17] have been obtained. It would be interesting to take this approach further and perhaps use analytical models related to the particle size distribution to provide an average coordination number and harmonic average.

The approach we outline here follows that by Flatt [20]. It consists in carrying out a force balance between shear forces and interparticle forces to determine the fraction of unbroken doublets at a given shear τ:

$$f_{k,l}(G/\tau) = 1 - \frac{\int_0^{\pi/2} 2\arctan\left\{\left(\frac{G}{\tau}\right)^{-1} \frac{\pi\left(a_k{}^2 + a_l{}^2\right)}{3\bar{a}} \frac{1}{\cos\varphi}\right\} d\varphi}{\pi \int_0^{\pi/2} d\varphi} \tag{11}$$

where a_k and a_l are the radii of the pair of interacting particles, τ is the yield stress.

Summation over all the interacting particles allows calculation of the additional volume fraction due to particles that cannot be separated by the applied shear force:

$$\Delta\Theta = \frac{\sum_k \sum_{l \geq k} n_{k,l} f_{k,l} \Delta V_{k,l}}{d^3} \tag{12}$$

Where d is the size of the box in which a given number of particles was placed to determine the number contacts $n_{k,l}$ between particles of sizes a_k and a_l.

In Figure 4, we plot for the same cement and w/c, the expected yield stress versus the thickness of the adsorbed layer. This figure was constructed for a particular cement at a w/c of 0.35. For the particle size distribution of that cement, the loose packing volume fraction is 65%. Since the true volume fraction is 48%, the difference of 17% can be given from unbroken interparticle bonds and would give G/τ = 1.7 μm. This additional volume fraction is plotted against the G/τ in Figure 5.

The sharp rise around 1.5 nm, corresponds to a layer thickness limit at the maximum attractive force at maximum compression of the adsorbed layers. The reason is that the combined effect of charge and steric hindrance as described in Eq. (8) are not sufficient to overcome van der Waals force and particles get pulled together until the layers cannot compress any further. In the case we are illustrating, it is obvious that a charge of +/- 10 mV at the exterior of an adsorbed layer will have important rheological consequences if that layer is smaller than 5 nm. Beyond that the effect is minor.

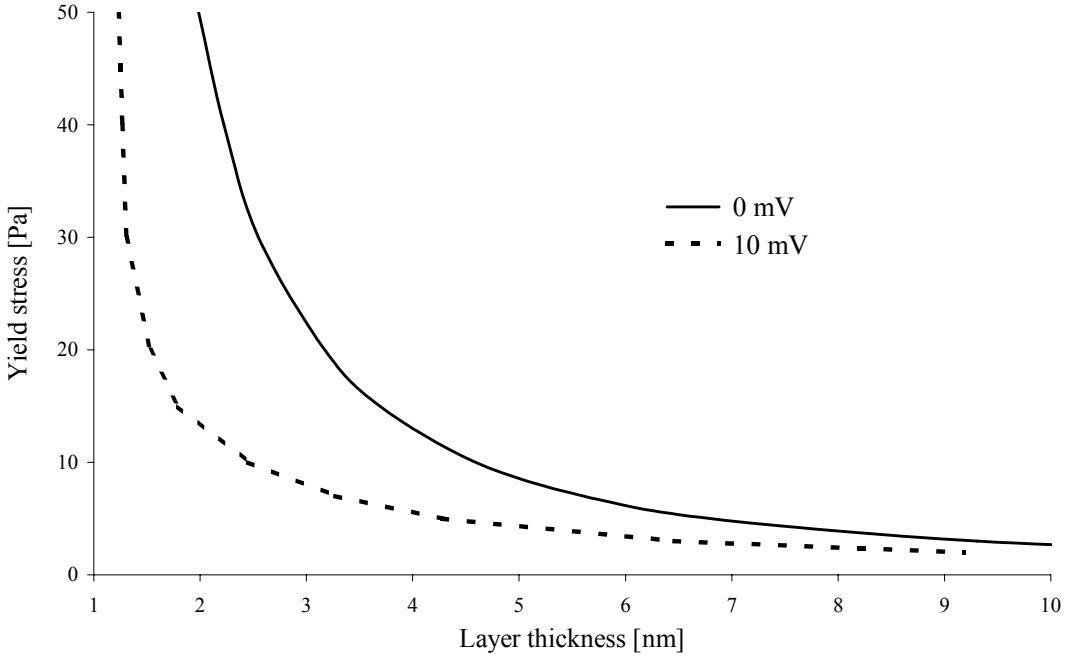

Figure 4. Expected yield stress of cement with specified PSD, for w/c = 0.35. The maximum compressibility is considered to be 0.7 nm.

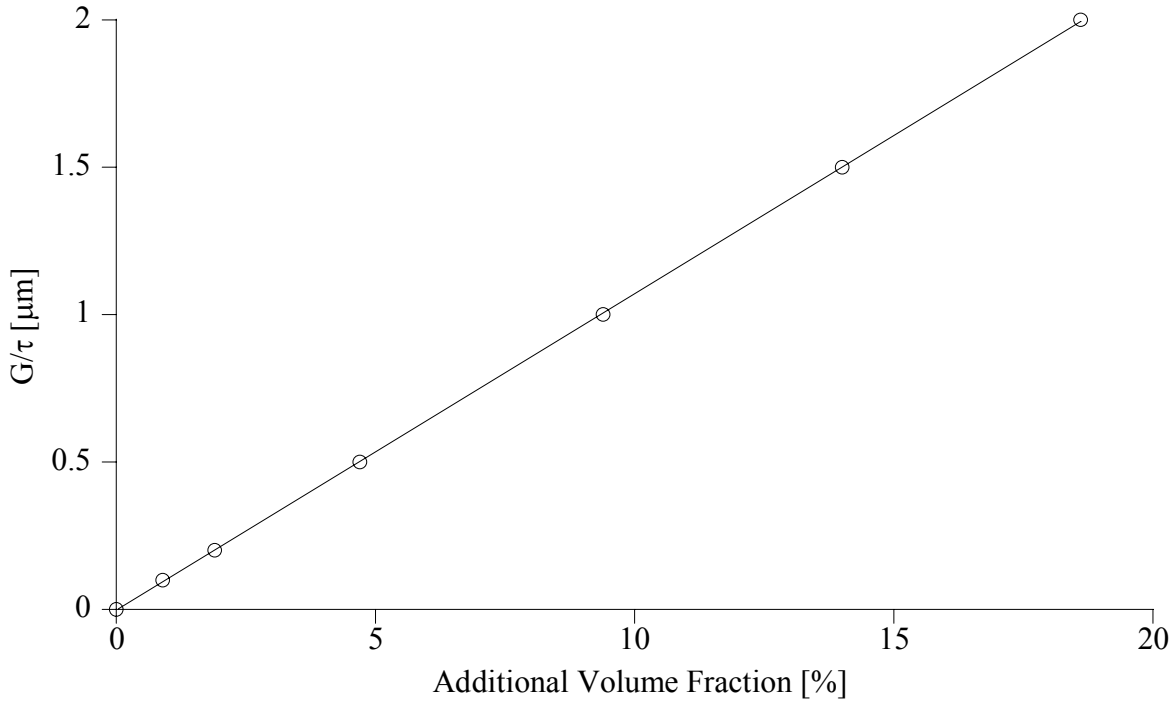

Figure 5. Relation between the interparticle force parameter G normalised by shear stress and the additional volume fraction expected to result from unbroken interparticle bonds.

The approach we have presented bears the important limitation in the determination of number of contacts $n_{k,}$ between particles of different sizes [20]. It also uses a semi-empirical approach to estimating the increase in volume fraction from non-dispersed particles. However, it leads to results that are coherent with the experimental observation that yield stresses of about 5-10 Pa are observed for polymers expected to have adsorbed layer thicknesses of the order of 2 nm for a 10 mV potential.

Future prospects would be to further investigate the various parameters, which are still uncertain to some degree, in the evaluation of the interparticle forces and need to be more accurately established. These include more reliable zeta potential measurements, maximum allowable effective volume fraction increase due to a non-dispersed doublet, the adsorbed polymer layer thickness, the plane of origin for electrostatic forces (placed at the surface of the adsorbed layer for the above calculations, but placed half way to the surface by Lewis et al. [4]), hydrodynamic forces which are expected to oppose dispersion, better Hamaker constants for the different cement phases (calculations done presently with MgO data, the fact that cement particles are multiphase and non-spherical).

5. CONCLUSIONS

It has been shown how colloidal theories can be applied to the very complex system of cement suspensions, though cement particles are not in the range of colloids. The interparticle forces, electrostatic, steric and dispersion, that act on cement particles were all found to scale on the harmonic diameter, $\bar{a} = \frac{2a_k a_l}{a_k + a_l}$, for un-equal spheres. Several parameters in the calculation of the interparticle force calculation have been reviewed and the importance of a small charge induced by superplasticiser adsorption shown to be important.

The particle size distribution can be taken into account by using a particle packing model which provides the harmonic diameter distribution of randomly packed cement particles. The possibility of taking into account the particle size distribution is an important step forward as it has often been cited as one of the stumbling blocks limiting the use of interparticle interaction energies for quantitative assessment of concentrated suspension rheology. The approach presented leads to reasonable coherence between molecular properties of dispersants, particle size distribution and measure yield stress. The limitations within this approach must be dealt with in the future to reach a fully consistent quantitative picture of how forces on the nano-level control in a predictable way the macroscopic rheological behaviour.

REFERENCES

[1] Horn, R.G. Surface forces and their action in ceramic materials, Journal of the American Ceramic Society, 1990, vol. 73, pp. 1117-1135.

[2] Russel, W.B., Saville, D., Schowalter, W.R. Colloidal dispersions, Cambridge University Press, 1991.

[3] Evans, D.F, Wennerström, H. The colloidal domain where physics, chemistry, biology, and technology meet, Wiley-VCH, New York, etc, 2nd ed., 1999.

[4] Lewis, J.A., Matsuyama, H., Kirby, G., Morissette, S., Young, J.F. Polyelectrolyte effects on the rheological properties of concentrated cement suspensions, Journal of the American Ceramic Society, 2000, vol. 83, pp. 1905-13.

[5] Flatt, R.J., Polymeric Dispersants in Concrete, Polymers in Particulate Systems: Properties and Applications, (Hackley V.A., Somasundaran P., Lewis J.A., Eds), Marcel Dekker, New York, 2001, pp. 247-294.

[6] Flatt, R.J., Houst, Y.F., Bowen, P., Hofmann, H. Electrosteric Repulsion induced by Superplasticizers Between Cement Particles : an Overlooked Mechanism ?, 6th CANMET/ACI International Conference on Superplasticizers and other Chemical Admixtures in Concrete, (Malhotra V.M. Ed.), SP 195, American Concrete Institute, Farmington Hills, Mi, USA, 2000, pp. 29-42.

[7] Sakai, E., Daimon, M. Dispersion Mechanisms of Alite Stabilized by Superplasticizers Containing Polyethylene Oxide Graft Chains, Proceedings of the 5th CANMET/ACI International Conference on Superplasticizers and other Chemical Admixtures in Concrete (V.M. Malhotra Ed.), ACI, Farmington Hills, Mi, USA, 1997, SP-173, pp. 187-201.

[8] Flatt, R.J., Houst, Y.F., Bowen, P., Hofmann, H., Widmer, J., Sulser, U., Maeder, U., Bürge, T.A. Interaction of superplasticizers with model powders in a highly alkaline medium , 5th Canmet/ACI International Conference on Superplasticizers and Other Chemical Admixtures in Concrete (editor: Malhotra V.M.), American Concrete Institute Farmington Hills, Mi, USA, 1997, SP-173, pp. 743-762.

[9] Flatt, R.J., Houst, Y.F., Bowen, P., Hofmann, H., Widmer, J., Sulser, U., Mäder, U., Bürge, T.A. Effect of Superplasticizers in Highly Alkaline Model Suspensions Containing Silica Fume, 6th CANMET/ACI

International Conference on Fly-Ash, Silica Fume, Slag and Natural Pozzolans in Concrete (Malhotra V.M. Ed.), American Concrete Institute, Farmington Hills, Mi, USA, 1998, SP 178, Vol. 2, pp. 911-930.

[10] Flatt, R.J., Bowen, P., Siebold, A., Houst, Y.F. Cement Model Powders for Superplasticizers Studies, Proceedings of the 11th ICCC, Durban, 2003.

[11] Flatt R.J., Bowen, P. Electrostatic Repulsion Between Particles in Cement Suspensions: Domain of Validity of Linearized Poisson-Boltzmann Equation for Non-Ideal Electrolytes, Cement and Concrete Research, 2002, vol. 32, (accepted) .

[12] De Gennes, P.G. Polymers at an interface: a simplified view, Advances in Colloid and Interfaces Science, 1987, vol. 27, pp. 189-209.

[13] Pedersen, H.G., Bergström, L. Forces Measured Between Zirconia Surfaces in Poly(acrylic acid) solutions, Journal of the American Ceramic Society, 1999, vol. 82, pp. 1137-45.

[14] Bergström, L., Schilling, C.H., Aksay I.A. Consolidation Behavior of Flocculated Alumina Suspension, Journal of the American Ceramic Society, vol. 75,1992, pp. 3305-14.

[15] Zhou Z., Solomon, M.J., Scales, P., Boger, D.V. The yield stress of concentrated flocculated suspensions of size distributed particles, Journal of Rheology, vol. 43, 1999, pp. 651-671.

[16] Houst, Y.F., Flatt, R.J., Bowen. P., Hofmann, H., Mäder, U., Widmer, J., Sulser, U., Bürge, T.A. Influence of Superplasticizer Adsorption on the Rheology of Cement paste, Proceedings of the International Conference The role of Chemical admixtures in high performance concrete (J.G. Cabrera and R. Rivera-Villareal, Editors), RILEM Publications S.A.R.L., Cachan, France, 1999, pp. 387-402

[17] Kapur, P.C., Scales, P.J., Boger, D.V, Healy, T.W. Yield Stress of suspensions loaded with size distributed particles, AIChE Journal, vol. 43, 1997, pp. 1171-1179.

[18] Staiger, M., Flatt, R.J., Bowen, P., Hofmann, H. Colloidal processing of nanosized ceramic dispersions : particle size distributions and their effect on colloid stability calculations and rheological behaviour, Ceramic Transactions - Ceramic Processing Science VI, American Ceramic Society, Westerville, USA, vol. 112, 2001, pp. 173-178.

[19] Navi, P., Pignat C. Three-dimensional Characterization of the Pore Structure of a Simulated Cement Paste, Cement and Concrete Research, vol. 29, 1999, pp. 507-514.

[20] Flatt, R.J., Interparticle Forces and Superplasticizers in Cement Suspensions, PhD Thesis No 2040, EPFL, Lausanne, Switzerland, 1999.

MODELLING INTERPARTICLE FORCES AND YIELD STRESS OF CEMENT SUSPENSIONS

Robert J. Flatt*, Paul Bowen, Yves F. Houst and Heinrich Hofmann

École polytechnique fédérale de Lausanne (EPFL), Laboratoire de technologie des poudres, MXD, CH 1015 Lausanne, Switzerland. E-mail: Paul.Bowen@epfl.ch , Yves.Houst@epfl.ch , Heinrich.Hofmann@epfl.ch
* Present address: SIKA A.G., Corporate Research and Analytics, P.O. Box 1300, CH 8048 Zürich, Switzerland. E-mail: flatt.robert@ch.sika.com

Robert J. Flatt

Robert Flatt received his diploma (1994) in chemical engineering and his PhD degree (1999) in materials science, both from the Swiss Federal Institute of Technology in Lausanne. He then spent 2.5 years as a research associate at Princeton University. Since May 2002, he is in charge of research on mineral/organic interactions at Sika A.G. in the division of Corporate Research and Analytics. His past research involved modelling the rheology of superplasticized cement suspensions, developing tailored mortars for the restoration of roman mosaics, identifying key factors in crystallization damage of porous materials and developing particle modified consolidants for the restoration of stone works.

THE DEVELOPMENT OF BLENDED SUPPLEMENTARY CEMENTING MATERIALS CONSISTING OF HIGH AND LOW CALCIUM FLY ASHES

Antiohos S.[1], Papadakis V.G.[2], Maganari K.[1] and Tsimas S.[1]

[1:] National Technical University of Athens, Chemical Engineering Dept., Labs of Inorganic and Analytical Chemistry, Athens, Greece. E-mail: stangits@central.ntua.gr
[2:] University of Patras, Chemical Engineering Dept., Greece. E-mail: vgp@pat.forthnet.gr

ABSTRACT

For overcoming the problems associated with the use of each type of fly ash (high and low calcium) in cementitious systems (low early strength, insufficient chemical resistance, expansion, etc), a development of new supplementary cementing materials consisting of blends of high and low-calcium fly ashes in various proportions was examined. Developing such blended pozzolans will result in coping with the mechanical and durability problems arising from each of the two types when these are added separately into cementitious systems and concrete.

The blended pozzolans resulted from the mixing of a low calcium fly ash with a high calcium fly ash, both generated in great quantities in Greece. The fly ashes were selected to cover a range of active silica and calcium oxide contents. Various mix proportions were adopted in order to find an optimum composition for the new pozzolan. The efficacy of the new combined supplementary material was examined in terms of active silica content, compressive strength and efficiency factor from the mechanical properties perspective.

Identification of hydration products was based on XR Diffraction of the corresponding pastes, while microstructure development was monitored by means of a SEM. Comparison between the overall performance of the new combined fly ash systems and the initial fly ashes was attempted in order to explain individual contributions and detect possible synergistic effects related to the different fly ashes used.

1. INTRODUCTION

Acute environmental problems created by the irresponsible disposal of fly ash [1] and the anticipation that sustainability [2] in the construction sector can only be achieved via the increased utilization of such by-products, has led to an ongoing research for the full exploration of their properties. The majority of the fly ashes generated in Greece possess significant lime contents, being therefore characterized as high-calcium ashes. A respectable amount of low-lime fly ashes is also produced contributing to the great diversity of this material in the local scene.

Despite the fact that advantages of both types of fly ashes are fairly well established, certain shortfalls that accompany each of them, especially when these are used as cement replacements, contribute to the skepticism with which they are still being handled by a part of the industry. In recognition of the significant differences in behaviour of the two types of fly ashes, Canadian Standards Association (CSA) recently revised the specification for fly ashes categorization, dividing them into three classes depending on their calcium content [3]. This is a classification scheme that is expected to be implemented in the national standards of other countries producing different types of fly ashes during the forthcoming years.

In the literature there is plentiful information regarding the distinctions in the chemical and mineralogical composition between low and high calcium fly ashes and the effect that these factors have on their reactivity. It is low-calcium fly ashes for example that react slower, especially during the early stages of hardening, mainly due to the higher presence of crystalline phases, which are considered chemically inert in concrete [4]. High calcium fly ashes on the other hand provide better early age strengths as a result of the cementitious compounds they possess. It is believed [3] that calcium substitution in the glass phase is generally increasing the reactivity of high-lime fly ashes providing for the formation of the calcium-silicate and calcium-aluminate phases in the absence of an external source of lime. It should be however pointed out that class C fly ashes differ from the class F ashes not only in that they contain more lime, but also the lime depolymerized glass phase [5].

Despite their increased reactivity and lower sensitivity to inadequate curing [6], high-lime fly ashes are generally less efficient in suppressing expansion due to ASR [7] and sulphate attack [8]. On the other hand, ashes of lower lime contents provide better resistance to ASR and sulphate attack and furthermore they usually guarantee better long term performance. Concerning additional durability properties, such as carbonation and chloride penetration [9,10], both low and high calcium ashes seem to have a similar beneficial effect, with the latter presenting a slightly better resistance.

To deal with the mutual shortcomings of each type of fly ash, the majority of the researchers have attempted to produce ternary blends by introducing in the fly ash/cement matrix an additional highly reactive pozzolanic material, such as silica fume [11] and metakaolin [12]. These policies however in most cases result in substantial cost increases putting obstacles to their wider acceptance as a routine tactic in the concrete sector. Keeping this in perspective, and to additionally control the rate of the hydration reaction, Naik et al. [13] prepared several mixtures of blends of class F and class C ashes. The constructed blends, that occupied 40% of the total cementitious material, showed either comparable or better results (in terms of both mechanical and durability properties) than either the reference mixture or mixture containing the class C fly ash only.

In the present study, new supplementary cementing materials (SCM) were prepared by mixing two types of fly ashes in several proportions. The main objective was to demonstrate that contributions of each type of fly ash in concrete could compensate for the handicaps of the other, while maintaining the production cost at low levels. The efficiency of the new products was examined in comparison with both the control mixture and the corresponding mixtures containing each type of fly ash.

2. EXPERIMENTATION

2.1 Materials

Two different fly ashes, a high-calcium (designated as T_f) from Ptolemais region, and a low-calcium one (T_m) from Megalopolis, representing the diversity of fly ashes derived in Greek power plants were used in the present work. A normal setting Portland cement was used (CEM I 42.5N according to European Standard EN 197-1) during the construction of the mortar and paste specimens. The chemical composition both for the fly ashes and the cement used are given in Table 1.

2.2 Preparation of mortars and pastes

2.2.1 Mixing proportions and construction of new blends

Both fly ashes were ground prior to use in a lab ball mill in order to obtain ashes of similar fineness. The requirement set during grinding was that 80% of the particles passed through the 45 μm sieve. Grinding of T_m fly ash proved to be more energy demanding since it consisted of more coarse particles in the as-received form. Therefore prolonged grinding was implemented in that case.

When the ashes were brought to the required fineness, they were mixed in a rotating blender until homogeneity of the new blend was achieved. The blended fly ash mixtures were prepared by using various dosages of the high (T_f) and low (T_m) fly ashes. The proportions applied were 75% T_f and 25% T_m (blend designated as T_1), 50% T_f and 50% T_m (for blend T_2) and 25% T_f and 75% T_m for the mix designated as T_3. The chemical composition of the new blends is given also in Table 1. An initial observation is that the blending procedure had a beneficial effect on the sulfate content of the blended fly ashes, as these either met the requirements stated in EN 450-1 'Fly ash for concrete' [14], or in the worst case (T_1) approached conformation with those.

Table 1. Chemical composition of raw materials (mass %)

	SiO_2	**Si_{re}***	**CaO**	**Al_2O_3**	**Fe_2O_3**	**MgO**	**SO_3**	**Na_2O**	**K_2O**
CEM I	20.28		65.01	4.75	3.76	1.61	2.55	0.17	0.35
T_f	36.92	29.13	29.79	13.50	7.06	2.69	5.10	0.92	0.5
T_m	51.36	31.36	13.80	16.73	8.75	2.26	1.49	0.77	1.52
T_1	40.38	29.60	24.89	14.65	7.50	2.56	4.02	0.88	0.75
T_2	44.08	30.36	21.50	15.70	8.75	2.45	3.18	0.81	0.93
T_3	48.00	32.02	17.96	15.92	8.92	2.36	2.39	0.78	1.26

* The method specified in European Standard EN 450-1 was followed for estimating the reactive silica content (Si_{re}) of fly ashes.

2.2.2 Curing procedures and compression test

In order to study the compressive strength, mortar mixes with the new blends were designed by adopting cementitious material-to-sand ratio of 1:3, water to binder ratio (w/b) of 0.5 and 10-30% by weight cement replacement. Keeping the w/b ratio constant, cement mortar without any fly ash or activator was prepared as the control one. Additionally, one mix with no fly ash addition (control specimen) and two mortars incorporating the two initial fly ashes (also replacing 10-30% by weight cement), were prepared for comparison purposes.

The dry mortars were mixed in a mixer machine and then water was added. After sufficient mixing, they were cast in 4x4x16 cm mortar prisms and vibrated for 20 sec on a vibration table. The molds were stripped after 24 h, and the specimens were immersed in lime-saturated water at 20^{o}C, until testing. The testing ages were 2, 7, 28, and 90 days. For each age, two specimens of each mixture were tested for compressive strength and the mean value of these measurements is reported.

Pastes were prepared using a similar procedure, adopting a representative 20% cement replacement at the same w/b ratio and curing under water at 23^{0}C, in order to monitor the hydration process of the constructed systems. At the dates of testing, the samples were fractured into pieces. The hydration was stopped with the addition of acetone and diethylethere followed by drying until constant weight in a vacuum pump. Finally, the specimens were placed into polypropylene bags and stored in a dryer until they were tested.

2.3 Efficiency factors

The concept of the efficiency factor (or *k-value* according to EN 206-1) has been introduced as a way to predict the effect of fly ashes (and other supplementary cementing materials) on the compressive strength of Portland cement systems that incorporate them. In other words, the efficiency factor is defined as the part of the fly ash, which can be considered as equivalent to Portland cement, having the same properties as the concrete without fly ash (obviously k=1 for Portland cement) [15]. In this work, the efficiency factors were determined in order to draw conclusions regarding the effectiveness of each new blended cementing material.

2.4 Evaluation of the Hydration Process

XRD patterns of the hydrated samples were recorded using a Siemens D 500 X-ray diffractometer (CuK_a radiation, 40KV, 30mA) in a scanning range of 5 to 65^0 in 2θ scale. The testing rate that was applied was 0.02^0/min for all specimens. The identification of the products was carried out by using a Diffrac-At Database. A XL 30 Philips ESEM equipped with an energy-dispersive X-ray analyzer (EDAX) was used both for the microstructure and quantitative elemental analysis of the hydration products.

3. RESULTS AND DISCUSSION

3.1 Compression test

The results of the compression test in the case of 20% cement replacement are presented in Figure 1. The compressive strength values for the control specimen and the mixtures incorporating the two initial ashes are plotted against the values of the blended fly ash specimens.

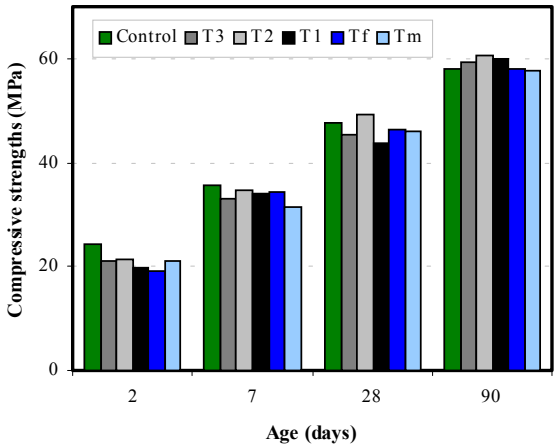

Figure 1. Compressive strengths with hydration age for 20% cement replacement

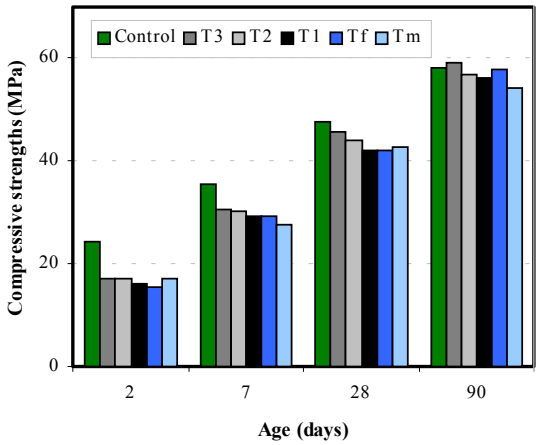

Figure 2. Compressive strengths with hydration age for 30% cement replacement

It is easily visible that during the first month of the hardening process, the control specimen (no fly ash addition) exhibited the highest value of almost all the mixtures tested. This is consistent with research establishments regarding the relatively slow evolution of the pozzolanic reaction, which mainly determines the strength development in fly ash-cement systems. The only mixture that presents higher strength value than the control after 4 weeks of hydration is T_2, constructed with 50% of class C T_f and 50% of class F T_m ashes. Somewhat surprisingly at the same age the strength values of the ashes that participate in the blend are noticeably lower. This is clearly an indication that a synergistic effect between the two ashes has taken place leading to a quicker initiation of the pozzolanic action.

After 2 days of hydration it is high lime fly ash T_f that exhibits the lowest strength value. This was unexpected since generally high calcium ashes behave better at early ages as a result of the hydration of their cementitious compounds. On the other hand, despite its low reactivity at this stage, low-lime ash T_m contributes substantially to the strength of the T_2 blend. Since the initial ashes were both ground to obtain similar finenesses, the superior performance of T_m ash cannot be attributed to that factor. However, the beneficial action of the filler effect [16] cannot be excluded, especially when the grain size distribution of T_m ash is improved due to prolonged grinding. It is clear that a small replacement (25%) of T_f ash by T_m ash at this age (blend T_3) induces positive consequences for the mix. However, the most efficient mix (T_2) contains respectable amounts of high-lime ash indicating that the synergy between the two different ashes occurs even at early ages.

The hydration of the cementitious compounds of high-lime ash T_f seems to occur during the next 5 days, accounting for the remarkable strength gain evident after 7 days of hydration. At that stage, the contribution of T_f ash in the blends is critical, since those blends incorporating over 50% T_f (T_1 and T_2) outperformed the ones with a limited T_f participation (T_3).

At the end of the first month of the hardening process, T_2 blend has exceeded the strength values of both the control mixture and the individual ashes, whilst the other blended specimens are not gaining substantial strength, remaining lower than the individual ashes and the reference mixture. On the contrary, during the forthcoming months (at 90 days), the compression test results exhibited excellent strength values for all the blended fly ash specimens compared to the control specimen. The fact that at the same age the ashes that consist the blends are not performing evenly, provides a guidepost that at elevated ages even small contributions from each fly ash are effective in producing superior fly ash systems. The incorporation of a different type of fly ash in each constructed blend obviously did much to offset the synergetic effect that was also detected in previous hydration stages.

At increased cement replacement (Fig. 2) the situation differs substantially. Despite the fact that synergistic effects are still detected, it is clear that the individual ashes used as well as their intermixtures retard the strength development, especially during the early ages. This is mainly associated with the increased cement content substituted in that case and the well-established incompetence of fly ashes to act drastically from the beginning of the hydration period. The initial ashes (T_f and T_m) are presenting a similar behavior to the previous replacement dosage, but the most efficient blend is the one with substantial participation of low-lime T_m (blend T_3). It is possible that a small participation of high-lime ash T_f reduced the period before the onset of the pozzolanic reaction leading to a notable strength increase at 28 days.

After 3 months, a dramatic improvement in the strength performance of all the examined blends occurs. This is substantiated by the fact that T_3 blend outperforms the no-fly ash mixture at this age, whilst T_1 and T_2 blends only fall slightly short of the control specimen. Especially noticeable is the fact that in the systems with an appreciable cement replacement, the strength of the blended fly ash mixtures is proportional to their active silica content from 7 days forward. This becomes even more pronounced after the first month of hardening, where the noteworthy strength improvement of the T_3 blend over the control specimen is the result of its high active silica, which binds CH forming accessory pozzolanic C-S-H. This is in agreement with the findings of Antiohos et al. [17], who observed that the role of reactive silica in the strength development of fly ash-cement systems becomes predominant after the first month of the hydration process.

To sum up, it must be pointed out that none of the constructed blended fly ash systems at any age presented the worst behavior. Generally, it can be deduced that at moderate fly ash additions, the blend that incorporated equal amounts of two different fly ashes exhibited the best behavior at all ages of hydration. On the contrary, when the fly ash contribution became more substantial (30% by weight cement replacement), the role of soluble silica in each fly ash blend was highlighted, providing for the strength superiority of T_3 blend at the age of 28 days and beyond.

3.2 Efficiency factors

For estimating the *k*-values, the procedure described by Papadakis et al. [18] was followed. In the case of mortars and concrete that incorporate supplementary cementing materials, the *k*-value derives from the following expression for the compressive strength (f_c) measured for the constructed systems:

$$f_c = K \left(\frac{1}{W / (C + kP)} - a \right) \quad (1)$$

where K is a parameter depending on the cement type (here 38,8MPa), C and P are the cement and fly ash contents respectively in the mortar (kg/m^3), W is the water content (kg/m^3) kept constant in all the mixes and α a parameter depending mainly on time and curing. Using this equation, the measured values of the compressive strength given in Figures 1 and 2, the *k*-values for the new blended SCM of the present work were calculated and are presented in Table 2.

Table 2. Efficiency factors (*k*-values) for initial and blended fly ashes

	***k*-values**									
	SCM dosage (% by cement weight)									
	20					**30**				
Age (days)	**T_f**	**T_m**	**T_1**	**T_2**	**T_3**	**T_f**	**T_m**	**T_1**	**T_2**	**T_3**
2	*0.67*	*0.81*	0.72	0.82	0.80	*0.63*	*0.71*	0.65	0.71	0.70
7	*0.92*	*0.72*	0.89	0.94	0.84	*0.73*	*0.65*	0.72	0.76	0.78
28	*0.92*	*0.88*	0.75	1.09	0.85	*0.76*	*0.78*	0.76	0.85	0.92
90	*0.99*	*0.97*	1.12	1.15	1.06	*0.99*	*0.82*	0.91	0.95	1.03

In previous attempts [19] dealing with Greek fly ashes the reported *k*-values were around unity during the early ages and they progressively exceed it as the hydration procedure evolved. This means that up to a certain level, those fly ashes could easily substitute, equivalently, for Portland cement. However, those values were calculated for a moderate level of cement replacement (i.e. 20% by weight). For a similar pozzolan addition applied here, the results given in Table 2 verify the aforementioned conclusions. Both initial ashes (T_f and T_m) have a *k*-value less than 1 at 7 days, but afterwards as fly ash is involved in the pozzolanic reactions, they reach unity. The beneficial role of the intermixing procedure is again highlighted through the concept of the efficiency factor. None of the constructed fly ash blends presents the smallest value during the early stages of hydration. On the contrary, the blends present decent early-age *k*-values and at 90 days they all exceed the corresponding values of the initial ashes used. It is of special importance to note that the *k*-value of the blend consisting of equal amounts of the initial fly ashes (T_2) is very close to unity after only 7 days of hydration and has significantly exceeded unity 3 weeks later. Furthermore, a small incorporation of a class F fly ash in a matrix redundant with class C ash (case of T_1 blend) can assist the strength development of such a system especially after the first month of hydration. This is clear from the dramatic increase of the *k*-value of the aforementioned blend during the last two months of the procedure.

When the replacement dosage increases (i.e. 30%), the *k*-values of all systems are normally diminished. Co-operation between initial fly ashes in the blends is still efficacious, providing *k*-values that are comparable even with the ones that the initial ashes exhibited at a lower replacement level during the early stages of hydration. As the hydration progresses, the blends are tardily reaching unity due to pozzolanic reaction taking place. Blend T_3 (with surplus of low-lime T_m) takes over from T_2 and performs better especially after the first week, reaching an impressive 1.03 factor at the end of the hydration period. This manifests the ability of blended fly ash systems owing appropriate active silica contents to substitute equal amounts of Portland cement even at high cement replacements, providing final products of the same quality.

3.3 Identification of hydration products

For investigating the role of the newly formed hydration products in the performance of the constructed blends, their XRD patterns were examined in comparison with the corresponding ones of the initial ashes at the same testing ages. Indicative images for the early (7 days) and later (90 days) stages of hydration are given in Figures 3 and 4 respectively.

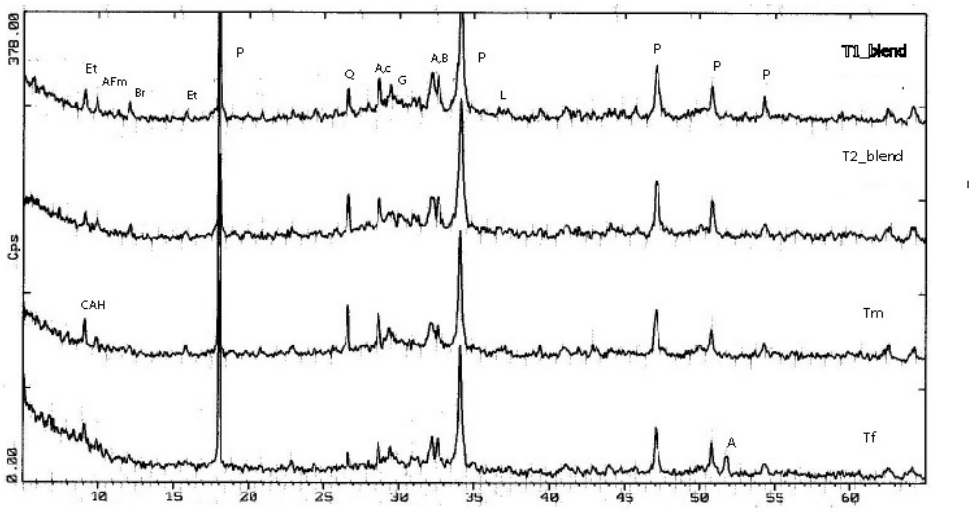

Figure 3. XRD patterns of hydrated pastes after 7 days of hydration.
The following notations were used for the various minerals identified: Et: ettringite, AF_m: monosulphate, P: portlandite, Br: Brownmillerite, Q: quartz, CAH: C_4AH_{13}, L: lime, c: calcite, G: gypsum, A: alite, B: belite.

Figure 3 shows the XRD patterns of the hardened fly ash-cement pastes at 7 days. Main hydration products observed for all specimens at this age were portlandite, AF_t, and AF_m. Especially for low-lime T_m ash and given that its SO_3 content is relatively low (1.49 percent), the unexpected intensification of the AF_m peaks can be attributed to the formation of C_4AH_{13} instead of AF_m, because AF_m and C_4AH_{13} have very similar diffraction peaks. Accessory differences between the initial fly ashes (such as variable intensity in the quartz and gypsum peaks) are mainly due to differences in their mineralogy. However, no other significant differences could be detected in the nature of the hydration products. The contribution of blended ashes seems to have no beneficial effect on the reaction rate of the minerals contained in the clinker. Moreover, portlandite is continuously produced in all samples, indicating the absence of pozzolanic reaction at such an early age. An important observation, that possibly denotes that synergetic action between the utilized ashes is not in full progress yet, is that the intensity of the various peaks is highly depended on the participating percentage of each ash in the blends. For example, when the contribution of T_f ash was increased in the blends (from 50% in T_2 to 75% in T_1 blend) an intensification of the AF_t and portlandite peaks was observed as a result of the excess of free lime and sulfur contained in this ash. In contrast, the intensity of crystalline silica (Quartz) diminished due to the limited T_m content in those blends.

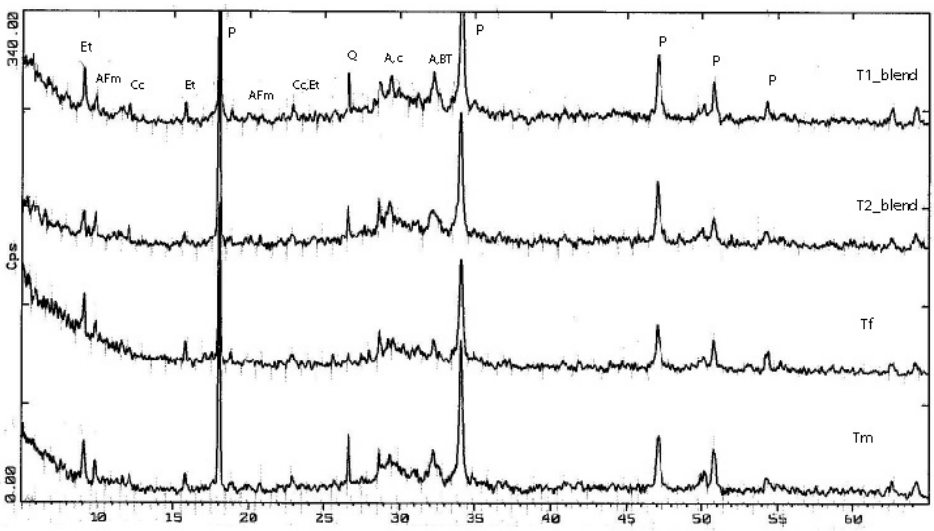

Figure 4. XRD patterns of hydrated pastes after 90 days of hydration.
The following notations were used for the various minerals identified: Et: ettringite, AF_m: monosulphate, P: portlandite, Q: quartz, Cc: $C_4A\underline{C}H_{11}$, c: calcite, A: alite, B: belite.

Three months after the start of the curing process, some changes in the XRD patterns of the specimens (Fig. 4) are easily detectable. The decrease of the portlandite peaks for instance, indicates the significant progress of the pozzolanic reaction mainly expressed as the consumption of crystalline CH by active silica of fly ashes. Carbonate hydrates are also appearing in both blended samples after 90 days. It is possible that a nontrivial part of CH was carbonated. Calcium silicate peaks are getting relatively smaller with hydration age, especially in the case of T_2 blend. However, the presence of alite and belite after 90 days indicates that the hydration of the two phases is not yet complete. Impressively, AF_t and AF_m peaks are not only increasingly generated, but contrary to what is stated in the literature [19] the AF_m peaks seem to grow independently of the AF_t ones. The fact that this phenomenon is more pronounced in the constructed blends constitutes an additional indication of the combined action of the initial ashes. The consistent production of pore-filling AF_t and AF_m phases, even at late stages, obviously contributes to the final strength of the blended systems.

3.4 ESEM and EDAX Examination

ESEM examination substantiated the results presented in the previous sections. Figures 5(a) and (b) depict the SEM images of the T_f and T_2 (the most effective) fly ash-cement systems respectively after 7 days curing. Despite the fact that some of the fly ash particles appear to be etched, or covered with hydration products, in both cases the majority retains its smooth shape indicating the absence of reaction. Voids visible in the images suggest that the systems are fairly porous.

When hydration progressed (28 days), the erosion of fly ash particles (fig. 5(c)) in T_2 blend has progressed dramatically, bringing about a breaking down of their glassy surface and release of additional active constituents inside the matrix. It is postulated that a substantial participation of a high-lime ash in the blend activated the ash particles in the matrix. A possible reason for that could be the high free lime contents of T_f ash that is easily dissolved from the outer shell of the glass, creating an excess of portlandite in the system.

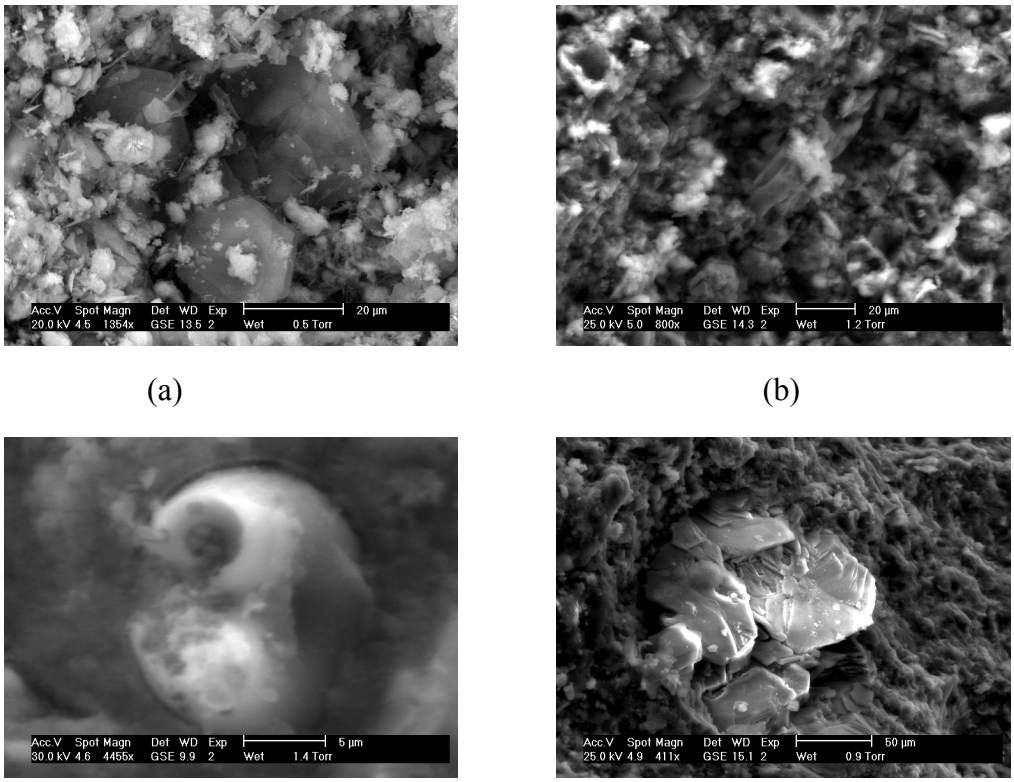

Figure 5**.** ESEM images of initial and blended fly ash systems

The increase in the alkalinity of the system initiates the corrosion of the so far inert particles contained in the T_m ash [20]. Accordingly the period before the initiation of the pozzolanic reaction is notably diminished, leading with sufficient curing (at 90 days), to a more compact structure (fig. 5(d)). The evident decrease in the porosity of the system accounts for the strength superiority of the T_2 blend, especially after the first month of the hardening process.

4. CONCLUSIONS

The use of blends of high-calcium and low-calcium fly ash is an effective means for dealing with mutual shortcomings related to each type of fly ash. It was demonstrated that blends with equal contributions from each fly ash was found to be the most effective in terms of mechanical properties for moderate cement substitution, whilst at advanced replacements the intermixture possessing the highest active silica content shows supremacy at all hydration ages. The encouraging performance of the constructed supplementary cementing materials was mainly attributed to synergistic effects detected between the utilized ashes. While such composite cements are not a panacea for all concrete problems, they constitute a unique opportunity to produce concrete avoiding non environmental-friendly tactics with excessive cost.

REFERENCES

[1] Cenni, R., Janisch, B., Splietho, H. and Hein K.R.G. Legislative and environmental issues on the use of ash from coal and municipal sewage sludge co-firing as construction material, Waste Management, vol. 21, 2001, pp. 17-31.

[2] Mehta, P.K. Role of pozzolanic and cementitious materials in sustainable development of the concrete industry, 6th CANMET/ACI international conference on fly ash, silica fume, slag and natural pozzolans in concrete, Bangkok, 1998, vol. 1, pp.1-20.

[3] Thomas, M.D.A, Shehata, M.H., and Shashiprakash, S.G. The use of fly ash in concrete: classification by composition, Cement and Concrete Aggregates, vol. 21, 1999, pp. 105-110.

[4] Hemmings, R.T. and Berry, E.E. On the glass in coal fly ashes: recent advances, MRS Symposium Proceedings, Pittsburgh, 1988, vol. 113, pp. 3-38.

[5] Ghosh, S.N., Sarkar, L.S. Mineral admixtures in cement and concrete. In: Progress in Cement and Concrete, 1st ed., ABI Books, New Delhi, 1993, p. 203, .

[6] Poon, C.S., Wong, Y.L. and Lam, L. The influence of different curing conditions on the pore structure and related properties of fly-ash cement pastes and mortars, Construction and Building Materials, vol. 11, 1997, pp. 383-393

[7] Smith, R.L. Is the available alkali test a good durability predictor for fly ash concrete incorporating reactive aggregate. MRS Symposium Proceedings, Pittsburgh, 1988, vol. 113, pp. 249-256.

[8] Dunstan, E.R. A possible method for identifying fly ashes that will improve the sulfate resistance of concretes. Cement and Concrete Aggregates, vol. 2, 1980, pp. 20-30.

[9] Papadakis, V.G. Effect of supplementary cementing materials on concrete resistance against carbonation and chloride ingress. Cement and Concrete Research, vol. 30, 2000, pp. 291-299.

[10] Zhang, M., Bilodeau, A., Malhotra, V.M., Kim, K. and Kim, J.C. Concrete incorporating supplementary cementing materials: effect on compressive strength and resistance to chloride-ion penetration. ACI Materials Journal, vol. 96, 1999, pp. 181-188.

[11] Lynsdale, C.J., Khan, M.I. Chloride and oxygen permeability of concrete incorporating fly ash and silica fume in ternary systems. 5th CANMET/ACI international conference on durability of concrete, Barcelona, 2000, vol. 2, pp.739-753.

[12] Bai, J., Sabir, B.B., Wild, S., and Kinuthia, J.M. Strength development in concrete incorporating PFA and metakaolin. Magazine of Concrete Research, vol. 52, 2000, pp. 153-162.

[13] Naik, T.R., Singh, S., and Ramme B. Mechanical properties and durability of concrete made with blended fly ash. ACI Materials Journal, vol. 95, 1998, pp. 454-462.

[14] European Standard EN 450-1. Fly ash for concrete - definitions, specifications and conformity criteria. Brussels: CEN, 2000.

[15] KEMA Environmental Technology. Determination of the k-value of fly ash, Report No. 00474-KET/R&B 97-4062, Arnhem, 1997, pp. 1-32.

[16] Yamazaki, K Fundamental studies of the effects of mineral fines on the strength of concrete. Transactions of Japanese Society of Civil Engineers, vol. 85, 1962, pp. 15-44.

[17] Antiohos, S. and Tsimas, S. Investigating the Role of Reactive Silica in the Hydration Mechanisms of High-calcium Fly Ash/Cement Systems. Cement and Concrete Composites (submitted), 2002.

[18] Papadakis, V.G., Tsimas, S. Supplementary Cementing Materials for Sustainable Building-Sector Growth, European Commission DGXII, Marie Curie Fellowship, Final Scientific Report, Project No HPMF-CT-1999-00370, National Technical University of Athens, Greece, 2001, pp. 23-27.

[19] Papadakis, V.G. Effect of fly ash on Portland cement systems. Part II: High-calcium fly ash. Cement and Concrete Research, vol. 30, 2000, pp. 1647-1654.

[20] Fraay, A.L.A, Bijen, J.M. and deHaan, Y.M. The Reaction of Fly Ash in Concrete. A Critical Examination. Cement and Concrete Research, vol. 19, 1989, pp. 235-246.

* All correspondence should be addressed to:
Professor Stamatis Tsimas, National Technical University of Athens, Department of Chemical Engineering, 9 Heroon Polytechniou, Zografou Campus, GR-15773, Athens, GREECE.

THE DEVELOPMENT OF BLENDED SUPPLEMENTARY CEMENTING MATERIALS CONSISTING OF HIGH AND LOW CALCIUM FLY ASHES

Antiohos S.[1], Papadakis V.G.[2], Maganari K.[1] and Tsimas S.[1]

[1:] National Technical University of Athens, Chemical Engineering Dept., Labs of Inorganic and Analytical Chemistry, Athens, Greece. E-mail: stangits@central.ntua.gr
[2:] University of Patras, Chemical Engineering Dept., Greece. E-mail: vgp@pat.forthnet.gr

Stelios Antiohos

S. Antiohos holds a diploma in Chemical Engineering acquired from the National Technical University of Athens. He was conferred a MSc diploma in Environmental Management from the E.A.E.M.E (European Association for Environmental Management Education), specializing in Hazardous Materials Transportation Management Schemes. At the moment he is a PhD Candidate at the National Technical University of Athens. His thesis focuses on the role of active silica on the pozzolanic reactivity of fly ashes. He is also associated with research activities and projects related with other supplementary cementing materials and their suitability as additives in cement and concrete.

EFFECT OF ALKALINE ACTIVATION ON THE MECHANICAL PROPERTIES OF NEW KIND OF LOW ENERGY CEMENT

A. Guerrero[1], M.P. Gutierrez[2], S. Goñi[1] and M.P. Lorenzo[2]

[1]Institute of Construction Science Eduardo Torroja (CSIC). C/ Serrrano Galvache s/n, 28033
E-mail: aguerrero@ietcc.csic.es and sgoni@ietcc.csic.es
[2]University of San Pablo CEU, Spain. E-mail: pazloga@ceu.es

ABSTRACT

A new kind of low-energy-belite cement has been synthesized by using, as raw material, two municipal solid waste incineration ashes (MSWIA). Mixtures were prepared in a proportion of 35.7% and 64.3% (by weight), respectively, to obtain a CaO/SiO_2 molar ratio of 2. To study the influence of temperature on the reactivity of cements, samples (synthesized from hydrothermal treatment, in water and KOH 0.5M, and then heated at 700, 800, 900 and 1000ºC), were hydrated for 28 days at room temperature. During this hydration time, the combined water content was evaluated, from thermal analyses. The high reactivity was reached for the sample hydrothermally treated in KOH 0.5M and then heated at 800ºC. This temperature is strongly lowered in comparison to 1450ºC of traditional belite cement manufacture. The alkaline activation was corroborated from the mechanical strength results, which improved strongly in comparison to those obtained in samples hydrothermally treated in water.

1. INTRODUCTION

Among the reasons that are actually advancing the development of new materials, especially new kinds of cement, are their higher performances and the environmental restriction of their fabrication processes. In the case of Ordinary Portland Cement, the large amounts of CO_2 emission produced during its traditional fabrication, together with the large quantities of natural raw materials consumed, are stimulating investigations relating to new low-energy-belite cement, produced through environmentally friendly processes, which avoid or at least decrease the problems aforementioned.

The use of industrial waste and by-products as alternative secondary raw materials is increasing considerably. Numerous investigations are being carried out on the search for potential applications of MSWIR in the construction field. Nevertheless, expansion and high chloride contents are serious problems with these wastes, which must be treated prior to their incorporation into construction materials [1-3].

This paper is the continuation of an extensive investigation on the use of municipal solid waste incineration ash (MSWIA) as a raw material for synthesising reactive low energy cement [3-5]. The synthesis is based on previous studies, carried out in our laboratory, on the use of fly ash, from coal combustion, as raw materials for synthesising reactive belite cement [6-8]. The fabrication process is based on previous work by Jiang and Roy [9]. The process involves two sequential steps. The first step consists of the hydrothermal treatment of fly ash to form the hydrated precursors of the cement. Subsequent dehydration of these phases, by controlled heating, gives rise to the highly reactive belite phases. During the hydrothermal treatment (200ºC for 4 hours and 1.24 MPa of

pressure) the fly ash pozzolanic reaction is strongly activated leading to hydraulic products: katoite ($Ca_3Al_2(SiO_4)(OH)_8$) together with CSH gel ($Ca_{1.5}SiO_{3.5}.xH_2O$) and α-C_2SH, which are the precursors of the cement. In the second step the hydrates are calcined at 800ºC.

In the present study, two types of municipal solid waste incineration ashes (MSWIA), one coming from fluidized bed combustion (called R1 in this paper) and the other from cleaning-gas devices (called R2 in this paper), were prepared in a proportion of 35.7% and 64.3% (by weight), respectively, to obtain a CaO/SiO_2 molar ratio of 2, similar to the Ca/Si molar ratio in low-energy-cement [6-8]. Cements were synthesised in a range of temperatures between 700ºC and 900ºC from the mixture of MSWIA aforementioned (R1+R2), which was previously activated by hydrothermal treatment at 200ºC, in an alkaline KOH 0.5M solution.

To evaluate the effect of the alkaline solution, we compared the results with the behaviour of sample treated with water. An improvement in the value of compressive strength of the mixture with alkaline activation was observed. The precursor phases and the effect of alkaline activation were characterised, among others, by X-ray diffraction. The reactivity of cements was evaluated from their combined water contents (estimated from thermogravimetric curves (TG)) for a period of 28 days.

2. EXPERIMENTAL PROCEDURE

The chemical compositions of two municipal solid waste incineration ashes (MSWIA) (one coming from fluidized bed combustion (called R1) and the other from cleaning-gas devices (called R2)) are given in Table 1 and Figure 1.

Table 1. Chemical Composition of Original MSWIA (% by weight)

	R1	**R2**
CaO	21.9	44.9
SiO_2	34.1	11.4
Al_2O_3	19.3	11.3
Fe_2O_3	6.6	1.1
MgO	2.6	1.9
SO_3	3.3	3.9
Na_2O	2.1	2.1
K_2O	1.9	1.9
Cl^-	3.6	13
Zn^{2+}	0.41	0.36
Cd^{2+}	0.0013	0.0017
Pb^{2+}	0.13	0.38
LOI*	4.6	17.6
IR*	5.2	0.1
Density	2.59	2.55
Blaine (cm^2/g)	2240	7275

* LOI= loss on ignition; IR= insoluble residue

The mixtures were prepared in a proportion of 35.7% and 64.3% (by weight), respectively, to obtain a CaO/SiO_2 molar ratio of 2.

The principal crystalline compounds detected in the starting MSWIA are: Halyte (NaCl), sylvite (KCl), $CaCl_2.Ca(OH)_2.H_2O$ whose X-ray reflections are more intense for MSWIA coming from the cleaning-gas-device (R2) in comparison with those of R1; Portlandite ($Ca(OH)_2$), anhydrite ($CaSO_4$), metallic aluminium and α-SiO_2 are mainly detected in R1. Intense gehlenite (C_2AS) reflections appeared in both R1 and R2.

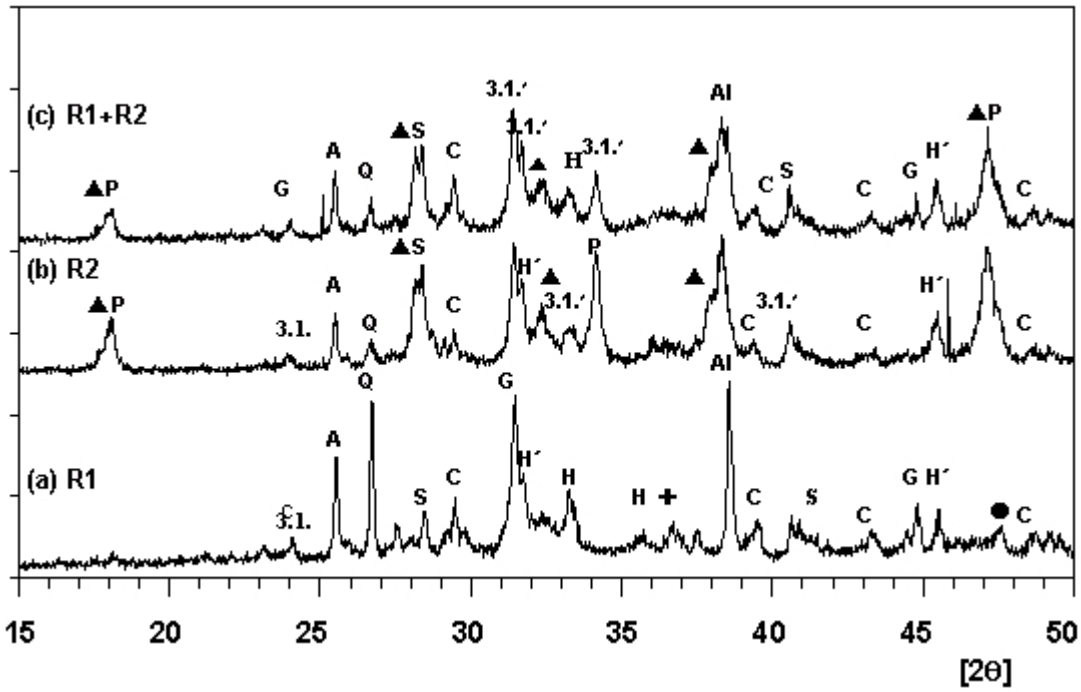

Figure 1. X-ray Diffraction Patterns of Original MSWIA: C calcite; Q α-quartz; P portlandite; G gehlenite; A Anhydrite; S sylvite; H hematite; Al metallic aluminium; H' halyte; ▲ $CaCl_2.Ca(OH)_2.H_2O$; ● C; ✚ Mg_2C_3

Alkaline solution (KOH 0.5M) and MSWIA (R1+R2) were mixed at an alkaline solution to R1+R2 ratio of 10. The mixture was maintained at room temperature for 24 hours to eliminate the H_2 gas, which is strongly formed from metallic aluminium dissolution. Thereafter, the alkaline mixture was hydrothermally treated at 200ºC and 1.24 MPa steam-pressure for periods of 1h, 2h, 4h and 6h, where the precursors of cement were obtained. The dried solid was heated at a rate of 10ºC/min. up to 600ºC and at 5ºC/min. from 600ºC to 900ºC.

Pastes of cements synthesised at 700ºC, 800ºC and 900ºC were prepared at water to cement ratio of 0.8 to evaluate their hydraulic activity. The pastes were kept at >90% RH and 21ºC±2ºC for a period of 28 days from mixing. The hydrothermal treatment was carried out with Parr Mod. 4522 pressure reactor equipment (1000 mL pump with split-ring closure and a PID Mod. 4842 temperature controller). The minor elements (Zn, Cd and Pb) were determined by Anodic Solution Voltamperometry (ASV) using a Mehtrom model 746.

The precursors and cement phases were characterised by X-ray diffraction (XRD), infrared spectroscopy (IR) and thermal analyses (TGA) [6]. X-ray diffraction (XRD) patterns were recorded with a diffractometer (Model PW-1730 Philips Research Laboratories, Eindhoven, The Netherlands) using a graphite monochromator and Cu $K\alpha_1$ radiation. IR study was carried out on a Perkin Elmer 783 instrument and KBr pellets containing 0.5% of sample. Thermal analyses were recorded with a Netzsch equipment with STA 409 simultaneous analysis system using 50 mg samples and a dynamic nitrogen stream (flow rate = 100 cm^3/min) at a heating rate of 10ºC/min.

For the mechanical study, several mortar samples of 5x5x5 cm were prepared using α-quartz. The sand-to-cement ratio was 3.0; the de-mineralized water-to-cement ratio was 0.9; 1 day after mixing, samples were demolded and stored at the temperature of 21±2ºC and >90% rh for 28 days.

3. RESULTS AND DISCUSSION

3.1 Effect of Alkaline Activation and Hydrothermal Treatment

As was mentioned in previous work [6] after 1 hour to 6 hours of hydrothermal treatment no significant changes could be observed in the sample, independent of the medium: water or alkaline solution. In spite of this behaviour, significant differences could be observed in the sample treated at room temperature for 24h in KOH 0.5M solution (Figure 2):

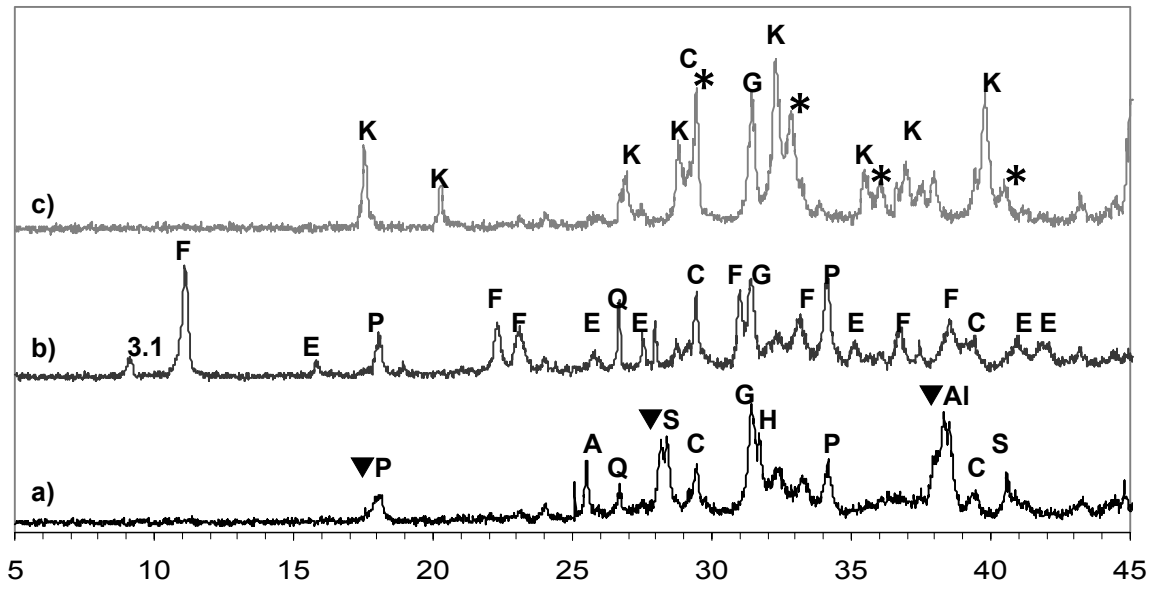

Figure 2. Evolution of X-ray diffraction patterns of MSWIA mixture pre-treated with alkaline solution and with hydrothermal treatment: a) starting R1+R2; b) ambient (with 0.5M KOH) and c) after 1h 200ºC (HT): K katoite; C calcite; ▼ $CaCl_2.Ca(OH)_2.2H_2O$; Q α-quartz; G gehlenite; A anhydrite; ∗ $Ca_3Al_2(SiO_4, CO_3, OH)_3$; Al metallic aluminium; S sylvite; H halite; E ettringite; F Friedel´s salt

First, the original crystalline compounds disappeared, with the exception of portlandite and calcite, which increased owing to the alkaline solution decreasing the solubility of portlandite and favouring its carbonation; and, second, the formation of crystalline Friedel´salt ($Ca_4Al_2O_6Cl_2.10H_2O$) and ettringite ($Ca_6Al_2(SO_4)_3(OH)_{12}.26H_2O$) of the AFm and AFt structural families, respectively. These two compounds are formed from the dissolution metallic aluminium, which provides the aluminate ion together with the sulphate ion provided by anhydrite in the case of ettringite; and chloride ion provided by sylvite, halyte and $CaCl_2.Ca(OH)_2.H_2O$ in the case of Friedel´salt.

After 1h of hydrothermal treatment (Figure 2 (c)), ettringite, Friedel´s salt and portlandite disappeared; and two types of katoites were formed: $Ca_3Al_2(SiO_4)(OH)_8$ (C_3ASH_4) and $Ca_3Al_2(SiO_4,CO_3,OH)_3$ ($C_3AS_3c_3H_{1.5}$). The presence of $Ca_{1.5}SiO_{3.5}.xH_2O$ and α-C_2SH (their main X-ray reflections (at 2θ = 29.4) are overlapped with those of calcite), was confirmed from IR analyses by the strong absorption band at 950 cm^{-1} [6].

3.2 Evolution of Precursors with Heating Temperature

The dehydration of cement precursors appears in Figures 3 and 4 and was carried out by heating up to 900ºC.

3.2.1 Samples Treated With Water

After HT (Figure 3(a)) intense X-ray reflections of katoite silication (C_3ASH_4) and $Ca_{1.5}SiO_{3.5}xH_2O$ (CSH gel) are formed. These phases have the property of incorporating a wide range of species via a solid solution mechanism, in the case of katoite silication, and via intercalation for CSH gel, providing, therefore, stabilisation mechanisms for minor toxic elements of MSWIA.

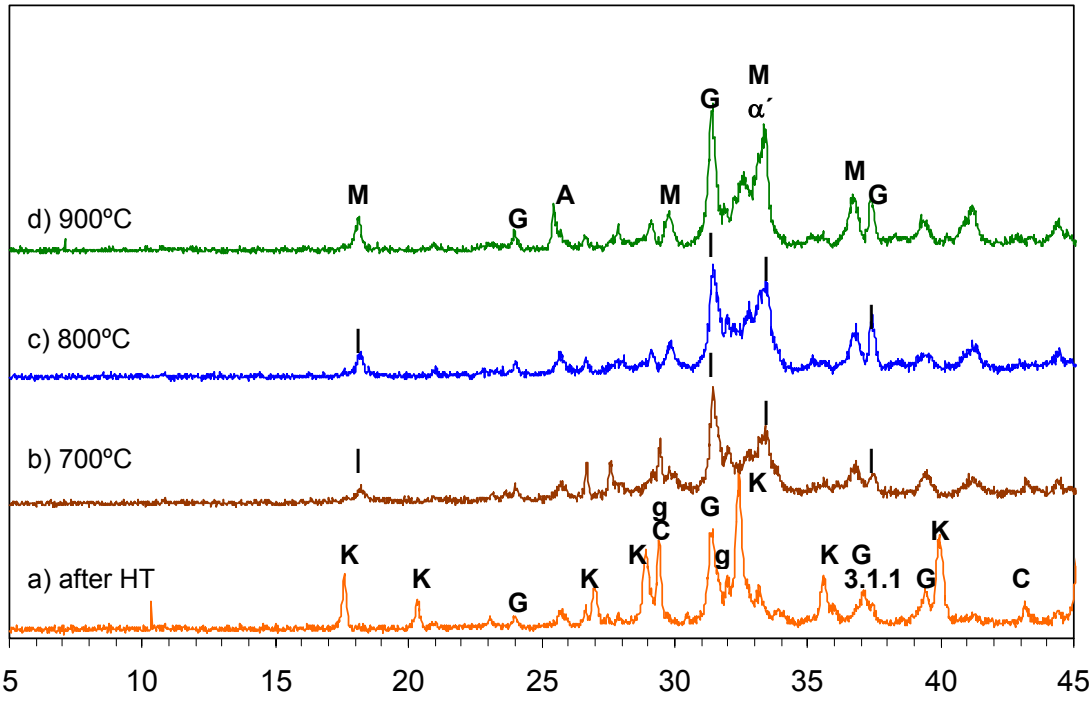

Figure 3. Evolution of Hydrated Precursors with Heating Temperature: K katoite; C calcite; M mayenite; ▲ CaO; Q α-quartz; G gehlenite; α´-α´$_L$ C_2S; A anhydrite; g $Ca_{1.5}SiO_{3.5}.xH_2O$ (CSH gel).

Sample heated at 700ºC (Figure 3(b)): the reflections of katoite: $Ca_3Al_2(SiO_4)(OH)_8$ and CSH gel disappeared, and those of calcite decreased. Gehlenite remains and new broad reflections began to be detected, which could be attributed to the α`$_L$-$C_2S$ and mayenite ($C_{12}A_7$). At 800ºC (Figure 3 (c)) the intensity of α`$_L$-C_2S and mayenite reflections increased; gehlenite reflections decrease; as expected by temperature, the calcite decreased significantly. After 900ºC (Fig. 3(d)), reflections of α`$_L$-C_2S and mayenite were better defined, and gehlenite (C_2AS) increased; Calcium oxide is detected from 800ºC.

The decrease of gehlenite reflections at 800ºC together the amorphous halo observed between 31 and 34 of 2θ angular zone is, among others, the reason for the use of this sample as raw material for synthesising low-energy cement.

3.2.2 Samples Heated With Alkaline Solution

The evolution of samples heating from 700ºC to 900ºC (Figure 4), is very similar to the case of the sample with water. The principal differences are: (i) after hydrothermal treatment, two types of katoite: $Ca_3Al_2(SiO_4)(OH)_8$ and $Ca_3Al_2(SiO_4, CO_3, OH)_3$, are detected which disappeared with heating; (ii) after heating a new broad reflection began to be detected, which could be attributed to the α`$_L$-C_2S and mayenite ($C_{12}A_7$), (iii) a decrease of calcite reflections that disappeared totally after 700ºC of heating. (iv) sample at 800ºC presented an amorphous halo was between 31 and 34 of 2θ angular zone, higher than the case of water, which could be attributed to recently dehydrated phases and the intensity of α`$_L$-C_2S and mayenite reflections increased.

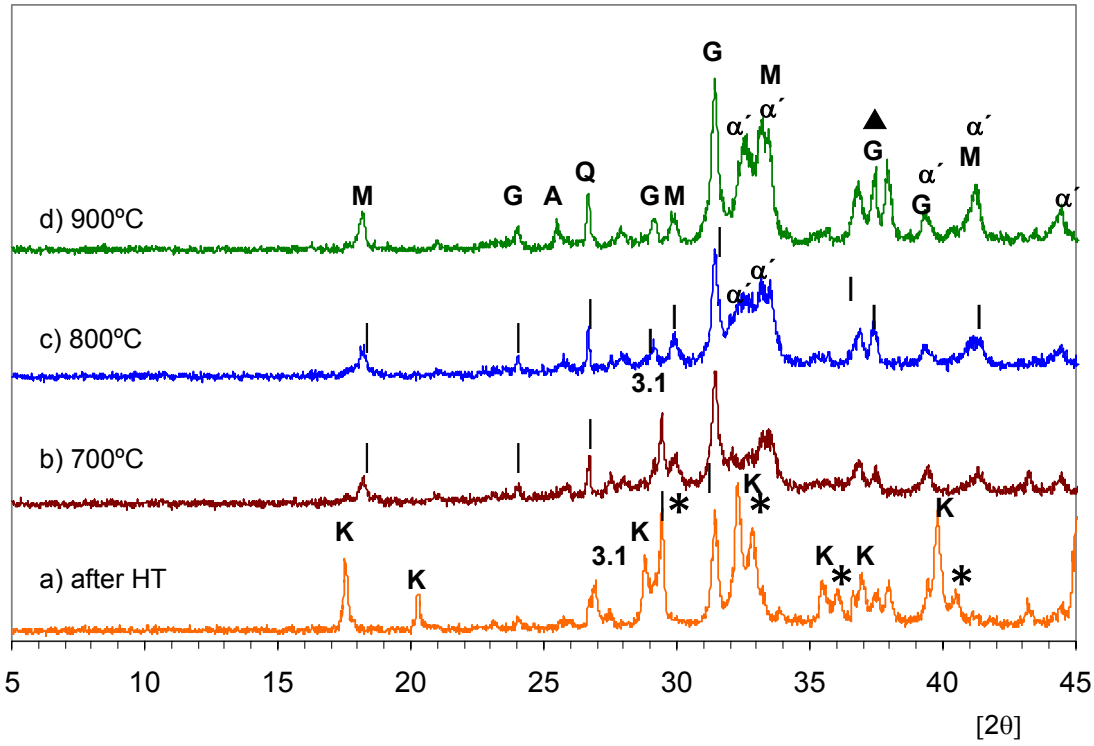

Figure 4. Evolution of Hydrated Precursors Activated with Heating Temperature: K katoite; C calcite; M mayenite; ▲ CaO; Q α-quartz; G gehlenite; α´-α´$_L$ C_2S; A anhydrite; ∗ $Ca_3Al_2(SiO_4, CO_3, OH)_3$.

These results are very similar to those obtained when fly ash from coal combustion instead of MSWIA was used as raw material for synthesising fly ash belite cement (FABC) [7]. In that case, better hydraulic activity (estimated by the combined water content) and mechanical strength were found at the temperature of heating of 800ºC. On the basis of those results, the authors applied the same methodology for the cements obtained here.

In both samples, the mayenite phase plays an important role, related to the hydration rate of cements.

3.3 Degree of hydraulicity of the New Cements

The degree of hydraulicity of cements obtained after hydrothermal treatment with water and KOH 0.5M of mixture R1+R2, was evaluated from the combined water content (evaluated from thermogravimetric curves). For this, pastes were prepared at a demineralized water to cement ratio of 0.8, which is similar to that used for fly-ash-belite-cement and municipal solid waste incineration ash cement in previous works [6, 9]. The pastes were maintained for 1, 7, 14 and 28 days from mixing of the cements obtained at 700º, 800º and 900ºC, after hydrothermal treatment with water and KOH 0.5M. As can be seen in Fig. 5, the rate of hydration is markedly fast for alkaline activated cement.

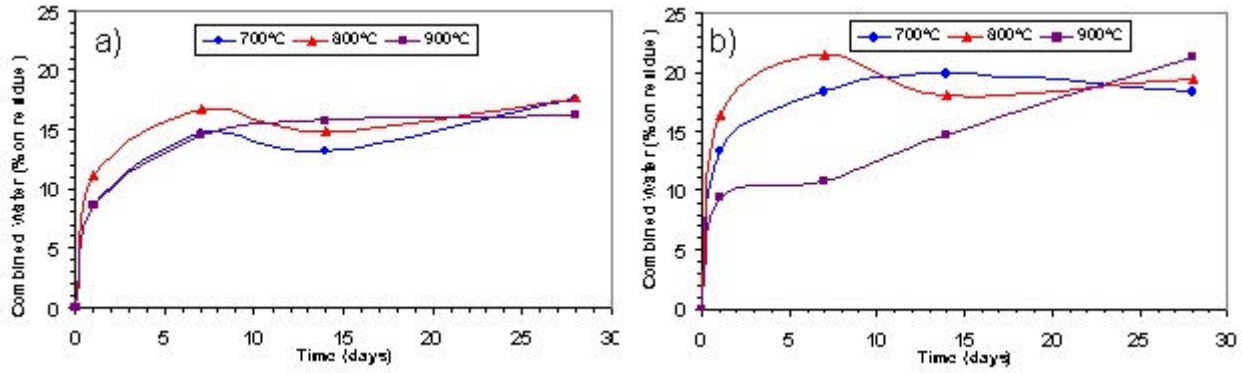

Figure 5. Evolution of Combined Water versus Hydration Time: a) Water, b) 0.5M K(OH)

Thus, the combined water content of the cements reach the maximum value by 7 days, at 800ºC, independent of the media. Nevertheless, the combined water content values of each cement at different temperatures is similar after 28 days of hydration.

This good behaviour of the cements obtained at 800ºC, at early ages, was corroborated by the mechanical strength results.

3.4 Compressive Mechanical Strength

The compressive mechanical strength data are represented in Fig. 6. Each value representing the average of three measurements

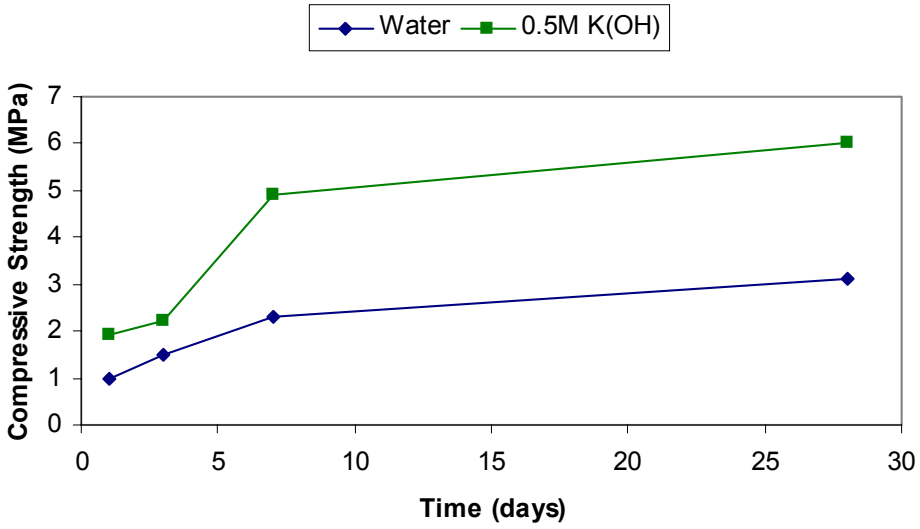

Figure 6. Compressive Strength of the two kinds of cements

At any time of hydration, the cement synthesised with alkali activation presents higher strength values than cement synthesised with water, principally from 7 days. This cement reached, after 28 days of hydration, a value of 6 MPa, which is comparable to that β-C_2S variety substituted by alkalis (K/Na y Fe) [11] and obtained at 1520ºC.

In this case, we obtained the cement with an important reduction of synthesis temperatures, that implies a considerable reduction of energy consumption.

This hydraulic activity could be attributed to the mayenite phase, besides, the α´-C_2S variety is not a pure phase, and, therefore, its reactivity will be higher in comparison to that of the pure phase obtained by traditional ways; together with the amorphous character of α´and β- C_2S phases in cement synthesised at 800ºC as consequence of alkaline activation (see Fig.4).

4. CONCLUSIONS

- Chloride and metallic aluminium of MSWIA represent one of the main problems and from the point of view of its potential valorisation towards construction materials. The alkaline treatment of MSWIA avoids such problems and, in addition, the new hydraulic phases formed have the property of incorporating a wide range of species via solid solution or intercalation mechanisms, providing, therefore, stabilisation mechanisms for minor toxic elements of MSWIA or other toxic wastes.
- Treatment with KOH 5.0M is an important tool to strongly improve the mechanical strength of cements synthesized from these new raw materials.

ACKNOWLEDGEMENTS

The authors are grateful for financial assistance from CAM and CICYT Projects: (07M/0052/1999)(MAT95-0054) (BQU2000-1357) and (PB 98-0516).

REFERENCES

[1] Alkemade, M.M.C.; Eymael, M.M.Th.; Mulder, E. and Wijs, W. De; "How to Prevent Expansion of MSWI Bottom Ash in Road Construction? Environmental Aspects of Construction with Waste Materials, JJJM Goumans, HA. Van der Sloot and ThG. Aalbers (Editors),1994, p. 863-876.

[2] Barbery, O. and Ghodsi, A.; "Trapping of Chloride, Sulfate and Heavy Metals", Proc. of the International Symposium on Sustainable Construction: Use of Incinerator Ash. Ed. by Ravindra K. Dhir, Tom D. Dyer and Kevin A. Paine, Publishers Thomas Telford, London, 2000, pp. 173-183.

[3] Guerrero, A.; Fernández, E.; Macías, A. and Goñi, S.; "Hydrothermal Treatment of Fly Ash from Municipal Solid Waste Incineration", Proceedings of Waste Materials in Construction: Science and Engineering of Recycling for Environmental Protection, Editors: G.R. Woolley, J:J:M: Goumans and P.J. Wainwright, Pergamon, Amsterdam, (ISBN: 0-08-043790-7), vol. 1, 2000, pp. 178-185.

[4] Guerrero, A.; Goñi, S.; Macías, A. and Fernández, E.; "Influence of Synthesis Temperature on the Hydration of New Cements from Fly Ash of Municipal Solid Wates Incineration", CANMENT/ACI International Symposium on Sustainable Development and Concrete Technology, Editor: V.M. Malhotra, vol. SP202, 2001, pp. 267-283.

[5] Jiménez, P.; Goñi, S.; Guerrero, A.; Lorenzo, M.P. and Macías, A.; "New Kind of Low Energy Friendly Environmentally Cement", Proceedings of Challenges of Concrete Construction, University of Dundee, Dundee (Scotland), 2002.

[6] Guerrero, A.; Goñi, S.; Macías, A. and Luxán, M.P., "Hydraulic Activity and Microstructural Characterization of New Fly Ash-Belite Cement Synthesised at Different Temperatures", J. Mater. Res., vol. 14, No. 6, 1999, pp. 2680-2687.

[7] Guerrero, A.; Goñi, S.; Macías, A. and Luxán, M.P., "Mechanical Properties, Pore-Size Distribution and Pore Solution of Fly Ash-Belite Cement Mortars", Cem. and Concr. Res., vol. 29, 1999, pp. 1753-1758.

[8] Guerrero, A.; Goñi, S.; Macías, A., "Durability of New Fly Ash-Belite Cement Mortars in Sulfated and Chloride Medium"., Cem. and Concr. Res., vol. 30, No. 8, 2000, pp. 1231-1238.

[9] Jiang, W. and Roy, D.M., "Hydrothermal Processing of New Fly Ash Cement", Ceramic Bulletin, vol. 71, No. 4, 1992, pp. 642-647.

[10] Goñi, S.; Guerrero, A.; Macías, A., Peña, R.; Fernández, E.; "Secondary Raw Materials for Synthesising New Kind of Cements", Materiales de Construcción, vol. 51, nº 263-264, 2001, pp. 71-84.

[11] Suzuki, K., Ito, S. and Shibata, S.; "Hydration and Strength of α-α´and β-Dicalcium Silicates Stabilized with Na-Al, K-Al, Na-Fe and K-Fe", in Proceedings of the 7th Int. Congr. of the Chemistry of Cement, Paris, 1980, II, p. II-47-51.

EFFECT OF ALKALINE ACTIVATION ON THE MECHANICAL PROPERTIES OF NEW KIND OF LOW ENERGY CEMENT

A. Guerrero[1], M.P. Gutierrez[2], S. Goñi[1] and M.P. Lorenzo[2]

[1]Institute of Construction Science Eduardo Torroja (CSIC). C/ Serrrano Galvache s/n, 28033 Madrid, Spain.
E-mail: aguerrero@ietcc.csic.es and sgoni@ietcc.csic.es
[2]University of San Pablo CEU, Spain. E-mail: pazloga@ceu.es

A. Guerrero

A. Guerrero is a Doctor of Chemistry, working at the Institute of Construction Science "Eduardo Torroja" (IETcc-CSIC) since 1992, in the field of the durability of cement-based materials in simulated liquid radioactive wastes the use and recycling of pozzolanic industrial by-products and, in general, on microstructure characterization of the materials.

HYDROTHERMAL TREATMENT OF INDUSTRIAL WASTES AND ITS IMPLICATION FOR IMMOBILIZING OTHER TOXIC WASTES

R. Peña[1], A. Guerrero[1], S. Goñi[1] and M.P. Lorenzo[2]

[1]Institute of Construction Science Eduardo Torroja (CSIC). C/ Serrrano Galvache s/n, 28033 Madrid, Spain. E-mail: sgoni@ietcc.csic.es; aguerrero@ietcc.csic.es and rpena@ietcc.csic.es
[2]University of San Pablo CEU, Spain. E-mail: pazloga@ceu.es

ABSTRACT

The influence of the temperature of hydrothermal treatment in water of fly ash and bottom ash from incineration of municipal solid wastes is presented in this work. The evolution of the liquid phase was characterized by pH and electric conductivity measurements, and that of the solid phase was characterized by X ray diffraction (XRD), FT infrared (FTIR) spectroscopy and surface area (BET-N_2) analyses. The results showed, in the case of the bottom ash, the formation of ettringite, α-C_2SH and gel CSH at low temperatures (ambient and 50ºC). Ettringite is converted to katoite after treatment at 100ºC. A zeolite type scolecite is detected at 200ºC. As a result, the surface area of the bottom ash increased. In the case of fly ash, Friedel´s salt is massively formed at 100ºC leading to an increase of 5 times the surface area. Hexagonal Friedel´s salt converted to cubic katoite after treatment at 150ºC, subsequently decreases its surface area. Gel CSH and $C_2SH_{0.35}$ were also formed.

1. INTRODUCTION

The capacity for trapping ionic species in the lattice of the Portland clinker phases or forming solid solutions with phases of higher solubility during the hydration of Ordinary Portland Cement (OPC), is one of its more important properties, which constitutes the main mechanisms for immobilizing toxic and radioactive wastes. That is the case of CSH gel; AFm and AFt phases; katoites; tobermorites etc., which can trap a wide variety of ionic species owing to their microstructural characteristics.

These phases were synthesized in the past through the hydrothermal treatment of two type of wastes coming from two different combustion processes, such as, coal fly ash [1-5] and ash from incineration of municipal solid wastes [6, 7]. The experimental conditions of temperature and pressure, which are inherent in the hydrothermal conditions favour the thermodynamic evolution of any process through to the more stable state. In this way, it is possible to obtain similar phases from different materials such as the combustion wastes aforementioned.

On the basis of those works, an extensive research project is being undertaken in our laboratory on the hydrothermal treatment of different industrial wastes and characterization of their hydrated phases for immobilizing Pb, Cd, Cr and Cs. In the present work, the influence of the temperature of hydrothermal treatment in water of two type of ashes from incineration of municipal solid wastes: fly ash from cleaning-gas-devices and bottom ash, are presented. The liquid phase was characterized by pH and electric conductivity measurements, and the solid phase was characterized by X ray diffraction (XRD), FT infrared (FTIR) spectroscopy and surface area (BET-N_2) analyses.

The possibility for extending to these wastes the capacity for trapping toxic elements constitutes an important application of using a waste to immobilize other wastes.

2. EXPERIMENTAL

Two ashes from municipal solid waste incineration, one from fluidized bed combustion (bottom ash) and other from cleaning-gas-devices (fly ash), called R1 and R2, whose chemical compositions are given in Table 1, were hydrothermally treated (without stirring), in demineralized water at a water to solid ratio of 10, for 12 hours at the following temperatures: Ambient, 50ºC, 100ºC, 150ºC and 200ºC. The solid was filtered and dried to constant weight at 50ºC.

The hydrothermal treatment was carried out without stirring with a Parr pressure reactor Model 4761, 300 mL bomb with split-ring closure and 4316 gage block assembly and a 4842 temperature controller. XRD patterns were recorded on a Philips PW 1730 diffractometer, graphite monochromator, Cu $K\alpha_1$ radiation. FTIR study was carried out on a Atimattson Genesis FTIR TM instrument and KBr pellets containing 0.5% of sample. The surface area measurements were made by the BET method with a Micromeritics ASAP 2010 device; a previous sample degasification at 50ºC during 24h up to 0.05 μm Hg pressure, and N_2 gas 95N as absorbate.

Table 1. Chemical composition of untreated ashes (% by weight).

	LOI	IR	SiO_2	Al_2O_3	Fe_2O_3	CaO	MgO	SO_3	Na_2O	K_2O	Cl^-	Surface area (m^2/g)
R1	4.6	5.2	34.1	19.3	6.6	21.9	2.6	3.3	2.1	1.9	3.6	0.798
R2	17.6	0.1	11.4	11.3	1.1	45	1.9	3.9	2.1	1.9	13	7.84

3. RESULTS AND DISCUSSION

3.1 Bottom Ash from incineration of municipal solid waste (R1)

3.1.1 X-Ray Diffraction and BET-N_2 Analyses

The main crystalline compounds of untreated ash R1 (Figure 1 (a)) are the following: $Ca_2Al_2SiO_7$ (gehlenite), SiO_2 (α-quartz), γ-$CaSO_4$ (soluble anhydrite), NaCl (halite), KCl (sylvite), α´L-Ca_2SiO_4, $CaCO_3$ (calcite) and metallic aluminium. The minority crystalline phases are: α-Fe_2O_3 (hematite), and probably Mg_2C_3.

After the treatment in water at room temperature and at 50ºC (Figures 1 (b) (c)), the starting chloride-compounds and anhydrite disappeared; the intensity of reflections of metallic aluminum and gehlenite decreased. Ettringite ($Ca_6Al_2(SO_4)_3(OH)_{12}.26H_2O$) is obtained from anhydrite and dissolved metallic aluminium. In addition, α-$Ca_2SiO_4.H_2O$ and C-S-H gel ($Ca_{1.5}SiO_{3.5}.xH_2O$) are formed from hydration of α´L-Ca_2SiO_4. As a result of the treatment at room temperature, the specific surface area of the bottom ash increased 6 times (from 0.798 m^2/g to 4.88 m^2/g for the untreated R1 and after the treatment at room temperature, respectively). The amount of ettringite begins to decrease at 100ºC (Figure 1 (d)) disappearing after 150ºC of hydrothermal treatment (Figure 1 (e)). At this temperature, Katoite, silication ($Ca_3Al_2(SiO_4)(OH)_8$) appeared together with anhydrite, which reprecipitated from the sulfates liberated by decomposition of ettringite. At 200ºC traces of $CaAl_2Si_3O_{10}.3H_2O$ zeolite structure type scolecite is detected (Figure 1 (f)). The surface area remains more or less constant between room temperature and 100ºC, increasing thereafter. So, after 150ºC the surface area is 5.15 m^2/g and 5.51 m^2/g, after 200ºC of treatment in water.

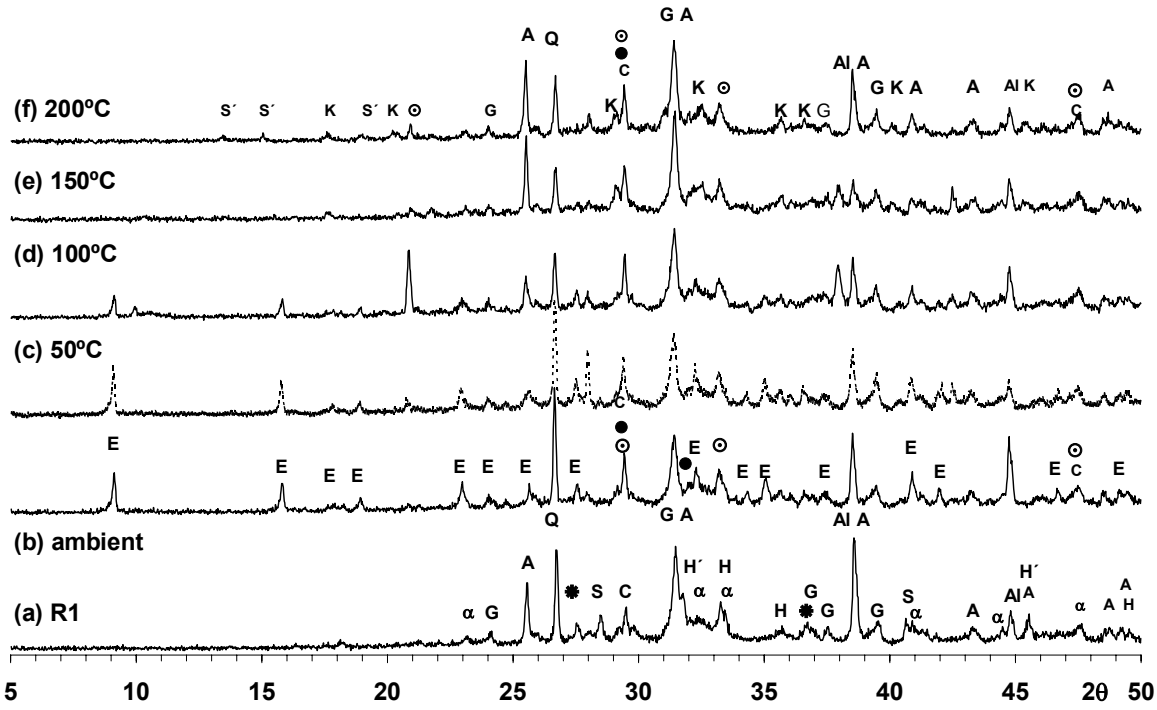

E ettringite; K katoite; G gehlenite; A anhydrite; S sylvite; H´ halite; H hematite; C calcite; Al metallic aluminium; α α´L-C_2S; ❋ Mg_2C_3; Q α-quartz; ⊙ α-C_2SH; ● $Ca_{1.5}SiO_{3.5}.xH_2O$; S´ scolecite.

Figure 1. Evolution of XRD Patterns of R1 with the Temperature of Hydrothermal Treatment in Water

3.1.2 FTIR Spectroscopy Analyses

The FTIR analyses corroborated the XRD conclusions. As can be seen in Figure 2, in the case of untreated R1 (Figure 2 (a)), the vibrations of lattice water produce the bands centered at 3450 cm^{-1} and 1650 cm^{-1}; $[CO_3]^{2-}$ group produces the bands centered at 1450 cm^{-1} and 877 cm^{-1}; the wide band appeared between 1350 cm^{-1} and 750 cm^{-1} is due to the vibration of $[SO_4]^{2-}$, $[SiO_4]^{4-}$ and $[AlO_2]^-$ groups.

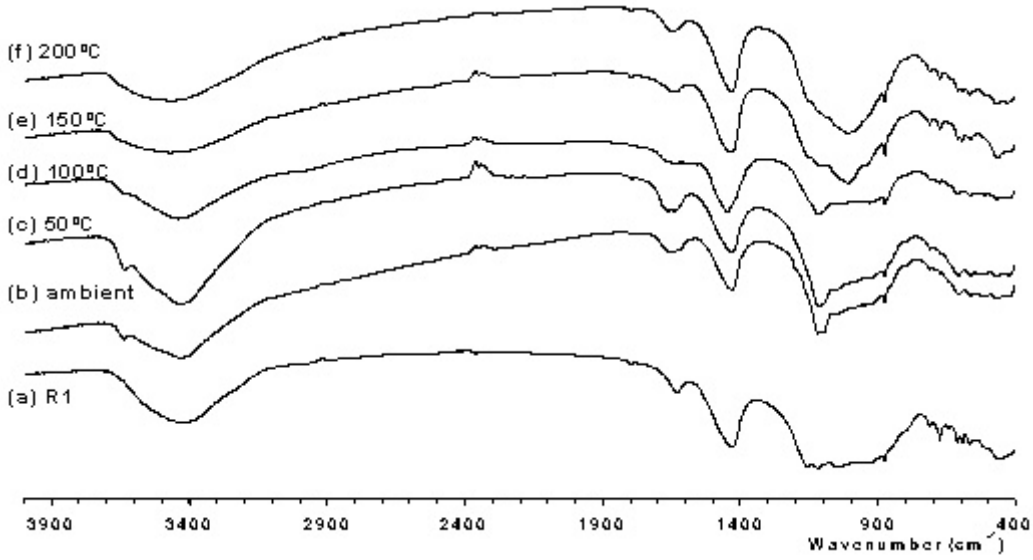

Figure 2. Evolution of FTIR spectrum of R1 with the Temperature of Hydrothermal Treatment in Water.

After the treatment in water at ambient temperature, 50ºC and 100ºC (Figures 2 (b-d)) the OH^- groups from ettringite produce a band centered at 3644 cm^{-1} and the band from $[SO_4]^2$ vibration is clearly detected at 1122 cm^{-1}. The main changes caused by the hydrothermal treatment at 150ºC and 200ºC (Figures 2 (e) and (f)) are the following: The band centered at 3644 cm^{-1} disappeared and the wide band located between 1350 cm^{-1} and 750 cm^{-1} has a maximum at 1018 cm^{-1}, which could corresponds to $[SiO_4]^{4-}$ from katoite, C-S-H gel and α-$Ca_2SiO_4.H_2O$.

3.1.3 Aqueous Phase Analyses

The evolution of the pH and conductivity is quite similar throughout the temperatures (Figure 3). After the treatment of the bottom ash R1 at the ambient temperature, the pH of the aqueous phase was 10.6, which at 50ºC decreased to 9.8, due to the precipitation of ettringite. Thereafter, the pH varied to a value of 10.1 after 200ºC. The conductivity reached a value of 9.7 mS, for the treatment at the ambient temperature, varying up to a value of 11.9 for 200ºC of treatment.

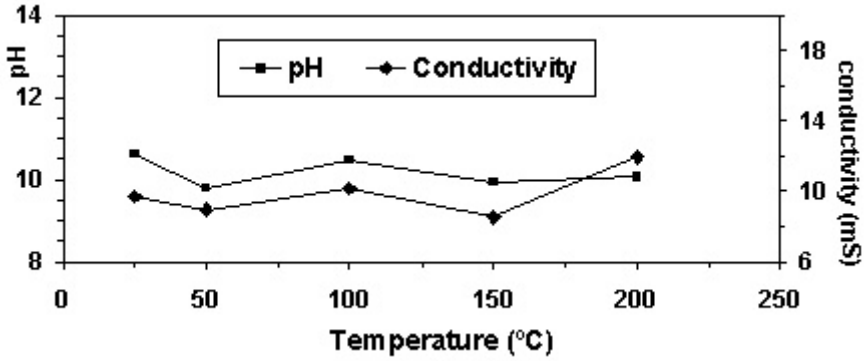

Figure 3. Evolution of pH and conductivity of the aqueous phase of R1 with the Temperature of Hydrothermal Treatment in Water.

3.2 Fly ash from cleaning-gas-devices of municipal solid waste incineration (R2)

3.2.1 X-Ray Diffraction and BET-N_2 Analyses

The fly ash coming from the cleaning-gas-device has high Ca^{2+} content (from the CaO used as adsorbent), high chloride and high SO_3 content. The main crystalline compounds (Figure 4 (a)) are the following: NaCl (halite), KCl (sylvite), $CaCl_2.Ca(OH)_2.H_2O$, γ-$CaSO_4$ (soluble anhydrite), $Ca(OH)_2$ (portlandite), $CaCO_3$ (calcite), α'L-Ca_2SiO_4, metallic Al and $Ca_2Al_2SiO_7$ (gehlenite). The minority crystalline phases are the following: α-Fe_2O_3 (hematite) and SiO_2 (α-quartz).

After the treatment in water at room temperature and at 50ºC (Figures 4 (b) (c)), the starting chloride-compounds, metallic aluminium and anhydrite disappeared. Ettringite ($Ca_6Al_2(SO_4)_3(OH)_{12}.26H_2O$) and α-Friedel´s salt ($Ca_4Al_2O_6Cl_2.10H_2O$) are formed from anhydrite; chloride-compounds and dissolved metallic aluminium. Besides, α-$Ca_2SiO_4.0.35H_2O$ and $Ca_{1.5}SiO_{3.5}.xH_2O$ are formed from hydration of α'L-Ca_2SiO_4. As a result of the treatment at room temperature, the specific surface area of the fly ash R2 increased 3 times (from 7.84 m^2/g to 24.9 m^2/g for the untreated R2 and after the treatment at room temperature, respectively). The amount of Friedel´s salt increased markedly at the temperature of 100ºC (Figure 4 (d)), where the α to β Friedel´s salt transformation is produced; portlandite disappeared. At this temperature, the specific surface area of the fly ash R2 increased 5 times (from 7.84 m^2/g to 40.1 m^2/g for the untreated R2 and after the treatment at 100ºC temperature, respectively) The XRD profiles are quite different after 150ºC and 200ºC of hydrothermal treatment (Figures 4 (e) (f)), with the following changes: (i) ettringite, β-Friedel´s salt and α-$Ca_2SiO_4.0.35H_2O$ disappeared; (ii) katoite, silicaton ($Ca_3Al_2(SiO_4)(OH)_8$) is formed, together with traces of $Ca_4Al_2O_6(CO_3)_{0.5}(OH).11.5H_2O$. The presence of $Ca_{1.5}SiO_{3.5}.xH_2O$ (its X-ray reflections are overlapped with those of calcite), was confirmed from IR analyses by the strong absorption band at 950 cm^{-1} (Figures 5 (e) (f)).

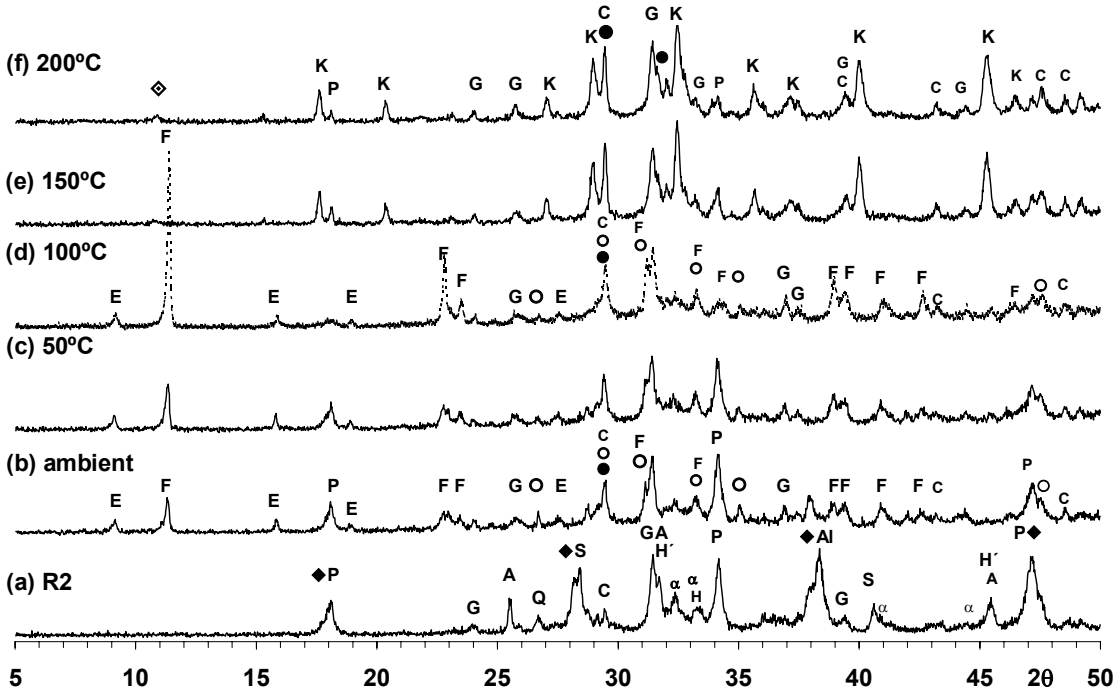

E ettringite; F β-Friedel´s Salt; P portlandite; K katoite; G gehlenite; A anhydrite; S sylvite; H´ halite; H hematite; C calcite; α α´L-C_2S; Q α-quartz; ◆ $CaCl_2.Ca(OH)_2.H_2O$; ○ $C_2SH_{0.35}$; ● $Ca_{1.5}SiO_{3.5}.xH_2O$; ◈ $Ca_4Al_2O_6(CO_3)_{0.5}(OH).11.5H_2O$; Al metallic aluminium

Figure 4. Evolution of XRD Patterns of R2 with the Temperature of Hydrothermal Treatment in Water

The surface area of the fly ash R2 decreased strongly after the hydrothermal treatment at 150ºC; 12.2 m^2/g and 10.3 m^2/g after the hydrothermal treatment at 200ºC. This decrease is attributed to the conversion of hexagonal Friedel´s salt to cubic katoite, which is produced at 150ºC.

3.2.2 FTIR Spectroscopy Analyses

In the case of untreated R2 (Figure 5 (a)), the vibrations of lattice water produce the bands centered at 3477 cm^{-1} and 1640 cm^{-1}; $[CO_3]^{2-}$ group produces the bands centered at 1471 cm^{-1} and 875 cm^{-1}; the wide band appeared between 1300 cm^{-1} and 750 cm^{-1} is due to the vibration of $[SO_4]^{2-}$, $[SiO_4]^{4-}$ and $[AlO_2]^-$ groups. After the treatment in water at ambient temperature (Figure 5 (b)) the OH^- groups from ettringite and Friedel´s salt produce a band centered at 3643 cm^{-1} and the band from $[SO_4]^2$ vibration is clearly detected at 1132 cm^{-1}. The new bands at 800 cm^{-1}, 540 cm^{-1} and 432 cm^{-1} can be attributed to the vibration of AlO_2^- group from Friedel´s salt. Their intensity increased with the heating temperature of hydrothermal treatment up to 100ºC, disappearing after 150ºC and 200ºC of treatment (see Figures 5 (e) and (f)). At these temperatures, the band centered at 950 cm^{-1} is clearly formed, which could corresponds to $[SiO_4]^{4-}$ from katoite and C-S-H gel.

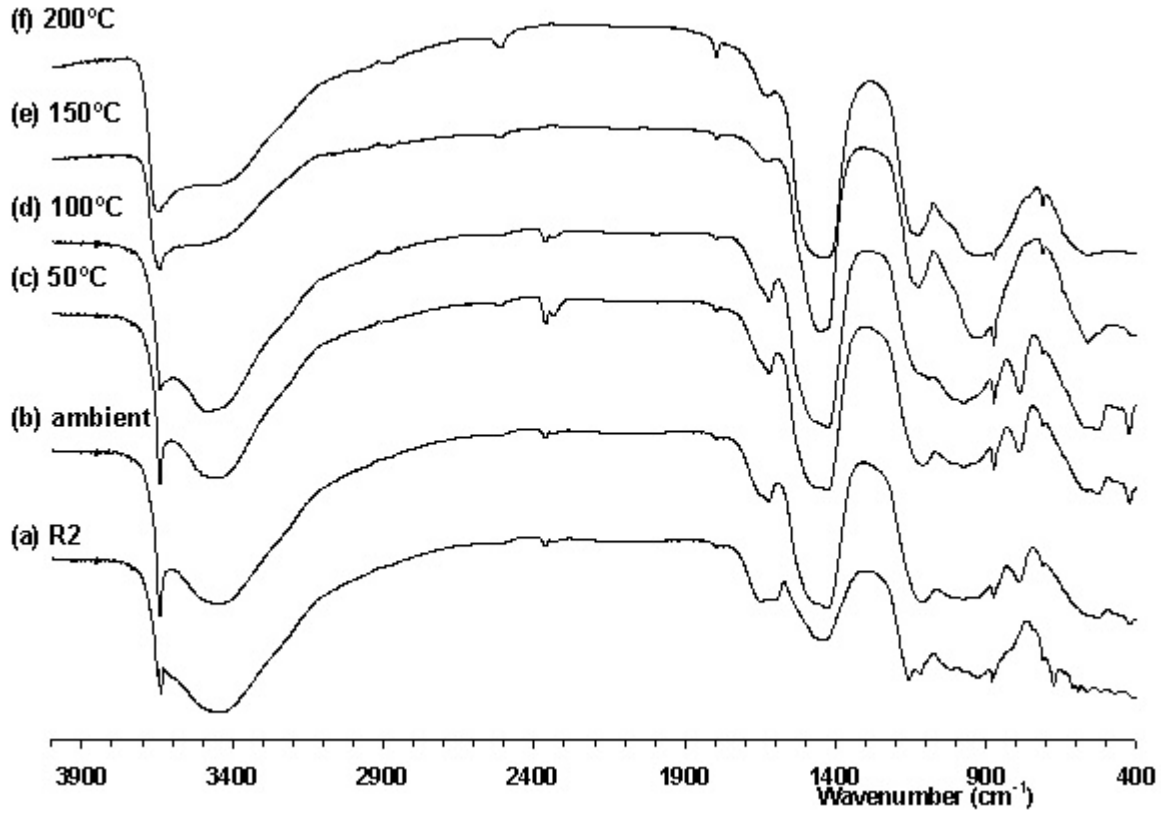

Figure 5. Evolution of FTIR spectrum of R2 with the Temperature of Hydrothermal Treatment in Water.

3.2.3 Aqueous Phase Analyses

As can be seen in Figure 6, there is no significant pH change of the aqueous phase of the fly ash R2 throughout the temperatures. After the ambient treatment the pH was 12.1 and the conductivity was 30 mS. At 50ºC the conductivity decreased up to 25 mS, increasing thereafter progressively with the temperature up to reach a value of 35 mS, after the hydrothermal treatment at 200ºC.

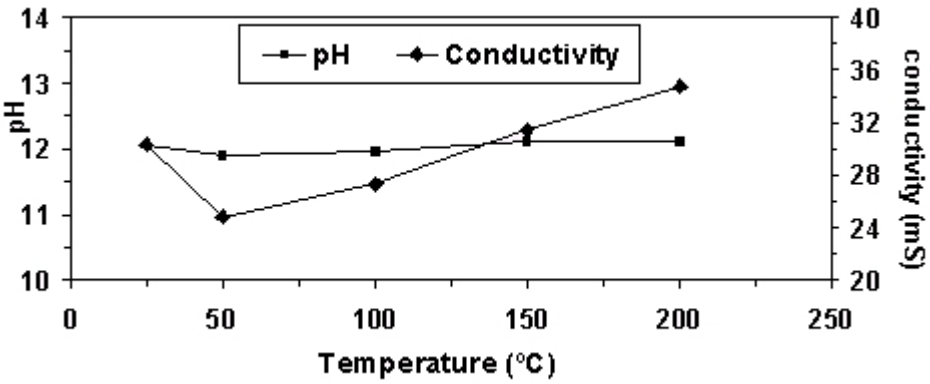

Figure 6. Evolution of pH and conductivity of the aqueous paase of R2 wit the Temperature of Hydrothermal Treatment.

4. CONCLUSIONS

The hydrothermal treatment of these wastes caused the formation of phases with the property of incorporating ionic species in their structures. These phases were different for fly ash and bottom ash:

- Bottom ash: Ettringite, α-C_2SH and gel CSH are formed from the bottom ash at the lower temperatures: ambient and 50ºC, leading to an increase of its surface area of 6 times. Ettringite converted in the more stable cubic katoite after 100ºC of treatment. A zeolite type scolecite is detected at 200ºC.
- Fly ash: Friedel´s salt is massively formed at 100ºC, in the case of fly ash, leading to an increase of 5 times of its surface area. Hexagonal Friedel´s salt converted in cubic katoite after 150ºC of treatment, decreasing consequently its surface area. Gel CSH and $C_2SH_{0.35}$ were also formed.

ACKNOWLEDGEMENTS

The authors are grateful for financial assistance from CICYT Project PB98-0516.

REFERENCES

[1] Jiang, W. and Roy, D.M. Hydrothermal processing of new fly ash cement, Ceramic Bulletin, vol.71 (4), 1992, pp. 642-647.

[2] Ma, W. and Brown, P.W. Sequestration of cesium and strontium by tobermorite synthesized from fly ashes", J. Am. Ceram. Soc., vol. 79, 1996, pp.1707-1710.

[3] Ma, W. and Brown, P.W. Hydrothermal reactions of fly ash with $Ca(OH)_2$ and $CaSO_4.2H_2O$, Cem. Concr. Res., vol. 27 (8), 1997, pp. 1237-1248.

[4] Ma, W. and Brown, P.W. Hydrothermal synthesis of tobermorite from fly ashes, Adv. Cem. Res., vol. 9 (33), 1997, pp. 9-16.

[5] Goñi, S., Guerrero, A., Luxán, MP., and Macías, A. Dehydration of pozzolanic products hydrothermally synthesized from fly ashes. Microstructure evolution". Materials Research Bulletin, vol. 35 (8), 2000, pp. 1333-1344.

[6] Guerrero, A., Fernández, E., Macías, A., and Goñi, S. Hydrothermal treatment of fly ash from municipal solid waste incineration, Proceedings of Waste Materials in Construction: Science and Engineering of Recycling for Environmental Protection, Editors: G.R. Woolley, J.J.M. Goumans and P.J. Wainwright, Pergamon, Amsterdam vol. 1, 2000, pp.178-185.

[7] Yao, Z., Tamura, C., Matsuda, M. And Miyake, M. Resource recovery of waste incineration fly ash: Synthesis of tobermorite as ion exchanger, J. Mater. Res., vol. 14 (11) 1999, pp. 4437-4442.

HYDROTHERMAL TREATMENT OF INDUSTRIAL WASTES AND ITS IMPLICATION FOR IMMOBILIZING OTHER TOXIC WASTES

R. Peña[1], A. Guerrero[1], S. Goñi[1] and M.P. Lorenzo[2]

[1]Institute of Construction Science Eduardo Torroja (CSIC). C/ Serrrano Galvache s/n, 28033 Madrid, Spain. E-mail: sgoni@ietcc.csic.es; aguerrero@ietcc.csic.es and rpena@ietcc.csic.es
[2]University of San Pablo CEU, Spain. E-mail: pazloga@ceu.es

Raúl Peña Penilla (Pre-Doctoral Student)

Institute of Construction Science Eduardo Torroja (CSIC).

C/ Serrrano Galvache s/n, 28033 Madrid, Spain.

E-mail: rpena@ietcc.csic.es

BIODETERIORATIVE PROCESSES ON AIR-EXPOSED CEMENT MATERIALS

Kondratyeva I.A.[1], Gorbushina A.A.[2] and Boikova A.I. [1]

[1]Institute of Silicate Chemistry, Russian Academy of Science, 199155 ul.Odoevskogo 24, korp.2, St.Petersburg, Russia.
Fax +7(812) 328-54-01
[2]Geomicrobiology, ICBM, Oldenburg University, 26111 Germany.
E-mail: lebed@isc.nw.ru, pulchinella77@mail.ru, ikondratyeva@mail.ru

Knowledge of the bioreceptivity of building materials for microbially induced decay processes has increased considerably in the last years. Indoor and outdoor atmosphere exposed building materials are widely recognized as a favorable environment for microbial biofilms in general and for microscopic fungi specifically.

An important role is played by the microscopic fungi in an atmosphere exposed environment. A series of experiments on industrial clinker samples were carried out to determine the behavior of cements under the influence of fungal growth in the air exposed environment.

The problem of increased durability of cement-based constructions can be solved only with a thorough understanding of the kinetics and microscopic mechanisms of deterioration. As it is known from other inorganic materials (stone, glass etc), special attention should be given to interactions of material with microorganisms and to the processes of their microbial degradation.

Interactions of cement-based materials with deteriorative microscopic fungi were investigated on samples of anhydrous industrial ordinary Portland cement clinkers and on hydrated cement samples (with and without SiO_2 sand) of varying chemical composition. Clinker samples of complex chemical composition included CaO, Al_2O_3, Fe_2O_3, SiO_2 as main components as well as Na, K, Mg, Ti, S as minor components.

These samples were inoculated with a number of microscopic fungal strains, commonly found on silicate rocks all over the world. For the experiment we selected a so-called ubiquitous isolate, the spores of which are frequently found in the air. Inoculation was done by the application of a fungal spore suspension on one side surface of cement cubes.

The samples were incubated at 70% relative humidity and room temperature. Incubation time has presently reached 1 year for anhydrous clinkers and 1.5 and 2.5 years for industrial hydrated cements. Short times of incubation (2-3 months) have shown no considerable material changes. Later, however, experimental growth was slightly accelerated by an addition of 50µl of organic nutrient medium per cement cube.

Scanning electron microscopy (SEM) and X-Ray powder diffraction were used in order to detect biodeteriorative processes on these building materials.

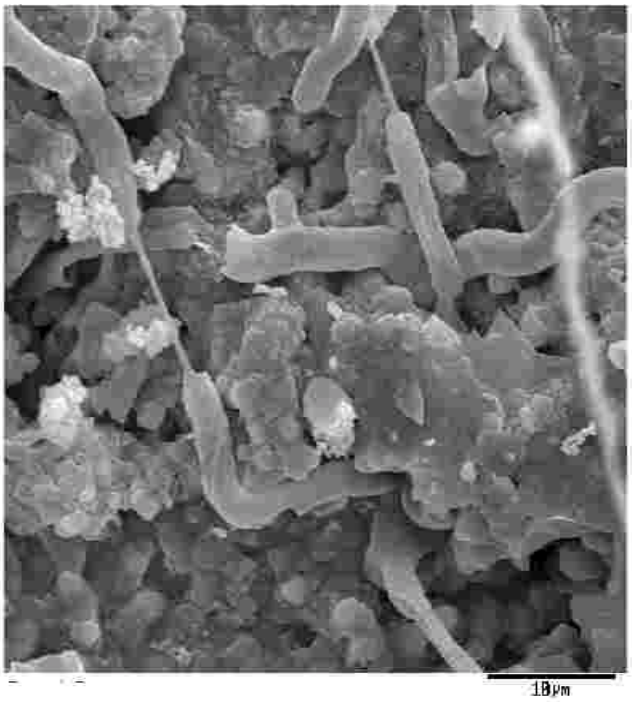

Figure 1.

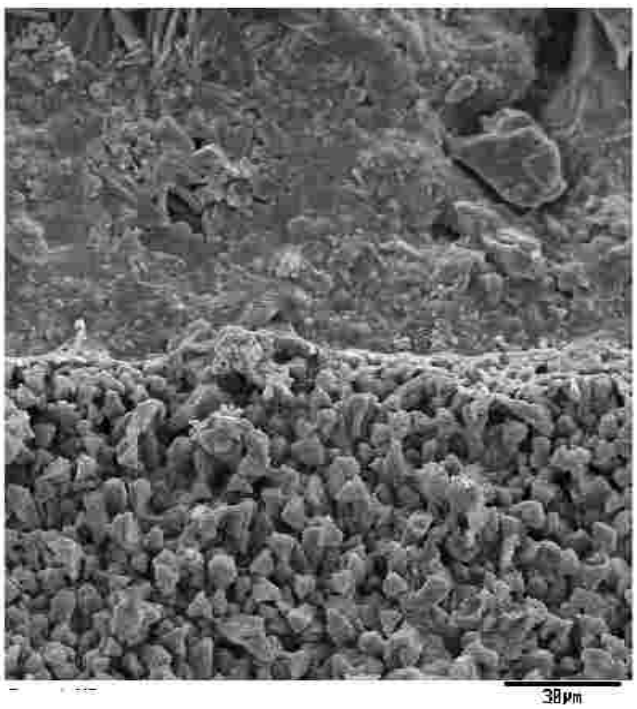

Figure 2.

SEM demonstrates the growth of fungal mycelium on all inoculated cement blocks (Figure1, 1.5 years exposure). Branching hyphae spread over the cement surface and frequently form very close contacts with the grains of material. Such contact might be important in the process of mechanical destruction and separation of cement grains. By the penetration of fungal structures between the grains, the crystals of the material can be diminished, which was additionally improved by the crystallographic analysis. Such mechanisms of mechanical destruction, which were previously also shown for marble and other mineral materials [1,2] could represent an important fact in changes of mechanical properties and cohesiveness of cement materials.

Figure 2 clearly demonstrates that fungi affect anhydrous minerals efficiently. It shows the border of the zones of ordinary clinker (upper part) and of clinker, which has been reacting with biological agents (1 year exposure). The differences in mineral composition of an intact clinker (alite, belite etc) and of the zone, which has reacted with microscopic fungi and their exudates (calcite) are extremely evident and were repeatedly demonstrated by both microscopic (SEM) and X-ray analysis. Previously Ribas Silva and Garcia indicated the following deteriorated compounds: calcium-based products - from cement, such as portlandite and calcium carbonate; siliceous products - from aggregates, such as quarz, feldspars, micas and other unidentified crystals.

While the direct products of the interaction between fungi and clinker phases (including their hydrates) remain currently unidentified, we hope to promote the respective study soon.

X-ray analysis of mineralogical changes has further demonstrated that hydration of cement phases was definitely stimulated by biological agents. During a short period of 1 year, anhydrous substances (clinkers) were hydrated and mineralogically changed by the presence of actively growing microscopic fungi. On the hydrated clinker cubes, the X-Ray analysis has demonstrated that chemical composition of the block surfaces has not been changed by microscopic fungi. However, the most important factor is the obvious decrease of intensities of maxima of all mineralogical phases on the cubes side interacting with growing micromycetes as well as broadening of all the reflections themselves.

Figures 3, 4 display the development of biofilms on the hydrated cement samples after 2.5 years exposure. Samples made from hydrated cements with SiO_2 sand are evidently (even by eye) more corroded by fungi than pure cement paste cubes. This difference can be ascribed to heterogeneity of sample texture provided by numerous pores in hydrated cements with SiO_2 sand. Several holes with a scale of about 1 mm are clearly visible in the surface of cement cubes (with SiO_2 sand) covered by fungi spores after 1.5 years exposure. Similar holes appear in hydrated cements without SiO_2 sand after longer exposure (2.5 years).

Microscopic fungi settle and grow on the surfaces of solid building materials, penetrate into the pores, interact with the minerals through production of organic acids or by a respiration process. Thus the growth of microscopic fungi on industrial Portland cement materials has been shown to represent a significant factor changing the mineral composition and mechanical properties of the material in question.

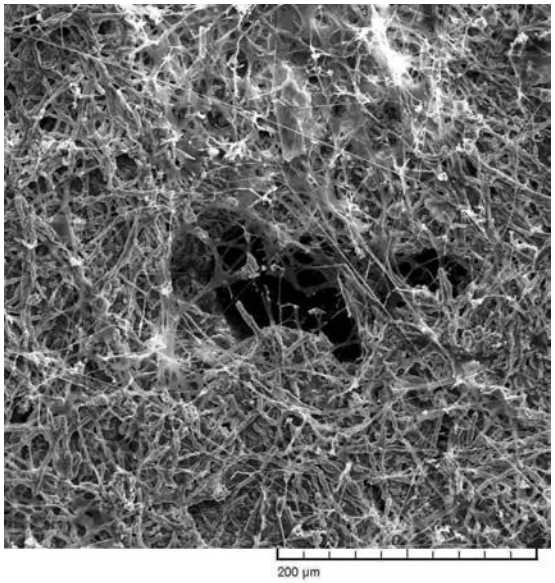

Figure 3a.

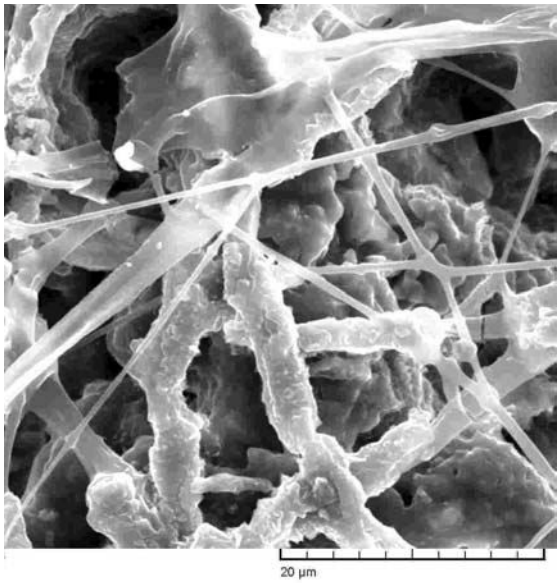

Figure 3b.

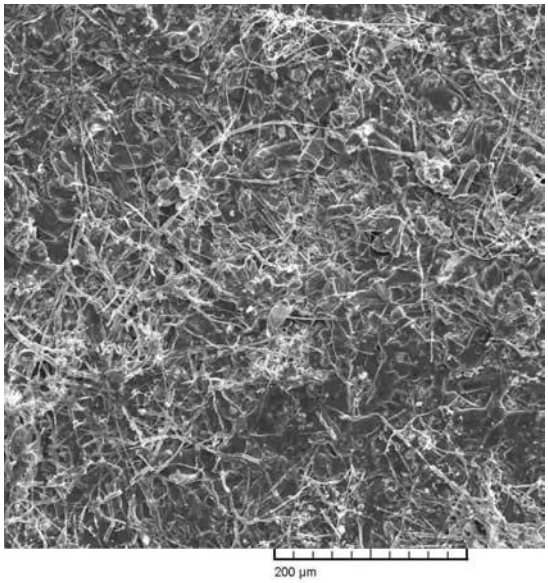

Figure 4a.

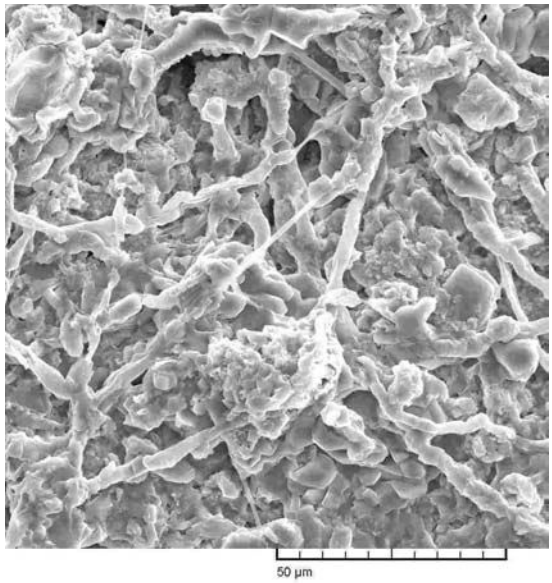

Figure 4b.

REFERENCES

[1] Dornieden, Th., Gorbushina, A.A., & Krumbein, W.E. (1997). Changes of the physical properties of marble as a result of fungal growth. *International Journal for Restoration of Buildings*, 3, 441-456.

[2] Sterflinger, K. & Krumbein, W.E. (1997). Dematiaceous fungi as the main agent of biopitting on mediterranean marbles and limestones. *Geomicrobiology Journal*, 22**,** 219-231.

[3] Ribas Silva, M., Garcia, L.A.M. (1997). Microbiological identification of microorganisms responsible for degradation of concrete. *10th International Congress on Chemistry of Cement, Gothenburg, Sweden, vol.4, 4iv037.*

EFFECT OF CALCIUM SULPHITE HEMIHYDRATE OR ITS MIXTURE WITH CALCIUM SULPHATE DIHYDRATE ON THE PROPERTIES OF CEMENTS CONTAINING VARIOUS CONTENTS OF C_3A

Artur Lagosz[1], Jan Malolepszy and Wiesława Nocun-Wczelik

University of Mining and Metallurgy, Faculty of Materials Science and Ceramics, Kraków, Poland.
E-mail: [1]arturlagosz@uci.agh.edu.pl

1. INTRODUCTION

Flue gas desulphurization wastes from wet methods are used nowadays as set controlling additives to cements, because of the high amount of $CaSO_4 \cdot 2H_2O$, exceeding 95%, and stability of other properties. The proper amount of calcium sulphate controls the initial and final setting of cement, heat of hydration as well as strength development [1].

Application of semi-dry methods of desulphurization, especially for smaller plants results in the formation of $CaSO_3 \cdot 0{,}5H_2O$ in the products as well as the presence of a residual absorber (usually calcium hydroxide) and chloride salts. The main desulphurization product content depends on the method of desulphurization used (from several to several dozen percent in waste product). The proportions between calcium sulphite, calcium hydroxide and chlorides vary within a wide range even for the same installation. They depend on the type of coal used and boiler rating in electric or power plants.

Significant differences in various semi-dry methods of desulphurization and differences in chemical constitution of the wastes thus produced, cause many difficulties with waste disposal. It is connected particularly with high activity of all phases included in the wastes.

The main component of desulphurization product obtained in semi-dry process - calcium sulphite hemihydrate $CaSO_3 \cdot 0.5H_2O$ - is not without influence on cement setting [2-3, 7-11]. The results of setting time measurements of cements including $CaSO_3 \cdot 0.5H_2O$ show this very clearly. There are also some reports dealing with the effect of wastes obtained in semi-dry installations on cement properties [8]. A large number of tests were carried out for cements from group CEM I – without mineral additions. It has been found that the retarding influence of sulphite and wastes containing calcium sulphite is bound with different reaction mechanism than observed in the case of calcium sulphate (gypsum) added as set retarder.

The analysis of the published works and our studies indicate that there is no equivocal opinion about calcium sulphite effect on cement hydration. The authors assumed that addition of mineral admixtures to cement clinker could improve the properties of cements due to the lower amount of clinker and, consequently, lower amount of tricalcium aluminate in cement.

Our studies point out some differences in the properties of cement properties produced based on different clinkers, with high and low amounts of a C_3A phase [12]. Lower content of C_3A in cements affects water/cement ratio and increases plasticity of cement mortars.

This paper shows the results of the studies on the effect of desulphurization products from semi-dry installation and natural gypsum mixed at different ratios, added as a set controlling agent, on the

properties of cements with different clinker and slag contents, produced as CEM I, CEM IIB/S and EM III/A, according to European standards.

2. EXPERIMENTAL

The studies covered the determination of standard properties of cements made on the base of one clinker with C_3A content 9.3%. As a setting time controlling agent the gypsum in its natural form ($CaSO_4 \cdot 2H_2O$ = 95.5%), a waste product containing $CaSO_3 \cdot 0.5H_2O$ ($CaSO_3 \cdot 0.5H_2O$ =61.4%) and the combination of these two materials in some different proportions were used. For preparing the cements from CEM II and CEM III groups granulated slag was used, added as 30 and 60% by weight of cement.

Cements were made with the following assumption: total content of sulphates or sulphites calculated as SO_3 was 3.5% of total weight of every cement. They were prepared from cements: type CEM I (containing gypsum), type CEM I (containing desulphurization product) – both prepared in laboratory, as well as ground slag, gypsum and desulphurization product in its natural form. The components for CEM I containing gypsum were pulverised in a laboratory ball mill to produce cement with specific surface of 330 ± 5 m^2/kg, as measured by Blaine method. Time of grinding with addition of slag and different retarders was the same. Because desulphurization product from the semi-dry method and slag exhibit high specific surface, the specific surface of cement blends is higher. The composition of cements and their specific surface areas are presented in Table 4.

All cement samples were produced by homogenisation of ingredients in amounts given in Table 4. Gypsum and waste product was added when cements from group CEM II and CEM III were prepared.

The chemical components of the clinker and mineral composition calculated using Bogue's formulas, the chemical components of the slag and the chemical as well as mineral composition of the waste products are presented in Tables 1-3.

Table 1. Chemical composition of clinker and slag and mineral composition of clinker.

Chemical composition	[wt. %]
LOI - 1100°C / 1h	0.52
SiO_2 + insoluble in HCl	21.96
Fe_2O_3	2.51
Al_2O_3	5.12
CaO_{total}	66.37
MgO	1.16
SO_3	0.66
Total:	98.30
Insoluble in HCl	0.61
CaO_{free} – glycol method	0.54
Mineral composition:	
C_3S	65.8
C_2S	11.9
C_3A	9.3
C_4AF	7.6

Table 2. Chemical and mineral composition of waste from desulphurization process.

Chemical composition	[wt. %]
SiO_2	1.00
CaO_{total}	45.50
CaO_{free} – glycol method	3.90
Fe_2O_3	0.27
Al_2O_3	0.45
MgO	0.65
S_{total} as SO_3	39.61
SO_3	1.72
SO_2	30.31
Cl_2	3.85
Mineral composition:	
$CaSO_3 \cdot 0.5H_2O$ (calculated)	61.1
$CaCl_2$ (calculated)	6.0
$Ca(OH)_2$ from TG	9.5
$CaCO_3$ from TG	13.5

Table 3. Chemical composition of slag.

Chemical composition	[wt. %]
CaO	43.50
SiO_2	39.22
Al_2O_3	6.82
Fe_2O_3	2.83
MgO	4.56
MnO	0.85
SO_3	0.96

The water demand, initial and final setting times (Vicat method) and stability of volume were determined in the pastes prepared from cements. The determination of compressive and flexural strength of cement mortars, at w/c ratio = 0.5 was carried out on 4×4×16 cm standard bars stored in water, at 18 ± 2°C. The strength of those mortars was determined after one day and after 2, 7 and 28 days respectively. Moreover, the plasticity of mortars at the shaking table was determined just after their preparation.

Microcalorimetric measurements were carried out with help of Polish BMR differential microcalorimeter on cement pastes. The heat evolution curves were produced and total heat output was calculated.

3. RESULTS AND DISCUSSION

The stability of volume tests for all cements using the standard Le-Chatelier rings show the measured distance t be less than 2 mm (acceptable level is below 10 mm). The results of the determination of setting time and the water demand calculated as w/c ratio are shown in Figures 1 and 2.

The plasticity tests of mortars just after their preparation were carried out at 15 “jumps” of the shaking table by measuring the diameter of spilled mortar cake previously formed as a cut cone of footing diameter = 10 cm. The results of this test are shown in Figure 3.

Table 4. Composition of cements.

Type of cement	SO_3/SO_2 (molar ratio)	Percentage of components [wt. %]					Specific surface area by Blaine [m^2/kg]
		CEM I (G)*	CEM I (W)**	Slag	Natural gypsum	Waste product	
CEM I / 1	100 / 0	100		-	-	-	325
CEM I / 2	70 / 30	70	30	-	-	-	335
CEM I / 3	50 / 50	50	50	-	-	-	340
CEM I / 4	0 / 100	-	100	-	-	-	350
CEM II / 1	100 / 0	67.4	-	30.0	2.6	-	360
CEM II / 2	70 / 30	47.2	20.1	30.0	1.8	0.9	370
CEM II / 3	50 / 50	33.7	33.5	30.0	1.3	1.5	375
CEM II / 4	0 / 100	-	67.1	30.0	-	2.9	385
CEM III / 1	100 / 0	34.9	-	60.0	5.36	-	395
CEM III / 2	70 / 30	24.4	10.2	60.0	3.6	1.8	400
CEM III / 3	50 / 50	17.4	17.1	60.0	2.6	2.9	410
CEM III / 4	0 / 100	-	37.1	60.0	-	5.8	425

*- CEM I (G): clinker 93.51%, natural gypsum 6.49%,
** - CEM I (W): clinker 92.71%, desulphurization product 7.29%.

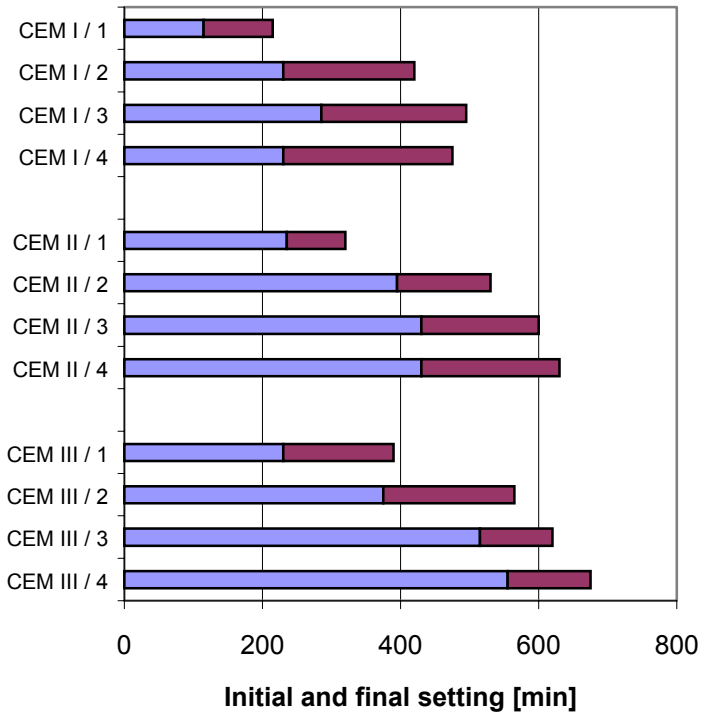

Figure 1. Initial and final setting of cements.

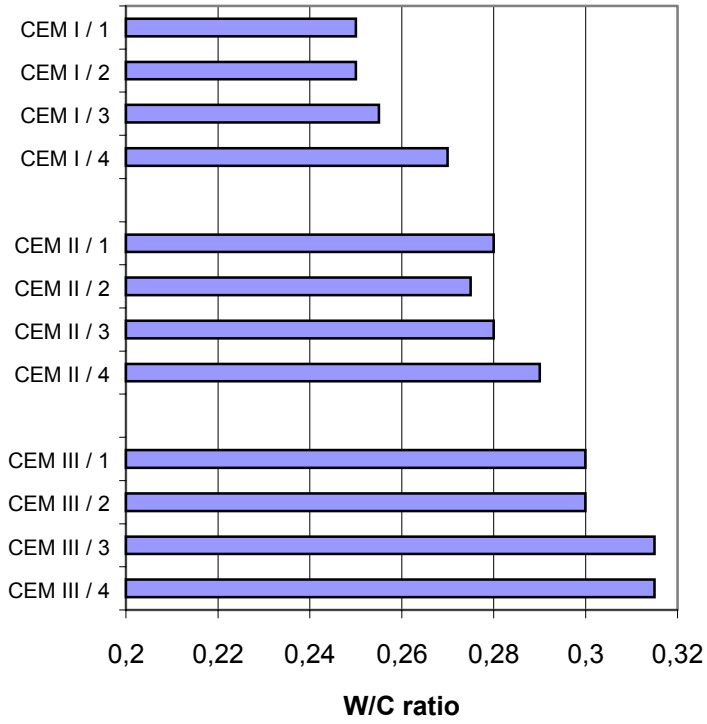

Figure 2. Water/cement ratio of cement pastes.

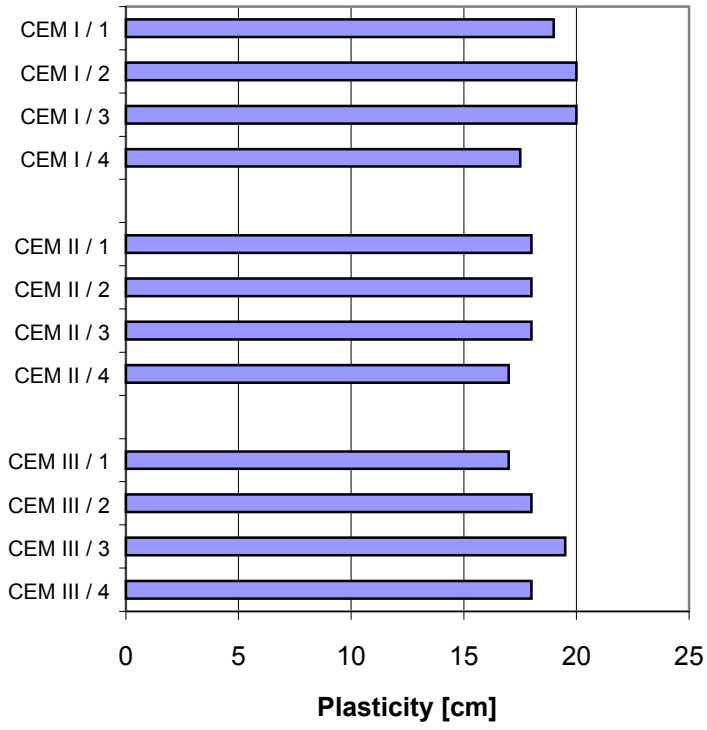

Figure 3. Plasticity of cement mortars (w/c = 0.5; sand/cement ratio = 3).

Partial and total replacement of gypsum by the waste containing calcium sulphite hemihydrate (see Table 1), brings about the elongation of both initial and final setting of cement irrespective of slag content. Only in the case of CEM III can we observe shortening of the time gap between initial and final setting time. The retarding effect is growing with growing waste and slag content, something that was easy to predict.

The addition of the mixture containing desulphurization product (mainly $CaSO_3 \cdot 0.5H_2O$, $Ca(OH)_2$ and $CaCl_2$) with calcium sulphate dihydrate influences the w/c ratio, especially for higher waste content. It can be also attributed to the higher specific surface area of those samples and C_3A reaction with other components of the waste product. Small additions of waste may even reduce w/c ratio (as for sample CEM II/2). Also the plasticity tests of the standard cement mortars (w/c=0.5, sand/cement=3) show slightly better results in the case of small additions of waste containing calcium sulphite. It is visible in case of CEM I as well as CEM III type cements.

Total replacement of gypsum with calcium sulphite containing waste affects negatively the properties of cement paste as well as the properties of ready mixed cement mortars. Only in the case of CEM III group the plasticity of mortar is slightly higher than in case of CEM II/1 containing pure gypsum. This change, observed for cements from group I and II containing waste material as retarder may be attributed to the higher specific surface of those cements and with – what we presented in our paper [12] - rapid C_3A hydration during the first minutes after mixing with water. The plasticity of cement mortars becomes lower and the water/cement ratio increases considerably. It is particularly visible for cements marked as CEM (I, II,) / 4.

The results of compressive and flexural strength of standard mortars are presented in figure 4 and 5. Initial strengths of mortars (after 1 day) strongly depend on the amount of gypsum replaced by the waste containing calcium sulphite hemihydrate. The strength development lowering is connected with the prolonged setting time of cements. After one day of hardening this strength is reduced from about 33 to 55% for the cements marked as CEM (I, II, III) /3 in relation to CEM (I, II, III) /1 corresponding to commercial cements. The strength differences observed in the first days of hardening are more pronounced when cements with gypsum are compared with cements containing the pure waste product as a retarder.

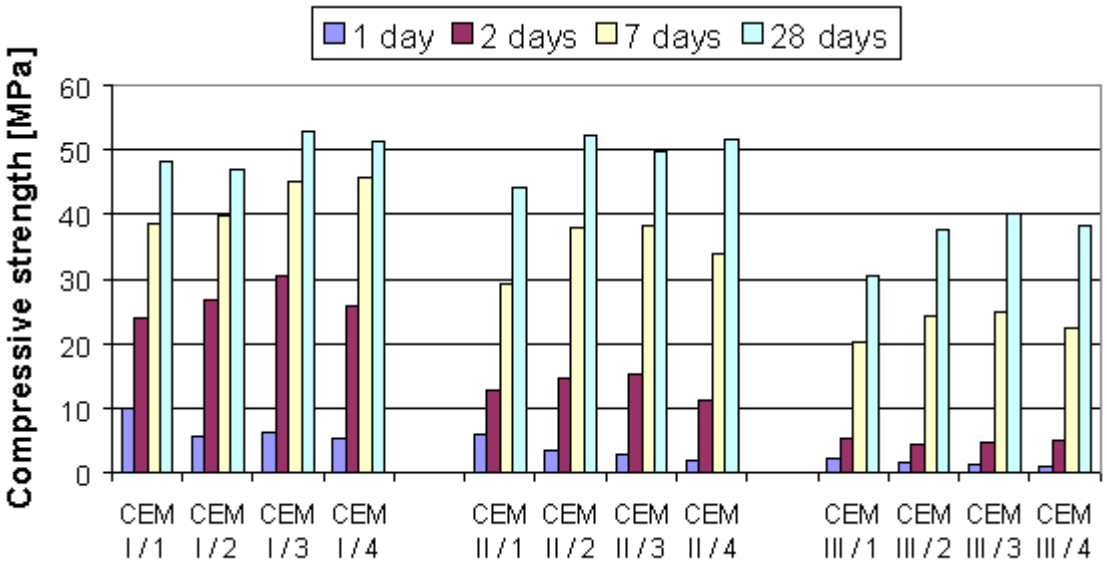

Figure 4. Compressive strength development of cements cements.

After two days of hardening we may observe not only the higher strength of cements containing additions of the waste (in contrast to cements containing pure gypsum as retarder) but also a significant acceleration of strength development. After 2 days of hydration the compressive strength may be higher in cements containing even 25% addition of waste. It means that the strength increase (especially compressive strength) between first and second day of hardening may be even 85% higher for cements containing mixtures of waste with gypsum.

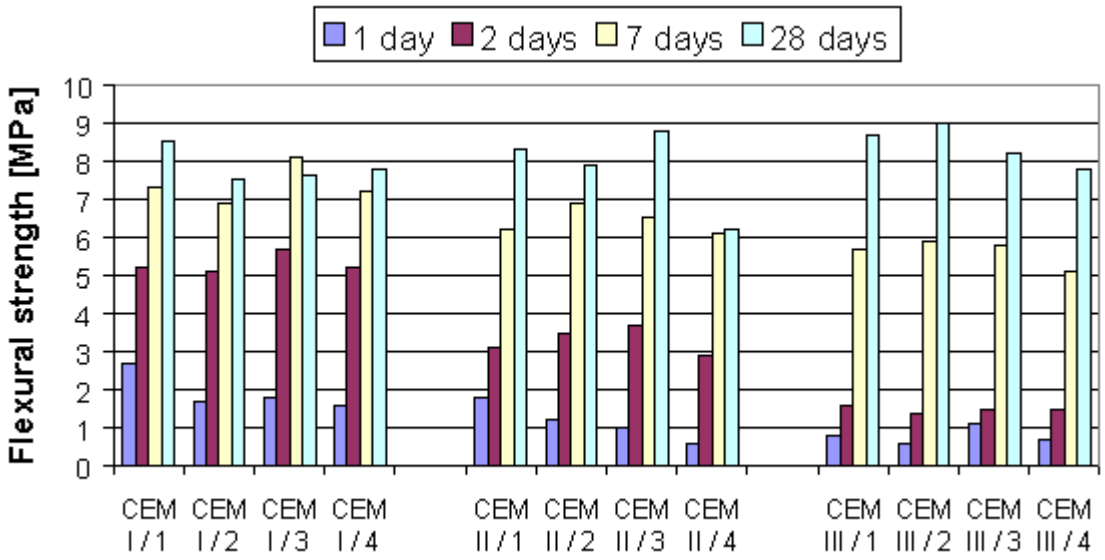

Figure 5. Flexural strength development of cements.

In the case of cements containing high amounts of slag – CEM III (low amount of clinker) the influence of waste product from desulphurization process is not so visible as in case of CEM I and CEM II. We cannot observe such differences between the strength values after 1, 2, and 7 days and it is easy to find that addition of mixture of waste with gypsum or even neat waste product increases the compressive strength after 28 days of hardening. It may caused by the presence of calcium hydroxide in the waste. Thus the slag hydration is strongly accelerated. However the flexural strength development is not observed.

Retardation of initial setting times and reduction of strength development during the first day of hydration in the presence of desulphurization by-product could be attributed not only to the effect of components included in it on C_3A hydration but also to the effect on the rate of alite (C_3S) hydration. As it is commonly known, strength development depends strongly on alite hydration in cements.

The slower strength development and prolonged setting time of cements containing lower and higher addition of desulphurisation waste material is correlated with smaller heat evolution rate. The microcalorimetric tests show significant differences in the extent of the so-called induction period in relation to cements containing pure gypsum as a retarder. It also influences the amount of heat produced during the first day.

A substantial strength increase observed between the 1-st and 2-nd day of hydration also complies well with differences between total heat output calculated after 3 days of hydration and heat output after 1 day.

Heat evolution curves of cements are presented in Figures 6-8. Heat-evolved values after 24 h and 72 h are illustrated in Figure 9.

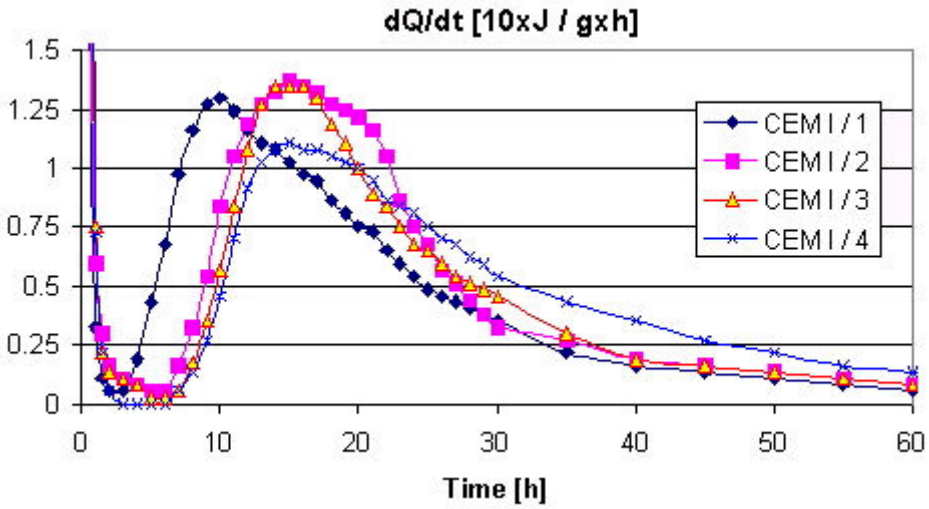

Figure 6. Hydration kinetic curves for cements from group CEM I with different waste to gypsum ratio.

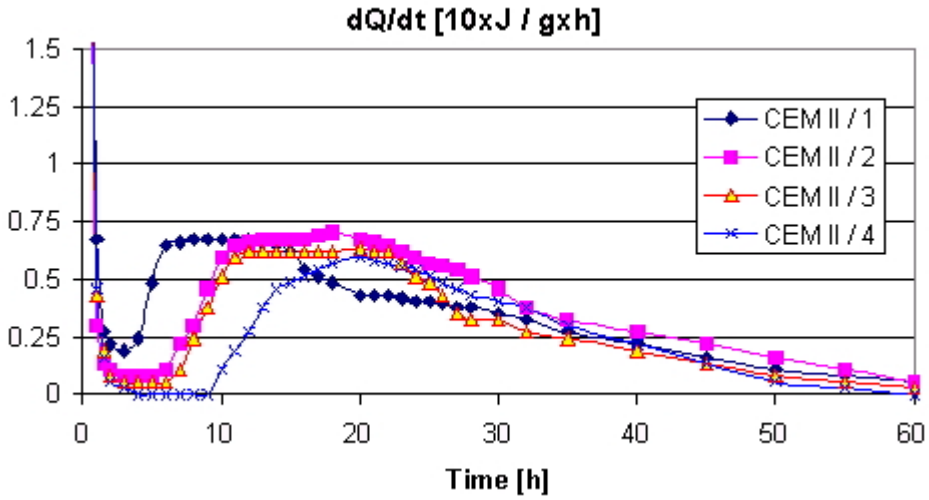

Figure 7. Heat evolution curves for CEM II B/S cements with different waste to gypsum ratio.

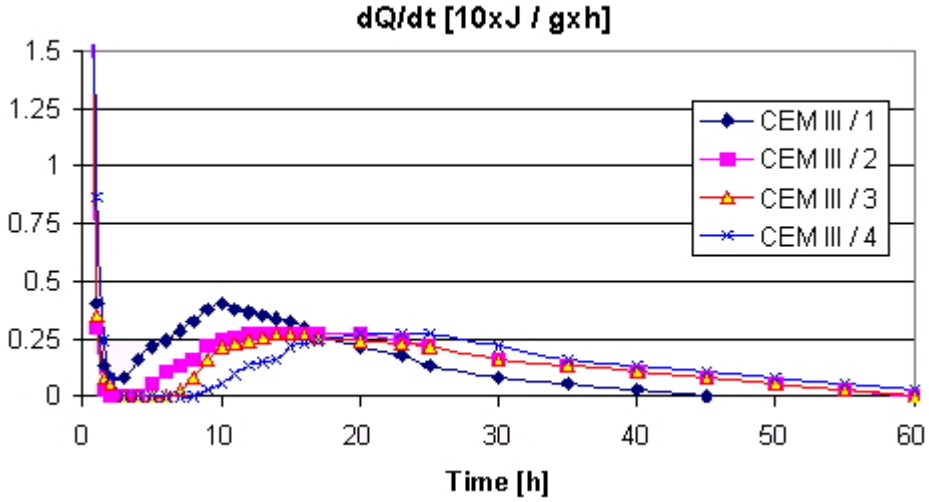

Figure 8. Heat evolution curves for CEM III A cements with different waste to gypsum ratio.

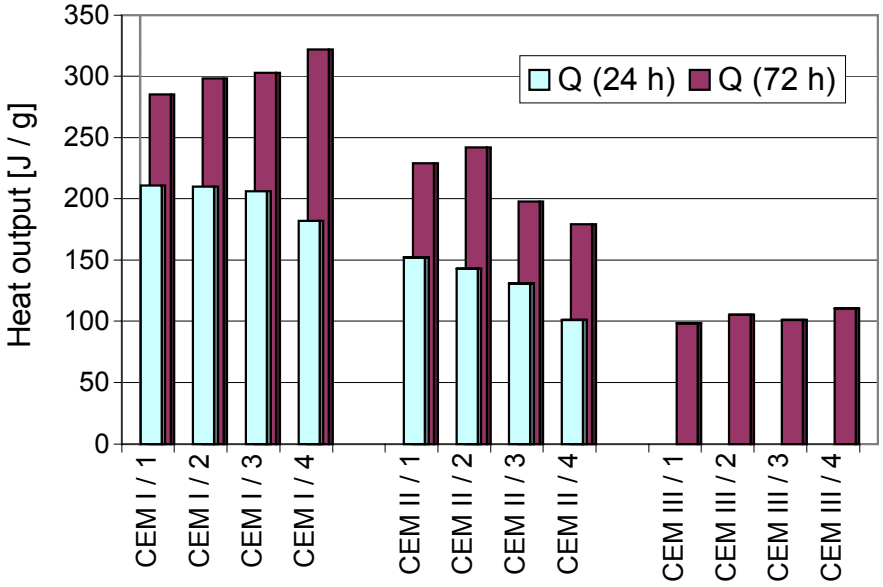

Figure 9. Heat output for cements after 24 and 72 hours of hydration.

Increased amounts of waste in cements brings about not only the elongation of the induction period during cement hydration, but also retards the reaction of the aluminate phase with water after consuming gypsum and /or calcium sulphite (the latter can be observed in case of CEM I cements). Addition of slag distinctly decreases the induction period, but only in the case of cements containing the mixture of gypsum with calcium sulphite containing waste. For cements CEM II/4 and CEM III/4 we observe longer induction periods. However, the total heat output shows no change after 3 days of hydration.

4. CONCLUSIONS

1. Total replacement of gypsum by calcium sulphite containing waste from semi-dry installation of desulphurization used as cement set controlling agent, results in prolonged setting time, considerably slower strength development during the first day of hardening, irrespective of slag content in cement.
2. After a longer period of time (28 days), we observe a decrease of flexural and an increase of compressive strength of cements as compared to cements prepared with pure gypsum as set retarder, irrespective of slag content.
3. Between 1-st and 2-nd day of hardening a substantial strength development in cement containing waste products is observed. Compressive strength after 2 days of hardening may be even 25% higher than in cement with gypsum. Such acceleration of strength development is observed in CEM III after a longer period of time (between 2-nd and 7-th days of reaction in water).
4. At lower content of waste in cements - 30%, calculated as calcium sulphite molar replacement of gypsum, the water to solid ratio and plasticity of cement mortars is affected only to a small extent; these properties seem to be even better than in the case of cement with gypsum. This is independent on slag content.
5. Prolonged setting time and lower strength within the first day of hydration are closely connected with elongation of induction period observed when calcium sulphite containing waste material is added.

ACKNOWLEDGEMENTS

This work is sponsored by the Polish Scientific Committee, (grant No. 7 T08D 048 21).

REFERENCES

[1] Brylicki W., Malolepszy J., Lagosz A.: Physicochemical properties of wastes produced in semi-dry method of desulphurization process and utilisation methods. Polish Conference on Sorbers for Desulphurization, Kamień Śląski 1997. (in Polish)

[2] Bloss W., Odler I.: Über die Möglichkeiten des Einsatzes von Calciumsulfit zur Regelung des Portlandzementerstarrens. TIZ Fachberichte vol. 106, Nr 9, pp. 644-647 (1982).

[3] Gawlicki M., Lagosz A., Malolepszy J.: Utilisation of fly ashes containing calcium sulphite in cement production. Polish Ceramic Bulletin, Edited by Polish Academy of Science, pp. 133-140, Kraków 1997. (in Polish)

[4] Brylicki W., Lagosz A.: Utilisation of desulphurization products in cellular concrete production.Proc. of Conference on Waste Disposal, Sopot 1995. (in Polish)

[5] Brylicki W., Gawlicki M., Malolepszy J.: Utilisation possibility of ash-sulphate-sulphite wastes in building materials production. Proc. of Conference on Waste Disposal, Sopot 1993. (in Polish)

[6] Kurdowski W.: „Handbook of cement technology", pp.92-95, ed.Arkady, Warszawa 1981.

[7] Gawlicki M., Lagosz A., Malolepszy J.: Utilisation of fly ashes containing calcium sulphite in cement production. 10th ICCC Goetheborg, 1997.

[8] Lagosz A.: Effect of calcium sulphite hemihydrate on hydration process of cement. PhD Dissertation. AGH, Krakow, Poland 2000.

[9] Shiino H., Yasue T., Arai Y.: Effect of Calcium Sulfite on Setting of Portland Cement. Gypsum and Lime Nr 188, s. 17-26 (1984)(in Japanese).

[10] Bloss W.: Verrendurg eines Gemishes aus Kalziumsulfit-Halbhydrat und Kalciumsulfat Dihydrat für die Herstellung von Zement. Patent RFN Nr 303756 (1.10.1980).

[11] Bloss W.: Verrendurg eines Alofallproduktes aus der Trockenen Rauchgasentachwefelung für die Herstellung von Flugaschezement. Patent RFN Nr 3038457 (11.10.1980).

[12] Lagosz A., Malolepszy J.: Effect of calcium sulphite hemihydrate or its mixture with calcium sulphate dihydrate on the properties of cements containing various contents of C_3A. 14th Int. Baustofftagung "Ibausil", Weimar 2000, vol. 1, pp.1-0465 – 1-0474.

MECHANISM OF PbO AND ZnO INTERACTION WITH CEMENT PASTE

Wieslawa Nocun-Wczelik[1] and Grzegorz Lój[2]

Faculty of Material Science and Ceramics, University of Mining and Metallurgy, Kraków, Poland. E-mail: [1]wiesia@uci.agh.edu.pl and [2]gloj@uci.agh.edu.pl

ABSTRACT

Effect of PbO on hydration and hardening of different cements was tested by standard methods. As a first step the standard setting time and compressive tests were done, followed by calorimetric measurements. Substantial retardation of reaction with water at early stages with subsequent intensification of the process was firstly found. The studies in model systems, including pure clinker minerals and other retarding agent - ZnO were carried out to find the mechanism of delayed formation of products in post-induction period. PbO and ZnO added to cement paste or mortar as fine-grained solid additives retard setting proportionally to their content in hydrating materials.

Effect of retardation by PbO is different for different cements; but for PbO additive not exceeding 0,5 wt. % the setting parameters meet the European standard requirements. PbO does not affect such parameters of fresh paste as w/c or volume changes. PbO brings about a significant change of heat evolution kinetics – at 2 – 5% PbO the induction period becomes many times longer, but when reaction starts again it seems that there is no special modification of hydration mechanism and kinetics. The effect of PbO on heat evolution may differ significantly for different cements. PbO does not hinder the heat evolution process of alite while ZnO does. Finely ground PbO gives a significant growth of heat output on pure alite hydration – presumably it plays a role of nucleating agent.

1. INTRODUCTION

As was reported over 30 years ago, small amounts of PbO or ZnO retard strongly the hydration of Portland cement [1]. This effect has been attributed to the formation of an impermeable layer of products – heavy metal hydroxides or amphoteric salts produced in the reaction between the oxides and C_3S. The strength decrease at later ages was not observed in the case of PbO, though a significantly retarded setting was found. The calorimetric studies revealed a prolonged dormant period with many hours shift of the second heat evolution peak. The author did not find a full explanation for the effect of PbO on the hydration process.

Further the effect of heavy metals was studied from the point of view of their immobilisation in the hardened cement matrix [2,3]. The researchers focused on the studies of the stabilisation mechanism and leaching of heavy metals from different cement based materials [4, 5]. A very high degree of Pb or Zn immobilisation was found as well as the formation of highly disordered C-S-H in the presence of heavy metal compounds [6, 7]. The retarding effect of Pb or Zn compounds (salts) on cement hydration was also proved in some later works [8 -10].

Proceedings of the 11th International Congress on the Chemistry of Cement (ICCC)
'Cement's Contribution to the Development in the 21st Century'
Hosted by: The Cement and Concrete Institute of South Africa
CD-ROM produced by: Document Transformation Technologies
11 - 16 May 2003, Durban, South Africa
ISBN Number: 0-9584085-8-0
Editors: Dr G. Grieve and G. Owens
Congress Organised by: Event Dynamics

2. EXPERIMENTAL

The experimental work was carried out step by step starting from the standard measurements on cements produced from commercial cement clinkers doped with PbO. Next, the calorimetric measurements were carried out, followed by some investigations using different methods to elucidate the mechanism of the retarding effect. Then the ZnO additive was introduced.

2.1 Materials

Two cements: "Cement 1" and "Cement 2" were produced in a laboratory ball mill from two clinkers from different cement plants in Poland. The clinkers were ground with gypsum (in proportions 95% clinker +5% gypsum) to the specific surface of 3000±50 cm^2/g (Blaine). The characteristics of the cement clinkers is given in Table 1 (chemical composition and phase composition calculated using Bogue's formulas). The analytical grade PbO or ZnO was used in cement paste (and mortar) preparation, added as 0,1%; 0,25%; 0,5%; 0,75%; 1%; 2% and 5% by weight of cement.

2.2 Methods

The following standard tests were carried out following the procedures given in European standards EN196-1 and EN 196-3:

- water demand of pastes with different PbO dosage
- setting time
- volume changes and consistency of pastes• compressive strength
- flexural strength.

The compressive and flexural strength development was monitored during the 360 - day curing on small 2,5x2,5x10 cm bars.

As a next step, the hydration kinetics was followed by microcalorimetry. Heat evolution measurements were carried out by the use of a differential microcalorimeter BMR (non-isothermal – non-adiabatic; constructed in the Institute of Physical Chemistry, Polish Academy of Science) on pastes produced at w/c ratio 0,5. The starting temperature was kept constant at 25°C.

Table 1. Chemical and phase composition of cement clinkers

Component	Content in wt. [%]	
	Cement clinker 1	Cement clinker 2
CaO	65,55	68,11
SiO_2	21,33	22,57
Al_2O_3	5,46	4,97
Fe_2O_3	2,65	2,13
MgO	1,06	0,82
SO_3	0,71	0,40
Alkalis	1,05	0,37
L.O.I		0,25
C_3S	64,2	68,05
C_2S	12,6	13,23
C_3A	9,9	6,79
C_4AF	8,1	7,28
CaO_{free}	1,2	0,68

2.3 Results

2.3.1 Standard tests

The results of standard tests are given in Tables 2 and 3 (w/c, Le Chatelier test, consistency of standard mortar), Figure 1 (setting data) and in Tables 4 – 7 (strength results). The strength tests were carried out with PbO additive up to 2%, because the samples with 5% PbO revealed no strength and very strong bleeding after 48 hours, so that the de-moulding of standard bars was not possible.

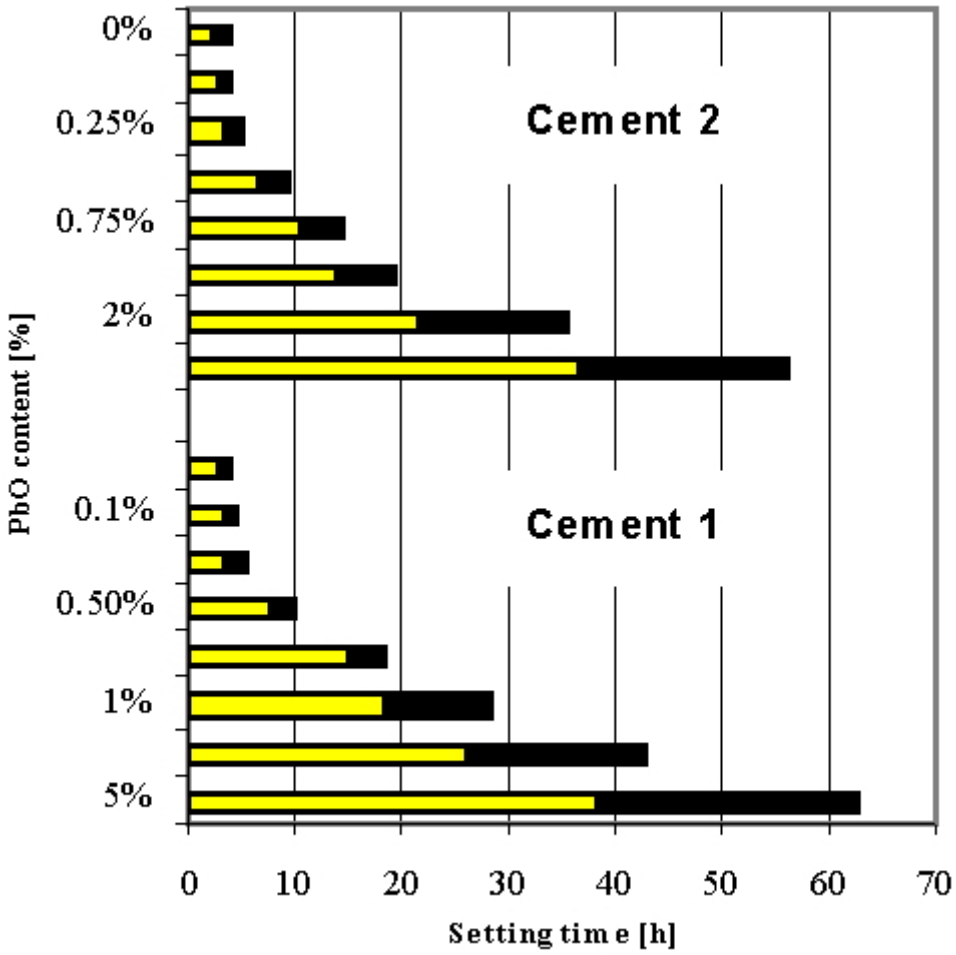

Figure 1. Setting time as a function of PbO content in cement pastes.
Yellow – initial setting; black – final setting.

Table 2. Cement 1 - determination of some standard properties of PbO doped pastes and mortars (water demand – volume changes – consistency)

PbO content in [%] by weight of cement	W/C	Volume changes (Le Chatelier test) in [mm]	Diameter of fresh mortar cake [mm]
0	0,28	0,0	170
0,1	0,28	0,5	170
0,25	0,28	0,0	170
0,5	0,27	0,0	170
0,75	0,27	0,0	165
1,0	0,28	0,5	165
2,0	0,28	0,0	175
5,0	0,27	0,5	185

Table 3. Cement 2 - determination of some standard properties of PbO doped pastes and mortars (water demand – volume changes – consistency)

PbO content in [%] by weight of cement	W/C	Volume changes (Le Chatelier test) in [mm]	Diameter of fresh mortar cake [mm]
0	0,28	0,0	170
0,1	0,28	0,0	170
0,25	0,28	0,0	170
0,5	0,28	0,5	175
0,75	0,29	0,0	175
1,0	0,28	0,5	170
2,0	0,29	0,0	180
5,0	0,29	0,5	175

Table 4. Cement 1 – compressive strength of PbO doped mortars

PbO content	Compressive strength [MPa] at age						
	1 day	2 days	7 days	28 days	90 days	180 days	360 days
0%	15,3	22,4	32,4	36,6	40,3	44,1	47,0
0,25%	15,0	24,7	33,5	40,2	42,1	46,5	48,0
0,5%	12,9	25,1	37,0	40,8	41,0	46,0	48,0
0,75%	8,25	22,3	35,4	40,2	38,3	44,2	46,4
1,0%	0,0	21,3	35,5	38,0	41,3	46,6	49,2
2,0%	0,0	10,4	29,9	36,8	40,0	42,9	45,1

Table 5. Cement 1 – flexural strength of PbO doped mortars

PbO content	Compressive strength [MPa] at age						
	1 day	2 days	7 days	28 days	90 days	180 days	360 days
0%	4,47	6,43	8,89	9,84	10,00	10,70	11,20
0,25%	4,46	7,04	8,54	9,95	10,16	10,90	11,35
0,5%	4,53	7,27	8,45	10,48	10,25	11,05	11,48
0,75%	2,93	6,42	8,56	10,11	10,17	10,92	11,25
1,0%	0,0	6,08	7,89	10,08	10,51	11,25	11,55
2,0%	0,0	3,13	8,05	9,49	9,53	10,28	10,63

Table 6. Cement 2 – compressive strength of PbO doped mortars

PbO content	Compressive strength [MPa] at age						
	1 day	2 days	7 days	28 days	90 days	180 days	360 days
0%	6,8	18,0	39,2	48,4	52,9	52,9	54,0
0,25%	6,8	18,2	38,7	48,6	50,0	54,0	55,2
0,5%	6,0	19,0	40,0	50,0	51,2	55,0	56,3
0,75%	4,5	17,9	38,9	48,8	49,9	53,6	54,5
1,0%	0,0	17,4	39,0	48,6	50,5	52,9	55,0
2,0%	0,0	9,2	36,2	44,1	47,2	49,5	49,9

Table7. Cement 2 – flexural strength of PbO doped mortars

PbO content	Compressive strength [MPa] at age						
	1 day	2 days	7 days	28 days	90 days	180 days	360 days
0%	2,1	4,2	6,7	7,7	8,0	9,9	10,3
0,25%	2,0	4,5	6,5	7,5	8,4	10,2	10,3
0,5%	1,9	4,5	6,5	7,9	8,3	10,5	11,0
0,75%	1,0	4,5	6,8	8,0	8,5	10,2	10,4
1,0%	0,0	4,0	6,8	7,7	8,0	10,1	10,3
2,0%	0,0	2,1	5,7	6,9	7,2	7,8	8,0

2.3.2 Calorimetric measurements

The calorimetric curves are presented as Figures 2 and 3.

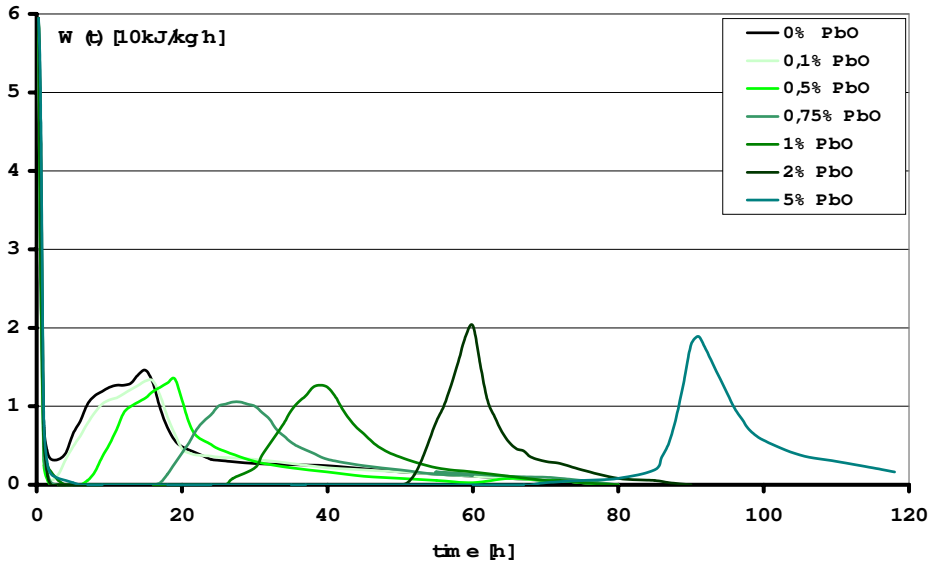

Figure 2. Heat evolution curves of Cement 1 doped with PbO.

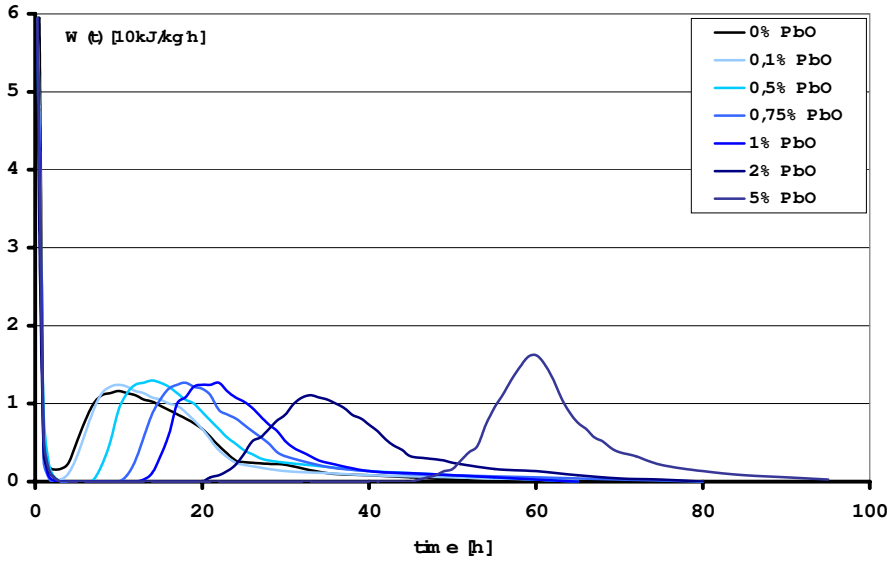

Figure 3. Heat evolution curves of Cement 2 doped with PbO.

2.4 Discussion

From the results from W/C and volume change determination, PbO gives neither the effect on water demand or consistency of mortar at the beginning of hydration produces expansive products (Le Chatelier test – see Table 1). The setting process is clearly disturbed with PbO additive; the pastes with up to 0,50% PbO meet the standard requirements. One can notice that initial and final setting, specially for higher PbO content, is less retarded in the case of Cement 2.

As the results from the compressive and flexural strength data show, PbO additive up to 0,5% gives generally no retarding effect on strength development. One can even notice a slight strength increase as compared to the control sample At higher amounts a delayed hardening at early ages is observed at standard 2-day measurements. At 1% and more PbO, it is impossible to de-mould the standard bars after 24h. The samples with 5% PbO were completely destroyed – exfoliated. Up to 1% the strength results are almost on the same level. At 2% PbO the strength of mortar is less or more reduced within 360-day measurements; it relates particularly to cement 2 and its flexural strength. However it seems that the difference becomes higher not only at early ages but also after prolonged curing (180, 369 days).

The calorimetric studies prove the systematic retardation of cement hydration with time, documented as Figures 2 and 3.

The data showed above would indicate the formation of a physical “barrier” which is effective at an early age, augments with PbO additive and becomes withdrawn after a shorter or longer time, depending on PbO content.

This barrier (impermeable layer of Pb containing material?) is presumably thicker and more stable at higher PbO contents and really must be once destroyed; after this the formation of products takes place in such a way that the microstructure is almost the same, thus giving very similar strength results to the reference. This is compatible with calorimetric observations, where we can observe a shift of the main peak along the time axis, but the height and shape of peak remains little changed. A diffusion process through the layer surrounding the cement grains seem to be rather of less importance. (In these cases the peaks would be broader and lowered with PbO)

It seems reasonable that the Pb containing compounds, if they are formed have no special influence on the mechanism and rate of hydration after the initial prolonged dormant period, when they are present in the paste. The incorporation of some Pb ions to the structure of hydration products (C-S-H) is also possible. Taking into account the w/c data and shape of calorimetric curves one can find that the effect of PbO on ettringite formation should be rather excluded.

According to the suggestion given in one previous work [1] the retarding effect of PbO is attributed to the blocking up of the alite surface presumably by the formation of an impermeable layer of product. The retardation depends on the alite content. However it is difficult to adapt this explanation to the differences between the data for cement 1 and 2. The setting and hydration kinetics of cement 1, that is of lower alite content is more retarded. There must be other phenomena and processes involved. Anyway, the authors of this first study cited here [1] clearly point out that there is no satisfactory explanation dealing with PbO’s influence on cement hydration and some points remain unclear (e.g. There is no defined product detected).

Let us discuss this taking into account our results:
PbO additive when retards alite hydration by formation of $Pb(OH)_2$ or other amphoteric compounds, must dissolve at first.

It dissolves better, at a higher rate with higher alkali content in cement paste – more OH^- available! – such a situation is in Cement 1 (see Table 1). Thus it dissolves in cement paste from Cement 1 better. It means that it would dissolve in "normal" (not very low alkali) cement paste better than the low alkali one or in pure alite paste.

Additional possible reaction affecting PbO interaction with cement paste - gypsum dissolution at early stage of hydration - gives sulphate ions which combine with Pb and $PbSO_4$ precipitation takes place and Ca ions release to the solution (hypothetical formation of Ca salts with Pb in anion). But this effect of gypsum seems to be less important, otherwise calcium aluminate hydration in cement paste to form ettringite would not be balanced and false setting would be observed or water demand changed in some way.

2.5 Supplementary studies – results and discussion

To elucidate some aspect of the PbO retarding mechanism, the authors carried out some further experiments. The calorimetric measurements were done with ZnO, the effect of which is better documented and explained by the formation of well defined compounds [1]. A stronger but similar-in-shape retarding effect was observed. Therefore the calorimetric studies to follow the hydration of alite with ZnO and PbO were carried out as a next step. The calorimetric curves are given as Figures 4 and 5.

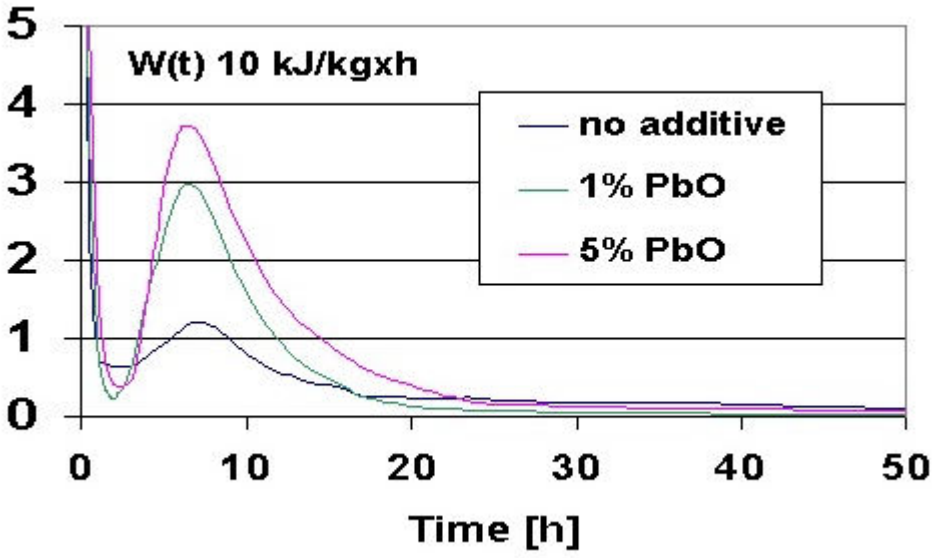

Figure 4. Calorimetric curves of alite with PbO.

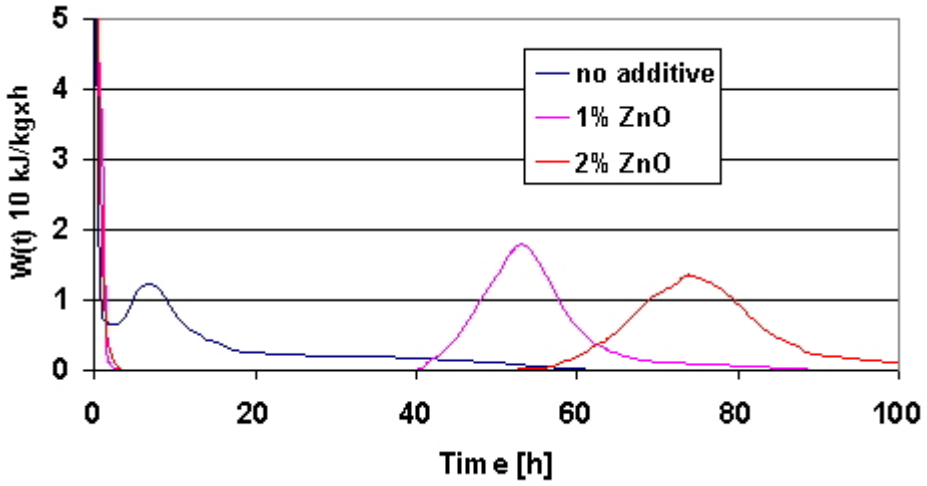

Figure 5. Calorimetric curves of alite with ZnO.

As we can see the hydration of alite sample in the presence of alite is not retarded by PbO while in the presence of ZnO it is! Perhaps the formation of any Pb containing compound by a through solution mechanism is fairly slow and, what is more, the dissolution of PbO is much slower in alite paste than in cement paste, where there is always some concentration of easily soluble alkalis and other ions, which may strongly accelerate this process. It seems quite reasonable that in the case of pure alite PbO plays a role of nucleating agent prior to retarding the process. The results for alite hydrating in the presence of ZnO seem to prove that ZnO is more easily soluble in the alkaline liquid formed on alite hydration and that the calcium hydroxozicate does precipitate on the surface of hydrating grains and efficiently covers the surface to protect alite against attack of water. Another reason is that perhaps early Pb containing coating if it exists in pure alite system, is weak and its thickness is insufficient and permeable. Therefore, as a further step the interaction alite – PbO – $CaSO_4$ was taken into account. The calorimetric measurements were done and they demonstrate the retarding effect of the gympsum on alite + PbO hydrating mixture (Figure 6).

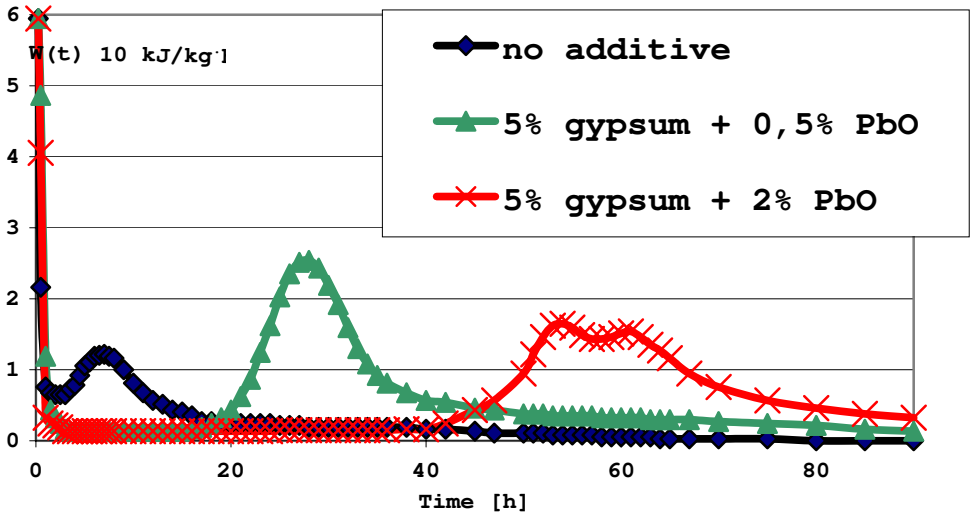

Figure 6. Calorimetric curves of alite with PbO and gypsum.

We can, therefore presume that the insoluble $PbSO_4$ layer can be formed; its thickness is a function of Pb content. After a time this layer collapses. Probably destroyed by osmotic pressure of hydrating silicate; Pb ions are partly consumed by poorly ordered C-S-H [11]. This layer is built up not only of sulphate; different energies of Pb bonds have been found in ESCA measurements in model systems [12], but $PbSO_4$ seem to be responsible for the retarding effect.

3. SUMMARY

The effect of PbO and ZnO interaction with cement pastes and mortars can be summarized as follows:

- PbO and ZnO added to cement paste or mortar as fine grained solid additives retard setting proportionally to their content in hydrating materials;
- effect of retardation by PbO is different for different cements; but for PbO additive not exceeding 0,5 wt. % the setting parameters meet the European standard requirements;
- PbO does not affect such parameters of fresh paste as w/c or volume changes;
- PbO brings about a significant change of heat evolution kinetics – at 2 – 5% PbO the induction period becomes many times longer, but when reaction starts again it seems that there is no special modification of hydration mechanism and kinetics;
- The effect of PbO on heat evolution may differ significantly for different cements;
- PbO does not hinder the heat evolution process of alite while ZnO does; PbO gives a significant growth of heat output – presumably it plays a role of nucleating agent.

- PbO hinders alite hydration in the presence of gypsum; $PbsO_4$ seems to be the main factor responsible for retarding effect.
- However, the retarding mechanism of PbO powder on cement hydration is complex. It seems that there is no one hypothesis which should be operative. This is not only the question of physical barrier on alite surface; the reason for this relates to the other components of cement paste.

ACKNOWLEDGEMENTS

Financial support from the Polish National Research Committee (grant No 4 T08D 011 22) is kindly acknowledged.

REFERENCES

[1] Lieber, W. The influence of lead and zinc compounds on the hydration of Portland cement, 5th international symposium on the chemistry of cement, Tokyo 1968, vol. 2, pp.444-454.
[2] Glasser, F.P. Immobilisation potential of cementitious materials, Environmental aspects of construction with waste material, Elsevier Science Publishers, Amsterdam, 1994, pp.77-86.
[3] Tamas, F.D., Csetenyi, L., Tritthart, J. Effect of adsorbents on the leachability of cement bonded electroplastic wastes, Cement and Concrete Research, vol.22, 1992, pp.399-407.
[4] Nocun-Wczelik, W., Małolepszy, J. Studies on immobilisation of heavy metals in cement paste – C-S-H leaching behaviour, 10th international symposium on the chemistry of cement, Goeteborg 1997, vol. 4, 4iv043.
[5] Rigo, E., Gies, H., Krug., M., Miskiewicz, K., Stade, H., Wieker, W. Beitrag zur Immobilisierung von Blei-, Zink- und Kupferionen in achlecht geordneten C-S-H -Phasen, Zement-Kalk-Gips, vol.53, 2000, pp.414-422.
[6] Nocun-Wczelik, W., Trybalska, B., Rakowska, A. The microstructure of C-S-H formed in the presence of heavy metal compounds, Polish Ceramic Bulletin 8, section Ceramics, vol. 46, 1994, pp.289-291.
[7] Nocun-Wczelik, W. Microstructure of some hydrated calcium silicate hydrates formed in hydrothermal conditions, 21th international conference on cement microscopy, Las Vegas, 1999.
[8] Rosetti, A., F. Medici, F. Inertization of toxic metals in cement matrices: effect on hydration, setting and hardening, Cement and Concrete Research, vol.25, 1992, pp.1147-1152.
[9] Gawlicki, M., Czamarska, D. Effect of ZnO on the hydration of portland cement, Journal of Thermal Analysis, vol.38, 1992, pp.2157-2161.
[10] Nocun-Wczelik, W., Małolepszy, Application of calorimetry in studies of the immobilization of heavy metals in cementitious materials, Thermochimica Acta, vol. 269/270, 1995, 613-619.
[11] Nocun-Wczelik, W., Loj, G., to be published.
[12] Nocun-Wczelik, W., Loj, G., Nocun M., to be published

MECHANISM OF PbO AND ZnO INTERACTION WITH CEMENT PASTE

Wieslawa Nocun-Wczelik[1] and Grzegorz Lój[2]

Faculty of Material Science and Ceramics, University of Mining and Metallurgy, Kraków, Poland. E-mail: [1]wiesia@uci.agh.edu.pl and [2]gloj@uci.agh.edu.pl

Wieslawa Nocun-Wczelik, Dr. Sc., Eng.

Research worker and lecturer at the Faculty of Material Science and Ceramics, University of Mining and Metallurgy, Kraków, Poland. She is working in the field of cement and concrete chemistry at the Department of Building Materials. Her scientific interests include basic studies on cement hydration: spectroscopy, microscopy and calorimetry of cements (head of laboratory), calcium silicate hydrates, calcium aluminate cements, waste materials disposal, specially practical implementation of different by-products and wastes to cement clinker and concrete. She was the member of different research teams working on research projects related to the alumina and cement production, high performance concretes, waste conditioning process and many others. She was the participant of congresses on cement chemistry in Paris (1980), Rio de Janeiro (1986), New Delhi (1992) and Goeteborg (1997), as well as many other international symposia.

FINELY DISPERSED ADDITIVES TO CEMENT

Wieslawa Nocun-Wczelik

Faculty of Material Science and Ceramics, University of Mining and Metallurgy, Kraków, Poland.
E-mail: wiesia@uci.agh.edu.pl

ABSTRACT

The hydration process of cementitious mixtures with some finely ground and/or finely dispersed additives of different origins has been followed using calorimetry and other methods to evaluate the scope of cement replacement as well as the effect on strengthening of structure. The nucleating action and chemical modification of hydrating systems will be discussed. The hydration products will be characterised by means of thermogravimetry and microscopy.

The experimental work, which is a part of larger project, was carried out step by step starting, by using fly ash admixtures, then silica fume, calcined clay, limestone and finely grained siliceous glassy admixture.

Obviously, the heat evolved decreases with admixture content, however the heat calculated for 1g of cement in every initial, blended anhydrous sample becomes higher in case of silica fume, glassy admixture and metakaolin and this fact seems to prove that intensive hydration takes place. One can draw conclusions about the significant contribution of admixtures used in this study to setting and hardening. Relatively high heat calculated value for 50 % SF and glassy admixture can be attributed to wetting and (ad)sorption of process water with dissolved ions on the silica-rich developed surface of the admixture, followed by C-S-H formation. TG data show that small amounts of SF or MK favours $Ca(OH)_2$ formation at an early age due to the nucleation effect and accelerated hydrolysis of silicates from cement. However, after 3 days the pozzolanic effect of calcium hydroxide consumption is evident in the case of silica fume but not yet in the case of metakaolin.

The differences between the particular admixtures are not only the question of specific surface development but also the active silica contribution to the C-S-H phase formation and role of alumina containing hydrates at later ages of hydration.

1. INTRODUCTION

The alumina and/or silica bearing admixtures of poorly ordered structure were used in ancient times to improve setting and hardening of mortars [1]. Nowadays, industrial by-products of different origins are used as admixtures, mainly slags and pulverised fuel ashes, but also silica fume and other artificial pozzolans [2].

Silica fume, delivered as a by-product in silicon alloy production, has been put into use in the seventies and is known as a very active pozzolanic admixture for high performance and self-compacting concrete [3].

Dehydrated clay, produced by heating at sufficiently low temperature, shows relatively high surface area and pozzolanic activity [4]. From the other side, the chemical composition of metakaolin is

very similar to the composition of many fly ashes. The dehydrated clay is not a component of standard pozzolanic cement itself, but its effect must be taken into account when we consider the use of some wastes containing the products of clayey mineral decomposition (e.g. coal shales, "mineral" part of the desulphurisation residue from some installations) [5].

Locally, some finely ground alumino-silicate materials are used as concrete admixtures, e.g. waste materials of zeolitic character or other vitrified substances [6].

The small particles of these admixtures are well distributed between the cement grains and easily absorb the calcium ions evolved on hydrolysis of silicate cement phases [7]. C-S-H phase produced as a result of pozzolanic reaction reveals a specific microstructure of initial amorphous component, very compact, "dense", with no large pores. Calcium hydroxide is consumed with time in the pozzolanic reaction and enters the C-S-H structure, improving its resistance to chemical attack. In such a way a composite material of high strength and durability can be produced [8].

The interaction of admixtures with cement paste is very often of various character, particularly when they are built of amorphous, glassy or very disordered silica and alumina bearing substances. The physical, nucleating effect of small particles incorporated into cement paste should also be taken into account. The addition of finely dispersed limestone is a good example. Very fine powders are used in the production of some special high performance concretes [3].

2. EXPERIMENTAL

The experimental work, which is a part of larger project, was carried out step by step starting by using fly ash admixtures, then the silica fume, calcined clay, limestone and finely grained siliceous glassy admixture. As a first part of research programme the calorimetric measurements were carried out, followed by some investigations using different methods to elucidate the mechanism of accelerating/cement replacement effect.

2.1. Materials

The following materials were used in this study:

- standard cement "52.5R" with no other admixtures (CEM 52.5),
- silica fume of SiO_2 content > 95 % and specific surface > 15 m^2/g (SF),
- pulverised fuel ash,
- siliceous admixture,
- metakaolin with 58.13 % SiO_2 and 38.12 % Al_2O_3 (MK)
- limestone (pure reagent grade).

The admixtures were used at 5 to 50% cement replacement (by weight) respectively. The pastes were produced at water to cement ratio = 0.5. The commonly known procedure was applied to stop the hydration as required (grinding or rinsing with acetone and drying).

2.2. Methods

The hydration kinetics was followed by microcalorimetry. Heat evolution measurements were carried out by use of differential microcalorimeter BMR (non-isothermal – non-adiabatic; constructed in the Institute of Physical Chemistry, Polish Academy of Science) on pastes produced at w/c ratio 0,5. The starting temperature was kept constant at 25°C. The selected samples were analysed using DTA-TG methods (differential thermoanalyser "Derivatograph Q 1500-C") and observed under SEM (JEOL electron microscope with LINK-ISIS microanalyser).

2.3. Results

The results of calorimetric measurements are shown in Figures 1-5.

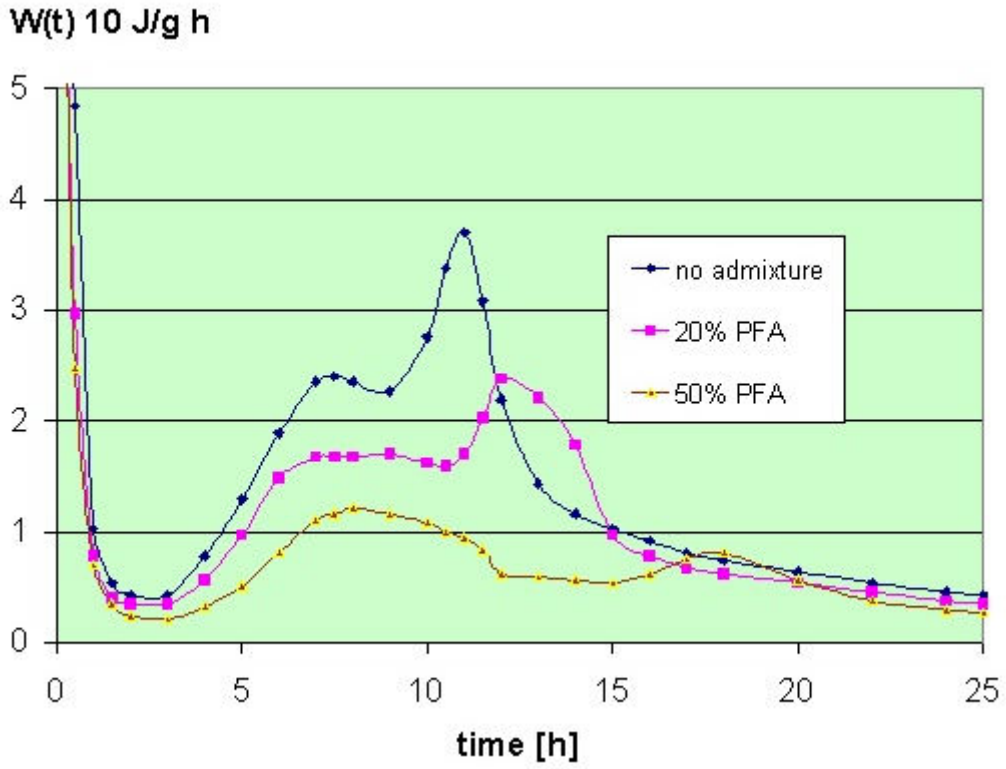

Figure 1. Heat evolution curves of cement pastes with fly ash

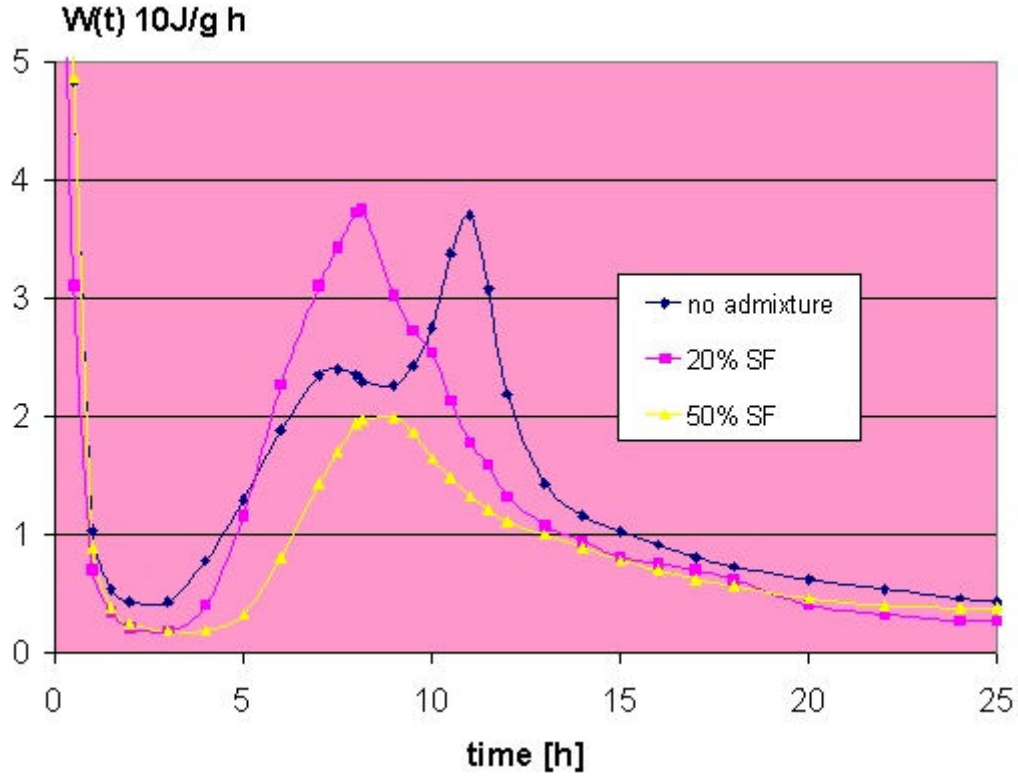

Figure 2. Heat evolution curves of cement pastes with silica fume

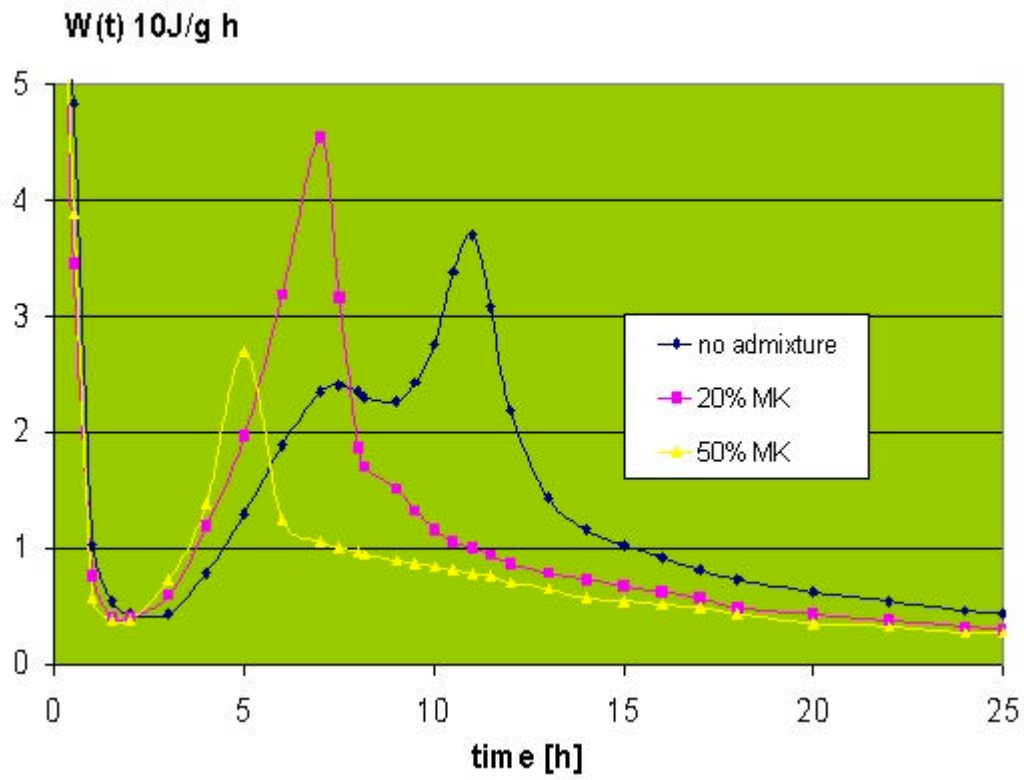

Figure 3. Heat evolution curves of cement pastes with metakaolin

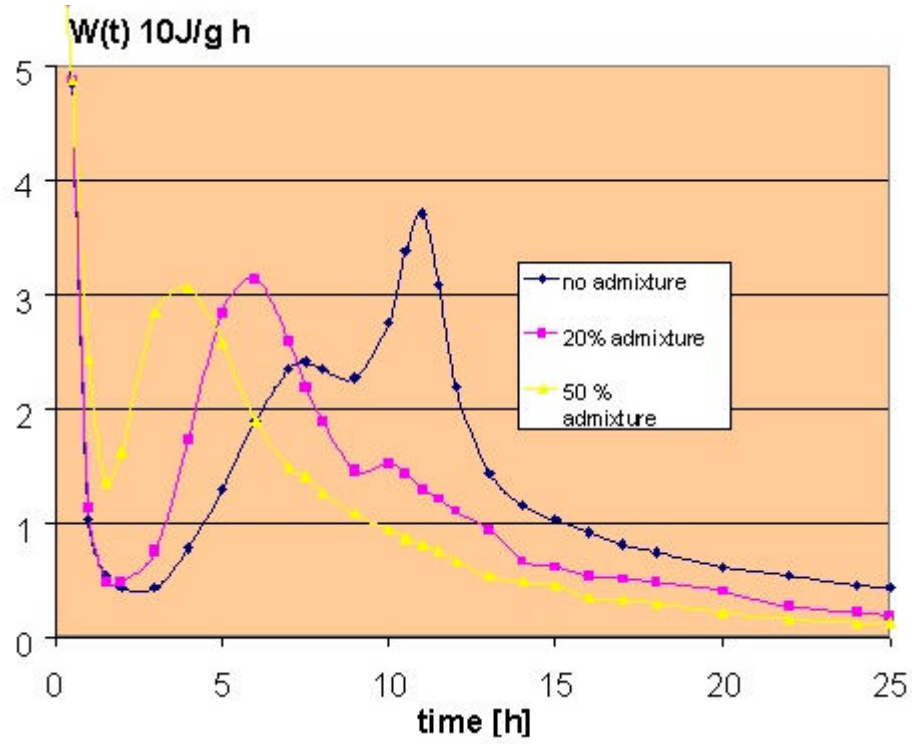

Figure 4. Heat evolution curves of cement pastes with fine-grained, glassy admixture

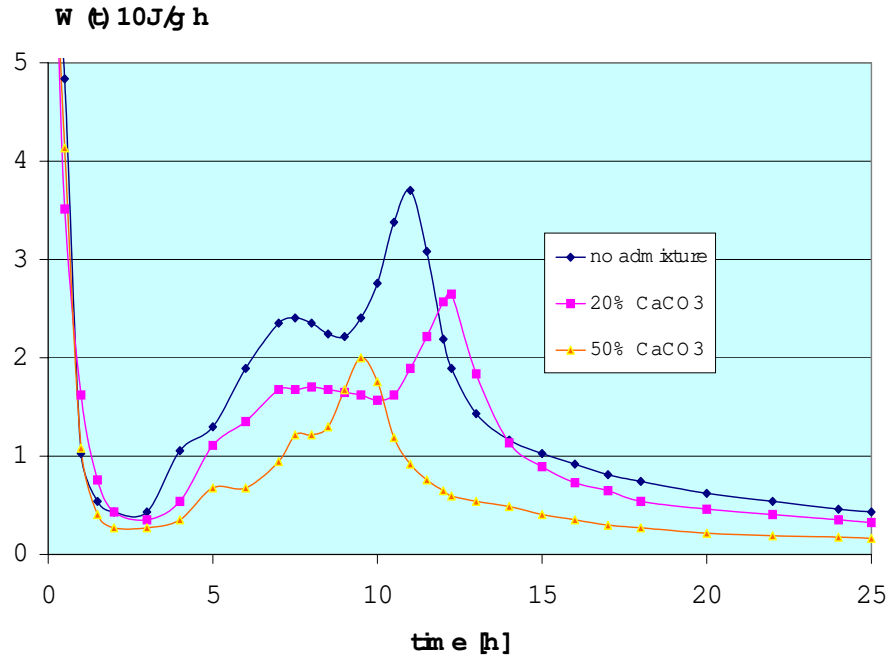

Figure 5. Heat evolution curves of cement pastes with calcium carbonate

Table 1. Heat evolved during 24h hydration of CEM I 52.5R samples with admixtures.

Sample code		Heat calculated for 1g of (cement + admixture) in initial sample [kJ/kg]	Heat calculated for 1g of pure cement in initial sample [kJ/kg]
1	No admixture	356	356
2	20 % PFA	275	344
3	50 % PFA	178	355
4	20 % SF	291	364
5	50 % SF	216	432
6	20 % MK	269	336
7	50 % MK	194	388
8	20 % GlAd*	290	363
9	50% GlAd*	274	548
10	20 % $CaCO_3$	266	332
11	50 % $CaCO_3$	174	348

* - fine-grained admixture of glassy phase

The examples of paste microstructure are shown in Figures 6 – 8.

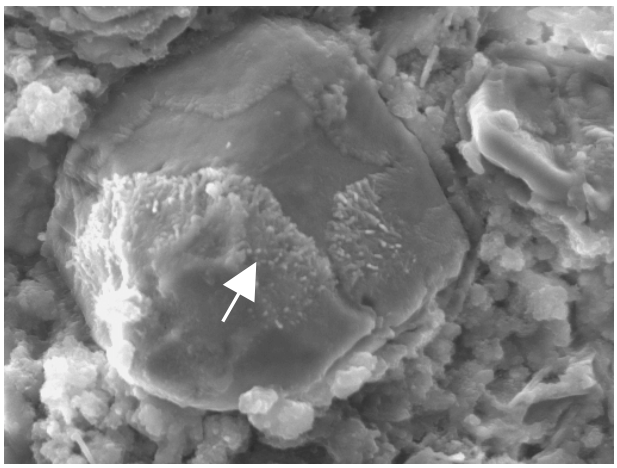

Figure 6a. SEM. Microstructure of paste with 10% SF, 1 day hydration; cement grain surrounded by C-S-H with C-S-H deposited on the surface.

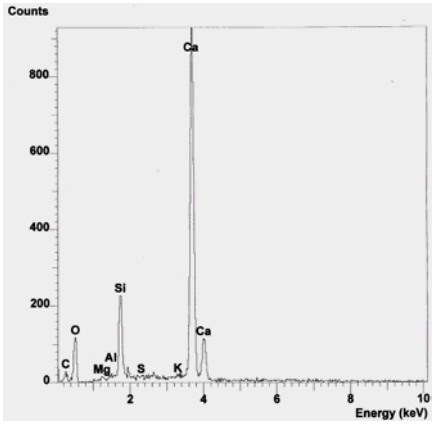

Figure 6b. EDS plot in the area indicated by an arrow, showing the components of C-S-H sur-facial product.

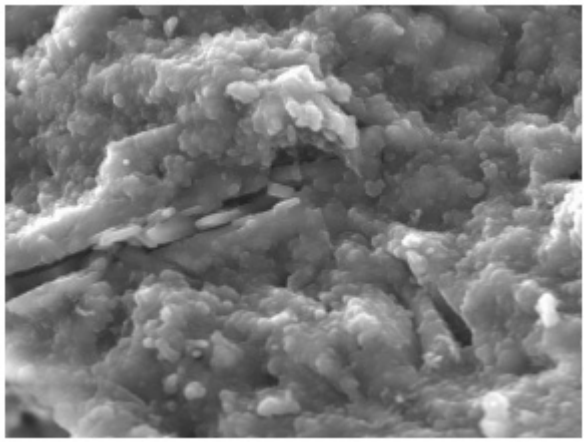

Figure 7. SEM. Microstructure of paste with 10% SF, 7-day hydration. C-S-H small grains and calcium hydroxide plate-like crystals.

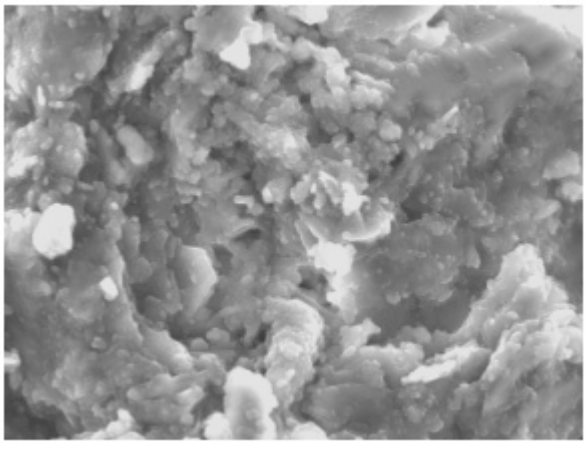

Figure 8. SEM. Microstructure of paste with 10% MK, 7-day hydration; the residual irregular metakaolinite plates and hexagonal portlandite formed in the pore.

Table 2. Calcium hydroxide content in selected cement pastes with admixtures.

Sample code	$Ca(OH)_2$ content as a function of time [wt. %]			
	1 day	3 days	7 days	28 days
No admixture	8.0	11.8	7.5	8.7
10 % SF	9.3	10.0	5.6	5.0
10 % MK	9.3	11.2	5.6	7.5

3. DISCUSSION

In this work the comparative studies of hydration process in cementitious systems with fly ash, calcined clay (metakaolin), silica fume, finely ground glassy siliceous admixture and calcium carbonate used as admixtures to cement were carried out. The details of hydration acceleration/retardation at early age have been clearly pointed out by microcalorimetry. The heat evolved values, calculated in relation to the "pure" cement content, show that at 20% admixture of siliceous admixtures or metakaolin, the accelerating effect on cement hydration, that is the shortening of induction period and shift of the main heat evolution peak is evident. Also the calcium carbonate fine grains, though almost non-reactive chemically, presumably play a role of nucleating agent; the effect of fly ash within the first 24h is similar.

Obviously, the heat evolved decreases with admixture content, however the heat calculated for 1g of cement in every initial, blended anhydrous sample becomes higher in case of silica fume, glassy admixture and metakaolin and this fact seems to prove that intensive hydration takes place. Though this simulation is based upon some simplified assumptions, one can draw conclusions about the significant contribution of admixtures used in this study on setting and hardening. The relatively high heat calculated value for 50 % SF and glassy admixture can be attributed to wetting and (ad)sorption of process water with dissolved ions on the silica-rich developed surface of admixture, followed by C-S-H formation. TG data show that small amount of SF or MK favours the $Ca(OH)_2$ formation at an early age due to the nucleation effect and accelerated hydrolysis of silicates from cement. However, after 3 days the pozzolanic effect of calcium hydroxide consumption is evident in case of silica fume but not yet in case of metakaolin. Metakaolin exhibits, in comparison with SF, more moderate action, as determined by several methods.

The differences between the particular admixtures are not only the question of specific surface development but also the active silica contribution to the C-S-H phase formation and role of alumina containing hydrates at later ages of hydration.

The SEM observations with EDS analysis are a good supplement to the calorimetric and TG measurements. In SF doped samples, C-S-H composed of small, spherical particles with Ca from hydrolysis of silicate phases is produced as a main component of paste (Figures 6-8) and shows a good adherence to cement grains, as can be seen in Figure 6. The metakaolin admixture is not so well dispersed in the paste. The plate-like metakaolin areas are however saturated with Ca and form Al containing C-S-H together with ettringite and calcium hydroxide. The particular phases can be distinguished only by means of EDS.

4. CONCLUSIONS

- Silica fume, metakaolin or every other aluminosilicate fine-grained admixture of disordered structure added to cement participates more or less actively in cement hydration as shown by the results of heat evolved calculated for 1 g of cement.
- The retarding effect of fly ash on heat evolution is similar to that of calcium carbonate, however the nucleating role of small particles is clearly seen at early age of hydration.
- The rate of calcium silicate hydration in pastes with silica fume or metakaolin increases, as shown by results from TG measurements showing the higher calcium hydroxide contents at an early age of hydration.
- The small particles of admixtures are dissolved and/or saturated with Ca (ad)sorbed from the liquid phase and C-S-H is thus formed as is documented in SEM+EDS studies.

ACKNOWLEDGEMENTS

Financial support from the Faculty of Material Science and Ceramics is acknowledged.

REFERENCES

[1] Supplementary Cementing Materials for Concrete, ed. V. M. Malhotra, Ottawa 1987.
[2] Mehta, P.K., Pozzolanic and cementitious byproducts as mineral admixtures for concrete – a review, Proc. of 1st Conference on Fly Ash, Silica Fume, Slag and Other Mineral By-products in Concrete, ed. V.M. Malhotra, Vol.1, Montebello-Canada, 1983, pp.1-46.
[3] Aitcin, P.C., High Performance Concrete, ed. E. &E.F. Spon, London and New York 1998.
[4] Liu, J.N., Silbee, M.R., Roy, D.M., Strength and hydration of activated alumino-silicate material, Proc. Of 10th International Congress on the Chemistry of Cement, Vol.3, Gothenburg-Sweden, 1997, 3ii114, pp. 6.
[5] Roszczynialski, W., Gawlicki, M., Nocuń-Wczelik, W., Production and use of by-product gypsum in construction, Waste Materials and By-products in the Manufacture of Concrete, ed. S. Chandra, Noyes Publications – New Jersey USA, 1997, pp.53-141.
[6] Pacewska, B., Wilińska, I., Bukowska, M., Nocuń-Wczelik, W., Effect of waste aluminosilicate material on cement hydration and properties of cement mortars, Cement and Concrete Research (in press)
[7] Kurdowski, W., Nocuń-Wczelik, W., The tricalcium silicate hydration in the presence of active silica, Cement and Concrete Research, Vol.13, 1983, pp.341-6.
[8] Koenig, R., Wagner, J.P., Mikrosilika – Baustoff aus der Zukunft, ed. Woermann, Darmstadt 2000.

FINELY DISPERSED ADDITIVES TO CEMENT

Wieslawa Nocun-Wczelik

Faculty of Material Science and Ceramics, University of Mining and Metallurgy, Kraków, Poland.
E-mail: wiesia@uci.agh.edu.pl

Wieslawa Nocun-Wczelik is a research worker and lecturer at the Faculty of Material Science and Ceramics, University of Mining and Metallurgy, Kraków, Poland. She is working in the field of cement and concrete chemistry at the Department of Building Materials. Her scientific interests include basic studies on cement hydration: spectroscopy, microscopy and calorimetry of cements (head of laboratory), calcium silicate hydrates, calcium aluminate cements, waste materials disposal, specially practical implementation of different by-products and wastes to concrete. She was the member of different research teams working on research projects related to the alumina and cement production, high performance concretes, waste conditioning process and many others. She was the participant of congresses on cement chemistry in Paris (1980), Rio de Janeiro (1986), New Delhi (1992) and Goeteborg (1997), as well as many other international symposia.

THE CONDITIONS OF THAUMASITE FORMATION AND ITS ROLE IN CONCRETE

J. Malolepszy* and R. Mróz*

*Department of Building Materials, Faculty of Materials Science and Ceramics,
University of Mining and Metallurgy, al. Mickiewicza 30, 30-059 Kraków, Poland.
Tel: (48 12) 617-22-37, Fax: (48 12) 633-15-9. E-mail: rmroz@uci.agh.edu.pl

ABSTRACT

The following report will mainly focus on the conditions of thaumasite formation in concrete and mortar. Until now there has been a predominant opinion that the destruction of concrete by sulphate ions is connected first of all with expansive ettringite and gypsum formation. The C_3A content in cement is the main parameter limiting the resistance of concrete to chemical corrosion. However, recent studies indicate that CSH undergoes also sulphate corrosion, especially in the presence of CO_2 and at lower temperatures. In this case thaumasite, which crystals are similar to those of ettringite, is produced. The formation of thaumasite also results in expansion followed by microcracks in concretes and mortars. In this work results of the experiments dealing with the influence of C/S ratio in CSH on the thaumasite formation are presented. The XRD, IR spectroscopy and SEM – EDS methods are used to characterize this phase.

1. INTRODUCTION

Concrete durability can be defined as a complex of concrete properties, which must be kept unchanged within the longest possible time of utilization [1,18].

There are a number of factors influencing concrete durability; among them are:

- Physical and chemical properties of components
- technology
- curing conditions
- mechanical load constant and/or variable
- aggressive environment
- maintenance / conservation.

In many cases the factors mentioned above interact to influence the concrete. Chemical corrosion belongs to the factors which change concrete durability in a significant way [1].

Concrete corrosion in sulphate environments is the most dangerous. As a result expansion with gypsum and ettringite formation takes place [1].The amount of gypsum and ettringite depends mainly on the content of calcium hydroxide and hydrated calcium aluminate [2]. In the case of magnesium sulphate attack the most durable CSH phase also undergoes decomposition [2].

Another example of CSH destruction in concrete occurs when thaumasite is produced [5]. Thaumasite forms as a result of alkali sulphates and CO_2 attack on concrete at lower temperatures and in conditions of high humidity [5,6,7].

Proceedings of the 11th International Congress on the Chemistry of Cement (ICCC)
'Cement's Contribution to the Development in the 21st Century'
Hosted by: The Cement and Concrete Institute of South Africa
CD-ROM produced by: Document Transformation Technologies
11 - 16 May 2003, Durban, South Africa
ISBN Number: 0-9584085-8-0
Editors: Dr G. Grieve and G. Owens
Congress Organised by: Event Dynamics

The influence of ammonium sulphate and magnesium sulphate can be considered even more destructive for concrete [3,4].

The investigations of many authors indicate that many concrete constructions may be deteriorated by thaumasite formation occuring as a result of sulphate attack.

Typical elements that may suffer from thaumasite sulphate attack are [5]:
- foundations, columns and pier bases
- ground slabs and buried pad foundation
- roads pavements
- trench fill and concrete drainage pipes
- concrete ground anchors
- tunnel linings

As a result of thaumasite sulphate attack on the elements mentioned above, potentially significant structural effects have been identified as [5]:
- loss of concrete cross-sectional area
- loss of cover concrete on the reinforcing bars
- loss of bond between reinforcement and concrete
- settlement, inducing structural damage
- loss of durability as a result of loss of protection against reinforcement corrosion.

Examples of the thaumasite sulphate attack mentioned above are widely described in literature.

The British authors point out numerous cases of the thaumasite sulphate attack phenomenon occurring mainly in concrete foundations of industrial buildings, flats, flyovers and bridges in Great Britain [5,6,7].

The damage caused by thaumasite formation have also been noticed in concrete surface and car and train tunnels in the Italian Alps [8]. Also very dangerous are the symptoms of thaumasite sulphate attack in concrete constructions in dams located in Italy [9]. There are also similar cases of sulphate attack on historical buildings in Greece and Turkey [10].

It seems reasonable that the thaumasite attack is more or less evident depending on the nature of base material exposed to low temperatures and corrosive media.

Thus the following report will present the preliminary results of research on the influence of C/S to CSH ratio on thaumasite formation.

2. EXPERIMENTAL

Concrete is produced from different cementitious materials. The differences may concern the mineral composition and mineral admixtures, such as slags, fly ashes and other pozzolans used.

As a result of cement hydration, CSH phase is formed with variable C/S ratio of 0,8 to 2,5. The lowest limit corresponds to the use of high volume silica bearing admixtures. Therefore in order to follow the C/S effect the CSH has been synthesized with C/S ratios of 0,8, 1,5, 2,0, 2,5 respectively.

2.1. CSH synthesis

The mechanism of calcium silicate hydrate synthesis has been studied by many authors [11,12,13,14,20].

This process includes the following stages:

- surface protonation of SiO_2 with OH^- formation
- slow migration of silicate anions into the solution
- reaction between Ca^{2+} from the solution and silicate ions with formation of a product rich in CaO (so-called CSH II of C/S ratio about 1,5 - 2,0)
- reaction of an initial product with SiO_2 dissolution product with CSH phase poorer in CaO synthesis (so-called CSH I of C/S ratio about 0,8 – 1,0)
- depending on the conditions of the synthesis and proportions between SiO_2 and CaO formation of more ordered phases.

The process of setting and hardening of the products containing calcium silicate can take place at normal temperature under atmospheric pressure or by using hydrothermal conditions, that is at temperatures above 100^0C and saturated water vapour. The process can be considered as a hydration reaction "through solution" in which we can identify, in the most general case, dissolving substrates and precipitation of products.

As a result of the reaction in the reacting mixture we get the products in the form of calcium silicate hydrates, characterized by having different degrees of order.

In the following research a synthesis of CSH phases was carried out in hydrothermal conditions as well as at ambient temperature under atmospheric pressure. The materials were put together in the proportions expressed by C/S mole ratios, 0,8, 1,5, 2,0 and 2,5.

In the process of CSH phase synthesis amorphous silica and burnt lime were used, mixed in proper C/S proportions. Then the mixture was homogenized to produce a paste with water to solid ratio equal 1,5. The mixtures were then put into containers where they were heated at 50^0C within 2 hours. After that they were subjected to the homogenization process again. The only variable parameter was C/S ratio. The samples prepared in such a way were subjected to thermal processing at 180^0C under saturated steam pressure. The samples prepared at ambient temperature were shaken for 8 days.

2.2. Preparation of pastes

Fresh CSH produced as mentioned above was mixed with some additives, such as $CaCO_3$, $Ca(OH)_2$ and $Na_2SO_4 \cdot 10H_2O$, used in variable quantities in relation to CSH phase. Thus the series of doped C-S-H were produced; their composition is given in Table 1.

Table 1. Composition of pastes produced from CSH of variable C/S ratio, cured at normal temperature under atmospheric pressure for 8 days.

No	Sample code	Composition of samples						
		C/S ratio in CSH phase				$CaCO_3$	$Ca(OH)_2$	$Na_2SO_4 \cdot 10H_2O$
		0,8	1,5	2,0	2,5			
		weight [%]						
1	P/C/1D	75	-	-	-	10	5	10
2	P/C/2D	-	75	-	-	10	5	10
3	P/C/3D	-	-	75	-	10	5	10
4	P/C/4D	-	-	-	75	10	5	10
5	P/C/1	100	-	-	-	-	-	-
6	P/C/2	-	100	-	-	-	-	-
7	P/C/3	-	-	100	-	-	-	-
8	P/C/4	-	-	-	100	-	-	-

From the mixtures the 12 x 8 mm pastilles were made by pressing at a pressure of 1kN. The samples were exposed for sulphate attack.

Table 2. Composition of pastes produced from CSH of variable C/S ratio, cured in hydrothermal conditions within 24 hours of the autoclaved process.

No	Sample code	Composition of samples						
		C/S ratio in CSH phase				$CaCO_3$	$Ca(OH)_2$	$Na_2SO_4 \cdot 10H_2O$
		0,8	1,5	2,0	2,5			
		weight [%]						
1	P/24/1D	75	-	-	-	10	5	10
2	P/24/2D	-	75	-	-	10	5	10
3	P/24/3D	-	-	75	-	10	5	10
4	P/24/4D	-	-	-	75	10	5	10
5	P/24/1	100	-	-	-	-	-	-
6	P/24/2	-	100	-	-	-	-	-
7	P/24/3	-	-	100	-	-	-	-
8	P/24/4	-	-	-	100	-	-	-

2.3. Conditions of curing

The CSH pastes doped with $CaCO_3$, $Ca(OH)_2$ and Na_2SO_4 were divided into two testing series and stored at two different temperature ranges [15,16,17]:

- I: 5 ± 1^0C range
- II: 20 ± 2^0C range.

The samples were stored in sealed containers at 95% RH. The testing took place after: 28, 90, 180, 270 and 360 days.

3. RESULTS

The effect of $CaCO_3$, $Ca(OH)_2$ and Na_2SO_4 additions used for preparation of CSH phases (with variable C/S ratio from 0,8 to 2,5) and conditions of curing (low temperature, autoclaving) on the formation of thaumasite were estimated based on the results produced by SEM – EDS, XRD and IR spectroscopy.

The results presented here show the effect of $CaCO_3$, $Ca(OH)_2$ and Na_2SO_4 additives, as well as curing temperature after 360 days storage. SEM observations reveal the crystallization of fibre – like form [Figures1a, 2a] in samples doped with $CaCO_3$, $Ca(OH)_2$ and Na_2SO_4 with C/S ratio 1,5 and stored at temperature 5^0C, regardless of the the origin of the CSH phase (produced at ambient temperature or by autoclaving) [19].

The crystallization takes place in the regions of cracks, gaps and voids. EDS analysis proves the thaumasite's character of these forms [Figures 1b, 2b].

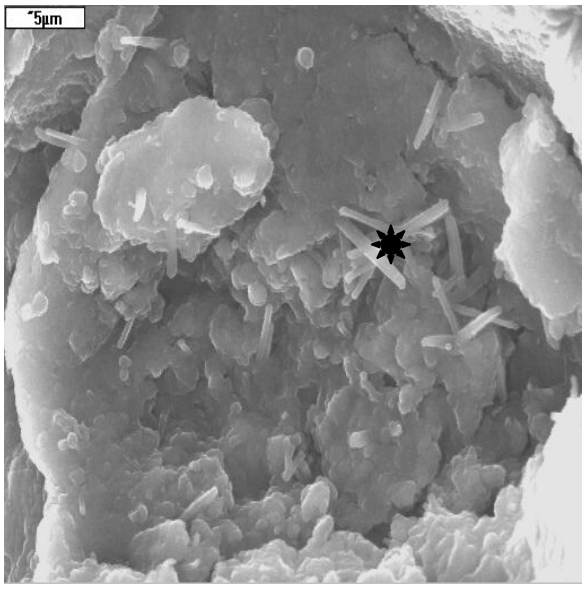

a) Crystallization of fibre – like thaumasite forms

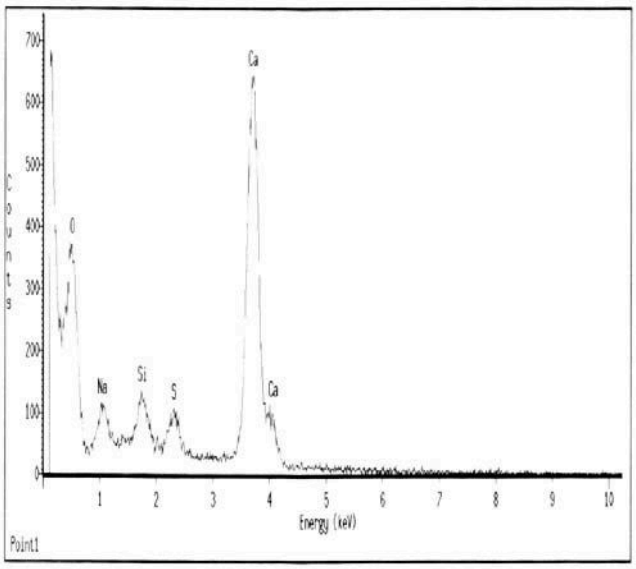

b) EDS analysis of thaumasite crystals (with incorporated Na from Na_2SO_4)

Figure 1. SEM-EDS. Sample (P/C/2D) - C/S ratio 1,5 doped with $CaCO_3$, $Ca(OH)_2$ and Na_2SO_4 , stored at 5^0C, after 12 months curing.

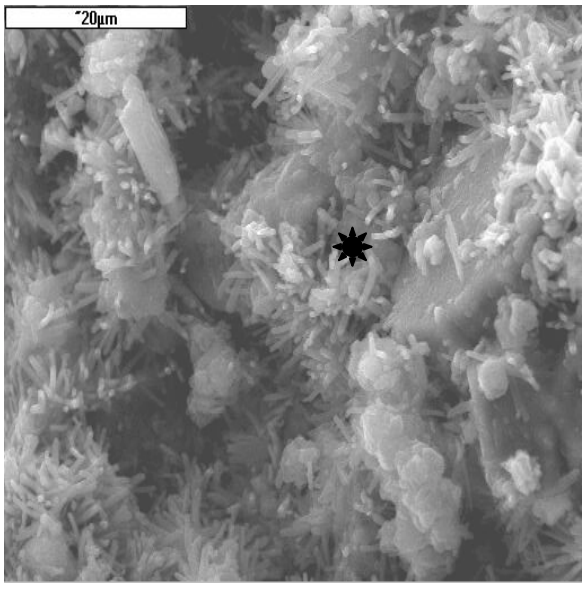

a) Crystallization of fibre – like thaumasite forms

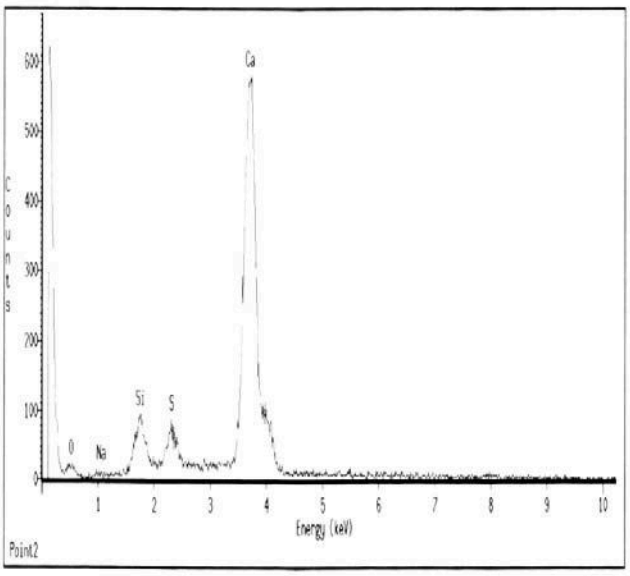

b) EDS analysis of thaumasite crystals

Figure 2. SEM-EDS. Sample (P/24/2D) - C/S ratio 1,5 doped with $CaCO_3$, $Ca(OH)_2$ and Na_2SO_4, stored at 5^0C, after 12 months curing.

Crystallization of similar product was observed in CSH samples with C/S ratio 2,0 doped with $CaCO_3$, $Ca(OH)_2$ and Na_2SO_4 and stored at 5^0C [Figures 3a, 4a]. Also in this case, chemical analysis by EDS proved the thaumasite-like character of these forms [Figures 3b, 4b].

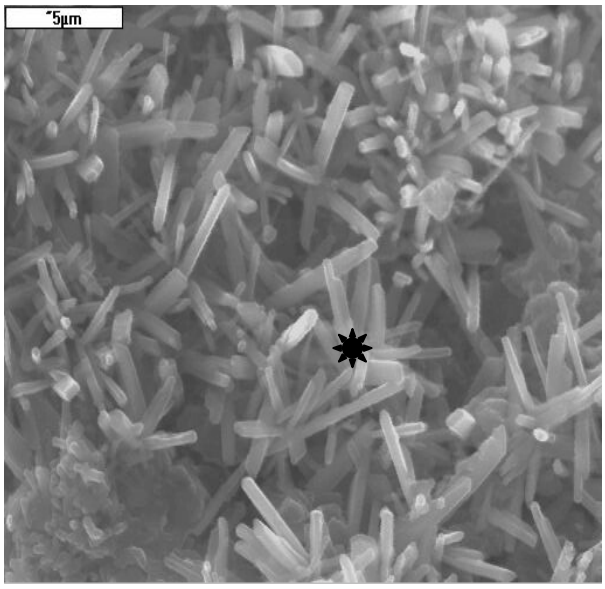

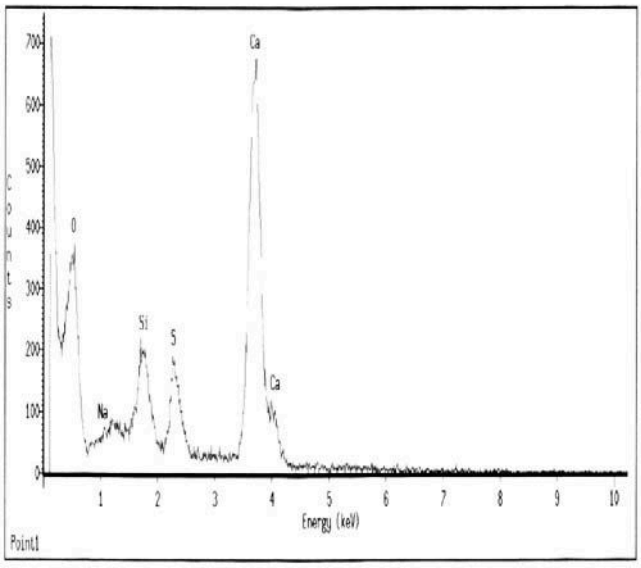

a) Crystallization in region of cracks and gaps b) EDS analysis of thaumasite crystals

Figure 3. SEM-EDS. Sample (P/C/3D) - C/S ratio 2,0 doped with $CaCO_3$, $Ca(OH)_2$ and Na_2SO_4 , stored at 5^0C, after 12 months curing.

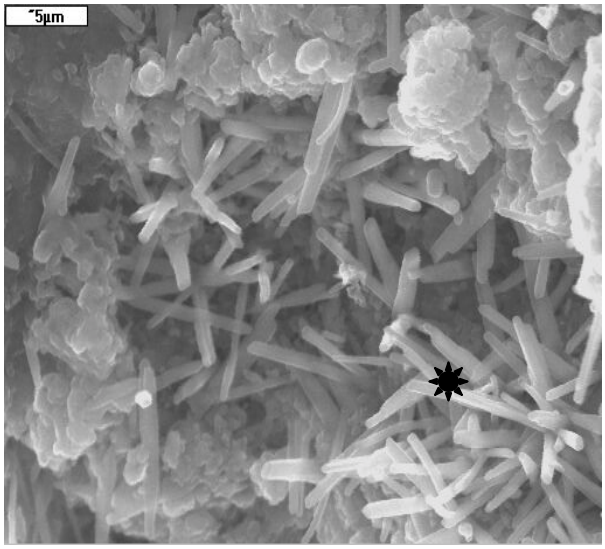

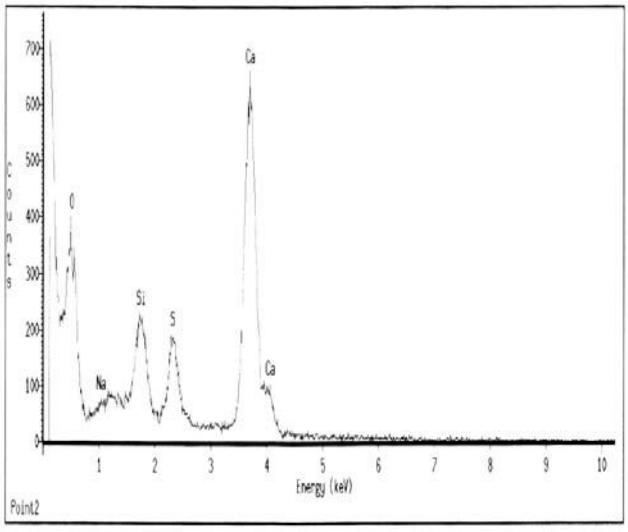

a) Crystallization in sample b) EDS analysis of thaumasite crystals

Figure 4. SEM-EDS. Sample (P/24/3D) - C/S ratio 2,0 doped with $CaCO_3$, $Ca(OH)_2$ and Na_2SO_4, stored at 5^0C, after 12 months curing.

Crystallization of fibre – like forms in samples produced at C/S ratio 2,5 with addition of $CaCO_3$, $Ca(OH)_2$ and Na_2SO_4, stored at temperature 5^0C shows the presence of better crystallized products [Figures 5a, 6a]. The EDS chemical analysis proves the thaumasite-like character of these forms in these samples [Figures 5b, 6b].

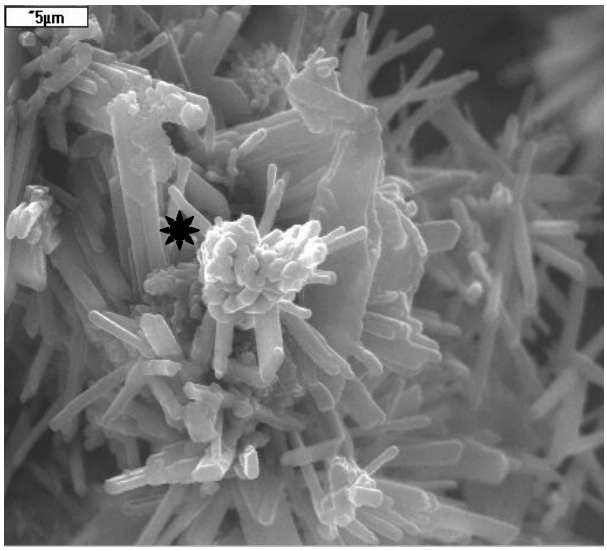

a) Formation of better crystallized products

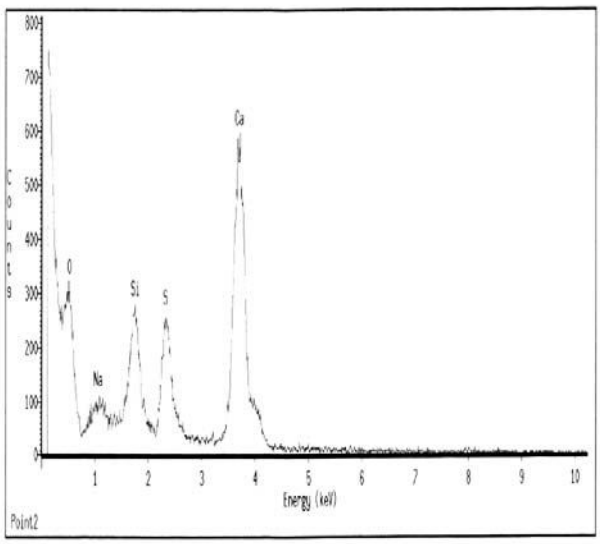

b) EDS analysis of thaumasite crystals

Figure 5. SEM-EDS. Sample (P/C/4D) - C/S ratio 2,5 doped with $CaCO_3$, $Ca(OH)_2$ and Na_2SO_4, stored at 5^0C, after 12 months curing.

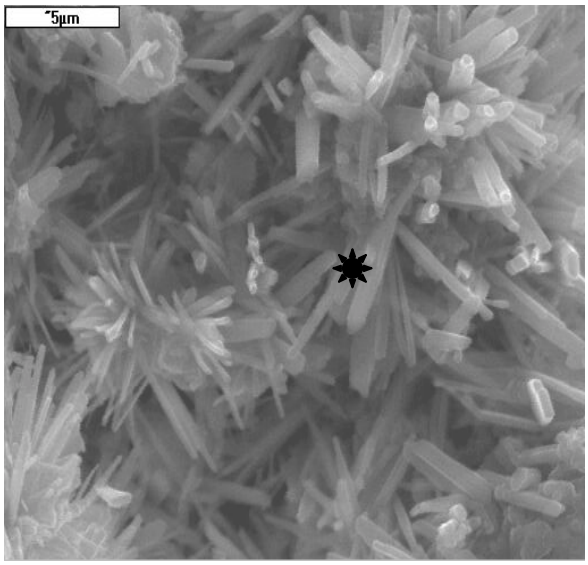

a) Formation of better crystallized products

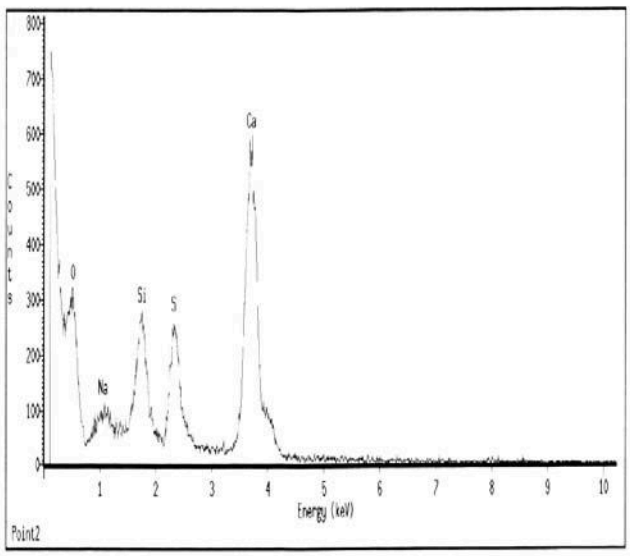

b) EDS analysis of thaumasite crystals

Figure 6. SEM-EDS. Sample (P/24/4D) - C/S ratio 2,5 doped with $CaCO_3$, $Ca(OH)_2$ and Na_2SO_4, stored at 5^0C, after 12 months curing.

The crystallization of thaumasite-like forms took place in areas of voids, cracks and gaps. SEM observations of CSH samples (C/S ratio 0,8 with additions of $CaCO_3$, $Ca(OH)_2$ and Na_2SO_4 , stored at 5^0C), in which fibre – like forms were not observed in cracks, gaps and voids, shows CSH phase and local crystallization of portlandite [Figures 7a, 8a], as identified by EDS [Figures 7b, 8b].

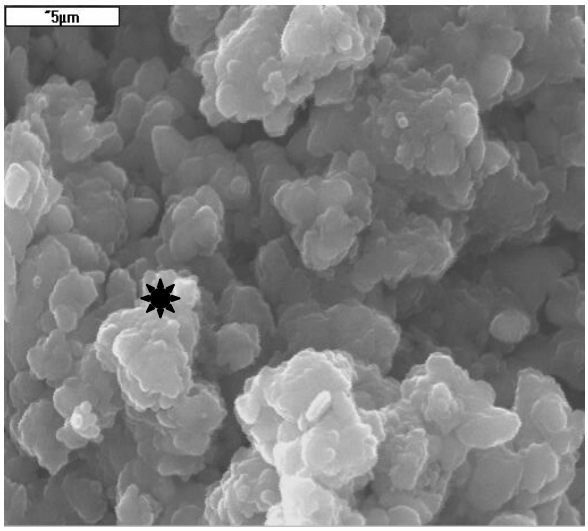

a) CSH phase without any crystallization

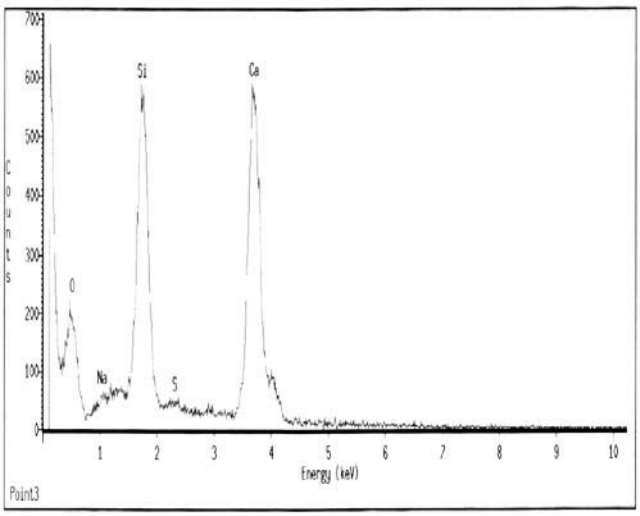

b) EDS analysis of these form

Figure 7. SEM-EDS. Sample (P/C/1D) - C/S ratio 0,8 doped with $CaCO_3$, $Ca(OH)_2$ and Na_2SO_4, stored at 5^0C, after 12 months curing.

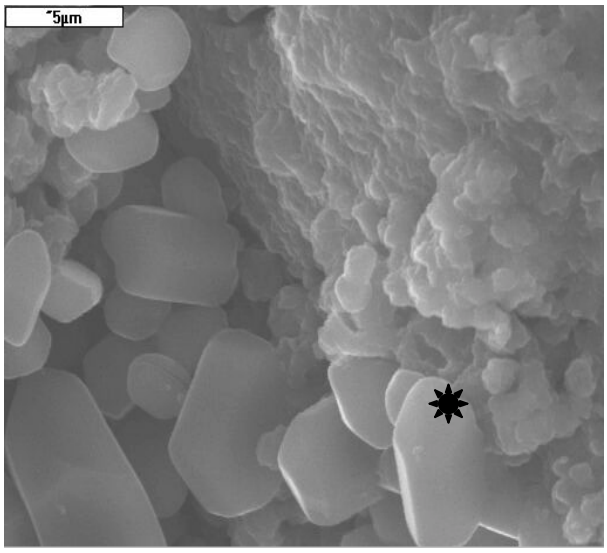

a) Crystallization of portlandite

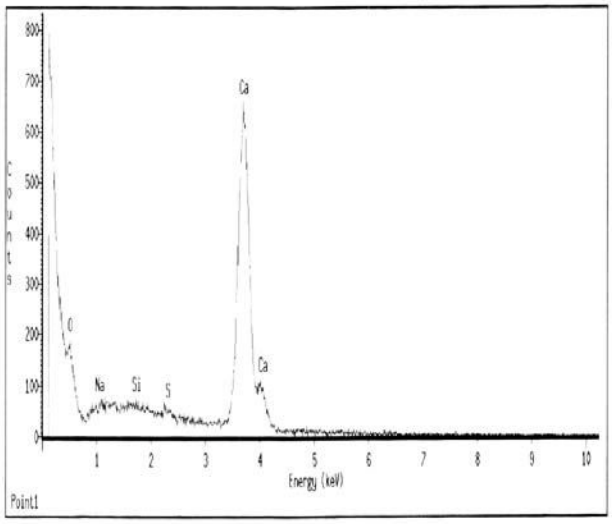

b) EDS analysis of these form

Figure 8. SEM-EDS. Sample (P/24/1D) - C/S ratio 0,8 doped with $CaCO_3$, $Ca(OH)_2$ and Na_2SO_4, stored at 5^0C, after 12 months curing.

The XRD data for the samples cured for 360 days were compared to those for the samples cured at shorter times, 90 and 180 days respectively. The intensities of peaks decreased less or more, the peaks of Na_2SO_4 completely disappeared after 360 days storage at 5^0C. Simultaneously an increase of $CaSO_4 \cdot 2H_2O$ content with time was observed, for the samples with lower C/S ratio. In the samples produced at higher C/S ratio the portlandite residue was observed all the time, while in those with low C/S ratios calcium hydroxide was significantly consumed.

The XRD data in each case indicate the formation of thaumasite [19].

The IR spectroscopy results for the samples cured for 360 days, compared to the control samples, show the analogous changes in the intensity of bands attributed to SO_4^{2-} and OH^- groups from $Ca(OH)_2$ structure as the XRD results.

4. CONCLUSIONS

The synthesised CSH phase, produced in this work was characterised by variable C/S ratio from 0,8 to 2,5. A variety of cements used in concrete production was a circumstance which decided about carrying out the research on the C-S-H of C/S variable in a wide range.

SEM observations confirm the presence of fibre – like forms in CSH of C/S ratio = 1,5; 2,0 and 2,5, doped with $CaCO_3$, $Ca(OH)_2$ and Na_2SO_4 and stored at 5^0C. XRD and EDS analysis proves the thaumasite-like character of these products.

The SEM observations of C-S-H samples show also the consequences of volume changes - cracks and scratches in which thaumasite fibrous forms are deposited. The cracks and scratches appear in samples stored in 5^0C.

The results of XRD analysis show also that in the samples containing CSH doped $CaCO_3$, $Ca(OH)_2$ and Na_2SO_4 and stored in 5^0C the calcite, gypsum and portlandite are detectable apart from the thaumasite.

There are no differences between the two series of samples – one produced initially at ambient temperature and the second synthesized in hydrothermal conditions. Finally, the results presented above seem to indicate that the ettringite is not necessary for the formation of thaumasite.

ACKNOWLEDGEMENTS

The financial support from Faculty of Minerals Science and Ceramics, University of Mining and Metallurgy (grant No 10.10.160.674) is fully acknowledged.

REFERENCES

[1] Neville A. M., “Properties of Concrete”, London 1997
[2] Taylor H. F. W., “Cement chemistry”, Academic Press, London 1990
[3] Oberholster R. E., Van Aardt I. H., Brandt M., “Structure and Performance of Cements”, Appl. Science Publ., s. 363, London 1983
[4] Roy D. M., 8th ICCC Rio de Janeiro, t I, s. 362, 1986
[5] Thaumasite Expert Group “The thaumasite from of sulfate attack: Risks, diagnosis, remedial works and guidance on new construction. Raport of the Thaumasite Expert Group”, DETR, Londyn, 1999
[6] Thaumasite Expert Group “Thaumasite form of sulfate attack”, Concrete Nr 2, s. 37 - 40, 1999
[7] Hobbs D. W., Taylor M. G., “Nature of the thaumasite sulfate attack mechanism in field concrete”, Cement Concrete Research 30, s. 529 - 533, 2000
[8] Hartshorn S., Sims I., “Thaumasite - a brief guide for engineers”, Concrete Nr 10, s. 24 - 27, 1998
[9] Berra M., Baronio G., “Thaumasite in Deteriorated Concretes in Presence of Sulfates”, Concrete Durability sp. 100 - 106, s. 2073 - 2089
[10] Papayianni I., “Durability lessons from the study of old mortars and concretes”, P. K. Mehta Symposium on Durability of Concrete, Nice 1994
[11] Taylor H. F. W., “The chemistry of Cements”, Academic Press, London 1964
[12] Uchikawa H., Proc 9th ICCC, Vol. 1, 797, New Delhi, 1992
[13] Kalousek G. L., J. Am. Ceram. Soc., 40, 74 1957
[14] Nocun-Wczelik W., “Structure and properties of calcium silicate hydrates”, Polish Ceramic Bulletin No 18,1999 (in Polish)
[15] Bensted J., “Scientific background to thaumasite formation in concrete”, World Cement Research 11,1998
[16] Bensted J., Varma S. P., “Studies of Thaumasite”, Sil. Ind. T 2, 1973

[17] Bensted J., Varma S. P., “Studies of thaumasite, part II”, Sil. Ind. T 39, 1974
[18] Krivenko P., “Mineralogical aspects of durability of concretes“, Kurdowski Symposium: Science of Cement and Concrete, Kraków, June 20-21, 2001
[19] Malolepszy J., Mróz R., “The conditions of Thaumasite formation and its role in concrete”, II International Scientific Conference: Quality and Reliability in Building Industry”, Levoca, September 24 – 26, 2001
[20] Rademaker P.D., Reiman V., Zement-Kalk-Gips, 47, 636 1994

NON-DESTRUCTIVE MEASUREMENT OF CHLORIDE DIFFUSION PROFILES IN MORTAR AND CEMENT PASTE SAMPLES USING RADIOTRACER METHOD AND AUTORADIOGRAPHY

M. Manera[1], H.M. Prasser[2], R. C. Perego[3], Z. I. Kolar[3], M. Marroccoli[1] and R. Cioffi[1]

[1]Dipartimento di Ingegneria e Fisica dell`Ambiente, Universita` degli Studi della Basilicata
C.da Macchia Romana, 85100, Potenza, Italy. E-mail: marcomane@libero.it
[2]Environment and Safety Research Institute, Research Center Rossendorf, Postfach 51 01 19,
D- 01314 Dresden, Germany. E-mail: h.m.prasser@fz-rossendorf.de
[3]Department of Radiochemistry, Interfaculty Reactor Institute, Delft University of Technology
Mekelweg 15, 2629 JB, Delft, The Netherlands. E-mail: r.perego@iri.tudelft.nl

ABSTRACT

In this study a radiotracer-based method is applied to follow the chloride transport in mortar and cement paste samples. Portland, blast furnace and limestone cements are used to cast prisms that, after curing, are sliced in 2.5 mm thick samples and then covered with a wax layer on all sides - except one. The samples are then put in contact with a ^{36}Cl-labelled NaCl solution. After a given time the samples are taken out of the solution and, after complete removal of the wax layer, placed on a beta particle sensitive film for the autoradiography. Densitometry, i.e. measurement of the degree of blackening of the film can provide qualitative and quantitative data on the two-dimensional diffusion profile attained.

1. INTRODUCTION

One of the problems affecting the durability of reinforced concrete structures is the corrosion of the steel bars. Normally these are protected from corrosion by a microscopic oxide layer which forms on the surface of the bars due the high alkalinity (pH = 13) of concrete. The protecting layer can disappear due to the carbonation of the surrounding concrete, i.e. the reaction between $Ca(OH)_2$ and CO_2, which causes acidification. Another factor that contributes to the destruction of the film is the reaction with free chloride ions dissolved in the pore water. In the presence of water and oxygen this causes corrosion, due to electrochemical between iron ions, water and oxygen [1]. The source of chlorides in concrete may be internal or external. In the former and less common case, the chlorides are present from the moment of mixing. This is the case if chloride containing mixtures are added to the concrete (e.g. $CaCl_2$ is added to accelerate the setting and hardening), or if seawater or beach aggregates are used in the concrete. Nevertheless the most common source of chloride ions is external. This is in roads and highways in cold countries where de-icing salts are applied. Another situation where chloride ions are abundant is in the marine environment. Here the structures may be situated partly below the sea level and partly above it. The breaking of the waves and the periodic tides gives rise to a situation characterised by cycles of wetting (increasing the amount of the reactant water), and drying (increasing the amount of the reactant oxygen), that form an ideal environment for the corrosion of the steel bars [2][3].

In order to predict the durability of concrete structures it is helpful to evaluate the diffusion of chloride ions in such structures. This is normally done by sample destruction followed by chemical analysis of the portions of interest [4]. In this study a radiotracer-based method is applied to follow the chloride transport in mortar and cement paste samples.

2. EXPERIMENTAL

2.1 Materials and Specimens

2.1.1 Materials

Ordinary Portland Cement (CEM I 32.5 R), Blastfurnace Slag Cement (CEM III/B 42.5 LHHS) and Limestone Cement (CEM II/A-L 42.5 R) were used in making mortars and only Ordinary Portland Cement (CEM I 32.5) was used in making cement paste. The sand used in mortars was 2 mm maximum aggregate size standard sand according to the EN 196/1-ISO 679 norm and the mixing water was demineralized water. Cement, sand and mixing water were at laboratory temperature.
The water/cement ratio was 0.5 and the aggregate /cement ratio was 3.

2.1.2 Test specimen preparation

The preparation of the mortars followed the EN 196/1-ISO 679 norm. The samples, cast in moulds soon after the preparation of the mortar and cement paste, were prisms having dimensions of 40mm x 40mm x 160mm. After 24 hours stored in a wet environment the prisms were demoulded and cured in water for 60 days. After curing, the prisms were sliced in 45mm x 40mm x 2.5mm specimens by means of a diamond saw cooled with water.

A total number of 30 test specimens were produced: 9 mortar specimens for each cement type and 3 cement paste specimens with Portland cement. The mortar and cement paste slices were then smoothed with water on a grinding machine in order to reach a constant thickness all along the specimen and then vacuum saturated with the same water in which they were cured. The specimens were kept under water until their sealing with wax. Each test specimen was coated by dipping for a few seconds in melted wax and then left in a controlled chamber at 20^{o}C to let the coating become hard and not sticky any longer. Once the coating was hard enough the test specimens were taken out of the controlled chamber and the wax was removed from one of their sides by grinding it on sandpaper with water. The prepared specimens were then kept, till the beginning of the test, with the wax-free side in water to prevent evaporation.

2.1.3 Labelled solution preparation

The problem of diffusion of chloride ions arises mainly in structures exposed to saline environment therefore a sodium chloride solution was prepared by dissolving 3.5 g of analytical grade NaCl in 100 ml of distilled water to make up a solution that would produce an equivalent chloride ion concentration to that of sea water. The advantage over seawater is the absence of sulphates, which could react with the tri-calcium aluminates instead of chloride.

Once the sodium chloride solution 3.5% (w/w) was prepared, ^{36}Cl in negligible quantity (^{36}Cl = 0.08% of inactive NaCl) was added as the radioactive tracer. ^{36}Cl is a long-lived radioisotope ($T_{1/2}$ = $3.5 \cdot 10^5$ a) decaying by emitting β^- radiation with a maximal energy of 0.7 MeV. The activity (number of radioactive nuclei in a unit of time) of the solution was 11.5kBq/ml. For each experiment 10 ml of this solution were used, with a total activity of 115 kBq.

2.2 Techniques and procedures

2.2.1 Autoradiography method

Autoradiography is a radiochemical technique that is often applied to physiological and medical studies on living organisms. Nevertheless it also finds large application in non-living systems where a measure of the localisation of the radionuclide tracers is required. Autoradiography is based on the production of an image of the radioactive source on a photographic emulsion, which is a suspension of silver bromide crystals in gelatine. The interaction between the silver bromide and the nuclear radiation produces ionisation of the silver bromide crystals. This provides electrons that are free to travel from one ion to another until they are trapped at defects within the silver bromide crystal structure. At a structural defect a silver ion absorbs the electron and becomes a silver atom. The crystals containing silver atoms become visible after the application of the chemical developer. This reduces all the silver atoms formed to metallic silver, which is characterised by a black colouring. In contrast, the crystals that did not undergo the above-described modification are washed out of the emulsion by the chemical fixer solution. The whole process results in a black-coloured image of the radioactive source [5].

2.2.2 Test procedure

The experiments were performed in 10 glass boxes, each containing three specimens held by a PETG grid to keep the samples separated from each other and suspended vertically in the solution. The right volume (10 ml) of labelled solution was poured into the glass boxes in order to allow contact between the solution and the sample only at the lower side of the sample free of the wax layer. Each box was sealed with a glass cap and two foils of self-sealing Parafilm “M” laboratory film (American National Can) to prevent solution evaporation. Three contact times, during which the specimens were immersed in the labelled solution, were chosen: 14 days, 33 days and 55 days. For each contact time three mortar samples (one for each cement) and one cement paste sample were taken out of the solution and, after removal of the wax layer, placed on a photographic film for the autoradiography. The beta radiation emitted by Cl-36 close to the sample surface interacts with the film emulsion, giving rise to blackening of the film that becomes visible after its development. Darker parts of the image indicate higher Cl-36 i.e. chloride ion concentration in the layer adjacent to the sample surface (Figures 1-2).

Figure 1. Autoradiography of cement mortar after 14, 33 and 55 days in labelled solution

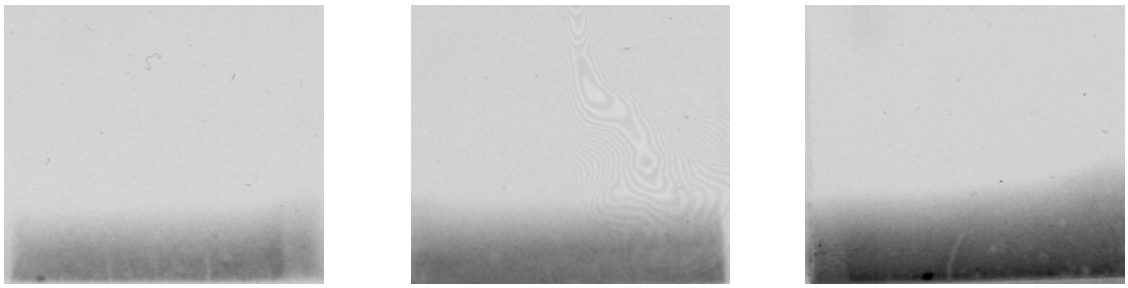

Figure 2. Autoradiography of cement paste after 14, 33 and 55 days in labelled solution

The images produced on the films were analysed as a grey scale using a computerised image process. Calibrating the grey level (degree of blackening) it would be possible to extract quantitative data on the amount of chloride that is diffused in the samples.

3. RESULTS AND DISCUSSION

3.1 Autoradiographic image analysis

By means of the autoradiography method 4 films were produced for each contact time, considering four different exposure time of the same set of samples to the beta particle sensitive film. Each film was scanned by means of a UMAX Mirage 2 scanner according to the scheme reported in Figure. 3.

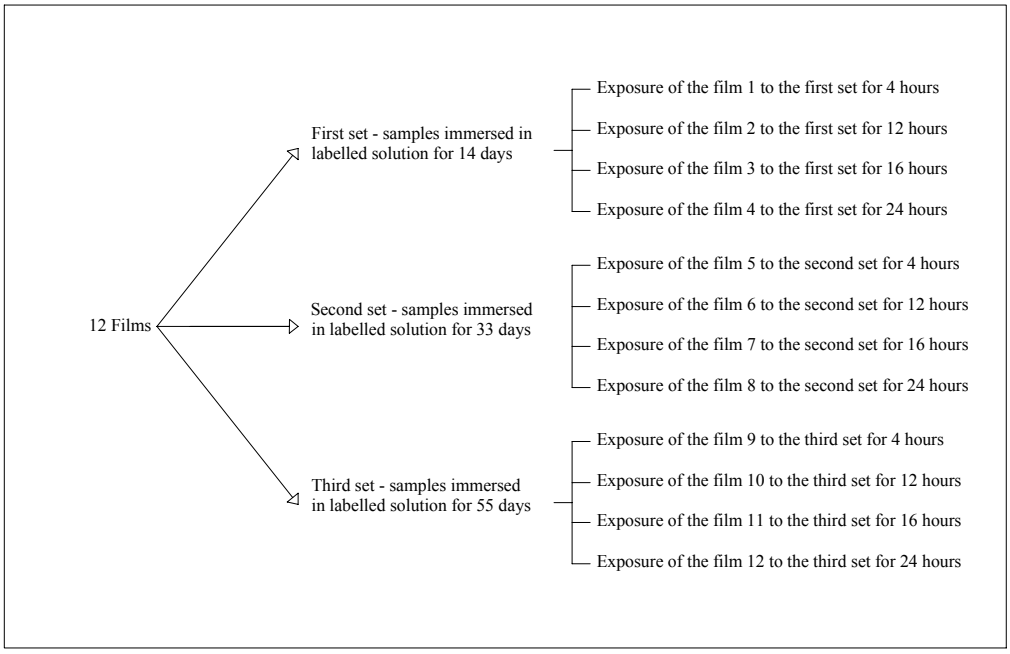

Figure 3. Scheme of the 12 films produced by exposing three set of samples to beta particle sensitive film for four different exposure time

The films were analysed by means of an in-house developed software, that could acquire the autoradiographic images of the samples according to the scale of greys of different intensity and respectively associated to numerical values ranging between 1 and 256.

The images thus produced showed both the different intensity of grey corresponding to the different chloride activity and the penetration depth of the chloride front.

Once the images had been acquired in grey scale, there was the need to find a calibration curve that could associate a value of activity of the penetrated chlorine to each grey value. For this purpose the cement paste sample, immersed in solution for 55 days, was taken as a reference.

The 55 days of immersion in the labelled solution ensured the maximum value of activity (and then the maximum value of grey) reached, while the cement paste ensured a more precise calibration curve owing to the lack of aggregate.

3.2. Calibration curve

3.2.1 Theoretical basis

The grey values are a measure of the reaction (blackening) of the film to the energy absorbed by the film itself, namely the dose.

This energy absorbed by the film (i.e. dose) is proportional to the number of radioactive nuclei decaying in a unit of time (i.e. activity) and to the exposure time of the film to this activity (i.e. to the time that the film is exposed to the radioactive sample). Since the activity is directly proportional to the chloride concentration, it is clear that the dose is a direct measure of the chloride concentration itself. Note, then, that the relative dose is equivalent to the relative concentration. The calibration curve was obtained with a computer program on the following basis:

Given:

$G_{i,j}$ - grey values taken from the calibration images (four images of the cement paste CP sample with different photo exposure time and equal solution exposure i.e. the contact time, preferably the largest solution exposure time)

i - index of the given location (horizontal stripe of averaging) in the image (i.e. different i correspond to different dose rates)

j - index of the applied film exposure time (j = [1..4])

t_j - film exposure time

Unknown:

d_i - dose rate at the given location of cement paste CP

$D_{i,j}$ - exposed dose at the location i of cement paste sample after the film exposure time t_j

For the dose holds:

$$D_{i,j} = t_j \cdot d_i \tag{1}$$

The dose should be a well-defined function of the grey value. Since we believe that a zero grey value corresponds to zero dose, we assume a polynomial:

$$D = \sum_{k=1}^{n_a} a_k \cdot G^k \tag{2}$$

To adapt the coefficients a_k we can use all available measuring information $G_{i,j}$ and t_i. Unfortunately, D is unknown. For an optimal approximation we apply the "minimum of the sum of the error squares" criterion:

$$\sum_{i,j} \left(t_j \cdot d_i - \sum_{k=1}^{n_a} a_k G_{i,j}^k \right)^2 \rightarrow \min \tag{3}$$

Since d_i is unknown, we must treat these values as variables during the minimum search according to (3), i.e. they have the same quality as the coefficients a_k. To linearize (3), we must introduce a new function $T_{k,j}$:

$$T_{k,j} = \begin{cases} t_j & \text{if } k = i \\ 0 & \text{if } k \neq i \end{cases} \tag{4}$$

With this substitution, eq. (3) takes the form:

$$\Psi = \sum_{i,j} \left(\sum_{k=1}^{n_d} d_k \cdot T_{k,j} - \sum_{k=1}^{n_a} a_k G_{i,j}^k \right)^2 \rightarrow \min \tag{5}$$

To find the minimum, derivatives of eq. (5) have to be found:

$$\frac{\partial \Psi}{\partial d_m} = \sum_{i,j} T_{m,j} \cdot \left(\sum_{k=1}^{n_d} d_k \cdot T_{k,j} - \sum_{k=1}^{n_a} a_k G_{i,j}^k \right) = 0 \tag{6}$$

$$\frac{\partial \Psi}{\partial a_m} = \sum_{i,j} G_{i,j}^m \cdot \left(\sum_{k=1}^{n_d} d_k \cdot T_{k,j} - \sum_{k=1}^{n_a} a_k G_{i,j}^k \right) = 0 \tag{7}$$

After changing the order of the summations in (6) we get:

$$\frac{\partial \Psi}{\partial d_m} = \sum_{k=1}^{n_d} d_k \cdot \sum_j T_{m,j} \cdot T_{k,j} - \sum_{k=1}^{n_a} a_k \cdot \sum_{i,j} T_{m,j} \cdot G_{i,j}^k = 0 \tag{8}$$

Here, according to (4) all products of $T_{m,j} \cdot T_{k,j}$ for $k \neq m$ are equal zero. The same is true for $T_{m,j} \cdot G_{i,j}$, when $i \neq m$:

$$\frac{\partial \Psi}{\partial d_m} = d_m \sum_j t_j^2 - \sum_{k=1}^{n_a} a_k \cdot \sum_j t_j \cdot G_{m,j}^k = 0 \tag{9}$$

After changing the order of the summations in (7) we get:

$$\frac{\partial \Psi}{\partial a_m} = \sum_{k=1}^{n_d} d_k \sum_j G_{k,j}^m \cdot t_j - \sum_{k=1}^{n_a} a_k \sum_{i,j} G_{i,j}^m \cdot G_{i,j}^k = 0 \tag{10}$$

The linear system of equations to be solved looks like follows:

$$\begin{pmatrix}
\sum_j t_j^2 & 0 & \cdots & 0 & \sum_j t_j G_{1,j} & \sum_j t_j G_{1,j}^2 & \cdots & \sum_j t_j G_{1,j}^{n_a} \\
0 & \sum_j t_j^2 & \cdots & 0 & \sum_j t_j G_{2,j} & \sum_j t_j G_{2,j}^2 & \cdots & \sum_j t_j G_{2,j}^{n_a} \\
\vdots & \vdots & & \vdots & \vdots & \vdots & & \vdots \\
0 & 0 & \cdots & \sum_j t_j^2 & \sum_j t_j G_{n_d,j} & \sum_j t_j G_{n_d,j}^2 & \cdots & \sum_j t_j G_{n_d,j}^{n_a} \\
\sum_j t_j G_{1,j} & \sum_j t_j G_{2,j} & \cdots & \sum_j t_j G_{n_d,j} & \sum_{i,j} G_{i,j}^2 & \sum_{i,j} G_{i,j}^3 & \cdots & \sum_{i,j} G_{i,j}^{n_a+1} \\
\sum_j t_j G_{1,j}^2 & \sum_j t_j G_{2,j}^2 & \cdots & \sum_j t_j G_{n_d,j}^2 & \sum_{i,j} G_{i,j}^3 & \sum_{i,j} G_{i,j}^4 & \cdots & \sum_{i,j} G_{i,j}^{n_a+2} \\
\vdots & \vdots & & \vdots & \vdots & \vdots & & \vdots \\
\sum_j t_j G_{1,j}^{n_a} & \sum_j t_j G_{2,j}^{n_a} & \cdots & \sum_j t_j G_{n_d,j}^{n_a} & \sum_{i,j} G_{i,j}^{n_a+1} & \sum_{i,j} G_{i,j}^{n_a+2} & \cdots & \sum_{i,j} G_{i,j}^{2n_a}
\end{pmatrix} \cdot \begin{pmatrix} d_1 \\ d_2 \\ \vdots \\ d_{n_d} \\ a_1 \\ a_2 \\ \vdots \\ a_{n_a} \end{pmatrix} = \begin{pmatrix} 0 \\ 0 \\ \vdots \\ 0 \\ 0 \\ 0 \\ \vdots \\ 0 \end{pmatrix} \tag{11}$$

The determinant of the main matrix is zero. Since the constant vector is also zero, the system is underdetermined and one of the variables can be freely chosen. This reduces the order by 1. I choose $d_1 = 1$. This means that the result will be not the absolute dose but the dose relative to a chosen value (in our case to d_1). In this case, the system reduces to:

$$\begin{pmatrix} \sum_j t_j^2 & 0 & . & 0 & \sum_j t_j G_{2,j} & \sum_j t_j G_{2,j}^2 & . & . & \sum_j t_j G_{2,j}^{n_a} \\ 0 & \sum_j t_j^2 & . & . & . & . & & & . \\ . & . & & . & . & . & & & . \\ 0 & 0 & . & \sum_j t_j^2 & \sum_j t_j G_{n_d,j} & \sum_j t_j G_{n_d,j}^2 & . & . & \sum_j t_j G_{n_d,j}^{n_a} \\ \sum_j t_j G_{2,j} & . & . & \sum_j t_j G_{n_a,j} & \sum_{i,j} G_{i,j}^2 & \sum_{i,j} G_{i,j}^3 & . & . & \sum_{i,j} G_{i,j}^{n_a+1} \\ \sum_j t_j G_{2,j}^2 & . & . & \sum_j t_j G_{n_a,j}^2 & \sum_{i,j} G_{i,j}^3 & \sum_{i,j} G_{i,j}^4 & . & . & \sum_{i,j} G_{i,j}^{n_a+2} \\ . & & & . & . & . & & & . \\ . & & & . & . & . & & & . \\ \sum_j t_j G_{2,j}^{n_a} & . & . & \sum_j t_j G_{n_d,j}^{n_a} & \sum_{i,j} G_{i,j}^{n_a+1} & \sum_{i,j} G_{i,j}^{n_a+2} & . & . & \sum_{i,j} G_{i,j}^{2n_a} \end{pmatrix} \cdot \begin{pmatrix} d_2 \\ . \\ . \\ d_{n_d} \\ a_1 \\ a_2 \\ . \\ . \\ a_{n_a} \end{pmatrix} = \begin{pmatrix} 0 \\ 0 \\ 0 \\ 0 \\ -\sum_j t_j G_{1,j} \\ -\sum_j t_j G_{1,j}^2 \\ . \\ . \\ -\sum_j t_j G_{1,j}^{n_a} \end{pmatrix} \qquad (12)$$

This system can be solved. In the result the relative dose rates d_2 - d_{nd} and the coefficients for the polynomial approximation are obtained. The dose rates are related to the arbitrarily chosen value for d_1 (i.e. $d = 1$).

3.2.2. Discussion

In the following graph the result of the polynomial approximation according eq. (2) for an order of 3 (three coefficients) is shown (Figure 4). From the image of sample CP, 125 successive pixel lines starting from line number 20 (maximum exposure) were evaluated. The points at the graph are products of relative dose rate multiplied by the photographic exposure time plotted over the corresponding grey value, i.e. $D_{i,j} = t_j \cdot d_i = f(G_{i,j})$, where d_i is a result of solving the system of eq. (12), and $d_1 = 1$.

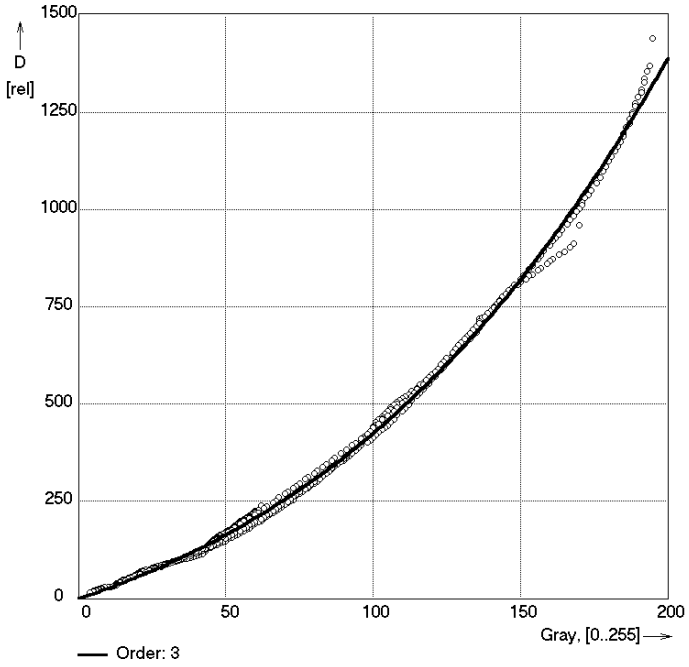

Figure 4. Polynomial approximation for an order of three

The influence of the order is illustrated in the following figure:

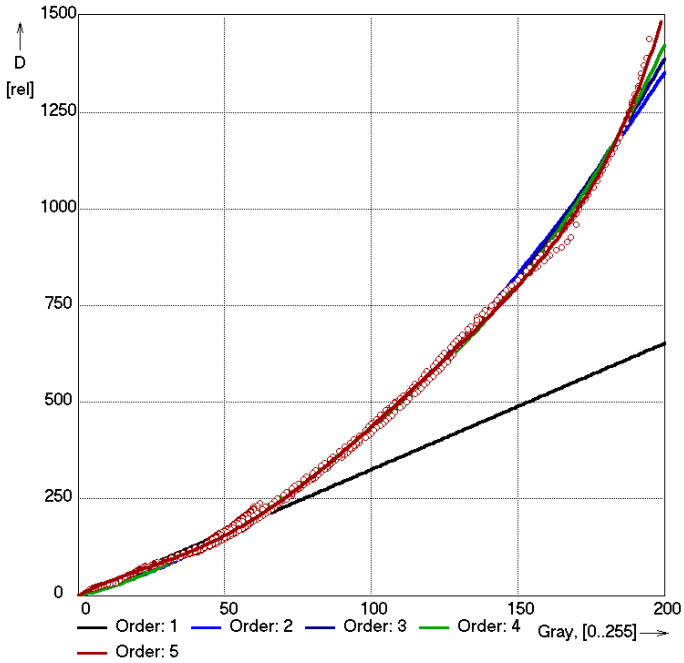

Figure 5. Different influence of the order

Here, the points are taken from the result for fifth order, just the lines are corresponding to different orders. Since the correction of the dose rates for the individual points is done applying the calculated values of d_i, the location of the individual measuring points at the plot differs for different orders (Figure 6).

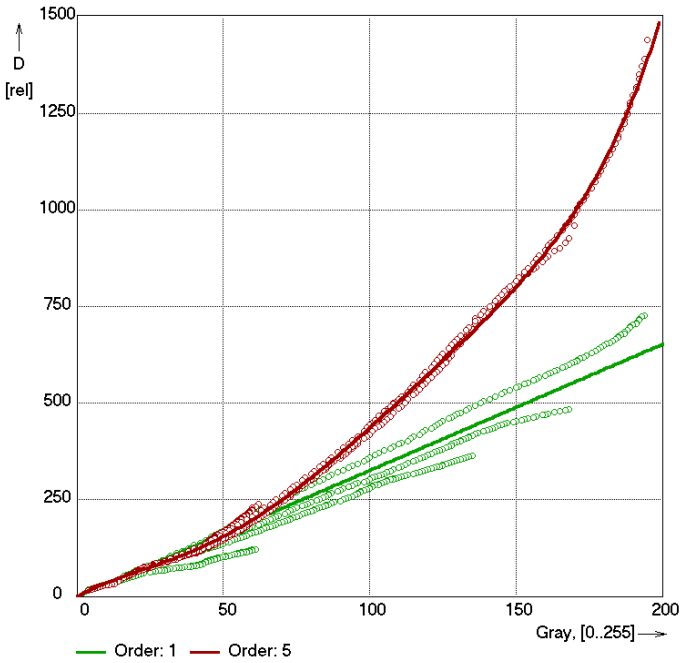

Figure 6. Comparison between order 1 and order 5

3.3 Results

The resulting relative dose curve (relative concentration curve) could be fitted with a polynomial of the 5th order. The equation obtained, linking the relative dose (or relative concentration) to the grey values, can be used now for all the other samples in order to get directly the relative concentration

curve, once the grey values are known by means of the software already mentioned. Therefore, for the cement paste sample taken as reference, the graph relating the relative dose to the penetration depth of the chloride can be seen in Figure 7.

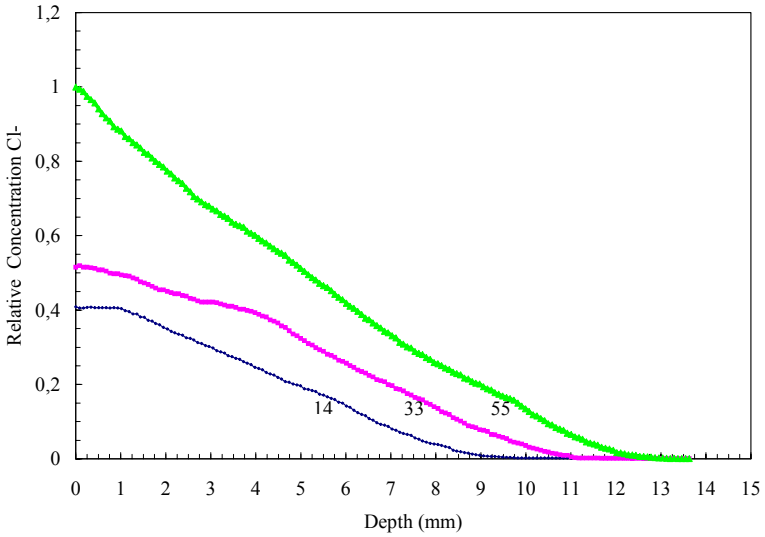

Figure 7. Influence of exposure time on chloride ingress. The exposure time in days is marked on the curves

A diffusion coefficient of about $2*10^{-12}$ m^2/s corresponds to the curves represented in the above graph (Figure 7).

4. CONCLUSIONS

The use of a radioactive chloride isotope offers the possibility of performing non-destructive measurements of the evolving chloride distribution within the samples locally exposed to aqueous sodium chloride solution (3.5 % NaCl). The present method has a number of advantages if compared with the current methods for chloride analysis, namely (1) it is a non-destructive technique; (2) it provides two-dimensional chloride diffusion profiles; (3) the spatial resolution is less then 1 mm; (4) it offers the possibility of using small samples because of high spatial resolution i.e. short diffusion lengths are sufficient; (5) it is less labour intensive as compared with other methods; (6) the developed autoradiographic films remain available for further investigations and for placing on document files.

REFERENCES

[1] Neville, A.M. Properties of concrete. 4th and final ed. London: Addison Wesley Longman Limited 1995.
[2] Papadakis, V.G., Fardis, M.N. and Vayenas, C.G. Chemical Engineering Science, vol.51 (4), 1996, pp.505-513.
[3] Frey, R., Balogh, T. and Balázs, G.L. Kinetic method to analyse chloride diffusion in various concretes, Cement and Concrete Research, vol.24 (5), 1994, pp.863-873.
[4] BS 1881:Part 6:1971, Methods of testing concrete, British Standards Institute, 1971.
[5] L'Annunziata, M.F. Radionuclide Tracers. Their detection and measurement, International Atomic Agency Vienna, Austria : Academic Press Harcourt Brace Jovanovich, 1987, p.321.

NON-DESTRUCTIVE MEASUREMENT OF CHLORIDE DIFFUSION PROFILES IN MORTAR AND CEMENT PASTE SAMPLES USING RADIOTRACER METHOD AND AUTORADIOGRAPHY

M. Manera[1], H.M. Prasser[2], R. C. Perego[3], Z. I. Kolar[3], M. Marroccoli[1] and R. Cioffi[1]

[1]Dipartimento di Ingegneria e Fisica dell`Ambiente, Universita` degli Studi della Basilicata C.da Macchia Romana, 85100, Potenza, Italy. E-mail: marcomane@libero.it
[2]Environment and Safety Research Institute, Research Center Rossendorf, Postfach 51 01 19, D- 01314 Dresden, Germany. E-mail: h.m.prasser@fz-rossendorf.de
[3]Department of Radiochemistry, Interfaculty Reactor Institute, Delft University of Technology Mekelweg 15, 2629 JB, Delft, The Netherlands. E-mail: r.perego@iri.tudelft.nl

Marco Manera

Affiliation:	Università degli Studi della Basilicata, Italy.
E-mail:	marcomane@libero.it
Contact details:	D.I.F.A. Dipartimento di Ingegneria e Fisica dell`Ambiente, Applied Chemistry and Materials Technology group, Universita` degli Studi della Basilicata, C.da Macchia Romana, 85100, Potenza, Italy.

THE DISPERSING MECHANISM AND APPLICATIONS OF POLYCARBOXYLATE-BASED SUPERPLASTICIZERS

Tomomi Sugiyama[1], Akira Ohta[1] and Taketo Uomoto[2]

[1]NMB Co., Ltd. Central Research Labs, Chigasaki, Japan. E-mail: t.sugiyama@nmb-pbk.co.jp
[2]The university of Tokyo, Institute of Industrial Science, Tokyo, Japan.

ABSTRACT

The demand for concrete that uses superplasticizer has increased in recent year, accompanying the diversification and the advances of concrete technology in the field of civil engineering. The most important superplasticizers are those that containing polycarboxylate-based dispersants (PCs) as their main component. The superplasticizers exhibit high dispersibility at low dosages and provide excellent slump retention. Much has been done on the adsorption and the dispersing properties of PC-based superplasticizers.

In this present paper, we studied 1) the relationship between the chemical structure of PC and dispersibility or dispersibility retention, and 2) the adsorption property of PC on inorganic fine particles such as cement particles. Furthermore, we describe some applications of PC-based superplasticizers.

1. INTRODUCTION

In recent years, with the expansion of the scale and application range of concrete construction, concomitantly new materials and new ways of execution have been developed. Therefore, features like high flowability, high strength, high durability, etc. were also required for performance. To satisfy such demands, chemical admixtures are essential. The importance of superplasticizers that have a high water reducing effect and good flowability retention is especially great

There are various types of dispersants such as β-naphthalene sulfonate formalin condensate (NS), melamine sulfonate formalin condensate (MS), aromatic aminosulfonic acid polymers (AS) and polycarboxylate-based polymers (PC), etc. as the main components of superplasticizers.

Especially, PCs draw attention as main components of superplasticizers, because they have high dispersibility at small dosage, and it is possible even to improve dispersibility and dispersibility retention by controlling the molecular structure.

In this paper, we focused on PCs as the main components of superplasticizers. We investigated the relationship between chemical structure and dispersibility or dispersibility retention. Furthermore, we studied the adsorption property of PC on inorganic fine particles.

Proceedings of the 11th International Congress on the Chemistry of Cement (ICCC)
'Cement's Contribution to the Development in the 21st Century'
Hosted by: The Cement and Concrete Institute of South Africa
CD-ROM produced by: Document Transformation Technologies
11 - 16 May 2003, Durban, South Africa
ISBN Number: 0-9584085-8-0
Editors: Dr G. Grieve and G. Owens
Congress Organised by: Event Dynamics

2. EXPERIMENT

2.1 Materials

2.1.1 Dispersant

Polycarboxylate-based dispersants (acrylic acid-based: PC-1, 2, 3 and 4), a dispersing component in polycarboxylate-based superplasticizers, were used. Figure 1 shows the chemical structures and monomer ratio of PC polymers.

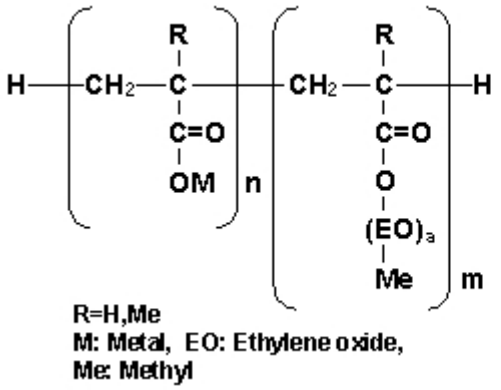

Polymer	Molar ratio		Side chain length (a)	Molecular weight
	n	m		
PC-1	2	1	12	36,000
PC-2	5	1	25	28,000
PC-3	3	1	25	26,000
PC-4	2	1	25	23,000

Figure 1. Chemical structure and monomer ratio of PC polymers

2.1.2 Inorganic fine particles

Ordinary Portland cement, two types of blast furnace slag (BF: specific surface area: 4000 and 10000 cm^2/g) and three types of limestone powders (LS: specific surface area: 4700, 11000 and 20000 cm^2/g) were used. Table 1 shows the chemical composition of the fine particles.

Table 1. Specific surface area and chemical compornents of fine particles

Fine Particles		Specific gravity	Specific * surface area	ig. loss	SiO_2	Al_2O_3	Fe_2O_3	CaO	MgO	SO_3	$CaCO_3$
		g/cm^3	cm^2/g	Mass %							
Cement	OPC	3.15	3160	0.6	21.6	5.3	2.3	64.5	2.1	1.8	-
Blast furnace slag	BF-4000	2.90	4110	-	32.1	13.2	0.2	42.5	6.6	2.1	-
	BF-10000	2.90	9800	-	32.6	12.9	0.2	42.6	6.6	2.0	-
Limestone powder	LS-4700	2.79	4730	-	0.5	0.1	0.1	54.9	0.5	0.0	98.0
	LS-11000	2.77	10970	-	2.7	0.2	0.2	53.3	0.9	0.0	95.1
	LS-20000	2.77	18180	-	1.7	0.1	0.2	54.0	0.8	0.0	96.3

* by Blaine method

2.2 Experimental method

2.2.1 Adsorbed amount

Paste with Water/Powder = 35% was mixed for 3 minutes with an ASTM mortar mixer. A suction filter filtered off the liquid phase. The organic carbon content in the filtrate was determined with a total organic carbon analyser (Shimadzu TOC 5000). The amount of dispersant adsorbed onto the fine particles (apparent adsorbed amount) was calculated by subtracting the dispersant amount calculated from the carbon content in the filtrate, from the dosage of dispersant.

The number of adsorbed PC molecules was estimated by calculating the adsorbed amount per unit area based on the BET specific surface area value, and subtracting the Avogadro number from the molecular weight of the dispersant polymer.

2.2.2 Measurement of root mean square radius (RMS radius)
RMS radius was measured by a light scattering instrument (DAWN-F; Wyatt Technology) connected to a GPC system. Tests were conducted in neutral and alkali (pH=11.0 by NaOH) environments.

2.2.3 Specific surface area
We produced plain paste and paste containing PC-3 at the dosage of 0.15% of powder weight, with W/C = 35%. Three minutes after the fine particles contacted the water, the paste was dispersed in acetone to stop further hydration. The liquid phase was filtered off with a suction filter and washed with acetone several times, then dried for 24 hours at 40℃ to prepare specimens.

The specific surface area by the BET method was found for the processed specimens and non-hydrated fine particles from measurements with a gas-flow automatic specific surface area measuring device (Shimadzu Flowsorb 2300).

3. RESULTS AND DISCUTIONS

3.1 Relation between chemical structure and dispersing effect

3.1.1 Adsorbed amount of PC polymers on the surface of OPC
The relation of dosage and adsorbed amount on the surfacw of OPC of PC polymers are shown in Figure 2. The adsorbed amount of PC-1 to 3 tended to increase as dosage of PC polymers increased. However, the adsorbed amount of PC-4 did not increase so much when dosage increased.

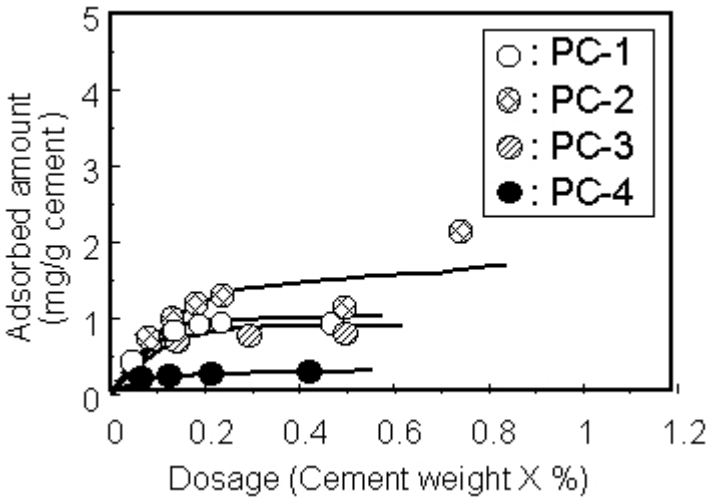

Figure 2. Relation between adsorbed amount and dosage

3.1.2 RMS radius of PC polymers
Figure 3 shows the RMS radius of PC polymers in neutral and alkali environments. In an alkali environment, the RMS radius of PC-2 and 3 which have low graft density increased compared with a neutral environment. However, in neutral and alkali environments, the RMS radius of PC-1 and PC-4 which have high graft density did not differ very much.

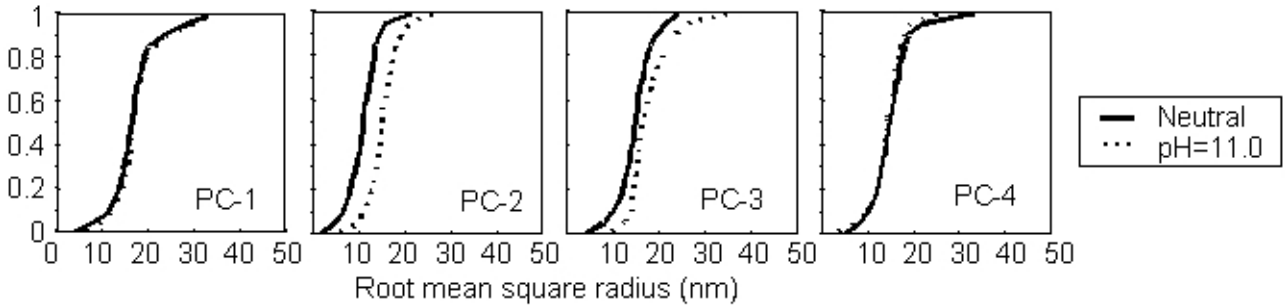

Figure 3. Cumulative RMS radious distribution

3.1.3 Dispersibility and dispersibility retention of PC polymers

Figure 4a) shows the relationship between the dosage and dispersibility in OPC mortar. In the figure, 100% on Y-axis indicates the flowability of plain mortar. The flowability of PC polymer modified mortar increased as the dosage increased. The flowability of PC-2 (long graft length, small number of grafts) increased most.

Figure 4b) shows the change in flowability over time. The flowability of mortar containing PC-4 does not change immediately after mixing and retains it at the age of 60 minutes. This is attributed to structural characteristics (long graft length, large number of grafts) of the PC polymer.

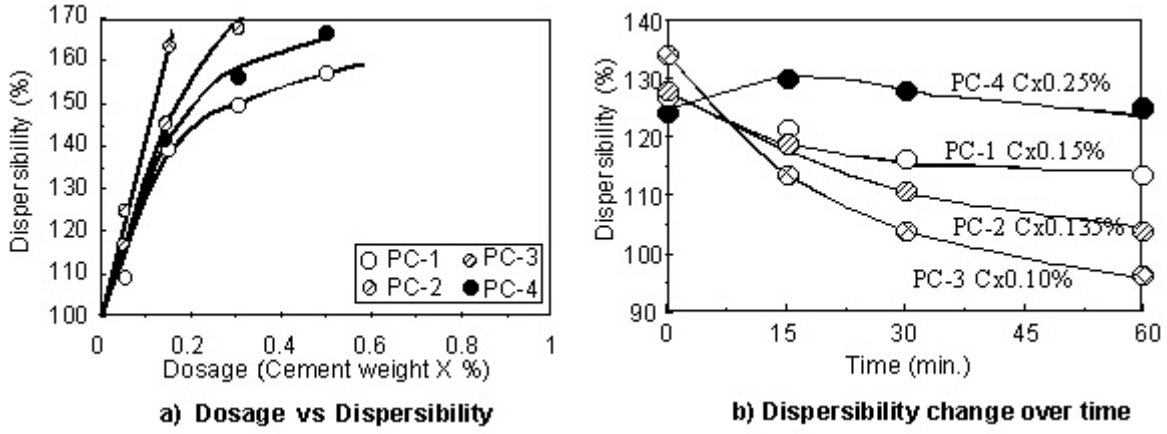

Figure 4. Dispersibility and dispersibility retention of PC polymers

3.1.4 Structural factors causing high dispersibility and long retention

Based on these results, Table 2 shows the structural factors of polymers in relation to dispersibility and dispersibility retention. In cases of low dispersibility and short dispersibility retention, the trunk polymer is long, the graft polymers are short, and the relative number of grafts is large. In the event of high dispersibility, the trunk polymer is short, the graft polymers are long, and the relative number of grafts is small. In cases of long dispersibility retention, the trunk polymer is even shorter, the graft polymers are long, and the relative number of grafts is large.

Table 2. Structural factors causing high and long dispersibility retention

Stractural factor / Dispersibility	Relative chain lendth of trunk plymer	Relative graft length	Relative number of grafts
Low dispersibility and short dispersibility retntion	Long	short	Large
High dispersibility	Short	Long	Small
Long dispersibility retention	Shorter	Long	Large

As shown in Table 2, we can control dispersibility and its retention immediately after mixing by varying the balance of length of the trunk polymer and length of grafts with regard to their quantitative ratio.

3.2 Adsorption properties of PC polymers on inorganic fine particles

3.2.1 Molecular size of PC polymer

The size of the PC-3, which is the general type of PC polymers was calculated based on the chemical structure and molecular weight of the PC polymer. The length of C-C-C in the main chain was assumed to be 2.51Å, which is the maximum stretched length of 3 carbon atoms according to the literature [4]. The length of an ethylene glycol side chain, according to the literature [4], is 19.5Å for a 7-unit chain elongated in a stable conformation. The length of the trunk polymer when stretched to its maximum length was calculated to be 20 nm, with a side chain length of 7 nm (Figure 5 (a)) by Figure 1 (n+m=70).

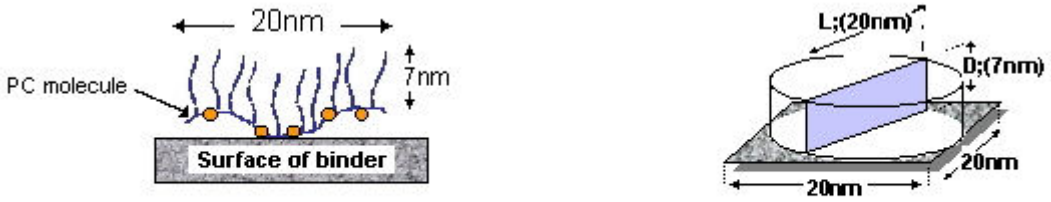

a) Stable conformation on surface

b) Effective thermodynamic volume

Figure 5. Stable conformation and thermodynamic effective volume of PC-3

When PC-3 is adsorbed onto the particle surface of the cement material, most side chains face into the water. The size of the dispersant at that time is presumed to be as shown in Figure 5 (a). The volume occupied by the molecule when it freely moves is equivalent to a column 7 nm in thickness and 20 nm in diameter: the effective thermodynamical volume of the column is equivalent to the volume of a cylinder with a diameter of 20 nm and a height of 7 nm (Figure 5 (b)) [5]. Due to the size of the molecule stretched to its full length, based on the molecular weight of the polycarboxylate-based dispersant, it is considered that one dispersant polymer occupies the volume of a cylinder with 20 nm in diameter and 7 nm high, excluding other molecules. Thus, one adsorbed polymer occupies 314nm^2 and at saturation adsorption the density of adsorption is believed to be one molecule of dispersing polymer molecule, allowing for packing considerations, per 400 nm^2 of the binding material surface (Figure 5 (b))[6].

3.2.2 Specific surface area of various inorganic fine particles

Table 3 shows the results of specific surface area measurment of particles by the BET method after water contact. The specific surface area of OPC before water contact was 0.71 m^2/g. However, three minutes after water contact, the specific surface area of plain OPC (without PC-3) increased to 1.04 m^2/g, that is, 1.5 times; and that of OPC containing PC-3 increased up to 1.29 m^2/g, that is, 1.8 times of that of non-hydrated OPC. On the other hand, the specific surface areas of less active BF and LS do not increase due to water contact.

Table 3. Specific surface area of several fine particles

Inorganic fine particles		Specific surface area		
		Before contact with water	3min. after from contact with water	
			Without PC	With PC
Cement	OPC	0.71	1.04	1.29
Blast furnace slag	BF-4000	0.87	0.89	0.90
	BF-10000	2.37	2.40	2.42
Lime-stone powder	LS-4700	1.03	1.04	1.03
	LS-11000	2.45	2.44	2.46
	LS-20000	4.06	4.07	4.08

3.2.3 Amount of PC-3 adsorbed on various inorganic fine particles

Table 4 shows the measurements of adsorption amount converted into unit weight and unit surface area, to various binding materials when the dosage of dispersing agent was fixed at 0.15% of the mass of binding material. In this paper, adsorption amount is related to the specific surface area after water contact when PC-3 was the fine powder.

3.2.4 Adsorbed number and occupied area of PC-3

Based on the adsorbed amount per unit surface area, and the molecular weight of the dispersant, a number of adsorbed PC-3 molecules per unit area of fine particles were calculated.

$$A = B / Mw \times N_A \quad (1)$$

Where A: adsorbed number of PC-3 per unit area
B: adsorbed amount of PC-3 per unit area
N_A: Avogadro number = 6.02×10^{23}
Mw: Weight-average molecular weight

Results are given in Table 4. The numbers of dispersant molecules adsorbed per unit area varied with the type of binding material. Adsorbed number on the unit surface area differs with the type of binding materials and the number of PC-3 per 100nm^2 surface area of OPC and BF are almost equal to 1.5, while that of LS is 0.8.

Table 4. Adsorbed amount of PC-3 on various fine particles

Inorganic fine particles		Adsorbed amount per unit weight (mg/g)	Adsorbed amount per unit *1 area (mg/cm^2)	Adsorbed *1 number (N/100nm^2)	Area occupied per molecule (nm^2)
Cement	OPC	0.84	0.65	1.51	66.2
Blast furnace slag	BF-4000	0.70	0.78	1.81	55.2
	BF-10000	1.25	0.52	1.21	82.6
Limestone powder	LS-4700	0.38	0.37	0.86	116.3
	LS-11000	0.91	0.37	0.86	116.3
	LS-20000	1.48	0.36	0.83	120.5

*1 Specific surface area of contact with water including PA

$$W=100/A$$

Where W: occupied area
A: adsorbed number of PC-3 per 100nm^2

Results are given in Table 4. In OPC and BF, occupied area per PC-3 molecule is approximately 70 nm^2 but in LS, this area is approximately 120 nm^2.

3.2.5 Adsorbed conformation of PC-3 on the surface of various fine particles

When PC-3 extends to full length, the length of the main chain is approximately 20 nm: one molecule of PC-3 therefore occupies an area of 314 nm^2. However, we presumed that real fine particles form fractal surface structures, and the adsorbing form of PC-3 cannot conform to it and consequently, requires a larger area.

On the contrary, the occupied area of one PC-3 molecule in the case of OPC and BF is approximately 70 nm^2, and in the case of LS is approximately 120 nm^2. If it is presumed that they

adsorb, the diameters of their thermodynamically effective volume are approximately 9nm and 12nm, respectively.

It was previously reported that the measurement results of the root mean square (RMS) radius of the molecule by a light scattering method indicates that the PC-3 polymer shrinks by about 60% as the sulfate ion concentration increases [7].

However, the length of PC-3 main chain is reduced by OPC and BF to 45% of its original length, and shrunk to 60% by LS, which does not contain sulfate ions. The reasons for the shrinkage of the polymer due to the effects of sulfate ions or other factors that reduce the thermo-mechanical effective volume are suggested, as follows:

- As seen in Figure 6 (b), the thermodynamically effective volumes of PC-3 overlap.
- As seen in Figure 6 (c), the thermodynamically effective volume of PC-3 is pressed, and PC-3 absorbs in an elongated form.

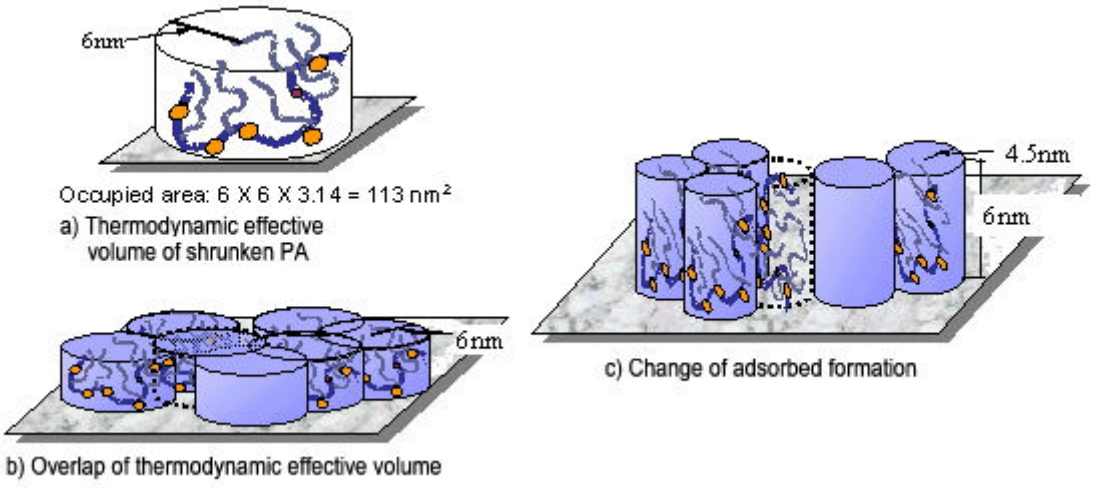

Figure 6. Various adsorbed configurations of PC-3

4. APPLICATIONS OF PC POLYMERS IN CONCRETE

Based on these mechanisms, we can control the dispersibility and dispersibility retention of concrete containing PC polymer based superplasticizers by controlling the balance of the length of the trunk polymer and the length of grafts.

We show two application examples of PC-based superplasticizer in concrete. One relates to high flowable concrete, using low heat Portland cement and limestone powder, another to ultra-high strength concrete using low heat Portland cement and silica fume.

4.1 High flowable concrete

Showing a demand performance and a mixing proportion in Table 5. To satisfy the demand performance, superplasticizer (SP-1) that combined PC-3 that shows high dispersion and PC-4 that has good dispersion maintenance was used.

Table 5. Demand performance and mixing proportion of high flowable concrete

Demand performance		Mixing proportion						
Slump Flow immediately after mixing	Slump flow after 90 min.	W/C (%)	s/a (%)	Unit weight (kg/m3)				
				Water	Cement	Limestone powder	Sand	Coarse aggregate
65 ± 5 cm	65 ± 5 cm	45	49	165	367	150	821	853

The change of concrete flow with time is shown in Figure 7. It is clear from Figure 7 that it becomes possible to retain high dispersion for a long time by combining the dispersion ability of PC-3 and the dispersion maintenance ability of PC-4.

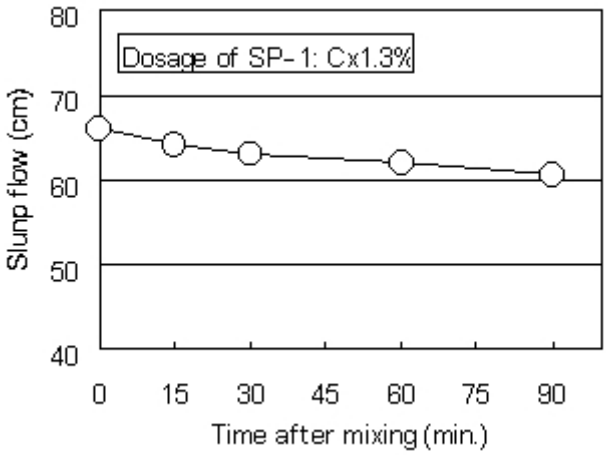

Figure 7. Change of slump flow

4.2 Ultra high strength concrete

Demand performance and mix proportions are shown in Table 6. In this study, to get ultra-high dispersibility, we used superplasticizer (SP-2) combined with PC-2 as they gave the highest dispersibility, and dispersibility improvement.

Table 6. Demand performance and mixing proportion of ultra-high strength concrete

Demand performance		Mixing proportion						
Slump Flow immediately after mixing	Compressive strength	W/C (%)	s/a (%)	Unit weight (kg/m3)				
				Water	Cement	Silica fume	Sand	Coarse aggregate
65 ± 5 cm	> 130N/mm^2 (91 days)	16	32.9	160	900	100	336	926

The concrete test results are shown in Figure 8. Based on these results, mixing of concrete with a very low water cement ratio, such as 16%, becomes possible by using a superplasticizer with a high

dispersing effect. As a result, the production of the ultra-high strength concrete with compressive strength exceeding 130 N/mm^2 at 91 days was possible.

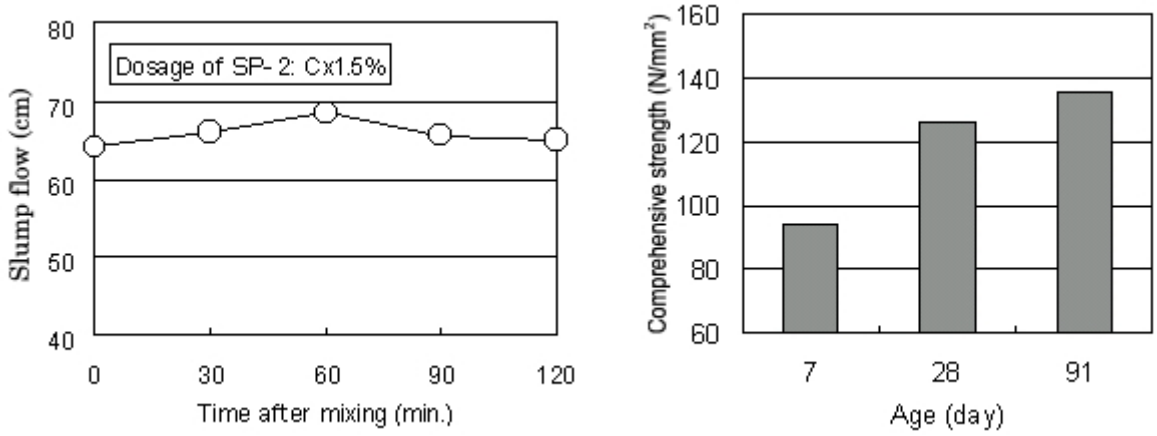

Figure 8. Concrete test results of ultra-high strength concrete

5. CONCLUSIONS

The findings from our research are as follows:

- Varying the balance between length of trunk polymer and length of grafts of their quantitative ratio can control dispersibility and its retention immediately after mixing.

- The appropriate area of PC calculated from measured values is 1/3 to 1/5 of the value that is calculated from the value of the polymer in its fully extended configuration. Therefore PC polymer is considered to be adsorbed in contracted form. In addition, it is suggested that the contraction of polymer occurs due to effects other than sulfate ion, suggesting a decrease in thermo-mechanical effective volume that is not due to the contraction of the polymer.

REFERENCES

[1] Moriya, Y. and Ohta A., The Trend of Air Entraining and High-Range Water Reducing Agents, J. Soc. Mat. Sci., Vol.43, No.491, 1994, pp.919-929

[2] Yoshioka, K., Sakai, E. and Daimon, M., Role of Steric Hindrance Effects of Superplasticizer on the Dispersibility of Cement Particles, Proceedings of the Japan Concrete Institute, Vol.19, No.1, 1997, pp.335-340

[3] Sato, T. and Ruch, R., Surfactant Science Series Vol.9, Stabilization of Colloidal Dispersion by Polymer Adsorption, Marcel Dekker, N.Y., 1980 and reference cited therein.

[4] Tadokoro, H., Structure of Polymer, 1976

[5] Colloid Science I, Basic and Dispersion and Adsorption, Japan Chemical Society pp.263-264

[6] Ohta, A., Sugiyama, T. and Uomoto, T., Study of Dispersing Effects of Polycarboxylate-Based Dispersant on Fine Particle, Proceedings 6th CANMET/ACI Int'l Conference Superplasticizers and Other Chemical Admixtures in Concrete, 2000, pp.211-227

[7] Ohta, A. and Uomoto, T., Study on the Dispersing Mechanism of Polycarboxylate-based Dispersing Agent to Binding Materials, Proceedings of the Japan Concrete Institute, Vol.19, No.2, 1998, pp.85-90

DURABILITY OF HEAT CURED MORTARS AND PASTES WITH PORTLAND LIMESTONE CEMENT

D. Heinz[1] and L. Urbonas[2]

[1]Mineral Engineering, University of Technology, TU München, Baumbachstr. 7, D-81245 München Germany. E-Mail: Heinz@bsi.bv.tum.de
[2]Inst.of Mineral Engineering, University of Technology Aachen, Mauerstr. 5, D-52064 Aachen, Germany. E-Mail: urbonas@ghi.rwth-aachen.de

ABSTRACT

In this study the influence of limestone addition on the length change and resonance frequency of mortars and paste samples was investigated under different curing conditions. The samples were prepared with a Portland cement, which resulted in significant expansion after heat curing in previous studies [1-3]. One part of the samples was cured for 4 hours at 95°C, the other part at 20°C until one day, and finally all samples were stored at 20°C and 5°C in water. The hydrated pastes and mortars were examined by means of x-ray diffraction and scanning electron microscopy. No ettringite was found after curing at 95°C. Only traces of AFm phases were identified as sulphate bearing phases. During the subsequent storage of these samples in water at 20°C and 5°C, expansion occurred. With increasing amounts of limestone in the cement the expansion effect was shifted to earlier times with decreasing maximum expansion values. Mortars showed higher expansions than pastes. The storage at 5°C in comparison with that at 20°C caused earlier expansion of the samples. The amount of ettringite determined by quantitative X-ray diffraction increased parallel to the expansion of the samples.

A fundamentally positive influence of an addition of limestone on the deleterious expansion of mortars and pastes after heat curing was not found. The mechanism of late ettringite formation in limestone cement is discussed.

1. INTRODUCTION

Delayed ettringite formation and the resulting structure changes in cement pastes and mortars is a very complex process. The expansion on the basis of delayed ettringite formation depends on several parameters, temperature of heat-treatment, chemical and mineralogical composition of the cement, storage conditions after heat-treatment, microstructure of mortar or paste etc.

Preliminary studies on the soundness of heat-treated Portland limestone cement (4h, 95°C) followed by 7 years storage under water at room temperature showed almost no length change [1]. One hypothesis for this phenomenon is based on the observation of stable ettringite formation caused by a parallel reaction of carbonate and sulphate with aluminate [2]. Therefore minor potential for delayed ettringite formation had been expected. On the other hand thaumasite can be formed at low temperatures during the hydration of heat-treated Portland limestone cements, whereby CSH phases act as a source of sulphate.

The aim of this research was to clarify the influence of limestone additions on the delayed ettringite formation and expansion in the mortars and neat pastes at 20°C and 5°C and to characterize the mechanisms of this influence.

2. MATERIALS AND METHODS OF TESTING

In the experiments a cement, type CEM I 42,5 R and its mixes with 15 and 30 wt-% limestone from Jurassic limestone (Jurakalk) was used. The limestone was milled to a degree of fineness similar to that of limestone in an industrial Portland-limestone cement according to own investigations (94% < 63 µm). The particle size of the original materials was characterised using air jet screening. The density was determined with a Helium pycnometer, the specific area was measured according to the Blaine method. The results are shown in Table 1.

The chemical analysis of the original materials was determined by x-ray fluorescence analysis after the samples had been ignited at 1000°C. The Na_2O, K_2O, SO_3 and Cl contents were determined according to DIN/EN 196, part 2 and part 21. The content of CO_2 was measured volumetrically. For the calculation of clinker-phases according to Bogue, it was supposed that all of the SO_3-content was bound as $CaSO_4$ and all of the CO_2 content was bound as $CaCO_3$. The results are shown in Table 2.

Powder XRD analysis showed the presence of the anhydrous phases in the cement: C_3S, β-C_2S, C_3A, periclase (MgO), anhydrite ($CaSO_4$), calcite ($CaCO_3$) and brownmillerite ($C_2(A,F)$). In addition to calcite, a small amount of dolomite, quartz, mica and illite was identified in the limestone. The mortars were prepared according to DIN/EN 196 part 1. The pastes were prepared in accordance to DIN/EN 196, part 3 with a water/cement ratio of 0.5.

For the investigations flat prisms (measuring: 1x4x16 cm) with gauge studs were cast using pure cement and mixes with 15 and 30% of limestone. Part of these samples were stored for 2 hours and then treated in water at 95°C for 4 hours. The rest of the samples were first stored for up to 24 hours in an environment of 20°C and 95% relative humidity. All the samples were then stored in water at 5°C and 20°C.

Table 1. Particle size distribution (air-jet screening), density and specific surface of cement limestone

Particle Size	Cement CEM I 42,5 R		Limestone	
	F	R	F	R
[mm]	[M.-%]			
> 0.09	-	-	0,6	0,6
0.09 – 0.063	-	-	5,2	5,8
0.063 – 0.04	-	-	4,4	10,2
0.04 – 0.032	1.2	1.2	9,7	19,9
0.032 – 0.025	7.2	8.4	6.2	26.1
0.025 – 0	91.6	100.0	73.9	100.0
Density [g/cm^3]	3.14		2.77	
Spec. surface acc. Blaine [cm^2/g]	4900		9000	

F – part of fraction; R – coarse on the screen

3. RESULTS OF INVESTIGATIONS

3.1 Strength, length change and resonance frequency of the samples

As expected the strength of mortar prisms decreases with increasing limestone addition (Table 3). Therefore the mortars without any limestone addition and with 15 wt.-% of limestone addition still belong to the range of the strength class 42.5 R. However, in case of the 30 wt.% addition limestone only 32.5 R equivalent is reached.

The length change and resonance frequency of the heat-treated samples were measured after different periods of hydration (Figures 1 to 4).

Table 2. Chemical composition of cement and limestone

Components	Cement CEM I 42.5 R	Limestone
SiO_2	20.80	7.59
Al_2O_3	4.90	2.76
Fe_2O_3	2.24	1.01
CaO	62.60	86.57
MgO	2.80	1.44
K_2O	1.41	0.18
Na_2O	0.11	0.03
TiO_2	0.31	0.16
ZnO	0.07	0.03
Mn_2O_3	0.44	0.06
P_2O_5	0.06	0.03
SO_3	3.85	0.03
Total	99.59	99.89
LOI 1000°C	3.05	41.18
CaO_{free}	0.60	-
CO_2	2.19	39.05
Na_2O_{eq}	1.04	0.15
C_3S	43.78	-
C_2S	26.63	-
C_3A	8.45	-
C_4AF	8.17	-

Table 3. Strength of mortars stored at room temperature (according to DIN/EN 196. part 1)

Amount of Limestone	Bending Strength		Compressive Strength	
[M.-%]	[MPa]			
	2d	28d	2d	28d
0	6.6	8.1	38.2	52.2
15	5.5	7.4	29.6	46.7
30	4.4	6.6	22.5	36.0

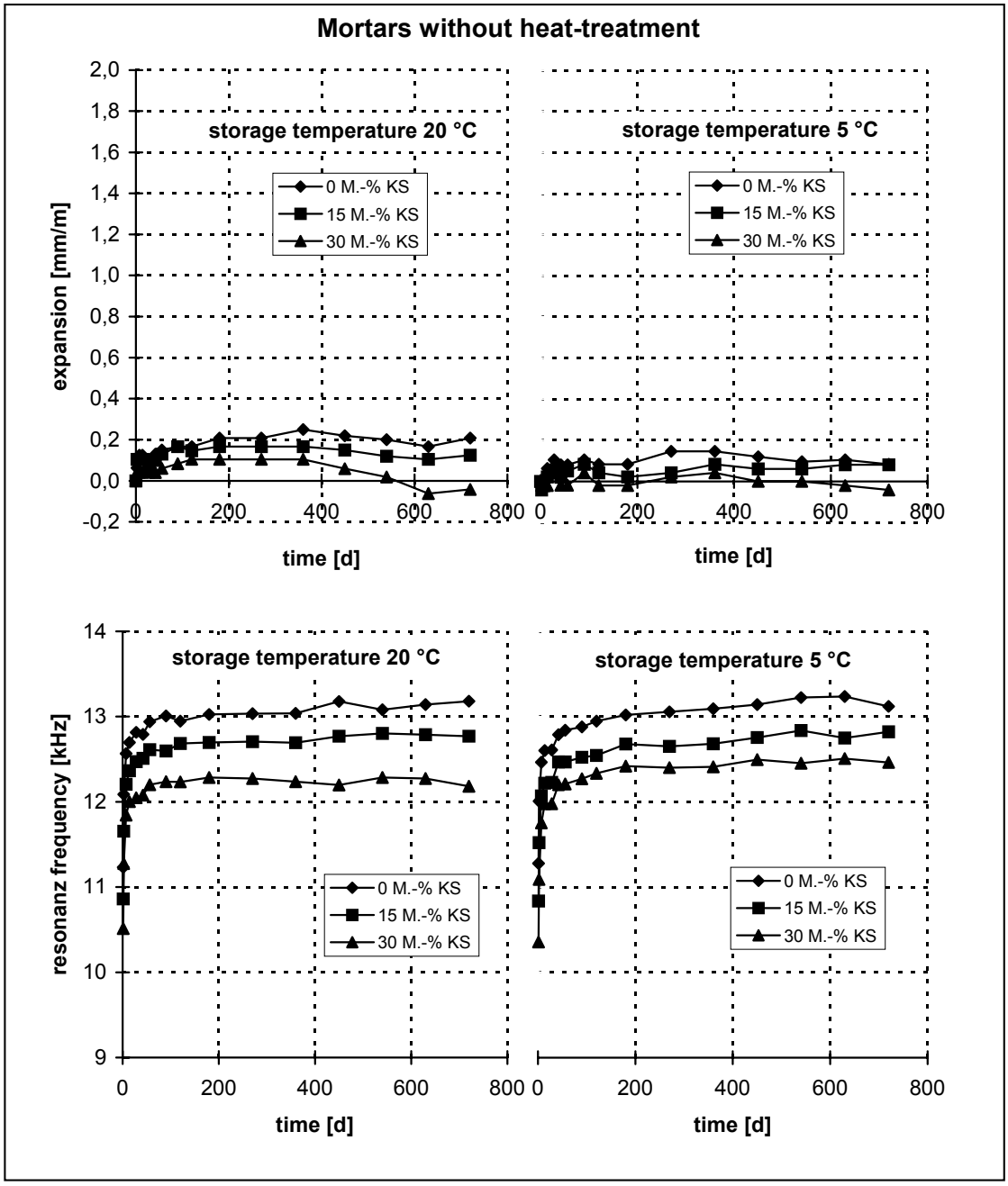

Figure 1. Length change and resonance frequency of mortars without heat-treatment. (KS = limestone)

After 720 days mortar samples without heat-treatment showed a low expansion of 0.20 mm/m at 20°C storage temperature and small shrinkage of 0.02 mm/m at 5°C. The expansion decreased with the limestone content. After increasing during the first 6 months, the resonance frequency remained almost constant for the following 18 months. The resonance frequency decreased as the limestone content increased.

Heat-treated mortar samples showed a high expansion of up to 11.3 mm/m during the time of examination. The evolution of the expansion depends on the amount of limestone and on storage conditions. An earlier commencement of the expansion was observed with an increasing amount of limestone and/or a decrease in storage temperature. The addition of limestone led to earlier termination of the main expansion phases and to slighter expansion after 720 days.

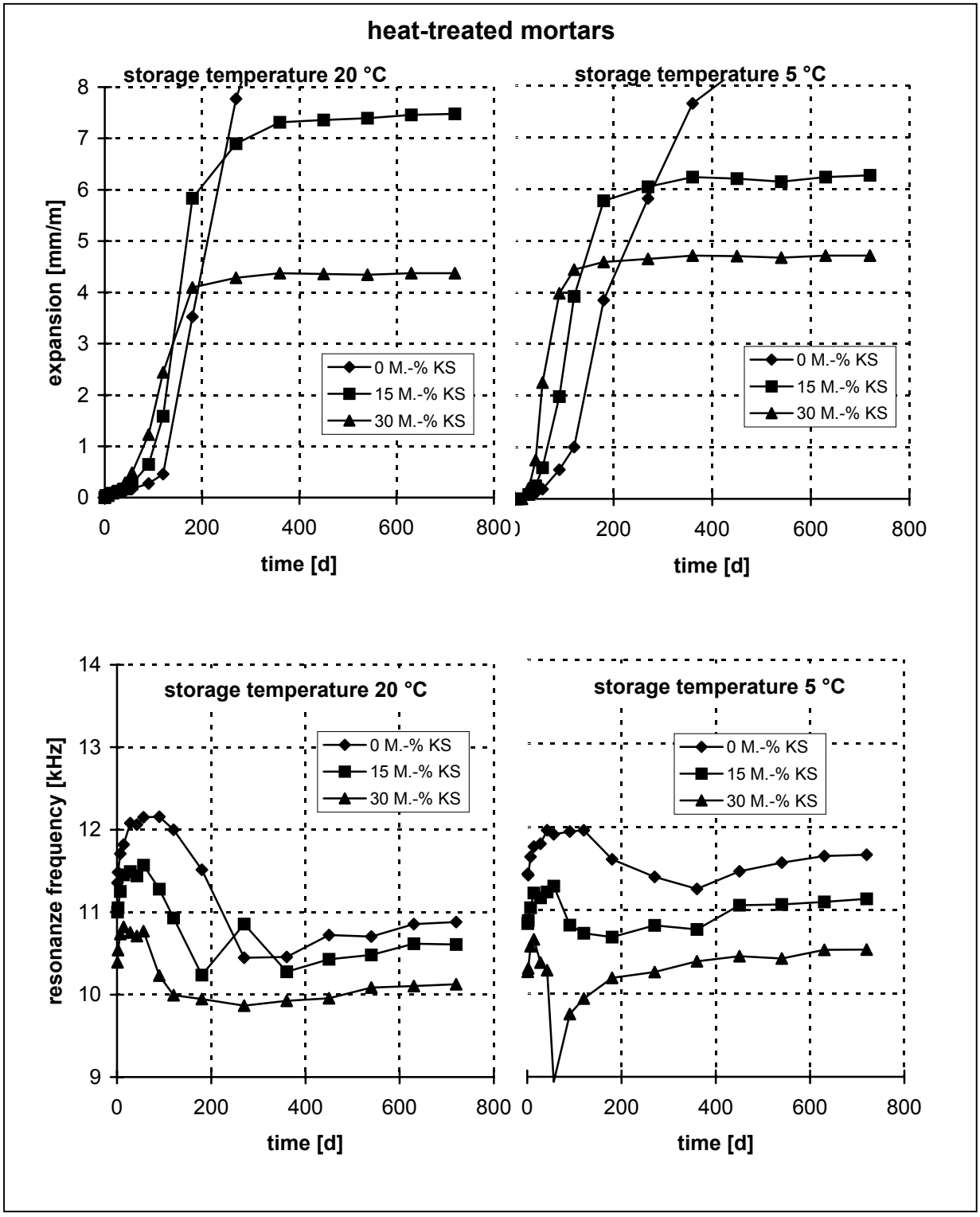

Figure 2. Length change and resonance frequency of mortars with heat-treatment (KS = limestone)

The resonance frequency decreased during the expansion period. Afterwards the resonance frequency remained constant or increased slightly. Cracks occurred in all the samples stored for longer than six months at 20°C.

For up to 720 days of storage, paste samples without heat-treatment showed higher rates of expansion than the mortar samples. Similarly to the mortar prisms, the expansion increased at lower limestone contents or higher temperature of storage. The resonance frequency increased for the first 180 days and then remained almost constant.

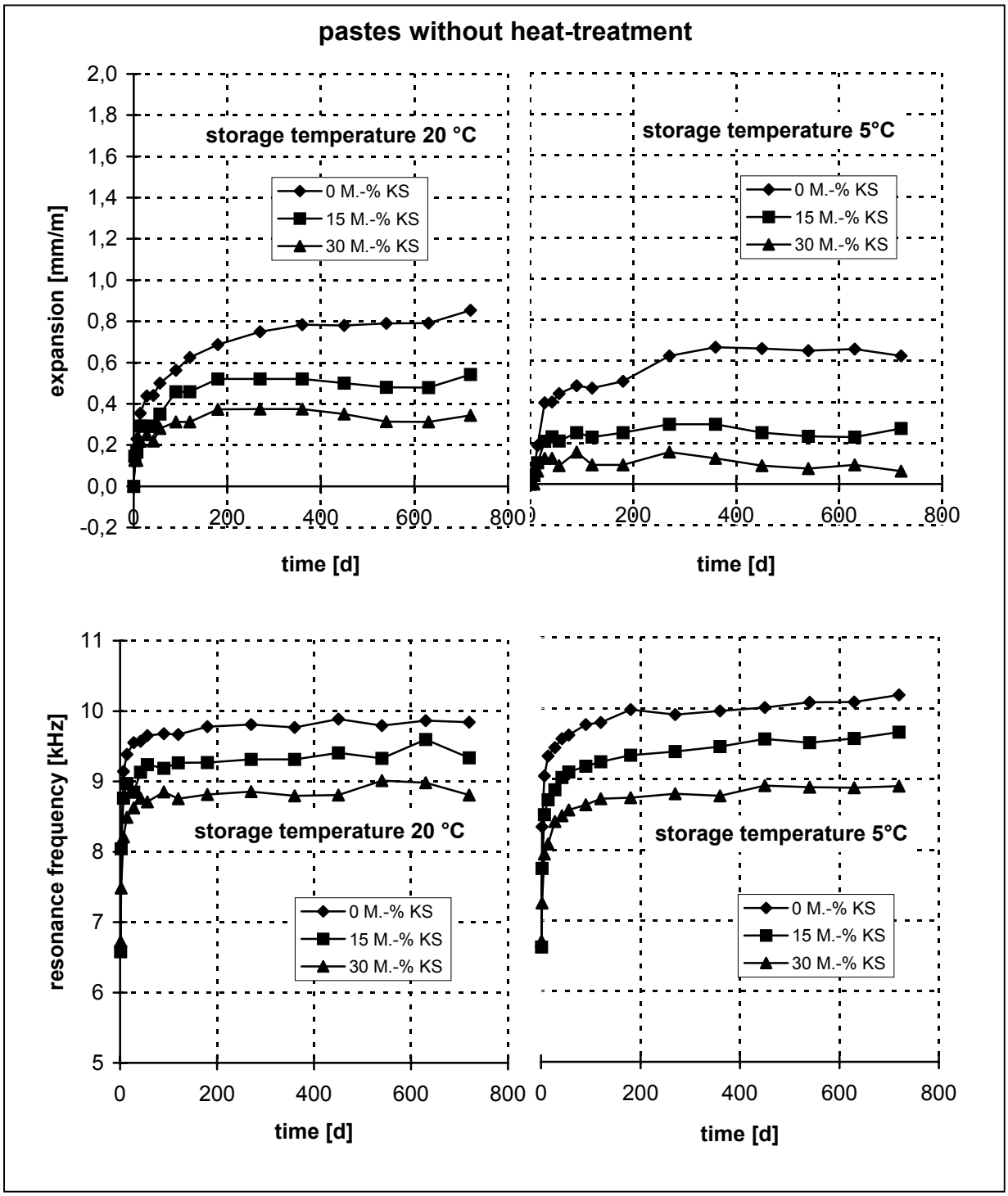

Figure 3. Length change and resonance frequency of pastes without heat-treatment (KS = limestone)

It was observed that after one year, in contrast to samples not subjected to heat-treatment, the heat-treated samples exhibited higher expansion rates with an increasing amount of limestone. For example samples with 30% of limestone expanded by 1.17 mm/m at 20°C and 0.90 mm/m at 5°C after one year. In the second year of storage at 20°C the samples with limestone showed distinct expansion. At 5°C the expansion remained at a low level. The resonance frequencies showed no significant decrease during that period.

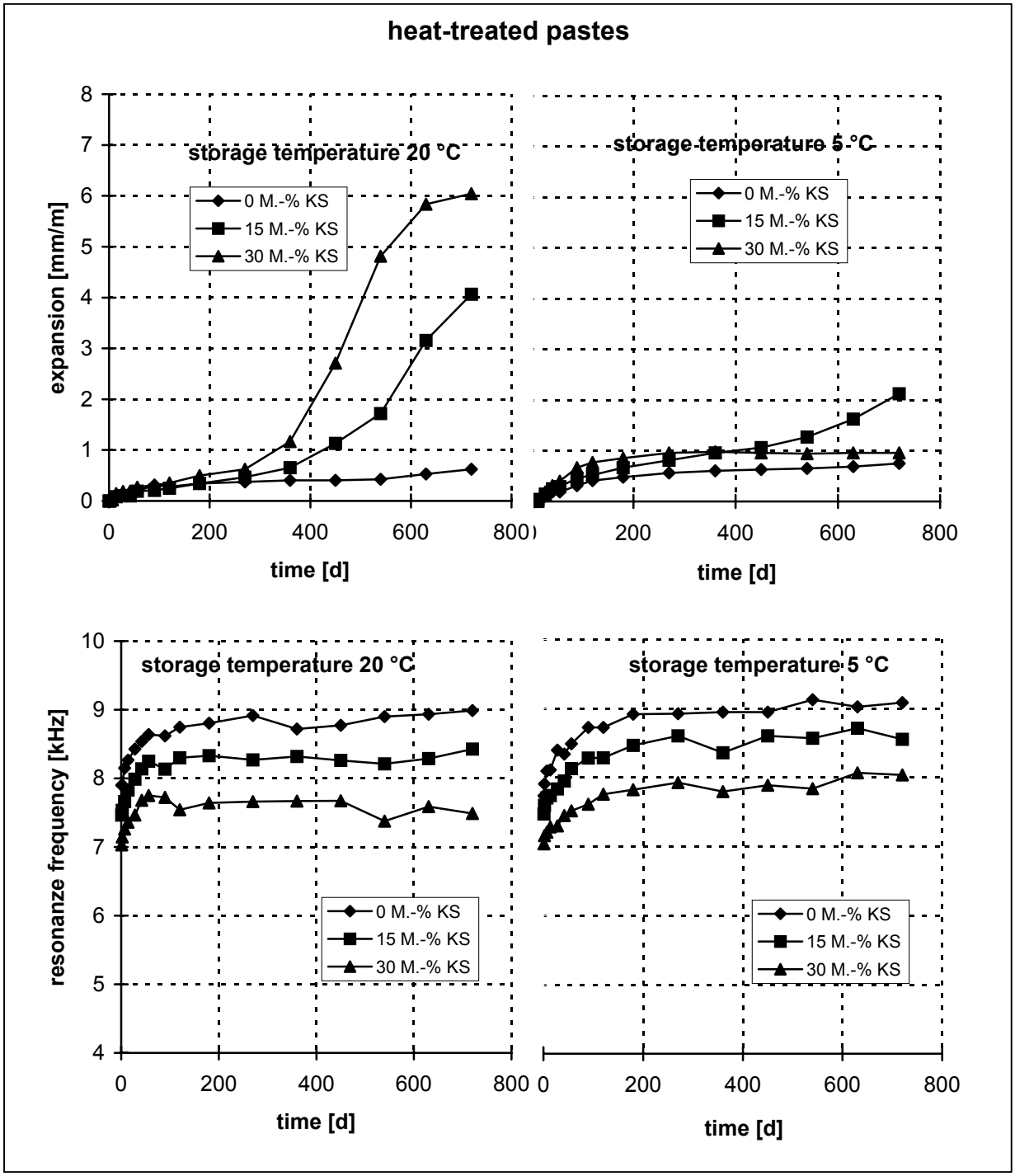

Figure 4. Length change and resonance frequency of pastes with heat-treatment (KS = limestone)

3.2 Mineralogical analyses

The hydrates formed in the aged samples were examined by X-ray diffraction analysis (XRD). scanning electron microscopy (SEM) and X-ray microanalysis. The content of ettringite in the hydrated samples was detected by using the method of internal standards. Calcium sulphate hemihydrate ($CaSO_4 \bullet 0.5H_2O$) was used as the internal standard (3).
For the XRD and X-ray microanalysis, fragments of the mortar and paste samples were sputtered with carbon.

Some results of the analyses are presented in Figures 5 to 9 and in Table 4.

Table 4. Amount of ettringite in the mortars and pastes (XRD determination)

Addition of Limestone	Storage Temperature	Amount of Ettringite [M.-%]			
[M.-%]	[°C]	2h	1d	28d	360d
		heat-treated mortar			
0	20	n.d.	n.m.	n.m.	3.1
0	5	-	-	0.60	3.3
15	20	n.d.	n.m.	0.90	3.3
15	5	-	-	0.90	2.6
30	20	n.d.	n.m.	0.90	2.9
30	5	-	-	1.10	2.4
		Pastes Without Heat-treatment			
0	20	2.5	5.5	6.6	7.3
0	5	-	-	6.4	8.0
15	20	2.2	6.0	6.6	6.7
15	5	-	-	6.6	7.4
30	20	1.8	4.6	5.4	4.9
30	5	-	-	5.6	5.4
		Heat-treated Pastes			
0	20	-	n.m.	2.2	2.9
0	5	-	-	2.0	3.6
15	20	-	n.m.	2.5	2.6
15	5	-	-	2.3	5.3
30	20	-	n.m.	2.9	6.4
30	5	-	-	3.6	5.4

n.d.- not determined; n.m.- not measurable

After two hours of hydration of pastes, only ettringite was identified as a hydrated phase of cement. During storage of mortars and pastes without heat-treatment at 20°C and 5°C monocarboaluminate hydrate and ettringite were observed after 28 days. The concentration of monocarboaluminate hydrate was found to increase with an increase of calciumcarbonate and with higher storage temperature (20°C). After 360 days the influence of the storage temperature (5°C or 20°C) for $C_3A \cdot CaCO_3 \cdot 11H_2O$ formation was no longer detectable. No monosulphoaluminate hydrate and thaumasite was identified for mortar and paste samples stored at 5°C and 20°C during the observation time.

Only traces of monosulphoaluminate hydrate were found in mortar and paste samples immediately after heat-treatment. Ettringite and monosulphoaluminate hydrates were formed during 28 days storage at 20°C and 5°C. Generally the amount of ettringite increased with increasing amount of carbonate in cement and is substantially lower in the samples without heat-treatment. The effect of

storage temperature is distinct only for mortar and paste samples with 30% limestone – with decreasing temperature the amount of ettringite increases. No monocarboaluminate hydrate was identified in heat-treated pastes and mortars after 28 days storage at 20°C and 5°C

Compared to the samples without heat-treatment a higher amount of ettringite and lower amount of monocarboaluminate was found in the heat-treated mortar samples after 360 days.

Monosulphoaluminate hydrate and a small amount of ettringite were identified in pastes containing no limestone and stored at 5°C and 20°C. The same hydrates were found in the pastes prepared with 15% limestone stored at 20°C. A higher amount of ettringite was identified in the paste prepared with 15% limestone and stored at 5°C. The same was found for the paste prepared with 30% limestone and stored at 5°C and 20°C. The amount of monocarboaluminate hydrate increases with increasing $CaCO_3$ content in the samples. The mortar samples contain substantially more ettringite in the paste (without sand) as the paste samples.

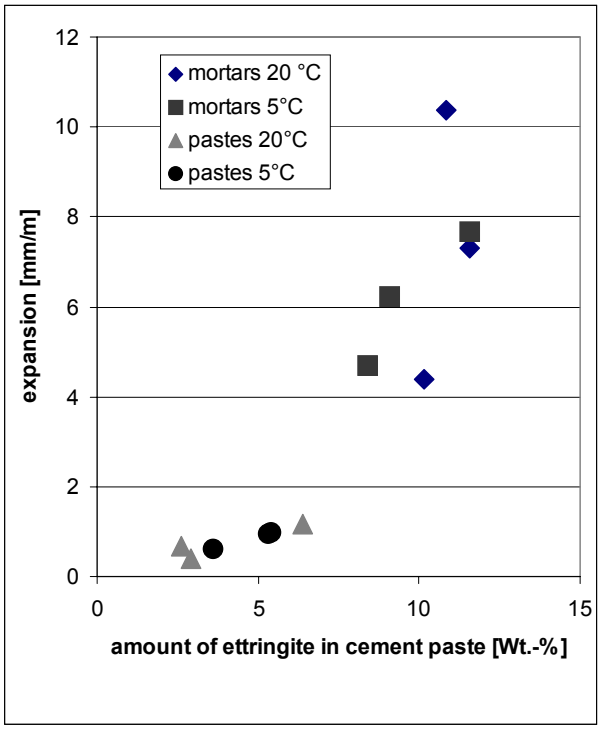

Figure 5. Correlation between expansion and ettringite amount in the cement paste

The expansion of mortar and paste samples correlated with the amount of ettringite in the cement matrix. Usually, with an increasing amount of ettringite, expansion of the samples increase (Figure 5).The results of SEM- and X-ray microanalysis of 360 days aged samples of mortars and pastes containing 30% of limestone, stored at 5°C are presented in the Figures 6 to 9.

Although particles with chemical composition high in sulphate were identified, no needle-like crystals of ettringite were found in the non heat-treated mortar samples. The irregular shaped particles found with an increased amount of sulphate are ettringite-like phases, mixed with calcium silicate hydrates, as is indicated by the chemical composition (Figure 6).

Given the low Al_2O_3 and Fe_2O_3 content, the high sulphate content, of the area marked by "1" (Figure 6) can not only be attributed to the presence of calcium sulphate-aluminate or ferrite phases. This may be a mixture of calcium silicate hydrate and thaumasite-like phases.

In the mortar samples treated at 95°C, needle-like crystals of ettringite could be identified. The chemical composition of these crystals showed only slight deviation from the theoretical composition. Based on the present results it cannot be stated whether the presence of SiO_2 and excess of CaO are due to traces of calcium silicate hydrates, calcite or portlandite respectively or a matter of accommodation of SiO_2 in the crystal structure of ettringite. In the same sample only one composition with SiO_2 and a higher molar SO_3/Al_2O_3 ratio (of 3.6) than expected for ettringite was found. The identified irregularly formed particle, which is rich in sulphate, is a mixture of ettringite, CSH-phases and possibly calcite or portlandite.

There are also irregularly formed particles in the non heat-treated paste samples. They are rich in sulphate and as well as the components typical for AFT-phases (CaO. Al_2O_3 and Fe_2O_3) they contain MgO and SiO_2. In the pore, needle-like ettringite crystals are apparent. The SO_3/Al_2O_3ratio

was found to be lower than the theoretical value typical for ettringite. Furthermore. no SiO_2 was detected (Figure 7).

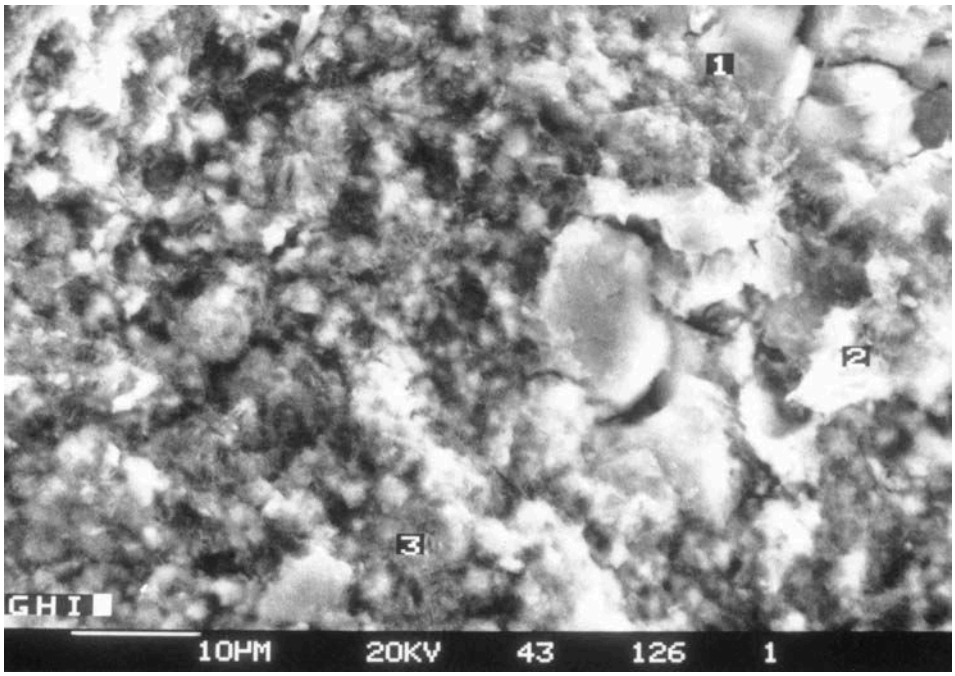

	1	2	3
	[M.-%]		
MgO	-	5.3	5.21
Al_2O_3	1.7	10.3	8.5
SiO_2	21.2	8.6	8.7
SO_3	8.5	13.3	20.3
CaO	66.5	52.5	54.0
Fe_2O_3	2.0	10.0	3.2

Figure 6. SEM and X-ray microanalysis of mortar with 30% limestone in cement after 360 days storage at 5°C

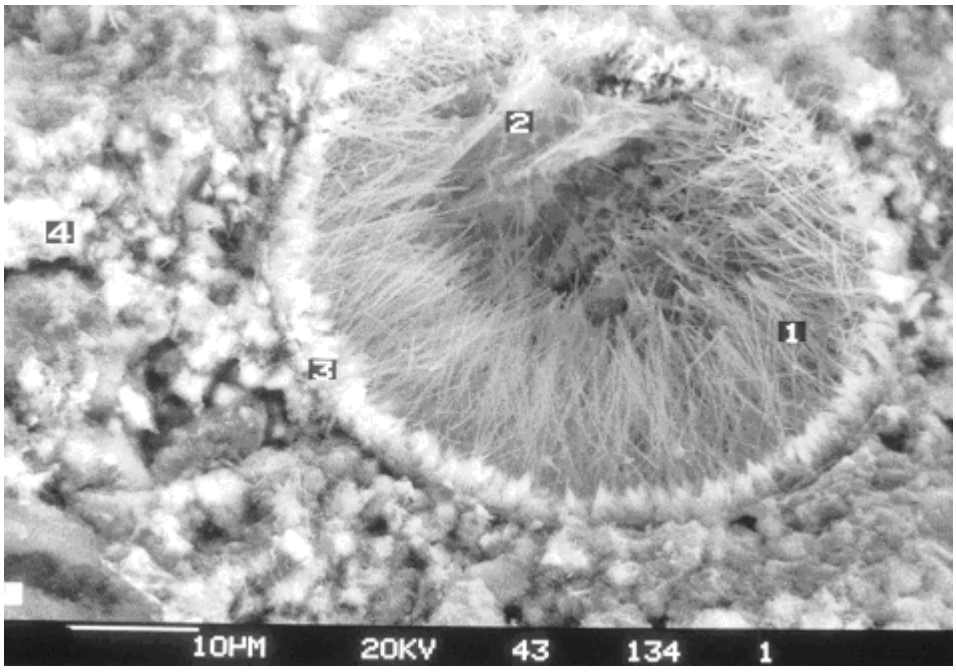

	1	2	3	4
	[M.-%]			
MgO	-	-	-	4,6
Al_2O_3	8.1	2.6	4.3	5.3
SiO_2	1.1	13.1	18.2	24.8
SO_3	14.0	5.8	8.8	7.9
CaO	76.8	78.5	68.7	55.5
Fe_2O_3	-	-	-	1.8

Figure 7. SEM and X-ray microanalysis of cement paste with 30% limestone in cement after 360 days storage at 5°C

No needle-like ettringite crystals appeared in the heat-treated paste samples. It was shown by X-ray microanalysis that areas rich in sulphate contain mainly mixes of different phases (Figures 8 and 9). The chemical composition at mark 1 (Figure 8) shows a much higher SO_3/Al_2O_3–molar ratio (of 4.22) than for ettringite which might indicate the presence of thaumasite or ettringite-thaumasite solid solutions.

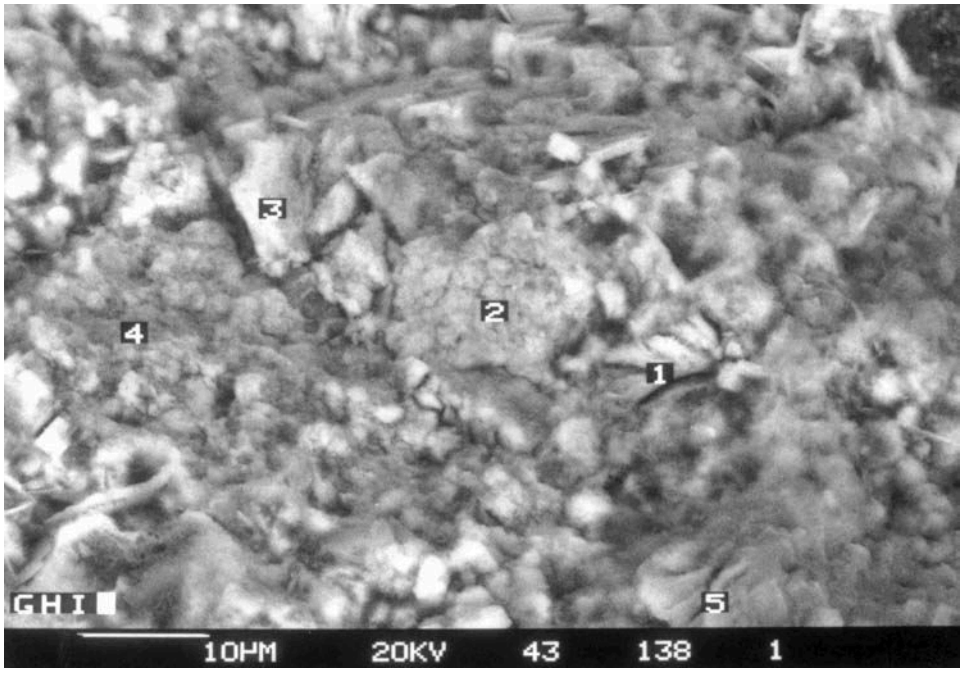

	1	2	3
	[M.-%]		
MgO	-	-	-
Al_2O_3	9,9	6,3	7,1
SiO_2	6,2	14,9	9,1
SO_3	29,0	-	13,6
CaO	55,0	77,8	70,2
Fe_2O_3	-	-	-
K_2O	-	1,0	-

	4	5
	[M.-%]	
MgO	1,6	6,9
Al_2O_3	12,8	4,3
SiO_2	-	35,9
SO_3	85,7	3,8
CaO	-	47,7
Fe_2O_3	-	1,4
K_2O	-	-

Figure 8. SEM and X-ray microanalysis of heat-treated cement paste with 30% limestone in cement after 360 days storage at 5°C

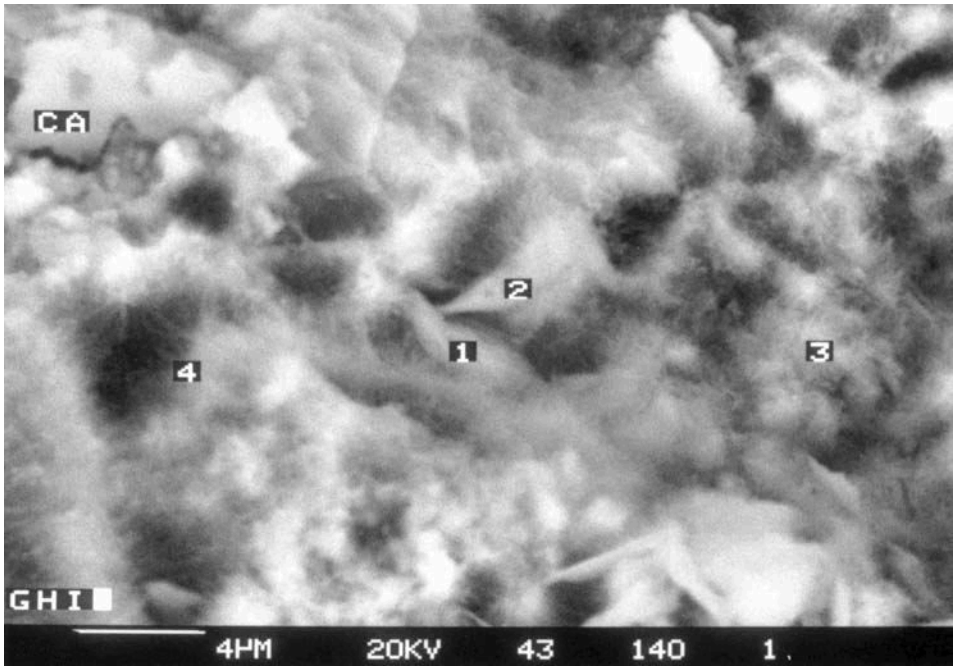

	1	2	3	4
	[M.-%]		[M.-%]	
MgO	-	-	-	2,5
Al_2O_3	4,7	4,8	3,9	2,6
SiO_2	8,1	11,5	25,4	24,2
SO_3	15,6	10,8	4,0	2,7
CaO	71,6	70,0	66,7	66,0
Fe_2O_3	-	3,0	-	2,1

Figure 9. SEM and X-ray microanalysis of heat-treated cement paste with 30% limestone in cement after 360 days storage at 5°C

4. DISCUSSION AND CONCLUSIONS

Delayed ettringite formation and the resulting structure changes in cement pastes and mortars is a very complex process. The expansion on the basis of delayed ettringite formation depends on several parameters, i.e. the temperature of heat-treatment, chemical and mineralogical composition of cement, storage conditions after heat-treatment and the microstructure of mortar or paste [4].
In the present work the effect of limestone addition on the soundness of cement pastes and mortars with and without heat-treatment was investigated.

The effects of the limestone during cement hydration are partly physical and partly chemical. Chemically it reacts with aluminate phase producing $C_3A.CaCO_3.11H_2O$ thus competing with the gypsum. Furthermore monocarboaluminate hydrate is formed because the dissolution of $CaCO_3$ takes place slowly in comparison with the ettringite formation. In the pastes and mortars monocarboaluminate hydrate was found at ages over 28 days. After 1 day of hydration this phase was not present. As expected, no monocarboaluminate hydrate phases were found in mortar and paste samples after heat-treatment. This corresponds with results of Ghorab et. al. [5] who found decomposition of $C_3A.CaCO_3.11H_2O$ at higher temperatures. In heat-treated samples reactions may occur as follows (in simplified form):

$$C_3AH_6 + CaSO_4\,(\text{from CSH}) + 6\,H_2O \rightarrow C_3A.CaSO_4.12H_2O \quad (1)$$
$$C_3A.CaSO_4.12H_2O + 2\,CaSO_4\,(\text{from CSH}) + 20\,H_2O \rightarrow C_3A.3CaSO_4.32H_2O \quad (2)$$
$$C_3AH_6 + 3\,CaSO_4\,(\text{from CSH}) + 26\,H_2O \rightarrow C_3A.3CaSO_4.32H_2O \quad (3)$$
$$C_3AH_6 + CaCO_3 + 5\,H_2O \rightarrow C_3A.\,CaCO_3.11H_2O \quad (4)$$
$$\text{C-S-H} + CaCO_3 + CaSO_4 + x\,H_2O \rightarrow CaSiO_3.CaSO_4.CaCO_3.15H_2O\ (\text{at } 5°C) \quad (5)$$

During the storage of cured samples the reactions 2 and 3 are normally expected. With this reactions a better crystallization of monosulfoaluminate hydrate during 28 days of hydration was observed. Until 28 days of hydration no reaction between aluminate hydrates and calcite was observed. The result of the competing reaction between carbonate and aluminate phases (reaction 4) was observed only between 28 and 360 days of hydration. Delayed ettringite formation was accelerated by lower temperature and $CaCO_3$ addition. Although $CaCO_3$ and sulphate compete to react with tricalciumaluminate hydrate after 28 days of hydration, a higher amount of ettringite was found as was expected. This phenomenon can presumable be attributed to differences of microstructure and strength characteristics of specimens with and without limestone addition. According to Taylor et al. [4] anything that weakens the material will lower its ability to resist expansion. More investigation is needed to identify and explain the latter reaction path.

Mortar samples showed higher rate and extent of expansion in comparison with neat paste samples. This corresponds with the observations of Yang et al. [6]. According to Taylor et al. [4] the paste material is strong enough to resist the stresses caused by ettringite formation to an extent that greatly retards the reaction and the resulting expansion. A weaker bond between aggregate and paste allows the reaction and expansion to proceed more quickly.

Some weakening in the structure of pastes and mortars can occur due thaumasite formation at 5°C. The formation of thaumasite in mortars and concretes is usually dependant on a surplus of sulphate-ions. the existence of $CaCO_3$ and humid storage conditions at low temperatures. If mortars are heat-treated (at 95°C), part of the sulphate-ions are accumulated in the CSH-phases. The presence of $CaCO_3$ in combination with low temperature storage may theoretically also lead to formation of thaumasite. This, in particuilar, is happening in micro-areas where CSH-phases rich in sulphate have close contact to $CaCO_3$ or it is due to carbonation of the CSH-phases. The investigations showed that crystal-mixes appeared in micro-areas of pastes with 30% (wt.) of limestone filler which were heat-treated and stored at 5°C. The amount of thaumasite or ettringite-thaumasite mixed crystals is so small that they could not be identified by XRD. Sulphate from the CSH-phases and

$CaCO_3$ which are both part of the cement in first place, react with calcium-aluminate-hydrate and form monocarboaluminatehydrate ($C_3A{\cdot}CaCO_3{\cdot}11H_2O$) and ettringite ($C_3A{\cdot}3CaSO_4{\cdot}32H_2O$).

The investigations showed that after heat-treatment the addition of fine limestone led to:

- an accelerated ettringite formation and expansion of the mortars and pastes
- a decrease in expansion of mortar
- a higher initial rate of expansion reactions of mortar samples during subsequent water storage at 5°C in comparison with that at 20°C

REFERENCES

[1] Kalde M. Heinz., D., Ludwig. U. Expansive DEF in cement paste, mortars and concrete (in German). Thesis, Scient. Journal Bauhaus-Universität Weimar. 1+2 Heft. 1998. 44. Jahrgang.

[2] Ghorab. H. Y., Ludwig.U. Model investigations on damages of heat-treated precast concrete, Part 1: Stability of monophases and ettringite(in German). TIZ-Fachberichte (105). 1981. Heft 9. S. 634-640

[3] Ludwig. U., Rüdiger. I. Quantitative analysis of ettringite in cement pastes, mortars and concretes (in German). Zement-Kalk-Gips Nr3. 1993. S. 150 – 153

[4] Taylor H. F. W., Famy. C., Scrivener K. L. Delayed entringite formation. Cement and Concrete Research. 31 (2001). pp. 683-693

[5] Ghorab.H.Y., Kishar.E.A., Abou Elfetouh. S. H. Studies on the stability of calciumsulfoaluminate hydrates. part III: the monophases. Cement and Concrete Research. 28 (1998). pp. 763-771

[6] Yang. R., Lawrence. C. D., Sharp. J. H. Delayed ettringite formation in 4-years old cement pastes. Cement and Concrete Research. 26 (1996). pp. 1649-1659

INFLUENCE OF LIMESTONE AND FLY ASH ADDITIONS TO CEMENT THAT CAUSED EXPANSION OF HEAT-TREATED MORTAR DUE TO DEF

Wiesław Kurdowski and Sylwester Duszak

University of Mining and Metallurgy, Cracow, Poland.

ABSTRACT

Ground limestone and fly ash were added to cement which showed a DEF expansion after thermal treatment of the mortar. The fifteen per cent addition decreased, but did not eliminate the expansion. However, the samples to which potassium hydroxide was also added revealed a distinctly lower expansion. The higher content of additions, namely 30%, was sufficient to practically eliminate DEF. However, when SO_3 content in blended cements was completed by gypsum addition close to 4%, i.e. to the content in pure Portland cement, the expansion is practically eliminated. The comparison of mortar expansion with XRD ettringite is discussed.

Keywords: DEF, Portland cement, fly ash, limestone, expansion

1. INTRODUCTION

Delayed ettringite formation (DEF) is a very stimulating topic and many problems remain unsolved especially the mechanism of expansion [1-4].

It is well known that the replacement of 30% of cement by fly ash and 50% by slag is very effective in elimination of the expansion caused by DEF [5-7]. However, only a few papers are devoted to the influence of limestone and Kelham [8], among others, examined this addition, but no comments have been given in his paper. Summarising one can conclude that the influence of limestone is relatively less familiar.

The principal goal of this investigation is the examination of the influence of limestone on the DEF and consequently on the expansion of the mortars. For the sake of comparison the same quantity of low lime fly ash was used.

The paper presents the results of the investigation of these additions on the expansion of mortars after heat treatment. Also the composition of the paste in these mortars was followed by the X-ray method.

2. MATERIALS AND METHODS

Portland cement clinker of composition presented in Table 1 was used. This clinker was ground with addition of gypsum giving 4% SO_3 in cement. The mortar of this cement after heat treatment at 90^{o}C (Figure 1) presented an expansion of about 6 mm/m [9].

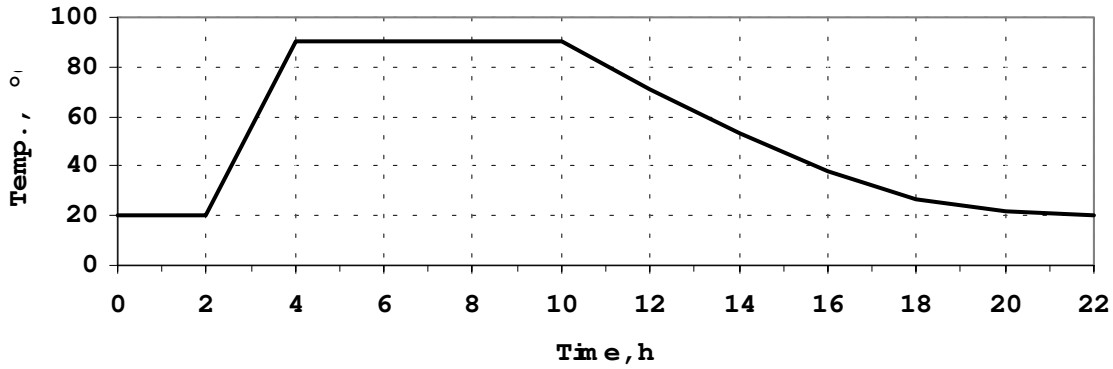

Figure 1. Programme of heat treatment

Fifteen and 30% of very pure limestone (L) and of fly ash (V) were added to this cement (for example 15L and 30L). The second series of cements containing 15% of addition was obtained by adding 0.22% KOH and 0.9% of gypsum to these cements (15LKG and 15 VKG). On the other hand to the cements containing 30% of addition 1.8% of gypsum was added (30LG or 30VG). Thus 8 cements were obtained, the ninth being the standard cement without addition.

In Table 1 chemical compositions of all materials used are presented and in Table 2 the contents of SO_3 and Na_2O_e in all cements are given.

Table 1. Chemical composition of materials

Component	Material		
	Clinker*, %	Fly ash, %	Limestone, %
Loss of ign.		1.13	42.79
SiO_2	21.75	50.33	0.42
Al_2O_3	4.92	29.22	0.32
Fe_2O_3	2.79	6.47	0.20
CaO	65.23	4.46	55.50
MgO	2.00	2.11	0.07
SO_3	1.23	0.74	0.05
Na_2O	0.16	1.95	0.02
K_2O	1.23	2.88	0.0
TiO_2	-	0.70	-

* Mineral composition C_3S - 55.3; C_2S - 20.6; C_3A - 8.3; C_4AF - 8.5

Table 2. Content of SO_3 and Na_2O_e in cements

Cement	Content of SO_3, %		Content of Na_2O_e, %	
	Portland cement	Total	Portland cement	Total
Portland cement	5.12	5.12	0.97	0.97
15L	4.35	4.35	0.82	0.82
15V	4.35	4.46	0.82	1.12
15LKG	4.35	4.76	0.82	0.95
15VKG	4.35	4.77	0.82	1.25
30L	3.58	3.58	0.68	0.68
30V	3.58	3.80	0.68	1.86
30LG	3.51	4.33	0.68	0.67
30VG	3.51	4.55	0.68	1.82

The solubility of alkalis of fly ash is very limited because not more than 5% is dissolved after 24 hours [10]. Therefore the content of soluble alkalis in cements containing fly ash will be practically the same as for the cements with limestone addition.

The mortars were prepared from these cements according to EN196-1 (one part of cement, three parts of sand). For all mortars, after different periods of water curing, the expansion was measured with the Graf-Kaufmann apparatus. [11]. For these measurements the mortar prisms of 4x4x16 cm were provided with two bolts, each one on the opposite longer end of the prism. The phase composition of the samples was followed by X-ray. For some samples porosity was measured using M I P.

3. RESULTS

The expansion of all mortars is presented in Figure 2. The highest expansion was found in the case of Portland cement. The mortar of cement with 15% of fly ash (15V) attained less than a half of the value for Portland cement and with 15% of limestone less than for 15V. The mortars of cements containing a small additional addition of gypsum and KOH (15LKG and 15VKG) presented a very small expansion.

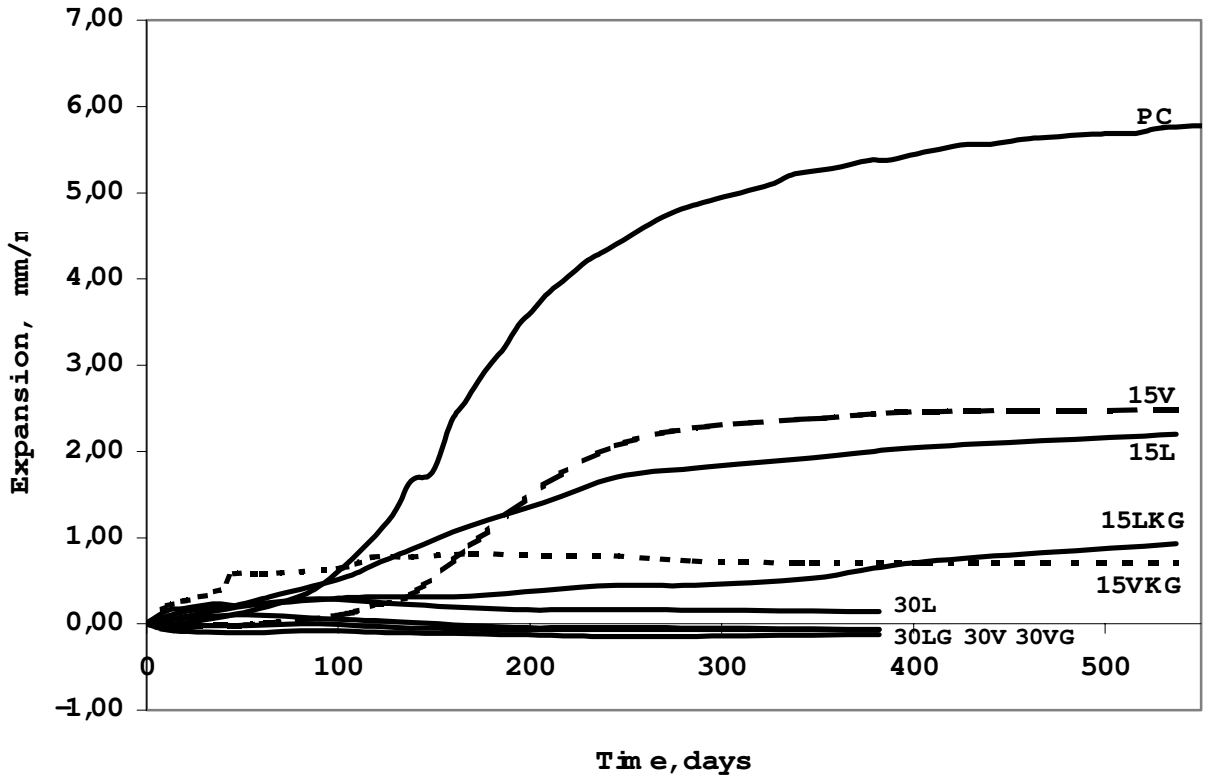

Figure 2. Expansion of the mortars after different times of water curing

Practically no expansion of mortars was observed in case of cements with a 30% addition without and with additional gypsum.

The changes in the phase composition of the samples were determined by the X-ray diffraction analysis. The mortars obtained from cements with the addition of fly ash (15V) give the following results:

After 7 days monosulfate prevails and its quantity decreases slightly for 200 days. Simultaneously, a small quantity of ettringite is formed in the mortar after 28 days of water curing and increases for 200 days (Figure 3).

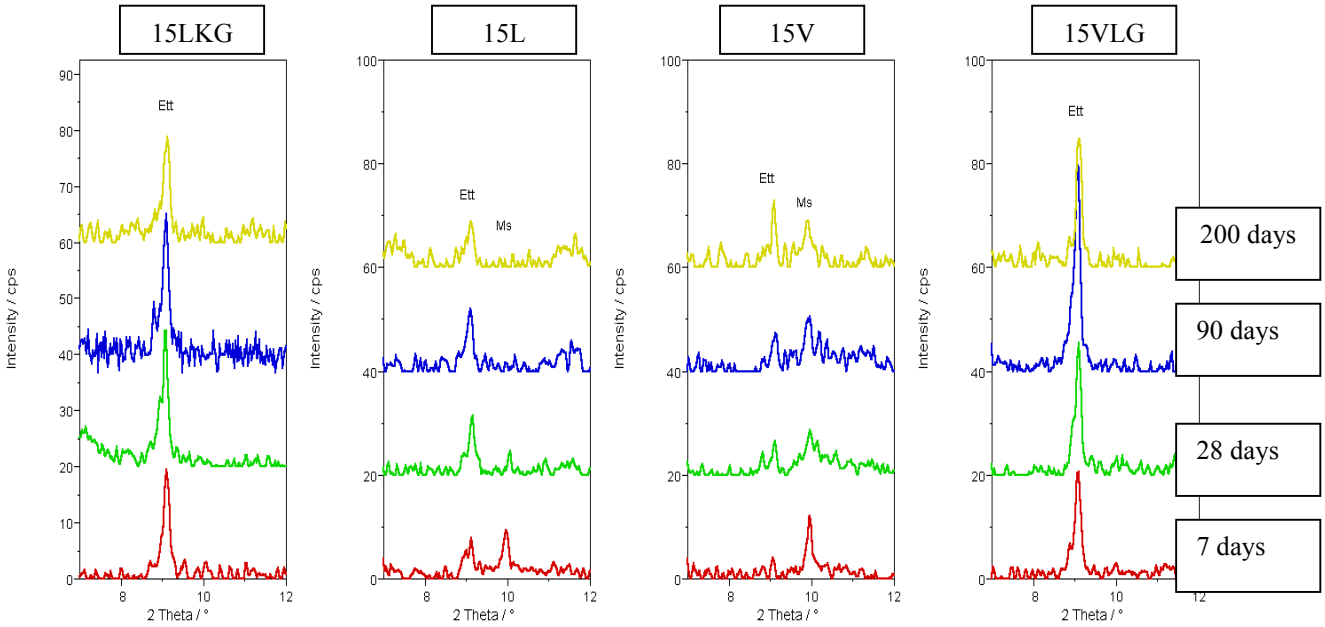

Figure 3. Section of X-ray pattern of the mortars after water curing

The content of ettringite is evidently higher already after 7 days of water curing and the intensity of its line on X-ray pattern increases from 7 days for 90 days in the mortar of cement containing an addition of fly ash together with KOH and an additional portion of gypsum (15VKG). Then, after 200 days, the ettringite content is a little smaller.

In the mortars prepared from cement with limestone, the content of ettringite is drastically higher in the case of cement 15LKG (Figure 3), and similarly to cement15 VKG, its content is high already after 7 days of water curing. In the mortar of cement 15L the content of ettringite is much lower, but after 7 days of water curing the line of monosulfate appears on the X-ray pattern (Figure 3). Its intensity decreases after 28 days and disappears after 90 days. The content of ettringite increases noticeably between 7 and 28 days.

In all mortars of cement with the limestone addition the content of calcite is high in all periods of curing and the intensity of its line on the X-ray pattern remains practically constant.

The X-ray examination of the mortars of cements with 30% of fly ash and limestone showed a similar behaviour. In the pastes containing limestone intensity of ettringite line is noticeably higher than in case of cements with fly ash. However, in the sample 30L, and especially 30LG, the line of gypsum is strong after 180 days of water curing (Figure 4). Probably it is due to the tricalcium aluminate reaction with calcite, but no carboaluminate line can be found in the X-ray examination. In samples with fly ash, namely 30V and 30VG, the strong line of monosulfate is visible after 180 days of water curing of mortars. In the mortar 30VG the content of ettringite was already high after 7 days of water curing.

The porosity of two mortars, namely of cements 15V and 15VKG, was measured after 450 days of water curing. The porosity of both mortars is low and essentially the same: for 15V it is equal to 8.37%, for 15VKG 8.45%. However, the content of capillary pores in the range 0.1 to 1 μm is higher in the case of mortar of cement 15VKG (Figure 5).

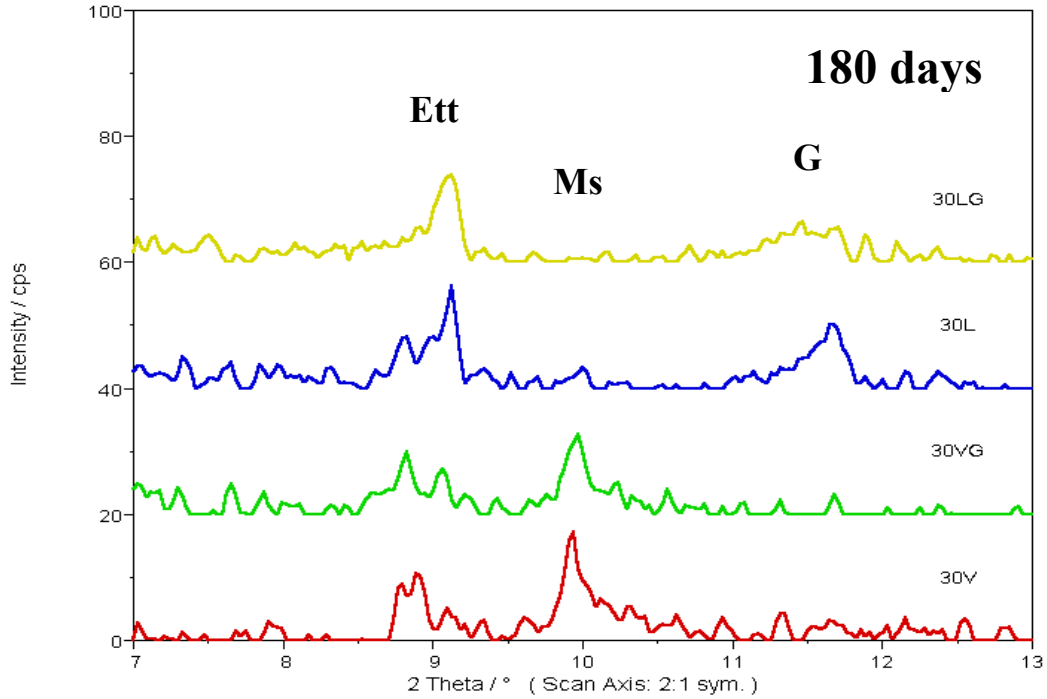

Figure 4. Section of X-ray pattern of mortars 30L and 30LG after 180 days

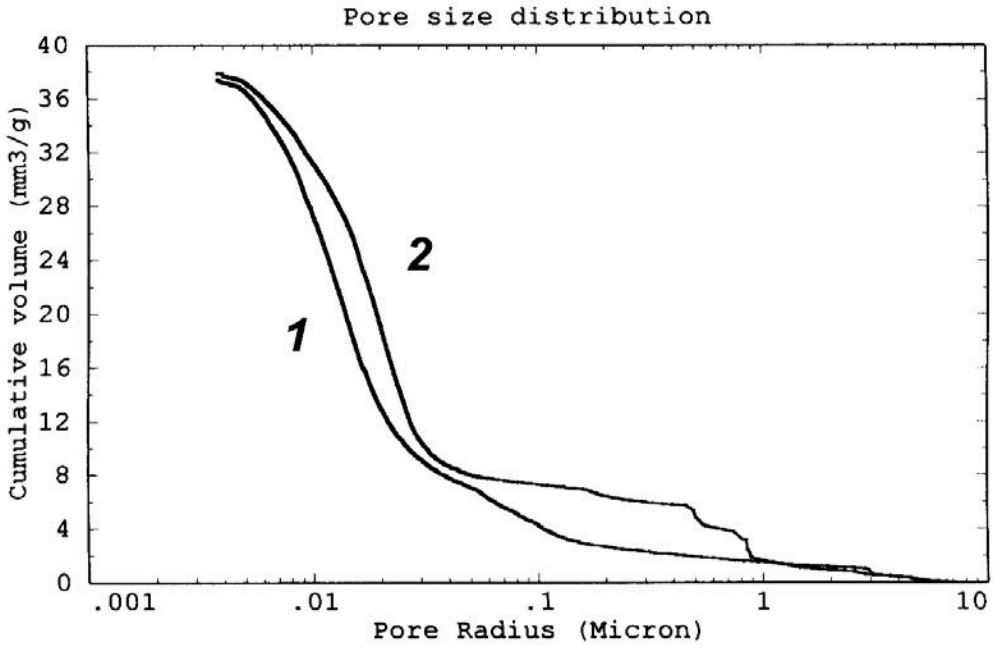

Figure 5. Cumulative porosity of mortars of cements 15V (1) and 15VKG (2)

4. DISCUSSION

In the light of results obtained it is clear that the addition of fly ash and limestone decreases or even eliminates the expansion of heat treated mortar after long water curing. In case of 15% addition the decrease of expansion is larger than 50%. From the content of monosulfate and ettringite found in X-ray patterns (Figure 3) it is evident that in the samples with the addition of KOH and gypsum (series 15LKG and 15VKG) ettringite is stable during heat treatment and its increase during longer water curing is small. It is in good correlation with the lack of expansion of these specimens. However, in the mortars of cements 15L and 15V after thermal treatment and water curing for 7

days, the monosulfate prevails and is progressively transformed into ettringite thus causing expansion. The reason for stability of ettringite in specimens 15LKG and 15VKG is not clear and the explanation of this phenomenon needs further study.

Also the content of capillary pores are higher in the mortars of cements with addition of KOH. The comparison of alkali content (Table 2) shows that it is also higher in the mortar presenting lower expansion (cements 15LKG and 15VKG).

The addition of 30% of fly ash or limestone essentially eliminates expansion and the quantity of gypsum has no evident influence on the behaviour of mortars. On the other hand, the paste composition is different for limestone and fly ash, which means that the chemical reactions of aluminates are different. In the case of cement 30V monosulfate prevails for 180 days. In contrast to this, in a mortar of cement 30L and 30LG, there are relatively high concentrations of ettringite. However, the remaining gypsum in the mortars of cement with limestone, especially 30L, presents a serious hazard and gives the potential for ettringite formation at later ages.

5. CONCLUSIONS

From the results of the investigation, the following conclusions can be drawn:

1. The addition of 15% limestone decreases the expansion of mortars to a larger degree than the low lime fly ash.
2. The addition of 30% of limestone and low lime fly ash practically eliminates the expansion of mortars.
3. The addition of a small quantity of potassium hydroxide solution (0.2% of KOH) and gypsum (0.9%) to cements with 15% of fly ash or limestone has a very pronounced effect on expansion but the explanation of this phenomenon needs further study.
4. The determination of the liquid phase composition in the mortar should give more information about the influence of the addition of KOH and gypsum to the system.
5. In case of cement 30L the high content of gypsum remains in the mortar after 180 days of water curing.
6. More light on the problem of gypsum in case of the limestone addition should give examination of the SO_4^{2-} concentration in the liquid phase of the mortar as well as following the paste composition over longer curing times.

REFERENCES

[1] Johansen V., Thaulow N., Skalny J., “Simultaneous presence of alkali-silica gel and ettringite in concrete”, Adv. Cem. Res. 5, pp. 23-29, 1993.

[2] Lewis M.C., Scrivener K.L., “Heat Curing and Delayed Ettringite Formation”, Mat. Res. Soc. Symp. Proc., pp. 243-250, Boston 1995.

[3] Scrivener K.L. and Lewis M.C., “A microstructure and microanalytical study of heat cured mortars and delayed ettringite formation”, 10th ICCC Göteborg 1997, vol. IV, paper 4IV061.

[4] Famy C., “Expansion of heat-cured mortars”, PhD Thesis, Imperial College Materials Department, London, UK, 1999.

[5] Ghorab H.Y., Heinz D., Ludwig U., Meskendahl T. and Wolter A., On the stability of calcium aluminate sulfate hydrates in pure system and in cements”, Proc. 7th ICCC, vol IV, Paris 1980, pp, 496 –503.

[6] Heinz D., Ludwig U. and Rudiger I., “Delayed ettringite formation in heat treated mortars and concretes”, Concr. Precas. Plant and Technol. Vol. 11, pp. 56-61, 1989.

[7] Fu Y. and Beaudoin J. J., “Microcracking as a precursor to delayed ettringite formation in cement systens”, Cem. Concr. Res., vol. 26, pp. 1493-1498, 1996.

[8] Kelham S., “The Effect of Cement Composition and Fineness on Expansion Associated with Delayed Ettringite Formation” Cem. Concr. Comp., vol 18, pp 171-179, 1996.

[9] Kurdowski W., Kurdowski Symposium, Kraków 2001, pp. 139-157.

[10] Kurdowski W. unpublished data.

[11] Graf Otto, ed., Handbuch der Werkstoffprufung, Springer Verlag, Berlin, 1941, p. 407.

MICROSTRUCTURE OF HAC PASTE AFTER FIFTEEN YEARS OF IMMERSION IN STRONG CHLORIDE SOLUTION

Wiesław Kurdowski[1], Sylwester Duszak[1] and Francois Sorrentino[2]

[1]University of Mining and Metallurgy, Cracow, Poland
[2]Lafarge, France

ABSTRACT

Bars of HAC paste showed high strength after fifteen years of immersion in a strong chloride solution. No evident trace of corrosion was seen. On the surface of the bars a skin was found which was detached in several places. The cross section of the bar revealed three zones: the superficial and intermediate layers of total thickness of about 3 mm and the "unchanged" interior of the paste. The superficial layer has a much higher porosity than the intermediate layer, but lower than the interior of the sample. The intermediate layer has the lowest porosity and seems to play a role of a diffusion barrier. The chloride ion content is the highest in superficial layer, but the differences are not very pronounced. Also the phase composition of all three zones of the sample is very similar and the main components are Friedel's salt, gibbsite and hydrogarnet. The composition of the skin is totally different and contains brucite and aragonite. The transformation of hexagonal aluminates to cubic had no negative influence on strength. Also the results of experiments clearly show that the formation of Friedel's salt has no destructive effect on cement paste. HAC paste is extremely durable in strong chloride solution.

Keywords: aragonite, basic calcium chloride, calcite, chloride corrosion, Friedel's salt, hydrogarnet, gibbsite, High Alumina Cement,

1. INTRODUCTION

During their hydration high aluminate cements (HAC) develop hexagonal crystals CAH_{10}, C_2AH_8 which transform to cubic hydrogarnet C_3AH_6. The ability of these hydrates to trap chloride ions (1) mainly as chloroaluminate $C_3A{\times}CaCl_2{\times}10\ H_2O$ (Friedel's salt) has led to several applications of this type of cement such as concreting in marine [2,3] or chemically severe environments [4,5] or stabilisation of waste [6,7] .

Another area of interest concerns the ability of HAC to prevent the corrosion of concrete reinforcement [8,9].

The good performance of HAC in a corrosive environment is mainly due to the development of a special microstructure [10]. Nevertheless, the problem relevant to the durability of the structures i.e. the formation and the stability of the Friedel's salt, deserves a definite answer.

Most of the studies which have been done in the past [2-11] have used a calcium aluminate cement produced by a smelting process. In the present study, we use a calcium aluminate produced by sintering

In 1990 during the HAC Conference in London the results of the investigations of corrosion of HAC paste immersed in strong chloride solution were presented [12]. The main conclusions of these investigations were that the good durability of the paste was caused by very low porosity. The only new phase formation found in the core of the paste was Friedel's salt.

After a further 12 years of immersion of the bars of HAC past, the samples were once more examined. The results of this examination are presented in this paper.

2. MATERIAL

The samples were the bars of HAC paste made in 1987 and immersed in strong chloride solution whose composition is presented in Table1 [12]. The solution was the mine water from the salt mine Kłodawa in north Poland. The dimension of bars was 4 x 4 x 16 cm and w/c ratio of the paste was 0.4.

Table 1. Chemical composition of chloride solution

Component	Concentration, g/l
NaCl	240
$MgCl_2$	65
KCl	15

The HAC cement used was Górkal 70 from the Polish plant and was produced by the sintering method. Its main mineralogical phases were CA and CA_2 and αA added during grinding. In very small amounts, gehlenite was also present.

In the bars crushed during compressive strength measurement, several layers can be distinguished even with naked eye. Thus the bars were cut in such a manner to obtain a sample including all layers formed in the bar during immersion in chloride solution. Simultaneously each layer was separated and constituted individual samples.

From all samples, polished sections were prepared for SEM examination. Independently, crushed pieces of the bar were also examined under SEM.

3. METHODS

Phase composition of the samples was determined by XRD which was the basic method.

The XRD results were supported by SEM examination connected with chemical analysis using EDAX.

For porosity measurements the Mercury Intrusion Porosimetry method was used.

4. EXPERIMENTAL RESULTS

The bars are in a very good state with no trace of destruction, even of surface corrosion.

The confirmation of this good state of samples was their high strength. The strength was as follows:

compressive strength 69.1 MPa
bending strength 17.3 MPa

On the surface of the bars a brighter skin deposited (Figure 1). This skin is very unstable and is detached in several places.

Under the skin there is a dark external layer about 2 - 3 mm thick. Then there is a bright transitional layer about 1 mm thick. This bright layer surrounds the “unchanged” core of the sample (Figure 2)

MIP shows that the porosity of the bright transitional layer is very low, much lower than the core. However, the average pore radius is the highest in this zone and drastically lower in the core. The results of the MIP measurements are presented in Table 2.

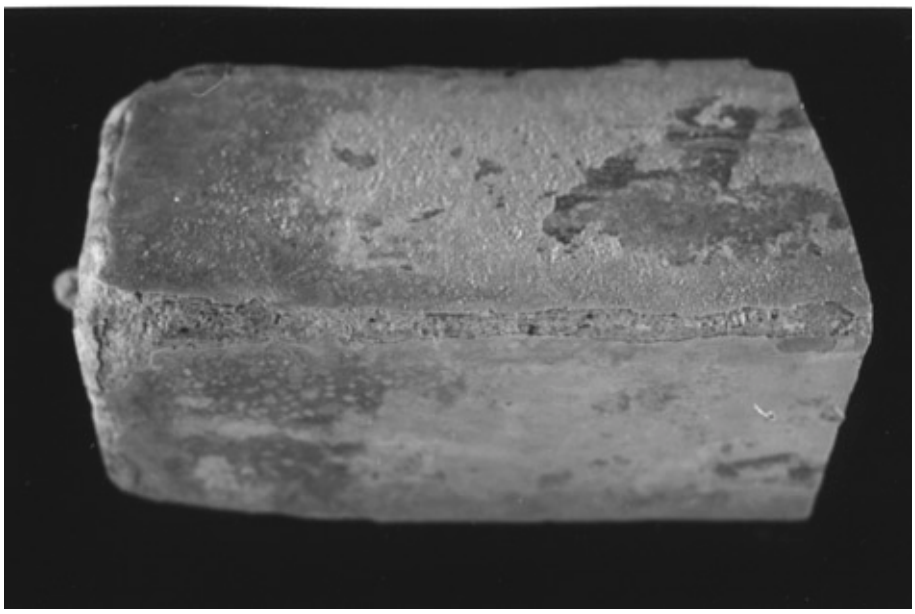

Figure 1. General view of the cut bar with partially detached skin

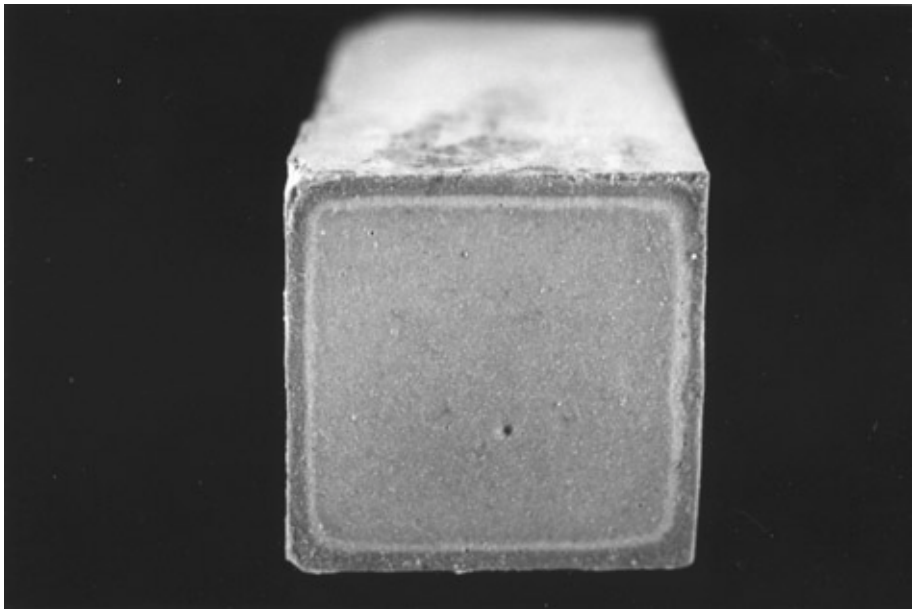

Figure 2. The section of the bar; the dark, the bright layers and the core are clearly visible

Table 2. Porosity of three zones of the bar

Layer	Total pore volume, mm^3/g	Porosity, %	Average pore radius, μm,
Core	3.00	0.66	0.016
Transitional	0.73	0.16	0.44
External	2.14	0.45	0.23

The chemical composition of the three zones of the bar was determined by EDAX. The results (Figure 3) show that the differences are very limited. It is seen that the content of three elements in question i.e. Ca, Al and Cl is practically the same in the transitional layer and in the core.

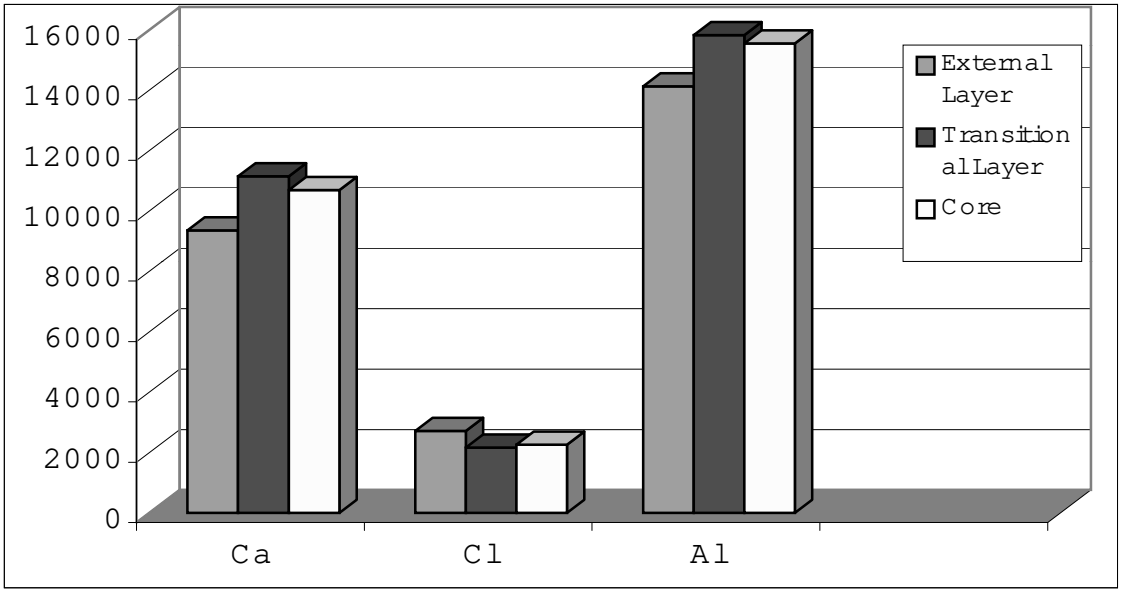

Figure 3. Content of three elements in different zones of the sample.

The X-ray examination of the skin shows that it is composed principally of brucite and aragonite. Two additional phases are calcite and Friedel's salt (Figure 4), but their content is drastically lower. A trace of halite is also found.

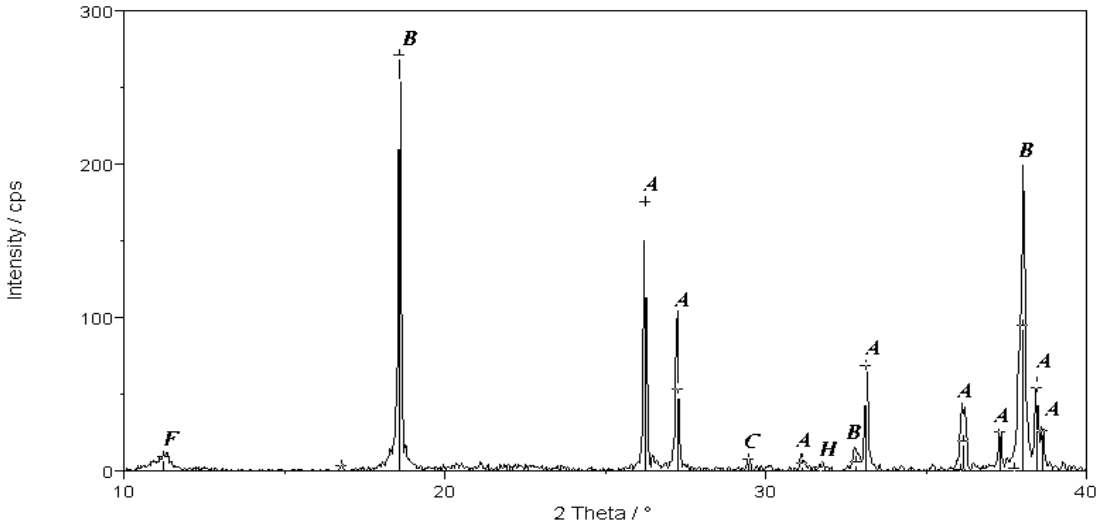

A – Aragonite, B –Brucite, C – Calcite, F – Friedel's salt, H – Halite

Figure 4. X-ray of skin

The phase composition of three other samples i.e. two layers and the core differ significantly from each other (Figure 5). The external layer contains low quantity of Friedel's salt but high content of calcite. The content of gibbsite is relatively high. These remaining phases are aragonite and CA_2.

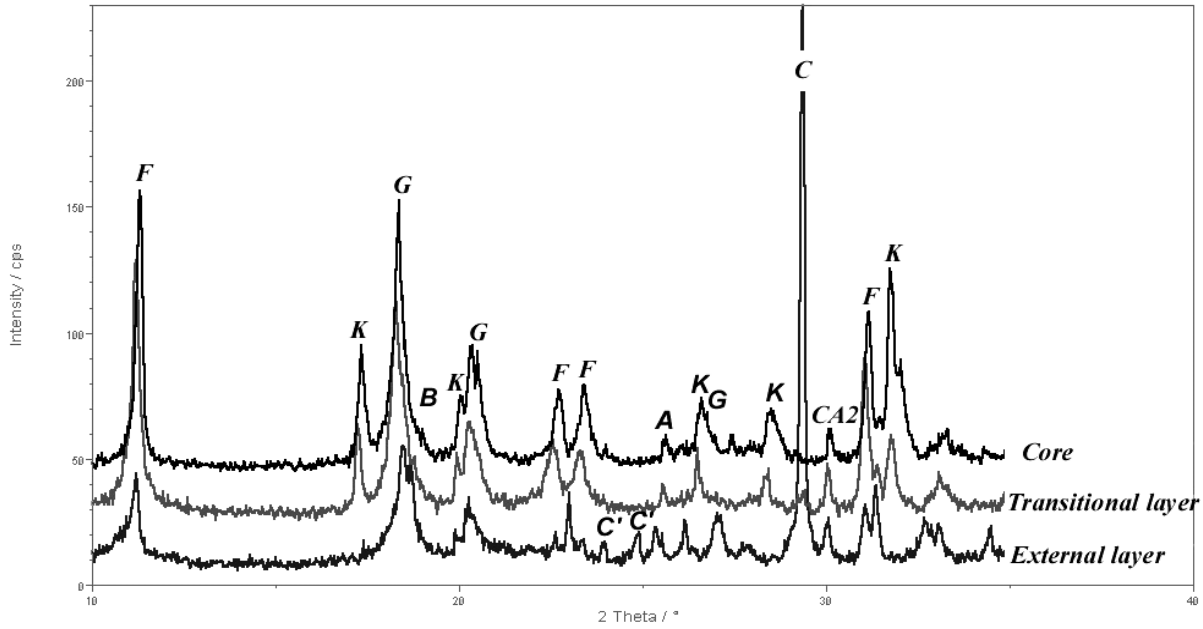

F – Friedel's salt *K - Hydrogarnet* *G – Gibsite* *C - Calcite*
A - Corundum *C' – Aragonite* *B –Brucite*

Figure 5. Phase composition of two layers and a core

The transitional layer is much richer in Friedel's salt. Also the X-ray lines of hydrogarnet have a high intensity. Gibbsite concentration is considerable.

The content of CA_2 seems to be on the same level in all three sample. Small quantities of calcite are to be noted.

The core is very rich in three phases namely: Friedel's salt, gibbsite and hydrogarnet.

The phase composition is summarised in Table 3.

Table 3. Phase composition of different zones of the bar

Layer	Main phases	Minor phaes
Skin	Aragonite, Brucite	Calcite, Friedel's salt, Halite
External layer	Calcite, Friedel's salt, Gibsite	CA_2, Corundum, Brucite, Aragonite
Transitional layer	Friedel's salt, Gibsite, Hydrogarnet	CA_2, Corundum,
Core	Friedel's salt, Gibsite, Hydrogarnet	CA_2, Corundum,

SEM observation supported but also enriched the results of XRD analysis. This observation shows that in the skin the basic calcium and magnesium chlorides are present (Figure 6).

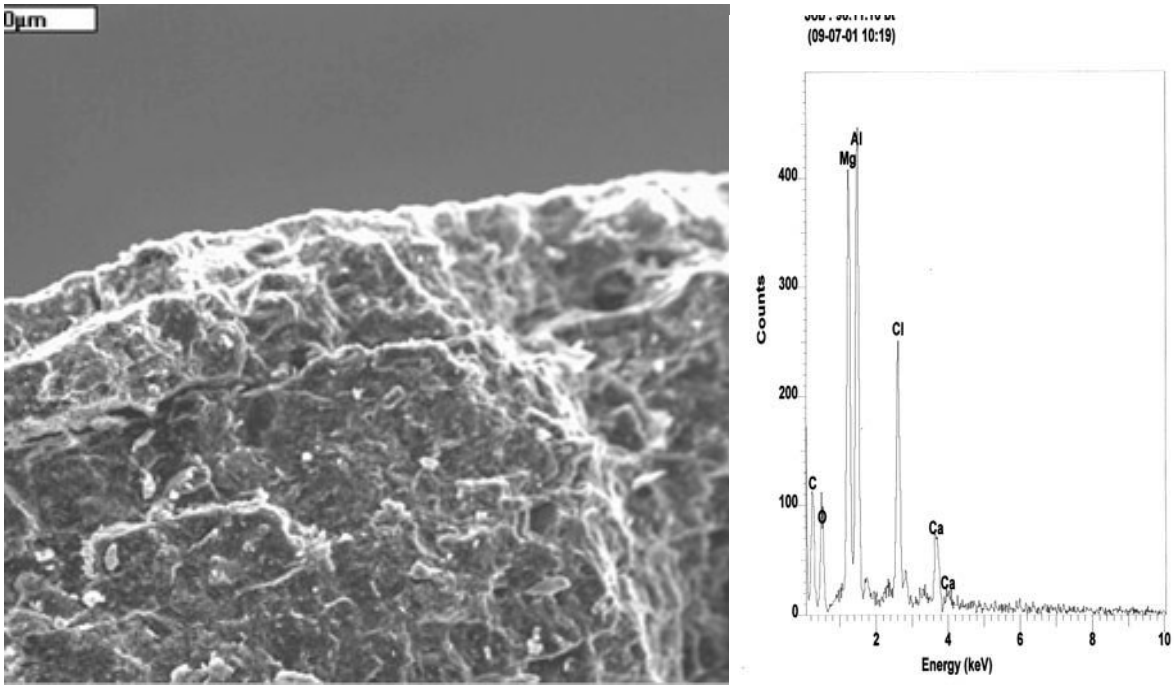

Figure 6. SEM image of the skin and two layers

These chlorides form very compact gel and it is the reason of inefficiency of XRD (Figure 7).

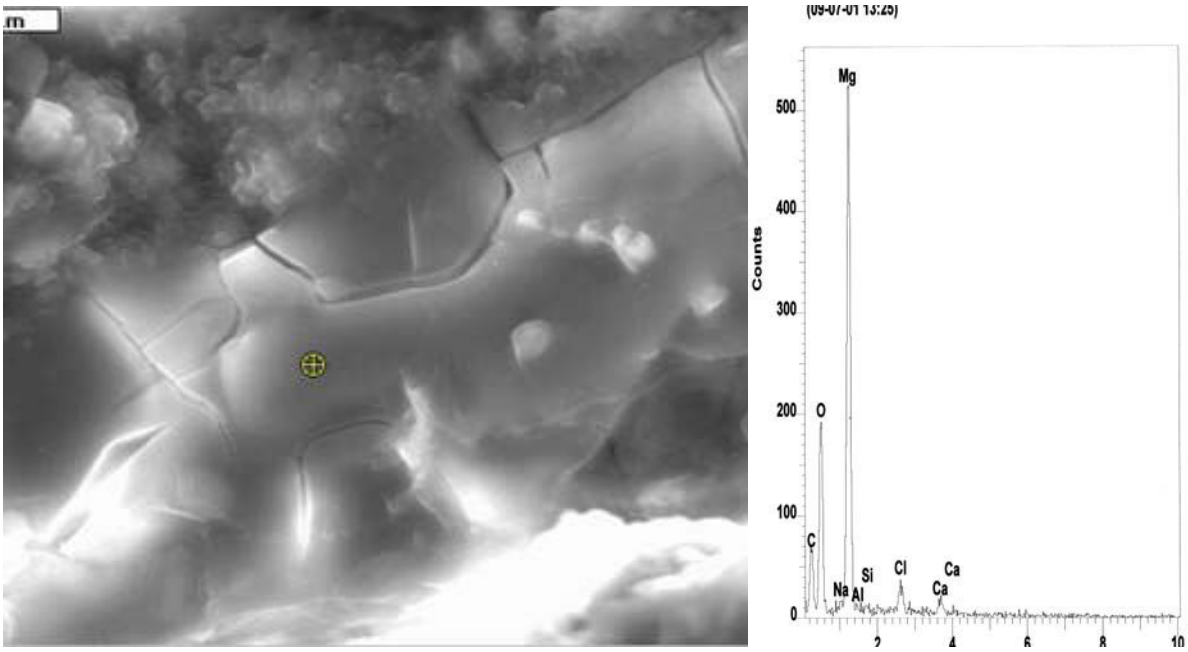

Figure 7. Compact layer of basic chlorides

The two remaining phases are aragonite and brucite (Figure 8).

CA_2 forms frequently forms large grains of about 100 µm (Figure 9) but can also be found in beautiful crystals.

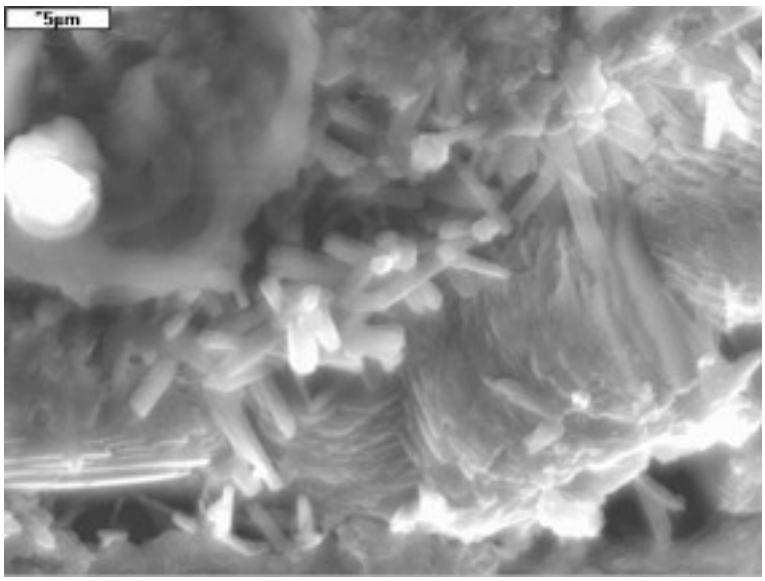

Figure 8. The composition of the skin under SEM,
low layer – brucite, midlle layer aragonite laths

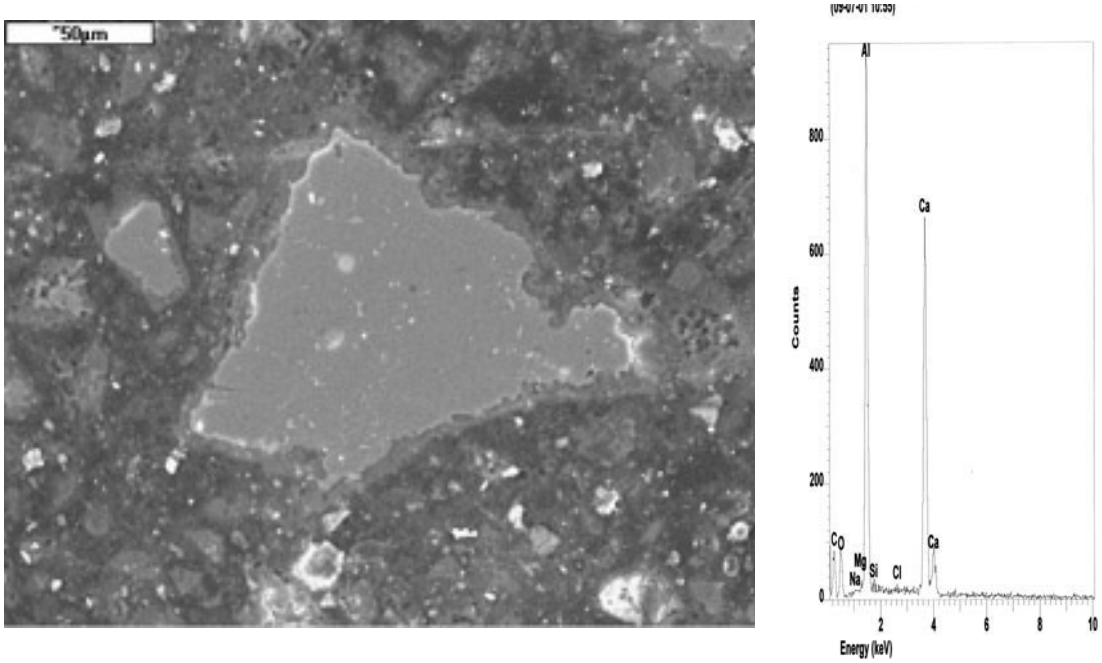

Figure 9. SEM picture of CA_2 big grain

The results of careful X-ray microanalysis give some interesting data. The layer of hydrates which surrounds the unhydrated cement grain which represents the Friedel's salt of low chloride content. One can suppose that there is a solid solution series $C_3A{\times}CaCl_2{\times}10H_2O$ - C_4AH_{13} [13]. The particles in this layer represents the content of chloride in the level 4.5 - 10.4% (Figure 10). It seems that this layer represents so called inner hydrate.

The process of transformation of cement grains into the Friedel's salt hydrate is shown in Figure 11. The central part of transformed grains is composed of particles of Friedel's salt but near the two ends the brighter relicts of unhydrated cement are clearly seen (Figure 11).

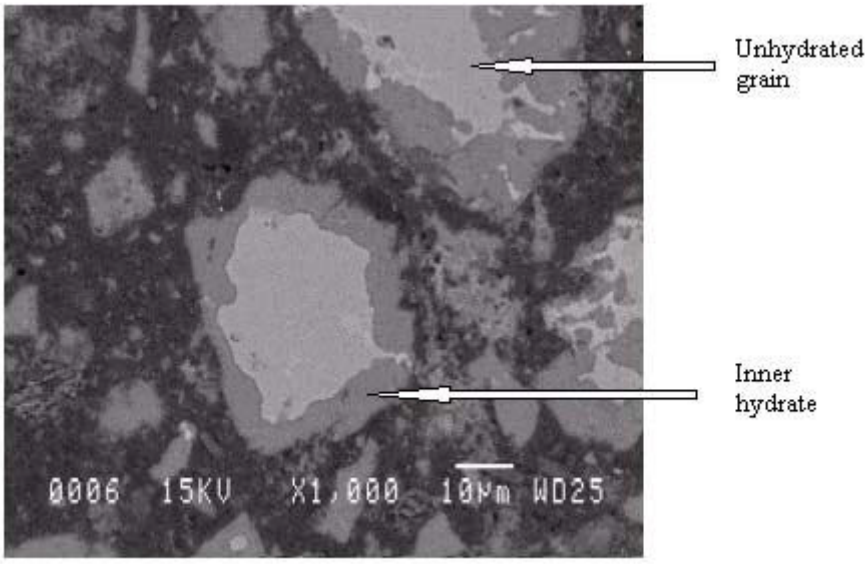

Figure 10. Solid solution Friedel's salt - C_4AH_{13}
around the unhydrated cement grain (inner hydrate)

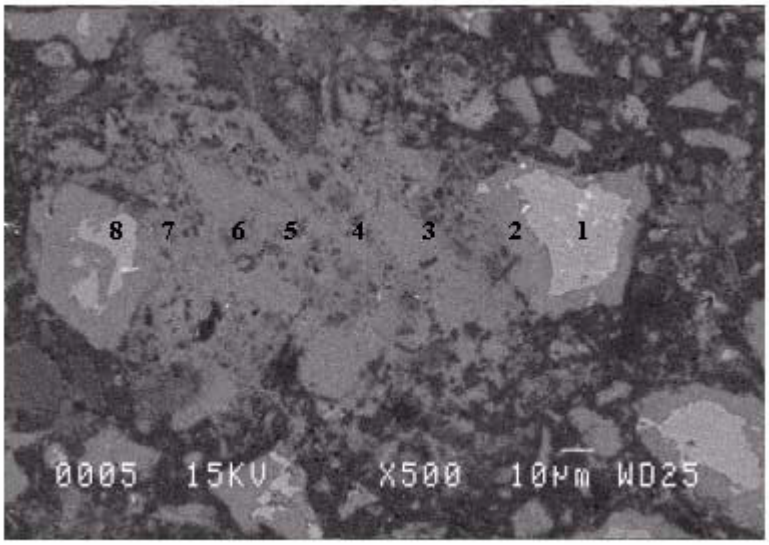

Figure 11. Transformation of unhydrated cement (1-8) in Friedel's salt (3-6), 2 and 7 represent a solid solution of Friedel's salt and calcium aluminate hydrates

In Table 4, some examples of typical analysis of different phases are shown.

Table 4. Typical analysis of different phases

Component	Kind of phase					
	cement	Friedel's salt	solid* solution	Alumina	Gehlenite	CA_2
	content, mass %					
CaO	36.3	57.5	59.3	3.5	41.9	18.4
SiO_2	0.3	0.3	0	1.0	20.0	1.2
Al_2O_3	62.9	25.6	34.5	93.7	37.6	72
Fe_2O_3	0.3	0	0.5	0	0	0
MgO	0	0	0	0	0	0
Cl_2	0	15.5	5.5	0.3	0.2	8.1

* solid solution Friedel's salt - C_4AH_{13}

The minor phase which is gehlenite contains practically no chloride and the same is valid for alumina. Contrary to this in CA_2 the content of chloride is relatively high. This is probably the beginning of the transformation of this phase into Friedel's salts.

5. DISCUSSION

The results of examinations show that the HAC paste is very durable when immersed in strong chloride solution. On the superficial zone of the bars the transitional layer is formed which is very dense and hinders the diffusion of chloride ions in the deeper part of the bar. The concentration of chloride ions in this transitional layer is significantly lower than in the external layer and is the same as in the core. Also the mineralogical composition of the transition zone is almost identical to that of the core and differs drastically from the external layer.

Contrary to this the skin is not very stable and seems to play a minor role as a corrosion barrier. Also its mineralogical composition changed significantly during the long period of aggressive action of the chloride solution. Previously the main constituents were basic chlorides and amorphous brucite [12]. Now under influence of atmosphere which enriched the solution in CO_2 aragonite prevails but also a crystalline brucite is in high concentration. The trace of halite can be caused by different nest formations under the skin which were found in our first study [12].

In the external layer no basic chlorides were found and the main corrosion products are calcite and Friedel's salt.

Also in the core of the sample Friedel's salt is formed preferentially on the surface of cement grains and frequently forms a solid solution with C_4AH_{13} and thus has a lower chloride concentration.

Results show that the HAC paste is very durable in chloride environments and the main corrosion product is Friedel's salt. Simultaneously the paste composition is changed from CAH_{10} hydrogarnet which became the main hydration phase. Also alumine hydroxide gel is transformed into gibbsite.

Despite the relatively high content of Friedel's salt in the core of the sample the porosity of this part of the bar is very low (Table 2). Without doubt it is the main reason for the very good durability of the paste [14]. It is also evident that the formation of Friedel's salt is not accompanied by crystallisation pressure and porosity increase. Average pore radius in the core is about 16 nm which means that the pores belong to the very small capillary pores. Because of the low porosity of the paste its strength is high, even after 12 years of immersion in chloride solution.

6. CONCLUSIONS

From the experimental results the following conclusions can be drawn:

1. HAC paste is very durable in chloride solution,
2. The main corrosion product in the bar, except in the superficial layer, is the Friedel's salt after 12 years corrosive action of chloride solution,
3. The formation of Friedel's salt does not cause an increase of porosity and the strength of cement paste remains high,
4. The hydration products underwent transformation i.e. the $Al(OH)_3$ gel formed gibbsite and the hexagonal hydrates were transformed into hydrogarnet.

REFERENCES

[1] G.M. Darr, U. Ludwig " The incorporation of chloride in calcium aluminate hydrate"
[2] Ind chim Belg 39, 687-692, (1974)
[3] P. C.Aitcin, F. Blais , C.M. George " Durability of calcium aluminate cement concrete: assessment of concrete from 60 year old marine structure of Halifax, NS, Canada " Symp. adv. Concr. technol. , Las Vegas 145-167, 1995
[4] N.C. Baker, P.F.G. Banfill " Durability of high cements mortars for the marine environnment" ACI SP 145, 409-422 (1994)
[5] S. Goni, M.T. Gaztanaga, J.L. Sagrera, M.S. Hernandez " The influence of Na Cl on the reactivity of high alumina cement in water : pore solution and solid phase characterization" J. of mater Res vol 9 N°6 June 1994 1533-1539
[6] M.A. Sanjuan " Formation of chloroaluminates in calcium aluminate cements cured at high temperatures and exposed to chloride solutions" Journal of materials science 32, 1997, 6207-6213
[7] B. Kessler, J. Letourneux, B. Robin, M. Testud " Finely divided waste incineration residue treatment" Patent EP 588689, 09/07/1993
[8] B. Jesus, B. Kessler, B. Robin, M. Rollet, F. Sorrentino" Waste incineration residue treatment by mixing with hydraulic binder additive and water and wet grinding" Patent EP 549492 12/18/1992
[9] M.A. Sanjuan " Overview on electrochemical parameters to assess the corrosion state of steel reinforcement in CAC mortar and concrete" J. mater. Sci. 35, 105-108, (2000)
[10] B. Reddy, G.K. Glass, P.L Lim, N.R. Buenfeld" On the corrosion risk by chloride bound in concrete" Cement, concrete composites , 24,2002,1-5
[11] S. Goni, A. Guerrero " Stability of Friedel's salt in calcium aluminate paste seven years old at 40°C " Conference on Calcium aluminate cements, Ed. R. J. Mangabhai , F.P. Glasser, Edimburgh, 2001, 385-394
[12] Y. Halse, P.L. Pratt " The development of microstructure of high alumina cement" 8th Intern. Conf Chem. f Cement 1986, theme 3, vol IV p 317-321 (Rio)
[13] W. Kurdowski, L. Taczuk and B. Trybalska, Calcium Aluminate Cements, Ed. R. J. Mangabhai, E. Spoon, 222-229, London 1990.
[14] C. M. George, “Structure and Performance of Cements” chapter IX, Ed. P. Barnes, Applied Science Pub., 417-470, London 1983.
[15] H. F. W. Taylor, Cement Chemistry, Academic Press, London 1990

EARLY-AGE HEAT EVOLUTION CHARACTERISTICS OF SOUTH AFRICAN CEMENTS IN RELATION TO CLINKER CHEMISTRY AND CRYSTALLOGRAPHY

Graham, P.C. and Ballim, Y.

School of Civil and Environmental Engineering, University of the Witwatersrand, Johannesburg, South Africa; E-mail: peterg@civil.wits.ac.za; ballim@civil.wits.ac.za

ABSTRACT

This paper presents the results of a test programme, which was undertaken to quantify and compare the heat characteristics of cement clinker obtained from most of the cement manufacturing facilities in South Africa. The clinkers were all ground to a uniform fineness, blended with a uniform gypsum and, using a uniform concrete mixture, were tested in an adiabatic calorimeter to determine the amount of heat and the rate of heat evolution during the early period of hydration. Cements obtained from the same manufacturing plants were also tested to separately indicate the effects of the actual manufacturing process on the heat characteristics of the cements. The heat results are also assessed in relation to the results of chemical analyses and optical microscopy of the clinkers.

The results show that the nine clinkers assessed can be categorised into low, medium and high heat clinkers. Also, for a given cement clinker, the heat characteristics of the manufactured cement appear to be related to a combination of fineness of grinding, amount of SO_3 and type of gypsum or additives used in the manufacturing process.

1. INTRODUCTION

The thermal response of concrete due to hydration of cement is a predominant factor in the potential for early-age cracking of large concrete elements. An analysis of this cracking potential requires an ability to quantify both the amount of heat that is evolved by the cement as well as the rate at which this heat is evolved [1]. Both these parameters are strongly influenced by the chemical and mineralogical composition of the cement, insofar as it affects the kinetics of the hydration reactions of cement. Furthermore, clinker morphology has been shown [2] to influence the compressive strength and, by inference, the hydration development of cement. Clearly, an ability to estimate the thermal response of cement in concrete, based on a knowledge of clinker characteristics would be of assistance to mass concrete designers and cement manufacturers seeking to control temperature development in such structures.

As a contribution to understanding the relationship between clinker characteristics and heat evolution, this paper presents the results of adiabatic calorimeter tests aimed at assessing the thermal response of a range of South African cements, nominally of the same quality and standard but drawn from different manufacturing facilities across the country. Nine clinker samples were obtained and a cement was produced from each clinker by grinding with a controlled amount of a uniform gypsum (laboratory cement). The laboratory cements were prepared in this manner (uniform specific surface area and SO_3 content) in order to render them as comparable as possible with respect to the thermal responses of the clinkers. Manufactured cement was also obtained from the same cement plants (factory cement) to provide a basis for determining the effects of the manufacturing process on the heat characteristics of the cement, as distinct from the clinker

chemistry. The chemical composition of the clinkers and the gypsum was determined using X-ray fluorescence (XRF) and samples of the raw clinkers were mounted, polished and etched for optical microscope study. These results were then used to characterise the crystallographic and chemical properties of the cements.

Each of the laboratory and factory cements was used to prepare a concrete with fixed mixture proportions and aggregate type. The concretes were tested in an adiabatic calorimeter in order to determine the rate and amount of heat evolved by the cements. Comparisons of the heat properties of the different cements were made on the basis of a maturity function rather than clock time.

2. CEMENT AND CLINKER SAMPLING AND PREPARATION

2.1 Sample Collection

Cement and clinker samples were drawn from nine production plants belonging to three cement companies operating in South Africa. Each of these production plants manufactures Type 1 cement that satisfies the requirements of the local standard specification, SABS EN 197-1 [3]. To ensure that the samples were representative of current production, the clinker was drawn from the moving stock just before entry into the grinding mill. Approximately 4 kg of clinker was drawn from each plant and 500 g of each sample was reserved for microscopy and chemical analysis. The remaining 3.5 kg was used to manufacture cement in the laboratory. At each factory, a 4 kg sample of manufactured cement was drawn from the exit end of the grinding mill approximately 20 minutes after the clinker sample was drawn. This ensured that, within reason, the clinker sample and the clinker component of the cement sample drawn from a production facility were of the same chemical composition.

2.2 Gypsum for Manufacturing the Laboratory Cements

In order to manufacture the cements in the laboratory, a sample of gypsum, with chemical composition as shown in Table 1, was obtained from one of the production plants.

Table 1. XRF analysis of the chemical composition of the gypsum used in the cements and the amount of gypsum added to each clinker

	% by Mass	Clinker Identification	% Gypsum added (by mass)
CaO	30.20	A	3.683
SiO_2	6.90	B	4.910
Fe_2O_3	0.44	C	5.031
Al_2O_3	0.60	D	5.010
MgO	0.80	E	5.147
TiO_2	0.04	F	4.490
Mn_2O_3	0.02	G	4.984
K_2O	0.19	H	5.120
Na_2O	0.25	K	4.490
SO_3	41.00		
P_2O_5	0.00		
LOI	18.25		

Based on this chemical analysis, the amount of gypsum added to each of the clinkers was adjusted so that each cement had an SO_3 content of 2.3%. Table 1 also shows the proportion of gypsum added to each of the cement clinkers. The SO_3 contents of the factory cements, determined from XRF analyses, are shown in Table 2.

2.3 Grinding and Fineness of the Cements

In manufacturing the laboratory cements, each clinker with the appropriate amount of gypsum was ground in a laboratory ball mill. The mill was periodically stopped and the specific area of the sample was determined using the Blaine test [4]. Grinding was stopped when the measured specific surface area of the sample was 3200 ± 50 cm^2/g. Using this procedure, the average fineness measured for the nine samples was 3198 cm^2/g with a standard deviation of 24 cm^2/g. The fineness of the factory cements was determined using the Blaine test and the results obtained are shown in Table 2.

Table 2. Fineness and SO_3 contents of the nine factory cements sampled

Clinker	A	B	C	D	E	F	G	H	K
Fineness (cm^2/g)	2956	3528	3197	3528	3756	2886	3650	3702	3573
SO_3 (%)	2.36	2.00	1.35	1.61	2.11	2.23	1.67	1.97	2.00

3. TEST METHODS

3.1 X-ray Fluorescence

XRF was used to determine the chemical compound composition of the clinkers. The analyses were conducted using ground clinker samples and these results were also used to determine the required amount of gypsum for each cement. This analysis was conducted in the laboratory of one of the cement producers, where XRF is used for routine quality control purposes. The instrument is regularly calibrated and checked for operational accuracy. The samples used in this project were placed in the automatic feed system of the instrument alongside the routine production sample analyses.

3.2 Optical Microscopy

A geological polarising microscope with reflected light capability, was used to assess the structure and morphology of polished and etched samples of each of the clinkers. The clinker samples were lightly crushed using a steel pestle and the –2.36 to +1.18 mm fraction was used to prepare the polished sections. The fragments were encapsulated in epoxy and one surface was polished, initially with 600 grit carborundum paper, followed by progressively finer abrasion systems, until a final polish with 0.25 mm diamond paste, on a lapping disk with a non-aqueous lubricant.

The polished samples were then etched using a procedure recommended by St John, et al [5] in order to differentiate the alite, belite and interstitial aluminate phases in the clinker. Digital photo-micrographs were then obtained of the etched surfaces and an image analysis system was used to measure crystal sizes and to provide a qualitative description of the clinker morphology.

3.3 Adiabatic Calorimetery

3.3.1 Expressions for the rate of heat evolution

The adiabatic calorimeter proposed by Gibbon, et al [6] was used to determine the amount and rate of heat evolved by each of the laboratory cement samples. In essence, the calorimeter uses a one-litre sample of concrete in a bath of water but separated from direct contact with the water by a 40 mm thick air space. A temperature probe in the concrete sample is monitored by a personal computer fitted with an analogue-to-digital input/output card. A heater element in the concrete bath is then turned on or off in response to the concrete temperature to maintain the water bath at the same temperature as that of the concrete. The concrete temperature is then monitored over time and the amount of heat per unit mass of cement (q_t) is determined from:

$$q_t = C_p.(T_t - T_o).\frac{m_s}{m_c} \quad (1)$$

where C_p is the specific heat capacity of the concrete, determined as the mass weighted average of the specific heat capacities of the concrete components and is assumed to be constant throughout the test [6]; T_t is the temperature of the concrete sample at time t during the adiabatic test and T_o is the sample temperature at the beginning of the test; m_s is the mass of the concrete test sample and m_c is the mass of cementitious binder in the sample.

The heat rate is conventionally determined by differentiating Equation 1 with respect to time, so that:

$$\dot{q}_t = \frac{dq_t}{dt} \quad (2)$$

The time basis of Equation 2 presents a problem because of the circular relationship between the rate of heat evolution, the extent of hydration, time and the temperature at which the hydration reactions take place. This is generally addressed by expressing the heat rate (as in Equation 2) as a function of maturity [7,8], rather than time. Hence, the heat rate applicable to a particular point in a structure at a given time is determined by the maturity (or time-temperature history) at that point. Stated differently, at a given point in time, the heat rate will vary across a concrete section in accordance with the variation in maturity across the section.

In order to normalise the heat curves to an equivalent degree of advance of hydration, the time axis is expressed in terms of Arrhenius maturity development [9], which, in its relative form, is written as:

$$t_{20} = \sum_{i=1}^{i=n} \exp\left[\left(\frac{E}{R}\right)\left(\frac{1}{293} - \frac{1}{273 + 0.5.\left(T_i + T_{i-1}\right)}\right)\right].\left(t_i - t_{i-1}\right) \quad (3)$$

The reference temperature in Equation 3 is taken as 20 ^{o}C and t_{20} is the equivalent maturity time (in hours); E is the activation energy parameter (33.5 kJ/mol, taken as constant [10]); R is the universal gas constant (8.314 J/mol.^{o}C); T_i is the temperature (^{o}C) at the end of the i^{th} time interval, t_i.

Noting that the rate of hydration and therefore, the rate of heat evolution, is dependent on the absolute temperature, Ballim and Graham [11] have shown that, since Equation 1 accounts only for temperature differences, the rate of heat evolution determined from an adiabatic calorimeter test should be normalised with respect to maturity, rather than time. This means that, rather than the form shown in Equation 2, the heat rate should be expressed as:

$$\dot{q}_M = \frac{dq_t}{dM} \quad (4)$$

Expressing the maturity heat rate (Equation 4) as a function of the cumulative maturity, allows the heat rate curve to be normalised so as to be independent of the starting temperatures in the adiabatic test.

3.3.2 Sample preparation and testing

The nine laboratory cements were each used to make a concrete sample with the mixture composition as shown in Table 2. All the mixture components, including the water, were stored in the same room as the calorimeter at least 24 hours before mixing. This allowed the temperature of the materials to equilibrate to the room temperature, which was controlled at 19±1 ^{o}C. A 1.2 litre sample of each concrete was prepared by manual mixing in a steel bowl and the adiabatic test was started within 15 minutes after the water was added to the mixture. All the tests were started at

temperatures between 18 and 20 ^{o}C and temperature measurement in the calorimeter was continued for approximately 4 days. The silica sand used in the concretes was obtained in four size fractions and these were recombined as needed for the mixing operation to ensure a uniform sand grading for each concrete.

Table 2. Mixture composition of the concrete used for the adiabatic calorimeter tests

Cement	350 kg/m^3
9.5 mm washed silica stone	850 kg/m^3
graded, washed silica sand	885 kg/m^3
Water	233 L/m^3

4. RESULTS AND DISCUSSION

4.1 XRF Analysis

Table 3 shows the results of the XRF analyses of each of the clinker samples. The table also shows the calculated proportions of the four main cement mineral phases in each clinker based on the Bogue analysis [12]. It was not thought necessary to apply the modifications to the Bogue analysis as proposed by Taylor [13] since the analysis was conducted on clinker samples. In this case, the error incurred in the analysis would not be significantly improved for rapidly cooled clinkers such as those tested in this investigation. Table 3 also shows the calculated values of the alumina and silica ratios as defined in reference 12.

The following points are noted from the results presented in Table 3:

- The chemical compound analysis of the clinkers generally lies within the limits proposed by Addis [14] for South African cements. This means that the nine clinker samples selected can be considered typical of South African clinkers intended for cement manufacture.
- Clinker E shows an unusually high content of Fe_2O_3 which explains the high calculated C_4AF content of this clinker.
- Clinker K is unusual in the group because of the significantly higher MgO content as well as the higher Al_2O_3 content.
- Accepting that the Bogue analysis indicates likely or potential compound development, the results indicate that the higher alite content of clinkers B, C, E and F is likely to result in relatively high early age heat results because of the strong influence of this compound on heat liberation during early hydration [13].
- The relatively high C_3A content of clinker K is also likely to add significantly to the early heat evolution of this clinker.
- With the exception of the cements from clinker A, all of the cements can be classed as low alkali [14]. The sodium equivalent values for clinkers B and C are however lower than the minimums cited by Addis [14] for South African cements.

Table 3. Results of XRF analysis of the clinker samples and Bogue calculation of crystalline phase composition.

	% Composition of clinker								
	A	B	C	D	E	F	G	H	K
CaO	66.50	68.16	66.50	65.57	68.40	67.60	67.60	65.06	65.6
SiO_2	22.30	23.03	21.20	22.15	22.10	22.20	22.80	22.26	21.90
Fe_2O_3	3.61	2.28	3.03	2.98	4.26	3.33	1.90	3.05	1.57
Al_2O_3	3.80	3.82	4.20	4.51	3.80	4.40	4.30	3.98	5.00
MgO	1.10	1.48	3.30	2.64	0.50	0.80	1.40	2.04	3.70
TiO_2	0.18	0.31	0.30	0.45	0.19	0.21	0.28	0.25	0.26
Mn_2O_3	0.05	0.17	0.61	0.22	0.09	0.06	0.24	0.99	0.72
K_2O	0.62	0.13	0.25	0.16	0.39	0.57	0.58	0.53	0.32
Na_2O	0.37	0.00	0.12	0.20	0.19	0.18	0.06	0.14	0.11
SO_3	0.82	0.30	0.25	0.26	0.20	0.48	0.27	0.21	0.48
P_2O_5	0.15	0.00	0.02	0.00	0.16	0.13	0.03	0.00	0.10
Free Lime	1.02	1.10	1.25	0.80	0.82	0.61	1.57	0.97	0.35
LOI	0.80	0.30	0.58	0.00	0.64	0.12	0.98	0.90	0.16
TOTAL	100.20	99.98	100.30	99.14	100.80	100.80	100.40	99.41	99.92
Alumina Ratio	1.05	1.67	1.39	1.51	0.89	1.32	2.25	1.31	3.16
Silica Ratio	3.03	3.80	2.96	2.98	2.77	2.90	3.70	3.19	3.36
Crystalline phase composition (%) by Bogue analysis									
C_3S	66	69	72	61	75	70	64	61	63
C_2S	14	14	7	18	6	11	17	18	15
C_3A	4	6	6	7	3	6	8	5	11
C_4AF	11	7	9	9	13	10	6	9	5

4.2 Optical Microscopy

Table 4 presents a summary of the observations made during the microscopic assessment of the clinkers.

4.3 Adiabatic Calorimetry

Figure 1(a) shows the calculated heat rates for the nine laboratory cements using the maturity heat rate form as described by Equation 4. The units of the heat rate in this figure are unconventional and are best described as “maturity watts” per kg of cement (J/maturity second per kg). This figure shows considerable overlap of the heat rate curves and only the clearly discernable curves are identified. Expressed in this form, clinker cement K stands out in the brief but significantly larger heat rate at between 15 and 20 maturity hours. The curves also show that, after 200 maturity hours, most of the maturity heat rates have reduced to less than 0.1 J/maturity second/kg.

Based on the heat rate curves shown in Figure 1(a), the laboratory cements fall into three distinct groups in terms of the maximum heat rate as follows:

- High heat – clinker cement K
- Medium heat – clinker cements A, B, E and F
- Low heat – clinker cements C, D, G and H

For clarity, representative curves of each of these three groups are extracted from Figure 1(a) and shown in Figure 1(b). Figure 2 shows the measured heat rates of the laboratory and factory cements made with clinker D as an example of the effect of the downstream production process on heat rate.

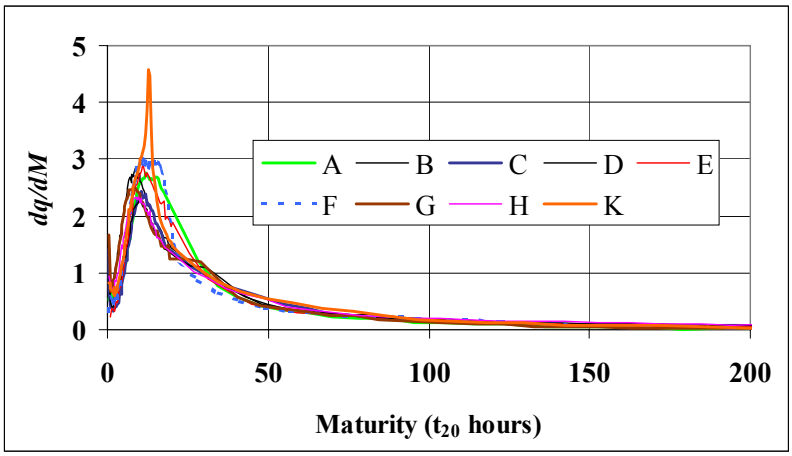

(a)

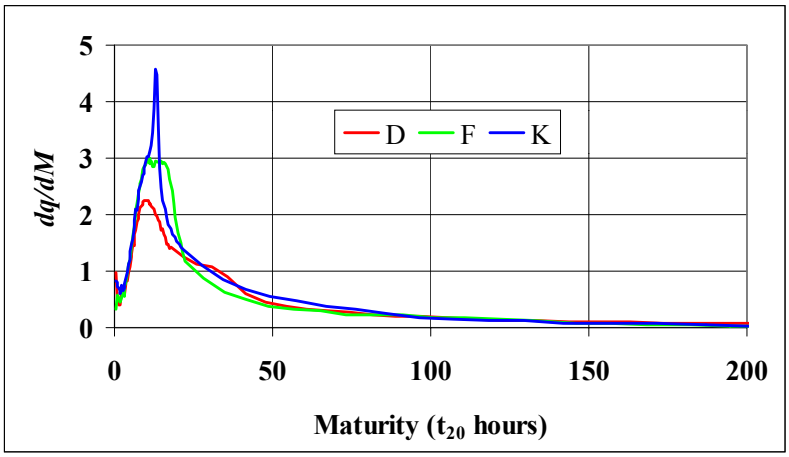

(b)

Figure 1. Measured heat rates of the nine laboratory cements showing (a) all the curves and (b) three curves representative of the three heat rate categories.

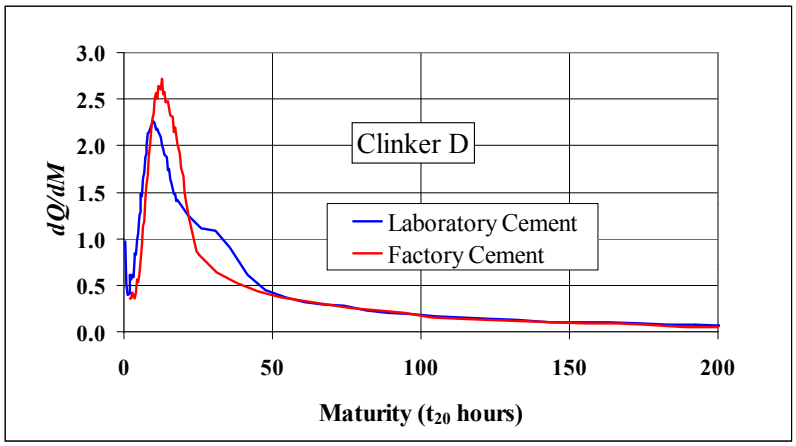

Figure 2. Measured heat rates of the laboratory and factory cements made with clinker D

Table 4. Summary of observations made during the microscopic examination of the clinker samples

Clinker	Alite	Belite	Interstitial phase
A	Angular, euhedral crystal shape, generally hexagonal; crystal size from 20 to 60 Φ*m*	Well distributed with occasional nests; rounded, oval or pear-shaped crystals; crystal size in the range 15 to 55 Φ*m*	Generally thinly distributed, especially in areas where C_3S and C_2S are tightly packed.
B	Angular, euhedral crystal shape, generally hexagonal; crystal size from 20 to 60 Φ*m*; most crystals have C_2S inclusions	Well distributed with occasional nests; rounded shapes with ragged edges; crystal size in the range 20 to 50 Φ*m*	Well distributed matrix with approximately equal aluminate and ferrite phases;
C	Dominant crystal form; many crystals have joined but retain the angular structure; crystal size from 10 to 50 Φ*m*	Sparse distribution; individual crystals rare and mainly occurs as flows between the C_3S crystals; crystal size from 3 to 15 Φ*m*	Well distributed matrix; aluminate clearly discernable and appears as localised patches or concentrated spots
D	Crystals usually angular with common pseudohexagonal shapes; crystal size from 10 to 50 Φ*m*; some large inclusions	Well distributed in small nests; rounded, oval or pear-shaped crystals; crystal size in range 10 to 30 Φ*m*; narrow rims on C_3S crystal edges	Well distributed throughout; poor distinction between phases; aluminates appear present as localised patches
E	Dominant crystal form; angular with pseudohexagonal shapes; crystal size from 10 to 55 Φ*m*; C_2S inclusions common	Well distributed in small nests; rounded to oval-shaped crystals; crystal size in range 10 to 35 Φ*m*; distinct lamellar structure	Good distribution with occasional abutting C_3S grains; aluminate in the form of narrow streaks – possibly dendritic
F	Tightly packed with much joining while retaining angular shape; small inclusions which are not common;	Well distributed in small nests; rounded to oval-shaped crystals; crystal size in range 20 to 30 Φ*m*; distinct lamellar structure	Good distribution; aluminate in the form of small patches and narrow streaks – possibly dendritic
G	Relatively small grains: 5 to 35 Φ*m*; angular with pseudohexagonal shapes; inclusions common	Rounded to oval; small crystals: 5 to 40 Φ*m*; thin zones on edges of C_3S.	Aluminate phase prevalent; large patches with small ferrite areas.
H	Tightly packed grains; joined to form subhedral shapes; 10 to 50 Φ*m*; some inclusions	Well distributed in small and large nests; rounded to pear shaped; 10 to 30 Φ*m*	Aluminate phase in dindritic form
K	Crystals angular euhedral; often joined; 10 to 40 Φ*m*; inclusions small and rare	Individual crystals rare; generally occurs in the matrix in dendritic crystals or as rims on C_3S grains	Well distributed and rich in aluminate; small amounts of periclase visible.

In general the difference between the heat rates of the laboratory and factory cements was in the peak heat rate obtained, with the ascending and descending limbs of the heat rate curves showing significant overlap. Hence, as a basis for comparison, Table 5 shows the maximum heat rate obtained for the laboratory cements and the corresponding factory cements.

Given the methods of sample preparation used in this project, the main production factors that are likely to differentiate the heat characteristics of the factory cements are the fineness and SO_3 content (shown in Table 2) and the additives (if any) added at the grinding stage in the factory. The extent and nature of any extraneous materials added at the grinding stage were not identified or quantified in this project nor was the actual gypsum used at each factory analysed to assess variations in the chemical compositions.

Table 5. Peak maturity heat rates measured for the laboratory and factory cements

Cement Type:	Peak heat rate (Watts/kg) using clinker:								
	A	B	C	D	E	F	G	H	K
Laboratory	2.75	2.85	2.44	2.26	2.91	3.00	2.50	2.34	4.58
Factory	2.56	2.55	3.00	2.72	3.45	2.69	2.93	1.52	6.72

Considering the results shown in Table 5 together with the measured fineness and SO_3 contents of the factory cements as shown in Table 2, it appears that, in general, a higher fineness and a lower SO_3 content results in higher peak heat rates. However, this observation is not valid for clinkers B and H. In particular, clinker H has a fineness of 3702 cm^2/g (compared to 3200 cm^2/g for the laboratory cement) and an SO_3 content of 1.97% (compared to 2.3% for the laboratory cement), yet the peak heat rate of the factory cement is 35% lower than that of the laboratory cement. The reason for this is likely to lie in the type of gypsum or the effects of possible additives used in the manufacture of this cement.

4.4 Relating heat rates to physico-chemical characteristics of the clinker

Considering the results of the XRF analysis presented in Table 3, the qualitative description of the clinker morphology characteristics presented in Table 4 and the heat rate classifications presented above, the following points are noted:

- The high heat rate performance of clinker K seems to be related to the high C_3A content, which is also reflected in a high alumina ratio. While working with significantly different cements at the time, Lerch [15] noted similar "spikes" in the rate of heat evolution of cements with high C_3A contents. He also noted that the magnitude of the heat rate "spike" decreased and the time of its occurrence increased as the SO_3 content of the cement increased. Macphee and Lachowski [16] note that the presence of periclase has the effect of reducing the hydration kinetics of the cement. However, in the case of clinker K, it appears that the effect of the relatively high MgO content and the resulting presence of periclase is overshadowed by the effect of the high C_3A content. Furthermore, the dendritic form of the belite in this clinker, may also encourage earlier hydration of this phase.
- There are very few common chemical or morphological characteristics between clinkers A, B, E, F and H to indicate that they should belong in a joint heat rate category as measured in the adiabatic calorimeter tests. This is particularly so when considering the clinkers that have been categorised as low-heat clinkers (C, D, G and H). These two groups of clinker are not distinguishable on the bases of the chemical analysis or the morphological descriptions.
- This point is further emphasised by the apparently anomalous peak heat rate performance of the factory cement produced with clinker H in comparison with the corresponding laboratory cement. This indicates that the nature of the gypsum and the possible effects of the additives used in the manufacture of the cement can have a larger influence than the (relatively small) variations in cement fineness and chemical/mineralogical composition of the clinker.
- Because of the relatively high alite contents, none of the clinkers assessed conform to the description of a "low-heat" cement as described by Jackson [17].

5. CONCLUSIONS

1 Considering the maturity rate of heat evolution, the nine clinker cements tested can be categorised into high, medium and low heat cements based on the maximum measured heat rate. The average maximum heat rates obtained in each of these categories were: 2.5 J/maturity second/kg, 3.0 J/maturity second/kg and 4.6 J/maturity second/kg respectively.

2 Within this categorisation, only clinker cement K was placed in the high heat category, clinker cements A, B, E and F were categorised as medium heat cements and clinker cements C, D, G and H were considered as low heat cements.

3 XRF analysis for chemical composition and qualitative microscopy for morphological characterisation of cement clinker, in themselves, do not provide sufficient information to allow a heat-rate characterisation of the cement derived from such a clinker. It is suggested that this information should be combined with further analysis of the clinker involving a thorough characterisation of the crystallographic forms and an assessment of the phase distribution in different size fractions of the ground cement.

4 Comparing the performance of the factory and corresponding laboratory cements, it appears that, in general, the peak value of the heat rate is strongly influenced by the fineness of grinding and amount of SO_3 in the cement. However, it is possible that factors such as the type of gypsum used and the effects of additives introduced at the grinding stage could have a larger effect than fineness and SO_3 content. This aspect requires further investigation.

ACKNOWLEDGEMENTS

The authors gratefully acknowledge the kind assistance of the three cement companies, PPC Co. (Pty) Ltd, Alpha (Pty) Ltd and Lafarge Cement (Pty) Ltd who provided the cement and clinker samples that were used in the tests.

REFERENCES

[1] Hughes B.P and Mahmood AT, Laboratory Investigation of Early Age Thermal Cracking of Concrete, ACI Materials Journal, May/June 1988

[2] Campbell D.H, A Summary of Ono's Method for Cement Quality Control With Emphasis on Belite Color, Petrography of Cementitious Materials, ASTM STP 1205, Sharon M de Hayes and David Stark Eds., American Society for Testing Materials, Philadelphia, 1994

[3] SABS EN 197-1:2000. Cement – Part 1: Composition, specifications and conformity criteria for common cements. South African Bureau of Standards, Pretoria, 2000

[4] SABS SM 748: 1971. Standard test method: Specific surface of cement, South African Bureau of Standards, Pretoria, 1971.

[5] St. John, D. A, Poole, A. W and Sims, I. Concrete Petrography: A handbook of investigative techniques. Arnold, London, 1998

[6] Gibbon G.J, Ballim and Grieve, A low-cost, computer-controlled adiabatic calorimeter for determining the heat of hydration of concrete. ASTM Journal of Testing and Evaluation, Vol. 25, No. 2, 1997. pp. 261-266

[7] Wang, Ch and Dilger, W.H. Prediction of temperature distribution in hardening concrete. In Thermal Cracking in Concrete at Early Ages. Springenschmid, R (ed.), E&FN Spon, London, 1994, pp. 21-28

[8] Van Breugel, K. Prediction of temperature development in hardening concrete. In: Prevention of Thermal Cracking in Concrete at Early Ages. Springenschmid, R (ed.), RILEM Report 15. Chapter 4. E&FN Spon, London, 1998, pp. 51-75.

[9] Naik T.R., Maturity Functions for Concrete During Winter Conditions, in: Temperature Effects on Concrete, ASTM STP 858, T.R. Naik, Ed., American Society for Testing and Materials, Philadelphia,1985

[10] Bamford, C. H. and Tipper, C. F. H. (eds.) Comprehensive chemical kinetics, Vol. 1: The practice of kinetics. Elsevier Publishing Company, London, 1969.

[11] Ballim, Y. and Graham, P. C. A maturity approach to the rate of heat evolution in concrete. Paper under review for publication 2002.

[12] Lawrence, C. D. The constitution and specification of Portland cements. In: Hewlett, P.C (Editor). Lea's Chemistry of Cement and Concrete, 4th Edition. London, Arnold. 1988. Chapter 4.

[13] Taylor, H. F. W. Cement chemistry. 2nd edition. Thomas Telford, London, 1997.

[14] Addis, BJ Cementitious materials. In: Addis, B. J. (editor), Fulton's Concrete Technology. Cement and Concrete Institute, Midrand, South Africa, 2001.Chapter 1.
[15] Lerch, W. The influence of gypsum on the hydration and properties of Portland cement pastes. Proceedings of ASTM – technical papers. Vol. 46, 1946, pp. 1252-1297
[16] Macphee, D. E and Lachowski, E. E. Cement components and their phase relations. In: Hewlett, P.C (Editor). Lea's Chemistry of Cement and Concrete, 4th Edition. London, Arnold. 1988. Chapter 3.
[17] Jackson, P. J. Portland cement: Classification and manufacture. In: Hewlett, P.C (Editor). Lea's Chemistry of Cement and Concrete, 4th Edition. London, Arnold. 1988. Chapter 2.

BINDING AND SOLIDIFICATION OF RADIOACTIVE WASTE BY HOT PRESSING USING CEMENTITIOUS SYSTEMS

V. V. Chistyakov[1] and V. N. Chernyak[2]

[1] Kiev National University of Construction and Architecture, Kiev, Ukraine.
E-mail: sribm@mail.kar.net
[2] State Specialized Company "Technocentre", Chernobyl, Kiev region, Ukraine.
E-mail: vladchern@technocentre.com.ua

ABSTRACT

In the paper some results of investigations of the processes of binding and solidification of the various kinds of both liquid and solid radwaste in cement paste by using a hot pressing method are presented. The efficiency of both various binding systems and hot pressing conditions has been discussed. The compositions of hydrated new-formations and properties of solidified cement paste (porosity, water-resistance, leach rate, etc.) have been investigated. The high efficiency of the use of hot pressing technology for radioactive waste solidification (in comparison with the traditional technology of radwaste cementation) has been demonstrated.

1. INTRODUCTION

The employment of effective technologies of manufacturing cement-based construction articles is increasing in the field of radioactive and other hazardous waste management. Current developments in the field of hot pressing were used to develop a new technology of immobilizing some low and middle level radioactive waste. According to that technology, both high temperature (100-200 C) and pressure (25-50 MPa) have an influence on the mix of cementitious binder and radwaste (at the same time) during certain time (30-45 minutes). Products obtained are characterized by decreased porosity (<10 %), increased strength (30-100 MPa) and low level of cesium-137 leach rate ($<10^{-5}$ g/cm^2·day). Some natural materials (e.g. clinoptilolite, bentonite, etc.), which have advanced surface and developed pore structure and hence have good sorption properties, can be used for the absorption of various toxic and radioactive substances. Their use as modifying admixtures for cementitious matrices also has been investigated.

2. EXPERIMENTAL PROCEDURE

The following radwastes were investigated: salt concentrate of the Chernobyl nuclear power plant (Chernobyl NPP), spent radioactive cation exchanger KU-2-8, and the bottom silt of Pripyat's creek (the Chernobyl Exclusion Zone). Because of the danger of working with radwaste in the laboratory, non-reactive components were made with the same chemical composition as the wastes to be investigated.

The salt concentrate of Chernobyl NPP is related to middle level active waste. The chemical composition of the salt concentrate after it was steamed is shown in Table 1. The simulator of the radioactive cation exchanger was prepared. Exception was made for the ground sediment (bottom silt) of Pripyat's creek: it was sampled from a place with very low activity but its average chemical composition was similar to that around the cistern.

Table 1. Mean chemical composition of an evaporated concentrate of Chernobyl NPP

Chemical compound	Concentration in a solution, g/L	Amount, mass %
$NaNO_3$	660-720	55-60
Na_2SO_4	96-120	8-10
NaCl	48-60	4-5
NaOH	120-180	10-15

For the investigations of the cesium leaching the composites, which simulate the radwaste, the non-active CsOH was added in the calculated quantity: for composites imitated low-level waste (silt and cation exchanger) — $5 \cdot 10^{-7}$ g/kg (calculated from the average activity $1 \cdot 10^{-5}$ Ci/kg according to the proportion 1 Ci^{Cs-137} = $1.26532344318937 \cdot 10^{-2}$ g Cs-137 [1]), for middle-active waste (salt concentrate) — $1 \cdot 10^{-4}$ g/kg (calculated from $2.5 \cdot 10^{-7}$ Ci/L)

The chemical composition of binder components is shown in Table 2. The composites of cement matrices for binding and solidifying waste are shown in Table 3.

Table 2. Chemical compositions of the binder components for preparation of the immobilization matrices

Component	Quantity of main oxides, mass %			
	CaO	Al_2O_3	SiO_2	Fe_2O_3
Blast Furnace Slag	41	11	36	2
Bentonite	10	14	46	2

Specimens for hot pressing, after cement binder and waste were mixed thoroughly, were placed in the hot pressing device (Figure 1). To prepare specimens the following optimized regime of hot pressing was used: the temperature of isothermal curing of 150 °C, pressure of 25 MPa, total time of hot pressing - 45 min. After hot pressing is finished, the specimens were being extracted out of the device and then placed in a desiccator with distilled water. The samples of water solution, taken at 1, 7 and 28 day, were investigated by the atomic-absorption method (device AAS-30) for cesium concentration determination.

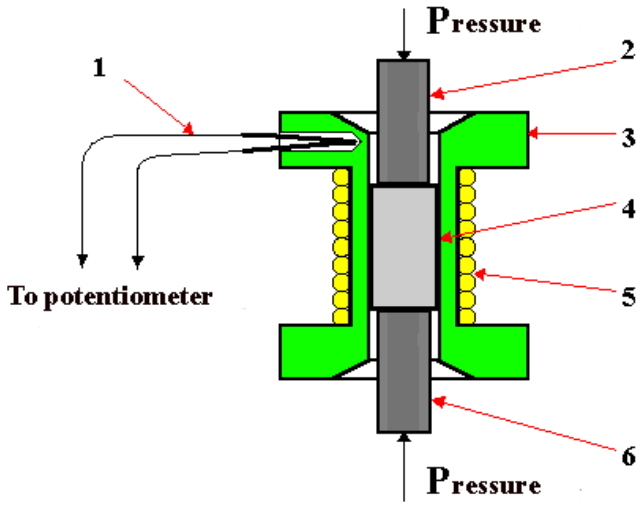

Where:

1 – the alumel-chromel thermocouple;
2 – upper plunger;
3 – metal matrix;
4 – a specimen;
5 – heating coil;
6 – lower plunger

Figure 1. The schematic model of the laboratory device for hot pressing

Table 3. Compositions of specimens contained the mixtures of binder and radwaste simulator

No of compo-sition	Composition
1	30 % SC+ 80 % OPC
2	20 % SC + 80 % OPC
3	30 % SC + 70 % (BFS:OPC:MB = 1:1:1)
4	25 % IER* + 75 % OPC
5	25 % IER** + 75 % OPC
6	30 % Silt*** + 70 % OPC

Where:
SC – the salt concentrate; OPC – the ordinary Portland cement; BFS – blast furnace slag; MB – heat-treated bentonite; IER – ion exchange resin KU-2-8; * – heat-treated at 300 C IER; ** – IER that was neutralized with CaO and "Silor" solution [2]; *** – initial silt that was treated with $Ca(OH)_2$ solution at 90°C.

3. RESULTS AND DISCUSSIONS

Some physical-mechanical properties of the specimens obtained are shown in Table 4. The advisability of using the binders on the basis of the mixture of OPC and heat-treated bentonite has been investigated in the work [2].

Table 4. Characteristics of specimens with the simulator of radioactive waste of Chernobyl Exclusion Zone

No of specimen (see Table 3)	Amount of a simulator of radwaste, mass %	W/C ratio	Hydration period	Density, g/cm^3	Compressive strength, MPa	Porosity, %
1	30	0.06	30 min	2.34	134	8.93
2	20	0.07	30 min	2.29	156	9.38
3	30	0.06	30 min	2.28	91	7.75
4	25	0.07	30 min	2.32	99	8.02
5	25	0.06	30 min	2.05	31	8.46
6	30	0.13	30 min	2.20	57	9.13

The obtained results of cesium and calcium concentration determination in the samples of leaching cement specimens with investigated kinds of radwaste are shown in Table 5 and in Figure 2.

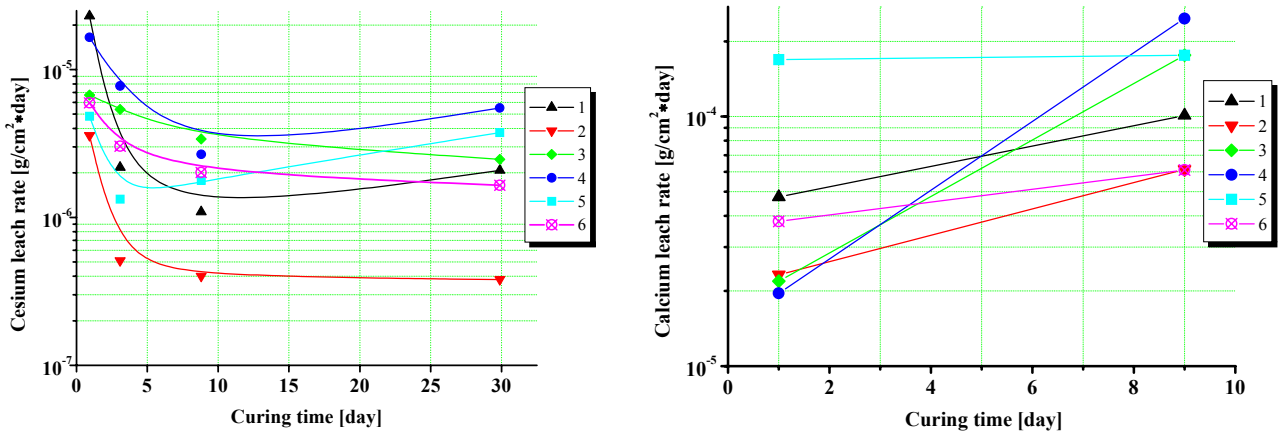

Figure 2. Determination of Cesium (left) and Calcium (right) leaching from cement matrixes with various compositions (see Table 3)

Table 5. Results of cesium and calcium concentration determination, leach rate determination in cement specimens with radwaste (by atomic-absorption spectroscope AAS-30, Germany)

No. of compo-sition	Sample No.	Method of preparation	Time, Day	Cs^{+}, mg/l	Ca^{2+}, mg/l	Cesium leach rate, $g/cm^2 \cdot day$	Calcium leach rate, $g/cm^2 \cdot day$
1	1	Hot Pressing	1	2.32	4.8	$2.30 \cdot 10^{-5}$	$4{,}76 \cdot 10^{-5}$
1	2	Hot Pressing	3	0.22	—	$2.18 \cdot 10^{-6}$	—
1	3	Hot Pressing	7	0.11	10.8	$1.09 \cdot 10^{-6}$	$1{,}01 \cdot 10^{-4}$
1	4	Hot Pressing	28	0.21	—	$2.08 \cdot 10^{-6}$	—
2	5	Hot Pressing	1	3.58	2.32	$3.58 \cdot 10^{-5}$	$2.32 \cdot 10^{-5}$
2	6	Hot Pressing	3	0.51	—	$5.10 \cdot 10^{-6}$	—
2	7	Hot Pressing	7	0.45	6.14	$4.42 \cdot 10^{-6}$	$6.14 \cdot 10^{-5}$
2	8	Hot Pressing	28	0.38	—	$3.80 \cdot 10^{-6}$	—
3	9	Hot Pressing	1	0.79	3.51	$6.73 \cdot 10^{-6}$	$2.19 \cdot 10^{-5}$
3	10	Hot Pressing	3	0.63	—	$5.37 \cdot 10^{-6}$	—
3	11	Hot Pressing	7	0.56	20.61	$4.77 \cdot 10^{-6}$	$1.76 \cdot 10^{-4}$
3	12	Hot Pressing	28	0.29	—	$2.47 \cdot 10^{-6}$	—
4	13	Cementation	1	1.98	2.35	$1.65 \cdot 10^{-5}$	$1.96 \cdot 10^{-5}$
4	14	Cementation	3	0.93	—	$7.75 \cdot 10^{-6}$	—
4	15	Cementation	7	0.32	29.73	$2.67 \cdot 10^{-6}$	$2.47 \cdot 10^{-4}$
4	16	Cementation	28	0.66	—	$5.50 \cdot 10^{-6}$	—
5	17	Cementation	1	0.58	20.31	$4.83 \cdot 10^{-6}$	$1.69 \cdot 10^{-4}$
5	18	Cementation	3	0.16	—	$1.33 \cdot 10^{-6}$	—
5	19	Cementation	7	2.14	21.12	$1.78 \cdot 10^{-5}$	$1.76 \cdot 10^{-4}$
5	20	Cementation	28	0.45	—	$3.75 \cdot 10^{-6}$	—
6	21	Hot Pressing	1	0.65	2.58	$5.95 \cdot 10^{-6}$	$3.80 \cdot 10^{-5}$
6	22	Hot Pressing	3	0.54	—	$3.03 \cdot 10^{-6}$	—
6	23	Hot Pressing	7	0.48	4.30	$2.01 \cdot 10^{-6}$	$6.10 \cdot 10^{-5}$
6	24	Hot Pressing	28	0.40	—	$1.65 \cdot 10^{-6}$	—

The obtained results of cesium leach rate determination show a decreasing outflow of this element out off the cementing matrix. It completely co-ordinates with the results of the determination of cesium leach rate. It is necessary to take into account that the real area of the leaching surface of cement specimens is much bigger that the one determined by usual geometric measurement due to the presence of the developed pore structure. In this case the specific cesium leach rate is even less.

The use of the atomic-absorbing method of analysis was dictated by following reason. The results, determined by direct measurement of the activity of a solution, did not mirror the real chemical concentration of cesium in this solution. That discrepancy is predetermined by the inequality of the left and right parts in the equation of the determination of leaching radioactive substances by the method of ISO 6961 [3]:

$$R_n^i = \frac{a_n^i}{A_0^i \times F \times t_n},$$

where R_n^i is the increment of the level of leach rate for i-th component, $kg/m^2 \cdot day$; a_n^i – radioactivity per second or weight (kg) of each component leached during each time interval; A_0^i – specific radioactivity or mass concentration of each component in the initial specimen, kg·day; F – area of specimen surface, m^2; t_n – duration of n-th period of leaching, day; n – time increment; A_0 and a_n are corrected according to the half-value period.

Increased physical-mechanical properties and low level of substances' leaching for the composites with the additives of bentonite and BFS could be explained by the formation of the additional products of hardening due to interaction between these components and the alkalis of salt waste. As a result zeolite-like new-formations are formed. Both increased temperature (150 °C) and pressure (25 MPa) promote these processes. On the x-ray diagrams of specimens obtained the gismondite-like zeolite Na-P can be noticed. Its internal volume is enough for disposal of the molecules of some substances (like sodium nitrate) inside it. Those compositions could be called "clathrate"-like [4]. However, this question needs further investigation. Determination of calcium leach rate showed the heterogeneity of the process of leaching of this element from cementitious matrices. Obviously, that behavior is predetermined by solubilization of calcium hydrosilicates, which is initiated after the pH level has decreased enough owing to calcium hydroxide leaching. The comparison of the determined values of calcium and cesium solubilities (see Table 4) shows that in all the cases leach rate of calcium is much less then relates as to its initial concentration and the high level of sorption of cesium on the active centers of new-formations of hydrosilicates' during the full process of hot pressing [5,6].

4. CONCLUSIONS

The use of cementitious compositions on the basis of OPC clinker, BFS and bentonite as the immobilizing matrices producers composites which contain the new-formations of hydrosilicates with included salt waste as in chemical compounds as by the "clathrate" principle.

The study of leaching cesium and calcium from cementitious specimens (with radwaste) by atomic-absorption method allowed us to determine that the values of leaching of these elements into environment are low enough and mainly satisfy the requirements for immobilizing matrices. The use of hot pressing decreased these negative indications that shows the important prospects of applying this method for immobilization various hazardous waste.

REFERENCES

[1] Shybetski, J. et al. Designing the base of coordinated thermodynamical values of radio-isotopic forms of hydrogen, carbon and strontium in the structure of the Program complex SELECTOR-A and its addenda for modeling geochemical systems in connection with radwaste management, Report on scientific and investigation work, Kiev, State scientific center of environmental radiogeochemistry, 1998, p. 45.

[2] Chistyakov, V., Chernyak, V. Cementitious systems for binding and solidifying radioactive waste, Proceedings of 4th Beijing international Symposium on Cement and Concrete, Beijing, China, 1998, pp. 134-139.

[3] ISO 6961. Long-term leach testing of solidified radioactive waste forms, 1st edition, 1982-10-15, p. 6.

[4] Veselovskij R. A., Kolesnikov A. V. A new point of view on impregnation problem, Proceedings of 2nd International Conference RILEM on the Rehabilitation of Structures, Australia, Melbourne, September 21-23, 1998, pp. 35-38.

[5] Barrer R. Hydrothermal chemistry of zeolites, Moscow: Mir published, 1985, p. 420.

[6] Chistyakov, V., Ledovskikh, V, Chernyak, V. Blended binders for immobilization of liquid radioactive waste, Proceedings of 2nd International Conference on Alkaline Cements and Concretes, Kiev, Ukraine, May 18-20 1999, pp. 643-648.

BINDING AND SOLIDIFICATION OF RADIOACTIVE WASTE BY HOT PRESSING USING CEMENTITIOUS SYSTEMS

Valerii V. Chistyakov[1] and Vladimir N. Chernyak[2]

[1] Kiev National University of Construction and Architecture, Kiev, Ukraine.
E-mail: sribm@mail.kar.net
[2] State Specialized Company "Technocentre", Chernobyl, Kiev region, Ukraine.
E-mail: vladchern@technocentre.com.ua

VALERIY V. CHISTYAKOV

Valeriy V. Chistyakov was born February 11, 1949 in Ukraine.

His M.Sc. Degree (building materials technology) he received at the Kiev Civil Engineering Institute (since 1995 – Kiev National University of Construction and Architecture), 1979.

His Ph.D. Degree (the technology of silicates and the refractory of nonmetallic materials) he received at the Kiev Polytechnic Institute (now National Technical University of Ukraine), 1986.

His Dr. Sc. Degree (Technical) he received in 1994. The title of his thesis was: "Physical-chemical aspects of intensification of hydrate- and structure-formation processes in mineral cementitious systems".

Since 1980 has worked as a staff member of the Department on Concrete and Reinforced Technology at the Kiev Civil Engineering Institute.

Since 1983 he worked as the chief scientist of the Department of Chemical Technology of Binding Substances at the Kiev Polytechnic Institute.

Since 1995 he is Professor of Department of Building Materials of Kiev National University of Construction and Architecture.

Professor Chistyakov contributed/published over 180 scientific articles, papers in various national and international journals, proceedings, seminar/congress volumes and 2 monographs. He granted 20 certificates of authorship. In 1994 he was a recipient J. Soros Grant No. K2X100, project "Physical-chemical bases for synthesis of analogues of natural minerals in the systems Me_2O-Me_2O_3-SiO_2-H_2O and Me_2O-MeO-Me_2O_3-SiO_2-H_2O".

Specialization:

1. Main field: inorganic chemistry of cementitious systems.
2. Other fields: radioactive and toxic waste management.
3. Current research interests: cement and mineral systems; cement composites and concrete; admixtures for cement systems; new cements; processes of hydrate- and structure-formations; high pressure and temperature reactions; nuclear and chemical waste management; chemically bonded ceramics; materials and technologies for producing the containers for synthesis of artificial diamonds.

ESTIMATION OF THE CAPACITY OF SOUTH AFRICAN COAL FLY ASH FOR PHOSPHATE ION REMOVAL FROM AQUEOUS SOLUTION

N.M. Agyei*[a], C.A. Strydom[b] and J.H. Potgieter[c]

[a]Department of Chemistry, University of Venda, Private Bag X5050,
Thohoyandou 0950, South Africa.
[b]Department of Chemistry, University of Pretoria, Pretoria 0002, South Africa.
[c]Department of Chemical and Metallurgical Engineering, Pretoria Technikon,
P.O. Box 56208, Arcadia,0007 Pretoria, South Africa .

ABSTRACT

Phosphate ions have been removed from aqueous solution by fly ash. Better removal was obtained at higher solute concentration, acidic pH and higher temperature. The effect of particle size and the speed of mixing were found not to be significant. A first-order kinetic model was used to obtain values for overall sorption rate constants and intra-particle diffusion constants. The Frumkin isotherm was found to be the appropriate equation for modelling isotherms from the experimental adsorption data, and values have been obtained for the isotherm constants. A 400 mg/l PO_4^{3-}(as P) solution was fed at a steady velocity of 2.0 cm/min through a 2.0 cm fixed-bed column (at pH 9.0 and 25°C), and breakthrough curves were constructed to obtain an estimated adsorption capacity value of 32 mg PO_4^{3-}/g fly ash.

1. INTRODUCTION

Environmental and economic concerns have led to an on-going search to find novel and effective ways to utilise the huge amounts of fly ash that is land-filled or stockpiled. In the year 2000, only 18 out of the over 56 million metric tons of fly ash generated in the U.S.A. were utilised [1], mostly in the cement and concrete industry. For South Africa the fractional utilisation was even lower, at 1.2 out of 25 million metric tons production [2].

Eutrophication, the gradual increase in the levels of nutrients such as phosphorous in an ageing ecosystem such as a lake, leads to an explosion in algae growth, which eventually results in a lack of light penetration and oxygen absorption that is necessary for underwater life. Cultural or man-made eutrophication, resulting from runoff containing excessive amounts of nutrients in the form of sewage, detergents, and fertilisers, is a well-known environmental concern. The most widely used method for phosphate removal from aqueous solution, namely, precipitation with lime, is expensive due to the high doses of lime required [3].

Due to the high percentages of alumina and silica, fly ash is a good candidate for use as an economic adsorbent for large-scale use. It has been found to remove F^- [4,5], Cr^{3+} [6], Cu^{2+}, Pb^{2+}, Cd^{2+} [7] ions as well as phenolic compounds [8,9] from aqueous solution. The study was used to investigate the feasibility of using fly ash, a by-product of coal combustion for electric power generation, to remove phosphate ions from aqueous solution, as a possible technique for wastewater treatment.

Proceedings of the 11th International Congress on the Chemistry of Cement (ICCC)
'Cement's Contribution to the Development in the 21st Century'
Hosted by: The Cement and Concrete Institute of South Africa
CD-ROM produced by: Document Transformation Technologies
11 - 16 May 2003, Durban, South Africa
ISBN Number: 0-9584085-8-0
Editors: Dr G. Grieve and G. Owens
Congress Organised by: Event Dynamics

An earlier study on the removal of phosphate ion from aqueous solution by fly ash and slag [10] suggested that the Frumkin isotherm (1) [11] is the appropriate equation for modelling the experimental adsorption data:

$$\upsilon = \log(\beta/55.55) + 2\alpha\Phi/2.303 \quad (1)$$

where $\upsilon = \log[\Phi/(1-\Phi)c]$, c = concentration of the solute that is in equilibrium with the adsorbent, $\Phi = M/M_{ads}$, M = mass of solute adsorbed at equilibrium, M_{ads} = the maximum mass of solute adsorbed at equilibrium, α = the lateral interaction coefficient, and β = a constant which describes the adsorption equilibrium ($\beta = \exp(-\Delta G^0_{ads}/RT)$, where ΔG^0_{ads} represents the standard free energy of adsorption). This equation is a useful isotherm for fitting non-ideal adsorption systems, and can be arrived at theoretically in terms of surface heterogeneity and in terms of repulsive forces between adsorbed molecules [12].

The sorption of solute from liquid phase to solid phase may be considered as a reversible reaction with equilibrium being established between two phases. If this can be described with a first order reversible kinetic model, then the overall rate constant for the process, k', and the intra-particle diffusion coefficient, D_i, can be determined, respectively, from the relations [13]:

$$\ln[1-U(t)] = -k' t \quad (2)$$

$$t_{1/2} = 0.030\, r^2/D_i \quad (3)$$

where the fractional attainment of equilibrium, $U(t) = X/X_e$, X = fraction of adsorbate sorbed at time t, X_e = fraction of adsorbate sorbed at equilibrium, $t_{1/2}$ = time at which $X/X_e = 0.5$ (given by $(\ln 2)/k'$), and r = mean radius of adsorbent particles (assuming spherical geometry for the adsorbent).

For a fixed-bed unit operating at a steady liquor flow rate, and for which a symmetrical breakthrough S-curve has been obtained experimentally, the height of the mass transfer zone, h_Z, and the specific dynamic adsorption capacity, C_T, are given, respectively, by the relations [14]:

$$h_Z = h_T[V_Z/(V_T - 0.5\, V_Z)] \quad (4)$$

$$C_T = \int_0^{V_T} (X_0 - X)\, dV/m \quad (5)$$

where h_T = bed height, V_T = volume of effluent collected upon exhaustion of the bed, V_E = volume of effluent collected up to breakthrough, $V_Z = V_T - V_E$, X_0 = influent concentration, X = effluent concentration, V = effluent volume, and m = mass of adsorbent.

2. EXPERIMENTAL

2.1 Materials and apparatus

The fly ash sample (Matla fly ash, M432) was obtained from PPC Technical Services (Germiston, South Africa). The sample was analysed there by XRF and XRD using Siemens SRS 3300 and D 5000 spectrometers, respectively. Particle sizes were also measured there with a Malvern Mastersizer instrument. A temperature-regulated Labcon platform shaker was used for solution agitation. A sieving system from Labquip was used for particle fractionation. Absorbance measurements were made using a Unicam UV-Visible spectrophotometer. All chemicals used were of analytical grade. De-ionised water was used for preparing solutions.

2.2 Procedures

The chemical oxide composition of the fly ash was determined by XRF spectrometry after being prepared as fused disks according to standard procedures. XRD scans were performed using Cu K_α radiation at a speed of 0.2 degrees 2 theta/min. For particle size analysis, 1 g of the material was suspended in water with sodium metaphosphate as dispersing agent and pumped past a laser beam. Laser Fraunhofer diffraction principles were used and an algorithm applied to the data collected by computer to calculate the parameters of interest.

The determination of phosphate (as phosphorous) was done spectrophotometrically using the yellow (λ= 470 nm) vanadomolybdo-phosphoric acid method [15]. The method is widely used to determine dissolved phosphorous in natural waters and wastewaters. The calibration curve obtained was linear up to *ca*. 55 mg/l P, with a detection limit (3σ) of 0.2 mg/l P.

2.2.1. Kinetics of phosphate removal

2-g samples of fly ash were weighed and placed in several 250-cm^3 Erlenmeyer flasks, each containing 200 ml of 80 mg/l PO_4^{3-}(as P) solution at pH 9.0 and 25°C (anhydrous KH_2PO_4 was used to prepare a 500 mg/l PO_4^{3-}(as P) stock solution). The flasks were stoppered and continuously shaken at a speed of 120 cycles per minute. The shaking was interrupted momentarily at pre-determined time intervals for a flask to be removed and the concentration of phosphate in the decanted and filtered (Whatman No. 42) supernatant solution to be determined. The phosphate monitoring was carried out at 10-minute intervals for the first 1 hour, then at longer intervals thereafter until the absorbance values levelled off.

2.2.2. Effect of concentration

Solutions of different initial concentrations- 20, 40, 60, 80 mg/l PO_4^{3-}(as P)- were used to investigate the effect of concentration on the kinetics of phosphate removal by 2 g of fly ash at pH 9.0 and 25°C following the procedure described in *2.2.1.*

2.2.3. Effect of particle size

400 g of fly ash were shaken mechanically for 20 minutes in a stack of sieves of various apertures to obtain fractions of different particle size. 2 g of 45-, 75-, 90-, 150- and 300-μm fractions were placed in Erlenmeyer flasks, each containing 200 ml of 80 mg/l PO_4^{3-}(as P) solution (pH 9.0 and 25°C). The flasks were then shaken continuously for 16 hours to attain equilibrium, after which the residual concentration of phosphate in the supernatant solutions was determined.

2.2.4. Effect of temperature

2 g of fly ash were placed in Erlenmeyer flasks, each containing 200 ml of 80 mg/l PO_4^{3-} (as P) solution at pH 9.0. The flasks were shaken continuously for 16 hours to attain equilibrium, surrounded by water set at various temperatures (25, 40, 50 and 60°C), after which the residual concentration of phosphate in the supernatant solutions was determined.

2.2.5. Effect of pH

2 g of fly ash were placed in Erlenmeyer flasks, each containing 200 ml of 80 mg/l PO_4^{3-} (as P) solution at 25°C and at initial pH values of 3.0, 5.0, 7.0, 9.0 and 11.0. The required pH values were obtained using 0.1 M HCl or 0.1 M NaOH. The flasks were shaken continuously for 16 hours to attain equilibrium, after which the residual concentration of phosphate in the supernatant solutions was determined.

2.2.6. Adsorption isotherms

0.5, 2, 3, 4 and 5 g of fly ash were shaken continuously with 200 ml of 100 mg/l PO_4^{3-} (as P) solution at pH 9.0 and 25°C for 16 hours to attain equilibrium, after which the residual concentration of phosphate in the supernatant solutions was determined.

2.2.7. Breakthrough curves

A glass column (4 cm I.D., 35 cm high) with a tap at one end was clamped vertically and a 10-mm layer of glass wool inserted near the bottom. The space above the plug was packed with a bed made by intricately mixing 5 g fly ash and 8 g inert sand (to improve the porosity) and another layer of glass wool was placed at the top of the bed. The space above the bed was filled with a 400 mg/l PO_4^{3-} (as P) solution (at pH 9.0, 25°C), which was then allowed to flow continuously through the bed at a steady velocity of 2.0 cm/min (volumetric flow rate of 25 cm^3/min). The concentration of phosphate in the effluent was monitored at half-minute intervals by collecting 5 cm^3 of it for analysis until the effluent concentration approached that of the influent.

3. RESULTS AND DISCUSSION

The chemical composition and particle dimensions of the fly ash are shown in Table 1. XRD analysis showed that the main mineral phase is quartz with smaller amounts of mullite and sillimanite. Figure 1 illustrates the variation of percent removal of PO_4^{3-} with time. It can be seen that the uptake of PO_4^{3-} virtually ceased after a contact time of about 6h.

Table 1. Chemical composition and physical characteristics of fly ash

Component	Mass %
SiO_2	52.4
Al_2O_3	33.7
Fe_2O_3	3.6
Mn_2O_3	<0.1
TiO_2	1.7
CaO	4.1
MgO	1.1
P_2O_5	0.3
SO_3	0.2
Cl	<0.1
K_2O	0.6
Na_2O	0.5
LOI @ 1000°C	0.8
Total	99.0
Specific surface area (m^2/g)	1.42
Mean particle diameter (μm)	25.7
Density (g/cm^3)	2.21

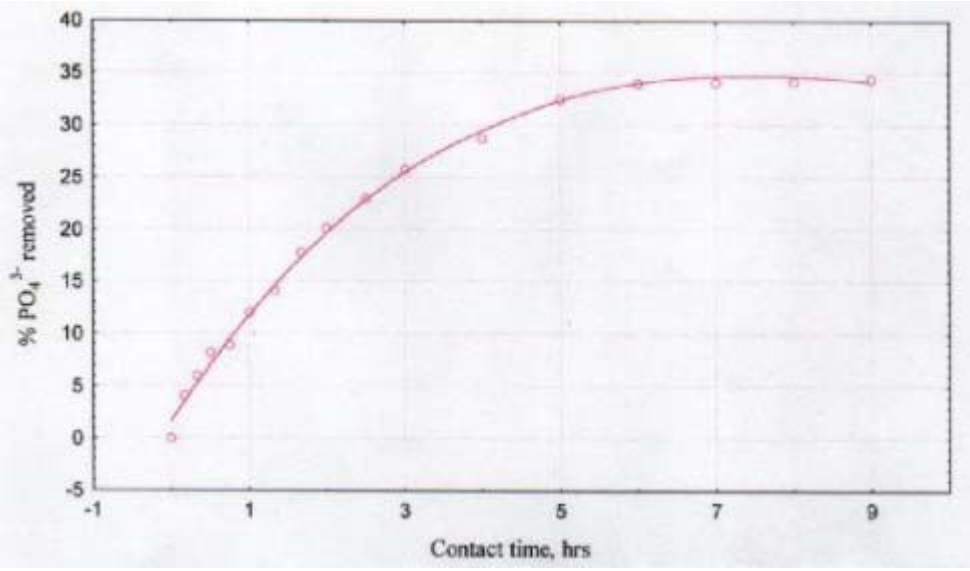

Figure 1. Kinetics of PO_4^{3-} removal from 80 mg/l solution
(Conditions: 2 g FA, pH 9.0, 25°C)

A plot according to Eq. (2) is presented in Figure 2. The good straight-line fit observed indicates that the sorption reaction may be approximated by first-order reversible kinetics. It was found that the adsorption rate was not significantly affected by the rate of mixing, providing evidence that intra-particle diffusion is the controlling resistance rather than the external diffusion. The values of the rate constant and intra-particle diffusion constants, calculated using Eq. (2) and Eq. (3), respectively, are given in Table 2.

Table 2. The values of first-order reaction rate constant and intra-particle diffusion coefficient

Parameter	Value
k' (per hour)	0.423
D_i (cm^2/s)	8.40×10^{-12}

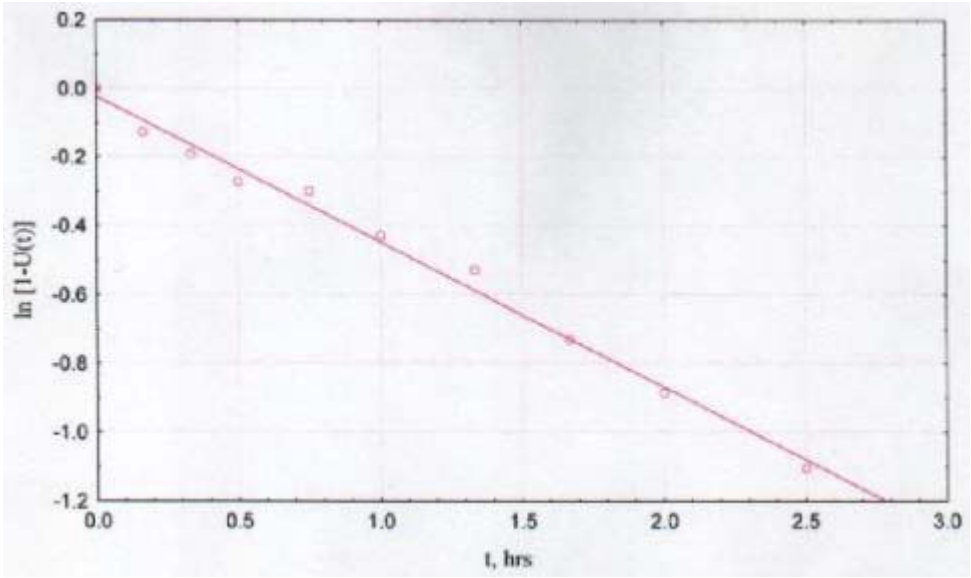

Figure 2. Application of first-order kinetics to the data in Figure 1

The rate and separation efficiency of PO_4^{3-} from aqueous solution was found to increase with the initial phosphate concentration over the concentration range studied; the data is shown in Figure 3.

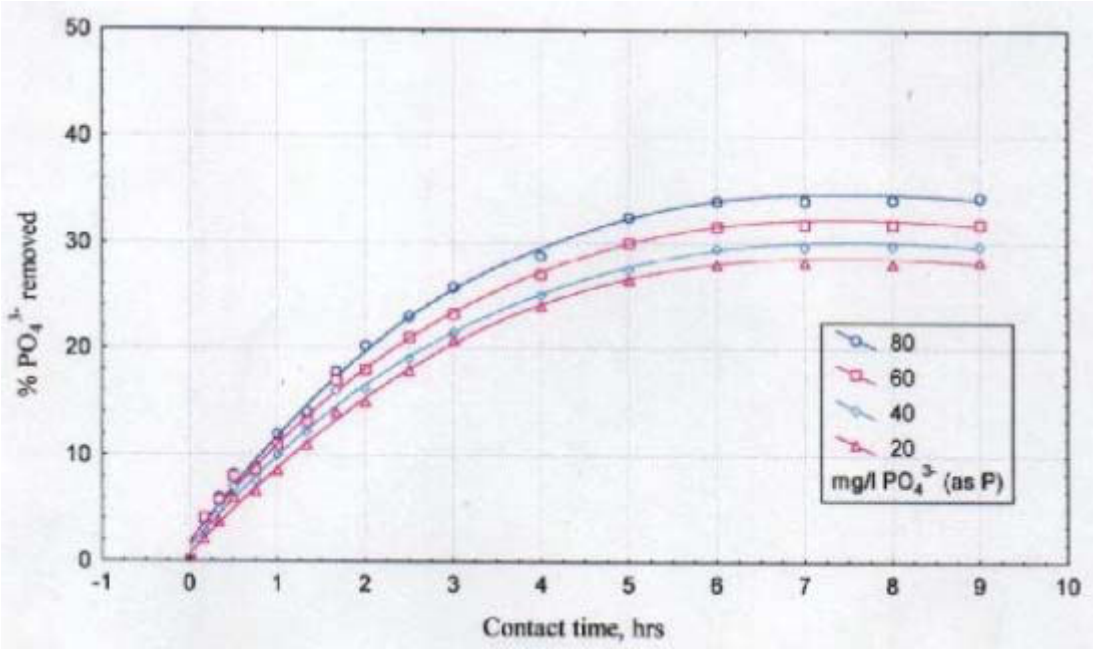

Figure 3. Effect of concentration on the kinetics of PO_4^{3-} removal
(Conditions: 2 g FA, pH 9.0, 25°C)

Although there was some increase in the percent PO_4^{3-} removed as the adsorbent particle size decreased (Figure 4), this increase was not proportionate to the increased surface area.

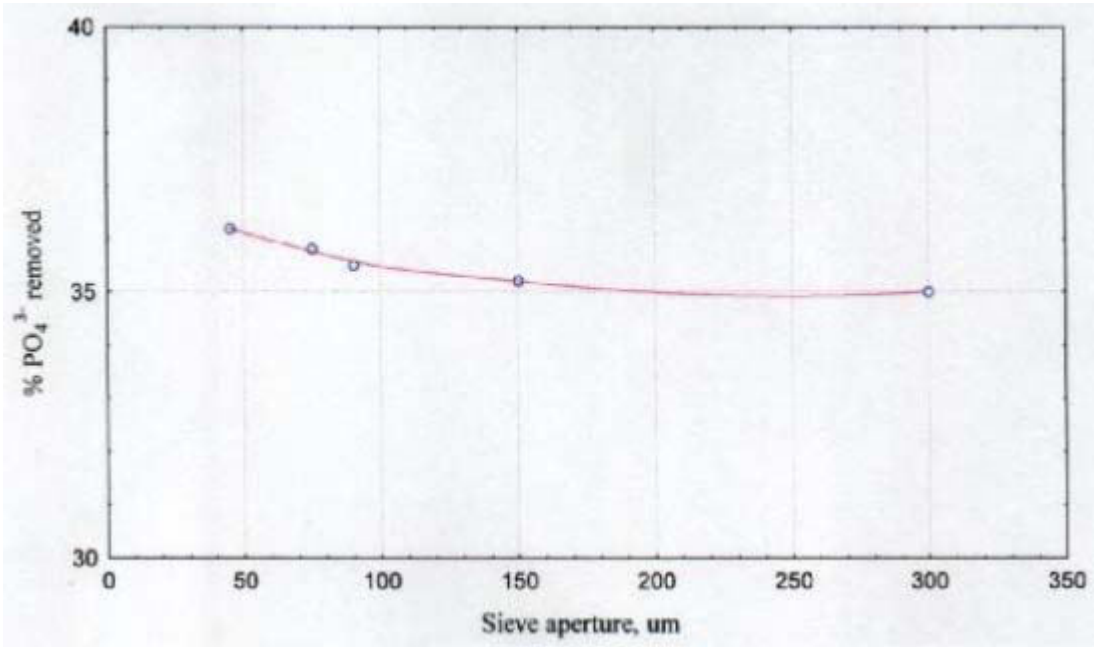

Figure 4. Effect of particle size on the efficiency of PO_4^{3-} removal
(Conditions: 80 mg/l PO_4^{3-} (as P), 2 g FA, pH 9.0, 25°C)

This gives an indication that for this adsorbent chemisorption is a more significant contributory phenomenon to the removal of PO_4^{3-} than physical adsorption. This observation is consistent with the findings of Johansson and Gustafsson [16], who suggested that Ca-P precipitation pre-dominates

surface adsorption as a mechanism for phosphate removal by slag. The effect of temperature on the efficiency of PO_4^{3-} removal by fly ash, slag and OPC is illustrated in Figure 5.

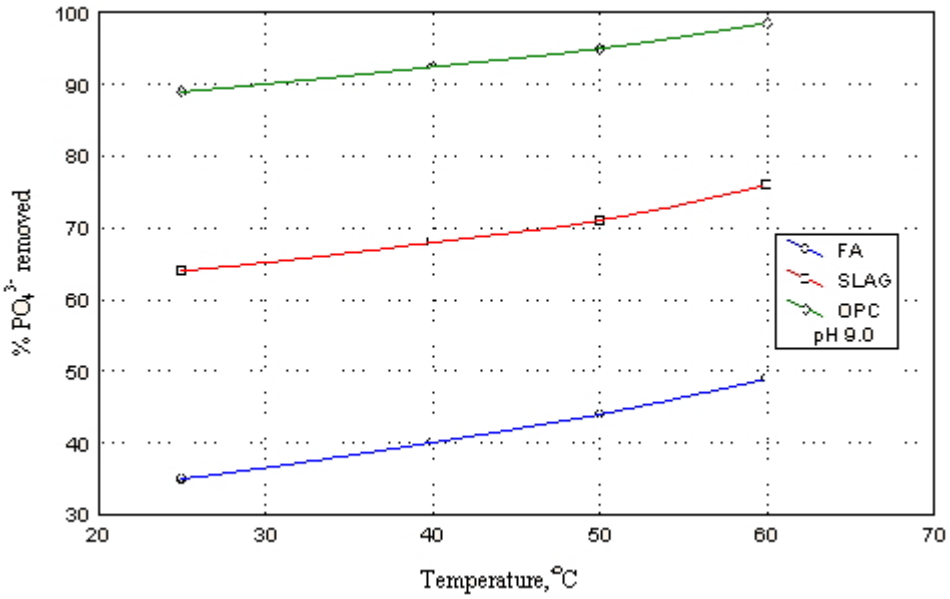

Figure 5. Effect of temperature on the efficiency of PO_4^{3-} removal.

The percent PO_4^{3-} removed was observed to increase with increasing temperature as expected, and it appears that some de-sorption may be occurring at higher temperatures. The decreasing slope of the temperature curve in the order fly ash, slag, OPC is indicative of decreasing activation energy for the PO_4^{3-} adsorption process.

Figure 6 illustrates the variation of percent PO_4^{3-} removed with the initial pH of the aqueous solution. It can be seen from the figure that the efficiency of PO_4^{3-} removal increases steadily in acidic pH.

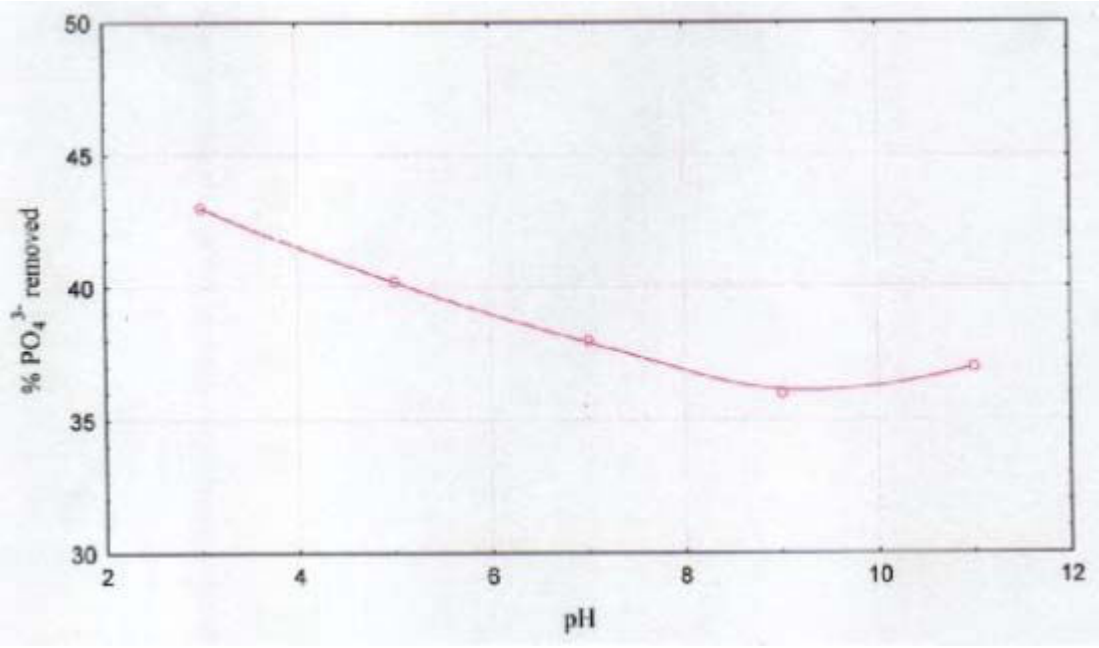

Figure 6. Effect of pH on the efficiency of PO_4^{3-} removal
(Conditions: 80 mg/l PO_4^{3-} (as P), 2 g FA, 25°C)

There could be two reasons for this. Firstly, it may be due to the accumulation of positive charge on the adsorbent surface that increases its affinity for the negatively charged phosphate ions. Secondly, an increased proportion of phosphate ions will be converted to the acidic forms ($H_2PO_4^-$ and HPO_4^{2-}), which may be more readily removed from solution via de-protonation and subsequent precipitation as $Ca_3(PO_4)_2$ as suggested by Tabikh and Miller [17]. The acidic pH would also release some Ca^{2+} ions from the fly ash via hydration to precipitate $Ca_3(PO_4)_2$. The observed slight increase in the efficiency of PO_4^{3-} removal beyond pH 9 could be due to the creation of favourable conditions for calcium phosphate precipitation at high pH, thus enhancing the removal of PO_4^{3-} by dissolved calcium, which is always present in the system.

Table 3 shows the experimentally obtained adsorption data. The fit of the data to the Frumkin isotherm is shown in Table 4, and the application of the Frumkin equation to the data is illustrated graphically in Figure 7. Attempts to fit the data to the Langmuir and Freundlich isotherms yielded non-linear plots with values of $R^2 < 0.4$. It is evident that the Frumkin isotherm is the appropriate one for fitting the data. The Frumkin constants were calculated and are shown in Table 4. The value of the lateral interaction coefficient α reflects the phosphate-adsorbent strength of interaction.

Table 3. Experimental adsorption data

mass of fly ash (g)	mg/l P[a] after adsorption	mg P[a] adsorbed
0.5	72.8	5.44
2	71.9	5.62
3	71.4	5.72
3.5	70.2	6.43
4	65.0	7.00
5	58.7	8.26

[a] PO_4^{3-}(as P)

Table 4. Frumkin isotherm constants and linear correlation coefficients

R^2	α	β
0.9918	3.061	0.0254

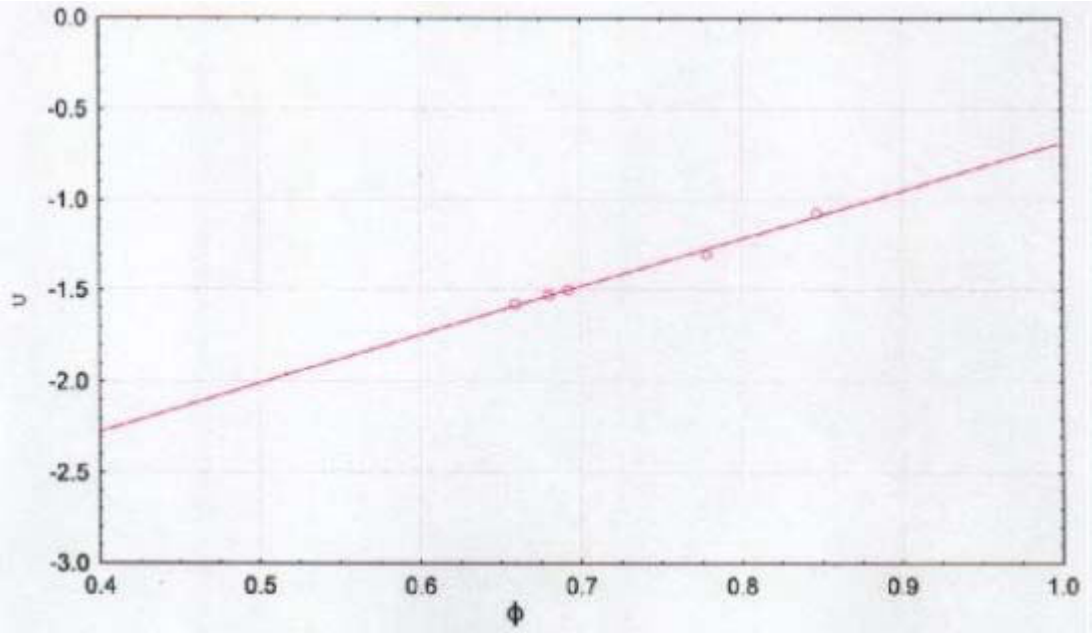

Figure 7. Application of the Frumkin isotherm to the data in Table 3 (Conditions: 100 mg/l PO_4^{3-} (as P), pH 9.0, 25°C)

The data obtained for the breakthrough experiments are shown in Table 5, and a typical breakthrough curve is represented in Figure 8.

Table 5. Breakthrough data

t_E[a] (min)	V_T (cm^3)	V_Z (cm^3)	h_Z (cm)	C_T (mg PO_4^{3-}/g)
2.8	187	116	1.742	32

[a]Breakthrough time

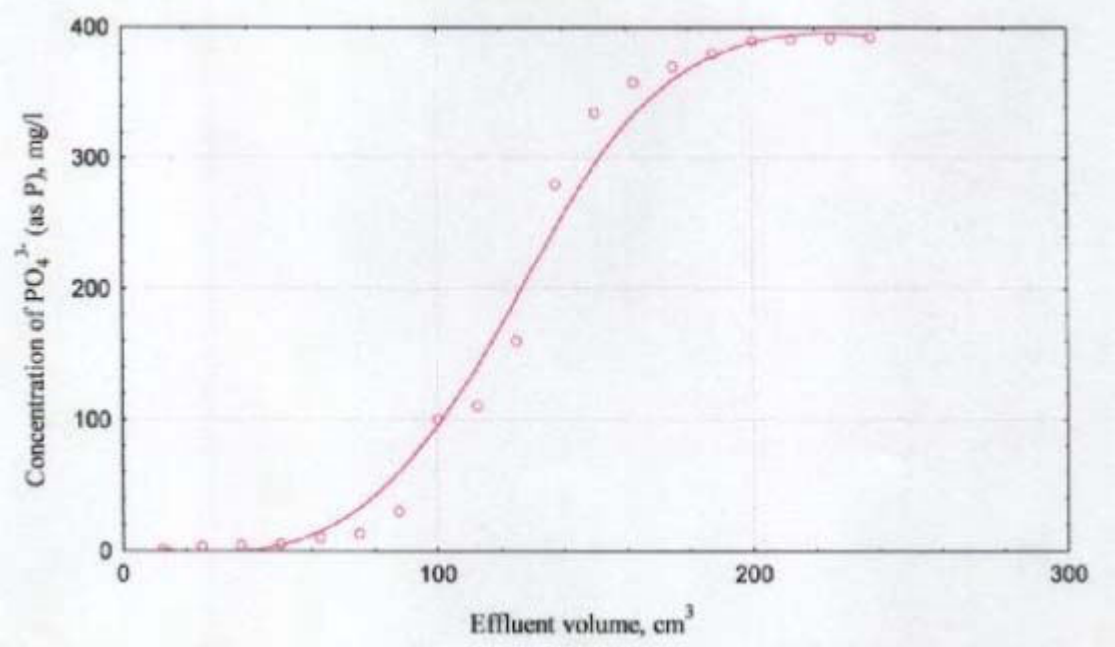

Figure 8. Breakthrough curve for PO_4^{3-} adsorption by fly ash
(Conditions: 5 g FA, pH 9.0, 25°C)

The curves obtained were good approximations for characteristic symmetrical breakthrough *S*-curves. For practical purposes the breakthrough and exhaustion times were taken to be the times at which the effluent concentration reached 5 and 95 %, respectively, of the influent concentration. The value of the height of the exchange zone h_Z (see Eq. (4)) is a measure of the rate of ion exchange and/or phosphate removal, while the value of the breakthrough time t_E is indicative of the adsorption capacity. The capacity value C_T was obtained by graphical integration of Eq.(5). This value (Table 5) is quite substantial, and is of a similar order of magnitude as the 67 mg/g (calculated from adsorption isotherms and not from breakthrough curves) reported by Akgerman and Zardkoohi [8] for the adsorption of phenol on fly ash. Capacity values obtained experimentally from breakthrough curves can be extrapolated to calculate the capacity of a large-scale bed [14].

4. CONCLUSIONS

The by-product fly ash has been successfully used for the removal of phosphate from aqueous solution. Potential economic utilisation of this materials might be either as a lining to slow down the seepage of nutrients such as phosphate from landfills or as a fixed-bed for treating agricultural and other waste waters. The phosphate-loaded solid waste may then be solidified by the addition of lime or Portland cement to a concrete mass that is stable and durable enough for safe disposal.

REFERENCES

[1] American Coal Ash Association (ACAA) 2000 Coal Combustion Product (CCP) Production and Use, http://www.ACAA-USA.org.

[2] R. Kruger, South African Coal Ash Association, Personal Communication, Johannesburg, 2002.

[3] R.L. Droste, Theory and Practice of water and wastewater treatment, john Wiley & Sons, Inc., New York, 1997.

[4] K. Mathe, MSc Thesis, University of the Transkei, South Africa, 1996.

[5] R. Piekos, S. Paslawska, Fluoride uptake characteristics of fly ash, Fluoride, 32(1), 1999, 14-19.

[6] G.P. Dasmahapatra, T.K. Pal, A.K. Bhadra, B. Bhattacharya, Studies on separation characteristics of hexavalent chromium from aqueous solution by fly ash, Sep. Sci. Technol., 31(14), 1996, 2001-2009.

[7] R. Apaka, E. Tutema, M. Hugula, J. Hizala, Heavy metal cation retention by unconventional sorbents (red muds and fly ashes), Water Res., 32(2), 1998, 430-440.

[8] Akgerman, M. Zardkoohi, Adsorption of phenolic compounds on fly ash, J. Chem. Eng. Data, 41, 1996, 185-187.

[9] P.C. Kao, J.H. Tzeng, T.L. Huang, Removal of chlorophenols from aqueous solution by fly ash, J. Haz. Mat., 76(2-3), 2000, 237-249.

[10] N.M. Agyei, C.A. Strydom, J.H. Potgieter, An investigation of phosphate ion adsorption from aqueous solution by fly ash and slag, Cem. Concr. Res., 30, 2000, 823-826.

[11] A.W. Adamson, Physical Chemistry of Surfaces, Wiley, New York, 1990.

[12] K.J. Laider, J.H. Meiser, Physical Chemistry, Benjamin/Cummings Publishing, London, 1982.

[13] F. Helfferich, Ion Exchange, McGraw Hill Book Company Inc., New York, 1962.

[14] A.S. Michaels, Simplified methods of interpreting kinetic data in fixed-bed ion exchange, Ind. Eng. Chem., 44(8), 1952, 1922-1930.

[15] E. Arnold (Ed.), Standard Methods for the Examination of Water and Wastewater, American Public Health Association, 1985, Washington, D.C., 445-446.

[16] L. Johansson and J.P. Gustafsson, Phosphate removal using blast furnace slags and opaka- Mechanisms, Wat. Res., 34(1), 2000, 259-265.

[17] A.A. Tabikh, F.M. Miller, The nature of phosphogypsum impurities and their influence on cement hydration, Cem. Concr. Res., 1(6), 1971, 663-678.

POZZOLANIC PROPERTIES OF CALCINED PAPER SLUDGE

Jean Péra[1] and Jean Ambroise[1]

[1]Unité de Recherche Génie Civil, Institut National des Sciences Appliquées, Villeurbanne, France.
E-mail: Jean.Pera@insa-lyon.fr

ABSTRACT

Worldwide, the paper industry produces more than 20 million t/y of residues from wastewater treatment and de-inking. Traditionally, papermills deposit these residues in landfills or burn combustible residues and landfill the resulting ash.

These sludges consist basically of water (50%), organic matter (25%), and minerals (25%). The organic matter contains binders and fibres that cannot be re-used in new paper products. The minerals consist of calcium carbonate and kaolin used for various quality reasons in the papermaking process.

Through a European research project, a thermally controlled process, in which these minerals were converted into a valuable product with pozzolanic properties, was developed.

This paper deals with the influence of the sludge composition and the calcination parameters on the pozzolanic activity of the calcined product. A multiple linear regression analysis shows that the main factors affecting the pozzolanic activity of the calcined sludge are: the kaolin content of the raw sludge, the quantity of lime produced during calcination, and the quantity of particles lower than 10 µm present in the product.

1. INTRODUCTION

The recycling of paper has become an important industry in the past decade. Recycling reduces the requirement for virgin fibre and energy and can lower the environmental impact of paper manufacture. Between 1983 and 1995, the amount of recovered paper utilized by the European paper industry increased from 14.4 to 30.7 million t/y [1]. The re-use of recovered paper in papermaking inevitably results in the generation of process residues that cannot be used in paper production. These residues most often are disposed of landfills. However, landfills are becoming increasingly undesirable and prohibitively expensive. Therefore, it is important to find alternate disposal means for these sludges.

Recovery of energy, useful materials, or both from the sludge could provide an economical alternative to landfill disposal. Many mills are choosing incineration as a way to handle sludge [2-4]. Air emissions are not a problem for combustion temperatures above 870°C. The ash produced is not a hazardous material. The volume of ash from the incineration process is significant, typically around 25 % of total dry solids. Disposal of incinerator ash is a problem that is becoming increasingly important. Few constructive uses for incineration ash have been developed, and none that are used by the pulp and paper industry. Typically, it is used for land-spreading or as a component of cement [5].

Proceedings of the 11th International Congress on the Chemistry of Cement (ICCC)
'Cement's Contribution to the Development in the 21st Century'
Hosted by: The Cement and Concrete Institute of South Africa
CD-ROM produced by: Document Transformation Technologies
11 - 16 May 2003, Durban, South Africa
ISBN Number: 0-9584085-8-0
Editors: Dr G. Grieve and G. Owens
Congress Organised by: Event Dynamics

The disposal option considered in the present paper is developing a controlled calcination process which utilizes the organic content of the sludge as fuel and allows the re-use of the resulting ash as a pozzolanic material usable in cement and concrete [6-7]. Such application is possible due to the composition of the sludge: 50 % water, 25 % organic matter and 25 % minerals consisting mainly of calcium carbonate and kaolin. When burnt in the range of 650 to 750°C, kaolin is transformed into metakaolin, a very reactive pozzolan. During the process, the following three main steps occur:

i) organic matter is incinerated, producing sufficient energy to keep the process running autothermally,
ii) water is evaporated,
iii) kaolin is transformed into metakaolin, while calcium carbonate is preserved.

This paper deals with the influence of the sludge composition and the calcination parameters on the pozzolanic activity of the resulting ash. The behavior of calcined sludge in concrete is also presented.

2. COMPOSITION OF RAW PAPER SLUDGES

Sixteen sludges supplied by different European facilities were investigated. The moisture content of the sludges as received was in the range of 35 to 60 % by weight. The average wet density of sludges was 600 kg/m^3. The mineralogy of dried sludges was assessed by means of X-ray diffraction (XRD), Infra-red spectrometry (FTIR), Differential thermal analysis (DTA) and chemical analysis. The results are shown in Table 1.

Table 1. Mineralogy of raw dried sludges (w_t %).

Sludge	Organic content	Inorganic components					
		Kaolinite	Talc	Muscovite	Quartz	Calcite	Total
S1	39.7	35.8	3.8	5.8	0.7	12.2	58.3
S2	35.0	26.3	12.8	2.0	0.6	18.6	60.3
S3	34.0	18.3	2.3	2.9	0.2	41.5	65.2
S4	47.7	23.9	1.2	1.4	0.0	25.4	51.9
S5	40.6	19.5	2.7	1.9	0.0	34.3	58.4
S6	31.6	17.4	1.9	1.3	0.0	47.8	68.4
S7	46.4	22.5	1.3	3.2	0.0	25.0	52.0
S8	23.8	20.9	3.2	2.0	0.0	49.3	75.4
S9	38.0	22.6	2.2	3.2	0.0	31.9	59.9
S10	28.6	19.7	2.7	1.9	1.0	46.1	71.4
S11	23.9	45.4	5.7	1.5	0.0	21.4	74.0
S12	39.5	26.2	1.6	1.4	0.0	31.3	60.5
S13	43.5	16.5	3.6	3.4	0.6	31.2	55.3
S14	33.5	18.7	2.7	2.3	0.0	42.1	65.8
S15	54.2	15.7	3.0	4.1	1.3	20.3	44.4
S16	32.3	26.5	2.6	1.7	0.8	36.1	67.7

The inorganic fraction of dried sludges is in the range of 45 to 75 %. It is mainly composed of kaolinite and calcite. The ratio between kaolinite and calcite varies from 0.36 (S8) to 2.94 (S1). In this inorganic fraction, the proportion of kaolinite reaches 61 % for S1 and S11, while it is only 25 % in S6 and S8. The calcium carbonate content is as low as 21 % in S1 and reaches 70 % in S6. Some sludges (S2 and S11) contain more than 5 % talc. The amounts of muscovite and quartz are generally low.

3. THERMAL PROCESSING OF SLUDGES

Sludges were burnt in a laboratory electrical fixed-bed furnace. The volume of the furnace was 125 L and 5 kg of wet sludge was calcined per batch. The temperature was limited to 700°C. A previous study has shown that higher temperatures led to significant decarbonation of calcite and yielded unreactive products (i.e, anorthite and gehlenite) [6].

The temperature was increased at a rate of 250°C/hr and the product was maintained at 700°C for 5 hours. Then, it was cooled, with the furnace being closed. Discharging took place as the furnace recovered to ambient conditions. The cooled burnt sludge was de-agglomerated to get particles smaller than 100 µm. Laser granulometry and BET surface area analyses were carried out to characterize the physical properties of residual ash. XRD and FTIR spectrometry analyses were also performed to investigate the transformation of kaolinite into metakaolinite, as well as the preservation of calcite during calcination.

The evolving gases were analyzed during the tests. The values recorded for SO_2 and NO_x were under the European standard limits; that for CO above the limit. This result needs the presence of a post-combustion chamber to decrease the CO content of gases. As sludges contain chlorides and heavy metals and the calcination occurs at about 700°C, the formation of dioxin-furans may be promoted during calcination. Within the sixteen sludges investigated, only two of them presented this risk. Therefore, emissions have to be treated by a post-combustion system in an industrial process.

4. CHARACTERIZATION OF CALCINED SLUDGES

XRD and FTIR spectrometry data show that kaolinite was completely dehydroxylated during incineration and transformed into metakaolinite. Calcite was somewhat decarbonated, especially in sludges containing the lowest proportions of kaolinite (i.e, S3 and S6). The presence of an IR band at 3645 cm^{-1} revealed the formation of $Ca(OH)_2$ after cooling. The intensity of the band allowed the determination of the quantity of calcium hydroxide present in the final product. The results obtained are shown in Table 2. Table 2 also presents the particle size distribution and the BET specific surface area of calcined sludges.

From Table 2, it appears that important agglomeration occurred during the incineration of S1, S9, S10 and S16, in which 14 to 27 % particles were found to be larger than 100 µm. The average diameter of the particle size distribution is in the range of 7 µm (S4) to 29 µm (S1). The ultra-fine particle content (< 5 µm) varies from 18 % (S8) to 40 % (S4) and the BET surface area ranges from 5.7 m^2/g (S10) to 15.9 m^2/g (S1).

5. POZZOLANIC ACTIVITY OF CALCINED SLUDGES

5.1 Assessment of the Pozzolanic Activity

The term "pozzolanic activity" includes two parameters, namely the maximum amount of lime that a pozzolan can combine and the rate at which such combination occurs. Therefore the pozzolanic activity of the thermally converted paper residues was measured on pastes containing 50 % calcium hydroxide and 50 % calcined sludge, hydrated at equivalent consistency (W/S = 0.70). The control paste was a mixture of 50 % calcium hydroxide and 50 % fine quartz. The residual DTA peak of calcium hydroxide was measured at different ages and the lime consumption was calculated by comparing the peak obtained in pastes containing quartz and calcined sludge. The behavior of calcined sludges was compared to that of a commercial metakaolin (MK) presenting the following properties: metakaolinite content: 97 %; D_{50} = 1 µm; BET surface area: 14 m^2/g.

Table 2. Quantity of $Ca(OH)_2$ present in calcined sludges (w_t %) and physical properties.

Sludge	$Ca(OH)_2$	Particle size distribution (%)			D_{50} (µm)	BET surface area (m^2/g)
		< 5 µm	< 10 µm	< 100 µm		
1	0	20	32	73	29	15.9
2	0	30	62	98	8	8.4
3	36	20	40	91	17	10.6
4	12	40	68	100	7	16.5
5	15	28	54	94	10	10.2
6	27	15	30	96	20	9.2
7	11	18	34	95	17	9.4
8	7	22	48	95	11	7.0
9	9	20	32	74	19	16.0
10	5	28	56	86	9	5.7
11	0	30	48	90	11	12.6
12	7	25	45	97	14	14.6
13	10	28	48	95	11	10.2
14	2	26	50	97	10	7.0
15	6	30	58	95	9	10.7
16	2	22	42	73	16	9.6

5.2 Lime Consumption

The results are shown in Figure 1.

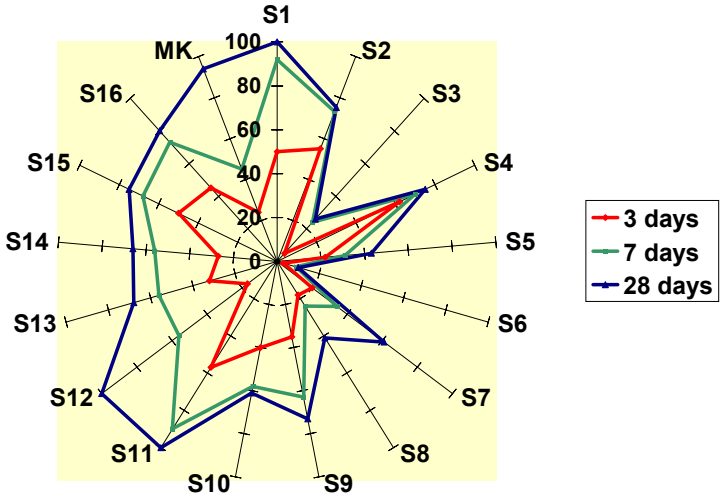

Figure 1. Lime consumption of calcined sludges and MK.

After 3 days of hydration, the best pozzolans are calcined S4, S11, S2, S1 and S15; the less reactive are calcined S3, S6, S7 and S8. This ranking is confirmed after 7 and 28 days, except for calcined S7 which consumes a lot of lime between 7 and 28 days. After 28 days of hydration, 100 % calcium hydroxide is consumed by calcined S1, S11 and S12 which present a kaolinite content varying from 43.3 to 61.4 % in the organic fraction. This result is remarkable compared to MK which consumes less lime than those pozzolans (only 94 % after 28 days). The kaolinite content itself seems to be insufficient to explain the reactivity of calcined sludges, as shown in Figure 2.

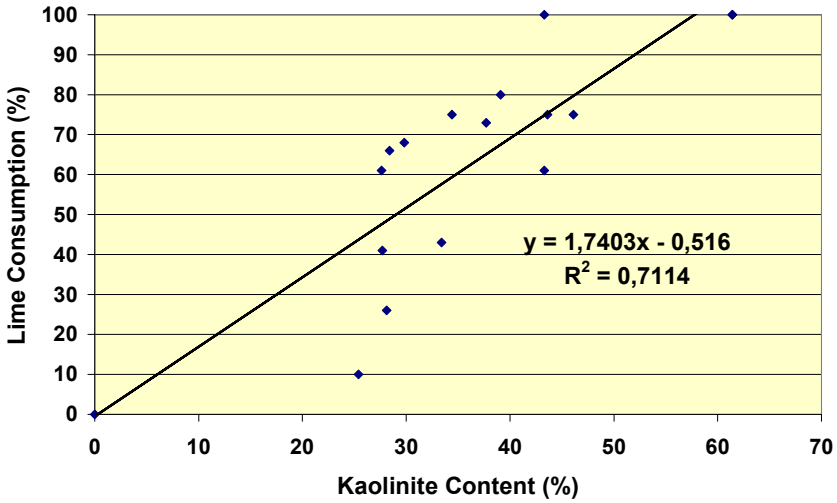

Figure 2. Relationship between the lime consumption and the kaolinite content of the inorganic fraction after 28 days of hydration.

A multiple linear regression analysis was therefore undertaken to explain the pozzolanic activity of calcined sludge at different hydration times: 3, 7 and 28 days. The parameters investigated were:

- the lime consumption: C,
- the quantity of calcium hydroxide present after cooling: D,
- the kaolinite content of the inorganic fraction: K,
- the BET specific surface area: S,
- the quantity of particles smaller than 10 µm: G10,
- the average diameter of the particle size distribution: D50.

The software used for this task was SPSS for MS Windows. The main findings of this investigation are as follows:

i) after 3 days of hydration, the pozzolanic activity of calcined sludge is explained by 4 parameters (D, K, G10 and D50):

$C_3 = - 0.77D + 0.61K + 1.67\ G10 + 2.30\ D50 - 89$ $\quad R^2 = 0.86$

ii) after 7 days of hydration, the main parameters are K and D:

$C_7 = 1.07K - 1.17D + 24.5$ $\quad R^2 = 0.76$

iii) after 28 days of hydration, the main parameters remain K and D:

$C_{28} = 1.18K - 1.42D + 34$ $\quad R^2 = 0.84$

A general conclusion may therefore be drawn for practical use. The main parameters influencing the pozzolanic activity of calcined sludge are:

- the quantity of kaolinite in the inorganic fraction,
- the quantity of calcium hydroxide produced during thermal treatment and which has to be minimized,
- the quantity of particles smaller than 10 µm, which has to be maintained at a certain level to get high activity at early ages.

The BET surface area does not play any role.

6. BEHAVIOR OF CALCINED SLUDGE IN CONCRETE

Calcined S1 was used for these experiments and compared to other pozzolans at a cement replacement of 15 %: commercial metakaolin (MK), fly ash (FA) and silica fume (SF). The cement was a Type CEM I CPA 52.5 according to European standards. The mixture proportions of the control concrete were:

- cement: 350 kg/m^3,
- sand (0/4 mm): 785 kg/m^3,
- coarse aggregate (14/20 mm): 1,070 kg/m^3,
- water: 177L/ m^3,
- superplasticizer in liquid form (SP): 9.8 L/m^3.

The slump was 160 mm. In other concretes, 15 % cement was replaced by each admixture, and the water and superplasticizer contents were adjusted to get about the same workability, as shown in Table 3.

Table 3. Properties of fresh concrete.

Mineral admixture	Water (L/m^3)	SP (L/m^3)	W/CM	Slump (mm)
S1	178	13.3	0.51	150
MK	177	13.3	0.51	150
FA	167	8.8	0.48	150
SF	200	10.9	0.57	165
Control	177	9.8	0.51	160

The compressive strength was measured on cylinders (∅ = 110 mm, h = 220 mm) at different ages: 2, 7, 28 and 90 days.

The results obtained are presented in Figure 3.

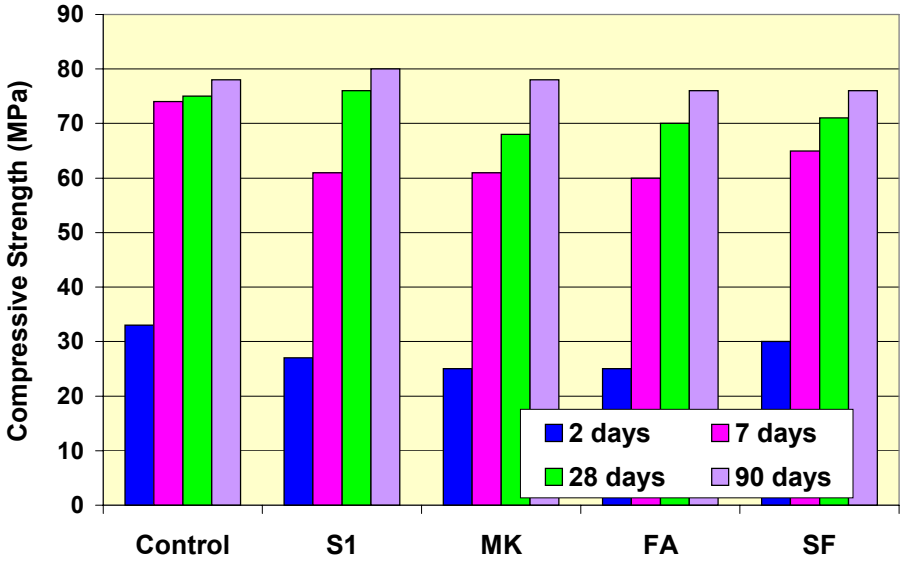

Figure 3. Compressive strength of different concretes.

Figure 3 points out that all admixtures behaved very well and led to high strength at 28 days. Calcined sludge (S1) developed the same performance as commercial metakaolin (MK).

7. PILOT TESTS OF INCINERATION

Pilot tests were undertaken using different types of combustors: rotary kiln, gas suspension calciner, screw-kiln, fluidized-bed combustor and multi-hearth furnace.

7.1 Rotary Kiln

Wet sludge was introduced in the colder part of the kiln heated by gas. The air admission, the kiln speed and the draught were adapted according to the characteristics of the product (calcite content, heat value) and the reactions that can occur.

A de-inking sludge was treated in such conditions. When the temperature reached 700°C, kaolinite disappeared and calcite was completely destroyed, yielding gehlenite and free lime. In any case, no pozzolanic material was formed. Suitable product was obtained as the temperature dropped to 650°C, but organics were not totally destroyed. Therefore, the color was too dark for applications in concrete. The control of the temperature profile seems very difficult in a rotary kiln.

7.2 Gas Suspension Calciner

Before being calcined, paper sludge had to be dried. A drier-crusher was used for this task. The moisture of the sludge dropped from 60 % to less than 1 % and a powder was handled during the calcination process. The temperatures measured at the top of the gas suspension riser pipe were in the range of 520°C to 630°C. The temperature close to the material inlet was up to 100°C higher than the average calcination temperature. At 520°C, a second heat treatment is necessary.

XRD analyses showed that kaolinite has been dehydroxylated and pointed out the formation of detectable amounts of free lime. Chemical analysis of ash confirmed the presence of approximately 2 % free lime in the heat treated product, and the conduction of a CaO balance showed that 7-8 % of the CaO present in the drier-crushed material cannot be accounted for and, thus it must be assumed to have reacted as a result of the heat treatment.

The pozzolanic activity of the final product was lower than that observed in laboratory tests: 83 % instead of 100 % lime consomption, for S1.

7.3 Screw Kiln

Screws are installed in the furnace heated by gas or fuel burners. The furnace is composed of two cells:

- the first one which receives the raw material, is used to dry the sludge,
- the second one is fed with dried sludge and used for calcination.

A sewage sludge was treated using this equipment. No decarbonation occurred and the kiln was very easy to manage. The kiln should be able to treat about 3 t/hr wet sludge. The main problem is that such equipment is still in development and has not yet been used in industrial applications. It allows low imputs of sludge.

7.4 Fluidized Bed Combustor

The wet sludge was discharged on a fluidized bed where it dried and burnt. The furnace was also equipped with a post-combustion chamber.

According to the conditions of the calcination process (temperature in the range of 550 to 700°C), the free lime content of the ash was lower than 2 % and the calcined sludge developed good pozzolanic properties.

When the sludge presented a heat value higher than 1500 kcal/kg, it could be burnt without any additional gas. The process was stable and the final product presented a suitable whitish color. However such equipment cannot treat more than 3 t/hr wet sludge.

7.5 Multi Hearth Furnace

The tests were done at NESA facilities (Belgium), using a Nichols Herreshoff Pyrolyser multi-hearth furnace. Development of the Nichols Herreshoff Pyrolyser started with the fact that in the conventional process of incinerating sludge and refuse, it is sometimes possible to start volatilizing organic matter at a temperature only slightly higher than that needed for the evaporation of free water.

In order to make use of this behaviour, a modified form of the Herreshoff multi-hearth furnace was applied. The furnace consisted of a vertical cylinder constructed of steel and lined with refractory brick. The sludge entered at the top and descended through a series of hearths until the final dry sterile ash was discharged at the bottom.

Circulating rabble teeth constantly turned and moved material on each hearth, exposing fresh surfaces for contact with the gas in order to ensure consistent processing during the various stages.
In the Nichols Herreshoff Pyrolyser the crucial processing stages start with the pre-drying of the sludge on the upper hearths. As the feed descends to the middle of the furnace its temperature rises, so that the organic materials drive off their volatile constituents in a strongly reducing atmosphere. As this stage, close control of solid and rising gas temperature is assured. A very stable process results.

Gases given off from the feed are led out of the furnace and into a separate post-combustion chamber, where complete burning of the volatile organics takes place. These gases are held at a minimum temperature of 800°C for half a second or more in order to achieve complete combustion of gases, thus ensuring that there is no possibility of odours in the off-gases.

In the case of pyrolysis followed by incineration of the solid product, excess air is provided to the bottom combustion zone of the furnace and to the post-combustion chamber. Exhaust gases from the post-combustion chamber are controlled in the range 20 to 30 per cent. That is to say, excess air is kept low, enabling high gas temperatures to be reached economically. In an alternative design there is no post-combustion chamber as such, the pyrolisis gas being ducted away for use as a separate source of fuel.

Meanwhile, inside the furnace itself, the residual solid material, having given off its volatiles, passes down into the third zone, where, with the addition of further pre-heated air, total oxidation is carried out and the residual fixed carbon is oxidized. No more than 0.3 per cent of original fixed carbon remains. Immediately before discharge there is a final cooling zone to provide thermal recovery from the ash.

The calcination with pyrolysis allowed a significant reduction of the air flow in the furnace (- 36 %) and the gas consumption (- 50 %). Therefore, it is possible to reduce the size of equipment needed for emission treatment. The quantity of dust present in the emissions was very low: about 4 % of the sludge weight.

In each case (with or without pyrolysis), the final product was very reactive. The temperature of treatment was 630°C and the free lime content of the ash was lower than 0.5 %.

7.6 Ranking of the Different Calciners

The criteria used to rank the different calciners used for the pilot tests were:

- the precision of the temperature,
- the quality of the final product,
- the stability of the process,
- the energy consumption,
- the investment cost.

Each criterion received a mark from 0 (bad) to 3 (excellent). The higher the final mark, the better the calciner. The results of this ranking are shown in Table 4.

Table 4. Ranking of the different calciners used for pilot tests.

Calciner	Criteria used for rating					Total	Rank
	Precision	Quality	Stability	Energy	Investment		
Gas suspension calciner	2	2	1	0	Non available	5	3
Fluidized-bed combustor	3	3	2	1	3	12	2
Rotary kiln	1	1	0	0	1	3	4
Multi-hearth furnace	3	3	3	2	2	13	1

From Table 4, it appears that the multi-hearth furnace and fluidized-bed combustor are the more suitable equipment to calcine paper sludge in order to get a highly reactive pozzolan. Therefore, they were chosen for industrial tests.

8. CONCLUSION

The transformation of paper sludges into a high-value added material represents a reliable and long-term issue for the paper industry. Despite a lower kaolinite content, some calcined sludges are able to develop higher pozzolanic activity than metakaolin obtained by calcination of clays. The main parameters playing a role in this activity are the kaolinite content in the organic fraction and the quantity of calcium hydroxide produced by calcite decarbonation during calcination. These two parameters are closely linked and, when considered separately, insufficient to describe the reactivity of calcined sludges. At early ages, the proportion of particles smaller than 10 µm also influences the reactivity. The average diameter of the particle size distribution and the BET specific surface area do not play a main role in this activity.

ACKNOWLEDGEMENT

The authors gratefully acknowledge support from the European Community which funded the project under the Brite/Euram Programme (BRE2 CT 94/0626, Project No. PL-8174).

REFERENCES

[1] Clark, D. Keynote address, PPI Paper Recycling '96 Conference, London, 1996.
[2] Pickell, J. and Wunderlich, R. Sludge disposal: current practices and future options, Pulp & Paper Canada, vol 96, n° 6, 1995, pp. 41-47.
[3] Reid, I. D. Solid residues generation and management by Canadian pulp and paper mills in 1995, Paprican Miscellaneous Report 32, 1997, pp. 1-31.
[4] Webb, L A host of options available for sludge, Pulp and Paper International, vol. 38, n° 11, 1996, pp. 44-48.
[5] Ernstbrunner, L. Reconstruction of a cement plant for fiber residue processing, Ciments, Bétons, Plâtres et Chaux, n° 815, 1995, pp. 244-48.
[6] Péra, J. and Amrouz, A. Development of highly reactive metakaolin from paper sludge, Journal of Advanced Cement Based Materials, vol. 7, n° 2, 1998, pp. 49-56.
[7] Péra, J., Ambroise, J., Biermann, J. and Voogt, N. Use of thermally converted paper residue as building material, 3rd international symposium on sustainable development of cement and concrete, San Francisco, 2001, pp. 111-123.

POZZOLANIC PROPERTIES OF CALCINED PAPER SLUDGE

Jean Péra[1] and Jean Ambroise[1]

[1]Unité de Recherche Génie Civil, Institut National des Sciences Appliquées, Villeurbanne, France.
E-mail: Jean.Pera@insa-lyon.fr

Jean Pera

Dr. Jean Péra is Professor of Civil Engineering at the National Institute of Applied Sciences of Lyon, France. He obtained his Engineer diploma in Urban and Civil Engineering (1970), Ph. D (1973) and "Docteur-ès-Sciences" (1979) degrees from this Institute. He has extensive teaching, research and consultancy experience of more than 32 years. He is expert at the European Union for the "Growth and Sustainable Development" program.

His areas of research include development and performance evaluation of new concrete and composite materials, waste management and low-cost building materials. He has published more than 200 papers in various journals and proceedings of national/international conferences. He is holder of 14 patents. He is member of the editorial board of two journals: Journal of Cement and Concrete Composites and Journal of Ferrocement. He also acts a reviewer for other journals: Cement and Concrete Research, Waste Management, Canadian Journal of Civil Engineering. He is member of various scientific and technical societies. He was awarded at the 5th CANMET/ACI International Conference, Barcelona, Spain, 2000, for his contributions in the field of concrete durability.

CONCRETE ANTICIPATED MIXTURE DESIGN AND CONTROL - PRACTICAL METHODS BASED ON CEMENT HYDRATION

Carlos E. S. Tango[1] and Francisco R. Andriolo[2]

[1] IPT – Technological Research Institute, São Paulo, Brazil. E-mail: tango@ipt.br
[2] Andriolo Ito Engenharia S.C. Ltda., São Paulo, Brazil. E-mail: fandrio@attglobal.net

ABSTRACT

This work presents the application of a mathematical model for predicting concrete strength in anticipated experimental concrete mix design and quality control. Strength development model is based on cement paste hydration and its relation with porosity in various levels of water-cement ratio. Using recent data as examples, with the use of silica fume and HRWR admixture, the main steps of an anticipated experimental concrete mix design method is briefly presented as an improvement of the traditional "IPT concrete mixture design method". Additionally, the "AMEBA" anticipated concrete strength control method, adapted to ACI quality control philosophy is illustrated, with data from a precast concrete plant using pozzolan to prevent effects from alkali-silica reactivity of cement with gravel aggregate.

1. INTRODUCTION

The Technological Research Institute (IPT) of the São Paulo State Government has continuously improved a concrete mixture design method since 1927 [1]. This dynamically changing procedure is intensively used and is well known as the "IPT Concrete Mixture Design Method" in the cement and concrete media of Brazil [2,3], as well being disseminated worldwide by old IPT collaborators [4].

Additionally, models for strength-time function were derived and verified with data from the Institute [5], and a derivative concrete strength prediction method was published and called "AMEBA Method" [6].

This work briefly presents the model's fundamentals, a practical example of mixture design method application with its strength anticipating improvements, as well anticipated concrete quality control results, adapted to the international ACI concrete control procedure with an example using pozzolan addition to ordinary portland cement for precast elements.

2. HYDRATION AND STRENGTH DEVELOPMENT MODELS

2.1 Basic mathematical model: strength versus w-c ratio versus time

One of Powers' approaches for compressive strength as a function of gel/space ratio, which is a function of the non-evaporable water and hydration degree in a cement paste, is similar to Abrams' "law" [7] and is given by equation 1 [8]:

$$f_{c,j} = A_p / B_p^{\,x / w_n} \qquad (1)$$

Where:
$f_{c,j}$ = compressive strength at age j;
A_P and B_P = Powers' constants for paste, depending on materials and test conditions;
x = water-cement ratio;
w_n = relative mass of non-evaporable water,
Equation 1 can be seen as a time generalization of Abram's "law", because it is valid for any age, and paste-aggregate transition zone effects, not considered for paste, can be regarded by adequately adjusted constants A_p and B_p also for concrete. From equation 1 it is possible to arrive at equation 2 [6]:

$$f_{c,j} = A / B^{\,x / h_j} \tag{2}$$

Where:
A and B = constants depending on materials (paste-aggregate transition zone included) and test conditions;
h_j = hydration degree at age j.
Inverse of hydration degree can be given by equation 3 [5]:

$$1 / h_j = 1 + j^{-n} . (h'^{-1}_{max} + h''^{-1}_{o} . x^{-1}) \tag{3}$$

Where:
j^{-n} = transformed time, age j elevated to -n, with n = 0.5 for no-slag or low-slag cements;
h'_{max} = maximum initial hydration "speed" considering the transformed time T;
h''_o = derivative of the initial hydration "speed" as a function of x, when x = 0.

Then, we can write equation 4 substituting equation 3 given values in equation 2:

$$f_{c,j} = A / B^{(x + x . j^{-n} / h'_{max} + j^{-n} / h''_o)} \tag{4}$$

We can write equation 4 as equation 5:

$$f_{c,j} = A / (B^x . E^{x.j^{-n}} . D^{j^{-n}}) \tag{5}$$

Where:
$E = B / h'_{max}$ = constant;
$D = B / h''_o$, = constant.
Equation 5 assumes the aspect shown in Figure 1 when graphically expressed.

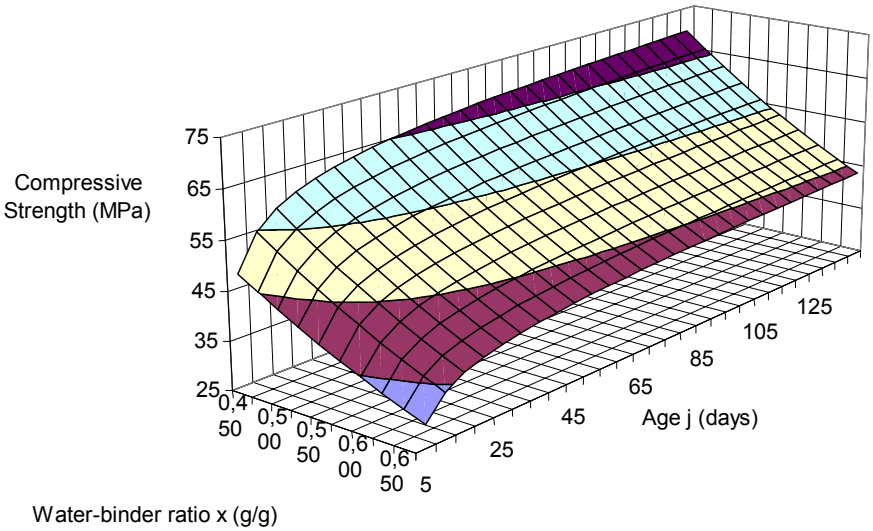

Figure 1. 3-D diagram representing equation 5, adjusted from concrete data using OPC, silica fume, and HRWR admixture.

2.2 Linearization for extrapolation and prediction of strength

Equations 4 and 5 are linearizable, that means, it is possible to transform a surface shown in Figure 1 to a ruled (composed by straight lines) surface, applying the logarithm function to compressive strength, and elevating age to exponent –n. Figure 2 shows a view of a linearized graphic with plotted real compressive strength data from three different concrete mixture proportions (with ingredients from the same samples) poured in 1935 by Ary Torres [9, 10]. Transformed time ($j^{-0.5}$) is represented on abscissa's axis, where real age grows from right to left and zero means infinite age.

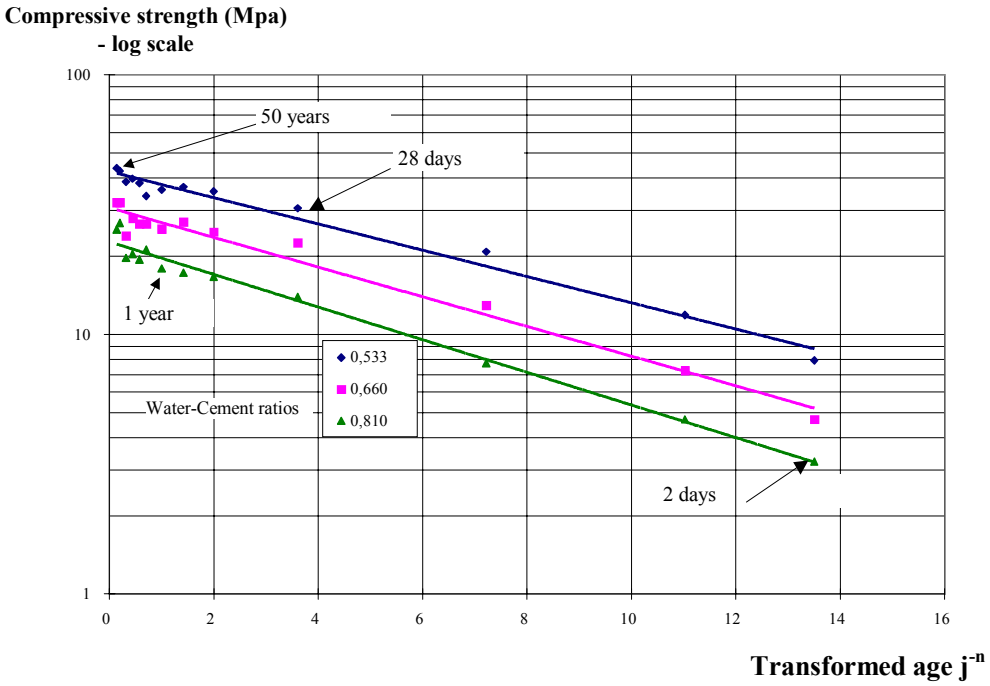

Figure 2. Transformed strength-transformed age diagram (n = 0.5)

3. DESCRIPTION WITH AN EXAMPLE OF ANTICIPATED EXPERIMENTAL MIXTURE DESIGN METHOD

The following steps briefly describe and exemplify the IPT concrete mixture design method [3]:

3.1 First step, rough estimative of concrete mixture proportions

First step utilizes the equation 5, and also equation 6, this last one as follows:

$$m_{est} = x_{est} / [F + G \cdot \log(d_{max}) + H \cdot a_{tc}] - 1 \qquad (6)$$

Where:

x_{est} = estimated water-binder ratio, in the example calculated as 0.362 kg/kg using equation 5 for compressive strength (f_{cj}) at age (j) of interest, (in the example, 49,1 MPa at 28 days, exponent n= 0.5) and constants with prior adjusted values for similar concretes, (in the example, for Brazilian type V-ARI cement with 10 % of silica fume, A = 106.7; B = 4.320; D = 19.81; and E = 1.260);

d_{max} = required maximum aggregate size, in the example, 19.0 mm;

a_{tc} = required slump, in the example 100 mm;

F, G, H, previously found empirical constants [2], in the example with the values 8.029×10^{-2}, -1.946×10^{-2}, and 7.447×10^{-5}, respectively, for ordinary portland cement with silica fume with HRWR admixture, crushed granite cubic aggregate;

m_{est} = roughly estimated aggregate-binder proportion, in the example calculated as 4.75 kg/kg.

3.2 Second step, experimental establishment of dry mortar-dry concrete proportion

The second step is an operation with fresh concretes [2], the procedure being to vary mortar content (dry mortar = cement + fine aggregate) in a mixer, (each tentative mixture varying 2%) with constant coarse aggregate amount and constant aggregate-binder proportion, making the mortar content choice for desired workability. In the example, experiments resulted in 50 % for mortar/concrete (dry basis, weight). A necessary amount of water for workability can be used without preoccupation at this step.

3.3 Third step, preparing of specimens with "rich", "medium" and "poor" mixture proportions

The third step consists of making experimental concretes with aggregate-binder proportions m_{est} ("medium"), $m_{est} - 1$ ("rich" in cement), and $m_{est} + 1$ ("poor" in cement). Each of these mixtures is made with mortar-concrete proportion above determined (50 %) and its water-binder ratio is tentatively established to obtain desired slump; practical binder consumption is calculated from density measuring of the fresh mixtures. Specimens are poured and cured to desired ages for each of the three mixtures. Table 1 shows results obtained for the given example.

Table 1. Example of fresh concrete data at third step

HRWR/ binder (% Weight)	Silica fume/ binder (% Weight)	Slump range (mm)	Aggregate/ binder (kg/kg)	Water/ binder (kg/kg)	Binder content (kg/m^3)
1.0	10	100 ± 10	3.75	0.454	461
			4.75	0.515	382
			5.75	0.614	325

Note: Binder = cement + silica fume

3.4 Fourth step, hardened concrete tests

Specimens are tested at different ages, as shown in table 2, that summarizes the results.

Table 2. Example of hardened concrete data at fourth step

Water/binder (kg/kg)	Mean Compressive strength of 3 tests, (MPa) at age					
	3 days	7 days	14 days	28 days	63 days	91 days
0.454	41.3	51.3	58.0	63.3	66.1	65.2
0.515	36.3	44.1	49.0	55.2	59.0	59.2
0.614	29.3	36.5	43.1	46.0	50.2	53.3

3.5 Fifth step, adjusted equations and mixture design diagram

At the end of this step, the anticipated or definitive experimental concrete proportioning is obtained for a specified job.

Equation 5 is the generalization of Abrams' "law" for any age, and above results lead to the following exemplificative situations when it is adjusted using Minimum Square Method and exponent n is assumed 0.5:

$$f_{c,j} = 189.1 / (7.615^{x} . 2.562^{x.j^{-0.5}} . 1.234^{j^{-0.5}}) \quad (5a)$$

When only results till 7 days where available (equation 5a is the anticipated equation), and

$$f_{c,j} = 141.6 / (4.179^{x} . 4.286 . E^{x.j^{-0.5}} . 1.399^{j^{-0.5}}) \quad (5b)$$

using all results in the regression.

For the desired compressive strength 49.1 MPa at 28 days, the above equations lead to necessary water/binder of respectively 0.593 (anticipated 21 days) and 0.584 (definitive).

Of course, the later result prevails for the establishment of designed definitive mixture proportions. For establishment of mixture proportions at 28 days, extrapolation from 3 and 7 days is acceptable and calculations agree reasonably [6].
Relating concrete proportions water/binder (x), aggregate/binder (m) and cement content (C) in the fresh state, equations 7 and 8 (called "Lyse's" and "Molinari's") are inferred [3, 4]:

$$x = 0.08016 \cdot m + 0.1466) \quad (7)$$

(Adjusted Lyse's equation [3] for the example)

$$1/C = 0.0004549 \cdot m + 0.0004623) \quad (8)$$

(Adjusted Molinari's equation [3] for the example)

Anticipated curves from the anticipated situation are graphically expressed in the IPT Mixture Design Diagram shown in Figure 3 (Diagram for a concrete family with OPC, silica fume, HWRA admixture, 19 mm crushed granite, river sand and 10 ± 1 cm slump. Curves without experimental points are extrapolations to the future).

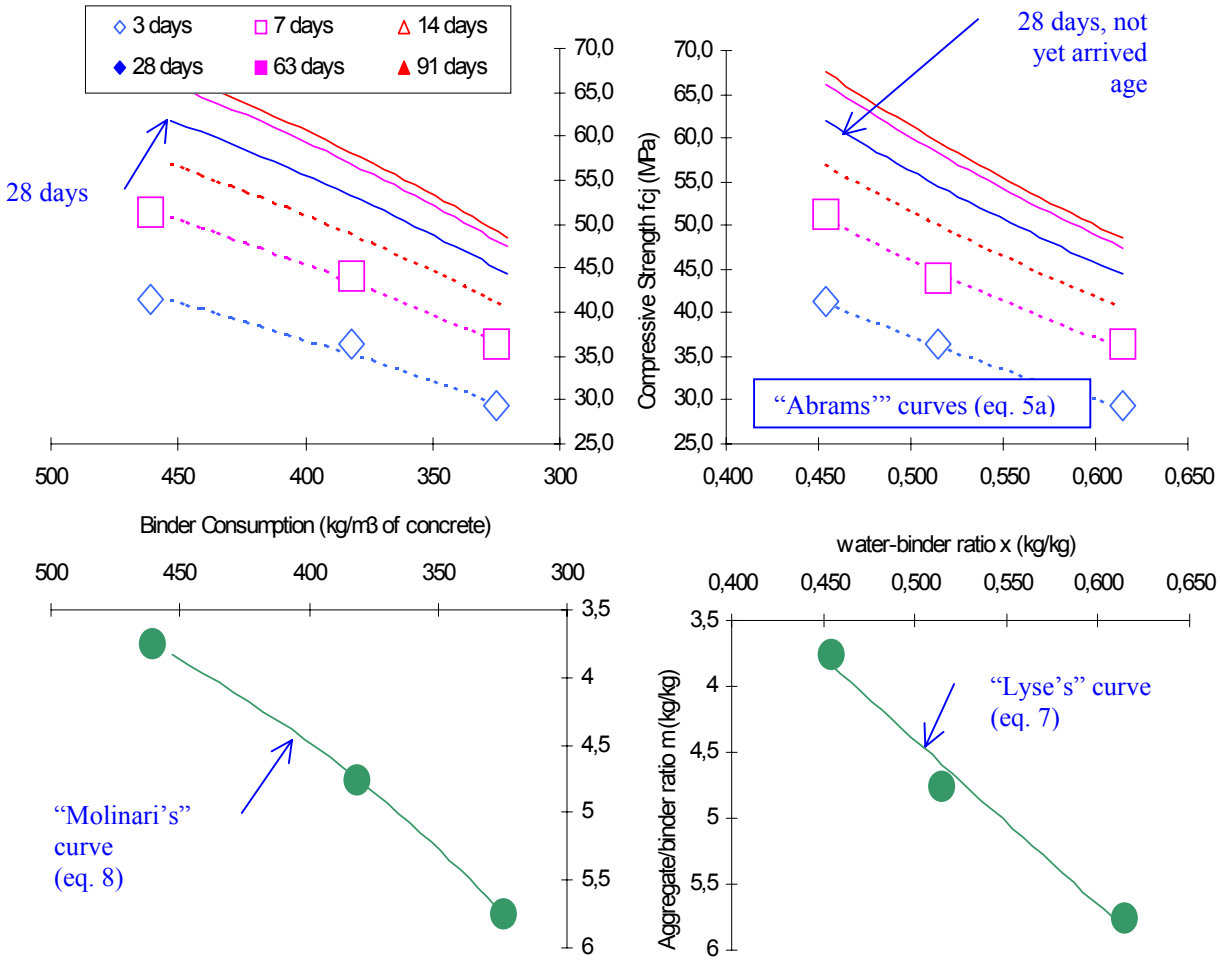

Figure 3. "IPT Mixture Design Diagram" [2, 3, 4] relating predicted (after 7 days) concrete compressive strength to mixture proportions.

In the example, it is possible to arrive to the mixture proportions given in table 3.

Table 3. Concrete mixture weight proportions for the example (binder is considered unity)

Status of mixture design	Used equations	Cement	Silica fume	HRWR admix.	Fine Aggr.	Coarse Aggr.	Water
Anticipated from 3 and 7 days ages only	5a and 7	0.900	0.100	0.010	2.283	3.283	0.593
Definitive after 91 days age	5b and 7	0.900	0.100	0.010	2.228	3.228	0.584

Note: proportions for obtention of 49.1 MPa at 28 days age, dry mortar/dry concrete = 50%.

4. ANTICIPATED CONTROL METHOD (E.G. FOR PRECAST POZZOLAN CONCRETE)

The "AMEBA" method name is due to the general principle of extrapolating compressive strength at a late or high ("Alta" in Portuguese) age with results obtained earlier at medium ("Média") and low ("Baixa") ages. It was demonstrated that the method applies to cement products such as concrete, grout or mortar, including cement plant control [6].

Basic principles reside on the linear aspect shown in Figure 2 for the strength-time transformed curve of a given set of constituents and mixture proportions, mainly water-binder ratio.
Prediction is made with a simple rule of three with transformed time and transformed strength differences; after re-transforming, calculation results in equation 9:

$$f_{ca} = f_{cm}^{\ AMEBA} / f_{cb}^{\ AMEBA\text{-}1} \quad (9)$$

Where:
f_{ca} = compressive strength at a late age "a" or control age, example, 28 days;
f_{cm} = compressive strength at a medium age "m", example, 7 days;
f_{cb} = compressive strength at a low age "b", example, 3 days.
AMEBA = function of the three ages in study, given by equation 10:

$$AMEBA = (a^{-n} - b^{-n}) / (m^{-n} - b^{-n}) \quad (10)$$

Equation 9 was used to simulate an anticipated control using the American Concrete Institute control principles [11], with the concrete production data of precast elements in the Ilha Solteira Hydroproject, Brazil, with the following characteristics:

4.1 Concrete design requirements for strength simulated control in the example

Practical control age: 3 days;
Required minimum (5 % percentile) compressive strength at practical control age: 14,7 MPa;
Design control age: 28 days (simulation);
Required ACI [11] minimum compressive strength f'_c at 28 days(simulation)= 36.6 MPa;
Initially estimated production standard deviation of compressive strength s_d = 7.0 MPa (simulation);
Mean mixture design target strength f'_{cr} = 46 MPa.
Concrete composition (weights for 1 m3 of concrete): Cement, 271 kg; Pozzolan, 53 kg; Water, 132 kg; Natural Sand, 571 kg; Gravel 19 mm, 690 kg; Gravel 38 mm, 690 kg; Plastifying Admixture, 0,810 kg.
Slump range: 40 $\pm$ 5 mm.

Available control results: 186 series with compressive strength average results at 3, 7, and 28 days corresponding to a period

4.2 Characterization of concrete constituents in the control example – need for pozzolan

Cement in the example was an ordinary portland type with Brazilian standard strengths 19.5, 27.8, 39.1, and 45.3 MPa at 3, 7, 28, and 90 days, respectively, and Blaine fineness 354 m^2/kg (averages of all the production).

Blaine fineness of the pozzolan was 790 m^2/kg; pozzolanic activity indexes were 84.7 % with cement and 7.3 MPa with lime, with a water requirement of 105 %. Reduction in expansion was 97.2 %. Results of all job averages for cement and pozzolan chemical analysis are given in table 4.

Table 4. Chemical analysis of cement and pozzolan (average values for the whole job)

Average for	Ignition loss	I.R.	SiO_2	Al_2O_3	Fe_2O_3	CaO	MgO	SO_3	Na_2O	K_2O	Eq. Alkalis
Cement (%)	1.14	0.13	21.36	-	3.53	63.77	2.47	1.65	0.15	0.66	0.58
Pozzolan (%)	1.39	-	66.65	24.45	5.36	-	1.10	Nihil	-	-	-

The concrete aggregates used were a blend of natural aggregates (river gravel and sand). In the studies carried out it was observed that the alluvial aggregates were made up of medium and coarse sand and gravel with a certain mineralogical uniformity and predominant presence of quartz, quartzite, agate, chalcedony, silicificated sandstone, silicificated limestone, chert and ferruginous concretions. The petrographic evaluation (ASTM-C-295), chemical analysis (ASTM- C-289) and mortar bar tests (ASTM-C-227) showed the presence of deleterious minerals and expansion due to the alkali-aggregate reaction. Because of the potential reactivity of the aggregates, a pozzolanic material, from calcined kaolinitic clay, was used as a partial cement replacement, including the use for precast elements with higher earlier strengths.

4.3 Concrete control simulation with example's real data

For 28, 7 and 3 days ages, n = -0.50, AMEBA can be calculated as 1.9478, and equation 9 is expressed as equation 9a:

$$f_{c28} = f_{c7}^{1.9478} / f_{c3}^{0.9478} \quad (9a)$$

The above equation was used with the first series (n exponent is 0.5, indicated when materials have not a previous background). At series number 72, n (see equation 9) was changed because in a real situation it would be reasonable to have sufficient available data for a better evaluation of the exponent. For subsequent series, equation 9b, which n value is 0.67, was used:

$$f_{c28} = f_{c7}^{1.7917} / f_{c3}^{0.7917} \quad (9b)$$

Effectively, exponent 0.67 was considered good for this condition as shows the linearity obtained in Figure 4.

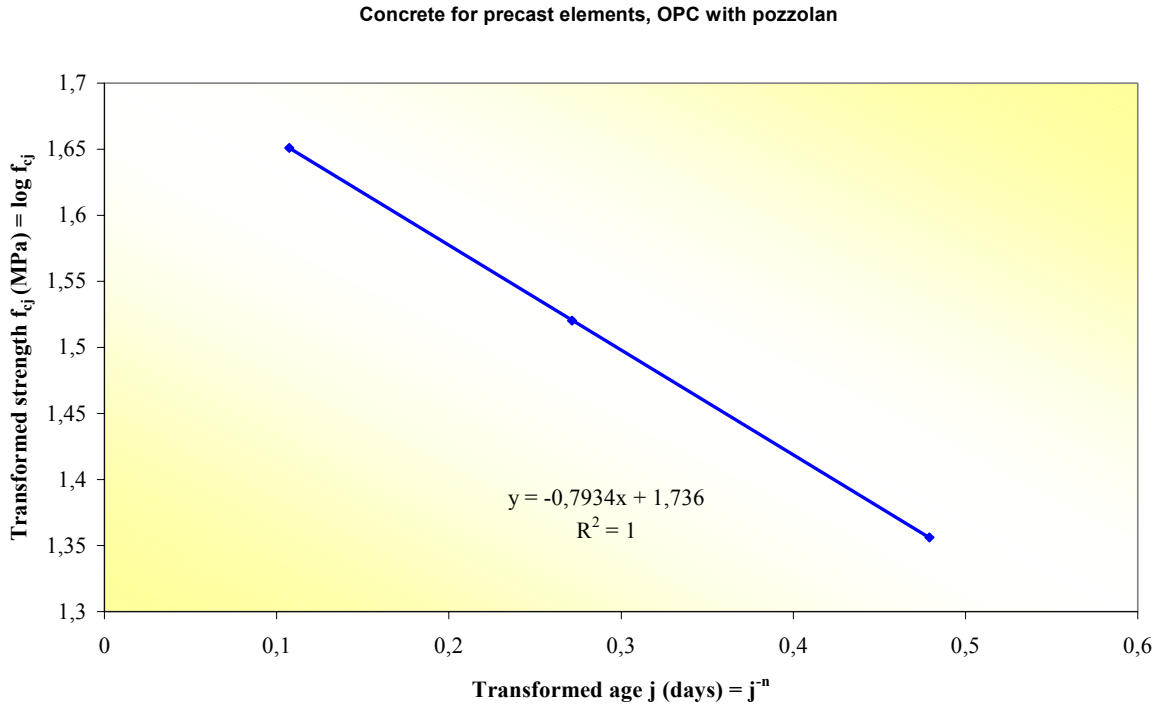

Figure 4. Transformed strength-time diagram for three points, each one being respectively the representation of all job average strengths at 3, 7 and 28 days, using n = 0.67 in time transforming.

Figures 5 and 6 show control charts for the job with simulated-predicted and effective results of tests at 28 days.

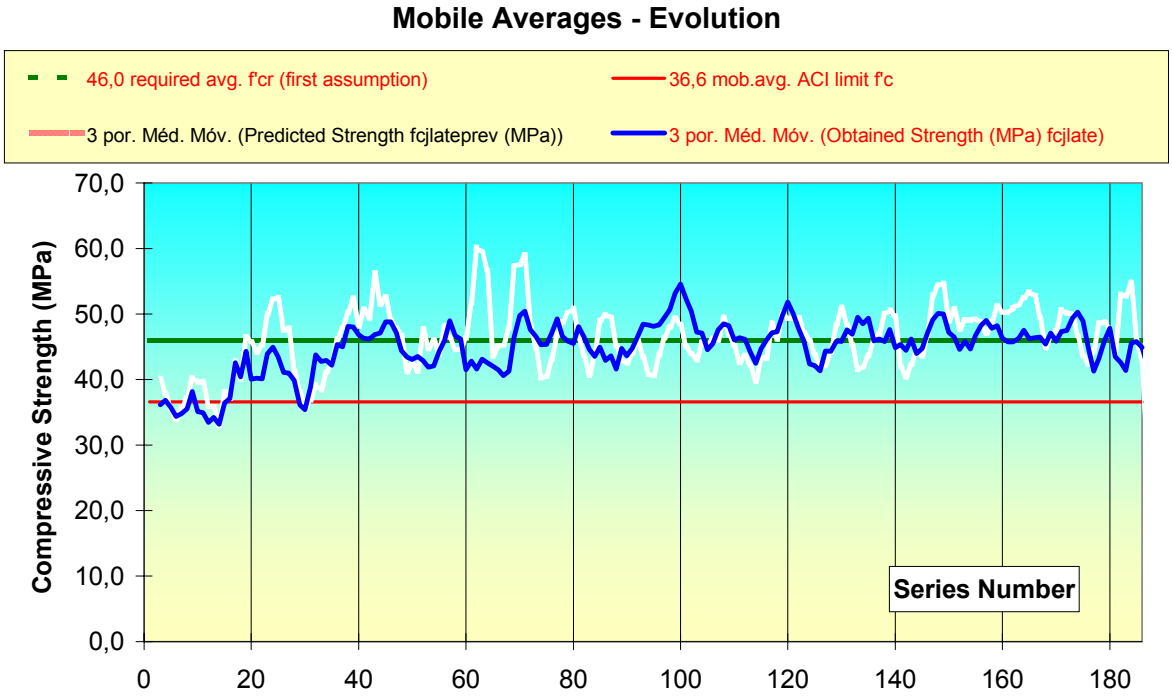

Figure 5. Predicted and effective mobile averages of 3 series along concrete production.

ACI lower limit f'$_c$ not being respected is an alert for changes in the production process. As seen in Figure 5, concrete became better at the beginning of production and remained stable after series about number 40.

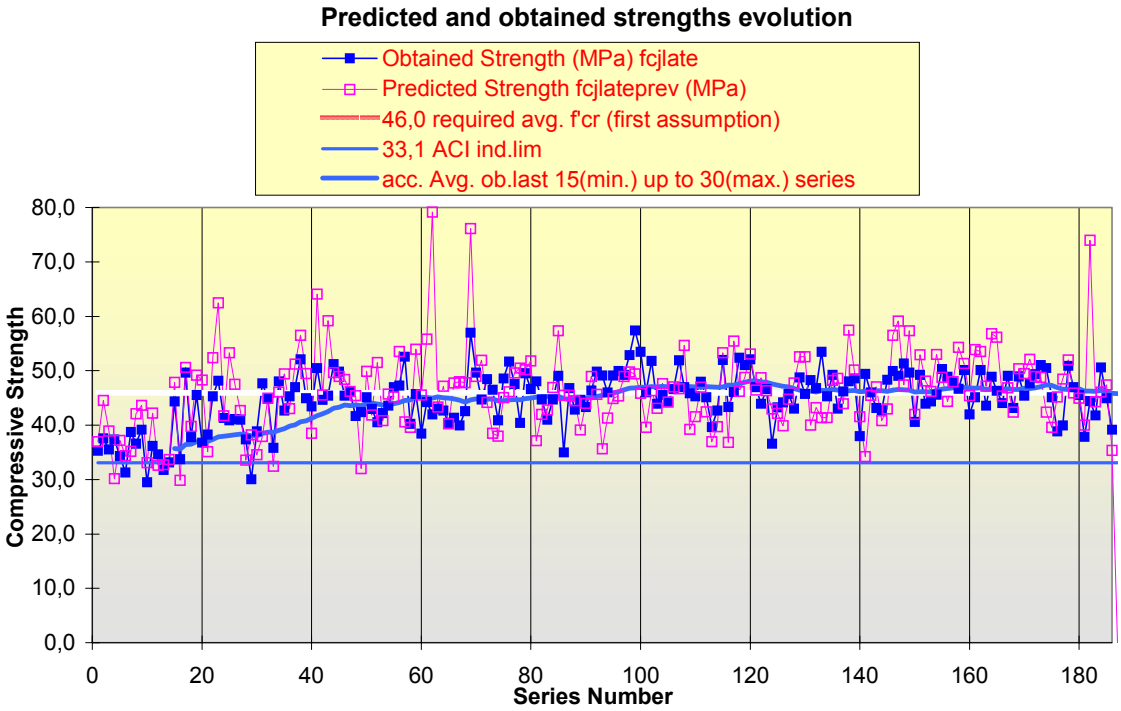

Figure 6. Predicted and effective individual values along concrete production.

In Figure 6, ACI individual limit is stated as f'_c – 3.0 MPa. One single value below this limit implies a revision of control, additional verification tests if judged necessary, and revision of corresponding concrete utilization or demolition in worst situations. Note that dispersion of prediction values is higher than of effective, but dispersion has a preference for higher values of strength.

5. CONCLUSIONS

This work summarizes and exemplifies methods for utilization in concrete technology of a linear model given by equation 5 and illustrated by Figure 1, derived from hydration evolution theories. Examples and refereed works permitted the conclusion that it is possible to use those methods efficiently for anticipated experimental concrete mixture design or for anticipated concrete control (in this work, specifically, with ordinary portland cement and pozzolan addition, and adapted to ACI control procedures).

Obviously a prediction method is not deterministic, and uncertainties are associated, as can be seen by observed differences and dispersion more accentuated for predictions than for effective values. As a result, the methods can be advantageously used with precautions, based on a reasonable knowledge of their principles and characteristics.

ACKNOWLEDGEMENTS

To IPT Concrete Laboratory and IPT Center of Professional Masters in Habitation Courses; as well to the Ilha Solteira Dam Project.

REFERENCES

[1] Torres, A.F. Dosagem dos Concretos [Concrete Mixture Design], Laboratorio de Ensaio de Materiaes, Escola Polytechnica, São Paulo, June, 1927. (LEM, Bulletin 1, in Portuguese old orthography).

[2] Priszkulnik, S. & Kirilos, J.P. Considerações sobre a resistência à compressão de concretos preparados com cimentos portland comum tipos CP-250, CP-320 e CP-400, e a sua durabilidade. [Considerations about compressive strength of concretes prepared with portland cement types CP-250, CP-320 and CP-400, and their durability] II Encontro Nacional da Construção - Clube de Engenharia e Câmara Brasileira da Indústria da Construção, Rio de Janeiro, Brazil – 8 – 13, Dec., 1974. (In Portuguese).

[3] Tango, C.E.S. & Saad, V.M.K. Incrementos no método de dosagem IPT para concretos de amplo espectro de desempenho [Improvements on IPT mixture design method for large-spectrum performance concrete], 43º Congresso Brasileiro do Concreto, Instituto Brasileiro do Concreto, Foz do Iguaçu, Brazil, Aug. 2001. (In Portuguese).

[4] Helene, P.R.L. & Monteiro, P.J.M. Designing Concrete Mixtures for Desired Mechanical Properties and Durability, ACI Special Publication SP-144, San Francisco, USA, 1994, pp. 519-543.

[5] Tango, C.E.S. Modelling and Verifying Portland Cement Concrete Strength-Time Relationship up to 50 Years Ages, 9th International Congress on the Chemistry of Cements, New Delhi, India, 1992.

[6] Tango, C.E.S. An Extrapolation Method for Compressive Strength Prediction of Hydraulic Cement Products, Cement and Concrete Research, ISSN 0008-8846, Volume 28, N. 07, USA, 22/Jul., 1998, pp.969-983

[7] Abrams, D.A. Design of Concrete Mixtures, Structural Materials Research Laboratory, Lewis Institute, Chicago, USA, Dec. 1918. (Lewis Institute, Bulletin 1).

[8] Powers, T.C. (1949) The Non-evaporable Water Content of Hardened Portland Cement Paste - It's Significance for Concrete Research and it's Method of Determination. American Society for Testing and Materials, USA, May 1949. (ASTM Bulletin n. 158, pp. 68-76).

[9] IPT Test Report 6.469, Ensaios de Longa Duração em Concreto [Long-term Concrete Tests], Instituto de Pesquisas Tecnológicas [Technological Research Institute], São Paulo, Brazil, 1935. (In Portuguese, restricted access document).

[10] IPT Test Report 773.521, Ensaios de Longa Duração em Concreto [Long-term Concrete Tests], Instituto de Pesquisas Tecnológicas [Technological Research Institute], São Paulo, Brazil, 1985. (In Portuguese, restricted access document).

[11] ACI (ACI 318-95 and Commentary ACI 318R-95) Building Code Requirements for Structural Concrete, American Concrete Institute, Farmington Hills, USA, 1995.

THERMODYNAMIC ANALYSIS OF THE SOLIDIFICATION PROCESS OF MIXED CEMENTS

M.S. Garkavi, D.M. Garkavi and E.A. Krishan

Magnitogorsk State Technical University, Magnitogorsk, Russia. E-mail: mgarkavi@mail.ru

ABSTRACT

The solidification of binding agents is the result of two interrelated processes - the formation of hydrates and the formation of structures. An artificial stone formed during this process undergoes a number of structural changes in its formation according to the evolution of the binding system which takes place continuously and only in one direction.

One can judge the thermodynamic stability of the structural state of the solidifying system by the value of the production of entropy, the minimum value of the production of entropy corresponding to a thermodynamically stable state.

The experimental study of the solidification of mixed cements on the basis of metallurgical slags and fly ashes shows the fact that the thermodynamic stability of the structure of the final stone depends on the content of mineral additives in the composition of the cement. The more mineral additive the less the thermodynamic stability of the structure of the cement stone. However, there is a certain mineral additive content range in mixed cements, which depends on their nature. The thermodynamic stability of cements with a certain content of mineral additive will be higher than that of the cement stone without any additive. Such mixed cements possess great strength and have a long life. It gives us an opportunity to use them successfully instead of Portland cement in different fields of construction.

According to the thermodynamic stability of the structure of the final stone, mixed cements are divided into a number of groups, and reasonable fields of application are proposed.

1. INTRODUCTION

The solidification of binding systems depends on thermodynamically irreversible interactive processes – the formation of hydrates and the formation of structure. The first process is determined by the chemical reaction between the binding agent and water and the specific products – hydrated new formations – are produced. The second process is connected with the formation of the spatial frame η (which shows the strength of an artificial stone).

While developing, this artificial stone undergoes a number of structural states, changing of which can be determined by the generalized thermodynamic coordinate the degree of the structure formation completion [1].

We may consider that the solidification process is a gradual change of different structures, i.e. the structures of the superior hierarchy arise from the structures of the inferior hierarchy [2,3]. In fact, the structure formation process may be considered as a process of formation and development of inter - particle contacts, and during this process their nature, type and strength change.

Mixed cements exist as two-component systems, consisting of PC clinker and mineral additive. During the solidification process several chemical reactions take place, connected with the different hydraulic activity of the components. At the same time, only one structure formation process that has physical nature, may take place in any isolated volume of the solidifying system. And every chemical reaction, taking place in the given binding system, is connected with the structure formation process and has influence on its development.

If the interaction of these chemical reactions with the structure formation process is separated in time, it can lead to the multi-stage process.

Multi-stage structure formation is in fact the formation of the separate structural states in binding system. This shows that inter – particle contacts of the same nature periodically take place. The number of stages in the structure formation depends on the correlation of hydraulic activity of components and their quantity in mixed cement.

1. EXPERIMENTAL RESULTS

In this paper we present the results of thermodynamic analysis of solidification of mixed cements on the basis of fly - ashes and waste metallurgical slags with different proportions of the slags in the investigated binding agents.

Figure 1 shows the change of the degree of completion of structure formation of mixed cements on the basis of fly ash.

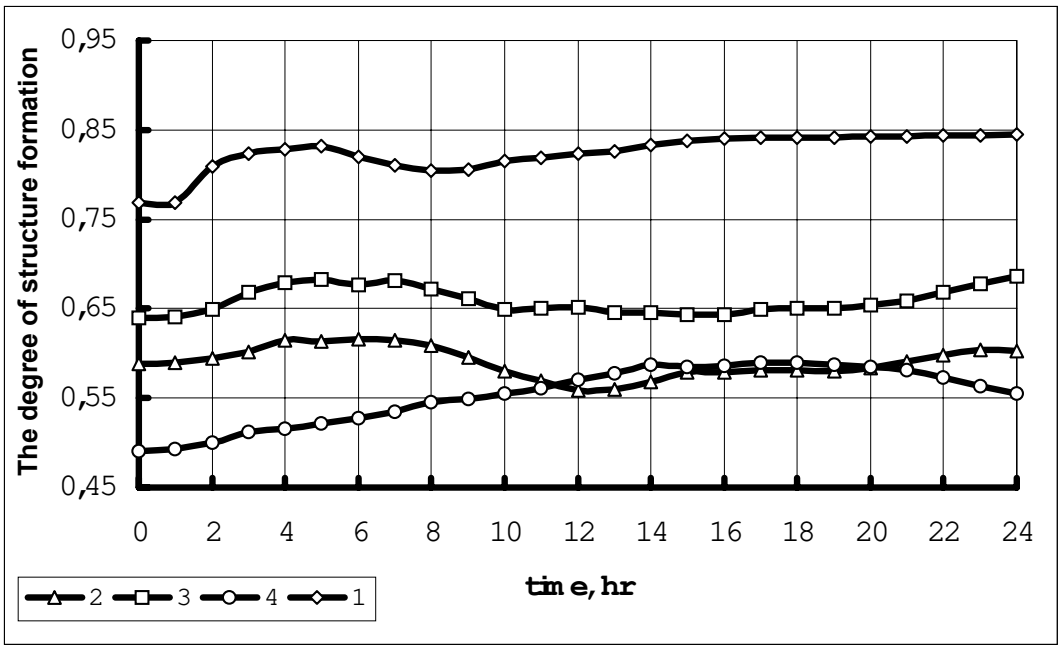

Figure 1. The completion degree of mixed cement structure formation on the basis of fly – ash (t = 20 ^{0}C): 1 – 100% PC; 2–4 – the content of fly - ash 20, 50,80% correspondingly

The process of solidification may be divided into several periods, characterized by different kinetics. These periods reflect the changes in structural conditions of the resulting cement stone.

In Figure 1, related to PC, one can separate three main periods:

- The first period is characterized by the increase of the degree of completion of structure formation η, which is connected with the formation of a coagulation structure in the binding system, and it coincides in time with the induction period of hydrate formation.

- The second period is accompanied by the reduction of the degree of completion of the structure formation process, which is connected with the destruction of the coagulation system owing to acceleration of the hydration process. During this period a transition coagulation– condensation structure takes place in the binding system.
- The third period is also characterized by the increase of the degree of completion of the structure formation, which is connected with the formation of the condensation – crystallization structure of the cement stone.

As it follows from Figure 1, mixed cements, containing 20 and 80 percent of fly–ash (curve 2, 4), have the nature of structure formation analogous to the structure formation of PC. Mixed cements, containing 50 percent of fly-ash (curve 3), have two maxima at the curve of changing of degree of completion of structure formation, that is the evidence of a multi stage process which takes place in the given binding system.

The mixed cement, containing 80 percent of dump steel-smelting slag, has the same nature of structure formation. When there is less quantity of steel-smelting slag in mixed cements, these cements have the nature of solidification analogous to PC (Figure 2).

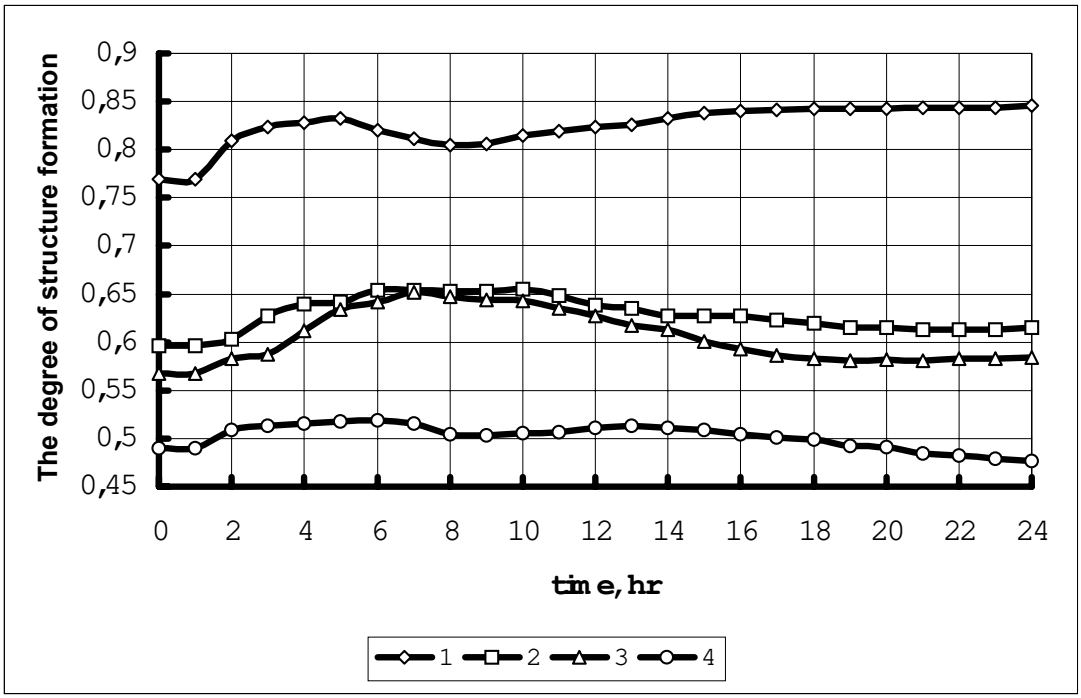

Figure 2. The completion degree of mixed cement structure formation on the basis of waste steel – smelting slag (t = 20 ^{0}C): 1 – 100% PC; 2-4 – the content of steel – smelting slag 20, 50, 80% correspondingly

The emergence of the second maximum on the curve of changing of degree of completion of the structure formation is connected with the intensification of the hydrate formation process owing to the pozzolanic reaction of mineral additives to the mixed cement. It prolongs the existence of transition coagulation – condensation structure in the solidification system. And so we can observe a competition between the appearing condensation – crystallization contacts and coagulation – condensation ones, which already exist. And it results in the emergence of the second maximum at the curve of changing of η (Figures 1 and 2).

If there is a low proportion of mineral additive in the mixed cement, the pozzolanic reaction develops practically synchronously with the hydration reaction of clinker component, i.e. the simultaneous interaction with the process of structure formation takes place and this process is

developed according to a single stage mechanism. If there is a high proportion of mineral additive, this synchrony is broken. This is connected with the fact, that apparent self-energy of mineral additive hydration activation considerably exceeds the activation energy of clinker components of the mixed cement [4]. It is important to mention, that when the solidification temperature increases owing to heat activation the asynchrony disappears and the structure formation process goes on according to single-stage mechanism.

According to all these facts, we can conclude that the precondition for the development of multi-stage structure formation during the solidification of mixed cement is the essential difference between apparent self-energies of activation of hydrate formation of these cement components.

In Figure 3 there are values of the apparent energy of hydration activation of mixed cement components. Figure 3, shows that the blast-furnace granulated slag has apparent self-energy of hydration activation similar to the activation energy of PC. This fact explains the absence of the multi-stage structure formation process in slag Portland cements even when there is a high proportion of slag in them.

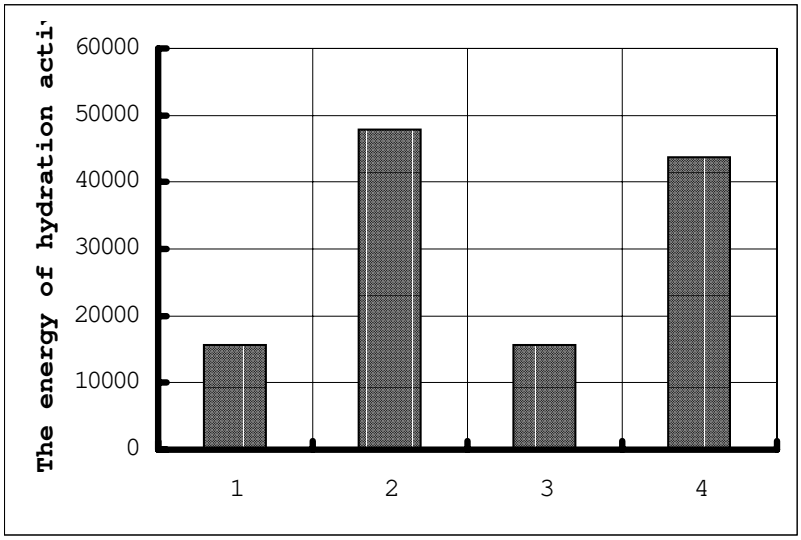

Figure 3. The apparent hydrate formation activation energy of mixed cement components:
1 – clinker; 2 – fly–ash; 3 – blast – furnace granulated slag; 4 – waste steel – smelting slag

As the hydrate formation is only one aspect of the cement stone formation, we should observe the structure formation criteria for developing multi – stage structure formation in a binding system.

The strength of the forming cement stone in mixed cements is determined by adhesion contacts. The hydrated new formations of both components take part in the formation of these contacts. The contribution of mixed cement components in the formation of contacts of the particular type structure development can be estimated by the quantity of the instantaneous power of structure formation $\mathbf{W_\eta}$, which is the product of the constant $\mathbf{K_\eta}$ of the process velocity and the quantity of its apparent activation energy $\mathbf{E_{A\eta}}$, i.e. $\mathbf{W_\eta = K_\eta E_{A\eta}}$ [4].

During the synchronous interaction of the hydrate formation and the structure formation processes, i.e. during the single – stage structure formation the following ratio is carried out:

$$\mathbf{W_{\eta\,[mix]} < W_{\eta[cl]} + W_{\eta\,[min.ad.]}} \qquad (1)$$

where $W_{\eta\ mix}$, $W_{\eta\ cl}$, $W_{\eta\ min.ad.}$ – the instant power of the structure formation of mixed cement, its clinker component and mineral additive.

Ratio 1 shows, that both components of mixed cements simultaneously take part in the process of cement stone structure formation. However the component which has greater instant power of structure formation, predominates.

When the synchronous interaction is interrupted during the indicated processes, i.e. during the multi-stage structure- formation process, this ratio is fulfilled:

$$W_{\eta\ [mix]} = W_{\eta[cl]} + W_{\eta\ [min.ad.]} \quad (2)$$

The given ratio means, that the components of mixed cements take part in the structure formation process in succession, and the first portion is carried out by the reactions of the component with greater instant power of structure formation.

Taking into account the content of mineral additive in the mixed cement, the ratio (2) will be:

$$W_{\eta\ [mix]} = (1-\varphi)\ W_{\eta[cl]} + \varphi W_{\eta\ [min.ad.]} \quad (3)$$

where φ - mass quota of mineral additive in mixed cement.

The experimental examination of the ratio (3) with the help of mixed cements on the basis of waste steel-smelting slag and fly – ash showed, that this ratio can be carried out in case of φ=0,8 for slag cement and φ=0,5 for fly - ash cement. It is well coordinated with the above mentioned character of changing of degree of completion of mixed cement structure formation η.

That is why equation (3) serves both as a ratio of values of apparent activation energy of hydrate formation of mixed cement components and as an index of multi stage process of structure formation in binding systems.

Note: With increased solidification temperature all mixed cements have the single stage structure formation process because in the following conditions the asynchrony of the hydrate formation and structure formation development is eliminated.

From the above we can consider that the structure formation character of mixed cements is determined by the quantity of mineral additive in it and its nature.

Evidently, during the solidification processes in mixed cements with different structure formation character final and intermediate structural states appear with different thermodynamic stability, and this predetermines their different physical, mechanical and performance qualities.

3. THE THERMODYNAMIC STABILITY OF STRUCTURAL STATES

The stability is the capacity of the binding system to keep its properties under the influence of internal and external factors [6,7].

The breach of stability of any structural state is connected with the removal of the last one from the balance, the degree of which is characterized by the value of entropy production. If the variation from equilibrium is small, the production of entropy serves as a criterion for establishing a stationary state, when this value is minimum, and in case of its equilibrium this value is equal to zero [6].

In binding systems the stability of developing structural states is determined by the quantity and sign of the redundant production of entropy. And the quantity of the redundant production of

entropy is determined by the interactive processes of structure and hydrate formation, and the sign is determined by the correlation of velocity and motive power of these processes.

In general, the quantity of the redundant production of entropy for a binding system is determined by the following ratio [8,9]:

$$\delta_x P = \delta_x P_\xi + \delta_x P_\eta \qquad (4)$$

where $\delta_x P_\xi$ - portion in the redundant production of entropy, which is determined by hydrate formation; $\delta_x P_\eta$ portion in the redundant production of entropy, which is determined by structure formation.

The instability of a binding system (when $\delta_x P < 0$) can appear in the following cases:

$$1)\ \ \delta_x P_\xi < 0,\ \ \delta_x P_\eta > 0,\ \ |\delta_x P_\xi| > |\delta_x P_\eta| \qquad (5)$$

i.e. in this case a " dangerous " portion in the redundant production of entropy is produced by the hydrate formation, which causes the instability of the binding system structure;

$$2)\ \ \delta_x P_\xi > 0,\ \ \delta_x P_\eta < 0,\ \ |\delta_x P_\xi| < |\delta_x P_\eta| \qquad (6)$$

in this case the instability of the binding system comes from the structure formation process;

$$3)\ \ \delta_x P_\xi < 0,\ \ \delta_x P_\eta < 0 \qquad (7)$$

In this case the instability of the binding system is determined by the joint influence of hydrate and structure formation processes.

During the solidification of mixed cements with single stage structure formation only one unstable structural state appears (Figure 4a).

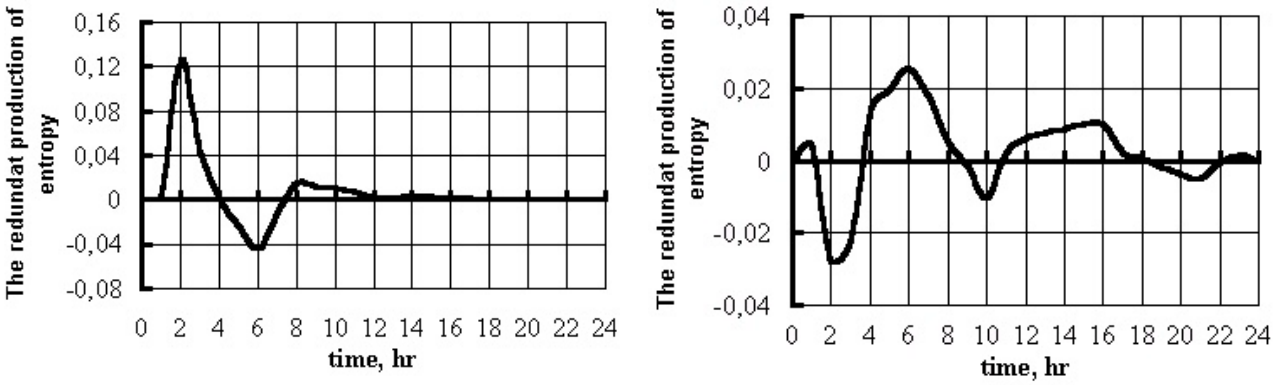

Figure 4. The redundant entropy production during the mixed cements solidification:
a) with single – stage structure formation;
b) with multi – stage structure formation

This thermodynamically unstable structural state corresponds to the formation of a transitional coagulation – condensation structure in the binding system. This structure represents a temporal - spatial dissipation structure, according to [6,7].

It is important that thermodynamic instability of the given structural state in all mixed cements with single stage structure formation comes from the joint influence of the hydrate and structure formation processes, and this is related to the ratio (6).

During the solidification of mixed cements with multi stage structure formation two thermodynamically unstable structural states appear and the second one is more stable, as it follows from Figure 4b. The origin of the second instability comes from a pozzolanic reaction, developing in the binding system, in which the elements of the thermodynamically stable condensation crystallization structure have already taken place.

The experiments of the solidification of mixed cements on the basis of fly ash showed that the most thermodynamically stable condensation crystallization structure forms during the solidification of cement, containing 20 percent of fly ash. Such mixed cement has the highest strength characteristics (Figure 5).

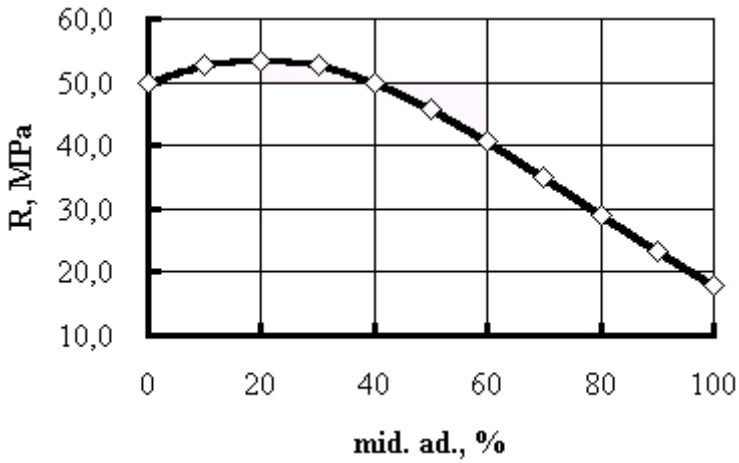

Figure 5. The correlation of the mixed cement strength and the mineral additive content (fly – ash)

When there is more fly ash in mixed cement the thermodynamic instability of structure of forming cement stone increases and the strength reduces.

4. CONCLUSION

According to the analysis of the solidification process of mixed cements one can divide them into three groups and determine areas of their application:

- 1st group mixed cements with the single stage structure formation and normal solidification conditions.
  These cements are characterized by high thermodynamic stability of the forming solidification structure. These cements are substitutes of PC.
- 2nd group mixed cements with the multi stage structure formation.
  It is expedient to use these cements for the production of concretes, which are solidifying during the heat treatment and for the production of slowly solidifying concretes for mass concrete.
- 3rd group highly filled mixed cements with high percentage of mineral additive.

These cements are characterized by the low thermodynamic stability of structure of the forming stone and its low strength. It is expedient to use these cements for the production of concretes and mortars of low strength.

Therefore, the thermodynamic analysis data of the mixed cements solidification can serve as the basis for the developing of rational compositions on the basis of various waste products.

REFERENCES

[1] Tsimermannis, L.B. Thermodynamic analysis of mineral binder hardening in closed system, 6th International congress on the chemistry of cement, Moscow, 1974, vol. II, book 1, pp. 25 – 26.

[2] Grankovsky, I.G. Structure formation in mineral binding systems, Kiev: Naukova dumca, 1984, p.300.

[3] Gladishev, G.P. Makrokinetics and thermodynamics of natural hierarchical process, Physical Chemistry Magazine, 61 №9, 1987, pp. 2289 – 2301.

[4] Khibitcheva, M.N. and Garkavi, M.S. and Belikh, V.T. The solidification of mixed binding with the use of fly – ash, Cement, №8, 1990, pp. 16-18.

[5] Sitchev, M.M. The cement adhesion, Cement, №11, 1969, pp.11-13.

[6] Prigogin, I. and Stengers, I. Order from chaos. New dialogue between man and nature, M.: Progress, 1986, p. 432.

[7] Ebeling, V. The structure formation during the irreversible process, M.: Mir, 1979, p. 280.

[8] Garkavi, M.S. and Sitchev, M.M. The self–organization in the solidifying cement pastes, Cement, №1 – 2, 1991, pp. 69 – 71.

[9] Sitchev, M.M. and Garkavi, M.S. The structure changes during the binding solidification and their thermodynamic analysis, The Applied Chemistry Magazine, 65 №6, 1992, pp. 1264 – 1265.

PERFORMANCE BASED DESIGN SYSTEM FOR CONCRETE MIXTURE WITH MULTI-OPTIMIZING GENETIC ALGORITHM

Takafumi Noguchi[1], Ippei Maruyama [1] and Manabu Kanematsu [1]

[1] Department of Architecture, University of Tokyo, Tokyo, Japan.
E-mail: noguchi@bme.arch.t.u-tokyo.ac.jp

ABSTRACT

This paper presents a method for optimizing concrete mixture proportions according to the required performance and also presents several case studies. Since various qualities are usually required of concrete, we characterize the proportioning problems as multi-criteria optimization problems. We dealt with the notion of Pareto optimality to derive the optimum solution and applied it to a genetic algorithm. In this contribution, two proportioning problems are solved by the genetic algorithm: a request of cost-performance at 60 MPa in strength as a simple problem, and a concrete mix for mass concrete in cold weather at the coast.

1. INTRODUCTION

Concrete is required to exhibit performance corresponding with applied environment. And nowadays, thanks to technological progress, it is possible to make the concrete meet those requirements. However, there has been no established method. Only a few attempts [1][2] have so far been made in relation to these problems. The main reason for few outcomes is that a wide variety of mixture proportions are possible and there is no way to optimize mathematically the problem under many criteria, which are represented by objective functions. This contribution describes the method of optimizing mixture proportions of concrete by application of the Genetic Algorithm (GA) and several engineering models representing the relationship between the properties of concrete and mix proportions.

Proportioning problems cannot be solved by the usual methods that consist of searching for the best solution with a single objective function, such as linear programming problems and nonlinear programming problems. The reason for this impossibility is that various performances are required of concrete corresponding to the environments in which the concrete is used, and it is impossible to express the plural requests in a single objective function. It follows from the features of the proportioning problem mentioned above that a proportioning problem is considered to be a multi-criteria optimization problem.

2. HOW TO APPLY GENETIC ALGORITHM TO MULTI-CRITERIA PROBLEMS

2.1 Genetic Algorithms

Genetic algorithms are optimizing, learning and searching algorithms based on the mechanism of natural selection and natural genetics. What is important in GA is that it is unnecessary to develop a method to solve the target problem. Because GA can solve the problem with the relative evaluation of the non-inferior set and is easier to formulate rules of evaluation than any other existing method, GA is widely applied to the engineering field, especially to combination problems. Since proportioning is a type of combination problem, there is a good reason to apply GA.

Proceedings of the 11th International Congress on the Chemistry of Cement (ICCC) 11 - 16 May 2003, Durban, South Africa
'Cement's Contribution to the Development in the 21st Century' ISBN Number: 0-9584085-8-0
Hosted by: The Cement and Concrete Institute of South Africa Editors: Dr G. Grieve and G. Owens
CD-ROM produced by: Document Transformation Technologies Congress Organised by: Event Dynamics

In GA “genotype” is the parameter set, which means a vector in the set of optimization problem, coded as a finite-length string with binary digits. The simple string is called “individual”. To apply GA to a proportioning problem, the genotype is designed to represent various components and various mixture proportions (see Fig.1). The genotype consists of two parts. One is a coded binary string and the other is a database containing components such as cement, aggregate, admixtures, and so on. As demonstrated in Figure 1, the string has linkage parts and volumetric ratio parts. The linkage parts have a connection to the database, which is used when the fitness is calculated with volumetric ratios. The volumetric ratio parts show the volumes of components in concrete as component/water ratios. In reality, the binary string is fixed as 256 bytes whereas it is not shown in Figure 1.

The algorithms make a “phenotype”, which demonstrates characteristic form and quality in the designed system, from each individual according to its genotype. Each designed genotype has its phenotype. In our system, the term phenotype means the concrete properties and performance that are estimated from mixture proportions coded in the genotype. The kinds of concrete properties and performance are also shown in Figure 1. Prediction formulas are formulated statistically for each property.

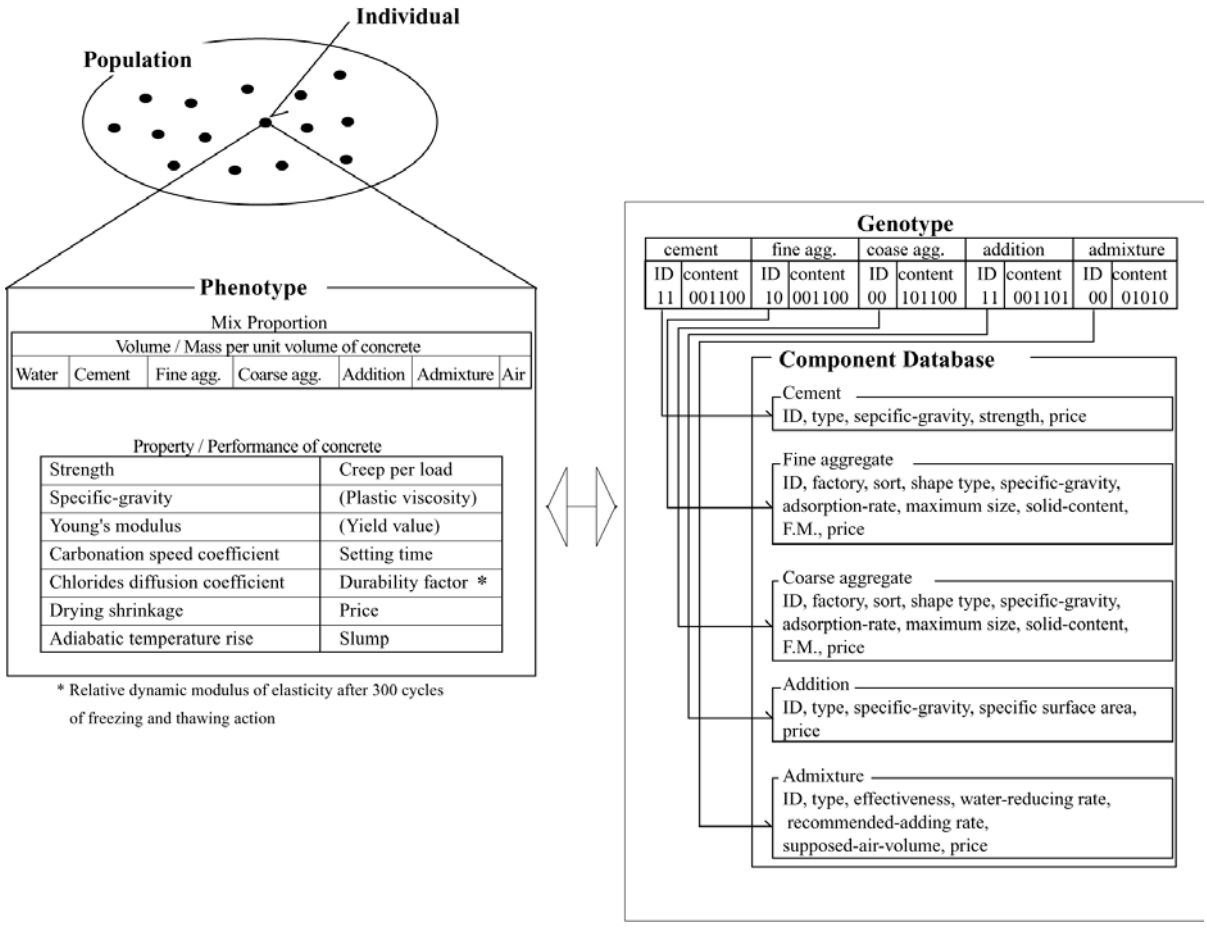

Figure 1. Schematic of GA applied for proportioning problem

“Fitness value” gives the numerical evaluation of each individual and each phenotype in the designed system. According to the fitness values, which can be plural in Pareto optimality problem, an individual in the “population” representing the set of individuals will be reproduced with crossover and mutation from generation to generation. Thus the individuals in the set become fitted under applied environment. In the developed algorithm, suitable functions are designed to meet the way of performance requesting and those are shown in Figure 2 together with the equations. U is the parameter representing the required performance of concrete mixture and T is the parameters

that determine shape of function. These two parameters express the allowable range of requirements for performance.

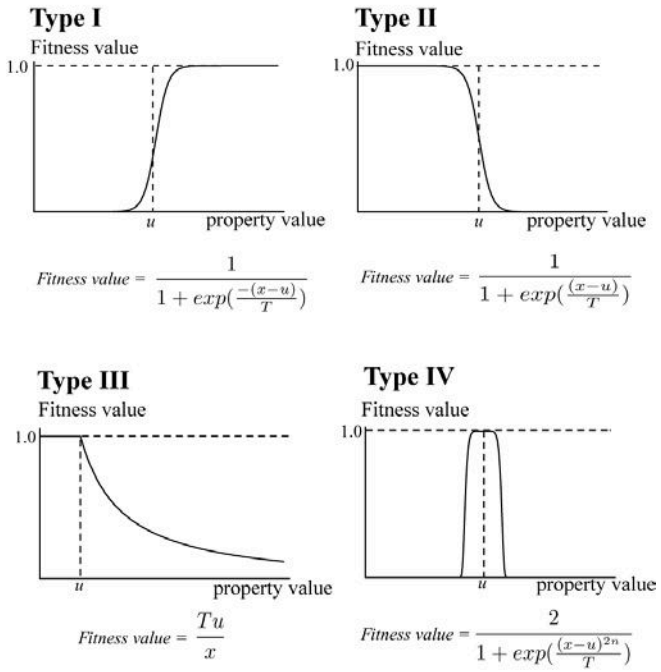

Figure 2. Fitness function and its shapes

2.2 Genetic Algorithms Applied to Multi-criteria Problem

In multi-criteria optimization, the notion of optimality is not obvious at all. For example, it is difficult to compare strength with fluidity. There does not exist the way to evaluate and compare different things. But the concept of Pareto optimality helps the evaluation of multiple criteria in a rational way. The Pareto optimal set is defined as stated below.

When a vector **x** is partially less than **y** and all criteria are minimizing criteria, the mathematical expression of the vector **x** in the Pareto optimal set is:

$$(\mathbf{x} < p\mathbf{y}) = (\forall i)(x_i < y_i) \wedge (\exists i)(x_i < y_i) \tag{1}$$

Under the condition of equation (1), point x "dominates" point y. If the point is not dominated by any other, that point is "non-inferior". The set of these non-inferior points is what we call a Pareto optimal set. According to this definition, if there is a point, which is not less than any other points by all criteria, only the best point will get a good evaluation. If there is no such a point, a set of non-inferior points, which trade off one of the set of points for another, will be evaluated as good.
To apply genetic algorithms to a multi-criteria problem, an algorithm that can derive the Pareto optimal set is developed. Goldberg [3] had designed similar algorithms. Improvement on Goldberg's algorithms and application to the proportioning problem are conducted. The developed program applied to concrete mixture problem is named MixGA. The program-flow of MixGA is detailed as follows.

1. Assume that there exist P criteria and N individuals
2. Make N individuals randomly.
3. Select criterion No. 1 and determine the fitness value of each individual's genotype.
   Choose parents A and B with the roulette method in which the probability of its selection is in proportion to fitness value.
   Crossover A and B, and reproduce child C and child D.
4. Repeat steps (2) and (3) from criteria No. 1 to No. P.

5. After getting N individuals in the new population (child generation) and N individuals in the old population (parent generation).
6. Produce a temporary generation with the child and parent generations.
7. Mutate genes by reversing the number at certain loci arbitrarily with a constant probability of 1%. (Loci is the plural word of locus. Locus means the position of the gene.)
8. Select Pareto individuals from the temporary generation and make the next generation that consists of N individuals. Reduction rule of population is dominated by two roles below.
   (i) If the number of Pareto individuals is less than N, then preserve all the Pareto individuals. Up to the number of all individuals becomes N, select individuals one by one from the rest with the criteria No. 1 to No. P. The probability of selection is in proportion to their fitness value. This method intends that the good genes in the remainder should be carried on in the next generation.
   (ii) On the other hand, if the number of Pareto individuals is N or more, select individuals from the Pareto individuals according to criteria No. 1 to No. P. The probability of selection is in proportion to their fitness in order.
9. Iterate steps (2) to (8) until the given number of times.
10. Conduct final selection.

The algorithm detailed above is characterized by the evolution of population with highly evaluated genes and Pareto optimal conditions. The highly evaluated individual has a good feature in a part of the binary string. And these parts of a binary string in individuals are inherited to next generation explicitly. An individual in the next generation inherits several good parts of a binary string that can be highly evaluated through phenotype. This process of evolution makes it possible to find out the optimal concrete mixture among an almost infinite number of combinations of materials and proportions; otherwise the process can be a random search and that will fail.

But it should be noted, however, that a Pareto optimum set is a set of non-inferior points. This definition implies it is possible that the evolved population has individuals, which have an outstanding performance by a certain performance criterion in exchange for bad fitness values of the others. The Pareto set conditions do not provide a single exact solution but help to search for an optimal set widely. Because of this undesirable aspect of Pareto optimality, the concept of "meta-property" is used. In MixGA the average of fitness values of target properties is used as one of properties and this kind of property of individual is called meta-property. With the meta-property concept it is possible to inherit another possibility in gene that shows balancing in target properties of concrete to the next generation. Besides a final process of evaluation, a final selection is conducted using the fitness values and eliminating the individuals that do not meet the required performance.

3. TRIAL OF MIXGA

The followings are two case studies, in which the mixture proportion of concrete is optimized under required conditions by using MixGA.

3.1 Case study 1

In case study 1, simple cost performance problem of strength property is examined. In detail, the concrete is required to have 60 MPa, Slump 18 cm and lower cost. Other properties are less significant.

3.1.1 Prediction of Strength of Concrete

As is mentioned above, predicting functions that enable us to calculate the properties of concrete with any mix proportion are formulated. Regarding the strength properties of concrete, the

formulating is partially based on the theoretical approach and partially based on the statistical approach. The formulas used are shown below.

Strength of mortar:

$$F_m = (a(B/W) + b) \cdot K \tag{2}$$

where F_m denotes the strength of mortar, a, b and K denote material parameter depending on cement, W denotes the water content per unit weight [kg/m^3], and B denotes the summation of cement and admix content per unit weight [kg/m^3]. In this contribution 4 kinds of cement are formulated; namely Ordinary Portland Cement (OPC), Low Heat Cement (LHC), Moderate Heat Cement (MHC) and High Early Strength Cement (HESC).

Effect of coarse aggregate on strength:

$$r_g = \left(1 - \left(d\left(\frac{1}{W/B+1}\right) \cdot \frac{V}{1000}\right)\right) \times \left(1 - \left(e \cdot B/W + f\right) \cdot \left(LogX - LogA\right)\right) \tag{3}$$

where r_g denotes the effect of coarse aggregate on strength, d, e and f denote material parameter depending on aggregate, V denotes the volume of coarse aggregate per unit weight, X denotes the maximum size of coarse aggregate and A denotes the minimum size of aggregate that is able to affect the loss of strength.

Effect of type of coarse aggregate focused on the paste interface:

$$r_{g2} = k \tag{4}$$

where r_{g2} denotes the effect of coarse aggregate type and k denotes the material parameter of aggregate type depending on crushed aggregate (CR) or gravel (GR).

Effect of air content:

$$r_{air} = 1 - k_2 \cdot V_{air} \tag{5}$$

where r_{air} denotes the effect of air content on strength, k_2 denotes the parameter depending on water to binder ratio and type of coarse aggregate, and V_{air} denotes the volume of air per unit volume of concrete.

Effect of addition of Ground Granulated Blast furnace Slag (GGBS):

$$X < 0.3: \quad r_{mix} = 1 + \left(\left(g(X_2 - h)^{3/2}\right) \cdot \left(\frac{1}{X_1 + 1}\right) + \left(lX_2 + m\right)\right) \times \frac{X}{0.3} \tag{6}$$

$$X \geq 0.3: \quad r_{0.3} \times \left(a_1 X_2 + b_1\right) \times \frac{X - 0.3}{0.4} \tag{7}$$

where r_{mix} denotes the effect of admixture on strength, g, h, l, m, a_1, b_1 denote the material parameter, X denotes the replacement ratio, X_1 denotes the water to binder ratio, X_2 denotes specific surface area of slag and $r_{0.3}$ denotes the value calculated by equation (6) with X of 0.3.

Effect of addition of Fly-Ash (FA):

$$X < 0.45: \quad r_{mix} = 1 - (a_2 X_1 - b_2) \times X \tag{8}$$

$$X \geq 0.45 \quad r_{mix} = 1.0 \tag{9}$$

where r_{mix} denotes the effect of admix on strength, a_2 and b_2 denote the material parameter, X denotes the replacement ratio and X_1 denotes the water to binder ratio.

Effect of addition of Silica Fume (SF):

$$X > 0.2 \quad r_{mix} = 1 + X \tag{10}$$

$$X \geq 0.2 \quad r_{mix} = 1.2 \tag{11}$$

where r_{mix} denotes the effect of admix on strength, X denotes the replacement ratio.

Strength of Concrete:

$$F_c = F_m \times r_g \times r_{g2} \times r_{air} \times r_{mix} \tag{12}$$

where F_c denotes the strength of concrete.

3.1.2 Prediction of cone slump

Function for predicting of the value of cone slump is developed statistically with rheological approach. Kikukawa [4] proposed equation (13), which expresses the rheological parameters of cement paste at 20 ^{o}C that are plastic viscosity and yield value, as a function of solid content of cement and volumetric density of cement paste. This expression was on the basis of study of Roscoe [5].

Plastic viscosity of cement paste:

$$\eta_p = \eta_w \left(1 - \frac{V}{c}\right)^{-(K_1 V + K_2)} \tag{13}$$

where η_p denotes plastic viscosity of cement paste [Pa s], η_w denotes plastic viscosity of water, V denotes volumetric density of cement paste, c denotes solid content of cement, K_1,K_2 denote constants affected by the properties of the cement paste. –17.5 and 12.0 are used respectively.

Yield value :

$$\tau_p = a\eta_p + b \tag{14}$$

where τ_p denotes yield value of cement paste [Pa], a and b denote constant parameters. 15.505 and 1.244 are used respectively

Temperature effect on the rheological parameters:

$$\eta_{pT} = 0.00387\eta_{p20} \cdot T + \eta_{p20} \tag{15}$$

$$\tau_{pT} = 3.03\tau_{p20} \cdot T + \tau_{p20} \tag{16}$$

where η_{p20} denotes plastic viscosity of cement paste at 20 ^{o}C, τ_{p20} denotes yield value of cement paste at 20 ^{o}C, T denotes temperature, η_{pT} denotes plastic viscosity of cement paste at T ^{o}C and τ_{pT} denotes yield value of cement paste at T ^{o}C.

Effect of admixtures and additions:
Collecting the result of experiments, the effects of the contents on the rheological parameters are integrated into the formulas statistically.

$$r_{admix,\eta} = f_i(X) \tag{17}$$

$$r_{admix,\tau} = G_i(X) \tag{18}$$

where $r_{admix,\eta}$ and $r_{admix,\tau}$ are the coefficient of viscosity and yield value depending on the admixtures and X is the admixture to cement ratio. In this contribution, 4 type of admixtures are formulated; namely High Range Water Reducer (HRWR), AE agent (AE), Accerelator (AC) and Retarder (RE)

$$r_{add,\eta} = f_j(X) \tag{19}$$

$$r_{add,\tau} = G_j(X) \tag{20}$$

where $r_{add,\eta}$ and $r_{add,\tau}$ are the coefficient of viscosity and yield value depending on the addition and X denotes the replacement ratio.

Solid content of aggregate:
Ooi [6] investigated the complex nature of packing particles with random shape and wide grading, and developed mathematical model predicting the compacted bulk density of aggregate. This model is expressed as a second order polynomial of the sieve residuals as follows:

$$Z = \sum_{i}^{n}\sum_{j}^{n} A_{ij} X_i X_j \tag{21}$$

where Z denotes solid content of combined fine aggregate and coarse aggregate, A_{ij} is coefficient representing the packing performance of combined aggregates of two different diameter, X_i and X_j express volumetric ratios of the aggregates at the representative sieve sizes.

Rheological parameters of fresh concrete:
Recently Oh [7] found a phenomenon that the rheological parameters of fresh concrete have good correlation to a relative thickness of excess paste on the basis of excess paste theory developed by Kennedy [8]. The relation between the relative thickness of excess paste and the rheological parameters of fresh concrete is formulated as follows:

$$P_e = 1 - V_a / Z \tag{22}$$

$$\Gamma = \frac{P_e}{\sum_i^n n_i s_i D_{pi}} \tag{23}$$

where P_e denotes volume of excess paste, V_a is volume of aggregate, Γ denotes relative thickness of excess paste, n_i is number of aggregate of size i, s_i denotes surface area of each aggregate of size i, D_{pi} is diameter of aggregate of size i.

Using relative thickness of excess paste and rheological parameters of cement paste, the viscosity and yield value of concrete can be calculated.

$$\eta_c = \eta_p \times (1 + 0.0705\Gamma^{-1.69}) \tag{23}$$

$$\tau_c = \tau_p \times (1 + 0.0705\Gamma^{-2.22}) \tag{24}$$

where η_c denotes plastic viscosity of fresh concrete and τ_c denotes yield value of fresh concrete

Cone slump:
Using the experimental data of slump predicted rheological values, the regression curve is formulated as the function of yield value and parameter of mix proportion as below:

$$S = a_3 \times Ln(\tau_c) \times \frac{1}{1 + W/B} + b_3 \tag{25}$$

where S denotes the value of slump, a_3 and b_3 are coefficients.

3.1.3 Costs
In this problem, the function of cost is simply the summation of material cost.

3.2 Case study 2
In case 2, assuming that construction site is in cool temperate zone and average temperature is 10 ^{o}C, concrete is required 15 cm of slump, 40 MPa of strength, 6.0x10^{-4} of drying shrinkage, 35^{o}C of adiabatic temperature rise at 7 day for mass concrete. Additionally 100 of durability factor, which means relative dynamic modulus of elasticity after 300 cycles of freezing and thawing actions, and 5.0x10^{-8} of Chlorides-diffusion-coefficient are required strictly. The other parameters are less important.

3.2.1 Adiabatic temperature rise
Adiabatic temperature rise is modelled as follows:

$$Q = Q_\infty (1 - Exp(-\gamma t)) \tag{26}$$

$$Q_\infty = a_4 B + b_4 \tag{27}$$

$$\gamma = a_5 B + b_5 \tag{28}$$

where Q denotes the adiabatic temperature rise at t day, a_4, b_4, a_5 and b_5 denote the material parameters and B denotes the weight of binder per unit volume.

3.3 Results

The required parameters of concrete in both cases are summarised in the same Table 1.

Table 1. Required performances

	Durability factor	Chlorides diffusion coefficient	Carbonation speed coefficient	Strength	Young's modulus	Drying shrinkage	Adiabatic temperature rise	Initial setting	Final setting	Slump	Cost
Unit		cm^2/year	$cm/year^{0.5}$	MPa	GPa	10^{-6}	K	hour	hour	cm	Yen
Case 1	0	1.00E-06	0.27	60	26	800	40	5	8	18	5000
Case 2	100	5.00E-08	0.25	40	25	600	35	5	8	15	10000

Case 1:

After running the MixGA with 120 individuals and 100 generations, mix proportions shown in Tables 2 are derived regarding with case 1. As final selection, elimination of the individuals, which do not meet required performance of strength and slump simultaneously, is conducted. Additionally in the final selection, as an index of cost performance, a value of strength divided by cost is used. Three mix proportions listed in Table 2 are top-to-third in strength-cost index. In left of Figure 3 shows the degree of conformity of three mix proportions listed in Table 2. Among three proportions, mix A has the best strength-cost index. It should be noted that, as is shown in left graph of Figure 3, mix C is much cheaper than mix A. The value of strength of mix A is higher than that of mix C. But in MixGA both mix A and Mix C is evaluated equally and they survive selections from generation to generation.

Table 2. Pareto optimal mixture proportions derived by MixGA

		W/B	Water	Cement (type)	Addition (type)	Fine aggregate (type)	Coarse aggregate (type)	Admixture 1 (type)	Admixture 2 (type)
Case 1	A	0.42	138	275 (OPC)	52 (GGBS)	936 (CR)	987 (GR)	0.000	0.000
	B	0.43	145	264 (HESC)	76 (GGBS)	967 (CR)	925 (GR)	0.232 (AC)	0.006 (AE)
	C	0.41	145	301 (MHC)	52 (GGBS)	962 (CR)	921 (CR)	0.000	0.048 (AE)
Case 2	D	0.47	132	280 (LHC)	0	1035 (CR)	898 (CR)	0.115 (HRWR)	0.512 (AE)
	E	0.47	132	281 (LHC)	0	1029 (CR)	893 (CR)	0.005 (HRWR)	0.526 (AE)
	F	0.47	131	281 (LHC)	0	1028 (CR)	906 (CR)	0.195 (HRWR)	0.512 (AE)
	G	0.48	132	273 (MHC)	0	1034 (CR)	898 (CR)	0.0215 (HRWR)	0.526 (AE)

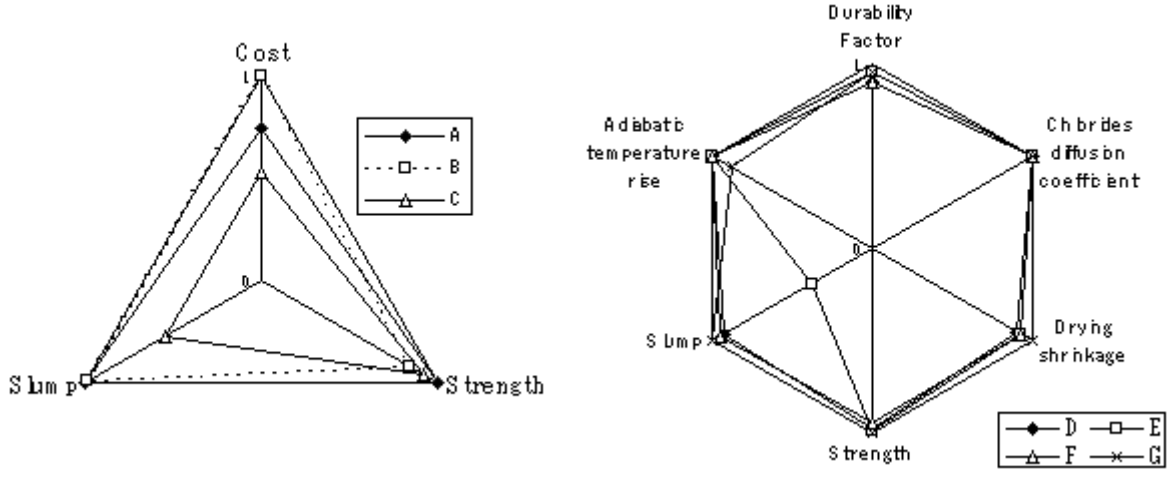

Figure 3. Ratio between phenotype and required performance of concrete mixtures derived by MixGA

Case 2:

After running the MixGA with 140 individuals and 200 generations with meta-property concept, mix proportions shown in Tables 2 are derived regarding with case 2. As final selection, elimination of the individuals, which do not meet required performance of strength, slump, drying shrinkage, chlorides diffusion coefficient, durability factor and adiabatic temperature simultaneously, is conducted. In right of Figure 3 shows the degree of conformity of four mix proportions listed in Table 2. As shown in Figure 3, almost all the mixtures meet the required performance. It should be noted here that mix E has low value in slump and this mix is evaluated equally from the Pareto optimal point of view. If only the Pareto optimization is used, it is possible that such undesirable individual that do not have good value in all several properties is able to survive the selection. The genetic algorithm with the notion of Pareto optimality has a good potential in initial convergence tendency but it has a risk of undesirable acceleration in a few properties as well. With meta property concept, which disappreciate the prominence and unbalancing it is possible to derive the sufficient set of mixture proportions. Using the suitable fitness function and evaluation method is important to get sufficient set.

4. CONCLUSIONS

The results of this contribution are summarized as follows:

1. A genetic algorithm system integrating the concept of Pareto optimality, which is named MixGA, was developed for solving multicriteria optimization problems in concrete mix proportioning.
2. As shown in the examples presented in this study, MixGA can derive the appropriate mix proportions from the vast combinations of sorts of content and proportions of mixture to explore. This system is maintained by suitable fitness evaluation, reasonable reproduction and correct prediction formulas.
3. The genetic algorithm with the notion of Pareto optimality has a good potential in initial convergence tendency but it has a risk of undesirable acceleration in a few properties as well. Using meta property concept, it is possible to compensate for this risk of the notion of Pareto optimality.

REFERENCES

[1] Marks, W. and Potrzebowski, J., Multicriteria optimization of structual concretemixes, Architecture and Civil Engineering 38(4), 1992, pp.77-01

[2] Piasta, Z. and Czarneski, L., Analysis of material efficiency of resin concrete. in Brittle Matrix Composite, Elsevier Apllied Science London and New York, 1989, pp.593-602

[3] Goldberg, A. E., Genetic Algorithms in Search Optimization & Machine Learning, Addison Wesley, 1989, pp.192-208

[4] Kikukawa, H., Studies on viscosity equation of Portland cement paste, Journal of Material, Concrete Structure and Pavements, V-2, 354, 1985, pp.109-118 (In Japanese)

[5] Roscoe, R., The Viscosity of Suspension of Rigid Spheres, British Jouranl of Applied Physics, Vol.3, 1952, pp.267-269

[6] Ooi, T., Comparted bulk density of aggregate with random shape and widely ranged particle size distribution, Journal of Structure and Construction Engineering. AIJ, No.423, 1991, pp.11-16 (In Japanese)

[7] Oh, S. G.., Noguchi, T., and Tomosawa, F., Toward Mix Design for Rheology of Self-Compacting Concrete, 1st International RILEM Symposium on Self-Compacting Concrete, Stockholm, 1999, pp.361-372

[8] Kennedy, C.T., The Design of Concrete Mixes, Proceedings of the American Concrete Institute, Vol.36, 1940, pp373-400

HIGH-BELITE PORTLAND CEMENT – AN UPDATE ON DEVELOPMENT, CHARACTERIZATION AND APPLICATIONS

Anjan Kumar Chatterjee

TCG, Kolkata, India. E-mail: dr_akc@vsnl.net

ABSTRACT

Interest in high-belite Portland cement has progressively grown over the last three decades for its anticipated multidimensional benefits like lower energy consumption, raw materials conservation and constructional durability of the resultant concrete. Notwithstanding prolonged research and development efforts, the product and its manufacturing technology are yet to be of extensive commercial significance as there are still no viable technologies to substantially enhance the intrinsic reactivity of the belite phase and to generate large surface area for the cement at a reasonable energy input to achieve a higher rate of hydration in concrete.

Since the last review made in early nineties, a substantial amount of information and data have been generated on doping and rapid cooling of the belite phase, on its NMR spectra for characterization, on remelting reactions to make belite softer to grind, on chemical processes to synthesize belite cements of very high surface area, and on the properties of such cements.

The present paper is an attempt to review the status of development of high-belite cements and draw up the emerging scenario of this class of binder.

1. INTRODUCTION

High-belite Portland Cements, in the context of the present paper, are those in which there is a reversal in the preponderance of alite by belite without any significant sacrifice of early age strength in mortar and concrete. Since this implies higher levels of early reactivity in belite, such cements are also termed as reactive or active belite cement. This definition of course excludes the modified Portland Cements in which alite is replaced by the calcium sulphoaluminate phase.

Interest in the high-belite Portland Cement was triggered by the energy crunch of early seventies as its production was expected to be less energy intensive. Subsequently the interest was enhanced by the potential of raw-material conservation but ultimately the growing interest in the product gravitated towards its capability of producing a more durable hydrated matrix with a very steady rate of strength gain with time. But the realization of the goal continues to elude the scientific and technical community primarily for two reasons:

- Search for a practical and viable means of improving the hydration rate of the belite phase, and
- Establishing the technology to overcome the high-energy consumption in grinding belite for surface generation.

A fairly comprehensive review on the subject was attempted by the author in mid nineties [1]. Over the last decade, sizeable information and data have been generated on the manufacturing, characterization and application of high-belite Portland Cement. The present paper is aimed at highlighting the essence of newer findings.

2. ADAPTING THE TRADITIONAL PROCESS TECNOLOGY

It goes without saying that there could be a rapid proliferation of the high-belite Portland Cement technology, if it could be adapted to the existing process of cement manufacture. The technological adaptations required are primarily for a rapid cooling process and homogeneous dispersion of dopants or chemical stabilizers used in small dosage [1]. In fact, it is known that at least in countries like India and Poland alkali-stabilized moderately high-belite (35 – 45%) cements have been in production and use with satisfactory performance. Taking cue from this and for faster exploitation of the high-belite cement technology, further studies were carried out at the author's erstwhile laboratories in the above perspectives. Experiments were conducted with raw mixes designed for two tentative levels of lime saturation factors (LSF) 0.82 and 0.78 and incorporating the dopants like K_2O, B_2O_3, Mn_2O_3, Cr_2O_3, SO_3, BaO. All firings were carried out in a pilot rotary kiln provided with a specially designed cooler that achieved a cooling rate of 500^o – 600^oC / min. Some of the relevant findings are summarized below.

2.1 Effect of Rapid Cooling

A representative set of experimental data is given in Table 1, from which the following observations could be made :

i) The effect of rapid cooling on the cement strength was visible, when the LSF was in the range of 0.81 – 0.82, the proportion of a given dopant was near-optimal and the C_2S/ C_3S ratio by the Bogue computation was not abnormally high (say, above 6).

Table 1. Effect of clinker cooling rate on the cement strength parameter

Type of Dopant	Rapid Cooling				Slow Cooling			
	Dopant (%)	C_2S/ C_3S (Bogue)	Clinker LSF	28-day Comp. Str. (N/mm^2)	28-day Comp. Str. (N/mm^2)	Clinker LSF	C_2S/ C_3S (Bogue)	Dopant (%)
None	-	4.85	0.813	54.5	46.5	0.813	3.98	-
	-	11.05	0.780	45.0	50.5	0.784	4.21	-
B_2O_3	0.68	1.84	0.823	78.6	67.0	0.814	2.89	0.65
	0.60	13.14	0.780	64.0	67.0	0.783	5.39	0.62
K_2O	0.28	2.26	0.819	78.0	61.2	0.824	2.00	0.31
	0.14	3.51	0.789	66.0	68.5	0.792	3.14	0.18
Mn_2O_3	1.24	3.59	0.820	61.0	54.0	0.820	2.04	1.19
	1.20	4.60	0.780	49.0	41.5	0.776	5.08	1.20
Cr_2O_3	0.70	3.47	0.820	61.5	56.0	0.813	2.31	0.70
	0.68	3.69	0.794	67.7	69.6	0.793	3.54	0.68
SO_3	0.39	3.07	0.820	69.0	55.0	0.820	2.14	0.21
	0.27	6.15	0.770	47.0	47.0	0.770	6.10	0.21
BaO	0.97	8.01	0.811	51.4	-	-	-	-

ii) The positive effect of rapid cooling was not observed in the case of samples having LSF below 0.80, even when the amount of dopant or the C_2S/ C_3S ratio was in the acceptable range.

iii) A high cooling rate appeared to be important for the retention of sulphate in the clinker but not so critical for B_2O_3 or K_2O retention. In some of our previous studies [1], however, it was seen that slow heating of clinker often led to higher losses of K_2O and consequently to its low retention in clinker.

On the whole, the need and relevance of rapid cooling from 1300° – 850°C have been phenomenologically reconfirmed. The higher the cooling rate, the more reactive is the stabilized belite phase as reflected by the cement strength parameter. It may be relevant to mention that rapid cooling did not result in any significant increase in the proportion of belite phase in clinker.

2.2 Effects of Dopants Incorporation

The optimal incorporation of dopants is expected to primarily influence the formation of clinker phases, stabilization of belite polymorphs, fixation of alite crystal systems, and the distortion of lattice structures of the stabilized phases. Based on a large number of experiments, now and earlier, attempts were made to retain the dopants in clinkers at the following levels:

$B_2O_3 \rightarrow 0.5\%$, $K_2O \rightarrow 0.3\%$, $Mn_2O_3 \rightarrow 1.2\%$,
$Cr_2O_3 \rightarrow 0.7\%$, $SO_3 \rightarrow 0.35\%$, $BaO \rightarrow 1.0\%$.

The subsequent data and discussions will relate to clinkers containing dopants at the above levels.

2.2.1 Phase quantification

The quantification of the belite phase, irrespective of its polymorphic form, was attempted by the usual techniques of x-ray diffractometry, optical microscopy and scanning electron microscopy. A set of typical results are given in Table 2 along with the Bogue composition for clinkers having LSF 0.82. The comparison revealed that the quantification of the belite phase by both the microscopic techniques appeared quite close and the deviations with reference to Bogue compositions were also not very high, except in the case of boron-doped clinker. The XRD values, however, showed larger variations.

Table 2. Quantification of the belite phase in clinker with LSF around 0.82

Clinker with	C_2S				C_3S				Non-silicate			
	B	X	O	E	B	X	O	E	B	X	O	E
No dopant	61.9	42.0	57.1	58.0	12.8	42.5	28.3	29.0	25.2	14.8	14.6	13.0
B_2O_3	49.8	53.8	61.3	60.0	27.1	26.9	24.3	25.0	23.1	18.9	14.4	15.0
K_2O	51.9	35.3	52.2	53.0	23.0	43.2	33.5	34.0	25.0	21.5	14.2	13.0
Mn_2O_3	58.1	47.1	55.5	56.0	16.4	33.9	26.8	27.0	25.4	19.0	17.7	17.0
Cr_2O_3	57.7	51.9	58.4	56.0	16.6	30.1	25.5	28.0	25.7	17.1	15.6	16.0
SO_3	56.4	45.5	54.4	57.0	18.3	39.1	29.7	29.0	25.1	15.2	15.9	14.0
BaO^+	54.2	-	49.0	-	20.8	-	30.0	-	27.1	-	17.7	-

Note : B = Bogue computation
X = X-ray diffractometry
O = Optical microscopy
E = Scanning electron microscopy
\+ = Clinker freelime high (around 3%)

Thus, relying more on the microscopic techniques, five high-belite clinkers with different dopants were produced from the same raw mix. The microscopically estimated amounts of the silicate phases (in comparison to the corresponding Bogue compositions) were used to grade the influence of the dopants on belite formation (Table 3), which can be summarized as follows:

$$B_2O_3 > K_2O > Cr_2O_3 \approx SO_3 > Mn_2O_3.$$

Needless to mention the reverse is the trend of influence on the alite formation.

Table 3. Influnce of dopants on the belite formation.

Phases	Clinkers doped with														
	B_2O_3			K_2O			Cr_2O_3			SO_3			Mn_2O_3		
	B	M	M/B	B	M	M/B	B	M	M/B	B	M	M/B	B	M	M/B
Alite	22.2	12.8	0.58	21.3	24.5	1.15	24.9	31.0	1.24	25.2	30.4	1.21	23.6	38.5	1.63
Belite	57.3	73.1	1.3	57.3	59.5	1.04	54.5	50.7	0.93	53.6	48.8	0.91	55.3	42.3	0.76
Nonsilicate matrix	20.5	14.1	0.69	21.1	16.0	0.76	20.5	18.3	0.89	21.2	20.8	0.98	21.1	19.2	0.91

2.2.2 Identification of polymorphic forms

Based on the precise measurement of 2θ values and their comparison with the reference data, the presence of different polymorphs of the belite phase was detected. The results are furnished in Table 4. From the table it is evident that in all the clinkers, irrespective of the dopants used, there was predominance of the β-phase. The α-phase appeared only in the K_2O-doped clinker, apart from the undoped reference clinker. In all the doped varieties α'_H phase was detected while the α'_L phase was noticed in all the doped clinkers except those, which contained SO_3 and BaO.

Table 4. Presence of belite polymorphs as detected by XRD in the rapidly cooled clinkers.

Clinker with	Clinker LSF	2θ values in degree			
		β	α	α'_H	α'_L
No dopant	0.82	31.100	31.669	-	-
No dopant	0.78	31.096	31.809	-	-
B_2O_3	0.82	31.058	-	32.197	32.073
B_2O_3	0.78	31.092	-	32.197	32.065
K_2O	0.82	31.092	31.669	32.196	32.074
K_2O	0.78	31.105	31.801	32.461	32.085
Mn_2O_3	0.82	31.102	-	32.465	32.076
Mn_2O_3	0.78	31.054	-	32.449	32.073
Cr_2O_3	0.82	31.063	-	32.201	32.076
SO_3	0.82	31.096	-	32.469	-
BaO	0.82	31.067	-	32.430	-

Further some attempts were made to assess the relative proportions of the different polymorphs. The β-phase appeared to vary from 88 to 96% of the total belite phase and no other discernible trends were noticed in the variously doped clinker samples.

2.2.3 Effect of doping on lattice parameters

The lattice parameters were measured for the β-belite phase in some of the doped clinker samples. The results are furnished in Table 5. It is evident from the table that the incorporation of B_2O_3 and Mn_2O_3 resulted in significant dimensional change in the cell parameters and consequently in the cell volumes. The changes were not so significant for potash doping.

Table 5. Changes in the cell parameters of the belite phase on doping in rapidly cooled clinker of LSF around 0.82.

Clinker with	Cell Parameters				Cell volume $(nm)^3$
	a (nm)	b (nm)	c (nm)	β	
No dopant	0.93761	0.66569	0.55124	91.5274°	0.34406
B_2O_3	0.94395	0.67595	0.56528	100.2715°	0.36068
Mn_2O_3	0.94545	0.67175	0.56589	94.4991°	0.35940
K_2O	0.92477	0.67384	0.55687	92.4015°	0.34701
Reference values (JCPDS)	0.93100	0.67565	0.55059	94.46°	0.34633

If one were to draw some conclusions by juxtaposing Tables 1, 3 and 5 on the reactivity of the different polymorphs of the belite phase, one would still be baffled as in the past. The variable reactivities of these polymorphs can be attributed to differences in ionicity of M-O bonds (where M is a cation) or to different levels of crystal imperfection. However, the effectiveness of boron in making the belite phase more reactive is worth noting, while the other dopants tend to give anomalous structure-property relationships.

3. NMR STUDIES OF THE HIGH-BELITE CLINKERS

During the last two decades, the nuclear magnetic resonance (NMR) spectroscopy has found wide application in cement science [2]. Nucleii with odd mass numbers (e.g. ^{17}O, ^{27}Al, ^{29}Si) have half integer spins and are of most interest in this method of characterization. It is also known that in many instances the isotropic chemical shift is the most important NMR parameter for structural investigations. Many NMR investigations of cement materials are based on it.

It has been reported [3] that the nine crystallographically distinct Si sites of high-purity C_3S resonate between –68.9 and –74.5 ppm and the Q^o sites of the various C_2S phases resonate between –70.1 and –73.5 ppm. The ^{29}Si peaks for the high-purity phases are quite narrow (<1 ppm), if they are well crystallized and if the spectra are well resolved. Since, however, the alite and belite phases of commercial Portland Cements are quite impure and since these impurities cause distortions in the electronic environments of Si, their spectra become broad and poorly resolved. Despite such resolution problems, the recent work has shown that quantitative spectral deconvolution of the ^{29}Si MAS-NMR spectra of Portland Cements provides reliable alite / belite ratios.

Based on such advances seen in the application of NMR spectroscopy of cement silicate phases, some of the high-belite clinkers of the present study were subjected to MAS-NMR spectroscopy on a varian INOVA-400 spectrometer using CP/MAS probes for 7 mm (^{29}Si). The spectra are given in Figure 1. The observed isotropic chemical shifts for belite showed that the polymorph was in the β-form [$\delta_{iso}(^{29}Si)$ = -71.32 ppm] in all the four doped clinker studies. There were no spectral features to identify the presence of α and α′ forms that were detected by XRD to be present below 10% of the total belite phase. The spectra were further subjected to deconvolution in order to determine the quantities of alite and belite using the method discussed in [4]. The values obtained have been compared in Table 6 with corresponding values determined by XRD and computed by the Bogue formula. It seems from the table that the mean NMR values of the belite phase are higher than the corresponding XRD values and closer to Bogue values, except in the case of chromia doping. On the other hand, the NMR values of alite are lower than XRD estimates, with the some exception for the Cr_2O_3 doped samples.

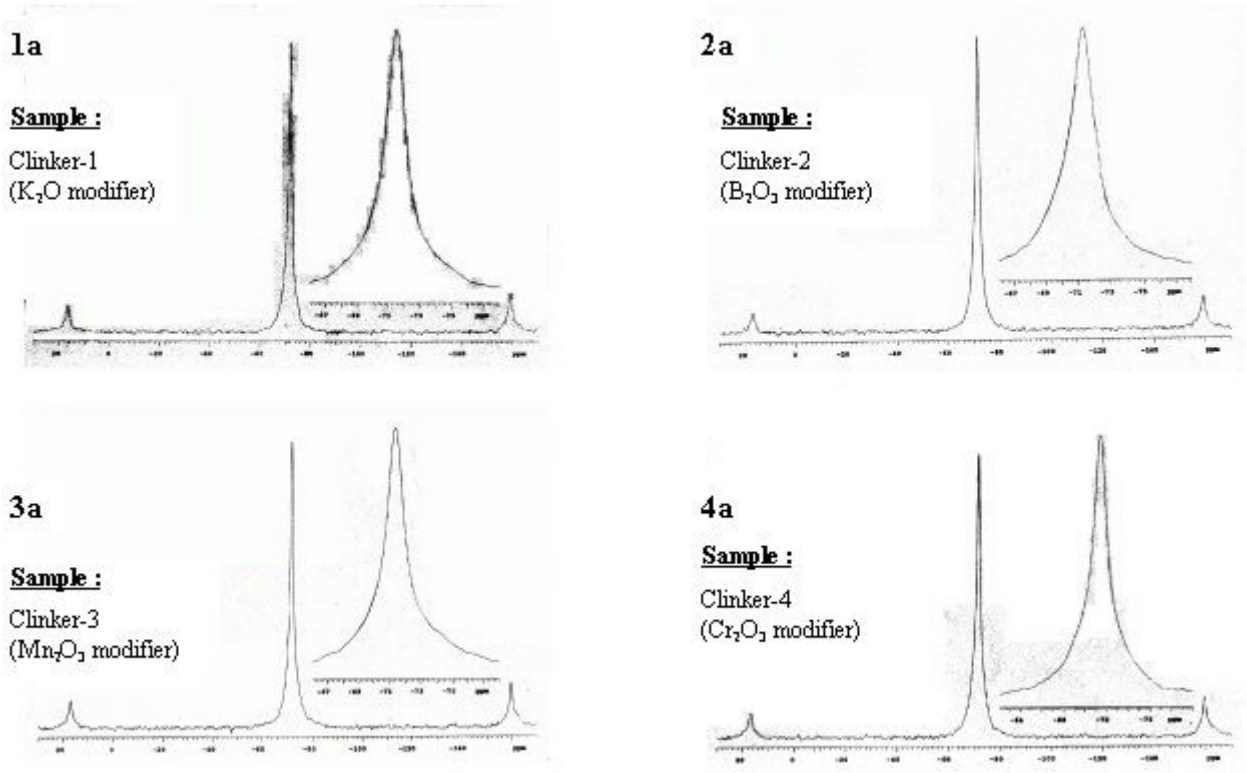

Figure 1. ^{29}Si MAS NMR (9.4 T, $v_r = 7.0$ kHz)

Table 6. Quantification of alite and belite in doped clinkers by NMR spectroscopy.

Dopant	Belite %			Alite %		
	NMR	XRD	Bogue	NMR	XRD	Bogue
K_2O	48.2 ± 5.0	42.87	55.4	29.9 ± 6.0	32.48	20.5
B_2O_3	53.0 ± 4.0	50.67	54.8	23.5 ± 5.0	27.37	21.2
Mn_2O_3	46.7 ± 4.0	44.30	52.7	30.4 ± 4.0	34.48	22.5
Cr_2O_3	41.5 ± 4.5	48.13	52.0	37.7 ± 5.0	30.19	23.5

3.1 Boron Incorporation in the Silicate Phases

In the present study, an attempt was made to separate out the silicate from the non-silicate portion of the doped clinkers and to estimate the distribution of the dopants in the above two fractions. In all the samples studied it was observed that the incorporation of B_2O_3 in the silicate fraction was the highest in the range of 95-96%, followed by K_2O 85-90%, Cr_2O_3 78-80%, and Mn_2O_3 65-70%, when tested under identical conditions. The high level of incorporation of B_2O_3 in the silicate phases also prompted a careful look at the NMR spectra of the clinker doped with B_2O_3. It was interesting to note that there was a unique second-order quadruple line-shape for ^{11}B spectra, which indicate that ^{11}B is incorporated in belite by substitution of Si. Some confirmatory studies are in progress.

4. GRINDABILITY OF BELITE-RICH CLINKERS

It has been shown by actual grindability tests that one of the most important parameters that determine clinker grindability is its belite content (Figure 2) [5]. This results in high-energy consumption in cement grinding, which has served as a major impediment in the popularization of the manufacturing technology for high-belite Portland Cement.

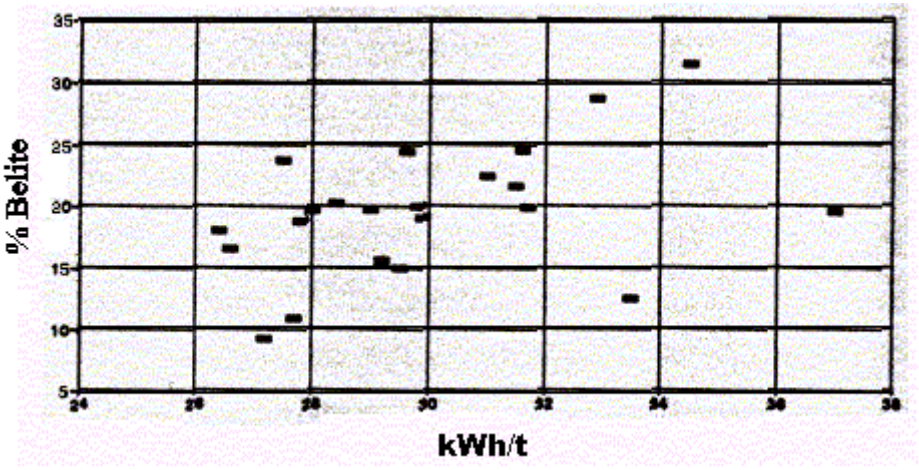

Figure 2. Relationship between belite content and power consumption.

Recently an interesting technological approach has been reported to make the high-belite clinker amenable to easier grinding. This is based on what has been termed as a "remelting reaction" for the belite phase [6]. The remelting reaction is an unusual decomposition reaction in which a solid decomposes into another solid and a liquid during cooling. When α-C_2S with a large amount of impurities is cooled from its stable temperature region, it decomposes into a liquid and α'_H-C_2S, which has a lower impurity concentration. The reaction is always preceded by the α - to - α'_H polymorphic transition, which forms six sets of α'_H-phase lermellae without a change in chemical composition. The subsequent remelting reaction requires an atomic diffusion process. The rate of the remelting reaction depends on the Al / Fe ratio of the parent α-phase and the temperature. In a recently conducted study with an industrially produced belite-rich clinker, two reheating and quenching regimes were adopted for two fractions of the same clinker so as to stabilize α-C_2S in one and α'-C_2S in another. When these two fractions were subjected to grindability and hydration studies under comparable conditions, the results showed marked improvements (Figures 3 and 4) [7].

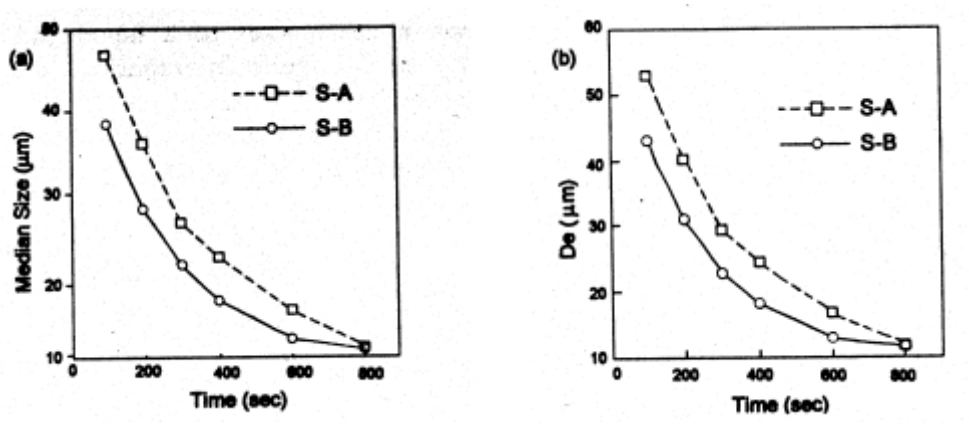

Figure 3. Change in (a) median size and (b) De of Rosin-Rammlar distribution with grinding time (S-A and S-B contain α- and α'-belite phases respectively**).**

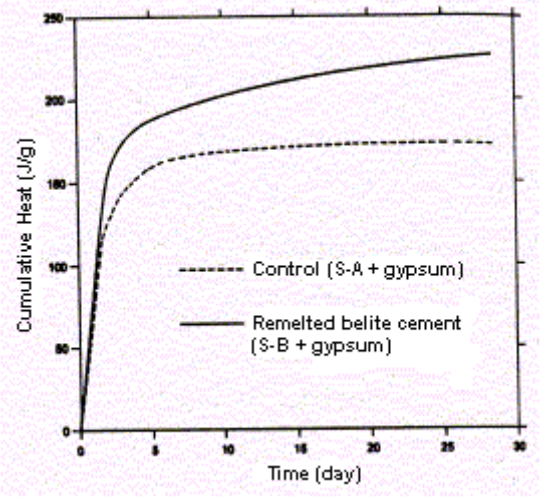

Figure 4. Cumulative heat evolution for 28 days at w/c=0.4 and 20°C
(S-A and S-B contain α- and α′-belite phases respectively).

5. CHEMICAL PROCESSES FOR REACTIVE BELITE

Apart for the technology of doping and cooling to produce reactive and easily comminutable belite, there are also options of obtaining reactive belite of high surface area by chemical processes. In addition to the sol-gel and hydrothermal routes of processing summarized in [1], β-C_2S has also been prepared by the Pechini process [8], a more popular synthesis technique for many ceramic phases, which utilizes a mixture of citric acid and ethylene glycol as the organic carrier phase. In all these preparations, the belite phase is stabilized in β-form. The Pechini process yields β-C_2S with surface area as high as 40 m^2/g with proportional increase in its rate of hydration reaction.

Although, prima facie, the chemical processes indicate some distinct potential advantages such as low temperature operation, low energy consumption and high reactivity, there are issues like the purity of raw materials, scale of operation, continuity of process, etc. which would determine the viability of the processes concerned. From the perspective of economic viability, these processes seem to be quite distant at present.

6. RESPONSE OF CHEMICAL ADMIXTURES TO BLENDED HIGH-BELITE CEMENTS

The durability properties of high-belite Portland cements and their blends with fly-ash have been illustrated earlier [1]. In continuation of these studies an attempt has been made to prepare a fly-ash blended cement from a commercially produced potash bearing high-belite clinker of the following phase composition as determined microscopically : 57.4% belite, 29.3% alite and 13.3% matrix. The blended cement was prepared by inter-grinding of 15% fly-ash and gypsum equivalent to 2.3% SO_3. In order to compensate the drop in early age strength, the effect of three different types of chemical admixtures were studied. The results are given in Table 7. From the table, one may observe that the effect of the three admixtures on improving the early as well as later age strengths can be rated as follows:

Acrylic Polymer-based > Melamine-based > Ligno-Sulphonate-based.

This is quite in line with the general expectation from these three varieties of chemical admixture.

Table 7. Effect of chemical admixtures on the physical properties of high-belite blended Portland cement.

Property Parameters	Cement without fly-ash	Cement with inter-ground fly-ash and no admixture	Cement with separately ground fly-ash and no admixture	Cement with inter-ground fly-ash plus		
				0.2% ligno-sulphonate based admixture	0.2% melamine based admixture	0.2% acrylic polymer based admixture
Specific Surface Area, m^2/kg	307.0	372.0	370.0	400.0	390.0	400.0
Normal Consistency, %	27.0	28.8	27.5	26.3	26.8	21.3
Setting Time (I), min	110.0	115.0	110.0	115.0	105.0	95.0
Setting Time (F), min	190.0	195.0	200.0	210.0	195.0	210.0
Compressive Strength, N/mm^2						
1-day	18.2	12.0	13.0	15.3	14.0	24.0
3-day	28.4	21.6	20.8	24.2	25.0	42.0
7-day	40.0	32.0	32.6	37.0	37.3	51.4
28-day	63.4	50.4	59.7	52.5	63.0	77.6

In order to ascertain the impact of the particle size distribution of the fly-ash on the cement properties, another batch of blended cement was prepared by blending 15% fly-ash ground separately to D_{50} size of 8.2 μm and 100% passing through 45 μm sieve. The properties obtained for this blended cement without any chemical admixture are also included in Table 7. It may be seen that with improved particle size distribution of fly-ash, although there was significant enhancement of the 28-day compressive strength, the early age strengths remained more or less unchanged.

In other words, for effecting a rise in the early age strength levels of the high-belite Portland cements, the use of chemical admixtures may provide an easy and practical solution. Needless to mention that the effects of the acrylic polymer-based admixture on setting, hardening and strength gain of the high-belite Portland cement are notworthy.

7. CONCLUSIONS

The present studies reconfirmed that the belite phase can be made more reactive to various degrees by incorporation of dopants or chemical modifiers along with rapid cooling of clinkers. Oxides like K_2O, B_2O_3, Mn_2O_3, Cr_2O_3, SO_3, and BaO were found to be variously effective. Of these dopants, the incorporation of B_2O_3 in the belite phase is almost total at a level of about a half a percent dosage with resultant distortion of the cell structure and high gain in later age strength.

Oxides like B_2O_3, K_2O and Cr_2O_3 do promote the formation of belite to a higher extent than SO_3 and Mn_2O_3. The incorporation of BaO may lead to higher free lime in clinker unless the dosage is very carefully optimized.

A rapid process of cooling at least in the range of 500^o – 600^oC / min improves the reactivity of high-belite clinkers, when their LSF is in the range of 0.81 – 0.82 and the dopants are present at optimal levels. At still lower LSF, this relationship could not be experimentally established.

The polymerphic form of the belite phase can be identified and quantified by both x-ray diffractometry and NMR spectroscopy. Both the techniques established the predominance of the β-form. Small presence of α, α'_H and α' were detected by x-ray diffractometry but not in NMR

spectra. The α-form was noticed in the K_2O-doped clinker only, while α'_L was absent in the SO_3 and BaO doped ones.

One of the ways of improving the reactivity of the belite phase is obviously to generate high surface area for rapid hydration. Since belite made by high-temperature pyroprocessing is hard to grind, chemical processes have been attempted. The Pechini process has yielded belites of high surface area of up to 40 m^2/g.

Recently, a technology has been developed based on "remelting reaction" to make even the high-temperature belite easy to grind. But the chemical processes as well as remelting technique are still in the experimental stage and would require further development.

The reactive belite manufacture based on doping and quenching continues to suffer from relatively poor early age strength, which can be compensated with the help of chemical admixtures, particularly, of the acrylic polymer-based type.

On the whole, the progress in perfecting the technologies for making reactive belite has been substantial. It appears that such technological features as clinker doping and quenching as well as use of appropriate chemical admixtures in grinding can be more easily adapted to the existing manufacturing process for immediate proliferation of the production technology of high-belite Portland cement. Optimization of the clinker cooling regime to realize the grinding benefits through remelting reactions will be an added advantage.

ACKNOWLEDGEMENTS

The paper is primarily based on the data generated by the author and his team in the laboratories of the Associated Cement Cos. Ltd., India. The contribution of Mr. S. A. Khadilkar and Dr. D. Venkateswaram in generating the experimental data is thankfully acknowledged. Thanks are also due to Dr. Pollemann of Germany and Dr. Skibsted of Denmark in helping the research program by providing valuable and relevant diffractometric and NMR spectroscopic data.

REFERENCES

[1] Chatterjee, A. K. High belite cements – present status and future technological options : Part I, Cement and Concrete Research, Vol. 26, No. 8, 1996, pp. 1213-1225; Part II, Cement and Concrete Research, Vol. 26, No. 8, 1996, pp. 1227-1237.

[2] Kirkpatrick, R. J. Nuclear Magnetic Resonance Spectroscopy in Handbook of Analytical Techniques in Concrete Science and Technology, Eds. V. S. Ramachandran and J. J. Beaudoin, Noyes Publications, New Jersey, USA, 2001, pp. 205-225.

[3] Skipsted, J. and Jakobsen, H. J., Characterization of the calcium silicate and aluminate phases of Portland cements by ^{27}Al and ^{29}Si MAS-NMR spectroscopy, Proceedings of the 2nd International Conference on NMR spectroscopy of Cement-Based Materials, Eds. P. Colombet, A. R. Grimmer and H. Zanni, Springer-Verlag, 1998.

[4] Skipsted, J. and Jakobsen, H. J., Quantification of calcium silicate phases in Portland cements by ^{29}Si MAS-NMR spectroscopy, Journal of Chemical Society Faraday Transactions, Vol. 91, No. 24, 1995, pp. 4423-4430.

[5] Theisen, K. Estimation of cement clinker grindability, World Cement, August, 1993, pp. 17-21.

[6] Fukuda, K., Maki, I. and Ito, S. Phase stability study on the remelting reaction in Ca_2SiO_4 solid solutions, Journal of American Ceramic Society, Vol. 78, No. 12, 1995, pp. 3387-3389.

[7] Fukuda, K. and Ito, S. Improvement in reactivity and grindability of belite-rich cement by remelting reaction, Journal of American Ceramic Society, Vol. 82, No. 8, 1999, pp. 2177-2180.

[8] Nettleship, I et al, Journal of European Ceramic Society, Vol. 11, 1993, pp. 291-298, referred to in "Hydration of Portland Cement" by E.M. Gartner, J.F. Young, D.A. Damidot and I. Jawed, Structure and Performance of Cements, Eds. Bensted, J. and Barnes, P., Spon Press, London, 2002.

CEMENT MODEL POWDER FOR SUPERPLASTICIZER PROPERTIES STUDIES

Robert J. Flatt[1,2], Paul Bowen[1], Alain Siebold[1] and Yves F. Houst[1]

[1] Ecole polytechnique fédérale de Lausanne (EPFL), Laboratoire de technologie des poudres, MXD, CH 1015 Lausanne, Switzerland.
E-mail : Paul.Bowen@epfl.ch, asiebold@club-internet.fr , Yves.Houst@epfl.ch
[2] Present address: SIKA A.G., Corporate Research and Analytics, P.O. Box 1300, CH 8048 Zürich, Switzerland. E-mail: flatt.robert@ch.sika.com

ABSTRACT

Studies on cement suspension rheology are often complicated because of the hydration reactions of cement, which modify surface properties over time. Less complex and better defined systems, model powders, have been used instead of cement for studies of interactions with superplasticizers. The powders previously proposed have all at least one major drawback: they cannot be used at high pH or do not have surface properties at this pH close to that of Portland cement suspensions. Dead burnt MgO and $Mg(OH)_2$ are good candidates. Their isoelectric points are around pH 12.4 and 12 respectively, in the same range as that of Portland cement. Unfortunately, $Mg(OH)_2$ powders initially chosen, produced by precipitation, were found to be porous and were rejected. Dead burnt MgO powders react with water, but they can be considered as non-reactive between 1/2 hour to 2 hours of contact with a basic solution. Such powders allowed us to study adsorption of superplasticizers, evolution of zeta potential as a function of adsorbed superplasticizer and rheology of suspensions. It is also possible to add different salts to study their influence on the preceding properties. MgO powders can be easily sintered to get compacts or single crystals which can be used for atomic force microscopy measurements with aqueous solutions of superplasticizers.

1. INTRODUCTION

Cement suspensions have an inherent complexity which is an obstacle to understanding cement/superplasticizer interactions. Indeed, cements are reactive multimineral powders, the surfaces of which evolve in time. Mineralogical and chemical compositions of the different particle size fractions can be different. Certain cements also contain mineral additions, like silica fume, fly ash, slag or filler. Organic grinding aids are generally used in the production route and remain on cement grain surfaces. Cements have variable C_3A content, the reactivity of which can also vary. The importance of the C_3A reactivity on the rheology of cement slurries is well known. Not only do the surfaces of the hydrating minerals evolve in time, but also the chemical composition of the solution is changing in the period between the mixing and placing of concrete.

Superplasticizers are anionic polyelectrolyte polymers with carboxylate and/or polysulfonate groups. The pH of the aqueous phase of cement suspensions being around 13, the acidic functions are completely dissociated. The conformation of these polymers is influenced by the pH and the ionic composition, and this point should be taken into consideration when trying to understand their performance.

Proceedings of the 11th International Congress on the Chemistry of Cement (ICCC)
'Cement's Contribution to the Development in the 21st Century'
Hosted by: The Cement and Concrete Institute of South Africa
CD-ROM produced by: Document Transformation Technologies
11 - 16 May 2003, Durban, South Africa
ISBN Number: 0-9584085-8-0
Editors: Dr G. Grieve and G. Owens
Congress Organised by: Event Dynamics

Dispersion of agglomerated cement particles is recognised to be the main way by which superplasticizers improve the workability of concrete. The fluidfying effect of superplasticizers is essentially linked to their adsorption onto cement surfaces. A major factor is to ensure that the polymer adsorbs onto the particles and maintains a similar configuration.

During cement hydration, a part of the superplasticizer can be consumed by the formation of organo-mineral phases [1]. This part will no longer be able to contribute to the dispersion of cement particles.

A characteristic of cement suspensions is that the electrostatic surface potential of the particles is very close to zero at this high pH. Getting exact values of surface potentials near the isolectric point (pH of zero zeta potential) is a difficult task and both slightly positive or negative ζ (zeta) potentials can be found reported in the literature. For what we are concerned with, however, it suffices to state that cement suspensions are very close to their isoelectric point and have a very small surface charge even though they are in a highly alkaline suspension.

2. DIFFERENT MODEL POWDERS PREVIOUSLY USED

The adsorption of a polynaphtalene sulfonate (PNS) has been measured on amorphous SiO_2 and quartz and found to be negligible [2, 3]. This is not surprising since amorphous SiO_2 has a very negative ζ potential at high pH (~ -60 mV at pH 12). Yet, the addition of silica fume to cement shows a higher adsorption than with the same amount of cement alone [4]. The same behaviour has been observed with a $Mg(OH)_2$ powder used instead of cement [5].The adsorption of PNS on TiO_2 strongly depends on the pH of the suspension [2, 6]. It has a maximum at pH 3 and the adsorption strongly decreases in the alkaline region. This behaviour is rationalised by taking into account the change in surface charge of TiO_2 with pH. Titanium dioxide has an isoelectric point around pH 6. Below this value, its ζ potential is positive and above, it is negative. This explains the pH dependent adsorption of the PNS which is an anionic polymer. Therefore, at high pH the significant viscosity decrease observed by Jolicoeur et al may be attributable to dispersion due to high surface charges [2].

α-Alumina has been used successfully for different measurements [2, 3, 7, 8]. Its isoelectric point is around pH 8.5. It should be noted that alumina reacts at high pH and forms soluble aluminates. Numerous other compounds like $Al(OH)_3$, gypsum, attapulgite, kaolin, portlandite and graphite have also been studied by Nkinamubazi [3].

$CaCO_3$ (calcite) has been used for adsorption and rheological measurements [9, 10]. Its isoelectric point is at pH 10. It is the highest value of the different powders used which should start approaching a surface behaviour not dissimilar to cement, especially as there is a high calcium content in cements.

A model system should mimic cement surfaces as closely as possible i.e. have a potential close to zero. In addition, the elevated pH seems an important criterion to assure a similar polymer conformation as would be found with cement. So, a model powder having an isoelectric point at a high pH should be used. Suspensions such as those containing titanium dioxide cannot simultaneously fulfil both conditions (high pH and positive zeta potential). Though they can provide some information on adsorption, it would not be wise to use such data to differentiate the effects involved in superplasticizing of concrete. As a matter of fact, very few systems can fulfil simultaneously the conditions mentioned above and conserve the essential inertness required for a model system. To the best of our knowledge, no adsorption experiments have been carried out at pH around 12 with model powders that are positively charged before the work of Flatt et al [5, 11].

The limitations linked to the powders cited above, led the preceding authors to examine carefully the different possibilities. Among the materials compiled by Parks [12] dead burnt magnesium oxide and magnesium hydroxide, which have nominal isoelectric points respectively at pH 12.4 and 12, were retained as candidates. They were used successfully to study the adsorption isotherms of different superplasticizers and their influence on zeta potential [11] and on rheology [5, 13].

It should be noted that the magnesium hydroxide used in [5] was found to be agglomerated and hence porous. Superplasticizers can adsorb onto the pore walls. In such a case, it is no longer possible to measure correct adsorption isotherms and the use of such porous powders should be avoided.

3. MAGNESIUM OXIDE

3.1 General properties

Magnesium, which lies above calcium in the periodic table, has a similar outer electronic shell and a smaller radius than calcium. This makes its bonding to oxygen much stronger than that of calcium. This stronger bond makes magnesium hydroxide almost insoluble. The rate of hydration of MgO can be further decreased by *dead burning*. This produces a very interesting model powder. The main cement phases (calcium silicates and calcium aluminates) contain calcium oxide, which is probably the dominant surface leading to the positive zeta potential of cement [14]. It is therefore possible that the initial effects involved in superplasticizing will be closely linked to the adsorption of superplasticizers on calcium oxide-like surfaces. This makes magnesium oxide an even more interesting model powder. As for magnesium hydroxide it offers a surface expected to offer many similarities to that of the hydrated cement phases.

We must point out that it is possible to add electrolytes to these model suspensions in order to obtain very similar ionic compositions of the pore solution. However, in the experimental work below, the suspensions were only prepared in 0.01 M NaOH in order to work at a pH close to the isoelectric point of the suspensions. Though loosing a little of the cement specificity, it is believed, however, that such suspensions maintain the three major features of interest, small zeta potential, high pH and inertness. MgO powders can be easily sintered to get compacts or single crystals which can be used for atomic force microscopy measurements with aqueous solutions of superplasticizers [15].

The promising results obtained [5, 11, 13] with MgO, led us to study in more detail the properties and physical characteristics of MgO. Its reactivity in contact with water and its ζ potential were more precisely studied. Finer powders are needed for ζ potential measurements (< 10 μm) and still finer powders for the determination of the adsorbed polymer layer thickness (median size ~ 100 nm or less). Corresponding MgO powders are included in the following study.

3.2 Thermodynamic properties

Magnesium oxide reacts with water to form magnesium hydroxide. Thermochemical calculations allowed us to draw Figure 1 which shows that the stability range of $Mg(OH)_2$ lies within the instability range of MgO. This confirms the irreversibility of the MgO hydration. A stable equilibrium in the system MgO-H_2O is established only after all MgO has been hydrated. The calculated pH is then equal to 11.95. At equilibrium, the calculated pH in the system $Mg(OH)_2$-H_2O is 10.36.

Heat treatments of MgO strongly reduce the rate of hydration. According to the temperature of the treatment, the powders are called *dead burnt* or *hard burnt*.

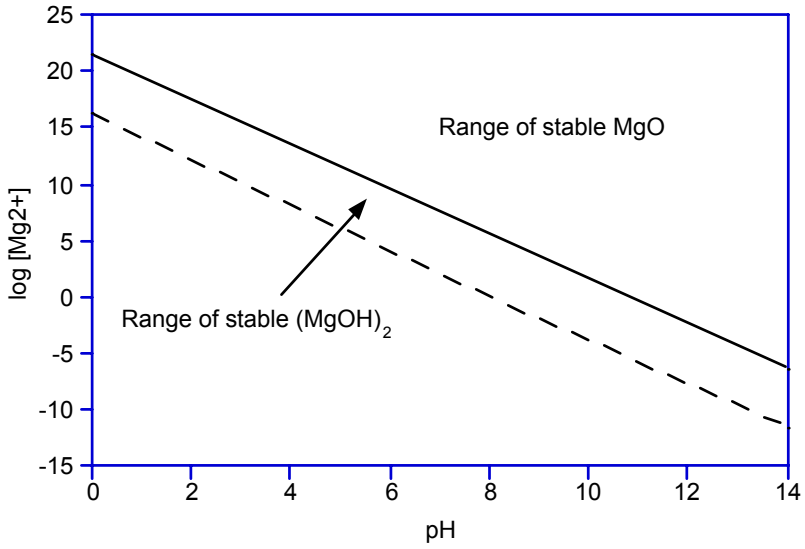

Figure 1. Stability range of MgO and $Mg(OH)_2$ in pure water at 25 °C.

3.3 Materials characterisation

3.3.1 General properties

Three MgO powders and one $Mg(OH)_2$ powder have been selected. Amoung the MgO's, one was *dead burnt*, another one was *hard burnt* and the last one is an ultrafine powder. The commercial name and type of powder are given in Table 1. A certain amount of the powder MagChem P-98 was classified by air in order to obtain a finer fraction < 10 μm (P98-C). Classification was preferred to grinding which may have increased the reactivity of the powder by creating new surfaces during the milling process.

3.3.2 Size characterisation

The particle-size distribution (PSD) of all these powders was measured by laser diffraction (Mastersizer S, Malvern, G.B.). The coarse powders MagChem P98 and P10 have a PSD close to that of cement. The volume diameter of the fraction finer than 10% of the total, D(v, 0.1), the median volume diameter D(v, 0.5), and the volume diameter of the fraction at 90% of the total cumulative distribution D(v, 0.9), as well as the span {[(D(v, 0.9) - D(v, 0.5)]/ D(v, 0.5)}, are reported in Table 2.

Table 1. Powders studied as possible model inert cement particles

Commercial name	Formula	Producer	Description
MagChem P-98	MgO	Martin Marietta Magnesia (USA)	Dead burnt
MagChem 10	MgO	Martin Marietta Magnesia (USA)	Hard burnt
UBE 500 Å	MgO	UBE Industries (Japan)	Ultrafine
MagChem MH-10	$Mg(OH)_2$	Martin Marietta Magnesia (USA)	

It appears that the *ultrafine* powder (UBE 500 Å) is not particularly fine despite its high surface area (31.5 m^2/g). A scanning electron microscopic examination of this powder has shown that it is heavy agglomerated. Despite powerful ultrasonic treatment, it was not possible to break these agglomerates.

Table 2. Percentile volume diameters of the powders measured by laser diffraction.

Name	D(v, 0.1) [µm]	D(v, 0.5) [µm]	D(v, 0.9) [µm]	Span
MagChem P-98	2.88	17.59	54.65	2.94
P98-C	0.33	1.82	5.40	2.78
MagChem 10	3.80	13.57	31.04	2.00
UBE 500 Å	2.01	5.91	11.87	1.67
MagChem MH-10	4.02	11.44	23.98	1.74

3.3.3 Reactivity

The reactivity of the different MgO powders was evaluated by contacting 10 g of powder with 200 ml of 0.01M NaOH solution. After given times, the powder was filtered on a 0.45 µm filter and dried at 110 °C. The evolution of the BET specific surface area over time was measured with a GEMINI 2375 (Micromeritics, USA) system. The results are given in Table 3. For MagCem P-98, old MagCem P-98 and P98-C, the final surface area after 24 hours is 3-4 times higher than the initial area. This factor is nearly 8 for MagCem P-10 indicating that this powder is much more reactive. A common characteristic for all these powders is that the surface remains roughly constant (within experimental error) between 30 and 60 minutes. The ultrafine UBE 500 Å powder exhibits a large surface area which surprisingly decreases after an initial increase as a function of time in NaOH. This could be due to the dissolution of small particles and to a re-precipitation phenomenon on the larger particles (Ostwald ripening),

Thermogravimetric analyses (Mettler TG50 thermobalance) were performed in order to quantify the amount of hydroxide present or formed during immersion in the NaOH solution. Samples were heated at 10 °C/min up to 800 °C in air. The results are given in Table 4.

Table 3. BET specific surface areas of the different powders versus treatment

S_{BET} (m^2/g)	As received	30 min in NaOH 0.01M	1 h in NaOH 0.01M	24 h in NaOH 0.01M
MagChem P-98	0.84 ± 0.05	2.48 ± 0.05	2.4 ± 0.5	2.24 ± 0.10
Old MagChem P-98	1.26 ± 0.20	1.74 ± 0.020	1.57 ± 0.10	4.68 ± 0.30
P98-C	2.44 ± 0.05	6.84 ± 0.40	6.90 ± 0.10	10.45 ± 0.10
MagChem 10	0.58 ± 0.05	1.14 ± 0.06	1.22 ± 0.05	4.40 ± 0.05
UBE 500Å	31.45 ± 0.43	47.8 ± 1.1	44.24 ± 0.33	34.61 ± 3.5

Considering the stoichiometric reaction of dehydration of magnesium hydroxide, the corresponding mass loss is 30.9 %. This allowed us to calculate the percentage of $Mg(OH)_2$ present in the raw powders or formed during NaOH treatment (table 4). For all powders, the amount of hydroxide has increased (some times significantly as with P98-C and UBE 500 Å) after 24 hours in NaOH compared to their raw content. All these results show, however, that our magnesium oxide powders are not really inert in NaOH solution (pH = 12). Hence, their use should be preceded by a pre-treatment (at least 30 min in NaOH).

Table 4. $Mg(OH)_2$ formed during contact in NaOH 0.01M solution at 20 °C.

% $Mg(OH)_2$ formed	As received	30 min in NaOH 0.01M	1 h in NaOH 0.01M	24 h in NaOH 0.01M
MagChem MH-P98	1.33	2.72	1.91	6.61
MagChem P-98	0.26	2.95	3.92	2.04
P98-C	3.56	9.36	8.71	24.88
MagChem 10	0.23	1.23	1.20	7.39
UBE 500Å	2.46	78.1	80.69	94.36

3.3.4 Acoustophoretic measurements

An Acoustosizer II device (Colloidal Dynamics, Warwick, RI, USA) was used on one hand to measure the isoelectric point of P98-C and, on the other hand, to follow the variation of zeta potential stemming from polymer adsorption. The characterisation of cement suspensions by acoustophoresis has been discussed recently [16]. Only particles with a diameter below about 10 μm give a signal with this instrument. Measurements with a coarse powder lead to erroneous results of ζ potentials. So, the use of P98-C is preferred.

The suspensions were prepared by dispersing 53 g of P-98C powder in 200 ml of freshly boiled aqueous solution (to ensure complete elimination of CO_2) containing 0.01 mol/l of KCl. The suspension (water/solid = 3.77) was kept under vigorous agitation and ultrasonic treatment for 15 minutes before the measurements. The suspension is then allowed to cool down to 25 °C for another 15 minutes (under magnetic agitation). The pH was close to 11.1. A NaOH (30 %) solution was progressively added by means of a micropipette. The results (points of 3 determinations) are given in Figure 2. The IEP measured at pH 12.45 on P98-C is close to the value commonly given in the literature, i.e. at pH 12.4 [12].

Similar suspensions (but with 18.5 g) were prepared and, instead of a NaOH solution, concentrated superplasticizer solutions were added. Four different superplasticizers (polycarboxylate based polymers) with equivalent chemical structures, but with different carboxylic group density and different side chain lengths were tested. The results are given in Figure 3. The variations of ζ potential are low comparatively to some preceding results [11]. The polymers tested here contain only carboxylate functions and the results are comparable to those obtained with a similar instrument, but on β-and γ-C_2S [17]. Such measurements allow us to estimate the adsorption isotherm plateau of superplasticizers. The adsorption plateau is situated at the beginning of the straight part of the curve [11].

3.3.5 Other utilisation of MgO powders

This study is part of a European research project and the powders have been used by different partners. An overview of some results is given in another article submitted for this Conference [15].

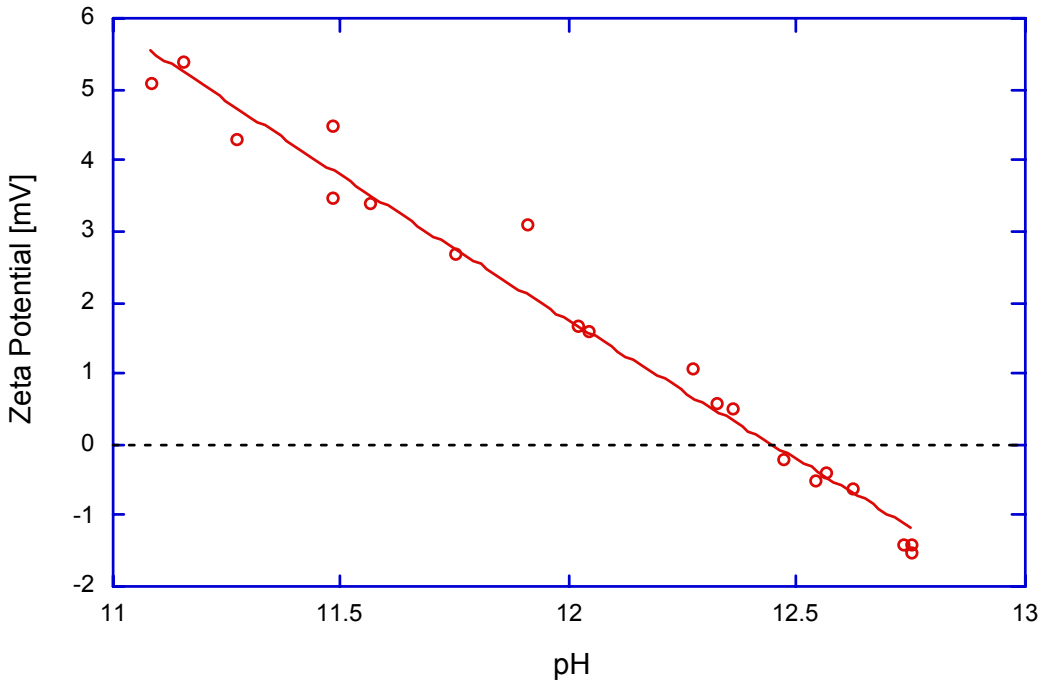

Figure 2. Variation of ζ potential of MgO P-98C as a function of pH.

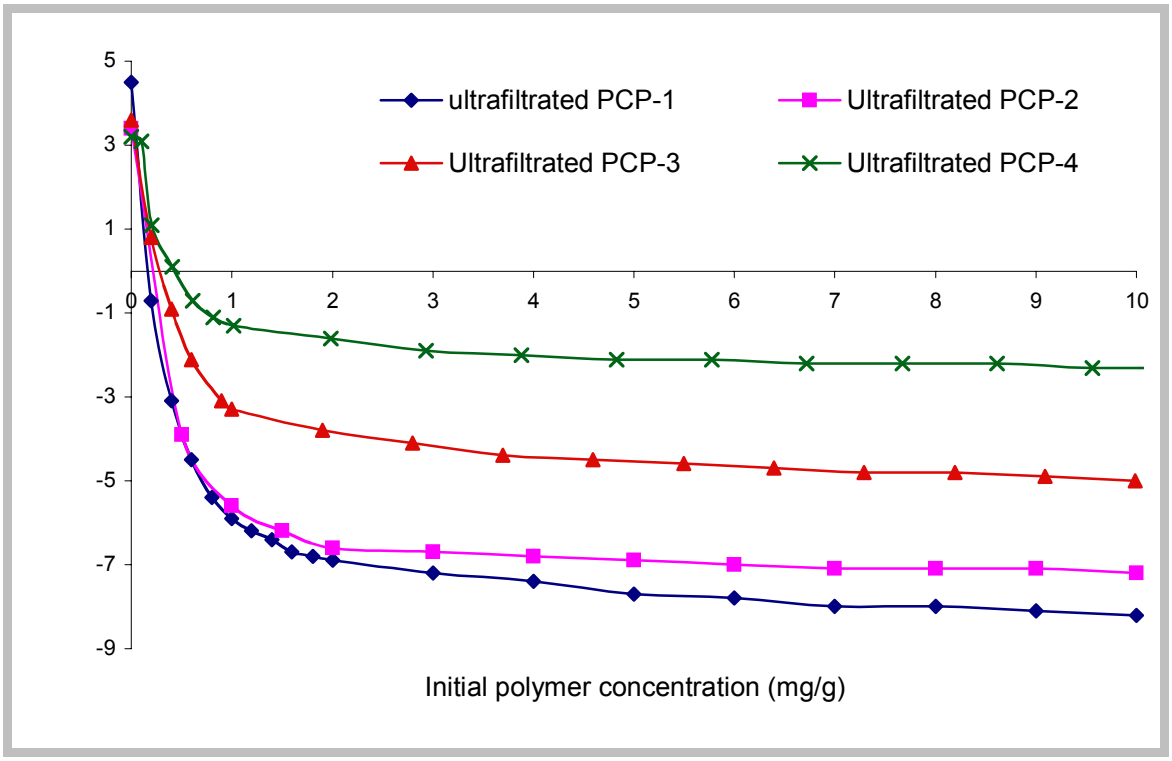

Figure 3. Variation of ζ potential of MgO P-98C as a function of added polymer.

4. CONCLUSIONS

The different model powders used in the place of cement have been reviewed. As Portland cement particles are slighly positively charged or neutral at the pH of the cement pore solution (pH around 13), model powders should have similar properties. It has been shown that all these powders, except MgO or $Mg(OH)_2$, have the drawback of having an isoelectric point either in acidic regions (SiO_2, TiO_2) or lower than the pH of the cement pore solution, like $\propto$-Al_2O_3, $Al(OH)_3$ or $CaCO_3$. That means that the powders are negatively charged at this pH and that their adsorptive properties of superplasticizers are different from that of cement.

Different MgO and $Mg(OH)_2$ powders have been determined. Despite the fact that MgO was dead or hard burnt, it was found that it reacts in contact with an aqueous solution. However, after between 30 and 120 minutes, the surface properties are reasonably stable and the powder can be considered as inert during this period of time.

The $Mg(OH)_2$ at our disposal had to be eliminated because of its non negligible internal porosity and a nano-size MgO (primary particles size of 50 nm) because of its very high reactivity and of its high degree of agglomeration.

It has been shown that the finer fraction of MgO (< 10 μm), obtained by air classification, is suitable for measurements by the acoustophoretic technique. It is particularly appropriate to estimate adsorption isotherms plateau of superplasticizers in a much shorter time than the traditional depletion method.

ACKNOWLEGEMENTS

This work was funded by the 5th European Framework Programme (Contract G5RD-CT-2001-00435) and received a financial support from the Swiss Federal Office for Education and Science (contract No 00.0273-1).

REFERENCES

[1] Flatt, R.J. and Houst, Y.F. A simplified view on chemical effects perturbing the action of superplasticizers, Cement and Concrete research, vol. 31, 2001, pp. 1169-1176.

[2] Jolicoeur, C., Nkinamubanzi, P.C., Simard, M.A., Piotte, M. Progress in Understanding the Functional Properties of Superplasticizers in Fresh Concrete, Proc. of the 4th CANMET/ACI International Conference on Superplasticizers and Other Chemical Admixtures (Malhotra, V.M., Ed.), American Concrete Institute, Farmington Hills, Mi, USA, 1994, SP 148, pp. 63-87.

[3] Nkinamubanzi, P.-C. Influence des dispersants polymériques (superplastifiants) sur les suspensions concentrées et les pâtes de ciment, Ph.D. thesis, Université de Sherbrooke, 1994.

[4] Diamond, S. and Struble, L. Interaction between naphtalene sulfonate and silica fume in Portland cement pastes, Materials Research Society Proceedings, vol. 114, 1988, pp.117-126.

[5] Flatt, R.J., Houst, Y.F., Bowen, P., Hoffmann, H., Widmer, J., Sulser, U., Maeder, U., Bürge T.A. Effect of superplasticizers in a highly alkaline model suspensions containing silica fume, Proceedings of the 6th Canmet/ACI International Conference Fly-Ash, Silica Fume, Slag and Natural Pozzolans in Concrete, (editor: Malhotra, V.M.), American Concrete Institute, Farmington Hills, Mi, USA, 1998, SP-178, pp. 911-930.

[6] Pierre, A., Carquille, C., Lamarche, J.M., Foissy, A. and Mercier, R. Adsorption d'un polycondensat d'acide naphtalène sulfonique (PNS) et de formaldéhyde sur le dioxyde de titane, Cement and Concrete Research, vol. 18, No 1, 1988, pp. 18-28.

[7] Chapuis, J. Physical Elementary Mechanisms of Fluidification by Superplasticizers or Water-Reducing Agents, Proc. 8th ICCC, Rio de Janeiro, vol. 6, 1986, pp. 544-549.

[8] Chapuis, J. Rheological Measurements with Cement Paste in Viscosimeters: A Comprehensive Approach, Rheology of Fresh Cement and Concrete (P.F.G. Banfill, Ed.), E. & F.N. SPON, London, etc., 1990, pp. 3-12.

[9] Pierre, A., Lamarche, J.M., Mercier, R. and Foissy, A. Adsorbtion d'un fluidifiant du ciment sur le carbonate de calcium, Cement and Concrete Research, vol. 19, 1989, pp. 692-702.

[10] Mosquet, M., Chevalier, Y., Brunel, S., Guiquero, J.-P., Le Perchec, P. Polyoxyethylen di-phosphonate as efficient dispersing polymers for aqueous suspensions, Journal of Applied Polymer Science, vol. 65, 1997, pp. 2545-2555.

[11] Flatt, R.J., Houst, Y.F., Bowen, P., Hofmann, H., Widmer, J., Sulser, U., Maeder, U., Bürge, T.A. Interaction of superplasticizers with model powders in a highly alkaline medium, Proceedings of the 5th Canmet/ACI International Conference on Superplasticizers and Other Chemical Admixtures in Concrete (Editor: Malhotra V.M.), American Concrete Institute, Farmington Hills, Mi, USA,1997, SP-173, pp. 743-762.

[12] Parks, G.A. The Isoelectric Points of Solid Oxides, Solid Hydroxides and Aqueous Hydroxo Complex Systems, Chemical Reviews, Vol. 65, 1965, pp. 177-198.

[13] Gustafsson, J. and Reknes, K. Adsorption and dispersing properties of lignosulfonates in model suspensions and cement paste, Proc. 6th CANMET/ACI International Conference on Superplasticizers and Other Chemical Admixtures in Concrete (Malhotra V.M. Ed.), American Concrete Institute, Farmington Hills, Mi, USA, 2000, SP-195, pp. 181-193.

[14] Sakai, E., Daimon, M. Mechanisms of Superplastification, Materials Science of Concrete IV (Skalny, J. and Mindess, S, Eds.), The American Ceramic Society, Westerville, OH, 1995, pp. 91-111.

[15] Kauppi A., Banfill, P.F.G., Bowen, P., Houst, Y.F., Lafuma, F., Mäder, U., Petersen, B.G., Reknes, K., Schober, I., Siebold, A., Swift, D. Improved Superplasticizers for High Performance Concrete, Submitted to the 11th ICCC.

[16] Flatt, R.J., Ferraris, C.F. Acoustophoretic characterization of cement suspensions, Materials and Structures, vol. 35, 2002, accepted.

[17] Lewis, J.A., Matsuyama, H., Kirby, G., Morissette, S., Young, J.F. Polyelectrolyte effects on the rheological properties of concentrated cement suspensions, Journal of the American Ceramic Society, vol. 83, 2000, pp. 1905-13.

CEMENT MODEL POWDER FOR SUPERPLASTICIZER PROPERTIES STUDIES

Robert J. Flatt[1,2], Paul Bowen[1], Alain Siebold[1] and Yves F. Houst[1]

[1] Ecole polytechnique fédérale de Lausanne (EPFL), Laboratoire de technologie des poudres, MXD, CH 1015 Lausanne, Switzerland.
E-mail : Paul.Bowen@epfl.ch, asiebold@club-internet.fr , Yves.Houst@epfl.ch
[2] Present address: SIKA A.G., Corporate Research and Analytics, P.O. Box 1300, CH 8048 Zürich, Switzerland. E-mail: flatt.robert@ch.sika.com

Robert J. Flatt

Robert Flatt received his diploma (1994) in chemical engineering and his PhD degree (1999) in materials science, both from the Swiss Federal Institute of Technology in Lausanne. He then spent 2.5 years as a research associate at Princeton University. Since May 2002, he is in charge of research on mineral/organic interactions at Sika A.G. in the division of Corporate Research and Analytics. His past research involved modelling the rheology of superplasticized cement suspensions, developing tailored mortars for the restoration of roman mosaics, identifying key factors in crystallization damage of porous materials and developing particle modified consolidants for the restoration of stone works.

PRODUCTION OF CONSTRUCTION-GRADE CEMENT FROM CONTAMINATED WASTES

Anil Goyal[1], Michael C. Mensinger[1], S. Peter Barone[2] and Anthony L. Lee[2]

[1]ENDESCO Services, Inc., Des Plaines, Illinois, U.S.A.
[2]Gas Technology Institute, Des Plaines, Illinois U.S.A.

ABSTRACT

As the world population increases and becomes concentrated in and around urban areas, the demand for habitable land and human services will drastically strain existing waste management systems. The quantities of wastes generated from construction and demolition, the chemical industry, healthcare, wastewater treatment plants, paper mills, refineries, incinerators, power plants, and contaminated sediments from lakes, rivers, and estuaries are all expected to increase.

Cement-Lock® Technology is a thermo-chemical manufacturing technology that transforms these wastes into construction-grade cement. The cement has properties similar to those of ordinary Portland cement. During processing all organic contaminants are completely destroyed and converted to innocuous carbon dioxide and water. Chlorine and sulfur compounds are sequestered and heavy metals are locked within the molten matrix to completely immobilize them. This paper describes the development of the this technology from laboratory testing to the current large-scale demonstration program.

1. INTRODUCTION

As the world population increases and becomes concentrated in and around urban areas, the demand for habitable land and human services will drastically strain existing waste management systems. The quantities of wastes generated from construction and demolition, the chemical industry, healthcare, wastewater treatment plants, paper mills, refineries, incinerators, power plants, and contaminated sediments from lakes, rivers, and estuaries are all expected to increase. With habitable land being at a premium, the shortage of appropriate land for landfills will become acute. An ecological alternative for integrated waste management is to consider these wastes as resources that can be utilized to benefit humanity. The technology has been specifically developed to accomplish this objective and for which patents have been obtained from the U.S. patent office (U.S. Patent Nos. 5,803,894 and 5,855,666).

2. TECHNOLOGY DESCRIPTION

The technology is a versatile, cost-effective, and environmentally friendly manufacturing technology capable of converting many types of contaminated wastes into salable commodities, namely, construction-grade cement, power, and/or steam [1, 2, 3]. The acceptable wastes include a wide variety of domestic, industrial, and contaminated as well as non-contaminated wastes. The technology provides a means to harness these wastes as resources for beneficial use. These wastes can be processed individually or in mixtures. In general, different types of wastes can be treated together so that the property associated with each waste can be utilized in achieving the goal of maximizing the desired products in the most cost-effective manner. For example, contaminated

Proceedings of the 11th International Congress on the Chemistry of Cement (ICCC) 11 - 16 May 2003, Durban, South Africa
'Cement's Contribution to the Development in the 21st Century' ISBN Number: 0-9584085-8-0
Hosted by: The Cement and Concrete Institute of South Africa Editors: Dr G. Grieve and G. Owens
CD-ROM produced by: Document Transformation Technologies Congress Organised by: Event Dynamics

soils, sediments, or ash can be co-processed with refinery sludge or tank bottoms to minimize fuel consumption while maximizing both power and cement production.

In the process as shown in (Figure 1) wastes are directed to a thermo-chemical transformation unit of the technology. The wastes are mixed with proprietary modifiers and subjected to temperatures in the range of 1260° to 1538°C (2300° to 2800°F) in the presence of oxygen. This step not only melts the mixture, but also facilitates chemical reactions between the waste and the modifiers that impart latent cementitious properties to the resulting melt upon quenching. The quenched melt is referred to as Ecomelt®.

The thermo-chemical transformation unit can be a rotary kiln melter, for example, or any other type of suitable melting unit; this unit is referred to as the Ecomelt® Generator (EG). Any fuel, including natural gas, petroleum sludge, sewage sludge, shredded tires, waste fuels from industry, and tailings from coal washing plants, can be used in the process. The fuel is burned in the EG using air, enriched air, or oxygen. Excess oxygen, that is, oxygen in excess of the stoichiometric requirement for fuel combustion, is maintained in the EG to produce a matrix of stable oxides. The melt generated in the EG is quenched, ground, pulverized, and blended with an additive to produce construction-grade cement. The flue gas from the EG is directed to a power generating section for heat recovery and flue gas cleanup. In this way the heat content of the flue gas is utilized for the production of the electricity. Other details of the Cement-Lock Technology are given by Rehmat *et al.* [2, 3].

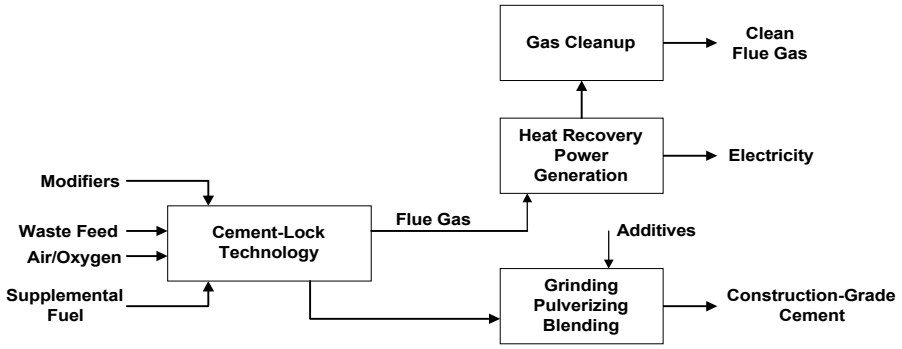

Figure 1. Integrated waste management system utilizing Cement-Lock® technology

3. BENCH-SCALE AND PILOT-SCALE DATA

The technology has produced construction-grade cement from a wide variety of waste materials including organic contaminated soils, dredged estuarine sediment, river sediment, contaminated debris/concrete, municipal incinerator fly ash, coal ash, municipal solid wastes, and PCB-contaminated wastes. The harbor sediments were contaminated with polynuclear aromatic hydrocarbons (PAHs), polychlorinated biphenyls (PCBs), pesticides, insecticides, chlorinated dioxins and furans, and heavy metals. The river sediments also contain similar contaminants. The concrete waste was spiked with oil and chromium.

For each of these applications, the contaminated material was decontaminated through this process and subsequently converted into construction-grade cement. The typical cements produced by this process have been tested independently by Construction Technology Laboratories (the technical arm of the Portland Cement Association, U.S.A.), a cement manufacturer, the New Jersey Department of Transportation, and another independent testing laboratory in New Jersey. In all cases the cement product exceeded the compressive strength requirements per ASTM (American

Society for Testing and Materials) C 150 standards. Therefore, the product can be used in general construction projects as a replacement for ordinary Portland cement. The compressive strengths of cements produced from various wastes are shown in Figures 2 through 4. It is significant to note that the cement product did not require use of any activators (performance enhancing additives). The properties of the cement product can be adjusted to meet application needs by varying the types and quantities of modifiers and additives.

Unlike stabilization and solidification processes that encapsulate heavy metal contaminants within an artificial matrix, in the Cement-Lock process these metals become part of the cement matrix through a process of ionic replacement and, therefore, do not leach. The results of the U.S. Environmental Protection Agency (U.S. EPA) Toxicity Characteristic Leaching Procedure (TCLP) tests on cement produced from several waste materials showed that the priority metal concentrations in the leachate were several orders of magnitude below the regulatory limits. These results are summarized in Table 1.

The organic contaminant destruction from several of the wastes processed in the Cement-Lock Technology is presented in Table 2. The organic destruction exceeds 99.99 percent, thereby maximizing energy recovery and minimizing risks to public health.

Since contaminated wastes are used to produce cement, concern may arise as to the concentration of trace elements in the cement product itself. A comparison of the concentrations of trace elements in cement produced by the Cement-Lock process from contaminated wastes showed that the trace metal concentration is within or close to the range normally found in Portland cement (Table 3). Therefore, the cement is free of adverse public perception.

The pilot-scale plant data were consistent with the laboratory-scale data in terms of organic destruction, leachability, and the quality of the cement generated from the estuarine sediment.

4. TECHNOLOGY STATUS

Following successful testing of the process at the bench-scale and pilot-scale levels, a large-scale demonstration plant with up to 22,937 cubic meters (30,000 cubic yards) of harbor sediment per year capacity is under construction in the New York/New Jersey harbor area. The plant shakedown is expected in December 2002. The primary objective of this program is to demonstrate integrated operation of the process while converting contaminated dredged estuarine sediment into construction-grade cement. The demonstration facility will be integrated with an off-site cement manufacturing company that will grind the Ecomelt and blend it with appropriate additives. The construction-grade cement will be utilized in selected beneficial use projects in the New York/New Jersey harbor area.

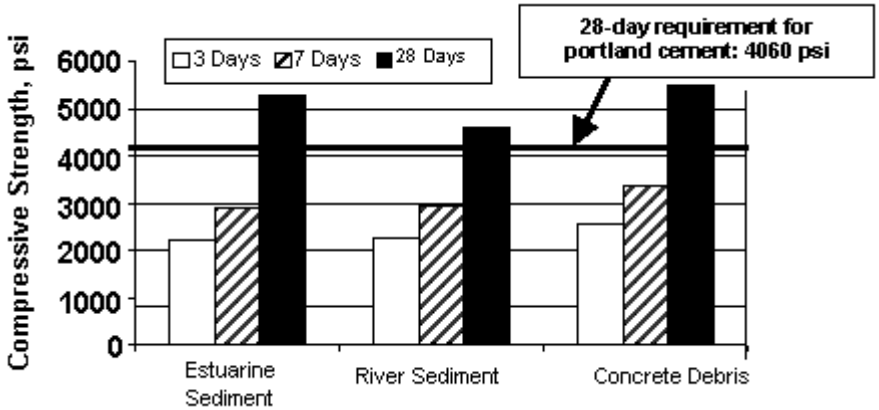

Figure 2. Compressive strength of cements produced from sediment and debris

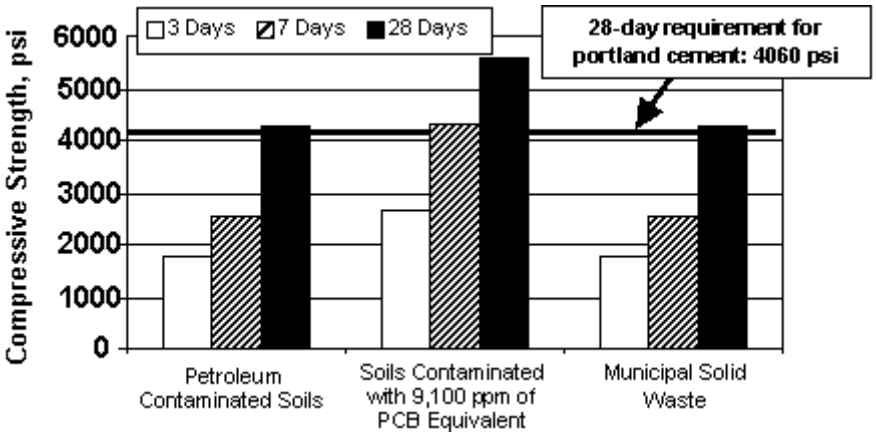

Figure 3. Compressive strength of cement produced from contaminated solids

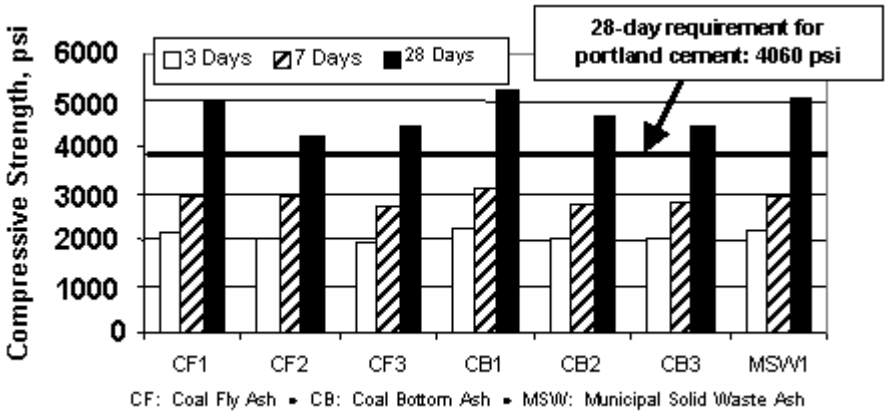

Figure 4. Compressive strength of cement produced from different ash materials

Table 1. Metal immobilization in construction-grade cement produced from different waste materials

				TCLP*			
	Untreated Material			Cement Produced From			
Metal	Estuarine Sediments	River Sediments	Concrete	Estuarine Sediments	River Sediments	Concrete	Regulatory Limit
	mg/kg (dry)			mg/L			
Arsenic	39	7.8	--	< 0.005**	< 0.01	--	5
Cadmium	27	9.5	--	< 0.001	< 0.002	--	1
Chromium	298	138	500	0.15	< 0.072	0.097	5
Copper	--	180	--	--	< 0.01	--	--
Lead	542	218	--	< 0.002	< 0.01	--	5
Mercury	2.9	0.55	--	< 0.0004	< 0.0004	--	0.2
Selenium	6.2	--	--	< 0.003	--	--	1
Silver	13	--	--	< 0.001	--	--	5

* Toxicity Characteristic Leaching Procedure.

** Less than the detection limit of the analytical procedure used.

Table 2. Organic contaminant destruction achieved with different waste materials

	------ Estuarine Sediments -------			---------- River Sediments ----------			-------------- Concrete --------------		
Contaminant	Untreated Sediment	Cement Product	DRE*	Untreated Sediments	Cement Product	DRE	Untreated Concrete	Cement Product	DRE
	----- mg/kg(dry) -----		-- % --	------ mg/kg(dry) ------		-- % --	------ mg/kg(dry) ------		-- % --
Oil & Grease	--	--	--	18,000	< D.L.**	> 99.99	5,000	< D.L.	> 99.9
SVOCs	370	0.22	99.93	51.2	< D.L.	> 99.99	--	--	--
	---------- µg/kg(dry) ----------								
PCBs	8,585	< D.L.	> 99.99	1,100	< D.L.	> 99.99	--	--	--
	---------- ng/kg(dry) ----------								
2,3,7,8-TCDD/TCDF	262	< D.L.	> 99.99	--	--	--	--	--	--
Total TCDD/F	2,871	< D.L.	> 99.99	--	--	--	--	--	--
Total PeCDD/F	4,363	< D.L.	> 99.99	--	--	--	--	--	--
Total Hx/Hp/OCDD/F	34,252	< D.L.	> 99.9	--	--	--	--	--	--

* Destruction and removal efficiency.
** Less than detection limit of the analytical procedure used.

Table 3. Priority trace elements in Cement-Lock cement and Portland cement

Element	Cement-Lock Cement	Portland Cement Range	
	---------- mg/kg ----------		
Mercury	< 0.07*	< 0.001	0.039
Selenium	< 0.94	0.62	2.23
Cadmium	1.59	0.03	1.12
Lead	35.8	1	75
Silver	2.66	6.75	19.9
Arsenic	9.22	5	71
Barium	--	91	1402
Chromium	196	25	422
Nickel	133	15	129

** Less than the detection limit of the analytical procedure used.

The demonstration will also confirm the environmental benefits of the technology through sustained operation; it will also demonstrate that the plant meets all the regulatory requirements and that no secondary waste streams are generated during processing, and the plant does not adversely impact the air quality in the surrounding neighborhood.

The rotary kiln melter for the demonstration-scale project (Figure 5) is 3.1 meter (10 feet) in diameter and 9.1 meter (30 feet) long. The entire system consists of raw sediment storage hopper, hoppers for modifiers, screw conveyors for moving material to the melter, a pug mill for blending all of the feed materials before charging, the rotary kiln melter, quench/granulator, secondary combustion chamber, flue gas quench system, lime injection, bag house, and activated carbon adsorption system for air pollution control.

Figure 5. Rotary Kiln Melter for Demonstration Plant

The demonstration plant will be capable of processing other materials including contaminated soils, petroleum refinery wastes, and various other industrial wastes. Also, with process enhancements and improvements, the capacity of the demonstration plant can be increased to 76,456 cubic meters (100,000 cubic yards) per year.

Significant public input has already been incorporated into this project based on numerous public outreach meetings.

The next stage of the process development will be the construction of a commercial-scale plant having a treatment capacity of 382,280 cubic meters/yr (500,000 yd^3/yr) of contaminated sediments and wastes. Other opportunities are also being pursued with different clients in the U.S. and around the world.

All equipment required for commercial applications is commercially available. Various vendors willing to provide turnkey production plants have already been identified.

5. CONCLUSIONS

The Cement-Lock Technology offers a significant improvement over conventional means of decontaminating many different types of wastes. The technology decontaminates and converts waste materials into products for beneficial use, namely, construction-grade cement, power, and/or steam. These commodities are among the most coveted commodities in all parts of the world. By converting wastes into useful products, we can conserve our natural resources for future generations while improving the condition of the environment for the present generation.

REFERENCES

[1] Rehmat, A., Lee, A., Mensinger, M.C., and Goyal, A., "Co-Production of Electricity and Cement From Coal," Paper presented at the Coal Power Project & Finance Workshop, Porto Alegre, Rio Grande do Sul, Brazil, February 27-March 1, 2000.

[2] Rehmat, A., Lee, A., Goyal, A., Mensinger, M.C., and Bhatty, J.I., "Production of Construction-Grade Cements From Contaminated Wastes," Paper presented at the Fifth International Conference on Concrete Technology, New Delhi, India, November 17-19, 1999.

[3] Rehmat, A., Lee, A., Goyal, A., Mensinger, M.C., Bhatty, J.I., and Barone, S.P., "Production of Construction-Grade Cements From Wastes Using Cement-Lock™ Technology," Paper presented at the Fourth Beijing International Symposium on Cement and Concrete, Beijing, China, October 27-30, 1998.

INVERSION OF THE CEMENT HYDRATION AS A NEW METHOD FOR IDENTIFICATION AND/OR RECYCLING?

F. Splittgerber [1] and A. Mueller [2]

[1] Department of Civil Engineering, Bauhaus-University Weimar, Weimar, Germany.
E-mail: frank.splittgerber@bauing.uni-weimar.de
[2] Department of Civil Engineering, Bauhaus-University Weimar, Weimar, Germany.
E-mail: anette-m.mueller@bauing.uni-weimar.de

1. INTRODUCTION

The starting point of the research projects which are the basis of this paper was the question, whether the hydration of the cement is completely reversible. Because this question was not asked till now there are hardly any answers although this topic could be interesting from different points of view:

- The first point of view is connected with the material testing. If the hydration is reversible, then it should be possible to get back the phases of the non-hydrated original cement by a heat treatment. These "secondary" clinker phases may be a tool for the identification of the original cement used in a concrete.
- The second point of view is concerned with recycling. From this angle, the reversibility would be one of the prerequisites for the generation of closed circles for all the constituents of concrete.

The following paper deals with both of these aspects. The results that were obtained by basic experiments with clinker phases, cement paste and mortars are presented here.

2. CEMENT IDENTIFICATION ON BASIS OF RECOVERED CLINKER PHASES

2.1 Motivation

Concrete damage, which occurs in structures during their service life, are frequently due to an insufficient durability of the hardened cement paste and a weak bond between the hardened cement paste and the aggregates. Since the repair of such damage is often connected with substantial costs, lawsuits appear frequently as a consequence. In these cases the determination of the cement type used in the concrete or mortar may be very helpful. Furthermore if a repair mixture must be designed it is also an indispensable prerequisite to know the composition of the original concrete.

In the literature only some descriptions of methods for the distinction of the type of cement of hardened concrete or mortars can be found [1,2,3,4]. A general identification of the cement type used, however, is not possible with all these methods.

2.2 Main Idea of the Method

The chemical and mineralogical compositions are, apart from the particle size distribution, the most important features of cement in the non-hydrated state. In this state the type of cement can be recognised by the mineralogical composition. By the hydration of the cement this composition is fundamentally changed. But the quantitative phase composition of the hydrated cement can hardly be determined. Furthermore the hydration mechanism is not yet well understood for all types of

cement, so conclusions from the hydration products to the original cement are practically impossible.

The method for the determination of the type of cement in hardened mortar and concrete described here aims at the recovery of the non-hydrated state by a heat treatment of the hardened specimen in order to recognise the type of cement by its original phases. The ideal case would be a complete dehydration of the hardened cement paste and a recovery of the phases of the original cement at temperatures up to the original cement burning temperature. With these phases then the type of cement can be recognised. Because aggregates are present this ideal case cannot be achieved. Because reactions between the aggregates and the paste may occur, or melting phases are formed, a burning temperature of 1400°C cannot be realized. So it is possible that the phase formation can only take place incompletely. Therefore additional analyses and features are required in order to capture the modifications in comparison with the original cement.

2.3 Test Sequence

The first experiments for the development of the new method were carried out with clinker phases as well as cements. The influences of the aggregates were excluded by using of pastes. In the experiments should be found out what kinds of non-hydrated phases are formed in dependence of the temperature. The tests were carried out in the following steps:

- Manufacturing of pastes from the clinker phases and cements and standard mortar prisms
- Hydration for a time of at least 180 days
- Sample preparation for the identification:
  - Pulverization of the pastes below a particle size of 63 µm
  - Crushing of the mortar below 1 mm and then separating the fraction below 63 µm for the further analyses.
- Heat treatment at following temperatures: 600°C, 900°C, 1100°C, 1200°C and 1400°C.
- Determination of the mineral phases formed by the heat treatment by X-ray diffraction.
- Additionally: chemical determination of the content of free lime by an extraction with ethyl acetoacetate.

This paper only deals with the experimental investigations in clinker phases. It is only one example given for the practical application of the cement identification by X-ray diffraction in a mortar.

2.4 Analyses of Clinker Phases

With the basic studies of the clinker phases the question should be answered first whether the hydration can be reversed completely by a heat treatment, and at which temperatures this reversibility can be achieved for the different phases. The nomenclature of the used samples is represented in Table 1.

Table 1. Used clinker phases and mineral admixtures

Sample	Content
C3S	100 % alite
C2S	100 % belite
C3A	100 % aluminate-phase
C4AF	100 % ferrite-phase
BFS	100 % blast-furnace slag

Technically manufactured clinker phases were used, so it can be assumed that the typical minor components are incorporated. Besides, mineral admixtures like blast-furnace slag were tested.

C3S-Sample

As shown in Figure 1, the only effect that can be clearly observed at a temperature of 600°C is the decomposition of the Portlandite. The free lime expected from this decomposition is hardly detectable. Also no other crystalline phases can be found out of the XRD-diagram. Interferences were found again in the sample that was treated at 900°C. On the basis of these peaks the crystalline phases belite (β-C_2S) and free lime (CaO) could be identified. Because this temperature was obviously not high enough for the formation of C_3S, the surplus of CaO is present as free lime. At 1000°C and 1100°C no modifications are observed in principle. However, compared with a heat treatment at 900°C, the intensities of the belite peaks and the CaO peaks increase.

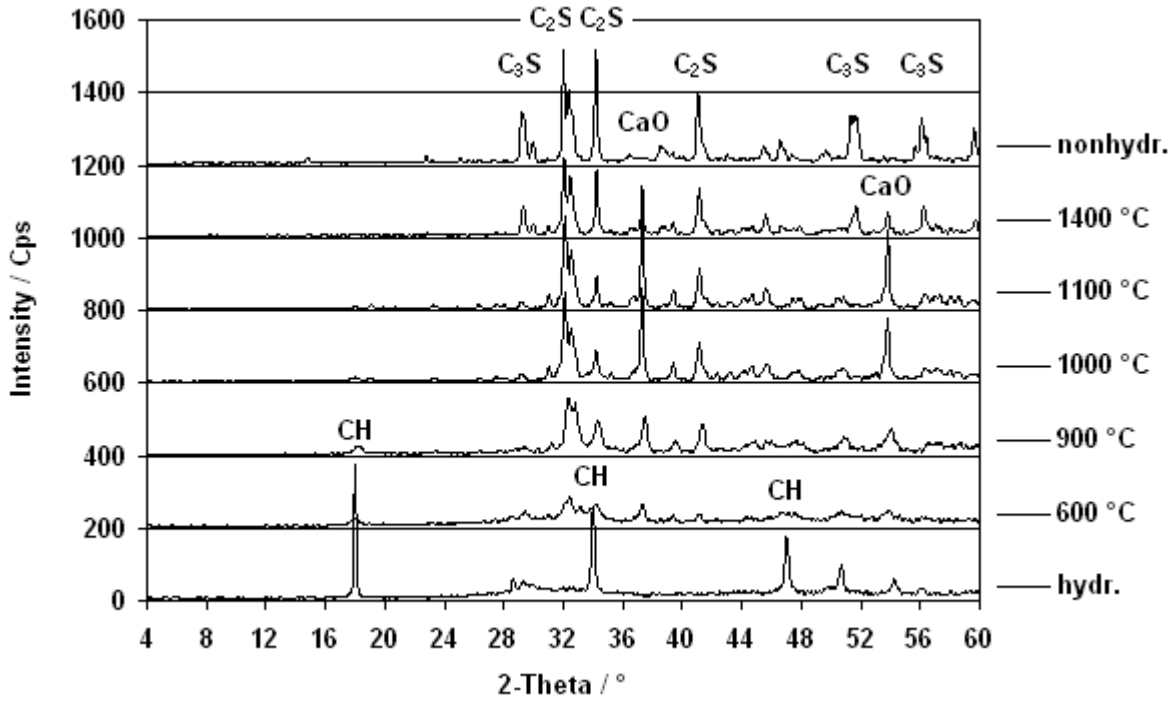

Figure 1. XRD curves of the C3S-sample

At 1400°C modifications occur. Alite was determined as additional component. Since only little free lime could be proved, the plausible conclusion is, that a part of the belite has reacted with the CaO under formation of alite. The fact that the alite is formed in nearly the same temperature range during the burning of cement supports this result. A good correspondence of both curves is noticeable if the XRD-diagram of 1400°C is compared with that of the non-hydrated material. The somewhat smaller intensities can be attributed to a not complete conversion, which explains also the presence of residues of free lime. However, by a further temperature increase on approximately 1450°C that corresponds to the temperature during the burning of cement, these differences should not occur longer.

C2S-Sample

Non-hydrated belite residues and a small amount of portlandite are proved in the hydrated C2S-sample. At a heat treatment at 600 °C the portlandite decomposes. During the further heat treatment at temperatures of 900, 1000, 1100 and 1400 °C no general mineralogical modifications are detected. Only the intensity of the belite peaks increases clearly with rising temperature and achieves nearly the level of the original sample at 1400°C. It can be observed that in this sample also at very high temperatures of 1400°C no alite is formed, since obviously no CaO is available for the reaction. Therefore also no CaO peaks occur at the temperatures of 900 to 1100°C.

C3A- and C4AF-Sample

In the hydration product of the C3A-sample only C_3AH_6 (hexahydrate) was detectable (Figure 2). At the treatment temperatures of 600, 900 and 1000°C the intermediate phase mayenite ($C_{12}A_7$) was formed. In this stage free lime is also existing, as the result of the difference of the CaO content of the aluminate and the mayenite. By a heat treatment at 1100°C the starting point is reached again, i.e. the hydration of C_3A with water is completely reversible. A further increase of the temperature up to 1400°C leads to a decrease of the crystallinity because of the beginning of the melting .

If the hydration of aluminate takes place in the presence of gypsum, an important difference occurs. Ettringite and monosulfate are generated as hydration products. During the decomposition in the temperature range between 900 and 1100°C the mineral ye'elimite ($4CaO \cdot 3Al_2O_3 \cdot SO_3$) is formed instead of $C_{12}A_7$.

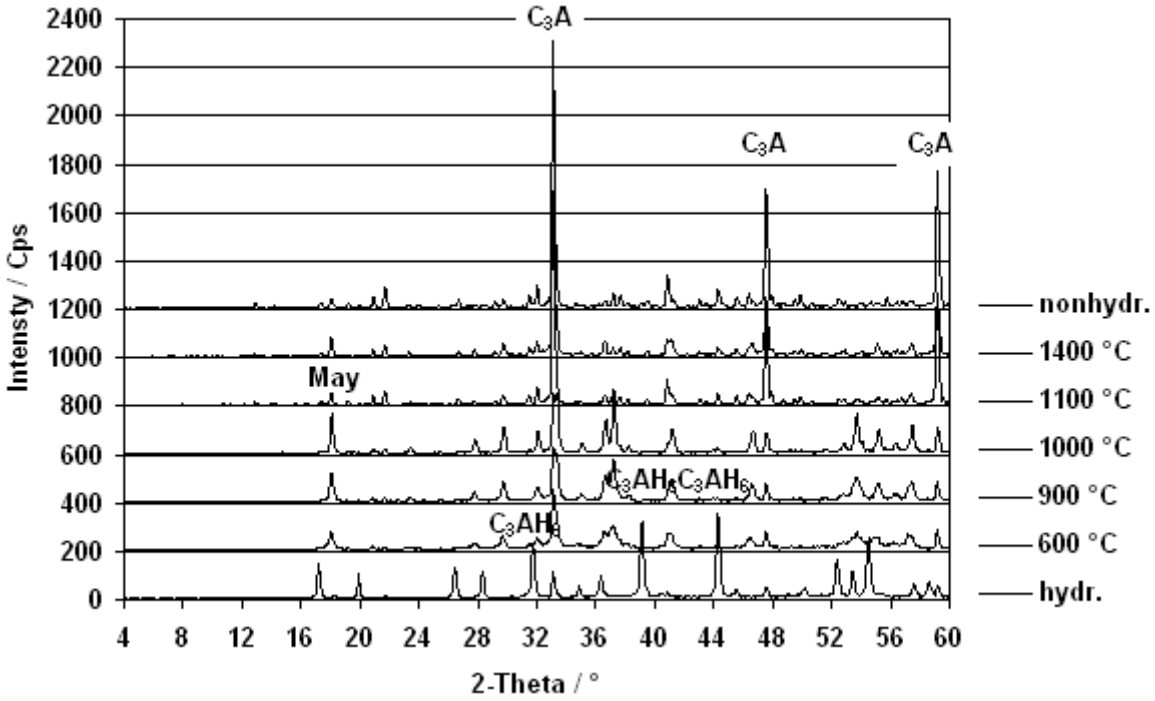

Figure 2. XRD curves of the C3A-sample

The hydration products of the C_4AF-phase can be distinguished hardly from those of the C_3A. As in the C3A-sample the dehydration at temperatures above 600°C takes place under formation of the mineral mayenite ($C_{12}A_7$). However, no free lime appears, due to the fact that the CaO content of the mayenite is higher than that of the brownmillerite. As a further difference in presence of sulphate no ye'elimite could be identified.

BFS-Sample

Opposite to the clinker phases the ground, granulated blast-furnace slag was mixed for the hydration with a saturated solution of $Ca(OH)_2$. No crystalline phases were found in the hydrated sample after a hydration time of 10 months as shown in Figure 3. Since Portlandite peaks are not visible in the hydration product, it can be concluded that the $Ca(OH)_2$ is consumed by the hydration. However, no predictions are possible about the degree of hydration. At heating temperatures above 900°C a crystalline phase occurs which can be identified as gehlenite. It has been formed either from residues of non-hydrated blast-furnace slag or from the hydration products. At higher temperatures the XRD-diagrams show no changes.

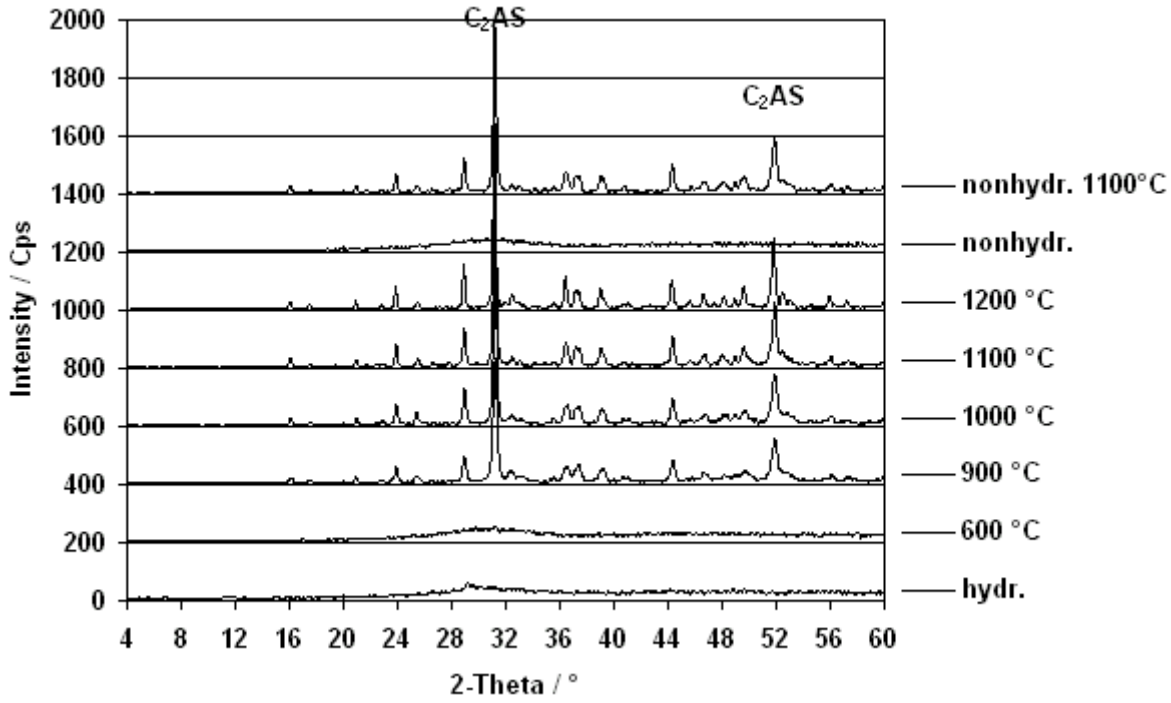

Figure 3. XRD curves of the BFS-sample

In the initial state the granulated blast-furnace slag has, due to the quenching process in the production, a very high proportion of glass phase. Therefore no crystalline phases were detected in this sample. In order to enable a comparison with the heat-treated samples an additional XRD-diagram was taken up in Figure 3 (upper curve). It shows the non-hydrated granulated blast-furnace slag after an annealing at 1100°C and a slow cooling, by that the slag undergoes crystallization. In this sample gehlenite could be identified as the main component of the granulated blast-furnace slag.

2.5 Analyses of Mortars

The investigations of the clinker phases result in the following possibilities of differentiation:

- Distinction between portland cements and cements containing mineral admixtures is possible by the identification of typical mineral phases for the admixture, e.g. gehlenite for granulated blast-furnace slag.
- Distinction between ordinary and sulphate-resistant portland cements is possible on the basis of the ye`elimite phase after a heat treatment at 1100°C.
- Estimation of the content of alite is possible indirectly by the content of free lime formed at temperature of 1100°C.

For the identification at least two temperature ranges must be regarded. The first temperature range is from 1100°C to 1200°C. It is important for aluminate and ferrite identification. Higher treatment temperatures from 1400°C to 1450°C are necessary for the identification of the silicates. Since this temperature range is hard to apply because melting phases are formed in the presence of some aggregates and admixtures, the alite content of the original cement must be estimated, as an alternative, from the contents of belite and free lime after a heat treatment at 1100°C.

For the application of the identification features on mortars or concrete it is furthermore important to prepare the sample in such manner that the cement paste is enriched as much as possible. Then it is possible to distinguish between the types of cements used in a mortar as demonstrated in Figure 4.

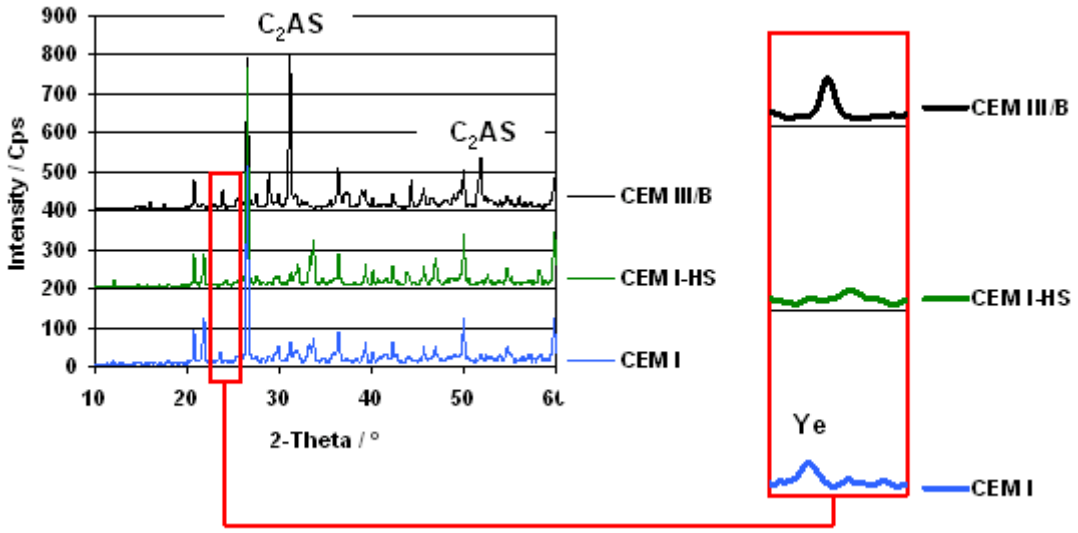

Figure 4. XRD-curves of cement pastes made from three different cements, heat treated at 1100°C and extracted with salicylic acid

This figure shows the XRD-curves of the enriched and heat treated cement pastes of mortars made from an ordinary portland cement (CEM I), a sulphate resistant portland cement (CEM I-HS) and a blastfurnace slag cement (CEM III). After the heat treatment the calcium silicates have been extracted by salicylic acid. The blast furnace slag cement can easily be identified by the large gehlenite peaks. Both Portland cements can be recognized by the interferences of free lime and belite. But there is an important difference between the two Portland cements too. While the sample from the ordinary Portland cement contains significant amounts of ye'elimite ($4CaO{\cdot}3Al_2O_3{\cdot}SO_3$), in the sample from the sulphate resistant one no ye'elimite could be identified. So the distinguishing features are also confirmed in the experiments on mortars.

3. RECYCLING ON BASIS OF REVERSIBILITY OF CEMENT HYDRATATION

3.1 Motivation

Recycling of concrete becomes more and more important on the one hand to reduce the use of resources and on the other hand to minimize the waste of landscape for landfilling. Concrete debris can be reused as aggregate in new concrete. But from the theoretical point of view this application results in an inevitable degradation with regard to the properties since concrete is a composite material. A more fundamental possibility would be the division of the concrete into its components, which can then be recycled separately. Only a very few papers [5,6] are known from the literature about this topic. Therefore first experiments were done with the target to get an orientation.

3.2 Test Sequence

The experiments were carried out with an ordinary Portland cement and a blastfurnace slag cement. The cements were processed to pastes (w/c = 0.4) and placed under water for 180 days. Then they are dried, crushed and ground. The powdered materials were burnt at 600°C, 1100°C, 1200°C and 1400°C in an electrical furnace. The specimens, made from blastfurnace slag cement could not be treated at 1400°C because they melted completely at this temperature. The secondary binders were examined with regard to the chemical composition and the reactivity. Furthermore mortar prisms were manufactured for testing the strength development. In the following only the results obtained with the Portland cement shall be presented.

3.3 Properties of the Treated Samples

3.3.1 Composition

With regard to the chemical composition there are only small differences between the original and the secondary cements. Only the content of SO_3 decreases slightly in the secondary cements treated at 1200°C and 1400°C due to the decomposition of calciumsulfate.

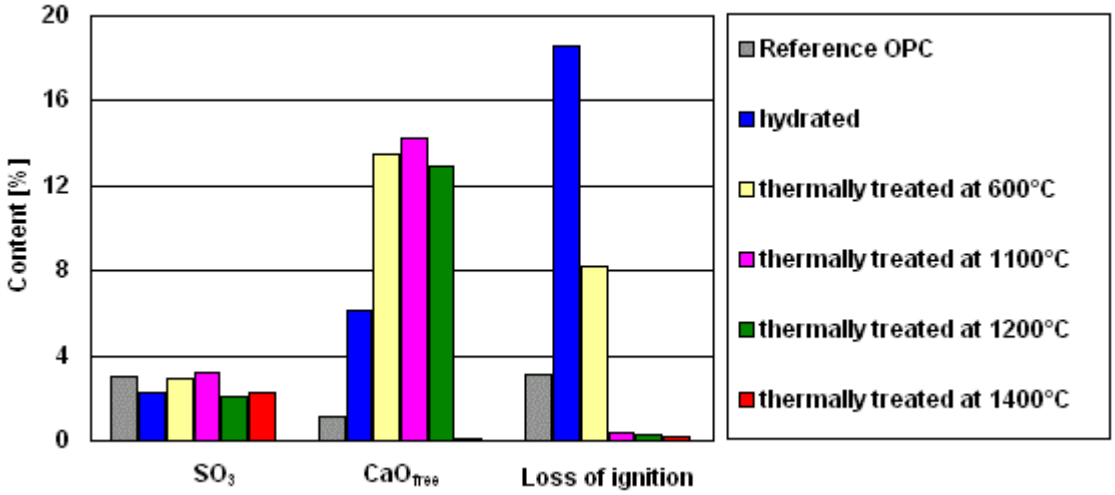

Figure 5. SO_3-content, CaO_{free}-content and loss of ignition of the samples

With regard to the phase composition there are considerable differences in dependence of the temperature. The loss on ignition as featured for the content of fixed water and the content of free lime is shown in Figure 5. As expected the loss on ignition decreases with increasing burning temperature. In contrast to this the free lime content shows a maximum at medium temperatures. The samples treated at 600°C, 1100°C and 1200°C have very high contents of free lime. Only when the specimens are burnt at 1400°C the free lime content drops below the limit of 2 %. These results are confirmed by the XRD analyses. In agreement with the results in the first part of this paper the reference cement and the sample, burnt at 1400°C have nearly the same XRD diagram. That means that the hydration as chemical reaction is reversible. The other samples show the following features: In the cement paste only portlandite is detectable. In the 600°C-sample only traces of portlandite remain. The free lime measured by the method according to FRANKE (Fig. 5) is not detectable with the XRD-measurements, i.e. it must be poorly crystalline. The samples, burnt at 1100°C or 1200°C contain belite, aluminate and ferrite. Because these temperatures are too low for the formation of alite, a considerable amount of free lime remains in these samples.

3.3.2 Granulometric Parameters

In Table 2 the specifications about the fineness and the density of the samples are summarized.

Table 2. Granulometric Parameters and absolute density of the samples

		Reference OPC	Heat Treated Samples	
			600°C	1400°C
Mean particle size[1]	[µm]	22,64	22,68	21,58
Specific surface[2]	[cm^2/g]	3000	15500	5440
Absolute density[3]	[g/cm^3]	3,20	2,75	3,22

[1]measured with laser granulometer [2]measured acc. to BLAINE [3]measured with helium pycnometer

The reference material and the 1400°C treated sample have rather similar parameters. Only the specific surface of the treated sample is higher than that of the reference material.

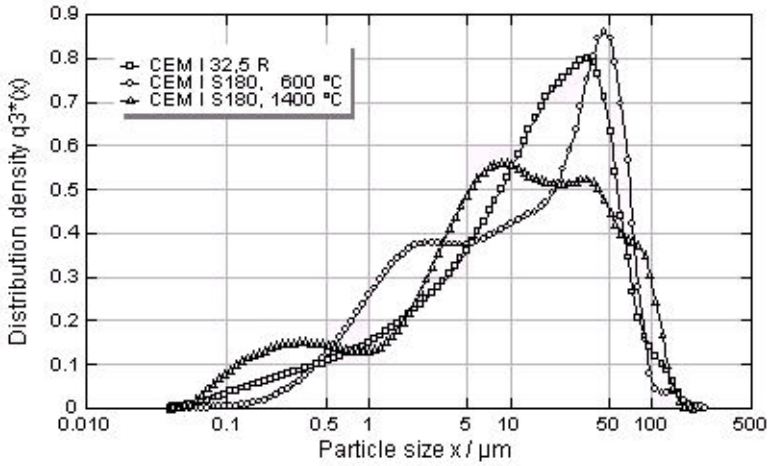

Figure 6. Particle size distribution

The reason can be the higher portion of particles < 1 µm (Figure 6). The 600°C-sample considerably differs from the others. Although the mean particle size is nearly the same the specific surface is more than three times higher. Besides the density is lower. Both point to the fact that this sample shows changes in its properties due to the high content of free lime.

3.3.3 Evolution of Heat of Hydration

The reactivity of the treated samples was measured by Differential Calorimetric Analyses. From the Figure 7 follows that there are considerable differences in the rate of heat evolution.

Compared with the reference cement in the first stage at 0,1 hours the rate is higher both for the sample heated on 600°C and for the sample heated on 1400°C. In the main stage at about 10 hours the reference cement has the highest rate of heat evolution. The following reasons may be responsible for the differences in the first stage:

- In the case of the 600°C-sample the reaction of the very reactive free lime with the water may be one of the reasons for the high rate of heat evolution.
- The difference between the reference cement and the 1400°C-sample points to a higher reactivity of the secondary cement either due to a higher activity of the recovered clinker phases or due to the higher portion of particles smaller than 1µm.

With regard to the main stage in which the order of the rate of heat evolution is inverted compared with the first stage no reasons can be given.

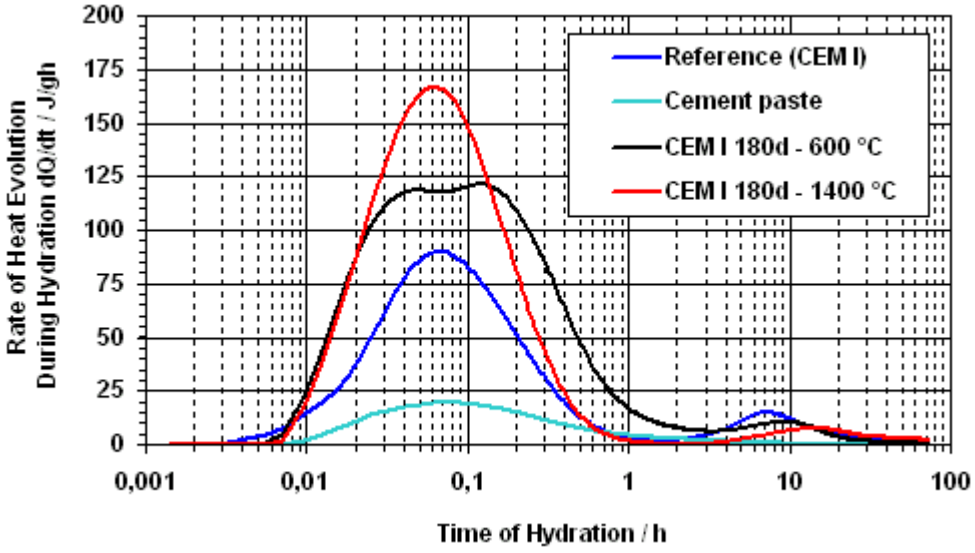

Figure 7. Rate of heat evolution during hydration

3.3.4 Strength Development

The development of the compressive strength shown in Figure 8 is very different for the mortars from the three tested binders. From the experiments follows that the 600°C-sample is workable only, if the portion of mixing water is increased.

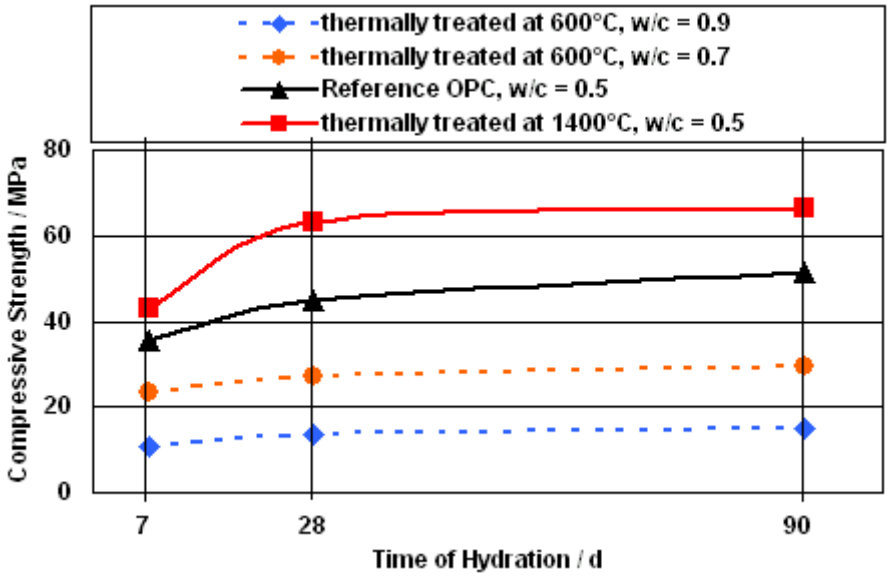

Figure 8. Strength development of the samples

The strength of these specimens is in the range from 11 MPa to 30 MPa. That is clearly more than the strength of a hydraulic lime mortar that may be one of the possible standards of comparison. On the other hand it is less than the strength of the original cement. The strength of the 1400°C-sample exceeds this one of the reference sample in the considered time of hydration. That means that the higher reactivity found in the DCA experiments for the initial stage of hydration at least is reflected also in the strength development.

4. CONCLUSIONS

With regard to the pure clinker or Portland cement the reactions of hydration are reversible completely if the material is heated to the burning temperature of cement. This reversibility is reduced if the temperatures are too low or if further materials are added. For instance the addition of gypsum can result already in the formation of an additional intermediary phase.

With regard to the identification of the type of cement used in concrete or mortars, three diagnostic features were figured out: After a heat treatment at 1100°C, a high content of belite and free lime points to a Portland cement; (i), the appearance of the ye'elimite phase points to a portland cement with high sulfate resistance; (ii) the appearance of gehlenite (iii) points to a blast furnace slag cement.

Concerning the inversion of the hydration, the presence of aggregates must be taken into consideration, because of their large amount in the mortar or concrete. Therefore it is necessary to enrich the cement paste as much as possible by special procedures.

Looking at the possibilities for the recycling of concrete or mortars, must be noticed that there is a start for using a heat-treated concrete or mortar at least as one component of a new binding material or as raw material for manufacturing of a binder because of their hydraulic potential. Generally it should be looked for a way which allows a recycling without a complete separation of the cement paste and the aggregates. This requires further research about the decomposition of heat treated concrete and mortar as well as the re-hydration behaviour.

REFERENCES AND CITATIONS

Standards

[1] British Standard 1881, Testing Concrete, Part 124 November 1988. Methods for analysis of hardened concrete.

Books

[2] H.W: Iken, Handbuch der Betonprüfung, Betonverlag, Düsseldorf, 1994.

[5] Müller, Christoph, Dora, Bernd: Verwertung von Brechsand aus Bauschutt. Deutscher Ausschuß für Stahlbeton, H. 506 Beuth-Verlag, Berlin.2000.

Journal Articles

[3] M.T. Blanco, F. Puertas, T. Vazquez, A. de la Fuente, The most suitable techniques and methods to identify high alumina cement and based portland cement in concrete. Materiales de construction 42**,** 51-64 (1992).

[4] Goguel, R.L.; St.John,D.A.: Chemical identification of Portland Cements in New Zealand concrete No. 1 & 2. Cem. Concr. Res. Vol. 23 S. 59-68 & 283-293.

Conferences

[6] Möbius, Anke, Müller, Anette. Untersuchungen zur Nutzung von zementgebundenem Recyclingmaterial als Primär- oder Sekundärbindemittel. Ibausil-Tagungsbericht, Band II, 2-0351-2-03600, Weimar 2000.

ACKNOWLEDGMENTS

The authors would like to acknowledge the support provided for the projects by the Deutsche Forschungsgemeinschaft.

THE STRUCTURE AND MICROSTRUCTURE OF AUTOCLAVED MATERIALS MODIFIED BY POZZOLANIC MINERAL ADMIXTURES

Pytel, Z. and Malolepszy, J.

Faculty of Material Science and Ceramics, Department of Building Materials, University of Mining and Metallurgy, Ave. Mickiewicza 30, PL-30-059, Cracow, Poland. E-mail: pytel@uci.agh.edu.pl

ABSTRACT

The structure and microstructure of autoclaved materials is mainly determined by the kind and amount of the chemical reaction products being formed. In the case of sand-lime bricks, the final products of hydration produced under hydrothermal conditions are hydrated calcium silicates (of various degrees of crystallization) which usually appear as amorphous C-S-H phase, and crystalline tobermorite. The presence of foreign ions in the reaction medium exerts a considerable influence on the morphology of these products. The presence of the ions may be due to impurities in raw materials, or they may be intentionally introduced as mineral additives. The influence of various mineral additives on the formation of the structure and microstructure of autoclaved materials was analysed in the course of model tests. The aforementioned autoclaved materials were obtained from the mixture of lime and silica (mixed at molar ratio CaO/SiO_2 = 0.83). This composition was subsequently modified by the introduction of a small amount of mineral additive. Fly ashes, flue gas desulphurisation products and the heat treatment products of silty materials were used as pozzolanic mineral additives. In order to heighten the chemical activity of the additives in question, they were activated by means of sulphates and alkalis.

The quality of the materials obtained was assessed on the basis of the results of the following studies: XRD analysis, SEM+EDS, mercury porosimetry and the study of physical characteristics. The cognitive effect of the studies is the presence of C-S-H phase and tobermorite in the materials obtained, which results directly from the introduction of mineral additives as well as the application of sulphates or alkalis in the chemical activation. The changes occurring in the morphology of basic/primary final products of hydration under hydrothermal conditions favourably modify the microstructure of autoclaved materials, as a result of which the improvement of application properties can be noted. It refers particularly to the strength development of such a kind of material which has a decisive influence on the application effects observed in the course of the studies conducted.

1. INTRODUCTION

Quartz sand and burnt lime are the traditional starting materials in sand-lime brick production [1,2]. These materials, mixed and formed, are subsequently autoclaved, to transform lime and silica into hydrated calcium silicates of a different structure [3,4,5]. The amorphous phase calcium silicate hydrate (C-S-H), being the first product, is the precursor of tobermorite and other phases synthesised in hydrothermal conditions [6]. In practice, the same impurities in the raw mixture can give the other products; in the presence of aluminium ions the stabilisation of tobermorite occurs [7] or even the formation of hydrogarnets takes place [8]. The latter phase affects significantly the strength of the final product.

The mechanical properties of autoclaved products are strongly related to the total amount of C-S-H and tobermorite [9]. Hence the materials should be processed with the aim of producing the highest content of these phases. Such an effect can be achieved by the incorporation of the same admixtures.

The phase composition and microstructure of autoclaved products is thus modified by the use of mineral additives such as fly ash, metakaolinite and by-products from fluidised bed combustion installations. These admixtures bring about the formation of additional C-S-H and subsequently tobermorite, as a result of the pozzolanic reaction. Simultaneously the capillary porosity of the products is reduced and consequently their strength and quality is increased [10].

The waste materials and by-products of pozzolanic character, e.g. fly ashes, slags, silica fume can be used in silicate building materials technology. Also very promising is the potential incorporation of a "new generation" of wastes (i.e. gypsum, etc) from desulphurization operations in the same fluidised bed combustion (FBC) installations [11].
These wastes exhibit high pozzolanic activity resulting from the presence of a decomposed clayey mineral - metakaolinite. The same amount of $CaSO_4$ and $CaCO_3$ can promote the formation of hydroellastadite [12] or scawtite [13,14] in hydrothermal conditions. The microstructure of materials is thus modified.

Some of the waste materials from the groups mentioned above show their pozzolanic activity under the presence of alkalis or sulphates [15,10]. Thus the determination of the effect of some ions on the formation and properties of hydration products during autoclaving is of special importance from both practical and scientific point of view.

2. CHARACTERISTICS OF STARTING MATERIALS

For the purpose of synthesis of autoclaved materials used as reference samples (T), quartz sand (MK) was applied as the silicate raw material. It was produced by Quartzwerke GmbH under the trade name of SIKRON-Feinstmehl SGL-300. The characteristic parameters of this raw material are as follows: specific density-2.65g/cm^3, bulk density- 0.72 g/cm^3, Blaine specific surface S_w = 550 m^2/kg and SiO_2 content = 99.2%. That's why this material is different to sand used in practice for the manufacture for calcium-silicate products. The other basic raw material was burnt lime obtained in the course of heat treatment of analytically pure $CaCO_3$ produced by Fluk Company (Firma Fluka). Thermal dissociation was conducted at 1050°C for 3 hours.

In order to modify the composition of the lime/sand mixture, the following pozzolanic mineral additives were used: metakaolinite (MU), fly-ash (S), and fluidised bed waste (ZFŻ). Although pozzolanic properties are typical of all the above-mentioned mineral additives, in each case pozzolanic activity is determined by different factors. In the case of fly-ash (S) such a factor is mainly its vitreous/glasslike phase, whereas the pozzolanic properties of fluidised bed waste (ZFŻ) are determined by the presence of dehydrated silty minerals. Metakaolinite (MU) was included in this study as a model material of high pozzolanic activity, obtained during thermal decomposition of kaolinite. The pozzolanic activity of the mineral additives was determined by the chemical method in the ASTM 379-565 Standard. This method consists of the analysis of components soluble in basic solutions. These components are considered as potentially active in the presence of calcium hydroxide. The ASTM method gives the ability to determine reactive of both silica and alumina to $Ca(OH)_2$. The results are presented in Table 1.

With the aim of increasing the pozzolanic activity of the additives, they were activated chemically by means of sulphates and alkalis. Sulphates were introduced into the samples in the form of natural

gypsum (G) and anhydrite (AN). Alkalis were introduced in the form of water solutions of NaOH (NH), KOH (KH) and Na_2CO_3 (NC).

Table 1. Pozzolanic properties of mineral additives

Sample symbol	Pozzolan content (in weight %)		Total
	SiO_2	Al_2O_3	
Fly ash (S)	9.24	3.4	12.64
Fluidised bed waste (ZFZ)	12.84	4.62	17.46
Metakaolinite (MU)	21.19	17.66	38.85

3. SAMPLE PREPARATION

The reference samples of autoclaved materials were obtained from the mixture of basic raw materials which were mixed at the molar ratio $CaO:SiO_2=0.83$. This value shows stoichiometric relations of both oxides in tobermorite. These raw materials, i.e. silica powder and burnt lime underwent the process of homogenization, at first without water and then with the appropriate amount of water. Water was added to the mixture of solid components in the amount necessary to slake the burnt lime component and to guarantee an increase in humidity until the weight ratio w/s = 0.2 was obtained. The mixture composition shown above was modified with an appropriate amount of a mineral additive. In most cases the amount of mineral additives introduced was 20% in relation to the total mass of solid components, although in the case of metakaolinite MU it was 2%. Chemical activators in the form of gypsum and anhydrite constituted 1% of the total mass of solid components. Alkalis, in turn, were introduced together with make-up water containing the dissolved equivalent amounts of NaOH, Na_2CO_3 or KOH, which, calculated respectively by Na_2O and K_2O constituted 5% of the solid components of the mixture.

After the process of homogenization was completed, each mass thus obtained was placed in a hermetic container in a laboratory drier at 60°C for 4 hours with the aim of slaking burnt lime. Following this treatment, the process of homogenization was resumed and afterwards samples were formed with the use of a press. The cylinder-shaped samples had the following parameters: d x h = 25 x 25 mm. The process of sample pressing was two-stage, i.e. pressing pressure was respectively 10 and 20 MPa including interstage deaeration. The prepared samples were subsequently treated under hydrothermal conditions. Autoclaving took place at 180°C for 8 or 72 hours for mineral additive-free samples, and 8 hours only for the samples containing additives.

4. STUDY RESULTS

4.1 Physical properties of autoclaved materials

The influence of pozzolanic mineral additives on the quality of autoclaved materials was estimated on the basis of the analysis results of the primary physical characteristics. Thus in the course of a study, compressive strength R_c as well as volume density C_0 were established. The results are shown in Table 2.

The data obtained clearly indicate that when only a pozzolanic mineral additive is introduced into the lime/silica mixture, it does not result directly in the strength improvement of the autoclaved materials obtained. Only when it is combined with additional chemical activators, can we observe a significant increase in strength.

4.2 Phase composition analysis of materials obtained.

The mineral composition of autoclaved materials in question was determined by means of XRD analysis with the use of a Philips PW 1040 diffractometer. XRD patterns were examined for the

angle range 2θ = 5 to 55°. The interpretation of the XRD diffraction spectrums was carried out in accordance with ICPDS data. The results of phase composition analysis is presented in Figure 1 in the form of all XRD patterns for the samples of additive-containing autoclaved materials with chemical activation, which were compared with reference samples. The abbreviations used in the diagram stand for the following: Q-quartz; CH- calcium hydrate; CSH- calcium silicates hydrate, type C-S-H (I) or C-S-H (II); CC- calcium carbonate; AN- anhydrite.

Table 2. Physical properties of autoclaved materials obtained

Sample symbol	Type of mineral additive	Type of chemical admixtures	Type of property studied	
			compressive strength R_c, MPa	density C_0, kg/m^3
T / 8	-	-	53,8	1475
S – 20	Fly ash (S) (20 wt. %)	-	35.1	1592
S – G		Gypsum (1 wt. %)	49.1	1643
S – AN		Anhydrite (1 wt. %)	49.8	1557
S – NH		NaOH (5 wt. % eqw. Na_2O)	104.6	1834
S – KH		KOH (5 wt. % eqw. K_2O)	85.1	1783
S - NC		Na_2CO_3 (5 wt. % eqw. Na_2O)	96.2	1805
ZFZ - 20	Fluidal waste (ZFZ) (20 wt. %)	-	27.3	1549
ZFZ– G		Gypsum (1 wt. %)	38.2	1445
ZFZ – AN		Anhydrite (1 wt. %)	45.5	1549
ZFZ – NH		NaOH (5 wt. % eqw. Na_2O)	70.6	1659
ZFZ – KH		KOH (5 wt. % eqw. K_2O)	75.1	1790
MU – 2	Metakaolinite (MU) (2 wt. %)	-	35.1	1404
MU – G		Gypsum (1 wt. %)	37.6	1393
MU – AN		Anhydrite (1 wt. %)	39.6	1399
MU – NH		NaOH (5 wt. % eqw. Na_2O)	100.6	1742
MU – KH		KOH (5 wt. % eqw. K_2O)	54.2	1623
MU - NC		Na_2CO_3 (5 wt. % eqw. Na_2O)	79.3	1617

In Figure 1 only the fragments of XRD patterns for the angle range 2θ = 15 to 40° were presented, these being the most interesting ones as far as the observed changes are concerned. The above-mentioned angle range comprises first of all the area of lines typical of the products being formed in the course of synthesis occurring at 180°C under hydrothermal conditions, as well as the highest intensity reflections coming from the reaction substrates. Thus, within the angle range mentioned the presence of a reaction product being formed as C-S-H phase can be corroborated on the basis of the highest intensity lines for the distance d = 0.3070 nm (2θ=29.09°). Similarly, the presence of reaction substrates in the form of quartz is detected due to reflections occurring when d = 0.4255 (2θ=20.88°), 0.3344 (2θ=26.66°), 0.2457 (2θ=36.58°) and 0.2283 (2θ=39.48°)nm (according to ICPDS file no. 33-1161). The presence of the unreacted calcium hydrate is corroborated by the lines occurring when d = 0.4902 (2θ=18.10°), 0.3115 (2θ=28.66°), 0.2625 (2θ=34.16°) and 0.2445 (2θ=36.76°) nm (according to ICPDS file no. 4-733). While comparing individual XRD patterns, one can easily notice considerable similarity, which may testify to a very similar mineral composition of the materials obtained, among which the dominant product is C-S-H phase.

However, after the in-depth intensity analysis of the appropriate reflections originating from the starting materials as well as the analysis of shape and intensity of the line coming from the main reaction product, an essential observation can be made. The additional chemical activation leads to an increase in the reaction rate; higher effectiveness, however, is connected with alkalis rather than with sulfates. The results of compressive strength analysis of the samples support this. It can be

seen from the results that the samples of alkali-activated materials exhibit the best strength properties (Table 2 data).

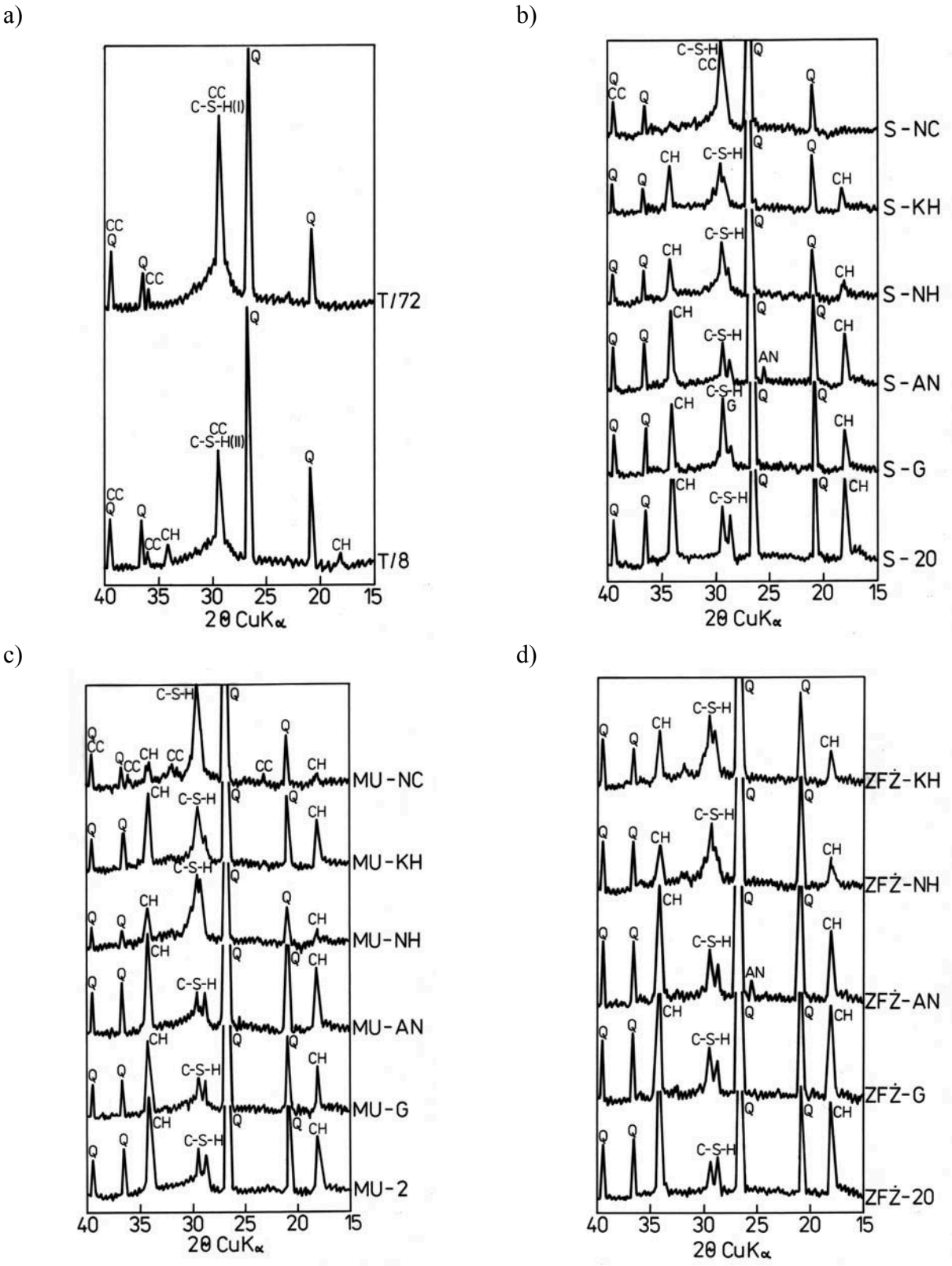

Figure 1. Analysis results of mineral composition of autoclaved materials
a) XRD pattern of reference sample (molar ratio C/S=0.8)
b) XRD patterns for fly ash (S) samples
c) XRD patterns for metakaolinite samples (MU)
d) XRD patterns for fluidised bed waste samples (ZFŻ)

4.3 Porosity analysis of autoclaved materials

Microporosity analysis was conducted by means of mercury porosimetry with the use of a Carlo-Erba PO-225 porosimeter. The measurements were taken for the mercury pressure range 0.1 to 200 MPa. Figure 2 presents the microporosity analysis results for the samples of autoclaved materials in the form of curves showing pore size distribution in the samples containing a mineral additive, in comparison to T/8 reference sample.

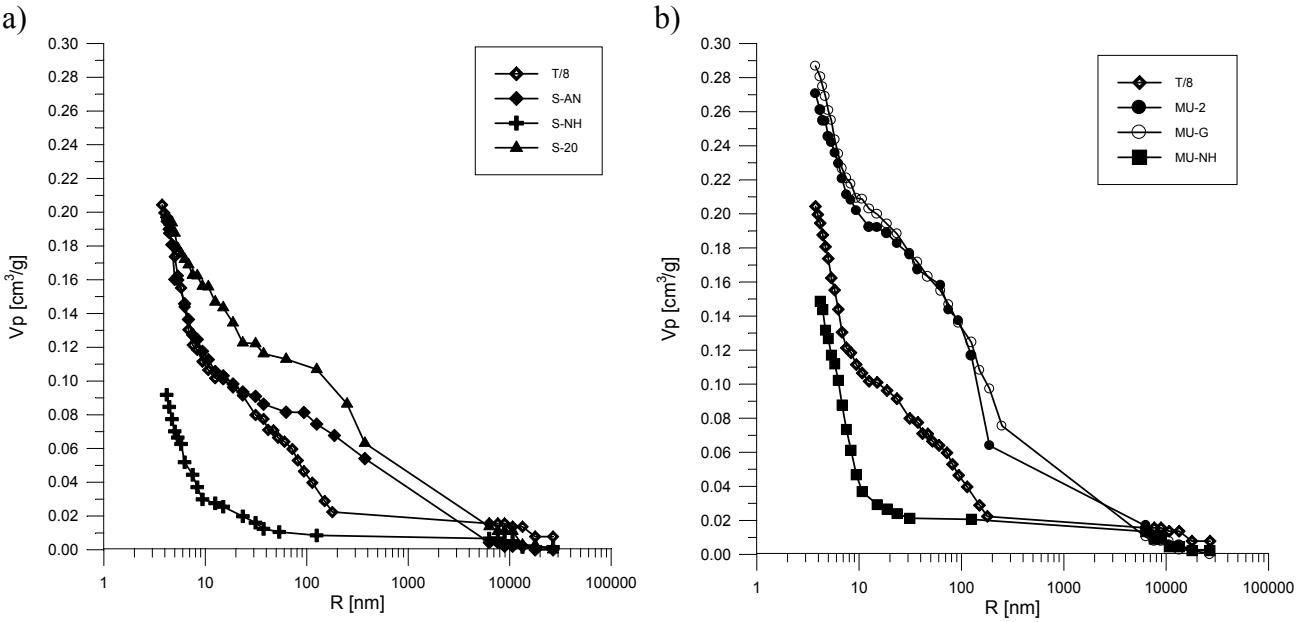

Figure 2. Pore size dystribution
a) samples containing fly ash (S)
b) samples containing metakaolinite (MU)

When comparing the curves showing the size distribution of pores in T/8 sample and in the samples of S and MU series, it can be stated that the introduction of a mineral additive into the quartz sand/lime mixture (molar ratio C/S = 0.83) without additional chemical activation did not result in any considerable changes in the structure of pores, both capillary and gel-like. An entirely different effect is observed in the additive-containing samples that were activated by alkali and sulfate ions. The detailed analysis indicated that the general porosity of these samples decreased and the structure of pores changed. It was observed that the volumetric participation of capillary pores decreased for the radius range 10 to 50 nm, whereas gel-like pores were on the increase. The latter type of pores is connected with the formation of an additional amount of C-S-H phase. The afore-mentioned tendency of changes in porosity is supported by the volume density values of the analyzed materials.

4.4 Microstructure analysis of autoclaved materials

In order to explain the differences occurring in the microstructure of the autoclaved materials in question, related to the presence of pozzolanic mineral additives as well as to the type of chemical activation used, the samples of the materials obtained were observed by means of scanning microscopy. For research purposes, a JSM 5400 scanning microscope was used produced by JEOL), which was equipped with a microanalyzer of XRD dispersion – EDS-Oxford Instruments LIKN-ISIS (serial number 300). The typical microstructure picture of an autoclaved material obtained from quartz sand/lime mixture with molar ratio C/S = 0.83 (T/8 reference sample) is shown in Figure 3, whereas the microstructure changes of autoclaved materials modified with mineral additives can be seen in Fig. 4. The influence of pozzolanic mineral additives as well as individual

types of chemical activation on the microstructure of the materials were presented on the basis of the sample series containing fluidised bed waste (ZFŻ).

a) b)

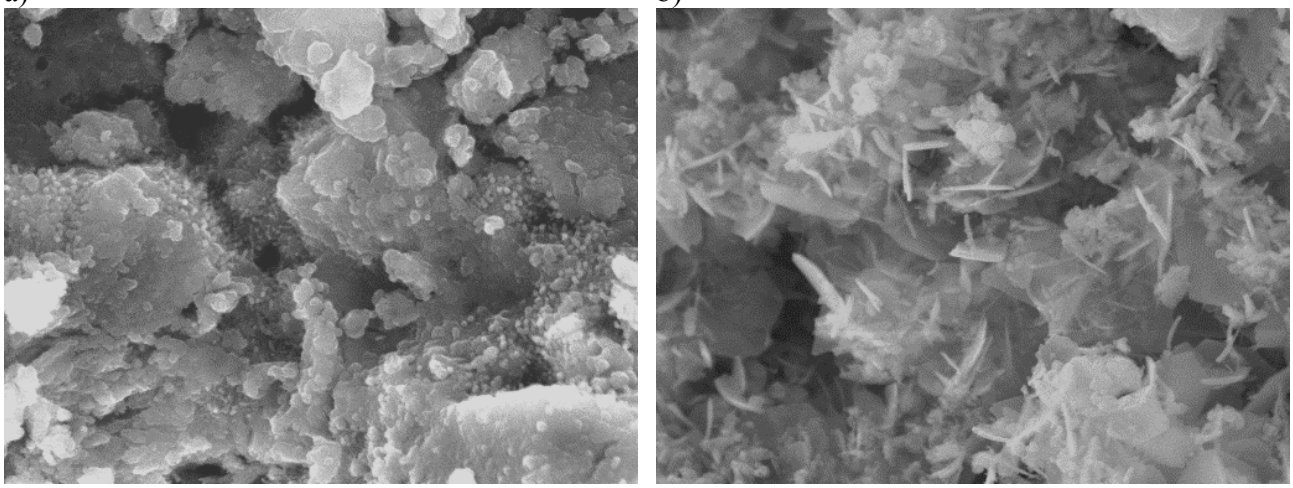

Figure 3. Microstructure of autoclaved material without mineral additives
a) sample obtained in 8-hour synthesis (T/8 sample)
b) sample obtained in 72-hour synthesis (T/72 sample)

While analyzing the microstructure pictures seen in Figure 3, it can be stated that the forming microstructure of the autoclaved materials results from the presence of a basic product of synthesis occurring under hydrothermal conditions, i.e. amorphous C-S-H phase with molar ratio C/S = 0.8 to 1.0. When this product is formed in the systems that are not activated additionally, it appears in its typical sponge-like form, known as “honeycomb”. However, with the prolonged time of synthesis, it shows tendency to the formation of crystalline tobermorite. This phenomenon is directly connected with the structure of the pores present in this type of material. Two main categories of pores can be distinguished, namely capillary pores (connected with the method of cast profile formation), and gel-like pores, typical of the synthesis products being formed, especially C-S-H phase.

When pozzolanic mineral additives are introduced into the quartz sand/lime mixture in the above-mentioned amounts, it leads, in the course of a pozzolanic reaction, to the formation of additional amounts of products such as hydrated silicates and calcium aluminosilicates, which slightly modifies the microstructure of the autoclaved materials obtained. The further changes in the microstructure of the materials are expected after small amounts of sulfates or alkalis are introduced into the system in the course of reaction. These changes are clearly seen in Figure 4, where the main product of a hydrothermal reaction, i.e. C-S-H phase, adopts various morphological forms (with dominant oblong-shaped forms) under the influence of chemical activation, particularly by alkalis.

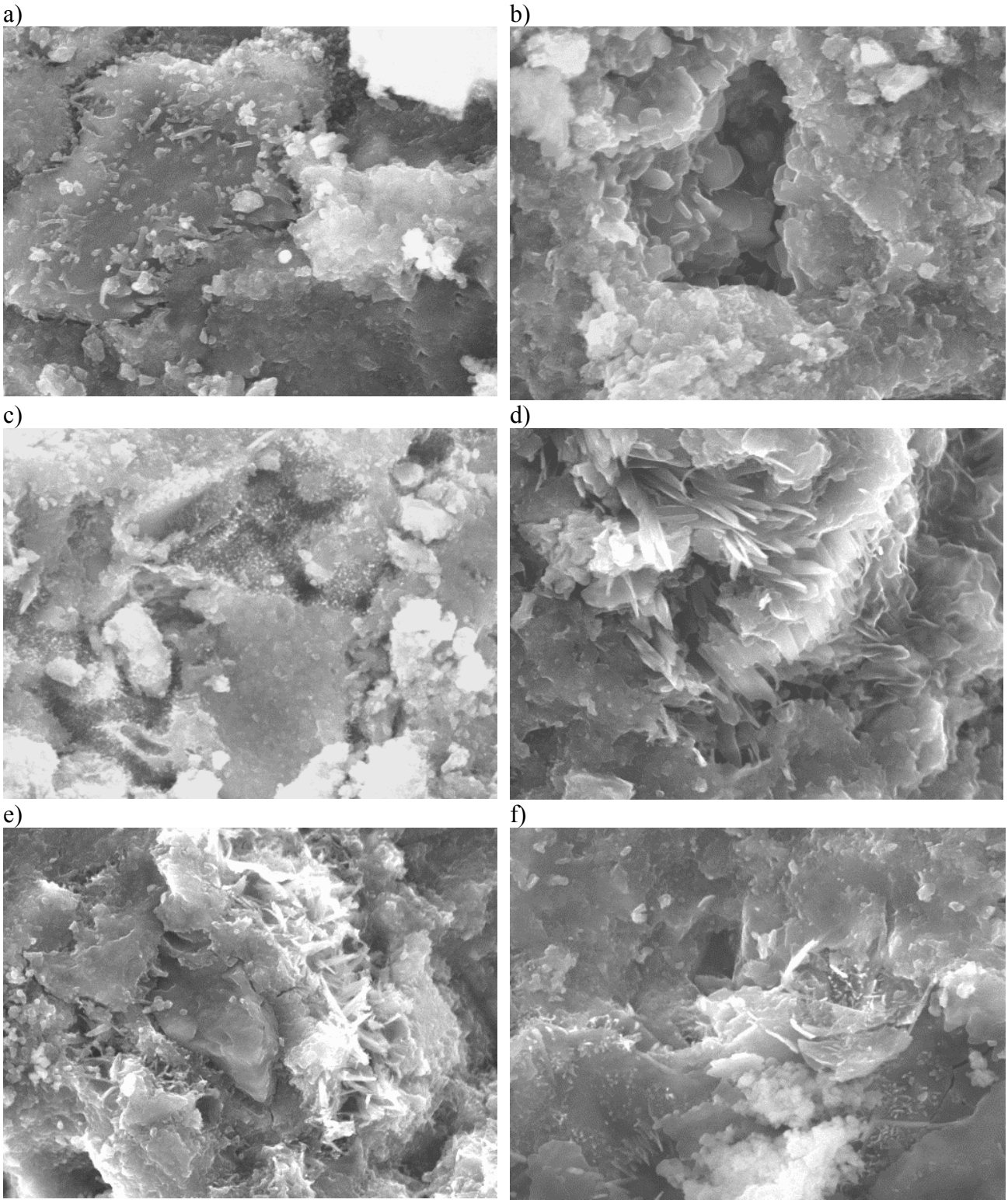

Figure 4. Microstructure of autoclaved materials with fluidal waste additive
a) microstructure of sample ZFZ-20 b) microstructure of sample ZFZ-G
c) microstructure of sample ZFZ-AN d) microstructure of sample ZFZ-NH,
e) microstructure of sample ZFZ-KH f)microstructure of sample ZFZ-NC

5. SUMMARY

When taking into account the configuration of interrelated factors that determine the structure and microstructure of the autoclaved materials in question, it must be stated that we can influence their practical properties to some extent by means of pozzolanic mineral additives. As can be seen from the research results, the introduction of such additives into quartz/lime mixture (molar ratio C/S = 0.83) combined with chemical activation by sulfate or alkali ions, exerts a positive influence on the strength properties of the autoclaved materials.

The strength development/increase of the samples that was observed, results from the fact that during the pozzolanic reaction the additional amounts of products (hydrated calcium silicates of amorphous C-S-H phase type) are formed. It is also due to the favourable modification of the morphological forms of this product, which is caused by the presence of the accessory ions in the product structure.

C-S-H phase being formed during a synthesis of short duration and without additional activation usually occurs in its typical sponge-like form (Figure 3a), whereas in the presence of chemical activators, particularly alkalis, it tends to develop oblong and more compact forms. This has an essential influence on the structure of pores in the material.

These observations can be corroborated by the porosity analysis results of the materials obtained (Figure 2). According to these results, chemical activation by means of alkalis, and to a lesser extent sulfate ions, contributes to a decrease in porosity in general as well as to the changes in porosity structure. The above-mentioned changes concern mostly a decrease in the volumetric participation of capillary pores in favour of gel-like ones. The direction of these changes can be rationally explained when taking into account the physical and chemical aspects of the additives function.

As far as the physical impact of pozzolanic additives is concerned, they function as micro-aggregate, which due to considerable size reduction exerts an influence on the resultant curve of grain-size distribution of the raw mixture in the process of pressing. However, the influence of pozzolanic mineral additives on the quality of autoclaved materials should be discussed mainly from the chemical point of view, as an active chemical admixture. Active SiO_2 and Al_2O_3 forms, pozzolans bound/set in amorphous phases, react in solution with calcium ions. As a result, the formation of products takes place, the structure of which shows some similarity to the typical products of pozzolanic cements hydration. The main representative of these products is amorphous C-S-H phase (Figure 1), the structure of which normally contains gel-like pores. When the additional amount of this phase is formed in the course of a pozzolanic reaction in hydrothermal conditions, at a much higher reaction rate, it contributes to an increase in this type of pores (diameter range 5÷10nm).

A wealth of information is also provided by the analysis results of phase composition of the materials; the results were obtained with the use of XRD diffraction. These data confirm the earlier observations, namely that additional chemical activation leads to an increase in substrates consumption rate. Such a conclusion can be drawn on the basis of the growing intensity of the reflex coming from the main product of synthesis in hydrothermal conditions, with the simultaneous decrease in lines typical of reaction substrates. It can be clearly seen from the above-mentioned data that as a result of the introduction of pozzolanic mineral additives, no considerable qualitative changes in the materials are observed, as the dominant product is, in each case, amorphous or semi-crystalline C-S-H phase (molar ratio C/S = 0.8 to 1.0) present in various morphological forms. There are, however, quantitative changes.

A good confirmation of the above-mentioned conclusions are the results of the microstructure observations of the materials in question, which were obtained by means of scanning microscopy. The analyzed patterns of microstructures for the fluidal waste samples series (ZFŻ), shown in Figure 4, point to the changes caused mainly by a type of activator used.

ACKNOWLEDGMENT

This work is performed with financial support by the Polish Scientific Research Committee under Grant No 7 T08D 02815.

REFERENCES

[1] G.E. Van Derburgh, British Pat. No. 2470 (1866).
[2] W. Michaelis, German Pat. No. 14195 (1880).
[3] H.F.W. Taylor, "The Chemistry of Cements", Academic Press, London (1964).
[4] H.F.W. Taylor, D.M. Roy, Proc. the 7th Int. Congr. Chem. Cem., Paris, Vol. I, p. II-2/1, Paris (1980).
[5] H.F.W. Taylor, "Cement Chemistry", Academic Press, London (1990).
[6] T. Mitsuda, S. Kobayakawa, H. Toray, Proc. the 8th Int. Congr. Chem. Cem., Rio de Janeiro, Vol. II, p. 173, Rio de Janeiro (1986).
[7] G.L. Kalousek, J. Am. Ceram. Soc., 40 (1957), p. 74.
[8] S. Diamond, J.L. White, W.L. Dolch, Amer. Min., 51 (1966), p. 388.
[9] J.M. Crennon, J.R.L. Dyczek, H.F.W Taylor, CCR 2 (1972), p. 277.
[10] J.R. Sersale, Proc. the 7th Int. Congr. Chem. Cem., Paris, Vol. I, p. IV-1/3, Paris (1980).
[11] Z. Pytel, J. Małolepszy, Pro. 3rd Int. Conf. WASCON 2000, Leeds, UK, Edited by G.R. Wooley, J.J.J.M. Goumans, P.J. Wainwright, Pergamon, Volume I, pp. 371÷382.
[12] N.C. Ludwig, S.A. Pence, J. Amer. Constr. Inst. **52** (1956), p. 673.
[13] H.F.W. Taylor, Proc. the 5th Int. Congr. Chem. Cem. Tokyo, Vol. II, p. 1, Tokyo (1968).
[14] W. Kurdowski, M. Pilch, Proc. the 9th Int. Congr. Chem. Cem. New Delhi, Vol. IV, p. 170, New Delhi (1992).
[15] J.A. Voinovitch, R. Dron, Silicates Ind., 41 (1976), p. 209.

PROPERTIES OF ACTIVATED PASTES CONTAINING METAKAOLIN AND OTHER MINERAL ADDITIVES

J. Deja[1]

[1]Faculty of Materials Science and Ceramics,
University of Mining and Metallurgy, Cracow, Poland
E-mail: deja@uci.agh.edu.pl

ABSTRACT

By-products as pozzolanic additions are now routinely used for the production of high-performance concrete. Recently some activated materials such as metakaolin have been shown to be excellent pozzolans.

Alkaline activation of metakaolin as well as mixtures of metakaolin, Portland cement, granulated blast furnace slag make it possible to produce very dense and high strength materials. The products formed in the alkaline activation reaction of metakaolin and its mixtures strongly depend on what type of activator is used. In the study described, properties of metakaolin pastes were determined after 3, 28, 90 and 180 days.

The influence of OPC, $Ca(OH)_2$, GBFS, $CaSO_4 \cdot ½H_2O$ and NaOH on the mechanical strength, microstructure and phase composition of the pastes was measured.

The most interesting properties were observed for metakaolin paste activated by mixture of OPC, gypsum and calcium hydroxide. Concentration of NaOH plays also very important role in the formation of dense microstructure. The pastes containing slag with higher glassy phase and Al_2O_3 content achieved significantly better mechanical properties.

The influence of curing conditions (natural, low pressure steam curing and autoclaving) on the mechanical properties and microstructure of the pastes was also very visible.

For samples cured in low-pressure steam conditions and autoclaved, the average pore radius is significantly lower.

XRD tests and SEM observations indicate that besides the C-S-H gel phase some amounts of amorphous alkaline aluminosilicates are present in activated pastes.

1. INTRODUCTION

Making newer and better materials is an inevitable process related to development of civilisation. In recent years, the research on the possibility of obtaining binders based on chemically activated metakaolinite has been intensified. Application of calcined clays as pozzolanic additive makes it possible to significantly alter the properties of the produced binders [1-5]. Their properties depend on the applied components, type and amount of the activator and curing conditions. Good activators of metakaolinite include calcium hydroxide, Portland cement or sodium hydroxide.

Water glass or gypsum may also be used as additional components. Numerous studies revealed that the metakaolinite activation involving sodium hydroxide requires an appropriate concentration of this substance [3, 5, 6]. Other factors that have an impact on the metakaolinite activation process are the temperature of kaolin clay calcinations and the curing temperature of hydrating pastes.

Application of appropriately high temperatures may contribute to the formation of additional phases. One of the binders that has recently been a subject of broad research includes so called alkali-activated slag binders that are composed of natural or artificial aluminosilicates activated by appropriate alkaline activators [7-9]. The production of hydraulic clinker-free binding materials combines the environmental and economic aspects. It is related to both the use of slags that are industrial waste and reduced power consumption in comparison with the production process of Portland cement. Appropriate activation of vitrified calcium and magnesium aluminosilicates gives a binding material that features high strength and resistance to chemical attack. A group of binders of this type includes so-called geocements containing metakaolinite [10, 11].

Alkaline activation of metakaolinite produces an inorganic polymer of good mechanical properties. Formation of this binder may be compared to the synthesis of zeolites. The structure of these materials consists of a three-dimension framework composed of SiO_4 and AlO_4 tetrahedrons bound together by common oxygen. The alkaline metal cation deriving from the added activator compensates for insufficient charge of aluminium. The difference, in comparison with the synthesis of zeolites, is the form in which it occurs - the alkaline activation of metakaolinite leads to the formation (in most cases) of the amorphous phase [5, 12, 13].

The materials of this type, apart from high strength, are resistant to the exposure to low and high temperatures, feature low shrinkage and a high resistance to corrosive attacks, as well as the ability to bind heavy metals and immobilise other noxious substances.

The objective of the conducted tests was to determine the properties of activated slag-cement-metakaolinite pastes. These tests included, but were not limited to, checking of strength properties of the samples with different activators added, the influence of curing conditions and testing of phase composition and microstructure of pastes.

2. EXPERIMENTATION

2.1 Characteristics of the applied materials

The tests involved the following raw materials: kaolin clay, crushed granulated blast-furnace slag, CEM I 32,5 R Portland cement, quick lime, β semi-hydrate gypsum.

2.1.1 Metakaolinite

Metakaolinite was obtained by roasting kaolin clay at high temperatures. For the requirements of this research, kaolin clay of the chemical composition presented in Table 1 was used to obtain this material.

Table 1. Chemical composition of kaolin clay.

Component	Share [mass %]
SiO_2	53.20
Al_2O_3	32.80
Fe_2O_3	0.55
TiO_2	0.45
CaO	0.30
MgO	0.25
K_2O	0.60
Na_2O	0.20
L.O.I.	11.6

The clay was calcined in different scenarios in the following environments:

750^0C for 24 h – denoted as MK1 or 850^0C for 2 h – denoted as MK2

Application of kaolin clays initially roasted in different conditions (750^0C and 850^0C) was aimed at testing the impact of the temperature of this process on the activity of metakaolinite.

2.1.2 Ground granulated blast-furnace slag

Two types of ground-granulated blast furnace slags were used in the research i.e. the Polish slag from Huta Sendzimira [Sendzimira Steelworks] (hereinafter denoted as SP) and the British slag from Scunthorpe (hereinafter denoted as SE). Chemical composition of slags is summarised in Table 2.

Table 2. Chemical composition of slags.

Component	Share [mass %]	
	SP slag	SE slag
SiO_2	38.8	35.7
Al_2O_3	7.1	12.6
Fe_2O_3	1.5	0.7
CaO	44.2	39.5
MgO	6.4	8.4
Others	2.0	1.69
Glass content	87	97

2.1.3 Portland cement

Another component applied to make pastes was CEM I 32.5 R Portland cement (according to EN – 197-1). The specific surface of cement was 310 m^2/kg (according to Blaine).

2.1.4 Quick lime and gypsum

A commercial product – quick lime (denoted as CH) and β semi-hydrate $CaSO_4$ were used in the research (denoted as G).

2.1.5 Alkaline activators

NaOH solutions (concentration: 5M, 12M and 15M) and sodium water glass with silicate modulus of 1.5 (denoted as WG) were used as alkaline activators.

2.1.6 Superplasticizer
Melamine-naphthalene superplasiticizer was used in the preparation of the pastes.

2.2 Characteristics of prepared pastes
The applied denotations of specific pastes and their compositions are summarised in Table 3.

Table 3. Denotations and compositions of specific pastes.

No.	Type of component [mass %]									SP	W/S
	MK1	MK2	CEM	SP	SE	G	CH	NaOH	WG		
1	50	-	50	-	-	-	-	-	-	3	0.45
2	45	-	-	-	45	-	5	-	5	3	0.45
3	45	-	-	45	-	-	5	-	5	3	0.45
4	45	-	45	-	-	5	5	-	-	3	0.45
5	40	-	-	-	45	-	10	-	5	3	0.45
6	40	-	-	-	45	-	10	5(12M)	-	3	0.45
6A	40	-	-	-	45	-	10	5(5M)	-	3	0.45
6B	40	-	-	-	45	-	10	5(15M)	-	3	0.45
7	-	50	50	-	-	-	-	-	-	3	0.45
8	-	45	-	-	45	-	5	-	5	3	0.45
9	-	45	-	45	-	-	5	-	5	3	0.45
10	-	45	45	-	-	5	5	-	-	3	0.45
11	-	40	-	-	45	-	10	-	5	3	0.45
12	-	40	-	-	45	-	10	5(12M)	-	3	0.45

The pastes were cured at $+20^0$C and relative ambient humidity of approximately 60%.

In order to determine the impact of curing conditions upon the properties of pastes, the samples marked as 6A and 6B underwent the process of low-pressure steam curing (4-2-6-2 cycle at the maximum temperature of 70ºC) or 6-hour autoclaving at the temperature of 180ºC.

3. RESULTS

The strengths of pastes were tested within the range of 1-180 days. The results of strength testing of the samples cured in natural conditions are presented in Figures 1 and 2.

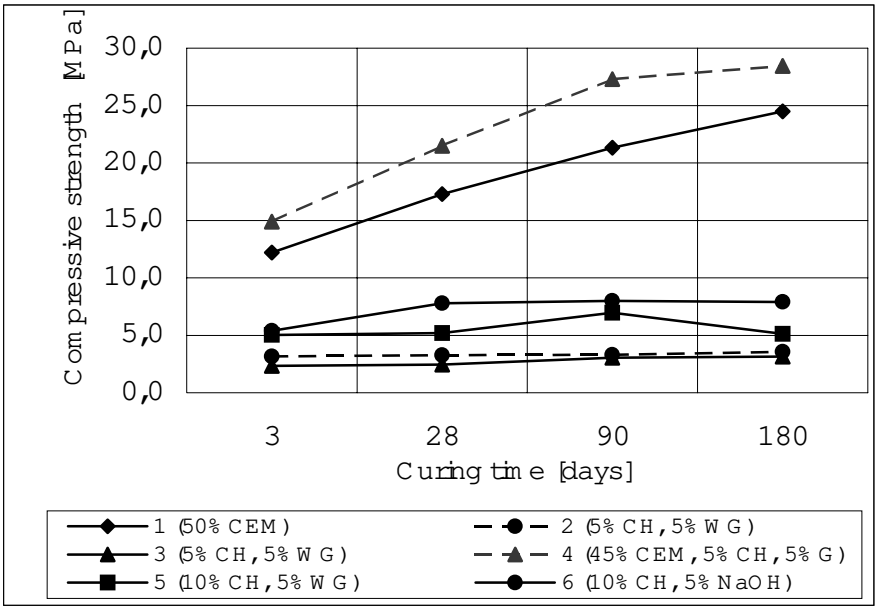

Figure1. Compressive strength of the samples containing different activators (clay calcination temperature - 850^{0}C)

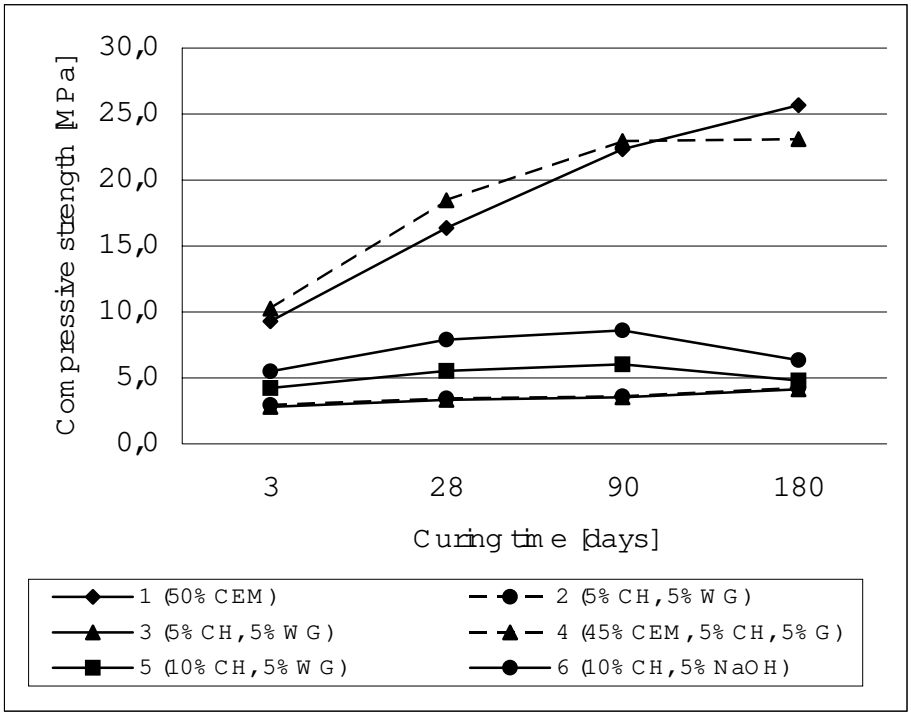

Figure 2. Compressive strength of the samples containing different activators (clay calcination temperature - 750^{0}C)

It is clear that the samples containing cement feature considerably higher mechanical strengths compared with "cement-free" samples. Addition of gypsum to the cement-containing samples causes a conspicuous increase in strength. It is also observed that the strength gain over time for "cement-free" mixtures is low. In some cases, the latter even demonstrate slight drops of strength after 180-day curing.

It may be observed that in most cases the impact of the temperature of initial kaolin clay treatment upon the strength of paste is negligible; it pertains mainly to "cement-free" pastes. In the case of samples that contain cement (nos 1 and 7 as well as 4 and 10), these differences are much more significant. These pastes, based on the clay calcined at the higher temperature, featured higher

strengths than the analogous samples containing clay calcined at the temperature of 750^0C. Thus, one may assume that the thermal treatment temperature did not impact their pozzolanic activity to a significant extent. On the basis of the conducted tests, it is possible to conclude that the slag-containing samples of higher contents of Al_2O_3 (SE) feature higher compressive strengths than analogous pastes prepared on the basis of the SP slag (lower Al_2O_3 content).

3.1 Impact of activator type on the microstructure and phase composition of pastes

The microstructure testing of hardened pastes was conducted using a scanning microscope for each type of mixture. The phases that occurred were identified by means of the EDS analysis.

The selected average pictures of the microscope observation are presented in Figures 3-5. A basis phase that occurs in all mixtures is an amorphous C-S-H phase. Etringite crystals can be seen in the cement-containing pastes.

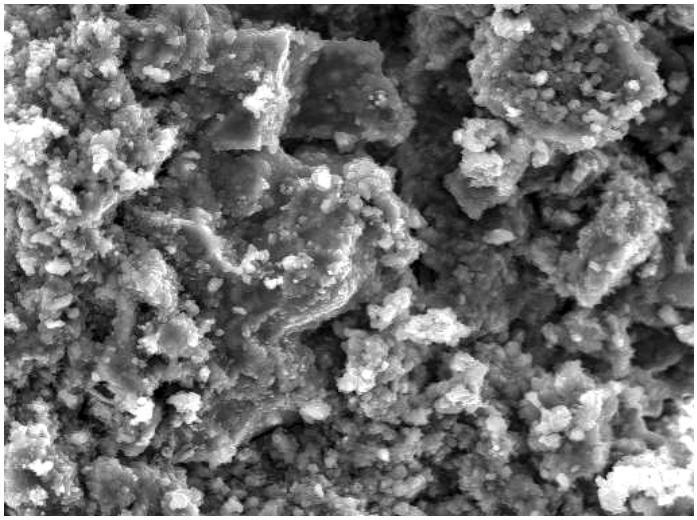

Figure 3. Microstructure of paste No. 1 - 50% MK, 50% CEM; amorphous C-S-H phase.

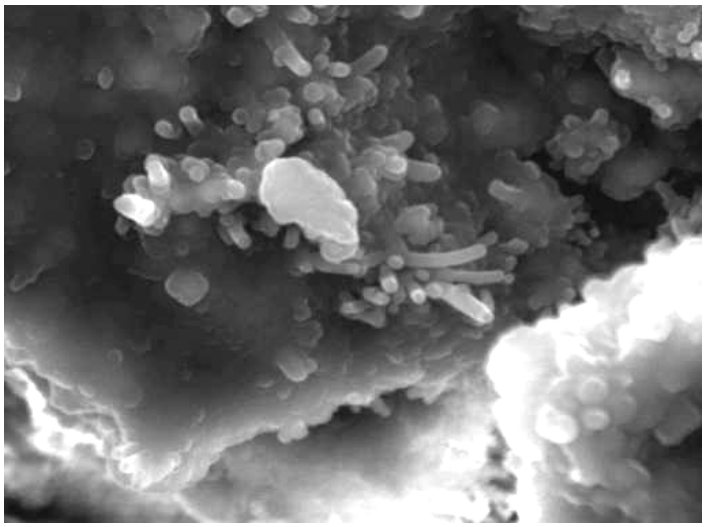

Figure 4. Microstructure of paste No.1 – etringite crystals

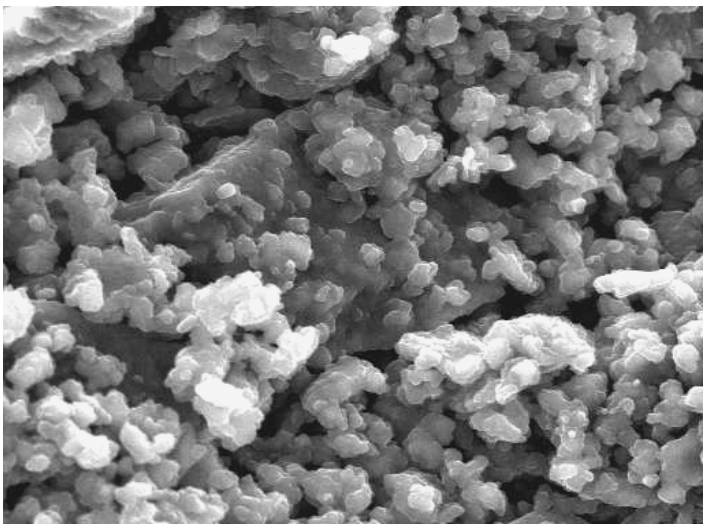

Figure 5. Microstructure of paste No. 3 – 45% MK1, 45%SP, 5% CH, 5% WG; amorphous C-S-H phase on the slag grains.

The X-ray test results (XRD) confirmed the observations conducted by means of the scanning microscope. XRD patterns of the pastes containing different activators are presented in Figure 6

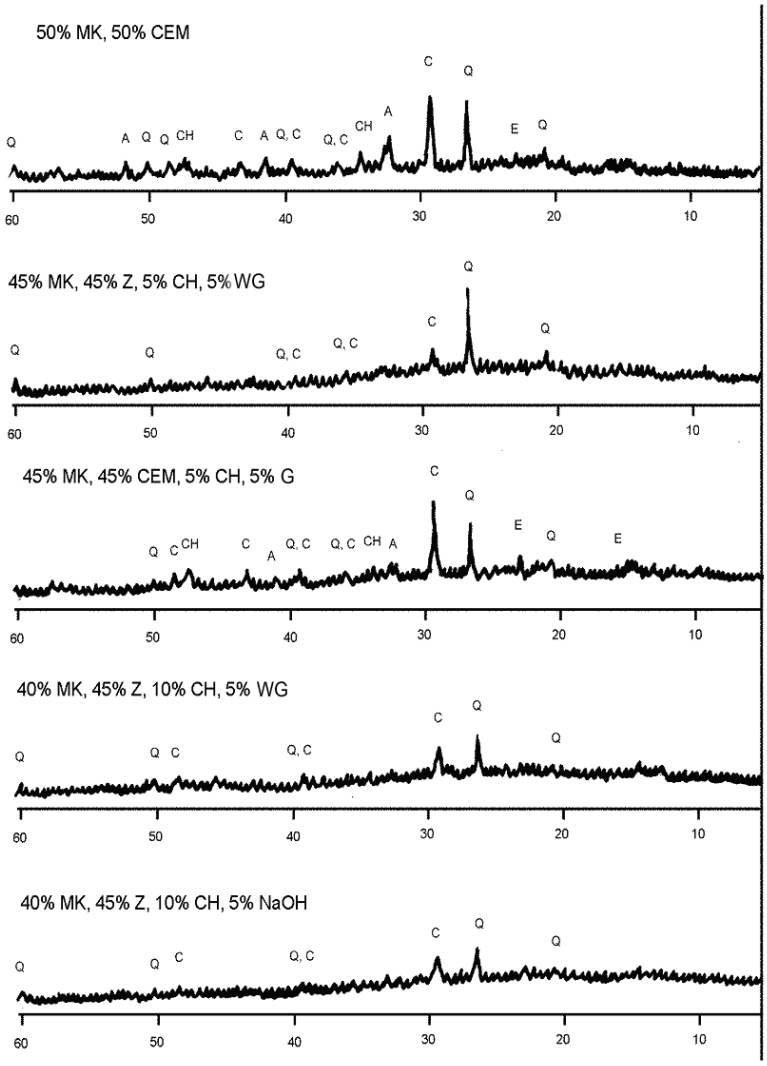

Figure 6. XRD patterns of the pastes (natural curing).

The following notations of phases are used in the figure: Q – quartz, CH – $Ca(OH)_2$, C – C-S-H ; $CaCO_3$, E – etringite, A – C_2S.

The hump in the XRD patterns indicates high contents of the amorphous phase in the tested samples.

3.2 Impact of alkaline activator concentration and curing conditions on the strength properties of pastes

Table 4 presents the strengths of activated NaOH pastes of different concentration and cured in different conditions.

Table 4. Influence of NaOH concentration and curing conditions on the strengths of pastes.

Type of paste	Compressive strength [MPa]			
	3 days	28 days	90 days	180 days
6 (natur)	5.4	7.8	8.0	7.9
6 (low press)	6.8	8.8	9.2	10.1
6 (autocl)	8.3	9.4	10.2	11.8
6A(natur)	5.0	7.0	7.2	7.3
6A (low press)	6.1	8.1	8.4	8.6
6A(autocl)	7.5	8.9	9.6	10.2
6B (natur)	6.4	8.9	9.4	10.3
6B(low press)	9.2	10.2	11.1	12.0
6B (autocl)	12.1	13.6	14.2	16.8

On the basis of the presented data, one may conclude that the concentration of the alkaline activators has an impact upon the properties of tested pastes. The samples activated with a 15M solution of NaOH featured higher strength than analogue pastes containing 5M and 12M activator.

It may be concluded that the samples that were steam cured or autoclaved featured higher mechanical strength than naturally cured samples. It pertains to both "cement-free" pastes as well as cement-containing samples.

The rise of the curing temperature of pastes also resulted in certain alterations of the microstructure view. The intergrain boundaries between the hydrating grains of slag and metakaolinite were significantly blurred and considerable amounts of the C-S-H of the "honey comb" type phases as well as some amounts of sodium zeolites occurred.

3.3 Impact of curing conditions on the porosity of pastes

The testing of pore size distribution was made by means of the mercury porosymetry. The tested 6A pastes were subject to natural curing, low pressure steam curing and autoclaving. Figure 6 presents the comparison of the pore size distribution for the three mentioned types of pastes.

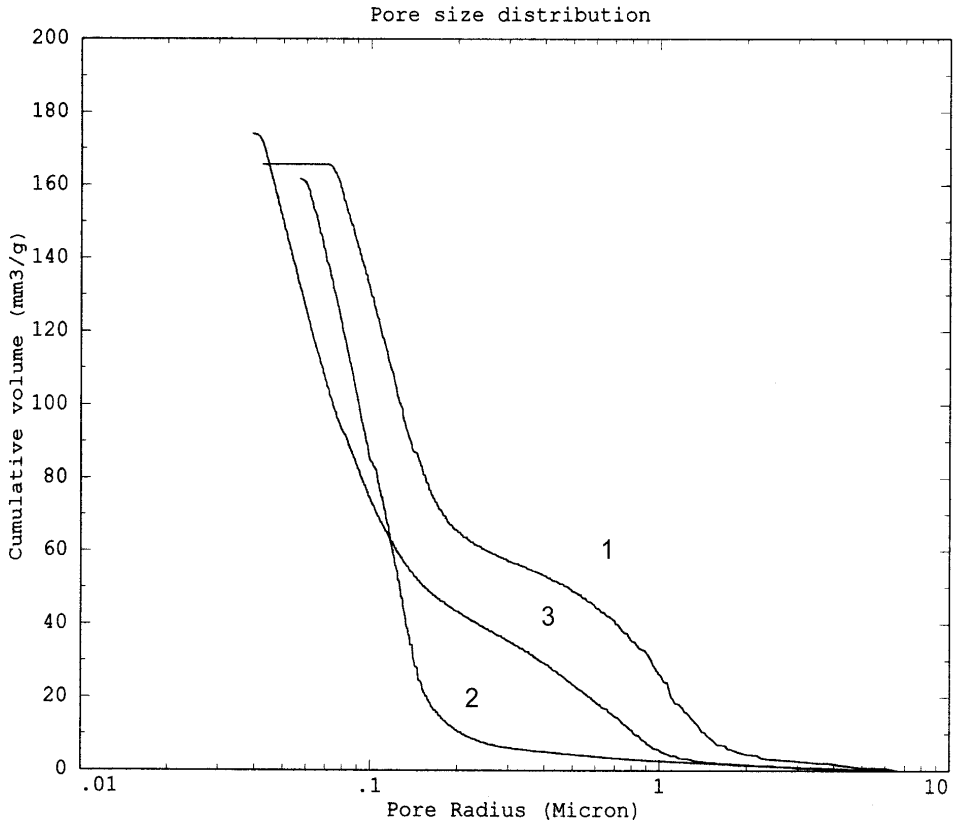

Figure 7. Pore size distribution for paste 6A: (1) - natural curing; (2) – low pressure steam curing; (3) - autoclaving.

The testing showed that the total porosity is comparable for all the samples. The temperature increase contributed to a reduction of the number of capillary pores. These differences pertain also to the average pore sizes that were 124.229 nm (natural curing), 120.249 nm (steam curing) and 55.462 nm (autoclaving), respectively.

4. CONCLUSIONS

[1] The testing confirmed the possibility of application of chemically activated metakaolinite as a slag and slag-cement binder component.
[2] Application of alkaline activator (NaOH) of the higher concentration resulted in a significant growth of paste strength.
[3] The pastes containing a several-ten-percent addition of Portland cement featured the highest strengths. The best mechanical properties were obtained for the mixtures containing 45% metakaolinite and cement and 5% of calcium hydroxide and gypsum.
[4] A major product of the reaction of naturally cured pastes was the C-S-H amorphous phase.
[5] The increase of the initial curing temperature (steam curing or autoclaving) leads to a significant (several-ten percent) growth of compressive strength of pastes and forming of the C-S-H I phase, calcium aluminosilicates and zeolites. Autoclaving of pastes resulted also in a two-fold reduction of an average pore radius.

REFERENCES

[1] P.S. De Silva, F.P. Glasser, Pozzolanic activation of metakaolin, Advances in Cement Research, 1992, 4, No. 16.

[2] P.S. De Silva, F.P. Glasser, Hydratation of cements based on metakaolin: thermochemistry, Advances in Cement Research, 1990, 3, No. 12.

[3] J. Cabrera, M.F. Rojas, Mechanism of hydratation of the metakaolin – lime – water system; Cement and Concrete Research 31 (2001) 177-182.

[4] J.N. Liu, M.R. Silsbee, D.M. Roy, Strength and hydratation of an activated alumino-silicate material, 10th ICCP, Gőteborg 1997.

[5] S. Alonso, A.Palomo, Calorimetric study of alkaline activation of calcium hydroxide – metakaolin solid mixtures, Cement and Concrete Research 31 (2001) 25-30.

[6] M. Murat, Hydratation reaction and hardening of calcined clays and related minerals: I. Preliminary investigations of mathakaolin, Cement and Concrete Research, 13 (2) (1983).

[7] V. D. Gluchowski, Alkali-Earth Binders and Concretes Produced with Them, Building Materials Institute, Kiev, USSR, 1979 (in Russian)

[8] J. Małolepszy, J. Deja, The Influence of Curing Conditions on the Mechanical Properties of Alkali Activated Slag Binders, Silicates Industriels 53 (11-12) (1988) 179-186.

[9] B. Talling, J. Brandstetr, Present state and future of alkali activated slag concretes, 3rd International Conference on Fly Ash, Silica Fume, Slag and Natural Pozzolans in Concrete, vol. 2, Tronheim, Norway, ACI SP 114, 1989, pp. 1519-1546.

[10] J. Davidovits, Alkaine cements and concretes: Properties of geopolymer cements, Proceedings of the first international Conference held at the Scientific-Research Institute on Binders and Materials named after V. D. Gluchowski, Kiev 1994.

[11] M.A. Mokhort, Formation of Structure and Properties of geopolymer cements, Proceedings of the first international Conference held at the Scientific-Research Institute on Binders and Materials named after V. D. Gluchowski, Kiev 1994

[12] Z. Pytel, J. Małolepszy, The influence of calcination conditions on the pozzolanic properties of kaolinite clay, CWB-3/99 (in Polish).

[13] F. Curcio, B.A. De Angelis, S. Pagliolcio, Metakaolin as pozzolanic microfiller for high-performance mortars, Cement and Concrete Research, Vol. 28. No. 6. 1998.

PROPERTIES OF ACTIVATED PASTES CONTAINING METAKAOLIN AND OTHER MINERAL ADDITIVES

J. Deja[1]

[1]Faculty of Materials Science and Ceramics,
University of Mining and Metallurgy, Cracow, Poland
E-mail: deja@uci.agh.edu.pl

Jan Deja

Born: 28. 07. 1955

1974-1979: University of Mining and Metallurgy, Cracow, Poland – student

1991: Ph.D.

1980: University of Mining and Metallurgy, Cracow
Faculty of Material Science and Ceramics, Department of Building Materials - scientific worker

Special Fields:
Binding materials and concrete technology. Technology of alkali-activated slag binders. Concrete durability.

Author or co-author of ca. 70 papers concerning binding materials and concrete technology. Many papers were presented during international conferences (for example: ACI/CANMET Conferences, ICCC).
Member of the Board of Polish Cement and Lime Association and President of the Board of "Polski Cement" Ltd. Member of Standing Committee 2 in CEMBUREAU (Brussels).

WATER PERMEABILITY OF SELF COMPACTING CONCRETE

Katrien Audenaert[1], Veerle Boel[1] and Geert De Schutter[1]

[1] Magnel Laboratory for Concrete Research, Ghent University,
Department of Structural Engineering,
Technologiepark-Zwijnaarde 9,
9052 Ghent, Belgium
E-mail: katrien.audenaert@rug.ac.be, veerle.boel@rug.ac.be, geert.deschutter@rug.ac.be

ABSTRACT

Self-compacting concrete (SCC) is a new kind of concrete that doesn't need any compaction. The two essential properties of SCC are a high flowability and a high segregation resistance obtained by a large amount of fine particles and the use of superplasticizers. It is known that the pore structure of SCC differs from the pore structure of traditional concrete. Many research programmes are already done concerning the fresh properties of SCC, but almost nothing is known about the durability of SCC. The durability of concrete is strongly affected by the water permeability, water absorption and capillary suction.

This project includes laboratory studies of the water permeability, water absorption and capillary suction of 7 SCC and 2 traditional concretes. A constant amount of cementitious materials (cement and filler), as well as a constant amount of water, sand and gravel was considered. The influence of the amount and type of cement and filler is studied (Portland cement, limestone filler, fly ash).
The results of this study are compared with models found in literature.

1. INTRODUCTION

Self-compacting concrete (SCC) was developed in Japan in the 1980's. The aim was to develop a concrete that could be placed without vibration. In this way, some health risks as well as environmental problems could be avoided. Also durability problems related with badly vibrated concrete structures could be reduced.

The two essential properties of SCC are a high flowability and a high segregation resistance obtained by a large amount of fine particles and the use of superplasticizers. Due to the high amount of fine particles, the pore structure of SCC concrete is somewhat different from the pore structure of traditional concrete [1]. The pore structure is one of the major influencing factors concerning durability. The actual application of SCC might be somewhat risky due to a lack of knowledge concerning the actual durability of the new cementitious material.

Many research programmes have already been carried out concerning the fresh properties of SCC, but little is known about the durability of SCC. Durability is not like strength a bulk property but (with some exceptions) in the first place a surface property, determined by composition and properties of the surface layers, indicated with the word 'skin'. Concrete has three skins: the cement skin (about 0.1mm thick), the mortar skin (about 5 mm) and the concrete skin (about 30mm). These are due to the wall effect, to sedimentation and segregation as a result of gravity and to permeation

Proceedings of the 11th International Congress on the Chemistry of Cement (ICCC)
'Cement's Contribution to the Development in the 21st Century'
Hosted by: The Cement and Concrete Institute of South Africa
CD-ROM produced by: Document Transformation Technologies
11 - 16 May 2003, Durban, South Africa
ISBN Number: 0-9584085-8-0
Editors: Dr G. Grieve and G. Owens
Congress Organised by: Event Dynamics

and evaporation of water in and out of concrete. Therefore durability is not only influenced by the concrete composition, but also by curing and the quality of the concrete cover.

The ease with which fluids enter and move through the concrete matrix influences largely thedurability of concrete (for example: deterioration due to chloride ions caused by the transport of a chloride solution into the material). There are two mechanisms controlling the transport of water into concrete: permeability and sorptivity. Permeability is a measure of the flow of water under pressure in a saturated medium and sorptivity is the ability to absorb water by capillary suction.

In this article results of water permeability, water absorption and capillary suction of SCC found in literature are described and the results of tests carried out at the Magnel Laboratory of Concrete Research on 7 SCC and 2 traditional concretes (TC) will be discussed. These test results will be compared with models found in literature predicting the water permeability and capillary suction for traditional concrete.

2. LITERATURE RESULTS OF SCC

Many test methods exist to determine the behaviour of concrete in the presence of water: capillary suction, absorption by immersion, vacuum absorption, water permeability, water penetration depth, etc. For each of these types of test, different procedures exist with regard to the dimensions of the test specimen, the preparation of the sample (which is extremely important with regard to the internal humidity), duration of the test. For SCC, some test results are available in literature but comparing these results is difficult because there is no standardized way to test. Generally, it appears that better results are found for the SCC-mixes compared to traditional concrete mixes. Table 1 presents a summary of results found in the literature.

Table 1. Summary of test results found in literature

reference	Test description	Test method	# SCC mixes	slump flow (mm)	compr. strength (N/mm²)	unit	Range of results
2	vacuum absorption	-	1	740	84 (90days)	vol %	14
3	water penetration	DIN 1048	4	-	35-65	mm	11-15
4-5-6	water penetration	DIN 1048	2	805-830	62-75	mm	2-18
7-8	water penetration	DIN 1048	3	780-790	50-64	mm	6-11
9	porosity	AFREM	2	580-600	56-58	%	12.7-13.2
	water absorption	RILEM	2			%	5.8-6.5
	capillary suction (24h)	AFREM	2			kg/m²	3.9-4.0
10	capillary suction	-	5	630-700	61-62	g/m²h	3.4-6.0

3. EXPERIMENTAL PROGRAMME

3.1 Concrete composition

At the Magnel Laboratory for Concrete Research, 7 SCC and 2 TC were investigated. In these mixes, a constant amount of fine material (cement and filler) is considered: 600kg/m³; as well as a constant amount of water, sand and gravel, respectively 165 kg/m³, 853 kg/m³ and 698 kg/m³. Three types of cement (CEM I 42.5 R, CEM I 52.5 and CEM I 52.5 HSR) and two types of filler (Betocarb P2 and Superfine S, the last having a much finer grading) were used. The amount of

superplasticizer was determined to obtain a suitable flowability without segregation. Also the value for the V-funnel was measured (values between 5s and 10s), air content (values between 1.5% and 3%) and the U-box requiring self levelling.

In Table 2 the mix compositions are given together with the slump flow and the compressive strength at 28 days measured on concrete cubes of 150mm.

Table 2. Mix design

	SCC							TC	
	1	2	3	4	5	6	7	1	2
CEM I 42.5 R [kg/m³]	360			300	400	450	360	360	400
CEM I 52.5 [kg/m³]		360							
CEM I 52.5 HSR [kg/m³]			360						
limestone filler S [kg/m³]							240		
limestone filler P2 [kg/m³]	240	240	240	300	200	150			
water [kg/m³]	165	165	165	165	165	165	165	165	165
sand 0/5 [kg/m³]	853	853	853	853	853	853	853	640	626
gravel 4/14 [kg/m³]	698	698	698	698	698	698	698	1225	1220
glenium 51 [l/m³]	2.3	2.5	2.2	2.2	2.2	2.3	2.8		
W/C [-]	0.46	0.46	0.46	0.55	0.41	0.37	0.46	0.46	0.41
W/(C+F) [-]	0.27	0.27	0.27	0.27	0.27	0.27	0.27	0.46	0.41
slump flow [mm]	685	740	820	750	840	780	785	-	-
compressive strength [MPa]	55	63	70	44	63	68	56	46	52

3.2 Test method

Three kind of tests were carried out: water absorption by immersion and capillary suction following the RILEM procedure [11,12] and water permeability test.

3.2.1 Water absorption by immersion

From the mixes described above, cubes 100 x 100 x 100mm were made. These concrete cubes were stored in a climate room at 20°C ± 2 °C and more than 90% R.H. At the age of 28 days, these concrete cubes were stored for 1 week at 20°C ± 3 °C and 60 ± 3 % R.H. The cubes were then immersed in water until the change in weight during 24 hours is less than 0.1%. The cubes were then placed in an oven at a temperature of 105 ± 5°C until the difference in weigth during 24 hours was less than 0.1%. These tests were carried out on three specimens for each concrete mix. This procedure was also carried out in water containing 3.5% by mass NaCl in order to verify if there was any difference. The results are given in Table 3.

Table 3. Water absorption by immersion

	absorption by immersion (% of dry mass)	
mix	in water	in water with 3.5% NaCl
SCC1	4.8	4.8
SCC2	4.9	4.5
SCC3	4.3	4.3
SCC4	5.0	5.0
SCC5	4.7	4.3
SCC6	4.2	4.3
SCC7	5.1	4.7
TC1	4.9	5.0
TC2	4.6	4.4

From this table the following can be concluded:

- the results for the absorption in the solution containing 3.5% NaCl are the same or somewhat lower than the results in water. This is in accordance with the formula given in [13] that predicts that the results of the absorption in water must be multiplied by 0.975 to obtain the results for the solution containing 3.5% NaCl.
- cement type: a cement type with a higher strength (SCC2, SCC3), resulting in a higher concrete strength (using the same W/C-ratio), does not necessarily give a lower water absorption. For SCC2 and SCC3, the water absorption is respectively somewhat higher and lower than water absorption for SCC1. In the presence of a solution containing NaCl, a higher strength for the cement type gives a lower water absorption.
- cement content: a higher cement content, resulting in a lower W/C-ratio and a higher strength gives a lower water absorption. This conclusion is valid for the absorption in water and in water containing 3.5% NaCl.
- type of filler: using a limestone filler with a finer grading gives a higher absorption in case of water without chlorides and a lower absorption in water containing chlorides.
- TC in comparison with SCC: the SCC give lower values for absorption than the corresponding TC (same amount and type of cement, same W/C-ratio). This conclusion is valid for the absorption in water and in water containing 3.5% NaCl.

3.2.2 Capillary suction

From the mixes described in section 3.1, cubes 150 x 150 x 150mm were made. These concrete cubes were stored in a climate room at 20°C ± 2 °C and more than 90% R.H. At the age of 28 days, these concrete cubes were stored for minimum 2 and maximum 3 weeks (the tests for capillary suction were started on Monday) at 40°C ± 5 °C and 40 ± 3 % R.H. The test was performed in an environment at 20°C ± 3 °C and 60 ± 3 % R.H. Then, the cubes were placed on stable supports in water, so that the water level is 5 ± 1 mm above the lower face of the specimen. Before the test and after 3, 6, 24, 72 and 168 hours the mass of the specimen is determined as well as the height of capillary rise (at the four sides of the cube in the middle).

These tests were carried out on three specimens for each concrete mix. This procedure is also carried out in water containing 3.5% by mass NaCl in order to verify if there is any difference. The results for the mass increase in water are given in Figure 1. In Table 4 the results are given of the mass increase after 24 hours in water and in water containing 3.5% NaCl. Also the height of capillary rise after 24 hours in these two cases is given. The measurements on the other moments follow the same trend.

From these results, the following conclusions can be made:

- water in comparison with water containing 3.5% NaCl: there is no distinct trend comparing these results.
- cement type: a cement type with a higher strength (SCC2, SCC3), resulting in a higher concrete strength (using the same W/C-ratio), gives in all cases a better result (decrease of the mass increase and decrease of the height of capillary rise)
- cement content: a higher cement content, resulting in a lower W/C-ratio and a higher strength gives a lower water absorption (lower mass increase and lower height of capillary rise). This conclusion is valid for the absorption in water and in water containing 3.5% NaCl.
- type of filler: using a limestone filler with a finer grading gives a lower mass increase and a lower height of capillary rise in both cases (water with and without chlorides).
- TC in comparison with SCC: the SCC give lower values for the mass increase and the height of capillary rise than the corresponding TC (same amount and type of cement, same W/C-ratio). This conclusion is valid for the absorption in water and in water containing 3.5% NaCl.

- a linear correlation exists between the mass increase and the height of capillary rise in the case of SCC ($R^2 \approx 0.95$ after 24, 72 and 168 hours). This correlation seems not to exists in case of TC. More testing will be carried out to verify this.

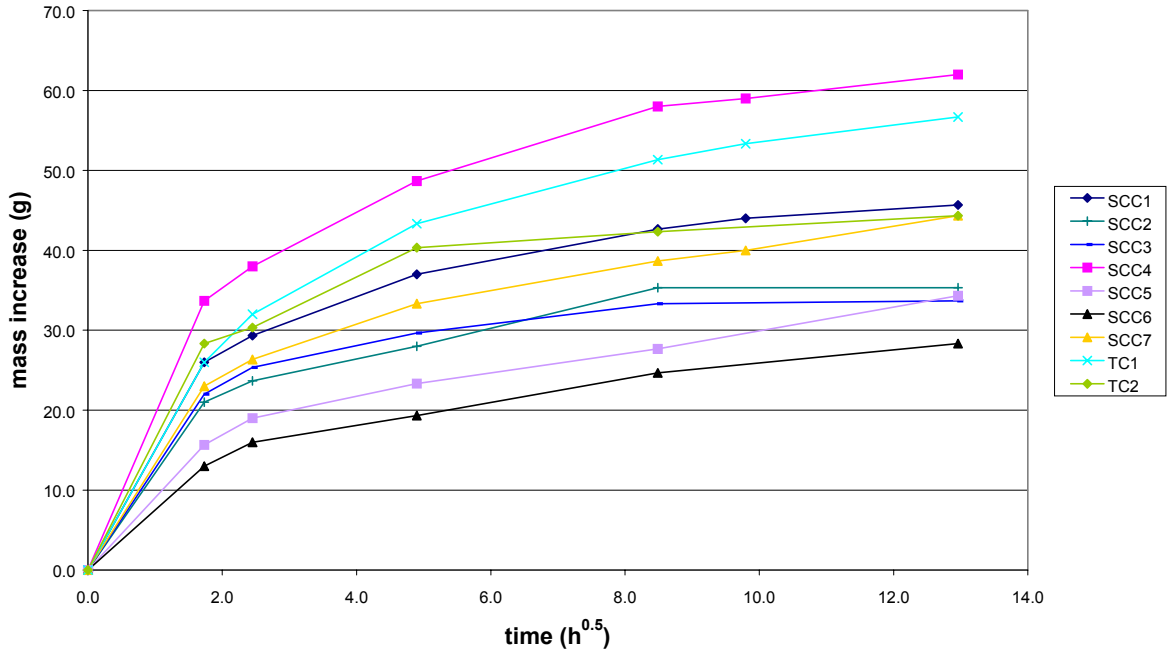

Figure 1. Mass increase by capillary suction

Table 4. Results capillary suction after 24 hours

	in water		in water containing 3.5% NaCl	
mix	mass increase (g)	height (mm)	mass increase (g)	height (mm)
SCC1	37	25	40	30
SCC2	28	23	27	23
SCC3	30	20	30	22
SCC4	49	31	44	28
SCC5	23	18	17	23
SCC6	19	17	15	19
SCC7	33	23	34	28
TC1	43	44	43	41
TC2	40	31	46	39

3.2.3 Water permeability

From the mixes described in section 3.1, cubes 150 x 150 x 150mm were made. These concrete cubes were stored in a climate room at 20°C ± 2 °C and more than 90% R.H. until the age of 56 days. Then, one core (diameter 80mm, height 25mm) from the center of each cube was taken. Afterwards, these cores were vacuum saturated in water. Then the water permeability test was performed in a testing device as shown in Figure 2. Water is present at the upper side of the specimen, on the lower side there is no water. Hence the pressure head is known and the water permeability can be calculated using the following formula:

$$K = \frac{A_t}{A_s}\frac{d}{t-t_0}\ln\left(\frac{h_0}{h}\right) \quad (1)$$

with K the coefficient of permeability, A_t the cross section of the tube, A_s the cross section of the specimen, d the thickness of the specimen, t the time and t_0 the starting time, h_0 the height of water in the tube at t_0 and h the height of water at time t.

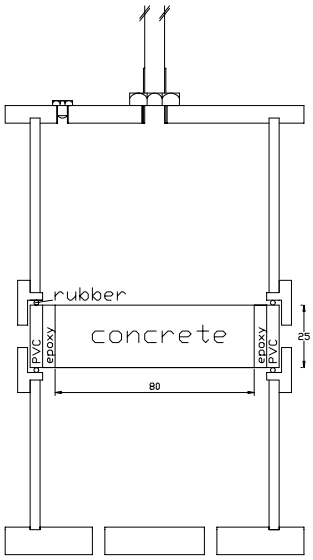

Figure 2. Testing device for water permeability

These tests were performed on three specimens for each concrete mix. In figure 3, the results are given for all mixes except SCC4, SCC7 and TC2 because these tests are not finished yet. In table 5 the value of K after 35 days is given.

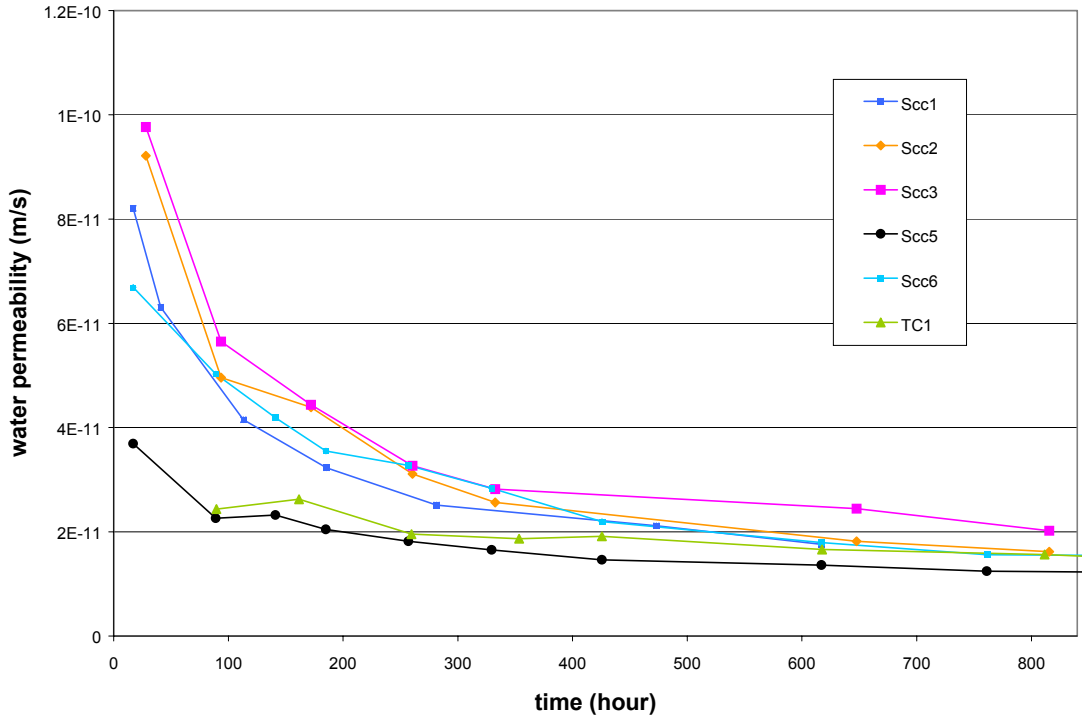

Figure 3. Water permeability

Table 5. Test results for water permeability

mix	K (10^{-11}m/s)
SCC1	1.8
SCC2	1.6
SCC3	2.0
SCC4	-
SCC5	1.2
SCC6	1.5
SCC7	-
TC1	1.6
TC2	-

The standard deviation on these test results varies between $1x10^{-12}$ m/s and $6x10^{-12}$ m/s, which corresponds with the values given in the literature [14]. In [14], the suggestion is made that only the order of magnitude or at the most the nearest $0.5x10^{-11}$ m/s should be mentioned. The conclusion is that the tests results obtained show very small differences. Also, all concrete mixes have a low water permeability and this test method is not suitable to compare 'good' concrete mixes.

4. MODELLING

4.1 Water absorption by immersion

No modelling was found in the literature for this kind of test. This is due to the differences in conditioning of the specimens before the test, the test conditions: drying at 40°C, 105°C, the duration of the test: a certain number of days or a criterium (e.g. difference in weight less than 0.1% in 24 hours).
For concrete in Belgium the criteria for water absorption, following the test method used in the tests described above, are that the individual result must be smaller than 6.5% and the mean value smaller than 6%. All test results given in Table 3 are good.

4.2 Capillary suction

For capillary suction, most models describing the absorption of water (in mass or in penetration depth) in function of time, suppose the following relation [15,16,17,18]:

$$i = A + S\,t^{1/2} \qquad (2)$$

with t the time and i the penetration height or the increase in mass, S is the sorptivity index. Some authors do not use the term A [19]. It is important to note that most researchers are only measuring in the first hour [15,18,19].
In [18], the equation $i = St^{1/2}$ for capillary suction is derived from the Darcy's equation for one dimensional flow in an unsaturated medium. The term A in equation (2) is added for the intercept that is usually found. The origin of this intercept is the filling of open surface porosity on the inflow surface and along the sides of adjacent faces. In Figure 4, the test results of SCC1 are given, together with the two types of modelling of equation (2) obtained by regression.

In [16] it is suggested that the sorptivity value is less than 3 mm/h$^{0.5}$ based on the requirement that the depth of water penetration in concrete exposed to rain must be smaller than the concrete cover. From the regression analysis using equation (2), the values for S are all between 0.5 mm/h$^{0.5}$ and 2.5 mm/h$^{0.5}$.

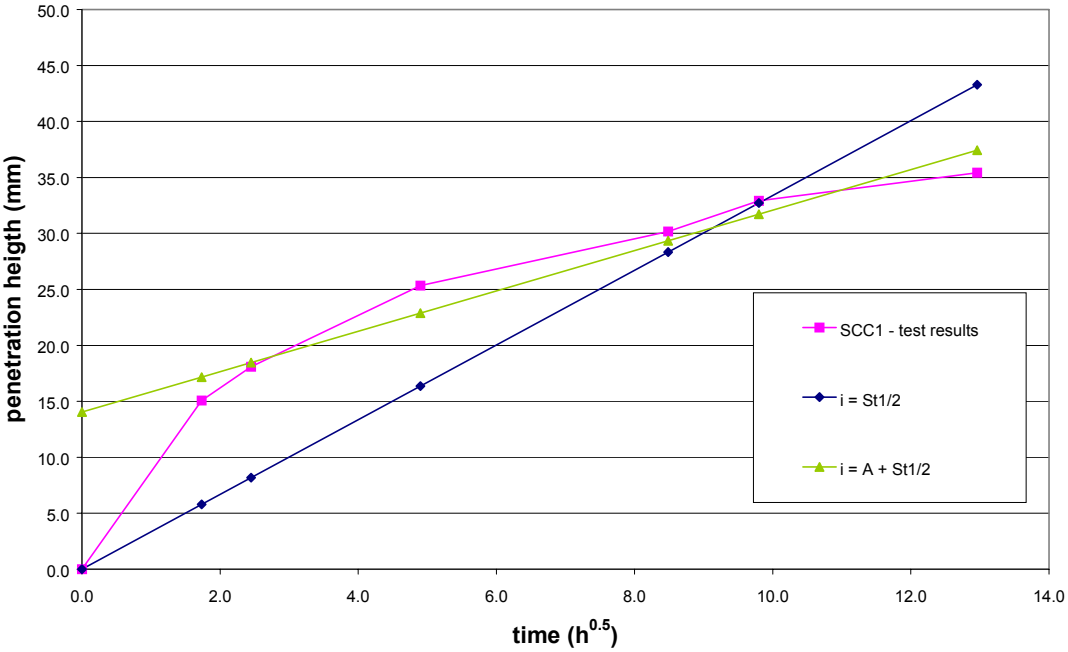

Figure 4. Test results SCC1, together with two types of modelling

All models described in this section are predicting the progress of the water absorption with time, but none of them are predicting the value of S. In the Model Code 90 [20], a formula is given to predict S in the relationship $i = St^{1/2}$:

$$\ln\left(S/S_0\right) = 0.2\, f_{ck}/f_{ck0} \tag{3}$$

with $S_0 = 10^{-4}$ m/s$^{0.5}$, f_{ck} the characteristic strength and f_{ck0} = 10MPa. In Figure 5, the experimental values and the predicted values based on equation (3) are given.

The predicted and experimental values, given in Figure 5, correspondings very well, giving the correct trend except for TC1, where the difference between the experimental and the predicted value is somewhat larger.

4.3 Water permeability

Two models for the value of K are found in literature: the model in MC90 [20]:

$$\ln\left(K/K_0\right) = -0.7\, f_{ck}/f_{ck0} \tag{4}$$

with K_0 is 10^{-10} m/s, f_{ck} the characteristic strength and f_{ck0} = 10MPa.; and the model of Wong et al. [21], but this model is only applicable for high hydrostatic pressures, which is not the case in the present study.

The experimental and predicted values are given in table 6.

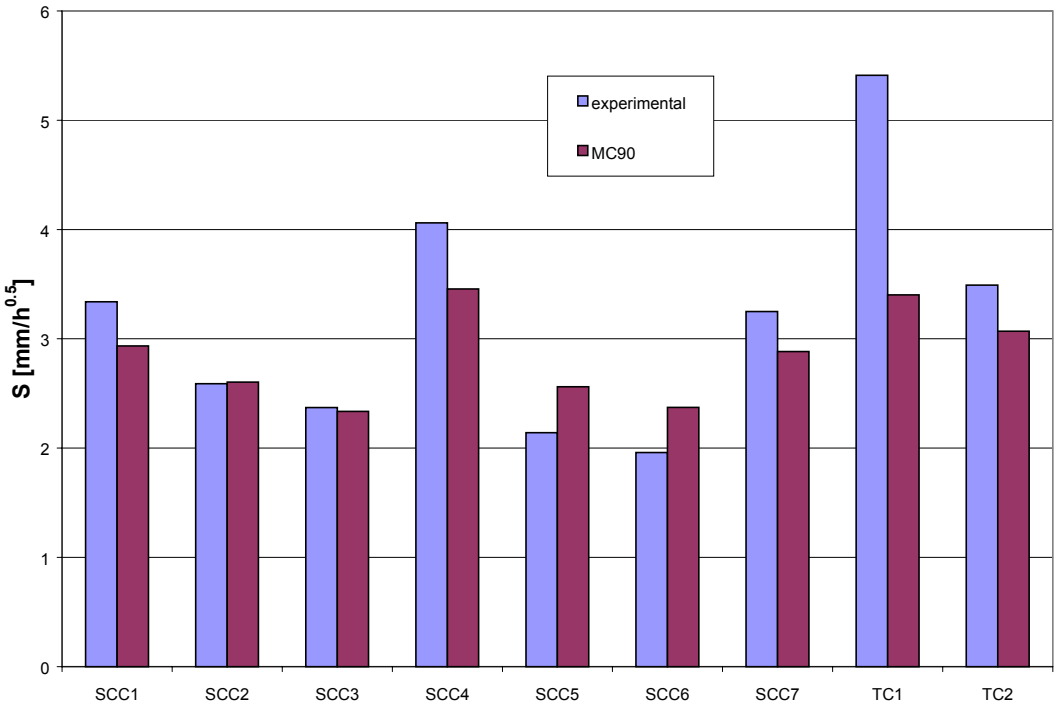

Figure 5. Experimental and predicted values for S

Table 6. Experimental and predicted values for K

	K (10^{-11}m/s)	
mix	measured	predicted
SCC1	1.8	0.8
SCC2	1.6	0.5
SCC3	2.0	0.4
SCC5	1.2	0.5
SCC6	1.5	0.4
TC1	1.6	1.4

From this table, it can be concluded that the values for the traditional concrete correspond very well. For the values of the SCC, the predicted values are lower than the experimental values.

5. CONCLUSIONS

Self-compacting concrete is a new type of cementitious material with a pore structure different from traditional concrete. This influences the durability and, more particularly, the behaviour with respect to water. In the literature, only a few test results were found concerning this subject and were summarized in this article.

In the Magnel Laboratory for Concrete Research, an experimental programme was carried out with 7 self-compacting concrete mixes and 2 traditional concretes. The type and amount of cement was studied, as was the amount of filler (two types of limestone filler were used). Also a comparison between self-compacting concrete and traditional concrete was made. Results are given for the water absorption by immersion and capillary suction and of the water permeability. These tests were carried out in water and in water containing 3.5 % NaCl. These results are compared with predictions obtained by literature models.

The main conclusion is that the self compacting concrete absorbs less water than traditional concrete.

REFERENCES

[1] Audenaert K., Boel V., De Schutter G., Poppe A.-M. Kennismaking met zelfverdichtend beton: duurzaamheid moet verder bestudeerd, Bouwkroniek, 22 february 2002, pp. 27-30.

[2] Lieberum K., Graubner C. Selbstverdichtender Beton für Fertigteile, BFT, 2/2002, pp. 28-30.

[3] Jacobs F., Hunkeler F. Design of self-compacting concrete for durable concrete structures, 1st international conference on self compacting concrete, Stockholm, 1999, pp. 397-407.

[4] Brameshuber W., Uebachs S., Tigges C. Selbstverdichtender Beton im Fertigteilwerk, BFT, 11/2001, pp. 80-89.

[5] Brameshuber W., Krüger T., Uebachs S. Selbstverdichtender Beton im Transportbetonwerk, Beton, 10/2001, pp. 546-550.

[6] Brameshuber W., Uebachs S., Eck T. Betontechnologische Grunlagen des Selbstverdichtenden Betons, Workshop self compacting concrete, Leipzig, november 2001, pp.11-23.

[7] Ludwig H. Dauerhaftigkeit selbstverdichtender Betone, Workshop self-compacting concrete, Leipzig, november 2001, pp. 175-190.

[8] Ludwig H.,Weise F., Hemrich W., Ehrlich N. Selbstverdichtender Beton-Grunlagen und Praxis, BFT, 6/2001, pp.58-67.

[9] Rougeau P., Maillard J., Mary-Dippe C. Comparitive study on the properties of self compacting and high performance concrete used in precast construction, 1st international conference on self compacting concrete, Stockholm 1999, pp. 251-261.

[10] Jacobs F. Erfahrungen mit SVB in der Schweiz, Workshop self-compacting concrete, Leipzig, november 2001, pp. 221-233.

[11] Concrete test methods – absorption of water by immersion, Material and Structures, 1974, pp. 291-293.

[12] Concrete test methods – absorption of water by capillarity, Materials and Structures, 1974, pp. 295-297.

[13] Steffens A., Dinkler D., Ahrens H. Modellierung und numerische Analyse von Karbonatisierung und Chloridbindung in Betonbauteilen, Beton – und Stahlbetonbau, 2001/3, pp. 138-146

[14] Neville, A. Properties of concrete, 4th and final edition London: Longman, 1995, p. 494.

[15] Hall, C. Water sorptivity of mortars and concretes: a review, Magazine of Concrete Research, 1989, June, pp. 51-61.

[16] Ho D., Hinczak I., Conroy J., Lewis R. Influence of slag cement on the water sorptivity of concrete, 2nd International Conference on Fly Ash, Silica Fume, Slag and Natural Pozzolans in Concrete, Madrid, ACI SP91-72, 1986, pp. 1463-1473.

[17] Potter R., Ho D. Quality of cover concrete and its influence on durability, 1st International Conference on Concrete Durability, Atlanta, ACI SP100-25, 1987, pp. 423-445.

[18] Reda Taha M., El-Dieb A., Shrive N. Sorptivity: a reliable measurement for surface absorption of masonry brick units, Materials and Structures, August-September 2001, pp.438-445.

[19] Neville, A. Properties of concrete, 4th and final edition London: Longman, 1995, p. 489.

[20] CEB-FIP Model Code 1990, Design Code, Thomas Telford, London, 1993

[21] Wong S., Wee T., Swaddiwudhipong S., Lee S. Study of water movement in concrete, Magazine of Concrete Research, 2001, June, pp. 205-220.

WATER PERMEABILITY OF SELF COMPACTING CONCRETE

Katrien Audenaert[1], Veerle Boel[1] and Geert De Schutter[1]

[1] Magnel Laboratory for Concrete Research, Ghent University,
Department of Structural Engineering,
Technologiepark-Zwijnaarde 9,
9052 Ghent, Belgium
E-mail: katrien.audenaert@rug.ac.be, veerle.boel@rug.ac.be, geert.deschutter@rug.ac.be

Name: Katrien Audenaert

Affiliation: Magnel Laboratory for Concrete Research
Department of Structural Engineering
Ghent University

E-mail: katrien.audenaert@rug.ac.be

Contact: Address: Technologiepark-Zwijnaarde 9,
9052 Ghent,
Belgium
Tel: 0032.9.264.55.32
Fax: 0032.9.264.58.45

INFLUENCE OF INORGANIC AND ORGANIC CORROSION INHIBITORS ON CARBONATION MECHANISM AND CORROSION OF STEEL REINFORCEMENT

G. Batis[1] and K.K. Sideris[2]

[1]Associate Professor, National Technical University of Athens, School of Chemical Engineering, Section of Materials Science and Engineering, Greece.
[2] Lecturer, Laboratory of Building Materials, Department of Civil Engineering, Democritus University of Thrace, Xanthi, Greece.
E-mail: kksider@civil.duth.gr

1. INTRODUCTION

Reinforced concrete is the most commonly used construction material worldwide. In the absence of aggressive media such as chlorides and carbon dioxide, good quality concrete with sufficient cover is all that is needed for the structure to achieve its design life with little or no maintenance. Due to the presence of $Ca(OH)_2$ in the pores of the cement matrix, the pH has an average value of 12.4 [1]. Under these circumstances a thin oxide layer is formed around the reinforcement helping it to remain uncorroded. Reinforcement corrodes only if the protective layer deteriorates. This may be happen either due to the fall of the pH value of the pore solution - if the pH value falls below 11 the protective layer starts cracking, and it deteriorates totally when the pH falls below the value 9 – or due to the great concentrations of chlorides around the steel reinforcement bar. Both phenomena – carbonation and chloride ingress-result in the corrosion of the reinforcement and the reduction of the designed service life of the structure.

High performance concrete mixtures significantly increase the corrosion initiation time. It was reported [2] that the corrosion initiation due to carbonation may be significantly extended when high quality concrete is used in combination with supplementary cementing materials. But even in this case, there finally comes a time at which the corrosion of steel initiates.

As it was reported that in many cases in severe environments even good quality concrete cannot provide sufficient protection, a number of additional corrosion protection systems are marketed to face the problem of corrosion in reinforced concrete. Corrosion inhibitors, coatings at the surface of reinforcing steel or at the surface of concrete, stainless steel and cathodic protection are some of the technologies developed. Among those corrosion protection systems the use of corrosion inhibitors as concrete admixtures is a very popular, easy and a relatively economical method. Calcium-nitrite (CNI)[3,4] and N,N'-dimethylaminoethanol is used as a corrosion-inhibitive admixture in concrete [5,6].

Although its action in inhibiting the corrosion due to chloride ingress is well investigated, there is limited research concerning its behavior against carbonation, especially when the inhibitor is added in blended cement mixtures. This is experimentally investigated in this paper. Mortar mixtures were prepared with portland and blended cements and were exposed to a curing room with 18-23 °C and 50-65% relative humidity and also in outdoor conditions. Carbonation depth and steel rebar loss versus time measurements were taken for a period up to three years for portland and blended mortar mixtures prepared with and without the addition (of inorganic and organic) corrosion inhibitors.

2. MATERIALS AND METHODS

The materials used were four types of cement (type I-35, I-45, blended cement II-35 and II-45). Chemical composition of those materials is presented in Table 1.

Table 1. Chemical composition of the materials used.

Oxide content (%)	Commercial cement I-35	Commercial Blended Cement II-35	Commercial Cement I-45	Commercial Blended Cement II-45
SiO_2	20.67	22.36	19,64	25,3
Al_2O_3	4,99	6.62	4,62	5,95
Fe_2O_3	3.18	4.08	3,27	4,44
CaO	63.60	56.55	63,59	55,7
MgO	2,79	3.52	1,91	2,98
SO3	2,44	2.44	3,03	3,00
Na_2O	0.29	0.53	0,38	0,30
K_2O	0.37	0.72	0,62	0,57

Mortar mixtures were produced according to DIN 1164 [7] by using EN-196-1 [8] standard sand. The water/cementitous material ratio was equal to 0.45 for each mixture. The ratio cement/sand was equal to 1/3. Two types of corrosion inhibitors were used: One inorganic corrosion inhibitor (ICI) based on $Ca(NO_2)_2$ and one organic (OCI) based on in N,N'-dimethylaminoethanol were added at a dosage of 20 l/m^3 of concrete and 4% per weight of cement respectively.

Resistance against carbonation was measured on cylinder (40x100 mm) mortar specimens. Six specimens were produced for each mixture. A 10mm diameter steel rebar was embedded in the middle of four specimens of each mixture produced with class 35 cements. Those specimens were initially cured for 28 days in a curing room with relative humidity ≥95% and temperature 20±2 °C. After this period, they were placed in an outdoor locations in Athens (Zografou campus). Carbonation depth was measured at different ages up to three years in two specimens using a phenolpthalein spray indicator. Gravimetric weight loss was measured at the same ages according to the procedure described in [9].

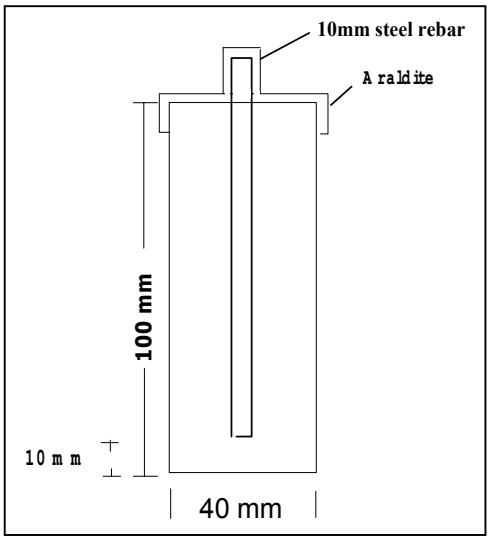

Figure 1. Cylindrical specimens used for carbonation measurements

Using class 45 cements produced additional specimens. Those specimens were cured for three days in a curing room with relative humidity ≥95% and temperature 20±2 °C. After this, they were

placed in a carbonation chamber with relative humidity of 60±5%, temperature of 20±2 °C and CO_2 concentration of 10%. Carbonation measurements were performed after five weeks.

3. TEST RESULTS

Carbonation measurements performed in outdoor conditions at different ages up to three years, are presented for all mixtures in Figures 1, 2 and 3. From Figure 2 is obvious that specimens with blended cement II-35 have greater carbonation depth than the specimen with I-35 cement. In Figure 3 is shown the carbonation depth of specimens with cement I-35 with and without corrosion inhibitors. The specimens with corrosion inhibitors have smaller carbonation depth in comparison with the specimens without inhibitors. The same event is shown in Figure 4.

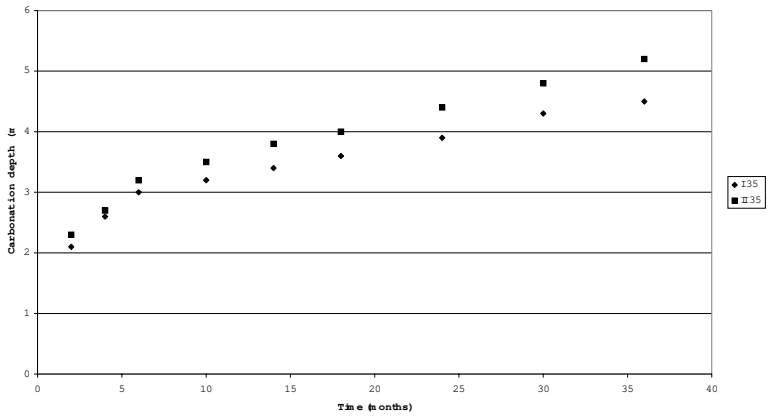

Figure 2. Carbonation depth of specimens with cement I-35 and II-35.

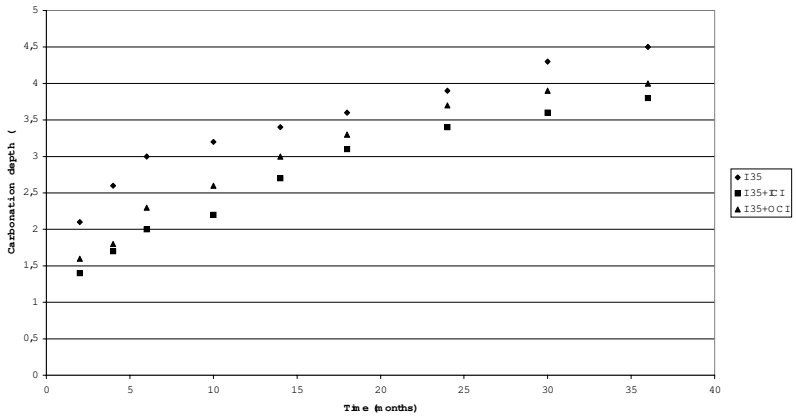

Figure 3. Carbonation depth of specimens with cement I-35 (with and without corrosion inhibitors).

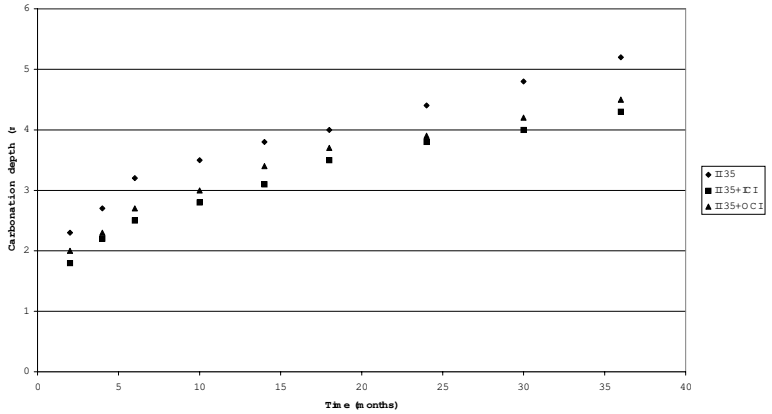

Figure 4. Carbonation depth of specimens with cement II-35 (with and without corrosion inhibitors).

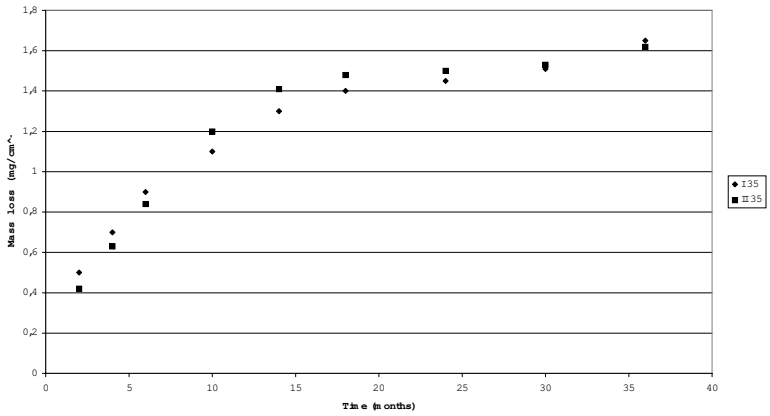

Figure 5. Rebars mass loss of specimens with cement I-35 and II-35.

Mass loss of specimens with I-35 and II-35 cement are shown in Figure 5. Difference of corrosion resistance between specimens with I-35 cement and II-35 cement is not shown in this experiment.

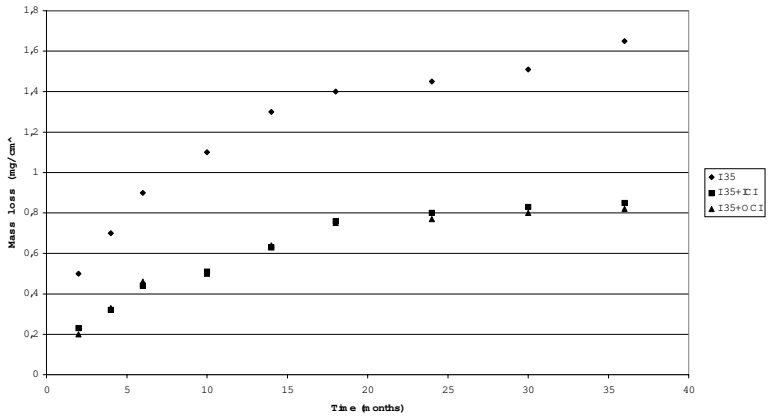

Figure 6. Rebars mass loss of specimens with cement I-35
(with and without corrosion inhibitors).

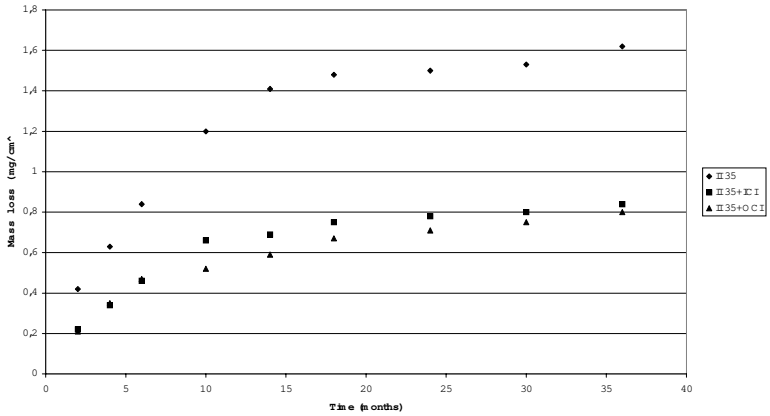

Figure 7. Rebars mass loss of specimens with cement II-35
(with and without corrosion inhibitors).

Mass loss of rebars specimens with and without corrosion inhibitors made with I-35 cement are shown in Figure 6. The presence of both corrosion inhibitors (ICI and OCI) decrease the mass loss of rebars about of 50%. The same phenomenon is observed in the specimens with cement II-35 (Figure 7).

Carbonation measurements performed on class 45 cement mortars placed in the carbonation chamber are presented in Figure 8. It is obvious that specimens with blended cement II-45 have greater carbonation depths than the specimen with I-45 cement. Also the specimens with corrosion inhibitors have smaller carbonation depths in comparison with the specimens without inhibitors.

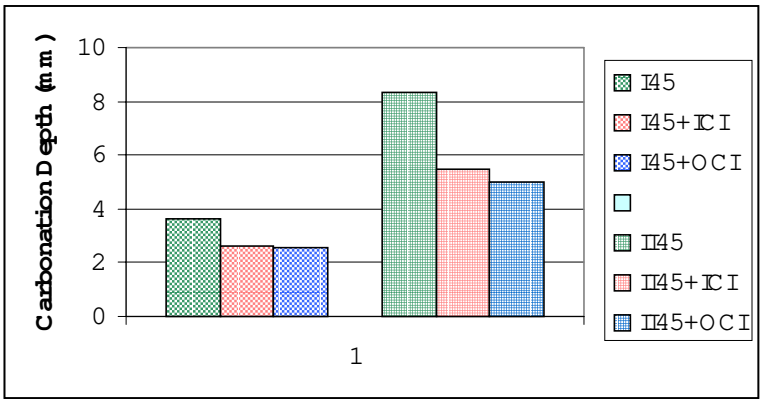

Figure 8. Carbonation depth of specimens with class 45 cements (with and without corrosion inhibitors) after 5 weeks exposure in carbonation chamber.

4. DISCUSSION

Carbonation depth of blended cement mortars is in general greater than the one of Portland cement mortars. This phenomenon is also mentioned elsewhere [10-11]. Carbonation depth of II-35 cement mixtures is almost equal to the one of the control mixtures with cement I-35 at the age of one year, but it significantly increases at the age of two and three years. This is mainly attributed to the reduction of OH^- caused by the pozzolanic reaction.

Addition of an inorganic corrosion inhibitor (calcium nitrite) slightly decreased the carbonation depth of all mixtures at all times, as it is also reported elsewhere [10,12]. The influence of the inhibitor is very significant in the case of gravimetric weight loss (Figures 6, 7). Although this was quantitatively low in any case, addition of calcium nitrite reduced the weight loss up to 50% for all mixtures. By the presence of $Ca(NO_2)_2$ a stable passive layer could be formed on the reinforcement, avoiding all the metastable forms, according to the following reaction [10,12]:

$$Fe^{+} + 2OH^{-} + 2NO_2^{-} \rightarrow \gamma\text{-}Fe_2O_3 + 2NO\uparrow + H_2O$$

The passive layer of γ-Fe_2O_3 decrease the formation of corrosion products. The rest of Ca^{2+} decrease the reduction of pH of all mortars containing corrosion inhibitors.

Addition of inorganic corrosion inhibitor also decreased the carbonation depth of all mixtures and reduced the gravimetric weight loss [Figures 6, 7]. The smaller carbonation depth observed in N,N'-dimethylaminoethanol specimens could be attributed to the lower water penetration of these mixtures. Further research is needed in order to obtain a clear explanation for this phenomenon. In all cases the addition of OCI, based on N,N'-dimethylaminoethanol, in fresh mortar has a protective effect. The effectiveness of this class of compounds has been shown by means of various experiments [5,6,13,14,15]. Earlier experiments have shown that aminoalcohol chemisorbs from aqueous solution onto oxidized steel surfaces [13].

The thickness and the composition of the absorbate phase, depend upon the composition and the concentration of the aminoalcohols solutions. The absorbate phase is formed, even if chlorides are present [13]. The corrosion inhibition effect is explained by the fact that aminoalcohol displaces,

due to its strong bonding, ionic species from the oxidized steel surface, in particular chlorides, and forms a durable passivating film [14,15].

5. CONCLUSIONS

Mixtures produced with blended cements exhibited greater carbonation depths compared with the control mixtures produced with Portland cements, irrespective of the class (35 or 45) of the cement used.

The addition of both corrosion inhibitors decreased the carbonation depth of all mixtures. However, their influence was stronger in reducing the gravimetric weight loss of steel rebars.

Both corrosion inhibitors offered significant protection against carbonation by reducing the carbonation depth and the gravimetric weight loss up to 50% for all mixtures. According to the results available so far, both inhibitors performed equally against carbonation at the dosages examined.

REFERENCES

[1] Broomfield J. P.: Corrosion of Steel in Concrete, 3rd edition, E&FN SPOON, 1997, pp.240.Papadakis V. G., Fardis M. N., Vayenas C. G.: Hydration and Carbonation of Pozzolanic Cements, ACI Materials Journal, Vol. 89, 1992, No2, pp. 119-130.

[2] Page C. L., Ngala V.T., Page M. N.: Corrosion inhibitors in concrete repair systems, Magazine of Concrete Research, Vol. 52, 2000, No 1, pp. 25-37.

[3] Gaidis G. M., Rosenberg A. M.: The Mechanism of Nitrite Inhibition of Chloride Attack on Reinforcing Steel in Alkaline Aqueous Environments, Materials Performance, Vol. 18, 1979, No 11, pp. 45-48.

[4] Maeder, U., A new Class of Corrosion Inhibitors, Corrosion and Corrosion Protection of Steel in Concrete, Vol. II, Editor R. N. Swammy, 1994, pp 215-232.

[5] Batis, G., Grigoriadis, Gr., Meletiou, C. A., «Protection of Steel Rebars in Lightweight Concrete with the Use of Corrosion Inhibitors, Modern Concrete Materials: binders, additions and admixtures, Editor Ravindra K. Dhir, 1999, pp 493-501.

[6] DIN 1164: DIN Taschenbuch 73, Zement.

[7] European Standard EN 196-1: Methods of Testing cement – Part 1: Determination of Strength.

[8] Kouloumbi N., Batis G.: Chloride Corrosion of Steel Rebars in Mortars with Fly Ash Admixtures, Cement and Concrete Composites, Vol. 14, 1992, pp. 199-207.

[9] Sideris K., Savva A: Influence of Calcium Nitrite based Corrosion Inhibitor on the Durability of Portland Blended Cements, Fifth CANMET/ACI International Conference on Recent Advances in Concrete Technology, Singapore, July 29 – August 1, 2001, Supplementary Volume, pp. 121-139.

[10] Malami Ch., Kaloidas V., Batis G., Kouloumbi N. Carbonation and Porosity of Mortar Specimens with Pozzolanic and Hydraulic Cement Admixtures, Cement and Concrete Research, Vol. 24, No 8, 1994, pp1444-1454.

[11] Berke N. S., Hicks M.C., Protection Mechanisms of Calcium Nitrite, Corrosion Conference on Understanding Corrosion Mechanism in Concrete: A Key to Improving Infrastructure Durability, MIT, Cambridge, MA (1997).

[12] Welle A, Liao J.D., Kaiser K., Grunze M., Maeder U. and Blank N.: Interactions of N,N'-dimethylaminoethanol with steel surfaces in alkaline and chlorine containing solutions, Applied Surface Science, Vol. 119, 1997, pp. 185-198.

[13] Mader U.: A mew class of corrosion inhibitor for reinforced concrete, 3rd CANMET/ACI International Conference on Concrete in Marine Environment, St. Andrews by-the-sea, Canada, 1996, SP-163.

[14] Batis G., Routoulas A., Maeder U.: Performance of Corrosion Inhibitors in the Protection of Reinforced Concrete in Seaside Environment, 14th International Corrosion Congress, Cape Town, South Africa, 1999.

INFLUENCE OF INORGANIC AND ORGANIC CORROSION INHIBITORS ON CARBONATION MECHANISM AND CORROSION OF STEEL REINFORCEMENT

G. Batis[1] and K.K. Sideris[2]

[1]Associate Professor, National Technical University of Athens, School of Chemical Engineering, Section of Materials Science and Engineering, Greece.
[2] Lecturer, Laboratory of Building Materials, Department of Civil Engineering, Democritus University of Thrace, Xanthi, Greece
E-mail: kksider@civil.duth.gr

K. K. Sideris

Dr. of Engineering, Laboratory of Building Materilas, Civil Engineering Department, Democritus University of Thrace, P.O. Box 252 Xanthi, 671 00 GREECE
20-5-1969 : Born in Athens, Greece

1992:	M.Sc. in Civil Engineering
1992 - 1994:	Military Service.
1992-1996:	Ph. D. candidate of Democritus Univercity of Thrace
1997-1998:	Research assistant at the laboratory of building materials, Democritus University of Thrace
02/ 1998:	Lecturer at the lab. Of Building Materials, Democritus University of Thrace

PROFESSIONAL EXPERIENCE

I have worked in several construction offices in Athens as a consultant in terms of concrete technology and durability aspects. During my military service, I have worked in the construction of a military airport in Greece (buildings, motorways, shelters etc).
Since 1997 I am teaching several lessons at the civil engineering department in the areas of Building Materials, Concrete Technology and Concrete Durability

My research interests are in the area of cement hydration (empacized in the hydration of blended cements), concrete technology and concrete durability.

Papers available on request.

DURABILITY OF CEMENT MORTARS IN SIMULATED SEWAGE ENVIRONMENT

T. Cerulli, C. Pistolesi, C. Maltese and D. Salvioni

Research & Development Laboratory, MAPEI S.p.A., via Cafiero 22, 20158, Milano, Italy.
E-mail: s_laboratorio@mapei.it

ABSTRACT

The corrosion of concrete sewage by the action of sulphuric acid is a worldwide problem both for industrialised and underdeveloped countries. Today there are several ways to repair degraded concrete in the sewage area but often these methods are ineffective or too expensive. In order to make effective cement mortars to repair concrete in sewage, a study was carried out on 3 different renders and a polymer modified mortar. The products were tested using a biogenic simulation chamber and a sulphuric acid immersion test. A comparison between these two techniques was pointed out. The progression of acid attack was followed by X-ray diffraction, B.E.T. specific surface area measurements, EDS and optical microscopy.

1. INTRODUCTION

The degradation of concrete in sewerage is a problem currently studied by many researchers [1,2,3,4,5]. One of the main reasons of such degradation is the sulphuric acid produced by bacterial oxidation of hydrogen sulphide (aerobic oxidation), formed by the anaerobic fermentation of civil and industrial waste-waters. Sulphuric acid has a deleterious effect on concrete structure being the cause of softening and spalling of the hardened cement phases [3,6,7]. Today, in Europe, two are the most important accelerated tests used to evaluate the resistance of cement mortars to sewage conditions. One technique is based on loss mass measurements of samples stored for one year in a chamber where an accelerated bacterial attack is simulated [8]. The other method is based on a residual strength determination of samples immersed for 14 days in a sulphuric acid solution at pH=0 and 70 days at pH=1 [12].

In order to develop cement-based materials resistant to aggressive sewage environment, four different mortars were prepared and tested with the mentioned accelerated methods. A physical-chemical study was carried out by X-ray diffraction, B.E.T., EDS and optical microscopy on mortar specimens dipped in a sulphuric acid solution (pH=0) to clarify the mechanism of acid attack.

2. EXPERIMENTAL

2.1 Specimens Preparation

The mortar composition is reported in Table1. The components were mixed according to ENV 196/1. The physical-mechanical properties of fresh mortars are reported in Table 2. On the same Table the neutralisation capacity [11] is shown.

Specimens of different sizes (according to the test method) were kept for 24 hours at 20°C and 95% R.H. Therefore the samples were demoulded and cured at 20°C and 95% R.H. for 28 days.

Proceedings of the 11th International Congress on the Chemistry of Cement (ICCC)
'Cement's Contribution to the Development in the 21st Century'
Hosted by: The Cement and Concrete Institute of South Africa
CD-ROM produced by: Document Transformation Technologies
11 - 16 May 2003, Durban, South Africa
ISBN Number: 0-9584085-8-0
Editors: Dr G. Grieve and G. Owens
Congress Organised by: Event Dynamics

Table 1. Mortar composition

Components	A	B	C	D	Characteristics
Cem.I 42,5 R (according ENV 196/1)	25	-	3	35	CaO=63,8 Al_2O_3=4,6 SO_3=4,0 Fe_2O_3=1,9 MgO=2,2
CEM III/C (according ENV 196/1)	-	32	-	-	Al_2O_3 =17,0 MgO=11,0 CaO=40,0 SiO_2=32
High alumina cement	-	-	27	-	Al_2O_3=40,0 Fe_2O_3=16,2 CaO=39,4
Superplasticizer	0,1	0,1	0,1	0,1	Naphthalene based superplasticizers
Normalised sand (according ENV 196/1)	74,9	67,9	64,9	64,9	Silica sand
Water (perceptual on the solid part)	12	15,5	15	-	-
Acrylic latex	-	-	-	19,5	Dry content = 14%

Table 2. Chemical physical properties

Sample	A	B	C	D
Specific gravity (kg/m^3)	2246	2140	2170	2150
Flow test (%-UNI 7044)	57	87	74	70
Compressive strength (MPa-28 days)	69	30	90	58
Calculated Neutralization Capacity	4,1	5,5	7,6	5,4

2.2 Chemical Sulphuric Acid Corrosion Test

Mortar specimens (40x40x160mm), after demoulding, were cut in two 40x40x80mm parts and cured. At the end of curing period the mortars were divided in three groups. A group was kept in water for 14 days. Another set of samples was dipped in a 1M solution of sulphuric acid (pH=0-10l) for 14 days. The remaining specimens were immersed in a 0,1 M sulphuric acid solution (pH=1-10l). The pH of the solution was computer controlled and kept constant by means of an electrode system interfaced with dosing pumps. When the pH exceeded the threshold value of 0,1 pH unit, the computer started the pumps that added automatically a 5M sulphuric acid solution to establish the initial pH conditions. The mixing of the solution was assured by means of an air pump; the mixing speed was set to avoid a mechanical abrasion of the samples.

The specimens, after acid treatment, were washed. Then their volume and mass change were determined. The reference specimens and the degraded ones were cut into 40mmx40mmx40mm cubes in order to obtain a regular shape. Their compressive strength was measured.

2.3 Biogenic Sulphuric Acid Corrosion

Mortar samples (30mmx30mmx30mm) were prepared as reported previously. At the end of curing period the mortars were subjected to biogenic acid corrosion. The test was performed at the University of Hamburg (Germany). The experimental details are deeply explained elsewhere [8,9]. The mass loss was detected after 2, 4, 6, 8, 10 and 12 months of bacteriological attack.

2.4. Chemical-Morphological Study

Cylindrical specimens (30mmx30mmx30mm) were subjected to chemical sulphuric acid test to analyse the mechanism of mortar degradation, cylindrical specimens (30mmx30mmx30mm) were subjected to chemical sulphuric acid test.

Specific surface area determination by B.E.T. method was carried out before and after acid attack. Sulphuric acid penetration was studied by a selective precipitation of lead sulphate on polished sections of degraded samples. Such salt was subsequently coloured by sodium rodizonate (0,2% water solution). The procedure is summarised below:

- The surface of degraded specimens was treated with a concentrated water solution of lead nitrate
  $CaSO_4$ (or other sulphates) + $Pb(NO_3)_2 \rightarrow PbSO_4$ (unsoluble) + $Ca(NO_3)_2$ (soluble)
  Lead Sulphate is white and cannot be easily detected;
- This compound was coloured by the addition of a water solution of sodium rodizonate
  $PbSO_4$ + Sodium Rodizonate → Lead Rodizonate + Na_2SO_4

Lead Rodizonate is a red complex which is clearly evident on the material surface.
A SEM (Scanning Electron Microscopy) analysis was also performed on the samples before and after acid corrosion.

Furthermore EDS line scan for SKα, CaKα, SiKα, was carried out on polished sections of the specimens after acid degradation. The study was focused on the border line between the unaltered region and the degraded one.

A set of samples (30mmx30mmx30mm), prepared according to the composition in Table 1 without the use of sand, were analysed by XRD analysis (Philips PW 1830 with Cu Kα radiation) before and after acid treatment.

RESULTS

3.1 Durability Test

Mass and compressive strength changes after acid attack are reported in Table 3.

Table 3. Sulphuric acid immersion test

pH=0				
Sample	A	B	C	D
Mass loss %	40	5	10	45
Residual strength (%)	56	77	82	53
Compressive strength MPa (acid/water)	41 / 73	24,6 / 32	76 / 93	32,3 / 61
pH=1				
Sample	A	B	C	D
Mass Increase %	1	5	4	6
Residual strength (%)	69	70	67	68
Compressive strength MPa (acid/water)	56 / 81	25,2 / 36	73 / 109	47,6 / 70

The strength loss is given by a parameter called “Residual resistance” calculated using the following formula:

$$R_r=(R_a x 100)/R_b \quad (1)$$

Where
R_a= Compressive strength of the specimen after acid attack (average on four specimens);
R_b= Compressive strength of the reference specimen (average on four specimens).

Mass loss was calculated according to the formula:

$$\text{Mass loss} = [(M_f-M_o)/M_f]100 \quad (2)$$

Where
M_f = Mass before acid attack
M_o = Mass after acid attack

At pH=0, the data reported in Table 3 showed the following order of acid resistance:

High alumina cement mortar > Slag cement mortar > Ordinary Portland cement mortar ≈ Polymer modified mortar.

Although these results are in agreement with a large part of published literature [8,10], Fourie [4,5] using hydrochloric acid, showed the higher resistance of a Portland cement system respect to slag and calcium aluminate cement based concretes.

At pH=1, we found a very similar resistance of mortar specimens.

Mass losses of the samples subjected to bacteriological attack are shown in Table 4. Such parameter was calculated as reported for acid immersion test. The order of resistance was:

Slag cement mortar > Polymer modified mortar > High alumina cement mortar > Portland cement mortar.

Table 4. Mass reduction in biogenic chamber

Incubation (week)	A (%)	B (%)	C(%)	D(%)
8	1,4	0	0	0
16	12,2	1,2	4	0,4
24	17,6	3,3	8,5	12,1
32	27,4	3,9	16,6	12,1
40	66,2	3,9	28,8	12,9
48	70,3	6,5	28,9	13,5

3.2 Morphological analysis

The specific surface area measurements are shown in Table 5. A substantial surface area increase was observed due to acid corrosion. Only SEM micrographs of specimens A and C were enclosed in the paper (Figures 2, 3, 4 and 5). In Figure 2 (undamaged part of sample A) a strongly carbonated and compact microstructure appears. Fibrillar C-S-H is not visible. In Figure 3 (corroded part of specimen A) the microstructure is completely changed. It is characterised by many cracks and a lower density. SEM micrographs of specimen C are shown in Figures 4 and 5. Crystals of hydrated calcium aluminates appear. In this case the microstructure was not strongly affected by acid aggression.

Table 5. Specific surface area before and after acid attack

Sample	Before (m^2/g)	After (m^2/g)
A	6,8	14,9
B	11,2	21,1
C	5,9	10,3
D	8,1	10,2

Acid penetration was emphasised by rodizonic acid test. Polished sections of mortar samples before and after acid degradation are presented in Figure 1.

Figure 1. Sodium Rodizonate Test (from the left: A; D; B; C)

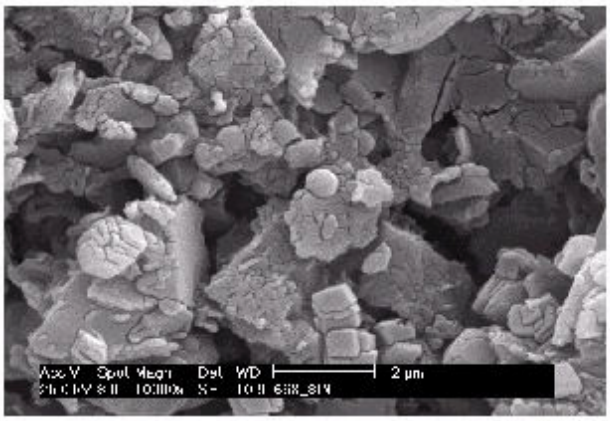

Figure 2. Undamaged part of sample A

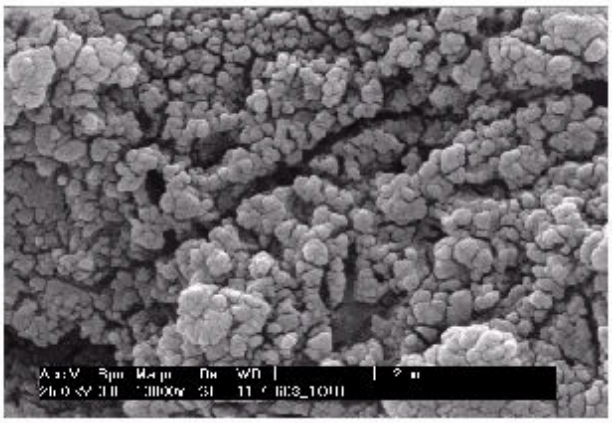

Figure 3. Degraded part of sample A

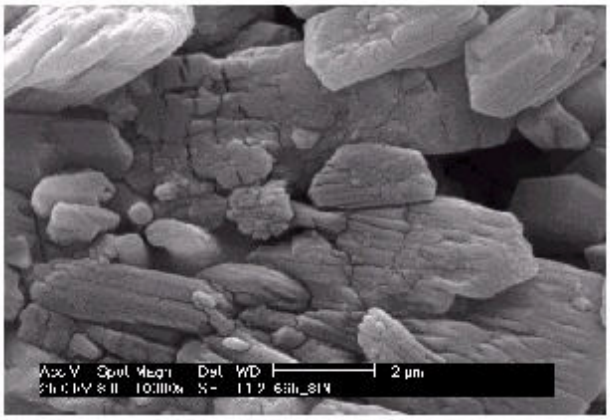

Figure 4. Undamaged part of sample C

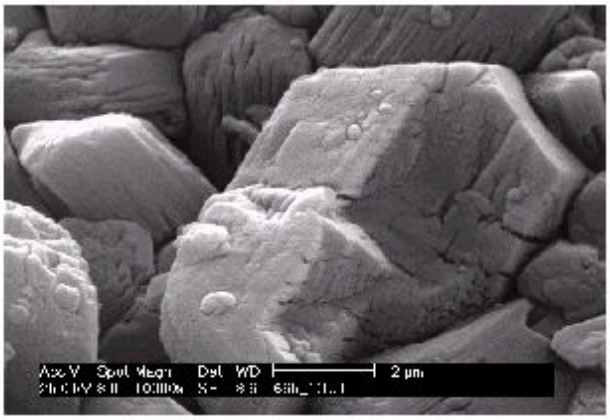

Figure 5. Degraded part of sample C

3.3 XRD Analysis

The diffraction patterns (E=Ettringite; P=Portlandite; G=Gypsum) are reported in Figures 6,7,8 and 9. Sample A is characterised by a large gypsum formation. Crystals of ettringite are also present. A sensible portlandite reduction occurs.

Acid treatment on slag based cement paste (B) causes gypsum precipitation. Portlandite is not evident.

Gypsum is again the main reaction product in the case of specimen C. A small amount of crystalline ettringite appears.

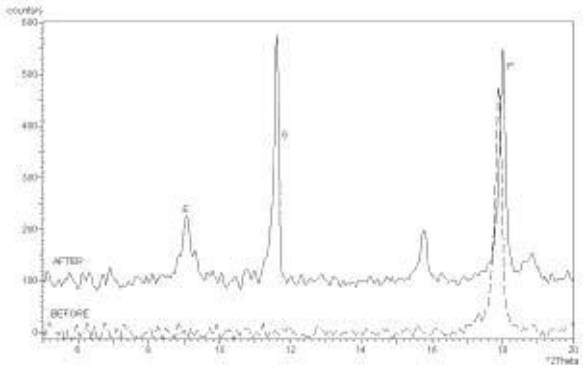

Figure 6. Specimen A before and after acid attack

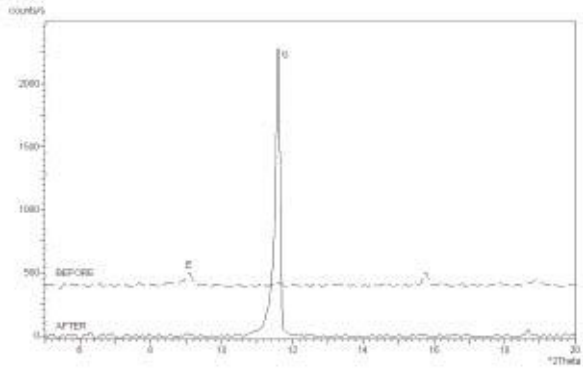

Figure 7. Specimen B before and after acid attack

XRD pattern in Figure 8 (sample D) is characterised by a large gypsum formation and portlandite reduction.

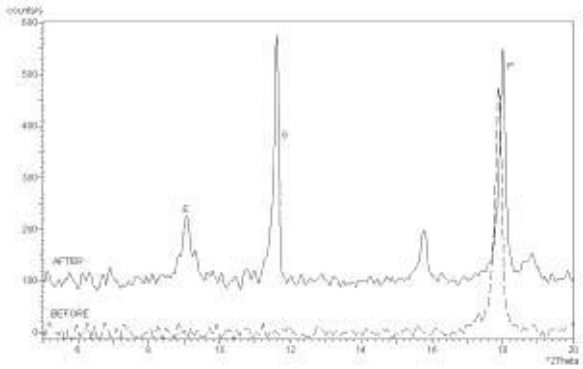

Figure 8. Specimen C before and after acid attack

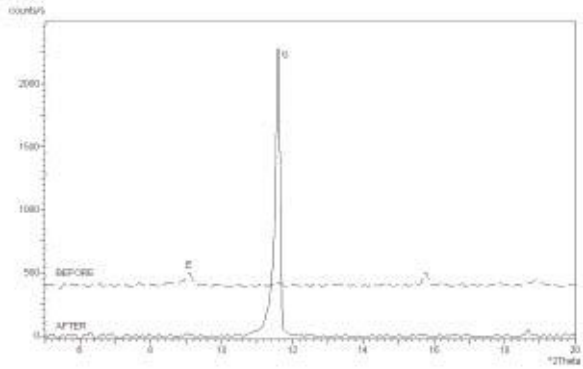

Figure 9. Specimen D before and after acid attack

From these results a substantial gypsum formation is evident in all the specimens. Ettringite is also formed in the case of samples A and C. Portlandite reduction was noted in Portland cement pastes.

3.4 EDS Analysis

From EDS analysis (Figure 10) the following chemical relationship were found toward the undamaged part of the sample:

1) Ca/S ratio increase;
2) Ca/Si ratio increase.

A similar trend was found on the other mortars. Therefore a single corrosion mechanism could be expected.

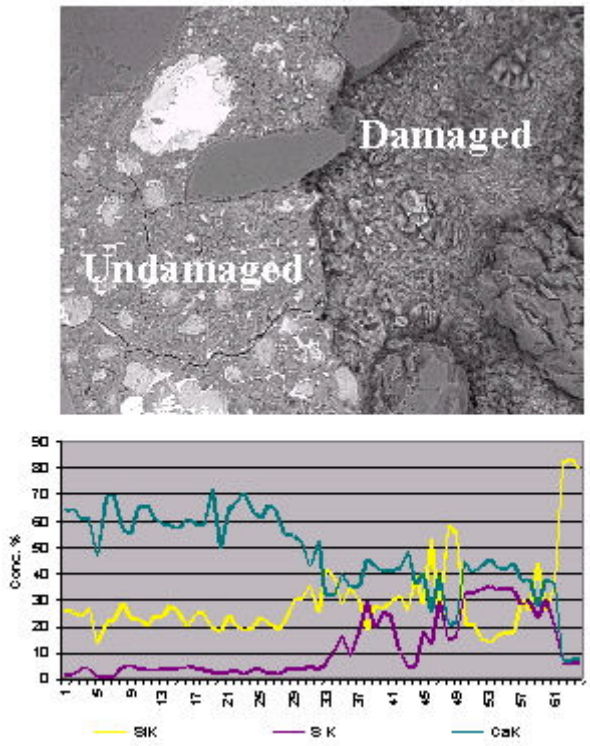

Figure 10. EDS Line Scan of Specimen B

3. DISCUSSION

4.1 Durability

The test conditions certainly affect final results. In fact calcium aluminate cement (CAC) mortar was the most resistant in sulphuric acid immersion test at pH 0 and slag mortar showed the highest resistance in bacteriological simulation chamber. Surprisingly at pH=1 all the mortars were corroded in a similar manner. Furthermore Fourie *et al.* [4,5], using hydrochloric acid and dolomite aggregates, outlined that high alumina cement was somewhat less resistant than Portland cement based mixtures. Such results are in contrast with our findings. Several reasons could explain these differences. In the cases studied by Fourie, the reaction between acid and binder is complicated by the high reactivity of dolomite in acidic environment respect to silica type aggregates. Choosing silica sand, we focalised our analysis only on the chemistry of reaction between binder and acid. The higher resistance of Portland cement could be connected to the stronger interfacial bond between hydrated calcium silicates and carbonate based aggregates [13]. Such hypothesis is confirmed by Fourie that observed a very high acid resistance of CAC/Alag mixture - aggregate with similar composition to alumina cement. In fact Alag type aggregates are not attacked by acid and they are able to bond strongly hydrated calcium aluminates [9]. Moreover the reaction product of hydrochloric acid aggression on hardened cement phase is mainly Calcium Chloride which is more soluble than gypsum (that is formed during sulphuric acid attack). Therefore different corrosion kinetics should be expected.

So acid type, pH and experimental procedure strongly influences acid resistance results.

In contrast with previous statements [8], neutralisation capacity alone cannot explain the different performances of mortars subjected to bacteriological and chemical aggression. The volume of acid added to keep the pH constant was very low and no significant differences were noted among the specimens. The kinetics of acid attack is presented in Figure 1. Sulphuric acid penetration in the alumina cement based mortar is very small. On the contrary in the case of slag mortar, it is much deeper. However acid aggression does not cause deleterious damages on these systems. Destructive

effect of acid is more evident for specimens A and D (Portland cement based renders) due to a larger mass reduction.

4.2 Chemical Morphological considerations and mechanism

XRD patterns pointed out that the main reaction product formed during acid degradation is gypsum. A significant specific surface area increase was also noted. Morphology variation is likely connected to gypsum precipitation and C-S-H alteration. Acid corrosion was further emphasised by SEM micrographs. Considering the small amount of ettringite detected during acid corrosion, we suppose that gypsum precipitation is the first cause of mortar degradation.

The involved reaction is:
$Ca(OH)_2$ (solution) + $H_2SO_4 \rightarrow CaSO_4 \bullet 2H_2O\downarrow$
Calcium hydroxide is provided by: 1)Initial cement hydration; 2)Dissolution of hydrated calcium silicates (Portland cement based mortar) or hydrated calcium aluminates (alumina based mortar).

At pH=0, that is a short time critical condition, the degradation process is governed by kinetics. The experimental results showed higher resistance of mortars with lower amount of portlandite. Therefore at pH=0, portlandite neutralisation is a reaction kinetically faster than the decomposition of hydrated cement phases. At pH=1, for longer immersion time, the degradation process is governed by thermodynamics and all hydrated phase are involved in the reaction (portlandite, hydrated calcium aluminates and hydrated calcium silicates). Afterwards substantial differences among mortars cannot be observed. Previous papers pointed out an increase of sulphuric acid resistance with water cement ratio [3,6]. The rise of water/cement ratio, which is connected to an increase of capillary pores, could balance the mechanical stress arising by gypsum crystallisation. Therefore concrete degradation due to acid attack could be very similar to damaging action of freeze-thaw cycles. The expansion, caused by gypsum crystalisation, could be the main reason of mortar failure.

4. CONCLUSION

The experimental work showed a larger selectivity of sulphuric acid immersion test at pH=0. Mortars resisting such test conditions also gave good results to bacteriological aggression. However, the bacteriological chamber is more similar to reality. Thus, the sulphuric acid immersion test could be a useful and fast experimental procedure to screen mortars before biogenic simulation chamber and field tests.

A mechanism of sulphuric acid degradation at pH=0 was supposed:

1) Acid reacts with portlandite to give gypsum;
2) Expansive gypsum formation causes internal stress determining mortar failure.

REFERENCES

[1] R.L. Islander, J. S. Devinny, F. Mansfeld, A. Postyn, H. Shih “Microbial Ecology of Crown Corrosion in Sewers”, Journal of Environmental Engineering, 117 (6), 1991, pp.751-770.

[2] S. Ehrich, E. Bock “Biogenic Sulphuric Acid Corrosion Test Procedure For Cement Bound Materials”, Proc. Int. Conf. Cem. Microsc., 1996, 18th, pp.331-341.

[3] T. Cerulli, C. Pistolesi, C. Maltese, D. Salvioni, G. Facchetti “Durability of Cement Mortars to Sulphuric Acid Attack”, Supplementary Papers CANMET/ACI on Durability of Concrete, 2000, Spain, pp.357-371.

[4] C.W. Fourie, M.G. Alexander “Acid Resistance of Sewer Pipe Concrete Mixtures” Proc. Fifth Intern. Canmet Conference, ACI Intern. Pub. SP-192, V.M. Malhotra Ed., 2, 2000, pp.705-719.

[5] M.G. Alexander, C.W. Fourier “Acid Resistance of Calcium Aluminate Cement in Concrete Sewer Pipe Manufacture” Calcium Aluminate Cement 2001, Proc. Intern. Conf. on CAC, July, 2000, R. D. Mangabhai and F.B. Glasser ed., Communication Ltd., London, 2001, pp.633-645.

[6] N.I. Fattuhi, B.P. Hughes “The Performances of Cement Paste and Concrete Subjected to Sulphuric Acid Attack”, Cem. Concr. Res., 18 (1992), pp.545-553.
[7] R.S. Ravindrarajah, C.M. Mercer “Sulphuric Acid Attack on High Strength Concrete” Durability of Building Materials and Components, Edited by S. Nagataki, T. Nireki and F. Tomosawa (1993).
[8] S. Ehrich, L. Helard, R. Letourneux, J. Willocq, E. Bock “Biogenic and Chemical Sulphuric Acid Corrosion of Mortars”, J. Materials in Civil Engineering, Nov. 99, pp.340-344.
[9] K.L. Scrivener, J.L. Cabiron, R. Letourneux “High Performance Concrete From Calcium Aluminate Cements”, Cem. Concr. Res., Vol.26, 1999, pp.1215-1223.
[10] N. De Belie, H.J. Verselder, B. De Blaere, D. Van Nieuwenburg and R. Verschoore “Influence of the Cement Type on the Resistance of Concrete to Feed Acids”, Cem. Concr. Res., Vol.26, N.11, 1996, pp.1717-1725.
[11] B. Espinosa, R. Letourneux, S. Marcdargent “Acid Attack of Hydraulic Cement Bound Materials: Corrosion Kinetics and Neutralisation Capacity”, 13thICC, 1996, paper 445.
[1] L. Franke, M. Oly, F. Pinsler “Richtlinie Für Die Prüfung Von Mörteln Für Den Einsatz IM Sielbau”, Tiefbau Ingenieur Bau Straβenbau, 4, 1997, 19-23.
[13] H.F.W. Taylor “Cement Chemistry”, 2nd edition, 1998, Thomas Telford ed., pp.354.

EFFECTS OF PREHYDRATION ON FINENESS CHARACTERIZATION OF GRANULATED BLASTFURNACE SLAG

B. Osbaeck

F.L.Smidth A/S, R&D, Laboratory, Copenhagen, Denmark. E-mail: bjarne.osbaeck@flsmidth.com

ABSTRACT

Like Portland cement clinker, granulated blastfurnace slag to be used as a cementitious material in mortar and concrete is ground to a certain fineness to achieve the reaction potential that is necessary for the desired strength development. Fineness characterisation based on measurement of the specific surface by air permeability is still the most widely used method in the cement and slag grinding industry. During the grinding process minor prehydration of the ground powder can take place even for granulated blastfurnace slag. This small prehydration can influence the results of the fineness measurement and can, when not taken into account, lead to erroneous conclusions e.g. in connection with grinding tests, mill comparisons and materials comparisons. The paper illustrates the character and magnitude of the effects based on analysis of data from a mill comparison test and from laboratory tests.

1. INTRODUCTION

The quality of cements and other cementitious products is judged primarily from their strength development potential as a binder in mortar or concrete. The strength producing potential is a matter of the inherent reactivity of the material(s) used as a basis for production of the cement or cementitious material, and the fineness to which it is ground in the finish grinding mill. Thus in industrial grinding of cements or cementitious materials one or more fineness parameters are used as control figures and indicators for expected strength performance. Also in evaluation of the grindability of different materials a fineness parameter is used to quantify the degree of fineness achieved by the grinding effort and thus becomes a key figure for evaluation.

In the cement industry a specific surface measured by the air permeability method is the most widely used fineness parameter. It is commonly performed according to the method developed by Blaine [1], but a similar method proposed by Lea and Parker [2] is used in some countries. They give similar results. Both methods are fairly simple and quick and give a figure correlated to the specific area and which – most importantly - usually gives a good correlation to the reactivity and strength development potential of the ground product.

However, when comparing e.g. products from different grinding installations one should be careful as the simple correlation to strength does not always hold. This is usually due to differences in particle size distribution of the final products but also other factors such as prehydration during grinding may influence the result. Due to its high reactivity towards water Portland cement is very susceptible to prehydration. But we have experienced that even a material such as granulated blastfurnace slag, though only characterized as latent hydraulic, can be prehydrated to a certain degree during storage and grinding. Furthermore this prehydration, even when very limited in magnitude, can have an influence on the results of fineness measurements and particularly on

Proceedings of the 11th International Congress on the Chemistry of Cement (ICCC)
'Cement's Contribution to the Development in the 21st Century'
Hosted by: The Cement and Concrete Institute of South Africa
CD-ROM produced by: Document Transformation Technologies
11 - 16 May 2003, Durban, South Africa
ISBN Number: 0-9584085-8-0
Editors: Dr G. Grieve and G. Owens
Congress Organised by: Event Dynamics

measurements of the specific area according to the air permeability method. Evidence of this feature is given in the following case study and from laboratory experiments.

2. COMPARISON OF SLAGS GROUND IN DIFFERENT MILLS

From a production of ground slag where different mills were in use for grinding of the product it was found out that using the same basic slag source one had to grind the slag to a substantially higher specific surface area as measured by air permeability in one mill than in another to achieve the same strength contribution figures of the final products.

To find the reason arrangements were made for comparative grindings using exactly the same slag source (Chemical characteristics in Table 1) .

Table 1. Chemical analyses (%), Modules and Glass content (%) of the slag.

CaO	SiO_2	Al_2O_3	MgO	Fe_2O_3	Mn_2O_3	TiO_2	K_2O	Na_2O	S-total
39.6	35.4	13.2	8.5	0.57	0.60	0.50	0.35	0.26	0.73

CaO / SiO_2	$(CaO + MgO) / SiO_2$	$(CaO+MgO+Al_2O_3)/SiO_2$	% Glass (BS 6699)
1.12	1.36	1.73	97

In addition to the two industrial mills in question (referred to in the following as “Mill A” and “Mill B”) tests were also performed in a pilot scale mill (“Mill C”) of the same type as Mill B. From experience it was found that the slag meals from Mill B had to be ground to a Blaine fineness 70-80 m^2/kg higher than those of Mill A to achieve the same strength figures in mixes with Portland cement. This difference was also used in the comparative test series. The products from Mill 3 were produced in the same Blaine range as those from Mill B.

Besides using the Blaine method the products were also characterized for fineness using laser diffraction spectrometry (LDS) to get a description of the particle size distribution (PSD). Supplementary fineness characterizations using air jet sieving and air elutriation were also applied.

The laser diffraction spectrometry were performed on Sympatec Helos equipment using wet dispersion in ethanol. The following key data were used from the particle size distribution measurement: the median size (d-50), the n- value according to the Rosin-Rammler-Sperling-Bennett (RRSB) distribution (n) and the calculated specific surface (SSA).

The air jet sieving was performed on an Alpine air jet sieving unit. The 32 µm and 45 µm residues were measured. The air elutriation was performed on an F.L.Smidth Flourmeter adjusted to separate at 10µm. The fine fraction thus achieved is designated AEF-10µm (AEF = Air Elutriation Fines). Key fineness results from the applied methods are found in Table 2.

Table 2. Fineness and LOI data on the ground slag samples

Mill	Sample	Blaine (m2/kg)	SSA (LDS) (m2/kg)	d50 (LDS) (µm)	n (LDS)	R 32µm (%)	AEF-10µm (%)	W 200 (%)	W 750 (%)
A	1	470	488	9.5	1.07	4.10	62.9	0.06	0.22
A	2	495	529	8.4	1.05	4.10	67.1	0.05	0.22
A	3	440	483	10.3	1.03	6.00	57.9	0.03	0.16
B	1	531	557	8.1	1.00	6.50	57.9	0.16	0.33
B	2	573	620	7.1	1.00	3.60	63.4	0.18	0.36
C	1	573	570	7.8	1.02	4.30	60.3	0.32	0.61
C	2	565	547	8.1	1.04	5.10	60.2	0.25	0.52
C	3	529	544	8.3	1.03	4.60	59.4	0.14	0.31

Knowing that particularly the Blaine measurement can be sensitive to prehydration of a cementitious material the state of prehydration had to be quantified. As basis for that a thermogravimetric analysis (TGA) of the samples was performed using a Stanton Redcroft thermobalance. The loss on heating up to 750°C in a nitrogen atmosphere (20°C per min.) was recorded. The results for the 8 samples are shown in Figure 1.

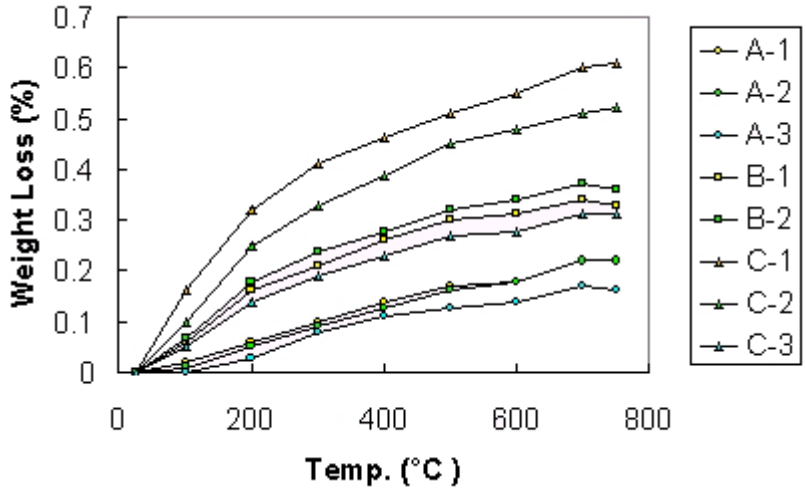

Figure 1. Thermogravimetric analysis of the ground slag samples (Cf. Table 1)

The loss occurs continuously over the temperature range, however, with a more pronounced increase up to 200°C. As key parameters the following are used: the cumulative weight loss up to 200°C (W 200) and 750°C (W 750). The values are found in Table 2.

Judged from these measurements it can be seen that the sequence of prehydration levels is as follows: Mill C > Mill B > Mill A. Sample 3 from mill C has lower loss values than the other two samples from that mill and is on the same levels as those from Mill B.

Comparison of the fineness results obtained by different method reveals some interesting features.

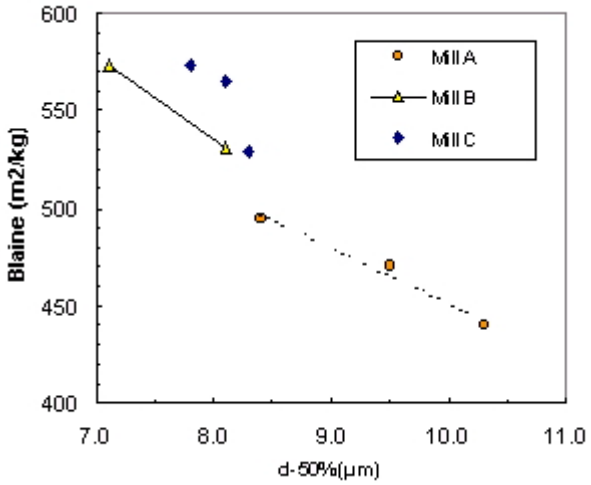

Figure 2. Specific surface (Blaine) versus median particle size (LDS)

Figure 2 shows the measured specific surface by the Blaine method plotted against the median particle size determined by laser diffraction. Both methods show Mill B and C products as being finer than Mill A products but there is a clear indication that at the same fineness level quantified by the d-50 value the Blaine value will follow the sequence Mill C > Mill B > Mill C, i.e. the same

sequence as for the prehydration level. Even the sample 3 from Mill C falls similarly as the Mill B samples just as for the prehydration values.

Since the spread of the PSD as indicated by the RRSB-n-values is not completely identical for the different mill products, differences in the Blaine values could be influenced by this factor. However, if we use a specific surface calculated from the whole PSD (SSA (LDS)) instead of the median particle size (d-50) we still see the same pattern (Cf. Figure 3).

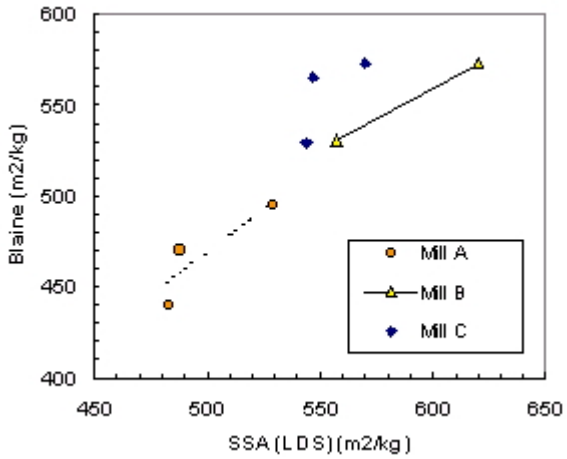

Figure 3. Specific surface (Blaine) versus specific surface (SSA) calculated from the PSD.

If we use the air elutriation fines (AEF-10µm) as fineness parameter we see a different situation (Cf. Figure 4).

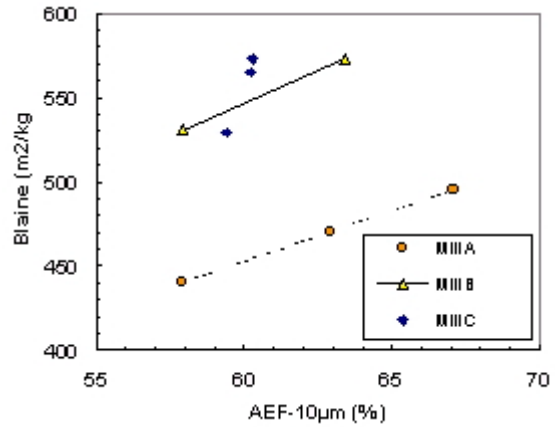

Figure 4. Specific surface (Blaine) versus air elutriation fines below 10 µm (AEF-10µm).

Judged from *this* fineness parameter the samples from Mill B and C are not generally finer than those from Mill A, and the Blaine sequence at equal AEF-10µm is similar but more accentuated than in the other comparisons.

From the comparisons above there seems to be a clear indication of the phenomenon that prehydration of slag the powder gives rise to an increased specific surface as measured by the air permeability method (Blaine method).

For quantification of the indicated effect regression analyses have been made on the present data expressing the measured Blaine value as a function of an alternative fineness parameter and the weight losses as measured by TGA. Regression models based on 200°C losses (W 200) are found in Table 3 and those on 750°C losses (W 750) in Table 4.

Table 3. Regression models. Blaine as a function of an alternative fineness parameter and 200°C loss.

Regres.	Model	r
(1.1)	Blaine = -29.9 * d50 + 232 * W200 + 740 (3.6) (35)	0.993
(1.2)	Blaine = 0.60 * SSA(LDS) + 264 * W200 + 157 (0.13) (58)	0.980
(1.3)	Blaine = 3.8 * AEF10 + 466 * W200 + 740 (2.8) (86)	0.924

Table 4. Regression models. Blaine as a function of alternative fineness parameter and 750°C loss.

Regres.	Model	r
(2.1)	Blaine = -32.1 * d50 + 141 * W750 + 745 (4.0) (35)	0.991
(2.2)	Blaine = 0.66 * SSA(LDS) + 164 * W750 + 106 (0.11) (32)	0.984
(2.3)	Blaine = 2.6 * AEF10 + 286 * W750 + 267 (3.5) (70)	0.876

The regressions turn out with high multiple correlation coefficients (r) and the individual regression coefficients (apart from those of AEF-10) are highly statistically significant (cf. the standard errors in the parenthesis below the regression coefficients).

There is a fairly large difference in magnitude between the specific effects of prehydration based on models with LDS parameters (d50 and SSA) as alternative fineness parameters and those obtained with AEF-10 as fineness parameter. This could be due to experimental errors or other non-recognized reasons, but it could also be a result of an effect of prehydration even on the LDS results.

Regression models expressing the selected *LDS fineness parameters* as a function of AEF-10 and the selected TGA losses turn out as shown in Table 5.

Table 5. Regression models. LDS parameters as a function of AEF-10µm and TGA losses.

Regres.	Model	r
(3.1)	d50(LDS) = -0.14 * AEF10 - 7.9 * W200 + 18.1 (0.08) (2.9)	0.816
(3.2)	d50(LDS) = -0.12 * AEF10 - 4.7 * W750 + 17.1 (0.10) (2.0)	0.746
(4.1)	SSA(LDS) = 4.2 * AEF10 + 321 * W200 + 328 (4.5) (138)	0.726
(4.2)	SSA(LDS) = 3.2 * AEF10 + 181 * W750 + 282 (4.9) (100)	0.636

Though the correlations are not impressive the regression coefficients for the loss values (W-values) are still generally statistically significant. This is an indication of a possible effect; however, a causal correlation still has to be demonstrated.

3. TESTING EFFECTS OF PREHYDRATION ON FINENESS RESULTS.

In order to verify the indicated effects of prehydration on Blaine fineness and possibly other fineness parameters, laboratory tests have been initiated with the aim of forcing a prehydration on slag powder and measuring the effect on fineness parameters. The first experiments performed have been based on simple treatments of a slag powder of low initial prehydration (W200=0.14%; W750=0.30 %) ground in a laboratory ball mill to a Blaine fineness of 480 m^2/kg.

One type of treatment was to expose a bed of slag powder to air at 100%RH for a short period of time. This did not give any significant prehydration of the slag meal. However, direct mixing with water at room temperature and at 100 °C followed by drying did. At present only preliminary results are available but they do indicate an effect on Blaine to support the findings of the mill products comparison presented above.

Figures 5 and 6 show the measured Blaine values as a function of weight losses up to 200°C (W200) and 750°C (W750). A marked effect is indicated on the Blaine as results of the prehydration, although these experiments show a higher prehydration level than measured in the mill comparison case.

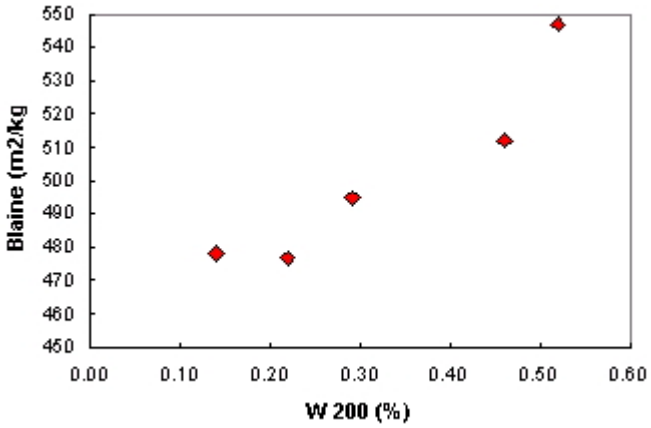

Figure 5. Specific surface (Blaine) versus TGA weight loss (25-200°C) on a ground slag sample submitted to different kinds of forced prehydration

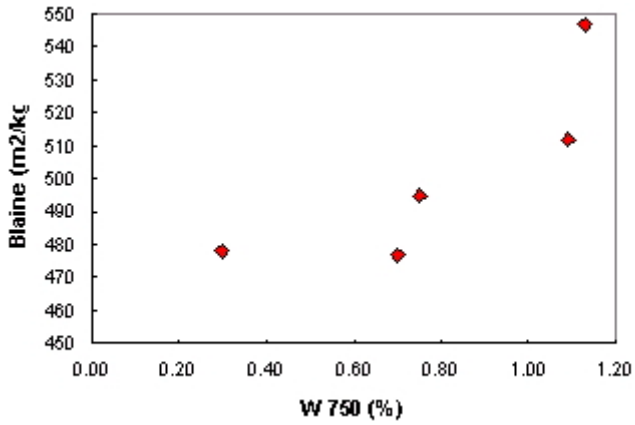

Figure 6. Specific surface (Blaine) versus TGA weight loss (25-750 °C) on a ground slag sample submitted to different kinds of forced prehydration

Estimates of the specific effects of prehydration on Blaine using the data above give the following approximate figures: + 160 m2/kg per percent. W200 and +70 m2/kg per percent. W750. If one takes the four data at highest W-level only the figures are: +190 m2/kg per percent. W200 and

+120 m2/kg per percent. W750, i.e. values approaching those estimated from the mill comparison data. Characterization of fineness by laser diffraction was also performed but no conclusive results were obtained.

4. DISCUSSION

The background for prehydration of slag is that a major part of slag used for cement and concrete has been granulated (rapidly cooled) by water and thus delivered and stored with a moisture content of typically up to 15%. During the storage of this product a certain amount of prehydration will take place. When grinding the slag it can be dried in a special drier before grinding. This is normally done in connection with grinding in a ball mill. When a vertical roller mill is used the drying is usually performed in the mill itself i.e. in combination with the grinding. Thus there will be a difference in the character of contact with water and water vapour dependent on the grinding procedure and equipment used and this can give rise to differences in the prehydration level of the ground products even if the raw slag used is the same. In the example above the A samples are from a ball mill using predried slag whereas the B and C samples are from vertical roller mills with combined drying and grinding.

Returning to the results of the present investigation it may seem surprising that a minute prehydration of a material should have such a marked effect on the measured Blaine fineness as indicated in the present study. But considering that the Blaine surface is measured by the resistance to an air flow through a packed bed of powder it could be argued, that a formation of hydrates on the surface of the particles could increase the resistance to the air flow and thus the resulting Blaine value. For ground slag particles where the surfaces in general are much smoother than those of ground Portland cement clinker particles due to the glassy character of the slag, the effect of such hydrate formations on the surface could be more pronounced.

To pursue the matter the samples from the mill product comparison have been investigated by scanning electron microscopy. This investigation revealed that distinct formations of hydrates were present on the surfaces of all samples even on the samples of lowest prehydration.

Figure 7 shows the surface of a particle from sample A-2 viewed under large magnification. Formations of hydrates on the otherwise smoothly looking surface are clearly visible.

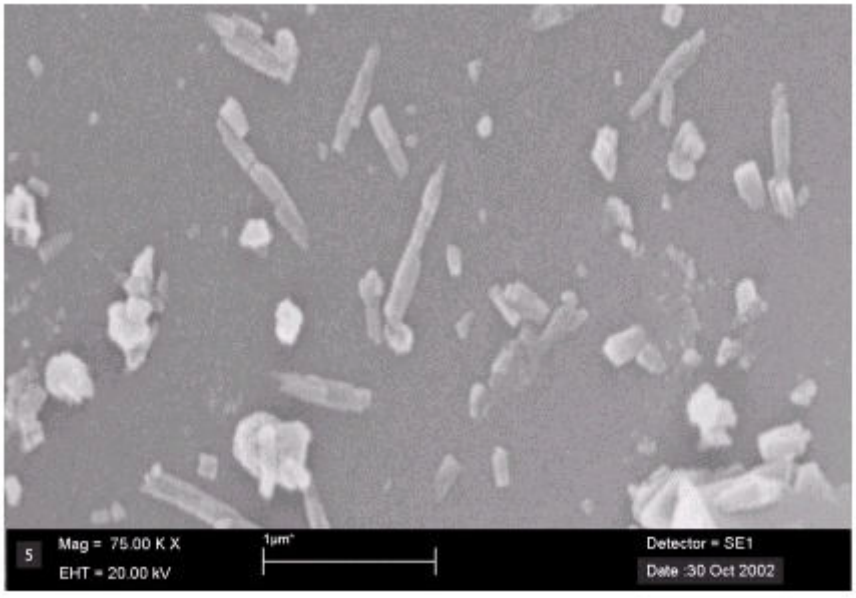

Figure 7. Scanning electron micrograph of surface of slag particle (Sample A-2) .
(1 µm bar indicated on the graph)

Particles from the B and C-series with a higher prehydration level in general had less clean surfaces and the hydrates formed on the surfaces seemed to be larger (Cf. Figure 8). On both micrographs small slag particles adhering to the surface are also visible but in general easy to distinguish from the tabular or rod-like hydrate formations.

The hydrate formations might also be able to influence the PSD measurements by laser diffraction since this technique is based on deflection of light by particles, but this has to be studied further.

The influence on the Blaine measurement results also deserves further investigations, but it is the opinion of the author that the data presented in this paper do indicate an influence of even small levels of prehydration.

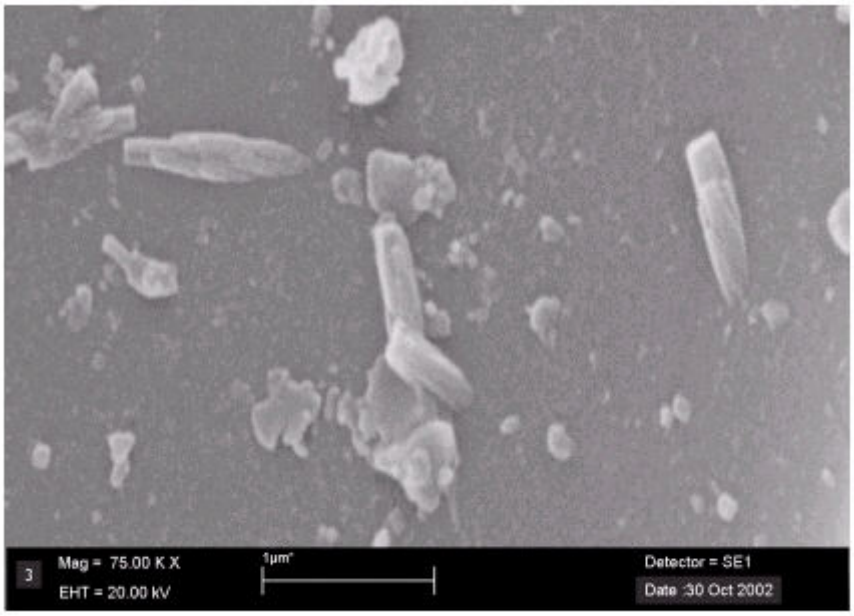

Figure 8. Scanning electron micrograph of surface of slag particle (Sample C-3) .
(1 µm bar indicated on the graph)

The magnitude of the effect is probably variable dependent on how the prehydration has taken place, so the quantifications attempted in the present investigation should only be considered as indicative of the order of magnitude that can prevail.

A standard measurement of loss-on-ignition on slag will not always be sufficient to reveal the state of prehydration of a slag powder since the measurement is disturbed by oxidations of constituents in a reduced state of oxidation. But a thermogravimetrical analysis performed in nitrogen seems to be a useful technique to reveal even small levels of prehydration.

The present paper has concentrated on the issue of the influence of prehydration of slag on the results of different fineness characterization methods. Another question is how prehydration may influence the reactivity of the slag when used a cementitious constituent. Investigations on this matter are taking place as well in our laboratory.

5. CONCLUSIONS

Prehydration of slag powder occurring during grinding seems to be able to give rise to increased values of the specific surface measured by the air permeability method (Blaine) even at small levels of prehydration. This is important to remember when comparing the performance of different mills and different materials, and when evaluating product performance with reference to fineness.

Indications were found to a possible effect of prehydration on the particle size distribution measured by laser diffraction spectrometry as well, but this needs further investigation.

The state of prehydration of slag, even at small levels of prehydration, can be measured by thermogravimetric analysis in nitrogen atmosphere.

REFERENCES

[1] ASTM C 204, Standard Test Method for Fineness of Hydraulic Cement by Air Permeability Apparatus. American Society for Testing and Materials.

[2] BS 4550: Part 3: Section 3.3: 1978 , Method of Testing Cement. Fineness Test. British Standards Institute.

SIMULATION OF CEMENT PASTE MICROSTRUCTURE DURING HYDRATION, CHARACTERIZATION OF THE PORE SPACE AND PERMEABILITY DETERMINATION

Christian Pignat, Parviz Navi and Karen Scrivener

Swiss Federal Institute of Technology, Department of Material Sciences
Laboratory of Construction Materials
MX-G Ecublens, CH-1015 Lausanne, Switzerland
E-mail: christian.pignat@epfl.ch, parviz.navi@epfl.ch, karen.scrivener@epfl.ch

ABSTRACT

An Integrated Particle Kinetics Model (IPKM) has been developed to simulate the evolution of cement microstructure during hydration. This model is not discrectized (based on pixels), so that features can be represented over several orders of magnitude of length. The capillary pore space is characterized by an analytical transformation into a network of cylindrical tubes, which allows a wide range of pore sizes to be described without resolution limits. The water permeability of the obtained network is then calculated by applying Darcy and Poiseuille laws.

1. INTRODUCTION

Empirical knowledge and experimental data on cement-based materials are well developed; nevertheless some phenomena are not well understood. Simulation in the field of cement-based materials can bring a better understanding and help to link microstructure with properties.

Based on a continuum approach, we have implemented an Integrated Particle Kinetics Model, (IPKM) for three-dimensional simulation of the evolution of tricalcium silicate (C_3S) microstructure during hydration [1,2,3]. This model considers spherical cement grains and hydrates. The model is vectorial because all the solid phases are described by a position and a radius. The hydration rate of each grain is controlled by three mechanisms in competition and depends on time, the radius of the anhydrous core and the thickness of hydrates.

In this paper the following aspects are presented: the microstructure formation, the hydration kinetics, the characterization of the pore space and the permeability calculations. Some numerical examples of pore size distributions and permeabilities are discussed. A general discussion of the model and perspectives are presented in conclusion.

2. MICROSTRUCTURE FORMATION

At the present stage of development the phase C_3S is considered because it is the main component of Portland cement and its hydration has been extensively studied. The particle-size distribution is similar to that of commercial cements in the range 1–60 µm. (At present limitations of computing power on the number of particles mean that particles below 1 µm in size are not considered.). The particles are placed at random in the computational volume at the desired water to cement ratio down to w/c = 0.4.

Proceedings of the 11th International Congress on the Chemistry of Cement (ICCC)
'Cement's Contribution to the Development in the 21st Century'
Hosted by: The Cement and Concrete Institute of South Africa
CD-ROM produced by: Document Transformation Technologies
11 - 16 May 2003, Durban, South Africa
ISBN Number: 0-9584085-8-0
Editors: Dr G. Grieve and G. Owens
Congress Organised by: Event Dynamics

Two hydration products are formed, calcium silicate hydrate (C-S-H) and calcium hydroxide (CH). The relative reaction volumes are shown in equation (1).

$$V_{C_3S} + 1.318\, V_{H_2O} \Rightarrow 1.57\, V_{C-S-H} + 0.596\, V_{CH} \quad (1)$$

The C-S-H grows on C_3S grains and the CH in the pore space. The C-S-H composition is considered constant during hydration and the "inner C-S-H" the same as the "outer C-S-H". A schematic representation of the different solid phases is shown in Figure 1.

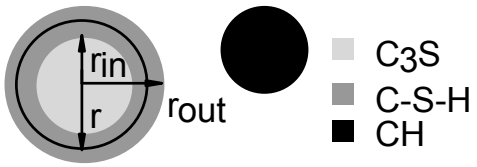

Figure 1. Schematic representation of the solid phases. r is the original anhydrous grain radius, r_{in} the radius of the remaining anhydrous core, r_{out} the radius of the C-S-H and r_{out} - r_{in} the thickness of C-S-H.

The number of CH grains is a function of time and the number of C_3S grains (equation (2)).

$$n(t) = n_{max}(1 - \exp^{-at}) \quad (2)$$

where: n(t) is the number of CH grains at time t, n_{max} is its maximum ($t=\infty$), a is a constant calculated from experimental data.

There is a random precipitation of small quantities of CH on the existing CH grains until the necessary amount given by the equation (1) is reached.

3. HYDRATION KINETICS

In this simulation the evolution of hydration is controlled by three different mechanisms, nucleation and growth, phase-boundary reaction and diffusion. The corresponding kinetics are described by equations (3)-(5), proposed in [4].

Nucleation and growth of products :

$$(-\ln(1-\alpha))^{1/3} = K_1 t \quad (3)$$

Phase-boundary reaction :

$$1-(1-\alpha)^{1/3} = \frac{K_2 t}{R_0} \quad (4)$$

Diffusion :

$$1-(1-\alpha)^{1/3} = \frac{\sqrt{K_3 t}}{R_0} \quad (5)$$

where α is the degree of hydration of the considered particle, R_0 its original radius, t the hydration time and K_1, K_2 and K_3 are parameters calculated through cement heat generation curves.

For spherical particles, the equations (3)-(5) can be re-formulated by replacing the degree of hydration by the rate of advancement of the reaction front dr_{in}/dt (equations. (6)-(8)).

$$dr_{in}(t) = -K_1^3 R_0 t^2 Exp(-K_1^3 t^3 / 3)\,dt \tag{6}$$

$$dr_{in}(t) = -K_2 dt \tag{7}$$

$$dr_{in}(t) = \frac{-\sqrt{K_3}}{2\sqrt{t}}\,dt \tag{8}$$

Since the third mechanism represented by equation (8) does not consider the thickness of the diffusion layer explicitly, we have replaced it by equation (9).

$$dr_{in}(t) = -\frac{K_3 dt}{r_{out} - r_{in}} \tag{9}$$

The rate of reaction (hydration) of each grain depends on the time, the original radius of the anhydrous core and the thickness of C-S-H. The passage from one kinetic regime to another occurs when two hydration rates become equal. Depending on original grain size, hydration may progress through the three mechanisms or only through the first and the third ones. A schematic representation of the three hydration kinetics for a single particle is shown in Figure 2. In this example the hydration of the considered grain is controlled by three mechanisms and the passage from the first mechanism to second one occurs in point A and from the second one to the third one in point B.

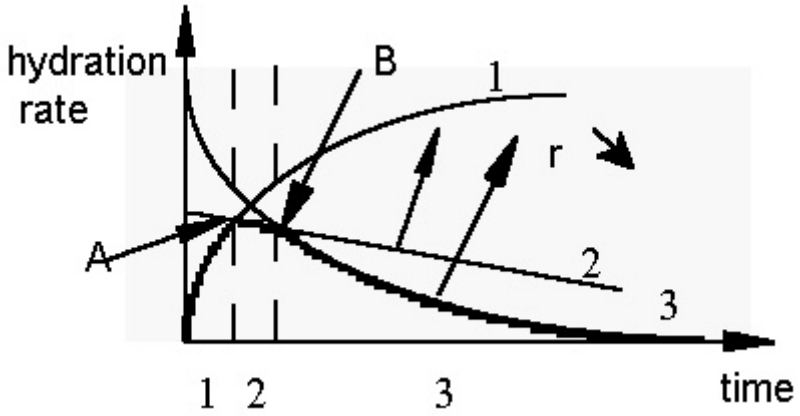

Figure 2. Schematic representation of the variation of three kinetic curves 1, 2, 3 with passage points from one mechanism to another one (points A and B).

After interparticle contacts take place, due to the increase of grain sizes, the hydration rate is diminished to take into account the effect of the diminution of the available space for the deposition of the C-S-H and the decrease of the overall amount of water to continue the hydration reaction (equation (10)).

$$(dr_{in}^{i}in(t))' = dr_{in}^{i}(t) \times \left(\frac{surface\ \ free}{surface\ \ total}\right)^{i} \times \left(1 - \frac{\alpha\nu}{\rho w_0 + \alpha}\right) \tag{10}$$

ν is the ratio between the products volumes (C-S-H + CH) and the reactant volume (C_3S), ρ is the density of cement and w_0 the water-to-cement ratio.

4. CHARACTERIZATION OF PORE SPACE

To characterize the pore space, a pore center is defined as a local maximum of the distance to the grains and a neck center (boundary between two pores) is defined as a local minimum of this distance. The pore centers are calculated analytically from algorithms developed in the field of molecular biology [5]. Extension of these algorithms, pore centers are defined as the center of a tangent sphere to four grains that can be placed without overlapping other grains. The pore network is represented by tubes linking adjacent pore centers and has a radius depending on the neck.

In Figure 3, a 2D illustration of two pore centers and one cylinder is presented. At each step of hydration the program controls the existence of pore centers and necks throughout the pore system and constructs the network of cylindrical tubes.

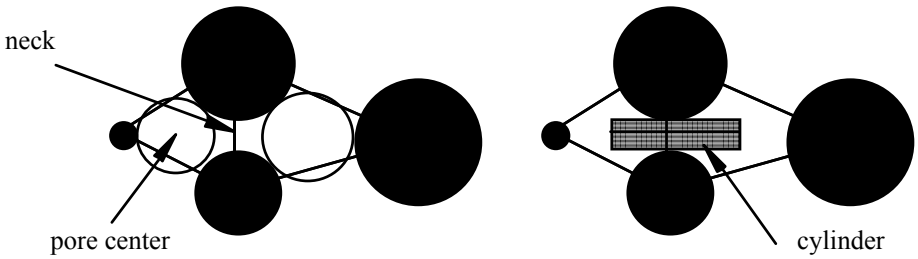

Figure 3. 2D schematic representation of two pores and one cylinder. The black circles represent cement particles.

The effective radius of a cylinder is the hydraulic radius of the neck; this value is defined by the equation (11).

$$R = \frac{2 * \text{area}}{\text{perimeter}} \tag{11}$$

This radius is equivalent to that of a circle the neck is circular.

5. PERMEABILITY CALCULATIONS

According to the Hagen-Poiseuille law, the flux q in a cylindrical tube of hydraulic conductivity g is given by equation (12):

$$q = \frac{g}{\mu}\Delta p \tag{12}$$

where: μ is the viscosity of fluid and Δp is the pressure difference between the two tube extremities.

The hydraulic conductivity is defined by equation (13) and the flux may be written by equation (14):

$$g = \frac{\pi r^4}{8l} \tag{13}$$

$$q = \frac{\pi r^4}{8l}\frac{\Delta p}{\mu} \tag{14}$$

To calculate the permeability, the principle of mass conservation is applied to each node i (tube extremity) of the network by equalizing the fluid flows that may enter or leave through the tubes connecting neighboring nodes j to the node i. By applying a Gauss-Seidel iterative method with

over-relaxation (equation (15)) all the nodal pressures are calculated. The flux direction can be chosen in one of the three directions.

$$p_i = \beta \frac{\sum_j g_{ij} p_j}{\sum_j g_{ij}} + (1-\beta) p_i \qquad (15)$$

p_i is the pressure at the node i and g_{ij} is the conductivity of the tube connecting nodes i and j, β is the over-relaxation parameter.

The over-relaxation considers the previous value to calculate the new one, β is between 1 and 2 and its optimal value, which permits the final solution to be found most rapidly, depends on the geometry.

At a given surface, by summing the fluids entering or leaving the surfaces exposed to the macroscopic pressure gradient ΔP and applying Darcy's law given by the equation (16), the permeability coefficient K can be calculated.

$$Q = K \frac{A}{\mu L} \Delta P \qquad (16)$$

where: Q is the macroscopic flow passing through the surface of area A and a length of L.

6. EXAMPLES: PORE SIZE DISTRIBUTIONS AND PERMEABILITY

The influence of particle size distributions (psd) on the pore size distribution of hydrated C_3S paste was studied through numerical simulation. Table 1 presents the size characteristics of four psds considered in this study. The cumulative weight distributions of the grains are also given in Figure 4. In this work the computational volume considered is 100μm*100μm*100μm and the water-to-cement ratio 0.42. We have simulated only the hydration of these four coarse cements D1, D2, D3 and D4 and examined their pore distribution.

Table 1. Size characteristics of the four psds considered in comparison with that of real cement: number of particles, specific surface, minimum and maximum radii

	Number of particles	Specific surface (cm^2/g)	ϕ_{max} (μm)	ϕ_{min} (μm)
D1	191	1058	40.4	10.9
D2	932	1597	40.4	5
D3	2556	1976	40.4	2.95
D4	4182	2085	40.4	2
real	110000	3585	40.4	0.5

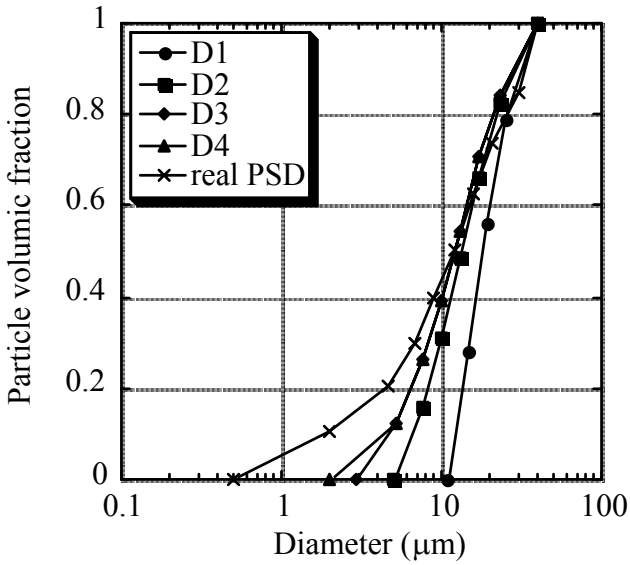

Figure 4. The four particle size distributions in comparison with a that of a real cement

The results before and after hydration for the pore size characteristics are given in Table 2. It presents the number of particles, cylinders, the minimum and maximum radii for the four cements. The reached hydration degree is around 0.95 and the porosity around 7 % for the four cements.

Table 2. The number of grains and cylinders, the maximum and minimum radii are presented for the four cements, before and after hydration. The hydration degrees at the end of simulation are around 0.95 for the four different cements, which gives a porosity around 7%.

	Number of grains	Number of cylinders	R_{max} (μm)	R_{min} (μm)
D1 before	191	2398	6.93	0.96
D2 before	932	11275	5.18	0.44
D3 before	2556	30662	4.01	0.24
D4 before	4182	49321	3.82	0.18
D1 after	229	1067	4.93	0.0039
D2 after	1118	3728	3.60	0.0011
D3 after	3067	11550	3.19	0.00045
D4 after	5018	16572	2.79	0.00023

Table 3. Number of cylinders smaller than the given size for the four cements before hydration

Radius in μm	D1 before	D2 before	D3 before	D4 before
10	2398	11275	30662	49321
5	2119	11275	30662	49321
2	125	4277	22350	42257
1	1	299	3158	8483
0.5		3	141	532
0.2				2

Table 4. Number of cylinders smaller than the given size for the four cements after hydration

Radius in μm	D1 after	D2 after	D3 after	D4 after
5	1067	3728	11550	16572
2	693	3200	11216	16382
1	316	1667	6847	11178
0.5	135	631	2903	4711
0.2	45	213	861	1420
0.1	20	91	355	637
0.05	7	43	146	314
0.02	3	16	46	100
0.01	3	6	31	50
0.005	2	2	9	23
0.002		2	2	70
0.001			1	6
0.0005			1	6

The number of cylinders as a function of size is shown in Tables 3 and 4, before and after hydration respectively.

For the permeability calculations, only the three coarsest particle size distributions were considered, due to the time and memory necessary for the calculations. To obtain lower porosities than can be by complete hydration, we have also dilated the solid structure by increasing all particle radii by the same amount. The permeability results for hydration are shown in Figure 5 compared with experimental results for C_3S pastes [6], and those for dilation of the solid structure are shown in Figure 6.

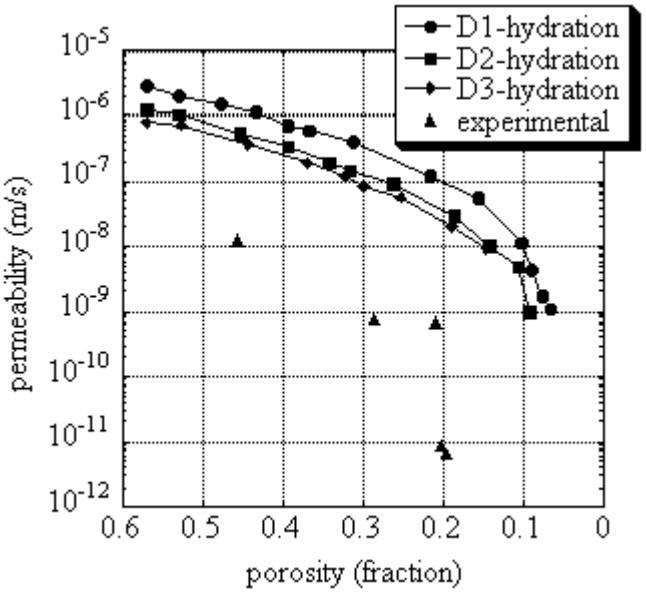

Figure 5. Experimental and calculated permeabilities during hydration. The specific surfaces are 1058 cm^2/g for D1, 1597 cm^2/g for D2, 1976 cm^2/g for D3 and 3200 cm^2/g for the real cement.

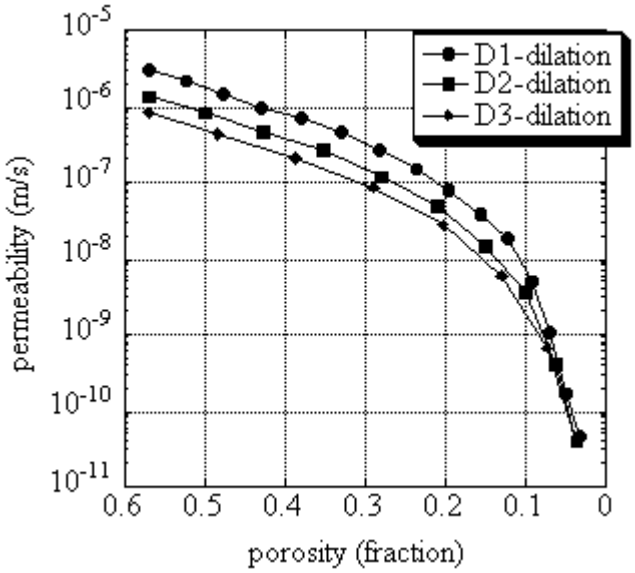

Figure 6. Calculated permeabilities for dilation of the solid structure

7. DISCUSSION

The particle size distributions for the simulation are coarser than real ones due to the limitations of calculation with a large number of particles. The number of grains increases considerably as smaller particles are taken into account (Table 1) and the calculation time is proportional to the square of this number. After hydration, this number of grains increases because grains of calcium hydroxide are created in the pore space. The number of cylinders is much greater than the number of particles. After hydration, of course, many pores and necks disappear because the pore space is reduced.

Regarding the cylinder sizes, the pore size distributions become finer during hydration (Tables 1-3) and the minimum values after hydration are around a nanometer. This analytical transformation of the pore space into a network of cylindrical tubes allows pores down to this nanometric size to be characterised, which avoids resolution problems and allows pertinent values for small pores to be considered.

The calculated permeabilities deviate considerably from the experimental values (Figure 5) but the main reason for this is that the specific surfaces are much smaller than in real cement. Another reason is that shrinkage responsible for the closure of small pores is neglected at this stage. During the simulation of hydration some problems arise due to changes in the pore connectivity as some pores are removed whereas others are created in the vicinity of these disappearing pores. When the structure is dilated such problems are avoided, indeed, the pore centers do not change position, decrease in size and then disappear progressively without creating other pores.

The percolation threshold of the porosity is found to be around 3 % (Figure 6), which is in agreement with the case of monosize spheres packing with overlapping [7]. The percolation threshold calculated for different models depends strongly on the type of structure and on the resolution of pixel based models: for sites in regular lattices the value is 15.4% [8], in the NIST model, results depend on pixel size (resolution), this value being 22 % for pixels of 1 μm, 17 % for pixels of 0.5 μm and 12 % for pixels of 0.25 μm [9].

8. CONCLUSION AND PERSPECTIVES

The model presented here allows the pore structure developed during hydration to be simulated. However, at present this IKPM model is still limited in several respects. Firstly, only C_3S and spherical solid phases are considered. It is intended in the future to introduce the other constituents of cement and their hydration products. The use of spheres is clearly an approximation of the real shapes of cement grains, but is necessary in a vectorial-based model and it is felt that the advantages of this approach outweigh the limitations. It is not so obvious that the shape has a strong influence on the microstructure and properties, but this point will be further explored by comparison with experimental results. The major advantage of such a “continuum” approach is that there is no lower limit on the pore size which can be represented, which opens up the possibility of studying shrinkage forces which arise during partial desaturation of the pores, as in drying or autogeneous shrinkage.

Concerning the hydration kinetics, the formula can be calibrated against experimental data. The parameters can be related to the particle size distribution and water-to-cement ratio in order to quantify the influence of these factors.

At present the major limitation is the difficulty in considering small particles due to the fact they are very numerous. The calculation time is proportional to the square of the number of particles and

this number increases enormously even when the minimum diameter is decreased by a small amount. The limit is actually around 2 μm when the computational volume is 100 μm*100 μm*100 μm. It may be possible to tackle this limit by imaging a different treatment of the small particles that react very quickly or by a multilevel.

ACKNOWLEDGMENTS

Financial support from Swiss National Science Foundation is gratefully acknowledged.

REFERENCES

[1] Navi, P.; Pignat, C., Simulation of cement hydration and the connectivity of the capillary pore space, Advances in Cement Based Materials, 4 (1996) 58-67.

[2] Navi, P.; Pignat, C., Three-dimensional characterization of the pore structure of a simulated cement paste, Cement and Concrete Research, 29 (1999) 507-514.

[3] Navi, P.; Pignat, C., Effects of cement size distribution on capillary pore structure of the simulated cement paste, Computational Materials Science, 16 (1999) 285-293.

[4] Bezjak, A.; Jelenic, I., On the determination of rate constants for hydration processes in cement pastes, Cement and Concrete Research, 10 (1980) 553-563

[5] Yeates, T. O., Algorithms for evaluating the long-range accessibility of protein surfaces, Journal of Molecular Biology, 249 (1995) 804-815

[6] Odler, I ; Köster, H., Investigation on the structure of fully hydrated Portland cement and tricalcium silicate pastes, III. Specific surface area and permeability, Cement and Concrete Research, 21 (1991) 975-982

[7] Elam, W. T.; Kerstein, A. R.; Rehr, J. J., Critical properties of the void percolation problem for spheres, Physical Review Letters, 52 (1984), 1516-1519

[8] Scher, H.; Zallen, R., Critical density in percolation processes, Journal of Chemical Physics, 53 (1970), 3759-3761

[9] Garboczi, E. J.; Bentz, D. P., The effect of statistical fluctuation, finite size error, and digital resolution on the phase percolation of the NIST cement hydration model, Cement and Concrete Research, 31 (2001), 1501-1514

INTERFACIAL ZONE ALKALI-ACTIVATED SLAG PASTE-SAND IN MORTARS CURED IN MAGNESIUM CHLORIDE SOLUTION

J. Deja[1] and K. Przybylski[1]

[1]Faculty of Materials Science and Ceramics,
University of Mining and Metallurgy, Cracow, Poland.
E-mail: deja@uci.agh.edu.pl and kaz@uci.agh.edu.pl

ABSTRACT

The transition zone between Portland cement paste and aggregate is the weakest region of the concrete which strongly influences strength, permeability and durability. It is commonly known that durability of alkali-activated slag mortars and concrete is very high. Very dense microstructure with very low content of the capillary pores is the main reason for the very high durability of AASC.

Ground granulated blast furnace slag activated by water glass was used for mortar preparation. Ordinary Portland cement mortars were used as reference samples. Tested mortars were cured in water and in a magnesium chloride solution respectively.

Diffusion coefficients of chloride ions and strength of the mortars were determined. Microscope observations with EDS microanalyses were also carried out.

Scanning electron microscope (SEM), X-ray diffraction, microporosity tests were used to investigate the interface between paste and sand.

The results show significantly lower diffusion coefficients and much denser interfacial zones between paste and quartz sand for alkali-activated slag mortars than for OPC mortars.

1. INTRODUCTION

It is generally accepted that alkali-activated slag cement, which consists of ground granulated slag and an alkaline activator, may exhibit higher strength, denser microstructure, and better durability than Portland cement [2-4].

It is commonly accepted that binding materials containing blast furnace slag are more resistant to the action of aggressive solutions. A good example is the resistance to chlorides. Impermeability decreases the chloride ions' diffusion coefficient in slag cement pastes. It is also important that some of the diffused chlorides become bound in the cement paste. Slag binder pastes show a higher chloride binding capability compared to OPC paste [5-7]. It reaches 1% of the cement mass.

Similar conclusions apply to the high chemical resistance of alkali-activated slag binding materials - products of hydrating these materials show lower dissolvability, which makes their durability higher than in case of products of hydrating Portland cement. The dissolvability of high alkali products of hydrating Portland cement, $Ca(OH)_2$, C_2SH_2, C_3AH_6 remains at the level of 0.3 - 0.5 g/l, whereas the dissolvability of low alkali lime hydrosilicates and hydrogarnets (main products of

hydrating AASC binders) remains in the range 0.035 - 0.05 g/l, and the dissolvability of carbonates and alkali aluminum silicates is even lower [8].

The interfacial zone between cement paste and aggregate in all concretes is the weakest region that controls permeability and durability. In the case of Portland cement concrete this interfacial zone is characterized by the prevalence of calcium hydroxide and higher porosity. The thickness of this zone in OPC concretes ranges from 50 to 100 μm [9].

There are only a few studies [9, 10, 11] where the transition zone in alkali-activated slag concretes have been investigated. Contrary to OPC mortars, in AASC mortars, dense and uniform transition zone was observed. The formation of the dense and uniform transition zone in alkali - activated slag mortars can be attributed to several factors such as the water reducing function of alkaline activators, the high initial concentration of $[SiO_4]^{4-}$ in the pore solution and increased dissolution of quartz in a high pH medium [9].

The objective of the study was to examine the properties of AASC mortars cured in $MgCl_2$ solution.

Comparative research on the diffusion of the chloride ions and the resistance to corrosion of AASC mortars and OPC mortars was carried out. Phase composition of the pastes and microscope observations were also carried out. Additionally, observations of paste-aggregate transition zones in 27 year old AASC concrete were conducted.

2. EXPERIMENTATION

2.1 Raw materials

The following materials were used in the research: granulated blast furnace slag, ordinary Portland cement, water glass, quartz sand and 27 year old AASC concrete.

2.1.1 Granulated blast furnace slag

A pelletized Polish blast furnace slag (BFS) was used in the research. The characteristics of the granulated blast furnace slag are given in Table 1. An XRD and microscopic analysis indicated that the slag consists mainly of glassy phase (ca. 85%) with some crystalline melilites. BFS was ground in ball mill to the specific surface ca. 400 m^2/kg.

2.1.2 Ordinary Portland Cement

A typical commercial ordinary Portland cement CEM I 32.5R (according to the European standard EN 197-1) was used in this study as a reference binder [1]. The chemical and some physical properties of the Portland cement are also given in Table 1.

Table 1. Chemical composition and physical properties of BFS and OPC.

Material	Chemical composition [mass %]							Specific gravity [kg/m^3]	Blaine Fineness [m^2/kg]
	CaO	SiO_2	Al_2O_3	MgO	Fe_2O_3	MnO	Na_2Oeq		
Granulated Blast Furnace Slag	43.76	39.38	6.13	8.25	0.35	0.47	1.09	2940	405
Ordinary Portland Cement	64.00	21.20	5.04	2.21	2.54	n.d.	0.78	3120	315

2.1.3 Water glass
Sodium water glass was used as the activator of the slag binder. Numerous previous studies have indicated that beside Na_2CO_3, water glass is the best activator for Polish granulated blast furnace slag [4, 6]. The silicate modulus of the water glass was 1.5.

2.1.4 Sand
Standardized quartz sand 0 - 2 mm was used in mortar preparation.

2.1.5 AASC concrete
The 100mm diameter cylinders were cut off from the 27 year old alkali - activated slag concrete. It was AASC concrete activated with Na_2CO_3 (6% of the slag mass) containing sand-gravel mix as the aggregate. The mean compressive strength of the AASC concrete after 27 years of curing was 43.2 MPa.

2.2 Preparation of mortars
The BFS and OPC, sand, water glass and water were used in mortars preparation. In alkali - activated slag mortar water glass was dissolved in the mixing water first and then mixed with the slag and sand. Constant water to binder ratio of 0.45 was used. The composition of mortars is presented in Table 2.

Table 2. Composition of the mortars

Mortar	Ingredients [g]				w/b
	Portland Cement	Slag	Water glass	Sand	
AASC	-	450	67.5	1350	0.45
OPC	450	-	-	1350	0.45

The fresh mortars were cast in 25x25x100 mm bars and plates of 80 mm in diameter and approx. 10 mm in thickness. Some pastes without sand (w/b=0.27) were also prepared for XRD analysis of hydration products. All the mortars and pastes were preliminarily cured for 28 days in water (temp. 20 +/- 1^{o}C).

2.3 Corrosion solution
The subject of the research was the effect of $MgCl_2$ solution on the described mortars. A solution with the concentration of 293g $MgCl_2/dm^3$ was used in the examination of diffusion and resistance to corrosion.

2.4 Examination of chloride diffusion through mortar plates
Prepared mortar rings (diameter 80 mm, thickness 10 mm) after 28 days of preliminary curing were used in diffusion measurements. The apparatus for measuring chloride diffusion through mortars consisted of two chambers, between which a plate made of the mortar was placed. The mortar plate was tightened with rubber gasket and silicon glue. The whole assembly was put together with screws located symmetrically around the mortar plate. The first chamber was filled with $MgCl_2$ the solution, whereas the second chamber was filled with saturated $Ca(OH)_2$ solution.

After 90, 120 and 180 days, a sample was taken from the chamber filled with the calcium hydroxide solution for chloride content analysis. Chloride content in the samples was determined by Mohr's method [12]. On the basis of the results of chloride ion concentrations in diffusion solutions, effective CL^- ion diffusion coefficients were calculated.

2.5 Sample durability tests
After 28 days of initial curing samples were moved to the corrosion environment. Tests on bars taken from chloride solutions and water (reference samples) were carried out after 28, 90, 180 and 365 days of curing.

2.6 Powder X-Ray Diffraction (XRD) Analysis
Powder XRD analysis was performed on OPC and AASC pastes after 28 days of hydration. The phases were identified from the characteristic peak database of the Powder Diffraction File of the Joint Committee on Powder Diffraction Standards.

2.7 Microporosity measurements
The microporosity of the mortars was determined by means of mercury porosimetry. The total porosity in the range of 4 to 7500 nm as well as average pore radius was measured. The samples were tested after 365 days of water curing.

2.8 Scanning Electron Microscope (SEM) Observations
The samples in the form of rectangular plates, with dimensions 2,5 x 1 x 1 cm, were cut using a diamond-wheel saw. They were mechanically abraded under kerosene with silicon carbide paper (up to 1200 grit No.). After polishing with diamond paste to a 1μm finish, the samples were ultrasonically cleaned with alcohol.

A careful attempt was made to monitor the development of the structures, morphologies and chemistry of samples formed under different conditions of experiments using scanning electron microscopy (SEM) with the backscattering electron image (BSE) mode together with energy dispersive X-ray spectroscopy (EDS) analysis.

2.9 Environmental Scanning Electron Microscope (ESEM) Observations
Pieces of 27 year old AASC concrete were used for ESEM observations. Microanalysis of the different interfacial zones (paste - aggregate) was also carried out.

3. EXPERIMENTAL RESULTS

3.1 Effective diffusion coefficients
The calculated “effective” chloride diffusion coefficients are presented in Table 3 and Figure 1.

Table 3. Values of “effective” diffusion coefficients of Cl ions.

Type of mortar	Time [days]	„Effective” diffusion coefficient [m^2/s] • 10^{-12}
AASC	0-90	2.20
	90-120	2.35
	120-180	2.48
OPC	0-90	21.21
	90-120	24.18
	120-180	31.17

It is well visible that “effective” diffusion coefficient of Cl ions for AASC mortar is much lower than for OPC. It confirms also the results of previous work [4, 6, 7] where the positive influence of granulated blast furnace slag on the chloride resistance of the mortars and concretes was observed.

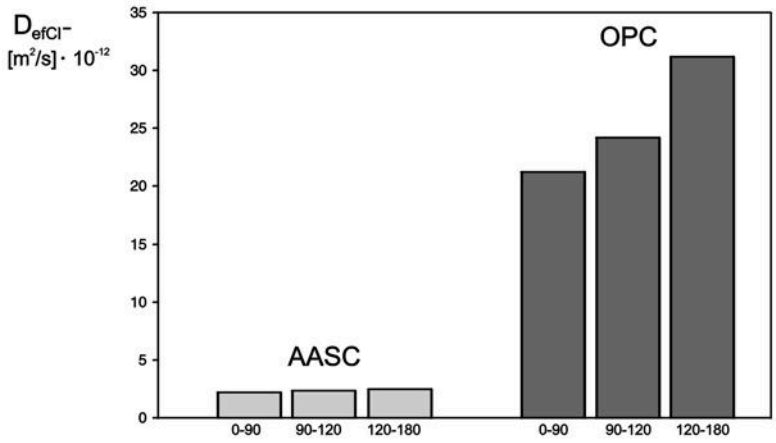

Figure 1. Values of "effective" diffusion coefficients of Cl ions.

3.2 Durability in $MgCl_2$ solution

The results of flexural and compressive strength measurements are presented in Table 4.

Table 4. Results of flexural and compressive strength tests.

Environment	Flexural/Compressive strength [MPa]					
	3 d	28 d	28+28 d	28+90 d	28+180 d	28+365 d
AASC						
Water	7.90 24.90	10.90 46.80	13.20 63.90	14.10 70.40	14.60 77.20	14.70 80.30
$MgCl_2$	-	-	12.90 62.40	13.80 66.95	13.70 69.45	13.60 66.90
OPC						
Water	8.30 21.20	14.40 41.80	11.60 43.70	11.70 44.90	11.80 49.60	11.85 52.10
$MgCl_2$	-	-	12.10 39.40	6.90 21.48	3.20 15.05	0.00 0.00

OPC mortars cured in the $MgCl_2$ solution showed clear corrosion changes after ca. 180 days. A substantial swell could be seen at the ends and along edges of the bars. After 180 days of curing significant reduction of the strength was noted (~ 50%). After one year the samples were completely destroyed. On the other hand AASC mortars confirmed very high resistance to the $MgCl_2$ action.

3.3 XRD Analysis of Hydration Products

For better understanding of the microstructural properties of the AASC mortars and concretes, the phase composition of the paste was determined. The XRD patterns of the AASC paste and OPC paste after 28 days of water curing are presented in Figure 2.

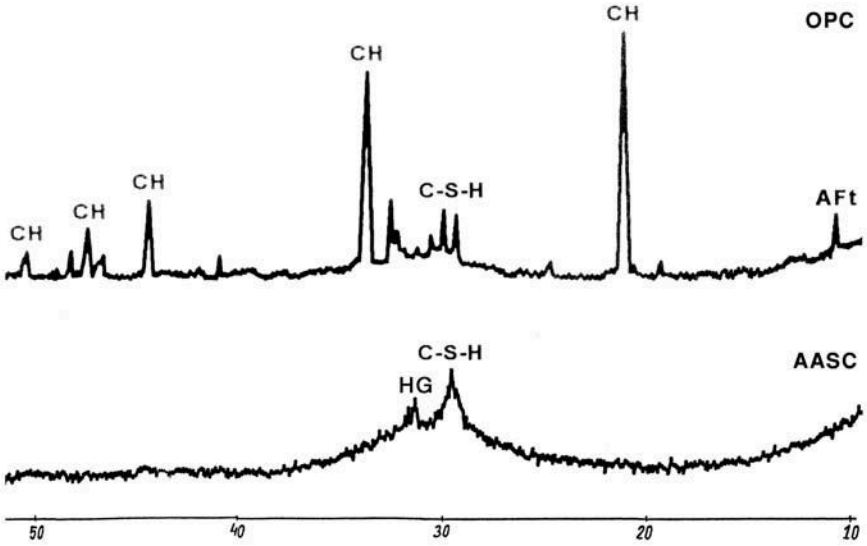

Figure 2. XRD patterns of OPC and AASC pastes after 28 days of curing.

The hydration products in OPC paste are typical: C-S-H phase, portlandite and ettringite. In AASC paste amorphous C-S-H phase is dominating the hydration product. Traces of hydrogarnets (HG) were also detected.

3.4 Microporosity

The microporosity of the mortars after 365 days of water curing is presented in Table 5 and Figure 3.

Table 5. Porosity of the mortars.

Type of mortar	Total porosity [mm^3/g]	Average pore radius [nm]
AASC	12.6	4
OPC	28.5	28

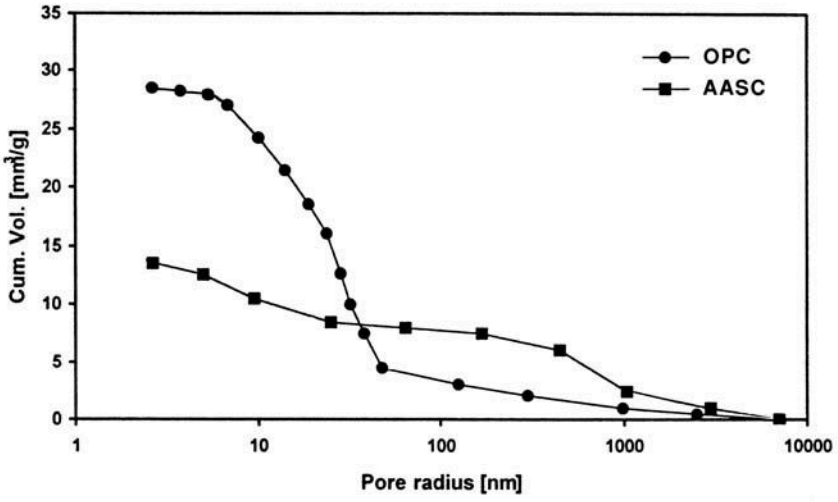

Figure 3. Pore size distribution.

It is very clear that the porosity of the AASC mortar is less than half of the porosity of the OPC mortar. The average pore radius for AASC mortar is also very low, which means that small gel pores dominate this mortar.

3.5 SEM observations

Morphologies of the mortar samples and the transition zone between Portland cement paste/quartz sand and alkali-activated slag cement/quartz sand after the corrosion test in $MgCl_2$ solution are shown in Figures 4-8. SEM observations were conducted for both 1 mm regions: saturated $Ca(OH)_2$ solution / mortar and $MgCl_2$ solution / mortar. In the case of Portland cement – $Ca(OH)_2$ contact region the material was dense without cracks and pores. On the other hand in the case of Portland cement mortar after reaction in $MgCl_2$ solution, the samples were completely corroded (see Table 4). Many cracks have been observed in the analysed region of the OPC (Figure 4). Contrary to the $Ca(OH)_2$ solution – mortar region, the interfacial zone between Portland cement paste and quartz sand in these samples was characterized by many regions rich in Al and Cl (Figure 5).

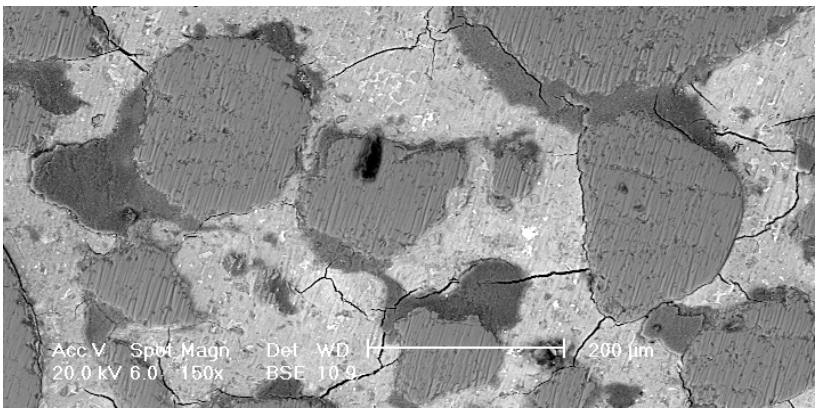

Figure 4. Microstructure of OPC mortar in the contact with $MgCl_2$ solution (1 year of exposure)

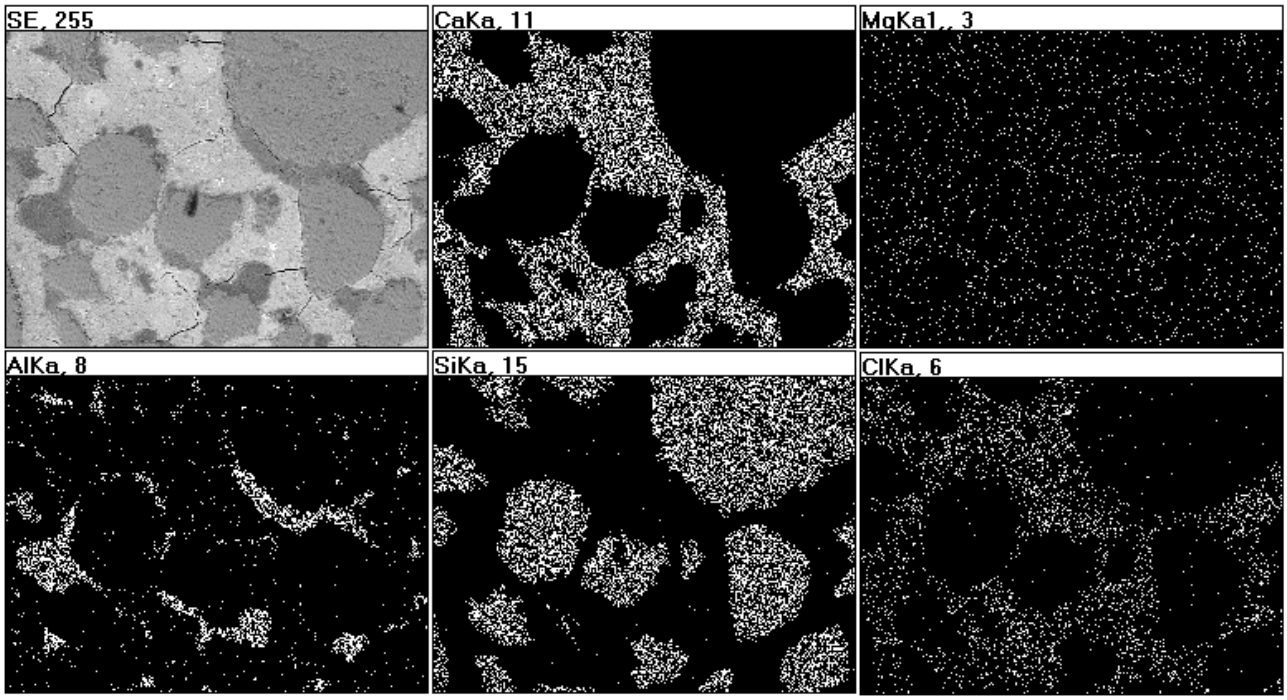

Figure 5. X-ray map in the region shown in Figure 4.

Figure 6(a) and 6(b) shows the surface morphology of AASC mortar in the contact region with $Ca(OH)_2$ solution. It can be seen that this material exhibits dense microstructure without cracks and excellent adhesion between paste and aggregate. It has also been observed that the paste/aggregate contact layer is very compact. It corresponds very well with the results presented in Table 4 (very low porosity of the AASC mortars cured in water). On the other hand in the case of AASC mortars after corrosion in $MgCl_2$ solution, the progress of corrosion and a large number of cracks in the outer part of the samples were observed. Figure 8 shows the X-ray maps of this region indicating strong accummulation of Mg and Cl in this zone (ca. 800μm distance from ASSC mortar vicinity – Fig.7a). It appears that in the presence of Mg^{2+} ions the replacement between these ions and Ca ions in C-S-H phase takes place. But, it is very evident that even after one year of corrosive exposure the development of corroded zone was limited and much smaller than for OPC mortar. Contrary to the OPC samples, no enrichment in Al, and Cl on the surface of the sand grains was observed.

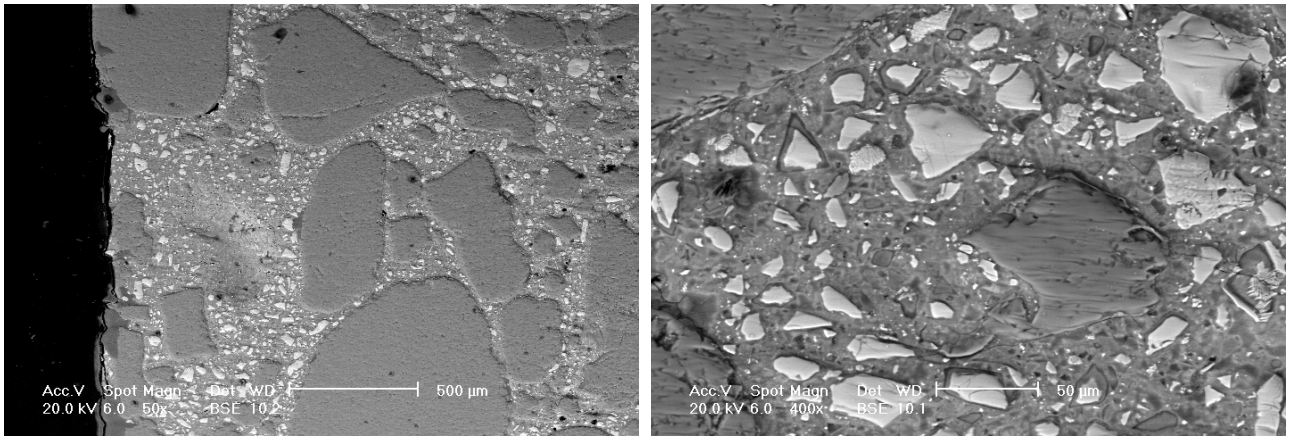

(a) (b)

Figure 6. Microstructure of AASC mortar in the contact with $Ca(OH)_2$ solution (1 year of exposure); (a) magnification 50x, (b) magnification 400x

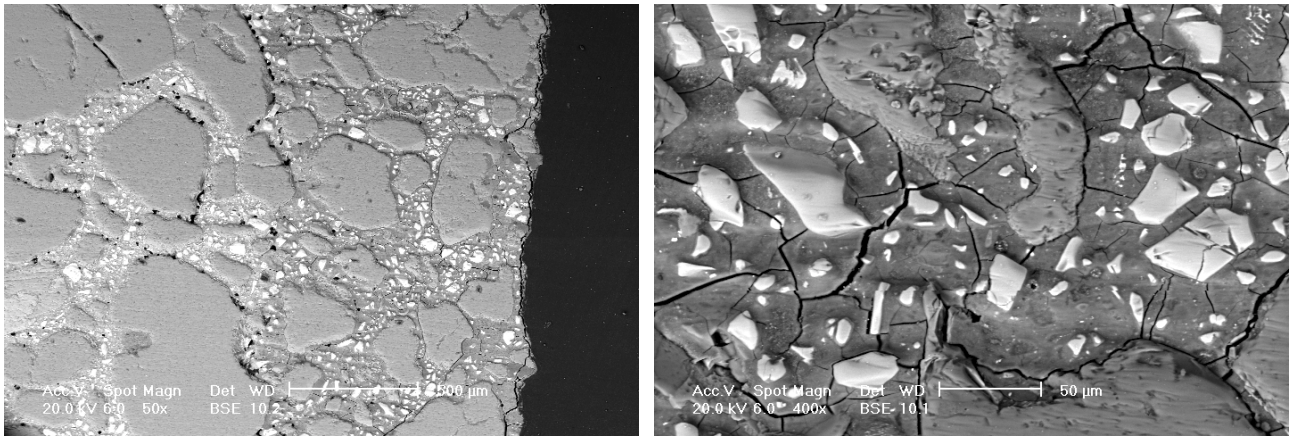

(a) (b)

Figure 7. Microstructure of AASC mortar in contact with $MgCl_2$ solution (1 year of exposure); (a) magnification 50x, (b) magnification 400x

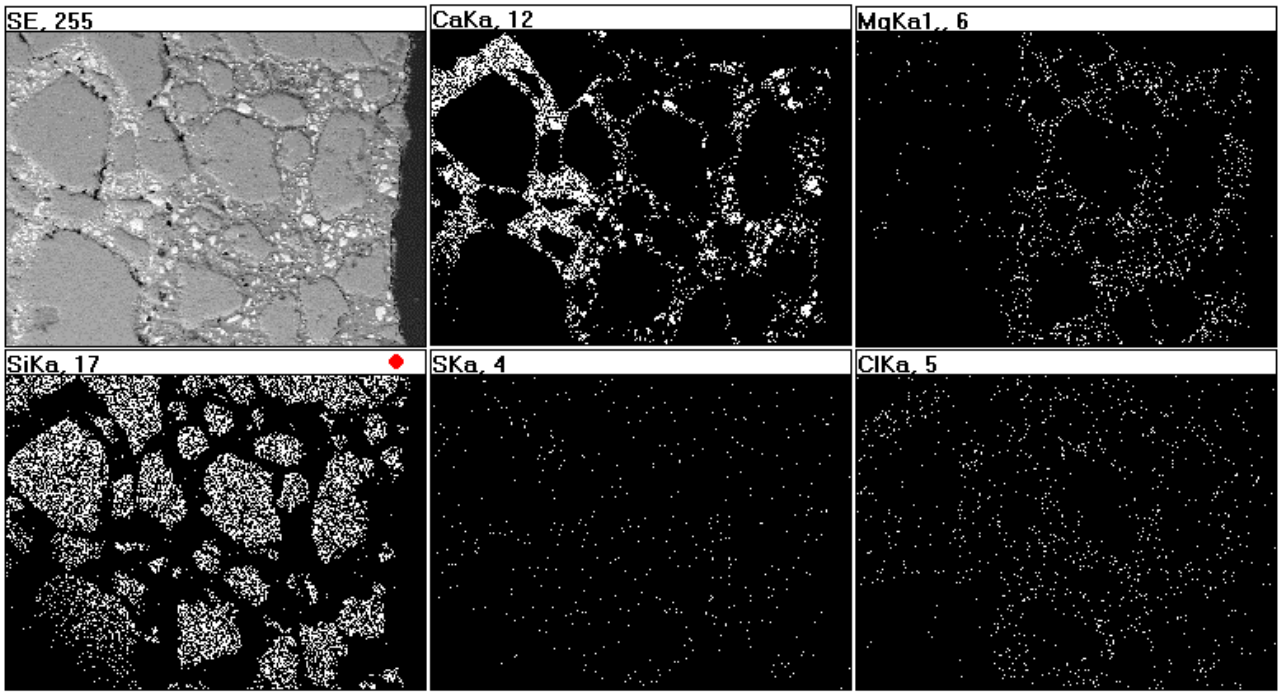

Figure 8. X-ray map in the region shown in Figure 7a.

3.6 ESEM observations

Generally, compact C-S-H phase was detected as a main product in 27 year old AASC paste. Some quantities of $CaCO_3$ and thomsonite were also present. The microstructure is highly densified with no microcracks. The interfacial zone between paste and gravel is very dense and even traces of interaction paste - grain were found (Figure 9.).

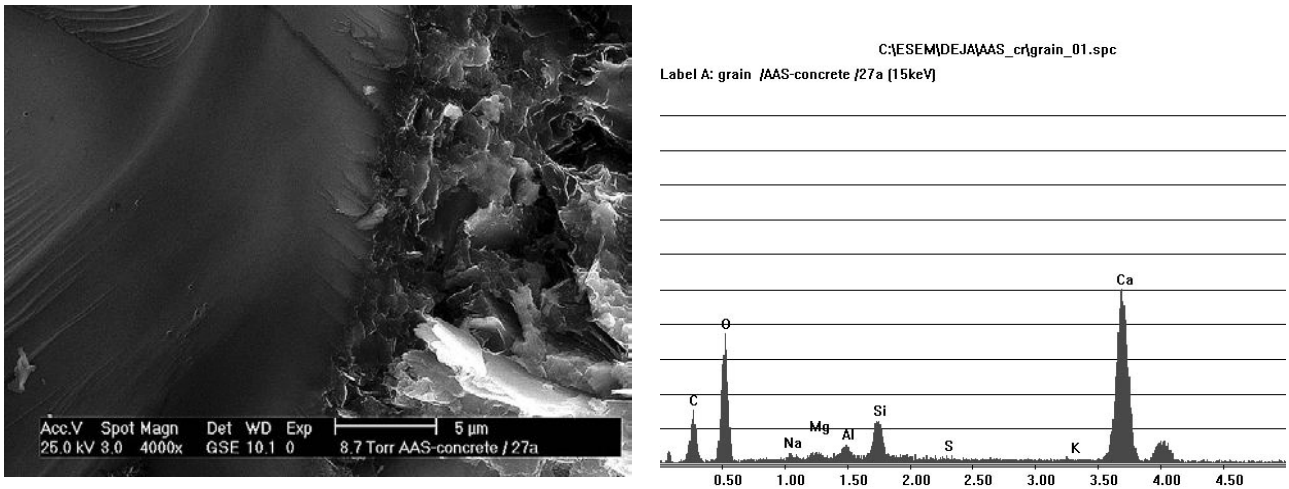

Figure 9. Interfacial zone grain - AASC paste (ESEM + EDS).

4. CONCLUSIONS

This study has investigated the resistance of alkali - activated slag mortar to the action of $MgCl_2$ solution. The “effective” diffusion coefficients of chloride ions in AASC mortar and OPC mortar were determined. The phase composition of the pastes, interfacial zone paste - aggregate in the mortars and 27 year old AASC concrete was also investigated.

The following conclusions can be drawn based on the experimental results:

(1) The "effective" diffusion coefficients of Cl ions in AASC mortars are lower by a class compared to OPC mortars.
(2) Durability of AASC mortars to the action of highly concentrated $MgCl_2$ solution is significantly higher than ordinary Portland cement mortars.
(3) The phase composition of the AASC paste, low porosity and very dense interfacial zone paste - aggregate are the main reasons for the very high durability of AASC mortars. The absence of portlandite and the low crystallinity of the C-S-H phase in these pastes form the dense and impermeable microstructure of the mortars and concretes.
(4) In the presence of Mg^{2+} ions in the aggressive medium the replacement between these ions and Ca^{2+} in C-S-H phase takes place. But, even after one year the development of the corroded zone is very limited.
(5) ESEM observations of 27 year old AASC concrete confirmed that interfacial zone paste - gravel is very dense with no microcracks. The observations confirm also Shi hypotheses that the presence of alkalis in AASC paste markedly increases the dissolution rate of quartz [9]. The surface dissolution of sand grains will enhance the bonding between quartz and alkali - activated slag paste.

REFERENCES

[1] EN-197-1, European Standard Cement - Part 1: Composition specifications and conformity criteria for common cements were tested, 2000.
[2] D.M. Roy, Alkali-activated cements. Opportunities and challenges, Cement and Concrete Research 29 (1999) 249-254.
[3] B. Talling, J. Brandstetr, Present state and future of alkali activated slag concretes, in: Fly Ash, Silica Fume, Slag and Natural Pozzolans in Concrete, Vol. 2, Proceedings of the 3rd International Conference, Trondheim, Norway, ACI SP114, 1989, pp. 1519-1545.
[4] J. Deja, J. Malolepszy, Effect of cementitious material on the corrosion of steel development in the environment of high chloride content, Proceedings of International Conference on Corrosion of Steel in Concrete, Sheffield 1994, Vol. II, pp. 684-687.
[5] S. Goto, M. Daimon, Roceedings of the 8th International Congress on the Chemistry of Cement, Rio de Janeiro, 1986, VI, 405-409.
[6] J. Deja, Chloride Resistance of Pastes and Mortars Containing Mineral Additives, Proceedings of the 10th International Congress on the Chemistry of Cement, IV, Gothenburg (1997) 4iv15.
[7] J. Deja, J. Malolepszy, Resistance to chlorides, Proceedings of International Conference, Trondheim, Norway, ACI SP 114, 1989, pp. 1547-1564.
[8] V.D. Gluchowski, Cement-Wapno-Gips, 4/1976 (in Polish)
[9] C. Shi, P. Xie, Interface Between Cement Paste and Quartz Sand in Alkali-Activated Slag Mortars, Cement and Concrete Research, vol. 28, No. 6, pp. 887-896, 1998.
[10] P.V. Krivenko, Proceedings of 1st International Conference on Alkaline Cements and Concretes, vol. 1, pp. 11-130, Kiev, 1994.
[11] J.Malolepszy, K.Przybylski,Effect of paste composition and microstructure on the durability of alkali activated slag concretes, Proceedings, 14th International Corrosion Congress Co-operation in Corrosion Control, Cape Town, South Africa, 26th September to 1st October 1999, Vol.122, paper 123,0 (pp.1-7).
[12] A. Bobrowski, B. Barchańska, Chemia Analityczna 24 (1979) 857-863 (in Polish).

EFFECT OF SILICA FUME ADMIXTURE ON THE PROPERTIES OF FLY ASH CEMENTS

Zbigniew Giergiczny

Górazdze Cement S.A., Technical University of Opole, Poland.
E-mail: zbigniew.giergiczny@gorazdze.pl

ABSTRACT

In this work the silica fume addition to fly ash cement was studied. Silica fume of high pozzolanic activity was considered as a good supplement of low-calcium fly ash. The progress of the reaction between fly ash and calcium hydroxide was investigated, as well as the rate of the process occurring in the system fly ash – silica fume – calcium hydroxide was analyzed. A significantly higher calcium hydroxide consumption in the presence of active microsilica was found using the thermogravimetric method. In this reaction the calcium silicate hydrates are preferentially produced.

The beneficial influence of silica fume addition on the strength of fly ash cement mortars should be attributed to its very high pozzolanic activity and fineness, giving a filler effect – small SF particles enter the space between cement grains. The "excess" gel-like C-S-H produced in the pozzolanic reaction can thus fill the pores in hardened paste and consequently the total porosity decreases. The mean pore diameter is also reduced.

This low calcium hydroxide content together with reduced porosity allows the assumption of a significantly higher corrosion resistance of these materials in an aggressive environment. The examination of mortars stored for a long time in sulphate solutions ($MgSO_4$, H_2SO_4), and in satured sodium chloride confirmed this.

1. INTRODUCTION

Fly ashes are commonly used in cement and concrete production, because of their ability to react with alkalis, mainly calcium hydroxide evolved during the hydrolysis of calcium silicates from cement clinker. The hydrated calcium silicates and aluminates are thus produced. This fly ash property is known as pozzolanic activity [1], [2], [3].

Cements and concretes produced with fly ash show low heat of hydration, lower shrinkage, better workability, high corrosion resistance and fairly good strength at later ages. The negative feature revealed in building practice, attributed to the presence of fly ash in cementitious materials is low strength development, as compared to the cements from standard group CEM I, as well as very poor strength development at low temperatures. This is attributed to the retarded pozzolanic process, strongly affecting the physical and mechanical characteristics of hardened fly ash composites.

There is no one opinion about the start of pozzolanic reaction between the glassy fly ash substance and calcium hydroxide. It seems however, that this is determined by the activity of the pozzolan. Therefore some operations, such as very fine grinding, grain size separation, alkali activation, chemical additives or thermal treatment are used to improve the pozzolanic properties [5], [6]. In this work the ways of modification of fly ash cement mechanical properties by silica fume are

Proceedings of the 11th International Congress on the Chemistry of Cement (ICCC) 11 - 16 May 2003, Durban, South Africa
'Cement's Contribution to the Development in the 21st Century' ISBN Number: 0-9584085-8-0
Hosted by: The Cement and Concrete Institute of South Africa Editors: Dr G. Grieve and G. Owens
CD-ROM produced by: Document Transformation Technologies Congress Organised by: Event Dynamics

presented. Silica fume, formed as a by-product from ferrosilicon alloy metallurgy, is known for its high pozzolanic activity and can be used as as supplement of poorly pozzolanic fly ash, modifying the hardening process at early ages.

The following studies were carried out in this work:

- kinetics of fly ash – $Ca(OH)_2$ pozzolanic reaction,
- effect of silica fume on the properties of fly ash cement.

2. MATERIALS

The samples of cements were prepared in laboratory from commercial Portland cement, fly ash and silica fume. The chemical composition of the materials used is given in Table 1.

Table1. Chemical composition of materials

Material	Percentage of component in wt. %									
	l.o.i.	SiO_2	Al_2O_3	Fe_2O_3	CaO	CaO_f	MgO	SO_3	Na_2O	K_2O
PFA	1,9	50,8	23,9	8,6	3,6	0,2	2,8	0,8	0,8	2,9
SF	0,1	91,4	1,24	3,4	0,4	---	---	---	0,63	1,6

Silica fume – a by-product from ferrosilicon metallurgy is formed as a result of reduction of quartz by carbon in an electric furnace and consists mainly of amorphous silica. The XRD pattern of silica fume is shown in Figure 1.

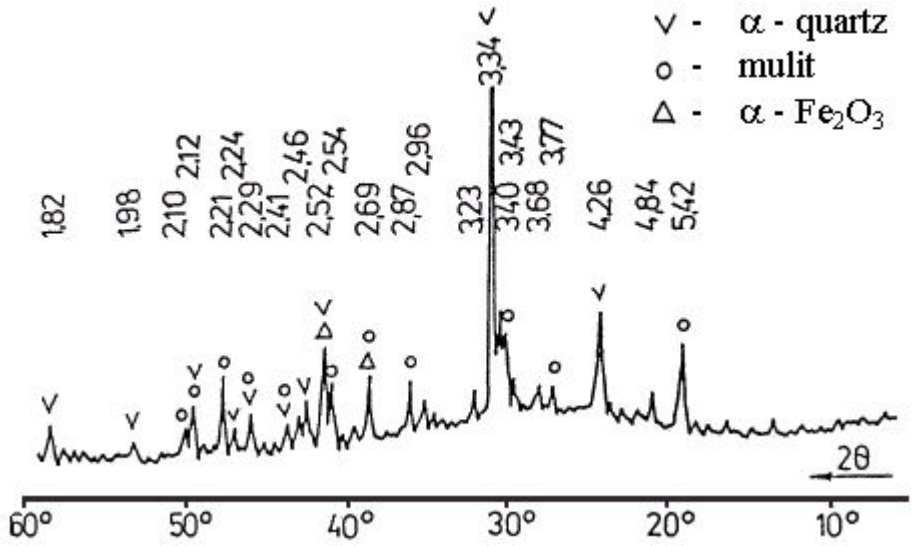

Figure 1. XRD pattern of fly ash

Fly ash, originating from black coal combustion reveals, apart from glassy phase, some amounts of quartz, mullite and haematite, as main crystalline components. The XRD pattern of fly ash is shown in Figure 2.

Cement was produced from Portland cement clinker of the following phase composition (calculated by Bogue method): C_3S – 57,5%; C_2S – 19,2%; C_3A – 9,8%; C_4AF – 6,7%; $CaSO_4$ – 1,5% and natural gypsum added as 4,0%.

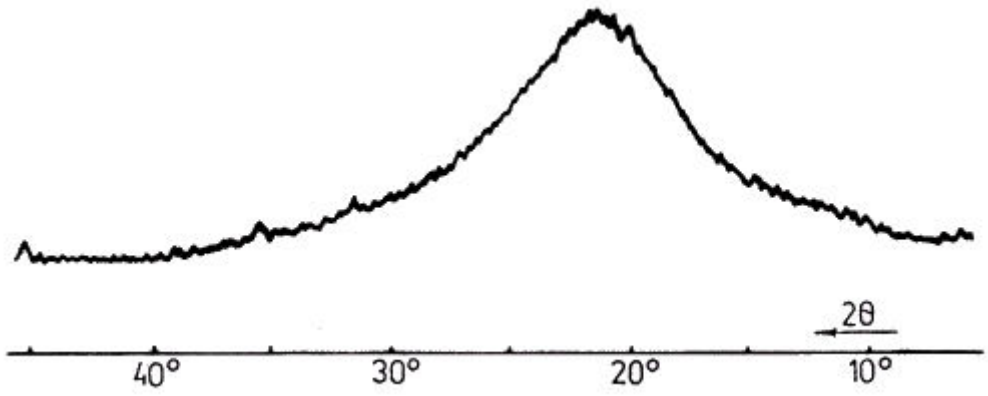

Figure 2. XRD pattern of silica fume

3. KINETICS OF FLY ASH – $CA(OH)_2$ POZZOLANIC REACTION

Two cementitious mixtures were produced to follow the course of the reaction between the fly ash admixture with silica fume and calcium hydroxide:

1) Mixture I – 70% PFA and 30% $Ca(OH)_2$ (in wt. %)
2) Mixture II – 10g SF added to 100g of mixture I.

The mixtures were hydrated at water to solid ratio 0,6. The pastes thus produced were stored in sealed containers. The hydration was stopped after 1, 3, 7,14, 28, 90 and 180 days respectively; the dried samples were investigated using differential thermal analysis, thermogravimetry and X-ray diffraction. In Figure 3, the DTA curves for mixtures I and II given above are plotted.

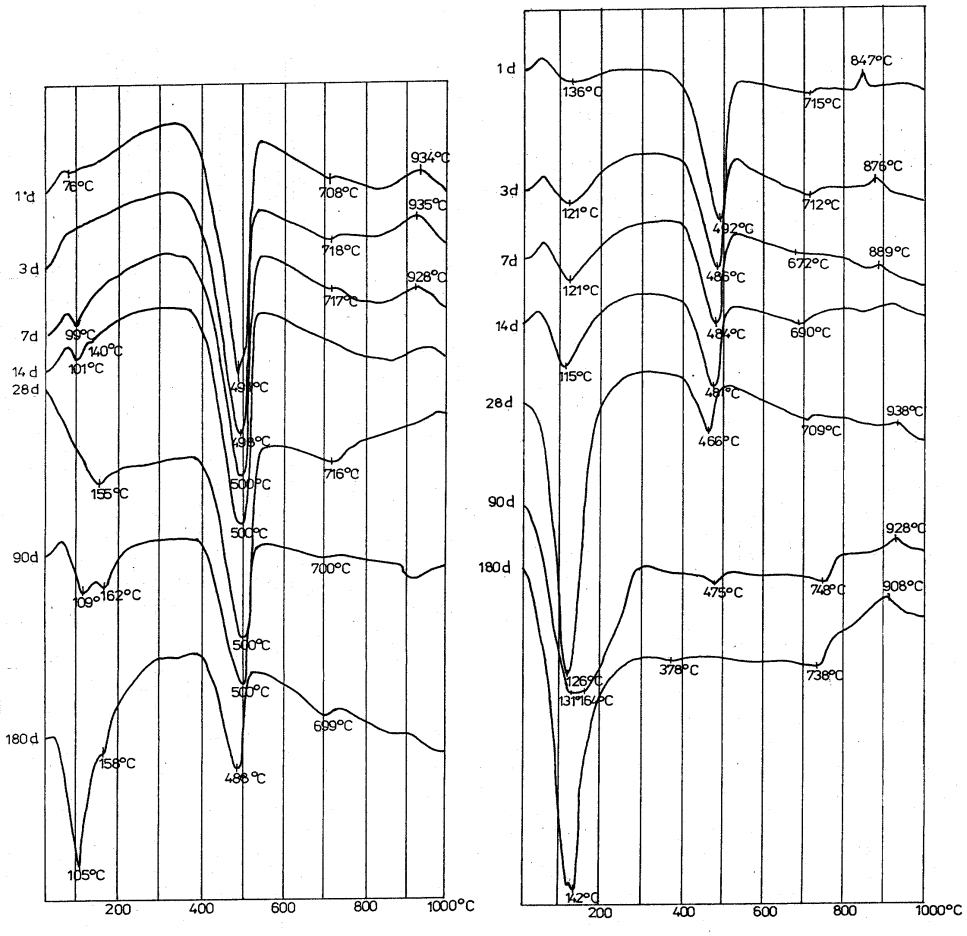

Mixture I Mixture II (with silica fume)

Figure 3. DTA curves of hydrated mixtures

From the set of DTA results it is evident that $Ca(OH)_2$ consumption in the mixtures with silica fume is significantly accelerated. The $Ca(OH)_2$ decomposition peaks in the temperature range of 475 - 490° are reduced and the endothermic peak in the range of 120 – 130° C increases with time. The latter one corresponds to the decomposition of gel-like pozzolanic reaction product. At 180-day hydration there is no calcium hydroxide in the sample admixture with silica fume – all $Ca(OH)_2$ was consumed by active fly ash and silica fume components. These results have been also confirmed by XRD studies where the $Ca(OH)_2$ and C-S-H peaks show the same trends (see Figure. 4).

The amount of $Ca(OH)_2$ consumed in the pozzolanic reaction, calculated based on TG data, is shown in Figure 5.

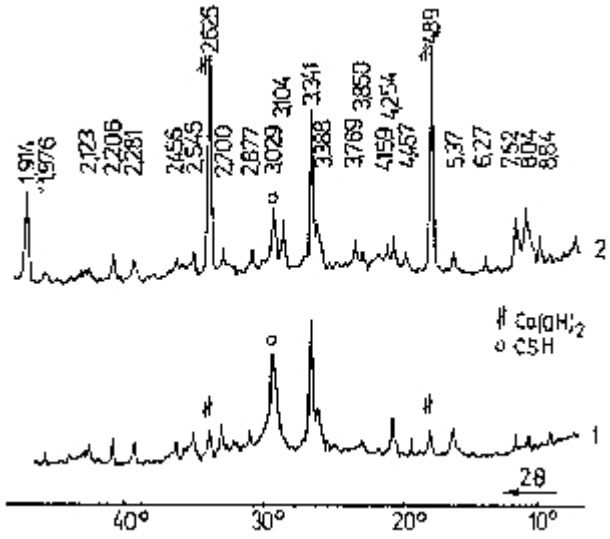

Figure 4. XRD patterns after 180 days hydration
1- mixture II (with silica fume), 2- mixture I

As is evident from DTA curves (see Figure 3) as well as from the data shown in Figures 4 and 5, the silica fume admixture plays a role of active supplement to the fly ash of low pozzolanic activity within the first days. The calcium silicate hydrates are mainly produced in this early reaction.

4. EFFECT OF SILICA FUME ON THE PROPERTIES OF FLY ASH CEMENT

4.1.Properties of fly ash cements tested with silica fume

The fly ash cements were produced by simultaneous grinding of clinker, fly ash and gypsum. The composition and properties of cements are shown in Table 2.

Table 2. Composition and properties of fly ash cements

Sample code	Composition of cements, wt.%			Density g/cm^3	Specific surface, m^2/kg
	Clinker	PFA	Gypsum		
Cement "0"	96	---	4	3,07	311,2
Cement 1	81	15	4	2,94	304,8
Cement 2	66	30	4	2,85	321,2
Cement 3	46	50	4	2,77	327,0

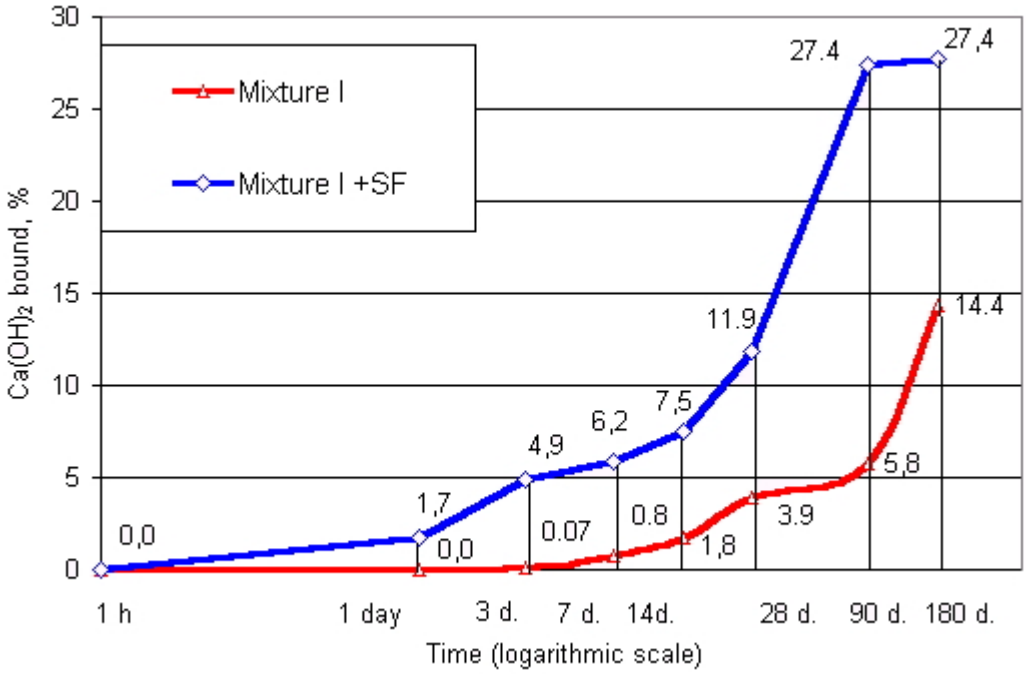

Figure 5. Rate of $Ca(OH)_2$ consumption in pozzolanic reaction.

Silica fume was added at 5 and 10% by mass of cement (mixing was done in a laboratory mill). The mortars were produced following the EN 196 standard. The compressive strength was tested on 4x4x16 cm bars following the procedure given in EN 196.
The results of the compressive strength tests are given in Table 3.

Table 3. Compressive strength of fly ash cements

Sample code	SF content in wt.%	Compressive strength in MPa at age			
		3 days	7 days	28 days	90 days
Cement 1	---	20,6	27,5	38,0	52,0
Cement 1	5	21,0	30,5	51,9	60,1
Cement 1	10	22,7	33,2	52,3	61,3
Cement 2	---	17,7	22,5	34,7	49,3
Cement 2	5	21,7	28,8	51,5	60,1
Cement 2	10	22,6	30,1	49,6	59,9
Cement 3	---	8,3	14,0	23,5	41,5
Cement 3	5	13,7	20,2	37,2	50,3
Cement 3	10	14,7	24,5	43,1	53,7

In Table 4 the total porosities and mean pore radii for 90-day matured paste produced using cement 1 (1% PFA) with or without the added 5% of silica fume are given. Both values decreased with silica addition and this is important from the durability point of view.

Table 4. Results of porosity measurements

Sample	Total porosity cm^3/g	Mean pore radius, nm
Cement 1(15% PFA)	0,2797	38; 650
Cement 1(15%PFA + 5%SF)	0,2478	4,8; 38

The durability of fly ash and silica fume containing mortars was also tested. For this purpose the following investigations were carried out:

- the mortars were stored in a sulphate aggressive environment,
- the mortars were produced using saturated NaCl solution and stored in such a solution (testing for possible use of mixed cementitious materials in some special works).

Sulphate resistance. This was evaluated based on the reduction of compressive strength for mortars stored in two different solutions:

- sulphuric acid of SO_4^{2-} concentration - 4800 mg/dm^3,
- magnesium sulphate solution of Mg^{2+} concentration – 3000 mg/dm^3.

The samples of mortars were put into the aggressive solution after 28-day maturing in standard conditions, in water. The observations were carried out within 2 years, for cement 2 and 3 admixture with 10% SF. The compressive strength of mortars is shown in Table 5.

Table 5. Compressive strength of mortars cured in different liquid media

Type of cement	Liquid environ-ment	Compressive strength in MPa at age			
		90 days	180 days	360 days	720 days
Cement "0" No admixture	Water	53,6	55,9	60,1	60,3
	H_2SO_4	53,6	49,3	42,7	40,7
	$MgSO_4$	53,9	52,1	39,5	37,6
Cement 2 30% PFA	Water	51,7	60,9	64,3	64,0
	H_2SO_4	54,4	59,7	62,9	58,8
	$MgSO_4$	52,7	56,7	55,5	55,0
Cement 2 30% PFA 10% SF	Water	57,3	61,8	62,3	63,9
	H_2SO_4	54,4	61,0	61,8	63,7
	$MgSO_4$	52,7	57,0	51,6	51,0
Cement 3 50% PFA	Water	31,2	37,0	42,0	42,1
	H_2SO_4	34,2	39,1	45,3	39,0
	$MgSO_4$	31,2	40,7	43,4	38,5
Cement 3 50% PFA 10% SF	Water	45,6	47,2	48,0	48,0
	H_2SO_4	45,5	47,0	48,4	45,6
	$MgSO_4$	40,6	40,3	34,5	31,4

As is evident from the data given in Table 6, the fly ash admixture is one way of improving sulphate resistance, while the silica fume addition brings about the modification of mechanical properties. The sulphate resistance, which is very good in H_2SO_4 solution, decreases significantly in $MgSO_4$. It should be derived from the mechanism of reaction between $MgSO_4$ and hydrated paste, where the decomposition of amorphous C-S-H occurs, apart from gypsum formation. Magnesium hydroxide and silica produced in this process have no cementitious properties [6]. The reactions of $MgSO_4$ with hydration products can written as follows:

$$Ca(OH)_2 + MgSO_4 + 2H_2O \rightarrow CaO_4 \cdot 2H_2O + Mg(OH)_2$$
$$3CaO \cdot 2SiO_2 \cdot nH_2O + 3MgSO_4 + 7H_2O \rightarrow 3CaO_4 \cdot 2H_2O + 3Mg(OH)_2 + 2SiO_2 \cdot nH_2O$$

Therefore in case of mortars produced from cements with fly ash and silica fume, at low calcium hydroxide content and very high amounts of C-S-H, the compressive strength decrease is the consequence of a detrimental $MgSO_4$ effect on gel-like C-S-H stability.

4.2 Properties of fly ash cements produced and stored using NaCl solutions

The studies were carried out for cement without admixture (cement "0"), cement 2 (30% PFA) and cement 2 modified with silica fume. The cement pastes were produced with NaCl solution of concentration 310 g NaCl/dm^3. After 2-day hardening the mortars were stored in a NaCl saturated solution. The compressive strength tests showed the differences between the "neat" cement and the pozzolanic cements. Cements with pozzolanic admixtures show continuous strength development, while cement without admixture does not. Additionally, cement with fly ash and silica fume exhibits very high strength after prolonged storage - 90 days and more, when the strength decrease is observed for mortar without pozzolanic admixture (Figure 6). This mortar reveals, on visual examination, some surface cracks being the results of swelling.

The following features were noticed during the DTA and XRD investigations (see Figures 7 and 8):

- in hardened cement paste produced from Portland cement, calcium chloroaluminate $3CaO{\cdot}Al_2O_3{\cdot}CaCl_2{\cdot}10H_2O$ and calcium hydroxide $Ca(OH)_2$ are detected,
- in cement – fly ash paste modified with silica fume there is no $Ca(OH)_2$ peak; the small $3CaO{\cdot}Al_2O_3{\cdot}CaCl_2{\cdot}10H_2O$ peak is detectable after 90 days curing; a significant amount of C-S-H is noticeable.

Such a situation can be attributed to the high ability of C-S-H formed preferentially in the presence of fly ash (and silica fume) to incorporate the chlorine ions. Another reason is presumably related to the change of concentrations in the liquid phase in the presence of pozzolanic - siliceous admixtures.

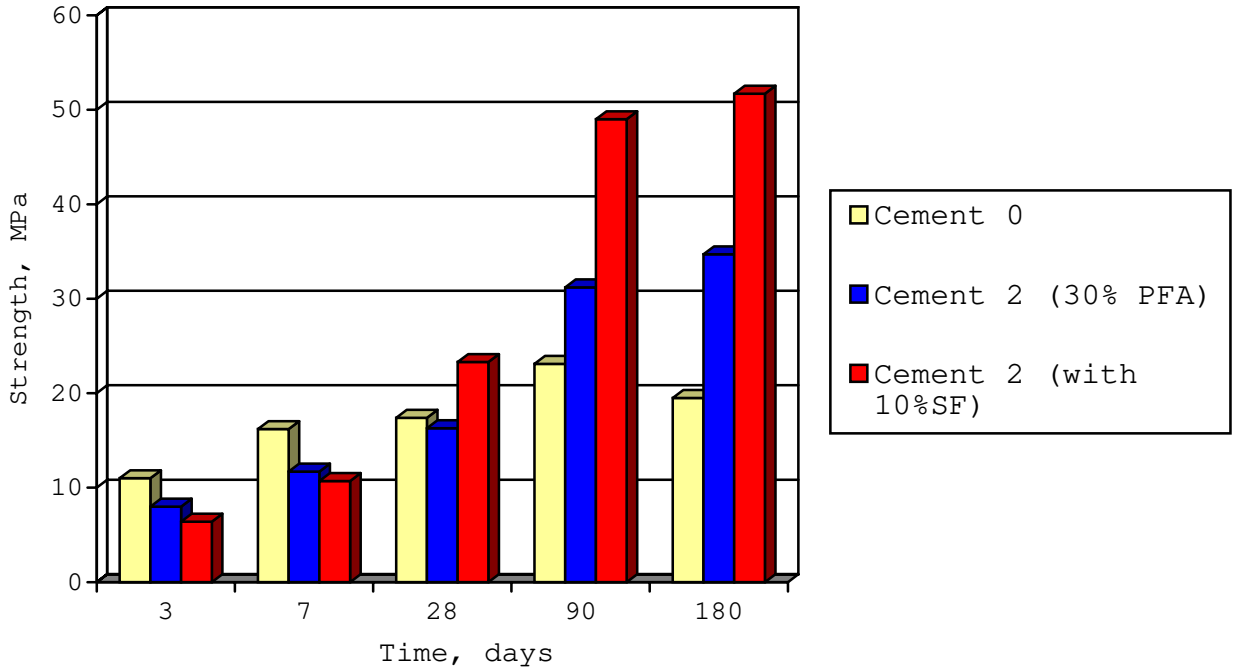

Figure 6. Compressive strength of mortars stored in NaCl solution.

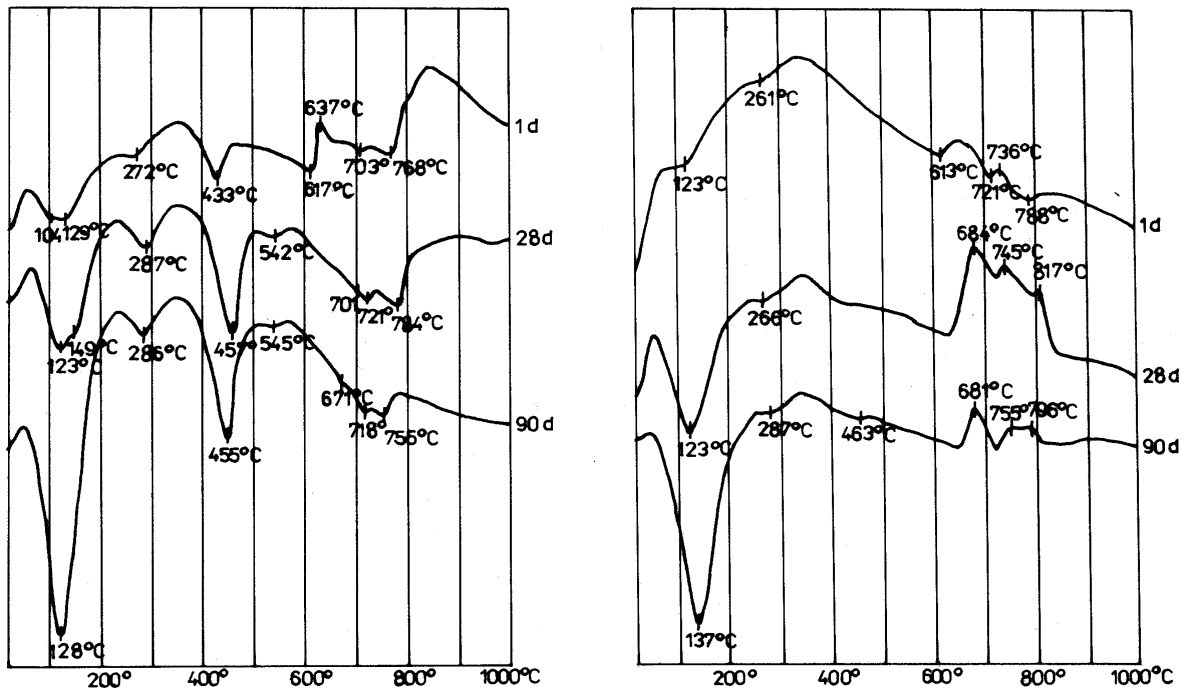

Cement "0" (Portland cement) Cement 2 with silica fume

Figure 7. DTA curves of hydrated cement pastes

o- NaCl; □-$Ca(OH)_2$; • - CSH; ▼- $3CaO{\cdot}Al_2O_3{\cdot}CaCl_2{\cdot}10H_2O$

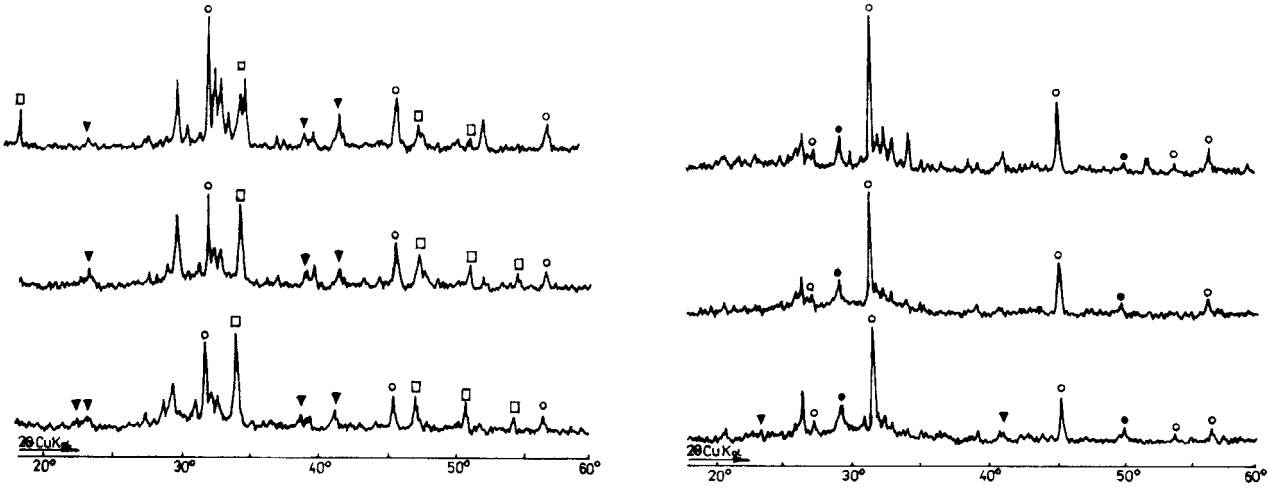

Cement "0" Cement 2 with silica fume

Figure 8. XRD patterns of hydrated cement pastes

5. DISCUSSION

Huge amounts of fly ash – a by-product of high fineness and pozzolanic activity are produced in those countries, where black coal is basic source of energy. Fly ashes are commonly used in cement and concrete manufacturing. A main feature related to siliceous fly ash's (denoted in EN 197-1

standard as “V”) practical implementation in cement, particularly when a higher admixture content is taken into account, is prolonged setting and low strength development (within the first 28 days), as compared to Portland cement CEM I of the same class. This may be improved by use of silica fume modifying admixture.

Silica fume is a very active pozzolanic material, quickly consuming the calcium hydroxide with the formation of calcium silicate hydrates (see Figure 5), revealing its activity at earlier ages, when fly ash is still relatively inert. Fly ash cement with silica fume shows higher compressive strength at all ages (see Table 3) and the differences are greater for higher fly ash contents (30 and 50% respectively). This advantageous influence of silica fume on fly ash cement strength can be attributed to the high pozzolanic activity of microsilica. In pozzolanic reaction the calcium silicate hydrates are produced as a main product, as confirmed in DTA measurements (see Figures 3 and 4). Additional C-S-H is distributed in pores, thus reducing the total porosities of pastes (Table 4). The mean pore radius decreases also. The fineness of fly ash and silica fume fill the empty spaces in the hardened system. This affects also the microstructure, which becomes more dense.

Hardened cement – fly ash – silica fume materials show low calcium hydroxide content and together with reduced porosity this strongly improves their corrosion resistance. The tests of cement – fly ash – silica fume mortars stored in sulphuric acid solution showed the stability of strength parameters (Table 5). On the other hand, in a $MgSO_4$ solution at later ages, the mortars exhibit reduction of strength and some destructive changes, this being the consequence of interaction between Mg^{2+} ions and C-S-H.

The fly ash and fly ash-silica fume cements show very good properties in the saturated NaCl solution (see Figure 6), while Portland cement mortars reveal destruction after a time (swelling, cracks). These results demonstrate the suitability of using fly ash and mixed pozzolanic materials in underground works in salt mines, in drilling and other “extreme” conditions.

6. CONCLUSIONS

1. Silica fume is a mineral additive complementing pozzolanic activity low calcium fly ashes.
2. Introducing silica fume as a component of fly ash cements improves their compressive strength in all examined hardening periods.
3. The hardened cement – fly ash paste with silica fume admixture shows lower content of $Ca(OH)_2$ and lower porosity, which is interesting, as it improves resistance to aggressive media.

REFERENCES

[1] Malhotra V.M., Ramezanianpour A.A. Fly in concrete, second ed.: CANMET, Natural Resources Canada,1994, p.307

[2] Massazza F. Pozzolana and pozzoloanic cements in Lea’s Chemistry of cement and concrete, 4th ed.,1998, pp. 471 – 631

[3] Kurdowski W. Chemistry of cement. Science Edittion PWN, Warsav, 1991, p. 480 (in Polish),

[4] Fan Y.Yin S., Wen Z., Zhong J. Activation of fly ash and its effects on cement properties, Cement and Concrete research, vol.29, 1999, pp.467-472

[5] Poon C.S., Kou S.C., Lam L., Lin Z.S. Activation of fly ash/cement systems using calcium sulfate anhydrite ($CaSO_4$), Cement and Concrete research, vol. 31, 2001, pp.873 – 881.

[6] Bapat J.D. Performance of cement concrete with mineral admixtures. Advances in Cement Research, vol. 13, 2001,pp. 139 – 155

PERFORMANCE OF METAKAOLIN AND PORTLAND CEMENTS FORMING ETTRINGITE: KINETIC AND MORPHOLOGICAL DIFFERENCES

R. Talero

Instituto de C.C.Eduardo Torroja-CSIC
Serrano Galvache, s/n,28033, Madrid, Spain.

ABSTRACT

This research intends to verify the XRD and Le Chatelier (L-A) experiments. For this purpose, 28 cements consisting of 7 Portland cements and 21 blended cements containing 20,30 and 40% metakaolin (M pozzolan) have been submitted to the L-A test for two years. With these cements, L-A specimens were manufactured. The parameter *Diameter Growth Rate*,Vcø(=ΔØ (%)/day) was not measured but it was obtained by dividing the **ΔØ**(%) measured by the relevant age. Other complementary determinations were: chemical anlysis, XDA patterns and SEM of ettringites and specific properties of some cements tested. The results have shown that:

(a_1) The formation rate of the ettringite resulting from reactive alumina, $Al_2O_3{}^{r-}$, present in M pozzolan, is considerably higher than the formation rate of ettringite from C_3A and much higher than ettringite from C_4AF, both present in OPC. These ettringites have been named: "rapid formation"(ett-rf), "slow formation" (ett-lf") and "very slow formation"(ett-vlf) ettringites, respectively.

(b_1) The size of the **ett-rf** crystals is considerably smaller than the size of the **ett-lf** ones (in accordance with the aforementioned conclusion).

On the other hand, these results have also shown that:

(a_2) Pozzolanic reactions derived from the reactive alumina,$Al_2O_3{}^{r-}$, present in M pozzolan, for a gypsum and water environment -L-A specimens- take place during the first 28 days – and even, during the first 7 days. This occurred for most POZC prepared with this M pozzolan (metakaolin), and **ett-rf** and **ett-lf** were the reaction products in all cases.

(b_2) Ett-rf and **ett-lf** formation, does not take place independently from one another, but interdependently or in a joint way or interactive way. That means that both ettringites appear, to a greater or lesser extent, when dealing with gypsum and water environments. Nevertheless, the reaction products are closer to **ett-rf** than to **ett-lf**, when more M pozzolan is added (40%) and vice versa(20%).

Keywords: Gypsum Attack, Portland Cements, Metakaolin, Ettringites, Formation rates, Kinetics, Sizes.

1. INTRODUCTION

The Le Chatelier-Ansttet (L-A) test (1) has been used in some European countries (2) (3) (4) (5) (6) as an accelerated test to predict cement behaviour against gypsum attack. However it was used here, mainly, to show differences between the ettringite formed from reactive alumina (tetra- or penta-

coordinated alumina), $Al_2O_3^{r-}$ (7), which is present in M pozzolan (from now on **"ett-rf"**), and the ettringite from C_3A and C_4AF, both present in OPC (from now on **"ett-lf"** and **"ett-vlf"**, respectively). These differences will be shown later on.

Researchers' disagreement regarding the influence of pozzolans on ettringite kinetochemestry led us to use the Le Chatelier-Ansttet (L-A) test (indirect or relative parameter **Vcø = ΔØ(%)/day**) in order to confirm phase formations previously obtained (8) (9).

On the other hand, experimental results also have shown that the L-A specimen overall dimensions change during water diffusion and chemical reactions(10), and in a recent international meeting on sulphate attack(11), other related effects were pointed out. Moreover Santhanam et al.(12) lately expressed dissatisfaction because of the fact that sulphate attack, that was given so much importance some years ago, has lost interest for researchers, and pleaded for setting up again the investigation to determine the service life of concrete foundations that have been attacked by sulphates. For this purpose, reagent substances and reaction products formed and possibly involved when pozzolanic additions are in contact with Portland cement attacked by gypsum, should be known first, as well as their respective morphologies, sizes, formation rates, inter-reaction or inter-connection during formation, technological consequences and other possible effects.

For all these reasons, the same experiments were carried out once again, but new indirect parameters and reasonings had to be considered to confirm that the formation rate of rapid formation ettringites (from reactive alumina present in M pozzolan)), must be greater than the formation rate of slow formation ettringites (from C_3A present in OPC), and consequently, their different sizes, as well. This indirect or relative parameter has been ***Diameter Growth Rate, Vcø,***(= ΔØ(%)/day) as well as pozzolanic reactions derived from the reactive alumina $Al_2O_3^{r-}$, present in M pozzolan for a gypsum and water environment - L-A specimens - taking place through the 28 days – and even as early as during the first 7 days. This occurred for most POZC prepared with this M pozzolan; **ett-rf** and **ett-lf** were the reaction products in all cases. Further their respective inter-relation or inter-connection during formation will be shown. For that purpose L-A specimens(1), manufactured with cement paste partially hydrated plus gypsum (ratio 1:2), were used.

2. OBJECTIVES

The main objectives of this research are the following:

1. To prove through the L-A test that the formation rate of ett-rf(V_f ett-rf) is higher than the formation rate of ett-lf(V_f ett-lf) and than the V_f ett-vlf (semi-quantitative or comparative analysis). Therefore:

$$\mathbf{V_f\ ett\text{-}rf\ is > V_f\ ett\text{-}lf\ is > V_f\ ett\text{-}vlf}$$

2. To confirm that **ett-rf** crystals are smaller than **ett-lf** ones, as well as to find a conclusive explanation for both of them.

3. To determine whether the greatest amount of pozzolanic reactions for the $Al_2O_3^{r-}$ present in M pozzolan, take place in L-A specimens during the first 28 days, and sometimes as early as 7 days, for most POZC tested.

4. To determine whether there is any relation or not between **ett-rf** and **ett-lf** and/or **ett-vlf** during their formation in gypsum and water environments.

3. EXPERIMENTAL

3.1 The starting materials used for this research are shown in Table 1:

TABLE 1.- CHEMICAL COMPOSITION OF CEMENTING MATERIALS

DETERMINATIONS (%)	PORTLAND CEMENTS							POZZOLAN
	OPC (P-nº)				SRPC (PY-nº)			
	P-1	P-2	P-31	P-5	PY-1	PY-4	PY-6	M
	(3,08)*	(3,06)	(3,06)	(3,09)	(3,12)	(3,16)	(3,21)	(2,55)
L.O.I.	1,60	2,91	3,45	2,31	2,28	1,64	1,11	0,60
I.R.	0,70	1,21	0,86	0,62	0,54	0,43	0,15	0,22
SiO_2	19,18	19,36	18,13	21,10	18,75	22,10	21,70	73,53
Al_2O_3	6,44	6,03	5,30	4,30	4,97	1,98	1,52	23,11
Fe_2O_3	1,75	2,89	3,80	2,70	5,52	4,46	4,11	1,19
CaO	63,94	59,49	61,68	64,40	60,82	65,59	67,97	0,63
MgO	1,48	1,21	1,82	1,31	2,59	0,83	0,42	0,03
Na_2O	0,90	1,23	0,76	0,81	0,56	0,15	0,43	0,07
K_2O	0,52	0,69	0,31	0,21	0,23	0,05	0,20	0,70
SO_3	3,50	4,94	3,86	2,30	3,72	2,78	2,34	
TOTAL	100,01	99,96	99,97	100,06	99,98	100,01	99,95	100,08
H_2O(105°C)	0,24	0,93	0,33	0,42	0,66	0,22	0,22	0,16
CaO free	1,90	0,70	0,63	0,90	0,68	1,20	1,75	

*.- Specific Weight (g/cm^3)

DETERMINATIONS (%)	POTENTIAL CALCULUS BOGUE (%)						
C_3S	51,05	33,47	58,70	58,84	50,44	58,19	79,43
C_2S	16,48	30,26	7,70	16,10	15,71	19,46	2,29
C_3A	14,11	11,09	7,62	6,83	3,83	0,00	0,00
$C_4AF(+C_2F)$ss	5,33	8,79	11,56	8,22	16,80	11,75	10,19
C_4AF+2C_3A (6)	33,55	30,97	26,80	21,88	24,46	11,75	10,19
C_4AF+C_3A (1)	19,44	19,88	19,18	15,05	20,63	11,75	10,19
Spf. Surf. Blaine(cm^2/g)	3192	3015	3248	3100	3811	3233	3287

Spf. Surf. Blaine(cm^2/g)	39 81

GYPSUM

MINERALOGICAL COMPOSITION (%)

H_2O(40°C a 217°C)	20,13	$CaSO_4.2H_2O$	95.58
CO_2(217°C a 1000°C)	0,75	$CaSO_4.1/2H_2O$ and/or $CaSO_4$	2.47
I.R.	0,26	$CaCO_3$	0.75
SiO_2	0,04	$MgCO_3$	0.81
SO_3	45.87	TOTAL	99.61
CaO	32.54		
MgO	0.36		
Na_2O	0,02		
K_2O	0.01		
TOTAL	99.98	H_2O at 40°C	0 41

In accordance with Eitel´s ternary diagram(15), the following materials have been chosen:

1. Four OPC -P-1, P-2, P-3 and P-5 (=P-nº)- and three SRPC -PY-1,PY-4 and PY-6 (=PY-nº).
2. Metakaolin prepared using kaolin (with ≈ 50% quartz content); calcination at 750°C.
3. Gypsum natural stone (with a high $CaSO_4.2H_2O$ content) used as aggressive media.

3.2 The operating procedure

First of all, 21 POZC specimens, with ratios 80%/20%, 70%/30% and 60%/40% (%P-nº/%M or %PY-nº/%M ratios), were prepared with 7 Portland cements -4 OPC and 3 SRPC- and M pozzolan. Secondly, all these POZC were analysed by the Frattini test (16) in order to confirm their pozzolanic characteristics at 7 and 28 days (later on related to sulphate attack) (Figure 1).

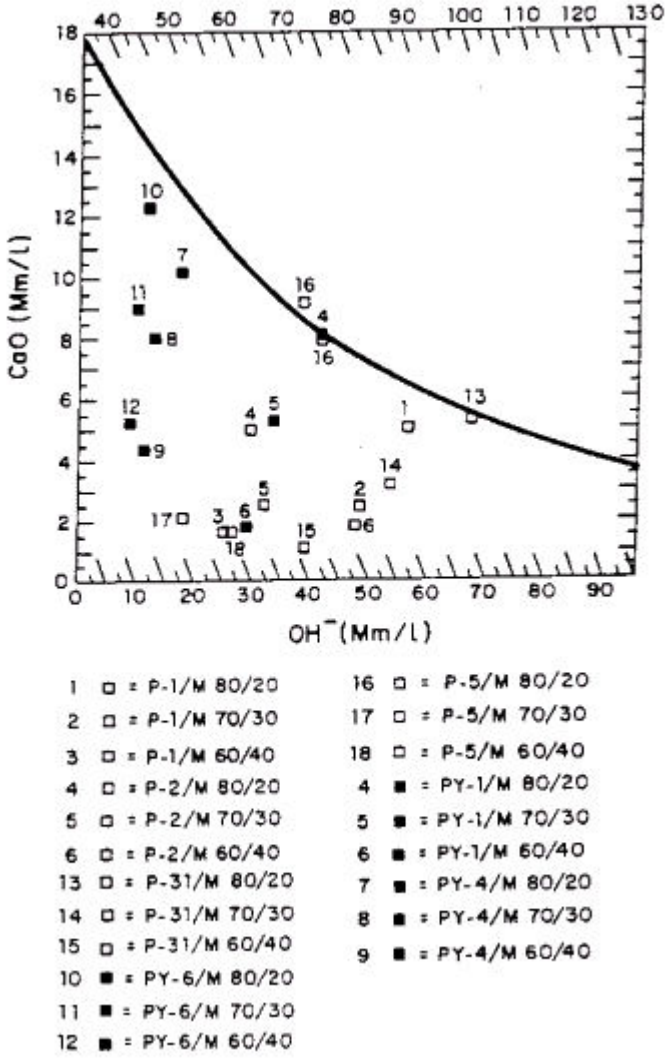

Figure 1. Fratini test of the 21 POZC

Thirdly, mechanical strengths (flexural and compressive strength) (17) and setting time (18) were determined (Table 2). Lastly, each POZC and each PC, were submitted to the L-A test(1). In it, the cement is firstly ground to make it pass through a sieve of approximately an 88 µm opening (a No. 170 sieve), and then the ground cement, 100.0 g, is used to make a 0.50 water-cement ratio paste, which will be allowed to harden for several weeks (usually 2), and then crushed into 5 mm size and dried at 40°C. Gypsum, 50.0 (as ≈ 50 percent of the dried set cement) is added, and the mixture is ground to pass through a sieve of approximately 212 µm opening (a No. 70 sieve). Six percent of distilled water by weight of solids is added, and the dampened paste is placed in an 80 x 30 cylindrical mould, and compressed under a pressure of 196 Pa/minute. The cylinder is placed on filter paper kept damp by allowing the ends to be dipped in water and covered with a bell jar to make an air-tight joint. The diameter was measured at 24h, 7 days, 28 days, 90 days or even later, according to the purpose. Thus, firstly, the direct parameter, **ΔØ(%)**, was measured (the maximum expansion acceptable is 1.25% at 28 days – physical requirement(15)(16) -, and secondly, the indirect or relative parameter, **Vcø = ΔØ(%)/day**, was calculated dividing the **ΔØ(%)** by the relevant age.

TABLE 2.- Mechanical strengths and times of setting from OPC, P-1, P-2, SRPC PY-6 and their POZC with M pozzolan.

CEMENTS	Mechanical strengths, MS(cement mortar type: EN 196-1)(13)				Setting Times (h, m)(14)		
	Flexural strength, FS(MPa)		Compressive strength, CS(MPa)		Initial Setting Time	Final Setting Time	Time of Setting (TS)
	28 days	90 days	28 days	90 days			
P-1	7.0	7.3	47.7	50.3	2h 00m	2h 39m	0h 39m
P-1/M 80/20	8.2	8.4	54.9	55.9	2h 10m	2h 05m	0h 40m
P-1/M 70/30	8.7	8.9	53.3	54.3	2h 25m	3h 10m	0h 45m
P-1/M 60/40	8.6	8.8	48.3	49.2	2h 15m	2h 55m	0h 50m
P-2	4.0	4.2	27.3	32.4	2h 10m	3h 09m	0h 59m
P-2/M 80/20	8.2	8.4	60.8	61.9	4h 15m	6h 55m	2h 40m
P-2/M 70/30	9.7	9.9	49.7	50.6	4h 55m	7h 40m	2h 45m
P-2/M 60/40	7.7	7.9	45.7	46.5	3h 55m	6h 45m	2h 50m
PY-6	7.8	7.3	54.3	63.0	0h 05m	0h 25m	0h 20m
PY-6/M 80/20	8.8	9.8	59.8	71.6	5h 50m	7h 35m	1h 45m
PY-6/M 70/30	9.5	10.4	57.2	68.4	5h 45m	7h 35m	1h 50m
PY-6/M 60/40	7.3	8.1	54.3	54.6	6h 15m	8h 10m	1h 55m

NOTE: The rest of the cements (OPC, SRPC and their POZC) reached MS and TS values of similar order.

Other complementary determinations were: chemical analysis of the cementing materials used(Table 1), XDA patterns(Figures 3, 4 and 5) and SEM analysis of ettringites (Figures 6 and 7).

4. RESULTS

Vcø values are shown in Figures 2 (a), (b), (c), (d), (e), (f) and (g). For discussion and interpretation, the curves shown in this Figure 2 were grouped according to their similarity to a Gauss curve (mainly, its right and/or left branch).

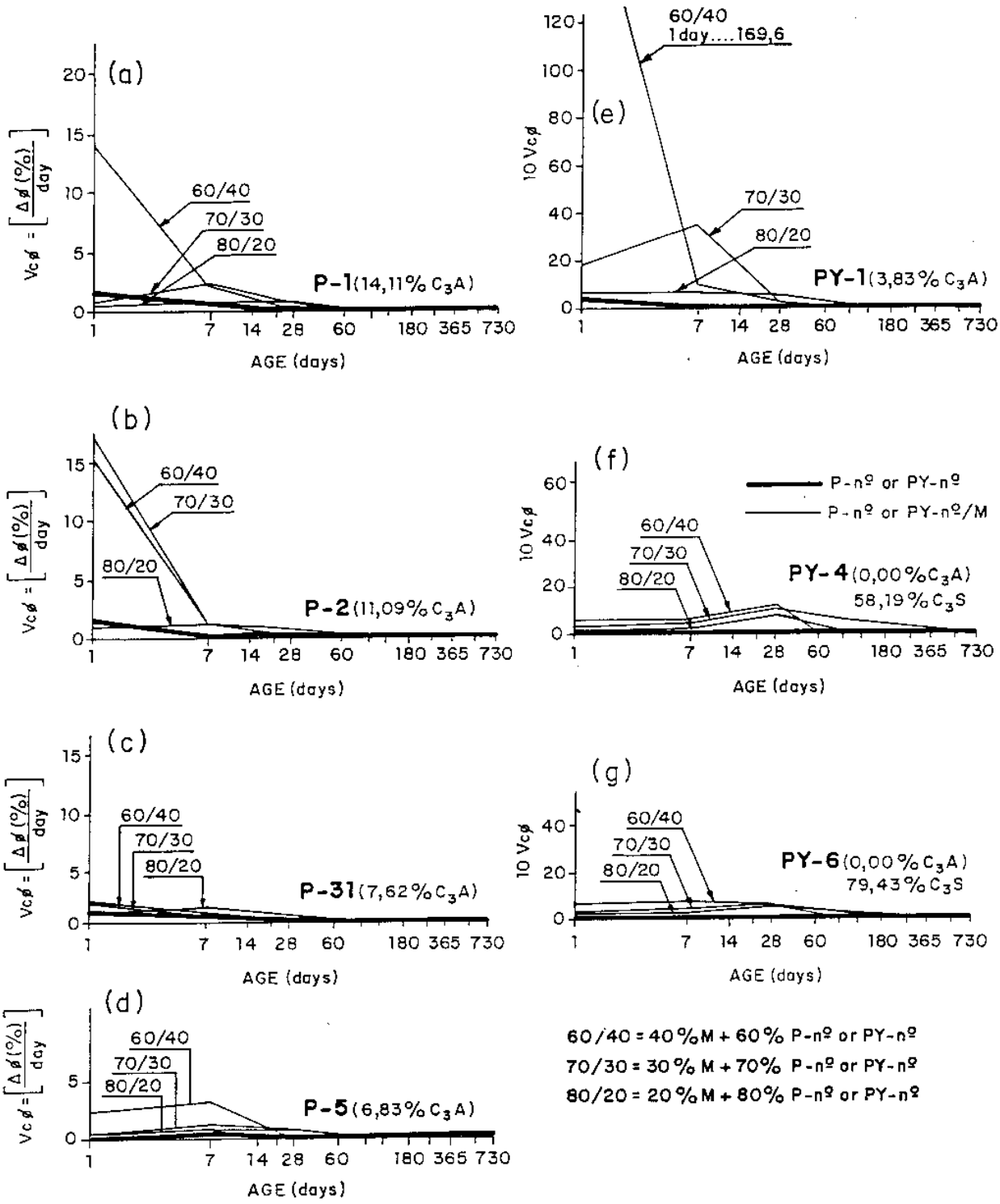

Fig.2- Parameter : Diameter Growth Rate, Vc Ø
Specimens : 80 mm Ø x 30mm h.
Pastes : Le Chatelier - Anstett (2)
Cements : 4 OPC (P-nº), 3 SRPC (PY-nº) and 21 POZ C
Pozzolan : M

4.1 Observations

4.1.1 (A) Plain OPC -4- and plain SRPC -3-:

Origin, evolution and development of **Vcø** values for the 7 PC tested -4 OPC and 3 SRPC- generally can be compared to a Gauss curve or, at least, to its right branch. These branches have a negative

slope and reach very small values, decreasing to zero in all cases, for a given age. Accordingly, the areas defined by plain PC curves are proportional to their C_3A content (in %).

NOTE**:** In these figures (Figure 2), no initial point has been represented since it would correspond to the specimens manufacture, thus, zero days. Therefore, the initial point of 1 day, **Vcø$_{1d}$**, should be considered linked by an imaginary line to the day 0 point, **Vcø$_{0d}$**. This imaginary line must be considered as well the left branch of the Gauss curve.

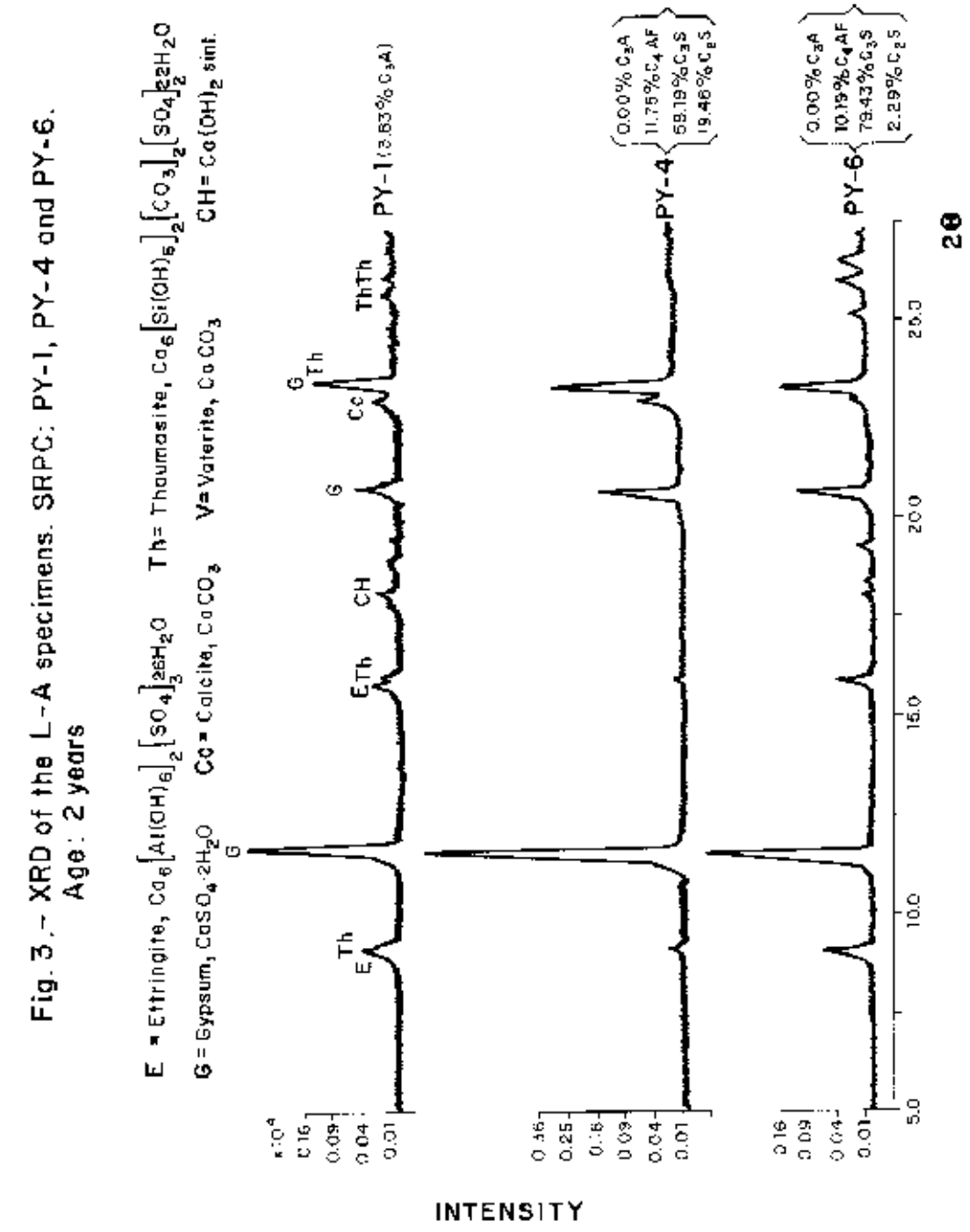

4.1.2 (B) POZC -21-:

1. In all L-A specimens for the 21 POZC, the origin, the evolution and the development of **Vcø** values have shown, at the end of the test, a decrease from age 1 day down to zero in all cases. This decrease was sometimes preceded by an increase. It is necessary to emphasize that no matter which of the 21 POZC is considered, since the highest **Vcø** values were always reached during the first 28 days, and most times, during the first 24 hours. This increase up to its respective highest **Vcø** value is generally

followed by a rapid and sharp decrease, sharper than the one for its plain OPC=P-nº or its SRPC=PY-nº, Figures 2(a), (b), (c), (d), (e), (f), (g), and the more M pozzolan (its $Al_2O_3^{r-}$) was added, the highest the C_3A(%) content the OPC had.

In short, **Vcø** diminished faster for any family of POZC than for its plain PC P-nº or PY-nº, and even faster as the addition of M pozzolan is higher. This decrease began after the maximum **Vcø** value, which was normally reached at the age of 1 to 7 days. Besides, the bigger the C_3A(%) content was for PC, P-nº or PY-nº, the higher the maximum **Vcø** value was for its POZC.

2. At age 1 day, **Vcø** values generally increased as the amount of M pozzolan increased for all OPC (=P-nº) or SRPC (=PY-nº) considered. For this reason, **Vcø** values satisfied the following order:

< Vcø < P-nº or PY-nº/M 100/00<80/20<70/30<60/40, at 1 day **[1]**.

Hence, relation **[1]** is a consequence of the direct chemical effect derived from the physical substitution of PC by M pozzolan. But after 7 days, until the age of 28 days and up, the opposite order took place:

> Vcø > P-nº or PY-nº/M 100/00>80/20>70/30>60/40, from 28 to 730 days **[2]**.

Furthermore, **Vcø** magnitude order was much smaller after 7 days, decreasing as the M pozzolan amount increased in every case, and sometimes with the opposite sign.

3. Vcø value for any plain OPC (=P-nº) or SRPC (=PY-nº) tested, was only a direct consequence of its daily **ΔØ**; this is due to the formation of **ett-lf** (Figure 3). Nevertheless, when M pozzolan was added, its **Vcø** values increased proportionally, and specially, at early test ages.

The main cause must be once again, the $Al_2O_3^{r-}$ present in M pozzolan, when transformed into **ettr-rf** due to its pozzolanic activity for a gypsum and water environment -L-A specimens- (Figures 4 and 5).

5. DISCUSSION AND INTERPRETATION

The aim of kinetic-chemistry is to study the evolution of chemical system(s) in terms of time. Kinetic chemistry deals particularly with measurement and interpretation of reaction rates which are to be defined as **R=dX/dt[3]**. For a reaction that takes place in a solid-liquid interface -as it occurs with ettringites-, if the interface area is not known, different definitions for the intensive **"rate"** should be used, such as: **R=(1/W)(dX/dt)[4]** or **r=(1/V´)(dX/dt)[5]**, where **W** and **V´** are weight and volume of the solid particles dispersed in the fluid phase. Nevertheless, **Vcø** was considered representative enough for our objective, since:

- **W** and **V´** parameters as well as the parameters for the corresponding reaction products formed (in this research, ettringites from different origins: $Al_2O_3^{r-}$, C_3A and C_4AF, respectively) are very difficult to separate and quantify exactly;

- the reaction rate has to be proportional to the derivative of the reaction advance versus time, in such a way that it does not matter which of the expressions **[4]** or **[5]** is used;

- the reaction development of ettringite formation can be represented by the daily "Total" specimen increase or by its greatest size; the evolution through time of the diameter growth, the **Diameter Growth Rate**=**ΔØ(%)**/day = **Vcø**, is represented for L-A specimens (Figure 2).

5.1 From observations (B) 1 and 2

According to observations **(B)1** and **(B)2**, the bigger/lower the negative slope of the **Vcø** curve is, the bigger/lower the correspondent positive slope must be. This positive slope corresponds to the first 24 hours. These observations allow the following reasoning: considering first only plain PC(OPC=P-nº and SRPC=PY-nº) curves, it can be seen that the maximum **Vcø** value for 1 day,$\mathbf{Vc\phi_{1d}}$ increases with PC C_3A content (%). According to this, for the P-1 specimen to reach the same $\mathbf{Vc\phi_{1d}}$ value than the P-1/M 60/40 specimen, C_3A(%) content of OPC P-1 should have been ≈ 91.72%, that is to say, this OPC should have been an expansive **S** type clinker(19), but it was not. Thence, the reason why 60% of OPC P-1 with 40% of M pozzolan, have given rise to 1 day higher $\mathbf{Vc\phi_{1d}}$ value than plain OPC P-1, is once again the M pozzolan (40%) forming **ett-rf**(8)(9). See Figures 4 and 5.

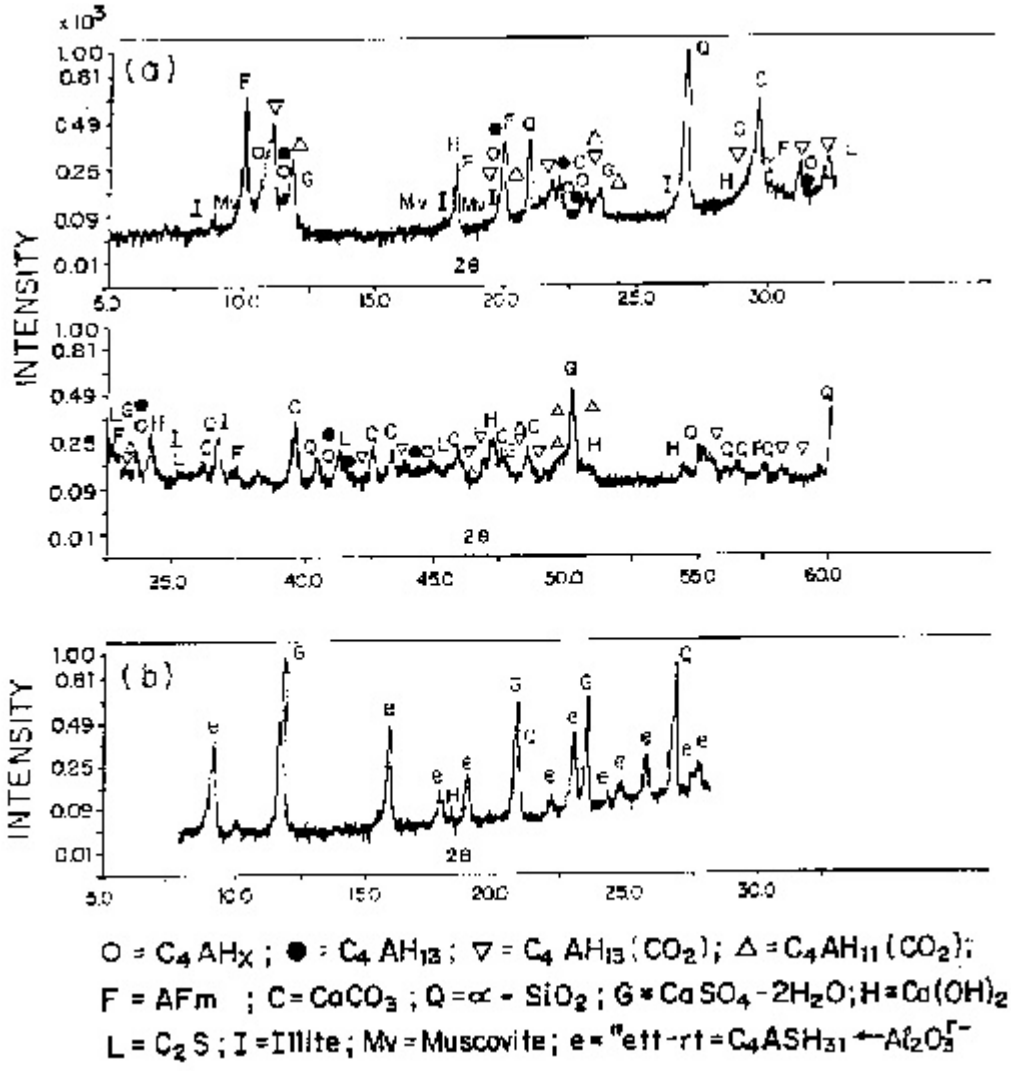

Figure 4. L-A specimens. XRD of the POZC:PY-6/M 60/40
a) partially hydrated according to the L-A test
b) L-A specimens. Age: 7 days

However, the most interesting thing of this reasoning is that the total area defined by OPC P-1 curve would correspond to the formation of 64.60 g of **ett-lf** from the C_3A present in OPC P-1(14.11%), whereas the corresponding areas for PY-4/M 60/40 and/or PY-6/M 60/40 curves, would match at the most with the formation of 55.23 g of **ett-rf**, mainly from Al_2O_3 present in M pozzolan (23.11%), assuming that all is reactive, and if all is not reactive, which probably would be the case(8)(9), it would still be better for the final conclusion of this reasoning. Nevertheless, both areas ratio is at the most ≈ 1:10. Here, it can be said once again(8)(9), that a great paradox can be seen(8)(9) between

behaviours (**Vcø** values v time) and theoretical stoichiometric calculations(8)(9), but behaviours holding priority.

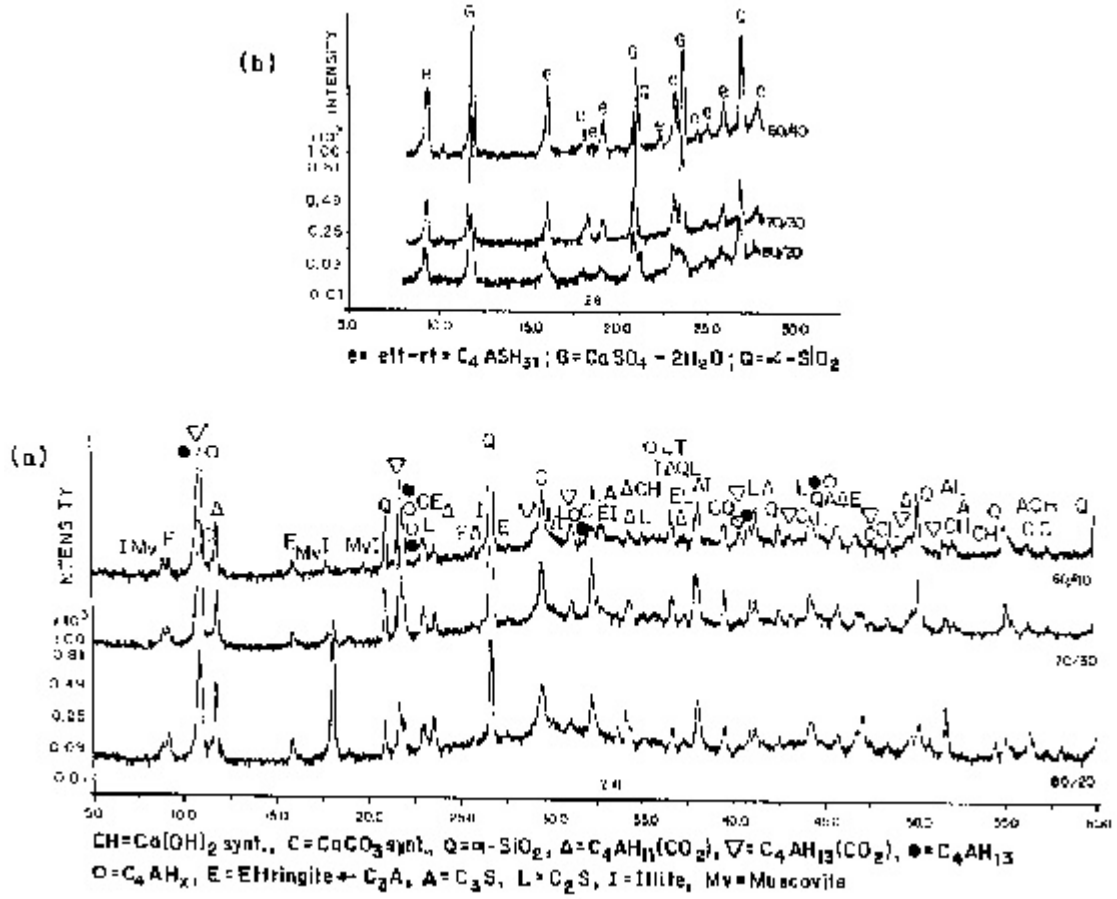

Figure 5. L-A specimens. XRD of the POZC:PY-4/M 80/20, 70/30 and 60/40
a) partially hydrated according to the L-A test
b) L-A specimens. a) + Gypsum + H_2O Age: 7 days

Therefore, the only possible explanation of such remarkable paradox is that the reactive alumina,$Al_2O_3^{r-}$ of M pozzolan reacting to form ettringite, must be notably higher than C_3A from the OPC P-1. For this reason, the M pozzolan would form the ettringite much faster than that of the C_3A from OPC, although the quantity formed in the first case is a bit greater than in the second. For this, it can be said that such a notable reactivity of the $Al_2O_3^{r-}$ could be found in the physical-chemistry ideal state for this process. The C_3A would be an opposite case, let's say, the non-ideal, or at least, a less ideal form from the same results. Consequently, it can also be said that the formation rate of its ettringite markedly decreases, thus, the C_3A will form it more slowly, and therefore, the C_4AF will be still much slower in forming it. That is to say,

V_f ett-rf must be > V_f ett-lf is > V_f ett-vlf [3]

But neverthless, it could be envisaged that **V_f ett-rf is = V_f ett-lf** and their common value would be the **V_f ett-lf**: With this supposition, whatever POZC family is considered, their curve should be their respective OPC curve. Let´s say, P-nº or PY-nº/M 80/20,70/30 and 60/40 curves should be the same that their respective plain P-nº or PY-nº curve. On the contrary, this behaviour has not happened but the behaviours or classifications (Eqs. **[1]** and **[2]**) have been achieved.

Both groups of curves were achieved by drawing **Vcø** versus time and all **Vcø** values were due to the ettringites´ expansion. On the other hand, the ettringite formation from C_3A present in OPC was

verified by a previous paper(8). Likewise, it was also shown that M pozzolan forms ettringite as well during their exposure to the same sulfate bearing solution(from gypsum)(8), for instance, in L-A specimens, see Figures 4(b) and 5(b).

To sum up, when comparative analysis was made between PY-6/M 60/40 and PY-4/M 60/40 curves with P-1 curve, areas, shapes and developments were different, and when made between P-1/M 80/20,70/30 and 60/40 curves with P-1 curve, were different as well. Besides, the more different the curves have been, the more OPC P-1 was replaced by M pozzolan and vice versa, or in other way, the greater the amount of M pozzolan added was, the earlier and greater high **Vcø** values were. Consequently, the initial supposition seems to be incorrect. Hence, or **V_f ett-rf is < V_f ett-lf,** or **V_f ett-rf is > V_f ett-lf**. But **V_f ett-rf** cannot be **< V_f ett-lf** for the
following reasons:

1ª.- If the two groups of curves obtained for both compared cases, are very different, the cause that gave rise to them is also very different. And if **Vcø** value of POZC P-1/M 60/40 - 14.46% -, is greater than **Vcø** value of OPC P-1 -1.62% -, or in other way, that 8.466% C_3A(= 14.11%x0.6) with M pozzolan (40%) brings about more **Vcø** than 14.11% C_3A(from plain OPC P-1), the cause is the M pozzolan when converted in **ett-rf** (Figures 4(b) and 5(b)) by means of its high pozzolanic activity at early ages (Fratini test(16) at 2 days: results,

- with gypsum(%SO_3 content = 7.0): $[CaO]_{2d}$ = 44.50 mM/l and $[OH^-]_{2d}$ = 5.45 mM/l, (**ett-rf** was formed, Figures 4(b) and 5(b)), and
- without gypsum: $[CaO]_{2d}$ = 35.00 mM/l and $[OH^-]_{2d}$ = 2.15 mM/l;

that is, both cements satisfied the Fratini test at 2 days).

2ª.- For this reason, the curves shown in Figures 2(a), (f) and (g) are needed: Even though the amounts of ettringite obtained for each case through theoretical stoichiometric calculations are relatively similar, their respective areas - defined by OPC P-1 curve and PY-4/M 60/40 and PY-6/M 60/40 curves- are completely different, and in addition, its shapes and developments as well. Consequently, their respective formation rates will be completely different, as well as their technological consequences once again, as well. For instance:

- **$Vcø_{1d}$** and **VNP_{1d}** values raised at 1 day: OPC P-1 were quite lesser than POZC P-1/M 60/40 (**$Vcø_{1d}$** values, see Figure 2(a): 1.62(%)/day against 14.46%/day) and **VNP_{1d}**, 14.25 mm against 34.30 mm), and
- **$Vcø_{7,28d}$** and **$VNP_{7,28d}$** values rised at 7 and 28 days: OPC P-1 were **$Vcø_{7,28d}$** also less than POZC PY-4/M 60/40 and PY-6/M 60/40, see Figure 2(a), (f) and (g): at 7 and 28 days, 0.52%/day and 0.17%/day against 0.54%/day and 0.32%/day, and 0.73%/day and 0.66%/day, respectively, and **$VNP_{7,28d}$** higher than POZC PY-4/M 60/40 and PY-6/M 60/40 (at 7 and 28 days, 23.8 mm and 26.4 mm against 0.00 mm, 0.00 mm, 0.00 mm and 17.0 mm, respectively).

This shows that formation rate of ettringite from reactive alumina $Al_2O_3^{r-}$ present in M pozzolan, would turn out to be significantly higher than formation rate of ettringite from C_3A (origin of PC), and as a result and according to the Von Weimarn´s and Garrido´s set patterns(20)(21), **ett-rf** would have to be a much smaller size than the **ett-lf**, as it occurred in this research, see Figures 6(a) and (b) and 7(a) and (b). Von Weimarn and Garrido demonstrated that precipitation rate for a salt is directly proportional to the super-saturation grade and inversely proportional to its solubility. Besides, the set pattern of Von Weimarn(20) and Garrido(21) underlines that the more insoluble a salt is (and so the ettringite solubility varies between 0.255 and 0.024 g ett/l for water solutions with $Ca(OH)_2$ content between 0.056 and 1.08 g CaO/l while $Ca(OH)_2$ solubility in water is 1.2 g CaO/l at 18°C) the more

difficult is to produce a slow precipitation and to form big and well shaped crystals as occurred in this research, see Figures 6 and 7.

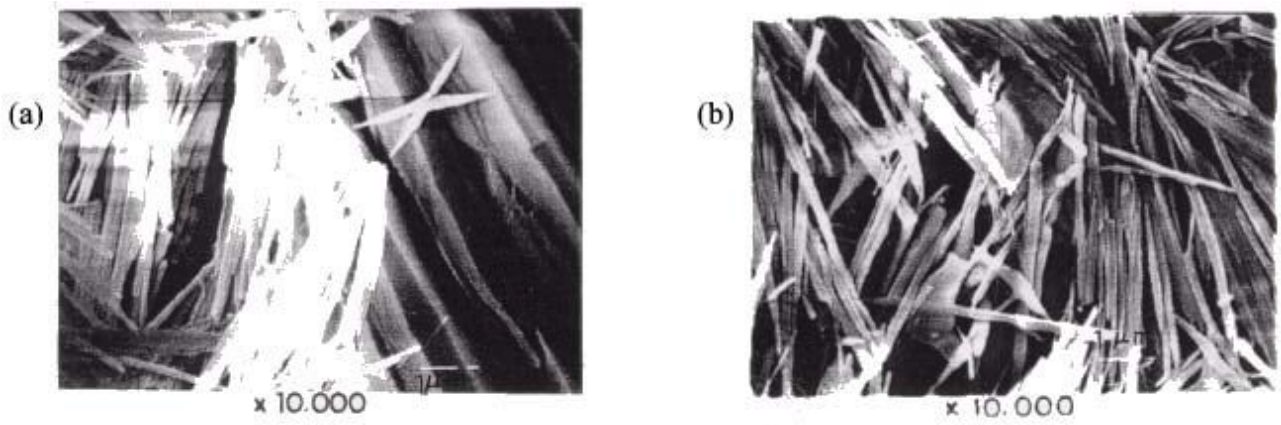

Figure 6. Ettringites of rapid formation, ett-rf

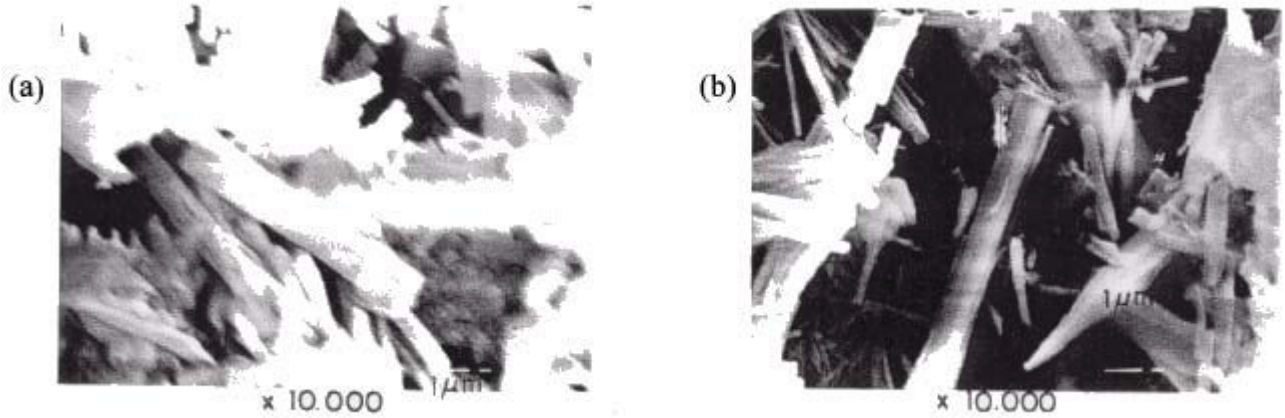

Figure 7. Ettringites of slow formation, ett-lf

Hence, according to Von Weimarn´s and Garrido´s set patterns, if reagents are mixed in such a way that high super-saturation takes place -as usually happens for the reactive alumina $Al_2O_3^{r-}$ present in some pozzolans - fast precipitation occurs and it results in a gelatinous precipitate. This creates small crystals which are quickly formed (**ett-rf**, in this case). In contrast, if the precipitating agent is slowely added in a diluted solution - as is required for the C_3A present in OPC– there is slow super-saturation, and a precipitate constituted by macro crystals slowly appears (**ett-lf**, in this case). This means that initial rate of precipitation is proportional to **[(Q-S)/S)]**, where **Q** is total concentration of the substance that precipitates, **S** is concentration of the solution in balance with the precipitate, and finally, **Q-S** is the super- saturation when the precipitation starts. Summing up, the particle size of the precipitate decreases (**ett-rf**, in this case) when the concentration of the reagent substances increases (M pozzolan or its reactive alumina, $Al_2O_3^{r-}$, in this case); and on the contrary, if crystalline precipitate (great and well-formed crystals) is preferred **[(Q-S)/S)]**, the concentration has to be as small as possible(OPC or its C_3A, in this case).

On the other hand and according to Garrido, crystals that result from weak super-saturation are the same as those resulting from that vapour phase gives rise (that is to say, without solvent) to smaller crystals and growth rates correspond to faces that have an electric field. However, an inversion of the growth order is originated when the growth is performed with strong super-saturation, and the faces with strong electric field have a minimum growth rate. This inversion can be explained taking into account that when solution is strongly super-saturated, ions in solution and dipoles assume a different

configuration than when the solution corresponds to saturation. In contact with crystal-solution a different phenomenon occurs. As the solution is poorer in solvent with strong super-saturation, it must result in dissolution. This is easier to obtain in reticular surfaces with a weak electric field, which makes these surfaces increase their growth rate, which will be able to exceed the rate of the surface with strong electric field. The higher the super-saturation grade (it brings about the change of faces), the stronger the solvent-crystal link is, and the salt solubility will also be lower (the ettringite is insoluble enough). Hence, there is a very marked interaction between solvent and crystal, and the **F** forms, which have appeared in balance stage, may be replaced by **S** or **K** forms.

3ª.- At 1 day,

- POZC PY-4/M 60/40 and PY-6/M 60/40, $\mathbf{Vc\phi_{1d}}$ values: 0.63%/day and 0.62%/day, respectively,
- OPC P-1, $\mathbf{Vc\phi_{1d}}$ value: 1.62%/day, being 60% = 0.972%/day and 40% = 0.648%/day, and
- POZC P-1/M 60/40, $\mathbf{Vc\phi_{1d}}$ value:
    - theoretical value: 0.972%/day + (0.63%/day + 0.62%/day)/2 = 1.597%/day, which is greater than 0.972%/day, and
    - real value: 14.46%/day, but 14.46%/day – 0.972%/day = 13,488%/day, which is greater than 0.972%/day, and than 1.62%/day, properly, that is to say, in any case, $\mathbf{Vc\phi_{1d}}$ of POZC P-1/M 60/40 is greater than $\mathbf{Vc\phi_{1d}}$ of OPC P-1; but according to results obtained, real values prevailed.

From these results, reasons and foundations, many questions about morphology and size differences of ettringites that Mehta brought up (22) can be now explained in detail.

When $\mathbf{Vc\phi_{xd}}$ is 0.00(%)/day after reaching the maximum value, the ettringite formation reaction is finished. Accordingly, it can be seen in Figure 2 that for all cements considered, most of the area defined by the curves correspond to ages from 0 to 28 days. Besides, if there is M pozzolan in L-A specimen, the larger the amount of M pozzolan present, the sooner the zero value is reached. This proves that:

1st. The greatest amount of pozzolanic reactions forming ettringite from the reactive alumina, $Al_2O_3^{r-}$, present in M pozzolan, takes place during the first 28 days.
2nd. The bigger the amount of M pozzolan added to the SRPC=PY-nº is, the sooner this reaction takes place -7 days.
3rd. The bigger the C_3A amount present in OPC or SRPC, the sooner this reaction takes place.

5.2 From observation (B) 3:
It can be proved that formation of **ett-rf** and **ett-lf** in L-A specimens does not take place independently from one another, but inter-dependently or in a joint or interactive way for the closer the $Al_2O_3^{r-}$ and C_3A particles were, the more inter-dependent this formation is. This situation of maximum proximity from each other would be achieved for maximum addition of M pozzolan and OPC with high C_3A content (%), as also happened in this research for POZC specimens, P-1/M 60/40 and P-2/M 70/30 and 60/40, see Figures (a) and (b). Thus, and in order to verify this hypothesis, it can be said that,

- when these OPC, P-1 and P-2 were present in a big amount (ratios 70/30 and 80/20, respectively), or
- when these OPC were replaced by other OPC or SRPC with small C_3A content(%) (this is the case of the P-31(7.63% C_3A), P-5(6,83% C_3A) and PY-1(3.83% C_3A)),

Vcø maximum value should have been reached after 1 day -at the age of 7 days in this case or even later- by their 60/40, 70/30 or even 80/20 POZC, which once again happened in this research for such POZC, see Figures 2(a), (b), (c), (d) and (e).

Therefore, when C_3A content was zero -case of PY-4/M and PY-6/M families-, the **Vcø** would reach the maximum value after 7 days, which in this research was reached at the age of 28 days, see Figures 2(e) -ratio 60/40 – 2(f) and 2(g).

6. CONCLUSIONS

Through interpretation and discussion of the **Vcø** values, the following conclusions were reached:

L-A test - parameter: **Vcø -**, has finally proved that:

- The V_f of ettringite from the $Al_2O_3^{r-}$ present in M pozzolan, or **ett-rf**, is considerably higher than the V_f of the ettringite from the C_3A present in OPC, or **ett-lf**, and even higher than the ettringite from C_4AF, or **ett-vlf**, which is according to conclusions and proposals from references (8)(9).
- The **ett-rf** has a much smaller size than the **ett-lf**. This is a direct consequence of the conclusion above.

The pozzolanic reactions from $Al_2O_3^{r-}$ present in M pozzolan in a gypsum and water environment -L-A specimens-, formed **ett-rf** and took place all through the 28 days, starting early during the first 7 days in most of the cases studied, and the larger the content in C_3A was for the PC, the sooner those reactions finished.

The combined formation of the **ett-rf** and **ett-lf** in L-A specimens, did not take place independently from one another, but they were more or less inter-dependent or in a joint or interactive way, and the reaction products are closer to **ett-rf** than **ett-lf** when more M pozzolan is added (40%), and vice versa(20%).

REFERENCES

[1] L.Blondiau: Considerations diverse relatives à l´éssai de resistance chimique au sulfate de alcium suivant le processus Le Chatelier-Anstett.- Rev.Mat.Constr.Trav.Publ.No.524 and No.546(1961).

[2] A.Río: Resistenza chimica dei cementi pozzolanici.-L´Ind.Ital.Cem.,ANN XXVII, nº 6, jun.(1957).

[3] A.Río,A.Celani and L.Angeletti:La composizione dei cementi pozzolanici e la loro resistenza alla acque solfatiche.- L´Ind.Ital.Cem.,ANN XXX nº4, april(1961).

[4] M.J.M.Jaspers:Contribution à l´étude experimentale de la mesure par l´essai Le Chatelier-Ansttet de la resistance des ciments aux sulfates et chlorures.- Rev.Mat.Constr.Trav.Publ. nº 633-634,jun.-jul.(1968).

[5] P.García Paredes: Inalterabilidad de los conglomerantes frente al ataque de los sulfatos.Comparación de métodos para apreciarla.-Booknotes nº 113.Inst."Eduardo Torroja"-CSIC,C/.Serrano Galvache,s/n,28033-MADRID-Spain.

[6] J.Calleja and P.García Paredes: Sobre los métodos para el estudio de la durabilidad de los conglomerantes hidráulicos.-Mat.Constr.nº137,jan-feb-mar.(1970),pp.51-77.

[7] J.S.Moya and al.:Aluminum-27 and Silicon-29 Magic-Angle Spinning Nuclear Magnetic Resonance Study of the Kaolinite-Mullite Transformation.-J.Am.Ceram.Soc., 71,[10],C418-21,(1988).

[8] R.Talero: Comparative XRD analysis ettringite originating from pozzolan and from Portland cement.-Cem.Concr.Res.,Vol.26,No.8,pp.1277-1283(1996).

[9] R.Talero: Kinetochemical and morphological differentiation of ettringites by Le Chatelier-Ansttet test.-Cement and Concrete Research 32 (2000) 707-717.

[10] N.Gospodinov,R.F.Kazandjiev,T.A.Partalin and M.K.Mironova: Difusion of sulfate ionscement stone regarding simultaneous chemical reactions and resulting effects.-Cem.Concr. Res.,Vol.29,pp.1591-1596(1999).

[11] Jacques Marchand and Jan P.Skalny: Materials Science of Concrete: Sulfate Attack Mechanisms.-Published by The American Ceramic Society,725, Ceramic Place, Westerville, OH 43081-USA(2002).

[12] M.Santhanam,M.D.Cohen and J.Olek: Sulfate attack research - wither now?.-Cem.Concr. Res.,31 (2001)845-851.

[13] R.Talero:Contribution to the Analytical and Physical-Chemistry Study of the System: Pozzozlanic Cements-Gypsum-Water(20°±3°C).-Ph.D.Thesis, Complutense University of Madrid-Spain(1986).

[14] R.Talero:Sulfate resistance of Portland cements. Accelerated test to determine it: Specifications.- Monograph No.399,Dic.1989:Inst."Eduardo Torroja"-CSIC., Calle Serrano Galvache, s/n, Apartado de Correos 19002,28033-MADRID-Spain (1989).

[15] W.Eitel:Recent Investigations of the System: Lime-Alumina-Calcium-Sulfate-Water and its importance in Building Research Problems.-Journal Am.Concr.Inst.,28 (7),679-98 (1957).

[16] EN 196-5 Standard: Pliego de Prescripciones Técnicas Generales para la Recepción de Cementos RC-75(BOE nº 206 de 28 de agosto de 1975) = N.Frattini:Ann.Chim.Applicata, 39,616-20(1949).

[17] EN 196-1:1996 Standard: Método de ensayo de cementos. Parte 1:Determinación de resistencias mecánicas(mechanical strentghs determination).- AENOR, Calle Génova nº 6,28004-MADRID-Spain.

[18] EN 196-3:1996 Standard: Método de ensayo de cementos. Parte 2:Determinación del tiempo de fraguado(setting times determination) y de la estabilidad de volumen(Le Chatelier´s needles).- AENOR.

[19] ASTM C 845-90 Standard: Standard Specification for Expansive Hydraulic Cement.- ANNUAL BOOK OF ASTM STANDARDS.-Sect.4 Construction,Vol.04.01,Cement; Lime;Gypsum,pp.391-393,1995.

[20] P.Von Weimarn: Principles and Methods of Chemical Analysis, H.F. Walton, Prentice Hall, Inc., New York,p.21,1952.

[21] J.Garrido: FORMA Y ESTRUCTURA DE LOS CRISTALES.-Ed.Alhambra, S.A., Printed in Spain, R.E.182,Calle Claudio Coello,76,Madrid (1973).

[22] P.K.Metha:Mechanism of sulfate attack on Portland cement concrete. Another look.-Cem. Concr.Res.,Vol.13,No.3,pp.401-06,1983.

CRITICAL COMPARATIVE ANALYSIS OF THE STEADY AND NON-STEADY- STATE CHLORIDE DIFFUSION COEFFICIENTS FOR SEVERAL TYPES OF CONCRETES

M. Castellote*, C. Andrade, I. LLorente and C. Alonso

Institute of Construction Science "Eduardo Torroja" (CSIC), Madrid, Spain;
E-mail: martaca@ietcc.csic.es

ABSTRACT

Chloride penetration into concrete may lead to the corrosion of reinforcement, which is recognized to be the main cause of the lack of durability of reinforced concrete. In recent years, the chloride ingress in concrete is being studied by the measurement of the so-called chloride Diffusion Coefficient which is being used for predicting the service life. However, in the calculation of the diffusion coefficient of chlorides through concrete there are several points that there need explicit recognition of their limitations and a critical analysis. In this paper, these points are undertaken from an experimental (considering 4 different types of concrete and 2 types of mortar with different kind of binders in steady and non steady tests) and theoretical (sensitivity analysis) point of view. As a result, it can be said that the D_{ns} values cannot be used simplistically for comparing concretes without been referred to the surface concentration and to binding capacity while the D_s values represent the transport ability in a reliable way. However, if the D_s is used for service life prediction, the binding ability and the resulting surface concentration in the real environment will have to be taken into account.

1. INTRODUCTION

One of the main concerns about service life of reinforced concrete is related to corrosion of reinforcements. This distress is responsible of very expensive repairs to maintain the function, safety and aesthetics of the structure. Therefore, the calculation of the time until depassivation of the rebars is becoming an urgent need due to the engineering demand of prediction of the service life of concrete structures. The service life of the rebars is composed of two periods [1]: initiation and propagation. The most widely used methodology for determining the initiation period consists on the calculation of the diffusion coefficient of the chlorides and then using it to extrapolate to longer periods using the Fick's second law.

However, in the calculation of the diffusion coefficient of chlorides through concrete there are several points that there need explicit recognition of their limitations and a critical analysis. As a first point, in the calculation of the diffusion coefficient of chlorides through concrete it is often neglected that at least two kind of coefficients can be obtained: one of them from steady state experiments using the so-called diffusion or migration cell [2-7], or by measuring the resistivity, and the other from non-stationary experiments [8, 10]. These coefficients are called in literature reversibly as effective, D_{eff}, or apparent, D_{app}. In order to avoid any confusion, in present paper they will be named as D_s= stationary value of diffusion coefficient and D_{ns}= non-stationary value. Concerning the meaning of these two coefficients, D_s tries to characterize the transport itself, assuming that the flux of chlorides is constant in time. On the other hand, D_{ns} takes into account not only the transport, but also the binding of chlorides with cement phases, and therefore it is used for predicting purposes.

As a second point, different experimental conditions in non steady state conditions lead to different diffusion coefficients [11,12,13], which makes the problem of obtaining realistic values of D_{ns} very difficult to be solved. In addition, it has been noticed that D_{ns} varies in function of the surface chloride concentration, and in function of the time. Regarding C_s, it will depend not only on the concrete composition, but also on the external concentration, which in many situations will be so unpredictable as the weather is. With respect to the time law of evolution of D_{ns}, it differs with the type of cement [14] and other circumstances still not well known, probably related to the evolution in the binding ability, which is the third point to take into account [15,16].

Taking this in mind, a comparative exercise of these coefficients as well as the possibility of using them for prediction purposes, or as input parameters for service life models, needs a critical analysis considering different types of concretes and binders, which is the objective of this paper. So, in this contribution some experimental results, as an illustration of the extensive discussion on the key points described above, for different types of concretes and binders at different times, are presented.

2. EXPERIMENTAL

2.1 Materials and procedures

In order to cover in this study a wide range of conditions, several types of cementitious matrix (4 different types of concrete and 2 types of mortar) with different kind of binders have been used. The design of the different mixes are detailed in table 1.

Table 1. Mixes of the materials used.

label	1	2	3	4	5	6
Type of matrix	C	C	C	C	M	M
Cement	I-42.5 R/SR	I-42.5 R/SR	I-42.5 R/SR	I-42.5 R/SR	IV-B/32.5 SR/BC	IV-B/32.5 SR/BC
Addition	none	140 (FA)	36 (SF)	140 (FA) 36 (SF)	FA (as part of the cement)	FA (as part of the cement)
w/c	0.45	0.45	0.45	0.45	0.37	0.49
cement (Kg/m^3)	400	260	364	224	708.3	
Cement + sand	-----	-----	-----	-----	-----	1948
sand (Kg/m^3)	911	911	911	925	1239.4	-----
Gravel (Kg/m^3)	949	949	949	885	-----	-----
Remarks: C: Concrete, M: Mortar, FA: Fly ash, SF: Silica Fume						

All the specimens were cylindrical of 75 mm in diameter and 150 mm in high. They were demoulded after 24 hours of being cast and were cured during 28 days in a humid chamber (95% HR). After this period, the porosity of each mix was evaluated by mercury porosimetry and two specimens of every mix were tested to determine the D_s, (by migration tests) according to the procedure in [17], and the D_{ns} (by diffusion tests with different durations of the exposure to the chloride solution) according to [18]. The rest of specimens were sealed. One year later, two specimens of every dosage were removed from storage, their porosity measured and the coefficients analysed. Some other specimens kept sealed for two years more and at the age of three years they were tested to determine the D_s.

Prior to the tests, the specimens were pre-treated for saturation under vacuum following the standard ASTM C1202-91. The experimental conditions of the tests were:

2.1.1 Migration tests

Distilled water was introduced in the compartment where the anode was placed (anolyte), while the cathodic compartment was filled with a solution 1 M NaCl. The voltage drop applied was of 12 V DC.

Black steel bars were used as electrodes. Periodically during the experiment, Cl^- concentration in the anodic compartment was monitored to know the flux of chlorides.

2.1.2 Diffusion tests

Sealed specimens in a ponding device full of a solution 1 M of NaCl. After different periods of exposure, the chloride profiles were measured by milling the surface of the specimen, exposed to the chloride solution, layer by layer and analysing the powdered samples obtained. From these profiles, the D_{ns} were calculated by fitting to the Fick´s second law.

3. RESULTS

The steady state diffusion coefficients, calculated according the procedure and equations given in [17], are presented in Figure 1, where it can be seen that for concrete mixes (1 to 4) there is not a noticeable decrease in the values obtained as the age of the matrixes increases. As long as the mortars are concerned, a more pronounced decrease has been produced.

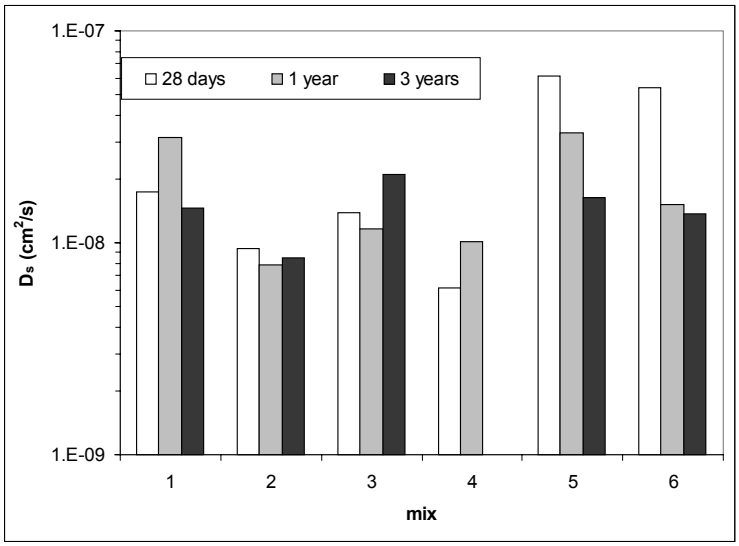

Figure 1. Steady state chloride diffusion coefficients obtained for the 6 mixes after curing in humid chamber for 28 days and after 1 and 3 years sealed.

The non-steady state diffusion coefficients calculated after milling the specimens and analysis the chloride content according the procedure and equations given in [18], are given in table 2 and in Figure 2. In table 2, the diffusion coefficients as well as the surface concentration and the correlation of the fitting to the Fick`s second law are given.

From Figure 2, it can be deduced that the data corresponding to concrete dosages (1 to 4) can be correlated (in function of the duration of the test) all together, independently of having been exposed to the chloride solution after curing for 28 days or after one year sealed. Therefore, for these concretes, it seems that there is not a significant influence in the delay of exposure to chlorides in the coefficient obtained. It can be also noticed that for the dosage 1, cast with OPC low in aluminates, there is not a decrease in the diffusion coefficient as long as the test or age of the specimens increases. The case of mortars is different (dosages 5 and 6) as there is a difference depending on the delay to the exposure to chlorides which, in addition, does not follow the same trend for the two mixes studied. The temporal evolutions of the coefficients given in table 2 have been fitted to potential equations. The factors encountered and the correlation coefficient are given in table 3. In the case of mortars only the data obtained after one year have been used in the fitting. From data of table 3 it can be deduced that the decreasing slope is different depending on the type of mix and binder (parameter b), and that a general rule can not be established.

Table 2. D_{ns} diffusion coefficients, surface concentration and correlation of the fitting to the Fick`s second law for the different mixes and conditions

Curing		28 days	28 days	28 days	1 year	1 year	1 year	1 year
Duration of the test		3 months	1 year	2 years	3 months	1 year	1.5 year	2 years
1	**D_{ns}**	**21.0 E-8**	**----**	**----**	**32.2 E-8**	**57.9 E-8**	**22 E-8**	**48.6 E-8**
	C_s (%)	0.35	----	----	0.22	0.43	0.423	0.38
	R^2	0.984	----	----	0.995	0.715	0.821	0.828
2	**D_{ns}**	**4.41 E-8**	**4.32 E-8**	**----**	**----**	**1.57 E-8**	**0.83 E-8**	**0.58 E-8**
	C_s (%)	0.35	0.2	----	----	0.26	0.50	0.42
	R^2	0.994	0.989	----	----	0.997	0.978	0.989
3	**D_{ns}**	**10.8 E-8**	**7.02 E-8**	**----**	**----**	**----**	**6.97 E-8**	**3.27 E-8**
	C_s (%)	0.31	0.21	----	----	----	0.36	0.38
	R^2	0.983	0.997	----	----	----	0.907	0.900
4	**D_{ns}**	**2.17 E-8**	**1.51 E-8**	**0.95 E-8**	**----**	**2.67 E-8**	**----**	**----**
	C_s (%)	0.21	0.25	0.28	----	0.23	----	----
	R^2	0.997	0.999	0.938	----	0.971	----	----
5	**D_{ns}**	**8.37 E-8**	**4.20 E-8**	**----**	**1.14 E-8**	**0.81 E-8**	**0.70 E-8**	**0.46 E-8**
	C_s (%)	0.57	0.48	----	0.72	0.89	0.96	1.10
	R^2	0.998	0.986	----	0.997	0.989	0.981	0.985
6	**D_{ns}**	**2.24 E-8**	**0.14 E-8**	**----**	**----**	**0.67 E-8**	**0.47 E-8**	**0.31 E-8**
	C_s (%)	0.57	0.51	----	----	0.84	0.93	0.87
	R^2	0.998	0.999	----	----	0.988	0.980	0.980

Table 3. D_{ns} in function of the duration of the test and correlation factors for the different dosages.

$D_{ns} = a * e^{-b * \text{time (years)}}$			
Mix	**a**	**b**	**r**
1	No correlation found		
2	7E-8	1.2625	0.887
3	1E-7	0.6129	0.922
4	3E-8	0.4931	0.783
5	1E-8	0.4929	0.980
6	1E-8	0.6914	0.922

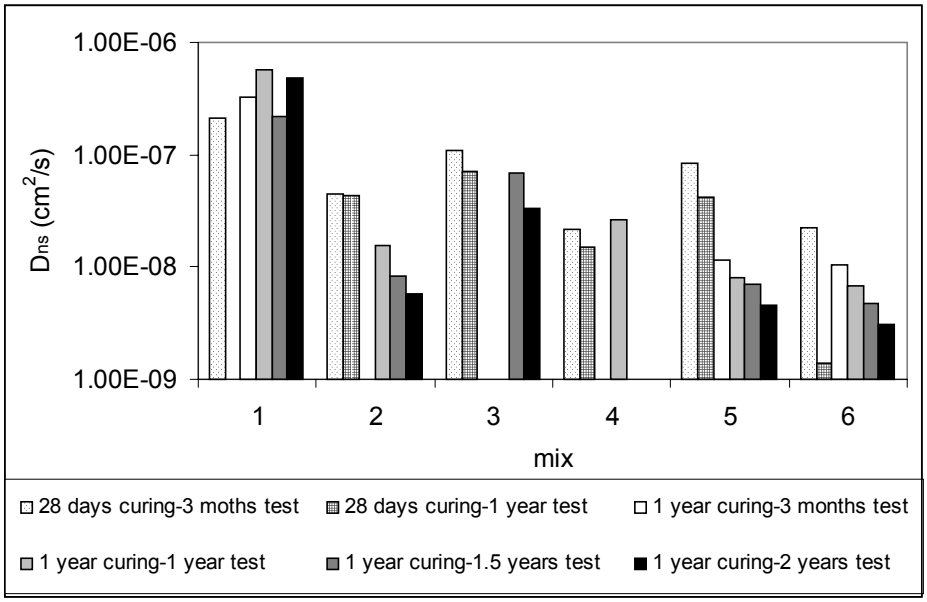

Figure 2. D_{ns} for different time of exposure to chlorides and at different delay in exposing them.

4. DISCUSSION

From the comparison of the two types of coefficients obtained, it could be said that the D_s is a more "reliable" coefficient, as provided that the material does not change, the values that are obtained are quite consequent and the scatter among them is reasonable (see Figure 1). This is due to the fact that it only accounts for the porous network of the material. So, it does not depend on so many parameters as the D_{ns}. The differences among these two kind of coefficients can be illustrated by depicting them in function of the porosity of the matrix (Figure 3 (a-b)).

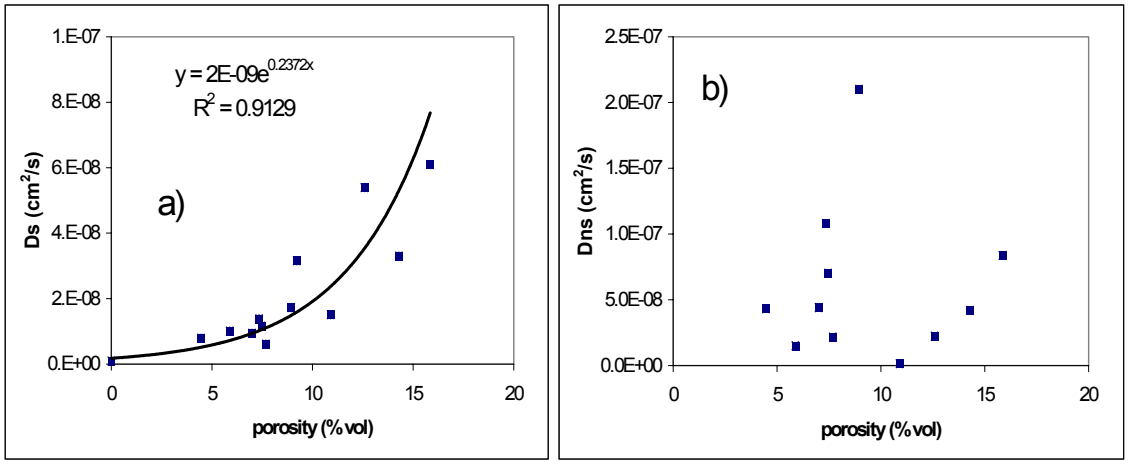

Figure 3. (a-b) a) D_s and b) D_{ns} in function of the porosity (% vol) of the cementitious matrix.

Figure 3, which includes the data for 28 days and after 1 year, shows very clearly that there is a relationship between the porosity and the steady state diffusion coefficient. However, there is no sign of relationship when trying to correlate with the D_{ns}. This is due to the fact that the D_{ns} depends on several factors, which are going to be analysed as follows:

4.1 Influence of time

The evolution of D_s with time was shown in Figure 1 and that of D_{ns} in Figure 2. In both cases, the D values either remain nearly constant or decrease with time, although the trends are not consistent with the cement type, as D_s remains almost constant in the four concrete mixes, while D_{ns} only does in the OPC-low C3A concrete. For the rest of the concretes, there is not a general trend to be established.

4.2 Influence of C_s

In present experiments, the C_s is different due to the mixes being different in spite of the fact that the external concentrations of the testing solutions are the same. Again porosity and binding ability influence the C_s values obtained. In the case of D_s values, their calculation is based in the external solution concentration and therefore, it could be deduced that they are independent of C_s. However, it has been demonstrated [18] that the D_s increase as the external concentration decrease. That is to say, as more diluted is the external solution, higher is the D_s value.

In order to understand the influence of C_s, in Figure 4 (a-d) several examples have been plotted. Figure 4-a shows the experimental C_s for the different concretes and binders tested. Figure 4-b illustrates that for the same C_s, the lower D_{ns}, the lower is the concentration of chlorides at a certain distance from the surface. Figure 4-c shows the profiles for the same D_{ns} but with 3 different C_s, where the deduction indicates that very different concentration of chlorides can be found at the same distance, lower as lower is the C_s, for the same D_{ns}. Finally, in Figure 4-d an extreme example is shown. In this case, a lower D_{ns} with higher C_s gives higher chloride concentration values until 9 mm depth. These examples

indicate that a value of D_{ns} not referred or standardized to a C_s value is certainly misleading from the point of view of the onset of reinforcement corrosion.

4.3 Influence of binding ability

The influence of binding in the values of D_s and D_{ns} can be studied by using the equation (1) given in [19], assuming a linear binding.

$$\frac{D_s}{D_{ns}} = \varepsilon + (1-\varepsilon)\frac{Cs}{Cl} = \varepsilon + (1-\varepsilon)\gamma \qquad (1)$$

ε is the volumetric fraction of pores and Cs and Cl are the concentrations (mol/cm^3) in the solid and liquid respectively. The ratio among these variables is γ.

Taking into account that D_s can be considered as dependent on the porosity (Figure 3-a), using the correlation obtained in present research this variable is put in function of the other and equation (1) can be plotted as in Figure 5, where the three-dimensional map showing the D_{ns} in function of D_s and Cs/Cl (γ).

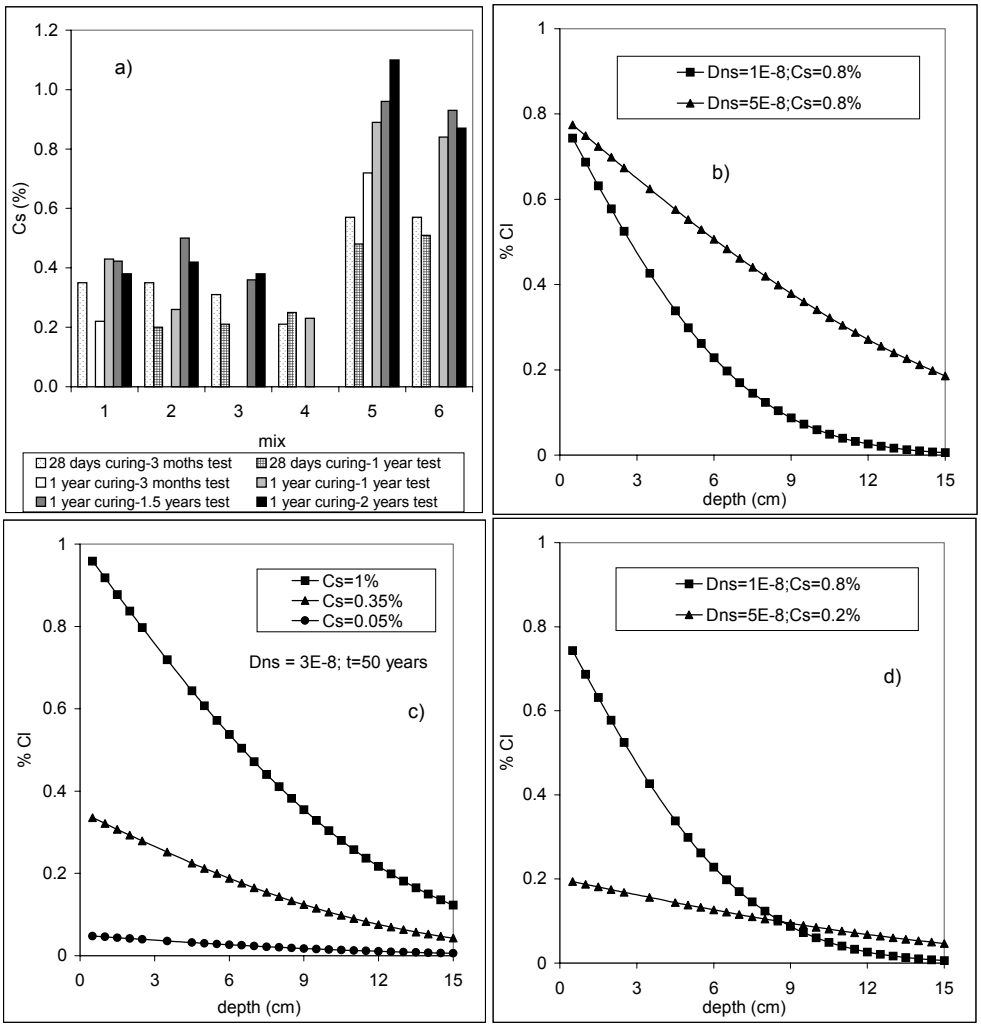

Figure 4. (a-d): Influence of C_s: a) experimental C_s for the different concretes and binders tested. B-d) Profiles of chlorides obtained, according to the second Fick´s law, after 50 years for : b) different D_{ns} and the same C_s, c) the same D_{ns} and three different C_s, and d) different D_{ns} and different C_s.

.

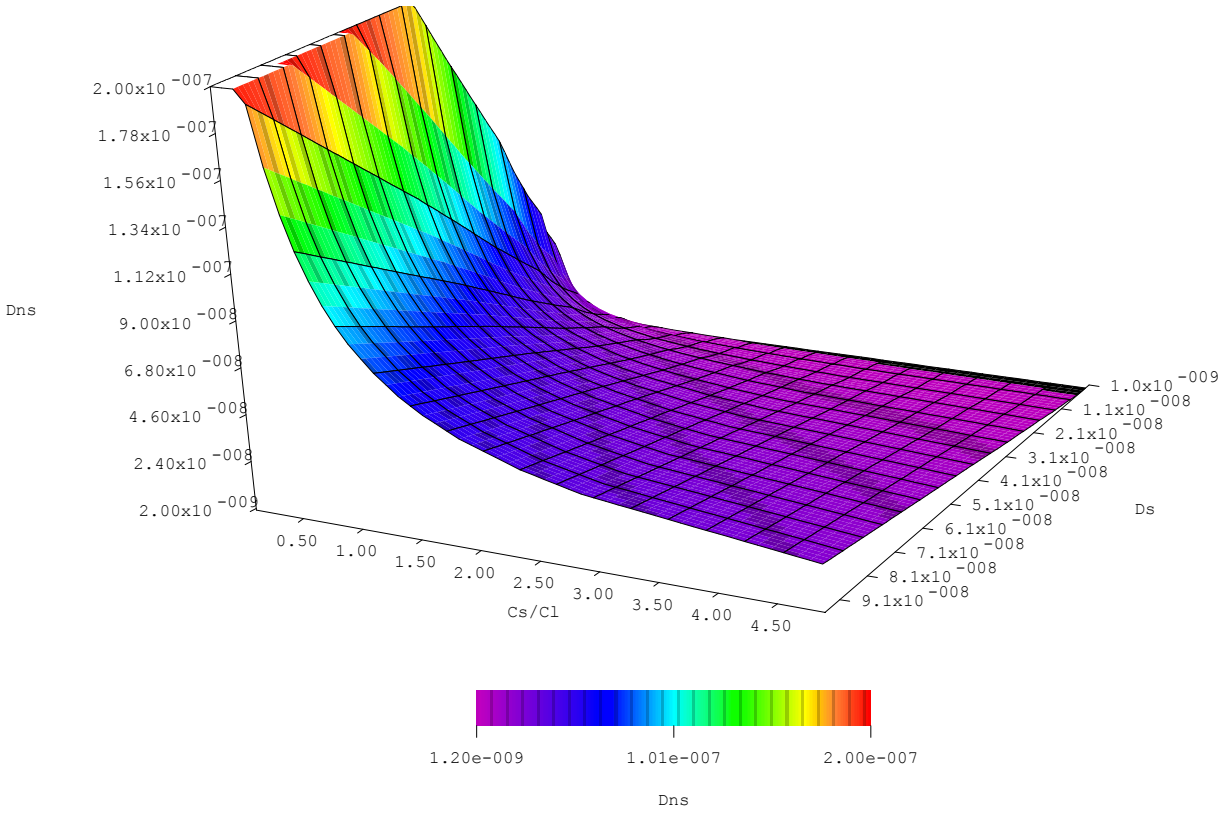

Figure 5. Three-dimensional plot of equation 1, giving D_{ns} in function of D_s and Cs/Cl.

From equation 1 and Figure 5, it can be deduced that if: a) Cs<Cl, $D_s < D_{ns}$; b) Cs=Cl $D_s = D_{ns}$ and c) Cs>Cl, $D_s > D_{ns}$. That is to say, the relation D_s/D_{ns} is determined by the binding ability.

As an example illustrating the influence of binding of chlorides with solid phases, the resulting profiles after 50 years of exposure to chlorides are depicted in Figure 6-a considering that they correspond to different concretes with the same capillary net or resistivity, which means the same D_s (3E-8 cm^2/s in this example), but having different binders and therefore different binding abilities.

For the same C_s, the Figure illustrates a logical trend that indicates that the chloride concentration is smaller at a certain depth as binding ability is higher, which deals to smaller D_{ns} values. However, again the trend might not be logical if instead of a constant C_s, the binding ability means also different C_s values. Let us consider two different γ values. For example 1) γ=0 and 2) γ=0.5. Assuming an external concentration of 0.5 M and so the same concentration in the pore solution of the most external layer of the concrete, for the same D_s (the same porosity) the C_s would result in 0.09% for γ=0 and C_s =0.43 for γ=0.5. Figure 6-b depicts the resulting profiles indicating that a higher γ would be negative because it would allow higher chloride concentrations at the same depth, that is , that higher amounts of chlorides will be found near the reinforcement in spite of the lower D_{ns} and higher binding ability.

This allows the deductions that the total amount of chlorides can be a misleading parameter and that the free amount of chloride ions in the pore solution has to be determined, and that it seems that the C_s is a very influencing parameter on the risk of reinforcement corrosion.

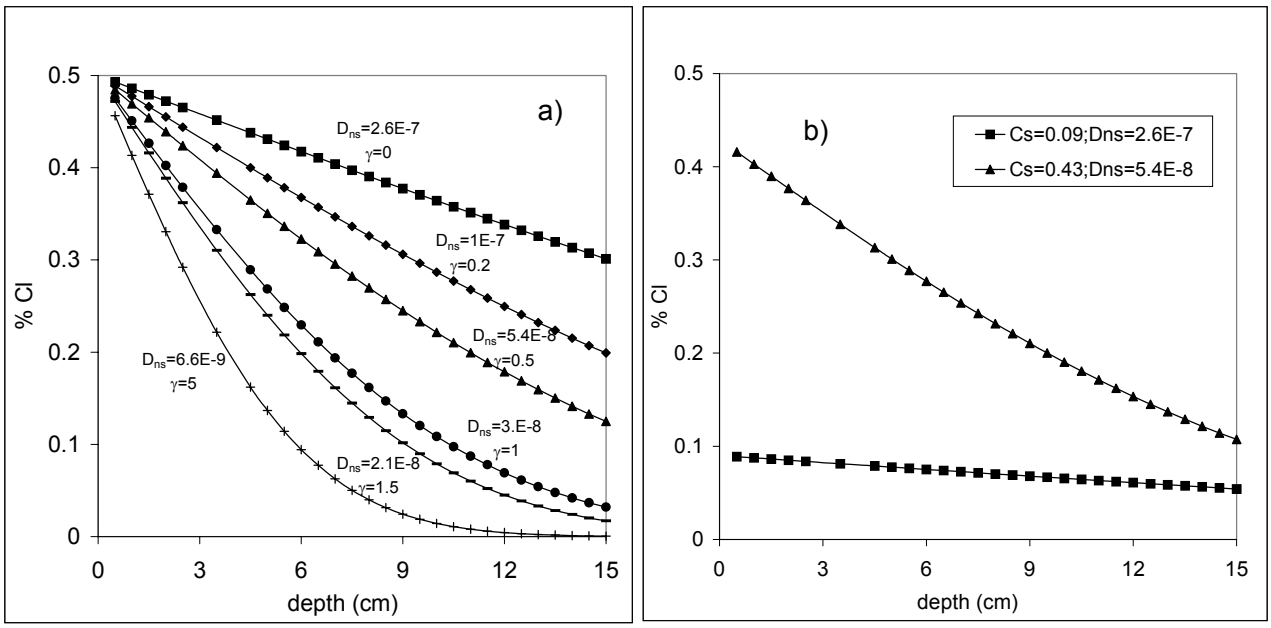

Figure 6. Profile of chlorides obtained, according to the second Fick´s law, after 50 years for concretes with the same D_s but different binding ability (γ) and therefore, different D_{ns} :a) without considering the influence of binding on C_s and b)considering the influence of binding on the C_s.

5. CONCLUSIONS

The main conclusions that have been drawn out form the results of present paper are:

1) The D_{ns} values cannot be used simplistically for comparing concretes without been referred to the surface concentration and to binding capacity. The D_{ns} values alone are misleading regarding the prediction of the onset of reinforcement corrosion.
2) The D_s values seem to be less misleading as they represent the connectivity of pores (transport capacity). However, binding and the resulting surface concentration in the real environment have to be accounted for the sake of service life prediction.

REFERENCES

[1] TuuttiI, K., Corrosion of steel in concrete, Swedish Cement and Concrete Research Institute (CBI), Report Fo 4.82. Stockholm. (1982)

[2] Whiting, D., "Rapid determination of the chloride permeability of concrete". Federal Highway Administration. Report nª FHWA/RD-81/119, (1981).

[3] Page, C.L. Short, N.R. and Tarras, A., "Diffusion of chloride ions in hardened cement pastes". *Cement and Concrete Research*, 11, (3) (1981) 395-406.

[4] Andrade, C., "Calculation of chloride diffusion coefficients in concrete from ionic migration measurements".*Cement and Concrete Research*, 23, (3) (1993) 724-742.

[5] Ollivier, J.P., Arsenault, J., Truc, O., Marchand, J., Mario Collepardi Symposium on Advances in Concrete Science and Technology, Rome, (1997).

[6] MacDonald, K.A.; Northwood, D.O, "Experimental measurements of chloride ion diffusion rates using a two-compartment diffusion cell: Effects of material and test variables". *Cement and Concrete Research*, 25, (7) (1995) 1407-1416.

[7] Gilleece, P.R.V.; Basheer, A.E.; Long, A.E.: "The effect of concentration on the accelerated chloride ion migration tests for modified concretes". Proceedings of the International RILEM Workshop, St- Rémy-les-Chevreuse, France (1995) pp 161.

[8] Tang, L., Nilsson, L.O., "Rapid determination of the chloride diffusivity in concrete by applying an eléctrical field". *ACI Materials Journal,* Technical Paper, (1992) 49-53.

[9] Andrade, C., Sanjuán, M.A., Recuero, A., Río, O.,"Calculation of chloride diffusivity in concrete from migration experiments, in non steady-state conditions". *Cement and Concrete Research*, 24, (7) (1994) 1214-1228.

[10] Andrade, C., Castellote, M., Alonso, C., González, C., "Comparison of testing methods on chloride diffusion into concrete". Proceedings of European Conference EUROMAT´98. Lisboa (Portugal); July (1998).
[11] Castellote, M., Andrade, C., Alonso, C,: "Measurement of the steady and non-steady-state chloride diffusion coefficients in a migration test by means of monitoring the conductivity in the anolyte chamber. Comparison with natural diffusion tests". Cement and Concrete Research, 31 (2001) 1411-1420.
[12] Andrade, C. Castellote, M. Alonso, C. and González, C. "Non-steady- state chloride diffusion coefficients obtained from migration and natural diffusion tests. Part I: Comparison between several methods of calculation", *Materials and Structures,* 33, January-February (2000) 21-28.
[13] Castellote, M, Andrade C and Alonso, C. "Non-steady- state chloride diffusion coefficients obtained from migration and natural diffusion tests. Part II: Different experimental conditions. Joint relations Materials and Structures, Vol 34, July 2001, pp 323-331.
[14] Bamfort, P.B., and Price, W, F,. Concrete 2000, Economic and durable construction through excellence, (E&F Spon, Dundee), Vol 2, September (1993), 1105-1118
[15] Martín-Pérez, B, Zibara, H., Hooton R. D and Thomas, M.D. A," A study of the effect of chloride binding on service life predictions, Cement and Concrete Research, 30 (2000) 1215-1223.
[16] Andrade, C. Alonso, C, Arteaga, A, Tanner, P. "Methodology based on the electrical resistivity for the calculation of reinforcement service life". Supplementary papers of the proceedings of the Fifth International CANMET/ACI Conference on Durability of concrete. Barcelona, Spain, 4-9 June 2000, pp 899-915.
[17] Andrade, C., 'Calculation of chloride diffusion coefficients in concrete from ionic migration measurements'. Cement and Concrete Research 23 (3) (1993) 724-742.
[18] Andrade, C.; Castellote, M.; Cervigón, D; Alonso, C.: "Influence of external concentration and testing time in chloride diffusion coefficient values of steady and non steady state migration experiments". Proceedings of the Fourth International Symposium on Corrosion of Reinforcement in Concrete Construction, SCI. Cambridge, (1996).
[19] A. Atkinson; A. K. Nickerson,: "The diffusion of ions through water-saturated cement". Journal of Materials Science, 19, (1984) 3068-3078.

CRITICAL COMPARATIVE ANALYSIS OF THE STEADY AND NON-STEADY-STATE CHLORIDE DIFFUSION COEFFICIENTS FOR SEVERAL TYPES OF CONCRETES

M. Castellote*, C. Andrade, I. LLorente and C. Alonso

Institute of Construction Science “Eduardo Torroja” (CSIC), Madrid, Spain;
E-mail: martaca@ietcc.csic.es

Marta Mª Castellote

The Author is a Doctor in Industrial Chemistry. She has been working in the Institute of Construction Science "Eduardo Torroja" (IETcc) from October 1993. She was awarded with the special distinction of the University of Zaragoza (Spain) for her PhD, in 1997. Her research has been mainly focussed in the application of electrical fields to concrete, for the characterisation of the ionic transport through concrete, as well as for decontamination purposes. In addition, she is working in the application of Advanced Techniques (Synchrotron Radiation and Neutron Diffraction) in the characterisation of solid cementitious materials.

RESEARCH ON A NEW KIND OF MINERAL ADDITIVE OF CONCRETE: FINE POWDER OF STEEL-MAKING SLAG

Yimin Chen, Hongtao Zhang, Zhen Lin, Suihua Guo and Wensheng Zhang

China Building Materials Academy, Beijing 100024; Email: chenym1@163.com

ABSTRACT

This paper gives the experiment results on a new kind of mineral additive made from steel-making slag. Experiment results show that the fine powder of steel-making slag may used to produce concrete with strength grade from C20 to C60. It can replace from 10% to 50% of cement in concrete and the best amount of replacement is between 20% to 25%. It can be used in plastic concrete and flowing concrete. The effect of fine powder of steel-making slag on strength and workability of concrete is similar to other mineral additives.

Keywords: fine powder of steel-making slag, concrete, mineral admixture

1. INTRODUCTION

Mineral additives, as a component part of concrete, play an increasingly important role in concrete. It not only decreases the cost of concrete but also improves the performance of concrete. High quality mineral additives, i.e. powder of blast furnace slag, 1st grade fly ash, silica fume, have become a necessary part of high performance concrete. In recent years, nearly all high strength concrete and high performance concrete contain part of fine powder of blast furnace slag or 1st grade fly ash.

Steel-making slag is the waste in steel production and its annual amount in China is more than 10 million tons. Steel-making slag has been used in cement as mineral additive[1] for more than 30 years and in China. There is a national standard for cement containing steel-making slag [2]. But only a little research on it as a concrete additive has been done[3], and it has not been successfully and widely used because its properties were not good enough; it is too difficult to be ground, its composition is changeable, it is not sufficiently reactive and not stable volume. This paper gives excellent results of powder of steel-making slag as an active mineral additive of concrete.

2. MATERIALS

Steel-making slag was taken from two steel corporations: one from Beijing (B) and the other from Wuhan (W). They were ground to finer than 400m^2/kg and became active mineral additives for concrete. Their chemical compositions are listed in Table 1. The ratio of $CaO/(SiO_2+P_2O_5)$ must be higher than 2.0 for high reactivity. The content of iron is less than 1% and free CaO is limited to less than 5% for the necessary of soundness. Autoclave testing shows that the soundness of cement with as high as 45% fine powder of steel-making slag is still good enough.

Three kinds of cement were used: 525 Portland cement P.525, 525 ordinary Portland cement (P.O.525) which containing less than 15% mineral additive, 425 ordinary Portland cement (P.O.425) which containing about 15% mineral additive. Table 2 lists the properties of cement. Four

kinds of commercial water-reducer, FDN, JSP-IV, HH-2, JYD-3, were used. Fine aggregate was sand and coarse aggregate was 5-25mm stone.

Table 1. Chemical compositions, specific gravity and specific area of steel-making slag powder

Chemical compositions (wt%)												Sp. gravity	Sp. area
No.	Loss	SiO_2	Al_2O_3	Fe_2O_3	CaO	MgO	SO_3	P_2O_5	R_2O	TiO_2	Fe	g/cm^3	m^2/kg
B	0.79	15.28	5.31	18.55	43.15	12.39	0.10	0.92	0.06	1.06	0.68	3.17	460
W	1.65	11.22	0.94	22.45	43.13	6.63	0.19	2.33	0.10	--	0.56	3.12	459

Table 2. Properties of cement

No.	Specific area m^2/kg	Water requirement of normal consistency %	Soundness	Setting time (h : min)		Compressive strength (MPa)			Flexural strength (MPa)		
				initial	final	3d	7d	28d	3d	7d	28d
P.525	323	27.6	Pass	3:15	4:35	5.2	-	9.0	34.7	-	61.5
P.O.525	335	27.3	Pass	4:13	5:38	6.0	7.9	9.2	33.2	48.1	61.8
P.O.425	310	26.7	Pass	4:18	5:50	4.0	5.6	7.1	26.4	38.7	49.8

3. EXPERIMENT RESULTS OF PLASTIC CONCRETE

Table 3 lists compositions, slump and strength grade of plastic concrete made from P.525 cement, in which 10~50% cement is replaced by W steel-making slag powder. The water/binding materials is 0.32 and the slump of concrete varies from 60mm to 80mm. FDN is high effective water-reducer, polymethylene naphthalene sulfonate. Figure1 gives the relationship between strength.

Table 3. Composition, slump and strength grade of plastic concrete

No.	Composition(kg/m^3)						W/B	Slump (mm)	Strength grade
	Cement	Steel-making slag	Water	Sand	Stone	FDN			
1-1	520	0	190	626	1113	3.6	0.32	78	C60
1-2	468	52	190	626	1113	3.6	0.32	75	C60
1-3	416	104	190	626	1113	3.6	0.32	72	C60
1-4	364	156	190	626	1113	3.6	0.32	70	C55
1-5	312	208	190	626	1113	3.6	0.32	68	C55
1-6	260	260	190	626	1113	3.6	0.32	60	C45

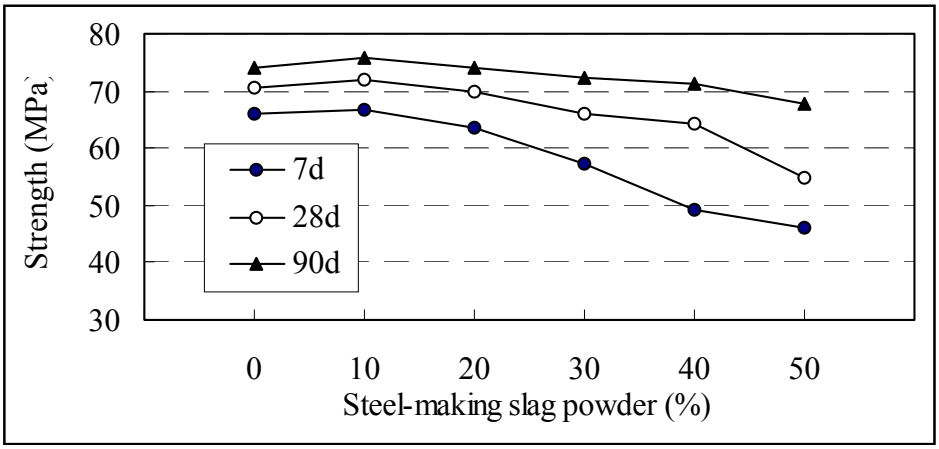

Figure 1. Concrete strength vs amount of steel-making slag powder replacing cement

It is shown that the strength of concrete did not obviously change when 10% or 20% cement is replaced by steel-making slag powder and the strength grade remains C60. When 30% to 50% cement is replaced, concrete strength decreases with the increasing of steel-making slag powder added. The early strength decreases more obviously than the long-term strength, which indicated that steel-making slag powder helps concrete strength increasing with time.

4. EXPERIMENT RESULTS OF FLOWING CONCRETE

4.1 Concrete adding 15%~35% steel-making slag powder from Beijing

Table 4 lists concrete composition with 10% to 35% steel-making slag powder from Beijing. In the compositions binding material (cement and mineral admixture) is 514kg/m^3 and the ratio of water/(cement + mineral additive) is 0.37. P.O.525 cement is used and from 10% to 35% of cement is replaced by steel-making slag powder. Slump of concrete is about 220mm.

Figure 2. gives the relationship of concrete strength with the amount of steel-making slag powder. Strength of the four samples at 28 day are higher than 55MPa. Between 15% to 25%, with steel-making slag powder increasing the concrete strength at 7 day does nearly not change and at 28 day gradually increases. When adding 25% steel-making slag powder, the strength of concrete reaches the highest one. When 35% cement is replaced by steel-making slag powder, 7 day strength of concrete decreases obviously and 28-day strength is similar to that with 15% steel-making slag powder. So, in this case, suitable content of steel-making slag powder as mineral admixture will improve concrete strength, especially the long term strength, and optimum amount is 25%. Even if 35% cement is replaced by steel-making slag powder, 28-day strength can be as high as that containing 15% steel-making slag powder.

Table 4. Composition and strength concrete with 15% to 35% steel-making slag powder

No.	Steel-making slag	Composition(kg/m^3)						Strength (MPa)	
		Cement	Steel slag	Water	Sand	Stone	JSP-IV	7d	28d
ZH-1	15%	437	77	190	681	1065	9.3	50.7	55.4
ZH-2	20%	411	103	190	681	1065	9.3	49.1	58.3
ZH-3	25%	385	129	190	681	1065	9.3	51.0	63.0
ZH-4	30%	360	154	190	681	1065	9.3	47.7	58.1
ZH-5	35%	334	180	190	681	1065	9.3	41.6	55.6

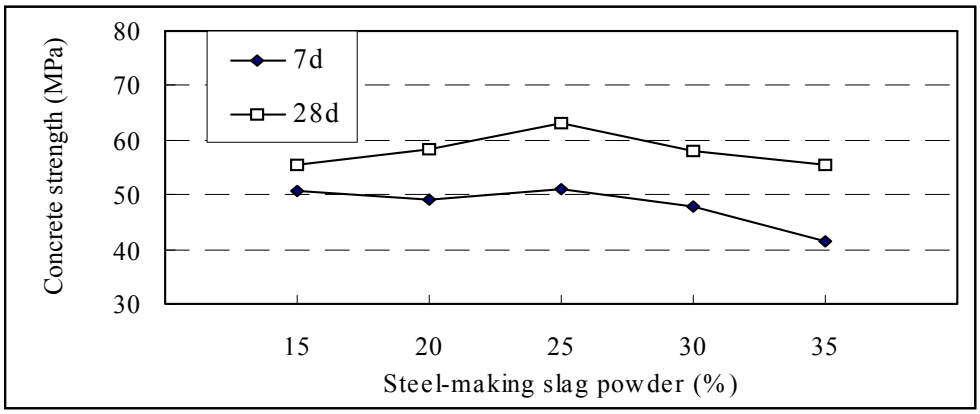

Figure 2. Effect of content of steel-making slag powder from Beijing to concrete strength

4.2 Concrete containing 30% steel-making slag powder from Beijing

In Table 5, concrete is made from 70% P.O.525 cement and 30% steel-making slag powder from Beijing. The water/ binding materials ratio changes during 0.35 and 0.47 and binding materials content changes during 550 kg/m^3 and 385 kg/m^3. Figure 3 shows that concrete strength increases with the increase of amount of binding materials containing 30% steel-making slag powder and with the decrease of water/binding material ratio, which is same to the regular pattern of concrete strength.

The strength grade of concrete in Table 5 locates in C30 to C40. When cement amount is 269kg/m^3, steel-making slag powder is 116 kg/m^3 and water/binding material is 0.47, concrete strength grade is C30. When cement is 291kg/m^3, steel-making slag powder is 124 kg/m^3 and water/binding material is 0.44, concrete strength grade is C35. When cement is 311kg/m^3 and 353kg/m^3, steel-making slag powder is 142kg/m^3 and 152kg/m^3, and water/binding material is 0.35 and 0.41, concrete strength grade is C40.

Table 5. Composition and strength of concrete with 30% steel-making slag powder and various amounts of binding materials and water/binding material ratio

No	W/B	Composition (kg/m^3)						Bind Material (kg/m^3)	Slump (mm)	Strength (MPa)	
		Cement	Steel slag	Water	Sand	Stone	HH-2			7d	28d
8-1	0.35	353	152	166	687	1031	15.15	505	210	44.0	52.1
8-2	0.38	333	142	171	715	1030	14.25	475	220	37.7	49.9
8-3	0.41	311	134	173	745	1028	13.35	445	230	34.4	49.6
8-4	0.44	291	124	174	775	1028	12.45	415	220	32.0	44.0
8-5	0.47	269	116	173	807	1027	11.55	385	210	30.1	37.8

Amount of P.O.525 cement and steel-making slag powder (kg/m^3)

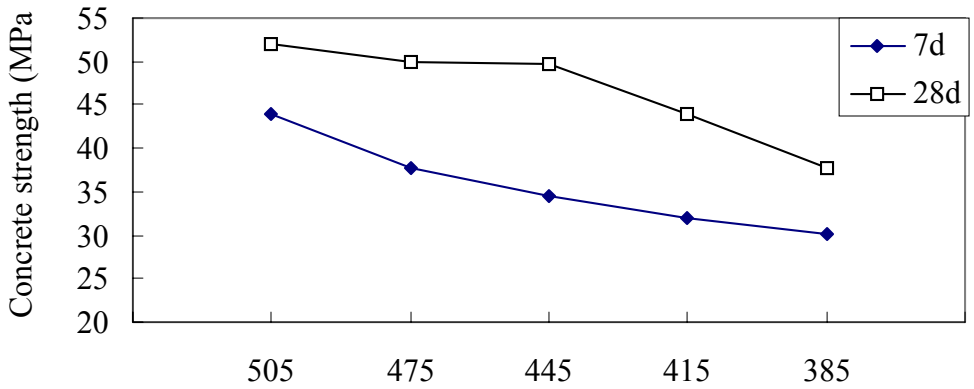

Figure 3. Concrete strength made from P.O.525 vs amount of binding materials with 30% steel-making slag powder

In the composition of concrete in Table 6, binding material is also combined with 30% steel-making slag powder from Beijing and 70% P.O.425 cement. The amount of cement and steel-making slag powder is between 510 kg/m^3 and 340kg/m^3. Water/binding ratio is between 0.375and 0.55. Figure 4 is the curves of concrete strength to amount of cement and steel-making slag powder.

The data shows the same regularity with the concrete adding other mineral admixtures and with Table 5 and Figure 3. Concrete strength grade is between C20 to C40. By comparing Table 5 and Table 6, it can be observed that, in the case adding 30% steel-making slag powder from Beijing, the

influence of water/binding material ratio on the strength of concrete is stronger than that of cement strength.

Table 6. Composition and strength of concrete made from 70% P.O.425 cement and 30% steel-making slag powder from Beijing

No.	W/B	Composition (kg/m^3)						Slump (mm)	Strength (MPa)		
		Cement	Steel slag	Water	Sand	Stone	JYD-3		3d	7d	28d
11-1	0.55	238	102	187	991	897	10.2	185	11.6	23.0	31.8
11-2	0.49	266	114	187	915	933	11.4	210	12.4	26.8	40.4
11-3	0.45	294	126	187	841	967	12.6	195	15.5	31.6	43.1
11-4	0.41	328	138	188	769	998	13.8	200	19.4	34.9	50.5
11-5	0.37	357	153	190	695	1020	15.3	205	25.1	40.5	51.9

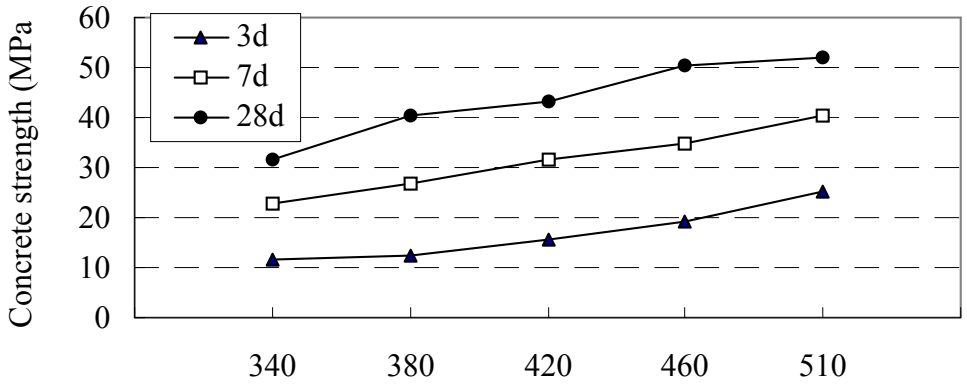

Figure 4. Strength of concrete made from 70% P.O.425 cement and 30% steel-making slag powder from Beijing vs amount of binding materials

4.3 Concrete containing 25% steel-making slag powder from Wuhan

Table 7 lists the composition of concrete made by 75% P.O.525 cement and 25% steel-making slag powder from Wuhan. Table 8 lists their slump and strength testing results. Figure 5 gives the relationship between concrete strength and amount of binding materials. In these compositions, water-reducer, FDN, is the pure polymethylene naphthalene sulfonate and does not contain set-retarding component, so the slump loss after 60 minutes may be a lot. From the results it is indicated that adding steel-making slag powder can effectively improve concrete workability. The strength grade is between C25 and C55, which is in the reasonable range.

Table 7. Composition of concrete with 25% steel-making slag powder from Wuhan

No.	Binding material (kg/m^3)	W/B	Composition (kg/m^3)					
			Cement	Steel-making slag powder	Sand	Stone	Water	FDN
12-1	582	0.33	436	146	582	1036	192	4.1
12-2	488	0.39	366	122	634	1083	190	3.4
12-3	386	0.48	289	97	677	1104	185	2.7
12-4	286	0.61	215	71	721	1124	174	2.0

Table 8. Slump and strength of concrete with 25% steel-making slag powder

No.	Binding material (kg/m^3)	Steel-making slag powder (%)	Slump (mm)		Strength(Mpa)			Strength grade
			Initial	60min	7d	28d	90d	
12-1	582	25	216	188	49.4	62.1	70.8	C55
12-2	488	25	210	176	45.6	53.3	66.2	C45
12-3	386	25	204	160	34.2	46.9	52.7	C40
12-4	286	25	198	144	21.7	31.8	39.4	C25

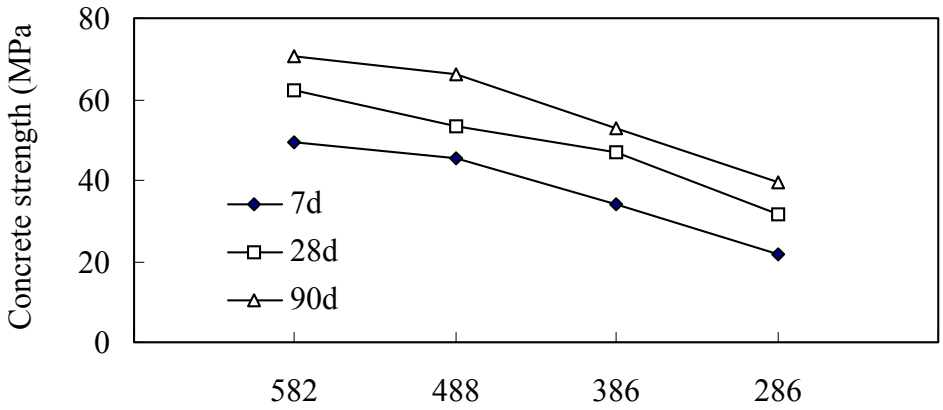

Figure 5. Concrete strength made from75% P.O.525 cement and 25% steel-making slag powder from Wuhan vs amount of binding materials

5. CONCLUSIONS

(1) After being ground to finer than $400m^2/kg$, fine powder of steel-making slag can be used as a mineral additive for concrete. It is suitable for both plastic concrete and flowing concrete.

(2) Fine powder of steel-making slag can be used in C20 to C60 grade concrete to replace cement from 10% to 50%. In some cases, its benefits are to improve concrete properties, and the optimum addition is 20% to 25%.

(3) The regularity of the effect of steel-making slag powder on concrete strength is similar to other mineral additives. It contributes to increasing long term strength of concrete and is favorable for decreasing the slump loss of concrete.

REFERENCES

[1] Chen Yimin, Zhang Hongtao, Guo Suihua, Lin Zhen, Zhang Wensheng; Study on the fine ground steel slag as high reactivity blending materials of cement, Cement (in Chinese), No. 5, 2001, pp.1-4

[2] GB 13590: 1992, Steel-making slag and blast furnace slag cement, P.R.China, 1992

[3] Zhong Xiaolin, Gong Wulun, Liang Fuzhi; Properties and application of steel-making slag powder used as mineral additive of pumpable concrete, Industry Construction (in Chinese), No.7,1993, pp.44-47

RESEARCH ON A NEW KIND OF MINERAL ADDITIVE OF CONCRETE: FINE POWDER OF STEEL-MAKING SLAG

Yimin Chen, Hongtao Zhang, Zhen Lin, Suihua Guo and Wensheng Zhang

China Building Materials Academy, Beijing 100024, Email: chenym1@163.com

Yimin Chen

Date of birth: Feb. 28, 1958
Place of birth: Yongkang City, Zhejiang province, P.R.China

Degree: Ph.D. of materials

Service Organization: China Building Materials Academy

Location:
Vice-chairman, Science and Technology Committee, China Building Materials Academy
Leader, Key Laboratory of Cement Based Materials, National Building Materials, Industry Bureau
Professor , Zhejiang University
Professor , Shenyang Building Technical College
Professor , Jinan University

THE USE OF FLY ASH TO TREAT WASTE FROM THE FERRO-ALLOY INDUSTRIES

J.Herman Potgieter[1], Sanja S. Potgieter[2], Maggi Loubser[3], Elsabé. Kearsley[4], Christien A. Strydom[5], D. de Waal[5] and S.O. Paul[6]

[1]Department of Chemical & Metallurgical Engineering, Technikon, Pretoria, Private Bag X 680, Pretoria, 0001, South Africa; E-mail: hermanp@techpta.ac.za
[2]Department of Chemistry & Physics, Technikon Pretoria, Private Bag X 680, Pretoria, 0001, South Africa; E-mail: potgieters@techpta.ac.za
[3]Department of Earth Sciences, University of Pretoria, Pretoria, 0001, South Africa.
[4]Department of Civil Engineering, University of Pretoria, Pretoria, 0001, South Africa[5]Department of Chemistry, University of Pretoria, Pretoria, 0001, South Africa.
[6]Department of Chemistry, University of South Africa, Pretoria, 0001, South Africa.

ABSTRACT

This paper describes the stabilisation of a ferro-vanadium waste in various ways. In each case a combination of the ferro-vanadium waste together with fly ash was employed for this purpose. The methods investigated ranged from physical encapsulation in different matrices to high temperature immobilisation in solid products.

Keywords: stabilisation/solidification, fly ash, environmental, ferro-vanadium waste.

1. INTRODUCTION

Fly ash produced from coal combustion possesses many physical and chemical properties that make it eminently suitable for use in the cement and concrete industries. The combination of fly ash and cement with hazardous waste offers a number of novel ways to treat side product streams from several industries. These treatments are based on the solidification, immobilisation and encapsulation of wastes through various physical, thermal and chemical mechanisms. South Africa is a major producer of various ferro-alloy raw materials, for example ferro-chrome, ferro-silicon and ferro-vanadium, to name but a few. These industries produce a number of waste products that can be potentially harmful to the environment and require treatment or controlled land filling to minimise their harmful effects.

It is well known that fly ash can be utilised as a component of raw meal in cement production [1]. Wastes combined with fly ash can be used as one option to immobilise harmful elements originating from the waste, after thermal treatment. However, a pre-requisite for this route of treatment, is that the burnability of the cement raw mix not be compromised by the addition of any foreign material added to it.

A further thermal treatment that renders waste harmless or at least decreases interaction with the environment is sintering with fly ash. Using this method it is possible to create useful products from the process, for example lightweight aggregates and ceramic filters/tiles (Kruger R, private communication).

The pozzolanicity of fly ash offers another route for the treatment of wastes. Together with a suitable activator, like lime, it can be mixed with the waste to harden in a solid cementitious matrix. In this way the potentially harmful elements present in the waste can be incorporated in a durable matrix, which can present both a physical as well as chemical barrier against its contact with the environment.

The addition of fly ash to concrete offers many potential advantages in different applications of concrete. Should the concrete be used to encapsulate waste of some form or another, the well-documented ability of fly ash to adsorb heavy metal elements [2], that can potentially be present in an untreated waste, would certainly enhance the effectiveness of this proposed treatment option. In addition, the greater durability imparted by the fly ash to the final concrete element [3] would further contribute to a reduced risk of potential leaching.

The current work will describe the application of all the above-mentioned options to utilise fly ash to render a waste from a South African ferro-vanadium producer less harmful to the environment.

2. EXPERIMENTAL PROCEDURE

Industrial materials were used in this investigation. Their compositions were measured by XRF analysis following the standard method used in the XRD & XRF laboratory of the University of Pretoria, as adapted from H. Bennett and G. Oliver's proposed methods and are given in Table 1.

Table 1. Chemical composition of the materials used in the investigation.

%	PPCLIME	LETHABO FA	WASTE
SiO_2	0.37	52.59	2.71
TiO_2	<0.01	1.68	11.96
Al_2O_3	0.20	34.59	3.70
Fe_2O_3	<0.01	3.15	75.91
MnO	0.71	0.04	0.35
MgO	1.13	1.06	0.98
CaO	71.57	4.08	0.56
Na_2O	<0.03	0.17	2.10
K_2O	<0.01	0.60	<0.01
P_2O_5	<0.01	0.28	<0.01
Cr_2O_3	<0.01	0.04	0.27
V_2O_5	<0.01	0.04	0.45
LOI	25.42	0.57	0.07
Total:	99.43	98.99	96.96

2.1 Immobilisation

A typical cement raw mix was compiled with various amounts of ferro-vanadium waste and fly ash in addition to the usual limestone and clay components. The burnability of these mixes was evaluated according to the F.L. Schmidt method[5] by measuring the residual amount of free lime[6] at various clinkering temperatures. For the production of cement clinker, an LSF (lime saturation factor) value of 95 was selected, together with a SR (silica ratio) of 2.7. Since the coal used to fire cement kilns result in a fly ash incorporation of typically 1.9 – 3.5% in the clinkers, 2.0% of the Lethabo fly ash was incorporated into all the cement raw meal mixtures investigated.

Ferro-vanadium waste additions varied between 0.5 to 2.0% by mass. The effects of the waste incorporation on the burnability of the clinkers are summarised in Table 2.

2.2 Solidification

For the thermal encapsulation of the waste, various proportions of fly ash and ferro-vanadium wastes were nodulised and then heated at different temperatures to form sintered lightweight aggregates. For lack of suitable apparatus to measure the abrasion resistance of the material manufactured, two crude in-house tests have been developed to determine the robustness of the lightweight aggregates produced in this way. In the first instance the materials were dropped 20 times from a standard height of 1.5 m onto a ceramic tiled concrete floor. If it did not break, it was considered tough enough for practical use and application. In the second test, 100 g of sintered nodules was stirred at 300 rpm in a steel container on a magnetic stirrer for 30 minutes and the mass of powdered material produced in this period measured by sieving it through a 1mm screen. The mass of powder passing the screen was expressed as a percentage of the original mass of material used. Sintered material producing less than 2.5% powder was considered suitable for use as lightweight aggregate. The mixtures used, clinkering temperatures investigated and the results obtained, are summarised in Table 3 and Figure 1.

2.3 Encapsulation

In an attempt to render the ferro-vanadium waste less exposed to the environment, encapsulation in various lime-fly ash mixtures, as well as in concrete mixtures were attempted. In the case of the lime-fly ash mixtures, curing after stripping from the moulds after one day was done at 45 ^{o}C, while in the case of concrete normal water curing was performed. Strength measurements after various time intervals were performed according to standard test methods [7]. The mixtures used and results obtained in each case, are summarised in Tables 4 and 5, as well as in Figures 2 and 3.

3. RESULTS AND DISCUSSION

From the results in Table 2, it can be seen that an increasing clinkering temperature leads to a decrease in the residual free lime present. This indicates that the phase forming reactions have been more complete at the higher temperatures than at the lower ones. In similar laboratory studies with normal production raw meal, lower free lime contents are normally encountered at all the clinkering temperatures investigated. The burnability of the raw meal containing waste should thus be optimised further before it can be considered for possible plant application. This can be accomplished by simultaneous adjustments to the LSF and SR to ensure the optimum amounts of silicate materials available to combine with the lime from the calcined limestone in the raw meal. Furthermore, an increase of the waste content at the same clinkering temperature increase the amount of free lime remaining unreacted. From this it can be concluded that the amount of waste in the raw mix should preferably be limited to no more than 1% and the clinkering temperature should preferably not be less than 1450^{o}C.

Table 2. Burnability of various clinkers incorporation fly ash and ferro-vanadium waste.

Clinkering Temperature (^{o}C)	% Ferro-vanadium waste	Residual Free CaO (%)
1350	0.5	11.8
1350	1.0	12.2
1350	1.5	13.0
1350	2.0	13.9
1250	0.5	19.2
1300	0.5	12.3
1350	0.5	11.8
1400	0.5	11.2
1450	0.5	10.2

The results presented in Table 3 and Figure 1 indicate that, by increasing the percentage waste in the lightweight aggregate by 10%, one saves some money on the raw materials used, but requires an additional 100°C thermal energy to achieve about the same degree of durability. The durability of the lightweight aggregate is a function of both the composition as well as the sintering temperature. In the lime-fly ash mixtures reasonable strengths for handling purposes can only be achieved if the amount of lime is at least 24% of the total mixture, i.e. roughly one quarter of the final mix.

Table 3. Mixes used for lightweight aggregate production.

% Fly ash	% Ferro-vanadium waste	Sintering temperature (°C)	"Drop – test" durability	% Powder
80	20	850	Friable and brittle	9.5
		900	Break after dropping twice	6.4
		950	Break after dropping 5-7 x	3.9
		1000	Break after dropping 14-17 x	1.8
		1050	Durable – doesn't break	0.5
		1100	Durable – doesn't break	0.3
90	10	850	Break after dropping 6-8x	3.6
		900	Break after dropping 15-18 x	1.3
		950	Durable – doesn't break	0.2
		1000	Durable – doesn't break	0.08
		1050	Durable – doesn't break	0.02
		1100	Durable – doesn't break	0.01

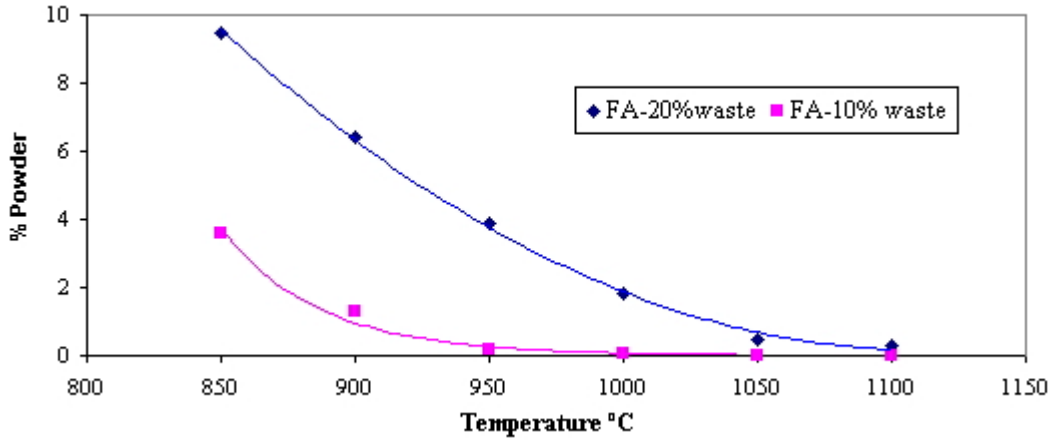

Figure 1. Durability of sintered lightweight aggregates

The compositions of the various lime-fly ash mixtures are given below in Table 4, while Figure 2 schematically represents the strength at various ages. The compositions of the concrete mixtures used in the investigation are given in Table 5. The strength obtained in each case is graphically represented in Figure 3.

Table 4. Compositions of the lime – fly ash mixtures used in the investigation.

Mix no.	% Lime	% Fly ash	% Fe-V waste
M1	23.75	71.25	5
M2	19.00	76.00	5
M3	14.25	80.75	5
M4	9.50	85.50	5

Table 5. Mix Compositions of the concrete investigated.

Components	Mix Design ($kg.m^{-3}$)					
	A 42.5R Cement	B 42.5R Cement & 5% Fe-V	C 42.5R Cement & 10% Fe-V	D 42.5R Cement & 15% Ash	E 42.5R Cement, 15% Ash & 5% Fe-V	F 42.5R Cement, 15% Ash & 10% Fe-V
Water	210	210	210	210	210	210
42.5R Cement (PPC)	350	341.25	332.5	297.5	290	283
Pozzfill (Lethabo)	0	0	0	105	100	95
Dolomite super sand	970	961	953	882	878	875
9.5 mm dolomite	970	970	970	970	970	970
Ferro-vanadium Waste	0	17.5	35	0	17.5	35

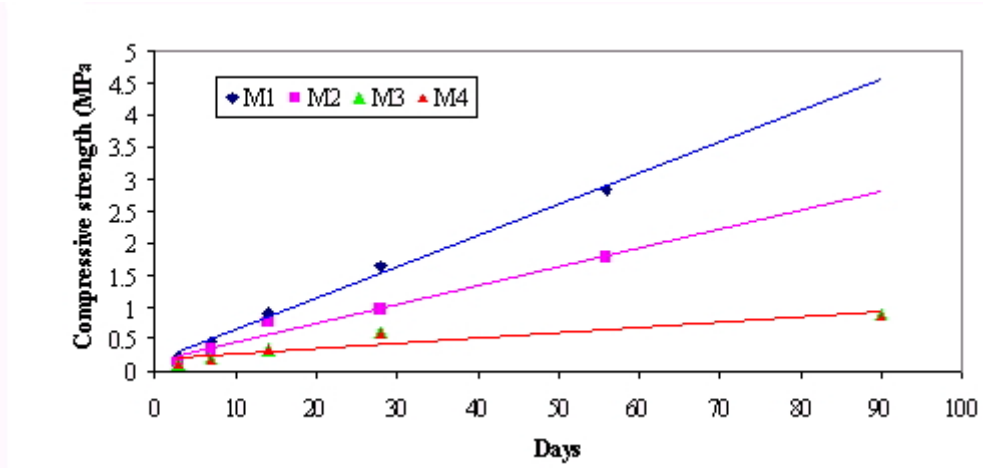

Figure 2. Strength developments in lime-fly ash-waste mixes

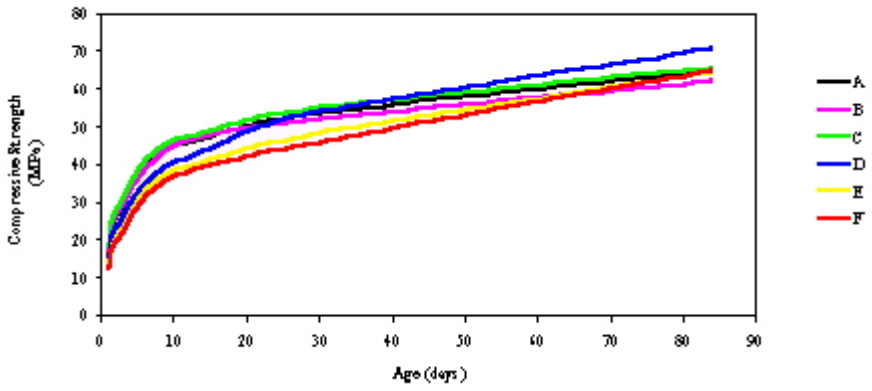

Figure 3. Compressive strengths of various concrete mixtures

The final strengths of all the concrete mixes were satisfactory for practical applications and the substitution of cement with a combination of fly ash and ferro-vanadium waste can result in a sizeable saving for the final mixture without compromising its performance. Table 6 indicates that the best possible savings can be achieved by encapsulating the ferro-vanadium waste with a combination of cement and fly ash. One will obviously have to assess the potential amount of leaching in each of the cases investigated before a final verdict can be given on the best treatment option future. This is currently under investigation in our laboratories.

Table 6. Economic comparison of various methods of treatment.

Treatment Method	**Normal raw materials costs (R/ton; R/m^3)**	**Raw materials costs with waste (R/ton; R/m^3)**	**% Savings**
Sintering as lightweight aggregate (20% vs 10 %)	R 45-00	R 43-00	4.4%
Immobilisation in cement clinker	R 80-00	R 78-50	1.9
Encapsulation in lime-fly ash (M1)	R 100-00	R 97-50	2.5
Encapsulation in concrete (A vs F)	R 300-00	R 280-00	6.7

In an effort to establish whether any chemical interactions have occurred between the solidified waste and the solid matrix, spectroscopic techniques have been used to study some of the lime/fly ash/ ferro-vanadium waste samples prepared. Infrared spectra of the processed samples dispersed in KBr pellets were recorded at Pretoria University; in general, all samples yielded very similar spectra, and no trend was observed. Only one sharp band was observed: it was in the 3640 wave number region and is indicative of a hydroxyl group. The remaining broad bands are in the 1400 and 1100 wave number region and consist of several closely overlapped bands, which have not yet been deconvoluted and hence not identified. A typical example of the spectra obtained is shown in Figure 4. The most striking observation is that there are hardly any changes in the spectra of the various samples.

The FT-Raman spectra were recorded at UNISA; no sample preparation was necessary. Unfortunately the feature that is common to cement samples in general was also observed with the present samples: an excessive amount of fluorescence. The samples were illuminated with only a few mW of laser power (1064 nm wavelength). The broad fluorescence band was centered at about 2000 wave numbers; it was possible to observe some broad band in the 750 wave number region, which varied in intensity from sample to sample - but no trend was evident. A few samples exhibited broad bands in the 1100 wave number region - again with no observable trend. A typical example of the spectra obtained is shown in Figure 5. It should be noted that intensity variations are common for Raman spectra, where the observed scatter is a function of the orientation and size of the crystallites.

When the Raman spectra were recorded at low temperature, the fluorescence was reduced, the observed broad bands sharpened considerably, and additional bands could be observed in the 1100 and 1400 wave number region. Further low temperature studies of cement-related compounds may be of interest.

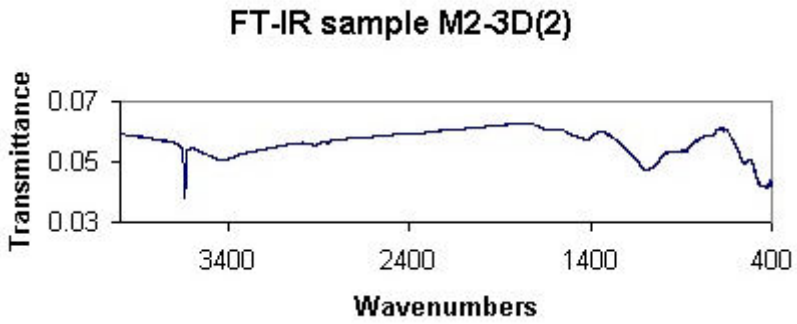

Figure 4. Typical IR spectra of a lime - fly ash – waste mixture

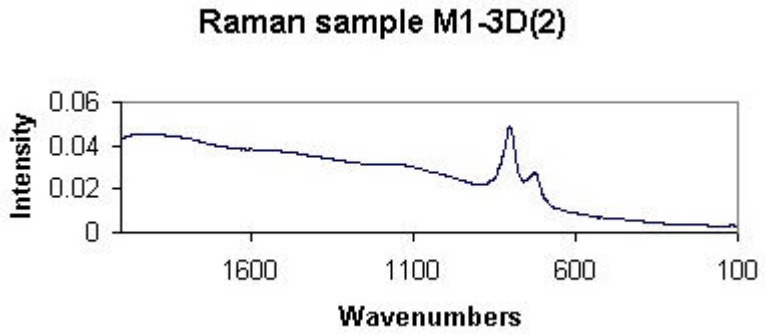

Figure 5. Typical Raman Spectra of a lime – fly ash – waste mixture

4. CONCLUSIONS

The following conclusions can be drawn from this investigation:

1. Increasing the percentage waste in the lightweight aggregate by 10% saves some money on the raw materials used, but requires an additional 100 ^{o}C thermal energy to achieve about the same degree of durability.
2. The durability of the lightweight aggregate is a function of both the composition as well as the sintering temperature.
3. In the lime-fly ash mixtures reasonable strengths for handling purposes can only be achieved if the amount of lime is at least 24% of the total mixture, i.e. roughly one quarter of the final mix.
4. The final strengths of all the concrete mixes were satisfactory for practical applications and the substitution of cement with a combination of fly ash and ferro-vanadium waste can result in a sizeable saving for the final mixture without compromising its performance.
5. The best possible savings can be achieved by encapsulating the ferro-vanadium waste with a combination of cement and fly ash. One will obviously have to assess the potential amount of leaching in each of the cases investigated before a final verdict can be given on the best treatment option future.
6. Spectroscopic techniques applied were not able to detect any interaction between the solid matrix used and the incorporated ferro-vanadium waste.
7. Incorporation of ferro-vanadium waste into a variety of solid matrices can successfully treat it and a reasonable savings can be achieved in the cost of the products produced. Leaching tests are currently underway to assess the success of incorporation of the Fe-V waste in various solid matrices.

ACKNOWLEDGEMENTS

Pretoria Portland Cement (PPC) is gratefully acknowledged for supplying the materials used in this investigation, while ESCOM (Electricity Supply Commission) and the NRF (National Research Foundation) kindly provided financial assistance. Students R. Komane, E. Ngobeni, J. Pretorius and C. Smith helped with the practical tests performed during the investigation.

REFERENCES

[1] Mullick A.K., "Advances in Portland Cements and utilisation of industrial wastes: Towards sustainable development", Proc. 9th International Chemistry of Cement Conference, New Dehli, India, 1, 199, pp 258 – 79.
[2] Mintek (Council for Mineral Technology) Report M352D, Fly ash as an absorbent – precipitation agent in the removal of ionic species from solution, 1988.
[3] Taylor H.F.W., Cement Chemistry, Academic Press Ltd, London, 1990.
[4] Bennett H and Oliver G., XRF Analysis of Ceramics, Minerals and Applied Materials. John Wiley & Son, 1992: p67-93.
[5] Johansen V., and Kristensen N.H., Laboratory burnability and practical kiln operation, 84th Annual Meeting of the American Ceramic society (Cement Division), Cincinnati, U.S.A., Paper 69, 1982, pp 4.
[6] SABS (South African Bureau of Standards) EN 196 –2, 1994a.
[7] SABS EN 196-1: Part 1, 1994b

THE EFFECT OF CHEMICAL MEASUREMENT UNCERTAINTIES ON CEMENT PRODUCTION COSTS – A CASE STUDY

J.H. Potgieter[1], H. Baloyi[1], D. J. Delport[1] and S.S. Potgieter[2]

[1]Department of Chemical and Metallurgical Engineering, Technikon Pretoria, Private Bag X 680, Pretoria, 0001, South Africa. E-mail: hermanp@techpta.ac.za
[2]Department of Chemistry and Physics, Technikon Pretoria, Private Bag X 680, Pretoria, 0001, South Africa. E-mail:potgieters@techpta.ac.za

ABSTRACT

Raw materials in cement manufacturing normally have varying chemical compositions and require regular analyses for plant control purposes. This is achieved by using several analytical instruments and methods. The values obtained for the major elements Ca, Si, Al and Fe are used to calculate the Lime Saturation Factor (LSF), Silica Ratio (SR) and Alumina Modulus (AM). These plant control parameters are used in production to regulate the mixing and blending of various raw meal components used in cement manufacture and to operate the plant optimally. It goes without saying that errors in these parameters not only influence the quality of the cement produced, but also have a major effect on the cost of production of cement clinker through their influence on the energy consumption and residence time in the kiln.

A fact seldom appreciated by plant operators and production managers, is that all analytical measurements suffer from inherent uncertainties. Whatever the source of error, it affects both the precision as well as accuracy of results obtained. This inevitably leads to varying analytical results obtained on samples with a constant composition. It can be especially severe in cases where only one analysis is performed on a sample at any particular time for quality or plant control purposes.

This paper investigated the effect of normal statistical variations in analytical results obtained in the main elements of interest in cement raw meal on the production costs of cement clinker. It was found that a combination of simultaneous variations in the concentrations of Ca, Si, Al and Fe can lower or increase the production costs of clinker by as much as 13% in some cases. The lowest percentage of variation in production costs was around 5%. If considered over a period of a year, these variations can amount to a significant sum of money.

1. INTRODUCTION

In a cement plant, professionals (usually engineers) in charge of the quarry, raw mix preparation, refractory procurement and kiln operations are sometimes poorly versed in chemistry, while most of the professionals (usually chemists) working in the laboratory are not very familiar with kiln and plant operations. The result is a technical gap that could cost the plant millions of Rands per year in unnecessary refractory repairs, kiln upsets and clinker quality problems.

A cement kiln can in fact be considered as a chemical reactor in which a series of complicated reactions take place. Just like any other reactor, it will only give optimum output in terms of cost and product quality if the feed is of as constant a composition as possible. In the cement industry, three plant

parameters are used to control the manufacturing process, namely [1]:

$$LSF = CaO/(2.8\ SiO_2 + 1.2\ Al_2O_3 + 0.65\ Fe_2O_3) \quad (1)$$

$$SR = SiO_2/(Al_2O_3 + Fe_2O_3) \quad (2)$$

$$AM = Al_2O_3/Fe_2O_3 \quad (3)$$

where LSF = lime saturation factor
SR = silica ratio
AM = alumina modulus

These three values are used to control both the raw material feed as well as the clinker (product) quality.

In order to understand the importance of the LSF, SR and AM, it is necessary to briefly state their influence on clinker quality and plant operation conditions. The tendency in a plant is to operate close to a LSF value of 100% to optimise the amount of alite or C_3S, which is responsible for the early strength of cement, and the grindability, which is related to the amount of C_3S, of the clinker. In practice the LSF is usually kept between 92% and 98%. If the LSF is above 99%, the raw mix could become hard to burn, which could result in more fuel usage and incomplete CaO reaction with the other components in the raw mix. If the LSF drops below 90%, refractory brick may be washed out or infiltrated with clinker melt and ring formation is enhanced.

The normal range for SR is 2-3. High SR reduces the amount of coating, produces dusty clinker and reduces clinker burnability. Low SR operational values lead to similar problems as those already mentioned with low LSF values. For most Portland cements, the AM varies between 1.5 and 2.5. The higher the AM, the higher the viscosity of the melt. High AM clinkers have a high heat of hydration, high reactivity and a tendency to high early strength, while low AM clinkers are usually hard to grind.

It is generally accepted that kiln feed composition is under control and constant if the LSF remains within $\forall$ 0.2 of the target value [2]. However, this will depend on the variation of chemical analyses with regard to the elemental oxides required to calculate the control parameters. This in turn will be affected by, amongst others, plant conditions like process feed conditions and variations in the raw materials, as well as instrumental measurement accuracy, calibration stability and statistical variations normally encountered in the collection of analytical data. A fact often forgotten is that a XRF spectrometer (or an ICP spectrometer used in some cases), measures element concentration, which is then converted to the equivalent oxide content with computer calculations performed as part of the analysis program. This means that a small error or change in an elemental concentration has a much larger effect in the expressed elemental oxide content.

The purpose of this paper is not to explore sources of possible determinate or indeterminate errors that can have an effect on the reported values of analytes, but to point out the effect that such errors or normal statistical variations in measurements can have on the calculation of the plant control parameters and subsequently the cost of production of cement clinker.

2. EXPERIMENTAL PROCEDURE

It is generally accepted [3] that measurements display a statistical variance in the form of a Gaussian distribution. In simple terms it translates to the observation that the larger the number of measurements conducted, the larger is the precision of the mean value of all the measurements. From XRF measurements conducted over a number of years [4], it was established that the precision of the values

used for the LSF, SR and AM in South African cement clinkers varies as follows:

CaO : 0.2 - 0.8
SiO_2 : 0.2 - 0.6
Fe_2O_3 : 0.1 - 0.5
Al_2O_3 : 0.2 - 0.4

For the purpose of this investigation, the average of the variations, i.e. the standard deviations of the mean values, were calculated and used.

It should be borne in mind that the measured values are further influenced by the number of repetitions on each sample, the number of samples prepared and measured for a particular determination, counting times on the XRF spectrometer, stability of the instrument, calibration accuracy and sample collection and preparation errors. Taking all this into account, the variations in the precision of measured values mentioned above are not only reasonable, but also fairly small.

The approach followed in this investigation was to calculate the variations in the LSF, SR and AM if a high, low and average value of each specific elemental oxide was used in the relevant formulas. Furthermore, it was assumed that if only average values were used in each case, that the production cost of a ton of clinker was R100. The change in the relevant parameter (LSF, SR or AM) that occurred when higher or lower values than the average of the specific elemental oxides were used, then resulted in a change from the standard (assumed) production cost. Because the latter value was R100/tonne, changes could easily be recognised as percentages.

It was furthermore assumed that the raw meal was a two-component mixture of limestone and clay in a ratio of 90 %:10 %. The composition of the limestone and clay used in this exercise was obtained from a real operational plant [5] and is given in Table 1 below, while Table 2 gives the raw meal composition made up from limestone and clay combined in the said 90%:10% ratio. It also indicates the variation in the different values of each specific elemental oxide used in the formulae calculations.

Table 1. The composition of raw materials, Limestone and Clay.

Compound	%Limestone	%Clay
SiO_2	8.06	66.83
Al_2O_3	1.93	10.28
Fe_2O_3	1.66	4.00
Mn_2O_3	0.07	0.07
CaO	48.48	5.41
MgO	0.38	1.26
LOI	38.53	7.39
Total	99.11	95.24

Table 2. The percent of compounds used to calculate the SR and AM feed compositions

Compound	Low	Average	High
SiO_2	13.14	13.64	14.14
Al_2O_3	2.52	2.72	2.92
Fe_2O_3	1.68	1.88	2.08
CaO	43.89	44.39	44.89

The approach taken meant that for the two elemental oxides used in the calculation of the AM at three values for each one, nine different combinations (3^2) are possible. Similarly, for the SR (3^3) 27 and for

the LSF (3^4) 81 possible combinations could be calculated. A spreadsheet was set up on Excel to do the necessary calculations and manipulation of the data.

3. RESULTS AND DISCUSSION

The design of a suitable mix is a fairly simple procedure, when only two raw materials are to be used. Most plants employ computer programs to calculate new mix compositions and designs, because it becomes a lot more complicated when three or four different raw materials are employed.

One can present the three parameters LSF, SR and AM as a three-dimensional combination with the x-axis being the SR, the y-axis the AM and the z-axis the LSF. For a two-component mix, which will be used in this paper, the model can be presented as follows in Figure 1:

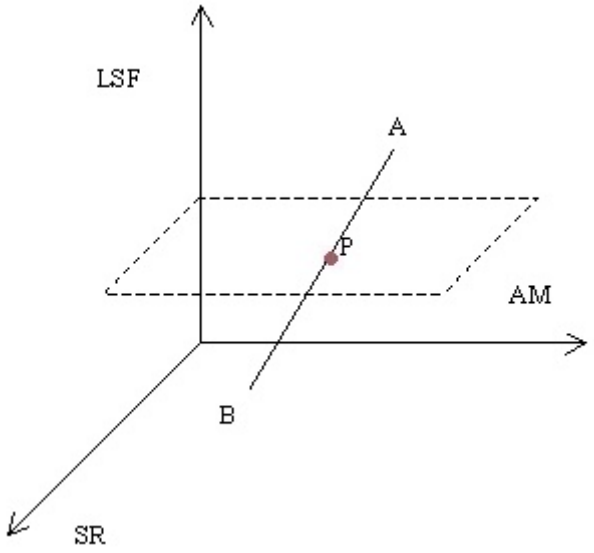

Figure 1. A two-component mix solution region diagram

Raw material, A has a higher LSF than the mix (e.g. the limestone), while material B (the clay), has a lower LSF than the final mix. A large number of mixes can be made between A and B and their LSF values will follow the line AB in Figure 1. This line is called the "solution region". If the LSF value is set at the plant, point P is obtained in the plane for that particular LSF and no other combinations of A and B will satisfy the set LSF requirement. This action then also fixes the SR and AM values. There is a particular cost associated with point P for the raw meal and thus the subsequent clinker production, and analytical variations and inaccuracies in the values used to calculate any of these production parameters (LSF, SR and AM) will have an effect on such costs. The subsequent discussion will illustrate the magnitude and cost implications of such variations.

The simplest case of possible changes in AM will be considered first and the demonstration then expanded to the more complicated cases of SR and eventually the LSF.

When the average values of Fe_2O_3 (1.88 %) and Al_2O_3 (2.72) in Table 2 were used to calculate the AM of the raw meal investigated, a value of 1.45 was obtained. For comparison purposes it was assumed that the cost of clinker produced from such a raw meal mixture was R100/tonne, and that changes in the AM because of higher or lower values of Fe_2O_3 and Al_2O_3 change the cost of the clinker in a directly proportional manner. Table 3 below illustrates the situation when changes in the elemental oxide concentrations due to analytical measurements occur. It also illustrates how the setpoint value of 1.45 (close to the preferred value of 1.50) can drift and change with uncertainties in the measured analytical determinations.

Table 3. Changes in calculated AM with corresponding changes in the comprising elemental oxides

AM variation	Production Cost (R/tonne)	Fe_2O_3 concentration			Al_2O_3 concentration		
		High	Average	Low	High	Average	Low
1.45	100.00		X			X	
1.31	90.38		X		X		
1.62	111.90		X				X
1.55	107.35	X				X	
1.40	97.03	X			X		
1.74	120.31	X					X
1.34	92.65			X		X	
1.21	83.74			X	X		
1.50	103.68			X			X

The values tabulated in Table 3 indicate that even if the CaO and SiO_2 concentrations stay constant, normal analytical variations in the measurement of Fe_2O_3 and Al_2O_3 concentrations could result in the AM drifting out of the acceptable level of change for plant control purposes (set AM [1.45] $\forall$ 0.2) on at least two occasions. Furthermore, the cost can decrease by more than 16% and increase by as much as 20.3% in such cases. One can of course argue that many measurements on the same raw meal or the same sample many times over make such a scenario unlikely. However, normal practice on a production plant where a single sample is taken once every two hours (or at even longer time intervals) and only run once through the analysing instrument makes it quite likely that the scenarios identified above can occur, with significant implications for the production costs of the clinker.

Table 4 summarizes the calculated values for the change in setpoint SR of 2.97 (which is <3) and production costs when the various combinations of changes in the measured elemental oxide concentrations were taken into account. From the results presented in Table 4, it can be deduced that the lowest cost production occurs when the SiO_2 value is at its lowest, with Al_2O_3 and Fe_2O_3 at their highest possible values in the variation. The percentage reduction in production costs is less dramatic than in the case when only the AM is considered and amounts to just 12%. In contrast with this, the increase observed when the SiO_2 value is at its highest and both Fe_2O_3 and Al_2O_3 have their lowest values respectively, is about 13.5%. However, normal analytical variations in the measurement of SiO_2, Fe_2O_3 and Al_2O_3 concentrations now result in the SR value being out of the acceptable level of change for plant control purposes (set SR [2.97] $\forall$ 0.2) on at least six occasions, compared to the previous two occasions when only the AM was considered.

A similar analysis exercise in the case of the LSF variations that can possibly be encountered, indicates that the lowest production cost of R94-94/tonne, or 5.06% lower than the baseline, can be achieved with the CaO value at its lowest, and SiO_2, Al_2O_3 and Fe_2O_3 all at their highest possible variations. A very similar increase of 5.5% in the production cost above the baseline value is produced when the CaO value is at its highest possible variation, and the rest all at their lowest possible values.

Table 4. Changes in calculated SR with corresponding changes in the comprising elemental oxides

SR variation	Production cost (R/tonne)	SiO_2 concentration			Fe_2O_3 concentration			Al_2O_3 concentration		
		High	Aver	Low	High	Aver	Low	High	Aver	Low
3.13	105.51			X			X			X
2.99	100.71			X		X				X
2.86	96.33			X	X					X
2.99	100.71			X			X		X	
2.86	96.33			X		X			X	
2.74	92.32			X	X				X	
2.86	96.33			X			X	X		
2.74	92.32			X		X		X		
2.63	88.63			X	X			X		
3.25	109.52		X				X			X
3.10	104.55		X			X				X
2.97	100.00		X		X					X
3.10	104.55		X				X		X	
2.97	100.00		X			X			X	
2.84	95.83		X		X				X	
2.97	100.00		X				X	X		
2.84	95.83		X			X		X		
2.73	92.00		X		X			X		
3.37	113.54	X					X			X
3.21	108.38	X				X				X
3.07	103.67	X			X					X
3.21	108.38	X					X		X	
3.07	103.67	X				X			X	
2.95	99.35	X			X				X	
3.07	103.67	X					X	X		
2.95	99.35	X				X		X		
2.83	95.37	X			X			X		

It therefore seems that a plant controlled on LSF and SR parameters can experience production cost variations ranging from 5 to 12 % below the baseline costs to between 5.5 to 13.5% above the baseline costs. For a plant producing 1 million tonnes of clinker a year this variation can result in an average of R8.5 million savings or R9.5 million loss. Figures like these emphasize the importance of statistical quality control and proper analytical control in no uncertain terms.

4. CONCLUSIONS

The possible variations in analytical results and continued imprecision of chemical analyses can lead to potentially significant losses in the production costs of clinker in a cement plant, as well as problems with the control of plant operational parameters within specified limits of variation.

REFERENCES

[1] H F W Taylor, Cement Chemistry, Thomas Telford Publishing, London, 1997.
[2] PPC Cement, Course notes: Production of Cement, 1994.
[3] D L Massart, B G M Vandeginste, S N Deming, Y Michotte and L Kaufman, Chemometrics: A Textbook, Elsevier, Amsterdam, 1988.
[4] H Potgieter, PPC Technical Services database, unpublished results; J P Willis, Dept. of Geochemistry, University of Cape Town, personal communication.
[5] PPC Port Elizabeth, Logsheets, 1996.

THE EFFECT OF MICROWAVE CURING ON STRENGTH DEVELOPMENT IN CEMENT MORTARS

J.H. Potgieter[1], S.S. Potgieter[2], A. Giyose[1] and C.A. Strydom[3]

[1]Department of Chemical & Metallurgical Engineering, Technikon Pretoria, Private Bag X680, Pretoria, 0001, South Africa, E-mail: hermanp@techpta.ac.za.
[2]Department of Chemistry & Physics, Technikon Pretoria, Private Bag X680, Pretoria, 0001, South Africa, E-mail: potgieters@techpta.ac.za.
[3]Department of Chemistry, University of Pretoria, Lynnwood Avenue, Pretoria, 0002, South Africa.

ABSTRACT

Curing is a very important factor influencing the strength development observed in mortars and concrete. For this reason the curing conditions in standard test procedures are very carefully specified and controlled. In practical applications steam curing is often employed to accelerate the strength development of mortar or concrete. In this sense it is widely used in the precasting of concrete products to ensure sufficient early strengths in casts to allow fast stripping and turn-around times of the available moulds. A common practice in this industry is to use steam curing at a temperature of approximately 80 ^{o}C to allow a production cycle of 24 hours for cast concrete products.

This paper investigated the use of microwave heating instead of normal and steam curing on the strength development of cement mortars. Intermittent heating, continuous heating, the effect of various w:c ratios and the behaviour of different types of cement were some of the variables investigated. Although it might sound like a far-fetched idea, it should be borne in mind that bricks in the brickmaking industry are already treated in large enough "microwave chambers" for drying and firing purposes. Should this type of technology be promising and easily manageable, there is no reason why such an approach cannot replace traditional steam curing in precast concrete in future.

1. INTRODUCTION

Accelerated curing in the concrete industry is no foreign phenomenon and is frequently applied in the production of prefabricated components. The medium normally used to affect such accelerated curing is steam, heated to a temperature of approximately 80ºC. Steam curing usually takes place in steps in a confined space and the moulds containing cast concrete undergo a stepped temperature increase over a period of about 1hour until the desired temperature is reached. After approximately 14 hours, the temperature is decreased again in a stepwise fashion until demoulding can begin. The whole process lasts about 24h and the purpose of such accelerated curing is to produce components with a sufficient strength for handling purposes in as short a time as possible.

Microwave energy is new technology application to drying, calcining, curing and manufacturing processes requiring thermal processing. Heating by microwave energy is based on the excitation of a molecular dipole at its resonant frequency. At 2.45 GHz, which is near the resonant rotational frequency of a liquid water molecule, the change in electrical field direction causes oscillation of the molecule, which exerts a torque on the molecule, whose resulting violent motion results in instant heating. The amount of heat generated in a material is directly proportional to the square of the electric field, the frequency and the loss factor [1].

This is expressed as the power absorbed per unit volume of material exposed to the energy:

$$P = 27.8 \text{ X } 10^{-12} E^2 f \varepsilon_r''$$

Where: f = frequency in Hz

E = rms local field intensity in V/m, and

ε''_r = relative dielectric loss factor

For a given frequency and field intensity, the relative dielectric loss factor is the dominant variable in determining the microwave power absorbed and therefore the resulting temperature rise in the material.

In a conventional gas or electric furnace, an object is warmed gradually by convection or radiation as heat penetrates from the outside inwards. Microwave energy, by contrast, is cold and heat is only produced when the microwave energy is absorbed by the sample. Since microwaves easily penetrate materials (with the exception of metals) they can be directed and uniformly absorbed throughout the entire volume of an object. This volumetric heating effect causes a material to heat up evenly and rapidly. Since the loss factor for cement is significantly lower than for water, the power absorbed in the water is much greater than that in the cement (and aggregates in the case of concrete) at a given power output and frequency. The power absorbed in the mixture is essentially concentrated in the water areas and decreases as evaporation nears completion, thus limiting the tendency to overheating.

The capabilities of microwave energy have opened up new opportunities in chemistry, materials science and other areas [2]. In the construction industry these include drying of gypsum [1], sample preparation for analyses [3, 4], curing of concrete [5] and syntheses of ceramics [6]. Very novel work is also done at the Materials Research Laboratory of Pennsylvania State University by various researchers on the manufacturing of different types of cement using microwave technology [6 - 10]. This paper will describe the effect of microwave irradiation on the strength development of cement mortars.

2. EXPERIENTIAL PROCEDURE

Mortars were made from OPC (ordinary Portland cement) and an OPC-fly ash mixture (82.5%: 17.5%) with standard sand in a ratio of 1:3. Different w/c ratios varying from 0.4 to 0.6 were used. The moulds used were standard ISO-moulds with dimensions of 40 x 40 x 160 mm and were constructed from PVC (polyvinylchloride).

After mixing the mortars in a Hobart mixer according to standard procedures [11], the PVC moulds were half-filled, vibrated for 1 minute on a vibrating table and then filled completely before another minute's final vibrating. The moulds were then covered with polypropylene and left to stand for 2 hours. After initial setting has taken place, the moulds were heated in a commercial microwave oven (Sharp Model) at 170 W for various time periods. The heating cycles were performed with either continuous or intermittent heating times varying between 1 minute to 20 minutes for continuous curing and 2.5 minutes to 5 minutes in the case of intermittent curing. In the latter case half an hour standing time was allowed between the intermittent heating intervals of one minute at a time.

Twenty-four hours after completion of heat curing, the moulds were stripped and the samples placed in a water bath for normal water curing until compressive strength tests were carried out on a Farnell press.

3. RESULTS AND DISCUSSION

Table 1 represents a summary of the results obtained when OPC and sand mixtures with a w/c ratio of 0.45 were heated continuously for varying time intervals and tested after 24 hours (1day).

Table 1. Compressive strength of cement mortars at 1 day after continuous microwave curing.

Curing Time (Minutes)	Compressive strength (MPa)
2.5	5.9
5.0	7.8
7.5	3.7
10.0	3.1
15.0	1.7
20.0	0.9

The highest strengths were obtained after short heating times, with 5 minutes' heat curing giving the best strength development. During continuous heating a certain amount of steam was evolved and a number of fine cracks were observed in the mortars. It increased with increased heating time and is probably the cause of the decrease in compressive strength observed with the longer microwave heating times.

Table 2 gives a summary of the results obtained when cement mortars with varying w/c ratios were microwave cured for 2.5 and 5 minutes intermittently at 170 W power output before normal water curing for different lengths of time.

Table 2. The effect of initial microwave curing on cement mortars with varying w/c ratios.

Microwave heating time (min)	Curing Time (Days)	Compressive strength (MPa) at a w/c ratio of		
		0.4	0.5	0.6
5.0	1	3.1	6.0	8.7
	7	10.2	8.8	13.2
	14	14.8	32.8	26.6
	28	22.7	40.6	35.2
2.5	1	3.1	5.1	5.2
	7	10.4	13.1	16.7
	14	13.3	18.7	22.5
	28	18.8	31.3	38.3

For the 2.5 minute intermittent microwave curing the highest strength obtained after 1 day was lower than in the case of continuous microwave heating followed by a day's water curing. The maximum compressive strength obtained after 28 days was in the mortar with a 0.6 w/c ratio. This is in contrast to the situation when 5 minutes of intermittent microwave curing was employed before the onset of the normal water curing. In the latter instance, the mortars with a 0.5 w/c ratio developed the highest compressive strength after 28 days.

For this particular mortar, the strength after one day was also higher than when continuous microwave heating was applied. No steam evolved from the moulds when the intermittent microwave-heating

mode was employed. It was noticed that the temperature of the exposed surface increased, but no visible cracks were observed after the microwave heating stage. It seems that the optimum strength development requires a balance between the amount of heat developed in the mortar during microwave heating and the w/c ratio. The former effect (heat development in the mortar) will be closely associated with the mode of heating (intermittent or continuous) and the time it was applied.

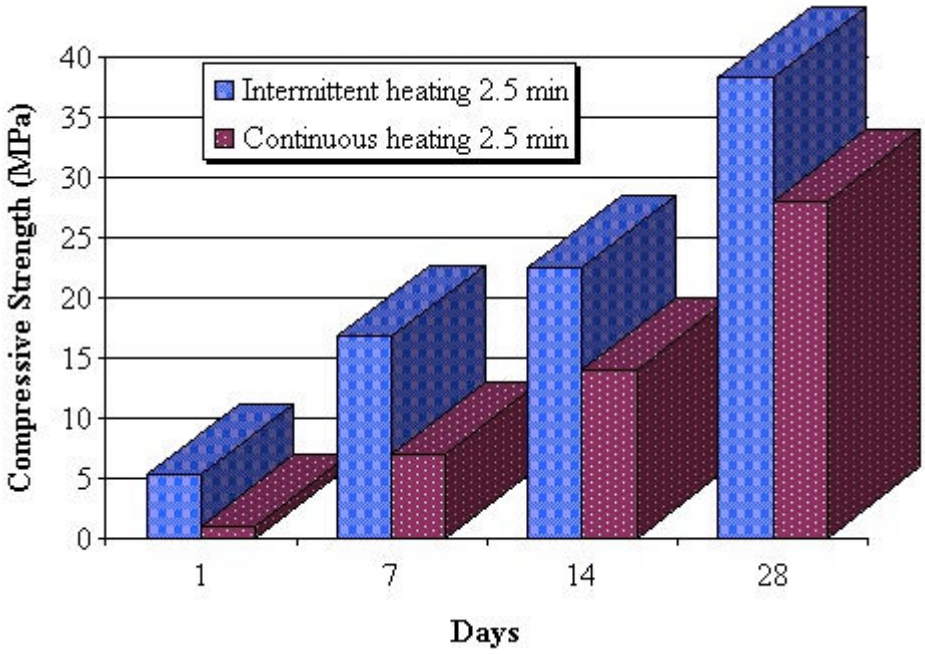

Figure 1. Comparison of achieved compressive strength for OPC mortars that were heated intermittently and continuously.

Figure 1 illustrates the difference in compressive strengths for OPC mortars with a w/c ratio of 0.6 that were microwave heated for 2.5 minutes intermittently and continuously, respectively. It seems that the intermittently heated mortars display a trend of having higher compressive strengths after additional water curing than the ones subjected to continuous heating before water curing.

The results obtained when the OPC-fly ash blend mortars were microwave cured continuously for different time intervals are given in Table 3.

Table 3. Compressive strengths of OPC-fly ash mortars microwave cured continuously at 170W

Microwave heating time (min)	Curing time (days)	Compressive strengths (MPa) at a w/c	
		0.5	0.6
2.5	1	4.9	4.7
	7	11.5	12.6
	14	18.9	21.6
	21	27.3	22.4
	28	30.8	36.9
5.0	1	6.9	7.3
	7	9.7	12.0
	14	18.6	18.5
	21	19.3	19.1
	28	21.8	20.4

When the blended mortars were heated continuously for longer than 2.5 minutes, steam evolution occurred. This probably caused fine cracks in the mortar and can be the reason why the mortars microwave cured continuously for 5 minutes displayed lower compressive strengths after subsequent water curing than the corresponding ones subjected to 2.5 minutes microwave curing. The trend that the highest compressive strength development occurred with a w/c ratio of 0.6 when the microwave heating period was 2.5 minutes and at 5 minutes heating time when the w/c ratio was 0.5, is the same as was observed when the microwave heating was applied intermittently. The fly ash - OPC blends generally show a slower strength gain than the straight OPC mortars, which is in agreement with behaviour normally observed under regular curing conditions [12].

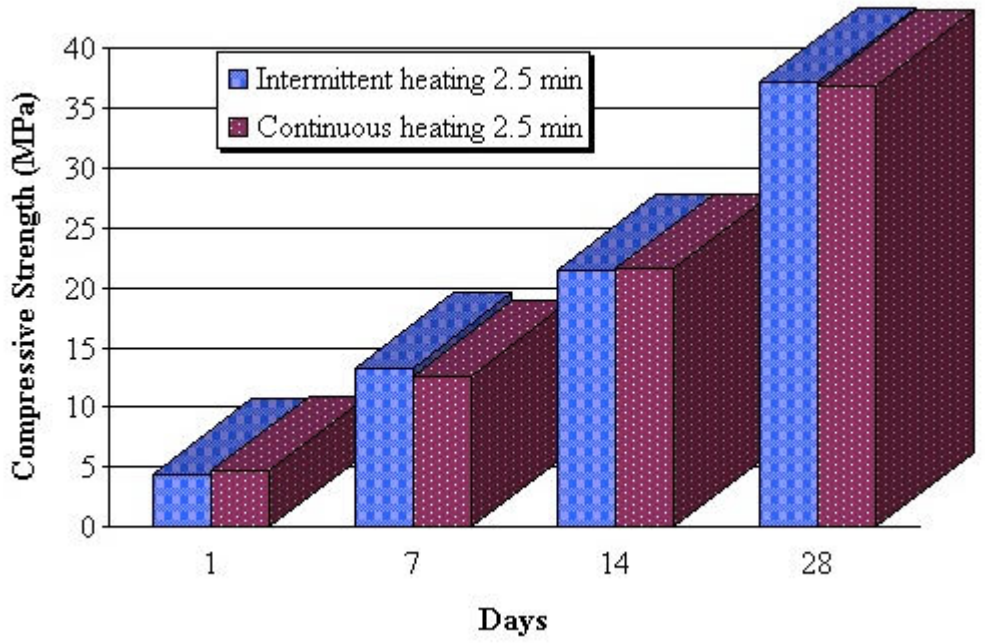

Figure 2. Comparison of achieved compressive strengths for OPC-Flyash mortars after heating continuously and intermittently.

Figure 2 is a schematic presentation of the effect of intermittent and continuous microwave heating of OPC-fly ash mortars, before subsequent normal curing, on the compressive strength after various time intervals. A similar pattern is observed as in the case of the OPC mortars. Similar strengths at the different curing ages were seen, with a trend to marginally higher values in the case of the intermittent heating.

4. CONCLUSIONS

This preliminary investigation yielded most interesting results and opened up some exciting possibilities for future investigations. However, it is of too introductory a nature to result in many definite conclusions.

It can definitely be concluded that:

1. Intermittent heating seems to produce better results than continuous heating, especially if the latter is associated with prolonged heating periods.
2. Excessive heating seems to lead to steam evolution from the mortars, which impairs hydration and compressive strength development.
3. Significant steam evolution led to crack formation in the mortars that were affected and this resulted in lower compressive strengths.

It is recommended that more work be done to differentiate more clearly what the effect of longer similar intermittent and continuous heating times are, that more w/c ratios be evaluated and that some method of measuring the temperature inside and on the top outside part of the mortar be developed, so that it can be correlated with the ultimate strength development behaviour of the material.

ACKNOWLEDGEMENTS

PPC Co. Ltd is gratefully acknowledged for supplying the materials used in the investigation. The NRF, Technikon Pretoria and the University of Pretoria supplied financial funding for this project.

REFERENCES

[1] D.P. Lindroth and W.R. Berglind, Microwave drying of the flue-gas desulphurized gypsum, Environmenttal and Mining Journal, Febr.1994, pp 34 - 38.
[2] R. Dagani, Molecular magic with microwaves, Chemical & Engineering News, Febr. 1997, pp 26 - 33.
[3] J. Figg, Microwave heating in concrete analysis, Journal Applied Chemical & Biotechnol, Vol. 24, 1973, pp 143-155.
[4] C.A. Strydom, J.H. Potgieter, W.J. Mhlongo and C. Masina, Extraction of Free lime from clinkers using microwave energy, World Cement, Vol. 30, No. 11, 1999, pp. 101 – 104.
[5] W. Xuequan, D. Jianbgo and J. Mingshu, Microwave curing technique in concrete manufacture, Cement & Concrete Research, Vol. 17, 1987, pp 205 - 210.
[6] Y. Fang, D.M. Roy and R. Roy, Microwave clinkering of ordinary and colored Portland cements, Cement & Conrete Research, Vol. 26, No 1, 1996, pp 41 – 47.
[7] Y. Fang, Y. Chen, M.R. Silsbee and D.M. Roy, Microwave sintering of fly ash, Materials Letters, Vol. 27, 1996, pp 159 - 159.
[8] H. Li, M.R. Silsbee, J. Cheng and D.K. Agrawal, Formation and hydration of C_3S prepared by microwave and comparison with the conventional method, Cement & Concrete Research, Vol. 29, No. 10, 1999, pp 1611 - 1618.
[9] H. Li, M.R. Silsbee, J. Cheng and D.K. Agrawal, Mircrowave preparation of tricalcium silicate by microwave sintering, Presentation at the 100th American Ceramic Society Annual Meeting, Ohio, 1998.
[10] H. Li, D.K. Agrawal, J. Cheng and M.R. Silsbee, Microwave sintering of sulphoalumina cement with utility waste, Cement & Concrete Research, Vol. 31, 2001, pp 1257 – 1261.
[11] SABS EN 196 - 1: Testing of Cement, 1994
[12] D.G. Mantel, The Manufacture, Properties and Applications of Portland Cements, Cement Additives and Blended Cements, PPC, 1992.

QUANTITATIVE IDENTIFICATION OF CEMENT BLEND COMPONENTS IN BINARY MIXTURES.

J.H. Potgieter[1], S.S. Potgieter[2], D.J. Delport[2] and A. Walker[3]

[1]Department of Chemical and Metallurgical Engineering, Technikon Pretoria, Private Bag X 680, Pretoria, 0001, South Africa. E-mail: hermanp@techpta.ac.za
[2]Department of Chemistry and Physics, Technikon Pretoria, Private Bag X 680, Pretoria, 0001, South Africa. E-mail: potgieters@techpta.ac.za
[3]Pretoria Portland Cement Co. Ltd, Deal Party Road, Port Elizabeth, 6000, South Africa.

ABSTRACT

The quantitative resolution of cement blends into the various proportions of their components is often of interest for plant control purposes and in forensic investigations. This goal can be accomplished in a number of different ways. An often used method involves the use of a noxious, hazardous reagent for heavy medium separation of cement components. This investigation will describe the use of alternative methods to achieve the same purpose. It involves an extraction procedure to selectively dissolve one of the components from a binary mixture, chemical analyses by XRF of individual cementitious material components and their combinations in binary mixtures and density measurements. Various binary mixtures of fly ash, slag and OPC have been investigated and will be reported on. It is foreseen that the approach taken could easily be implemented on plant level for production control purposes.

1. INTRODUCTION

The adoption of the new cement specifications [1] in South Africa in 1996, governing the composition of cements being sold in the country, has drastically changed the local market. Not only did the three major cement producing companies, namely Pretoria Portland Cement Co. Ltd. (PPC), Alpha and Lafarge South Africa, start to produce a larger variety of blended cements, but new players in the form of so-called third party blenders also entered the market. This led to a lot of confusion for especially the un-informed consumer buying the cheapest possible product in the retail market for his/her "do-it yourself" projects.

After much campaigning on behalf of all the role players in the market, legislation was adopted at the turn of the century, that made it illegal for anyone to sell cement not bearing the S.A. Bureau of Standard's mark of performance. This reduced the number of competitors in the market. However, it did not eliminate third part blenders, who bought all their ingredients separately and blended it themselves, from the building and construction market. Due to these circumstances, a need arose for the qualitative and even quantitative identification of the ingredients in blended cements.

One of the methods recommended in the EN cement standards, and which have been applied for many years prior to its introduction in the S.A cement industry, to separate components like fly ash and slag from cement blends, is based on heavy medium density separation. In this procedure bromoform is used to separate Ordinary Portland cement (OPC) from either fly ash or slag, based on their differences in density. However, it is a tedious method, not very accurate and the medium used, bromoform, is carcinogenic. An optical microscope can also be employed, but has the drawback that it is at best qualitative in the identification of the components of a blended cement. Other crude qualitative

chemical tests included the addition of dilute acid to a blended cement in order to detect the liberation of CO_2 gas if a limestone filler has been used in the blend, or H_2S gas when slag (especially from a steel works) has been blended with OPC. However, none of these are accurate or infallible, so it was clearly necessary to find another means or way to detect the presence of mineral admixtures in cement qualitatively and quantitatively.

Our laboratory recently published a paper [2] to illustrate the fast and simple quantitative determination of limestone in blended cements by employing FT - IR spectroscopy. This paper will describe a variety of other approaches applied to quantify the amount of fly ash or slag in binary blended cements.

2. EXPERIMENTAL PROCEDURE

2.1 Selective dissolution

Previously published work [3] indicated that maleic or salicylic acid selectively dissolves the two silicate phases, alite (tricalciumsilicate) and belite (dicalciumsilicate), as well as CaO, in cement. The C_3A, C_4AF and gypsum are insoluble in any one of these media. It was therefore assumed that both fly ash and slag would also be fairly insoluble if treated with any of the two acids mentioned.

One gram of sample was treated with 25 ml of a 20% (m/m) solution of maleic acid in methanol and stirred at room temperature for 10 minutes. The resultant solution was filtered through a fine paper or a pre-weighed sintered glass crucible. The collected residue was washed with 4 portions of 25 ml each of methanol. Then the crucible was dried at 150 ºC and the residue weighed after cooling. The percentage residue was calculated and a calibration curve of the % insoluble residue vs % pozzolan / mineral admixture (fly ash, slag) was constructed for a variety of blends investigated.

2.2 Colorimetry

It was noticed that a distinct yellow colour was present each time in the collected alcohol filtrate. It was therefore endeavoured to establish whether a correlation existed between the intensity of the colour of the filtrate and the mineral admixture addition in the brinary blends investigated. The absorption of light at a wavelength of 320 nm by the coloured filtrates was measured on a Spectronic 601 UV - VIS spectrometer.

2.3 XRF

Suitable masses of the composed binary blends and virgin materials were milled for 3 minutes in a ring mill using hexane as a grinding aid. The resultant powders were dried on hotplates at either 45 ^oC (OPC) or 150 ^oC (fly ash) and pressed pellets for XRF analyses were prepared on a Herzog press set to a pressure of 20 tonnes. The pressed pellets were analysed on a Siemens 400 MP spectrometer, employing Rh Kα radiation at 50 kV and 30 mA. The concentration of calcium, expressed as CaO, was used to construct a calibration curve of count rate vs the % mineral admixture (usually fly ash) in the blend. From count rates for CaO on commercial samples their mineral admixture content could be established from the calibration curve and correlated with some of the other methods investigated.

2.4 Density measurements

Four grams of sample of various binary blends were compacted under a pressure of 30 tonnes on a Herzog press and their densities measured on a Grabner Mini densitometer. This was used to construct a calibration curve of the measured density versus the mineral admixture content. Production samples were analysed with this instrument and the results compared with those obtained by XRF measurements, as described in the previous method. In selected cases 3g of sample powder was put into an aluminium cup and measured on the densitometer without any prior compaction in order to establish whether compaction is essential for the success of the measurement.

2.5 Raw materials

All materials used in the investigation were analysed by preparing fused beads according to standard procedures [4] and measuring it on a Siemens 400 MP XRF spectrometer.

3. RESULTS AND DISCUSSION

The chemical compositions of the materials used in this investigation are given in Table 1.

Table 1. Chemical compositions of various cement-related materials.

Component	Cement 1 (OPC)	Cement 2 (OPC)	Cement 3 (OPC)	Fly ash	Slag (Vanderbijlpark)
SiO_2	21.30	21.60	21.99	42.00	30.40
Al_2O_3	3.38	3.59	3.63	28.10	10.40
Fe_2O_3	2.08	2.39	3.03	5.60	1.60
Mn_2O_3	1.00	0.92	0.43	0.07	0.70
TiO_2	0.29	0.33	0.36	1.61	0.40
CaO	63.72	63.63	63.52	13.18	47.10
MgO	4.42	4.12	2.73	3.64	6.50
P_2O_5	0.013	0.022	0.096	1.640	0.060
K_2O	0.68	0.73	0.56	0.95	0.86
Na_2O	0.08	0.09	-	0.50	-

The results obtained with the selective dissolution approach are graphically illustrated in Figure 1. There is an excellent linear correlation between the percentage insoluble residue remaining on the filter after the dissolution procedure and the amount of fly ash added to the blend.

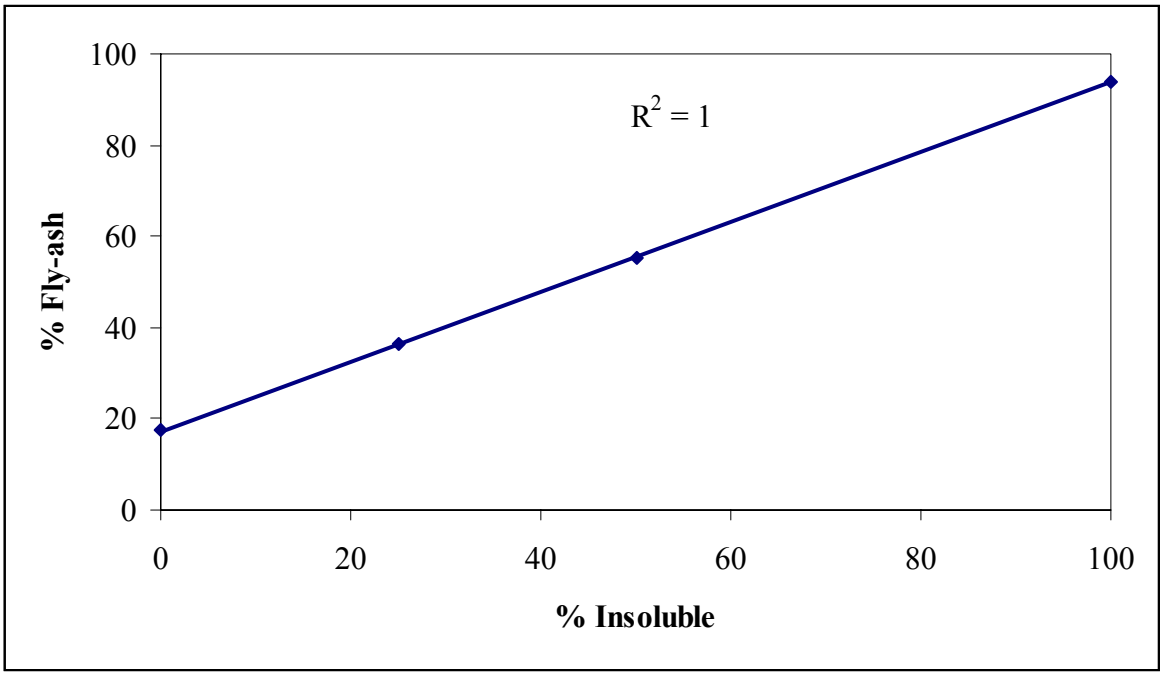

Figure 1. Fly ash contents in a binary cement blend determined by selective dissolution.

When all three cements (no. 1-3) were used to produce binary blends with fly ash, the resultant calibration graph in Figure 2 indicates that the curves obtained when applying the selective dissolution approach depend on the origin of the cement. Cements 1 and 2 were produced by PPC, while no. 3 was an Alpha cement. The observed shift in the calibration curve of % insoluble residue versus the amount

of fly ash in the blend is to be expected, because different cements contain different amounts of alite and belite phases.

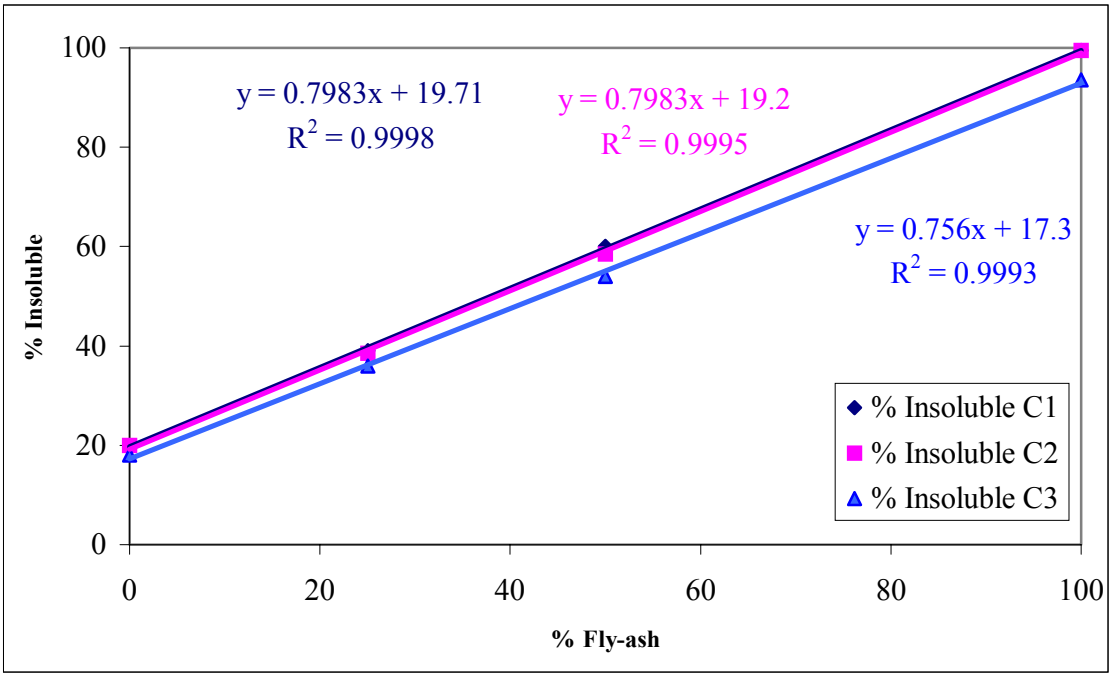

Figure 2. Fly ash contents in binary blends composed from different OPC's

A comparison in Figure 3 between the application of this procedure with either fly ash or slag added to the binary blends, shows that there again is a small difference in the calibration curves obtained. When selective dissolution is selected as the procedure of choice, care will have to be exercised when the source of cement or mineral admixture changes. However, it should work well when the cement and mineral admixture used in the blend have a reasonably constant composition. Furthermore, it is cheap and easy to use at plant level for quality control purposes. The procedure does not require complicated equipment and can easily be prepared by trained unskilled personnel.

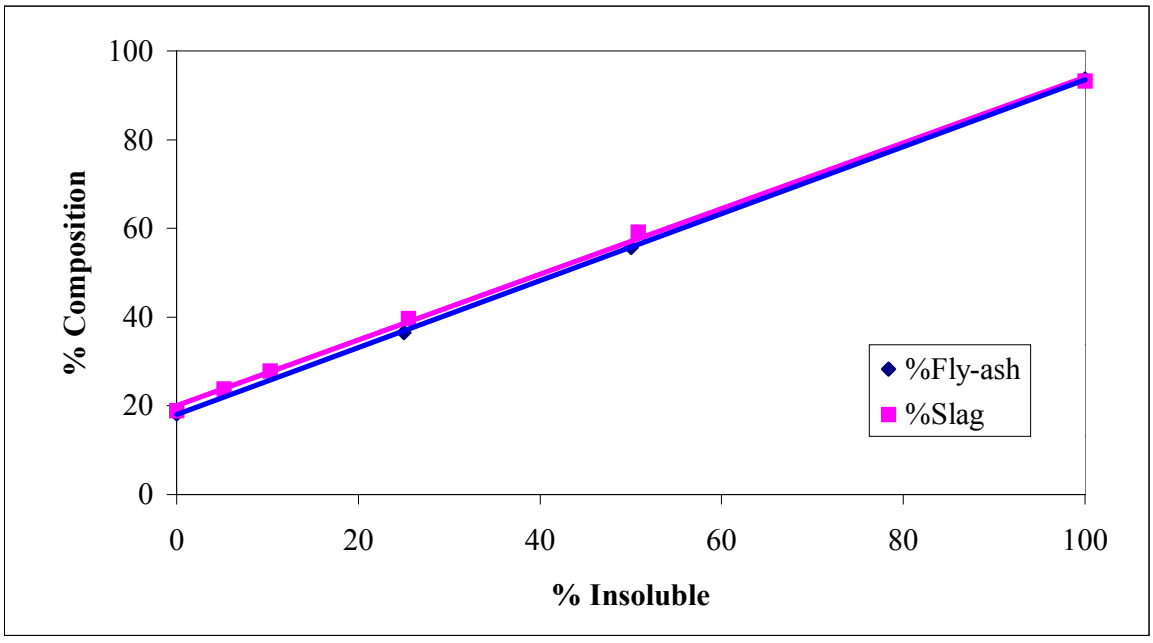

Figure 3. A comparison of results obtained for the selective dissolution method with two different binary mixtures.

A preliminary estimation of the degree of variability in a cement (OPC) and fly ash used regularly to

produce binary blends has yielded the results summarized in Table 2. The selective dissolution procedure was applied in turn to each material collected over a period of six weeks.

Table 2. Estimation of the variability of raw materials used for the production of binary cement blends.

Sample no.	**Insoluble residue (%) in**	
	Fly ash	OPC no. 3
1	94.2	18.0
2	94.6	18.8
3	95.0	18.4
4	93.8	17.4
5	93.7	18.2
6	95.5	18.8
Average	94.5 ± 0.7	18.3 ± 0.5

From the preliminary investigation conducted over a period of six weeks, it seems that the materials' compositions remain constant enough to allow the selective dissolution method to be employed for plant and quality control. The method will, however, require regular calibration curves to be constructed to ensure that unknown blends that are investigated will be analysed accurately.

An attempt to correlate the amount of fly ash in the binary blend with the light absorbance of the filtrate solution after application of the selective dissolution procedure, proved to be unsuccessful, as can be seen from Figure 4. No linear correlation could be established between the absorbance of the filtrate and the amount of fly ash added to the blend.

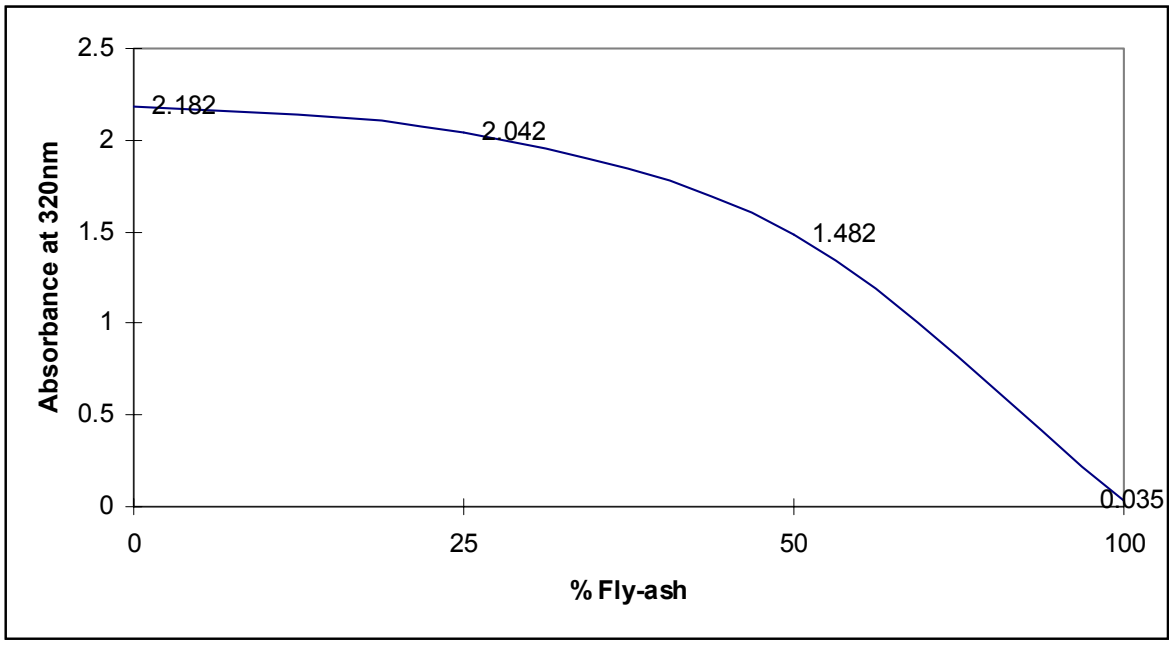

Figure 4. Absorbance results for a binary mixture of OPC and fly ash.

A number of binary blended plant samples were analysed on the XRF spectrometer. Each time a calibration curve was constructed from the OPC and fly ash used to prepare the blended cement. For this purpose laboratory mixes containing 0, 25, 50 and 100% fly ash were composed and the fly ash content graphically represented against the number of counts obtained for the CaO in each specimen. This procedure implies that five samples had to be prepared as pressed pellets for measurement on the XRF spectrometer every time a plant sample of the blended cement were to be analysed. A comparison of a set of results obtained when using selective dissolution with maleic acid and XRF measurements

is given in Table 3.

Table 3. A comparison of the resolution of binary OPC-fly-ash blends.

Sample no.	Cement used in blend (no.)	Linearity of calibration	Fly ash by XRF (%)	Fly ash by selective dissolution	Δ (% - %)
1	3	1.000	13.7	13.3	+0.4
2	3	1.000	29.6	29.2	+0.4
3	3	0.999	29.1	28.9	+0.2
4	3	1.000	29.3	29.3	0
5	3	0.999	29.3	29.6	-0.3
6	3	1.000	30.1	29.9	+0.2
7	2	1.000	29.8	30.1	-0.3
8	1	0.999	30.3	29.1	+1.2

The fly ash content obtained by XRF measurements and an application of the selective dissolution method compares very well with each other. In all but one of the samples the inter-method difference was less than 0.5 percentage points, which is quite acceptable for plant purposes.

The results summarized in Table 4 were obtained from density measurements on OPC no. 3 and fly ash. XRF measurements were also done on the samples from the plant in a similar way as described above.

Table 4. Summarized Results

Sample no.	Fly ash density (g mL^{-1})	OPC no.3 density (g mL^{-1})	Fly ash content estimated from compressed density (%)	Fly ash content estimated from Powder density (%)	Fly ash content by XRF (%)	Δ (% - %)
1	2.551	3.297	14.0	12.3	13.5	+0.5
2	2.559	3.301	13.5		13.3	+0.2
3	2.500	3.245	12.8	11.8	12.9	-0.1
4	2.489	3.254	12.6	11.4	13.2	-0.6
5	2.513	3.314	22.4		23.1	-0.7
6	2.466	3.265	22.2		22.5	-0.3
7	2.533	3.308	15.7	14.1	15.0	+0.7
8	2.530	3.304	15.3		15.4	-0.1
9	2.504	3.304	15.4	13.7	15.7	-0.3
10	2.506	3.290	23.1		23.6	-0.5
11	2.500	3.285	15.8		16.1	-0.3
12	2.505	3.305	21.9	21.0	22.5	-0.6
13	2.529	3.273	15.8		16.3	-0.5
14	2.515	3.305	22.9		23.8	-0.9
15	2.515	3.305	24.0	22.1	24.4	-0.4
16	2.522	3.308	16.9		16.3	+0.6
17	2.472	3.290	17.0		16.6	+0.4
18	2.526	3.263	25.2		24.4	+0.8
19	2.484	3.303	15.7		15.4	+0.3
20	2.493	3.293	16.4		16.6	-0.2
21	2.503	3.266	23.8	22.5	24.7	-0.9
22	2.439	3.235	25.1		25.2	-0.1

A reasonable degree of similarity is observed between values obtained with the XRF in Table 4 and the measurements done with the densitometer. The differences are small enough to be satisfactory for plant control purposes. The use of powder samples in the uncompressed form is not recommended, as the measured density values differ quite a bit from those of similar compressed samples. This approach is faster than XRF measurements, because for the latter method samples first needed to be milled and dried before any measurements can be done. The densitometer is also much cheaper than a XRF spectrometer and does not require the same extensive maintenance required by XRF instruments. With proper training operator bias could be eliminated from determinations done with a densitometer to yield a fast and inexpensive plant control procedure for binary cement blends.

4. CONCLUSIONS

Three methods of measuring mineral admixture content in binary cement blends have been investigated. Reasonable degrees of similarity between the results obtained with all three procedures were found that are considered satisfactory for plant and quality control purposes. Two of the methods, namely selective dissolution and densitometer measurements, are very suitable for use by unskilled labour and do not require highly skilled operators. Furthermore, both are quite inexpensive and easy to implement without a large capital layout. These methods are recommended for use by third party blenders who do not have the extensive infrastructure of well-equipped laboratories for plant and quality control purposes. The applicability of some of the above-mentioned methods should be investigated to determine their stability to resolve ternary cement blends.

ACKNOWLEDGEMENTS

PPC Co. Ltd., Alpha, Slagment and Ash Resources are thanked for the supply of samples used in the investigation. PPC is also gratefully acknowledged for the use of their XRF equipment. The NRF and Technikon Pretoria financially supported Herman and Sanja Potgieter, as well as Dawie Delport, while conducting this research.

REFERENCES

[1] SABS ENV 197:1, Cement: Composition, specifications and conformity criteria, Part I: Common Cements, 1992.
[2] M.A. Legodi, D. De Waal and J.H. Potgieter, Quantitative determination of $CaCO_3$ in cement blends by FT - IR, Applied Spectroscopy, Vol. 55, No. 3, 2001, pp. 361 - 365.
[3] A.A. Tabikh and R.I. Weht, An X-ray diffraction analysis of Portland cement, Cement & Concrete Research, Vol. 9, 1971, pp. 317 - 328.
[4] K. Norrish and J.T. Hutton, An accurate spectrographic method for the analysis of a wide range of geological samples, Geochimicia et Cosmochimica Acta, Vol. 33, 1969, pp. 431-453.

PRODUCT-BASED ASSESSMENT TO BURNING WASTE DERIVED FUEL IN CEMENT KILNS – CASE STUDY IN BRAZIL

V. Maringolo[1], Y. Kihara[1, 2] and A. J. Suto[1]

[1] Brazilian Portland Cement Association, São Paulo, Brazil. E-mail: vagner.maringolo@abcp.org.br
[2] Geosciences Institute, University of Sao Paulo, Brazil. E-mail: yushiro@usp.br

ABSTRACT

An increasing number of cement plants in Brazil are getting the permits to burn hazardous wastes as substitutes for fossil fuels. In the present case study, a waste derived fuel (WDF) from different waste streams is supplied. The trace elements introduced in the system with WDF are – depending on their volatility and compatibility to solid solutions – either emitted and retained in electrostatic precipitators or incorporated into the clinker crystal lattices. A product-based assessment of clinker integrity and mechanical performance of cements resulting from burning WDF was carried out. Analytical techniques comprised reflected-light microscopy, atomic absorption and X-ray spectrometry, leaching and mechanical strength tests. Results evidenced similarity between products from burning either conventional fuel or WDF. Clinker microstructures were alike. Mechanical strengths of cements kept above standard values. Trace elements – even Cd and Hg – showed compatibility with clinker, although Co and especially Pb were rather incompatible. No elements were significantly soluble from cements, thus attesting retention of environmentally relevant elements in the crystal lattice of clinker mineral phases.

1. INTRODUCTION

The environmental implications of burning hazardous wastes in cement kilns are mostly related to atmospheric emissions, which are subject to highly restrictive regulatory limits. Antimony (Sb), arsenic, barium, beryllium, cadmium, chromium, cobalt, copper, lead, molybdenum, nickel, selenium, silver, thallium, vanadium, and zinc are toxic elements that, once introduced in high amounts in the kiln, bring up for the cement industry not only environmental implications but also technological and economical concerns by virtue of the influences that may be favorable or adverse to the process itself and ultimately to the rheological performance of the final product.

The present work derives from the author's unpublished PhD thesis [1] whose research followed a product-centered approach of a case-study – the Tupi Cement Group's Companhia de Cimento Ribeirao Grande plant – burning a waste derived fuel (WDF) in one of its two kilns, substituting for up to 30% the conventional fuel. The plant is located in the State of Sao Paulo, Brazil. It is made up of two suspension preheater kilns and satellite cooler, with daily production capacity of 3000 tons of clinker and a thermal throughput of 910kcal/kg of clinker.

The bulk of the samples comprised 50 clinkers taken from the production line, corresponding to a systematic gathering over three years, from December 1997 to December 2000, 8 of them burned with 100% fuel oil. The clinkers were analysed at the laboratory of the Brazilian Portland Cement Association for their microtexture by reflected light microscopy, total chemical composition by X-ray spectrometry, and trace element components by atomic absorption spectrometry. Leaching tests

Proceedings of the 11th International Congress on the Chemistry of Cement (ICCC)
'Cement's Contribution to the Development in the 21st Century'
Hosted by: The Cement and Concrete Institute of South Africa
CD-ROM produced by: Document Transformation Technologies
11 - 16 May 2003, Durban, South Africa
ISBN Number: 0-9584085-8-0
Editors: Dr G. Grieve and G. Owens
Congress Organised by: Event Dynamics

were carried out on 14 laboratory composite cements prepared exclusively with WDF-burned clinkers. Mechanical strength tests of 685 industrial cements at 1, 3, 7 and 28 days were carried out, covering the production span from 1996, prior to the beginning of waste combustion, to 1998, when cements were made up from a mix of both conventional and waste-burned clinkers.

2. SAMPLING AND SAMPLE PREPARATION

The clinker samples were in a few cases grabbed during test burns with WDF substituting for 15% or 30% of the oil fuel, but mostly were compound samples, representing monthly production at roughly 10% substitution. Approximately 30kg of clinker were collected. Each sample was homogenized and then parted until 1,5kg to 2,0kg. This quantity was sifted in 19mm, 9.5mm, 4.8mm and 2.4mm mesh apertures. Each grain fraction (F1>19mm, 9.5mm<F2>19mm, 4.8mm<F3>9.5mm, 2.4mm<F4>4.8mm and F5<2.4mm) was weighed separately and its percentage calculated. A mean fraction of each clinker was prepared by mixing proportional quotas of all grain fractions. The grains were hammer-ground for the making of polished sections for microscopy, and ground in a swinging mill for five minutes for atomic absorption spectrometry, and for the preparation of fusion beads for X-ray fluorescence spectrometry.

Fourteen cement samples for the leaching test were prepared in the laboratory using 14 different clinkers burned with WDF in the following proportions: 71.3% clinker; 7% carbonate matter; 18% blast-furnace slag and 3.7% calcium sulfate.

3. WASTE DERIVED FUEL (WDF)

The rate of WDF substitution for fuel at the Companhia de Cimento Ribeirao Grande was based on the consumption of 6100kg/h fuel oil at 100% load. The burner was designed for simultaneous injection of oil and WDF allowing burning from 870kg/h to 4,640kg/h WDF – representing substitution for oil ranging from 15% to 40% [2].

The WDF is regularly supplied by a facility that operates the waste handling, pre-treatment, blending and transportation to the cement plant, and is accountable for unloading, storing and injecting WDF into the kiln.

Different waste streams are characterized and pre-selected. The blend is processed from paints, thinners, resins, greases, wash-up solvents and waste oils. The manufacturer keeps analytical control of all WDF shipments in order to check for their compliance with the permit specifications. The analysis included gross and net heat value, humidity, viscosity, flash point, ash content, volatile compounds, heavy metal and sulfur contents, and the amount of solids in suspension. Variations in fuel properties require kiln operation adjustment; therefore WDF must be as uniform as possible. General characteristics are included in Table 1 [3].

Table 1. Specifications for waste derived fuel

Parameters	Characteristics
Water content	Approximately 35%
Content of solids in suspension	<25%
Maximum dimension of solid particles	Non deformable: 3mm Deformable: 8mm
Net heat value	Minimum: 5.000kcal/kg Mean: 8.500kcal/kg
Maximum kinematics viscosity	300cSt
Flash point	<80°C

Table 2 shows average characteristics of WDF used in test burns and of WDF burned regularly from December 1997 to August 1998 [4].

Table 2. Average characteristics of WDF used in test burns and regularly supplied

Characteristics	Unit	test burns WDF	regular supply WDF
Number of samples		3	339
Rate of substitution	%	30	9.2
Net heat value	kcal/kg	5,860	6,434
Cl	%	1.85	0.76
S	%	0.60	0.45
Water	%	26.19	23.23
pH		6.91	7.21
Inorganic class I	g/h	Not detected *	Not detected *
Inorganic class II	g/h	451.00	102.61
Inorganic class III	g/h	12,917.90	2,877.36

* Detection limit of the analytical method not specified

The permit specifications of element maximum concentration in WDF and feed rate (g/h) into the kiln were set based on the test burns and are given in Table 3.

Table 3. Permit limits for element input in WDF and feed rate

Element	Quantity (ppm)	Feed rate (g/h)
Cadmium	0.35	<1.0
Mercury	0.35	<1.0
Thallium	0.35	<1.0
Arsenic	200	560
Cobalt	0.6	<1.7
Nickel	260	750
Selenium	0.6	<1.7
Tellurium	0.6	<1.7
Barium	5,000	14,000
Chromium	1,000	2,800
Copper	1,000	2,800
Lead	1,500	4,200
Antimony	200	560
Manganese	250	700
Vanadium	8.9	<25
Tin	8.9	<25
Rhodium	8.9	<25
Platinum	8.9	<25
Palladium	8.9	<25
Sulfur	10,000	28,000
Chlorine	20,000	56,000
Fluorides	8.9	<25
Cyanides	100	280

4. RESULTS

4.1 Chemistry

Trace elements enter the kiln with the raw meal and fuels. They will move to the stack with the exhaust gases and concentrate in the electrostatic precipitator dust or incorporate into the clinker.

Table 4 shows comparative chemical compositions of the raw meals, electrostatic precipitator dusts and clinkers collected during conventional kiln operation with oil and test burns with WDF substituting for 30% oil. Also shown are the trace element ranges in the bulk 50 industrial samples separated into 42 clinkers burned with WDF and 8 clinkers burned without WDF.

Table 4. Chemistry of materials from test burns and average trace element contents of samples

Elements		Materials							
		Test burns						Bulk of samples	
		Without WDF			With 30% WDF			Without WDF	With ~9.2% WDF
		Raw meal	EP dust	Clinker	Raw meal	EP dust	Clinker	8 clinkers	42 clinkers
CaO		40.20	38.74	62.22	39.62	41.06	63.30		
SiO_2		12.50	12.42	20.66	10.28	12.34	21.29		
Al_2O_3		3.12	5.10	5.00	4.56	3.18	4.52		
Fe_2O_3		1.95	2.63	2.93	2.47	2.19	3.41		
SO_3		0.42	0.97	1.17	1.21	0.36	0.57		
MgO		4.22	3.50	5.30	3.63	3.56	5.33		
K_2O		0.75	1.35	1.13	1.40	0.55	0,82		
Na_2O		0.08	0.11	0.10	0.19	0.06			
LOI		36.18	34.44	1.30	35.70	36.02			
LSF		100,47			110,48				
SR		2,46			1,46				
AR		1,60			1,85				
Cd	ppb	47	100	18	120	408	62	26 – 154	32 – 187
Hg	ppb	140	780	70	134	964	72	n.d. – 45	n.d. – 380
Ta	ppb	n.d.	n.d.	n.d.	274	586	62	n.d. – 119	n.d. – 228
As	ppm	4.3	6.2	4.9	3.9	7.3	5.6	4.5 – 6.7	3.9 – 10.1
Co	ppm	3.0	4.3	2.8	9.3	11.5	17.0	10.6 – 63.1	7.3 – 67.2
Ni	ppm	13.3	21.0	2.,6	19.4	32.1	61.3	11.8 – 36.6	10.2 – 61.3
Se	ppb	0.3	1.8	n.d.	0.6	6.9	0.3	n.d. – 97	n.d. – 358
Te	ppm	n.d.	n.d.	n.d.	n.d.	n.d.	n.d.	n.d.	n.d.
Ba	%	0.03	0.04	0.11	0.02	0.03	0.04	0.04 – 0.07	0.03 – 0.09
Cr	ppm	23.7	36.0	54.5	25.7	41.6	99.2	39.8 – 174.4	41.9 – 155.4
Cu	ppm	10.5	8.5	5.8	14.1	13.5	80.2	5.0 – 29.6	10.7 – 85.7
Pb	ppm	5.6	12.4	5.7	11.9	118.7	4.1	1.9 – 16.9	2.8 – 39.9
Sb	ppb	82	142	45	33	90	54	n.d. – 68	n.d. – 482
Mn	%	0.02	0.02	0.08	0.02	0.03	0.04	0.03 – 0.04	0.03 – 0.05
V	ppm	19.2	31.2	45.2	37.5	35.2	64.3	22.3 – 78.4	17.9 – 78.3
Sn	ppm	2.2	0.9	14.3	2.0	4.0	15.3	n.d. – 3.1	0.6 – 29.3
Pt	ppm	n.d.	n.d.	n.d.	18.3	26.1	12.5	n.d. – 3.7	n.d. – 39.2
Pd	ppm	n.d.	36	n.d.	n.d.	n.d.	n.d.	n.d. – 118	n.d. – 1729
Ag	ppb	14	50	32	n.d.	226	n.d.	10 – 100	13 – 844
Zn	ppm	16.2	22.5	21,3	24,4	29,5	158,4	27.3 – 49.6	25.9 – 133.5
Be	ppb	n.d.	n.d.	n.d.	n.d.	n.d.	n.d.	n.d.	n.d.
S	ppm	80	150	1300	100	100	200	70 – 340	n.d. – 400
Cl-	ppm	300	3700	400	300	8800	100	20 – 200	20 – 300
F-	%	0.13	0.18	022	0,10	0,11	0,16	0.15 – 0.24	0.11 – 0.27
CN-	ppm	9.1	3.1	10,9	0,4	26,6	n.d.	n.d. – 3.9	n.d. – 5.8

n.d. = not detected

Detection limits: Be = 0.02ppb; Pt = 1ppm; Pd = 0.7ppb; Te = 0.12ppb; Ag = 0.1ppb; Hg = 0.10ppb; CN^- = 0.1ppm; Se = 0.10ppb

Volatile chlorine concentrated in the electrostatic precipitator dust. As alkali sulfates were not observed in the clinkers, available sulfur must have entered solid solutions in silicates and aluminates. The hazardous wastes account for the higher content of chlorine in the dust when operating with WDF. As a matter of fact, chlorine contents in WDF used in test burns (Table 2) were not possible to record due to clogging of the kiln.

Figure 1 shows comparatively the correlation of element mass concentrations in clinker and in electrostatic precipitator dust, to that in the raw meal for both situations with and without WDF, as seen in Table 4.

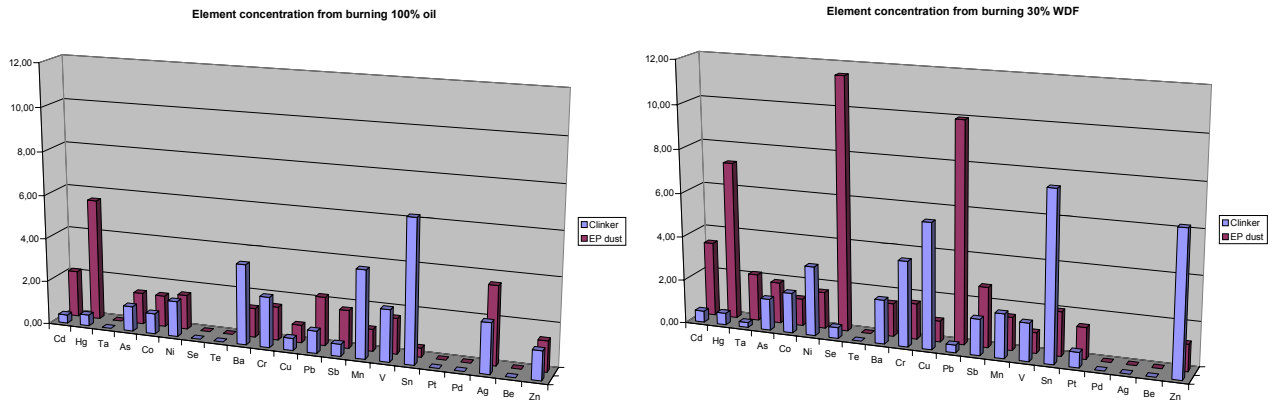

Figure 1. Element concentration in clinker and electrostatic precipitator dust from test burns with and without WDF

Tellurium, Pd and Be were not detected. Cadmium, Hg, Pb, Sb, Ta, Se, Pt and Ag concentrated preferentially in the electrostatic precipitator dusts. Higher degrees of incorporation in to the Portland clinker structure are seen with the transition elements Co, V, Mn, Ni, Cr, Cu, Zn, Ba and Sn.

The graphs demonstrate the varying input accounted for by the raw materials themselves. Nonetheless, the wide ranges for Cd, Th, Sb, Pt and V contents are likely due to the hot air from the cooler used in the preheater. Variation in Zn, Cu, Ni, Co, and V are attributed to the fuel oil and WDF input.

Volatile elements show intense and increasing recirculation within the kiln system. This should be the reason why there are high variations in Cd, Hg and Th in the electrostatic precipitator dust. Lead and Ag apparently also behave as volatile elements in the kiln.

The amounts of trace elements in the industrial clinkers are discontinuous. The scattered values proved easier to interpret on a spider diagram, commonly used in igneous petrology [4]. Elements are placed on the X-axis. All samples are normalized to a reference composition, so that on the Y-axis the logarithmic scale does not express contents but actually the ratio between the contents (either percentage, parts per million or parts per billion) of a particular element in the sample and in the reference composition. The points located above or below the baseline “1” on the Y-axis mean the sample is either enriched or depleted in a particular element in comparison to the reference.

For the bulk of clinkers, a sample with the lowest content of trace elements was chosen as reference; values are given on the X-axis under each element. The element sequence on the X-axis was arranged in such a way as to provide a clear visual interpretation of the results. Tellurium, Be, Ta and Se were not, or only occasionally, detected in the samples, and were not included.

Figure 2 shows the distribution of trace elements in the two sets of clinker samples, those burned with and those without WDF, and the overlapping areas of both the graphs.

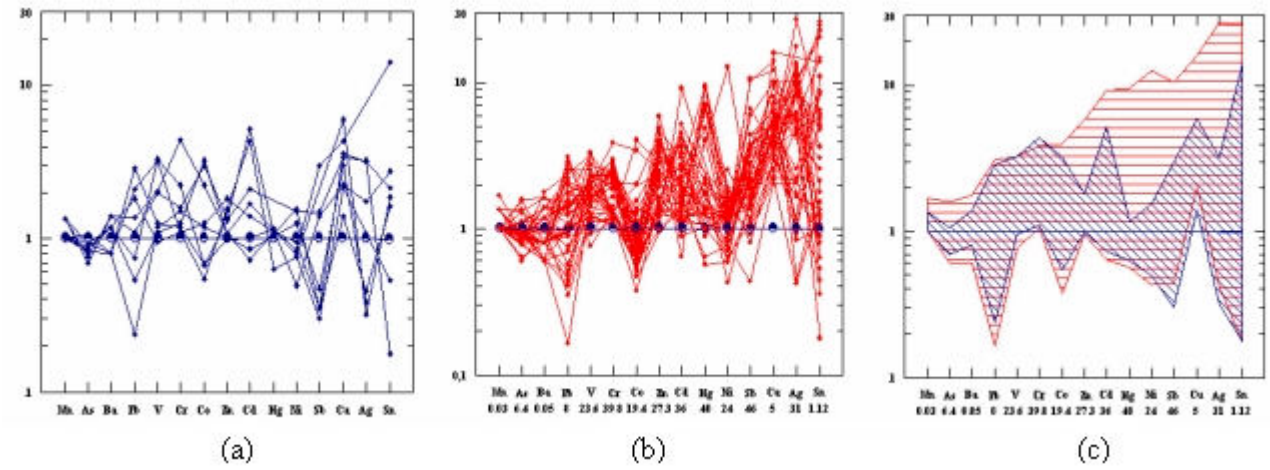

Figure 2. Distribution of trace elements in the industrial clinker samples: (a) burned without WDF, (b) burned with WDF, (c) overlapping areas of (a) and (b)

Despite the limited number of clinkers burned without WDF, Figure 2a clearly demonstrates the element variation in the raw materials and conventional fuel, which are the only input in the kiln system. There is little variability for Mn, As, Ba and Hg. Lead, Co and Ni are distributed both above and below the baseline. Silver and Sb tend to depletion while V, Cr, Cd and Cu display enrichment. Tin shows no definite trends.

Similarly, Mn, As and Ba showed small variation in the clinkers burned with WDF (Figure 2b). Nickel remained similar (with the exception of a much enriched sample), but Pb and Co highlighted their strong depletion. All of the remaining elements – even Sn – are found to be enriched. The behavior of Hg, Ag and Sb inverted their trend, and Cu intensified the enrichment.

The intersection of graphs (Figure 2c) shows the element trends in both situations – only Ni presents a biased behavior because of one much enriched sample. The diagram emphasizes the trace element enrichment in clinkers when burning WDF, which is expected as WDF manufacture involves various hazardous wastes from different streams whose input will add to that of the raw materials and fuels.

4.2 Clinker Microstructure

Microscopic analysis was carried out on 37 clinkers burned with WDF and 6 without WDF, in order to check for the influence of the introduction of WDF on their texture and mineral composition.

The trace element contents involved in the case-study did not reach levels high enough to influence the kinetics of reactions. The clinkers did not show any distinct feature. On average, the clinkers contained 73% alite, a high proportion of silicates (81%), and a high alite/belite ratio (11) and low free lime content (1.25%). The optimal combination of components resulted from adequate LSF, SR and AR, good grinding and homogenization of raw materials, and optimized burning conditions.

While alite crystals displayed either straight or sub-straight borders, with generally incipient generation of a fringe of secondary belite, belite crystals in zones were invariably internally disorganized. Belite is also present in clinkers as amoeboid crystals in the matrix, surrounding alite crystals and following their contour, but these crystals are clearly not products of alite decomposition.

Characteristic of all clinkers studied is the slightly high potassium content (≥0.75%) giving rise to crystallization of prismatic alkali aluminates. Also typical is the occurrence of periclase as a consequence of the high (over 4%) content of magnesium in the raw meal.

The clinker textural features are illustrated in Figures 3a – 3f.

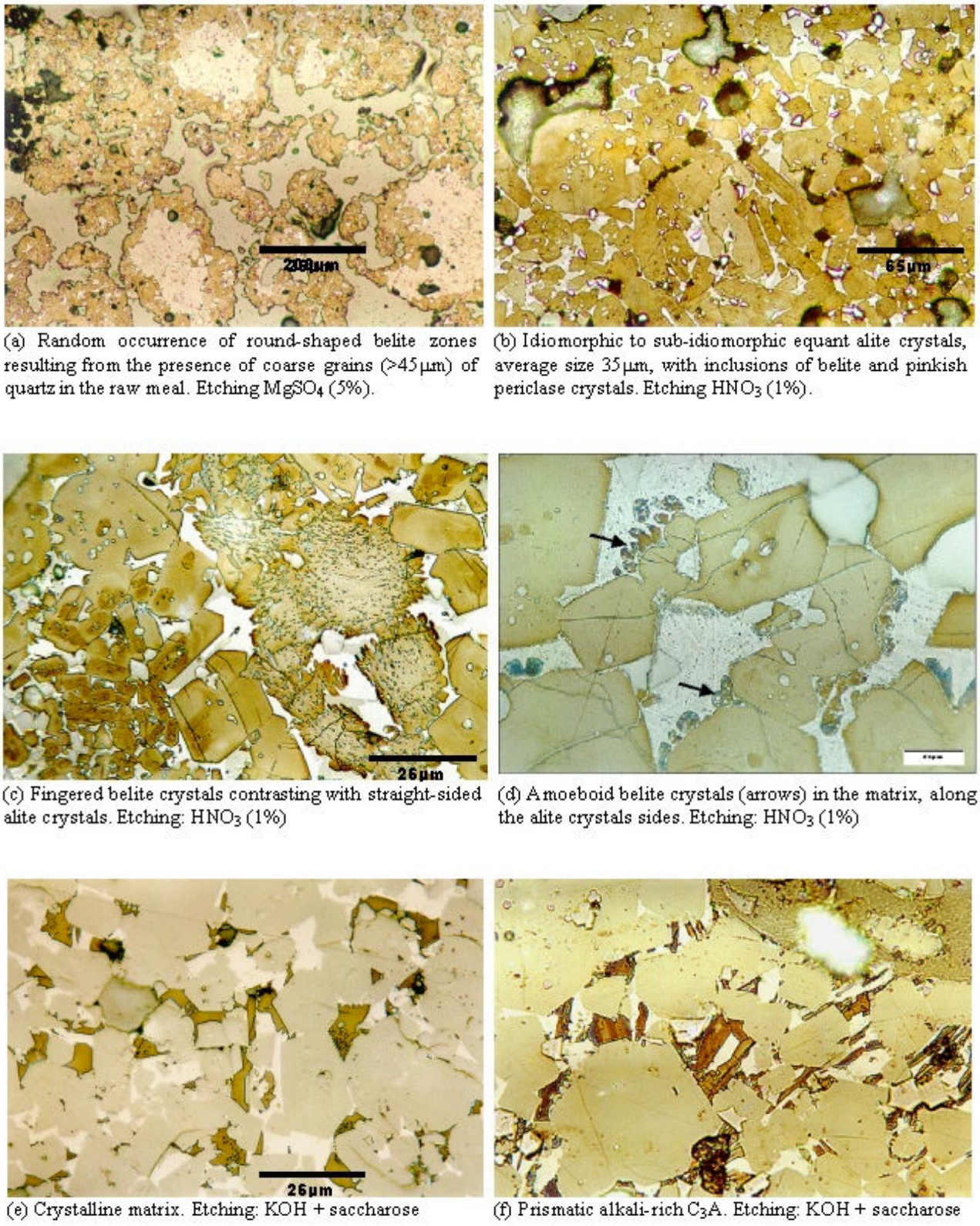

(a) Random occurrence of round-shaped belite zones resulting from the presence of coarse grains (>45µm) of quartz in the raw meal. Etching $MgSO_4$ (5%).

(b) Idiomorphic to sub-idiomorphic equant alite crystals, average size 35µm, with inclusions of belite and pinkish periclase crystals. Etching HNO_3 (1%).

(c) Fingered belite crystals contrasting with straight-sided alite crystals. Etching: HNO_3 (1%)

(d) Amoeboid belite crystals (arrows) in the matrix, along the alite crystals sides. Etching: HNO_3 (1%)

(e) Crystalline matrix. Etching: KOH + saccharose

(f) Prismatic alkali-rich C_3A. Etching: KOH + saccharose

Figure 3. Textural and mineralogical features of clinker burned with WDF

4.3 Leaching

The leaching tests followed the U.S. EPA method [5]. The concentrations of Sb, As, Ba, Be, Cd, Cr, Pb, Hg, Ni, Ag, Se and Ta were determined in the leached extract for each of the 14 laboratory cements (Table 5).

Table 5. Concentration data (ppb) of metals obtained in the leaching tests

Element	Leached metal content (ppb)													
	1	2	3	4	5	6	7	8	9	10	11	12	13	14
Sb	0.20	0.20	0.30	0.20	n.d.	0.60	n.d.	n.d.	n.d.	n.d.	n.d.	n.d.	n.d.	n.d.
As	n.d.	n.d.	n.d.	n.d.	n.d.	n.d.	n.d.	n.d.	n.d.	n.d.	n.d.	n.d.	n.d.	n.d.
Ba	2,100	1,100	3,800	9,300	5,600	3,800	4,500	3,300	5,000	6,800	1,200	1,700	690	3,580
Be	n.d.	n.d.	n.d.	n.d.	n.d.	n.d.	n.d.	n.d.	n.d.	n.d.	n.d.	n.d.	n.d.	n.d.
Cd	n.d.	n.d.	n.d.	n.d.	n.d.	n.d.	n.d.	0.03	n.d.	0.18	n.d.	n.d.	0.23	n.d.
Pb	n.d.	n.d.	1.7	2.4	5	1.7	0.9	5.0	0.8	6.4	0.7	1.4	2.6	600
Cr	32	102	600	68.3	300	600	400	800	180	86.5	400	96	200	150
Hg	n.d.	n.d.	0.6	0.7	n.d.	1.2	1.4	1.2	0.6	n.d.	2.2	1.4	1.8	n.d.
Ni	1.5	n.d.	13	18	4.2	13	13	11	4.3	4.5	4	0.9	n.d.	5.8
Ag	n.d.	n.d.	n.d.	n.d.	n.d.	n.d.	n.d.	n.d.	n.d.	n.d.	n.d.	n.d.	n.d.	n.d.
Se	n.d.	n.d.	n.d.	n.d.	0.8	n.d.	n.d.	n.d.	n.d.	n.d.	n.d.	n.d.	n.d.	n.d.
Ta	n.d.	n.d.	n.d.	n.d.	n.d.	n.d.	n.d.	n.d.	n.d.	n.d.	n.d.	n.d.	n.d.	n.d.

Detection limits: Se = 0.10ppb, Sb = 0.10ppb, Hg = 0.10ppb, Be = 0.02ppb, Tl = 0.5ppb, Ag = 0.05ppb, As = 0.10ppb

In over half of the analyses, the element contents in the leached extract were below detection limits. Arsenic, Be, Ag and Ta were not detected in any of the samples, while Se was detected in only one. All other values fall far below the U.S. EPA standards. Table 6 lists the highest values found.

Table 6. Highest leaching values opposed to the standards

Metal	Standard limits (ppb)	Highest value (ppb)
Antimony	1,000	0.60
Arsenic	5,000	Not detected
Barium	100,000	9,300
Beryllium	7	Not detected
Cadmium	1,000	0.23
Lead	5,000	600
Chromium	5,000	800
Mercury	2,00	2.2
Nickel	70,000	18
Silver	5,000	Not detected
Selenium	1,000	0.8
Thallium	7,000	Not detected

Regarding the admissible limits, Sb, Cd, Hg, Ni and Se highest values are extremely low. Barium and Pb showed figures that represent 9.3% and 12% of respective standards. The most significant value was a single Cr analysis of 800ppb, which makes up 16% of the permissible limit.

The leaching results confirm the retention of environmentally relevant trace elements in the crystal lattices of clinker mineral phases. No significant solubility of any element occurred; the highest values observed in most of the analyses were about 99% lower than the standard limits. Those found for Ba, Pb and Cr were lower - 91%, 88% and 84%.

4.4 Mechanical Performance of Cements

Composite Portland cements account for about 70% of the production in Brazil. Cement type CP II-E 32 consists of 56% to 94% clinker and gypsum, 6% to 34% blast-furnace slag, and up to 10% carbonate material [6]. Mechanical strength tests of industrial cements followed the Brazilian Test Method NBR 7215 [7] with cylindrical test specimens of 50x100mm, in proportion 1:3 (slag : sand), water cured at 23ºC, s/alk sol.=0.5.

Compressive strengths at 1, 3, 7 and 28 days of 685 industrial CP II-E 32 cements are shown in diagrams (Figures 4a – 4c) and cover the period 1996 – 1998, from the time that the plant was not

burning WDF until 1998, the time that cements were made of a mix of clinkers burned with and without WDF.

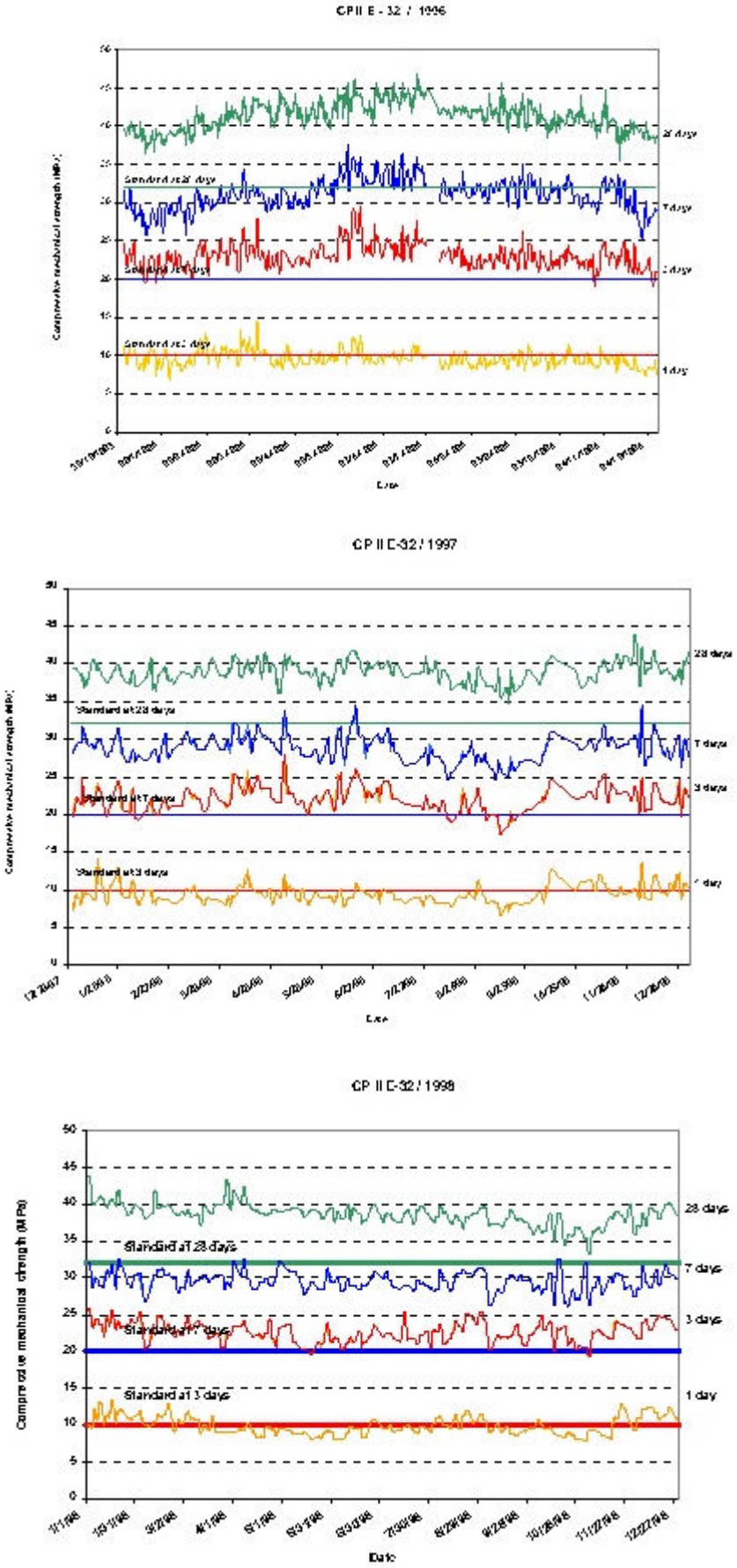

Figure 4. Cement mechanical strength at 1, 3, 7 and 28 days for 1996, 1997 and 1998

The mechanical strengths at all ages are above the standards required [9]. The performance of cements at 1 day is equivalent to the standard set for 3 days. The same tendency is verified for performance at 3 days, which is higher than the normative limit at 7 days. The input of clinkers burned with WDF in the composition of CP II-E 32 is not even noticeable on the diagrams, which clearly implies that wastes introduced in the clinkering process do not affect cement performance.

5. DISCUSSION

Energy efficiency is a key issue for an energy intensive industry such as the cement industry. The use of WDF as partial substitutes for fossil fuels in cement kilns is strategic for the business and plays a significant role in hazardous wastes management.

On the other hand, WDF inputs an additional amount of elements of environmental concern in to the kiln system. The present work has shown however that higher contents of trace elements in the kiln imply higher contents in the clinker structure. Element entrapping in crystal lattices is done through solid solutions with major elements Ca, Si, Al and Fe up to the each mineral's limit of solubility. The results showed that there is a general compatibility of trace elements, even volatile ones, with clinker. The transition metals Cd, Zn, Cu, Mn, Cr and V were especially compatible, while Ni, Co and also Pb were comparatively less so, suggesting that they do not enter the clinker microstructure as readily.

No distinctive textural features were found in clinker either burned with or without WDF. Moduli LSF, SR and AR and control of the burning conditions in the kiln are surely the main factors to account for the clinkers textural and mineralogical characteristics. The optimal compressive strengths of cements were warranted by maintenance of the clinker quality throughout the time span from when only fuel oil was burned until lately when WDF has been used routinely in the kiln.

Composite cements, prepared exclusively with clinkers burned with WDF, did not leach detectable amounts of As, Be, Ag and Tl, while Sb, Cd, Hg, Ni and Se were extremely low. Slightly higher but still 91%, 88% and 84%, lower than the correspondent standard leaching limits, were Ba, Pb and Cr.

The potential release of toxic constituents is the most appropriate control parameter to check for the environmental impact of cement-based products. The response of cements to the extreme conditions of the leaching test corroborated the retention of trace elements in the crystal lattices of Portland clinker minerals. Because of this, cements made up of clinkers burned with WDF can be seen as environmentally sensitive building materials, meeting performance requirements while safely keeping metals within its structure.

REFERENCES

[1] Maringolo, V. Clínquer co-processado: produto de tecnologia integrada para sustentabilidade e competitividade da indústria de cimento, PhD Thesis, Universidade de São Paulo, 2000.

[2] C.Greco Térmica e Fluidos Consultoria Ltda. Um projeto bem sucedido de co-processamento em cimenteira. Informativo C.Greco, São Paulo, n. 10, 2000.

[3] Barbosa, A.M. and Santos, M.C. Utilização de resíduos industriais na Cimento Ribeirão Grande, 5th Brazilian Conference on Portland Cement, São Paulo, Proceedings of..., 1999.

[4] Wilson, M. Igneous petrogenesis, London: Unwin Hyman, 1989, 466p.

[5] U.S. EPA Method 1311, Revision 0: 1990, Toxicity characteristic leaching procedure, 1990.

[6] ABNT NBR 11578:1991, Cimento Portland composto, Rio de Janeiro, 1991.

[7] ABNT NBR 7215: 1996, Cimento Portland – determinação da resistência à compressão; Rio de Janeiro, 1996.

PRODUCT-BASED ASSESSMENT TO BURNING WASTE DERIVED FUEL IN CEMENT KILNS – CASE STUDY IN BRAZIL

V. Maringolo[1], Y. Kihara[1, 2] and A.J. Suto[1]

[1] Brazilian Portland Cement Association, São Paulo, Brazil. E-mail: vagner.maringolo@abcp.org.br
[2] Geosciences Institute, University of Sao Paulo, Brazil. E-mail: yushiro@usp.br

Vagner Maringolo

E-mail: vagner.maringolo@abcp.org.br

Address: Torres de Oliveira Avenue, 76, CEP 05347 São Paulo, Brazil

Affiliation: Brazilian Portland Cement.Association

SHORT BIOGRAPHY

- PhD in Applied Mineralogy by the Institute of Geosciences, University of Sao Paulo, Brazil. Thesis on environmental issues related to clinker burned with hazardous waste derived fuel and correspondent cements.
- Member of environmental committees for elaboration of regulations to burning hazardous wastes as substitutes for fuels and raw materials in cement kilns.
- Technical Assistant at the Brazilian Portland Cement Association since 1994.

INFLUENCE OF THE TYPE OF CALCIUM SULFATE ON THE PROPERTIES OF CALCIUM SULFOALUMINATE CEMENT

Jean Péra[1], Jean Ambroise[1], Eric Holard[2] and Guy Beauvent[2]

[1] Unité de Recherche Génie Civil, Institut National des Sciences Appliquées, Villeurbanne, France.
E-mail: Jean.Pera@insa-lyon.fr
[2] Carrières du Boulonnais, Ferques, France. E-mail: ericholard@cybelithe.com

ABSTRACT

This laboratory investigation focuses on the influence of the calcium sulfate source used to prepare sulfoaluminate cement. A sulfoaluminate clinker was ground at a Blaine fineness of 545 m^2/kg and mixed with four types of calcium sulfate (phosphogypsum, borogypsum, natural gypsum and fluoroanhydrite) to get anhydrite sulfoaluminate cements. Five amounts of calcium sulfate were used: 5, 10, 15, 20, 25, and 30%.

The wettability of these cements was studied by means of the measurement of the instantaneous spread of a paste (W/C = 0.44). Whatever the sulfate content might be, borogypsum and fluoroanhydrite led to the lowest spreads.

The compressive strength was assessed on standard mortars. No strength gain was recorded with fluoroanhydrite after 6 hours of hydration. With other calcium sulfates, the 6-hr maximum strength was obtained using 5% natural gypsum. After 24 hours of hydration, the use of 20 to 25% fluoroanhydrite led to the best strength. With other calcium sulfates, the maximum strength was reached incorporating 20% calcium sulfate. After 28 days of hydration, the cement containing 20 to 30 % fluoroanhydrite presented the best strength. With other calcium sulfates, the strength was 30% lower.

This research points out that the choice of the calcium sulfate source is very important for the strength development of calcium sulfoaluminate cements.

1. INTRODUCTION

Calcium sulfoaluminate cements have essentially been developed in China and production has now expanded to more than one million tonnes per year [1-14]. The main constituent of calcium sulfoaluminate clinker is yeelimite ($C_4A_3\bar{S}$). Belite (C_2S) and ferrite (C_4AF) are both present in calcium sulfoaluminate and Portland clinkers, while C_3S and C_3A, characteristic of Portland clinker are absent in calcium sulfoaluminate clinker. Calcium sulfoaluminate clinker is generally interground with 16-25 % gypsum to get calcium sulfoaluminate cement. Such cement is seen as a potentially very attractive high-performance material. Rapid strength gain and durability in a range of aggressive environments make it applicable to civil engineering needs [15-16].

This laboratory investigation focuses on the influence of the calcium sulfate source used to be mixed with calcium sulfoaluminate clinker on the strength development of calcium sulfoaluminate cement.

2. EXPERIMENTAL

2.1 Starting Materials

A calcium sulfoaluminate clinker was manufactured in a rotary kiln by Carrières du Boulonnais. Its phase composition was as follows:

- $C_4A_3\bar{S}$: 53.5 %,
- C_2S: 21.2 %
- C_4AF: 16.3 %
- perovskite 9.0 %

It was ground at a Blaine specific surface area of 545 m^2/kg and mixed with four sources of calcium sulfate to prepare calcium sulfoaluminate cement: borogypsum, phosphogypsum, natural gypsum and fluoroanhydrite.

The physical properties of these materials are presented in Table 1. The main impurities found in the calcium sulfates were respectively:

- borogypsum: traces of quartz,
- phosphogypsum: none,
- natural gypsum: traces of anhydrite,
- fluoroanhydrite: traces of calcium hydroxide and calcium carbonate.

Table 1. Physical properties of starting materials.

Material	Density (g/cm^3)	Blaine specific surface area (m^2/kg)	Average diameter of the particle size distribution (D_{50} (µm)
Clinker	2.74	545	12.5
Borogypsum	2.30	280	24.4
Phosphogypsum	2.31	264	14.1
Natural gypsum	2.26	240	17.6
Fluoroanhydrite	2.79	346	10.4

The particle size distribution of the calcium sulfates is shown in Figure 1. Fluoroanhydrite presents a particle size distribution quite different from other sulfates: there are large quantities of particles smaller than 10 µm (50 %) and higher than 50 µm (35 %).

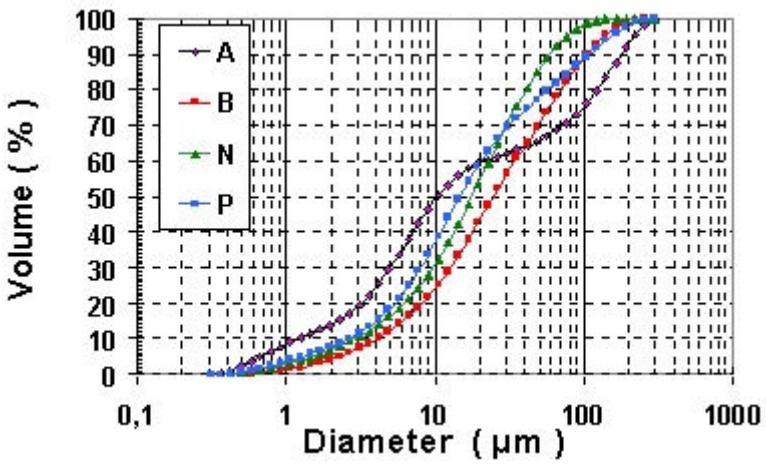

Figure 1. Particle size distribution of calcium sulfates.

2.2. Composition of Calcium Sulfoaluminate Cements

Each of the four calcium sulfates was mixed with clinker at the following contents: 5, 10, 15, 20, 25 and 30 %. Therefore, 24 cements were investigated for their physical and mechanical properties.

2.3 Testing Program

Each cement was hydrated at W/C = 0.44 and its workability was assessed by the measurement of the instantaneous spread of a truncated cone ($\varnothing_{sup}$ = 70 mm, $\varnothing_{inf}$ = 80 mm, h = 40 mm).
In a second series of tests, the compressive strength of standard mortars was measured at different ages: 6 hours, 24 hours and 28 days. The composition of mortars was: cement/sand = 1/3; water/cement = 1/2.

3. RESULTS AND DISCUSSION

3.1 Workability of Pastes

As shown in Figure 2, the presence of borogypsum and anhydrite reduces the spread of pastes, especially at contents higher than 15 %.

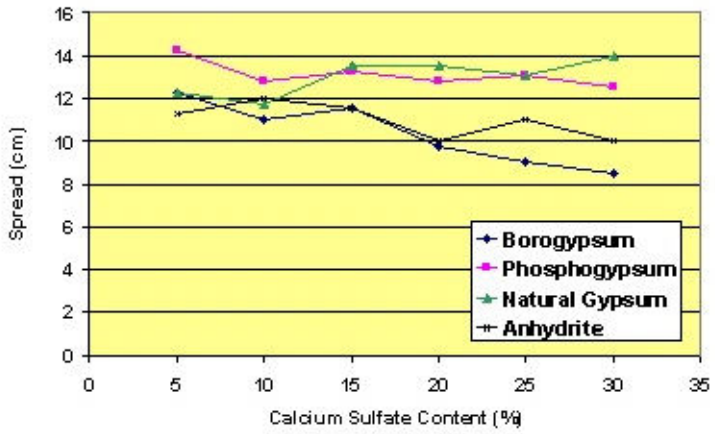

Figure 2. Initial spread of hydrated cements.

3.2 Compressive Strength of Mortars

At 6 hours of age (Figure 3), not any strength was recorded when anhydrite was used.

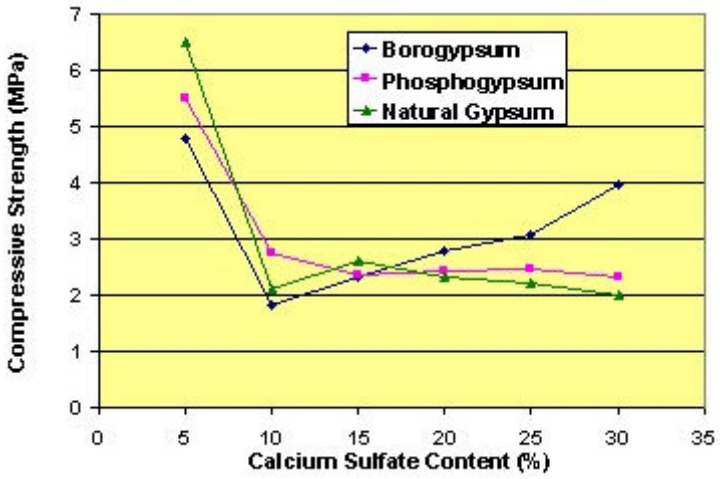

Figure 3. Compressive strength after 6 hours of hydration.

To explain this result, conductivity tests were carried out on suspensions (Water/Cement = 4/1). The results obtained for cements containing 20 % calcium sulfate are presented in Figures 4 to 7.

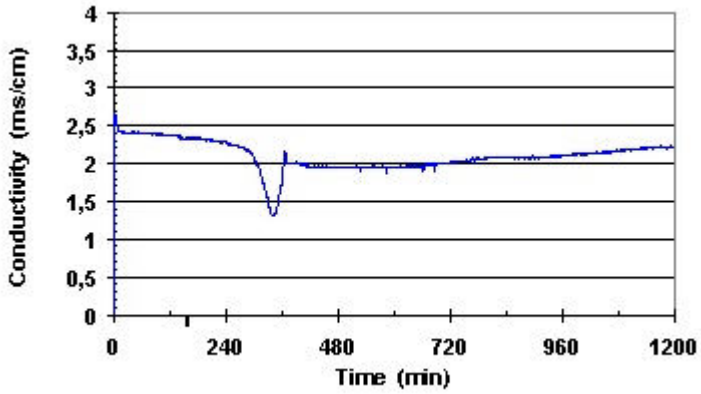

Figure 4. Conductivity of cement containing 20% borogypsum.

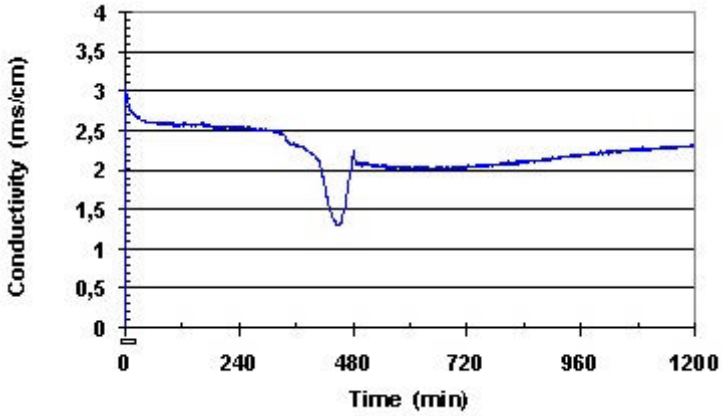

Figure 5. Conductivity of cement containing 20% phosphogypsum.

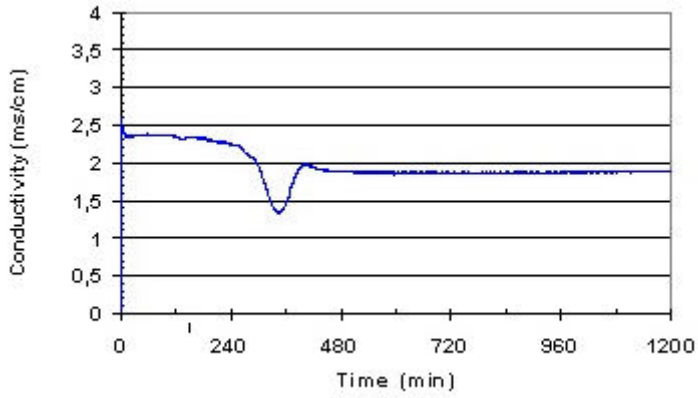

Figure 6. Conductivity of cement containing 20% natural gypsum.

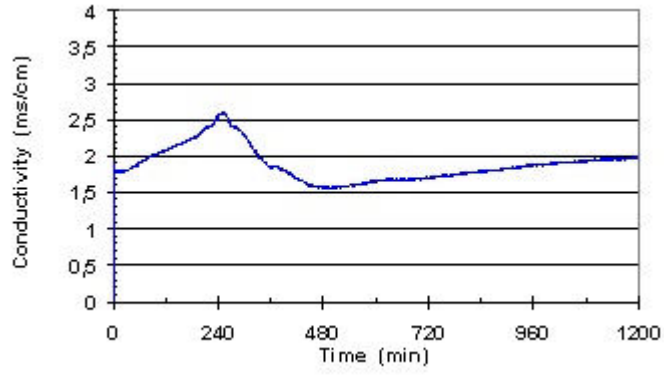

Figure 7. Conductivity of cement containing 20% anhydrite.

The curves obtained for borogypsum, phosphogypsum and natural gypsum are similar: a slight decrease of conductivity, followed by a sudden drop which corresponds to the precipitation of ettringite, and then a new increase of conductivity. The conductivity drop appears after 340 minutes for borogypsum and phosphogypsum and 450 minutes for natural gypsum. When anhydrite is used, the curve is totally different: conductivity first increases and reaches a peak after 250 minutes, then it decreases and a minimum conductivity is obtained after 480 minutes. This phenomenon is less marked than for other sulfates and proves that ettringite precipitates later and explains why no strength is recorded after 6 hours. In order to enhance the dissolution of anhydrite, a mixture of calcium hydroxide and potassium sulfate (2 % by weight of anhydrite) was added to cement. A 6 hr-compressive strength was therefore recorded: 2.4 MPa for the cement containing 20 % anhydrite.

After 24 hours of hydration (Figure 8), best strengths are obtained when anhydrite is used, and they are higher than 40 MPa when anhydrite content reaches 15 %.

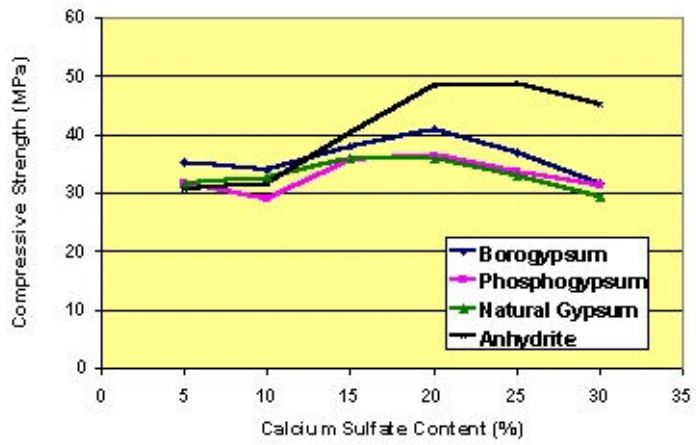

Figure 8. Compressive strength after 24 hours of hydration.

At 28 days of age (Figure 9), compressive strength as high as 75 MPa is obtained when anhydrite content reaches 20 % other calcium sulfates lead to strength in the range of 50 to 60 MPa at a dosage of 20-25 %.

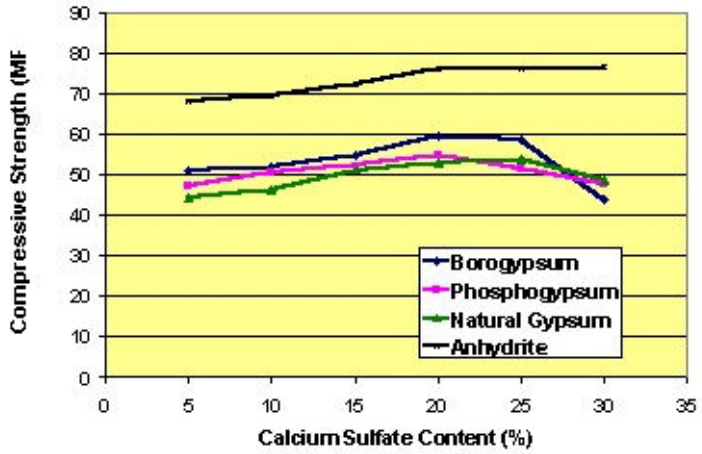

Figure 9. Compressive strength after 28 days of hydration.

The strength development of cements containing 20 % calcium sulfate is shown in Figure 10. This Figure clearly points out the positive influence of anhydrite on strength after one day of hydration.

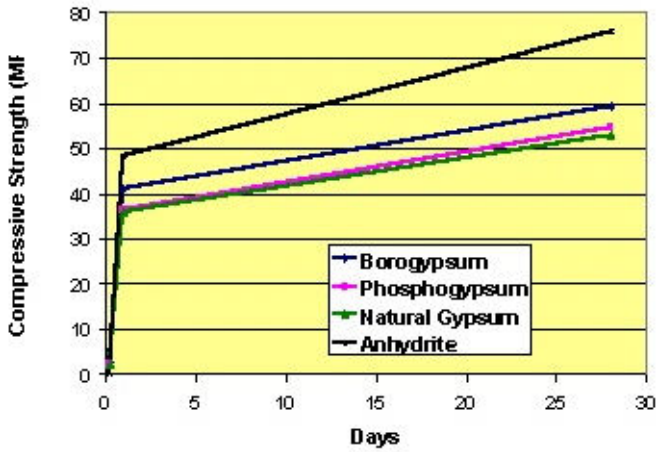

Figure 10. Evolution of compressive strength versus time.
Cement containing 20% calcium sulfate.

4. CONCLUSIONS

From this limited investigation, the following conclusions can be drawn:

1. The nature of the calcium source has an influence on the workability of calcium sulfoaluminate cement: borogypsum and fluoroanhydrite reduce the workability.
2. No strength is recorded at 6 hours of age when anhydrite is used, due to a delay in ettringite precipitation. Anhydrite has to be activated to get some strength.
3. The use of borogypsum and anhydrite leads to the best strength after one day of hydration.
4. A calcium sulfate content of 20 % is recommended to get the maximum strength. The use of anhydrite leads to strength 30 % higher than other sulfates.

REFERENCES

[1] Deng, J., Ge, W., Su, M. and Ying, L. Sulfoaluminate series, 7th international congress on the chemistry of cement, Paris, 1980, vol. 4, pp. 381-386

[2] Su, M., Wang, Y., Zhang, L. and Li, D. Preliminary study on the durability of sulfo/ferroaluminates cements, 10th international congress on the chemistry of cement, Gothenburg, 1997, vol. 4, 4 iv 029, 12 p.

[3] Park, C.K., Kim B.K., Hong, S.Y. and Shin, G.Y. Microstructural change of calcium sulfoaluminate cement paste due to temperature, 10 th international congress on the chemistry of cement, Gothenburgh, 1997, vol. 4, 4 iv 068, 6 p.

[4] Zhang, L., Su, M. and Wang, Y. Development of the use of sulfo and ferroaluminate cements in China, Advances in Concrete Research, 1999, vol 11, n° 1, pp. 15-21.

[5] Zhang, L., Glasser, F.P. New concretes based on calcium sulfoaluminate cement, international conference on modern concrete materials, binders, additions and admixtures, Dundee, 1999,pp. 261-274.

[6] Beretka, J., Sherman, N., Maroccoli, M., Pompo, A. and Valenti, G.L. Effect of composition on the hydration properties of rapid-hardening sulfoaluminate cements, 10th international congress on the chemistry of cement, Gothenburg, 1997, vol. 2, 2 ii 029, 8 p.

[7] Brown, A.D.R. Application of calcium sulfoaluminate cements in the 21th century, Concrete 2000, Dundee, 1993, vol. 2, pp. 1773-178.

[8] Sherman, N., Beretka, J., Santoro, L. and Valenti, G.L. Long term behavior of hydraulic binders based on calcium sulfoaluminate and calcium sulfosilicate, Cement and Concrete Research, 1995, vol. 25, n° 1, pp. 113-126.

[9] Kurdowski, W., George, C.M. and Sorrentino, F.P. Special cements, 8th international congress on the chemistry of cement, Rio de Janeiro, 1986, vol. 1, pp. 292-318.

[10] Muudbhaktal, G.A., Parmeswaran, P.S., Heble, A.S., Pat, B.V.K. and Chatterjee, A.K. Non alitic cement from calcium sulfoaluminate clinker; optimisation for high-strength and low-temperature application, 8th international congress on the chemistry of cement, Rio de Janeiro, 1986, vol. 4, pp. 364-370.

[11] Mehta, P.K. Investigations on energy-saving cements, World Cement Technology, 1980, May, pp. 166-177.

[12] Beretka, J., Santoro, L., Sherman, N. and Valenti, G.L. Synthesis and properties of low energy cements based on $4CaO.3Al_2O_3.SO_3$, 9th international congress on the chemistry of cement, New Delhi, 1992, vol. 1, pp. 292-318.

[13] Sharp, J.H., Lawrence, C.D. and Yang, R. Calcium sulfoaluminate cements - Low energy cements, special cement or what, Advances in Cement Research, 1999, vol. 11, n° 1, 3-13.
[14] Beretka, J., de Vito, B., Santoro, L. Sherman, N. and Valenti, G.L. Hydraulic behaviour of calcium sulfoaluminate based cements derived from industrial process wastes, Cement and Concrete Research, 1993, vol. 23, pp. 1205-1214.
[15] Glasser, F.P. and Zhang, L. High Performance cement matrices based on calcium sulfoaluminate-belite compositions, Cement and Concrete Research, 2001, vol. 31., n° 12, pp. 1881-1886.
[16] Quillin, K. Performance of belite-sulfoaluminate cements, Cement and Concrete Research, 2001, vol. 31, n° 9, pp. 1341-1349.

DEVELOPMENT OF GLASS FIBRE REINFORCED COMPOSITES USING WHITE SULFOALUMINATE CEMENT

Jean Péra[1], Jean Ambroise[1], Eric Holard[2] and Guy Beauvent[2]

[1] Unité de Recherche Génie Civil, Institut National des Sciences Appliquées, Villeurbanne, France.
E-mail: Jean.Pera@insa-lyon.fr
[2] Carrières du Boulonnais, Ferques, France; E-mail: ericholard@cybelithe.com

ABSTRACT

As the hydration of calcium sulfoaluminate cement does not yield any calcium hydroxide, it should be interesting to use such cement in the production of glass fibre reinforced composites. Moreover, in such matrices efflorescences due to the carbonation of calcium hydroxide cannot appear.

A white sulfoaluminate cement was prepared and introduced in a matrix having the following weight composition:

- cement: 50 %,
- siliceous fine sand: 50 %,
- chemical admixtures

The AR-glass fibre (l = 11 mm) content was 2.8% of the matrix mass. The water to matrix ratio was 0.187. The composite was prepared by the premix method. Some specimens contained a mesh in addition to fibres.

The samples were subjected to three-point flexural loading at 3 hours, 24 hours, 7 days, and 28 days.

After 3 hours of hydration, the average maximum stress (MOR) reached 8 MPa. The composite developed ductile behaviour. At 24 hours of age, it reached 9.3 MPa. The presence of a mesh increased this value to 20.2 MPa. At later ages, the performances were: 16.5 MPa at 7 days and 20.5 MPa at 28 days.

These results show that high-performance composites can be obtained using calcium sulfoaluminate cement instead of Portland cement. The main finding is that the initial strength (3 hours) is very high and allows both quick demolding and rapid rotation of molds.

1. INTRODUCTION

Glass fibre reinforced cement (GFRC) is an interesting construction material of considerable potential. But its development has been lower than expected due to the high alkalinity or Portland cement matrices. Borosilicate E-glass is chemically destroyed in Portland cement and even alkali-resistant glass fibre is subjected to physical attack by calcium hydroxide crystals. Pozzolanic additions like metakaolin or microsilica are used to decrease the calcium hydroxide content and therefore guarantee the durability of GFRC composites [1-2]. Less alkaline non-Portland cement matrices have been developed for reinforcement by glass fibres: high-alumina cement, supersulfated

Proceedings of the 11th International Congress on the Chemistry of Cement (ICCC)
'Cement's Contribution to the Development in the 21st Century'
Hosted by: The Cement and Concrete Institute of South Africa
CD-ROM produced by: Document Transformation Technologies
11 - 16 May 2003, Durban, South Africa
ISBN Number: 0-9584085-8-0
Editors: Dr G. Grieve and G. Owens
Congress Organised by: Event Dynamics

cement and calcium sulfoaluminate cement [3-5]. Accelerated ageing tests have shown that AR glass fibres are more durable in calcium sulfoaluminate cement than in Portland cement.

As no calcium hydroxide is produced during calcium sulfoaluminate cement hydration, efflorescences due to the carbonation of calcium hydroxide are avoided. Therefore, decorative GFRC composites can be developed with guaranted tint. That is the second advantage of calcium sulfoaluminate cement versus Portland cement

This paper presents the preliminary results obtained on white sulfoaluminate cement reinforced AR glass fibres.

2. EXPERIMENTAL

A white calcium sulfoaluminate clinker was prepared by Carrières du Boulonnais in a rotary kiln, from a mixture of residual aluminium hydroxide and phosphogypsum. The phase composition of this clinker was as follows:
- belite (C_2S): 11 %,
- yeelimite ($C_4A_3\overline{S}$): 84 %,
- ferrite (C_4AF): 4 %,
- perovskite (C_3FT_2): 1 %.

Calcium sulfoaluminate cement was obtained by intergrinding 70 % of that clinker and 30 % phosphogypsum.

The hydration of such cement is described by the following equations:

$$C_4A_3\overline{S} + 2C\overline{S}H_2 + 34\,H \rightarrow \underset{\text{ettringite}}{C_3A3C\overline{S}H_{32}} + \underset{\text{gibbsite}}{2AH_3},$$ in absence of calcium hydroxide.

$$C_4A_3\overline{S} + 6CH + 8\,C\overline{S}H_2 + 80H \rightarrow 3C_3A3C\overline{S}H_{32},$$ in presence of calcium hydroxide yielded by C_2S hydration.

In each case, the main product of hydration is ettringite. The mixture proportions of the matrix are shown in Table 1.

Table 1. Mixture proportions of the matrix.

Cement/Sand	1.00
Water/Cement	0.37
Superplasticizer (% cement)	1.00
Accelerator (% cement)	0.05
Retarder (% cement)	0.27
Water-retaining agent (% cement)	0.06

The sand was a very fine siliceous sand (< 500 µm). All chemical admixtures were powdered products:
- superplasticizer: polycarboxylate,
- accelerator: lithium chloride,
- retarder: sodium tetraborate,
- water-retaining agent: polyethylene-glycol.

Short fibres (l = 11 mm) and mesh derived from the same AR-glass (Vetrotex - Cem-Fil). The properties of fibres are presented in Table 2.

Table 2. Properties of short fibres.

Filament diameter	14 µm
Strand tensile strength	1700 MPa
Elastic modulus	72 GPa
Density	2.68g/cm^3
Strand	38 tex (102 filaments)

Cem-Fil 120/1 had a nominal weight of 120 g/m^2 and was produced using 320 tex and 640 tex Cem-Fil direct rovings. The mesh density was 8 x 8 strands per 10 cm.

The short fibre content was 2.83 % of total weight (cement + sand). The mesh was placed at 5 mm from the extreme tensile fiber of the composite.

Thin plates (350 mm x 350 mm x 14 mm) were cast and cured at ambient temperature. They were demolded 90 minutes after casting. Specimens of 70 mm in width were cut from each plate and subjected to 3-point loading on a span of 200 mm at a cross-head speed of 1 mm/min. The load deflection was recorded during the test and allowed the calculation of the following parameters:
- limit of proportionality (LOP): stress corresponding to the first crack of the matrix,
- modulus of rupture (MOR): maximum stress recorded,
- several toughness indices.

These indices were those described by the ASTM C 1018 85 [6]: I_5, I_{10}, $I_{20}$and I_{30}. The residual strength factors $R_{20,10} = 10\ (I_{20} - I_{10})$ and $R_{10\text{-}5} = 20(I_{10} - I_5)$ were also calculated.
Tests were performed at different ages: 3 hours, 24 hours, 7 and 28 days. Specimens tested after 3 hours were sealed in plastic bags at 20°C until the date of tests.

3. RESULTS AND DISCUSSION

3.1 Mechanical Properties

From the load-deflection curves recorded, equivalent elastic bending stress versus deflection curves were derived. Typical stress-deflection curves are shown in Figures 1 to 3. These are average values, each obtained from six samples.
All composites developed ductile behaviour as shown in Figure 4: all indices are higher than required values and remain constant with time.

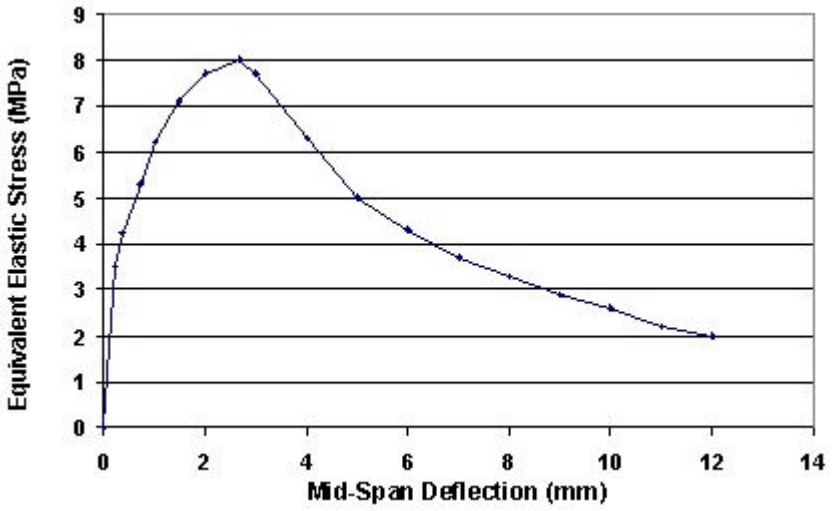

Figure 1. Flexural behaviour after 3 hours of hydration.

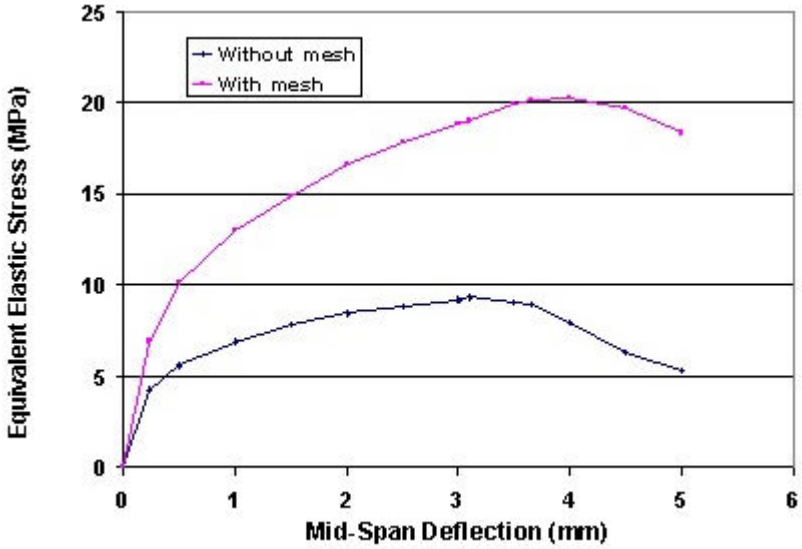

Figure 2. Flexural behaviour after 24 hours of hydration.

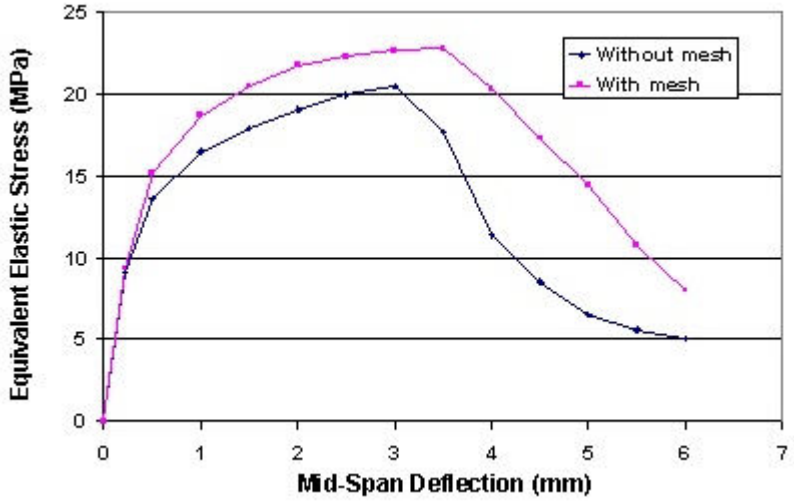

Figure 3. Flexural behaviour after 28 days of hydration.

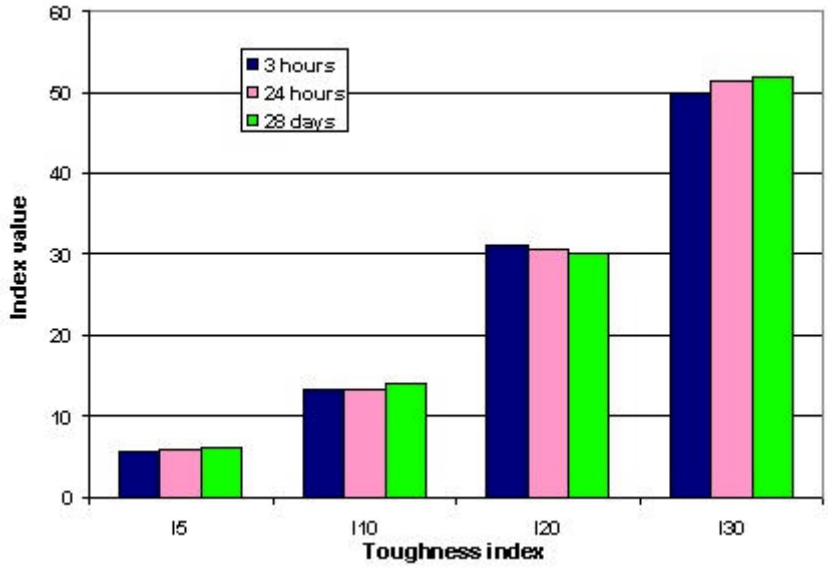

Figure 4. Indices of toughness at different ages for composites reinforced by short fibres.

As shown in Figures 2 and 3, the presence of mesh increases the performances of the composites, and especially at 24 hours. The MOR values obtained at different ages are summarized in Table 3.

Table 3. MOR values recorded at different ages.

Age	MOR (MPa)
3 hours	8.0
24 hours	9.3
24 hours with mesh	20.2
28 days	20.5
28 days with mesh	22.8

The main remarkable result is the performance obtained after 3 hours of hydration: MOR = 8 MPa, ductile behaviour. This is very important for the precast industry: such performance allows quick demolding and rapid rotation of molds.

At 28 days, the performances of the composite are similar to those obtained for a white OPC composite, reinforced 3 % fibres and mesh, containing metakaolin and a polymer. To get such results, the composite had to be cured at 40°C for 3 days, before being stored at 20°C in sealed plastic bags. Its mechanical behaviour is shown in Figure 5.

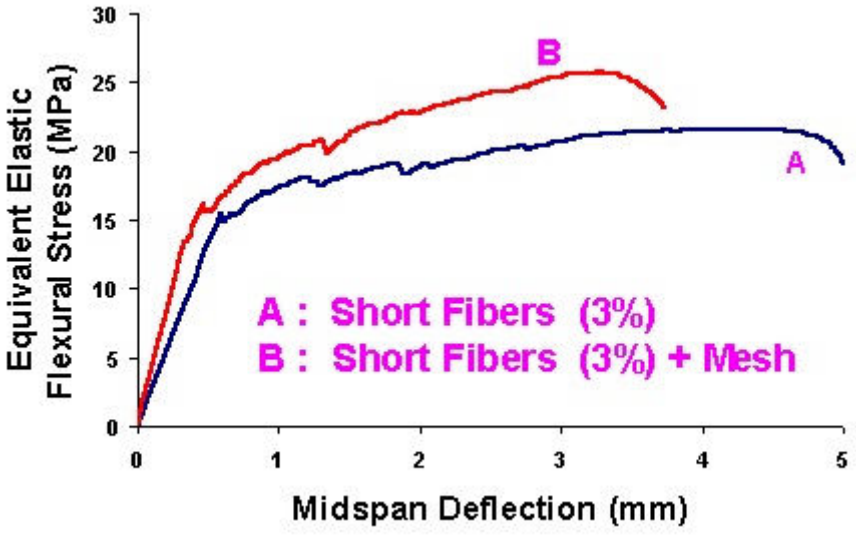

Figure 5. Performance of OPC composite.

3.2 Microstructure

Figures 6 and 7 show a good bond between fibres and matrix. Ettringite is present in the matrix and there is no calcium hydroxide.

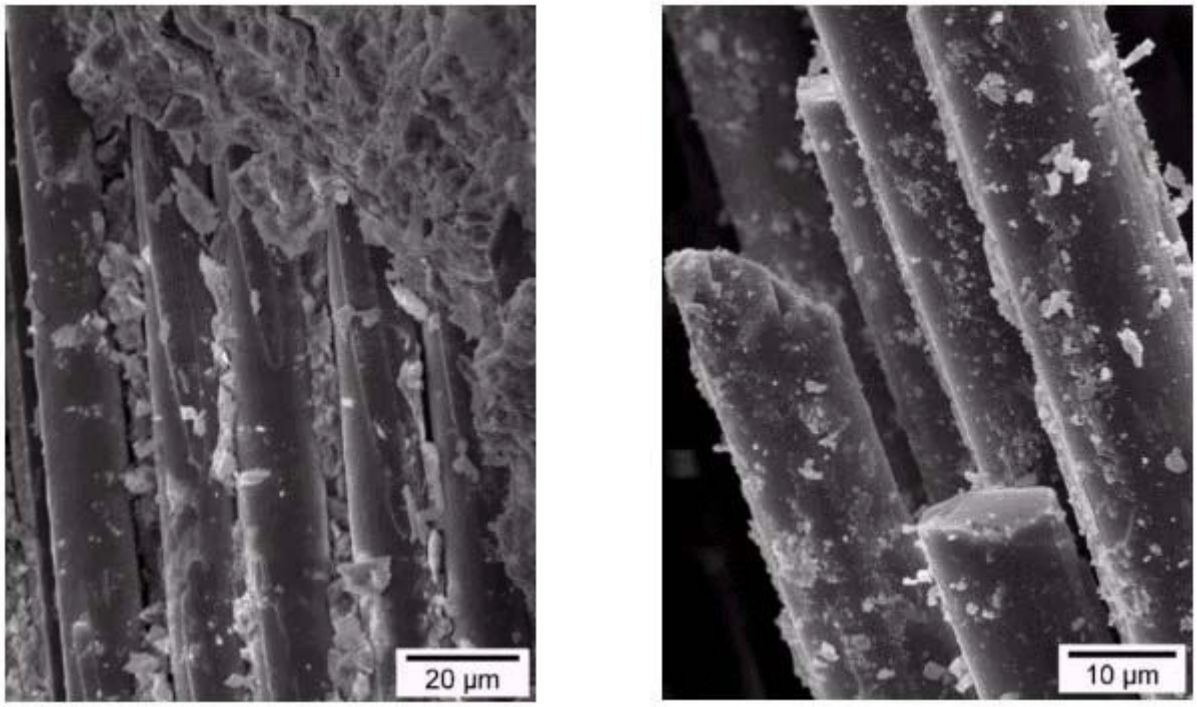

(a) (b)

Figure 6. Unattacked fibres well embedded in the matrix.

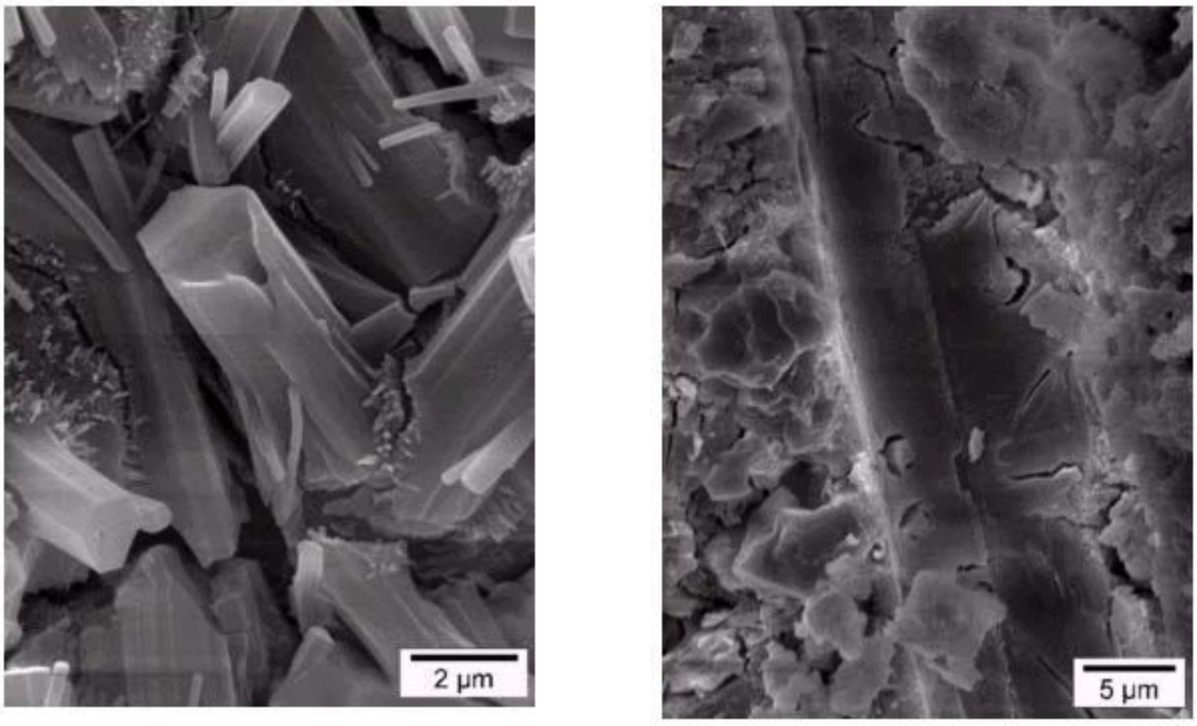

(a) (b)

Figure 7. Microstructure: crystals of ettringite (a); trace of fibre showing the absence of calcium hydroxide within de matrix (b).

4. CONCLUSIONS

This preliminary investigation points out the following:

[1] White calcium sulfoaluminate cement can be developed from waste materials: residual aluminium hydroxide and phosphogypsum.
[2] This cement can be used to prepare high-performance fibre-reinforced composites.
[3] Without any temperature curing, those composites develop high bending stress and ductile behaviour, after only 3 hours.
[4] The use of such composites is of interest to the precast industry: it allows quick demolding and rapid rotation of molds.
[5] Ductile behaviour is maintained with time at ambient conditions. Ageing tests are needed to confirm these results.

REFERENCES

[1] Ambroise, J., Dejean, J. and Péra, J. Metakaolin blended cements: an efficient way to improve GRC durability and ductility, 6th biennal congress of the GRCA, Edinburgh, 1987, pp. 19-27.
[2] Bentur, A. and Diamond, S. Effects of direct incorporation of microsilica into GFRC composites on retention of mechanical properties after ageing, Symposium on durability of glass-fibre reinforced concrete, Chicago, 1985, p. 337-347.
[3] Majumdar, A.J. and Laws, V. Glass fibre reinforced cement, Oxford, BSP Professional Books, 1991, pp. 130-142.
[4] Shen, R. Research and development of some new fibre reinforced cement composites in China, RILEM symposium on developments in fibre reinforced cement and concrete, Sheffield, 1986, vol. 2, pp. 32-40.
[5] Hyashi, M, Sato, S. and Funjii, H. Some ways to improve GFRC, Symposium on durability of glass-fibre reinforced concrete, Chicago, 1985, p. 270-279.
[6] Johnson, C.D. Methods of evaluating the performance of fibre-reinforced concrete, Symposium on fiber-reinforced cementitious materials, Materials Research Society, Boston, 1990, vol. 211, pp. 15-24.

QUALITY CONTROL IN CEMENT LABORATORIES

Gerardo Díaz[1], Pablo Kittl[2] and Marco Rosales[3]

[1] Department of Material Engineering, IDIEM, Faculty of Physical Science and Mathematics, University of Chile, P.O. Box 1420, Santiago, Chile. E-mail: gediaz@cec.uchile.cl
[2] Department of Mechanical Engineering, Faculty of Physical Science and Mathematics, University of Chile, P.O. Box 2777, Santiago, Chile.
[3] Institute of Innovation in Mining and Metallurgy, IM2, Avda. del Parque 4980, Of. 31, Huechuraba, Santiago, Chile.

ABSTRACT

Probabilistic strength of materials was used to determine the number of compacted neat cement paste samples to be tested to carry out a probabilistic mechanical characterization of a particular cement, when the fracture probability and its particular tolerance are known. Weibull's parameters were determined from compacted neat cement paste samples. Parameter dispersions were determined through a numerical simulation. A functional relation between parameter deviations and the number of samples tested was estimated with Fischer's matrix. Finally an estimate was made of the necessary number of samples to be tested to meet the tolerance admissible to a predetermined fracture probability by linking the parameters dispersions and their deviations. The number of samples required to be tested when the tolerance in the cumulative fracture probability is much less than the probability was found to be excessively large. In order to get an acceptable number of samples to be tested, both from the point of view of the statistical significance of the results and of the feasibility of testing, the tolerance of the cumulative fracture probability must be of the same order as that of the probability.

1. INTRODUCTION

The quality control tests carried out by the cement laboratories of cement plants, universities and research centers all over the world usually emphasize the physical, chemical and mechanical characterization of the cement. Quality control is carried out by cement plants to monitor their manufacturing processes. It is also performed whenever certification of the cement is sought, either through the control of external-to-the-plant laboratories or through the control of third party laboratories. The dynamics imposed by globalization, in a wide range of markets, has also reached the cement sector. Nowadays, globalization has shortened distances and manufactured products are required from distant points in the planet.

In Chile, in particular, clinker, as well as cement have been imported from remote places. Hence, the necessity of complying with different control standards on intermediate and final products arises, both in the origin places and the destination places. It is within this setting that control standards must work as facilitating agents for commercial exchange, and not as barriers to it. In accordance to this, there exists today a worldwide trend toward the homogenization of control standards in cements.

Nowadays, a great number of countries are adopting modern accreditation systems for laboratories that control a wide range of products. Accreditation has constituted itself into a tool of an economic

nature that increases competitiveness in various industries thus facilitating commercial exchange. As an articulating agent in this process the ISO standards stand out. In particular in [1] the basic guidelines through which a laboratory can perform as an accredited laboratory and, then, offer its services as such are established. One of the advantages of the accreditation system is its practical universal validity. Therefore, laboratory accreditation provides advantages both to laboratories and to users or potential users of laboratory services.

Laboratories benefit by receiving national and international recognition of their competence and qualifications by using the evaluation process as a quality assurance feature and by saving both time and money through the possible elimination of multiple audits from many potential clients. Users of laboratory services benefit by having an independent and objective means of selecting a laboratory for the required services, an easy way to provide specifications for laboratory services, and also by saving both time and money by not having to perform extensive evaluations on their own [2].

For the particular case of cements, the quality controls are aimed at determining certain physical, chemical and mechanical properties. Standardized procedures are followed for the aforesaid; these, through the testing of a particular number of samples, representative of a certain production volume, allow for the characterization of a particular cement. Certain characteristic parameters of cement are estimated from these samples.

One of these estimates relates to the mechanical characterization of the cement, which is one of the most significant variables at the moment of designing structures to be built with a given type of cement. This mechanical characterization is made starting with the preparation, curing and testing of mortars subjected to flexure and compression, and the determination of the fracture strengths. This is also done by using standardized procedures as a function of the curing age of the mortar samples made. Most countries have local standards to carry out these testing procedures; most of them are based on North American, ASTM, or European standards.

The question of the statistical validity of the results obtained from small samples that should be representative for thousands of tons of production appears when considering the present cement production volumes in different factories. Probabilistic strength of materials provides an answer for the aforesaid. The probabilistic treatment of materials or probabilistic strength of materials [3,4] foundations are laid on the impossibility of unequivocally characterizing a material considering the values of characteristic properties with no dispersion.

Fracture strength [5] and the critical stress intensity factor in mode I [6] have been treated as typical properties in compacted cement pastes and in cement mortars. Even when measurement methods have become greatly sophisticated and refined, precision and accuracy of experimental measurements improved, the resultant dispersion phenomenon continues to be present. Taking this into account Weibull [3] proposed the statistical analysis of the experimental results of brittle materials fracture. In this way the experimental results are described through probability distribution functions. These probability distribution functions are defined by means of a certain number of parameters, and it is from the experimental evidence that indicates how many correspond for each particular case. The application diversity and the parameter determination methods can be found in Kittl and Díaz [4].

For some material subjected to any given stress field, the speed of the application of external loads also influences the probability distribution functions. In [7] the applicability of models that use Weibull's distribution functions when the external loads are applied gradually is discussed. Both analytical methods and graphic methods have been used in the estimation of the parameters that describe the probability distribution functions. Graphic methods present the advantage of their simplicity of application according to what was shown by León and Kittl [8].

Estimating the parameters of probability distribution function is not enough; their respective dispersions also have to be estimated. Through Fischer's information matrix it is possible to estimate such dispersions [9]. Then, not only is there variability in the material characteristic properties or stress, which we can represent through their mean values and their corresponding dispersions, but also the parameters of the probability distribution functions present dispersion. For the results obtained from the testing of a certain number of samples to have statistical validity it is necessary to count on a minimum number of these. The aforesaid calls, sometimes, for severe restrictions on the execution of testing. That is why simulation methods which allow for the estimation of the parameters of the probability distribution functions along with their respective dispersions have been developed [9].

The purpose of the present work is estimating, through numerical simulation, the parameter dispersion of Weibull's cumulative probability of fracture function in compacted neat cement paste. And then, with Fischer's matrix, estimating the necessary number of samples to be tested to meet the tolerance admissible to a pre-established fracture probability.

2. EXPERIMENTAL PROCEDURE

In the manufacture of the compacted neat cement paste samples a commercial portland cement devoid of admixtures was used. Its composition was as follows: 20.42% SiO_2, 7,16% Al_2O_3, 2,76% Fe_2O_3, 61,4% CaO and 1,72% MgO having a specific surface of 305 m^2/kg and a retention of 13,6% in a moist 45μm sieve.

The cement was mixed with 5% in weight of water and was introduced in a rectangular steel mould 55x20mm in dimension. Then a compacting pressure of 25.6 MPa was applied to it in order to obtain samples 5mm high. The samples were stored in a moist room, with 99% humidity and at 23ºC for 24 hours. Once the 24 hours were over the samples were submerged in water until saturation, for their process of hydration to advance as fast as possible. Afterwards, the samples were again entered into the moist room until completing 14 days of hydration. The hydration process was stopped by putting the samples into an oven at 110ºC for 24 hours. Later they were stored in a dessicator until the moment of testing. In this way, 32 samples were made. All samples were subjected to the three-point bending test, with a testing span of 40mm.

3. PROBABILISTIC CHARACTERIZATION

According to the probabilistic strength of materials, Weibull's fracture cumulative probability distribution function F is given by:

$$F(\sigma, V) = 1 - \exp\{-\frac{V}{V_o}\phi(\sigma)\} \tag{1}$$

where V is the volume of the material subjected to the stress field σ, V_0 is the volume unit, and ϕ is the Weibull´s specific risk of fracture function. Experimental data usually adjusts quite well to two-or-three parameter specific risk functions:

$$\phi(\sigma) = \left(\frac{\sigma}{\sigma_0}\right)^m \qquad \sigma \geq 0 \tag{2}$$

$$\begin{cases} \phi(\sigma) = \left(\dfrac{\sigma - \sigma_L}{\sigma_o}\right)^m & \sigma_L < \sigma \le \infty \\ \phi(\sigma) = 0 & 0 \le \sigma \le \sigma_L \end{cases} \tag{3}$$

where m, σ_0 and σ_L are the Weibull´s parameters determined from the experimental data, and are representative of the genesis process or the material manufacturing process. σ_L is the stress under which there is no fracture, σ_0 is a normalization parameter and m is Weibull´s modulus.
Considering a three-parameter specific risk of fracture function the equation (1) can be rewritten as follows:

$$\xi(\sigma) = \ln \frac{1}{1 - F(\sigma)} = \frac{V}{V_0} \left(\frac{\sigma - \sigma_L}{\sigma_0} \right)^m \tag{4}$$

Weibull's diagram is obtained by making a graph of $\ln\xi(\sigma)$ versus $\ln\sigma$ for a group of experimental data from samples of material similarly made in size and geometry. Then, Weibull's parameters m, σ_0 and σ_L can be estimated.

Once Weibull's specific risk function parameters are estimated, the estimation of the dispersions associated to each one of them can be carried out, in such a way that each parameter is expressed in terms of its estimated mean value plus its dispersion. When big samples or statistically valid samples to estimate the parameters exist, the maximum likelihood estimators are approximately distributed through a multivaried normal distribution with mean values m, σ_0 and σ_L. This last function has a symmetrical R Fischer's information matrix, which is a quadratic form, its elements are given by:

$$\begin{aligned} r_{ij} &= -NE\left[\frac{\partial^2 \ln f(\sigma_i; m, \sigma_0, \sigma_L)}{\partial\theta_i \partial\theta_j} \right] \\ \{\theta\} &= \{m, \sigma_0, \sigma_L\} \\ E(g) &= \int_{\sigma_L}^{\infty} g(\sigma) \frac{dF}{d\sigma} d\sigma \end{aligned} \tag{5}$$

In this matrix, after its inversion, the variances in the diagonal and the co-variances of the estimators are expressed as $(1/N)\ R^{-1}$, where N is the number of tests carried out.

4. NUMERICAL SIMULATION

With the purpose of illustrating the method, a pair of simplifying hypothesis were used. The first of them is the direct use of Weibull's cumulative probability distribution function, as expressed in equation (1). The second one, since the volume of all the samples remained constant, is $V = V_0$ in the aforementioned equation.

Weibull's parameters were estimated from the fracture strength of the compacted neat cement paste samples through the use of a nomogram [8]. This is a graphic method that allows for the estimation of the parameters in a simple way and with great accuracy. The parameter values are shown in Table 1.

Table 1. Weibull's parameters for compacted cement paste

Weibull's parameters	
m	3.00
σ_0 MPa	0.06
σ_L MPa	6.96

After that a group of 30 random numbers were generated, λ_i. The corresponding value of σ_i was calculated with each one of them according to the following equation:

$$\lambda_i = 1 - \exp\{-\frac{V}{V_o}\left(\frac{\sigma_i - \sigma_L}{\sigma_0}\right)^m\} \quad (6)$$

using those of Weibull's parameters included in Table 1 for the equation (6). Afterwards the respective σ_i were set in an ascending way and Weibull's diagram was made, using the following expression as an estimator for the fracture cumulative probability:

$$F = \frac{n - 0.5}{N} \quad (7)$$

in which n is the sequence number in the ascending ranking, and N is the total number of σ_i values, 30 in this case. In Figure 1 the respective Weibull diagram is shown, fracture strength data generated at random.

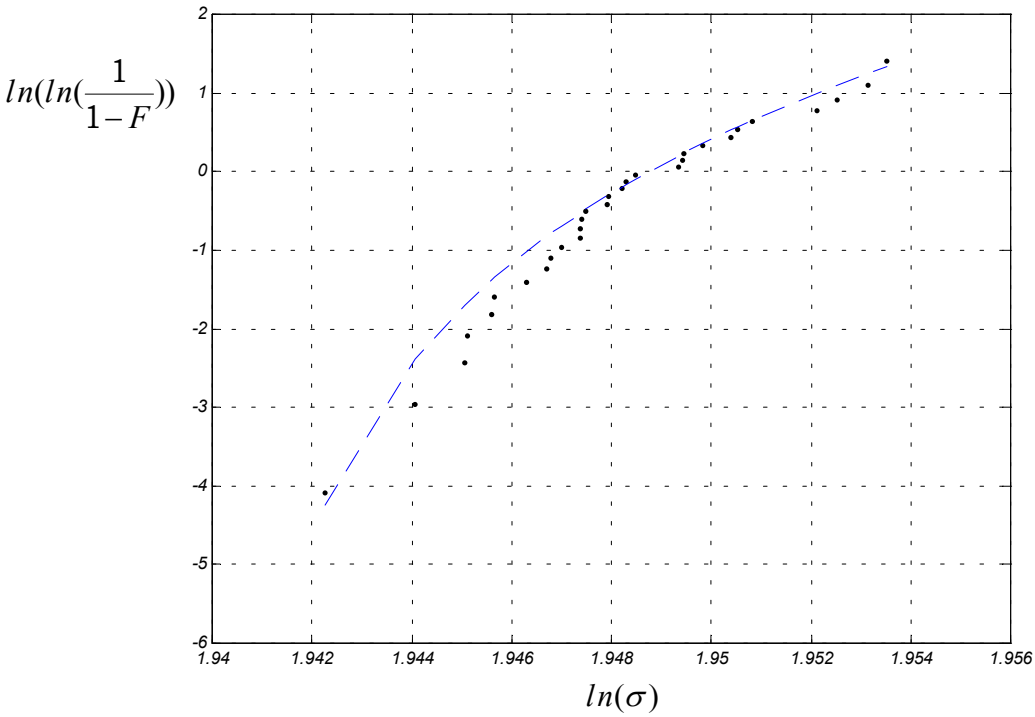

Figure 1. Weibull's diagram obtained from generating random numbers for the compacted neat cement paste samples.

In Weibull's diagrams of this nature it is possible to make an estimate of the value of $\ln\sigma_L$ the first approximation directly from the graph, corresponding to the asymptote of the inferior branch of the curve. For this case an asymptote near 1.941. Then, several numbers around that asymptote value were taken and a diagram was made for each one of them, using $\ln(\sigma-\sigma_L)$ as an independent variable, for the expression:

$$\ln(\ln(\frac{1}{1-F})) = m\ \ln(\sigma - \sigma_L) - m\ \ln(\sigma_o) \quad (8)$$

In each case, the linear correlation coefficient, R^2, was determined using minimum square method and the respective values for parameters m and σ_0 in function of the different σ_L values used. Figures 2, 3 and 4 illustrate such functional variations respectively.

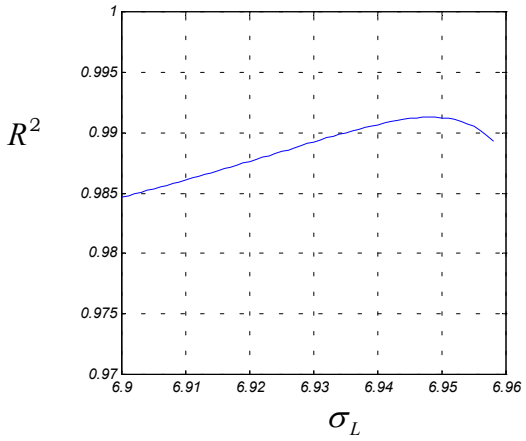

Figure 2. Linear correlation coefficient as a function of σ_L for the randomly generated data of compacted neat cement paste samples.

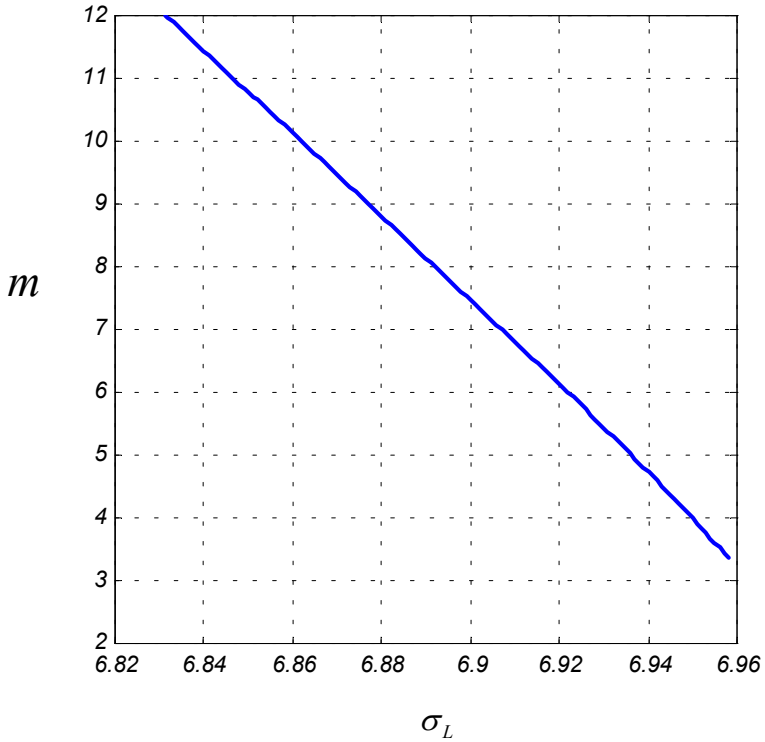

Figure 3. Weibull's parameter m as a function of σ_L for the randomly generated data of compacted neat cement paste samples.

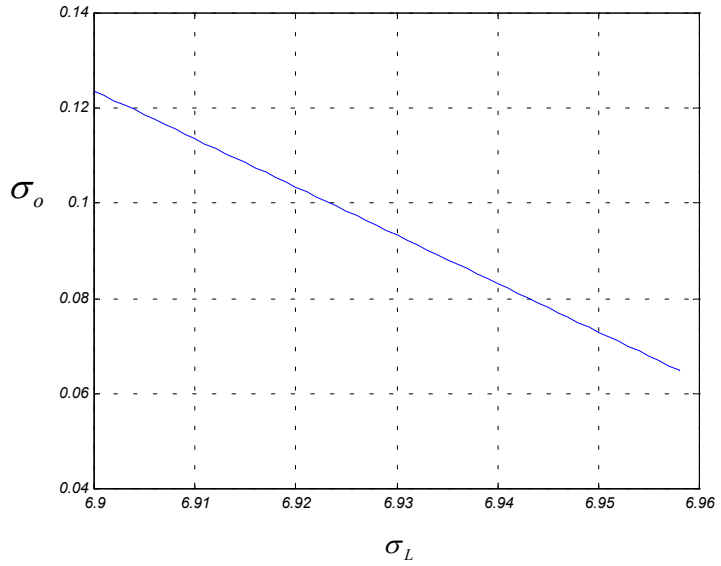

Figure 4. Weibull's parameter σ_0 as a function of σ_L for the randomly generated data of compacted neat cement paste samples.

Using the maximum correlation coefficient in the square minimums adjustments of randomly generated data from the parameters estimation of compacted neat cement paste samples subjected to the three point bending test, according to Figure 2, parameter σ_L = 6.948 MPa. Therefore, from Figures 3 and 4 respectively, the remaining Weibull´s parameters m = 4.1 and σ_0 = 0.077 MPa are obtained.

The simulation process, described here with an example, was repeated one thousand times, starting by generating random numbers λ_i again and determining the respective Weibull's parameters m, σ_0 and σ_L in every stage. For each Weibull´s parameters the mean values and their corresponding dispersions were calculated from this set of one thousand repetitions (m, σ_0, σ_L) using the following expressions, respectively:

$$\bar{x} = \frac{1}{N}\sum_{i=1}^{N} x_i \tag{9}$$

$$\Delta x = \sqrt{\frac{1}{N}\sum_{i=1}^{N}(x_i - \bar{x})^2} \tag{10}$$

Equations (9) and (10) allows one to obtain the mean value of m, σ_0 and σ_L and their dispersions Δm, $\Delta\sigma_0$ and $\Delta\sigma_L$, respectively. Here N = 1000. Table 2 shows the mean value of the parameters thus obtained with their respective dispersions.

Table 2. Weibull's parameters m, σ_0 and σ_L, their mean values and their dispersions for compacted neat cement paste samples randomly generated in numerical simulation process with 1000 iterations.

Weibull's parameter	Mean value	Dispersion
m	3.371	Δm = 0.510
σ_0	0.065 MPa	$\Delta\sigma_0$ = 0.0071 MPa
σ_L	6.955 MPa	$\Delta\sigma_L$= 0.0057 MPa

According to Fischer' information matrix defined in the equation (5) the following expressions for Weibull's parameters dispersions can be determined:

$$\Delta m = \frac{1}{\sqrt{N}} f(m,\sigma_L,\sigma_0)$$
$$\Delta \sigma_L = \frac{1}{\sqrt{N}} g(m,\sigma_L,\sigma_0) \qquad (11)$$
$$\Delta \sigma_0 = \frac{1}{\sqrt{N}} h(m,\sigma_L,\sigma_0)$$

where f, g and h are functions which depend on the parameters and N is the number of testing. Therefore, using the parameter dispersions indicated in Table 2 in the equation (11), the values for f, g and h are 2.79, 0.0031MPa and 0.0039 MPa, respectively.

For a determined fixed value of the cumulative fracture probability F the respective fracture strength value, or calculated strength, σ_c, can be determined from the following equation:

$$F = 1 - \exp\left\{-\left(\frac{\sigma_c - \sigma_L}{\sigma_0}\right)^m\right\} \qquad (12)$$

If an ΔF tolerance in cumulative fracture probability F for a calculated fracture strength value, σ_c, is admitted then the Weibull´s parameters will also be modified. Parameters m, σ_0 , and σ_L suffer deviations δm, $\delta\sigma_0$ and $\delta\sigma_L$ respectively. That is to say, they become $m + \delta m$, $\sigma_0 + \delta\sigma_0$ and $\sigma_L + \delta\sigma_L$. The cumulative fracture probability changes to $F + \Delta F$. The equation (12) can be written for each of these deviations which allows one to determine the following expressions for the variations of each parameter:

$$\delta m = \left\{\frac{\ln\left[\ln\left(\frac{1}{1-(F+\Delta F)}\right)\right]}{\ln\left[\ln\left(\frac{1}{1-F}\right)\right]} - 1\right\} m \quad ; \delta\sigma_L = \left\{\frac{\sigma_c - \sigma_0\left[\ln\left(\frac{1}{1-(F+\Delta F)}\right)\right]^{1/m}}{\sigma_c - \sigma_0\left[\ln\left(\frac{1}{1-F}\right)\right]^{1/m}} - 1\right\}\sigma_L$$
$$\delta\sigma_0 = \left\{\left[\frac{\ln\left(\frac{1}{1-F}\right)}{\ln\frac{1}{1-(F+\Delta F)}}\right]^{1/m} - 1\right\}\sigma_0 \qquad (13)$$

The number of samples to be tested to perform with tolerance ΔF with a pre- established fracture probability F is determined by equating $\delta m = \lambda\Delta m$, $\delta\sigma_0 = \lambda\Delta\sigma_0$ and $\delta\sigma_L = \lambda\Delta\sigma_L$, where λ is, in general, a number higher than one. When λ=1, 70% of the fracture strength values falls within the acceptance range. Therefore, considering the equations (13) and the dispersion equality with their respective parameters deviations, the expressions for determining the number of samples to be tested are:

$$Nm = \frac{f^2}{\delta m^2}; N\sigma_L = \frac{g^2}{\delta \sigma_L^2}; N\sigma_0 = \frac{h^2}{\delta \sigma_0^2} \quad (14)$$

where Nm, $N\sigma_L$ and $N\sigma_0$ are the number of samples to be tested that allow to determine the respective parameters, m, σ_0 and σ_L, with a pre-established probability and an admissible tolerance. For the results to be statistically valid the highest value defined by the equation (14) must be taken as the number of samples to be tested. Table 3 shows the number of samples required to be tested to perform the fracture probability and its tolerance in compacted neat cement paste subjected to three-point bending test.

Table 3. Number of samples to be tested to estimate Weibull's parameters m, σ_0 and σ_L with a fixed cumulative fracture probability F and admissible tolerance ΔF for compacted neat cement paste subjected to the three-point bending test.

Cumulative fracture probability.	Cumulative fracture probability with admissible tolerance.	Number of samples to estimate the corresponding Weibull´s parameters.		
F	F+ΔF	Nm	$N\sigma_0$	$N\sigma_L$
10^{-7}	10^{-6}	43	2	9297
10^{-6}	10^{-5}	31	2	2000
10^{-5}	10^{-4}	22	2	432
10^{-4}	10^{-3}	14	2	93
10^{-3}	10^{-2}	8	2	20

In accordance with Table 3 it was found that when the tolerance in the cumulative fracture probability, ΔF, is much less than that probability, the required number of samples to be tested is excessively large. In order to get an acceptable number of samples to be tested, both from the point of view of the statistical significance of the results and of the feasibility of testing, the tolerance of the cumulative fracture probability must be of the same order as that of the probability.

5. CONCLUSIONS

The assurance of the quality in the manufacture of cement requires strict and rigorous controls. The existence of accredited laboratories that control the properties that characterize cements is fundamental to this. By using probabilistic strength of materials it was possible to determine Weibull's parameters in compacted neat cement paste samples subjected to the three-point bending test, and through numeric simulation the number of samples to be tested for all parameters to be statistically valid with a pre-established probability and with an admissible tolerance was determined.

It was found that when the tolerance in the cumulative fracture probability, is much less than that probability, the required number of samples to be tested is excessively large. In order to get an acceptable number of samples to be tested, both from the point of view of the statistical significance of the results and of the feasibility of testing, the tolerance of the cumulative fracture probability must be of the same order as that of the probability. The choice of probability fracture and its tolerance will depend on the demands, complexities, safety and costs of the structures to be built with a certain cement.

ACKNOWLEDGEMENTS

One of the authors, G. D., wishes to thank the Fondo Nacional de Desarrollo Científico y Tecnológico, FONDECYT, for Grant Nº 1020127.

REFERENCES

[1] ISO 17.025 (2000), General requirements for the competence of calibration and testing laboratories, Ginebra, Suiza.

[2] Gladhill, R. L. (1989), Advantages of laboratory accreditation. In: Accreditation Practices for Inspections, Test, and Laboratories. Ed. H. E. Schock, Jr. ASTM, STP 1057, American Society for Testing and Materials. Philadelphia. pp. 19-23.

[3] Weibull, W. (1939), A statistical theory of the strength of materials. Ing. Vetenskaps Akad. Handl, Vol 151, pp. 1-45.

[4] Kittl, P. and Díaz, G. (1988), Weibull´s fracture mechanics or probabilistic strength of materials: State of the art. Res Mechanica, Vol. 24, pp. 99-207.

[5] Díaz, G. and Carracedo, M. I. (1999), The size effect on fracture mechanics of cement mortar: A statistical analysis. Ciencia abierta. Vol. 5, 13 pp. http://www.cec.uchile.cl/~cabierta/revista/5/mortero.htm.

[6] Díaz, G., Kittl, P. and Martínez, V. (1997), On the mechanical properties of compacted neat cement paste, cement mortar and gypsum paste. 10th International Congress on the Chemistry of Cement. Gothenburg, Sweden. Vol 3v023, 8 pp.

[7] Kittl, P. Díaz, G. and Martínez, V. (1994), Applicability of Weibullian model of fracture by application of a slowly gradual load. In: Probabilities and Materials Test, Models and Applications. Ed. D. Breysse. Kluwer Academic Publishers. London. pp. 439-449.

[8] León, M. And Kittl, P. (1985), On the estimation of Weibull´s parameters in brittle materials. Journal of Materials Science, Vol. 20, pp. 3778- 3782.

DURABILITY OF MORTARS MADE WITH ALKALI ACTIVATED SLAG

R. M. De Gutiérrez[1], J. Maldonado[1], S. Delvasto[1], F. Puertas[2], and A. Fernández-Jiménez[2]

[1]R. M. De Gutiérrez, J. Maldonado, S. Delvasto, Escuela de Ingeniería de Materiales, Universidad del Valle, Cali, Colombia.
[2]F. Puertas, A. Fernández-Jiménez, Eduardo Torroja Institute (CSIC), Madrid, Spain.

ABSTRACT

Scientific groups have studied a new type of binder obtained by the alkaline activation of granulated blast furnace slag in order to get alternative materials to traditional Portland cements, which are characterized by their high negative environmental impact. Previous studies proved that the nature of the activator is the main process factor to get alkali-activated slag (AAS) cements of appropriate quality, these being waterglass ($Na_2SiO_3.nH_2O$+NaOH) with a concentration of 4 % Na_2O as the best activator. The aim of this research was to study the durability of AAS mortars using the mentioned alkaline activator. A blast furnace slag from Spain was activated using an alkaline solution/slag ratio of 0.51. Mortars with sand/slag ratio 2/1 were prepared to cast different specimen sizes according to the properties to be measured, such as compressive strength, absorption and total porosity, capillary absorption, ability to resist Chloride penetration, Chloride diffusion coefficient, sulphate resistance and electrochemical corrosion tests. The results showed that AAS mortars had half of the absorption of a mortar prepared with an Ordinary Portland Cement (OPC) used as reference. The capillary absorption coefficient was 70 % inferior to that of the reference cement and presented also a lower coefficient than reported for a cement blended with silica fume. AAS mortars reported a Chloride diffusion coefficient 95 % lower than that of the reference hardened mortar. The Kock-Steinegger test showed that the AAS cement is resistant to sulphate environments. The total porosity and pore size decreased with time in all mortars independently of aggressive media. Electrochemical valuation done on steel bars embedded in the alkali-activated slag mortars showed no corrosion after 1 year of exposure to a Chloride medium. These results demonstrate that the AAS mortars when the alkaline activator is $Na_2SiO_3.nH_2O$+NaOH have high durability when exposed to sulphate and Chloride media.

Keywords: Alkali-activated slag cement mortars, Ground Granulated Blast Furnace Slag, Durability, Chloride diffusion, steel corrosion, aggressive environments.

1. INTRODUCTION

By now, it has been proved that blending cements with high performance pozzolans or with blast furnace slag augments the long-term durability of concrete structures in marine environments. The necessity of using industrial by-products and also of lowering the energy cost of the production of cements and its environmental impact on the atmosphere has switched the attention of the researchers, since 1960, to researching of new types of binders based on the alkaline activation of blast furnace slag[1,2]. Glukhosky[3] in Ukraine first developed these cements from alkali-activated slag (AAS).

Previous studies proved that the nature of an alkaline activator is the most significant factor on the development of mechanical strengths, and showed $Na_2SiO_3{\cdot}nH_2O$+NaOH (with a concentration of 4% Na_2O) to be the best activator for good properties[2,4]. The microstructure of the products of reaction of these materials differs from that of Portland cements. Its high early strength and low permeability are characteristic. Additionally, the resistance of ASS concrete to different aggressive

environments has been studied by different authors[5-9]. This paper presents the results of research into the durability of mortars with alkali-activated slag (AAS) using $Na_2SiO_3.nH_2O$ + NaOH as the alkaline activator.

2. EXPERIMENTAL METHODS

2.1. Materials

Table 1 shows the chemical composition of a blast furnace slag from Ensidesa, Avilés, Spain was found to be 95%. Its glass content determined by XRD[10] and microscopy techniques[11]. Its specific surface area was 460 m^2/kg. A Portland cement was used as reference material and its chemical composition is also presented in Table 1.

Table 1. Chemical Composition (% wt)

Component	OPC	SLAG
SiO_2	20.75	35.50
Al_2O_3	6.53	12.15
Fe_2O_3	3.64	1.01
CaO	60.13	41.45
MgO	2.56	8.34
SO_3	1.97	0.18
Na_2O	-	0.58
K_2O	-	0.64

Mortars of the alkali-activated slag were prepared by mixing waterglass (SiO_2/Na_2O = 1.5) with 4% of Na_2O to the slag. Following other studies[4,12], the sand/slag ratio used was 2/1 and the alkaline solution/slag ratio was 0.51. The sand used was a siliceous material with a purity higher than 95% in quartz.

2.2. Testing

The experimental procedure was done according to:

- ASTM C109, Compressive Mechanical Strength[13]
- ASTM C642, Absorption and total porosity[14]
- Fagerlund and Swiss Standard Methods, capillary absorption [15,16]
- ASTM C1202, Ability to Resist Chloride Ion Penetration[17]
- Chloride Diffusion Coefficient Method[18]
- Kock and Steinegger Techniques[19] and ASTM C1012[20], sulphate resistance
- ASTM C876[21] and ASTM G59[22], Corrosion Tests

50.8 mm cubic prisms were used to study the mechanical strength, the total absorption and the sulphate resistance behaviour of mortar specimens. The Koch-Steinegger procedure undertaken using specimens of 100 x 100 x 600 mm. 76.2 x 152 mm cylinders were cast for the rest of the tests. A corrugated steel bar was embedded in each cylinder prepared for corrosion testing. All specimens were cured at ambient temperature in a humid chamber (98%) until the testing day.

3. RESULTS AND DISCUSSION

The evolution of the compressive strengths at ages of 28, 60, 90 and 120 days is shown in Figure 1. Each data point is an average of three specimens. Alkali-activated slag mortars (AAS) yield 75.8% higher strength than the OPC mortar at 28 curing days. The strength increases up to 94.4% at 120 curing days. It is to be noted that OPC blended cements with 70% w/w blast furnace slag or 10%

w/w silica fume reported 50% lower results than for the AAS mortar and that is in agreement with the findings by Deja[23].

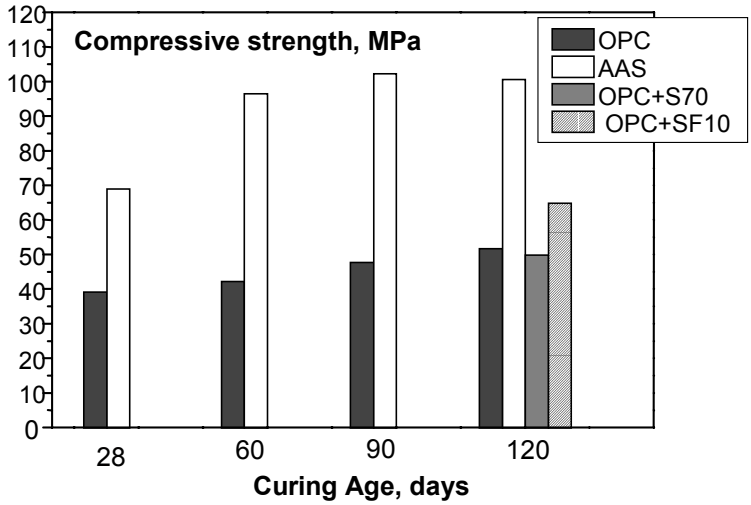

Figure 1. Compressive Strength Development

Total absorption results of mortars at different curing days are presented in Table 2. The absorption was evaluated following ASTM C642[14] after drying specimens at 100°C and then by immersing the samples under water for 24 hr. Included in Table 2 is the total percentage of pores and the specific density at 28 curing days. It is noticeable in the AAS mortar a diminishing of the absorption at higher curing days that agreed with greater compactness and strength increases. At 90 curing days there was a reduction of 61% in absorption when compared with OPC mortars. The total porosity was reduced by about 50%, although the density was comparable with that obtained in OPC mortars. These results agree with those reported by Roy et al.[24] and Wu et al.[25].

Absorption and porosity values lower than 3 and 10% respectively are considered acceptable as parameters of compaction and durability for mortars.

Table 2. Results of Tests according to ASTM C642.

Material	Total Absorption, % Curing age, days			Porosity, % (28 days)	Specific Density, K/m^3 (28 days)
	28	60	90		
AAS	4.96	2.67	2.04	5.78	2183
OPC	5.28	6.26	5.28	11.42	2186

The permeability of mortars was evaluated using the capillary suction technique done in specimens conditioned at 60°C for 48 hours[15,16]. The results of capillary absorption were calculated as a square root time function, as shown in Figure 2. The capillary Index or the absorption coefficient (k) and the resistance to water penetration (m) are reported in Table 3. Also, the saturation time (t_n) and the capacity of capillary suction at 3 and 24 hours exposure are included. The k values of the AAS mortars is 70 % less than the index showed by the OPC mortar. The observed behaviour is comparable with that found in pozzolans of high reactivity. The index of the mortar blended with 10% of silica fume was 30% higher than that of the AAS mortars. A lower k indicates the refinement of the capillary pores and therefore a reduction of the pore connectivity. The shape of the graph in Figure 2, shows it is more difficult to reach saturation of the AAS specimens when compared to the OPC prisms.

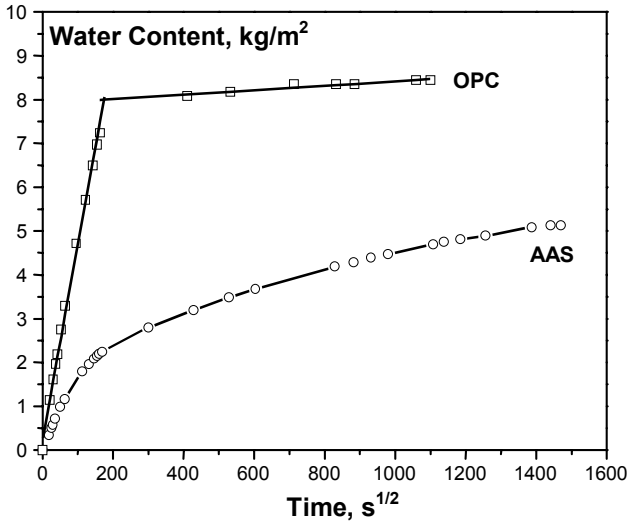

Figure 2. Water Suction Test.

Table 3. Results of Capillary Absorption testing

Material	k $kg/m^2s^{1/2}$	m s/m^2	t_n s	Kg/m^2 (3 hours)	Kg/m^2 (24 hours)
AAS	0.0130	-	-	1.69	2.58
OPC	0.0445	1.56×10^7	30.1×10^3	4.90	8.06
OPC+Silica Fume 10%	0.0170	10.3×10^7	243×10^3	-	-

Hakkinen[26] determined the pore size distribution of AAS mortars by means of mercury porosimetry finding a dense microstructure with fine pores between 5 and 30 nm. Roy et al.[24] reported up to 80% in reduction of the median pore size compared with that obtained in OPC mortar. Previous work on AAS mortars, prepared with the same slag used in this research, show that the distribution of the pores is bimodal, a high percentage of the pores had sizes between 0.1 and 10 μm and other presented sizes lower than 0.01 μm[12].

Permeability to Chloride ions was evaluated following the ASTM C1202 procedure[17], in order to monitor the amount of electric current passing through a 51 mm thick specimen put between two solutions, one of them containing NaCl. The results of this test are presented in Figure 3. The total charge passed is related to the material resistance to chloride ion penetration. AAS mortars gave a charge of 1329 coulombs against 4938 coulombs reported by the reference mortar. This reduction of 73% was obtained at 28 curing days of the specimens. Douglas et al.[27], reported similar values working on AAS concrete samples. The ASTM standard defines passing charges in the range of 1000 – 2000 coulombs as materials with low chloride permeability.

The diffusion coefficient of chloride ions was evaluated in a diffusion cell by using plates thinner than 10 mm. 12 V was applied in order to accelerate the process of diffusion. The diffusion coefficient was calculated by using the first law of Ficks, the concept of stationary state flux and the equation of Nernst and Planck[28,29]. In Figure 4 it is seen that AAS mortars present a diffusion coefficient 95% lower than that of the reference mortar. This is also lower than reports on mortars with additions such as metakaolinite (MK), silica fume (SF) and blast furnace slag (S)[23,30,31]. Roy et al.[24] and Byfors et al.[8] reported similar values. Byfors working on paste specimens showed coefficients 30 to 40 times lower than those determined in OPC pastes. The same author evaluated the binding capacity of these materials in order to assign the observed behaviour to the formation of Friedel salt; however, the results are not conclusive.

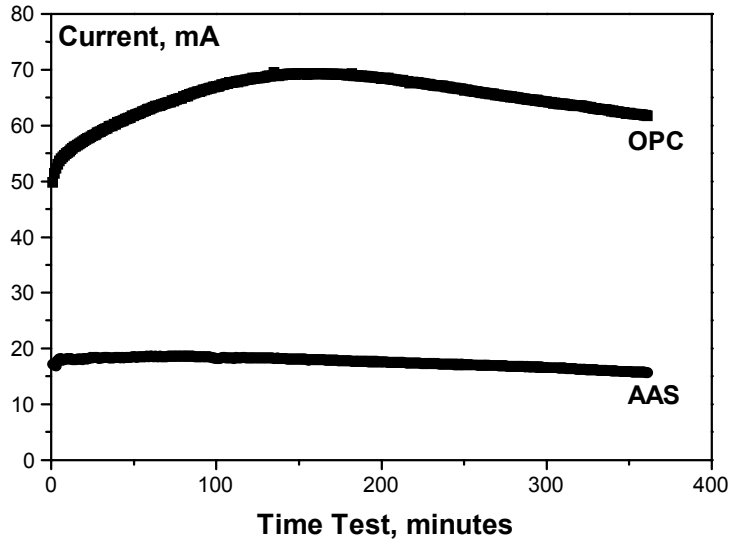

Figure 3. Ability to Resist Chloride Ion Penetration

AAS mortar specimens exposed to sulphates showed reduced values of total porosity when compared to the mortar specimens immersed in the reference solution. Additionally, their pore size decreased about ten times, while the proportion of small size increased significantly. This fact is associated with the kinetics of the activation process and also to the variation of composition and structure of the main product of reaction, hydrated calcium silicate[33]. When prisms of hardened AAS mortars were submerged in a Na_2SO_4 solution, the analysis of the microstructure of the reaction products, by means of SEM/EDX and DRX showed neither sulphur nor gypsum. Also, free $Ca(OH)_2$ as Portlandite was not found[33].

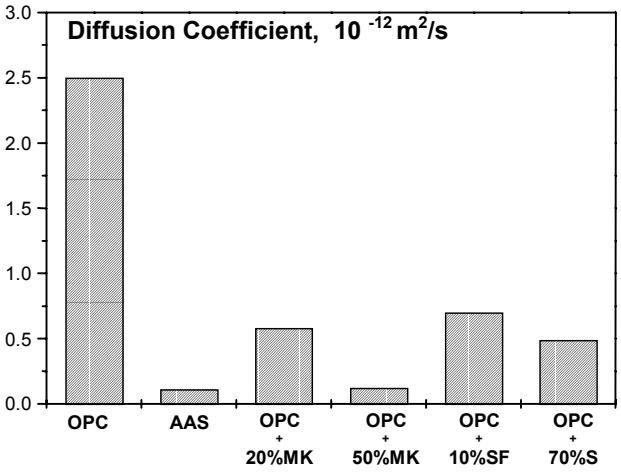

Figure 4. Comparative Analysis of Chloride Diffusion Coefficient

Flexural and compressive strength results of AAS mortar prisms submerged in aggressive solutions containing sulphates did not show negative effects when compared with those conserved in the reference medium, which was deionised water, as is observed in Figure 5. On the contrary the compressive strength increased, which agrees with the observation reported by Xuequan et al[33].

AAS mortars presented expansion values of 0.016% after 200 days of exposure to a Na_2SO_4 solution. The visual aspect of the mortar specimens after the testing is presented in Figure 6. These findings are in accordance with those reported by other researchers[34,35].

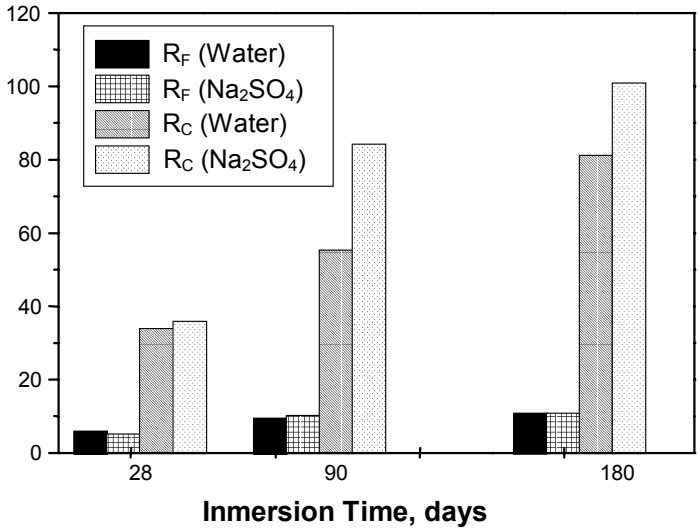

Figure 5. Flexural (R_F) and Compressive (R_C) Strength (MPa)

Steel bars embedded in OPC and AAS mortars, exposed to partial immersion in 3.5% NaCl, were evaluated, in order to determine their corrosion behaviour by of half cell potential and linear polarisation resistance techniques. The results of these tests and the visual observation of these specimens, after one year of exposure, indicate that the AAS material gives protection against steel corrosion. This could be attributed to its reduced permeability. Deja[34] concluded that AAS mortars are highly resistant to corrosion based on electrochemical techniques and weight losses of the steel bar reinforcement after 365 days of exposition to chlorides environment.

Figure 6. OPC and AAS mortars after 180 days of exposition to Sulphates

4. CONCLUSIONS

The results of the experimental work carried out until now confirm the excellent durability of AAS mortars prepared with waterglass as an alkaline activator when exposed to sulphate and chloride environments. It is noted that the protection of the steel bars embedded in the AAS mortar after 1 year of exposition to chlorides environment is satisfactory. This is mainly attributed to the reduced capillary absorption and low chloride permeability.

REFERENCES

[1] Puertas, F. "Cementos de Escorias Activadas Alcalinamente: Situación Actual y Perspectivas de Futuro". Materiales de Construcción, Vol. 45, No. 239, 1995, pp.53-64.

[2] Wang, S.D., et al. "Alkali Activated Slag Cement and Concrete: A Review of its Properties and Problems". Advances in Cement Research, 7, No. 27, 1995, pp. 93-102.

[3] Glukhovsky, V.D., Rostovskaja, G.S., Rumyna, G.V. "High Strength Slag-alkaline Cements". 7th Intern. Congr. Chem. Cem. (Paris), 3, V164-168, 1980.

[4] Fernández-Jiménez, A., Palomo, J.G., and Puertas, F. "Alkali-activated Slag Mortars Mechanical Strength Behaviour". Cement and Concrete Research, 29, 1999, pp 1313-1321.

[5] Krivenko, P.V. "Alkaline Cements and Concretes: Problems of Durability". 2nd Intern. Conf. Alkaline Cements and Concretes (Kiev), 1999.

[6] Pera, J., and Chabannet, M. “Durability of Alkali-activated Slag Cements”. Proc. Mat. Res. Society. Symp. on Mechanisms of Chemical Degradation of Cement-based System (Boston), 1995, pp. 281-288.
[7] Deja, J., Malolpeszy, J. “Resistance of Alkali-activated Slag Mortars to Chloride Solution”. 3rd Intern. Conf. on Fly-ash, Silica Fume, Slag, and Natural Pozzolans in Concrete, Trondheim, V 2, SP 114-75, 1989, pp. 1547-1563.
[8] Byfors, K., et al. “Durability of Concrete made with Alkali Activated slag”. 3rd Intern. Conf. on Fly-ash, Silica Fume, Slag, and Natural Pozzolans in Concrete, Trondheim, V2, 1989, pp. 1429-1466.
[9] Bakharev, T., Sanjayan, J.G., and Cheng, Y-B. “Resistance of Alkali-activated Slag Concrete to Carbonation”. Cement and Concrete Research 31, 2001, pp. 1277-1283.
[10] Hooton, R.D., Emery, J.J. “Glass Content Determination and Strength Development Predictions for Vitrified Blast Furnace Slag”. First Int. Conference Fly Ash, Silica Fume, Slag and other Mineral by Products in Concrete. Montebello, Quebec, Canada, SP 79-SO, 1983, pp. 943-962
[11] British Standard Institution BSI- BS6699-92.
[12] Fernández-Jiménez, A., Puertas, F. “Morteros de Escoria Activada Alcalinamente. Comportamiento Mecánico y Estabilidad de Volumen”, Sostenibilidad y Tendencia de Diseño y Construcción, Coloquia 2001, Madrid.
[13] ASTM C 109. Standard Test Method for compressive Strength of Hydraulic Cements Mortars.
[14] ASTM C 642. Standard Test Method for Density, Absorption, and Voids in Hardened Concrete.
[15] Fagerlund, G., “On the Capillarity of Concrete”, Nordic Concrete Research N°1, Oslo, Paper N°6, 1982, 20p.
[16] EMPA – SIA 162/1, Test No. 5 – Water Conductivity, Suiza, 1989.
[17] ASTM C1202, Standard Test Method for Electrical Indication of Concrete’s Ability to Resist Chloride Ion Penetration.
[18] Kock, A., and Steinegger, H. “Ein Schnellprüfverfahren für Zemente auf ihr verhalten bei sulfatangriff”. ZKG INTERNATIONAL, 13 Nº 7, 1960, pp. 317-324
[19] De Gutiérrez, R., and Rodríguez, P. “Durabilidad y Corrosión de Materiales Cementicios”, CYTED, Seminario Internacional, Costa Rica, 1999.
[20] ASTM C1012, Standard Test Method for Length Change of Hydraulic-cement Mortars exposed to a Sulphate Solution.
[21] ASTM C876. Standard Test method for half-cell Potentials of uncoated Reinforcing Steel in Concrete.
[22] ASTM G59. Standard Practice for Conducting Potentiodynamic Polarization Resistance Measurements.
[23] Deja, J. “Chloride Resistance of the Pastes and Mortars containing Mineral Additives”. Proceedings of the 10th Int. Congress on the Chemistry of Cement, Goteborg Sweden, (4iv015),1997, 8p.
[24] Roy, D. M., Jiang, W., and Silsbee, M.R. “Chloride Diffusion in Ordinary, Blended, and Alkali-activated Cement Pastes and its Relation to other Properties”. Cement and Concrete Research 30, 2000, pp. 1879-1884.
[25] Wu, X. et al., “Alkali Activated Slag Cement Based Radioactive Waste Forms”. Cement and Concrete Research, V21, 1991, pp.16-20.
[26] Häkkinen, T. “The Influence of Slag Content on the Microstructure Permeability and Mechanical Properties of Concrete, Part 1: Microstructural studies and basic mechanical properties”. Cement and Concrete Research, Vol. 23, 1993, pp. 407-421.
[27] Douglas, E., Bilodeau, A., and Malhotra, V.M. “Properties and Durability of Alkali-activated Slag Concrete”. ACI Materials Journal, Vol. 89, No. 5, 1992, pp. 509-516.
[28] Streicher, P.F. and Alexander, M.G., “A Critical Evaluation of Chloride Test Methods for Concrete”, Third Canmet/ACI International Conference of Durability of Concrete Supplementary Papers, Nice France, 1994, pp.517-530.
[29] De Gutierrez, R. M. et al., “Chloride Diffusion Coefficient by a modified Permeability Test and its Application in Normal and Blended Cements Mortars”. Proc. 13TH International Conference, Melbourne, Australia, 1996
[30] De Gutierrez, R. M., Delvasto, S. and Talero, R. “Properties of Cement Mortar Blended with Silica Fume, Fly Ash and Blast Furnace Slag”, Marine Corrosion in Tropical Environments, ASTM STP 1399, A. B. Smith and C. D. Jones, Eds., American Society for Testing and Materials, West Conshohocken, PA., 2000, pp.190-196.
[31] International Conference, Melbourne, Australia, 1996
[32] De Gutierrez, R. M., Delvasto, S. and Talero, R. “Una Nueva Puzolana para Materiales Cementicios de elevadas Prestaciones”, Materiales de Construcción, V 52, N°260, 2000, pp.5-14.
[33] Puertas, F., De Gutierrez, R., Fernández-Jiménez, A., Delvasto, A., Maldonado, J. “Alkali-Activated Slag And Flyash/Slag Cement Mortars: Chemical Resistance To Sulphate And Sea Water Attack”. Materiales de Construcción (in press).
[34] Xuequan, X. et al., “Alkali-activated Slag Cement based Radioactive Waste Forms”. Cement and Concrete Research, V21, 1991, pp.16-20
[35] Kukko, H. and Mannonen, R. “Chemical and mechanical properties of alkali-activate blast furnace slag (F-Concrete)”. Nordic Concrete Research, Pub. No. 1, Oslo, 1982.
[36] Deja, J., Malolepszy, J. and Jaskiewicz, G. “Influence of chloride corrosion on the durability of reinforcement in the concrete”. Proc. Third International Conference Fly Ash, S, slag and natural Pozzolans in Concrete, Trondheim, Norway, Sp 126-27, 1989, pp. 511-525.

DURABILITY OF MORTARS MADE WITH ALKALI ACTIVATED SLAG

R. M. De Gutiérrez[1], J. Maldonado[1], S. Delvasto[1], F. Puertas[2], and A. Fernández-Jiménez[2]

[1]R. M. De Gutiérrez, J. Maldonado, S. Delvasto, Escuela de Ingeniería de Materiales, Universidad del Valle, Cali, Colombia.
[2]F. Puertas, A. Fernández-Jiménez, Eduardo Torroja Institute (CSIC), Madrid, Spain.

F. Puertas

Torroja Institute (CSIC), Madrid, Spain.
Author E-mail: puertasf@ietcc.csic.es

EFFECT OF THE ADDITION OF ULTRAFINE CEMENT ON THE PROPERTIES OF FIBER REINFORCED COMPOSITES

Josef Kaufmann, Thomas Matschei and Daniela Hesselbarth

Swiss Federal Laboratories for Materials Testing and Research (EMPA)
Concrete / Construction Chemistry Lab, Duebendorf, Switzerland.
E-mail: Josef.Kaufmann@empa.ch and Daniela.Hesselbarth@empa.ch

ABSTRACT

Mixing powders of different mean grain size at certain mix proportions may increase the packing density. This packing effect is used in concrete technology by adding fine fly ash or microsilica to the coarser cement, leading to denser materials. In this paper the effect of the addition of ultrafine cement, mostly based on blast furnace slag, to normal grain sized Portland cement is presented. A decrease of the porosity and hence an improvement of the mechanical properties of the hardened paste is observed. Additionally the rheological properties of the fresh paste are influenced positively, leading to much improved workability. Such dense materials generally are very brittle. The use of fiber, increases the ductility significantly and leads to a further improvement of the strength properties. The excellent rheological properties allow the conventional mixing of composites with a high fiber content and low w/c ratio.

1. INTRODUCTION

Most material properties such as mechanical properties, gas and water transport, shrinkage, frost resistance and hence durability are influenced by the porosity [1].

In fiber reinforced composites the porosity of the fiber-matrix interface is of crucial importance. High interfacial porosity leads to a poor bond between matrix and fiber and hence a loss of strength. Additionally, high porosity may create connected pathways along the fibers, increasing permeability and therefore gas, water and ion transport which may cause serious durability problems. The quality of a fiber-matrix interface can be improved either by a surface treatment of the fiber itself or by adjusting the matrix properties like rheology, shrinkage and porosity [2].

Porosity depends on the chemical composition of the raw materials, their hydration processes and the packing properties of the different components (sand, cement, filler). Packing density may be increased by combining two or more components with different particle size distribution [3]. Especially fine particles may improve the density of a fiber-matrix or aggregate-matrix interface, as they can be packed closer to the surface of the fiber or the aggregate [4].

New concrete mix designs like DSP (densified small particle) are based on this concept. They involve a dense granular matrix with high superplasticizer and silica fume content and extremely hard aggregates (granite, calcined bauxite etc.) [5]. Due to the higher water demand and the susceptibility to shrinkage, a new concept of replacing silica fume by ultrafine cement and/or pozzolanic active and non-active fillers was tested.

Proceedings of the 11th International Congress on the Chemistry of Cement (ICCC)
'Cement's Contribution to the Development in the 21st Century'
Hosted by: The Cement and Concrete Institute of South Africa
CD-ROM produced by: Document Transformation Technologies
11 - 16 May 2003, Durban, South Africa
ISBN Number: 0-9584085-8-0
Editors: Dr G. Grieve and G. Owens
Congress Organised by: Event Dynamics

The influence of microfillers on enhancement of concrete strength and fluidity has been demonstrated [6,7]. Different amounts of ultrafine cement and filler were added to ordinary Portland cement. A conventional mixing process was used. The application of superplasticizers allowed the preparation of cement slurries and mortars with very low water-cement-ratios [6]. Mechanical, rheological and length change properties of these binder systems and the effect of fiber reinforcement was studied.

2. EXPERIMENTAL

Ordinary Portland cement CEM I 42.5 N according to European Standard EN 197-1, ultrafine cement (Portland cement blended with blastfurnace slag), limestone filler and fly ash were used as part of the binder system. The chemical composition of the cementitious binder compounds are given in Table 1. Figure 1 shows the particle size distributions obtained by laser diffraction. As water-reducing agent a polycarboxylate type superplasticizer was used.

Table 1. Chemical composition of the cements used

	CaO	MgO	SiO_2	Al_2O_3	Fe_2O_3	Na_2O	K_2O	SO_3	L.O.I.
CEM I 42.5 N	62.8	2.0	19.9	5.4	2.8	0.13	1.0	2.8	2.5
Ultrafine cement	45.3	8.1	32.6	9.9	0.6	0.3	0.4	2.6	1.5

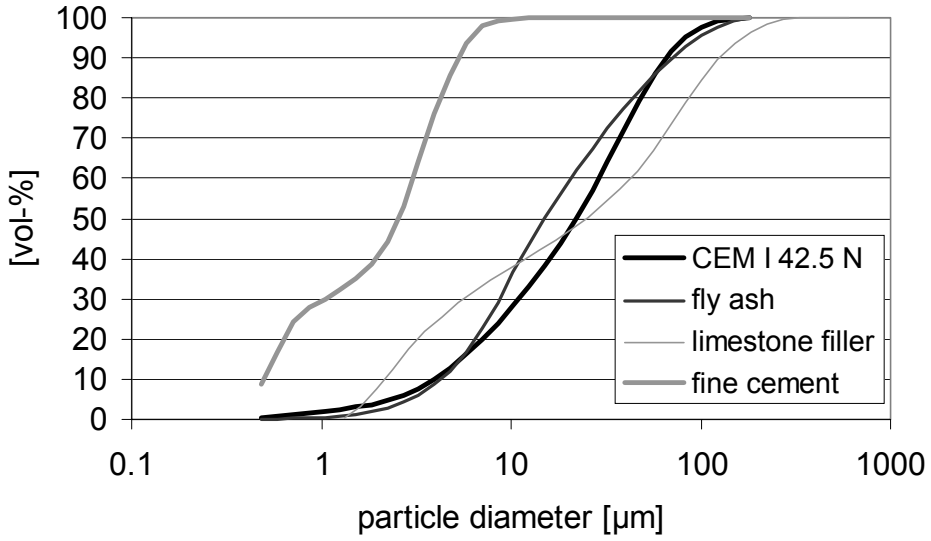

Figure 1. Grain size distribution of the raw materials

3. RESULTS

3.1 Rheology

In a first test series Portland cement CEM I 42.5 N pastes were prepared with different fillers - ultrafine cement, limestone filler and fly ash. The water/binder ratio was 0.20, and 2.0% superplasticizer in respect of the binder was used. Mixtures with a filler content of 10%, 20%, 30% and 50 weight-% were tested.

For the rheological measurements a rheometer (Paar Physica MCR 300) in controlled shear rate mode was used. It was equipped with a spherical measuring system, developed especially for cement pastes and mortars [8].

The pastes were mixed as described above. Immediately after mixing a flow curve with shear rates from 0.01 s^{-1} to 100 s^{-1} was recorded. Apparent yield stress and plastic viscosity were calculated according to the Bingham model. Ultrafine cement and limestone filler showed the best results concerning workability (see Figure 2) leading to low plastic viscosity and apparent yield stress. Low fly ash content (10% - 20%) led to significantly higher values.

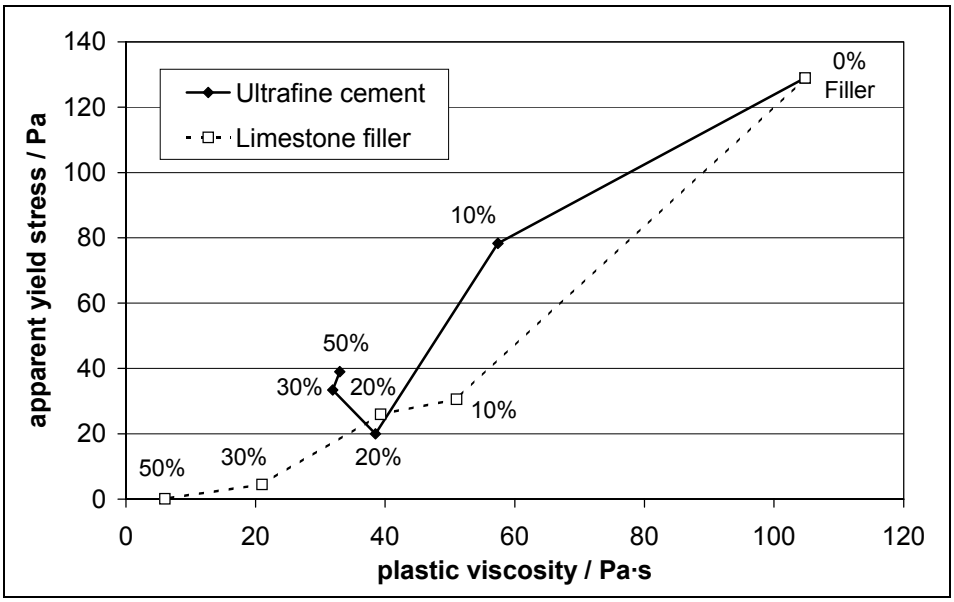

Figure 2. Bingham parameters of the investigated cement pastes with different filler contents

3.2 Mercury intrusion porosimetry

The positive packing effect of the ultrafine cement is demonstrated in the mercury porosimetry measurement (Figure 3) of hardened cement pastes. Ordinary Portland cement CEM I 42.5 N was blended with 25 vol.-% of different fillers. Superplasticizer dosage (2 weight-% of binder) and slump flow (230 cm) was kept constant, while water-binder-ratio was adjusted. The specimens, which were cured under water, were measured at an age of 7 days. Previously to the measurement the specimens were dried at 110°C. The use of ultrafine cement significantly reduces total porosity and shifts the pore size distribution towards smaller pores.

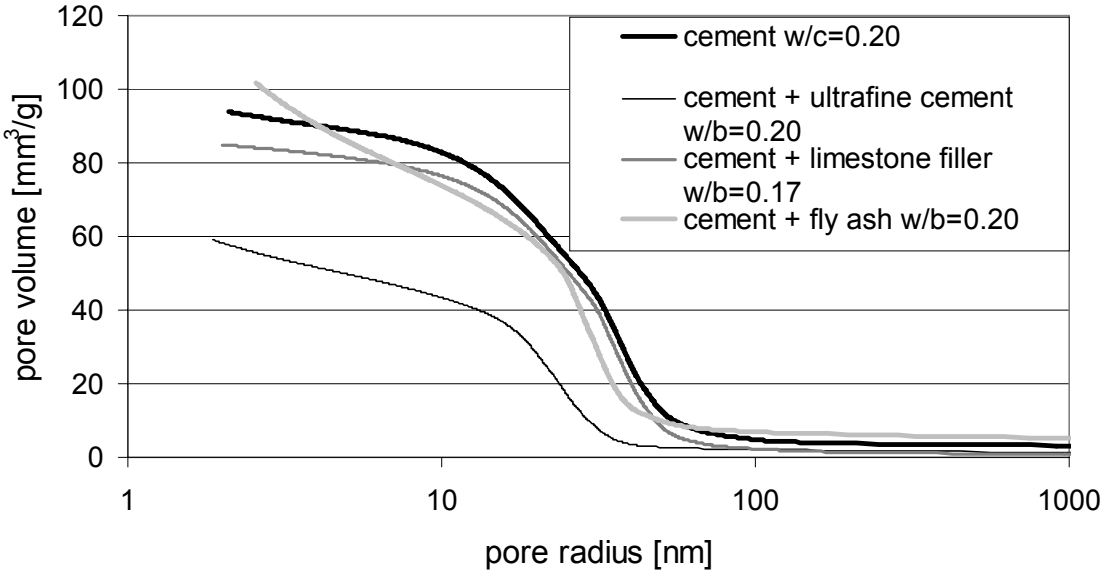

Figure 3. Pore size distribution (mercury intrusion) of hardened cement pastes containing 25 vol-% of filler

3.3 Influence of ultrafine cement on shrinkage and strength properties

Because of its positive effects on rheology and density, the system ordinary Portland cement/ultrafine cement was studied in further detail. In a test series, length change behavior of hardened cement pastes containing different amounts of ultrafine cement was studied. Slump flow (200 mm) and superplasticizer content (2 weight-% of binder) were kept constant and water content was adjusted. Length change was measured on steel plates fixed on the specimens (40 mm x 40 mm x 160 mm) directly after demoulding at an age of one day. After that, a series of three specimens were stored under water.

Table 2. Mix proportions of pastes for length change measurement

No.	CEM I 42.5 N [%]	Ultrafine cement [%]	Superplasticizer [%]	w/b -
1	100	0	2.0	0.19
2	90	10	2.0	0.17
3	80	20	2.0	0.155
4	70	30	2.0	0.145

While for pure Portland cement pastes expansion is observed, hardened cement pastes containing low amounts of ultrafine cement (10% , 20%) show some shrinkage during the first seven days (Figure 4). After that, expansion dominates. This might be owing to the very fine powder and hence accelerated hydration kinetics leading to self desiccation within the sample. At higher ages the water then is replaced by suction from the outside. This may induce stress.

At higher contents of ultrafine cement (30 weight-%) significant swelling, beginning on the first day, is measured. This effect possibly originates from the very low w/b ratio (0.145).

Total length change is influenced positively in each case by the addition of ultrafine cement [9].

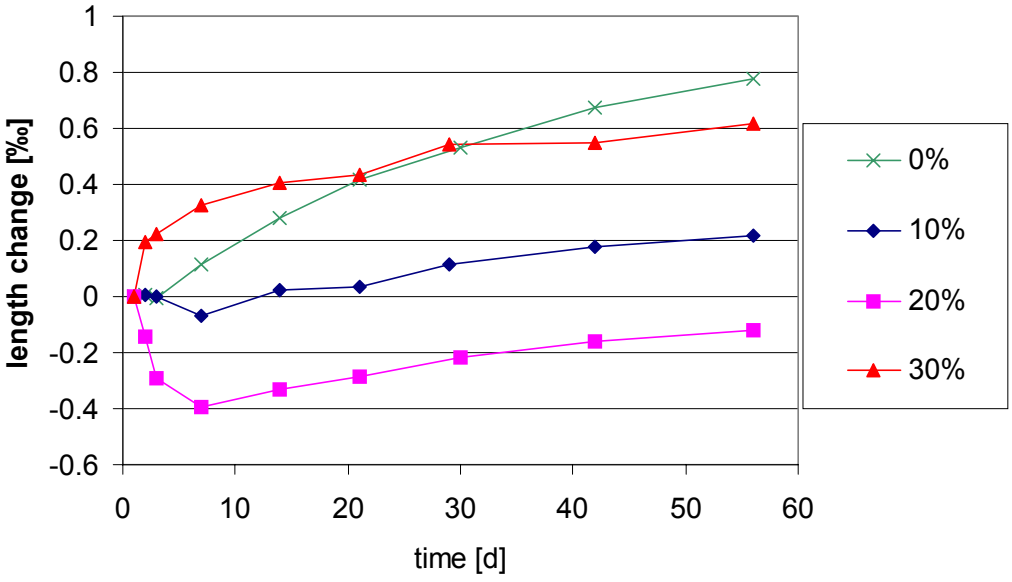

Figure 4. Influence of ultrafine cement content on length change (curing under water)

Mechanical properties (compressive strength and flexural strength) were determined on a series of 3 specimens (40 mm x 40 mm x 160 mm). The effect of the addition of ultrafine cement on the

compressive strength at ages 7 and 28 days under water is shown in Figure 5. The addition of ultrafine cement leads to a significant increase of compressive strength. The addition of medium amounts of ultrafine cement (10%, 20%) has a positive effect on the flexural strength (see Figure 5) determined in a three point bending test arrangement, meanwhile a high content (30%) of ultrafine cement has a detrimental effect on this property. The loss of flexural strength with age might be caused by microcrack formation initiated by shrinkage stress.

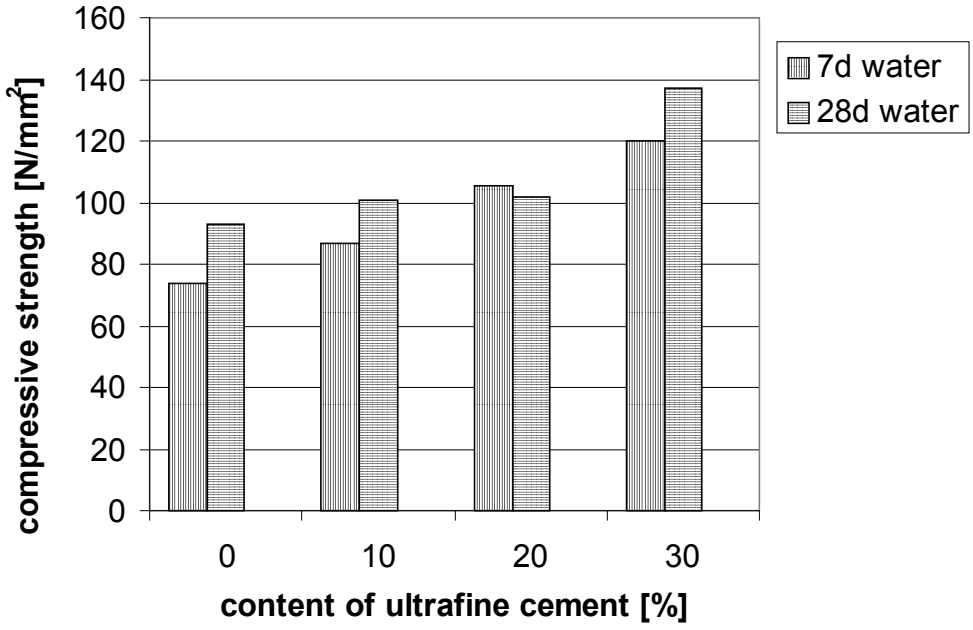

Figure 5. Compressive strength of hardened cement pastes containing different amounts of ultrafine cement

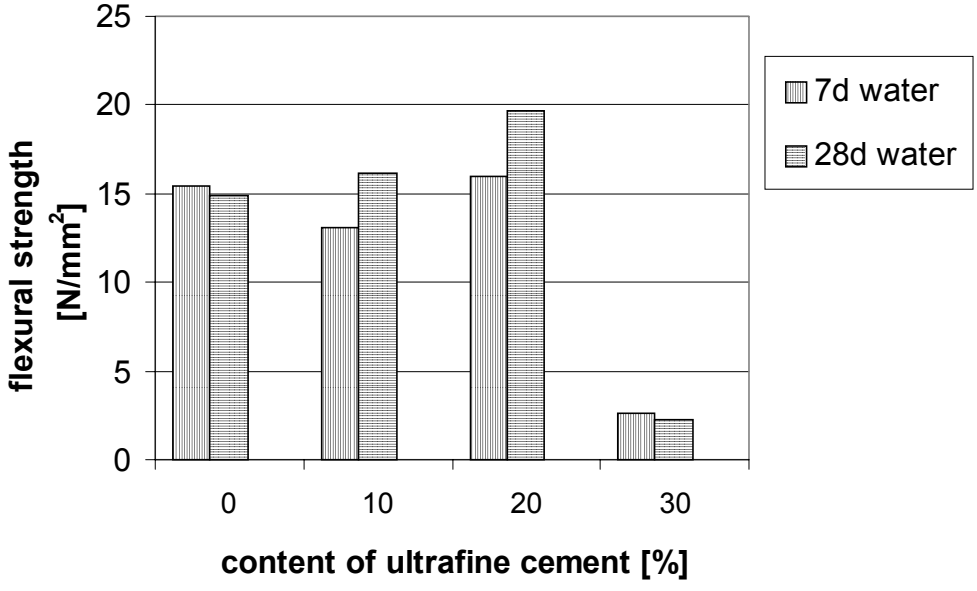

Figure 6. Flexural strength of fiber reinforced composites containing different amounts of ultrafine cement

The influence of different curing regimes on the strength properties was further analyzed. Ordinary Portland cement was blended with 25 vol-% of ultrafine cement. Water-binder ratio was 0.20. After

demoulding, the specimens were stored at different curing conditions at 20°C. The reference was pure Portland cement paste. The addition of ultrafine cement has a positive effect on the compressive strength of hardened cement paste independent of curing regime. Low standard deviations ranging from 1 to 5 N/mm^2 were observed. The best results for compressive strength are obtained for specimens that are stored under water during the first 7 days.

The influence of the storage regime on the flexural strength (three point) is shown in Figure 8. For some curing regimes high standard deviations up to 5 N/mm^2 are observed, originating from some specimens having significantly lower values. This indicates a cracking tendency for these sets of specimens. For illustration besides the mean value, the lowest value of a specimen set is also plotted (asterisk in Figure 8). The flexural strength is negatively influenced by initial curing, under water, during the first 7 days. Microscopic studies revealed crack formation beginning between 1 and 7 days. Gradual water supply from the outside may prevent stress formation between the outer and the inner paste. Hence increased flexural strength is observed for specimens cured at wet (98% RH) conditions at an early age.

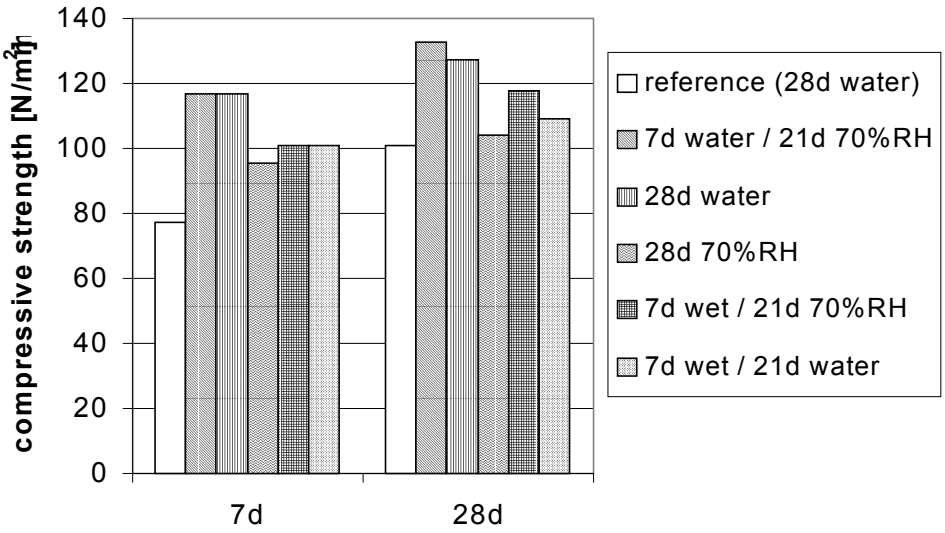

Figure 7. Compressive strength of hardened cement pastes containing 25 vol-% of ultrafine cement

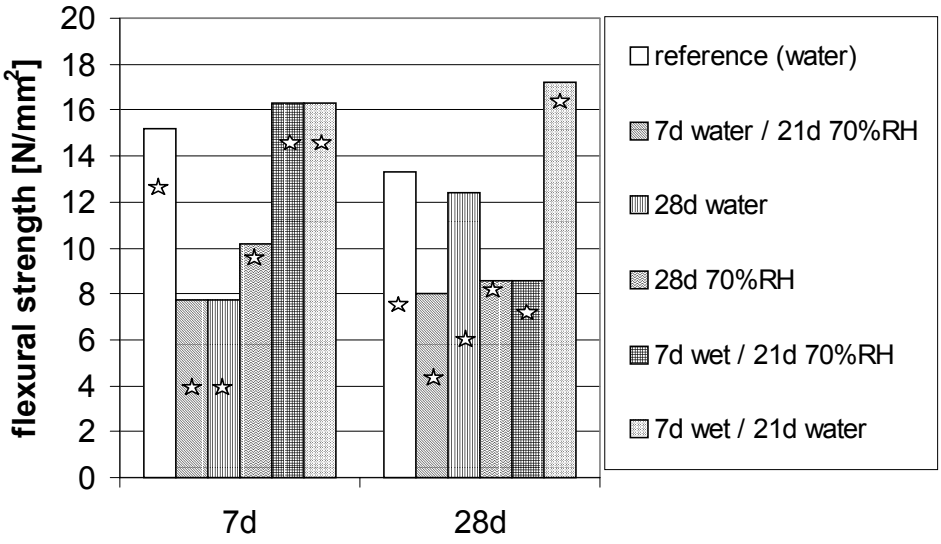

Figure 8. Flexural strength of hardened cement pastes containing 25 vol-% of ultrafine cement (asterisk indicating lowest values)

3.4 Effect of fiber reinforcement

Owing to the great sensitivity to microcrack formation and hence loss of tensile strength, reinforcement with low content (1 vol-%) of different short fibers was studied. The properties of the fibers used are given in table 3. The matrix consisted of Portland cement blended with 25 vol-% of ultrafine cement. Water-binder-ratio was 0.20 and superplasticizer content was 2 weight-%. Curing was under water.

Table 3. Fiber properties

	modulus of elasticity [GPa]	tensile strength [GPa]	density [g/cm^3]	diameter [µm]	length [µm]
carbon	238	3.95	1.77	7	6
polypropylene	8.5	0.34-0.15	0.91	35x250-600	6
metal	not tested	>2	7.5	160	13

The influence of fiber reinforcement on the compressive strength was negligible. While the polypropylene fibers even have a negative effect, the use of metallic or carbon fibers increases the flexural strength significantly (see Figure 9) compared to the reference without fiber reinforcement. The strong influence of the fiber properties, e.g. tensile strength, however indicates that the fiber mostly acts as reinforcement and does not necessarily control crack tendency.

Microscopic analysis revealed that crack formation is not prevented by the introduction of short fibers as is shown in Figure 10 (left). The observed cracks are mostly very long and discrete, e.g. the matrix in the vicinity of the cracks is completely intact and very dense. The crack path follows an array of carbon fibers and goes around unhydrated cement grains. This indicates that the fiber is effective, absorbing part of the fracture energy and that the cement grains are tougher than the hydration products. The good fiber-matrix bond also is demonstrated in Figure 10 (right).

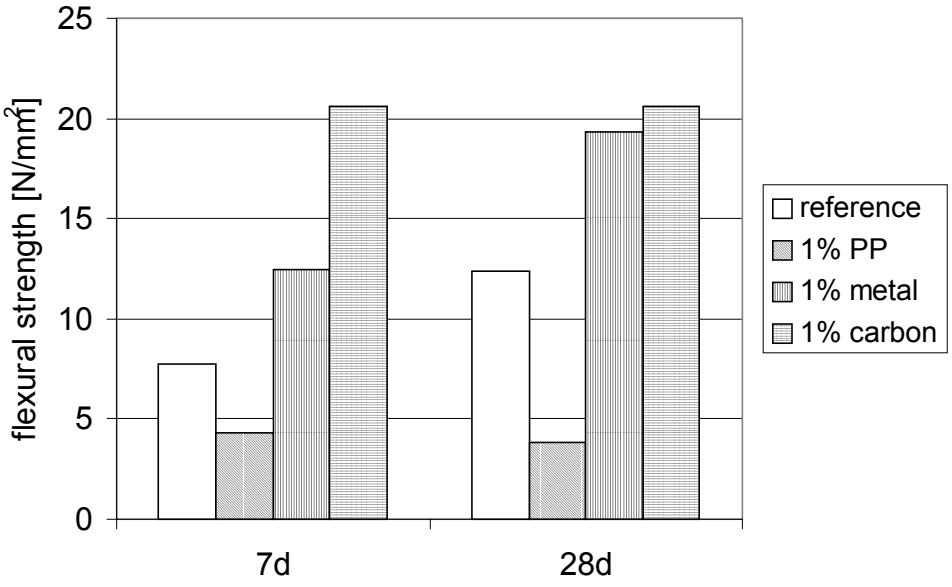

Figure. 9. Flexural strength of fiber reinforced composites containing 25 vol-% of ultrafine cement (curing under water)

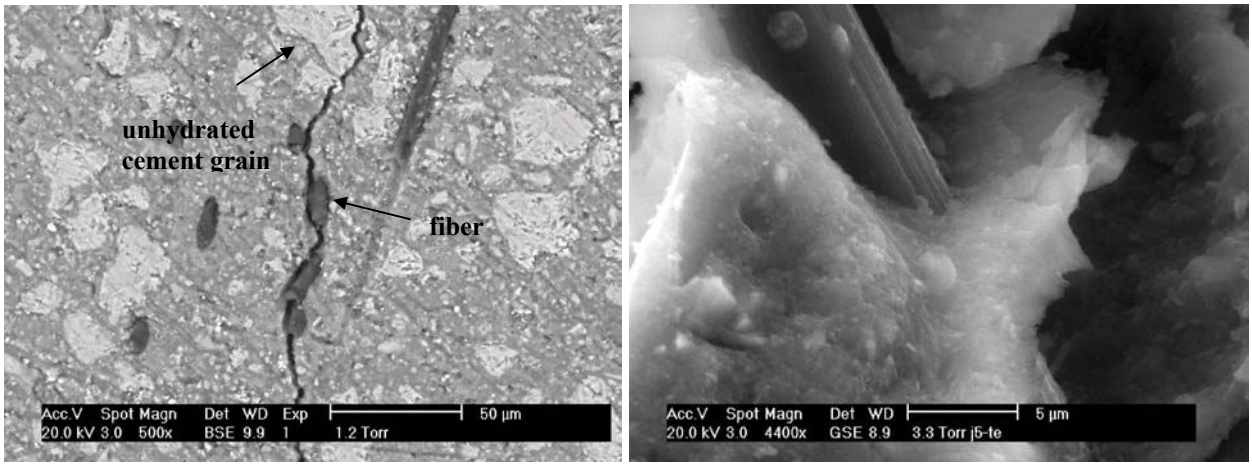

Figure 10. ESEM micrograph of carbon fiber reinforced hardened cement paste containing 25 vol-% of ultrafine cement at an age of 7 days left: crack right: matrix-fiber interface

3.5 Application

The good rheological properties and the very dense packing of cement blended with ultrafine cement may be used for mixing high performance composites with very good mechanical properties. For example, bending properties of hardened cement pastes containing different amounts of metal fiber are shown in Figure 11. Such materials even fulfil the requirements for steel bar replacement in concrete. Additionally, the very dense matrix may improve durability of such composites compared to other mixing concepts. Extension of service life, replacement of cost and energy intensive parts as well as weight considerations may make such materials, despite the higher material costs, a sustainable alternative to actual technology.

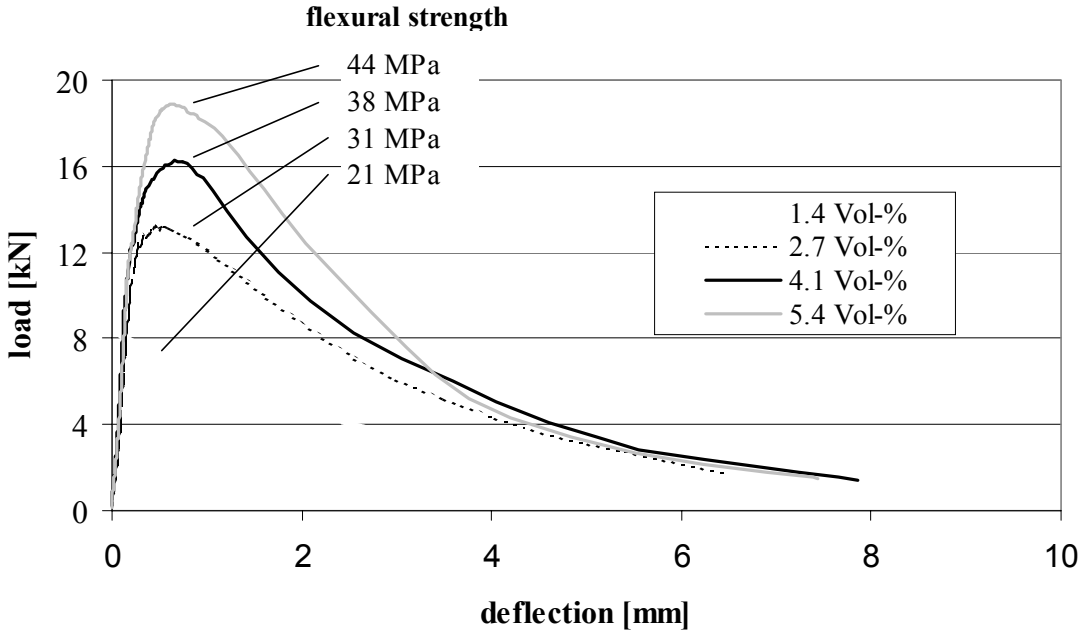

Figure 11. Load-deflection response of metal fiber reinforced composites (40mm x 40mm x 160mm) containing 20 weight-% of ultrafine cement (3 point bending)

4. CONCLUSIONS

The effect of the addition of ultrafine cement on rheology, mechanical properties and length change behavior of hardened cement paste was studied. Rheological properties, viscosity and yield value, can be improved by blending ordinary Portland cement with ultrafine cement. The bimodal grain size distribution also leads to a high packing density. Consequently, in combination with superplasticizers, very dense materials with very low porosity can be produced even with conventional mixing and casting techniques.

The addition of ultrafine cement to normal Portland cement improves the compressive strength, especially early strength, of hardened cement pastes. Flexural strength however strongly depends on curing conditions. This indicates microcrack formation caused by shrinkage at an early age. Flexural strength may be improved by early wet (98% RH.) curing, which is preferable to full immersion in water.

In fiber reinforced composites this dense matrix leads to a good fiber-matrix bond. The fibers however do not necessarily control crack tendency. Strong and stiff fibers may bridge such shrinkage cracks and a good tensile behavior is obtained. High amounts of metallic fibers for instance lead to very high flexural strength and ductile materials.

REFERENCES

[1] Collepardi,S. et al, Durability of high-performance Concretes with pozzolanic and composite Cements, Proc. 5th Int. Conf. on Durability of Concrete, Barcelona, Spain 2000, p. 159ff

[2] Bentur ,A. and Mindess, S., Fibre reinforced cementitious composites, London and New York ,1990.

[3] German, R., Particle Packing Characteristics, Metal powder industries federation, Princeton,1989

[4] Richard P. et Cheyrezy M., Les Bétons de Poudres Réactives, Annales de l'ITBTP 532, p. 85ff. 1995

[5] Bache, H., Densified cement ultrafine based materials, Int. Conference on Superplasticizers in Concrete, Ottawa, 1981, p. 33ff

[6] Feng, N., Influence of ultrafine powder on the fluidity and strength of cement paste, Advances in Cement Research, 12, 2000, pp. 89-95

[7] Goldman, A., Bentur, A., The Influence of Microfillers on Enhancement of Concrete Strength, Cement and Concrete Research, 23, 1993, pp. 962-972

[8] Müller, M., Tyrach, J., Brunn, P. O., Rheological Characterisation of machine-applied plasters, cement-lime-gypsum international, 52, 1999, pp. 252-258

[9] Martschuk,V., Rudert,V., Stark, J., Hochleistungsbindemittel mit Feinstzementen, 14. Internationale Baustofftagung (Ibausil), September 20-23, 2000, Weimar, Germany, Vol. 1, pp. 315-326

Super-Pozz®:
AN ULTRA-FINE POZZOLANIC CLASS F FLY ASH FOR SUPERIOR CONCRETE

E.Y. Seedat and R.A. Kruger

Sphere-Fill (Pty) Ltd, South Africa.

ABSTRACT

"Super-Pozz®" is a unique, ultra-fine, highly reactive Class F fly ash, which can be beneficially applied to variety of cementitious systems. This paper presents the results of an investigation into the characteristics and quality of concrete when Portland cement is replaced by a reactive ultra-fine pozzolan such as Super-Pozz®. In particular its effect on water demand, and the amount of high range water reducer (superplasticiser) is discussed. Data is presented which illustrates strength development and durability characteristics similar to that achieved when silica fume (microsilica) is used as a pozzolan.

The work also highlights the morphological particle size characteristics of the ultra-fine fly ash (UFFA) and illustrates how these can be utilized to produce superior quality concrete. Results obtained confirm that astutely designed mixes exhibit properties similar to formulations containing silica fume. Of major benefit over silica fume is however the reduction in water and/or admixture dosage required for a given workability. The lower water: binder ratio improves durability.

Finally, three examples where UFFA was used in mining applications are discussed.

1. INTRODUCTION

Fly ash of high quality and consistency is an integral part of the civil engineering and construction industries. Its benefits in concrete are well documented and it is widely utilized where quality and durability are of concern.

The air classification of fly ash to extract the more reactive fine fraction is used to improve its performance, increase consistency and thus ensure compliance to the stringent specifications necessary for high quality concrete. In South Africa, classified fly ash with a maximum retention of 12,5% on a 45-micron sieve has been commercially produced for more than 25 years.

Recently beneficiation technology has been developed to produce an ultra-fine fly ash (UFFA), where in excess of 85% of the particles are below 10μm. Such a product is now commercially marketed under the trade name, Super-Pozz®. In this study the technical performance of concrete using this UFFA has been found to be equal to or exceeding that where silica fume is utilized.

2. CHARACTERISTICS AND PROPERTIES

As can be seen in the chemical composition and physical characteristics listed in Tables 1 and 2, Super-Pozz® is extremely fine. The D_{90} value of 11 micron indicates the particle size below which 90% of the particles are to be found. Figure 1, illustrates the comparative particle size distribution

analysis of silica fume as well as the UFFA and conventional SABS (1491 Part 2) fly ash. As can be seen the Super-Pozz has a particle size distribution intermediate to the other two pozzolans.

Table 1.Typical chemical composition

Chemical Analysis	Mass %
SiO_2	53.5
Al_2O_3	34.3
CaO	4.4
Fe_2O_3	3.6
K_2O	0.8
MgO	1.0
TiO_2	1.7
LOI @ 950°C	< 1

Table 2. Typical physical characteristics

Physical Analysis	Mass %
Relative Density	2.20
Surface Area (cm^2/g)	13000
Colour	Light grey
Particle Shape	Spherical
Particle Size, D_{90}	11 μm
D_{99}	25 μm
Mean Particle Size	4.0 μm

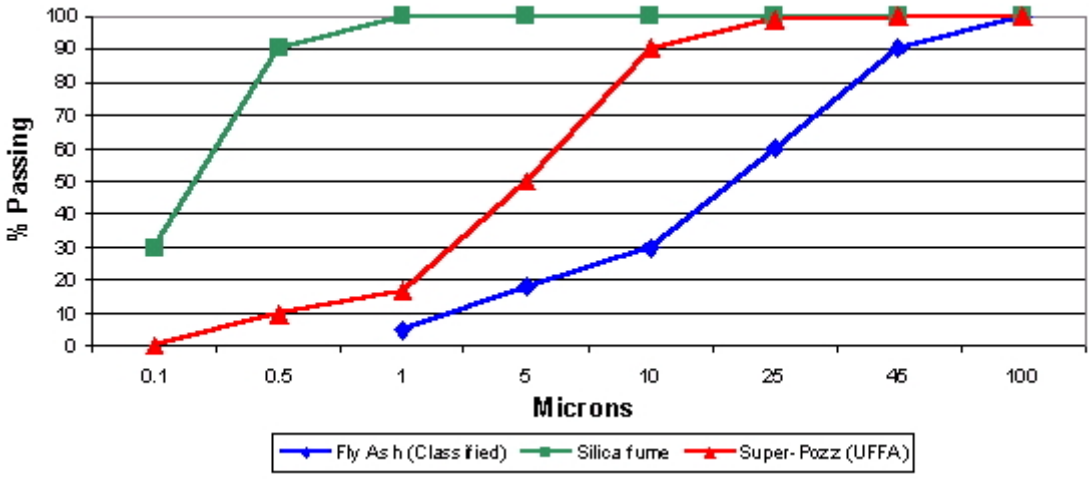

Figure 1. Particle Size Distribution

3. CONCRETE QUALITY AND MIX DESIGN

The quality and impermeability of high-performance concrete are, inter alia, determined by the amount of water utilized in the mix design i.e. the water/binder ratio. High range water reducers (HRWR) are extensively used to ensure effective consolidation during placement with low water contents. Ultra-fine pozzolanic materials such as silica fume are often utilized in high performance

concrete where the presence of the extremely fine particles decreases the permeability and improves durability.

In order to measure the effect of the UFFA on the workability, water requirement and HRWR dosage, three series of concrete mixes were prepared, based on the following mix design methodology:

A. Workability: Keeping the w/b ratio (binder=cement + pozzolan) and HRWR content constant and measuring the variation of the slump
B. Water Demand: Keeping HRWR dosage the same and varying the amount of water required to achieve the same slump
C. Admixture Requirement: Keeping the w/b ratio the same and varying the amount of HRWR required to maintain similar slump measurements.

In all 3 series, the UFFA was used at replacement levels of 5%, 10%, 15% and 20% of the total binder content. For silica fume mixes, replacement levels of 5% and 10% were used. The total binder content was kept constant at 400kg/m^3. Crushed dolerite with a specific gravity of 2.92 served as the coarse aggregate. The sand content was a blend of dolerite crusher sand and filler sand with a specific gravity of 2.82. Prior to their use, the materials were completely dried. The cement used was CEM I 42.5. The HRWR was a naphthalene-based admixture.

On all mixes, compressive strengths were measured at 1, 3, 7, 28, 56 and 90 days. Water permeability and absorption as well as chloride permeability were used to evaluate durability. Workability was measured in terms of slump. The target slump was 125mm.

4. EXPERIMENTAL PROGRAMME

With the exception of HRWR and water, the mass of the mix constituents remained the same in all 3 series (Table 3). Using this as a starting point, the design for a specific series A, B, C was then characterized by a particular water and HRWR content. Mix 1, using plain PC (CEM I 42.5) as the binder served as the control mix.

Table 3. Mix formulations of dry constituents used to prepare specimens in all series

Mass of Constituents							
Reference	**1**	**2**	**3**	**4**	**5**	**6**	**7**
Extender	Nil	5% CSF	10% CSF	5% UFFA	10% UFFA	15% UFFA	20% UFFA
CEM I 42.5	400	380	360	380	360	340	320
Silica Fume	-	20	40	-	-	-	-
Super-Pozz (UFFA)	-	-	-	20	40	60	80
Crusher Sand	600	600	600	600	600	600	600
Filler Sand	195	175	155	175	155	155	155
Coarse Aggregate	1080	1100	1120	1100	1120	1120	1120

*CEM I 42.5 – Ordinary Portland Cement *CSF – Silica Fume *UFFA – Ultra-fine Fly Ash

5. SERIES A: EVALUATION OF WORKABILITY

Table 4 and Figure 2 shows that the replacement of a portion of cement with UFFA, improves the workability of the concrete substantially. If all constituents of the mix proportion are kept constant i.e. w/b ratio and admixture content, the introduction of UFFA provides a major increase in workability. For series A, 5.2 ltrs/m^3 of HRWR and 152 ltrs/m^3 of water (w/b 0.38) were used

throughout. As can be seen from the data in Table 4 the slump increased with the amount of UFFA used. The increase in workability can be ascribed to the morphology of the UFFA. In particular the sphericity of the particles enables them to “roll” in the concrete mix. This ball-bearing or lubricating effect aids flow and increases the slump. Furthermore the specific particle size distribution and efficient dispersion of Super-Pozz allows for effective packing in the interces and thus facilitates consolidation.

Table 4. Workability data for concrete specimens of equal w/b ratio and containing the same amount of HRWR

EVALUATION OF WORKABILITY							
Reference	A1	A2	A3	A4	A5	A6	A7
Extender	Nil	5% CSF	10% CSF	5% UFFA	10% UFFA	15% UFFA	20% UFFA
Water content (liters)	152	152	152	152	152	152	152
HRWR (liters)	5.2	5.2	5.2	5.2	5.2	5.2	5.2
Slump (mm)	**50**	**55**	**50**	**80**	**130**	**170**	**190**

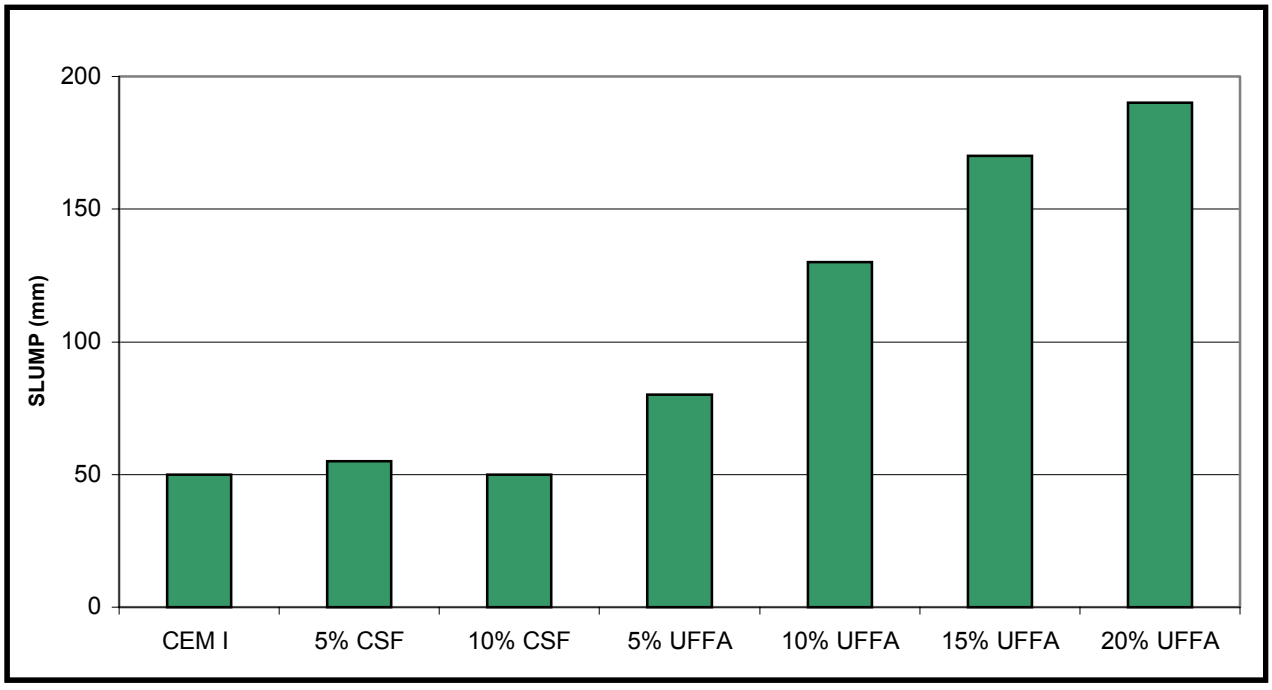

Figure 2. Evaluation of Workability: Slump recorded for constant water content of 152 l/m_3 and 5,2l/m_3 of HRNR

The rates of strength development of these concrete mixes (Series A) are given in Table 5. It will be noted that while the specimens containing silica fume initially developed strength more rapidly, at 90 days the compressive strength of the specimens containing the UFFA was the same. This indicates that the UFFA exhibits latent pozzolanicity.

Table 5. The effect of the addition of UFFA on the rate of development of compressive strength for concrete specimens of equal w/b ratio and containing the same amount of HRWR.

COMPRESSIVE STRENGTH (MPa)							
Reference	**A1**	**A2**	**A3**	**A4**	**A5**	**A6**	**A7**
Extender	Nil	5% CSF	10% CSF	5% UFFA	10% UFFA	15% UFFA	20% UFFA
1 day	18.5	19.5	19.5	16.0	15.0	14.0	13.5
3 day	38.5	38.5	38.5	35.0	31.5	30.0	28.0
7 day	55.5	53.0	57.0	52.5	46.5	46.5	44.5
28 day	72.5	81.0	88.0	69.5	73.0	73.0	71.5
56 day	81.0	88.0	94.0	79.0	81.0	87.5	79.5
90 day	82.0	88.5	98.5	91.5	91.0	92.0	97.5

6. SERIES B. EVALUATION OF WATER DEMAND

One of the main features expected of the UFFA is, by virtue of its sphericity and ideal particle size distribution, is to reduce the amount of water required to achieve a specific slump value. In this series, the binder content, HRWR content and work ability were kept constant and the effect of water requirement measured. The HRWR was dosed at 5.2ltrs/m^3 (1.3% wt of binder).

Table 6. The effect of UFFA on the water required to maintain a constant slump

EVALUATION ON WATER REQUIREMENT							
Reference	**B1**	**B2**	**B3**	**B4**	**B5**	**B6**	**B7**
Extender	Nil	5% CSF	10% CSF	5% UFFA	10% UFFA	15% UFFA	20% UFFA
Water (liters)	**163**	**169**	**171**	**153**	**141**	**137**	**134**
HRWR (liters)	5.2	5.2	5.2	5.2	5.2	5.2	5.2
W/b ratio	0.41	0.42	0.43	0.38	0.35	0.34	0.33
Slump (mm)	130	130	125	140	125	130	140

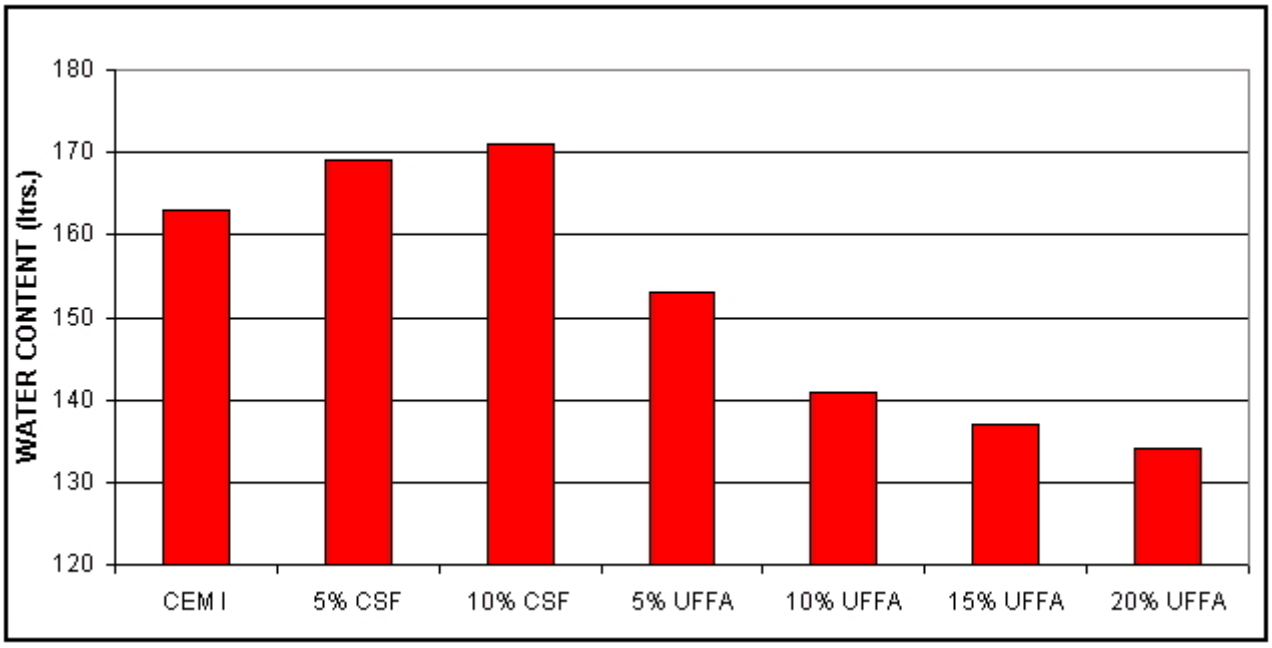

Figure 3. Evaluation of Water Requirement: Water content/m_3 of fluxes with constant slump and HRWR dosage

The results from Table 6 and Figure 3 shows that the formulations containing silica fume required more water than their UFFA counterparts to achieve a slump of about 125mm. The water demand of concrete decreased along with the amount of cement replaced by UFFA.

Table 7. The compressive strength for concrete specimens of equal HRWR and slump

COMPRESSIVE STRENGTH (MPa)							
Reference	**B1**	**B2**	**B3**	**B4**	**B5**	**B6**	**B7**
Extender	Nil	5% CSF	10% CSF	5% UFFA	10% UFFA	15% UFFA	20% UFFA
1 day	15.5	15.5	13.5	15.0	20.5	17.0	15.0
3 day	35.0	32.5	30.0	35.0	40.0	36.5	35.0
7 day	52.0	48.5	47.0	50.58	58.5	56.5	52.5
28 day	70.5	77.5	78.5	69.5	82.0	85.0	81.0
56 day	80.0	80.5	84.0	84.0	91.5	91.5	97.0
90 day	81.0	81.0	79.0	86.0	93.5	102.5	93.5

At constant binder content, the compressive strength of concrete increased along with a reduction in the w/b ratio. The incorporation of UFFA in concrete facilitates a lower w/b ratio and as a result, improved compressive strength is achieved at all ages. After 56 days the compressive strength achieved by the mixes containing UFFA exceeded that of the mixes containing silica fume.

As a result of the ongoing pozzolanic reaction the concrete specimens containing the UFFA showed a far higher rate of gain in strength between 28 and 90 days than their silica fume counterparts.

7. SERIES C: EVALUATION OF HRWR REQUIREMENT

For concrete where compressive strength is easily achievable, lower admixture content can be used to attain the desired workability. Due to the particle shape and size of the UFFA, workable concrete can be made using less admixture content.

For the C series, both workability and water content (152 liters/m^3) were kept constant and the amount of HRWR required for a slump of about 125mm was measured.

Table 8. Evaluation of the amount of HRWR required to maintain similar slumps in concrete containing UFFA and silica fume

EVALUATION OF HRWR REQUIREMENT							
Reference	C1	C2	C3	C4	C5	C6	C7
Extender	Nil	5% CSF	10% CSF	5% UFFA	10% UFFA	15% UFFA	20% UFFA
W/b ratio	0.38	0.38	0.38	0.38	0.38	0.38	0.38
HRWR (liters)	**5.3**	**6.3**	**6.8**	**5.1**	**3.7**	**2.9**	**2.5**
Slump (mm)	150	140	130	135	130	125	125

From the results in Table 8 and Figure 4, it can be seen that in order to maintain the same workability, concrete containing 10% UFFA reducers the HRWR requirement whilst silica fume increases it. Generally, when silica fume is used in concrete, its performance is enhanced by the variable HRWR addition used to control water demand. With UFFA, the situation is changed. UFFA provides a lower HRWR dosage or alternatively a normal water-reducing admixture (plasticiser) can be used instead as a minimum to achieve the desired workability.

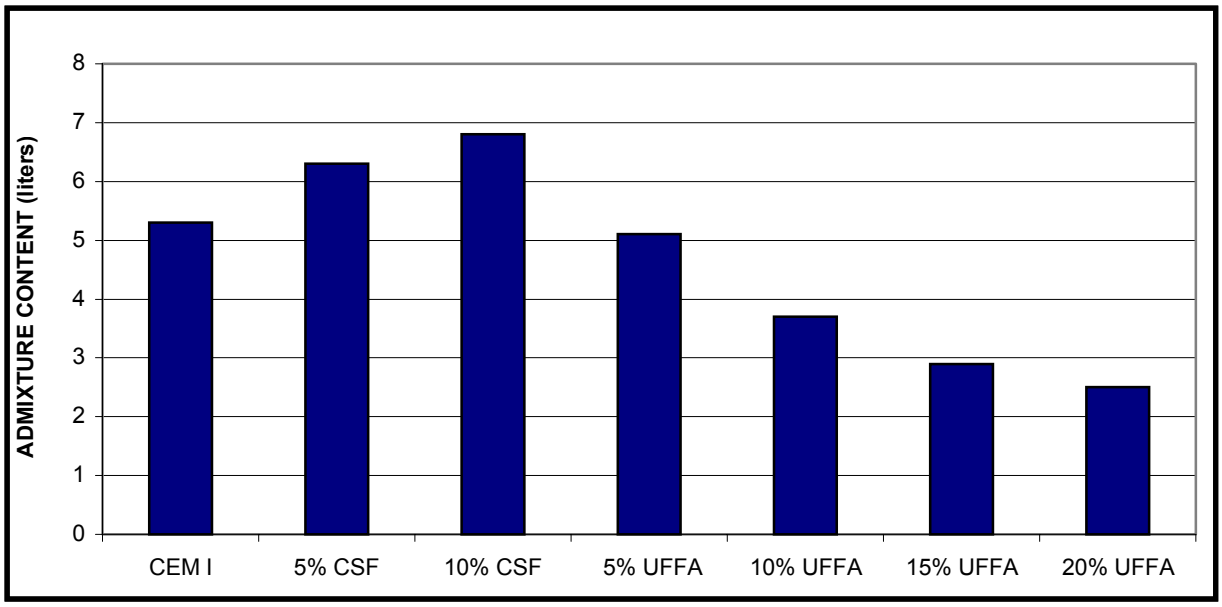

Figure 4. Evaluation of Admixture Requirement Variation in admixture content for constant slump of W/b ratio

At all ages, mixes containing comparable amounts of UFFA and silica fume exhibited similar rates of strength development (Table 9). At higher replacement levels the pozzolanic behavior of the UFFA is responsible for significant rates of gain in strength at later ages.

Table 9. The compressive strengths for concrete specimens of equal slump and w/b ratio

COMPRESSIVE STRENGTH (MPa)							
Reference	**C1**	**C2**	**C3**	**C4**	**C5**	**C6**	**C7**
Extender	Nil	5% CSF	10% CSF	5% UFFA	10% UFFA	15% UFFA	20% UFFA
1 day	17.0	25.0	22.5	24.0	20.0	21.5	16.5
3 day	44.5	55.0	49.5	53.0	46.0	43.0	37.5
7 day	60.0	70.5	69.0	75.0	65.0	59.0	57.5
28 day	83.5	92.0	97.0	92.0	80.0	87.5	82.5
56 day	91.5	101.0	99.5	99.0	99.5	99.5	95.0
90 day	93.0	89.0	105.0	103.5	100.0	106.0	103.0

8. DISCUSSION OF MIX DESIGN CRITERIA AND THEIR TEST RESULTS

The foregoing vividly illustrates the importance of understanding the factors that influence the rate of strength development in concrete mixes containing UFFA. In order to maximise the benefits of fineness, sphericity and pozzolanic activity of UFFA, particular attention must be given to mix design criteria.

In the first instance, using the same amount of water and superplasticiser in concrete mixes containing the UFFA, as used in comparable concrete with silica fume, results in large increase in slump. This is mainly due to the sphericity of the UFFA, which facilitates flow. As can be expected, the concrete with higher slumps exhibited a slower initial rate of strength development. At later ages (90 days) the compressive strength of concretes with UFFA was similar to those containing silica fume.

If, however the amount of water or superplasticiser used in the mix is adjusted and the concretes are designed to have similar slumps, the picture changes entirely. Not only are the rates of strength development comparable but also due to its latent pozzolanic activity, the compressive strength of the mixes containing UFFA exceeds those with silica fume.

The long-term pozzolanic activity of the UFFA can be seen as a function of its particle size distribution. Silica fume is much finer than the UFFA. As a result of the higher surface area the pozzolanic reaction proceeds rapidly and strength is quickly developed. The downside of this is that as the surface of the silica fume becomes covered with the reaction products the $Ca(OH)_2$ can no longer reach and the pozzolanic reaction slows down. UFFA on the other hand has a wider range of particles sizes. As the finer particles are covered and thus prevented from participation in further reaction, the larger particles still remain available. The pozzolanic reaction can thus still proceed at later ages.

The above is certainly not the definitive explanation since the glass content of the pozzolan as well as the composition and concentration of both alkaline and alkali hydroxides influence the rate and extent of the pozzolanic reaction. Nevertheless the higher rate of strength development exhibited at later ages by the UFFA must necessarily take the difference of particle size distribution into account.

9. DURABILTY

While strength development is an important criterion for concrete performance, it fails to give an insight into durability. Durability was assessed by means of a series of tests designed to measure the density and impermeability of the binder paste microstructure. Water permeability and absorption as well as chloride permeability were measured. Probably the most important consideration when using UFFA, is its ability to improve the durability of concrete by decreasing the water demand without adversely affecting the workability. Thus, samples for the durability tests were prepared using series “A” specimen’s i.e. constant slump and HRWR, taking into effect the water reducing properties of the UFFA.

9.1 Water permeability

The DIN 1048 test method was used to measure the impermeability of concrete. In this test, slabs initially water-cured for 28 days, are then exposed to a water pressure of 5 bars for 72 hours after which the slab is split and the depth of water penetration measured. Penetration of less than 25mm is generally considered to be impermeable concrete

Table 10. Water permeability (DIN 1048)

WATER PERMEABILITY (mm)					
CEM I 42.5	**5% CSF**	**10% CSF**	**5% UFFA**	**10% UFFA**	**15% UFFA**
19	8	14	12	6	18

As can be seen, the results achieved generally fell within the range of 5 to 20mm with the 10% UFFA mix showing the best resistance to water penetration.

9.2 Water Absorption

In this test the cubes are initially water cured for 28 days, following which cores are drilled out and oven dried for 72 hours before once again being immersed in water. The increase in mass resulting from the immersion is expressed as a percentage of the dry specimen. Higher water absorption figures are indicative of permeable concrete.

As can be seen from the results obtained in Table 11, concrete specimens containing the UFFA have the lowest absorption values. This is indicative of a denser microstructure. The decrease in values from 28 to 56 days reflects an increase in density as the result of the refinement of the pore structure.

Table 11. Water Absorption (BS 1881: Part 118)

WATER ABSORPTION (%)						
	CEM I 42.5	**5% CSF**	**10% CSF**	**5% UFFA**	**10% UFFA**	**15% UFFA**
28 day	1.70	1.61	1.56	1.53	1.41	1.38
56 day	1.67	1.58	1.45	1.47	1.32	1.25

9.3 Chloride Permeability

The Rapid Chloride Permeability Test (ASTM 1202) measures the total charge (coulombs) flowing though a 2 inch thick concrete specimen during 6 hours of applied potential of 60V. The test is conducted on cores, cured in water for 28 days or longer. The one end of the specimen is immersed in NaCl solution, the other in NaOH. The total charge passing through is regarded as a measure of the resistance of concrete to the diffusion of chloride ions. The higher the charge the easier the ions migrate and the poorer the concrete.

Table 12. Chloride permeability (ASTM C1202)

CHLORIDE PERMEABILITY (Coulombs)						
	CEM I 42.5	**5% CSF**	**10% CSF**	**5% UFFA**	**10% UFFA**	**15% UFFA**
28 day	2206	1329	598	2008	1769	1681
56 day	1798	772	279	1699	972	816

The results obtained (Table 12), substantiates the fact that cement extenders decreases the permeability of concrete. This is mainly attributed to the conversion of $Ca(OH)_2$ to calcium silicate hydrates. Although it would appear that silica fume mixes are more resistant to chloride diffusion, the mixes containing UFFA continue to develop strength at later ages. This on-going refinement of the pore structure will be accompanied by a concomitant reduction in chloride diffusion.

10. CURRENT APPLICATIONS

During the last year extensive trials have been conducted both locally and internationally to demonstrate the benefits of UFFA in high performance concrete. The following are some typical examples.

10.1 Ore-Pass Lining

Ore passes are key elements in underground mining. They are subject to harsh environmental conditions and are designed to the highest standards to limit the effect of impact and abrasion, blasting shock, geological stress and aggressive waters. With high durability and low maintenance being crucial much attention is paid in optimizing the concrete mix design. It is widely accepted that calcium aluminate cement based concrete will outperform other equivalent cementitious base concretes in terms of abrasion resistance. However, the use of Portland cement based mixes provided a viable alternative in terms of material cost and performance. In a study carried out at a south african gold mine it was shown that the use of Portland cement with UFFA and silica fume has a great potential in achieving very high strengths, particularly over longer periods. The total addition of these pozzolans was 15% of the total binder content with the ratio of UFFA/silica fume at 1:1. The primary benefits found, with the use of UFFA was a mix of lower water demand and improved workability. Additionally, the UFFA preserved the integrity of the paste matrix both with regard to prevention of cracking and the resistance to aggressive attack.

10.2 HPC for Underground Roads

High performance concrete is essential for underground roads in order to withstand the abrasion and impact loading caused by the grinding action of the LHD (front end loader) wheels and buckets. In two very large underground operations, UFFA was used to compliment the mix to meet the design requirements. Based on the success with the ore-pass lining referred to above, a concrete using 15% Super-Pozz as the only cement extender was designed. Compressive strength in excess of 80 MPa was achieved with a concrete that had high initial flow and maintained its placeability for an extended period. Abrasion resistance and impact criteria were achieved.

10.3 Use in HPC as Steel fibre reinforced shotcrete (SFRS)

The application of SFRS is a well-known concept and method of support within the tunneling industry. With the growing use of sprayed concrete as a permanent construction material, demands on its durability characteristics have increased proportionately. In a very deep shaft, located in dynamic rock conditions, SFRS was specified as a permanent rock support system. The design parameters assessed included early and long-term compressive strength, in-situ strength, energy absorption capabilities and yield. Additionally the placed shotcrete was required to be sufficiently impermeable to ensure long-term durability. The design compressive strength target was a minimum 60 MPa. Using the EFNARC (European Federation for Sprayed Concrete) specifications, the energy absorption criteria, was set at 1000 J (Joules) for a 28-day plate test. Sporadic incidences of strain bursting of the shaft sidewalls required an early age strength of 5 MPa after 48 hours and the ability to absorb 400 J of energy after 4 – 8 hours.

Following the trial mix process, the mix finally adopted was a complex blend of very high quality materials. UFFA was added to the mix to reduce water demand, assist pumpability, increase resistance to chemical attack and provide long-term strength gain. By incorporating UFFA, the cohesion and adhesion properties were also enhanced. The SFRS was successfully applied for this project; a total of 7500m^3 being placed within the shaft barrels.

11. SUMMARY AND CONCLUSIONS

Results obtained show that UFFA such as Super-Pozz can be used as a viable substitute for silica fume. If the advantages of the UFFA are exploited in the concrete mix design, the initial rate of strength development was found to be the same or similar to those of silica fume mixes. At later ages, however, the pozzolanic activity of the UFFA leads to higher compressive strength values.

Durability test measuring the water permeability and absorption as well as chloride permeability showed comparable values for both silica fume and the UFFA mixes.

The use of UFFA, as an alternative to silica fume can be effective in enhancing the properties of concrete, both in its fresh and hardened state. Due to the lower water demand required, UFFA can be ideally used to:

- Lower the water/binder ratio
- Lower the amount of HRWR required; or
- A combination of the above

Super-Pozz is not only a new-generation cement extender offering exciting opportunities to the design high performance concrete. With its unique properties, there are other additional applications that will certainly benefit the use of Super-Pozz. Some that spring to mind are:

- Specialist Grouts
- Ready mix concrete
- Precast Concrete
- Self-leveling flooring

- Self Compacting Concrete (SCC)
- Cement modified Pre-mix bagged materials

Future developments could possibly see the co-utilization of UFFA and silica fume, as this will provide civil engineers with the opportunity to simultaneously exploit the best properties of both products.

REFERENCES

[1] Processed Fly Ash for High Performance Concrete. H.A.W. Cornelissen, R.E. Hellewaard, J.L.J. Vissers, 5th CANMET/ ACI Conference, Wisconsin, USA, 1995, Vol. 1, Pg. 67 – 81

[2] Superfine Fly Ash in High Strength Concrete.W.B. Butler, Concrete 2000, 7 – 9 September1993, Vol. 2, Pg. 1825 – 1831

[3] Specifications for Silica Fume to Produce Durable Concrete. King Fahad University of Petroleum & Minerals, Saudi Arabia, 2000

[4] BS 1881: Part 122. Method for determination of Water Absorption

[5] A Framework for Durable Concrete. G.R. Summers, Gulf Construction, September 2001

BLAST FURNACE SLAG WEATHERING STUDY

Battagin, Arnaldo Forti[1] and Pecchio, Marcelo[2]

Brazilian Portland Cement Association, São Paulo, Brazil.
[1]E-mail: arnaldo.battagin@abcp.org.br and [2]marcelo.pecchio@abcp.org.br

ABSTRACT

Blast-furnace slag as an addition to Portland cement is extensively used in Brazil. In spite of the high addition content (up to 70 mass %), the cement industry cannot absorb the total slag production, leading to storage of millions of tons in open air. Slag is thus exposed to weathering for years.

This paper presents the study carried out on three long-stored slag samples compared to two new ones, aimed at checking their degree of aging and its influence on their reactivity, and consequently on the mechanical performance of the corresponding blended cement.

Old slag samples showed lower hydration heat liberation and significant - in some cases reaching 30% to 40% - loss in performance, followed by changes in setting times.

1. INTRODUCTION

About 7.3 million tons of blast furnace slag was produced in Brazil in 2000 [1] and around 6 million tons was converted into granulated blast furnace slag (GBFS).

Granulation is obtained by quenching the molten slag into glass using high pressure water jets. The rapid cooling prevents crystallization producing a granular glassy material that, after grinding, has good hydraulic properties making it a Portland clinker substitute or extender.

GBFS in slag cement or blended Portland slag cement has been extensively used in Brazil for more than 50 years [2] but the cement industry cannot absorb the whole slag production. Although consumption in 2000 was about 4.9 million tons there was an excess 1.1 million tons that was not used. Due to this, around 12 million tons of GBFS are stockpiled mainly in cement plants.

Many publications have dealt with the use of fresh-made GBFS as a cementitious material but less work has been done about the use of weathered slag. In fact, there is only one known contribution of Hiroshima and Igarashi [3] that studied the effect of weathering of GBFS and concluded that there was a loss of 28-day compressive strength and an increase in setting times of cements containing “old” slag. On the other hand, Brazilian cement manufacturers have reported an improvement in slag grindability.

It is generally agreed that slag reactivity is due to both inherent characteristics and external factors. Inherent characteristics are related to operational conditions of blast furnace, temperature and viscosity of molten slag, granulation process and installation, etc.

Proceedings of the 11th International Congress on the Chemistry of Cement (ICCC)
‘Cement’s Contribution to the Development in the 21st Century’
Hosted by: The Cement and Concrete Institute of South Africa
CD-ROM produced by: Document Transformation Technologies
11 - 16 May 2003, Durban, South Africa
ISBN Number: 0-9584085-8-0
Editors: Dr G. Grieve and G. Owens
Congress Organised by: Event Dynamics

External factors are characteristics that are imposed to slag by means of handling, storage and grinding. For practical purposes and quality control, we can summarize as inherent slag characteristics their chemical composition and their glass content. External factors determining slag reactivity are mainly slag fineness, alkali concentrations of the reacting system, temperature during early phases of the hydration process, and degree of weathering.

This paper reports results from a laboratory study on the weathering effects on slag reactivity using chemical analysis, microscopy examination, conduction calorimeter, accelerated compressive strength tests by NaOH activation and cement compressive strength tests with partial slag replacement.

2. EXPERIMENTAL DETAILS AND RESULTS

2.1 Chemical Composition and Glass Content

Five slag samples were selected: UV1, UV2 and UN produced by USIMINAS, a Brazilian steel plant located in Minas Gerais State, VRV and VRN produced by Companhia Siderurgica Nacional (CSN) located in Volta Redonda, Rio de Janeiro. UV1, UV2 and VRV were stockpiled in un-ground form for more than 10 years and UN and VRN have just been produced. Chemical compositions are given in Table 1.

Table 1. Chemical composition

Oxide	% in mass				
	UV1	UV2	UN	VRV	VRN
CaO	42.54	42.28	41.91	42.50	42.47
SiO_2	34.68	35.10	35.10	35.65	34.31
Al_2O_3	12.23	12.08	12.54	11.32	11.42
Fe_2O_3	0.96	0.84	0.53	1.14	3.26
SO_3	2.40	2.44	2.65	2.45	2.58
MgO	6.18	6.38	6.39	6.09	5.08
K_2O	0.37	0.40	0.39	0.52	0.28
Na_2O	0.11	0.10	0.11	0.113	0.12
TiO_2	0.52	0.40	0.37	0.19	0.46
Total	99.99	100.02	99.99	99.973	99.98
IB1(*)	1.76	1.73	1.73	1.68	1.72
IB2(**)	1.23	1.20	1.19	1.19	1.24

(*)IB1 – $I = \frac{CaO + MgO + Al_2O_3}{SiO_2} > 1$ (**)IB2 - i = CaO/SiO_2

Results show that slags are basic and comply with the requirements of Brazilian Standards. There are no significant differences among slag chemical compositions. Although expressed as SO_3, sulphur is mostly present as sulphide, especially for UN and VRN slag samples. Sulphide oxidation is supposedly more expressive in old slags (UV1, UV2 and VRV).

The glass content was determined by means of optical polarizing microscope according to the method proposed by McMaster [4]. Results are given in Table 2.

Table 2. Slag glass content

Slag	%
UV1	95.2
UV2	93.6
UN	97.9
VRV	92.9
VRN	86.9

The slag melt has a high content of thermal energy. If this energy is fully dissipated by slow cooling a stable crystalline and non-hydraulic slag is formed. On the other hand, if quick cooling is used, a glassy slag with latent hydraulic properties is obtained. It is generally agreed that slag should have a high glass content to develop cementitious properties. As shown in Table 2, samples present a high glass content, most of them higher than 90%. Only VRN exhibited a glass content below 90% but it seems that small amounts of crystalline material in vitreous slag will not have very detrimental effects. Demoulian and collaborators [5] have even reported that crystal nuclei have an advantageous effect.

2.2 Loss on Ignition (LOI), Insoluble Residue (IR) and Scanning Electron Microscopy

In order to evaluate the effect of storage conditions on slag LOI and IR were determined in all samples. LOI value could detect a certain stage of hydration/carbonation because it is known that slags are formed after solidification of high temperature molten material and do not present any LOI. However, vitreous slags are soluble in HCl solution and any IR value detected could be related to contaminations of slag during storage. Table 3 presents the results of LOI and IR.

Table 3. LOI and IR values

Sample	Insoluble Residue (%)	Loss of Ignition (%)
UV1	0.70	2.30
UV2	0.25	0.90
UN	0.25	-0.50
VRV	0.49	2.50
VRN	0.25	-1.70

(Obs.) Negative sign indicates a gain of mass due to an oxidation process

Table 3 shows that “old” slags presented higher values of LOI and IR compared to new ones. Figures 1 and 2, obtained by sample observation under scanning electron microscope show that weathered slag exhibits grains with a coating surface of hydration/carbonation and probably sulphate products. It is believed that the hydrated layer is thin but tends to increase the longer the time of storage in an open-air environment.

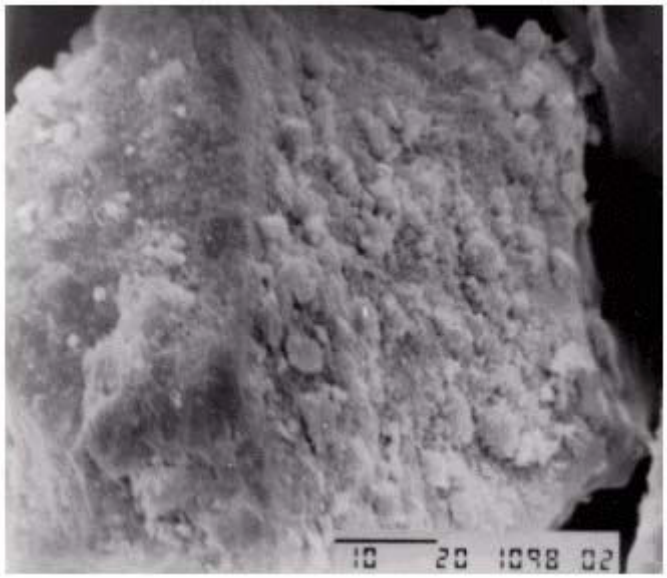

Figure 1. Slag grains with coating surface of hydration/carbonation and probably sulphate products

Figure 2. Slag grains with coating surface of hydration/carbonation and probably sulphate products

2.3 Hydraulic Activity of Slag by Reaction with Alkali: Compressive Strength Tests and Heat of Hydration

Accelerated strength tests using sodium hydroxide solution as mixing water were employed. Slags were ground to a fineness of (4000 ± 150)cm^2/g. Cylindrical test specimens of 50x100mm, in proportion 1:3 (slag: sand), water cured at 23ºC, s/alk sol.=0.5, according to an adaptation of Brazilian Standard NBR 7215 [6] were carried out. Alkali solution (20%) was prepared by dissolving 200g of sodium hydroxide in 1 liter of distilled water and cooled to room temperature. Average strength results at 48h are given in Table 4.

Table 4. Slag hydraulic activity with NaOH

Samples	Density ($g.cm^{-3}$)	Blaine surface area ($cm^2.g^{-1}$)	Hydraulic activity with NaOH (MPa)
UV1	2.79	3950	7.4
UV2	2.84	4120	12.2
UN	2.91	3980	15.0
VRV	2.80	4040	8.6
VRN	2.94	4030	12.8

A conduction calorimeter was used to measure the evolution of heat of hydration. Slag pastes with slag/alkaline solution equal to 0.4 and curing temperature 23ºC were adopted. Results of total heat liberation up to 72 hours are shown in Figure 3.

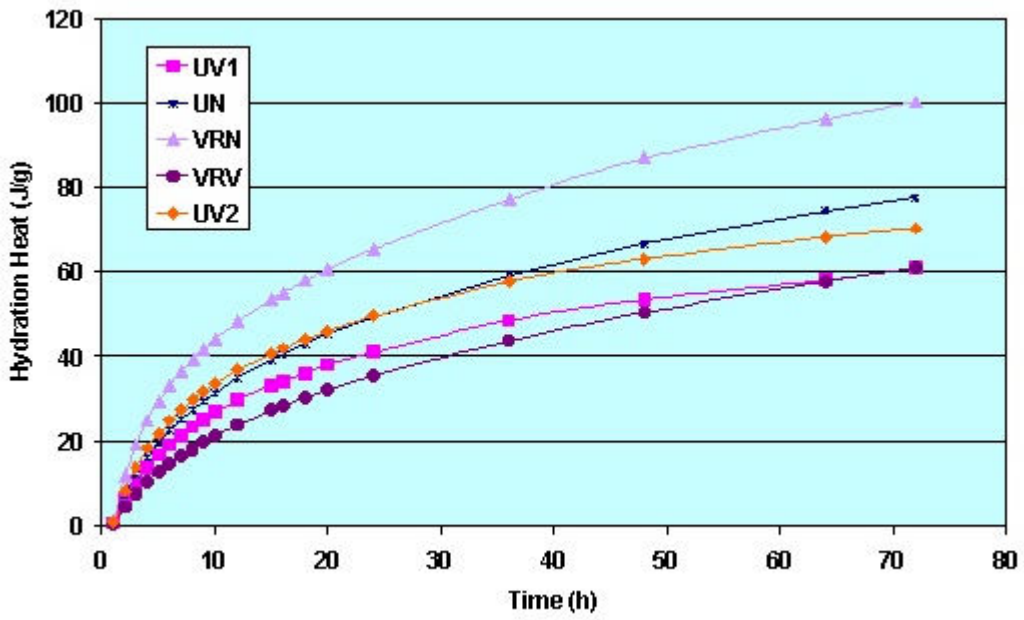

Figure 3. Total heat of hydration liberation

From Figure 3 we conclude that the total heat liberated by "new" slag from a single source is higher than that of the corresponding weathered slag. Accordingly, the same conclusion can be deduced from results of hydraulic activity with NaOH shown in Table 4. Weathered slags both from USIMINAS (UV1 and UV2) and Companhia Siderurgica Nacional (VRV) presented lower values of hydraulic activity with NaOH compared to the new slags from the same origin.

Brazilian former studies [7] have shown that typical compressive strengths for good quality slags are expected in range of 9 to 11MPa. We can deduce that "new" slags comply with these values while weathered slags presented values below of these limits. It should be noted, however, that slag UV2 presented a good behavior perhaps due to its higher fineness.

2.4 Cement Compressive Strength Test and Setting Time

In order to evaluate the mechanical performance behavior, each slag sample after being ground to a fineness (4000±150)cm^2/g was mixed with an industrial ordinary Portland cement with Blaine fineness 4400cm^2/g.

The proportions of mixes were 0, 20%, 30%, 40%, 50% and 60% of slag replacement. Test specimens were prepared and tested for 7 and 28 day compressive strength in accordance with NBR 7215. Results obtained are given in Table 5 and Figures 4 and 5.

Table 5. Compressive Strength (MPa)

Slag content (%)	UV1		UV2		UN		VRV		VRN		Reference	
	7 days	28 days	7 days	28 days	7 days	28 days	7 days	28 days	7 days	28 days	7 days	28 days
0	-	-	-	-	-	-	-	-	-	-	40.3	47.1
20	34.9	44.6	38.2	46.2	40.8	51.0	37.4	44.6	41.1	50.7	-	-
30	33.4	43.1	35.8	46.4	40.5	53.4	36.0	44.9	38.3	50.1	-	-
40	29.6	40.8	33.9	44.9	41.3	54.3	37.0	42.3	37.2	52.3	-	-
50	25.3	37.2	29.9	42.1	35.8	51.9	29.4	40.7	34.4	51.4	-	--
60	21.4	34.0	25.2	39.9	33.6	50.6	25.1	36.6	29.3	49.2	-	-

Figure 4 shows the 7-day compressive strength of cement mortars *versus* slag replacement from 20% to 60%. It is showed that the higher the slag replacement, the higher the strength loss for both weathered and new slags. However, it seems that strength loss is higher for weathered slags compared to "new" slags.

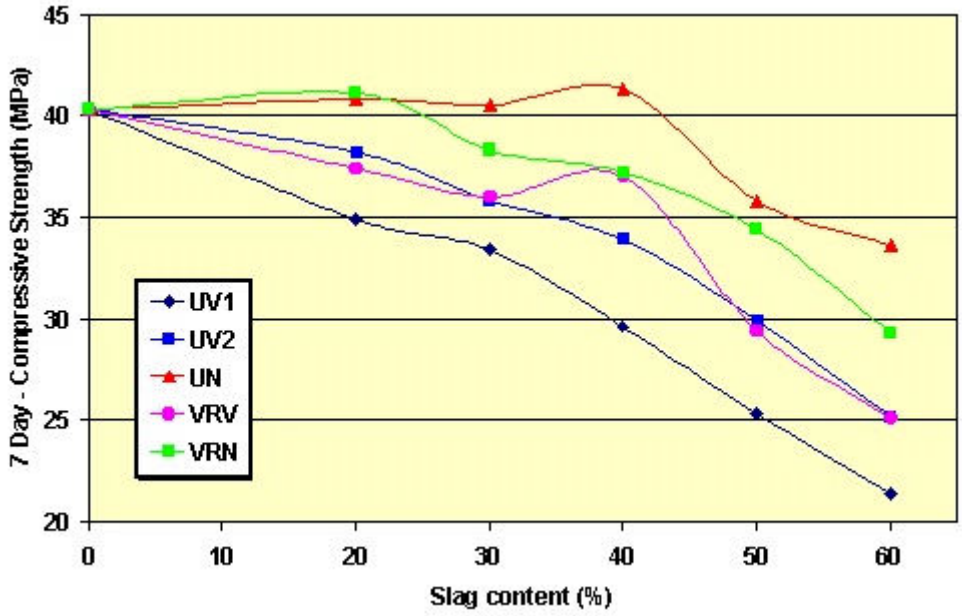

Figure 4. Slag contents *versus* 7-day compressive strength

A different behavior was found for 28-day compressive strength, Figure 5. Accordingly, a strength gain was obtained for mixes containing new slags. For 40% slag replacement strength gains are 15% and 10%, compared to reference for UN and VRN, respectively.

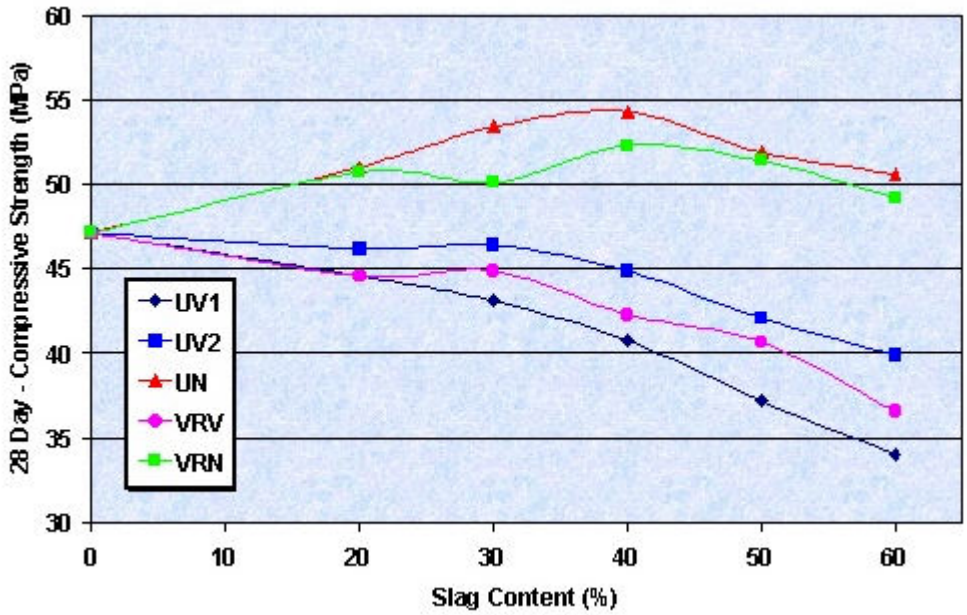

Figure 5. Slag contents *versus* 28-day compressive strength

By comparing mortar strength of mixes with same slag replacement and from a single source, results showed that strength losses are higher for weathered slags. For instance, for 60% slag replacement, UV1 presented a loss of 36% compared to UN at 7 days.

Table 6 clearly shows that raising the slag replacement there is an increase in setting time for both weathered and new slags. By comparing weathered and new slags from the same source, there is a slight decrease of initial setting time and a shortening of final setting time for mixtures containing weathered slag that reached up to 85 minutes.

Table 6 shows the results of initial and final setting times

Table 6. Setting Time (min)

Slag content (%)	UV1		UV2		UN		VRV		VRN	
	Initial	Final	Initial	Final	Initial	Final	Initial	Final	Initial	Final
20	155	235	165	235	175	245	175	235	155	235
30	185	245	165	235	200	240	145	205	215	245
40	170	260	175	245	170	240	175	225	185	275
50	185	275	195	265	205	265	155	215	235	295
60	195	275	145	245	205	275	170	220	225	305

3. CONCLUSIONS

From the results of tests carried out in this investigation the following conclusions may be drawn.

- Slag weathering is linked to a hydration/carbonation/oxidation process that causes a loss of slag reactivity;
- By comparing weathered and new slags from a single source tests showed a decrease of heat of hydration liberation as well as a decrease of alkali accelerated strength in weathered slag;
- LOI and IR tests, for its simplicity, could be used for quality control of slag weathered degree;
- For 7-day compressive strength, test of mixes with slag replacement from 20% to 60% showed that the higher the slag replacement, the higher the strength loss for both weathered and news slags compared to the reference. However, it seems that strength loss is higher for weathered slags;
- A different behavior was found for 28-day compressive strength tests. In spite of mixes containing weathered slags having exhibited a strength loss for all slag replacement, mixes containing new slags presented a strength gain of 10% to 15% with replacement from 30% to 50%;
- For some slag replacement, mixes presented strength loss of up to 40% by comparing new and weathered slags from a single source.

- Finally, by raising the slag replacement, there is an increase of setting time for both weathered and news slags. By comparing weathered and new slags from a single source there was a slight decrease of initial setting time and a shortening of final setting time for mixes containing weathered slag that reached up to 85 minutes.

REFERENCES

[1] Annual Report 2000 – National Institute of Siderurgy

[2] Battagin,A.F. et all – Contribution to the knowledge of Blast Furnace Slag Cement Properties. Technical Report nº 90. Brazilian Cement Association, 1987. (in Portuguese)

[3] Hiroshima, A; Igarashi,T. Effect by Weathering of Granulated Blast Furnace Slag Powder on the Quality of Portland Blast Furnace Slag Cement, CAJ Review, 1983, p. 65-66.

[4] Hooton,D.R. and Emery, J.J. Glass content determination and strength development predictors for vitrified Blast Furnace Slag. In Fly ash, silica fume, slag and other mineral by-products in concrete. ACI SP-79, vol. II, pages 943-962.
[5] Demoulian, E.;Vernet,C.;Hawthorn,F.;Gourdin,P. Détermination de la teneur en laitier dans le ciments par dissolucion seletive. In. Int. Congr. Chemistry of Cement,7th . Paris, 1980. Proceedings. v II, p 151-156.
[6] NBR 7215, Determination on Cement Compressive Strength, Brazilian Association of Technical Standards, 1996. (in Portuguese)
[7] Cincotto, M.A. and Battagin, A.F. – Characteristics of blast furnace slag and its use as a cimentitious material and as concrete aggregate. Technical Research Institute Bulletin 65, 1992 p.18 (in Portuguese)
[8] Demolian, E et al – Influence de la composition chimique et de la texture des laitiers sur leur hidraulicité. In: Int. Congress on Chemistry of Cement, 7th, Paris, 1980 V4, p17-20.

BLAST FURNACE SLAG WEATHERING STUDY

Battagin, Arnaldo Forti[1] and Pecchio, Marcelo[2]

Brazilian Portland Cement Association, São Paulo, Brazil.
[1]E-mail:[1]arnaldo.battagin@abcp.org.br , [2]marcelo.pecchio@abcp.org.br

SHORT BIOGRAPHY

Reinhold Amtsbüchler, a Professional Engineer, is manager – Product Assistance Department - at Lafarge SA Cement. He graduated as a civil engineer from Vienna University in 1973. Prior to joining the present group in 1982, he worked with consulting civil engineers in Austria and South Africa, as well as project engineer in Iran, and as group concrete technologist for the RMC Group in Austria. He has been closely associated with the promotion of fly ash in southern Africa. His doctorate in technical science was awarded by Innsbruck University in 1993 for a thesis on the effect of different binder combinations on the cracking behaviour of tunnel linings. He is the author of 16 concrete related papers.

EFFECT OF HIGH TEMPERATURE ON THE PORE STRUCTURE AND STRENGTH OF GRANULATED BLASTFURNACE SLAG MODIFIED CEMENT PASTE

Juha Komonen[1] and Vesa Penttala[2]

[1]Helsinki University of Technology, Laboratory of Building Materials, Finland.
E-mail: juha.komonen@hut.fi
[2]Helsinki University of Technology, Laboratory of Building Materials, Finland.
E-mail: vesa.penttala@hut.fi

ABSTRACT

The effect of high temperature on the residual properties of granulated blastfurnace slag modified cement paste was investigated. Portland cement paste with a slag content of 60 % and water binder ratio of 0.32, was exposed to temperatures of 20, 50, 75, 100, 120, 150, 200, 300, 400, 440, 520, 600, 700, 800, and 1000°C. The unsealed specimens were heated at a rate of 4ºC/min to test temperature, were kept there for 60 minutes, were cooled at a rate of 4ºC/min to 20°C, and were tested. Residual compressive and flexural strengths were measured and pore structure of the pastes was determined by mercury porosimetry. Tests were performed at the age of 90 days. The total porosity of the pastes more than doubled when exposure temperature was increased from 20°C to 1000°C. The gradual heating coarsened the pore structure. The most notable coarsening of pore structure - together with strength loss and decomposition of hydration products - took place at exposure temperatures higher than 440°C. After 600°C the residual compressive capacity ($f_{c600°C}/f_{c20°C}$) was still over 57 %. Strength loss due to the increase of temperature was not linear. According to the tests it seems that exposure temperatures from 50°C to 120°C can be as dangerous as exposure temperature of 440°C to the residual compressive strength when granulated blastfurnace slag modified cement paste with low water binder ratio is in question.

1. INTRODUCTION

Properties of clinker minerals, hydrated clinker minerals, hydration products, hardened cement paste, mortar and concrete at high temperatures as well as their residual properties have been extensively investigated. The basic phenomena governing changes of cement based materials at high temperature are known: desiccation of pore system, diversified and opposite thermal deformations, chemical phase transformations, decomposition of hydration products, and destruction of microstructure [1-8]. In general, phases present in hardened cement paste expand in the temperature range 20-200°C, but above 200°C shrinkage with different intensity prevails [1,2]. All changes seem to coarsen pore structure [3], which is one basic factor controlling the strength of any material.

Finely ground granulated blast furnace slag is utilized to control fresh and hardened properties of cement based materials. A partial replacement of cement decreases water requirement, slows down evolution of heat of hydration and strength gain. It has to be activated by e.g. $Ca(OH)_2$ produced during hydration of Portland cement. This produces different mineralogical and structural composition of paste, which has been reported to have advantageous high temperature behaviour [2].

2. MATERIALS AND TEST SPECIMEN MANUFACTURING

2.1 Materials

The binders used in the research project were a normal Portland cement CEM I 42.5 R and a granulated blast furnace slag (GBFS), both of local origin. The chemical compositions of the binders are given in Table 1. Blaine specific surface area of the cement was 497 m²/kg. Initial and final setting times of the cement were 90 and 180 minutes, respectively. At the age of 1, 7 and 28 days the compressive strength of standard cement mortar prisms were 27, 45 and 54 MPa, respectively. City tap water was used. Particle size distribution of the binders was analysed using a laser diffraction granulometer (LDG). The LDG specific surface areas of the cement and GBFS were 372 m²/kg and 525 m²/kg, respectively.

Table 1. The chemical composition of the binders.

Binder		Portland cement CEM 42.5 R	Granulated blast Furnace slag
Chemical analysis			
SiO_2	(%)	19.72	36.59
Al_2O_3	(%)	5.15	8.77
Fe_2O_3	(%)	2.39	0.81
MgO	(%)	3.05	9.75
CaO	(%)	61.7	36.71
Na_2O	(%)	0.73	1.19
K_2O	(%)	0.82	0.58
TiO_2	(%)	-	3.58
MnO	(%)	-	0.70
S	(%)	-	1.56
SO_3	(%)	3.02	-
Insoluble	(%)	1.11	1.1
Ignition loss 950º C	(%)	3.02	0.01

2.2 Paste manufacturing

Mixing was performed by a Hobart 200 mixer. In the mixing procedure the dry ingredients were mixed for 30 seconds before water was added into the rotating mixer and thereafter mixing was continued at speed 1 for two minutes. Then the mixer was stopped and mixing was continued at speed 2 for two additional minutes. The total mixing time was four and half minutes. The water binder ratio of the paste specimens was 0.32.

2.3 Test specimens and curing

Paste prisms having dimensions of 40 mm x 40 mm x 160 mm were produced for flexural strength and compressive strength tests. The prisms were cast in steel moulds containing three parallel prisms. The prisms were compacted on a vibrating table in two layers. After trowelling, the specimens were covered by two plastic sheets. The specimens were in the steel moulds for the first 22 ± 2 hours after which they were cured in water at 20º C for six days. After water curing, the prisms were moved into the climate room to a temperature of 20º C and relative humidity of 45%. There they were stored until testing. Tests were performed at the age of 90 days.

3. HEATING PROCESS AND HARDENED PASTE TESTS

3.1 Heating device

Heating oven used is Ceramotherm® N 300 by Nabertherm GmbH. The inside dimensions of the oven are 550 mm x 700 mm x 780 mm. The maximum operating temperature is 1280º C. The heating of the device was performed from all walls, door, and bottom of the kiln, which produced a uniform temperature distribution. The bottom heating elements were covered by a silicon-carbide-plate having a thickness of 20 mm. The temperature of the kiln was measured by a platinum-rhodium-thermocouple mounted on the back wall of the kiln (height of 10 cm from the bottom). The temperature and heating of the kiln were controlled by Program Controller S19 by Nabertherm.

3.2 Heating procedure and strength tests

The prisms were moved from the curing environment half an hour before heating started. The unsealed specimens, prisms and mercury intrusion porosimeter (MIP) samples were heated at the same time. They were subjected to continuous heating at a rate of 4º C/min to the test temperature in question. The maximum test temperature was kept constant for a period of 60 minutes. Figure 1 presents a photograph of test specimens in the kiln at 1000° C. The specimens were cooled in the kiln at the rate of 4º C/min to the ambient temperature (20° C) after which they were immediately tested. From each prism both flexural and compressive strengths were measured. After the four-point flexural strength test, the compressive strength was measured from the end parts of the prism.

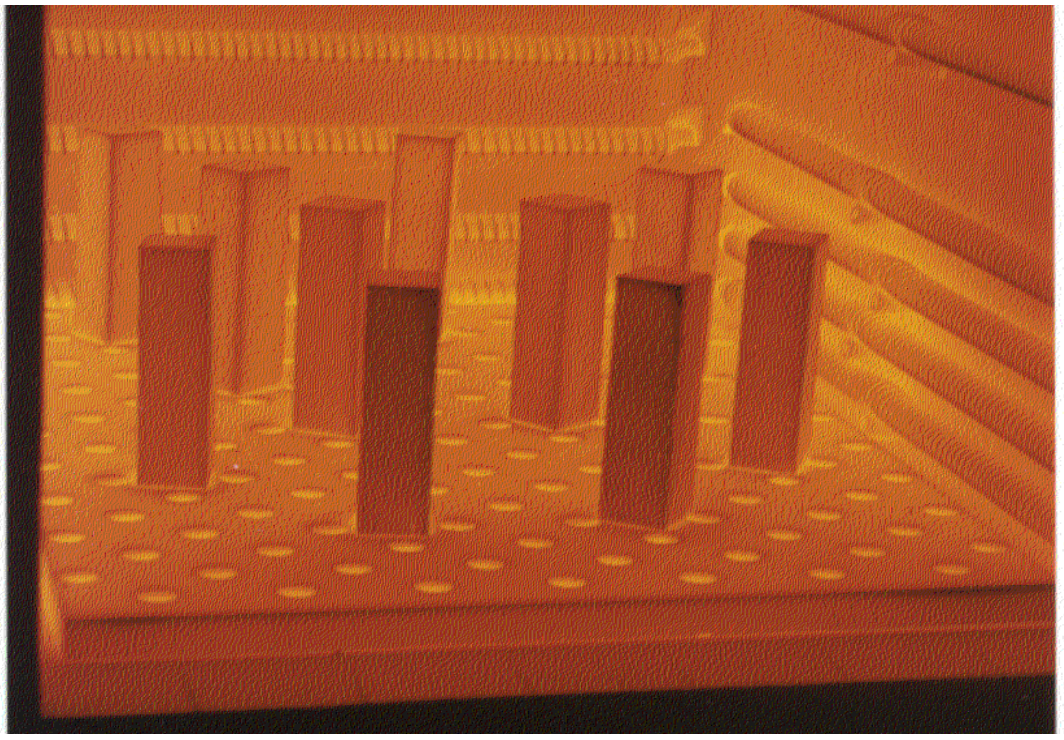

Figure 1. Test specimens in kiln at 1000° C.

3.3 MIP test

MIP samples with dimensions of 15 mm x 15 mm x 15 mm were sawed using diamond saw (water as a lubricant agent) from the centre of the 40 mm x 40 mm x 160 mm test prisms. The intact, non-cracked and non-carbonated material was required and therefore the surface layer of about 12 mm of the prisms was not used. After sawing, the surfaces of the MIP samples were dried with compressed air. Then the samples were weighed and transferred into the kiln. The temperature exposure program (temperatures from 50 to 1000º C) was started not later than half an hour from the sawing. After cooling, the specimens were weighed and stored in vacuum until testing. The control samples (stored at 20°C) and the samples, which were heated to the temperatures below 200ºC, were stored in vacuum for at least 36 days before their pore structure was determined.

3.4 XRD test

The mineralogical composition of the binders, their chemical phase transformations and decompositions were analysed by X-ray diffraction. A Philips PW1710 diffractometer with CuKα radiation was used (40 kV and 40 mA). The measurements were carried out from 2θ angles from 5° to 60° with a step of 0.02°. Each step took 0.5 s. Tests were carried out three times. The investigated material was collected from the temperature exposed test prisms. After the strength tests, the fragments of three crushed prisms were collected into two Pyrex® 26 x 100 SVL 25 culture tubes, which were equipped with teflon gaskets. The fragments were stored in the tubes before they were powdered by a Herzog laboratory mill. The powdered sample and an internal standard of CaF_2 (5% of the sample weight) were ground manually using mortar and pestle. After grinding, the sample was dispersed in ethanol, the suspension was dropped onto a sample holder PW 1817/32 and the ethanol was allowed to evaporate. The analysed sample weight was about 10 mg. Residual paste diffractograms were determined after the temperature exposures of 20, 120, 150, 200, 440, 520, 600, 700, 800, and 1000° C.

4. TEST RESULTS AND DISCUSSION

4.1 Residual crystal structure

Residual crystal structure of the paste was surprisingly stable. The residual diffractogram was quite changeless when the paste was exposed to the temperatures of 120, 200, and even up to 440° C. Minor phase transformations took place at these temperatures, but were overlapped by the background hump of GBFS (due to the amorphous and vitreous nature of GBFS). After the exposure temperature of 520° C, decomposition of $Ca(OH)_2$ and development of CaO were registered. The residual diffractogram peaks of these two phases are shown in detail in Figure 2. The higher exposure temperature of 600° C did not change the composition of paste, but 700° C caused some changes in crystalline phases. After 800° C, the whole amorphous nature of GBFS disappeared. New peaks in the residual diffractogram indicated crystallizations and transformations in phases of the paste matrix. After temperature exposure of 1000° C, the residual diffractogram intensities (due to more complete crystal transformations) increased and crystallization of new phases also took place.

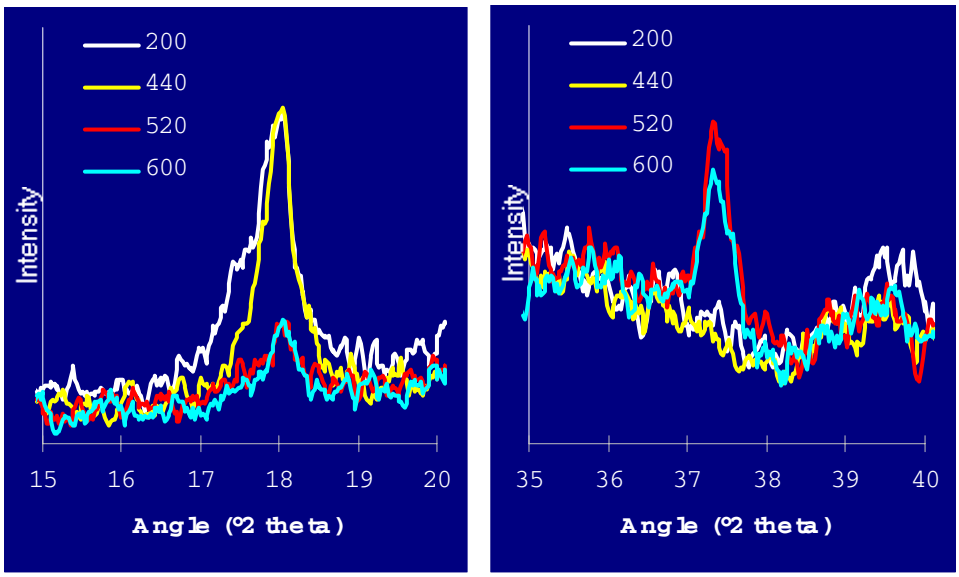

Figure 2. Residual XRD diffractogram peaks of the paste. Destruction of $Ca(OH)_2$ is shown on the left and formation of CaO is apparent on the right. Each curve is an average of three measurements. The sample exposure temperatures are shown in the pictures.

4.2 Residual compressive strength

Strength loss due to the increase of temperature was non-linear. In the temperature range from 50 to 120° C strength losses could be noticed, Figure 3. Significant loss of residual compressive strength at about 100° C confirms literature findings [4,5]. Residual compressive strength of the paste also fluctuated as a function of exposure temperature. After temperature exposures of 150° C, 400° C and 440° C, the residual compressive strengths equalled the reference strength at 20º C. After higher exposure temperatures (from 520° C to 1000° C), the residual compressive strengths of the paste decreased. After the temperature exposure of 600° C the residual compressive capacity ($f_{c600°C}/f_{c20°C}$) of paste was still 57 %.

4.3 Residual flexural strength

The effect of high temperature on the residual flexural strength was very non-linear. When the temperature was increased from 50 up to 120° C, the residual flexural capacity decreased to a local minimum value of 42 %. However, the exposure temperatures of 20, 50, 150 and even 400° C gave identical residual flexural strengths. Flexural strength seems to be more sensitive to cracks and other defects of the material. The flexural test appears to describe this strength loss more clearly, (the maximum loss was noticed at 120° C), which can be attributed to the swelling of water layers in the paste causing weakening of the bonds [6] ,or it can be caused by water evaporating from the pore structure of the specimens [7]. Temperature range from 150° C to 440° C increased residual flexural strengths. The higher exposure temperatures from 520 to 700° C decreased residual flexural strengths. Comparing residual flexural strengths in Figure 3, it can be noticed that temperatures around 120° C are as dangerous as temperatures from 520° C to 700° C to residual flexural strength, when GBFS modified Portland cement paste with low water binder ratio is in question. The highest exposure temperatures 800° C and 1000º C had equal residual compressive and residual flexural strengths.

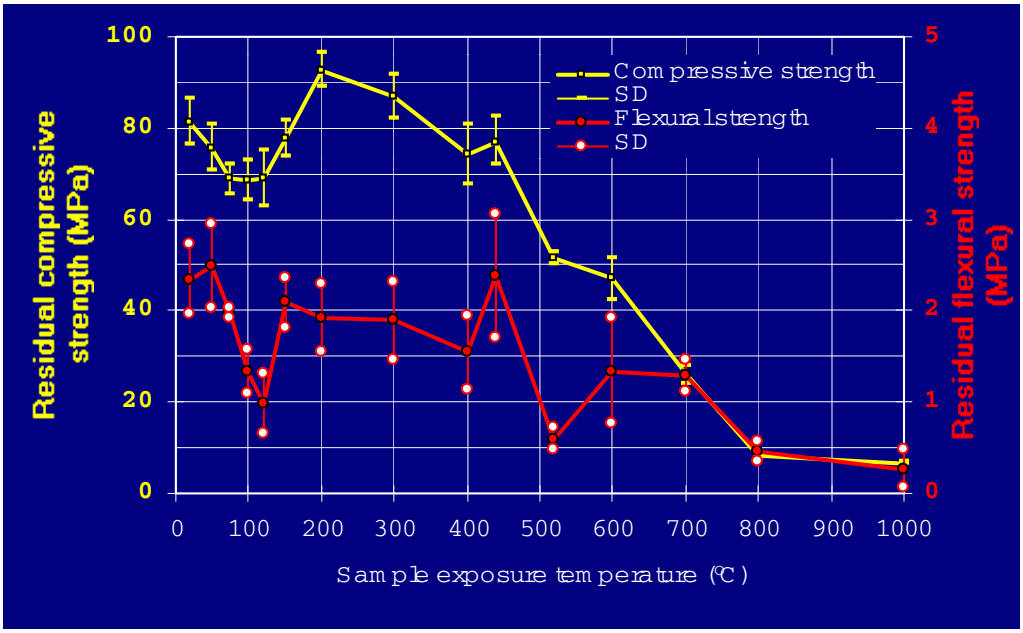

Figure 3. Residual strengths of the test prisms. Residual compressive strength is an average of six test results and residual flexural strength is an average of three test results. Standard deviations are also shown.

4.4 Residual porosity

The residual porosity of the paste increased with the increase of exposure temperature. Total porosity increase from 14,7 % to 42,3 % when the exposure temperature was raised from 20° C to 1000° C. The increase of pore volume of paste specimens heated up to 300° C was significantly

smaller than could be expected from the weight losses. This confirms the findings with mortar specimen [3]. At exposure temperatures above 300° C the residual pore volume clearly increased. The effect can be caused by the significant increase of microcracks [1]. This is also detectable as an increase of porosity at about 10 nm range in Figure 5 (particularly above 400° C). Gel porosity (radii 2 nm) is also quite stable in this temperature range (from 150° C to 350° C) [2] but increases after higher exposure temperatures. In general, it seems that sample weight losses in the exposure temperature range from 100° C to 500° C does not explain changes of pore structure (detectable with MIP) when GBFS modified cement paste with water binder ratio of 0.32 is studied.

4.5 Residual pore size distribution

The gradual heating coarsened the pore size distribution of the paste. Already with a thermal load of 50º C the mean pore radius was shifted a bit towards larger pore radii due to the water evaporation, Figure 4. Increased microcracking is already observed after exposure temperature of 40º C [7]. With increasing temperature from 50º C to 75º C and to 100° C caused a temperature gradient large enough to clearly coarsen the pore structure. This coarsening effect might originate also from decrystallization of ettringite [9]. With a temperature increase up to 120 and 150 a small increase in the zone from 40 nm to 100 nm was observed. After dewatering, the porosity changes originate mainly from decomposition of the paste components.

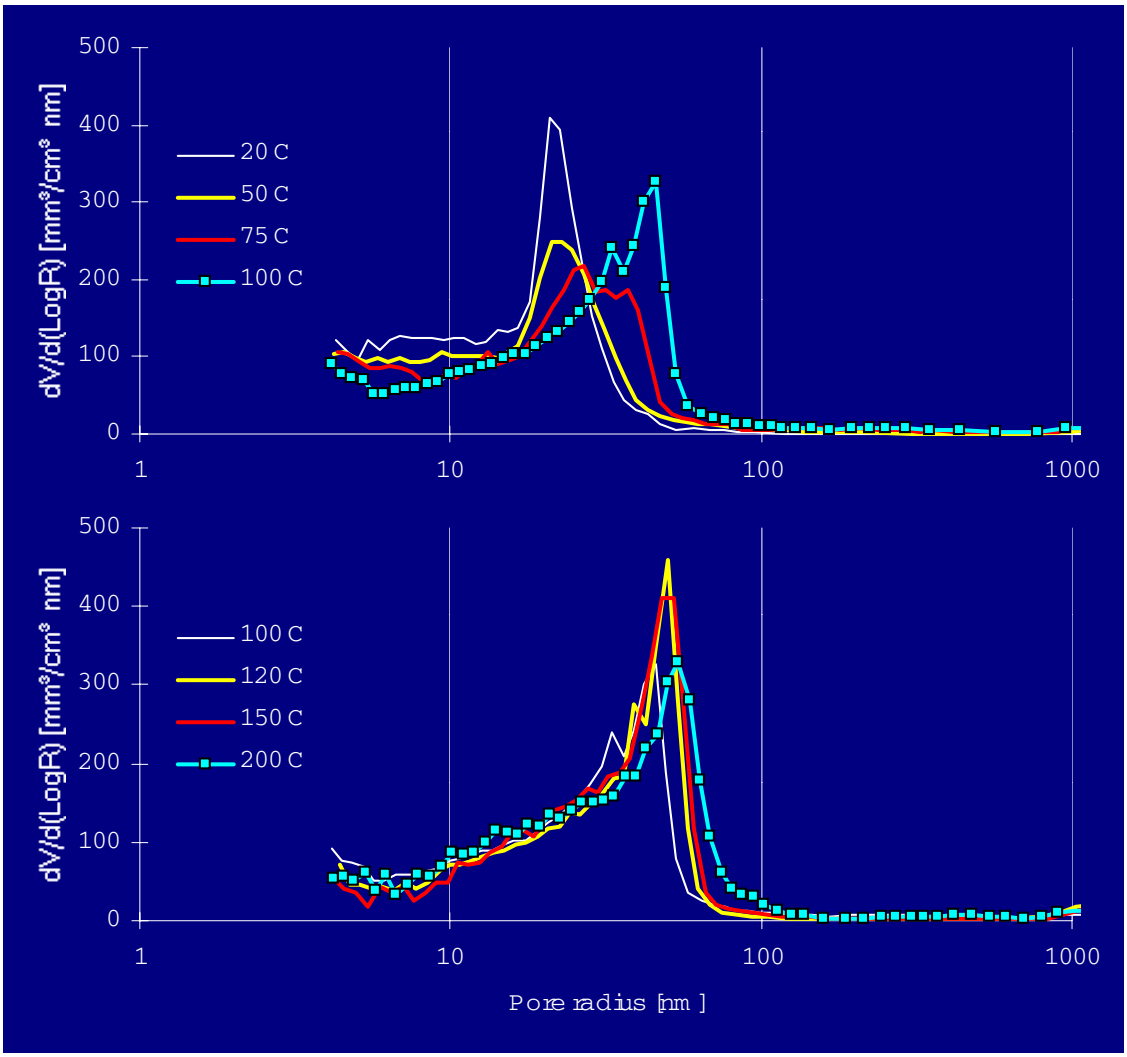

Figure 4. Residual pore size distributions of the test pastes. Sample exposure temperature is given in the legend. Each curve is an average of two measurements.

The pore structure of paste was quite stable in the temperature range from 200º C to 300º C, Figure 5. The increase in sample exposure temperature from 300º C to 400º C or to 440º C had only a minor effect on the pore size distribution of paste. Only a little increase of porosity around 10 nm was observed. The residual pore size distribution of the paste was characterised by one distinct peak at temperatures up to 440º C. Beyond 440º C, at temperature 520º C, a new growth in the pore volume from 5 nm to 15 nm was observed. It might originate from the porosity of CaO formed during dehydration of $Ca(OH_2)$ [1,7,8], which is also verified in Figure 2. In addition, the porosity in the pore radius zone from 70 nm to 120 nm increased. After 600º C, a new capillary pore structure with two peaks (one at about 20 nm and the other at 80 nm) was formed. At higher temperatures the residual pore size distribution consisted of two peaks.

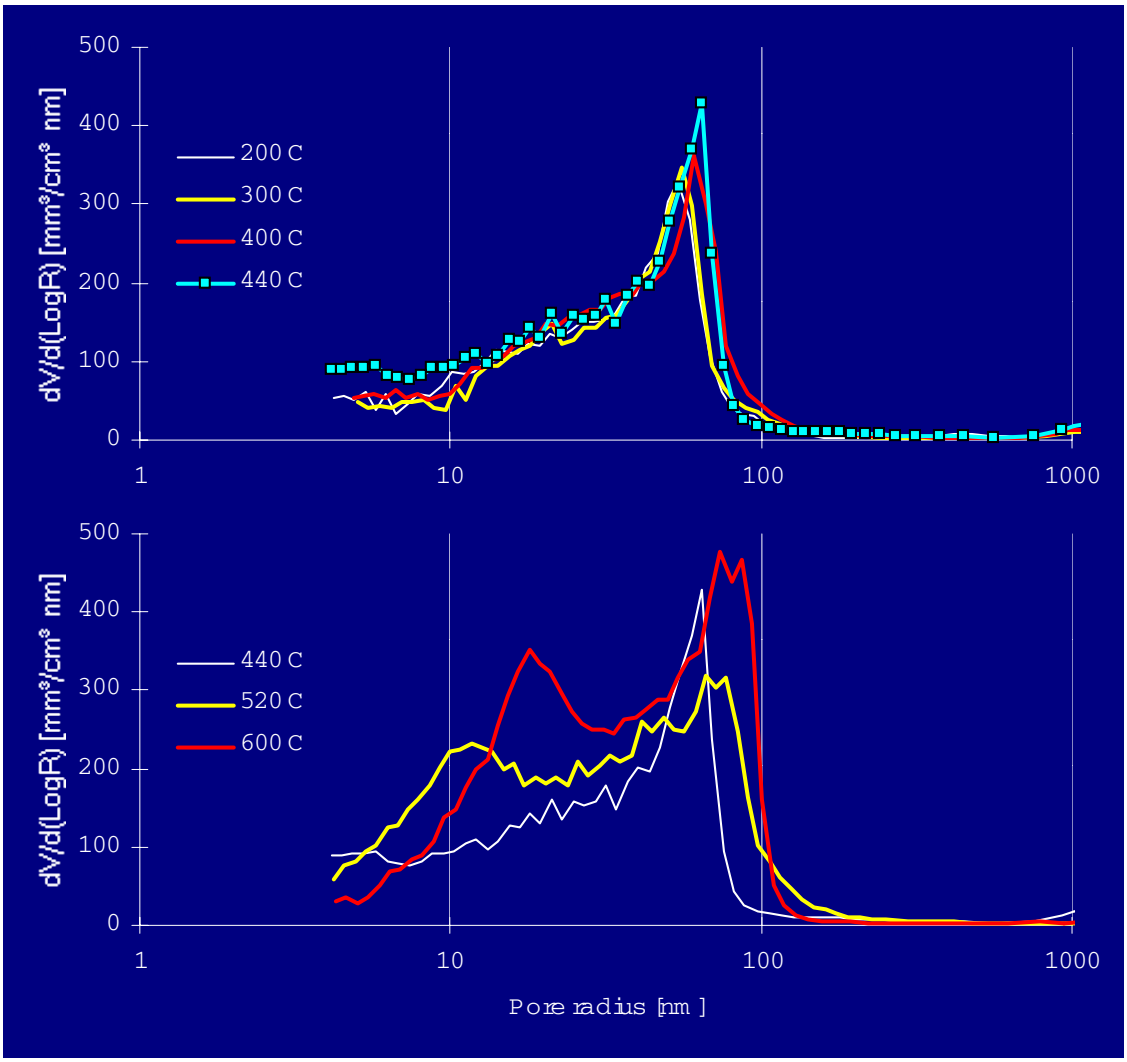

Figure 5. Residual pore size distributions of the test pastes. Sample exposure temperature is given in the legend. Each curve is an average of two measurements.

At exposure temperatures beyond 600° C the total pore volume and the mean pore radius were continuously increased, Figure 6. Especially the macropore volume, pore radii > 100 nm, showed a more distinct increase at sample exposure temperatures of 700, 800, and 1000º C.

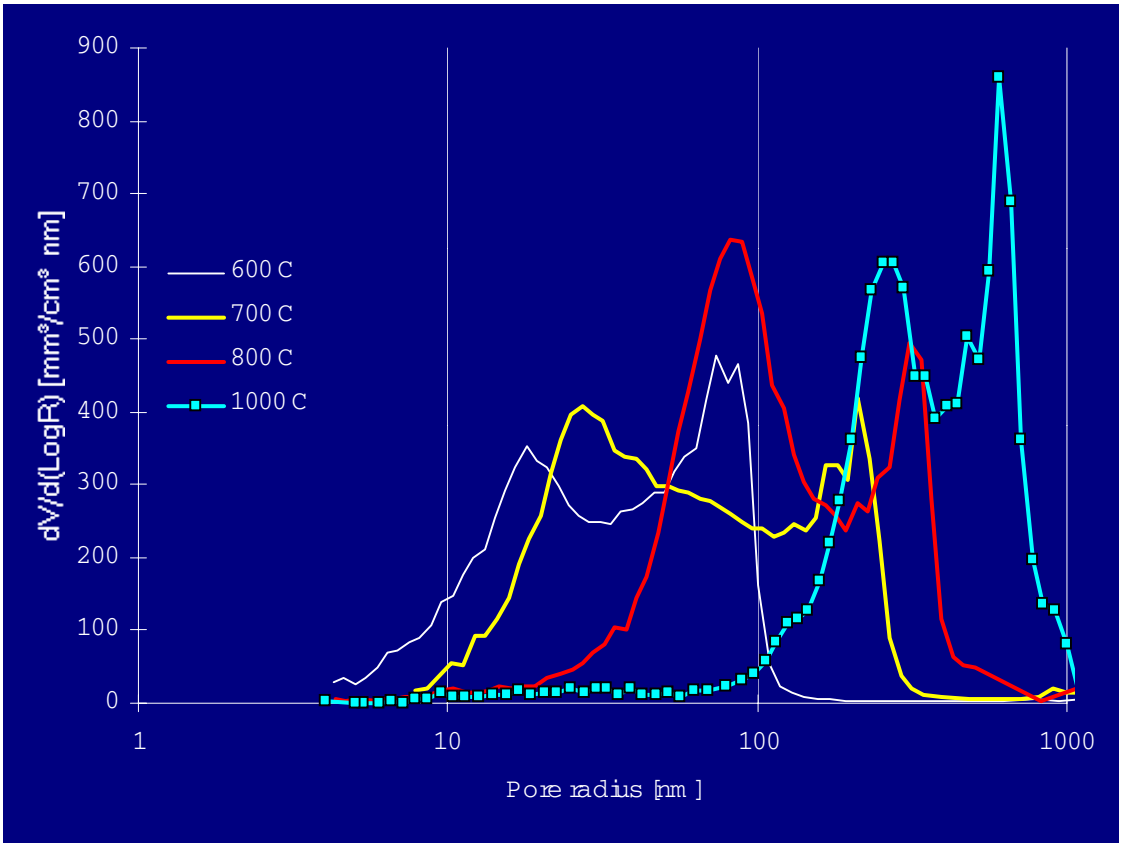

Figure 6. Residual pore size distributions of the test pastes. Sample exposure temperature is given in the legend. Each curve is an average of two measurements.

4.6 Porosity and strength

Exposure temperatures above 600ºC caused strength losses together with a significant coarsening of the pore size distribution. More notable loss of residual compressive strength can be connected to the increase of total porosity of the cement paste from 21 % to 32 % after the exposure temperatures of 400ºC and 520ºC, respectively.

5. CONCLUSIONS

The pore volume and the mean pore radii of the GBFS modified Portland cement paste increased continuously with the increase of exposure temperature. These changes were not linear with respect to the temperature increase. The changes of pore size distributions were mainly caused by the capillar porosity (radii below 100 nm) changes below the exposure temperature of 520ºC. Higher exposure temperatures increased the volume of macropores (pore radii > 100 nm). Beyond 1000ºC the residual pore structure consisted of macropores.

Total porosity almost trebled when exposure temperature was increased from 20°C to 1000°C. The gradual heating coarsened the pore structure. The most notable coarsening of pore size distribution together with a strength loss took place at exposure temperatures higher than 440° C. XRD diffractograms verified decomposition of $Ca(OH)_2$ at these temperatures.

Strength loss due to the increase of temperature was also non-linear. It appears that exposure temperatures from 100°C to 120°C can be as dangerous as exposure temperature of 440° C to residual compressive strength. After 600° C the residual compressive capacity ($f_{c600°C}/f_{c20°C}$) of the paste was still over 57 %. Residual flexural strength fluctuated considerably. Temperature exposure of 120°C decreased residual flexural capacity ($f_{f\,120°C}/f_{f\,20°C}$) to local minimum value of 42 %. This temperature (120° C) caused residual flexural strength equal to residual strength after temperature exposure of 700° C.

Cement based materials are much weaker under tension than under compression. When properties of cementitious materials are investigated after temperature exposure the flexural or tensile strength should be studied, because in this respect all the material defects seems to be noticed more sensitively.

REFERENCES

[1] Piasta, J. Heat deformations of cement paste phases and the microstructure of cement paste, Materials and Structures: Research and Testing, vol.17, 1984, pp.415-420.

[2] Jumppanen, U-M., Dieterichs, U. and Hinrichsmeyer, K. Material properties of F-concrete at high temperatures, Espoo, Technical Research Centre of Finland, 1986. (Research Reports 452).

[3] Rostásy, F. S., Weiss, R. and Wiedemann, G. Changes of pore structure of cement mortars due to temperature, Cement and Concrete Research, vol. 10, 1980, pp.157-164.

[4] Sarshar, R. and Khoury, G. A. Material and environmental factors influencing the compressive strength of unsealed cement paste and concrete at high temperatures, Magazine of Concrete Research, vol. 45, 1993, pp.51-61.

[5] Sarshar, R. Effect of elevated temperatures on the strength of different cement pastes and concretes, London, University of London, 1989, PhD Thesis.

[6] Dias, W. P. S., Khoury, G. A. and Sullivan, P. J. E. Mechanical properties of hardened cement paste exposed to temperatures up to 700 C (1292 F), ACI Materials Journal, vol. 87, 1990, pp.160-166.

[7] Khoury, G. A. Compressive strength of concrete at high temperatures: a reassessment, Magazine of Concrete Research, vol.. 44, 1992, pp.291-309.

[8] Diederichs, U., Jumppanen, U-M. and Penttala, V. Behaviour of high strength concrete at high temperatures, Espoo, Helsinki University of Technology, 1989. (Faculty of Civil Engineering and Surveying, Concrete Technology, Report 92).

[9] Zhang, L., Glasser, F. P. Critical examination of drying damage to cement pastes, Advances in Cement Research, vol. 12, 2000, pp.79-88.

EFFECT OF HIGH TEMPERATURE ON THE PORE STRUCTURE AND STRENGTH OF GRANULATED BLASTFURNACE SLAG MODIFIED CEMENT PASTE

Juha Komonen[1] and Vesa Penttala[2]

[1]Helsinki University of Technology, Laboratory of Building Materials, Finland.
E-mail: juha.komonen@hut.fi
[2]Helsinki University of Technology, Laboratory of Building Materials, Finland.
E-mail: vesa.penttala@hut.fi

Juha Komonen is a senior assistant in the Department of Civil and Environmental Engineering at Helsinki University of Technology, Helsinki, Finland. He is a lecturer in the Laboratory of Building Materials Technology.

EVALUATION OF THE INTER-LABORATORY PRECISION FOR THREE SOUTH AFRICAN DEVELOPED DURABILITY INDEX TEST METHODS

G R H Grieve[1], M Alexander[2], Y Ballim[3], and R Amtsbüchler[4]

[1]Executive Director, Cement & Concrete Institute, P O Box 168, Halfway House, South Africa, 1685. E-mail: Graham@cnci.org.za
[2]Head of Civil Engineering Department, University of Cape Town, Private Bag, Rondebosch, Cape Town, South Africa, 8000. E-mail: Mark@ebe.uct.ac.za
[3]Head of School, Department of Civil Engineering, University of the Witwatersrand, P O Wits, South Africa, 2050. E-mail: ballim@civil1.civil.wits.ac.za
[4]Manager Product Assistance, Lafarge South Africa (Pty) Ltd, Private Bag X26, Gallo Manor, South Africa, 2052. E-mail: Reinhold.Amtsbuchler@lafarge-za.lafarge.com.

ABSTRACT

As part of a concrete durability research programme undertaken by two universities, three durability index tests were developed. When practitioners tried to use these methods problems were experienced with achieving the specified index values when in-situ concrete was tested. An inter-laboratory precision evaluation was undertaken for these tests. The results were analysed and recommendations were made about the test methods and the recommended limits for results. The rewritten test methods were used in a second round of testing, the results of which will be reported later.

1. INTRODUCTION

The Cement and Concrete Institute (C&CI) has administered and managed the investment by cement producers in research projects on concrete durability at the Universities of Cape Town and The Witwatersrand for more than a decade. Amongst the projects tackled by the researchers have been those in which some method of determining concrete permeability and its resistance to ingress of harmful gasses and fluids has been required. This work led to the publication of a series of monographs on the issue of durability index testing[1,2,3]. When this information became incorporated into contract specifications certain practical implementation problems occurred, such as measurement differences between laboratories for the same test, and difficulty in achieving the required index values under site conditions.

These implementation problems were discussed at a workshop of interested parties. It was agreed that further work was required to determine the reproducibility and repeatability of the test methods, which, until then, had been methods in development at the research facilities. It was agreed that the C&CI laboratory would manufacture and distribute to participating laboratories a number of sets of test specimens, and that C&CI would collate and analyse the test results from all participants. This paper covers this test programme.

It was also agreed that to exploit the full potential of the test methods, it would be desirable to try to provide guidance on the desirable limits for test results for tests carried out on site concrete. The latter would be investigated as another project, as it was anticipated that there would be a need to

Proceedings of the 11th International Congress on the Chemistry of Cement (ICCC) 11 - 16 May 2003, Durban, South Africa
'Cement's Contribution to the Development in the 21st Century' ISBN Number: 0-9584085-8-0
Hosted by: The Cement and Concrete Institute of South Africa Editors: Dr G. Grieve and G. Owens
CD-ROM produced by: Document Transformation Technologies Congress Organised by: Event Dynamics

evaluate conditions in three or four different curing zones across South Africa, namely Eastern Coastal, Western Coastal and Moist and Dry Interior.

2. TEST METHODS

The researchers developed three test methods, namely an oxygen permeability test, a water sorptivity test and a rapid chloride conductivity test. In each case a set of test specimens consisting of 25-mm thick slices from a 68-mm core are used.

The details of these tests are as follows:

2.1 Oxygen Permeability Test

This test is a falling head permeameter test. Oven dried specimens are subject to a head of 100 kPa of oxygen pressure and the pressure decay with time is recorded. The coefficient of permeability is determined from the slope of the line produced when the natural log of the ratio of initial pressure to pressure at any time is plotted against time. The oxygen permeability index (OPI) is defined as the negative log of the coefficient of permeability.

2.2 Water Sorptivity Test

This is a unidirectional absorption test and involves placing the test specimens (the edges of which have been sealed) in a shallow layer of water. The test uses the mass of water absorbed from the bottom face of the sample (in mm/√h) as a measure of sorptivity.

2.3 Rapid Chloride Conductivity Test

This test involves determining the DC conductivity of test specimens, which have been saturated with a sodium chloride solution. The test provides a rapid indication of the resistance of concrete to the penetration of chloride ions. The values are stated in milliSiemens per centimetre (mS/cm).

The full details of the test methods are given in reference 3.

3. THE TEST PROGRAMME

The working group participants agreed that C&CI would manufacture the concrete cubes and prepare the test specimens for all the laboratories from these cubes after the required curing period.

The following mix proportions were used in making the concrete in the laboratory:

Table 1. Mix proportions used for test program

Material	Mass of dry material (kg/m^3)	
Water	205	220
CEM I 42,5N	315	489
19-mm andesite coarse aggregate	1174	1174
Granite crusher sand	769	584
Water:cement ratio	0,65	0.45

Cubes were made from the laboratory mixes and these were all subjected to either 1 or 14 days of curing submerged in water at 22 to 25 °C. After completing the water curing process, the cubes were exposed to the laboratory air at 22 to 25 °C at a relative humidity of 65%. At 28 days, core drilling was done horizontally into each of two opposite vertical faces (as cast) of each cube and then the outer 5 mm was trimmed off each side before the two 25-mm thick test specimens were cut

off the two opposite cores. The sides of the test specimens were coated with epoxy resin to seal them.

The test specimens were then placed in an oven at 50 ± 2°C for a minimum of 7 days and relative humidity below 20% and then sets of these specimens were sealed in plastic bags before being distributed to all participating laboratories. Each laboratory received the following specimens:

Table 2. Numbers of test specimens made for each test laboratory

Test method	Number of test specimens
OPI	4
Sorptivity	4
Chloride conductivity	3

On receipt, each laboratory was expected to recondition the test specimens in an oven for a further 7 days at 50 ± 2°C and relative humidity below 20% before initiating the tests.

In each case the laboratory was required to report their results to C&CI. In the case of the OPI and Sorptivity tests the laboratories were also asked to submit the correlation coefficients for the regression analysis on the data from each test.

4. PARTICIPATING LABORATORIES

All South African laboratories that had the equipment to do these tests, at the end of 2001, participated in this inter-laboratory evaluation. It should be noted that not all laboratories were equipped to undertake all of the tests under consideration. These details are included in the table overleaf.

Table 3. Test undertaken by the participating laboratories

Laboratory	Tests undertaken		
	OPI	Sorptivity	Chloride conductivity
Lab 1	Y	Y	Y
Lab 2	Y	Y	Y
Lab 3	Y	Y	Y
Lab 4	N	N	Y
Lab 5	Y	Y	Y
Lab 6	Y	Y	Y
Lab 7	Y	Y	N

5. TEST RESULTS

Table 4 gives the suggested ranges for durability classification using these index values for the three tests from reference 1. (It should be noted that one of the reasons for undertaking this testing programme was to generate information which could help with a review of these suggested ranges.) These ranges have been used to categorise the values reported by each laboratory. Colour has been used to emphasise these categories

Table 4. Suggested ranges for durability classification

Durability class	OPI (log scale)	Sorptivity (mm/√h)	Chloride Conductivity (mS/cm)
Excellent	>10	<6	<0,75
Good	9,5-10	6-10	0,75-1,50
Poor	9,0-9,5	10-15	1,50-2,50
Very poor	<9,0	>15	>2,50

Tables 5a to 5d give the summarised average test results and coefficients of variation for the four different test conditions from each laboratory.

Table 5a. Test results for specimens made to w/c=0,45: curing 1d

Laboratory	OPI (log scale)		Sorptivity (mm/√h)		Chloride Conductivity (mS/cm)	
	Average	CoV	Average	CoV	Average	CoV
Lab 1	9.50	1.63	12.66	13.84	0.72	7.19
Lab 2	9.46	1.35	13.38	13.47	0.80	2.59
Lab 3	9.43	1.46	12.11	7.95	0.80	12.50
Lab 4					0.99	17.00
Lab 5	9.44	1.10	10.15	2.06	1.07	8.31
Lab 6	9.38	1.30	10.10	4.07	1.23	8.72
Lab 7	9.50	2.27	11.58	15.23		
Mean	9.45	1.52	11.66	9.44	0.93	9.38
CoV (%)	0.48		11.43		20.71	

Table 5b. Test results for specimens made to w/c=0,65: curing 1d

Laboratory	OPI (log scale)		Sorptivity (mm/√h)		Chloride Conductivity (mS/cm)	
	Average	CoV	Average	CoV	Average	CoV
Lab 1	9.35	2.63	14.76	1.95	1.57	6.08
Lab 2	9.36	0.86	12.85	7.31	1.50	5.34
Lab 3	9.22	0.64	13.19	9.52	1.89	23.63
Lab 4					1.63	11.33
Lab 5	9.43	0.90	10.31	6.83	1.87	4.44
Lab 6	9.41	0.61	12.07	7.94	1.95	4.95
Lab 7	9.98	0.87	12.35	5.78		
Mean	9.46	1.09	12.59	6.56	1.74	9.29
CoV (%)	2.80		11.62		10.90	

Table 5c. Test results for specimens made to w/c=0,45: curing 14d

Laboratory	OPI (log scale)		Sorptivity (mm/√h)		Chloride Conductivity (mS/cm)	
	Average	CoV	Average	CoV	Average	CoV
Lab 1	9.88	1.30	14.16	11.92	0.85	5.46
Lab 2	9.81	0.85	11.62	17.82	0.85	5.94
Lab 3	9.74	1.56	9.70	9.12	2.11	57.44
Lab 4					1.04	12.28
Lab 5	9.76	1.14	8.09	0.17	1.06	5.66
Lab 6	9.82	0.43	9.35	3.48	1.24	7.88
Lab 7	9.83	0.97	9.13	4.93		
Mean	9.81	1.04	10.34	7.91	1.19	15.78
CoV (%)	0.51		21.26		39.71	

Table 5d. Test results for specimens made to w/c=0,65: curing 14d

Laboratory	OPI (log scale)		Sorptivity (mm/√h)		Chloride Conductivity (mS/cm)	
	Average	CoV	Average	CoV	Average	CoV
Lab 1	9.87	0.63	14.23	15.25	1.40	3.25
Lab 2	9.87	2.84	10.48	7.84	1.44	1.39
Lab 3	9.93	1.82	9.48	4.42	1.41	25.05
Lab 4					1.66	9.12
Lab 5	10.00	2.28	9.36	7.74	1.75	8.24
Lab 6	10.13	0.85	8.03	6.95	1.80	8.01
Lab 7	9.98	0.96	8.33	7.99		
Mean	9.96	1.56	9.98	8.36	1.58	9.18
CoV (%)	0.97		22.60		11.52	

6. DISCUSSION OF TEST RESULTS

6.1 Internal Precision of Test Method (Within Laboratory Precision)

The internal precision of the test results from each laboratory was assessed from the coefficient of variation CoV (%) of each set of results from each laboratory presented in tables 5a to 5d above.

6.1.1 OPI

In general, the coefficients of variation for the results of the OPI tests are very low indicating that within each laboratory the results of the tests of the four different specimens are very similar. This suggests that the OPI test has a good internal precision. There does not appear to be any trend in this precision for the different mix types or curing regimes.

6.1.2 Sorptivity

The coefficients of variation recorded for this test are much higher indicating that the internal precision of the method is rather poor. Although the differences are small, it does seem that the repeatability of this test improves as the curing period is increased.

6.1.3 Chloride Conductivity
For this test the coefficients of variation are higher than might be considered acceptable (although a limit for this acceptability has yet to be established) and the internal precision is considered to be unsatisfactory. It should be noted that in all cases laboratories 3 and 4 have significantly higher CoV values than the other laboratories. Omitting these two sets of values still leaves the mean CoV higher than 5% and therefore unsatisfactory. However, it was suggested that laboratories 3 and 4 should investigate their laboratory procedures to determine if there might be ascribable causes for the poor repeatability.

6.2 External Precision of Test Method (Between Laboratory Precision)
The between laboratory precision of the test results from each laboratory was assessed from the coefficient of variation CoV (%) of the results for each test method for all laboratories is presented in the bottom row in tables 5a to 5d above.

6.2.1 OPI
The between laboratory precision of this test is very good with a CoV of substantially less than 5%. There is however a concern that the classification resulting from the results from different laboratories differs in two cases in tables 5b and 5d.

6.2.2 Sorptivity
The between laboratory precision for this method is poor. In addition, there seems to be a deterioration of the precision as the curing period is increased. The same problem occurs with this test where different laboratories arrived at different classifications in some cases.

6.2.3 Chloride Conductivity
Again, the between laboratory precision for this method is poor. The precision does however appear to be better for the mixes with the higher w/c ratio. While the internal precision of this test for laboratories 3 and 4 was shown to be very low, it does not appear to have affected the mean values reported. The same problem occurs with this test where different laboratories arrived at different classifications in some cases.

7. RECOMMENDATIONS

It is recommended that the test methods be rewritten giving more detail and restricting the possibility of different interpretation or practice.

In addition, it is recommended that the user of this information be provided with guidance to the interpretation of the results in a different format. For example, instead of applying terms such as “excellent”, “good” or “poor”, estimates should be provided of the life expectancy of concrete given certain index values. While a specifier might be unwilling to specify concrete that had poor durability for his client he might be more comfortable to recommend that it was not necessary to opt for a higher durability than the design life required.

8. CONCLUSION

The test methods have been rewritten as recommended above and are included as appendices 1 to 4.

These rewritten procedures have been used in a second round of inter-laboratory precision evaluation tests. It is hoped the results of the second round will be presented in the final submission of this paper or a later paper.

REFERENCES

[1] Alexander, M.G., MacKechnie, J.R. and Ballim, Y. Guide to the use of durability indexes for achieving durability in concrete structures, Cape Town: University of Cape Town, Dept. of Civil Engineering, 1999. (Research Monograph 2).

[2] Alexander, M.G., Streicher, P.E. and MacKechnie, J.R. Rapid chloride conductivity testing of concrete, Cape Town: University of Cape Town, Dept. of Civil Engineering, 1999. (Research Monograph 3).

[3] Alexander, M.G., Ballim, Y. and Mackechinie, J.R. Concrete durability index testing manual, Cape Town: University of Cape Town, Dept. of Civil Engineering, 1999. (Research Monograph 4).

Appendix 1

PROPOSED TEST METHOD FOR SAMPLE CUTTING AND PREPARATION PRIOR TO DETERMINING DURABILITY INDEX VALUES

1. SCOPE

This test method describes how to cut and prepare test specimens in order to carry out tests for determining the durability indices of concrete as described by Alexander, Ballim and Mackechnie [(1)].

Each test specimen shall consist of a 68mm diameter concrete disc cut in a direction perpendicular to the direction of casting from a shuttered surface of a concrete member or laboratory specimen.

The thickness of the specimen should be 5mm greater than the maximum nominal aggregate size and ± 2mm tolerance is allowed. Thus for concrete with a nominal aggregate size of 19mm a 25 ± 2mm thick by 68mm diameter sample will be required. As far as possible try to keep specimen thickness standardised at 25 mm.

2. APPARATUS

a) A water-cooled diamond tipped core barrel with an inner diameter of 68mm, attached to a suitable coring drill.
b) In the case of preparing test specimens from cubes: A holding device in which cubes can be clamped to ensure they remain in position while coring takes place.
c) A water-cooled moveable bed diamond saw using an un-notched, thin (circa 2mm) blade
e) A facing machine (if possible) or other machine capable of removing the outer 5mm of surface of the specimens but without changing the orientation or flatness of the face.
f) A sample holding device in which samples can be held in position on the movable bed of the diamond saw but which can allow rotation of the sample while facing and cutting.
g) An oven capable of maintaining a temperature of 50 ± 2ºC and relative humidity below 20%. The relative humidity can be maintained by the inclusion of trays of saturated calcium chloride solution. The trays should provide a total exposed area of at least $1m^2$ per $1m^3$of volume of the drying facility and should contain sufficient calcium chloride to show above the surface of the solution throughout the test.

3. TEST SPECIMEN PREPARATION FROM CUBES

a) If samples are prepared from cubes they need to be cut from the surfaces perpendicular to the trowelled face of the cube.
b) Clamp the specimen firmly into the holding device and place the core barrel perpendicular to the concrete face.
c) If only one specimen per cube is required, core aproximately 40mm into the sample.
   Two specimens may be cored from one cube:
   i) One behind the other to asess the effects of curing, core aproximately 80mm into the cube.
   ii) Another specimen may be cored from the other side of the cube, core aproximately 40mm on both sides perpendicular to the trowelled face.
d) Secure the sample tightly on the movable bed of the diamond saw. Cut or grind the first 5mm from the cored face of the cube. Cut the required thickness of the test specimen from the cube.

e) Mark the test specimens with the correct reference number on the non test face. The test face is the outside or exposed face of the concrete cube.
f) The results of this process is a 68mm diameter by aggregate size +5mm thick specimen marked with the correct reference number. The test face is that face of the specimen that has no marking on.

4. TEST SPECIMEN PREPARATION FROM CORES FROM SITE CONCRETE

a) Place the core barrel perpendicular to the surface of the concrete, and secure so that it can not move.
b) Core to a depth of 60-80mm.
c) Carefully remove the core from the concrete face by breaking it off with a hammer and chisel.
d) Mark each core and remove to the laboratory.
e) Follow steps 3 d) to 3 f) above.

5. CURING AND AIR DRYING OF LABORATORY SPECIMENS

The duration of moist curing of laboratory specimens should be either 7 days or 28 days. In the case of site concrete, the age at which the specimens are taken for testing is generally specified by the consultant or project specification.

After the above period of "moist" curing the specimens should be air-dried until 28-days old before sample conditioning can commence.

Cutting of the specimens can take place after 21 days.

6. SEALING OF SAMPLE EDGES

The edges of the sample discs for sorptivity testing still have to be sealed. This is done using ABE Epidermix 365 epoxy, or similar, which is carefully applied to the curved surfaces with a sponge to completely coat and seal them. Care must be taken not to get the epoxy on the flat test surfaces.

Put the samples back in the oven after the epoxy have touch dried.

While this process can be used to seal the edges of all specimens it may be omitted in the case of OPI and Chloride Conductivity testing.

REFERENCES

[1] Alexander MG, Ballim Y, Mackechnie JM, ' Concrete durability index testing manual' Research Monograph no. 4, Departments of Civil Engineering University of Cape Town and University of the Witwatersrand, March 1999

Appendix 2

STANDARD PROCEDURE FOR OXYGEN PERMEABILITY TEST

1. SCOPE

This test method sets out the procedure for determining the oxygen permeability index as described by Alexander, Ballim and Mackechnie [1].

The test is suitable for the evaluation of materials and mix proportions for design purposes as well as research and development. Care should be taken in interpreting the results of this test when it is used on surface treated concrete's, or on concrete that has been exposed to environmental influences such as carbonation or marine salts.

2. APPARATUS

a) A water-cooled diamond tipped core barrel with an inner diameter of 68mm, attached to a suitable coring drill.
b) In the case of preparing test specimens from cubes: A holding device in which cubes can be clamped to ensure they remain in position while coring takes place.
c) A water-cooled moveable bed diamond saw
d) A facing machine.
e) A sample holding device in which samples can be held in position on the movable bed of the diamond saw but which can allow rotation of the sample while facing and cutting.
f) An oven capable of maintaining a temperature of 50 ± 2ºC and relative humidity below 20%. The relative humidity can be maintained by the inclusion of trays of saturated calcium chloride solution. The trays should provide a total exposed area of at least $1m^2$ per $1m^3$ of volume of the drying facility and should contain sufficient calcium chloride to show above the surface of the solution throughout the test.
g) Permeability test arrangement as described in [1] page 8-10, housed in a room where the temperature is controlled at 23 ± 2ºC and relative humidity at 60 ± 5%. The air-tightness of the equipment needs to be tested on a regular basis using impermeable test specimens. If there is zero drop in pressure of 100kPa over an eight-hour period the equipment is considered to be in good working order.
h) Silicone rubber collars for each cell made of silicon with Shore hardness 39A. The collars need to be replaced when cracks and tears occur.
i) Standard grade 99.8% oxygen supply and regulator capable to regulate flow to 100kPa.
j) Vernier calliper

3. TEST SPECIMENS

The test specimen shall consist of a 68mm diameter concrete disc cut in a direction perpendicular to the direction of casting from a shuttered surface of a concrete member or laboratory specimen using test method AAA

Four test specimens are required per test.

4. CONDITIONING OF THE SAMPLES

After cutting and coring store the specimens in the oven at 50 ± 2°C and less than 20% relative humidity for seven days, or until dried to a constant mass.

5. TESTING OF SAMPLES

a) After drying, take the samples out of the oven and cool on a steel tray for 45 minutes.
b) After 45 minutes mark the samples of the same mix 1,2 3 and 4 on the inner face.
d) Measure the thickness of each sample with the vernier at 4 points equally spaced around the perimeter of the sample and record on the data sheet to the nearest 0.1mm.
e) Place the sample in the rubber collar with the test face (outer face) at the bottom.
f) Place the rubber collar in the PVC sheath with the wooden ring on top of the collar.
g) Place on top of the permeability cell.
h) Place the coverplate in position and fasten . Repeat for samples 2, 3 and 4
f) Start the test exactly 1 hour after removing the specimens from the oven, turn the gas on the regulator to 120 kPa.
g) Open the gas inlet and outlet valves of the permeability cells and allow oxygen to flow through the permeameters for 5 seconds.
h) Close the gas outlet valve of all four permeability cells.
i) Wait till pressure rises above 100 kPa on the gauge of the permeability cell and close the inlet valve.
j) Tap the gauge and release air by opening the outlet valve slighty untill the pressure on the permeability cell gauge is 100 kPa . Record the time and pressure.
k) Repeat for all cells.
l) After 5 minutes tap the gauge and record the time and reading; Continue to check the pressure.
m) Subsequent readings should be taken before a pressure drop of 5 kPa occurs. Record the pressure and time on a standard form.
n) The test may be terminated when the pressure has dropped to 50 kPa.
o) In the case of automated sytems, pressure readings should be recorded on the computer at 15 minute intervals for two to eight hours.

6. CALCULATION OF THE OXYGEN PERMEABILITY INDEX

The calculation involves conducting a linear regression analysis on the best fit line obtained by plotting values of $\ln(P_o/P_t)$ against t where:

P_o = initial pressure at start of test (at time t_o) kPa
P_t = subsequant readings in pressure kPa at time t, measured from t_o,
t = in seconds

The simplest way to calculate the slope of the regression line is by entering the data in a Microsoft Excell range and use the function SLOPE {(data range of ($\ln(P_o/P_t)$) ; (data range of time)}. The correlatation coefficient can be obtained by using the CORREL {(data range of $\ln(P_o/P_t)$) ; (data range of time)} function.

The coefficient of correlation should be greater than 0.99. Where the correlation is less than 0.99 a retest should be done on the same sample.

The D'arcy coefficient of permeability is given by:

$$k = \frac{\omega . V . g . d . z}{R . A . \text{ø}}$$

k = coefficient of permeability of test sample (m/s)
ω = molecular mass of oxygen = 32 g/mol
V = volume of oxygen under pressure in permeameter (m^3)

g = acceleration due to gravity (m/s^2)
R = universal gas constant = 8313 (Nm/K mol)
d = sample thickness (m)
ø = absolute temperature (K)
z = slope of the line determined in the regression analysis

The coefficient of permeability is calculated for each of the test samples. The permeability index is given as the negative log of the average of the coefficient of permeabilitty of the samples, which for four samples is:

Permeability index = - $\log_{10}$ [¼ (k_1+k_2+k_3+k_4)]

7. REPORTING

Report the following, if known:

a) source of the specimen.
b) Identification number of specimen .
c) Location of specimen within core or cylinder.
d) Type of concrete, including binder type , water/cement ratio and other relevant data supplied with the sample.
e) Description of specimen.
f) Curing history.
i) Unsual specimen preparation eg removal of surface treatment.
j) Test results.

REFERENCES

[1] Alexander MG, Ballim Y, Mackechnie JM, ‘ Concrete durability index testing manual’ Research Monograph no. 4, Departments of Civil Engineering University of Cape Town and University of the Witwatersrand, March 1999

Appendix 3

STANDARD PROCEDURE FOR WATER SORPTIVITY TEST

1. SCOPE

This test method sets out the procedure for determining the water sorptivity index as described by Alexander, Ballim and Mackechnie [1].

The test is suitable for the evaluation of materials and mix proportions for design purposes as well as research and development. Sample age may have a significant effect on the test results, depending on the type of concrete and the curing procedure. Care should be taken in interpreting the results of this test when it is used on surface treated concrete's, or on concrete that has been exposed to environmental influences such as carbonation or marine salts.

2. APPARATUS

a) Vacuum saturation facility as described in [1] page 18.
b) Plastic or stainless steel tray 20mm deep and large enough to hold six test specimens.
c) Absorbent paper towel.
d) Vernier calliper
e) Weighing scale with accuracy to 0.01g
f) Tap water saturated with calcium hydroxide. (180grams of $Ca(OH)_2$ per 1 liter of water).
g) A stopwatch for each sample being tested
h) Epoxy paint and paintbrush. (Suitable products are ABE Epidermix 365 or Sikaguard Wetseal A+B)
i) The water sorptivity test must be conducted in a room in which the temperature is controlled at 23 ± 2ºC and relative humidity at 60 ± 5%.

3. TEST SPECIMENS

The test specimen shall consist of a 68mm diameter concrete disc cut in a direction perpendicular to the direction of casting from a shuttered surface of a concrete member or laboratory specimen using test method AAA

Four test specimens are required per test.

4. CONDITIONING OF THE SAMPLES

a) After cutting and coring store the specimens in the oven at 50 ± 2°C and less than 20% relative humidity for seven days, or until dried to a constant mass.
b) During the seven day drying period take the specimen out of the oven end let it cool for an hour.

5. TESTING OF SAMPLES

a) After drying, take the samples out of the oven and cool on a steel tray for 45 minutes.
b) After 45 minutes mark the samples of the same mix 1, 2, 3 and 4 on the inner face.
c) Measure the thickness of each sample with the vernier at 4 points equally spaced around the perimeter of the sample and record the measurements to the nearest 0.1mm on the data sheet.

d) Place 10 layers of tissue paper on the tray leaving a gap between the sides of the tray and the edge of the paper.
e) Pour calcuim hydroxide solution into the tray untill the tissue paper is properly wet and a 1mm layer of water is visible on top. Remove all the air bubbles by smoothing the paper pad towards the edges.
f) After exactly one hour of cooling weigh the samples to an accuracy of 0.01g and record the weight as the dry mass at time 0.
g) Place the samples with the test face (outer face) on the wet paper start the stopwatch.
h) 30 seconds later place the 2^{nd} sample test face at the bottom on wet paper and start the second stop watch.
i) Weigh the samples at 1, 2, 4, 8, 16, 32 and 64 minutes, after patting it once on a damp piece of absorbent paper.
j) Record weights to the nearest 0.01g on a standard form replacing the samples each time with the test face on the wet paper.
k) After weighing of the samples is complete, place the samples in the vacuum saturation tank. Seal the lid with petroleum jelly and close it.
l) Evacuate the tank to –75±3 kPa and leave the samples under vacuum of –75±3 kPa for 2 hours.
m) After 2 hours, isolate the tank and allow calcuim hydroxide saturated water to flow into the chamber untill the water level is approximatly 40mm above the top of the samples .
n) Reconnect the vacuum pump to the tank and maintain the vacuum for 24 hours at –75±3 kPa.
o) After 24 hours remove the samples from the water, dry the surface with a paper towel and immediately weigh to a accuracy og 0.01g. Record this as the saturated weight of the sample on a standard form.

6. CALCULATION OF THE WATER SORPTIVITY INDEX

The mass of the water absorbed at each weighing period (M_{wt}) is given by:

$M_{wt} = M_{st} - M_{so}$

M_{st} = mass of the sample at time t
M_{so} = mass of the sample at time t=0

By conducting a linear regression analysis determine the value of F given by:

$M_{wt} = F \times \sqrt{t}$

F = the slope of the best fit line obtained by plotting M_{wt} against $\sqrt{t}$
t = time in hours after a sample is first exposed to water on its lower face

The simplest way to calculate the slope of the regression line is by entering the data in a Microsoft Excell range and use the function SLOPE {data range of M_{wt}; data range $\sqrt{t}$}. The correlation coefficient can be obtained by using the CORREL {data range M_{wt}; data range of $\sqrt{t}$ } function.

The coefficient of correlation should be greater than 0.99. Where the correlation is less than 0.99 it is recommended to plote the curve M_{wt} against $\sqrt{t}$ and examine the curve for non-linear sections. Carry out further regression analysis selecting the linear portion of the plot. At least 5 points are required to obtain a reliable regression analysis.

The water sorptivity (S) is given by:

$$S = \frac{F.\ d.}{M_{sv} - M_{so}}$$

F = the slope of the regression line (g/√h)
d = average sample thickness (mm)
M_{sv} = the vacuum saturation mass of the sample (g)
M_{so} = Mass of sample at t=0 (g)

The water sorptivity is calculated for each of the test samples. The sorptivity index is given as the average of the water sorptivity of the four samples.

7. REPORTING

Report the following, if known:

a) Source of the specimen.
b) Identification number of specimen .
c) Location of specimen within core or cylinder.
d) Type of concrete, including binder type , water/cement ratio and other relevant data supplied with the sample.
e) Description of specimen.
f) Curing history.
i) Unsual specimen preparation eg removal of surface treatment.
j) Test results.

REFERENCES

[1] Alexander MG, Ballim Y, Mackechnie JM, ‘ Concrete durability index testing manual’ Research Monograph no. 4, Departments of Civil Engineering University of Cape Town and University of the Witwatersrand, March 1999

Appendix 4

STANDARD PROCEDURE FOR CHLORIDE CONDUCTIVITY TEST – RESEARCH MONOGRAPH NO 4

1. SCOPE

This test method sets out the procedure for determining the chloride conductivity index as described by Alexander, Ballim and Mackechnie [1].

The test is suitable for the evaluation of materials and mix proportions for design purposes as well as research and development. Sample age may have a significant effect on the test results, depending on the type of concrete and the curing procedure. Care should be taken in interpreting the results of this test when it is used on surface treated concrete's, or on concrete that has been exposed to environmental influences such as carbonation or marine salts.

Since the test results is a function of the electrical resistance of the specimen, the presence of reinforcing steel or other embedded electrical conductive material may have a significant effect.

2. APPARATUS

a) Vacuum saturation facility as described in [1] page 28.
b) Conduction cell as shown in Figure 3.2 page 29[1]. The anode and cathode part of the cell should be permanently marked on the outside of the cell.
c) DC power supply 0-12 Volt, 0-1 Ampere stabilised.
d) Digital Voltmeter and ammeter (2 multi-meters), 4 digits, 0-20 V range, 0-300 mA, rated accuracy 0.1%
e) Electrical cables and plugs.
f) Weighing scale 0.01g.
g) Due to the highly corrosive solutions used during the test all equipment has to be cleaned thoroughly with warm soapy water after each use. The copper electrodes and banana plugs need to be cleaned with sandpaper or an acidic solution. Replacement electrical connections might be necessary from time to time.
h) 10 liter container with a lid.
i) CP grade NaCl (99% purity).

3. SOLUTIONS

a) Sodium chloride solution: Add 2.93 kg of NaCl (salt) to the 10-liter container. Add tap water up to the 10-liter mark. Stir occasionally for 1 day or until all the salt has dissolved. Seal the lid of the container.
b) Saturated calcium hydroxide solution: Add 180 grams of $Ca(OH)_2$ to 1 liter of water.
c) Saturated copper sulfate solution.

4. TEST SPECIMENS

The test specimen shall consist of a 68mm diameter concrete disc cut in a direction perpendicular to the direction of casting from a shuttered surface of a concrete member or laboratory specimen using test method AAA

Four test specimens are required per test.

The samples should be discarded after testing and cannot be retested.

5. CONDITIONING OF THE SAMPLES

a) After cutting and coring store the specimens in the oven at 50 ± 2°C and less than 20% relative humidity for seven days, or until dried to a constant mass.
b) After drying, take the samples out of the oven and cool on a steel tray for 45 minutes.
c) After 45 minutes mark the samples of the same mix 1, 2, and 3 on the inner face.
d) Measure the thickness of each sample with the vernier caliper at 4 points equally spaced around the perimeter of the sample and record the measurements to the nearest 0.1mm on the data sheet.
e) Place the samples in the vacuum tank , seal the tank and evacuate to 75±3 kPa. Maintain the vacuum for 3 hours.
f) After exactly 3 hours allow the salt solution to enter the vacuum tank and cover all the samples. Maintain the vacuum of 75±3 kPa for another 5 hours.
g) After 5 hours allow the samples to soak for another 18±1 hours
h) The above implies that the samples are ready to be tested 27 hours after being taken from the oven.

6. TESTING OF SAMPLES

a) First fill the capillaries of the chloride cell and then both parts of the cell with the salt solution.
b) Take a sample and place it in the rubber ring
c) Place the rubber ring into the central section of the cell and screw it onto the cathode part of the cell. Turn around and screw on the anode part of the cell. Tighten both parts
d) Place the chloride cell horizontally.
e) Pour copper sulphate solution into the connecting points.
f) Connect the ammeter and voltmeter as shown in figure 3.2[(1)]
g) Adjust the DC power supply until the voltmeter reads 5 or 10 Volts.
h) Record the ammeter and voltmeter reading on a standard form.
i) Samples can be discarded after testing.

7. CALCULATION OF THE CHLORIDE CONDUCTIVITY INDEX

The chloride conductivity is given by:

$$\sigma = \frac{i.\,t}{V.\,A}$$

σ = conductivity of the sample (mS/cm)
i = electric current (mA)
V = potential difference (V)
t = thickness of sample (cm)
A = cross-sectional area of the sample (cm^2)

The chloride conductivity is calculated for each of the test samples. The chloride conductivity index is given as the average of the chloride conductivity of the four samples.

8. REPORTING

Report the following, if known:

a) source of the specimen
b) Identification number of specimen
c) Location of specimen within core or cylinder
d) Type of concrete, including binder type, water/cement ratio and other relevant data supplied with the sample.
e) Description of specimen.
f) Curing history.
i) Unsual specimen preparation eg removal of surface treatment.
j) Test results.

REFERENCES

[1] Alexander MG, Ballim Y, Mackechnie JM, ‘ Concrete durability index testing manual’ Research Monograph no. 4, Departments of Civil Engineering University of Cape Town and University of the Witwatersrand, March 1999

SETTING BEHAVIOUR OF SEPARATELY GROUND AND INTERGROUND SLAG CEMENT PRODUCED THROUGH DIFFERENT COMBINATION OF CLINKER AND SLAG

D.K. Mitra and J.D. Panda

Dalmia Institute of Scientific & Industrial Research
Rajgangpur-770017, Orissa, India
E-mail: rkl_disirrgp@sancharnet.in, disirrgp@rediffmail.com

ABSTRACT

The present market trend for early setting of Portland Slag Cement (PSC) has necessitated the need to look for certain controlling parameters keeping the cost factor intact. For this purpose, three different qualities of industrial clinker with C_3S=45, 50 and 59.3% having a grain density of 2.66, 2.70 and 2.54 g/cc with its degree of sulphatization (SD) = 47.3, 29.0 and 35.7 % respectively, along with a batch of granulated slag with its glass content as 97 % collected from a nearby source, are taken to produce PSC prepared by both intergrinding (IG) and separately grinding, followed by intermixing (SGIM) the different combinations of clinker and slag.

It is found that by separately grinding a suitable combination of clinker and slag % (by volume) and intermixing, the resultant cement shows set acceleration, which is in contrast to interground cement wherein selection of suitable clinker/slag combination is not possible, and hence cannot give rise to the required Particle Size Distribution (PSD) of cement and thereby exhibits maximum set retardation. It is observed that irrespective of the process by which cement is ground, it needs to have wide PSD and suitable clinker chemistry with respect to C_3A and SD % in order to get set acceleration. It is also found that with the difference in clinker grain density by 0.04 g/cc there is subsequent increase or decrease by 5.5 % (by vol.) in the clinker/slag composition.

1. INTRODUCTION

In consideration of the increasing demands of the cement customers with regard to quality and efficiency of the products, the technology of the cement grinding process in most of the cement industries have switched over to separate grinding and subsequent mixing process [1]. With respect to set control parameters since it depends on the PSD of cement and clinker chemistry, it is obvious that the proportion of clinker/slag should be such that it can provide the required PSD during grinding that favours the process of coagulation and rigidification [2,3 & 5] in the presence of required level of SD % [4].

This relates to fundamental aspects of grain density of the components as it reflects its volume and thereby brings changes in the clinker/slag proportion which after grinding to a respective fineness shows either narrow or wide PSD, accordingly with the availability of C_3A and SD % setting commences as the hydration of cement progresses.

2. RAW MATERIALS AND TEST PROCEDURES

Three different qualities of clinker- A, B and C, a batch of granulated slag and by-product gypsum are characterized with respect to oxide constituents, clinker phases, degree of sulphatization, grain

density of slag and clinker and SO_3 content in gypsum, Table 1. Each quality of clinker along with the granulated slag and by-product gypsum in the weight proportion of 48.5 %, 50 % and 1.5 % respectively, is interground and separately ground and intermixed to a specific surface area of 350 m^2/kg in the laboratory ball mill, and each fraction of ground components and finished cements are subjected to particle size analysis through FRITSCH analysette 22 and the setting time of each finished cement is determined. Two compositions each with clinker- A and C representing low and high grain density as 2.54 and 2.70 g/cc respectively, are prepared using different combination of clinker and slag and put on trial after separate grinding to 350 m^2/kg and subsequent intermixing and based on its results, the volume % of clinker and slag that is required to reduce the setting time is determined with respect to clinker-B representing grain density 2.66 g/cc and is ground to a fineness of 350 m^2/kg. The results of its particle size distribution with respect to gradient n and setting time are then compared with the relationship drawn between the difference in clinker grain density and subsequent changes in the volume proportion of clinker and slag while using clinker-A and C. In the case of interground cement, all the components are taken together and ground to fineness identical to cements produced through separate grinding and subsequent intermixing. Irrespective of the process of grinding the composition of the finished cements are kept same all through the trials.

Table 1. Raw materials characterization

Constituents %	Clinker A	Clinker B	Clinker C	Granulated slag	By- product gypsum
SiO_2	19.11	20.40	19.28	34.80	ND
Al_2O_3	6.01	6.20	5.93	21.10	ND
Fe_2O_3	3.26	3.70	4.28	0.46	ND
CaO	62.30	61.65	60.80	29.10	ND
MgO	5.16	5.23	5.28	10.20	ND
K_2O	1.22	1.13	1.28	ND	ND
Na_2O	0.13	0.14	0.12	ND	ND
SO_3 (clinker)	0.43	0.54	0.36	-	-
SO_3 (gypsum)	-		-	-	43.20
C_3S %	59.30	45.00	50.00	-	-
C_2S %	10.00	24.50	16.90	-	-
C_3A %	10.40	10.10	8.50	-	-
C_4AF %	9.90	11.30	13.00	-	-
Sulphatization %	35.70	47.30	29.00	-	-
Grain density, g/cc	2.54	2.66	2.70	1.97	-
Glass content in slag, %	-	-	-	97.00	-

3. RESULTS AND DISCUSSIONS

Clinker-A: The intermixed cement no.07 records 45 % reduction in the initial setting time with respect to interground cement no.90 as because one of its separately ground fraction no.31 shows n and x^1 value as 0.202 and 17.10 μm respectively representing wide particle size distribution (PSD) whereas cement no.26 attributes to set retardation due to comparatively narrow PSD and is almost the same as interground cement, Table 2.

It is certain that this difference in setting time is due to the change in the volume % of clinker and slag incorporated into the composition nos.76 and 77 as a result the trend represented by the line FG in Figure 1 takes the position towards the composition made with clinker-B and C.

Table 2. Properties of interground and separately ground PSC prepared by using clinker-A

Composition No.	Composition (Clinker+slag+gypsum)		Grinding Process	Blains (m^2/kg)	PSD		Setting time (minutes)	
	Weight %	Vol. %			Gradient n	Position x^1 µm	Initial	Final
90	48.5+50+1.5	43+57	IG*	352	0.215	16.27	275	305
30	20+20	43.5+56.5	SG*	350	0.215	16.38		
31	28.5+30+1.5	42.4+57.6	SG	351	0.202	17.10		
07(30+31)	48.5+50+1.5	43+57	IM*	350	0.212	16.45	150	205
76	15+30	28+72	SG	351	0.215	15.35		
77	33.5+20+1.5	56.5+43.5	SG	350	0.226	16.27		
26(76+77)	48.5+50+1.5	43+57	IM	351	0.220	16.00	260	285

*IG, SG & IM represents intergrinding, separate grinding & intermixing

Clinker-B: The volume % of clinker and slag required to reduce the setting time is calculated for the nos.72 and 73 based on the results obtained using clinker-A and C and the finished cement no.106 on being tested for setting time records set acceleration by 31 % with respect to interground cement no.176, Table 3. This is represented by the trend line HI in Figure 1.

Table 3. Properties of interground and separately ground PSC prepared by using clinker-B

Composition No.	Composition (Clinker+slag+gypsum)		Grinding Process	Blains (m^2/kg)	PSD		Setting time (minutes)	
	Weight %	Vol. %			Gradient n	Position x^1 µm	Initial	Final
176	48.5+50+1.5	41.7+58.3	IG*	350	0.227	15.90	225	265
72	15+30	27+73	SG*	352	0.205	17.50		
73	33.5+20+1.5	55.4+44.6	SG	351	0.227	15.88		
106(72+73)	48.5+50	41.7+58.3	IM	351	0.217	16.10	155	190

*IG, SG & IM represents intergrinding, separate grinding & intermixing

Clinker-C: Two compositions (48, 51 & 197) and (65, 66 & 145) representing two different combinations of clinker and slag by volume prepared by using clinker-C, out of which the compositions nos. 65, 66 & 145 have a tendency towards reduction in setting time because one of its fraction composition no.65 indicates wide PSD, comparatively the nos. 48, 51 & 197 records narrow PSD and thereby maximum retardation in setting time results with respect to interground cement no.177, Table 4.

Table 4. Properties of Interground and Separately ground PSC prepared by using clinker-C

Composition No.	Composition (Clinker+slag+gypsum)		Grinding Process	Blains (m^2/kg)	PSD		Setting time (minutes)	
	Weight %	Vol. %			Gradient n	Position x^1 µm	Initial	Final
177	48.5+50+1.5	41.5+58.5	IG*	352	0.226	15.85	205	
48	20+20	42.2+57.8	SG*	350	0.214	16.53		
51	28.5+30+1.5	41+59	SG	352	0.231	15.59		
197 (48+51)	48.5+50+1.5	41.5+58.5	IM*	351	0.226	15.76	285	310
65	12.3+32.7	21.5+78.5	SG	351	0.201	17.25		
66	36.2+17.3+1.5	60.2+39.8	SG	352	0.236	15.12		
145(65+66)	48.5+50+1.5	41.5+58.5	IM	351	0.219	15.83	190	220

* IG, SG & IM represents intergrinding, separate grinding & intermixing

However, compared to clinker-A and B, the composition made with clinker-C does not give rise to an appreciable amount of set reduction because C_3A content is only 8.5 % compared to 10.4 and 10.1 % in clinker-A and B respectively. As a result more C_3A could not react despite having high K_2O and low sulphatization % [4]. This accordingly has reflected in the orientation of the trend lines JK and LM representing the composition nos.48, 51, 197 and 65, 66, 145 respectively, Figure 1.The reasons for having same trend of HI and LM joining the compositions 72,73,106 and 65, 66, 145 respectively is because of having less difference in the volume % of clinker and slag.

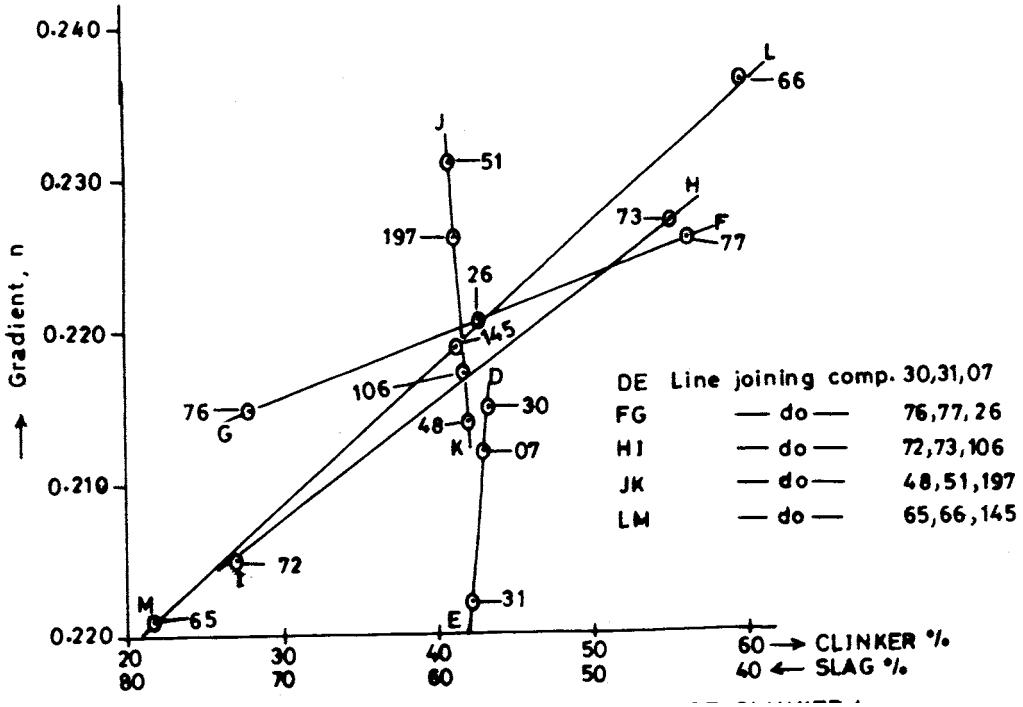

Figure 1. Gradient n as a function of clinker / slag volume %.

It is clear from the compositions contributing to set reduction, Table 2, 3 & 4, that with the difference in clinker grain density by 0.04 g/cc there is simultaneous increase or decrease by 5.5 % (by vol.) in the clinker/slag composition. This linear relationship is shown in Figure 2 where I and II represents two fractions of separate grinding.

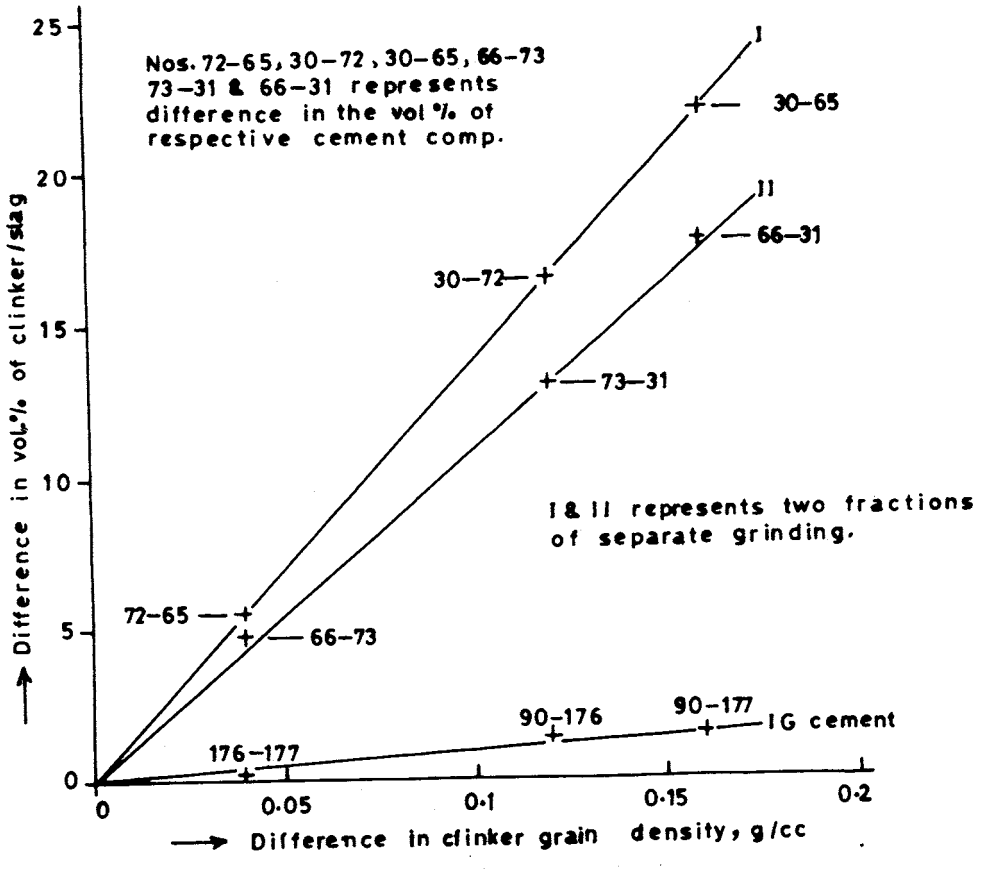

Figure 2. Difference in clinker grain density as a function of difference in clinker / slag volume %.

4. CONCLUSION

It is possible to accelerate the setting time of PSC by separately grinding a suitable combination of clinker and slag % by volume and subsequent mixing which provides the required particle size distribution in cement and the clinker chemistry with respect to C_3A and sulphatization of alkalis. By suitable combination of clinker and slag does not mean to have an approach in acquiring equal grindabilities; rather it is to be referred as an attempt towards achieving favourable PSD in cement. Such combinations, however, are found to vary with the grain density of clinker, which decides the intake of volume of each component that are to be ground. This suggests a linear relationship wherein it is found that with a difference in clinker grain density by 0.04 g/cc there is subsequent increase or decrease in the volume % of clinker/slag by 5.5 %. Further a definite trend is found to exist between the compositions that indicate set acceleration; its gradient n and grain density of clinker, which highlights identical trend for the compositions prepared with the clinkers having less difference in their grain density. Selection of a suitable combination of clinker/slag is however not possible in an interground cement, and hence cannot be aimed for a required PSD which leads to having no control over its setting characteristics.

REFERENCES

[1] Trenkwalder, J and Ludwig, H.M. Conversion of the grinding process for producing cements containing blast furnace slag to separate grinding and mixing at the Karlstadt works, ZKG International,Vol.53, No.10/(2000), P.A24.

[2] Ellerbrock, H.G, Sprung, S and Kuhlmann, K. Particle size distribution and properties of cement- part III, Influence of the grinding process, ZKG International, Vol.43, No.1/(1990),PP.13-19.

[3] Muller- Pfeiffer, M, Ellerbrock, H.G and Sprung, S. Factors affecting the properties of cements with several main constituents, ZKG International, Vol.53, No.5/(2000), PP.241-250.

[4] Richartz, W. Effect of K_2O content and degree of sulphatization on the setting and hardening of cement, ZKG International, Vol.39, No.12/(1986), PP.678-687.

[5] Jiang, S.P, Mutin, J.C and Nonat, A. Studies on mechanism and physico-chemical parameters at the origin of cement setting- I. The fundamental processes involved during the cement setting, Cem. Cocr. Res., Vol.25, No.4 (1995), PP.779-789.

SETTING BEHAVIOUR OF SEPARATELY GROUND AND INTERGROUND SLAG CEMENT PRODUCED THROUGH DIFFERENT COMBINATION OF CLINKER AND SLAG

D.K. Mitra and J.D. Panda

Dalmia Institute of Scientific & Industrial Research
Rajgangpur-770017, Orissa, India
E-mail: rkl_disirrgp@sancharnet.in, disirrgp@rediffmail.com

Dr. J.D. Panda

Dr.Panda after completion of his post graduation in Applied Chemistry from Calcutta University and Dr.Ing.Degree in Ceramics-Technical from University of Clausthal, West Germany, served as Research Chemist with Dr.C.Otto and Company, W.Germany, as Manager Refractory Division with OCL India Limited and since 1975 onwards leading a group of Scientists engaged in the field of Cement and Ceramics as Director, DISIR,Rajgangpur, India. He has visited number of countries and have published 100 research papers in National and International Journal, have attended 80 seminars and conferences and also chaired conferences in number of occasions. He has been awarded Refractory Technologist of the year-1993 by Indian Ceramic Society, Import substitution Award in 1987, 1992 and 1999 and awarded with a Silver Shield by The Invention Promotion Board for import substitution work in 1975. He is a member of Indian ceramic Society, Indian Institute of Ceramic, German Ceramic Society and a Corporate member of American Ceramic Society.

Dr. D.K. Mitra

Dr.Mitra after completion of his post graduation and Ph.D degree in the field of applied geology from IIT., Kharagpur, India, served in different capacity in the field of cement and refractory for the last more than 16 years. Presently as a Sr.Scientist with DISIR, he is actively associated with the fundamental research and developmental work in cement. He has published 6 scientific papers in National and International journal and have attended many seminars/conferences/workshop.

WHAT TRIGGERS CONCRETE DETERIORATION IN AQUEOUS UNDERGROUND ENVIRONMENTS?

Michael Romer and Lorenz Holzer

Swiss Federal Laboratories for Materials Testing and Research (EMPA),
Concrete / Construction Chemistry Lab, PO Box, CH-8600 Duebendorf,
Switzerland. E-mail: bauchemie@empa.ch

ABSTRACT

Interactions of concrete with percolating water produce complicated deterioration-textures and chemical zonations. Although concrete corrosion has many different faces, there are some general phenomena, which are observed in most field studies of deteriorated concrete. As can be estimated from field evidence, many of these parameters (pH-value, chemistry of percolating water and of pore solution) vary with time and place. At a fixed point of consideration different corrosive processes follow each other because the reactive front is moving with time. These processes include dissolution of cementitious phases, transportation of dissolved chemical species and (re-)precipitation of secondary minerals. Further complicated reactions include various kinds of carbonation and sulfate attack. In detail these processes are difficult to predict, because there are a large number of chemical parameters which are difficult to quantify.

The observed textural relationships indicate that chemical attack is triggered by permeable inhomogeneities which serve as pathways for the percolating water. Leaching and dissolution of the cement paste seem to be restricted to the neighborhood of these pathways. Depending on the size of the pathway and the flow rate large amounts of aggressive substances may be brought far into the system and lead to serious degradation. The performance of a defined concrete based on laboratory tests may therefore lead to over optimistic prognoses.

1. INTRODUCTION

Cement based materials are generally characterized by durability qualities. Durability criteria are defined for laboratory tests and bulk properties of material samples. In contrast to these circumstances, situations in reality look quite different and are complicated by a number of factors.

First, the severity of concrete deterioration is related to the risk of failure on one hand and to the costs of repair on the other, but service life of buildings is not related to the average quality of its building materials.

Second, the action of the environment is composed of many different physical and chemical components which generally vary in their intensities over time and within short distances.

Third, the factor of time is of crucial importance. Laboratory tests as a matter of fact have to accelerate the deterioration processes, physical and chemical test conditions are intensified accordingly. The resulting mechanism may therefore be different from the mechanisms during long time interaction.

Proceedings of the 11th International Congress on the Chemistry of Cement (ICCC)
'Cement's Contribution to the Development in the 21st Century'
Hosted by: The Cement and Concrete Institute of South Africa
CD-ROM produced by: Document Transformation Technologies
11 - 16 May 2003, Durban, South Africa
ISBN Number: 0-9584085-8-0
Editors: Dr G. Grieve and G. Owens
Congress Organised by: Event Dynamics

In order to initiate protective countermeasures against all the different forms of chemical interaction it is important to understand the underlying deterioration processes. Because modeling of chemical interaction is complicated by a vast number of variables and manyassumptions have to be made, we try to derive some evidence about the interaction mechanisms on the basis of microscopical investigation of field samples.

2. CHEMICAL INTERACTION OVER SPACE AND TIME

Building materials based on Portland cement always interact with aqueous environments. The porous space inside these materials contains partly or completely an aqueous solution. The chemical composition of this solution is derived from cement and its hydration products and is in equilibrium with the solid components of the system[1]. In contact with an environment of different composition, chemical gradients develop in the building material as well as in the environment leading to diffusion and mass transfer interactions between the ground water and the saturated cement paste [2,3].

The chemical composition of the environment (chemical gradients, diffusion) and the kind of water flow (advective flux) are the promoters of the chemical interaction. The latter is very much dependent on the permeation properties of the building material, capillary suction being the most important driving factor in cases of Portland cement based systems. On the other hand, the transportation of chemical ingredients through the porous system is only possible for those not reacting with the pore solution to form stable solids [4]. The composition of the pore solution as well as the density of the porous structure will both be affected and changed with ongoing chemical interaction.

Water of the environment may principally penetrate porous materials continuously throughout the connected pore space or along local inhomogeneities with larger permeability. The latter pathways have the potential of bringing chemically reactive components far into the material system and of maintaining the diffusion steep gradients. In reality, one can often find locations with advanced degrees of concrete deterioration being related to cracks, joints or interfaces whereas efflorescence on the overall concrete surface gives evidence of a water movement through the porous structure of the building material towards its surface. Most of the concrete damages in underground constructions which require repair or maintenance are related to chemical degradation along local inhomogeneities.

3. SURFACE PHENOMENA

Elevated water saturation of concrete is often associated with pathways (joints, cracks) through the concrete component. The formation of layers of secondary minerals on the surface of concrete could only be observed with relatively thin shotcrete and sodium sulfate hydrates (Figure 1) [5]. Surface scaling of concrete due to the crystallization of salt near the surface is rare in tunnels (maybe due to high levels of humidity). In most cases water is moving along local and permeable inhomogeneities through the concrete. Low flows of water are accompanied by formation of calcite and/or water soluble salts on the surface of the concrete close to the intersection (Figure 2) [6]. Larger flows of water are frequently conducted by biofilms (Figure 3) on the concrete surface and water soluble salts may form in the lateral drying region of the wet concrete. Under biofilms the concrete surface may show phenomena of cement paste dissolution and erosion due to acid attack (Figure 4).

In contrast to these surface phenomena the back of underground constructions is much less accessible for investigation but more pronounced for interactions.

Figure 1. Shotcrete lining in the service tunnel "St. Gotthard" (upper part of the wall) showing a more or less uniform cover with bright efflorescence. Dark (wet) regions within the shotcrete mark localities with water transport and evaporation through the shotcrete.

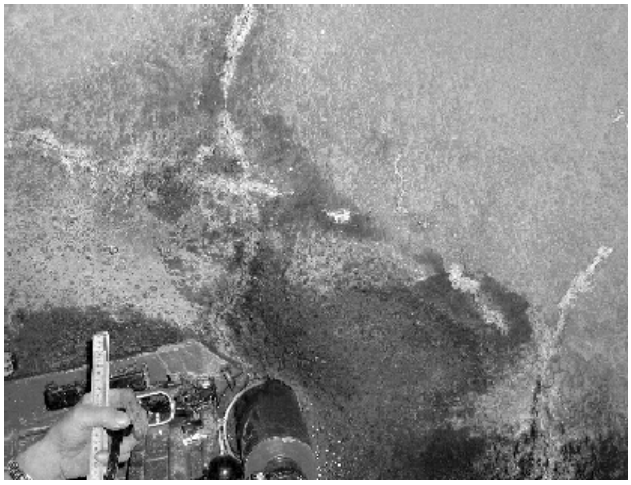

Figure 2. Shotcrete lining in the "Bauen" Tunnel showing formation of a calcite crust directly on the intersection of small deformation induced cracks through the concrete. There are no signs of water running over the concrete surface.

Figure 3. "Gotschna" tunnel: ground water locally penetrating the shotcrete lining. Depending on the amount of running water large amounts of biomass may form. The white mass in the center of the picture represents a colony of sulfur bacteria.

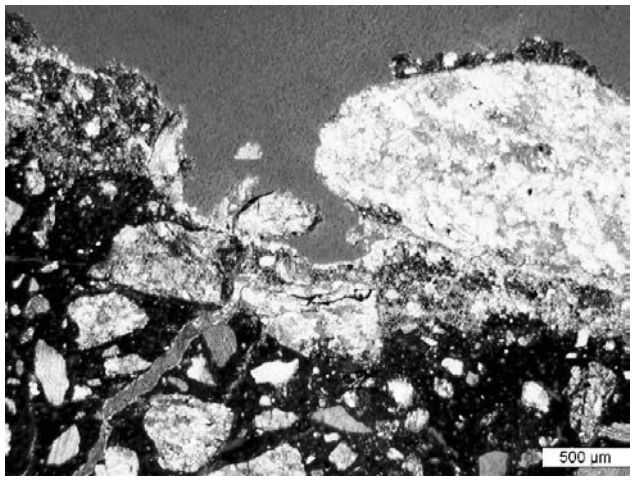

Figure 4. Shotcrete surface from underneath the biomass of Figure 3 (thin section perpendicular to the surface): portlandite in the hardened cement paste is leached off, the top layer of the paste is extensively carbonated whereas part of the original paste is eroded and aggregates are exposed on the surface.

4. CONCRETE DETERIORATION IN CONTACT WITH GROUND WATER

On the surface of concrete exposed to ground water we find the evidence of aggressive components of this water. In a simplified view two processes may be distinguished: 1st - components of the hardened cement paste are dissolved and leached off by the ground water. 2nd - components of the ground water may form stable compounds with constituents of the pore solution or the cement paste. Components of the environment like magnesium or sulfate will react fast with original concrete due to the possibility of the formation of stable reaction products. Therefore only dilute concentrations of water-soluble reactive components may be transported together with pore solution through the concrete, as a consequence this process is followed by substantial leaching. Potassium,

sodium and chloride may be transported in higher concentrations due to their more or less inert behavior.

Phenomena on the inner (accessible) surface of tunnel linings may or may not give indications of severe deterioration processes regarding interactions with ground water. Detailed examination of localities in the concrete with high permeabilities (pathways for ground water) may deliver indirect evidence of corrosive interactions on the outer surface of the concrete exposed to ground water.

Samples of shotcrete and massive concrete of tunnel structures representing different situations in Switzerland have been investigated. The samples were cored carefully in locations showing representative deterioration phenomena as well as at positions without any evidence of deterioration serving as reference samples. After cutting and drying, fractions of the material were chosen for microscopical or analytical investigation.

4.1 Shotcrete

Shotcrete is mostly characterized by a diffuse layering due to the spraying procedure (Figure 5). Alteration by interacting with percolating water produces complicated deterioration-textures and chemical zonations along the contact to the shotcrete support and to a lesser extent along the layer contacts within the concrete. On a microscopic profile starting in the unchanged shotcrete towards the above mentioned contacts the alteration increases and 3 distinct zones can be distinguished (Figure 6). In the zone of leached cement paste the lack of portlandite and the general grain size reduction of cementitious phases give evidence for general dissolution processes. The corrosion zone is characterized by complete dissolution of cement paste resulting in a highly porous and mechanically weak material. The transitions between the regions of different state of alteration are quite sharp. A detailed description of the microscopic and chemical aspects of zonations in deteriorated shotcrete (tunnel lining) is given in [7].

Figure 5. Sample of shotcrete lining of "Koblenz" railway tunnel showing several distinct layers parallel to the support (bottom) due to irregular accumulations of sand, aggregate, paste and air voids.

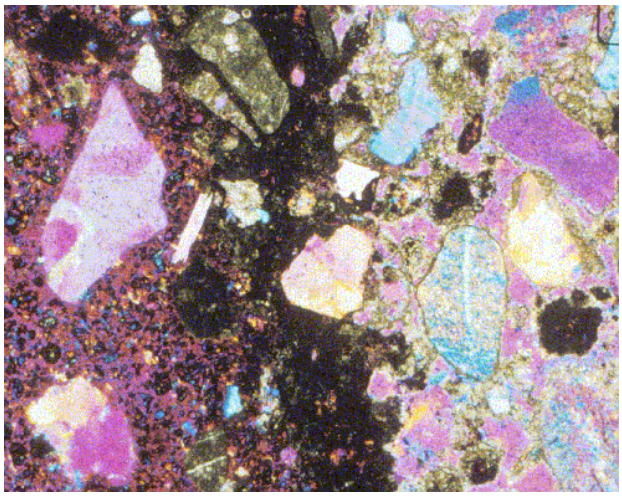

Figure 6. Thin section perpendicular to the crack surface with layering on microscopy scale within one mm (picture size). Leaching zone to the left, corrosion zone to the right with a distinct layer of carbonation in-between (dark). Zonations are propagating to the left with time.

In intensely deteriorated samples the growth of secondary minerals in small veins is superimposed onto the chemical dissolution phenomena. Cracks, veins and pore spaces are filled with very fine and fibrous matter. In relation to the interaction of ground water in tunnel concrete the formation of sulfate containing minerals was dominated by thaumasite. Ettringite on the other hand could be

detected as recrystallized needles in air voids surrounded by unaltered paste that is interpreted as a ordinary consequence of high degrees of water saturation over longer periods of time [8]. Thaumasite in contrast is associated with different kind of chemically altered or deteriorated concrete[9].

4.2 Massive concrete

After more than 30 years of interaction with percolating sulfate-rich groundwater the concrete of a road tunnel locally displays massive corrosive damage up to complete chemical disintegration reaching up to 20 cm thickness. Chemical and mineralogical alteration along the rock-concrete contact leads to cracking and loss of attachment with the underlying rock, giving way to contact-parallel migration of groundwater. Corrosive interactions along primary inhomogeneities within the concrete are taking place in a similar way. The pattern of interaction phenomena may change drastically along a single intersection though the concrete showing evidence of extensive leaching or the formation of new mineral solids like brucite or gypsum (Figure 7). As a result of long time interaction over decades, larger volumes of concrete may be affected starting from these primary inhomogeneites whereas the majority of the concrete structure is more or less unaffected by interactions with ground water (Figure 8).

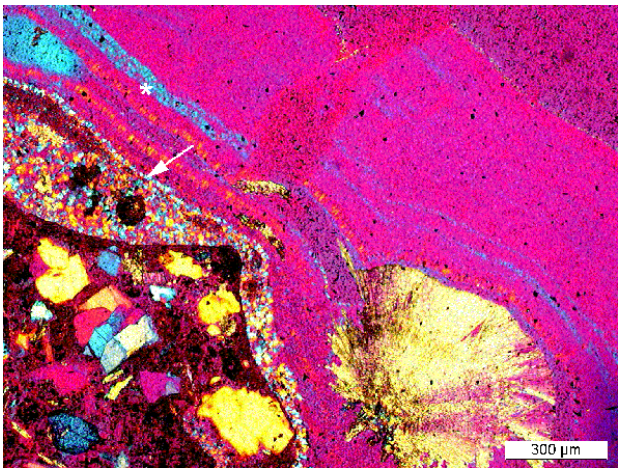

Figure 7. Layers of brucite(*) and thaumasite (arrow) together with a rosette of aragonite/calcite on the concrete crack surface (bottom left).

Figure 8. Concrete lining of “San Bernardino” tunnel: depending on whether the altered concrete is wet or dry it shows properties of a mush or a crumbly material.

5. DISCUSSION

The observed textural relationships indicate that chemical attack is triggered by permeable inhomogeneities which serve as pathways for the percolating water. Shotcrete linings are rather thin and inhomogeneous regarding the distribution of porosity. Therefore shotcrete is quite often found to be substantially affected by ground water whereas the deterioration in ordinary concrete is mostly restricted to primary inhomogeneities like joints, cracks or regions with poor compaction. Leaching and dissolution of the cement paste seem to be restricted to the neighborhood of these pathways.

The stability of hydration products in hardened cement paste is dependent on the chemical composition of the pore solution which itself is chemically buffered by the latter. As a consequence the interaction with an aqueous environment of different composition is not resulting in a continuous alteration over distance but in the formation of a zonation pattern: regions with different solid compositions show relatively sharp transitions between them. This gives evidence of a moving boundary behavior in the opposite direction of the diffusion flux [4].

At a fixed point of consideration different corrosive processes follow each other because the reactive front is moving with time. These processes include dissolution of cementitious phases, transportation of dissolved chemical species and (re-)precipitation of secondary minerals. The flow of water through a crack always leads to leaching of the crack walls.

Depending on the flow rate and the density of the concrete as well as on its state of leaching the water in the crack is shifting its composition in the direction of the chemical composition of pore solution. At the same time the chemical concentration of the percolating ground water is important for the diffusion of aggressive components like sulfate into the neighboring paste. Depending on the flow rate through the crack, leaching effects and formation of new reaction products are superimposed (Figure 9). For the same original composition of interacting water different phenomena and reaction products may be formed dependent on the pathway and whether the composition of the local cement paste is leached at the same time or not [10].

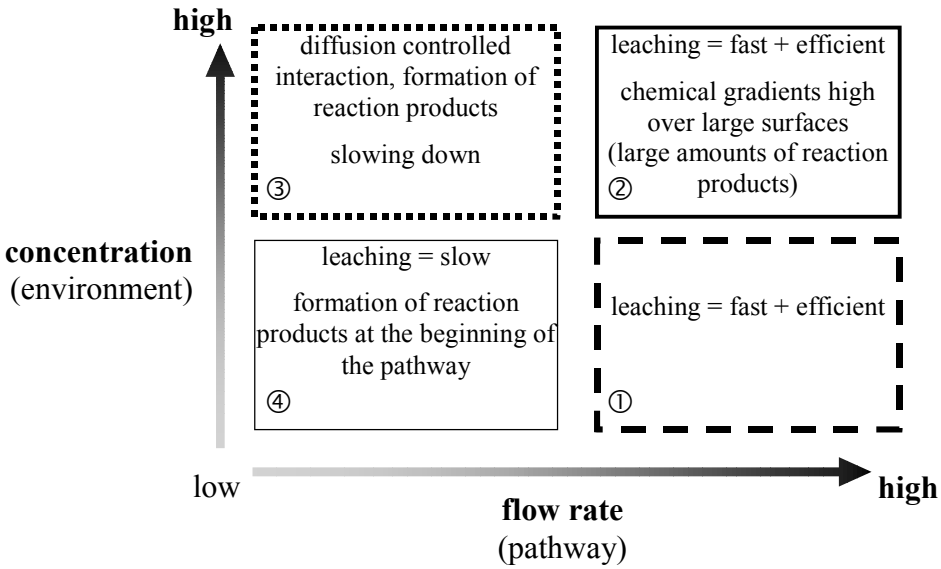

Figure 9. Schematic presentation of the parameters flow rate and chemical concentration of the percolating water and the interaction patterns resulting in different combinations of these parameters.

Extensive leaching of concrete in underground constructions (pattern ① and ② in Figure 9) is not only important for the degradation of the building material itself, it may also cause the formation of precipitates in the drainage system. This process leads to the failure of the drainage and to a pressure increase which itself will force the water to penetrate new pathways. Pattern ③ represents the situation in laboratory test conditions and pattern ④ could be illustrated with the situation of a dam wall. The latter patterns are related to decelerating processes whereas extended leaching may lead to accelerating interaction mechanisms.

6. CONCLUSIONS

The observed textural relationships of deteriorated concrete in underground constructions indicate that chemical attack is triggered by permeable inhomogeneities which serve as pathways for the percolating water.

It is therefore important to note that physical parameters like permeability or inhomogeneities are at least as important as chemical parameters like the composition of the paste, pH-values and composition of the interacting water. Performance test in general don't take into account the effects of cracks and other pathways of percolating water and may therefore lead to over optimistic prognosis.

The flow rate of percolating water in a defined cavity is defining the route of chemical interaction by having a major impact on the bringing in of reactive constituents, the formation of diffusion gradients and the advective transport of soluble paste components out of the system. Because of different sizes of intersections and resulting flow rates, interaction phenomena may be quite different within short distances.

In all investigated tunnel structures with concrete in contact with ground water, the processes of leaching and the formation of sulfate minerals, predominantly thaumasite, have been detected. As a consequence thaumasite may be a very common finding in a large number of underground constructions. The concentration of sulfate in the ground water as well as the use of cement with low contents of aluminum seem to be less important.

The adhesion of shotcrete linings may be affected by small amounts of interactions on the interface. In this regard not only water described as ”aggressive” corresponding to regulations has to be considered but a wide range of chemical compositions, severe conditions may therefore be related to ground water not considered as aggressive corresponding to current standards.

The workmanship in the production of concrete as well as in the placement and after-car are crucial for the bulk properties of the concrete components as well as for tight joints between them. In aggressive environments the contact of ground water with concrete has to be prevented by sealing off the concrete structure.

ACKNOWLEDGMENTS

The projects have been funded by the Swiss Federal Roads Authority (ASTRA) and by the Swiss Federal Laboratories for Materials Testing and Research (EMPA). We would also like to thank Marcel Pfiffner and Andreas Leemann for contributing with field work and microscopical investigations.

REFERENCES

[1] Mehta, P.K., Schiessl, P. and Raupach, M. Performance and Durability of concrete systems, 9th International Congress on the Chemistry of Cement pp.571-659 (New Delhi, 1992).
[2] Diamond, S. Concrete pore solutions. Cement and Concrete Research 11, pp.383-392 (1981).
[3] Andac, M. and Glasser, F.P. Long-term leaching mechanisms of Portland cement-stabilized municipal solid waste fly ash in carbonated water. Cement and Concrete Research 29, pp.179-186 (1999).
[4] Samson, E., Marchand, J. and Beaudoin, J.J. Modeling the influence of chemical reactions on the mechanisms of ionic transport in porous materials An overview. Cement and Concrete Research 30, pp.1895-1902 (2000).
[5] Romer, M. and Lienemann, P. Versalzung und Korrosion von Spritzbeton (Sicherheitsstollen des Gotthard-Strassentunnels). Chimia, Neue Schweizerische Chemische Gesellschaft 52, pp.197-201 (1998).
[6] Romer, M., Holzer, L. and Pfiffner, M. Interaction of water with concrete: Deterioration Mechanisms, CONSEC'01: Concrete Under Severe Conditions (eds. Banthia, N. et al.) pp.1075-1082 (Vancouver, BC, Canada, 2001).
[7] Holzer, L. and Romer, M. Corrosion of concrete: Assessing the mechanisms, 7th Euroseminar on Microscopy Applied to Building Materials (eds. Pietersen, H.S. et al.) pp.67-79 (Technical University of Delft, The Netherlands, Faculty of Civil Engineering and Geosciences, Delft, NL, 1999).
[8] Famy, C. and Taylor, H.F.W. Ettringite in hydration of portland cement concrete and its occurence in mature concretes. ACI Materials Journal 98, pp.350-356 (2001).
[9] Romer, M., Holzer, L. and Pfiffner, M. Swiss tunnel structures: concrete demage by formation of thaumasite, 1st international conference on thaumasite in cementitious materials pp.(in press) (London, England, 2002).
[10] Taylor, H.F.W. and Gollop, R.S. Some chemical and microstructural aspects of concrete durability in Mechansisms of chemical degradation of cement-based systems (eds. Scrivener, K.L. and Young, J.F.) pp.177-184 (E & FN Spon, London, 1997).

WHAT TRIGGERS CONCRETE DETERIORATION IN AQUEOUS UNDERGROUND ENVIRONMENTS?

Michael Romer and Lorenz Holzer

Swiss Federal Laboratories for Materials Testing and Research (EMPA),
Concrete / Construction Chemistry Lab, PO Box, CH-8600 Duebendorf,
Switzerland. E-mail: bauchemie@empa.ch

Michael Romer
PhD. in Earth Science

Affiliation: Swiss Federal Laboratories for Materials Testing and Research (EMPA)

Function: Head of Concrete / Construction Chemistry Lab

E-mail address: michael.romer@empa.ch

Contact details: PO Box
CH-8600 Duebendorf
Switzerland
Tel: +41 1 823 41 35, fax +41 1 823 40 35

INFLUENCE OF CEMENT EXTENDERS ON THE CORROSION RATE OF STEEL IN CRACKED CONCRETE

Scott, A.[1] and Alexander, M. G.[1]

[1] Department of Civil Engineering, University of Cape Town, RSA, E-mail: mark@eng.uct.ac.za

ABSTRACT

In-service cracking in reinforced concrete structures allows for the rapid onset of corrosion due to chloride ion ingress. The impact of cracking on the subsequent corrosion rate is, however, less clear, particularly where different cementitous materials are used.

The influence of cement extenders on the corrosion of steel in cracked beam specimens exposed to chloride solutions is being investigated in a research program at the University of Cape Town. As part of a wider program, four concrete mixes comprising OPC, 50% slag, 30% FA and 7% SF were studied. Specimens were loaded to produce a centrally located crack with a nominal width of 0.2mm. The results showed a significant dependence of corrosion rate on the type of extender.

1. INTRODUCTION

The corrosion of reinforcing steel in concrete has been the subject of extensive investigations for many years. There are numerous articles that describe the fundamental principles and mechanisms relating to the corrosion of steel reinforcing [1,2,3]. Cement extenders have been shown to improve the time to initiation of corrosion given adequate curing and cover [4,5]. There is however less understanding and agreement on the influence of cement extenders on the corrosion rate of steel in concrete. The subject of cracking is another area that tends to complicate the corrosion issue and one that has also been the subject of much debate. Relatively little work has been done on the influence of cement extenders on the corrosion of steel in cracked concrete.

Slag concretes in particular have been the focus of concern primarily due to the presence of sulphides in the pore water. Tromans [6] has suggested that sulphides may be incorporated into the oxide layer thus reducing its ability to protect the steel. Valentini et al [7] conducted an investigation into the corrosion rates of steel in blastfurnace slag mortars, at slag replacement levels of 20, 45 and 75%. A water:binder (w/b) ratio of 0.5 was used with covers of 10 mm and water curing for 28 days prior to storage at 50% and 100% relative humidity (RH). Their results showed that immediately after curing the slag-containing samples had a corrosion rate 10 times higher than the Ordinary Portland Cement (OPC) control. This difference decreased with time but the slag-containing samples generally maintained somewhat higher passive corrosion rates at 50% RH. These articles note that tests performed at different ages may give contradictory results, and this may be attributed to the variation in sulphide pore solution concentration which is not constant with time.

Arya and Xu [8] examined a number of cement extenders using steel anodes with cast-in chlorides at 1 and 3% coupled by a Zero Resistance Ammeter to a chloride free cathode. For 3% chlorides it was shown that corrosion rates occurred in decreasing order of Fly Ash > OPC > Slag > Silica Fume, for cement replacement levels of 35, 0, 65 and 10% respectively. The FA and OPC samples

Proceedings of the 11th International Congress on the Chemistry of Cement (ICCC)
'Cement's Contribution to the Development in the 21st Century'
Hosted by: The Cement and Concrete Institute of South Africa
CD-ROM produced by: Document Transformation Technologies
11 - 16 May 2003, Durban, South Africa
ISBN Number: 0-9584085-8-0
Editors: Dr G. Grieve and G. Owens
Congress Organised by: Event Dynamics

displayed similar corrosion rates with the Slag and SF samples both showing much lower rates. Sirivivatnanon et al [9] investigated the influence of similar cement extenders in mortar samples and found different results. Mild steel samples were cast into blocks of mortar with a w/b ratio of 0.8, 10 mm cover and a number of cement replacement levels. After initial curing, the samples were exposed to a 3% NaCl solution. The macrocell corrosion rates at 6 months were in the order of OPC > FA > Slag > SF as shown in Table 1. There was however a significant difference in corrosion rate between the 5% and 10% SF replacement levels, which would alter the corrosion ranking order.

Table 1. Corrosion rate as a function of binder type [9]

Binder Type	*Approx Rate (uA/cm^2)*
OPC	2.25
20-40% FA	0.75
40-60% Slag	0.5
5% SF	1
10% SF	0.2

The results of Sirivivatnanon et al [9] showed a variation in order of corrosion rates, based on cement replacements, which differed from those of Arya and Xu [8]. The presence of chlorides from the onset may inhibit the formation of the passive layer and have further effects on the concrete microstructure which would otherwise not have occurred thus giving different results as noted.

The presence of cracks and their impact on corrosion is equally contentious. Beeby [10] and Arya and Wood [11] suggest that there is no direct relationship between crack width and corrosion rate. They refute other claims of a correlation by stating that the cracks may accelerate corrosion initiation, but not necessarily the propagation rate. Assuming two cracks A and B, which become active at 1 and 2 years, after 3 years there is 100% more corrosion at crack A, this falls to 50% at 4 years and 5% after 20 years. Thus the time at which the measurements are taken will affect the comparison. Arya and Wood [11] state that the more important considerations are: 1) crack properties, for instance whether the crack is active or dormant, 2) concrete – steel properties, whereby low permeability of the concrete will limit ionic transport, high moisture limits oxygen ingress and increased strength leads to better bond and less slip at the steel-concrete interface, 3) service environment. Controlling the environment around the steel concrete interface is seen to be more important than the presence of the crack itself.

The work of Francois and Arliguie [12] and Suzuki et al [13] also supports the argument of limited effect of crack width on corrosion rate. Suzuki et al. [13] however showed that there are some early-age differences in corrosion rate based on crack width but these decrease with time. It was found that the w/c ratio had a more significant impact on corrosion rate. Pettersson and Jorgensen [14] looked at a number of crack width and cover combinations using both OPC and SF concrete. For a w/b of 0.3 it was found that cover had an effect on corrosion rates for crack widths of 0.4 mm. For cracks widths above this value cover had negligible effect on corrosion. The smaller crack widths would be more likely to benefit from autogenous healing and thus limit the effect of the crack. The corrosion rate was shown to vary with addition of micro silica from a value of 10 μm/year for OPC, 5 μm/year for 5% replacement and approximately 2.3 μm/year for 10 and 15% replacements at 300 days. Marcotte and Hansson [15] have also shown reductions in corrosion rates associated with cracked high performance concrete (HPC). They state however that the use of HPC resulted in less than expected performance improvements. The greater degree of microcracking in the HPC may have been responsible.

The focus of the current investigation therefore is directed towards an improved understanding of the influence of cement extenders on the corrosion rate of steel in concrete. Since cracks clearly represent a point of easy access of chlorides to the steel, thus circumventing the normal requirement for diffusion of chlorides or carbonation, it was deemed necessary to examine what further effects they would have coupled with the use of cement extenders. Four binder types consisting of OPC, slag, FA and SF were used in the current investigation. A surface crack width of less than 0.2 mm was chosen which would be considered allowable under most environmental conditions.

2. EXPERIMENTAL METHOD

The corrosion of steel was investigated in concretes, using four different binder types, and subjected to cyclic wetting and drying. Identical samples of OPC, slag (50%), FA (30%) and CSF (7%), at a water: binder ratio of 0.58, were prepared. The oxide analyses of the materials used are presented in Table 2. The mix proportions and 28 day strengths for the concretes are given in Table 3.

Table 2. Oxide analyses of binder materials (%)

Oxide	*OPC*	*SLAG*	*FA*	*SF*
SiO_2	21.5	35.4	53.1	91.9
CaO	65.9	33.5	4.2	0.0
Al_2O_3	3.7	15.8	33.7	0.7
Fe_2O_3	3.6	0.9	3.6	0.8
Mn_2O_3	0.06	0.90	0.05	0.09
TiO_2	0.18	1.20	1.77	0.11
MgO	0.88	11.10	1.02	0.26
SO_3	2.44	0.60	0.30	0.46
K_2O	0.54	0.90	0.75	1.33
Na_2O	0.19	0.30	0.40	0.42

Table 3. Mix proportions and 28 day strengths

Materials	OPC	Slag	FA	SF *
Water (ℓ/m^3)	175	175	175	175
Cement (kg/m^3)	302	151	211	281
Extenders (kg/m^3)		151	91	21
Sand (kg/m^3)	750	750	750	750
Stone (kg/m^3)	1050	1050	1050	1050
Strength (MPa)	47	44	40	53

* Superplasticiser used to ensure particle dispersion

Mild steel bars of diameter 16 mm were cast into the samples at a cover depth of 20 mm. The bars were first brushed to remove the mill scale and thoroughly cleaned. A wire was attached to one end of the bar and both ends were heat shrink-wrapped and epoxy-coated to provide an exposed surface area of 158 cm^2. Prior to casting, the bars were again cleaned and degreased with acetone. The overall dimensions of the concrete samples were 375 x 120 x 120 mm.

The specimens were demoulded after 24 hours and water-cured for another 14 days at 20^{o}C. A centrally located transverse crack was created in the samples by three-point bending. There was some relaxation of the crack once the load was removed and thus it was necessary to initially overload the sample. The crack widths were measured and those corresponding to a surface crack width of approximately 0.2 mm were chosen. The cracks were maintained through partial slipping of the round bar. The crack widths have been reasonably constant over the initial exposure period.

A reservoir was created on the surface and specimens exposed to a weekly cycle of three days wetting with a 5% NaCl, solution and four days drying, at 30 ^{o}C. A number of identical non-cracked specimens were also cast and subjected to the same exposure conditions for comparative purposes.

The samples were monitored bi-weekly for corrosion potential, rate and resistivity. Resistivity measurements were taken using a 4 probe Wenner system. Corrosion rate data was obtained by means of coulostatic technique whereby a small charge was applied to the steel and the relaxation of the potential monitored over a fairly short period of time, see Figure 1. The characteristic profile of the decay curve as given by equation 1 was then used to determine the time constant

$$n_t = n_o \exp\left(\frac{-t}{\tau_c}\right) \tag{1}$$

where n_t is the potential shift at time t, n_o is the initial potential shift and τ_c is the time constant [16]. The polarization resistance (Rp) is then obtained from the time constant and capacitance (C) information, equations 2 and 3, with q_s being the applied charge.

$$\tau_c = CR_p \tag{2}$$

$$C = \frac{q_s}{n_o} \tag{3}$$

The polarization resistance was then converted into a corrosion rate (i_{corr}) by means of the Stern Geary relationship, equation 4 [2], with an assumed constant value B of 26 as suggested by Andrade and Alonso [17].

$$i_{corr} = \frac{B}{R_p} \tag{4}$$

The potential was monitored against a Ag/AgCl reference electrode and recorded using an HP 34970A data acquisition unit. The perturbation was produced by means of a single shot pulse generator capable of supplying a charge of up to 30 mA over a defined period, usually less than 30 milliseconds.

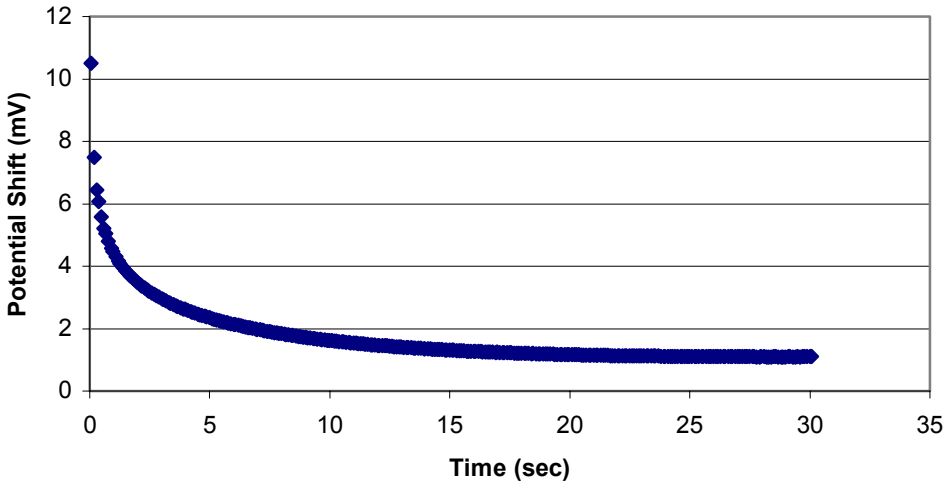

Figure 1. Coulostatic potential transients

3. RESULTS

3.1 Resistivity Data

Resistivity measurements were taken on three occasions: at the start of the drying cycle, at the same time as the corrosion rate measurements (taken during the drying period), and finally at the end of the drying period just before ponding. The results reported are based on a moving average of three periods corresponding to time of corrosion rate measurements. The results of resistivity measurements for the four binder types are shown in Figure 2. It can be seen that mineral extenders have a marked effect on the resistivity of the concrete. The FA samples had the highest resistivity stabilizing at approximately 75 kOhm.cm after steadily increasing for the first 26 weeks. The resistivity of the slag samples increased fairly slowly from their initial value of 20 kOhm.cm to a high of 50 kOhm.cm before reducing somewhat to 40 kOhm.cm. SF showed an initial rapid rise of resistivity similar to that of FA but subsequently leveled off after approximately 14 weeks at about 35 kOhm.cm. There was a very slow and minor increase in the resistivity of OPC concrete and values remained well below those of the other three binder types. The decrease in resistivity measurements after week 40 may be a result of some climate control problems that were experienced; it is not clear at this stage whether the subsequent downward trend may be due to chloride ingress.

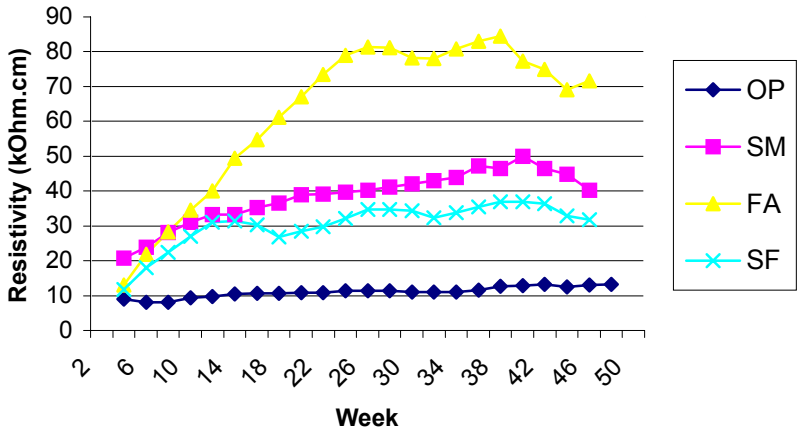

Figure 2. Resistivity measurements

The measurements of resistivity over each weekly drying cycle showed significant variability, dependant on binder type. The OPC samples showed the least variability in resistivity, about 19 percent, over a typical weekly cycle, with the SF, slag and FA samples displaying typical variations of 28, 30 and 31 percent respectively.

3.2 Corrosion Rate Data

The results for the cracked samples are shown in Figure 3 as a moving average of three readings. The corrosion rate of steel in cracked concrete appears to be strongly influenced by the use of cement extenders. The OPC samples displayed the highest initial corrosion rate of approximately 0.67 $\mu A/cm^2$ and continued to increase over the study period to a maximum of about 2.5 $\mu A/cm^2$. The samples containing cement extenders had initial corrosion rates of 0.15, 0.25 and 0.43 for the SF, slag and FA samples respectively. The rates for the SF samples increased fairly rapidly and settled at a similar value to FA of approximately 0.45 $\mu A/cm^2$ by week 26. During this same period the OPC samples increased from their initial value of 0.67 to over 1.4 $\mu A/cm^2$. The slag samples showed a minor increase in corrosion rate from 0.25 $\mu A/cm^2$ to a reasonably steady value of 0.35 $\mu A/cm^2$.

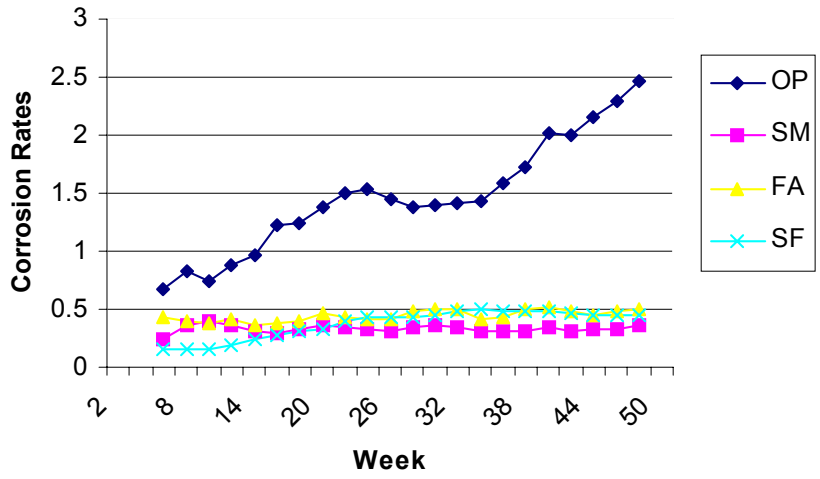

Figure 3. Corrosion rates (μA/cm^2) of 0.2 mm cracked samples

The corrosion rates of cracked and uncracked concretes were also compared for OPC samples only. The onset of active corrosion was marked by a substantial increase in both corrosion potential and rate. Corrosion initiation for cracked concrete was almost immediate upon exposure to the chloride solution, whereas the steel in the uncracked concrete only started to corrode when sufficient chlorides had diffused through the concrete and reach the steel (a period of approximately 25 weeks). The comparison of corrosion rates for cracked concrete and uncracked concrete adjusted to similar times for initiation are shown in Figure 4. There is clearly a more gradual increase in corrosion rate for the uncracked specimens.

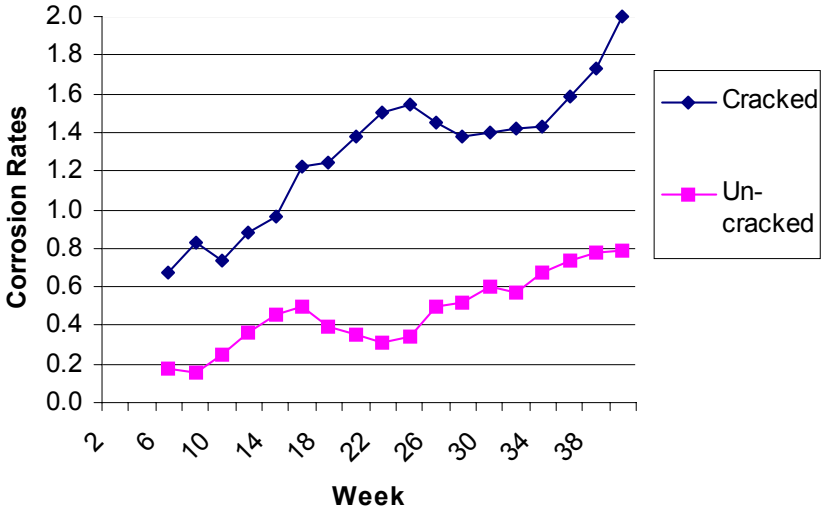

Figure 4. Corrosion rates (μA/cm^2) for cracked and uncracked OPC concrete

3.3 Pre-Ponding Potential Data

It was observed that prior to cracking, and before ponding, the samples containing slag had a significantly higher negative potential value compared with the other samples, which then fell rapidly after cracking. A limited and ongoing investigation into the effects of cracking on the

potential of slag-containing concretes was then conducted. The potentials of samples after two weeks of wet curing showed that SF had the least negative of -90 mV, followed by FA and OPC at about -190 to -250 mV and finally slag at –600 mV. Two subsequent set of mixes (SL, SH) containing 25 and 75 % slags were then cast and the potentials immediately following cracking are shown in Figure 5.

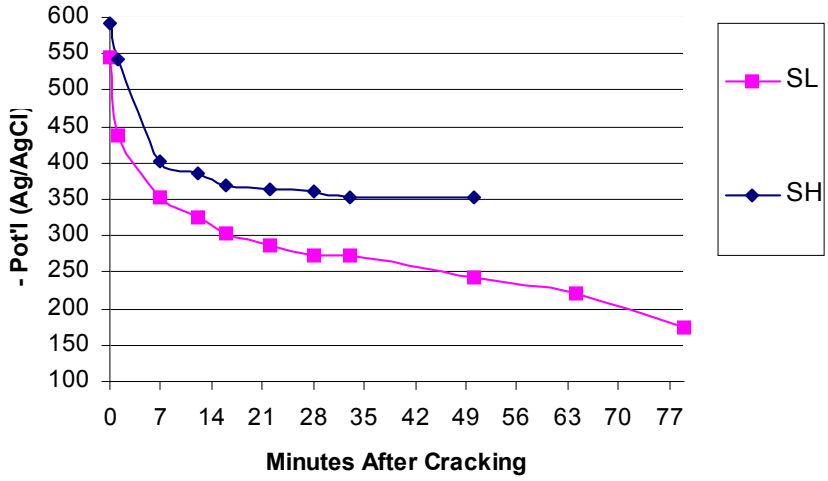

Figure 5. Post-crack potentials of slag concrete

The potentials values of the slag concretes rose rapidly, from an initial potential of approximately –550 mV before cracking, to –300 mV or more after thirty minutes for SL. Twenty four hours after cracking the potentials of SL and SH had further increased to more than –200 mV. This rapid rise in potential was only observed in the slag bearing concretes.

4. DISCUSSION

The development of cracking, as previously noted, was obtained through limited slipping of the bar which in turn could act as a preferential site for the movement of chlorides and subsequent corrosion. Ingress of chloride ions along slipped versus un-slipped bars was investigated separately using a silver nitrate, ultra-violet test method adapted from Schoppel et al [18]. The preliminary results indicate that while there is preferential movement of chlorides along the bar interface, compared to the bulk concrete, there was no significant difference between the slipped and un-slipped bars. Furthermore as cracking was introduced at 14 days there was still some time for subsequent healing of the bond interface due to continued hydration. The SF and OPC would have the least reserve capacity for continued hydration, followed by slag and FA. An examination of the corrosion rates reveals that OPC had significantly the highest corrosion rate followed by FA and SF and then slag with the lowest. As the continued hydration of the FA should limit the impact of the early bar slip it is clear that factors other than degree of slip and subsequent healing are the more important parameters.

It has long been argued that resistivity of the concrete plays a significant role in the corrosion rate of steel in concrete [19]. While this generally appears to be true, a significant variation can be seen with respect to the FA samples. FA concretes had a resistivity approximately 2 times greater than the SF concrete despite having nominally the same corrosion rate, and 1.5 times greater than slag concrete while having a higher corrosion rate. The resistivity ratios for OPC, FA, and SF are similar to those given by Baweja et al [20].

The results of 28 day chloride conductivity tests, as given by Alexander et al [21] and Magee [22], generally correlate with the corrosion rates obtained for the current study. The approximate values given in Table 4 for chloride conductivity show the highest values for OPC and FA with similar values for Slag and SF.

Table 4. Chloride conductivity measurements
(14d curing, w/b 0.6)

Binder Type	*Chloride Conductivity (mS/cm)*
OPC	2.0
FA	1.5
Slag	1.1
SF	1.0

The use of chloride conductivity measurements therefore may offer some additional insight into the corrosion rates of steel and is currently being investigated.

A clear relationship has been demonstrated between increasing pH and chloride levels required for the initiation of corrosion [23]. The impact of cement extenders on pH levels has been shown by Arya and Xu [8] with OPC having the highest OH^- concentration followed by similar levels for slags and FA and considerably reduced levels for SF. The reduced OH^- concentration in SF concretes may offset the improved physical properties of the material thus accounting for the similar corrosion rates to FA concrete which are higher compared to slag. The variations in corrosion rates between any of the cement extenders is however relatively small when compared to the substantial reduction in rate they offer over OPC concrete.

The impact of pore water chemistry on corrosion rates must also be considered. Salvarezza et al [24] demonstrated a relationship between SH-/OH- ratio and nature of the passive layer, such that at high SH^-/OH^- ratios a more porous sulphide-containing layer dominates the composition. Cao et al [25] however stated that the passivation of steel is more stable in slag solutions than OPC. The exact role of sulphides present in slag concretes is still not entirely understood and further investigations are necessary. The presence of sulphides in the slag may account for the high negative potentials just prior to cracking. It was observed that once the samples were cracked these values very quickly reduced to more passive conditions. The cracks could allow an easy pathway for the movement of oxygen thus overcoming the more reducing environment associated with the sulphides at the steel. These rapid reductions in potentials were only observed in the slag-bearing concretes. Further research is currently being conducted to more accurately quantify these phenomena.

5. CONCLUSION

The addition of cement extenders has a significant impact upon the corrosion rate of mild steel in cracked concrete, in the order of OPC>FA>SF>slag. The OPC concrete had corrosion rates at least 5 times higher than any of the other extended cement concretes at week 48. All cracked extended concretes therefore displayed superior performance compared even to un-cracked OPC concrete. The magnitude of resistivity measurements did not adequately explain the variations in corrosion rate with FA having by far the highest resistivity and yet the second highest corrosion rate (0.50 $\mu A/cm^2$). It appears that chloride conductivity measurements may offer some help in explaining the likely corrosion rates in the light of the cement chemistry of the pore solution. Of particular interest is the rapid decline in corrosion potential of slag concretes following initial cracking which has been attributed to oxidation of sulphides at the steel concrete interface.

REFERENCES:

[1] Tuutti, K. Corrosion of steel in concrete, Swedish Cement and Concrete Research Institute, 1982.

[2] Schiessl, P. ed. Corrosion of steel in concrete: Report of the Technical Committee 60-CSC RILEM, Chapman & Hall, 1988.

[3] Glass, G. and Buenfeld, N. The presentation of the choride threshold level for corrosion of steel in concrete, Corrosion Science, Vol 39, No. 5, 1997, pp. 1001-1013.

[4] Mangat, P. et al. Microstructure, chloride diffusion and reinforcement corrosion in blended cement paste and concrete, Cement and Concrete Composites, Vol. 16, 1994, pp. 73-81.

[5] Mackechnie, J. and Alexander, M. G. Marine exposure of concrete under selected South African conditions, Proceedings third ACI/CANMET Int. conference on the performance of concrete in marine environment, St. Andrews by-the-Sea, Canada, 1996 pp. 205-216.

[6] Tromans, D. Anodic polarization behavior of mild steel in hot alkaline sulfide solutions, Journal of Electrochemical Society, June, 1980, pp. 1253-1256.

[7] Valentini, C. et al. Influence of blast furnace slags on the corrosion rate of steel in concrete, Corrosion Rates of Steel in Concrete: ASTM STP 1065, Philadelphia, 1990, pp. 17-28.

[8] Arya, C. and Xu, Y. Effects of cement type on chloride binding and corrosion of steel in concrete, Cement and Concrete Research, Vol. 25, No. 4, 1995, pp. 893-902.

[9] Sirivivatnanon, V. et al. Influence of fly ash, ground granulated blast furnace slag and silica fume on chloride induced corrosion of steel in reinforcement, 2nd International Symposium on Blended Cements, Malaysia, 1994, pp. 114-120.

[10] Beeby, A. Cracking, cover and corrosion of reinforcement, Concrete International, February, 1983, pp. 35-40.

[11] Arya, C. and Wood, L. The relevance of cracking in concrete to corrosion of reinforcement, (Concrete Society Technical Report No. 44), 1995.

[12] Francois, R. and Arliguie, G. Influence of service cracking on reinforcement steel corrosion, Journal of Materials in Civil Engineering, February, 1998, pp. 14-20.

[13] Suzuki, K. et al. Mechanism of steel corrosion in cracked concrete, Corrosion of reinforcement in concrete, third international symposium on corrosion of reinforcement in concrete construction, Warwickshire, 1990, pp. 19-28.

[14] Pettersson, K. and Jorgensen, O. The effect of cracks on reinforcement corrosion in high-performance concrete in a marine environment, Proceedings third ACI/CANMET Int. conference on the performance of concrete in marine environment, St. Andrews by-the-Sea, Canada, 1996, pp. 185-200.

[15] Marcotte, T. and Hansson, C. A comparison of chloride-induced corrosion products from steel-reinforced industrial standard versus high performance concrete exposed to simulated sea water,International Symposium on High Performance and Reactive Powder Concrete, Sherbrooke, 1998, pp. 145-162.

[16] Hassanein, A. et al. The use of small electrochemical perturbations to assess the corrosion of steel in concrete, NDT&E International, Vol 31, No. 4, 1998, pp. 265-272.

[17] Andrade, C. and Alonso, C. Corrosion rate monitoring in the laboratory and on-site, Corrosion and Building Materials, Vol 10. No. 5. 1996, pp. 315-328.

[18] Schoppel, K. et al. Indication of free chloride ions on concrete surfaces by the UV-test, Betonwerk and Fertigteil-Technik, Heft 11, 1988, pp. 80-85.

[19] Bentur, A. et al. Steel corrosion in concrete: fundamentals and civil engineering practice, London: E&FN Spon, 1997.

[20] Baweja, D. et al. Chloride-induced steel corrosion in concrete: part 2-gravimetric and electrochemical comparisons, ACI Materials Journal, May-June, 1999, pp. 306-313.

[21] Alexander, M. G. et al. Guide to use of durability indexes for achieving durability in concrete structures: research monograph No. 2, Cape Town, University of Cape Town, 2001

[22] Magee, B. Performance of Silica Fume Concrete, University of Cape Town, 1998, Research Report 1/98, pp. 56-57.

[23] Page, C. and Vennesland, O. Pore solution composition and chloride binding capacity of silica-fume cement pastes, Materials and Structures, Vol. 16, No 19, 1983, pp. 19-25

[24] Salvarezza, R. et al. The electrodissolution and passivation of mild steel in alkaline sulphide solutions, Corrosion Science, Vol. 22, No. 9, 1982, pp. 815-829.

[25] Cao, H. et al. Corrosion characteristics of steel in solutions derived from cements and blended cements, Cement and Concrete Research, Vol. 20, 1990, pp. 325-334.

[26] Glass, G. K. et al. (1993), An Investigation of Galvanostatic Transient Methods Used to Monitor the Corrosion Rate of Steel in Concrete, Corrosion Science, Vol. 35, No 5-9, pp. 1585-1592.

[27] Rodriguez, P. and Gonzalez, J. (1994), Use of the Coulostatic Method for Measuring Corrosion Rates of Embedded Metal in Concrete, Magazine of Concrete Research, Vol. 46, No. 167, pp. 91-97.

MODELLING THE DURABILITY PROPERTIES OF CONCRETE COVER

E.J. Griesel and M.G. Alexander

Department of Civil Engineering, University of Cape Town,
P O Rondebosch, 7701, South Africa. E-mail: ejg@mweb.co.za

ABSTRACT

Durability properties of reinforced concrete are governed by the characteristics of the concrete cover layer, sometimes called the covercrete. Three durability indexes have been developed to quantify the properties of this layer, and include measures of oxygen permeability, chloride conductivity and water sorptivity of concrete specimens. However, the relationships between the various microstructural properties of the covercrete and these indexes are not yet fully understood.

A model is proposed which takes into account the dynamic interaction of cement hydration, microstructure formation and moisture transport. The hydration process is based on a multi-mineral hydration-heat model, and is dependent on sufficient pore moisture. Pore structure development is modelled as a function of the average degree of hydration, which is also used as a basis for moisture transport processes. The dynamic coupling of these models makes it possible to approximate microstructure development for arbitrary initial and boundary conditions.

This model is to be encapsulated into finite element computer code, which will be experimentally verified and used to investigate the influence of the various microstructural properties on the durability indexes.

Keywords: durability, durability indexes, hydration, microstructure, moisture transport, covercrete, drying, dynamic interaction.

1. INTRODUCTION

At present, there is sustained interest in problems of concrete durability, due to premature deterioration of many structures worldwide. Regarding reinforced concrete in particular, it is now realised that the primary determinant of durability is often the quality of the concrete cover layer, sometimes called the covercrete. The properties of this layer, and in particular its transport properties, govern the durability performance of the structure.

The need has arisen for practical design parameters that can be used for durability, in much the same way as the compressive strength test has been used up until now for quality control purposes. In response to this need, three durability index tests have been developed, which provide measures of oxygen permeability, water sorptivity and chloride conductivity of concrete specimens [1]. Thus far these tests have been researched extensively, and fledgling efforts are being made to incorporate them as design parameters into construction specifications. However, the influence of many important variables on the development of covercrete properties, including exposure conditions, is not yet fully understood. In the context of hot and dry climates such as exist in South Africa, it is particularly important to be able to characterise the influence of drying at early ages on the properties of the covercrete.

This paper considers the essential links between the microstructure of the cover layer and the engineering parameters describing its transport properties. It discusses the modelling of the microstructure and its development with time, using a multi-variable approach, based on fundamental relationships of cement chemistry and physics. The variables considered include cement (binder) type, mix proportions, exposure conditions, and time. Once this fundamental modelling is complete, the relationships between the microstructural properties and the engineering covercrete properties can be explored. This will aid in a better understanding of the important factors governing covercrete quality, and assist in arriving at improved specifications and construction practices so as to ensure long-term durability of concrete structures.

2. OVERVIEW OF DURABILITY INDEXES

The durability index tests provide measures for the chloride conductivity, water sorptivity and oxygen permeability of standard concrete samples [2]. These are cylindrical cores of 68 mm diameter and 25 mm thickness, which are oven dried at 50°C and 15% relative humidity prior to testing. Samples are dried until the change in mass is less than 0.1% over a 24 hour period.

2.1 Water Sorptivity Index Test

The samples are placed onto saturated layers of absorbent material in a plastic tray, and their mass gain monitored at prescribed time intervals. To ensure uniaxial absorption, the sides of the samples are sealed prior to testing. The water sorptivity index is calculated using the dimensions of the specimen, its porosity and the absorption rate, and is interpreted as the rate of penetration of the water front, in mm/√hr.

2.2 Oxygen permeability index test

This test involves determining the rate at which oxygen permeates through a pre-conditioned concrete sample, using a falling head permeameter [2]. An initial oxygen pressure differential of approximately 100 kPa is applied across the sample. The pressure decay with time is measured, and the Darcy coefficient of permeability is determined. The oxygen permeability index is the negative logarithm of the coefficient of permeability.

2.3 Chloride conductivity index test

This test determines the conductivity of concrete samples, from their dimensions and electrical resistance. The samples are saturated with a 5 M NaCl solution prior to testing, by immersion under vacuum (-80 kPa) for 24 hours. The test procedure involves applying a potential of 10 V across the ends of the specimen and measuring the electrical current (DC) passing through, using a conduction cell filled with 5 M NaCl solution.

3. RELATIONSHIPS BETWEEN CAPILLARY POROSITY AND THE DURABILITY INDEXES

In a previous study a theory on concrete drying was formulated, which was based on the reduction of pore relative humidity (PRH) with time and depth from exposed surfaces, and its influence on cement hydration and subsequently the development of microstructural properties [3].

The influence of drying processes was obtained from an empirical expression formulated by Parrott [4], which described the changes in PRH with time and concrete depth, while cement hydration was roughly estimated from work done by Soroka [5]. The theory was based on the fact that hydration rates are very sensitive to changes in PRH, and that significant changes in porosity of the cement paste take place above 95% PRH [4]. Rough estimations were calculated on the variation of capillary and gel porosity with depth from exposed surfaces, and these were related to the results from the durability indexes.

Good correlations were found between the calculated capillary porosity and the durability indexes. These findings appeared promising enough to justify a more thorough investigation of early age development of the covercrete microstructure, and the influence thereof on the durability indexes.

4. MODELLING OF COVERCRETE PROPERTIES

Microstructure formation of concrete exposed to the environment is a complex problem, and incorporates a large number of variables. It is reasonable to assume that the potential service life of a reinforced concrete structure is largely established during the early stages of construction, typically within the first 10 days after casting [6]. At this stage the covercrete has a dynamic microstructure, which is highly sensitive to proper curing and initial exposure conditions [3].

The major processes involved in microstructure formation are cement hydration and moisture transport, which are dynamically linked, especially at early ages [3, 6]. Hydration is responsible for the development of the microstructure, and is very sensitive to the availability of sufficient pore moisture. The properties of the resulting microstructure, on the other hand, govern moisture transport processes, particularly drying, and thus the availability of pore water for further hydration. In order to model microstructure formation for arbitrary mix proportions and exposure conditions, it is necessary to take the dynamic interaction of these processes into consideration.

In a recent publication [6], analytical models were developed for microstructure formation, cement hydration and moisture transport, which are based on fundamental material models for the individual processes. Formulations are simplified as much as possible, for the purpose of integrating them into real-time computational schemes of heat and moisture transport of real-sized structures.

The hydration process is based on a multi-mineral hydration-heat model, and is dependent on sufficient pore moisture. Pore structure development is modelled as a function of the average degree of hydration, which is used again as basis for moisture transport processes. The dynamic coupling of these models makes it possible to approximate microstructure development for arbitrary initial and boundary conditions.

4.1 Cement Hydration

The hydration model in this study is based on the process of hydration-heat generation of cement in concrete, for any arbitrary temperature history, as quantified by Suzuki et al [7]. Hydration reactions in Portland cement are described for each clinker mineral, and interdependencies among them are evaluated separately. The total amount of hydration-heat is then obtained as the sum of the individual reactions, in proportion to the weight fractions of the clinker minerals. The cement minerals included are alite (C_3S), belite (C_2S), an aluminate phase (C_3A), a ferrite phase (C_4AF) and gypsum.

This approach makes it easy to include additional mineral components, e.g. in the case of blended cements. The extenders included in this model are fly ash (FA) and slag (SG), as single-phase hydration minerals. They are not classified like Portland cement, and it is assumed that the part reacting is only the glass phase at normal temperature, and is regarded as a homogeneous material [8]. The reactions of these extenders are described in terms of the amount of calcium hydroxide produced by hydration, and their delaying effect on hydration is taken into account. At this stage, the hydration of slag is assumed to be unaffected by the presence of gypsum.

The hydration process is described as the weighted sum of the individual mineral reactions, thus

$$\begin{aligned} H &= \sum p_i H_i \\ &= p_{C_3A}(H_{C_3AET} + H_{C_3A}) + p_{C_4AF}(H_{C_4AFET} + H_{C_4AF}) + \\ &\quad p_{C_3S}H_{C_3S} + p_{C_2S}H_{C_2S} + p_{SG}H_{SG} + p_{FA}H_{FA} \end{aligned} \tag{1}$$

where p_i = weight fraction of component i
H_i = heat-generation rate of component i
H_{C3AET} and H_{C4AFET} are both heat rates resulting from the formation of ettringite

It has been confirmed by Uchida and Sakakibara [9] and Suzuki et al [7] that Arrhenius's Law is applicable to cement hydration, and the heat generation rate (H_i) of each mineral component is described by the following equation:

$$\begin{aligned} H_i &= \gamma_i \beta_i \mu H_{i,T0} e^{-\frac{E_i}{R}(\frac{1}{T}-\frac{1}{T_0})} \\ Q_i &\equiv \int H_i dt \end{aligned} \tag{2}$$

where E_i = activation energy of component i
R = gas constant
Q_i = accumulated heat of component i
$H_{i,T0}$ = reference heat generation rate of component i at constant temperature T_0, and is also a function of Q_i
γ_i = coefficient which expresses the delaying factor of organic admixtures
β_i = coefficient which expresses the reduction in heat generation due to the reduced availability of free water
μ = coefficient which expresses changes in heat generation with the concentration of calcium hydroxide
$-E_i/R$ = definition of the thermal activity of component i

The reference heat generation rate ($H_{i,T0}$) is set as a material function for each reaction (Figure 1), with T_0 taken as 293 K, and is assumed to be under conditions where sufficient water (and calcium hydroxide for slag and fly ash) is available.

The hydration process is modelled as a step-wise function of time and temperature, using the above information. A time interval is chosen, and for each reaction (and time-step) a value for its accumulated heat is calculated from the relationship

$$Q_i = H_{i,T0} t_{tot} \tag{3}$$

where t_{tot} = total time elapsed since the start of hydration (hours)

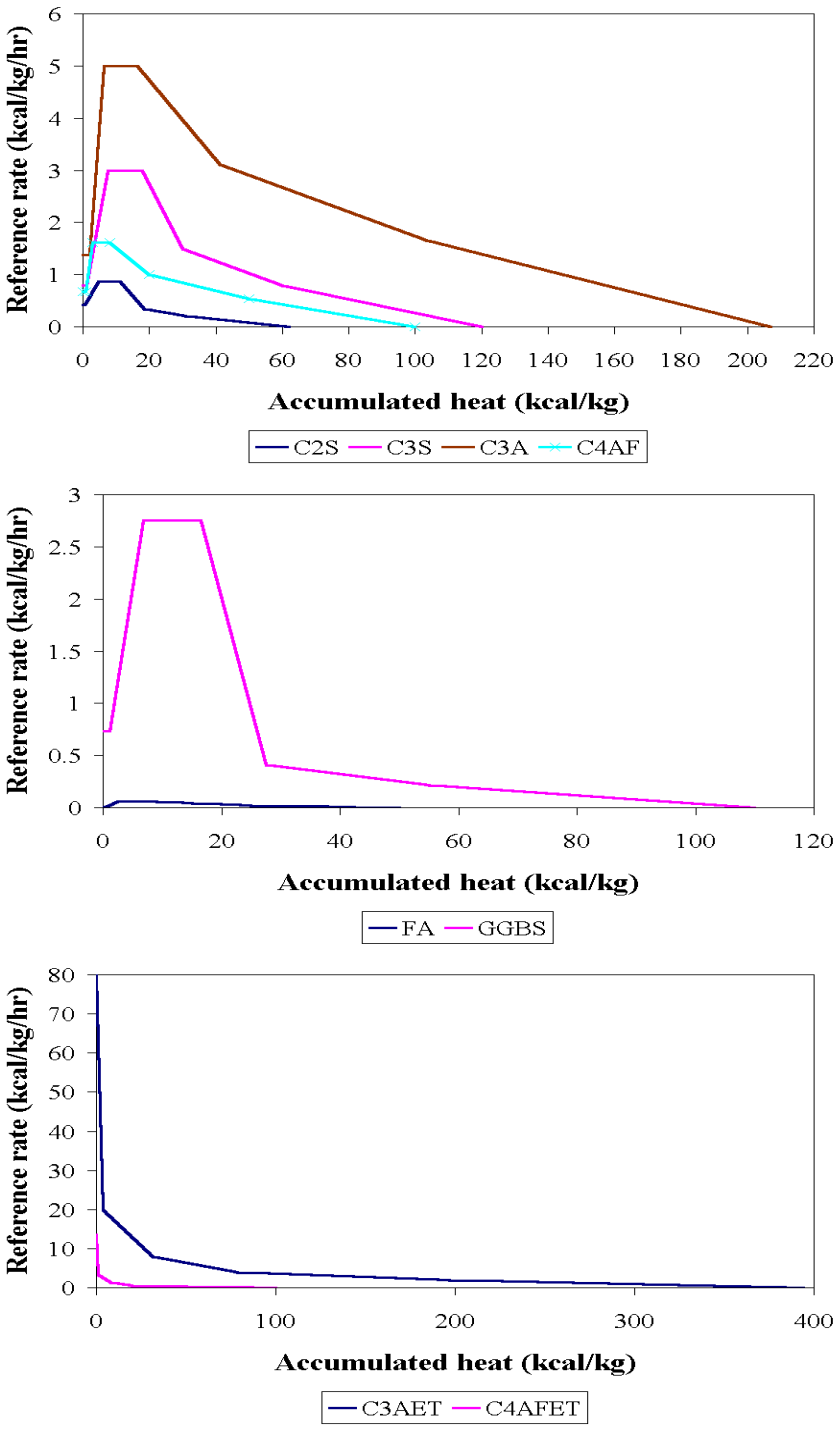

Figure 1. Reference heat generation rates of cement minerals

The value used for $H_{i,To}$ in this calculation is obtained from the appropriate part of the curve in Figure 1. The degree of hydration for each reaction is calculated from

$$\alpha = \frac{Q_i}{Q_{i,\infty}} \tag{4}$$

where a = degree of hydration

$Q_{i,\infty}$ = maximum amount of accumulated heat for reaction i (Figure 1)

Using the calculated value for Q_i, the thermal activities of the individual reactions (E_i/R) are calculated from the relationships illustrated in Figure 2. Finally, coefficients γ_i, β_i and μ are calculated, and the final heat generation is obtained from Equation 1.

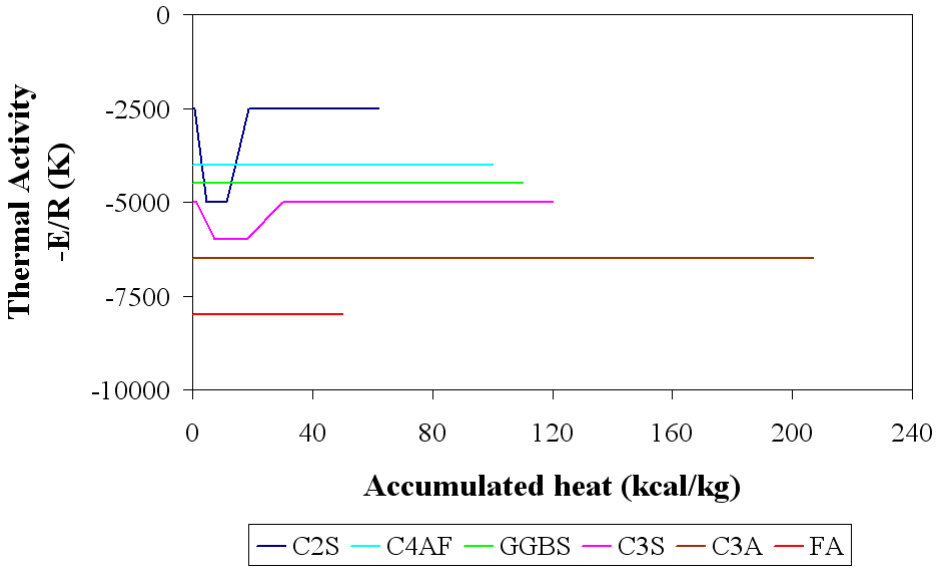

Figure 2. Thermal activities of component reactions

The system temperature used in Equation 2 (T) is calculated at the end of each time step, using the total amount of heat generated (Equation 1) and a heat conduction analysis to take environmental temperature into account.

4.2 Microstructure Formation

The degree of hydration and amount of chemically combined water, calculated from the hydration model, are used to calculate the development of the cement paste microstructure. This part of the model is based on the concept of cement particle growth, as computed from the state of maturity of the cement paste matrix, as illustrated in Figure 3 [6].

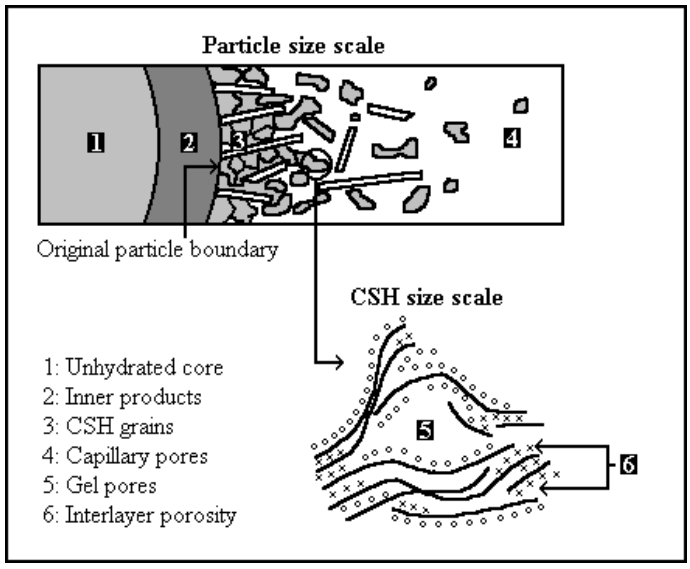

Figure 3. Cement particle growth

Important assumptions made here are that cement particles are spherical, uniform in size and uniformly distributed in the initial state of the mix. These may seem like gross approximations,

taking into account the fact that the particle size distribution (PSD) of commercially available cements varies over at least two orders of magnitude.

However, the dispersion characteristics of the cement paste are more important than the particle distribution itself [6]. For water:powder ratios in the normal range, it has been found that the distance between powder particles is of the same order of magnitude as the average particle size. In the case of flocculation of powder particles, the average size of flocculated clusters can be used as the representative size of particles. While a model that takes the entire PSD into account would be more accurate and theoretically preferable, the above assumptions make it possible to deal with any initial configuration of the dispersed system. Also, the evaluation of the microstructural properties of real structures can be evaluated without using extensive computational resources.

The porosity of the cement paste is subdivided into three categories, namely interlayer porosity, gel porosity and capillary porosity. These can be calculated from the degree of hydration, the volume of gel products, characteristic gel porosity and assumptions regarding interlayer thickness, interlayer specific surface area and the density of chemically bound water. The porosity of the inner products (Figure 3) is assumed to be constant, and the capillary porosity in the outer product is assumed to vary linearly (with the option to extend this to a polynomial function) from the particle boundary to the outer region of the expanding clusters.

This information is used to calculate the total amount of hydration products for any given degree of hydration, which is further used to obtain the volume of capillary and gel pores present in the cement paste. The specific surface areas (or surface area per unit volume of cement paste) of capillary and gel porosities are obtained next, in order to be able to formulate an expression for the pore size distribution (or porosity as a function of pore radius) of the cement paste.

It is assumed that moisture transport takes place only in the gel and capillary pores, because interlayer moisture is physically bound and unable to move under normal pressure gradients [6]. Therefore, the porosity distribution function takes the form

$$\phi(r) = \phi_{lr} + \phi_{gl}\left(1 - e^{-B_{gl}r}\right) + \phi_{cp}\left(1 - e^{-B_{cp}r}\right) \tag{5}$$

where $\phi(r)$ = porosity distribution
r = pore radius (m)
ϕ_{lr} = interlayer porosity
ϕ_{gl} = gel porosity
ϕ_{cp} = capillary porosity
B_{gl} = porosity parameter for gel pores
B_{cp} = porosity parameter for capillaries

The parameters B_{gl} and B_{cp} are obtained from an explicit relationship, which relates B_i as a function of S_i/ϕ_i [6].

4.3 Moisture Transport

Due to the dynamic nature of the developing cement paste microstructure, the hydration and microstructure formation described in the previous sections are included in the formulation of an expression for moisture transport. This implies that the rate of change of pore water content is not only a function of pore pressure gradients, but also of chemical fixation during hydration, as well as the rates of change of porosity, density of pore water and degree of saturation [6].

The authors of [6] used the conventional energy conservation principles to obtain an expression that describes concrete water content in terms of pressure gradients and diffusivity and permeability coefficients. This expression was further extended into a pore pressure based formulation (Equation 6), with an additional term to account for self-desiccation (Q_{hyd}) and porosity changes (Q_{pd}). This process is illustrated in Figure 4 [6].

$$\alpha_P \frac{\partial P}{\partial t} - div\left(D_P \nabla P\right) + Q_P = 0 \tag{6}$$

where P = pore pressure (Pa)
t = time (s)
α_P = specific fluid mass capacity parameter, and approximately equal to the amount of water the concrete can absorb (or release) for a unit change in the liquid pore pressure potential
D_P = macroscopic moisture (liquid and vapour) conductivity (m^2/s)
Q_P =rate of moisture loss due to hydration and microstructure formation

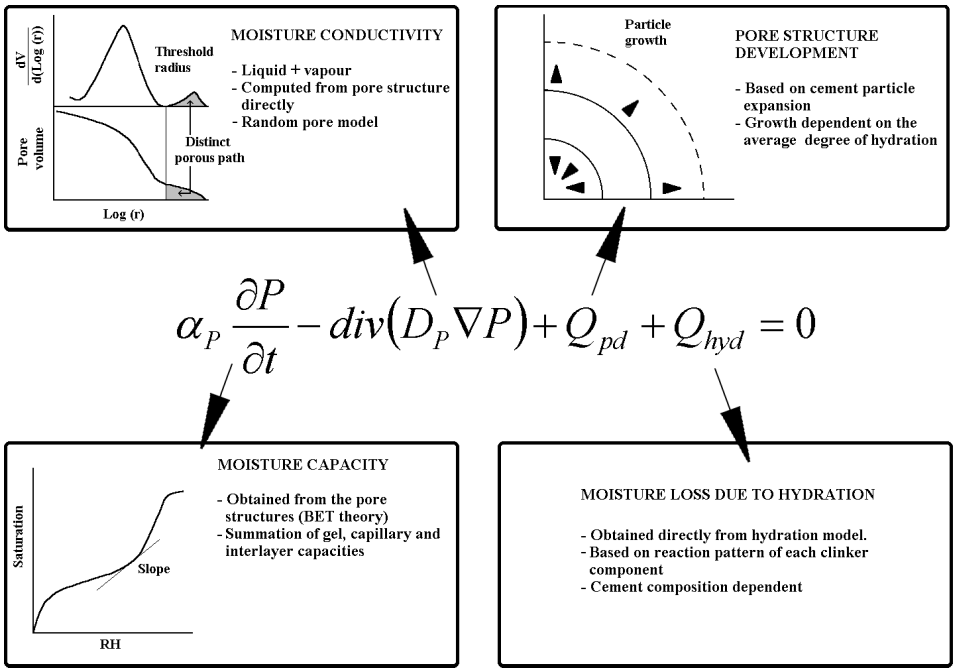

Figure 4. Schematic representation of the calculation of moisture conditions in concrete

In order to use the above expression for computational use, it was necessary to quantify a number of phenomena observed for moisture conditions in cementitous materials. These include the hysteresis effect observed during wetting and drying cycles, moisture retention under normal environmental conditions and simplified expressions for moisture conductivity coefficients.

4.4 Concrete as a composite material

The hardened cement paste matrix in concrete is but one of the three major components considered during moisture transport. The zone connecting the cement paste and the aggregates, called the interfacial transition zone (ITZ), is another important contributing component, while the role of the aggregates themselves become significant when considering high porosity aggregates (typically used for light-weight concretes or to compensate for self-desiccation at low water:binder ratios).

For any given aggregate grading, it has been found that there exists a crucial aggregate content, usually above 45%, at which percolation of interfacial transition zones (ITZ) occurs [6]. This means that neighbouring ITZs of different aggregate particles come into contact with each other, and form

at least one continuous path to exposed surfaces. These paths are generally more porous than the neighbouring cement paste matrix, due to insufficient packing of powder particles next to relatively large aggregate particles [6]. For normal mix proportions, the characteristics of the ITZ are crucial in defining the moisture transport behaviour in concrete.

In order to quantify the moisture transport in concrete, a multi-component model is considered. The assumption is made that thermodynamic equilibrium holds for moisture transport in each of the separate components of interest. These are evaluated individually and summed to obtain the net effect. Finally, expressions are evaluated and included in the result, to compensate for the interactions (or local moisture transfer) between individual components.

5. COMPUTER MODEL AND EXPERIMENTAL VERIFICATION

The theory as discussed above is to be encapsulated into a finite element computer model, in order to generate large quantities of microstructural data and investigate the influence of various covercrete properties on the durability indexes.

Firstly, however, the output generated by the model must be verified experimentally, and conditions that produce inaccurate results, identified. The purpose of the model is not to model extreme mix designs and environmental conditions, but rather to get a feel for the influence of 'normal' designs, construction practice and environments on the microstructural properties of the covercrete.

The calculated properties that will be verified experimentally include degree of hydration, porosity distributions and moisture distributions of fully cured samples, as well as samples exposed to controlled drying conditions. The latter might call for some sort of 'layered' experimental approach, where the covercrete is divided into several layers of uniform thickness, and evaluated separately. The experimental technique to be used has not yet been finalised.

6. CONCLUSIONS

Three durability indexes have been developed, providing measures of oxygen permeability, chloride conductivity and water sorptivity of concrete specimens. However, the relationships between the various microstructural properties of the covercrete and these indexes are not fully understood.

A model is proposed which takes the dynamic interaction of cement hydration, microstructure formation and moisture transport into consideration. Cement hydration is based on a multi-mineral hydration-heat model. Hydration reactions are described for each clinker mineral, and interdependencies among them are evaluated separately. The total amount of hydration-heat is then obtained as the sum of the individual reactions, in proportion to the weight fractions of the clinker minerals. The cement minerals included are alite, belite, an aluminate phase, a ferrite phase and gypsum. Fly ash and slag are included in the model as single-phase hydration minerals.

Microstructure formation is based on the concept of cement particle growth, as computed from the state of maturity of the cement paste matrix. The cement particles are assumed to be uniformly sized and distributed in the initial state of the mix. The porosity of the hydrating cement paste is sub-divided into interlayer-, gel- and capillary porosity. The amount of hydration products is calculated, and used to obtain the volume of capillary and gel pores present in the cement paste. This information is used to calculate the specific surface areas of the pores, and finally the porosity distribution of the cement paste.

A multiphase formulation is used to describe the combined transport processes of both liquid and vapour, and thus the overall moisture transport process is reduced to Fick's second law. This called for simplified expressions for moisture conductivity coefficients, and phenomena such as the hysteresis effect of moisture isotherms and moisture retention under normal environmental conditions were quantified [5].

In order to quantify the moisture transport in concrete, a multi-component model is considered. The assumption is made that thermodynamic equilibrium holds for moisture transport in each of the separate components of interest, which are the hardened cement paste, the aggregates and the ITZ. These are evaluated individually and summed to obtain the net effect. Finally, expressions are evaluated and included in the result, to compensate for the interactions (or local moisture transfer) between individual components.

A computer model is to be developed, experimentally verified and used to generate large quantities of data, in order or identify and quantify the microstructural properties that influence the durability indexes. The purpose of the model is to get a feel for the influence of general designs, construction practice and environments on the microstructural properties of the covercrete.

REFERENCES

[1] Alexander, M.G. 1997. An indexing approach to achieving durability in concrete structures, FIP '97 Symposium: The Concrete Way to Development, Johannesburg, March 1997, Concrete Society of Southern Africa, pp. 571-576.

[2] Griesel, E.J. and Alexander, M.G. June 2001. Effect of Controlled Environmental Conditions on Durability Index Parameters of Portland Cement Concretes. Cement, Concrete and Aggregates, Vol. 23, No. 1, pp. 44-49.

[3] Griesel, E.J. 1999. The influence of controlled environmental conditions on potential concrete durability. MSc(Eng) Thesis, University of Stellenbosch.

[4] Parrott L.J. 1988. Moisture Profiles in Drying Concrete. Advances in Cement Research, Vol. 1, No. 3, pp. 164-170.

[5] Soroka, I. 1979. Portland Cement Paste and Concrete. MacMillan Press Ltd., London and Basingstoke, pp. 30-36.

[6] Maekawa, K., Chaube, R. and Ksihi, T. 1999. Modelling of Concrete Performance: Hydration, microstructure formation and mass transport. London: Routledge. 308p.

[7] Suzuki, Y., Tsuji, I., Maekawa, K. and Okamura, H. 1990. Quantification of Hydration-heat Generation Process of Cement in Concrete. Concrete Library of JSCE (Japan Society of Civil Engineers). No 16.

[8] Maekawa, K. and Kishi, T. November. 1996. Multi-component model for hydration heating of blended cement with blast furnace slag and fly ash. Translation from Proceedings of JSCE (Japan Society of Civil Engineers). No. 550, V-33.

[9] Uchida, K. and Sakakibara, H. 1987. Formulation of the heat liberation rate of cement and prediction method of temperature rise based on cumulative heat liberation. Concrete Library of JSCE (Japan Society of Civil Engineers). No 9.

MODELLING THE DURABILITY PROPERTIES OF CONCRETE COVER

E.J. Griesel and M.G. Alexander

Department of Civil Engineering, University of Cape Town,
PO Rondebosch, 7701, South Africa. E-mail: ejg@mweb.co.za

PERSONAL INFORMATION

Marital status:	Single
Full Names:	Eben Johannes Griesel
Nationality:	South Africa
Date of Birth:	7 July 1970
Age:	32
Place of Birth:	Germiston, Gauteng, South Africa
Phone:	(082) 563-6835
Fax:	(011) 807-1468
E-mail:	ejg@mweb.co.za

EDUCATION

1991 - 1995	University of Pretoria (undergraduate)
1996 - 1999	University of Stellenbosch (MSc Eng*)
2000 – 2002	University of Cape Town (PhD)

* Passed with distinction

LANGUAGES

English, Afrikaans

WORK EXPERIENCE

2000 - 2002	GenusSoft, Johannesburg Software developer

PUBLICATIONS

[1] Griesel, E.J. 1999. *The influence of controlled environmental conditions on potential concrete durability.* MSc(Eng) Thesis, University of Stellenbosch.

[2] Griesel, E.J. and Alexander, M.G. June 2001. *Effect of Controlled Environmental Conditions on Durability Index Parameters of Portland Cement Concretes.* Cement, Concrete and Aggregates, Vol. 23, No. 1, pp. 44-49.

[3] Bentz, D.P, K.K. Hansen, Madsen, H.D., Vallée, F. and Griesel, E.J. November 2001. *Drying / Hydration in Cement Pastes During Curing*. Materials and Structures, Vol. 34, pp. 557-565

PORTLAND CEMENT AND CALCIUM ALUMINATE CEMENT IN SEWER ENVIRONMENTS

Clyde W. Fourie[1] and Mark G. Alexander[2]

[1]PhD student, Department of Civil Engineering, University of Cape Town, Private Bag, Rondebosch, 7700, South Africa. E-mail: frxcly001@mail.uct.ac.za
[2]Professor, Department of Civil Engineering, University of Cape Town, Private Bag, Rondebosch, 7700, South Africa. E-mail: mark@ebe.uct.ac.za

ABSTRACT

Concrete for use in sewers that are prone to the biological production of sulphuric acid needs to be manufactured using materials capable of resisting acid attack. The acid readily attacks certain constituents in the concrete, such as cements and calcareous materials, exposing the steel reinforcing, which can lead to collapse of the pipe.

Altering the nature of the binder can significantly improve the acid resistance of the concrete. The physical and chemical nature of the binder can be modified by incorporating mineral extenders into the mixture or by replacing the normal Portland Cement with Calcium Aluminate Cement.

Generally, acid-soluble calcareous aggregates are used in concrete mixtures to prolong the life of pipes exposed to acidic environments. The dissolution of the calcareous aggregate neutralises a mild sulphuric acid environment (pH = 3,00) and ensures that the acid attack is spread over the entire surface of the concrete, and is not only concentrated on the binder portion. It is speculated that the neutralisation of the acid environment not only slows down the rate of the sulphuric acid attack but also reduces the activity of the acid-loving thiobacillus bacteria, thus decreasing the rate of sulphuric acid production.

However, in aggressive sulphuric acid environments (pH = 1,00) the calcareous layer is dissolved rapidly. Under these conditions, Calcium Aluminate Cement is more effective in improving the acid resistance of the concrete. The chemistry of the Calcium Aluminate Cement is such that it is claimed to have a higher neutralisation capacity than Portland Cement, and the Calcium Aluminate Cement appears to be toxic to the thiobacillus bacteria. The acid resistance of the mixture is further improved by using a synthetic aggregate such as Alag™ in place of the calcareous aggregate.

Keywords: acid resistance, Portland Cement, Calcium Aluminate Cement, calcium hydroxide, mineral acid tests, bacteriological tests

1. INTRODUCTION

Concrete, the material conventionally used for manufacture of sewer pipes, performs poorly if subjected to a sulphuric acid environment such as that found in certain sewer systems. In areas having a flat topography and warm climate, sewer systems often cannot be designed to eliminate the factors responsible for the biological generation of sulphuric acid. The acid produced by the thiobacillus bacteria existing on the concrete above the sewage level attacks the alkaline constituents of the concrete exposing the steel reinforcing to the corrosive environment.

In such cases, the concrete must be modified to resist the sulphuric acid attack. A common practice is to use calcareous aggregates in the concrete mixture [1]. The acid-soluble calcareous aggregates ensure that the sulphuric acid generated by the bacteria is effectively neutralised and that the acid attack is spread over the entire surface of the concrete, and not only concentrated on the cement binder. It is speculated that the neutralisation of the sulphuric acid by the calcareous aggregate affects the metabolism and growth of the thiobacillus bacteria [2]. The bacteria are known to thrive best in an acidic environment, and as a result, the continuous neutralisation of the sulphuric acid stifles the growth of the bacteria.

Calcareous aggregate mixtures have proved to substantially increase the performance of concrete sewer pipes in mild sulphuric acid environments [2]. In aggressive acid environments, a sacrificial lining is sometimes cast on the inside of the concrete pipe to improve performance. In extreme circumstances, the sacrificial lining is insufficient, and alternative methods are sought to obtain a concrete that can resist the biologically-induced sulphuric acid attack in sewers.

The performance of concrete in acidic mediums is significantly improved by modifying the cement binder of the mixture. The addition of condensed silica fume improves the integrity of the Portland Cement (PC) binder in an inorganic acid medium, and in so doing, improves the performance of the concrete [3]. The silica fume reduces the amount of calcium hydroxide precipitated during the hydration of the PC, and leads to the refinement of pores in the hydrated cement binder. Calcium hydroxide is leached out of the cement binder in acidic mediums initiating the degradation of the concrete.

An alternative approach is to use Calcium Aluminate Cement (CAC) as a replacement for the PC to improve performance in a strong acidic environment. The hydrated CAC produces no calcium hydroxide [4,5], in contrast with PC. In addition, the CAC is stated to have a higher neutralisation capacity than PC [6]. The mineral phases formed during the hydration of the CAC are theoretically more effective in neutralising acidic mediums than the mineral phases formed during the hydration of PC.

CAC concrete is expected to perform better in biologically induced sulphuric acid environments. The higher neutralisation capacity of the CAC is reported to substantially reduce the aggressiveness of the sulphuric acid environment [6], thus reducing the metabolic rate and growth of the thiobacillus bacteria. It is speculated that the CAC is toxic towards the thiobacillus bacteria, which is of great significance in explaining the good performance of CAC in biologically-induced sulphuric acid environments.

The acid-resisting performance of CAC and PC mixtures is currently being investigated at the University of Cape Town (UCT). Results to date [3,7] have indicated that concrete containing CAC and a calcareous aggregate performs comparably to a PC/calcareous aggregate concrete, when immersed in hydrochloric acid solution at a pH of 1,00. On the other hand, concrete with CAC and a synthetic Alag™ aggregate better resists the attack of the hydrochloric acid solution [7]. These tests relate purely to attack of the concrete by strong mineral acids.

Investigations of bacterial attack on concrete are also being undertaken at UCT. Preliminary results indicate that concrete containing CAC shows no sign of attack compared to concrete with PC, over a period of several months in a bacterial chamber. Investigations in a sewer system having an extremely corrosive sulphuric acid environment show that concrete containing CAC and Alag™ is not attacked over a period of 16 months. Results of the on-going work will be reported subsequently.

2. CEMENT CHEMISTRY

The chemistry of cement plays an important role in determining the performance of concrete in chemical environments. The hydration products of cement are all compounds of relatively low solubility but are not stable when in contact with acidic mediums.

PC is composed mainly of lime (C) and silica (S) as well as a small portion of alumina (A) and iron oxide (F); refer to Table 1 [4]. The oxides interact with each other to form complex binary and ternary compounds, tricalcium silicate (C_3S), dicalcium silicate (C_2S), tricalcium aluminate (C_3A), and tetracalcium aluminoferrite (C_4AF). The major constituent in PC is calcium silicate. The reaction of PC with water mainly forms a hydrated calcium silicate gel (*C-S-H*) and calcium hydroxide ($CaO.H_2O$ or *CH*) is precipitated out of the pore solution due to its low solubility.

Table 1. Typical oxide composition of cements

Compound	*Portland (%)*	*Calcium Aluminate (%)*
CaO *(lime)*	64,1	37,7
Al_2O_3 *(alumina)*	5,5	38,5
Fe_2O_3 *(ferrite)*	3,0	12,7
FeO *(ferrous)*	-	3,9
SiO_2 *(silica)*	22,0	5,3
MgO *(magnesia)*	1,4	0,1
SO_3	1,75	0,1

CAC is composed essentially of equal portions of alumina and lime and a large portion of iron oxide; refer to Table 1 [4]. The binary and ternary compounds expected in CAC are $C_{12}A_7$, CA and C_2S. The major constituent in CAC is mono-calcium aluminate (CA). The reaction of CAC with water at normal temperatures forms alumina gel (AH_3), and the hydrates CAH_{10} and C_2AH_8. The monocalcium aluminate hydrate and dicalcium aluminate hydrate are metastable hexagonal products that, on ageing of the cement, change into the more stable cubic tricalcium aluminate hydrate compound and alumina gel. The conversion leads to a volume change, and the expansive cubical form creates a marked loss in strength and increase in porosity of the converted cement.

3. INFLUENCE OF CEMENT CHEMISTRY ON INORGANIC ACID RESISTANCE

The hydration products of the cements indicate that CAC has the potential to be more resistant to acidic environments than PC. CAC contains mainly alumina gel, which only becomes unstable at a pH below 4. On the other hand, no hydrated compound of PC is stable at a pH below 11. It is stated that in practice, CAC materials have proved to be more resistant to soft water environments and weak acidic environments (pH > 4) than PC materials [4]. The poorer resistance of the PC is ascribed to the instability of the calcium hydroxide, which readily leaches out of the cement in soft waters and weak acidic environments. No conclusive evidence exists as to the cause of the good performance of CAC in weak acid environments but it is known that the increased porosity due to the conversion reaction that can occur in CAC may significantly reduce the performance of the CAC in aggressive environments.

In sewers, the sulphuric acid environment is either mild (pH of 2 to 4) or strong (pH < 2), and there is a lack of clarity on whether CAC materials are more resistant to such environments than PC materials. Test methods developed to study the resistance of concrete in mild and strong mineral acid solutions produce conflicting results as to whether a CAC material performs better than a PC material. The test methods are the subject of controversy since it is difficult to interpret the performance of a concrete in a biologically-induced sulphuric acid environment from these tests.

Mineral acid tests [6] indicate that CAC mortars perform better than PC mortars in mild sulphuric acid solutions having an initial pH of both 2 and 3. The results indicate that the CAC mortars consume more hydrogen ions than the PC mortars, thus reducing the corrosiveness of the mild sulphuric acid solutions at a faster rate with a correspondingly lower mass loss than the PC mortar. It is stated that CAC has the ability to neutralise an acid environment more effectively than PC. The calculated neutralisation capacity indicates that CAC neutralises approximately double the amount of hydrogen ions compared with equivalent amounts of PC. In addition, it is suggested that the alumina gel, which forms due to the reaction of the hydrogen ions with the CA hydrate, hinders the sulphuric acid attack at these pH levels.

Similar tests in a strong sulphuric acid solution having a pH of 1 showed that the CAC materials were more aggressively attacked [6]. The CAC mortars showed a higher mass loss and hydrogen ion consumption than the PC materials. In the same reference it is suggested that the abnormality observed at a pH of 1 is due to the slightly soluble by-product, calcium sulphate, which precipitates onto the PC mortar more readily in a strong sulphuric acid solution, thus stifling the acid attack. No calcium sulphate is precipitated onto the CAC mortar due to the absence of calcium hydroxide. In addition, the alumina gel formed during the acid attack is readily decomposed at a pH of 1.

A reliable test method, the hydrochloric acid resistance test [8] developed at the University of Cape Town, is used extensively to determine the performance of different materials in a hydrochloric acid environment at a pH of 1. The hydrochloric acid medium eliminates the effects of the calcium sulphate precipitating onto the samples tested and determines the ability of the materials to resist a corrosive inorganic acid solution. The test is more representative of actual acid attack on concrete sewer pipes in practice, since it better simulates the real mixtures and mimics both physical and chemical aspects of the problem. The concrete samples tested are prepared in a manner similar to that of concrete pipes. The heavy mechanical compaction produces a dense matrix largely impermeable to gases and fluids.

The hydrochloric acid tests indicate that concrete mixtures of CAC and Dolomite aggregates [3,7] are somewhat less resistant than similar PC mixtures in the mineral acid solution at a pH of 1. The percentage mass loss is highest for mixtures CAC and Dolomite aggregate (Figure 1), the values recorded for the 18 % cement and 23 % cement mixtures after 72 hours being 38,2 % and 37,8 % respectively. The PC mixtures with Dolomite aggregate are also readily attacked by the hydrochloric acid solution. The percentage mass loss of the 23 % PC mixture (32,4 %) is slightly higher than that for the 18 % PC mixture (30,0 %), presumably due to its higher calcium hydroxide content resulting in a greater mass loss. Noticeably, the mixture containing 23 % CAC and the synthetic Alag™ aggregate showed the greatest resistance to hydrochloric acid attack, the percentage mass loss after 72 hours being only 11,8 %, which is substantially lower than the other mixtures.

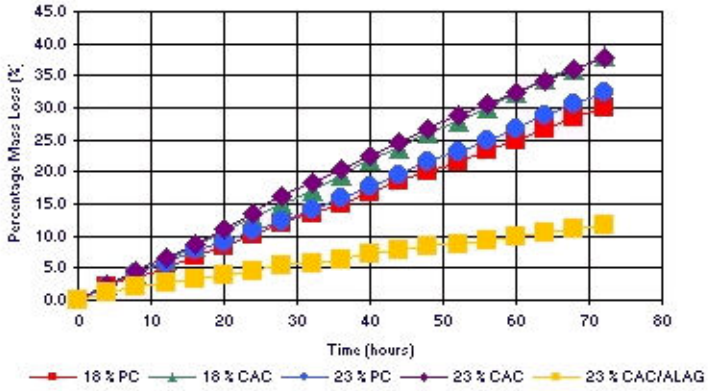

Figure 1. Percentage mass loss with time of concrete samples containing Dolomite aggregates at a pH of 1

The hydrogen ion consumption (Figure 2) of the mixtures follows similar trends to the percentage mass loss results. The exception is that the hydrogen ion consumption of the 23 % PC/Dolomite aggregate mixture ($3{,}12 \times 10^{-2}$ g/cm^2) was similar to the hydrogen ion consumption of the mixtures containing 18 % and 23 % CAC and Dolomite aggregate ($3{,}11 \times 10^{-2}$ g/cm^2 and $3{,}04 \times 10^{-2}$ g/cm^2 respectively). The increase in calcium hydroxide due to the higher PC content is probably responsible for the increased hydrogen ion consumption compared to the 18 % PC mixture ($2{,}62 \times 10^{-2}$ g/cm^2). The 23 % CAC/synthetic Alag™ aggregate mixture had considerably lower hydrogen ion consumption ($0{,}6 \times 10^{-2}$ g/cm^2) than the other mixtures.

The significant difference between the test procedures, other than the mineral acid medium, is in the samples tested. In the hydrochloric acid resistance test, the concrete samples consist of a large portion of Dolomite aggregate (77 %) and a smaller portion of cement (23 %). The mortar samples in the strong sulphuric acid solution test consist of a siliceous aggregate (67 %) and a larger portion of cement (33 %). The large portion of Dolomite stone in the concrete, which readily dissolves in the hydrochloric acid solution, can mask the effect that the neutralisation capacity of the CAC should have on the hydrogen ion consumption.

On the other hand, the hydrochloric acid resistance test shows that a CAC/Alag™ concrete is significantly more resistant to a strong acid environment than the CAC/Dolomite and OPC/Dolomite concrete. The CAC/Alag™ concrete should show the highest neutralisation capacity [7] but it has the lowest hydrogen ion consumption and corresponding mass loss. At this stage, conclusive reasons for the excellent acid resistance of the CAC/Alag™ mixture are not immediately evident. Tests to determine the acid resistance in granular form of the Alag™ aggregate may show a superior acid resistance of these aggregates. A further reason may be the creation of a good interfacial bond between the aggregate and the cement binder. The material is dense with a low porosity indicating that very durable concrete can be achieved with these materials.

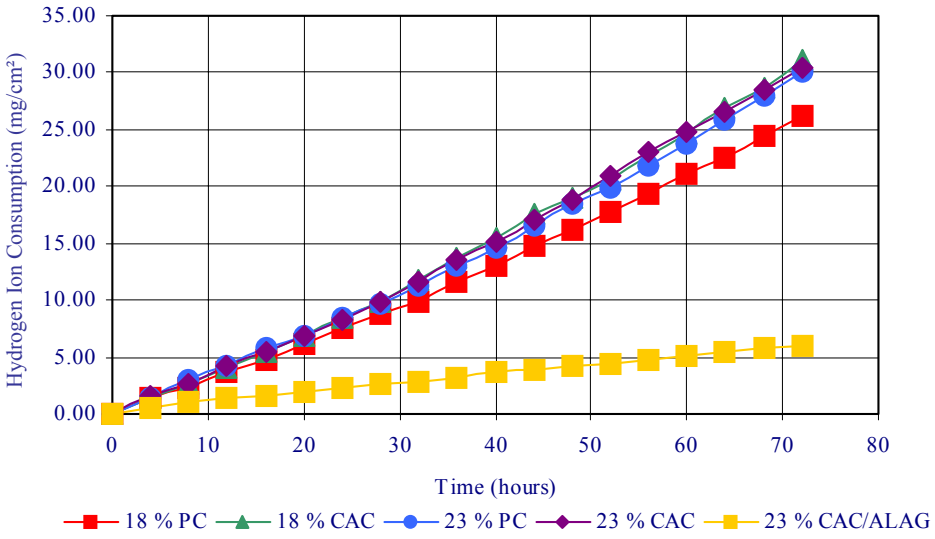

Figure 2. H^+ ion consumption with time for concrete samples containing Dolomite aggregates, at a pH of 1

4. DISCUSSION

It is of concern that the results obtained from hydrochloric acid resistance testing do not entirely agree with the statements discussed in the literature. The hydrogen ion consumption does not show that CAC has a neutralisation capacity double that of PC, but that the values are similar. No calcium sulphate is precipitated on the PC materials in the hydrochloric acid solution as with the

strong sulphuric acid solution. The absence of the calcium sulphate allows a direct comparison to be made between the hydrogen ion consumptions of the two cement materials.

The calculated neutralisation capacity is based solely on the alumina and the lime composition of the cements [6]. In one kilogram of PC there is approximately 0,3 moles of alumina and 12,1 moles of lime. In comparison, one kilogram of CAC contains approximately 5,1 moles of alumina and 6,8 moles of lime. The higher alumina content in CAC is accountable for the more efficient hydrogen ion consumption. A mole of alumina reacts with 6 moles of hydrogen ions whereas a mole of lime only reacts with 2 moles, thus one kg of CAC neutralises 44 moles of hydrogen ions compared to 26 moles with one kg of PC.

Strictly, the theoretical neutralisation capacity calculation is incorrect since it is only based on the oxide composition of the cement. The properties of cement do not simply depend on the proportions of lime, magnesia, silica, alumina and other compounds contained in the ground clinker, but depend also on the stability of the hydration products formed from ternary and binary oxide systems of the cements. The neutralisation capacity and its effect on acid resistance of CAC at a higher pH are currently being investigated at UCT using the hydrochloric acid resistance test method. Work completed indicates that sewer pipe materials used in South Africa are resistant to a mineral acid solution at a pH of 2.

Further, much of the work reported in the literature has been done on materials that may not be representative of the physical and chemical properties of the mixtures as used in industry. The degree of mineral acid attack depends on the chemical and physical properties of the material, with the physical properties often being of equal importance to the chemical properties. If the material is not produced using materials and mixture proportions similar to those used in industry, or in a manner similar to that of industry, the acid resistance will not be representative of that occurring in reality. The sample preparation method is particularly relevant in the study of sewer pipe concrete made using the roller suspension method. The concrete pipes are heavily compacted often detrimentally affecting the integrity of calcareous aggregates in an acidic environment. The heavy mechanical compaction tends to fracture calcareous aggregates of low physical strength allowing rapid dissolution in acidic environments and deterioration of the concrete matrix.

5. VIRGINIA SEWER EXPERIMENTS

Investigations at UCT into the performance of concrete in biologically induced sulphuric acid environments are a major part of the research into the acid resistance of concrete for use in sewer pipes. The conditions in South Africa are such that biologically induced sulphuric acid environments having a pH of 1 are fairly common. An experimental sewer at Virginia in the Free State with these conditions has been used for various sewer experiments for over a decade, and is also being used in the current work. The hydrochloric acid resistance test simulates such environments, and together with the on-site testing at Virginia, reliable results are obtained within a short period. The Virginia experimental sewer site is an ideal location for accelerated biological acid testing. Preliminary investigations during summer revealed that within a period of 5 months, samples showed signs of thiobacillus bacterial growth, and pHs of less than one were recorded in the sulphuric acid environments present on some of the samples. The samples are placed directly above the maximum daily sewage level in a sewer environment having a hydrogen sulphide content of between 70 ppm in the cold winter months and 150 ppm in the hot summer months. The samples are kept continuously moist by the evaporation and condensation of the sewage. Literature [6] indicates that accelerated biological tests conducted in a laboratory can produce results within one year. The hydrogen sulphide of the laboratory environment reported in reference [6] is only 10 ppm, which occurs in many sewer systems throughout South Africa.

Information obtained from field studies on the Virginia test sewer in South Africa indicates that concrete materials containing 23 % cement similar to those tested in the hydrochloric acid resistance test show little signs of sulphuric acid attack, refer to Table 2. The materials are typical of those used for the lining of concrete sewer pipes in the Gauteng region. No mass loss is recorded for the CAC/Alag™ and CAC/Dolomite samples installed in the highly corrosive sulphuric acid environment over a period of 16 months. The percentage mass loss of the PC/Dolomite sample is small (2,9 %). The pH on the surface of the three samples is approximately 6,5 indicating that the sulphuric acid microenvironment is weak. Samples containing 18 % PC and 82 % Dolomite stone showed noticeable signs of sulphuric acid attack. The percentage mass loss recorded for these samples is approximately 5,0 %. The pH recorded on the surface of the samples is between 4,0 and 4,5 indicating that the sulphuric acid environment is mild and more corrosive. The most attacked samples installed in the sewer are samples containing 18 % and 23 % PC and siliceous aggregate. The pH on these samples is between 1,0 and 1,2 indicating that the sulphuric acid environment is strong and extremely corrosive towards concrete. The mass loss recorded for these samples is 5,3 % and 6,6 % respectively.

Observations at Virginia indicate that CAC and concrete containing Dolomite appear to retard the biological sulphuric acid attack. The CAC mixtures are expected to give good performance as the materials have the ability to effectively neutralise the biologically induced sulphuric acid environment. It is speculated that the CAC materials are toxic towards the thiobacillus bacteria curbing their growth. The good performance of the 23 % PC/Dolomite concrete is not fully understood, except that the material is expected to effectively neutralise the sulphuric acid environment. The poor performance of the PC/ siliceous concrete is related to the inability of the siliceous aggregate to dissolve in the biologically-induced sulphuric acid and as expected all the acid attack is concentrated on the small portion of the PC binder. Although the percentage mass loss is low, poor performance is noticeable in the protrusion of the siliceous aggregate from the attack surface compared to the smooth attacked surface of the Dolomite samples.

Table 2. Percentage mass loss of concrete samples in the Virginia Sewer Experimental Section, over a period of 16 months

Samples	*Mass Loss (%)*
23 % CAC/Alag™	0,0
23 % CAC/Gauteng Dolomite	0,8
23 % PC/Gauteng Dolomite	2,9
23 % PC/siliceous	6,6
18 % PC/Western Cape Dolomite	5,0
18 % PC/siliceous	5,3
18 % PC/Gauteng Dolomite	7,1

6. CONCLUSION

The performance of concrete in sulphuric acid environments such as those encountered in sewers can only be fully determined from tests done to ascertain the mineral acid resistance, and resistance to biologically-induced sulphuric acid environments. The tests must be conducted on materials similar to those used in industry and in conditions likely to be met in areas prone to the biological generation of sulphuric acid. Indications from work done thus far are that CAC materials perform better in biologically-generated sulphuric acid environments.

ACKNOWLEDGEMENTS

The authors gratefully acknowledge the financial support of the Concrete Pipe Association of Southern Africa, the National Research Foundation, and Lafarge Aluminates.

REFERENCES

[1] South African Council for Scientific and Industrial Research, Corrosion of Concrete Sewers, 1958.
[2] Parker C.D. The Corrosion of Concrete: 2. The Function of Thiobacillus Concretivorus in the Corrosion of concrete Exposed to Atmosphere Containing Hydrogen Sulphide, Australian Journal of Experimental Biological and Medical Science, vol. 23, 1942, pp. 91-98.
[3] Fourie, C.W. and Alexander, M.G. Acid resistance of Sewer Pipe concrete Mixtures, Proceedings of Fifth International Canmet Conference, Barcelona, 2000, vol. 2, pp. 705-719.
[4] Lea, F.M The Chemistry of Cement and Concrete, 3rd ed. Edward Arnold (Publishers) Ltd, 1970
[5] Scrivener, K.L. Cabiron, J.L. and Letourneux, R. High-performnace concretes from calcium aluminate cements, Cement and Concrete Research, vol. 29, 1999, pp. 1215-1223.
[6] Ehrich, S. Helard, L. Letourneux, R. Willoq, J.and Boch, E. Biogenic and Chemical Sulphuric Acid Corrosion of Mortars, Journal of Materials in Civil Engineering, November 1999, pp. 1-5.
[7] Fourie, C.W. and Alexander, M.G. Acid resistance of Calcium Aluminate Cement in Concrete Sewer Pipe Mixtures, Proceedings of the International Conference on Calcium Aluminate Cements, Edinborough, 2001, pp. 633-645.
[8] Fourie, C.W. and Alexander, M.G. Method Statement for the Hydrochloric Acid Test, Unpublished Report, Department of Civil Engineering, University of Cape Town, 1999.

PORTLAND CEMENT AND CALCIUM ALUMINATE CEMENT IN SEWER ENVIRONMENTS

Clyde W. Fourie[1] and Mark G. Alexander[2]

[1]PhD student, Department of Civil Engineering, University of Cape Town, Private Bag, Rondebosch, 7700, South Africa. E-mail: frxcly001@mail.uct.ac.za

[2]Professor, Department of Civil Engineering, University of Cape Town, Private Bag, Rondebosch, 7700, South Africa. E-mail: mark@ebe.uct.ac.za

C W Fourie

CW Fourie is a PhD student in the Department of Civil Engineering at the University of Cape Town. He holds a BSc Chemistry and Materials Science degree. He has worked as a Chemist for Sappi Paper and as a Mill Chemist for Nampak Paper.

Mr Clyde William Fourie
PhD Student
Department of Civil Engineering
University of Cape Town
Private Bag
Rondebosch
7700
South Africa

E-mail: frxcly001@mail.uct.ac.za
Tel: +27 21 6502584
Fax: +27 21 6897471
Cell: +27 82 2230514

A MULTI-CHANNEL ISOTHERMAL HEAT CONDUCTION CALORIMETER FOR CEMENT HYDRATION STUDIES

L. Wadsö

Building Materials, Lund University, Box 118, 221 00 Lund, Sweden.
E-mail: lars.wadso@byggtek.lth.se

ABSTRACT

When cement hydrates heat is produced and different methods to measure this heat are interesting ways of studying the cement hydration process. There are essentially two types of calorimeters (heat measuring devices) used today: (semi)adiabatic calorimeters in which the temperature increase in an insulated sample is measured, and isothermal (conduction) and calorimeters in which the heat flow from a sample is measured. Although isothermal calorimeters have many advantages over the other type (more well defined conditions, less corrections needed etc.) such instruments have not been as widely used, at least partly because some such calorimeters have had large baseline drifts and other problems.

The paper presents the design of a new multi channel heat conduction calorimeter for cement hydration studies under essentially isothermal conditions. Each calorimeter within the multi channel instrument is both sensitive (precision ±10 μW) and stable (<20 μW over 24 h) so that it is possible to perform both long-term measurements (1 month) and use small samples (<1 g of cement paste). The instrument is placed in an air thermostat that can operate between 5 and 60°C.

1. INTRODUCTION

The instrument described in this paper is a heat conduction calorimeter, i.e. the heat produced in the sample is conducted away from the sample into a heat sink. In this way the sample temperature does not increase and the calorimeter type is therefore also called an isothermal calorimeter. The heat production rate (thermal power; units: watts) is measured with a heat-flow sensor positioned between the sample and a heat-sink. It is actually not the heat flow that is measured, but the temperature difference over the heat flow sensor, but this is proportional to the heat-flow, so the result is an output signal that is proportional to the heat-flow from the sample. This gives much higher stability than if separate temperatures are measured in the sample and the heat sink.

All processes (physical, chemical, biological) produce heat. Calorimetry is therefore a very general method to study different kinds of processes. Isothermal calorimeters are therefore used in many different fields of science and technology, e.g.:

- To detect compatibility problems between products and packages.
- To monitor microbial growth in foodstuffs.
- To measure vapor sorption properties of materials.
- To study drug interactions in the pharmaceutical industry.
- To determine shelf life of active compounds.

In the field of cement and concrete isothermal calorimetry can also have many uses [1-4]:

- Measure total heat of hydration.
- Assess admixture retardation.
- Quality control of cement production.
- Determine cement-admixture incompatibility.

The instrument described in this paper has been commercialized by Thermometric AB (Järfälla, Sweden; www.thermometric.com) under the name TAM Air [4].

2. DESCRIPTION OF THE INSTRUMENT

As it is often of interest to run many samples simultaneously, e.g. to measure the retardation as a function of admixture concentration, the present instrument has eight calorimeters in one thermostat. Each of the calorimeters is easily assessable from the top of the instrument. Figure 1 shows a cut-away drawing of the instrument.

The heat flow sensors used are solid-state Peltier thermocouple plates that have a comparatively high voltage output for the very low temperature differences of the calorimeters. The sample and reference ampoules are placed in ampoule holders that are fastened to the topsides of the heat flow sensors. The calorimeters have two sensitivity ranges: ±60 mW and ±600 mW. The 600 mW range is advantageous to use for measurements of early hydration as one does not want the output signal to go out of range when a sample is charged into the calorimeter. The higher sensitivity is useful for long-term measurements of cement hydration.

The instrument is modular. Each calorimeter in manufactured as a unit of its own. In the instrument described here eight modules are used together, but it is possible to only use from just one module as a single-channel calorimeter up to as many modules as one can practically handle. A major advantage with modular design is that if a calorimeter needs to be serviced, one may remove only that module or directly exchange it for a new module.

Each calorimeter module has its own reference that is differentially connected to the sample, i.e. the output signal is the difference between the signal from the sample and the signal from the reference. The primary importance of a reference is to decrease the noise level. When a thermal disturbance enters the calorimeter it will reach both the sample heat-flow sensor and the reference heat-flow sensor at the same time, and if the thermal properties (mainly heat capacity) of the sample and the reference are similar, these disturbance signals will cancel out. The reference also makes the calorimeter react faster and in a more predictable way to rapid changes in heat production rate.

All heat conduction calorimeters have heat sinks into which the produced heat is deposited (before being transferred out into the thermostat). It is normally an advantage to have a large heat-sink as this will decrease the temperature variations and the noise. The drawback of a large heat sink is that the calorimeter will become larger, heavier and take longer time to thermostat to a new temperature. In the present design the calorimeters have a partially shared heat sink. The heat produced in a sample will first be conducted out into a small primary heat sink in that calorimeter and then further into to a larger secondary heat sink that is common for all the calorimeters in the instrument. By optimizing the sizes of the primary and secondary heat sinks one will get a rather small multi-channel instrument with low noise. This is further discussed in the next section.

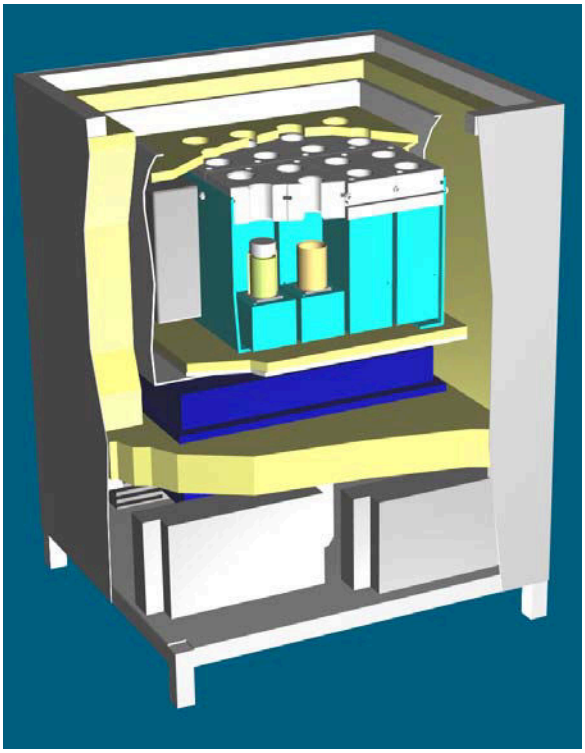

Figure 1. A cut-away drawing of the instrument.
The eight calorimeters are shown in blue and white with two calorimeters cut open to show the ampoule holders (one of which has a sample in it). The grey box to the left of the calorimeters is the data logger. Below the calorimeter is the air thermostat equipment.

An air thermostat that can keep the calorimeter at temperatures between 5 and 60°C surrounds the multi-channel calorimeter. The heating and cooling is made by a Peltier heater/cooler, i.e. the same type of solid-state device that is used as a heat flow sensor in the calorimeters. The temperature stability of the air thermostat is ±0.02 K.

3. PROPERTIES OF THE INSTRUMENT

3.1 Temperature increase in sample

Heat conduction calorimeters are essentially isothermal instruments and it is important that the heat produced in the sample is conducted away so that the temperature increases in the sample are low. Using a procedure described in reference[5] the temperature increase in the center of a cement paste sample has been calculated. At maximal thermal power (at the main peak) the center temperature will be elevated less than 0.3 K for a 5 g sample of cement paste. Smaller samples will have less over-temperature.

3.2 Time constant

The time constant of an ampoule with 5 g cement paste is in the order of 200 s, i.e. it takes 200 seconds for the output signal to drop from a value to 38% of that value (when there is no heat produced in the sample). The time constant (measured or calculated) may be used to correct the output signal for the thermal inertia of the calorimeter using the Tian equation[6]:

$$P = \varepsilon\left(U + \tau\frac{dU}{dt}\right) \qquad (1)$$

Here, P (W) is the thermal power produced in the sample, U (V) is the voltage output of the heat-flow sensors, ε (W/V) is the calibration coefficient, and τ (s) is the time constant.

3.3 Cross-talk

As eight calorimeters are placed in contact with each other there is a risk that heat produced in one sample will influence the output from the other samples (cross-talk). The cross-talk may be minimized by a careful selection of references. A reference with closely matched heat capacity will substantially decrease the cross-talk. Figure 2 shows the result from a test of cross-talk. Computer simulations of the thermal behavior of the instrument have given similar results. If the references are well matched cross-talk is generally not a problem. However, charging of a room temperature sample into a calorimeter working at a very different temperature will give larger disturbances than shown in Fig. 2. Careful matching of heat capacities and pre-thermostating of samples and will decrease the cross-talk.

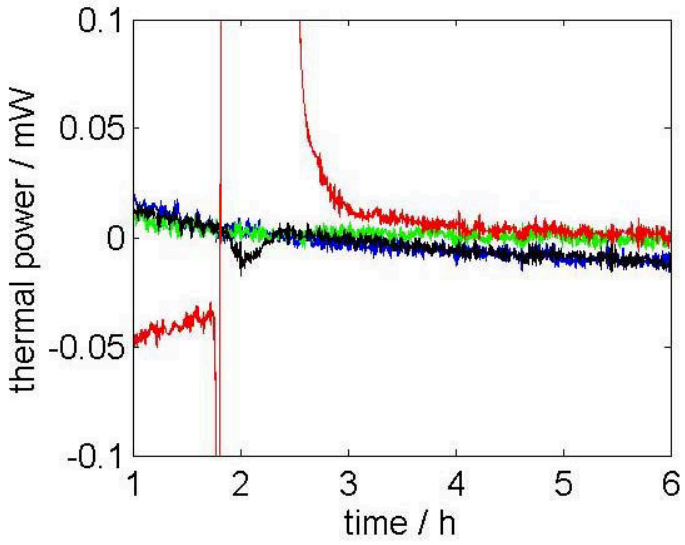

Figure 2. Result from a test of cross-talk in an instrument in which all calorimeters have about 14% difference in heat capacity between the sample and the reference sides.

In Figure 3, the red curve shows the output from a calorimeter that was charged with a sample with an excess heat of 13 J at about 1.7 h. The output from the calorimeter closest to that calorimeter (black line) is slightly disturbed (the maximal deviation is about 17 μW).
The temperature of the thermostat having been changed before this measurement causes the sloping baselines.

3.4 Baseline stability

At the higher amplification (max 60 mW) the least significant bit of the A/D-converter is about 1 μW and the short-term baseline (less than 1 hour) is usually within a few microwatts when the instrument is working at close to room temperature. Over a longer time period (e.g. 1 week) the baseline will be within ±3 μW. The baseline values are very constant and do not change (e.g. over a period of a year). The above values are when the calorimeter is working near room temperature; at higher or lower temperatures one will see a slight deterioration of performance. The manufacturer guarantees a sensitivity (precision) of ±10 μW and a 24-hour stability of better than 20 μW under all conditions.

3.5 Calibration coefficients

Calibration coefficients are determined from electrical calibrations with heaters that are either fixed in the ampoule holders or inserted into ampoules. The instrument should be calibrated regularly; more often if it is used for different types of measurements, at different temperatures, or placed in a dusty environment. Under normal laboratory conditions the calibration coefficients are very stable. A change in a calibration coefficient indicates a broken calorimeter.

4. TYPICAL USES OF THE INSTRUMENT

Below are given some typical types of measurements that can be made with the present instrument.

4.1 Measuring the total heat produced

By charging the samples into the calorimeter as soon as possible (typically 200 s) after water and cement has been mixed (or mix water and cement inside the calorimeter) it is possible to measure the total heat produced during seven days (or any other time period), a value that should be equal to the result from the standardized solution calorimeter. An advantage with the isothermal calorimeter is that it gives not only the total heat, but also the thermal power as a function of time during the seven days. A Tian correction (Eq. 1) may be applied to correct for the influence of the time constant.

4.2 Measurements at different temperatures

From measurements of cement paste or mortar hydration at different constant temperatures the rate of hydration as a function of temperature and degree of hydration (defined as the ratio between the produced heat and the maximal heat produced) may be determined [3]. The activation energies may also be evaluated. From such data the temperature field during hardening of a massive construction may be calculated with less calculations than is needed when (semi)adiabatic measurement results are used.

Figure 3 shows the specific thermal power (watts per gram cement) as a function of produced heat (joules per gram cement). This is both a convenient and illustrative way to compare calorimetric cement hydration curves. The produced heat Q (J/g(cement)) on the x-axis can be seen as the extent of reaction ξ (g(reacted cement)/g(cement)); more produced heat means that the hydration reaction has preceded further:

$$\xi = \frac{Q}{\Delta h} \tag{2}$$

Here, Δh (J/g(reacted cement)) is the specific reaction enthalpy. The specific thermal power P (W/g(cement)) on the y-axis is proportional to the rate of reaction ν (g/s):

$$\nu = \frac{P}{\Delta h} \tag{3}$$

These relations are useful in modelling the cement hydration process as solid-state kinetic models usually have the form:

$$\nu = f(\xi) \tag{4}$$

This can easily be rewritten using the calorimetrically measured parameters P and Q [7, 8]:

$$Q = f_2(P) \tag{5}$$

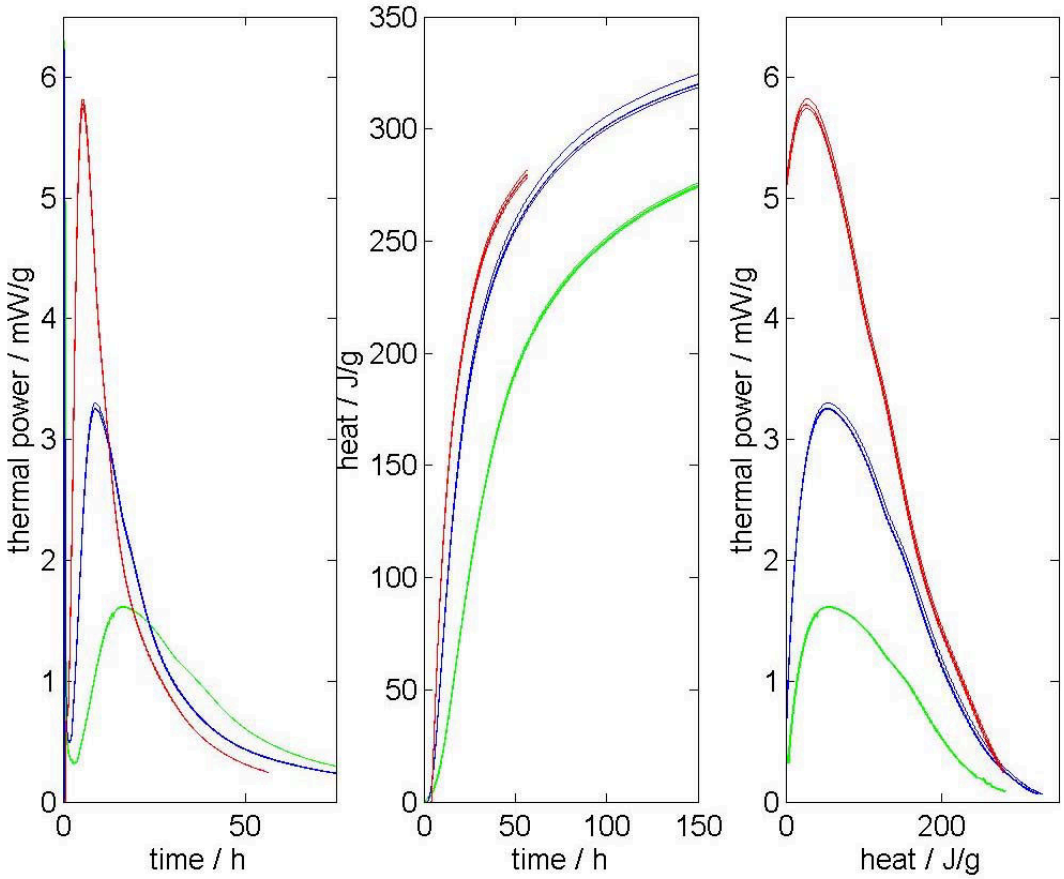

Figure 3. Three different ways of viewing the results from measurements at three temperatures (green: 10°C; blue: 20°C; red: 30°C). At each temperature the results from four measurements with samples from the same mix are shown. The left subplot shows the primary result from the calorimeters; the middle subplot shows the same result integrated; the right subplot essentially shows reaction rate as a function of extent of reaction.

Data from a calorimetric measurement can therefore be used to test kinetic models. A problem with this use of these equations is that the reaction enthalpy Δh may have different values at different times of the hydration process. Note that the 30°C-results in the right subplot are slightly shifted to the left, indicating there is a change in reaction path when the temperature is increased.

4.3 Assessment of retardation

Many admixtures retard the hydration process. By making measurements on cement paste or mortar with different percentages of an admixture it is possible to construct a diagram of retardation (time) as a function of admixture content [9]. Figure 4 shows an example of such a measurement. It is also possible to make a measurement with different recipes (cement, filler, admixtures etc.) to see when the main hydration process starts.

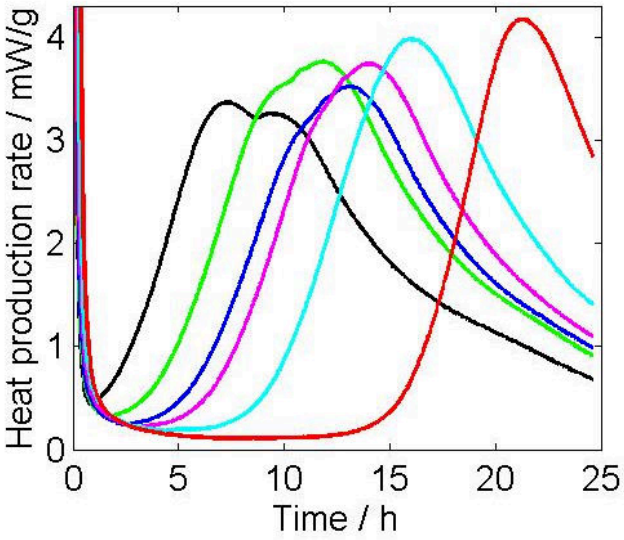

Figure 4. An example of the influence of an admixture on the hydration kinetics of a cement. From left to right the curves are from samples with 0, 0.1, 0.15, 0.20, 0.30, 0.50% of an admixture.

ACKNOWLEDGMENTS

The author acknowledges the help from Thermometric AB in designing the instrument.

REFERENCES

[1] Bronswijk, J. P., Loo, M. d., and Loo, W. v., Heat measurement with the Thermal Activity Monitor, World Cement, 1993, pp.23-26.

[2] Bensted, J., Some applications of conduction calorimetry to cement hydration, Adv. Cement Res., vol.1, 1987, pp.35-44.

[3] Reinhardt, H. W., "On the heat of hydration of cements," Department of Engineering, Delft University, The Netherlands., 5-79-1, 1979.

[4] Anon., "TAM Air cement - an 8 channel Thermal Activity Monitor for research and quality control in cement and concrete production (product brochure)," Thermometric ABJärfälla, Sweden, 2002.

[5] Wadsö, L., Temperature changes within samples in heat conduction calorimeters, Thermochim. Acta, vol.366, 2000, pp.121-127.

[6] Cembureau, "Recommended procedure for the measurement of the heat of hydration of cement by the conduction method," U.D.C. 666.94.015.45: 620.1., 1977.

[7] Willson, R. J., Beezer, A. E., Mitchell, J. C., and Loh, W., Determination of thermodynamic and kinetic parameters from isothermal heat conduction microcalorimetry: applications to long-term-reaction studies, JJ Phys Chem, vol.99, 1995.

[8] Willson, R. J., Beezer, A. E., and Mitchell, J. C., Solid state reactions studied by isothermal microcalorimetry; the solid state oxidation of ascorbic acid, Int. J. Pharmaceutics, vol.132, 1996, pp.45-51.

[9] Wadsö, L., "The study of cement hydration by isothermal calorimetry," Thermometric ABJärfälla, Sweden, 2000.

A MULTI-CHANNEL ISOTHERMAL HEAT CONDUCTION CALORIMETER FOR CEMENT HYDRATION STUDIES

Lars Wadsö

Building Materials, Lund University, Box 118, 221 00 Lund, Sweden.
E-mail: lars.wadso@byggtek.lth.se

Dr. Lars Wadsö is a senior researcher at Building Materials at Lund University in Sweden. His thesis was on wood-water relations, but his main current scientific interest is in development of calorimetric instruments and methods. He has designed a number of isothermal calorimeters and methods for such calorimeters for use in various fields. He is also engaged in the indoor air quality field through the industrial research school The Building and Its Indoor Environment at Lund University.

WORK TOWARDS A STANDARD FOR ISOTHERMAL (CONDUCTION) CALORIMETRY FOR CEMENT HYDRATION

Lars Wadsö

Building Materials, Lund University, Box 118, 221 00 Lund, Sweden.
E-mail: lars.wadso@byggtek.lth.se

ABSTRACT

This paper presents work done to prepare a draft for a Nordic (NORDTEST) standard for measurement of the heat of hydration with isothermal (conduction) calorimetry. The main aim of the work is to produce a standard for measurements of 2-, 3- and 7-day (isothehrmal) heats as an alternative to (semi) adiabatic calorimetry and solution calorimetry. It is also thought that large parts of the standard may be used when planning other types of experiments with isothermal calorimetry.

1. INTRODUCTION

When cement hydrates, heat is produced and different methods to measure this heat are interesting ways of studying the cement hydration process. There are essentially four different calorimetric techniques used today to study cement hydration:

1.1 Isothermal calorimetry

The heat production in the sample is monitored while the sample temperature is unchanged. This type of calorimeter is usually a heat conduction (flow) calorimeter in which the heat produced in the sample is measured as it is conducted out from the sample through heat flow meters. There are today several types of commercial instruments used in the pharmaceutical industry and elsewhere (references [1, 2] discuss different uses of isothermal calorimetry), and some instruments that are limited to cement science. No cement standards exist for isothermal calorimetry, although Cembureau have issued recommendations how to use it [3] and there have been (and are) a few manufacturers of such instruments. Figure 1 shows a schematic description of a twin heat conduction calorimeter and Fig. 2 shows the instrument used in the present study (TAM Air, Thermometric AB, Järfälla, Sweden).

1.2 Adiabatic calorimetry

In this type of calorimetry the sample is perfectly insulated so that all heat produced is used to heat the sample. The temperature increase of the sample is measured and the rate of temperature increase is a measure of the heat production rate in the sample. So-called adiabatic shields are usually used to stop the heat form leaving the sample

1.2.1 Semiadiabatic calorimetry

This is an insulated calorimeter in which the insulation is not perfect so a certain fraction of the heat produced is allowed to escape from the sample (how much may also be measured by measuring the temperature gradient through the insulation). In practice the sample is placed in an insulation made of polystyrene. There are several standards on semiadiabatic calorimetry.

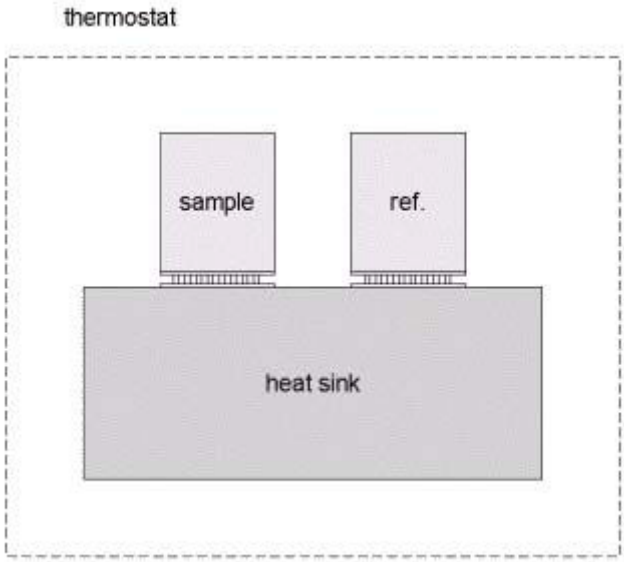

Figure 1. A schematic drawing of a heat conduction calorimeter. When heat is produced in the sample the temperature of the sample is slightly increased. The temperature difference between the sample and the heat sink will then generate a signal from the heat flow sensor (a thermocouple plate positioned between the sample and the heat sink). An identical reference side contains an inert reference sample (water or dry sand) with the same heat capacity as the sample. The sample and reference heat flow sensors are differentially connected so that disturbances entering the calorimeter will be reduced (because they will influence the sample and reference sides in similar ways). The whole calorimeter is placed in a thermostat.

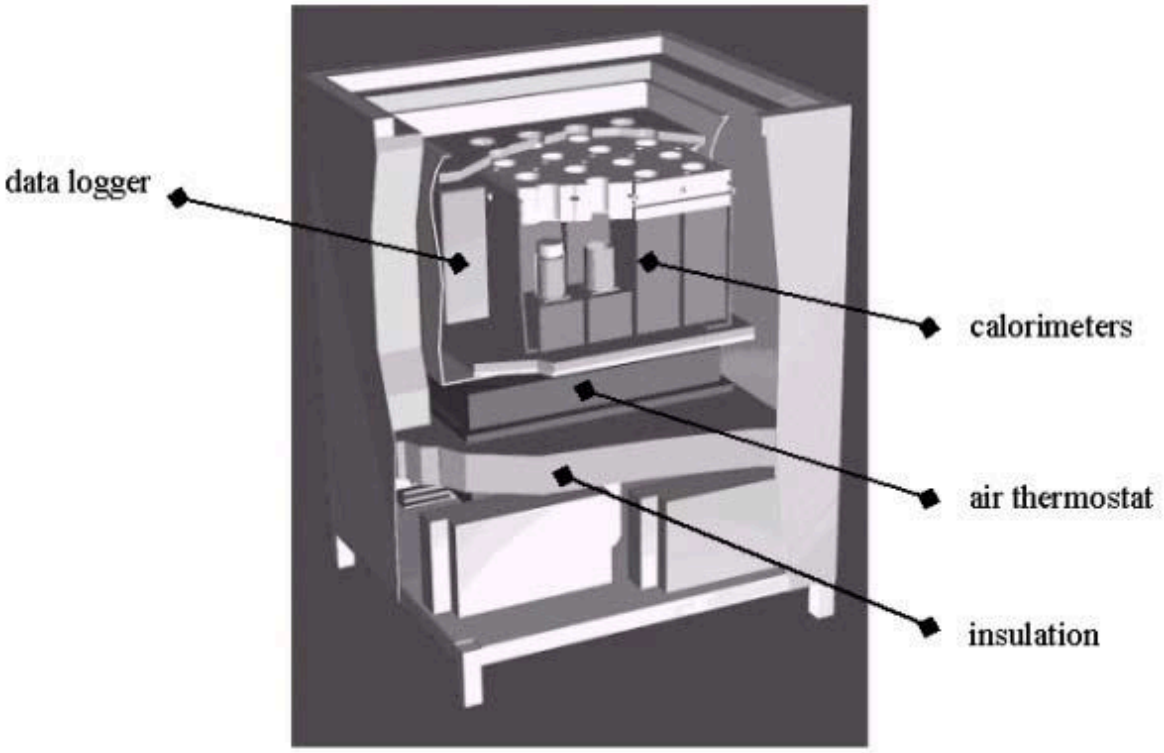

Figure 2. A cut-away drawing of the TAM Air instrument (Thermometric AB, Järfälla, Sweden) that was used in the present study. The calorimetric block contains eight separate isothermal calorimeters, each with a baseline-stability better than 10 microwatts. The data logger is placed in the thermostat and connected to the serial port of a computer. The air thermostat and the 50 mm polystyrene insulation give a temperature stability of 0.02 K.

1.2.2 Solution calorimetery
In this method, which is actually a type of semi-adiabatic calorimeter, the total heat of hydration at a certain time is determined as the difference between the heat liberated when an un-hydrated sample and the sample under investigation are dissolved in mixtures of hydrofluoric and nitric acid. The use of this old standardised technique is decreasing because of the hazardous materials used.

This paper is about a proposal for a standard for isothermal calorimetry of cement hydration. Isothermal calorimeters, often called heat conduction calorimeters, have seen significant development the last decades and they have a wide use in science and industry. Such instruments have many advantages over the standardized and presently used (semi) adiabatic calorimeters:

- Isothermal calorimeters directly measure the heat production rate that is proportional to the rate of the reaction (adiabatic calorimeters measure temperature (change) that is recalculated to give heat produced).
- In isothermal calorimetry it is not necessary to know the heat capacity of the sample, as is required in adiabatic calorimetry.
- For the evaluation of isothermal measurements it is not necessary to know the activation energy; on the contrary isothermal calorimetry can be used to measure activation energies.
- Isothermal calorimeters are very stable and seldom need to be calibrated more than a few times a year (adiabatic calorimeters are often calibrated before each run).
- Isothermal heat conduction calorimeters for cement hydration studies are more sensitive than adiabatic calorimeters and have a higher time-resolution of events taking place. Measurements may therefore be made on much smaller samples than are used in (semi) adiabatic calorimetry.
- The temperature never increases to unrealistic temperatures in an isothermal calorimeter (final temperatures during measurements in adiabatic calorimeters can be very high, e.g. 80^{o}C; far above what is desirable in real construction).
- Isothermal calorimetric experiments are easy to perform and need little operator training and operator time (in contrast especially to the solution calorimetric method described above).
- Isothermal calorimeters are widely used in science and industry and one may therefore expect that such instruments have higher performance/cost-ratios than instruments made specifically for the cement or concrete market.

Isothermal calorimetry has many advantages over conventional cement calorimetry, but a possible drawback is that only small samples may be used. For measurements on large samples of concrete one therefore needs adiabatic or semi-adiabatic calorimeters. However, most measurements can be made on cement pastes, mortar or micro-concrete since normal coarse aggregate does not influence the heat development in the cement paste (approx. 30% of the concrete volume).

Testing of concrete is costly and time-consuming, both because of the large quantities of material that have to be handled and because many of the measurement techniques, e.g. strength measurements, are work-intensive. Some of the measurements that today are made on concrete could instead be done in a much smaller scale on cement paste in isothermal calorimeters. Testing for unwanted excessive retardation is one example. Mixing and charging eight cement paste samples with different concentrations of an admixture into an isothermal calorimeter takes about one man-hour.

Adiabatic and semi-adiabatic calorimeters are sometimes advocated because the temperature increases during a measurement, just like it does in a massive construction. However, this is not of any real advantage since there are very different temperature increases in different parts of a massive construction. The isothermal measurement is the most well defined calorimetric measurement, and to completely describe the hydration of a cement paste or a mortar the best way is to take isothermal hydration measurements at different temperatures.

2. THE PRESENT STANDARDISATION PROJECT

NORDTEST, a Nordic organisation for development of test methods and conformity assessment (www.nordtest.org), is funding an effort to develop a standard for cement hydration measurements by isothermal calorimetry. The project group has the following partners:

1. Building Materials, Lund University, Sweden (Lars Wadsö, coordinator)
2. The Norwegian Building Research Institute, Norway
3. SP, The Swedish National Testing and Research Institute, Borås, Sweden
4. Cementa AB, Sweden
5. Grace Construction Products, USA

The project has two parts. In the first part, parts of which are reported here, the present author at Building Materials at Lund University, Sweden tested different aspects of isothermal calorimetry. In the second ongoing part, the following different types of calorimetric measurements will be performed on two cements:

- Isothermal calorimetry with and without fine aggregate (partners 1, 3 and 5).
- Semi-adiabatic calorimetry (partners 2 and 3).
- Solution calorimetry (partner 4).

The aims of the project are:

- To investigate different aspects of isothermal calorimetry of cement hydration.
- To compare the result of isothermal measurements with those from semi-adiabatic and solution calorimetry.
- To draft a standard for 2-, 3- and 7-days heat of hydration measured by isothermal calorimetry.

Isothermal calorimetry is a very versatile and general measurement technique that can have dozens of uses within the fields of cement and concrete. We have, however, chosen to write a standard only on the determination of 2-, 3- and 7-day heat of hydration. The reason for this is that this type of measurement is today made with semi-adiabatic and solution calorimetry and it is therefore possible to compare our isothermal results with results with these methods. As the standard text will be rather detailed and discusses different aspects of isothermal calorimetry (e.g. calibration and choice of instrument) it may also be used as a base for developing methods for other purposes, e.g. assessment of retardation, determination of activation energy, indicating false set etc.

The standard text will be written in such a way that different models of isothermal calorimeters can be used, but it must also clearly define which properties such a device should have to work well. In the present project all isothermal calorimetry is done in TAM Air calorimeters (Thermometric AB, Järfälla, Sweden; www.thermometric.se). This is a newly developed eight-channel isothermal heat conduction calorimeter which is well suited for cement hydration studies.

3. ASPECTS OF ISOTHERMAL CALORIMETRY OF CEMENT HYDRATION

In this section I discuss some aspects of isothermal calorimetry that were investigated in the first part of the NORDTEST project. Some of these issues discussed concern isothermal calorimetry in relation to present standardised techniques, e.g. measurements of strength. It is obvious that it is necessary to strictly control the use of aggregate when making samples for strength measurement, as the strength of a mortar is dependent on the properties of the aggregate. Present standards therefore prescribe the use of an expensive standardised sand. It would then be natural to suggest

that one also use this sand when making isothermal calorimetry specimens. However, it is not obvious that the aggregate has much influence on the rate of cement hydration, and if one could use cement paste without sand one would decrease the cost and simplify the measurement procedure.

Note that all the results are given in watts per gram cement or joules per gram cement. By this it is possible to directly compare measurements of mortar and cement paste. Also note that not all aspects discussed below may or can be incorporated into the draft standard.

3.1 Sample size

There are two aspects of sample size to be discussed in connection with isothermal calorimetry:

1. In isothermal calorimetry the sample size is limited because if the sample becomes too large it will no longer be at isothermal conditions. This is discussed below (subsection 3.9).
2. Sample size may in also have a direct effect on the result of a heat conduction calorimetric experiment as it may change the heat loss paths from the sample, e.g. with a larger, and therefore higher, sample an increased fraction of the heat produced may be conducted away without passing through the heat flow sensor. For good isothermal calorimeters this is not a problem, e.g. with the TAM Air used in the present project we see no differences between results (expressed as mW/g(cement)) from cement paste samples in the range 2-10 g. In the present study I have used about 5 g of cement paste and 10-15 g of mortar in the experiments and have found that this gives reproducible results.

3.2 Aggregate influence (paste vs. mortar)

Some types of calorimetry (semi-adiabatic) are usually made on concrete with large aggregate, whereas other types (solution calorimetry) require cement paste without any aggregate. In the isothermal calorimeters we have used, it is possible to include aggregate up to about 5 mm in diameter. The spread in data will, however, increase if 5 mm aggregate is used.

We have made measurements of cement paste hydration with and without fine sand and only found minor differences. This is natural as it is in the cement paste that the reaction takes place; the aggregate can usually be considered to be inert. In isothermal calorimeters it is therefore often possible to leave out the aggregate and work with cement pastes. This facilitates sample preparation.

However, note the following:

- It is possible to include some sand to decrease segregation at high water-cement ratios or high plasticiser concentrations, but it is in many cases also possible instead to decrease the water-cement ratio if one can accept a slightly longer time until the main reactions start.
- When sand is included, the start of the main hydration reaction is often slightly more rapid than without the sand. This is probably because the sand grains can act as seeds for the hydration reaction. For 2-7 days heat of hydration this is of no importance.
- It is probable that filler materials like silica fume and finely ground limestone will influence hydration. Such materials can be incorporated without any problem in a measurement.
- If one expects that a large size aggregate could influence hydration by substances/ contaminants on its surface one may, for test purposes, wash these off into the mixing water.

3.3 Glass ampoules (vials)

In heat conduction calorimetry it is essential that there is good contact between the sample and the heat flow sensors and one normally uses ampoules of stainless steel or glass that tightly fits into an ampoule holder in the calorimeter. For cement hydration studies disposable glass ampoules (chromatographic vials) are the most rational choice. However, the very alkaline pore solution of

cement paste may partly dissolve the surface of a glass ampoule. Will the heat from this reaction influence the measurement of the heat from the cement hydration reaction? To test this I made parallel measurement with cement paste in glass ampoules and in polyethylene bags placed into glass ampoules. The result was both integrated for the total heat and examined visually and there was no observable trend in any direction. The relative standard deviation of the integrals up to 40 h was about 3% for the whole data set, as well as for the samples in glass ampoules and the samples in polyethylene bags, respectively. The conclusion is that the glass-cement paste reaction does not significantly influence the result of the calorimetric measurements.

3.4 Deriving the total heat

When the result from a calorimetric measurement is to be integrated so that one can compare it with solution calorimetric results it is important that the measurement is started as soon as possible after the water is mixed with the cement. I have found that it is no problem to charge samples into the calorimeter in less than 180 seconds after the water was added.

When the sample is charged into the calorimeter it is never at exactly the same temperature as the calorimeter. There will therefore be an initial disturbance, most of which can be removed by the application of the Tian equation [3]:

$$P = \varepsilon (U + \tau \frac{dU}{dt}) \qquad (1)$$

The Tian equation is useful for processes with rapidly changing heat production to find the true shape of the $P(t)$-curve from the U-output from the heat flow sensors, but for calculating the true *integral* a simpler approach may be used. The heat Q is the integral of the thermal power P:

$$Q = \int_{t=t_1}^{t_2} P dt = \varepsilon \int_{t=t_1}^{t_2} U dt + \varepsilon\tau \int_{t=t_1}^{t_2} \frac{dU}{dt} dt \qquad (2)$$

Here, t_1 is the start of the integration a few minutes after the water was added and t_2 is the end of the integration, typically 2, 3 or 7 days after water was added. The second integral is trivial and Eq. 2 can be rewritten as:

$$Q = \varepsilon \int_{t=t_1}^{t_2} U dt + \varepsilon\tau \left(U(t_2) - U(t_1)\right) \qquad (3)$$

Normally, $U(t_2)$ is very small compared to $U(t_1)$ and we finally arrive at the following simplified expression for the heat integral from a isothermal calorimetric measurement:

$$Q = \varepsilon \int_{t=t_1}^{t_2} U dt - \varepsilon\tau U(t_1) \qquad (4)$$

The time constant τ needed for the Tian correction may be determined from calibrations or calculated from knowledge of the thermal properties of the calorimeter and the sample. The most practical way is probably to calculate it as the ratio of the sum of the heat capacities of the sample components (cement, sand and water), the ampoule and the ampoule holder divided by the thermal conductivity of the heat flow sensor. Such a procedure will probably give a value within 10% of the true value.

3.5 Influence of the mixing procedure

In mortar standards the mixing procedure is important and particularly when one is interested in measuring the total heat with isothermal calorimetry the mixing has to be quick. We have tested mixing small amounts of cement paste and mortar by hand. Typically, we mix about 50 g of cement paste or about 100 g of mortar by hand in a plastic cup or glass cup. Mixing is usually done with a stainless steel teaspoon and takes about 15 seconds. We have found that hand mixing is efficient and we see no differences between samples mixed for 30 seconds and samples that are mixed for a longer time. Mixing with an electrical hand mixer (household type) may possibly be more reproducible and can be made in as short time as hand mixing. Note that it is essential that the sample be efficiently mixed for some time after the last dry cement is gone. Also note that it is probable that samples containing fine fillers like silica need more aggressive mixing than hand mixing.

3.6 Calibration

Isothermal calorimeters are normally calibrated electrically by sending a known current through a resistor (heater) that is placed close to where the samples are placed. Calibrations may be made with built-in heaters (usually attached to the sample holders) or with heaters that are placed in ampoules. It is probable that the placement and construction of such heaters to some extent will influence the result of a calibration [4], but this has not been specifically investigated for the types of calorimeters used in this project.

Calibration should be done regularly and the generated calibration coefficients and baselines (offset) should not differ substantially from calibration to calibration. Rules for calibration intervals and acceptance of calibration results need to be discussed. Monthly calibration is advisable, particularly when a calorimeter is used continuously. Our experience from the Thermometric TAM Air is that its calibration coefficients and baseline offsets are very stable with time.

3.7 Test experiments

Test experiments are experiments designed to test the whole measurement procedure, i.e. the instrument, the calibration coefficient, the mixing and charging procedures etc. For a multi-channel calorimeter like the TAM Air we recommend the following experiment. Make a mix of 100 g cement and 50 g water. Charge between 3 and 8 g into each of the eight calorimeters and measure until the main hydration peak has passed. The test experiment is successful if the curves look similar and all peak values are within +/-5% of the mean peak value. This test measurement takes less than one day and confirms that the whole measurement procedure works as intended.

3.8 Measurements at different temperatures

When measuring the total heat of hydration it is important that the measurement is started soon after the mixing. When the measurement is made at a temperature that is different from that of the room where the mixing is made, the sample may carry a substantial amount of (positive or negative) heat into the calorimeter making it go out of range for a time during which data about the heat production is lost. This is mostly a problem at elevated temperatures where the reaction rate is higher. It is therefore recommended that one uses pre-heated ingredients and work in such a way that the sample has approximately the measurement temperature when it is charged into the calorimeter. One can for example test how much one has to pre-heat the water to get a final ampoule temperature that is the same as that of the calorimeter temperature.

3.9 Temperature changes in an isothermal calorimeter

Heat conduction calorimetry is often referred to as isothermal calorimetry because one tries to keep the temperature of the sample constant by removing the produced heat by conduction (cf. (semi) adiabatic calorimetry it which one insulates the sample in order to be able to measure its temperature increase). Heat conduction calorimetry is, however never perfectly isothermal as there

will always be a small temperature difference between the sample and the thermostat. The present author [5] has given a procedure to calculate the temperature increase in a sample during a measurement in a heat conduction calorimeter. A cement hydration standard for heat conduction calorimetry should demand that the temperature increase caused by the heat production in the sample should be limited, e.g. below 0.5 K, during a measurement.

4. DISCUSSION AND CONCLUSIONS

Isothermal calorimetry is a useful method to solve problems in cement and concrete science and technology, but its use has been limited by the lack of standardised method for its use in the cement and concrete field. The aim of this work is to propose a Nordic standard for measurements of total heat of hydration (usually 2, 3 or 7 days) with the following limitations:

- Temperature 20^{o}C.
- Water-cement ratio 0.5.
- Cement paste (no sand)

The procedures stated in this standard can then be modified and used also for other types of measurements of cement hydration. For example, if one wants to quantify retardation as a function of admixture concentration one can modify the standard procedure so that one adds the admixture with the mixing water. If this needs to be done at different temperatures one can modify the temperature conditions in the standard.

The first stage of this work has been to test if a number of procedures required by other standards are necessary to implement in the new standard. The main result of this was that:

- Samples of 5g cement paste give reproducible results.
- The influence of the aggregate is very small (fillers are probably an exception).
- Glass ampoules may be used.
- The total heat can be derived with a simplified Tian-expression.
- Hand mixing produced reproducible results.

5. NOMENCLATURE

P	thermal power	W
Q	heat	J
U	voltage*	V
ε	calibration coefficient*	W/V
τ	time constants	s

* The output from a heat conduction calorimeter in normally a voltage

REFERENCES

[1] Wadsö, I., Isothermal microcalorimetry near ambient temperature: An overview and discussion, Thermochem. Acta, vol.294, 1997, pp.1-11.

[2] Wadsö, I., Trends in isothermal microcalorimetry, Chem. Soc. Rev., 1997, pp.79-86.

[3] Cembureau, Recommended procedure for the measurement of the heat of hydration of cement by the conduction method, U.D.C. 666.94.015.45: 620.1., 1977.

[4] Bäckman, P., Bastos, M., Hallen, D., Lönnbro, P., and Wadsö, I., Heat conduction calorimeters: time constants, sensitivity and fast titration experiments, J. Biochem. Biophys. Methods, vol.28, 1994, pp.85-100.

[5] Wadsö, L., Temperature changes within samples in heat conduction calorimeters, Thermochim. Acta, vol.366, 2000, pp.121-127.

MONITORING EARLY CEMENT HYDRATION BY RHEOLOGICAL MEASUREMENTS

F. Winnefeld[1] and L. Holzer[1]

[1]Swiss Federal Laboratories for Materials Testing and Research, Section Concrete/Construction Chemistry, 8600 Dübendorf, Switzerland. E-mail: frank.winnefeld@empa.ch

ABSTRACT

This contribution focuses on the structural changes of cement paste from mixing to setting, determined by rheological measurements and ESEM-observations. Initially after adding of water, the cement starts to hydrate. During the induction period the rate of hydration is very low. The cement paste is still workable and behaves like a fluid. At the beginning of the acceleration period, the structure of the cement paste changes, it stiffens. By measuring the rheological properties during cement hydration, information on the structural growth during the hydration process can be obtained. But it is important that the structure of the paste is not influenced by the measurement itself. Cement paste before setting is a flocculated suspension that is very sensitive to the applied shear. Its microstructure breaks down very easily. The usual rheological techniques - for example flow curves - are not suitable for a continuous monitoring of cement hydration, as the yield stress of the paste is exceeded during measurement, causing a structural breakdown. With a special dynamic measurement technique, low-amplitude oscillatory shear, the structural growth of cement pastes can be studied continuously from mixing until setting. As an application example of the method the influence of superplasticizers was examined. The results correlate well with ESEM and calorimetry data.

1. INTRODUCTION

Rheology is defined as the science of flow and deformation of matter. Regarding fresh cement paste, mortar and concrete, it is a powerful tool to determine their workability properties. Viscometric flow of a homogeneous liquid is usually explained using the two plate model (Figure 1). The sample is placed between two parallel plates. The upper plate is moved with a constant velocity, the force needed is F. The lower plate is fixed. If the liquid adheres to the plates, a laminar flow in x-direction occurs. Shear stress and rate of shear are given by the equations shown in Figure 1. In commercial rheometers, the simplified plate geometry is replaced by a rotating plate-plate-, cone-plate- or concentric cylinder-geometry.

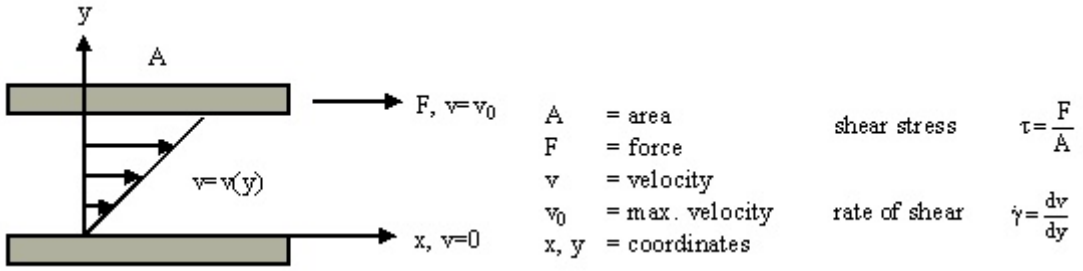

Figure 1. Two plate model - definition of rheological parameters

Usually, the flow behavior of a liquid or a suspension is characterized by a flow curve. The sample is sheared at different levels of rate of shear and the resulting stress is measured. The opposite, different preset levels of stress and measuring the resulting rate of shear is also possible. The flow curve, usually stress versus rate of shear, shows a typical behavior, depending on the tested material. For Newtonian liquids such as water, stress is proportional to rate of shear. The slope of the curve is the viscosity. Cement pastes, mortars and concretes are approximately Bingham- or Herschel-Bulkley-fluids with a yield stress [1], there are some other models reported in literature [2,3]. The flow behavior of these materials is strongly dependant on mixture composition, e. g. type and amount of cement, aggregate, admixture, but also water/cement-ratio, temperature and intensity of the previous mixing process.

The rheology of cement paste (as well as mortar or concrete) is also depending on hydration time. Like in other suspensions, the cement particles start to form agglomerations via diffusion-induced collisions [4] immediately after mixing. The cause of the flocculation process is interparticle (van der Waals-) forces. If the particle concentration is low, the aggregates will settle. At higher concentrations, the flocculation process forms a network that is quite stable with regard to sedimentation. This material behaves to small amplitude deformations like an elastic solid. At later hydration times, the cement particles begin to interact also mechanically due to the formation of hydration products.

It is obvious that the change in rheological properties can provide information on the hydration progress and workability time. Hydration causes an increase in viscosity and especially in yield stress [1]. However, the measurement of sequential flow curves on the same sample with a rheometer or of the shear stress as a function of the rate of shear are not suitable methods. Their disadvantage is, that the material is influenced by the measurement itself. Therefore, a non-destructive rheological method is needed that measures the structural strength of cement paste without allowing it to flow, at stresses below the yield point. A special dynamic method, low-amplitude oscillatory shear, can be applied. Again, the two plate model is useful to explain the method (Figure 2).

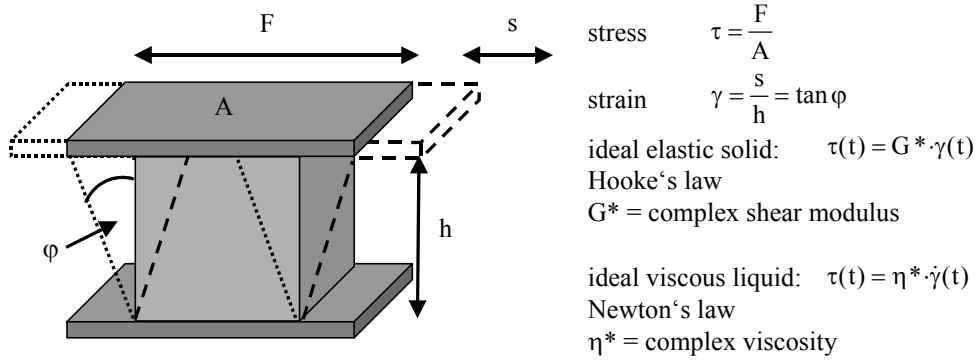

Figure 2. Two plate model - oscillatory shear experiment

Strain (or stress) is oscillated according to a sine function (Figure 3):

$$\gamma(t) = \gamma_A \cdot \sin(\omega \cdot t) \quad \text{(with } \omega = \text{angular frequency)} \tag{1}$$

The resulting stress (strain resp.) and the lag between applied stress and resulting strain (phase angle) is measured:

$$\tau(t) = \tau_A \cdot \sin(\omega \cdot t + \delta) = \gamma_A \cdot [G' \cdot \sin(\omega \cdot t) + G'' \cdot \cos(\omega \cdot t)] \quad (2)$$

(with the complex shear modulus G* = G' + i·G")

For an ideal elastic solid, strain and the resulting stress are in phase. For an ideal viscous liquid, however, the stress sine curve is delayed by a phase angle of 90° compared to the strain sine curve. Viscoelastic substances such as cement paste show a behavior that ranges between an ideal liquid and an ideal solid. The lag between strain and stress curve is $0 < \delta < 90°$. δ is called the phase or the loss angle. The storage modulus G' calculated from the data represents the elastic (or solid-like, reversible) response of the material to a strain or a stress, the loss modulus G" describes the viscous (or liquid-like, irreversible) response. The ratio G"/G' = tan(δ) represents the ratio of viscous and elastic properties. Therefore, the measurement of G' and G" of cement paste can provide information on the structural growth during the first hours of cement hydration. There are only few reliable data in world-wide literature on the application of this method to cement pastes [6-11], because the material is so very sensitive to shear.

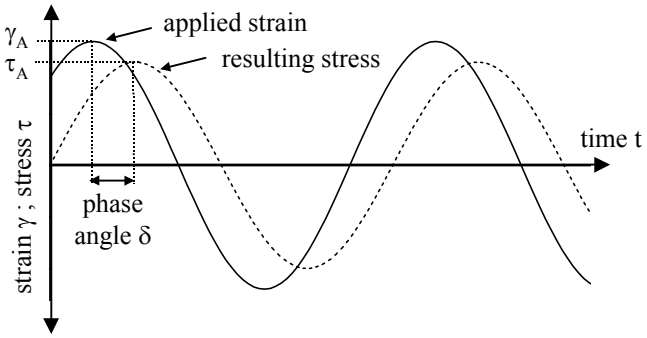

Figure 3. Applied oscillatory strain, resulting stress and phase angle for a viscoelastic material

2. EXPERIMENTAL

2.1 Materials

An Ordinary Portland cement CEM I 42.5 N according to European Standard EN 197-1 with a specific of 2840 cm^2/g (Blaine method) was used. The chemical composition is given in table 1.

Table 1. Chemical composition of the used Ordinary Portland cement CEM I 42.5 N

CaO wt.-%	MgO wt.-%	SiO_2 wt.-%	Al_2O_3 wt.-%	Fe_2O_3 wt.-%	Na_2O wt.-%	K_2O wt.-%	SO_3 wt.-%	CO_2 wt.-%	L.O.I. wt.-%	free lime wt.-%
63.2	2.1	19.5	5.3	3.1	0.13	1.1	3.1	2.1	2.7	0.43

The influence of admixtures on cement hydration was examined using three superplasticizers with different chemistry (Table 2). The adsorption of the admixtures on the cement was studied preparing pore solutions under nitrogen atmosphere (glove box). Cement and distilled water containing the superplasticizer were mixed by hand for one minute. The dosage of admixtures was 0.45% referred to cement, water/cement ratio was 0.40. The pore solution was extracted by suction filtration after 5 min and in a second series after 30 min of hydration.

Table 2. Properties of the used superplasticizers

abbreviation	chemistry	solid content	adsorption of admixture (dosage 0.45%, w/c = 0.40) on cement	
			after 5 min	after 30 min
PC	Polycarboxylate	approx. 35%	52 %	59 %
NS	Naphthalene sulfonate	approx. 35%	84 %	85 %
LS	Ligno sulfonate	approx. 35%	70 %	71 %

2.2 Rheology

A rheometer (Paar Physica MCR 300) that enables both stress- and strain-controlled experiments was used. A cylindrical measuring geometry according to ISO 3219 with a cup and a rotating bob was used (Searle geometry), the measuring gap was 1.13 mm. The measuring system was connected to the rheometer by an air bearing. A special, newly developed technique (direct strain oscillation [11]) was applied that allows measurements at very low torques (< 0.1 µNm) and very small deflection angles (< 0.1 µrad). Such a high sensitivity is necessary due to the very low torques and deflection angles that have to be measured for the examination of very weak structures.

Cement pastes were prepared with w/c ratio of 0.40. The admixtures were dissolved in the mixing water. Mixing was done according to EN 196-3. The paste was transferred into the rheometer cup with a spoon. The measuring bob was then slowly lowered into the paste. The cup was covered with a solvent trap to keep relative humidity above the paste to over 90%. The temperature of the sample was maintained to 20°C by means of a circulating water bath. The measurement started 5 min after the addition of water to cement. In the hydration experiments, data were collected every 60 seconds.

2.3 Heat flow calorimetry

The heat flow during hydration of the cement pastes was determined by means of isothermal conduction calorimetry. Water/cement ratio and dosages of superplasticizer were the same as described in 2.1.

2.4 Electron microscopy

To determine whether changes in rheological properties are related to microstructural changes of the cement pastes, the morphology of the hydration products was studied using an environmental scanning electron microscope (ESEM). Pastes were prepared under nitrogen as described in 2.1. At different hydration times (30 min, 2 and 5 hours) the pore solution was separated. A sample of the filter residue was then immediately transferred into the ESEM.

3. RESULTS

3.1 Determination of the linear viscoelastic region

The prerequisite of the oscillatory shear experiments is, that the strain level during measurement stays below a critical strain in the so-called "linear-viscoelastic region" (LVR), so that the structure of the flocculated network will not be disturbed. Higher stresses outside the LVR will cause a structural breakdown of the paste. The sample then begins to flow like a liquid. To determine the LVR, a strain sweep with increasing strain amplitude and an angular frequency of 2.5 s^{-1} was performed (Figure 4).

Within the LVR in the low-strain region, the G'- and G"-curves are both independent of the strain level. That means, that the microstructure of the suspension is not disturbed. G' (14 kPa) is higher than G" (7 kPa), indicating that the paste shows mainly a gel-like or solid-like behavior. The critical strain is $6x10^{-5}$. Above the critical strain, a structural breakdown occurs, G' and G" decrease rapidly. The critical strain corresponds to the yield stress. Actually, yield stresses can be determined in a more accurate way by oscillatory stress or strain sweeps than by calculation from flow curves with

the Bingham- or the Herschel-Bulkley-model. The critical stress of all examined samples was between $5x10^{-5}$ and $2x10^{-4}$. This corresponds well with the data from [5,6]. In [8] a critical strain of 1.3 10^{-4} for C_3S-pastes with w/c ratio of 0.50 is reported. For the further hydration experiments in 3.2 and 3.3. a strain amplitude of $\gamma = 5x10^{-5}$ was used.

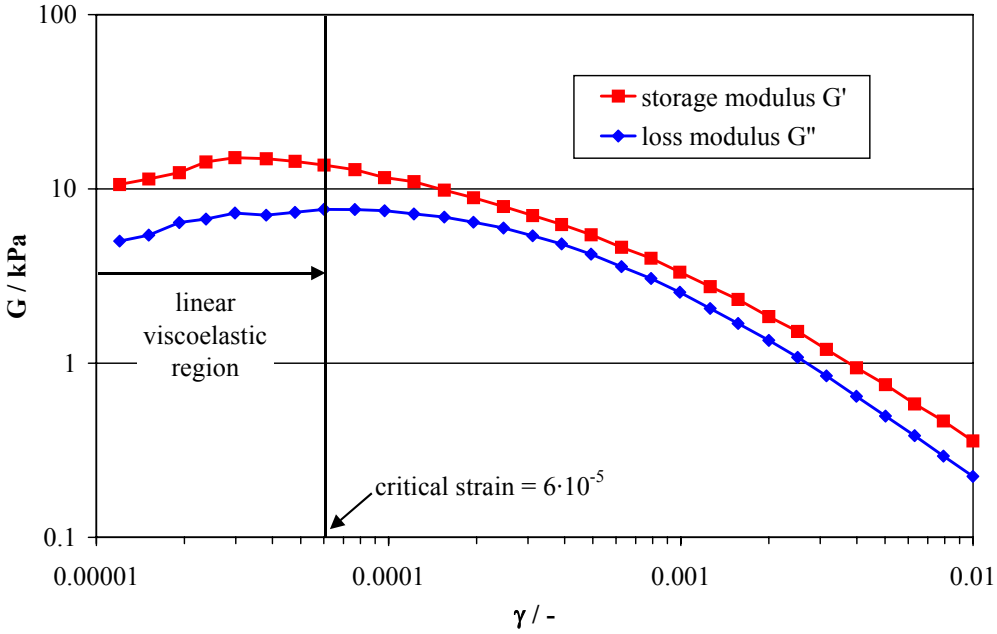

Figure 4. Strain sweep of Portland cement paste with w/c = 0.40; angular frequency = 2.5 s^{-1}

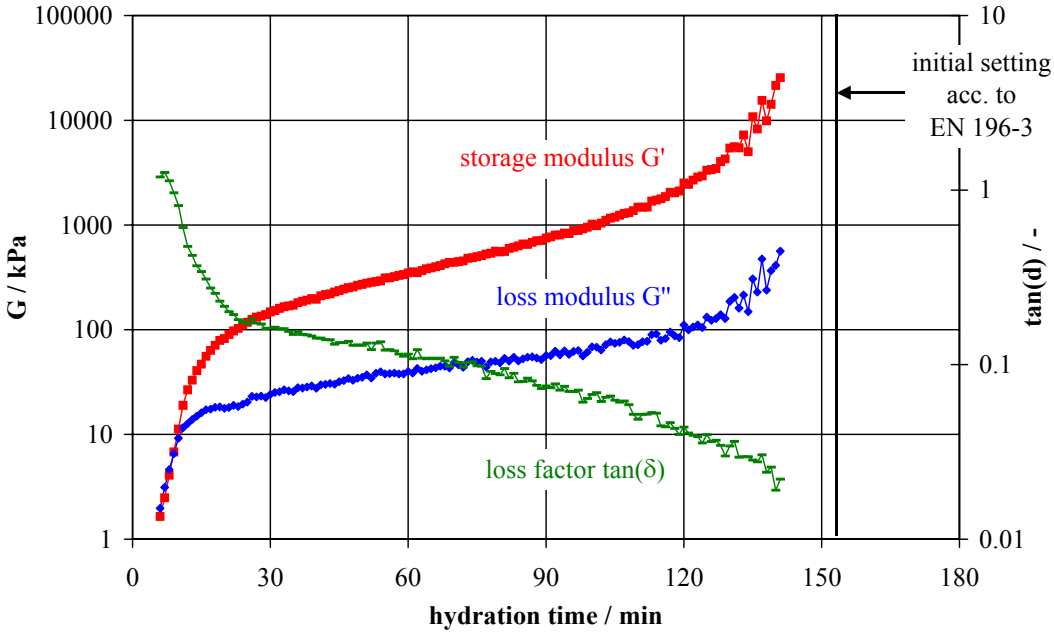

Figure 5. Change of storage modulus, loss modulus and loss angle during early hydration of Portland cement paste with w/c = 0.40; strain = $5x10^{-5}$, angular frequency = 2.5 s^{-1}

3.2 Time behavior of Portland cement paste

Figure 5 shows the time behavior of a Portland cement during an oscillatory shear experiment. At the beginning of the measurement (5 minutes after the addition of water to the cement), the paste shows a both liquid- and solid-like behavior with tan(δ) at about 1. The values for G' and G" are approximately 2 kPa. Then G" and especially G' increase rapidly, because the structure of the paste

recovers from the structural breakdown due to the mixing process. The flocculation of the cement particles is responsible for this thixotropic effect. The increase in G' is stronger than the increase in G", the character of the paste becomes more solid-like. At the end of this period after 30 minutes of hydration, the values for G' are 150 kPa and for G" 25 kPa.

After this thixotropic structural gain, the increase of G' and G" gets slower, with a linear gradient in relation to the logarithmic scale of G. This indicates that the paste slowly begins to stiffen. At about 110 min hydration time, the increase of the storage modulus and also of the loss modulus gets stronger. The reason for the increase of G' is the increasing amount of solids in the suspension due to hydration, but also the interaction of the hydration products [5]. This workability loss occurs at an earlier time compared to the initial setting determined by the Vicat test method according to European Standard EN 196-3. This can be explained by the fact that the result of the Vicat test is caused by a certain, quite high viscosity or stiffness of the paste and not by a significant shift of the structural development.

After the beginning of this strong increase in G’ and G”, the measurement had to be stopped. The stiffness of the sample caused first an increasing scattering of the data, then very low values for G' were measured. It can be suggested that the measuring bob had lost adhesion to the cement paste and wall slip occurred. The reproducibility of the oscillatory shear experiments is quite good [12], indicating that no problems like wall slip occurred, as discussed in [10]. This could be expected because of the narrow gap used and the very low strains applied in the experiments. The experimental data is quite comparable to those determined by [5-7], considering the first 90 minutes of hydration. The decrease in G” reported in their papers, however, could not be observed. It can be suggested that this decrease is an artifact due to the increasing stiffness of the paste, as discussed in [6]. A rapid rise in G' and G" at the beginning of the acceleration period was determined by [13]. Other authors report much lower (1/100) values for G’ and G” for oilwell cement slurries with high w/c ratios around 1.0 [14]. In [14], the authors did not find the decrease in G”. But in the last two cases it is very uncertain, if they worked within the linear viscoelastic region.

3.3 Influence of superplasticizers

The influence of a polycarboxylate-based superplasticizer (PC), commonly used in self-compacting concrete, was tested (Figure 6). Generally, the storage modulus is lower with increasing dosage of the superplasticizer at a certain hydration time. The paste has less structural strength and is more fluid. The rise of the storage modulus after the initial thixotropic structural gain is also less strong in the case of the superplasticizer-containing pastes. G" shows the same effect as G'. The greater fluidity of the superplasticizer-modified pastes is caused by the adsorption of the polymer on the clinker surfaces leading to steric and to a less extent electrostatic repulsion between the cement grains [15]. The more superplasticizer added to the paste, the more the workability time increases. The adsorption of the polymer on the cement also causes this prolongation of workability time. The retarding effect of the polycarboxylate-based superplasticizer was also confirmed using a conduction calorimeter. A good correlation was found between the end of workability time determined by oscillatory shear and the end of the dormant period measured by calorimetry (Figure 7).

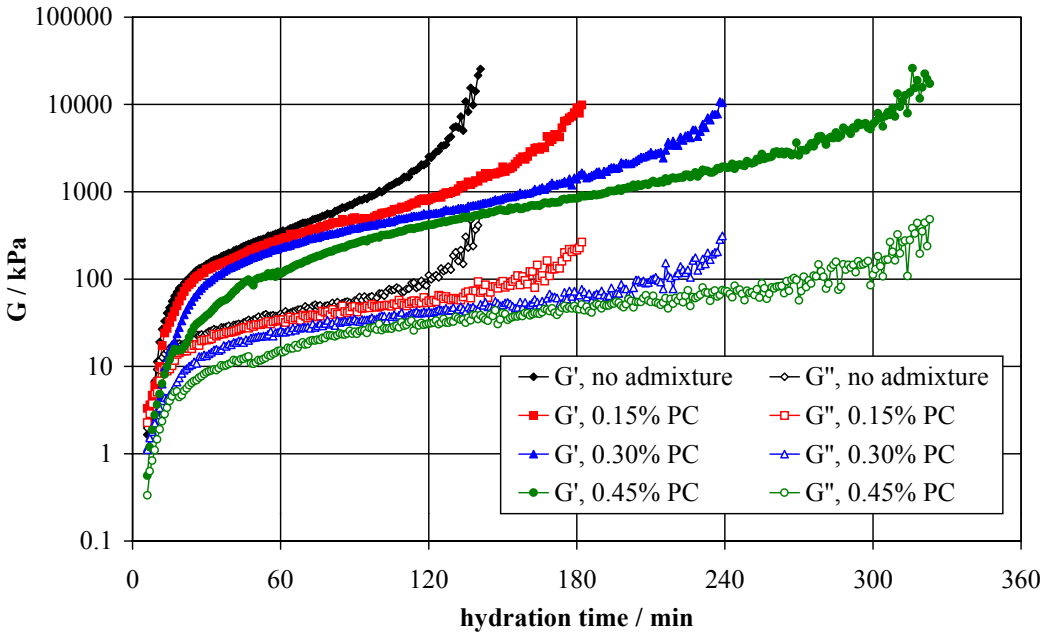

Figure 6. Influence of polycarboxylate-based superplasticizer on storage and loss modulus depending on hydration time; w/c = 0.40; strain = $5x10^{-5}$, angular frequency = 2.5 s^{-1}

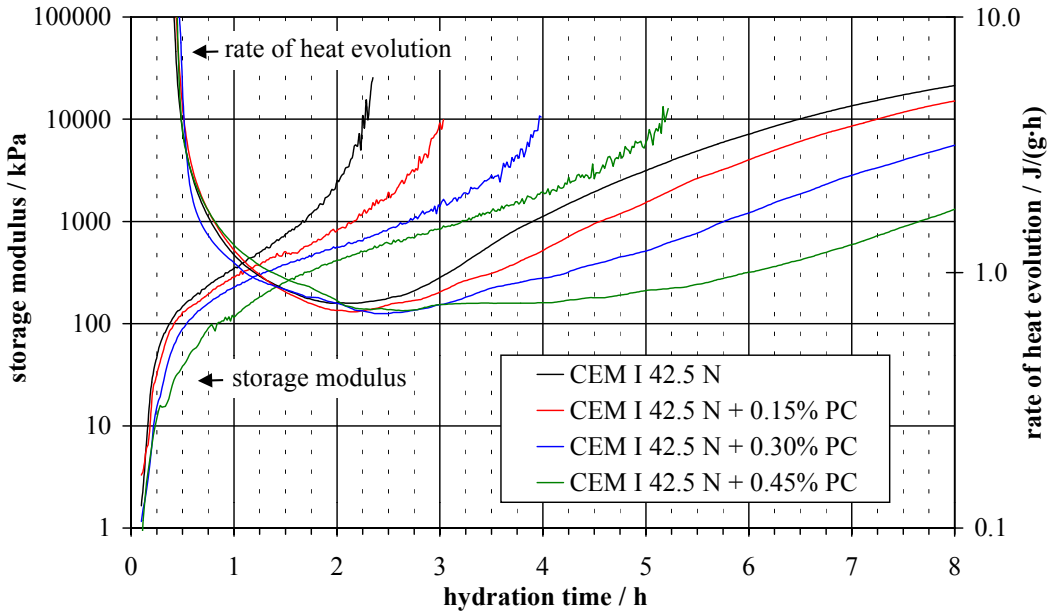

Figure 7. Comparison between rheological and calorimetric data on the hydration progress of PC-containing cement pastes

The microstructures of the pure cement paste and the paste with 0.45% PC were investigated in the environmental scanning electron microscopy (ESEM) at hydration times 30 min (end of thixotropic structural gain, 2 hours (beginning workability loss of pure cement paste) and 5 hours (beginning workability loss of the paste with 0.45% PC).

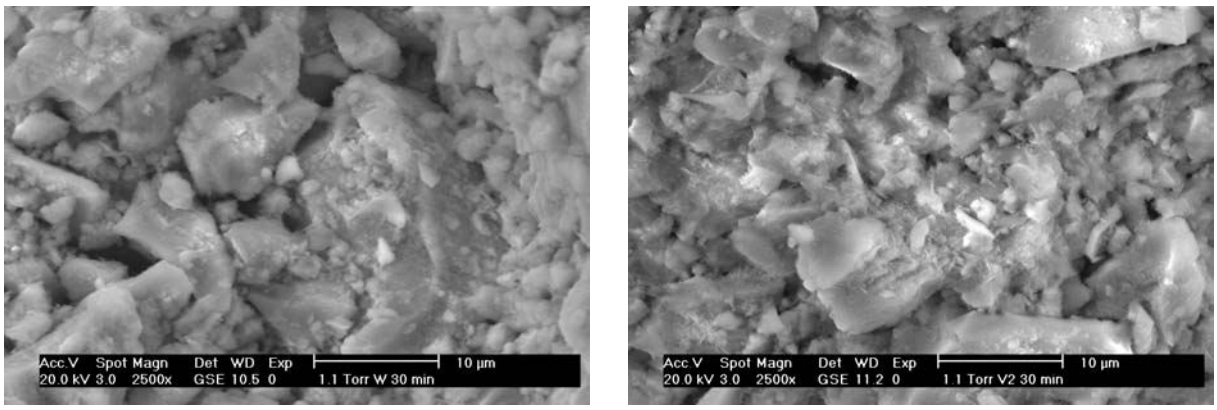

Figure 7. ESEM-micrograph of Ordinary Portland cement paste with w/c 0.40 without admixture (left) and with 0.45% PC (right) after 30 min of hydration

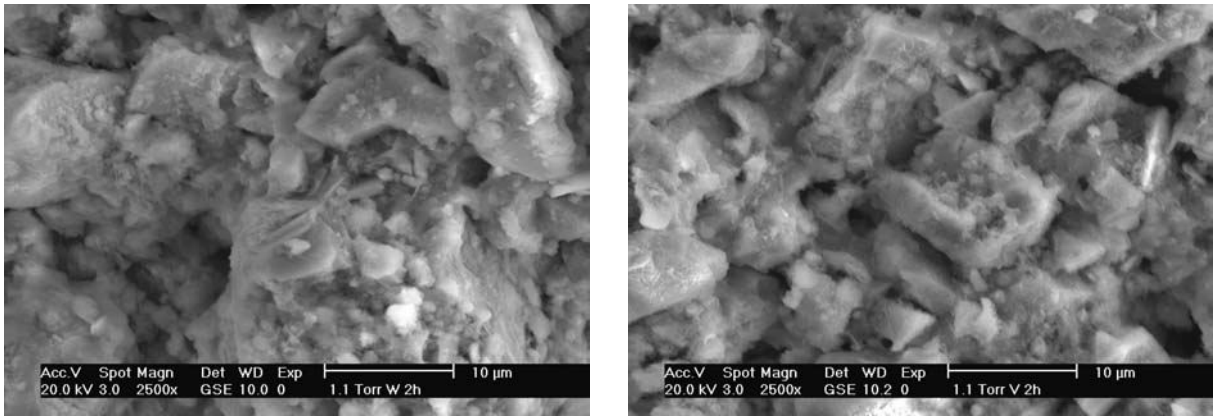

Figure 8. ESEM-micrograph of Ordinary Portland cement paste with w/c 0.40 without admixture (left) and with 0.45% PC (right) after 2 hours of hydration

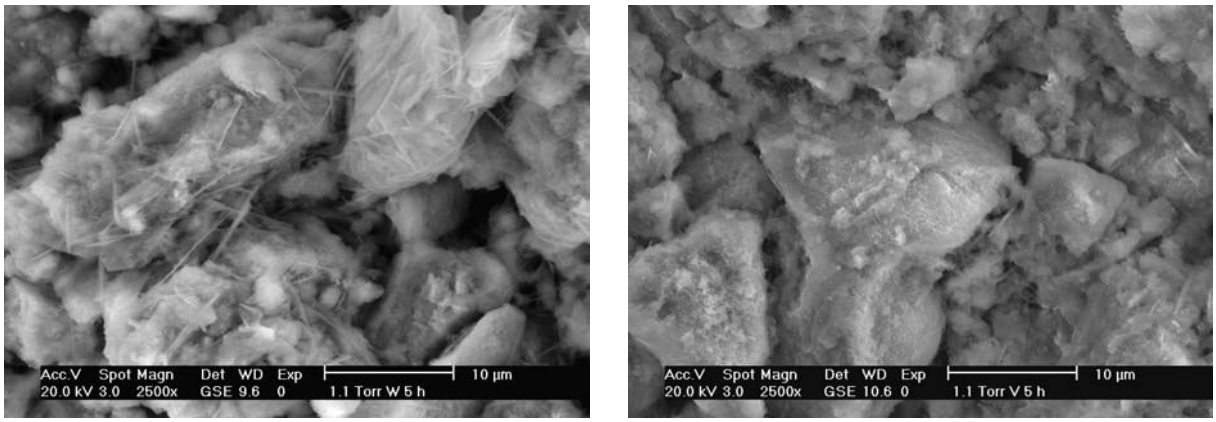

Figure 9. ESEM-micrograph of Ordinary Portland cement paste with w/c 0.40 without admixture (left) and with 0.45% PC (right) after 5 hours of hydration

Figure 7 shows the microstructure of the two pastes at an age of 30 minutes. In both cases initial hydration products have formed on the surface of the cement clinker grains. The hydration products, however, are not big enough to connect the larger cement particles. At a hydration time of two hours (Figure 8), larger crystals can be found on the clinker surfaces. The hydration products now start to bridge the space between the particles, causing the workability loss determined by the oscillatory shear measurements. The paste with PC however shows after two hours mainly the same structure than after 30 minutes of hydration. The beginning of a significant bridging of the space between the particles can be observed at a hydration time of five hours (Figure 9.). In comparison to that, the particles in the paste without admixture are connected by a network of hydration products.

Beside the polycarboxylate-superplasticizer, two other products based on naphthalene sulfonate (NS) and on ligno sulfonate (LS) were tested at a dosage of 0.45%. Figure 10 shows the results of the oscillatory shear experiments in comparison to the data for the pure and the PC-modified pastes. It is obvious, that in spite of the greater adsorption on the cement grains both products are less effective in plastification of the cement paste compared to the polycarboxylate. The decrease in storage modulus compared to the control mix is less compared to the polycarboxylate. The increase of G' at the end of workability time marking strong structural gain, is remarkably earlier, 150 min for 0.45% NS and 140 min for 0.45% LS, compared to 270 min for 0.45% PC-superplasticizer. This effect corresponds to data obtained from the Vicat-test, heat flow calorimetry and ESEM experiments.

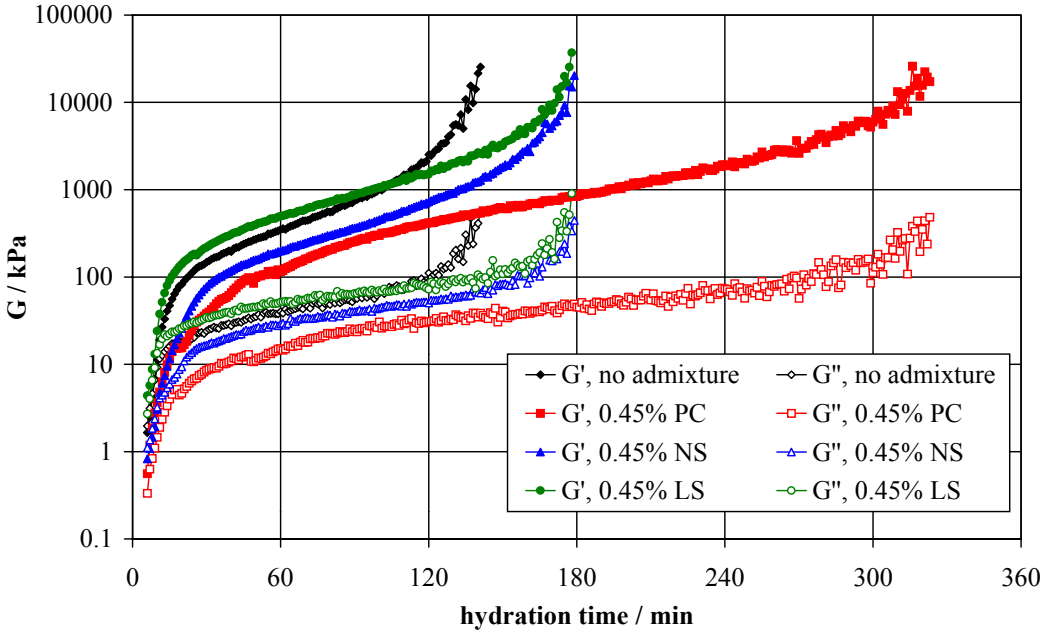

Figure 10. Influence of polycarboxylate-based superplasticizer on storage and loss modulus depending on hydration time; w/c = 0.40; strain = $5x10^{-5}$, angular frequency = 2.5 s^{-1}

4. CONCLUSIONS

It could be shown that oscillatory shear experiments are a suitable method for studying the structural growth of cement paste during early hydration. Storage modulus G' and loss modulus G", representing solid- and liquid-like behavior, can be measured continuously without influencing the very shear-sensitive structure of the paste. The experiments have to be carried out in the linear viscoelastic region below a critical strain. The critical strain for the examined cement pastes ranges from $5 \cdot 10^{-5}$ to $2 \cdot 10^{-4}$.

Freshly mixed cement paste with water/cement-ration of 0.40 shows both solid- and liquid-like behavior, with values for G' and G" of approximately 2 kPa. The greatest increase in storage modulus G' occurs on one hand within the first 30 minutes of hydration due to thixotropic effects caused by flocculation of the cement particles. On the other hand, the end of workability time is marked by a strong increase of G' at about 110 min of hydration in the case of the examined Ordinary Portland cement paste without admixture.

The influence of three different superplasticizers was studied. Effects like workability time, plastification or retardation could be determined. The end of workability time could be linked on one hand with the end of the dormant period measured using a heat flow calorimeter, on the other hand with structural changes observed in the ESEM.

REFERENCES

[1] Tattersall, G.H. and Banfill, P.F.G. The Rheology of fresh concrete, Boston, London, Melbourne: Pitman Advanced Publishing, 1983.

[2] Quemada, D. Models for rheological behaviour of concentrated disperse media under shear, IX. International Congress on Rheology, Mexico, 1984, pp.571-582.

[3] Atzeni, C.; Massidda, L. and Sanna, U.: Comparison between rheological models for cement pastes, Cement and Concrete Research, vol.15, 1985, pp.511-519.

[4] Sonntag, R.C. and Russel, W.B. Elastic properties of flocculated networks, Journal of Colloid and Interface Science, Vol.116, 1987, pp.485-489.

[5] Schultz, M.A. and Struble, L.J. Use of oscillatory shear to study flow behavior of fresh cement paste, Cement and Concrete Research, vol.23, 1993, pp.273-282.

[6] Struble, L.J.; Zhang, H.; Sun, G.-K. and Lei, W.-G. Oscillatory shear behavior of Portland cement paste during early hydration, Concrete Science and Engineering, Vol.2, 2000, pp.141-149.

[7] Blask, O., Knöfel, D., Sandor, M. and Pakusch, J. Connection between rheological and microstructural changes during hydration of cement pastes, 23rd International Conference on Cement Microscopy, Albuquerque, 2001, pp.104-116.

[8] Mansoutre, S., Colombet, P. and Van Damme, H.: Water retention and granular rheological behavior of fresh C_3S paste as a function of concentration, Cement and Concrete Research, Vol.29, 1999, pp.1441-1453.

[9] Schmidt, G. and Schlegel, E. Rheological characterization of C-S-H-phases-water suspensions, Cement and Concrete Research, Vol.32, 2002, pp.593-599.

[10] Saak, A.W., Jennings, H.M., Shah, S.P. The influence of wall slip on yield stress and viscoelastic measurements of cement paste, Cement and Concrete Research, Vol.31, 2001, pp.205-212.

[11] Läuger, J., Wollny, K. and Huck, S. Direct Strain Oscillation - A new oscillation method enabling measurements at very small deflection angles and torques, Annual Transactions of the Nordic Rheology Society, Nordic Rheology Conference, Trondheim, 2001, Norway, Vol.8/9, 2000/2001, pp.97-100.

[12] Winnefeld, F. Rheological behavior of Portland cement pastes during early hydration, 24th International Conference on Cement Microscopy, San Diego, 2002, pp.18-31.

[13] Banfill, P.F.G., Carter, E. and Weaver, P.J. Simultaneous rheological and kinetic measurements on cement pastes, Cement and Concrete Research, Vol.21, 1991, pp.1148-1154.

[14] Saasen, A., Marken, C., Dawson, J. and Rogers, M. Oscillating rheometer measurements on oilfield cement slurries, Cement and Concrete Research, Vol.21, 1991, pp.109-119.

[15] Uchikawa, H., Hanehara, S., Sawaki, D. Effect of electrostatic and steric repulsive force of organic admixture on the dispersion of cement particles in fresh cement paste, Proceedings 10th International Conference on the Chemistry of Cement, Gothenburg, 1997, Vol.3, paper 3iii001, 8 pp.

MONITORING EARLY CEMENT HYDRATION BY RHEOLOGICAL MEASUREMENTS

F. Winnefeld[1] and L. Holzer[1]

[1]Swiss Federal Laboratories for Materials Testing and Research, Section Concrete/Construction Chemistry, 8600 Dübendorf, Switzerland. E-mail: frank.winnefeld@empa.ch

Dr. Frank Winnefeld
Swiss Federal Laboratories for Materials Testing and Research
Section Concrete/Construction Chemistry
Überlandstrasse 129
8600 Dübendorf
Switzerland
phone: +41 (0)1 823 4535
fax: +41 (0)1 823 4035

Curriculum Vitae:

Study in Chemistry at the University of Siegen / Germany:
- Diploma in Chemical Engeneering 1991
- Diploma in Chemistry 1994
- PhD in Chemistry on "Mortars for restoration of historical brickwork buildings"
- from 1993-2000 employed as PhD student and later as senior researcher at the Institute for the chemitry of building materials under the headship of Prof. Knöfel

Since 2000 senior researcher at the Section Concrete/Construction Chemistry of the Swiss Federal Laboratories for Materials Testing and Research (EMPA). The research focuses mainly on the development, chemistry and hydration of binder systems, mortars and concrete.

THE EARLY CEMENT HYDRATION: A MULTI-METHOD APPROACH

L. Holzer[1], F. Winnefeld[1], B. Lothenbach[1] and D. Zampini[2]

[1] EMPA Swiss Federal Laboratories for Materials Testing and Research,
Concrete / Construction Chemistry Lab, 8600 Dübendorf, Switzerland. E-mail: esem@empa.ch
[2] MBT (Schweiz) AG, R&D Switzerland, 8048 Zürich, Switzerland.

ABSTRACT

During cement hydration chemical processes and structural changes in nano- and micrometer ranges induce a specific physical behaviour of the material on a macroscopic scale. In the ideal case a profound understanding of the link between these aspects enables the design of materials with specific characteristics. In order to improve such an integral understanding of the hydration process, fresh Portland cement pastes are investigated during the early hydration period (1 minute to several days) by means of various complementary methods: rheology, calorimetry, glove-box experiments, ESEM-investigations of the microstructure, Backscattered imaging (BSI) on polished sections, X-ray powder diffraction (XRD) and analysis of pore solution chemistry. The comparison of the different results, calibrated to the same timescale, helps to clarify the relationships of micro and macroscopic aspects and explains some connections between physical properties and chemical or mineralogical processes, which dominate the hydration process of fresh cement pastes.

1. INTRODUCTION

Most important material properties of cementitious materials such as workability, setting behaviour, strength but also durability qualities are strongly related to the hydration process [1]. Therefore a profound understanding of the early hydration period is a prerequisite for a specific material design. However the link of physical properties with the microstructural development is difficult for several reasons: Firstly, the elaboration of relationships at different scales is a challenge. C-S-H and gelpores are nanoscale structures [2]. The very fine hydration products form networks on a µm- to mm-range. Aggregates reach diameters of several cm, while concrete structures are generally in the range of several meters. Thus, for a thorough understanding of the system a wide range of meter scales has to be taken into consideration. Secondly, the change from a suspension to a solid material leads to variable measuring conditions, for which no single and simple method of characterisation can be applied. The dynamic aspects of the process must be encountered by methods with a sufficient time resolution. Thirdly, the wet or moist system is prone to produce artefacts. Hydration products may become unstable during the investigation (e.g. in high vacuum). During the investigations uncontrolled reactions may take place between the highly concentrated pore solutions and reactive cementitious components [3]. Because of its complexity, an integral view of the cement system is very difficult. Many studies are based on single characterisation methods and thus the interest is often focused on isolated aspects of cement hydration. In this study, we try to correlate information from different methods, which were applied to fresh paste. Based on an internally consistent set of data from several methods an integral description of the hydration process arises.

Proceedings of the 11th International Congress on the Chemistry of Cement (ICCC)
'Cement's Contribution to the Development in the 21st Century'
Hosted by: The Cement and Concrete Institute of South Africa
CD-ROM produced by: Document Transformation Technologies
11 - 16 May 2003, Durban, South Africa
ISBN Number: 0-9584085-8-0
Editors: Dr G. Grieve and G. Owens
Congress Organised by: Event Dynamics

2. MATERIALS AND METHODS

All experiments are carried out with pastes from ordinary Portland cement (OPC) CEM I 42.5 with a water/cement(w/c)-ratio of 0.5. The composition of the cement is given in Table 1.

Table 1. Composition of OPC, CEM I 42.5

Chemical analysis		Normative phase composition (modified after Bogue)	
	g/100g		g/100g
SiO_2	20.60	C_3S	48.23
Al_2O_3	4.80	C_2S	22.67
Fe2O3	2.70	C_3A	10.41
CaO	63.60	C_4AF	8.22
MgO	1.90	$CaSO_4$	4.09
Na_2O	0.10	$(K,Na)_2SO_4$	1.38
K_2O	1.00	CaO	0.58
CaO (free)	0.58	$CaCO_3$	3.53
CO_2	1.55		
SO_3	3.12	Bogue calculations according to [1]	
Total	99.95		

The following section is a summary of methods used. The methods are described in more detail in [4].

2.1 Rheology

Viscoelastic properties of fresh paste are measured with a Paar Physica MCR 300-rheometer that enables dynamic measurement of low-amplitude oscillatory shear [5], [6] with a cylindrical measuring geometry. Measuring conditions: Temp. 20°C, RH>90%, pre-shearing: 1 minute/100s-1 shear rate, strain amplitude: 5*10-5, angular frequency: 2.5s-1, measuring rate 1/min, dynamic measurement during the first 220 minutes.

2.2 Calorimetry

Hand mixed pastes are measured in a calorimeter under isothermal conditions at 20°C. The evolution of heat flow as a response to exothermal hydration reactions is documented over the first 60 hours.

2.3 Glove box experiments

Hydration experiments are performed in a glove box under nitrogen gas atmosphere in order to prevent carbonation. For each hydration step (1, 20, 30 min. 1, 1.5, 2, 4, 6 hrs. 1, 2, 7, 28 days) a batch of paste is mixed seperately. For hydration steps less than 1 day, hydration is stopped by pore solution extraction with vacuum filteration through a 0.45 µm membrane filter. Subsequently filter residues and pore solutions are prepared for further investigations. For samples older than 6 hours, hydration is stopped by evaporation of free water at 50 °C.

2.4 ESEM (Environmental Scanning Electron Microscope; Philips XL30 FEG) [7]

Microstructural aspects are investigated qualitatively by Secondary Electron Imaging (SEI) [8], [9], [10], [11], [12] on fractured surfaces from filter residues, which are transferred from the glove box in a moist state immediately after pore solution extraction. For each time step phase fractions of hydrates are estimated relative to the total of the hydration products. Conditions in ESEM: H2O vapour pressure 3-6 mbar, Temp <10°C, RH 60-95%.

2.5 ESEM: Back Scattered Imaging (BSI)

From one part of each filter residue polished sections are prepared (drying 110°C, impregnation, lapping, polishing [13]). From BSI the degree of hydration is estimated and EDX analyses are performed (the latter are not presented in this paper).

2.6 X-ray powder diffraction (XRD) and soluble calcium ("free lime")

Material from fresh filter residues (<1day) and from crushed samples (>1day) are washed with acetone twice, then filtered (<63 µm) and dryed at 50°C for 24 hours. From these samples XRD-patterns are determined with a Siemens D500 (5-65° 2 È, 1.2°/min.). For each spectrum the major peaks are summarized. From this, relative peak intensities of the different cristalline phases are calculated. In addition "free lime" is determined after the method of Franke [14]. Thereby soluble calcium is extracted with ethylene glycol mainly from portlandite and from calciumoxide in clinker.

2.7 Chemical composition of pore solution

OH- concentrations are determined with a combined pH-electrode. Concentrations of Al, Ca, Fe, Mg, Na, K, SO4 and Si are determined by ICP-OES.

3. RESULTS AND DISCUSSION

3.1 Rheology and Calorimetry

During the transformation of fresh paste from a suspension to a solid material four characteristic periods are generally distinguished. The induction period during the first few minutes is characterised by an exothermal peak (see Figure 1, heat flow), which is attributed to the dissolution of soluble cement components (compare section 3.4: pore solution chemistry).

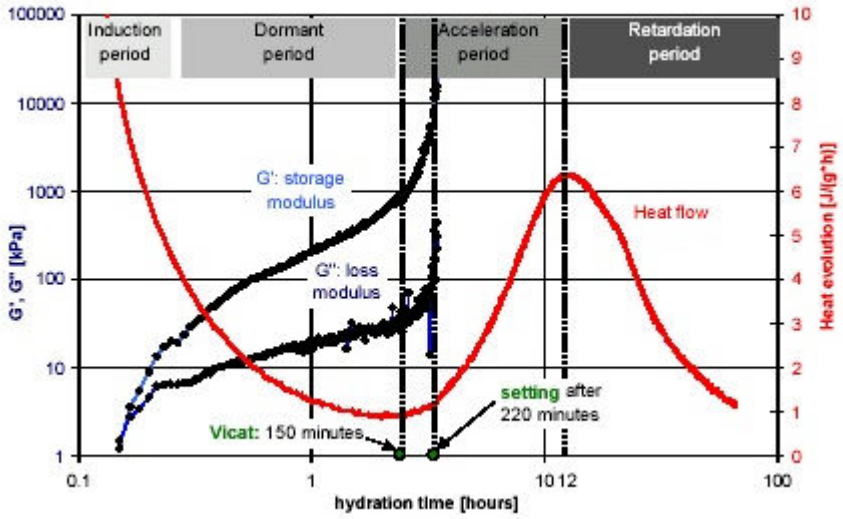

Figure 1. Changing properties of fresh paste, consisting of ordinary PC (CEM I 42.5, w/c-ratio 0.5), monitored by the measurement of heat flow in an isothermal calorimeter and of visco-elasticity in a rheometer by lowamplitude oscillatory shear method.

For the dormant period significantly lower heat flow indicates strongly reduced reaction rates. This is also reflected by slow changes of the rheological properties (see Figure 1, G' and G"). The storage modulus G' represents the elastic (reversible, solid-like) response of the material to the oscillating strain. The loss modulus G" describes the viscous (irreversible, liquid-like) response [5]. In the dormant period G' and G" show an increasing gradient, which indicates a slow stiffening of the paste. The start of the acceleration period is then characterised by an exponential increase of G' and G" which reflects a more "rigid" behaviour due to the interaction of newly formed hydration

products. The faster growth of G' compared to G" indicates that the paste becomes more solid-like. This stiffening, which is not correlated with significant development of compressive strength, is called setting and it is not a strictly defined physical state. In our experiments setting can be attributed to the time span between first hindrance of Vicat-indentation at 150 +/-10 min. and the "rheometer wall slip" after 219 min. A further typical feature of the acceleration period is the strong increase of heat evolution between 2.5 and 12 hours which reflects faster hydration rates. Afterwards decreasing hydration rates lead to a thermal relaxation in the retardation period. Strength development slowly starts after the setting, is relatively fast during the first days and slowly continues for months and years.

3.2 Microstructural Investigation

3.2.1 Estimation of hydration rates and degree of hydration

In a paste with ordinary PC (eg. CEM I 42.5) only a few % of the clinker grains are transformed into new hydration products during the first hours. It is thus very difficult to quantify the degree of hydration in young cement pastes with a satisfying accuracy [15]. By means of Back Scattered Imaging (BSI) the progress of hydration can be documented qualitatively (See Figure 2):

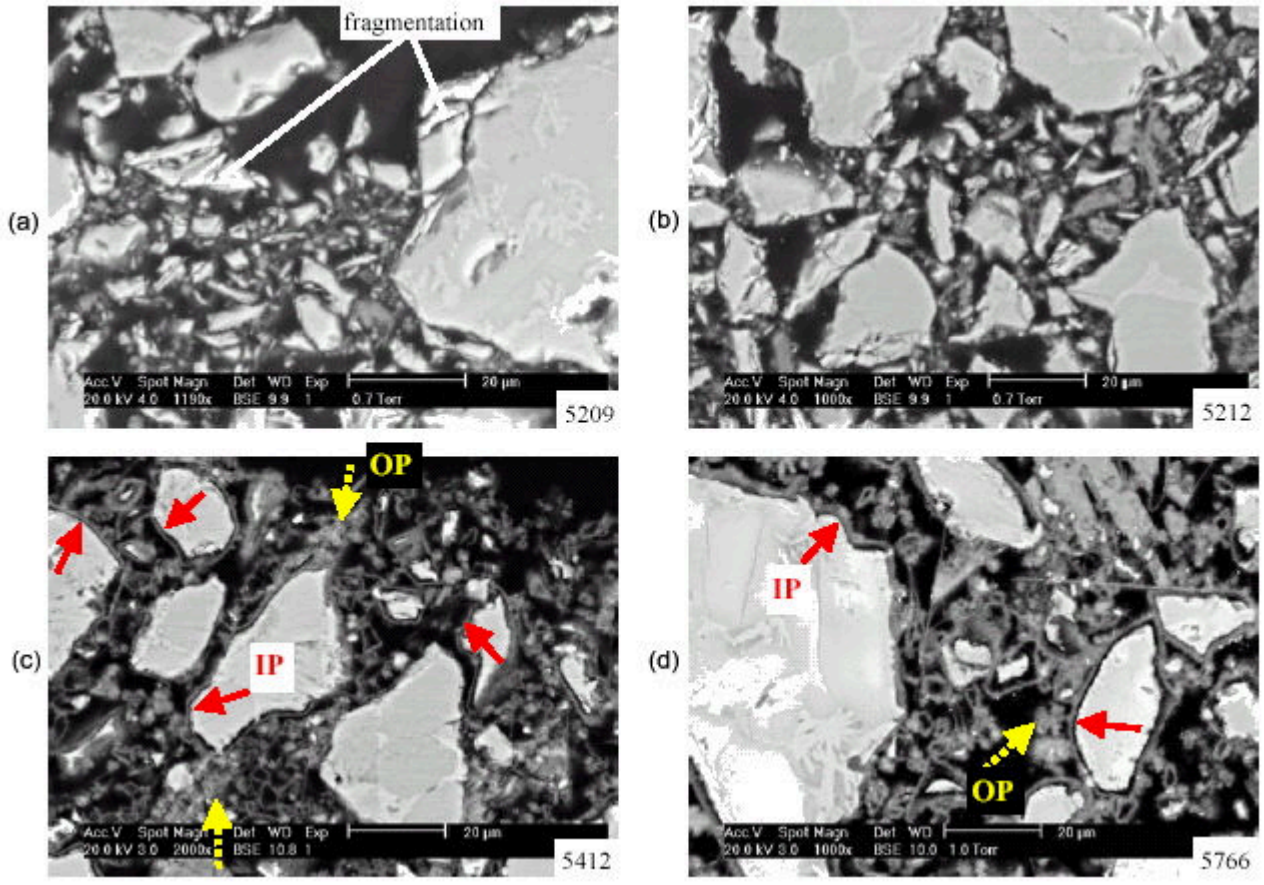

Figure 2. Back Scattered Imaging (BSI) in ESEM: Growth of hydration products in a paste with ordinary PC (CEM I 42.5), w/c-ratio 0.5. Legend: black=porosity, dark grey=hydration products, bright grey=unhydrated clinker, IP=Inner Product, OP=Outer Product.

2(a) after 2 hours: Dissolution preferentially attacks edges and cracks. This leads to a fragmentation of yet unhydrated clinker grains. **2(b)** after 2 hours: The thickness of the hydration layer is below 0.5 µm. **2(c)** after 6 hours: Clinker grains are covered by 0.5-1 µm C-S-H (VI), called Inner Product. Less than 5 % of the clinker are transformed into hydrate phases. **2(d)** after 24 hours: The IP layer reaches a thicknes of 1-2 µm. In the interstitial space OP is formed. The degree of hydration is estimated to 0.2.

Within the first minutes dissolution is the dominating process [1]. Thereby cement grains are not uniformly dissolved. “High energy sites” along edges or cracks are preferentially eroded. This leads to a fragmentation of those clinker grains with a lot of inherited cracks (Figure 2a). At this stage the cement grains are hardly hydrated and there is only a thin hydration layer of a few 100 nm recognisable (Figure 2b). Within the next hours the hydration layer is growing constantly and it reaches a uniform thickness of 0.5 to 1µm after 4 to 6 hours (Figure 2c) and 2 µm after 24 hours (Figure 2d). Based on the microstructural observations the degree of hydration is estimated to <0.05 after 6 hours and to 0.2 after 24 hours.

The evolution in the degree of hydration based on two simple hydration models with a constant (0.833 %/hr) and variable hydration rates (0-4 hrs: 0.417 %/hr, 4-12 hrs: 1.666 %/hr, >12hrs: 0.417 %/hr) is shown in Figure 3.

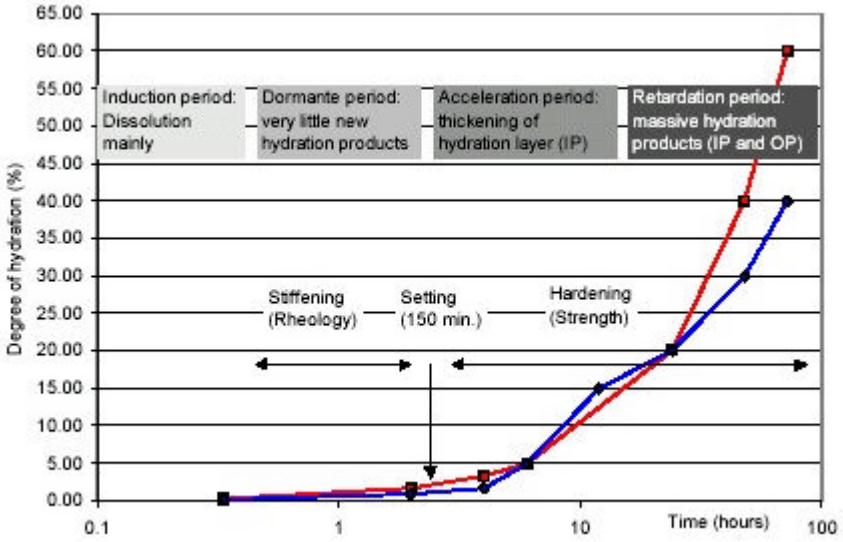

Figure 3. Two models for the degree of hydration as a function of time: Red squares: constant hydration rate. Blue diamonds: variable hydration rate The hydration rates of the corresponding periods are given below.

Both curves are forced through the estimated degree of hydration of 0.2
after 24 hours. This value reflects an estimation which is based on BSI (Figure 2). The curves for the degree of hydration obtained from the two models are not significantly different during the early hydration period.

3.2.2 Description and quantitative estimation of hydration phases
C-S-H is the main hydration phase in ordinary PC. Various models exist for the nanoscale structure [16], [17], [18], [19], [20]. Although nuclei with a crystalline structure are generally accepted, C-SH has an amorphous behaviour with respect to X-rays. The quantification of C-S-H by means of XRD is therefore difficult. An alternative approach for an approximate quantification of hydration products is the estimation of phase fractions based on ESEM-investigations (Figure 4).

During the first 20 minutes clinker grains are covered by a very thin layer (Figure 5a) of amorphous C-S-H (IV) (C-S-H types according to [21]). Within this gel layer tiny crystals of short prismatic ettringite (average length: 300 nm) can be observed (Figure 5b). In the first 4 hours amorphous C-H (IV) (80%) and ettringite (20%) are the dominant hydration products (Figure 4). After four hours locally a new type of C-S-H (II) with a spongy appearence is observed (ca. 7%) (Figure 5c). At the same time also first flakes of portlandite precipitate (ca. 3%).

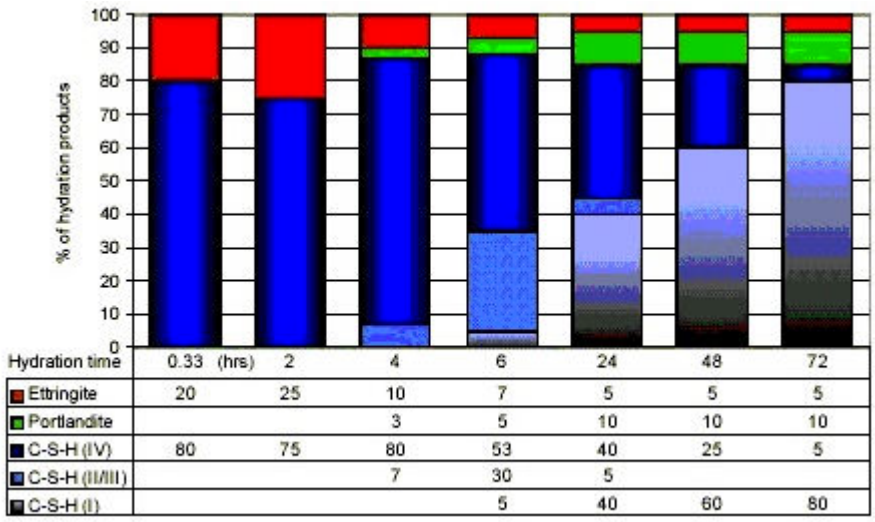

Hydration time	0.33 (hrs)	2	4	6	24	48	72
Ettringite	20	25	10	7	5	5	5
Portlandite			3	5	10	10	10
C-S-H (IV)	80	75	80	53	40	25	5
C-S-H (II/III)			7	30	5		
C-S-H (I)				5	40	60	80

Figure 4. Volumetric fractions of hydration phases in the cement matrix as a function of time. The estimated compositions are based on microstructural observations in the ESEM.

After six to seven hours the amount of spongy C-S-H (II) increases (max. 30%), together with the formation of a new, fibrous or needle like type of C-S-H (I) (Figure 5d). Obviously a transformation of C-S-H types occurs between 4 and 24 hours. The amorphous C-S-H (IV) is dominant during the dormant period. A transitional spongy type C-S-H (II) grows during the setting and early acceleration period. Finally, fibrous C-S-H (I) becomes the dominant phase in mature pastes (up to 80 %). However, no strict stability fields can be defined for the different C-S-H types, which can also be formed contemporaneously. A new generation of long prismatic ettringite (> 1.5 µm) is formed between 6 and 24 hours. At the same time the relative amount of portlandite is increasing constantly and is then stabilising after 24 hours at approximately 10 % of the total amount of hydration products.

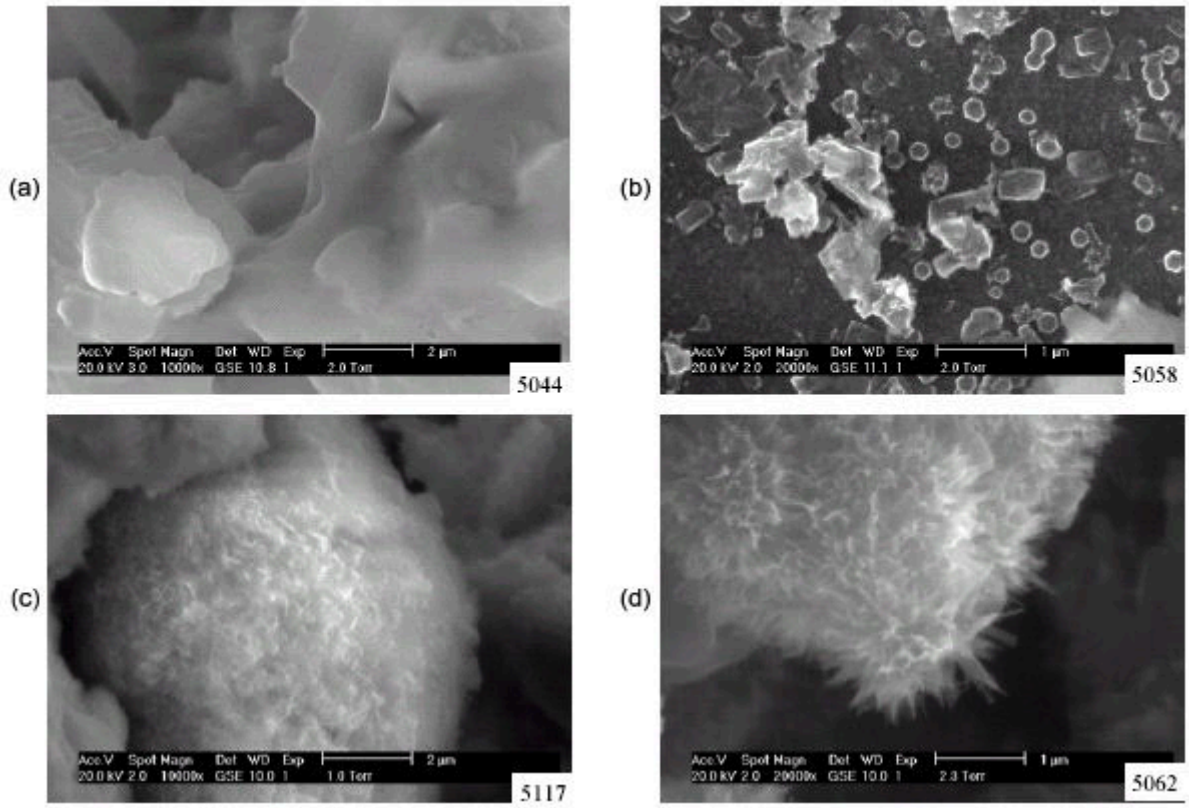

Figure 5. Morphology of typical hydration products in a paste of ordinary PC (w/c 0.5), observed in ESEM with gaseous Secondary Electron Imaging (SEI) under 60 to 95 % relative humidity.

5(a) After 20 minutes: A thin layer of amorphous C-S-H (IV) covers the cement grains. **5(b)** After 2 hours: Hexagonal ettringite prisms (~300 nm length) embedded in a layer of amorphous CS-H (IV). **5(c)** After 4 hours: Spongy type of C-S-H (II). **5(d)** After 24 hours: Fibrous type of C-S-H (I).

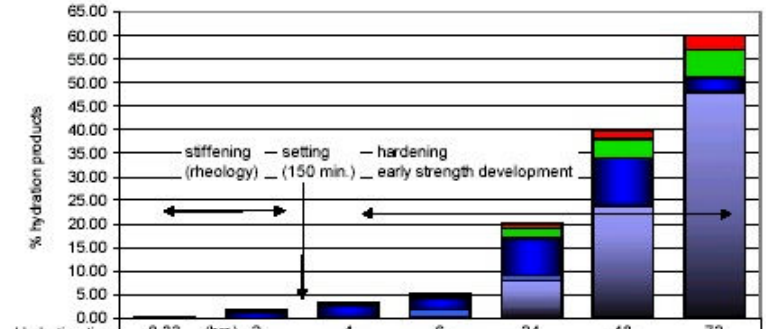

Hydration time	0.33 (hrs)	2	4	6	24	48	72
Ettringite	0.06	0.42	0.33	0.35	1.00	2.00	3.00
Portlandite	0.00	0.00	0.10	0.25	2.00	4.00	6.00
C-S-H (IV)	0.22	1.25	2.67	2.65	8.00	10.00	3.00
C-S-H (II/III)	0.00	0.00	0.23	1.50	1.00	0.00	0.00
C-S-H (I)	0.00	0.00	0.00	0.25	8.00	24.00	48.00

Figure 6. Volumetric phase fractions of hydration products, normalised by the degree of hydration at the corresponding time. (100 % = total of solid phases). Qantitative estimation of phase fractions from Figure 4, multiplied by the degree of hydration from Figure 3 (constant hydration rate).

3.2.3 Inner Product (IP), Outer Product (OP) and Hollow shell hydration

According to the geometric relationship with unhydrated clinker grains, two different types of hydration products can be distinguished: Inner Product (IP) and Outer Product (OP) as documented in Figure 7.

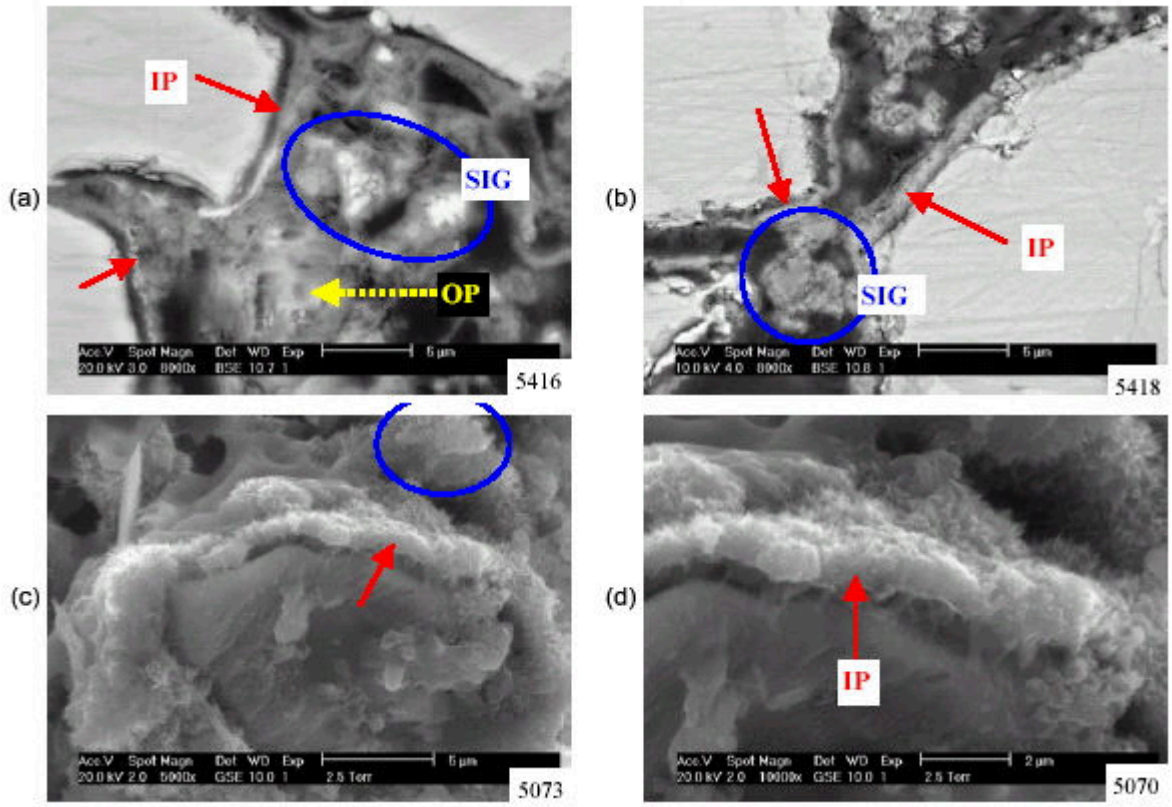

Figure 7. Inner Product (IP), Outer Product (OP) and Small Intersitital grains (SIG) in a paste of ordinary PC (w/c 0.5) observed in ESEM.

7(a) BSI after 6 hours: The IP layer covering unhydrated cement grains has a uniform thickness of less than 1 µm. In this locality first fibrous OP is observed. 7**(b)** BSI after 6 hours: Locality without OP. Small interstitial grains (SIG) between larger cement grains form an interstitial meniscus. **7(c)** and **7(d)** SEI after 24 hours: Part of the IP is broken away and gives insight to the unhydrated clinker core. Within the hollow space between IP shell and clinker core, ettringite and portlandite are precipitating. The surface of IP is covered by fibrous C-S-H (I). Amorphous C-S-H (IV) is also present.

The IP partially or fully replaces the formerly unhydrated cement grains. After the first two hours only a thin gel layer (<<500 nm) covers the cement grains. From this boundary layer the IP grows concentrically towards the center. After 4 to 6 hours the IP has a uniform thickness of 1 µm (Figure 7 a and b). Between the IP shell and the unhydrated clinker core empty space is formed (Fig. 7 c and d). Dissolution of the clinker core thus seems to be faster than the growth of the IP.

This phenomena is termed "hollow shell hydration" [22], [23]. Within the hollow space ettringite and portlandite are precipitating (Fig. 7 d) before the space is filled with C-S-H. As a result IP replaces the initial clinker grains by forming a dense pseudomorph.

Initially the interstitial space between the clinker grains is filled with pore solution. In a mature paste the interstitial space is overgrown by porous and heterogeneous hydration products, i.e. the OP. First local accumulations of OP are observed after 6 hours (Figure 7a). This is contemporaneous with the first appearance of fibrous C-S-H (I). In contrast to the short fibrous C-S-H (I) in IP (Length ~200 nm), OP is characterised by longer C-S-H fibres (>500 nm). After 24 hours the fibrous OP forms an interstitial matrix in which portlandite, ettringite but also small interstitial cement grains (SIG) are embedded.

In summary the terms IP and OP reflect a concept for the description of the cement microstructure on a µm- to mm-scale. The size of most hydrate phases however is below 1 µm and what is considered as IP or OP, frequently represents a mixture of C-S-H with other phases like portlandite, ettringite or C-A-H. In summary, the boundaries of IP and OP are not strictly defined [24]. It is often impossible to distinguish IP of small cement grains from the surrounding OP-matrix. IP and OP should therefore not be considered as distinct phases with fix properties (porosity, density, chemistry). These properties depend on the composition and structure on a sub-µm scale, where IP and OP are heterogeneous.

3.2.4 Small Interstitial Grains (SIG)

As shown in Figure 2, small interstitial cement grains (SIG) with a diameter below 5 µm react faster than larger cement grains (>10 µm). Already after 2 hours the small cement grains are embedded in a diffuse gel layer. The apparent higher reactivity of small cement grains can be explained by a higher surface/volume-ratio. As a consequence the gel layer covering SIG is relatively voluminous compared to the distinct IP-layer on large cement grains (Figures 8a and 8b).

In addition SIG tend to form multi-grain agglomerations which act as a connecting meniscus between larger cement grains (Figure 7b). After 4 to 6 hours spheroids with a typical diameter of 2 µm are frequently observed (Figure 8c and 8d). It is suggested that the reactive multi grain agglomerations (initially consisting of SIG) represent precursors or nuclei of the spheroids.

Together with the slowly precipitating OP these reaction products represent the major connecting elements between the larger cement grains during the first hours of hydration. At this stage the small interstitial products may be a dominant factor with respect to the interparticle forces. This should be be taken into consideration when microstructural aspects are discussed in relation to properties of fresh paste (rheology, stiffening, setting and early strength development).

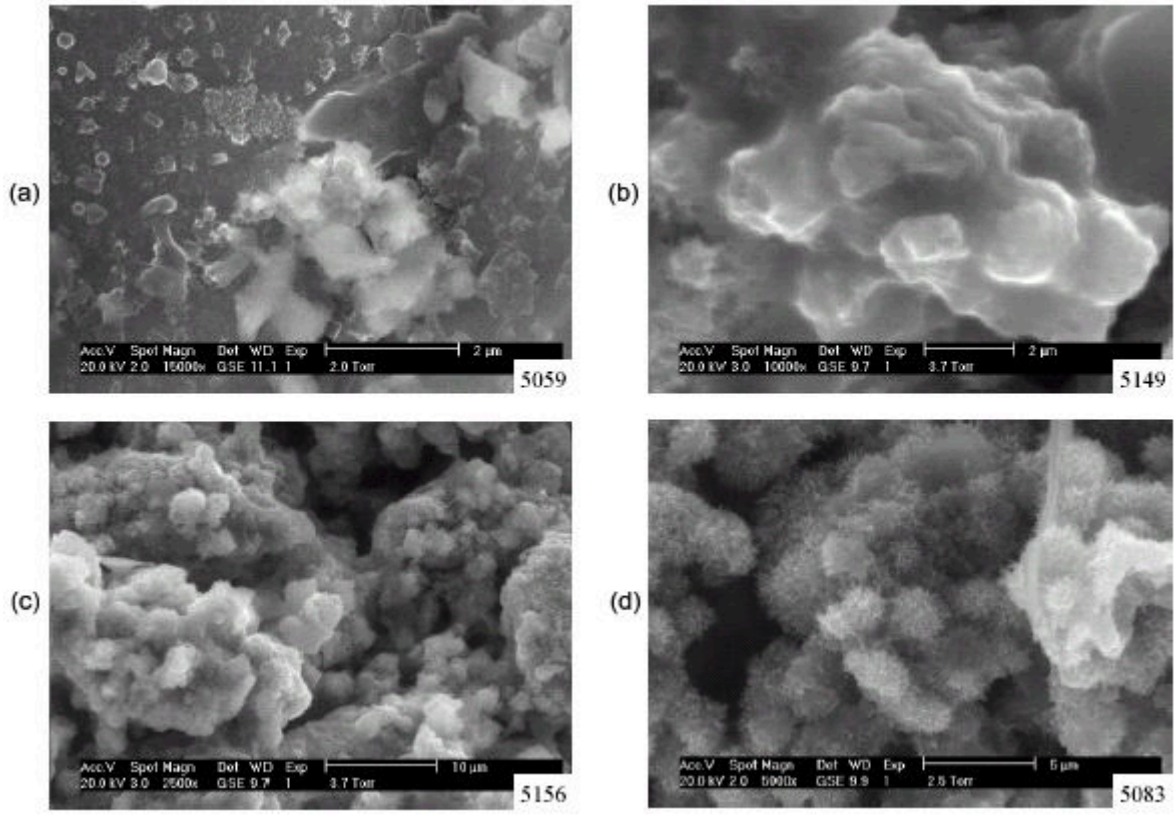

Figure 8. Agglomeration and hydration of Small Interstitial Grains (SIG) observed in ESEM.

8(a) after 2 hours: Small clinker grains with a diameter of 1µm (or less) form agglomerations. The small grains are embedded in a diffuse hydration layer consisting of amorphous C-S-H (IV). **8(b)** after 6 hours: A large number of fully hydrated grains, typically with a diameter of 2 µm form agglomerations in the interstitial space between larger cement grains. The "2 µm spheroids" are connected by a massive gel of C-S-H (IV). **8(c)** after 6 hours: Numerous "2 µm spheroids" form an interstitial matrix which connects the larger cement grains. **8(d)** after 24 hours: Due to the fibrous C-S-H (I) the spheroids become a hedgehog-appearence.

3.3 X-Ray powder diffraction (XRD) and soluble calcium

The results from X-Ray diffraction are summarised in Figures 9 and 10. During the induction and dormant periods (first 4 hours) the relative intensities of the clinker phases remain nearly stable. Only for C3A a slight decrease is indicated within the first minutes. C3S shows a significant decrease between 6 and 24 hours (acceleration period). Between 6 hours and 28 days 80 to 90 % of C3A are decaying. For C2S and C4AF only little changes can be recognised even after 28 days.

Hemihydrate is the most reactive sulfate carrier. Within the first 30 minutes it disappears completely. A part of it seems to be transformed into gypsum, which increases significantly during the first two hours. Between 4 to 6 hours and one day gypsum and anhydrite are almost completely dissolved.

The first reaction product, which precipitates after 1 minute, is ettringite. Between six hours and 7 days a second generation of ettringite is formed. Small quantities of portlandite (Ca(OH)2) can be detected after 4 hours and in the following period it is growing constantly. This is compatible with the concentrations of soluble calcium ("free lime") which are determined after the method of Franke [14]:

hydration time:	1min	0.5	1	1.5	2	4	5	6	hrs
"free lime":	0.59	0.57	0.59	0.63	0.66	0.99	1.41	1.82	wt-%

From the comparison of the two methods it follows that the detection limit of Ca(OH)2 in XRD corresponds to 0.6 - 1.0 % soluble calcium.

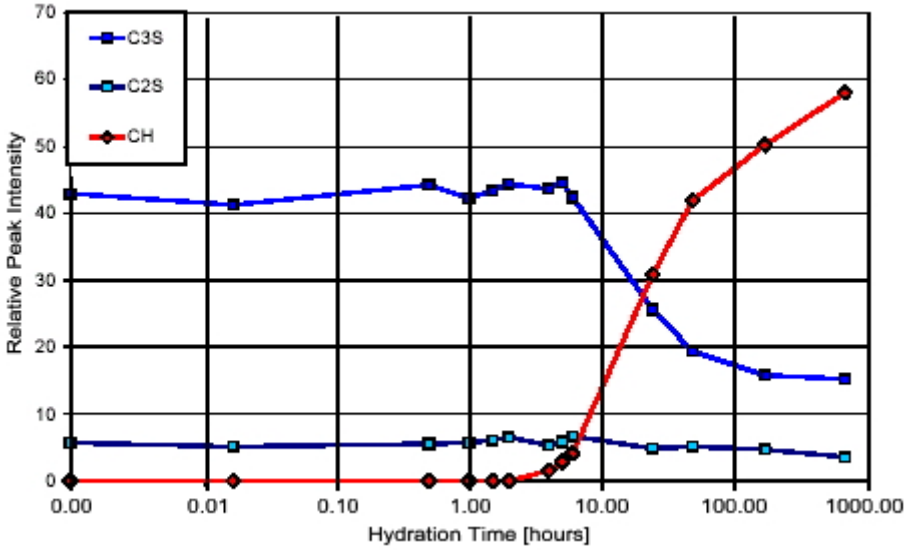

Figure 9. XRD results showing relative peak intensities as a function of hydration time for the following cristalline phases:- C3S: alite, C2S: belite, CH: portlandite.

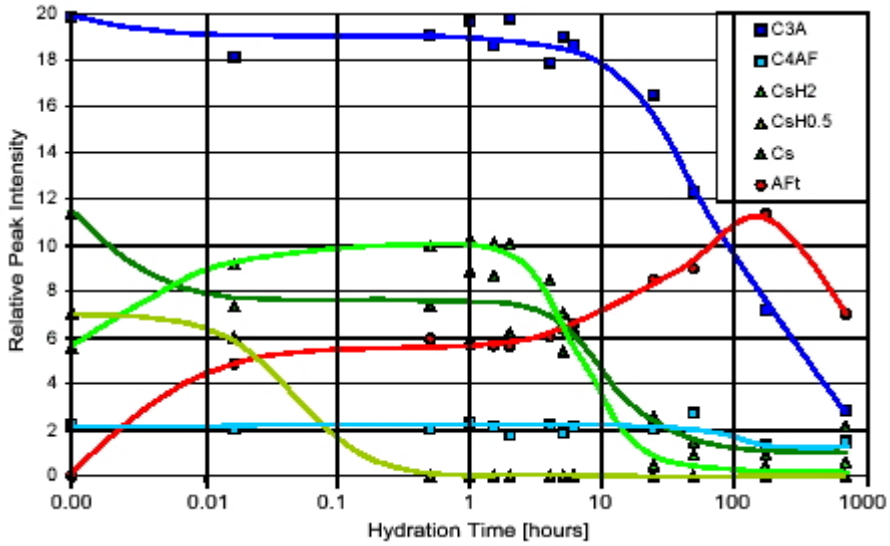

Figure 10. XRD results for:- C3A: aluminate, C4AF: ferrite, CsH2: gypsum, CsH0.5: hemihydrate, Cs: anhydrite, AFt: ettringite.

3.4 Pore Solution Chemistry

Pore solution was collected using the vacuum filtration technique during the first 8 hours. A comparison with published pore solution data form more mature OPC pastes [25], [26] indicates comparable ion-concentrations, except for K, Na and SO4, which vary with the corresponding cement compositions. The comparison of different sets of data indicates that the temporal development of pore solutions generally follows similar trends. Data from the literature [25, 26] data are therefore used in Figure 11 to extrapolate from the measured pore solution compositions (¡Ü8 hours) to concentrations at longer hydration times.

The changes of ionic concentrations in solution are related to dissolution and precipitation of solid phases (compare Figures 9, 10 and 11). K, OH- and SO4 show the highest concentrations in pore solutions from fresh paste, while Na, Ca and Si are present at somewhat lower concentrations.

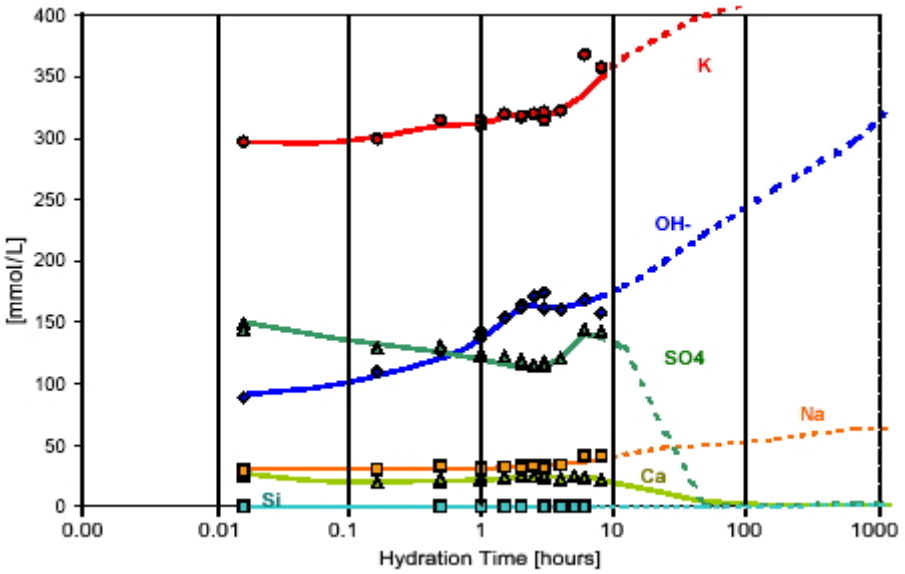

Figure 11. Measured concentrations in the pore solution of ordinary PC as a function of time. Data given in [25] and [26] were used to draw the approximate development of pore solution compositions at hydration times longer than 8 hours.

The relatively high concentrations of K and Na after a few minutes are largely due to the dissolution of alkali-sulphate phases (K2SO4, 3K2SO4·Na2SO4) in cement. Over time the concentrations of alkalis increase complementary to the hydration rate of clinker phases. The release of K and Na is attributed mainly to the dissolution of C3A and gypsum.

Similarly, the high initial sulphate concentrations stem from the ready dissolution of the alkalisulphate phases as well as from the presence of the Ca-sulphate phases. Sulphate concentrations slowly decrease during the first hours of hydration due to the precipitation of ettringite. After 1 to 2 days, sulphate concentrations in OPC pore solutions decrease drastically. At this time gypsum and anhydrite disappear, while the precipitation of ettringite continues until the sulphate present in solution is consumed (see Figures 10 and 11).

The hydroxide concentrations increase constantly from initially 90 mmol/L (1 min.) over 150 mmol/L (6 to 8 hours) to 300 mmol/L in mature pastes. Measured calcium concentrations increase from initially 15 mmol/L to 20-25 mmol/L after 4-6 hours. Afterwards calcium decreases again because portlandite is limiting its solubility with increasing OH- concentrations.

Silicate and magnesium concentrations are low and little changes can be observed during the first hours of hydration. The concentration of Al and Fe are below the respective detection limits (Al < 0.04 mmol/L; Fe < 0.01 mmol/L), as the precipitation of ettringite and Fe-bearing phases efficiently removes Al and Fe from the pore solution.

4. CONCLUSIONS

There is no single method which can describe the different aspects of hydration processes sufficiently. For physico-chemical investigations of cement hydration a correlation between complementary methods has to be applied. Major changes of early paste properties such as stiffening and setting are related to very small changes of the hydration products. The degree of hydration during setting is below 0.05. These minor changes are difficult to measure quantitatively. However they can be documented by qualitative microstructural investigations with ESEM.

The main hydration product is C-S-H which can be described as a solid phase with characteristics of

a gel [27]. C-S-H is a non-stochiometric phase for which the following morphological types can be distinguished: structureless/amorphous (IV), spongy-type (II) and fibrous (I). During the dormant period structureless C-S-H prevails. In mature pastes C-S-H mainly consists of a fibrous type.

From the microstructural investigations it follows that changes of the material properties are not exclusively determined by the amount and type of hydration phases. Of major importance are structural elements, such as small interstitial grains (SIG) which form a meniscus of hydration products between larger cement grains. Because hydration rates of small particles are faster, SIG can form agglomerations of hydration products in the interstitial space within a short time. In this way SIG influence the interactions between the cement particles significantly and therfore they are interpreted as dominant factors which control physical properties in fresh pastes, eg. viscoelasticity.

Another view on the hydration processes considers chemical solid-liquid interactions. The chemistry of pore solutions during the first hours is dominated by the dissolution of reactive cement phases such as alkali-sulphate phases in clinker or $CaSO4 \cdot 0.5H2O$ and the simultaneous precipitation of ettringite, gypsum, portlandite and the C-S-H phases. Significant changes of the pore solution chemistry during the acceleration period can be correlated with the dissolution of C3A, C3S and gypsum and the precipitation of ettringite, portlandite and C-S-H. However, the low solubility of $SiO2$ puts limitations on the link with microstructural observations on C-S-H. In summary, most significant changes of the pore solution chemistry occur subsequent to the setting, contemporaneous with important compositional changes, as observed with XRD. In this period considerable reaction volumes are affected by the hydration process which can be linked on a macroscopic scale with the increase of strength. In contrast, properties of fresh, viscous pastes depend on minimal volumetric changes, which are difficult to show by chemical measurements and phase quantifications. Thus for the early hydration period qualitative investigations of the microstructure with ESEM are of major importance.

ACKNOWLEDGEMENTS

This study was financed by Swiss Federal Institute of Materials Testing and Research (EMPA) and by MBT (Schweiz) AG. The authors would like to thank L. Brunetti for assistance with glove box experiments, M. Guecheva for ICP-OES- and U. Gfeller for XRD-measurements. Fruitful discussions with J. Kaufmann contributed a lot to this paper.

REFERENCES

[1] Taylor, H.W.F., Cement chemistry. 1997, London: Thomas Telford Publishing.
[2] Richardson, I.G., The nature of the hydration products in hardened cement pastes. Cement & Concrete Composites, 2000. 22(2): p. 97-113.
[3] Damidot, D. and F. Sorrentino. Observation of the hydration of cement paste by ESEM: Care needed to study the early hydration. in Proceedings of the 18th international conference on cement microscopy. 1996. Houston, USA: ICMA.
[4] Holzer, L., Chemical and microstructural investigation of cement hydration, 2002, report Nr. 202'305, EMPA Swiss Federal Laboratories for Materials Testing and Research, Dübendorf., CH.
[5] Schultz, M.A. and L.J. Struble, Use of oscillatory shear to study flow behaviour of fresh cement paste. Cement and Concrete Research, 1993. 23: p. 273-282.
[6] Struble, L.J., et al., Oscillatory shear behaviour of Portland cement paste during early hydration. Concrete Science and Engineering, 2000. 2: p. 141-149.
[7] Danilatos, G.D., Foundations of Environmental Scanning Electron Microscopy. Advances in Electronics and Electron Physics, Academic Press, 1988. 71: p. 109-250.
[8] Sujata, K., T.B. Bergstrom, and H.M. Jennings, Preliminary studies of wet cement pastes by an environmental scanning electron microscope, in Microbeam Analysis, D.G. Howitt, Editor. 1991, San Francisco Press, Inc.: San Francisco. p. 195-198.
[9] Neubauer, C.M. and H.M. Jennings, The Role of the Environmental Scanning Electron Microscope in the Investigation of Cement-Based Materials. SCANNING, 1996. 18: p. 515-521.
[10] Möser, B. Betrachtung der frühen Hydratation von Klinkerphasen im ESEM-FEG. in 13. Internationale

Baustofftagung Ibausil. 1997. Weimar: Bauhaus-Universität Weimar.
[11] Zampini, D., S.P. Shah, and H.M. Jennings, Early age microstructure of the paste-aggregate interface and its evolution. Journal of Materials Research, 1998. 13(7): p. 1888-1898.
[12] Radonjic, M., et al. ESEM study of the hydration of the silicate, aluminate and ferrite single phases from Portland Cement. in Proceedings of the 22nd international conference on cement microscopy. 2000. Montreal, Canada: ICMA.
[13] Crumbie, A.K. SEM microstructural studies of cementitious materials: Sample preparation of polished sections and microstructural observations with backscattered images – artefacts and practical considerations. in Proceedings of the 23rd international conference on cement microscopy. 2001. Albuquerque, USA: ICMA.
[14] Franke, A., Bestimmung von Calciumoxid und Calciumhydroxid neben wasserfreiem und wasserhaltigem Calciumsilikat. Zeitschrift für Anorganische und Allgemeine Chemie, 1941. 241: p. 180-184.
[15] Scrivener, K.L. and P. Pratt. Backscattered electron images of polished cement sections in the scanning electron microscope. in 6th international conference on cement microscopy. 1984. Albuquerque, USA: ICMA.
[16] Feldman, R.F. and P.J. Sereda, A new model for hydrated Portland Cement and its practical implications. Engineering Journal (Can), 1970. 53/8-9: p. 53-59.
[17] Jennings, H.M. and P.D. Tennis, Model For the Developing Microstructure in Portland Cement Pastes. Journal of the American Ceramic Society, 1994. 77(12): p. 3161-3172.
[18] Richardson, I.G., The nature of C-S-H in hardened cements. Cement and Concrete Research, 1999. 29(8): p. 1131-1147.
[19] Tennis, P.D. and H.M. Jennings, A model for two types of calcium silicate hydrate in the microstructure of Portland cement pastes. Cement and Concrete Research, 2000. 30(6): p. 855-863.
[20] Jennings, H.M., A model for the microstructure of calcium silicate hydrate in cement paste. Cement and Concrete Research, 2000. 30: p. 101-116.
[21] Diamond, S., Identification of hydrated cement constituents using a scanning electron microscope - energy dispersive x-ray spectrometer combination. Cement and Concrete Research, 1972. 2: p. 617-632.
[22] Hadley, D.W., W.L. Dolch, and S. Diamond, On the occurrence of hollow-shell hydration grains in hydrated cement paste. Cement and Concrete Research, 2000. 30: p. 1-6.
[23] Kjellsen, K.O., B. Lagerblad, and H.M. Jennings, Hollow-shell formation - an important mode in the hydration of Portland cement. Journal of Materials Science, 1997. 32: p. 2921- 2927.
[24] Groves, G.W. TEM studies of cement hyddration. in Mat. Res. Soc. Symp. 1987.
[25] Gunkel, P., Die Zusammensetzung der flüssigen Phase erstarrender und erhärtender Zemente. Beton-Informationen, 1983. 23(1): p. 3-8.
[26] Locher, F.W., et al., Erstarren von Zement IV: Einfluss der Lösungszusammensetzung. ZKG, 1983. 36(4): p. 224-231.
[27] Scherer, G.W., Structure and properties of gels. Cement and Concrete Research, 1999. 29: p. 1149-1157.

FIXATION OF CHROMATE FROM BAG FILTER DUST (BFD) IN LAMELLAR CALCIUM ALUMINATE HYDRATES (AFM-PHASES) AND ITS RECYCLING PROCESS

Göske, J.[1], Pöllmann, H.[1] and de Villiers, J.P.[2]

[1]Department of Mineralogy / Geochemistry, Martin-Luther-University Halle (Saale), Domstr. 5, D - 06108 Halle (Saale), Germany. E-mail: goeske@geologie.uni-halle.de
[2]Department of Geology, University of Pretoria, Pretoria 0002, Republic of South Africa. E-mail: jpdev@postinoup.ac.za

1. INTRODUCTION

Some compounds among the group of layered Calcium aluminate hydrates are important for the process of cement manufacturing. Their chemical composition can be described by the following general formulae:

$3CaO*Al_2O_3*CaX*nH_2O$ and $3CaO*Al_2O_3*CaY_2*nH_2O$
with X= SO_4^{2-}, CO_3^{2-}, CrO_4^{2-} [1] ... and Y= OH^-, Cl^-,$NO3^-$

Structurally they consist of positively charged layers of $[Ca_2Al(OH)_6]^+$ and negatively charged interlayers of $[OH*nH_2O]^-$. Detailed structural studies were done with Monosulfate ($3CaO*Al_2O_3*CaSO_4*12H_2O$) and Monochloride ($3CaO*Al_2O_3*CaCl2*12H_2O$). The structure is shown in Figure 1.

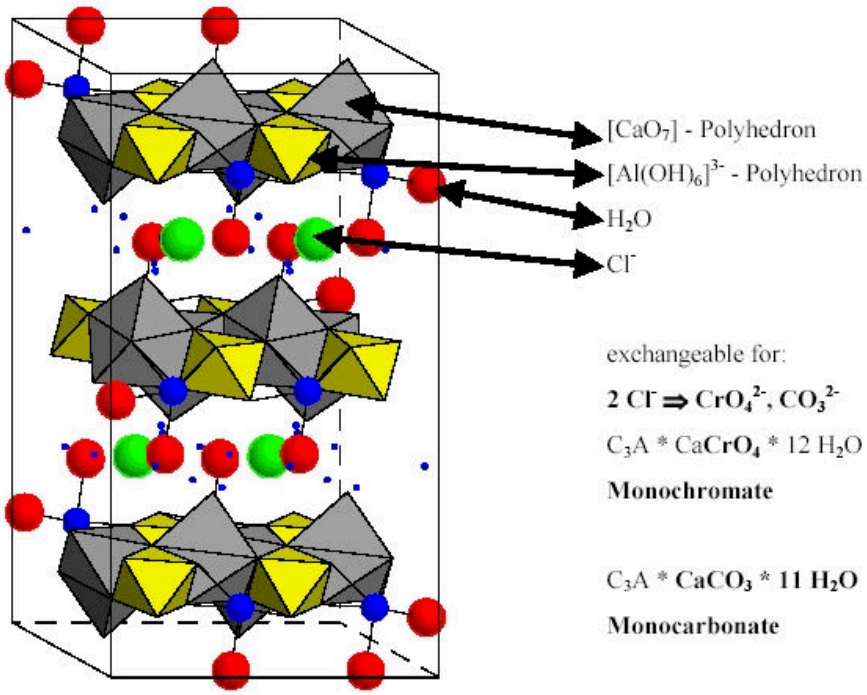

Figure 1. Structure of α-Monochloride

Tetra Calcium Aluminate Hydrate with the formula $C_3A*Ca(OH)_2*nH_2O$ is especially suitable as storage mineral, because of its layered structure[2,3,4,5,6]. It is widely used to incorporate efficiently for example heavy metals, because the OH-group in the interlayers can be exchanged for 1^+- or 2^+-anions (Figure 1).

Tetra Calcium Aluminate Hydrate with the formula $C_3A*Ca(OH)_2*nH_2O$ is especially suitable as storage mineral, because of its layered structure[2,3,4,5,6]. It is widely used to incorporate efficiently for example heavy metals, because the OH-group in the interlayers can be exchanged for 1^+- or 2^+-anions (Figure 1).

It is well known that chromates are capable of accelerating cement hydration. Chromate is the reason for the so called "Cement- or Bricklayer-eczema". Formation of these lamellar calcium aluminate hydrates (in connection with hydration of calcium aluminates) can proceed under variable conditions:

1. Formation in concrete due to harmful substances in the environment.
2. Formation due to additives controlling cement hydration
3. Formation under controlled conditions as storage minerals

Monosulfates also form in nature, as was shown by Pöllmann, who described natural Monosulfate ("Kuzelite") as alteration products in basalts (i.e. Zeilberg by Maroldsweisach in Lower Franconia/Germany)[7].

2. METHODS

Mixtures with different loading agents and BFD in various parts were investigated:

fresh heated lime + technical calcium aluminate : BFD = 0.5 : 1 M%
1 : 1 M%
1 : 0.5 M%

The amounts were filled into polyethylene vials and reacted with distilled water (solid-to-liquid ratio = 1:15) for variable times. After 1, 5, 10 and 24 hours the samples were filtered. The filtrates were analyzed for their chromate content with ICP, the insoluble residues were investigated with XRD and SEM.

3. RESULTS

3.1 Investigation of the chromate content in the filtrates after reaction with agents

The chromate content in the component ratio is:
0.5 : 1 = 17.34 [mg/l]
1 : 1 = 35.11 [mg/l]
1 : 0.5 = 68.99 [mg/l]

The content of chromate in the filtrates after different times is shown in table 1.

Table 1. Content of chromate in the filtrates after different times. 0.03 [mg/l] ≈detection limit

	Chromate content (mg/l)		
mixture / time (h)	**1 : 0.5**	**1 : 1**	**0.5 : 1**
0h	17.34	35.11	68.99
1h	0.08	16.86	49.82
5h	**≤0.03**	0.17	39.94
10h	**≤0.03**	**≤0.03**	0.12
24h	**≤0.03**	**≤0.03**	**≤0.03**

3.2 Investigation of the insoluble residues by X-ray diffraction

Figure 2 shows the XRD diagrams of residues after different periods of reaction.

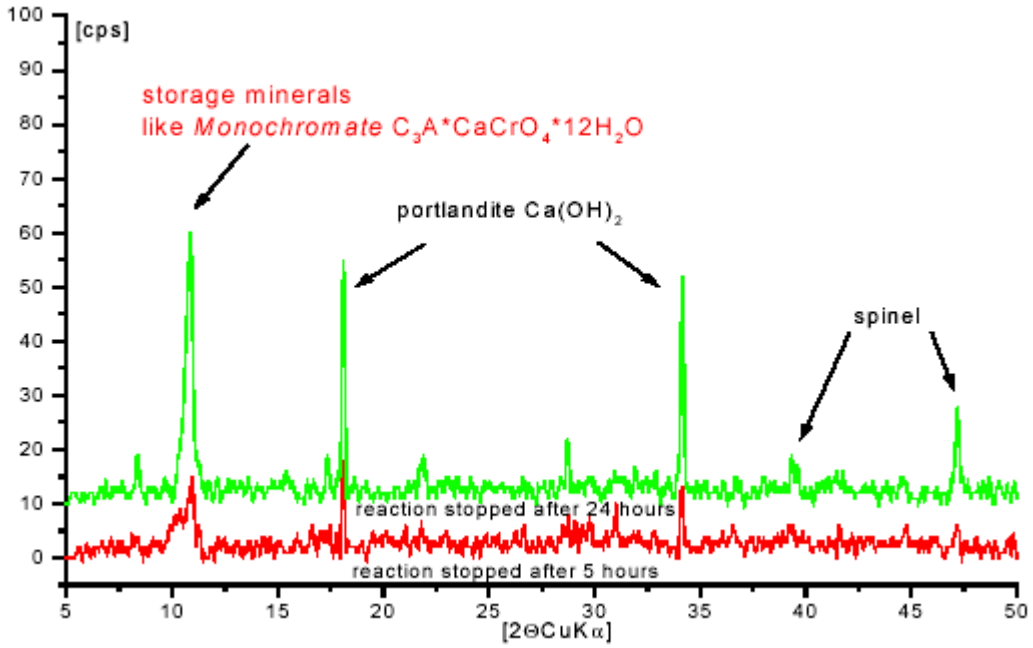

Figure 2. XRD diagrams of residues after different times of reaction

3.3 Examination of the storage minerals and reaction products in the residues by SEM

Figure 3 shows a Cryo-SEM picture of a residue after a reaction time of 24 h. Portlandite and lamellar Calcium aluminate hydrate (storage mineral) can be seen as hexagonal platy crystals near phases of BFD.

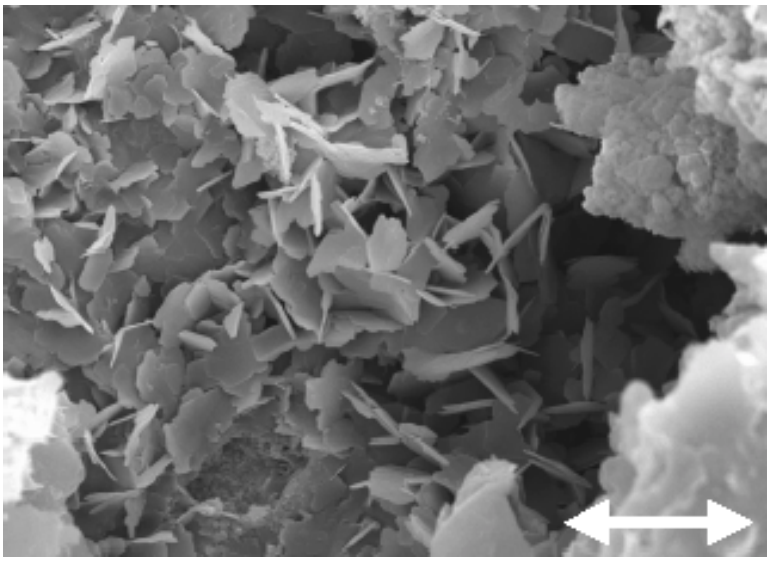

Figure 3. Cryo-SEM image of a residue, reaction stopped after 24h, scale bar = 10 µm

4. DISCUSSION AND CONCLUSION

Amounts of chromium (VI) in mixtures with BFD originally containing 70 mg/l, were less than 0.03 mg/l after conversion of TCAH into a lamellar storage mineral like Monochromate. Suitable procedures can be transferred from laboratory scale to the scale of technical industry processing. TCAH can be synthesized through stoichiometric compositions of various educts.

The possibility for chromate removal from BFD-solutions and for recycling is illustrated in the following scheme[8]:

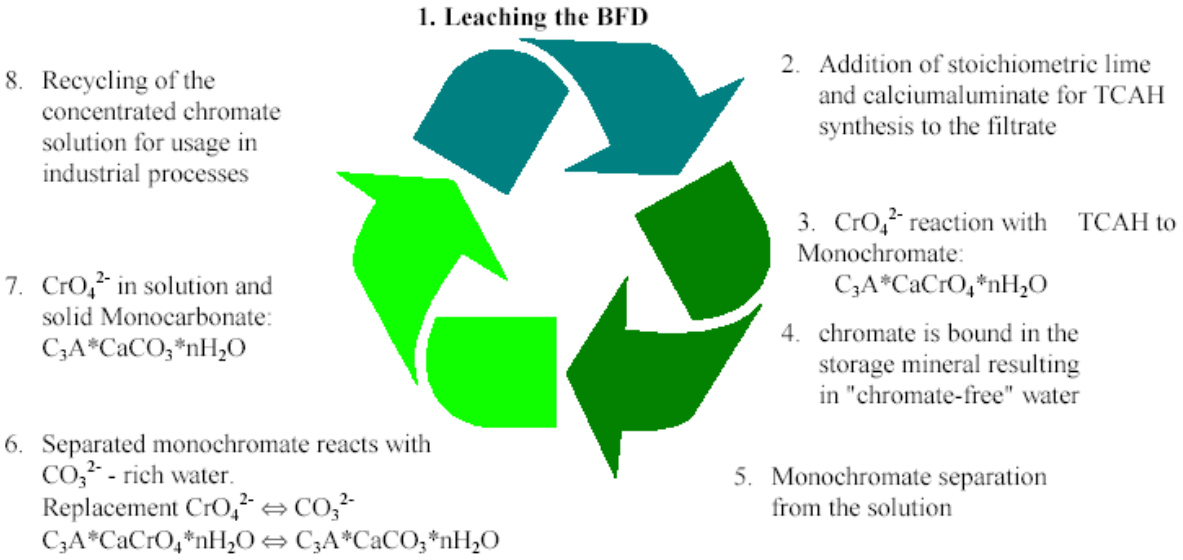

REFERENCES

[1] S. Auer. N. Jb. Min. Mh. (1990),1,7
[2] H. Pöllmann: Fachtagung Innsbruck-Igls, (1993), 51-59
[3] J. Göske, H. Pöllmann: 15th ICAM, (1996), 211
[4] J. Göske, H. Pöllmann: VI Congr. Brasil. Geoquímica (1997), Vol. I, 196-200
[5] J. Göske, H. Pöllmann: Eur. J. Min. Bh., Vol. 7(1) (1995), 87
[6] J. Göske Dissertation, Halle, Germany (1998)
[7] H. Pöllmann: N. Jb. Min. Mh. (1997)
[8] J. Göske, H. Pöllmann: Short course IMA COM (1999), Pretoria / Südafrika, 52-56

FIXATION PROPERTIES OF NO_3^-, SO_4^{2-} AND CL^- IN TCAH AS A FUNCTION OF THE CONCENTRATION: UNDER THE INFLUENCE OF THE CATIONS NA^+ AND K^+ IN VARIABLE CONCENTRATIONS

J. Göske and H. Pöllmann

Department of Mineralogy / Geochemistry, Martin-Luther-University Halle (Saale)
Domstr. 5, D - 06108 Halle (Saale), GERMANY. E-mail: goeske@geologie.uni-halle.de

ABSTRACT

Lamellar Calcium aluminate hydrates are hydration products in ordinary Portland cements and play an important role in the hardening process. Due to the fixation ability of organic and inorganic ions the technical features of lamellar phases are important as reservoir minerals for pollutants. Formation of these hydrates can proceed under variable conditions:

- Formation in concrete due to harmful substances in the environment
- Formation due to additives controlling cement-hydration
- Formation under controlled conditions as storage minerals

1. INTRODUCTION

Some compounds among the group of layered Calcium aluminate hydrates are important for the process of cement manufacturing. Their chemical composition can be described by the following general formula: $3CaO*Al_2O_3*CaX*nH_2O$ and $3CaO*Al_2O_3*CaY_2*nH_2O$ with X= SO_4^{2-}, CO_3^{2-}, CrO_4^{2-}, ... and Y= OH^-, Cl^-, NO_3^-, .[1,2,3]. Structurally they consist of positively charged layers of $[Ca_2Al(OH)_6]^+$ and negatively charged interlayers of $[OH * nH_2O]^-$.

Detailed structural studies were done with Monosulfate ($3CaO*Al_2O_3 *CaSO_4*12\ H_2O$) and Monochloride ($3CaO*Al_2O_3*CaCl_2*12\ H_2O$).

Tetra Calcium Aluminate Hydrate (**TCAH**) with the formula $C_3A*Ca(OH)_2*nH_2O$ is especially suitable as storage mineral, because of its layered structure. It is widely used to incorporate efficiently for example heavy metals, because the OH-group in the interlayers can be exchanged for 1^+- or 2^+-anions [4,5].

Storage minerals can be used or added for the immobilization of inorganic and organic substances in contaminated water, gas and soil. The composition of the harmful substance to be immobilized depends on the structure and the kind of the compounds. The immobilization of toxic substances is based on the crystallo-chemical fixation and physical aggregation due to the crystallization of metal-metal-hydroxy salts. These compounds offer a great possibility for diadochism of cations and anions. The fixation of non-polar and polar molecules is guaranteed by additional bonding mechanisms (hydrogen bond, residual bond, etc.) and crystallo-chemical replacement.

Proceedings of the 11th International Congress on the Chemistry of Cement (ICCC)
'Cement's Contribution to the Development in the 21st Century'
Hosted by: The Cement and Concrete Institute of South Africa
CD-ROM produced by: Document Transformation Technologies
11 - 16 May 2003, Durban, South Africa
ISBN Number: 0-9584085-8-0
Editors: Dr G. Grieve and G. Owens
Congress Organised by: Event Dynamics

The idealized composition of the metal-metal-hydroxy salts are :

$$[\ Me_{(u)}\ \ Me_{(v)}\ \ (OH)_{(w)}\ ]\ *\ [\ X_{(x)}\ \ n\ H_2O\ \ (A_{(y)})\ \ (B_{(z)})\ ]$$

1. 2. 3. 4. 5. 6. 7.

The following cations and anions can be partially or completely replaced:

	Cu^{2+}		Co^{3+}		CrO_4^{2-}	BrO_3^-	MnO_4^-	$Mo_7O_{24}^{6-}$
	Ni^{2+}		Mn^{3+}		SeO_4^{2-}	Br^-	CN^-	$Fe(CN)_6^{3-}$
	Zn^{2+}		Ga^{3+}		SeO_3^{2-}	CO_3^{2-}	$HCOO^-$	$Fe(CN)_6^{4-}$
	Ca^{2+}		Cr^{3+}		SiO_3^{2-}	ClO_4^-	OCN^-	
1. :	Cd^{2+}	**2. :**	Al^{3+}	**4. :**	ClO_3^-	SO_3^{2-}	$S_2O_3^{2-}$	
	Mg^{2+}		Fe^{3+}		$B(OH)_4^-$	NO_3^-	WO_4^{2-}	
	Fe^{2+}		In^{3+}		OH^-	J^-	C_6H_5-(CH_2)n-COO-	
	Co^{2+}		Ni^{3+}		NO_2^-	SCN^-	(CH_3)n-(CH_2)n-COO-	
	Mn^{2+}		Ga^{3+}		Cl^-	SO_4^{2-}	-OOC-(CH_2)n-COO-	
					JO_3^-	$Al(OH)_4^-$	$H_2W_{12}O_{40}^{6-}$	

3. **:** Adsorption of (in)organic, (non)polar molecules
5. **:** Fixation instead of H_2O
6. **:** Additional fixation of e.g. : Na_2SO_4, $KClO_4$, Na_2CrO_4, etc.
7. **:** Additional incorporation of (non)polar molecules

This paper shows the examination of the fixation of NO_3^-, SO_4^{2-} and Cl^- in TCAH as a function of different educt concentrations. In addition an estimate is presented on the fixation in TCAH under the influence of the cations Na^+ and K^+ (in variable concentrations) /6/.

Detailed statements about the disturbing effects of the cations on the anions in different concentrations in solution are given, with regard to preferred immobilisation of the anions in the crystalline residue.

2. METHODS

Stoichiometric amounts were filled into polyethylene vials and reacted with CO_2-free water under a protective gas filling for 14 days. The mineral phases studied are eager to exchange CO_2 for any other anions. Therefore care was taken to use CO_2-free water. Reactions, drying and further sample preparation were done in a glove-box filled with nitrogen.

X-ray diffraction techniques were used to identify the reaction products and to determine their lattice parameters. In order to inhibit carbonate formation during x-ray analysis, the counting was done at 100% humidity, without air inside a TTK camera, which was flushed with nitrogen gas of technical quality. A wet piece of cloth inside the chamber during the measurements guaranteed almost 100% humidity.

3. RESULTS

Various concentrations of the cations just mentioned have a substantial influence on the formation of TCAH containing nitrate, chloride and sulphate in the presence of the anions NO_3^-, SO_4^{2-} and Cl^-.

Fixation [mg/l] and mineral identification by X-ray-diffraction by 100% r.H., after 14 days reaction time:

anion concentration [mg/l]					fixation [mg/l] (in solid compound)			mineral identification under X-ray-diffraction by 100% r.H.
Na_2SO_4	+	NaCl	+	$NaNO_3$	SO_4^{2-}	Cl^-	NO_3^-	
96060	+	35450	+	62010	54160	16490	29300	$C_3A*3CaSO_4*30\text{-}36H_2O$
96060	+	35450	+	31005	43790	11080	8800	$C_3A*3CaSO_4*30\text{-}36H_2O$
96060	+	35450	+	6200	42530	10360	200	$C_3A*3CaSO_4*30\text{-}36H_2O$
96060	+	17725	+	62010	58870	8420	29730	$C_3A*3CaSO_4*30\text{-}36H_2O$
96060	+	17725	+	31005	45730	6460	10600	$C_3A*3CaSO_4*30\text{-}36H_2O$
96060	+	17725	+	6200	60830	6840	1960	$C_3A*3CaSO_4*30\text{-}36H_2O$
96060	+	3545	+	62010	45870	1460	25530	$C_3A*3CaSO_4*30\text{-}36H_2O$
96060	+	3545	+	31005	49230	540	9620	$C_3A*3CaSO_4*30\text{-}36H_2O$
96060	+	3545	+	6200	57370	1860	3000	$C_3A*3CaSO_4*30\text{-}36H_2O$
48030	+	35450	+	62010	25220	10580	19650	$C_3A*3CaSO_4*30\text{-}36H_2O$
48030	+	35450	+	31005	34230	16360	12350	$C_3A*3CaSO_4*30\text{-}36H_2O$
48030	+	35450	+	6200	30810	11690	1830	$C_3A*3CaSO_4*30\text{-}36H_2O$
48030	+	17725	+	62010	25410	4690	18250	$C_3A*3CaSO_4*30\text{-}36H_2O$
48030	+	17725	+	31005	32860	12980	1280	$C_3A*3CaSO_4*30\text{-}36H_2O$
48030	+	17725	+	6200	36890	8320	3010	$C_3A*3CaSO_4*30\text{-}36H_2O$
48030	+	3545	+	62010	31570	860	14670	$C_3A*3CaSO_4*30\text{-}36H_2O$
48030	+	3545	+	31005	36750	1420	17440	$C_3A*3CaSO_4*30\text{-}36H_2O$
48030	+	3545	+	6200	31330	920	2040	$C_3A*3CaSO_4*30\text{-}36H_2O$
9606	+	35450	+	62010	8930	12290	19190	$C_3A*3CaSO_4*30\text{-}36H_2O$, $C_3A*(1x)CaCl_2*(x)Ca(OH)_2*nH_2O$ $(0 \le x \le 0.17)$
9606	+	35450	+	31005	9450	13400	25690	$C_3A*3CaSO_4*30\text{-}36H_2O$, $C_3A*(1\text{-}x)CaCl_2*(x)Ca(OH)_2*nH_2O$ $(0 \le x \le 0.17)$
9606	+	35450	+	6200	9060	13140	1370	$C_3A*(1\text{-}x)CaCl_2*(x)Ca(OH)_2*nH_2O$ $(0 \le x \le 0.17)$, $C_3A*3CaSO_4*30\text{-}36H_2O$
9606	+	17725	+	62010	8940	6330	21930	$C_3A*3CaSO_4*30\text{-}36H_2O$, $C_3A*(1\text{-}x)CaCl_2*(x)Ca(OH)_2*nH_2O$ $(0\le x\le 0.17)$,$C_3A*(1\text{-}x)Ca(NO_3)_2*(x)Ca(OH)_2*nH_2O$ $(0\le x\le 0.34)$
9606	+	17725	+	31005	8970	9120	18330	$C_3A*3CaSO_4*30\text{-}36H_2O$, $C_3A*(1\text{-}x)CaCl_2*(x)Ca(OH)_2*nH_2O$ $(0 \le x \le 0.17)$

9606	+	17725	+	6200	9300	5450	1770	$C_3A*3CaSO_4*30\text{-}36H_2O$, $C_3A*(1\text{-}x)CaCl_2*(x)Ca(OH)_2*nH_2O$ $(0 \le x \le 0.17)$
9606	+	3545	+	62010	8830	920	39040	$C_3A*3CaSO_4*30\text{-}36H_2O$, $C_3A*(1\text{-}x)CaCl_2*(x)Ca(OH)_2*nH_2O$ $(0\le x\le 0.17)$, $C_3A*(1\text{-}x)Ca(NO_3)_2*(x)Ca(OH)_2*nH_2O$ $(0\le x\le 0.34)$
9606	+	3545	+	31005	9030	820	16590	$C_3A*3CaSO_4*30\text{-}36H_2O$, $C_3A*(1\text{-}x)Ca(NO_3)_2*(x)Ca(OH)_2*nH_2O$ $(0\le x \le 0.34)$, $C_3A*(1\text{-}x)CaCl_2*(x)Ca(OH)_2*nH_2O$ $(0 \le x \le 0.17)$
9606	+	3545	+	6200	8730	940	1430	$C_3A*3CaSO_4*30\text{-}36H_2O$, $C_3A*(1\text{-}x)CaCl_2*(x)Ca(OH)_2*nH_2O$ $(0\le x\le 0.17)$, $C_3A*(1\text{-}x)Ca(NO_3)_2*(x)Ca(OH)_2*nH_2O$ $(0\le x\le 0.34)$

anion concentration [mg/l]					**fixation [mg/l]** (in solid compound)			**mineral identification by X-ray-diffraction by 100% r.H.**
K_2SO_4	**+**	**KCl**	**+**	**KNO_3**	**SO_4^{2-}**	**Cl^-**	**NO_3^-**	
96060	+	35450	+	62010	79320	9490	19670	$C_3A*3CaSO_4*30\text{-}36H_2O$
96060	+	35450	+	31005	79730	7630	5850	$C_3A*3CaSO_4*30\text{-}36H_2O$
96060	+	35450	+	6200	78680	8970	1900	$C_3A*3CaSO_4*30\text{-}36H_2O$
96060	+	17725	+	62010	78720	4760	16840	$C_3A*3CaSO_4*30\text{-}36H_2O$
96060	+	17725	+	31005	75210	3390	8180	$C_3A*3CaSO_4*30\text{-}36H_2O$
96060	+	17725	+	6200	68040	4570	1660	$C_3A*3CaSO_4*30\text{-}36H_2O$
96060	+	3545	+	62010	75030	490	18880	$C_3A*3CaSO_4*30\text{-}36H_2O$
96060	+	3545	+	31005	68310	40	7930	$C_3A*3CaSO_4*30\text{-}36H_2O$
96060	+	3545	+	6200	64720	770	150	$C_3A*3CaSO_4*30\text{-}36H_2O$
48030	+	35450	+	62010	30240	11060	18910	$C_3A*3CaSO_4*30\text{-}36H_2O$
48030	+	35450	+	31005	32950	6430	6770	$C_3A*3CaSO_4*30\text{-}36H_2O$
48030	+	35450	+	6200	32550	7060	190	$C_3A*3CaSO_4*30\text{-}36H_2O$
48030	+	17725	+	62010	35270	7540	27170	$C_3A*3CaSO_4*30\text{-}36H_2O$
48030	+	17725	+	31005	31330	1190	7140	$C_3A*3CaSO_4*30\text{-}36H_2O$
48030	+	17725	+	6200	33950	5310	460	$C_3A*3CaSO_4*30\text{-}36H_2O$
48030	+	3545	+	62010	31660	640	18180	$C_3A*3CaSO_4*30\text{-}36H_2O$
48030	+	3545	+	31005	33440	770	8240	$C_3A*3CaSO_4*30\text{-}36H_2O$
48030	+	3545	+	6200	31710	800	620	$C_3A*3CaSO_4*30\text{-}36H_2O$
9606	+	35450	+	62010	8550	12870	15610	$C_3A*3CaSO_4*30\text{-}36H_2O$, $C_3A*(1\text{-}x)CaCl_2*(x)Ca(OH)_2*nH_2O$ $(0 \le x \le 0.17)$

9606	+	35450	+	31005	8610	11320	7030	$C_3A*3CaSO_4*30\text{-}36H_2O$, $C_3A*(1\text{-}x)CaCl_2*(x)Ca(OH)_2*nH_2O$ $(0 \le x \le 0.17)$
9606	+	35450	+	6200	8740	12490	1280	$C_3A*(1\text{-}x)CaCl_2*(x)Ca(OH)_2*nH_2O$ $(0 \le x \le 0.17)$, $C_3A*3CaSO_4*30\text{-}36H_2O$
9606	+	17725	+	62010	9030	5800	16340	$C_3A*3CaSO_4*30\text{-}36H_2O$, $C_3A*(1\text{-}x)Ca(NO_3)_2*(x)Ca(OH)_2*nH_2O$ $(0 \le x \le 0.34)$
9606	+	17725	+	31005	8990	3700	4280	$C_3A*3CaSO_4*30\text{-}36H_2O$, $C_3A*(1\text{-}x)CaCl_2*(x)Ca(OH)_2*nH_2O$ $(0\le x\le 0.17)$, $C_3A*(1\text{-}x)Ca(NO_3)_2*(x)Ca(OH)_2*nH_2O$ $(0\le x\le 0.34)$
9606	+	17725	+	6200	8970	6330	310	$C_3A*3CaSO_4*30\text{-}36H_2O$, $C_3A*(1\text{-}x)CaCl_2*(x)Ca(OH)_2*nH_2O$ $(0 \le x \le 0.17)$
9606	+	3545	+	62010	9080	100	19750	$C_3A*3CaSO_4*30\text{-}36H_2O$, $C_3A*(1\text{-}x)CaCl_2*(x)Ca(OH)_2*nH_2O$ $(0\le x\le 0.17)$, $C_3A*(1\text{-}x)Ca(NO_3)_2*(x)Ca(OH)_2*nH_2O$ $(0\le x\le 0.34)$
9606	+	3545	+	31005	9230	970	21760	$C_3A*3CaSO_4*30\text{-}36H_2O$, $C_3A*(1\text{-}x)Ca(NO_3)_2*(x)Ca(OH)_2*nH_2O(0 \le x \le 0.34)$, $C_3A*(1\text{-}x)CaCl_2*(x)Ca(OH)_2*nH_2O$ $(0 \le x \le 0.17)$
9606	+	3545	+	6200	9180	650	1300	$C_3A*3CaSO_4*30\text{-}36H_2O$, $C_3A*(1\text{-}x)CaCl_2*(x)Ca(OH)_2*nH_2O$ $(0\le x\le 0.17)$, $C_3A*(1\text{-}x)Ca(NO_3)_2*(x)Ca(OH)_2*nH_2O$ $(0\le x\le 0.34)$

$CaSO_4*2H_2O$:	Gypsum
$C_3A*3CaSO_4*nH_2O$:	Sulphate-Ettringite
$C_3A*CaSO_4*nH_2O$:	Monosulfate
$C_3A*(1\text{-}x)CaCl_2*(x)Ca(OH)_2*nH_2O$:	Chloride containing, lamellar phase
$C_3A*(1\text{-}x)Ca(NO_3)_2*(x)Ca(OH)_2*nH_2O$:	Nitrate containing lamellar phase

Comparison of the fixation of nitrate, chloride and sulphate in [ppm] as a function of the conc. of sodium:

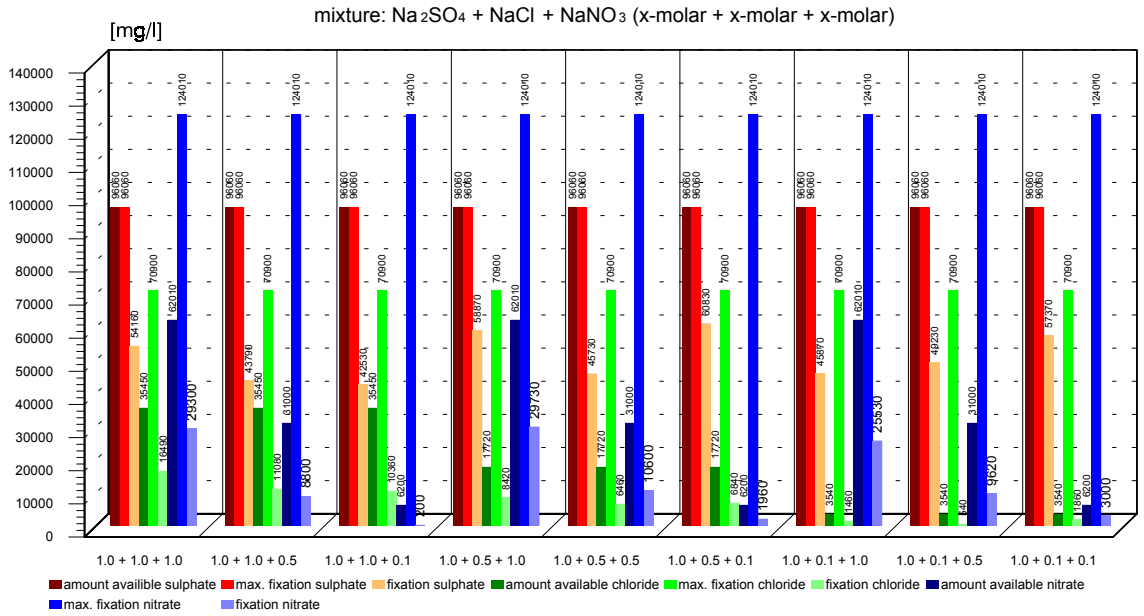

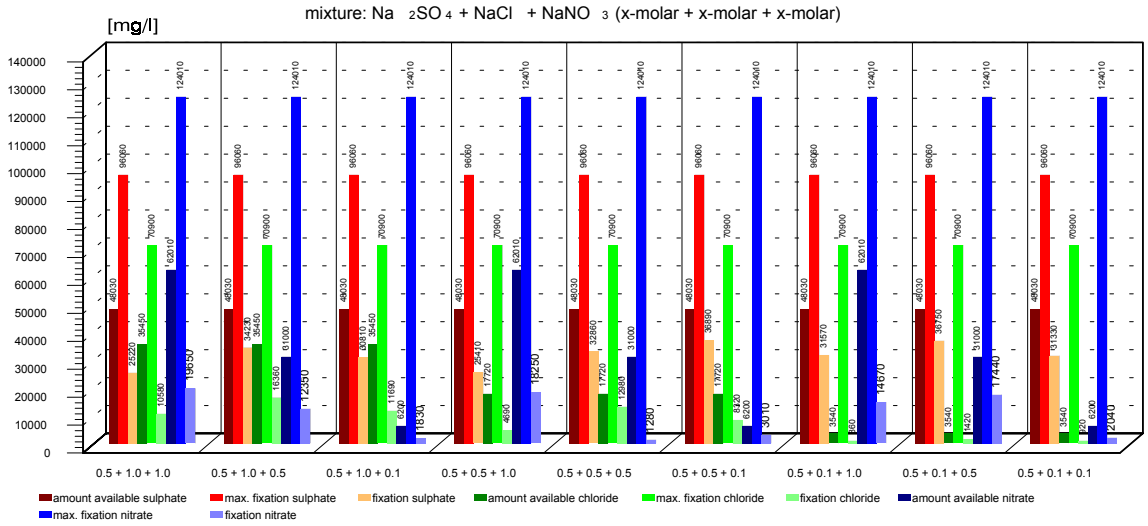

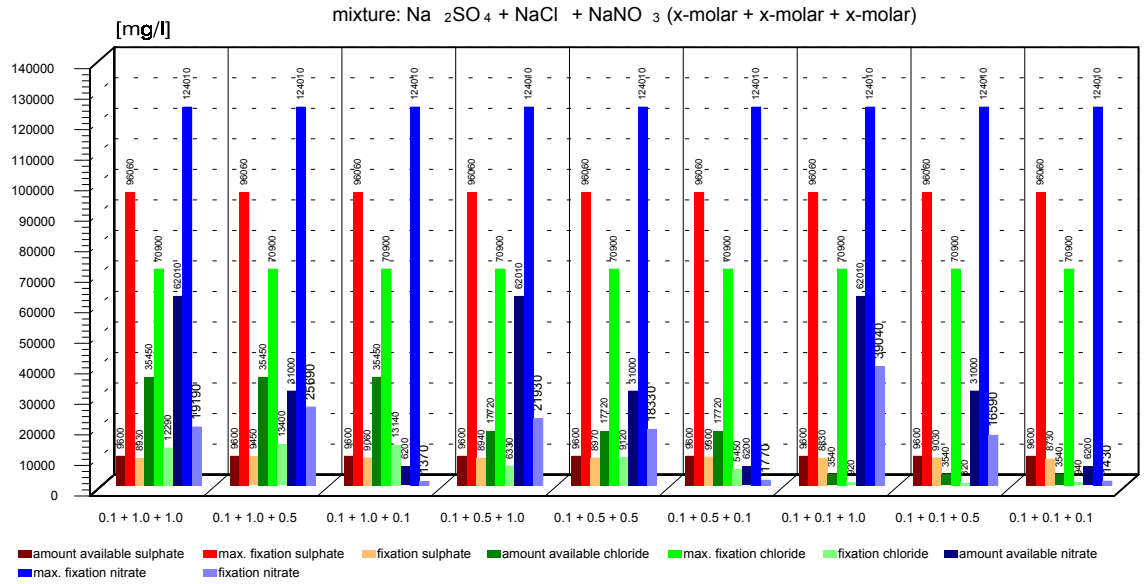

Comparison of the fixation of nitrate, chloride and sulphate in [ppm] as a function of the conc. of potassium:

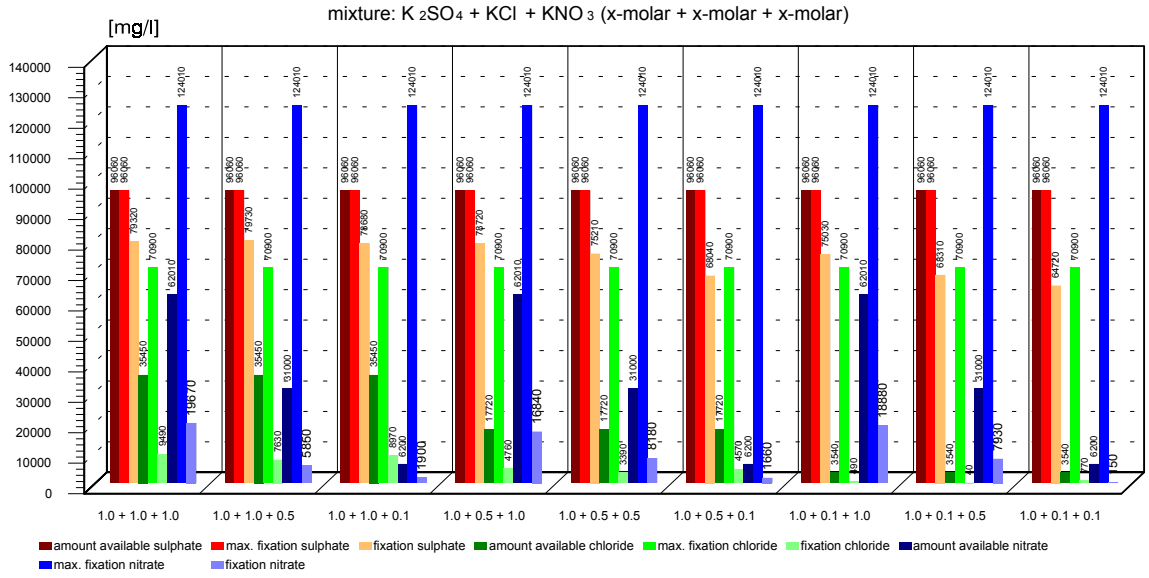
mixture: K 2SO4 + KCl + KNO3 (x-molar + x-molar + x-molar)
[mg/l]
1.0 + 1.0 + 1.0
1.0 + 1.0 + 0.5
1.0 + 1.0 + 0.1
1.0 + 0.5 + 1.0
1.0 + 0.5 + 0.5
1.0 + 0.5 + 0.1
1.0 + 0.1 + 1.0
1.0 + 0.1 + 0.5
1.0 + 0.1 + 0.1
amount available sulphate
max. fixation sulphate
fixation sulphate
amount available chloride
max. fixation chloride
fixation chloride
amount available nitrate
max. fixation nitrate
fixation nitrate

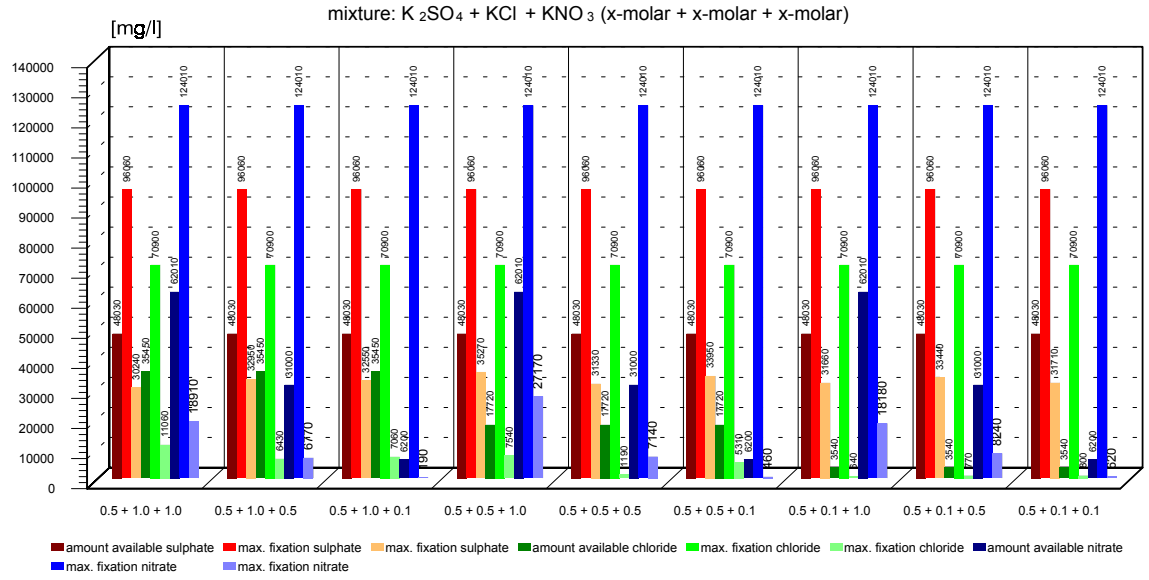
mixture: K 2SO4 + KCl + KNO3 (x-molar + x-molar + x-molar)
[mg/l]
0.5 + 1.0 + 1.0
0.5 + 1.0 + 0.5
0.5 + 1.0 + 0.1
0.5 + 0.5 + 1.0
0.5 + 0.5 + 0.5
0.5 + 0.5 + 0.1
0.5 + 0.1 + 1.0
0.5 + 0.1 + 0.5
0.5 + 0.1 + 0.1
amount available sulphate
max. fixation sulphate
max. fixation sulphate
amount available chloride
max. fixation chloride
max. fixation chloride
amount available nitrate
max. fixation nitrate
max. fixation nitrate

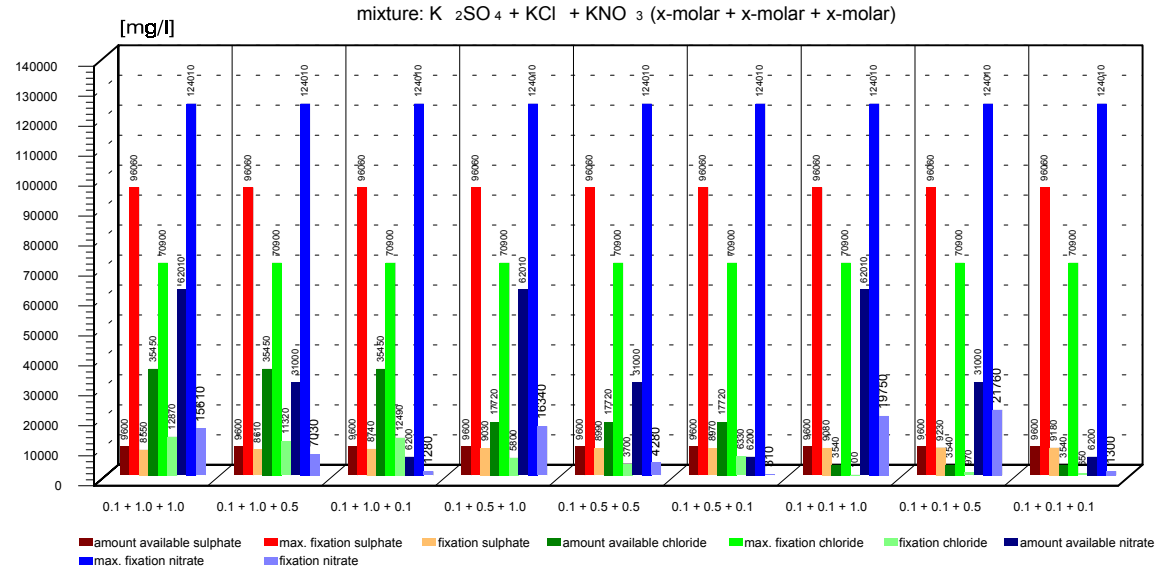
mixture: K 2SO4 + KCl + KNO3 (x-molar + x-molar + x-molar)
[mg/l]
0.1 + 1.0 + 1.0
0.1 + 1.0 + 0.5
0.1 + 1.0 + 0.1
0.1 + 0.5 + 1.0
0.1 + 0.5 + 0.5
0.1 + 0.5 + 0.1
0.1 + 0.1 + 1.0
0.1 + 0.1 + 0.5
0.1 + 0.1 + 0.1
amount available sulphate
max. fixation sulphate
fixation sulphate
amount available chloride
max. fixation chloride
fixation chloride
amount available nitrate
max. fixation nitrate
fixation nitrate

4. CONCLUSIONS

- Fixation behaviour of sulphate, chloride and nitrate in presence of sodium or potassium:

  1.0 mol Sodium : Chloride > Nitrate > Sulphate
  0.5 mol Sodium : Chloride > Nitrate > Sulphate
  0.1 mol Sodium : Sulphate > Chloride > Nitrate

  1.0 mol Potassium : Chloride > Nitrate > Sulphate
  0.5 mol Potassium : Chloride > Nitrate > Sulphate
  0.1 mol Potassium : Sulphate > Nitrate > Chloride
- High sulphate contents disturb the crystallisation of lamellar calcium aluminate hydroxy salts.
- Lower sulphate contents give preferential the crystallisation of nitrate and chloride containing lamellar phases.
- Chloride containing lamellar phases were identified in the presence of primary crystallised sulphate-ettringite and near gypsum
- A chloride containing lamellar phase in the presence of sulphate-ettringite exclusively forms at high sulphate and low chloride concentration.
- In comparison to sodium, potassium prefers the fixation of sulphate in sulphate-ettringite by different concentrations of nitrate, chloride amd sulphate.

REFERENCES

[1] F.G. Buttler et al.,J. Amer. Ceram. Soc. 42 (1959), 121-126
[2] R. Allmann, N. Jb. Min. Mh. (3) (1977), 136-144
[3] A. Terzis et al.,Z. Krist. 181(1987), 29-34
[4] H. Pöllmann, Professional dissertation, Erlangen, (1989)
[5] J. Göske, H. Pöllmann, Eur. J. Min. Bh., Vol. 7(1) (1995), 87
[6] J. Göske, Dissertation, Halle, Germany (1998)

BASIC INVESTIGATIONS ON THE CRYSTAL CHEMISTRY OF SULFONATE CONTAINING AFM-PHASES

Stöber, S. and Pöllmann, H.

Institut für Geologische Wissenschaften der Martin - Luther Universität Halle - Wittenberg
Mineralogie/Geochemie, Domstraße 5, 06108 Halle (Saale).
E-mail: stoeber@geologie.uni-halle.de
Institut für Geologische Wissenschaften der Martin - Luther Universität Halle - Wittenberg
Mineralogie/Geochemie, Domstraße 5, 06108 Halle (Saale).
E-mail: poellmann@geologie.uni-halle.de

ABSTRACT

Three different groups of lamellar calcium aluminate sulfonate hydrates were purely synthesized. Metric parameters were refined and structural properties of the new Afm – phases were discussed. The influences of different relative humidities in the range of 100…35 % and the influence of different temperatures on the stability of the Afm – salts was studied in detail. In addition, binary systems of $C_3A{\cdot}Ca(OH)_2{\cdot}nH_2O$ - $C_3A{\cdot}Ca(X)_2{\cdot}nH_2O$ were investigated at different r.h. in order to determine phase compositions and the crystal chemistry of newly formed Afm-phases.

1. INTRODUCTION

In Ordinary Portland Cements (OPC) the aluminate phase of the clinker reacts together with $CaSO_4$ nH_2O and water to ettringite (Aft-phase) and in a second step to monosulfate, which belongs to the family of lamellar calcium aluminate hydrate (Afm-phases). Calcium Aluminate Cements (CAC) crystallize C_2AH_8 and AH_3 as reaction products of CA at intermediate temperatures. C_2AH_8 itself belongs to the group of Afm – phases. In comparison to monosulfate, $Al(OH)_4^-$ ions are fixed in the so called interlayer of the structure. As indicated, Afm-phases [1], [2], [3] are based on layered structures, built up of main layers $[Ca_2Al(OH)_6]^+$ and interlayers $[X{\cdot}nH_2O]^-$ or $[1/2\ Y{\cdot}nH_2O]^-$ ordered in the direction [00l]. X and Y are placeholders for inorganic or organic anions. In the main layer Al-atoms form a distorted brucite lattice. The octahedral sites are occupied by Ca-atoms. Whereas the coordination of Al is 6 the coordination of Ca is 7, which results in an additional coordination with an O-atom of a water molecule of the interlayer. The interlayer is a fragile area, built up of weakly bonded water – anion frameworks. Water molecules can be easily removed and the anion exchanged against further inorganic or organic anions. Because of the application of different additives in cement chemistry to manipulate the properties of the cement paste and the concrete, the kinetics of the hydration process and rheology were influenced [5], [6], [7]. The presented investigations deal with the influence of additives on the influence on the crystal chemistry of Afm-phases.

2. EXPERIMENTAL

2.1 Synthesis of the reactants

CaO was synthesised by sintering pure $CaCO_3$ (Merck p.a.) at 1000°C for 1h. The loss of ignition of γ-Al_2O_3 was determined at 1000°C for 1h, in order to correct the concentration of γ-Al_2O_3 for the

Proceedings of the 11th International Congress on the Chemistry of Cement (ICCC)
'Cement's Contribution to the Development in the 21st Century'
Hosted by: The Cement and Concrete Institute of South Africa
CD-ROM produced by: Document Transformation Technologies
11 - 16 May 2003, Durban, South Africa
ISBN Number: 0-9584085-8-0
Editors: Dr G. Grieve and G. Owens
Congress Organised by: Event Dynamics

synthesis of CA. For the synthesis of CA, stoichiometric concentrations of CaO and Al_2O_3 were sintered at 1350°C several times for 1h with ball milling in between.

2.2 Synthesis of different Calciumsulfonatehydrates

Principally, stoichiometric concentrations of $CaCO_3$ and different sulfonic acids (Table 1) reacted in moist atmosphere. $CaCO_3$ was mixed with water to obtain a slurry. The sulfonic acid was added drop wise. After the combination of $CaCO_3$ and acid the solution became transparent under the formation of CO_2. In order to accelerate the reaction the synthesis was performed at 40°C and was stirred carefully. The measured pH-value at the end of the reaction $CaCO_3$ + sulfonic acid was 7. Afterwards the solution was evaporated in a drying oven at 30-40°C. After 5 days, transparent idiomorphic crystals were obtained and the chemical composition was determined, immediately.

Table 1. Sulfonic acids

Chemical formula	Description
Alkanesulfonic acids	
CH_3SO_3H	Methane sulfonic acid
$C_2H_3SO_3H$	Ethane sulfonic acid
$C_3H_3SO_3H$	Propane-1-sulfonic acid
$C_4H_3SO_3H$	Buthane -1-sulfonic acid
Benzene sulfonic acids	
$C_6H_5SO_3H$	Benzene sulfonic acid
$C_7H_7SO_3H$	Toluene-p-sulfonic acid
$C_8H_9SO_3H$	Xylene sulfonic acid
$C_9H_{10}SO_3H$	Mesitylene sulfonic acid
Naphthalene sulfonic acids	
$C_{10}H_7SO_3H$	Naphthalene-1-sulfonic acid
$C_{10}H_7SO_3H$	Naphthalene-2-sulfonic acid

2.3 Instrumentation

The XRD measurements were performed on a SIEMENS 5000 Diffractometer with Cuk_a radiation. For the temperature and humidity controlled measurements a TDK camera from PAAR was used. During the measurements the interior of the camera was purged with N_2. In order to install different relative humidities the N_2 was pumped slowly through saturated salt solutions. The following parameters in Table 2 were used for the measurements.

Table 2. Parameters for XRD measurements

Parameters	Values
2Theta [°]	3…80
Voltage [kV]	40
Current strength [mA]	30
Step 2Theta [°]	0.01
Count time [s]	1
Scatter- and Antiscatter slit	Variable

In order to determine the loss in weight and to determine the onset temperatures of the different dehydration reactions a TG/DTG 320CU and a DSC 220 of SEIKO were used. For the specific determination of the water concentrations Karl-Fischer instrument of Methrom with an oven was applied. Chemical analyses of the different lamellar calcium aluminate sulfonate hydrates were performed by AAS and ICP/OES. The sulfonic compounds were directly determined by the total organic carbon method.

3. RESULTS

After synthesis of 4 months, the precipitates of all samples were filtered under N_2-atmosphere in the glove box and investigated immediately at 100 % r.h. by XRD. For the studies the salts were dried step by step to 35% r.h. and the chemical composition of each salt was determined.

The habit of the crystals showed in the case of the fixation of benzene- alkane- or naphthalenesulfonic acid anions in the crystal structure idiomorphic well crystallized individuals with the typical platy hexagonal habit. Especially calcium aluminate alkanesulfonate hydrates crystallize as platy aggregates (Figure 1).

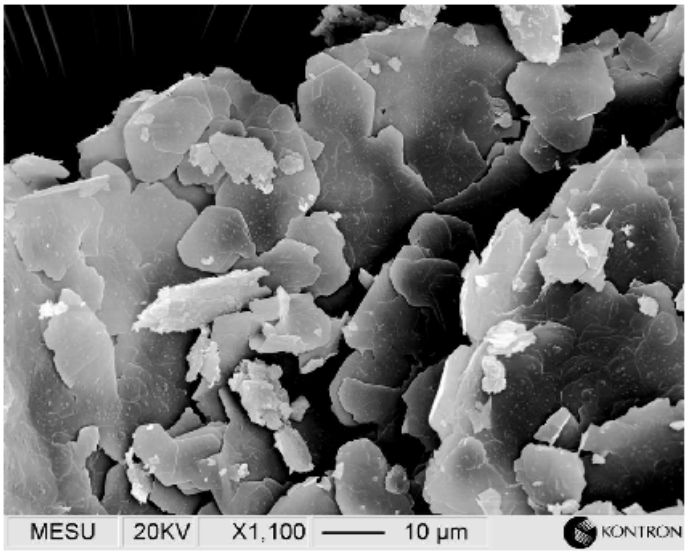

Figure 1. SEM image of $C_3A{\cdot}Ca(CH_3SO_3)_2{\cdot}15H_2O$

3.1 Metric parameters of lamellar Calcium aluminate sulfonate hydrates

3.1.1 Metric parameters of lamellar calcium aluminate alkanesulfonate hydrates

The least-squares-refinements of the metric parameters of Afm phases (Table 3) is based on the structures of calcium aluminate sulphate hydrate [1] and the monoclinic calcium aluminate chloride hydrate [2]. Lamellar calcium aluminate alkanesulfonate hydrates crystallized in the trigonal system with possible space groups R3 R-3, R3m and R-3m. The unit cell contained 6 sequences $[Ca_2Al(OH)_6]^+[X{\cdot}nH_2O]^-$ (X = alkanesulfonic ion) perpendicular [00l] at 100 % and 35 % r.h.

On the basis of the hexagonal setting of the unit cell the lattice parameter $a_o = b_o$ varies in the region 0.577±002 nm. Due to the chemical fixation of different long chained alkanesulfonic acid ions the layer distance c´ = c/6 will be increased approximately linearly (Figure 2). STERN et al. (1996) showed that the chemical fixation of alkanesulfonic acid ions $C_nH_{2n-1}SO_3^-$ with n > 4 in the interlayer let the interlayer distance c´ approach a saturation value for n = 12 at approximately 22 nm.

Table 3. Metric parameters of calcium aluminate alkanesulfonate hydrates

Afm-Phase	a_o [nm]	c_o [nm]	c´ [nm]	r.h. [%]
$C_3A{\cdot}Ca(CH_3SO_3)_2{\cdot}15H_2O$	0.5776	7.6723	1.2787	100
	-.-	6.5610	1.0935	35
$C_3A{\cdot}Ca(C_2H_5SO_3)_2{\cdot}14H_2O$	0.5772	8.1297	1.3549	100
	0.5752	8.1916	1.3653	35
$C_3A{\cdot}Ca(C_3H_7SO_3)_2{\cdot}16H_2O$	0.5764	8.1972	1.3662	100
	-.-	9.1470	1.5245	35
$C_3A{\cdot}Ca(C_4H_9SO_3)_2{\cdot}16H_2O$	0.5760	9.0989	1.5165	100
	-.-	9,4800	1.580	35

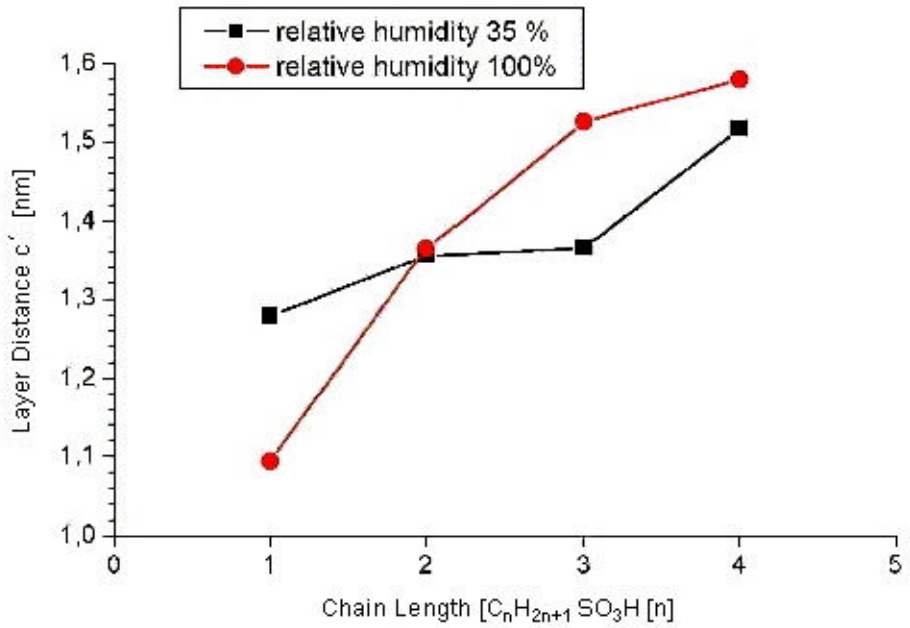

Figure 2. Variable layer distance c´ due to increased chain length of alkane sulfonic acid anions.

3.1.2 Metric parameters of lamellar calcium aluminate benzene sulfonate hydrates

At 100 and 35% r.h, calcium aluminate benzene sulfonate hydrate and calcium aluminate toluene-p-sulfonate hydrate crystallized on the basis of a hexagonal primitive unit cell with a sequence $[Ca_2Al(OH)_6]^+[X{\cdot}nH_2O]^-$ per unit cell perpendicular [00l]. However the fixation of xylene sulfonic ions in the interlayer of the Afm-phase forced the formation of a salt with a trigonal lattice, comparable to the lattices of lamellar calcium aluminate alkane sulfonate hydrates. In opposition, calcium aluminate mesitylene sulfonate hydrate crystallized monoclinic. The refined metric parameters of the different investigated lamellar calcium aluminate benzene sulfonate hydrates are summarized in Table 3. At 100 and 35% r.h, calcium aluminate benzene sulfonate hydrate and calcium aluminate toluene-p-sulfonate hydrate crystallized on the basis of a hexagonal primitive unit cell with a sequence $[Ca_2Al(OH)_6]^+[X{\cdot}nH_2O]^-$ per unit cell perpendicular [00l]. However the fixation of xylene sulfonic ions in the interlayer of the Afm-phase forced the formation of a salt with a trigonal lattice, comparable to the lattices of lamellar calcium aluminate alkane sulfonate hydrates. In opposition, calcium aluminate mesitylene sulfonate hydrate crystallized monoclinic. The refined metric parameters of the different investigated lamellar calcium aluminate benzene sulfonate hydrates are summarized in Table 4.

Table 4. Metric parameters of calcium aluminate benzene sulfonate hydrates

Afm-phase	a_o [nm]	b_o [nm]	c_o [nm]	c´ [nm]	β [°]	r.h. [%]
$C_3A{\cdot}Ca(C_7H_7SO_3)_2{\cdot}15H_2O$	0.5779	0.5779	1.7202	1.7202	90.000	35
	-.-	-.-	1.7177	1.7177	90.000	100
$C_3A{\cdot}Ca(C_8H_9SO_3)_2{\cdot}14H_2O$	0.5797	0.5797	9.7986	1.6331	90.000	35
	-.-	-.-	9.7734	1,6289	90.000	100
$C_3A{\cdot}Ca(C_9H_{11}SO_3)_2{\cdot}15H_2O$	0.9783	1.1369	1.8038	1.7544	103.445	35
	0.9355	1.1453	1.7555	1.7554	90.548	100

3.1.3 Metric parameters of lamellar calcium aluminate naphthalenesulfonate hydrates

The lattices of Afm - phases containing naphthalenesulfonic acid anions in the crystal structure are founded on a hexagonal metric with one sequence $[Ca_2Al(OH)_6]^+[X{\cdot}nH_2O]^-$ (X = naphthalenesulfonic ion) per unit cell (Table 5).

Table 5. Metric parameters of calcium aluminate naphthalenesulfonate hydrates

Afm-phase	a_o [nm]	c_o [nm]	c´ [nm]	r.h. [%]
$C_3A{\cdot}Ca(C_{10}H_7\text{-}1\text{-}SO_3)_2{\cdot}14H_2O$	-.-	1.6611	1.6611	100
	-.-	1.5350	1.5350	35
$C_3A{\cdot}Ca(C_{10}H_7\text{-}2\text{-}SO_3)_2{\cdot}14H_2O$	-.-	1.8325	1.8325	100
	0.5781	1.8213	1.8213	35

3.2 Stability of Afm-phases

3.2.1 Influence of variable relative humidities r.h. on the crystal chemistry of Afm - phases

In the interval 100…35% r.h. the salts were dried to 95%, 86%, 75%, 55% and 35% r.h. On each hydration level they were investigated by XRD. The water concentrations of the phases were determined by thermogravimetry (TG/DTG) and the Karl-Fischer Method. It could be proved that calcium aluminate buthane-1-sulfonate hydrate started dehydrating with the decrease of the relative humidity. Further dehydration reactions occurred hand in hand with lower r.h. atmospheres Consequently, the layer distance decreased nearly linearly as a result of lower H_2O concentration in the interlayer region. According to the dehydration of butane-1-sulfonate containing Afm-phase, the processes of further investigated calcium aluminate alkanesulfonate hydrates took place. (See Figure 3)

The influence of variable relative humidities on the group of different calcium aluminate benzene sulfonate hydrates in the interval [100…35] caused a totally different behaviour against variable relative humidities (Figure 4). In opposition to the dehydration of calcium aluminate alkanesulfonate hydrates, the layer distances of calcium aluminate benzene sulfonate hydrates remained stable. Thermal analysis performed on the salts at different relative humidities gave the result, that the same H_2O concentrations always remained in the interlayer. Because of the stronger O – H bondings between H_2O molecules and the hydrogen atoms of the benzene ring and its CH_3-substituents the water molecule were more strongly fixed than in the interlayer of calcium aluminate alkanesulfonate hydrates.

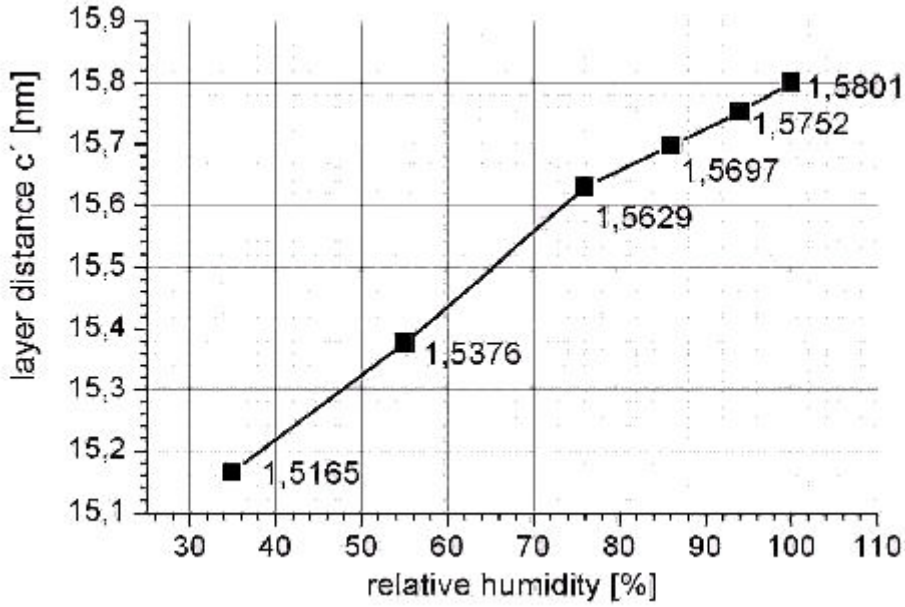

Figure 3. Variation of the interlayer water concentration of calcium aluminate alkanesulfonate hydrates as a function of r.h.

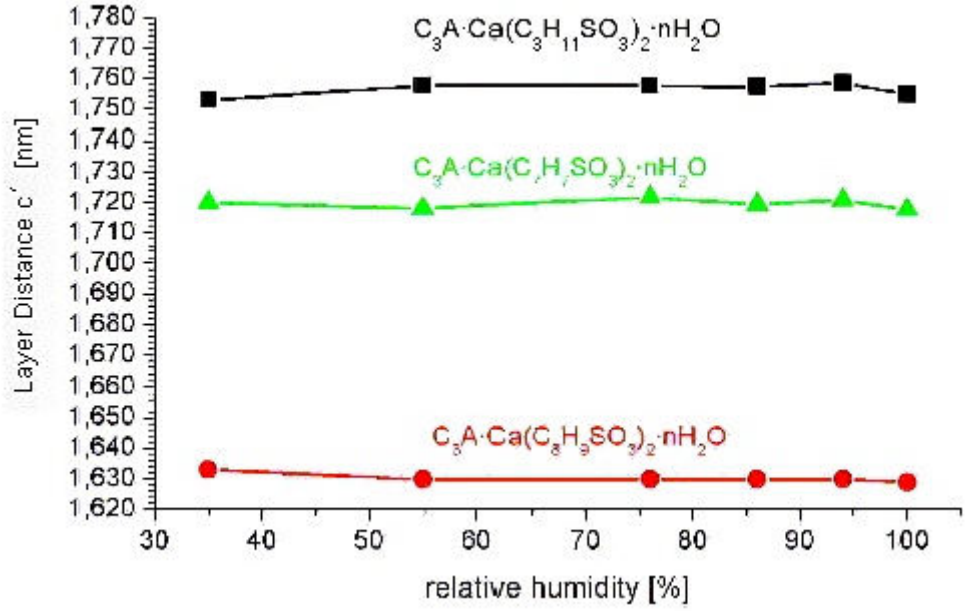

Figure 4. Variation of the interlayer water concentration of different calcium aluminate benzene sulfonate hydrates as a function of r.h.

3.2.2 Thermal stability of Calcium aluminate sulfonate hydrates

Thermal investigations of Afm - phases are divided into the dehydration processes of the interlayer $X{\cdot}nH_2O]^-$ X = sulfonic acid ion and the main layer $[Ca_2Al(OH)_6]^+$. All 3 groups, calcium aluminate alkane-, benzene- and naphthalenesulfonate hydrates started dehydrating at 30-35°C. The interlayer water was released in several steps. According to the properties of the crystal structure of each salt, the major concentration was dehydrated as separate reactions between 30…120°C. More strongly fixed water molecules resisted the temperature increase until 150 °C. FISCHER (1982) [8] postulated, that these strongest bonded interlayer water molecules are the 7th coordination of calcium atoms of the main layer.

The main layer $[Ca_2Al(OH)_6]^+$ of the crystal structure dehydrated at higher temperatures approximately 250°C. It could be proved, that the dehydration process contained one or several reactions; hence not all of them were determined by TG/DTG because of the simultaneous dehydration processes and exothermal pyrolysis of the organic compound. Therefore, two dehydration processes should be discussed.

The interlayer area of calcium aluminate xylene sulfonate hydrate dehydrates in 4 steps (interlayer) at 34°C, 66°C, 86°C and 161°C. The main layer dehydrated in 1 step according to the loss in weight of the TG graph, water molecules were removed from the interlayer of the structure during heating. The chemical composition of the interlayer changed from $[(C_8H_9SO_3)_2{\cdot}8H_2O]^{2-}$ to $[(C_8H_9SO_3)_2{\cdot}5.5H_2O]^{2-}$, $[(C_8H_9SO_3)_2{\cdot}4H_2O]^{2-}$, $[(C_8H_9SO_3)_2{\cdot}2H_2O]^{2-}$ and consequently to $[(C_8H_9SO_3)_2{\cdot}0H_2O]^{2-}$. Therefore the layer distance decreased from originally 1.633nm to lastly 1.434nm (Figure 5).

As a further example the dehydration process of calcium aluminate naphthalene-1-sulfonate hydrate $[Ca_2Al(OH)_6]^+[C_{10}H_7\text{-}1\text{-}SO_3{\cdot}14H_2O]^-$ should be discussed. This salt dehydrated in the range of 25…100°C and 125…150°C. The dehydration of the main layer started at 217°C. However the c´ values refined on the basis of temperature controlled XRD measurements, did not agree with the loss in weight and the heat flow (DSC). The interlayer dimension c´ was not changed systematically as a function of increased temperature. Naphthalene-1-sulfonic acid anions changed slightly with increasing temperatures their orientation in the interlayer until a certain threshold value of the H_2O

concentration was reached. At approximately 112 °C the layer distance shrank drastically, the orientation of the naphthalene-1-sulfonic acid anions changed and the layer distance c´ became extremely low (Figure 6).

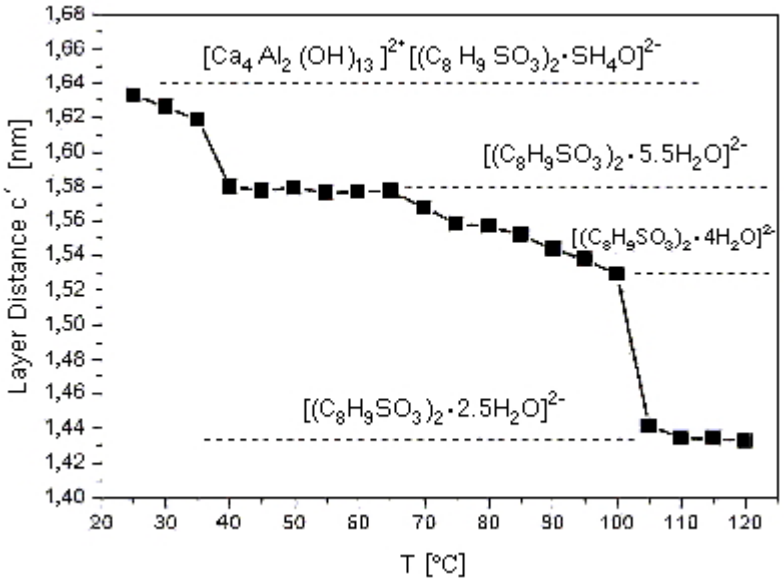

Figure 5. Refinement of c´ of temperature controlled XRD measurements of $Ca(C_8H_9SO_3)_2 \cdot 14H_2O$

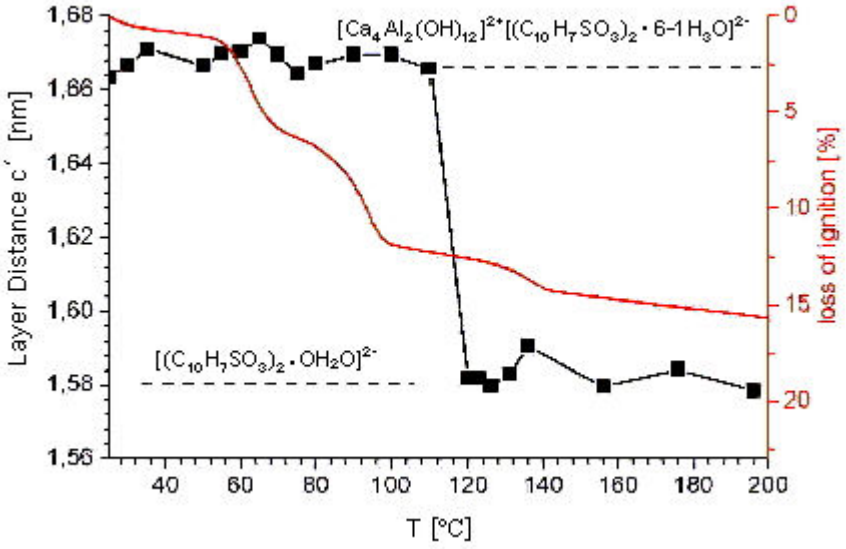

Figure 6. Refinement of c´ of temperature controlled XRD measurements of $C_3A \cdot Ca(C_{10}H_7\text{-}1\text{-}SO_3)_2 \cdot 14H_2O$ at 35 r.h.

3.3 Investigations in systems $[Ca_2Al(OH)_6]^+[OH \cdot nH_2O]^-$ - $[Ca_2Al(OH)_6]^+[C_{10}H_7SO_3 \cdot nH_2O]^-$

In the systems $[Ca_2Al(OH)_6]^+[OH \cdot nH_2O]^-$ - $[Ca_2Al(OH)_6]^+[X \cdot nH_2O]^-$ no solid solution $[Ca_2Al(OH)_6]^+[xX \cdot (1\text{-}x)Y?H_2O]^-$ (X = sulfonic acid anions, $Y = OH^-$) in the range of 10…90 mole-% X were detected. At 100 % r.h., an Afm phase, identified as a pure calcium aluminate sulfonate hydrate on the basis of powder patterns determined during the investigations of pure Afm-phases, was identified by XRD. With the Afm-phase a Gel phase stood in chemical equilibrium and re-crystallized at lower r.h to pure calcium aluminate hydroxide hydrate (Figure 7).

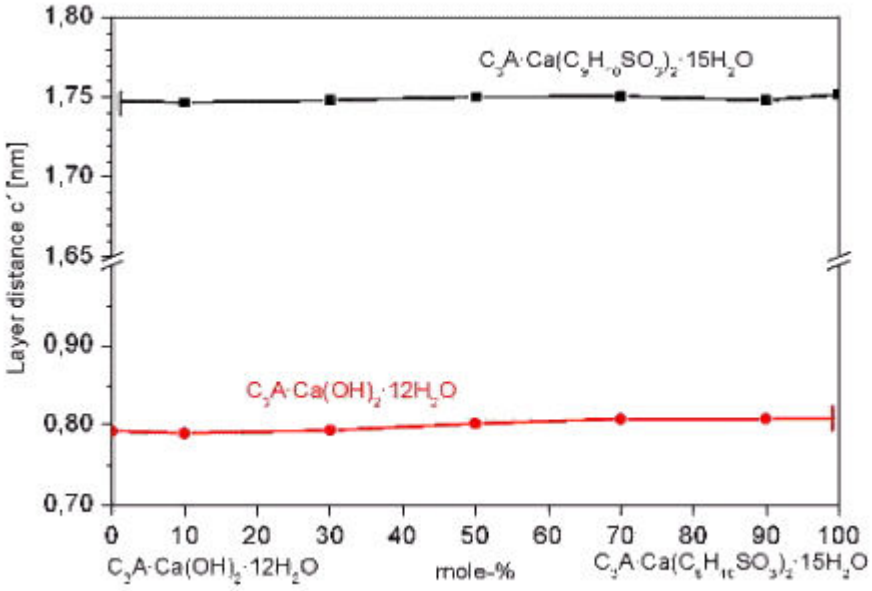

Figure 7. System $C_3A{\cdot}Ca(OH)_2{\cdot}12H_2O$ - $C_3A{\cdot}Ca(C_9H_{11}SO_3){\cdot}15H_2O$ at 35 % r.h.

However, in the system calcium aluminate hydroxide hydrate – calcium aluminate naphthalene-2-sulfonate $[Ca_2Al(OH)_6]^+[OH{\cdot}nH_2O]^-$ - $[Ca_2Al(OH)_6]^+[C_{10}H_7SO_3{\cdot}nH_2O]^-$ at 100 and 35% r.h. a intermediate phase beside the pure phases was stable in the concentration range 10-70 mole-% $C_{1O}H_7SO_3^-$. The composition of the intermediate phase varied respectively the concentration ratio $C_{10}H_7SO_3^-/OH^-$. The chemical formula is $[Ca_2Al(OH)_6]^+[xOH{\cdot}(1\text{-}x)C_{10}H_7SO_3{\cdot}nH_2O]^-$. The structure of the phase is built up of 2 different sequences $[Ca_2Al(OH)_6]^+[C_{10}H_7SO_3{\cdot}nH_2O]^-$ and $[Ca_2Al(OH)_6]^+[OH{\cdot}nH_2O]^-$. Because of the immiscibility of inorganic and sulfonic acid ions in the crystal structure, the interlayer contained only naphthalene-2-sulfonic or hydroxide ions in one layer. The systematic distribution of hydroxide and naphthalene-1-sulfonic acid ions in separate interlayers caused the formation of a superstructure. (Figure 8)

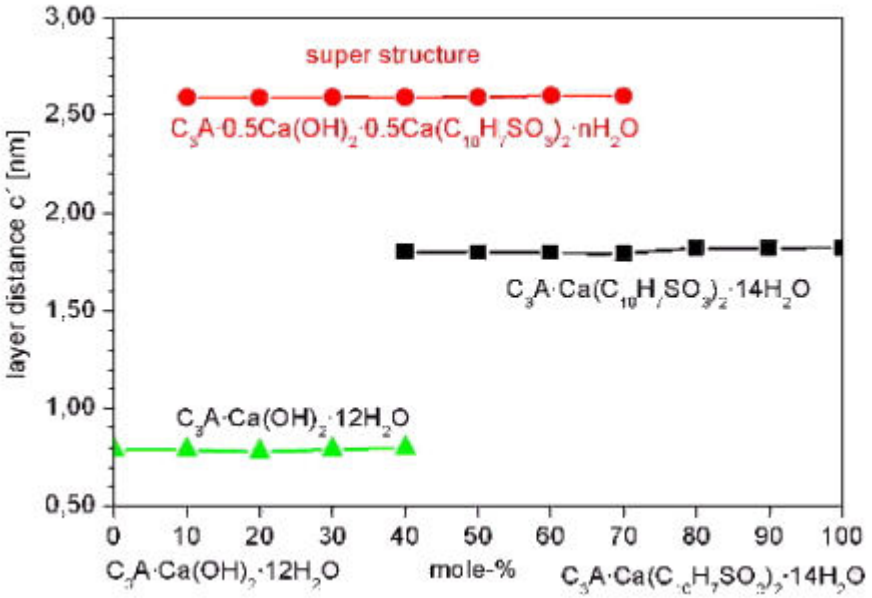

Figure 8. System $C_3A{\cdot}Ca(OH)_2{\cdot}12H_2O$ - $C_3A{\cdot}Ca(C_{10}H_7\text{-}1\text{-}SO_3){\cdot}14H_2O$ at 35 % r.h.

4. DISCUSSION AND CONCLUSIONS

Pure phases of lamellar calcium aluminate alkanesulfonate hydrates, calcium aluminate benzene sulfonate hydrate and calcium aluminate naphthalenesulfonate hydrates were synthesized by paste reaction under equal conditions in the range of 4 months. All salts are built up of a layered structure based in most cases on a trigonal or hexagonal metric. Just calcium aluminate mesitylene sulfonate hydrate crystallized in the monoclinic crystal system. The unit cells of the synthesised phases contain one or 6 sequences of $[Ca_2Al(OH)_6]^+[X{\cdot}nH_2O]^-$ X = sulfonic anion perpendicular c_o.

The central point of these investigations dealt with the weak bondings between H_2O and the sulfonic anions in the interlayer of the structure. Water molecules and sulfonic ions built frameworks, where the molecules were kept together by O-H bondings. In the interlayer of calcium aluminate benzene sulfonate hydrates, water molecules were stronger bonded due to O-H of the benzene and CH_3 - substituent than in interlayer with chemically fixed alkanesulfonic acid anions. Not only the relative humidity, but also variable temperatures decrease the H_2O concentration in the interlayer. As a result the layer distance decreased. Therefore it was possible to detect and identify different stable hydration stages. In the other case the naphthalene-1-sulfonic ion kept its orientation in the interlayer during the dehydration process and the layer distance could not be applied as an indicator for dehydration activities. Thus the layer distances of the different hydration stages were not refined. The phase composition and the crystal chemistry of the phases were investigated in binary systems $[Ca_2Al(OH)_6]^+[OH{\cdot}nH_2O]^-$ - $[Ca_2Al(OH)_6]^+[X{\cdot}nH_2O]^-$ X = sulfonic ion. It could be proved that two different salts, the “inorganic” calcium aluminate hydroxide hydrate and the “organic” calcium aluminate sulfonate hydrate were stable. No solid solution series were determined in any of the investigated binary systems. Only in the system $[Ca_2Al(OH)_6]^+[OH{\cdot}nH_2O]^-$ - $[Ca_2Al(OH)_6]^+[C_{10}H_7\text{-}2\text{-}SO_3{\cdot}nH_2O]^-$ at 100 and 35% r.h. naphthalene-2-sulfonic acid anions and hydroxide ions are chemically fixed systematically in separate layers in one phase. The distribution of the different ions resulted in the formation of a superstructure $[Ca_2Al(OH)_6]^+[x\ OH\ (1\text{-}x)C_{10}H_7\text{-}2\text{-}SO_3{\cdot}nH_2O]^-$.

REFERENCES

[1] Allmann, R.: Die Doppelschichtstruktur der plättchenförmigen Calcium - Aluminium - Hydroxisalze am Beispiel des $3CaO{\cdot}Al_2O_3{\cdot}CaSO_4{\cdot}12H_2O$ N. Jb. -Min. Mh.vol.140 (1968) pp. 144.

[2] Terzis, A., Fillipakis S., Kuzel, H.-J. & Burzlaff, H.: The Crystal structure of $Ca_2Al(OH)_6Cl{\cdot}2H_2O$ Z. Krist., vol. 189, (1987), pp. 29 – 34

[3] Renaudin,G., Francois,M. & Evrad,O.: Order and disorder in the lamellar hydrated teracalcium monocarboaluminate ocompound, Cem. Concr. Res., vol. 29, (1999), pp. 63-69

[4] Pöllmann, H.: Carboxylic acids and their reaction products and mechanisms with the aluminate phase of cement - Proc. Int. Conf. Chem. Cem., New Dehli, vol. 6, (1992), pp.198 - 204.

[5] Pöllmann, H. & Stöber, S.: Hydration Characteristics and New Hydrates Using Organic Additives (Carboxylates and Sulfonates). - Proc. of the 10th. Int. Congr. on Chem. Cem. Göteborg, (1997), 3iii032

[6] Pöllmann, H.: Study of the Hydration Mechanisms and Formation of new Hydrates applying organic Additives to the Aluminate Phase of Cement., Proc. 11th. Conf. on Cem. Micr., New Orleans, Louisiana, vol. 324, (1989), pp. 343.

[7] Pöllmann, H.: Organische Derivate des TCAH mit Schichtstrukturen vom Typus $Ca_2[Al(OH)_6]+[RCOO{\cdot}nH_2O]^-$ Z. Krist. vol. 186, (1989), pp. 236 - 237.

[8] Fischer, R. & Kuzel, H.-J.: Reinvestigation of the system $C_4A{\cdot}nH_2O$ - $C_4A{\cdot}CO_2 \cdot nH_2O$. - Cem. Concr. Res., Vol. 12 (6), (1982), pp. 517-526.

SYNTHESIS OF ALINITE-CEMENT OUT OF COPPERSLAG AND MUNICIPAL-SOLID-WASTE-INCINERATION (MSWI) RESIDUES

M. Tewelde[1] and H. Pöllmann[1]

[1]Department of Mineralogy/Geochemistry, Martin-Luther-University, Halle, Germany.
E-mail: Tewelde@geologie.uni-halle.de and Pöllmann@geologie.uni-halle.de

ABSTRACT

Through an addition of $CaCl_2$ to an ordinary Portland cement clinker, an alinite phase originates instead of alite [Number]. And the temperature of clinker formation could be reduced by 400-500°C. A cement, based on these cement phases, has been produced commercially in the previous USSR by burning the raw-mix at 1150°C after adding 6-25% $CaCl_2$ as a sintering aid to an ordinary Portland cement clinker [1]

This paper will demonstrate that through an appropriate mixing of industrial residues (copper slag, municipal solid waste incineration residues (MSWI) and limestone fines) and thermal treatment a synthesis of alinite can take place.

1. INTRODUCTION

The copper mining industries in the Mansfeld area have left a lot of waste dumps. About 50 million tons of applicable copper slag which are remains of the 800 years of copper production are stored in the area of Eisleben/Helbra (Germany) [2]. From an environmental technical point of view, the copper slag of Mansfeld do not cause any harm if utilized properly. So far, the application of this copper slag is limited to use in road stone constructions [3].

On the other hand, there are a lot of other industrial wastes (residues) which are detrimental to the environment if not treated correctly. Therefore, it is the aim of this research to contribute to this idea, that is: to synthesise, among others, a hydraulic substance, alinite in this case, out of mainly industrial residues. During the hydration of alinite a C-S-H-gel appears which can enable the incorporation of detrimental elements [4]. This leads to an improvement of the leachability behaviour and accordingly to the possibility of immobilizing hazardous substances by using hydraulic binders.

Oberste-Padtberg & Neubauer [5] carried out experiments in 1989 to synthesise Alinite-cement out of industrial-residues. Neubauer [4] gave the chemical formula of Alinite as $Ca_{10}Mg_{1-x/2}\square_{x/2}[(SiO_4)_{3+x}(AlO_4)_{1-x/2}/O_2/Cl]$; ($0{,}35 < x < 0{,}45$; $\square$ = lattice vacancy). A typical Alinite cement contains the following main mineralogical phases: alinite (65%), belite (20%), mayenite ($C_{11}A_7.CaCl_2$; 10%) and C_4AF (5%)

2. EXPERIMENTAL METHODS

2.1 Synthesis

An appropriate mixing of a copper slag from the Mansfeld area (Germany) (Table 1), municipal solid waste incineration (MSWI) (Table 2) residues and correction of the raw mix by adding

limestone fines and a subsequent thermal treatment of the mixture leads to the synthesis of alinite cement (hydraulic binder) (Table 3).

Table 1. Chemical composition of copper slag from Mansfeld (Germany)

Oxides [weight %]		Oxides [weight %]		Oxides [mg/Kg]		Oxides [mg/Kg]	
SiO_2	49,10	BaO	0,41	Fe_2O_3	50900	PbO	257
CaO	17,40	P_2O_5	0,28	MnO	4260	ZrO_2	213
Al_2O_3	13,50	SO_3	0,26	ZnO	3200	CoO	136
MgO	6,69	SrO	0,06	CuO	2210	UO_2	96
K_2O	3,69	Rb_2O	0,02	V_2O_5	1410	MoO_3	108
Na_2O	1,40	Y_2O_3	0,01	Cr_2O_3	1110	NiO	91
TiO_2	0,79			SnO_2	329	Ga_2O_3	51
Total = 100,01 %							

Table 2. Chemical composition of MSWI

Oxides [weight %]		Oxides [weight %]		Accessory elements [mg/Kg]	
SiO_2	9,1	TiO_2	0,7	Cu	557
CaO	37,2	MnO	0,1	Ni	<10
MgO	1,0	P_2O_5	0,4	Cr	122
Fe_2O_3	1,0	SO_3	5,8	Zn	9420
Al_2O_3	3,6	LOI (1000°C)	32,8	Cd	109
Na_2O	1,7	LOI (700°C)	19,5	Pb	2016
K_2O	2,4			As	2
				Total	98%

In order to make the synthesis of alinite a reality, an alinite cement was synthesised first from pure chemical components which were gradually replaced, during the course of the investigation, by the above-mentioned industrial wastes (residues) and treated thermally by various temperatures and durations, as well, so as to optimise the synthesis parameters. All compositions were fired in Corrundum crucibles.

Table 3. Composition of typical Alinite cement [1]

	Alinite
CaO	45-55%
SiO2	13-19%
Al2O3	9-12%
Fe2O3	4-10%
MgO	1-10
CaCl2	6-18

3. CHARACTERISATION

3.1 X-ray Diffraction Analysis

The phase compositions of the synthesised sample were determined using a Philips powder diffractometer D5000. Operating conditions were 40kV accelerating voltage and 30 mA beam

current on a copper anode. Diffractograms were taken in increments of 0,04° with a counting time of 2s.

3.2 Heat Flow Calorimeter Analysis

The calorimetric measurements were done using a heat flow calorimeter which was constructed and later developed in the institute of Erlangen (Germany) [6]. Three samples can be measured simultaneously with this equipment against an empty reference-cell and the resulting data can be collected online on a PC. During the measuring process, the samples and the reference-cell are protected from exposure to air.

4. RESULTS

4.1 X-ray Diffaction Results

Figure 1 shows the x-ray diffraction pattern of the sample B19 on which alinite (main phase), chlorellestadite and chloromayenite (both are primary mineral-reservoirs) are illustrated. The minerals, chlorellestadite and chloromayenite, are capable of fixing detrimental elements like heavy metals in their lattice. This behaviour is very useful, taking the composition of the constituents we have into consideration. As already mentioned above, during the hydration of alinite (Figure 2) there originates $Ca(OH)_2$ (portlandite), $C_3A.CaCl_2.10H_2O$ (Friedel's salt -monochloride-) and C-S-H gel (which enables also to incorprate heavy metals [4]). This is another important side of alinite, which is the behaviour of fixing detrimental substances in its structure during the hardening process by immobilising them.

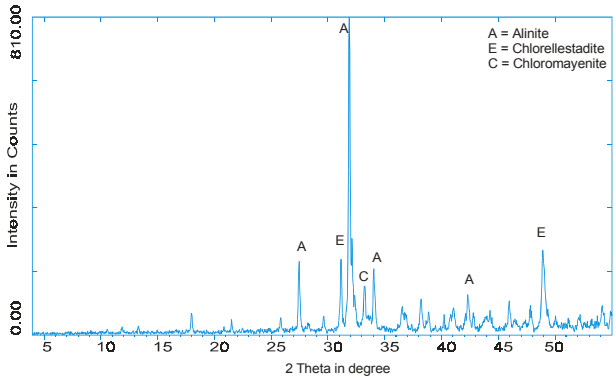

Figure 1. X-ray powder diffraction pattern of B19.

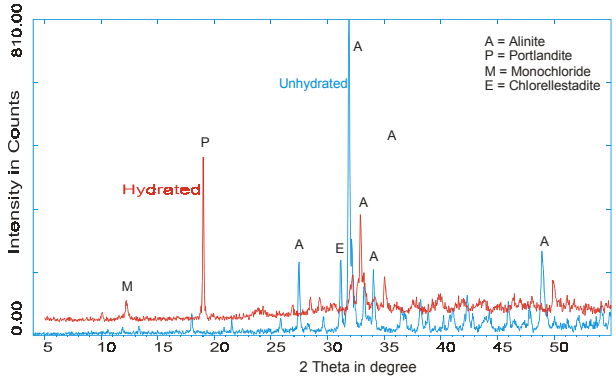

Figure 2. X-ray powder diffraction pattern of hydrated and unhydrated sample (B19).

4.2 Heat flow calorimeter results

The hydraulic properties of the sample -B19- were measured using the above-mentioned heat flow calorimeter at a water/solid ratio (w/s) of 1 and by a hydration time of 24 hours.
Figure 3 shows the heat evolution curve for sample B19 which was fired at different temperatures for one hour. It can be seen from the diagram that the tendency to hydraulicity in all samples exists. The hydration process occurs during the first two hours which is very fast in comparison to that of an ordinary Portland cement and it ceases after approximately four hours.

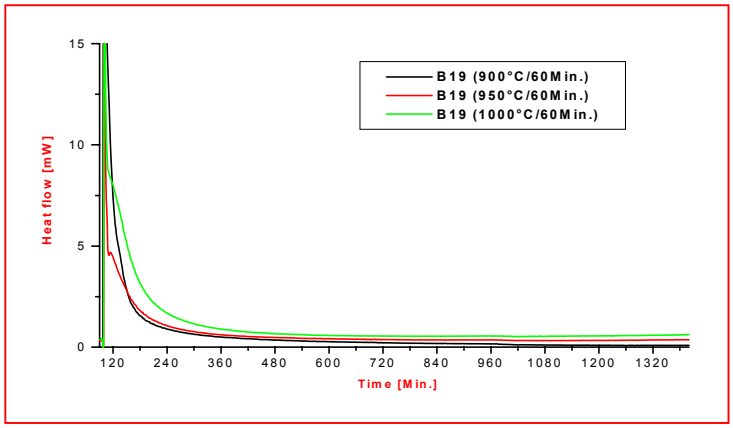

Figure 3. Hydration heat evolution of sample B19

An image, produced using a cryo-transfer scanning electron microscope (cryo-SEM), of the hydrated sample of B19 after a hydration time of 10 minutes is shown in Figure 4.

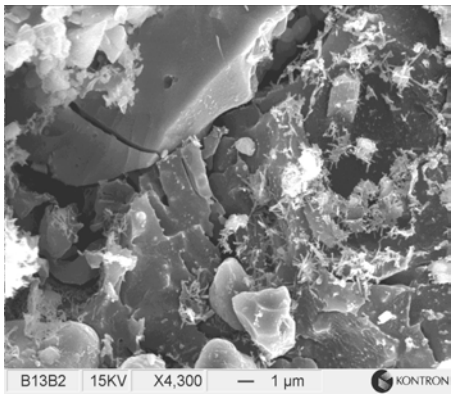

Figure 4. Cryo-SEM image of a hydrated sample of B19
(w/z = 0,5; after a hydration time of 10 Min.)

Regarding the strength development of the sample, it behaves like those cements which contain alimite (after a hydration time of 1d ~ 17 N/mm^2 ; 7 days ~ 24 N/mm^2) [7] and it is believed that 1-3% boric acid (H^3BO^3) or tartaric acid ($C^4H^6O^6$) can influence the setting time of alinite.

4.3 Results of the leaching behaviour test

The leaching behaviour of the sample was examined according to the German standard DEV-S4 test in which a finely ground sample is mixed with water in a ratio of 1:10 (sample : water) and shaken for 24 hours. After filtrating the solution, it is then examined using ICP-OES for possible heavy metalcontent.

Table 4. Element contents of B19 in ppb

	Pb	Ni	Cd
B19	3200	20	340
B19A (900°C/60 Min.)	2500	10	290
L of B19A	*	*	*
TA-Kl. 2	<1000	<1000	<1000

TA-Kl.2 = German regulation for technical instructions on waste handling
* = below detection limit; B19 = not thermally treated; B19A = thermally treated by 900°C/60 Min.; L of B19A = Leachate of B19A

Table 4 shows that the leaching of heavy metals in the leachate (L of B19A) is almost non-existent. This is an indication of the incorporation of these metals in the minerals like alinite, chlorellestdite and chloromayenite.

5. CONCLUSIONS

From the above results, it can be seen that through an approprate mixing of Industrial residues such as copper-slag, municipal solid waste incineration (MSWI) and correcting the mixture by adding limestone fines and sintering it at an adequate temperature as well duration, the synthesis of a hydraulic substance like alinite is possible. This is demonstrated by the results of the heat flow calorimeter- and powder diffraction-analysis.

The results of the heat flow calorimeter show that the hydration of alinite is very fast and it takes place during the first hour and is finished after approximately four hours. The powder diffraction analysis of the hydrated sample delivers a result which shows the formation of hydrated phases such as $Ca(OH)_2$ and $C_3A.CaCl_2.10H_2O$; chlorellestadite ($Ca_{10}(SiO_4)_3(SO_4)_3Cl_2$) remains unchanged. And the leaching behaviour of the sample shows that the content of heavy metals in the leachates is almost zero which gives an indication to their incorporation in the mineral phases formed.

REFERENCES

[1] C. Hewlett, P. LEA's Chemistry of Cement and Concrete, 4th Edition, New York. Toronto: Arnold publishers, 1998, pp.423; 436, 790 & 822-823

[2] Schreck, P. Schadstoffausträge aus den Halden der Kupferschieferverhüttung, UFZ – Bericht, Nr. 23, 1997, pp.9-14

[3] Pentinghaus, H.J., Istrate, G. und Schreck, P. Mansfelder Kupferschlackenpflaster-Phasenbestand, Gefüge und Verwitterung, UFZ- Bericht, Nr. 23, 1997, pp.37-45.

[4] Neubauer, J. Realisierung des Deponiekonzeptes der „inneren Barriere" für Rauchgasreinigungsrückstände aus Müllverbrennungsanlage.- Dissertation, 1992, Erlangen (Germany), pp.74-89.

[5] Oberste-Padtberg, R. & Neubauer, J. Laborversuche zur Herstellung von Alinitzement aus Müllverbrennungsrückständen, WLB, Wasser, Luft und Boden, Heft 10, 1989, pp.63-65.

[6] Pöllmann, H., Kuzel, H.-J. und Meyer, H. W. Heat-flow calorimetry in cement chemistry construction and application of a low cost high-sensitive calorimeter – proc. of the 13th int. conf. on cement microscopy, Tampa, USA, 1991, pp.254-272.

SYNTHESIS OF ALINITE-CEMENT OUT OF COPPERSLAG AND MUNICIPAL-SOLID-WASTE-INCENERATION (MSWI) RESIDUES

M. Tewelde[1] and H. Pöllmann[1]

[1]Department of Mineralogy/Geochemistry, Martin-Luther-University, Halle, Germany.
E-mail: Tewelde@geologie.uni-halle.de and Pöllmann@geologie.uni-halle.de

Mulugheta Tewelde

Date of place and birth:	October 22, 1959; Asmara, Eritrea
Nationality:	Eritrean
Address:	Lerchenfeld Str. 6; 06110-Halle (Saale), Germany
E-mail:	tewelde@geologie.uni-halle.de
Marital Status:	Married July 24, 1994, to Medhin Andemeskel, two children
1987 – 1993:	Westfälische Wilhelms-University, in Münster (Germany), Master of Science, Mineralogy
1994 – 1995:	Polisius-Research and Development Center for Cement-Plants
1995 – 1997:	I have been working in different areas
1998 – to date:	PhD student in Institut for Geochemistry in Halle, Germany

INVESTIGATIONS ON THE HYDRATION OF CAC AT 25…45°C BY ISOPERIBOLIC HEAT FLOW CALORIMETRY AND XRAY DIFFRACTION (XRD)

Stöber, S. and Pöllmann, H.

Institut für Geologische Wissenschaften der Martin – Luther Universität Halle – Wittenberg
Mineralogie/Geochemie, Domstraße 5, 06108 Halle (Saale).
E-mail: stoeber@geologie.uni-halle.de and poellmann@geologie.uni-halle.de

ABSTRACT

The hydration of a CAC (Secar 51) with and without 0.01 m $LiCO_3$ was monitored with a modified Heat-Flow calorimeter at 25, 30, 35, 40 and 45°C. Beside acceleration and retardation of the cement hydration kinetics the heat liberation of the cement pastes as a function of the temperature was detected. Furthermore the phase formation of different pastes was investigated online at higher temperatures and the efficiency of the X'Celerator detector for detecting very fast hydration reactions was proven.

1. INTRODUCTION

In 1983 a new Heat Flow calorimeter based on semiconductor elements was developed by KUZEL [3]. The instrument improved the determination of the heat of reactions of cements, mortars, lime and other cement based materials. In the following years the calorimeter was equipped with a computer controlled data collection and an online data calculation [4].

Cements and especially formulated systems based on the reciprocity of their compounds are highly specialized products and should always guarantee the same performance. However, different climates, with cold or hot temperatures influence the properties of such building products. Hydration reactions will be retarded or accelerated. In order to control the quality and properties of building products the heat flow calorimeter the, was remodelled and combined with a thermostat to perform measurements at different temperature levels in the range of 5…80°C.

This paper demonstrates the capability of the improved calorimeter in combination with an X´Pert Theta-Theta Diffractometer plus the new X'Celerator on the determination of hydration reactions and the phase formation at different temperatures with and without admixtures.

2. EXPERIMENTAL

2.1 Construction principles and sample preparation for Heat-Flow calorimetry

The heat flow calorimeter [2], [3] [5] consists of an aluminium block, sited in an isolated box with a cover. The aluminium block contains 4 openings for the measuring cells, a construction of a copper plate with BiTe- semiconductors sited below. Three cells can be used for the measurement of the sample heat-flow and one cell is occupied by the reference. In this case 1g of a hydrated CAC cement, Secar 51, (w/s = 0.5) for 20 days at 40°C was used as a reference. Just after the combination of the water with the cement, the heat of reaction (exothermic reactions) is measured in difference with the reference to exclude background heat effects. Heat values were detected as mV per time by a multimeter of PREMA 5017 multimeter, which was able to scan three channels in a

certain preinstalled time interval. The raw data stored on the hard drive of a personal computer(PC) was afterwards plotted and analysed. The online measurement program used to direct PC, multimeter, and calorimeter was OMI (Online Measurement and Interpretation) written by ECKER [6].

For the detection of the course of hydration at different temperatures, the construction of the calorimeter was improved. An RM6-thermostat from LAUDA was used to condition the water temperature, and this was pumped through a channel system in the aluminium block and the aluminium top.

The samples for the measurement were produced the following way. 1g cement powder was weighed into the copper pot. Top and cover pot were closely sealed using a commercial Vaseline. The samples were put onto the copper plates of the cells. In order to improve the heat transport between copper vessel and the copper plate of the cell special water free oil was introduced between the two parts. Finally the aluminium cover was put on the aluminium block and the water was filled into syringes on the surface of the aluminium cover to equilibrate cement powder and water on the same temperature for 12h. In order to determine the heat flow quantitatively for a certain time range the raw data must be multiplied by the calibration factor. Because, the calibration constant is depended on the temperature, K must be determined for every temperature separately [2].

For the measurement of the heat flow of the cement paste, the parameters in Table 1 were used.

Table 1. Parameters for the determination of the heat flow by calorimetry

Parameters	**Values**
Temperatures [°C]	25, 30, 35, 40, 45
Time interval [min]	1
Activity of the channels [s]	20
Data collection [s]	20

2.2 Parameters and sample preparation for X-ray analyses

In order to determine the phase formation of the Secar 51 pastes, freshly prepared samples were mixed with water or admixture and immediately shrink-wrapped in a PE film. The pastes could not dehydrate during the hydration process. In order to make XRD measurements the samples were fixed and heated in a HTK-16 camera from PAAR. The X´Pert Theta-Theta Diffractometer with copper radiation CuK□ from Philips was equipped with a new X'Celerator detector. It made it possible to make measurements in the range of 3…40 degrees 2 Theta with a step of 0.017 degrees 2 Theta and a count time of 10s in 6 minutes. For the investigations of the course of hydration of pastes Secar 51 + 0.1 mole/l Li_2CO_3 measurements between 3…40 degrees 2 Theta, with a step of 0.033 degrees 2 Theta and a count time of 5s were used. The measurement took approximately 49s. Therefore fast non-ambient measurements made it possible to determine fast hydration reactions, especially at 40°C.

3. RESULTS

3.1 Determination of the calibration values K at different temperatures

For each temperature the calibration constant was determined three times in order to reproduce the results. The most important point was to bring the calorimeter to equilibrium. Under a calibration time of 12 h at constant temperatures, the reproducibility of the calibration values was not sufficiently good. In Figure 1 K was plotted against the temperature. It is quite clear that K will decrease linearly with high temperatures and increase with low temperatures. Now, a precise determination of K for different temperatures makes it possible to calculate further K values by the regression equation.

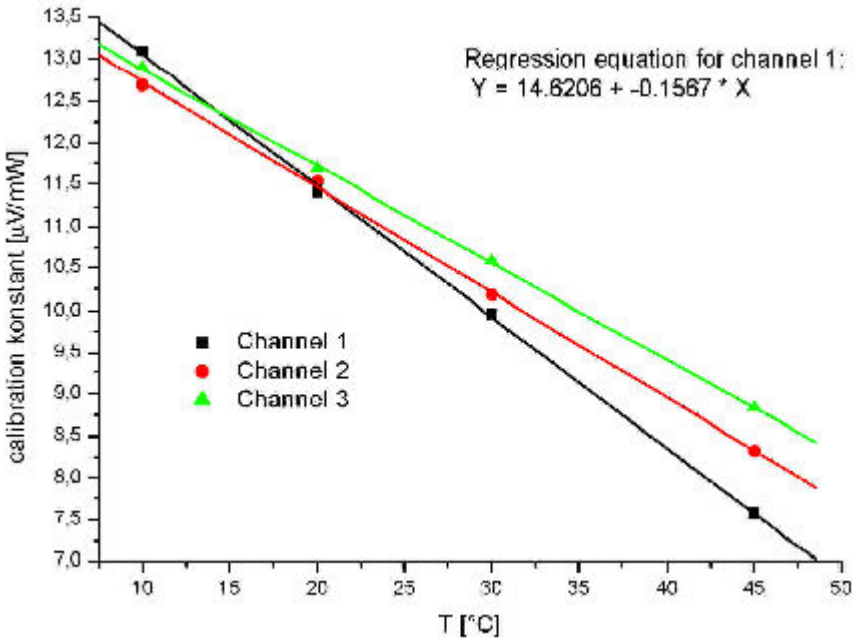

Figure 1. K values plotted against the temperature

3.2 Determination of the heat flow of Sec. 51+H_2O at 25…45 °C by isoperibolic calorimetry

The induction period decreased with increased temperatures during the hydration process (Figure 1). In the calorimeter curve Sec. 51 + H_2O T =25 °C the induction period took approximately 18 h and was finally decreased step by step to less than 20 minutes. The maximum values of the main hydrations were shifted to lower times with increased temperatures. Figure 3 described an approximately linear correlation. Especially at low ambient temperatures 25…30 °C small differences of the hydration maxima positions were detected although the pastes hydrated under comparable conditions. Thirdly, the course of the heat-flow as a function of the temperature changed completely. At 25°C heat was immediately set free at approximately 20h as one peak. Higher ambient temperatures caused the formation of different separately detectable heat processes before the start of the main hydration and as a long fade out of the heat evolution at the end of the main hydration. This effect was firstly visible in the calorimeter curve heated at 30°C of a Secar 51+H_2O. The heat evolution during the main hydration occurred in a smaller time interval, which resulted in a sharper heat evolution. This tendency was reinforced with the increased temperatures.

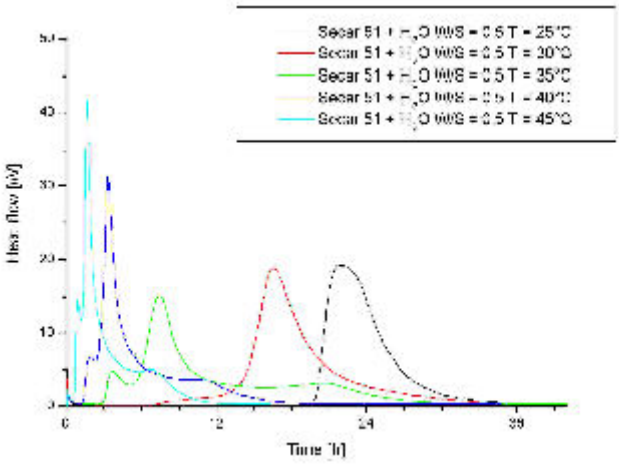

Figure 2. Calorimeter curves: Sec.51+ H_2O w/s = 0.5 T =25, 30, 35, 40, 45°C

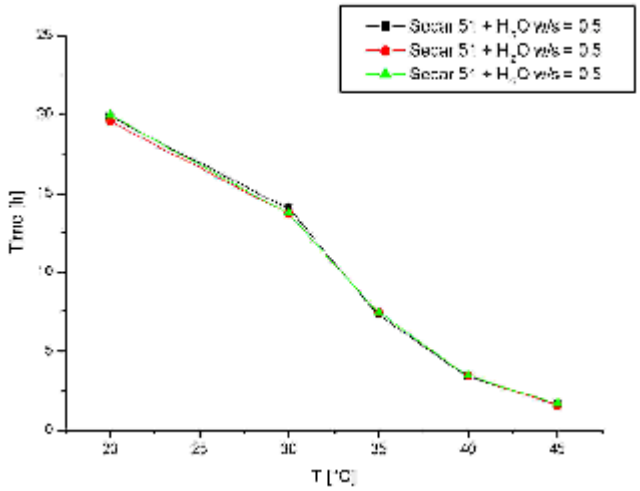

Figure 3. Hydration maxima variation of calorimeter curves: Sec.51+ H_2O w/s = 0.5 as a function of the temperature

The phase formation of cement pastes heated at 25 °C showed the typical course of phase formation (Figure 4). CA reacted with water to CAH_{10} after 18h and to C_2AH_8 + AH_3 after 16h of hydration [7]. Higher ambient temperatures at 30 and 35°C hindered the formation of CAH_{10}. C_2AH_8 crystallized as the predominant reaction product together with AH_3 of CA. At 30 °C, two different hydration stages of the calcium aluminate hydrate, the C_2AH_8 and $C_2AH_{7,5}$ were stable. $C_2AH_{7,5}$ was transformed after approximately 14 h to C_2AH_8 indicated by the shift of the (006) peak to lower 2 Theta values in the XRD pattern (Figure 5). At 40 °C, CA reacted very fast with water to C_2AH_8. After approximately 2.5h first (006) and (0012) reflections were detected with a net area of 2 and 3 cps·deg respectively. Just 4 h later, the net area of the (006) counted 70.3 cps·deg. After 9…10 h, the (211) peak at 17.29 2 Theta indicated the formation of C_3AH_6.

On one side C_3AH_6 resulted in the conversion reaction $3C_2AH_8$ => 2 C_3AH_6 + $2AH_3$ + 9H and one the other side hydrogrossularite crystallized primarily according to the reaction: 3CA + 12H => 2 C_3AH_6 + 2 AH_3 [7]. Monocarbonate $C_3A{\cdot}CaCO_3{\cdot}11H_2O$ crystallised after approximately 6.6h. Monocarbonate crystallized due to the substitution of $Al(OH)_4^-$ ions in the interlayer of C_2AH_8.by CO_3^{2-} ions of the paste. As part of the conversion reaction, AH_3 crystallized (Figure 6). Due to the conversion of C_2AH_8 to monocarbonate and C_3AH_6 the intensity of both, the (006) peak and (0012) peak of C_2AH_8 decreased.

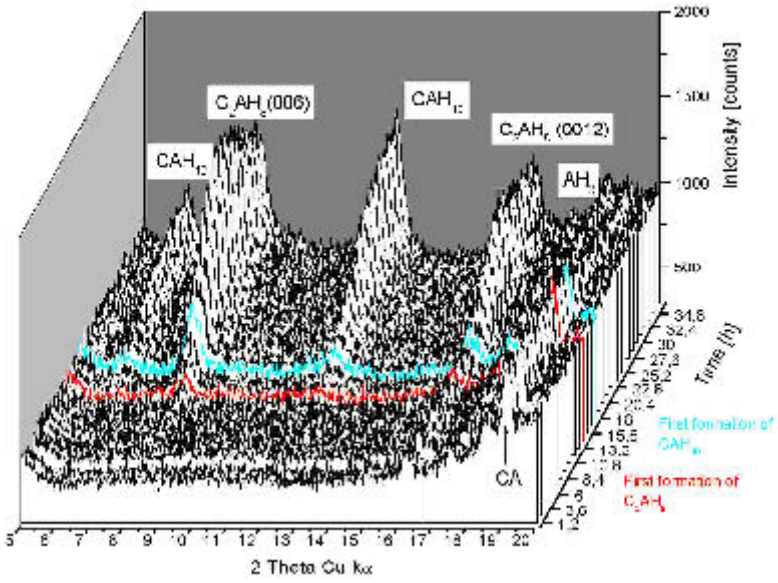

Figure 4. Phase formation Sec 51+ H_2O w/s =0.5 T = **25°C**

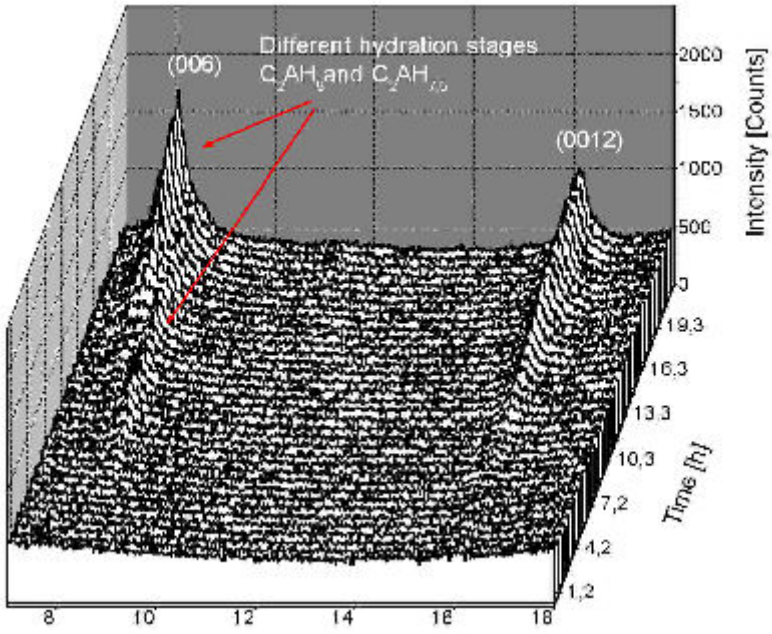

Figure 5. Change of the hydration stage C_2AH_8 – $C_2AH_{7.5}$ at **30** °C during the hydration

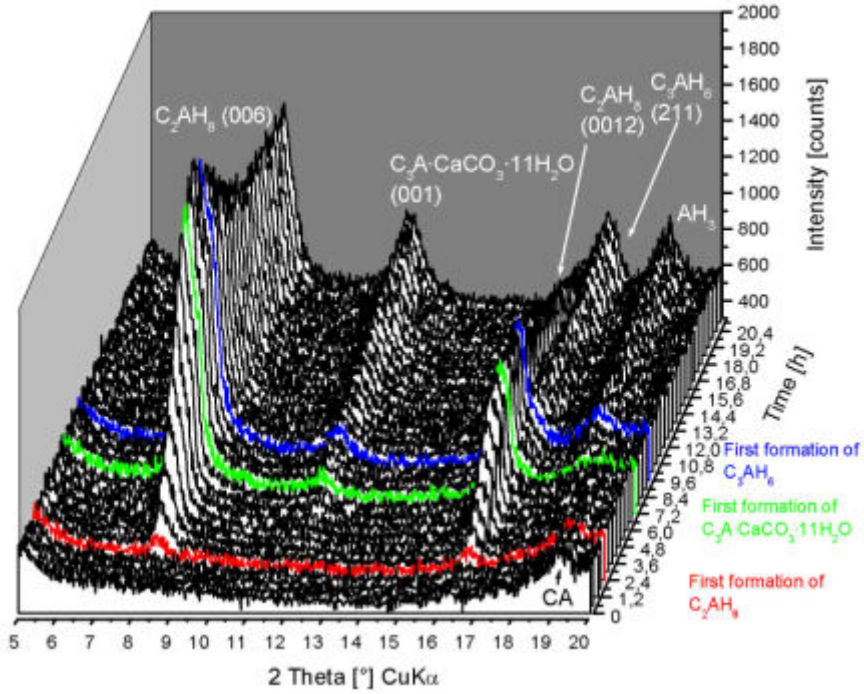

Figure 6. Phase formation Sec 51+ H_2O w/c =0.5 T = **40°C**

3.3 Determination of the heat flow of a Secar 51 + 0.01 mole/l Li_2CO_3 at 40 °C by isoperibolic calorimetry

The application of different Lithium salts like LiCl or Li_2CO_3 [1] used as a set accelerator were widely investigated.

Figure 7 shows the heat evolution of Secar 51 pastes mixed with 0.1…0.001 mole/l at a w/s ratio of 0.5 and T = 40°C. The addition of Li_2CO_3 concentrations > 0.01 m accelerated the CAC (calcium aluminate cement) hydration vigorously. Neither an induction period, nor the main hydration is fully visible in the plot of the calorimeter curves.

The detection of the phase assemblage per time for such fast hydration reactions by XRD, was always a problem because of high count times per step 2 Theta and long measuring times in order to obtain a suitable pattern. The application of an X'Celerator improved the determination of the hydration phase formation.

The addition of 0.01 mole/l Li_2CO_3 accelerated the formation of C_2AH_8 drastically. Just after 1 minute of mixing Secar 51 with 0.1 m Li_2CO_3 solution, a small peak at 8,11 degree 2-Theta indicated the formation of C_2AH_8 in the cement paste (Figure 8). After 1 minute the determined net area of the (006) peak of C_2AH_8 had a value of 5.9 cps·deg and after 59 minutes of hydration the net area value of the (006) peak was 95.2 cps·deg. At higher hydration times until 1.5 h the hydration seemed to be retarded, because, the intensity of the monocarbonate and C_2AH_8 peaks did not grow. In contrast, the earliest detected formation of C_2AH_8 occurred in Li_2CO_3-free pastes (Secar 51 + H_2O paste, heated at 40°C) after 2.4h! Furthermore, the formation of C_3AH_6 was not detected in between 0…1.5h of hydration. Monocarbonate was formed at approximately 40 minutes, as a result of the carbonation process of C_2AH_8. $Al(OH)_4^-$ ions were substituted by carbonate ions in the inter layer of the C_2AH_8 structure and $Al(OH)_3$ was formed with a low degree of cristallinity.

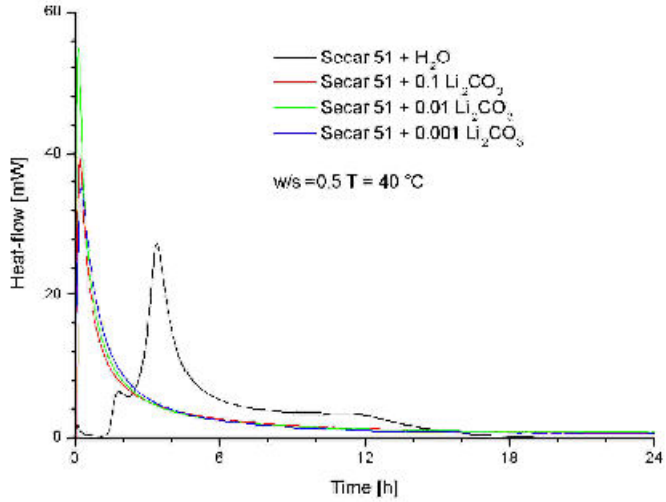

Figure 7. Heat flow calorimetry: Sec 51 + 0.01 m Li_2CO_3 w/c = 0.5

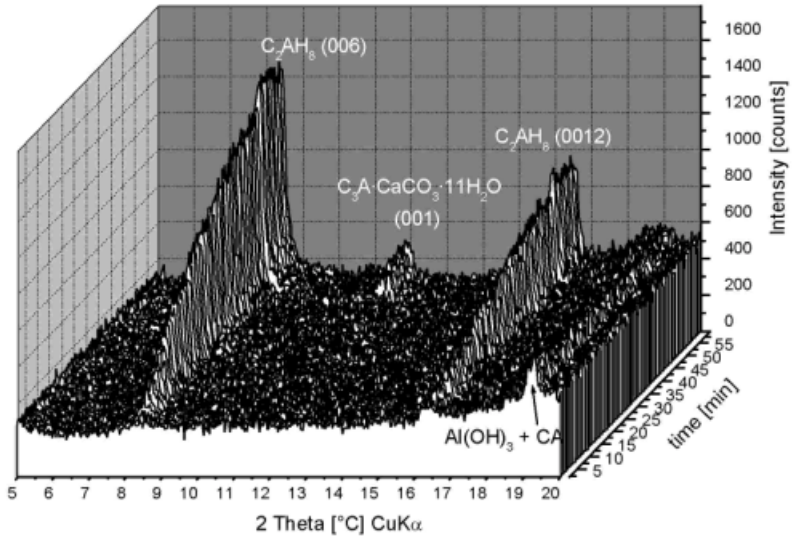

Figure 8. Early phase formation (1h): Sec 51 + 0.01 m Li_2CO_3 w/s = 0.5 T = **40 °C**

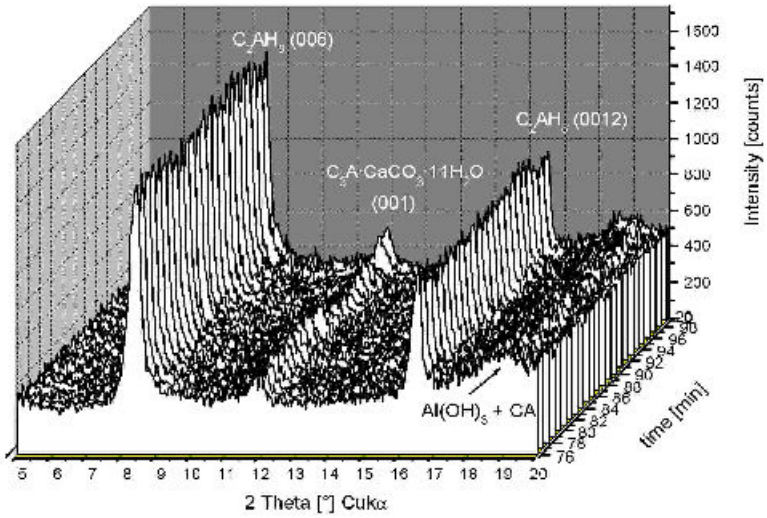

Figure 9. Intermediate phase formation (1-11h): Sec 51 + 0.01 m Li_2CO_3 w/s = 0.5 T = **40 °C**

4. CONCLUSIONS

Calorimetric studies demonstrated that increased temperatures shortened the distinct induction period from approximately 16.7h (Sec.51.H_2O 25°C) to 0.2h (Sec.51.H_2O 45°C). Increased temperatures shifted the maxima of the main hydration to lower hydration times and the heat flow during the main hydration was set free in a shorter time interval.

At 25 °C, the exothermic hydration of Secar 51 reacted with water was detected as one sharp peak between.19…33h. Higher temperatures manipulated the heat evolution systematically. In the calorigrams of Sec51 + H_2O at 30, 35, 40 and 45 °C the main reactions were split into 2 reactions, a smoother exothermic reaction, just after the end of the induction period and a following stronger hydration reaction. The heat liberation at the end of the main hydration of Sec51. + H_2O at 30, 35, 40 and 45 °C did not approach values near zero, but faded out as a function of the temperature.

Briefly said, all facts pointed out that the increase of temperature from 25°C to 40°C accelerated the overall cement hydration of the Secar 51 pastes, but distributed the heat liberation over a larger time range. The phase assemblage of the heated pastes, investigated by time resolved XRD, changed. CAH_{10}+C_2AH_8+AH_3 crystallized at 25°C as reaction product of CA. At 30°C C_2AH_8+AH_3 crystallized as the main hydration product. At 40 and 45 °C, $Al(OH)_4^-$ ions of the C_2AH_8 inter layer were substituted by carbonate ions due to increased temperature. Monocarbonate and additional AH_3 crystallized. Furthermore, C_3AH_6 crystallized after 10 h and C_2AH_8 was converted to C_3AH_6, the stable phase in the system CaO-Al_2O_3-H_2O.

Variable high temperature, did not only change the phase assemblages, but accelerated the crystallisation of the hydration phases. At 25 °C the (006) reflection of C_2AH_8 was first detected at approximately 12h. In the XRD pattern of a Secar 51+ H_2O paste, heated to 40°C, the (006) reflection was present after approximately 2.4h.

In order to analyze the hydration of Sec 51 + H_2O to 40 °C with 0.01 m $LiCO_3$ solution the application of heat flow calorimetry was not sufficient, because the reaction was too fast to resolve the 3 main phases of hydration, the heat of wetting, the induction period and the period of main hydration. However XRD measurements with the new X'Celerator made it possible to follow the incredibly fast hydration of CA to C_2AH_8 and AH_3 and at later times to monocarbonate.

REFERENCES

[1] Sharp, J.H., Bushnell-Watson, S.M. & Payne,D.R.: The effect of Admixtures on the hydration of Refractory Calcium Aluminate cements Proc. Int.Symp of CAC London (1990) pp.127-141

[2] Kuzel, H.-J.: Ein einfaches Wärmeleitungskalorimeter mit hoher Empfindlichkeit. - Fortschr. Miner., Beihefte, vol. 60 (1),(1982), pp. 128 - 129.

[3] Kuzel, H.-J.: Ein leistungsfähiges Wärmeleitungskalorimeter, TIZ – Fachberichte, Vol. 108 No.1,(1984), pp. 46 - 51.

[4] Pöllmann,H., Kuzel, H.-J. und Meyer, H.W.: Heat-Flow Calorimetry in Cement Chemistry - Construction and Application of a low cost, high sensitive Calorimeter. - Proc. 13th Int. Conf. Cem. Micr., (1993) pp. 254-272, Tampa

[5] Kuzel, H.-J, Baier,H.: Hydration of calcium aluminate cements in the presence of calcium carbonate Eur. Jour. Min. vol. 8 (1996) pp.129-143

[6] Ecker, M.: (OMI) Online Measurement and Imaging program. A efficient software for the supervision of Heat-Flow calorimeters (mich.ecker@t-online.de)

[7] Scrivener,K.L.: Historical and Present Day Applications of Calcium Aluminate Cements. Proc. Int. Conf. on CAC Heriot-Watt University Edinburgh Scotland pp.3-23

MANGANESE IN HIGH ALUMINA CEMENT

H. Pöllmann and R. Oberste-Padtberg

ABSTRACT

Manganese can be used in two different ways for HAC-applications : Manganese ore can be added to the raw meal, but manganese sulphate can also be added to HAC`s to form stable hydrated mineral assemblages.

Manganese is not normally used in HAC production because the similar phase to monocalcium aluminate (CA), Ca_2MnO_4 (marokite) crystallizes in a distorted spinel structure type and shows no hydraulic behaviour.

New investigations have shown that the addition of manganese ore to the raw meal composed of bauxite and lime leads to the formation of highly reactive HAC`s. Lowered production temperatures and lower costs of raw material are also obtained.

Depending on the composition of the raw materials, clinkering temperature and handling, new phases are formed, but also solid solutions with brownmillerite, monocalciumaluminate and larnite can occur.

The hydration of manganese containing HAC`s leads to the formation of hydrates incorporating manganese in their crystal lattices. In technical applications, when calcium sulphate is added the formation of manganese containing ettringites may occur. The use of manganese sulphate instead of calcium sulphate leads to the formation of shigaite.

Keywords: High Alumina cement, manganese, manganese sulfate, shigaite

1. INTRODUCTION

In the past manganese seemed to have no impact on HAC production because the phase chemically analogous to monocalciumaluminate (CA), $CaMn_2O_4$ (marokite) crystallizes in a distorted spinel structure type and is therefore not hydraulic. In the meantime new investigations proved that the addition of manganese oxides to the raw meal of a typical HAC leads to the formation of highly reactive HAC´s. Obviously lowered production temperatures and lower costs of raw materials are added advantages. Depending on the raw materials and the temperature applied the new formed phases are solid solutions of manganese with the primary minerals of a HAC, like CA and C_4AF, but also calcium manganates and different Ca-Al-Si-Fe-Mn-oxides with varying stochiometry are formed.

The hydration of these primary minerals leads to different new hydrates partially also incorporating manganese in their crystal lattices.

In technical applications of HAC´s calcium sulfate is often added. In the course of hydration of these systems ettringite is formed. The use of $MnSO_4$, instead of gypsum leads to the formation of shigaite, a lamellar metal-metal hydroxysalt with good water binding capacities.

It is possible to create optimal HAC and manganese sulfate mixtures for use in the building industry.

2. RESULTS

The formation of manganese containing HAC is based on mixtures of raw materials like limestone, bauxite and manganese ore as sources for calcium, aluminium and manganese. But other raw materials and wastes can also be used. In manganese-free High Alumina cements the overall composition lies close to a ratio of CaO/Al_2O_3 = 1.0 with varying contents of Fe_2O_3. The iron-content is normally provided by the Fe-content of the bauxites used. In Figure 1 the raw materials for the production of manganese-containing cements are shown.

Figure 1. Bauxite (left), limestone (bottom) and manganese ore (middle) – the raw materials for production of manganese containing cements

The chemical composition for the production of manganese-containing cements can be illustrated within a tetrahedron CaO – Al_2O_3 – Mn_2O_3 and Fe_2O_3 (Figure 2). The content of manganese should be below 50 %, otherwise the non-hydraulic phases dominate and only poorly reacting mixtures are crystallizing.

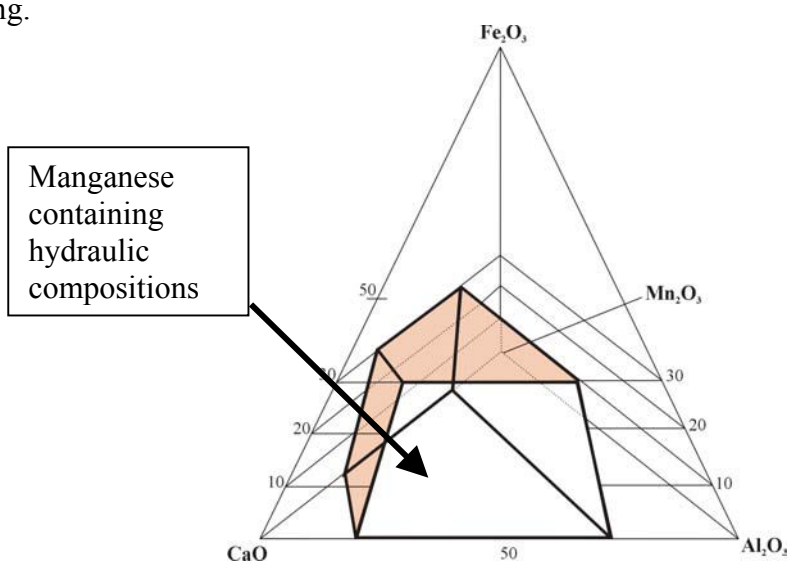

Figure 2. Tetrahedron CaO – Al_2O_3 – Mn_2O_3 – Fe_2O_3 with the region of hydraulic manganese-containing mixtures including classic HAC

2.1 Synthesis of manganese containing cement

By using the raw materials in different compositions and after sintering at different temperatures from 1050°C to 1350°C, various HAC-clinkers were obtained composed of various cementitious minerals with various tendencies for hydraulicity. The mixtures were also investigated due to varying sintering times from 0.5 hours to 10 hours.

Different calcium aluminates and calcium aluminium ferrites crystallizing in HAC-systems are shown in Table 1. Due to increasing contents of manganese other phases and solid solutions are additionally formed.

Table 1. Phases of High Alumina cement

Name	Simplified Formula	Formula	Limits
Monocalcium -aluminate	Ca	$CaAl_2$-x$FexO_4$	$0 \le x \le 0,2$
Mayenite	$C_{12}A_7$	$Ca_{11}Al_{14}O_{33} \cdot CaX_2$	$X = F^-, Cl^-, OH^-$, etc.
Grossite	CA_2	$CaAl_{4-x}Fe_xO_7$	$0 \le x \le 0,4$
Gehlenite	C_2AS	$Ca_2Al_{2-x}Fe_xSiO_7$	$0 \le x \le 0,4$
Brownmillerite	C_4AF	$Ca_2Al_{2x}Fe_{2-x}O_5$	$0 \le x \le 0,8$
Pleochroite	$C_{20}f_3A_{13}S_3$	$Ca_{20}Al_{32-2x}(Mg,Fe)_xSi_xO_{68}$	$2,5 < x < 3,5$
Magnetite	fF	$(Fe,Mg)(Fe,Al)_2O_3$	
Wüstite, Iron	f	FeO, Fe	
Larnite		C_2S	
Perovskite	CT	$CaTiO_3$	
Ye'elimite	C_4A_3S	$Ca_4Al_6O_{12}SO_4$	
Corundum	A	α-Al_2O_3	
Lime	C	CaO	

In the presence of manganese other hydraulic phases are formed like:

$CA_{(ss)}$, C_4(A, Mn, F), Ca (Mn, Fe) O_{3-x}, C_x (A, Mn) S_y, ($C_{12}A_7$), C(A, Mn)$_2$, minor phases containing (Si, Ti).

Depending on the mineralogical compositions, different hydraulic behaviour is obtained. It is highly important to avoid compositions with high amounts of calcium manganates with perovskite or spinel structure types, because these phases are only poorly hydraulic. The hydraulic behaviour of manganese-containing cements with different contents of manganese is shown by heat flow

calorimetric measurements, but also the strength development of mortars using manganese-containing cements was investigated.

Different ratios of $CaO/Al_2O_3/Mn_2O_3$ were homogenized and treated thermally at 3 different temperatures. The ratios were varied according Figure 2, whereas the times of treatment varied between 0.5 hours up to 10 hours with intermediate grinding. Pt- and Al_2O_3-crucibles were used for the heat treatment. All mixtures were sintered at 1350°C, 1250°C and 1100°C.

The clinkers were ground and investigated by heat flow calorimetry. As can be seen from Figure 3 depending on oxide ratios, different grades of hydraulicity occur, depending on the phase assemblage formed. In presence of Iron oxide in manganese-containing cements the sintering temperatures are lowered drastically to less than 1100°C. Due to these reduced temperatures optimised clinkers can also be produced. Less energy is necessary to sinter these clinkers (Figure 4). Different quaternary eutectica were found.

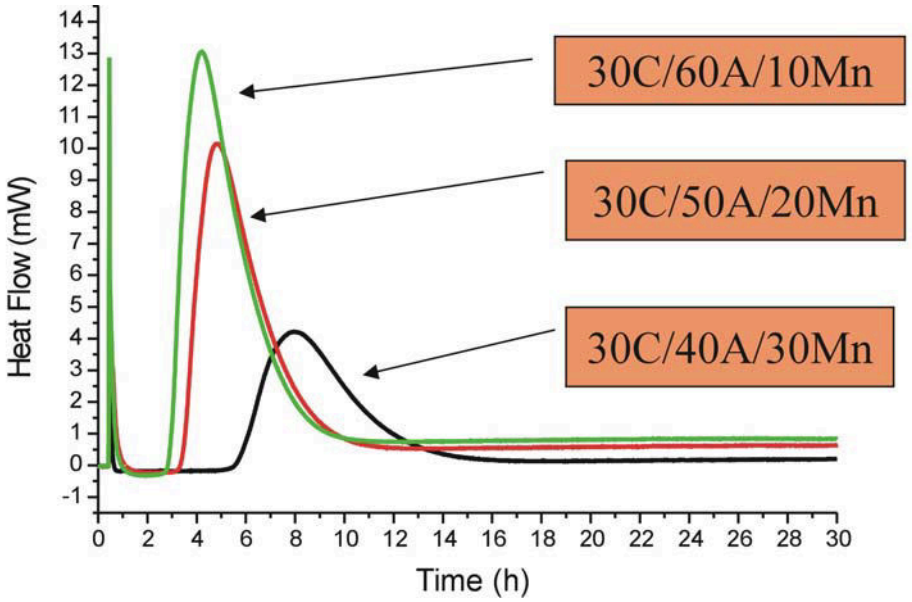

Figure 3. Heat flow calorimetry of different ratios $CaO / Al_2O_3 / Mn_2O_3$

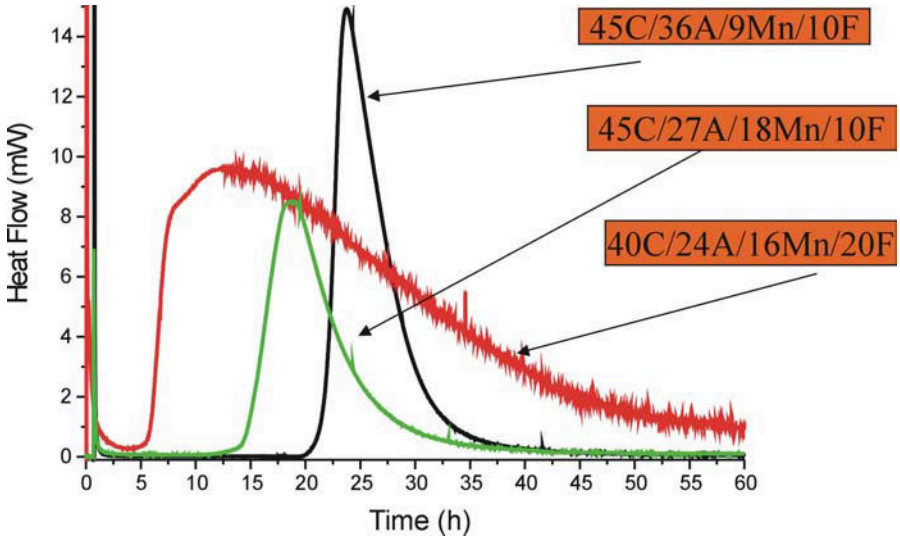

Figure 4. Heat flow calorimetry of different ratios of $CaO / Al_2O_3 / Mn_2O_3 / Fe_2O_3$

2.2 Phase formation in pure systems

The complicated phase formations were investigated mainly based on complex solid solutions of the brownmillerite type structures. The presence of other manganese-containing phases like perovskites and spinels must be avoided because they do not react with water. The lower the content of the clinker is in perovskites and spinels, the better is the reactivity with water. The results on the ternary phase diagram is shown in Figure 5 (Zötzl & Pöllmann).

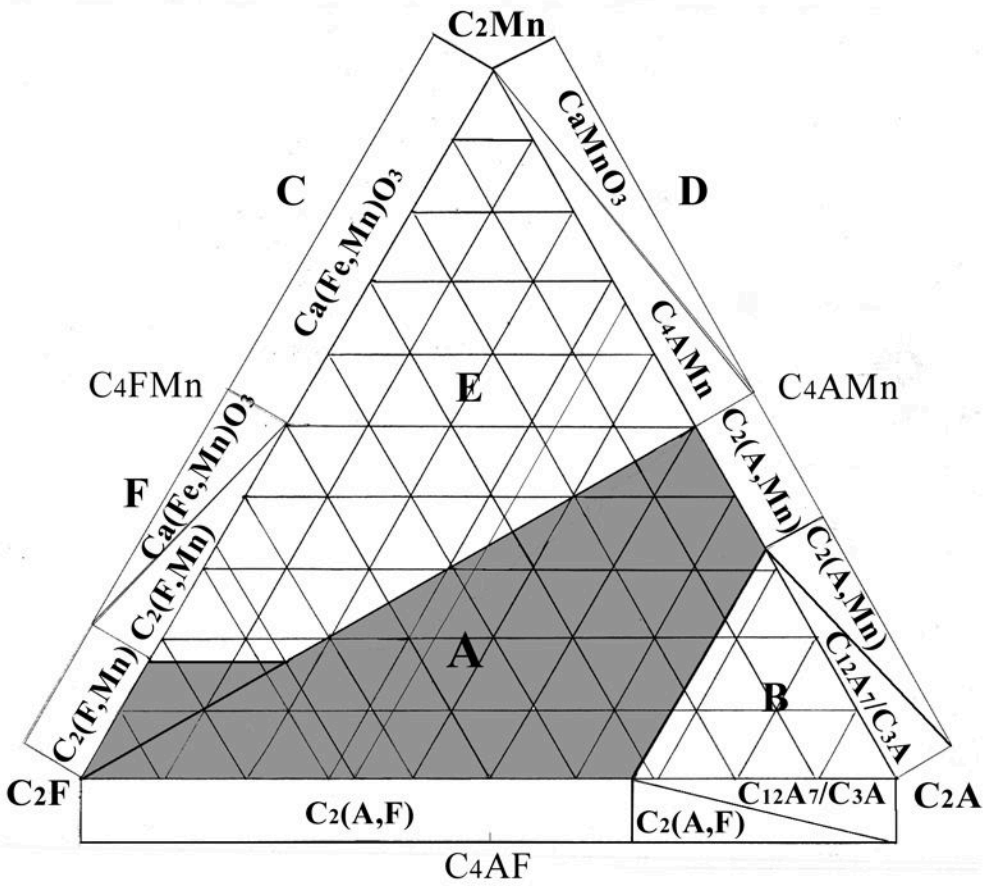

Figure 5. Phase relations in the pseudoternary diagram C_2F – "C_2A" – C_2Mn

The dark area is characterized by ternary solid solutions of the brownmillerite structure, whereas in the other fields different other phases coexist, some of these are not hydraulic in any case. In area A only solid solutions of brownmillerite are crystallizing with varying contents of iron, manganese and aluminium. In area B brownmillerite and $C_{12}A_7$ and/or C_3A are coexisting. Area E can be characterized by the coexistence of brownmillerites and coexisting perovskites and marokite, depending on the amount of manganese and conditions used. On the rims of the triangle the phases and their amounts are given schematically with increasing and decreasing tendency.

The complex phase relations are being investigated, but it is already obvious that there are upper limits of the addition of manganese at approximately 50 % to the mixtures to obtain a useful hydraulic clinker and also that the oxidation control of the sintering conditions can play a very important role to avoid crystallization of inert phases.

3. HYDRATION CHARACTERISTICS

The replacement of Al by Mn in HAC influences the reaction characteristics of HAC/water suspensions, and, as can be seen from Figure 6, the hydration intensity (determined by the total heat development due to the hydration) is affected by this substitution:

The commercial HAC without Mn-substitution showed initial hydration after 13 hours, whereas the HAC with a 20 wt-% Mn-substitution showed, after 8 hours, a beginning of hydration, the maximum hydration intensity (i. e. the maximum heat flow) being lower than that of the former one. The HAC with a 50 wt.-% Mn-substitution showed the highest heat flow, whereas the total heat evolution of all the three samples were in the same order of magnitude.

The HAC without Mn-substitution showed initial hydration after 10 hours, whereas the HAC with a 20 wt-% Mn-substitution showed, after 13 hours, the beginning of hydration, the maximum hydration intensity (i. e. the maximum heat flow) being lower than that of the former one. The HAC with a 50 wt.-% Mn-substitution showed the highest heat flow, whereas the total heat evolution of all the three samples were in the same order of magnitude.
(Pöllmann, H. & Oberste-Padtberg, R.).

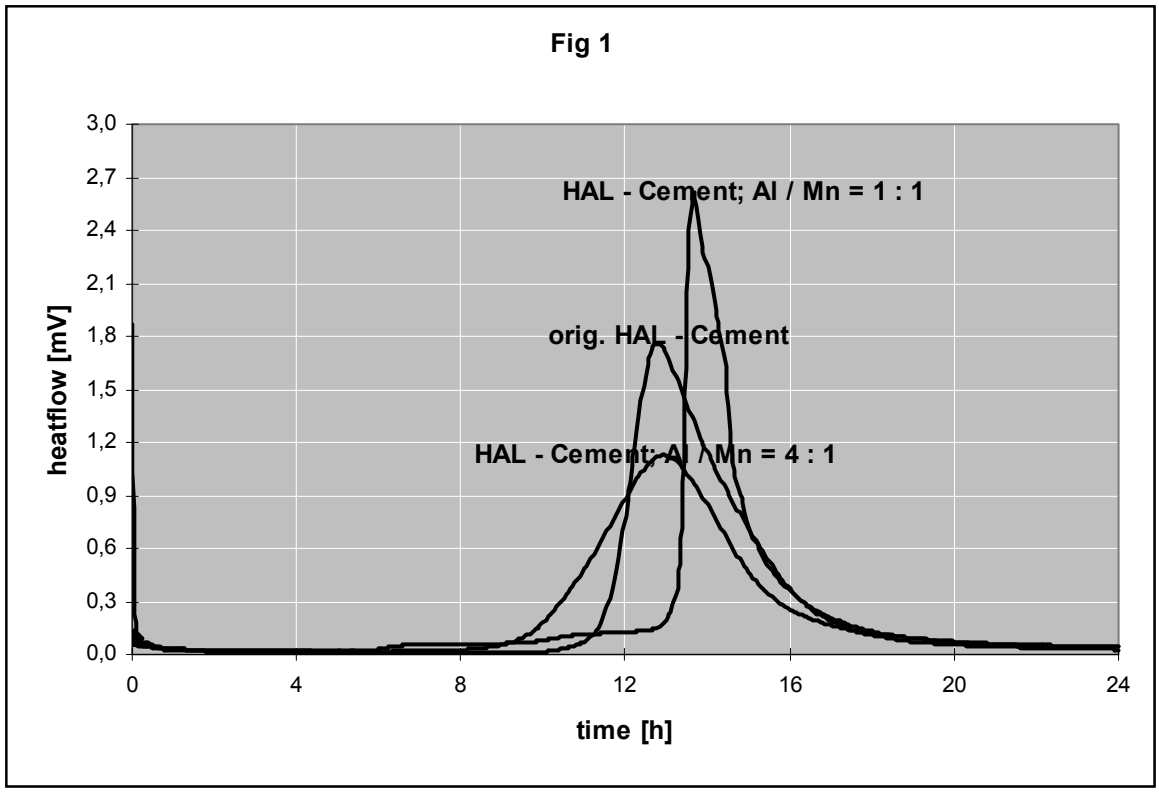

Figure 6. Hydration characteristics of Cements as compared a typical HAC to cements where the aluminium is replaced by manganese up to equivalent ratios of aluminium and manganese

3.1 Hydration behaviour of cements and building mixtures using $MnSO_4$

The manganese –cement systems were designed in the form such that the anhydrous active matter consisted uniquely of pure classic HAC (HAC component minerals) or with newly synthesized manganese-substituted cements (new manganese-containing components) on one hand, and , on the other hand, they consisted of so-called ternal systems, consisting of HAC, Ca- or Mn-sulfate and a CaO-containing material (either $Ca(OH)_2$ or ordinary Portland cement). The hydration of these mixtures are controlled by the addition of organic retarders such as citric acid, sodium gluconate or –tartrates.

Applications and use of these ternal mixtures are mortars which were designed on the basis of sand (0 – 8 mm) at a sand/active matter-ratio of 4 : 1 and a water/active matter ratio (equivalent to water/cement-ratio) of 0,44 : 1.

The hydration behaviour was investigated using a calorimeter (Pöllmann, H., Kuzel, H.-J. & Meyer, H.)

As can be seen from Figure 7, the hydration characteristics, i. e. the hydration velocity as well as the hydration intensity in ternal systems, containing conventional HAC and $MnSO_4$, can significantly be influenced by the amount of manganese sulfate:

Here, a powder, consisting of (70 parts HAC, 15 parts OPC, 1.5 parts sodiumcarbonate, 2 parts organic retarders, and 23 parts of Ca-sulfate, partly being replaced by Mn-sulfate), was mixed with water (water/solid: 0,44 : 1) and then permitted to hydrate in an isothermal calorimeter. As can be seen from Figure 7, the above mentioned powder mix showed the fastest heat evolution, when it contained 11 parts of Mn-sulfate. Increasing and decreasing manganese contents led to a retardation of the hydration and to a decrease in hydration intensity. The control of hydration can be followed directly due to the amount of manganese sulfate added. The main peak of heat evolution can be followed very precisely showing acceleration and retardation due to the amount added.

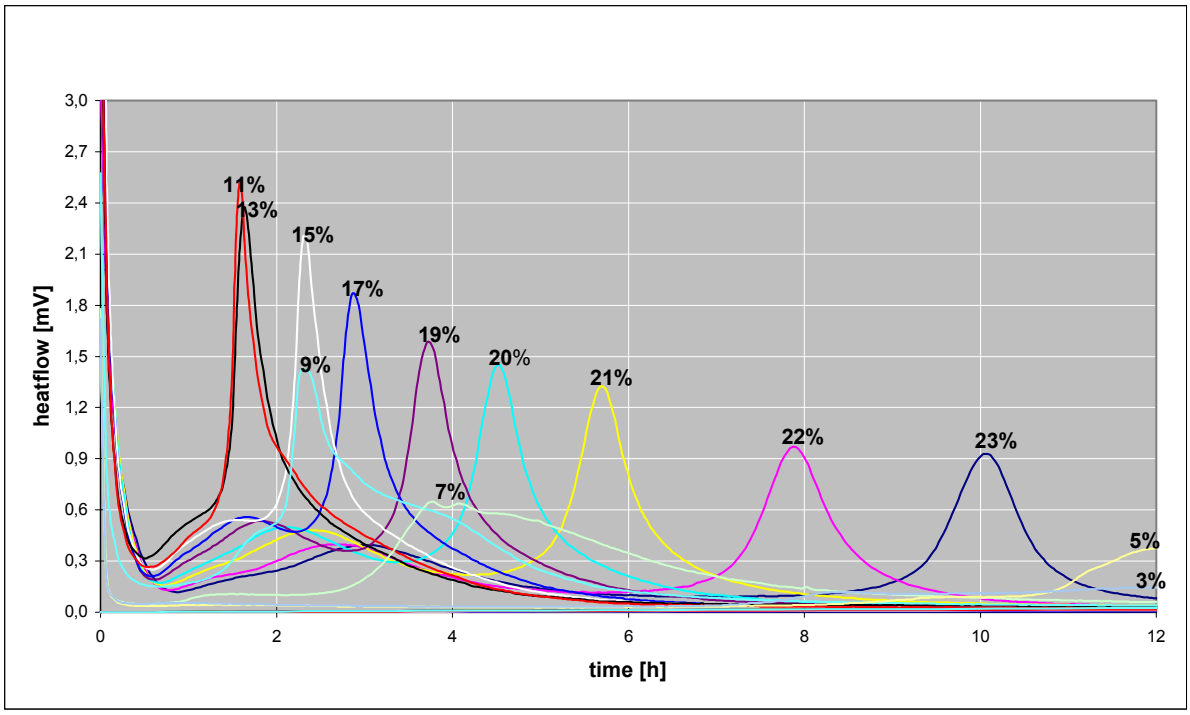

Figure 7. Influence of the amount of $MnSO_4$ on the hydration velocity of ternal HAC-mixes

Basically these mixtures have a complicated hydration chemistry and various hydrates form, including crystalline and amorphous phases. In manganese-free systems the main newly formed hydrate is ettringite. In manganese-containing mixtures ettringite and the mineral shigaite, a lamellar metal-metal hydroxy salt were identified.

The time of maxima of heat evolution is strongly dependant on the amount of sulfate and type of sulfate (calcium sulfates, manganese sulfate) added (Figure 8). It must be mentioned, that other metal sulfates, besides calcium sulfate do not have a similar effect on the hydration.

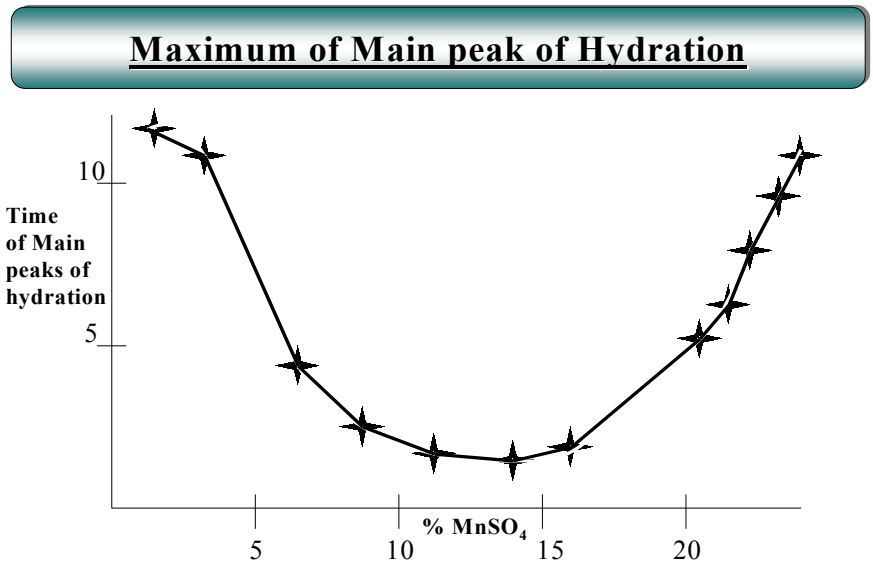

Figure 8. Time of maxima from peaks of heat evolution as a function of manganese sulfate content of the ternal mixtures

The hydration characteristics were also determined in the above mentioned ternal systems, where the HAC was Mn-substituted. As an example in comparison to an ordinary manganese-free HAC, other HAC`s, with an Al/Mn-ratio of 4:1 and 1:1 were tested.

As can be seen from Figure 9, the Mn-substituted HAC`s had a slight retardation of hydration but, especially the HAC with an Al/Mn-ratio of 4:1 showed within the first 10 hours of hydration the maximum amount of heat evolution.

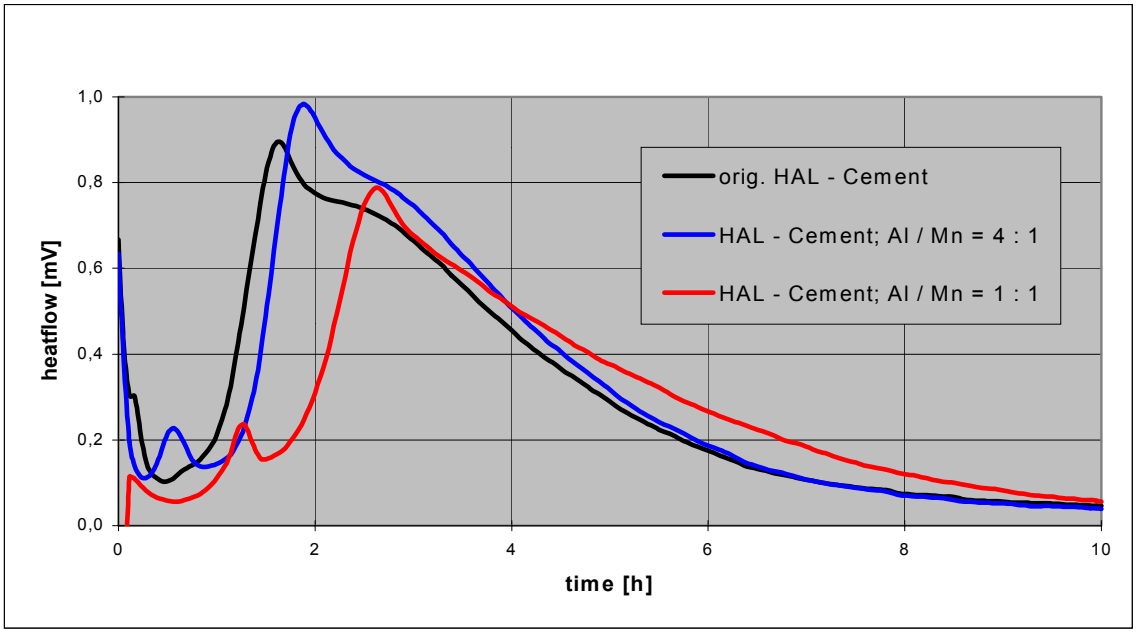

Figure 9. Heat evolution of ternal mixtures using manganese-containing HAC`s

3.2 Strength Development

The development of the strength was determined in mortars on the basis of the above mentioned ternal systems (HAC, Ca-sulfate, Mn-Sulfate, OPC and organic retarders). These mortars were mixed with sand (0 - 8 mm) and water (water/cement = 0.41 : 1).

Table 2 shows the formulation of the different binders, which were created because their compositions are close to actual binders using calcium sulfate as a component, whereas Figure 10 shows the results of the strength development in the mixes tested.

Table 2. Formulations whose strength development is shown in Figure 10

	HAC	OPC	Ca-sulfate	Mn-sulfate	Na-carbonate	org. additives
Mix 1	64	11	22	0.0	0.3	2.7
Mix 2	62	11	6	18	0.3	2.7
Mix 3	65	11	0.0	21.3	0.0	2.7

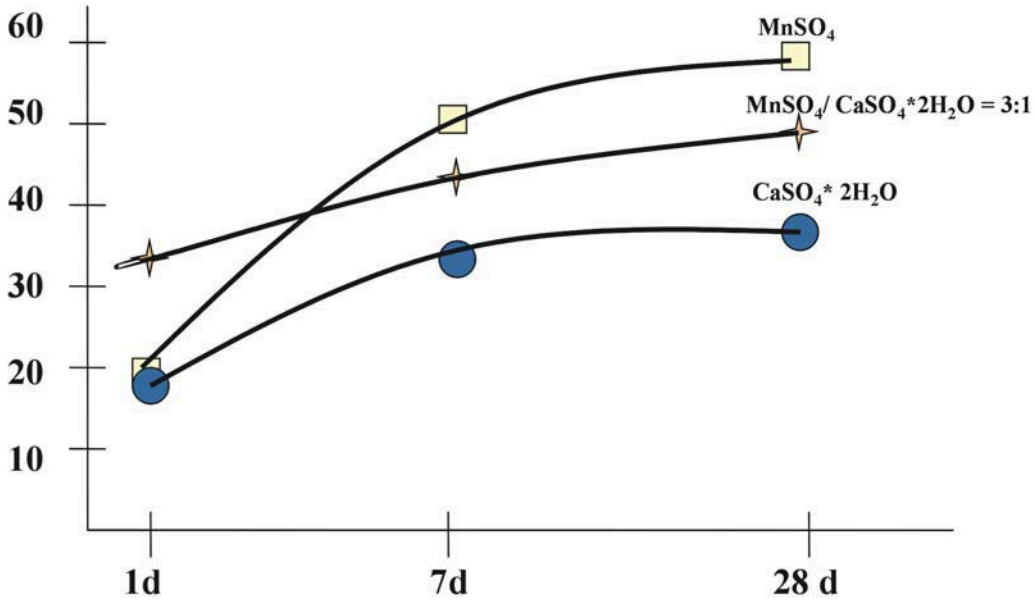

Figure 10. Compressive strength development (in N/mm^2) at 20^o C/65 % r. h. of mixes 1- 3 from Table 2

As can easily be seen from Figure 10, a substitution of a part of the $CaSO_4$ – content in the ternal mixes (closely related to technical mixes in the case of gypsum addition) by $MnSO_4$ leads to an increase in compressive strength development of mortars. In the case of $MnSO_4$ a mixture is given without Na-carbonate, so that no influence of a potential activator is included.

3.3 Stability of newly formed hydrates

In order to determine the leachability of different ternal HAC-systems, the binders of Table 3 were mixed with water (water/solid = 0.44 : 1) and then permitted to harden for 7 days. The hardened materials were then crushed and sieved at 1 mm, and the fines were leached for 1 week with water (ratio 10 wt.-parts of water : 1 part of crushed material) and then analysed for Mn. In all the cases, the Mn-content was below the detection limit of << 0.1 ppm.

Table 3. Composition of HAC-Mixes for the determination of Mn-leachability (see text)

	HAC	OPC	Org. additives	$MnSO_4$	$CaSO_4$
HAC-mix 1	64	12	2		22
HAC-mix 2	64	12	2	22	
HAC-mix 3	64	12	2	16	6

The advantages of manganese for production of HAC`s can be summarized as follows :

1) Lowered sintering temperatures (by 100 ^{o}C – 300 ^{o}C) (due to high amounts (20-30%) of manganese present, own phases are formed and no additional fluxes were used)
2) Use of widely available and cheap raw materials
3) High strength development
4) High early strength development
5) Weathering stability
6) High water bonding capacity due to phase formation of metal-metal hydroxy salts with high water bonding capacities
7) Complex use of this cement in construction industry possible due to good strength development
8) Use of this cement in environmental applications for immobilization of soluble manganese salts to form insoluble hydrates
9) High chemical resistance, low leaching rates
10) Workability at low temperatures possible due to high heat evolution
11) Admixture control of hydraulic properties in applications possible similar to HAC

REFERENCES

[1] Bayoux, J.B., A. Bonin & M. Verschaeve: Study of the Hydration Properties of Aluminous Cement and Calcium Sulphate Mixes, Calcium Aluminate Cements, R.J. Mangabhai, ed., E. & FN Spon, London, pp. 320-334.

[2] Füllmann, Th.: Quantitative Rietveld-Phasenanalyse von Tonerdezementen, Dissertation Erlangen, 1997.

[3] Harben, P., C. Raleigh & J. Harris: Manganese Uses and Markets, Industrial Minerals Information Ltd., London, 1998.

[4] Mangabhai, R.J. ed.: Calcium Aluminate Cements, E & FN Spon, London, 1990.

[5] Motzet, H.: Entwicklung eines Sinterverfahrens zur Herstellung von eisenreichen Tonerdezementen, Dissertation, Halle/Saale.

[6] Motzet, H. & H. Pöllmann: Quantitative Phase Analysis of High Alumina Cements, Proceedings of International Conference Cement Micr., 1998, pp. 187-206.

[7] Peacor,D.R., Dunn,P.J.,Kato,A. & Wicks,F.J.: Shigaite, a new manganese aluminum sulfate mineral fom the Ioi mine, Shiga, Japan, N. Jb. Min., Mh., 1985, 453-457.

[8] Pöllmann, H., H.J. Kuzel & H.W. Meyer: Heat-Flow Calorimeter in Cement Chemistry-Construction and Application of a Low Cost High Sensitive Calorimeter, Proc. 13th International Conference on Cement Chemistry, Tampa, 1991, pp. 254-272.

[9] Pöllmann, H.: Shigait-Synthese, Eigenschaften und Anwendung – Z. Krist., 2001.

[10] Pöllmann, H. & Oberste-Padtberg, R.: Manganese in High Alumina Cement, Calcium Aluminate Cements, (2001), IOM Communications, 139-148

[11] Puertas,F., Blanco-Varela, M.T. & Dominguez,R.: Characterization of Ca_2AlMnO_5. A comparative study between Ca_2AlMnO_5 and Ca_2AlFeO_5 – Cem.Concr.Res. 20, 429-438, (1990).

[12] Scrivener, K.L. & A. Capmas: Calcium Aluminate Cements in Lea`s Chemistry of Cements and Conrete, PC Hewlett, ed., Arnold, London, 1998, pp. 709-778.

[13] SOURIE, A. & F.P. GLASSER: Studies on the Mineralogy of High Alumina Cements, British Ceramics, Trans. Journal, 90, 1991, pp. 1772-1776.

[14] WALENTA, G.: Synthesen und Rietveld Verfeinerung der Einzelphasen von Tonerdezementen – Dissertation Erlangen, 1997.

[15] ZÖTZL, M. & PÖLLMANN, H.: Diadochiebeziehungen im System $Ca_2Fe_2O_5$ – $Ca_2Mn_2O_5$ – $Ca_2Al_2O_5$ – Ber. Dt. Min. Ges., 206, (2001)

[16] ZÖTZL, M. & PÖLLMANN, H.: Phasenstabilitätsbereiche im System $CaMnO_{2.8}$ – „$CaAlO_{2.5}$“ bei 1300 ^{o}C – Ber. Dt. Min. Ges., (2002).

STUDY OF THE HYDRATION OF OPC UNDER THE INFLUENCE OF DIFFERENT ORGANIC ANIONS BY HEAT-FLOW CALORIMETRY

Stöber, S. and Pöllmann, H.

Institut für Geologische Wissenschaften der Martin - Luther Universität Halle - Wittenberg
Mineralogie/Geochemie, Domstraße 5, 06108 Halle (Saale).
E-mail: stoeber@geologie.uni-halle.de and pollmann@geologie.uni-halle.de

ABSTRACT

The main purpose of this investigation was, to demonstrate how different admixtures (benzene sulfonic acids and alkanesulfonic acid sodium salts) systematically change the setting times of ordinary Portland cement pastes (OPC) due to different concentrations, systematic changes of chain lengths of alkanesulfonic acids sodium salts and systematic variations in number and orientation of CH_3 - substituents on the benzene ring. Furthermore the crystallisation of OPC pastes under the influence of these admixtures was investigated. The course of hydration of the OPC pastes was determined by isoperibolic heat-flow calorimetry. For the investigation of the bulk phase composition of the cement pastes, differential scanning calorimetry (DSC) and X-ray powder diffraction techniques (XRD) were applied.

Both, alkanesulfonic and different benzenesulfonic acid anions showed retardation or acceleration effects on the hydration process depending on the variation of the chain-length or the molecular structure of the different benzenesulfonic acid anions. Under the presence of admixtures newly Afm-phases crystallized containing alkanesulfonic or benzenesulfonic acid anions in the crystal structure.

1. INTRODUCTION

There is widespread use of admixtures in cement chemistry. It is estimated that more than 80% of the concrete production in North America contains one or more admixtures. Today organic and inorganic substances are added to the concrete batch immediately before or during mixing. They are used to modify the properties of the cement paste or concrete, to make them more suitable for particular applications and to save energy for economic purposes. Different effects like acceleration or retardation of the setting tunes, decreased water requirements without a change in workability, durability enhancements, and increased rate of strength development and many more effects are provided by admixtures. The different properties of admixtures are defined by different standards and specifications provided by RILEM, ACI, ASTM or CSA [1].

The raw materials for most admixtures are by-products or waste materials resulting from technical processes. For example the retarding effect of Calcium- or Sodium lignosulfonates depends on their sugar impurities. Sugar-free lignosulfonates are poor retarders and sugar rich lignosulfonates are good retarders.

In this work, pure benzene sulfonic acids and different sodium alkane sulfonates were applied to investigate the direct effect of the systematic variation of the molecular structure on the cement or concrete hydration.

The following parameters were raised:

- Variation of number and orientation of CH_3 - substituents on the benzene ring of different benzene sulfonic acids
- Variation of the chain length of alkanesulfonic acids sodium salts $C_nH_{2n-1}SO_3Na$ n = 1, 3, 5, 7, 8, 9

2. EXPERIMENTAL

For the investigations on the effects of sulfonic acids and sodium salt additions, a commercial OPC CEM I 32,5 R with a measured specific surface of 3870 cm^2/g was used. The composition of the main phases in the clinker is summarized in Table 1. As admixtures, commercial alkanesulfonic acid sodium salts and different benzene sulfonic acids (Table 2) were used.

Table 1. Composition of the OPC (Clinker phases and Calcium sulphate dihydrate)

C_3A [wt.-%]	C_2S [wt.-%]	C_3S [wt.-%]	C_4AF [wt.-%]	Gypsum [wt.-%]
7.5	9.8	72.5	2.6	3.0

Table 2. Admixtures: Different sulfonic acids and sodium salts

Alkane sulfonic acid Sodium salts	
CH_3SO_3Na	Methane sulfonic acid sodium salt
$C_2H_5SO_3Na$	Ethane sulfonic acid sodium salt
$C_3H_7SO_3Na$	Propane-1- sulfonic acid sodium salt
$C_4H_9SO_3Na$	Butane-1- sulfonic acid sodium salt
$C_5H_{11}SO_3Na$	Pentane-1-sulfonic acid sodium salt
$C_7H_{15}SO_3Na$	Heptane-1-sulfonic acid sodium salt
$C_8H_{17}SO_3Na$	Octane-1-sulfonic acid sodium salt
$C_9H_{19}SO_3Na$	Nonane-1-sulfonic acid sodium salt
Benzene sulfonic acids	
$C_6H_5SO_3H$	Benzene sulfonic acid
$C_7H_7SO_3H$	Toluene-p-sulfonic acid
$C_8H_9SO_3H$	Xylene sulfonic acid
$C_9H_{11}SO_3H$	Mesitylene sulfonic acid

In order to determine the course of hydration, an isothermal heat flow calorimeter designed by KUZEL [2][3] was applied. The instrument consists of 4 measuring cells sited in an aluminum block. One cell is occupied by the reference, in this case a copper vessel and cover closely sealed and filled with 1 ml H_2O. The other cells are used to determine the hydration of cement pastes. Due to the exothermal heat evolution of the cement hydration, the evolved heat is measured in difference ($Heat_{Sample}$-$Heat_{Reference}$). This construction allows the determination of corrected heats per time as voltage (mV) without background heat effects. The heat is detected by BiTe semiconductors and registered by a digital multimeter from PREMA. The measured mV-values are stored on the hard disk of a computer and were analysed and interpreted by commercial scientific software. The illustration of the calorimeter files of an OPC (Figure 1) showed a typical heat flow diagram. In order to determine the heat flow quantitatively the heat flow data must be multiplied by the calibration factor K, in order to equalise inhomogeneities of the calorimeter construction.

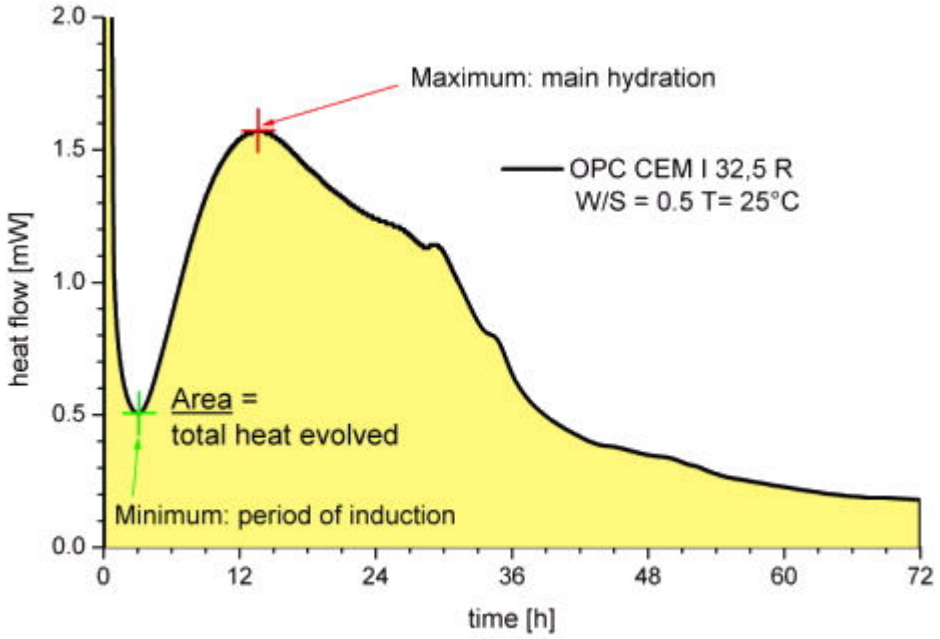

Figure 1. Typical calorimeter curve of OPC and H_2O (Reference)

In order to determine the effect of admixture addition on the cement paste hydration, the minimum of the period of induction (mpi) and the maximum of the main hydration (mmh) were determined. Additionally, the area under the calorimeter curve was integrated, because the area is directly proportional to the heat flow per time and consequently directly proportional to the phase formation. The partition of the area in different segments gave the ability to determine in which segments the admixtures have had their strongest influences on the hydration of the cement paste.
The phase formation as a function of time was firstly determined by Differential Scanning Calorimetry (DSC) and secondly by X-ray diffraction (XRD), because C-S-H is formed as amorphous gel phases [4], [5].

For DSC measurements, cement paste samples of constant mass 10 mg were taken at different hydration times and dried at 35 % r.h. over a saturated $CaCl_2$ concentration in a desiccator for 4 weeks. The same dried samples were investigated by XRD in order to identify the dehydration reactions of the DSC graphs and to determine changes in the crystal chemistry of Afm- or Aft-phases. For the measurements a Si-single crystal sample carrier for small sample material was used.

3. RESULTS

3.1 The influence of variable chain lengths on the hydration of an OPC

In order to demonstrate the effect of variable chain lengths on the cement paste hydration under the influence of sodium alkane sulfonates $C_nH_{2n+1}SO_3Na$ with n = 1,3,5,6,7,8,9 the properties of 0.25 mole/l will be discussed (Figure 2). In comparison to the reference (OPC and H_2O) the addition of sodium alkane sulfonates shifted the mpi to higher hydration times. Moreover, the time ranges of the induction period of different calorimeter curves were affected. Longer aliphatic chains of the alkanesulfonic acid sodium salt increased the induction periods. Hand in hand with the minimum of the induction period, the maximum of the main hydration compared to the reference were shifted to higher hydration times, too. In relation to these 2 points the bulk heat of hydration during the main hydration was liberated at higher times. The addition of 0.25 molar sodium alkane sulfonic acid solutions to OPC caused the distribution of the heat of hydration over a larger time interval. The evolved heat in the range 0 to 72h showed, that the influence of the admixtures with $C_nH_{2n+1}SO_3Na$ with n = 1,3,5 and 6 is predominantly strong during the end of the induction period up to 36 h (Figure 3). However, for cement pastes mixed with admixtures $C_nH_{2n+1}SO_3Na$ with n = 7,8 and 9

most of the heat was liberated between 36 to 72h. The total heat of hydration was decreased due to the addition of increased chain lengths. Not only retardation effects are visible, in the calorimetric graph of OPC and 0,25 m CH_3SO_3Na accelerates hydration reactions in the range of 0 to 36h, which can be seen due to a higher heat of hydration.

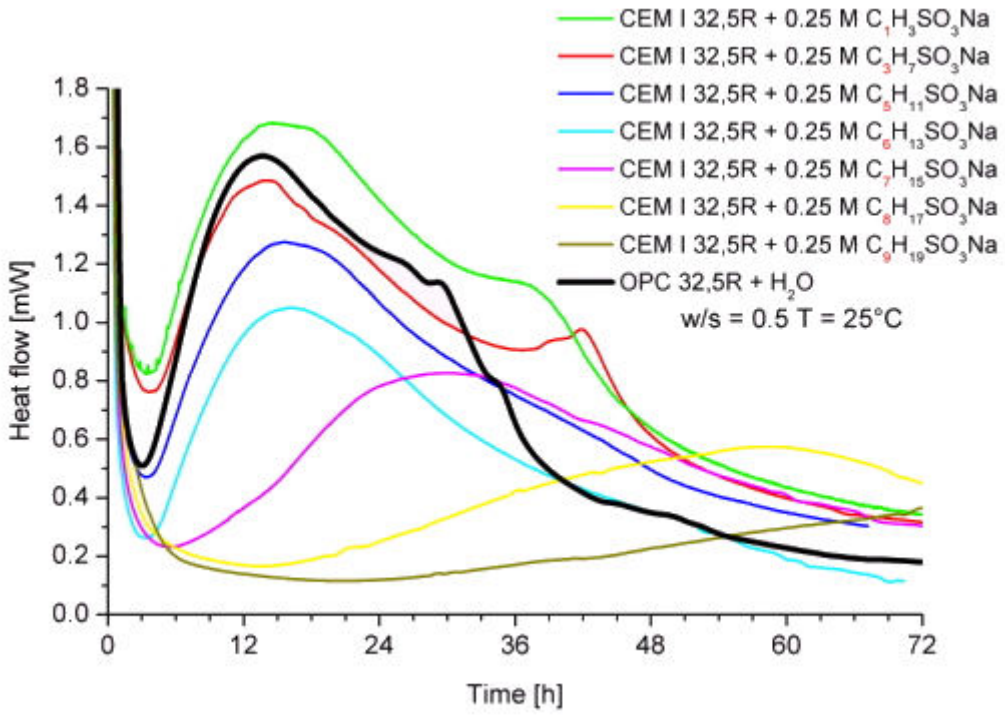

Figure 2. Calorimeter curves: OPC and 0.25 M $C_nH_{2n-1}SO_3Na$ n = 1,3,5,7,8,9

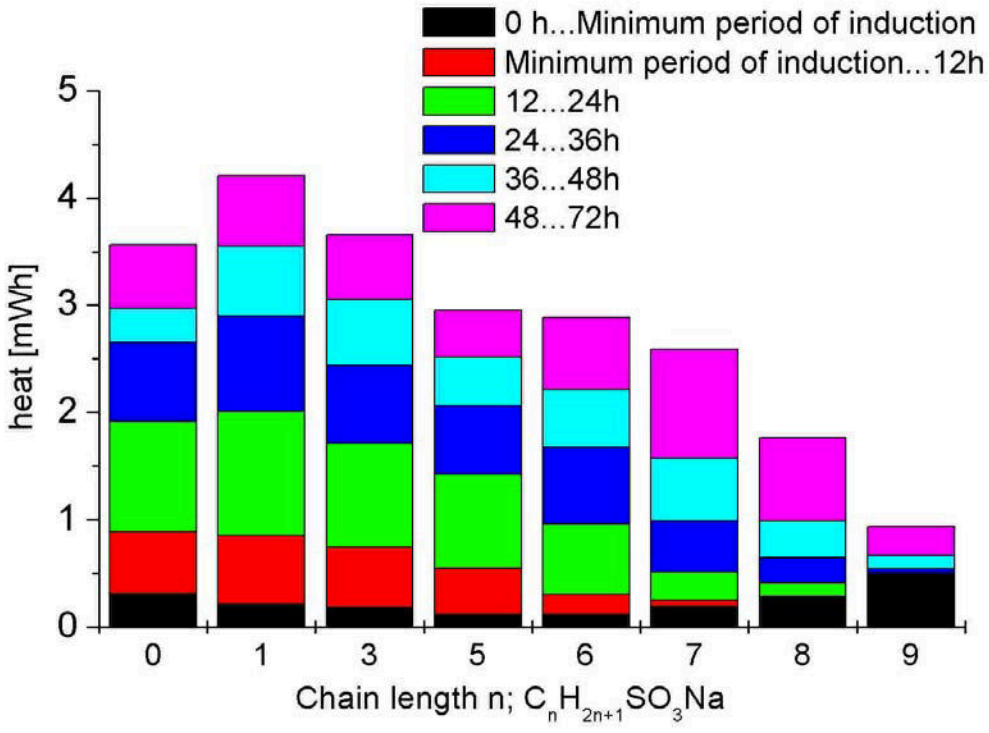

Figure 3. Heat of OPC - pastes: OPC and 0.25 M $C_nH_{2n-1}SO_3Na$ n = 1, 3, 5, 7, 8 and 9

3.2 The influence of CH_3-substituents on the cement hydration

The addition of 1M benzenesulfonic acid $C_6H_5SO_3H$, toluene-p-sulfonic acid $C_7H_7SO_3H$, xylenesulfonic acid $C_8H_9SO_3H$ and mesitylenesulfonic acid $C_9H_{11}SO_3H$ to an OPC paste diminished the bulk heat evolution in the interval 0 to 72h (Figure 4.) in general.

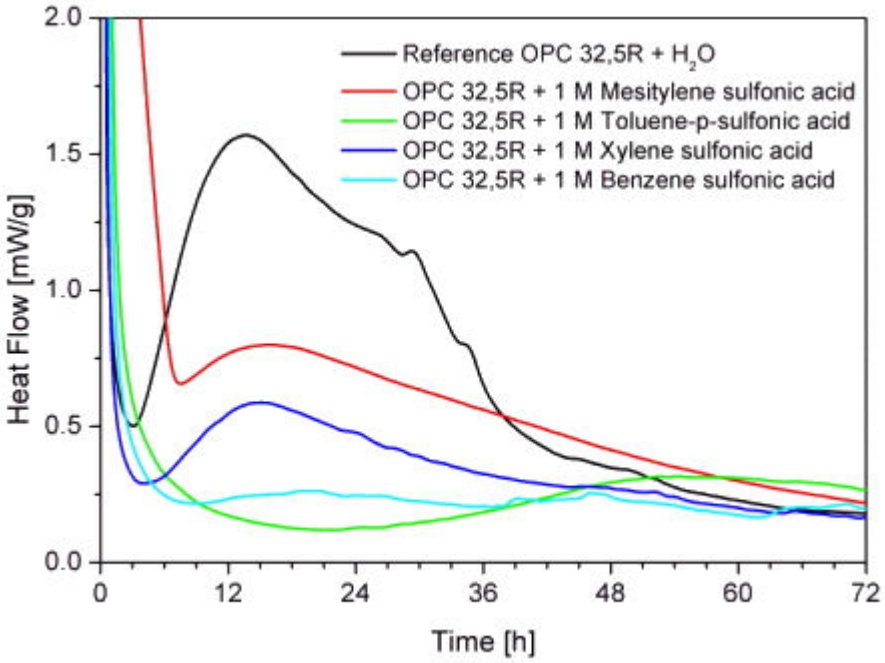

Figure 4. Calorimeter curves: OPC and 1 M benzene sulfonic acids

The addition of $C_6H_5SO_3H$ produced 32 %, $C_7H_7SO_3H$ 33%, $C_8H_9SO_3H$ 57% and $C_9H_{11}SO_3H$ 75% heat of the reference paste. On the basis of the influence of the admixture addition on the mpi, mmh and the heat flow, the 4 different benzenesulfonic acids must be divided in 2 groups. It can be seen that sulfonic acids without CH_3 substitution ($C_6H_5SO_3H$) and the sulfonic acid with one CH_3-group, substituted in opposite orientation to the sulfonate group (SO_3H), had a strong retarding effect on the cement hydration. The continuous increase of the CH_3-number at the benzene ring ($C_8H_9SO_3H$ and $C_9H_{11}SO_3H$), where CH_3 groups are asymmetrically ($C_8H_9SO_3H$) and symmetrically ($C_9H_{11}SO_3H$) substituted on the benzene ring, lowered the retarding effect (Figure 5).

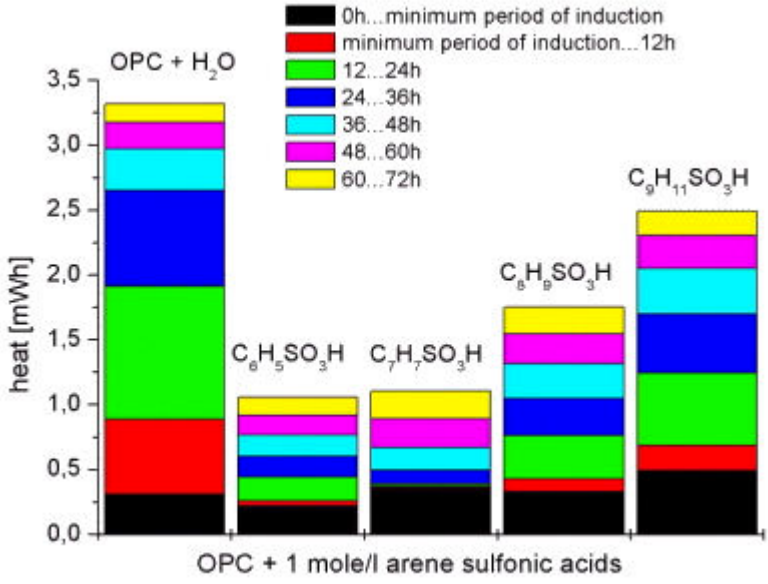

Figure 5. Heat evolution: OPC and 1M benzene sulfonic acids

Not only high benzenesulfonic acid concentrations had significant influence on the cement hydration. 10^{-3} to 10^{-6} mole/l additions increased the heat flow of cement pastes, investigated by heat-flow calorimetry. This time sulfonic acids with an asymmetrical and a symmetric distribution of the CH_3 substituents accelerated the cement hydration, whereas admixtures of group 1 with an opposite orientation of CH_3 and SO_3H group ($C_7H_7SO_3H$) and ($C_6H_5SO_3H$) did not accelerate as well as group 2 compared to the reference (Figure 6).

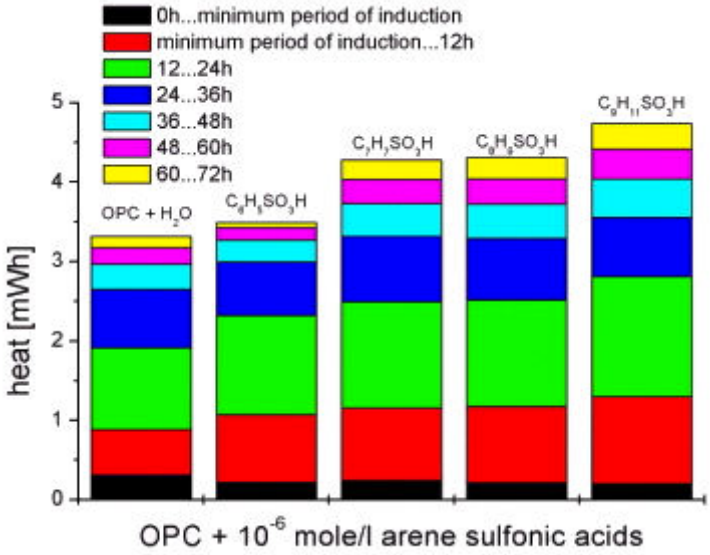

Figure 6. Heat evolution: OPC and 10^{-6} M benzene sulfonic acids

3.3 Investigations on sulfonic acid influences on the phase assemblage of a cement paste

3.3.1 Phase formation of OPC pastes investigated by DSC

The measurement of dried cement pastes by DSC made it possible to determine the dehydration reaction of the different main hydration phases indirectly (Figure 7).

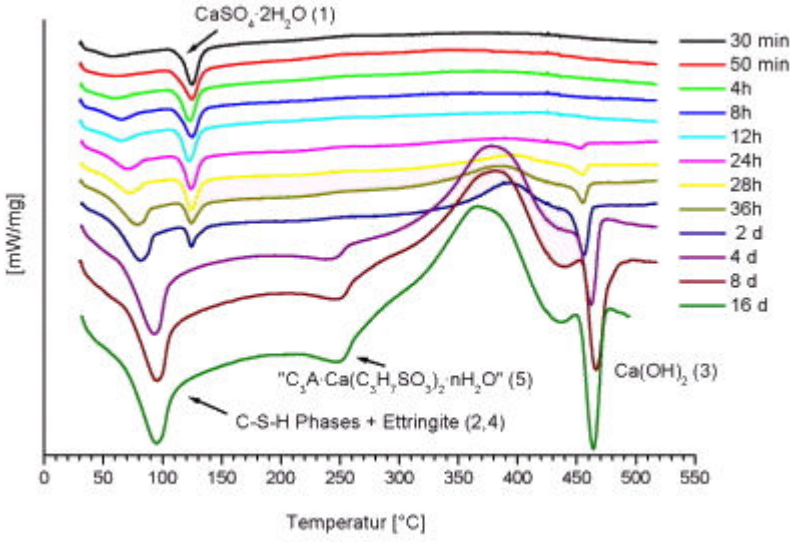

Figure 7. DSC graphs of OPC and 1 M $C_3H_7SO_3H$ w/s =0.5 T = 25°C

In the temperature range 35 to 120°C the dehydration process of the C-S-H phase and the ettringite dehydration reactions progressed. Therefore it was not possible to determine the C-S-H and ettringite concentrations separately. However, the formation of ettringite was followed indirectly on the dehydration of gypsum. If more gypsum was used for the ettringite crystallisation, the peak area of the gypsum dehydration peak became smaller. Furthermore, the endothermic peak in the region

260 to 320°C was identified as the dehydration of the main layer of an Afm-phase. Due to the pyrolysis of the benzene ring or the aliphatic chain of the alkanesulfonic acid most of the DSC graphs showed a big exothermic peak at approximately 250°C. The dehydration of portlandite started at about 430 °C Although, the portlandite formation is a result of the hydration reaction of calciumsilicates, the integration of the area of the endothermic portlandite dehydration peaks did not give sufficient results for quantification of the C-S-H concentrations.

3.3.2 Phase formation of OPC pastes investigated by XRD

Different cement pastes were investigated as a function of the hydration time (Figure 8 and Figure 9). C_3A and the ferrite phase reacted with gypsum to ettringite, which was detected after 15 minutes of cement hydration. The crystal structure of ettringite was not influenced because of the presence of sulfonic acid anions. The 2 Theta values of ettringite were not shifted to higher or lower 2 Theta-values and the refinement of the metric parameters gave the values of the common sulphate ettringite.

Instead of the formation of monosulfate or monocarbonate, new AFm–phases crystallized, because the sulfonic acid ions of the alkanesulfonic acids $C_nH_{2n+1}SO_3^-$ with n = 1,2,3,4 and the different benzenesulfonic acid ions were chemically fixed in the interlayer of the AFm-structure instead of sulphate or carbonate ions [6], [7]. The ion exchange is visible due to the 2 Theta shift of the (00l)-base reflections. Most of the time only 3 to 5 (00l) reflections could be detected and used for the refinement of metric parameters due to the low grade of cristallinity. Therefore only the c-dimensions were refined (Table 3).

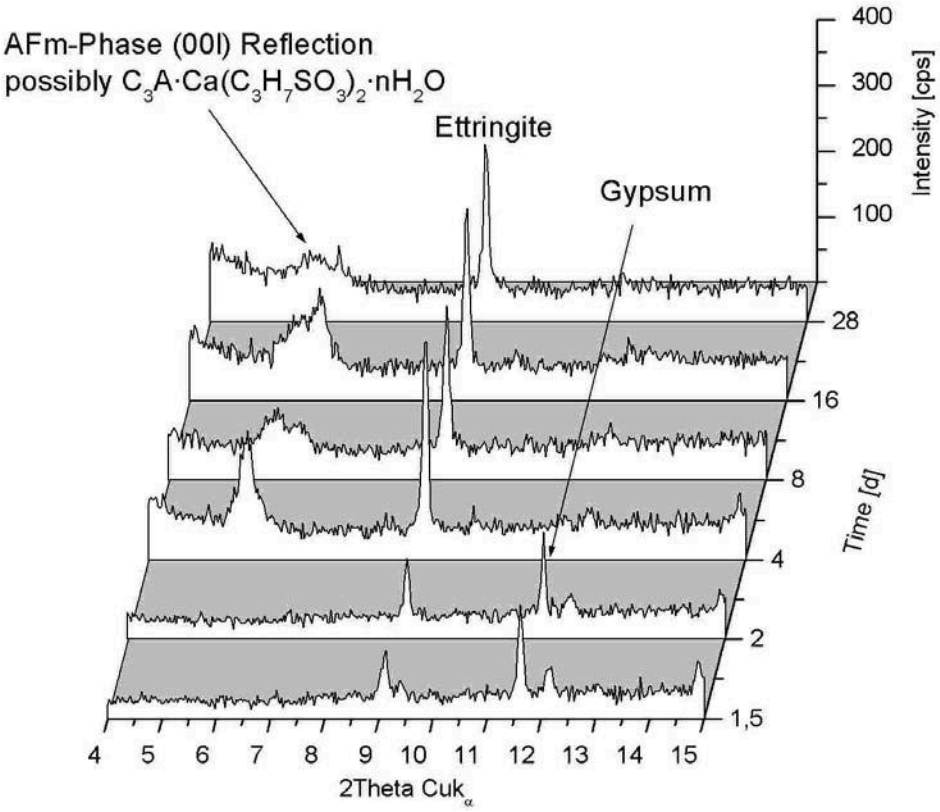

Figure 8. Phase formation: OPC and 1 M $C_3H_7SO_3H$

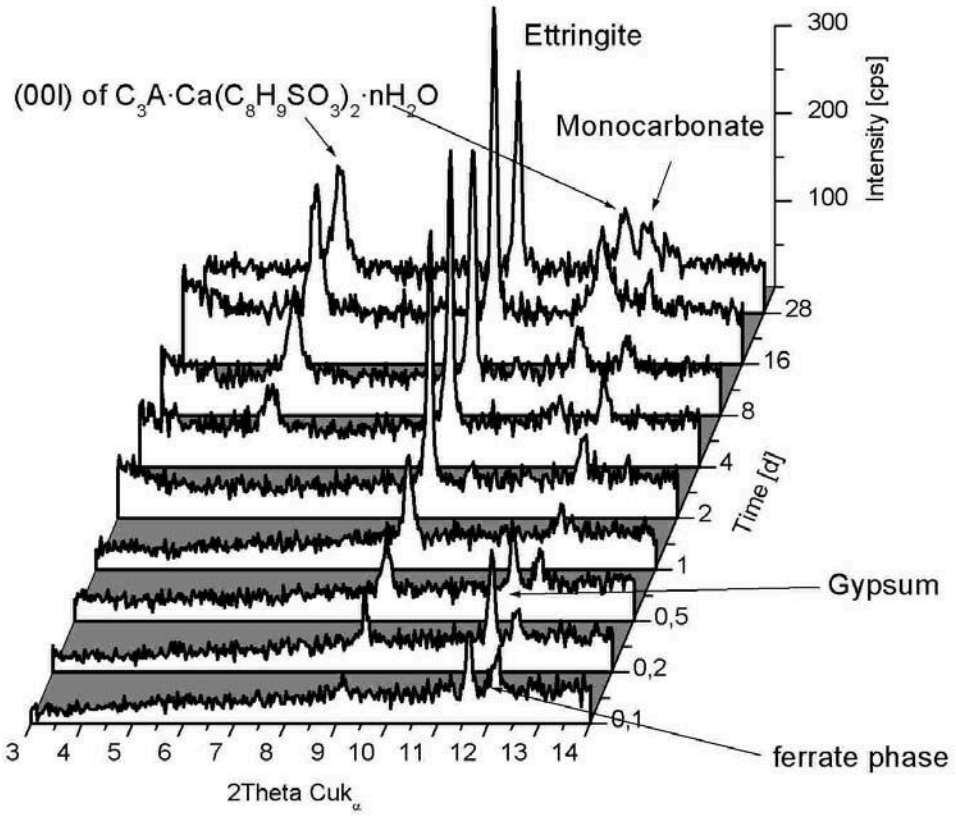

Figure 9. Phase formation: OPC and 0.25 M $C_8H_9SO_3H$

Table 3. Layer distances of in situ formed Afm-phases

Afm-phases	Layer distance c´ [nm]
$C_3A{\cdot}Ca(C_7H_7SO_3)_2{\cdot}nH_2O$	1.714
$C_3A{\cdot}Ca(C_8H_9SO_3)_2{\cdot}nH_2O$	1.583
$C_3A{\cdot}Ca(C_9H_{11}SO_3)_2{\cdot}nH_2O$	1.761
$C_3A{\cdot}Ca(CH_3SO_3)_2{\cdot}nH_2O$	1.255
$C_3A{\cdot}Ca(C_3H_7SO_3)_2{\cdot}nH_2O$	1.385

4. DISCUSSION AND CONCLUSIONS

The addition of different benzene sulfonic acids and alkanesulfonic acid sodium salts modified the hydration kinetics of an OPC. Benzene sulfonic acids accelerated or retarded the OPC hydration. Low admixture concentrations (10^{-6} to 10^{-3} mole/l) activated the hydration reactions; the minima of the period of induction of the calorimeter curves were shifted approx. 2h in comparison to the reference to lower hydration times. Higher admixture concentrations (10^{-2} to 1 mole/l) retarded the cement hydration strongly.

The interpretation of the heat flow, determined on the basis of calorimeter curve areas, showed that the time at the end of the induction period to 36h was most influenced by the admixture. Alkane sulfonic acid sodium salts acted as only retarders.

Methane sulfonic acid sodium salt concentrations (10^{-4} to 0.25 mole/l) accelerated the cement hydration. High concentrations of long chained alkane sulfonic acid sodium salts (0.25 and 1 mole/l) showed strong retarding effects. Not only the minimum of the induction period also the maximum of the main hydration were shifted to higher times. The total heat flow of the cement

pastes, measured between 0 to 72 h decreased successively with the addition of long chained sodium alkane sulfonates.

Retardation or acceleration of the OPC hydration kinetics pastes existed due to the orientation and number of CH_3-substituents at the benzene ring of different benzene sulfonic acids and the variation of the length of alkanesulfonic acid sodium salts $C_nH_{2n-1}SO_3Na$ n = 1,3,5,7,8,9 The different molecular structure of benzene sulfonic acids showed that 2 groups one the one side $C_7H_7SO_3H$ and $C_6H_5SO_3H$ and on the other side $C_8H_9SO_3H$ and $C_9H_{11}SO_3H$ existed. The addition of group 1 admixtures retarded strongly and the addition of admixtures of group 2 retarded too, but not as strong as group 1.

The effects of the acids are based on the number and different orientation of the CH_3 substituents against the sulfonate group. Toluene-p-sulfonic acid has an opposite arrangement of the substituents, the benzene sulfonic acid has no CH_3 substituents. Mesitylene sulfonic acid and xylene sulfonic acid have a symmetric and asymmetric distribution of the CH_3 substituents.

The variation of the chain length of alkanesulfonic acids showed strong retarding effect with longer chain lengths. The comparison of both, alkane- and benzene sulfonic acids gave the result, that strong retarders, as long we talk about these sulfonic acids, are preferably based on an opposite distribution of a sulfonate group and an aliphatic C_nH_{2n-1} chain. It is not too important if a benzene ring is put between the C_nH_{2n-1} chain and the sulfonate group, the more important is the chain length. The quantitative investigation of the C-S-H phase in the cement pastes by DSC was not possible, because the dehydration reactions of ettringite and the C-S-H phases overlapped during heating in the range 30 to 120 °C. However, the formation of newly formed Calcium aluminate sulfonate hydrates was detected in OPC pastes and 0.25 M $C_6H_5SO_3H$, $C_7H_7SO_3H$, $C_8H_9SO_3H$ or $C_9H_{11}SO_3H$ and OPC pastes and 1 M $C_nH_{2n-1}SO_3Na$. The phases were identified and the metric parameters refined.

REFERENCES

[1] Ramachandran, V.S.: Concrete Admixtures Handbook 2nd edition New Jersey: Noyes Publications 1995 p.4 and 82

[2] Kuzel, H.-J.: Ein einfaches Wärmeleitungskalorimeter mit hoher Empfindlichkeit. - - Fortschr. Miner., Beihefte, vol. 60 (1),(1982), pp. 128 - 129.

[3] Kuzel, H.-J.: Ein leistungsfähiges Wärmeleitungskalorimeter, TIZ – Fachberichte, Vol. 108 No.1, (1984), pp. 46-51.

[4] Bensted, J.: Effect of accelerator additives on the early hydration of Portland cement. Il cemento, vol. 75 (1), (1978), pp. 13-20

[5] Yaoxing Chen.: Untersuchungen über die Hydratation und das Zustandekommen des Erstarren von Portlandzementen *Dissertation TU Clausthal* (1990)

[6] Pöllmann, H., H.-J. Kuzel & H. Meyer. Heat flow calorimetry in cement chemistry - Proc. 13th. Int. Con. Cem. Micr., Tampa,(1991) pp. 254-272

[7] Allmann, R.: Refinement of the hybrid layer structure $[Ca_2Al(OH)_6]^+ \cdot [1/2\ SO_4 \cdot 3H_2O]$, N. Jb. Min. Mh., Vol. (3) (1977), pp. 136 - 144.

QUANTITATIVE MICROFABRIC ANALYSIS OF POLYMER-MODIFIED HIGH-POROUS MORTARS

Andreas Jenni[1], Roger Zurbriggen[2], Marco Herwegh[1] and Lorenz Holzer[3]

[1] Institute of Geological Sciences, University of Berne, Berne, Switzerland.
E-mail: andreas.jenni@geo.unibe.ch
[2] Elotex AG, Sempach Station, Switzerland. E-mail: roger.zurbriggen@elotex.com
[3] EMPA, Dübendorf, Switzerland. E-mail: lorenz.holzer@empa.ch

ABSTRACT

Redispersible powder (RP) and cellulose ether (CE) are two standard additives for ceramic tile adhesives to improve (a) the performance with respect to workability and water retention (mainly given by CE) of the fresh paste, as well as (b) final strength and flexibility properties of the hardened mortar (mainly improved by RP). In addition to established methods for visualisation and quantification of mortar components like pores, fillers and cement minerals, new methods had to be developed for the polymer phases. Based on stained polymers in combination with fluorescence and electron microscopy, digital images can be generated which are processed by image analysis resulting in distribution diagrams of the different polymers in the mortar.

The distributions of all mortar phases can be used to investigate the time dependent changes of processes occurring during preparation, application and hardening of mortars. It becomes evident that individual polymers show specific behaviours during the different stages. During an early stage, CE and latices become locally enriched at the cement matrix/air interfaces due to their high surface activity. In case of CE, the migration of the pore water into the porous substrate induces an enrichment towards the mortar base. In contrast, latices tend to stay in place. Therefore, CE is soluble, whereas latex is not redispersible in the pore water.

The data resulting from the distribution diagrams of different formulations will be compared with their physical properties (e.g. adhesion strength). The quantitative distribution pattern of an additive is one key to understand its performance in the application including the influence on the final mechanical properties of the mortar.

1. INTRODUCTION

Polymer-modified cement mortars, namely, tile adhesives, can be described and classified either by their compositions, working parameters (e.g., application, workability, storage conditions) or final physical properties. All these parameters are closely related to the time-dependent interaction of the individual components (polymers, cement phases, mineral fillers, pores). From initial mixing to the hardened end product (Figure 1) the microfabric evolution in this complex polyphase system links all the different stages and their physicochemical aspects. Therefore, detailed microscopy of polymer-modified mortars is regarded as a key tool for a profound understanding of such composite materials.

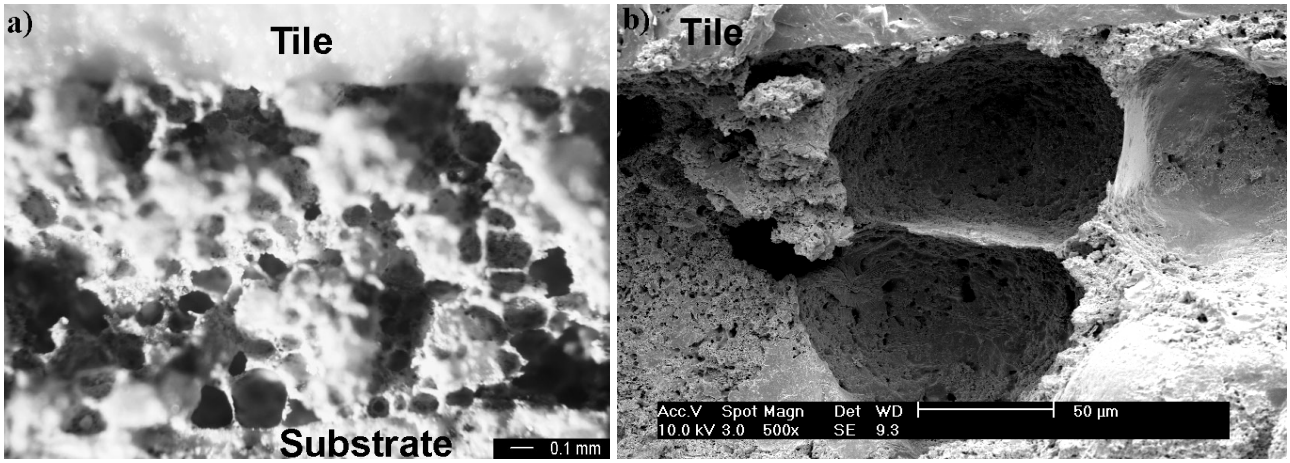

Figure 1: a) Reflected light microscope image of a polymer-modified mortar. Fracture surface from tile (top) through highly porous mortar to concrete substrate (bottom); b) environmental scanning electron microscope image of an uncoated fracture surface across a tile (top) mortar interface. Three air voids are separated by a polymer film (vertical) and a cement-polymer composite wall (horizontal).

Common tile adhesives are commercially available as premixed dry compounds. At the construction site only a predefined amount of water must be added and mixed to achieve a ready-to-use fresh mortar. The components of such an instant dry mortar can basically be grouped into binders, fillers and additives. Ordinary Portland cement (OPC) is the most typical binder, which is added in the amount of 20-40 wt%. Other types of cement, hemihydrate, natural and industrial puzzolana can be combined with OPC or even replace it completely. 60-80 wt% are composed of filler materials, typically siliceous and/or carbonate sand and finer grained fractions (<100 µm), but also various light weight fillers can be contained. Typical additives are cellulose ether (CE) and redispersible powder (RP). In order to achieve a good workability and water retention, approx. 0.5 wt% CE is added. RP (0.5-5 wt%) further improves the workability of the fresh mortar and finally provides an increased adhesive strength of the hardened end product.

2. METHODS AND RESULTS

Planar and polished sections of the high-porous mortars (bulk porosity of up to 40 vol%) are required for quantitative microfabric analysis. Unfortunately, conventional impregnation and polishing techniques often affect the polymer phase causing severe artefacts by dissolution and redispersion followed by redistribution and leaching, as well as mechanical damaging of the fragile microstructure (Figure 1). In order to prevent these artefacts various impregnation resins, polishing and cleaning aids were evaluated according to their dissolution effect on the polymer phases (CE, latices and polyvinyl alcohol). Chemical elements (e.g., Cl) occurring exclusively in some polymers or selective staining of the polymers allow their discrimination in the mortar by element mapping (electron microscopy) or fluorescence microscopy.

With these newly developed methods, we can allocate and quantify the polymer phases in addition to the conventionally measured mortar components like pores, fillers and cement minerals (anhydrous clinker and hydrates) [1], [2], [3]. Figure 2, for example, presents a micrograph taken by fluorescence microscopy. Prior to mixing the dry components (35.0 wt% OPC, 42.0 wt% quartz sand, 22.5 wt% carbonate powder, 0.5 wt% CE), CE had been stained by a fluorescence dye, following a similar procedure described by [4]. Under fluorescent light, the occurrence of CE is manifest by very bright yellow colour. Additionally, fillers, air voids and the cement matrix can be distinguished by their different fluorescence behaviour. The segmentation of the phases via image

analysis allows a distribution diagram (Figure 2) to be reconstructed showing the full width of the mortar bed (5 cm). In this way, each horizontal bar of the diagram represents the mortar composition, summarised over the entire image length for a specific depth interval. The diagram shows enrichments of CE and distribution variations of fillers, air voids and the cement matrix through the mortar profile.

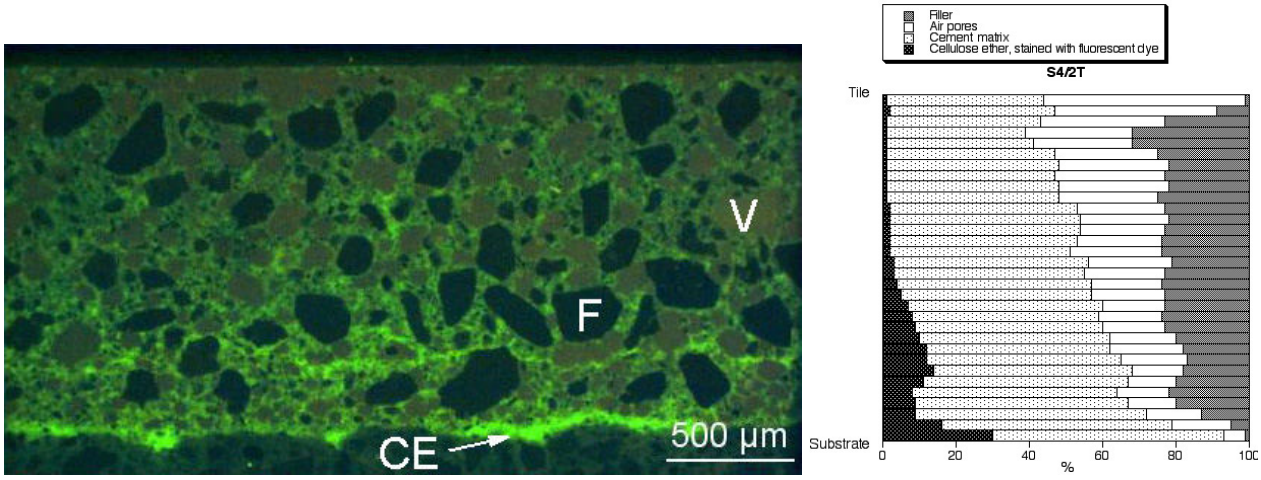

Figure 2: left: mortar with tile (top) and concrete substrate (bottom), F: mineral filler, V: air void, CE: cellulose ether stained with fluorescent dye; right: profile across the mortar ranging from the concrete substrate to the ceramic tile. The diagram shows the distribution of CE (including an overshining effect), the cement matrix (cement phases, capillary porosity), filler and air voids in area%. The phases were segmented according to their specific colour range on the micrograph and are not normalised with respect to their initial composition (wt%).

Allocation and quantification of latices is shown by a mortar which has been modified with ethylene/vinyl acetate/vinyl chloride latex (35.0 wt% OPC, 40.0 wt% quartz sand, 22.5% wt carbonate powder, 2.0 wt% latex, 0.5 wt% CE). In order to visualise the spatial distribution of the latex, chlorine mappings were acquired on an electron microprobe by wavelength dispersive spectroscopy. The small chlorine concentration requires long dwell times which leads to a total acquisition time of approx. 8 h for an image with a size of 750x750 pixels, i.e., 1500x1500 µm. Figure 3 shows the chlorine map and the corresponding distribution diagram of the latex. The latter was normalised with respect to the cement matrix to avoid an influence of air void and filler distribution on the latex distribution.

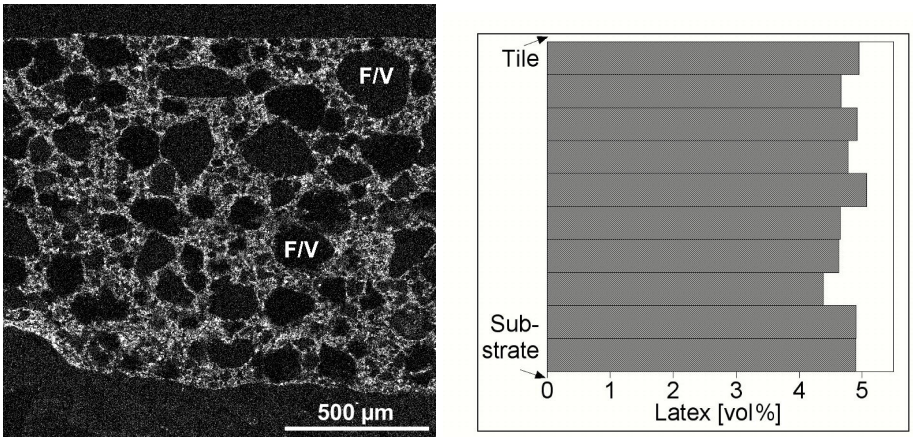

Figure 3: left: mortar with tile (top) and concrete substrate (bottom), mortar with mineral fillers and air voids (black, F/V) and the chlorine distribution (latex) in the cement matrix; right: profile across the mortar ranging from the concrete substrate to the ceramic tile. The diagram shows the distribution of latex in the cement matrix in vol%, normalised with respect to its initial composition.

3. DISCUSSION

Fluorescence light microscopy of FITC-stained CE revealed a strong enrichment of CE towards the porous concrete substrate in mortars without latex-modification. This strong segregation, which causes large concentration gradients (Figure 2), must be related to the migration of free pore water in the first minutes to hours after application. Hence, CE must be dissolved in the pore water rather than being adsorbed to mineralic surfaces of filler and cement grains. On the other hand, the air entraining ability indicates that CE partly occupies the air/slurry interface to stabilise air bubbles. CE trapped at air/slurry interfaces is regarded as stationary whereas CE dissolved in the pore water can be transported together with the migrating capillary water. The accumulation of CE in the lowermost part of the mortar bed creates a CE-rich contact layer with increased water retention. Interestingly, only a limited amount of CE is able to enter the porous concrete substrate over short distances. This penetration is in particular concentrated along microcracks in the concrete substrate. It is as yet unknown, the extent to which the CE enrichment affects cement hydration in the lowermost part of the mortar and the consequences for the final adhesion properties of the substrate.

In mortars containing CE and latex, the CE distribution pattern is different from mortars without latex. The strong enrichment towards the substrate is less evident, but there is an additional enrichment towards the uppermost 30 µm of the mortar layer, directly underneath the mortar/tile interface. We believe, therefore, that latices stop the large-scale migration of CE and/or reduce the migration of the free pore water, but allow small-scale migration due to the high surfaces activity of CE which enhances a CE accumulation at the mortar air interface.

Latices seem to be homogeneously distributed throughout the cement matrix. As the latex particles have a defined particle size of about 1 µm, they cannot pass the capillary pores, and are, therefore, restricted to very local migration. However, some latices tend to be enriched at the mortar-tile interfaces, which significantly increases adhesion strength. These enrichments result from a local fractionation mechanism, which must be attributed to an early stage of mortar evolution, i.e., to the time interval between mortar application on the substrate and the inlaying of the tile.

Our new microstructure analysis techniques have also been applied to water stored samples. The distribution pattern of the ethylene/vinyl acetate/vinyl chloride latex did not change. However, the CE is remobilised and now enriched towards the concrete substrate. This in agreement with conclusions drawn from wetting experiments on in-situ polymer films [5], which showed that latices cannot be remobilised, but CE is redissolved in water. For that reason, the remobilisation and migration of CE in the hardened mortar during wet storage is not hindered by latex films.

In addition, distribution patterns of the non-polymeric phases can also be used to detect processes occurring during preparation, application and hardening of mortars. For example, the enrichment of air voids towards the tile interface (Figure 2) is related to additional air entrapment between the pre-applied mortar with its uneven surface and the tile. The amount of entrapped air is supposed to increase with both longer open time and the tendency of the mortar to form a skin. The mechanism of air entrapment generates a mechanically weak zone and might induce decreased adhesion strength at the mortar-tile interface.

4. CONCLUSIONS

This study demonstrates that even in a highly viscous mortar, phases strongly fractionate and can produce large concentration gradients across the mortar bed. The quantitative distribution pattern of an additive is a major key to understand its performance in the application.

Each quantitative microscopic technique is dedicated to a certain additive chemistry requiring specific staining methods. Therefore, different staining and scanning microscopy techniques must be combined to generate a global picture of the whole mortar microstructure, which is valid over the entire range of thickness and composition.

In the future, these newly developed methods will be applied to a wider range of mortar types subjected to different storage types (dry vs. wet storage). The resulting data will be compared with the physical properties (e.g. adhesion strength) of the different samples.

In order to understand the physical properties, and to develop new products with specific performance profiles, the quantitative microscopy of polymer structures is regarded as an important step in the study of the entire evolution of the microfabric of such composite materials.

REFERENCES

[1] Scrivener, K.L., Patel, H.H., Pratt, P.L. and Parrott, L.J. Analysis of phases in cement paste using backscattered electron images, methanol adsorption and thermogravimetric analysis, Materials Research Society Symposium, Boston, 1986, vol. 85, pp. 67-76.

[2] Kjellsen, K.O. and Detwiler, R.J. A quantitative S.E.M. image analysis of cement paste microstructure. VTT Symposium, Espoo, 1992, vol. 136, pp. 28-40.

[3] Yang, R. and Buenfeld, N.R. Binary segmentation of aggregate in SEM image analysis of concrete, Cement and Concrete Research, vol. 31, 2001, pp. 437-441.

[4] De Belder, A.N. and Granath, K. Preparation and properties of fluorescein-labelled dextrans, Carbohydr. Res., vol. 30, 1973, pp. 375-378.

[5] Holzer, L., Jenni, A. and Zurbriggen, R. Eine in-situ ESEM-Studie über mikrostrukturelle Veränderungen polymervergüteter Mörtel während der Wasserlagerung, 3. Tagung Bauchemie, Würzburg, 2001, GDCh Monographie, vol. 24, pp. 156-159.

QUANTITATIVE MICROFABRIC ANALYSIS OF POLYMER-MODIFIED HIGH-POROUS MORTARS

Andreas Jenni[1], Roger Zurbriggen[2], Marco Herwegh[1] and Lorenz Holzer[3]

[1] Institute of Geological Sciences, University of Berne, Berne, Switzerland.
E-mail: andreas.jenni@geo.unibe.ch
[2] Elotex AG, Sempach Station, Switzerland. E-mail: roger.zurbriggen@elotex.com
[3] EMPA, Dübendorf, Switzerland. E-mail: lorenz.holzer@empa.ch

Andreas Jenni

Institute of Geological Sciences, University of Berne, Baltzerstrasse 1, CH-3012 Berne, Switzerland

Telephone:	0041 31 631 87 58 Fax: 0041 31 631 48 43
E-mail:	andreas.jenni@geo.unibe.ch
Present Affiliation:	PhD position at the Geological Institute, University of Berne; research project founded by the Swiss Commission for Technology and Innovation in cooperation with Elotex AG, Switzerland, and the Swiss Laboratories for Materials
Testing and Research:	Microstructures of polymer-modified cement mortars
Education:	Masters degree in earth sciences
Experience:	Characterisation of microstructures (M. Herwegh, A. Jenni: Granular flow in polymineralic rocks bearing sheet silicates: new evidence from natural examples.- Tectonophysics 332, Pages 309-320, 2001.); light, fluorescence, laser scanning and electron (SEM, ESEM, TEM) microscopy combined with digital image analysis.

ON THE STATE AND ROLE OF ALKAL'S DURING THE ACTIVATION OF ALKALI-ACTIVATED SLAG CEMENT

Caijun Shi

CJS Technology Inc., 2116 Upland Dr., Burlington, Ontario, Canada L7M 2Z2
E-mail: caijunshi@yahoo.com

ABSTRACT

This paper reviews the hydration and hydration products of alkali-activated slag cements, interactions between alkali ions and calcium silicate hydrate (C-S-H), and leachability of alkalis from C-S-H. The presence of alkali ions of the activator ensures a high alkaline environment for vitreous slag to initiate and to continue hydration. C-S-H, with a low C/S ratio and a significant amount of alkalis, is the major hydration product of alkali-activated slag cements although some minor hydration products may vary with the nature of the slag and activator used. The amount of alkalis in C-S-H increases with the increase of alkali concentration in the solution and with the decrease of C/S ratio. Alkalis incorporate into C-S-H in three different mechanisms. One or another mechanism may dominate depending on the C/S ratio of C-S-H. However, the three mechanisms co-exist. The incorporation of alkalis into C-S-H changes its solubility curve. Alkalis in C-S-H can leach out easily. The solubility curve of C-S-H changes to its original shape when alkalis leach out. Thus, alkalis provide a high pH environment and act as catalysts rather than reactants during the hydration of alkali-activated slag cements.

1. INTRODUCTION

Alkali-activated slag cements are drawing more and more attention because of their high performance and utilization of by-product materials in their manufacture. The principle of alkaline activation of slag has been known since the 1940's [1]. Although many attempts have been made to explain the hydration process of alkali-activated slag cement, the roles of activators are still not well understood.

It is generally agreed that the performance and microstructure of alkali-activated slag cements are determined by the chemical and mineralogical compositions of the slag and the dosage and nature of the activator(s) used. Thus, it is not surprising that different results are obtained in different laboratories since the raw materials used in various laboratories could be very different. Different mechanisms have been proposed to explain the roles of activators. For example, Kondo regarded NaOH as a catalyst during the activation of slag [2]. However, Narang and Chopra [3] believed that NaOH took part in the reactions in much the same way as lime and gypsum but, due to strong cationic influence, acts relatively strongly.

In this paper, the author reviews the hydration and hydration products of alkali-activated slag cements, interactions between alkalis and C-S-H, leachability of alkalis in C-S-H, and tries to clarify the status and role of alkalis in alkali-activated slag cements.

Proceedings of the 11th International Congress on the Chemistry of Cement (ICCC)
'Cement's Contribution to the Development in the 21st Century'
Hosted by: The Cement and Concrete Institute of South Africa
CD-ROM produced by: Document Transformation Technologies
11 - 16 May 2003, Durban, South Africa
ISBN Number: 0-9584085-8-0
Editors: Dr G. Grieve and G. Owens
Congress Organised by: Event Dynamics

2. LIHYDRATION BEHAVIOUR OF ALKALI-ACTIVATED SLAG CEMENTS

Many researchers have tried different means to investigate the early hydration of alkali-activated slag cements. Shi and Day [4, 5] conducted a systematic study on the early hydration behaviour of alkali-activated slag cements containing different activators using a calorimeter.

The hydration behaviour of alkali-activated slag cements can be classified into three types as shown in Figure 1. For type I, one peak occurs during the first few minutes and no peaks appear thereafter. Hydration of the slag in water or in Na_2HPO_4 solution at both 25 and 50°C is an example. In this case, the slag usually does not set and harden during the testing period. For Type II, only one initial peak appears before the induction period and one accelerated hydration peak appears after the induction period. The hydration of slag activated by alkali hydroxides belongs to this type. For Type III, two peaks, one initial and one additional, appear before the induction period and one accelerated hydration peak appears after the induction period. The initial peak could be lower or higher than the additional initial peak depending on the nature of activators and hydration temperature. This type of hydration includes the cements activated by alkali weak acid salts including silicates, carbonates, phosphates and fluorides.

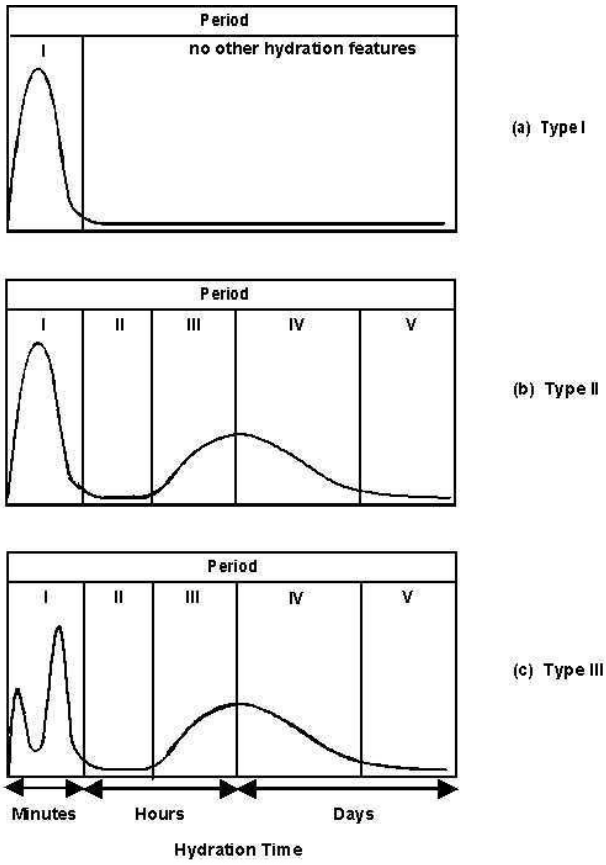

Figure 1. Hydration Models for Alkali-Activated Slag Cements [4]

Although alkali fluoride has a low pH, it can still activate the potential hydraulic reactivity very obviously. The hydration behaviours of slag are in agreement with the statement that any alkaline compound, whose anion or anion group can react with Ca^{2+} to form a less soluble or hardly soluble Ca-compound, can act as an activator for a slag [6]. The initial pH has an effect on the initial dissolution and hydration of the slag. However, the further hydration of the slag is determined by the formation of a hardly soluble Ca-compound.

When an alkali weak acid salt is used, it has a low initial pH, so that the initial dissolution and hydration of the slag will be slow. However, the formation of the hardly soluble Ca-compound will leave free alkalis in the solution and increases the alkalinity of the solution, which then accelerates the hydration of the slag. If an alkali salt solution has a low pH, and no hardly soluble Ca-compound can form, the alkali salt cannot be used as an activator. It has been noted that the Ca-Compound has a great effect on the structure formation and properties of hardened cement pastes [4]. The anion or anion group plays a critical role the hydration of alkali-activated slag cements in two aspects: initial pH and the formation of hardly soluble Ca-compound.

3. HYDRATION PRODUCTS OF ALKALI-ACTIVATED SLAG CEMENT

Many researchers have investigated the hydration products of alkali-activated slag cements and it is generally agreed that the major hydration product of alkali-activated slag cements is calcium silicate hydrate (C-S-H) with a low C/S ratio [7-10]. However, a variety of minor hydration products such as

C_2ASH_8, $C_3AS_xH_{6-2x}$, C_4AH_{13}, M_4AH_{13}, $C_3A.CaCO_3.12H_2O$, etc, have been reported. There is no doubt that the minor hydration products vary with the composition of both slag and activator.

3.1 Effect Of Chemical Composition Of Slag On Hydration Products

The chemical compositions of a slag vary among ore bodies and furnace operations. Osborne et al. [11] conducted a large-scale test of practical furnace operation and determined the composition of blast furnace slag for optimum furnace operation in CaO-MgO-Al_2O_3-SiO_2 system (Table 1).

Table 1 Optimum Chemical Composition of Blast Furnace Slag for Furnace Operation (% by mass) [11]

No.	Al_2O_3	SiO_2	CaO	MgO
1	5.0	36.0	43.0	16.0
2	10.0	32.0	44.0	14.0
3	15.0	28.5	44.0	12.5
4	20.0	24.0	45.0	11.0
5	25.0	19.0	48.0	8.0
6	25.0	12.0	57.0	6.0
7	30.0	9.0	56.0	5.0
8	35.0	7.0	54.0	4.0

Experimental results have indicated that the chemical composition of blast furnace slag has a significant effect on its hydration process due to the formation of different hydration products [12]. In many cases the MgO content of blast furnace slag is low and the slag can be described by the CaO-SiO_2-Al_2O_3 system. The phase diagram of CaO-Al_2O_3-SiO_2-H_2O system, as shown in Figure 2 indicates that five different products such as C-S-H, $Ca(OH)_2$, C_4AH_{13}, C_2ASH_8 and CS_2H_3 could appear in this system, while calcium hydroxide and gehlenite hydrate cannot co-exist at equilibrium [13]. In reality, equilibrium is attained only locally on a scale of microns or less due to difficulty of ionic transport within the pastes [14]. It must also be recognized that some calcium hydroxide may be made essentially non-reactive by the formation of an impermeable coating of C-S-H [15]. Thus, it is not surprising that calcium hydroxide and gehlenite hydrate have been detected at the same time [16].

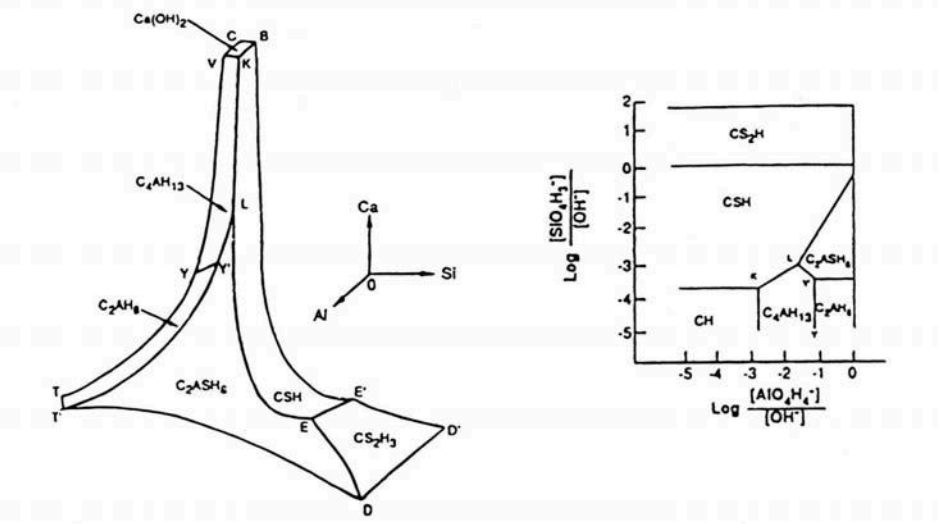

Figure 2. Phase Diagram in CaO-Al_2O_3-SiO_2-H_2O system [13]

It can also be expected that hydration products vary with the chemical composition of the slag in the presence of an activator. Granulated phosphorus slag consists mainly of CaO and SiO_2, and its Al_2O_3

and MgO content is usually very low. X-ray diffraction analysis and scanning electron microscopic observations have indicated that C-S-H is the only hydration product of activated ground granulated phosphorus slag when NaOH is used as an activator [17, 18]. However, C_2ASH_8 and C_4AH_{13} have also been detected in NaOH activated blast-furnace slag in addition to C-S-H [19]. C_2ASH_8 or gehlenite hydrate is an AFm phase which has an interlayer aluminosilicate anion [20]. M_4AH_{13}, instead of C_4AH_{13}, occurs if the MgO content of the slag is high. Since strength depends on initial porosity, the degree of reaction and space filling, and the intrinsic strength of the reaction products [21], the chemical composition of slag will have a direct influence on strength development of alkali-activated slag cement.

3.2 Effect Of Chemical Activators On Hydration Products

The nature of the chemical activator influences the hydration products. It was found that C-S-H, C_4AH_{13} and C_2ASH_8 are products of NaOH and lime-activated slag, and ettringite forms when sulphates are present [19]. X-ray diffraction patterns of alkali-activated slag and ASTM Type III Portland cement pastes hydrated for 540 days at 23°C are shown in Figure 3. Hydration products of alkali-activated slag are different from those of Portland cement pastes. The main hydration product of the three alkali-slag cement pastes is C-S-H, but minor hydration products vary with the nature of activators. C_4AH_{13} appears in $Na_2O.SiO_2$-activated slag, $C_3A.CaCO_3.12H_2O$ in Na_2CO_3 activated slag and C_4AH_{13} and C_2ASH_8 in NaOH-activated slag [22]. Other research found that the addition of different activators changes hydration products of lime-natural pozzolan, lime-fly ash and lime-slag blends [23]. Change in hydration products due to the presence of different activators will change the hydration process and microstructure formation, which affect the strength development of the cement in turn.

Wang and Scrivener [8, 24] examined NaOH- and waterglass-activated slag cement pastes using XRD. As hydration time increases, the diffuse peak attributed to the $CaO\text{-}SiO_2\text{-}Al_2O_3$ vitreous structure decreases, but a peak belonging to C-S-H intensifies. The crystallinity of C-S-H in NaOH-activated slag cement is obviously higher that that in waterglass-activated slag cement. A crystalline compound $Mg_6Al_2CO_3(OH)_{16}.4H_2O$ also appears in NaOH-activated slag cement.

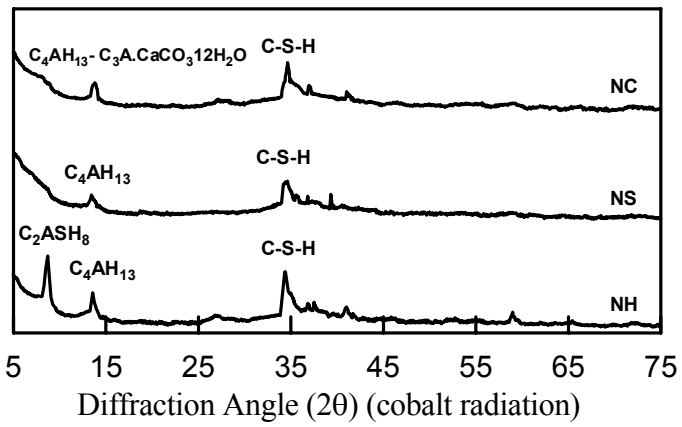

Figure 3. XRD Patterns of Alkali-Slag Cement Pastes Hydrated for 540 Days at 23°C [22]

Glukhovsky et al [7] reported a series of crystalline compounds such as hydrogarnet, zeolitic phases, mica phases including nepheline, natrolite, analcite, paragonite and gismondite, from the hydration of alkali-activated slag cements based on XRD analyses. However, many researchers [17, 25, 26, 8] could not identify those crystalline phases in hardened alkali-activated slag cement pastes cured at room temperatures, even after 15 years of curing [10]. Crystalline compounds such as xonotlite, tobermorite, sodium-zeolite, such as NAS_2H_3 could be identified in hydrothermal treated alkali-activated slag cement pastes [10, 27].

4. INTERACTIONS BETWEEN ALKALIS AND C-S-H

Stade [28] suggested that the incorporation of alkalis into C-S-H, from room to elevated temperatures, follow the following three mechanisms:

(1) Neutralization of acidic Si-OH groups by Na^+ or K^+:

$$C\text{-}S\text{-}H + M^+ \text{---> } M\text{-}C\text{-}S\text{-} \quad (1)$$

(2) Ion exchange of Na/K for Ca. This process would increase with increasing C/S ratio.

$$C\text{-}S\text{-}H + M^+ \text{---> } M\text{-}C\text{-}S\text{-}H + Ca^{2+} \quad (2)$$

(3) cleavage of Si-O-Si bonds by Na^+ or /K^+, with the attachment of Na^+ or /K^+ to Si, represented by:

$$Si\text{-}O\text{-}Si + 2M^+ \text{ ---> } 2Si\text{-}O\text{-}M \quad (3)$$

The first mechanism happens mainly to C-S-H with a low C/S ratio because it contains a high concentration of acidic Si-OH group. The second mechanism is applied mainly to C-S-H with a high C/S ratio. The third mechanism depends on the surface area of C-S-H. Due to the complexity of the system, it is also suggested that multiple mechanisms at any one time may be operating to uptake alkaline ions.

It is agreed that the incorporation of alkalis into C-S-H increases as the C/S ratio of C-S-H decreases. It was found [29] that there is almost a linear relationship between the log scale of the Na/Ca and the C/S ratios of the C-S-H, ranging from 0.85 to 1.8, as shown in Figure 4. This means that the incorporation of alkalis into C-S-H decreases swiftly as the C/S ratio of C-S-H increases. The alkali incorporated into C-S-H is almost linearly proportional to the initial concentration of the alkali in the solution. Kalousek [30] found that the limited composition for N-C-S-H system is $0.25Na_2O.CaO.SiO_2.xH_2O$. Taylor [31] found that the Na/Ca atom ratio is about 0.01 in hydrated Portland cement pastes, since the C/S ratio of C-S-H in hydrated Portland cement paste usually ranges from 1.2 to 2.3 depending on the cement composition, water to cement ratio, hydration temperature, age, etc. [32]. The incorporation of impurities into a crystalline structure is usually governed by crystallochemical restraints that limit the number of possible replacement mechanisms and their stoichiometry, while C-S-H is a poorly crystallized version of the mineral tobermorite and the main restriction for the incorporation of alkali into the structure of C-S-H is probably the condition of electroneutrality [33].

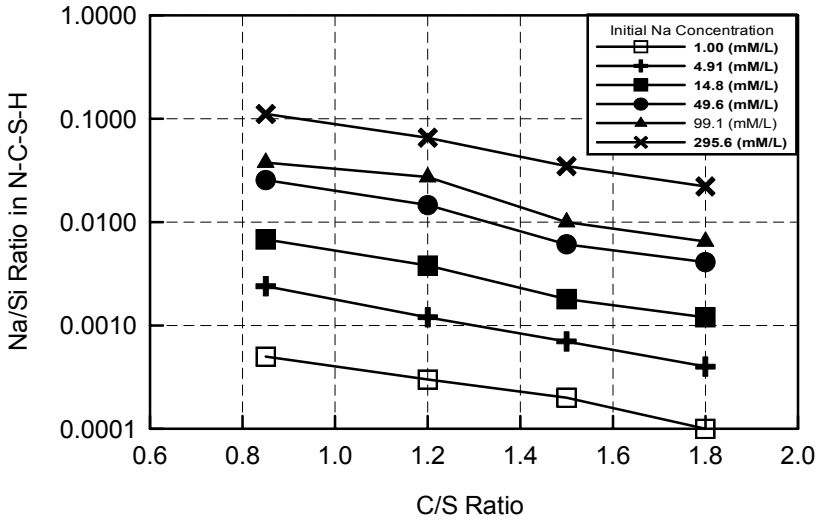

Figure 4. Effect of C/S Ratio and Initial Alkali Concentrations on Na/Si Ratio in C-S-H Phase [29]

Curing temperature can have a significant effect on the alkali retention capacity of C-S-H. For a given C/S ratio, C-S-H formed at elevated temperatures has a higher crystallinity and lower surface area, and will bind smaller amounts of alkalis than that formed at lower temperatures. ^{29}Si NMR spectroscopy indicated that there is little difference between Na-free and Na-contained C-S-H gel with a high C/S ratio, however, some differences were found in C-S-H gels with a low C/S ratio. Q_2/Q_1 ratio decreases as the Na content increases [34]. This indicates that the presence of Na decreases the Si chain lengths in C-S-H.

Taylor concluded from his analysis of pore solution data that sodium was significantly better bound into hydrated cement paste than potassium [31]. Experimental results obtained by Stade [28], and Hong and Glasser [29] indicated that there is no significant difference in uptake of Na and K by C-S-H.

C-S-H in NaOH activated-slag cement pastes has a similar C/S ratio, but waterglass-activated slag cement paste has a C/S ratio lower than that of the slag due to the addition of SiO_2 from the waterglass [8]. The initial alkali concentration in alkali-activated slag pastes can be as high as several moles. It can be expected that the alkalis bound by C-S-H are higher that that by Portland cement.

Hong et al [26] monitored the concentration of Na_2O in the liquid phase of 0.3 N NaOH and Na_2SiO_3 activated-slag cements with a water to slag ratio of 20 from 3 hours to 28 days. It was found that the Na_2O concentration in the liquid did not change with time in Na_2SiO_3-activated slag cements, but decreased slightly with time in the NaOH activated-slag cement. In another study, it was found that 80 to 90% of initial alkali could be detected in the liquid phase of the hardened alkali activated slag cement (Figure 5). The author proposed that the alkaline cation acts as a destruction catalyst, based on the wave character of the change of Na_2O concentration in the liquid phase of hardened alkali-activated slag cement, during the destruction of the glassy slag structure and the formation of hydrates [35].

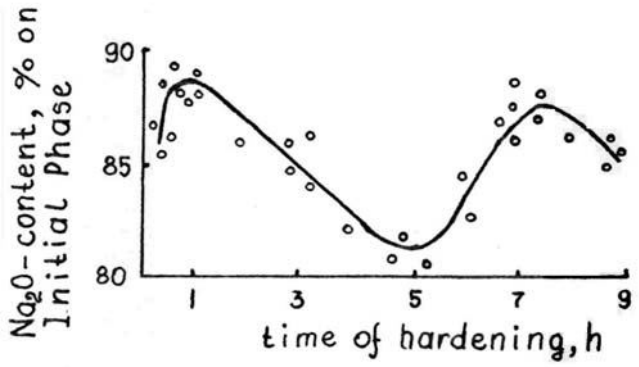

Figure 5. Wave character of the change of Na_2O concentration in the liquid phase of hardened alkali-activated slag cement [35]

5. SOLUBILITY OF C-S-H AND LEACHABILITY OF ALKALIS FROM C-S-H

The presence of alkalis significantly increases the solubility of Si and decreases the solubility of Ca due to common ion effect. However, it does not change the K_{sp} of C-S-H. The solubility curve of N-C-S-H is very different from that of C-S-H (Figure 6), but is closer to that of C-S-H after the leaching test. Analysis of liquid and solid phases indicated that the Na/Ca molar ratio in leachates is much higher than that in the solid phase, which means that Na is preferably leached from the solid phase. The Na/Ca molar ratio in the leachate consistently increases with decreasing C/S ration of N-C-S-H gel. This is attributed to the fact that lower C/S ratio gels are relatively enriched in Na.

Several studies have been conducted on the leachable alkalis in alkali-activated slag cement pastes in order to understand the activation mechanism of slag cements. Belitsky et al [36] measured the non-

leachable amount of Na_2O by immersing 2 grams of 1 - 2 mm size crushed hardened $Na_2O.nSiO_2$ activated slag cement pastes in 100 ml of distilled water for 7 days. The total alkali content was determined by dissolving the pastes in 1 N HCl solution. Experimental results indicated that the non-leachable Na_2O varied only from 0.17 to 0.37% by mass of slag, depending on the age, molar ratio n and dosage of $Na_2O.nSiO_2$.

Eight batches of hardened alkali-activated slag cement pastes were prepared using four types of slag - gelhlenite, akermanite, diopside and melilite, and two types of activators – NaOH and Na_2CO_3 and cured at 80, 200 and 250°C for 28, 90, 360 and 720 days [10]. The cement pastes were ground in a agate mill and the ground samples washed with distilled water until it showed pH=7. The measured soluble alkali content varied from about 16% to 46% and changed slightly with the type of activator and the composition of slag, but decreased significantly as the curing temperature increased.

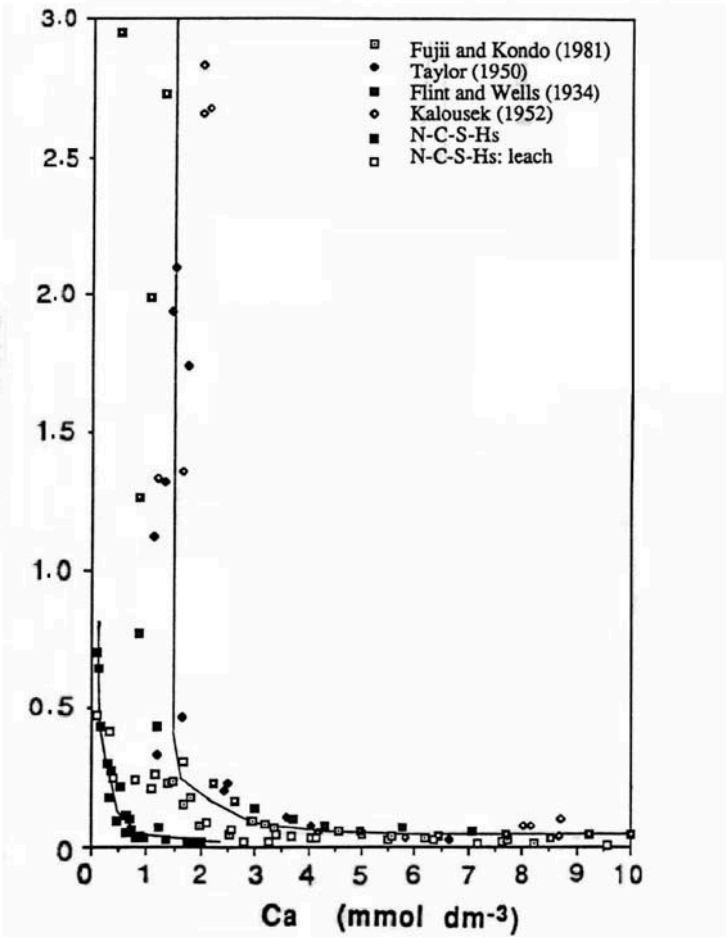

Figure 6. Solubility Curves of C-S-H and N-C-S-H [34]

6. SUMMARY

The hydration of alkali-activated slag cements falls into three cataegories: For type I, one peak occurs during the first few minutes and no peaks appear thereafter. In this case, the slag usually does not set and harden during the testing period. For Type II, only one initial peak appears before the induction period and one accelerated hydration peak appears after the induction period. For Type III, two peaks, one initial and one additional initial peaks, appear before the induction period and one accelerated hydration peak appears after the induction period.

C-S-H with a low C/S ratio is the major hydration product of alkali-activated slag cements although other minor hydration products may vary with the nature of the slag and activator used. Solubility Curves of C-S-H and N-C-S-H [34] incorporate into C-S-H in three different mechanisms: (1) neutralization of acidic Si-OH groups by Na^+ or K^+, (2) ion exchange of Na/K for Ca, and (3) cleavage of Si-O-Si bonds by Na^+ or K^+, with attachment of Na^+ or K^+ to Si. Depending on the C/S ratio of C-S-H, one or another mechanism may dominate, however, the three mechanisms co-exist.

The incorporation of alkalis into C-S-H increases as the alkali concentration in the solution increases and as the C/S ratio of the C-S-H decreases. The main restriction for the incorporation of alkali into the structure of C-S-H is probably the condition of electroneutrality. The incorporation of alkalis affects the solubility curve of C-S-H. However, alkalis in C-S-H can be leached out easily. The leaching out of alkali from C-S-H moves its solubility curve toward its original curves.

The presence of alkalis keeps a high pH value in the solution, which is important to initiate and to continue the hydration of the slag. However, the alkalis are not really involved in the hydration process and hydration products. Alkalis can be simply regarded as catalysts rather than reactants. However, the anion or anion groups of activators have a great effect on the hydration, structure formation and properties of hardened alkali-activated slag cements.

REFERENCES

[1] Pudon, A. O., The action of alkalies on blast-furnace slag, Journal of the Society of Chemical Industry, 1940, Vol.59, pp.191-202.

[2] Kondo, R. Goto, G. and Diamon, M., The Latent Property of Granulated Blast Furnace Slag by Various Activators, Tetsu to Hagane, 1979, Vol.65, pp.1825-1829.

[3] Narang, K. C. and Chopra, S. K., Studies on Alkaline Activation of BF, Steel and Alloy Slags, Silicates Industriels, 1983, Vol.48, No.9, pp.175-182.

[4] Shi, C. and Day, R. L., A Calorimetric Study of Early Hydration of Alkali-Slag Cements, Cement and Concrete Research, 1995, Vol.25, No.6, pp.1333-1346.

[5] Shi, C. and Day, R. L., Factors Affecting Early Hydration Characteristics of Alkali-Slag Cements, Cement and Concrete Research, 1996, Vol.26, No.3, pp.439-448.

[6] Shi, C. and Li, Y. Investigation on Some Factors Affecting the Characteristics of Alkali-Phosphorus Slag Cement, Cement and Concrete Research, 1989, Vol.19, No.4, pp.527-533.

[7] Gluhovsky, V. D., Rostovkaja, G. S., and Rumyna, G. V., High Strength Slag-Alkali Cement, Proceedings of 7th International Congress on the Chemistry of Cements, Vol.III, pp.V-164-168, Paris, 1980.

[8] Wang S., Scrivene, K. L, Hydration Products of Alkali Activated Slag Cement, Cement and Concrete Research, 1995, Vol.25, No.3, pp.561-571.

[9] Shi, C., Day, R. L., Wu, X. and Tang, M., Comparison of the Microstructure and Performance of Alkali-slag and Portland Cement pastes, Proceedings of 9th International Congress on the Chemistry of Cement, New Delhi, India, 1992, Vol.3, pp.298-304.

[10] Malolepszy, J., Some Aspects of Alklai Activated Cementitious Materials Setting and Hardening, Proceedings of 3rd Beijing International Symposium on Cement and Concrete, International Academic Publishers, 1993, Vol.2, pp.1043-1046.

[11] Osborn, E. F, et al, Optimum Composition of Blast-Furnace slag as Deduced from Liquids Data for the Quaternary System CaO-MgO-Al_2O_3-SiO_2, Journal of Metal, 1954, Vol.6, No.1, pp.33-45.

[12] Hommertgen, C. and Odler, I., Investigation on Hydraulically Reactive Glass in the System CaO-Al_2O_3-SiO_2, Symposium Proceedings of Materials Research Society, ed. by Glasser, F. P., McCarthy, G. J., Young, J. F., Mason, T. O. and Pratt, P. L., 1991, pp165-172.

[13] Dron, R., Experimental and Theoretical Study of the CaO-Al_2O_3-SiO_2-H_2O System, Proceedings of 6th International Congress on the Chemistry of Cement, Moscow, 1974, supplementary paper 9-5.

[14] Lachowski, E. E., Mohan, K. and Taylor, H. F. W., Analytical Electron Microscopy of Cement Pastes, II. Pastes of Portland Cement and Clinkers, Journal of American Ceramic Society, 1980, Vol.63, No.7-8, pp.447-452.

[15] Malquori, G., Portland-Pozzolan Cement, Proceedings of 4th International Symposium on the Chemistry of Cement, Washington, 1960, Vol.II, pp.983-1000.

[16] Shi, C. and Day, R. L., Chemical Activation of Lime-Slag Blend, Proceedings of 5th International Conference on Fly Ash, Silica Fume, Slag and Natural Pozzolans in Concrete, SP153-61, 1995, Vol.2, pp.1165-1177.

[17] Shi, C., Studies on Alkaline Activation of Reactivity of Granulated Phosphorus Slag, Southeast University, M. Eng. Thesis, 1987 (in Chinese).

[18] Shi, C., Li, Y. and Tang, X.; Preliminary Investigation on the Activation Mechanism of Phosphorus Slag, Journal of Southeast University (in Chinese), 1989, Vol.19, No.1, pp.141-145.

[19] Regourd, M., Structure and Behaviour of Slag Portland Cement Hydrates, Proceedings of the 7th International Congress on the Chemistry of Cement, Paris, 1980, Vol.1, III-2/11-26.

[20] Taylor, H. F. W., Cement Chemistry, Academic Press, London, 1990.

[21] Helmuth, R., Fly Ashes in Cement and Concrete, Portland Cement Association, 1987.

[22] Shi, C. and Day, R. L., Alkali-slag Cements For The Solidification of Radioactive Wastes, Stabilization and Solidification of Hazardous, Radioactive, and Mixed Wastes, ASTM STP 1240, T. Michael Gilliam and Carlton C. Wiles, Eds. American Society for Testing and Materials, Philadelphia, 1996, pp.163-173.

[23] Shi, C., Activation of Natural Pozzolans, Fly Ashes and Blast Furnace Slag, University of Calgary, 1992.

[24] Wang, S. D. and Scrivener, K. L., Microchemistry of Alkaline Activation of Slag, Vol.2, pp.1047-1053, Proceedings of 3rd Beijing International Symposium on Cement and Concrete, International Academic Publishers, October 27-30, 1993, Beijing, China.

[25] Yu, S. and Wang, W., Hardening Mechanism of Clinker-free Sodium Silicate Slag Cement, Journal of Chinese Silicate Society (in Chinese), 1990, Vol.18, No.2, pp104-109.

[26] Hong, S. Y., Kia, J. C. and Kim, J. K., Studies on the Hydration of Alkali-Activated Slag, Proceedings of 3rd Beijing International Symposium on Cement and Concrete, International Academic Publishers, Beijing, China, 1993, Vol.2, pp.1059-1063.
[27] Shi, C., Wu, X. and Tang, M.; Hydration of Alkali-Slag Cements at 150°C, Cement and Concrete Research, 1991, Vol.21, No.1, pp.91-100.
[28] Stade, H., On the Reaction of C-S-H (Di, Poly) With Alkali Hydroxide, Cement and Concrete Research, 1989, Vol.19, No.5, pp.802-810.
[29] Hong, S. Y. and Glasser, F. P., Alkali Binding in Cement Pastes, Cement and Concrete Research, 1999, Vol. 29, No.12, pp.1893-1904.
[30] Kalousek, G. L., Studies of portions of the quaternary system soda-lime-silica-water at 25°C, Journal of Research of the National Bureau of Standards, 1944, Vol. 32, pp. 285-502.
[31] Taylor, H. F. W., A method for predicting alkali ion concentrations in cement pore solutions, Advances in Cement Research, 1987, Vol.1, No.1, pp.5-16.
[32] Odler, I., Hydration, Setting and Hardening of Portland Cement, in Lea's Chemistry of Cement and Concrete, Ed. By P. C. Hewlett, pp.241-189, Arnold, London, 1998.
[33] Ramachandran, V. S., Feldman, R. F. and Beaudoin, J. J., Concrete Science - Treatise on Current Research, Heyden & Son Ltd, 426p, 1981.
[34] Atkins, M. et al., A Thermodynamic Model for Blended Cements, Research Report for Department of Environment, DoE/HMIP/RR/92/005, 1991.
[35] Krivenko, P. V., Alkaline Cements, Proceedings of 9th International Congress on the Chemistry of Cement, New Delhi, India, 1992, Vol.3, pp.482-488.
[36] Belitsky, I. V., Sakata, A. and Goto, S., The Role and Behaviour of Alkaline Activators in the Slag-Alkaline Cement Based on the Soluble Silicate Glass, Vol.2, pp.1038-1042, Proceedings of 3rd Beijing International Symposium on Cement and Concrete, International Academic Publishers, October 27-30, 1993, Beijing, China

COMBINED EFFECT OF CHEMICAL, MECHANICAL, AND THERMAL ACTIVATION OF LOW CALCIUM FLY ASH

P. Arjunan[1], M. R. Silsbee[2] and D. M. Roy[2]

[1]Custom Building Products, 6515, Salt Lake Ave, Bell, CA 90201, U.S.A.
E-mail Arjun@cbpmail.net
[2]Materials Research Institute, The Pennsylvania State University, PA 16802, U.S.A.
E-mail: Silsbee@psu.edu and DellaRoy@psu.edu

ABSTRACT

In previous studies (1-4) the authors have discussed the identification of suitable chemical and mechanical activation systems for low calcium fly ash activation, and the role of mineralogical and chemical compositions of the fly ash on the chemical and mechanical activation. The goal of the present study is to characterize the performance of chemically and mechanically activated fly ash - cement materials when exposed to a simulated steam curing environment. The effect of simulated steam curing conditions on the compressive strength was evaluated up to 350ºC with and without the chemical and mechanical activation system. Heat of hydration, BET surface area measurement, and x-ray diffraction studies were used as the other characterization techniques. The studies clearly show that the steam curing increases the compressive strength development of fly ash - cement materials during the early hydration period. No acceleration of compressive strength development was observed at 28-day hydration. The steam cured fly ash-cement materials exhibit the same order of influence of chemical and mechanical activation as observed for room temperature curing.

1. INTRODUCTION

Fly ashes are fine powders formed from pulverized coal combustion process. Fly ashes pose a major solid waste disposal problem all over the world. Fly ashes are widely used in blended cements or with Portland cement. Properties of fly ashes vary significantly with coal composition and plant operating conditions. Alkali activation of cementitious materials has been the subject of research for the last few decades (1- 6). In the previous studies of low calcium fly ash activation studies by the authors (7,8), combined effects of chemical and mechanical activation of the fly ash at 20 wt % replacements level were identified using various chemical activators. It has been demonstrated that the addition of NaOH in small concentrations (0.5-1wt % of fly ash) produced equal or higher compressive strengths than the 100% OPC control mixture. The mechanically activated fine ash produced higher strengths than the respective non-activated ash. A low concentration of sodium hydroxide was an effective chemical activator for all the fly ashes studied. The chemical and the mineralogical composition of the low calcium fly ashes did not influence the alkali activation. The treatment of the fly ash particles with NaOH prior to paste formation with OPC is necessary for early strength development. Morphological and heat evolution studies revealed that the possible surface renewal effect of the fly ash particles may be key to the effective chemical activation. The optimization studies showed that the sodium hydroxide concentration between 0.05 N and 0.1N produces the best alkali activation effect for the low calcium fly ash.

Proceedings of the 11th International Congress on the Chemistry of Cement (ICCC)
'Cement's Contribution to the Development in the 21st Century'
Hosted by: The Cement and Concrete Institute of South Africa
CD-ROM produced by: Document Transformation Technologies
11 - 16 May 2003, Durban, South Africa
ISBN Number: 0-9584085-8-0
Editors: Dr G. Grieve and G. Owens
Congress Organised by: Event Dynamics

Among the most important factors to be considered on concreting are curing temperature and humidity. Temperature and humidity can have a major effect on the mechanical properties of concrete.

Temperature can accelerate or decrease the rate of strength development of concrete at early stages (9-11). It has long been known that elevated curing temperatures, while accelerating the early strength gain of concrete, reduce the ultimate strength (12). In this study, the effect of simulated steam curing conditions on the mechanical properties was evaluated on low calcium fly ash with and without the chemical activation system identified in the previous study. The study also discusses the procedures and conditions used for the simulated steam curing and the results obtained therein.

2. MATERIALS

The materials and methods used for the alkali activation of low calcium fly ash are described elsewhere (7,8). The various inorganic salts used in this study were either AR/GR or Reagent Grade chemicals. The superplasticizer used was a sulfonated naphthalene formaldehyde condensate supplied by Boremco, trade name Mighty 150. X-ray diffraction and hydration calorimetric evaluations were carried out on the cured and uncured samples.

2.1 Milling

Milling of the coarse fly ash was carried out in an attrition mill using zirconia balls in an isopropanol medium. Milling of the fly ash was carried out at room temperature and 90ºC.

2.1.1 Room Temperature Milling

Forty grams of the ash was dispersed in 60 grams of de-ionized water and transferred into the grinding pot containing zirconia balls. Appropriate concentrations of sodium hydroxide were added wherever applicable. The slurry were milled for 15 minutes and transferred quantitatively into the beaker. The slurries were allowed to stand for 12 hours before mixing with OPC.

2.1.2 Milling at 90ºC

Forty grams of the ash was dispersed in 60 grams of hot deionized water (90ºC) and transferred into the grinding pot containing zirconia balls. Appropriate concentrations of sodium hydroxide were added wherever applicable. The slurries were milled for 15 minutes and transferred quantitatively into the beaker. The slurry was allowed to stand for 12 hours before mixing with OPC.

2.2 Reactive fly ash preparation

A novel method was used for the preparation of chemically activated fly ash suspension. A forty-gram portion of the as received or milled ash was dispersed in 60 grams of de-ionized water in a 500 ml glass beaker. The various activators (inorganic salts) were added to the slurry in different concentrations. The contents were covered with a watch glass and digested with magnetic stirring for 2 hours at 90ºC using a hot plate. The contents were cooled and the water lost during the digestion was replaced. The treated ashes were blended with OPC in the slurry form to make cement paste.

2.3 Cement - Fly Ash Paste Preparation

Ordinary Portland Cement (OPC), and OPC and untreated and treated coarse and fine fly ashes were mixed in the ratio of 80:20. The water content was maintained at the ratio of W/S= 0.30 for all the studies. When used in the slurry form, the liquid phase was the same solution as used during the chemical treatment of the ashes. The slurry was allowed to stand for 12 hours before mixing with OPC. The cement (OPC-1) and the various treated fly ashes were mixed in the ratio of 80:20 (by

weight of solids), with the W/S=0.30. The batch compositions of the formulations used in the steam curing treatment are given in Table 1.

Table 1. Batch Composition of different Formulations used in Steam Curing Treatment

Sample Code	OPC (g)	Fly ash (g)	Water (g)	NaOH (g)	Mighty 150
S1	160	40	60	Nil	Nil
S2	160	40	60	Nil	Nil
S3	160	40	60	Nil	Nil
T1	160	40	60	0.2	1
T2	160	40	60	0.2	Nil
T3	160	40	60	0.2	Nil
T4	160	40	60	0.2	Nil
T5	160	40	60	0.4	Nil
T6	160	40	60	0.6	Nil

S 1 = 100% OPC; S 2 = OPC + Coarse fly ash; S 3 = OPC + Coarse fly ash milled at 90ºC in water; T 1 = OPC + Coarse fly ash + 0.5 wt% NaOH of fly ash (digested at 90ºC); T 2 = OPC + Coarse fly ash 0.5 wt % NaOH of fly ash + 0.5% superplasticizer (digested at 90ºC); T 3 = OPC + Coarse fly ash milled at room temperature in water with 0.5 Wt% NaOH of fly ash; T 4 = OPC + Coarse fly ash milled at 90ºC in water with 0.5 Wt% NaOH of fly ash; T 5 = OPC + Coarse fly ash milled at 90ºC in water with 1.0 wt% NaOH of fly ash; T 6 = OPC + Australian coarse milled at 90ºC in water with 1.5 wt% NaOH of fly ash

The compositions S1 to S3 were used as control mixtures against which the performances of test mixtures (T1 to T6) were compared.

2.4 Curing Schedule

Simulated steam curing experiments were conducted at 65°± 5°C. Initially the temperature rise in the cube with respect to curing chamber temperature was optimized using a model cube prepared from OPC: Coarse ash (80: 20). It has been noted that the cube temperature reaches the curing chamber temperature of 65°C within two hours and thereafter stays constantly within 2°C of the chamber temperature till the end of 350°C - hours (65 °C x 5.4 hours) curing. Delay between mixing and application of steam was maintained at 30 minutes for all samples. Paste temperature during mixing was 20+ 5°C and cube temperature at the stripping time was less than 40°C. The humidity of the curing chamber was maintained above 95% R.H. throughout the curing cycle. The curing conditions used in this study are given in Table 2.

Table 2. Curing Conditions used in the Study

Curing Cycle	Time for each Cycle*	Total Cubes for each Curing Cycle
100ºC curing hours	92.3 minutes	4
200ºC curing hours	184.6 minutes	4
300ºC curing hours	276.9 minutes	4
400ºC curing hours	323.0 minutes	4

*: One Curing hour is equivalent to 65ºC-hour.

3. RESULTS AND DISCUSSION

3.1 Compressive Strength

The compressive strengths of steam-cured cubes were measured after the respective curing cycles up to 350ºC-hours curing. After 350ºC-hours, the samples for 28-day strength were removed from the curing chamber and stored at 25ºC + 5ºC for 27 days. Results of compressive strength development after accelerated curing of different OPC: ash formulations are given in Figure 1. In agreement with the general trend, steam curing accelerates the early strength (12).

The comparison of 1-day strength obtained for room temperature curing as reported earlier (7,8) and the results of 350ºC-hours shows that, by steam curing, 1-day strength can be obtained within 5 to 6 hours. Likewise, the influence of alkali activation by NaOH and mechanical activation by grinding on compressive strength has been observed in the same order as in the case of room temperature curing. However, the comparison between ambient curing (7,8) and steam curing shows that steam curing did not have a positive effect on compressive strength at 28-day hydration. This observation is in agreement with the earlier reported studies on high temperature curing of concrete (9-12). Sample code T4, T5, and T6 represents the results for OPC: ash activated by three different NaOH concentrations. The result shows that overdose of NaOH has a negative effect at all curing ages, and the optimum seems to be around 0.5 Wt% (0.0833 N) NaOH. This observation also in agreement with the earlier data obtained with different NaOH concentrations (7,8).

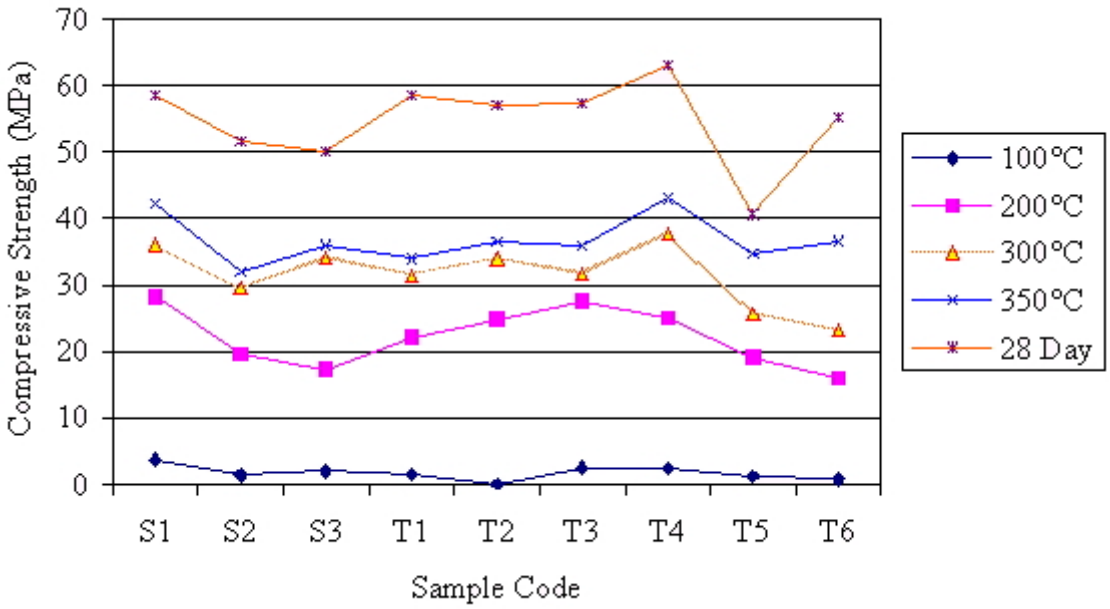

Figure 1. Development of Compressive Strength as a Function of Curing Temperature for the Various Activated OPC: Ash Paste Mixtures.

3.2 X-Ray Phase Analysis

XRD phase analysis has been done on 350ºC-hour steam cured and 28-day hydrated samples. The major phases present in the samples and their respective intensities are given Table 3. Portlandite and calcium silicate are the major crystalline phases observed in all the samples. Minor amount of ettringite also observed in most of the hydrated samples. The 350ºC-hour steam cured pastes and 28-day hydrated samples show no difference in phase formation but provide a slight variation in their quantity. X-ray diffraction powder patterns for 28-day cured samples are more amorphous in nature. There is no appreciable difference in intensities of the phases formed between 100% OPC, and non-activated OPC: ash mixture and activated OPC: ash mixture (S1 to T6).

Table 3. Cement Hydration Phases and their Respective Intensities Present in 350ºC-hour Steam Cured and 28-day Hydrated Samples

Sample Code	C_3S		Portlandite		Ettringite	
	350ºC-hour	28-Day	350ºC-hour	28-Day	350ºC-hour	28-Day
S1	Very Strong	Strong	Medium	Strong	Very Weak	Weak
S2	Very Strong	Strong	Medium	Strong	Very Weak	Weak
S3	Very Strong	Strong	Medium	Strong	Very Weak	Very Weak
T1	Strong	Strong	Medium	Strong	-	N.D
T2	Strong	N.D	Strong	N.D	Very Weak	Very Weak
T3	Very Strong	Strong	-	Weak	Very Weak	Very Weak
T4	Strong	Very Strong	Weak	Strong	Very Weak	Very Weak
T5	Strong	Strong	Strong	Strong	Very Weak	Very Weak
T6	Strong	Strong	Strong	Strong	Very Weak	Very Weak

3.3 Hydration Calorimetry

A series of hydration calorimetric studies were conducted to investigate the reason for the high early compressive strength gains of the elevated-temperature-cured OPC: fly ash mixtures. In the first series the effect of alkali concentration on the fly ash activation was evaluated using isothermal calorimetry. The results of this study are given in Figure 2. The heat evolution profiles did not clearly distinguish the effect of various sodium hydroxide concentrations on the fly ash activation. In the second series of isothermal calorimetric studies, the effect of elevated temperature on the fly ash activation was performed for the paste samples containing non activated fly ash: OPC mixture (Figure 3) and 0.5% NaOH activated (Figure 4) fly ash: OPC. The heat evolution profiles were obtained at 25, 35, 45, and 55ºC for both the as received and 0.5% NaOH activated OPC: ash pastes. High early heat evolution profiles clearly confirm in both the cases (Figure 3 and 4) the high temperature curing has a positive effect on the activation and hydration of fly ash cement paste.

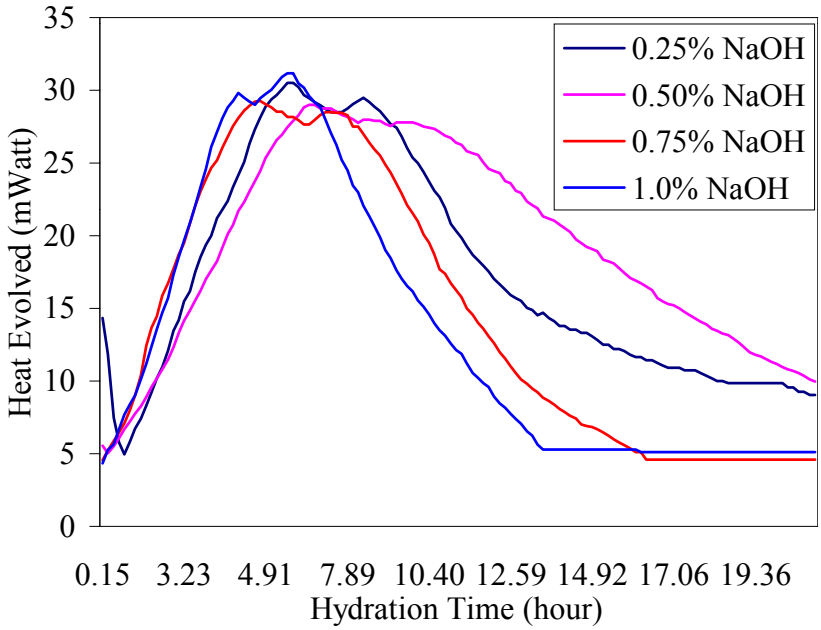

Figure 2. Isothermal Heat Evolution Profiles

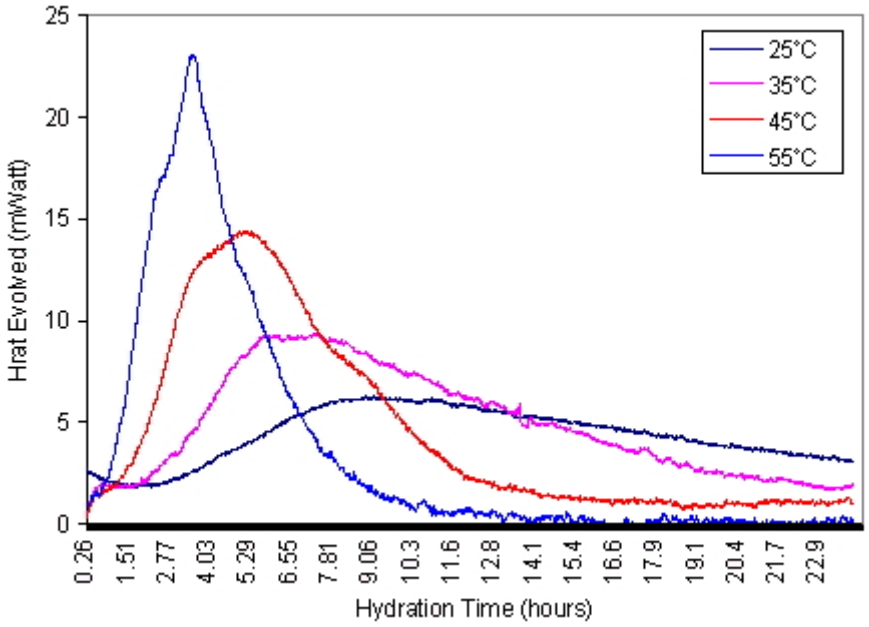

Figure 3. Isothermal Heat Evolution Profiles for as Received OPC: Fly Ash Mixture Cured at Various Temperatures.

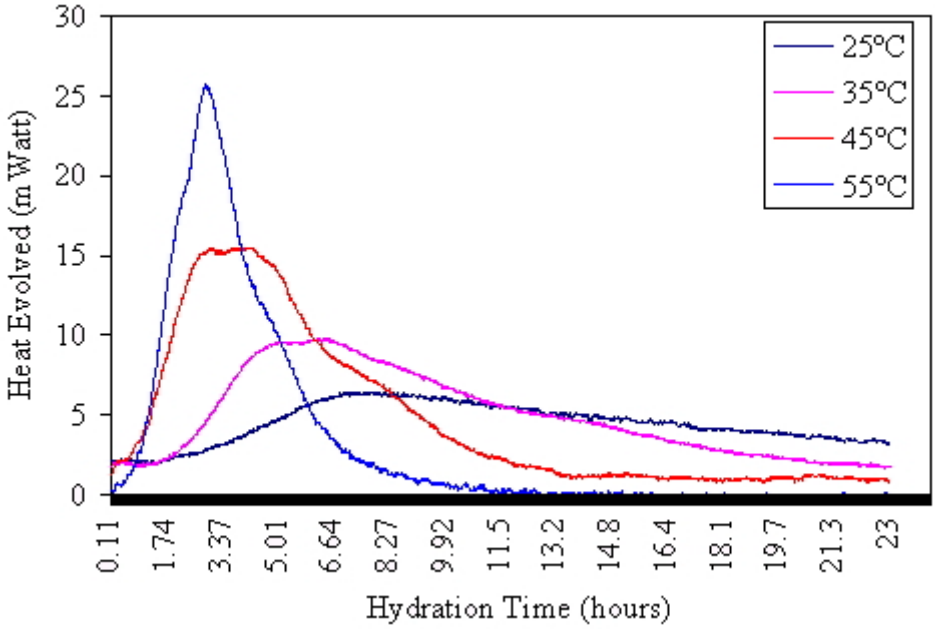

Figure 4. Isothermal Heat Evolution Profiles for 0.5 Wt% NaOH Activated OPC: Fly Ash Mixture Cured at Various Temperatures.

4. SUMMARY

This study describes the effects of steam curing at elevated temperatures on chemical and mechanical activation of a low calcium fly ash. It has been clearly shown that the steam curing increases the strength development during early hydration period. The study also stresses the importance of using the optimum dosage of NaOH concentration for alkali activation. The results of the steam curing at elevated temperatures show the influence of chemical and mechanical activation in the same order as observed for room temperature curing. The acceleration of strength by steam curing is not observed for 28-day hydration. Hydration calorimetric studies confirm the positive effect of elevated temperature on the 0.5% NaOH activated fly ash. X-ray powder diffraction studies on 350ºC-hour curing and 28-day hydration samples indicate that the formation of calcium silicate and portlandite as the major crystalline phases and ettringite as the major crystalline phase is completed at 350ºC-hour curing itself.

ACKNOWLEDGEMENTS

Authors wish to acknowledge the partial financial support provided by ROCLA Inc. to carry out this investigation.

REFERENCES

[1] Mehta, P. K., Cement and Concrete Research., Vol.15, 51-64,1985.

[2] Talling, B., "Effect of curing conditions on alkali-Activated Slags", Fly Ash, Silica Fume, slag, and Natural Pozzolans in concrete, Proceedings of 3rd Intl. Conf., Trondheim, Norway, pp. 1485-1500, 1989.

[3] Tasjiro, C., and Yoshimoto, T., "Effect of Sodium Compounds on the Strength and Microstructural Development of Blast-furnace Slag Cement Mortars", ACI SP 114, Vol. 2., V.M. Malhotra, ed., 1989, pp.1307-23.

[4] Jiang, W. and Roy, D.M., "Hydrothermal Processing of New Fly Ash Cement", Bulletin of the American Ceramic Society, Vol.17, No.4, 1992.

[5] Roy, D. M., and Silsbee, M.R., Material Research Society Symposiums, Proceedings, Vol.245, pp. 153-164, 1992.

[6] Caijun Shi and Robert L. Day, "Acceleration of the Reactivity of Fly Ash by Chemical Activation", Cement and Concrete Research., Vol.25, No. 1, pp.15-21, 1995.

[7] Arjunan, P., Silsbee, M.R., and Roy, D.M., "Chemical Activation of Low Calcium Fly Ash: Part I: Identification of suitable Activator", Proceedings of the Intl. Ash Utilization Conf, 2001, Kentucky.

[8] Arjunan, P., Silsbee, M.R., and Roy, D.M., "Chemical Activation of Low Calcium Fly Ash: Part II: Effect of Mineralogical Composition on Alkali Activation", Proceedings of the Intl. Ash Utilization, 2001, Kentucky.

[9] Paul Zia, Shuaib Ahmad, and Michael Leming., "High-Performance Concretes",

[10] A State-of-Art Report (1989-1994), FHWA-RD-97-030.

[11] Castillo, C. and Durrani, A. "Effect of Transient High Temperature on High-Strength Concrete", ACI Materials Journal, Jan-Feb, Vol. 87, No. 1, pp. 47-53, 1990.

[12] Sandvik, M., and Gjorv, O. E., "High Curing Temperatures in Lightweight High-Strength Concrete", Concrete International, Dec, Vol. 14, No. 12, pp 40-42. 1992.

[13] Detwiler, R. J., Fapohunda, C. A., and Natale, J., "Use of Supplementary Cementing Materials to Increase the resistance to Chloride Ion Penetration of Concretes Cured at Elevated Temperatures", ACI Materials Journal, Vol. 91, No. 1, pp 63-66, Jan-Feb 1994.

DELAYED ETTRINGITE FORMATION AND THE INFLUENCE OF CEMENT CHARACTERISTICS

Barry E. Scheetz[2*], Della M. Roy[2], Paul J. Tikalsky[1] and Tara Cavalline[3]

[1]Department of Civil Engineering, The Pennsylvania State University, PA 16802, U.S.A.
[2]Materials Research Laboratory, Pennsylvania State University, PA 16802, U.S.A.
[3]Law Engineering, Charlotte, North Carolina, 28227, U.S.A.

ABSTRACT

Among the mechanisms of degradation of concrete from the presence of excess sulfate identified in recent years has been the phenomenon of delayed ettringite formation (DEF). This phenomenon is a degradation process that sometimes is identified in concrete that has been exposed to curing at temperatures above 70° C. The process, however, is complex and is still not thoroughly understood, even with intense research interest in the past decade that focused on understanding the process. According to the latest interpretation, any ettringite formed prior to curing at above 70° C is destroyed during the initial heat treatment, and the damage in the concrete structure is associated with the formation or reformation of ettringite during the subsequent service at ambient temperatures. To explore the influence of variation in cement composition upon possible damage, twenty-one Type I and Type II portland cements from North America were investigated, that represented a statistical variation in range of sulfate, equivalent alkali, C3A and fineness. These were evaluated for DEF following a modification of the J. Stark procedure. The results and evaluations will be discussed in detail.

1. BACKGROUND

Cement manufacture has changed significantly in the past two decades, mainly because of environmental and energy concerns (1). As a consequence, rising concerns have raised questions in various scientific forums as to how far these changes in cement compositions have affected the performance of modern concretes. According to Mehta (2), while many 50-90 year old concrete structures are still in good condition, there are numerous cases of deterioration in recently built structures. Skalny (3) indicated that "*... that there are some 253,000 bridge decks ...in varying states of deterioration and approximately 35,000 are being added to this list every year in the United States alone.*" The condition in Europe and other parts of the world is no better (4,5).

An NCHRP study has been conducted on the composition of Portland cement, the important physical characteristics of Portland cement and the role played by these various chemical and physical properties of Portland cement on performance of concrete and their influence on the durability of concrete. In this paper, we focus on one aspect of durability, i.e. the relation of cement composition to secondary ettringite formation/delayed ettringite formation, SEF/DEF.

2. INTRODUCTION

Delayed ettringite formation is a complex process, not wholly understood (6,7,8,9). In recent years, a number of failures have been reported for concrete products precast at elevated temperatures. They have been characterized by cracking after some years of service in environments exposed to

Proceedings of the 11th International Congress on the Chemistry of Cement (ICCC)
'Cement's Contribution to the Development in the 21st Century'
Hosted by: The Cement and Concrete Institute of South Africa
CD-ROM produced by: Document Transformation Technologies
11 - 16 May 2003, Durban, South Africa
ISBN Number: 0-9584085-8-0
Editors: Dr G. Grieve and G. Owens
Congress Organised by: Event Dynamics

the weather. This cracking is related to the presence of abundant ettringite at paste-aggregate boundaries and elsewhere. Kennerly(10), was one of the first to report possible problems with delayed ettringite formation. However, the more detailed and pioneering work of Ludwig and co-workers (11,12,13) has confirmed the damage caused by ettringite formation in heat-treated concrete structures. According to these studies, any ettringite formed prior to curing at temperatures of above about 70° C is destroyed during the heat treatment, and that the damage is associated with the formation or reformation of this phase during the subsequent service at ambient temperature. The term 'delayed ettringite formation', or DEF is widely taken to denote this phenomenon, but some investigators include the late formation of ettringite in material that has been cured at ordinary temperatures

The most comprehensive and extensive literature review of DEF was done by Day (14). According to Day, the term "delayed ettringite formation" is not accurate and "secondary ettringite formation" is more correct. Delayed formation of ettringite may cause expansion of the concrete, loss of strength, and ultimately deterioration. As described above, it has been observed that a number of conditions must be present for delayed ettringite formation to occur (6,8,11,15,16). The temperature of the concrete at early ages must be at least 65-70° C, and during its lifetime, the concrete must be either completely or nearly saturated intermittently or continuously. An excess of SO_4 also facilitates the reaction (15)

The phenomena of alkali-silica reactivity (ASR) and DEF have often been shown to be linked (8,17,18,19,20). These results are in accord with the observations on field concretes and also with those of (19), who found that a limestone mortar did not expand significantly after curing at 95°C. However, if reactive silica was added to the mix, marked expansion occurred, initially from ASR, and was later exacerbated by the effect of DEF. Diamond (7) reports that damage from DEF can occur in normally cured concrete. He attributes this effect to high contents of SO_3 (4-5 %) in the cement and more specifically in the clinker and indicates that ASR almost always precedes DEF. Brown and Bothe [20] have suggested that the ettringite formation cannot occur in pore solutions with high alkalinity. Influence of cement composition on the delayed ettringite formation was studied recently by many authors among the these are studies by (21,22,23). The Glasser (23) study approaches the DEF mainly in terms of thermodynamic modeling and pore fluid analysis.

Odler and Chen (24) reported that significant expansion occurred only with cement that was high in both SO_3 (4.9%) and C_3A. Famy et al. (25) emphasize the effect of the microstructural characteristics. Contrary to the findings of Taylor (15), Klemm and Miller (6) claims that high SO_3 content in clinker and silicate phases of cement paste are innocuous in the formation of secondary ettringite. C_3A was also targeted as a parameter influencing DEF, but research by (26). shows no clear correlation between the amount of potentially damaging monosulfate crystals and the original C_3A content of the cement. Kelham (22) also contends that sulfate-resisting cements with low C_3A contents are not susceptible to DEF, and that the addition of KOH or K_2SO_4 accelerates expansions at elevated temperatures.

Other researchers have focused their efforts on how characteristics other than SO_3 and C_3A such as increased fineness, Na_2O, MgO, C_3A, and C_3S can be correlated with increased expansion. Stark [26] points out, however, that the combined action of frost and deicing salt can also aggravate the problem. Therefore, in view of the controversies concerning causes and mechanisms of SEF/DEF deterioration, the investigations described below were undertaken, in an attempt to relate cement composition from a wide variety of sources in the U.S. to the potential for concrete deterioration.

3. EXPERIMENTAL

Twenty-one cements that represent the compositional extremes for all 114 Type I and Type II Portland cements manufactured in the United States were employed in this study (27). Bogue

mineralogies for each are detailed in Table 1. For this study both air-entrained and non-air-entrained mortar specimens were prepared according to ASTM C 305 as detailed in Table 2.

Table 1. Bulk Mineralogical Composition of Type I and Type II Cements

Cement #	PCA #	C3S	C2S	C3A	C4AF
1	**2414**	58.4	15.9	5.5	9.1
2	**2312**	60.7	15.7	3.8	12.2
3	**2403**	59.5	13.2	6.4	9.7
4	**1056**	62.4	9.7	11.7	4.9
5	**1043**	59.1	14.4	10.0	5.9
6	**1016**	54.5	17.5	10.0	8.8
7	**1013**	59.0	12.2	11.7	7.7
8	**1024**	57.2	14.4	9.6	8.8
9	**1039**	52.0	19.5	9.3	7.7
10	**1015**	58.3	16.5	7.5	7.5
11	**1028**	53.7	15.7	9.5	7.9
12	**1051**	47.2	23.3	6.7	9.7
13	**1104**	58.9	16.7	5.8	8.8
14	**1060**	56.5	17.8	7.2	9.5
15	**1027**	57.8	14.3	7.8	7.9
16	**1059**	60.1	14.2	9.5	4.6
17	**1017**	55.1	19.4	7.2	7.4
18	**1007**	59.2	11.9	10.6	6.0
19	**1020**	61.1	12.0	9.8	8.8
20	**2322**	60.6	13.6	7.4	9.8
21	**2334**	52.0	19.2	7.3	8.9

Table 2. Proportions of Mixtures Prepared for DEF Studies

components	***Air-entrained***	***Non-air-entrained***
Sand	1650g	1650g
Cement	600g	600g
Water	319g	319g
Air-entraining admixture	0.55mL	

3.1 Studies of Delayed Ettringite Formation

In order to evaluate delayed/secondary ettringite formation for each of the 21 cements, a testing regime involving both air-entrained and non-air-entrained mortar bars and both 60°C and 80°C elevated temperatures was generated, as can be seen in Table 3.

The variation in temperatures provides microcracking, and the elevated temperatures and varying humidity levels provide conditions that encourage crystal formation.

Previous work done by (27) was used to develop a cycle of alternating temperature and moisture conditions. Samples were initially allowed to cure for 28 days at room temperature in saturated lime water in order to provide adequate strength. Samples were then transferred to drying ovens at either 60°C or 80°C for two weeks and then returned to room temperature lime water for eight weeks, in the hope of allowing crystals to form. After eight weeks in room temperature lime water, bars were transferred to a freeze-thaw tester, where they underwent a ramped freeze-thaw protocol

that varied temperature between 20°C and -20°C over a period of 24 hours. This testing cycle was repeated three times, and can be seen in Table 3. The testing protocol for delayed ettringite formation outlined above was followed, and length and mass measurements at each stage in the cycling were recorded.

4. RESULTS

4.1 Secondary/Delayed Ettringite Formation

Modified Stark method (26) was used to evaluate the expansion produced by SEF/DEF. The mortar bar samples were treated in three different exposure conditions. After initial curing at room temperature in saturated lime water, 1) air-entrained mortar bar samples cured at 60ºC (A60), 2) air-entrained mortar bar samples cured at 80ºC (A80), 3) and non-air-entrained mortar bar samples cured at 60ºC (NA60). Each drying period was followed by room temperature saturation and then freezing and thawing. The time for the total 3 cycles of curing/exposure was 242 days.

The data obtained for the total dimensional change in the SEF/DEF mortar bar by modified Stark test for 21 cements after 3 cycles of the different exposure conditions are given in Table 5. It is first noted that only very limited net expansions were generally observed; and then in only a few of the 21 cements (including the three cements shown in Figures 1, 2 and 3).

5. DISCUSSION

Indeed, after an analysis of the final averaged expansion data for three test specimens for each of the 21 cements, only five of the twenty-one cements used in this program showed a positive expansion and then only in the non-air-entrained sample series. One cement expanded nearly an order of magnitude larger than the remaining four. This single cement, #11, represented a star point for both SO_3 and alkali and content with among the highest Blaine fineness. As such, it represents a unique extreme outlier in all Type I and II cements manufactured in the United States.

Table 3. Modified Stark SEF/DEF test

Cycle #	***Days***	***Action***
Initial	1 to 28	curing in RT saturated limewater
	29 to 43	drying at 60° C or 80° C
1	43 to 99	curing at RT in saturated limewater
	100	24 hour freeze-thaw cycling
	101 to 114	drying at 60° C or 80° C
2	115 to 170	curing at RT in saturated limewater
	171	24 hour freeze-thaw cycling
	172 to 185	drying at 60° C or 80° C
3	186 to 241	curing at RT in saturated limewater
	242	24 hour freeze-thaw cycling

The majority of the cements, seventeen in all, exhibited a net shrinkage, as a result of the 172-185 day thermal cycle in the testing sequence, that was larger than any expansion caused by ettringite formation. Statistical modeling with all twenty seven of the chemical and mineralogical variables examined in this program resulted in a positive single variable correlation between expansion and sulfate of 70% for the air-entrained samples cured at 80° C of the form:

$$Exp = 1.27 \times 10^{-2} - 5.66 \times 10^{-2} \times SO_3 + 1.19 \times 10^{-2} \times (SO_3)^2$$

and 67% for the non-air-entrained samples cured at 60°C, with the form:

$$Exp = -7.9 \times 10^{-2} + 3.24 \times 10^{-3} \times SO_3 + 4.74 \times 10^{-3} \times (SO_3)^2.$$

A weak negative trend with CaO, R^2 -42%, is represented in the non-air-entrained data as

$$Exp = -21.6870 + 0.70058 \times CaO - 5.66 \times 10^{-3} \times (CaO)^2$$

Among the major oxides of the Portland cement compositons, SO_3 content showed a significant positive correlation and CaO exhibited a negative correlation with the 242 day DEF expansion for all of the test specimens. Correlations were observed for C_3S, P_2O_5 and Blaine fineness but did not necessarily apply to all of the test specimens studied. The best correlation was observed between DEF expansion and the ratio of SO_3/Al_2O_3 for all three sets of test specimens even though Al_2O_3 alone does not correlate with the observed expansions**.** This relationship took the form:

$$Exp = 1.9 \times 10^{-1} + 0.363346 \times SO_3/Al_2O_3 - 0.153024 \times (SO_3/Al_2O_3)^2$$

Additionally, the ratio between SO_3/CaO also exhibited a significant correlation to all after 242 days at 80° C which took the form:

$$Exp = 5.28 \times 10^{-3} - 3.32353 \times SO_3/CaO + 45.478 \times (SO_3/CaO)^2$$

In addition to evaluating the final averaged expansion data, if the individual samples are tracked through each cycle of the testing protocol, a more detailed pattern emerges. Figures 1, 2 and 3 are normalized expansion data for three of the five cements [#1, #11 and #12] that demonstrated expansive behavior at the end of the full 3 cycle testing. Supporting data for each of these figures are presented in tables 3, 4 and 5, respectively.

Very little happens through the end of the first cycle; however by the time that the second cycle is completed the non-air-entrained samples can be differentiated from the air-entrained samples. By the termination of the testing cycle at 242 days, a clear separation between the two classes of cements can be seen. In all cases, the non-air-entrained specimens are exhibiting greater expansion than the air-entrained specimens. In contrast, figure 4 is a typical example of comparable data for a cement [#19] that did not exhibit expansion. Clearly no differentiation between air-entrained vs. non-air-entrained specimens can be seen.

Examination of the data presented in figures 1 to 3 also points out the lack of impact that the ultimate temperature of the heating cycle had upon the observed shrinkage/expansion behavior of the test cements. The air-entrained specimens heated to 60° C are virtually indistinguishable from those heated to 80°C. The heating cycles manifest changes in the masses of the test specimens as detailed in figure 5 for cement #12.

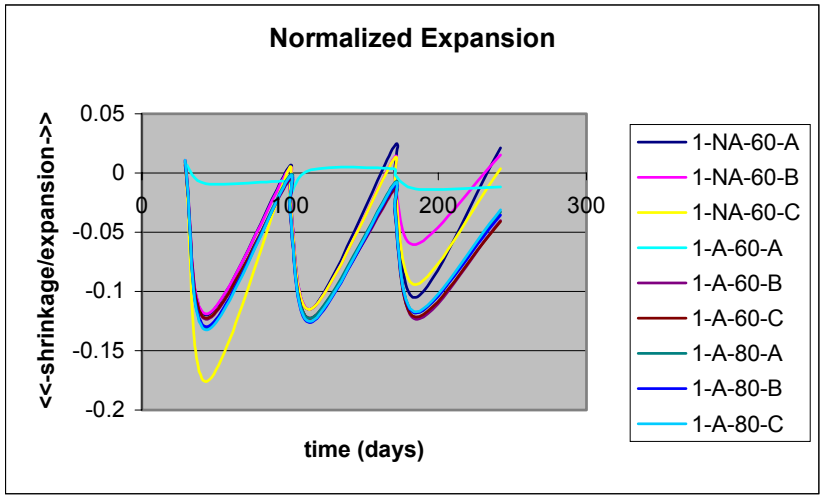

Figure 1. Normalized expansion data for Cement #1 after 3 cycles of DEF testing. [*data for sample 1-A-60-A are the result of experimental difficulties during the testing protocol and are not valid*].

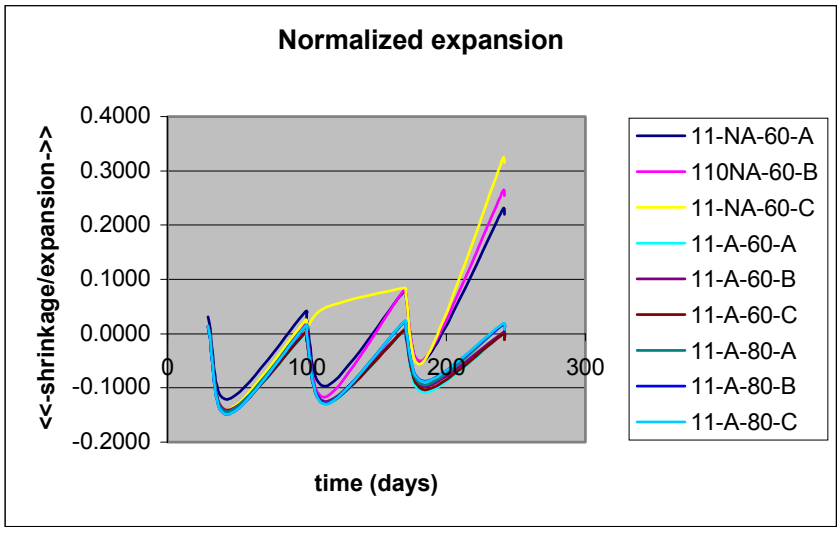

Figure 2. Normalized expansion data for Cement #11 for 3 cycles of DEF testing.

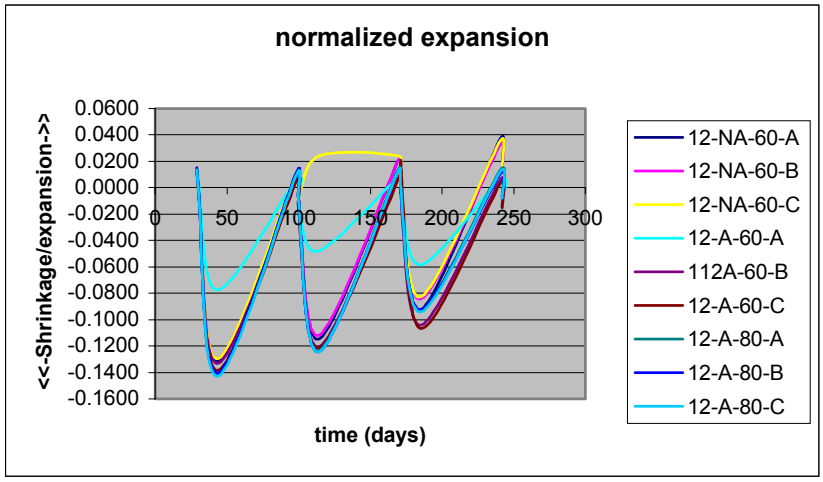

Figure 3. Normalized expansion data for Cement #12 for 3 cycles of DEF testing.

The influence of the air-entraining agent separates the specimens into two sets with the air-entrained specimens generally being about 7% lighter than the non-air-entrained specimens. The heating cycle results in a loss of mass for the specimens of approximately 7 to 8% of the original mass. Upon rehydrating, the cements test specimens take up only about 5 to 6% of the mass lost relative to the initial weight.

Scanning electron microscopic [SEM] characterization coupled with energy dispersive x-ray [EDX] analyses of the non-air-entrained specimens identified massive ettringite formation in extrinsic porosity formed in the specimens. The chemistry of the pore filling was determined by EDX to be consistent with ettringite. In these studies, only massive formation was observed in open porosity (cements #11 and #13). Note the extensively developed micro-cracking adjacent to the ettringite from cement #11 and cement #13. (see figures 6 and 7)

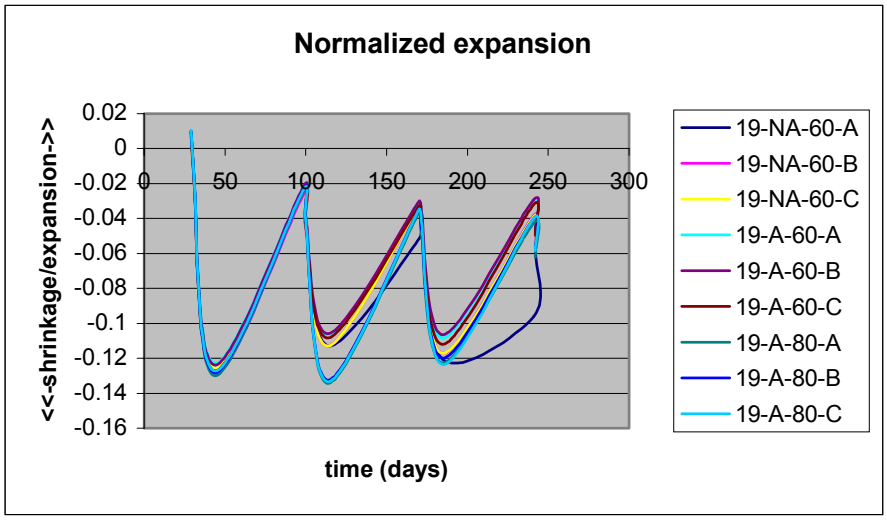

Figure 4. Normalized expansion data for cement #19 for 3 cycles of DEF testing.

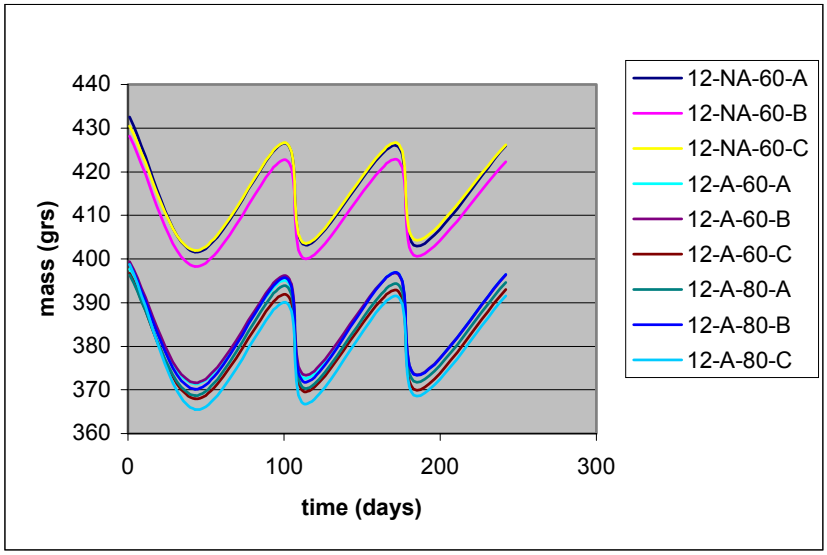

Figure 5. Change in mass of cement #12 as a result of thermal cycling in the DEF testing protocol.

An example of an air void filling in the non-expanding cement [#19] which showed extensive development of monocalciumsulfoaluminate phase in the large voids.

Figure 6. Scanning electron micrograph of massive ettringite filling pore space in cement #11. Note the presence of cracks radiating out from this ettringite-filled pore.

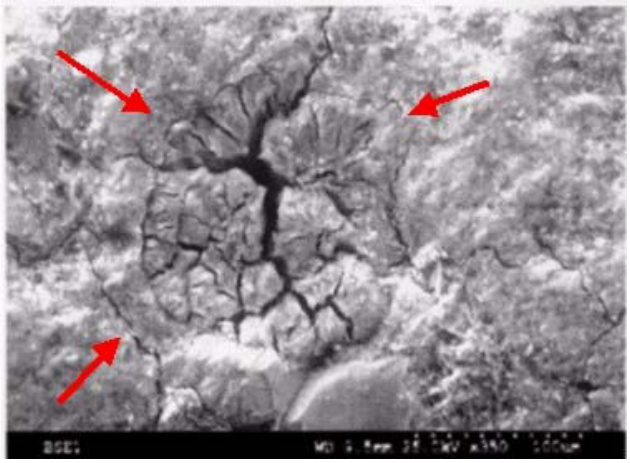

Figure 7. Low magnification [450x] of the surface of cement #13 showing distribution of extrinsic pores filled with massive ettringite. Note predominant cross-cutting micro-cracks.

6. CONCLUSIONS

The experimental design for the DEF studies was structured to limit the extremes of environmental conditions that were/are known to contribute to ettringite formation by restricting the use of reactive aggregates, emphasizing air-entrained specimens and limiting the non-air-entrained samples to the lowest of the test temperatures. The purpose of this action was to address only the extremes of the DEF reactions from the chemistry of the cement. Based on the current observations, DEF should not be a concern if the concrete is manufactured from cements with typical chemical and mineralogical characteristics for Type I or Type II Portland cements. Only if extremes in properties, notably equivalent alkali and sulfate or in Blaine fineness, are approached should concern be warranted. For samples cured at elevated temperatures [80^{o}C] as a means of exacerbating the DEF formation, only a weak correlation was noted with single chemical factor sulfate for the air-entrained samples at 80^{o}C. A slightly better correlation with the ratio of sulfate to calcium oxide for the same sample sets was noted. For the non-air-entrained specimens cured at 60° C single factor correlations were noted for sulfate and a negative correlation with calcium oxide; both of which were weak correlations at best. Finally, the second best fit to the data occurred with a ratio of sulfate to alumina for these non-air-entrained specimens.

ACKNOWLEDGEMENTS

The authors gratefully acknowledge the support of the National Cooperative Highway Research Program for funding this project under Project NCHRP 18-05.

REFERENCES

[1] Osborne, G.J., and Hardcastle, J.L. (1997), “Changes in Properties of Portland Cement and Their Effects on Concrete Durability,” Proceedings, 4th CANMET/ACI International Conference on the Durability of Concrete, Sydney, Australia, Vol. 2, pp. 1411-1432.

[2] Mehta, P.K. "Durability of Concrete - Fifty Years of Progress?" Durability of Concrete, Second International Conference, Montreal, Canada. Vol. I. 1991. Pp. 1-31.

[3] Skalny, J.P. (1987), “Concrete Durability – an Issue of National Importance”, Editor: J.M. Scanlon, ACI SP-100, pp.265-279.

[4] O'Brien, T, R. Cather and J. Figg (1987) "Concrete durability: the interface between research and practice," Editor: J.M. Scanlon, ACI SP-100, pp 255-278.

[5] Seabrook, P.(1989), "Discussion of papers on physical and chemical causes of deterioration of concrete in seawater," Proc. Ben Gerwick Symposium on International Experience with durability of concrete in Marine Environment,University of California at Berkley, Editor: P.K. Metha, pp 73-74.

[6] Klemm, S. and F.M.Miller (1999), Internal sulfate attack: distress mechanism at ambient and elevated temperatures,"Ettringite, the sometimes host of destruction, Ed. B. Ertin, ACI SP-177,pp 81-92.
[7] Diamond, S (1996). “Delayed Ettringite Formation – Processes and Problems”, Cement and concrete Composites, 1`8, 205-215.
[8] Meland, I., H. Justnes, J. Lindgard, S. Smeplass. "Durability Problems Related to Delayed Ettringite Formation and/or Alkali Aggregate Reactions." Proceedings of the 10th International Congress on the Chemistry of Cement. 1997
[9] Hime, W.B. "Delayed Ettringite Formation - A Concern for Precast Concrete?" PCI Journal Vol. 4 No. 4. July-Aug. 1996. Pp. 26-30.
[10] Kennerly, R.A. (1965), "Ettringite formation in dam gallery," J.Am. Concr. Inst., Vol 62, No 5, pp 559-574.
[11] Ghorab, H.Y., Heinz, D., and Ludwig, U., Meskendahl, T., and Wolter, A. (1980), “On the Stability of Calcium Aluminate Sulfate Hydrates in Pure Systems and in Cements,” 7th International Congress on the Chemistry of Cement, Paris, Vol. 4, pp.496-503.
[12] Heinz, D., and Ludwig, U. (1986), “Mechanism of Subsequent Ettringite Formation in Mortars and Concretes after Heat Treatment,” 8th Intl. Congress on the Chemistry of Cement, Rio de Janerio, Vol. 5, pp.189-194.
[13] Heinz, D., U. Ludwig and I. Rudiger,(1989), "Delayed ettringite formation in heat treated mortars and concretes," concretes Precasting Plant and Technology,11.56-60.
[14] Day, R.L. (1992)"The effect of secondary ettringite formation on the durability of concrete: a literature analysis, " PCA Res and Dev. Bulliten, RD108T.
[15] Taylor, H.F.W. Cement Chemistry. Thomas Telford. 1997.
[16] Stark, D. "The Moisture Condition of Field Concrete Exhibiting Alkali-Silica Reactivity." Durability of Concrete, Second International Conference, Montreal, Canada. 1991. Pp. 973-988.Stark, (1991),
[17] Wieker, W., R. Herr, and C. Huebert. "Alkali-Silica Reaction - A Risk for the Long Term Stability?" Betonwerk und Fertigteil-Technik. Vol. 60. No. 11. Nov. 1994. Pp. 86-91.
[18] Shayan, A., and Ivanusec, I. (1996), “An Experimental Clarification of the Association of Delayed Ettringite Formation with Alkali-Aggregate Reaction,” Cement and Concrete Composites, 18, 161-170.
[19] Diamond, S., and Ong, S. (1994), “Combined Effects of Alkali Silica Reaction and Secondary Ettringite Deposition in Steam Cured Mortars,” Cement Technology (Ceramic Transactions), Vol. 40; Edited by E.M. Gartner and H. Uchikawa. American Ceramic Society, Westerville, Ohio,
[20] Brown, P.W. and Bothe, J.V. "The Stability of Ettringite." Advances in Cement Research. Vol. 5. 1993. Pp. 47-63.
[21] Odler, I., and Chen, Y. (1996), “On the Delayed Expansion of Heat Cured Portland Cement Pastes and Concretes,” Cement and Concrete Composites, 18, 181-185.
[22] Kelham, S. (1996), "The effect of cement compositon and fineness on expansion associated with delayed ettringite formation," Cement and concrete Composites, 18, 171-179.
[23] Glasser, F.P. (1996), “The Role of Sulfate Mineralogy and Cure Temperature in Delayed Ettringite Formation,” Cement and Concrete Composites, 18, 187-193.
[24] Odler, I. and J. Colan (1999), Investigations on cement expansion associated with ettringite formation, Cem. Concr. Res, Vol. 29,pp 731-735.
[25] Famy, C., A. Atkinson, K.L. Serinona, A.R. Brough, E, Lachoroski, (2000) "Characterization of calcium silicate hydrate products in expansive and non-expansive heat-cured mortars -- electron microscope study," Durability of Concrete, Proc. 5th Intl. Conf. Barcelona, Spain, ed. V. Malhotra
[26] Yan, R., C.D. Laurence, C.J. Lynsdale and J.H. Sharp, "Delayed ettringite formation in heat cured Portland cement mortars, Cem. Concr. Res., Vol 29, 17-25. (2000),
[27] Stark, J, and Bollmann, K, (1997) “Ettringite Formation- A durability Problem of Concrete Pavements,” 10th ICCC, Gothernburg, Sweden, 4iv062.
[28] Roy, Della M. et al. (2001) “Relationship of Portland Cement Characteristics to Concrete Durability, final report, NCHRP 18-5.

RELATIONSHIP BETWEEN CEMENT CHARACTERISTICS, HEAT OF HYDRATION AND CONCRETE STRENGTH

Paul J. Tikalsky[1], Barry E. Scheetz[2*], Della M. Roy[2], James Rosenberger[3], P. Arjunan[4] and Tara Cavalline[5]

[1]Department of Civil Engineering, The Pennsylvania State University, PA 16802, U.S.A.
[2]Materials Research Laboratory, Pennsylvania State University, PA 16802, U.S.A.
[3]Department of Statistics, Pennsylvania State University, PA 16802, U.S.A.
[4]Custom Building Products, 6515 Salt Lake Avenue, Bell, CA 90201, U.S.A.
[5]Law Engineering, Charlotte, North Carolina, 28227, U.S.A.

ABSTRACT

The study was conducted as part of a comprehensive effort directed at examining the effects of cement composition on concrete durability. Detailed characterization was performed on 21 statistically diverse Type I and II Portland cements manufactured in North America. The cements were studied and derivative properties were determined including heats of hydration. In addition, physical characteristics such as compressive strength were also determined. Analyses of the relationships between 72 measured cement characteristics and various properties were performed. Multi-variant and response surface modeling were conducted on this data set. Combination of four variables (C_3A, Blaine surface area, potential CH and equivalent alkali) showed the greatest correlation with 1-day isothermal heat of hydration. The highest correlation with single variable correlated with C_3S, as expected. The strongest single variable correlation of compressive strength with any of the cement characteristics was with equivalent alkalis at both 28 and 90 days of curing. This was a negative correlation. A multi-variant, center-weighted response surface modeling approach showed a significant relationship between compressive strength measured at 28 days and 180 days to equivalent alkali and Fe_2O_3. Similarly, a significant correlation was found between the ratio of 28/7 day heats of hydration, equivalent alkali and 180 day compressive strength.

1. INTRODUCTION

Cement manufacture has changed significantly in the past two decades, mainly as a result of environmental and energy concerns (1). Environmental concerns have resulted in the use of alternative fuels and fuels with reduced sulfur; in addition, kiln dust, which is rich in alkalis, is routinely collected and returned to the kiln as raw feed, resulting in cements with a higher alkali contents. It has being reported that modern cements are not as durable as older cements (2).

The important question is being raised in various scientific forums as to how far changes in cement compositions have affected the performance of modern concrete versus how changes in loadings, maintenance practices and environmental conditions have affected the performance of concrete structures. This paper investigates the correlation of chemical composition and heat of hydration on compressive strength. Other concrete properties are addressed in separate papers.

Proceedings of the 11th International Congress on the Chemistry of Cement (ICCC)
'Cement's Contribution to the Development in the 21st Century'
Hosted by: The Cement and Concrete Institute of South Africa
CD-ROM produced by: Document Transformation Technologies
11 - 16 May 2003, Durban, South Africa
ISBN Number: 0-9584085-8-0
Editors: Dr G. Grieve and G. Owens
Congress Organised by: Event Dynamics

2. COMPRESSIVE STRENGTH OF CONCRETE

The compressive strength of concrete is related to a wide variety of factors, including: w/cm ratio, cement type and content, aggregate type and gradation, air content, compaction, and curing. However, at a more fundamental level, the strength of concrete is related to the chemical and physical properties of the Portland cement used. Tricalcium silicate and dicalcium silicate play the most decisive roles in compressive strength development. The tricalcium silicate is the more soluble form and contributes to the early age strength development and dicalcium silicate increases the compressive strength of concrete at later ages. The strength development of the four major Portland cement compounds as reported for pure components is illustrated in Figure 1 (3). Past research has primarily been conducted on the effects of isolated variables (4). However, the compounding effects have not been analyzed because of the limited nature of computational hardware. A complete discussion of past studies on cement hydration and reactions is available in another reference (5). The past work has emphasized the importance of particle fineness, SO_3 content, alkalis, heat of hydration, along with C_3S and C_2S content in the development of compressive strength. This past work lays the ground work for the study undertaken by the authors for the National Cooperative Highway Research Program. Strength development is not just a function of four chemical compounds.

Many researchers have investigated the dependence of compressive strength of cement pastes or concrete on fineness of cement. Helmuth (6) stressed the importance of minimum and maximum particle sizes as well as particle size distributions in determining the strength development of cements. According to Valenta (7), and Alexander (8), fineness is important for high compressive strength, but the actual particle size distributions of the cements are of even more importance. Kumar and Roy (9) found that the fineness of Portland cement plays an important role on strength development up to 28 days of hydration, but the fineness of normal Portland cements produced no pronounced effect on strength at later ages.

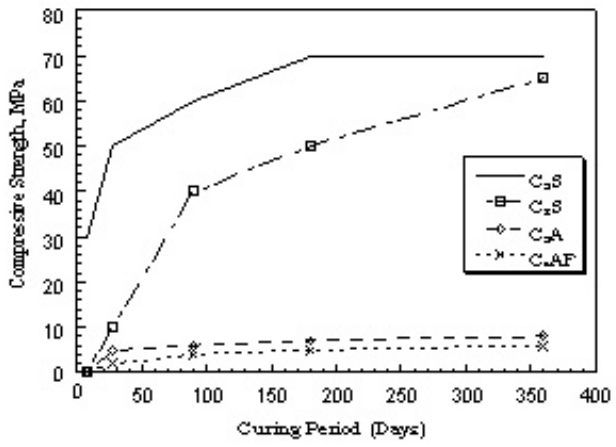

Figure 1. Development of Compressive Strength of Pure Phases of Portland Cement (3)

The chemical reactions that occur during the early stages of hydration of the phases in Portland cement concrete are responsible for the setting and hardening of mortar and concrete. The heat generated by the exothermic reactions play a role in the rate of hydration of the remaining Portland cement. The liberation of heat occurs most rapidly during the first hours and days after mixing. Heat of hydration of hydraulic cement measures the difference in heat of solution of anhydrous cement to that which has been hydrated for different ages between 7 and 28 days. The heat of hydration provides a convenient way to monitor hydration using either isothermal or adiabatic calorimetry (10). As hydration progresses the compressive strength of concrete increases. However the amount of increase of compressive strength is not strictly a function of heat evolution, since some hydration reactions generate a lot of heat and very little strength. With this in mind, the maturity of a particular concrete must include both the heat generated and chemical composition of a particular Portland cement. The advantage of using an isothermal method is that information would be obtained concerning other aspects of hydration such as initial and final setting time. Jawed et al. (11) reported the contribution of

individual hydration reactions to the heats of hydration of Portland cement. The heats of hydration of individual reactions for complete hydration are given Table 1.

Lerch (12) established the important influence of SO_3 content of cement on the strength and drying shrinkage. Since then the relationship between optimum SO_3 content for strength and fineness, C_3A content and equivalent alkalis were studied by many other researchers. Lerch (12) reported that the optimum requirement of SO_3 for properly retarded cement increased with an increase in both C_3A and alkali contents. Meissner (13), Equation 1, and Haskell (14), Equation 2, generated linear regression equations for optimum SO_3 contents and strength of cement.

Table 1. Heats of Individual Hydration Reactions of Cement Compounds (11)

Reactions	- ΔH (J/g) for complete hydration		
	Pure compounds	Clinker measured	Cement measured
$C_3S \rightarrow$ C-S-H + CH	~ 500	570	490
$C_2S \rightarrow$ C-S-H + CH	~250	260	225
$C_3A \rightarrow C_4AH_{13} + C_2AH_8$	-	-	-
$C_3A \rightarrow C_3AH_6$ + CH	880	840	-
C_3A + Gyp. → monosulfo-aluminate hydrate	-	-	~1160
$C_4AF \rightarrow C_3(A,F)H_6$	420	335	-

$$SO_3\ (\%) = 0.789 + 0.1149\ (C_3A\ \%) + 1.872\ (Na_2O_{eq.}\ \%) \quad (1)$$

$$SO_3\ (\%) = 1.841 + 0.0950\ (C_3A\ \%) + 1.6364\ (Na_2O_{eq.}\ \%) \quad (2)$$

Later, Ost (15), extended Haskell's treatment to include cement fineness. He obtained the Equation 3 in which fineness, Na_2O, and Fe_2O_3 content were the factors determining the optimum SO_3 content with respect to compressive strength.

$$SO_3(\%) = 0.556\ (Na_2O_{eq.}\ \%)+0.0017659(\text{Blaine},cm^2/g)-0.1072(Fe_2O_3\%)– 3.6004 \quad (3)$$

Alkali compounds, in general, accelerate the rate of early hydration of Portland cement and give high early compressive strength, although the final strengths are lower than those of the low alkali cements. Alkalis seem to act as catalysts in forming calcium silicate hydrate from lime and silica. This is due to the formation of sodium silicate which reacts with $Ca(OH)_2$ to form calcium silicate hydrate (C-S-H). On mixing the cement with water, alkali ions readily pass into solution and influence the early hydration reactions of cement, particularly of C_3A.

3. EXPERIMENTAL PROGRAM

A multi-variant, center-weighted response surface modeling approach was used to evaluate statistical correlations between the 32 Portland cement variables, as well as ratios of related properties in order to explain the dependence of compressive strength upon these variables. The data obtained used 21 statistically diverse Type I and II Portland cements manufactured in North America. The cements were selected using a center cube model using and containing a full range of four variables, SO_3, C_3A, fineness and equivalent alkalis. The statistical variations in compressive strength of concrete made with the 21 Portland cement concretes for different curing periods are given in Table 2. This table provides the minimum, maximum, and mean of compressive strength calculated for all cements at various curing periods. The highest increase in compressive strength was reported for all cements between the 3 and 28 days of curing. This increase was similar for

most of the cements. Similarly, uniform increase was observed for most of the cements at 90 and 180 days of curing. However, the rate increase decreased as the curing period increased.

Multi-variant and single-regression analysis was conducted on combinations of Portland cement properties and the dependency of compressive strength. R^2 and p values were documented to isolate potential statistical correlations. While many of the more than a million computer correlations showed no reliable relationship, there are certain variables that act in concert to contribute to the strength development of concrete. Some of the multi-variant analysis data for the dependency of compressive strength on the combination of 9 trace and minor elements are given in Table 3. Multi-variant combinations were run on more than 300,000 combinations including all nine elements simultaneously, any eight of the nine, through single variable evaluations. Combined trace and minor elements show a strong correlation to 3 and 28 day compressive strengths. This correlation generally increased as the curing period increased. While some of these models would appear to be quality prediction tools, the number of data points is insufficient to make 9 or 8 variable equations valid, especially since the chemical ranges of trace elements were not used in the selection of the cements for the study. The center point model used in this study provides for valid models with 4 or less chemical or physical factors. The individual trace element oxides showed very poor correlation to the compressive strength except for that of chlorine. Since the percentage of chlorine was very low and similar for all the cements, the high R^2 for chlorine alone does not represent a reliable correlation. The value of looking at this set of data for a relationship between trace elements and compressive strength is to validate the concept that they play a role in the development of compressive strength in Portland cement. Additional work must be conducted to verify the significance of this role.

The similar increase in compressive strength among the cements shows that the greater variations in SO_3, equivalent Na_2O, C_3A, and Blaine fineness observed in these cements have relatively little influence on the compressive strength. However, there was a reasonable (negative) correlation between equivalent Na_2O and the compressive strength at 28, 90, and 180 days.

Table 2. Compressive Strengths of Concrete Specimens Derived from all Cements at 3, 28, 90, and 180 Days of Curing.

Property	3-day (MPa)	28-day (MPa)	90-day (MPa)	180-day (MPa)
Minimum	22.68	41.43	48.29	50.48
Maximum	33.93	51.72	61.36	65.2
Mean	27.67	46.37	53.28	57.11
Std Deviation	3.45	3.01	3.65	4.28

Multi-regression and single-regression analysis data for the dependency of compressive strength on the combination of SO_3 + equivalent Na_2O + C_3A + Blaine fineness + C_3S/C_2S ratio are given in Table 4. Combined SO_3 + equivalent Na_2O + C_3A + Blaine fineness showed increasing correlation to 28 to 90 to 180 day compressive strengths. Further analysis of this combination suggests that this correlation (negative) was dominantly due to equivalent Na_2O content of the Portland cement.

Multi-regression and single-regression analysis data for the dependency of compressive strength on the combination of C_3S/C_2S and the calcium hydroxide associated with C_3S and C_2S, showed no reasonable correlation between the compressive strength and the combination of C_3S/C_2S ratio + CH from C_3S and C_2S. Similarly, there was no correlation observed between the individual or combination of cement phases and the compressive strength of the Portland cement, including C_3S, as shown in Figure 2.

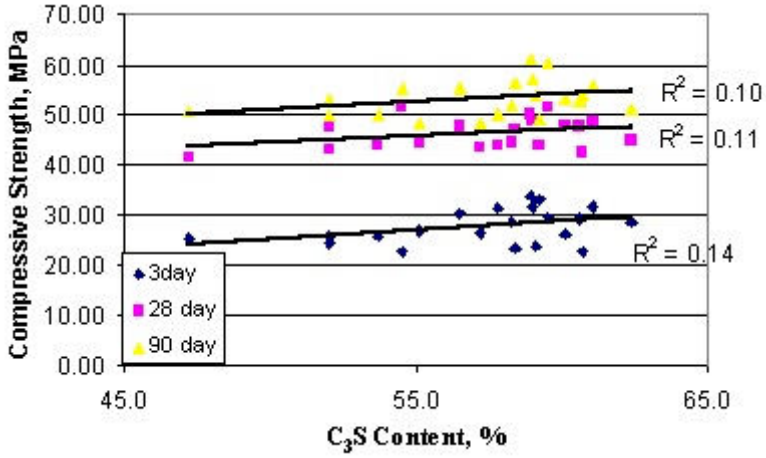

Figure 2. Compressive Strength vs. C_3S %.

All cements showed an increase in compressive strength as the equivalent Na_2O decreases; however, this correlation was less strong as the curing period increased. This correlation decreased from about 60 percent at 28 and 90 days curing to 51 percent at 180 days curing (Table 4). As 90 percent of the compressive strength development of the Portland cement is completed at 90 days curing, the influence of alkalis at 28 and 90 days on the compressive strength is very significant on the compressive strength. Analysis of the data shows that total equivalent Na_2O above 0.60 percent or K_2O content above 0.70 percent adversely affected the compressive strength. Distributions of 28, 90, and 180 days compressive strength as a function of total equivalent Na_2O content of the Portland cement are plotted in Figure 3. R^2 values for K_2O and Na_2O suggest that the compressive strength was mainly influenced by the K_2O content of Portland cement.

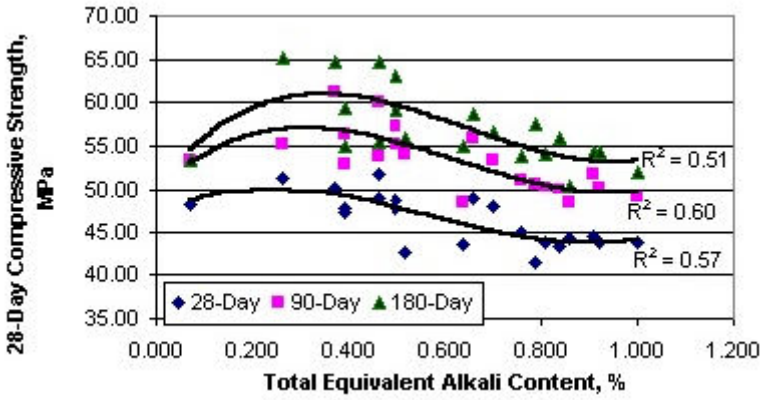

Figure 3. Distribution of compressive strength as a function of total equivalent alkali content of Portland cement

As was noted in the linear and quadratic statistical analyses, alkali demonstrated a strong negative correlation with strength. The negative correlation with alkali content is apparent, and when coupled with Fe_2O_3, which also agrees with the work done by Ost (17). In the response surface modeling, this observation carried through, and it was determined that the best correlation to the observed unconfined compressive strengths was achieved with equivalent alkali and Fe_2O_3 at 28 days of hydration. Figure 4 is a plot of the actual surface calculated for these data.

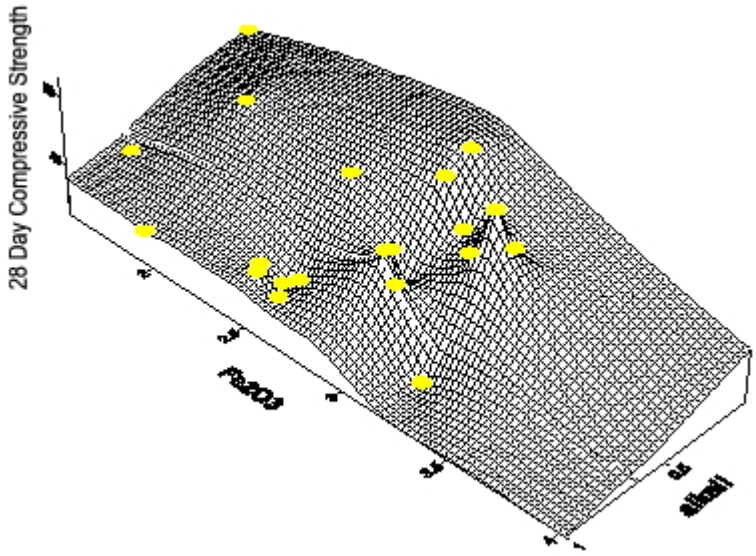

Figure 4. Surface for 28-Day Compressive Strength vs. Equivalent Alkali (Na_2O) and Iron (III) Oxide.

The response surface can be simplified as modeled, shown in Figure 5 according to Equation 4. At 180 days, a similar relationship with Na_2O_{eq} and Fe_2O_3 was observed. This is provided in Equation 5 and Figure 6.

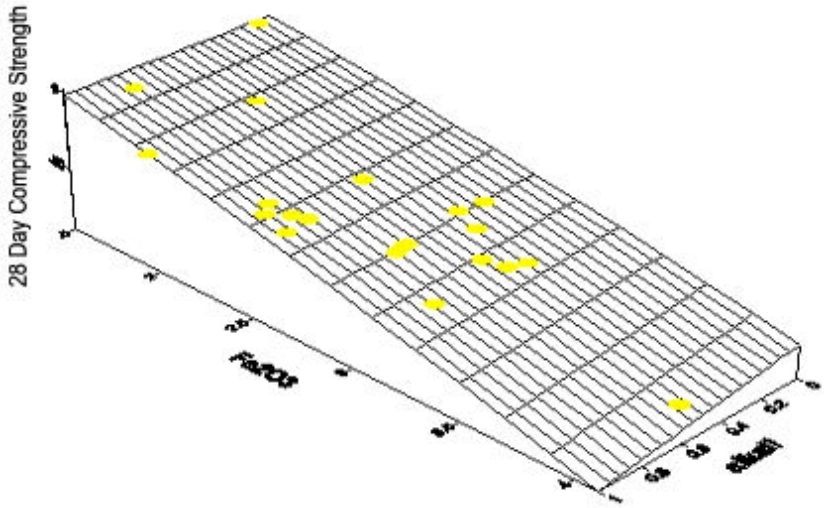

Figure 5. Response Surface Model for 28-Day Compressive Strength vs. Equivalent Alkali and Iron (III) Oxide.

$$28\ d\ F_c = 31.325 + 4.29\ Na_2Oeq. + 15.09Fe_2O_3 - 2.37(Fe_2O_3)^2 - 6.28(Na_2O_{eq} \times Fe_2O_3) \quad (4)$$

$$180\ d\ F_c = 32.75 - 10.65\ Na_2O_{eq} + 21.67Fe_2O_3 - 3.63(Fe_2O_3)^2 \quad (5)$$

The correlation with iron oxide Fe_2O_3 was observed to also be functionally correlated with C_4AF in a related manner. This suggests that, indeed, iron oxide is not the variable directly responsible for the observed correlation, but rather C_4AF.

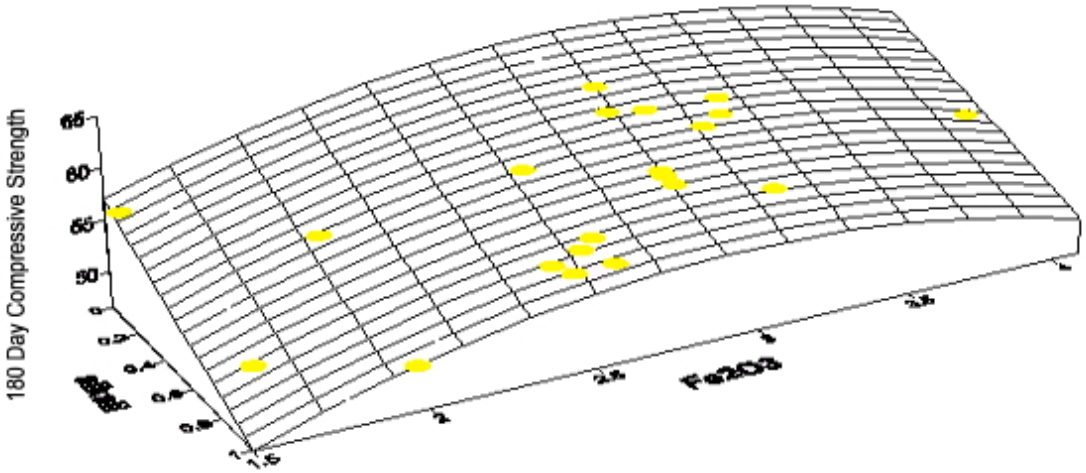

Figure 6. Response Surface Model for 180-Day Compressive Strength vs. Equivalent Alkali and Fe_2O_3.

Table 3. Dependence of Compressive Strength (AASHTO T 22) of Concrete on the Combination of Minor and Trace Elements of Cement

Independent Variables									3-day	28-day	90-day	180-day
P_2O_5	ZnO	Mn_2O_3	B_2O_3	BaO	Cr_2O_3	NiO	SrO	Cl	R^2	R^2	R^2	R^2
x	x	x	x	x	x	x	x	x	0.65	0.79	0.62	0.71
x	x	x	x	x	x	x	x	-	0.49	0.58	0.41	0.49
x	x	x	x	x	x	x	-	x	0.65	0.74	0.45	0.66
x	x	x	x	x	x	-	x	x	0.46	0.74	0.62	0.70
x	x	x	x	x	-	x	x	x	0.51	0.77	0.6	0.66
x	x	x	x	-	x	x	x	x	0.5	0.74	0.61	0.68
x	x	x	-	x	x	x	x	x	0.5	0.53	0.58	0.57
x	x	-	x	x	x	x	x	x	0.5	0.75	0.62	0.71
x	-	x	x	x	x	x	x	x	0.65	0.79	0.61	0.73
-	x	x	x	x	x	x	x	x	0.38	0.71	0.55	0.7

In the linear and quadratic analyses, the heat of hydration, which reflects the degree to which the chemical reaction has proceeded, was never correlated to strength. In the response surface modeling, this correlation was identified as being statistically significant. Unlike the correlation with iron oxide, there appears to be a pessimum where modest levels of alkali are important. The correlation with the ratio of 28-day to 7-day heats of hydration suggests that as this value increases at moderate alkali content, the 180 days compressive strength increases. The ratio of heats of hydrations between 28 and 7 day would suggest the relative importance of the contribution of C_2S hydration, relative to C_3S although neither of these two phases individually was significantly correlated, but are known to be the most significant cementing compounds. Figure 7 is the model response surface for this data, and Equation 6 is the mathematical surface.

$$180d\ strength = 47.87 + 18.63Na_2O_{eq.}\ 5.95\ [28/7\ day\ heat\ of\ hydration] - 23.78[Na_2O_{eq}]^2 \qquad (6)$$

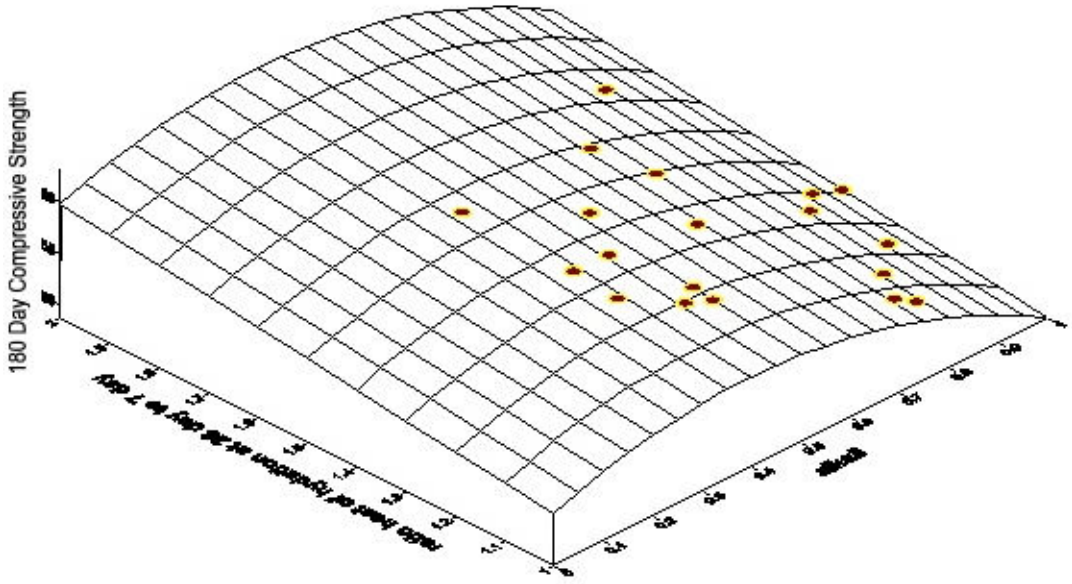

Figure 7. Relation Of 180-Day Compressive Strength vs. Alkali and Ratios of the Heat of Hydration at 28 and 7 Days.

4. SUMMARY

The strongest single variable correlation of compressive strength with any of the cement characteristics was with equivalent alkalis at both 28 and 90 days of curing. This was a negative correlation. A multi-variant, center-weighted response surface modeling approach showed a significant relationship between compressive strength measured at 28 days and 180 days to equivalent alkali and Fe_2O_3. Similarly, a significant correlation was found between the ratio of 28/7 day heats of hydration, equivalent alkali and 180 day compressive strength. Isothermal calorimetry measurements were used to determine the kinetics of hydration reactions taking place within the first 24 hours of hydration. Isothermal calorimetry data for 24 hours provide a general trend of early hydration behavior regarding setting time, but not a correlation to compressive strength development.

Table 4. Dependence of Compressive Strength (AASHTO T 22) of Concretes on the Combination of Physical and Chemical Characteristics of Cement.

Independent Variables					3-day	28-day	90-day	180-day
SO_3	Eq.Na_2O	C_3A	Blaine	C_3S/C_2S	R^2	R^2	R^2	R^2
x	x	x	x	x	0.14	0.54	0.46	0.31
x	x	x	x	-	<0.10	0.54	0.46	0.31
x	x	x	-	x	0.14	0.54	0.64	0.31
x	x	-	x	x	0.14	0.52	0.62	0.31
x	-	x	x	x	<0.10	<0.10	<0.10	<0.10
-	x	x	x	x	0.11	0.54	0.62	0.29
x	-	-	-	-	<0.10	<0.10	0.45	0.11
-	x	-	-	-	<0.10	0.57	0.60	0.51
-	-	x	-	-	0.17	<0.10	0.24	0.13
-	-	-	x	-	<0.10	<0.10	<0.10	<0.10
-	-	-	-	x	<0.10	<0.10	<0.10	<0.10

Heat of solution calorimetry (adiabatic) was used to determine the longer-term heat of hydration of partially hydrated cement samples at 7, 14 and 28-day hydration periods. R^2 values for the four

major cement phases suggested that 7-day hydration was negatively correlated to C_2S or C_4AF content.

As the C_2S or C_4AF content increased, the 7-day heat of hydration decreased. C_3S content by itself showed no significant correlation to compressive strength.

ACNOWLEDGEMENTS

The authors gratefully acknowledge the support of the National Cooperative Highway Research Program for funding this project under Project NCHRP 18-05.

REFERENCES

[1] Osborne, G. J., and J. L. Hardcastle. "Changes in Properties of Portland Cement and Their Effects on Concrete Durability." Proceedings of the 4th CANMET/ACI International Conference on the Durability of Concrete, Sydney, Australia, Vol. 2, pp. 1411-1432 (1997).

[2] Neville, A. M. "Why we have Concrete Durability Problems?" Special Publication SP-100, 21. Detroit: American Concrete Institute. Pp.21-30 (1987).

[3] Cannon, R. P. "Effects of Changes in Cement Properties on the Temperature of Concrete." Concrete 20 (2): 26-29 (1986).

[4] Blaine, R.L., H. T. Arni, and D. N. Evans. "Compressive Strengths of Portland Cement Test Mortars and Steam-Cured Mortars." Interrelations Between Cement and Concrete Properties, Part 3, National Bureau of Standards, Building Science Series 8 (1968).

[5] Lea, F. M. The Chemistry of Cement and Concrete, 4th Edition, Peter C. Hewlett, editor; London, UK, Arnold Publishing (1998)

[6] Helmuth, R. A. "Improved Cement and Energy Savings with Particle Size Control." Handout, Proceedings of the Institute of Electrical and Electronics Engineers Cement Industry Conference (1981).

[7] Valenta, O. "Durability of Concrete." Proceedings of the 5th International Symposium on the Chemistry of Cement, Cement Association of Japan, Vol.3, Tokyo, 7-11, pp.193-228 (1968).

[8] Alexander, K. M. "The Relationship Between Structure and the Composition and Fineness of Cement." Cement and Concrete Research 2 (6): pp. 663-680 (1972).

[9] Kumar, A., and Roy, D. M. (1984), "Effect of Fineness on Properties of Classified Cements," Cement, Concrete, and Aggregates, CCAGDP, Vol.6, No.1, pp 47-51.

[10] Struble, L. and P. Hawkins. "Hydraulic Cements-Physical Properties." Tests and Properties of Concrete, ASTM STP 169: 449-461 (1994).

[11] Jawed, I., Skalny, J., and Young J.F. (1983), "Hydration of Portland Cement", Chapter 6 in Structure and Performance of Cements, Edited by P.Barnes, Applied Science Publishers Ltd., London.

[12] Lerch, W. "The Influence of Gypsum on the Hydration and Properties of Portland Cement Pastes." Proceedings of the American Society for Testing and Materials, Vol. 46, pp. 1252-1292 (1946).

[13] Meissner, H. S. ASTM Bulletin No. 169, 39 (1950).

[14] Haskell W. E., (1959), Rock Products, 62, 110, 146

[15] Ost, B.W. (1974), Ceramic Bulletin, 53, pp. 579.

QUANTITATIVE PHASE ANALYSIS OF PORTLAND CEMENT

P. Arjunan[1], Della M. Roy[2], Barry E. Scheetz[2]*, Paul J. Tikalsky[3] and Steven Badger[2]

[1]Custom Building Products, 6515, Salt Lake Ave, Bell, CA 90201, U.S.A.
[2]Material Research Laboratory, The Pennsylvania State University, PA 16802, U.S.A.
[3]Department of Civil and Environmental Engineering, The Pennsylvania State University, University Park, PA 16802, U.S.A.

1. INTRODUCTION

Phases in Portland cement can be quantified by conventional approaches such as Bogue, optical microscopy, or X-ray diffraction (XRD) methods (1). The Bogue method is a normative calculation reconstructed from the chemical analysis, while the optical microscopy point counting method is tedious and time consuming. In Bogue calculation, the phases calculated may be in either crystalline or partially crystalline form. The most direct way to quantify the cement phases would appear to be XRD. QXRD quantifies the cement phases that are crystalline. Good agreement between the Bogue and XRD methods will provide the extent of crystallinity and completion of the phase formation during clinker processing. In addition, QXRD can identify the presence of minor and impurity phases other than the four major cement phases. Because the cement phases exist in various polymorphic forms, quantification of these polymorphic forms would be useful in studying the influence of cement phases on the concrete durability. Computer controlled scanning electron microscopy (CCSEM) with quantitative energy dispersive X-rayspectroscopy (EDS) was also utilized. The automated CCSEM point counting approach can truly identify all particles including minor or trace phases by using chemical compositions. The CCSEM approach also allows for discrete elemental discrimination of variations within a specific phase within a clinker as well as other parameters such as porosity.

The present study has combined selective dissolution techniques, MATCHDB, GMQUANT, and Rietveld methods to identify and quantify the cement phases; GMQUANT results were compared with Rietveld method results. Identification of phases by MATCHDB uses the whole-pattern database (2), wherein the basic procedure is to compare each pattern in the database with the pattern of the unknown. GMQUANT employs the full diffraction pattern collected over a specified 2 Θ range pre-selected to cover all of the major peaks of all of the phases to be studied (3).

2. MATERIALS AND METHODS

A total of 21 Type I and Type II Portland cements, which represent a statistical selection of cements based on the full range of four variables, sulfate, tri-calcium aluminate, fineness and equivalent alkali, were used for phase analysis.

Proceedings of the 11th International Congress on the Chemistry of Cement (ICCC)
'Cement's Contribution to the Development in the 21st Century'
Hosted by: The Cement and Concrete Institute of South Africa
CD-ROM produced by: Document Transformation Technologies
11 - 16 May 2003, Durban, South Africa
ISBN Number: 0-9584085-8-0
Editors: Dr G. Grieve and G. Owens
Congress Organised by: Event Dynamics

2.1 Qualitative X-Ray Diffraction

The samples were ground and sieved to pass 325 mesh and then slurry mounted on a zero background quartz plate using ethanol. A Scintag PDS, automated X-ray diffractometer, was used for all of the X-ray measurements. The X-ray generator was operated with a copper target X-ray tube (wavelength of 1.5406 Å) at 45 kV and 40 mA. The powder patterns were measured over the range of 5^{o} to 60^{o} 2Θ at a scanning rate of 2^{o} 2Θ per minute. The data were processed using an automated graphics workstation.

2.2 Quantitative XRD of Cement Samples

Quantitative determinations of four major cement phases, C_3S, C_2S, C_3A, and C_4AF, were carried out for all of the 21 cement samples. Analysis of the cement phases was done using the full pattern fitting method, which was performed using GMQUANT method (3) and Rietveld QXRD method (4) using the Young's software system (DBWS –9411). The following sections describe the various steps involved in the sample preparation and raw data collection and quantitative determination of cement phases.

2.2.1 Sample Preparation

Each as-received cement sample was mixed with pure aluminum oxide (corundum, as an internal standard) in the ratio of 1:1 and ground very finely to pass through 325-mesh sieve. The dry powder was then introduced into a glass jar, wrapping the jar with paper towels, and the jar was placed into a small paint can, which was then rolled for 3 minutes. The samples were loaded in the sample holders pressed against filter paper (Whatman, #50). The filter paper had a textured surface that helped to reduce preferred orientation (3).

2.2.2 Data Processing

MATCHDB software was first used to identify the component phases of the cement. A database of "full spectrum" cement and hydration product phases is maintained with the search/match program. The user is given the opportunity to evaluate the "goodness" of fit for each identified phase and is also allowed to compensate for line broadening induced by particle size effects. Once identification of all of the phases in the cement has been completed, GMQUANT software is used to determine the percentage of each phase identified. For processing the unknown samples with the Young Rietveld analyses program, four major cement phases (C_3S, C_2S, C_3A, and C_4AF) and the reference were used, Table 1. Table 2 summarizes the most frequently encountered phases.

Table 1. Crystal structure data for Rietveld Analyses

Phase	Space group	a_o	b_o	c_o	reference
C_3S	R_{3mh}	7.078	7.078	24.94	(7)
C_2S	$P2_{1/n}$	5.51	6.758	9.314	(8)
C_3A	P_{A3}	15.26	15.26	15.26	(9)
C_4AF	I_{BM3}	5.588	14.61	5.38	(10)

2.3 Selective Dissolution

Selective dissolution techniques were used to improve precision in the phase identification and quantification using QXRD methods. GMQUANT tends to overestimate/underestimate cement phases with poorly resolved XRD patterns having overlapping by the adjacent peaks. For example, the results of the aluminate and ferrite phases that are present in small amounts in comparison to silicate phases may be overestimated by the influence of silicate phases. Similarly, the closeness of XRD patterns of various forms of dicalcium silicate phases-alpha, beta, and alpha prime and tricalcium aluminate phases-makes it difficult to resolve by QXRD. To resolve these difficulties, two types of selective procedures were used. The first technique (5) dissolves the silicate phases preferentially, leaving interstitial phases in the sample.

Table 2. Phases Identified Using MATCHDB Program
for All the Cements after the Peak Shift Correction

PSU Sample Code	C_3S		C_2S			C_3A		C_4AF
	42-0551	31-0301	24-0234	33-0303	33-0302	38-1429	32-0150	30-0226
	Monoclinic	Triclinic	α'	α	β	Cubic	Ortho	Brownmillerite
1	x	x			x	x		x
2	x				x	x		
3	x				x	x		
4	x		x		x	x	x	
5	x				x	x		
6	x				x	x		
7	x	x			x	x		x
8	x			x	x	x		
9	x		x		x	x		
10	x				x	x	x	
11	x				x	x		x
12	x				x	x		
13	x				x	x		
14	x	x			x	x		x
15	x				x	x		x
16	x				x	x		
17	x				x	x		
18	x				x	x		
19	x				x	x		
20	x	x			x	x		x
21	x				x	x	x	

The second technique (6) dissolves the interstitial phases preferentially and leaves the silicate phases in the samples.

2.4 SEM quantification methods

The SEM is an analytical tool that uses a focused beam of electrons to form magnified images. Under ideal conditions, the SEM is capable of producing images with a feature resolution at the nanometer (10^{-9} m) level. In addition to detailed image capabilities, the SEM can provide information on the elemental composition of microscopic features. Information on the image and elemental characteristics of a sample is obtained through the interaction of the electron beam with the sample, which produces various effects that can be monitored with suitable detectors. The resulting signals, which include secondary and backscattered electrons along with characteristic X-rays, can be collected in synchronization with the position of the electron beam to provide highly detailed spatial and compositional information. Simply stated, secondary and backscattered electron signals provide image information, while characteristic X-rays are used to determine elemental composition.

Point counting is commonly used on non-homogeneous solids, such as geological cores and concrete sections. It is extremely useful for determining the volume fractions of the constituents of the sample, without regard for the size and shape of individual features. During the CCSEM analysis, fields on the samples were analyzed “in order”. Grid points were detected on the polished clinker by moving the electron beam in discrete increments (“x, y” pattern) across the sample. At each point, the computer directed the electron beam to pause and a chemistry of each point was collected. This point-by-point approach permitted the CCSEM analysis to be performed in an automated mode. Therefore, a grid of equally spaced points is superimposed upon each field-of-view; the beam is placed at each point in turn, and EDS characterization proceeds in the normal way, using vectors and classification rules. In this way, each point can be assigned to a particular

mineral or other classification. Stereological principles are then applied to relate the proportion of points of each particular classification (relative to the total points) to the volume fraction of that classification in the sample. Depending upon the application, a threshold may be used to discriminate points to be analyzed. When a threshold is used, points at which the grayscale (brightness) is out of threshold will be discarded, i.e., not analyzed, and not counted in the total number of points used for volume fraction calculations.

3. RESULTS AND DISCUSSION

The X-ray powder pattern of an original cement sample is shown in Figure 1. The exact identification of all of the phases is very difficult in the sample due to the close proximity and overlap of peaks of cement phases. Two types of selective dissolution techniques were used to solve this problem. In the first method, the cement samples were subjected to a selective dissolution technique using the salicylic acid-methanol-acetone mixture to concentrate the aluminate and ferrite portions; here, the calcium silicate phases (C_3S and C_2S) were dissolved preferentially (5). The X-ray powder pattern of the sample after the salicylic acid–methanol-acetone mixture selective dissolution is compared with the untreated powder pattern in Figure 1. The pattern shows the peaks in the 2 Θ range 30 to 35 degrees. Usually, this is the region in which all four major cement phases show their strongest peaks. The pattern clearly shows that the salicylic acid-methanol mixture removes the silicate phases by preferential dissolution. This process retains the interstitial phases in the sample, making them easy to identify. By this dissolution method, it is possible to quantify the interstitial phases from the residue obtained after the removal of silicates. Total silicates can also be quantified by mass balance calculation.

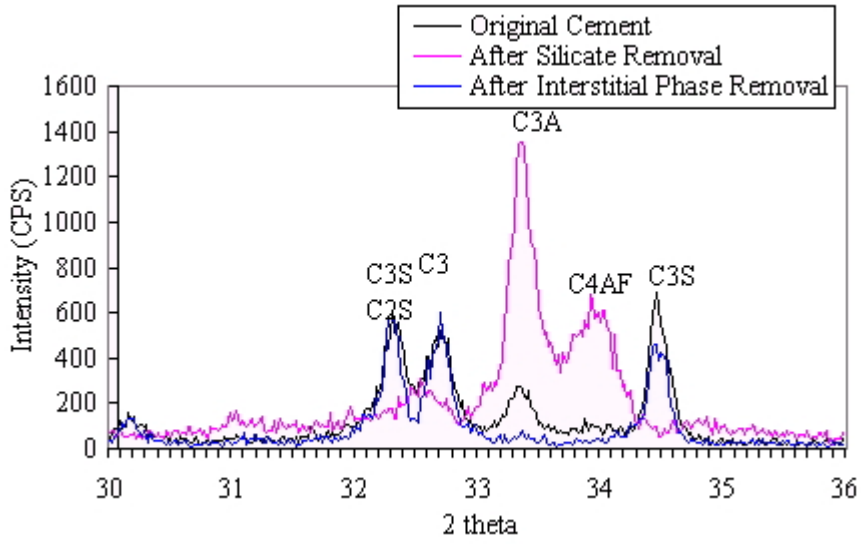

Figure 1. XRD Patterns before and after Selective Dissolution of Phases

In the second method, the cement samples were subjected to a selective dissolution using a solution containing 30 g of potassium hydroxide and 30 g of sucrose in 300 ml water to remove the interstitial phases. The X-ray powder pattern of the sample after the potassium hydroxide and sucrose solution treatment is shown in Figure 1. The KOH-sucrose method is useful in resolving the silicate and aluminate peaks present in the 2 Θ range 32 to 34 degrees. For example, the resolution of the peak at 2 Θ 33.17 is in question in the untreated powder pattern because this peak belongs to 100 percent intensity peaks of both cubic C_3A and α' C_2S. The absence of a peak at 33.17 ° 2 Θ in the XRD powder pattern after the potassium hydroxide and sucrose solution treatment confirms that there is no α' C_2S present in the sample.

3.1 MATCHDB Program

The MATCHDB identification program complemented the results of the selective dissolution techniques; identification of phases by MATCHDB uses the whole-pattern database (2). Before the MATCHDB routine, any shift in the peak during the data collection was corrected using the automatic peak correction routine. MATCHDB results obtained for all the cement samples are given in Table 2, although only the phases that show the figure of merit (FOM) above 0.500 are given. Apart from these major phases, small amounts of the MgO (periclase), calcite, and gypsum were also found in the samples; however, since the figure of merit was below 0.500 for these minor phases, they are not included in Table 2.

3.2.Quantification of C_3A and C_4AF by Salicylic Acid-Methanol Dissolution Method

After removing the silicate phases by the salicylic acid-methanol mixture, the residue left in the process was dried and quantified as the interstitial phases (aluminate and ferrite) in two ways. First, C_3A and

C_4AF contents were calculated as the total interstitial phases from the weight of residue obtained after the salicylic acid-methanol dissolution. From the mass balance calculation, C_3S and C_2S were reported as the total silicates. Second, the residue obtained from the dissolution technique was used to quantify the aluminate and ferrite phases by GMQUANT method. The X-ray diffraction data were collected for the residue after mixing the residue with corundum in the ratio of 1:1. The data treatment and quantification procedures were the same as the original cement samples. The results of the above calculations are given in Table 3.

Table 3. Results of Major Cement Phases Determined by GMQUANT Method after Preferential Dissolution of Silicates

PSU Sample Code	Percentage				
	C_3A	C_4AF	Total Interstitial Phases	Total Silicates from Mass Balance	Total Silicates (C_3S + C_2S) from Bogue
1	6.0	10.0	17.1	83.0	74.3
2	2.0	13.0	20.0	80.0	76.4
3	4.0	13.0	18.5	81.5	72.7
4	10.0	7.0	27.0	73.0	72.1
5	8.0	8.0	26.6	73.4	73.5
6	9.0	13.0	26.2	73.8	72.0
7	10.0	9.0	23.0	77.0	71.2
8	7.0	11.0	26.1	73.9	71.6
9	11.5	7.9	27.1	72.9	71.5
10	7.0	11.8	27.8	72.2	74.8
11	12.0	5.0	28.1	71.9	69.4
12	7.0	11.0	26.0	74.0	70.5
13	4.0	10.0	22.6	77.4	75.6
14	10.0	12.0	25.4	74.6	74.3
15	9.0	14.0	27.1	72.9	72.1
16	7.0	6.0	23.0	77.0	74.3
17	10.0	11.0	20.3	79.7	74.5
18	14.0	5.4	26.9	73.1	71.1
19	11.7	13.7	28.1	71.9	73.1
20	4.5	13.0	20.0	80.0	74.2
21	9.5	11.0	18.3	81.7	71.2

3.3 Results of X-Ray Phase Analysis

The results of phase analysis of cement samples by X-ray methods are given in Table 4. The Rietveld program normalized the values to 100% based on the phases specified in the calculated reference program. Therefore, a correction for minor phases not specified in the program was applied before computing the exact amount of the four major phases. Bogue values were taken as the base value for this calculation.

3.4 Discussion of Phase Analysis

The data presented in Table 4 are graphically summarized in Figure 2 for C_3S, Figure 3 for C_2S and Figure 4 for a combination of C_3A + C_4AF. The averages and standard deviations for C_3S presented in Figure 2 show that within the experimental error of the determinations, all five quantification methods overlapped. The Bogue determination most nearly approximates the results determined by the Rietveld method and of the point counting method but this latter method and the CCSEM both experience large standard deviations. GMQUANT underestimated the C_3S value by approximately 13%.

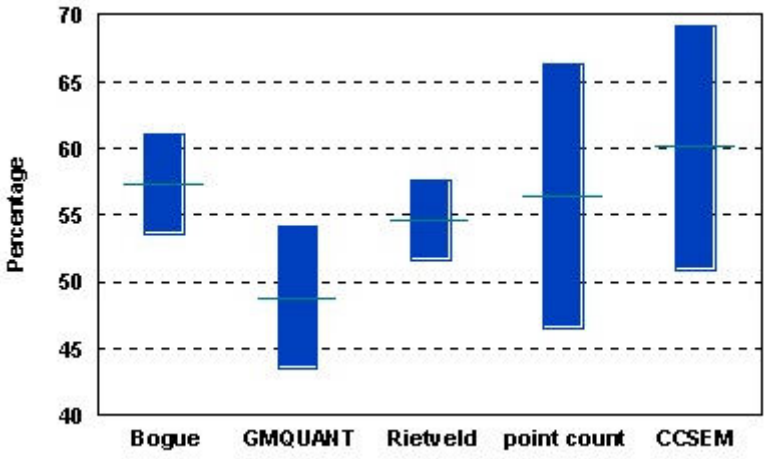

Figure 2. Comparison of the average and standard deviation for C_3S for each quantification method

For C_2S determination, again the experimental errors for all five methods overlapped. Point counting and CCSEM methods again both have large standard deviations with average values that closely approximate each other and are only slightly lower than the Rietveld determination. GMQUANT and Bogue methods very closely agree but are about 20% smaller than the other methods.

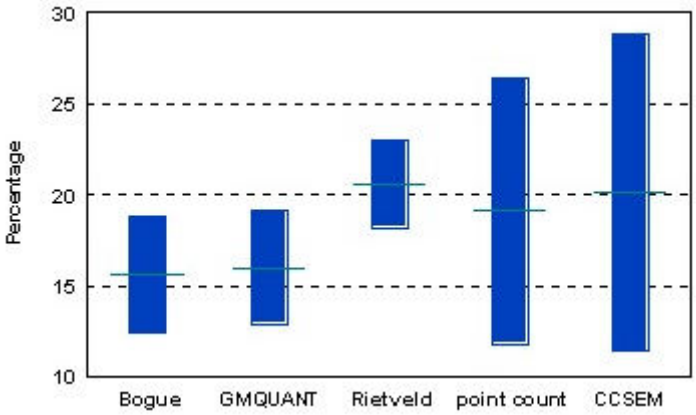

Figure 3. Comparison of the average and standard deviations for C_2S for each quantification method

Table 4. Results of the quantification of individual cements as a function of method

	C3S					C2S					C3A + C4AF				
sample #	Bogue	GMQUANT	Rietveld	point count	CCSEM	Bogue	GMQUANT	Rietveld	point count	CCSEM	Bogue	GMQUANT	Rietveld	point count	CCSEM
1	58.4	58.0	56.9	69.3	70.7	15.9	12.0	17.3	10.6	10.5	14.6	16.0	15.8	19.2	18.8
2	60.7	52.0	59.2	73.2	74.2	15.7	21.0	18.7	10.0	10.5	16.0	12.0	11.1	16.6	15.3
3	59.5	50.0	48.9	n/a	n/a	13.2	16.0	18.2	n/a	n/a	16.1	16.0	19.0	n/a	n/a
4	62.4	52.0	54.3	54.0	58.9	9.7	15.0	20.7	22.9	22.0	16.6	18.0	13.6	20.8	19.1
5	59.1	59.0	59.5	66.7	67.4	14.4	15.0	16.7	13.9	16.4	15.9	14.0	13.6	18.5	16.2
6	54.5	44.0	50.0	61.3	63.9	17.5	17.0	24.1	20.8	20.3	18.8	18.0	16.7	17.3	15.8
7	59.0	50.0	54.0	58.7	62.6	12.2	15.0	21.6	15.9	15.1	19.4	18.0	14.9	24.5	22.8
8	57.2	50.0	54.7	49.8	62.8	14.4	16.0	20.4	19.7	13.3	18.4	16.0	14.6	28.2	23.9
9	52.0	42.0	50.5	43.0	44.5	19.5	23.0	24.5	30.6	35.0	17.0	19.0	13.2	25.4	20.5
10	58.3	52.0	55.0	61.4	60.6	16.5	14.0	21.0	19.9	24.5	15.0	12.0	13.8	18.2	14.8
11	53.7	42.0	56.2	67.4	69.5	15.7	12.0	17.5	12.0	12.7	17.4	14.0	13.6	20.4	17.8
12	47.2	47.0	52.8	37.8	38.5	23.3	16.0	22.6	34.7	42.4	16.4	16.0	11.5	21.9	19.1
13	58.9	47.0	55.6	53.0	57.6	16.7	19.0	21.3	20.2	19.2	14.6	14.0	13.3	25.2	23.2
14	56.5	42.0	52.3	62.6	67.0	17.8	21.0	25.5	9.5	9.5	21.5	19.0	17.9	26.6	23.5
15	57.8	42.0	50.7	46.3	52.0	14.3	14.0	22.5	28.6	26.0	15.7	13.0	14.0	24.2	22.0
16	60.1	58.0	56.3	59.1	64.1	14.2	13.0	20.2	14.3	15.2	14.1	10.0	11.8	21.5	20.7
17	55.1	45.0	55.8	50.6	52.9	19.4	19.0	21.1	24.0	25.5	14.6	18.0	12.1	25.0	21.6
18	59.2	48.0	54.0	56.2	59.4	11.9	13.0	17.4	19.0	21.9	16.6	17.0	16.1	21.7	18.7
19	61.1	50.0	57.4	66.1	70.4	12.0	15.0	19.0	11.7	10.3	18.6	21.0	14.3	21.7	19.2
20	60.6	51.0	58.3	50.2	53.4	13.6	16.0	21.0	28.3	27.4	17.2	16.0	11.9	21.2	19.2
21	52.0	44.0	53.4	40.6	51.7	19.2	13.0	20.4	15.9	23.8	16.2	15.0	15.1	24.1	24.6
avg.	57.3	48.8	54.6	56.4	60.1	15.6	16.0	20.6	19.1	20.1	16.7	15.8	14.2	22.1	19.8
std	3.7	5.3	3.0	9.9	9.2	3.2	3.1	2.4	7.3	8.7	1.8	2.7	2.1	3.2	3.0

Figure 4 summarizes the combined data for C_3A and C_4AF. As in the tri- and di-calcium silicates, the point counting and CCSEM methods tend to provide a high value with relatively close agreement between the two methods. GMQUANT, Rietveld and the Bogue methods more closely agree for the interstitial phases.

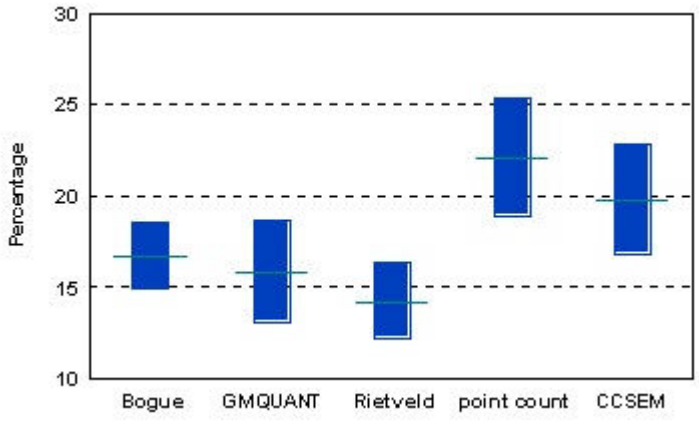

Figure 4. Comparison of the average and standard deviations for $C_3A + C_4AF$ for each quantification method

Each quantification approach has strong points and weaknesses associated with the method. GMQUANT and Rietveld X-ray methods are "full pattern" fitting routines. In the case of GMQUANT, the approach is interactive and relies upon the operator to fit the particle size broadening and crystal chemically induced peak shifts to the data. To be effective, reference full spectra data sets need to be contained in the database that is used to identify the contents. This approach is effective in fitting overlapping peaks and in general is easy to use. The Rietveld's program is a theoretical modeling program, which relies upon a precise knowledge of the clinker mineralogy. Its drawbacks are that it requires an intimate familiarity with the program to generate quality data and will only include in the analyses those phases that you program into the calculation.

The CCSEM point count method is very useful for the determination of the concentration of the various clinker phases. A larger standard deviation between samples was noted by the CCSEM technique due to the small area of analysis. Light microscopy studies have shown that error from counting statistics depends on the number of points, the size of the grid, and the grain sizes of the phases. In general, 4000 points has shown to give reasonable precision (11). Although the grain sizes of each phase do not cause a significant error in the analysis by SEM, the grid spacing is of great importance. Future analyses using CCSEM point counting should include a larger grid spacing than utilized within this study. The CCSEM approach also allows for discrete elemental discrimination of variations within a specific phase within a clinker as well as other parameters such as porosity. The SEM-based method has the potential to be the most accurate approach to quantification because they are based on non-biased analyses. Additionally, new technology allows for chemical acquisition to be collected in fractions of a second, which allows for short analysis times. The approach, however, will not differentiate polymorphs and is restricted by rather limited availability.

4. SUMMARY

The present study has combined selective dissolution techniques, QXRD methods - MATCHDB, GMQUANT, Rietveld, SEM based point counting and CCSEM methods to identify and quantify the cement phases. Selective dissolution techniques were used to improve precision in the phase identification and quantification using QXRD methods. QXRD analysis show that except for the C_2S content, the phase contents determined by QXRD were lower than the potential phases calculated by the Bogue method. A relatively close match is observed for C_4AF content from the Bogue and QXRD calculations. The values for interstitial phases determined by the dissolution technique, Bogue, GMQUANT, and Rietveld value compare within the precision range of the methods. The accuracy of the QXRD methods highly depended on the better resolution of C_3S and C_2S peaks. In general, GMQUANT and Bogue more nearly agreed. This agreement is in contrast to the SEM-based method which tended to produce higher values than did the other methods. Overall though, when the results were normalized to 100%, as the reported by the SEM method, the results were very similar.

Normalized Compositions of the 21 clinkers by each Technique

	C3S	C2S	C3A/C4AF
Bogue	64.1	17.5	18.4
GMQuant	60.6	19.8	19.6
Rietveld	61.1	23	15.9
CCSEM	60.1	20.1	19.8

ACKNOWLEDGEMENTS

The authors wish to thank Dr. J. Johnson and the late Dr. D. K. Smith of Pennsylvania State University for their advice and help in QXRD analysis. The authors also gratefully acknowledge the financial support provided by the Transportation Research Board through the project NCHRP 18-5.

REFERENCES

[1] Theisen, K. (1999), "Phase Composition of Clinker Measured by Microscopy Compared with Quantitative X-Ray Diffraction (Rietveld) and Bogue Results," Proceedings of the 21st Intl. Conf. on Cement Microscopy, Intl. Cem. Microscopic Association, Las Vegas, Nevada, pp. 353-366.

[2] Smith, D. K., Johnson, G. C., and Susan Q. Hoyle (1991), "MATCHDB – A Program for the Identification of Phases Using a Digitized Diffraction-Pattern Database," Advances in X-Ray Analysis, Vol.34, Edited by C.S. Barrett et al, Plenum Press, New York, pp. 377-385.

[3] Smith, D.K., Johnson, Jr., G.G., Scheible, A., Wims, A.M., Johnson, J.L., Ullmann, G (1987), "Quantitative X-Ray Powder Diffraction Method Using the Full Diffraction Pattern," Powder Diffraction, Vol. 2, No. 2, pp. 73-77.

[4] Rietveld, H.M. (1969), "A Profile Refinement Method for Nuclear and Magnetic Structures", J. Appl. Cryst., 2, pp. 65-71.

[5] Takasima, S. (1961), Semento Gijutsu Nenpo, 15, pp. 19-25.
[6] Gutteridge, W. A. (1979), “On the Dissolution of the Interstitial Phases,” Cement and Concrete Research, Vol. 9, pp. 319-324.
[7] O’Daniel, H. and E. Helluer (1950), “Zur struktur von $3CaO.SiO_2$,” *Neus Jahrb Maineral.* Montatsh University, pp 108-111
[8] Mumme, W.G., Hill, R.J., Bushnell-Wye G, and Segnite, E.R, (1995), "Rietveld Crystal Structure Refinements, Crystal Chemistry and Calculated Powder Diffraction Data for the Polymorphs of Dicalcium Silicate and Related Phases," Neus Jahrb Mineral, Abh, 169, Issue 1, pp.35-68.
[9] Mondal, P and J.W. Jeffery (1975) “Crystal structures of the tricalcium aluminate, $Ca_3Al_2O_6$,” Acta. Crystallog., Sec B, 31: 689-697.
[10] Colville A.A., and Geller, S (1972), "Crystal Structures of Ca_2 $Fe_{1.43}$ $Al_{0.57}$ O_5", Acta Crystallogr., Sec B, Vol. 28, pp. 3196-3200.
[11] Hofmanner, F., (1975) “Microstructure of Portland Cement Clinker,” Rheintaler Druckerei und Verlagg, Heerbrugg, Switzerland, pp 1-48.

CONTROL OF THE MICROSTRUCTURE OF CONCRETE: A CASE FOR NANOMETER-SIZED SEEDING

Barry E. Scheetz[1], Paul J. Tikalsky[2] and Steven Badger[3]

[1]Materials Research Institute The Pennsylvania State University, University Park, PA. E-mail: se6@psu.edu; [2]Department of Civil and Environmental Engineering, The Pennsylvania State University, University Park, PA. E-mail: tikalsky@psu.edu; [3]RJ Lee Group, Inc., 350 Hochberg Rd, Monroeville, PA, E-mail: sbadger@rjlg.com.

ABSTRACT

An aqueous dispersion of chemically precipitated C-S-H has been used as an addition to Portland cement concrete as a means of increasing durability and service life. The C-S-H, when used in this application, has been determined to act as seeds which template the nucleation and growth of the hydration products of di- and tri-valent calcium silicate in the Portland cement concrete. The C-S-H seeds have been determined to be x-ray amorphous, similar to conventional C-S-H, with particles measuring ~5nm in size. The dosage of these seeds is typically 400 parts per million by mass of concrete. The mechanism by which they function has been interpreted as a modification to the pore structure of the hydrating concrete resulting in an increase in its tortuosity. This increased tortuosity increases service life by controlling the ingress of water. Microstructual evidence on laboratory concretes and 25-year-old in-service concretes support the proposed theory.

1. BACKGROUND

The admixture that will be the focus of the discussion in this paper is a commercial product that is marketed under the trade name IPANEX. This product has been marketed in the United States for 30 years by IPA Systems. IPANEX is a chemically precipitated C-S-H that is sold in the form of a redispersable solid/liquid suspension which can be added to concrete in the final mixing just before placing. The presented performance behavior of concretes containing IPANEX has been based on field observations. Anecdotal evidence exists that supports the following observations: extremely low flow rate of water, the reduction in alkali induced expansion in ASTM C 441 testing [Figure 1], the reduction or elimination of bleed water, the reduction in autogenous cracking [Figure 2], depth of penetration of chloride ions, air flow, and reduced water absorption.

Proceedings of the 11th International Congress on the Chemistry of Cement (ICCC)
'Cement's Contribution to the Development in the 21st Century'
Hosted by: The Cement and Concrete Institute of South Africa
CD-ROM produced by: Document Transformation Technologies
11 - 16 May 2003, Durban, South Africa
ISBN Number: 0-9584085-8-0
Editors: Dr G. Grieve and G. Owens
Congress Organised by: Event Dynamics

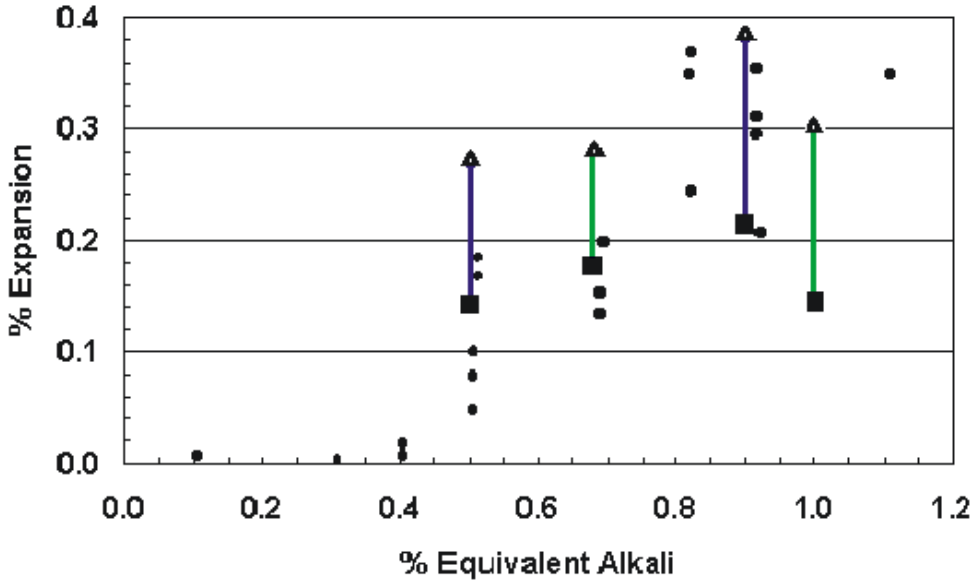

Figure 1. Comparison of ASTM C 441 expansion data for cements of varying alkali content contrasting the expansion in specimens with (filled squares) and without (filled triangles) IPANEX. Data representative of all 114 Type I and II United States manufactured cements are presented for comparison.

Figure 2. Comparison of two pre-stressed double "Tees" prepared by the same manufacturer with the same concrete formulation and cured under identical condition for the same period of time. The Tee on the left was prepared with the admixture and the Tee on the right was prepared without the admixture.

2. DISCUSSION

2.1 Characterization of admixture

Characterization of the IPANEX suspension showed that it is a hydrous calcium silicate with a calcium to silicon ratio of just slightly less than 1:1. Phase identification based on X-ray diffraction characterization does not indicate any crystalline component to the IPANEX. This observation is supported by TEM studies showing individual particles of the admixture measuring approximately 5 nanometers in length [Figure 3], well below the minimum 200-nanometer size necessary to diffract x-rays.

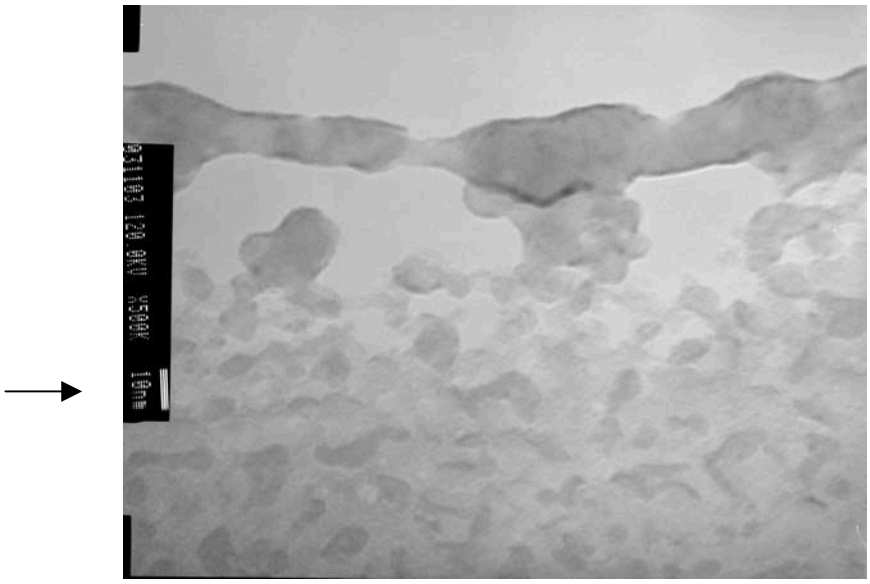

Figure 3. Transmission electron microscopic image of IPANEX seeds.
The white bar on the left [see arrow] represents 10 nm scale.

2.2 Characterization of hardened concrete

Field inspections of fourteen box culverts on the Pennsylvania Turnpike between mile marker 133 through 137 was conducted by Miss Jenny Elstner in 1993 [1] revealed severe degradation of the roof members of the culverts in thirteen of the fourteen culverts. Figure 4 clearly reveals the contrast between the one durable culvert and a typical example of the remaining thirteen compromised structures. The WJE study quantified the degradation into area spalled, cracks and area delaminated. These individual measurements were merely summed to reflect a degradation factor presented in Figure 5.

(a) (b)

Figure 4. Panel a (-top) is a photograph of the box culvert at milepost 133.4 of the PA Turnpike that was prepared by Pennsylvania Turnpike personnel using IPANEX. Panel b (bottom) from milepost 135.3 is typical of the remaining box culverts that were commercially prepared. The concrete formulations and curing were for all practical purposes identical.

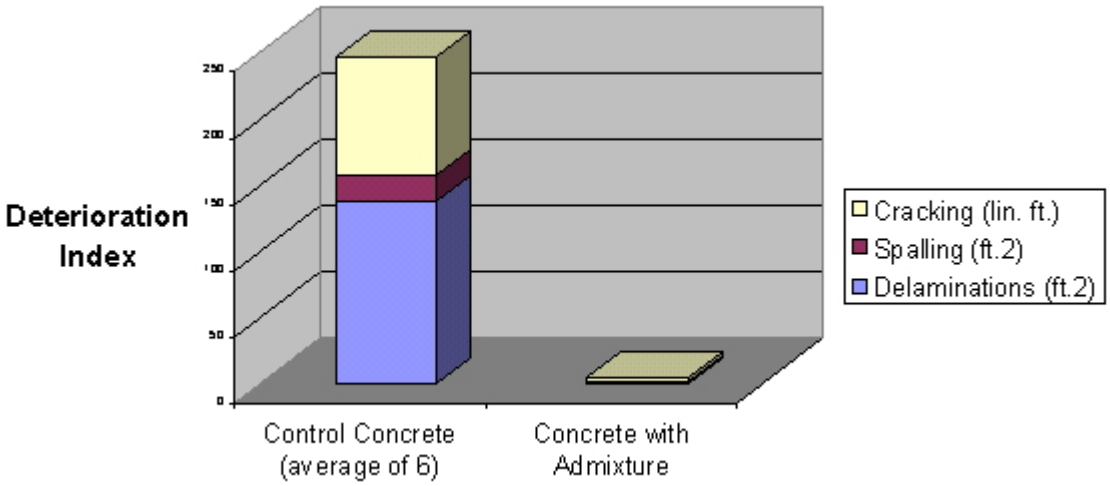

Figure 5. WJE quantification of the deterioration of the box culverts.

The initial characterization studies by Garvey [2] of the microstructures of Portland cement concrete from the PA Turnpike bridges with and without IPANEX were striking [Figure 6]. In the control specimen (B), individual cement particles with hydration products can readily be seen. The hydration products contacted adjacent particles and formed an interconnecting tangle of C-S-H fibrils which is hydrated Portland cement concrete. These specimens also contained discernable pores between the cement particles. By contrast, the bridge sample containing IPANEX (A) similarly contained discernable cement particles also with hydration products but in these specimens, the microstructure did not contain large discernable pores.

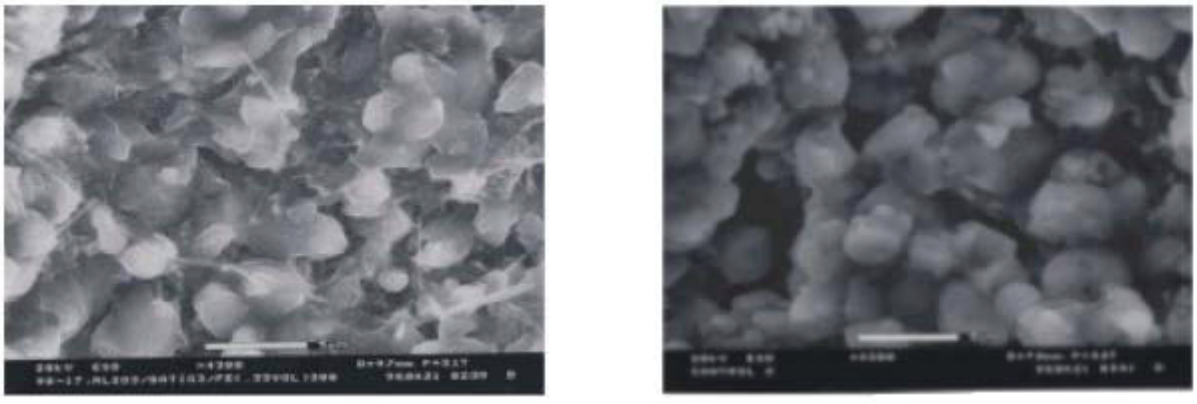

(a) (b)

Figure 6. Contrast of scanning electron microscopic images of (a) 25-year-old concrete containing IPANEX and (b) similar concrete exposed under identical conditions but without IPANEX.

It can more graphically be described as a homogeneous microstructure in which the C-S-H particles are uniformly distributed minimizing the appearance of large open pores. This same appearance has been confirmed on all examples of field placed concrete that have subsequently been characterized.

3. Mechanism for the performance of IPANEX

To achieve this degree of homogeneity in the microstructure, the formation of the C-S-H particles in the hydrating concrete would need to be "controlled" to grow evenly throughout the body of the concrete. Control over microstructure is routinely engineered into ceramics by "seeding" the green body. The development of the microstructure of the ceramic occurs during processing where the nucleation and growth of the ceramic phase is carefully controlled by the thermal history of the object [Kholkin, A.L (2001) [3], Tartaj, J (2001) [4], Huling, J.C. (1992) [5]]. Seeded, controlled nucleation and growth of the microstructure of structural Portland cement concretes in field applications has never been suggested nor demonstrated in the context of structural concrete.

At first blush, it is not obvious that a material that is admixed at 400 ppm by mass of concrete will have any effect on the properties of the concrete. However, preliminary modeling on the "micrometer" scale at NIST suggests that significant improvement in the properties of concrete are achievable from this approach. Preliminary modeling [NIST, 2002] [6] suggests that the seeding of concrete with C-S-H can increase the degree of hydration [Figure 7], which is consistent with our interpretation of the hydration mechanism, where the supersaturation of the pore fluid relative to the hydration products is eliminated [or restricted] by direct growth on the pre-existing seeds. The model also suggests that a modest increase in strength would be anticipated [Figure 7]. The increase is seldom seen in practice.

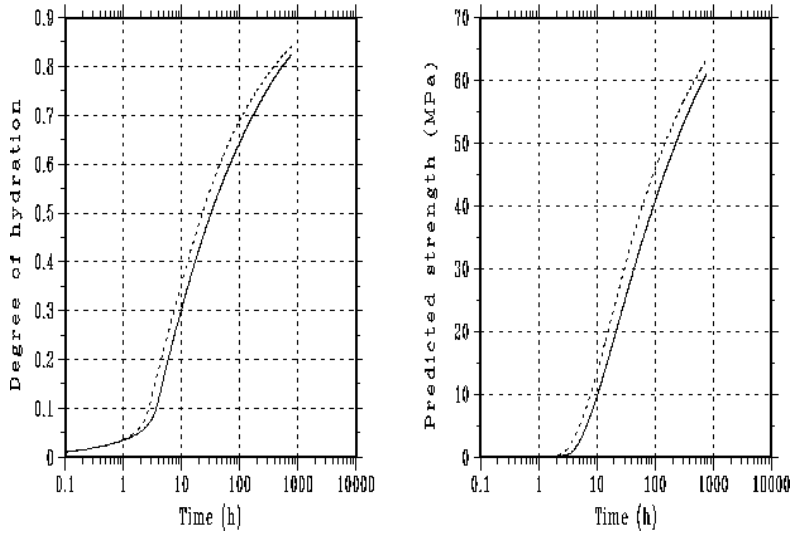

Figure 7. Predicted increase in hydration and compressive strength due to "seeding" microstructure with 1 μm *C-S-H* particle.

Taking into consideration that the average particle size of the IPANEX seed is just 5 unit cells of the crystalline counter part of C-S-H, tobermorite [approximately 10 molecules], 400 ppm corresponds to approximately 5 x 10^{23}seeds per hundred weight of concrete. On the "nanometer" scale, the shear number of IPANEX particles interacting with the hydrating cement particles in the concrete can readily be visualized as controlling the microstructural development. Since the total mass of additional C-S-H added to the concrete is very small, no great influence in mechanical properties should ensue.

The research reported by Garrault-Gauffinet and Nonat (1999) [6] on the determination of the nucleation mechanisms of C-S-H support the observations that were used in this model. Their findings determined that critical radii for nucleation of C-S-H ranged from 2 to as many as 50 molecules or 1 to 25 unit cells and that the process for both tri- and di-calcium silicate is a heterogeneous process. Their

study quantified the degree to which the pore fluids must become supersaturated with respect to C-S-H before the sufficient nuclei were formed and the process of growth would occur. They defined a relationship for the supersaturation as:

$$\beta = K_{super}/K_{solubility}$$

in which:

K_{super} is the activity product in the supersaturated solution,
$K_{solubility}$ is the solubility product.

They reported spontaneous nucleation from tri-calcium silicate hydration at a degree of supersaturation in which $\beta = 15$. The primary influence of the addition of C-S-H seed is to eliminate the supersaturation and provide a lower free energy surface to initiate the growth as soon as the solution concentration reached the saturation concentrations for C-S-H.

In the proposed model for the seeding of the microstucture, there is insufficient material added to the concrete to influence the mechanical properties. The impact of the seeding is manifested in a homogenizing of the C-S-H development. It does not necessarily influence the pore size distribution but does have a direct impact on the connectivity of the pore structure. Concretes fail by the ingress of deleterious components, usually contained in water, into the interior of the concrete via the accessible pore structure. Porosity in concrete can be described in terms of composite models as being a 3-3 composite. That is to say, there are two intertwining three-dimensional structures; one the porosity and the other is the matrix of the concrete. As a first approximation, ingress to the interior of the concrete specimen can be easily visualized as water entering and moving through the pores. If the pathway that the water must take is not convoluted and connected directly to the depth of the specimen, deleterious agents can be deposited deep within the specimen. However, if the pathway that the water must take is highly convoluted, movement of water, over the same period of time as the previously described "control" specimen, would only allow a minimal depth of penetration into the interior of the specimen.

The length of the pore pathway can be described as:

$$D_{eff} = \theta \gamma D_{intrinsic}$$

where:

D_{eff} is the effective diffusivity
θ is porosity
γ is tortuosity
$D_{intrinsic}$ is the intrinsic diffusivity of the concrete

The degree to which the flow pathway is lengthened by the seed nucleation and growth of the microstructure is tortuosity, the proportionality constant that along with the porosity of the concrete equates intrinsic diffusivity to effective diffusivity. The concept of tortuosity is depicted in Figure 8.

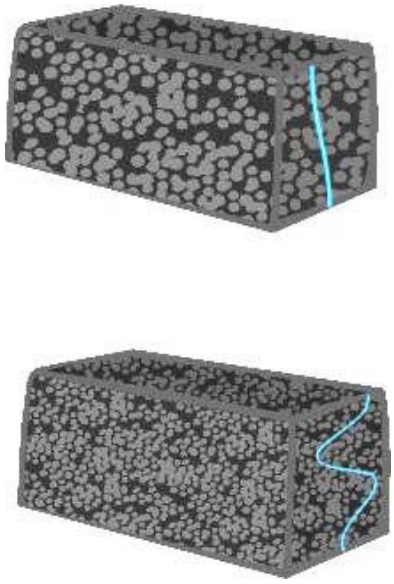

Figure 8. Tortuosity will effect the ease or difficulty for fluids/ions to flow through the concrete structure. The top image shows a flow path through the concrete showing low resistance and hense a lower overall tortuosity. The bottom image indicates a more difficult flow path and therefore a higher tortuosity.

Field observations as in Figure 2, suggest that for exposed concrete surfaces, the ingress of water on a diurnal basis, does not penetrate as far into the seeded concrete as for the unseeded concrete.

4. CONCLUSIONS

A mechanistic model has been developed that describes the role of IPANEX in structural concrete and adequately addresses 30 years of field observations of the durability of concrete formulated with this additive. The mechanism is based on the presence of C-S-H seeds in the admixture that are dispersed throughout the fresh concrete. The seeds act as nucleation sites for the growth of additional C-S-H from aqueous calcium and silicate species present in the pore solution as a result of the hydration of tri- and di-calcium silicates in the cement. Seeded at only 400ppm by mass of concrete little direct influence on mechanical properties of the concrete occurs. The primary influence of the seeding, which contains in excess of 10^{23} seeds per hundred eight of cement, is on the development of a homogenous microstructure in the concrete and is manifested in the inter-conductivity of the pore structure. This inter-conductivity is defined as tortuosity and in practice limits ingress of water and hence deleterious agents into the interior of concrete structures extending the service life and durability.

REFERENCES

[1] Wiss, Janny Elstner, Evaluation of Bridge Deck Slabs Incorporating IPANEX Concrete, WJE Report No. 901046 (1991).

[2] Kholkin, A.L.; Gruverman, A; Wu, A; Avdeev, M; Vilarinho, PM; Salvado, IMM; Baptista, Seeding effect on micro- and domain structure of sol-gel -derived PZT thin films, MATERIALS LETTERS, Vol.50 N° 4, 219 –224, 2001.

[3] Tartaj, J; Moure, C; Lascano, L; Duran, P. Sintering of dense ceramics bodies of pure lead titanate obtained by seeding-assisted chemical sol-gel, MATERIALS RESEARCH BULLETIN, Vol.36 N° 13-14, 2301-2310, 2001.

[4] Huling, Jeffrey Chase, Controlled Crystallization of Sol-Gel Mullite, Ph.D. Penn State Univ (1992).

[5] NIST (2002) --User's Guide to the NIST Virtual Cement and Concrete Testing, Figure 30: Predicted increase in hydration and compressive strength due to "seeding" microstructure with 1 µm CSH particles. [ciks.cbt.nist.gov/vcctl/vcctlman/node26.html].
[6] Garrault-Gauffinet, S. and A. Nonat, Experimental investigation of calcium silicate hydrate (C-S-H) nucleation, Journal of Crystal Growth, vol 200, pp 565-574 (1999).

Sources Consulted

[1] Garvey, John J., M.S. Thesis, the Pennsylvania State University (1999).
[2] Garvey, John J., Paul J. Tikalsky and Barry E. Scheetz. "Influence of Alkaline Earth Silicate Admixture on Durability of Pennsylvania Turnpike Bridges," Transportation Research Record, Journal of the TRB No., 1668 (19__).
[3] Scheetz, Barry E., Paul J. Tikalsky, John J. Garvey, Bruce Grant and Judy Thompson, Proceedings of the 21st International Conference on Cement Microscopy. Cd Rom (1999)
[4] Scheetz, Barry E., Paul J. Tikalsky, John J. Garvey, Bruce Grant and Judy Thompson, Proceedings of the 24th International Conference on Cement Microscopy. Cd Rom (2002)

INFLUENCE OF CLINKER FABRIC ON PROPERTIES OF CONCRETE

R.I. Malek[1], B. E. Scheetz[1], D.M. Roy[1] and P.J. Tikalsky[2]

[1]Materials Research Laboratory, E.mail: rqm@psu.edu
[2]Department of Civil and Environmental Engineering, E.mail: tikalsky@psu.edu
Pennsylvania State University, University Park, PA 16802, USA.

ABSTRACT

Twenty-one diverse clinkers were selected from 114 commercially available type I & II North American cements. Microscopic characterization of the clinkers was conducted without the knowledge of the manufacturing process, and the equipment or the manufacturer nor the source of raw materials. The results illustrate clinker differences and their effect on differences in cement performance in mortars and concrete. The clinkers were examined by an assemblage of analytical microscopic techniques including polarized light microscopy, reflected light microscopy, and scanning electron microscopy provided with back-scattered electron imaging. The samples were chemically etched in order to impart variation in color and textures among and within the various crystal phases. Several general observations can be made that pertain to the suite of clinkers examined and used to augment the information derived from strictly chemical data. It can be inferred from the microscopic analysis that a variety of different processing environments were represented in the data set. This included microstructures that are interpreted to be indicative of well-processed "normal" Portland cement. Additionally, large clusters of belite crystals are observed in many of the clinkers, which suggest inhomogeneity in the raw feed mix. Some of the clinkers exhibited what could be interpreted as reducing kiln atmosphere conditions. The observed size of the alite crystals suggested that the clinkers that give rise to cement with average properties possess predominantly smaller crystals. In contrast, clinkers that give rise to cements with poor properties possessed average and large size alites.

1. EXPERIMENTAL

Twenty-one North American clinkers were obtained from commercially available Type I and II Portland cements. The set of specimens included in this study was statistically chosen to span the range of characteristics that were identified as most significantly impacting the long-term durability of concretes manufactured from them (Table I). An experimental study was conducted to better understand the breadth of variation in manufacturing Portland cement. Statistically based samples of Portland cement clinker with a wide variety in properties were selected in the experimental design. The experimental design of this study is based on a center weighted response surface model in which the concentrations of equivalent alkali, C_3A, SO_3 and fineness were taken to represent four properties in the cement that could most differentiate one cement from another in terms of field performance. The *"Center"* cements represent a statistical average over all of the 114 available cements of the four characteristics in question. The *"Corner"* cements represent examples in which the four properties varied by one standard deviation high and low. Finally, the *"Star"* points represent extreme compositional variation of the four properties. Specimens from each of the clinker samples were examined with multiple-microscopic techniques including polarized light microscopy, reflected light microscopy, Nomarski differential interference microscopy (which is utilized for

Proceedings of the 11th International Congress on the Chemistry of Cement (ICCC)
'Cement's Contribution to the Development in the 21st Century'
Hosted by: The Cement and Concrete Institute of South Africa
CD-ROM produced by: Document Transformation Technologies
11 - 16 May 2003, Durban, South Africa
ISBN Number: 0-9584085-8-0
Editors: Dr G. Grieve and G. Owens
Congress Organised by: Event Dynamics

examining subtle variations in surface), scanning electron microscopy, and back-scattered electron imaging. A minimum of five samples of each clinker was randomly selected, epoxy impregnated and polished to a 0.3-micron diamond paste finish. The final polish was achieved by stepwise reduction in corundum grit to 1 micron and with diamond paste to 0.3 microns. The samples were chemically etched in order to impart variation in color and textures among and within the various crystal phases. The polished sections were etched using dilute solution of potassium hydroxide (0.1 molar aqueous KOH) followed by Nital solution (mixture of 1.0 ml nitric acid and 99 ml isopropyl alcohol) for 20 and 10 seconds, respectively. This combination will turn alite crystals to light blue to green and belite to brown to green. Both silicates will show details of internal structures. The tricalcium aluminate phase will turn to light brown.

2. RESULTS AND DISCUSSION

2.1 Center Points Clinkers

Some of the center point clinkers show nests of belite surrounded by ill-defined and rough-surfaced alite crystals (Figure 1a). This microstructure represents a heterogeneous distribution of phases with large belite nests. The belite nests are an indication of ash shortage, excessive quartz grain size, or presence of feldspar and blast furnace slag [1]. It also indicates an inadequately mixed raw material, which may lead to a decline of mortar strength [2]. The development of belite in the form of a ring around a central pore shown in the optical micrograph is probably formed by silica mobilization during sintering of coarse quartz in the feed [3]. The large number of belite clusters with rough textures may also be an indication of overheating or overburning [4]. The large, irregularly shaped belite crystals are attributed to: prolonged heating below liquid-formation temperature [5]; coarse quartz or quartzite in feed; or very slow cooling [6]. The observed multidirectional lamellar structure of belite is due to its formation and coarsening during alpha to alpha-prime transition during cooling [7]; or alternatively is due to clinker burned at greater than 1420^{o}C [8].

Some alite crystals are elongated and show broad twin green and brown zones. The interstices are composed of brown aluminate phase and the brighter brown to tan ferrite phase. Some other specimens show large clusters of belite associated with relatively high contents of free lime, as indicated from the chemical analysis, which may indicate a high lime saturation factor [9]. The simple twinning in alite crystals has been reported as a result of the rhombohedral to monoclinic transition at approximately 1050^{o}C [7].

The back-scattered electron micrograph (Figure 1b) shows the euhedral alite of average size of 40 µm with inclusions. The interstitial phase is composed of distinct aluminate and aluminoferrite phases. The EDX analysis of the ferrite phases demonstrates a higher percentage of Al relative to Fe due to its distribution between two phases. The back-scattered electron micrographs much more clearly reveal the microstructure showing belite grains with crossed-striated lamellae. Most of the belite grains are "ragged" and some can be seen to be dismembered, that is, the belite grain is broken into much smaller grains along the lamellae boundaries (Figure 1c). The microstructure represents a suite of homogeneously distributed phases of idiomorphic alite, rounded belite, and a finely differentiated matrix with rare small free-lime crystals. This microstructure is indicative of optimized manufacturing conditions: a “correct” chemical composition of well mixed raw feed, with no coarse particles, and satisfactory maintenance of sintering and cooling temperatures, *i.e.* good production conditions [9].

The increase in amount of small alite, decrease in large alite may represent a rapid burning at high temperature [6], resulting in growth rate of crystals slower than formation of nuclei [10]. The matrix is composed of aluminate and ferrite phases. The fine structure of aluminate and ferrite phases shown in the SEM micrographs is indicative of a rapid cooling from high temperature [7, 11]. The rough belite surface, prominent lamellae, segmented finger-like sections shown in the SEM

micrographs may indicate a reducing condition [4] in the kiln atmosphere. The ragged belite microstructure is indicative of a slow cooling [1, 12, 13, and 14].

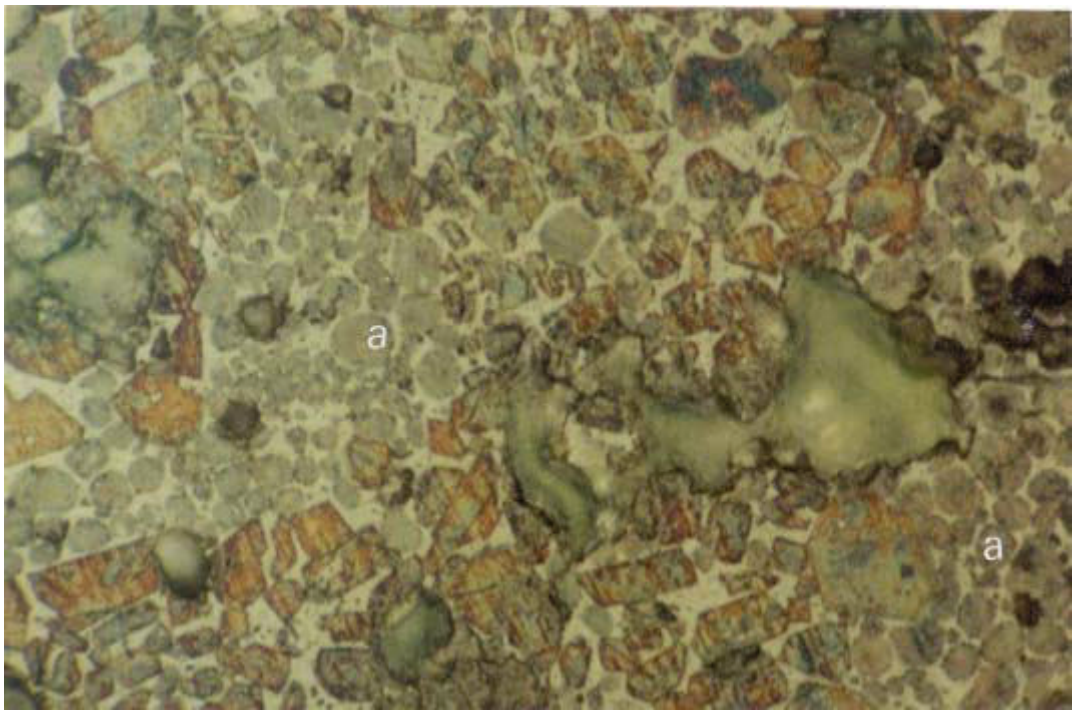

(a)

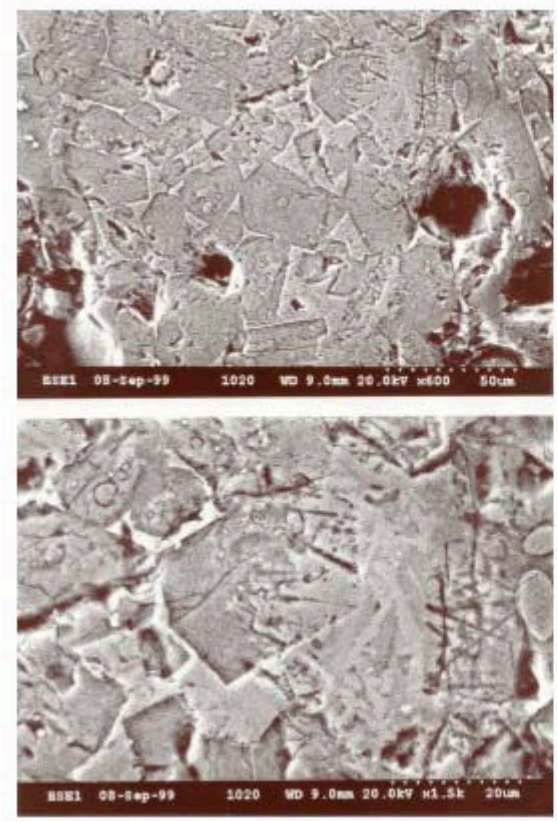

(b)

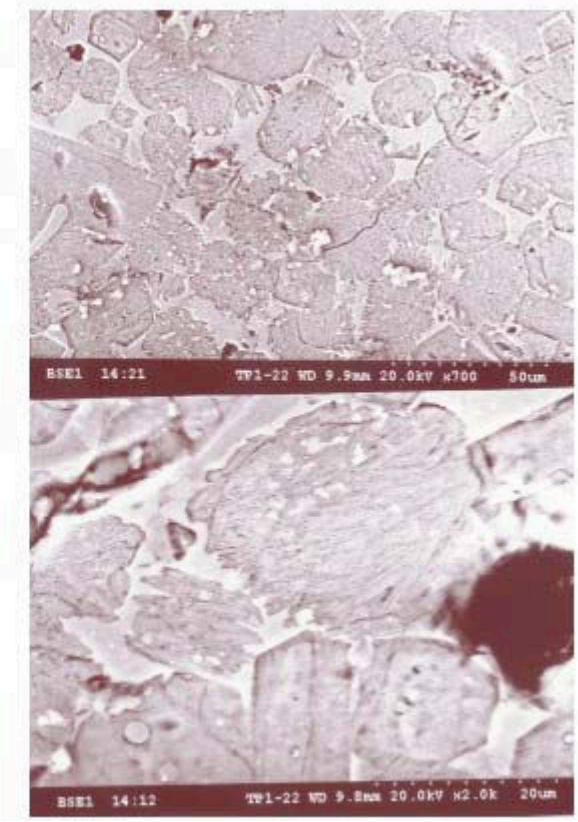

(c)

Figure 1. Optical and SEM micrographs representative of microstructures of the Center clinkers

2.2 Corner Points Clinkers

Reflected light microscopy of the Nital over KOH etched polished section shows coarsely crystalline blue-green alite of an average size 70 μm. Belite appears to be intergrown with alite and some very small belite crystals are growing from alite edges. The interstices are composed of brown aluminate phase, and the brighter brown to tan ferrite phase with also tiny tan-brown blebs (belite) in interstitial phase (Figure 2a).

Some clinkers in this category show coarsely crystalline euhedral relatively clear blue-green alite of an average size 60 μm. Belite is present as rounded twinned crystals. The interstices are composed of brown aluminate phase, and the brighter brown to tan ferrite phase. The black spots distributed over all of the micrograph are probably free lime (Figure 2b).

The Nomarski interference microscopy shows cross striations and the presence of islands or blotches within the boundaries of the belite grain. In addition, dark cores are observed in the center of the belite grains [can not distinguish lime by its dark appearance with this technique]. Also, some belite grains with "ragged" edges are readily observed (Figure 2c). This microstructure represents a homogeneous distribution of silicate phases which indicates an optimized manufacturing condition. The large alite is due to a number of factors including: longer burning time, higher temperature, lime-poor environment in the vicinity of belite; coarse raw mix; and high-viscosity liquid due to alkali or sulfate [4]; or extreme hard burning and porous shell on clinker nodule [15]. Larger alite crystal size, however, may have a greater effect in accelerating the very early strength development of cement [16, 17].

The presence of free lime is attributed to large pieces of raw mix, indicating insufficient fineness of grinding and uniformity of raw mix [18], insufficient homogenization of raw mix [19], local concentration of limestone [2], or pure calcite particles [9]. The observed multidirectional lamellar structure of belite is formed and coarsened during alpha to alpha-prime transition during cooling [7] of clinker burned at greater than 1420^{o}C [8]. The large belite with rough exterior is ascribed to the overheating or overburning [4]. The outgrowth on the surface of belite crystals crystals observed in the Nomarski interference micrographs can be ascribed to high alkali (K-feldspar) in raw mix [1]; Low primary air volume or pressure, excessive burning-zone temperature, slow cooling rate [4].

The ragged dismembered belite structure, which appears in the Nomarski micrographs, may originate during the alpha to alpha prime-inversion in with melt and slow cooling [20]. The large aluminate (C_3A) crystals are indicative of an extremely slow cooling and exsolution of lime from silicates [21]. Some coarsely crystalline euhedral blue-green alite, some with cores, and sizes ranging from 40 to 60 μm. Alite crystals exhibit mottled, rough surfaces, reflecting inclusions. Some of the large alite grains exhibit striations. The interstices are composed of brown aluminate phase and the brighter brown to tan ferrite phase. The back-scattered electron micrograph shows large alite crystals with rough surfaces and the average size is 50 μm (Figure 2d).

Some with cross-striated lamella belite grains with ragged edge reacting protrusions appear as typical morphology of reacting belite. The coarsely crystalline alite is typical of longer burning time, higher temperature, lime-poor environment in the vicinity of belite; coarse raw mix; and high-viscosity liquid due to alkali or sulfate [4]; or extreme hard burning and porous shell on clinker nodule [11]. Larger alite crystal size, however, may have a greater effect in accelerating the very early strength development of cement [16, 17]. The fine inclusions are probably due to pseudomorphic resorption of alite from lime-poor melt; slow cooling [1, 2], or perhaps excess solid solution [22].

The ragged belite microstructure is indicative of slow cooling [1, 12, 13, and 14]. The rough texture of the belite contains prominent lamellae, segmented finger-like sections shown in the SEM

micrographs is indicative of reducing conditions [4] in the kiln during processing. Nomarski interference microscopy shows details of the interstitial phases and it contrasts the darker tricalcium aluminate from the lighter ferrite phases. The tricalcium aluminate appears to dominate the ferrite phase. Two patterns are observed, one in which the ferrite phase forms rims around the outer surface of the tricalcium aluminate phase and one in which it appears as alternate banding between the two phases. The ferrite is never observed as being totally encapsulated within the calcium aluminate phase. The large aluminate (C_3A) crystals observed in the Nomarski interference micrographs is indicative of an extremely slow cooling and exsolution of lime from silicates [21].

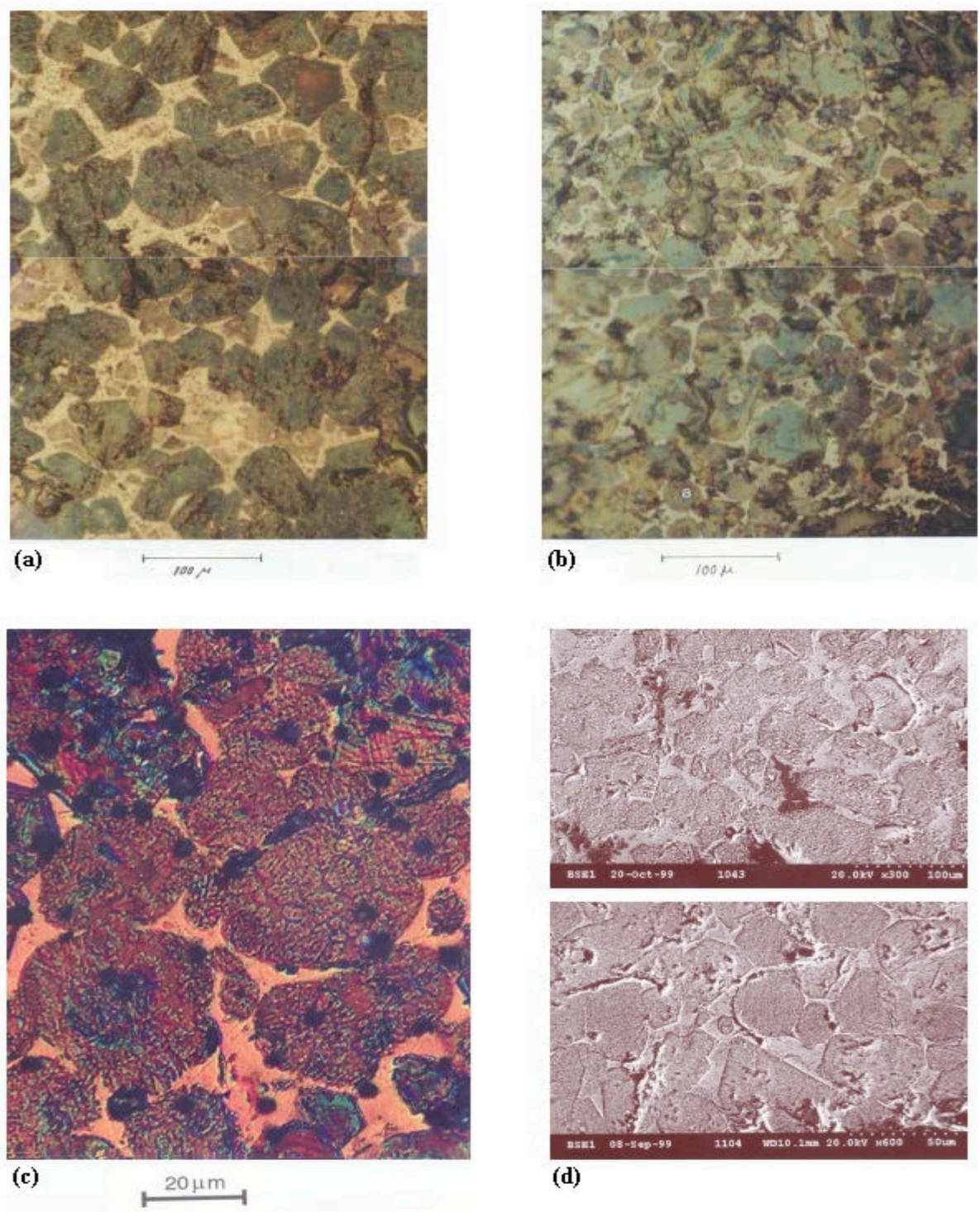

Figure 2. Optical, SEM, and Nomarski micrographs representative of microstructures of the Corner clinkers

Some sections show crystalline euhedral green alite of average size 40 um but isolated alite crystals can be quite large approaching 70 to 100 um. Belite exists as rounded brownish twinned grains as well as small rounded, dark grains of CaO. The interstices are composed of brown aluminate phase, and brighter brown to tan ferrite phase, and contain blebs of belite. The back-scattered electron micrograph shows the belite much more clearly as rounded grains with parallel- to crossed-striated lamellae.

This microstructure represents a homogeneous distribution of silicate phases; medium sized alite and rounded belite; finely differentiated matrix; scarce, small free-lime crystals. It may represent optimized manufacturing conditions: "correct" chemical composition of raw feed, well mixed and satisfactory maintenance of sintering and cooling temperatures [7], which generally represents good production conditions [9]. The variation in alite size indicates a non-homogeneous raw mix as well as locally high lime saturation factor [9]. Simple twinning in alite crystals forms as a result of rhombohedral to monoclinic transition at approximately 1050^{o}C during cooling [7]. The multidirectional lamellar structure of belite forms and coarsens during alpha to alpha-prime transition during cooling [7] of clinker burned at greater than 1420^{o}C [8]. The matrix is composed of dark aluminate phase and yellow ferrite, which may represent a normal clinker [1]. The dendritic intergrowth of the matrix phases is probably due to the relatively rapidly cooled clinker [1].

2.3 Star Points Clinkers

Reflected light microscopy of the Nital over KOH etched polished section shows coarsely euhedral blue-green alite of an average size 60 μm (Figure 3). Alite crystals are largely in contact with each other. At the point marked (a), belite is present in conjunction with a large crystal of alite, which has been interpreted as an incomplete conversion of the belite to alite. Alite contains some inclusions. Throughout the figure, belite is rounded or irregular in appearance and always associated with alite crystals. The interstices are composed of brown aluminate phase, and the brighter brown to tan ferrite phase. This microstructure represents a suite of homogeneously distributed phases of idiomorphic alite, rounded belite, and a finely differentiated matrix with rare small free-lime crystals. This texture is indicative of optimized manufacturing conditions: "correct" chemical sintering and cooling temperatures, *i.e*. good production conditions [9].

The large alite develops due to longer burning time, higher temperature, lime-poor environment in the vicinity of belite; coarse raw mix; and high-viscosity liquid due to alkali or sulfate [4]; or extreme hard burning and porous shell on clinker nodule [15]. It is estimated that this alite crystal size represents the optimal size for greatest effect on cement properties [16]. The small-scale inclusions are probably due to pseudomorphic resorption of alite from lime-poor melt; slow cooling [1,2], or excess solid solution [22]. The belite inclusion in alite is attributed to residual original belite [18]. The matrix is composed of very small brown aluminate phase and yellow ferrite which may represent a low aluminate matrix [1]. Few clinkers in this category possess belite nests which is an indication of ash shortage, excessive quartz grain size, or presence of feldspar and blast furnace slag in the raw feed. Some ragged belite structure was also observed which may originate during the alpha to alpha-prime which suggests inhomogeneity in the raw feed mix.

Figure 3. Optical micrograph representative of microstructures of the Star clinkers

Table 1. Generalized microscopic description of clinker

Sample ID	***Type***	***Description of cement characteristics***	***Microscopic Observations of clinker***
19	Center	Average cement	Avg. alite//*belite hard to see*//normal
9	Center	Average cement	Small alite//nested belite//normal
20	Center	Average cement	Small alite//*belite hard to see*//slow cool
8	Center	Average cement	//belite cross striated//slow cool
21	Center	Average cement	Small alite//nested belite//
1	Corner	Low SO_3/low alkali/low C_3A/low fineness	Large alite//*belite hard to see*//hard burning
3	Corner	high SO_3/low alkali/low C_3A/high fineness	Large alite//belite twinned//normal
10	Corner	Low SO_3/high alkali/low C_3A/high fineness	Avg. alite//belite nested//slow cool
18	Corner	high SO_3/high alkali/low C_3A/low fineness	Avg. alite//*belite hard to see*//normal
6	Corner	Low SO_3/low alkali/high C_3A/high fineness	Small alite//*belite ragged edges*//slow cool
13	Corner	high SO_3/low alkali/high C_3A/low fineness	Avg. alite // belite twinned//rapid cool
5	Corner	Low SO_3/high alkali/high C_3A/low fineness	Large alite//*belite hard to see*//long burning
4	Corner	high SO_3/high alkali/high C_3A/high fineness	Avg. alite//nested belite//
2	Star	Extremely low SO_3	Large alite//belite assoc w/ alite//normal
11	Star	Extremely high SO_3	Small alite//nested belite//abundant matrix
16	Star	Extremely low alkali	Large alite//*belite hard to see*//rapid cool
15	Star	Extremely high alkali	Large alite//*belite hard to see*//slow cool
12	Star	Extremely low C_3A	Avg. alite//*belite hard to see*//slow cool
7	Star	Extremely high C_3A	Avg. alite//belite twinned//normal
17	Star	Extremely low fineness	Small alite//nested belite//slow cool
14	Star	Extremely high fineness	Avg. alite//belite twinned//

3. GENERAL OBSERVATIONS

Several general observations can be made that pertain to the suite of clinkers examined. It can be inferred from the microscopic analysis that a variety of different processing environments were represented in the data set. This included microstructures that are interpreted to be indicative of well-processed "normal" Portland cement, [14%]. Additionally, large clusters of belite crystals are observed in many of the clinkers [28%]. Ten percent of the clinkers exhibited what could be interpreted as reducing kiln atmosphere conditions. This non-standard processing condition was not characteristic of any one of the individual statistical types of cements [center, corner or star] but, in fact, distributed evenly amongst the types. The observed size of the alite crystals suggested that the "average clinkers", the so-called center cements, possess predominantly smaller crystals. In contrast, the corner and star cements possessed average and large size alites.

In an attempt to relate the different clinker fabric to the bulk chemistry and properties of mortars and concrete made from them, the following observations can be made:

- ***Alkali content:*** For clinkers with low alkali content (<0.60 %), 80% of the clinkers contain large to average sized alite crystals and all of them possess belite grains that are twinned, hard to see, associated with alite or having ragged edges. For clinkers with high alkali content (>0.60 %), 90% of the clinkers contain small to average sized alite crystals and 55% of possess nested belite.
- ***Mortar strength:*** 60% of the mortars showing above average compressive strength (at 8 days) are made from clinkers with average sized alite crystals, whereas 85% of the mortars showing below average compressive strength (at 8 days) are made from clinkers with large to average sized alite crystals. On the other hand, 85% of the mortars showing above average compressive strength (at 121 days) are made from clinkers with large to average sized alite crystals, and 85% of those showing below average compressive strength (at 121 days) are made from clinkers with small to average sized alite crystals.
- ***Concrete strength:*** 50% of concretes that show below average compressive strength (at 180 days) are made from clinkers with nested belite.
- ***Heats of hydration:*** 40% of cements giving higher than average heat of hydration are made from clinkers with nested belite.

REFERENCES

[1] Gille, F. et al., Microskopie des Zementklinkers, Bilderatlas, Association of the German Cement Industry, Beton-Verlag, Düsseldorf, West Germany, 1965, 75 pp.

[2] Tsuboi, T., and Ogawa, T., "Microscopic Studies of Clinker for Evaluating the Sintering Process," Zement-Kalk-Gips, Vol. 25, No. 6, 1972, pp. 292-294.

[3] Campbell, D. H., "Microscopical Examination and Interpretation of Portland cement and Clinker," Portland Cement Association, SP030, 1999.

[4] Dorn, J.D., "The Use of Microscopy for Quality Control in the Manufacturing Process," Kiln Optimization Course, Portland Cement Association, Skokie, Illinois, March 1979, 9 pp.

[5] Maki, I., and Goto, K., "Factors Influencing the Phase Constitution of Alite in Portland Cement Clinker," Cement and Concrete Research, Vol. 12, 1982, pp. 301-308.

[6] Ono, Y.; Kawamura, S.; and Soda, Y., "Microscopic Observations of Alite and Belite and Hydraulic Strength of Cement," 5th ICCC, Tokyo, 1968; 1-79, Vol. 1, 1969, pp. 275-284.

[7] Hofmänner, F., Microstructure of Portland Cement Clinker, Holderbank Management and Consulting, Ltd., Holderbank, Switzerland, 1973, 48 pp.

[8] Ono, Y., "Microscopic Analysis of Clinker," Onoda Cement Co., Central Research Laboratory, 1973/ 12/15 and 1975/6/22. Paper supplied to students at Hawaiian seminar in 1975.

[9] Fundal, E., Microscopy of Cement Raw Mix and Clinker, FLS-Review 25, F.L. Smidth Laboratories, Copenhagen, Denmark, 1980, 15 pp.

[10] Butt, Y.M.; Timashev, V.V.; and Starke, J., "Phase Composition and Crystal Size of Quickly Fired Portland Cement Clinkers," Silikattechnik, Vol. 24, 1973, pp. 10-12.

[11] Long, G.R., “Clinker Quality Characterization by Reflected Light Techniques,” Proceedings of the Fourth International Conference on Cement Microscopy, ICMA, 1982, pp. 92-109.
[12] Taylor, H.F.W., The Chemistry of Cements, Academic Press, 1964, Vol. 1, 460.; Vol. 2, 442.
[13] DeLisle, F.A., “Microscopic Analysis of Clinker and Cement,” Cement Technology, Vol. 7, May/June 1976, pp. 93-96 and 98-99.
[14] DeLisle, F.A., “Application of Microscopy to the Various Structures of Clinker and Raw Mix,” Advanced Microscopy Seminar, Portland Cement Association, Skokie, Illinois, 1979, 19 pp.
[15] Long, G.R., “Clinker Fineness: Its Causes and Effects,” Proceedings of the Sixth International Conference on Cement Microscopy, ICMA, Albuquerque, New Mexico, 1984, pp. 243-250.
[16] Okorokov, S.D., “Interrelationship Among Composition, Structure, and Properties of Clinker,” Cement, No. 6, Leningrad, 1975.
[17] Odler, I. and Maula, Abdul S., “The Effect of Burning conditions on the Structures of Portland Clinker and the Reactivity of the Resultant Cement,” 8th ICCt, Brazil,II, pp. 265-269 (1986).
[18] Brown, L.S., “Microscopical Study of Clinkers,” Long-Time Study of Cement Performance in Concrete, RX026, 1948, pp. 877-923;
[19] Krämer, H., “Comparative Microscopic Investigations on Cement Clinkers,” Zement-Kalk-Gips, Vol. 13, No. 12, 1960, pp. 572-579.
[20] Ono, Y., “Microscopical Observation of Clinker for the Estimation of Burning Condition, Grindability, and Hydraulic Activity,” Third ICMA, Houston, Texas, 1981, pp. 198-210.
[21] Eby, C., “Clinker Granulometry,” Kiln Paper No. 15, Kiln Optimization Course, Portland Cement Association, Skokie, Illinois, 1985, 7 pp.
[22] Ono, Y., Ono’s Method, Fundamental Microscopy of Portland Cement Clinker, Chichibu Onoda Cement Corp., No. 2-4-2, Ohsaku, Sakura, Chiba, 285, Japan, 1995, 229 pp.

EFFECT OF DIFFERENT ACTIVATORS TYPE AND DOSAGES AND RELATION TO AUTOGENOUS SHRINKAGE OF ACTIVATED BLAST FURNACE SLAG CEMENT

Cincotto M. A [1], Melo A. A.[1] and Repette W. L.[1]

[1] Escola Politécnica, Departamento de Engenharia de Construção, University of São Paulo, Brazil.
E-mail: maria.cincotto@poli.usp.br, antonio.melo@poli.usp.br and wellington.repette@poli.usp.br

ABSTRACT

This article reports on the investigation of the relation between the activated blast-furnace slag cement hydration and unrestrained autogenous shrinkage development on mortar specimens. The chemical and microstructure changes due to hydration were determined on pastes by conduction calorimetry, mercury porosimetry and thermogravimetric analysis. Samples were prepared with ground blast furnace slag activated with sodium hydroxide (5% of Na_2O) and sodium silicate (silica modulus of 1,7) with 2.5, 3.5 and 4.5% of Na_2O, all them by slag mass. The high early strength Portland cement was used for comparison. Autogenous shrinkage for all activated slag mixes was higher than HESC; early hydration makes an important contribution to the total result that increases with the silica content of the mix. The calorimetry results show that as Na_2O content increases induction period decreases. The degree of reaction increases with the silica content as does autogenous shrinkage and the percentage of non-evaporable water measured by thermogravimetry.

1. INTRODUCTION

Activated slag cement (ASC) is a blend of blast furnace slag and activators, which are chemical species capable of enhancing the slag reactivity during hydration. In addition to the benefit of the use of an industrial residue, ASC based materials show, in many other aspects, advantages over the normally employed Portland cement. It is possible to develop ASC compositions that show extremely fast development of mechanical properties [1, 2] that, for instance, could be advantageous for diminishing operation downtimes during repair of roads or industrial structures. The nature of its hydrates confers to ASC a high resistance to chemical attack, especially under acidic conditions [3, 4]. ASC could be the main component of protection overlays. Adding to the technical advantages, the ASC material cost can be as low as a half of that of Portland cement.

Shrinkage of activated slag cement is reported to be greater than that of Portland cement, and it may represent the most serious limitation for the use of this material [5, 8]. During hydration, changes in chemical composition and microstructure take place, and shrinkage relates to both chemical and physical aspects [9, 10,]. Different studies have identified the main parameters involved with ASC shrinkage, namely the activator chemical species and dosage [11]; the ASC fineness [12]; and the curing conditions [13]. In general, shrinkage increases with higher activator dosages and ASC fineness, and it is greater for sodium silicate (waterglass) based activators compared with sodium hydroxide and sodium carbonate based materials.

The shrinkage mechanism of this cement is not yet very well understood. Published results on ASC do not relate shrinkage and hydration evolution. The majority of the reported earlier shrinkage measurements refer to seven days of hydration and an important period of the phenomenon is missed, as pointed out by Collins; Sanjayan [14].

Proceedings of the 11th International Congress on the Chemistry of Cement (ICCC)
'Cement's Contribution to the Development in the 21st Century'
Hosted by: The Cement and Concrete Institute of South Africa
CD-ROM produced by: Document Transformation Technologies
11 - 16 May 2003, Durban, South Africa
ISBN Number: 0-9584085-8-0
Editors: Dr G. Grieve and G. Owens
Congress Organised by: Event Dynamics

The results of an ongoing investigation at University of São Paulo show that autogenous shrinkage is significant in ASC, and can represent 50% of the shrinkage measured by the drying shrinkage method. Because autogenous shrinkage happens mainly at very early ages, it can be responsible for the reported early age cracking of ASC based elements. The understanding of autogenous shrinkage development and its relation to hydration evolution is essential for the development of casting procedures and admixtures intended to reduce or compensate the shrinkage of ASC. This article reports on the relationship between autogenous shrinkage and hydration evolution for different types and amounts of activators.

2. EXPERIMENTAL

2.1 Materials and mix proportion of mortars and pastes

The granulated blast furnace slag was supplied by Companhia Siderúrgica de Tubarão, with a basicity coefficient Kb = (CaO + MgO)/(SiO_2 + Al_2O_3) = 1,06. The slag consisted of 99,5 % of glass and some crystalline components such as gehlenite and merwinite. It was ground to a Blaine fineness of 500 m^2/kg. The mass percentage composition was: SiO_2 - 33.78; Al_2O_3 - 13.11; Fe_2O_3 - 0.51; CaO - 42.47; MgO - 7.46; K_2O - 0.32; Na_2O - 0.16; SO_3 - 0.15; S^{2-} 1.14; free lime - 0.1; loss on ignition - 1.67; insoluble residue - 0.53. For comparison, samples were also tested with a high early age strength Portland cement – HESC whose mass percent composition was SiO_2 - 19,45; Al_2O_3 - 4,86; Fe_2O_3 - 3,12; CaO - 64,44; MgO - 0,62; SO_3 - 2,94; K_2O - 0,70; LOI - 2,92; CO_2 – 2,45. The Blaine fineness was 461,8 m^2/kg, not too much lower than the slag. Other characteristics were: initial set: 138 min; final set: 200 min.; compressive strength (MPa): 1 day – 29,2; 3 days – 42,6; 7 days – 46,9; 28 days – 56,1. The sand used was a Brazilian standard sand composed of four equal proportions of the fractions sieved: 2.4-1.2 mm, 1.2-0.6 mm, 0.6-0.3 and 0.3-0.15 mm.

Mortar samples were prepared with a mass proportion of HESC or cementitious binder:sand:water of 1:2:0.48, while the paste samples were prepared with mass proportion of 1:0.48. The cementitious binder corresponds to the total mass of slag and the solid fraction of the activator combined; the water contained in the activators was deducted of the total amount of water. The ground blast furnace slag was activated with sodium silicate having a silica modulus of 1.7, with 2.5, 3.5 and 4.5 % of Na_2O, and sodium hydroxide (5% of Na_2O), by slag mass. The different alkali activators and their composition are summarized in Table 1. Mortars and paste samples are named according to the activator's name.

Table 1. Composition of activators

Name	Type	Composition	Silica Modulus
2NS	Sodium silicate	2,5%Na_2O+4,25%SiO_2	1,7
3NS		3,5%Na_2O+5,95%SiO_2	1,7
4NS		4,5%Na_2O+7,65%SiO_2	1,7
5N	Sodium hydroxide	5% Na_2O	-

2.2 Testing methods

2.2.1 Autogenous shrinkage

Nine mortar prisms (25x25x285 mm) were cast for each binder and the measuring of length change was according to ASTM C490 after 6, 8, 10, 12 hours and 1, 2, 3, 4, 5, 6, 7, 9, 11, 14, 21, 28 days. Because hardening is faster for the mortars 3NS and 4NS, the first shrinkage measurement happened 2 hours after mixing. To avoid moisture evaporating from the mortar, the prisms were wrapped with an inner layer of plastic sheet and an outer layer of aluminium foil. Aluminium foil should not be in contact with the highly alkaline mortar, since air bubbles are formed and this can

affect the shrinkage measurements. The protective wrapping sheets were applied over the moulding before casting.

Each prism was tightly sealed with an aluminum tape, guaranteeing a maximum moisture loss of 0.2% after 56 days. After demoulding, the prisms were stored in the dry room at a constant temperature of 24ºC and 50% RH. The first length reading was taken just after demoulding, and the results were expressed as mm/mm x 10^{-6}. The maximum temperature rise due to the heat of hydration was 3°C and the calculated thermal expansion coefficient was $15x10^{-6}$/°C. Because the temperature variation was too small, autogenous shrinkage results were not corrected for temperature effects.

2.2.2 Hydration evolution tests

Conduction calorimetry, thermogravimetric analyses, mercury porosimetry and X-Ray diffraction were performed for the investigation of the hydration evolution on paste samples prepared with water/binder ratio of 0.48. After each period corresponding to autogenous measurements, the hydration of the pastes was stopped by freezing in liquid nitrogen and then freeze dried. All mixes were tested after 6, 8, 10, 12 hours and 1, 2, 3, 7, 14, 28 days. For the calorimetry tests, samples of paste were prepared by mixing 20g of slag and water+activator in a plastic bag and immediately transferred to a JAF Wexham conduction calorimeter at 20°C. The heat output was recorded after 30 minutes, time needed for the system to reach equilibrium. The heat of hydration was determined up to 72 hours after mixing. For thermogravimetric analyses, the tests were made with ground samples of paste using only the 75 µm to 150 µm fraction sieved. Tests were performed in a NETSZCH TG 209-C thermobalance, with a heating ratio of 10ºC/min and under a nitrogen atmosphere with a gas flux of 30 ml/min. The pore size distribution was determined using a Micromeritics Autopore III 9410 porosimeter under pressures ranging from 0 to 414 MPa. The assumed surface tension of the mercury was 0.485 N/m at 25°C (ASTM D 4404-84). The density of the mercury was 13.5413 g/ml and the assumed contact angle was 130°. The X-Ray diffraction was performed on ground samples of paste using a Philips powder diffractometer with Cu Kα radiation, in sample holder with zero background.

3. RESULTS AND DISCUSSION

3.1 Autogenous shrinkage

The plotted results in Figure 1 confirm that the cumulative autogenous shrinkage for all activated slag mixes is higher than HESC and that it increases with the silica content of the mix. It can also be seen that most of the total autogenous shrinkage takes place during the early hydration stages after hardening.

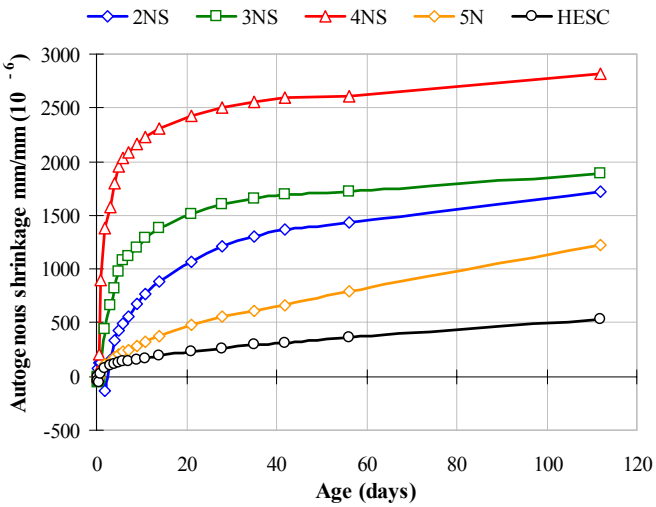

Figure 1. Comparative and cumulative autogenous shrinkage of activated slag and HESC.

The average results of the autogenous shrinkage of the silicate mixes increase with the SiO_2 content, but the difference between the 3NS and 2NS mixes are only statistically significant until 21 days. The 4NS mix shrinkage is 4.5 times greater than the one presented by HESC.

3.2 Conduction calorimetry

Figure 2(a) shows the profile of the heat liberation during 72 hours. The 5N mix shows the fastest heat evolution, with a maximum at 6 hours and no induction period. The HESC has also no induction period, and the highest rate of heat evolution, being the maximum around 18 hours. The induction period of all slag activated mixes correlates well with the Na_2O content, increasing as its content decreases, showing the effect of the alkaline media on the solubility of the slag and hydration evolution.

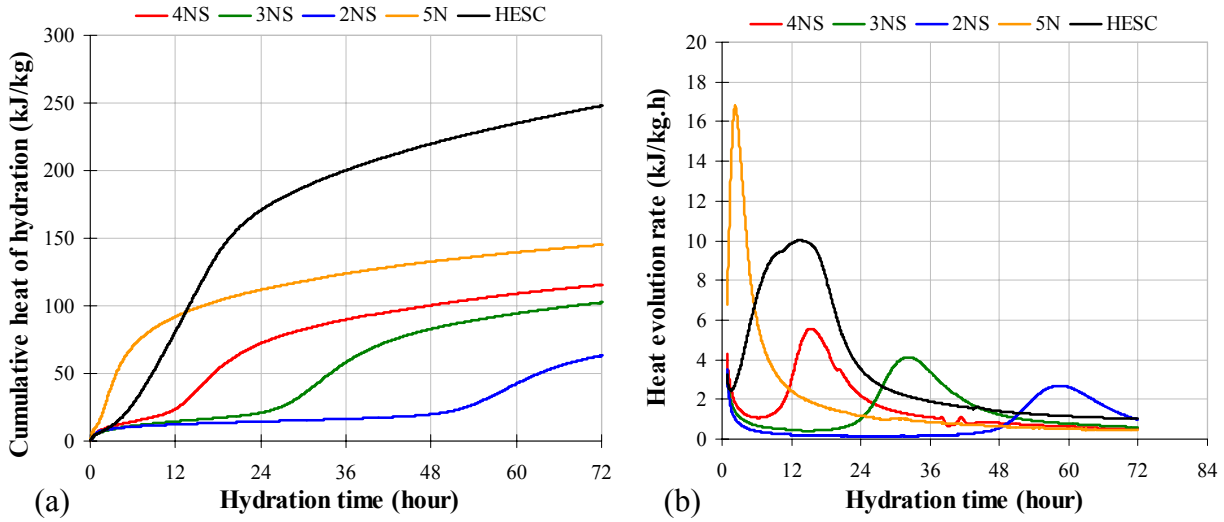

Figure 2. Cumulative heat of hydration (a) and heat evolution rate (b) of activated slag and HESC.

After the induction period, diffusion is the mechanism that controls hydration [15-17]. The slag solubility also influences the reaction sequence, and the total cumulative heat diminishes as Na_2O content decreases, as shown in Figure 2(b). Because the silica modulus is constant, it can be said that the degree of reaction increases with silica content. The influence of the activators on heat evolution rates is clear: a) for the soda mix, the induction period was not observed, but an acceleration period peak; b) for sodium silicate mixes it can be seen that as the Na_2O content decreases, the induction period increases and the magnitude of the peak corresponding to the main product formation decreases.

3.3 Thermogravimetry and X R D analyses

X Ray diffraction patterns of 4NS and 5N are shown in figure 3. The more evident differences between them are (a) the cristallinity of the hydrated products of the 5N mix and the amorphous structure of the silicate mixes and (b) the more evident presence of aluminate phases in the 5N mix, here illustrated by the diffractogram of the 4NS and 5N mixes.

Figure 4 shows the DTGA curves. The hydration reactions start on the first day, and continue to occur during the period studied of 28 days. Silicate activated mixes show only one peak observed between 30°C and 220°C attributed to C-S-H (I) and aluminates; and a smooth loss of mass observed between 275°C and 425°C due to hydrotalcyte formation, better defined for the soda activated mix. The main difference observed between silicate and soda activators is the shoulder of the main peak between 125°C and 185°C, due to aluminates formed on soda mix. The HESC presents peaks for C-S-H, AFm species, Portlandite and calcium carbonate.

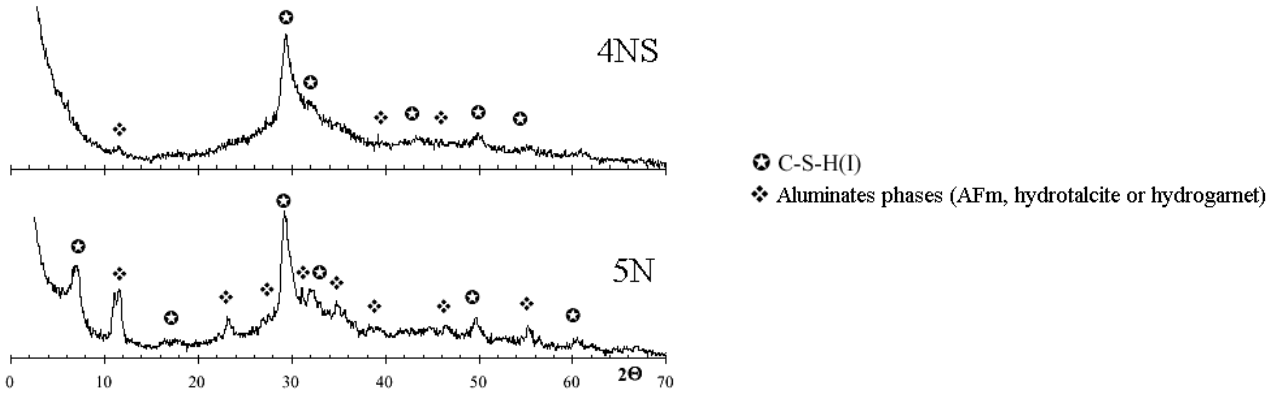

Figure 3. X Ray diffractogram of 4NS and 5N 28 days-old.

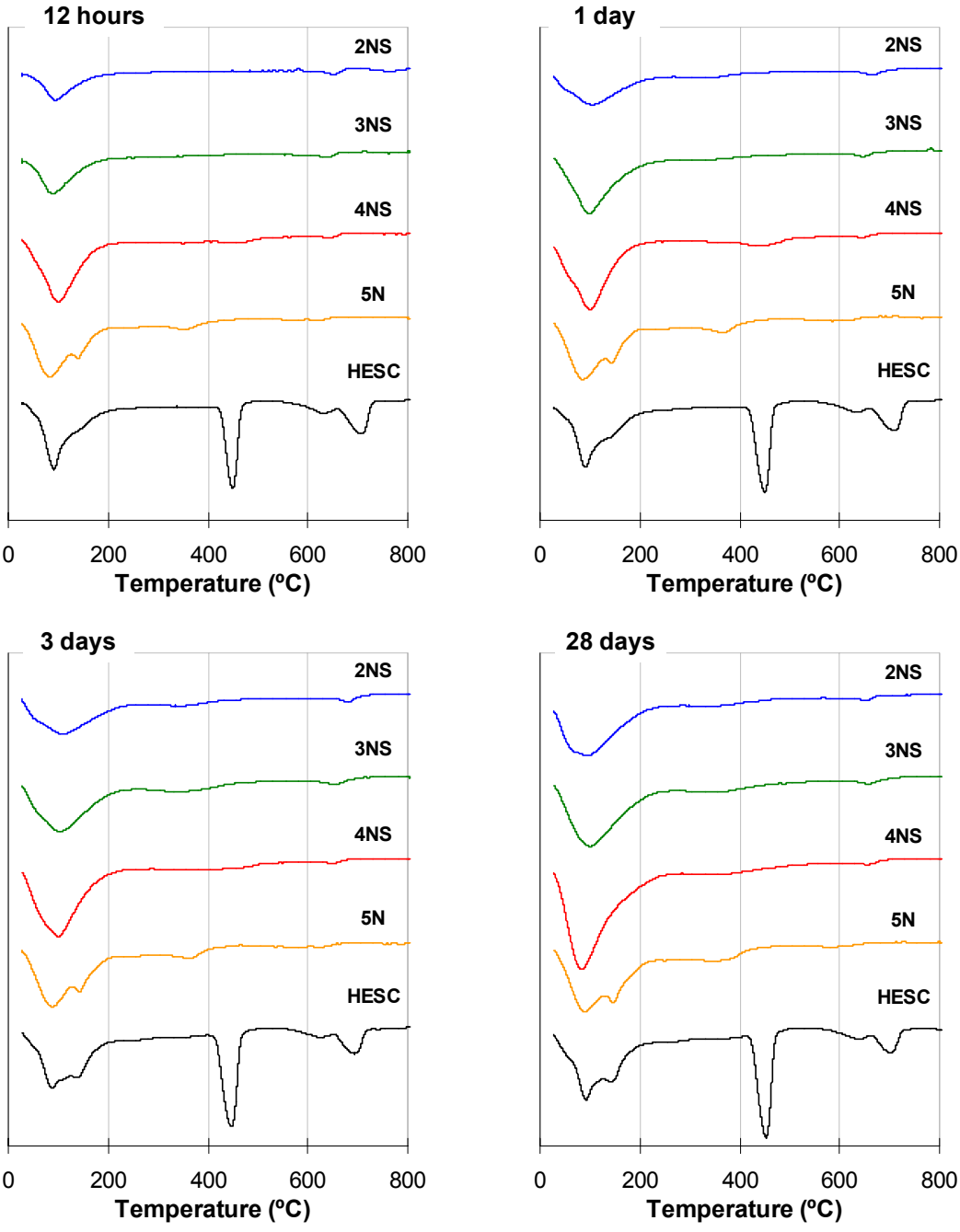

Figure 4. DTGA curves of activated slag and HESC.

3.4 Porosity

In Figure 5(a) the cumulative curves of pore size distribution show the different profile of HESC and soda activated and silicate activated slag. The total volume of pores at 28 days follows the order: 2NS > HESC ≅ 5N > 3NS > 4NS. The incremental pore size curves show the quantitative distribution frequency of the pore sizes in the range of mesopores and macropores (Figure 5(b)). The 4NS and 3NS is practically unimodal as the 2NS and HESC are bimodal and 5N three modal. It can be seen that silica plays an important role in the gel densification, being the maximum pore sizes of 25 nm for the 3N mix and of 15 nm for the 4N mix. The activated slag systems have a typical microstructure, which differs from that of hydrated OPC. In the case of alkali-activated slag, the volume of pores in the micropore size range tends to be bigger than that of HESC. The volume of pores within the capillary range is smaller than that of HESC. Under normal application conditions shrinkage depends on loss of water from macropores and mainly from mesopores [18, 19]. The volume of smaller pores is larger for the silicate mixes than for HESC and 5N. The threshold limit for silicate mixes are in the region of mesopores, whose value diminishes as the silica content increases. From the total pore volume the percentage of mesopores is 90-95% for the silicate mixes while for 5N and HESC are 58% and 54%, respectively. The results obtained are in good agreement with other studies on ASC porosity [15, 20, 21].

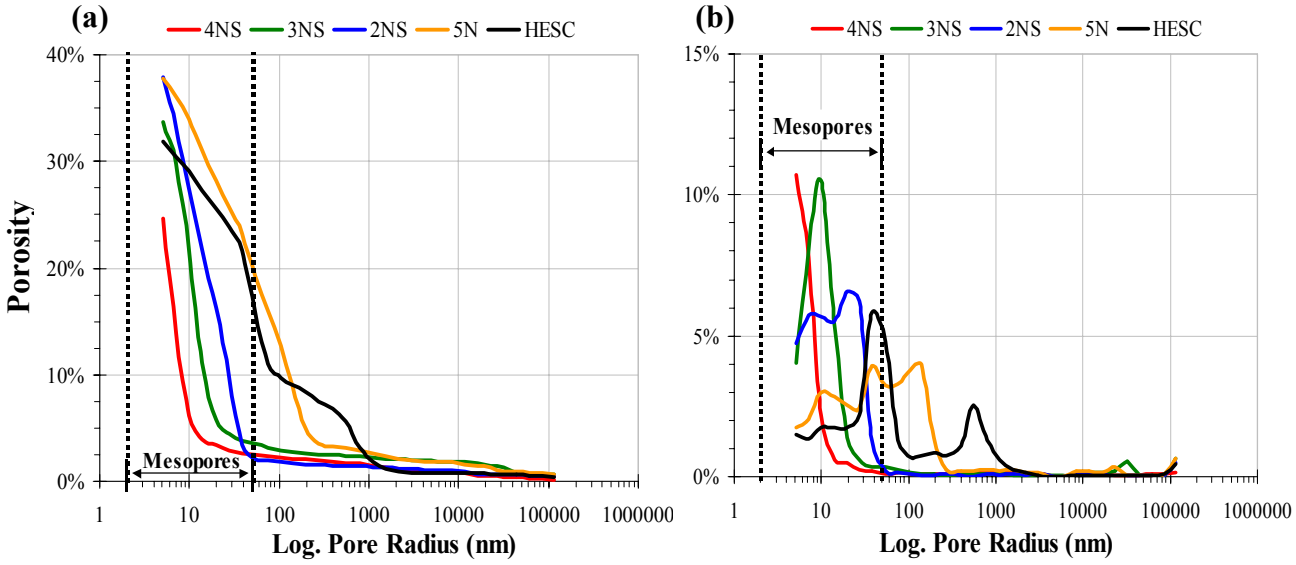

Figure 5. Cumulative (a) and incremental (b) pore size distribution of 4NS, 3NS, 2NS, 5N and HESC pastes at 28 days, with autogenous curing.

4. ANALYSIS OF RESULTS

Figure 6 shows results up to 28 days of autogenous shrinkage; cumulative heat of hydration (H); the total weight loss between 30 and 230 °C, the range in which the most part of C-S-H and AFm formed dehydrates; and the total volume of mesopores, assumed to have diameters between 3nm and 50 nm, expressed as a percentage of the sample bulk volume. Autogenous shrinkage is significant, and values as high as 2400 με were measured for the mortar samples 28 days after casting. In general, at all ages up to 28 days, autogenous shrinkage increases according to the following: HESC < 5N < 2NS < 3NS < 4NS. The larger the amount of silicates in the silicate activators, the bigger the autogenous shrinkage, and the sooner it takes place. Soda activated ASC did not show significant autogenous shrinkage up to 28 days, and compared well with the HESC mortar mix.

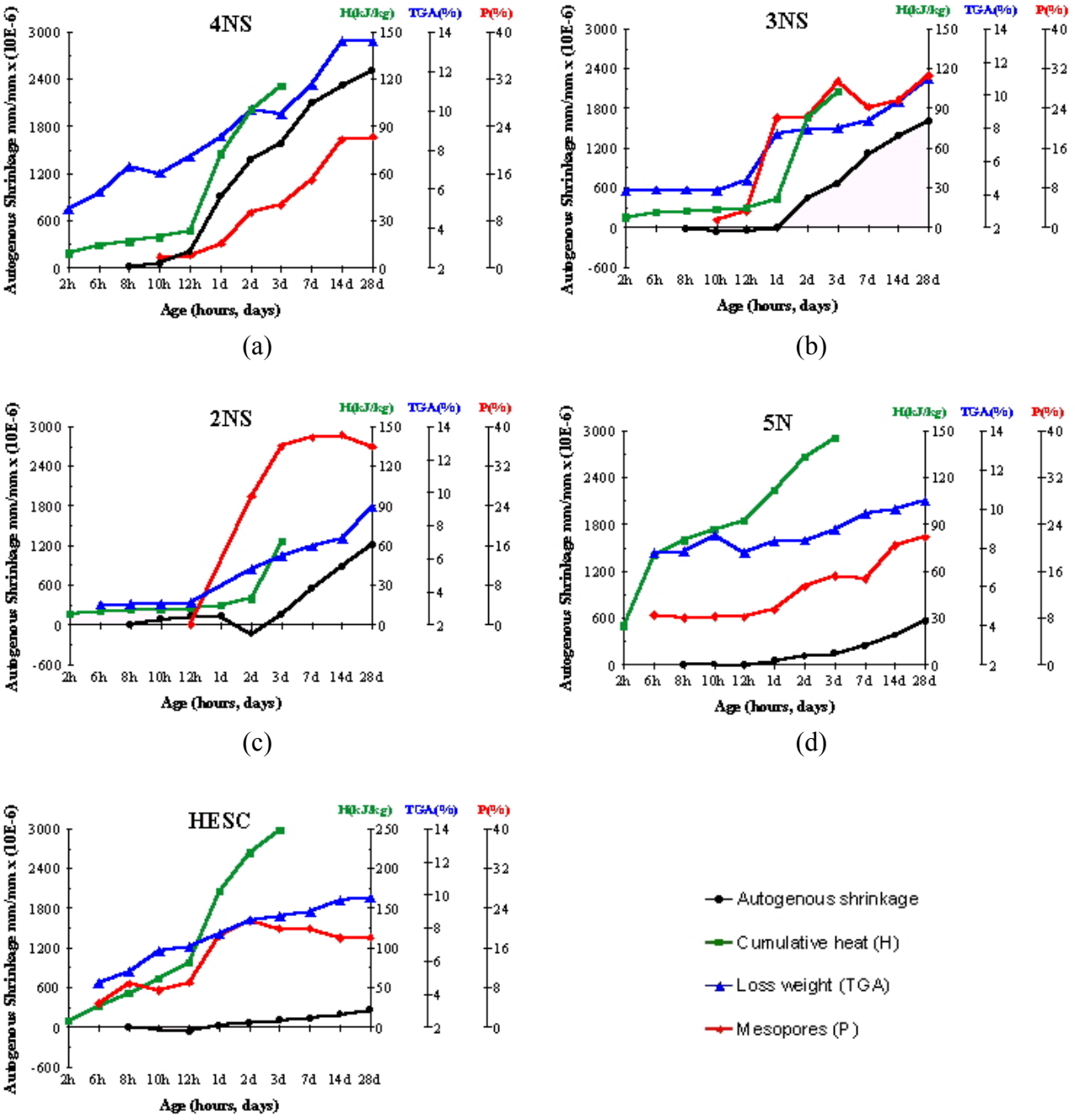

Figure 6. Comparative curves of autogenous shrinkage, cumulative heat (H), loss weight (TGA) and mesopores (P) for 4NS(a), 3NS(b), 2NS(c), 5N(d) and HESC(e) mixes.(Cont.)

When autogenous shrinkage and heat of hydration evolution curves of ASC activated with silicate are compared, it is possible to see that the beginning of the acceleration period of hydration and the initiation of autogenous shrinkage practically coincides. This shows that during the induction period, hydration is very slow and so too is the formation of a more rigid microstructure and the consumption of water capable of causing autogenous shrinkage due to self-desiccation or chemical contraction. Once the hydration becomes more intense, autogenous shrinkage increases rapidly and it is more evident.

The evolution of mesopores also coincides with the beginning of the acceleration period of the hydration. A linear correlation between the evolution of autogenous shrinkage and mesopore volume was found only for the 4NS mix (coefficient of correlation of 0.92). It is more evident in this mix that autogenous shrinkage results from the synergic effect of chemical shrinkage and the physical phenomenon of self-desiccation, mainly occurring at mesopores size pores.

The relation between autogenous shrinkage evolution and the volume of formed mesopores becomes less evident as the amount of silicate diminishes in the activators. It is possible to observe that the volume of mesopores also does not agree well with the heat of hydration and the weight loss evolution associated with the degree of hydration for the pastes prepared with less silicate. One should expect that the larger the heat of hydration, the larger would be the volume of formed mesopores and the weight loss associated with C-S-H content. All of these parameters should relate to the amount of autogenous shrinkage. This apparent discrepancy is probably due to the fact that although hydration evolves through the 28 days tested, part of the hydrated products does not cause the refinement of the pores, but the formation of inner particle hydrated products. Autogenous shrinkage still increases even after the formation of mesopores diminishes. The most likely cause is the consumption of water, or self-desiccation, promoted by the inner particles' hydration. This effect is more evident for the mixes prepared with activators with smaller amounts of silicate. It can be also said that the volume of outer product diminishes with the silicate activator content. As the hydration evolves, the inner products are formed, with migration out of Ca, Al and Si of the slag into the outer product and densifying it [20]. For the 2NS mix, after the acceleration period, the hydration does not contribute to the increase in mesopores' volume.

The 5N mix has a high heat of hydration just after mixing followed by a low ratio of reaction. The shrinkage is very low, increasing after 24 hours. If the total percentage of non-evaporable water for all mixes is compared, it can be observed that the result for mix 5N is equal to or higher than that for silicate mixes, although no correspondence to the autogenous shrinkage was observed.

On the other hand, there was a good correlation with the increase of mesopores. As it was concluded the contribution of silicate on the shrinkage, this can explain the lower result observed for this mix.

The HESC has a high porosity at early hydration that diminishes as the new hydrated products fill in the pores. However, from the total volume, the mesopore evolution practically stabilizes. The autogenous shrinkage on the contrary increases but very slowly and there is no correlation between these properties. A very high correlation exists with heat of hydration and non-evaporable weight loss, considered until 220°C. The 5N and HESC have both, similar products identified by XRD, and also similar volumes of mesopores (57% for 5N and 54% for HESC), and lower shrinkage if compared to silicate mixes.

5. CONCLUSIONS

The conclusions of this study are:

- Determinations indicated that autogenous shrinkage is a significant part of the total dimensional changes observed for these cements. This can explain the fact that the amount of water loss by evaporation does not account for the total measured shrinkage values.
- The silicate content in the activators has an important role on autogenous shrinkage. At 28 days, shrinkage of the mortar prepared with ASC activated with higher silicate content (4NS) was 4.5 times greater than that of HESC; the 3NS mix was 3,9 times greater and the 2NS mix 3,6 times greater.

- Given that autogenous shrinkage is the macroscopic effect of both chemical shrinkage and self-desiccation, the volume of mesopores has an important effect on autogenous shrinkage development. The total volume of mesopores increases as the non-evaporable water loss weight and the activator silicate content increase. The volume of mesopores is much bigger for the silicate activated than the soda activated ASC. Mesopores are approximately 95% of the total volume of the high dosage silicate activated ASC, and only approximately 54% of the Portland cement porosity, both at 28 days.
- Autogenous shrinkage of ASC does not always agree with hydration heat evolution, mesopore formation and degree of hydration. The degree of correlation among these parameters depends not only on the activator's chemical species, but also on the number of active elements that compose the activators.
- Autogenous shrinkage in ASC is a complex phenomenon that results form the synergic effect of chemical and physical parameters. From the comparisons of porosimetry, TGA and XRD results, it can be said that there is some evidence of the effect of microstructure on shrinkage results between silicate activated mixes and soda mix or HESC

ACKNOWLEDGEMENTS

The authors acknowledge the financial support for this project, provided by FAPESP- Fundação de Amparo à Pesquisa do Estado de São Paulo, and to CAPES – Fundação Coordenação de Aperfeiçoamento de Pessoas de Nível Superior for the scholarship provided to the second author.

REFERENCES

[1] Douglas, E.; Bilodeau, A. and Malhotra, V.M. Properties and durability of alkali-activated slag concrete. ACI Materials Journal, vol. 89, nº5, 1992, pp.509-516.
[2] John, V.M. Cimentos de escória ativada com silicatos de sódio (Cements from slag activated with sodium silicate). São Paulo, 1995. 189p. (Doctor Thesis) – Escola Politécnica, Universidade de São Paulo.
[3] Glukhovsky, V.D. Ancient, modern and future concretes. 1st International Conference on Alkaline Cements and Concretes, Kiev, 1994, vol.1, pp.1-9.
[4] Shi, C. and Stegemann, J.A. Acid corrosion resistance of different cementing materials. Cement and Concrete Research, vol.30, n.5, 2000, pp. 803-808.
[5] Collins, F. and Sanjayan, J.G. Microcracking and strength development of alkali activated slag concrete. Cement and Concrete Composites, vol.23, n.4-5, 2001, pp. 345-352.
[6] Wang, S.D. and Pu, X.C. and Scrivener, K.L. and Pratt, P.L. Alkali-activated slag cement and concrete: a review of properties and problems. Advances in cement research, vol.7, n.27, 1995, pp. 93-102.
[7] Taylor, H.F.W. Cement chemistry. 2th, ed.Thomas Telford House, 1997, p.480.
[8] Collins, F. and Sanjayan, J.G. Microcracking and strength development of alkali activated slag concrete. Cement and Concrete Composites, vol.23, n.4-5, 2001, pp. 345-352.
[9] Shi, C. Strength, pore structure and permeability of alkali-activated slag mortars. Cement and Concrete Research, vol. 26, n. 12, 1996, pp. 1789-1799.
[10] ShI, C and Day, R.L. Some factors affecting early hydration of alkali-slag cements. Cement and Concrete Research. vol. 26, n. 3, 1996, pp. 439-447.
[11] Bakharev, T.; Sanjayan, J.G. and Cheng, Y. Alkali activation of Australian slag cements. Cement and Concrete Research, vol. 29, 1999, pp.113-120.
[12] Andersson, R. and Gram, H.E. Properties of alkali-activated slag. In: Alkali activated slag (part I). Stockholm: Swedish Cement and Concrete Research Institute, 1988. pp.9-63. (CBI Research to 1-88).
[13] Yongde, L. and Yao, S. Preliminary study on combined-alkali-slag paste materials. Cement and Concrete Research, vol.30, n.6, 2000, pp. 963-966.
[14] Collins, F.G. and Sanjayan, J.G. Effect of admixtures on properties of alkali-activated slag concrete. Cement and Concrete Research. vol. 30, n. 9, 2000b, pp. 1367-1374.
[15] Jiménez, A.F. and Puertas, F. Alkali-activated slag cements: Kinetic studies. Cement and Concrete Research, vol.27, n.3, 1997, pp. 359-368.
[16] Shi, C. Early hydration and microstructure development of alkali-activated slag cement pastes. 10th International Congress on The Chemistry Of Cement, Gothenburg, 1997, vol.3, pp. 3ii0099 (8p.).
[17] Richardson, I.G. and Cabrera, J.G. The nature of C-S-H in model slag-cements. Cement and Concrete Composites. vol. 22, n. 4, 2000, pp. 259-266.

[18] Xi, Y. and Jennings, H.M. Relationships between microstructure and creep and shrinkage of cement paste. Materials science of concrete III, Ed. Jan Skalny, 1989, pp. 37-69.
[19] Wittmann, F.H. Creep and shrinkage mechanisms. In: Z.P. Bazant, F.H. Wittmann (Eds.), Creep and Shrinkage in Concrete Structures, Wiley, Chichester, 1982, pp. 129-161.
[20] Brough, A.R. and Atkinson, A. Sodium silicate-based, alkali-activated slag mortars Part I. Strength, hydration and microstructure. Cement and Concrete Research, vol.32, 2002, pp.865-879.

EFFECT OF DIFFERENT ACTIVATORS TYPE AND DOSAGES AND RELATION TO AUTOGENOUS SHRINKAGE OF ACTIVATED BLAST FURNACE SLAG CEMENT

Cincotto M. A [1], Melo A. A.[1] and Repette W. L.[1]

[1] Escola Politécnica, Departamento de Engenharia de Construção, University of São Paulo, Brazil.
E-mail: maria.cincotto@poli.usp.br, antonio.melo@poli.usp.br and wellington.repette@poli.usp.br

Maria Alba Cincotto

Maria Alba Cincotto is lecturer of post-graduation courses of Polytecnical School – Department of Civil Engineering, University of São Paulo, Brazil, with experience on chemistry of materials.

EFFECT OF SOLID SOLUTION OF AFm PHASES ON CHLORIDE BINDING

Erik P. Nielsen[1], Duncan Herfort[1], Mette R. Geiker[2] and R. Doug Hooton[3]

[1]R&D centre, Aalborg Portland, Denmark.
E-mail: epn@aalborg-portland.dk, dhe@aalborg-portland.dk
[2] Technical University of Denmark, Dept. of Civil Engineering, Denmark.
E-mail: mge@byg.dtu.dk
[3] University of Toronto, Dept. of Civil Engineering, Canada.
E-mail: d.hooton@utoronto.ca

ABSTRACT

The phase rule has been applied to model the binding of chlorides in hydrated Portland cements. The model predicts the solid solution of at least two AFm phases. It was tested in the laboratory on cement pastes prepared from white Portland cements containing 4 and 12% C_3A, and a grey Portland cement containing 7% C_3A. 1% calcite was added to all cements. The pastes were stored in solutions of different Cl (from $CaCl_2$) and Na (from NaOH) concentrations. When equilibrium was reached the mineralogy of the pastes was investigated by XRD and EDS analysis on the SEM. The solution was also analysed for Cl in addition to all other major components. The distribution of chloride between the solution and the solid phases was found to be controlled by an AFm solid solution phase consisting of monocarbonate and Friedel's salt. Higher contents of Friedel's salt in this solid solution phase corresponded to higher concentrations of Cl in the aqueous solution. Chloride was also bound by the C-S-H phase, but this too was governed by the content of Friedel's salt in the solid solution phase. All of the results obtained can be predicted by applying the phase rule and assuming equilibrium conditions.

1. INTRODUCTION

The harshest conditions that concrete can be subjected to usually involve some form of attack by chlorides. These include marine environments, roads and bridges exposed to de-icing salt, etc. In the case of reinforced concrete, the time it takes for the chlorides to migrate to the reinforcement is the main parameter used to predict the service life of the concrete.

It is generally agreed that when chlorides migrate into concrete they become partially fixed by the hydrate phases through one or more processes collectively referred to as binding. The binding capacity of the cement paste system has a significant effect on the service life of reinforced concrete, where only chlorides in solution can be transported towards the reinforcement where at some critical concentration they initiate corrosion.

The mechanisms that result in binding of chloride ions are still not entirely clear [1], but it is assumed that it is mainly the aluminium-bearing hydration products that react chemically with the chloride ions to form Friedel's salt, or solid solutions which include Friedel's salt [3]. Competition for the aluminates by the sulfate and carbonate ions will affect the capacity of the system to bind chlorides. The very high specific surface area of the C-S-H phase is often believed to substantially contribute to binding through physical adsorption [7], although evidence that it plays little or no role is also convincing [4].

Proceedings of the 11th International Congress on the Chemistry of Cement (ICCC)
'Cement's Contribution to the Development in the 21st Century'
Hosted by: The Cement and Concrete Institute of South Africa
CD-ROM produced by: Document Transformation Technologies
11 - 16 May 2003, Durban, South Africa
ISBN Number: 0-9584085-8-0
Editors: Dr G. Grieve and G. Owens
Congress Organised by: Event Dynamics

The binding process is normally examined by determining the contents of chlorides bound in cement paste as a function of the concentration of chlorides in an external solution over a wide range of total chloride contents. The results are then expressed by means of the so-called Langmuir or Freundlich isotherms [5], depending on which of these provides the best fit over the range of concentrations examined. In this paper we describe a thermodynamic model based on the phase rule for predicting the stable or metastable equilibrium phase assemblages in cement paste. The model is specifically applied to binding of chloride ions in presence of carbonates at constant alkali contents. The model is then tested experimentally in the laboratory.

2. THERMODYNAMIC MODEL BASED ON THE PHASE RULE

Although the 'Phase Rule' is valid for all chemical systems in equilibrium, only a handful of workers have used it to describe hydrated cement [2,8,9]. The rule states that the number of *phases (P)* plus the *degrees of freedom (F)* in a system is equal to the number of *components (C)* plus *n*. In the standard form *n* is equal to 2, but at constant temperature and pressure *n* can be reduced to 0, so that the phase rule becomes $P + F = C$.

The main components in hydrated Portland cement are CaO, SiO_2, Al_2O_3, Fe_2O_3, SO_3 and H_2O.

The maximum number of phases that can form in the fully hydrated system (for the invariant assemblage where F=0) is, therefore, six. For a typical Portland cement these phases would be the C-S-H phase, portlandite, monosulfate, ettringite, an iron oxide phase (possibly FH_3) and the pore solution. From the chemical composition of the system, and standard chemical compositions of the individual hydrate phases, the contents of phases in wt. % within any invariant system can be calculated by solving 'n' equations for 'n' unknowns, where 'n' is the number of components and phases. As a first approximation the composition of the pore solution is set to that of pure H_2O. This is valid as long as the weight fraction of components dissolved is negligible compared to the weight fraction that has reacted to form solid phases.

The introduction of chloride and carbonate adds two extra components to the system allowing up to eight phases at constant temperature and pressure. At small additions of these components the two additional phases would normally be the AFm phases, monocarbonate, and Friedel's salt. For convenience, $CaCl_2$, $CaCO_3$, $CaSO_4$ and C_3A are chosen as components in this paper rather than Cl, CO_2, SO_3 , and Al_2O_3. This is valid as long as these components occur as stoichiometric units in all hydrate phases. The presence of sodium (or potassium) introduces a degree of freedom rather than an extra phase, except at very high concentrations, but this can be disregarded when the alkali content is held constant. When $CaCO_3$ and $CaCl_2$ (and additional $CaSO_4$) are introduced to the 6-component system for hydrated Portland cement, all of the changes in phase assemblages (except at very high contents) take place within the subsystem for C_3A-$CaSO_4$-$CaCl_2$-$CaCO_3$. The other phases (i.e. C-S-H, $Ca(OH)_2$, FH_3, pore solution) occur as excess phases which participate in all phase assemblages, and as long as invariant conditions prevail remain constant in composition within any given assemblage. The 4-component sub-system C_3A-$CaSO_4$-$CaCl_2$-$CaCO_3$ is illustrated in Figure1 by means of the two 3-component sub-systems for chloride attack (Figure 1a), and carbonate addition (Figure 1b).

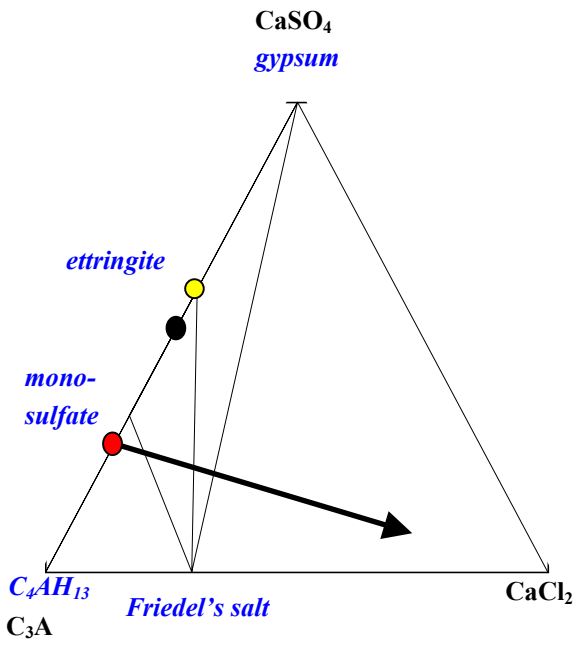

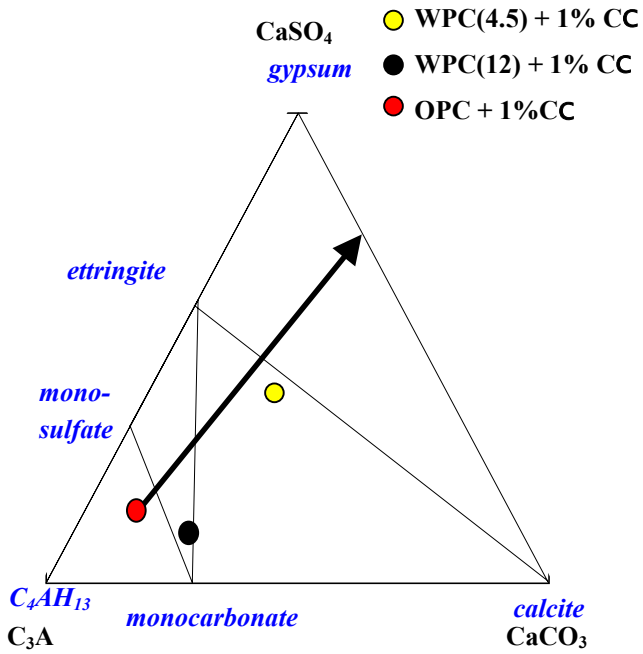

Figure 1a. Sub-system for C_3A-$CaSO_4$-$CaCl_2$ Figure 1b. Sub-system for C_3A-$CaSO_4$-$CaCO_3$. Arrow schematises the change in phase contents with increased $CaCl_2$. Filled circles indicate initial composition for all three pastes examined (see table 2) before chloride addition.

The addition of $CaCl_2$ to an under-sulfated Portland cement consisting of hydroxy AFm and monosulfate shown in Figure 1a for the sub-system C_3A-$CaSO_4$-$CaCl_2$ would initially form Friedel's salt. Further addition results in a depletion in the hydroxy AFm phase until it is eventually exhausted. Ettringite can only form at this point and continues to form alongside Friedel's salt with further addition of $CaCl_2$. In all, four different 3-phase assemblages are possible with increasing $CaCl_2$ contents. Four 3-phase assemblages are also possible in the C_3A-$CaSO_4$-$CaCO_3$ shown in Figure 1b. By combining the two diagrams, addition of $CaCl_2$ to a system starting out with a mixture of monosulfate, hydroxy AFm and monocarbonate, should result in the sequence of five 4-phase assemblages shown in table 1.

Table 1. Predicted sequence of phase assemblages resulting from $CaCl_2$ addition to hydrated Portland cement with relative high $C_3A/CaSO_4$ ratio.

1.	**Hydroxy-AFm, Monosulfate, Monocarbonate and Friedel's salt**	**Phases in excess:** C-S-H, Calcium hydroxide, Goethite and Pore solution
2.	**Monosulfate, Ettringite, Monocarbonate and Friedel's salt**	
3.	**Ettringite, Calcite, Monocarbonate and Friedel's salt**	
4.	**Ettringite, Calcite, Gypsum and Friedel's salt**	
5.	**Calcite, Gypsum, Friedel's salt, + degree of freedom (i.e. ↑ of Cl in PS)**	

According to the phase rule, no degrees of freedom are possible in assemblages 1 to 4 since each assemblage consists of eight components and the maximum number of phases (i.e. eight). An important constraint imposed by this invariance is that the composition of all phases must remain constant within each assemblage. However, once the total binding capacity is exhausted, i.e. when all the ettringite has reacted to form gypsum and Friedel's salt (assemblage no.5), only seven phases exist giving one degree of freedom. This degree of freedom would allow the $CaCl_2$ concentration to increase in the pore solution upon further addition, until it eventually becomes saturated with respect to $CaCl_2.2H_2O$.

A $CaCl_2$-binding isotherm for the sequence of reactions described above, at a constant level of alkalis, would be expected to develop as illustrated in Figure 2. The small increases in concentration of free chloride ions are the result of probable differences in the composition of the pore solution between assemblages.

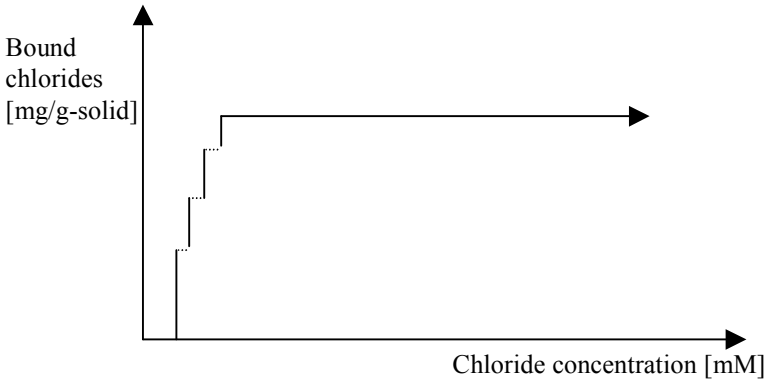

Figure 2. Schematised development of a $CaCl_2$ binding isotherm in an invariant system.

Significantly, this hypothetical isotherm for $CaCl_2$ has not been reported in the literature. Instead, the relationship between bound and free chlorides is invariably described as a continuous curve best described by the Langmuir or Freundlich models [2,6]. This implies either non-equilibrium conditions, which in our view is unlikely, or solid solution between two or more phases. The latter would reduce the number of phases and, therefore, provide one or more degrees of freedom, which would allow the chloride concentration to increase in the pore solution as a function of the total chloride content in the system. In the absence of sulfate and carbonate, a likely candidate for this solid solution would be the hydroxy-AFm - Friedel's salt solid solution phase reported in [3]. In the presence of carbonate, a solid solution between monocarbonate and Friedel's salt has also been reported [10,11], and this, in our view, would be the most likely phase to occur in realistic systems which must always contain some carbonate. The possible solid solution of monocarbonate and Friedel's salt forms the basis of the model which is tested in this study.

3. EXPERIMENTAL

Three Portland cement pastes were examined: two white Portland cements with Bogue-C_3A contents of approx. 4 and 12%, and a grey ASTM type II Portland cement. All the pastes were prepared at a w/s ratio of 0.70 after replacement of the cement by 1.0 wt. % calcite (note that all of the cements already contain some CO_2, present of course as carbonate). Compositions of the cements (determined by XRF) are shown in table 2.

Table 2. Composition of the Portland cements tested

Cement id.	SiO_2	Al_2O_3	Fe_2O_3	CaO	SO_3	MgO	Na_2O	K_2O	CO_2*
WPC(4)	24.8	1.87	0.33	68.9	2.20	0.52	0.16	0.11	0.14
WPC(12)	23.6	4.49	0.21	65.9	2.38	0.97	0.03	0.20	0.72
OPC	21.0	4.90	3.64	65.1	3.00	0.89	0.30	0.41	0.08
* Determined by DTG.									

Cement id.	C_3S	C_2S	C_3A	C_4AF
WPC(4)	72.2	16.8	4.4	1.0
WPC(12)	51.7	28.6	11.5	0.6
OPC	59.1	15.6	6.8	11.1

The cement pastes were cast in 2 cm^3 centrifuge tubes, sealed and kept at a constant temperature of 20^oC for one month. The samples were then de-moulded and crushed to between 2-4 mm in size. The crushed paste of approximately 8.25 g was then weighed before being placed in 12.5 ml. solution for 5 months at 20^oC. For each type of cement paste, the specimens were exposed to solutions of increasing $CaCl_2$ concentration, allowing progressively higher degrees of reaction, but at a constant alkali content. WPC(4) was stored at a sodium concentration (by addition of NaOH) of either 250 or 550 mM, whilst the OPC specimens were stored at 550mM and the WPC(12) specimens at 250mM.

After six months when the pastes had fully reacted with the solutions to equilibrium, the phase equilibria was examined by a combination of EDS (Energy Dispersive Scanning, at 15keV, 25µA and measuring time of 40 s.) and XRD (X-Ray Diffraction) analysis. As well as analysis of the solutions by titration (chloride and pH), ICP (Inductively Coupled Plasma Atomic Emission Spectrometry), and AA (Atomic Absorption), for all major components after removal of the solid phases by filtration.

4. RESULTS AND DISCUSSION

The Al/Ca and S/Ca ratios were found by EDS analysis to be fairly constant in the C-S-H at approximately 0.40 and 0.30, respectively.

A combination of XRD and EDS analysis verified the sequence of phase assemblages 1, 2 and 3, listed in table 1, except that Friedel's salt and monocarbonate occurred in solid solution, instead of as two separate phases. As predicted, the initial assemblage to form at low contents of $CaCl_2$ in the paste prepared from the low C_3A white cement (WPC(4)), was ettringite + calcite + monocarbonate + Friedel's salt (assemblage no. 3 in table 1), or more correctly ettringite + calcite + AFm_{ss}, where the solid solution phase is a mixture of monocarbonate and Friedel's salt. The initial assemblage formed from the high C_3A white PC, (WPC(12)) corresponds to assemblage no. 2 in table 1. Assemblage no. 3 formed at higher concentrations. The initial assemblage formed at small contents of $CaCl_2$ in the paste prepared from the grey Portland cement (OPC) corresponds to assemblage no. 1 in table 1. Assemblage no. 2 followed by assemblage no. 3 formed at higher $CaCl_2$ contents for this cement. In no case was the content of $CaCl_2$ high enough to form assemblage nos. 4 and 5, although preliminary results not included here indicate that these assemblages form as well.

Solid solution was found between Friedel's salt and monocarbonate for all of the specimens examined. This is illustrated by plotting the Cl/Ca vs. Al/Ca ratios determined from EDS analysis shown in Figure 3. Only two data sets are plotted here, i.e. for the low C_3A white PC (WPC(4)) with Na =550mM, at two different Cl contents. Figure 4 shows the same data, but plotted as S/Ca vs. Al/Ca. Since assemblage no 3 persisted at all chloride contents investigated for this cement, neither monosulfate nor Kuzel's salt were identified. Monosulfate was identified in assemblages 1 and 2 for the two other cements, where it invariably occurred as a pure phase without forming a solid solution with any of the other AFm phases.

XRD-patterns for the pastes examined confirmed the assemblages described above (not shown). For the AFm_{ss} phase, the same type of ordered stacking of layers of monocarbonate and Friedel's salt described in [11] was observed.

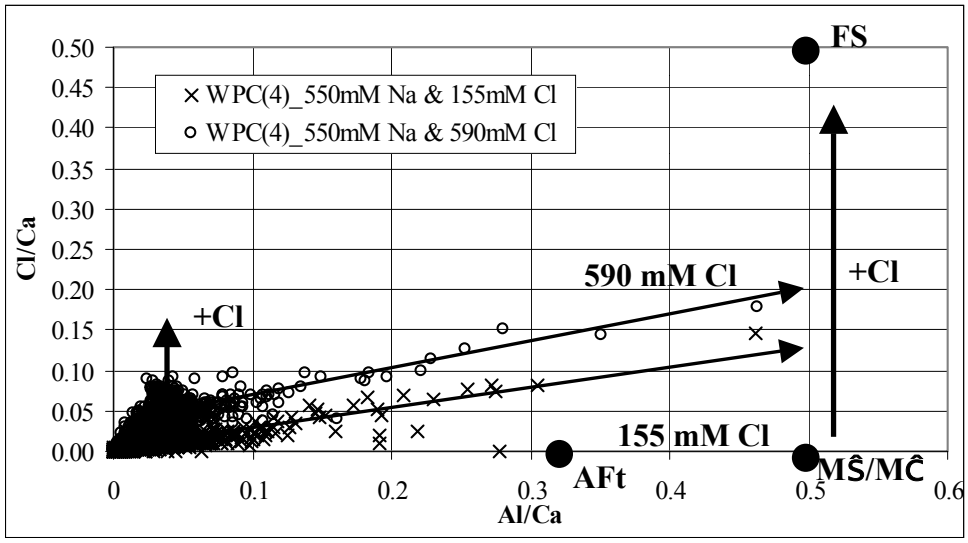

Figure 3. EDS-data illustrating the development of Cl/Ca in the AFm_{ss} phase between monocarbonate (MĈ) and Friedel's salt (FS) and in C-S-H, at increasing Cl additions.

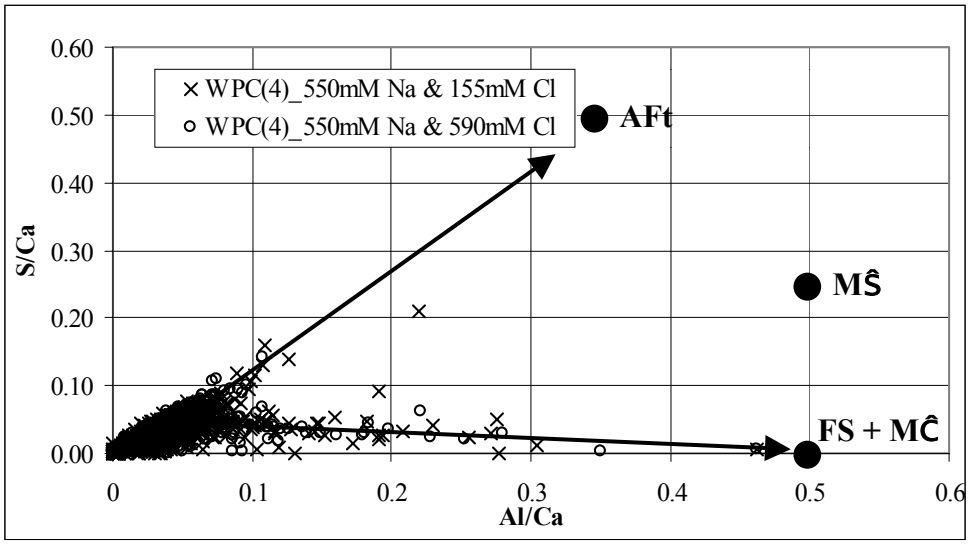

Figure 4. S/Ca vs. Al/Ca from EDS analyses. Actual plots are the same as the presented in Figure 3.

The solid solution of Friedel's salt and monocarbonate introduces a degree of freedom to the system. This permits the relative content of Friedel's salt to increase in the AFm solid solution, along with a concomitant increase in the concentration of chloride ions in both the pore solution and in the C-S-H phase. The phase rule is satisfied as long as a single relationship exists for the distribution of Cl between all three phases regardless of C_3A and C-S-H contents. That such a relationship exists at constant alkali content for the two white cements can be seen in Figures 5 and 6 where, despite a marked difference in C_3A contents (as well as C-S-H contents due to the significant difference in C_3S contents in the clinker), almost exactly the same distribution is found between all three phases at the constant alkali content of 250 mM Na. Lower concentrations are found in the C-S-H phase and AFm_{ss} phase at the higher concentration of 550mM Na in the solution. The slight difference in binding in the AFm_{ss} and C-S-H phase between the white and grey cements is possibly due to the presence of iron in the grey cement which adds an extra degree of freedom to the system. The relationship between the concentration of Cl in the C-S-H phase and the AFm_{ss} phase (Figure 6), appears to be independent of the alkali content.

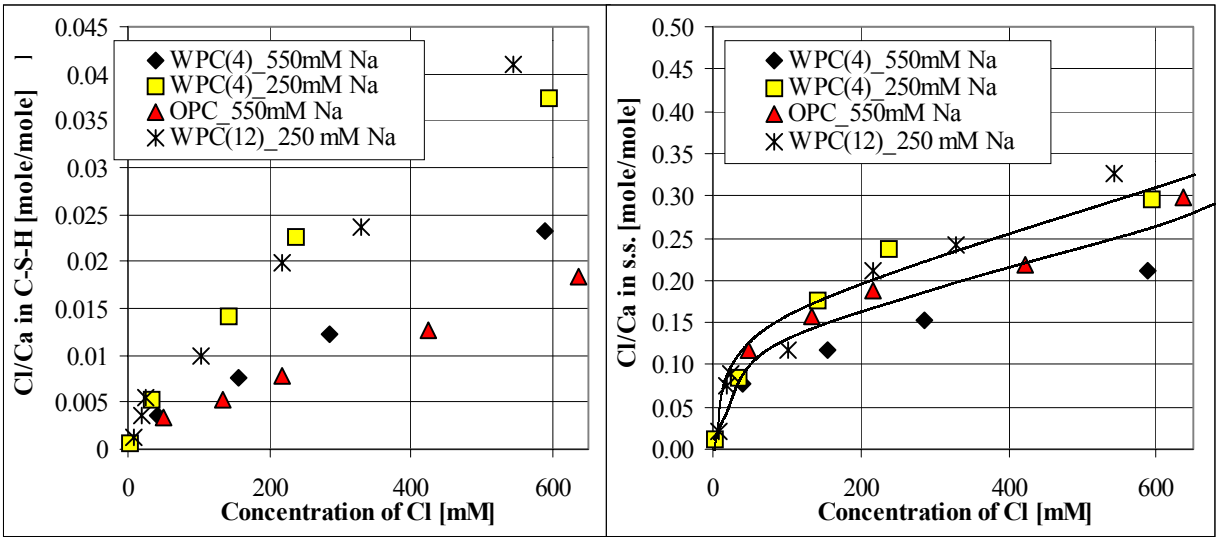

Figure 5. Cl/Ca ratio in the C-S-H and AFm_{ss} phases versus the concentration of chlorides in solution.

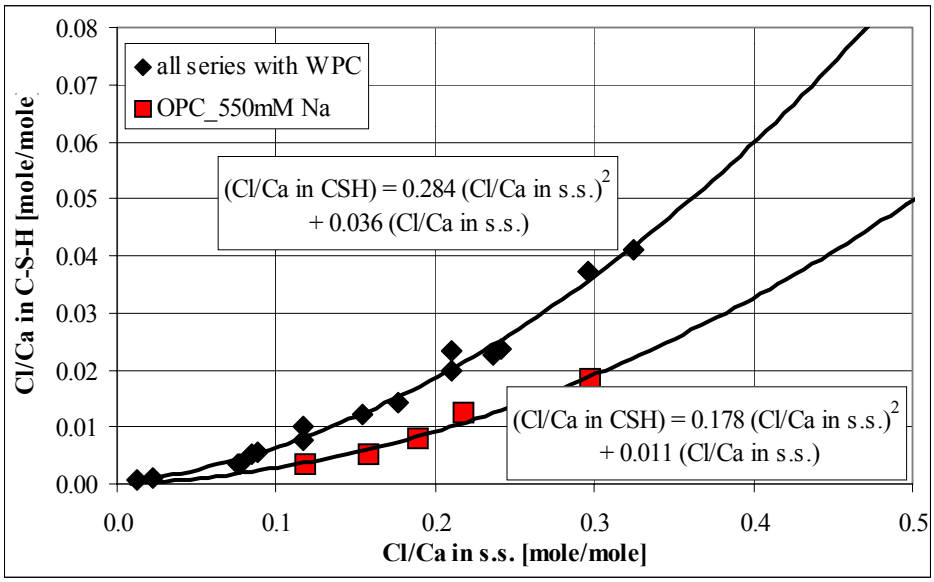

Figure 6. Cl/C ratio in the C-S-H versus the Cl/Ca ratio in the AFm_{ss} phase for all cements and alkali contents.

The above relationships apply to the distribution of chloride between the individual phases, but not to the ratio of total bound and free chlorides, since this will of course vary depending on cement composition (i.e. C_3A content etc.). This is clear from the traditional Cl isotherm shown in Figure 7 (for the same data used in Figures 5 and 6), where different isotherms clearly exist for the two white cements.

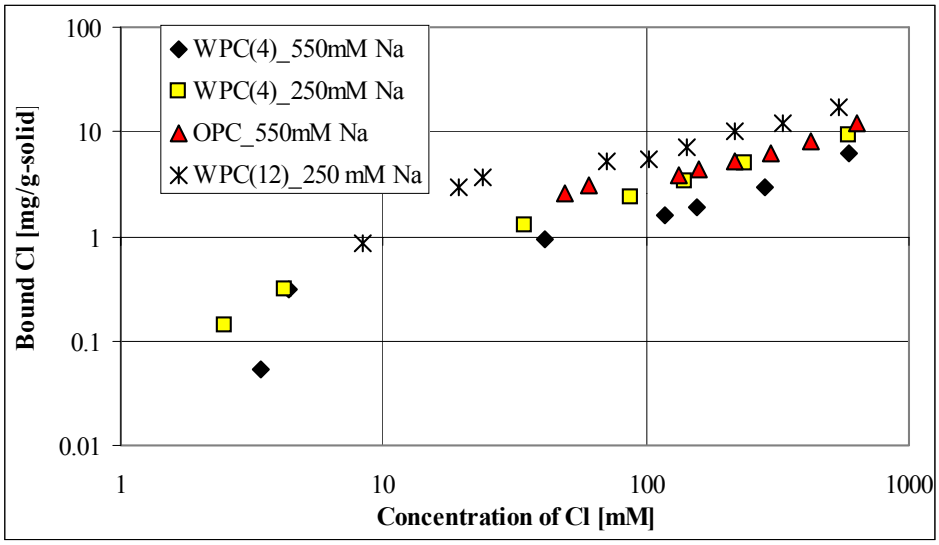

Figure 7. Chloride binding isotherms for the same data shown in Figures 5 and 6.

The above relationship can be understood more readily from the ternary subsystem shown in Figure 8 which is constructed from Figures 5 and 6. This diagram should apply to any Portland cement in which the concentration of Na in the pore solution is fixed at 250 mM. At higher alkali contents, concentrations of Cl (or Friedel's salt) in the AFm_{ss} phase and C-S-H phase will be lower for the same concentration of Cl in the pore solution. The same relationship should apply regardless of the relative content of C_3A, C-S-H, sulfate, carbonate and pore solution. The relationship can be used to calculate the overall binding capacity, i.e. the relationship between the free and bound chlorides, from the overall hydrate phase assemblage (which can in turn be calculated quantitatively from the chemical composition of the cement and water cement ratio as described above for the thermodynamic model).

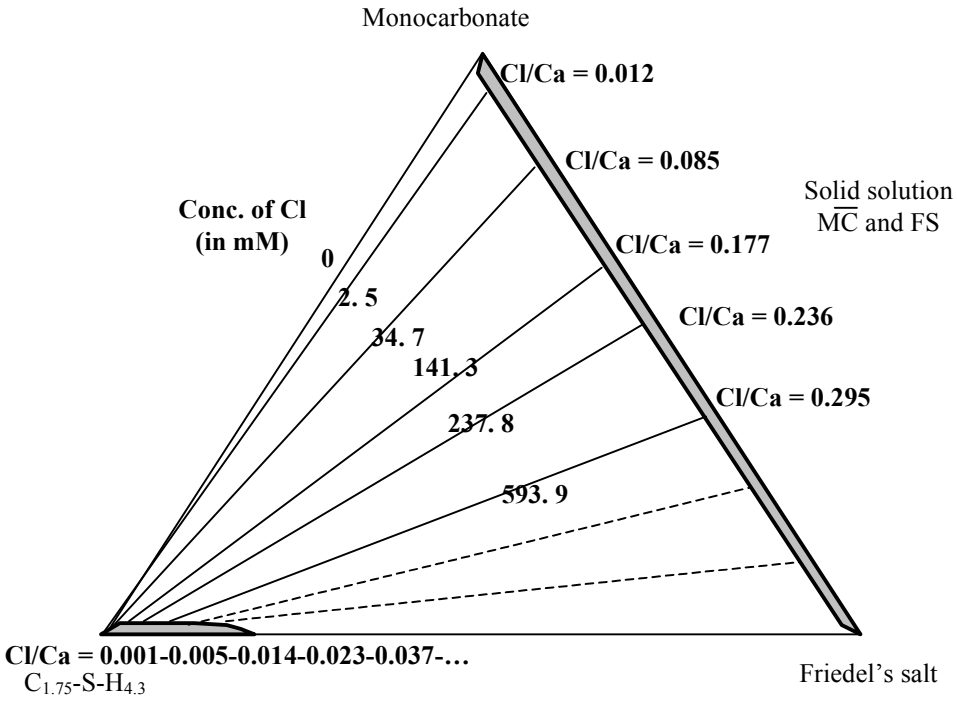

Figure 8. Pseudo ternary system for 'C-S-H'-Friedel's salt-Monocarbonate at a constant Na concentration in solution of 250 mM. Solid tie lines and corresponding chloride concentrations were determined in this study. The dashed lines are extrapolated from this.

The above relationship predicts that for a given aluminate content, low sulfate contents and high carbonate contents should be beneficial to binding since both would effectively increase the content of monocarbonate and therefore lower the mole fraction of Friedel's salt in the AFm_{ss} phase. Lower contents of Friedel's salt in the AFm_{ss} phase are beneficial because they lower the concentration of Cl in the pore solution (and C-S-H phase). Sulfate that invariably accompanies chloride intrusion from sea water, effectively lowers the mole fraction of monocarbonate in the AFm_{ss} phase, increasing the mole fraction of Friedel's salt and the chloride concentration in the pore solution. The reduction in binding capacity caused by sulfate attack, however, can be mitigated by the presence of carbonates which have the opposite effect.

5. CONCLUSIONS

Solid solution between Friedel's salt and monocarbonate reported elsewhere has been confirmed for hydrated Portland cement containing 1% calcite and different contents of C_3A.

The relationship between free and bound chlorides is governed by this solid solution.

Chlorides are also bound by the C-S-H phase, with a well defined distribution of chloride between all three phases (i.e. the AFm solid solution phase, the pore solution and the C-S-H phase) at any given alkali content.

Higher alkali and sulfate contents reduce the binding capacity of hydrated Portland cement. Carbonates increase the binding capacity.

All these results can be predicted by applying the phase rule.

REFERENCES

Books

[1] Glasser,F.P. Role of Chemical Binding in Diffusion and Mass Transport. In Ion and Mass Transport in Cement-Based Materials, Materials Science of Concrete, Ed. R.D.Hooton M.D.A Thomas, J.Marchand, J.J.Beaudoin. Pub. The American Ceramic Society, pp.129-154, 2001

[2] Glasser, F.P., "Application of the Phase Rule to Cement Chemistry", Chapter 5 in Refractory Materials Volume 6-II, Ed. Allen M. Alper, pub. Academic Press, 1970.

Journal articles

[3] Birnin-Yauri, U.A. and Glasser, F.P. Friedel's salt, $Ca_2Al(OH)_6(Cl,OH).\ 2H_2O$: Its solid solution and their role in chloride binding. Cement and Concrete Research, vol.28, pp. 1713-1723, 1998

[4] Lambert, P., Page, C.L. and Short, N.R. Pore solution chemistry of the hydrated system Tricalcium silicate/Sodium chloride/water. Cement and Concrete Research, vol.15, 1985.

[5] Martin-Perez,B, Zibara,H., Hooton,R.D. and Thomas,M.D.A. A study of the effect of chloride binding on service life predictions. Cement and Concrete Research, vol.30, 200, p. 121-1223.

[6] Tang,L. and Nilsson,O. Chloride binding capacity and binding isotherms of OPC pates and mortars, Cement and Concrete Research, vol.23, pp.247-253, 1993.

Conferences

[7] Yamato, T., Soeda, M. and Emoto, Y. Chemical resistance of concrete containing condensed silica fume. In: ACI Special Publication 114: Proceedings of the 3rd International Congress on fly ash, silica fume, slag, and natural pozzolans in concrete, ACI, Trondheim, 1989, p.897-913.

[8] Herfort , D., Porsborg, A.T., Grundvig, S., Jakobsen, H.J. and Skibsted, J. Hydrate Phase Assemblages of Portland Cement Pastes Stored at 5 and 20°C. Proceedings of the 20th IOM Cement and Concrete Science Conference. Sheffield, 2000.

[9] Juel,I., Herfort,D, Gollop,R, Konnerup-Madsen,J, Jakobsen,H.J. and Skibsted,J. A thermodynamic model for predicting the stability of thaumasite. Proceedings of the 1st international conference on thaumasite in cementitious materials. Building Research establishment UK, 2002.

[10] Herfort,D and Juel,I.A., The mineralogy of sulfate and sea water attack on concrete interpreted from EPMA analysis. Proceedings of the 23rd International Conference on Cement Microscopy, Albuquerque, New Mexico, 2001.

[11] Juel,I.A. and Herfort,D. The mineralogy of chloride attack on concrete containing limestone filler. Proceedings of the 24th International Conference on Cement Microscopy, San Diego, California, 2002.

EFFECT OF SOLID SOLUTION OF AFm PHASES ON CHLORIDE BINDING

Erik P. Nielsen[1], Duncan Herfort[1], Mette R. Geiker[2] and R. Doug Hooton[3]

[1]R&D centre, Aalborg Portland, Denmark.
E-mail: epn@aalborg-portland.dk, dhe@aalborg-portland.dk
[2] Technical University of Denmark, Dept. of Civil Engineering, Denmark.
E-mail: mge@byg.dtu.dk
[3] University of Toronto, Dept. of Civil Engineering, Canada.
E-mail: d.hooton@utoronto.ca

Erik Pram Nielsen

Erik Pram Nielsen has been an industrial Ph.D. student at the Research and Development Centre at Aalborg Portland A/S, Denmark, since July 2001, and is affiliated to the Technical University of Denmark.

The current research is focusing on the performance of concrete produced from white Portland cement to sulfate and sea water attack. His interests include corrosion mechanisms, concrete microstructure and transport mechanisms, and the thermodynamics and mineralogy involved in chemical attack.

Contact Details:

Aalborg Portland A/S
Research and Development Centre
Phone: (+45) 98 77 76 85
E-mail: epn@aalborg-portland.dk

THE EFFECT OF 4 ALKANOLAMINES ON PORE WATER COMPOSITION AND STRENGTH DEVELOPMENT OF MORTAR

Paul J. Sandberg[1]

[1] Grace Construction Products, Cambridge, MA, USA. E-mail: paul.j.sandberg@grace.com

ABSTRACT

The combined effect on cement hydration of adding 4 alkanolamines and soluble alkali and/or sulfate was studied for an undersulfated Portland cement, by means of pore solution analysis and compressive strength development at 1, 7 and 28 days. The results indicated some correlation between 7 and 28 day strength enhancement and iron solubilization, although 2 alkanolamines were able to enhance strength without any strong iron solubilization. 1 day strength enhancement did not correlate with soluble iron for any alkanolamine. A synergistic strength enhancing effect was found when the alkanolamines were combined with soluble alkali and sulfate. The results indicate that while iron solubilization seems important for strength enhancement after several days of hydration, other mechanisms may be important to explain the strength enhancing effect of the alkanolamines studied.

1. INTRODUCTION

The effect of 2 proprietary alkanolamines, referred to as CB 200 and CB 300, on EN 196 mortar strength development and iron solubilization, were studied and compared to the effects of Triethanolamine (TEA) and Triisopropanolamine (TIPA). TEA is the most basic alkanolamine, commonly used in grinding aids. TIPA is a proprietary alkanolamine used in the CBA® series of strength enhancing cement additives.

It has previously been shown that the alkanolamine TIPA, and to some extent TEA, has the ability to enhance the strength of hydrating cement [1]. The strength enhancing effect of TIPA has been linked to its ability to solubilize iron, and thus enhance the dissolution and hydration of anhydrous ferrite and hydrated iron compounds, which otherwise tend to block the strength-giving hydration of the silicate phases [2].

The purpose of this study was to conduct parallel studies of the pore solution chemistry on cement paste and strength development on mortar, both with and without the addition of soluble alkali hydroxide and alkali sulfate. The Portland cement used was ground to a Blaine surface area of 300 m^2/kg in a laboratory ball mill, with added hemihydrate to a cement SO_3 of 1.65%. This represents the unusually low SO_3 in the commercial low alkali cement, which was known to be very responsive to TIPA.

The clinker chemistry is shown in Table 1, which includes XRF analysis of the clinker sample used and a QRDA analysis using Rietveld refinement on a sister clinker, produced at the same plant but at a different date.

Table 1. Clinker chemistry

Chemical analysis % By XRF	CaO	65.27	
	SiO_2	22.86	
	Al_2O_3	4.56	
	Fe_2O_3	2.68	
	MgO	2.55	
	SO_3	0.37	
	K_2O	0.17	
	Na_2O	0.12	
Calculated compounds per ASTM C 150-97	C_3S	56	
	C_2S	23	
	C_3A	8	
	C_4AF	8	
QXRD Rietveld refinement on a sister clinker sample		Alite	51
		Belite	27
		Aluminate	6
		Ferrite	15
		Magnesium oxide	1.0
		Free lime	not detected

2. EXPERIMENTAL

2.1 Preparation of mix water compositions

High dosages of alklanolamine, 200 ppm, were chosen to ensure that any changes in porewater chemistry were readily detectable. Note that 200 ppm alkanolamine is a 2-4 times higher dosage than usually required to achieve strength gains in industrial cement additive applications.

Additives were dissolved in mix water for EN 196 mortar and cement paste at water - cement ratio 0.50 using the following mix water solutions conditioned to + 10 ^{o}C, Table 2.

- Deionized water.
- 0.25 mol/l KOH (equivalent to addition of 0.3875 % soluble Na_2O eqv to the cement).
- 0.50 mol/l KOH (equivalent to addition of 0.775% soluble Na_2O eqv to the cement).
- 0.125 mol/l K_2SO_4 (equivalent to addition of 0.50% soluble SO_3 and 0.3875 % soluble Na_2O eqv to the cement).
- 0.25 mol/l K_2SO_4 (equivalent to addition of 1.0 % soluble SO_3 and 0.775 % soluble Na_2O eqv to the cement).

Table 2. Compositions of 25 mix water solutions (% and ppm by weight of cement)

Additive	KOH conc. Mol/l			K_2SO_4 conc. Mol/l	
	None	0.25 mol/l	0.5 mol/l	0.125 mol/l	0.25 mol/l
Soluble Na_2Oeqv added	None	0.3875 %	0.775%	0.3875 %	0.775%
Soluble SO_3 added	None	-	-	0.5 %	1.0 %
NONE					
TEA @ 200 ppm					
CB 200 @ 200 ppm					
CB 300 @ 200 ppm					
TIPA @ 200 ppm					

2.2 Preparation of cement paste for pore solution studies

Mixing was done using 100 g cement and 50 g mix water, using a commercial planetary mixer for 30 seconds initial mixing, followed by 30 seconds mixing using a high speed mixer at 3000 rpm. The cement paste was cured sealed in a container at room temperature until the ages: 30 minutes, 210 minutes, 28 hours, 7 days and 28 days. Pastes were kept rotating until set in order to avoid excess bleeding and segregation.

2.3 Pore solution expression and composition analysis

Pore solutions from cement pastes 30 minutes and 210 minutes old (before set) were collected by means of vacuum filtration. The pore solution expression method [3] was used for extraction of pore solution from hardened cement paste, Figure 1.

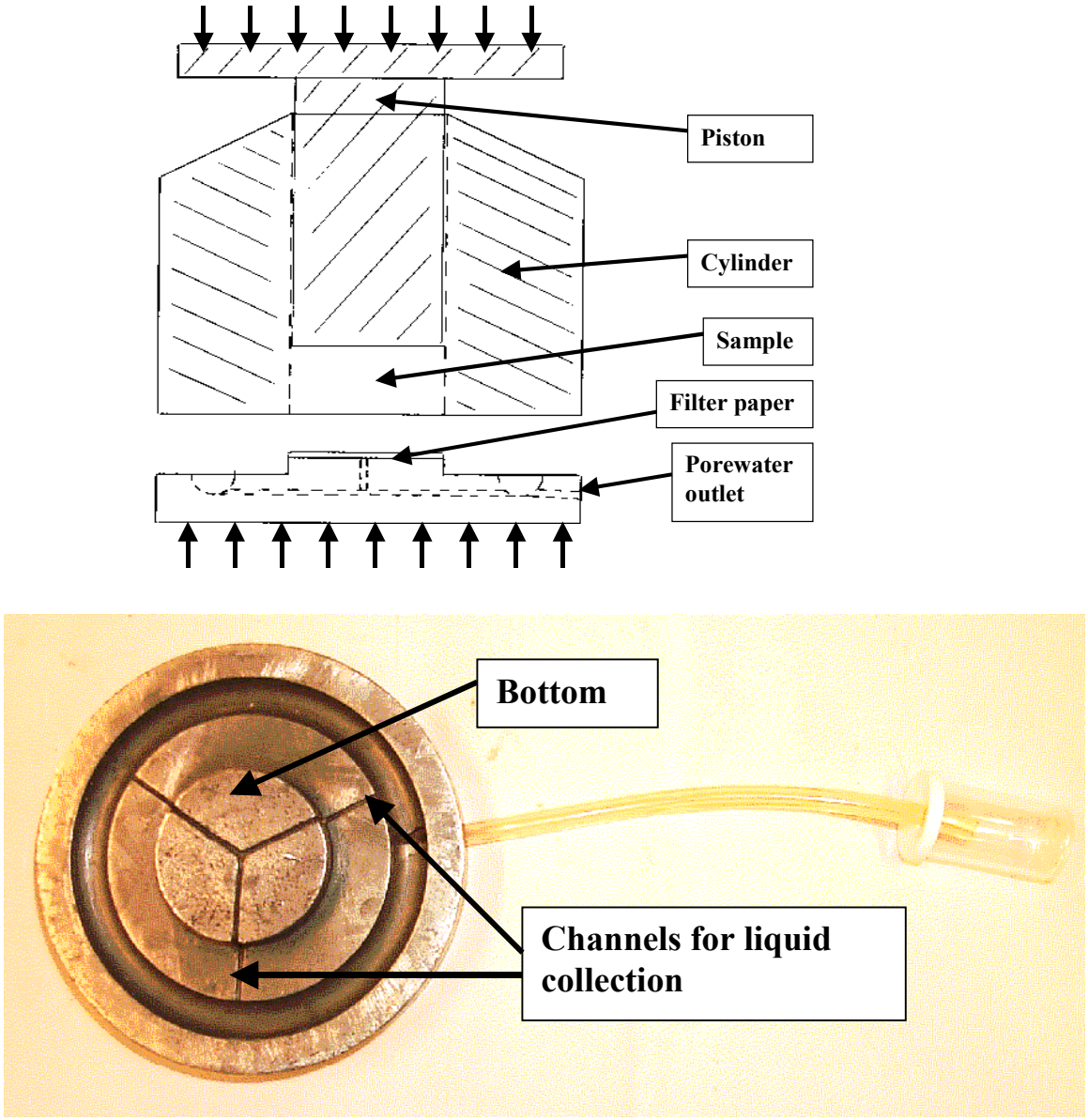

Figure 1. Pore solution expression device.

.

Following the pore solution extraction, 2.0 ml of filtered pore solution was immediately analysed for hydroxide ion concentration by titration with 0.1 mol/l HCl. Remaining filtered pore solution was immediately acidified to pH < 4 with a measured addition of HNO_3 (conc.) to avoid precipitation of the supersaturated pore solution.

ICP was used for the analysis of Fe, Al, Ca, Na, K and S in the expressed pore solution. It was assumed that all S was present as sulfate ions, because of the highly oxidising Portland cement environment. A total charge balance was computed for each pore solution analysed as a control of the validity of the results, using the ions Ca^{2+}, Na^{+}, K^{+}, SO_4^{2-} and OH^{-} (from hydroxide ion titration). The concentration of Fe and Al in solution is orders of magnitudes less than the alkali ions, and was therefore omitted from total charge balance computation. A deviation of 10% from the computed charge balance was considered acceptable, based on a pre-study involving triplicate mixes with 200 ppm TIPA and TEA added to plain portland cement. All data reported are from single measurements with less than 10% error in the computed charge balance.

2.4 Preparation and determination of compressive strength of EN 196 mortar

Mortar prisms of w/c 0.50 were manufactured for all mixes according to the European cement standard EN196. The compressive strength of EN196 prisms was determined after 1, 7 and 28 days hydration.

3. RESULTS

3.1 Pore solution analysis

The pore solution compositions for the blank cement are shown in Figure 2, at the hydration times 30 minutes, 210 minutes, 28 hours, 7 days and 28 days.

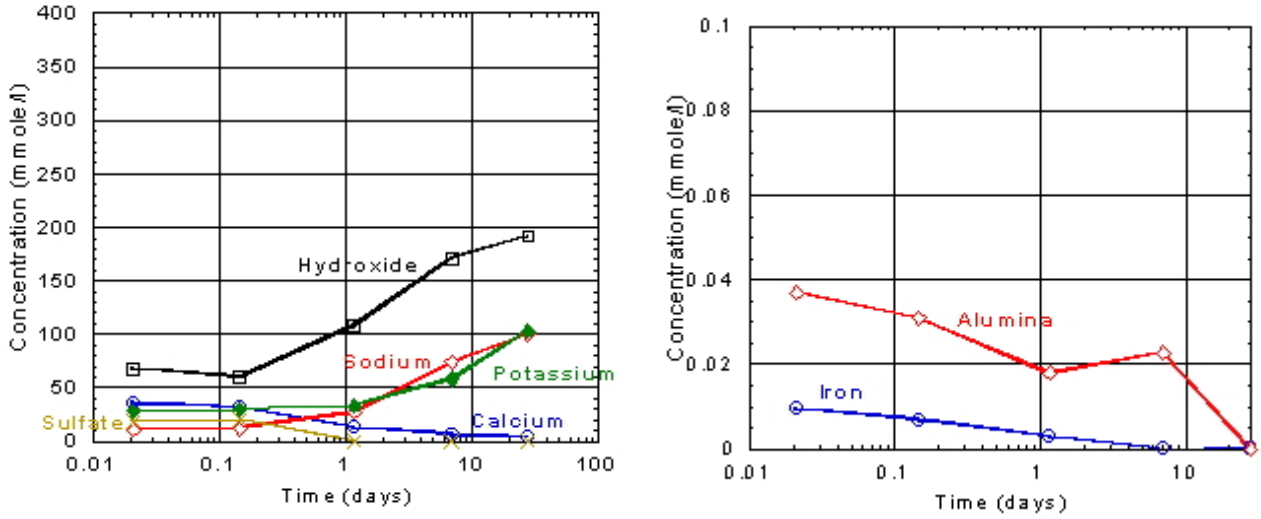

Figure 2. Pore solution composition of blank cement as a function of hydration time.

An example of the effect of soluble alkali sulfate on the pore solution composition is shown in Figure 3. 0.125 mol/l added potassium sulfate corresponds to 0.3875% soluble Na_2Oeqv and 0.5% soluble SO_3. Note the difference in scale in the y-axis.

The addition of a higher concentration of potassium sulfate or concentrations of potassium hydroxide generated very similar results as shown in Figure 3, and the data are not shown here. The effect of soluble alkali hydroxide and sulfate affected mainly the concentration of calcium, sulfate and hydroxide in the porewater as illustrated in Figure 4.

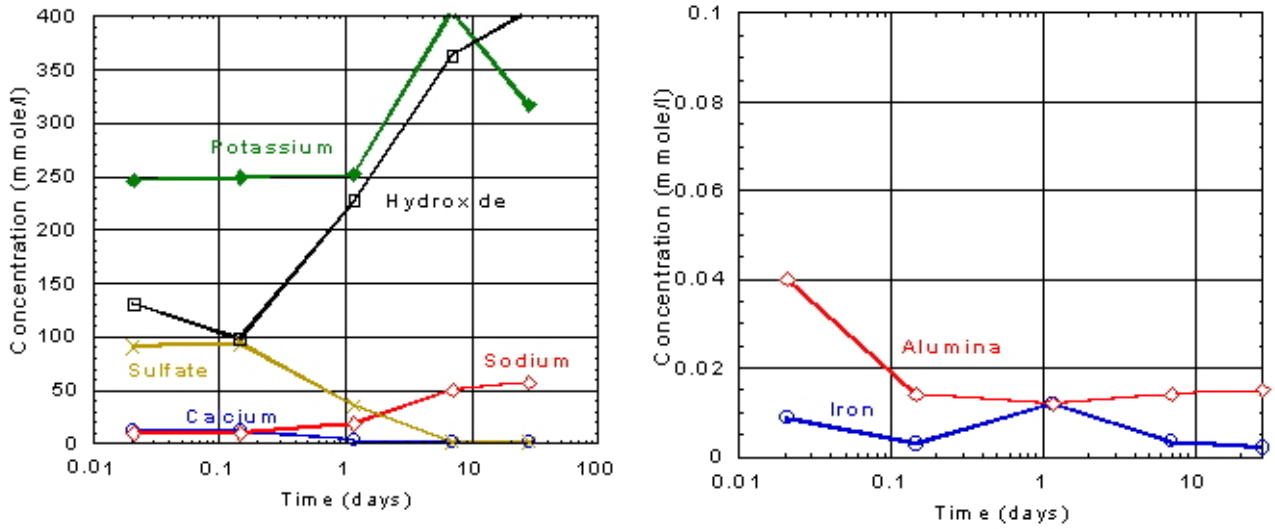

Figure 3. Pore solution composition of cement with 0.3875% soluble Na_2Oeqv and 0.5% soluble SO_3 added as potassium sulfate.

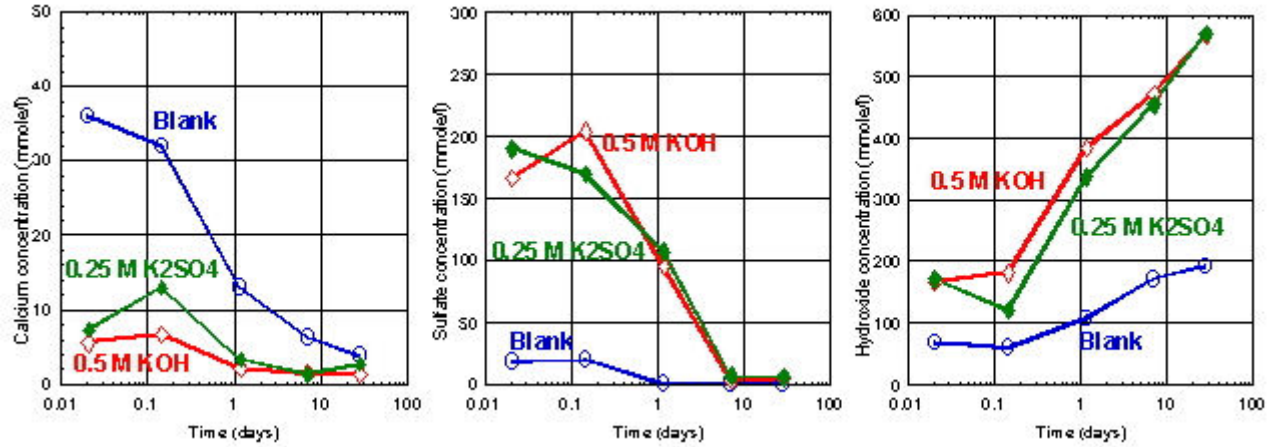

Figure 4. Effect of adding soluble alkali hydroxide or sulfate on the concentration of calcium (left), sulfate (middle) and hydroxide (right) in the porewater.

The effect of alkanolamines on the pore solution composition was small with the exception for iron, as illustrated for of calcium, sulfate and hydroxide in the porewater in Figure 5.

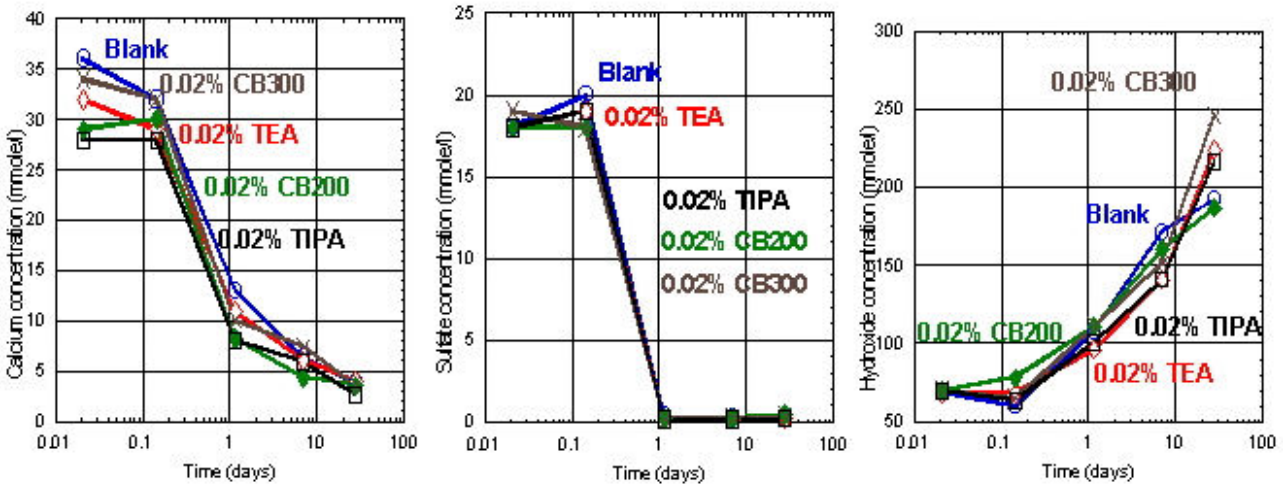

Figure 5. Effect of alkanolamines on the concentration of calcium (left), sulfate (middle) and hydroxide (right) measured in porewater.

3.2 Iron in expressed pore solution

The effect of the alkanolamines on the solubility of iron is shown in Figure 6, for cement with and without addition of soluble alkali sulfate.

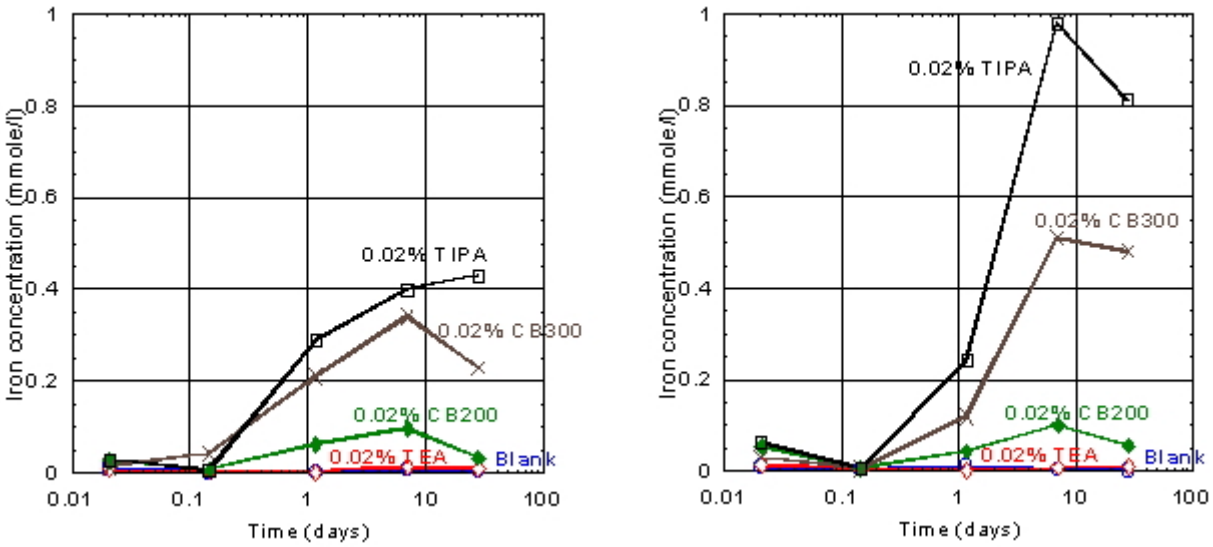

Figure 6. Effect of alkanolamines on the concentration of iron in the pore water. Cement with alkanolamine only (left), cement with alkanolamine and 0.3875% soluble Na_2Oeqv and 0.5% soluble SO_3 added as potassium sulfate (right).

3.3 EN196 mortar compressive strength

The EN196 mortar compressive strengths are shown in Table 3.

Table 3. Cement mortar strengths, EN196 (w/c 0.5)

Alkanol-amine	Comp. Strength (MPa)			% over No Alkanolamine			Coefficient of variation %		
	1 d	7 d	28 d	1 d	7 d	28 d	1 d	7 d	28 d
No addition of soluble alkali or sulfate									
None	9.3	34.7	61.9	100	100	100	1.8	2.7	2.0
TEA	11.2	37.3	63.3	120	107	102	2.7	3.0	2.2
CB 200	9.7	42.7	70	104	123	113	1.9	2.2	1.5
CB 300	8.6	40.9	67.9	92	118	110	3.2	2.8	2.3
TIPA	9.1	36.5	66.4	98	105	107	2.5	2.1	1.7
0.25 mol/l KOH added = 0.3875 % Soluble Na_2Oeqv									
None	11.5	34.4	52.9	100	100	100	2.5	2.6	1.9
TEA	12.3	33.5	54.9	107	97	104	2.3	1.8	1.7
CB 200	13.2	40.6	62.5	115	118	118	3.8	3.1	3.4
CB 300	11	40.4	63	96	117	119	3.3	3.7	2.8
TIPA	11.3	37.2	63.8	98	108	121	1.9	1.7	1.6
0.50 mol/l KOH added = 0.775 % Soluble Na_2Oeqv									
None	11	28.4	43.4	100	100	100	2.7	2.4	2.7
TEA	13.9	32.8	49.1	126	115	113	3.8	2.9	1.9
CB 200	11.9	35.5	52.2	108	125	120	3.8	2.9	2.5
CB 300	10.1	35.2	53.9	92	124	124	3.7	1.9	2.7
TIPA	12	38.6	56.2	109	136	129	2.6	2.6	1.8

.
.

Alkanol-amine	Comp. Strength (MPa) 1 d	7 d	28 d	% over No Alkanolamine 1 d	7 d	28 d	Coefficient of variation % 1 d	7 d	28 d
0.125 mol/l K_2SO_4 added = 0.3875 % Soluble Na_2Oeqv and 0.5 % Soluble SO_3									
None	13.7	37.4	53.8	100	100	100	3.7	2.4	2.8
TEA	16.2	38.7	56.5	118	103	105	1.9	3.8	3.2
CB 200	16.3	43.2	63.6	119	116	118	2.9	3.3	1.8
CB 300	14.5	44.3	66.1	106	118	123	2.8	3.2	1.6
TIPA	14.8	41	64.4	108	110	120	3.3	2.8	3.1
0.25 mol/l K_2SO_4 added = 0.775 % Soluble Na_2Oeqv and 1.0 % Soluble SO_3									
None	15.5	38.3	48.7	100	100	100	2.2	2.1	1.9
TEA	17.6	35.6	47.8	114	93	98	3.6	4.3	1.8
CB 200	18.7	37.8	51.4	121	99	106	3.8	3.6	2.5
CB 300	17.5	39.5	53.7	113	103	110	2.5	2.8	2.2
TIPA	16.4	39.4	52.9	106	103	109	2.1	2.7	1.2

4. DISCUSSION

4.1 Effect of alkanolamines on soluble iron and strength enhancement

The iron solubilizing effect of the alkanolamines studied was shown in Figure 6. The strength enhancing effect was shown in Table 3. Unfortunately no air content measurements were done on the prisms, but simple aircup measurements on parallel mortar mixes indicated that in no case was more than 1% air entrained in the mortar as an effect of the alkanolamine. It was assumed that 1% air increase in mortar corresponds to 4% loss of strength. As the coefficient of variation was approximately 3%, a strength response of 7% or more can be considered significant.

Individual measurements of iron in porewater had a coefficient of variation in the order of several tens of percent. Nevertheless, the iron solubilization effect of alkanolamines TIPA, CB 200 and CB 300 was found to be far greater than the variability.

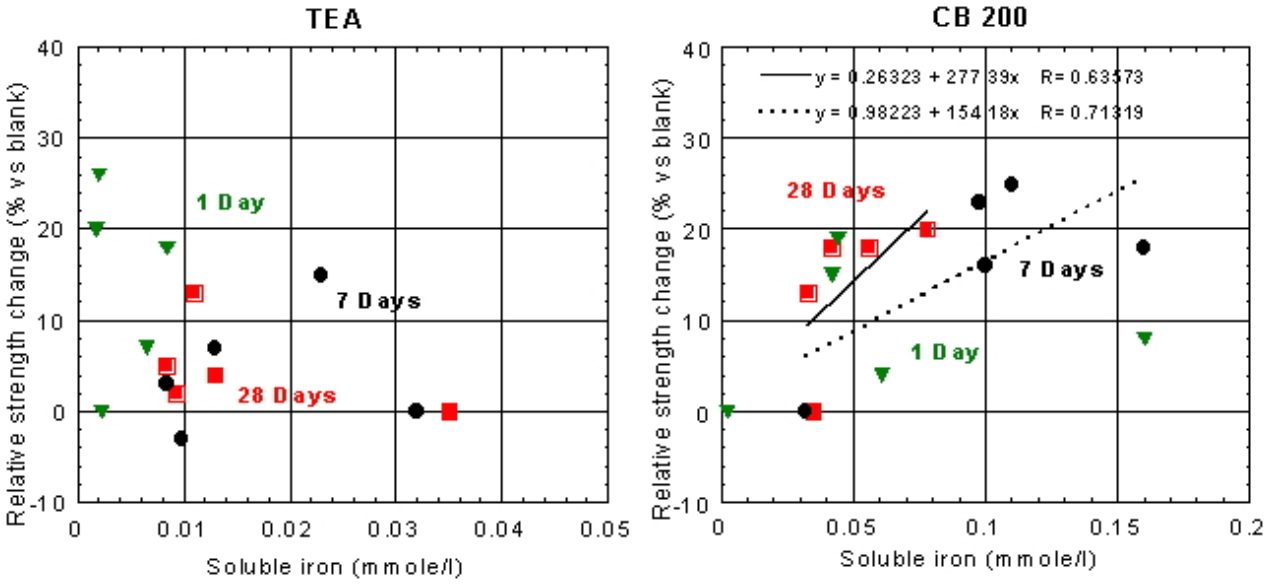

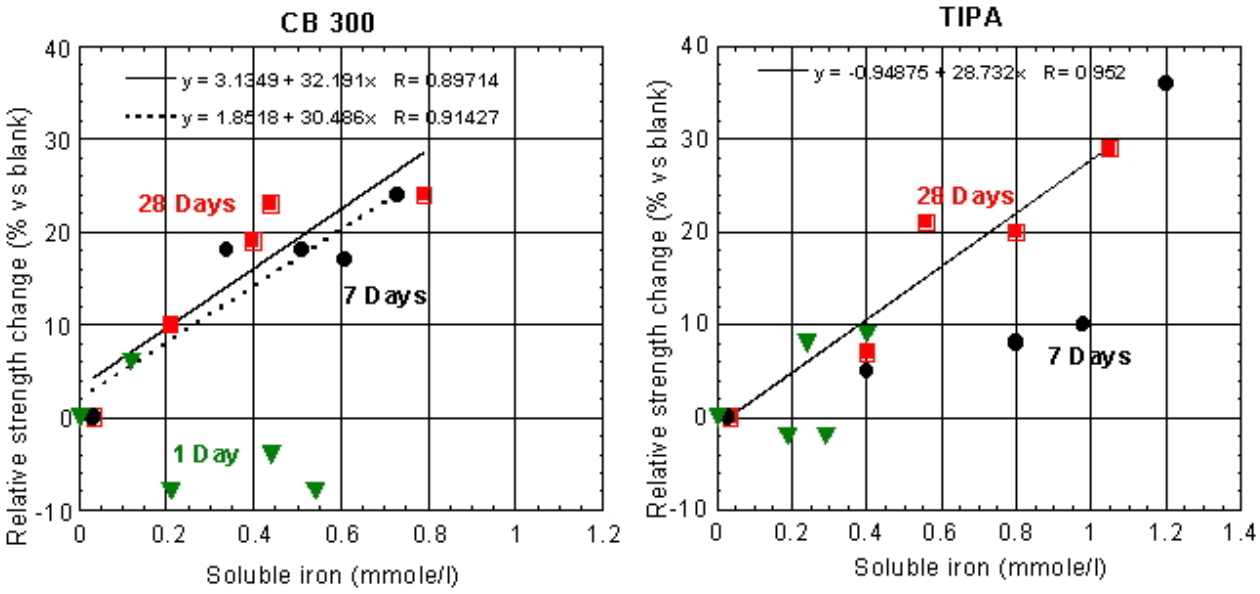

Figure 7. Correlation between strength enhancement and iron in porewater for the 4 alkanolamines. Note the differences in X-axis scale. A straight line indicates correlation between soluble iron and strength at 28 days. A dotted line indicates correlation between soluble iron and strength at 7 days. In no case was correlation found between soluble iron and strength at 1 day.

Figure 7 shows the correlation between strength enhancement and iron in porewater at 1, 7 and 28 days. All data for 0.25 mol/l K_2SO_4 added = 0.775 % soluble Na_2Oeqv and 1.0 % soluble SO_3 was excluded because of signs of strength loss caused by exceeding optimum SO_3.

The strong iron solubilizing alkanolamines TIPA and CB 300 showed relatively strong correlation between iron in porewater and strength enhancement at 28 days, as expected. The weaker iron solubilizing alkanolamines TEA and CB 200 showed poor correlation between iron in porewater and strength enhancement. However, CB 200 demonstrated significant strength enhancement also at 7 and 28 days in spite of less iron solubilizing effect as compared to TIPA. Thus it seems probable that iron solubilization, while clearly important, is not the only mechanisms responsible for 7 and 28 days strength enhancement in this study.

It is worth noting that TEA and CB 200 are stronger 1 day strength enhancers but also weak iron solubilizers as compared to TIPA and CB 300. Thus it appears that there is no correlation between the additives' ability to solubilize iron and the early strength enhancement. A possible explanation is that sulfate ions also solubilize iron, thus diminishing the solubilizing effect of the additive until all soluble sulfate has been consumed by the cement hydration.

Addition of soluble alkali or alkali sulfate both resulted in an increased hydroxide concentration in the pore solution, Figure 4. This was expected as sulfate binds into hydrates and release hydroxide. The addition of soluble alkali or sulfate and alkanolamines seem to have synergistic effects on the concentration of iron in expressed pore solution, Figure 6. Furthermore, as seen when comparing Table 3 and Figure 6, the synergistic effect of alkali and iron solubilization also resulted in higher relative strength enhancing effects of the alkanolamines at 28 days. The synergistic effect was predominant for TIPA, CB 200 and CB 300 for all alkali additions except for the highest level of alkali sulfate, which might have been the effect of exceeding the optimum SO_3.

5. CONCLUSIONS

The combined effect on cement hydration of added 4 alkanolamines, and soluble alkali and/or sulfate was studied, for an undersulfated Portland cement by means of pore solution analysis and compressive strength development at 1, 7 and 28 days. The results indicated some correlation between 7 and 28 day strength enhancement and iron solubilization, although 2 alkanolamines were able to enhance strength without any strong iron solubilization. 1 day strength enhancement did not correlate with soluble iron for any alkanolamine. A synergistic strength enhancing effect was found when the alkanolamines were combined with soluble alkali and sulfate.

The results indicate that while iron solubilization seems important for strength enhancement after several days of hydration, other mechanisms may be important to explain the strength enhancing effect of the alkanolamines studied.

ACKNOWLEDGEMENTS

The clinker used was kindly provided by Lafarge at Lichtenberg, South Africa. The experimental work was carried out in Sweden under a research agreement with Cementa Research, Sweden.

REFERENCES

[1] Gartner, E.M. and Myers D.F., Influence of tertiary alkanolamines on Portland cement hydration, Journal American Ceramic Society, vol. 76, 1993, pp.1521-1530.

[2] Chiesi, C.W., Myers, D.F. and Gartner E.M. Relationship between clinker properties and strength development in the presence of additives, 14th international conference on cement microscopy, Costa Mesa, California, 1992, pp.388-401. (International Cement Microscopy Association, Duncanville, Texas, 1992).

[3] Strelkov, M.I. Changes in the true state of the liquid phase during hardening of cements and the mechanism of their hardening, Reports of Symposium on the Chemistry of Cements, ed. P.P. Budnikov, Y.M. Butt, S.M. Royak, M.O. Yushkevich, Moscow, 1956, pp.183-200. State Publication of Literature on Structural Materials, translated by M. Corbin.

EXPANSIVE AGENTS OF CONCRETE MADE FROM BURNT BAUXITE

Yaozhong Xi[1] and **Shuxia Ren**[2]

[1]China Building Materials Academy, Beijing, 100024, China. -mail: xyz888@a-1.net.cn
[2]Tongji University, Shanghai, 200092, China. -mail: bluesummer@263.net

ABSTRACT

China is now the leading manufacturer and user of expansive agents (EA) for concrete. The most extensively used EA in China belongs to the ettringite type, which is manufactured with sulphoaluminate and aluminate clinkers made from high-grade bauxite and burnt at high temperatures. The aim of this research is to explore using low-grade bauxite for EA making, which is calcined at low temperatures. The bauxite expansive agent (BEA) consists of calcined bauxite and calcium sulfate. The physical properties of BEA + Portland Cement (PC) pastes show that the pastes expand sufficiently for shrinkage–compensating purposes. The properties of bauxite, calcined at 950°C can be significantly improved by mixing with alunite or by adding lime. The expansion and compressive strength of BEA expansive pastes are mainly affected by mineral and chemical compositions, the calcining regime of the bauxite as well as the type, content and fineness of the calcium sulfate. The environmental significance of utilising low-grade bauxite not only reduces the cost, but also improves concrete durability by lowering the heat generated by hydrating cement and the amount of calcium hydroxide in hardened cement paste. Results of semi-quantitative XRD and SEM microanalysis confirm that most of the SO_3 from calcium sulfate and Al_2O_3, SiO_2 from calcined bauxite enter the C-S-H gel. It is suggested that the C-S-H with considerable amount of Al_2O_3 and SO_3 is the major hydrate causing expansion.

1. INTRODUCTION

China is the largest producer and user of expansive agents for concrete (EA): more than 300 000 tons of EA are produced and about 8 million cubic meters of shrinkage-compensating concrete is used every year. Shrinkage compensating concrete is made by mixing 8-15% EA (of the PC component) with Portland Cement, sand and gravel and is used to reduce cracks and leakages in buildings and other structures.
Shrinkage compensating concrete [1] is mainly used in:

a) Structural self-waterproofing for base-plates of large structures, basements of high-rise buildings, airports, subways, tunnels, railway stations, etc.
b) EA strengthened zones substitute for post-filled joints of extra long structures, continuous placing is carried out so that the construction period is significantly reduced.
c) Crack control for structural mass concrete (C40 to C60). The addition of EA compensates for drying shrinkage and contraction shrinkage.
d) Roof waterproofing.

More than ten different types of expansive agents, including united expansive agent (UEA), composite expansive agent (CEA) and aluminate expansive agent (AEA) have been developed in China. These EA's consist mainly of expansive clinkers with different mineralogical compositions and $CaSO_4$. The expansive clinkers containing sulphoaluminate or aluminate are made by burning raw meal mixes with different compositions at about 1350°C. In this research, bauxite, heated to

relatively low temperatures is used to replace expansive clinkers for making EA. The results obtained show that this is feasible. The dehydration of bauxite and its hydration reaction in an expansive cement system are discussed in the paper.

MATERIALS AND EXPERIMENTAL

Bauxite from seven different origins (B1-B7, Table 1) was heated at 800°C for one hour and then ground in a small agate ball mill.
Two modified bauxites were also made:
M1, a mixture of ground burnt B2 and ground alunite (A, Table 2) with B2: A = 2: 1;
M2, a ground mixture of B2 and reagent $CaCO_3$ (B2: $CaCO_3$ = 2.3: 1) fired at 950°C for 2.5 hours.

Anhydrite (G1, Table 2) or gypsum (G2) or phosphogypsum (G3) is used as a source of $CaSO_4$ to make bauxite expansive agent (BEA) with G1 (or G2, G3): calcined bauxite (or modified bauxite) = 1: 1.

The fineness of the BEA's is 8% retained on a 0.08mm sieve. Expansive cements were made of Portland Cement and BEA (PC : BEA = 10 : 1).

Table 1. Chemical and mineral composition of bauxites

Code	Origin	SiO_2	Al_2O_3	Fe_2O_3	CaO	MgO	TiO_2	LOI	Minerals*	Appearance
B1	Mixian	27.95	43.83	8.19	0.92	0.81	1.42	15.04	K-ms; Py-mr; D-m; I-l	Black, firm
B2	Mixian	5.79	72.38	1.61	0.50	0.60	3.60	14.58	D-ms; K-mr; P, A-l	Black earth-like, loose
B3	Dengfeng	18.93	61.17	1.55	0.84	0.84	2.56	13.40	D-ms; K-m; P, M, A-l	Gray, firm
B4	Dengfeng	27.73	48.95	1.73	0.50	1.20	2.11	12.24	D-ms; K-mr; M-m; P, A-l	Pale gray with brown, loose
B5	Lincheng	31.90	45.84	4.32	1.80	0.52	1.31	13.39	D-ms; K-mr; P-l	Pale brown
B6	Yangquan	6.81	69.33	2.36	2.01	SO_3 1.32		15.19	D-ms; K, Q-l	Earth-yellow
B7	Jiyuan	44.16	37.75	1.91	0.45	0.87	1.40	12.42	K-ms; P-m; M, C-l	Pale gray with red-brown, loose

*Based on XRD. Abbreviations: D = Diaspore, K = Kaolinite, P = Pyrophyllite, I = Illite, M = Muscovite, G = Goethite, C = Clinochlore, Py = Pyrite A = Anatase, Q = Quarts; comparative quantities: ms (most) > mr (more) > m (much) > l (a little)

Table 2. Physico-chemical properties of anhydrite, gypsum, phosphogypsum and alunite

Code	Material	Origin	SiO_2	Al_2O_3	Fe_2O_3	CaO	MgO	SO_3	K_2O	Na_2O	LOI	Appearance
G1	Anhydrite	Xixian	3.48	1.05	0.54	35.38	3.32	49.84	/	/	6.06	Gray stone
G2	Gypsum	Taiyuan	4.58	1.09	0.59	31.37	4.08	38.51	/	/	19.82	Grayish white
G3	Phosphogypsum	Mixian	4.18	0.98	0.53	28.94	0.63	42.20	/	/	22.18	Dark gray
A	Alunite	Rujiang	42.17	22.10	1.98	0.61	0.22	18.52	4.67	0.71	8.32	Pale red

The reference PC used, was Jidong P·II 525 cement which contains 1.97% SO_3, 1.14% K_2O and 0.18% Na_2O, its strength approximates that of the 42,5 strength class of ENV 197-1:1995. The free expansion magnitude was determined using specimen prisms 7×7×50 mm with steel studs at both ends for measuring). The compressive strength was determined (specimen cubes 20×20×20 mm) using neat paste for the above prepared expansive cements. W:C for neat paste was 0.30.

Specimens were kept in their moulds for one day in a moisture cabinet at 20°C. Immediately after demoulding, the initial length was determined using a 50-75mm outer diameter micrometer, and then the specimens were stored in a water tank at 20°C. The lengths of the prisms were then measured at the pre-determined intervals. Comparison tests of specimens made with materials from different origins, varying quantities and different degrees of fineness of calcium sulphate were also carried out.

The bauxites used were examined by XRD and DTA, using the RIGAKU D/MAX-A diffractometer and the RIGAKU TA 100 DTA/TG thermal analyzer.

To investigate the BEA expansive cement hydration, three series specimens of neat paste (20×20×20 mm cubes) were prepared for each series:

- #0 (9% anhydrite + 91% P·II525 cement);
- #B6 (6% calcined B6 + 9% anhydrite + 85% P·II 525 cement);
- #B7 (6% calcined B7 + 9% anhydrite + 85% P·II 525 cement).

Cubes were removed from the curing water after 1, 3, 7, 14 and 28 days. These were crushed to < 5mm grains, immersed in absolute alcohol to stop hydration, ground to completely pass a 45μm sieve and then dried in a vacuum of 160 mm Hg (absolute pressure). The dried samples then were mixed with 10% of silicon powder (internal standard) for XRD semi-quantitative analysis.

Cubes hydrated for 90days, were fractured and carbon-coated for observation under the KYKY AMRAY 1000B SEM with TN5500 series-II EDXA.

3. RESULTS AND DISCUSSIONS

3.1 Activation of Bauxites

Chinese bauxites contain diaspore, kaolinite, pyrophyllite, muscovite, illite, chlorite, rutile, anatase, iron ores, etc. and have little pozzolanic reactivity. The chemical and mineral compositions for bauxites B1-B7 are given in Table 1 and this shows that diaspore and kaolinite are the most prominent minerals in bauxite. Heating is an effective means to activate bauxite. Figure 1 shows DTA curves up to 1000°C for seven bauxites. The largest endothermic peaks on each curve in the temperature range 508 to 530°C are caused by removing structural water from diaspore and kaolinite:

$$2\alpha\text{-AlO(OH)} \xrightarrow{450-650^\circ C} \alpha\text{-}Al_2O_3 + H_2O\uparrow$$

$$Al_2Si_2O_5(OH)_4 \xrightarrow{550-650^\circ C} Al_2Si_2O_7 + 2H_2O\uparrow$$

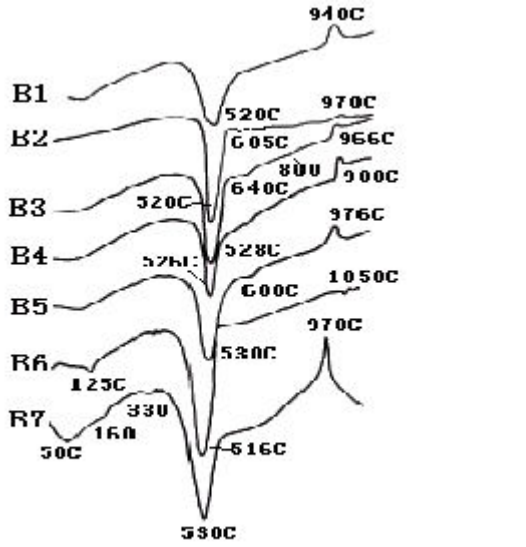

Figure 1. DTA curves for B1-B7 bauxites

The exothermal peaks in the 940-1050°C range on each curve are due to the phase transformation of metakaolinite to silica-alumina spinel[2]:

$$2Al_2Si_2O_7 \xrightarrow{925^\circ C} Al_2Si_3O_{12} + SiO_2\,(\text{amorphous})$$

Therefore, for the purpose of activation, the calcination temperature must not exceed 900°C (generally 750°C is used). The approximate amount of kaolinite in the bauxite can be estimated by

examination of the exothermic peak at about 950°C. Thus bauxites B1 and B7 contain more kaolinite. The blunt and small endothermic peak at 520°C in curve B1 is attributable to the exothermic effect of pyrite oxidation. Other than diaspore and kaolinite, paragenetic pyrophyllite, muscovite, illite and goethite will lose crystal water during heating: the 605-680°C endothermic peaks in curves B2, B3 and B5 are due to dehydration of pyrophyllite, and the endothermic peaks at 160°C and 330°C in curve B7 are due to losing water from illite and clinochlore respectively. Dehydrated products metakaolinite, α-Al_2O_3 and other aluminosilicates have pozzolanic reactivity. Another means to activate bauxite is heating bauxite with addition of limestone at 950°C and the XRD confirms the formation of active mineral $C_{12}A_7$ through reaction of CaO from decarbonation of $CaCO_3$ with Al_2O_3 and $Al_2O_3 \cdot 2SiO_2$ from calcination of bauxite [3].

Table 3. Free expansion magnitude and compressive strength of expansive neat pastes[1]

No	Expansive cements	Free expansion, %				Compressive strength, MPa		
		3d	7d	28d	90d	3d	7d	28d
0	PC, 100	0.022	0.043	0.061	0.083	36.9	51.5	59.3
1	PC, 100 + calcined B1, 5 + G1, 5	0.060	0.099	0.155	0.208	32.1	66.6	67.4
2	PC, 100 + calcined B2, 5 + G1, 5	0.065	0.094	0.167	0.232	26.6	70.6	79.9
3	PC, 100 + calcined B3, 5 + G1, 5	0.050	0.076	0.127	0.189	24.8	64.9	100.0
4	PC, 100 + calcined B4, 5 + G1, 5	0.084	0.117	0.208	0.230	31.4	62.5	95.8
5	PC, 100 + calcined B5, 5 + G1, 5	0.077	0.117	0.170	0.207	28.9	65.2	92.5
M1	PC, 100 + B2A[2], 6 + G1, 4	0.083	0.113	0.158	0.199	48.0	80.9	90.4
M2	PC, 100 + B2C[3], 5 + G1, 5	0.091	0.139	0.210	0.290	41.4	56.6	85.3

[1] Specimens with moulds cured in a moisture cabinet at 19°C for one day, after demoulding they are stored in water at 13°C;
[2] B2A consists of 66.7% calcined B2 and 33.3% alunite;
[3] B2C made by burning a mixture of B2 and $CaCO_3$ (B2:$CaCO_3$ = 2.3:1) at 950°C for 2.5 hours.

3.2 Free Expansion and Compressive Strength of three types of BEA

The neat paste of pure Portland Cement expands marginally (Table 3, 0).
With the addition of 10% BEA of the PC mass, the free expansion of expansive cements 1-5 (Table 3) increases significantly, the compressive strength at 3d decreases, however it increases at 7d and 28days.

With the addition of 16.7% alunite of the PC mass (M1, Table3), the expansion and compressive strengths are increased, because SO^{2-}_4 and $Al(OH)_4^-$ can dissolve out of alunite $KAl_3(SO_4)_2(OH)_6$ and react with $Ca(OH)_2$ to form ettringite.

The expansion and compressive strength for lime-combined expansive cement (M2, Table 3) are also significantly improved, since $C_{12}A_7$ in B2C reacts with $CaSO_4$, $Ca(OH)_2$ forming ettringite.

It is interesting to note that the physical proprieties of expansive cements No.4 and No.5, which were made from low grade bauxites B4 and B5 with the Al_2O_3 content below 50%, are better than those of the No.2 cement which was made from a high grade bauxite with an Al_2O_3 content of 72.4%.

3.3 Effect of Species, Content and Fineness of $CaSO_4$ as well as Fineness of Calcined Bauxite

3.3.1 Effect of anhydrite, gypsum and phosphogypsum

In Figure 2, G1, G2 and G3 denote the free expansion for BEA expansive pastes with addition of anhydrite, gypsum and phosphogypsum respectively, and S1, S2 and S3 the compressive strength for the pastes with anhydrite, gypsum and phosphogypsum. Figure 2 shows that specimens with addition of phosphogypsum (G3) have the largest expansion and those with gypsum (S2) have the largest compressive strength. The free expansion of anhydrite (G1) exceeds that of gypsum (G2) after 14d. The three types of $CaSO_4$ are all suitable as a main component for BEA.

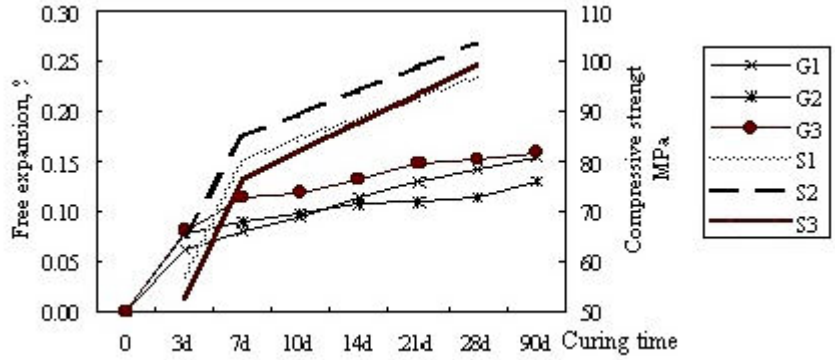

Figure 2. Effect of species of $CaSO_4$

3.3.3 Effect of anhydrite content

The effect of anhydrite content 40 in Figure 3 means that BEA consists of 60% calcined B4 (fineness 10%) and 40% anhydrite (fineness 6%). The 50 and 60 mean 50% and 60% addition of anhydrite to BEA, E represents free expansion and R compressive strength. Figure 3 indicates that, with an increase of anhydrite content, the free expansion increases and the compressive strength decreases.

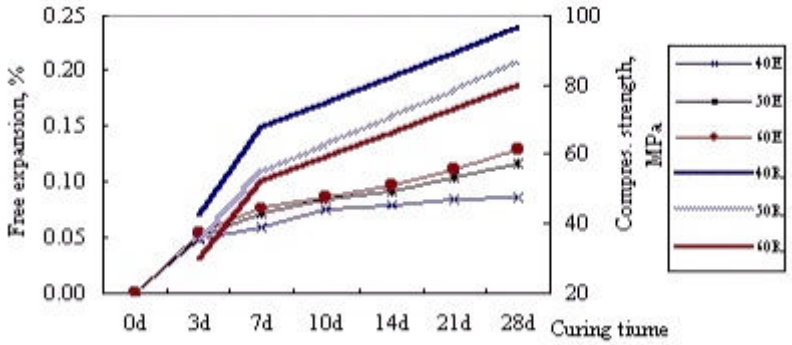

Figure 3. Effect of anhydrite content

3.3.4 Effect of anhydrite fineness

The BEA used for this test consists of 40% calcined B4 and 60% anhydrite. Figure 4 shows that the specimens with coarser anhydrite (10E, 0.08mm sieve residue10%) have larger free expansion compared to those with finer anhydrite (6E, fineness 6%), the compressive strength is not significantly influenced.

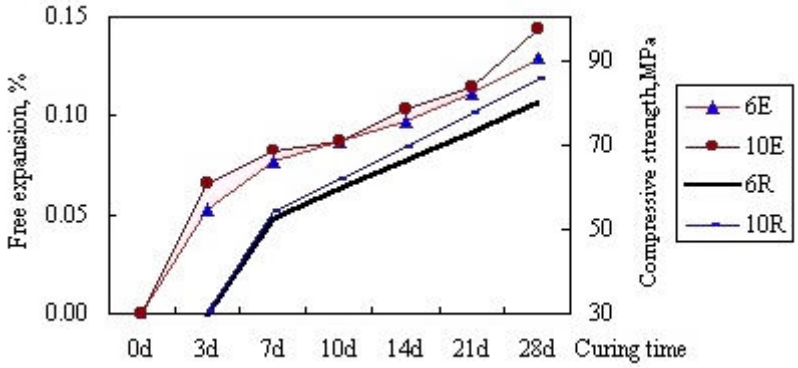

Figure 4. Effect of anhydrite fineness

3.3.5 Effect of fineness of calcined bauxite

The BEA used for this test consists of 40% calcined B4 and 60% anhydrite. Figure 5 demonstrates that the fineness of calcined bauxite (fineness 5% and 10%) does not have marked effect on physical properties of expansive cement within bauxite fineness range tested.

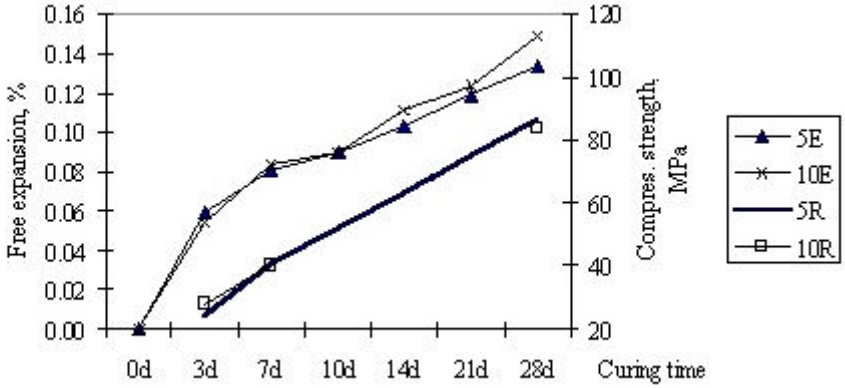

Figure 5. Effect of calcined bauxte fineness

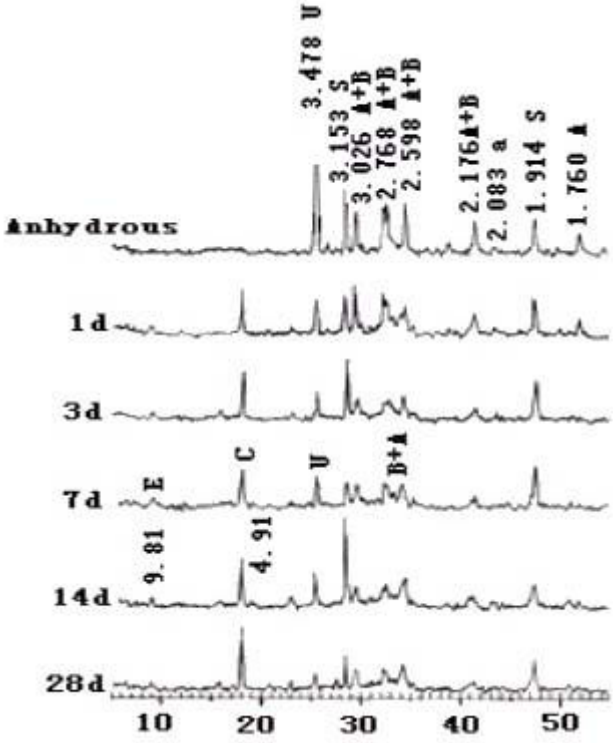

Figure 6. XRD powder patterns for anhydrous and hydrated #B6 expansive cement: E=ettringite, C=calcium hydroxide, U=anhydrite, a=α-Al_2O_3, A=alite, B=belite & S=silicon powder (reference).

3.4 Hydration of BEA Expansive Cement

3.4.1 Hydration products

The hardened cement pastes of BEA expansive cements #0, #B6 and #B7 at various ages were examined by XRD. The XRD powder patterns for hydrated #B6 in Figure 6 indicates main crystalline hydration products CH (4.91Å) and ettringite (9.81 Å) as well as the consumption of anhydrite (3.478Å), alite, belite and α-Al_2O_3 (2.083 Å dehydrated from diaspore

The relative quantities of CH, ettringite and remaining anhydrite are based on measuring peak heights in X-ray powder patterns. Figure 7 shows these plotted against curing time.

The results in Figure 7 confirm that with the addition of calcined B6 and B7, less anhydrite (Figure 7A) and less CH (Figure 7B) is found in cements #B6 and #B7 when compared with cement #0 without calcined bauxite. This indicates that hydration products α-Al_2O_3 and metakaolinite of bauxite participate in the hydration reaction. It is surprising that the ettringite formed in #B6 and #B7 cement pastes is less than that in #0 paste (Figure 7C); this implies that the α-Al_2O_3 and metakaolinite are not involved in the formation of ettringite. De Silva and Glasser [4] reported metakaolinite to react with $Ca(OH)_2$ forming C-S-H, C_4AH_{13}, C_2ASH_8 and in presence of calcium sulfate forming ettringite. Data by EDXA microanalysis [3] show that C-S-H formed in #B6 and #B7 pastes contain considerable amount of Al_2O_3 and SO_3, which apparently come from calcined bauxite, anhydrite, C_3A and C_4AF.

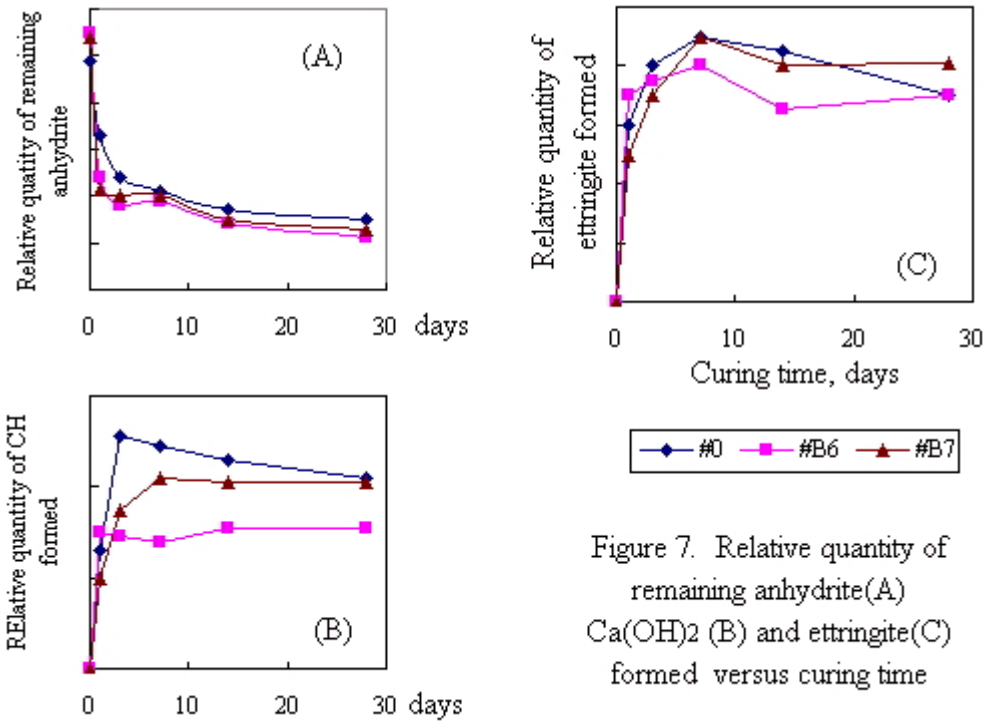

Figure 7. Relative quantity of remaining anhydrite(A) Ca(OH)2 (B) and ettringite(C) formed versus curing time

3.4.2 Morphology of hydration products

SEM secondary electron images of the #B7 paste hydrated for 90d show an earth-like matrix C-S-H gel with varying Al_2O_3 and SO_3 contents (see Figure 8A; 64 and 65 are unhydrated calcium silicates). Large clusters of piled $Ca(OH)_2$ plates are sometimes observed (Figure 8B). Occasionally hydrating calcined bauxite grains are seen: Figure 8C shows an oolitic grain with surrounding amorphous hydrate; Figure 8D shows a smaller metakaolinite grain with its rim of C-S-H containing 16.5% Al_2O_3 and 8.7% SO_3. Ettringite crystals consisting of 8-10μm needles and rods are seldom seen.

3.5 Mechanism of Expansion

Is all the SO_3 released from the anhydrite and the P·II 525 cement combined in ettringite? A rough calculation can answer this question.

According to the peak height of the 9.81Å diffraction line, the estimated ettringite content in hydrated cement at 28d is about 8% at most referred to anhydrous cement (the same below; for typical OPC pastes, the maximum ettringite formed is 7-11% (as determined by LOI). The 3.5% of SO_3 released from anhydrite at 28d (estimated on Figure 7(A)); in addition, 1.7% of that released from P·II 525 is 5.2%. Therefore, the SO_3 entering the ettringite phase is about 31% (1.6/5.2 × 100%), i.e. more than half of the SO_3 released from the anhydrite in the PC enters the C-S-H.

This result is in agreement with the estimation by Taylor [5].

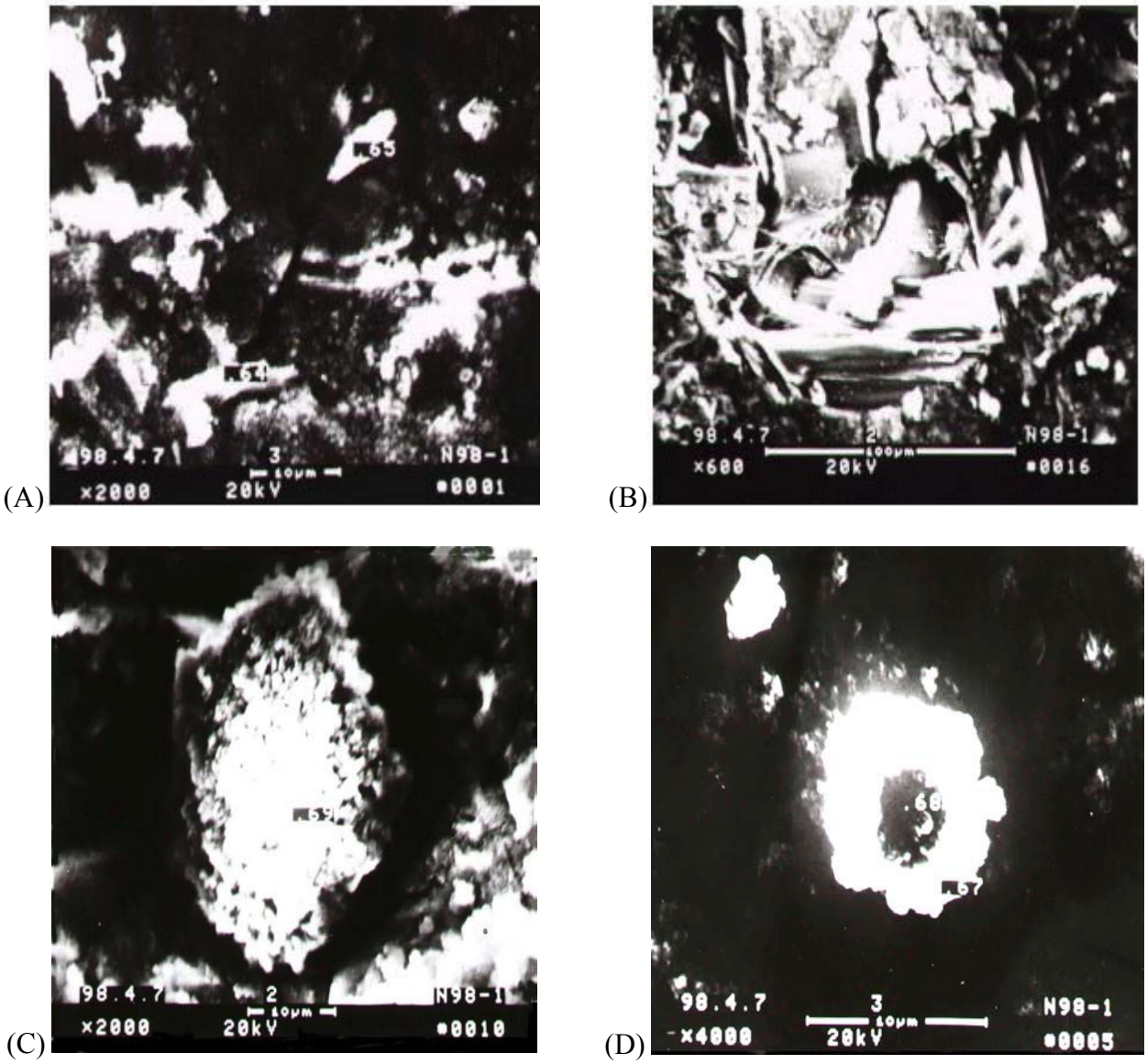

Figure 8. Secondary electron images of B7 expansive cement paste hydrated for 90d

A number of hypotheses have been proposed to explain the cause of expansion, the important ones are as follows:

(a) directed or anisotropic growth pressure of crystals, e.g. ettringite, CaO and MgO formed through topochemical reaction[6] or through solution;
(b) absorbing water by the negatively charged colloidal ettringite[7] or cement gel[8];
(c) expansion due to osmotic phenomena[9].

As known from section 2.4.1, only a small amount of ettringite crystallizes in hardened BEA expansive cement and large amounts of C-S-H gel with rich Al_2O_3, SO_3 forms and this appears to play a major roll in producing expansion. The backscattered electron images show the expansive nature of the inner product of C-S-H with appreciable quantity of Al_2O_3, SO_3 formed during early heat treatment of a Portland Cement mortar [10]. There is additional evidence for the expansive properties of C-S-H- $\bar{S}$-A: In the hydration of C_3S, C-S-H grows directly over the C_3S surfaces; the hydration of cement differs, in that a space develops between the C-S-H shells and the anhydrous clinker particles. i.e. the C-S-H shells expand since the C-S-H shells formed during cement hydration contain a certain amount of Al_2O_3, SO_3.

Further studies are required to understand the essentials of the C-S-H- $\bar{S}$-A expansion.

4. CONCLUSIONS

Based on the results obtained the following points are concluded:

- Expansive cements with calcined bauxites and modified bauxites have a free expansion of 0.06 to 0.09% at 3 days (0.02% for PC without BEA), 0.13 to 0.21% at 28 days (0.06% for PC without BEA). Thus the use of calcined bauxite or modified bauxite for EA manufacture is possible.
- The suitability of calcined bauxite for making EA is related to its chemical and mineralogical composition. Low-grade bauxite with rich kaolinite is as good as the high-grade bauxite with rich diaspore.
- Calcined bauxite, increases expansion at all ages, after three days the compressive strength exceeds that of PC by about 30%. The modified bauxites are activated on account for alunite (M1, alunite releases SO_4^{2-} and $Al(OH)_4^-$) and lime-added $C_{12}A_7$ (M2), and can increase 3 day and 7 day expansions and compressive strength at all ages by about 30% when compared to PC.
- Anhydrite, gypsum and phosphogypsum are the main components of EA for expansion. Phosphogypsum produces the largest free expansion with the lowest 3 day and 7 day compressive strengths among the three calcium sulfate materials.
- With an increase of anhydrite content in BEA, the free expansion of the BEA expansive cement pastes increases whilst their compressive strength decreases. The BEA expansive cement pastes with the coarser anhydrite have larger free expansion compared with those with finer anhydrite. The fineness of calcined bauxite does not have a marked effect on the physical properties of expansive cements.
- The results of XRD and SEM microanalysis indicate that in BEA expansive cement pastes, only a small amount of ettringite forms. Most of the Al_2O_3 and SiO_2 released from calcined products (α-Al_2O_3, metakaolinite) of bauxite and SO_3 released from calcium sulfate are combined in C-S-H formed during the hydration of C_3S and C_2S. The sulpho-aluminous C-S-H (C-S-H- $\bar{S}$-A) has expansion potential. It is suggested that C-S-H- $\bar{S}$-A is the major hydrate to cause the expansion BEA expansive cement.

REFERENCES

[1] You, B. Development and application of shrinkage-compensating concrete in China, The Beijing International Symposium on Cement and Concrete, 1998, Vol. 1, pp. 788-792.
[2] Huang, B. Handbook of Minerals Detection by DTA, science Press, 1987, P.516.
[3] Ren, S. An Investigation on Bauxite Expansive Agents, 1995, Beijing, MS dissertation, p. 33.
[4] De Silva P. S. and Glasser F. P. Pozzolanic activation of metakaolin, Advances in Cement Research, 1992, Vol. 4, No.16, pp. 167-178.
[5] Taylor, H. F. W., Cement Chemistry, Thomas Telford, London, 1997, p. 190.
[6] Lafuma, H. Théorie de l'expansion des liants hydrauliques, Rev. Mat. Constr. Trav. Publ., No.243, 441-444; No.244, pp. 4-8.
[7] Mehta, P. K. Mechanism of expansion associated with ettringite formation, Cem. Concr. Res. Vol. 3, No. 1, pp.1-6.
[8] Taylor, H. F. W., Cement Chemistry, Thomas Telford, London, 1997, p. 373.
[9] Hansen, W. C. Mechanism of the expansion of concrete, ACI Journal, 15, pp.213-227.
[10] Scrivener, K. L. and M. Lewis, A microstructural and microanalytical study of heat cured mortar and delayed ettringite formation, Proc 10th Int Congr Chem Cem, Goteborg, Sweden, 1997, Vol. 4, 4iv061, 8pp.

EXPANSIVE AGENTS OF CONCRETE MADE FROM BURNT BAUXITE

Yaozhong Xi[1] and **Shuxia Ren**[2]

[1]China Building Materials Academy, Beijing, 100024, China. -mail: xyz888@a-1.net.cn
[2]Tongji University, Shanghai, 200092, China. -mail: bluesummer@263.net

Yaozhong Xi

Currently Professor of the China Building Materials Academy. He has worked as a research fellow in the Department of Chemistry, University of Aberdeen in 1981-1984 as well as a visiting professor in the Materials Research Laboratory at the Pennsylvania State University from 1993-1995.

HYDROGEL PROCESS - A NOVEL PROCESS FOR LOW TEMPERATURE CLINKERISATION

M.V. Karandikar, S.A. Khadilkar and R.M. Cursetji

The Associated Cement Cos. Ltd., Research and Consultancy Directorate, CRS Complex, L.B.S. Marg, Thane 400 604, India, E-mail: rd3@bom3.vsnl.net.in

ABSTRACT

The Research and Development Division of the Associated Cement Cos. Ltd., India had pursued a comprehensive programme on bulk usage of fly ash. Considering the chemistry of low lime Class-F Indian Fly ashes, one approach, which was successfully attempted at the author's laboratory, was development of a process route (Hydrogel Process) of clinkerisation based on the fundamental principle of fly ash activation.

The Process involves activation of fly ash with alkali under non-hydrothermal conditions. The activated fly ash is reacted with Hydrated lime/ Limestone in predetermined proportions to produce the calcium silicate / aluminate hydrate gels, which are de-watered, dried and sintered at 800-1350^{o}C to produce the cement clinker. The sintering temperature depends on the type of cementitious system intended (Cementitious binder / Belite rich or Alite rich cement) to be produced. The process makes it possible to use about 20-50 % fly ash.

The authors have also attempted to evolve the possible mechanism of phase formation in the hydrogel process, through studies on microstructure and mineralogy of the calcined material at periodic intervals of temperature.

The paper also illustrates the experimental data generated on the compositional parameters and the compressive strengths of neat cements and its behavior in a sulphate environment for cementitious binder, indicating this cementitious binder to have more sulphate resistance than the conventional Portland cement.

Keywords: Hydrogel, Alkali activated fly ash, Reactivity, Clinkerisation

1. INTRODUCTION

In India approximately 95 million tonnes per annum of fly ash is generated from the thermal power plants. Disposal/utilization of these fly ashes is a major issue. It is a challenge to the Research Scientists to convert these fly ash into suitable products. The Research and Development Division of The Associated Cement Companies Limited have been pursuing several approaches for converting fly ash to suitable value added products. One of such approaches investigated in detail was conversion of fly ash (Class-F) to cementitious products through the Hydrogel Process of clinkerisation [1,2]

The Hydrogel is based on alkali activation of the low lime class – F fly ash. The alkali activated fly ash is reacted with hydrated lime (the proportion of the hydrated lime depends on the type of cementitious system to be produced) to produce the Hydrogel (a gelated mass-produced having

calcium silicate and calcium silicate-aluminate hydrates). The hydrogel on calcination/sintering (temperature dependent on the type of cementitious system to be produced) produces the sinter/ clinker, which on intergrinding with gypsum produces the cement/ cementitious binder. The process makes it possible to use about 20-50 % fly ash.

The paper discusses the mechanism of the hydrogel process of clinkerisation indicating the observed mineralogical and micro-structural changes in the hydrogel during the thermal processing. The hydrogel compositions can be tailor made to produce either (i) Low temperature Cementitious Binder or (ii) Belite or Alite rich Ordinary Portland cement Clinker.

The paper presents the optimized composition of the hydrogels, temperature of calcination / sintering of these cementitious systems discussing in detail the hydraulic properties of the resultant cements / binder.

1.1 Hydrogel Process – Mechanism

The possible mechanism [3] of the hydrogel process is summarised below:

- The alkali reacts with quartz converting to glassy silicates
- Amorphous alumino- silicates of fly ash react to form sodium alumino- silicate hydrates
- When the alkali activated fly ash is suspended in water the meta stable glassy phases are partially solubilised thus producing zeolitic hydrophilic sites with Na^+ ions which act as cation exchangers
- On addition of Hydrated Lime, the Ca^{++} ion gets exchanged forming Calcium Silicate - Aluminate Hydrates, the sequence of reactions can be represented as:

$$\text{Si - O}^- + \text{Na}^+ \longrightarrow \text{Si- O - Na}$$

$$\text{Si- O - Na} + \text{OH}^- + \text{Ca}^{++} \longrightarrow \text{Si - O - Ca - OH} + \text{Na}^+$$

Similar reactions would be expected to occur with the aluminates

The processing steps of the Hydrogel process are schematically represented in Figure 1.
The chemico-mineralogical composition of fly ash and hydrated lime used for Hydrogel preparation is given in Table 1. The mineralogical changes produced in fly ash on activation are shown in Figure 2.

Table 1. Chemico-mineralogical composition of fly ash and hydrated lime

% Oxides	Fly ash	Alkali Activated Fly ash	Hydrated lime
SiO_2	65.2	63.6	3.0
Al_2O_3	24.8	24.2	1.3
Fe_2O_3	4.8	4.6	1.2
CaO	0.8	0.7	60.4
MgO	0.4	0.3	0.1
LOI	1.4	1.8	33.8
TiO_2	1.4	1.3	-
Na_2O	0.06	2.5	-
K_2O	0.2	0.2	-
Mineralogy	α - Quartz Amorphous phase Mullite Magnetite	α - Quartz Amorphous phase Analcime, Mullite Magnetite	Calcite Calcium hydroxide CaO

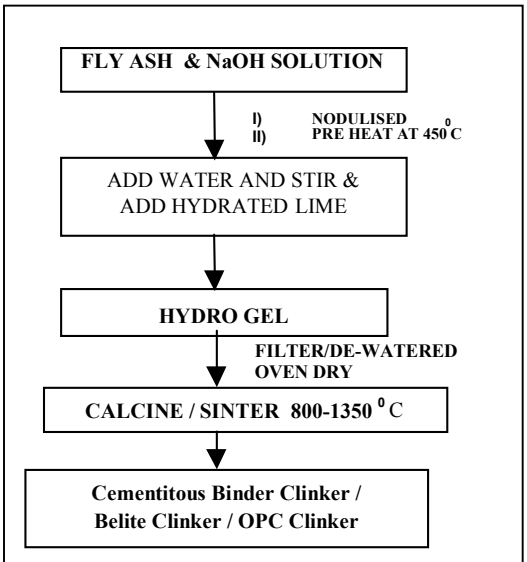

Figure 1. Schematic representation of Hydrogel Process

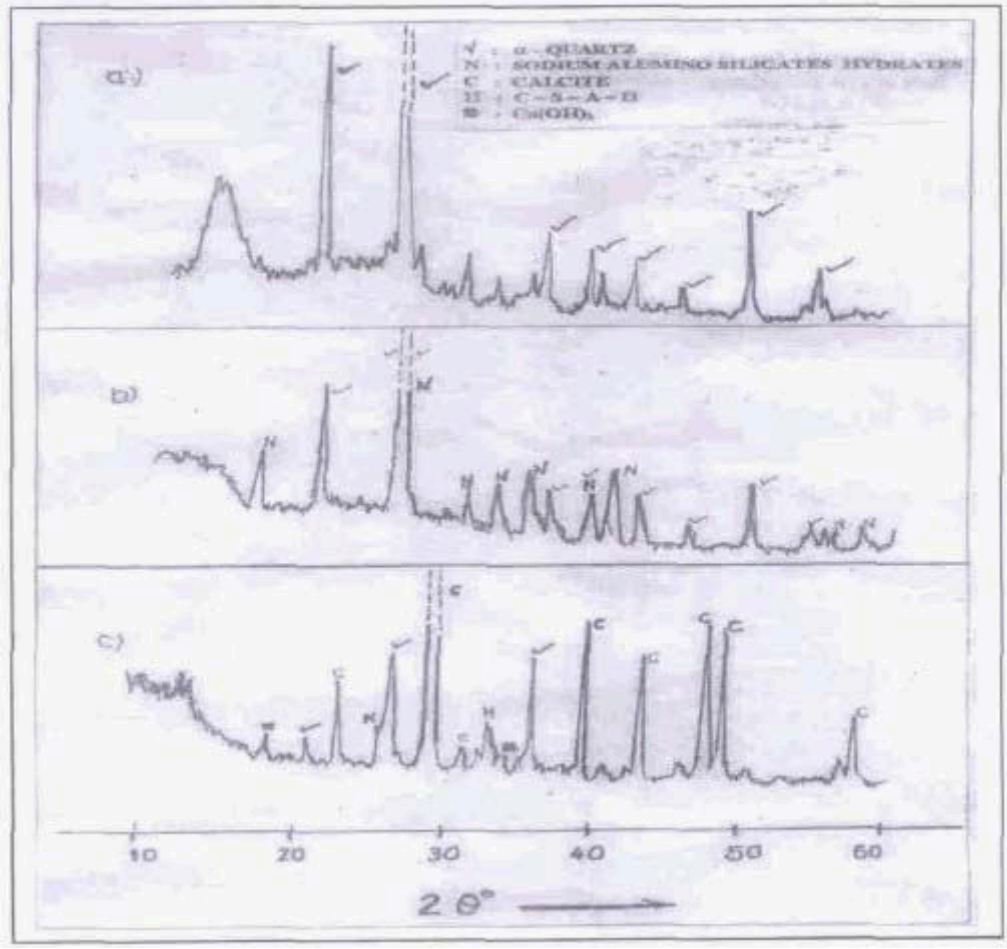

Figure 2. XRD scan of a) Fly ash b) Alkali Activated Fly ash c) Hydrogel

1.2 Mineralogical and Microstructure Characteristics of Hydrogel during Thermal Processing

1.2.1 Dried hydrogel and hydrogel fired at 600^0 C

- The content of Calcium - Silicate - Aluminate Hydrates (of Hydroglosular series C_3AH_6, $C_3AS_2H_2$ etc.) along with its crystallinity increases as the gel is heated to 600^0 C
- The calcite /Calcium hydroxide contents decreases

The morphological and microstructural features are similar except that the gel fired at 600^0 C shows a greater degree of interlinking and cross linking with higher compaction of the spherical/ aggregated grains of the dried gel (Figures 3 (a) and 3 (b).

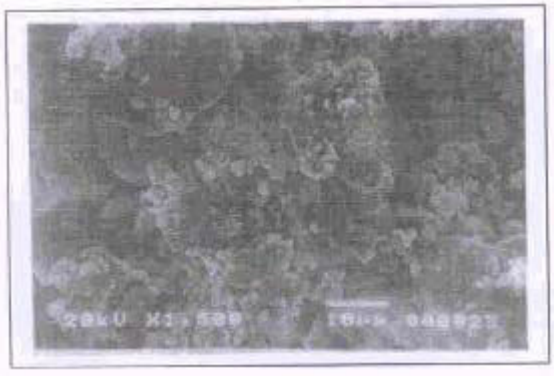

Figure 3 (a). SEM Photomicrograph of dried Hydrogel

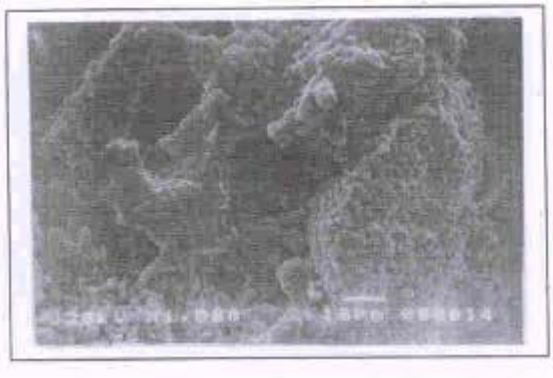

Figure 3 (b). SEM Photomicrograph of Hydrogel showing Interlinking and Cross linking of spherical grains

1.2.2 Hydrogel fired at 700^0 C and 800^0 C

- The content and crystallinity of the Calcium-Silicate-Aluminate Hydrates (C-S-A-H) increases indicating crystallisation of the Hydrates from its amorphous precursors in Hydrogel
- Further decrease in calcite /Calcium hydroxide contents
- Further inter-linking and cross linking of the spherical / aggregated grains is observed
- Microfine β-C_2S grains are observed which are compacted , inter-linked and crosslinked similar in habit to their (C-S-A-H) precursors (Figure 3 (c))

The changes up to 800^0 C are in hydrogel compositions for Low teperature Cementitious Binder system. The thermal changes in hydrogel compositions for Belite rich and alite rich Ordinary Portland Cement clinker are summarised below:

1.2.3 Hydrogel fired at 900^0 C and 1000^0 C

- The calcium - silicate -Aluminate Hydrate (C-S-A-H) decreases from 900^0 C to 1000^0 C, till at 1000^0 C it is absent. This disappearance of the hydrates is also substantiated by the loss observed at 900 - 950^0 C
- Appearance of C_2S and C_2AS phases at 900^0 C and an increase in their contents at 1000^0 C

1.2.4 Hydrogel fired at 1100^0 C and 1200^0 C

- The C_2AS phase decreases from 1100^0 C to 1200^0 C till at 1200^0 C it is absent.
- Presence of C_3S and C_3A is observed along with increased C_2S contents at 1100^0 C
- At 1200^0 C the microstructure depicts well formed clinker phases.

1.2.5 Hydrogel fired at 1300^0 C and 1350^0 C

- Further increase in phase formation (C_3S and C_3A) (Figure 3 (d))
- At 1350^0 C the clinker shows well crystallized cement clinker phases with α form of belite, the aluminates are coarsely crystallized and lathic in shape. The clinker is observed to be porous.

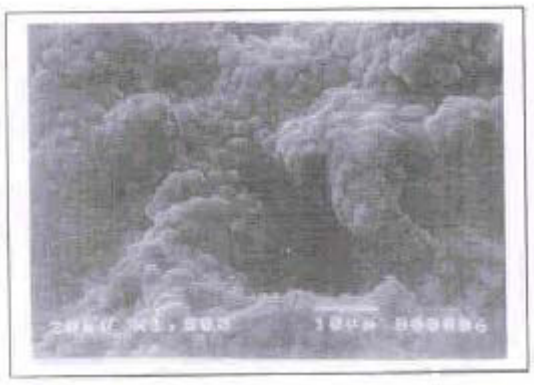

Figure 3 (c). SEM Photomicrograph of microfine β-C_2S grains

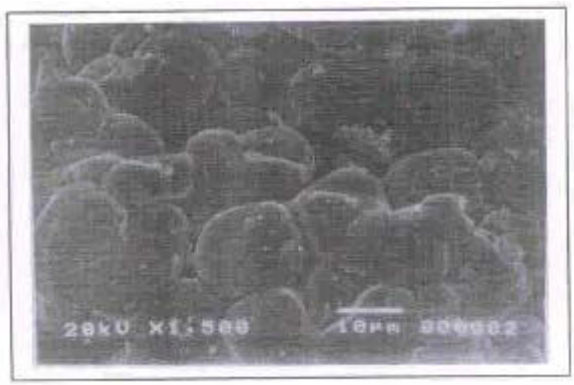

Figure 3 (d). SEM Photomicrograph of well formed Clinker phases

The mineralogical changes during the thermal processing are summarised in Figure 4.

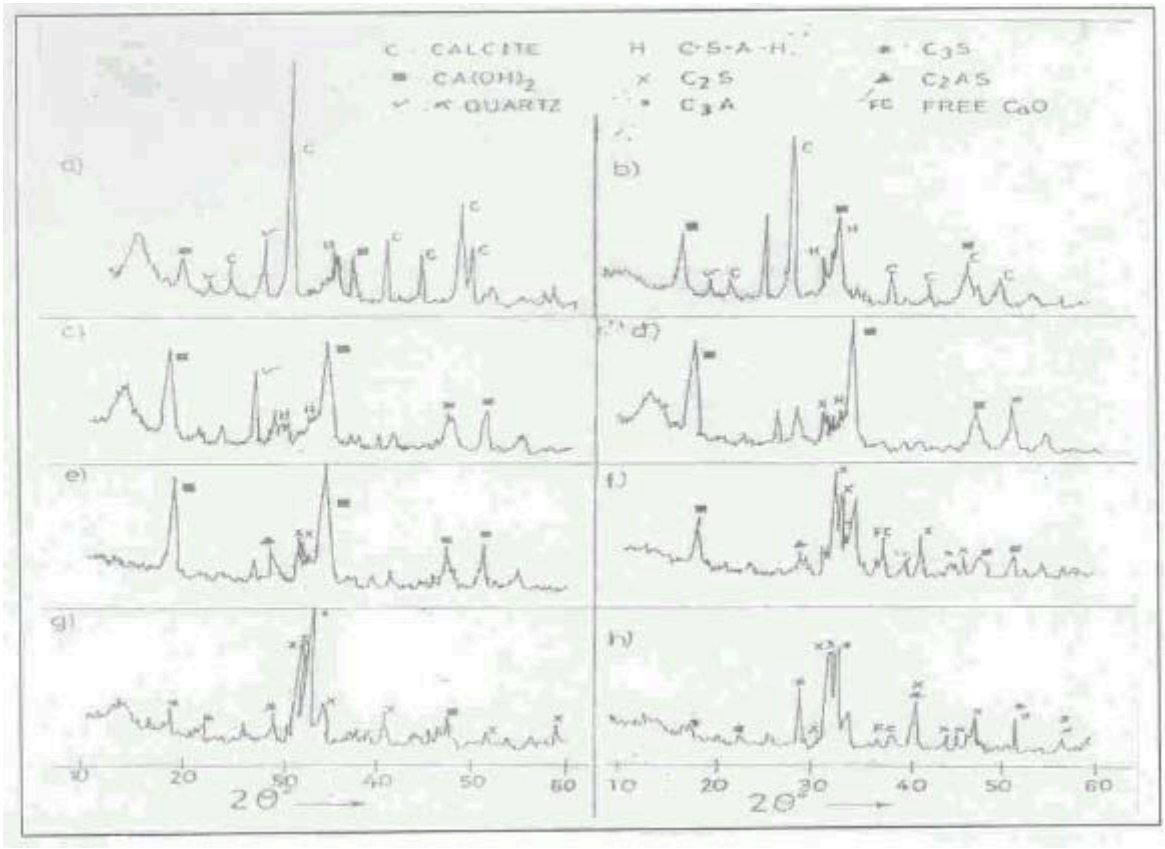

Figure 4. XRD Scans of Hydrogel fired at different temperatures

a) 600^0 C b) 700^0 C c) 800^0 C d) 900^0 C
e) 1000^0 C f) 1100^0 C g) 1200^0 C h) 1350^0 C

2. MANUFACTURE OF BELITE AND ALITE RICH OPC CLINKERS

The proportions of the activated fly ashes and hydrated lime along with chemical composition of the corresponding Hydrogels and resultant clinkers is given in Tables 2 and 3.

Table 2. Raw material proportions and gel compositions

	Hydrogel Clinker I mix	Hydrogel Clinker II mix
Raw material proportions		
Activated fly ash	23.5	--
Activated flyash + Siliceous corrective		20.7
Hydrated lime	76.5	79.3
Chemical Composition		
% Oxides		
SiO_2	17.2	16.58
Al_2O_3	6.68	4.35
Fe_2O_3	2.02	2.96
CaO	46.14	48.01
MgO	0.17	0.13
LOI	26.19	27.11
Na_2O	0.61	0.34
Modulus Conditions		
LSF	0.80	0.90
SM	1.98	2.27
AM	3.3	1.47

Table 3. Chemical Composition of Clinkers

% Oxides	Clinker - I	Clinker - II
SiO_2	23.36	22.75
Al_2O_3	9.05	5.97
Fe_2O_3	2.74	4.07
CaO	62.51	65.87
MgO	0.23	0.20
Na_2O	0.83	0.47
Free CaO	1.0	1.0
Modulus Conditions		
LSF	0.80	0.90
SM	1.98	2.27
AM	3.3	1.47
Potential phase composition		
C_3S	8.1	45.2
C_2S	60.9	31.2
C_3A	19.4	8.9
C_4AF	8.3	12.4
C/S Ratio	2.68	2.9

2.1 Reactivity and phase formation during sintering

The reactivity (lime combining ability) of the hydrogel at different temperatures was compared with raw mix prepared from fly ash (unactivated) and hydrated lime. The two mixes were fired at different temperatures from 600 - 1350^{0}C at intervals of 100^{0}C and a retention time of 20 minutes at each temperature. The fired samples at each temperature were analysed for free lime to assess the degree of reaction. The plot of free CaO v/s temperature of the mixes is shown in Figure 5. The results indicate a substantially improved reactivity of the hydrogel compositions.

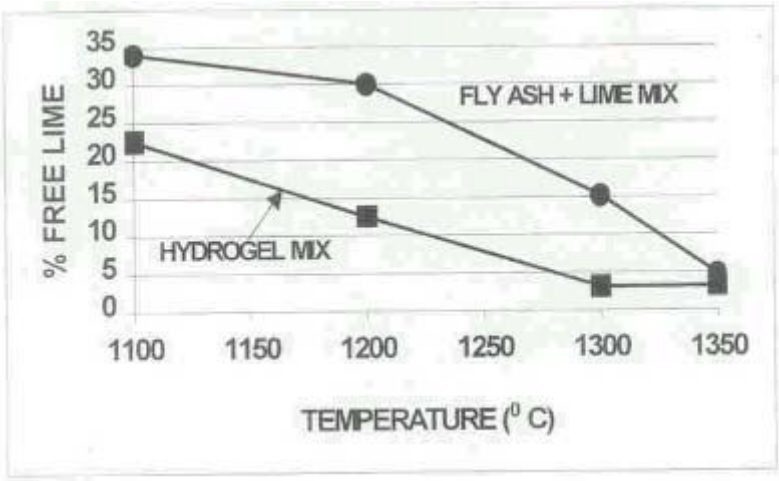

Figure 5. Comparative Reactivity of Hydrogel Mix and Fly Ash +Lime Mix

2.2 Preparation and Charaterisation of clinkers

Using the Hydrogel process clinkers were produced at pilot scale level. The optimum compositional parameters of the alite rich and belite rich clinkers are as follows:

	LSF	SM	AM	POTENTIAL PHASES			
				C_3S	C_2S	C_3A	C_4AF
CLINKER – I (Belite Clinker)	**0.80**	1.98	3.3	8.1	60.9	19.4	8.3
CLINKER – II (Alit rich Clinker)	**0.90**	2.27	1.47	45.2	31.2	8.9	12.4

Clinker – I (Belite Clinker) and Clinker – II (Alite rich Clinker) were prepared from the hydrogel prepared from alkali activated fly ash. The microstructure of the clinkers is presented in Figures 6 (a) and 6 (b).

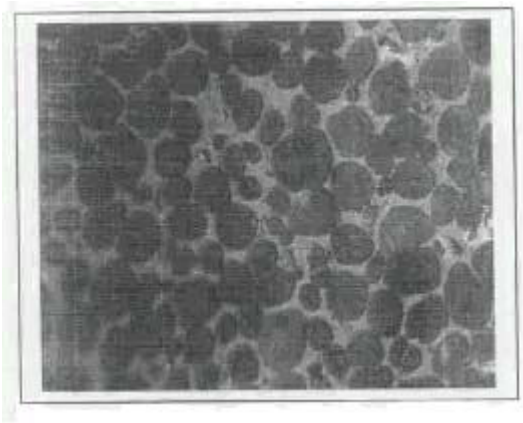

Figure 6 (a). Photomicrograph of Clinker – I showing well developed C_2S

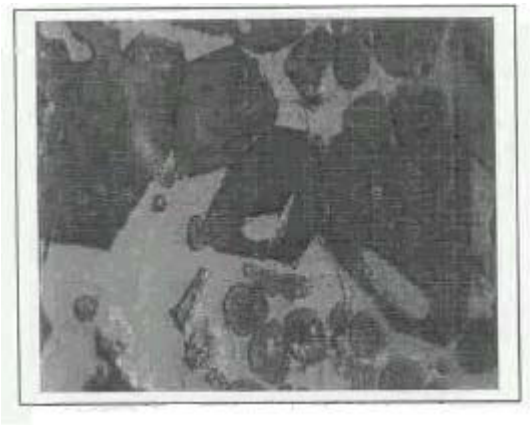

Figure 6 (b). SEM Photomicrograph of Clinker– II showing well developed C_3S

The clinkers were co-ground with gypsum in a laboratory ball mill to cements with a fineness of 320 m^2/Kg and SO_3 content of 2.7%.The physical properties of cements are given in Table 4.

Table 4. Physical Properties of Cements (Indian Standards)

Physical tests	Belite rich Cement	Alite rich Cement
Blaine's Specific surface (M^2/Kg)	320	320
SO_3 (%)	2.7	2.6
Consistancy (%)	28.3	25.6
Setting Time(mins.)		
Initial	75	110
Final	115	165
Compressive strengths (MPa)		
1 Day	11.0	24.5
3 Days	16.0	42.0
7 Days	22.0	58.5
28 Days	33.0	79.5

3. MANUFACTURE OF LOW TEMPERATURE CEMENTITIOUS BINDER(CB)

The raw materials used for the study were of the same composition as those given in Table 1. The detail investigation is reported in [4] and the optimum clinker (chemical and mineralogical) composition of hydrogel sintered at 800^0 C is shown in Table 5, whereas SEM photomicrograph of clinker in Figure 7 and compressive strength of neat cement paste with optimum gypsum is shown in Figure 8.

Table 5. Chemical and Mineralogical Composition of Optimum low temperature belite Clinker (on loss free basis)

% Oxides	Clinker
SiO_2	32.51
Al_2O_3	16.74
Fe_2O_3	2.78
CaO	45.15
MgO	0.63
Na_2O	0.04
K_2O	0.55
SO_3	0.11
CaO/SiO_2	**1.39**
Mineralogical Composition	C_2S , C_3A , α-Quartz, f CaO, $Ca(OH)_2$

Figure 7. Hydrogel at 800^0 C showing microfine β-C_2S

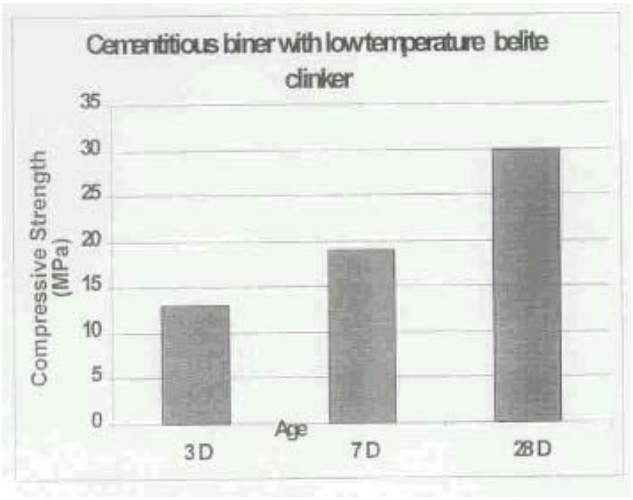

Figure 8. Compressive strength of low temperature belite clinker

3.1 Effect of Aggressive Environment on the Cementitious Binder[4,5]

Mortars prisms were cast with cementitious binder and were cured by immersing in the aggressive solution (0.5M Na_2SO_4+ 0.5 M NaCl solution) after 2 days of hydration in de-mineralised water, and after 3, 7 and 28 days of hydration they were tested for compressive strengths and flexural strengths .

- X-ray diffraction analysis by Philips X'pert MPD
- Chloride and sulphate content of the Outer coat and inner cores of the prisms were analysed by conventional methods.
- SEM analysis of the fractured surface of the mortar prisms cured at 28 days in water and in aggressive environments was carried out on a Jeol JSM 5400 microscope.
- Pore size distribution of the hydrated mortar cubes cured at 28 days in water and the aggressive environment was determined by Hg porosimeter.

3.1.1 Effect of sulphate + chloride solution on cementitious binder mortar

The flexural and compressive strengths of the mortars cured in de-mineralised water and the aggressive environment are graphically shown in Figures 9 and 10.

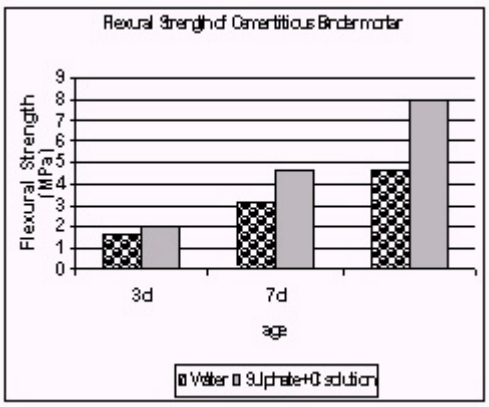

Figure 9. Flexural strength of Cementitious Binder mortar in water and aggressive environment

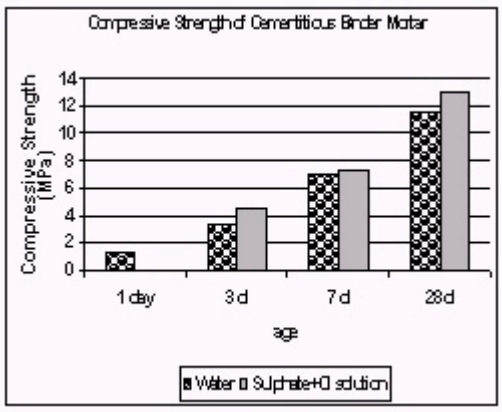

Figure 10. Compressive strength of Cementitious Binder mortar in water and aggressive environment

The outer coat of prisms were cut at a distance of 1 cm along all the faces and the averaged outer coat along with the central core was tested for sulphate and chloride concentration and compared with that of the prisms cured in de-mineralised water. The results are tabulated in Table 6.

Table 6. Sulphate and chloride content of the mortar prisms

	3 days Hydration		**7 days Hydration**		**28 days Hydration**	
	In Aggr. environment		**In Aggr. environment**		**In Aggr. environment**	
	% SO_3	**% Cl**	**% SO_3**	**% Cl**	**% SO_3**	**% Cl**
Av. External Coat of all faces of the prism	1.5	0.09	1.5	0.10	1.5	0.09
Core	1.7	0.06	1.6	0.08	1.6	0.06

The SEM photomicrographs showing the hydrated microstructure [6,7] of the mortars cured in water and in aggressive environment at 28 days are shown in Figures 11 (a) and 11 (b).

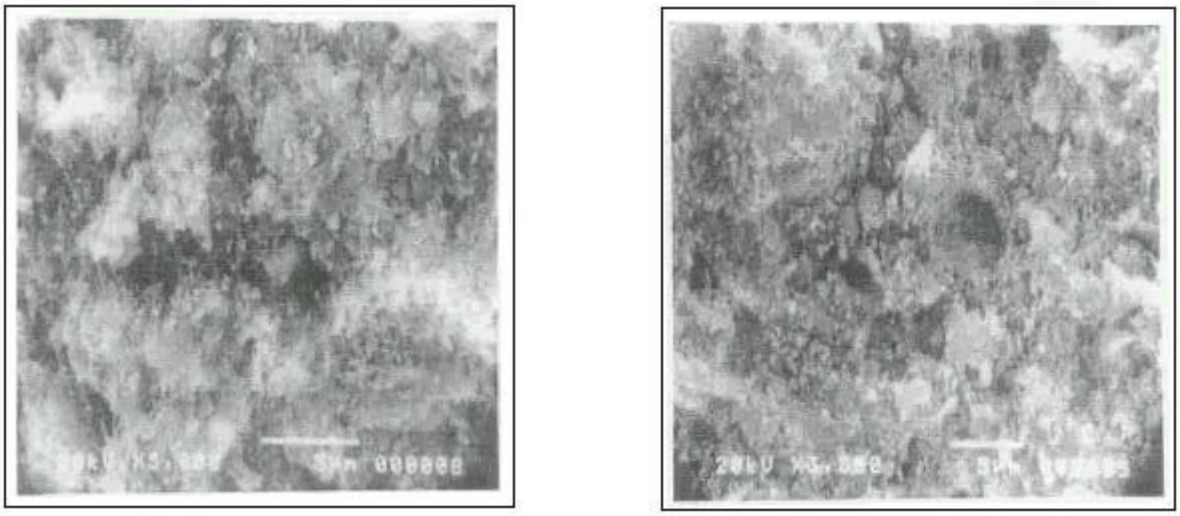

(a) Cured in de-mineralised water (b) Cured in aggressive medium

Figure 11. Microstructure of the Cementitious binder mortars cured in water and in aggressive medium showing compacted microstructure

The studies indicate that

- Considering the sulphate contents of the cement in the mortars, the SO_3 contents of the mortars is marginally more and it increases with age of hydration in the aggressive medium. The chloride levels in mortars are more or less constant with age of hydration indicating that the diffused chloride in the pore solution is in equilibrium with the curing solution and with age the penetration of chloride seems to have been hindered indicated by precipitation of traces of chloride based compounds in pores at 28 days.
- The XRD of the cementitious binder clinker shows amorphous contents along with C_2S,C_3A, calcium hydroxide, calcite and α-quartz, hydrated mortars in water shows formation of Ettringite $Ca_6Al_2(SO_4)_3$,$(OH)_{12}.26.H_2O$,Hillbrandite(C-S-H) and Hydroglossular $Ca_6Al_2(SiO_4,CO_3,OH)_3$ with lesser intensities while in aggressive medium the mortars show much higher levels of these phases along with traces of Hydrocalumite ($Ca_4Al_2O_6Cl_2.10H_2O$)

- Due to interaction of the water soluble sulphate from the aggressive medium in presence of sodium ions present in the cementitious binder, there is gradual increase in the compaction i.e. decrease in the porosity of the mortar prisms from 7 days to 28 days, this is attributed to the accelerated formation of Ettringite $Ca_6Al_2(SO_4)_3,(OH)_{12}.26.H_2O$ and Hydroglossular $Ca_6Al_2(SiO_4,CO_3,OH)_3$ and Gismondite $CaAl_2Si_2O_8.4H_2O$ and the subsequent precipitation of the phases inside the pores. Such increased phase formation is not observed in the mortar prisms cured in water and so the porosity is observed to be high - Figures 11 (a) and 11 (b).
- The flexural strengths of the mortar prisms in aggressive medium shows a substantial increase from 3 days to 7 days and to 28 days as compared to those cured in water.
- The porosity of the mortars at 28 days of hydration in aggressive medium is much less, it was observed to have lower porosity in the range of micro pores as compared to those cured in water. (Figure 12)

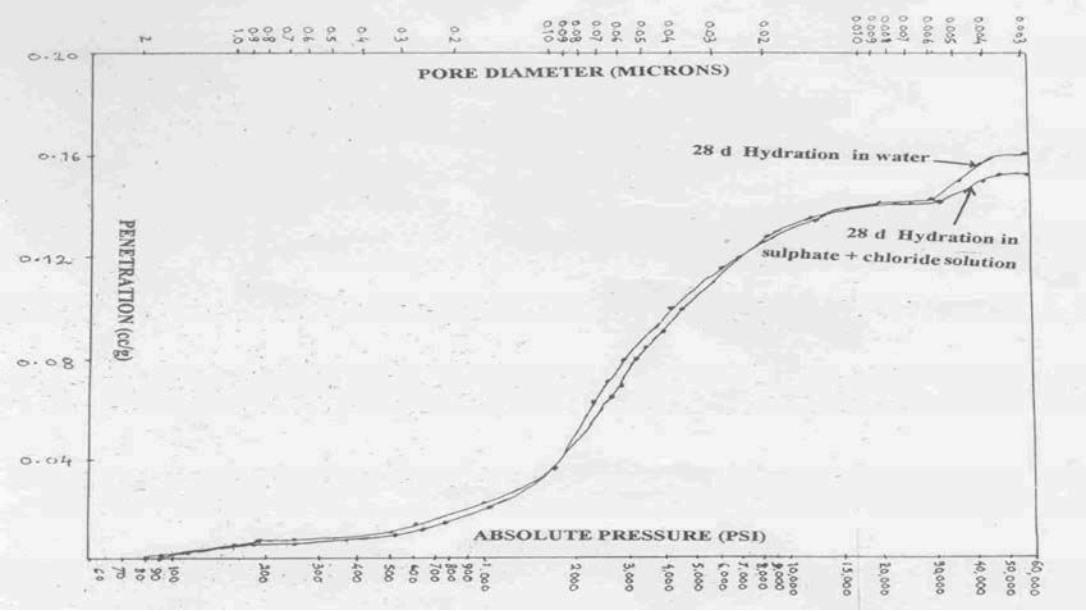

Figure 12. Pore size distribution of cementitious binder mortars cured in water and in an aggressive medium

CONCLUSIONS

- The Hydrogel process of clinkerisation utilises fly ash up to 50% and opens new avenues for its utilization. The optimum alkali levels required for activation being dependent on the nature of fly ash. The process does not involve hydrothermal activation.
- Depending upon type of Cementitious system intended to be produced viz. Cementitious binder clinker / belite rich or alite rich clinker, the temperature for thermal processing ranges from 800 -1350^0 C.
- The study establishes the possible mechanism of the Hydrogel process. Alkali activation of fly ash produces sodium alumino silicate hydrates, these zeolitic structures with hydrophilic sites act as cation exchangers exchanging the alkali ion with the Calcium ion, thus forming calcium–alumino silicate hydrates. These semi amorphous precursors present in the hydrogel dehydrate to produce the cement clinker minerals.
- The principle of alkali activation can be extended to activation of white china clay for manufacture of white cement, initial experiments have indicated the feasibility of white cement manufacture at lower temperature using this hydrogel process.
- The resistance of cementitious binder to aggressive environment is excellent. Such a binder could have specialised applications.

REFERENCES

[1] Jiang, W. and Roy, D.M., "Hydrothermal processing of new fly ash cement", Ceram.Bull., Vol.71 No.4, 1992, pp.642-647.

[2] Khadilkar.S.A, Karandikar.M.V, Ghosh.D and Chatterjee.A.K, "A Novel clinkerisation Process for Fly ash Utilisation" , 6 th International Conference on Fly ash, Silica Fume and Natural Pozzolanas in Concrete,Thiland, ACI SP- 178,Vol.1,1998, pp.225-237.

[3] Khadilkar.S.A, Karandikar.M.V, Ghosh.D and Chatterjee.A.K, "Alkali Activated Fly ash Cement under Non Hydrothermal Conditions– Some Results on Mechanism", 2nd International Conference on Alkaline Cements and Concretes, Kyiv, Ukraine,1999,pp.18-20.

[4] Karandikar.M.V, Khadilkar.S.A, Cursetji. R.M. and Chatterjee.A.K, " Fly ash based Cementitious Binder by Hydrogel Process ", 7th NCB International Seminar on Cement and Building Materials, New Delhi, India, 21-24 November 2000, Vol.4, pp.XI-50-57.

[5] Karandikar.M.V, Jatty.S.K., Khadilkar.S.A, and Cursetji.R.M., " Manufacture of Fly Ash Belite Cement Through Use of Alkali Activated Fly Ash", 7th CANMET/ACI International Conference on Fly Ash, Silica Fume, Slag and Natural Pozzolanas in Concrete, July 22-27,2001, Madras, India, pp.429-442.

[6] Guerrero.A., Goni.S., Macias,A. and Luxan M.P., "Hydraulic activity and microstructural characterization of new fly ash-belite cements synthesized at different temperatures" J.Mater. Res., Vol.14, No.6, Jun.1999, pp.2680-2687.

[7] Guerrero.A., Goni.S.,Macias. A. and Ferenindis E., " Microstructure of New Fly ash-Belite Cement Mortar: Changes Provoked by Sulphate, Chloride and Sodium ions", 21st International Conference on Cement Microscopy, Las Vegas, Nevada, USA, April 25-29,1999, pp.230-237.

ASSESSMENT OF POZZOLANIC REACTIVITY - AN ATTEMPT ON FORMULATING A POZZOLANIC INDEX

S.A. Khadilkar, M.V. Karandikar and R.M. Cursetji

The Associated Cement Cos. Ltd., Research and Consultancy Directorate, R & D Division,
CRS Complex, L.B.S. Marg, Thane 400 604, India.
E-mail: rd3@bom3.vsnl.net.in

ABSTRACT

The use of mineral admixtures, such as fly ash, micro-silica, metakaolin, calcined clay pozzolana, volcanic ashes etc. as a blending component in OPC, alters the hydration kinetics of the resultant blended cement. Due to the secondary hydration reactions of these admixtures with the available calcium hydroxide, their use results in a decreased availability of the calcium hydroxide in the hydrated cement matrix, thus forming a much compacted, less pervious hydrated cement paste matrix on hydration. These aspects are however a function of the nature, fineness and pozzolanicity of the mineral admixtures / Supplementary Cementitious Materials (SCM).

At the authors' laboratory, substantial work has been carried out to assess the efficacy of the different blending components through evaluation of the hydrated OPC and the blended cement pastes (made with the blending materials) at different ages of hydration. The evaluations include analysis of free calcium hydroxide, mineralogy of the hydrated products, analysis of the % unhydrated blending materials in the hydrated cement pastes at different ages of hydration viz. 1, 3, 7, 28, 60, 100 days.

Based on these studies the authors evolved a Pozzolanic Index (Q_H). The details of these findings and the comparison of the Q_H with the conventional compressive strength based Hydraulic Index (H_{in}) were discussed in the paper put forward at the PAC RIM IV conference[5]. A summary of the findings is also presented in this paper.

The Q_H could be used to assess the efficacy / pozzolanic reactivity of blending materials for selection of the reactive size fraction, and also for optimizing the fineness levels of the blending materials like fly ash for improved pozzolanic properties. The paper discusses these applications for fly ashes of different sources.

Keywords: Pozzolanic reactivity, hydraulic index, fly ash

1. INTRODUCTION

The methods of testing the pozzolanic activity of pozzolans or supplementary cementitious materials (SCMs) have been studied by many researchers for over 100 years. However pozzolans are so myriad and of different quality, it is difficult to establish appropriate test methods for assessing the pozzolanic activity. Lea[1] summarised and discussed various methods of testing the pozzolanic activity at the International symposium on the chemistry of Cement in 1938, while Malquori[2] discussed the test methods at the Fourth International symposium on chemistry of cement in 1960, which serve as an useful guides for the research on methods of testing the

pozzolanic activity of pozzolans. Moran and Gilliland[3] divided the test methods into three categories of tests:

- Tests on the Pozzolans alone
- Tests on Pozzolans lime mixtures
- Tests on Pozzolan Portland cement blends

In the light of present knowledge of test methods and techniques, which are a combination of various methods such a classification is difficult, however the relatively frequently used methods could be categorized in the form shown in Table 1.

Some of the test methods are observed to be suitable and correlate well with the strength results of lime mortars. However, they do not correlate to the behavior of cement pozzolan blends. In the widely used standards of various countries, the chemical methods of testing pozzolanic activity are more suited for judging activity of the pozzolanic materials and some of which are time consuming and do not provide a yard-stick to correlate to the strength of standard - cured mortar or concrete. For example, the pozzolanic activity test in the different standards provides the degree to which a pozzolan (fly ash) contributes to strength development of the resultant blended cement mortar, but does not provide a measure of the pozzolanic reaction of the used pozzolans. The compressive strengths of a blended cement mortar / concrete are partly due to the pozzolanic activity and partly due to the packing effect of the added pozzolans.

The estimation of the amount of free calcium hydroxide remaining in the hydrated pozzolana cement has also been used as an indication of the pozzolanic reactivity of the pozzolans. A number of methods[4] (as shown in Table 2), have been used to determine the free calcium hydroxide content in the hydrated lime pozzolana or pozzolana cement mortar or concrete.

Table 1. Classification of methods of testing pozzolanic activity which are relatively frequently used

Classification		**Example of Test Method**
Method testing of strength by accelerated curing of pozzolan lime or pozzolan cement mortar		ASTM C 593-66T, ASTM C 402-65T
Method adding Pozzolan to lime solution	Quantitative measurement of lime	Chapelle's Method, Moran and Gilliland's method
	Quantitative measurement of lime and alkali	AFNOR P 15 - 462 Italian standards ISO recommendation No 1156
Method treating pozzolan or pozzolan lime mixture with acid or alkali	Quantitative determination of SiO_2	Florentin's method
	Quantitative measurement of SiO_2+ Al_2O_3	ASTM C 379 - 56T, Poliet and Chausson's method, Austrian standards Charisius method
	Quantitative measurement of SiO_2+ Fe_2O_3	Steopoe's method
	Quantitative measurement of SiO_2+ Al_2O_3+ Fe_2O_3	Sestini and Santarelli's modification of Baire's method Feret - Florentin method
	Quantitative measurement of insoluble residue	Guillaume's method AFNOR P - 15 - 301
Method measuring development of dissolution heat of pozzolan		Jambors method
Measurement of electrical conductivity of lime pozzolan solutions		Lea's method

Table 2. Methods used for estimation of free calcium hydroxide

Method	Originally described by	Applied to Pozzolanic Mixes by
Sugar	--	Sestini and Santarelli
Glycerol	Emley, Lerch and Bogue	Katherein; Rodt
Ethylene Glycol	Schlapfer and Bokowski	Forsen; Rodt
Phenol	Konarzewski and Lukaszewicz	Sestini and Santarelli; Witterkindt
Lime solution	Bake well and Bessey; Forsen	Forsen; Lea
Calorimetric	Bessey	Lea; Vittori

In such methods presence of the unhydrated cement compounds prevents use of aqueous solutions, as further hydration would occur during extraction. In pozzolana cement mixes most of these methods do not give results having any precise accuracy. However, the methods have been observed to be consistent in themselves and are valuable for comparison of the hydration characteristics.

The pozzolanic activity of the pozzolana has also been reportedly monitored through estimation of the un-reacted pozzolana content of the hydrated blended cement pastes at different ages of hydration. Different chemical extraction methods have been studied by researchers for different pozzolans[4] and the studies have revealed suitability of specific methods for a given type of pozzolana.

At the authors' laboratory substantial work has been carried out[5] to assess the efficacy of the different blending components and attempts were made to assess the pozzolanic activity of the different pozzolans in the blended cement hydration through evaluation of the OPC and the blended cement pastes (with the blending materials) at different ages of hydration. The evaluations include analysis of free calcium hydroxide and analysis of the contents of unhydrated blending materials in the hydrated cement pastes at different ages of hydration viz.1, 3,7,28 and 60 days of hydration.

The % hydration of the Pozzolans can be related to the free calcium hydroxide content of the hydrated cement at different ages of hydration and through a comparison of the free calcium hydroxide values for hydrated blended cements with that obtained with the hydration of OPC - sand blends (control). Based on these comparisons the authors have evolved a hydraulic index, to rate the pozzolanic efficacy of the blending materials.

The hydraulic Index can identify differentially the contributions of the pozzolanic reactivity and the packing effect of the blending components, the Index could also be used for selection of the reactive size fraction as also for optimizing the fineness levels of the blending materials like fly ash for improved pozzolanic properties. The paper discusses these applications for fly ashes of different sources in some details.

1.1 Experimental

The Blended cements PPC (with fly ash of two varieties at absorption levels of 20%), PSF (with 7 % Silica Fume), PMK (with 7 % Metakaolin of two varieties, fine and coarse) were prepared by blending Industrial Ordinary Portland Cement with the fly ash, Silica Fume and Metakaolin. The requisite amount of gypsum was added to maintain the % SO_3 in cement to ~2.5%. The chemical composition of OPC, fly ash, Silica fume and Metakaolin GGBS is given in Table 3.

Table 3. Chemical composition of OPC, Fly Ash, Silica Fume, Metakaolin

% Oxides	OPC	Fly Ash	Silica Fume	Meta kaolin I	Meta kaolin II
SiO_2	21.2	62.4	97.9	51.6	50.8
Al_2O_3	4.4	24.3	0.15	45.7	43.7
Fe_2O_3	4.0	6.3	0.03	0.9	0.7
CaO	64.5	1.6	0.2	<0.1	0.2
MgO	1.0	0.10	0.01	0.1	0.1
LOI	2.0	1.7	1.1	0.9	3.4
Na_2O	0.1	0.54	0.01	0.06	0.09
K_2O	0.4	1.34	0.3	0.13	0.05
TiO_2	0.07	1.30	0.01	0.51	1.1
SO_3	2.3	<0.10	0.2	--	--
I.R	0.7	91.9	--	--	--

The physical properties of mortars of OPC,PPC-I (20% fly ash at 15% residue on 350#) and PPC- II (20% fly ash at 1% residue on 350#), PSF (7% silica fume), PMK-I (7% Fine meta kaolin) and PMK-II (7% coarse Metakaolin 20 micron size) at 1,3,7,28 and 60 days tested as per Indian Standards and are shown in Table 4.

1.2 Hydration studies of OPC, PPC, PSF,PMK

The authors at the 7th NCBM International conference, New Delhi, 2000[6], published results of the comparative hydration studies of OPC, PPC and PSC.

Table 4. Physical properties of OPC, PPC, PSF and PMK (Indian Standards)

	OPC	PPC-I	PPC-II	PSF	PMK-I	PMK-II
Sp.Surface (m^2/kg)	330	344	352	476	498	522
N.C (%)	25.5	28.5	28.8	29.3	30.8	27.8
Setting Time (minutes)						
Initial	95	110	110	95	140	115
Final	135	155	155	135	175	160
Compressive Strength (MPa)						
1 Day	20.0	20.5	19.5	26.5	24.5	24.5
3 Days	39.5	31.0	29.5	44.5	38.0	39.0
7 Days	44.5	34.0	37.5	47.5	48.5	53.0
28 Days	56.5	46.5	49.0	59.5	57.5	59.0
60 Days	64.0	52.0	54.5	63.0	54.0	56.5

The same methodology was followed for assessing the degree of hydration in the neat cements. The neat cement pastes were cast and de-molded after 1 day and were kept at >90% Rh, 27 ± 2 ^{o} C for 1,3,7,28 and 60 days. After each age of hydration, the neat cements were analysed for:

- Free $Ca(OH)_2$ content
- Unhydrated Pozzolan (SCM) content (unreacted mineral admixture or Blending Component)

The above hydration studies were also carried out on corresponding control samples for comparison, the control samples were prepared by blending OPC and ground quartz at the same percentage additions and same fineness as the corresponding blending component, i.e. (PPC-C) with OPC + 20% Fine quartz (of particle size distribution similar to fly ash), (PSFMK-C) with OPC+ 7% fine quartz.

1.3 Analysis methods

1.3.1 Free calcium hydroxide

The free calcium hydroxide content of the hydrated cement at each age of hydration was analysed by using the glycol extraction method as per IS 4032(Indian Standards). The free calcium hydroxide content of the different hydrated blended cements were also compared through XRD quantification so that any errors due to extraction of lower hydrates by the reagent could be corrected.

1.3.2 Analysis of Unhydrated blending components (Fly ash, Metakaolin and Silica Fume)

Mineral admixture (fly ash, silica fume and metakaolin) content in the unhydrated cements and hydrated blended cements at different ages of hydration were analysed by a selective dissolution method using picric acid - methanol as reported by Li et al[7]. The brief method is given below:

A known weight the hydrated neat cement was treated with aqueous - methanolic picric acid solution with magnetic stirring for a fixed time of 30 minutes. The residue was filtered and washed free of picric acid with methanol and subsequently washed with 300 ml of water at 50^0 C. The residue was dried and ignited at 1000 ^{o} C. The residue was weighed after cooling. The residue in the blending components and unhydrated cement was determined by the same method separately. Based on the residues of the blending component and the blended cement at each age of hydration the % unhydrated Blending component was determined from which the % hydration of the blending component was computed.

2. RESULTS AND DISCUSSIONS

The free calcium hydroxide contents of the different blended cements and corresponding control blended cements (with fine quartz of same fineness as the blending component) at different ages of hydration is graphically shown in Figures 1 and 2.

The unhydrated blending component in the cements at different ages of hydration was analysed by the selective dissolution method and the % hydration of blending component in the different cements was calculated and is graphically shown in Figure 3.

The pozzolanic reactions of the blending component gradually results in consumption of the calcium hydroxide produced from the hydration of the OPC part of the blending cement as a result there is a decrease in the calcium hydroxide contents of the hydrated cements, due to which the free calcium hydroxide contents of the blended cement would be comparatively lower than the hydrated OPC at the corresponding ages of hydration. Thus the difference in the free calcium hydroxide contents of the hydrated blended cements and OPC would be related to the pozzolanic reactivity of the blending component at that age of hydration.

The generated data indicates that % hydration of the blending component in the blended cement corresponds to the decrease in free calcium hydroxide content at each age of hydration. The higher the degree of hydration, the lower the free calcium hydroxide content. Thus, in order to quantify the pozzolanic reactivity of the blending components, the authors have evolved the Pozzolanic Index (Q_H).

$$\text{Pozzolanic Index} = Q_H = \frac{\text{(Calcium Hydroxide in OPC - Calcium Hydroxide in PBC)}}{\text{(Calcium Hydroxide in OPC - Calcium Hydroxide in PBC – control)}}$$

The Q_H of the different blending components calculated at 7 days of hydration is given in Figure 4.

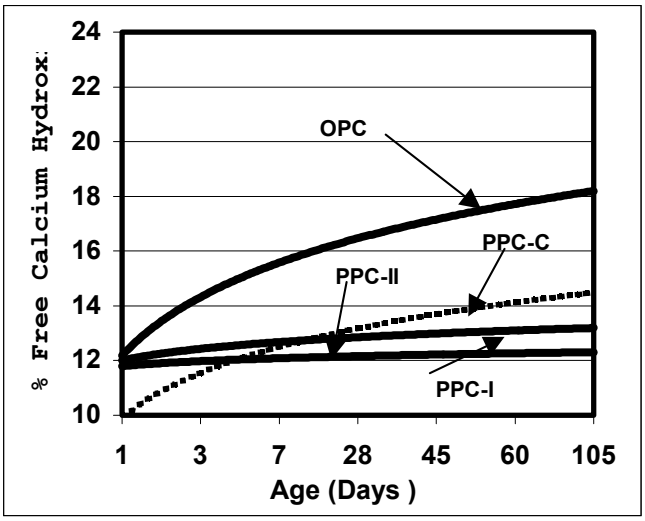

Figure 1. Comparison of Free Calcium hydroxide content in OPC, PPC and PPC-control

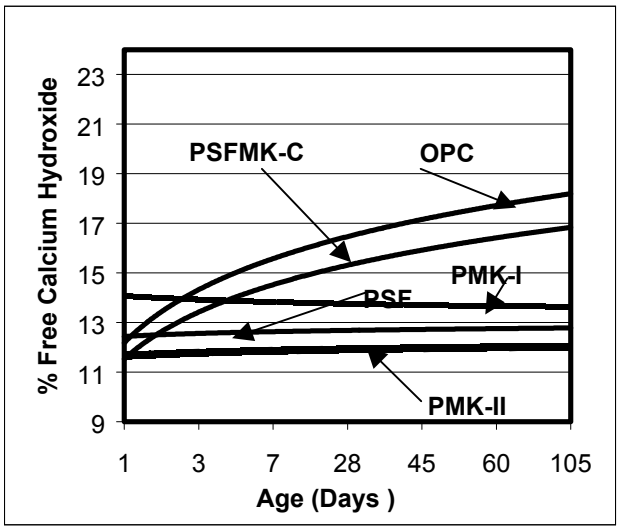

Figure 2. Comparison of Free Calcium Hydroxide content in OPC, PSF, PMK and PSFMK-control

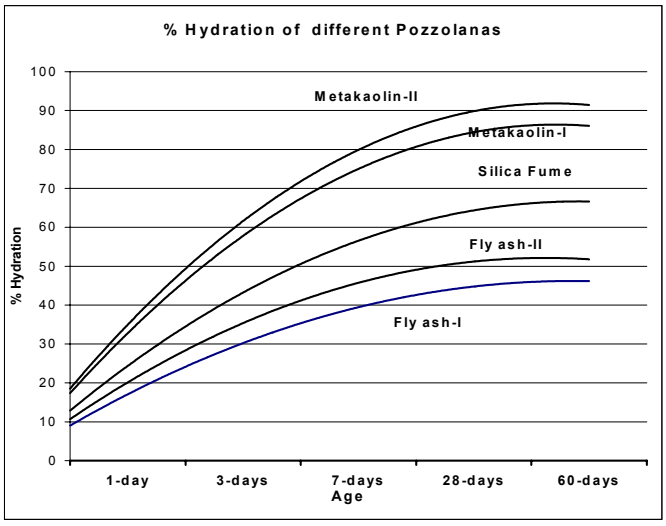

Figure 3. % Hydration of different blending components at different ages of hydration

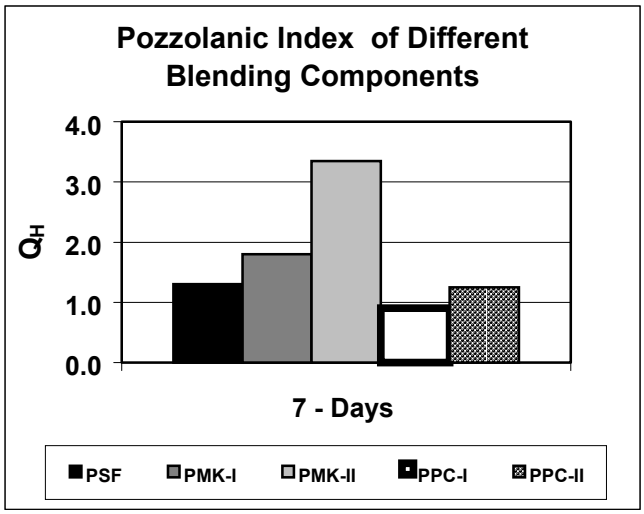

Figure 4. Pozzolanic Index of the different blending components at 7 days

The Hydraulic Index (H_{In}) based on compressive strength (as reported in literature) of OPC, Blended cements and their control samples at 28 and 60 days was also calculated from the data on the physical properties of cements and a comparison was made of the applicability of the two indexes.

The formula used for the Hydraulic index (H_{in}) based on compressive strengths is given below.

$$\text{Hydraulic Index } H_{in} = \frac{\text{Strength of PBC} - \text{Strength of PBC-Control}}{\text{Strength of OPC} - \text{Strength of PBC-Control}}$$

The pozzolanic activity of the different blending components based on H_{In} at 7 days and 28 days can be rated as follows:

At 7 days: Fly ash I < Fly ash II < MK I < MK II < Silica fume (1)

At 28 days: Fly ash I < Fly ash II < MK I < MK II < Silica fume (2)

Attempts were also made to correlate the Q_H of 7 days and H_{in} (Hydraulic Index based on compressive strength) at 28 and 60 days of hydration, the data shows a correlation coefficient of 0.91 and 0.72 respectively and is graphically shown in Figures 5 and 6.

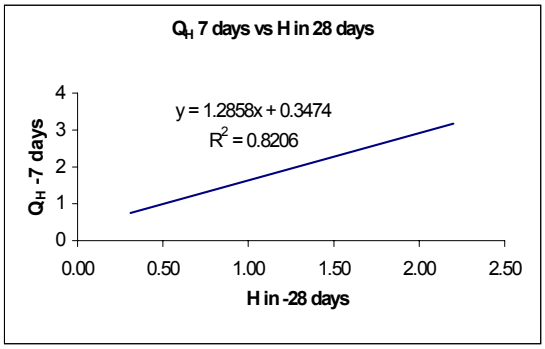

Figure 5. Q_H – 7 days v/s H_{In} 28-days

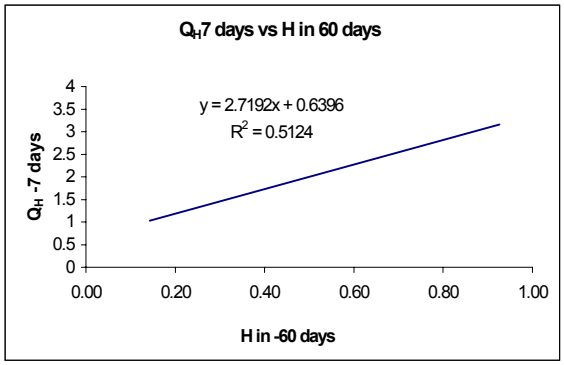

Figure 6. Q_H – 7 days v/s H_{In} 60 days

The results indicates that:

- The Pozzolanic Index (Q_H) at 7 days relates very well with H_{in} at 28 days.
- A comparison of the Q_H and H_{In} indicates that the former relates to reactivity while the latter relates to the resultant effect of reactivity and packing effect of the blending component.

Thus the Q_H index at 7 days is related to the pozzolanic reactivity of the blending component. The pozzolanic reactivity of the different blending components (Mineral admixture / SCMs) under study can be rated on the basis of the Q_H as follows:

Fly ash I < Fly ash II < SF < MK I < MK II (3)

While on the basis of % Hydration of the blending components with age shown in Figure 4 indicates the pozzolanic activity of the blending components to be of the following order:

Fly ash I < Fly ash II < SF < MK I < MK II (4)

The pozzolanic activity of the blended component as indicated by Q_H matches well with the % hydration of the blending component (Figure 4). The index however relates very well to the reactivity of the fly ash.

The indexes (Q_H and H_{In}) rate the fly ash II to be more reactive than fly ash I, which is also substantiated by the ~ 7-10% more hydration of the fly ash II at 28 days. This is due to more surface area of fly ash exposed during the hydration of the finer fly ash as compared to coarse fly ash leading to more pozzolanic reaction and lowering of free calcium hydroxide in the hydrated sample (Figure 1). The higher strength gain after 7 days can be partly attributed to improved packing. This observation is in congruence with that reported by Ducreux and Jarriage[8] who studied the pozzolanic activity of finer fraction by Feret's method.

2.1 Use of Pozzolanic Index (Q_H) for assessing the pozzolanicity of fly ash of different sources

Three fly ash samples of different sources were taken for the evaluation of the Pozzolanic Reactivity. The fly ash A and U is comparatively coarser while fly ash D is finer in its particle size distribution. The fly ash U is different in its nature of amorphous phase having the maxima of the amorphous hump at 2θ value of 26 ^{o} while the other two fly ash have the maxima at a 2θ value of 23^{o} indicating a possible difference in composition of the amorphous phase[9].

The amorphous / glassy content of the fly ashes as determined by chemical 1% HF dissolution method[10] are given below:

% Amorphous glassy content	Fly ash D	Fly ash A	Fly ash U
Chemical method	49.7	64.5	50.9

The morphological features of the fly ashes as observed under Scanning electron Microscope indicates relatively coarser to fine spherical particles (cenospheres) in fly ash A and U as compared to fly ash D. The percentage occurrence of the spherical particles is also higher in fly ash A and U. The chemical analysis and particle size distribution of fly ashes is shown in Tables 5 and 6.

Using the method described above the pozzolanic index at 7 days was determined along with % Reaction (% Hydration of the fly ash at different age of hydration as described above. The Q_H and the% reaction of the fly ash at different ages of hydration in PPC is depicted in Figures 7 and 8 respectively.

The pozzolanicity of the fly ashes can be rated as:

Fly ash U > Fly ash D > Fly ash A

Table 5. Chemical composition of fly ash of different sources

%	Fly ash D	Fly ash A	Fly ash U
SiO_2	58.4	63.2	48.0
Al_2O_3	31.1	24.8	27.8
Fe_2O_3	5.2	3.9	9.9
CaO	0.3	1.2	1.2
MgO	0.7	0.7	1.5
LOI	1.5	1.4	4.6
Na_2O	0.08	0.62	1.5
K_2O	1.05	2.0	3.6
TiO_2	1.4	1.0	1.0
SO_3	0.2	0.3	0.6
I.R	91.7	85.0	66.0

Table 6. Particle size distribution of fly ash of different sources

Size (Micron)	Fly ash D		Fly ash A		Fly ash U	
	within	Cum	within	Cum	within	Cum.
> 210	0	0	0.4	0.4	0.1	0.1
210-150	0	0	0.8	1.2	0.2	0.3
150-90	0	0	1.7	2.9	0.5	0.8
90-60	0	0	6.3	9.2	6.3	7.1
60-45	0	0	6.4	15.6	5.4	12.5
45-30	0.6	0.6	9	24.6	6	18.5
30-20	4.3	4.9	13	37.6	9.3	27.8
20-10	20.4	25.3	23.6	61.2	21.8	49.6
10-5	47.4	72.7	22.6	83.8	27.8	77.4
5-2	19.5	92.2	13.6	97.4	18.8	96.2
< 2	7.8	--	2.6	--	3.8	--
D_{50}	9.5μ		17.5μ		10.5μ	

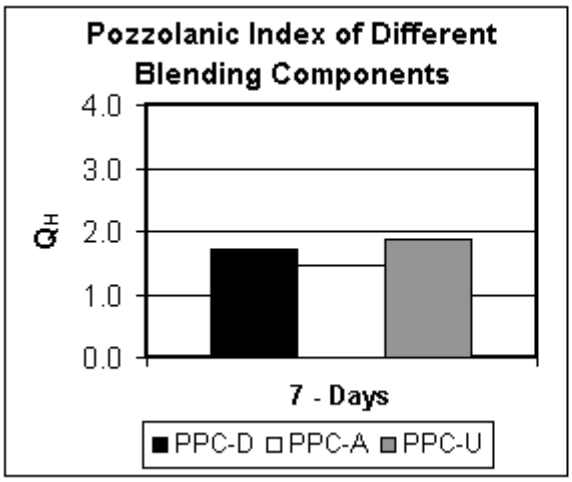

Figure 7. Q_H of the different fly ash at 7 days

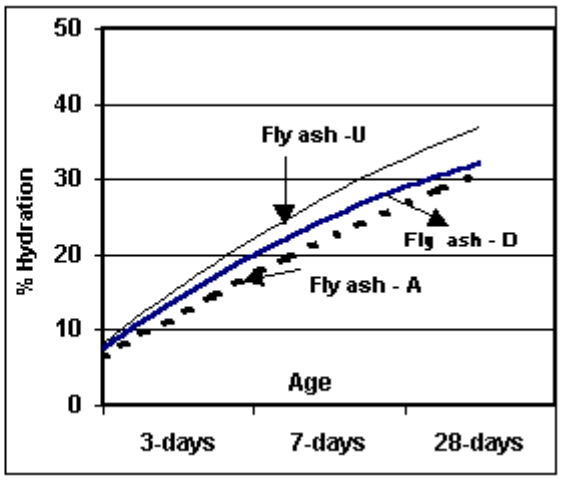

Figure 8. % Hydration of the fly ash in PPC

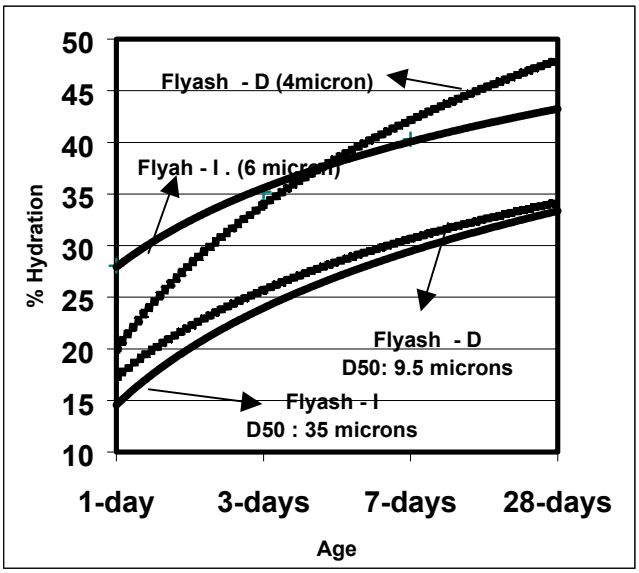

Figure 9. % hydration of fly ash with increased fineness

2.2 Optimisation of fineness of pozzolana/fly ash:

The reactivity of pozzolana/ fly ash is a function of its fineness and at an optimum fineness maximum reactivity can be achieved. Determination of the Q_H could be useful for optimizing the fineness of pozzolana / fly ash.

Figure 9 illustrates the change in pozzolanic reactivity and the % hydration with increased fineness of fly ash I and D. The fly ash I (D-50 of 35 microns) was ground to D-50 of 6 microns while fly ash D (D – 50 of 9.5 microns) was ground to D-50 of 4 microns.

The grinding of the fly ash produces a substantial change in the reactivity of the fly ashes. Thus the Q_H at 7 days could be used to optimize the fineness of the fly ash for maximized pozzolanicity.

3. CONCLUSIONS

- The Pozzolanic index (Q_H) evolved by the authors based on the free hydrated lime content of the neat cement pastes appears to applicable for assessment of the pozzolanic activity of the mineral admixtures. The method is comparatively rapid and is applicable for assessing the pozzolanic activity at the absorption levels used in the blended cement or blended concrete and is an indirect measure of the calcium hydroxide consumption by the pozzolanic component.
- The Pozzolanic index (Q_H) at 7 days can be mathematically stated as follows:

All measurements are done at the hydration age of 7 days and a control blended cement is also made at the same absorption levels using fine quartz of similar particle size distribution as that of the blending component under study:

- The reactivity as predicted by Q_H 7 days matches well with the % Hydration (% reaction) of the blending component.

- On the basis of Q_H at 7 days, the efficacy of the different blending components studied could be rated as follows:

  Fly ash I < Fly ash II < Silica fume < Metakaolin I < Metakaolin II

- As exemplified by the case study in the paper the determination of Q_H can be used for assessing the pozzolanic reactivity of the pozzolan (fly ash), and also for optimizing the fineness of the pozzolan.

- Further studies are in progress to evolve a rapid analytical technique for analysis of the % hydration (% Reaction), of the blending component at 7 days of hydration of the blended cement for predicting its pozzolanic activity, which would not require a hydration study on control blended cement made with fine quartz.

REFERENCES

[1] Lea. F.M "The Chemistry of Pozzolanas" Proc.Int. Sym. on the Chemistry of Cements, Stockholm, 1938, pp.460-483.

[2] Malquori G., "Portland- Pozzolana Cement" Proc. 4th Int.Symp. on Chem. of Cement, Washington, Vol.II, 1960, pp.983-1000.

[3] Moran W.T and Gilliland J.L "Summary of methods for determining pozzolanic activity", Special Technical Publication,ASTM,No.99,1949,pp.109-130.

[4] Bessey. G.E., "The Estimation of Free Calcium Hydroxide in Pozzolana Mixes" Proc.Sym. on the Chemistry of Cements, Stockholm, 1938. pp.484

[5] Karandikar.M.V., KhadilkarS.A.and Cursetji. R.M., "Assessment of Hydraulic Property of Different Mineral Admixtures through studies on the Hydration Characteristics of the Blended Cements", PAC RIM IV - International conference on Advanced Ceramics and Glasses, Nov.4-8 2001, Hawaii.

[6] Karandikar.M.V,Mukhopadhyay.A.K.,Gandhe.S.P., "ComparativeHydration Characteristics of OPC and Blended Cements", 7th NCB International Seminar on Cement and Building Materials, New Delhi, India, 21-24 November 2000,Vol.3, pp.X-66-77.

[7] Li. S., Roy.D.M and Amithab Kumar " Quantitative Determination of Pozzolanas in Hydrated Systems of Cement or $Ca(OH)_2$ with fly ash or Silica Fume" Cement and Concrete Research., Vol.15, 1985,pp.1079-1086.

[8] Ducreux R and Jarrige A., " Influence of fineness of fly ash on behavior of fly ash cement", Silicate Inds., 27, No.11,1962, (in french)

[9] Karandikar.M.V., KhadilkarS.A.and Cursetji. R.M.,"Comparative Assessment of Pozzolanicity of Low Lime Class-F Fly Ashes of Varying Amorphous Content", 5th Int.Sym. Cement and Concrete, to be held on oct.28-Nov.12002, Shanghai, China. (paper accepted for oral presentation)

[10] Arjunan. P., Silsbee M.R., Roy D.M., "Rapid Evaluation of Pozzolanic Reactivity in Coal Fly Ashes by a Wet Chemical Method" Sym. Structure-Property Relationships in Hardened Cement paste and composites, Dec.2-4, 1996.

REDUCTION OF PORTLAND CEMENT PASTE POROSITY BY TEOS IMPREGNATION

Hebert L. Rossetto and Milton F. de Souza

CEPOF, Laboratory of Materials Science, São Carlos Institute of Physics, University of São Paulo, São Carlos, SP, Brazil. E-mail: hebert@if.sc.usp.br

ABSTRACT

Pore-reduced cements, PRC, were prepared by uniaxial pressing of Portland cement powders wetted by the incipient wetting method. Hardened and dried PRC samples were impregnated by tetraethyl orthosilicate, TEOS. Impregnation caused porosity to drop from 8.8% to 0.9% (a 90% decrease) and compressive strength to increase simultaneously from 267 to 317 MPa (a 20% increase). Impedance Spectroscopy measurements showed an almost tenfold increase in resistance. Scanning Electron Microscopy revealed that the impregnated samples' surfaces were more uniform than those of the control samples.

1. INTRODUCTION

Impervious cement surfaces provide the first barrier against attack by deleterious substances, increasing concrete durability. It is well known that porosity is decreased when the water/cement, w/c, ratio of the cement-based products is reduced. Pore reduction can be increased [1] by choosing adequate conformation techniques that can operate with low water/cement ratio powders. One such technique is the uniaxial (or isostatic) pressing of cement powders wetted by the incipient-wetting method, which allows for w/c ratios of close to 0.10. By this method, small water droplets are sprayed on revolving cement particles to produce a thin water layer on each particle; this wetted layer acts as the binder among particles during the pressing operation. These binding forces are sufficiently strong to maintain the body's shape immediately after pressing and to produce bodies sufficiently strong for handling after 24 hours. Further immersion in limewater completes the cement hydration.

Although pore-reduced cements already have little porosity, the introduction of silica via molecular species, such as TEOS, further reduces porosity because this liquid is able to penetrate the cementitious body and to reach nano-sized pores. It is well known, from the literature [2], that TEOS undergoes hydrolysis in basic pH environments, producing highly reactive silica. The cementitious body provides the calcium hydroxide necessary to raise the pH for TEOS hydrolysis and to immediately react chemically with the silic acid produced. Voids and pores within the cement can, thus, be filled by the calcium silicate hydrates that are formed and calcium hydroxide content is reduced.

2. BACKGROUND

2.1 Incipient-Wetting Technique

Although it is often employed in ceramics processing, the incipient-wetting technique is not normally used in cement applications and, to the best of our knowledge, this is the first time it has been used within this scope. This technique plays a potentially important role in the development of

low-porosity and ultra high-strength cement-based products because it allows for the addition of a minimum amount of water necessary for the application of the dry pressing method without causing powder delamination, concomitantly producing sufficient adhesion among cement particles. It also prevents water and calcium hydroxide losses during uniaxial pressing and increases the mechanical strength before full hydration, among other advantages.

Basically, this technique consists of uniformly wetting the cement powder with a minimum amount of water. With the help of a spraying device, which produces micron-sized water droplets, water is uniformly spread all over the Portland cement particles, while the powder is kept under continuous movement during the wetting process. Values of w/c around 0.10 are achieved with this method, corresponding to a deposition of a ≈ 2.0 μm water layer on each cement particle.

2.2 TEOS

Tetraethyl orthosilicate, TEOS, is being used, for the first time, to the authors' knowledge, in cementitious products to produce nanometric silica particles inside the cement body's microstructure. Under base-catalyzed conditions, water dissociates to produce nucleophilic hydroxyl anions in a rapid first step. The hydroxyl anion then attacks the silicon atom of the TEOS molecule [3]. This hydrolysis reaction is described as follows:

$$Si(OC_2H_5)_4 + 4H^+ + 4OH^- \rightarrow Si(OH)_4 + 4C_2H_5OH \quad (1)$$

Such silicic acid gels react promptly with the calcium hydroxide, provided by the hydration of the C_3S from cement particles and by the limewater, resulting in calcium silicate hydrate (C-S-H) formation as follows below:

$$Si(OH)_4 + 4Ca(OH)_2 \rightarrow Si(OCa)_4^{4+} + 4H_2O \quad (2)$$

In contrast, if partially hydrolyzed TEOS is used in the impregnation process, silicic acid polymers are introduced into the pores of the cementitious body, leading to the corresponding chemical reaction of this polymer with calcium hydroxide. Therefore, different results should be expected if pre-hydrolyzed TEOS is used in the impregnation process.

3. EXPERIMENTAL METHODS

3.1 Materials Preparation and Impregnation

PRC samples were produced by uniaxial pressing of incipient-wetted Portland cement powder (see chemical composition in Table 1), with w/c = 0.12, at 20 and 40 MPa compaction pressures. Immediately after compaction, the samples were cured in a room-temperature humidity chamber for 24 hours, followed by curing immersed in a saturated limewater solution.

Table 1. Chemical composition of the Portland cement used.

Components	Weight %
$CaSO_4.2H_2O$ (CSH_2)	7.68
$4CaO.Al_2O_3.Fe_2O_3$ (C_4AF)	7.05
$3CaO.Al_2O_3$ (C_3A)	11.50
$3CaO.SiO_2$ (C_3S)	64.50
$2CaO.SiO_2$ (C_2S)	3.78

In a first approach, one set of samples was oven-dried at 105ºC for 24 hours and another was vacuum-dried at 10^{-3} torr for 4 hours and then placed in a desiccator at 20% humidity for 20 hours. Oven-drying at 105ºC may affect the cement pore structure by rearranging the hydrated products

due to internal stresses induced by the removal of adsorbed and free water [4-5]. Although many researchers consider this the standard drying procedure because it is simple, fast and results in effective water removal, a second approach was used in the work reported on here: the samples were oven-dried at 50ºC for 24 hours, which permitted the total porosity to be estimated more realistically.

Finally, each set of dried samples was impregnated by immersion for five minutes in TEOS either 28 or 40% SiO_2 (see TEOS properties in Table 2), the one with higher density being the pre-hydrolyzed product. Thereafter, all TEOS-impregnated samples were kept in a limewater chamber for 30 days and then characterized by the techniques below. Samples that were dried by the first method were characterized only through their porosity before and after impregnation, while samples dried by the second method were characterized in terms of their porosity, compressive strength, electrical resistance and the microstructure, observed by SEM.

Table 2. TEOS[#] properties.

Properties	Siliethyl TS 28	Siliethyl TS 40
Density at 25ºC	0.930-0.940	1.055-1.065
SiO_2	28.5-29.5	41- 42

[#] Hergrand Limited, Brazil.

3.2 Characterization

3.2.1 Mechanical Properties

Although the mechanical performance of TEOS impregnated samples was not the main focus of this work, there is a strength-porosity relationship that needs investigating. Sample pieces with parallel faces were cut from a 90-day larger sample using a slow speed water cooled cutting diamond disc to size them down to 20 x 10 x10 mm^3, and their mechanical strength was measured using an Instron machine.

3.2.2 Porosity

Measurements by Mercury Intrusion Porosimetry (MIP) (Porosizer 9320, Micromeritics) require the complete removal of water from the sample; this was accomplished by oven-drying it for 24 hours, either at 50ºC or 105ºC. Because of "bottleneck pores" in cementitious materials, MIP measurements are the subject of much criticism from a great many researchers [6-7], who claim that the pore size distribution is not accurately represented. Nitrogen adsorption measurements were taken to check the predominant pore shapes existing in impregnated and non-impregnated PRC.

Samples from the same large piece used to measure the mechanical properties were sized to 20x10x10 mm^3 for MIP measurements. For the nitrogen adsorption tests, samples with dimensions close to that used for the MIP measurements were crushed with a hammer and the fragments collected.

3.2.3 Microstructural Investigation

Changes caused by TEOS impregnation on the surface microstructure of 10x10x4 mm^3 samples were observed by SEM (DSM 960, Zeiss).

3.2.4 Electrical Properties

Impedance Spectroscopy is a noninvasive and nondestructive technique that has been applied to study cement-based materials [8] and can sample the microstructure without recourse of water removal by heating, which is known to alter the paste microstructure. 20x10x4 mm^3 sample pieces were cut from larger 90-day pieces, TEOS impregnated, cured in limewater for 30 days and then kept at room temperature in the air to reach humidity equilibrium. Control samples were prepared likewise. Thereafter, both types of samples were prepared by applying silver painted electrodes on

the 20x10 mm^2 faces. Measurements were taken at room temperature using an Impedance Analyzer (Solartron 1296) in the 1.0Hz to 1.0 MHz frequency range.

The measurement of electrical conductivity is related to pore interconnectivity and can be used to predict durability of cement-based materials. In this study, we propose an equivalent electrical circuit model for PRC, based on earlier literature. According to MacPhee et al. [9], four conduction pathways are possible as follows: (i) continuous electrolyte-filled pores connecting the electrodes (CP); (ii) discontinuous or blocked porosity electrolyte-filled pores (BP); (iii) hydration products (HP); and (iv) unreacted cement (UC). As hydration proceeds, the proportion of CP will reduce and the conductivity will occur increasingly through BP and HP. In the present case UC is strongly reduced because the samples are ninety days old. This brought us to the equivalent circuit, Figure 1, in which indexes 1, 2 and 3 represent BP, HP and electrode features, respectively.

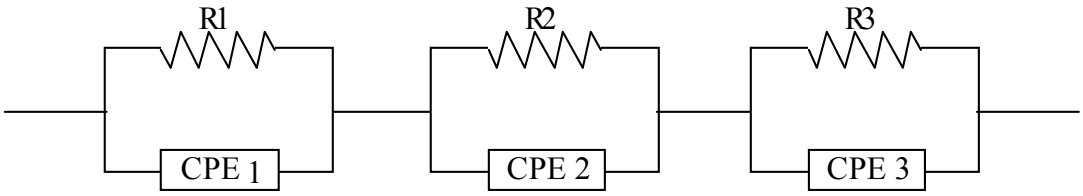

Figure 1. Equivalent electrical circuit model for 90-day PRC pastes.

4. RESULTS AND DISCUSSION

4.1 Evaluation of the First Approach

Firstly, the effects of two drying methods (oven-drying at 105ºC and vacuum-drying at room temperature), two impregnators (TEOS 28 and 40) and two compaction pressure values of the PRC samples (20 and 40 MPa) on porosity reduction, measured by MIP, were analyzed as the first step in defining the best experimental procedures to achieve the most effective porosity reduction. At this point, it should be noted that the above-mentioned drying methods involve the penetration ability of TEOS. We consider that the dryer the sample, the higher the TEOS intrusion and, hence, the greater the reduction in porosity. Nevertheless, both samples were oven-dried at 105°C before the MIP test so as to complete the removal of water, which revealed the samples' total porosity. The total porosity of the control samples pressed at 20 and 40 MPa were 13.1% and 12.7%, respectively.

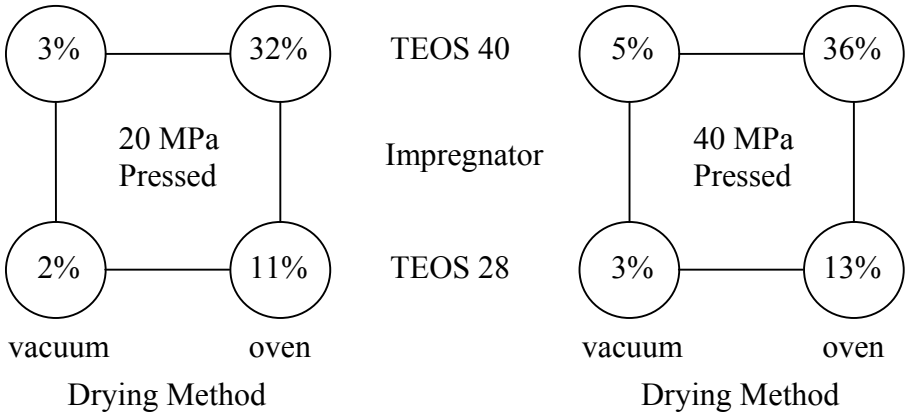

Figure 2. Porosity reduction efficiency of TEOS impregnated samples.

Figure 2 shows the efficiency of TEOS impregnation in reducing the porosity of PRC (average of two samples). Note that there is no evidence that compaction pressure on the samples plays any significant role in the reduction of porosity, at least at these levels, unlike the difference between the drying methods and pre-hydrolysis of TEOS, which exert a strong influence.

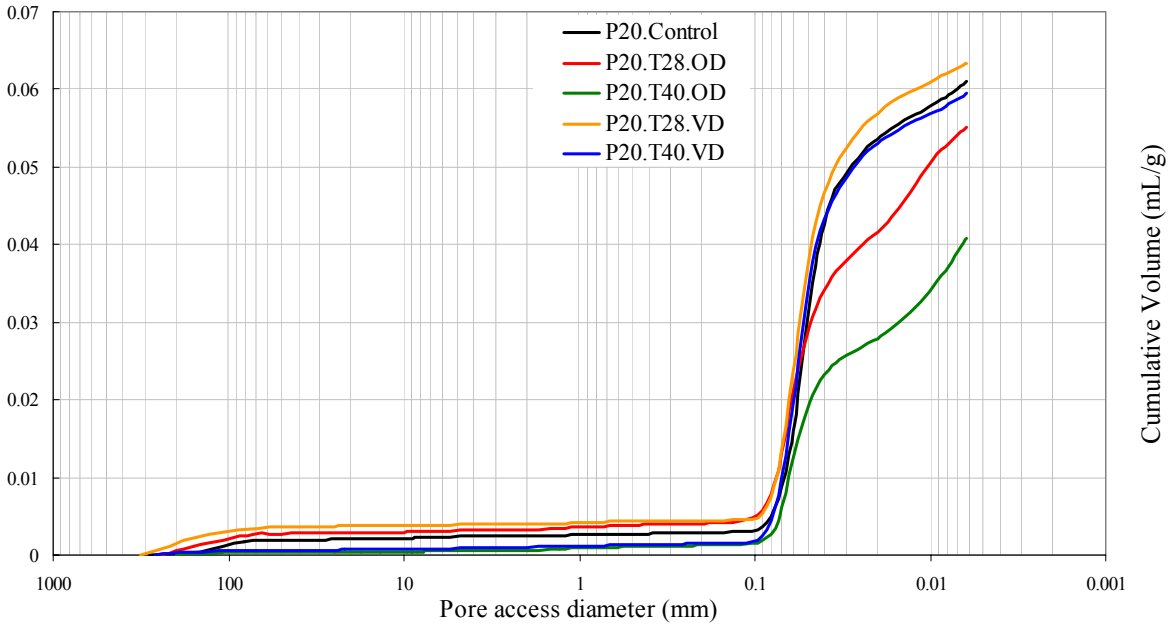

Figure 3. Mercury intrusion volume curve for 20 MPa pressed samples (T28 and T40 mean TEOS 28 and TEOS 40, OD and VD mean oven-dried and vacuum-dried samples, respectively).

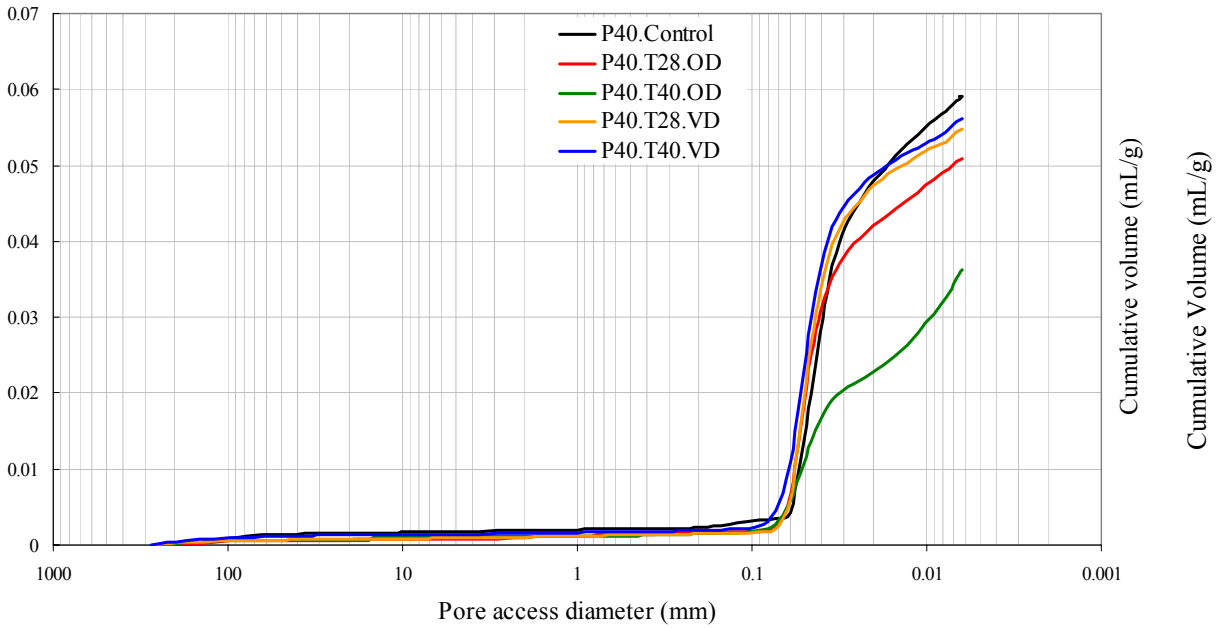

Figure 4. Mercury intrusion volume curve for 40 MPa pressed samples (T28 and T40 mean TEOS 28 and TEOS 40, OD and VD mean oven-dried and vacuum-dried samples, respectively).

The following conclusions were therefore drawn: (i) Vacuum-drying at room temperature does not permit substantial TEOS impregnation; hence, neither of the TEOS types effectively provided total porosity reduction of the PRC samples. (ii) Whereas oven drying is the method that most favors extensive TEOS impregnation, TEOS 40 – with its higher silica content – proved to reduce porosity

more effectively than TEOS 28. These findings, which are illustrated in figures 3 and 4, motivated us redouble our efforts in studying TEOS 40 impregnation.

4.2 Evaluation of the Second Approach

In this approach, samples were oven-dried at 50ºC for 24 hours before TEOS 40 impregnation and MIP tests. This procedure appears to be more realistic because only removal of free water occurs at this temperature. Table 3 shows the results of the MIP tests (average of two samples). It can be noted that the final porosity of both the 20 and the 40 MPa pressed samples impregnated with TEOS was around 1%. Moreover, the median pore diameter also dropped by more than one order of magnitude. Table 4 presents the results of compressive strength tests, which confirm the same trend of porosity measurements: an improvement of around 22%. Therefore, this approach produced the best results for TEOS impregnation of PRC pastes, as is illustrated in Figure 5.

Table 3. MIP results for TEOS 40 impregnated samples oven dried at 50ºC.

Sample	Pressed at 20 MPa		Pressed at 40 MPa	
	Control	Impregnated	Control	Impregnated
Total Intrusion Volume (mL/g)	0.0387	0.0036	0.0280	0.0048
% Porosity	8.8	0.9	6.0	1.1
Bulk Density (g/mL)	2.2761	2.3315	2.2058	2.3129
Median Pore Diameter (μm)	0.0243	0.0074	0.0295	0.0084

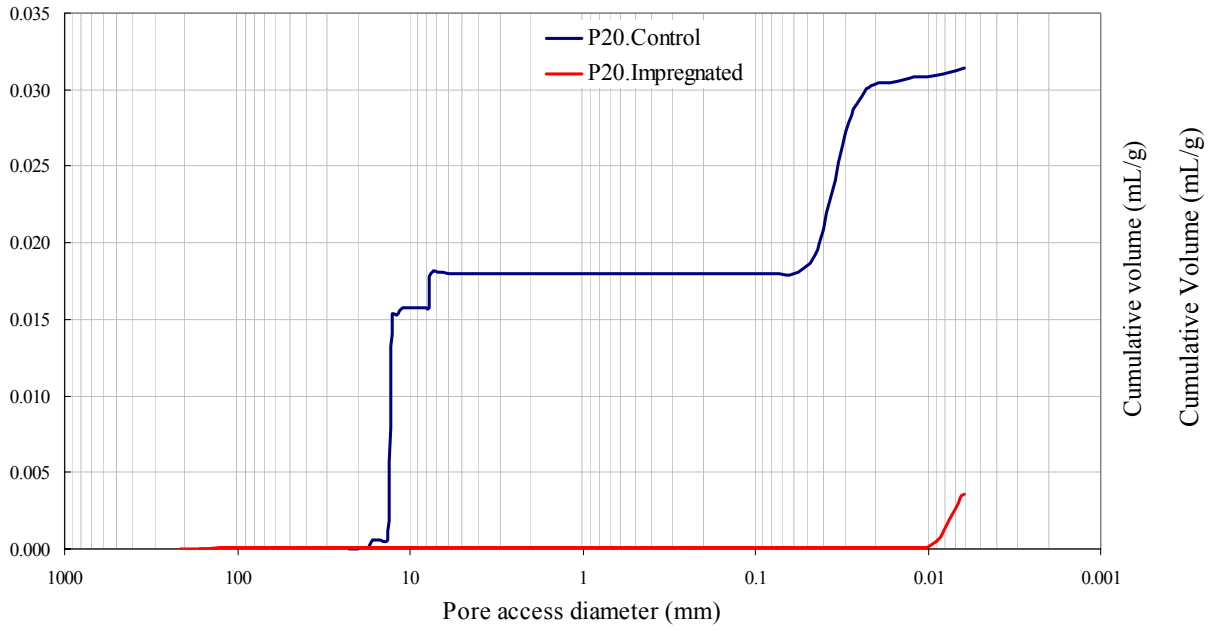

Figure 5. Mercury intrusion volume curve for 20 MPa pressed samples oven-dried at 50ºC.

Table 4. Compressive strength results for TEOS 40 impregnated samples oven dried at 50ºC.

Sample	Pressed at 20 MPa		Pressed at 40 MPa	
	Control	Impregnated	Control	Impregnated
Compressive Strength (MPa)	238	298	266	317

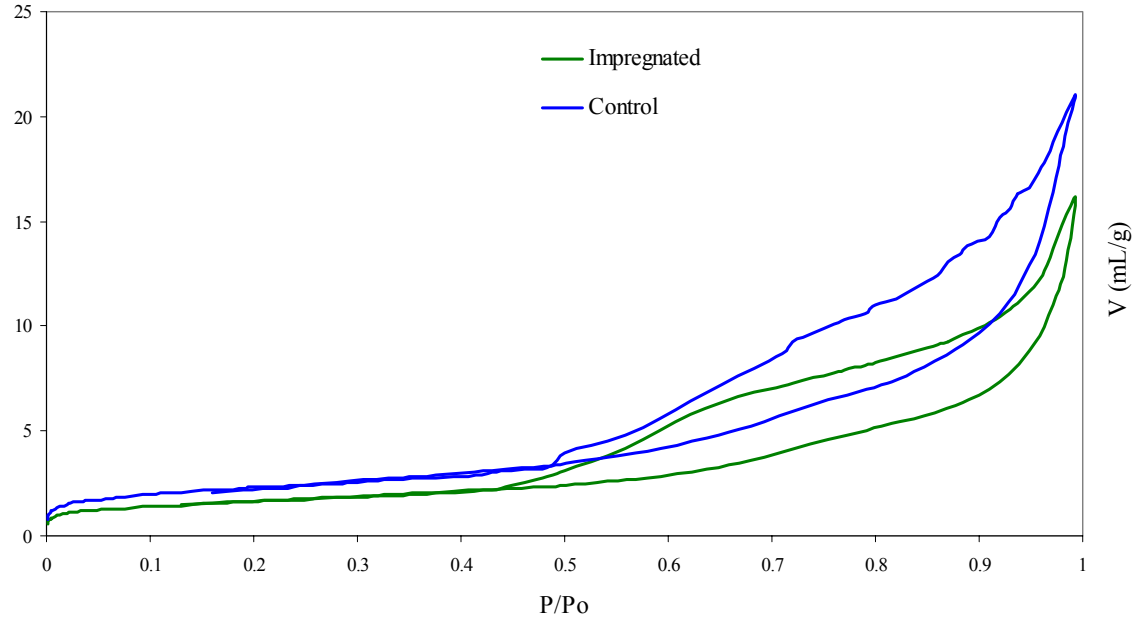

Figure 6. Adsorption-desorption isotherms of samples oven-dried at 50ºC.

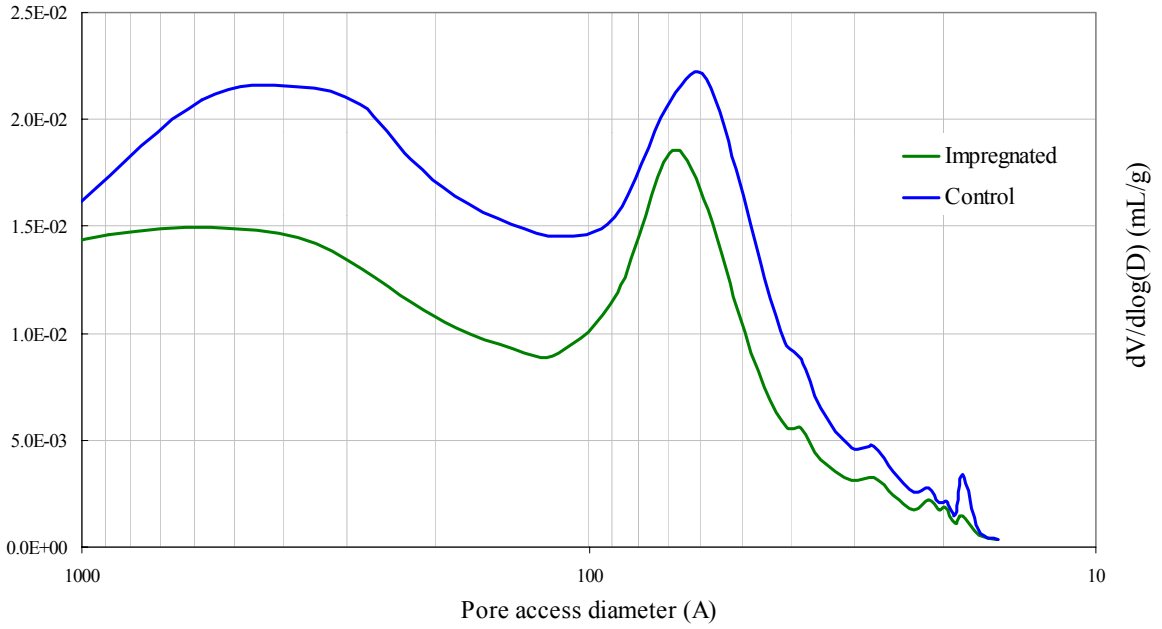

Figure 7. Nanopore size distribution of samples oven-dried at 50ºC.

The results given by N_2 adsorption tests are shown in Figure 6. Both samples oven-dried at 50ºC, pressed at 20 and 40 MPa, displayed similar adsorption-desorption isotherms. In comparison with the classical adsorption-desorption isotherms [10], the PRC paste isotherm is close to type H3, which is characteristic of mesoporous materials with a conical pore shape. With respect to pore size

distribution, TEOS 40 impregnated samples showed a lower nanopore volume than the control samples, as depicted in Figure 7.

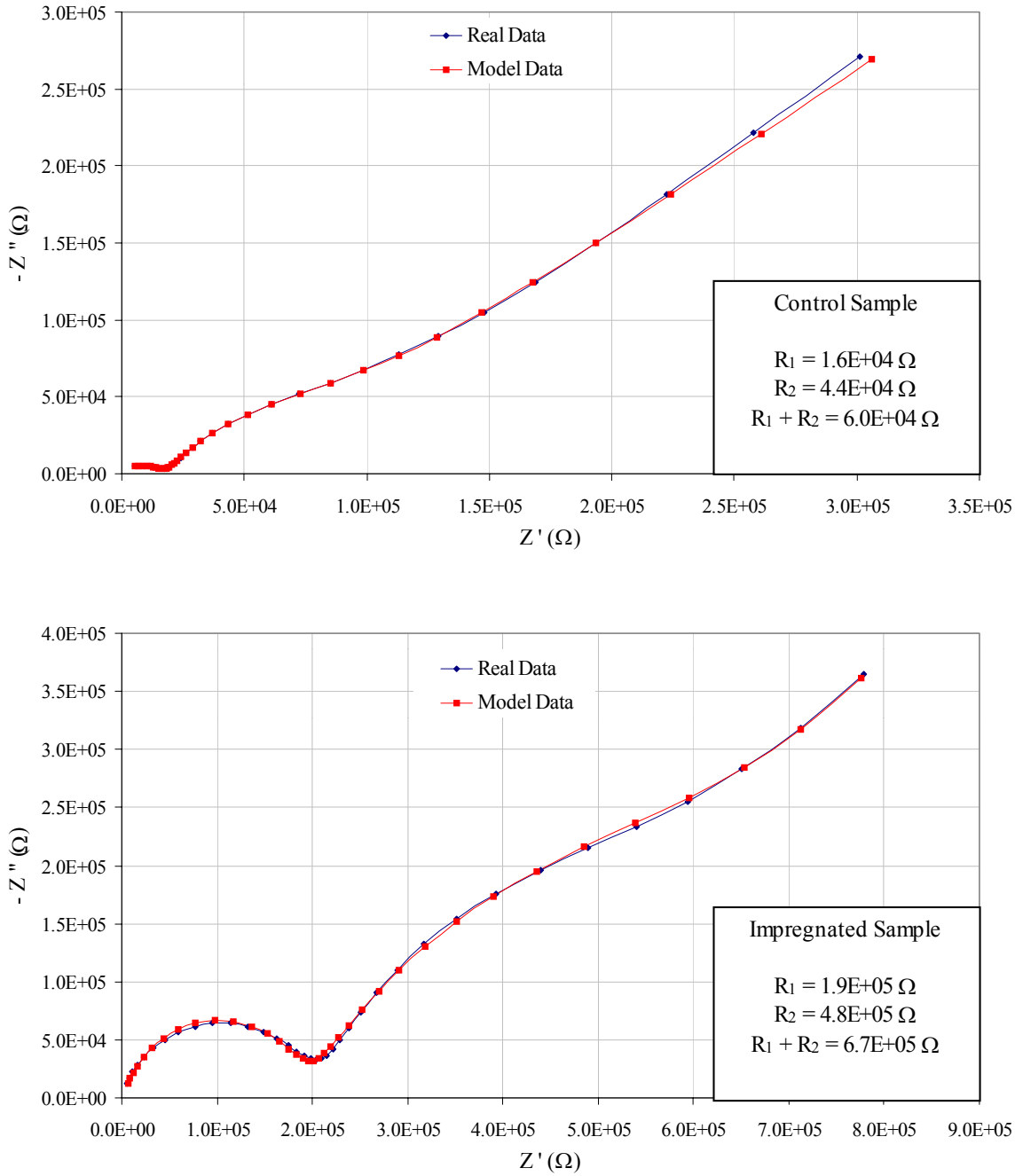

Figure 8. Nyquist plots for samples oven-dried at 50ºC.

According to the equivalent electrical circuit model proposed earlier, we proceeded to perform IS measurements to verify the effectiveness of TEOS impregnation. Figure 8 shows typical Nyquist plots for PRC paste. There is a good agreement between the samples data measured and the simulated model results. The spectras exhibit two high-frequency arcs contributed by BP and HP, with R_1 and R_2 resistances respectively, and a "tail" or low-frequency arc corresponding to the effect of cement-electrode interfacial capacitance.

The electric properties can be obtained by a simple calculation (see inserts in the Figure 8), demonstrating that electrical resistance increases with TEOS 40 impregnation. It can be concluded that electrical conductivity dropped sharply, indicating that pore interconnectivity was reduced.

Figure 9 shows the differences between the surface layers of the control and TEOS 40 impregnated samples, revealing a strong reduction in large pores.

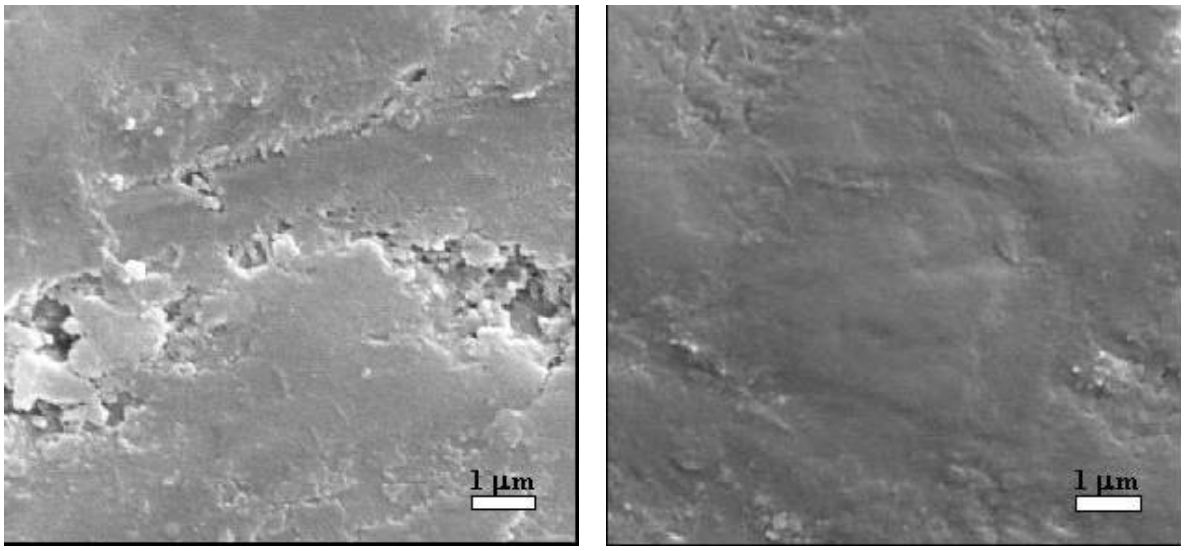

Figure 9. Surface layer of control (left) and TEOS 40 impregnated (right) samples.

Thus, we can foresee the application of TEOS-impregnated cement-based materials for buildings, dams, bridges and industrial storage facilities, by the advantageous durability feature. Furthermore, the rather high compressive strength achieved can lead to a structure lightening, what results in cost savings.

5. CONCLUSIONS

Impregnation by TEOS was shown to reduce the porosity and improve the mechanical properties of hardened PRC pastes, indicating that this procedure can be used to increase their durability and to lighten the structure. It was also found that oven drying at 50ºC is an effective method to prepare samples for TEOS impregnation. The application of TEOS through the surface layer of cured cementitious materials can result in an almost completely sealed surface layer, providing them with greater protection. The previous partial hydrolysis of TEOS (TEOS 40) with a higher silica concentration is more efficient than the monomeric molecule (TEOS 28).

ACKNOWLEDGEMENTS

The authors gratefully acknowledge the financial support of FAPESP. Our special thanks go to Dr. Jean-Claude M'Peko for his assistance in the use of the IS technique. We also thank the Brazilian company Hergrand Ltd. and Datiquim Ltd. for providing the TEOS for this study.

REFERENCES

[1] Pedersen, J., Macphee, D.E. and Chandler, H.W. Cold isostatic pressing of cement pastes to produce pore-reduced cement (PRC), J. Europ. Cer. Soc., vol.18, 1998, pp. 2089-93.
[2] Brinker, C.J., Scherer, G.W. Sol-gel processing: the physics and chemistry of sol-gel processing, San Diego: Academic Press, Inc., 1990.
[3] Iler, R.K. The chemistry of silica, New York: Jon Wiley & Sons, Inc., 1978.
[4] Moukwa, M., Aïtcin, P.-C.The effect of drying on cement pastes pore structure as determined by mercury porosimetry, Cem. Concr. Res., vol. 18, 1988, pp. 745-52.

[5] Gallé, C. Effect of drying on cement-based materials pore structure as identified by mercury intrusion porosimetry – a comparative study between oven-, vacuum-, and freeze-drying, Cem. Concr. Res., vol. 31, 2001, pp. 1467-77.
[6] Olson, R.A., Neubauer, C.M. and Jennings, H.M. Damage to the pore structure of hardened Portland cement paste by mercury intrusion, J. Am. Cer. Soc., vol. 80, 1997, pp. 2454-458.
[7] Diamond, S. Mercury porosimetry – an inappropriate method for the measurement of pore size distributions in cement-based materials, Cem. Concr. Res., vol. 30, 2000, pp. 1517-25.
[8] Christensen, B.J., Coverdale, R.T., Olson, R.A., Ford, S.J., Garboczi, E.J., Jennings, H.M. and Mason, T.O. Impedance spectroscopy of hydrating cement-based materials: measurement, interpretation and application, J. Am. Cer. Soc., vol. 77, 1994, pp. 2789-804.
[9] Macphee, D.E., Sinclair, D.C. and Stubbs, S.L. Electrical characterization of pore reduced cement by impedance spectroscopy, J. Mater. Sci. Lett., vol. 15, 1996, pp. 1566-68.
[10] Webb, P. Analytical methods in fine particle technology, Norcross, Micromeritics Instrument Corp., 1997.

REDUCTION OF PORTLAND CEMENT PASTE POROSITY BY TEOS IMPREGNATION

Hebert L. Rossetto and Milton F. de Souza

CEPOF, Laboratory of Materials Science, São Carlos Institute of Physics, University of São Paulo, São Carlos, SP, Brazil. E-mail: hebert@if.sc.usp.br

H.L. Rossetto

Hebert Luis Rossetto, post-graduate student of materials science and engineering, is a civil engineer graduated from EESC-USP. His major research interests are cement and related materials for civil engineering.

Milton Ferreira de Souza, Professor of Physics, Visiting Scientist of CEPOF, Institute of Physics of São Carlos – University of São Paulo. His major research interest lies in Materials Science.

ZEOLITE CEMENT BLEND FOR TRAPPING RADIOACTIVE WASTE

Gaëlle Nicolas[1], Nicolas Lequeux[1], Stéphanie Prene[2] and Philippe Boch[1]

[1]Gaëlle Nicolas, Laboratoire de Céramiques et Matériaux Minéraux - ESPCI 10 rue Vauquelin 75005 Paris, France, gaelle.nicolas@espci.fr
[1]Nicolas Lequeux, Laboratoire de Céramiques et Matériaux Minéraux - ESPCI 10 rue Vauquelin 75005 Paris, France, nicolas.lequeux@espci.fr
[2]Stéphanie Prene, Centre des Renardières – EDF 77250 MORET SUR LOING France, stephanie.prene@edf.fr
[1]Philippe Boch, Laboratoire de Céramiques et Matériaux Minéraux - ESPCI 10 rue Vauquelin 75005 Paris, France, philippe.boch@espci.fr

ABSTRACT

Concerning the management of long life radioactive waste, two options are available: storage in surface sites in sealed containers or burying in deep deposits. In both cases, cementitious materials are used as mechanical barriers. The present study was devoted to another aspect: the use of cementitious materials to immobilize pollutants (" chemical barriers "). ^{135}Cs constitutes the predominant nuisance of long-life fission products.

Water is the main cause of pollutant dissemination but the mobility of a polluted solution or suspension can be strongly reduced in cementitious environments. Two mechanisms are possible:

1. Reaction between the polluted water and an anhydrous cement to form a trapping phase;
2. Reaction between the polluted water and a reactive aggregate enclosed in cement, which constitutes the trapping phase.

For caesium trapping, we choose the second mechanism with zeolite as reactive aggregate.

1. MATERIALS

The large size of Cs^+ (1.65 Å) makes its insertion within crystallized minerals difficult. We have shown ([1], [2]) that ceramized cementitious compositions can immobilize caesium within pollucite. Moreover, caesium can be accommodated within zeolites, in particular in large-pore mordenite, clinoptilolite, chabazite, and zeolite P [3]. The present study was conducted using cheap and easy-supply natural chabazite ($Ca_6(Al_{12}Si_{24}O_{72}).40H_2O$), from Bowie (Arizona) [4], in a 6 µm size. We used three cements: an aluminous cement (*SECAR 71*), an ordinary Portland cement (CPA CEM I 52.5), and a white Portland cement (CPA CEM I - 55). The cement/zeolite ratio was 1.5. The water/solid ratio was 0.6. The cure temperature was 50°C. Various cure times were investigated, at the end of which the solids were ground, dried, and rinsed with acetone, then ether.

2. CHARACTERIZATION

Materials were characterised by XRD and MAS-NMR (^{27}Al or ^{29}Si). Caesium retention was studied by static retention batches. The Cs content in liquid was measured by atomic absorption and the Cs content in solid phase by PIXE (Particle Induced X-ray Emission).

3. RESULTS AND DISCUSSION

3.1 Caesium retention

Caesium retention tests were carried out on ground material (grain size < 200µm), by measuring the mass of caesium immobilized per gram of material. The results are in agreement with Langmuir's adsorption ($M_{Cs} = M_0 + A.\exp[-x/t]$). The fit of experimental data gives M_0, A, and t, M_0 corresponding to saturation. Results (table I) show that the caesium retention is high in mixes of aluminous or portland cement and zeolite. Several studies ([5], [6], [7]) have proved that caesium is poorly trapped by cement materials. Therefore, caesium retention must be due to the chabazite encapsulated in the blend.

Table 1. Cs retention(mg per gram of mortar) – Function of curing time

Curing time (days)	Portland cement	Aluminous cement
7	95 ± 7	81 ± 6
36	97 ± 6	82 ± 10
74	aberrant	80 ± 7
116	92 ± 10	94 ± 12
408	88 ± 11	120 ± 13
500	86 ± 6	aberrant

3.2 Zeolite-cement reaction

The problem with a zeolite aggregate is its reactivity with cement, but things are improved when using materials with a high zeolite/cement ratio and an adapted composition. One must point out that the pozzolanic reaction can degrade zeolites in cementitious materials [8]; they can also be formed as long-term phases in certain cements [9]. In materials made with aluminous cement, XRD can be used to follow the reaction between zeolite and cement, thanks to the development of crystallized stratlingite C_2ASH_8 (figure 1). Experiments of ^{29}Si NMR confirm that zeolite is still present after 408 days (figure 2).

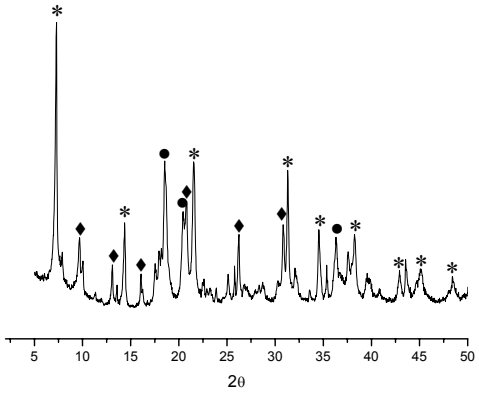

Figure 1. XRD Aluminous cement + zeolite - Cure time = 50 days.
* stratlingite, ● gibbsite, ♦ chabazite

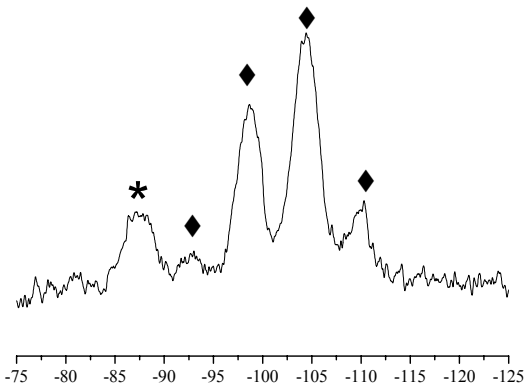

Figure 2. ^{29}Si NMR Aluminous cement + zeolite - Cure time = 408 days.
* stratlingite, ♦ chabazite

In materials made with Portland cements, the reaction product is poorly crystallized C-S-H, which can be characterized by ^{27}Al and ^{29}Si MAS-NMR. Figures 3 and 4 show that the residual content of chabazite is high.

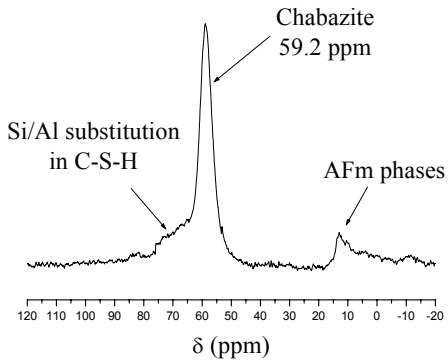

Figure 3. ^{27}Al MAS-NMR - White cement + chabazite.
Cure time = 50 days.

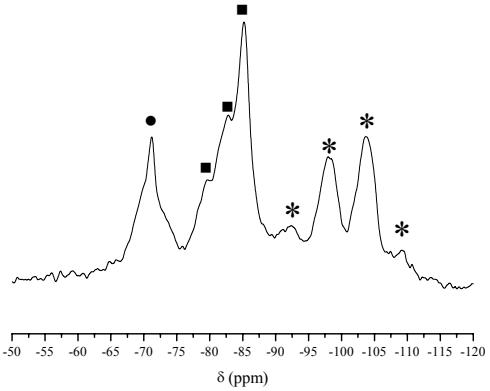

Figure 4. ^{29}Si MAS-NMR - Portland cement + chabazite.
Cure time = 116 days.
* chabazite, ● anhydrous cement, ■ C-S-H

On the time scale of our study, Cs retention measurements, XRD and MAS NMR proved that zeolite is still in the aged blend. But materials used to trap radioactive waste have to be stable for at least one thousand years. Based on the work done by Damidot and Glasser [10], we have built the 4-D CaO-SiO_2-Al_2O_3-H_2O diagram.

Starting with cement phases and zeolite, thermodynamic calculations were conducted to find stable phase assemblages of the system. Ten phases were chosen:

- Simple phases containing only Ca, Al or Si : portlandite CH, an amorphous silica gel SH, gibbsite AH_3.
- Phases containing Si and Ca or Ca and Al : CSH with two different C/S ratios CSH(I) with C/S= 1.8 and CSH(II) with C/S = 1.1, hydrogarnet C_3H_6 (no stable phase is know with Al and Si only).
- Phases containing Ca, Al and Si : $C_3AS_xH_{6-2x}$ with x=0.3 et 0.8 representing a solid solution between C_3AH_6 and C_3AS_3 (grossular), a zeolitic phase : a calcic Clinoptilolite $Ca_{0.56}Si_{4.88}Al_{1.12}O_{13}.12H_2O$.

The thermodynamic data come from Damidot and Glasser [10] for cement phases and from Bennings and al. [11] for zeolitic phases. To find stable assemblages, a thermodynamical and geochemical software –CHESS– is used.

An invariant point of the diagram is a point with an equilibrium between three solids and an aqueous phase. With ten starting solids, 120 points are possible. With CHESS, the equilibrium at each point can be calculated. If three starting solids are equal to the finishing ones, the point is considered to be an invariant. Finally, twelve invariant points were found (Table 2).

Table 2. Invariant points of the zeolite – cement system

Solid 1	Solid 2	Solid 3
CH	C_3AH_6	$C_3AS_{0.3}H_{10.8}$
CH	CSH(II)	$C_3AS_{0.3}H_{10.8}$
C_2ASH_8	$C_3AS_{0.3}H_{10.8}$	$C_3AS_{0.8}H_{9.6}$
C_2ASH_8	$C_3AS_{0.3}H_{10.8}$	AH_3
C_2ASH_8	$C_3AS_{0.8}H_{9.6}$	CSH(I)
C_2ASH_8	AH_3	Clinoptilolite
C_2ASH_8	CSH(I)	Clinoptilolite
C_3AH	$C_3AS_{0.3}H_{10.8}$	AH3
$C_3AS_{0.3}H_{10.8}$	$C_3AS_{0.8}H_{9.6}$	CSH(I)
$C_3AS_{0.3}H_{10.8}$	CSH(I)	CSH(II)
AH3	SH	Clinoptilolite
SH	CSH(I)	Clinoptilolite

These calculations confirm that the zeolitic phase can coexist with the cement. The representation of the stable phase diagram is shown in figure 5.

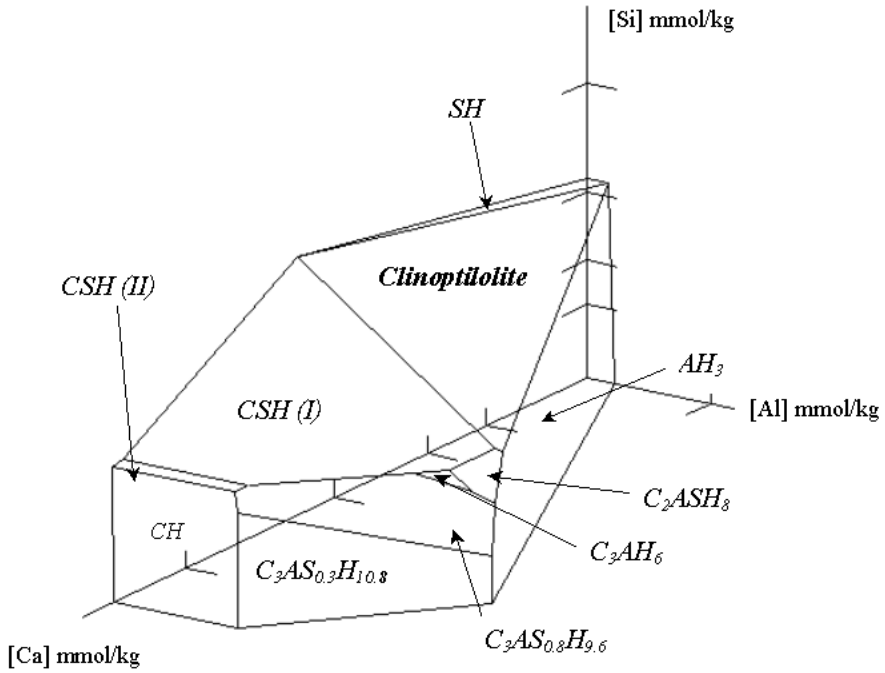

Figure 5. $CaO\text{-}SiO_2\text{-}Al_2O_3\text{-}H_2O$ phase diagram containing both cement phases and zeolite

4. CONCLUSIONS

Hazardous elements can be immobilized in cement hydrates, in ceramized cementitious materials, or in reactive aggregate. The present paper has shown that :

- Chabazite-cement blends offer potential as reactive aggregates to immobilize caesium ;
- In spite of the pozzolanic reaction, zeolite can be thermodynamically stable in a cement system.

REFERENCES

[1] P. Boch, M. Seiss, G. Vetter and M. Jacquin, *High-alumina cements for caesium trapping*, Cement and concrete research, 22, 369-374, 1992.

[2] H. Fryda, G. Vetter, R. Ollitrault-Fichet, P. Boch and A. Capmas, *Formation of chabazite in mixes of calcium aluminate cement and silica fume used for caesium immobilization*, Advances in cement research, 8, [29], 29-39, 1996.

[3] M. Atkins and F. P. Glasser, *Application of Portland cement-based materials to radioactive waste immobilization*, Waste Management, 12, 105-131, 1992.

[4] K. D. Mondale, F. A. Mumpton and F. F. Aplan, *Beneficiation of natural zeolites from Bowie, Arizona : a preliminary report*, Natural Zeolites : Occurence, Properties, Use, Pergamon Press, 527-537, 1978.

[5] S. Komarmeni and D. M. Roy, *Mechanisms of immobilization of nuclear waste elements by cement minerals*, Cement and Concrete Research, 11, 789-794, 1981.

[6] R. W. Crawford, F. P. Glasser, A. A. Rahman and M. J. Angus, *Diffusion mechanisms and factors affecting leaching of caesium-134 from cement based waste matrices*, Radioactive Waste Management and the Nuclear Fuel Cycle, 6, [2], 177-196, 1985.

[7] J. M. Lameille, G. Goutière, J.-C. Petit and M. Regourd, *Retention of cobalt, caesium and strontium in the hydrates of C3S, C3A and gypsum*, Journal of the American Ceramic Society, 70, [8], 604-614, 1987.

[8] H. F. W. Taylor, *Cement chemistry*, Academic Press, London, 1990, Academic Press.

[9] D. M. Roy, *Alkali-activated cements - Opportunities and challenge*, Cement and concrete research, 29, 249-254, 1999.

[10] D. Damidot and F. P. Glasser, *Investigation of the CaO-Al_2O_3-SiO_2-H_2O system at 25°C by thermodynamic calculations*, Cement and Concrete Research, 25, [1], 22-28, 1995.

[11] L. G. Bennings, R. T. Wilkin and H. L. Barnes, *Solubility and stabilty of zeolites in aqueous solution : II. Calcic clinoptilolite and mordenite*, American Mineralogist, 85, 495-508, 2000.

ZEOLITE CEMENT BLEND FOR TRAPPING RADIOACTIVE WASTE

Gaëlle Nicolas[1], Nicolas Lequeux[1], Stéphanie Prene[2] and Philippe Boch[1]

[1]Gaëlle NICOLAS, Laboratoire de Céramiques et Matériaux Minéraux - ESPCI 10 rue Vauquelin 75005 PARIS France, gaelle.nicolas@espci.fr
[1]Nicolas LEQUEUX, Laboratoire de Céramiques et Matériaux Minéraux - ESPCI 10 rue Vauquelin 75005 PARIS France, nicolas.lequeux@espci.fr
[2]Stéphanie PRENE, Centre des Renardières – EDF 77250 MORET SUR LOING France, stephanie.prene@edf.fr
[1]Philippe BOCH, Laboratoire de Céramiques et Matériaux Minéraux - ESPCI 10 rue Vauquelin 75005 PARIS France, philippe.boch@espci.fr

Nicolas Lequeux

Nicolas Lequeux is an Associate Professor in the *Laboratoire de Céramiques et Matériaux Minéraux* at the *Ecole Supérieure de Physique et Chimie Industrielles de la Ville de Paris* in France. Before coming to Paris, he received his Ph.D. in Physic Science from the *Université de Paris-Sud* in 1990. His research interests include the sintering of ceramics (in particular the low-shrinkage sintering, the microwave sintering and the sintering of calcium aluminate cements), and the structure of cement hydrates using spectroscopic methods as NMR and X-ray Absorption. His recent work is concerned with the speciation of pollutants in cement phases, the description of the nanostructure of CSH gels and the development of nanostructured organic-inorganic hybrid cementitious materials. He has published about 20 papers in the field of cement science.

A NEW APPROACH FOR THE ORGANIC-INORGANIC C-S-H

J. Minet, N. Lequeux and P. Boch

ESPCI, Laboratoire Céramiques et Matériaux Minéraux, 10 rue Vauquelin 75231 Paris, France.
E-mail: nicolas.lequeux@espci.fr

ABSTRACT

In order to synthesize organic layered calcium silicate hydrates (C-S-H), an alternative approach to the intercalation has been used. This approach allows covalent graft of organics on the dreierketten silicium-sheets of C-S-H, to create a true hybrid C-S-H.

This work presents a synthesis of an aminopropyl-hybrid C-S-H and its characterisation by X-ray diffraction and nuclear magnetic resonance. Although high aminopropyl contents have been investigated, the samples did not present evidence of demixion. It was possible to suggest structural models for these hybrids.

1. INTRODUCTION

Organic additives are commonly used to modify concrete properties, as for example fluidity, ease of placement, hardness, etc. Water-soluble polymers are designed to interact with the surface of hydrated Portland cement particles, and particularly with its major component: the calcium silicate hydrates (C-S-H). It has been proved, however, that the interactions between the polymers and the C-S-H are not the same as those found in clays [1, 2, 3]. More precisely, the intercalation onto the inner interlayer surface of the C-S-H is not clear, and may vary strongly with the nature of the polymer and the way the C-S-H is formed [4, 5].

One consequence is that we cannot ascertain that the adjunction of water-soluble polymer is a sure way to create an organic layered C-S-H, able to modify the whole material properties (since the macroscopic properties of a material are intimately linked to its structure).

An alternative to create a stable layered organic-inorganic C-S-H is to covalently graft organics on the dreierketten Si-sheets as shown in figure 1, to make a true hybrid C-S-H (h-C-S-H).

Proceedings of the 11th International Congress on the Chemistry of Cement (ICCC)
'Cement's Contribution to the Development in the 21st Century'
Hosted by: The Cement and Concrete Institute of South Africa
CD-ROM produced by: Document Transformation Technologies
11 - 16 May 2003, Durban, South Africa
ISBN Number: 0-9584085-8-0
Editors: Dr G. Grieve and G. Owens
Congress Organised by: Event Dynamics

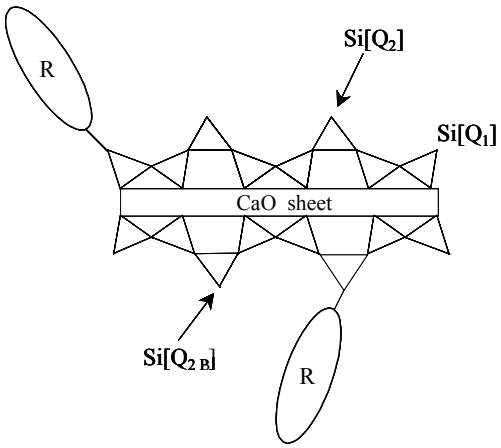

Figure 1. layer of hybrid C-S-H, with $Si[Q_n] = Si(OSi)_n$

This approach has already been used to create various hybrid materials [6, 7, 8, 9], including organoclays [10, 11], and has led to various applications in ion exchange, catalysis, photonics, and coatings [12, 13].

Recently, Suzuki and Sinn synthesized a well-defined C-S-H with a Ca/Si ratio of 5/6 using sol-gel route [14]. This room-temperature three-step synthesis consists in: (a) hydrolysis of tetraethyl orthosilicate (TEOS) in solution, (b) addition of an aqueous solution of $CaCl_2$, and (c) precipitation of C-S-H by addition of NaOH.

Using this method, the creation of h-C-S-H is possible by addition of trialkoxyorganosilane ($RSi(OR')_3$) in solution with TEOS during the first stage, which leads to the co-condensation of silicon alkoxides and the precipitation of h-C-S-H during the third stage.

This article reports the synthesis of hybrid C-S-H with various trialkoxyorganosilane/TEOS ratios, and their subsequent characterisation. The organic investigated (R) is the 3-aminopropyltriethoxysilane (ATES) $NH_2C_3H_6Si(OC_2H_5)_3$. The length of the aminopropyl radical is about 5 Å.

As the hybridation of C-S-H should result in some structural changes, X-ray diffraction was used to follow the modifications of the structural parameters, in particular to follow the expected increase in the c-axis spacing (d00*l*).
The local environment of silicon, i.e. the way the atoms are connected to each other, was investigated by nuclear magnetic resonance (NMR), with $Q_n = Si(OSi)_n$, and $T_m = CSi(OSi)_m$.

2. EXPERIMENTAL

2.1. Synthesis

All the h-C-S-H samples have a fixed Ca/Si ratio of 5/6 but the C/Si ratio is variable. For each synthesis, the starting materials were commercial grades.

TEOS and trialkoxyorganosilane were pre-hydrolysed in an ethanol-water mixture at pH=1 for 1h (with ethanol/water ratio = 2). An aqueous solution of $CaCl_2$ was added to give a Ca/Si ratio of 5/6 and a water/alcohol ratio = 24, to completely hydrolyse the alkoxysilanes. The solution was then stirred for 1h. Next, 6 ml of a 8,3 M NaOH solution were added dropwise and the solution was stirred and aged for 12h.

The precipitate was separated by centrifugation, redispersed and washed in deionized water and centrifuged again, twice. Finally, the samples were dried with LiCl under relative vacuum.

2.2. Characterisation

X-ray measurements were made with an Inel CPS 120 detector (resolution of 0,029°), with a germanium monochromator to select the Cu $K_{\alpha 1}$ radiation. Powder samples were placed in 0,5 mm quartz capillary tubes.

Solid state ^{29}Si magic angle spinning nuclear magnetic resonance (^{29}Si-MAS-NMR) experiments were carried out on a Brucker DMX-300 spectrometer, operating at the frequency of 59,63 MHz, with a sample spinning frequency of 4 kHz. Tetramethylsilane was used as a standard.

3. RESULTS AND ANALYSIS

A C-S-H with Ca/Si ratio of 5/6 was synthesized as a reference. X-ray diffraction (figure 2) shows that the material is well defined, with broad reflections consistent with the low Ca/Si ratio tobermorite-like ordered C-S-H [15]. The basal reflection is at 13 Å.

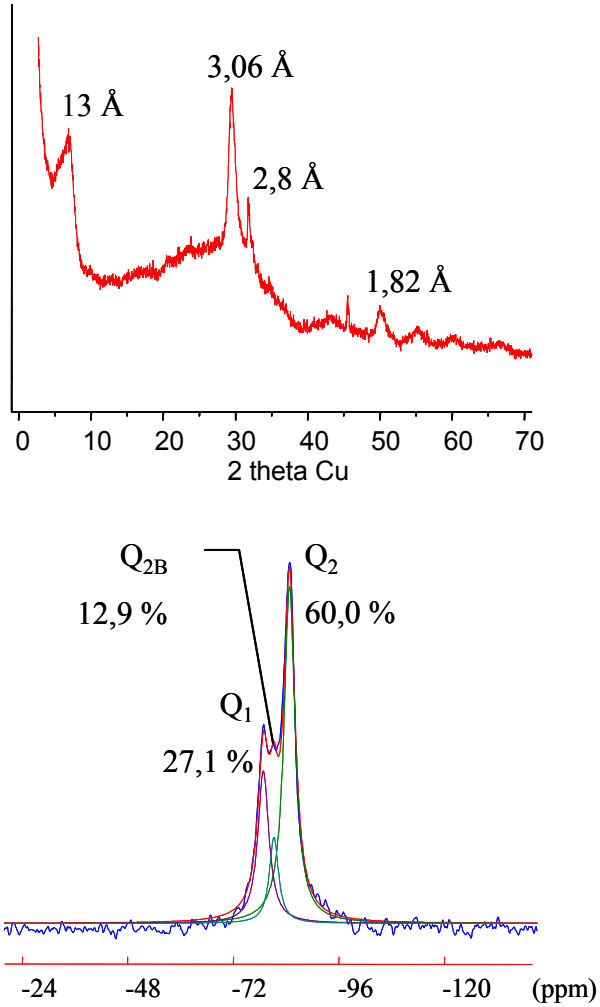

Figure 2. Top: X-ray diffraction, Bottom: ^{29}Si MAS-NMR of the reference C-S-H (Ca/Si= 5/6)

^{29}Si MAS-NMR of the reference (figure 2) presents three distinct environments for the silicon: Q_1 at –78,3 ppm, Q_2 at –84,2 ppm, and Q_{2B} at –80,7 ppm. The relative proportions of those environments are Si[Q_1]=27,1% (the terminal site), Si[Q_2]=60,0% (dimer site), and Si[Q_{2B}]=12,9% (bridging site), which is in good agreement with the dreierketten structure with 5/6 Ca/Si ratio C-S-H [16, 17], as shown in figure 1. The proportion between Q_1 and the (Q_2+Q_{2B}) sites indicates that the average chain length is relatively short (seven silicon atoms), which is similar to the length of the Si chain in pozzolanic synthesized C-S-H.

Two compositions are presented for each of the organics: 20% and 40%, plus a 100% 3-aminopropyltriethoxysilane reference.

The XRD patterns (figure 3) of the 20 % and 40% aminopropyl samples are consistent with the pattern of the C-S-H reference, but they present atypical basal spacings: 16,5 Å for the 20% and 20Å for the 40%. The 100% ATES XRD pattern is not consistent with the C-S-H reference, although it presents a broad basal spacing at 16,3 Å. It may be interpreted as an organoclay [10].

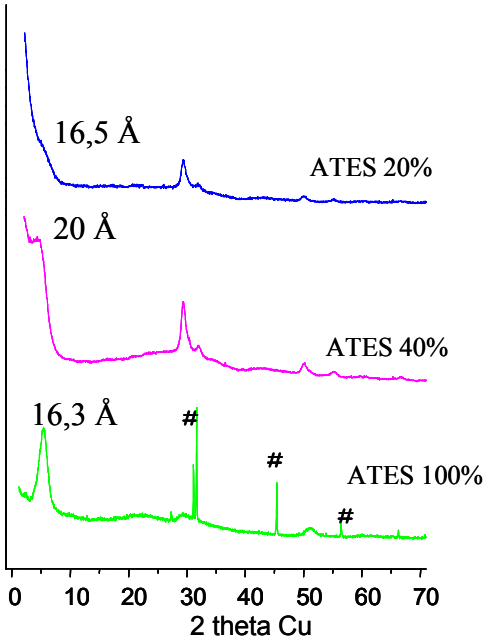

Figure 3. X-ray diffraction of ATES samples (with: # NaCl)

Thus, the observable effects on the structure of the presence of ATES of C-S-H are: no modifications in the [hk0] reflections (2θ>15°) and increase of the basal spacing [00*l*], function of the ATES content. As no disorder is created in the lamella structure of the C-S-H, and as the basal spacing increases, this demonstrates the hybridation of C-S-H.

^{29}Si-MAS-NMR experiments (figure 4) confirmed the XRD results. The characteristic sites Q_1 , Q_2 , and Q_{2B} are still observable (at the same chemical shift observed in the reference), as well as a site T_1 at –49,5 ppm, which is related to an C*Si*OSi environment.

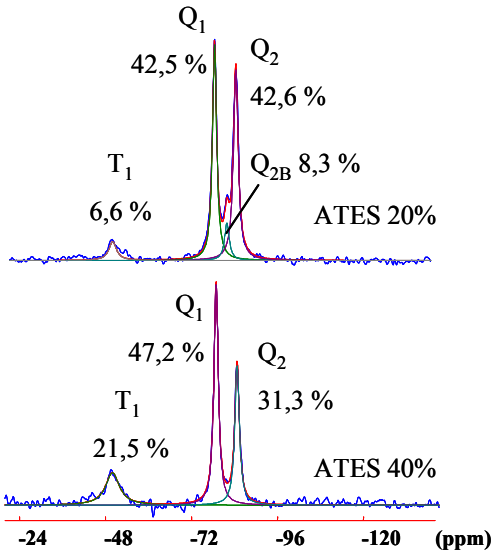

Figure 4. ^{29}Si-MAS-NMR experiments of ATES samples

The peak intensities change as the ATES content changes: an increase in the proportions of the Si[Q_1] and Si[T_1] sites are observable, as the proportions of Si[Q_2] and Si[Q_{2B}] sites decrease with the amount of ATES. Thus, the presence of ATES decreases the length of silicon chains. So an average chain in the 20% ATES sample is composed of four silicon atoms, whereas an average chain is reduced to three silicon atoms in the 40% ATES sample.

Without modifying the global structure of the C-S-H, the insertion of Si[T_1] in the dreierketten structure modifies the local environment, thus the silicium chain length decreases as the ATES content increases. This is consistent with the presence of the organic C*Si*OSi group at the single Si[T_1] site, i.e. at the end of the silicon chain, which confirms the hybridation of the C-S-H.

The evolution of the basal distances can be explained by using an h-C-S-H model: at low ATES contents, the interlayer between two neighbouring lamellae is not completely occupied by the aminopropyl radicals. Each radical can point out freely in the interlayer without steric restrictions due to facing radicals. The aminopropyl radicals are in a shifted configuration, and the basal distance increase is 3,5Å, compared to the reference. At higher ATES contents, the radicals are mainly in a face-to-face configuration, so the basal distance increase is doubled to 7Å (figure 5).

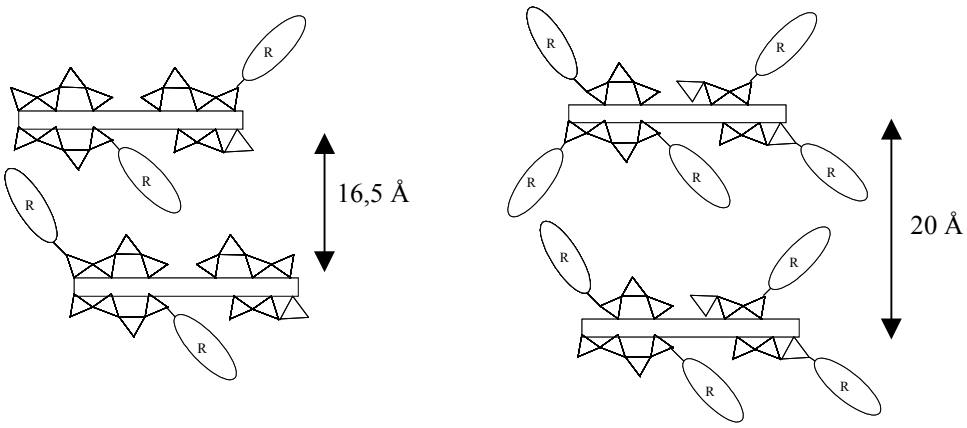

Figure 5. h-C-S-H models, left: radical shifted configuration for low ATES contents; right: radical face-to-face configuration for high ATES contents

4. CONCLUSIONS

Hybrid calcium silicate hydrates were synthesized by co-condensation of 3-aminopropyltriethoxysilane (ATES) and tetraethyl orthosilicate (TEOS) by a sol-gel route. The materials obtained were layered organic-inorganic C-S-H, even for the high ATES content (40%), and did not present evidence of demixing. We proposed structural models consistent with the changes in basal distance: a radical shifted model for low ATES contents, and a radical face-to-face model for high ATES contents.

This simple processing route offers opportunities to explore the influence of nature, length, and quantity of radicals introduced in the nanostructure of C-S-H.

ACKNOWLEDGMENTS

The authors wish to thank B. Besson and F. Babonneau for assistance and discussions on the NMR experiments.

REFERENCES

[1] P. LeBaron, Z. Wang, T. Pinnavaia. Polymer-layered silicate nanocomposites: an overview, Applied Clays Science, vol.15, 1999, pp.11-29.
[2] A. Okada, A. Usuki. The chemistry of polymer-clays hybrids, Materials Science and Engineering, vol.C3, 1995, pp.109-115.
[3] K. Carraro, L. Xu, R. Csencsits. Use of organo- and alkoxysilanes in the synthesis of grafted and pristine clays, Chem. Materials, vol.13, 2001, pp.3766-3773.
[4] A. Popova, G. Geoffroy. Interactions between polymeric dispersants and calcium silicate hydrates, J. Am. Ceram. Soc., vol.83, 2000, pp.2556-60.
[5] H. Matsuyama, J. Young. Intercalation of polymers in C-S-H: a new synthetic approach to biocomosites ?, Chem. Materials, vol.11, 1999, pp.16-19.
[6] C. Sanchez, B. Lebeau. Design and properties of hybrid organic-inorganic nanocomposites for photonics, MRS Bulletin, vol.may, 2001, pp.377-85.
[7] K. Shea, D. Loy. Bridged polysilsesquioxanes: molecular engineering of hybrid organic-inorganic materials, MRS Bulletin, vol.may, 2001, pp.368-75.
[8] Y. Chujo, R. Tamaki. New preparation methods for organic-inorganic polymer hybrids, MRS Bulletin, vol.may, 2001, pp.389-92.
[9] D. Loy. Hybrid organic-inorganic materials, MRS Bulletin, vol.may, 2001, pp.364-65.
[10] S. Burkett, A. Press, S. Mann. Synthesis, characterisation, and reactivity of layered organic-inorganic nanocomposites based on 2:1 trioctahedral phyllosilicates Chem. Materials, vol.9, 1997, pp.1071-1073.
[11] S. Mann, S. Burkett, S. Davis. Sol-gel synthesis of organized matter, Chem. Materials, vol.9, 1997, pp.2300-2310.
[12] R. Vaia, E. Giannelis. Polymer nanocomposites: status and opportunities, MRS Bulletin, vol.may, 2001, pp.394-401.
[13] B. Arkles. Commercial applications of sol-gel-derived hybrid materials, MRS Bulletin, vol.may, 2001, pp.402-07.
[14] S. Suzuki, E. Sinn. 1,4 nm tobermorite-like calcium silicate hydrate prepared at room temperature from $Si(OH)_4$ and $CaCl_2$ solutions, J. Mat. Science Letters, vol. 12, 1993, pp.542-544.
[15] H. Taylor. Cement chemistry, Academic Press, London, U.K., 1990.
[16] I. Klur. Etude par RMN de la structure des silicates de calcium hydratés, PhD thesis Université de Paris VI, Paris, France, 1996.
[17] M. Grutzeck, A. Benesi, B. Fanning. Silicon-29 magic angle spinning nuclear magnetic resonance study of calcium silicate hydrate, J. Am. Ceram. Soc., vol.72, 1989, pp.665-668.

ESTABLISHING THE CAUSE AND SOLVING THE PROBLEM OF POPPING OF PLASTER MADE WITH A CEM II/A-L 32.5

N. Govender[1], R.E. Oberholster[2], D.S. Scott[3] and M.J. Kearns[4]

[1]PPC Group Process Engineering Services, Johannesburg, South Africa.
E-mail: ngovender@ppc.co.za
[2]PPC Group Quality Services, Johannesburg, South Africa. E-mail: boberholster@ppc.co.za
[3]PPC Parktown, Johannesburg, South Africa. E-mail: dscott@ppc.co.za
[4]PPC Group Quality Services, Johannesburg, South Africa. E-mail: mkearns@ppc.co.za

ABSTRACT

During the period 1997 – 1999, "popping" of plaster made with CEM II/A-L from the PPC Slurry factory was experienced. Pops typically 20- to 40 mm in diameter, but occasionally as large as 90 mm, appeared approximately three months after plastering. The number varied from building to building and even on the same wall. The nodules apparently responsible for the popping were visible in the pop craters and were up to 5 mm in diameter.

Initial analysis showed that the core of the popped material consisted predominantly of CaO and $Ca(OH)_2$. It was therefore concluded that the popping was caused by the hydration of free lime. However, the origin of nodules with high free lime content was not immediately apparent. It was reasoned that it was unlikely to be from the cement, since large particles could not pass through the trommel screens after the finishing mills.

Reflected light microscopy conducted on polished and etched specimens of the nodules showed the presence of clinker minerals and free lime. It was thought that these could represent lumps of cement that formed in the bagged cement. However, careful microscopic analysis proved that the nodules were solid clinker particles and chemical analysis showed that the nodules had a high LSF value.

Further investigation revealed that a small percentage of large clinker nodules and limestone particles had found their way into the cement. A systematic investigation was therefore carried out to establish why the large particles were not screened out after the finishing mill and also the reason for the high LSF value. Process control measures were immediately instituted to remove large particles from the finished cement.

1. BACKGROUND

Towards the end of 1997 popping of internal and external plaster (where CEM II/A-L 32.5 sold under the trade name "Surebuild" was used) was reported from most of the 60 units of a luxury townhouse development. Sporadic reports of plaster popping followed early in 1998. Soon complaints were received almost daily and by the first quarter of 2002 the total number of claims received was greater than 240.

Popping occurred mainly in the Midlands of Kwazulu-Natal, the provinces of Gauteng, Northern Cape and Free State and in Namibia. All the incidences could be linked to Surebuild manufactured at the PPC Slurry factory during the period 1997 – 1998.

Proceedings of the 11th International Congress on the Chemistry of Cement (ICCC)
'Cement's Contribution to the Development in the 21st Century'
Hosted by: The Cement and Concrete Institute of South Africa
CD-ROM produced by: Document Transformation Technologies
11 - 16 May 2003, Durban, South Africa
ISBN Number: 0-9584085-8-0
Editors: Dr G. Grieve and G. Owens
Congress Organised by: Event Dynamics

2. MANIFESTATION

Popping was manifested by an almost circular piece of plaster, about 30 mm in diameter being pushed off leaving a cone-shaped crater (Figure 1 and 2). Either a black or yellowish orange nodule was usually found in the bottom centre of the crater. The nodules were up to 5 mm in diameter. In many cases they had disintegrated into an off-white powder. As many as 94 pops over an area of 4 m x 9 m were recorded.

Figure 1. Typical incidence of pops in plaster

Figure 2. Pop, 40-mm in diameter, with nodule of about 5-mm diameter in centre

3. NODULES

3.1 X-ray diffraction analysis

XRDA revealed that the nodules contained free lime, $Ca(OH)_2$ and clinker minerals.

3.2 XRFA

The analysis of the yellowish-orange nodules, the black nodules and clinker particles in the 212-micron residue of Slurry Surebuild is presented in Table 1. Both nodule types had a typical clinker composition but the yellowish-orange type had an unusually high SO_3 content of 1.7%.

3.3 Reflected light microscopy

Microscopy confirmed that the nodules consisted of Portland cement clinker. The yellowish-orange nodules appeared to be under-burnt while the black nodules showed fusion of C_3S (Figures 5) All the nodules contained a high amount of free lime (Figure 7). Clinker particles in the surrounding plaster matrix were relatively coarse, had a normal clinker structure and were different in appearance from the nodules. The differences between the clinker composition of the cement used for the plaster and the two types of nodules that caused the popping were as follows.

Table 1. Chemical composition of a the two types of nodules clinker particles in the +212-µm residue of Slurry Surebuild

Analyte	Result, % (m/m), loss free:		
	Yellow nodule	Black nodule	Clinker
SiO_2	20.0	23.3	23.3
Al_2O_3	3.9	3.1	3.1
Fe_2O_3	2.4	2.2	2.2
Mn_2O_3	0.4	0.2	0.2
TiO_2	0.3	0.2	0.2
CaO	64.3	69.0	69.0
MgO	2.4	1.9	1.9
SO_3	1.7	0.2	0.2
K_2O	0.8	0.8	0.8
Total	96.3	100.9	100.9

3.3.1 Plaster matrix surrounding pops (Figure 4)

a) Alite crystals predominated.
b) Alite crystal size varied from fairly large (40 µm) to medium (20 µm) to small (less than 10 µm).
c) Many alite crystals were fused (Figure 8).
d) Small belite crystals were deposited on the fringes of the alite crystals.
e) Very few regular alite crystals were observed.
f) The interstitial phase, consisting of C_3A and C_4AF, was clearly visible.
g) Very little free lime was observed

3.3.2 Soft, yellowish-orange nodules (Figure 3,5)

a) The microstructure was very different from the average clinker microstructure.
b) Regular alite and belite crystals did not form.
c) Free lime was visible in the microstructure.
d) The free lime hydrated very quickly on exposure to the atmosphere.

3.3.3 Black nodules (Figure 7 - the majority of nodules)

a) The nodules consisted mainly of alite crystals that varied in size from 20 µm to 60 µm, the majority being between 20 µm and 30 µm.
b) Many alite crystals were fused (Figure 8).
c) Very few to no belite crystals were observed.
d) The interstitial phase of C_3A and C_4AF was clearly visible throughout the nodules.
e) The free lime content was very high and occurred both in clusters and as individual particles.
f) It took about three weeks' exposure to the atmosphere to hydrate (etch) lime particles for identification by reflected light microscopy.

Figure 3. Polished specimen of yellowish nodule in plaster

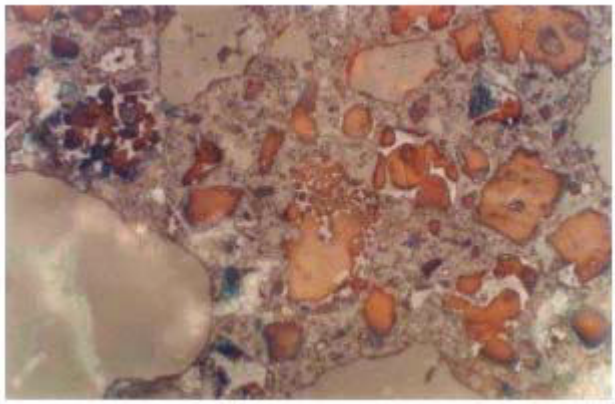

Figure 4. Brown alite crystals in plaster matrix

Figure 5. Under-burnt clinker of yellow nodule

Figure 6. Black nodule with gray plaster adhering to it

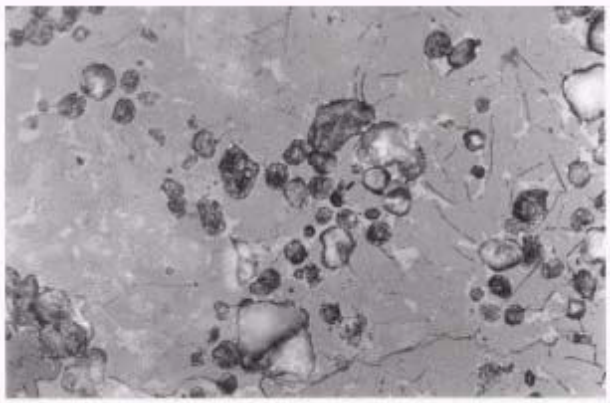

Figure 7. Multi-coloured free lime crystals in Black nodule

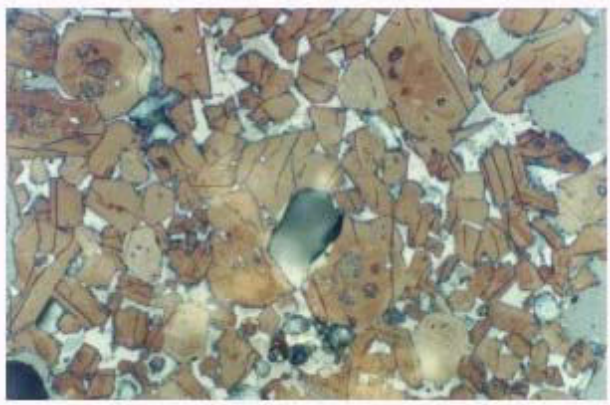

Figure 8. Brown, fused alite with some free lime in black nodule

4. CAUSE OF POPPING

The popping of the plaster was caused by large clinker particles (nodules) with a high free lime content. When the CaO reacted with moisture, expansion occurred locally according to the well-known reaction:

		CaO +	H_2O →	$Ca(OH)_2$
Molecular weight, g	:	56.08	18	74.08
Relative density	:	3.30	1.00	2.24
Molecular volume, cm^3	:	16.99	18	33.08

The rate at which the popping occurred after plastering depended, amongst other factors, on whether the nodules were hard-burnt. Free lime that results from the under-burning of clinker during upset kiln conditions is usually reactive enough to hydrate during cement grinding or storage. The hard-burnt CaO, which can result from inadequate proportioning or blending of the raw mix, is generally responsible for the delayed hydration and expansion encountered during normal service conditions. Even hard-burnt lime, when milled fine enough and present in a relatively small amount, will not cause problems in practice on hydration. However, when the free lime is concentrated in large nodules, hydration will result in expansion in its immediate vicinity and consequent popping.

4.1 Process Control Investigations

As a result of these problems an audit of cement mills' operation was carried out. During this audit it was noted that there were pebbles in large quantities discharging from the mills. It was also observed that there were significant numbers of pebbles discharging from the packer screen discharge pipes. The members of the audit team found that it was an unusual event and required investigation. The pebbles were grey or brown internally and samples from the packer screen were taken to test for breakability. Reference samples were taken from the mill clinker feed systems and tested.

The findings of the tests were:

- All the nodules were clinker pieces and there were no dolomite or chert pieces, contrary to expectations
- The free lime was very much higher in the nodules than the clinker samples.

- The particles were somewhat elongated and smoothed as a result of their passage through the mills. The width of the particles was commonly 3 to 7mm and the length between 5 and 10mm.
- Hence it was concluded that the particles were passing through the mill screens into the product.
- Microscopic examination showed little or no belite but plenty of alite.
- Under 6.5X magnification there was a huge difference in the appearance of the clinker particles and the packer samples. The clinker was normal grey crystalline while the packer nodules were reddish brown and the brown colour was often streaky.
- Particles were often seen to consist of brown and black layers.

Mill inspections were carried out and a clear indication of the nature of the problem was evident from these inspections when it was clearly observed that clinker particles persisted through the mill first chambers.

Figure 9. Clinker particles in mill

Figure 10. Clinker particles from mill

On breaking them it was found that they appeared to be hard-burnt nodules having brown cores. On attempting to break these in the mill it was also obvious that they required an exceptional effort to break.

Inspection of the hardness of burning on the rotary kilns as measured by the litre weights showed that short periods of hard burning were common and observation of the samples with high results showed that they were brown inside and were hard to break. It was now obvious that a part of the clinker being produced was too hard for the mill's grinding ability. The observations led us to believe that hardness of burning was connected with the problem in some way. It was also obvious that the mill charge levels and unit masses were not suitable under these conditions.

In order to effect the grinding of these hard particles, mill average ball masses were increased and screen cloth in all screens were changed to a smaller size. As a second measure the kiln mix design and control of burning were changed to eliminate hard burning. Finally the highest possible proportion of cement was ground on closed circuit mills.

The pebbles arising from the cement mills were weighed routinely and expressed as a percentage of mill output. The clinker particles were removed and "steamed" in an open pan. The expansive nodules (those that disintegrated) were measured as a percentage of all the clinker nodules. This was used to calculate the potential pops per 10 m^2 of plaster. The graph below shows how effective the corrective action was on the cement mills.

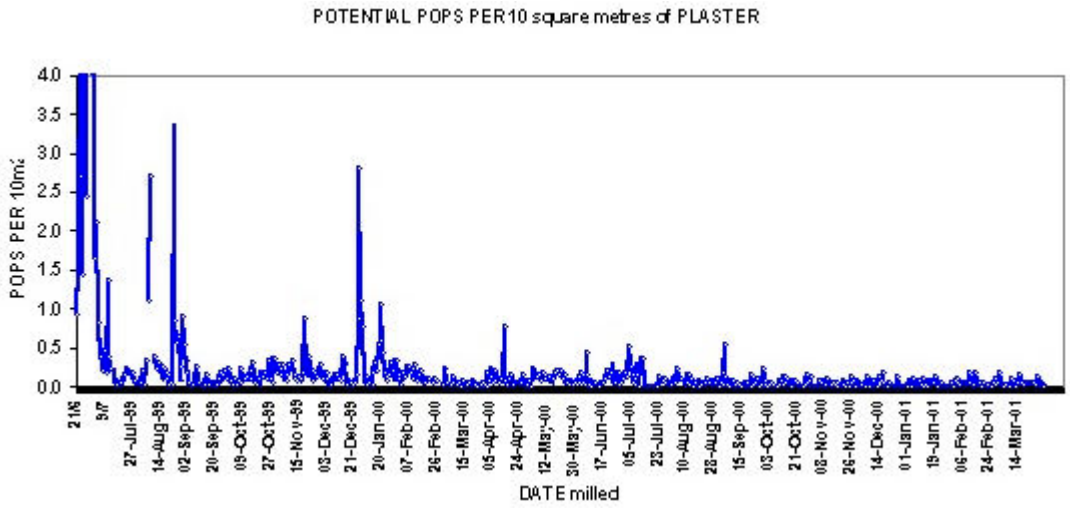

4.2 Investigations to Find the Source of the Expansive Nodules.
A number of investigations were undertaken to locate the source of these particles. These are briefly explained below.

4.2.1 Hard burnt particles
The particles found in the mills were very hard and it was first thought that they were caused by overburning. As a result a sampling program was carried out to isolate "Hard Burnt High Free CaO" particles. After some months of sampling some nodules were found on one kiln, but none were found on a larger kiln. The frequency and quantity just did not explain the severity of the problem in the cement. Also the presence of free lime just did not make sense with hard burning.

4.2.2 Testing of individual particles
A special Micro-XRF method was developed to individually analyse the particles discharging from the mills (particle masses were around 0,2 grams). This enabled a small sample to be used to categorise the particles into classes. These categories can be termed "High Free Lime High Lime" and " High Free Lime High Sulphur". This is given below in Table 2. A features which should be noted is the high free lime especially in the high lime family.

It could now be seen that these particles were of quite unusual composition and certainly unlike any normal clinker. Since the composition was similar to kiln dust, it was postulated that the origin could be as a result of kiln ring material originating in the alkali sulphate circulation phenomenon in rotary kilns.

Table 2. Chemistry of two families of particle: "High Free lime High Lime" and "High Free Lime High Sulphur"

	HFL HL	HFLHS
SiO_2	15	21
Al_2O_3	3	4
Fe_2O_3	2	2
CaO	75	65
SO_3	0	2
K_2O	0	1
TOTAL	98	98
FCaO	28	13
LSF	1.6	1.0
SR	2.7	30
AM	1.4	2.1
CaO/SiO_2	4.9	3.1

4.2.3 Sampling of Ring Material Discharging from Rotary Kilns
Rotary kilns suffer instability due to the collapse of ring material which releases large volumes of kiln charge material which has built up behind the ring towards the feed end of the kiln and very close to the burning zone. These rings are due to the deposition of material entrained in the kiln gas stream.

The sampling of the ring material gave results very similar to the material of the individual particles analysed by the micro-XRF method. It was quite obvious that this was the culprit material and was assumed that it was from rings.

4.2.4 Sampling of in situ Rotary Kiln Rings
It was decided to confirm the findings by sampling in situ rings during kiln reline stops. These confirmed the findings. In fact it became clear that the rings nearest the burning zone were the source of the hard particles. These rings are hard and consist of layered brownish and black material. This layering had been observed in individual particles when subject to microscopic observation.

5. CONCLUSION

The hard particles were derived from the hard material in the rings, which form near the burning zone coating (but behind - the feed side). These would collapse at irregular intervals, particularly in large diameter kilns and would find their way into normal production clinker as small slabs and chunks. On entering the cement mills, this material would not be ground without special precautions described earlier.

We could now theorise that the material, which became entrapped in the kiln gas-stream consisted of volatile matter and the finer particles in the raw meal. Due to the poor homogeneity of the raw meal with respect to particle size of silica and calcite particles, the calcite would be preferentially entrained, resulting in material which is high in alkalis, sulfate and lime(CaO). Combination of the CaO could therefore not take place, resulting in very high free lime particles.

The hardness can be explained by the fact that the material had been exposed to near flame conditions and on deposition created these hard plate-like rings in the kiln.

Although it took time to identify the source of this material, the corrective action taken early at the cement milling stage completely cured the problem. Corrective action at the burning stage may be possible, but has not been attempted, as it would be complicated if not impossible.

ALKALI ACTIVATED FLY ASHES: PROPERTIES AND CHARACTERISTICS

A. Fernández-Jiménez[1] and A. Palomo[2]

"Eduardo Torroja" Institute (CSIC). PO Box 19002, 28080 Madrid, Spain.
E-mail: [1]pesfj18@ietcc.csic.es and [2]Palomo@ietcc.csic.es

ABSTRACT

The alkali activation of fly ashes is a chemical process by which the glassy structure of this material is transformed into a very well compacted cement. In general terms the activation process may be considered as a set of destruction-condensation reactions (including the destruction of the initial solid substance) that initially leads to a series of unstable structure units and later produces the formation of thixotropic coagulation structures which can condense to form the hydrated products. The main objective of the present investigation was to determine the existing relationship between the mineralogical and microstructural characteristics of pastes and mortars of activated fly ash and the mechanical properties of said materials as a function of the curing time and temperature. For this purpose a Spanish fly ash and a 8M NaOH solution were used. The results obtained show: (a) the curing time and temperature are especially important; (b) mechanical strengths are notably increased when particles with size higher than 45 μm are eliminated; (c) the main reaction product is an amorphous aluminosilicate gel having a structure similar to that of some zeolitic precursors: 3-dimensional glassy structures in which the Si occurs in a variety of environments with a predominance of $Q^4(3Al)$ units at short curing times (5 and 8h) and $Q^4(2Al)$ at long curing times (7 days). The Al is essentially tetrahedrally coordinated.

Keywords: Alkali activation, fly ash, polymerisation degree, mechanical strengths.

1. INTRODUCTION

The production of Portland cement consumes a lot of resources and energy and involves the emission to the atmosphere of CO_2, SO_2 and NOx. So, it is very important to look for new resources, (especially industrial by-products) and new environmental friendly technologies. Alkaline cements are interesting and alternative cementitious materials (1-10).

The alkali activation of fly ashes is a chemical process by which the fly ash (FA), when mixed with certain alkaline activators and cured under mild temperature conditions, generates very compact materials. In general terms the activation process may be considered as a set of destruction-condensation reactions (including the destruction of the initial solid substance) that initially leads to a series of unstable structure units and later produces the formation of thixotropic coagulation structures which can condense to form the hydrated products. This set of reactions can be divided into three consecutive stages: (1) Destruction-Coagulation; (2) Coagulation-Condensation; (3) Condensation Crystallisation (8).

With respect to the technological properties of the activated fly ashes it is worthy to mention that:

- A strong material with a network structure is obtained
- It looks like a ceramic: Smooth, glassy and shiny

- Waste materials are used for its fabrication
- The workability of the fresh mixture is very good at low liquid/solid ratios
- Short curing time (a few hours) is needed.

However the chemical and mineralogical composition of the reaction products from the activation of fly ashes have not still been studied in detail, and therefore, the hardening mechanisms of this material are not fully understood. It is partly due to the existence of a wide variety of compositions of fly ashes as well as to the different types of activators that can be used, and also because of the difficulty of studying the amorphous reaction products. Additionally it is also important to emphasize the importance of the curing conditions (time and temperature) in the activation of fly ash (9).

For this the main objective of the present investigation was to determine the existing relationship between the mineralogical and microstructural characteristics of pastes and mortars of an activated fly ash and the mechanical properties of said materials. The factors considered in this research were: curing time, curing temperature and particle size distribution of fly ash.

2. EXPERIMENTAL

A Spanish fly ash was used (the chemical composition is presented in Table 1) together with an 8M NaOH solution as alkaline activator. This fly ash is made up of cenospheres and pleurospheres with a fraction of 78.5 wt % of particles sizes less than 45μm.

Table 1. Chemical composition of fly ash

	LoI	**IR**	**SiO_2**	**Al_2O_3**	**Fe_2O_3**	**CaO**	**MgO**	**SO_3**	**K_2O**	**Na_2O**
Fly ash	1.80	0.40	51.51	27.47	7.23	4.39	1.86	0.15	3.46	0.70

*Loss on Ignition *IR= Insoluble Residue

Mechanical properties of mortars made with activated fly ashes were determined from prisms (4x4x16 cm). The aggregate/fly ash ratio was always = 2/1, and the activating solution / fly ash ratio = 0.38. Some different curing conditions were applied to the prisms: two temperatures (65ºC and 85ºC), and some different times of reaction. Also, mortars with sieved fly ash (all particles smaller than 45μm) were prepared.

The mineralogical and microstructural characteristics of the final products were studied on small samples from pastes and mortars of alkaline activated fly ash. Pastes (cured at 85ºC at different times of reaction) were frozen with acetone and ethanol, and finally vacuum dried. Later they were studied by XRD, FTIR, MAS-NMR (9, 11). The pore size distribution was determined in mortars samples by mercury porosimetry. Theses mortars were also studied by SEM/EDX techniques.

Finally the amount of water-soluble sodium of samples was analysed by ion chromatography. For this purpose three grams of alkali activated paste dried under vacuum to a constant weight, were mixed with 250 ml of desionised water. The mix was mechanically shaken during 3 hours and then filtered and leveled up to 500ml with deionised water.

3. RESULTS

3.1. Characterization of alkali activated fly ash

According to the XRD data the fly ash is basically a vitreous material with some minor crystalline phases: mullite ($Al_6Si_2O_{13}$) quartz (SiO_2), magnetite (Fe_3O_4) and hematite (Fe_2O_3) (see Figure 1 **A**). In Figure 1 the XRD patterns of the alkali-activated fly ash cured (with NaOH 8M at 85ºC) for

different periods of time (2, 5, 8, 20h. and 7 days), are shown. The difractogramme of a sample cured 20h at 85ºC and then 6 days at 25ºC is also shown in the same figure.

When the fly ash is put in contact with the NaOH solution and thermally cured an amorphous product is formed (alkaline aluminosilicate); the typical halo appearing in the XRD difractogrammes gives evidence of this. Comparing the XRD pattern of the original fly ash with those of the hardened paste, it can be seen that the hardened materials contains quartz, mullite, etc (already existing in the starting ash); but also some new minor crystalline phases: hidroxisodalite and herchelite. The intensity of the peaks corresponding to these zeolites increases with the curing time (see Figure 1). Herchelite can be detected after 2 hours of reaction but hidroxisodalite was not detected until 8 hours. Formation of crystalline sodium carbonate was never detected.

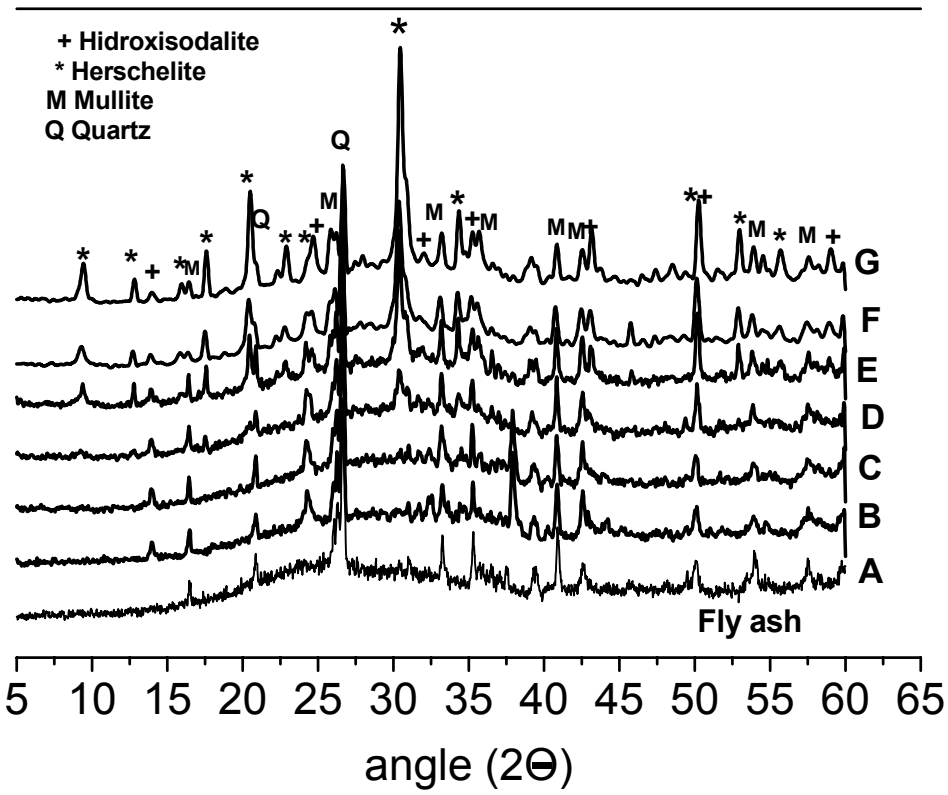

Figure 1. XRD patterns: **A,** starting fly ash; **B**, alkali activated fly ash (AAFA) 2h. 85ºC; **C**, AAFA 5h. 85ºC; **D**, AAFA 8h. 85ºC; **E**, AAFA 20h. 85ºC; **F**, AAFA 20h. 85ºC and then 6 days at 25ºC; **G,** AAFA 7 days 85ºC.

The FTIR spectrum of the starting fly ash as well as the spectra of AAFA materials are shown in Figure 2. The fly ash FTIR spectra is formed by one broad band at 1060 cm^{-1}, assigned to Si-O and Al-O vibrations and one small band at 454 cm^{-1} assigned to ν_4(O-Si-O) bending modes of SiO_4 tetrahedra (12). In the activated fly ash samples the 1060 cm^{-1} band moves towards lower frequencies (~1000 cm^{-1}) and the ν_4(O-Si-O) band towards higher values (465cm^{-1}). Additionally the band at 789 cm^{-1} in the starting fly ash due to AlO_4 vibrations disappears and a new band at around 730 cm^{-1} (associated with the presence of Al tetrahedrally coordinated in the alkaline aluminosilicate) appear (9).

The FTIR results (see Figure 2) are, once again, indicating the absence of formation of sodium carbonates. We consider it means that the polymerisation of aluminosilicate has consumed all the

sodium hydroxide present in the system. Finally stretching and deformation modes of water were detected at 3500 and 1600 cm^{-1}.

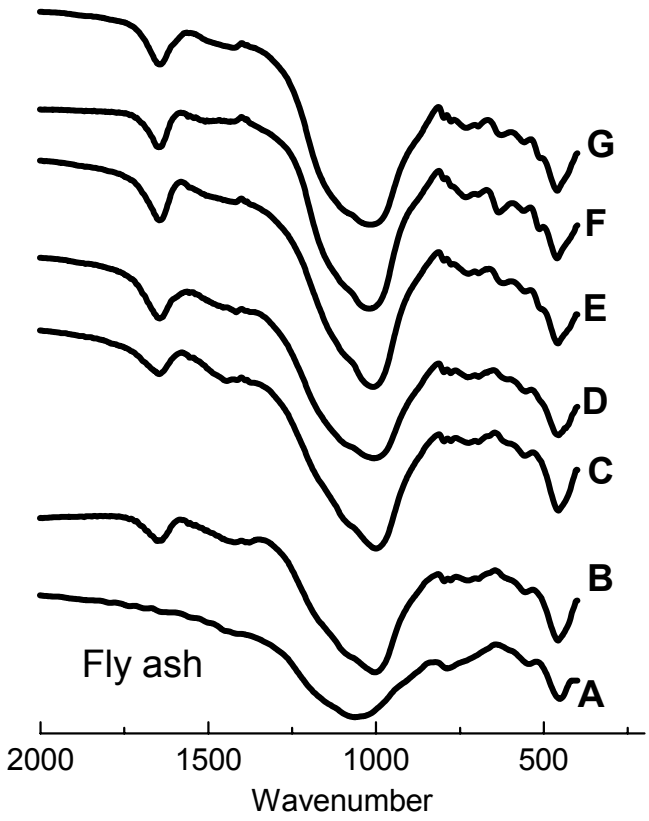

Figure 2. FTIR spectra: **A**, starting fly ash; **B**, alkali activated fly ash (AAFA) 2h. 85ºC; **C**, AAFA 5h. 85ºC; **D**, AAFA 8h. 85ºC; **E**, AAFA 20h. 85ºC; **F**, AAFA 20h 85ºC and then 6 days at 25ºC; **G,** AAFA 7 days 85ºC.

The ^{29}Si MAS NMR spectrum of the starting fly ash displays a wide asymmetric signal formed by seven components (see Figure 3 **A** and Table 2). The peaks appearing to –84, -93.6, -98.6, -103.4 ppm are assigned to the glassy part of the fly ash (15,16). The peak at –88 ppm is assigned to crystalline mullite (13) and finally the peaks respectively appearing at –108 and –115 are assigned to different crystalline silicates.

With respect to ^{29}Si NMR MAS spectrum of fly ash activated at 85ºC for 2h (Figure 3, **B**) it can be observed that the intense signals of the starting fly ash at –84 –93.6, -98.6 (previously assigned to the vitreous phase) have disappeared and a new peak at –96.5 ppm appeared. It can be thought that this transformation corresponds with the first stage of the reaction process of the fly ash in which the destruction of the bonds Me-O, Si-O-Si, Al-O-Al y Al-O-Si takes place as a consequence of the modification of the ionic force of the system (8).

After 5 hours curing time two peaks at –92.6 and –98.8 ppm appear (Figure 3 **C**). These peaks together with the one at –86 ppm can be assigned to formation of an intermediate amorphous alkaline aluminosilicate gel. This could correspond to the "s*econd coagulation-condensation stage*" (8).

The ^{29}Si NMR MAS spectra of fly ash activated at 85ºC for 8 hours (Figure 3 **D**) shows intense signals about –93.5 ppm and –98.8 ppm and –103.9 ppm assigned to the formation of an amorphous alkaline aluminosilicate gel similar to natural minerals of the zeolite or feldspar types.

For curing times longer than 8 hours the position of the spectra signals does not modify significatively for the fact of increasing curing time; but the intensity of the peaks can change notably. For example, short curing times (5, 8h) (spectra **C** and **D**) involves the signal at –93/94 ppm being the most intense one. However for longer curing times (spectra **E**, **F** and **G)** the most intense peak is the one at –98/-99 ppm. These different intensities can be associated to different degrees of polymerisation of the alkaline aluminosilicate hydrate. It might mean that after 8 hours curing time (at 85ºC), the last and long "*reaction stage of condensation-crystallisation*" (8) would have begun.

Therefore, sample cured 7 days at 85ºC should have developed the maximum reaction degree. Effectively, this particular sample is the one presenting the maximum mechanical strength (Figure 6). The NMR spectra of this material (Figure 3 G) shows sharp peaks at –98 ppm, –93 ppm, and –104 ppm, all of them associated with the formation of the alkaline silicoaluminate. The assignment of these peaks is not still clear but according to published data (15,16), the peak appearing at –104 ppm could be assigned to $Q^4(1Al)$ units, the peak appearing near –98 ppm to $Q^4(2Al)$ and the one at -93 ppm to $Q^4(3Al)$. These results would indicate that the main reaction products present a 3-dimensional glassy structure in which the Si occurs in a variety of environments but predominantly those of framework structures saturated in Al (i.e. ($Q^4(2Al)$ and $Q^4(3Al)$) where the Al is essentially in the tetrahedral site.

In all cases the peak appearing at –88 ppm is assigned to inert mullite. By deconvoluting these spectra (see Table 2) it can be observed that the percentage of mullite in the fly ash (~ 11%) is similar to that obtained in the fly ash sample activated for 7 days at 85ºC (11.79%). Finally the bands at –108/-109 ppm and –112 ppm are assigned to unreacted different crystalline silica, and the –81 and –84 ppm signals are assigned to the presence of residual silanol groups.

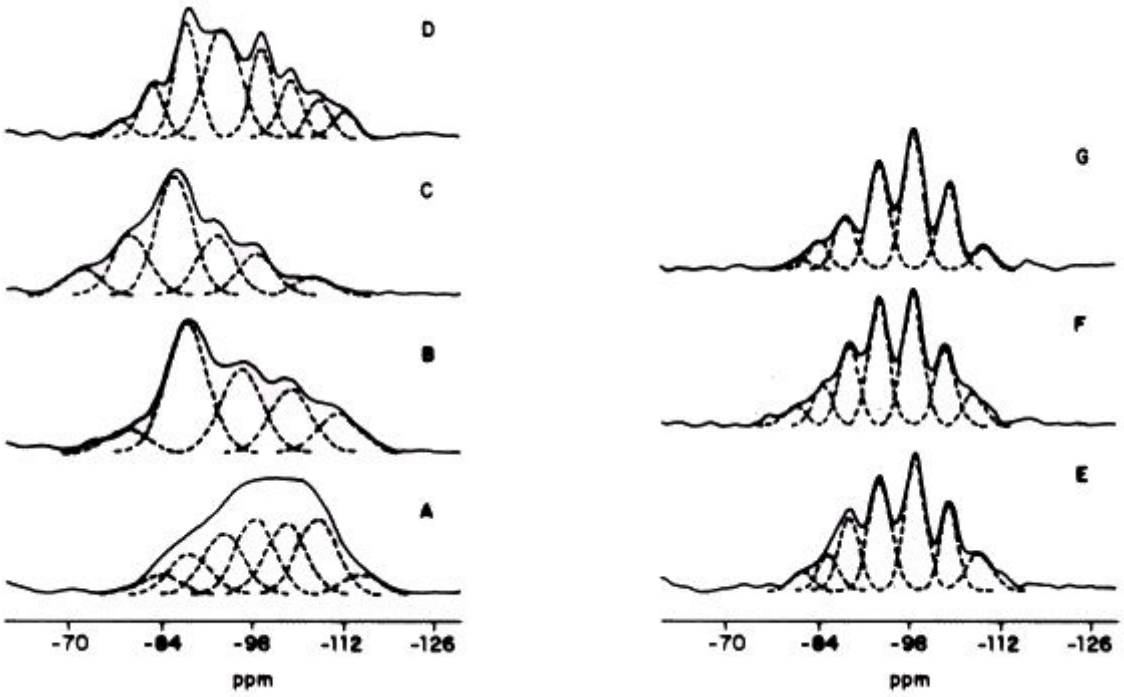

Figure 3. ^{29}Si MAS NMR spectra: **A**, starting fly ash; **B**, alkali activated fly ash (AAFA) 2h. 85ºC; **C**, AAFA 5h. 85ºC; **D**, AAFA 8h. 85ºC; **E,** AAFA 20h. 85ºC; **F**, AAFA 20h 85ºC and then 6 days at 25ºC; **G** AAFA 7 days 85ºC.

Table 2. Results obtained from deconvolution of ^{29}Si MAS NMR spectra of alkali activated fly ash pastes.

Sample			79/80	84	86	88/89	93	98/99	104	108	112
Fly ash	***Pos. (ppm)***			-84		-88.3	-93.6	-98.6	-103.4	-108	-115
	Width			7.15		7.15	7.15	7.15	7.15	7.15	7.15
	Integral (%)			5.32		11.0	16.98	20.66	19.46	20.9	5.61
2h.	***Pos. (ppm)***		***-79***			***-88.0***		-96.5	-104		-111
	Width		7.58			7.58		7.58	7.58		7.58
	Integral (%)		6.80			38.17		24.4	18.7		11.9
5h.	***Pos. (ppm)***	***-71.9***	***-79.3***		***-86***		***-92.6***	***-98.8***		***-107.5***	
	Width	6.56	6.56		6.56		6.56	6.56		6.56	
	Integral (%)	8.07	18.45		36.46		18.36	12.75		5.90	
8h.	***Pos. (ppm)***	***-77.5***	***-82.7***			***-88.2***	***-93.5***	***-99.1***	***-103.9***	***-107***	***-112.2***
	Width	4.80	4.80			4.80	4.80	4.80	4.69	4.80	4.80
	Integral (%)	2.72	9.87			24.31	20.80	20.53	9.19	6.95	5.63
20h.	***Pos. (ppm)***		***-81.7***		***-85.8***	***-89.7***	***-93.9***	***-99.2***	***-104.6***	***-109***	
	Width		3.93		3.93	3.93	3.93	3.93	3.93	3.93	
	Integral (%)		4.01		7.16	14.92	22.68	27.56	15.06	8.60	
20h.85ºC	***Pos. (ppm)***		***-81.0***		***-85.0***	***-89.0***	***-93.6***	***-98.9***	***-104***	***-108***	
6days	Width		3.70		3.70	3.70	3.70	3.70	3.70	3.70	
25ºC	Integral (%)		3.76		7.73	15.47	24.62	26.17	15.39	6.89	
7 days	***Pos. (ppm)***		***-81.2***		***-84.3***	***-88.5***	***-93.7***	***-98.9***	***-104.5***	***-109***	
85ºC	Width		3.62		3.62	3.62	3.62	3.62	3.62	3.62	
	Integral (%)		2.37		5.98	11.79	24.25	31.62	19.01	5.00	

In Figures 4 and 5 some micro structural characteristics (studied through SEM/EDX) of alkali activated fly ash mortars are shown. The studied samples contain spheres (from the fly ash) joined to each other with a continuous mass of reaction product acting like a cement. On said matrix the presence of pores as well as some tracks left by the reacted ash spheres, can be observed. Inside these hemispherical tracks some groups of crystals (associated with the formation of zeolites, already detected through XRD) can be seen. Finally some crystals of mullite and some unreacted spheres (having high proportions of Al and/or Fe) have also been detected.

From Figure 4 it can be deduced that the main reaction product corresponds to a glassy (6, 9, 17) alkaline aluminosilicate whose average atomic ratios are close to: Si/Al = 1.8-2.0 and Na/Al = 0.6-0.7 (point **A**). Point **B** corresponds to some un-reacted fly ash (Si/Al=1.38, Na/Al= 0.1).) and point **C** corresponds to a crystalline zeolitic structure with Si/Al = 2.23 and Na/Al = 1.47. In pastes activated for 7 days at 85ºC (see Figure 5) the main reaction product presents less Al (Si/Al = 2.0-2.2 and Na/Al = 0.8-0.9 (point **A**). Points **B** and **C** respectively correspond to crystalline zeolite (point **B**, Si/Al = 2.72 and Na/Al = 1.06; point **C**, Si/Al = 2.08 and Na/Al = 1.48), and finally point **D** corresponds to crystalline mullite.

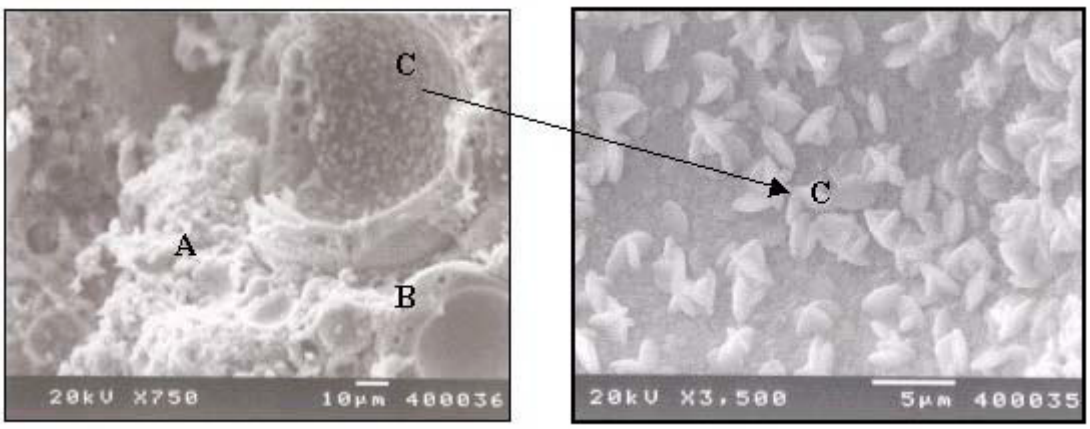

Figure 4. Mortars samples of alkali activated fly ash. Activator: 8M NaOH. Curing: 20 hours at 85ºC.

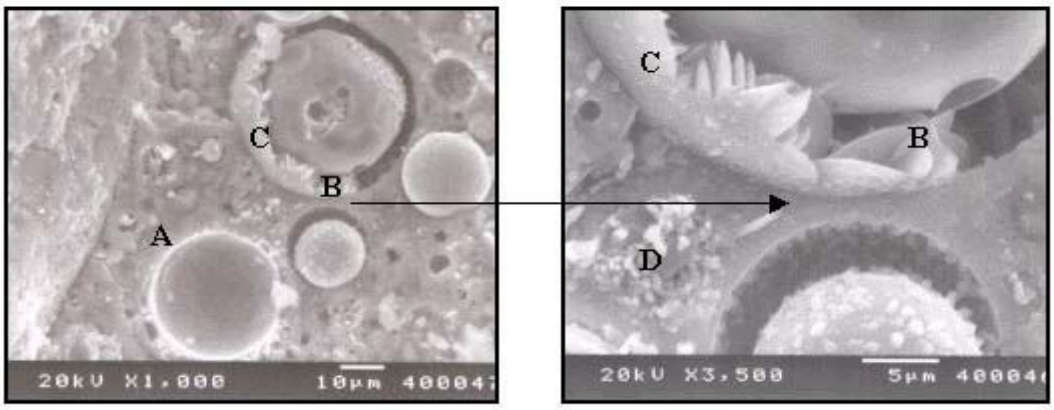

Figure 5. Mortars samples of alkali activated fly ash. Activator: 8M NaOH. Curing: 7 days at 85ºC.

In Table 3 percentages of Na fixed in the activated fly ash pastes are shown. These results show that the percentage of fixed sodium increases with the curing time. After 2 hours of curing at 85ºC (sample **B**) the percentage of fixed Na is higher than 55% of the Na initially added to the alkaline solution, but for a curing time of 7 days at 85ºC (sample **G**), this percentage increases to 77.17%.

Table 3. Na content in the activated fly ash pastes.

	Samples					
	B 2h. 85ºC	**C 5h. 85ºC**	**D 8h. 85ºC**	**E 20h. 85ºC**	**F 20h. 85ºC 6d. 25ºC**	**G 7d. 85ºC**
Na total (%	5.3%	5.3%	5.3%	5.3%	5.3%	5.3%
% Na lixiviated	2.29	2.27	2.27	1.94	1.84	1.21
% Na Fixed	56.8	57.17	57.17	63.4	65.28	77.17

3.2 Mechanical strength and porosity of AAFA mortars

In Figure 6, values of flexural and compressive strengths of mortars prisms made of alkali activated fly ash are given as a function of the curing temperature and the reaction time. The results obtained show that both factors time and curing temperature, play a very important role in the fly ash activation process. When curing time and curing temperature increase, the mechanical strengths increase too. The most important variation of strength takes place between 5 and 20 hours of curing. After that the mechanical strengths increase slowly. Additionally, it can be observed that the increase of strengths at 65ºC is not as quick as in the case of samples cured at 85ºC.

An important factor that has been considered in this study is the particle size of the starting fly ash. In this fly ash the percentage of particles with a size bigger than 45 µm is about 20%. When these coarse particles are eliminated the mechanical strengths of the activated material increase by about 15% (flexural) and 30% (compressive) (see Figure 6).

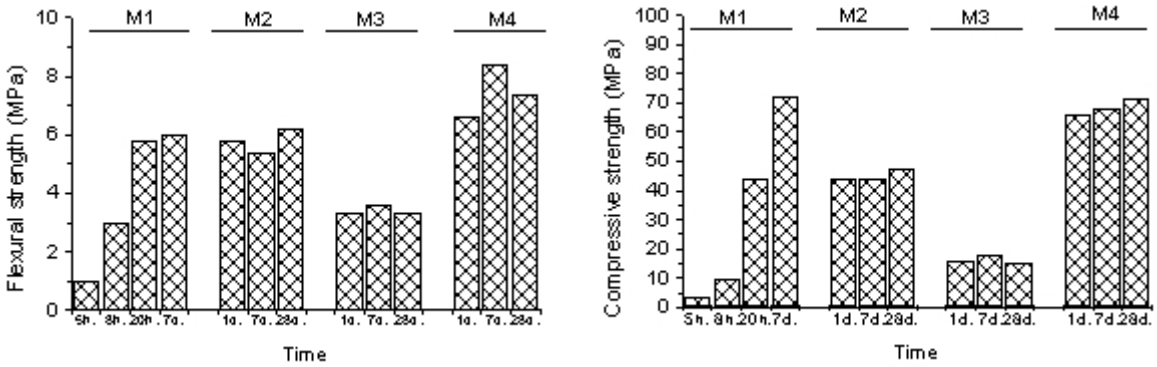

Figure 6. Mechanical strength. The curing conditions were: **M1**, all time at 85ºC; **M2**, 20h 85ºC and then 25ºC; **M3**, 20h 65ºC and then 25ºC; **M4**, mortars of activated sieved fly ash (<45 µm) cured 20h. 85ºC and then 25ºC.

In Figure 7 the total porosity and the pore size distribution are presented. It can be seen that mortars presenting the highest mechanical strengths are those presenting the lowest porosity and the highest percentage of small pores (between 0.1-0.01 μm).

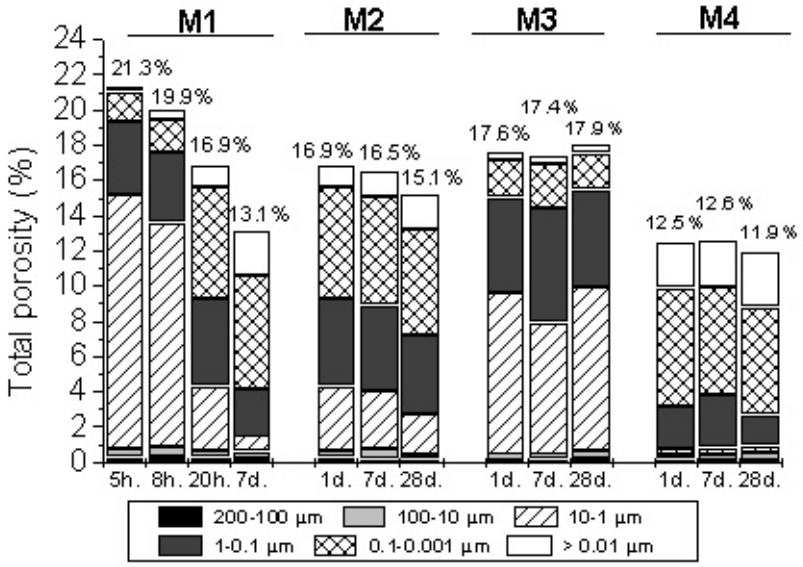

Figure 7. Total porosity and pore size distribution of alkaline activated fly ash mortars. The curing conditions were: M1, all time at 85ºC; M2, 20h 85ºC and then 25ºC; M3, 20h 65ºC and then 25ºC; M4, mortars of activated sieved fly ash (<45 μm) cured 20h. 85ºC and then 25ºC.

4. DISCUSSION AND CONCLUSIONS

The fly ash used in this study has a high fraction of glassy components together with a minor presence of crystalline phases: mullite ($Al_6Si_2O_{13}$) quartz (SiO_2), magnetite (Fe_3O_4) and hematite (Fe_2O_3). It means that it has high potential reactivity with alkalis. The reactivity can be enhanced by applying appropriate curing conditions and by controlling the specific surface of the fly ash.

The experimental results indicate that the curing time and the curing temperature play a determining role in the process of alkaline activation of fly ash. Increasing the time and the curing temperature the activation reactions are notably accelerated and consequently the gaining of mechanical strengths of the material is stimulated. Other important factor considered in this study (it will be reported with detail in a forthcoming publication) is the effect of particle size average of the starting fly ash on the development of activation reactions. The mechanical strengths are notably increased when particle sizes bigger than 45 μm. are eliminated. In this case compressive strengths reach 66 MPa for 1 day of curing (see Figure 6).

The main reaction product of alkali-activated fly ash is an alkaline aluminosilicate hydrate (6-10). Different microstructures can develop as a consequence of the reactive process. These products are amorphous to XRD but FTIR and ^{29}Si RMN MAS spectra show interesting information: The alkaline aluminosilicate presents a 3-dimensional glassy structure in which the Si occurs in a variety of environments. According with others authors (9,15) the structure contains Si and Al tetrahedra randomly distributed along the polymeric chains that are cross-linked so as to provide cavities of sufficient size to accommodate the charge balancing sodium ions. This arrangement leads to Si environments such as $Q^4(1Al)$, $Q^4(2Al)$ and $Q^4(3Al)$. The predominance of the $Q^4(2Al)$ or $Q^4(3Al)$ depends on the polymerisation degree which depends on the curing conditions.

A relationship between the mineralogical and micro structural characteristics and the mechanical properties of pastes and mortars of activated fly ash has been established: At short curing times

(<8h), the percentage of $Q^4(3Al)$ units is higher than the percentage of $Q^4(2Al)$ units and the mechanical strength is relatively low. However when the curing time increases the percentage of $Q^4(3Al)$ is lower than $Q^4(2Al)$ and the mechanical strength goes up.

The study performed through SEM/EDX has also confirmed the existence of minor crystalline reaction products already detected by XRD (herchelite and hidroxisodalite) and non reacted cenospheres from fly ash (rich in Al and Fe).

Finally, results obtained from leaching tests of pastes have proved that the reaction products fix about 56% of the initial Na added to the system, after 2 hours curing. This percentage increases with the curing time (77.17% for 7 days at 85ºC, see Table 3). However sodium carbonate was never detected at any of the studied samples.

ACKNOWLEDGEMENTS

The authors wish to thank the General Direction of Scientific Investigation for funding this research through the project COO-1999-AX-038 and the Comunidad de Madrid by the concession a postdoctoral grant associated with this investigation. They also thank Dr J Sanz and Dr I. Sobrados for the recording and discussion of MAS NMR spectra and J.L. Garcia and A. Gil for collaboration with mechanical tests.

REFERENCES

[1] B. Talling and J. Brandster. “Present state and future of alkali-activated slag concretes” 3rd International Conference of Fly Ash, Silica Fume, Slag and Natural Pozzolans in Concrete. Tondheim. SP 114-74, pp. 1519-1546 (1989).

[2] V.D. Glukhovsky, G.S. Rostovskaja and G.V. Rumyna. “High strength slag-alkaline cements”. 7th International Congress on the Chemistry of Cement. Paris. 3, V-164-168 (1980).

[3] F. Puertas “Cementos de escorias activadas alclinamente; situación actual y perspectivas de futuro” Materiales de Construcción, Vol 45, nº239, pp.53-64, (1995).

[4] R.I.A. Malek and D.M. Roy. “Structure and properties of alakaline activated cementitious materials” 97th annual meeting of the American Ceramic Society. Cincinati, OH (1995).

[5] Fernández-Jiménez, F. Puertas, J.G Palomo. “Alkali-Activated Slag Mortars: Mechanical Strength Behaviour” Cem. and Concr. Res. Vol. 29, pp.1313-1321, (1999).

[6] J. Davidovits. “Geopolymers: Inorganic polymeric new materials” J. Thermal Anal. 37, pp. 1633-1656 (1991).

[7] M.L. Granizo, S. Alonso, M.T. Blanco-Varela, and A. Palomo, “ Alkaline activation of metakaolin: effect of calcium hydroxide in the products of reaction” J. Am. Ceram. Soc. 85, [1], pp. 225-31 (2002).

[8] P.V. Krivenko. “Alkaline cements”, in: P.V. Krivenko (Ed.). Alkaline cements and concretes. 1. Vipol Stock Company. Kiev. (1994). pp 11-129.

[9] Palomo, M.W. Grutzeck, M.T. Blanco, "Alkali-activated fly ashes a cement for the future" Cement and Concrete Research, Vol 29, pp.1323-1329, (1999).

[10] J.G.S. Van Jaarsveld and J.S.J. Van Deventer “Effect of the alkali metal activator on the properties of fly ash based geopolymers”. Ind. Eng. Chem. Res., 38, No 10, pp 3932-3941 (1999).

[11] Fernández-Jiménez, F. Puertas “Structure of calcium silicate hydrate formed in alkaline acctivated slag. Influence f the alkaline activator nature” J. Am. Ceramic Soc. (in press), (2001).

[12] P Yu, R.J Kirkpatrick, B. Poe, P.F. McMillan and X. Cong. “Structure of Calcium Silicate Hydrate (C-S-H): Near-, Mid-, and Far-infrared Spectroscopy” J. Am. Ceramic Soc. Vol. 82, Nº 3, pp742-748, (1999).

[13] S. Gomes and M. François “ Characterization of mullite in silicoaluminous fly ash by XRD, TEM, and 29Si MAS NMR Cem. and Concr. Res. Vol. 30, pp.175-181, (2000).

[14] G. Engelhardth and D. Michel “High Resolution solid state NMR of silicates and zeolites” Ed. John Wiley and sons (1987).

[15] F.F. V. Barbosa, J.D.K. MacKenzie and C. Thaumaturgo “Synthesis and Characterisation of Materials Based on Inorganic Polymers of alumina and silica: sodium polysialate polymers” Int. J. of Inorganic Materials, 2, pp.309-317, (2000).

[16] Palomo and S. Alonso “Alkaline activation of fly ashes. A NMR study of the reaction products”. Cem. Concr. Res. (Submitted for publication).

[17] X. Zhaohui and X. Yunping “Hardenig mechanisms of an alkaline-activated class F fly ash” Cem. and Concr. Res. Vol. 31, pp.1245-1249, (2001).

NMR STUDY OF ALKALINE ACTIVATED "CALCIUM HYDROXIDE - METAKAOLIN" SOLID MIXTURES

A. Palomo*, T. Blanco-Varela, S. Alonso and L. Granizo

Eduardo Torroja Institute (CSIC), P.O. Box 19002, 28080 Madrid, Spain.
*Tel: +34-913020440 Fax: 0034-913026047 E-mail: Palomo@ietcc.csic.es

ABSTRACT

The activation of metakaolin by alkaline solutions produces the formation of an inorganic polymer with excellent mechanical properties. When calcium hydroxide is mixed with the metakaolin, the reaction produced in the alkaline activation is somewhat different and the products formed consist of the inorganic polymer and C-S-H gel in different proportions (depending on the reaction parameters). Also the type of activator and its concentration result to have a determinant influence on the final product formed.

Metakaolin and metakaolin + calcium hydroxide mixes were activated with NaOH and NaOH+waterglass solutions of different concentrations and they were cured in an oven at temperatures lower than 85ºC for between 2 and 24 hours

The aim of the investigation was to structurally characterise the materials formed in the process. Due to the amorphous character of the reaction products, NMR-MAS technique appeared to be the most suitable approach to characterise them, although supplementary studies were done by means of XRD and FTIR.

When the activator concentration is 5M or less, metakaolin activation (in the experimental conditions) occurs only to a minor extent. However, if lime is present in the system, activation takes place, CSH gel being the main reaction product. But if activator concentration is 8M or higher, metakaolin dissolution is very fast and the main reaction product is an alkaline aluminosilicate with high mechanical performance. The formation of CSH gel as the main or secondary reaction product (depending on the activation concentration) is also observed when lime has been added to the reaction mixture.

Therefore, a threshold OH^- concentration exists above which (independently of the lime presence among the reactants) the alkaline polymer is mainly formed. Beneath this [OH] threshold (in the systems containing lime), CSH gel is the main reaction product.

The data collected from the NMR study provides a suitable information for establishing the different routes followed by the activation reactions of metakaolin depending on both the hydroxyl ion concentration of the system and the presence (or not) of lime in the reaction mixture.

Keywords: Metakaolin, Alkaline Activation, MAS NMR, CSH gel

1. INTRODUCTION

Thermal treatment of kaolin at temperatures between 450º and 750ºC produces its complete dehydroxilation. This process involves the breakdown of kaolin structure and the formation of a quasi-amorphous material, named metakaolin (1).

Mackenzie et al (2) studied the process of dehydroxilation of kaolinite as a function of temperature. The increas of the temperature is responsible for the evolution of the coordination number of aluminium (octahedral in the original kaolin, pentahedral and tetrahedral in the resulting metakaolin), and is also responsible for the distortion of the original SiO_4 tetrahedra.

Granizo (3) characterised the metakaolín (produced by heating the kaolin at 750ºC for 24 hours) by means of MAS-NMR. She observed in the ^{29}Si NMR spectrum a broad band centred at –107 ppm confirming the diversity of network environments and also the predominance of tetrahedra of SiO_4 in a three-dimensional structure. Additionally she observed the presence of 3 peaks in the ^{27}Al NMR spectrum (at 2.8, 28.3 and 56.1) respectively indicating the existence in the metakaolin of the three possible coordination states.

The activation of metakaolin by means of alkaline (caustic) solutions leads to high mechanical performance inorganic polymer (4). This polymer (alkaline aluminosilicate) can be considered as a precursor of other crystalline structures like zeolites or feldspars (5)**.**

Glasser et al (6) point out that the alkaline activation of metakaolin (with [NaOH] = 0,5M), when in presence of $Ca(OH)_2$, goes through very different ways. They observed the CSH gel being the main reaction product.

It is also very well known the formation of CSH gel when metakaolin is used as an admixture with Portland cement (7).

The authors of the present paper already showed (8) that the nature of the reaction products depend on the concentration of the alkaline solution used for activating the system (when concentration is higher than 10M, the main reaction product is the alkaline aluminosilicate; but if [OH] concentration drops, then the main reaction product is the CSH gel.

The fact of dealing with amorphous compounds (not only the most important raw material but also most of the reaction products), makes difficult the characterisation studies. However MAS-NMR has proved to be a very efficient tool for solving the characterisation problem. In fact, bibliography on microstructural investigations of CSH gel through MAS-NMR is rapidly increasing (9, 10). The number of papers published on this alkaline aluminosilicate phase is small (11-13).

The aim of this investigation was to characterise through MAS-NMR the different products formed during the metakaolin activation (in the presence and the absence of calcium hydroxide) as a function of the Na_2O concentration.

2. EXPERIMENTAL

A number of metakaolin samples as well as metakaolin plus $Ca(OH)_2$ samples, were activated with different NaOH solutions or with different sodium silicate + NaOH solutions.

The metakaolin was obtained after treating a Spanish kaolin (57% SiO_2 and 41,5% Al_2O_3) at 750ºC for 24 hours.

In the case of the systems not including $Ca(OH)_2$, the metakaolin was mixed with the activating liquid (NaOH or waterglass + NaOH) in a liquid/solid ratio of 0.55 The resulting paste was kept at 85ºC for 2 hours.

For the systems including calcium hydroxide first of all the homogenisation of solids was carried out (ratio: 1/1). After that, the activating solution was added (liquid:solid = 0.7) and the resulting paste cured at 45ºC for 24 hours.

Whatever the system studied, the concentration of the NaOH solution used was 5M and 12M. The sodium concentration of the waterglass +NaOH solution was always 8M and 12M.

Finally, the whole of samples were studied through ^{29}Si and ^{27}Al MAS-NMR. Results were complemented by additional data obtained by means of XRD and FTIR.

3. RESULTS AND DISCUSSION

3.1 Activation with NaOH 5M

In the activation process of metakaolin with 5M sodium hydroxide, the hardening of the material is not achieved; there is insufficient precipitation of reaction products to produce mechanical strength.

Figures 1a) and 1b) show the spectra found for the starting material. From the NMR spectra given in Figures 2a) and 2b) it can be deduced that most of original metakaolin has not been attacked by the alkaline dissolution: the broad band at –107 ppm in the ^{29}Si spectrum and the octahedral signal of aluminium appearing at the ^{27}Al spectrum, are both signals which are found in the starting material. (Seen in Figures 1a) and 1b) and consequently confirm the low level of reaction of the metakaolin.

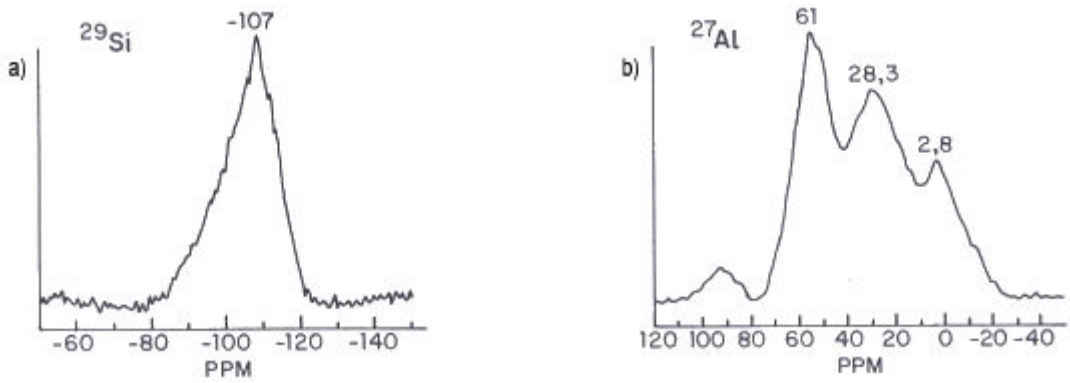

Figure 1. Original no activated Metakaolin (3).
a) ^{29}Si MAS-NMR spectrum and b) ^{27}Al MAS-NMR spectrum

It is true that the presence of (OH) groups in the system should favour the metakaolin dissolution due to the attack on the covalent bonds Al-O and Si-O (14); but it is also true that at this level of (OH) concentration the activation of the material is slow. Effectively, the absence of pentahedral aluminium (see spectrum ^{27}Al of Figure 2b) is indicating that the attack has taken place but it is also indicating that the solubilisation of aluminium selectively occurs as a function of the coordination number. Finally the modifications observed in the position of the signals of these spectra when compared with the starting material spectrum can be interpreted in terms of a deformation of the

silicon tetrahedra and aluminium pentahedra and octahedra of metakaolin because of its partial dissolution.

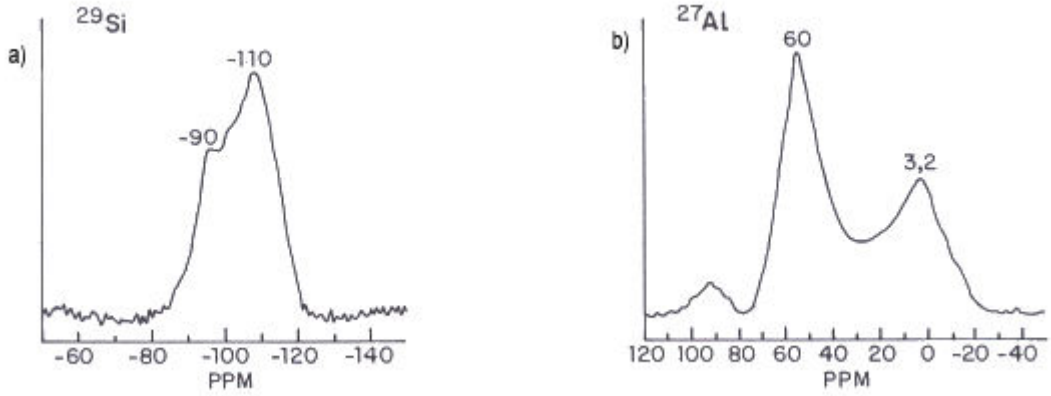

Figure 2. Metakaolin + (5M NaOH solution); 85ºC for 2 hours.
a) ^{29}Si MAS-NMR spectrum and b) ^{27}Al MAS-NMR spectrum

However, when the material to be activated is a mixture of metakaolin and calcium hydroxide and the activator is again a 5M NaOH solution, the material becomes hardened. The NMR ^{29}Si spectrum of the reaction product (Figure 3a) shows three sharp and very well defined peaks at –82, -84 and –89 ppm, a broad band at -107 ppm and a small shoulder at –77 ppm. This last signal clearly modifies the slope of the spectral line.

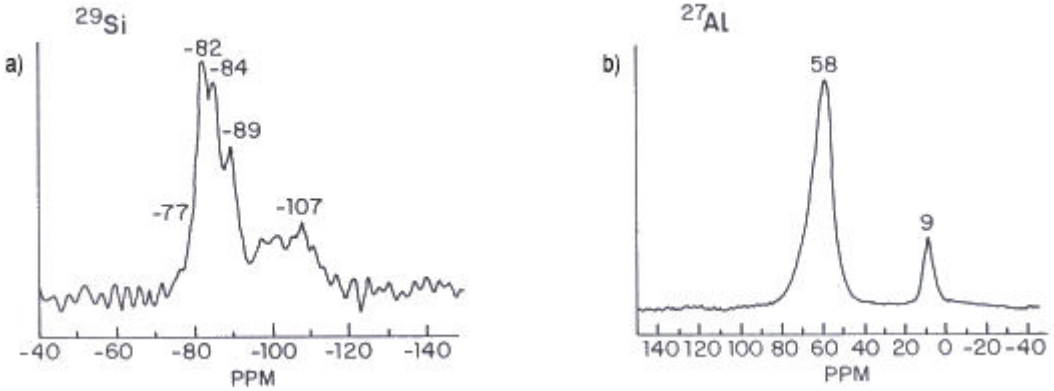

Figure 3. Metakaolin + $Ca(OH)_2$ + (5M NaOH solution); 45ºC for 24 hours.
a) ^{29}Si MAS-NMR spectrum and b) ^{27}Al MAS-NMR spectrum

The broad band at –107 ppm can be assigned to a Q^4 structure with no substitution of aluminium, and can be due to the existence in the sample of a fraction of metakaolin which has not still been activated.

With respect to the three sharp peaks the following can be established: The signal at –89 ppm could correspond to the response originated by the presence in the samples of Q^2(0Al) units; the signal at –84 ppm, it could be assigned to a Q^2(1Al) structure; and finally the signal at –82 ppm could be interpreted as the presence of Q^2(2Al) structural units. The shoulder at –77 ppm could indicate the existence of Q^1(1Al) units.

This interpretation of the NMR ^{29}Si spectrum of Figure 3a) is in good agreement with the interpretations given by other authors (15, 16); and it reveals a very important fact: the main product of reaction when a mixture of metakaolin and $Ca(OH)_2$ is activated with a 5M NaOH

solution, is a calcium silicate hydrate (CSH gel) very similar to that produced during the hydration of Portland cement (17). The structure of this product corresponds to a model of chains of SiO_4 tetrahedra which are partially substituted by AlO_4 tetrehedra. Said isomorphic Al substitutions could be responsible for the slight modification observed in the chemical shifts.

The NMR ^{27}Al spectrum of this sample presents two peaks at 9 and 58 ppm (see Figure 3b), respectively representing two types of coordination number of aluminium. The signal at 9 ppm is assigned to an octahedral network environment, and the signal at 58 ppm is indicating the existence of tetrahedral aluminium. This tetrahedral aluminium corresponds not only to the substitutions in the silicate chains but also to the aluminates in the non reacted metakaolin.

3.2 Activation with sodium hydroxide 12M

If we now increase the concentration of the activating solution to12M and the solution is put in contact with the metakaolin (and calcium hydroxide is not present in the system), then a material with high mechanical properties is obtained. This is the opposite situation to that created when the NaOH activating dissolution was 5M.

The NMR ^{29}Si spectrum of the reaction product basically presents two sharp peaks respectively at –89.8 and –86.7 ppm (Figure 4a). Both peaks can be attributed to three-dimensional structures of SiO_4 tetrahedra with abundant aluminium substitutions: $Q^4(3Al)$ units for the case of the peak at –89.8 (these units have been associated to a crystalline structure of the type of a zeolite like Hydroxisodalite or Faujasite, both compounds identified in the samples by means of XRD), and $Q^4(4Al)$ units for the case of the peak at –86.7 (indicating the existence of an amorphous polymer with cementing properties and with a three-dimensional structure made of almost the same number of SiO_4 and AlO_4 tetrahedra.

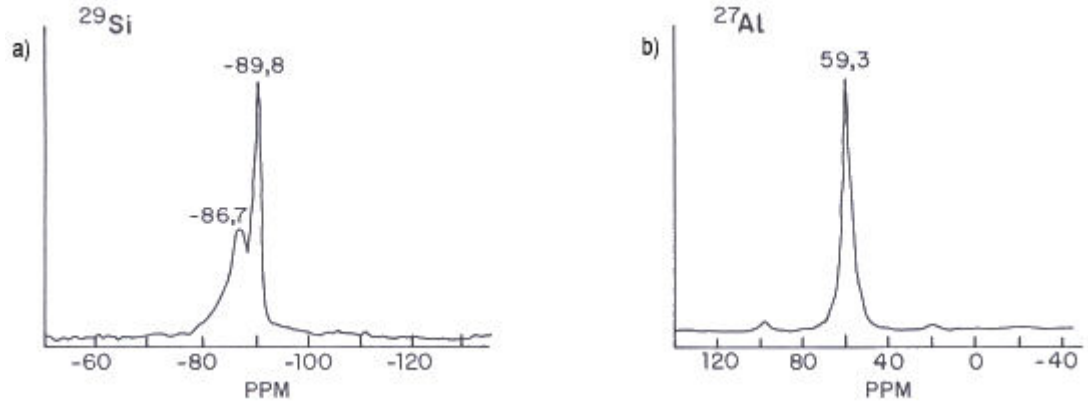

Figure 4. Metakaolin + (12M NaOH solution); 85ºC for 2 hours.
a) ^{29}Si MAS-NMR spectrum and b) ^{27}Al MAS-NMR spectrum

On the other hand, the absence of signals above –100 ppm, in the NMR ^{29}Si spectrum (Figure 4a), as well as the appearance of one only band in the NMR ^{27}Al spectrum, corresponding to the tetrahedral coordination of Al, (Figure 4b), are indicating the high degree of reaction reached by the system.

When activation of metakaolin is carried out with a 12M NaOH solution but in presence of calcium hydroxide, then in the NMR ^{29}Si spectrum appears an intense signal at –86.7 ppm (Figure 5a). It again indicates the formation of a product with three-dimensional structure at which the maximum aluminium substitutions takes place. Other less intense signal also appears at –82 ppm. It is associated with the presence of a phase with lineal structure and incorporating some AlO_4 tetrahedra

and basically formed by $Q^2(2Al)$ units. And finally a small shoulder at -78 ppm is interpreted as due to $Q^1(1Al)$ units.

The NMR ^{27}Al spectrum of this material (Figure 5b) presents only one peak at 61 ppm, characteristic of tetrahedral aluminium.

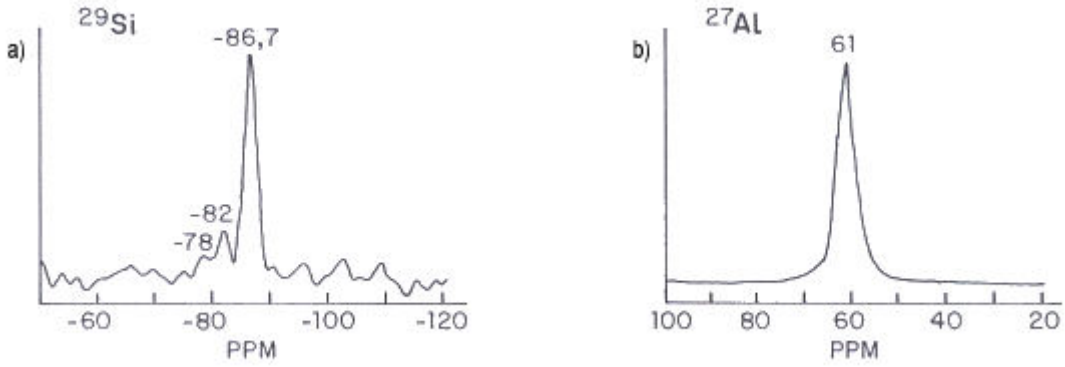

Figure 5. Metakaolin + $Ca(OH)_2$ + (12 M, NaOH solution); 45ºC for 24 hours.
a) ^{29}Si MAS-NMR spectrum and b) ^{27}Al MAS-NMR spectrum

In few words: when the alkaline activation of metakaolin is carried out in the presence of calcium hydroxide, the main reaction product is that alkaline polymer of three-dimensional structure which is also produced in the absence of calcium hydroxide. It could be even thought that both materials, due to the similarity of ^{29}Si spectra of Figures 4 and 5, posses the same Si/Al ratio.

But the spectrum ^{29}Si of Figure 5 also presents a signal at –82ppm. It has been interpreted as a signal belonging to the lineal structure typical of CSH gel. Additionally, the ^{27}Al spectrum shows the peak of the tetrahedral aluminium (there is no signs of non reacted metakaolin).

Therefore, it can be concluded that the alkaline activation of metakaolin with a NaOH solution (independently on the presence or absence of calcium hydroxide in the system) involves the formation of different products of reaction as a function of the concentration of the dissolution:

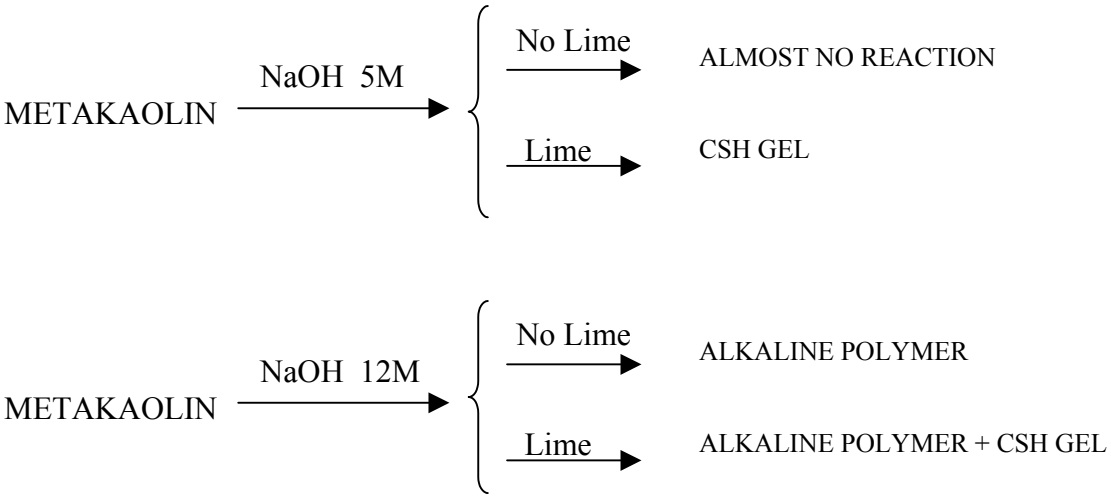

The presence of calcium hydroxide makes the CSH being the main reaction product in “low” alkaline medium (5M); but when [OH] increases, the total desegregation of metakaolin is accelerated and because of the effect of the common ion the dissolution of the calcium hydroxide becomes impeded. In this situation, the only way for the reaction to progress is the formation of the alkaline aluminosilicate. The precipitation of this product involves the fixation of the OH groups

and consequently the hydroxyl ion concentration in solution drops; it means that more calcium hydroxide is dissolved and that calcium is now fixed with the still non precipitated silicates in the form of CSH gel.

3.3 Activation with a mixture of Waterglass + NaOH

When the activation of metakaolin is carried out with a mixture of waterglass and NaOH (concentration of the mixture = 8M), it could be initially thought that a mechanism of reaction similar to that previously mentioned would take place, since the [OH] value of this mixture is lower than the 5M NaOH solution. However, the material hardens regardless of the presence or absence of calcium hydroxide.

When the system is formed by metakaolin and [Na] = 8M (waterglass + NaOH), then the NMR spectrum ^{29}Si of the reaction product (see Figure 6a) presents a broad band at –90.7 representative of a structure containing Q^4 (3Al) units (three-dimensional structure of SiO_4 tetrahedra with 3 substitutions of aluminium). Additionally, the NMR ^{27}Al spectrum shows that the transformation undergone by metakaolin has been a very intense one since the tetrahedral peak of aluminium is the only signal appearing in such a spectrum (Figure 6b).

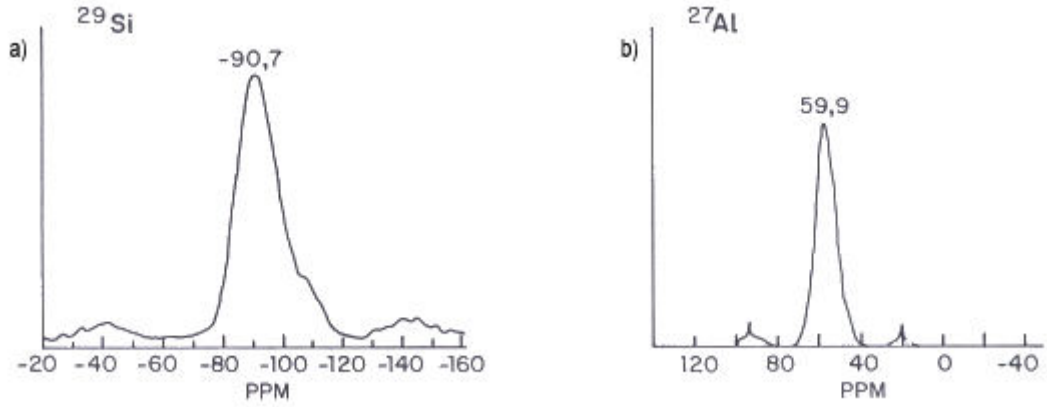

Figure 6. Metakaolin +([Na] = 8M, NaOH+Waterglass solution); 85ºC for 2 hours.
a) ^{29}Si MAS-NMR spectrum and b) ^{27}Al MAS-NMR spectrum

The presence of soluble silicates in the activating solution and the quick dissolution of the aluminium from the metakaolin supplies enough reactant species to the aqueous phase for producing the formation of the alkaline polymer. This early precipitation involves the displacement of chemical equilibrium towards a massive formation of reaction products.

The addition of soluble silicates to the activating solution slightly modifies the three-dimensional structure of the final reaction product when compared with the product obtained through activation with NaOH solution. The presence of soluble silicates produces Q^4(3Al) structures, however the activation with NaOH solutions leads to structures mainly formed by Q^4(4Al) units.

When calcium hydroxide is added to the system, the observed phenomenon is quite similar to the case of activation with a 5M NaOH dissolution. The NMR ^{29}Si spectrum of the reaction product (Figure 7a) shows a main peak at –81.8 ppm, interpreted as a signal corresponding to a Q^2(2Al) structure, and other peak at –84.3 ppm also interpreted as a lineal structure formed by SiO_4 chain with few aluminium substitutions [Q^2(1Al) units]. Finally the presence of a small shoulder at 78 ppm is interpreted as due to Q^1(1Al) units.

The ^{27}Al NMR spectrum (Figure 7b) shows the tetrahedral coordination of aluminium in the reaction products (signal at 60.1 ppm) but no other coordination number.

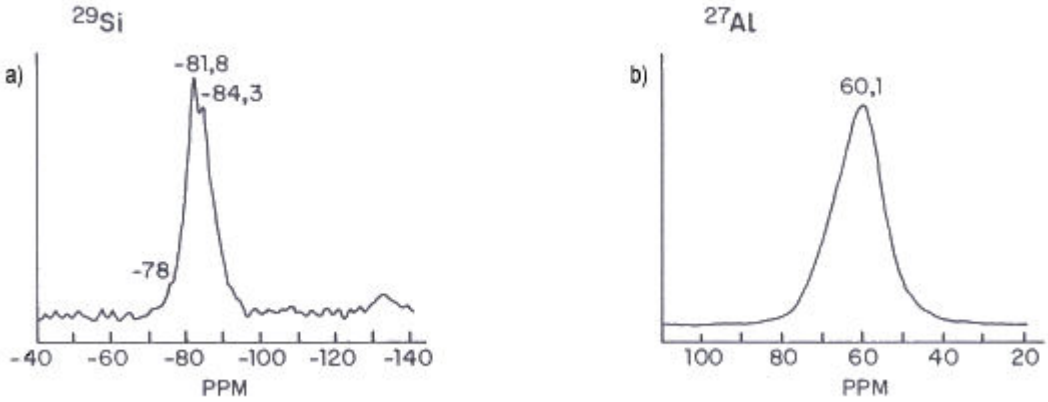

Figure 7. Metakaolin + $Ca(OH)_2$ + ([Na] = 8M, NaOH+Waterglass solution); 45ºC for 24 hours. a) ^{29}Si MAS-NMR spectrum and b) ^{27}Al MAS-NMR spectrum

The explanation of the formation of a structure like the one of CSH gel instead of the alkaline polymer (main reaction product in the system without calcium hydroxide) should be again looked for in the [OH] value. The [OH] of the waterglass+NaOH dissolution used in this part of the investigation is lower than the NaOH dissolution used in the former part; and it means that the dissolution of the calcium hydroxide is not inhibited. Therefore, the existence of calcium ions in the aqueous phase together with silicate ions (from the waterglass) makes the CSH gel precipitate. This precipitation favours the dissolution of more calcium hydroxide and consequently the increase of pH. This pH increase accelerates the dissolution of metakaolin giving place to a intense formation of reaction products..... And this is the reason for which signals from unreacted metakaolin (-107 ppm in the ^{29}Si spectrum and 2.8 and 28.3 in the ^{27}Al spectrum) cannot be observed in Figure 7.

When the system of work is constituted by metakaolin (no presence of calcium hydroxide) and the activating dissolution is a mixture of waterglass and NaOH with a sodium concentration 12M, again the three-dimensional alkaline polymer is formed as deduced from the signal at –90.7 [Q^4(3Al) units] appearing in the NMR ^{29}Si spectrum of Figure 8a). This reaction product is similar to the one obtained in the same system but activating with lower Na_2O concentration.

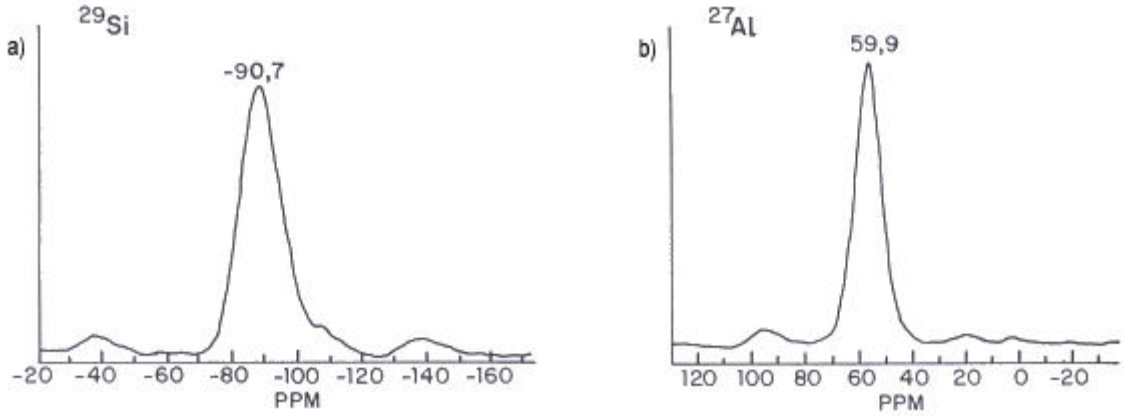

Figure 8. Metakaolin + ([Na] = 12M, NaOH+Waterglass solution); 85ºC for 2 hours. a) ^{29}Si MAS-NMR spectrum and b) ^{27}Al MAS-NMR spectrum

When calcium hydroxide is present in the system the NMR ^{29}Si spectrum shows an intense signal at –81.8 ppm and a second signal at –85.2 ppm (Figure 9a). The NMR ^{27}Al spectrum presents one only signal at 61.7 ppm corresponding to the tetrahedral coordination of aluminium, (Figure 9b).

The main reaction product is the CSH gel with aluminium substitutions in the silicate chain (conclusion extracted from the signal at –81.8 ppm in the NMR ^{29}Si spectrum of Figure 9a). The shoulder at –85.1 ppm (same figure) is indicating the formation of a three-dimensional structure of SiO_4 tetrahedra linked to AlO_4 tetrahedra [Q^4 units] corresponding to the alkaline polymer. Again, the different proportion at which the reaction products appear (due to the presence of calcium ions) is a consequence of the chemical priority of CSH gel to be formed against the alkaline polymer in the presence of the dissolved ions.

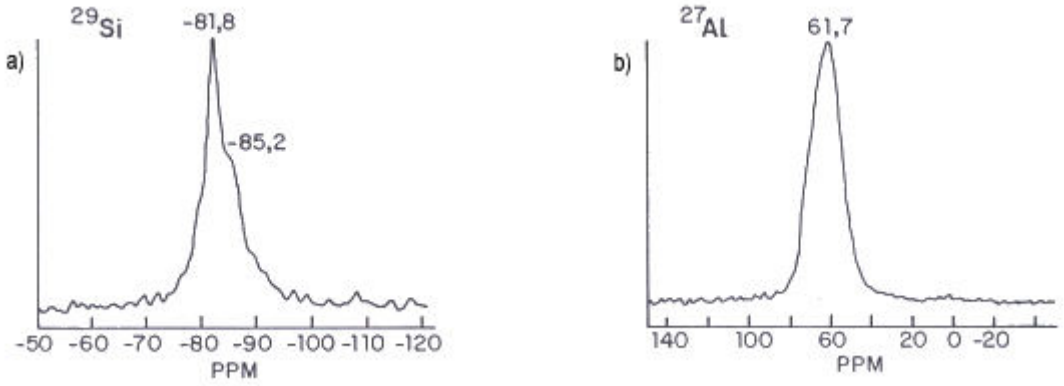

Figure 9. Metakaolin + $Ca(OH)_2$ +([Na] = 12M, NaOH+Waterglass solution); 45ºC for 24 hours. a) ^{29}Si MAS-NMR spectrum and b) ^{27}Al MAS-NMR spectrum

This very important difference can also be observed when we modify the type of activator. In the presence of calcium hydroxide, when activation is carried out with NaOH, the main reaction product is the alkaline polymer (there is no dissolution of calcium hydroxide because of the "common ion" effect); but if the activator is a mixture of NaOH and waterglass the precipitation of CSH gel is easier than the precipitation of the alkaline silicoaluminate. However this difference does not exist when calcium hydroxide is not present at the system because in such a case the alkaline polymer is always formed.

Finally it is important to emphasise that the alkaline polymer is richer in aluminium when activation is carried out with NaOH than when is carried out with a mixture of waterglass and NaOH.

4. CONCLUSIONS

- Alkaline activation of metakaolin requires strong concentration of alkaline activator, which depends on the type of activator used. In the experimental conditions a [Na] = 8M concentration of a mixture of NaOH + waterglass is needed and a 12M concentration if only NaOH is used.
- In absence of portlandite, the alkaline polymer obtained during the activation reaction is an amorphous compound. It is basically a three-dimensional network of SiO_4 tetrahedra [Q^4] at which Si atoms are partially replaced by Al atoms. The substitution is maximum $Q^4(4Al)$ when the activator is NaOH and less if the activator is a mixture of waterglass + NaOH.
- The alkaline activation of mixtures of metakaolin + $Ca(OH)_2$ produces CSH gel and/or alkaline polymer. The relative proportion of the reaction products depends on the concentration and type of activator. Then, the alkaline polymer will be the major phase when [OH] inhibits (due to the common ion effect) the initial dissolution of calcium hydroxide.
- The alkaline polymer is always network structured presenting maximum substitution of SiO_4 by AlO_4; independently of the type of activator used.

ACKNOWLEDGEMENT

To the CICYT for funding the projects MAT93-0282 and MAT96-0598

REFERENCES

[1] Murat, M. “Hydration reaction of hardening of calcinated clays and related minerals. II. Influence on mineralogical properties of the raw kaolinite of the reactivity of metakaolin” Cem. Concr. Res. Vol. 13, pp 511-518 (1983).

[2] Mackenzie, K.J.D.; Brown, I.W.M.; Meinhold, R.H. and Bowden M.E. “Outstanding problems in the kaolinite-mullite reaction sequence investigated by ^{29}Si and ^{27}Al solid state nuclear magnetic resonance: I, metakaolinite”. J. Am. Cer. Soc. 68, pp 293-297 (1985).

[3] Granizo, M.L. “Activación Alcalina de Metacaolín: Desarrollo de Nuevos Materiales Cementantes”. Report presented to get the doctor degree on Chemistries Sciences. Universidad Autónoma , Madrid, (1998).

[4] Palomo A. and.Glasser F.P “Chemically-bonded cementitious materials based on metakaolin”. British Ceramic Transactions. Vol.91pp. 107-112. . (1992)

[5] Palomo, M.T. Blanco, M.L. Granizo, F. Puertas, T Vazquez. and M.W. Grutzeck “Chemical stability of cementitious materials based on metakaolin” Cem. Concr. Res. (1999).

[6] P.S. De Silva and F.P. Glasser. Hydration of cements based on metakaolin: thermochemistry. Advances in Cement Research. 12. pp.167-177. (1990).

[7] KHATIB, J.M.; SABIR,B.B. and WILD, S. "Some properties of metakaolin paste and mortar" (pp 637-644) and "On the workability and strength development of metakaolin concrete" (pp 651-662). Proc. Of the Int. Conf. "Concrete in the service of mankind" Vol: Concrete for Environment and Protection. Ed. By R.K. Dhir and T.D. Dyer. Dundee(Scotland)(1996).

[8] M.L. Granizo, S. Alonso, M.T. Blanco-Varela and A. Palomo. “Alkaline activation of metakaolin. Effect of calcium hydroxide in the products of reaction”. J. Am. Ceram. Soc. 85, pp.225-231, (2002)

[9] M. Grutzeck, A. Benesi and B. Fanning. “Silicon – 29 magic angle nuclear magnetic resonance. Study of calcium silicate hidrates”. J. Am. Ceram. Soc. 72. pp. 665-668 (1989)

[10] I.G. Richardson, A. Brough, R. Brydson, G. Groves and C. M. Dobson. “Location of Al in substituted calcium silicate hydrate (CSH) gels as determinated by ^{29}Si and ^{27}Al NMR and EELS”. J. Am. Ceram. Soc, 76. pp. 2285-2288, (1993).

[11] N. Shigemoto, ; S. Sugiyama; H. Hayashi and K. Miyaura "Characterization of Na-X, Na-A, and coal fly ash zeolites and their amorphous precursor by IR, MAS NMR and XPS". J. Mat. Sci. Vol 30, pp 5777-5783 (1995).

[12] J. Davidovits. “Geopolymers: Inorganic polymeric new materials” J. Thermal Anal. 37, pp. 1633-1656 (1991).

[13] J.G.S. Van Jaarsveld and J.S.J. Van Deventer “Effect of the alkali metal activator on the properties of fly ash based geopolymers”. Ind. Eng. Chem. Res., 38, No 10, pp 3932-3941 (1999).

[14] P.V. Krivenko. Alkaline cements, in: P.V. Krivenko (Ed.). Alkaline cements and concretes. 1. Vipol Stock Company. Kiev, Ukraine, pp 11-129, (1994).

[15] Xian-Dong Cong and R.J. Kirpatrick. “^{29}Si MAS NMR Spectroscopic investigation on alkali silica reaction product gels”. Cem. Concr. Res. Vol 23, pp. 811-823 (1993)

[16] W. Wieker “Recent results of solid state NMR investigations and their possibilities of use in cement chemistry” 10th Int. Cong. on the Chemistry of Cement. Vol 1. Goteborg (1997)

[17] Xian-Dong Cong and R.J. Kirpatrick. J. Am. Cer. Soc. 79, p.1585 (1996).

INVESTIGATION OF HYDRATION BEHAVIOR OF FERRITE PHASE $C_6A_XF_{3-X}$ WITH DIFFERENT AL^{3+}-CONTENT IN MIXES WITH C_3A AND GYPSUM USING A REVISED HIGHLY EFFICIENT ISOTHERMAL CALORIMETER

J. Neubauer, F. Goetz-Neunhoeffer and I. Lindner

Department of Mineralogy, Friedrich-Alexander Universität Erlangen-Nürnberg, Germany.
E-mail: neubauer@geol.uni-erlangen.de

ABSTRACT

Seven different pure Ferrites ($C_6A_XF_{3-X}$) with x = 0; 0.5; 1; 1.25; 1.5; 1.75 and 2 were synthesized at 1250°C. All synthesis products were characterized by X-ray diffraction including Rietveld-refinement and granulometry. The hydration behavior of pure Ferrites was checked by calorimetric investigation. The calorimeter used is a fully revised, more accurate and more user friendly apparatus based on an arrangement first described by Kuzel 1984 [1]. The improvements are: Sample pans made of polystyrene, defined docking of sample vessels to the thermopile, defined sample compaction, and use of a water dispensing aid. All measurements were carried out under isothermal condition at a temperature of 23.0 ± 0.2 °C over a time range between 0 and 72 hours. Ferrites were hydrated with water and additionally in the presence of C_3A, Gypsum and water. Ferrites hydrated with water show a strong heat evolution and clear dependence on chemical composition of hydration heat during the first 72 hours and of time of maximum heat flow. Higher iron contents lead to lower heat evolution at later times. Ferrites hydrated with C_3A and Gypsum show two heat evolution maxima and increasing hydration heat with increasing iron content of Ferrites.

1. INTRODUCTION

The description of hydration properties – beside of rheologic properties - of formulations for construction chemistry products are important for their further optimization. Most of such formulations contain OPC in mixture with further inorganic and organic additives and mainly non reactive aggregates. The prediction of the influence of the inorganic and organic admixtures on the OPC is poor because the reaction mechanisms are misunderstood. This forced engineers to a mainly empirical procedure during the development of new binders. Basic research is necessary to understand the reactions of the hydraulic binders – in the given case of OPC – first with water and then with inorganic and organic additives. For this reason the hydration behavior of the main phases of OPC (Alite, Belite, Tricalciumaluminate and Ferrite) should be regarded in dependence of their chemical composition and their crystallographic modification.

Calcium aluminate ferrite phases are main phases not only in OPC but also in iron containing CAC. They form the solid solution series $C_6A_xF_{3-x}$ with $0 \leq x \leq 2.1$ [2,3]. Figure 1 shows a part of the ternary system CaO – CA – C_2F after Newkirk and Thwaite 1958 where the solid solution series of Ferrites is located. Aluminum and iron are located at 2 different sites in the structure (Figure 2). One site is octahedrally coordinated by oxygen the other tetrahedrally. Depending on the cooling rate the ratio of aluminum and iron which is coordinated tetrahedrally or octahedrally can be changed. Due to the different scattering factors of Al^{3+} and Fe^{3+} the refinement of the occupancy

factors of both elements on tetrahedral and octahedral sites leads to a total amount of iron and aluminum in the structure. This allows calculation of the chemical composition of the Ferrite phase using Rietveld refinement of XRD data.

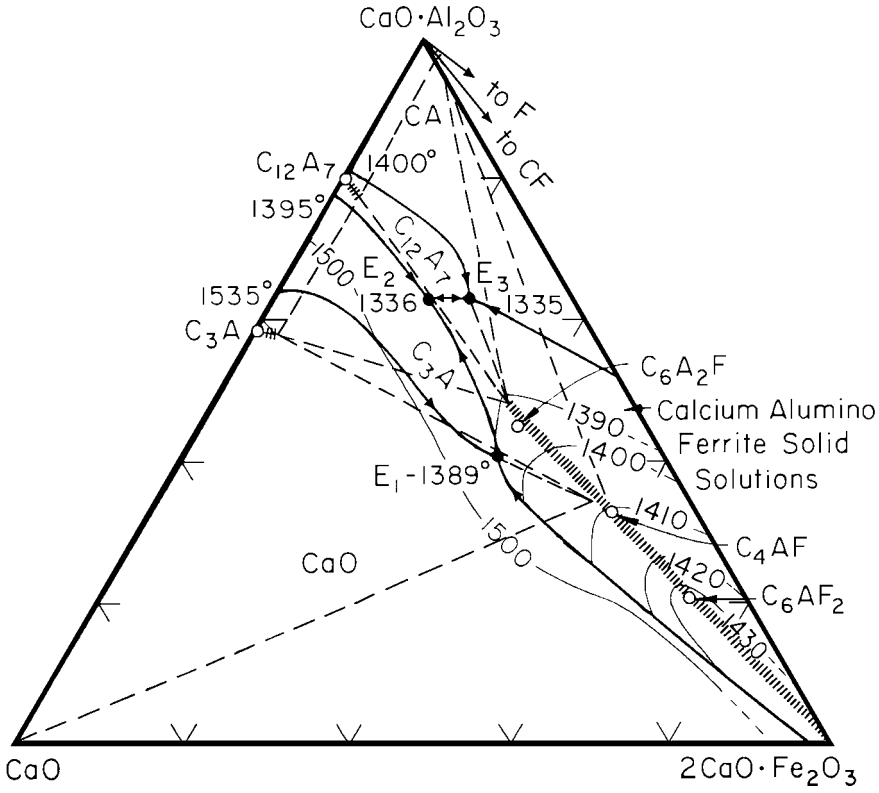

Figure 1. Pseudo ternary system CaO – CA – C_2F after Newkirk and Thwaite 1958

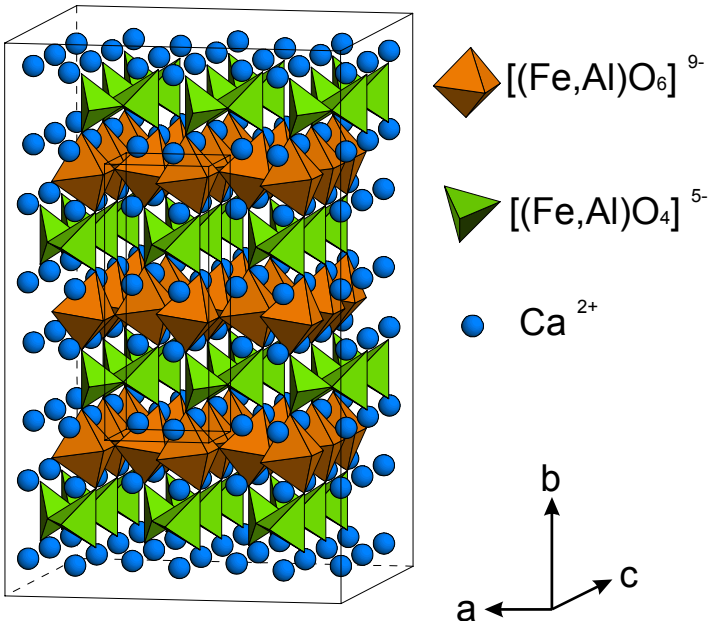

Figure 2. Orthorhombic (Ibm2) structure of Brownmillerite ($C_6A_{1.5}F_{1.5}$) given by [2]

The Al-rich members C_6A_2F to C_4AF constitute together with C_3A the so called interstitial phase in OPC clinker and give rise to very rapid setting. For that reason normally Ca-sulfate is added as a retarding agent.

The intention of this investigation was to collect data on the hydration behavior of the complete solid solution series of single phase compounds $C_6A_xF_{3-x}$ with $0 \leq x \leq 2$ by heat flow calorimetry. Furthermore ternary mixtures of $C_6A_xF_{3-x}$ (x = 1.25/ 1.5/ 1.75/ 2) with C_3A and gypsum (40ma.%:40ma.%:20ma.%) were investigated with a highly sensitive calorimeter [1,4]. Pure Ferrites were produced on a synthetic basis and characterized very well by means of chemical, granulometric and diffraction methods.

2. EXPERIMENTAL

2.1 Synthesis of Ferrites and C_3A

All syntheses were carried out in platinum crucibles using reagent grade chemicals:

$CaCO_3$
α-Al_2O_3
Fe_2O_3

20g batches of stochiometric ratios of oxides and carbonates were mixed in a disc mill and heated in a laboratory furnace in a first step at 1000°C for calcining purposes. Further sintering was proceeded at 1250°C for 39h to 118h depending on chemical composition of the batch. Sintering was interuppted after 3-41 hours in the laboratory furnace. The duration is increasing with increasing aluminum content of the solid solution. Synthesis was finished after complete reaction to pure Ferrite, which was controlled by X-ray diffraction. Table 1 summarizes sintering time and number of grinding steps for all air quenched syntheses.

Table 1. Sintering duration and number of grinding steps

ss member	Sinter time [h]	Grinding steps
C_6F_3 (C_2F)	39	4
$C_6A_{0.5}F_{2.5}$	36	6
C_6AF_2	36	6
$C_6A_{1.25}F_{1.75}$	43	4
$C_6A_{1.5}F_{1.5}$	69	5
$C_6A_{1.75}F_{1.25}$	118	9
C_6A_2F	118	9

C_3A was synthesized by mixing stochiometric ratios of Calcite and Corundum in a disc mill. The mixture was sintered using a platinum crucible inside a laboratory furnace which was heated to 1250°C for 118 hours interrupted by 5 grinding steps. Syntheses were air quenched.

2.2 XRD and Rietveld refinement

Pure Ferrites were checked by X-ray diffraction combined with Rietveld-refinement. X-ray diffraction was carried out on a Siemens D5000 using the following adjustments and front loading preparation technique:

Generator: 40 mA, 30 kV
Tube: fine focus
X-ray: Cu Kα
Filter: Ni
Slits: fixed 0.5°
Detector slit: 0.2°
Detector: scintillation
Step/Time: 0.02° 2θ / 3s
Range: 10° - 65° 2θ

All Rietveld calculations were performed using Topas 2.0 with fundamental parameter approach (FPA). The following parameters were refined:

- Background (Chebychev 5th order), zero shift, lattice parameters, scale factor, crystallite size, micro strain and occupancy factors for Al and Fe on tetrahedral and octahedral sites.

- Starting stuctural data for refinements were obtained from Colville (1970) [5] (SG Pcmn, ICSD 14296) for C_6F_3 and $C_6A_{0.5}F_{2.5}$ and from Colville and Geller (1971) [2] (SG Ibm2, ICSD 9197) for aluminum rich solid solution members.

2.3 Microcalorimetry

A new type of microcalorimeter to determine heat of reaction from hydration of hydraulic binders was described by Kuzel 1984 [1]. The isothermal calorimeter is based on the heat conduction technique. The heat, which is produced during a reaction has to pass a defined heat conduction path. Part of this defined path is a thermopile, which contains 71 in series connected BiTe semi conductor elements. Figure 3 displays a thermopile with the dimensions 32 mm x 32 mm x 4 mm.

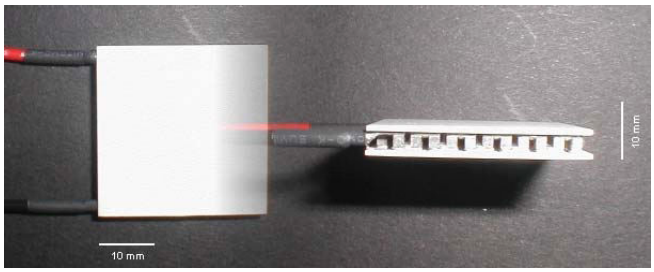

Figure 3. Thermopile with 71 BiTe semi conductor elements in planar configuration

The change in temperature, caused by the heat evolution during the hydration, results in a thermovoltage of the thermopile, which can be measured by a digital voltmeter. These µV or nV data are recorded online by a PC. This thermovoltage can be transformed into heat flow by calibration. The noise threshold can be reduced strongly by connecting two thermopiles in difference. One thermopile is used by the sample the other by an inert reference. Sample and reference are placed in vessels on top of the sample holder which is pasted onto the thermopile. Figure 4 shows a sketch of the measuring system setup.

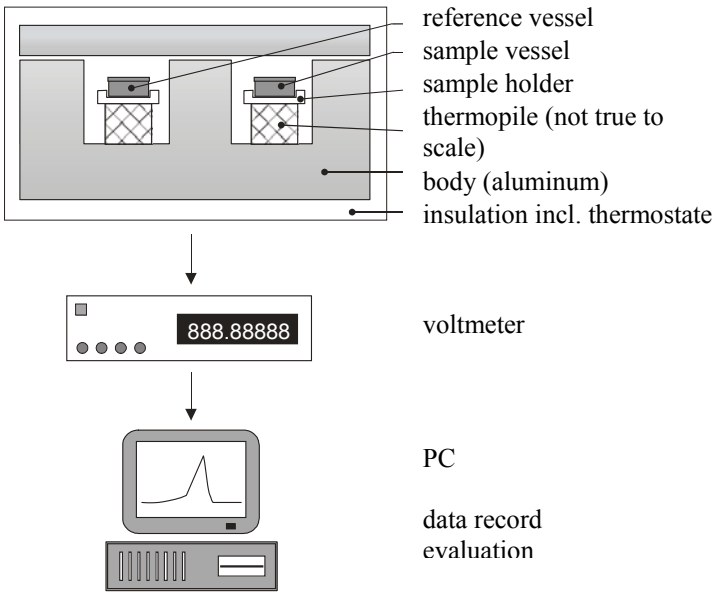

Figure 4. Complete calorimeter measuring system setup

The described calorimeter system is highly sensitive. A change of temperature in the sample vessel of 0.00002 °C can by detected properly. Further development of the calorimeter equipment [4] led to the following improvements:

⇒ Polystyrene vessels replaced copper or gilded copper vessels. Neither sensitivity nor time constant was affected. Advantages are:
- Vessels can be replaced after each measurement (no contamination)
- polystyrene is proved to be inert under hydration conditions
- sample can be observed during injection (translucent vessels)

⇒ Application of 75 µl thermal conduction paste between vessel and sample holder with the help of a "HandyStep". Advantages are:
- strictly defined heat conduction path with a highly repetitive docking area
- no pollution of the thermopile by oil of low viscosity

⇒ Application of a dispensing aid on top of the cement powder. Advantages are:
- defined sample surface
- no splashing of cement paste during injection of water
- perfect lateral spreading of water in the sample vessel
- fast and perfect mixing of solid and fluid components
- injection of water is possible down to w/c ratio of 0.35
- no contamination during compaction

⇒ Application of a compaction piston. Advantages are:
- defined sample surface
- defined density of the powder

⇒ User-friendly data acquisition and data evaluation by OMI and SEP software

The following specifications for the renewed configuration can be given:

Number of calorimetric channels	3
Operating temperature range	5 - 50 °C
Sensitivity at 23°C	about 90 µV/mW
Time constant (polystyrene vessel)	75 s
Resolution	< 2 µW
Noise level	1 µW
Precision (heat flow)	< ± 2 %
Liqiud thermostat temperature fluctuation	± 0,02 °C
Maximum sample volume	9 ml
Measuring range (maximum)	2000 mW
Limit of detectibility	2 µW

1g of Ferrite of different chemical composition was filled into polystyrene vessels after sample splitting. For Ferrite–Aluminate–Gypsum (40ma.%:40ma.%:20ma.%) mixtures 1.25 g batches were homogenized in a sealed bottle followed by manually stirring in an agate mortar. Homogenized batches were filled into polystyrene vessels. Before filling polystyrene vessels have been cleaned with isopropyl and deionized water and were dried at 45°C. Powders were subsequently covered with a dispenser-paper which was exactly fitted to the interior dimensions of the vessel and were compressed by a piston. Afterwards vessels are sealed with polystyrene lids. Deionized water is injected by a syringe. Water/solid ratio was 0.7 in all cases. Hydration temperature was 23.0±0.3°C.

3. RESULTS

3.1 Characterization of Ferrites

3.1.1 Characterization by XRD of the Ferrites

No additional phases (CF, C, C_3A, $C_{12}A_7$, CA) could be detected by quantitative Rietveld-analysis. Phase contents were in any case below the detection limits for all possible additional phases. Assuming equilibrium because of the long sintering times, the purity of all Ferrites is higher than 99.4 ma.%. Table 2 summarizes the refined lattice parameters and elementary cell volumina for synthesized Ferrites of different chemical composition.

Table 2. Refined lattice parameters and elementary cell volumina of Ferrites

SS	Lattice parameter in [Å] ± 0.001			V_{EC} [Å^3] ± 0.1
	a	b	c	
C_6F_3 (C_2F)	5.600	14.767	5.428	448.8
$C_6A_{0.5}F_{2.5}$	5.595	14.679	5.403	443.7
C_6AF_2	5.588	14.587 ± 0.002	5.375	438.1
$C_6A_{1.25}F_{1.75}$	5.579	14.550 ± 0.002	5.361	435.1
$C_6A_{1.5}F_{1.5}$	5.565	14.514	5.346	431.8
$C_6A_{1.75}F_{1.25}$	5.548	14.490	5.331	428.5
C_6A_2F	5.526	14.469	5.314	424.8

Elementary cell volumina decrease with increasing aluminum content. Lattice parameters show the same behavior. Lattice parameter c is linearly correlated to the chemical composition, while parameter a is over normal and b is under normal. Lattice parameter and elementary cell volumina simulate a perfect solid solution series. But there is a change in space group from $C_6A_{0.5}F_{2.5}$ to C_6AF_2. The distribution of aluminum and iron might influence hydration properties of Ferrites. The result of the refinement of occupancy factors is displayed in Figure 5.

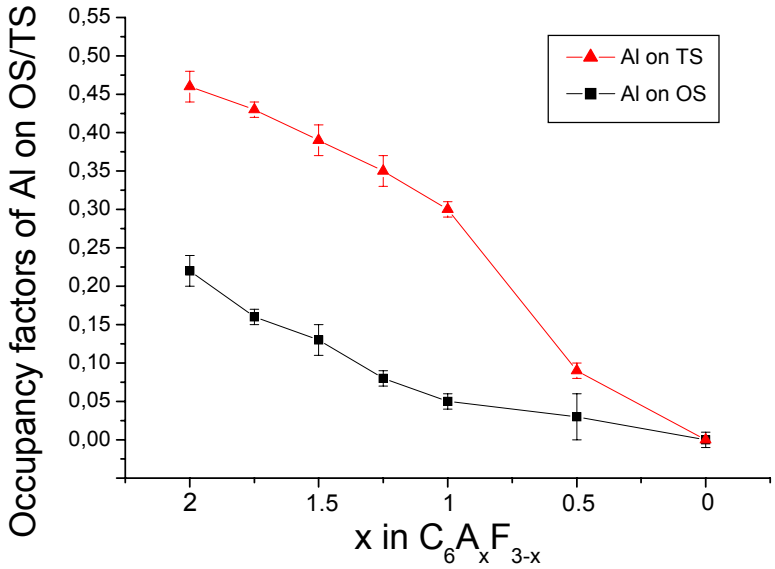

Figure 5. Refined occupancy factors of aluminum on tetrahedral (TS) and octahedral sites (OS)

Aluminum prefers tetrahedral sites. Ferrite of the chemical composition C_6A_2F is characterized by a nearly completely occupied tetrahedral site. In Table 3 the actual chemical composition of Ferrites are compared with the chemical composition calculated from refined occupancy factors.

Table 3. Comparison of actual chemical composition of $C_6A_xF_{3-x}$ and chemical composition calculated from refined occupancy factors

Actual	Calculated
C_6F_3	$C_6A_{0.03 \pm 0.02}F_{2.97 \pm 0.02}$
$C_6A_{0.5}F_{2.5}$	$C_6A_{0.33 \pm 0.10}F_{2.67 \pm 0.10}$
C_6AF_2	$C_6A_{1.04 \pm 0.06}F_{1.96 \pm 0.06}$
$C_6A_{1.25}F_{1.75}$	$C_6A_{1.30 \pm 0.03}F_{1.70 \pm 0.03}$
$C_6A_{1.5}F_{1.5}$	$C_6A_{1.57 \pm 0.07}F_{1.43 \pm 0.07}$
$C_6A_{1.75}F_{1.25}$	$C_6A_{1.74 \pm 0.05}F_{1.26 \pm 0.05}$
C_6A_2F	$C_6A_{2.04 \pm 0.10}F_{0.96 \pm 0.10}$

Chemical composition calculated from occupancy factors is in any case in very good accordance to the actual chemical composition.

3.1.2 Specific surface area of Ferrites and C_3A

The Ferrites were ground to a comparable specific surface. The specific surface of Ferrites and C_3A was determined according to Blaine method (Table 4).

Table 4. Specific surfaces of Ferrites and C_3A according to Blaine

SS	Density [g/cm^3]	Spec. surface [cm^2/g]
C_6F_3	4.02	3820 ± 10
$C_6A_{0.5}F_{2.5}$	3.93	3810 ± 10
C_6AF_2	3.83	3830 ± 10
$C_6A_{1.25}F_{1.75}$	3.78	3820 ± 20
$C_6A_{1.5}F_{1.5}$	3.74	3840 ± 10
$C_6A_{1.75}F_{1.25}$	3.69	3830 ± 20
C_6A_2F	3.65	3820 ± 30
C_3A	3.03	5010 ± 30

3.1.3 Ferrous iron content

At a sintering temperature of 1250°C ferrous iron might be present due to reduction. Therefore Fe^{2+} content was checked by colorimetric method (Table 5).

Table 5. Fe^{2+} content of synthesized Ferrites

SS	Fe_2O_3 [ma.%]	FeO [ma.%]	Fe^{2+}/Fe^{3+} [%]
C_6F_3	58.7	0.65	1.1
$C_6A_{0.5}F_{2.5}$	50.7	1.32	2.6
C_6AF_2	42.1	1.57	3.7
$C_6A_{1.25}F_{1.75}$	37.6	1.07	2.9
$C_6A_{1.5}F_{1.5}$	32.9	0.80	2.4
$C_6A_{1.75}F_{1.25}$	27.9	0.83	3.0
C_6A_2F	22.8	0.97	4.3

Ferrous iron could be detected in all synthesized Ferrite samples. The content of ferrous iron is not coupled to the chemical composition of the Ferrite solid solution member. Lowest relative content of Fe^{2+}/Fe^{3+} was detected for C_6F_3 with 1.1 % and the highest for C_6A_2F with 4.3 %.

3.2 Heat flow calorimetry

3.2.1 Hydration of pure Ferrites

Ferrites of the composition $C_6A_XF_{3-X}$ were hydrated using a water/solid-ratio of 0.7 at a temperature of 23.0±0.3°C. All measurements were repeated 2-4 times. Precision of measurements was in any case excellent. Representative calorimetric plots are shown in Figure 6. Hydration of Ferrites is very fast for all chemical compositions. For aluminum rich members the main heat evolution period is finished within the first 20 minutes. Only the heat flow of C_6F_3 stays for 1 hour in the main period. The time of maximum heat evolution is shifted towards later times with increasing iron content. The maximum heat flow of the main reaction is reduced with increasing iron content. Only $C_6A_{1.75}F_{1.25}$ does not follow this trend (Table 6). The specific heat evolution of Ferrites of different chemical composition shows a different behavior. The heat of hydration up to 72 h is increasing from C_6F_3 towards $C_6A_{1.25}F_{1.75}$. Ferrites with higher aluminum content do not produce significantly higher heat of hydration during the first 72 h excepted sample C_6A_2F (Figure 7). The heat of hydration reaches its maximum for C_6A_2F after 72 hours with 485 J/g. C_6F_3 shows the lowest heat of hydration after 72 hours with 307 J/g.

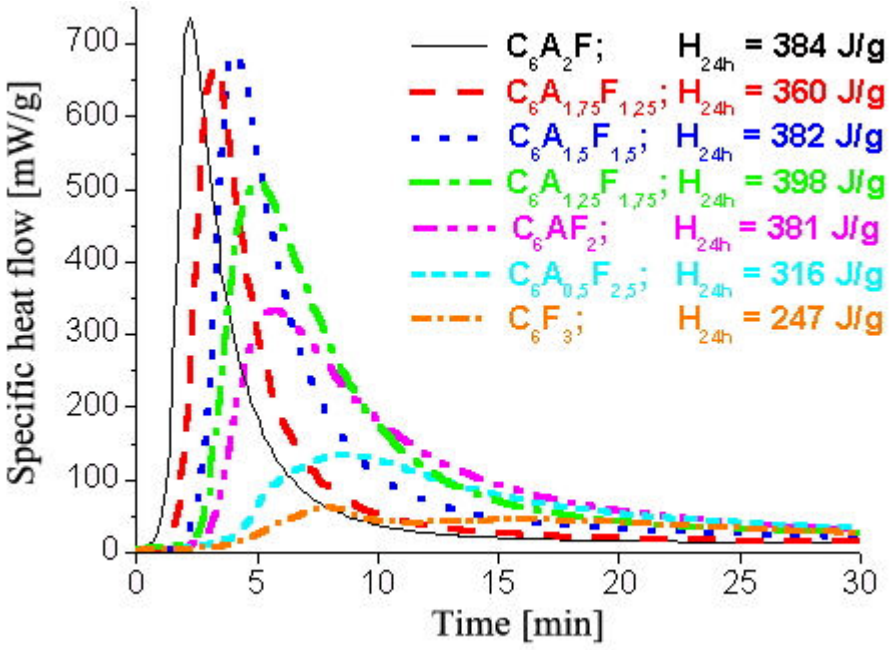

Figure 6. Specific heat flow of Ferrites during the first 30 minutes after contact with water, w/s=0.7.

Table 6. Maximum of specific heat flow of Ferrites

SS	max. of spec. heat flow [mW/g]
C_6F_3	61 ± 2
$C_6A_{0.5}F_{2.5}$	138 ± 3
C_6AF_2	338 ± 4
$C_6A_{1.25}F_{1.75}$	520 ± 9
$C_6A_{1.5}F_{1.5}$	708 ± 19
$C_6A_{1.75}F_{1.25}$	654 ± 19
C_6A_2F	706 ± 30

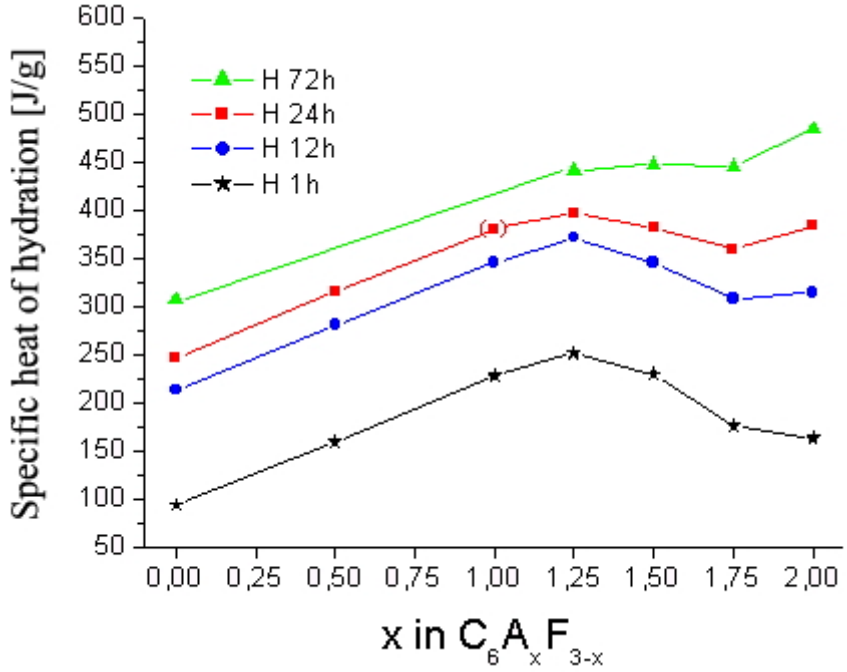

Figure 7. Specific heat of hydration of Ferrites with increasing hydration times, (■) vessel broken

3.2.2 Hydration of Ferrite - C_3A - Gypsum mixtures

Ferrites with the chemical composition $C_6A_XF_{3-X}$ 1.25 < x < 2 were hydrated with C_3A and Gypsum (40 ma.% : 40 ma.% : 20 ma.%) using a w/s-ratio of 0.7 at a temperature of 23.0 ± 0.3 °C. Figure 8 displays the heat evolution of Ferrite mixtures during the first 2 hours after contact with water.

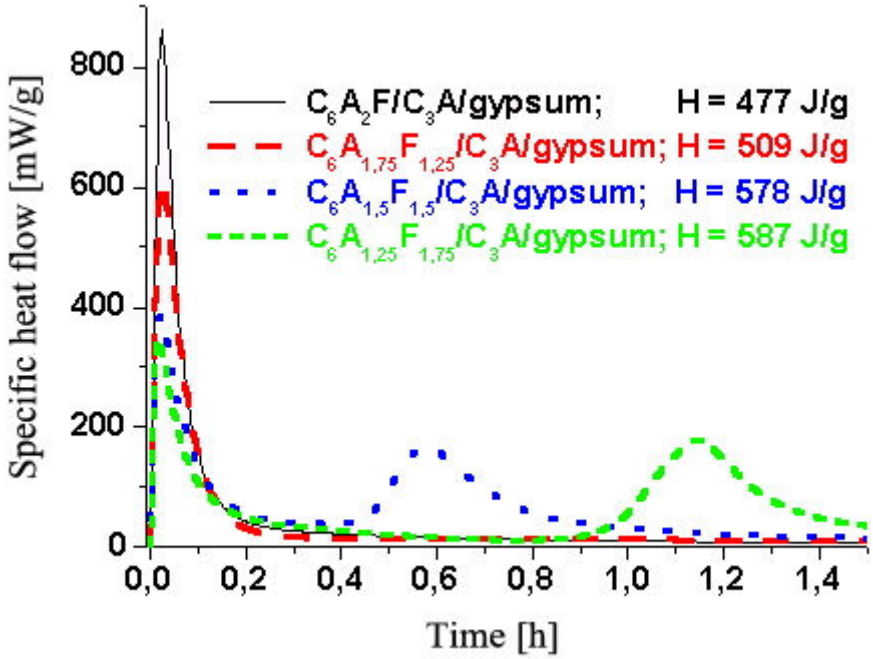

Figure 8. Heat evolution of Ferrite mixtures during hydration w/s=0.7, 23°

Mixtures with C_6A_2F or $C_6A_{1.75}F_{1.25}$ are showing only one maximum of heat like the pure Ferrites. In contrast to this hydration of ternary mixtures of $C_6A_{1.5}F_{1.5}$ and $C_6A_{1,25}F_{1,75}$ with C_3A and gypsum is different. Both hydration reactions are characterized by a 2nd maximum of heat evolution within 1.5h. The overall heat flow is increasing with Fe-content of the solid solution members (Table 7).

Table 7. Specific heat of hydration during the first 72 h for Ferrite mixtures

Mixture		C_6A_2F C_3A Gypsum	$C_6A_{1.75}F_{1.25}$ C_3A Gypsum	$C_6A_{1.5}F_{1.5}$ C_3A Gypsum	$C_6A_{1.25}F_{1.75}$ C_3A Gypsum
Specific heat evolution [J/g] during 72 h	Average value	477	509	578	587
	max. deviation from average value	19	8	9	19

4. DISCUSSION

Hydration reaction with w/s ratio of 0.7 is always characterized by a maximum of heat flow within the first quarter of an hour of reaction. This is corresponding with the investigations of Drabik (1988) [6]. Puertas (1992) [7] determined the maximum heat flow of $C_6A_{1.5}F_{1.5}$ with comparable specific surface as 700 mW/g at 0.5 h which is in very good accordance to this work with 708 ± 19 mW/g. Only the heat flow maximum is shifted towards earlier times by about 5 minutes. The time of maximum heat flow is increasing from Al-rich to Fe-rich calcium aluminate ferrate phases, which is in accordance with former investigations [8,9,10]. XRD analysis of the hydrated samples of the single phase compounds $C_6A_xF_{3-x}$ with x = 0/ 0.5/ 1.0/ 1.25/ 1.5/ 1.75/ 2 yielded different hexagonal calcium aluminate hydrates like Mono-/Hemicarbonate, C_3AH_6, as well as Goethite as crystalline hydration products. XRD investigation of hydrated Ferrites $C_6A_xF_{3-x}$ ($1 \leq x \leq 2$) after 96h showed predominantly iron substituted C_3AH_6 (compare Fortune (1983)[11]). Whereas

hydration of Al-rich C_6A_2F and $C_6A_{1.75}F_{1.25}$ leads to additional hexagonal calcium aluminate hydrates. In hydrated samples with Ferrites (x>1.5) no hexagonal aluminate hydrates could be detected. This allows the assumption that higher iron content in Ferrites support the conversion from laminar hexagonal hydrates to Hydrogarnet. The only crystalline phases in hydrated C_6F_3 and $C_6A_{0.5}F_{2.5}$ could be determined as Goethite and Fe-Monocarbonate. Hydrogarnet could not be formed because of the low aluminum content and the low maximum heat of hydration which was lower than 140 mW/g. This interpretation is supported by the results of Ecker (1998) [12]. The 1st maximum of heat flow can presumably be attributed to formation of the hexagonal calcium aluminate hydrates and its conversion to C_3AH_6, which is promoted at higher temperatures [7]. The specific heat of hydration of $C_6A_{1.5}F_{1.5}$ was 380 J/g after 24 hours and 420 J/g after 48 hours at 23°C. The 48 hours value is in fairly good agreement with the 500 J/g at 20°C published by Drabik (1988) [6]. But the comparison of heat of hydration is problematic because of the strong influence from parameters like specific surface, grain size distribution, w/s-ratio and temperature.

Reaction of Ferrite or C_3A with Gypsum was reported in [6,7,8,13]. Mixtures of C_3A and Gypsum show two heat flow maxima during hydration. The first one is attributed to the formation of Ettringite the second one to the conversion of Ettringite to Monosulfate (if sulfate content is too low). Mixtures of Ferrites, C_3A and Gypsum containing Ferrites of the composition $C_6A_{1.50}F_{1.50}$ and $C_6A_{1.25}F_{1.75}$ show the same behavior as C_3A - Gypsum mixtures. There is a first strong heat evolution after a few minutes caused by hydration of Ferrite, C_3A and Gypsum and the Formation of Ettringite. After 0.4 hours a second heat flow maximum is observed which can be attributed clearly to further hydration of Ferrite and C_3A and the conversion from Ettringite to Monosulfate. XRD investigations of 72 h hydrated products confirm this statement. The mixtures containing aluminum rich C_6A_2F and $C_6A_{1.75}F_{1.25}$ are missing a second heat flow maximum. XRD investigation of hydrated products after 72 h yielded Monosulfate as main hydration product. This proves that conversion from Ettringite to Monosulfate is accelerated by aluminum rich Ferrites. The specific heat evolution of mixtures containing Ferrites, C_3A and Gypsum after 72 h is increasing from 477 J/g to 587 J/g with increasing iron content of the Ferrites.

REFERENCES

[1] Kuzel, H.-J. Ein leistungsfähiges Wärmeleitungskalorimeter, TIZ-Fachberichte, vol. 108, no. 1, 1984, pp. 46-51

[2] Colville A.A. and Geller S., Crystal structures of $Ca_2Fe_{1.43}Al_{0.57}O_5$ and $Ca_2Fe_{1.28}Al_{0.72}O_5$, Acta Cryst., B 27, 2311-2315, 1971

[3] Mayerhofer W., Rietveldanalyse der Ferratphase – Vom Laborsystem zum technischen Portlandzement, Diplomarbeit Mineralogie Erlangen, 1996

[4] Neubauer, J. and Götz-Neunhoeffer, F. Efficiency of highly sensitive heat flow calorimetry in examination of OPC hydration, Proc. 24th Int. Conf. on Cem. Microscopy, San Diego, 2002

[5] Colville A.A., Crystal structures of $Ca_2Fe_2O_5$ and its relation to the nuclear electric field gradient at the iron sites, Acta Cryst. B 26, 1469-1473, 1970

[6] Drabik, M., Conversion and heat evolution during hydration of aluminum and iron containing clinker phases in presence of sulphate, J. of Thermal Analysis, 33, 679-684, 1988

[7] Puertas F., Hydration of $4CaO{\cdot}Al_2O_3{\cdot}Mn_2O_3$ in the absence and presence of gypsum. A comparative study with the hydration of $4CaO{\cdot}Al_2O_3{\cdot}Fe_2O_3$, Cem.Con.Res., 3, 20-32, 1992

[8] DeKeyser W., The hydration of ferrite phase of cements, Vth Int. Symp. on Chem. of Cem., Tokyo, Sup. Paper, II, 378-386, 1968

[9] Negro, A., Über die Hydratation der Calcium-Ferrite und Calciumaluminat-Ferrite, ZKG, 32, 83-88, 1979

[10] Christensen N., A time resolved powder neutron diffraction investigation of reactions of portland cement components with water, Acta Chem. Scandinavica, A 39, 593-604, 1985

[11] Fortune J.M. and Coey, J.M.D., Hydration products of calcium aluminoferrite, Cem. Con. Res., 11, 407-414, 1983

[12] Ecker M., Diadochiebezieungen in Calciumaluminatferraten und deren Hydratationsprodukten, Hallesches Jahrbuch f. Geowissenschaften, ReiheB, Beiheift 3, 1998

[13] Kemethmüller, S, Synthese und Charakterisierung von eisenhaltigem Tricalciumaluminat und dessen Hydratationsverhalten, Diplomarbeit Mineralogie Erlangen, 2001

EFFECT OF INORGANIC ADMIXTURES ON THE EARLY HYDRATION OF MONOCALCIUM ALUMINATE ($CA_{1-X}F_X$)

F. Goetz-Neunhoeffer and J. Neubauer

Department of Mineralogy, University Erlangen, Schlossgarten 5a, 91054 Erlangen, Germany
E-mail: goetz@geol.uni-erlangen.de

ABSTRACT

The main phase of high alumina cements Monocalcium aluminate (CA) is determining the setting behaviour of formulations in building chemistry applications. Until recently it was not completely understood what factors favour good performance of CA in technical products. In order to solve mechanisms occurring in technical systems with Calcium Aluminate cements (CAC) neat CA and several binary model systems of CA with admixtures of Li_2CO_3 and Ferrite phase $C_6A_yF_{3-y}$ ($0 \leq y \leq 1$) were analysed.

CA, iron doped $CA_{1-x}F_x$ solid solutions and three Fe-rich Ferrite solid solutions were synthesised in laboratory furnaces at 1250°C from reagent grade chemicals. All phases were checked for minor phases and characterised by X-ray powder diffraction analysis. Lattice and structural parameter refinement by Rietveld analysis with fundamental parameter approach (TOPAS) was employed for crystallographic characterisation of the anhydrous phases.

The neat compounds CA and iron doped $CA_{1-x}F_x$ and mixtures with Ferrite phases $C_6A_yF_{3-y}$ were hydrated at 23°C in a heat flow calorimeter based on a quadruple arrangement first described by [1] and fully revised by [2]. In accordance with calorimetric data the hydrating mixtures were investigated by X-ray powder diffraction analysis in order to interpret the recorded caloric effects of the first 48 hours of hydration.

1. INTRODUCTION

Monocalcium aluminate determines the setting behaviour of Calcium Aluminate Cements. CACs with different Fe-contents are used in a wide range of formulations for building chemistry applications because of their very rapid early strength. Hydration behaviour of formulations for construction chemistry products is a very important property for their further optimisation. Most formulations with CAC in the mixture are combined with inorganic and organic additives and non reactive aggregates. Until recently it was not completely understood how CA reacts in a cement paste and what factors favour good performance in technical products. The influence of admixtures on CAC is poor because reaction mechanisms depend on a combination of factors like homogenisation, grain size, hydration temperature, and w/s values.

In order to get an overview on mechanisms occurring in technical systems with Calcium aluminate cements (CAC), neat CA and three binary model systems of CA with Ferrite phases $C_6A_yF_{3-y}$ ($0 \leq y \leq 1$) were studied by heat flow calorimetry in combination with kinetic XRD investigations.

Proceedings of the 11th International Congress on the Chemistry of Cement (ICCC)
'Cement's Contribution to the Development in the 21st Century'
Hosted by: The Cement and Concrete Institute of South Africa
CD-ROM produced by: Document Transformation Technologies
11 - 16 May 2003, Durban, South Africa
ISBN Number: 0-9584085-8-0
Editors: Dr G. Grieve and G. Owens
Congress Organised by: Event Dynamics

Table 1. Investigated model systems

Model system		Additive	w/s ratio
$CA_{1-x}F_x$ with x = 0, 0.03, 0.06, 0.1		---	0.45
$CA_{1-x}F_x$ with x = 0, 0.05, 0.1	+	Li_2CO_3	0.45
CA	+	$C_6A_yF_{3-y}$ with y = 0, 0.5, 1.0	0.5

2. EXPERIMENTAL PARAMETERS

2.1 Synthesis of the calcium iron ferrites $CA_{1-x}F_x$ and $C_6A_yF_{3-y}$

CA, iron doped $CA_{1-x}F_x$ solid solutions and three Fe-rich Ferrite solid solutions were synthesised in laboratory furnaces at 1250°C from reagent grade chemicals by solid state reaction.

Table 2. Synthesis parameter for the synthetic CAC clinker phases

Phase	Trivial name	Temperature [°C]	Synthesis time [h]	Grinding
$CA_{1-x}F_x$	Monocalcium-aluminate	1250	16	5 min every 4h
$C_6A_yF_{3-y}$	Ferrite phase	1250	70	10 min every 12h

All pure synthesised phases were ground in a disk mill (agate, 50g, 30min) and sieved <36µm prior to all the following experimental procedures.

2.2 X-ray diffraction powder analysis

The synthesis products from $CA_{1-x}F_x$ and $C_6A_yF_{3-y}$ solid solutions were checked for minor phases and characterised by X-ray powder diffraction analysis. Preparation of the investigated samples, which were ground in a disc mill to get the required grain sizes for X-ray powder diffraction, was performed in frontloading technique. XRD data were collected using a D5000 Bragg-Brentano diffractometer with $Cu_{K\alpha}$-radiation.

For XRD data collection for Rietveld analysis the fixed slit arrangement was utilised. The qualitative phase composition of hydrated samples from calorimetric experiments was investigated after 4 days. XRD patterns were recorded with V20 slit and 0.6mm receiving slit arrangement.

Table 3. XRD instrumental conditions

	Rietveld refinement	Qualitative phase analysis of hydrated samples
Tube voltage	40 kV	40 kV
Tube current	30mA	35mA
Time/step	3s	2s
Step width	0.02° 2θ	0.02 °2θ
Divergence slit	0.5°	V20
Receiving slit	0.2 mm	0.6mm
Monochromator	Ni-filter	Secondary graphite
Range of scan	10-65 °2θ	5-60 °2θ

2.3 Rietveld refinement of XRD data

Lattice and structural parameter refinement by Rietveld analysis with fundamental parameter approach (TOPAS) was employed for crystallographic characterisation and for determination of the solid solution limit of the calcium aluminate ferrite solid solutions. The following ICSD-data were used for the structural refinement:

Table 4. Used structure models from the ICSD- database [3]

Phase	ICSD- Code	Reference
CA	260	Hörkner & Müller-Buschbaum (1976) [4]
$C_6(A,F)_3$	9197	Colville & Geller (1971) [5]
C_2F	14296	Colville (1970)[6]
CaO	61550	Natta & Passerini (1929) [7]

2.4 Specific area analysis

The specific area of the synthesised calcium aluminate ferrites was determined by Blaine method.

2.5 Heat flow calorimetry

For the hydration of the model systems a heat flow calorimeter operating in isothermal mode was employed [2]. Three samples can be investigated simultaneously. The temperature during hydration was kept constant at a value of 23.0°C±0.3°. The deionised water used for hydration experiments was injected with a syringe through the top of polystyrene vessels. Table 5 summarises the instrumental parameter.

Table 5. Instrumental parameter of the heat flow calorimeter

Hydration time [h]	48-100
Integration time / cell [s]	5
Interval time [s]	19

3. RESULTS

3.1 Characterisation of $CA_{1-x}F_x$ by XRD-analysis

The substitution limit of $CA_{1-x}F_x$ was determined from the refined cell volume of the solid solutions with x = 0, 0.3, 0.5, 0.6, 0.1, 0,15, and 0.20. In Figure 1 the determined cell volumes are plotted against the iron oxide ratio in the synthesis mixture. Standard deviation from six independent preparations and refinements was ± 0.015Å^3. The cell volumes increase with rising iron ratio, up to a composition of 11.7±0.2 mole% Fe_2O_3 substitution. With higher Fe_2O_3 contents no further increase of the lattice parameter could be detected but increasing amounts of $C_2(A,F)$ and CF_3A.

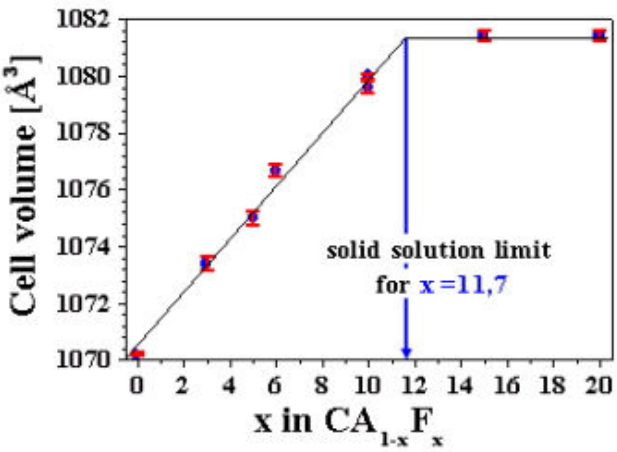

Figure 1. Determination of substitution limit of Fe_2O_3 in $CA_{1-x}F_x$

3.2 Characterisation of $C_6A_yF_{3-y}$ by XRD-analysis

For refinement of $C_6A_yF_{3-y}$ with y=0 and 0.5 the structure data of Colville [6] and for y=1 the data of Colville and Geller [5] were used. Figure 2 shows the average values of lattice parameter refinements from four measurements of each of the three solid solution members plotted versus to the chemical composition. Standard deviations of lattice parameter and of the cell volumes are very low with 0.001 Å and 0.1 $Å^3$.

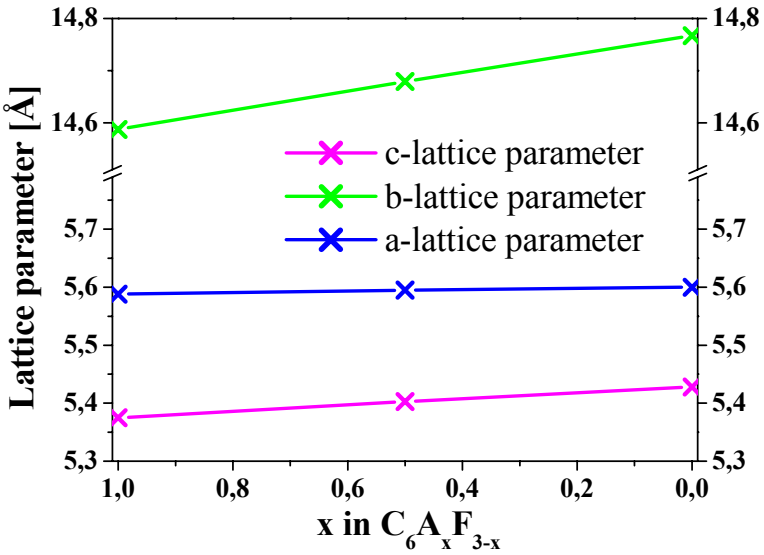

Figure 2. Average values of lattice parameter refinements from four measurements of each of the three solid solution members plotted versus the chemical composition

3.3 Heat flow calorimetry of $CA_{1-x}F_x$ pastes at w/s=0.45

Neat CA pastes with w/s ratio of 0.45 and specific surface area of 4000 cm^2/g show no reproducibility with respect to the length of induction period and the time of maximum heat evolution t_{max} (Figure 3). During the induction period heat flow is very low. Additionally to the results in Figure 3, another batch of CA was hydrated at different w/s values from 0.4 to 2.5 and a specific surface area of 2200 cm^2/g. The determined average values from 245 to 264 J/g ± 20 J/g give rise to the assumption that neither constant w/s nor specific area values play a dominating role with respect to reproducibility of CA hydration.

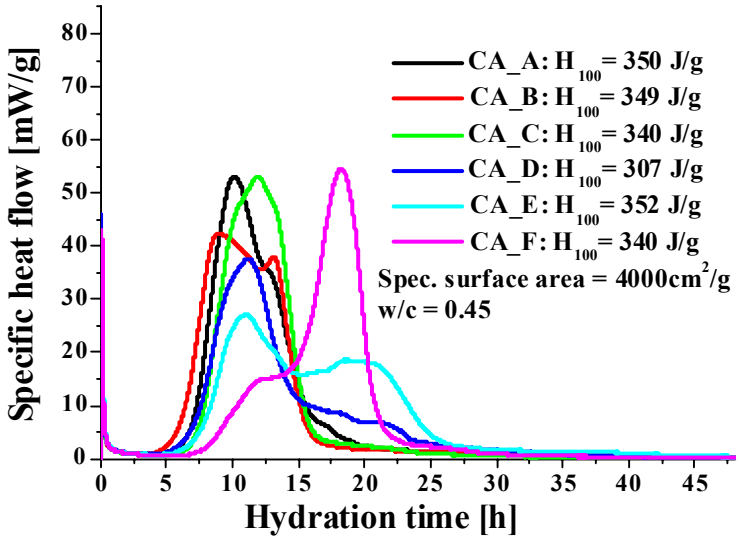

Figure 3. Heat flow diagrams of CA(T = 23°C, 100h, w/s = 0.45)

With increasing iron content of the solid solution, e.g. $CA_{0.94}F_{0.06}$, with w/s ratio of 0.45 and specific surface area of 4000 cm^2/g the hydration again shows no reproducibility with respect to the length of the induction period and the time of maximum heat evolution (Figure 4).

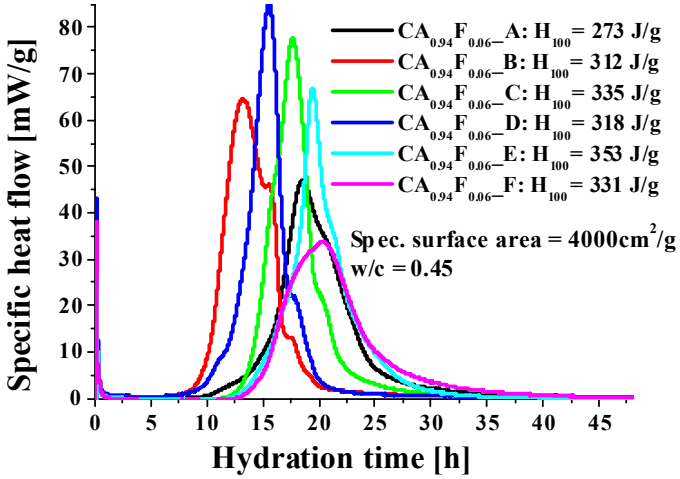

Figure 4. Heat flow diagrams of $CA_{0.94}F_{0.06}$ (T = 23°C, 100h, w/s = 0.45)

The induction period lies between 11.9h (CA) and 16.9h ($CA_{0.94}F_{0.06}$). After investigation of the different solid solution members of $CA_{1-X}F_X$ with x= 0, 0.03, 0.06, 0.1 with w/s=0.45 we could not determine a correlation of average specific heat and the time of maximum heat flow with the Fe-content (Figure 5). The average value of maximum heat flow increases up to $CA_{0.94}F_{0.06}$ and slightly decreases for $CA_{0.90}F_{0.10}$ but the standard deviations are overlapping and therefore no general statement on a correlation can be concluded. An influence of Fe-content on hydration behaviour of $CA_{1-X}F_X$ could not be observed.

Table 6. Heat flow values of CA and iron doped $CA_{1-x}F_x$

Specific heat flow [J/g] of $CA_{1-X}F_X$ with x= 0, 0.03, 0.06, 0.1				
T = 23°C, 100h, w/s = 0.45				
Composition of solid solution	**CA**	**$CA_{0.97}F_{0.03}$**	**$CA_{0.94}F_{0.06}$**	**$CA_{0.90}F_{0.10}$**
Specific surface area [cm²/g]	4000	4024	3999	4091
∅ Specific heat flow H_{100} (6 data sets) [J/g]	340	331	320	358
Minimum value[J/g]	307	308	273	343
Maximum value[J/g]	352	346	353	372
Max. deviation from ∅ specific heat flow	33	23	47	26
Standard deviation[J/g]	15	14	25	11

The average values of overall heat evolution after 100h with a standard deviation determined from six measurements of 11-25 J/g (Table 6) is better reproducible than the time of maximum heat flow t_{max} (Figure 5).

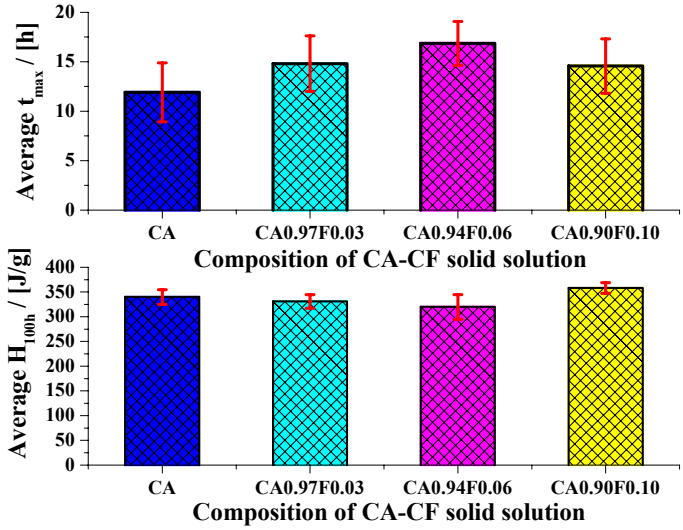

Figure 5. Comparison of average H_{100h} and t_{max} of $CA_{1-X}F_X$ with x= 0, 0.03, 0.06, 0.1 at w/s=0.45

3.4 Heat flow calorimetry of $CA_{1-x}F_x$ pastes with 0.02%Li_2CO_3-solution at w/s=0.45

With the application of aqueous 0.02%Li_2CO_3-solution instead of pure H_2O for heat flow calorimetry of the solid solution $CA_{1-x}F_x$ (x = 0, 0.05, 0.1) with w/s ratio of 0.45 and specific surface area of 3266 to 3421 cm^2/g, the hydration shows good reproducibility with respect to the average values for the heat flow of $CA_{1-X}F_X$. In Figure 6 the heat flow diagram of CA hydrated with aqueous 0.02%Li_2CO_3-solution is plotted. After injection only a short induction period was observed with heat flows from 2.5-6.5 mW/g.

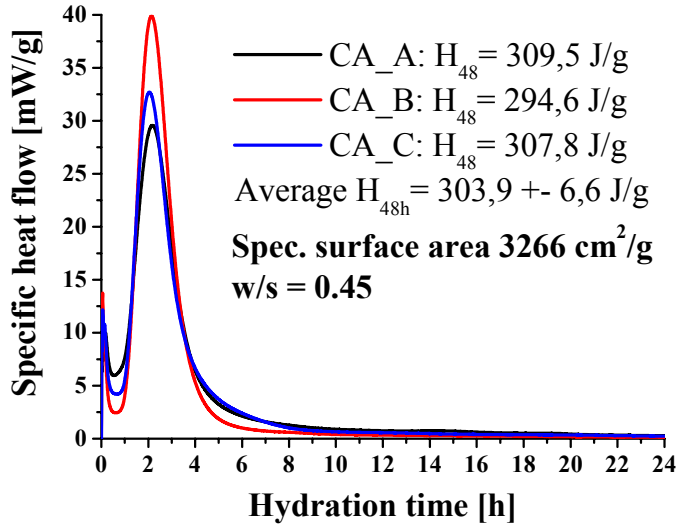

Figure 6. Heat flow diagram of CA accelerated with Li_2CO_3-solution

The standard deviations and the values for maximum deviation from average specific heat are noticeably lower than for hydration with pure H_2O. The time of maximum heat evolution is shifting to 2.1h (CA), 3.7h ($CA_{0.95}F_{0.05}$), and 3.1h for $CA_{0.90}F_{0.10}$ solid solution (Figure 7). The induction period is reduced and the times are much more reproducible by addition of Li_2CO_3-solution.

But again no correlation time of maximum heat evolution with the Fe-content of the solid solution could be observed.

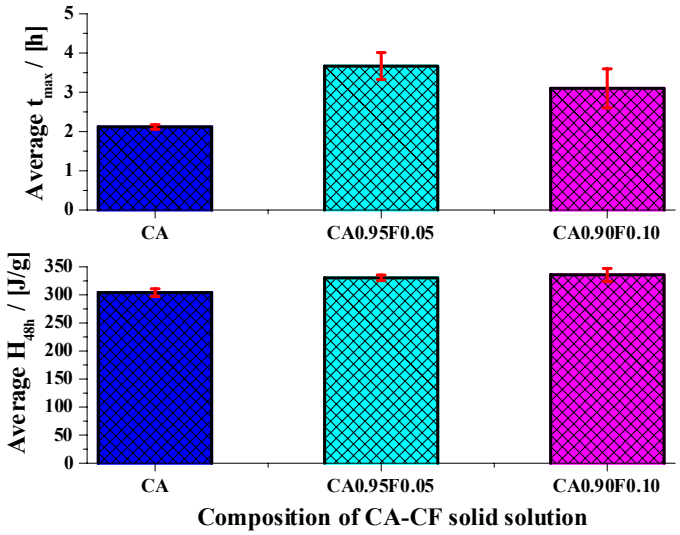

Figure 7. Comparison of average H_{48h} and t_{max} of $CA_{1-X}F_X$ with x= 0, 0.03, 0.06, 0.1 at w/s=0.45 with aqueous Li_2CO_3-solution

The average values for overall heat flow has the lowest values for CA and is increasing with the Fe-content of the hydrated $CA_{1-x}F_x$ solid solution member from 304 to 331 J/g. But standard deviations of $CA_{0.95}F_{0.05}$ and $CA_{0.90}F_{0.10}$ are overlapping slightly and specific surface area of $CA_{0.90}F_{0.10}$ is higher than for $CA_{0.95}F_{0.05}$. Because of the experimental data only the difference between CA and $CA_{0.95}F_{0.05}$ could be determined by heat flow calorimetry.

Table 7. Heat flow values of CA and iron doped $CA_{1-x}F_x$ accelerated with Li_2CO_3-solution

Specific heat flow [J/g] of $CA_{1-X}F_X$ x= 0, 0.05, 0.1			
T = 23°C, 48h, w/s = 0.45, 0.02% Li_2CO_3-solution			
Composition of solid solution	**CA**	**$CA_{0.95}F_{0.05}$**	**$CA_{0.90}F_{0.10}$**
Specific surface area [cm²/g]	3266	3287	3421
∅ Specific heat flow H_{48} (from 3 data sets) [J/g]	304	331	336
Minimum value[J/g]	295	326	321
Maximum value[J/g]	310	338	350
Maximum deviation from ∅ specific heat flow [J/g]	7	5	11
Standard deviation [J/g]	8	6	14

3.5 Heat flow calorimetry of CA with different Ferrite solid solutions at w/s=0.7

Ferrites of composition C_6F_3, $C_6A_{0.5}F_{2.5}$ and C_6AF_2 (spec. surface area ~ 3800 cm^2/g) were mixed with CA (spec. surface area ~ 4400 cm^2/g). Ferrite to CA ratio of the mixes was 30:70. Three mixes were hydrated at 23°C with w/s value of 0.5 in the heat flow calorimeter from 0-72h.

For Ferrite $C_6A_{0.5}F_{2.5}$ in mix with CA the induction period of hydration is finished after 6.5h and the time of maximum evolution can be set at 15.7-17.4h. After 25h the heat flow is very low with 0.4 ± 0.1 mW/g. In Figure 8 are plotted the heat flow diagrams of this mix for three measurements. The maximum heat flow and the times of maximum heat flow show good reproducibility.

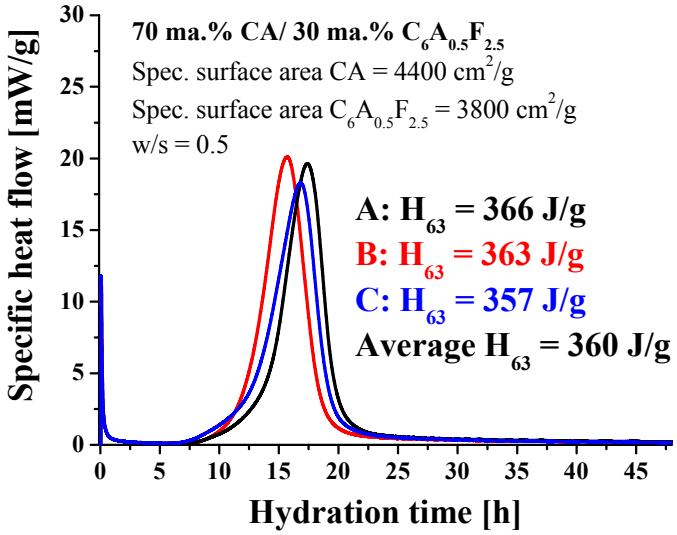

Figure 8. Heat flow diagrams of CA-$C_6A_{0.5}F_{2.5}$ –mix70:30 (T = 23°C, 72h, w/s = 0.5)

Hydration reactions of CA in mixes with the three Fe-rich Ferrites are not very different with respect to the value and the time of maximum heat flow (Figure 9). The overall heat of hydration after 63 h decreases slightly with the Fe-content of the Ferrites in the mixture with CA (Table 8). During the induction period the heat flow is very low.

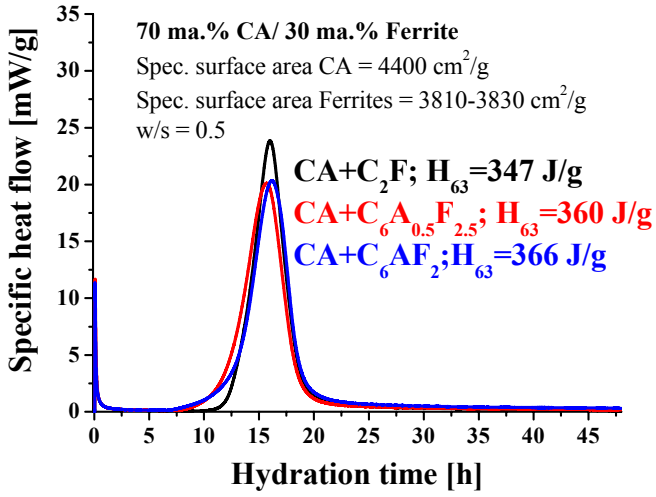

Figure 9. Heat flow diagrams of all mixes of CA with different Ferrite solid solutions; w/s = 0.5

Table 8. Specific heat flow H_{63} of CA with different Ferrite solid solutions; w/s = 0.5

Specific heat flow [J/g] of CA with $C_6A_yF_{3-y}$ y= 0, 0.5, 1.0			
T = 23°C, 63h, w/s = 0.5			
Composition of mix	**70ma.%CA + 30ma.%C_6F_3**	**70ma.%CA + 30ma.%$C_6A_{0.5}F_{2.5}$**	**70ma.%CA + 30ma.%C_6AF_2**
Specific surface area [cm²/g]	4400/3820	4400/3810	4400/3830
∅ Spec. heat flow H_{63} (3 data sets) [J/g]	347	360	361
Minimum value[J/g]	343	357	359
Maximum value[J/g]	350	363	379
Max. deviation from ∅ spec. heat flow	4	3	13
Standard deviation[J/g]	4	3	11

3.6 Qualitative XRD-analysis of the hydration products from heat flow calorimetry

Qualitative XRD investigation of the hydrated samples could show that C_2AH_y, CAH_x and AH_3 are forming from $CA_{1-x}F_x$ and mixtures with $C_6A_yF_{3-y}$. Although C/A value of the mixture of CA with ferrite was greater than for pure $CA_{1-x}F_x$ no difference in phase composition of the hydrated phases could be determined for this two-model system. In the case of the samples $CA_{1-x}F_x$ hydrated with 0.02% Li_2CO_3 the phase CAH_x could not be observed.

Table 9. Phase composition of hydrated samples from calorimetric investigations

Model system	w/s ratio	$CA_{1-x}F_x$	$C_6A_yF_{3-y}$	C_2AH_y	CAH_x	AH_3
$CA_{1-x}F_x$ (x = 0, 0.03, 0.06, 0.1)	0.45	**X**	**-.-**	**X**	**X**	**X**
$CA_{1-x}F_x$ (x = 0, 0.05, 0.1) + 0.02% Li_2CO_3	0.45	**X**	**-.-**	**X**	**-.-**	**X**
CA + ($C_6A_yF_{3-y}$ with y = 0, 0.5)	0.5	**X**	**X**	**X**	**X**	**X**

4. DISCUSSION

Neat pastes of $CA_{1-x}F_x$ (x = 0, 0.03, 0.06, 0.1) with w/s ratio of 0.45 and specific surface area of 4000 cm^2/g are showing no reproducibility of hydration behaviour. Neither length of induction period, overall heat of hydration nor time of maximum heat flow are showing a clear trend with increasing Fe-content of the solid solution [8]. This has not been reported yet and has absolutely to be taken into account when discussing hydration of CA. Our investigation could show that in spite of constant temperature, grain size distribution, and w/s value, the hydration can not be characterised to follow a certain course. Under the assumption of ideal reproducibility of preparation and taking into account the highly sensitive calorimeter arrangement with outstanding reproducibility we could only attribute this to phase depending on local and global effects. After hydration of $CA_{1-x}F_x$ at 23°C the hydrates CAH_x (x=7-10) and C_2AH_y (y≈8) were identified by X-ray diffraction analysis. C_2AH_y is known for better nucleation properties than the less CaO-containing CAH_x [9]. Investigation of synthetic iron free CAC mixtures led to the same not reproducible results for length of induction period and time of maximum heat evolution [10]. The observed formation of predominantly CAH_x in our investigated hydrated samples is another indicator for too low CaO/Al_2O_3-ratio being responsible for poor reproducibility of hydration.

Hydration experiments of the other two model systems are showing the expected increase in reproducibility with addition of Li_2CO_3-solution and with addition of Ferrites. Hydration of CA is little accelerated by Ferrite phase and very strongly accelerated by 0.02% Li_2CO_3-solution.

The accelerative effect of Li-salts is attributed to an elimination of the nucleation barrier by formation of Li-metahydrate, which is acting as nucleus for heterogeneous nucleation [9]. In the Li-accelerated system C_2AH_y could be determined as the only calcium aluminate hydrate phase. The absence of CAH_x is indicative of a more reproducible hydration behaviour.

Hydration reactions of CA in mixes with three Fe-rich Ferrites (70:30) exhibit only small differences. The mixtures were chosen to simulate hydration of Fe-rich CAC. In any mix with Ferrite CA is influenced by addition of the CaO-rich phase with shortening of the induction period and by producing a more repeatable course of hydration. Heat evolution and the time of maximum heat flow are not dependent on Fe-content of the Ferrite [11]. With our experiments we could show that CA hydrates more reproducibly in the presence of a CaO-rich phase. From investigations of several calcium aluminates (C_3A, CA, CA_2) it is known that CA_2 is hydrating less reactively than CA and C_3A is more reactive than CA [12]. This allows the conclusion that CaO/Al_2O_3-ratio of the

bulk composition favours the formation of C_2AH_y which is more spontaneous forming than CAH_x. But Ferrites are less accelerative than 0.02% Li_2CO_3-solution.

From our studies on hydration of CA with inorganic additives we can conclude that there are at least two mechanisms responsible for accelerating CA and getting more repeatable hydration behaviour:

- CaO-content of the bulk composition which must support higher CaO-concentration after addition of H_2O
- Nucleation of C_2AH_y is processing more reproducibly than nucleation of CAH_x. For that reason any change in the hydrating system which is favouring the formation of C_2AH_y leads to acceleration and better repeatability (as shown with addition of Li_2CO_3-solution)

ACKNOWLEDGEMENTS

Thanks are due to Dipl.-Min. I. Lindner, Dipl.-Min. A. Neumann and R. Enderle for their experimental support with synthesis, mineralogical characterisation and with heat flow calorimetry.

REFERENCES

[1] Kuzel, H. J. Ein leistungsfähiges Wärmeleitungskalorimeter, TIZ-Fachberichte, 108, 1, 1984, 46-51.
[2] Neubauer, J. & Goetz-Neunhoeffer, F. Efficiency of highly sensitive heat flow calorimetry in examination of OPC hydration, Proceedings of the 24th conference on cement microscopy, San Diego, 2002, pp 58-68
[3] FIZ Karlsruhe, ICSD, Inorganic Crystal Structure Database, 1995
[4] Hörkner W. & Müller-Buschbaum, H. Zur Kristallstruktur von $CaAl_2O_4$, Journal of Inorg. Nucl. Chemistry, 38, 1976, 983-984
[5] Colville A.A. and Geller S., Crystal structures of $Ca_2Fe_{1.43}Al_{0.57}O_5$ and $Ca_2Fe_{1.28}Al_{0.72}O_5$, Acta Cryst., B 27, 1971, 3196-3200
[6] Colville A.A., Crystal structures of $Ca_2Fe_2O_5$ and its relation to the nuclear electric field gradient at the iron sites, Acta Cryst., B 26, 1970, 1469-1473
[7] Natta, G. & Passerini, L. Gazetta Chimica Italiana, 59, 1929, 129-154
[8] Neumann, A. Hydratationsversuche an eisendotiertem Monocalciumaluminat, Master Thesis Mineralogy Erlangen, 2001, pp 101
[9] Rodger, S. A. & Double, D. D. The Chemistry of Hydration of High Alumina Cements in the Presence of accelerating and retarding Admixtures, Cement and Concrete Research, Vol. 14, 1984, 73-82.
[10] Schmid et al., ICCC 2003, Effect of $Ca(OH)_2$ and Li_2CO_3 on hydration behavior of synthetic Calcium Aluminate Cements,
[11] Lindner, I. Charakterisierung der Kalziumaluminatferrat-Mischkristallgleider und Untersuchung des Hydratationsverhaltens, Master Thesis Mineralogy Erlangen, 2002, pp 84
[12] Kudryavtsev, A. B., Kouznetsova, T.V., Linert, W. and Hunter, G. On the possibilities of in situ studies of the hydration of aluminate cements using wideline ^{27}Al NMR spectroscopy, Cement and Concrete Research, 1997, vol 27, no. 4, 501-513

EFFECT OF INORGANIC ADMIXTURES ON THE EARLY HYDRATION OF MONOCALCIUM ALUMINATE ($CA_{1-X}F_X$)

F. Goetz-Neunhoeffer and J. Neubauer

Department of Mineralogy, University Erlangen, Schlossgarten 5a, 91054 Erlangen, Germany
E-mail: goetz@geol.uni-erlangen.de

Dr. Friedlinde Goetz-Neunhoeffer

PERSONAL DATA

Name:	Friedlinde Goetz-Neunhoeffer
Address:	Schloßgarten 5a, 91054 Erlangen, Germany
	Tel. 09131/855780
E-mail:	goetz@geol.uni-erlangen.de

UNIVERSITY EDUCATION

1984-1987	BSc Student of Mineralogy, University Erlangen-Nueremberg
1987-1988	MSc Course in Mineral Processing & Ore Petrology, University College Cardiff, Department of Mineral Exploitation
1988	Master of Science (Univ. Wales) Master Thesis: Alluvial PGM: A mineralogical investigation of a panned cencentrate from Borneo
1987-1990	MSc Student of Mineralogy, University Erlangen-Nueremberg
1990:	Diploma in Mineralogy Master Thesis: Production of High Alumina Cement from iron rich Bauxite and Limestone by sintering in a rotary kiln.
1996:	PhD in Applied Mineralogy PhD Thesis: Synthesis and mineralogical characterization of calcium ferrate hydrates and their application as reservoir minerals in waste dumps

POST DOCTORAL SCIENTIFIC CAREER

Since 1997	Assistant Professor at the Department of Mineralogy, University Erlangen-Nuremberg

RESEARCH TOPICS

Available on request

QUANTITATIVE PHASE ANALYSIS OF VARIOUS FE-RICH CALCIUM ALUMINATE CEMENT CLINKERS BY SELECTIVE DISSOLUTION AND XRPD

Friedlinde Goetz-Neunhoeffer

Department of Mineralogy, University Erlangen, Germany.
E-mail: goetz@geol.uni-erlangen.de

ABSTRACT

A technical problem of manufacturing Fe-rich Calcium Aluminate Cement (CAC) by fusion, which was not considered, is that phase composition depends strongly on production conditions. Chemical composition of the raw meal mixture (chemical parameter) together with kiln type, kiln atmosphere, and cooling of the clinker (process parameter) are the most determining parameters for phase composition and solid solutions with ferric or ferrous iron. Since constant quality is very important for usage in building chemistry applications of CAC, many attempts for quantitative phase analysis have been started in the last years.

For this investigation quantitative phase compositions of four Fe-rich CAC clinkers from different manufacturers were determined by calibrated Rietveld analysis using TOPAS. Some of the minor phases could only be detected in CAC clinker after selective dissolution of the main phases C(A,F) and Ferrite phase $C_4A_{2-x}F_x$. The range of C(A,F) content lies within 45-51ma.% whereas the Ferrite phase varyied between 10 and 21ma.%, which implies higher dependence of the Ferrite phase on chemical and production parameters. Perovskite together with the structural related C_3FT-phase could be quantified in all Fe-rich CAC clinkers with 5-13ma.%.

1. INTRODUCTION

Almost all producers use the fusion process to produce Fe-rich CAC from the raw mixture of limestone and bauxite in L-shaped reverbatory kilns. The molten product is cast into pans and allowed to cool and solidify as clinker. Lime and Al_2O_3 as the principal oxides combine to give Monocalcium aluminate C(A,F) as the principal reactive phase in the cement, which reacts with water to form calcium aluminate hydrates. The alumina content of the raw materials mixture dictates the amount of hydraulic C(A,F) in the clinker. Selection of raw materials and the optimised chemical composition of the raw mix therefore play a major role for final product properties. From investigation of new production methods it is now known, that kiln atmosphere also very much determines the mineralogical phase composition of Fe-rich CAC [5]. The same raw meal can lead to quite different phase compositions in reducing kiln atmospheres. In order to guarantee constant quality of Fe-rich CAC, the amount of the main hydraulic phases, like C(A,F) and $C_4A_{2-x}F_x$, must be controlled by the producer. The need for constant quality is very high for application of Fe-rich CAC in building chemistry special products (e.g. tile adhesives, tile grouts, floor levelling compounds, rapid floor screeds, repair mortars).

Proceedings of the 11th International Congress on the Chemistry of Cement (ICCC)
'Cement's Contribution to the Development in the 21st Century'
Hosted by: The Cement and Concrete Institute of South Africa
CD-ROM produced by: Document Transformation Technologies
11 - 16 May 2003, Durban, South Africa
ISBN Number: 0-9584085-8-0
Editors: Dr G. Grieve and G. Owens
Congress Organised by: Event Dynamics

2. PREFACE TO EXPERIMENTAL PROCEDURE

Besides C(A,F) and $C_4A_{2-x}F_x$ up to 9 minor phases occur in Fe-rich CAC clinker, which leads to strong peak overlapping in X-ray powder patterns. A very powerful method to solve peak overlapping is Rietveld refinement of X-ray powder diffraction data from CAC clinker, which was reported by several authors in the past [1, 2, 3, 4]. Before Rietveld quantification can be applied, full qualitative phase analysis of all clinker minerals must be performed.

Some of the minor phases can not be detected directly in CAC clinker but only after selective dissolution of the main phases C(A,F) and $C_4A_{2-x}F_x$ [5]. For the investigation of four CAC clinkers enrichment of minor phases was performed by different solvents, for different times, and in successive combinations.

Most of the clinker phases form solid solutions and tend to incorporate foreign ions, which has direct influence on their density. Rietveld quantification is strongly related to phase density and therefore the exact chemical compositions even of minor phases are needed for determination of phase amounts in the mixture. Chemical composition of the main phases of all investigated Fe-rich CAC clinker was determined by EPMA or Rietveld refinement of occupancy factors in the structure.

For calibration of the Rietveld quantification all identified phases were synthesised from reagent grade chemicals for the determined composition. XRD pattern of the pure phases were checked for impurities of minor phases. Mixes with known amounts of 8-10 phases were prepared and the recorded diagrams were quantified by Rietveld method with a fundamental parameter approach (TOPAS).

In the following all essential steps performed for development of a quantitative phase analysis of Fe-rich CAC clinker are listed:

- Investigation of the main phases C(A,F) and $C_4A_{2-x}F_x$ in the clinker
- Enrichment and investigation of the minor phases
- Rietveld refinement of the all identified minor phases in the residues
- Synthesis of all phases with the determined chemical composition
- Rietveld refinement of the pure synthetic phases
- Mixing of different clinker-like phase compositions from single phases
- Calibration of Rietveld quantification and determination of accuracy and precision for any phase
- Transfer of quantification method on each technical CAC clinker with use of residues from selective dissolution

3. EXPERIMENTAL PARAMETER

3.1 Selective dissolution methods

Four different solvents were applied to each technical clinker with solution times from 15min to 1h. The less active solvent 1n acetic acid was used to dissolve Mayenite ($C_{12}A_7$) from CAC clinker. The mixture of Salicylic acid /Methanol is known to dissolve Calcium silicate phases. For our purposes 20g Salicylic acid was dissolved in 200ml Methanol and 5g CAC clinker was added. The beaker was covered and at 60°C stirred for 1h. The residue was filtered, washed with Methanol, and dried at 100°C. The most effective method to dissolve the main phases C(A,F) and $C_4A_{2-x}F_x$ from the clinker was a solution of 20g KOH and 20g Sucrose in 200ml H_2O. The mixture was heated in a covered beaker to 95°C and after adding 5g CAC clinker the solution was stirred for 30 min. The residues were filtered, washed with 50ml H_2O, and finally with 100ml Methanol. For the application of 1n HCl as dissolving agent 20g CAC clinker was needed. The HCl/clinker suspension was stirred for 30min at 60°C. The residue of Magnetite and Wuestite can be washed with H_2O and dried prior to XRD investigation.

Table 1. Effects of different solvents on phase enrichment resp. selective dissolution of Fe-rich CAC clinker

Solvent	1n HCl	1n Acetic acid	1g Salicylic acid in 10ml Methanol	10% KOH/ Sacch.-Solution
Solution time	30 min, 1h	30 min, 1 h	1h	15 min, 30 min, 1h
Predominantly **enriched** phases (residues)	Fe_3O_4 Magnetite FeO Wuestite		$Ca_4A_{0,5}F_{1.5}$Ferrate	Magnetite FeO Wuestite ß-Ca_2SiO_4 Belite Ca_2AS Gehlenite $Ca_3Fe_2TiO_8$ $CaTiO_3$ Perovskite
Predominantly **dissolved** phases		$Ca_{12}Al_{14}O_{33}$ Mayenite	ß-Ca_2SiO_4 Belite	

3.2 Synthesis of CAC clinker phases

For the calibration of quantitative phase analysis all identified CAC clinker phases were synthesized from reagent grade chemicals in a laboratory furnace in air. The chemical compositions of solid solutions were chosen according to the compositions determined in the technical clinker (ref. 4.1.2). The quenched mixtures were ground several times in a disk mill (agate) during the synthesis procedure.

Table 2. Synthesis parameter for the synthetic CAC clinker phases

Phase	Trivial name	Temperature [°C]	Synthesis time [h]	Grinding
$CA_{0.94}F_{0.06}$	Monocalcium-aluminate	1250	16	5 min every 4h
$C_4A_{1.5}F_{0.5}$	Ferrite phase	1250	70	10 min every 12h
$C_{12}A_7$	Mayenite	1150	70	15 min every 24h
ß-C_2S (Al-doped)	Belite	1550/ 1350(final step)	8	15 min every 2h
$C_2A_{0.8}F_{0.2}S$	Gehlenite	1250	8	5 min every 2h
CT	Perovskite	1250	10	5 min every 2h
C_3FT		1350/ 950 (final step)	14	15 min every 3h
$C_{20}M_3A_{13}S_3$	Pleochroite	1300	60	5 min every 10h

All pure synthetic phases were ground in a disk mill and sieved <36µm prior to the following experimental procedures.

3.3 X-ray diffraction powder analysis

3.3.1 Sample preparation for X-ray diffraction analysis

Preparation of the samples was standardized. The four technical Fe-rich CAC samples and their residues after selective dissolution were ground in a disc mill (Tungsten Carbide, 50g, 30min) to get the required grain sizes for X-ray powder diffraction. The specific area (Blaine) of the clinker was determined to 3600 ± 100 cm^2/g. Samples of the calibration mixtures were homogenized in a disc mill (agate, 20g, 3min).

3.3.2 Accuracy and precision of quantitative mineralogical phase analysis

Accuracy (absolute error E_a) and precision (standard deviation s) of Rietveld quantification for Fe-rich CAC phase composition was verified on eight different synthetic mixtures, which were prepared from the pure synthetic clinker phases. Measurement of ten independent preparations led to determination of the values for accuracy and precision as shown in Table 3.

Table 3. Accuracy and precision for CAC quantification of synthetic mixtures with Rietveld analysis. Measurement of ten independent preparation (all data in ma.%)

$CA_{0.94}F_{0.06}$	Theoret. Value	**0,0**	**20,0**	**28,0**	**40,0**	**42,9**	**50,0**	**55,0**	**55,6**
	Mean value	0,6	20,0	27,1	39,3	42,2	51,5	55,6	55,9
	Accuracy E_a	**-0,6**	**0,0**	**0,9**	**0,7**	**0,7**	**-1,5**	**-0,6**	**-0,3**
	Precision s	**0,4**	**0,4**	**0,9**	**0,6**	**0,9**	**1,5**	**0,6**	**1,3**
$C_4A_{1.5}F_{0.5}$	Theoret. Value	**0,0**	**8,0**	**10,0**	**15,0**	**16,0**	**22,2**		
(Ferrite phase)	Mean value	0,2	7,6	8,8	14,9	14,8	21,3		
	Accuracy E_a	**-0,2**	**0,4**	**1,2**	**0,1**	**1,2**	**0,9**		
	Precision s	**0,1**	**0,7**	**1,1**	**1,3**	**1,6**	**1,6**		
$C_{12}A_7$	Theoret. Value	**0,0**	**0,5**	**1,0**	**1,5**	**6,0**	**8,0**	**15,0**	
(Mayenite)	Mean value	0,1	0,7	0,8	1,4	5,1	7,2	13,5	
	Accuracy E_a	**-0,1**	**-0,2**	**0,2**	**0,1**	**0,9**	**0,8**	**1,5**	
	Precision s	**0,1**	**0,3**	**0,3**	**0,2**	**0,6**	**0,7**	**1,1**	
ß-C_2S	Theoret. Value	**0,0**	**2,0**	**4,0**	**5,1**	**7,0**	**10,0**	**15,0**	**20,0**
(Belite)	Mean value	0,2	1,8	4,8	5,6	6,8	9,6	15,0	20,4
	Accuracy E_a	**-0,2**	**0,2**	**-0,8**	**-0,5**	**0,2**	**0,4**	**0,0**	**-0,4**
	Precision s	**0,2**	**0,7**	**0,7**	**0,6**	**0,6**	**0,9**	**0,8**	**1,1**
$C_2A_{0.8}F_{0.2}S$	Theoret. Value	**0,0**	**6,0**	**10,0**	**15,0**	**20,0**	**25,5**		
(Gehlenite)	Mean value	0	6,4	10	14,7	20	25,6		
	Accuracy E_a	**0,0**	**-0,4**	**0,0**	**0,3**	**0,0**	**-0,1**		
	Precision s	**0,1**	**0,4**	**0,5**	**0,6**	**0,6**	**0,4**		
$C_{20}M_3A_{13}S_3$	Theoret. Value	**0,0**	**3,0**	**5,0**	**13,8**	**15,0**			
(Pleochroite)	Mean value	0,3	3,1	5,2	13,4	14,9			
	Accuracy E_a	**-0,3**	**-0,1**	**-0,2**	**0,4**	**0,1**			
	Precision s	**0,2**	**0,4**	**0,6**	**0,4**	**0,6**			
CT	Theoret. Value	**0,0**	**1,0**	**3,0**	**8,0**	**10,0**			
(Perovskite)	Mean value	0,4	1,4	3,0	7,1	8,8			
	Accuracy E_a	**-0,4**	**-0,4**	**0,0**	**0,9**	**1,2**			
	Precision s	**0,3**	**0,2**	**0,5**	**0,8**	**0,9**			
C_3FT	Theoret. Value	**0,0**	**3,1**	**6,1**	**8,0**	**12,0**	**15,0**	**17,0**	**25,0**
	Mean value	0,9	3,1	6,9	8,4	13,4	16,4	18	25,8
	Accuracy E_a	**-0,9**	**0,0**	**-0,8**	**-0,4**	**-1,4**	**-1,4**	**-1,0**	**-0,8**
	Precision s	**0,6**	**0,7**	**1,3**	**0,8**	**1,4**	**1,3**	**0,9**	**0,9**
$M_{0.5}f_{0.5}F$	Theoret. Value	**0,0**	**3,5**	**5,0**	**8,2**				
(Magnetite)	Mean value	0,0	3,9	5,4	7,6				
	Accuracy E_a	**0,0**	**-0,4**	**-0,4**	**0,6**				
	Precision s	**0,1**	**0,5**	**0,5**	**0,9**				

4. RESULTS

4.1 Qualitative phase composition of Fe-rich CAC clinker and residues from selective dissolution by X-Ray powder diffraction analysis

Comparison of XRD diagrams of residues from KOH selective dissolution gave a much better insight into the differences of qualitative phase composition of CAC clinker from four producers (Figure 1) than analysis of the untreated clinker. In clinker CAC-4 neither Mayenite nor Wuestite could be detected in the residues. But instead quite a lot of Gehlenite could be observed in the clinker, where CA and Ferrite phase are dissolved by the KOH dissolution technique.

After successive removal of Belite (Salicylic acid /Methanol) and Mayenite (Acetic acid) the from the KOH-residues, the samples were comprised of Magnetite, Wuestite, C_3FT-phase and Perovskite and residue from clinker CAC-4 additionally Gehlenite (Figure 2).

Qualitative phase composition of the analysed clinker was found to be variable. Some phases like Gehlenite (C_2AS) and Wuestite (f) did not occur in all Fe-rich CAC clinkers investigated.

Table 4. Qualitative phase composition of Fe-rich CAC Clinker

Phase in Fe-rich CAC Clinker	**Abbreviation**	**Phase in Fe-rich CAC Clinker**	**Abbreviation**
Monocalcium-aluminate	CA bzw. C(A,F)	C_3FT-phase	C_3FT ($Ca_3Fe_2TiO_8$)
Ferrite	$C_6A_xF_{3-x}$	Gehlenite	C_2AS
Mayenite	$C_{12}A_7$	Pleochroite	$C_{20}f_3A_{13}S_3$
Belite	ß-C_2S	Magnetite/ Magnesioferrite	Ff/MF
Perovskite	CT	Wuestite	f

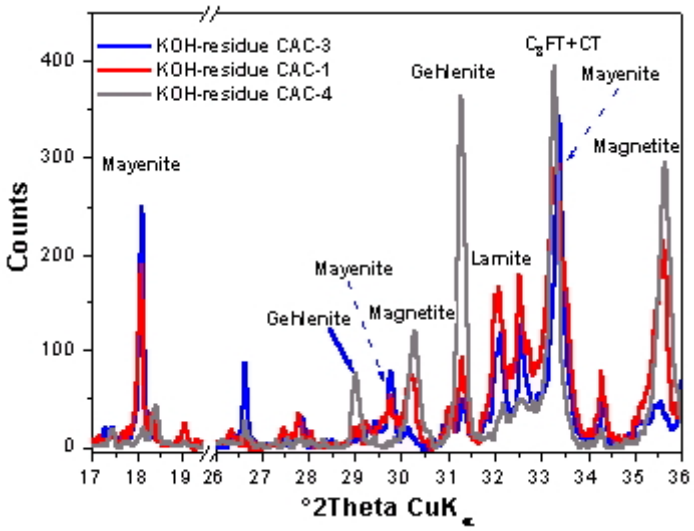

Figure 1. Comparison of residues from KOH dissolution of Fe-rich CAC clinker

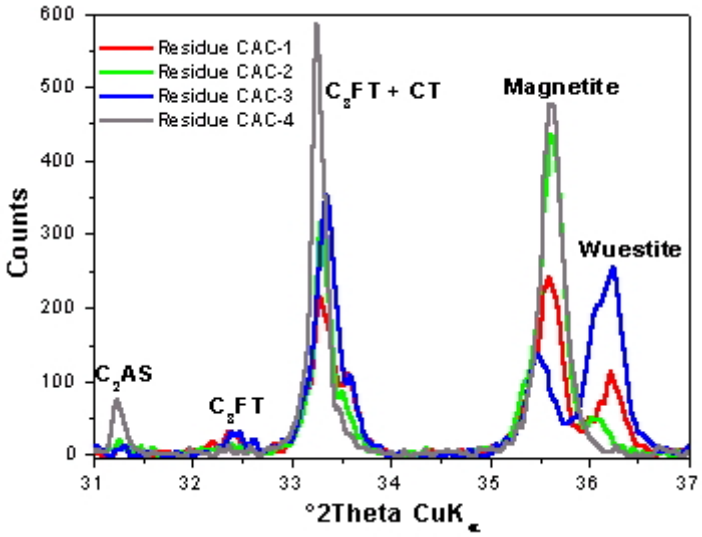

Figure 2. Comparison of residues from combined KOH, Salicylic/Methanol, Acetic acid dissolution of Fe-rich CAC clinker

4.2 Chemical composition of main clinker phases

Chemical compositions of the main phases of all investigated Fe-rich CAC clinkers were determined either by EPMA or Rietveld refinement of occupancy factors in the structure and found to be variable within the following ranges:

Monocalciumaluminate	$CA_{0.95}F_{0.05} \Leftrightarrow CA_{0.88}F_{0.12}$
Ferrite phase	$C_4A_{0.9}F_{1.1} \Leftrightarrow C_4A_{0.7}F_{1.3}$

Structural data and occupancies of minor phases were refined from the XRD pattern of the different residues of selective enrichment for clinker CAC-1 to CAC-4. Because of different chemical compositions of main and minor phases from clinker to clinker a specially adapted quantification method had to be designed for each of the four investigated Fe-rich CAC clinkers.

4.3 Chemical analysis of the clinker

Chemical analysis of the four Fe-rich clinkers by XRF-analysis could prove that there are only small differences in chemical composition of the clinker from the different producers. The contents of SiO_2 are higher for CAC-2 and CAC-4. TiO_2-content ranges between 1.60 and 1.80 ma.%, Al_2O_3 between 38.07 and 40.83ma.%. Fe_2O_3 shows the largest relative difference and values for CaO are all lying within 36.29 and 38.72 ma.%. CAC-2 and CAC-4 have MnO-contents of about 1 ma.%. Remarkable are the very low LOI of all samples due to oxidation of ferrous iron during analysis.

Table 5. Quantitative chemical composition of the investigated Fe-rich CAC Clinker

	CAC-1	CAC-2	CAC-3	CAC-4
SiO_2	2.65	3.45	2.70	3.70
TiO_2	1.84	1.60	1.82	1.67
Al_2O_3	40.8	38.1	40.3	39.5
Fe_2O_3	15.4	16.7	14.7	16.7
MnO	0.03	0.96	0.02	1.03
MgO	0.30	0.72	0.52	0.85
CaO	38.7	37.5	38.4	36.3
Na_2O	< 0.12	< 0.12	< 0.12	< 0.12
K_2O	< 0.12	< 0.12	< 0.12	< 0.12
P_2O_5	0.03	0.20	0.06	0.26
LOI	0.00	1.17	0.95	0.55

4.4 Quantification results of the technical clinker

All results are average values from ten independent preparations followed by Rietveld quantification of XRD-pattern. None of the values for precision exceeded 1 ma.%. The results of calibrated Rietveld quantification of four Fe-rich CAC clinkers are presented in Table 5 and Figure 2.

The dominating phases in all investigated Fe-rich CAC clinkers are CA and Ferrite phases. In clinker CAC-1 the highest CA content was determined with 51.1 ma.% whereas the lowest content could be found in clinker CAC-3 with 45.8 ma.%. The highest values for the Ferrite phase were observed again in clinker CAC-1 (21.2 ma.%).

For CAC-3 the highest content for Mayenite with 5.9 ma.% could be determined and for clinker CAC-4 the lowest content with 0.9 ma.%. Belite content is not much different for CAC-1, CAC-2, and CAC-3 with 5-6.5 ma.%. And again clinker CAC-4 is marked by low Belite content of 3.1 ma.%.

Table 6. Results of quantitative phase composition of four different Fe-rich CAC clinker determined by calibrated Rietveld analysis

Phase	CAC-1 [ma.%]	CAC-2 [ma.%]	CAC-3 [ma.%]	CAC-4 [ma.%]	Precision
CA	51.1	47.7	45.8	48.4	0.6-1.0
Ferrite phase	21.2	12.2	18.3	10.4	0.4-0.5
Mayenite	2.9	3.4	5.9	0.9	0.2-0.4
Belite	5.0	6.5	5.7	3.1	0.3-0.4
Sum hydraulic phases	***80.2***	***69.8***	***75.7***	***62.7***	
Gehlenite	1.3	2.0	1.4	8.7	0.2-0.5
Pleochroite	3.6	7.4	5.9	1.7	0.1-0.5
Perovskite	2.3	4.1	3.6	6.2	0.2-0.6
C_3FT-phase	3.3	6.3	2.5	6.6	0.4-1.0
Magnetite	5.7	8.4	3.0	14.0	0.4-0.6
Wuestite	3.5	1.8	7.3	0.0	0.1-0.5

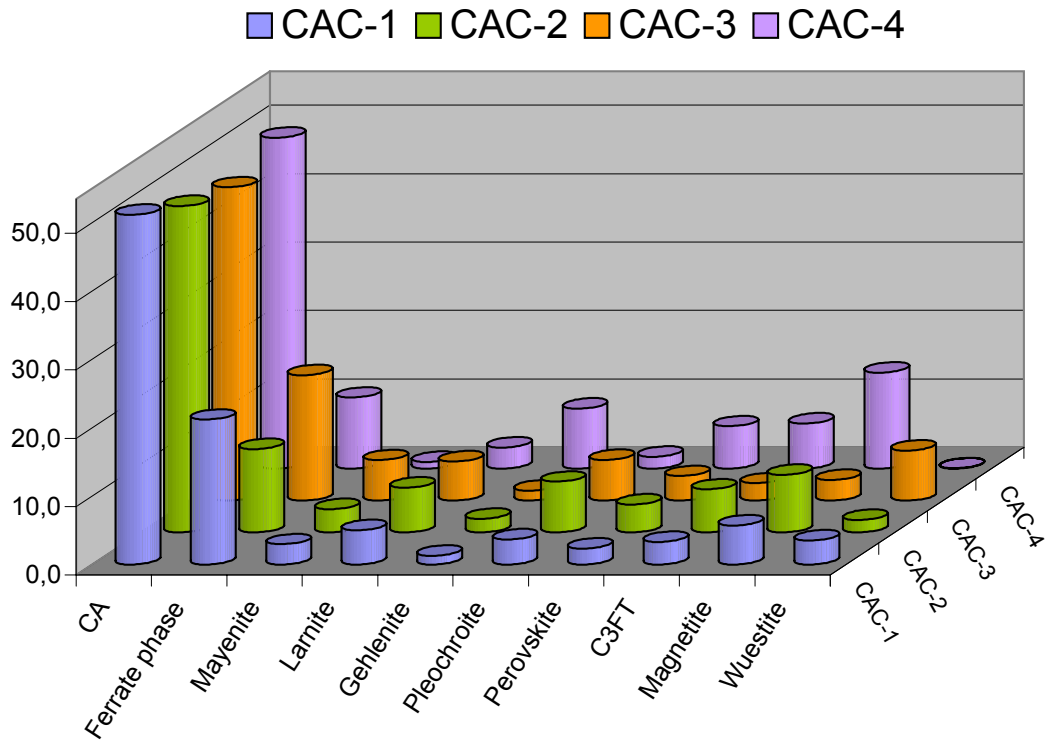

Figure 3. Quantitative phase composition, determined by calibrated Rietveld analysis of four different Fe-rich CAC clinkers

As a very interesting result of the quantification of four different Fe-rich CAC clinkers it can be shown that the sum of the hydraulic phases CA, Ferrite phase, Mayenite, and Belite varyies within 80.2 and 62.2 ma.%. In CAC-4 with 8.7 ma.% Gehelenite and 14 ma.% Magnetite the ratio between hydraulic and non hydraulic phases is about 2:1, whereas the phase composition of clinker CAC-1 is characterised by a ratio of about 4:1 (hydraulic:non hydraulic).

The non hydraulic minor phases of the Fe-rich CAC-clinkers differ more than the hydraulic main phases. Two Titatnium-containing phases could be quantified in all clinkers, Perovskite (CT) and a ternary phase C_3FT. Both phases are structurally related with each other and therefore can not be

quantified with the same high precision and accuracy as the other minor phases like Gehlenite. In all of the Fe-rich CAC clinkers Magnetite could be quantified from 3.0 (CAC-3) to 14.0 ma.% (CAC-4). Wuestite could be observed at the highest concentration of 7.3 ma.% in CAC-3.

5. DISCUSSION AND CONCLUSIONS

After performing full qualitative phase analysis of all clinker minerals a clinker specific Rietveld quantification method was developed by mixing of phases with chemical compositions determined from the technical clinker. With this calibration the values of quantitative phase analysis can be taken as true values. Systematic errors can only be excluded by calibration, which is the most time consuming part of any quantitative phase analysis. The calibrated quantification method needs further adaptation to the technical product by refining the residues from selective dissolution.

Although only small differences in chemical composition of the four investigated clinkers could be found the phase composition is much more different. Quantitative phase analysis of clinker CAC-2 and CAC-4, which are of very similar chemistry, show quite strong differences. In CAC- 4 only Magnetite and no Wuestite was found, which indicates less reducing atmosphere during fusion. But the sintering atmosphere is only one of the process parameters that affect phase composition of Fe-rich CAC. In CAC-4 the Mayenite content is reduced to very low values whereas the non hydraulic Gehlenite has a much higher value than in all other investigated clinkers. It is well known from experimental clinker with CAC composition [6] that cooling rate is a decisive parameter for some clinker phases like CA and probably the Ferrite phase and Gehlenite, which can incorporate more Fe^{3+} in the crystal lattice phases on very rapid cooling. Faster cooling enhances iron in the aluminate phases.

The difference in the amount of hydraulic phases to non hydraulic phases is, surprisingly, very high. In clinker CAC-1 the highest values for CA as well as for Ferrite phase were determined. But chemical composition of the clinker is not characterised by higher iron or calcium oxide content than the other CAC clinker.

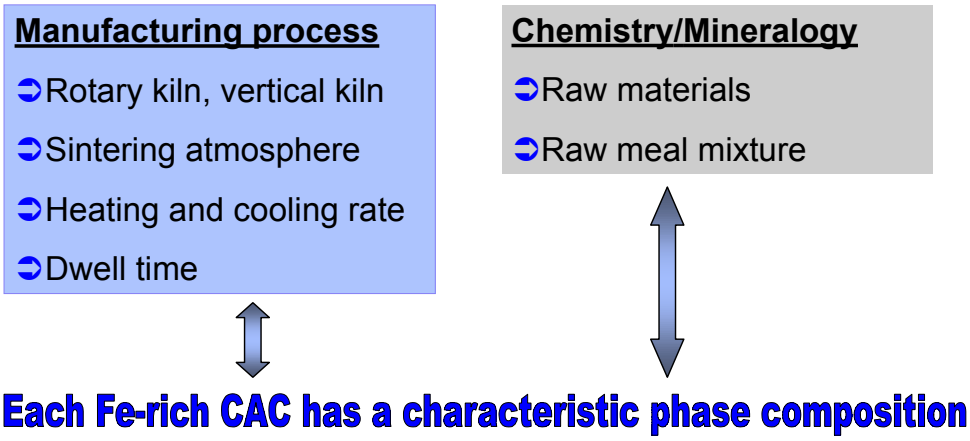

Figure 4. Influencing factors on phase composition of Fe-rich CAC-clinker

These complex interactions with an influence on phase composition (Figure 4) is only playing a role for Fe-rich CAC clinker, with ions like Fe and Mn which can be incorporated in crystal lattices of different phases in more than one valence.

The possibility of phase composition determination gives very useful information for producers on optimising the production process. Less desired phases in the clinker can be eliminated and other favourable phases can be enhanced by changing the raw mix chemistry or by varying process parameters. From our investigations it is known that iron content of Ferrite phase solid solution

determines hydration behaviour. With the knowledge of phase composition, correlation with hydration behaviour is made possible. New or special products can be developed by using data from hydration experiments together with phase compositions during hydration.

The most important perspectives of quantitative phase analysis of Fe-rich CAC-clinker are:

- On-line process and quality control
- Optimisation of product quality
- Development of special cements
- Research on hydration kinetics
- Investigation of hydrated CAC in building chemistry

REFERENCES

[1] Füllmann, Th. Quantitative Rietveld-Phasenanalyse von Tonerdezementen, PhD Thesis, University of Erlangen, Germany, 1997, 100p.

[2] Guirado, F., Gali, S, and Chinchon, S. Quantitative Rietveld analysis of aluminous cement clinker phases, Cem. Conc. Res. 30, 2000, 1023-29.

[3] Motzet, H. & Pöllmann, H. Quantitative phase analysis of high alumina cements, 20th Int. Conf. Cem. Micr., Guadalajara, 1998, 187-206

[4] Walenta, G. Synthesen und Rietveld-Verfeinerungen der Einzelphasen von Tonerdezementen, PhD Thesis, University of Erlangen, Germany, 1997, 119p.

[5] Motzet, H. Entwicklung eines Sinterverfahrens zur Herstellung von eisenreichem Tonerdezement im Drehrohrofen, PhD Thesis, University of Halle, Germany, 1998, 175p.

[6] Sourie, A. & Glasser, F.P. Studies of the Mineralogy of high Alumina Cement Clinkers, Br. Ceram. Trans. J., 90, 71-76, 1991

QUANTITATIVE PHASE ANALYSIS OF VARIOUS FE-RICH CALCIUM ALUMINATE CEMENT CLINKERS BY SELECTIVE DISSOLUTION AND XRPD

Friedlinde Goetz-Neunhoeffer

Department of Mineralogy, University Erlangen, Germany.
E-mail: goetz@geol.uni-erlangen.de

Friedlinde Goetz-Neunhoeffer

Name: Friedlinde Goetz-Neunhoeffer
Address: Schloßgarten 5a, 91054 Erlangen, Germany
Tel: 09131/855780
E-mail: goetz@geol.uni-erlangen.de

UNIVERSITY EDUCATION

1984-1987	BSc Student of Mineralogy, University Erlangen-Nueremberg
1987-1988	MSc Course in Mineral Processing & Ore Petrology, University College Cardiff, Department of Mineral Exploitation
1988	Master of Science (Univ. Wales)
Master Thesis:	Alluvial PGM: A mineralogical investigation of a panned cencentrate from Borneo
1987-1990	MSc Student of Mineralogy, University Erlangen-Nueremberg
1990:	Diploma in Mineralogy
Master Thesis:	Production of High Alumina Cement from iron rich Bauxite and Limestone by sintering in a rotary kiln.
1996:	PhD in Applied Mineralogy
	PhD Thesis: Synthesis and mineralogical characterization of calcium ferrite hydrates and their application as reservoir minerals in waste dumps

POST DOCTORAL SCIENTIFIC CAREER

Since 1997 Assistant Professor at the Department of Mineralogy, University Erlangen-Nuremberg Institution

EFFECTS OF PHOSPHATE-RICH RAW MATERIALS ON THE CRYSTALLOGRAPHIC AND HYDRAULIC PROPERTIES OF DICALCIUM SILICATE

R. Müller, J. Neubauer and F. Götz-Neunhoeffer

Department of Mineralogy, University Erlangen-Nuremberg, Erlangen, Germany.
E-mail: rmueller@geol.uni-erlangen.de

ABSTRACT

Samples with different phosphate contents were prepared at 1720 K and 1820 K in air to form the γ-, β-, α´-, and α-modifications of dicalcium silicate. Determination of the phase content by XRD showed that the stability fields of the phases in the quenched system differ considerably from the phase diagram in equilibrium. Samples which consist only of one C_2S polymorph were X-rayed and the structure models were refined by the Rietveld method. Refinements of the γ- and β-modifications yielded good results. Data from the α´-modification were refined with different structure models of which a distorted α'_L-C_2S structure led to the best results. The refinement of α-C_2S structural data was not satisfactory, because all models for this structure were determined from high-temperature X-ray diffraction. So the lattice parameters and structural data differ considerably from those at room temperature. Hydraulic behaviour of the single phase samples was investigated with the help of a heat conduction calorimeter, which was developed and revised at our department. All samples show very low hydration energies and remarkably different hydration behaviour.

1. INTRODUCTION

It is increasingly common to use high temperatures in the cement manufacturing process to burn waste materials. Burning materials like scrap tires or waste oil saves some of the fuel used in the clinkering process [1]. Substances like sewer sludge or meat and bone meals, however, can save fuel *and* raw meal. These materials have organic components which burn without residues in the rotary kiln and form a substitute for fuel. Their inorganic components can act as a substitute for raw meal, because of their similar chemical composition (after the addition of lime) [2]. However, these substances have a high phosphate content, which is usually not present in Portland cement raw meals. Therefore, the effect of phosphate on the clinker has to be examined.

It has been known for years that phosphate in Portland cement clinkers is incorporated mainly in the dicalcium silicate phase (C_2S, Belite) [3]. C_2S shows a relatively complex pattern of phase transformations (figure 1; [4], altered after [5]).

Proceedings of the 11th International Congress on the Chemistry of Cement (ICCC)
'Cement's Contribution to the Development in the 21st Century'
Hosted by: The Cement and Concrete Institute of South Africa
CD-ROM produced by: Document Transformation Technologies
11 - 16 May 2003, Durban, South Africa
ISBN Number: 0-9584085-8-0
Editors: Dr G. Grieve and G. Owens
Congress Organised by: Event Dynamics

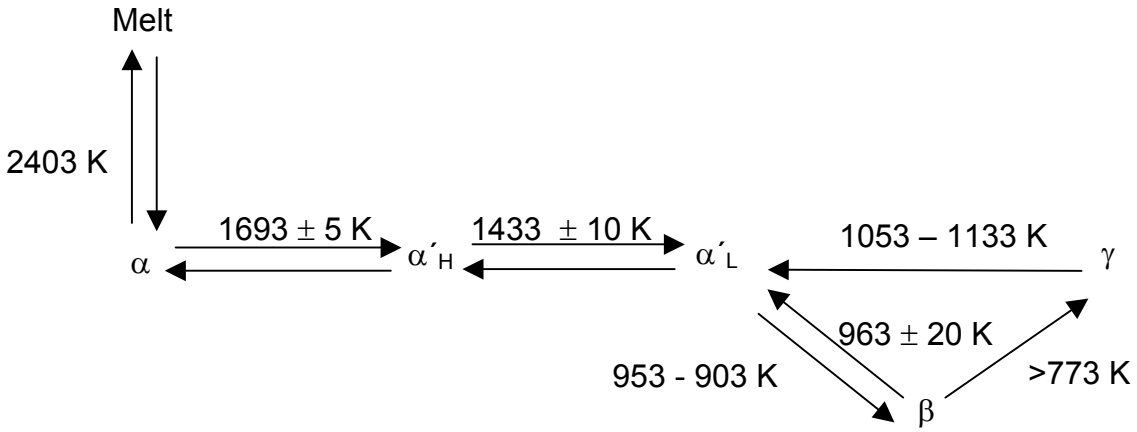

Figure 1. Phase transformations of C_2S

All C_2S polymorphs are nesosilicates. Investigations of the crystal structures of the high temperature polymorphs are often difficult, because some of them show complex twinning and hardly any single crystals can be obtained [6]. Also the high temperatures at which these phases are stable lead to experimental difficulties. Therefore, the crystal structure of α-C_2S has not yet been fully determined [7], [8]. There have been proposals of structures in the space groups P -3 m 1 [9], [12], P 6_3 m c [10], and P 6_3/m m c [11], [7], [12]. These structure models differ in the orientation of the $[SiO_4]^{4-}$-tetrahedra [12]. The crystal structure of α'_H-C_2S is a derivative of the β-K_2SO_4 structure type (space group P n m a) [9], while α'_L-C_2S shows a superstructure based on α'_H-C_2S [13], [14], [15]. β-C_2S has a monoclinic structure (space group P 1 2_1/n 1) [16] and γ-C_2S shows a crystal structure of the olivine type (space group P b n m) [17], [18]. The phase transformation from β-C_2S to γ-C_2S is associated with a significant increase of volume which leads to the effect known as "dusting".

γ-C_2S is the thermodynamically stable phase at room temperature while β-C_2S forms the Belite component in clinkers. Here this polymorph is stabilized by rapid cooling and the incorporation of foreign ions. Most of the C_2S-polymorphs can be stabilized at room temperature by incorporation of phosphate. The phase diagram dicalcium silicate - tricalcium phosphate (C_3P) is presented in figure 2. It can be seen that with increasing phosphate content phases are present which are structure derivatives of high temperature modifications of C_2S. Probably just one of the α'-C_2S modifications can be stabilized by phosphate [7], [22]. Phosphorus is incorporated in C_2S by replacing the silicon atoms on tetrahedra positions by the following mechanism [20]:

$$2SiO_4^{4-} \rightarrow 2PO_4^{3-} + \square_{Ca} \qquad (1)$$

$\square_{Ca}$ represents a Ca^{2+} vacancy.

Because of the Ca^{2+} vacancies and the shorter P-O bonds, the structures of the phosphate stabilized C_2S phases are distorted with respect to the pure C_2S polymorphs [20], [21], [22]. This process leads to the formation of commensurate and incommensurate superstructures at higher phosphate contents [20], [22].

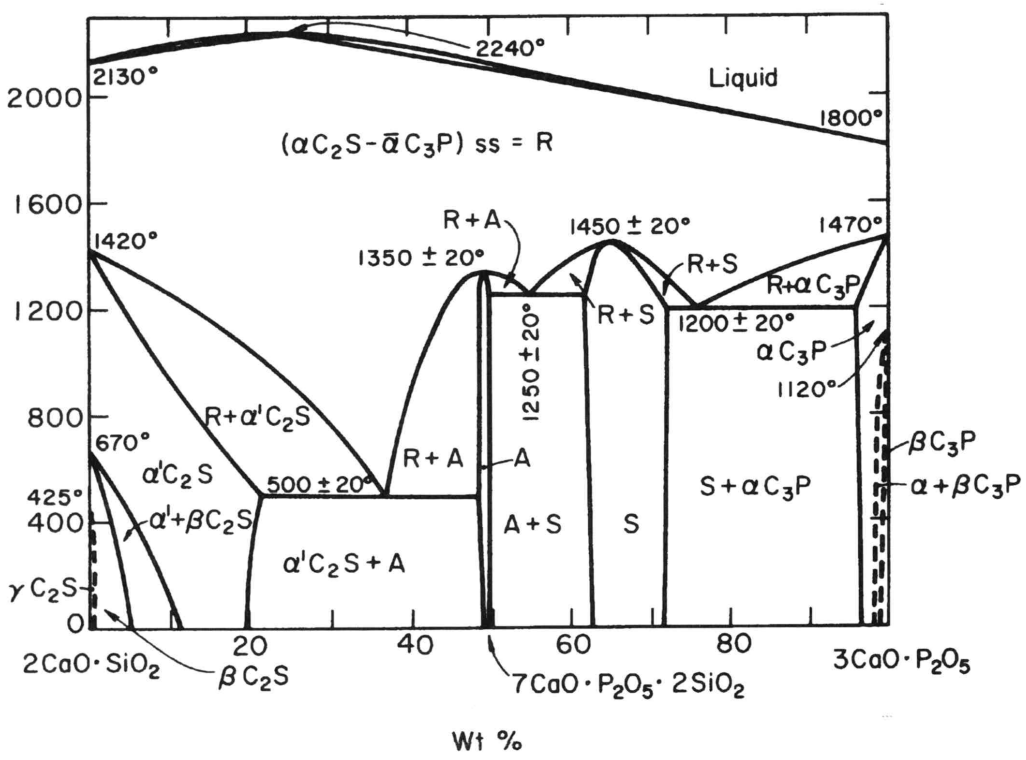

Figure 2. Pseudobinary phase diagram C_2S - C_3P [19]

R: C_2S/C_3P mixed crystal
S: silico-carnotite
A: A-Phase $Ca_7 (PO_4)_2 Si_2O_8$

While all polymorphs form CSH gel and $Ca(OH)_2$ (Portlandite) during hydration, their reactivity towards water is different [23], [24], [25]. It has been observed that α-C_2S and γ-C_2S are almost not hydraulically active [23], [24].α´-C_2S shows a slower reaction than β-C_2S but results in higher strength [26], [27], [28]. Remarkably, the stabilizing ion has a stronger effect on the reactivity than the fact which polymorph was stabilized [29], [30], [37]. For example, the reactivity of BaO and P_2O_5 stabilized C_2S polymorphs descends in the following order (stabilizer in parenthesis): α´-C_2S (BaO) > β-C_2S (BaO) > α´-C_2S (P_2O_5) > β-C_2S (P_2O_5).

2. EXPERIMENTAL

2.1 Sample preparation

Reagent grade C_2S and C_3P were mixed in the relations given in table 1. The samples were homogenized in an agate vibratory disk mill (RETSCH) and filled in platinum crucibles. Synthesises were carried out in a chamber furnace in air. Samples were calcined over night at 1270 K and ground in a tungsten carbide vibratory disk mill. All samples except RM 0.00 were sintered at 1720 K for six hours with two intermediate grinding steps. After that, samples were taken out of the furnace, cooled rapidly on a refractory brick in air and ground in a tungsten carbide vibratory disk mill to a grain size of < 36 µm, which was controlled by sieving.

Table 1. Sample composition in Mol-%

sample	Ca_2SiO_4	$Ca_3(PO_4)_2$	formula of the synthesized phase
RM 0.00	100.00	0.00	$Ca_2 \square_0 Si_1 P_0 O_4$
RM 0.03	98.25	1.75	$Ca_{1.9828} \square_{0.0172} Si_{0.9656} P_{0.0344} O_4$
RM 0.06	96.91	3.09	$Ca_{1.9700} \square_{0.0300} Si_{0.9400} P_{0.0600} O_4$
RM 0.11	94.29	5.71	$Ca_{1.9460} \square_{0.0540} Si_{0.8920} P_{0.1080} O_4$
RM 0.20	89.00	11.00	$Ca_{1.9009} \square_{0.0991} Si_{0.8018} P_{0.1982} O_4$
RM 0.25	85.71	14.29	$Ca_{1.8750} \square_{0.1250} Si_{0.7500} P_{0.2500} O_4$
RM 0.31	82.00	18.00	$Ca_{1.8475} \square_{0.1526} Si_{0.6949} P_{0.3051} O_4$
RM 0.42	73.42	26.58	$Ca_{1.7900} \square_{0.2100} Si_{0.5800} P_{0.4200} O_4$
RM 0.50	66.67	33.33	$Ca_{1.7500} \square_{0.2500} Si_{0.5000} P_{0.5000} O_4$

Sample RM 0.00 was sintered twice for two hours at 1820 K with intermediate grinding. Then it was sintered for 1.5 hours at 1820 K and cooled with 1 K/min to 1620 K. After that, it was taken out of the furnace and treated like the other samples. This procedure was chosen to ensure a complete transformation to γ-C_2S (after [31]).

2.2 Investigation methods

X-ray powder diffraction measurements were carried out with a D5000 diffractometer (SIEMENS) using Ni-filtered $Cu_{K\alpha}$ radiation. Samples were prepared in front and side loading technique to investigate possible preferred orientation effects. Qualitative phase analysis was used to determine samples containing only a single phase. Rietveld structure refinement was carried out on these single phase samples with the program TOPAS (BRUKER) using a fundamental parameters approach (FPA). By this method, the peak profile is calculated based on physical properties of the measurement device instead of using pure mathematical peak shape functions. Different structure models and refinement procedures were used (cf. 3.2).

Hydration of the single phase samples was investigated. For this purpose, all samples were ground to a comparable specific surface, which was determined by the BLAINE method. After that, they were measured in a differential heat conduction calorimeter designed in our department [32], [33]. In this device, three samples can be measured simultaneously connected in difference to an inert reference sample (quartz powder). Of each single phase sample, three measurements of 1 g were carried out with a water/cement ratio of 0.45 and a measurement time of 145 hours. Temperature during the measurements was kept constant at 296.7 ± 0.5 K.

3. RESULTS

3.1 Investigation of the phase compositions

The phosphate content of the samples was confirmed by chemical analysis. Qualitative phase analysis yielded the results given in table 2. The single phase samples on which further investigations were performed are marked separately. Of the two samples containing only the β-C_2S polymorph, RM 0.03 was chosen because the composition of RM 0.06 is located at the edge of the β-C_2S phase field in the phase diagram (cf. figure 2). There are considerable differences between the powder diffraction diagram of RM 0.11 and RM 0.20. RM 0.11 shows broader peak profiles and slightly different peak positions. Additional sintering could not produce sharper profiles. Therefore, RM 0.20 was chosen for further investigations.

Table 2. Results of the qualitative phase analysis with the help of X-ray powder diffraction

sample	phase composition	further investigated sample
RM 0.00	γ-C_2S	+
RM 0.03	β-C_2S	+
RM 0.06	β-C_2S	
RM 0.11	α'-C_2S	
RM 0.20	α'-C_2S	+
RM 0.25	α'-C_2S + α-C_2S	
RM 0.31	α-C_2S	+
RM 0.42	α-C_2S + ?	
RM 0.50	α-C_2S + ?	

In sample RM 0.42 and sample RM 0.50, the occurrence of additional reflexes compared to RM 0.31 was detected. The intensities of these peaks increase with increasing phosphate content. They could not be assigned to any phase known to be present in the system. Especially they are not related to the silico-carnotite phase, which should occur at higher phosphate contents.

By comparing diffraction diagrams of in front and side loading technique prepared samples and from structure data calculated diagrams, different reflex intensity distributions could be detected in diagrams of α-C_2S and γ-C_2S. A preferred orientation effect was presumed in these samples.

3.2 Rietveld analysis

Refined parameters for all refinements were: scale factor, zero displacement, background as Chebyshev polynomial of the 5th grade, crystallite size, microstrain, lattice parameters, and atomic coordinates on general positions. All parameters were refined simultaneously. Refinement of γ-C_2S (RM 0.00) included the March-Dollase correction of a preferred orientation on the (1 3 0) plane. During refinement of α-C_2S (RM 0.31) the correction of a preferred orientation on the (2 -1 0) plane led to the best results. For each silicon position, a phosphorous position was included in the refinements of RM 0.03, RM 0.20, and RM 0.31. Because of the similar scattering factor of Si and P, the refinement of the occupancy factors yielded no sensible results. The occupancy factors of the Ca, Si, and P positions were calculated from the chemical composition and distributed statistically.

Refinement of the samples RM 0.00 and RM 0.03 yielded good results, while the refinements of RM 0.20 and RM 0.31 were not satisfactory. Therefore, different structure models and refinement strategies were tested for both samples. For the refinements of RM 0.20 given in table 3, scale factor, zero displacement, background as Chebyshev polynomial of the 5th grade, crystallite size, microstrain, and lattice parameters were refined in one step and atom coordinates on general positions were refined in a second step. It can be seen that the structure models for α'_L-C_2S yielded better results than the models for α'_H-C_2S. The best fit can be obtained with a structure model for a *a 4b c* superstructure based on α'_H-C_2S (last line of table 3). Here the R-values and the fit were quite good, but a structure plot of the refined data showed physically untrustworthy bond distances. Therefore, additional constraints were introduced by defining the $[SiO_4]^{4-}$-tetrahedra as rigid bodies. The Si-O bond distances and bond angles were defined as variable in boundaries of 15.4 nm - 16.2 nm and 94° - 126°, respectively. Because of the already distorted $[SiO_4]^{4-}$-tetrahedra, the initial orientation of the tetrahedra could not be calculated without significant effort. Therefore, the tetrahedra were rotated near their initial position using a trial and error method.

Table 3. Results of different Rietveld refinements of sample RM 0.20

structure model	polymorph	stabilizing ion in structure model	R_{wp}	R_{Bragg}	GOF
[7]	α'_H	P^{5+}	17.20	11.435	3.44
[12]	α'_H	-	30.98	23.317	6.21
[13]	α'_H	Sr^{2+}	30.86	24.779	6.18
[34]	α'_L	Sr^{2+}	15.98	11.520	3.22
[12]	α'_L	-	15.88	10.197	3.20
[35]	α'_L	Sr^{2+}	15.64	10.065	3.15
[20]	distorted α'_L	P^{5+}	11.39	4.869	2.31

For the refinements of RM 0.31, different structure models were tested [7], [12], [36]. The best results were achieved using the trigonal structure data from [12].The used structure models and the results of the final Rietveld refinements are given in table 4.

Table 4. Results of the Rietveld structure refinements

sample	space group	lattice parameters	R_{wp}	R_{Bragg}	GOF	structure model
RM 0.00 (γ-C_2S)	P b n m	a = 50.806 nm b = 112.22 nm c = 67.621 nm	10.16	5.84	2.01	[17]
RM 0.03 (β-C_2S)	P 1 2_1/n 1	a = 55.076 nm b = 67.564 nm c = 93.173 nm β = 94.28°	8.95	3.72	1.78	[16]
RM 0.20 (α'-C_2S)	P n m 2_1	a = 93.921 nm b = 217.16 nm c = 68.282 nm	13.29	8.55	2.69	[20]
RM 0.31 (α-C_2S)	P -3 m 1	a = 54.040 nm b = 71.182 nm	13.07	11.60	2.56	[12]

3.3 Investigation of the hydration behaviour

The specific surface of samples RM 0.00, RM 0.03, RM 0.20, and RM 0.31 was determined by the BLAINE method. It was recognized that sample RM 0.00 had a high specific surface of 5650 cm^2/g caused by the dusting process. The other samples were ground to a comparable specific surface of 3190 - 3250 cm^2/g. (cf. table 5). It was refrained from grinding all samples to the high specific surface of RM 0.00 because this value is not common for ordinary cement phases. Calorimetric investigations showed that all four samples develop very low heat of hydration. It can also be seen that the individual polymorphs show distinctly different heat flow development. Heat flow graphs of the different phosphate stabilized C_2S polymorphs are given in figure 3, while determined values for heat of hydration are given in table 5. In figure 3, one of the three measured heat flow graphs for each sample was chosen. The heat flow graphs show remarkably high instrumental noise (cf. 4.3).

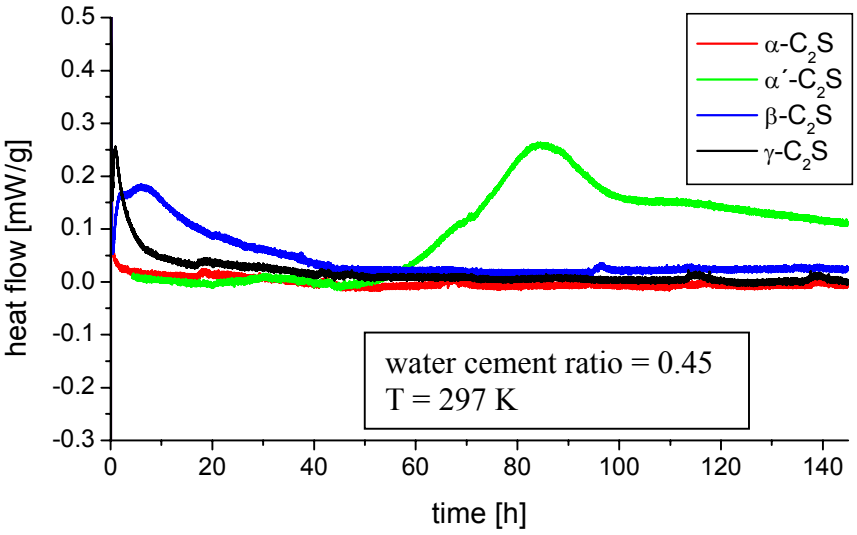

Figure 3. Heat flow graphs of the different dicalcium silicate modifications stabilized by phosphate

It is visible that α-C_2S shows no detectable heat of hydration during the measurement, while γ-C_2S develops a considerable heat at the beginning of the reaction (compared to β-C_2S). After about 20 hours, no further reaction is visible. β-C_2S has a short induction period and low heat of hydration, which is developed until the end of the measurement. α'-C_2S shows no hydraulic activity in the first 50 hours, but reaches the highest heat of hydration of the examined polymorphs.

Table 5. Results of the calorimetric investigations of dicalcium silicate modifications stabilized by phosphate

sample	start of reaction [h]	heat of hydration after 72 hours [J/g]	heat of hydration after 140 hours [J/g]	time of max. heat flow [h]	specific surface in cm^2/g
α-C_2S	-	0	0	-	5650
α´-C_2S	53	4	45	84	3250
β-C_2S	0.7	17	22	6	3260
γ-C_2S	0.3	8	9	0.9	3190

4. DISCUSSION

4.1 Phase composition of the samples

It was recognized that the phase composition of the samples differs considerably from the phase composition derived from the phase diagram and other literature data [19], [20]. With increasing phosphate content, phases were detected which should occur further towards the phosphate rich side of the phase diagram. Also, the additional reflexes in the diffraction diagrams of RM 0.42 and RM 0.50 could not be explained by literature data. The detected phase relations are in better agreement with results of FUKUDA et al. [22], [26]. In the work of FIX et al., the samples were cooled very slowly, while in the work of FUKUDA et al., the samples were quenched. In this work, the samples were cooled rapidly (about 25 g sample material in a platinum crucible was put on a cold refractory) but not in a controlled way. Probably the high temperature polymorphs of C_2S can be stabilized at lower phosphate contents if cooled more rapidly. It could not be determined whether the additional reflexes can be assigned to a new structure type or if an additional phase is present.

4.2 Rietveld structure refinement

Rietveld refinements of RM 0.00 (γ-C_2S) and RM 0.03 (β-C_2S) led to good results. It can be seen that the structure models used correspond with the synthesized phases. Refinements of RM 0.20 (α´-C_2S) and RM 0.31 (α-C_2S) raised certain difficulties. In the case of α´-C_2S, a relatively good fit could be achieved, but the structure model was strongly distorted. After the introduction of the rigid bodies refinement model, bond lengths and angles had satisfactory values. However, the given limit for some of them was reached. Furthermore, simplified structure data had to be used in the refinements: In literature data, not all tetrahedra positions have the same occupation factor. The occupation factors of Si and P had to be calculated, because they could not be sensibly refined (cf. 3.2), and distributed statistically. The refined structure model can be regarded as an approximation to the real crystal structure of phosphate stabilized α´-C_2S. Therefore, it could not be determined definitely whether the stabilized phase has an α´$_H$-C_2S or an α´$_L$-C_2S structure. Because the α´$_L$-C_2S structure models yielded better results, a crystal structure based on the α´$_L$-C_2S type is probable for this phase. Refinement of sample RM 0.31 (α-C_2S) showed the highest R-values of all polymorphs and a plot with considerable differences between calculated and observed intensities. Difficulties arise from the fact that the crystal structure of α-C_2S is not yet definitively known and that all available structure models were determined at temperatures of about 1800 K. At these temperatures, lattice parameters differ considerably from those of a phosphate stabilized polymorph at room temperature. Also, no structure model determined for samples with foreign ions was available, which would include certain distortions similar to those in the phosphate stabilized phase. It can be concluded that the crystal structure of phosphate stabilized α-C_2S can not be sufficiently described by the used literature data. Also, the formation of a commensurate superstructure is possible [22].

4.3 Hydration behaviour

It is clearly visible that the individual phosphate stabilized C_2S polymorphs show different hydration behaviour. It is common for all samples investigated that just very low heat flows are set free on hydration. The high amount of un-reacted water in the samples and the low heat flows lead to the effect that instrumental noise is visible in the heat flow graphs in figure 3. Therefore, it was difficult to determine a zero heat flow value for these experiments. Remarkably, γ-C_2S, which is mostly described as not reactive in the literature, shows more heat development than phosphate stabilized α-C_2S, which is still very low. These results are in accordance with long term experiments [23], [24], although the α-C_2S phase was stabilized here by incorporation of Al^{3+}, Fe^{3+}, and K^+. It has to be noted that the specific surface of γ-C_2S was much higher than that of the other samples. Overall and maximum heat of hydration during the first 145 hours was determined to be much higher for α´-C_2S than for β-C_2S which was reported in literature [27], [28]. Also the remarkably long induction period of α´-C_2S is in accordance to literature data [26]. Comparison between hydration data from sample RM 0.03 (β-C_2S) with data from earlier investigations of Al_2O_3 stabilized β-C_2S at this department [38], [33] showed distinctly different heat flow development: Al_2O_3 stabilized β-C_2S has a notably high initial heat of hydration and shows two further peaks at about three hours and at about eleven hours. Furthermore, the overall heat of hydration after 72 hours is 22 J/g. This value is reached by sample RM 0.03 only after 140 hours. The decisive effect of the stabilizing agent on the hydration behaviour of individual C_2S polymorphs was reported in the literature (cf. 1).

5. CONCLUSIONS

Different phases in the system C_2S – C_3P could be synthesized. The crystal structures of these substances are derivates of polymorphs of C_2S (namely γ-C_2S, β-C_2S, α-C_2S, and probably α´$_L$-C_2S). Because of the different experimental parameters, the phase relations were shifted towards the C_2S rich side in relation to the phase diagram in equilibrium from literature data. Rietveld refinements of the single-phase samples were carried out. It was noted that with increasing

phosphate content the structure fit was more difficult. γ-C_2S and β-C_2S structure models could be refined to good results, while in the case of α´-C_2S additional restraints had to be induced. The refinement of α-C_2S structure models determined at high temperature experiments yielded unsatisfactory results. Increasing structure distortions with increasing phosphate content lead at a certain phosphate level, to crystal structures which are too different from the ideal models for a reliable refinement. Hydration behaviour of the different phosphate stabilized C_2S polymorphs differs distinctly from each other. While α-C_2S and γ-C_2S show almost no reaction with water, β-C_2S develops low heat of hydration over a long time. α´-C_2S shows the highest maximum and overall heat of hydration and a remarkably long induction period of over 50 hours. Also, the comparison between phosphate and Al_2O_3 stabilized β-C_2S shows that the stabilizing ion is more decisive for the hydration behaviour than the stabilized polymorph.

REFERENCES

[1] Trezza, M. A. and Scian, A. N. Burning wastes as an industrial resource. Their effect on Portland cement clinker, Cement and Concrete Research, vol.30, 2000, pp.137-144.

[2] Götz-Neunhoeffer, F. and Neubauer, J. Effects of Raw Meal Substitution by Sewage Sludge on OPC Clinker studied by Rietveld Analysis, Proceedings of the 20th International Conference on Cement Microscopy, Guadalajara, 1998, pp.130-138.

[3] Nurse, R. W. The effect of phosphate on the constitution and hardening of Portland cement, Journal of Applied Chemistriy, vol.2, 1952, pp.708-716.

[4] Niesel, K. and Thormann, P. Die Stabilitätsbereiche der Modifikationen des Dicalciumsilicats, Tonindustrie-Zeitung, vol.91, 1967, pp.362-369.

[5] Taylor, H. F. W. (1997): Cement Chemistry, 2nd ed. London: Thomas Telford, 1995, p.459.

[6] Il´inets, A. M. and Bikbau, M. Y. Structural mechanism of polymorphic transitions of dicalcium silicate, Ca_2SiO_4. Part I: Atomic structures of polymorphic modifications, Kristallografiya, vol.35, 1990, pp.84-90.

[7] Mumme, W. G., Hill, R. J., Bushnell-Wye, G. and Segnit, E. R. Rietveld crystal structure refinements, crystal chemistry and calculated powder diffraction data for the polymorphs of dicalcium silicates and related phases, Neues Jahrbuch für Mineralogie Abhandlungen, vol.169, 1995, pp.35-68.

[8] Remy, C., Andrault, D. and Madon, M. High-Temperature, High-Pressure X-ray Investigation of Dicalcium Silicate, Journal of the American Ceramic Society, vol.80, 1997, pp.851-860.

[9] Yamaguchi, G., Ono, Y., Kawamura, S. and Soda, Y. Synthesis of the Modifications of Ca_2SiO_4 and the Determination of their Powder X-ray Diffraction Patterns, Journal of the Ceramic Association of Japan, vol.71, 1963, pp.21-26.

[10] Eysel, W. and Hahn, T. Polymorphism and solid solution of Ca_2GeO_4 and Ca_2SiO_4, Zeitschrift für Kristallographie, vol.131, 1970, pp.322-341.

[11] van den Berg, A. and Tuinstra, F. The Space Group and Structure of α'-K_2SO_4, Acta Crysallographica B, vol.34, 1978, pp.3177-3181.

[12] Mumme, W., Cranswick, L. and Chakoumakos, B. Rietveld crystal structure refinements from high temperature neutron powder diffraction data for the polymorphs of dicalcium silicate, Neues Jahrbuch für Mineralogie Abhandlungen, vol.170, 1996, pp.171-188.

[13] Catti, M., Gazzoni, G. and Ivaldi, G. Order-Disorder in the α'-$(Ca, Sr)_2SiO_4$ Solid Solution: A Structural and Statistical-Thermodynamics Analysis, Acta Crystallographica B, vol.40, 1984, pp.537-544.

[14] Suzuki, K. and Yamaguchi, G. A Structural Study on α'-Ca_2SiO_4, Proceedings of the 5th International Symposium on the Chemistry of Cement, Tokyo, 1968, pp.67-73.

[15] Kim, Y. J., Nettleship, I. and Kriven, W. Phase Transformations in Dicalcium Silicate: II, TEM Studies of Crystallography, Microstructure and Mechanisms, Journal of the American Ceramic Society, vol.75, 1992, pp.2407-2419.

[16] Jost, K. H., Ziemer, B. and Seydel, R. Redetermination of the Structure of β-Dicalcium Silicate, Acta Crystallographica B, vol.33, 1977, pp.1696-1700.

[17] Smith, D., Majumdar, A. and Ordway, F. The Crystal Structure of y-Dicalcium Silicate, Acta Crystallographica, vol.18, 1965, pp.787-795.

[18] Udagawa, S., Urabe, K., Natsume, M. and Yano, T. Refinement of the crystal structure of y-Ca_2SiO_4, Cement and Concrete Research, vol.10, 1980, pp.139-144.

[19] Fix, W., Heymann, H. and Heinke, R. Subsolidus Relations in the System $2CaO \cdot SiO_2$ - $3CaO \cdot P_2O_5$, Journal of the American Ceramic Society, vol.52, 1969, pp.346-347.

[20] Saalfeld, H. and Klaska, K. H. The crystal structure of $6\ Ca_2SiO_4 \cdot 1\ Ca_3(PO_4)_2$. Zeitschrift für Kristallographie, vol.155, 1981, pp.65-73.

[21] Saalfeld, H. Kristallchemische Untersuchungen im System Ca_2SiO_4 - $Ca_3(PO_4)_2$. Beitrag zur Frage der Diadochie des Siliciums und Phosphors, Zeitschrift für Kristallographie, vol.133, 1971, pp.396-404.
[22] Fukuda, K., Maki, I., Ito, S. and Miyake, T. Structural Change in Phosphorus-Bearing Dicalcium Silicates, Journal of the Ceramic Society of Japan, vol.105, 1997, pp.117-121.
[23] Bensted, J. y-dicalcium silicate and its hydraulicity, Cement and Concrete Research, vol.8, 1978, pp.73-76.
[24] Bensted, J. Some hydration studies of α'-dicalcium silicate, Cement and Concrete Research, vol.9, 1979, pp.97-102.
[25] Jelenic, I. Hydration of B_2O_3-stabilized α'- and β-modifications of dicalcium silicate, Cement and Concrete Research, vol.8, 1978, pp.173-180.
[26] Fukuda, K. and Taguchi, H. Hydration of α'_L- and β-dicalcium silicates with identical concentration of phosphorus oxide, Cement and Concrete Research, vol.29, 1999, pp.503-506.
[27] Matkovic, B., Carin, V., Gacesa, T. and Halle, R. Reactivity of belite stabilized by $Ca_5(PO_4)_3OH$, Proceedings of the 7th International Congress on the Chemistry of Cement, Paris, 1980, pp.189-194.
[28] Matkovic, B., Carin, V., Halle, R. and Young, J. F. Dicalcium Silicates Doped with Phosphates, Proceedings of the 8th International Symposium on the Chemistry of Cement, Rio de Janeiro, 1986, pp.276-281.
[29] Matkovic, B., Carin, V., Gacesa, T., Halle, R., Jelenic, I. and Young, J. F. Influence of Ba_2SO_4 on the Formation and Hydration Properties of Calcium Silicates: I, Doped Dicalcium Silicates, American Ceramic Society Bulletin, vol.60, 1981, pp.825-829.
[30] Ghose, A., Chopra, S. K. and Young, J. F. Microstructural characterization of doped dicalcium silicate polymorphs, Journal of Materials Science, vol.18, 1983, pp.2905-2914.
[31] Guinier, A. and Regourd, M. Structure of Portland Cement Minerals, Proceedings of the Fifth International Symposium on the Chemistry of Cement, Tokyo, 1968, pp.1-31.
[32] Kuzel, H. J. Ein leistungsfähiges Wärmeleitungskalorimeter, TIZ-Fachberichte, vol.108, 1984, pp.46-51.
[33] Neubauer, J. and Götz-Neunhoeffer, F. Efficiency of highly sensitive heat flow calorimetry in examination of OPC hydration, Proceedings of the 24th International Conference on Cement Microscopy, San Diego, 2002, pp.58-68.
[34] Udagawa, S., Urabe, K., Yano, T. and Natsume, M. Studies on the dusting of calcium silicate (Ca_2SiO_4). The crystal structure of α'-Ca_2SiO_4, Semento Gijutsu Nenpo, vol.33, 1979, pp.35-38.
[35] Il´inets, A. M. and Bikbau, M. Y. Structural mechanism of polymorphic transitions of dicalcium silicate, Ca_2SiO_4. Part II: Refinement of crystal structure of high-temperature α'_L modification of dicalcium silicate Ca_2SiO_4, Kristallografiya, vol.35, 1990, pp.91-93.
[36] Udagawa, S., Urabe, K. and Yano, T. The Crystal Structure of α-Ca_2SiO_4, Semento Gijutsu Nenpo, vol.31, 1977, pp.23-25.
[37] Chatterjee, A. K. High belite cements - present status and future technological options: Part I., Cement and Concrete Research, vol.26, 1996, pp.1213-1225.
[38] Schmitt, D., Gotz-Neunhoeffer, F. and Neubauer, J. Untersuchungen zum Hydratationsverhalten der synthetischen Portlandzementphasen Alit und Belit mittels eines weiterentwickelten Wärmeleistungskalorimeters, 3. Tagung der GDCh-Fachgruppe Bauchemie, Würzburg, 2001, pp.146-150.

EFFECTS OF PHOSPHATE-RICH RAW MATERIALS ON THE CRYSTALLOGRAPHIC AND HYDRAULIC PROPERTIES OF DICALCIUM SILICATE

R. Müller, J. Neubauer and F. Götz-Neunhoeffer

Department of Mineralogy, University Erlangen-Nuremberg, Erlangen, Germany.
E-mail: rmueller@geol.uni-erlangen.de

Jürgen Michael Georg Neubauer

Schloßgarten 5a, 91054 Erlangen, Germany, Tel. 09131/853986

Date of birth:	21.02.62
Birthplace	Fürth, Bavaria

School:

1968-1972	Basic school in Fürth
1972-1981	Secondary school "Qualification for university entrance"

Services:

1981-1983	Military and alternative national service

University:

1983-1984	Study of mechanical engineering at the FH Nürnberg
1984-1986	Study of Mineralogy at the Friedrich-Alexander University Erlangen (FAU) intermediate Examination "Vordiplom" Mineralogy
1986-1988	Study of Mineralogy at the FAU
1988-1989	Master thesis at Wülfrather Cement Topic: Development of special cements from secondary raw materials
7/1989	Master degree "Diplom-Mineraloge Univ." (Applied Mineralogy, Geochemistry)

Post graduation:

1989-1992	Assistant of Prof. Dr. Dr. H. Poellmann at the department of Mineralogy (FAU)
12/1992	PHD (Dr. rer. nat.) Topic: Immobilization and solidification of hazardous wastes
1992-1994	Assistant of Prof. Kuzel at the Department of Mineralogy (FAU)
since 8/1994	Assistant Professor at the Department of Mineralogy (FAU)
1999	Habilitation Topic: Quantitative phase analysis of OPC clinkers by X-ray diffraction (Rietveld) methods

MICROSTRUCTURAL DEVELOPMENT IN HYDRATED AND CARBONATED CALCIUM ALUMINATE CEMENT: INFLUENCE OF ALKALIS AND STRENGTH BEHAVIOUR

L.Fernández-Carrasco[1], F. Puertas, M.T. Blanco-Varela and T. Vázquez

[1]Institut de ciència de Materials de Barcelona, (C.S.I.C.), Campus de la UAB. E-08193- Bellaterra, Spain. E-mail: lfernandez@icmab.es
Instituto de Ciencias de la Construcción Eduardo Torroja, (C.S.I.C.), c/ Serrano Galvache s/n, 28033 Madrid, Spain. E-mail: tvazquez@ietcc.csic.es

ABSTRACT

This research is a microstructural study of calcium aluminate cements, hydrated with water and alkaline solutions. Further microstructural alterations due to carbonation have also been studied in those systems. Finally, a relationship between developed microstructure and final material strength has been evaluated.

The presence of KOH solutions has an effect over hydrated calcium aluminate formation. This effect generates a different microstructure from the ones produced by the hydration with water. There is no proof of the direct relationship between alkali presence and the $CaCO_3$ type obtained on the later carbonation. However, it can be proved that there is an indirect relationship, considering that the presence of alkalis modifies the morphology of the hydrated phase and, therefore, the $CaCO_3$ type generated in such carbonation.

The mechanical strength of pastes shows a relationship with the hydrate morphologies. The accelerated carbonation process over the calcium aluminate hydrates always affects the mechanical strength positively, without any dependence over the developed $CaCO_3$ polymorph. The weathering carbonation process does not always affecting the mix in the same way as the mechanical strength. After carbonation process, the strength evolution has shown a relationship with aluminium hydroxide morphology formed in hydration and carbonation reactions.

Keywords: Calcium aluminate cement, carbonation, alkalis effect, morphology development, mechanical strength.

1. INTRODUCTION

In the past, Calcium Aluminate Cement (CAC) had been largely used thanks to its special properties, such as rapid hardening, resistance to aggression acids, and sulphates [1], refractory properties, an ability to withstand low temperatures and abrasion and impact resistance [2].

However, further research has shown that CAC, as well as Portland Cement (PC), can be susceptible to CO_2; provoking calcium aluminate hydrate carbonation [3-11]. Although that carbonation process might increase mechanical strength, it could also promote steel corrosion.

Other special processes can take place with CAC such as cement carbonation in the presence of alkalis (alkaline hydrolysis) [12-19]. According to the latest researche into the alkaline hydrolysis process, calcium aluminate hydrates react with alkalis and CO_2 developing calcium carbonate and

an alkali aluminium carbonate similar to dawsonite; later that alkali aluminium carbonate evolves into aluminium hydroxide and alkali bicarbonate [20, 21].

However, there are several issues to be clarified when studying the carbonation with or without the presence of alkalis. Such issues are basically the parameters determining one or more calcium carbonate polymorph formations and also the relationship between the calcium carbonate polymorph and mechanical strength evolution.

The aim of this work is to establish the alkali effect on the nature and morphology of developed calcium aluminate hydrates, as well as to determine the final products generated in the carbonation processes of these hydrates. Moreover, a relationship between the developed morphologies and the material strength evolution is established.

2. EXPERIMENTAL

1x1x6 cm prismatic cement paste specimens were manufactured. The CAC chemical composition and specific surface are given in Table 1. The water/cement ratio used for pastes manufacture was 0.8.

Table 1. CAC Chemical Composition (%) and Specific Surface.

CaO	Al_2O_3	Fe_2O_3	SiO_2	CaO free	I.R. (UNE)	L.O.I.	Na_2O equivalent	Specific Surface (m^2/Kg)
40.21	40.60	15.84	3.89	0.07	2.82	0.36	0.129	321.5

L.O.I.: loss of ignition. I.R.: Insoluble residue.

Three mixing liquids were used for paste manufacture: distilled water and two KOH solutions of 1M and 3M concentration, respectively.

The specimens were cured at 4º and 40ºC. During a 14 days curing process, specimens were placed inside sealed boxes where relative humidity (RH) was close to 99%. Table 2 shows prepared samples and the nomenclature used.

Table 2. Non Carbonated Samples.

Temperature (º C)	Distilled water	KOH solution	
		1M	3M
4	P_4^0	P_4^1	P_4^3
40	P_{40}^0	P_{40}^1	P_{40}^3

After the curing process, specimens went through an accelerated carbonation process inside a carbonation chamber. The conditions inside the carbonation chamber were: CO_2 saturation, 20 ± 1ºC and RH of 75%.

The samples, after the curing process, were characterised by X Ray Diffraction (XRD), Fourier Transform Infrared Spectroscopy (FTIR) and Scanning Electron Microscopy (SEM). The samples were analysed on the 2^{nd} and 6^{th} month of CO_2 exposure.

Twelve specimens of each type were mechanically tested (compression), at the end of curing period and also at specified carbonation times. The average strength values for each type and age were determined.

3. RESULTS AND DISCUSSION

3.1. Mineralogical Composition of Pastes

Calcium aluminate hydrates formed in specimens and analysed after curing period by XRD and FTIR are shown in Table 3.

Table 3. Hydrates Formed in Pastes.

Sample	P_4^0	P_4^1	P_4^3	P_{40}^0	P_{40}^1	P_{40}^3
Hydrates	CAH_{10}	CAH_{10} C_2AH_8	C_3AH_6	C_3AH_6	C_3AH_6	C_3AH_6

The results show that KOH presence in mixed liquid provokes alterations in the formed calcium aluminate hydrate. At 4ºC, when 1M KOH concentration is used, C_2AH_8 is the main hydrate formed while when KOH concentration is 3M, even at 4ºC, the final product generated is the stable cubic hydrate C_3AH_6. At 40ºC; cubic hydrate is generated in all pastes.

The hydration products of P_{40}^3 sample are identical to those of P_{40}^1 and also calcium aluminate hydrate, C_3AH_6, is developed with the same morphology, in plate form without a preferential orientation. Due to this identical result, only the carbonation of the P_{40}^1sample is displayed, as carbonation products are similar in both samples.

Mineralogical characterisation of 2 months' carbonated samples shows that only the alkali hydrated samples presented calcite (see Table 4). The vaterite and also aragonite were the carbonates generated in the other samples; that is, in those pastes made without alkalis.

Table 4. Calcium Carbonates and Aluminium Hydroxide Formed in Pastes.

Exposition time (months)	P_4^0	P_4^1	P_4^3	P_{40}^0	P_{40}^1
2	vaterite aragonite AH_3 gel	vaterite aragonite ¤calcite b	vaterite calcite aragonite* n	vaterite aragonite* g	calcite aragonite* g
6	vaterite aragonite g, b*,n*	vaterite aragonite ¤calcite n	vaterite aragonite* calcite* n, b, g	vaterite aragonite* g, b*, n*	calcite aragonite* g, b*, n*

g: gibbsite, b: bayerite, n: nordstrandite.
*Minor phases, likely from the evolution of vaterite with time.
¤ Only in the external part of pastes.

Nevertheless at 6 months of carbonation (Table 4), in hydrated samples without an alkalis content, and not only 4º C but also at 40º C, calcium carbonate polymorphs detected were vaterite and aragonite.

On the other hand those samples made with alkalis contained a high proportion of calcite. With regard to aluminium hydroxide, at 4º C all polymorphic forms were detected but gibbsite was the main AH_3 developed; however in the presence of alkalis, the bayerite portion was greater and evolved towards nordstrandite. At 40º C, the gibbsite was the polymorphic form mainly detected.

The bibliography contains reference to the existence of a notable difference between the gibbsite and bayerite precipitation rate [22]. A fast precipitation would ease the formation of bayerite type structures whilst slow precipitation would tend to the gibbsite type. It has been described too that

nordstrandite is formed from bayerite aging [23], structure being an intermediate state between gibbsite and bayerite.

The carbonation of 4ºC water prepared samples appears to happen more slowly than those without an alkali presence. Therefore, in the P^0_4 specimens, the aluminium hydroxide precipitation is slow, and generates gibbsite. Nevertheless, the presence of other AH_3 polymorphic forms can also be caused by high pH of the CAC pastes, as a high pH tends to help the formation of bayerite and gibbsite.

It is important to mention that carbonation without alkalis, at 4º and 40ºC, did not generate calcite. Moreover, either CAH_{10}, C_2AH_8 or C_3AH_6 carbonation generate the same polymorphic forms of $CaCO_3$. With reference to the aluminium hydroxide, gibbsite is the polymorph mainly generated.

3.2 Mechanical Strength Development.
Table 5 gives the values obtained from the compressive tests carried out on the specimens.

Table 5. Pastes Compressive Strength (N/mm^2)

Sample	P_4^0	P_4^1	P_4^3	P_{40}^0	P_4^1
Non carbonated	31	6.6	---	13.9	---
2 months carbonated	49.3	11.2	5.3	15.7	3.2
6 months carbonated	65.2	10.1	10.2	18.6	3.6

Alkali presence in the mixing water has a very negative effect on the paste's strength development, both cured at 4º and 40º C. At high KOH concentrations, alterations in nature and rate of formation of hydrated compounds are produced. Those alterations are responsible for the resistance decrease. A comparative study of the total heat and the maximum rate of heat evolution curves, through the isothermal calorimetry technique, shows that CAC hydration reactions are accelerated with temperature but also in the presence of KOH [21, 24].

The samples that are carbonated in a CO_2 saturated chamber always show an increase of compressive mechanical strength as time goes by. The mass deposition of carbonation products in all the cases studied leads to a reduction of porosity of the pastes, and as a consequence a progressive increase of the mechanical strengths is produced [25].

In general, it can be seen in Table 5, that samples show a better mechanical behaviour as a consequence of specimen' exposure to CO_2. Only those samples made without alkalis at low temperature presented an acceptable strength value and also the gain with CO_2 exposure is significant.

An important strength increase was observed in those samples which initially presented AH_3 on a non crystalline form (P^0_4) and evolving to gibbsite by crystallisation. Such samples initially presented AH_3 on a non-crystalline form, evolving to gibbsite by crystallisation. It is for this reason that the strength increase of the P^0_4 specimens between two and four months of carbonation ascribed to the AH_3 crystallisation.

3.3 Microstructural Studies
In P_4^0 sample, the CAH_{10} is developed initially as a needle form but after 14 curing days the sample was mainly constituted by parallel oriented plates [26]. Due to the carbonation chemical process it can be proved, using XRD and FTIR, that the sample evolves towards the formation of calcium carbonate in vaterite and, in minor portion, into the aragonite form. In addition, there is aluminium hydroxide. Figure 1 shows developed morphologies in samples prior and after the carbonation process.

The P_4^0 carbonated sample was highly compacted, even though it could be found the calcium carbonate morphology mainly as plates (Figure 1b). Aluminium hydroxide was developed as a smooth film.

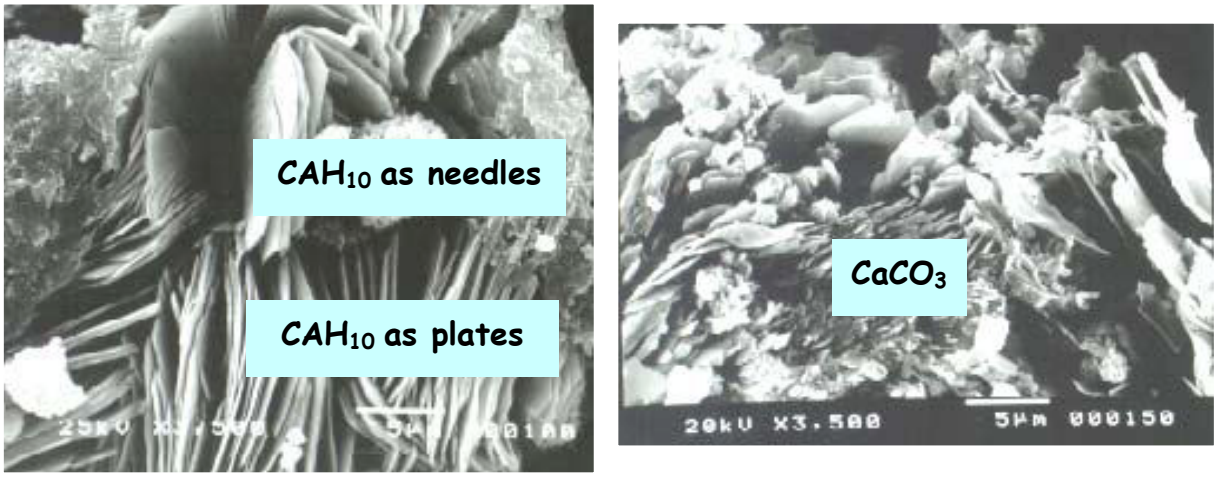

Figure 1. Morphology of sample P_4^0. a) prior carbonation b) carbonated.

When CAC was hydrated with 1M KOH solution at 4ºC, the developed morphology was mainly a plate and needle structure without any preferential orientation. At 14 days of curing the plates were the main constituents. TEM analysis showed the needles were CAH_{10} and plates were C_2AH_8 [26]. Carbonation specimen study through XRD and FTIR indicated that calcium aluminate hydrate evolved into vaterite, aragonite and also calcite and aluminium hydroxide. In Figure 2, P_4^1 sample microstructure can be seen.

The element average composition of CAH_{10}, C_2AH_8 and C_3AH_6 was analysed by TEM. The percentage of calcium and aluminium reduces at the same time the percentage of iron and potassium increases, for the CAH_{10} formed in the presence of potassium; nevertheless the developed morphology is not modified. The presence of potassium does not favour isomorphic substitution of Al^{3+} ions by Fe^{3+} ions in the C_3AH_6 hydrated phase. It was also found that gel phases in samples mixed with KOH solution have higher potassium and iron contents [26].

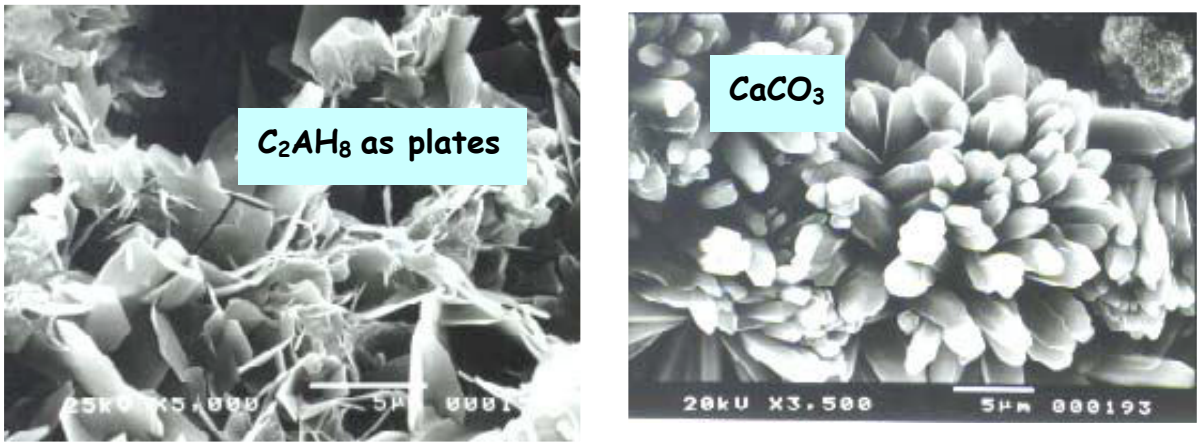

Figure 2. Morphology of sample P_4^1. a) prior carbonation b) carbonated.

After carbonation, P_4^1 surface was formed by groups of large polyhedric shapes of calcium carbonate (Figure 2b). A smooth film was also detected as $CaCO_3$ and dense prisms of AH_3.

The P_4^3 sample was formed by C_3AH_6 plate-like morphology placed with no order -roselike- and aluminium hydroxide. Due to CO_2 action over the sample, calcium carbonate in calcite, vaterite but also aragonite forms were developed. Figure 3 presents C_3AH_6 and $CaCO_3$ morphologies.

The calcium carbonate developed in the P_4^3 sample was as needle and plate morphology as can be seen in Figure 3b.

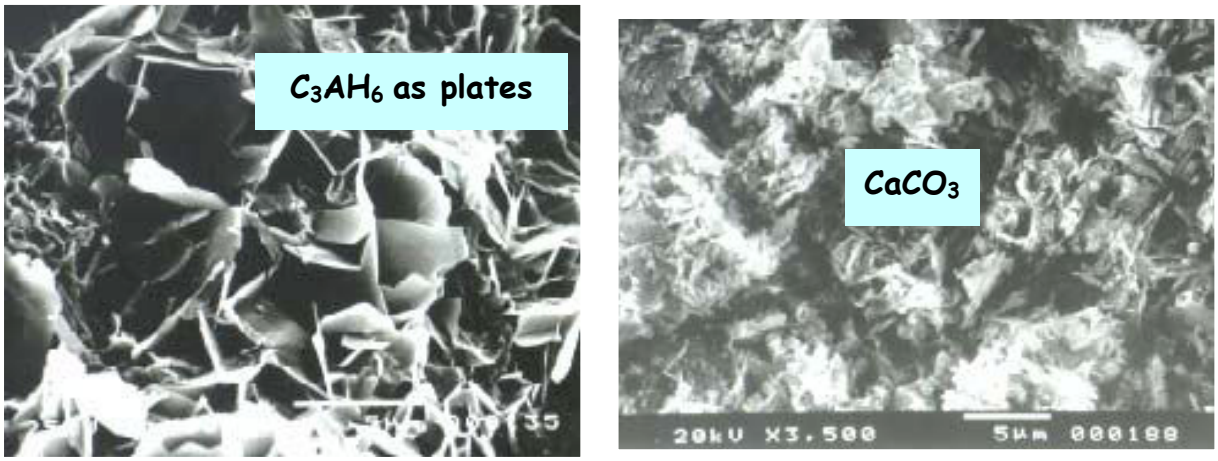

Figure 3. Morphology of sample P_4^3. a) prior carbonation b) carbonated.

At the highest temperature, 40ºC, with and without alkali presence, the calcium aluminate hydrate developed was C_3AH_6 as well as AH_3 (gibbsite). In the absence of alkalis the cubic hydrate was developed as parallel plates and aluminium hydroxide was disposed between the plates. Figure 4 displays the mentioned C_3AH_6 morphologies formed in the absence of alkalis. In alkali presence, C_3AH_6 was developed as spheres.

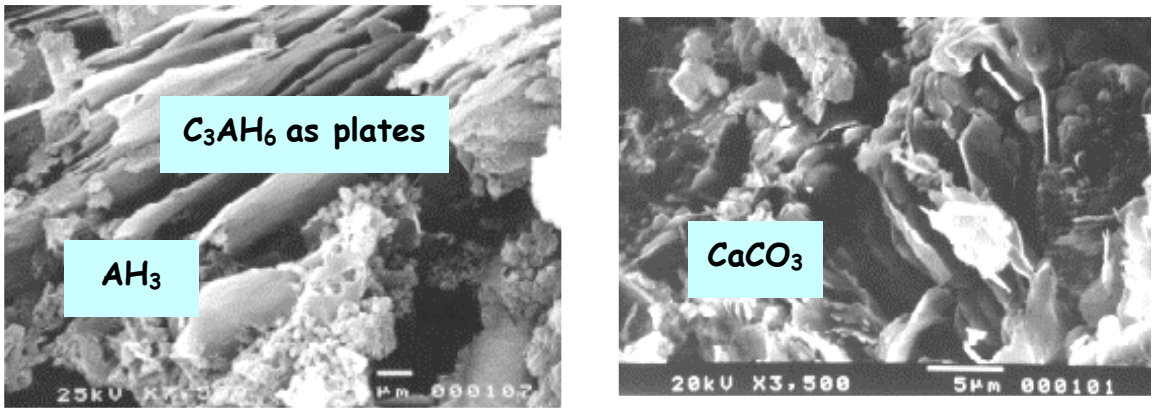

Figure 4. Morphology of sample P_{40}^0. a) prior carbonation b) carbonated.

In the P_{40}^0 sample, the calcium carbonate was developed as little plates disposed following an ordered orientation. Aluminium hydroxide was found shaped as dense microstructures in rounded form between the plates.

Different morphologies of calcium carbonate in sample P_{40}^1 were observed: as grouped plates and as grouped needles and also $CaCO_3$ was seen as needle form growing from spherical particles with a high aluminium and potassium content (Figure 5b).

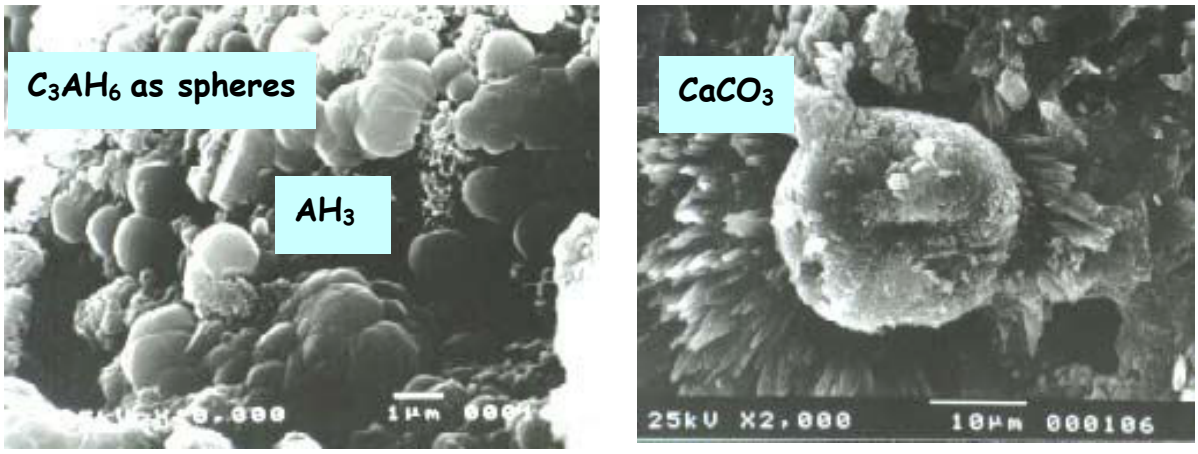

Figure 5. Morphology of sample P_{40}^{1}. a) prior carbonation b) carbonated.

From microstructural studies it was possible to determine the existence of a relationship between the morphology of the formed hydrate of either hexagonal or cubic structure, and the calcium carbonate, developed due to CO_2 action over such hydrates (see Table 6). Calcium aluminate hydrates with needle and/or ordered plate morphology due to CO_2 effect, evolve towards the formation of calcium carbonate as vaterite and aragonite. Those hydrates with disordered plate or sphere morphology evolve towards calcite formation. Afterwards, the vaterite form evolves towards calcite and aragonite.

Table 4. Calcium Aluminate Hydrate and Calcium Carbonate Morphologies

Sample	Hydrate type	Morphology	Carbonate Type
P_4^0	CAH_{10}	needles/ordered plates	vaterite/aragonite
P_4^1	C_2AH_8	disordered plates	vaterite/aragonite/calcite
P_4^3	C_3AH_6	disordered plates	calcite/vaterita/aragonite *
P_{40}^0	C_3AH_6	ordered plates	vaterite/aragonite *
P_{40}^1	C_3AH_6	spheres	calcite/aragonite *

* Minor phases.

From the results obtained, a relationship between the developed morphology of hydrated phases and mechanical strength was observed. Those samples constituted by hydrates with morphology in spherical form presented the minor strength value. When calcium aluminate hydrates were developed as plates without a preferential orientation, the specimens did not have good strength behaviour and only those samples with morphology developed as ordered plates gave high strength values.

4. CONCLUSIONS

Hydration of CAC with alkalis provokes a modification in the developed calcium aluminate hydrate and also the hydrate's morphology is different. Therefore the alkali presence modifies the calcium carbonate type developed.

The mechanical strength behaviour can be explained through the sample's morphology. Those samples with a needle or ordered plate morphology show the best mechanical strength behaviour; while those samples with a spherical or disordered plate spherical morphology gave the worst strength behaviour.

As illustrated in this paper, a relationship between calcium aluminate hydrate morphology and the developed calcium carbonate type is established. This is to say that those calcium aluminate hydrate with needle or plate morphology evolve towards vaterite and/or aragonite and those hydrated calcium aluminates with sphere morphology generate calcite.

Mechanical strength evolution over time is positively influenced by aluminium hydroxide: the morphological change of aluminium hydroxide from amorphous towards crystalline shape is reflected by an increase in mechanical strength.

ACKNOWLEDGMENTS

The authors wish to thanks to the Dirección General de Enseñanza Superior e Investigación Científica, of Spain, for the support given trough the Project PB97-1144 from the Promoción General del Conocimiento.

REFERENCES

[1] Bied, J., Brit. Pat. 8193, (1909).
[2] Taylor, H.F.W., "Cement Chemistry" 2nd edition, edited by Thomas Telford, (1997).
[3] Midgley, H.G., Woodward, B.M., RILEM Int. Symp. "Carbonation of Concrete", Wexham Springs, England, 4/4 5-6 April (1976).
[4] Raask, E., ib [3], 5-6, (1976).
[5] Blenkinsop, R.D., Currel, B.R., Midgley, H.G., Parsonage, J.R., Cem. Concr. Res., Vol. 15, pp. 276-284, pp. 385-390, (1985).
[6] Murat, M., Negro, A., Bachiorrini, A., C.R. Acad. Sci. Paris 291, C, 287 (1980).
[7] Bachiorrini, A, Murat, M., Cement Concr. Research, vol. 17, pp. 242-248, (1987).
[8] Lach, V., Matousek, M., Seminario Inter. Calcium Aluminates, Vol. V, pp. 305-313, Torino (Italia), (1982).Gfr
[9] Vázquez, T., Triviño, F., Ruiz de Gauna, A., Monografía nº 334 del Instituto Eduardo Torroja de la Construcción, (1976).
[10] Pérez, M., Tesis Doctoral, Universidad Complutense de Madrid, Sección Químicas, (1981).
[11] P. Barnes, J. Bensted, "Structure & Performance of Cements" published by E & F N Spon, 2nd edition (January 15, 2002).
[12] García Alcocel, E., Garcés, P., Chinchón, S., "General Study of Alkaline Hydrolysis in Calcium Aluminate Cement Mortars Under a Broad Range of Experimental Conditions". Cem. Concr. Res. Vol. 30, pp. 1689-1699, 2000.
[13] Stiglitz, P., "Utilisation du ciment alumineux dans la construction. Élimination des risques d'altération". Revue des Matériaux de Construction, nº 671-672, (1971).
[14] Rengade, L'Hopitallier, Fontmagne, "Recherches sur les causes de certains phénomènes d'altération des bétons de ciment alumineux". Reveu de Matériaux de Construction nº 378, 379. (1936).
[15] Lafuma, H., "Quelques aspects de la physico-chimie des ciments alumineux". Reveu Générale de Sciences Appliquées, Vol. 1, nº 3, pp. 66-74. (1952).
[16] Duriez, M., "Traité des Materiaux de Construction". Editions du Moniteur des Travaux Publics, Paris, (1957).
[17] Ciments Lafarge. Determination of freeable alkalis contained in sands. Le Tiel, Central Laboratory, November, pp. 9, nº 33C. (1966).
[18] Dunster, A. M., Crammond, N. J., "Alkaline Hydrolysis with Carbonation in High Alumina Cement Concrete Beams" X Symposium International In The Chemistry of Cements, Gothenburg (1997).
[19] Scrivener, K.L., Lewis, M., Houghton, J., "Microstructural Investigation of Calcium Aluminate Cement Concrete from Structures" X Symposium International In The Chemistry of Cements, Gothenburg (1997).
[20] Fernández-Carrasco, L., Puertas, F., Blanco-Varela, M.T. Vázquez, T., "Pottasium Dawsonite formation in Calcium Aluminate Cements". Conference on Calcium Aluminate Cements, Edinburgh (UK), pp. 379-384, (2001).
[21] L. Fernández-Carrasco. "Procesos de Hidratación y Carbonatación del Cemento de Aluminato de Calcio; Influencia de los Álcalis. Alteraciones Microestructurales y Relación con sus Propiedades Mecánicas". Tesis Doctoral, Universidad Autónoma de Madrid, Facultad de Ciencias (2000).
[22] Richardson, M., "Carbonation of Reinforced Concrete. It Causes and Management" Dublín, (1988).
[23] Hsu, P. H., Bates, T.F., Mineral. Mag., 33, pp. 749-768, (1964).
[24] Fernández-Carrasco, L., Puertas, F., Blanco-Varela, M.T. Vázquez, T., "CAC hydration. Alkali and temperature effect". In press.

[25] Puertas, F., Fernández-Carrasco, L., Blanco-Varela, M.T., Vázquez, T., De la Fuente, A., "Influence of KOH solution on the hydration and carbonation of high alumina cement mortars" Journal Mat. Sci. Vol. 31, pp. 2819-2827, (1996).
[26] Fernández-Carrasco, L., Blanco-Varela, M.T., Puertas, F., Vázquez, T., Glasser, F.P., Lachowski, E., "Hydration of High Alumina Cement in the Presence of Alkalis" Adv. Cem. Res., vol. 12, nº 4, pp. 143-152, (2000).

EFFECT OF $Ca(OH)_2$ AND Li_2CO_3 ON HYDRATION BEHAVIOR OF SYNTHETIC CALCIUM ALUMINATE CEMENTS

M. Schmid, F. Goetz-Neunhoeffer and J. Neubauer

Department of Mineralogy, University of Erlangen-Nuremberg,
Schlossgarten 5a, 91054 Erlangen, Germany. E-mail: M.Schmid@geol.uni-erlangen.de

ABSTRACT

Synthetic Calcium Aluminate Cements (CAC) were prepared from pure synthesised CA, CA_2 and/or corundum to investigate the influence of accelerating additives on the hydration and the development of the hydration products of Calcium Aluminate Cements. The hydration experiments of two synthetic mixtures were performed with a isothermal heat flow calorimeter [1] over a period of 72h at 23.0°C ±0.3°C (w/c=0.45). Synthetic CAC M3 was mixed from 50 ma.% CA and 50 ma.% CA_2 whereas the composition of mixture M4 was formulated to resemble technical CAC clinker with 60 ma.% CA, 34 ma.% CA_2 and 6 ma.% A. Each calorimeteric measurement was performed three times. By adding inorganic additives to the synthetic CAC, either 5 ma.% CH or 0.02% Li_2CO_3-solution, the maximum of heat flow is shifting to shorter hydration times and the measurement becomes very reproducible. The combination of heat flow calorimetry with in-situ XRD of the synthetic CAC proved that the heat of hydration can be related to the dissolution of CA and CH (only one mixture) and the formation of hydration products, C_2AH_8 and $C_2AH_{7.5}$.

1. INTRODUCTION

According to the results of several authors [2,3,4] the setting time of a Calcium Aluminate Cement is influenced by the addition of small amounts of inorganic additives. The influence of the ions acting as accelerator can be put in the following order [5]:

$$\text{cations: } Li^+ << Na^+ < K^+ < Ca^{2+} < Mg^{2+} < Sr^{2+} < NH_4^+$$
$$\text{anions: } OH^- < Cl^- < NO_3^- < Br^- < \text{acetate}$$

To get more basic information about the influence of the accelerating additives on hydration of Calcium Aluminate Cements and on the development of hydration products an investigation of the hydration behaviour of two synthetic mixtures was carried out. One composition of the two synthetic Calcium Aluminate Cements, prepared from pure synthesised phases, are defined in Table 1.

Table 1. Composition of the synthetic mixtures

phase	M3 [ma.%]	M4 [ma.%]
CA	50	60
CA_2	50	34
A	-	6

As accelerating additives 5 ma.% CH and 0.02% Li_2CO_3-solution were chosen.

2. EXPERIMENTAL

2.1 Synthesis and characterisation

The pure phases for the synthetic mixtures CA and CA_2 were obtained by sintering an equimolar mixture of $CaCO_3$ and Al_2O_3 in a laboratory furnace at 1400°C in platinum crucibles interrupted by several grinding procedures. The CA phase was free of minor phases after 8h and CA_2 after 16h. The corundum used for the mixtures contained a slight amount of θ-Al_2O_3 which disappeared after a short thermal treatment of 15 min at 1200°C. The CH used as an accelerator was synthesised by slow diffusion by keeping freshly prepared CaO and deionised CO_2-free water over 8 weeks in a sealed glass. After drying for 8h at 35% r.h. over a supersaturated $CaCl_2$-solution the remaining free water content of the CH was below 0.4 ma.%. The synthesised CA, CA_2, and CH were checked by XRD for minor phases. The purity was determined by Rietveld quantification to be higher than 99.7 ma.%.

The specific surface area was determined to be 3735±14 cm^2/g for CA and 4810±12 cm^2/g for CA_2 (blaine). The corundum used for the synthetic mixtures was sieved to minus 25µm and SEM confirmed that the apparent particle size was below 10µm.

The synthetic mixtures were homogenised in an agate mortar over a period of 15 minutes.

2.2 Heat flow calorimetry

For the hydration of the synthetic Calcium Aluminate Cements a heat flow calorimeter operating in isothermal mode as described by [5], was employed. Each synthetic CAC was measured three times. The temperature during hydration was kept constant at a value of 23.0°C±0.3°. The water used for hydration experiments was injected with a syringe. Table 2 shows the instrumental parameters.

Table 2. Instrumental parameter of the heat flow calorimeter

Hydration time [h]	72
Integration time / cell [s]	5
Interval time [s]	19

2.3 In-situ XRD-analysis of hydration

The examination of the hydrated mixtures and the in-situ XRD were performed with a Siemens D5000 diffractometer. The mixtures for hydration experiments were stirred manually and filled in a sample holder for XRD. To prevent carbonation the sample surface was covered with Capton foil. Another portion of the same batch of sample was used for the calorimetric investigation. Measurement parameters for X-ray diffraction are given in Table 3.

Table 3. XRD parameters

Radiation	Cu Kα
Tube voltage	40 kV
Tube curent	30mA
Time/step	2s
Stepwidth	0.02° 2θ
Divergence slit	V20
Receiving slit	0.2 mm

The qualitative phase composition of samples hydrated in the calorimeter was investigated after 4 days. XRD pattern were recorded from 5 to 65° 2 θ.

Quantitative phase development of sample M3 using CH as additive was recorded by scanning CA from 29.5 to 30.7° 2θ and C_2AH_x (C_2AH_8 + $C_2AH_{7.5}$) from 5.0 to 9.8° 2θ. The scan was repeated every 10 minutes.

Quantitative phase development in sample M4 with addition of Li_2CO_3 was detected by scanning from 5.5 to 30.5° 2θ. The scan was repeated every 40 minutes.

3. RESULTS

3.1 Hydration of the synthetic mixtures

Heat evolution of synthetic mixture M3 measured by calorimetric investigation is presented in Figure 1. The values of the heat of hydration after 72 hours and the time of the maximum heat flow are the average values of three measurements.

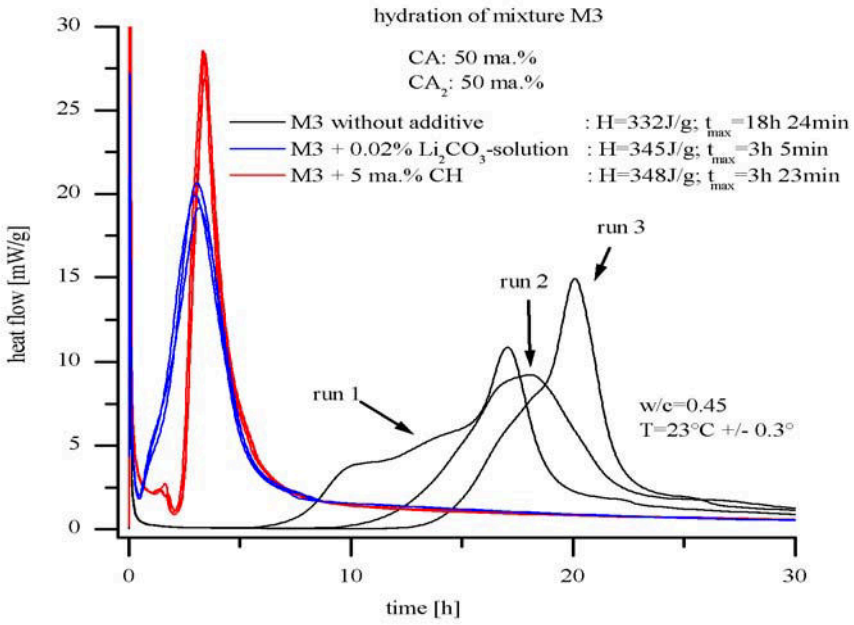

Figure 1. Hydration of mixture M3 without additives, with Li_2CO_3-solution and with CH (each mixture was measured three times)

The hydration of the synthetic mixture M3 without any additive shows poor reproducibility; note the time to the maximum heat flow and to the total heat of hydration (Figure 1). After injection of water the heat flow decreases and stays very low during the induction period, which lasts for several hours. The begin of the acceleration period of each sample of M3 without additive is variable. After the maximum of heat development the heat flow decreases but the hydration is not finished after 72h (>0.1mW/g).

By adding inorganic additives to the synthetic mixtures a different hydration behaviour can be observed. Hydration of mixture M3 with 0.02% Li_2CO_3-solution shows a very short induction period and an acceleration period starting at 0.5h after injection of water. The course of hydration of mixture M3, using 5 ma.% CH, shows a low heat flow during induction period up to 2h. After a slight decrease in heat flow the acceleration is very rapid.

For mixture M3 the course of hydration is decelerated showing humps in the heat flow suggesting several overlapping reactions. The heat evolution for mixture M3 with Li_2CO_3-solution is strongly accelerated and seems to belong to one homogenous reaction. Heat evolution after induction period

of mixture M3 with 5 ma.% CH starts at later times than the Li_2CO_3 accelerated sample but has even faster peat heat flow.

Figure 2 demonstrates the influence of the admixtures on the maximum of heat flow during the first 0.5h.

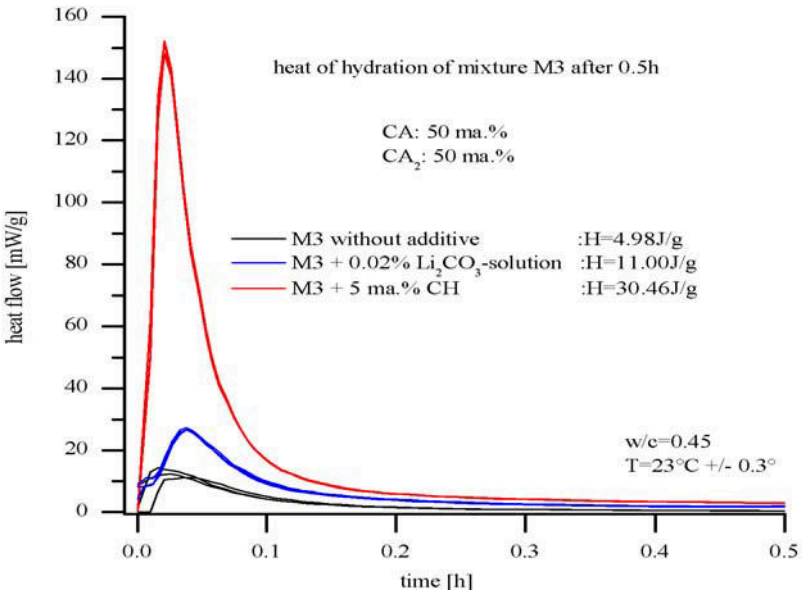

Figure 2. Hydration of mixture M3 during the first 0.5h
(each mixture was measured three times)

Heat evolution for M4 (Figure 3) with corundum is nearly comparable with mixture M3. Only M4 without additive is slightly different to M3 because of added corundum which seems to promote crystallization. The time to the acceleration of M4 without additives is more reproducible than M3 without additives. Hydration of mixture M4

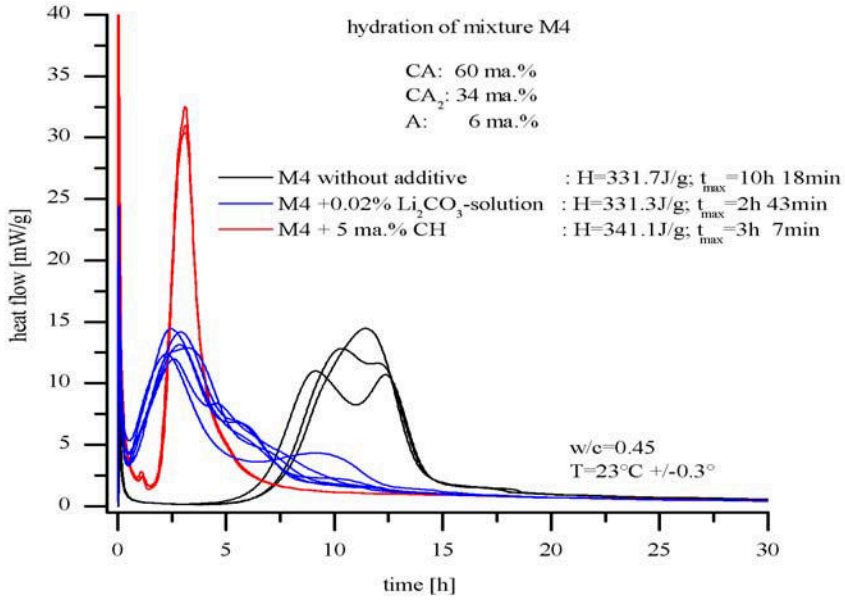

Figure 3. Hydration of mixture M4 without additives, with Li_2CO_3-solution and with CH
(each mixture was measured three times)

Table 4 summarizes that the heat of hydration during the first 0.5h is doubled by adding 0.02% Li_2CO_3-solution and is six times larger by adding 5 ma.% CH compared to M3 without additives.

Table 4. Heat of hydration of mixture M3 during the first 0.5h after injecting (mean of three measurements)

	M3 without additive	M3 0.02% Li_2CO_3-solution	M3 5 ma.% CH
heat of hydration after 0.5h [J/g]	4.9	11.0	30.5
maximum of heat flow [mW/g]	12	27	150

The maximum heat flow is reached during the first six minutes and is twice as high by the use of Li_2CO_3 and is over 12 times larger by adding 5 ma.% CH compared to the mixture M3 without additive.

Figure 4 shows that the heat of hydration of all mixtures lies in a narrow a range from 328 to 352 J/g. The maximum of heat evolution t_{max} is shown for all investigated mixtures in Figure 5. It is notable that no distinction between M3 and M4 can be made from heat of hydration and t_{max} because of the overlapping maximum and minimum values of three measurements.

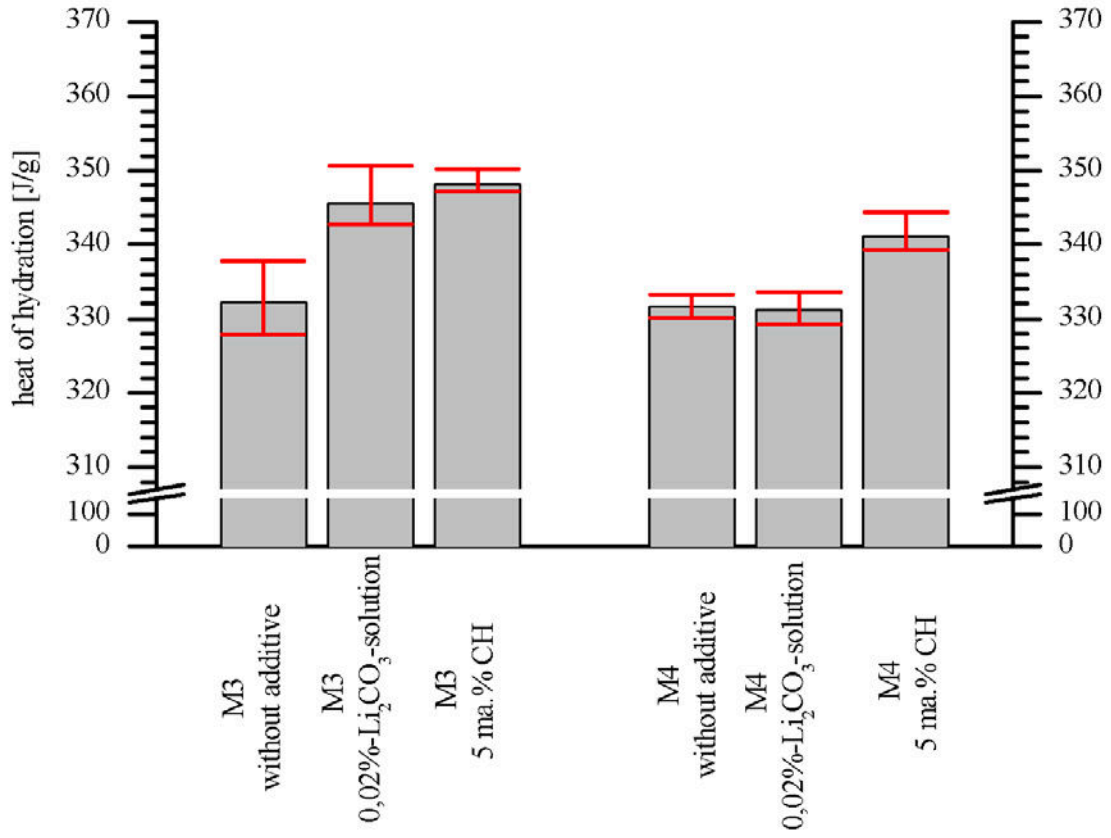

Figure 4. Heat of hydration of hydrated synthetic calcium aluminate cements M3 and M4

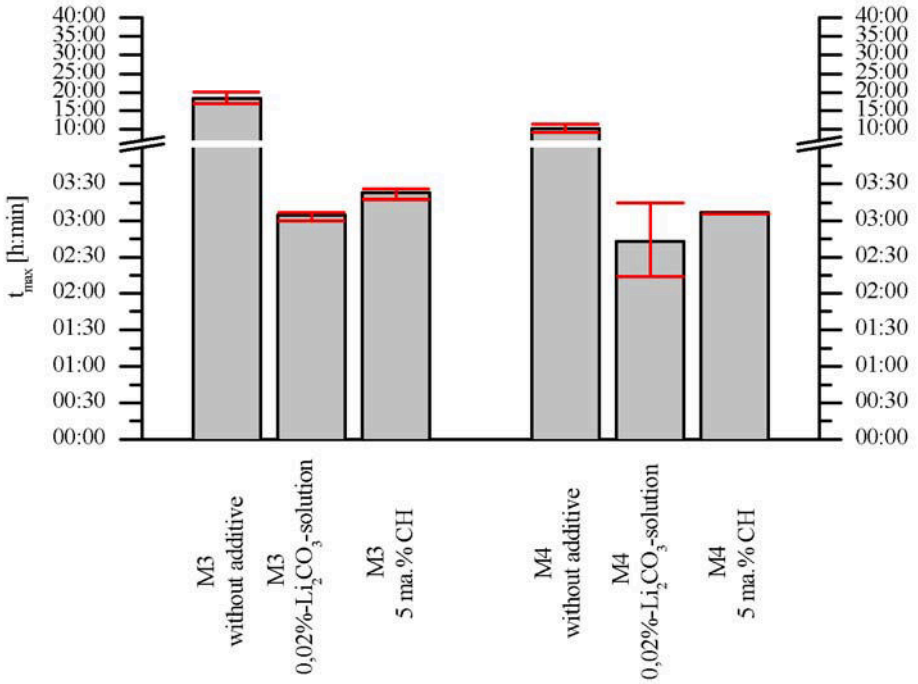

Figure 5. Maximum of heat development t_{max} of all hydrated mixtures

3.2 Hydration products of the synthetic mixtures

The phase composition of hydrated samples were determined after 4 days (Tables 5 and 6).

Table 5. Phase assemblage in the hydrated mixture M3

mixture	identified phases					
	CA	**CA_2**	**$C_2AH_{7.5}$**	**CAH_{10}**	**AH_3**	**CH**
M3 without additive	**X**	**X**	**X**	**X**	**X**	-
M3 0.02% Li_2CO_3-solution	**X**	**X**	**X**	**X**	**X**	-
M3 5 ma.% CH	**X**	**X**	**X**	**X**	**X**	**X**

Table 6. Phase assemblage in the hydrated mixture M4

mixture	identified phases						
	CA	**CA_2**	**A**	**$C_2AH_{7.5}$**	**CAH_{10}**	**AH_3**	**CH**
M4 without additive	**X**	**X**	**X**	**X**	**X**	**X**	-
M4 0.02% Li_2CO_3-solution	**X**	**X**	**X**	**X**	**X**	**X**	-
M4 5 ma.% CH	**X**	**X**	**X**	**X**	**X**	**X**	**X**

The hydration products C_2AH_8, C_4AH_{19} and C_3AH_6 were not detected, but $C_2AH_{7.5}$ a phase described by SCHELLER & KUZEL[6], was identified as a hydration product with lower water content than C_2AH_8.

3.3 In-situ-XRD of the synthetic mixtures

The in-situ measurement of the hydration reaction by XRD was performed for mixtures which are reproducible according to t_{max} and heat of hydration. Therefore only mixtures accelerated with additives were investigated.

No other hydration products other than C_2AH_8, $C_2AH_{7.5}$, AH_3 occur and the CA_2 content remains constant. Even CAH_{10} was not detected during the first twelve hours of measurement. Table 7 gives the single peaks used for peak area measurement. The temperature during in-situ measurement was 25°C +/- 2°C.

Table 7. Peak areas analysed during hydration

phase	peak (hkl)	peak area [° 2θ CuKα]
CA	triplet (12-3), (123), (220)	29.5-30.5
C_2AH_8	(006)	7.0-9.3
$C_2AH_{7.5}$	(004)	7.0-9.3

Before determining the peak area, the background was subtracted from each scan. In case of C_2AH_8, and $C_2AH_{7.5}$ not a single peak area but the whole area under both peaks was integrated. Figure 6 shows the continuous transformation from C_2AH_8 to $C_2AH_{7.5}$ of mixture M3 with 0.02%Li_2CO_3 at the beginning of the measurement (red line) and after a period of 12h (blue line).

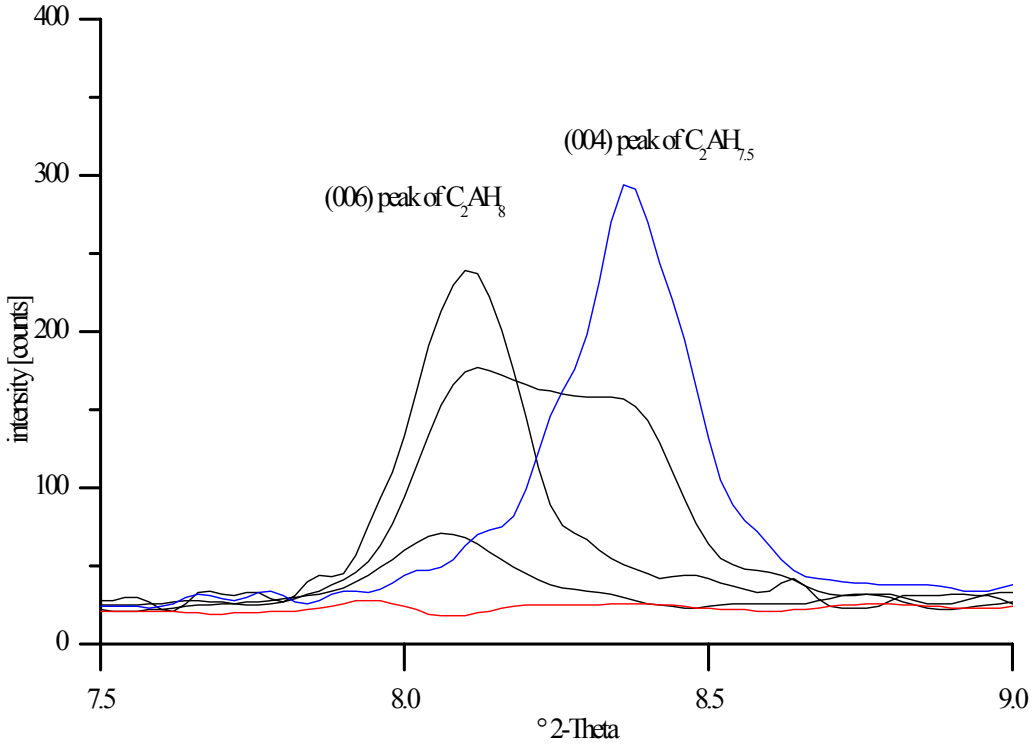

Figure 6. Transformation of C_2AH_8 to $C_2AH_{7.5}$ in M3 with 0.02% Li_2CO_3-solution

3.4 Hydration development of mixture M3 with 5ma.% CH

In Figure 7 two different investigations are plotted together: Heat flow calorimetry and quantitative XRD analysis of hydration of M3 with 5 ma.% CH. The decrease of CA and the increase of C_2AH_x were determined as described by peak area measurement; in situ measurements allow quantitative measurements.

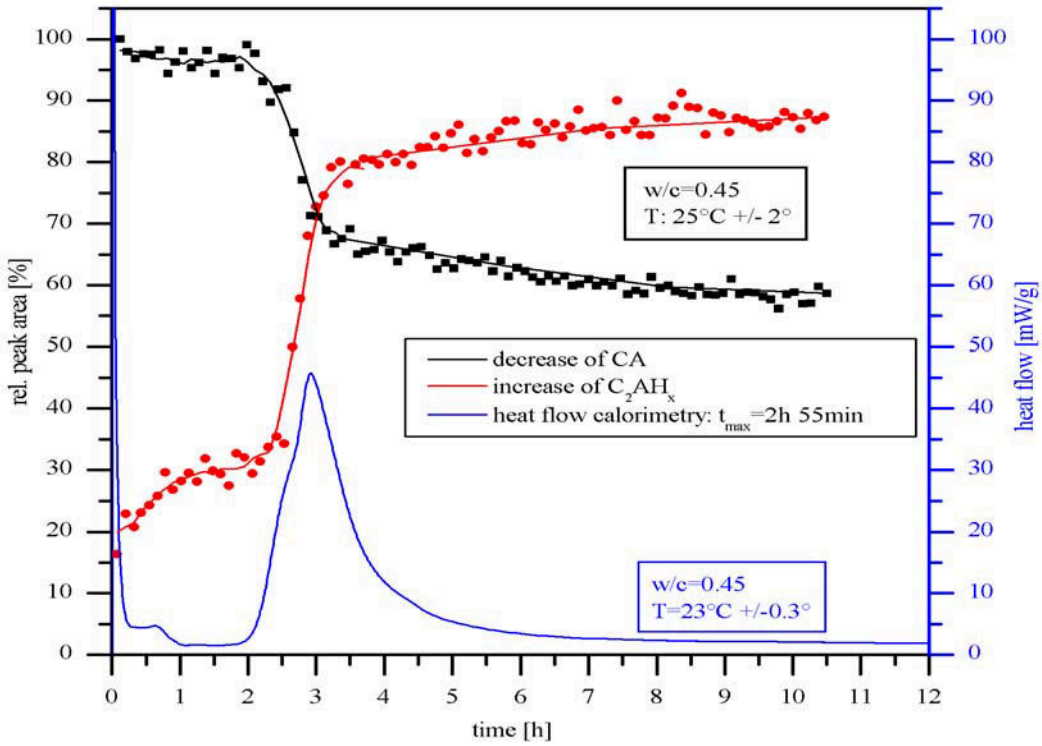

Figure 7. Quantitative in-situ XRD of M3 with 5 ma.% CH combined with heat flow calorimetry

For M3 with 5 ma.% CH the reaction can be divided into four different stages:

- t=0-10min: C_2AH_8 is present from the very early contact of the dry mixture with water. A minor amount of $C_2AH_{7.5}$ was also detected as a asymmetric broadening of the (006) peak of C_2AH_8 towards higher 2θ-values (Figure 6). The transformation from C_2AH_8 to $C_2AH_{7.5}$ is taking place immediately after mixing with water. No statement about dissolution of CA is possible because the first measurement of CA peak was performed after more than 10 min. Heat evolution is very strong (initial period) during the first 10 minutes.
- 10min<t<2h: In this period the amount of CA present in the paste remains nearly constant. The amount of crystallised C_2AH_x increases slightly during this period. At the same time the heat evolution is low (induction period).
- 2h<t<3h: After about 2 hours the decrease of the CA content accelerates very strongly. At the same time the amount of C_2AH_x increases. The heat evolution shows that the maximum of heat development correlates with the maximum rate of CA decrease and increase of C_2AH_x (end of acceleration period).
- 3h<t<11h: The decrease of CA decelerates; only small amounts of C_2AH_x crystallize. The heat flow shows a constant decrease at the same time (deceleration period).

3.5 Hydration development of mixture M4 with 0,02% Li_2CO_3-solution

Mixture M4, with Li_2CO_3-solution, displays a different hydration. Figure 8 summarises the quantitative phase content of CA and C_2AH_x combined with the heat evolution of the paste from calorimetric investigation.

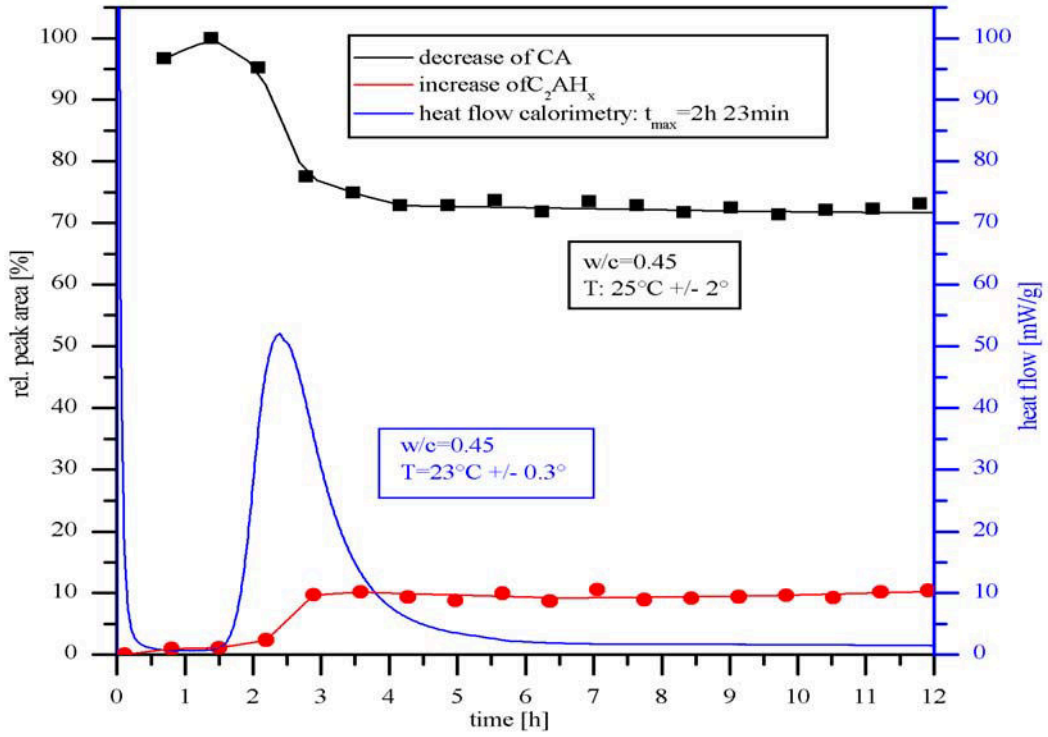

Figure 8. In-situ XRD of M4 with 0,02% Li_2CO_3-solution (left-hand scale) combined with heat flow calorimetry (right-hand scale)

- t=0-10min: Neither C_2AH_8 nor $C_2AH_{7.5}$ are detected. No statement about the decrease of CA content can be made because the first measurement of CA peak was performed after 10min. The heat flow is very strong during this period (initial period).
- 10min<t<2h: The amount of dissolution of CA remains constant during this period (first detection of CA was after 42 minutes). Crystallisation of C_2AH_x can be detected during this period. The heat evolution during this period is low (induction period).
- 2h<t<3h: During this period the content of CA decreases strongly. The content of C_2AH_x is increasing. C_2AH_8 is dehydrating and converting to $C_2AH_{7.5}$. The maximum of heat flow coincides with the maximum change in CA and C_2AH_x content (end of acceleration period).
- 3h<t<12h: During this period the CA content is nearly constant like the C_2AH_x content. The heat evolution decelerates very fast to low values (deceleration period).

4. CONCLUSION AND DISCUSSION

The results in this paper show that the combination of two methods, heat flow calorimetry and in-situ XRD-analyses of hydration, are in good agreement according to the maximum heat flow. For the in-situ XRD-analyses the error for each measured value is ±5% of the peak area. The maximum rate of transformation and dissolution may be shifted ±1h because of the temperature difference between in-situ XRD and heat flow calorimetry.

We could show that by adding small amounts of inorganic admixture, whether Li_2CO_3-solution or 5 ma.% CH, to a synthetic calcium aluminate cement mixture the measurement becomes very precise and accurate. The maximum heat flow is shifted to shorter times by adding Li_2CO_3-solution or 5 ma.% CH. The course of phase development during the in-situ XRD does not depend very much on the composition of the mixtures but on the additive used, which also has a dramatic influence on the total heat of hydration at very early stages. For that reason the heat of hydration

from two different sample preparation methods for heat flow calorimetry (injection of water with a syringe or stirring the mixture manually) cannot be compared with each other directly.

The accelerating effect of both additives is a combination of C_2AH_8 transformation to $C_2AH_{7.5}$, which is accompanied by a release of H_2O, with the rapid dissolution of CA. The peak of heat flow calorimetry can be attributed to two overlapping exothermic reactions: first of all dissolution of CH and CA and secondly crystallization of C_2AH_8 together with formation of $C_2AH_{7.5}$. By ongoing dehydration of formed C_2AH_8 to $C_2AH_{7.5}$ some H_2O is liberated which can react with CA to more calcium aluminate hydrate. The H_2O-content added to the anhydrous mixture determines how much CA can react, because for the low w/c ratio of 0.45 not all of the CA in the mixture can be hydrated. Therefore the H_2O-content and the C/H ratio of the hydrates formed determine the overall heat flow during hydration.

REFERENCES

[1] Neubauer, J. & Goetz-Neunhoeffer, F., Efficiency of highly sensitive heat flow calorimetry in examination of OPC hydration, Proceedings of the 24th Conference on Cement Microscopy, San Diego, 2002, pp.58-68.

[2] Rodger, S. A. & Double, D. D., The chemistry of high alumina cement in the presence of accelerating and retarding admixtures, Cement and Concrete Research, vol.14, 1983, pp.73-82.

[3] Curell et al., The acceleration and retardation of set of high alumina cement by additives, Cement and Concrete Research, vol.7, 1987, pp.420-432.

[4] Matusinovic, T. & Curlin, D., Lithium salts as set accelerators for high alumina cement, Cement and Concrete Research, vol.23, 1993, pp.885-895.

[5] Lea, F. Lea´s Chemistry of Cement and Concrete, 4th edition, John Wiley and Sons, New York, 1998

[6] Scheller, Th. & Kuzel, H. J., Studies on dicalcium aluminate hydrates, The VI International Congress on the Chemistry of Cement, Section II, Moscow, 1974

INFLUENCE OF FE^{3+}- DOPING OF C_3A ON ITS HYDRATION BEHAVIOR IN THE PRESENCE OF GYPSUM

S. Kemethmüller[1], J. Neubauer[2] and F. Goetz-Neunhoeffer[2]

[1]Department of Material Science -Glass and Ceramics-, University of Erlangen-Nuremberg.
[2]Department of Mineralogy, University of Erlangen-Nuremberg, Germany.
E-mail: goetz@geol.uni-erlangen.de

ABSTRACT

In OPC clinker, C_3A forms solid solutions with some minor components such as alkali oxides, Fe_2O_3 etc., present in OPC clinker. In the cubic crystal structure of C_3A, Fe^{3+} can substitute Al^{3+} up to a certain concentration.

For this investigation syntheses of $C_3A_{1-x}F_x$ in the range of $0 \leq x \leq 0.20$ were performed at 1250°C in a laboratory furnace. By Rietveld refinement of the $C_3A_{1-x}F_x$ lattice parameters a limit of $Fe^{3+} \rightarrow Al^{3+}$ substitution of 6 ± 0.2 mole% has been determined for the used synthesis parameter employed.

Influence of Fe^{3+}-doping of C_3A on its hydration behaviour was investigated with and without gypsum as retarding agent (w/c= 0.7; t= 72h; 23°C) with a heat flow calorimeter. The investigation has shown that overall heat flow and the ferric content of $C_3A_{1-x}F_x$ are correlated. Irrespective of the addition of gypsum as retarding agent, the heat of hydration declines with increasing ferric content. Reduction of overall heat flow is notably stronger when gypsum is added to $C_3A_{1-x}F_{x,}$ whereas the maximum heat flow and its point of time do not depend on the ferric content of $C_3A_{1-x}F_x$ solid solutions. Similarly, the ferric part does not influence the beginning of the transformation from Ettringite to Monosulfate.

1. INTRODUCTION

The setting of cement products is a property of particular importance for consumer and manufacturer, which is determined by the requirements of the market. Because there are several clinker phases present together with a large number of additives, which are altogether involved in the reaction with water, only the hydration behaviour of one separate clinker phase, Tricalciumaluminate (C_3A) was investigated in this study.

C_3A reacts very intensively with water and it is responsible for the initial reaction of OPC clinker [1]. To avoid a too early setting of the OPC (flash-set) it is necessary to add a retarding agent, like gypsum or anhydrite to the cement.

Iron oxide is one of the main oxides in the raw materials utilised for OPC. Iron oxide is not exclusively incorporated in the Ferrite phase, but also in C_3A. Normally C_3A crystallises in the cubic space group Pa3. The structure of cubic C_3A is built of six-fold rings of two types of distorted AlO_4-tetrahedra centered on threefold axes. The rings of $(Al_6O_{18})^{18-}$ are arranged closely, so that the aluminum atoms are almost placed near to six of the corners of a cube. [2]

Proceedings of the 11th International Congress on the Chemistry of Cement (ICCC)
'Cement's Contribution to the Development in the 21st Century'
Hosted by: The Cement and Concrete Institute of South Africa
CD-ROM produced by: Document Transformation Technologies
11 - 16 May 2003, Durban, South Africa
ISBN Number: 0-9584085-8-0
Editors: Dr G. Grieve and G. Owens
Congress Organised by: Event Dynamics

In the C_3A cubic crystal structure Fe^{3+} can substitute for Al^{3+} up to a certain concentration. (substitution limit). If the Fe-concentration exceeds this substitution limit, $C_3A_{1-x}F_x$ solid solution with constant composition coexists together with Ferrite phase $C_2(A_{0.48}F_{0.52})$ and CaO [3,4,5,6].

In this study the substitution of the Fe^{3+} in C_3A was investigated and the hydration behaviour of iron- substituted C_3A was observed. Lattice parameter of the $C_3A_{1-x}F_x$ solid solution members and the substitution limit for the synthesis parameters used was determined by Rietveld refinement. Influence of Fe^{3+}-doping of C_3A on its hydration behaviour was investigated with a heat flow calorimeter [7,8]. Measurements with and without gypsum as retarding agent were performed.

2. EXPERIMENTAL

2.1 Synthesis Parameter

The samples were prepared from mixtures of $CaCO_3$, Al_2O_3 and Fe_2O_3. As a first step, the samples were homogenised in a disk mill (agate, 10 min, 700 rpm). After that the mixture was decarbonated in a platinum crucible at 1000°C for 12 hours in a laboratory furnace and sintered at 1250°C in air atmosphere.
Then the sinter cake was cooled in a desiccator, crushed and re-sintered. This procedure was repeated at least three times. The total sinter time was 42 hours.

2.2 Characterisation of the Samples

All samples were sieved to <36 µm and prepared with front loading technique for XRD investigations. The qualitative examination was performed with the software DIFFRAC^{Plus} EVA 4.0 from BRUKER AXS. For reproducibility all samples were prepared and measured at least three times with a X-ray diffractometer (D 5000) with Cu Kα radiation.

For the qualitative examination of the hydration products after the setting in the heat flow calorimeter the samples were dried 12h in a CO_2- free atmosphere to a relative humidity of 35%.
The refinement of the structure data was performed with the Rietveld method with the software TOPAS 2.0 from BRUKER AXS. The program works with the fundamental parameter approach from Cheary & Coelho [9]. Table 1 shows the structure models used in the analysis.

Table 1. Structure models from the ICSD- database [10]

Phase	ICSD- Code/ Reference/ Year
C_3A	1841 Mondal & Jeffery (1975)
CaO	61550 Natta & Passerini (1929)
$C_2(A,F)$	9197 Colville & Geller (1971)
C_3AH_6	202315 Lager, Armbruster, Fabery (1987)

2.2.1 Surface Area Measurements

The surface area of all samples was measured by Blaine method. The samples were ground to a specify surface area between 3560-3690 cm^2/g.

2.2.2 Heat Flow Calorimetry

Hydration behaviour was investigated in a revised heat flow calorimeter after Kuzel [7,8].

The following parameters were used:

- temperature in the calorimeter 23.0 °C (±0.3°C)
- w/c ratio 0.7
- measurement time 72h

All iron- doped C_3A samples were hydrated for two ways. One with distilled water alone an another with gypsum and distilled water. The optimal gypsum ratio of 21.6 mass% was calculated (after Haskell in Stark & Wicht [11]).

3. RESULTS AND DISCUSSION

3.1 X- Ray Powder Diffraction Measurements

The structure of Mondal & Jeffery [2] was used for the Rietveld refinement of the pure C_3A structure. Figure 1 shows the good fit of the calculated and the measured profiles.

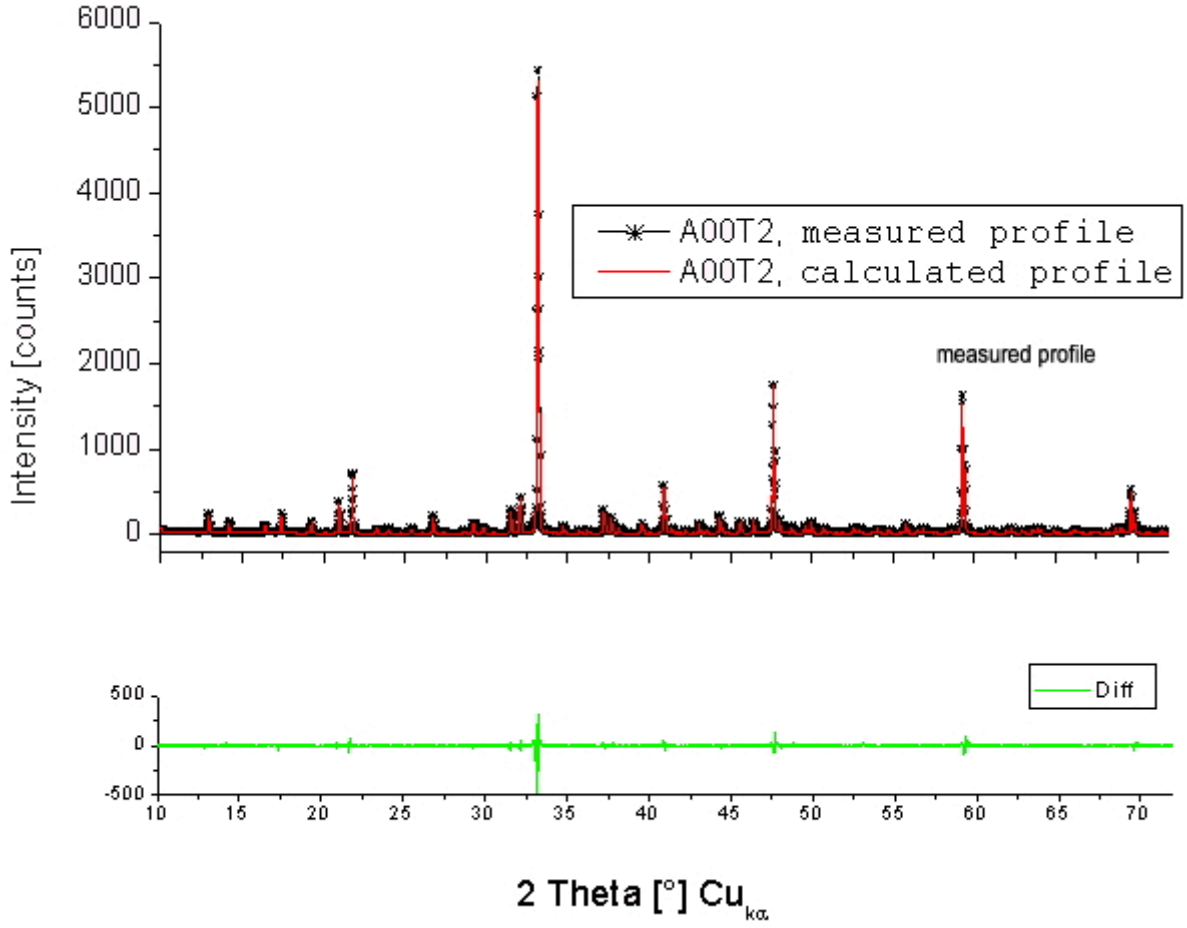

Figure 1. Measured and calculated profiles and difference plot of iron free sample A00

The substitution limit was determined from the refined a-lattice parameter of the $C_3A_{1-x}F_x$- solid solutions. In Figure 2 the determined a-lattice parameter is plotted against the iron oxide ratio in the synthesis mixture. The lattice parameter increases with rising iron ratio, up to a composition of 6±0.2 mole% (3.5±0.1 mass%) Fe_2O_3 substitution. No further increase of the parameter could be detected with higher Fe_2O_3 contents.

The noticeable rise of the minor phases CaO and $C_2(A,F)$ in the samples with higher iron oxide content than 6 mole%, also indicates a substitution limit of 6±0.2 mole% (3.5±0.1 mass%) Fe_2O_3. The ratio of Ferrite phase increases from 5±1.5 mass% (sample A08) to 29.5±1.5 mass% of sample A20 (Table 2). The CaO ratio also increases from 0.9±0.8 mass% to 6.5±0.8 mass%. The growing amount of minor phases also explains the different value of the lattice parameter of sample A20. The higher amounts of the minor phases reduces the quality of the refinement of the $C_3A_{1-x}F_x$ solid solution structure.

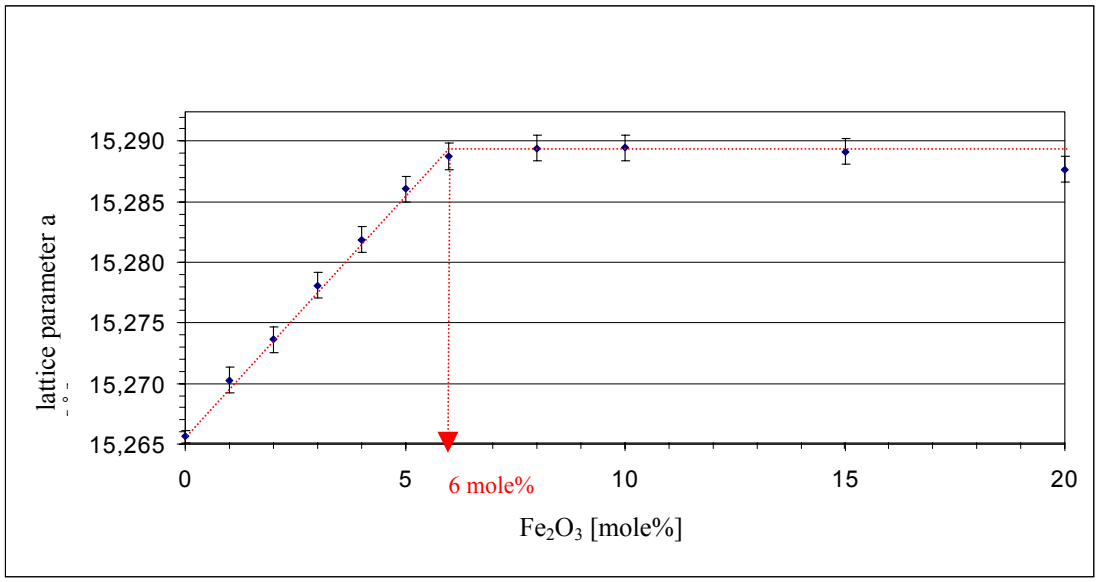

Figure 2. Determined a-lattice parameter of $C_3A_{1-x}F_x$ solid solutions increasing with substitution up to the limit of 6 mole%

Table 2. Quantitative phase composition (mass%) of the synthesis products of $C_3A_{1-x}F_x$ solid solutions with increasing x

Sample	Theoretical chemical composition	$C_3A_{1-x}F_x$ [mass%]	$C_2(A,F)$ [mass%]	CaO [mass%]
A00	C_3A	99.4 ± 2.0	---	< 0.8
A01	$C_3A_{0.99}F_{0.01}$	99.2 ± 2.0	< 1.5	< 0.8
A02	$C_3A_{0.98}F_{0.02}$	99.2 ± 2.0	< 1.5	< 0.8
A03	$C_3A_{0.97}F_{0.03}$	99.3 ± 2.0	< 1.5	< 0.8
A04	$C_3A_{0.96}F_{0.04}$	99.2 ± 2.0	< 1.5	< 0.8
A05	$C_3A_{0.95}F_{0.05}$	99.2 ± 2.0	< 1.5	< 0.8
A06	$C_3A_{0.94}F_{0.06}$	98.9 ± 2.0	< 1.5	0.8 ± 0.8
A08	$C_3A_{0.92}F_{0.08}$	94.1 ± 2.0	5.0 ± 1.5	0.9 ± 0.8
A10	$C_3A_{0.90}F_{0.10}$	92.9 ± 2.0	6.1 ± 1.5	1.0 ± 0.8
A15	$C_3A_{0.85}F_{0.15}$	76.9 ± 2.0	19.2 ± 1.5	3.9 ± 0.8
A20	$C_3A_{0.80}F_{0.20}$	64.0 ± 2.0	29.5 ± 1.5	6.5 ± 0.8

The determined substitution limit applies to the chosen synthesis parameter (see section 2.1). The limit is lower than comparable data reported in the literature. Table 3 lists the determined iron oxide limits of some authors at different synthesis temperatures.

In sample A20 29.5±1.5 mass% Ferrite phase was detected. From the occupancy factors for Fe/Al a composition of $C_2(A_{0.54}F_{0.46}) \pm 0.04F$ was calculated. The results match very well with the data of Majumdar, Taylor and Lee et al. [4,6,12], who determined a composition of 48 mole% Al_2O_3 and 52 mole% $Fe_2O_3$of the Ferrite phase coexisting with the $C_3A_{1-x}F_x$ solid solution.

Table 3. Substitution limits and sinter temperatures of $C_3A_{1-x}F_x$ solid solutions of different authors

Author	Substitution limit [mole%]	Sinter temperature in air [°C]
MAJUMDAR (1965) [4]	7.0	1325
TAYLOR (1990) [6]	7.6	1325
IMLACH & GLASSER (1973) [3]	<10	1150
TARTE (1965) [5]	10.0	1310
This study	6.0	1250

3.2. Investigations of the hydration behaviour of synthesised $C_3A_{1-x}F_x$

Each synthesised $C_3A_{1-x}F_x$ sample was investigated in the heat flow calorimeter three times with and without addition of gypsum.

3.2.1 Investigations of synthesised $C_3A_{1-x}F_x$ without gypsum

The hydration of the $C_3A_{1-x}F_x$- solid solution are featured by an extremely high heat of hydration within the first hour. Collepardi et al. also observed this effect [13]. The heat of hydration within the first hour is half the value of the total heat of hydration over 72 hours (Table 4).

The hydration of C_3A usually leads after the formation of hexagonal metastable hydration products C_2AH_8 and C_3AH_{13}- to the cubic C_3AH_6 (Scrivener & Pratt [14]). The transformation time to C_3AH_6 hydration products depends on temperature and can be achieved after minutes, hours or days (Lea [15] and Feldman & Ramachandran [16]). In this study by qualitative X-ray analysis of the hydration products after more than 72 hours only cubic C_3AH_6 was identified.

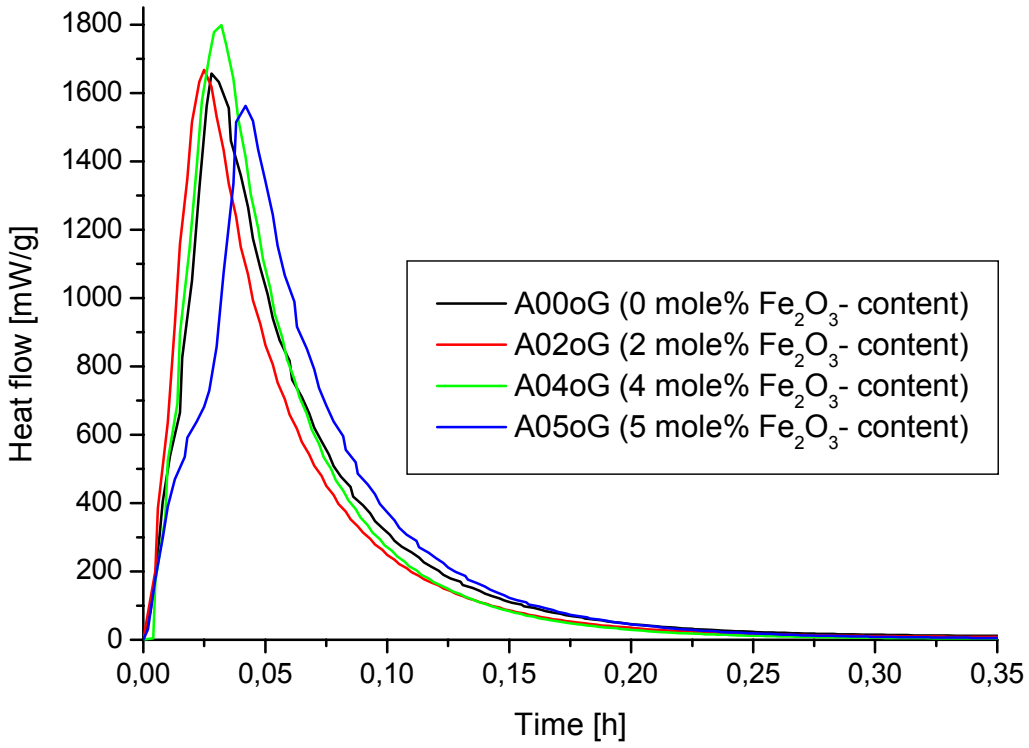

Figure 3. Part (0-0.35h) of representative heat flow curves of $C_3A_{1-x}F_x$ solid solution ($0 \leq x \leq 0.05$) without gypsum addition and for increasing iron oxide content (w/c=0.7; T=23.0°C)

No influence could be detected of the increasing iron oxide content in the $C_3A_{1-x}F_x$ solid solution on the height and the time of the maximum heat flow. But the total heat of hydration decreases with increasing iron oxide content from 793.7 J/g (Sample A00oG without Fe_2O_3) to 567.0 J/g (sample A05oG with 5mole% Fe_2O_3) (Table 4).

Table 4. Comparison of the hydration heat of the $C_3A_{1-x}F_x$ solid solutions ($0 \leq x \leq 0.05$) without gypsum addition and increasing Fe_2O_3 content (w/c=0.7; T=23.0°C)

Fe_2O_3- content	0 mole%	2 mole%	4 mole%	5 mole%
W_{max} [mW/g]	1714.9	1601.0	1770.1	1572.2
t_{max} [h]	0.029	0.028	0.032	0.041
Hydratation heat [J/g]				
After 72h	**793.7**	**702.7**	**642.3**	**567.0**
After 1h	366.2	346.4	361.1	349.0
Ratio [%]	46.1	49.3	56.2	61.6

3.2.2 Investigations of synthesised $C_3A_{1-x}F_x$ with gypsum

For the hydration with gypsum addition two reactions were recognised (Figures 4 and 5). A first reaction during the first 0.35h and a second reaction after about 4h. Many authors [6,13,15,17,18] have described the second reaction as the transformation of Ettringite to Monosulfate. The starting point of this transformation could not be correlated with the Fe_2O_3 content of the $C_3A_{1-x}F_x$- solid solutions. (Figure 5)

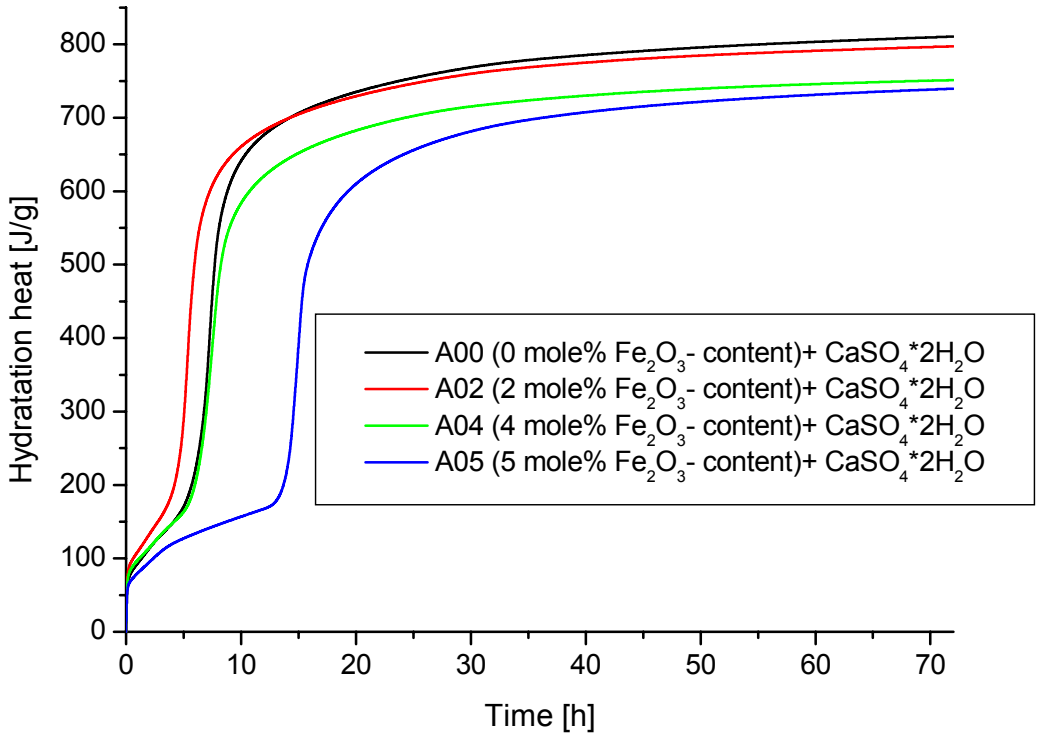

Figure 4. Time dependent heat of hydration (0-72h) of the $C_3A_{1-x}F_x$- solid solutions ($0 \leq x \leq 0.05$) with increasing iron oxide content and with gypsum (w/c=0.7; T=23.0°C; 21.6 ma.% gypsum)

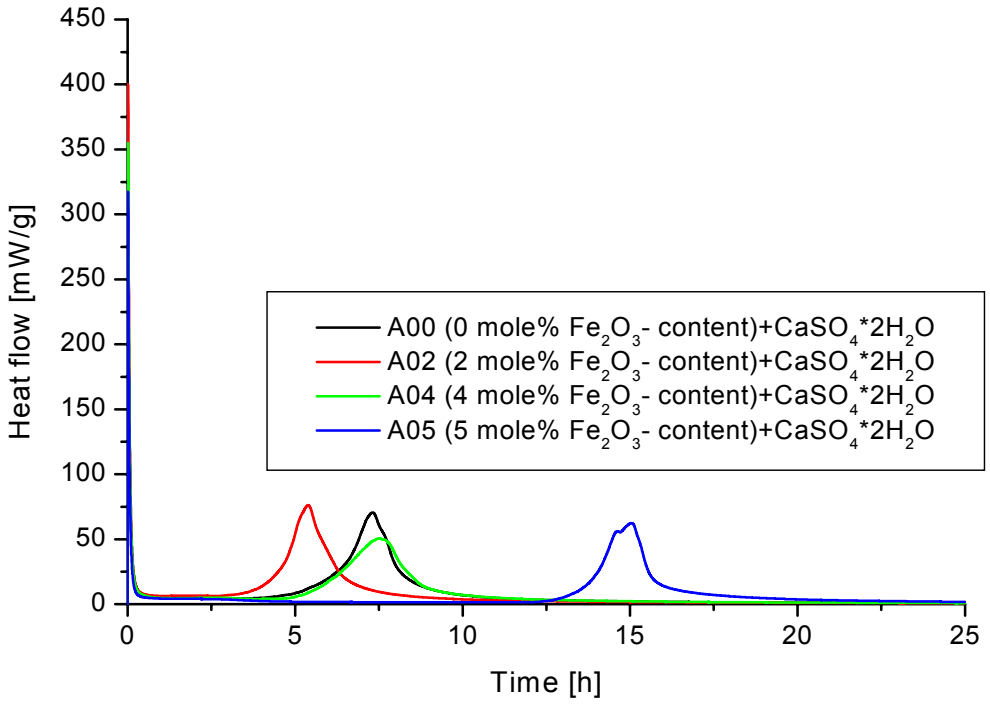

Figure 5. Part (0-25h) of the heat flow curves of the $C_3A_{1-x}F_x$- solid solutions ($0 \leq x \leq 0.05$) with increasing iron oxide content and gypsum addition (w/c=0.7; T=23.0°C; 21.6 mass% gypsum)

Sample A02 (2 mole% Fe_2O_3- content) shows a second reaction after about 3h, the samples A00 (0 mole% Fe_2O_3) and A04 (4 mole% Fe_2O_3) after about 5h and sample A05 (5mole% Fe_2O_3) after about 13h. Scrivener & Wieker [18] stated that the kinetics of the transformation from Ettringite to Monosulfate depends on other factors, like gypsum/C_3A- ratio, the grain spectrum, grain size distribution or the presence of CO_2. The qualitative X-ray investigations of the hydration products with gypsum showed Monosulfate, un-reacted $C_3A_{1-x}F_x$- solid solutions and a laminar phase of TCAH- type. Cubic hydrate could not be detected. The same phase composition was observed by Collepardi et al. [13].

The observed heat of the hydration is correlating with the iron oxide content of the $C_3A_{1-x}F_x$- solid solutions (Figure 5, Table 5). According to the investigations without gypsum heat of hydration $C_3A_{1-x}F_x$- solid solutions with gypsum after 72h of is decreasing with increasing Fe_2O_3- content.

Table 5. Comparison of the hydration heat of $C_3A_{1-x}F_x$ solid solutions ($0 \leq x \leq 0.05$) with gypsum for increasing Fe_2O_3 content (w/c=0.7; T=23.0°C; 21,6 mass% gypsum)

Fe_2O_3- content	**0 mole%**	**2 mole%**	**4 mole%**	**5 mole%**
W_{max} [mW/g]	309.1	380.5	347.3	296.8
t_{max} [h]	0.014	0.014	0.014	0.012
Hydratation heat [J/g]				
After 72h	**807.1**	**796.2**	**756.5**	**739.5**
After 1h	95.8	105.0	96,9	78.1

3.2.3 Comparison of the $C_3A_{1-x}F_x$ hydration with and without gypsum

The main difference when comparing the hydration with and without gypsum are the noticeable lower heat flows with gypsum at the beginning of the reaction (Figures 3 and 5) and the second peak after about 4h.

The heat of hydration after 72h of hydration samples without gypsum is always lower than for the samples when gypsum was added to $C_3A_{1-x}F_x$ (Table 6 and Figure 6). Furthermore, the reduction of the hydration heat with increasing iron oxide content of $C_3A_{1-x}F_x$-solid solution with gypsum is lower than for the hydrated samples without gypsum (Figure 6). The total heat of hydration after 72h of the samples with gypsum decreases from 807.1 J/g to 739.5 J/g, in contrast to the samples without gypsum (793.7 J/g to 567.0 J/g).

The ratio of the heat release after 72h without gypsum to the heat release of the samples with gypsum (Table 6) decreases from 98% (iron free C_3A samples) to 77% (Sample with 5 mole% Fe_2O_3).

Table 6. Comparison of W_{max}, t_{max} and the hydration heat (H) after 1h and 72h of all investigated $C_3A_{1-x}F_x$- solid solutions with and without gypsum addition

Sample (Fe_2O_3-content)	A00oG (0 mole%)	A00 (0 mole%) + gypsum	A02oG (2 mole%)	A02 (2 mole%) + gypsum	A04oG (4 mole%)	A04 (4 mole%) + gypsum	A05oG (5 mole%)	A05 (5 mole%) + gypsum
W_{max} [mW/g]	1714.9	309.1	1601.0	380.5	1770.1	347.3	1572.2	296.8
H after 72h	793.7	807.1	702.7	796.2	642.3	756.5	567.0	739.5
H after 1h	366.2	95.8	346.4	105.0	361.1	96.9	349.0	78.1
Ratio [%] H^{72h} with/without gypsum	98	100	88	100	85	100	77	100

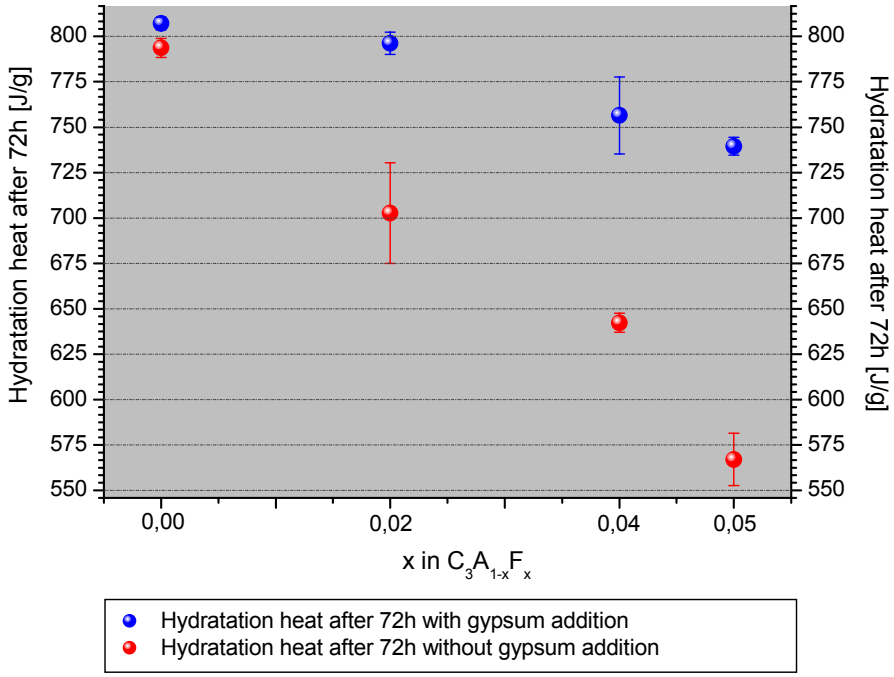

Figure 6. Comparison of the hydration heat after 72h of the $C_3A_{1-x}F_x$- solid solutions with and without gypsum (w/c= 0.7; T=23.0°C)

The addition of gypsum noticeably improves the total heat volume of the $C_3A_{1-x}F_x$- solid solutions richer in iron oxide. The iron substitution is clearly showing a correlation to the hydration behaviour of the $C_3A_{1-x}F_x$- solid solutions. For the hydration without gypsum the influence is stronger than for the hydration with gypsum.

4. CONCLUSIONS

The substitution limit for the exchange of $Fe^{3+} \rightarrow Al^{3+}$ in C_3A was found to be 6.0± 0.2 mole% at 1250°C in air in this study. By exceeding the substitution limit additional to $C_3A_{0.94}F_{0.06}$ increasing amounts of CaO and $C_2(A_{0.54}F_{0.46})$ ±0.04F are formed in the samples. This is consistent with the investigations from Majumdar, Taylor and Lee et al. [4,6,12].

The hydration process of the $C_3A_{1-x}F_x$- solid solutions is as described in literature [1,13,14,16,17,18]. $C_3AH_6$was observed as the main phases after 72h hydration in case of gypsum-free hydration. Monosulfate phase was found in the hydration products of $C_3A_{1-x}F_x$- solid solutions with gypsum. A correlation between the iron oxide content and the hydration heat could be detected. The hydration heat decreases with rising Fe_2O_3-content of the $C_3A_{1-x}F_x$- solid solutions. This dependence is higher without gypsum than for gypsum addition. This effect is probably due to the different hydration products. C_3AH_6 does not form a complete solid solution with C_3FH_6. The substitution limit lies between 0.8 mole%, Strassen [19], and at 0.2 mole% ,Schwiete & Iwai [20] at room temperature. Whereas Ettringite and Monosulfate are forming a complete solid solution with increasing Fe_2O_3-content [21]. Because the $Al^{3+} \rightarrow Fe^{3+}$ substitution for Monosulfate phase is higher than for Hydrogrossular ($C_3(A,F)H_6$), more $C_3A_{1-x}F_x$ phase can be hydrated with increasing iron content, which leads to higher hydration heat. Monosulfate can easily incorporate the liberated iron but in case of gypsum-free hydration probably non crystalline iron hydroxides are formed during hydration. The iron oxides are inhibiting further hydration of $C_3A_{1-x}F_x$ due to the reduction of available H_2O in the samples. Furthermore we are assuming that iron oxides are forming an gel like shell around the $C_3A_{1-x}F_x$ particles. Both effects reduce the hydration heat in the system without gypsum. When sulfate is available the hydration of $C_3A_{1-x}F_x$ is less affected by iron content.

An influence of the iron content on the time point of the transformation of Ettringite to Monosulfate could not be detected. The kinetics of this transformation seems to depend on other factors like temperature, w/c- ratio, surface area, grain spectrum, grain size distribution and the gyspum/C_3A ratio [18].

REFERENCES

[1] Eckart, A., Zur Hydratation der 4 Hauptklinkerphasen des PZ, ZKG, 48, 443-452, 1995

[2] Mondal, P. & Jeffery, J.W., The Crystal Structure of Tricalcium Aluminate, Acta Crystallogr., B 31, 689-696, 1975

[3] Imlach, J.A. & Glasser, F.P., System Fe- CaO-Al_2O_3-Fe_2O_3, Trans. Brit. Ceram. Soc., 70 [6] 227, 1971, ibid., 72 [5] 221, 1973

[4] Majumdar, A.J., System CaO-CaO*Al_2O_3-2CaO*Fe_2O_3, Trans. Brit. Ceram. Soc., 64 [2] 111, 1965

[5] Tarte, P., Al- Fe Isomorphic Substitution in 3CaO-Al_2O_3 and 2CaO-Fe_2O_3, and Interactions between the So-called C_3A and C_4AF Phases, Nature, Vol. 207, (5000), 973-974, 1965

[6] Taylor, H. F. W., Cement Chemistry, Academic Press, London, 1990

[7] Kuzel, H.-J., Ein leistungsfähiges Wärmeleitungskalorimeter, TIZ- Fachberichte 108, 46-51, 1984

[8] Neubauer, J. & Goetz-Neunhoeffer, F.: Efficiency of highly sensitive heat flow calorimetry in examination of OPC hydration, Proceedings of the 24th conference on cement microscopy, San Diego, 58-68, 2002

[9] Cheary, R. W. & Coelho, A. A., A Fundamental Parameters Approach to X-Ray Line-Profile Fitting,J. Appl. Cryst., Vol. 25, 109-121, 1992

[10] FIZ Karlsruhe, ICSD, Inorganic Crystal Structure Database, 1995

[11] Stark, J. & Wicht, B., Anorganische Bindemittel, Schriften der Bauhaus – Universität Weimar, 1998

[12] Lee, F.C.; Banda, H.M. & Glasser, F.P., Substitution of Na, Fe and Si in Tricalcium Aluminate and the Polymorphism of solid solutions, Cem. Concr. Res. 12, 237-246, 1982

[13] Collepardi, M.; Baldini, G. & Pauri, M., Tricalcium Aluminate Hydration in the Presence of Lime, Gypsum and Sodiumsulphate, Cem. Concr. Res. 8, 571-580, 1978
[14] Scrivener, K.L. & Pratt, P.L, Microstructural Studies of the Hydration of C_3A and C_4AF Independently and in Cement Paste, Br. Ceram. Proc., 35, 207, 1984
[15] Lea, F., Lea's Chemistry of Cement and Concrete, 4th Edition, John Wiley and sons, New York, 1998
[16] Feldman, R.F. & Ramachandran, V.S., Character of Hydration of C_3A, J. Am. Cer. Soc. 49, 5, 268-273, 1966
[17] Brown, P.W., Kinetics of Tricalcium Aluminate and Tetracalcium Aluminoferrite Hydration in the Presence of Calcium Sulfate, J. Am. Ceram. Soc. 76 [12] 2971-76, 1993
[18] Scrivener K.L. & Wieker, W., Advances in Hydratation at low, ambient and elevated Temperatures,9th ICCC, New Dehli, Vol I, 460 ff.,1992. Zur Strassen, H., Die chemischen Reaktionen bei der Zementerhärtung, ZKG 11, 137-143, 1958
[19] Schwiete, H.E. & Iwai, T., Über das Verhalten der ferritischen Phase im Zement während der Hydratation, ZKG, 17, 379-386, 1964
[21] Ecker, M., Diadochiebeziehungen in Calciumaluminatferraten und deren Hydratationsprodukten, Hallesches Jahrbuch für Geowissenschaften Reihe B: Geologie, Paläontologie, Mineralogie, Beiheft 3, 1998

INVESTIGATIONS ON THE HYDRATION BEHAVIOUR OF SYNTHETIC OPC-PHASES ALITE AND BELITE BY HEAT-FLOW CALORIMETRY

Dirk Schmitt[1], Friedlinde Goetz-Neunhoeffer[1] and Jürgen Neubauer[1]

[1]Department of Mineralogy, Friedrich-Alexander Universität, Erlangen, Germany.
E-mail: dschmitt@geol.uni-erlangen.de

ABSTRACT

The application of heat-flow calorimetry in qualitative and quantitative analysis of hydration reactions of hydraulic binders became vastly important during the last years. The calorimeter, which has been developed and continuously improved at the Department of Mineralogy, has proven its accuracy and reliability in academic and industrial use. The following investigations deal with synthesis and hydration of pure Alite and Belite of OPC clinker like composition and synthetic mixtures of both. The hydration reactions were measured over a period of 72 hours with different W/C-ratios at a temperature of 23°C ± 0.2°C. Weighed amounts of deionized water were filled in single-use syringes and injected into the sample vessels through a hole in the lid. The evaluation of the hydration process resulted in a very good reproducibility for all measurements performed. It also could be shown that the hydration of Alite is retarded by the addition of Belite.

1. INTRODUCTION

Within this contribution heat-flow calorimetric studies of the synthetic OPC-phases Alite, Belite and mixtures of both will be presented.

Alite is the most important component of all common OPC clinkers with an average content of about 60 ma.% [4]. Chemically, Alite is tricalcium silicate C_3S (Ca_3SiO_5). The composition and crystal structure may vary by the incorporation of up to 3 – 4 ma.% of foreign ions [5], especially MgO, Al_2O_3 and Fe_2O_3. Alite reacts relatively fast with water and dominates the hydraulic activity of the clinker, being the most abundant component. It determines the level of the initial and early strength during hydration.

The average content of Belite in normal OPC clinker is approximately about 15 ma.% [4]. The chemical composition of the dicalcium silicate C_2S (Ca_2SiO_4) varies by the incorporation of about 5 ma.% of foreign ions like MgO, Al_2O_3, Fe_2O_3, K_2O into the crystal lattice. In Portland cement clinker Belite occurs almost entirely in the β-modification [5]. Belite reacts slowly with water and contributes only little to initial and early strength in comparison to Alite, but is assumed to have influence on the final strength [4].

The hydration process of Alite, which has been examined by several authors [5,6,7,8,9,10,11,12] can be divided into four stages. These are the initial reaction, the induction period, the main reaction and the final, slow periods [5]. The mechanism of Belite hydration is similar to those of Alite but with a slower rate of reaction [3,13,14,15,16,17,18] and a lower content of produced CH (Portlandite, $Ca(OH)_2$). The rates of heat liberation during the different hydration stages of both Alite and Belite can be investigated using heat-flow calorimetry.

Proceedings of the 11th International Congress on the Chemistry of Cement (ICCC) 11 - 16 May 2003, Durban, South Africa
'Cement's Contribution to the Development in the 21st Century' ISBN Number: 0-9584085-8-0
Hosted by: The Cement and Concrete Institute of South Africa Editors: Dr G. Grieve and G. Owens
CD-ROM produced by: Document Transformation Technologies Congress Organised by: Event Dynamics

In order to examine the hydration behaviour of synthesized Alite and Belite and their mutual interaction during hydration, an improved highly sensitive heat-flow calorimeter [1,2] has been applied.

2. EXPERIMENTAL

2.1. Preparation of synthetic Alite and Belite

The OPC clinker phases Alite and Belite have been synthesized by sintering stoichiometric amounts of their corresponding oxides, respectively CaO, SiO_2, α-Al_2O_3, MgO. All chemicals used were of "reagent grade" quality. The composition of Alite, according to Regourd [19], is shown in Table 1.

Table 1. Composition of synthetic Alite in ma.%

CaO [ma.%]	SiO_2 [ma.%]	Al_2O_3 [ma.%]	MgO [ma.%]
71.7	25.9	0.6	1.8

Synthetic Belite has been stabilized using α-Al_2O_3 as minor oxide [20]. Its composition is shown in Table 2.

Table 2. Composition of synthetic Belite in ma.%

CaO [ma.%]	SiO_2 [ma.%]	Al_2O_3 [ma.%]
65.32	32.90	1.78

The initial substances were homogenized in an agate disk mill (Retsch, Type RS1) with a speed of 700 rpm and then transferred into platinum crucibles. Sintering was carried out in a high-temperature chamber furnace (Nabertherm, Type HT 1750) three times for two hours at a temperature of 1550°C for both Alite and Belite. Between each sintering period the samples were rapidly cooled in air and ground and homogenized in an agate disk mill. After the last sintering stage, samples were ground to a defined specific surface (after Blaine) as shown in Table 3.

Table 3. Specific surface (after Blaine) with standard deviation of synthetic Alite and Belite

	Alite	Belite
Specific surface [cm^2/g] ± SD	2851 ± 24	2760 ± 14

The purity of the synthesized phases was verified by qualitative X-ray powder diffraction (Siemens, Kristalloflex D5000) in combination with quantitative Rietveld-approach. In addition a particle size analysis (Malvern Instruments, MasterSizer) was carried out on both samples. The results are shown in Table 4.

Table 4. Grain size analysis of synthetic Alite and Belite

d (%)	Alite 1 min. dispersed	Belite 1 min. dispersed
10	≤ 2.3 µm	≤ 1.9 µm
50	≤ 13.4 µm	≤ 16.7 µm
97	≤ 63.5 µm	≤ 59.1 µm

The samples have been stored in polyethene bottles inside an exsiccator until further use.

2.2. Calorimetry

For the calorimetric investigations different synthetic mixtures of Alite and Belite, as shown in Table 5, have been prepared. Both synthesized phases were, according to their weight ratios, weighed in polyethene bottles and homogenized manually for about one hour. For calorimetry

single-use polystyrene vessels with lid have been used. Before being filled with the sample substance, the polystyrene vessels have been cleaned with isopropyl and deionized water and were dried at 45°C. As initial weight for Alite, Belite and the synthetic mixtures 2 has been chosen. The substances in powder form were weighed into the polystyrene vessels and were subsequently covered with a dispenser-paper which was exactly fitted to the interior dimensions of the vessels. This piece of paper prevents a spraying of the sample to the walls of the vessel during injection of the hydration liquid. After that the samples have been compressed with a press and closed with the lid which contained a closeable hole in the center of its diameter for the injection of deionized water as hydration liquid. The water has been weighed in single-use syringes with a w/s-ratios of 0.40, 0.45 and 0.50.

Table 5. Synthetic mixtures of Alite and Belite

	Mixture 1	Mixture 2	Mixture 3
Alite : Belite [ma.%]	90 : 10	75 : 25	60 : 40

For the realization of the calorimetric measurements a quadruplet-calorimeter in isothermal operation mode was used which has been developed [1] and continuously improved [2] at the Department of Mineralogy. The polystyrene vessels were coupled to heat-sensitive semi-conductors with a reproducible amount of a thermal transfer compound. To guarantee a constant temperature inside the calorimeter (23°C ± 0.2°C) an external liquid-thermostat was connected. After the adjustment of a thermal equilibrium inside the calorimeter, measurement was started with the data collection and device control software, followed by the immediate injection of the deionized water into the sample vessels. The hydration reactions of Alite, Belite and the synthetic mixtures were recorded over a period of 72 hours.

3. RESULTS AND DISCUSSION

3.1 Hydration of synthetic Alite

The hydration behaviour of synthetic Alite in polystyrene vessels with a w/c-ratio of 0.45 is shown in Figure 1.

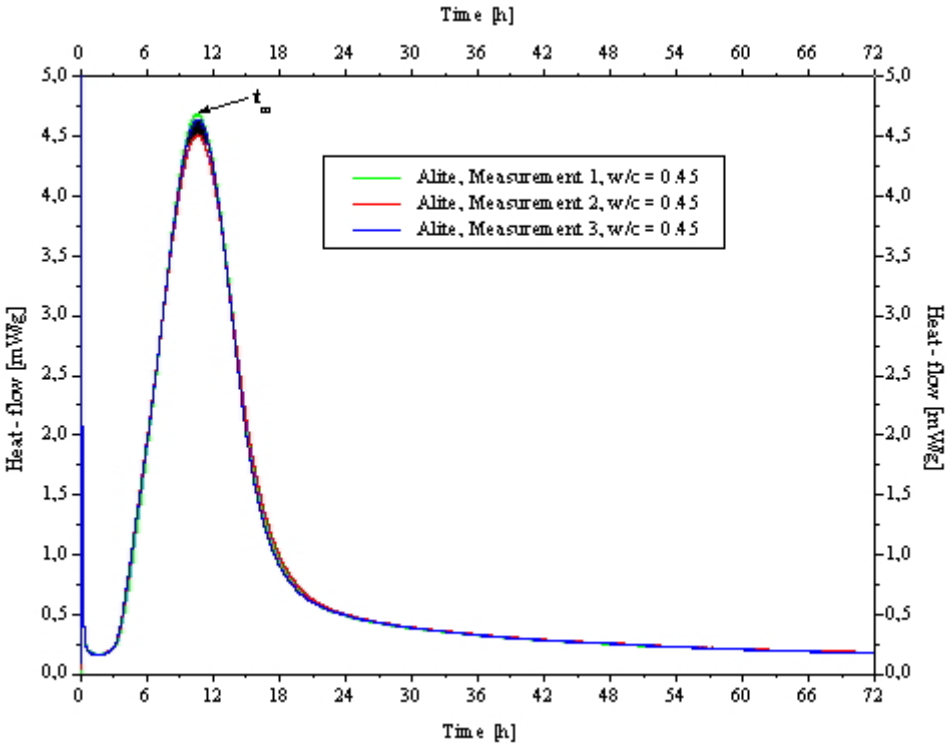

Figure 1. Heat-flow diagram of Alite in polystyrene vessels with w/c=0.45

The initial reaction is characterized by a relatively high heat-flow of about 8.4 mW/g during the first 0.5 hours. This corresponds to a heat of hydration of 1.77 J/g. The proportion of this first hydration period within the totally released heat of hydration after 72 hours amounts to about 1%. This observed initial, short hydration reaction has been reported earlier by Kondo and Daimon [21] as well as by Tadros et. al. [22]. The consumed amount of Alite during this period seems to be very low. This corresponds with the results of Fujii and Kondo [23], who reported a consumption of about 0,1%. Kondo and Daimon [21] supposed that the amount of Alite consumed before the induction period is less than 2%.

The induction period from this synthesized Alite is marked very shortly. The rate of hydration during this period decreases significantly. This corresponds to a period with low heat evolution as described before from calorimetric investigations by Kondo and Daimon [21].

At the beginning of the main reaction, the induction period gets replaced by a phase of rapid hydration. The examined Alite shows maximum heat-flow with a w/c-ratio of 0.45 after about 10.5 hours. Table 6 shows the time of the maximum of main reaction (in hours), the corresponding maximum heat-flow (in mW/g) and heat of hydration (in J/g) as well as the percentage of heat of hydration until t_m in relation to the total heat of hydration after 72 hours.

Table 6. Data of the main reaction period of Alite in polystyrene vessels

	Maximum of main reaction t_m [h]	Maximum heat-flow at t_m [mW/g]	Heat of hydration until t_m [J/g]	Heat of hydration until t_m [%]
Alite, w/c =0.45 Measurement 1	10.49	4.68	70.66	34.4
Alite, w/c =0.45 Measurement 2	10.50	4.51	71.00	34.4
Alite, w/c =0.45 Measurement 3	10.55	4.65	73.09	35.6
Mean value ∅	10.51	4.61	71.58	34.8
Standard deviation SD	± 0.03	± 0.09	± 1.32	± 0.7
Maximum deviation Δ_{max}	0.04	0.10	1.51	0.8

On closer inspection of the reproducibility of the Alite measurements shown above, a very good result can be reported as shown in Table 7. The average total heat of hydration after 72 hours of the Alite is 205.69 J/g with a standard deviation of ± 0.75 J/g or, as a total percentage, of 0.42%.

Table 7. Total heat of hydration of Alite in polystyrene vessels with w/c=0.45

	Heat of hydration [J/g]					
	Measurement 1	Measurement 2	Measurement 3	∅	SD	Δ_{max} [J/g]
Alite w/s = 0.45	205.37	206.55	205.16	205.69	± 0.75	0.86

To determine the influence of the w/c-ratio on the hydration behaviour of the synthetic Alite additional investigations with w/c-values of 0.40 and 0.50 have been performed. The results are shown in Figure 2, where measurements of three different w/s-ratios are compared. By comparing the main reaction periods, a possible dependence on the w/c-value may be observed. A higher w/c-value therefore accelerates this period of hydration.

This trend could be observed in all measurements performed. A relation to the maximum value of the heat-flow (t_m) could not be found. The total heat of hydration after 72 hours at a w/c-value of 0.50 is about 3.07 J/g lower than that at a w/c-value of 0.45. But there is no distinction between the w/s-values of 0.40 and 0.45 within the scope of the determined reproducibility (see Table 7).

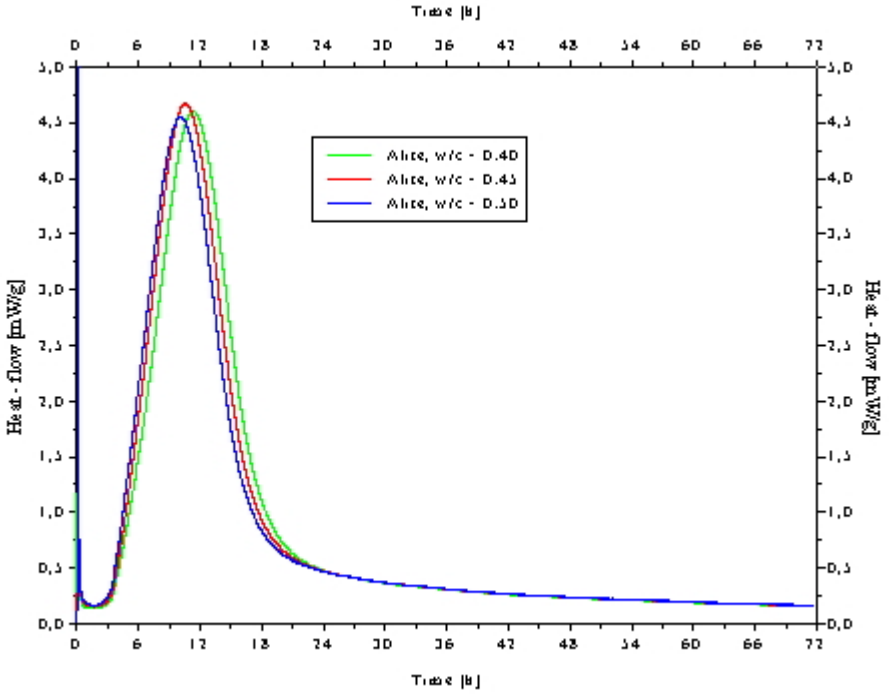

Figure 2. Heat-flow diagram of Alite in polystyrene vessels with different w/c-values

3.2 Hydration of synthetic Belite

The hydration behaviour of synthetic Belite doped with Al_2O_3 has been studied in polystyrene vessels at a w/c-value of 0.45. The relatively high heat evolution during the initial reaction, as shown in Figure 3, is noticeable. The initial reaction of this Belite shows a maximum heat-flow of about 48 mW/g, which exceeds that of Alite with the factor six. After 0.5 hours the average heat of hydration amounts about 12.74 J/g (± 0.28 J/g). This corresponds to a proportion of 58.8% of the total heat of hydration after 72 hours, as shown in Table 8.

Table 8. Heat of hydration of synthetic Belite in polystyrene vessels with w/c=0.45

	Heat of hydration [J/g]					
Time [h]	Belite Measurement 1	Belite Measurement 2	Belite Measurement 3	∅	SD	Δ_{max} [J/g]
0.5	12.46	12.73	13.02	12.74	± 0.28	0.28
24	18.97	19.42	19.41	19.27	± 0.26	0.30
48	19.90	21.00	21.17	20.69	± 0.69	0.79
72	20.21	22.26	22.52	21.66	± 1.27	1.45

The occurrence of such a high heat-flow at the very beginning of hydration could be related to the presence of the aluminate-phase. Because of the stabilization of Belite with Al_2O_3, the formation of aluminate-phase could be possible in the event of incomplete reaction of the educts. However, this case has been excluded by examining the synthesized phases with X-ray powder diffraction in combination with a quantitative Rietveld analysis. Because of the present results, this behaviour seems to be typical for this Belite stabilized by Al_2O_3. Among the high heat-flow at the beginning of hydration the appearance of two more maxima is remarkable. Figure 4 shows the comparison of the hydration process of Belite and Alite.

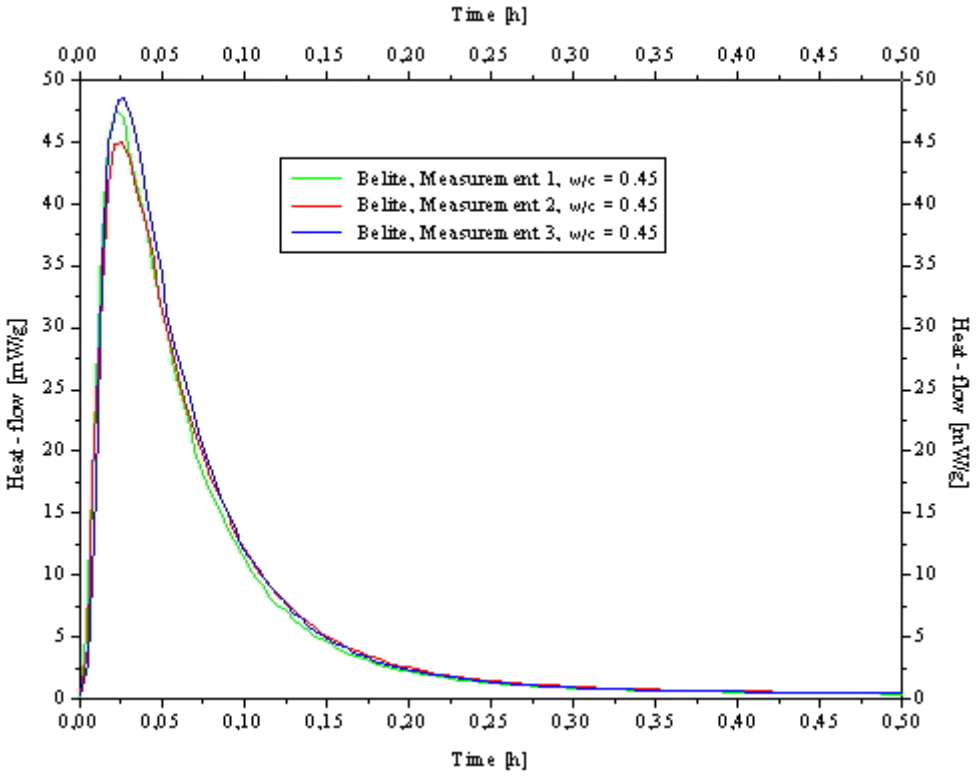

Figure 3. Heat-flow of Belite in polystyrene vessels with w/c=0.45 between the first 0.5 hours

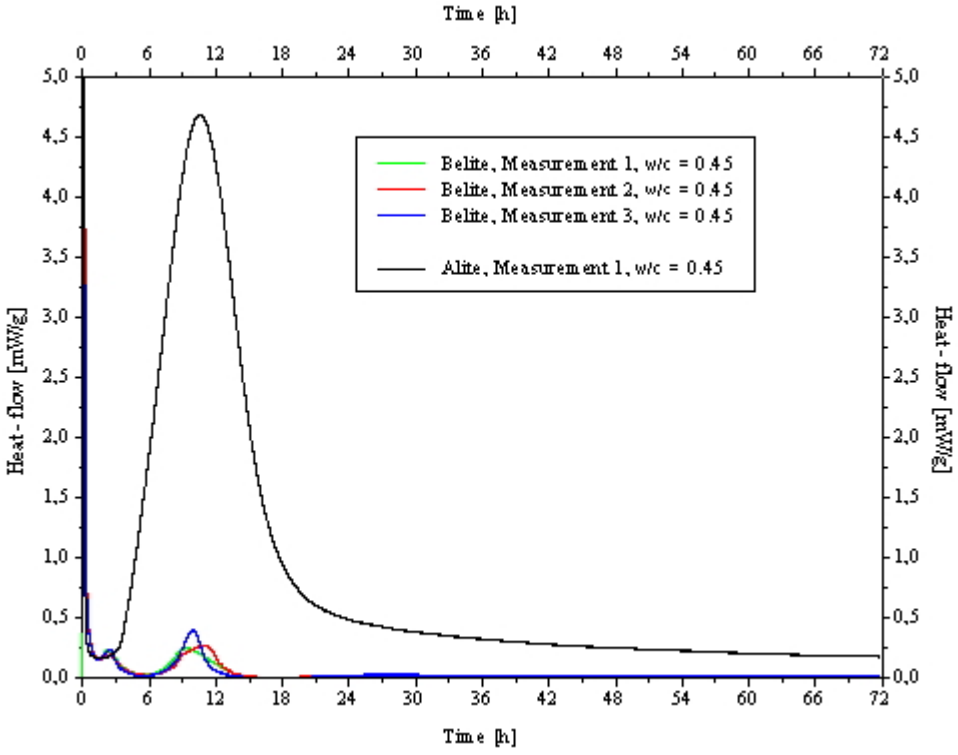

Figure 4. Comparison of hydration behaviour of synthetic Alite and Belite with w/c=0.45

The hydration of Belite shows similarities to that of Alite. Belite, in the same way as Alite, shows an elevated heat-flow between 9.5 and 11 hours after the initiation of hydration. However, the value of the maximum heat-flow of Alite (4.68 mW/g) during this period exceeds that of Belite (0.40 mW/g) by about 11 times. The mechanisms of these observed hydration reactions of Belite stabilized with Al_2O_3 have to be clarified in further investigations.

3.3 Hydration of synthetic mixtures of Alite and Belite

Comparing the hydration behaviour of the single phases Alite and Belite with the one of the synthetic mixtures, it could be shown that there is a correlation between the content of Belite and the hydration rate of Alite. Figure 5 shows the development of heat evolution.

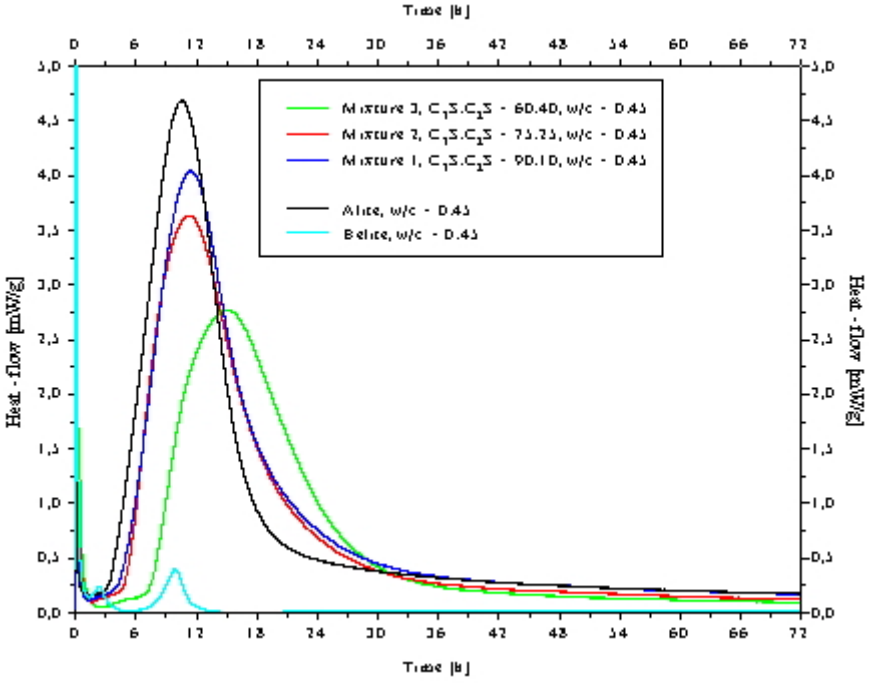

Figure 5. Heat-flow diagram of Alite, Belite and synthetic mixtures with w/c=0.45

The maximum heat-flow at the main reaction period is decreasing and is getting delayed with an increasing amount of Belite, as shown in Table 9.

Table 9. Average time and value of maximum heat-flow of the main reaction of Alite, Belite and synthetic mixtures with w/c=0.45; each three measurements

	Time of maximum heat-flow t_m [h], with SD	Maximum heat-flow at the main reaction [mW/g], with SD
Alite	10.51 ± 0.03	4.61 ± 0.09
Mixture 1 (90:10)	11.46 ± 0.07	4.06 ± 0.02
Mixture 2 (75:25)	11.33 ± 0.10	3.71 ± 0.08
Mixture 3 (60:40)	14.94 ± 0.13	2.77 ± 0.02
Belite	10.01 ± 0.77	0.31 ± 0.09

The results also indicate that there is no significant difference in delay between mixture 1 and mixture 2. However, the delay of mixture 3 with 40 ma.% of Belite of about more than 4 hours is very high. Also, the maximum heat-flow at the main reaction shows a continuous decrease with an increasing amount of Belite. The total heat of hydration after 72 hours is shown in Table 10, where the influence of an increasing amount of Belite results in a continuous decrease.

Table 10. Heat of hydration of Alite, Belite and synthetic mixtures with w/c=0.45

	Average heat of hydration after 72 hours [J/g]	SD	Δ_{max} [J/g]	Δ_{max} [%]
Alite	205.69	± 0.75	0.86	0.42
Mixture 1 (90:10)	204.38	± 1.59	1.13	0.55
Mixture 2 (75:25)	189.38	± 0.26	0.30	0.16
Mixture 3 (60:40)	165.55	± 1.08	1.19	0.72
Belite	21.66	± 1.27	1.45	6.69

The qualitative development shows, in comparison to pure Alite, a slight prolongation of the initial period. The adjacent induction period, which is hardly developed for Alite, gets prolonged with an increasing amount of Belite. The development of the recorded hydration-curves in this area shows, however, a slightly increasing heat-flow until the start of the main reaction. Because of that, this period should better be assigned to the main reaction. The beginning is first of all delayed by an increasing amount of Belite and the formation of CH is inhibited. This stage of hydration is shown explicitly in Figure 6.

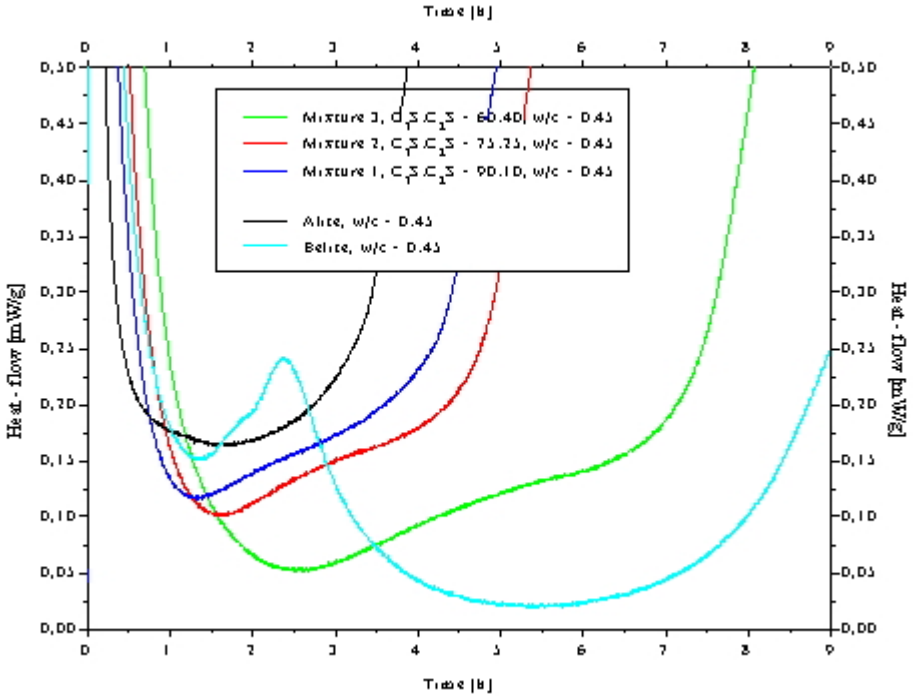

Figure 6. Heat-flow diagram of Alite, Belite and synthetic mixtures with w/c=0.45, closer view of the induction period from Figure 5

The above results confirmed those reported by Odler and Schüppstuhl [3] who also studied the mutual interaction of Alite and Belite during hydration process. The retardation of the hydration of Alite by an increasing amount of Belite could be shown clearly with heat-flow calorimetry. The unexpected results within the hydration process of synthetic Belite stabilized by α-Al_2O_3 have to be investigated by further studies.

REFERENCES

[1] Kuzel, H.-J. Ein leistungsfähiges Wärmeleitungskalorimeter, TIZ-Fachberichte, vol. 108, no. 1, 1984, pp. 46-51

[2] Neubauer, J. and Götz-Neunhoeffer, F. Efficiency of highly sensitive heat flow calorimetry in examination of OPC hydration, Proc. 24th Int. Conf. on Cem. Microscopy, San Diego, 2002

[3] Odler, I. and Schüppstuhl, J. Combined hydration of tricalcium silicate and β-dicalcium silicate, Cement and Concrete Research, vol. 12, 1982, pp. 13-20

[4] Stark, J. and Wicht, B. Anorganische Bindemittel, Schriften der Bauhaus-Universität Weimar, no. 109, 1998

[5] Taylor, H.F.W. Cement Chemistry, 2nd printing, London: Academic Press Limited, 1992

[6] Katyal, N.K., Ahluwalia, S.C. and Parkash, R. Solid solution and hydration behaviour of magnesium-bearing tricalcium silicate phase, Cement and Concrete Research, vol. 28, 1998, pp. 867-875

[7] Stephan, D., Maleki, H., Knöfel, D., Eber, B. and Härdtl, R. Influence of Cr, Ni and Zn on the properties of pure clinker phases, Part I. C_3S, Cement and Concrete Research, vol. 29, 1999, pp. 545-552

[8] Ménétrier, D., Jawed, I., Sun, T.S. and Skalny, J. ESCA and SEM studies on early C_3S hydration, Cement and Concrete Research, vol. 9, 1979, 473-482

[9] Regourd, M., Thomassin, J.H., Baillif, P. and Touray, J.C. Study of the early hydration of Ca_3SiO_5 by photoelectron spectrometry, Cement and Concrete Research, vol. 10, 1980, pp. 223-230

[10] Odler, I. and Schüppstuhl, J. Early hydration of tricalcium silicate: III. Control of the induction period, Cement and Concrete Research, vol. 12, 1982, pp. 13-20

[11] Odler, I. and Dörr, H. Early hydration of tricalcium silicate: I. Kinetics of the hydration process and the stoichiometry of the hydration products, Cement and Concrete Research, vol. 9, 1979, pp. 239-248

[12] Gartner, E.M. and Gaidis, J.M. Materials Science of Concrete I (ed. J.P. Skalny), Westerville, OH, USA: American Ceramic Society, 1989, p. 95

[13] Maycock, J.N., Skalny, J. and Kalyoncu, R.S. Crystal defects and hydration. I. Influence of lattice defects, Cement and Concrete Research, vol. 4, 1974, pp. 835-847

[14] Tong, H.S. and Young, J.F. Composition of solutions in contact with hydrating β-dicalcium silicate, Journal of the American Ceramic Society, vol. 60, 1977, pp. 321-323

[15] Fierens, P. and Tirlocq, J. Effect of synthesis temperature and cooling conditions of Beta-dicalcium silicate on its hydration rate, Cement and Concrete Research, vol. 13, 1983, pp. 41-48

[16] Pritts, I.M. and Daugherty, K.E. The effect of stabilizing agents on the hydration rate of β-C_2S, Cement and Concrete Research, vol. 6, 1976, pp. 783-796

[17] Shibata, S., Kishi, K., Asaga, K. and Daimon, M. Preparation and hydration of β-C_2S without stabilizer, Cement and Concrete Research, vol. 14, 1984, pp. 323-328

[18] Lu, Z. and Tan, K. Activity of β-C_2S under different sintering conditions, Cement and Concrete Research, vol. 27, 1997, pp. 989-993

[19] PDF-N° 42-0551, Regourd, M. Private communication, Centre Technique Industrielle, Paris, France, 1979

[20] Lai, G.-C., Nojiri, T. and Nakano, K. Studies of the stability of β-Ca_2SiO_4 doped by minor ions, Cement and Concrete Research, vol. 22, 1992, pp. 743-754

[21] Kondo, R. and Daimon, M. Early hydration of tricalcium silicate: A solid reaction with induction and acceleration periods, Journal of the American Ceramic Society, vol. 52, 1969, pp. 503-508

[22] Tadros, M.E., Skalny, J. and Kalyoncu, R.S. Early hydration of tricalcium silicate, Journal of the American Ceramic Society, vol. 59, 1976, pp. 344-347

[23] Fujii, K. and Kondo, W. Kinetics of the hydration of tricalcium silicate, Journal of the American Ceramic Society, vol. 57, 1974, pp. 492-497

INVESTIGATIONS ON THE HYDRATION BEHAVIOUR OF SYNTHETIC OPC-PHASES ALITE AND BELITE BY HEAT-FLOW CALORIMETRY

Dirk Schmitt[1], Friedlinde Goetz-Neunhoeffer[1] and Jürgen Neubauer[1]

[1] Department of Mineralogy, Friedrich-Alexander Universität, Erlangen, Germany.
E-mail: dschmitt@geol.uni-erlangen.de

Dirk Schmitt

Address:	Schlossgarten 5a 91054 Erlangen, Germany
Telephone:	+499131 / 8526198
Date of Birth:	18 December 1968
Nationality:	German

Education:

1991 - 1992	Friedrich - Alexander - Universität Erlangen Nürnberg Studies of Chemistry
1992 – 2000	Friedrich - Alexander - Universität Erlangen Nürnberg Studies of Mineralogy
Since 2000	Friedrich - Alexander - Universität Erlangen Nürnberg Scientific assistant at the Department of Mineralogy

Additional Information:

Well-grounded education and experience with analytical problems (Microscopy, REM, RFA, AAS, UV-VIS-Spectroscopy, IR-Spectroscopy and Ion-Chromatography).

Experience in Thermal Analysis (DSC, DTA, TG) and Calorimetry (DCA).

Excellent knowledge of Heat-flow Calorimetry related with hydraulic binders.

Well-grounded information in X-ray Analysis (Powder- and Single-crystal - Methods).

Well-grounded knowledge of Quantitative Rietveld Phase Analysis of cements.

Experience with MS-DOS, MS-Windows and several scientific programs (Excel, Origin, Diffrac AT, Rietveld-Software, Atoms, etc.)

A DYNAMIC MODEL AS A TOOL FOR THE DEVELOPMENT OF A SUSTAINABLE CEMENT CLINKER PROCESS

J. Görtzen[1] and G. Brem[2]

[1] Department of Energy Systems, TNO-MEP, Apeldoorn, The Netherlands.
E-mail: j.gortzen@mep.tno.nl
[2] Department of Energy Systems, TNO-MEP, Apeldoorn, The Netherlands.
E-mail: g.brem@mep.tno.nl

ABSTRACT

A dynamic model for the description of the cement clinker production process was developed. The model is based on the first principles of mass and energy conservation for gas, dust and solid flows in all apparatus under consideration. It comprises all relevant thermal processes that contribute to the formation of emissions. The model was adapted from a commercial plant and was validated statically and dynamically. Stationary validation of the model yields agreement with practical data within 10 % accuracy for all chemical components and key indicators. The dynamic validation shows a good similarity between model and practice for both trends and levels of all variables. The calculated and measured signals for the output variables also showed similar timescales as was proven by spectral analysis of the signals. It is now possible to investigate the effects of new control concepts and implementation of new processes, like mid-kiln firing, precalcination and pregasification of fuels, within the process. Further model improvement will be carried out in the future by using process identification experiments in practice.

1. INTRODUCTION

The production of cement clinker is an energy-intensive and raw material consuming process. By replacing the fossil fuels (coal, natural gas) with biomass and waste residues the costs can substantially be reduced. Also the raw materials can be replaced by secondary materials such as furnace slag, fly ash, etc. The use of these alternative fuels and raw materials may also contribute to the reduction of CO_2, known as an important greenhouse gas. However, the use of secondary fuels and raw materials may also result in higher emissions of harmful components, such as CO, NO_x, SO_2, HCl, heavy metals, etc. Besides increased emissions, process control can easily be disturbed using all kinds of inhomogeneous alternative fuels and raw materials. In order to investigate the consequences of application of secondary fuels and raw materials a mathematical model can be a helpful tool.

In contrast to many other industrial processes, such as drying technologies and waste and coal combustion, the development of numerical tools for the cement industry is relatively scarce. A possible explanation for this phenomenon lies in the complexity of the chemical and thermal processes that occur within the production process of cement clinker. Another important factor is the difficulty or (mostly) impossibility of measuring the key process indicators. However, as a result of increased knowledge of the different parts of the clinker production process the possibilities of a descriptive dynamic model which covers the entire process are increasing, with the emphasis laid on the rotary kiln. The modeling of rotary kilns started with the development of empirical relations for heat transfer [1-3]. More extensive modeling of rotary kilns comprised chemical reactions and different types of heat transfer [4,5]. Modern research focused on the development of dynamic and

Proceedings of the 11th International Congress on the Chemistry of Cement (ICCC) 11 - 16 May 2003, Durban, South Africa
'Cement's Contribution to the Development in the 21st Century' ISBN Number: 0-9584085-8-0
Hosted by: The Cement and Concrete Institute of South Africa Editors: Dr G. Grieve and G. Owens
CD-ROM produced by: Document Transformation Technologies Congress Organised by: Event Dynamics

static tools for cement production plant engineering and design [1,6-8]. Although research has led to an inceased understanding of the various parts of the clinker production process a general purpose model that simulates process dynamics related to input of primary and secondary fuels and raw materials has not been presented in literature yet.

In this paper a dynamic mathematical model is presented that can be used as a tool in the development of a sustainable cement clinker process with a maximum use of sustainable fuels and raw materials, a minimum of emissions and an optimal process control.

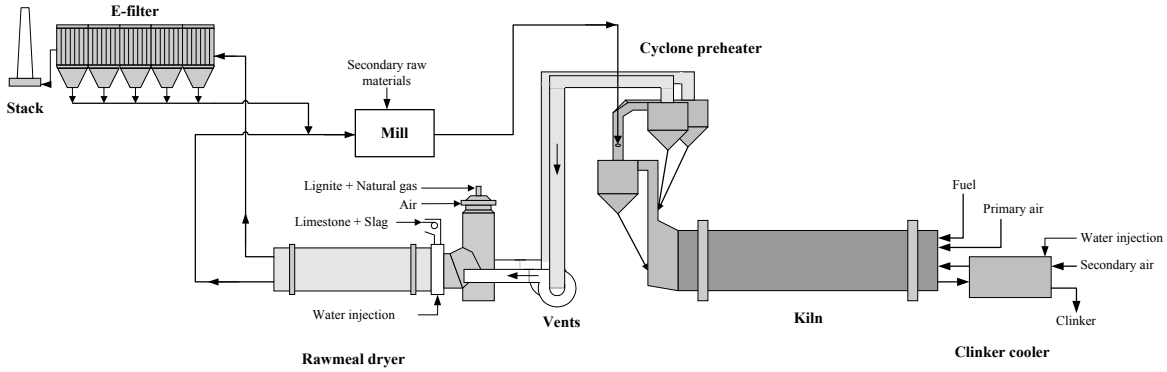

Figure 1. Overview of the modeled parts of the clinker production process.

2. MODEL DESCRIPTION

The core of the mathematical model includes a clinker cement kiln, a preheater section, a dryer and a satellite cooler as depicted in Figure 1. The model is completed with a model for an E-filter and meal mill to provide necessary material in- and outputs serving recycle calculations. The layout is adapted to the clinker production process of ENCI Maastricht, The Netherlands. Due to the modular structure of the computer code the configuration of the process scheme can easily be changed to alternative layouts and can be extended with other types of equipment. Therefor, each piece of equipment has distinct, predefined in- and output of heat and mass. The model is based on the principles of mass and energy conservation and supplemented with experimental and empirical relationships for heat and mass transfer as well as for reaction kinetics. Each part of the process is modeled in a different manner dictated by the type of operation performed in the corresponding equipment.

Table 1. Thermal relevant reactions, that are incorporated in the model.

Reaction	Ref.	Kiln	Cooler	Preheater	Dryer
Calcination	[9,10]	+	-	+	-
Sulphate (de-) composition	[11,12]	+	-	+	-
Sintering	[13]	+	-	-	-
Drying	[14,15]	+	+	+	+
Solid phase transition	[13]	+	+	-	-
Evaporation and condensation	[16]	+	+	+	+
Fuel decomposition	[16-18]	+	-	-	+
Gas phase kinetics	[19-22]	+	-	+	-

The overall process is governed mainly by thermal processes. It is therefore presumed that only the phenomena that have significant thermal effect are taken into account in the model. An overview of relevant chemical reactions as well as the different process components is shown in Table 1.

2.1 The rotary kiln

The actual burning of the clinker takes place in a rotary kiln in which gas and solid material are transported in a countercurrent fashion. The fuels are burned at the hot side of the kiln with preheated secondary air from the clinker cooler. The secondary airflow contains a substantial amount of dust, that originates from the cooler. To describe the conservation of mass for the gas, solid material and dust the following balances were used:

$$\frac{\partial \rho_g}{\partial t} = \frac{\partial \left(V_g \rho_g\right)}{\partial z} + \Phi_{\text{sec}} \frac{\partial R_g}{\partial z} + \sum_{i=1}^{nc} \Psi_i + \sum_{j=1}^{nf} F_{g,j} \tag{1}$$

$$\frac{\partial M_s}{\partial t} = \frac{\partial \left(V_s M_s\right)}{\partial z} + \frac{\partial}{\partial z}\left(D_s \frac{\partial M_s}{\partial z}\right) - \sum_{i=1}^{nc} \Psi_i + \Gamma_s + \sum_{j=1}^{nf} F_{g,j} \tag{2}$$

$$\frac{\partial M_d}{\partial t} = \frac{\partial \left(V_g M_d\right)}{\partial z} - \Gamma_s + \sum_{j=1}^{nf} F_{d,j} \tag{3}$$

The nomenclature used above is defined in Section 5 of this paper. The mass balance for the gas phase only contains convective transport, since the effects of diffusion can be neglected. Furthermore, it can be proven that the plug flow approach is justified based on the large Reynolds and Péclet numbers for the gas phase, indicating large radial mixing. In order to account for the transversel mixing of solids, a diffusion term arises in Equation (2). The diffusion coefficient and the solid axial convective velocity can be estimated from previous experimental work [23-25]. The opposite signs for summation terms on the right-hand-side of Equations (1) and (2) denote the exchange of mass between gasphase and solids, that arise from decompositions in the solid phase as well as from condensation and evaporation of volatile chemical components. The transport of dust is determined by the convective velocity of the gasphase because of the high level of acceleration of the fine dust particles and small relaxation times. The local degree of mixing with the solid phase is implemented empirically based on experimental values for the solid kiln feed and the cooled clinker. The decomposition of fuels has a contribution to all three mass balances via gaseous reaction products and fuel ashes.

Since the formation of gaseous emissions is related to temperature and local concentrations of reactants like oxygen and nitrogen it was decided to apply a semi two-dimensional flame approach that enables the staged mixing of secondary air with the kiln gasphase [26,27]. The actual shape of the flame is determined by the cross-sectional area for flow, A_g. With the application of different types of fuels several fuel decomposition models that contribute to the mass balances by the term F were incorporated. In Table 2 an overview of fuel models is given. The fuels are injected into the kiln for which motion balances are incorporated. For large fuel particles the burn-out is allowed to take place in the clinkerbed. The products of the fuel decomposition models are added to the kiln gasphase, which comprises extensive kinetic mechanismes for the formation of various chemical components, such as NO_x, CO, CO_2 and SO_2 [19-22].

Table 2. Overview of applied fuel decomposition models.

Fuel	Model	Ref.	Applied to
Gas	Mixing	-	Natural gas, producer gas
Liquids	Evaporation	[16]	Spent-glycol
Volatile solid	Pyrolysis	[18]	Paper residue, sludge, scrap tires
Heavy solid	Coal combustion	[17]	Bedcokes, finecoke, slate, lignite

The heat balance contains equations for the gasphase and the solid phase. The dust contribution to the heat balances of the kiln is taken into account in the gasphase balance:

$$\frac{\partial\left(\rho_g C_{p,g} T_g\right)}{\partial t} + \frac{\partial\left(X_d C_{p,s} T_g\right)}{\partial t} = \frac{\partial\left(\rho_g C_{p,g} V_g T_g\right)}{\partial z} + \frac{\partial\left(X_d C_{p,s} V_g T_g\right)}{\partial z} +$$

$$+ \sum_{i=1}^{nr} H_{g,i} + \Omega_{g,w} + \Omega_{g,s} + \sum_{j=1}^{nf} H_{f,j} \tag{4}$$

$$\frac{\partial\left(\rho_s C_{p,s} T_s\right)}{\partial t} = \frac{\partial\left(\rho_s C_{p,s} V_s T_s\right)}{\partial z} + \frac{\partial}{\partial z}\left(\lambda_s \frac{\partial T_s}{\partial z}\right) - \sum_{i=1}^{nr} H_{s,i} + \Omega_{s,w} + \Omega_{g,s} \tag{5}$$

The transfer of heat is given by Ω and represents direct and indirect exchange as well as radiation and heat loss to the surroundings via the kiln wall. The external heat loss is modeled by conduction through the kiln lining and wall and forced convection, radiation and natural convection at the outside of the kiln. The change in chemical enthalpy due to decomposition of fuels is added to the gasphase balance. The density of the gasphase is calculated by the ideal gas approach. Heat capacities for both gas and solids are mean, concentration-based values of the single component values.

2.2 Preheater

The cyclone preheater is a combination of cyclones and risers that operate at different temperature levels. The hot kiln exhaust gas is cooled as the dried raw meal is preheated for feeding into the kiln. The cyclones separate dust leaving the kiln, and hot kiln gas. In the configuration shown in Figure 2. the raw meal is heated in a two-stage preheater, containing three cyclones and two risers. Heating up the meal up to 750 °C can cause various emissions, such as CO and C_xH_y, that add to the emissions from the kiln.

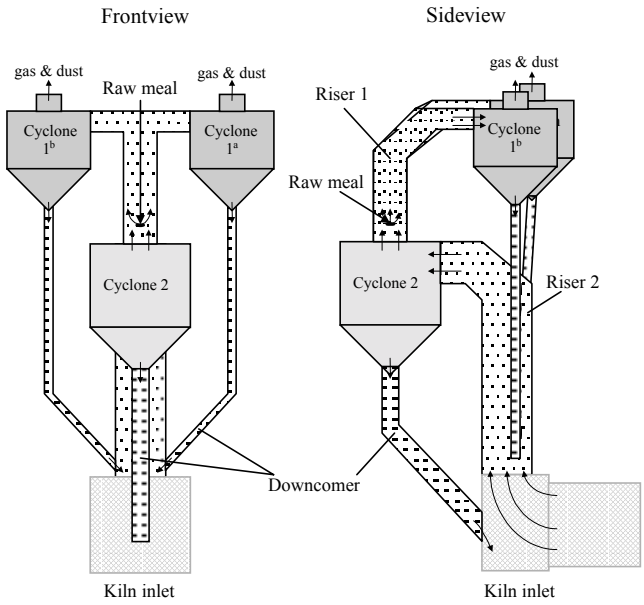

Figure 2. Setup of the two-stage cyclonepreheater

The cyclones are modeled using the CSTR-approach with an infinite heat transfer, while the risers contain an axial temperature gradient with radial temperature equivalence between the two phases. Mass transfer between the two phases is limited by heat or mass transfer to the meal particles. Sulphur capture and condensation of volatile components like alkali halogenes are the main

reactions that occur in the preheater. The cyclones operate at separation efficiencies that are calculated by semi-empirical modeling [28,29].

A new experimental method has been developed to get insight in the release of CO and C_xH_y from the raw material in the preheater cyclones [30]. For this purpose a so-called entrained flow reactor is used, resulting in different experimental relationships for the different emissions, process conditions and raw materials. New experimental results with the entrained flow reactor can easily be integrated in the model. The detailed results of this new experimental method will be published elsewhere.

2.3 Cooler

The cooler is used to cool down the clinker from the kiln and to preheat the secondary air. The modeling of the cooler was adapted from the kiln approach (see Paragraph 2.1). Parts of this model that were deleted for the description of the cooler are secondary air mixing, fuel decomposition and several reactions. The cooler contains extensive dust exchange between solid material and gasphase as well as water injection at the cooler exit to cool down the clinker material. An important process in the satellite coolers is the solidification of the partly melted clinker material. The configuration cooler is built up with nine satellites.

2.4 Dryer

In contrast to the clinker cooler and the cement kiln, the solid material and the gas move concurrently in the dryer. In literature many mathematical models are described to calculate the drying process. Our mathematical model consists of heat and mass balances [31], solid transport and flying of dust [32,33], completed with combined mass and heat transfer for the release of water from the particles. As implemented in the clinker process the dryer is equipped with water injection and burners to compensate for fluctuations in entering gas temperatures and water content of the wet meal. The configuration of the dryer is shown in Figure 3.

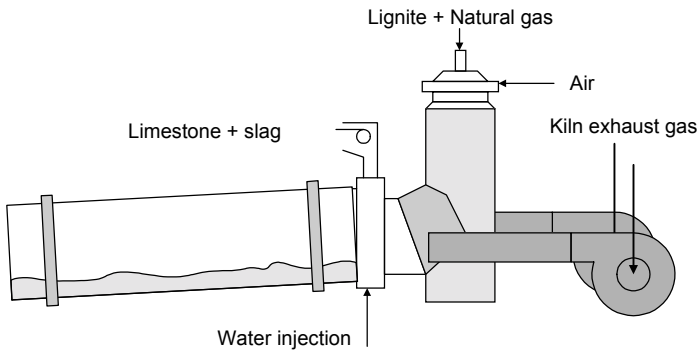

Figure 3. Setup of the dryer, including water injection and additional preheating of exhaust gases from the cyclone preheater.

2.5 Numerical methods

The balances that were set in the building of the model were discretisized according to a finite difference scheme with an upwind approach for the convective contributions. Up to 50 grid points were used per apparatus. The complete set of linear equations is then solved with fifth order Rung-Kutta method with variable stepsize in time. For the convenience of the user the mathematical model is supplied by a graphical user interface. On a standard 1 Ghz pentium machine the model calculation speed is 8 times faster than real-time.

3. MODEL RESULTS

In order to validate the model practical data of the plant of ENCI Maastricht are used. The model is validated stationary and dynamically. The stationary validation was performed using mean annual pratical data as input for the model. The model was calculated to a stationary situation, after which the outcome of the model was compared to the data of ENCI Maastricht. The dynamic validation of the model was conducted by usage of realtime practical data on a ten-second basis, that served as input for the model.

3.1 Stationary validation

The stationary validation of the model is used to investigate the magnitude of the chemical and physical operations that are comprised by the model. If any of these operations are not in order with practice, then stationary values are not predicted correctly. In Table 3. the results of the validation are shown. In this table model calculations are presented with the corresponding practical data. For the practical data standard deviations for the process output are given as well as deviations of the model results from practical data.

Table 3. Results of the stationary validation of the model, using mean practical data for all inputs of the year 1999. Concentrations are calculated for dry conditions and 10% O2.

Process variable	Unit	Model	ENCI	s.d. ENCI	Model vs. ENCI
Clinker production	t/h	114	122	7.6	-7.9
T kiln inlet	ºC	876	876	21.0	0
T after preheater	ºC	495	493	6.0	2.0
CO_2 kiln inlet	vol%	25.8	28.0	1.1	-2.2
NO_x kiln inlet	ppm	978	965	149	13
O_2 kiln inlet	vol%	1.58	1.60	0.3	-0.02
Max. melt fraction	%	23.2	23.1	0.4	0.1
SO_2 at stack	mg/Nm^3	37.8	36.0	30.0	1.8
NO_x at stack	mg/Nm^3	824	797	156	27
CO at stack	mg/Nm^3	120	119	11	1

It shows that all calculated values, except the clinker production, are well within the range of the practical data. Since the model was focused on the gasphase, good agreement for temperatures and concentrations is obtained for the stationary situation. The results for the prediction of gasphase concentrations at kiln inlet are somewhat better than at the stack because of slight underestimation of air leakage into the system downstream of the kiln, as can be seen in both concentrations for NO_x. The model predicts NO_x at the stack with a relatively small error of 4%. The model prediction for the clinker production is less then the value from practice. The reason for this could be found in the accuracy of the input data, since errors in raw meal composition and fuel ash fractions add up to errors in the clinker production. Also, overestimated dust release from the kiln and clinker cooler have large impact on the accuracy of the calculated clinker production. However, measured dust concentration in the exhaust gas of the cyclone preheater and calculated values match up to 2 tonnes per hour, indicating that the deviation is caused by erroneous input.

3.2 Dynamic validation

The dynamic validation is used to investigate the dynamic responses of the model to the required input. For a period of 24 hours practical data of ENCI Maastricht were gathered and were used as input for the mathematical model. In order to reflect the results of these calculations the NO_x signal at the kiln inlet is compared to the measured signal. This signal is affected by all thermal processes that take place within the cement clinker production process. The results are shown in Figure 4.

The match between calculations and practical data is reasonable. The magnitude of the signals are comparable, as was already proven in the stationary validation. The figure also shows that the clinker production process is very dynamic and contains various cycles in the low and high frequency domain. However, in contrast to the results of the static validation, where the signal for both calculation and measurement for NO_x were integrated over a long period of time, the model predictions deviate from measurements.

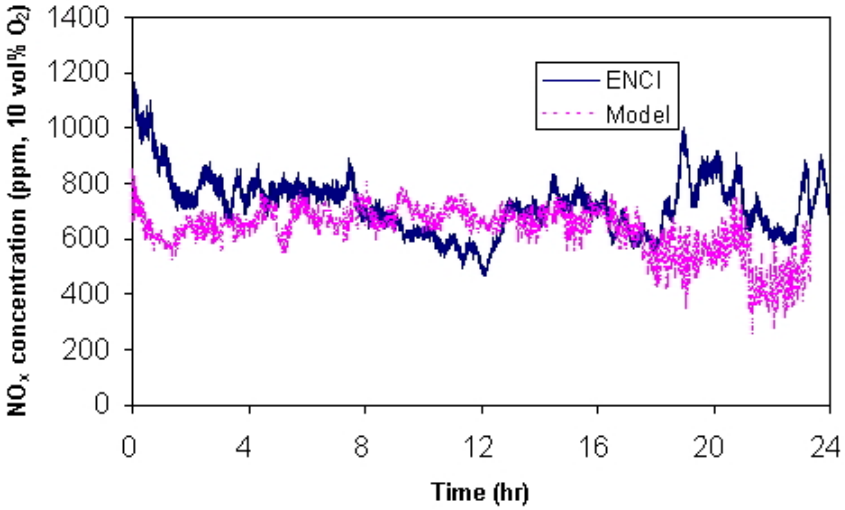

Figure 4. Result of the dynamic validation of the model, represented by the NO_x concentration at the stack. Practical data were obtained from ENCI, Maastricht.

The possible causes can be found in the long-term dynamics of the process. Historic trends that are present in the process are not covered by the model and can only be calculated on a long-term basis. Induced by this historic trend, the deviations in the stationary situation from which the model starts its calculation are reflected for long period. Another reason for the differences in both signals can be found in the input data. In Figure 5. the fuel input in the kiln and the O_2 concentration at the kiln inlet show that there exist large errors in fuel composition, which has direct influence on the NO_x and O_2 signals. Further refinement of the model input should have a positive influence on the accuracy of the model calculations.

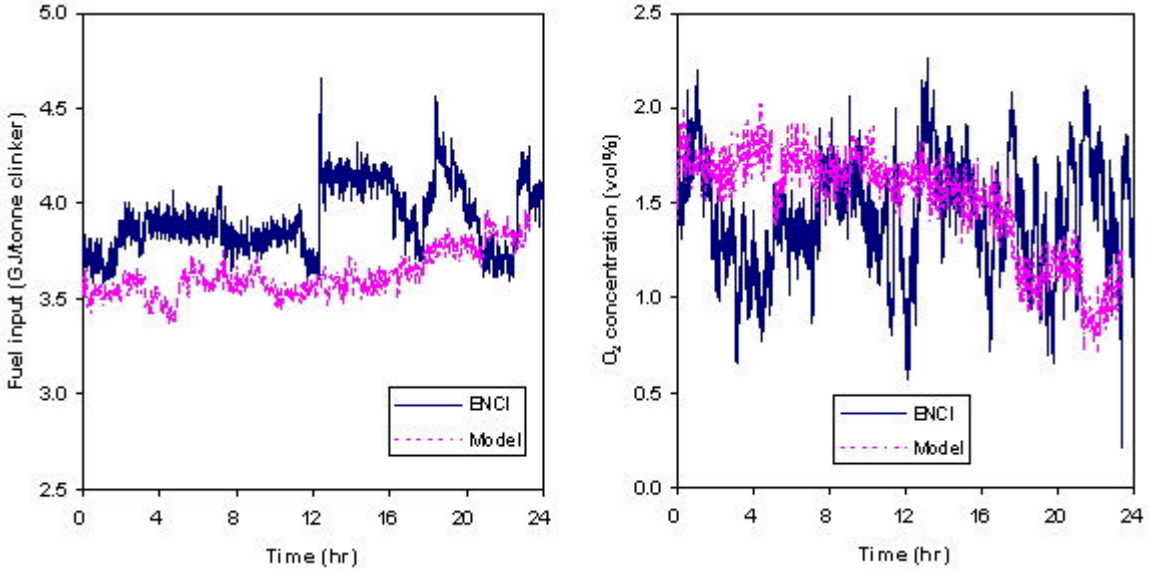

Figure 5. Result of the dynamic validation of the model, represented by the NO_x concentration at the stack. Practical data were obtained from ENCI, Maastricht.

The dynamic responses of the model can be investigated furthermore by looking at the emission spectra of the signal. Since the cement clinker production process contains several interactions in and between process apparatus the spectrum can be usefull. In Figure 6. the Bode plot for the calculated and the measured NO_x signal are presented. At time scales of 500 to 5000 seconds the dynamics of both are comparable. The high frequency domain is ruled by aliasing of the signal and is not representative. Low frequency domains cannot be compared because of the short calculation period of 24 hours.

The most important cycles in the process at time scales 3600 and 7200 seconds, representing kiln interactions with clinker cooler and cyclonepreheater, correlate well indicating correct residence time distribution for the solid phase.

Further research is needed on the dynamic of the process concentrates on dynamic process identification. By application of process identification, better understanding of the interactions in the kiln and between kiln, clinker cooler and cyclone preheater will be obtained, which can be used in the model. Especially flow behavior of the melted material and influences of the dust on the heat transfer from gasphase to solid phase must be demonstrated more thoroughly. Also the cycles of chlorine and sulphur as a direct result of thermal processes within the clinker production process will be investigated further.

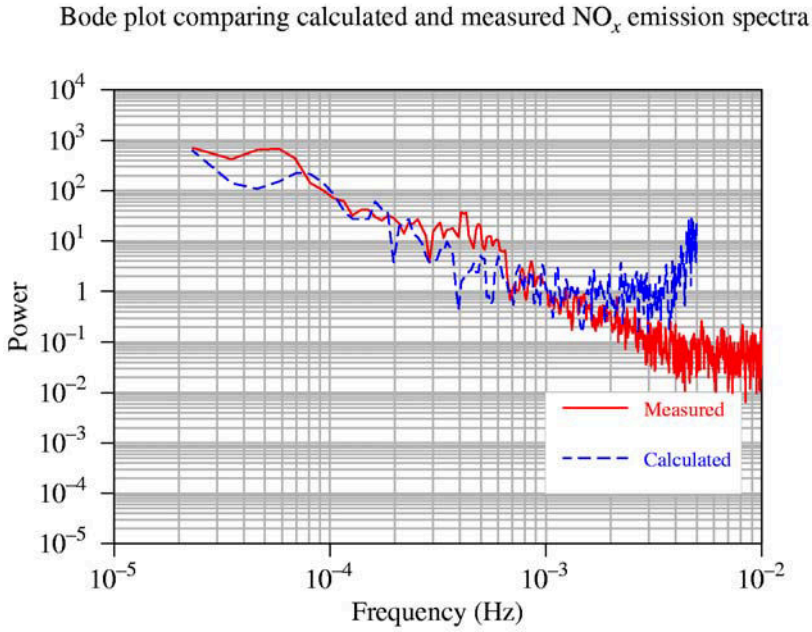

Figure 6. Bode plot of the measured and calculated NO_x emission spectra.

Because of the modular approach in the modeling process it is possible to incorperate several new processes. At this moment optional implementation of mid-kiln firing, precalcining and gasification of biomass are modeled and the effects of implementation on the process emissions and stability are calculated with the mathematical model.

4. CONCLUSIONS

A dynamic model for the description of the cement clinker production process was developed. The model contains all relevant apparatus and processes for the prediction of exhaust gas and clinker emissions for the main components like NO_x, CO and SO_x resulting from the deployment of primary and secondary raw materials and fuels.

Agreement between practical data and calculations with the model is fair. The stationary comparison showed that the magnitude of the output signals lies well within the range of large-scale process data. Within the dynamic validation agreement was found on magnitude as well as timescales of the signals.

Further research is concentrated on dynamic process identification and large-scale measurements of components like chlorine and sulphur, as well as implemenation of new process concepts like mid-kiln firing, precalcining and biomass gasification. Also, the dynamic modeling enables research on thermal and mass cycles and kiln instability, resulting in a better understanding of consequences and control issues.

5. NOMENCLATURE

Symbols			*Greek symbols*		
A	Square surface	(m^2)	Γ	Dust mass transfer	(kg s^{-1})
C_p	Specific heat coefficient	(kJ kg^{-1} K^{-1})	Φ	Mass flow	(kg s^{-1})
D	Diffusion coefficient	(m2 s^{-1})	λ	Heat conduction coefficient	(kJ m^{-1} s^{-1})
F	Fuel decomposition	(kg s^{-1})	Ω	Heat transfer rate	(kJ m^{-3} s^{-1})
H	Reaction enthalpy	(kJ kg^{-1})	ρ	Density	(kg m^{-3})
i	Chemical component index		ψ	Reaction rate	(kg s^{-1})
j	Fuel index				
M	Mass	(kg)	*Subscripts*		
nc	Number of chemical components		d	Dust	
nf	Number of fuels		g	Gas	
R	Gasphase flow area radius	(m)	s	Solid	
t	Time	(s)	sec	Secondary air	
T	Temperature	(K)			
V	Velocity	(m s^{-1})			
X	Concentration	(kg m^{-3})			
z	Axial coordinate	(m)			

REFERENCES

[1] Frankenberger, R. Beitrag zur Berechnung des Wärmeübergangs in Zementdrehofen, ZKG Intl., vol.24, 1971, pp.152-156.

[2] Rosa, J. Mathematische Formulierung des Wärmeubergangs im Drehofen, ZKG Intl., vol.23, 1970, pp.368-377.

[3] Onissi, T.R. Betrachtungen zum Wärmeubergang im Zementdrehofen, ZKG Intl., vol.33, 1980, pp.639-647.

[4] Gardeik, H.O. Vereinfachte mathematische Modelle zur Berechnung der Wärmeubertragung in innenbeheizte, adiabaten Drehroheren (Konvektionsmodelle). Teil 1: Idealisiertes Drehrohr mit unendlich grossem Wärmeleitkoeffizienten der Wand, ZKG Intl., vol.32, 1979, pp.201-210.

[5] Gardeik, H.O. Vereinfachte mathematische Modelle zur Berechnung der Wärmeubertragung in innenbeheizte, adiabaten Drehroheren (Konvektionsmodelle). Teil 2: Drehrohr mit endlichem Wert des Wärmeleitkoeffizienten der Wand, ZKG Intl., vol.32, 1979, pp.434-441.

[6] Locher, G. Mathematische Modelle zum Prozess des Brennens von Zementklinker: Teil 1: Reaktionen und Grundoperationen, ZKG Intl., vol.54, 2002, pp.29-38.

[7] Locher, G. Mathematische Modelle zum Prozess des Brennens von Zementklinker: Teil 2: Vorwärmer, Calcinator und Bypass, ZKG Intl., vol.55, 2002, pp.39-50.

[8] Locher, G. Mathematische Modelle zum Prozess des Brennens von Zementklinker: Teil 3: Drehrohrofen, ZKG Intl. vol.55, 2002, pp.68-80.

[9] Bapat, J.D. , Visvesraraya, H.C., Rao, T.R. and Subba Rao,m D. Kinetics of calcination in cement raw meal nodules, ZKG Intl., vol.47, 1994, pp.156-160.

[10] Khinast, J., Krammer, G.F., Brunner, Ch. and Staudinger, G. Decomposition of limestone: The influence of CO_2 and particle size on the reaction rate, Chem. Eng. Sci., vol.51, 1996, pp.623-634.

[11] Adanez, J., Gayan, P. and Garcia-Labiano, F. Comparison of mechanical models for the sulfation reaction in a broad range of particle sizes of sorbents, Journal of Industrial, Eng. Chem. Res., vol. 35, 1996, pp.2190-2197.

[12] Fuertes, A.B. and Fernandez, M.J. Kinetics of the calcium sulphate decomposition, Trans. IChemE., vol.73, 1995, pp.854-862.

[13] Barry, T.I. and Glasser, F.P. Calculations of portland cement clinkering reactions, Adv. Cem. Res., vol.12, 2000, pp.19-28.

[14] Chen, P. and Pei, D.C.T. A mathematical model for drying processes, Int. J. Heat Mass Transfer, vol.32, 1989, pp.297-310.
[15] Duchesne, C., Thibault, J. and Bazin, C. Modelling and dynamic simulation of an industrial rotary dryer, Dev. Chem. Eng. Mineral Process., vol.5, 1997, pp.155-182.
[16] Westerterp K.R., Van Swaaij, W.P.M.and Beenackers, A.A.C.M. Chemical reactor desing and operation, New York: John Wiley & Sons, 1993.
[17] Brem, G. Mathematical modeling of coal conversion processes, Thesis University of Twente, 1990.
[18] Van Berkel, A.I., Brem, G. and Valk, M. A Dynamic model of Biomass gasification in a circulating fluidized bed as a tool for optimising design and operation, 10th European conference and technology exhibition: Biomass for energy and industry, Würzburg, 1998.
[19] Visona, S.P. and Stanmore, B.R. Modelling NO formation in a swirling pulverized coal flame, Chem.Eng.Sci., vol.53, 1998, 2013-2027.
[20] Rizk, N.K. and Mongia, H.C. A semi-analytical emission model for diffusion flame, Rich/Lean and premixed lean combustors, J. Eng. Gas Turb. Power, vol.117, 1995, pp.290-301.
[21] Courtemanche, B. and Levendis, Y.A. A laboratory study on the NO, NO_2, SO_2, CO and CO_2 emissions from the cumbustion of pulverized coal, municipal waste plastics and tires, Fuel, vol.77, 1998, pp.183-196.
[22] Westbrook, C.K. and Dryer, F.L. Chemical kinetic modeling of hydrocarbon combustion, Prog. Energy Combust. Sci., vol.10, 1984, pp.1-57.
[23] Lebas, E., Hanrot, F. and Houzelot, J.L. Experimental study of residence time, particle movement and bed depth profile in rotary kilns, Can. J. Chem. Eng., vol.73, 1995, pp.173-180.
[24] Perron, J. and Bui, R.T. Rotary cylinders: Solid transport prediction by dimensional and rheological analysis, Can. J. Chem. Eng., vol.68, 1990, pp.61-68.
[25] Saj, P.S.T., Surender, G.D., Damodaran, A.D., Suresh, V., Philip, Z.G. and Sankaran, K. Residence time distribution and material flow studies in a rotary kiln, Metall. Trans., vol.21, 1990, pp.1005-1011.
[26] Echekki, T. A quasi-one-dimensional premixed flame model with cross-stream diffusion, Comb. Flame, vol.110, 1997, pp.335-350.
[27] Servert, J., Crespo, A., and Hernandez, J. A one-dimensional model of a turbulent jet diffusion flame in an ambient atmospheric flow, derived from a three-dimensional model, Combust. Sci. Tech., vol.124, 1997, pp.83-114.
[28] Lidn, G. and Gudmundsson, A. Semi-empirical modelling to generalise the dependence of cyclone collection efficiency on operating conditions and cyclone design, J. Aerosol Sci. vol.28, 1997, pp.853-874.
[29] Bohnet, M. Zyklonabscheider zum trennen von Gas/Feststoff-Strömungen, Chem.- Ing.-Tech., vol.54, 1982, pp.621-630.
[30] Bos, G.M. and Brem, G. Experimental characterisation of raw meal for the production of cement clinker, to be submitted, 2002.
[31] Douglas, P.L., Kwade, A., Lee, P.L. and Mallick, S.K. Simulation of a rotary dryer for sugar crystalline, Drying Tech., vol.11, 1993, pp.129-155.
[32] Wang, F.Y., Cameron, I.T., Litster, J.D. and Douglas, P.L. A distributed parameter approach to the dynamics of rotary drying processes, Drying Tech., vol.11, 1993, pp.1641-1656.
[33] Famke, F.A. and Wilson, J.B. Computer simulation of a rotary dryer: Part I: Retention time, IChE J., vol.32, 1986, pp.263-268.

RIETVELD MINERALOGICAL ANALYSIS OF PORTLAND CEMENTS

Ángeles G. de la Torre and Miguel A.G. Aranda*

Departamento de Química Inorgánica, Cristalografía y Mineralogía, Universidad de Málaga, 29071 Málaga, Spain. E-mail: g_aranda@uma.es

ABSTRACT

There is a great interest in the Quantitative Phase Analysis (QPA) of complex crystalline mixtures such as clinkers or cements. Final performances of these materials mainly depend on their mineralogical compositions and textures and not on the elemental compositions, as determined by x-ray fluorescence, XRF. X-ray Powder Diffraction (XRPD) combined with the Rietveld method is the most powerful tool to obtain the QPA of the cement samples. Here, we present mineralogical analyses for white Portland clinkers, gray Portland clinkers and gray Portland cements, using laboratory XRPD and the Rietveld method. The complexity of the systems is variable with the easiest mixture having three crystalline phases. Nevertheless, the toughest case can contain up to nine phases. Some effects such as good/poor particle statistics, preferred orientation or microabsorption have to be borne in mind in order to get accurate results. So, data collection strategy is very important. Moreover, it is possible to quantify the amorphous/non-diffracting content of the building materials by adding a suitable standard, for example Al_2O_3. Some results and guidelines to carry out the refinements of these mixtures will be given.

1. INTRODUCTION

The mineralogical phase analysis of materials of world importance such as cements is necessary to predict and understand their final performances. In the cement industry, Bogue calculations [1] are used to estimate the mineralogical composition by means of the elemental analysis obtained by XRF. This method is used worldwide to know the main phase fractions as quality control. However, it has well known problems [2] mainly due to the lack thermodynamical equilibrium in the kiln. Mineralogical composition of simple systems can be straightforwardly measured by Laboratory X-Ray Powder Diffraction (LXRPD) combined with the Rietveld method [3]. This methodology is the most powerful tool to obtain the Quantitative Phase Analysis, QPA [4]. This method is standardless but the crystal structures of all the phases must be known as the process consists in the comparison of the measured and calculated patterns. It has even adapted to follow online the cement samples in the factory [5,6]. QPA using the Rietveld method has been successfully used to analyze simple crystalline mixtures [7,8] and recently applied to gray Portland clinkers of different complexities [9-12], aluminous cements [13], calcium sulpho-aluminate cements [14] and mineralized white Portland clinkers [15]. To set up a contrasted technology to carry out fast and robust mineralogical quantitative analyses of these systems is a step forward for both the use of the Rietveld method and the Portland cement quality controls.

On the other hand, building materials contain amorphous/non-diffracting phases in variable amounts that may have an important role in the hydration processes. The quantification of an amorphous component in a crystalline sample by adding a suitable standard is being established [16,17]. In order to carry out a good quantitative analysis of the amorphous content, it is necessary

Proceedings of the 11th International Congress on the Chemistry of Cement (ICCC)
'Cement's Contribution to the Development in the 21st Century'
Hosted by: The Cement and Concrete Institute of South Africa
CD-ROM produced by: Document Transformation Technologies
11 - 16 May 2003, Durban, South Africa
ISBN Number: 0-9584085-8-0
Editors: Dr G. Grieve and G. Owens
Congress Organised by: Event Dynamics

to minimized all systematic errors in the powder diffraction data that causes deviations in the results, such as the choice of an adequate standard, preferred orientation, microabsorption, etc. [17].

2. EXPERIMENTAL SECTION

Three industrial samples have been analyzed: A white Portland clinker (W), a gray Portland clinker (G) and a gray Portland cement type I 42.5 R (C). The LXRPD patterns were recorded on a Siemens D5000 θ/2θ diffractometer (flat reflection mode) by using $CuK_{\alpha 1,2}$ radiation (1.542 Å) with a secondary curved graphite monochromator at room temperature. The samples were loaded in a methacrylate holder by sample-front pressing and they were spun during data collection at 15 rpm. The scanned 2θ range was 10º to 70º in all cases, in 0.03º steps, counting by 15s per step. The optics of the diffractometer was: two sets of Soller slits in the incident and diffracted paths, and three slits of 2, 2 and 0.2 mm (divergence, antidivergence, and receiving, respectively). The X-ray tube worked at 40 kV and 30 mA.

A high resolution powder diffraction pattern for a gray Portland clinker mixed with standard Al_2O_3 was recorded on a Stoe/Stadi-P powder diffractometer with Ge(111) monochromatized $CuK_{\alpha 1}$ radiation (1.540589 Å). The sample was loaded in a borosilicate glass capillary (0.3mm of diameter) and rotated during data collection. A position sensitive detector, PSD, was used in the angular range 10-70° [step 0.1° counting for 60s], with data transformed to 0.02° steps. The X-ray tube worked at 40 kV and 25 mA.

The elemental compositions were determined by XRF on a Philips PW 1660 spectrometer using the borate glass bead sample preparation method which minimizes matrix effects. Na and K chemical analyses were carried out by atomic emission spectroscopy. The sulfate content was determined gravimetrically as $BaSO_4$.

3. RESULTS AND DISCUSSION

3.1 Common features in the refinements

The powder patterns were analyzed by the Rietveld method with the GSAS suite of programs [18] by using the pseudo-Voigt peak shape function for all phases [19] corrected for axial divergency [20]. To fit the peakshape of the phases we have refined GW (the Gaussian part) and LY (the Lorentzian part) for most phases. For phases that showed anisotropic peak broadening, i.e. sharper and wider peaks depending upon the (hkl) indexes, a third parameter STEC (the anisotropic correction of the Lorentzian width) was refined along the adequate axis. The background was fitted by linear interpolation function. The goniometer zero was also optimized. Lattice parameters were refined for all phases.

The complexity of building materials is variable, the easiest mixture having three phases. Nevertheless, the toughest case can contain up to nine phases. Sample **W** had three phases, Ca_3SiO_5 or C_3S, Ca_2SiO_4 or C_2S and $Ca_3Al_2O_6$ or C_3A. Sample **G** contained five phases C_3S, C_2S, C_3A, $Ca_2(AlFe)_2O_5$ or C_4AF and aphthitalite $NaK_3(SO_4)_2$ or $K_3N\bar{S}_4$. Sample **C** was the most complex, it contained nine crystalline phases C_3S, C_2S, C_3A, C_4AF, $K_3N\bar{S}_4$, gypsum $CaSO_4{\cdot}2H_2O$ or $C\bar{S}H_2$, bassanite, $CaSO_4{\cdot}½H_2O$ or $C_2\bar{S}_2H$, calcite $CaCO_3$ and MgO or M. Table 1 shows some crystallographic information about these phases.

All mixtures contained C_3S as the main phase. Stoichiometric Ca_3SiO_5 presents polymorphism but the presence of foreign ions in the samples stabilizes high temperature MIII polymorph. It was suggested [2] that the monoclinic MIII form, called alite, is the one contained in the clinkers. We could unambiguously confirm this using ultra-high resolution synchrotron powder diffraction data

[9]. Alite crystallizes as pseudohexagonal multitwinned plaquets with large dimensions. Because of these large particle sizes, it usually presents strong preferred orientation when working in reflection geometry, i.e θ/2θ. This behavior is exacerbated if the sample is processed as pellets prior to the LXRPD experiment. Preferred orientation has been taken into account in all samples by using the spherical-harmonic correction [21]. This method yields much better fits than the March-Dollase algorithm [22]. Cylindrical symmetry was used with an order for the spherical harmonics of 8. The final texture indexes were 4.79, 2.79 and 2.50 for W, G and C samples, respectively. A value of 1 for the texture index represents an ideal random powder whereas ∞ stands for a single crystal. Hence, higher values of this index indicate more oriented samples. Clinker pellets usually give even higher texture indexes. On the other hand, if the LXRPD experiments are carried out in Debye-Scherrer geometry (transmission, with the sample contained in a rotating capillary), then the texture index is much smaller and sometimes negligible.

In addition to the preferred orientation, alite also presents anisotropic peak broadening. The broadening of the diffraction peaks slightly depends on the (hkl) indexes. This was taken into account using the ellipsoidal correction implemented in GSAS with the STEC parameter and the anisotropic axis running along the [1 0 0] direction.

Table 1**.** Crystallographic information of the phases in the analyzed samples.

Phase	Nomenclature	Space group	μ/cm^{-1} *	References
Ca_3SiO_5	C_3S	Monoclinic, C m	314	[23]
Ca_2SiO_4	C_2S	Monoclinic, P $2_1/n$	303	[24]
$Ca_2(AlFe)_2O_5$	C_4AF	Orthorhombic, I bm2	495	[25]
$Ca_3Al_2O_6$	C_3A	Cubic, P -3a	267	[26]
$NaK_3(SO_4)_2$	$K_3N\bar{S}_4$	Trigonal, P -3m	248	[27]
$CaSO_4{\cdot}2H_2O$	$C\bar{S}H_2$	Monoclinic, I 2/c	140	[28]
$CaSO_4{\cdot}½H_2O$	$C_2\bar{S}_2H$	Monoclinic, I 2	195	[29]
$CaCO_3$	$C\bar{C}$	Rhombohedral, R -3c	197	[30]
MgO	M	Cubic, F m-3m	97	[31]
Al_2O_3	A	Rhombohedral, R -3c	120	[32]

* Absorption coefficients for CuK_α

3.2 Refinement for a white Portland clinker

The Rietveld plot for a white Portland clinker is given in Figure 1. This sample contains only three crystalline phases, C_3S, C_2S and C_3A. The inset of Figure 1 displays the most informative peaks of the sample. It should be noted that the diffraction peaks due to C_3S and C_2S are very overlapped and the peak of C_2S at 31º 2θ is essential to de-correlate the scale factors for these phases, and so, the phase fractions.

Due to the strong peak overlapping and the limited information present in the powder pattern for low concentration phases, it is not advisable to refine the peak shape parameters for low content phases. So, the peak shape function for phases at concentration lower than 10% w/w were kept fixed to previously established values [9]. The final disagreement factors, as defined in references [3, 18] were R_{WP}=10.7% and R_P=7.8%. Removing the background contribution to these factors led to R_{WP}=8.5% and R_P=6.8%. The fit is remarkably good as the difference between the observed pattern (red crosses) and the calculated one (green line) is the very flat, pink bottom line in Figure 1.

The mineralogical composition for sample **W** obtained from the Rietveld analysis of the LXRPD data is given in Table 2. The elemental analysis, measured as reported in the experimental section, is also given in Table 2. In order to compare the mineralogical composition (Rietveld study) with the elemental composition from the XRF analysis, the phase analysis is also expressed as oxides

(derived elemental composition) in Table 2. This comparison should be exercised with care as these two techniques do not measure the same quantities. XRF tests the full sample while the LXRPD only tests the crystalline fraction. So the results should be similar only if the non-diffracting part of the sample is negligible. This is not always the case, see below.

The results showed in Table 2 indicate that both Ca and Si contents are overestimated when comparing the Rietveld and the XRF analyses. This is rationalized as the consequence of two effects: a) the unmodeled partial solid solution Ca by Mg and Si by Al: b) the presence of a non-diffracting fraction in the sample which is richer in aluminates. However, the difference in the Al_2O_3 percentages is striking. In fact, the C_3A content calculated by Bogue [1] is much higher than that determined by the Rietveld method. This is a real effect that we have measured in many other white Portland clinkers and this must be borne in mind when correlating the sulfate resistance and the aluminum content of these types of materials.

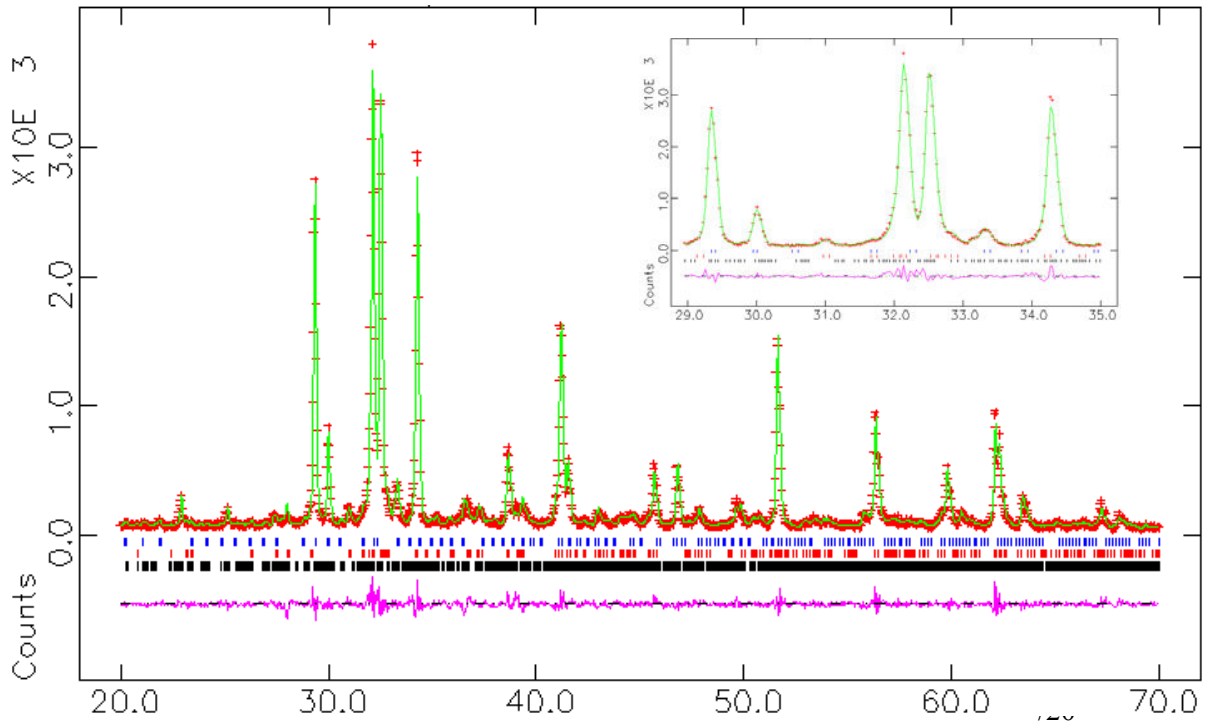

Figure 1. LXRPD Rietveld plot for the white Portland clinker with observed (red crosses), calculated (green line) and difference (pink bottom line) powder patterns. The marks correspond to the Bragg peaks of the different phases; from bottom to top: C_3S (black), C_2S (red) and C_3A (blue). The inset shows the most representative region (29-35º 2θ) with some peaks labeled

The non-diffracting part includes the sub-cooled liquid fraction, but also includes the defects in the crystalline particles such as micro-twining, dislocations, grain boundaries, etc. Hence, the measurable non-diffraction part is always higher than the sub-cooled liquid fraction. We have recently reported a methodology to quantify the non-diffracting/amorphous content of simple systems [17]. This protocol is based on the slight overestimation of a suitable fully crystalline standard when mixed with a sample containing an amorphous fraction. From the differences between the Rietveld and the weighted phase fractions, the quantification of the amorphous part is possible.

We are carrying out the non-diffracting part analysis for white Portland clinkers. The results will be reported elsewhere but we can advance that this part exceeded 20% w/w for several white Portland clinkers. This number includes the sub-cooled amorphous aluminates and many other defects in the

crystalline particles. We have annealed the white Portland clinkers at high temperatures and the C_3A phase fraction increases notably.

Table 2. Mineralogical composition for a white Portland clinker obtained by the Rietveld method. Derived elemental composition from Rietveld results and elemental composition measured by XRF expressed as oxide content.

Phases/elements	LXRPD-Rietveld /% w/w	XRF * /% w/w
C_3S	77.3(2)	-
C_2S	19.8(4)	-
C_3A	2.9(1)	-
CaO	71.66	68.90
SiO_2	27.25	22.98
Al_2O_3	1.09	5.08
Fe_2O_3	-	0.24
SO_3	-	0.9
MgO	-	0.58

* Na_2O and K_2O contents not determined

3.3 Refinement for a gray Portland clinker

The Rietveld plot for a gray Portland clinker is given in Figure 2. This sample contains five crystalline phases, C_3S, C_2S, C_4AF, C_3A and $K_3N\bar{S}_4$. The inset of Figure 2 displays the most informative peaks of the sample. Due to the real nature of the phases, the crystallinity and so the peak shape of the different phases is not the same. This has to be taken into account to correctly describe the peak profiles. For instance, alkaline sulfates are the last crystallizing fraction from the melt in the kiln and it has the broadest diffraction peaks. So, $K_3N\bar{S}_4$ is poorly crystalline and their peaks were described with a Lorentzian. C_4AF peaks are also quite wide and present anisotropic broadening which was corrected refining STEC along [1 2 0].

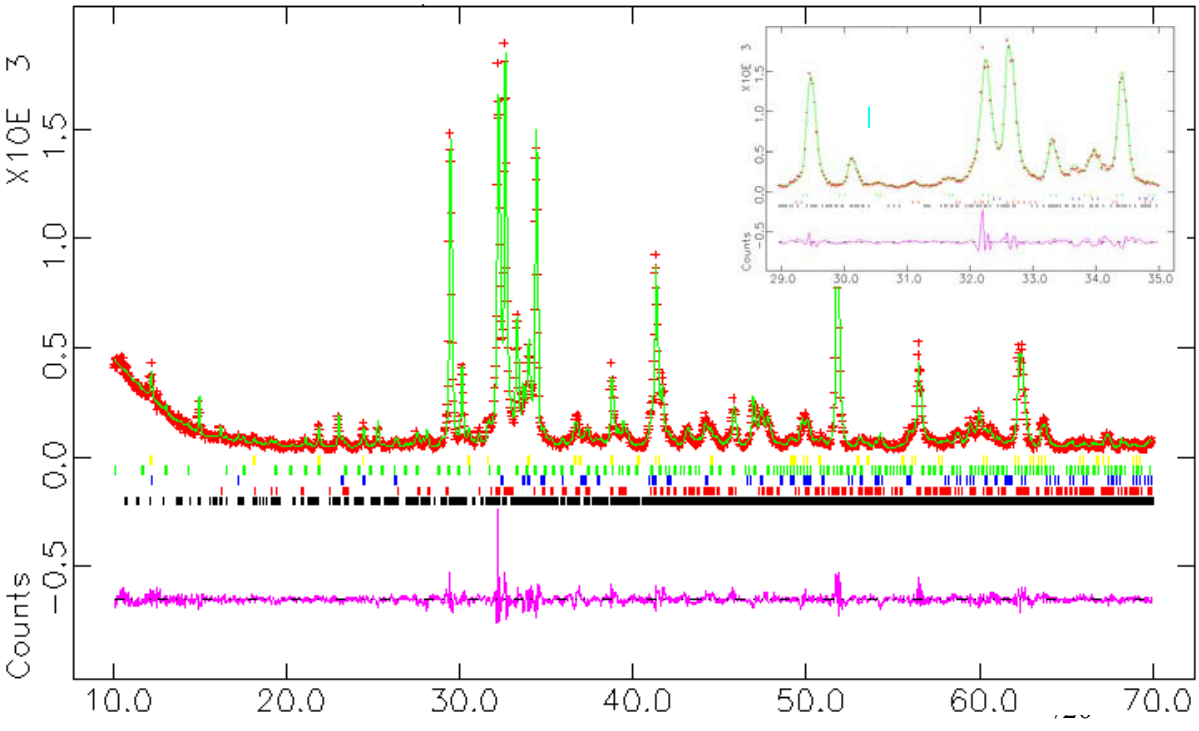

Figure 2. LXRPD Rietveld plot for a gray Portland clinker as in Figure 1. Phases from bottom to top: C_3S (black), C_2S (red), C_4AF (blue), C_3A (green) and $K_3N\bar{S}_4$ (yellow). The inset shows the most representative region (29-35º 2θ) with some peaks labeled

The mineralogical composition for the gray Portland clinker is given in Table 3. The final disagreement factors were R_{WP}=11.4% and R_P=8.7%. Without the background contribution, these values were R_{WP}=10.4% and R_P=8.5%. The good quality of the fit is evidenced in Figure 2 by the relatively flatness of the pink difference curve.

Consistently with the results shown above for sample W, both Ca and Si contents are also overestimated for this sample. However, the difference in the Al_2O_3 percentages is much smaller. This is likely due to the lower content of sub-cooled fraction in the gray Portland clinkers. A detailed diffraction study which includes the comparison between the amorphous contents of the white and gray Portland clinkers is in progress but it is out of the scope of the present work.

Table 3. Mineralogical composition for a gray Portland clinker obtained by the Rietveld method. Derived elemental composition from Rietveld results and elemental composition measured by XRF expressed as oxide content.

Phases/elements	LXRPD-Rietveld /% w/w	XRF /% w/w
C_3S	68.1(3)	-
C_2S	12.1(5)	-
C_4AF	11.6(2)	-
C_3A	6.8(2)	-
$K_3N\bar{S}_4$	1.4(1)	-
CaO	67.71	64.83
SiO_2	22.14	20.52
Al_2O_3	5.04	5.55
Fe_2O_3	3.81	3.28
Na_2O	0.13	0.26
K_2O	0.60	0.93
SO_3	0.67	1.35
MgO	-	1.30

3.4 Refinement for a gray Portland clinker with standard Al_2O_3

A high resolution pattern, strictly monochromatic CuKα_1 radiation, was collected for a gray Portland clinker mixed with Al_2O_3. The Rietveld plot for this sample is given in Figure 3. This sample contains six crystalline phases, C_3S, C_2S, C_4AF, C_3A, $K_3N\bar{S}_4$ and Al_2O_3. The inset of this Figure displays again the most informative peaks of the sample.

The final disagreement factors for this refinement were R_{WP}=5.7% and R_P=5.4%. Without the background contribution, these values were R_{WP}=5.4% and R_P=4.4%. The good quality of the fit is again evidenced in Figure 3 by the flat pink difference curve. It must be noted that working in transmission with a rotating capillary the phases should not show strong preferred orientation. In fact, we tested the spherical-harmonic correction and the texture index of C_3S converged to 1.07. So, it was not applied as the improvement in the refinement was negligible. The fit showed in Figure 3 was obtained with our structural model for C_3S [23] and without correcting the diffraction peak intensities.

From the overestimation in the Rietveld refined Al_2O_3 ratio with respect to the weighted fraction, we can estimate the non-diffracting content. However, this type of study has to be carried out with extreme care as microabsorption can lead to erroneous results. This work is in progress and it will be reported elsewhere.

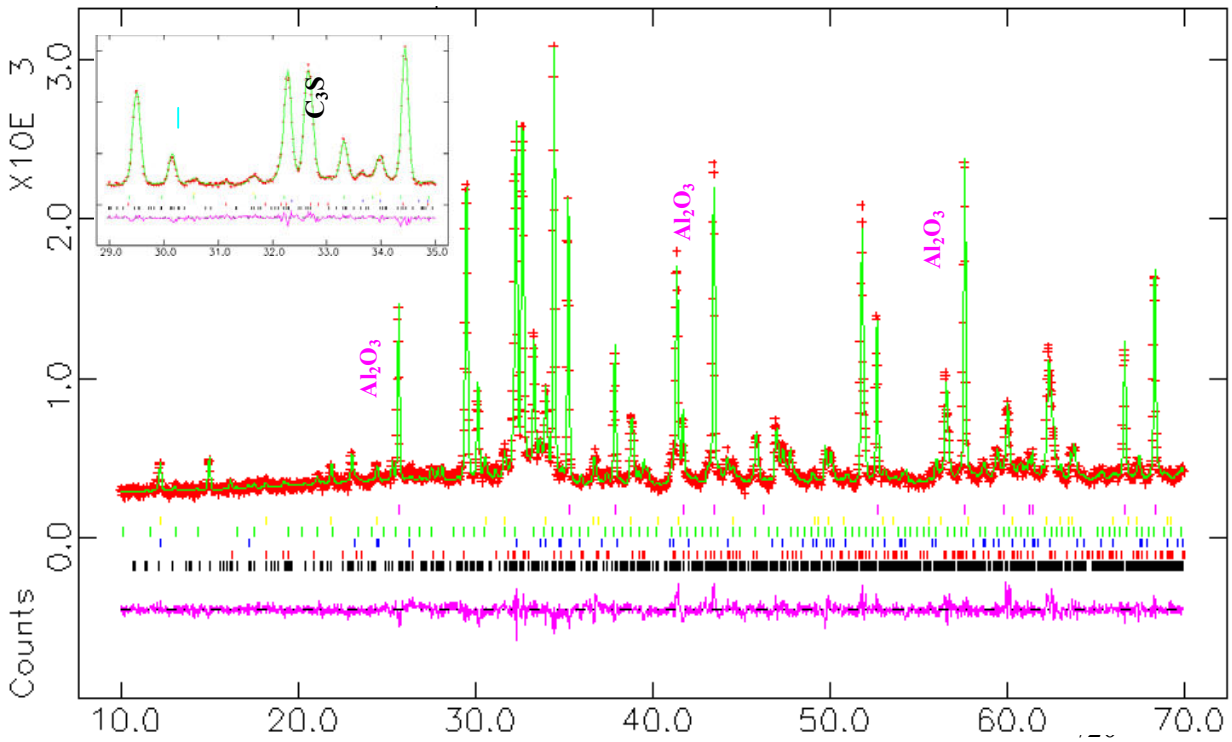

Figure 3. High-resolution LXRPD Rietveld plot for a gray Portland clinker as in Figure 1. Phases from bottom to top: C_3S (black), C_2S (red), C_4AF (blue), C_3A (green), $K_3N\bar{S}_4$ (yellow) and Al_2O_3 (pink). The inset shows the most representative region (29-35º 2θ) with some peaks labeled

3.5 Refinement for a gray Portland cement

The Rietveld plot for a gray Portland cement is given in Figure 4. This sample contains nine crystalline phases, C_3S, C_2S, C_4AF, C_3A, $K_3N\bar{S}_4$, $CaSO_4{\cdot}½H_2O$, $CaSO_4{\cdot}2H_2O$, $CaCO_3$ and MgO. The inset of Figure 4 displays the low angle region of the pattern where the peaks due to the set-retarder agents, gypsum and bassanite, are evident.

The mineralogical composition for this sample is given in Table 4. $CaSO_4{\cdot}2H_2O$ and $CaSO_4{\cdot}½H_2O$ showed strong preferred orientation due to their layered structures that yield plaquets for the microparticle shapes. This was corrected using March-Dollase algorithm [22] along [0 1 0] axis. Due to their low phase contents, the peak shape function was not refined and the values were kept fixed to those obtained in previous studies. The final disagreement factors were R_{WP}=11.7% and R_P=8.8%. Without the background contribution, these values were R_{WP}=10.1% and R_P=8.1%. Again, the pink difference curve is quite flat.

These studies show that mineralogical analyses of Portland cements with up to nine phases are feasible. Furthermore, the results are consistent, if $CaSO_4{\cdot}2H_2O$ was detected, then a lower content of $CaSO_4{\cdot}½H_2O$ was measured. We systematically detect bassanite in higher contents than gypsum in the analyzed Portland cements. Therefore, quantitative mineralogical analyses allow even to follow the dehydration reactions of gypsum in the cement ball mills. The content range for all phases in the studied cements were within the expected limits.

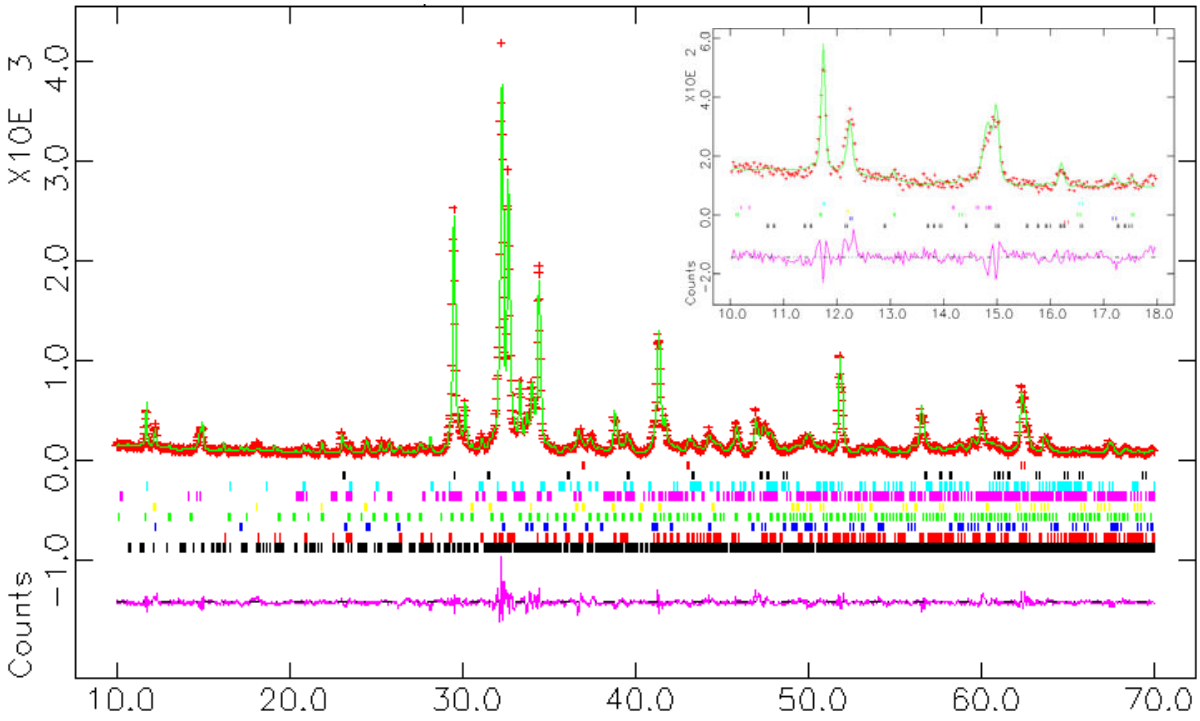

Figure 4. LXRPD Rietveld plot for a gray Portland cement as in Figure 1. Phases from bottom to top: C_3S (black), C_2S (red), C_4AF (blue), C_3A (green), $K_3N\bar{S}_4$ (yellow), $CaSO_4{\cdot}½H_2O$ (pink), $CaSO_4{\cdot}2H_2O$ (light blue), $CaCO_3$ (black) and MgO (red). The inset shows the low angle region (10-18º 2θ) with the conspicuous peaks for gypsum and bassanite also labeled

Table 4. Mineralogical composition for a gray Portland cement obtained by the Rietveld method.

Phases	LXRPD-Rietveld /% w/w
C_3S	58.7(3)
C_2S	16.7(5)
C_3A	5.1(2)
C_4AF	11.3(3)
$K_3N\bar{S}_4$	0.8(1)
$CaSO_4{\cdot}2H_2O$	0.9(1)
$CaSO_4{\cdot}½H_2O$	4.3(2)
$CaCO_3$	1.6(2)
MgO	0.6(1)

3.6 Errors in the mineralogical analysis by the Rietveld method

The errors in the analyses are variable and mainly due to poor particle statistics. So, rotation of the sample is essential in order to get accurate results for point quality control analysis. However, for on-line systems where many analyses are carried out, the results can be averaged and the particle statistics is not the main concern. Another important issue is microabsorption. A correction for this effect cannot be easily implemented in an on-line system. The preferred orientation and the overlapping of the peaks are other error sources.

It should be noted that the errors stated in Tables 2-4 are those only arising from the counting statistics in the patterns. The other sources of errors should increase the reported values by approximately 3-4. Taking all together, relative precision of 1% can be obtained for C_3S. For low

content phases, the relative errors are higher. Finally, it should be noted that the crystalline C_3S content can be measured with an overall error lower than 2% w/w.

4. CONCLUSIONS

Rietveld mineralogical analyses of building materials are shown to be feasible. As an example, we have presented three cases of different complexities: white Portland clinker, gray Portland clinker, gray Portland cement. The complexity increases in the series as the samples contained three, five and nine crystallines phases, respectively. The fits to the powder pattern are good as evidenced by flat difference curves. The disagreement factors are low indicating a suitable modeling. Subtle features such as the partial dehydration process in the cement ball mill can be investigated. With LXRPD data and the Rietveld method it is possible to quantify the bassanite and gypsum content in the cement and it can be satisfactorily related to the dosage.

ACKNOWLEDGEMENTS

We thank Dr. S. Bruque (Universidad de Málaga) and Dr. M.T. Blanco-Varela (CSIC-Madrid) for their fruitful discussions. We thank Dr. Zuñiga (Universidad del Pais Vasco) for collecting the high resolution X-ray pattern. This work has been supported by the FEDER 1FD97-0894 research grant. A. G. De la Torre acknowledges a studentship from Junta de Andalucía (Spain).

REFERENCES

[1] Bogue, R.H. Industrial Engineering Chemistry (Analytical Edition), 1929, vol 1, pp 192.
[2] Taylor, H.F.W. Cement Chemistry, 2nd ed. London: Thomas Telford Ltd, 1997, pp. 102.
[3] Rietveld, H.M. "A profile refinement method for nuclear and magnetics structures", J. Appl. Crystallogr., vol. 2, 1969, pp. 65-71.
[4] Madsen, I.C., Scarlett, N.V.Y., Cranswick, L.M.D. and Lwin, T. "Outcomes of the International Union of Crystallography Commission on powder diffraction round robin on quantitative phase analysis: samples 1a to 1h", J. Appl. Crystallogr., vol. 34, 2001,pp. 409-426.
[5] Manias, C., Retallack, D. and Madsen, I. "XRD for on-line analysis and control" World Cement, February 2000, pp. 78-81.
[6] Scarlett, N. V. Y. and Madsen, I. C. "On-line X-ray diffraction for quantitative phase analysis: Application in the Portland cement industry" Powder Diffraction, vol. 16, 2001, pp. 71-80.
[7] Hill, R.J. and Howard, C.J. "Quantitative phase analysis from neutron powder diffraction data using the Rietveld method", J. Appl. Crystallogr., vol. 20, 1987, pp. 467-474.
[8] Bish, D.L. and Howard, S.A. "Quantitative phase analysis using the Rietveld method", J. Appl. Crystallogr., vol. 21, 1988, pp. 86-91.
[9] De la Torre, A.G., Cabeza, A., Calvente, A., Bruque, S. and Aranda, M.A.G. "Full phase analysis of Portland clinker by penetrating synchrotron powder diffraction", Anal. Chem., vol. 73, 2001, pp. 151-156.
[10] Schmidt, R. and Kern, A. "Quantitative XRD phase analysis", World Cement, February 2001, pp. 2-8.
[11] Taylor, J.C., Hinczak, I. and Matulis, C. E. "Rietveld full-profile quantification of Portland cement clinker: The importance of including a full crystallography of the major phase polymorphs", Powder diffraction, vol. 1, 2000, pp. 7-18.
[12] Neubauer, J. and Sieber, R. "Quantification of synthetic alite and belite by the Rietveld method", Materials Science Forum, vol. 228-231, 1996, pp. 807-812.
[13] Guirado, F., Galí, S. and Chinchón, S. "Quantitative Rietveld analysis of aluminous cement clinker phases", Cem. Concr. Res., vol. 30, 2000, pp.1023-1029.
[14] Schmidt, R. and Pöllmann, H. "Quantification of calcium sulpho-aluminate cement by Rietveld analysis", Mat. Sci. Forum, vols. 321-324, 2000, pp. 1022-1027.
[15] Pajares, I., De la Torre, A.G. Martínez-Ramírez, S., Puertas,F., Blanco-Varela, M.T. and Aranda, M.A.G. "Quantitative analysis of mineralised white Portland clinkers: the structure of Fluorellestadite" Powder Diffraction, 2002, submitted.
[16] Winburn, R.S., Lerach, S.L., Jarabek, B.R. Wisdom, M.A., Grier, D.G. and McCarthy, G.J. "Quantitative XRD analysis of coal combustion by-products by the Rietveld method. Testing with standard mixtures", Adv. X-ray Anal., vol.42, 1998, pp. 387-396.
[17] De la Torre, A.G., Bruque, S. and Aranda, M.A.G. "Rietveld quantitative amorphous content", J. Appl. Crystallogr., vol. 34, 2001,pp. 196-202.

[18] Larson, A.C. and Von Dreele, R.B. “General Structural Analysis System”, Los Alamos National Lab. Rep. No. LA-UR-86-748. GSAS program @ http://public.lanl.gov:80/gsas/, 1994.
[19] Thompson, P., Cox, D.E. and Hasting, J.B. “Rietveld refinement of Debye-Scherrer synchrotron X-ray data from Al_2O_3”, J. Appl. Crystallogr., vol. 20, 1987, pp. 79-83.
[20] Finger, L.W., Cox, D.E. and Jephcoat, A.P. “A correction for powder diffraction peak asymmetry due to diaxial divergence”, J. Appl. Crystallogr., vol. 27, 1994, pp. 892-900.
[21] Von Dreele, R. B. “Quantitative texture analysis by Rietveld refinement,” J. Appl. Crystallogr., vol. 30, 1997, pp. 517-525.
[22] Dollase, W. A. “Correction of intensities for preferred orientation in powder diffractometry: application of the March model,” J. Appl. Crystallogr., vol. 19, 1986, pp. 267-272.
[23] De la Torre, A.G., Bruque, S., Campo, J. and Aranda, M.A.G. “The superstructure of C_3S from synchrotron and neutron powder diffraction and its role in quantitative phase analyses”, Cem. Concr. Res., 2002. In press.
[24] Mumme, W.G. “Crystal structure of tricalcium silicate from a Portland cement clinker and its application to quantitative XRD analysis”, Neues Jahrbuch fuer Mineralogie, vol. 4, 1995, pp. 145-160.
[25] Coville, A.A. and Geller, S. “The crystal structure of Brownmillerite, Ca_2FeAlO_5”, Acta Cryst., B27, 1971, pp. 2311-2315.
[26] Mondal, P. and Jeffery, J.W. “The crystal structure of tricalcium aluminate, $Ca_3Al_2O_6$”, Acta. Cryst., B31, 1975, pp. 689-697.
[27] Okada, K. and Ossaka, J. “Structures of potassium sodium sulphate and tripotassium sodium disulphate”, Acta Cryst., B36, 1980, pp. 919-921.
[28] Schofield, P. F., Knight, K. S. and Stretton, I. C. “Thermal expansion of gypsum investigation by neutron powder diffraction”, American Mineralogist, vol. 81, 1996, pp.847-851.
[29] Bezou, C., Nonat, A., Mutin, J. C., Christensen, A. N. and Lehmann, M. S. “Investigation of the crystal structure of gamma-$CaSO_4$, $CaSO_4 \cdot 0.5H_2O$ and $CaSO_4 \cdot 0.6H_2O$ by powder diffraction methods”, J. Solid State Chem., vol. 117, 1995, pp. 165-176.
[30] Maslen, E. N., Streltsov, V. A., Streltsova, N. R. and Ishizawa, N. “Electron density and optical anisotropy in rhombohedral carbonates. III. Synchrotron X-ray studies of $CaCO_3$, $MgCO_3$ and $MnCO_3$”, Acta Cryst., B51, 1995, pp. 929-939.
[31] Sasaki, S., Fujino, K. and Takeuchi, Y. “X-ray determination of electron-density distributions in oxides, MgO, MnO, CoO, and NiO, and atomic scattering factors of their constituent atoms”, Proceedings of Japan Academy, vol. 55, 1979, pp. 43-48.
[32] Maslen, E. N., Streltsov, V. A., Streltsova, N. R., Ishizawa, N. and Satow, Y. “Synchrotron X-ray study of the electron density in □-Al_2O_3”, Acta Cryst. B49, 1993, pp. 973-980.

RIETVELD MINERALOGICAL ANALYSIS OF PORTLAND CEMENTS

Ángeles G. de la Torre and Miguel A.G. Aranda*

Departamento de Química Inorgánica, Cristalografía y Mineralogía, Universidad de Málaga, 29071 Málaga, Spain. E-mail: g_aranda@uma.es

Short CURRICULUM VITAE for Dr. Miguel Angel García Aranda

Dr. Miguel Angel García Aranda
Departamento de Química Inorgánica, Cristalografía y Mineralogía
Universidad de Málaga
29071-MALAGA
Spain
Phone: Int- 34-952131874
Fax: Int- 34-952132000
e-mail: g_aranda@uma.es
www: http://webdeptos.uma.es/qicm/maga.htm

Dr. Aranda obtained his D. Phil. at the University of Málaga, Spain, in 1992 with a complementary doctoral training at the Chemical Crystallography Laboratory, University of Oxford, UK. His postdoctoral stay (1992-1993) was carried out in the "Interdisciplinary Research Centre in Superconductivity", University of Cambridge, UK. In 1994 he came back to the University of Málaga as an Assistant Lecturer and became Lecturer in Inorganic Chemistry on 1999.

He has interest in the structural elucidation of compounds from powder diffraction as well as quantitative phase analyses of industrial materials. These tools include laboratory and synchrotron X-rays and neutrons with the Rietveld method. His primary interests are in the synthesis and properties transition metal oxides such as manganites and novel open-framework systems, especially phosphonates.

He organizes a Summer school devoted of the Rietveld method and participates in the design, construction and commissioning of the powder diffraction facility of the Spanish-CRG at ESRF (European Synchrotron Research Facility), SPLINE. He belongs to the International Centre for Diffraction Data, ICDD, since 1997 and Real Sociedad Española de Química, RSEQ, since 1997.

He is co-author of more than 80 research articles in international Journals.

STUDY OF MAGNESIUM ION ATTACK IN PORTLAND CEMENT MORTARS

Manu Santhanam[1], Menashi Cohen[2], and Jan Olek[3]

[1] Department of Civil Engineering, IIT Madras, Chennai, India – 600036;
E-mail: manu@civil.iitm.ernet.in
[2] School of Civil Engineering, Purdue University, W. Lafayette, IN 47907, USA;
E-mail: mcohen@ecn.purdue.edu
[2] School of Civil Engineering, Purdue University, W. Lafayette, IN 47907, USA;
E-mail: olek@ecn.purdue.edu

ABSTRACT

Portland cement mortars prepared in accordance with ASTM C109 were subjected to immersion in magnesium sulfate and magnesium chloride solutions. Periodic monitoring of the physical properties, such as length, mass, compressive strength and dynamic modulus, was performed. The amounts of the primary reaction products formed were detected by thermal analysis, while microstructural observations were conducted by scanning electron microscopy.

Results from the studies indicate that the primary effect of Magnesium ions is the formation of magnesium hydroxide, or brucite, on the surface of the mortar specimens, soon after immersion. The mechanism of attack is then dictated by the nature of the solution. In the case of magnesium sulfate solution, the consumption of calcium hydroxide (for brucite formation) is matched by the deposition of gypsum. Expansion gradually increases and compressive strength drops with the increased formation of gypsum and ettringite. On the other hand, in the case of magnesium chloride solution, there are no secondary products formed. Thus, the removal of calcium hydroxide causes an increase in the porosity of the mortar, leading to a rapid drop in strength. At advanced stages of the attack, decalcification of calcium silicate hydrate (C-S-H) and its conversion to magnesium silicate hydrate (M-S-H) is observed for both the attacking solutions.

1. INTRODUCTION

The reactions involved in sulfate and chloride attack are well understood by researchers [1,2]. Magnesium sulfate ($MgSO_4$) and magnesium chloride ($MgCl_2$) solutions react with the hydrated cement paste to form gypsum ($CaSO_4.2H_2O$), ettringite ($6CaO.Al_2O_3.3SO_3.32H_2O$), brucite ($Mg(OH)_2$), and chloroaluminate salts, according to the following approximate equations:

$$Ca(OH)_2 + MgSO_4 + 2H_2O \rightarrow \underset{\text{Gypsum}}{CaSO_4.2H_2O} + \underset{\text{Brucite}}{Mg(OH)_2} \quad (1)$$

$$Ca(OH)_2 + MgCl_2 \rightarrow CaCl_2 + \underset{\text{Brucite}}{Mg(OH)_2} \quad (2)$$

The gypsum that forms in reaction (1) can further combine with aluminates and their hydration products in cement paste to form ettringite. The formation of ettringite causes expansion [3, 4], although the mechanism of expansion is still debated by researchers. In the case of magnesium

Proceedings of the 11th International Congress on the Chemistry of Cement (ICCC)
'Cement's Contribution to the Development in the 21st Century'
Hosted by: The Cement and Concrete Institute of South Africa
CD-ROM produced by: Document Transformation Technologies
11 - 16 May 2003, Durban, South Africa
ISBN Number: 0-9584085-8-0
Editors: Dr G. Grieve and G. Owens
Congress Organised by: Event Dynamics

chloride solution, the chloride ions can combine with the aluminates in the paste to form chloroaluminate compounds such as Friedel's salt, which are similar in structure to ettringite, but do not cause any expansion [5].

The brucite layer that forms on the surface has a very low solubility. Thus, the formation of brucite according to equations (1) and (2) will continue until the $Ca(OH)_2$ is depleted. With the consumption of $Ca(OH)_2$, a gradual decrease of pH occurs. This renders the calcium silicate hydrate (C-S-H) gel unstable, and causes it to liberate some $Ca(OH)_2$ into the surrounding solution to increase the pH. This can once again go into reaction with the attacking solutions. Thus, a progressive reduction of the CaO to SiO_2 ratio occurs in the C-S-H. At advanced stages of the attack, the Mg^{2+} ion can replace Ca^{2+} in the C-S-H to form magnesium silicate hydrate (M-S-H), which is reported to be non-cementitious [6]. The formation of M-S-H is the last stage of magnesium ion attack. A direct attack of the C-S-H by $MgSO_4$ can also cause the formation of M-S-H and secondary gypsum [7]. The M-S-H and gypsum are precipitated in bands parallel to the surface of the specimen [7, 8, 9].

Bonen and Cohen [7] investigated the effect of magnesium sulfate solutions on Portland cement pastes. They suggested that the attack by magnesium ions primarily leads to the formation of a brucite layer at the surface. A layer of gypsum underneath the brucite layer is also formed, by a two-way diffusion of ions. The SO_4 ions from the solution diffuse inwards, while the OH ions from the cement paste move outwards. Because of the low solubility of brucite, the penetration of Mg^{2+} beneath the brucite layer into the interior of the paste specimen is restricted.

A comparative study of attack of Portland cement mortars by magnesium sulfate and magnesium chloride solutions was conducted by Moukwa [10]. Pore structure analysis by Mercury Intrusion Porosimetry (MIP) showed that the attack by magnesium sulfate actually led to a densification of the pore structure at early ages, and a corresponding increase in strength. On the other hand, attack by magnesium chloride caused an increase in the porosity of the mortar, as well as in the threshold diameter.

This study described in this paper is an attempt to analyze Mg ion attack by combining physical, chemical, and microstructural studies.

2. EXPERIMENTAL MEHODS AND MATERIALS

Portland cement mortars were prepared using ASTM Type I cement in accordance with ASTM C109 [11]. The types of specimens cast are listed in Table 1. The specimens were stored within the molds in a moist condition for 24 hours. The molds were then removed, and the specimens transferred to a container with saturated limewater solution. At the age of 14 days after casting, the initial measurements for length, mass, compressive strength, and dynamic modulus were performed. Subsequently, the mortar specimens were stored in three different solutions at a temperature of 21 ^oC: (1) LW - saturated limewater solution (control), (2) MS - 3.8 mass percent $MgSO_4$ solution (Mg^{2+} = 7600 ppm, SO_3 = 25000 ppm), and (3) MC - 3.0 mass percent $MgCl_2$ solution (Mg^{2+} = 7600 ppm, Cl^- = 22200 ppm).

Table 1. Details of mortar specimens

Type	Dimensions	Test
1	Cube - 25 mm side	Compressive strength
2	Prism – 4 mm x 14 mm x 60 mm	DSC
3	Prism – 6 mm x 15 mm x 80 mm with plastic end pieces (described in Figure 1)	Length
4	Cylinder – 23 mm diameter, 80 mm height	Mass, Dynamic modulus, SEM

Measurements of physical properties were performed periodically. For all the physical measurements, the mortar specimens were dried using a cloth to bring them to a saturated surface dry (SSD) condition. The length of the prismatic specimens was measured using a comparator. Compressive strength was measured using a 60,000 lb. capacity universal testing machine. Dynamic modulus was calculated from measurements of the velocity of ultrasonic pulse transmitted through concrete, in accordance with ASTM C 597 [12].

Thermal analyses by differential scanning calorimetry (DSC) and microstructural studies by scanning electron microscopy (SEM) were performed after 32 weeks of immersion. The mortar specimens were removed from the solution and stored in acetone for one day in order to stop the hydration. The specimens for DSC were then ground using mortar and pestle and the fraction passing the 75 μm sieve was used for testing. For SEM studies, a 10 mm thick section was cut from the cylindrical specimens using a saw, and this section was then dried at 70 ^{o}C for at least 12 hours. This dried specimen was then impregnated by a low modulus epoxy, inside a cylindrical plastic mold, by evacuating to a low vacuum for two to three hours. The epoxy was then cured in an oven at 70 ^{o}C for at least eight hours. The hardened epoxy polymer was then cut with a fine diamond-tipped saw to expose the cross-section of the specimen. This was followed by grinding of the exposed surface on progressively fine grids. The adequacy of polishing was confirmed after each step using an optical microscope. After polishing, the surface was coated with a layer of gold-palladium. The prepared specimens were then stored in desiccators until testing.

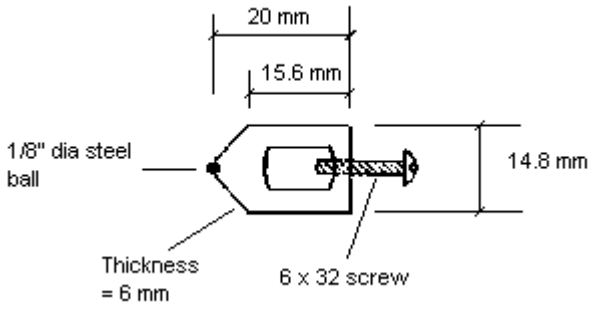

Figure 1. Plastic end pieces for mortar length change specimens [13]

3. RESULTS

3.1. Physical properties

The results of the tests for physical properties are shown in Figures 2 to 5. Each point in the plots represents an average of three measurements. According to the data in Figure 2, the mortar specimens in LW and MC exhibit a small amount of shrinkage, while the specimens in MS show a gradually increasing expansion.

As shown in Figure 3, the specimens in MS exhibit a steady increase in mass with time. On the other hand, the specimens in MC show a rapid increase in mass in the early stage, followed by a slower rate of mass gain. The control specimens in LW also show a slight gain in mass, presumably due to absorption. Compressive strength data, plotted in Figure 4, indicate that the specimens in MS undergo a steady decline in strength with immersion, while the specimens in MC show a rapid drop in strength at the early stages. Dynamic modulus of specimens in MS shows an increase in the early stages, followed by a sharp decline. The behaviour is similar in the case of MC; however, the drop in modulus is not as high as in MS. The control specimens exhibit an increase in modulus at the early stages, and then maintain a steady value.

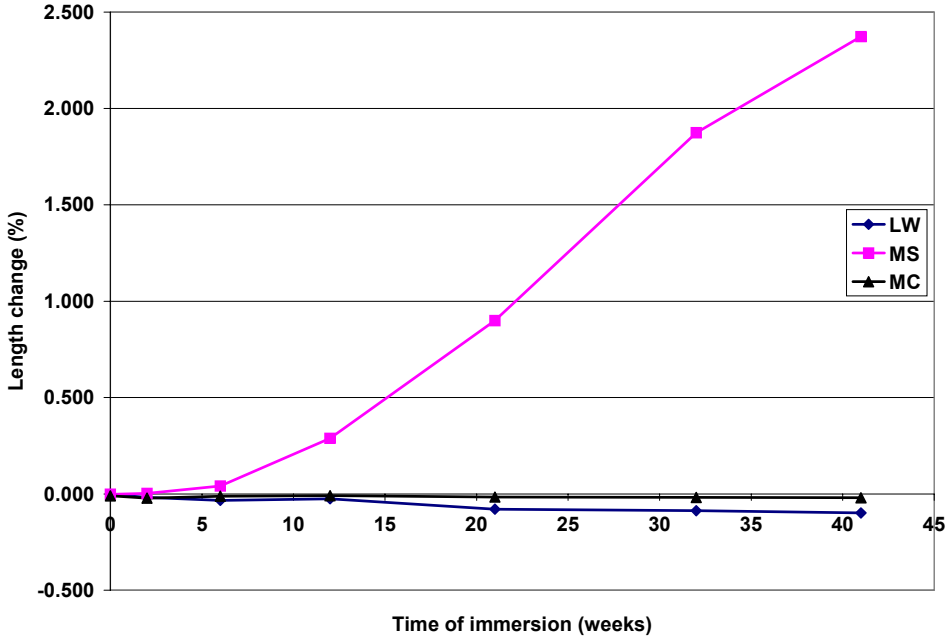

Figure 2. Length change of prismatic mortar specimens

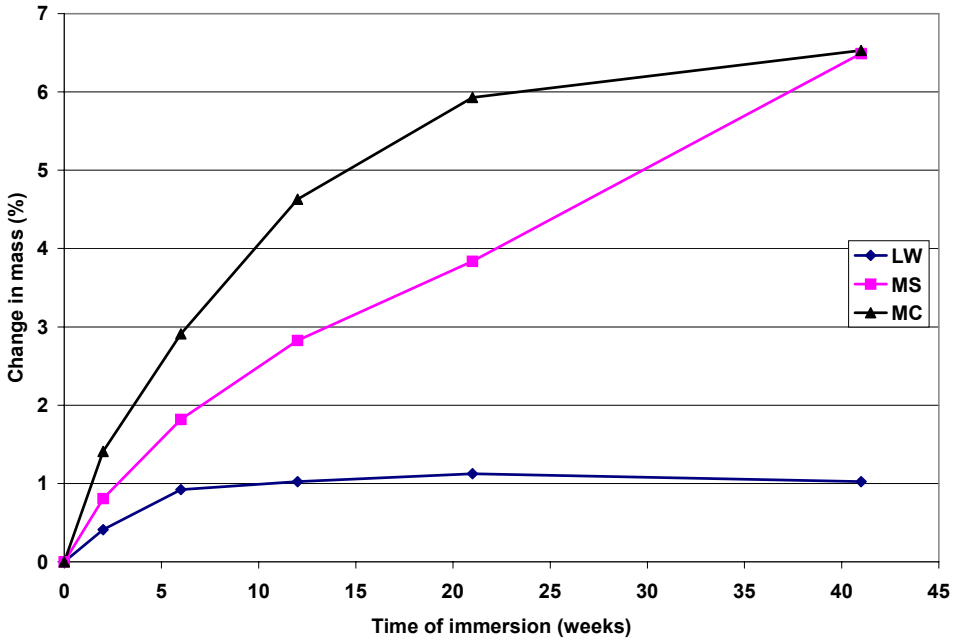

Figure 3. Change in mass of mortar specimens

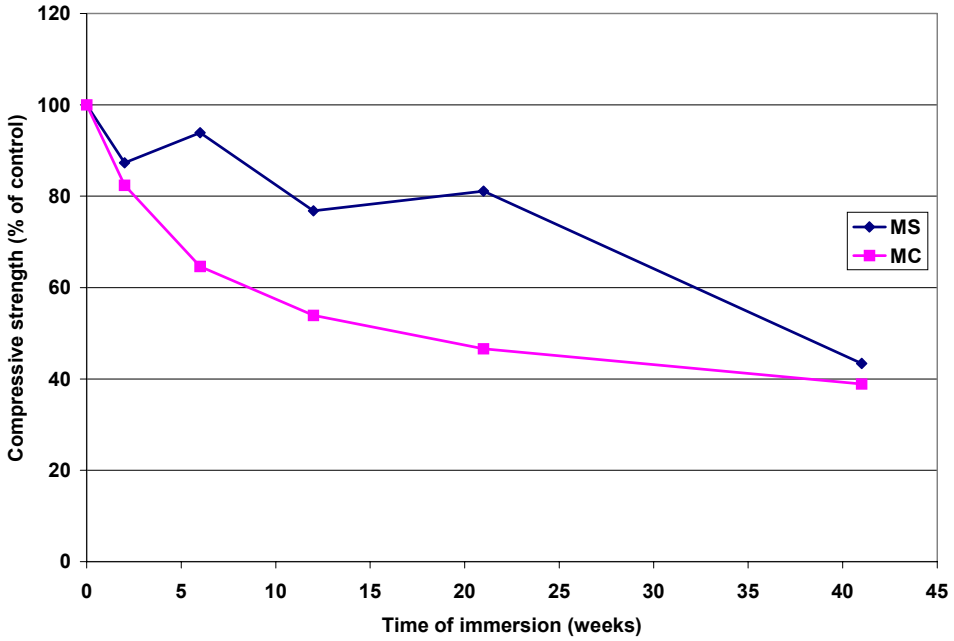

Figure 4. Compressive strength of mortar cubes

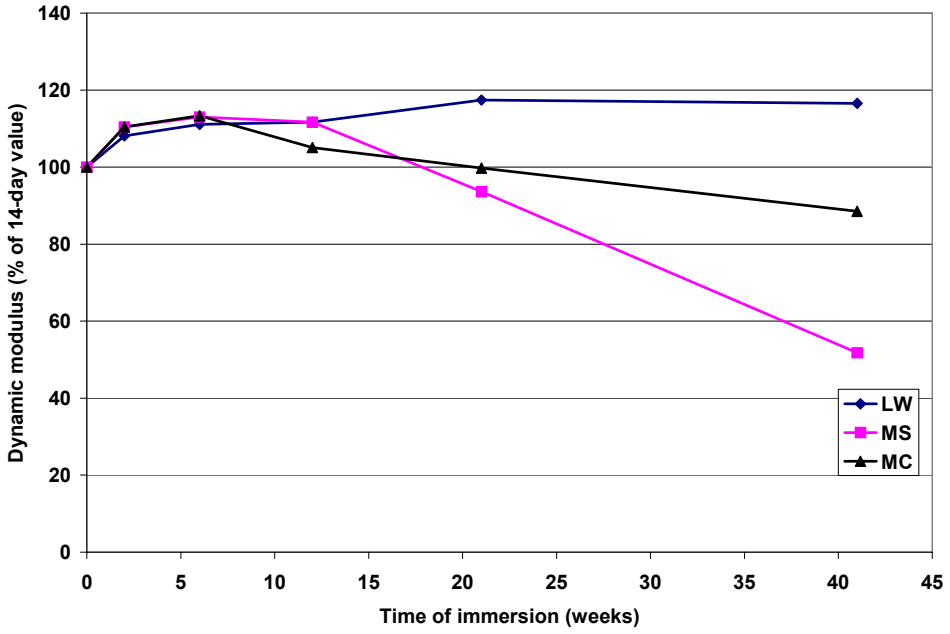

Figure 5. Dynamic modulus by pulse velocity of mortar specimens

3.2. Thermal analysis by DSC

Figures 6 and 7 show the results of the thermal analyses by DSC. The quantities of brucite formed are greater in $MgCl_2$ compared to $MgSO_4$. The high degree of brucite formation in $MgCl_2$ could be a possible explanation for the high initial mass increase observed in these mortars. The quantity of brucite increases steadily, although by a very small degree, in $MgSO_4$. In $MgCl_2$, there is an initial increase followed by a steady decline in the quantity of brucite.

At early ages, the depletion of CH in $MgSO_4$ matches the increase in the quantity of gypsum formed. The quantity of ettringite formed first increases and then decreases with age. The decrease in ettringite could possibly occur as a result of an unfavorable environment (low pH) for ettringite to be stable. The unstable ettringite could also decompose to form secondary gypsum. The high amounts of gypsum forming at later ages (32 weeks) seem to support this argument. Another reason

for the detection of large quantities of gypsum could be the direct attack of the C-S-H by the $MgSO_4$ solution.

Rapid consumption of calcium hydroxide occurs with $MgCl_2$, and no CH is left after 6 weeks of immersion. In $MgSO_4$, the CH becomes depleted only after 32 weeks of immersion.

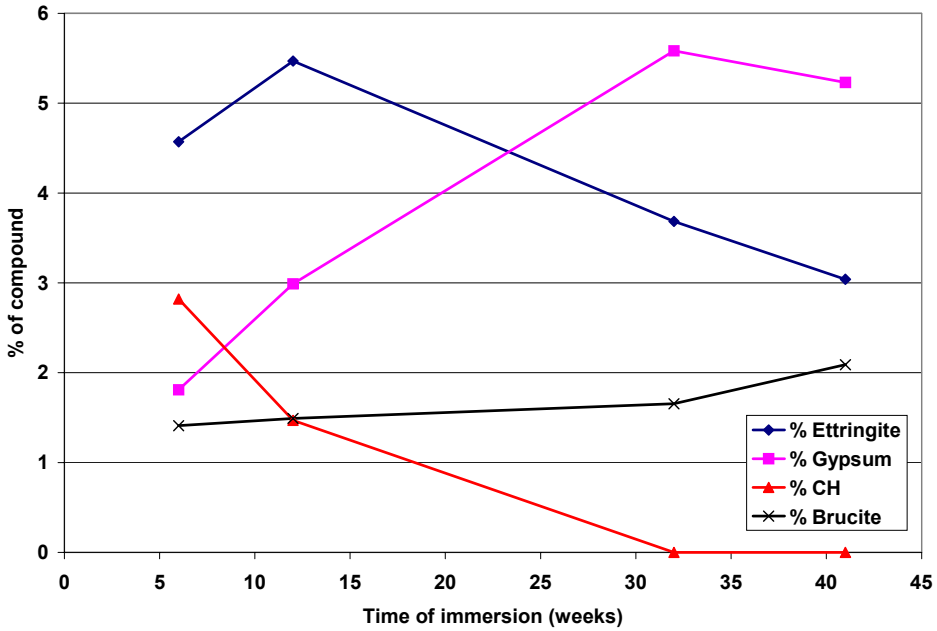

Figure 6. DSC results for PC mortar in magnesium sulfate solution

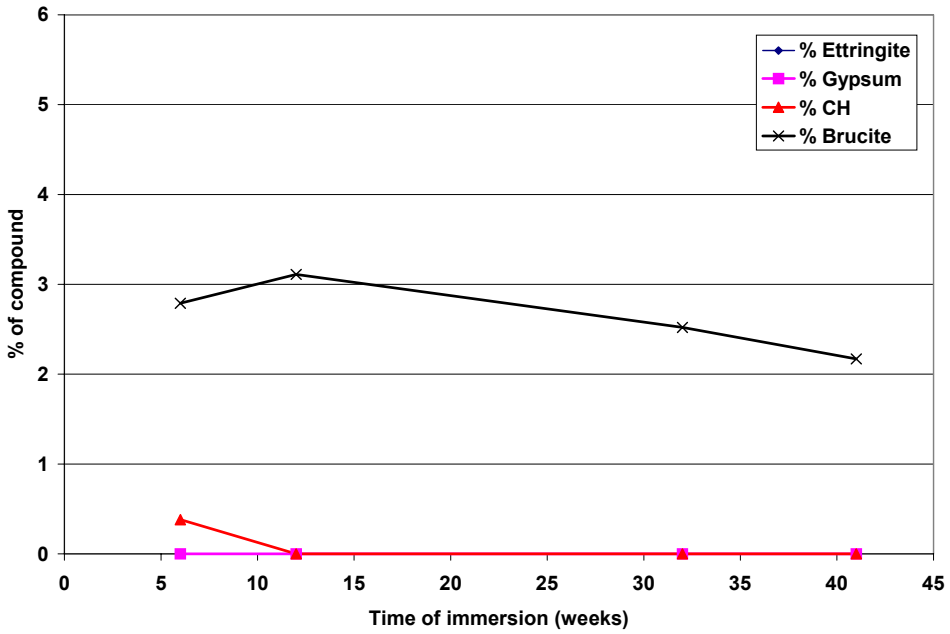

Figure 7. DSC results for PC mortar in magnesium chloride solution

3.3. Microstructural investigations by SEM

The micrographs for PC mortars attacked by $MgSO_4$ and $MgCl_2$ are shown in Figures 8 through 18. Figure 8 shows the micrograph of the PC mortar in $MgSO_4$ after 12 weeks of immersion. From the low magnification image on the left, the mortar does not appear to be damaged except in the near surface regions. The magnified view of a deteriorated surface region on the right side shows the presence of a brucite-gypsum double layer, and the formation of M-S-H. In Figure 9, a micrograph

of the PC mortar immersed for 32 weeks in $MgSO_4$ is shown. The high magnification image on the right represents a region about 500 μm from the surface of the mortar specimen, as shown by the highlighted area on the low magnification image on the left. Gypsum deposits around an aggregate can be observed, and small inclusions of thaumasite (corresponding X-ray spectrum shown at the bottom) are also found.

Figure 10 depicts a region near the surface of the mortar where the C-S-H has been completely transformed to M-S-H. Bands of gypsum are also observed. Thick layers of gypsum and brucite have precipitated underneath this surface region, presumably due to the penetration of the solution through the cracked region. Another region of the paste showing complete conversion to M-S-H has been shown in Figure 11. Figure 12 shows an overview of the mortar attacked by magnesium sulfate. The paste within this near-surface region appears dense, with abundant deposits of gypsum around aggregates and in air voids. Some cracks are also observed around aggregates and in the paste. Figure 13 is a high magnification image of the mortar in $MgSO_4$ showing a dense but cracked microstructure of the paste.

In Figure 14, the surface region of the mortar attacked by magnesium chloride is shown. From the low magnification image on the left, the brucite layer appears more than 100 μm thick. In the high magnification image on the right, a deposit of Friedel's salt can be observed. The paste in this surface region has a porous appearance. An intimate mixture of C-S-H and Friedel's salt is seen in Figure 15. Formation of M-S-H was also detected for the PC mortars in $MgCl_2$, as shown in Figure 16. Figure 17 shows an overview of the surface zone in the PC mortar attacked by $MgCl_2$. The paste in this region appears porous, although there are fewer cracks compared to the mortar in $MgSO_4$. A high magnification image shown in Figure 18 shows the nature of the paste in $MgCl_2$. This paste is marked by the presence of numerous voids resembling Hadley grains, which are the main cause of the porous appearance.

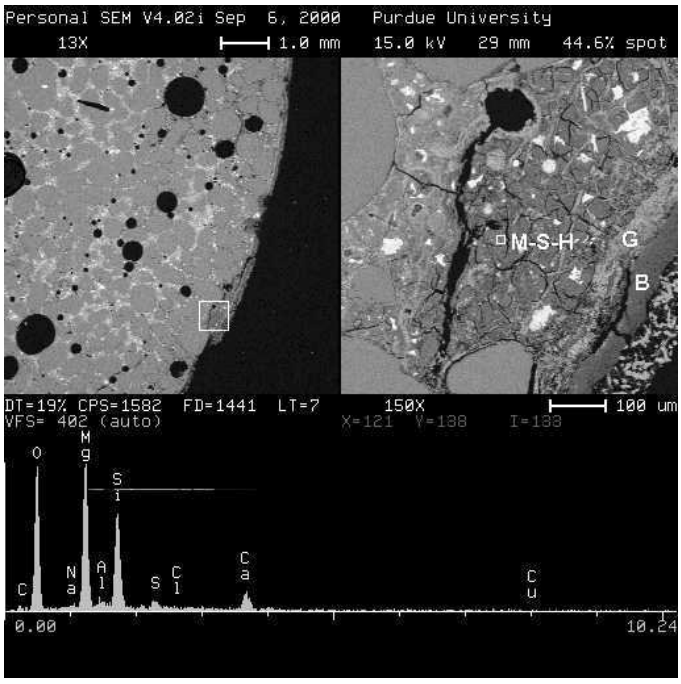

Figure 8. PC mortar after 12 weeks of immersion in $MgSO_4$ solution, showing the brucite-gypsum double layer, and M-S-H

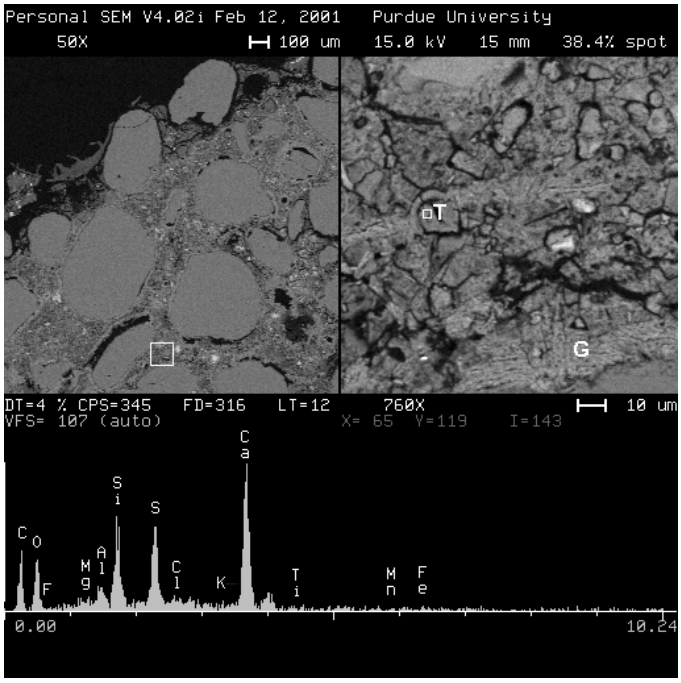

Figure 9. PC mortar in $MgSO_4$ solution after 32 weeks of immersion, showing evidence of thaumasite formation (T) along with abundant gypsum deposits (G)

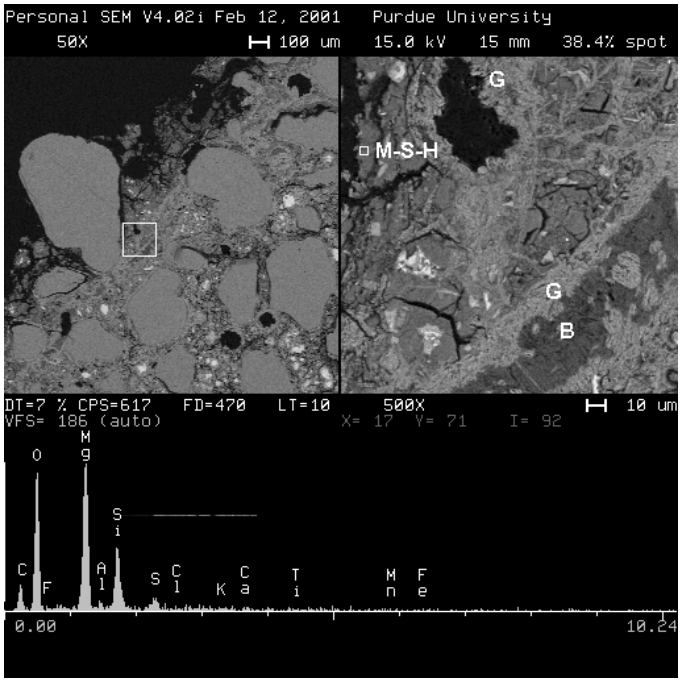

Figure 10. MSH and gypsum bands near the surface of the specimen in $MgSO_4$ solution (A layer of brucite (B) has also precipitated in between the white layers of gypsum)

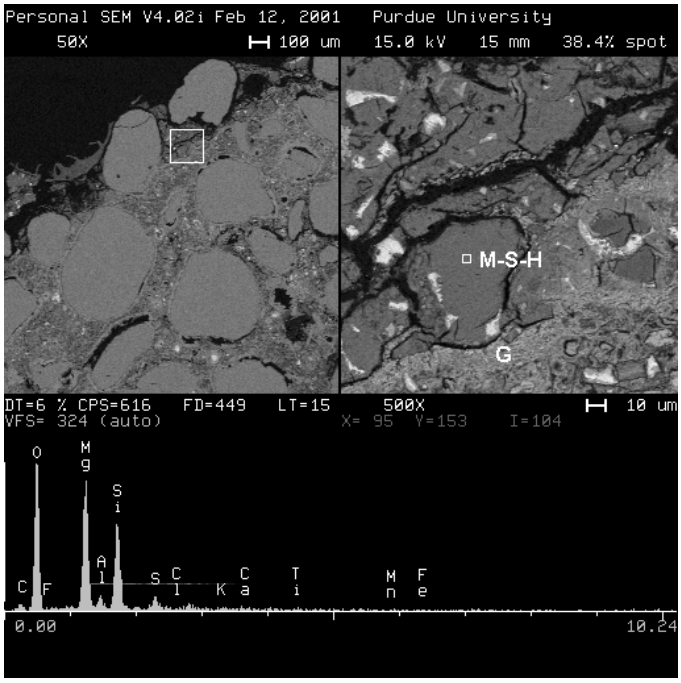

Figure 11. Another view of the deteriorated mortar in $MgSO_4$ solution, showing dark areas of MSH along with bands of gypsum

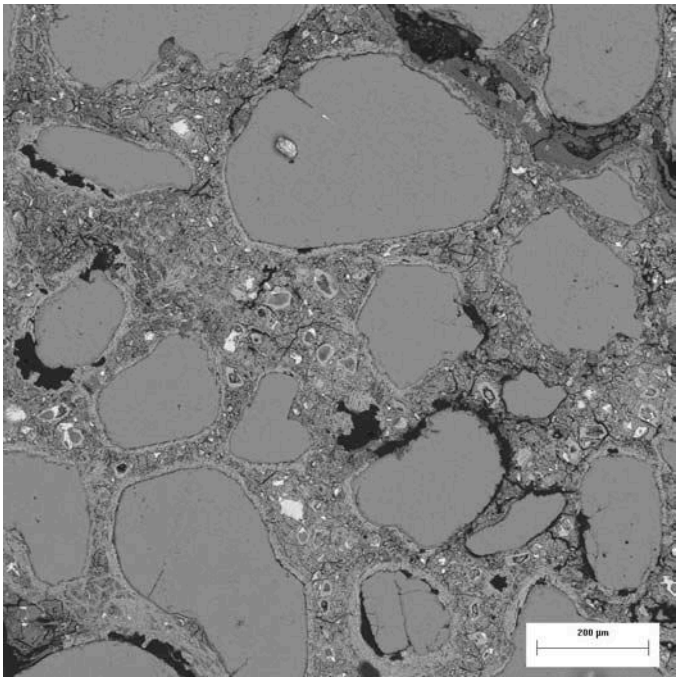

Figure 12. Micrograph showing the dense surface zone full of attack products (primarily gypsum deposits around the aggregates) in the mortar in $MgSO_4$ solution

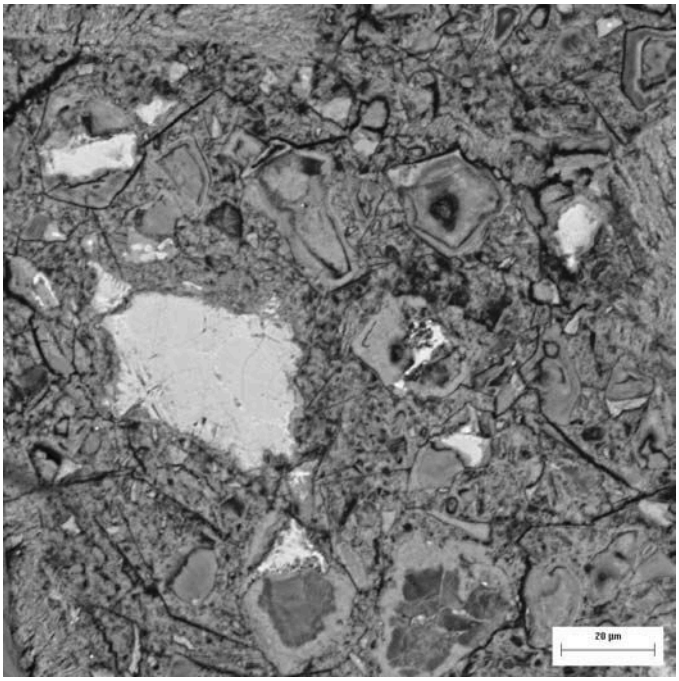

Figure 13. Dense but cracked paste in the mortar in $MgSO_4$ solution showing gypsum deposits

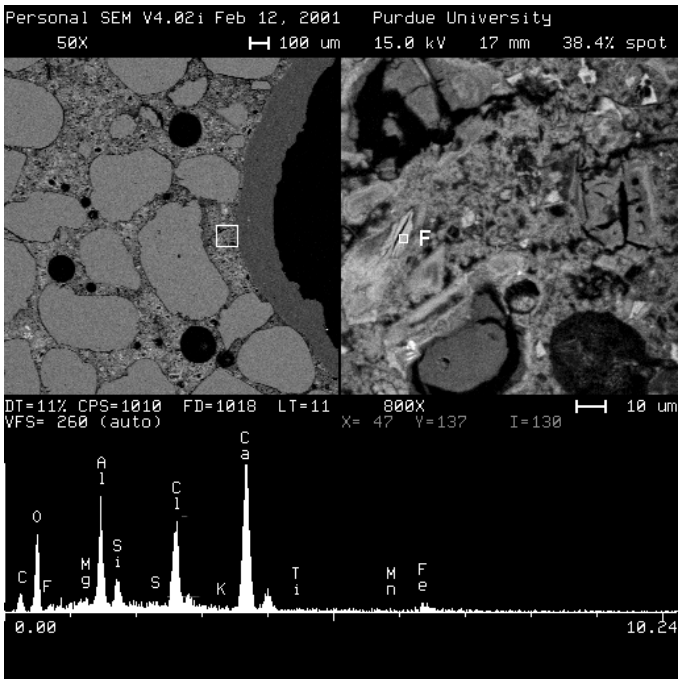

Figure 14. PC mortar stored for 32 weeks in $MgCl_2$ solution, showing a very thick brucite layer on the surface, as well as the formation of chloroaluminate compounds in the paste (F- Friedel's salt)

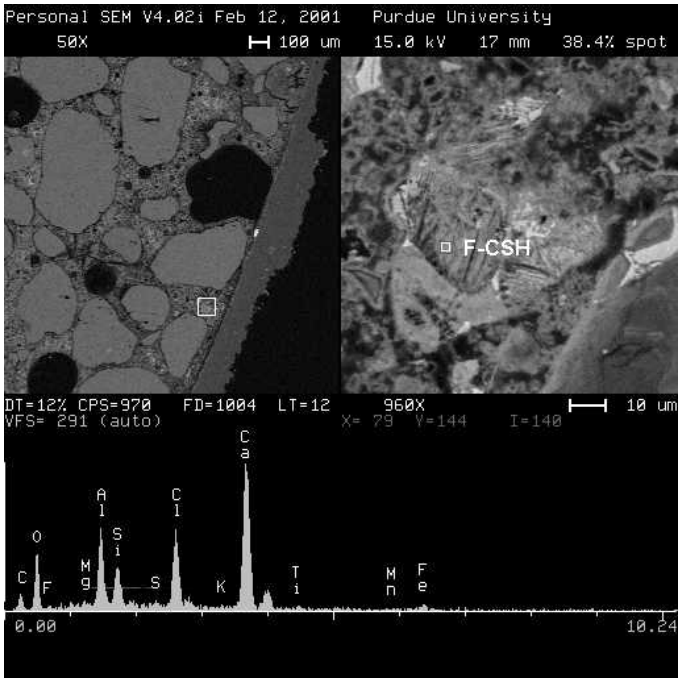

Figure 15. PC mortar stored for 32 weeks in $MgCl_2$ solution, showing an intimate mixture of chloroaluminate (possibly Friedel's salt) and C-S-H

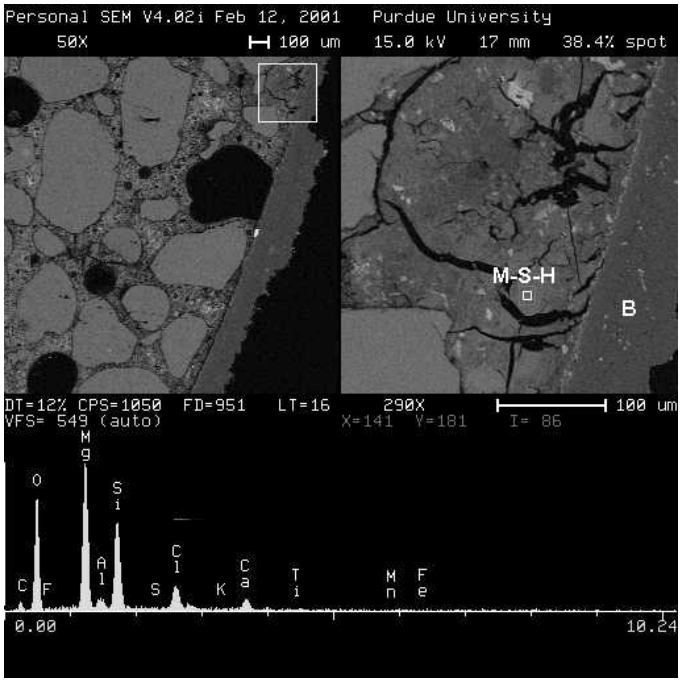

Figure 16. PC mortar stored for 32 weeks in $MgCl_2$ solution, showing the formation of M-S-H under the surface brucite layer

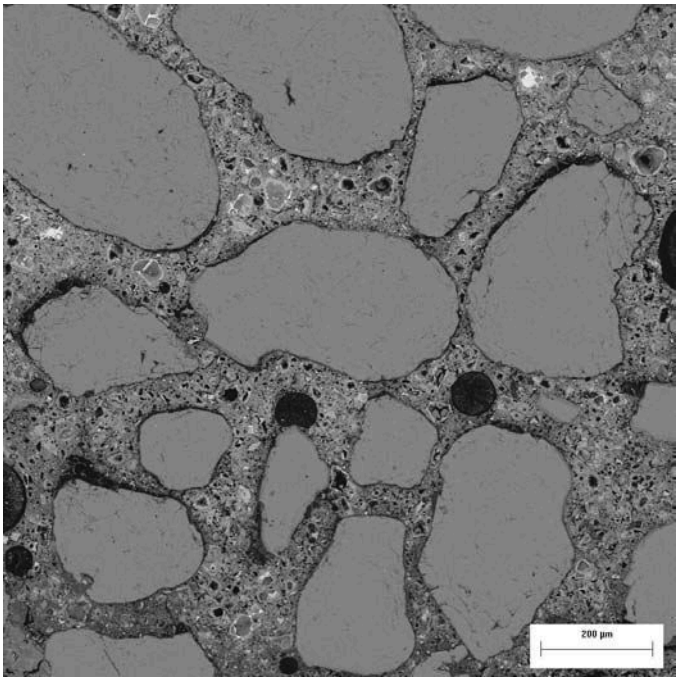

Figure 17. The highly porous surface zone in the mortar in $MgCl_2$ solution

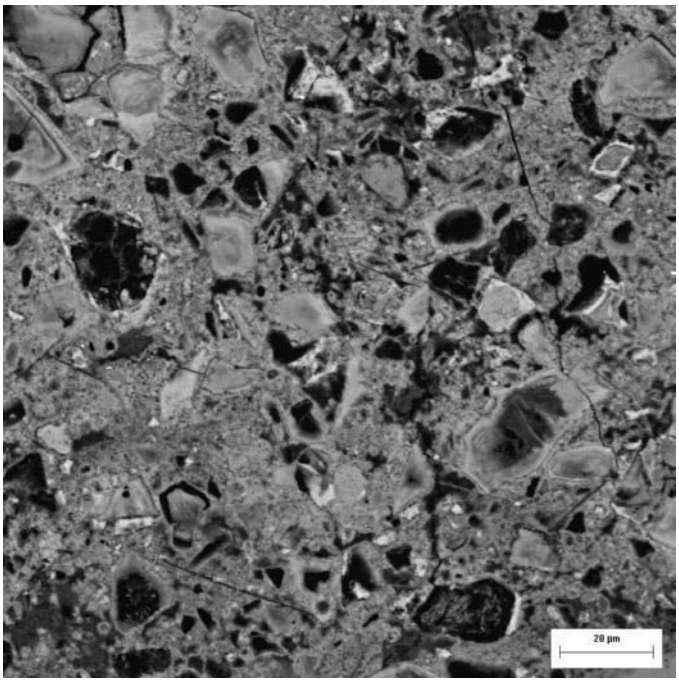

Figure 18. Paste in the mortar in $MgCl_2$ solution showing highly porous regions, which look like fully developed Hadley grains

4. DISCUSSION

The primary difference in the pattern of attack by magnesium sulfate and magnesium chloride is seen in the rates of deterioration. The attack by $MgSO_4$ starts slowly, owing to the limited penetration of the sulfate ions into the mortar because of the formation of a surface layer of brucite. The reaction at this stage becomes diffusion controlled. The sulfate ions diffusing through the brucite layer react with the hydrated cement products to produce gypsum and ettringite. The reduction in pH due to the consumption of calcium hydroxide (CH) can ultimately lead to the decalcification of the C-S-H. The formation of M-S-H occurs when the C-S-H is directly attacked by the magnesium sulfate solution. The brucite layer tends to break down leading to an increased penetration at later ages. This is reflected in the increased rate of attack as seen from the sudden jump in mass, and a sudden drop in the compressive strength seen at later ages with $MgSO_4$ attack. The presence of M-S-H is primarily in those areas within the specimen where the brucite layer is cracked. This implies that the damaging effects of the attack can be delayed considerably if a thick brucite layer is formed.

Cementitious systems having large replacement levels of pozzolans have been reported to perform poorly during magnesium sulfate attack [1, 14]. This can be attributed to the consumption of calcium hydroxide by the pozzolanic reaction. Thus, only small amounts of brucite can form in such systems. This can lead to a quicker direct attack on C-S-H. However, at optimal dosages, the reduced permeability and pore refinement that is obtained by pozzolanic replacement can effectively offset the negative effects of the pozzolanic reaction during magnesium sulfate attack [14].

$MgCl_2$ attack occurs very rapidly at first, but then slows down ultimately. The high quantity of brucite formed in $MgCl_2$ attack, along with the rapid consumption of CH indicates that the primary effect of the Mg ion is to drive the reaction towards brucite formation. The rate of attack, as seen from the mass change and compressive strength measurements, slows down at later ages, possibly because of a decreased formation of brucite. $MgCl_2$ attack depletes the CH very fast to form brucite, and triggers the decalcification of C-S-H, thus rendering the paste porous. Due to the absence of sulfate ions, the only secondary product that forms as a result of decalcification is M-S-H. Because no other secondary products are deposited, the structure is rendered porous, causing a rapid drop in strength at early ages. The chlorides enter into reaction with C_3A to produce chloroaluminate compounds such as Friedel's salt. These chloroaluminate compounds are reported to be similar in appearance to ettringite but do not cause any expansion [5]. Chlorides also get incorporated within the C-S-H. The $CaCl_2$ that is formed as a result of the reaction between $MgCl_2$ and CH is highly soluble and does not precipitate.

5. CONCLUSIONS

Magnesium ion attack of PC mortars was studied by monitoring physical, chemical, and microstructural properties of mortar specimens immersed in magnesium sulfate and magnesium chloride solutions.

The presence of the Mg ion is responsible for the following:

(1) Formation of an insoluble surface layer of brucite on the surface of the mortar specimens that temporarily prevents further ingress of the attacking solution. However, the formation of brucite leads to a rapid consumption of calcium hydroxide. When no secondary products (such as gypsum) are precipitated, the consumption of calcium hydroxide can render the structure porous leading to a rapid drop in strength.
(2) Direct or indirect attack of C-S-H and its subsequent conversion to M-S-H (reported to be non-cementitious) that causes the ultimate degradation of the mortars. In the case of a direct

attack, such as that happening in case of magnesium sulfate solution, the C-S-H is transformed progressively into silica hydrate and M-S-H through reactions with the attacking solution. On the other hand, indirect attack pertains to the situation where decalcification of C-S-H occurs as a result of the prevalent low pH levels (created by the consumption of calcium hydroxide). Subsequent conversion of decalcified C-S-H to M-S-H causes the ultimate failure.

REFERENCES

[1] Cohen, M.D. and Bentur, A., "Durability of Portland Cement - Silica Fume Pastes in Magnesium Sulfate and Sodium Sulfate Solutions", ACI Materials Journal Vol. 85-M3, 1988, pp. 148 - 157.

[2] Brown, P. W., and Badger, S., "The Distributions of Bound Sulfates and Chlorides Subjected to Mixed NaCl, $MgSO_4$, Na_2SO_4 Attack," Cement and Concrete Research Vol. 30, 2000, pp. 1535 – 1542.

[3] Mehta, P.K., Mechanism of Expansion Associated with Ettringite Formation, Cement and Concrete Research Vol. 13, 1983, pp. 401 - 406.

[4] Brown, P. W., and Taylor, H. F. W., The Role of Ettringite in External Sulfate Attack, Material Science of Concrete - Sulfate Attack Mechanisms, J. Skalny and J. Marchand, Eds., American Ceramic Society, Westerville, OH, 1999, pp. 73 - 98.

[5] Verbeck, G. J., Mechanisms of Corrosion of Steel in Concrete, Corrosion of Metals in Concrete, ACI Publication SP-49, 1975, pp. 21 – 38.

[6] Bonen, D., "Composition and Appearance of Magnesium Silicate Hydrate and its Relation to Deterioration of Cement Based Materials," Journal of the American Ceramic Society Vol. 75, No. 10, 1992, pp. 2904 – 2906.

[7] Bonen, D., and Cohen M.D., "Magnesium Sulfate Attack on Portland Cement Paste – I. Microstructural Analysis," Cement and Concrete Research Vol. 22, 1992, pp. 169 - 180.

[8] Gollop, R. S. and Taylor, H. F. W., Microstructural and Microanalytical Studies of Sulfate Attack: I. Ordinary Portland Cement Paste, Cement and Concrete Research Vol. 22, 1992, pp. 1027 - 1038.

[9] Diamond, S., and Lee, R. J., "Microstructural Alterations Associated with Sulfate Attack in Permeable Concretes," Material Science of Concrete - Sulfate Attack Mechanisms, J. Skalny and J. Marchand, Eds., American Ceramic Society, Westerville, OH, 1999, pp. 123 – 173.

[10] Moukwa, M., Characteristics of the Attack of Cement Paste by $MgSO_4$ and $MgCl_2$ from the Pore Structure Measurements, Cement and Concrete Research, Vol. 20, 1990, pp. 148 – 158.

[11] ASTM Standard Designation C 109, Test Method for Compressive Strength of Hydraulic Cement Mortars, The American Society of Testing and Materials, 1995.

[12] ASTM Standard Designation C 597, Test Method for Pulse Velocity Through Concrete, The American Society of Testing and Materials, 1995.

[13] Kerdegari, A., The Role of Gypsum in Portland Cement and Expansive Cements, Ph.D. Dissertation, Department of Civil Engineering, Stanford University, Stanford, CA, September 1978.

[14] Santhanam, M., Studies on Sulfate Attack: Mechanisms, Test Methods, and Modeling, Ph.D. Dissertation, School of Civil Engineering, Purdue University, W. Lafayette, IN, August 2001.

STUDY OF MAGNESIUM ION ATTACK IN PORTLAND CEMENT MORTARS

Manu Santhanam[1], Menashi Cohen[2], and Jan Olek[3]

[1] Department of Civil Engineering, IIT Madras, Chennai, India – 600036;
E-mail: manu@civil.iitm.ernet.in
[2] School of Civil Engineering, Purdue University, W. Lafayette, IN 47907, USA;
E-mail: mcohen@ecn.purdue.edu
[2] School of Civil Engineering, Purdue University, W. Lafayette, IN 47907, USA;
E-mail: olek@ecn.purdue.edu

Manu Santhanam

Education
Ph.D., Purdue University, August 2001
Thesis Title: Studies on Sulphate Attack: Mechanisms, Testing Methods, and Modeling

M.S. in Civil Engineering, Purdue University, May 1996
Thesis Title: Influence of Slag and Mineral Admixtures on Sulphate Resistance of Cement Mortars

B. Tech in Civil Engineering, IIT Chennai (Madras), July 1994
Senior Project: Design and Testing of High Strength Concrete

Teaching Experience

October 2001 – present:	Visiting Faculty, IIT Madras
June 2001 – August 2001:	Instructor, Purdue University
January 1999 – May 2001:	Teaching Assistant, Purdue University
August 1994 – May 1996:	Teaching Assistant, Purdue University

Work Experience

May 1996 – December 1998:	Senior Research and Development Chemist, Chemical Admixtures, Sika Corporation

Research Interests
- Chemical and mineral admixtures in concrete – optimization of mix designs and procedures, new product development
- Self Compacting concrete – rheology
- High performance concrete – production, quality assurance
- Durability – corrosion and chemical attack on concrete
- Repair and rehabilitation methods
- Non-destructive testing techniques – Ultrasonics, imaging
- Microanalytical investigations – X-ray diffraction, Scanning electron microscopy, thermal analysis by Differential Scanning Calorimetry
- Forensic analysis of material-related failures

Publications available on request.

ALKALI-ACTIVATED FLY ASH GEOPOLYMERIC MATERIALS

František Škvára, Jan Šlosar, Jan Bohunek and Alena Marková

Department of Glass and Ceramics, ICT Prague
CZ-166 28 Prague 6, Technická 5, Czech Republic.
E-mail: skvaraf@vscht.cz

ABSTRACT

Alkaline activation of fly ash yields materials whose strength exceeds that of standard Portland cements. Alkaline activation (AA) of fly ash in aqueous medium at pH>12, when the material sets and hardens, is a process differing from hydration of inorganic binders such as Portland cement. In the former process (mostly taking place by the "through solution" mechanism) the atoms of Al (and probably also those of Ca) penetrate the originally silicate lattice of fly ash, producing a 2D-3D inorganic hydrated polymer (geopolymer) having the general formula $M_n[-(Si-O)_z-Al-O]_n.wH_2O$. The hydration products of alkali-activated fly ash are amorphous in character, with prevailing $Q^4(2Al)$ arrangement and minority crystalline phases. The properties of alkali-activated fly ash depend on the way of preparing the mix, in particular on the concentration of the alkaline activator and on ambient moisture conditions. The optimum conditions were attained by curing at 60 – 90°C in open atmosphere. Additions of blast-furnace slag to alkali-activated mixes bring about significant increases in strength (more than 150 MPa in compression) under hydrothermal conditions at 60 – 90°C when also the C-S-H phase is formed apart from the geopolymeric one. Materials based on AA fly ash can be characterized as "chemically bonded ceramics", or as geopolymers, or as low-temperature hydrated aluminosilicate glasses.

Key words: Fly ash, geopolymer, high strength, new materials

1. INTRODUCTION

Slag-alkali cements[1,2], alkali-activated gypsum-free cement [3], cements of the Pyrament [4] type or geopolymeric binders [5,6,7] are new types of inorganic binding agents whose common feature is alkaline activation of clinker or substances with latent hydraulic properties, such as slag or fly ash. The effect of solutions of alkaline compounds (such as NaOH, Na_2CO_3 or Na_2SiO_3) on hydraulically active substances consists of disrupting the Si-O-Si bonds and producing hydrates of alkali-lime aluminosilicates similar to zeolites, and hydrates of the type C-S-H phase, gehlenite hydrate and hydrogarnates. Alkali-activated binders provide the possibility of utilizing waste materials, because the properties of materials based on alkali-activated binders are often superior to those of concrete and mortar prepared from standard Portland cement. The presence of zeolite-type substances is responsible for modifying the properties of the alkali-activated binders, for instance by increasing their resistance to acids [8] or improving their ability to immobilise heavy metals [9,10].

The literature presents relatively little information on binders based on alkali-activated fly ash. However, the results published recently [11,12,13] show that alkaline activation is also applicable to materials such as fly ash, similarly to the case of blast-furnace slag.

The Czech Republic produces annually more than 10 million tons of fly ash. Some of it is utilized as an additive to cements and concrete, but the majority is disposed of on dumps (for instance in a mixture with waste gypsum). For this reason we have been dealing with other possibilities of using waste power station fly ash, and with the development of new materials based on alkali-activated fly ash.

The present study is concerned with the effect of alkaline activators of the type NaOH and Na_2SiO_3 on aqueous suspensions of fly ash, also in the presence of ground granulated blast-furnace slag.

2. EXPERIMENTAL

The raw materials employed in the study were power station fly ash and granulated blast-furnace slag. Their chemical compositions are given in Table 1.

Table 1.

wt.%	SiO_2	Al_2O_3	Fe_2O_3	CaO	MgO	SO_3	K_2O	Na_2O	TiO_2	P_2O_5	Combustible substances
Slag	40.46	7.31	0.25	41.93	6.82	0.95	0.63	0.41	0.19		
Fly ash	53.79	32.97	5.51	1.84	0.92	0.46	1.76	0.37	2.1	0.15	0.74

In the experiments, use was made of non-ground fly ash with a specific surface area of 210 m^2/kg (Blaine), and of fly ash samples ground to a specific surface area of 450 - 600 m^2/kg. The slag was ground to a surface area of 350 m^2/kg and 520 m^2/kg respectively. The binder was prepared by mixing the fly ash and the slag in proportions over the range from 100 to 5 wt.% fly ash and from 0 to 95 wt% slag. The alkaline activator was added in the form of solution to the dry mixture of fly ash and slag. The SiO_2/Na_2O ratio (module M_S) of the alkaline activator was adjusted by adding NaOH to water glass having the module $M_S = 1.68$ so as to obtain values over the range of $M_S = 0.6$ - 1.6. The water glass employed had the composition 25.98% SiO_2, 15.49% Na_2O a 58.53% H_2O. The total concentration of the alkaline activator was varied over the range of 4 to 10% Na_2O of the binder weight. The pastes prepared in the experiments had mostly a w of 0.30 (w = weight of H_2O /weight of fly ash+ slag).

The binder pastes were moulded into specimens 20x20x20 mm in size, which were kept for 24 hours in an environment of 95% relative humidity and then unmoulded. The subsequent curing was carried out under various conditions of temperature and relative humidity. The “moisture cured” specimens were kept in an environment of 95% R.H. up to the time of compressive strength testing. Some specimens was subjected to “hydrothermal curing”, namely after the 24 hours of curing at 95% R.H. they were heated up to 60°C during 1 hour, up to 40 – 90°C during 2 hours and kept at the respective temperatures for an additional 4 hours. In the course of the hydrothermal curing process the specimens were kept in an enclosed space where the water vapour pressure corresponded to the respective temperature. Following this hydrothermal treatment the specimens were kept at 20°C and 40-50% R.H. up to the term of strength testing. The remaining part of the specimens were exposed to “dry curing”, when following their preparation they were placed in a drying oven at a temperature of 60 – 90°C (in open atmosphere) for 4 to 24 hours and then kept in air at 40 – 50% R.H. up to the time of testing. The compressive strength was tested after 2, 7 and 28 days. The fragments from the compressive strength tests were studied by X-ray diffraction, FTIR and thermal analysis and by high-pressure mercury porosimetry. The NMR MAS spectra (^{29}Si, ^{27}Al) were also measured. The microstructure was studied on fracture surfaces by the scanning electron microscope, and ED spectrometric analysis was carried out at selected points.

2.1 Results and Discussion

It may be generally said that the strength of alkali-activated (hereinafter AA) fly ash is influenced by the M_S modulus and the concentration of Na_2O in the alkaline activator, where the optimum performance was achieved at Na_2O concentration of 7 to 10% and at M_S of 0.6 to 1. The curing conditions are the dominant factor controlling the strength of AA fly ash. The initial strength of the AA fly ash system (for "moist curing" at 25°C) is very low and essentially independent of Na_2O concentration and the M_S module. The 28-day strength of the systems after curing at 20°C is also relatively low. A considerable increase in strength of the AA fly ash system was due to hydrothermal curing. The "dry curing" brought about a significant increase in strength (Figure 1) when the 24-hour strength exceeded the 28-day strength of standard Portland cement.

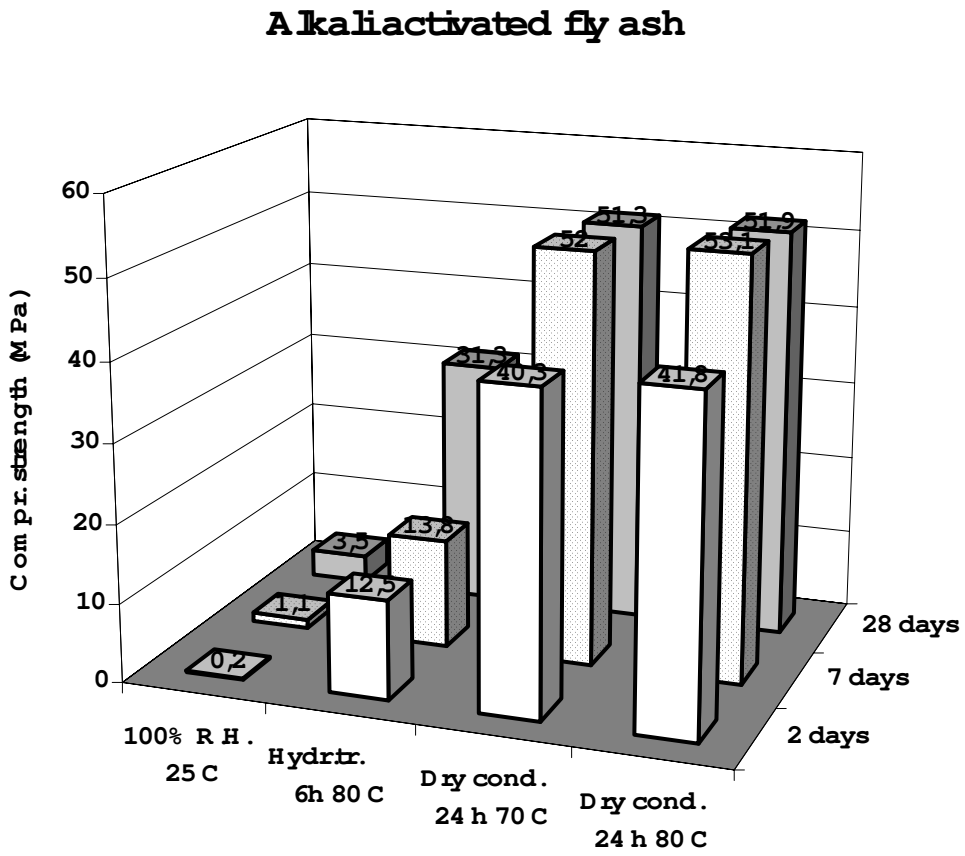

Figure 1. Compressive strength of alkali activated fly ash.

A very rapid increase in strength was found with mixes containing 50 – 70% fly ash and 50 – 30% slag, cured under hydrothermal conditions (Figure 2). However, relatively low strengths were achieved with systems of AA fly ash and slag under "dry curing conditions". Under "hydrothermal conditions of curing" the effect of grinding fineness of slag and fly ash was significant. With the system composed of 50% fly ash and 50% slag, 28-day strengths of up to 170 MPa were achieved by hydrothermal curing. These strengths are comparable to those of the new bonding materials (DSP materials 120 to 130 MPa, MDF materials 100 – 300 MPa).

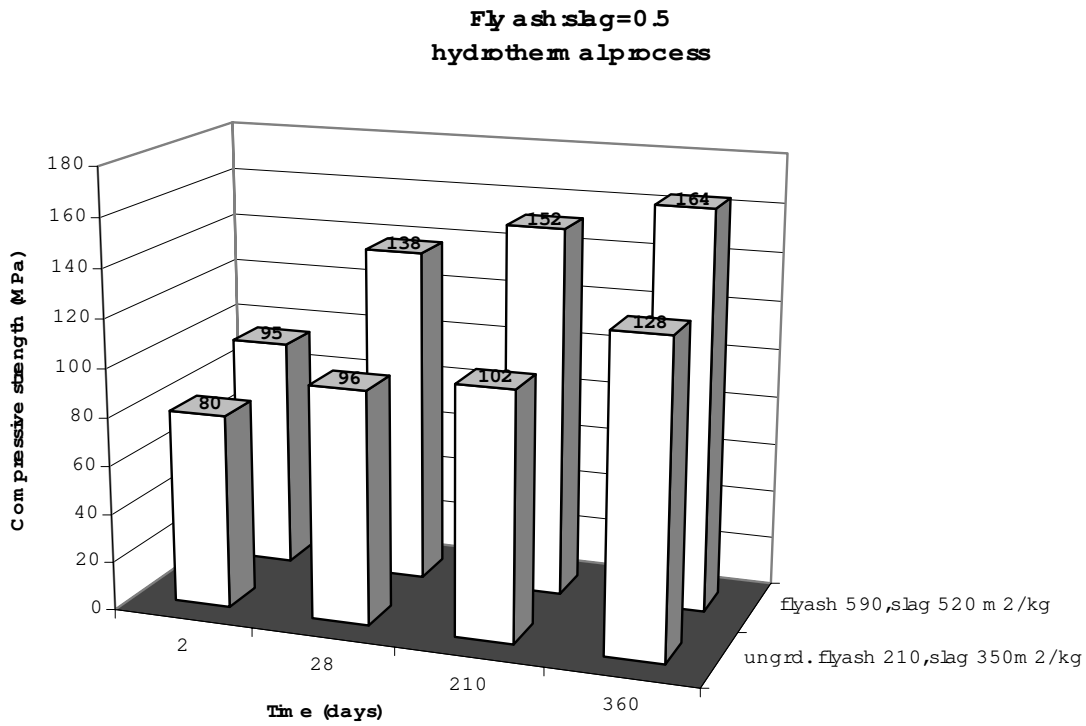

Figure 2. Compressive strength of alkali activated fly ash with slag.

The information obtained on the properties of the systems being studied indicates that the principle of alkaline activation is likewise applicable to power station fly ash. However, the formation of hydrates by alkaline activation of mixes comprising 100% fly ash is distinctly slower under both moisture and hydrothermal curing conditions than in the case of slag. Under the conditions of alkaline activation, the higher content of CaO in slag compared to fly ash obviously contributes to faster formation of bonding hydrates, particularly zeolite-like substances.

The basic hydration products in alkali-activated materials were identified in specimens hydrated at 20^{o}C, in those cured under hydrothermal conditions, and in specimens first treated by “dry curing” and subsequently moisture-cured for additional 28 days.

The X-ray diffraction patterns (Figure 3) show that the hydration products are mostly of X-ray amorphous character, where the sole diffraction (apart from that of mullite and quartz from the original material) is that of d = 0.304 nm, and that only in the systems with a high content of slag. This line obviously corresponds to the C-S-H phase formed. The results of thermal analysis (Figure 4) likewise indicate the presence of hydrated amorphous (gel-like) products, showing a continuous loss of H_2O in terms of temperature. The loss in weight of the products is listed in Table 2.

Table 2.

Curing conditions	Δm (%)	
	20-200 ^{o}C	200-600 ^{o}C
Dry conditions	8.21	2.53
Hydrothermal curing	8.56	2.68

The TA data show that the H_2O content in the products is virtually identical regardless of the conditions of curing.

Regardless of the curing conditions, the basic matter of the hydrates is positively of amorphous glassy character, only rarely containing acicular minority formations (Figures 5, 6). The results of ED spectrometer analyses of the fracture surfaces show that most of the hydrates are sodium

aluminosilicate ones. The minority of hydrates are probably composed of polymerized water glass in which Al was partially substituted for Ca.

The hydrates contain residues of the original fly ash particles on which the effects of gradual dissolution are apparent. The AA fly ash was found to exhibit a relatively high porosity (of up to 50%) regardless of the curing conditions. The material contains closed spherical pores formed by dissolution of the original ash particles and possibly by air entrapped during the preparation. A distinctly lower porosity is shown by the AA fly ash–slag mixes, where the total porosity amounted to 2-10% and there was a shift towards smaller pore sizes (Figure 7 vs. Figure 8).

On FTIR spectra (Figure 9) one can find the differences due to different conditions of alkaline activation. The band corresponding to Si-O and Al-O vibrations [14,15] of the original fly ash at 1080-1090 cm^{-1} is shifted towards lower values by alkaline activation. This shift is explained as a result of incorporation of aluminium into the original structure of the Si-O-Si lattice, similarly as has been found in the case of zeolites [18] . The more distinct the shift, the higher degree of aluminium penetration from the original mullite into the $[SiO_4]^{4-}$ lattice.

Analogous results have been obtained by NMR measurements of AA fly ash in solid phase. Table 3 presents evaluation ^{29}Si MAS NMR spectra (deconvulence of the spectra obtained).

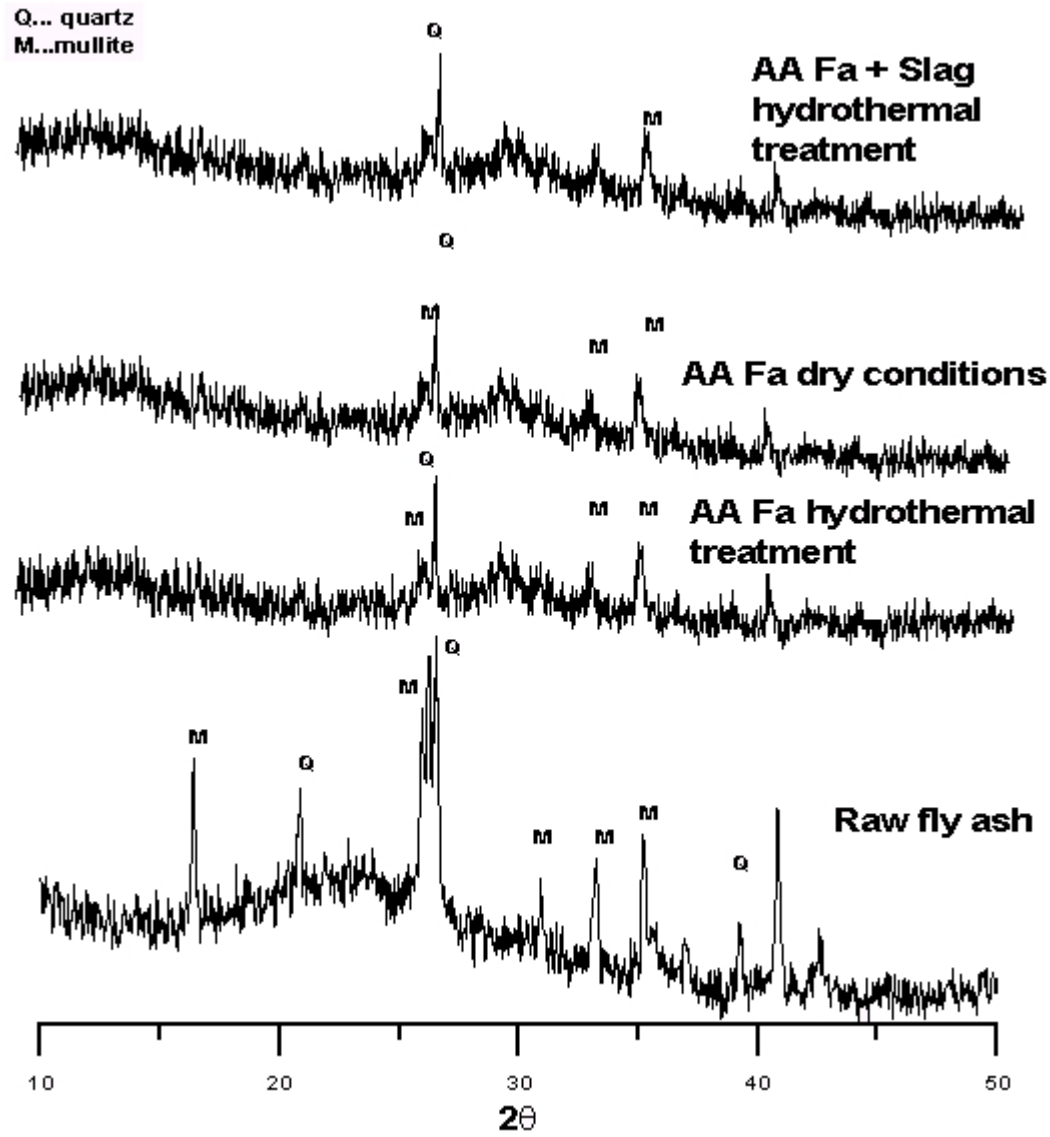

Figure 3. X-ray spectrum of alkali activated materials.

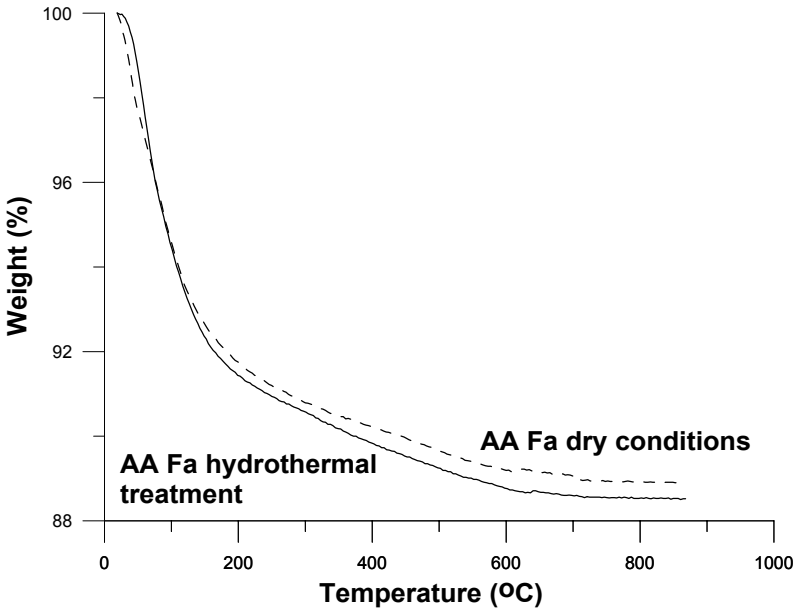

Figure 4. TG analysis of alkali activated fly ash.

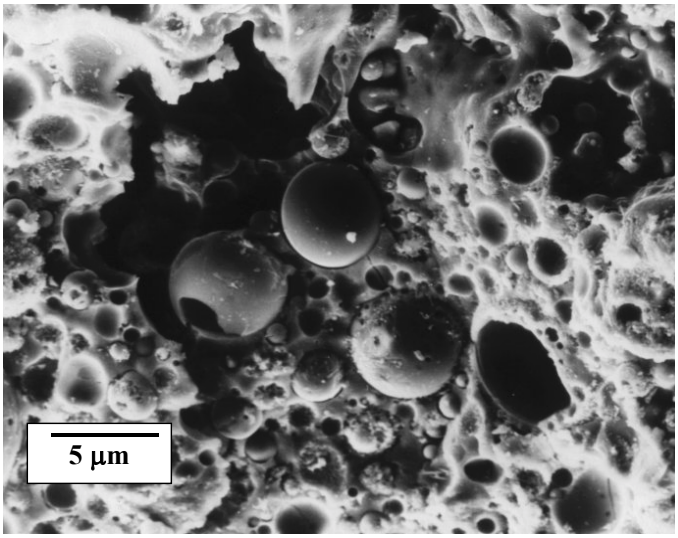

Figure 5. Microstructure of alkali activated fly ash.

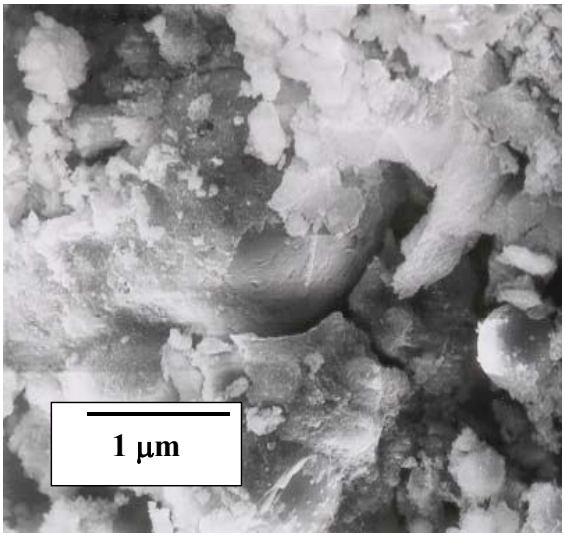

Figure 6. Microstructure of alkali activated fly ash (detail).

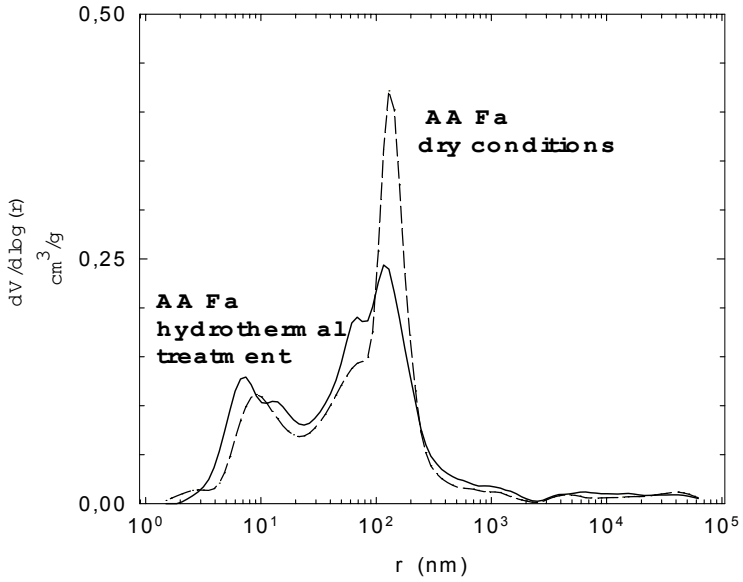

Figure 7. Pore size distribution of alkali activated fly ash.

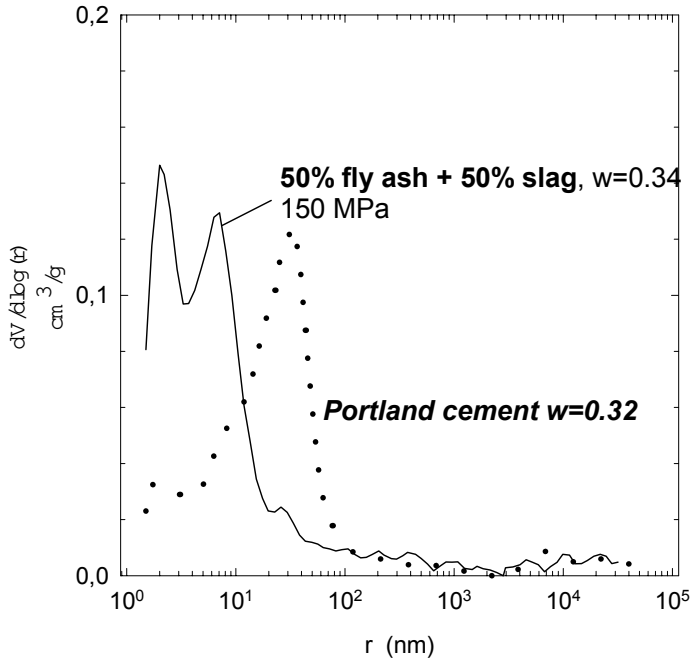

Figure 8. Pore size distribution of alkali activated fly ash with slag.

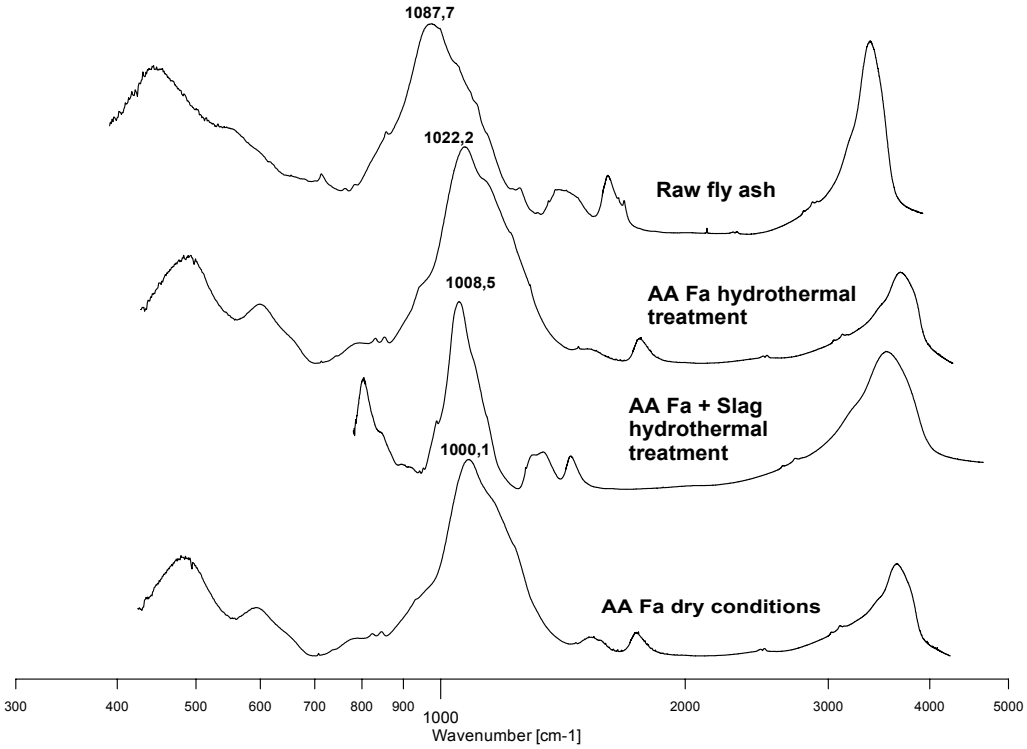

Figure 9. Infrared spectrum of alkali activated materials.

Table 3. Evaluation of ^{29}Si MAS NMR spectra

Co-ordination Si,Al [16,17]	Si(4Al)	Si(3Al,1Si)	Si(2Al,2Si)	Si(0Al)	
Raw fly ash	-79.1 8%	-87.6 23%	-95.8 8%	-107.4 61%	shift (ppm) % in spectrum
AA fly ash hydrothermal curing		-88.5 40%	-96.2 23%	-107.3 32%	
AA fly ash dry curing		-90.1 52%	-98.7 17%	-106.0 28%	
AA fly ash + slag	-81.2 6%	-90.4 51%	-98.9 16%	-104.9 25%	

The deconvolution yielded signals with a very close value of the shift and with various representations in percent. The majority signal of the original fly ash was attributed to tetrahedral $[SiO_4]^{4-}$ (Si(0Al)); the co-ordination Si(2-3Al), also established for this spectrum, probably corresponds to the mullitic phase. A sample of AA fly ash that underwent hydrothermal curing exhibited a quite different structure. The Si(OAl) was eliminated down to 5% (in contrast to 61% in the fly ash), new formations appear in the structure, co-ordination Si(4Al) has a representation of 40% and the content of Si(4Al) was more than 50%. This shift is still more distinct with the sample of AA fly ash cured under "dry conditions". In this case more than 50% of the bonds show Si(4Al) co-ordination and the rest the Si(2-3Al) co-ordination. The ^{27}Al spectra are almost identical, which confirms the similarity of the two materials, where the only difference arises in the signal intensity of about 10 ppm (beyond the framework of the experimental error).

Alkaline activation of fly ash in an aqueous medium at pH >12, which causes the material to set and harden, differs from the processes of hydration of inorganic binders, for example of Portland cement. The former process obviously proceeds by the "through solution" mechanism where the fly

ash particles (SiO_2 and mullite) first dissolve in the strongly alkaline medium and a new geopolymeric structure is formed from the solution. A 2D-3D inorganic hydrated polymer (geopolymer) having the general formula $M_n[-(Si-O)_z-Al-O]_n.wH_2O$ is produced. An elevated temperature of 40 to 95°C is necessary for establishing an adequately interconnected lattice of bonds in the geopolymer. A significant part is played by the moisture conditions, where "hydrothermal curing" yields lower strengths than the "dry curing" conditions. According to the FTIR and NMR results, the "dry curing" causes more Al atoms to become incorporated in the originally silicate lattice of fly ash and to create a more interconnected lattice structure of the geopolymer. According to the results of TA the water content is virtually the same after heating up in open atmosphere and after hydrothermal curing. However, it is possible that the small loss of H_2O due to heating in open atmosphere ("dry curing" conditions) affects positively the process of incorporation of Al atoms and the degree of higher interconnection of the structure.

On the other hand, the hydrothermal curing conditions are optimal in the presence of another hydraulically active substance, namely the slag. In that case the strengths achieved by "dry curing" conditions are distinctly lower (by 30-50%). Under hydrothermal curing and alkaline activation conditions, blast-furnace slag is even capable of forming additional hydrates of type CSH and CAH phases that can contribute to higher strength.

The materials based on alkali-activated substances exhibiting latent hydraulic properties (fly ash, slag) obviously belong among the materials which, due to their high strengths and prevailingly amorphous structure, constitute a transition between the classical inorganic binders and ceramics, and can be affiliated to the group called "chemically bonded ceramics". The materials based on AA fly ash can be characterized as an inorganic polymer similar to zeolitic precursors. The materials can also be described as low-temperature hydrated aluminosilicate glasses.

It should be emphasized that the materials of the type of "chemically bonded ceramics", such as the MDF or DSP modifications, are frequently prepared by special methods such as isostatic pressing, vacuum compaction, etc. In contrast to this, in our experiments the materials based on chemically activated substances with latent hydraulic properties were prepared by standard methods, have acceptable rheological properties and acceptable times of early set.

3. CONCLUSIONS

The products of hydration of alkali-activated fly ash are of amorphous character and contain minority crystalline phases. The FTIR demonstrates the difference between the non-hydrated and the alkali-activated fly ash, where the main band corresponding to SiO and AlO vibrations is shifted towards the lower values. In the Si^{29} MAS NHR spectrum, the hydration products of alkali-activated fly ash exhibit a three-dimensional glassy structure with prevailing $Q^4(2Al)$ arrangement. Alkaline activation brings about penetration of Al atoms into the original silicate network of fly ash.

The properties of alkali-activated fly ash depend on the way the mix has been prepared and treated, particularly on the concentration of the alkaline activator and on moisture conditions. The optimum results were obtained under the "dry curing conditions".

Considerable increases in strength were obtained when blast-furnace slag was added to mixes of alkali-activated slag. "Hydrothermal curing" has proved as being the optimum one for these mixes, as apart from the geopolymeric phase, also C-S-H phases are formed under these conditions, with the resulting compressive strength of more than 150 MPa.

The alkali-activated binders provide the possibility of utilizing waste inorganic materials, and the properties of the resulting binders often surpass those of standard Portland cement. The materials

based on AA fly ash can be characterized as “chemically bonded ceramics”, or as geopolymers, or as low-temperature hydrated aluminosilicate glasses.

ACKNOWLEDGMENTS

This study was a part of the research project CEZ:MSM 223100002: Preparation and properties of modern materials, modelling, characterisation, technology.

The authors should like to thank Dr. J. Brus (Institute of Macromolecular Chemistry, Academy of Sciences of the Czech Republic) for NMR measurements and helpful discussions.

REFERENCES

[1] Talling B., Brandštetr J. in: Progress in Cement and Concrete, Volume 4: Mineral admixtures in cement and concrete, p. 297-339, editors S.L.Sarkar and S.N.Ghosh, ABI Books Private Ltd., New Delhi 1993.
[2] Krivenko P.: “Alkaline cements”, Proc. 1st Intern.Conf. “Alkaline cements and concretes”, Vol.1. p. 11-130, VIPOL Stock Comp. Kiev 1994
[3] Škvára F.: “Gypsum-free portland cement pastes with low water-to-cement ratio”, MRS Symp.Proc. Vol. 370 "Microstructure of Cement-based systems/Bonding and Interfaces in Cementitious Materials", p. 153-158, editors S.Diamond, S.Mindess, Materials Research Society, Pittsburgh 1994
[4] Heitzmann R.F., Gravit B.B., K.J.L. Sawyer : US patent 4,842,649
[5] Davidovits J.: „Properties of geopolymer cements“, Proc. 1st Intern.Conf. „Alkaline cements and concretes“, Vol.1., p.131-150, VIPOL Stock Comp. Kiev 1994
[6] Davidovits J.: “Geopolymers - inorganic polymeric new materials”, J. Therm. Anal. 37, p. 1633-1656, 1991
[7] Davidovits J.: “Chemistry of geopolymeric systems, terminology”, Proc. Geopolymer Inter.Conf. (1999)
[8] Allahverdi A., Škvára F.:“Acid corrosion of geopolymeric cements”, Proc. 7th CANMET Intern. Conf on Fly Ash, Silica Fume, Slag and Pozzolans in Concrete 2001, Vol. 2. p. 561-579
[9] Van Jaarsveld J.G.S, Van Deventer J.S.J., Lorenzen L.: The potential use of geoplymeric materials to immobilise toxic materials, Part I., Miner. Eng. 10, 659-669 (1997), Part II ,12, 75-91(1999)
[10] Rostami H., Silvestrim T.: “Chemically activated fly ash, CAFA”, Proc. 13th Ann. Int. Pittsburgh Coal Conf., Vol.2, p. 1074-1079, University of Pittsburgh, Pittsburgh 1996
[11] Blaakmer J., van Loo W.: “Diabind, an alkali-activated slag fly ash binder”, Proc. 1st Intern.Conf. “Alkaline cements and concretes”, Vol.1., p. 347-360, VIPOL Stock Comp. Kiev 1994
[12] Škvára F., Bohunek J.:“ Chemical activation of substances with latent hydraulic properties”, Ceramics 43, 111-116 (1999)
[13] Palomo A., Grutzeck M., Blanco M.: “Alkali-activated fly ashes - A cement for the future”, Cem. Con. Res. 29, 1323-1329 (1999)
[14] Derouane E.: “Infra-red structural study of aluminium deficient zeolites’, J. Chem. Soc., Far. Trans. I, 70, 1402-1407 (1974)
[15] Querol X., Plana F., Alastuey A.: “Synthesis of Na-zeolites from fly ash”, Inst. of Earth. Sci., 46, 793-799 (1996)
[16] Lippmaa E., Mägi M., Samoson A., Tarmak M.: Investigation of structure of zeolites by solid-state high-resolution ^{29}Si NMR spectroscopy, J. Am. Chem. Soc. 103, 4992-4996 (1981)
[17] Pfeifer H., Ernst H: “NMR studies of Zeolites”, Universität Leipzig, Germany, p. 91-187, 1994
[18] Pichat P., Beaumont R., Barthomeuf D.: “Infra-red structural study of aluminium-deficient Y zeolites”, J.Chem.Soc. Far.Trans.I 70, 1402-1407 (1974)

ISOTHERMAL CONDUCTION CALORIMETRY OF PORTLAND-BLASTFURNACE SLAG BLENDED CEMENTS AT ELEVATED TEMPERATURES

Joanne Hill[1], Ben R Whittle[1], John H Sharp[1], Martin Hayes[2]

[1] University of Sheffield, Department of Engineering Materials, Mappin Street, Sheffield, S1 3JD, UK. E-mail: joanne.hill@sheffield.ac.uk and j.h.sharp@sheffield.ac.uk
[2] BNFL PLC, Sellafield, Seascale, Cumbria, CA20 1PG, UK.
E-mail: martin.hayes@bnfl.com

ABSTRACT

The effect of temperature over the range 20–80°C on the heat output of a number of Portland-blastfurnace slag blended cements has been studied by isothermal conduction calorimetry (ICC). The materials used were 100% ordinary Portland cement (OPC), 1:1, BFS:OPC, 9:1 BFS:OPC and, as a preliminary study, 100% ground granulated blast furnace slag (BFS). A superplasticiser was incorporated, allowing a very low water:powder ratio of 0.31 to be used. Results indicate that the setting of the cement was accelerated both with increasing temperature and decreasing slag content, although even 100% BFS at 20°C set within 48 hours. The presence of a peak 'S' was not observed at 60°C or 80°C. It was also noted that, as the curing temperature was increased, the contribution of the slag fraction to the total heat evolved increased.

1. INTRODUCTION

The use of composite cements based on the partial replacement of Portland cement by waste materials has become commonplace because they offer cost reduction, energy saving and, often, superior longer term products. These replacement materials fall into two nominal groups, pozzolanic and latently hydraulic. The first group includes pulverised fuel ash (PFA), rice husk ash, volcanic ash and silica fume. Ground granulated blast furnace slag (BFS) is the most notable material from the second group and the one used for this study. Cements containing up to about 65% BFS are well established and characterised in the literature [1-2]. However, cements with higher levels of replacement are less well documented [3] as they are more likely to be used for specific applications, for example, when low heat evolution is important, rather than in general construction.

The safe and cost effective storage and disposal of radioactive waste is a major problem facing all countries with nuclear power generating capacity. While the high level waste is likely to be vitrified prior to final disposal, cementation is the favoured method in the U.K. for disposal of low and intermediate level waste. It is essential to have a full and fundamental understanding of the effects that these waste materials have on the hydration behaviour and microstructural development of cement pastes, in order that reasonable predictions can be made concerning the long term storage of these products.

Due to the exothermic nature of cement hydration it is desirable, for the prediction of the long-term performance of packaged immobilised radioactive waste, to measure the exotherm produced. Many nuclear waste encapsulation processes use composite cements with high

replacement levels in part because of the reduced amount of heat generation of these systems. However, due to the scale of the encapsulation, temperatures within a package can rise significantly above ambient. It is also known that blast furnace slag can contribute to the total heat generation, especially at higher temperatures [4-8].

Isothermal conduction calorimetry (ICC) can provide valuable information on the early hydration of cements as well as the heat evolution during this hydration. The heat evolution plots obtained are not only affected by the composition of the cement but also by the presence of replacement materials and are strongly dependent on the temperature of hydration. Previously reported calorimetric studies [4-9] have examined the effect of temperature up to 60°C, but in this study, curing temperatures up to 80°C have been used to establish the contribution to the evolution of heat from the BFS. The data will be used in modelling studies to predict the temperature rise after various curing times in composite cements based on high levels of replacement of OPC by BFS, and to validate models being developed to predict thermal characteristics of cemented mixed waste products.

2. EXPERIMENTAL

Four cement systems were studied during this investigation. These were 100% ground granulated blast furnace slag (BFS), 100% ordinary Portland cement (OPC), 1:1 BFS:OPC and 9:1 BFS:OPC. The OPC was supplied by Castle Cement with the coarse ground BFS being sourced at Redcar Steelworks. All powders were prepared to comply with the specification of BNFL plc. The typical chemical analyses for these materials are given in Table I**,** and correspond to a potential phase composition for the OPC, based on the Bogue calculation, of C_3S, 53.5%; C_2S, 19.1%; C_3A, 7.7%; and C_4AF, 9.4%.

Table 1. Typical chemical analyses of materials used during the investigation

Component	OPC	BFS
CaO	64.4	42.1
SiO_2	20.7	32.3
Al_2O_3	4.9	13.1
Fe_2O_3	3.1	0.5
MgO	2.2	6.5
SO_3	2.9	–
K_2O	0.5	0.4
Na_2O	0.2	0.3
Chloride	0.02	0.03
Sulphide	-	0.9
Loss on ignition	0.9	0.8
Free lime	1.4	–

The powders were hydrated with deionised water containing a naphthalene sodium sulphonate admixture. A constant liquid:powder ratio of 0.31 was chosen. The admixture was added to the deionised water in such a quantity that the concentration of admixture in the paste was 0.65 ± 0.01 ml per 100 g of powder. Since the amount of cement in each system was different, and since the liquid used for hydration contained water and the plasticiser, the w:c ratio was not constant at 0.31. The true w:c ratios are presented in Table 2

Table 2. True w:c ratios for the cements studied

System	w:c ratio
100 % BFS	-
100 % OPC	0.3035
1:1 BFS/OPC	0.607
9:1 BFS/OPC	3.035

Two JAF calorimeters, supplied by Wexham Developments, were used and external mixing employed throughout. Internal mixing was not used as the design of this equipment only allows for very small samples (2g of powder) which resulted in very weak outputs, especially for samples with high levels of cement replacement. At temperatures up to and including 60°C a water-filled bath and perspex cells were used and maintained at a constant temperature ± 0.1°C. A diagram of a typical cell can be seen in Figure 1. At higher temperatures a silicone-oil filled bath and stainless steel cells were used. The stability of the temperature of this bath at 80°C was ± 0.5°C. Using this apparatus it was possible to observe the rate of heat evolution and the cumulative heat of hydration for treatments lasting either 72 hours (for temperatures 40°C and below) or 48 hours (for temperatures 60°C and above).

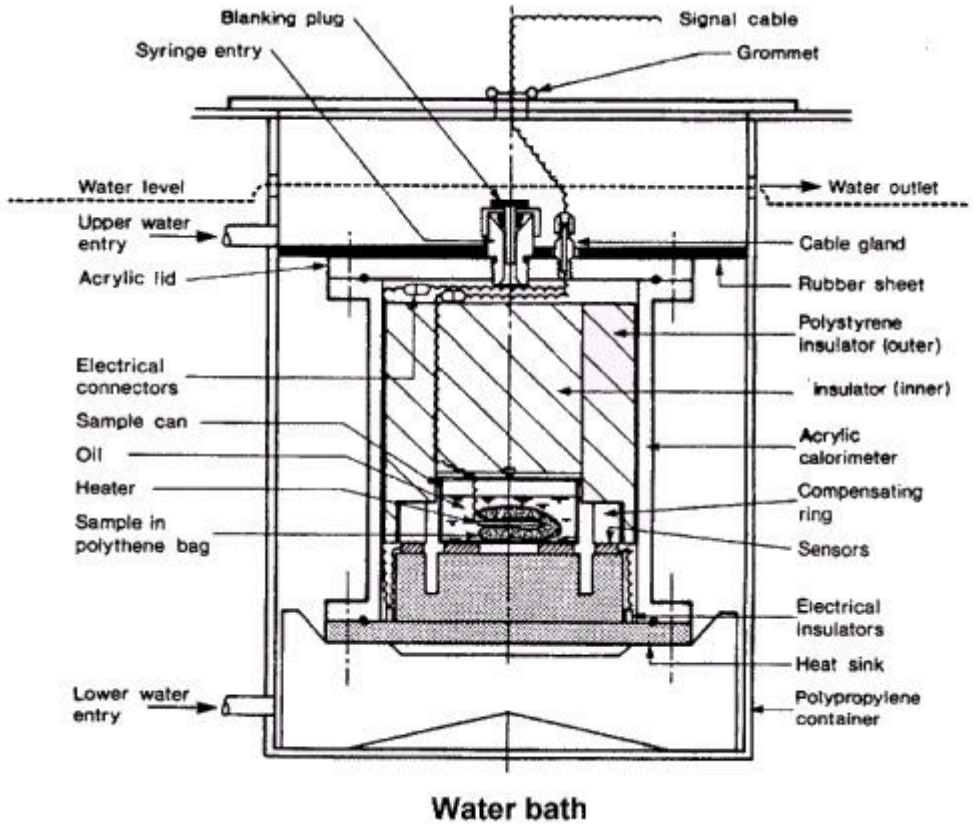

Figure 1. Calorimeter cell

Pastes consisting of 15 ± 0.001 g of powder and 4.65 ± 0.002 g of the water/admixture solution were mixed in polythene bags until homogeneous (approximately 2 minutes). The bags were then closed using adhesive tape, placed into sample cans containing transformer oil, and sealed inside the calorimeter cells. The cells were then immersed in the water/oil bath within 10 minutes of mixing having taken place. Prior to sample insertion, the cells were placed in the baths for a sufficient period of time to allow acclimatisation to the bath temperature. However, for experiments taking place at elevated temperatures, the cells cooled as the specimens were introduced, resulting in an initial endothermic response as the

relatively cooler cell re-heated to the bath temperature. The period of reheating lasted up to 2 hours and completely obscured the exothermic heat of wetting. This 'reheating endotherm', which has been removed from the results, affected the runs carried out at higher temperatures (60°C and 80°C) more than those at the lower temperatures. However, the reproducibility of the results at these temperatures was good, although there was increased noise on the trace**,** believed to be a consequence of the need to use stainless steel calorimeter cells rather than perspex. The rate of heat flux for a given temperature difference is a function of the heat transfer coefficient of the fluid and the thermal conductivity of the barrier. The thermal conductivity of stainless steel is two hundred times higher than that of perspex and, therefore, fluctuations in the temperature of the water bath are more strongly relayed to the thermopiles inside the cells, imparting greater noise.

3. RESULTS

Isothermal conduction calorimetry results are presented in Figures 2-9 for all the cement systems used. There were distinct differences in the rate of heat output of the individual cements at the different temperatures and also between the different cement systems at the same temperature (Table 3).

The effect of temperature on the rate of heat output of ordinary Portland cement can be seen in Figure 2. The sharpness of the peak and the amount of heat generated when considering the values of Q_m, the value of the maximum rate of heat output, (Table 3) increased with increasing temperature. However, t_m, the time at which Q_m occurred, decreased with increasing temperature. This demonstrates that increasing the temperature caused a classic acceleration of the set of the cement. When considering the total heat output (Figure 3) it can be seen that the shape of the curves at 40 and 60°C were similar but displaced, with the sample cured at the higher temperature generating more heat. At 20°C, there was a delay in the initial heat output followed by an acceleration in heat generation, so that, by around 35 hours, this sample had generated more heat than that at 40°C. At 80°C there was rapid initial heat evolution to 8 hours followed by a dropping off of the curve possibly due to evaporation of transformer oil and/or degradation of the sample bag and, therefore, mixing of the oil with the cement. After 60 hours hydration the sample cured at 60°C had generated more heat than at 80°C. This is a similar trend to the one seen between the 20°C and 40°C results. This is illustrated clearly in Table 3 and Figure 3.

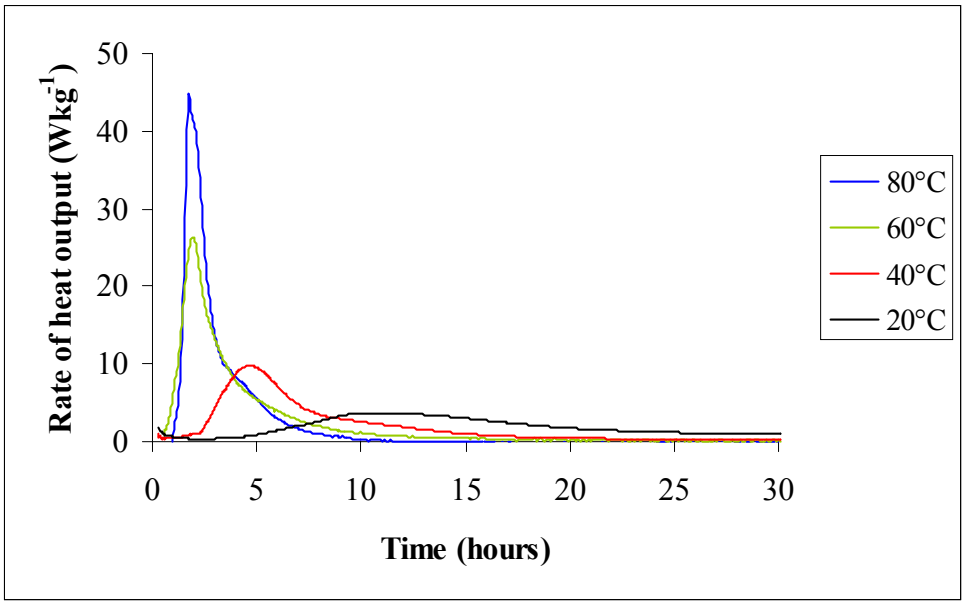

Figure 2. 100% OPC

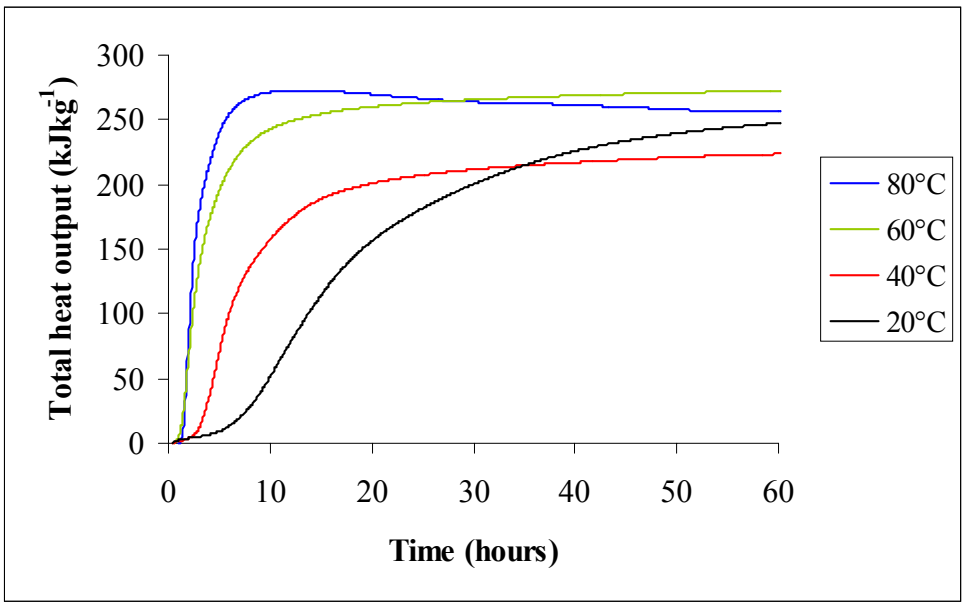

Figure 3. 100% OPC

Replacing 50% of the OPC with BFS (Figures 4 and 5) had the effect of decreasing the value of Q_m by just over half (Table 3). Again, it can be seen that the effect of decreasing temperature was to retard the set of the cement. However, unlike the neat Portland cement, there was no overlap in the total heat outputs of the slag cements but there was a longer initial delay at 20°C than at either 40, 60 or 80°C. If the slag fraction of the cement did not contribute to the cement hydration it would be expected that the total amount of heat generated would be half that of the OPC. At 20°C, the amount of heat generated by the slag cement was less than half that of the OPC. As the temperature was increased, however, the total amount of heat generated by the slag-containing cement also increased, so that, after 40 hours hydration at 80°C, the amount of heat generated was not dissimilar; 262 $kJkg^{-1}$ compared with 255 $kJkg^{-1}$ (Table 3).

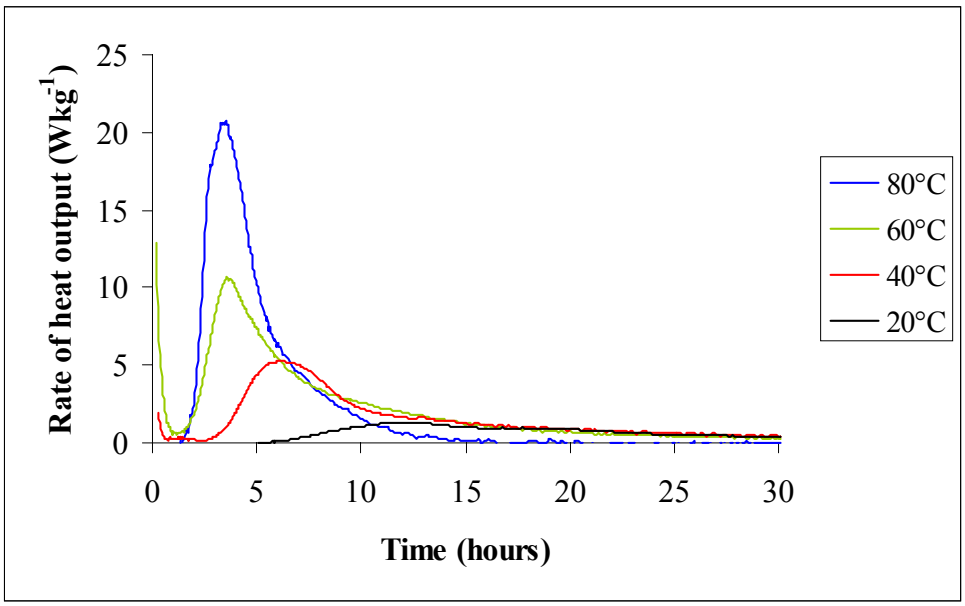

Figure 4. 1:1 BFS:OPC

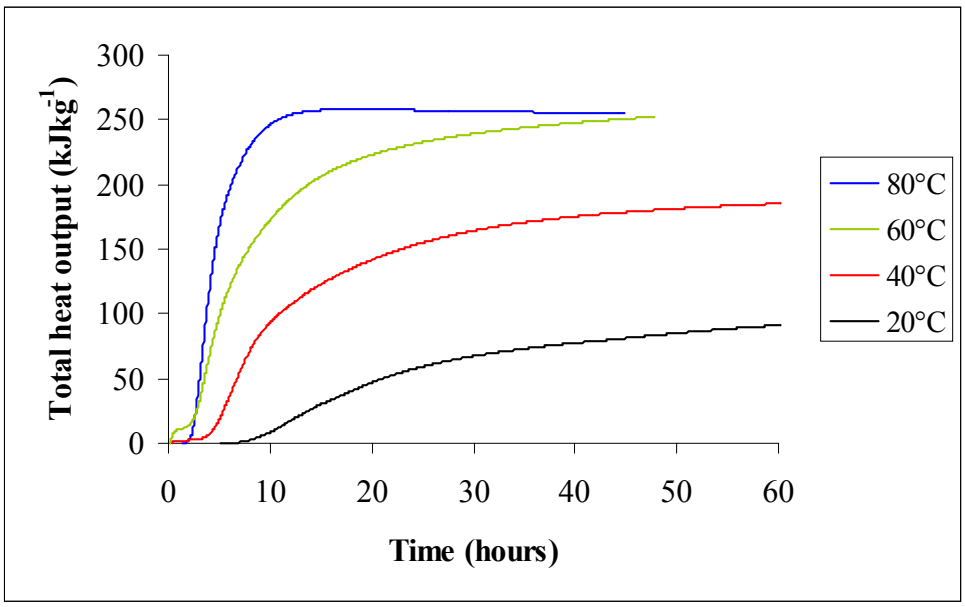

Figure 5. 1:1 BFS:OPC

The addition of 90% BFS to the cement (Figures 6 and 7) also had the effect of reducing the rate of heat generated (Q_m values decreased when compared to both OPC and 1:1 BFS:OPC) and reducing the total amount of heat generated at all temperatures (Table 3). Applying the same assumption that the slag acted merely as an inert diluent, there should have been only one tenth of the amount of heat generated when compared to 100% OPC. It can be seen from Table 3 that this was not the case at any of the temperatures studied. The heat generated from the 9:1 BFS:OPC system was consistently higher than one tenth. It can be concluded from the results of the 1:1 and 9:1 BFS:OPC systems that the slag fraction of the cement did contribute to the overall heat generated and, at higher hydration temperatures, this contribution was greater than at ambient temperature. Another interesting feature of these systems incorporating BFS was that the evidence for a peak 'S' (as reported elsewhere, e.g. [5-8,10,12], and discussed below) was not very strong, even at the 90% replacement level, although there was a broadening of the peaks at lower temperatures. The total heat output curves (Figure 7) followed the same trend as that observed for the 1:1 BFS:OPC cements.

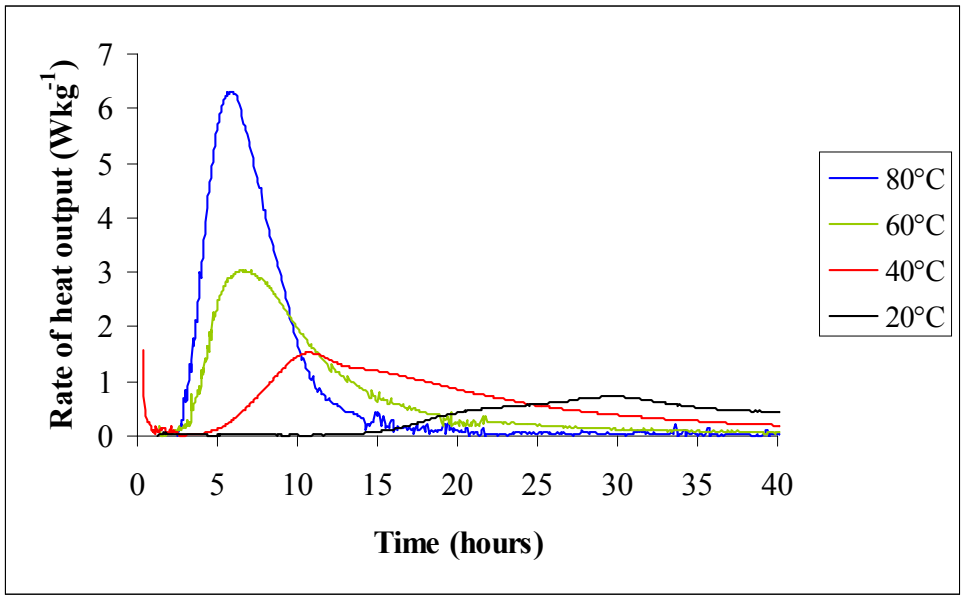

Figure 6. 9:1 BFS:OPC

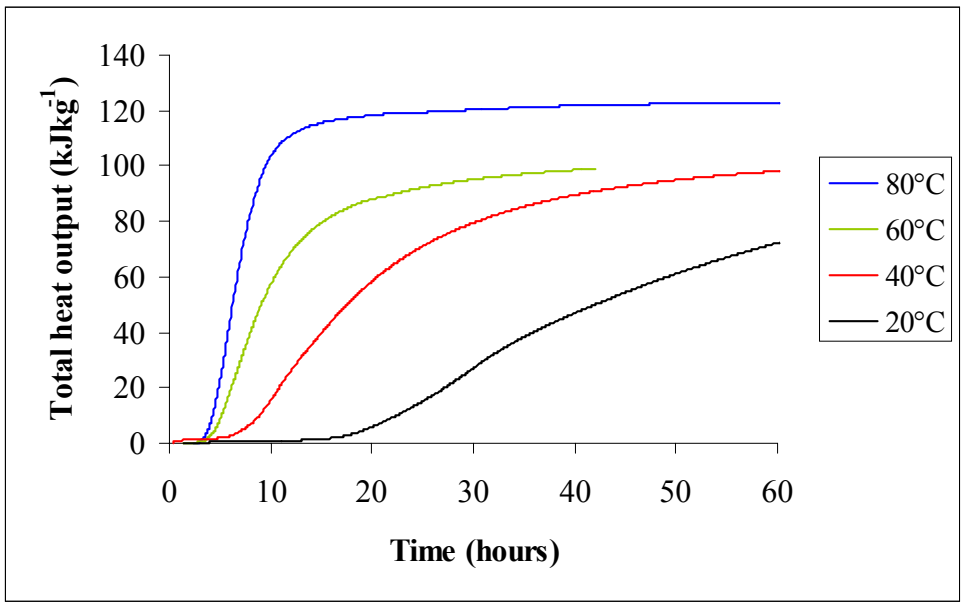

Figure 7. 9:1 BFS:OPC

The results of the hydration of the 100% BFS sample are shown in Figures 8 and 9. Although data for hydration at 80°C have been obtained they are not shown because they are not felt to be as reliable as the other data presented in this paper due to problems with the sensitivity of the stainless steel cells and the sensitive nature of the heat output. Further experimentation is continuing to obtain more reliable quantitative data. It can be seen that even at 20°C a definite peak was observed (Figure 8) but with a very low rate of heat output. This would be expected for a slag that was not being strongly activated by calcium hydroxide. The total heat of hydration was also low but, even at 20°C, it can be seen that heat was still generated and, therefore, that some hydration was taking place. The Q_m values (Table 3) at all temperatures were very similar to those of the 9:1 BFS:OPC system. However, the t_m values changed with temperature. At 20°C, the value for the 9:1 BFS:OPC cement was less than that for the pure BFS system. At 40°C and 60°C the opposite is true, which suggests that the increase in temperature has a greater effect on the hydration of BFS than that of the OPC.

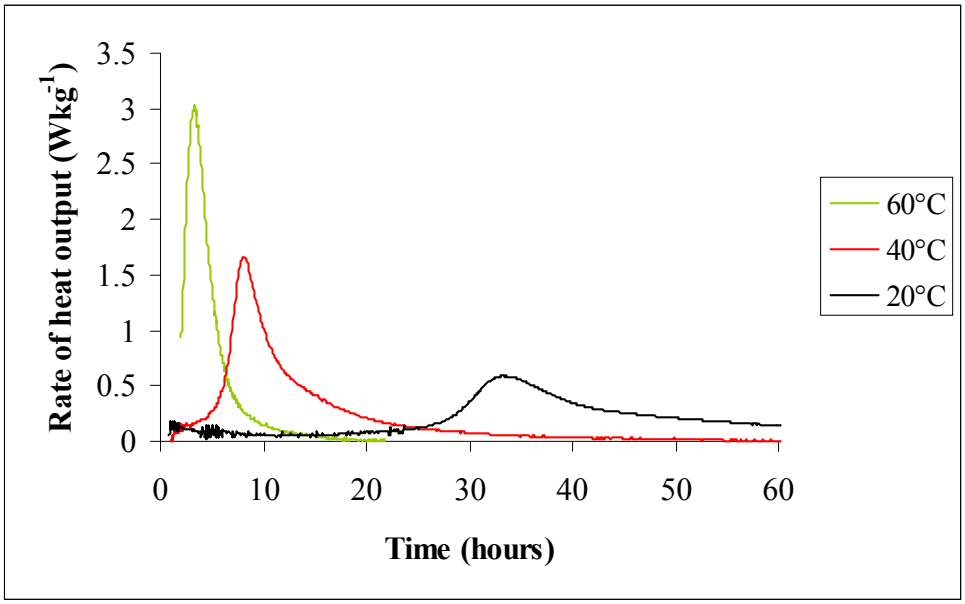

Figure 8. 100% BFS

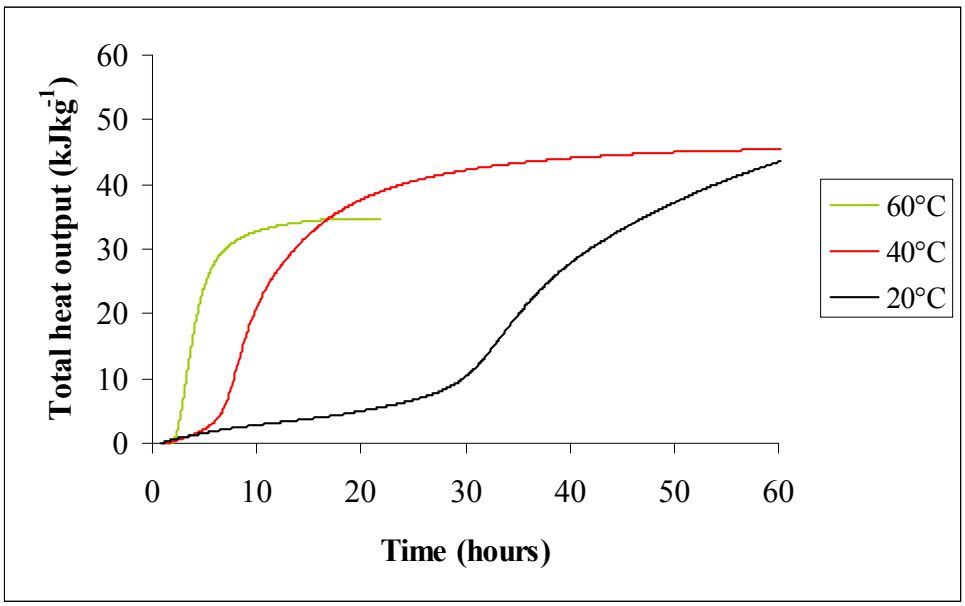

Figure 9. 100% BFS

The general trend between the different cement systems (Table 3) is that the maximum amount of heat generated decreased and the time taken to reach this maximum increased with increasing slag content. The opposite trend was observed as the curing temperature increased. All data need to be interpreted with care because in a number of systems (especially at lower curing temperatures) heat evolution was continuing beyond 72 hours, so the total heat recorded in Table 3 is incomplete. This, however, has no bearing on the general trends of the results.

Table 3. Values of Q_m (value of maximum rate of heat output), t_m (time at which Q_m occurs) and total heat evolved

Temp (°C)	Cement	t_m (hours)	Q_m (Wkg^{-1})	Total heat evolved (kJkg-1) @Q_m	24 hours	40 hours	60 hours
20	100% OPC	10.8	3.7	62.5	177.3	225.8	247.3
	1:1 BFS:OPC	11.9	1.3	16.7	57.3	77.6	91.3
	9:1 BFS:OPC	29.5	0.7	25.7	13.0	46.9	72.3
	100% BFS	33.3	0.6	16.3	6.3	27.8	43.5
40	100% OPC	4.7	9.8	59.8	206.3	217.1	223.5
	1:1 BFS:OPC	6.2	5.3	40.4	152.9	175.2	185.1
	9:1 BFS:OPC	10.7	1.5	19.3	69.1	89.6	98.1
	100% BFS	8.1	1.7	11.8	40.1	44.1	45.4
60	100% OPC	1.9	26.3	58.8	262.8	270.5	272.6
	1:1 BFS:OPC	3.5	10.7	48.4	231.1	247.7	-
	9:1 BFS:OPC	6.5	3.1	23.9	91.5	98.5	-
	100% BFS	3.3	3.0	10.7	34.8	-	-
80	100% OPC	1.8	44.7	48.1	266.9	261.6	256.1
	1:1 BFS:OPC	3.5	20.7	258.6	257.5	255.1	-
	9:1 BFS:OPC	5.6	6.3	51.3	119.2	121.7	122.9

4. DISCUSSION

Isothermal conduction calorimetry provides valuable quantitative information about the hydration reactions that occur during the early stages of hydration of cements. The most obvious information given is the amount of heat released. Additionally, the shape of the curves and other features in the plot can also provide information about the relative rates of hydration and the occurrence of other reactions (such as slag hydration). There is some disagreement as to the reactions associated with each peak but generally they are as follows. Peak I is due to the initial interaction and wetting of the cement powder with water and early stage reactions (not seen in this study because of the use of external mixing). After this initial peak there is the dormant period (also known as the induction period) during which little heat is evolved and the stiffness of the paste increases**,** followed by acceleration in heat evolution during which setting occurs [11]. The main peak, known as peak II, occurs after this acceleratory period and is generally believed to be due to the hydration of C_3S and generation of C-S-H gel and CH. In composite cements incorporating significant amounts of blast furnace slag, a peak 'S' occurring after peak II has been attributed to the hydration of the slag fraction [2,11] because this requires activation by the alkali which, in this case, is the calcium hydroxide liberated during the hydration of the C_3S [2,11]. It has also been reported, however, that, as the curing temperature increases, the occurrence of peak 'S' disappears as the slag hydration becomes increasingly thermally activated until peaks II and 'S' merge [4-8].

Perhaps the two most relevant previous studies of the heat evolution from OPC-BFS composite cements at elevated temperatures are those by Ma et al. [4], who studied a cement with 65% replacement by BFS in the temperature range from 10 to 55^{o}C, and Escalante and Sharp [5], who studied a cement with 60% replacement by BFS in the temperature range from 10 to 60^{o}C. There are, therefore, two novel features to this investigation. The first is the application of ICC at the very high curing temperature of 80^{o}C, while the second relates to the high replacement level (90%) of OPC by BFS, previously studied by Richardson et al [7] and Hill and Sharp [3,10]. The results were obtained to provide reliable quantitative data for theoretical models to be developed to predict the temperature variations in composite cement systems incorporating radioactive wastes. There is concern that if the heat of hydration is excessive and that the thermal profile within a package results in high thermal stresses, the integrity of the package may be adversely affected.

The results obtained are an extension of, and mostly similar to, those reported in previous studies [4-8,10,12]. It is confirmed that:

- the time to reach t_m, corresponding to the maximum in the heat evolution curve, for OPC, for the composite cements containing BFS, and indeed for ground, granulated BFS itself, decreases with increasing temperature
- the intensity of the main peak (often referred to as peak II and attributed to the hydration of alite to form C-S-H gel and calcium hydroxide) increases substantially with increasing curing temperature
- peak II is rather broad and shallow at 20^{o}C, becoming stronger and sharper at higher temperatures (as can be seen in Figures 2, 4 and 6)
- the induction, acceleratory and decay periods in the hydration of cement can be clearly distinguished.
- the BFS is hydraulic and its reactivity increases markedly with increase in curing temperature (see Figure 8)

Although a pronounced asymmetry of the endothermic peaks is evident in Figure 6, and to a lesser extent in Figure 4, especially at 40 and 60°C, the presence of a definite peak 'S' attributed to the hydration of the BFS after activation by calcium hydroxide formed in the reaction occurring at peak II, is not as apparent as in previous studies. For example, using similar equipment and experimental procedures (except for the use of internal mixing), Ma et al. [4], Bland and Sharp [12], and Escalante and Sharp [5] had obtained a second peak or shoulder in OPC-BFS composite cements, especially in the temperature range from 30 to 55°C. In addition, Hill and Sharp [10], using external mixing and one of the calorimeters used in the present investigation, and a similar 9:1 BFS:OPC composite cement with a w:s ratio of 0.35 reported a clear peak 'S' at 35°C. There are three factors that may contribute to this observation, namely the mixing procedure adopted, the coarse nature of the BFS used, and the incorporation of the naphthalene-sulfonate admixture, allowing the use of a very low liquid:powder ratio (0.31). When the superplasticiser was omitted from the 1:1 BFS:OPC system at 60°C, t_m and Q_m were both reduced, while peak 'S' was evident as a shoulder followed by a tail for several hours on the right-hand side of peak II. The presence of the admixture resulted in very strong retardation in the 9:1 BFS:OPC mix, which was particularly evident at 40 and 60°C, because the relative amount of superplasticiser to Portland cement was very high in this composite cement.

If blast furnace slag were an inert diluent, it would be expected that, as Portland cement were replaced by slag, the heat generated would decrease accordingly. Therefore, in a 1:1 BFS:OPC cement, it would be expected that the total amount of heat generated at a given temperature would be half that of the Portland cement. However, it can be seen from Table 3 that this was not observed at any replacement level. The total amount of heat generated by the composite cement systems was generally greater than that which would have been predicted. Also, this effect became more pronounced as the curing temperature increased. This indicates that an increase in temperature has a greater effect on the slag fraction than on Portland cement. This has been observed in the literature [6-8] where activation energies have been calculated and been found to be higher for blast furnace slag than for Portland cement. This has implications for predicting the thermal characteristics of composite cement systems incorporating blast furnace slag. From the results presented here, it can be seen that simple adaptation of a model for Portland cement hydration would not be sufficient for predicting the thermal events of blast furnace slag cement. The continuing study into the neat blast furnace slag hydration will provide valuable data for validation of predictive models.

5. CONCLUSIONS

1. This study has shown that it is possible to obtain reliable quantitative data at elevated temperatures up to 80°C.
2. Thermal activation of the cements especially those incorporating BFS, increases with increasing temperature.

ACKNOWLEDGEMENTS

The authors would like to acknowledge BNFL plc for the financial support for this work and the supply of materials used. We are grateful to Mr E Miller for many helpful discussions.

REFERENCES

[1] Hewlett, P.C. Lea's chemistry of cement and concrete, 4th edition., London: Arnold, 1998, pp 633-74.

[2] Taylor, H.F.W. Cement chemistry, 2nd edition. London: Thomas Telford, 1997, pp 261-94.

[3] Hill, J. and Sharp, J.H. The mineralogy and microstructure of three composite cements with high replacement levels, Cement and Concrete Composites, vol. 24, 2002, pp 191-199.

[4] Ma, W., Sample, D., Martin, R and Brown, P. Calorimetric study of cement blends containing fly ash, silica fume and slag at elevated temperatures, Cement, Concrete and Aggregates, vol. 16, 1992, pp 93-99.

[5] Escalante-Garcia, J.I. and Sharp, J.H., The effect of temperature on the early hydration of Portland cement and blended cements, Advances in Cement Research, vol. 11, 2000, pp 121-130.

[6] Wu, X., Roy, D.M. and Langton, C.A., Early stage hydration of slag-cement, Cement and Concrete Research, vol.13, 1983, pp 277-286.

[7] Richardson, I.G., Wilding, C.R. and Dickson, M.J., The hydration of blastfurnace slag cements, Advances in Cement Research, vol. 2, 1989, pp 147-157.

[8] Roy, D.M. and Idorn, G.M., Hydration, structure and properties of blast furnace slag cements, mortars and concrete, ACI Journal, 1982, pp 444-457.

[9] Shi, C. and Day, R.L., A calorimetric study of early hydration of alkali-slag cements, Cement and Concrete Research, vol.25, 1995, pp 1333-1346.

[10] Hill, J. and Sharp, J.H., Heat evolution in composite cements with additions of Sn(II) and Sn(IV) chlorides, Advances in Cement Research, submitted.

[11] Bye, G.C., Portland cement: Composition, production and properties, Pergamon Press, Oxford

[12] Bland, C.H. and Sharp, J.H., A conduction calorimetric study of gasifier slag-Portland cement blends, Cement and Concrete Research, vol.21, 1991, pp 359-367.

ULTRASONIC STUDY OF STRUCTURE FORMATION PROCESS IN CEMENT GROUT

A.A. Klyusov[1], A.A. Rybokon[2], A.A. Frolov[3] and I.A. Klyusov[4]

[1]Prof. Dr. Sci. (Chemistry), Head of Laboratory. VNIIGAZ, Razvilka, Lenynsky Raion, Moskovskaya oblast, 142717, Russia.
[2]Deputy head of Department of Gazprom, Moscow, Nametkina 17, Russia.
[3]Dr, Director of Orenburgaz, Orenburg, "Orenburggaz", Russia.
[4]PhD, Senior researcher, VNIIGAZ, Razvilka, Lenynsky Raion, Moskovskaya oblast, 142717, Russia.

ABSTRACT

The paper deals with ultrasonic investigation of the structure formation process in cement grout prepared on the basis of water and 8 % $CaCl_2$ and NaCl solutions at a water-to-cement ratio of 0.5. The comparison of curves of structure formation, with and without additives, shows that the increase in frequency of ultrasonic signal from 100 kHz to 1.2 MHz leads to a sufficient increase of sonic speed (by 2 – 10 times). At the same time this increase demonstrates more distinctly the minimums that correspond to the periods of cement grout setting. If for the initial setting period the increase of ultrasonic frequency does not have any sufficient effect, then the period of final set reduces (approximately by 2 hours). This fact confirms once more that any impact on the process of cementing agent hydration at the initial stage has a sufficient effect on the further flow of cementing system structure formation process.

1. INTRODUCTION

Ultrasonic methods have found extensive application for studying the structure formation process in mineral cementing agents [1,2] and non-destructive testing strength properties of artificial stone taking into consideration the size of internal defects of the structure [3,4]. However, this method is rarely used for studying the kinetics of structure formation, especially at the initial stage of the cementing agent's hydration. This is due to the fact that a measurement of propagation speed of sonic waves and signal amplitude is a difficult experimental task, especially for systems with a high rate of structure formation of e.g. cement grout with hardeners.

The purpose of this work is ultrasonic investigation of the structure formation process in cement grout prepared on the basis of water and 8 % $CaCl_2$ and NaCl solutions at a water-to-cement ratio of 0.5.

2. ULTRASONIC STUDY OF STRUCTURE FORMATION PROCESS IN CEMENT GROUT

The ultrasonic measuring chamber is a 200 cm^3 Plexiglas cylinder mounted on microscope support. To avoid measurement errors arising due to volumetric changes of the cement grout during hardening, the receiver was fastened at the bottom of the acoustic chamber while the emitter was allowed to move freely along the height of the cylinder with the help of a microscrew. A clock-type indicator and IZV-2 unit measured the distance between acoustic delays, taking into account linear

deformations of the object concerned, with accuracy up to 0.001 mm. The principle of the test stand's operation is as follows. A reference pulse of the G5-4B generator starts horizontal scanning of the C1-54 oscillator. A pulse of negative polarity from one of the channels of the generator is fed to a radio pulse generator input. Then the pulse with basic frequency corresponding to a resonance frequency of the transducer is fed to a piezoelectric cell. The cell after having been exited by electric pulse forms an elastic pulse which, after passing the medium investigated, is transformed again into an electric pulse by the other piezoelectric cell. Then the signal amplified in the receiver is fed simultaneously to the B4-1A pulse millivoltmeter and the C1-54 oscillator and then analyzed.

The method of measuring ultrasonic wave parameters is as follows. Amplitude and speed of wave propagation in the grouting liquid (water or $CaCl_2$ and NaCl solutions) are measured in the acoustic chamber at 22 ± 2^0C followed by Portland cement addition and mixing for 1 minute to a homogenous grout. The measurements are carried out at frequencies of 1.2 MHz and 100 kHz (for the purpose of comparison). Due to the problem of determination of the leading edge of the pulse because of considerable attenuation of the sonic wave at the early stage of hydration, the maximum of 2d and 3d half waves are taken as a reference. The following equation can be used for estimating the speed of acoustic vibration propagation:

$$c = L/(\tau_1 - \tau_2)$$

where L is the length of acoustic path in the medium considered; τ_1 is a total delay time of signal along the whole path; and τ_2 is the propagation time in acoustic delays. A maximum error of sonic propagation and signal amplitude measurement is respectively 1% and 5 %.

The first section on time vs. sonic speed graphs (Figure 1) characterized by sonic speed increase is the result of intensive wetting, dissolution and interaction of particles of cementing agent on the surface with the formation of external hydrates. The results of phase analysis show that the main hydrate phases having a high level of anisometricity during this period are ettringite (in water) and CSH (I) and ettringite (in chloride solutions).

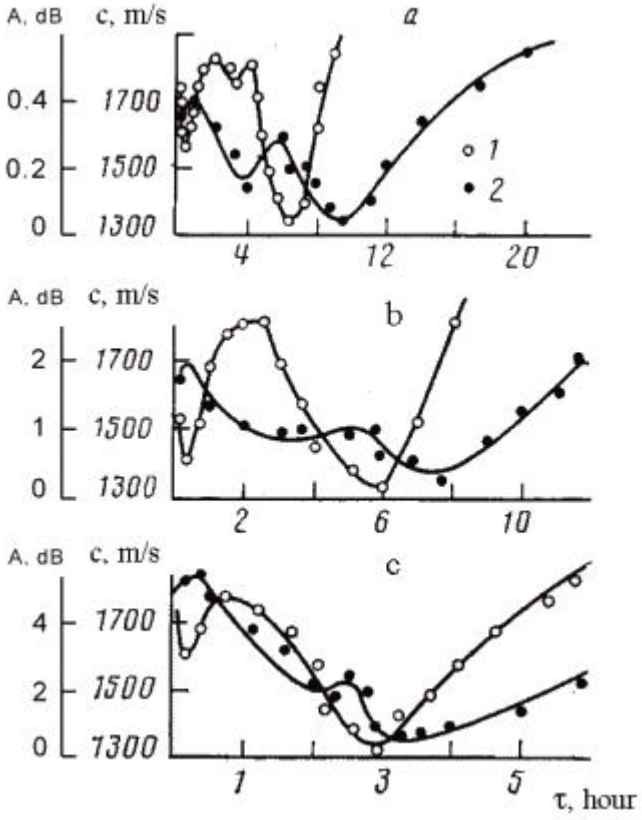

Figure 1. Amplitude (1) and speed (2) of ultrasound (f = 1.2 MHz) in cement grout without additive (a) and with sodium (b) and calcium (c) chloride vs. hardening time

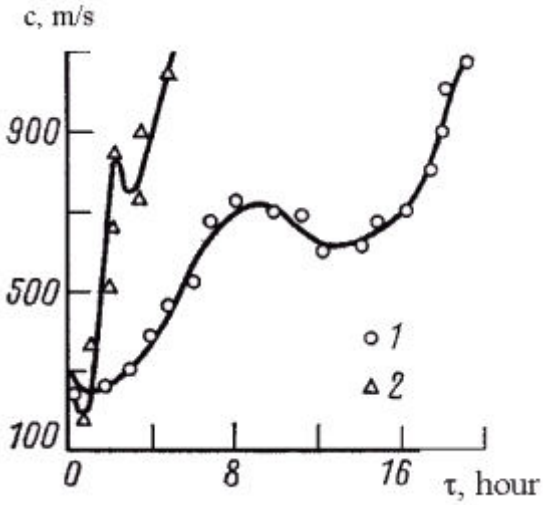

Figure 2. Sonic speed (f = 100 kHz) in cement grout without additive (1) and with calcium chloride (2) vs. hardening time

The next period is characterized by the formation of hydrosulfoaluminate (partially hydrosilicate) coatings. During this period the process of hydration slows down sharply, as reflected by the decrease in ultrasonic speed. Following the destruction of the blocking coating by crystalline pressure of the internal hydrates has the dominant effect on the decrease of sonic speed (due to a constant loss of contact between solid phase particles) as compared to the intensification of hydration. The latter is a result of more free diffusion of water to the unhydrated grains and the formation of periodic colloidal structures (PCS) with typical forces of molecular attraction and forces of interaction related to a polarization effect under the condition of restricted volume of the system [5]. The sonic speed slows down until the formation of a more or less stable spatial skeleton of coagulation structure from hydrate new formations including those growing on the surface of hydrating particles.

As the coagulation structure strengthens and phase contacts appear, sonic speed again increases. The first minimum on the curve corresponds to the initial setting of cement grout by Vical needle. Under the conditions of gradual increase in the number of phase contacts, filling voids with new formations and their interlinkage, the sonic speed increases as well. However, with time and with continued increase of plastic strength, caused by the transition of the coagulated structure into crystalline structure, sonic speed drops sharply. The comparison of data obtained with the results of the thermokinetic investigation shows that the minimum on the sonic speed curve, that approximately corresponds to the final set of cement grout by the Vical needle, coinciding with the maximum on the temperature vs. setting time curve. In this case the drop of sonic speed is caused, in our opinion, by a sharp increase of cement grout temperature. This, in turn, enhances thermal motion of particles of solid and liquid phases preventing the sonic pulse passing through the medium investigated. However, some researchers [4] think that temperature does not have a pronounced effect on this process.

After reaching the highest exothermal effect (during temperature drop) the thermal motion slows down and sonic speed increases again with the formation of rigid crystalline bonds. It should be noted that if the increase in ultrasonic signal amplitude during the formation of the coagulated structure of the cement grout results from a prevailing influence of new formations dispersion and a large quantity of free water, then, after commencing a final set, this is a result of the crystalline skeleton formation leading to the decrease of fluctuation absorption together with the decrease of transit time of the leading front of sonic wave. Besides, the decrease of free moisture and the increase of adsorbed moisture density (in pores and capillaries), as well as fibrous (or laminar) form

of new formations as compared to rounded grains of initial cementing agent at the initial stage of hydration lead to the decrease of sonic energy absorption. The introduction of sodium and calcium chloride into a cement grout leads to the increase in ultrasonic signal amplitude and reduction of specific periods on the curves of structure formation in accordance with the classical mechanism of accelerating action of the additives.

The comparison of structure formation curves, Figures 1 and 2, shows that the increase in frequency of the ultrasonic signal from 100 kHz to 1.2 MHz leads to a sufficient increase of sonic speed (by 2 – 10 times) and more distinct demonstration of minimums corresponding to the periods of cement grout setting. If for the initial setting period the increase of ultrasonic frequency does not have any significant effect, then the period of final set reduces (approximately by 2 hours). Data on sonic speed increase with the increase in signal frequency in cement grout obtained in these experiments agree with the opinion of the majority of experts [3]. The mechanism of the above phenomenon can be explained from the position of physical and chemical mechanics of dispersion. The increase in ultrasonic impact frequency in cement grout being kinetically active system as compared to inert one intensifies the process of hydration and hardening. As a result, we observe the increase of supersaturation with CaO and the formation of a large number of nuclei followed by crystallization of a large number of highly dispersed crystals of new formations in a unit of the system's volume. This results in the formation of amore dense structure with a large number of coalescence contacts.

3. CONCLUSION

The structure formation kinetics investigated with the help of the ultrasonic method reflects the main periods of cement grout hydration and hardening.

The introduction of chlorides into a cementing grout promotes a decrease in ultrasound absorption at the expense of intensive nucleus-formation and formation of more crystallized structure of the stone.

The increase of ultrasonic signal frequency from 100 kHz to 1.2 MHz leads to a significant increase of sonic speed and reduction of cement grout setting time.

REFERENCES

[1] Stepišnik J., Lukač M., Kocuvan J. Measurement of cement hydration by ultrasonics// Amer. Ceram. Soc. Bull. 1981. v. 60. № 4. p. 481.

[2] Lasiš D., Stepišnik J. An investigation of the osmotic model of cement curing by ultrasonics// Cem. and Concr. Res. 1984. v. 14. № 3. p. 345.

[3] Dzenis V.V. et al. Ultrasonic control of hardening concrete// 1971. Moscow.

[4] Jones R., Facarrow I. Non-destructive methods of concrete testing// 1974. Moscow.

[5] Grankovsky I.G. The formation of dispersion structure of mineral cementing systems// Inter. Congress on Cement Chemistry. 1976. v. 2. p. 189.

ULTRASONIC STUDY OF STRUCTURE FORMATION PROCESS IN CEMENT GROUT

A.A. Klyusov[1], A.A. Rybokon[2], A.A. Frolov[3] and I.A. Klyusov[4]

[1]Prof. Dr. Sci. (Chemistry), Head of Laboratory. VNIIGAZ, Razvilka, Lenynsky Raion, Moskovskaya oblast, 142717, Russia.
[2]Deputy head of Department of Gazprom, Moscow, Nametkina 17, Russia.
[3]Dr, Director of Orenburgaz, Orenburg, "Orenburggaz", Russia.
[4]PhD, Senior researcher, VNIIGAZ, Razvilka, Lenynsky Raion, Moskovskaya oblast, 142717, Russia.

Presenting author:

Klyusov Anatoly, b. 2 July 1940, Jenisejsk, Russia. Chemistry Researcher. Education: Degree, Engineering, Technical Institute, St Petersburg, 1963; PhD, Mendeleev Chemical and Technical Institute, Moscow, 1973; DSc, Mendeleev Chemical and Technical University, 1993; Professorial Degree, 1995. Appointments: All Russian Scientific Research Institute for Gas Technology, Moscow. Publications: 10 scientific reviews, 180 scientific articles and 43 patents in the field of Arctic oil and gas cements. Membership: Academician, President of the Regional Office, International Informatization Academy, New York Academy of Sciences, Fellow Cchem FRSC.

HYDRATION OF PORTLANDITE-METAKAOLIN AND PORTLAND CEMENT-METAKAOLIN SYSTEMS

A. Shvarzman [1], K. Kovler [2], G. S. Grader [3] and G. E. Shter [4]

[1] Faculty of Civil Engineering, Technion - Israel Institute of Technology, Haifa, Israel
E-mail: cvasia@tx.technion.ac.il
[2] Faculty of Civil Engineering, Technion - Israel Institute of Technology, Haifa, Israel
E-mail: cvrkost@tx.technion.ac.il
[3] Faculty of Chemical Engineering, Technion - Israel Institute of Technology, Haifa, Israel
E-mail: grader@tx.technion.ac.il
[4] Faculty of Chemical Engineering, Technion - Israel Institute of Technology, Haifa, Israel
E-mail: shter@tx.technion.ac.il

ABSTRACT

The kinetics of metakaolin - calcium hydroxide reactions, effects of portlandite/metakaolin ratio on compressive strength and microstructural development were investigated. Portlandite - metakaolin pastes containing 25%, 50%, 65%, 80%, 90% and 95% of metakaolin were prepared at water/solid ratios of 1. The reaction kinetics was investigated using differential thermal analysis. The nature and quantity of hydration products were determined. In an additional series the hydration process of metakaolin - Portland cement pastes was studied by examining the hydration products. The replacement percentage of metakaolinite was 8.4% and 15% by weight, respectively. The water to binder ratio was 0.33 in all the pastes. The relationship between the content of hydration products and strength development was obtained and discussed.

1. INTRODUCTION

In recent years the use of high-performance concrete (HPC) in structures has been greatly increased. Pozzolanic admixtures such as silica fume, fly ash, and metakaolin are used for the production of HPC [1 - 5]. In practice, a pozzolanic admixture can be introduced into concrete in one of two ways: as a partial replacement of cement and/or fine sand. It is known that the content of pozzolanic admixture influences properties of fresh concrete, mechanical properties and durability of hardened concrete. One of the engineering problems facing the technological engineer centers on the rational use of pozzolanic admixtures (i.e. choosing the optimal content of pozzolanic admixture) in the preparation of concrete and mortars. The pozzolanic admixtures such as silica fume and metakaolin are expensive materials. The non-rational use of pozzolanic admixtures will increase the cost of the mixture and/or reflect negatively on physical and mechanical properties of the concrete. It is known that pozzolanic admixture acts as chemically reactive material (able to react with portlandite) on the one hand and as microfiller, on the other hand. Quality and quantity of the active phases, the type of treatment, Si/Al molar ratio, the lime/pozzolana ratio in the mix, water to binder ratio, curing conditions, shape and size of particles, particle size distribution and specific surface area influence the activity of the admixture.

It is also well known that properties of concrete or paste are closely related to its microstructure and products of hydration. Of late, numerous studies have been reported related to the hydration of fly ash - cement, fly ash - lime, silica fume – cement and metakaolin - cement pastes [6 - 10].

Proceedings of the 11th International Congress on the Chemistry of Cement (ICCC)
'Cement's Contribution to the Development in the 21st Century'
Hosted by: The Cement and Concrete Institute of South Africa
CD-ROM produced by: Document Transformation Technologies
11 - 16 May 2003, Durban, South Africa
ISBN Number: 0-9584085-8-0
Editors: Dr G. Grieve and G. Owens
Congress Organised by: Event Dynamics

Formation of calcium hydroxide (portlandite) and non-evaporated water in the system are usually the main criteria for estimating hydration process. Some researchers have also investigated the fraction of reacted fly ash and the alkalinity of pore solution in fly ash - cement pastes. However, the influence of quality and quantity of hydration products on compressive strength development has not been studied adequately yet.

The main objectives of this research were to investigate the influence of metakaolin/portlandite molar ratio on the kinetics of the hydration process, to determine the optimal molar ratio from the viewpoint of chemical activity and to find out the relationships between the content of hydration products and compressive strength. This information will facilitate the rational use of metakaolinite for designing concrete mixes.

2. EXPERIMENTAL WORK

2.1 Materials and properties

An ordinary Portland cement (ASTM Type 1) was used throughout this work. A commercial metakaolin (MK1) produced by Engelhard Corporation (USA) and heat-treated local kaolin clay (MK2) were used in this study. The chemical composition, amorphous phase content (A.P.C.) and specific surface area (S.A.) of admixtures and cement are given in Table 1. The portlandite was analytical grade $Ca(OH)_2$.

Table 1. Chemical compositions of cement and additives (% wt.) and specific surface area (m^2/g)

	Portland cement	MK1	MK2
SiO_2	19.38	52.18	59.34
Al_2O_3	4.30	43.36	37.68
Fe_2O_3	1.95	0.25	1.86
TiO_2	0.38	4.21	1.12
CaO	64.8	0	0
MgO	1.09	0	0
Na_2O	0.19	0	0
K_2O	0.25	0	0
SO_3+Cl	1.92	0	0
P_2O_5	0	0	0
S.A.	0.35	11.4	18.3
A.P.C.		85	75

2.2 Chemical activity

Chemical activity, i.e. the ability to react with portlandite, $Ca(OH)_2$, in the presence of an excess of water, was determined indirectly – using the results of the compressive test of the paste. Six compositions with different portlandite/metakaolin ratios were prepared (Table 2). Metakaolin (MK1) and portlandite were dry-mixed for 5 min in the pan mixer. Later water was added to the metakaolin - portlandite mixture and mixed for 5 min. The water to solid ratio (W/S) in the paste specimens was 1.

The pastes mixed with a pan mixer were cast as cube samples of 25-mm size and cured in air (RH=65%, at 20ºC) until demolding. The samples were demolded after 6 days and then cured in humidity room (RH=100%, at 20ºC) until testing at 3, 7, 14, 21, 28 and 90 days.

Three cubes were tested in compression at every testing age and the average strength was determined, with the individual values varying within ±5% of the mean.

Table 2. Mix compositions

Content of Admixture (% wt.)	Content of Meta-kaolinite (%)	Content of Portlandite (% wt)	$CaO/(Al_2O_3 \cdot 2SiO_2)$ Molar Ratio
25	21	75	12.3
50	42.5	50	4.1
65	55	35	2.2
80	68	20	1.0
90	76.5	10	0.5
95	81	5	0.2

2.3 Compressive strength of cement - metakaolin pastes

The water to binder ratio was 0.33 in the paste specimens. Heat-treated kaolin clay was used as admixture. The replacement ratio of admixture was 20% by weight; the content of amorphous phase was 8.4% and 15%.

The pastes mixed with a pan mixer were cast as cube samples of 25-mm size. The samples containing heat-treated kaolin clay (MK2) and the reference sample were demolded after 24 hours and cured in lime-saturated water at 20ºC until the day of testing at 1, 3, 7, 14, 28 and 360 days.

2.4 Sample characterization

The weight change, energetic transformations and a gas evolution under elevated temperature were performed by simultaneous Differential Thermal and Thermogravimetric Analysis (DTA/TGA - Setaram TG 92-16.12, France). During DTA/TGA analysis the samples were heated at the rate of 5°C min^{-1} to a maximum temperature of 1000°C in airflow of 30 cm^3/min.

2.5 Hydration products

DTA/TGA analysis was used to study the nature of the reaction products, their content and the kinetics of the hydration process.

To investigate the effect of $CaO/Al_2O_3 \cdot 2SiO_2$ molar ratio on the kinetics of reaction portlandite and metakaolinite, DTA/ TGA analysis was performed at age of 90 days for different mixtures and at age of 14, 28 and 90 days for the mixture that was found optimal from the viewpoint of chemical activity.

3. RESULTS AND DISCUSSION

3.1 Effect of $CaO/(Al_2O_3 \cdot 2SiO_2)$ molar ratio on chemical activity

The compressive strength development of the pastes with different $CaO/(Al_2O_3 \cdot 2SiO_2)$ molar ratio [MR] is presented in Figure 1.

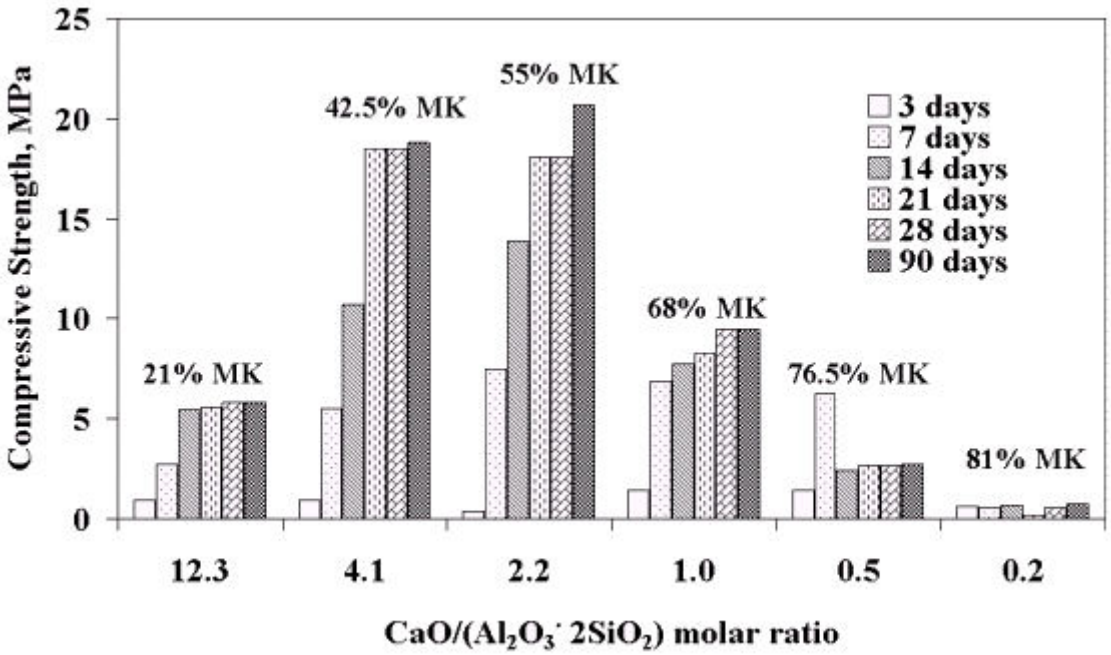

Figure 1. Compressive strength vs. $CaO/(Al_2O_3 \cdot 2SiO_2)$ molar ratio

As can be seen, the molar ratio influences compressive strength development. There is a parabolic dependence between compressive strength and [MR]. The $CaO/Al_2O_3 \cdot 2SiO_2$ molar ratio of 2.2÷4.1 is optimal from the viewpoint of compressive strength or chemical activity. In the range of 0.2 to 4.1 of [MR] a drastic increase in compressive strength was observed. However at MR>4.1 a severe decrease in compressive strength occurred. As can be seen from Figure 1, such intensive strength growth was observed within a very short aging time.

3.2 Effect of portlandite/metakaolin ratio on phase formation

The DTA - curves for portlandite-metakaolin paste with different molar ratios at age 90 days are shown in Figure 2. Content of hydration products was calculated from the TG curves. Figure 3 shows the weight loss associated with the disintegration of hydration products as a function of the portlandite/metakaolin molar ratio [MR].

As can be seen from Figure 2, the main phases formed at hydration are C_2ASH_8 (gehlenite hydrate) and C-S-H. In the range of [MR] = 0.45…4.1 an increase in the weight loss and, respectively, in the content of hydration products, such as C_2ASH_8 and C-S-H is observed (see Figure 3).

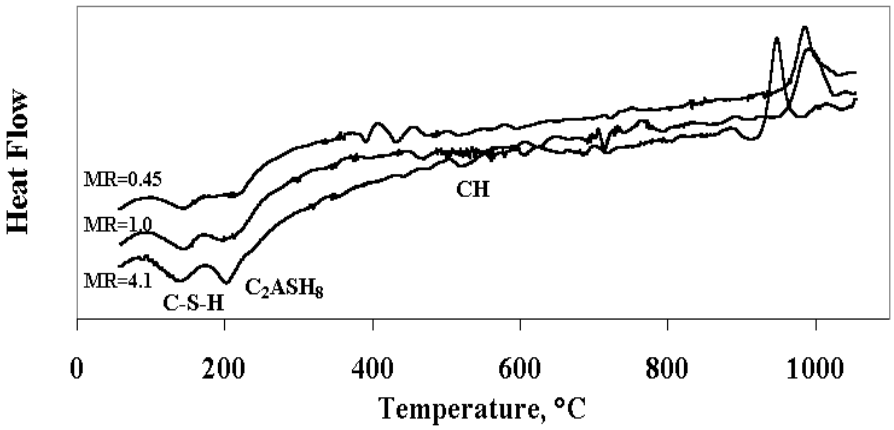

Figure 2. DTA-curves for portlandite - metakaolin paste with different $CaO/(Al_2O_3 \cdot 2SiO_2)$ molar ratios

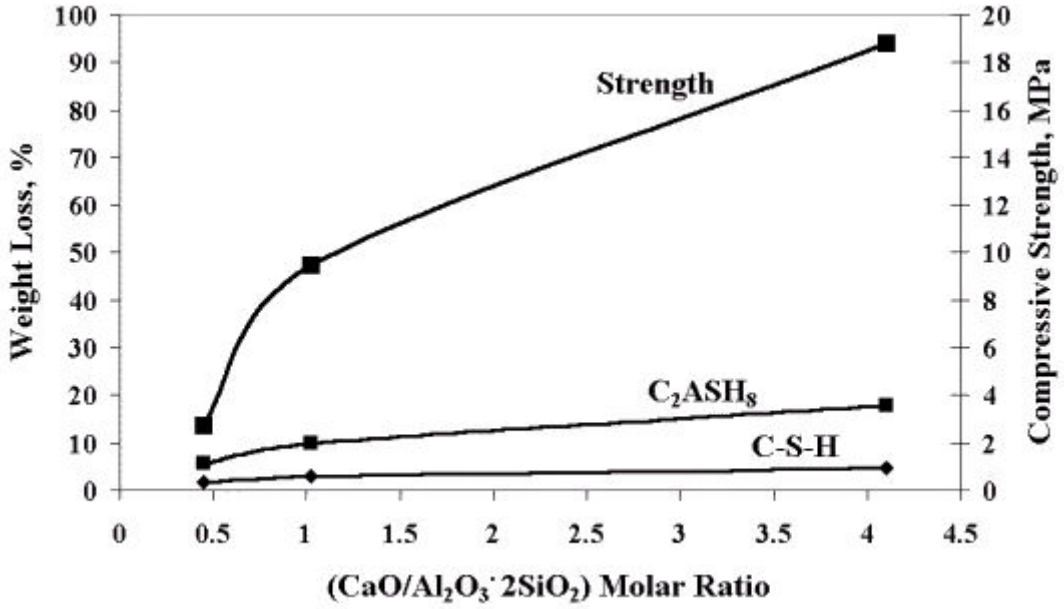

Figure 3. Influence of $CaO/(Al_2O_3 \cdot 2SiO_2)$ molar ratio on weight loss and compressive strength (age of 90 days)

3.3 Kinetics of hydration process of portlandite–metakaolin system

The DTA and TG-curves for portlandite - metakaolin paste with MR=4.1 at age 14, 28, and 90 days are shown in Figures 4 and 5. Kinetics of hydration process (the rate of the change of the weight loss), and the rate of strength development and content of hydration products are presented in Figures 6 and 7, respectively. The relationship between compressive strength and hydration products (gehlenite hydrate and calcium – silicate hydrate is shown in Figure 8.

As can be seen from Figure 6, the hydration process was very intensive at early ages. The rate of both strength development and hydration products formation was maximal at 14 days. According to Figure 6, the development of compressive strength is associated with the increase in C_2ASH_8 and C-S-H content, and the decrease in CH content, respectively. It was found (see Figure 8) that compressive strength of metakaolin - portlandite pastes with W/S=1 could be expressed as a linear function of the gehlenite hydrate and calcium silicate content. C-S-H and C_2ASH_8 are interdependent parameters. At the present stage of research it is not possible to determine the leading role of either of them.

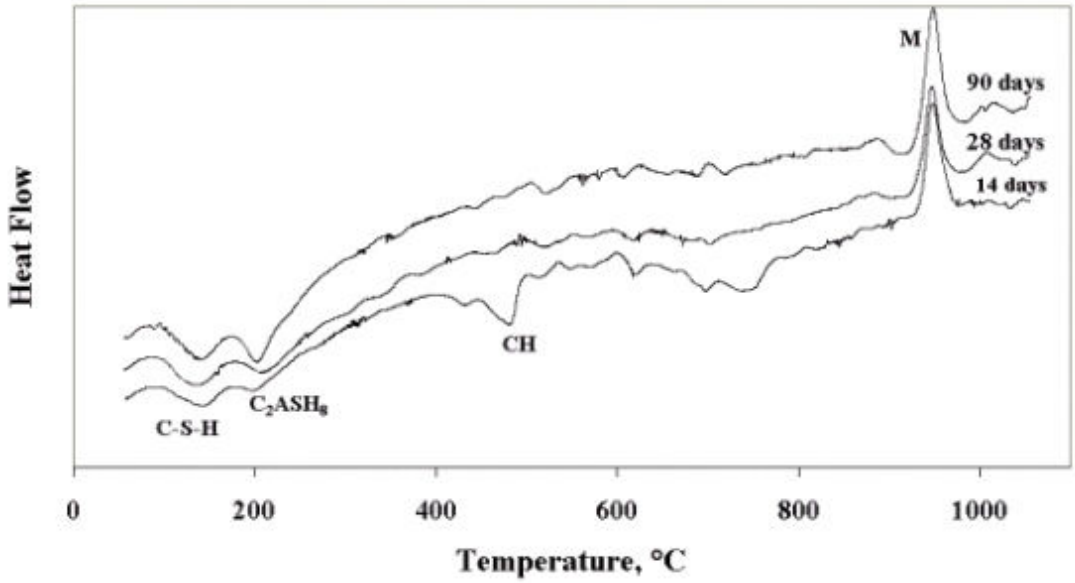

Figure 4. DTA-curves of CH/MK mixture with MR=4.1 at different hydration time

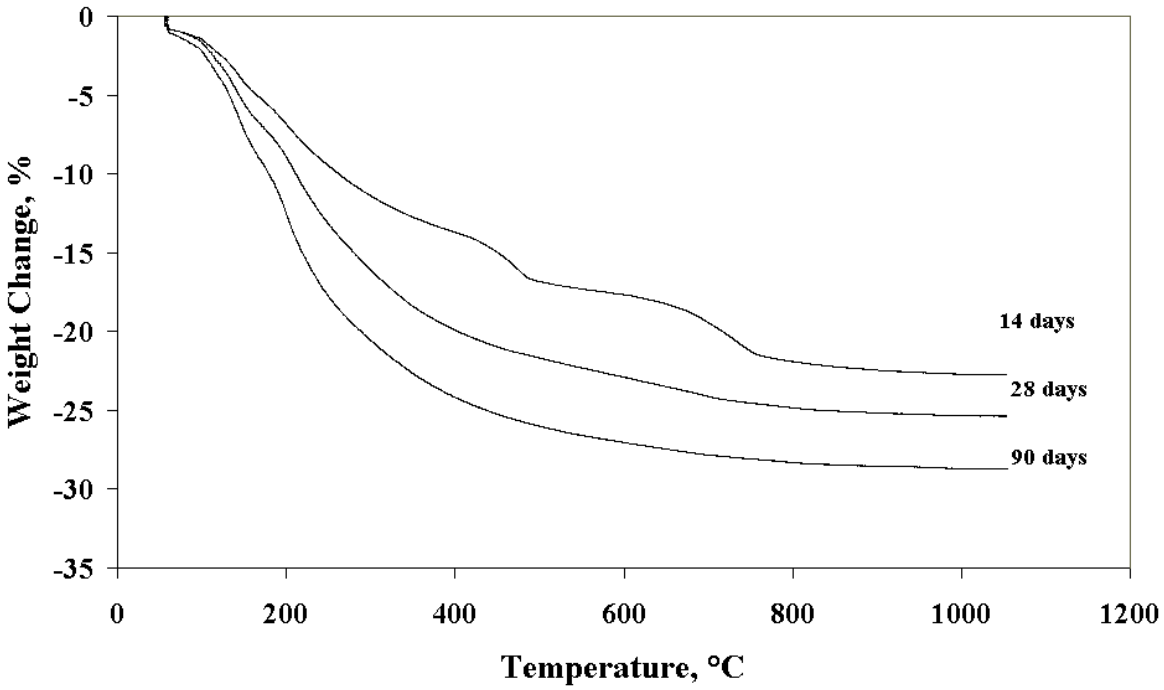

Figure 5. TG-curves of CH/MK mixture with MR=4.1 at different hydration time

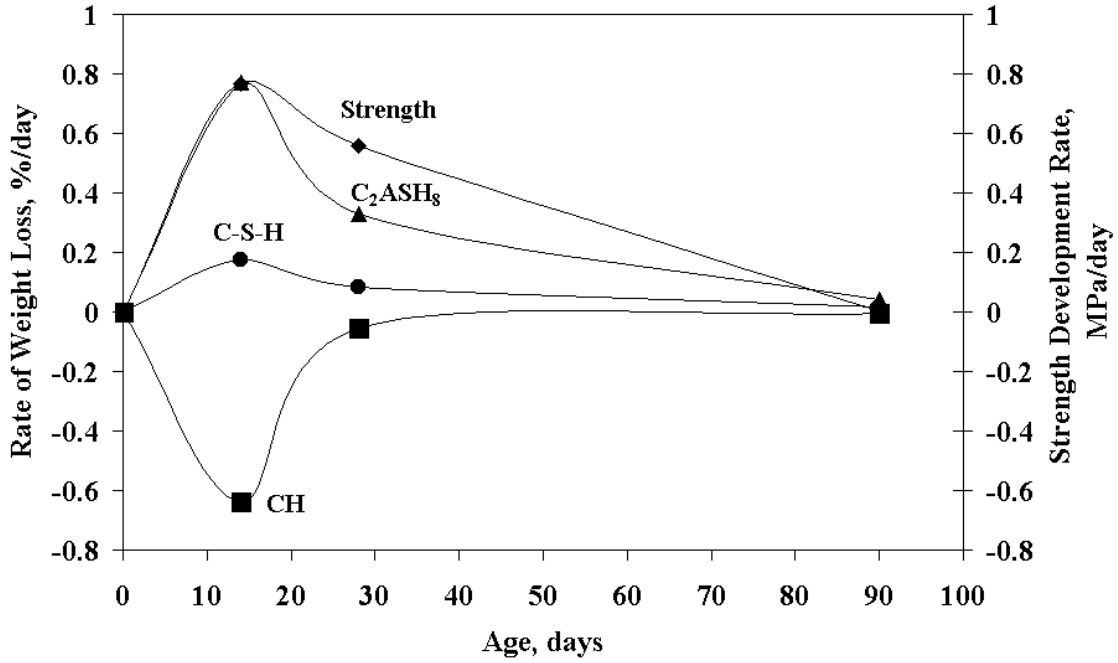

Figure 6. Kinetics of hydration process (MR=4.1)

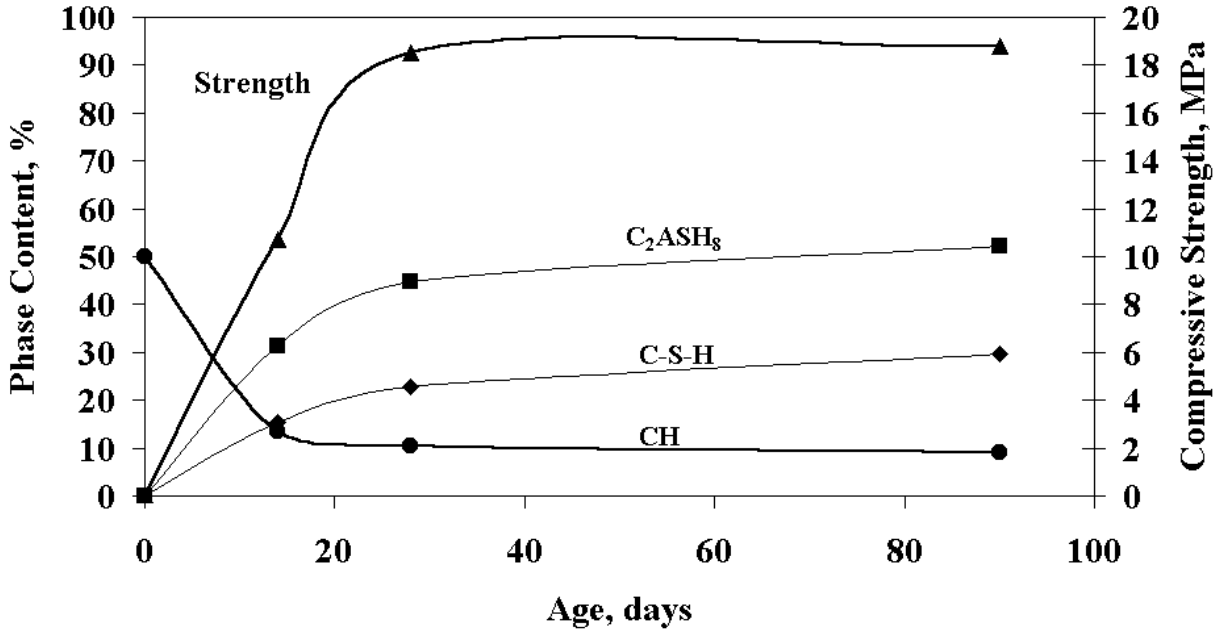

Figure 7. Influence of time on content of hydration products and compressive strength (MR=4.1)

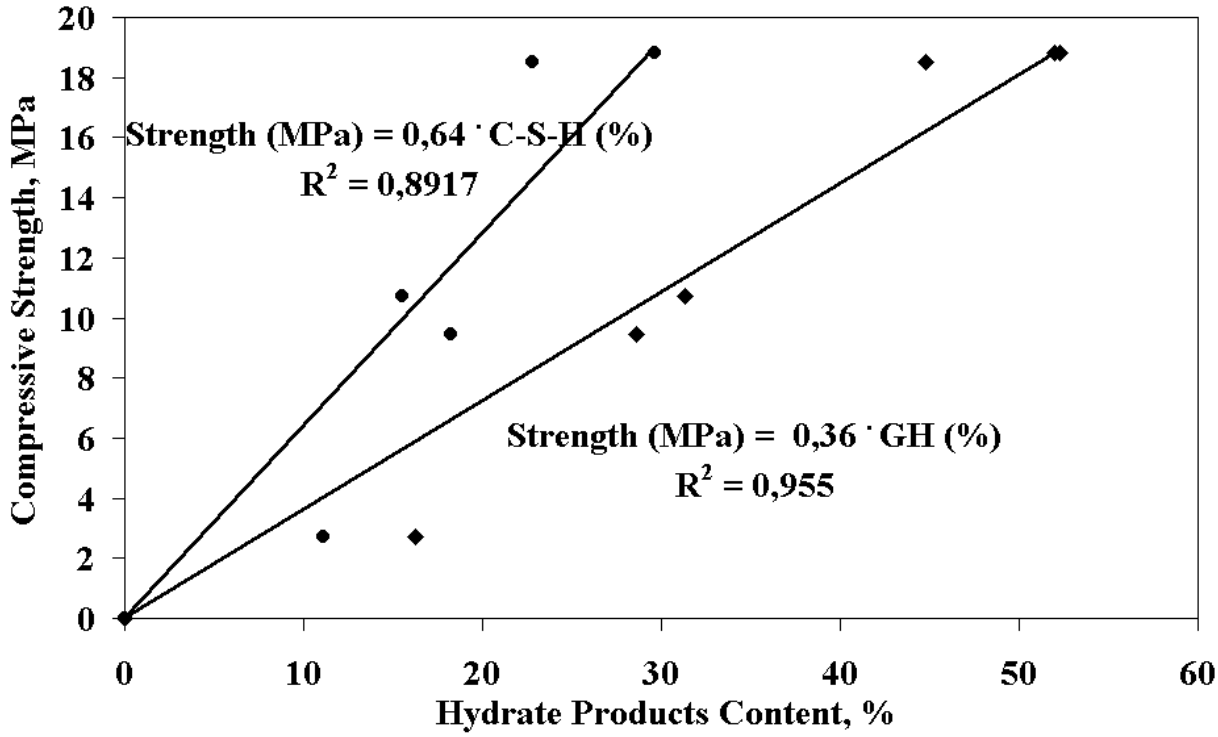

Figure 8. Relationship between compressive strength and gehlenite hydrate content and calcium silicate hydrate

3.4 Influence of metakaolin content on the mechanism of hydration in cement system

Figure 9 shows the evolution in the DTA curves at age of 28 days as a function of metakaolin content. The content of hydration products, such as gehlenite hydrate and portlandite, vs. metakaolin content at age of 28 and 360 days is shown in Figure 10. Compressive strength development for cement pastes with different content of metakaolin is shown in Figure 11.

As observed in Figure 9, the main phases present in the system are CSH and CH (portlandite). In MK- cement system gehlenite hydrate is also present, in addition to CSH and CH. It can be also seen that the content of metakaolin influences phase composition of the hydrating system. The increase in metakaolin content results in the decrease of CH content and the formation of gehlenite hydrate. There is a linear correlation between CH and C_2ASH_8 phase contents on the one hand, and metakaolin content on the other hand (see Figure 10). As in the case of metakaolin/portlandite systems, the increase in content of hydration products such as C_2ASH_8 and C-S-H corresponds to the increase of compressive strength. The compressive strength of pastes incorporating heat-treated kaolin is somewhat lower than that of reference pastes (see Figure 11). This phenomenon seems to be related to the amount of amorphous phase.

As can be found earlier, the $CaO/Al_2O_3 \cdot 2SiO_2$ molar ratio of 2.2÷4.1 is optimal from the viewpoint of compressive strength for metakaolin-portlandite systems. Analogical phenomenon was observed for metakaolin – cement systems. For example: the compressive strength of the paste with MK=8.4% (MR=7.4) was significantly lower than the compressive strength of the paste with MK=15% (MR=4.1).

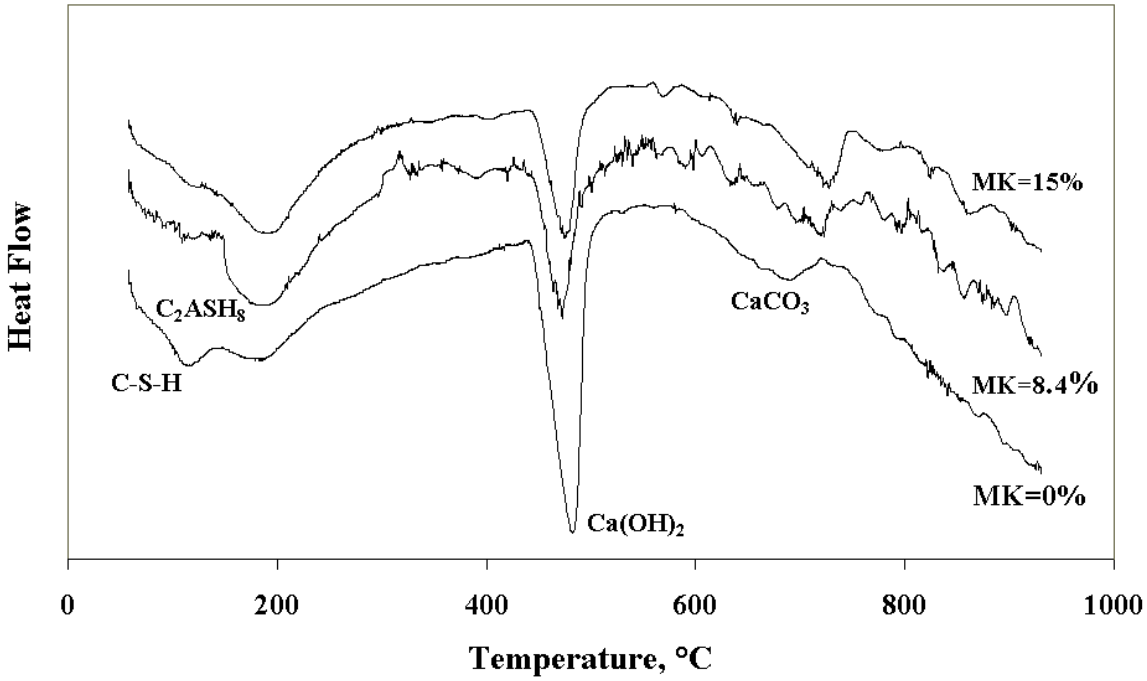

Figure 9. DTA-curves of paste with different content of metakaolin (Age: 28 days)

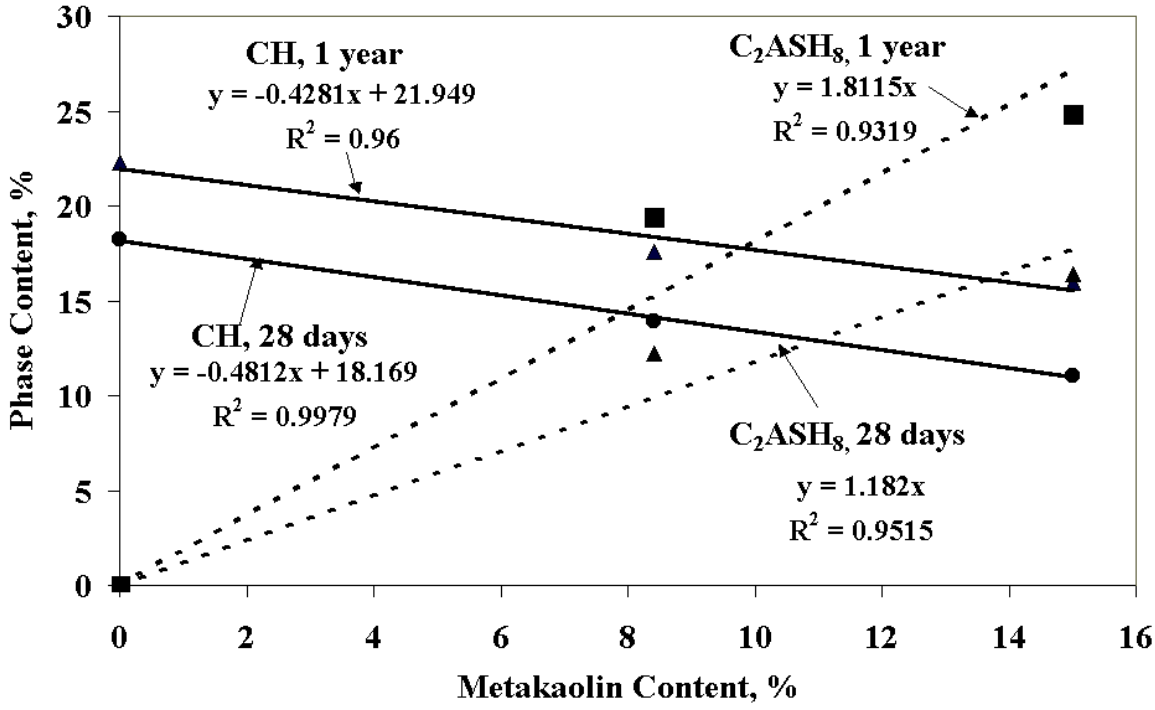

Figure 10. Influence of metakaolin content on the hydration products content (age of 28 and 360 days)

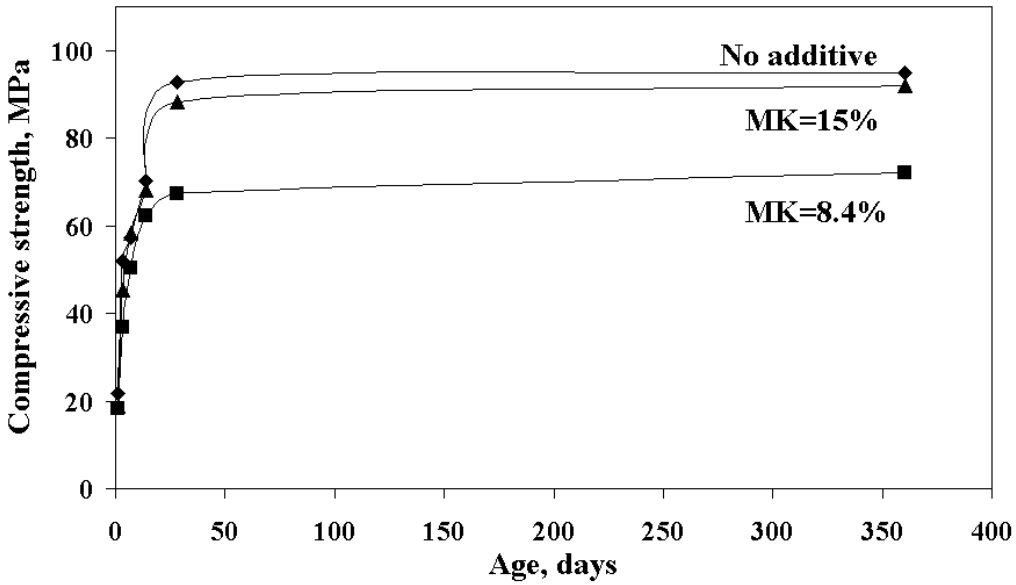

Figure 11. Strength development of cement pastes with different content of metakaolin

4. CONCLUSIONS

- The main phases that form in the hydrated MK-portlandite system are C_2ASH_8 and C-S-H.
- The hydration process is very intensive at early age. The rate of both strength development and hydration products formation was maximal at 14 days.
- Portlandite/metakaolin molar ratio influences the hydration rate, the content of hydration phases and strength development.

- In MK–cement systems an increase in C_2ASH_8 and C-S-H content corresponds to the growth of compressive strength, as in the case of MK-portlandite systems. An increase of metakaolin content leads to the growth of gehlenite hydrate and reduction of portlandite content.
- The $CaO/Al_2O_3 \cdot 2SiO_2$ molar ratio of 2.2÷4.1 is optimal from the viewpoint of compressive strength for both metakaolin-portlandite systems and cement-metakaolin system.

REFERENCES

[1] Hassan, K.E., Cabrera, J.G., Maliehe, R.S., The effect of mineral admixtures on the properties of high performance concrete, Cement and Concrete Composites, V. 22, 2000, pp. 267-271.

[2] Vu, D.D., Stroeven, P., Bui, V.B., Strength and durability aspects of calcined kaolin-blended Portland cement mortar and concrete, Cement and Concrete Composites, V. 23, 2001, pp. 471-478.

[3] Dhir, R.K., Jones, M.R., Development of chloride-resisting concrete using fly ash, Fuel, V. 78, 1999, pp. 137-142.

[4] Malhotra, V.M., Ramezanianpour, A.A., Fly ash in concrete, 2nd Ed., CANMET, Canada, 1994

[5] Sabir, B., Wild, S., Baj, J. Metakaolin and calcined clays as pozzolans for concrete: a review, Cement and Concrete Composites, V. 23, 2001, pp. 441-454.

[6] Lam, L., Wong, Y. L., Poon, C.S., Degree of hydration and gel/space ratio of high volume fly ash/cement systems, Cement and Concrete Research, V. 30, 2000, pp. 747-756.

[7] Biernacki, J., Williams, P., Stutzman, P., Kinetics of reaction of calcium hydroxide and fly ash, ACI Materials Journal, V. 98, N. 4, 2001, pp. 340-349.

[8] Silva, P.S., Glasser, F.P., Phase relation in the system $CaO\text{-}Al_2O_3\text{-}SiO_2\text{-}H_2O$ relevant to MK-lime hydration, Cement and Concrete Research, V. 23, 1993, pp. 627-639.

[9] Frias, M., Cabrera, J., Pore size distribution and degree of hydration of metakaolin-cement pastes, Cement and Concrete Research, V. 30, 2000, pp. 561-569.

[10] Cabrera, J., Frias, M., Mechanism of hydration of the metakaolin-lime-water system, Cement and Concrete Research, V. 31, 2001, pp. 177-182.

ALKALI ACTIVATED AUTOCLAVED AERATED CONCRETE MADE WITH FLY ASH DERIVED CENOSPHERES: EFFECT OF FLY ASH AND PRECURING TEMPERATURE

Michael W. Grutzeck[1], Stephen Kwan[2] and Maria DiCola[3]

Materials Research Institute, MRL Building, The Pennsylvania State University, University Park, PA 16802, USA. E-mail: [1]gur@psu.edu, [2]sxk13@psu.edu and [3]mld7@psu.edu

ABSTRACT

It is possible to make reduced density autoclaved aerated concrete (AAC) - like materials without foaming by adding fly ash derived cenospheres to the formulation. The cenospheres are robust enough to allow all types of mixing including shear mixing associated with macro defect free processing (MDF). Work has demonstrated that fly ash derived AAC can be produced with and without alkali activation. Sodium hydroxide activated samples produced various zeolites within the matrix whereas conventional lime based AAC produced tobermorite and katoite. Strengths of the samples are related to the nature of the precuring conditions, which ultimately affect microstructure and strength development during final autoclave processing.

Keywords: autoclaved aerated concrete, AAC, alkali activated, fly ash, cenospheres

1. INTRODUCTION

Autoclaved aerated concrete (AAC) is a popular building material in use all over the world. It has a 50-year history of successful use in all environments for all types of buildings (Wittmann, 1983, 1992). Two types of AAC are commonly being manufactured. Both use combinations of lime and Portland cement mixed with either ground quartz sand or Class F fly ash. AAC offers a wide array of positive attributes vis à vis concrete block and insulated wood frame construction for residents of North America. However, the final decision to use AAC instead of more conventional building materials will ultimately hinge on the cost of making, transporting and assembling AAC at its point of use. To date, even after intensive lobbying by the AAC industry, the North American consumer has not made the switch. In fact two of the original German manufacturers have pulled up stakes and gone home.

Environmentally speaking, AAC is less material and energy consumptive than many construction materials. It is estimated that the total amount of energy consumed during production (including energy invested in making Portland cement, lime and aluminum powder) is on the order of 1000 MJ/m^3 (Aroni et al., 1993). It achieves this status because some AAC manufacturers already use fly ash and other industrial waste in their formulations coupled with the traditional low energy processing in an autoclave at ~12 bars and 180°C. The introduction of a cellular structure during initial formation of the AAC allows one to produce 3-4 m^3 of AAC from 1 m^3 starting materials (Aroni et al., 1993). When making lime-silica AAC, ground quartz flour is mixed with lime (CaO), Portland cement and water to make thin slurry. At the last moment, aluminum powder is added to the mixture. The mixture is then transferred to a massive steel mold wherein the slurry begins to foam. The foaming causes it to rise in the mold much like a cake leavened with baking powder will rise in an oven. After 45 minutes or so, the AAC "cake" occupies approximately 3-4 times as much space as it did when it was first poured. It has also developed enough green strength to be

demolded, cut with wire saws to a variety of shapes (blocks and/or panels), and placed in a steam-heated autoclave. After treating at 180°C for 10-18 hours the block or panel is removed and ready for use. Densities are on the order of 400-600 kg/m^3 and compressive strengths range from 2 to 5 MPa (Aroni et al, 1993). AAC can also be made from Class F fly ash. The use of fly ash in this manner saves the AAC manufacturer the time and cost of ball milling quartz sand and also keeps the fly ash out of the World's landfills. However due to the Al_2O_3 content of the fly ash, using it instead of quartz does introduce a second phase in the final product, in addition to tobermorite fly ash based AAC contains aluminum substituted hydrogarnet (katoite).

In light of the above, the promotion of fly ash-based AAC as an environmentally friendly "green material" is reasonable. In addition to fly ash, AAC formulations can also include other by-product materials such as silica rich mine tailings and recycled glass cullet as well as alternate sources of lime and Portland cement including ground granulated blast furnace slag and cement kiln dust. In fact, it is possible to produce AAC entirely from these by-products. The latter substitutions are environmentally desirable in as much as the manufacture of Portland cement and lime require a great deal of energy and produce a great deal of carbon dioxide gas.

Given the many advantages of AAC, the issue at hand at this point in time in North America is customer appeal, which is ultimately linked to cost. The outward appearance and livability of an AAC and conventional house are nearly identical, but the similarity ends there. An AAC house is self-insulating, fireproof, and insect and mildew resistant, while not containing known allergens such as VOCs or fiberglass. The current building industry is well established and much of the cost of a wood framed house is labor. In contrast, AAC walls (exterior and interior) can be assembled with thin-set mortar in a week or less. Window and door openings as well as channels for interior wiring and plumbing can be cut after the fact using carbide tipped woodworking equipment: hand saws, routers and the like. Outer wall finishes can be stucco or brick. Interior finishes can be conventional dry wall or plaster. A motivated "do-it-your selfer" could assemble an AAC house from a kit, much like a Sears house kit of the 1930s. AAC could make affordable housing a reality.

The overall objective of the currently funded work is to find a means of toughening AAC in order to make it less prone to breakage and edge damage that often takes place during handling and placing. The damage problem is costly, but even more important is the fact that the builder/customer is left with a negative impression that is hard to overcome. Adoption of a new building material in North America will take time as first impressions are replaced by more favorable ones. If the proposed work is successful, it will provide a deeper understanding of the underlying chemistry of AAC and the feasibility of the proposed toughening process. If implemented by the industry, the proposed technology could provide builders with a more robust AAC resulting in greater user satisfaction and possibly new market penetration, e.g. using AAC to adsorb energy under extraordinary circumstances (runaway trucks and/or blast protection).

The work described below examines the feasibility of using alkali activation of fly ash based AAC to bring about a phase change, and alternate methods of introducing cellular structure to the material. It is known that micrometer-sized wollastonite and xonotlite particles can be used to toughen cement pastes (Low and Beaudoin, 1993a and b). Thus it was hypothesized that insitu growth of well dispersed micrometer sized zeolites in place of larger katoite crystals normally present in the matrix could serve a similar purpose. Sodium hydroxide (NaOH) was used to supply the needed alkali. At first all formulations contained only Class F fly ash and small amounts of either a concentrated NaOH solution or a molar equivalent $Ca(OH)_2$ slurry. These samples were precured and then autoclaved. The data were used to contrast behavior of materials resulting from a conventional pozzolanic reaction compared with those resulting from an alkali activated reaction. Due to the difficulty of foaming alkali containing mixtures with aluminum powder, cenospheres derived from Class F fly ash were used in a second series of samples to lower the density of the

final product. The cenospheres imparted voids as well as a degree of robustness to the mixtures, which made it possible to use shear mixing to prepare a reduced density material. Finally Portland cement was added to the alkali containing mixtures. It was anticipated that phase behavior would parallel those in a traditionally foamed AAC and that findings would be directly applicable to conventional AAC manufacturing. It was also anticipated that the new processing techniques employed to make reduced density AAC-like materials might possibly lead to the development of a new technology and new markets.

2. EXPERIMENTAL METHOD AND RESULTS

2.1 100% Fly Ash and Cenosphere Samples

100% Class F fly ash (Ft. Martin-Allegheny Power-Table 1) was mixed with just enough 12 M NaOH containing a few drops of superplasticizer (Mighty RD-1) to make a thick (modeling clay-like consistency) paste. The paste was manually kneaded, much like bread dough, on a counter top until smooth and then it was compacted into a 2-inch mineral oil coated brass cube mode.

Table 1. Composition and Characteristics of Starting Materials (wt %)

Component	Ft. Martin Fly Ash	Bruce Mansfield Cenospheres
SiO_2	52.74	55.
TiO_2	-nd-	1.27
Al_2O_3	24.31	34.
Fe_2O_3	11.47	2.75
Cr_2O_3	-nd-	0.04
CaO	3.36	0.09
MgO	0.81	0.34
MnO	-nd-	0.06
ZnO	-nd-	0.02
Alkalis	1.87	3.37
SO_3	0.70	-nd-
105°C H_2O	0.20	-nd-
LOI	1.92	-nd-
#325 Sieve	24.90	-nd-
Density (g/cc)	2.37	-nd-
Strength at 28 days (%)	79.75	-nd-

-nd- not determined

The sample was troweled off and then covered with a glass plate. The mold was placed in a 38°C walk-in curing chamber overnight. After precuring, it was demolded and then autoclaved at 180°C for an additional 16 hours. The compressive strength of the sample was 59 MPa, which is similar to the strength reported by Palomo et al. (1999) for a similar material. The X-ray diffraction pattern of the alkali activated fly ash sample (see Figure 1a) indicates that it contains residual glass (amorphous hump centered at ≈22°2θ), residual quartz and mullite, crystalline zeolites (Na-P1, hydroxysodalite and Na-chabazite), and X-ray amorphous tectosilicates (amorphous hump centered at ≈29°2θ).

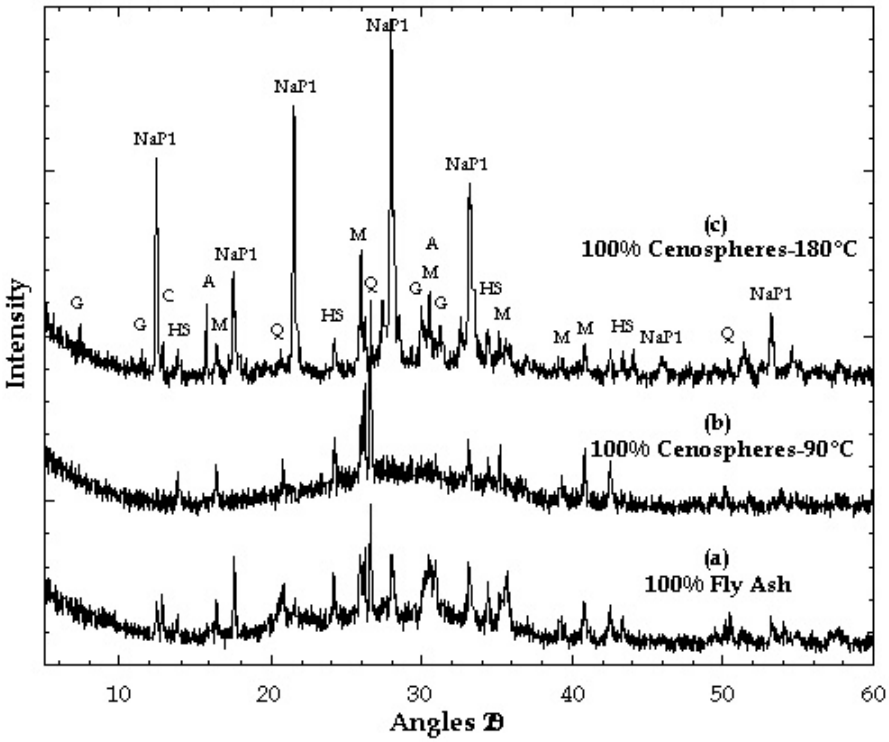

Figure 1. X-ray diffraction patterns of samples made from fly ash and cenospheres cured as a function of temperature. (M = Mullite, Q = Quartz, NaP1 = Na-P1, HS = Hydroxysodalite, G = Gmelinite, C=Na-Chabazite, A=Analcime.)

The accompanying microstructure for this sample is given in Figure 2. The matrix is dense and exhibits very little evidence of crystal growth at both levels of magnification (Photos 2A and 2B). The matrix seems more "gel-like" than crystalline, a characteristic in keeping with its strength and X-ray diffraction pattern.

(A) 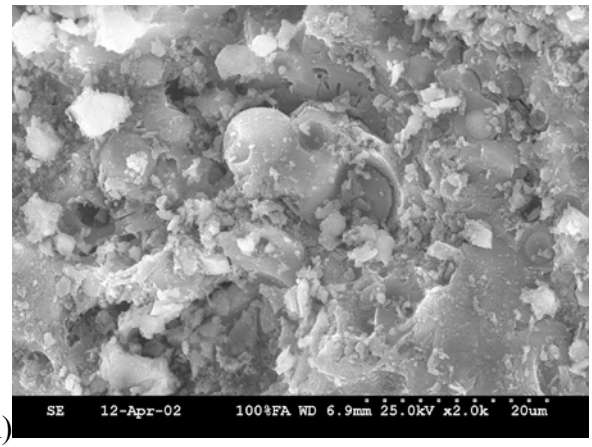

(B) 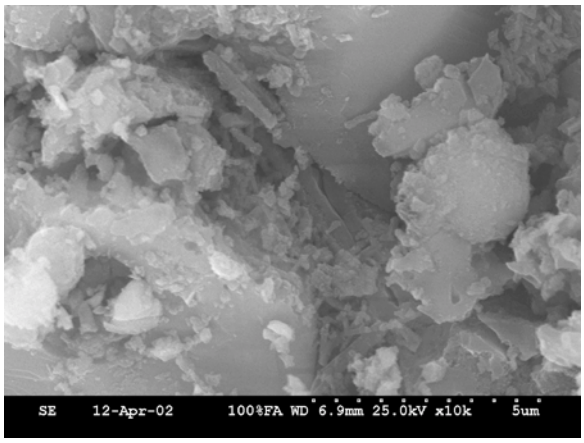

Figure 2. Microstructure of autoclaved 100% Class F fly ash sample made with 12M NaOH. Original magnifications: (A) 2000X and (B) 10000X

Due to the high specific gravity of the sample (~1700 kg/m^3), a second sample was made using 100% cenospheres derived from a Class F fly ash. These are commercially available from First Energy's Bruce Mansfield plant available through US Natural Resources, Inc. (Table 1). The cenospheres were mixed with the same 12M NaOH (containing Mighty RD-1) used previously and again kneaded by hand with the caveat that a few extra grams of NaOH solution were necessary to attain a similar "play dough" consistency. The mix, which now occupied about twice as much volume, was packed into two 2-inch mineral oil coated brass molds rather than one, and again

precured at 38°C overnight. After precuring, the two cubes were demolded. One was autoclaved for an additional 16 hours at 180°C and the other was placed on a platform in a desiccator containing water and cured at 90°C over night (~16 hours). Interestingly, the 90°C sample was twice as strong (2 MPa) as the 180°C autoclaved sample (1 MPa). X-ray diffraction data for these two samples are given in Figures 1b and 1c. The 90°C sample (Figure 1b) is generally devoid of secondary crystalline zeolites, save a trace of hydroxysodalite. Instead the pattern is dominated by a large X-ray amorphous hump with superimposed peaks representing residual quartz and mullite found in the Class F fly ash starting material. More salient is the shift of the maximum of the amorphous hump from ≈22°2θ to one centered near ≈29°2θ. This shift is a result of the development of a sodium-modified hydroxylated tectosilicate network structure (zeolite-like) in the sample during the curing process. These precursors represent nanoscale structures that will ultimately crystallize at higher temperatures. The X-ray diffraction pattern for the 180°C sample (Figure 1c) contains significantly more crystalline material than its 90°C counterpart. Autoclaving at 180°C caused most of the glass in the cenospheres to react (dissolve) and nucleate and grow into crystalline zeolites: Na-P1, hydroxysodalite, gmelinite, Na-chabazite and analcime. The phase development is similar to that observed for the 100% fly ash sample (Figure 1a), but it is better developed and the sample as a whole contains less residual glass. It is worth noting however that the sample cured at 90°C was stronger than the autoclaved sample. These differences are reflected in their microstructures (see Figure 3).

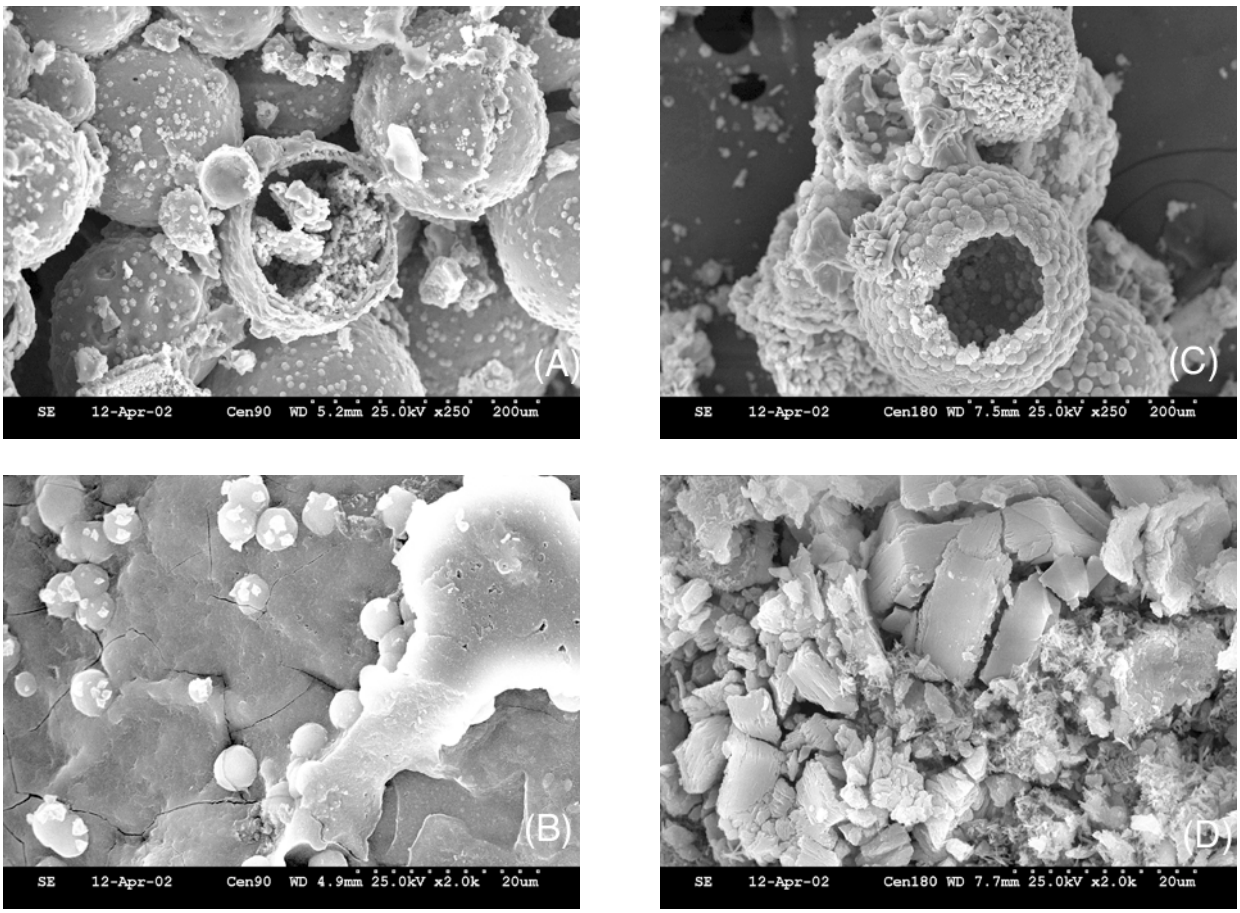

Figure 3. Micrographs of a 100% cenosphere sample cured at different temperatures. (samples A and B) were precured at 38°C and cured at 90°C, and (samples C and D) were precured at 38°C and autoclaved at 180°. Original magnifications: (A,C) 250X and (B,D) 2000X.

Photos A and B represent a sample precured at 38°C followed by curing at 90°C overnight. The cenospheres show varying amounts of dissolution due to the high alkaline mixing solution, but significant amounts of residual glass still remain (note cross section of cenospheres in Photo A).

The cenospheres are covered with a continuous "gel-like" coating. It is suggested that this coating is holding the cenospheres together. Photos C and D are micrographs of a 100% cenosphere sample precured at 38°C followed by autoclaving at 180°C overnight. The dissolution and subsequent reaction of the cenospheres is much more evident in this sample. The shells now consist entirely of zeolite crystals. Massive crystals are also evident in Photo D. The formation of zeolite crystals seems to have a negative impact on the compressive strength of the autoclaved sample.

Apparently the glassy cenospheres are better held together by the precursor gel that formed at 90°C, the lower reactivity at 90°C provides more continuous coverage and more strength than the nearly completely zeolitized sample. The 180°C cured samples are almost totally crystalline and have a very porous, almost lacy structure that seems to impart weakness rather than strength. The specific gravity of the 90°C cured sample was 618 kg/m^3; a conventional AAC sample would have been much stronger. As a result of the very low compressive strength, it was decided to examine a 50:50 blend of fly ash and cenospheres as a mean of providing strength and a more moderate density.

2.2 50:50 Cenosphere:Fly Ash Samples

A 50:50 by weight fly ash/cenosphere sample was again mixed and kneaded by hand as described above. In this instance, overnight precuring took place in the brass mold at 90°C instead of 38°C. Two samples were prepared. One was tested after curing at 90°C overnight, whereas the other sample was autoclaved at 180°C for an additional 16 hours. Unlike the earlier samples, analysis of these X-ray diffraction patterns indicated that curing temperature had made a significant difference in the phase development of the two samples, see Figure 4.

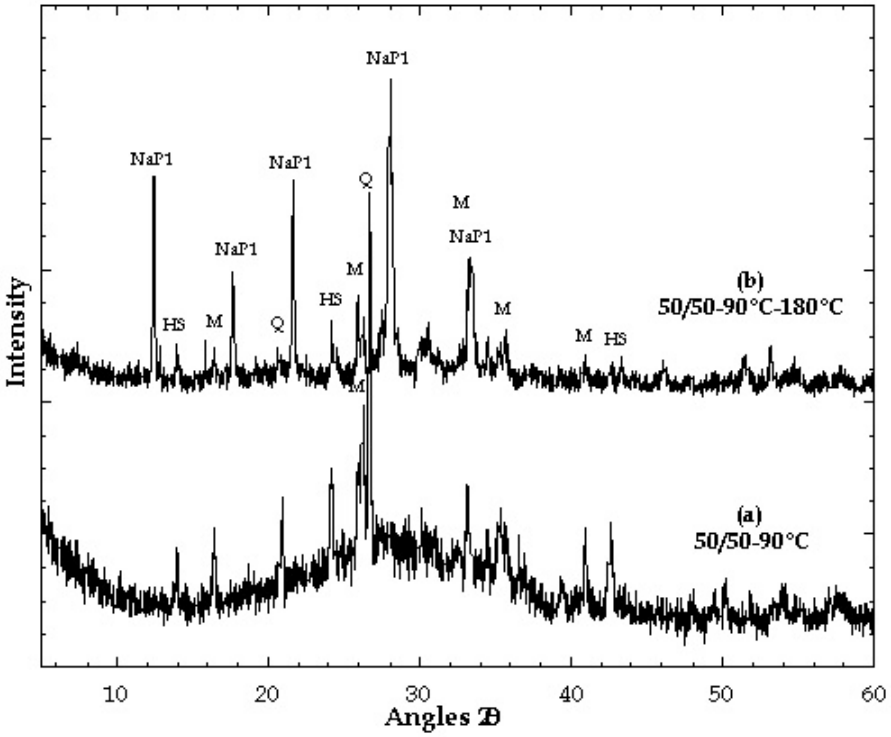

Figure 4. X-ray diffraction patterns of 50:50 samples of fly ash and cenospheres cured under different conditions. (M = Mullite, Q = Quartz, NaP1 = Na-P1, HS = Hydroxysodalite)

The 90°C sample contains residual glass and residual quartz and mullite. The pattern is dominated by a large X-ray amorphous hump centered at ≈27-28°2θ. Only trace amounts of hydroxysodalite can be detected. See Figure 4a. The 90°C plus 180°C autoclaving sample was radically different. Although it still contains a trace of mullite and hydroxysodalite, the quartz peak and most if not all of the amorphous background are gone. The pattern is more crystalline. See Figure 4b. The

sample consists of nearly pure Na-P1 zeolite with small amounts hydroxysodalite and residual quartz and mullite.

Micrographs for the two 50:50 samples are given in Figure 5. The difference in density of the samples is quite obvious from the micrographs. The appearance of the samples at 250x magnification closely resembles that of AAC. At higher magnifications (2000x and 1000x) however, the not so obvious differences become quite apparent. The 90°C sample (Figure 5A and 5B) contains a significant amount of residual glass and open porosity. The 90°/180°C cured sample (Figure 5C and 5D) is considerably more crystalline. Crystals are part of the matrix and fill once open pores. Using a blend of fly ash and cenospheres could provide an alternate method of developing a cellular structure on the microscale.

The interesting outcome, which may be due to a phase change, is the radical difference in compressive strength of these samples. Although specific gravities were nearly the same (924 kg/m^3 (90°C) versus 976 kg/m^3 (90°/180°C), the strength fell from 21 MPa for the 90°C sample to 9 MPa when the 90°C sample was subsequently autoclaved at 180°C.

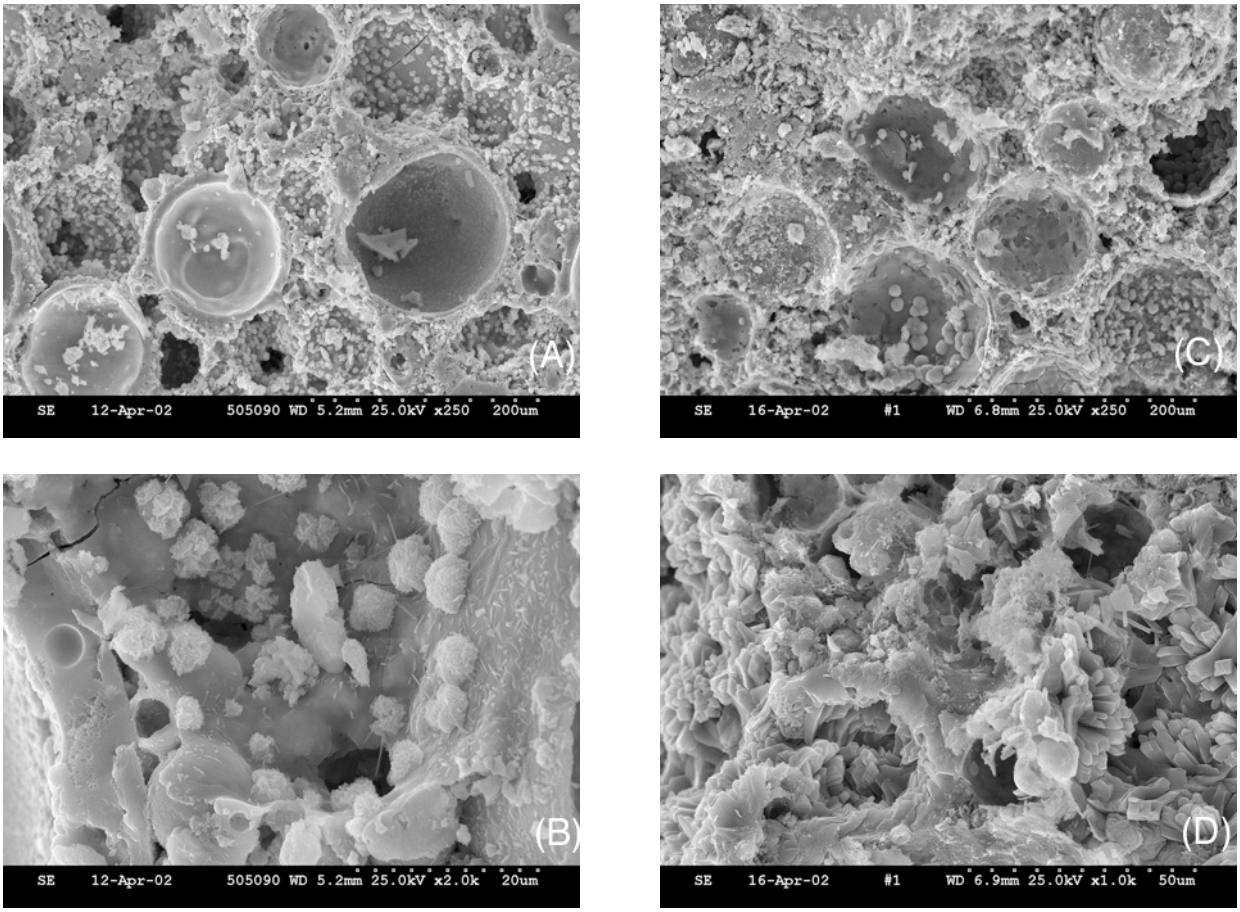

Figure 5. Comparison of microstructure of a 50:50 fly ash:cenosphere sample cured at various temperatures.

It is suggested that the 90°C cure caused the sample to develop initial strength and X-ray amorphous precursor phases that subsequently crystallized at 180°C. The crystallization process disrupted the continuity of the structure resulting in the lower strength of the 180°C sample. Although the 9 MPa value is still in keeping with the expected values for a 900 kg/m^3 sample (Aroni et al., 1993), the possibility of manufacturing a stronger material at 90°C seems attractive because an autoclave would not be needed to cure the material.

2.3 40:40:100 Portland Cement:Cenospheres:Fly Ash Mixtures

In conventional lime based AAC, tobermorite is the phase responsible for strength. Due to the complete lack of crystalline tobermorite in the above mixtures, it was decided to add Portland cement to the mixture in order to increase the calcium oxide content enough to produce tobermorite along with the zeolite. The recipe chosen contained the following materials:

- 40g Portland cement (Type III) Southdown Plant, Wampum, PA.
- 40g First Energy - Bruce Mansfield cenospheres (US Natural Resources)
- 100g Ft. Martin fly ash (Allegheny Power)

The dry ingredients were pre-blended and then mixed with 20g NaOH mixed in 40g H_2O containing a few drops of Mighty RD-1 (~12 M NaOH). A few extra drops of the ~12 M NaOH solution was added during the mixing and kneading process to obtain the same workability as above. For the sake of comparison, a duplicate sample was made in which the NaOH was replaced by a molar equivalent of CaO. In this instance 14g CaO was added to 40 g of DI water (containing a few drops of Mighty RD-1) in order to slake the lime prior to mixing. The dry ingredients were then mixed with the liquid and the resulting paste kneaded as before. A few grams of extra water were added to make a workable clay-like paste. Both mixtures were placed in glass covered 2-inch brass cube molds and precured overnight at 90°C. Both samples were already extremely hard on de-molding. Both 90°C cured samples were then autoclaved at 180°C overnight (approximately 16 hours).

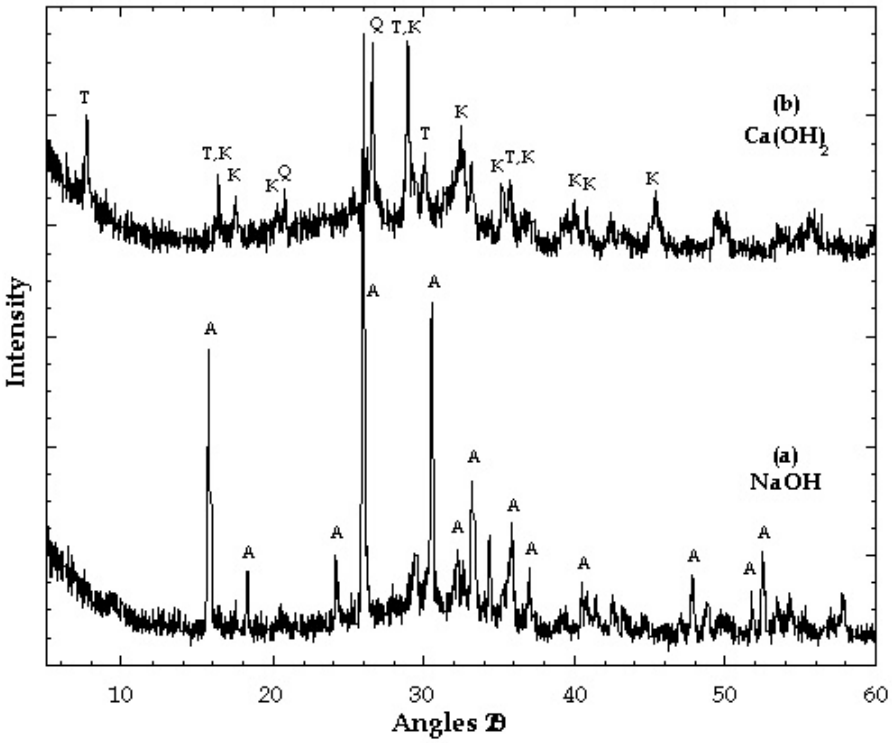

Figure 6. X-ray diffraction patterns of Portland cement containing mixtures (40:40:100) cured at various temperatures. (T=Tobermorite, K = Katoite, A = Analcime, Q = Quartz)

The specific gravity before and after autoclaving did not change significantly: Final values were approximately the same as their initial ones, i.e. 1526 kg/m^3 (NaOH sample) vs. 1335 kg/m^3 (CaO sample), suggesting that water vapor from the autoclave did not contribute water to the hydration reaction to any great extent. The X-ray diffraction patterns for the NaOH autoclaved sample are dominated by analcime while the CaO autoclaved sample consists primarily of tobermorite and partially silica substituted hydrogarnet (katoite). Both samples contain residual mullite and quartz. See Figure 6 above.

Microstructure of the samples are given in Figure 7. At low magnifications the samples look alike (A and C), but at higher magnifications the NaOH sample (B) appears massive and tends to contain zeolites growing inside of cenosphere cavities. The CaO sample (D) ends to consist of a lower porosity matrix that contains less cenosphere casts and little if any zeolites. Instead it is dominated by abundant tobermorite crystals filling space and leaving little porosity. Strength behavior was as follows: the NaOH-containing sample maxed out at 14 MPa. The companion lime-containing sample reached 32 MPa. If correct, the lower strength of the 90°C precured NaOH sample might be attributed to the development of precursor phases at 90°C that subsequently changed to analcime on curing to 180°C. The phase change could cause matrix weakness if there is a volume change associated with it. Conversely, the CaO containing sample developed tobermorite at 90°C and continued to improve its crystallinity and strength at 180°C, no phase change occurred. In this instance, the tobermorite sample is about twice as strong as one might expect for an AAC sample having a similar density (Aroni et al., 1993).

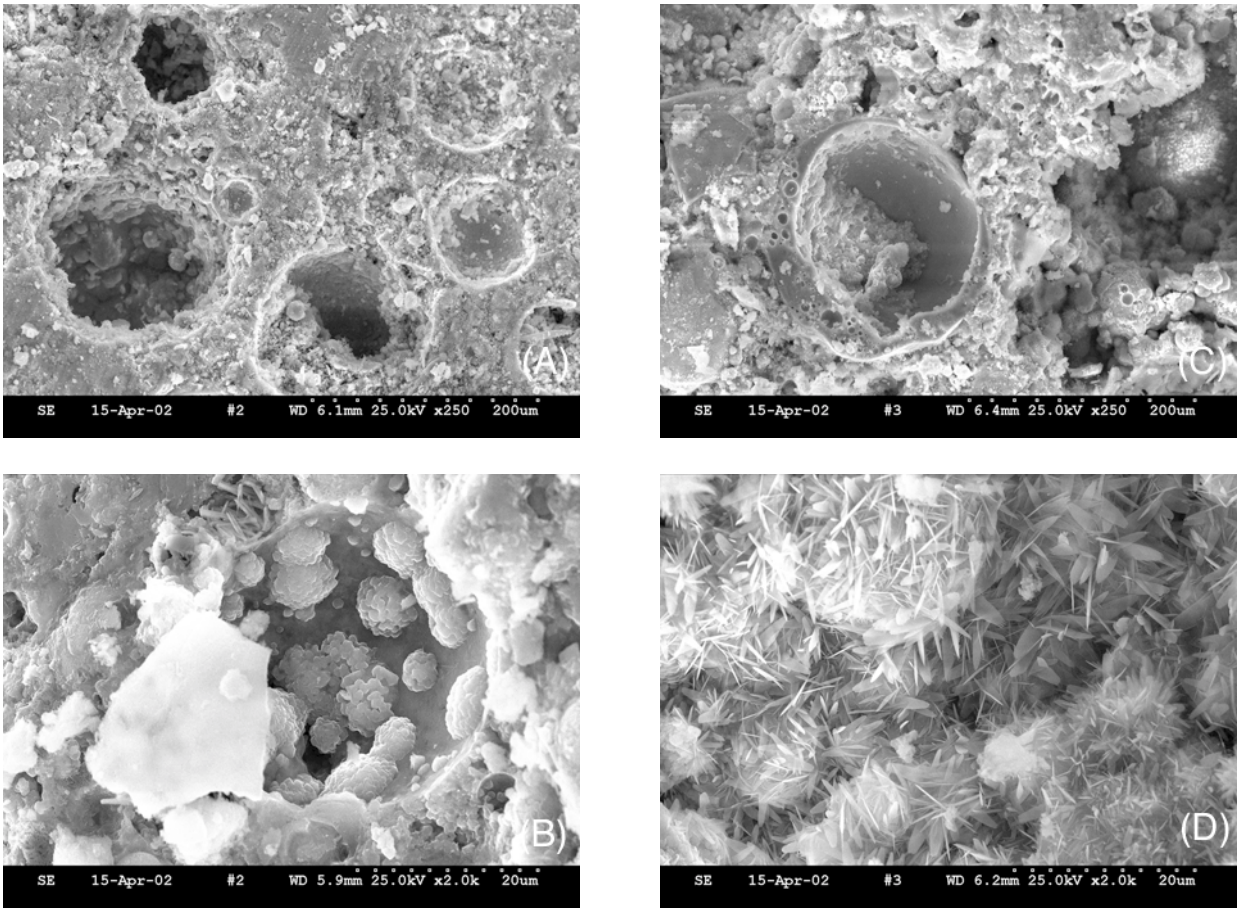

Figure 7. Comparison of microstructure of 40-40-100 samples made with NaOH and $Ca(OH)_2$. (A,C) 200X and (B,D) 2000X

In order to test this hypothesis, the same two samples were prepared again, but this time they were precured overnight at 38°C instead of 90°C prior to autoclaving. X-ray diffraction traces are given in Figure 8. Phase development for the lime-containing sample (Figure 8b) is identical to that for the 90°C precured sample depicted in Figure 6b.

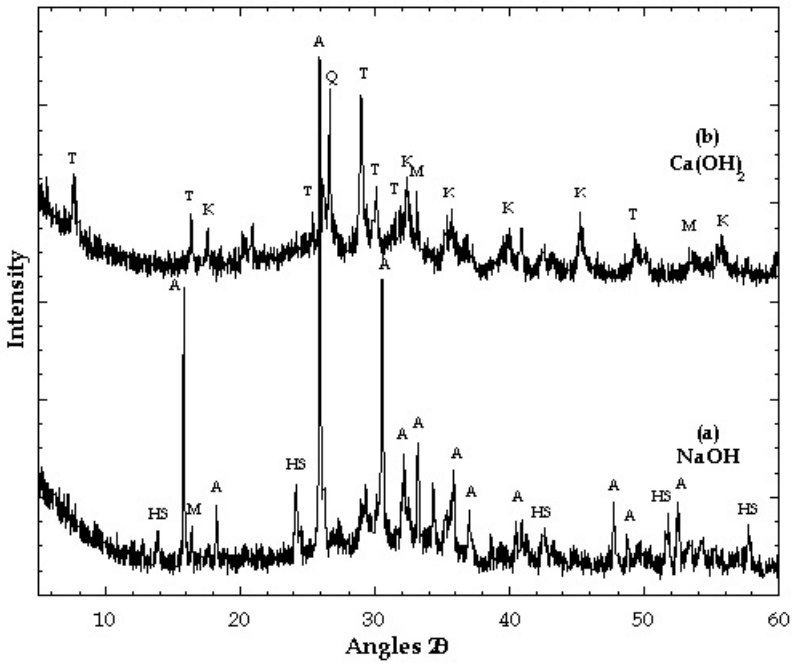

Figure 8. X-ray diffraction patterns of Portland cement containing mixtures cured at various temperatures. (T = Tobermorite, K = Katoite, M = Mullite, HS = Hydroxysodalite, A = Analcime, Q = Quartz)

Both traces contain tobermorite and katoite. The NaOH sample (Figure 8a) is also nearly identical, containing mostly analcime but now also a trace of hydroxysodalite. In both cases the change in precuring temperatures did not affect phase development to any great extent, but it radically affected the development of strength. The NaOH sample maxed out at 28 MPa and the lime sample attained 16 MPa, a complete reversal in behavior compared to the 90°C precured samples. The microstructures of the samples are given in Figure 9.

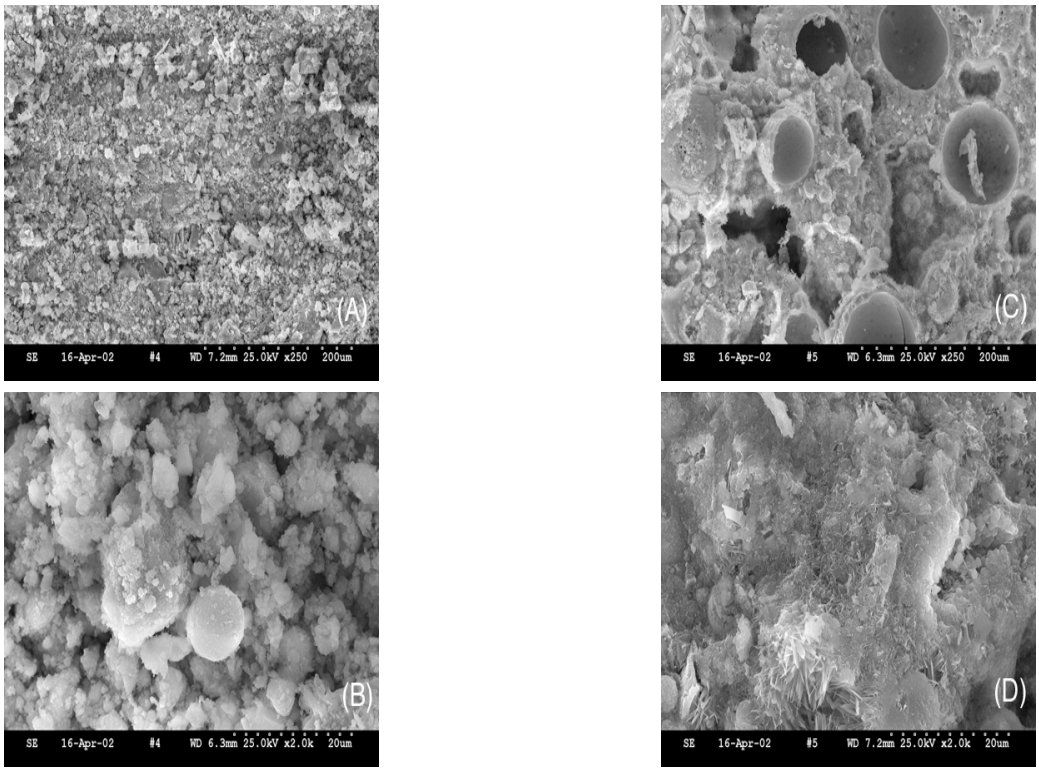

Figure 9. Comparison of the microstructure of 40-40-100 samples containing NaOH and $Ca(OH)_2$ cured at different temperatures

They are significantly different from their counterparts given in Figure 7. Cenospheres and most of the fly ash particles in the NaOH containing sample (Figure 8A and 8B) have reacted and been replaced by a large quantity of irregular crystalline masses. The lime-containing sample consists of less well defined tobermorite crystals (Figure 8C and 8D) compared to its 90°C precured counterpart presented earlier .The NaOH cured sample is rather interesting. All traces of cenospheres are gone and only a few fly ash spheres remain.

The matrix is dominated by small irregular crystalline masses that must interlock on the microscale and provide the increased strength noted for this sample. It is suggested that precuring at 38°C allowed significant dissolution and gel formation and that the gel subsequently nucleated and crystallized when heated to 180°C. Crystallization normally does not occur at 38°C, but, when the sample was precured at 90°C rather than 38°C, the nucleation and growth process occurred directly without the formation of a large amount of gel phase. This apparently reduced the degree of reactivity and the total amount of zeolite that formed. The sample still contains glassy material and an AAC like structure, which is not as strong. The CaO sample appears much like its Figure 7 counterpart except it was harder to find distinct tobermorite crystals. In addition, once they were identified, they did not exhibit the same degree of crystallinity as the sample precured at 90°C (compare Figures 7D and 9D). Unexpectedly, the 38°C cured CaO-cured sample was half as strong as its 90°C counterpart. It is suggested that a lime rich sorosilicate C-S-H formed initially at 38°C and then subsequently crystallized to tobermorite when it was heated to 180°C (Sato and Grutzeck, 1992). C-S-H is the normal precursor phase for tobermorite, but in this instance the sample had already developed enough strength that the conversion process disrupted the matrix. Normally AAC is autoclaved within a few hours of demolding while it is still relatively soft. This sample had cured overnight at 38°C and was already quite hard prior to autoclaving. The specific gravity of the 38°C sample (1500 kg/m^3) was slightly lower than the sample precured at 90°C (1526 kg/m^3). This is not really significant, and a priori one would not anticipate the drop in compressive strength from 32 MPa to 16 MPa unless some other mechanism were operative. It is suggested that the 38°C precure had locked in some other phase, which changed on further heating; it is suggested that C-S-H was this phase. The increase in strength of the NaOH sample seems justified, in light of our previously discussed hypothesis. Analcime formed directly from a well-developed gel having little strength, therefore the matrix was not disrupted.

3. CONCLUSIONS

Autoclaving shear mixed samples containing fly ash and/or cenospheres mixed with concentrated sodium hydroxide solution provides a means of producing a range of materials having varying densities and strengths that are based upon the development of zeolites as the binder phase. Although the objective of the work was to produce both tobermorite and zeolites at the same time, this has not yet been achieved. Further experiments are in progress. However, it was shown that shear mixing a paste formulated with Class F cenospheres, Class F fly ash, Portland cement and either concentrated lime water or sodium hydroxide solution allows one to make an extrudable AAC - like material without a foaming step. The material contains voids similar to those found in AAC that result from the added cenospheres, but the voids occur at the micrometer scale. Density is reduced even though MDF mixing technology is employed. Although precuring conditions did not affect phase development, it did affect microstructure and strength. When NaOH is used, precuring at 38°C prior to autoclaving allows for maximum aluminosilicate gel formation prior to crystallization. Nearly all of the cenospheres and fly ash particles are consumed during this process. If the sample is activated with CaO, an initial precure at 90°C seems to provide greater strength.

The following explanation for the observed behavior of the CaO system is based upon a new model for the hydration process (Grutzeck, 1999). When a lime-rich sample is precured at 38°C, the lime

will react with the fly ash and form a predominantly dimeric sorosilicate C-S-H on the surfaces of the fly ash. At 90°C, the situation is similar, but because of the lowered solubility of $Ca(OH)_2$ at elevated temperatures and the fact that sorosilicate C-S-H is not stable at temperatures above 80°C, dreierkette chains found in tobermorite form directly without the sorosilicate intermediary that forms at 38°C. Upon autoclaving, the 90°C precured sample will continue to build crystallinity of the already existing phase (tobermorite). The situation at 38°C is slightly different in as much as autoclaving necessitates the change of the original sorosilicate C-S-H into one dominated by chains (tobermorite).

In the case of the NaOH sample, precuring tends to allow the solution phase to dissolve significant quantities of alumina and silica from the fly ash and at the same time depress the Ca^{2+} ion solubility. Once in solution, the solvated sodium aluminosilicates ions tend to combine and the form insoluble gels. When heated the gel tends to crystallize as zeolites. Both samples formed precursor gels, but in the case of the 38°C sample, the process was nearly complete. The gel occupied formally open spaces and, once it crystallized, became a rather continuous fine-grained matrix. The sample precured at 90°C crystallized almost immediately without significant gel formation. This caused much of the sodium to enter the zeolite structure at early times while much of the glassy phase still remained. The zeolites tend to form coatings on the surfaces of cenospheres and fly ash grains rather than consume them.

It is concluded that the precuring step plays a significant role in determining early micro-structural development of these materials, which in turn ultimately impacts the performance of the final product. In a lime-based AAC, it is suggested that a 90°C precure could in fact increase the strength of the final product by a factor of two. Likewise in an alkali activated zeolite-containing system a 38°C precure leads to similar two-fold increase in strength versus a precure at 90°C.

ACKNOWLEDGMENT

This material is based upon work supported by the National Science Foundation under Grant No. CMS-9988534.

REFERENCES

[1] Low, N.M.P. and J.J. Beaudoin, " Flexural Strength and Microstructure of Cement Binders Reinforced with Wollastonite Fibres," Cement Concrete Research 23, 905-916 (1993a).

[2] Low, N.M.P. and J.J. Beaudoin, " Mechanical Properties and Microstructure of Cement Binders Reinforced with Synthesized Xonotlite Micro-Fibres," Cement Concrete Research 23, 1016-1028 (1993b).

[3] Aroni,S.,G.J. de Groot, M.J. Robinson, G. Svanholm and F.H. Wittman (eds), Autoclaved Aerated Concrete Properties, Testing and Design, RILEM Recommended Practice, 404 pp, E & FN Spoon, London (1993).

[4] Palomo, A., M.W. Grutzeck and M.T. Blanco, "Alkali-Activated Fly Ashes: A Cement for the Future," Cement Concrete Research 29, 1323-1330 (1999).

[5] Sato, H. and M.W.Grutzeck, "Effect of Starting Materials on the Synthesis of Tobermorite" Materials Research Society Symposium Proceedings 245, 235-240, Materials Research Society, Pittsburgh (1992).

[6] Grutzeck, M.W., "A New Model for the Formation of Calcium Silicate Hydrate (C-S-H)," Materials Research Innovation 3, 160-170 (1999)

[7] Wittmann, F.H. (ed.), Advances in Autoclaved Aerated Concrete, Proceedings 3rd RILEM International Symposium on Autoclaved Aerated Concrete, ETH Zurich, 364 pp., A.A. Balkema, Rotterdam (1992).

[8] Wittmann,F.H.(ed.), Autoclaved Aerated Concrete, Moisture and Properties, Developments in Civil Engineering Vol. 6, 380 pp., Elsevier, Amsterdam (1983).

INFLUENCE OF TRIISOPROPANOLAMINE ON THE PHYSICO-CHEMICAL AND MECHANICAL PROPERTIES OF PURE CEMENT PASTES AND MORTARS

J. Perez[1], A. Nonat[1], S. Garrault-Gauffinet[1], S. Pourchet[1], M. Mosquet[2] and C. Canevet[2]

[1]LRRS, UMR CNRS-Université de Bourgogne 5613, Faculté des Sciences Mirande
9 avenue Alain Savary, BP 47870, 21078 Dijon Cedex
E-mail : jean-philippe.perez@u-bourgogne.fr
[2]Chryso SAS, 7rue de l'Europe, 45300 Sermaises du loiret

ABSTRACT

Concrete and mortars are porous composite materials resulting from a mix of cement, aggregates and water. Addition of an organic additive, currently used as grinding aid (Triisopropanolamine named TIPA), generates a mechanical strength increase of concrete and mortars with respect to samples hydrated without additive. The physico-chemical study we have carried out in order to explain this macroscopic observation has led us to dismiss the assumption of a possible increase of the cement paste hydration degree despite a soluble complex formation between TIPA and iron hydroxide. A change of the cement paste microstructure has been emphasised in presence of TIPA but this modification involves no effect on the mechanical properties of cement pastes.

A modification of the cement paste - aggregate interface in presence of TIPA has to be taken into account as a result of mechanical compressive tests made on pure cement pastes and mortars.

1. INTRODUCTION

Concrete is a resistant material obtained by mixing cement, aggregates and water. This composite material is composed by a cement matrix where hydrated phases form from anhydrous cement grains hydration. The hydration reactions take place following a dissolution-precipitation mechanism. Calcium silicate hydrate (C-S-H) and Portlandite ($Ca(OH)_2$) precipitate from the dissolution of the silicate phases (C_3S and C_2S) which are the main component of a Portland cement with respect to the aluminate phase (C_3A et C_4AF). This is the C-S-H formation on anhydrous grains which mainly leads to the cohesive structure(1). The higher the hydration degree at a given time, the higher the mechanical properties(2) (3).

For a cement paste blended with aggregates, a part of the contact hydrates – hydrates will be replaced by new contacts hydrates - aggregates. This substitution could be at the origin of the lower mechanical strength of mortars because of the weak link of the hydrate – aggregate bond where cracks can initiate and propagate(4).

Moreover, cement manufacturers add grinding aids such as Triisopropanolamine (TIPA) in small amounts to increase grinder productivity. Besides this effect, TIPA is also particularly known to enhance mechanical strength of mortars at 7 and 28 days(5). A mechanism based on a soluble iron-TIPA complex formation which could increase the hydration degree of the cement paste has been proposed(6) (7). Iron hydroxide ($Fe(OH)_3$) is able to form in the C_4AF hydration process according to the mechanism proposed in (6). This precipitation could limit water and ionic species diffusion

and this could limit the hydration degree of a cement paste. TIPA, according to a facilitated transport modelcould solubilise iron hydroxide because of a soluble complex formation. Therefore, the aluminoferrite phase hydration degree could increase as well as the cement paste hydration degree and could lead to an enhancement of the mechanical properties of mortars.

But some basic questions can be expressed as follow:

- Can we link the mechanical strength enhancement to the only increase of the aluminoferrite phase hydration degree knowing that the mechanical properties are directly join up to the quantity of the C-S-H formed?
- Or, is the hydration degree increase of the silicate phases with TIPA a result to explain this macroscopic effect?
- Is the evolution of these mechanical properties observed on mortars samples identical on pure cement paste?
- Clear answers have not been yet proposed, so the aim of this work is to verify these assumptions in order to lead to a better understanding on the actual effect of TIPA on the mechanical properties of concrete and mortars.

First, the physico-chemical evolution of a cement diluted suspension with and without additive were studied by isothermal calorimetry and measurements of ionic concentration in solution.

Then, the microstructure of pure cement pastes was characterised by mercury intrusion porosimetry experiments. The hydration degree of cement paste was also determined by XRD analysis and calorimetry coupled with thermogravimetry measurements.

At last, mechanical compressive tests were carried out in the same way on both pure cement pastes and on mortars.

2. EXPERIMENTAL

2.1 Materials

A model clinker (synthesised by Lafarge) composed solely by the four principal phases with gypsum added (1.63% SO_3 by weight) was used for the physico-chemical experiments and for the hydration and porosimetry determination. An industrial clinker (Lafarge) with gypsum added (2.33% SO_3 by weight) was used for the mechanical tests because of the great quantities required. The chemical and mineralogical composition of both materials are given in the table 1.

Table 1. Chemical and mineralogical composition (% mass)

	CaO	SiO_2	Al_2O_3	Fe_2O_3	Na_2O	K_2O
Model clinker	68	23	5	4	0.05	0.1
clinker	65	20	5	3	0.1	0.8

	C_3S	C_2S	C_3A	C_4AF
Model clinker	62.7	18.7	6.5	12.1
clinker	67.5	6.5	8	8

The Blaine fineness of both clinkers are respectively 3500 cm²/g (model clinker) and 2500 cm²/g. TIPA solutions were obtained by dissolving trialkanolamine (Fluka) in deionized water.

2.2 Experimental methods

2.2.1 Cement diluted suspensions

The model clinker - gypsum mix was hydrated at 25°C with a w/c ratio equal to 5 under N_2 atmosphere to avoid carbonation. The chemical evolution was followed by isothermal calorimetry (Tian-Calvet Setaram). Furthermore, iron concentrations in solution were followed after 0.3 µm filtration using an atomic absorption spectrophotometer (Perkin-Elmer 3030).

2.2.2 Pure cement pastes and mortars

Two kinds of samples have been prepared, on the one hand, for hydration degree measurements and porosimetry experiments, and on the other hand, for mechanical compressive tests.

Cement pastes were mixed by hand for two minutes respectively with a saturated solution with respect to Portlandite and with the same solution containing TIPA ([TIPA] = 4.2 mmol/l). The water to cement ratio w/c is equal to 0.4. Pastes were then cast in Teflon moulds, kept at a relative humidity of 100% before demoulding and cured in a saturated solution of Portlandite at 25°C. Hydration was stopped and pastes were dried (alcohol-water and alcohol) at 7, 14 and 28 days. The pore size distribution of hardened cement pastes was determined using a mercury intrusion porosimeter (Micrometrics Autopore III). Samples were ground before diffractometry analysis (Inel XRG 3000) and thermal analysis (TG-DSC 111 Setaram).

For mechanical tests, cylindrical micro-samples (pure cement pastes and mortars) were hydrated in the same conditions but with a higher additive concentration ([TIPA]=17 mmol/l). The water to cement ratio was fixed at 0.35 and 0.6 for pure cement pastes and mortars respectively. For mortars, limestone aggregates have been used with a 50-50 cement – aggregate proportion ($0 < D_{aggregates} <$ 315 µm). At the appropriate time, samples were polished to obtain parallel sides before the compressive tests were carried out at a constant load rate (0.25 MPa/sec). For each time, 7 samples were crushed and the average was calculated.

3. RESULTS AND DISCUSSION

3.1 Chemical evolution of a cement suspension

The influence of TIPA (17 mmol/l) on the calorimetric and iron concentrations evolution is depicted respectively on Figures 1 and 2. The Figure 3 shows the cumulated flux for both hydrations.

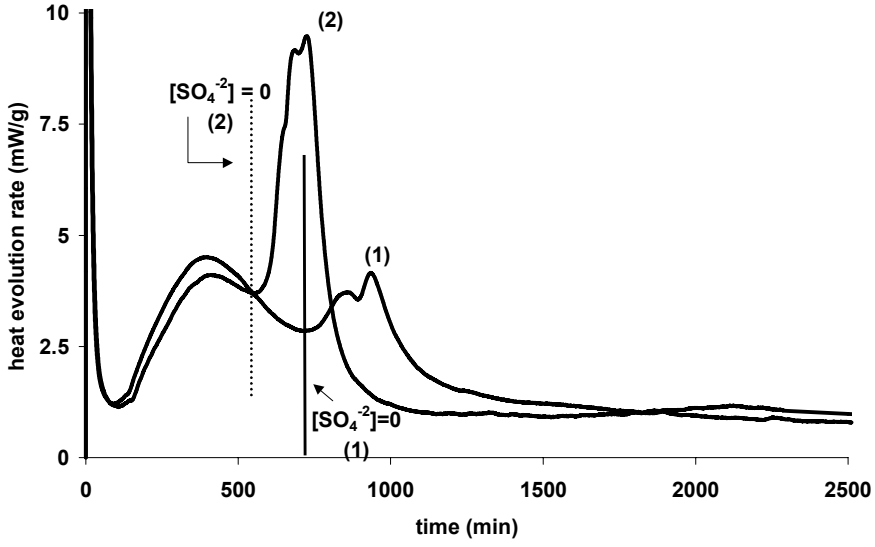

Figure 1. Heat evolution rate versus time for a cement hydration without (1) and with TIPA (2), w/c = 5 at 25°C.

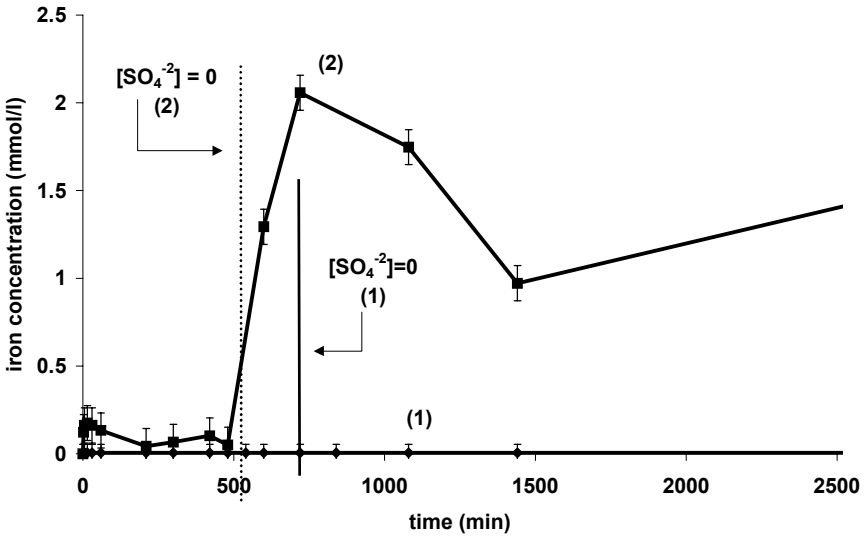

Figure 2. Iron concentrations evolution versus time for a cement hydration without (1) and with TIPA (2), w/c = 5 at 25°C.

The calorimetric curve (Figure 1) obtained for an hydration in a solution saturated with respect to Portlandite is described by three peaks which can be ascribed to the following different reaction steps. First, the initial peak corresponds to the different anhydrous phases dissolution followed by hydrates precipitation such as ettringite and C-S-H. Then, the second peak is ascribed to the acceleration of the silicate phases hydration and, at last the total sulphate ions consumption leads to the third multi-component peak corresponding to the aluminate phases hydration without gypsum. This last reaction leads to calcium hydroaluminate precipitation and to the ettringite dissolution following by the calcium monosulphoaluminate precipitation.

TIPA influences the kinetic evolution of cement hydration since the initial peak is more exothermic with the additive (Figure 3). Then, the acceleration of the silicate phase hydration starts at the same time and the hydration degree of these silicate phases seems to be similar for an hydration with TIPA than without additive (cumulated heat curves superposition). Moreover, the aluminate phases hydration is strongly modified. The third peak ($[SO_4^{-2}] = 0$) arises earlier but even if a strong acceleration of the aluminate phase hydration degree is underscored in the presence of TIPA at a given time (t = 600 min) (Figure 3), later the hydration degree of the cement suspension became similar.

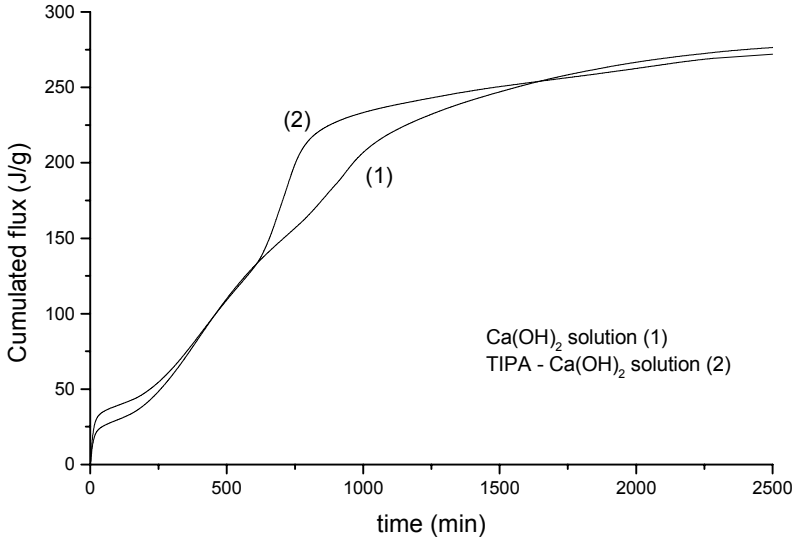

Figure 3. Heat evolution versus time for a cement hydration without (1) and with TIPA (2), w/c = 5 at 25°C.

Figure 2 represents the evolution of iron concentration in solution. Without TIPA, iron concentration is very low (10 µmol/l) and corresponds to the solubility of iron hydroxide $Fe(OH)_3$ which precipitates during cement hydration. This iron concentration remains constant during the whole hydration. TIPA addition leads to higher iron concentration in solution due to the formation of a soluble complex (Eq(1)) as predicted by Gartner et al[6]. However, the iron concentration in solution does not remain constant and evolves during the cement hydration. Two domains should also be considered, the first one when sulphate ions are present in solution, and the second one, after the total sulphate ions consumption. In the first domain, ettringite, as well as $Fe(OH)_3$, precipitates from the C_3A and C_4AF phases hydration and ettringite is able to incorporate iron in its structure[8].

Two oversimplified equilibria Eq(1) and Eq(2) should also be taken into account:

$$Fe(OH)_3 + TIPA \quad \varsigma \quad \text{soluble complex iron-TIPA} \qquad \text{Eq(1)}$$

and

$$6Ca^{2+} + xAl^{3+} + (2-x)Fe^{3+} + 3SO_4^{-2} + 12OH^- + yH_2O \quad \varsigma \quad Ca_6Al_xFe_{(2-x)}(SO_4)_3(OH)_{12},yH_2O \qquad \text{Eq(2)}$$

In presence of sulphate ions, the fact that iron concentration remains low, but higher than that observed for a hydration without additive, means the iron affinity for the ettringite structure (Eq(2)) is stronger than that of the soluble complex (Eq(1)). When sulphate ions are completely consumed (ettringite does not precipitate any more), iron concentration increases quickly in solution as a result of the C_4AF hydration continuation characterised by the third peak on the calorimetric curves (Figure 1). Iron concentration in solution became high (approximately 2 mmol/l), evidence at this time of the important C_4AF phase hydration. Then, the weak iron concentration decrease can be ascribed to a slight incorporation of iron in the calcium hydroaluminate or calcium monosulphoaluminate structure as for ettringite. At last, iron concentration remains constant until 28 days close to 1.5 mmol/l.

So, a soluble complex is able to form but what happens to the microstructure and the hydration degree of a cement paste, and more particularly that of the silicate phases responsible of the mechanical properties, in presence of TIPA and its complex?

3.2 Pore size distribution of pure cement pastes

The microstructure of pure cement pastes hydrated respectively without additive and with TIPA at 14 and 28 days was followed by mercury intrusion porosimetry (2 bars to 4000 bars intrusion pressure) to determine the pore size distribution. Figures 4 and 5 describe the cumulative pore volume versus the pores diameter. Well-defined threshold pore width was evident from 0.1 µm to approximately 5 nm. This pore size can be ascribed to the hydrates porosity and particularly to that of C-S-H, numerous hydrates in a cement paste. It also clearly appears that a modification of the pore distribution occurs for a cement paste hydrated in presence of TIPA with respect to a paste hydrated without additive. A largest pores distribution is characterised in presence of TIPA. This can be explained by a modification of the microstructure of the hydrated paste in presence of TIPA.

3.3 Hydration degree measurements of pure cement pastes

The hydration degree of pure cement pastes hydrated respectively without additive and with TIPA at 7 and 28 days was followed by X-ray diffractometry ($\lambda_{CuK\alpha 1}$ = 1.54056 Å) to characterise solid phases and by thermal analysis (ATG-DSC) to follow the dehydration of different hydrates precipitated.

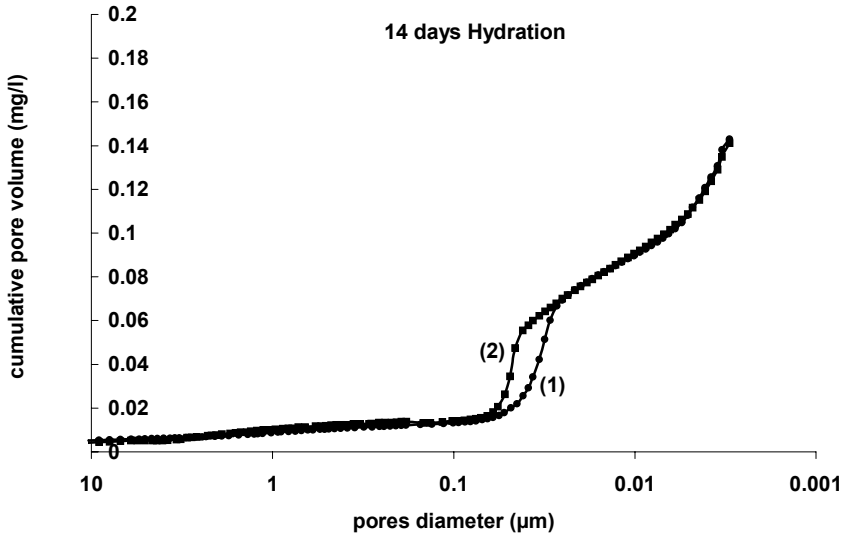

Figure 4. Cumulative pore volume versus pores diameter for cement pastes hydrated 14 days without (1) and with TIPA (2), w/c = 0.4 at 25°C.

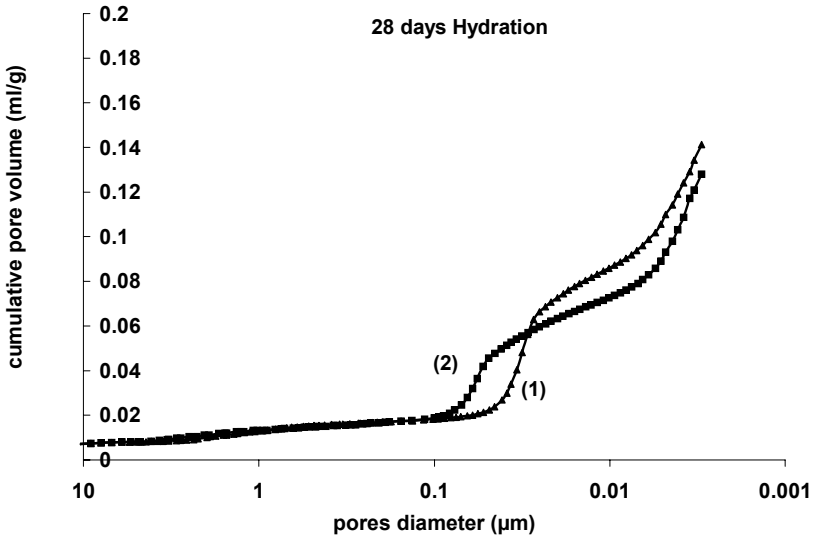

Figure 5. Cumulative pore volume versus pores diameter for cement pastes hydrated 28 days without (1) and with TIPA (2), w/c = 0.4 at 25°C.

In Figures 6 and 7, four diffraction peaks, in 2 theta increasing order, can be ascribed respectively to ettringite (2θ = 9.1 degree), calcium monosulphoaluminate (2θ = 10 degree), C_4AF (2θ = 12.2 degree) and Portlandite (2θ = 18.3 degree). No clear information can be extracted from the Portlandite peak. Otherwise, the C_4AF peak intensity is lower in presence of TIPA than with water whatever the hydration time (7 or 28 days) that means that C_4AF hydration is increased by TIPA certainly due to the complex formation. Similar conclusions have been reached by Schwarz[9] for a specific study of the citrate action on the ferrite phase hydration, because of a soluble complex formation between iron and citrate. Moreover, TIPA promotes the calcium monosulphoaluminate formation with respect to ettringite as has already been noted by Ichikawa[10] since calcium monosulphoaluminate peak intensity is higher and the ettringite peak is lower for hydration with TIPA than one with water.

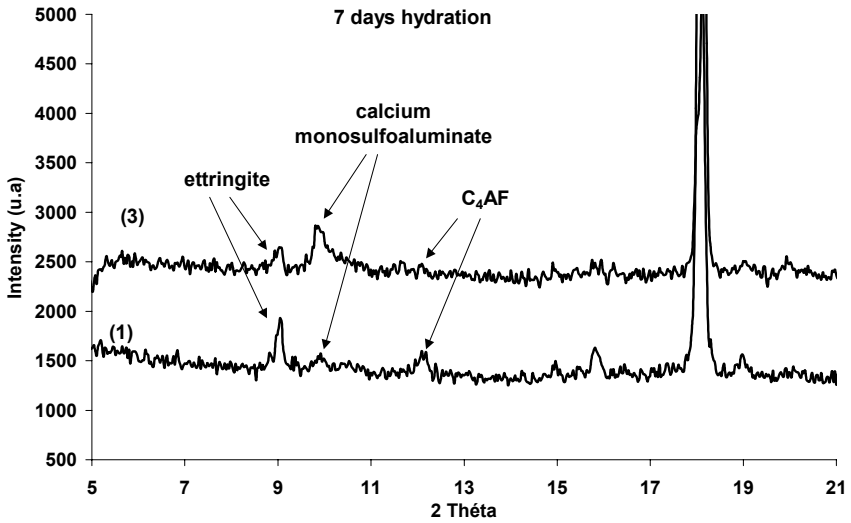

Figure 6. XRD patterns obtained for pure cement pastes hydrated 7 days respectively without (1) and with TIPA (2), w/c = 0.4 at 25°C.

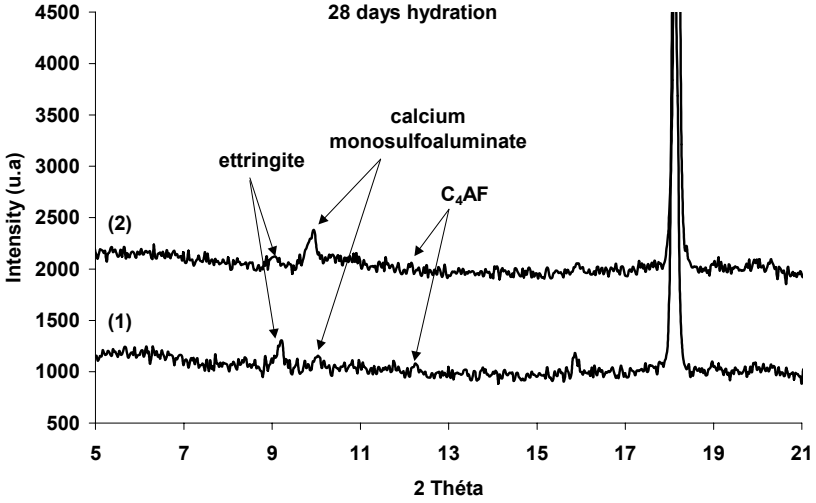

Figure 7. XRD patterns obtained for pure cement pastes hydrated 28 days respectively without (1) and with TIPA (2), w/c = 0.4 at 25°C.

Thermal analysis, Figures 8 and 9 represent the heat evolution and the weight loss associated with the heat release for 7 and 28 days hydration time. Taken as a whole, the dehydration heats and the associated weight losses are quasi similar between both samples since the total weight loss is the same, at any hydration time, for samples hydrated with TIPA and with water. On these thermal patterns, two peaks can be identified, the first one corresponding to the dehydration of C-S-H and the aluminate hydration products and the second one to the dehydration of the Portlandite which occurs in a 450°C - 550°C range of temperature. If many contributions should be considered in the first peak, a shoulder for hydration carried out with TIPA can be emphasised in a 180°C - 220°C range of temperature. This peak corresponds to the calcium monosulphoaluminate dehydration which confirms the results obtained by XRD analysis.

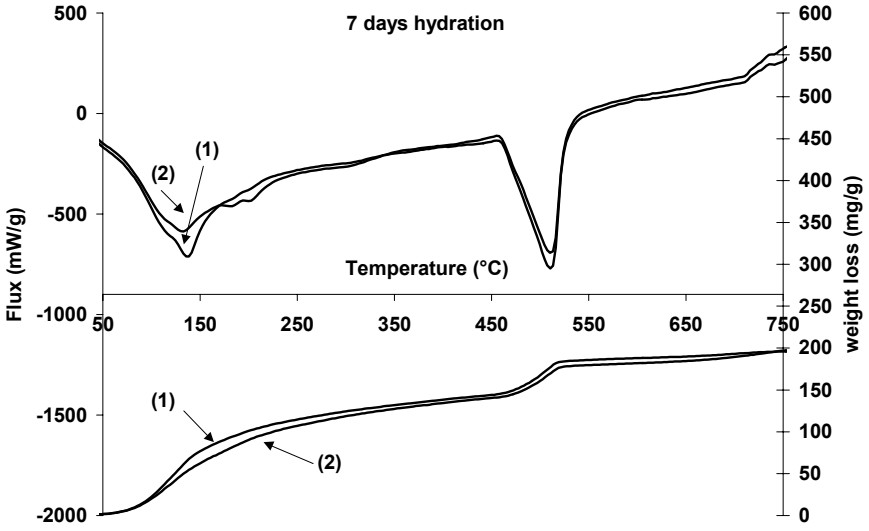

Figure 8. Thermograms obtained for pure cement pastes hydrated 7 days respectively without (1) and with TIPA (2) (10°C/min temperature ramp under N_2), w/c = 0.4 at 25°C.

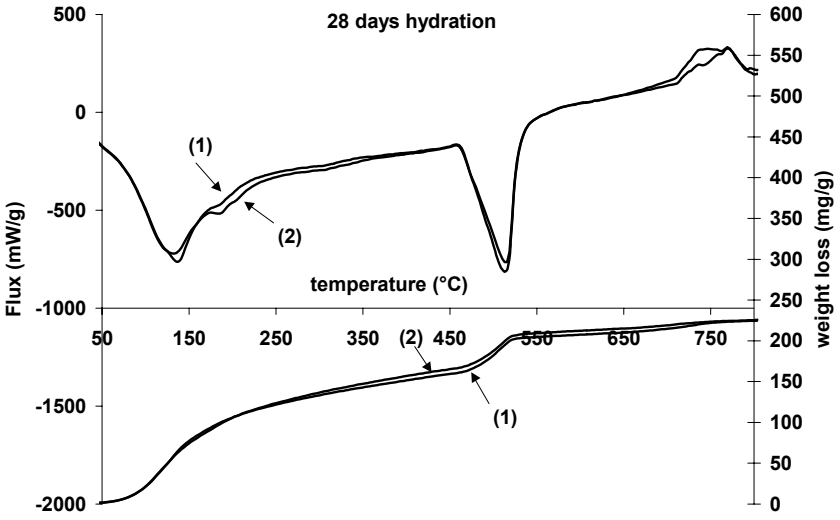

Figure 9. Thermograms obtained for pure cement pastes hydrated 28 days respectively without (1) and with TIPA (2) (10°C/min temperature ramp under N_2), w/c = 0.4 at 25°C.

Since Portlandite is one of the silicate phase hydration product, the heat and the weight loss associated with its dehydration are directly proportional to the hydration degree of these silicates phases. Whatever the hydration time, the second peak area and the weight loss are identical for an hydration carried out with TIPA or with water. So, it means that the hydration degree of the silicate phases, which are responsible for the mechanical strength development, is similar and therefore can not explain the mechanical strength enhancement observed in presence of TIPA.

3.4 Compressive tests on pure cement pastes and mortars

All compressive tests are carried out on mortars and no studies were made on pure cement pastes. Because of the strong exothermicity hydration reactions, micro-cracks are able to be generated in pure cement samples because of the sample size used for standard tests (4 x 4 x 16 cm^3). In this way, specific micro-samples of pure cement (cylinders ϕ = 6 mm) and mortars (cylinders ϕ = 8 mm) have been prepared in order to obtain a good dissipation of the hydration reaction heats.

Figures 10 and 11 depict the breaking strain evolution versus hydration time for pure cement pastes and mortars.

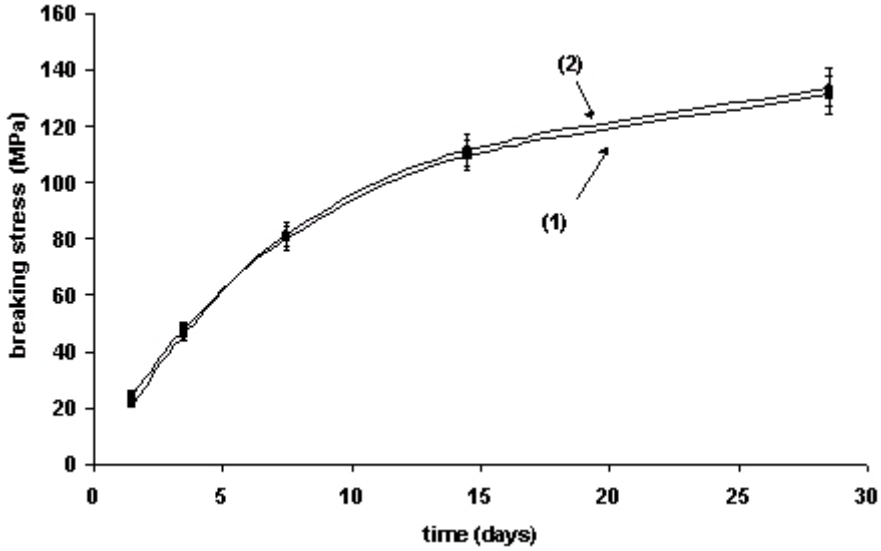

Figure 10. Breaking stress evolution versus time on pure cement paste micro-samples hydrated without (1) and with TIPA (2), w/c = 0.35 at 25°C.

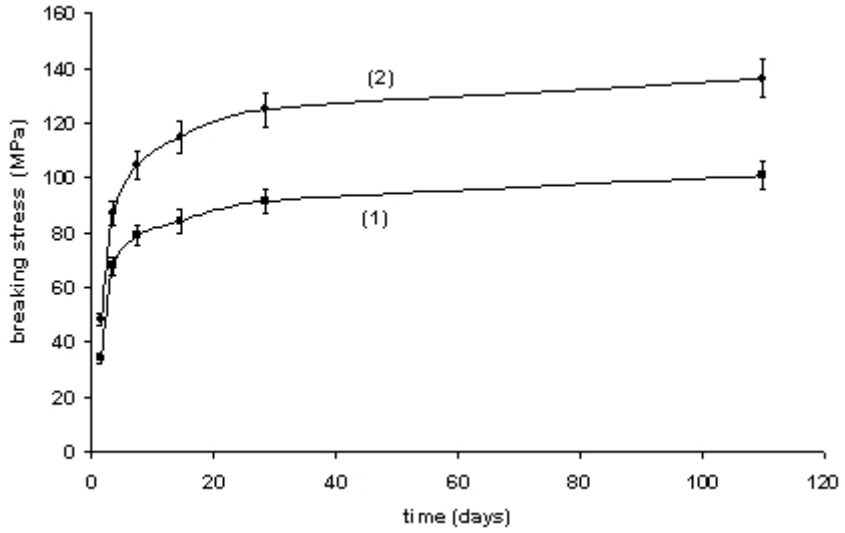

Figure 11. Breaking stress evolution versus time on mortars micro-samples hydrated without (1) and with TIPA (2) (50% cement – 50% limestone), w/c = 0.6 at 25°C.

Results obtained on pure cement pastes are very interesting because breaking strain remains similar during the whole hydration period for both samples series despite the soluble complex formation during the cement hydration in presence of TIPA. These results confirm that the silicate phase hydration degree is not modified by TIPA addition at any time, and that the complex formation has no effect on the mechanical properties of cement pastes. On the other hand, the change of the paste microstructure determined by mercury intrusion porosimetry has no effect on the mechanical properties of pure cement pastes.

But, compared to hydration with water, TIPA strongly increases the mechanical properties of mortars (limestone aggregates), from the beginning of hydration. The mechanical strength gap increases until 14 days and then remains constant until 3 months where the cement paste hydration degree approaches 100%. The gap which remains constant between mortars hydrated with TIPA

and those hydrated with water after 14 days of hydration is in agreement with precedent results which dismiss the assumption of an increase of the hydration degree in presence of TIPA since an increase of the hydration degree had to lead to convergence of mechanical properties.

So, it appears clearly the aggregate insertion in the cement matrix is at the origin of the mechanical strength enhancement implying probably a modification of the Interfacial Transition Zone (ITZ) due to the complex formation of the mortar hydrated with TIPA.

4. CONCLUSIONS

A soluble complex is able to form during the C_4AF hydration with TIPA. Even if this complex formation generates an increase of the alumino-ferrite phase hydration degree, it does not influence the hydration degree of the silicate phases which are responsible for the mechanical properties of the cement paste. Moreover, TIPA promotes the calcium monosulphoaluminate formation with respect to ettringite. A change of the microstructure of the hydrates of the cement paste hydrated in presence of TIPA has been emphasised but this modification involves no effect on the mechanical properties of pure cement paste hydrated without or with TIPA which remain similar during the whole hydration.

On the other hand, TIPA addition leads to an increase of the mechanical properties of mortars with respect to mortars hydrated without additive.

So, a modification of the interfacial properties, probably due to the complex presence in the interfacial zone, between the paste and the aggregate must be considered in order to explain the mechanical strength enhancement of mortars in presence of TIPA.

REFERENCES

[1] A. Nonat, J. C. Mutin, "From hydration to setting", Proceedings of the International RILEM Workshop, E&F Spon London, Dijon, (1992).

[2] T. C. Powers, T. L. Brownyard, "Studies on the physical properties of hardened cement paste", *Bulletin* , 845-864 (1948).

[3] S. P. Jiang, J. C. Mutin, A. Nonat, "Studies on mechanism and physico-chemical parameters at the origin of the cement setting. I: The fundamental processes involved during the cement setting", *Cement and Concrete Research* **25**, 779-789 (1995).

[4] J. C. Maso, "The bond between aggregates and hydrated cement pastes", 7th International congress on the chemistry of cement, Paris, (1980).

[5] U.S.Patents, "4,943,323". (W.R.Grace & Co, 1990).

[6] E. M. Gartner, D. M. Myers, "Influence of tertiary alkanolamines on Portland cement hydration", *Journal of the American Ceramic Society* **76**, 1521-1530 (1993).

[7] C. W. Chiesi, D. F. Myers, E. M. Gartner, "Relationship between clinker properties and strength development in the presence of additives", 14th.International Conference on Cement Microscopy, Costa Mesa, Californie, USA, (1992).

[8] M. Fukuhara, S. Goto, K. Asaga, M. Daimon, R. Kondo, "Mechanisms and kinetics of C_4AF hydration with gypsum", *Cement and Concrete Research* **11**, 407-414 (1981).

[9] W. Schwarz, "Novel cement matrices by accelerated hydration of the ferrite phase in Portland cement via chemical activation: Kinetics and cementitious properties", NATO/RILEM workshop, St Remy les chevreuses, (1994).

[10] M. Ichikawa, M. Kanaya, S. Sano, "Effect of Triisopropanolamine on hydration and strength development of cements with different character", 10th International Congress Chemistry of Cement, Suede, (1997).

INFLUENCE OF TRIISOPROPANOLAMINE ON THE PHYSICO-CHEMICAL AND MECHANICAL PROPERTIES OF PURE CEMENT PASTES AND MORTARS

J. Perez[1], A. Nonat[1], S. Garrault-Gauffinet[1], S. Pourchet[1], M. Mosquet[2] and C. Canevet[2]

[1]LRRS, UMR CNRS-Université de Bourgogne 5613, Faculté des Sciences Mirande
9 avenue Alain Savary, BP 47870, 21078 Dijon Cedex
E-mail : jean-philippe.perez@u-bourgogne.fr
[2]Chryso SAS, 7rue de l'Europe, 45300 Sermaises du loiret

PEREZ Jean-Philippe

1972/01/07, Talence (33), France.
French Citizenship

I joined the University of Bourgogne in the Fall of 1998 as a Ph.D student. I received the Ph.D. degree from University of Bourgogne in 2002. I spent a year as a post-doctoral researcher at the University of Bourgogne in 2003.

Areas of Interest

Research: On cement chemistry, with special interest in studying the interaction between organic additives and main cement phases and the properties of cement paste – aggregate interface.

Ph.D research: "Study of the hydration of the main phases of Portland cement and of the mechanical strength of cement pastes and mortars: Influence of trialkanolamines

Post-doctoral research: " Study of the properties of the cement – paste agrregate interface

Business Address

Université de Bourgogne, LRRS, UFR Sciences et Techniques, BP 47870, 21078 Dijon Cedex, France
Tel : (33) 0380396147 Fax : (33) 0380396132
E-mail: jean-philippe.perez@u-bourgogne.fr

UTILIZATION OF FLUORSPAR, $CaSO_4$ AND $CaCl_2$ FOR THE PRODUCTION OF LOW ENERGY CEMENT

H.U.Shah (Dr)[1], Arif Bashir (Dr)[2] and Zaka-ud-Din[3]

[1] DG Khan Cement Company Ltd., D.G Khan, Pakistan. E-mail: drshah@dgcement.com
[2] DG Khan Cement Company Ltd., D.G Khan, Pakistan. E-mail: abashir@dgcement.com
[3] DG Khan Cement Co. Ltd. Nishat House, Lahore, Pakistan. E-mail: zaka@dgcement.com

ABSTRACT

In this paper test results are presented from investigations conducted at laboratory level to utilize about 4% of SO_3 present in lime bearing component of an industrial white cement mix for producing white cements at lower burning temperature. Fluorspar and the composite mineralizer, fluorspar + $CaCl_2$ were added in varying proportions to the mix and their effect on the burnability, initial melt formation and mineral formation of the resulting low energy clinkers was evaluated. The performance of low energy white cements produced in the laboratory was studied in respect of physical properties and whiteness indices vis-à-vis plant cement.

1. INTRODUCTION

The use of $CaSO_4$ and fluorspar as fluxes and/or mineralizers in cement production for the sake of energy conservation is well established. In the literature is reported the production of Portland cement at a temperature of 1300°C which contained maximum alite phase together with β-C_2S, C_4A_3S, C_3A and $CaSO_4$ (1). High quality white mineralized clinker, with 10% less energy consumption than the traditional process was synthesized on an industrial scale by using CaF_2 and $CaSO_4.2H_2O$ fluxing and mineralizing pair (2). The good reactivity and burnability of special white cement mixes, possessing a silica modulus as high as 14, was achieved at the low temperature of 1350°C which is about 200°C less than the clinkering temperature of traditional white cement raw mixes (3). Portland cement clinkers containing alite as main phase were obtained in a laboratory rotary kiln at 1300°C by adding 5% $CaCl_2$ and chlorine was combined entirely in $C_{11}A_7CaCl_2$ phase. (4)

The new energy white cement prepared by us at laboratory level at 1300°C by adding fluorspar and fluorspar + $CaCl_2$ to the industrial mix, showed better mechanical properties and whiteness indices. DTA/TGA, XRD and SEM were used to study the clinkerization process.

2. MATERIALS AND EXPERIMENTAL PROCEDURE

The materials used were industrial white cement raw mix, laboratory mix, fluorspar (88% pure and prepared to a residue of less than 5% on 172 mesh) and commercial grade calcium chloride. The composition of raw mixes was determined by chemical analysis and is given in Table 1.

Table 1. Chemical Composition of White Cement Mixes

Composition of Oxides (weight %)										
Raw Mixes	SiO_2	Al_2O_3	Fe_2O_3	CaO	MgO	K_2O	Na_2O	SO_3	Chloride	LOI
Industrial Mix	14.8	2.98	0.30	42.42	1.92	0.16	0.10	4.00	0.00	33.40
Laboratory Mix	14.82	3.70	0. 40	42.80	2.00	0.52	0.24	0.12	0.00	35.40

The nodules of raw mixes containing varying proportions of fluorspar and fluorspar/$CaCl_2$ composite mineralizers were prepared and fired separately in platinum dishes in an electronic furnace of high precision at a heating rate of 10^{o}C/minute and retained at a final temperature of 1300^{o}C for 30 minutes. The resulting clinkers were allowed to cool initially within the furnace up to 1280^{o}C and then were rapidly quenched. The level of the uncombined lime was determined by the hot ethylene glycol extraction method. The burning behavior and mineralogical composition of the clinkers was followed by XRD and DTA/TGA studies. Physical-mechanical and other hydration properties of new white cements were studied and compared with reference white cement from the plant.

3. RESULTS AND DISCUSSION

3.1 Influence of mineralizers on burnability of raw mixes

The results of burnability studies of the plant and laboratory mixes with and without fluorspar and fluorspar/$CaCl_2$ are summarized in Table 2.

Table 2. Influence of Mineralizers on combinability of Industrial & Laboratory mixes

Mineralizer Added Weight (%)	Free Lime (%)	Heating rate ^{o}C/minute	Residence time at 1300^{o}C temperature minute
Industrial Mix	4.26	10	30
0.25% fluorspar	3.00	10	30
0.50% fluorspar	0.92	10	30
1.0% fluorspar	0.80	10	30
0.25% fluorspar + 1.00 $CaCl_2$	1.29	10	30
0.50% fluorspar + 2.00 $CaCl_2$	0.70	10	30
1.00% fluorspar + 2.00 $CalC_2$	Nil	10	30
Laboratory mix *	11	10	30

* *Raw Mix prepared by adding limestone in place of lime sludge in the industrial mix.*

It is apparent from the results that the addition of 0.25% of fluorspar to the industrial mix reduces the free lime content of the burnt mass from 4.26% to 3.0%. By increasing the fluorspar addition to 0.5% and 1.0 % the corresponding decrease in free lime content of the burnt masses is observed as 0.92% and 0.80% respectively.

The addition of composite mineralizer fluorspar/$CaCl_2$ to the mix in the range 0.25% fluorspar and 1.0% $CaCl_2$ reduces the free lime contents to 1.29%. Increasing the addition of fluorspar to 0.50% and $CaCl_2$ to 2% in the mix decreases the free lime of the clinker to 0.70%. Free lime in the clinker completely disappeared when 1% fluorspar with 2% $CaCl_2$ is added to the mix. In contrast, maximum free lime contents of 11% were observed in the clinker made under the same burning conditions from the laboratory mix where lime sludge in the industrial mix is replaced with pure

limestone containing 0.12% SO_3. The results obtained for free lime contents of burnt masses in the presence of mineralizers; $CaSO_4$, fluorspar and $CaCl_2$ confirm the previous studies carried out by Balanco (5), Klemm (6) and Wei (7). The order of effectiveness for the investigated fluxes and mineralizers pertaining to burnability of white cement mixes at 1300°C is found in the descending order, $CaCl_2$ + Fluorspar > Fluorspar > $CaSO_4$

4. THE EFFECT OF MINERALIZERS ON MELT AND MINERAL FORMATION PROPERTIES

The first formation of liquid, marking the start of clinkering, occurs in Ordinary Portland Cement at much lower temperatures than white cement. The absence of fluxes in white cement accentuates the need to add to the mix certain fluxes, which could reduce the clinkering temperature. The burning behavior of investigated fluxes and mineralizers on an industrial white cement mix was studied with the help of Differential Thermal (DTA) and Thermo-gravimetric Analyzer (TGA). The effect of these mineralizers on de-carbonation, melt formation and mineral formation of the mixes studied is depicted in the thermograms shown in Figure 1.

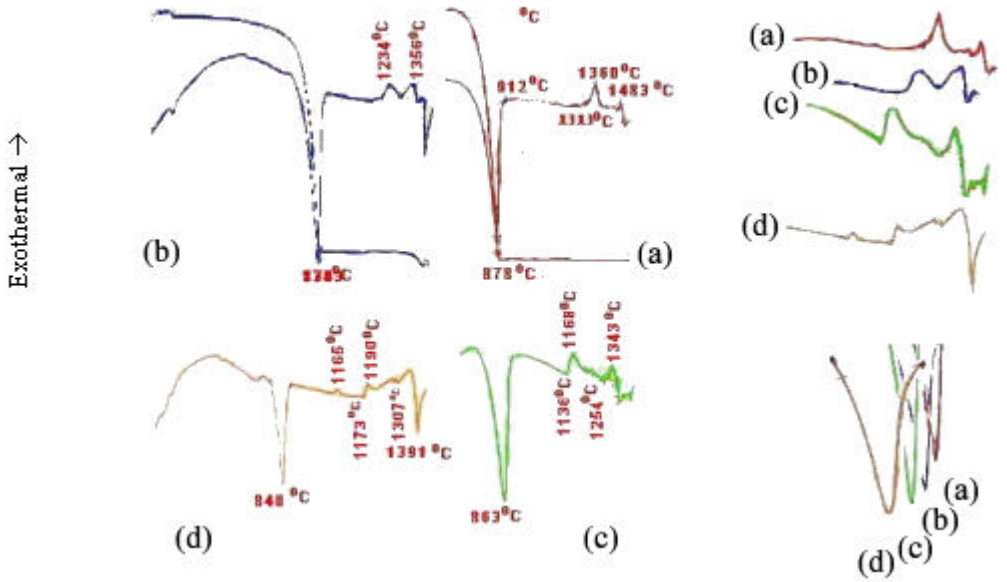

Figure 1. Thermograms of cement raw mixes (a) Laboratory mix, (b) Industrial raw mix (c) Industrial raw mix + 0.50% Fluorspar (d) Industrial mix + 0.50% Fluorspar + 2% $CaCl_2$

The parameters selected for DTA/TGA studies of these mixes are described in Table 3.

Table 3. Instrumental Condition for DTA/TGA

Atmosphere	Air
Reference Crucible	Al_2O_3
Sample Crucible	Al_2O_3
DTA Range	50.0 µv
TG Range	100.0 mg
Heating Rate	10°C/min.

The laboratory mix (a) Figure 1 prepared by replacing lime sludge in the industrial mix with pure limestone, shows peak de-carbonation temperature at 878°C. The initial melt formation temperature of the laboratory mix is completed at about 1312°C. The strong exothermic peak indicating the formation of C_3S is observed at the temperature of 1360°C.

The de-carbonation temperature in industrial white cement mix (b) Figure 1, is observed at 780°C. In this case the initial melt formation temperature appears at 1140°C, which is 172°C less than the laboratory mix. There is seen an exothermic peak corresponding to C_3S formation at temperature of 1234°C. The 126°C drop in C_3S formation temperature as compared with laboratory mix, is the result of SO_3 present in the industrial mix. $CaSO_4$ being an effective flux and mineralizer, lowers liquid phase temperature by over 100°C, decreases its viscosity and surface tension and increases the mobility of Ca^{2+}, $Si_xO_y^{2-}$, Fe^{3+} ions (8). Thus it helps initiate C_3S formation at earlier temperatures than is usually observed in the case of normal cement mixes.

The addition of 0.5% fluorspar to the industrial mix (c) Figure 1, reduces the peak de-carbonation temperature to 863°C and initial melt formation temperature of the mix to 1136°C. The strong exothermic peak appearing at 1168°C confirms the early studies (9) where addition of fluorides to sulphate containing mixes, is found to speed up the formation of alite through formation of the transition phase. It restrains the unfavorable effect of SO_3 while strengthening its favorable effects in clinkering process. The addition of fluorspar and $CaCl_2$ to the industrial mix is found most effective in reducing de-carbonation temperature of the mix (d) Figure 1. The intensification of the clinkering process in the presence of fluorides (F) is further augmented because of the addition of Cl to the mix.

The mineralogical composition of low energy white cement clinkers, burnt with investigated fluxes and mineralizers, is given in Table 4 and the corresponding X-ray diffractograms of clinkers are shown in Figure 2.

Table 4. Minerals formed during the process of burning of industrial white cement mix at 1300°C with mineralizers.

Added flux Wt (%)	C_3S	β-C_2S	C_3A	F-CaO	$C_{11}A_7CaCl_2$	C_4A_3S
0	+ +	+ + +	-	+	-	+ +
0.5% Fluorspar	+ + + +	+ +	+	+	+ +	+
0.5% Fluorspar + 2% $CaCl_2$	+ + + +	+ +	+ +	-	+ +	+

+ + + + = Major Phase, + + + = Normal Phase, + + = Medium Phase, + =Minor Phase, - = Absent

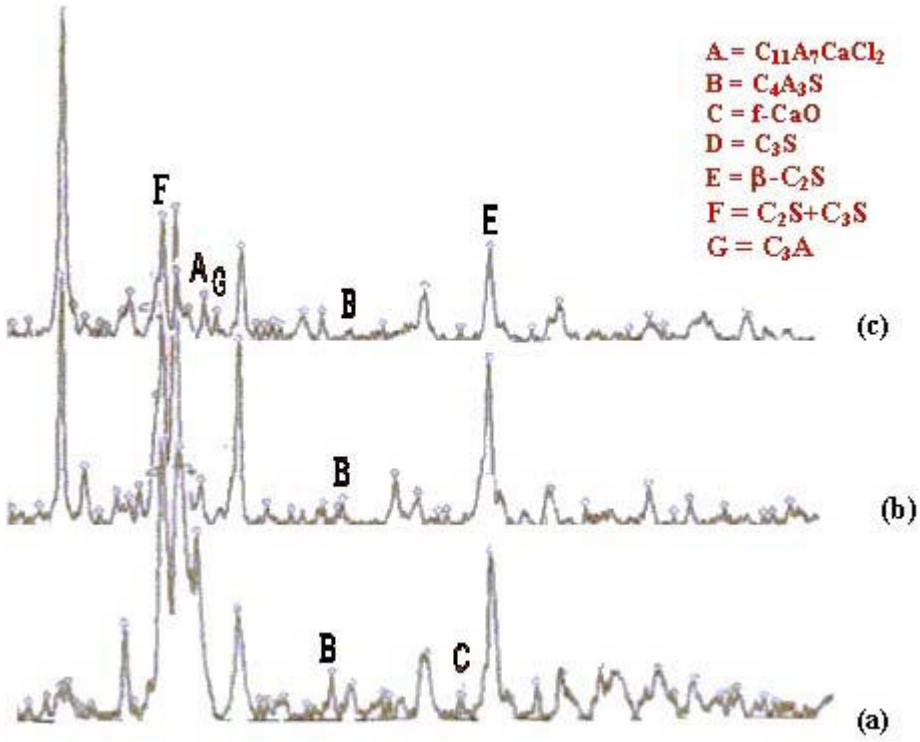

Figure 2. XRD Grams of different cement minerals observed at (a) 0%, (b) 0.50% Fluorspar and (c) 0.50% Fluorspar + 2% $CaCl_2$

The clinker made from the industrial mix (a) Figure 2, is found to attain minimum level of C_3S because of the stabilization effect of SO_3 on β-C_2S and the preferred reaction of SO_3 with lime to form C_4A_3S (9). The accelerated formation of C_3S at further lower temperatures because of 0.50% fluorspar addition is manifested from the prominent peak (D) in x-ray diffractogram (b) Figure 2. The compound mineralizer fluorspar and $CaSO_4$ is of great benefit in the cement manufacturing process as it activates SiO_2, promotes the decomposition of $CaCO_3$, decreases temperature of melt formation and viscosity of the melt and speeds up the formation of alite through transition phases. Furthermore, the unfavorable effects of SO_3 in the clinkering of cement mixes are effectively offset in the presence of fluorides (10). X-ray diffraction studies of clinker, made by adding composite mineralizer Fluorspar and $CaCl_2$ to the industrial mix, revealed the presence of all major phases like C_3S, C_2S, C_3A, C_4A_3S, $C_{11}A_7CaCl_2$.

From x-ray diffractograms (c) Figure 2, it is evident that clinker produced at 1300^oC, as a result of composite mineralizer fluorspar/$CaCl_2$, attains maximum level of alite phases. X-ray diffraction studies of clinkers support the results obtained during the burnability and DTA/TG studies of white cement mixes.

5. PHYSICAL CHARACTERISTICS, HYDRATION BEHAVIOUR AND STRENGTH PROPERTIES OF LOW ENERGY WHITE CEMENTS.

The physical characteristics, strength properties and hydration behaviour of low energy white cements and plant cement were evaluated with same set of standard conditions as shown in Table 5.

Table 5. Physical characteristics of low energy white cements.

Sample Code	Blaine (M^2/Kg)	Gypsum added	Initial set (minutes)	Final set (minutes)	Soundness (mm)	Whiteness index
C1	387	2% 4%	181 200	240 270	4.8 5.6	85
C2	380	2% 4%	54.0 90.0	95 112	4.81 6.00	88
Plant Cement	440	5%	160	220	2.0	86

C1 = Cement from industrial raw mix containing 4% SO_3 + 0.5% fluorspar
C2 = Cement from industrial raw mix containing 4% SO_3 + 0.5% fluorspar + 2% $CaCl_2$
Plant Cement = Cement made at the plant with above referred industrial raw mix

The mineralized cements show rapid set behaviour in the absence of gypsum addition. However, by adding 2% gypsum in the clinkers, both initial and final set of the resulting cement C1 is found in close proximity with the setting time of plant cement. The decrease in initial and final setting times registered in the set behaviour of cement C2, in the presence of 2 and 4% gypsum may be ascribed to accelerating effect of chloride.

The soundness of the low energy cement ground with 2 and 4% gypsum pass the soundness standard limits prescribed in BS or Pakistan Standard Specifications (PSI).

The whiteness indices of cement C1 and C2 are better than the plant cement despite the lower Blaine values. The mineralizer addition to the white cement mix results in the formation of C_3S almost at the same time when C_2S is formed. The simultaneous appearance of C_3S and C_2S results in the build up of minor elements in totally different pattern, thereby, improving the whiteness of cements C1 and C2 (11). The highest whiteness indices in case of cement-C2 could be the result of $CaCl_2$, which was used as a bleaching agent for improving the whiteness of cement.

The compressive strength at 3, 7 and 28 days of cement-C1 as shown in Table 6, is considerably less than cement-C1, cement-C2 and plant cement.

Table 6. Compressive strength of 1" mortar cubes (Mpa)

Cement No.	Gypsum weight%	3 Days	7 Days	28 Days	% Increase in strength between 3 and 7 days
C1	2	12.56	17.05	23.42	35.75
C2	4	15.5	22.4	27.0	44.5
Plant Cement	5	9.40	11.34	19.83	20.60

The difference in the compressive strength between cement C1 and cement C2 is attributed to the higher alite contents permitted by the strong mineralizing action of composite mineralizer fluorspar and $CaC1_2$.

The highest intensity of the C_3S peak appeared in x-ray diffractogram (c) Figure 2, bears ample proof to the effectiveness of the composite mineralizer as compared to fluorspar and/or $CaSO_4$. Higher 3,7 and 28 day compressive strength of cement-C1 and cement-C2 than the plant cement are due to the hydration characteristics of more active alite, β-C_2S, C_4A_3S and other mineral phases crystallized in the low energy clinkers. It is also evident from the test results shown in Table 6 that theincrease in compressive strength between 3 and 7 days in case of plant cement is 20.60% whereas for cements C1 and C2 is 37.75% and 44.5% respectively. This behaviour of low energy

cement is discernable from the hydration characteristics of C_4AS_3 together with active alite, belite and other minerals formed as a result of added fluxes and mineralizers.

6. HYDRATION STUDIES

The hydration of different cement pastes was arrested at 7 days by crushing the specimen, washing them with acetone and vacuum drying at room temperature. Figure 3 represents the amount of $Ca(OH)_2$ released at 450°C-520°C due of dehydration of $Ca(OH)_2$ found in cement pastes prepared from low energy cements-C1,C2 and plant cement. The amount of $Ca(OH)_2$ is found to be maximum for cement-C2 and minimum of plant cement. The higher contents of $Ca(OH)_2$ in cement C3 are attributed to the higher hydraulic activity of calcium sulpho-aluminates and other minerals formed in the presence of SO_3, fluorspar and $CaCl_2$ mineralizers.

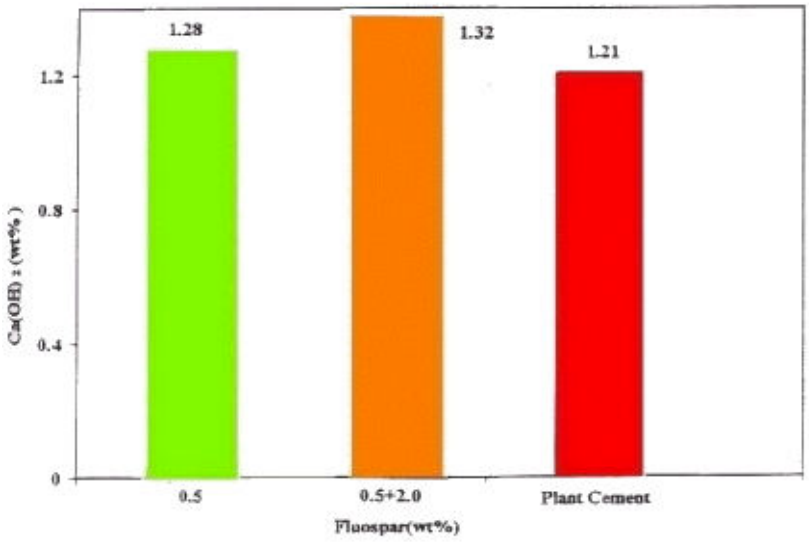

Figure 3. $Ca(OH)_2$ liberated at hydration of cement C1, C2 and Plant cement

The higher strength of cement-C1 and cement-C2 as compared to plant cement was further studied by scanning electron microscope (SEM). Figure 4, represents SEM micrographs (a) and (b) of cement pastes prepared from cement-C2 and plant cement respectively.

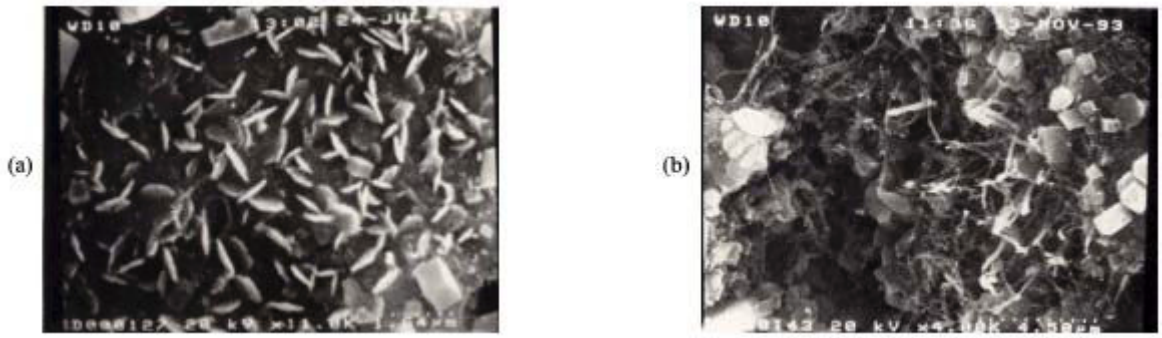

Figure 4. SEM Micrographs of cements-C2 (a) and plant cement (b)

The high temperature environment caused by the hydration of $C_4A_3\bar{S}$, $C_{11}A_7CaCl_2$, C_3S, β-C_2S and other minerals in low energy cement-C1 and cement-C2 is responsible for the higher early strength of mineralized cements. It can be observed through micrograph (b) that in the presence of excess sulphates, ettringite seems to be the stable hydration product. The intrusion C_3S, β-C_2S and other hydrates into the ettringite skeleton gives a very compact and dense structure to cement-C1 and cement-C2 pastes. In plant cement, monosulphualuminates are formed more stably than ettringite.

The formation of hexagonal plates Figure 4 (plant cement), with characteristic face to edge contacts having large vacant spaces are not completely filled by the hydration products of C_2S, C_3S, etc. Thus mechanical properties of such system will be inferior to cement-C1 and cement-C2.

7. CONCLUSIONS

1. It is possible to produce white cement of comparable or better performance even at a temperature of 1300°C with the addition of fluorspar and/or fluorspar & $CaCl_2$ from the raw mix containing about 4% SO_3 as $CaSO_4$.
2. The clinkering of white cement mix at 1300°C would lead to considerable energy savings in overall cost of production of the cement.
3. Increase in the production output is expected due to mineralizing action of investigated fluxes and mineralizes.
4. Reduction in burning temperature in the range of 250 – 300°C would lower the dust losses pollutant gases and energy losses encountered in the production of white cement.

REFERENCES

[1] Wang Tiandi etal, "Low temperature sintering mechanism of fast hardening cement clinker produced by Gangue & Coal slag," Collected papers of congress on cement, China, 1980-1981, P.185.

[2] Francisca Puertas etal, "Burnability of mineralized white cement: optimization of raw meal," 10th Int. Congr. Chem. Cement, Sweden, 1997, vol.1, LiO34, PP8.

[3] M.T. Blanco-Varela etal, "Modeling of the burnability of white cement raw mixes made with CaF_2 and $CaSO_4$, "Cement and Concrete Research, vol.26, No.3, PP 457-464, 1996.

[4] W.kurdowski and A.Garbacik, "$CaCl_2$ utilization in clinker burning" 7th Int. Congr. Chem. Cement, France, 1980, Vol.IV, PP.702-706.

[5] M & Blanco etal, "Production and Behaviour of new white sulphates resistant Cement," Concrete 2000, Proc. Int. Conf.. Univ. Dundee Scotland, UK, 7-9 Sept.1993, Vol.2, PP.1325-1337.

[6] W.A. Klemm etal, "The effect of Fluxes and Mineralizers in lowering cement kiln temperature, "Prog. Report No.1, Feb.31-July 31, 1997 Martin Mareeta Corpn. Baltimore, Maryland 21227, P.15.

[7] S.Wei and F.Mingfen, "A study of the effect of CaF_2 on clinker doped with compound mineralizer, "Proc. 8th Intl. Congr. Chem. Cement, Brazil, 1986, Vol. II, P.113.

[8] R.BCCHI, "Influence of the nature of preparation of raw materials on the reactivity of raw mixes," Proc. 7th Int. Congr.Chem. Cement, France, 1980,Vol.2 PP. 1-1/3 – 1-1/43.

[9] H.M. Cheong etal, "Effect of sulphates on the reaction of C_3S formation, "Proc. 9th Intl. Congr. Chem. Cement, India, 1992, Vol. II, P.385.

[10] S.U.Dagen etal, "Effect of SO_3 on mineral formation and properties of clinker, "Proc. 9th Intl. Cong. Chem, Cement, India, 1992, Vol. II, PP. 322-328.

[11] J.Waanders, "New Production techniques can smash price barrier in white cement Production, "Rock Products Mining and Processing, May 1964, PP. 89-91.

UTILIZATION OF FLUORSPAR, $CaSO_4$ AND $CaCl_2$ FOR THE PRODUCTION OF LOW ENERGY CEMENT

H.U.Shah (Dr) One[1], Arif Bashir (Dr) [2] and Zaka-ud-Din. [3]

[1] DG Khan Cement Company Ltd., D.G Khan, Pakistan. E-mail: drshah@dgcement.com
[2] DG Khan Cement Company Ltd., D.G Khan, Pakistan. E-mail: abashir@dgcement.com
[3] DG Khan Cement Co. Ltd. Nishat House, Lahore, Pakistan. E-mail: zaka@dgcement.com

Muhammad Hafeez Ullah Shah

Sr. Manager (QC) DG Khan Cement Co. Ltd, Pakistan.
Date of Birth: April 1, 1954
Language: English, Urdu

Higher Education: 1979-81 Ph.D (Chemistry), Low energy white cements) University of Punjab, Lahore, Pakistan.

Previous Activities: 1984-95 Worked in Cement Research and Development Institute, Lahore, Pakistan.

1995 - To date: Sr. Manager (QC) D.G. Khan Cement Company Pakistan.

Areas of Interest:

- Evaluation of clinkering process parameters and their impact on cement quality, Blending Cements, Using Fluxes & mineralizers for producing low energy cement.

Research Publications:

- H.U. Shah and Zafar Iqbal, "Evaluation of an optimum percentage addition of fluorspar in white cement raw mixes containing 4% SO3, "9th Congr. Chem. Cement, India, 1992, Vol. 11, pp.
- H.U. Shah et al, "production and Behaviour of low energy white cement. "4th NCB seminar, India, 1993.
- H.U. Shah et al, "Utilization of Fluorspar and SO3 for production of low energy white cement" International energy conference, Lahore, Pakistan, 1994.

EFFICIENCY OF HIGHLY ACTIVE RICE HUSK ASH ON THE HIGH-STRENGTH CONCRETE

Qingge Feng, Hirohito Yamamichi, Masami Shoya and Shuichi Sugita

Department of Environmental and civil Engineering, Hachinohe Institute of Technology, 88-1, Myo, Hachinohe 031-8501, Japan. E-mail: Fengqg@stud.hi-tech.ac.jp

1. INTRODUCTION

As an agricultural product, rice husk contains considerable amounts of SiO_2 [1,2]. Recently, many researches have investigated the production of the rice husk ash (RHA) with high pozzolanic activity and its possible application in cement and concrete. [3,4,5,6]. The results reveal that a well-burnt and well-ground rice husk ash is very active and considerably improve the durability of cement and concrete. In previous research [1,5,6,7], RHA with 2.0-3.0mS/cm by the change of electrical conductivity that is one of the rapid evaluations of the pozzolanic activity index of rice husk ash had been used. In this study, RHA with high pozzolanic activity (the change of electrical conductivity was 4.50-4.75mS/cm) can be obtained by controlling the firing temperature using a commercial furnace. The efficiency of highly active RHA on high-strength concrete is investigated.

2. MATERIALS AND MIXTURE PROPORTIONS

In this study RHA was obtained by burning rice husks in a commercial furnace. The XRD pattern of the RHA shows that the silica in it is amorphous in form. Its chemical composition and physical properties are presented in Table 1.

Table 1. Chemical composition* and physical properties of RHA and cements used

	RHA	Cement
Loss of ignition	2.31	3.10
S_iO_2	92.40	21.29
Al_2O_3	0.30	5.60
Fe_2O_3	0.40	3.00
CaO	0.70	62.69
MgO	0.30	2.24
Na_2O	0.07	0.30
K_2O	2.54	0.31
SO_3		1.47
P_2O_5	0.51	
MnO	0.11	
Cl	0.11	
specific gravity	2.10	3.16
specific surface, Blaine, m^2/kg		330
nitrogen adsorption, m^2/g	164	
median grain size, um	7.40	26
change in electrical conductivity, mS/cm	4.75	

*Conducted by X-ray fluorescence analysis

An ordinary Portland cement with a specific gravity of 3.16 specified in JIS R 5210 (Portland cement) was used. The coarse aggregate (density 2.64g/cm^3) was a crushed sand stone with the maximum size of 20mm. The fine aggregate was river sand (density 2.60g/cm^3, F.M. 2.84, for W/B of 0.30 and 0.35) and crushed sand (density 2.88g/cm^3, F.M. 2.69, for W/B of 0.45 and 0.55).

In order to control the air volume and the slump of all the fresh concrete added with RHA to be 5% and 8cm respectively, an air entraining agent and superplasticizers (Polycarboxylic acid system) were used.

The concrete mixtures were made at RHA blending ratios of 0,10,20,30% and W/B of 0.30, 0.35, 0.45, and 0.55 respectively. The proportions of the concrete mixture are summarized in Table 2.

Table 2. Mixture proportions of RHA blended concrete

W/B	RHA content,%	s/a,%	Unit content, kg/m^3						AE,%	SP,%
			water	RHA	cement	stone	crused sand	river sand		
0.55	0	43	170	0	309	1027	845		0.030	0.000
	10			31	278	1019	839		0.030	0.350
	20			62	247	1012	833		0.035	0.600
	30			93	216	1005	827		0.040	0.800
0.45	0	40	170	0	378	1046	761		0.030	0.000
	10			38	340	1037	754		0.035	0.600
	20			76	302	1028	747		0.055	1.200
	30			113	264	1018	740		0.075	1.800
0.35	0	40	178	0	509	968		636	0.030	0.175
	10			51	458	956		628	0.045	0.800
	20			102	407	944		620	0.060	1.600
	30			153	356	932		612	0.070	2.720
0.3	0	39	180	0	600	934		588	0.030	0.250
	10			60	540	920		579	0.060	1.400
	20			120	480	906		570	0.120	2.600

3. TESTING PROCEDURES

3.1 Pozzolanic activity of RHA

The evaluation of pozzolanic activity of RHA was determined by comparing the strength of mortar made with and without RHA, tested in accordance with JIS R5201 (Physical testing methods of cement, Japanese industrial standards, 1997). At the same time, measurements of heat evolution and hydration heat of cement with 0, 10, and 30% RHA or ground silica sand were conducted using the thermal conductivity calorimeter (Calvet calorimeter), at W/C=1.0, and 25ºC.

3.2 Compressive strength

The slump test and the air content test were conducted according to JIS A1101 (Method of test for slump of concrete, Japanese industrial standards, 1998), JIS A1128 (Method of test for air content of fresh concrete by pressure method, Japanese industrial standards, 1999). The concrete 100 200mm Φ specimens were placed to moist-cure at 20ºC and 85% relative humidity for 2 days, and water cure at 20ºC till the data of strength were tested.

The compressive strength of the concrete specimens was tested at the age of 3, 7, 28, and 91 days respectively according to JIS A 1108 (Method of test for compressive strength of concrete, in Japanese industrial standards, 1999), 3.3 $Ca(OH)_2$ content

Because of the determination of the $Ca(OH)_2$ content in the concrete, the cured mortar specimens were cut into approximately 5mm cubes, washed with acetone to stop further hydration and treated by D-drying for one week. The $Ca(OH)_2$ content is calculated using TG curves. The TG analyses were carried out at the temperature from 30 to 1050ºC and the heating rate of 10ºC /min.

4. RESULTS AND DISCUSSION

4.1 Pozzolanic activity of RHA

The determination of the heat evolution rate is a sensitive and useful tool to characterize the way in which pozzolans influence the early hydration of cement [8]. In this study, heat evolution and hydration heat of cement pastes containing 0, 10, and 30 percent of RHA or ground silica sand were studied with the thermal conductivity calorimeter. The curves of the rate of heat evolution and heat conversion of samples are shown in Figure 1 and Figure 2 respectively.

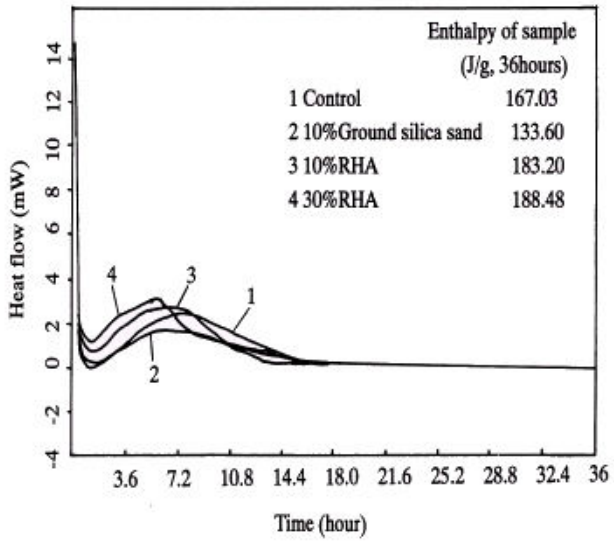

Figure 1. Calormetric curves from the hydration of cement

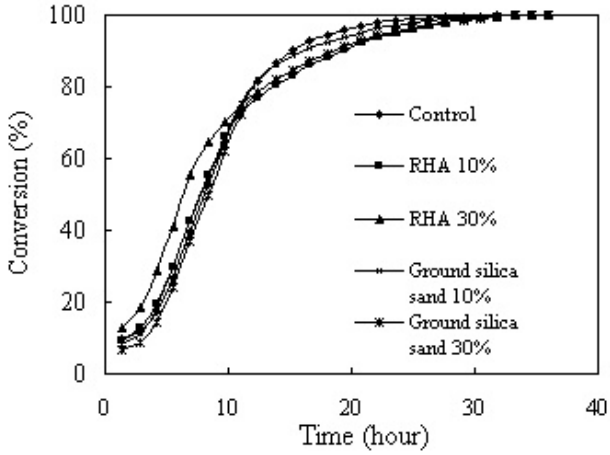

Figure 2. Hydration heat conversion of the samples

It can be seen that during the 12 hours, RHA showed an increase of hydration heat (positive values). The reason for the increase of hydration heat of cement with added RHA is due to two reactions taking place as follows: one is acceleration of the early hydration of C_3S. It is ascribed to the fineness and the high surface area of RHA, which is the availability of a large number of nucleation sites for precipitation of hydration products of C_3S (C-S-H). Another is a pozzolanic reaction. It corresponds to the second peak on the exothermic curve. The height of the second peak initially showed marked increases for cements incorporating RHA compared with the control cement, but then decreases. At the same time, the sample with added RHA was shown to shorten the dormant period. It was caused by the large amount of amorphous SiO_2. Silica from RHA could react with Ca^{2+}, OH^- ions, and calcium hydroxide liberated from the hydration of cement minerals to form more C-S-H gel. In concrete, these reactions were known to contribute to improving the properties of concrete [8,9,10]. The results also confirmed that the pozzolanic activity of RHA is high.

In the strength test procedure, RHA replaced 10% of the cement by mass. The result is shown in Table 3. It can be seen that, compared with the control, from the beginning of hydration (third day) a significant increase in the RHA specimens' strengths is observed. This is because of the large

quantity of amorphous SiO_2 and highly activite RHA, which can react with calcium hydroxide produced from cement hydration. This increased ratio does not decrease with the hydration time. As a result, this RHA is a very highly active pozzolan.

Table 3. Strength* of cement-rice husk ash Mortar

Sample	Rice husk ash(%)	Compressive Strength (MPa)				Flexural Strength (MPa)			
		3d	7d	28d	91d	3d	7d	28d	91d
Control	0	21.9 (100)**	32.4 (100)	39.3 (100)	44.0 (100)	5.16 (100)	6.40 (100)	8.10 (100)	8.45 (100)
RHA	10	26.6 (122)	44.3 (137)	52.3 (133)	55.7 (126)	5.71 (111)	7.61 (119)	9.45 (117)	10.00 (117)

*JIS R 5201 mix proportions are used, Cement/sand=1:3, water/cement=0.5

**Figure in parenthesis shows relative strength of cement-rice husk ash mortar to the strength of respective control mortar with no rice husk ash, expressed in percent.

4.2 The property of fresh concrete

The segregation of concrete with added RHA was not observed. At W/B of 0.30, 0.35, as RHA content increased the concrete appeared to become sticky. Although the slump and air content of concrete were under the control, the workability was not very good.

Because of the high specific surface area of the RHA, the RHA concrete required more superplasticizer and more air-entraining admixture compared with the control concrete to obtain the desired slump and air content, respectively (Figures 3 and 4).

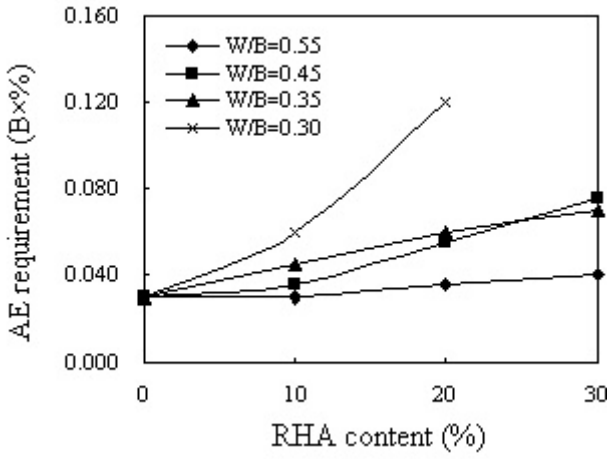

Figure 3. Relationship between requirement of air-entraining admixture and RHA content

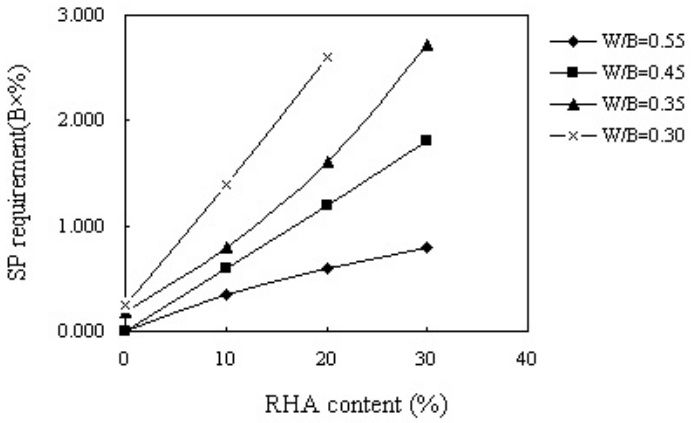

Figure 4. Relationship between requirement superplasticizer and RHA content

4.3 Strength property

The compressive strength and the compressive strength development ratio of concrete are shown in Table 4 and Figure 5. Not only at the age of 3 days, but also at the age of 28 days, the compressive strength of concrete incorporating RHA increased with the increase of RHA content. The maximum ratio of compressive strength development was found at the age of 7 days. The concrete with W/B of 0.35 containing RHA contents of 0%, 10%, 20%, and 30% at 28 days showed the compressive strength of 51.2MPa, 66.2MPa, 75.2MPa, and 82.2MPa, respectively. Its compressive strength was approximately 29-61% higher than that of the control concrete. In pace with curing time higher strength development was observed. A similar tendency of strength development of concrete incorporating RHA was observed with W/B of 0.30 and 0.45. Even at the high W/B of 0.55, the concrete with added 30 percent RHA had a compressive strength of 39.9MPa at the age of 28 days, which was still high.

Table 4. Compressive strength of the RHA concretes

W/B	RHA content,%	Compressive strength, N/mm^2			
		3 days	7 days	28 days	91 days
0.55	0	11.3	18.9	25.1	29.1
	10	12.7	20.8	30.6	35.0
	20	13.5	26.2	38.7	41.3
	30	16.0	29.8	39.9	41.0
0.45	0	18.6	27.1	36.3	43.8
	10	22.0	31.6	40.4	45.8
	20	26.4	39.5	46.4	50.4
	30	31.3	46.2	53.0	60.1
0.35	0	30.4	39.6	51.2	56.9
	10	41.4	53.0	66.2	73.3
	20	43.5	65.0	75.2	77.8
	30	49.0	70.9	82.2	88.1
0.3	0	35.7	41.8	52.3	60.5
	10	48.9	61.4	75.1	80.9
	20	52.5	65.7	77.8	78.9

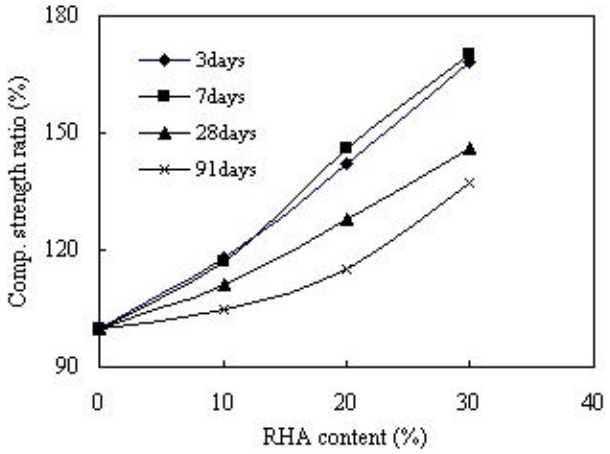

Figure 5. Relative compressive strength of RHA blended concrete vs RHA content (W/B=0.45)

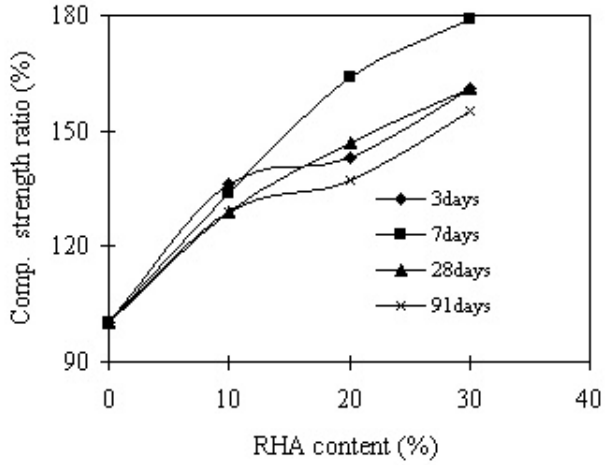

Figure 6. Relative compressive strength of RHA blended concrete vs RHA content (W/B=0.35)

Past research reported that RHA was ineffective in enhancing the properties of rich mix concrete [1,5,6]. Now high strengths in rich mix concrete incorporating RHA can be obtained because of the use of a new polycarboxylic acid-based superplasticizer and the highly pozzolanic activity of the RHA used for this research. It showed that the RHA was suitable for use as a supplementary cementing material to produce high-strength concrete.

4.4 $Ca(OH)_2$ content

The results of $Ca(OH)_2$ content in the RHA concrete with W/B of 0.35 and 0.45 are shown in Figures 7 and 8. Irrespective of the W/B, the $Ca(OH)_2$ content in the RHA concrete decreased visibly with the increasing addition of RHA. No $Ca(OH)_2$ content was observed in the sample with 30% added RHA. It also indicated this RHA is a highly active pozzolan and the silica in RHA could react rapidly with calcium hydroxide liberated from the hydration of cement minerals to form more C-S-H gel. In concrete, these reactions are known to contribute to improvement in the properties of concrete and the RHA concrete had shown the property of high strength.

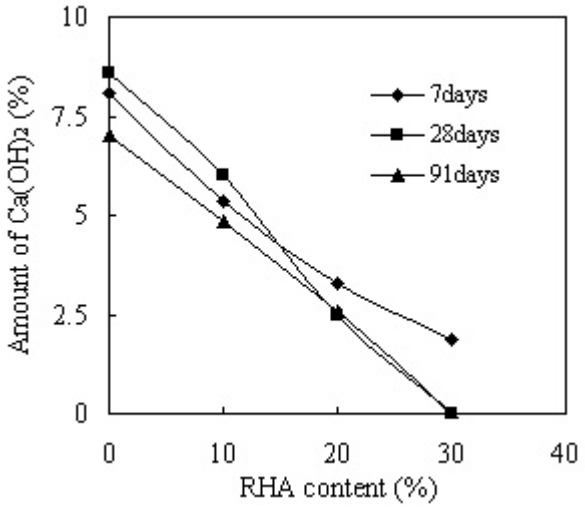

Figure 7. Amount of $Ca(OH)_2$ in the RHA concrete (W/B=0.35)

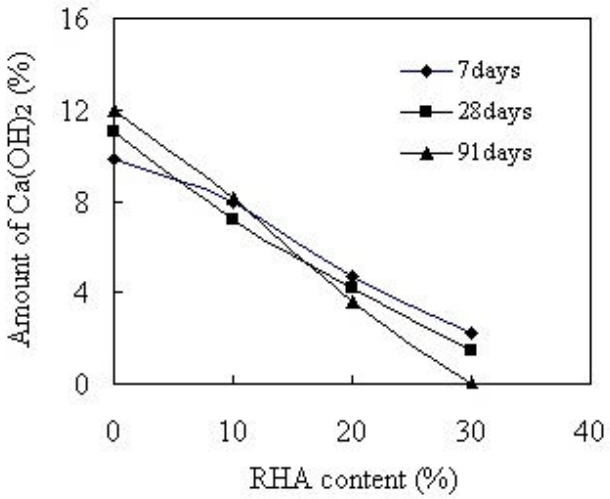

Figure 8. Amount of $Ca(OH)_2$ in the RHA concrete (W/B=0.45)

A high pH is important for the durability of reinforced concrete, and the reduced content of $Ca(OH)_2$ can cause reduced resistance to carbonation because $Ca(OH)_2$ acts as a buffer on the total carbonation reaction. It is necessary to maintain a certain amount of $Ca(OH)_2$ in concrete. So the maximum mixing ratio of the highly activite RHA in concrete was limited to below 30%.

5. CONCLUSIONS

By mean of studying the pozzolanic activity of RHA and the efficiency of a highly active RHA on high-strength concrete, conclusions are as follows:

1. RHA is highly active pozzolan and can be suitable for use as a supplementary cementing material to produce high-strength concrete.
2. RHA showed the behavior in the increase of hydration heat and the cement with added RHA has shown to shorten the dormant period.
3. Though the RHA concrete required more superplasticizer and more air-entraining admixture compared with the control concrete to obtain the desired slump and air content, the compressive strength of concrete incorporating RHA increased distinctly with the increase of RHA content and with decreasing W/B.
4. The reason for the improved strength in RHA concrete is that cement hydration is improved with the increase of RHA content and the rapidly pozzolanic reaction between the silica in the RHA and the $Ca(OH)_2$ liberated from the hydration of cement.

REFERENCES

[1] Sugita, S. “Fundamental Study on the Effective Utilization of Rice Husk Ash as Concrete Material”, Ph. D Thesis, Hokkaido University, 1996.

[2] James, J., and Rao, S., Characterization of silica in RHA, Ceramic Bulletin, V.65, No. 8, 1986, pp. 1177-1180.

[3] P.K. Mehta, Rice husk ash—a unique supplementary cementing material, Adv. Concr. Technol., Proc. CANMET, 1994, 419-444

[4] M.H. Zhang, V.M. Malhotra, High-performance concrete incorporating rice husk ash as a supplementary cementing material. ACI Mater. J. 93 (6) (1996) 629-636

[5] S. Sugita, M. Shoya, H. Tokuda, Evaluation of Pozzolanic activity of rice husk ash. Proceedings of the 4th CANMET/ACI International Conference on Fly Ash, Silica Fume, Slag and Natural Pozzolans in Concrete, Istanbul, Amer. Concr. Inst., Detroit, USA, vol. 1, 1992, 495-512 (ACI SP-132)

[6] S. Sugita, Q. Yu, M. Shayo, ect.,On the semi-industrial production of highly reactivity rice husk ash and its effect on cement and concrete properties. 10th Int. Cong. On Chemical of Cements, Gothenburg (Sweden) 1997

[7] M.P. Luxan, M. Mndruga, J. Seavedra, Rapid evaluation of pozzolanic activity of natural products by conductivity measurement. Cem. Concr. Res. 19 (1989) 63-68

[8] Peter C. Hewlett, Lea's Chemistry of Cement and Concrete, John Wiley and Sons Inc., 605 Third Avenue, New York NY 10158-0012, 1998, pp.471-601
[9] Reported by ACI committee 234, "Guide for the Use of Silica Fume in Concrete", ACI 234R-96, 1996, pp. 8-11
[10] Qijun Yu, K. Sawayama, S. Sugita, etc., The reaction between rice husk and $Ca(OH)_2$ solution and the nature of its product. Cem. Concr. Res. 29 (1999) 37-43

INFLUENCE OF THE STRUCTURAL CHANGE OF GRANULATED BLAST-FURNACE SLAG ON THE HYDRAULIC REACTIVITY

P. Z. Wang [1], R. Trettin [1] and V. Rudert [2]

[1]Institute for Building and Material Chemistry, University of Siegen, Germany.
[2] Wilhelm Dyckerhoff Institute for Building Material Technology, Germany.

ABSTRACT

The paper presents the experimental results of work on the influence of the structural change of granulated blast-furnace slag on its hydraulic reactivity. The investigations were carried out on technical granulated blast-furnace slags that were modified structurally by heating. It is demonstrated that, due to heating up to 700°C, there was a change of structure of the granulated blast-furnace slag, although the x-ray determinable crystallinity of the samples remained unchanged. The hydraulic reactivity of the investigated granulated blast-furnace slags and the associated compressive strength of the slag cements decrease with increasing temperature, according to the structural changes of the granulated blast-furnace slags.

1. INTRODUCTION

It is well known that basic blast-furnace slag with a suitable chemical composition possesses hydraulic characteristics, if it is obtained by rapid cooling in water to form a glasslike solid, which is then granulated. In contrast to that, basic blast-furnace slag which is slowly cooled in air, is not hydraulic because it is completely crystallized and has a thermodynamically stable structure. The hydraulic reactivity of the granulated blast-furnace slags therefore depends strongly on the structure. Therefore it is important to explain the relationship between the structure and the hydraulic reactivity of the granulated blast-furnace slag. To explain this relationship a great deal of reasearch on synthetic and technical granulated blast-furnace slags has been undertaken in the past [1-7]. However, so far no clear connection between the structure of granulated blast-furnace slags and their hydraulicity had been shown. The reactivity of granulated blast-furnace slag results from different characteristics, e.g. chemical composition, structure as well as crystallinity. Moreover the grinding fineness also plays an important role. In this paper an investigation on the influence of the structural change of granulated blast-furnace slag on the hydraulicity was carried out on a structurally modified sample series of technical granulated blast-furnace slags. Further influencing factors, like chemical composition, crystallinity as well as grinding fineness were kept constant. The results obtained so far are presented in the following sections.

2. MATERIALS AND PREPARATION

In order to examine the influence of the structural change of granulated blast-furnace slag on the reactivity, two industrial granulated blast-furnace slags (slag S1 and S2) with very different chemical compositions (Table 1) were used in the investigation. The granulated blast-furnace slags were first ground to a fineness less 63 µm with a ball mill and than heated in a PC-controlled electrical furnace to the relevant temperature 300°C, 400°C, 500°C, 600°C, 700°C, 750°C, 800°C and 1000°C at a heating rate of 20K/min, tempered for two hours at constant temperature and than cooled slowly to 100°C at a rate of 10°K/min. Subsequently, crystallinity was determined by

Proceedings of the 11th International Congress on the Chemistry of Cement (ICCC) 11 - 16 May 2003, Durban, South Africa
'Cement's Contribution to the Development in the 21st Century' ISBN Number: 0-9584085-8-0
Hosted by: The Cement and Concrete Institute of South Africa Editors: Dr G. Grieve and G. Owens
CD-ROM produced by: Document Transformation Technologies Congress Organised by: Event Dynamics

microscope and x-ray diffractometer. The crystallinity of the samples remained unchanged at temperatures up to 700°C (Figure 1), while they were completely crystallized at tempering above 800°C (Figure 2). The granulated blast-furnace slags that were tempered up to 700°C were structurally modified, whereas the chemical composition, crystallinity as well as grinding fineness were kept constant.

Table 1. Chemical composition of the granulated blast-furnace slags

Constituent [Wt.-%]	Granulated blast-furnace slag	
	S1	S2
SiO_2	34,5	40,3
Al_2O_3	11,3	9,4
Fe_2O_3	0,3	0,3
CaO	43,9	37,5
MgO	7,4	8,2
K_2O	0,4	1,2
TiO_2	0,5	0,7
MnO	0,2	1,2
Sulfide	1,2	1,4
CaO/SiO_2	1,27	0,93
$(CaO+MgO)/SiO_2$	1,49	1,13

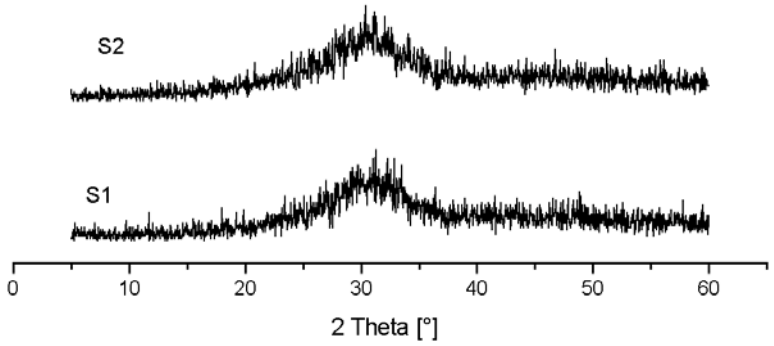

Figure 1. X-ray diagram of granulated blast-furnace slags after tempering at 700°C

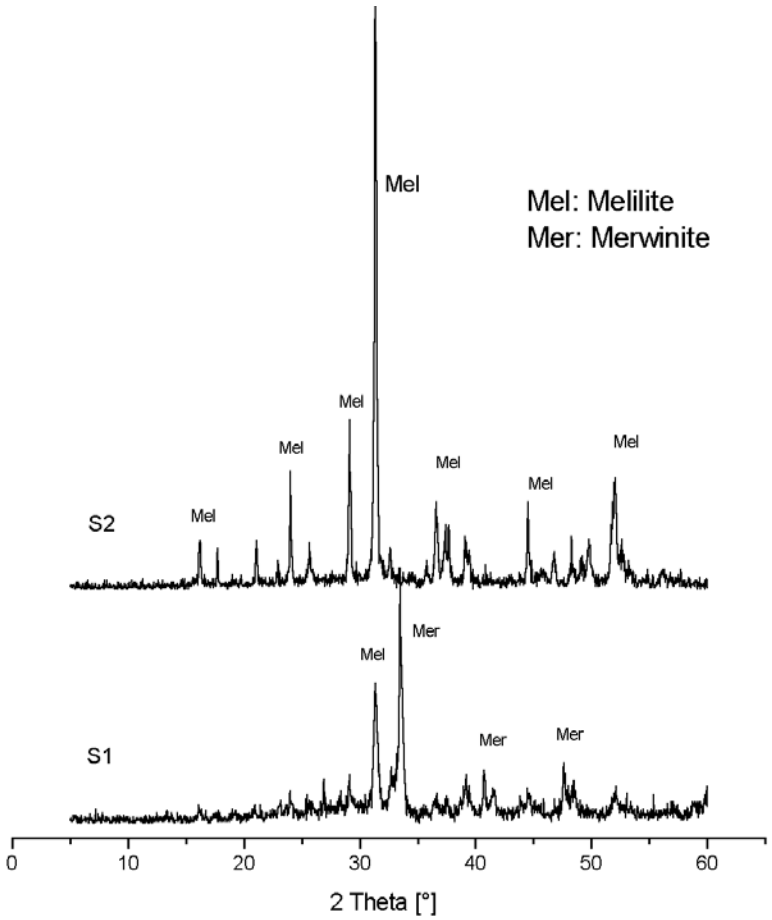

Figure 2. X-ray diagram of granulated blast-furnace slags after tempering at 800°C

3. INVESTIGATION RESULTS AND DISCUSSION

Granulated blast-furnace slag is a glassy solid product, which is formed by rapid cooling in water during the granulation of the blast-furnace slag. In the physicochemical sense the granulated blast-furnace slag is therefore in an unstable state, which is responsible for its hydraulic characteristics. In its glassy state granulated blast-furnace slag has no ordered crystal structure; except that merely a short-range order can be accepted. This short-range orderly structure is an important characteristic for the reactivity of granulated blast-furnace slag.

If a granulated blast-furnace slag is heated by raising the temperature, devitrification is known to occur. With rising temperature the glassy state passes on to a crystalline state. Probably the degree of structural order of the granulated blast-furnace slags was increased by the heat treatment, although x-ray detectable crystallinity remained unchanged during tempering up to 700°C. These structural changes can be confirmed by the density changes at different temperatures.

Figure 3 shows the density changes of the granulated blast-furnace slags with increasing temperature. It is shown that the densities of both slags (S1 and S2) were continuously increased during tempering up to 700°C. This indicates that the structure of the granulated blast-furnace slag was changed with rising temperature and thus the associated packing density was also continuously increased.

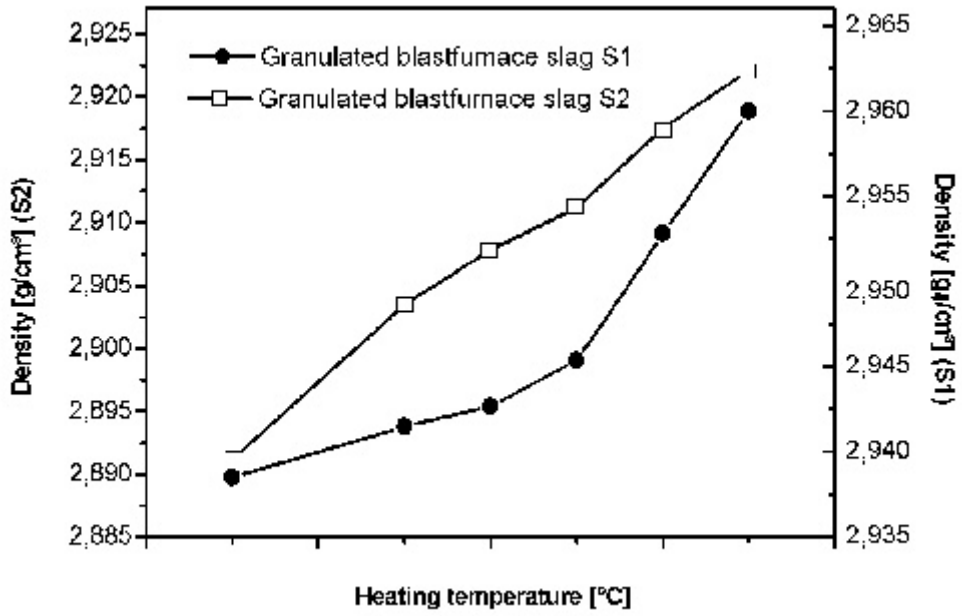

Figure 3. Density changes of the granulated blastfurnace slags with increasing temperature

The heat evolution of granulated blast-furnace slag S1 after heating at different temperatures is represented in Figure 4. As it can be seen from the diagram, the intensity of the heat evolution of the granulated blast-furnace slag decreases with increasing temperature although chemical composition, glass content and grinding fineness remain unchanged under the same conditions. The main reaction peaks became wide with rising temperature, i.e. the reaction is retarded. Further, the heat evolution curves show clearly two maxima after tempering at 600°C and 700°C. At 750°C only a retarded second maximum is recognizable, which disappears after tempering at 800°C.

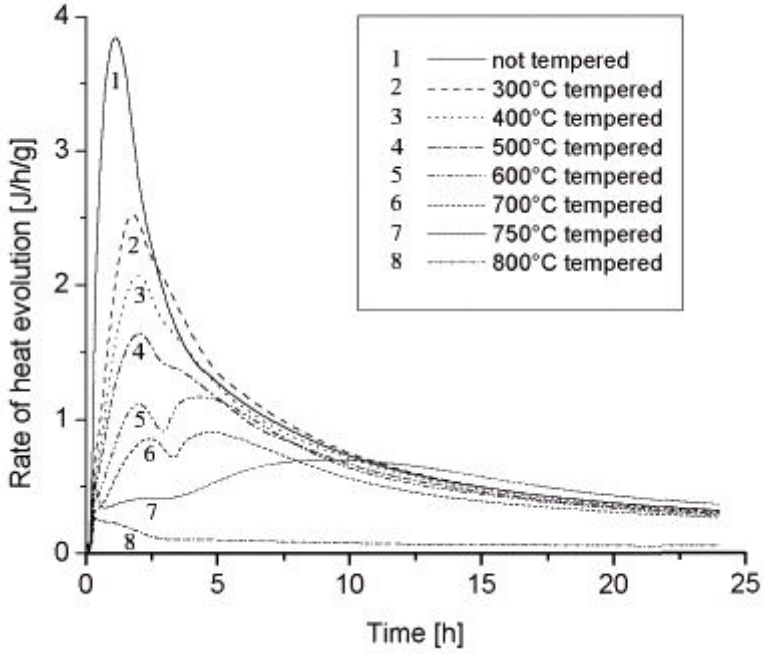

Figure 4. Heat evolution of the granulated blast-furnace slag S1 after tempering at different temperature

It is obvious that the structural changes of the granulated blast-furnace slag took place during the thermal treatments, and the associated reactivity for the hydration was significantly decreased,

although the content of glass remained unchanged. This indicates that the glassy state or the structural order of the granulated blast-furnace slag plays an important role in hydration. During the tempering the glass state develops more and more short-range order with increasing temperature. This leads to a strong reduction of the hydraulic reactivity of the granulated blast-furnace slag.

For direct observation of hydration products on the surface of the granulated blast-furnace slag a scanning electron microscope (SEM) was used. In Figure 5 the SEM-micrographs of the granulated blast-furnace slag S1 tempered at different temperatures are shown after hydration for two hours in a NaOH-solution. The visible hydration products decrease significantly with increasing temperature. This shows that the hydraulic reactivity of the granulated blast-furnace slag has clearly decreased due to structural changes by heating to various temperatures.

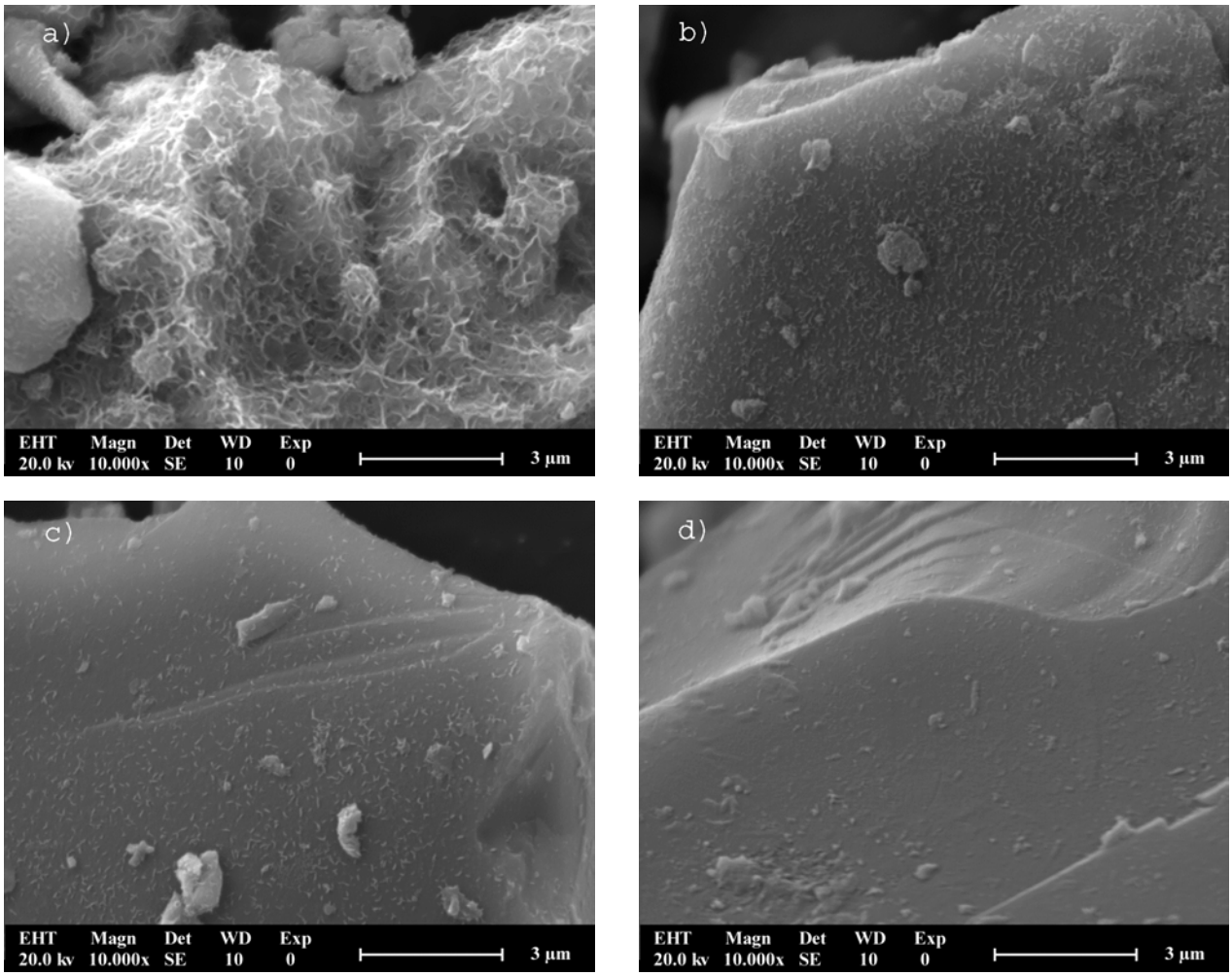

Figure 5. SEM-micrograph of the granulated blast-furnace slag S1 after 2 h hydration in 2n-NaOH a) not tempered, b) tempered at 300°C, c) tempered at 500°C, d) tempered at 700°C

Seven laboratory slag cements were prepared from the samples of granulated blast-furnace slag S1 by heating them to different temperatures 300, 400, 500, 600, 700 and 1000°C, which were subsequently subjected to compressive testing after 2 and 28 days under the same laboratory conditions. The results are shown in Figure 6. It becomes clear that compressive strength decreases with increasing temperature. The laboratory slag cement made from the granulated blast-furnace slag tempered at 700°C has e.g. only a compressive strength of 5,1 MPa after 2 days and 33,6 MPa after 28 days, while the laboratory slag cement made from the original granulated blast-furnace slag (only dried at 100°C) shows a compressive strength of 9,3 MPa after 2 days and 47,4 MPa after 28 days. The compressive strength of the slag cement, which was made from the granulated blast-

furnace slag tempered at 1000°C, which was completely crystallized, shows only 1,3 MPa after 2 days and 2,4 MPa after 28 days. This is attributed to the fact that the degree of structural order of the granulated blast-furnace slag was increased during the tempering and the associated hydraulic reactivity was strongly reduced. Therefore one should take note of this during the drying process of granulated blast-furnace slag.

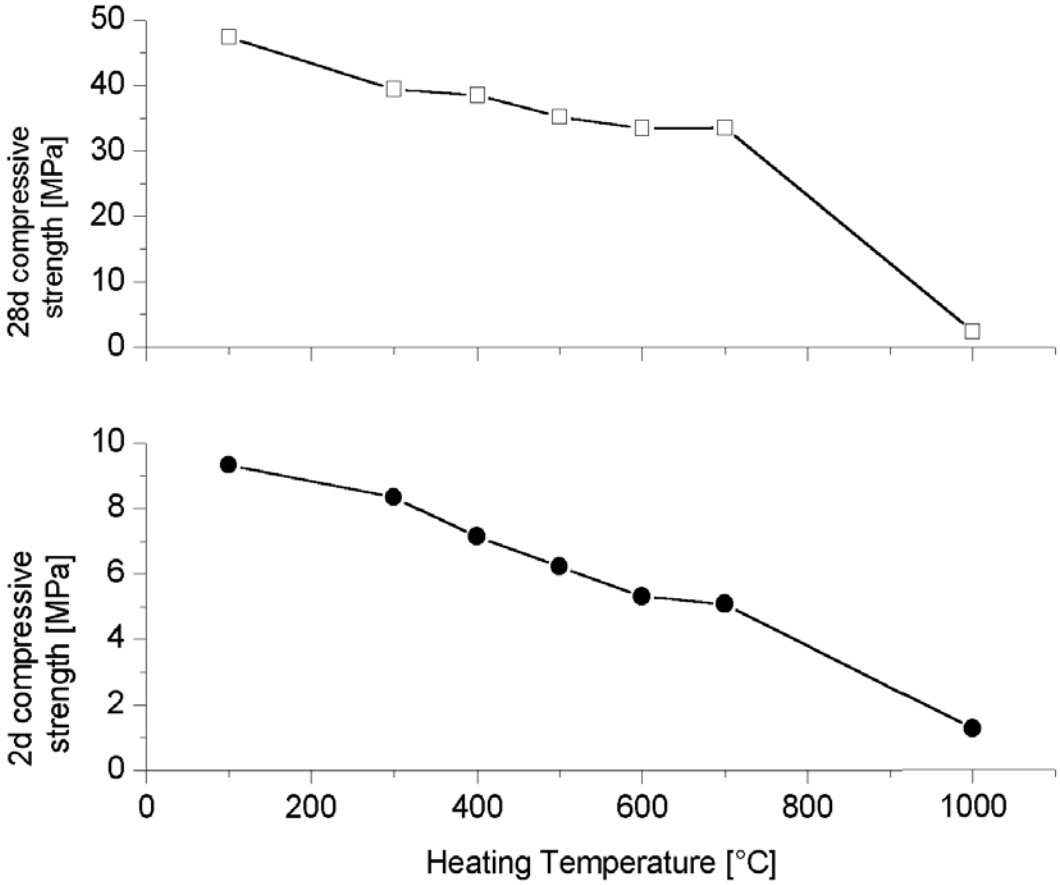

Figure 6. Compressive strength development of the laboratory cements with increasing temperature; slag/clinker=79/21, w/c=0,5

4. CONCLUSIONS

The influence of the structural change of granulated blast-furnace slag on hydraulic reactivity was examined on a series of samples that had been structurally modified by heating. During heating up to 700°C the degree of structural order of granulated blast-furnace slag increased unmistakably, although the x-ray determinable crystallinity of the samples remained unchanged.

The intensity of the heat evolution curve decreased with increasing degree of structural order of the granulated blast-furnace slag and the main reaction peak became wide. The samples tempered at 600°C and 700°C are characterised by two maxima on the heat flow diagrams, while the sample tempered at 750°C shows only a temporally retarded maximum. This difference occurred due to the structural changes of the granulated blast-furnace slag.

Hydraulic reactivity depends to a large extent on the structure of the granulated blast-furnace slag. With increasing temperature or degree of structural order of granulated blast-furnace slag, a strong reduction of the compressive strength of the blastfurnace cement is observed.

REFERENCES

[1] Keil, F. und Locher, W.: Hydraulische Eigenschaften von Gläsern. Zement-Kalk-Gips. 11 (1958) H. 6, S. 245-253

[2] Busch, H. und Petzold, A.: Phasentrennung in basischen Schlackengläsern. Silikattechnik 20 (1969) Heft 2, S. 47-49

[3] Busch, H. und Petzold, A.: Struktur und Hydraulizität basischer Hochofenschlacken. Silikattechnik 22 (1971) Heft1, S. 13-14.

[4] Locher,F.W.:Hydraulische Eigenschaften von kalkreichen Gläsern des Systems CaO-Al2O3-SiO2. Schriftenreihe der Zementindustrie H.25, (1960)

[5] Regourd, M.: Caracteristiques et activation des produits d'addition. 8th International Congress on the Chemistry of Cement.Rio de Janeiro-Brasil, 1986, Principal Reports, Theme 3, pp1-30.

[6] Smolczyk, H -G.: Slag structure and identification of slags. Proceedings of the 7th International Congress on the Chemistry of Cement, Paris (1980) Vol. I, III-I, pp. 3-17

[7] Solacolu, S.: Die Bedeutung der thermischen Gleichgewichte des Systems MgO-CaO-Al2O3-SiO2 für das Schmelzen und Granulieren der Hochofenschlacken. Zement-Kalk-Gips, Nr. 4/1958

RECENT PROGRESS IN SPECIAL CEMENTS IN CHINA

Tangbo Sui and Yan Yao

China Building Materials Academy, Guanzhuang, Choayang District, Beijing 100024, P.R. China.

ABSTRACT

Great progress has been made since the 1970s concerning the research and development of special cements. This paper is a review of the current status of special cements in China. Some low energy special cements with unique engineering performance and development trends in the future are also introduced.

Keywords: Special cements, Performance, Current status

1. INTRODUCTION

General purpose Portland cement has become one of the most widely used building materials since its invention in 1824 due to its better durability and lower cost. Based on the statistics of the China State Administration of Building Materials Industry, the annual output of cement in China in 2001 was close to 600 million tons, which accounts for about one-third of the total world cement production. General purpose Portland cement, however, can not completely satisfy the requirements of multi-function and high performance for different construction projects. Besides, in consideration of the conservation of energy and natural resources and of environmental protection, greater efforts have been made in the research and development of cements with special performance or functions, i.e. special cements. China has many advantages in this aspect. The main reason lies in the fact that there are many small production lines with an annual capacity of less than 100 thousand tons of cement for a single unit, which is very convenient for the production of different types of special cements. The abundance of raw materials is another benefit for the manufacturing of special cements in China.

This paper is a brief review of the research and development of special cements in China. Properties of some typical low energy special cements and development trends in the future are also introduced.

2. CLASSIFICATION

So far there is no common definition in the world concerning the classification of special cements. In China cements are divided into two categories, i.e. general purpose Portland cement and special cement. The former includes Portland cement (PC), ordinary Portland cement (OPC), Portland slag cement (PSC), Portland fly-ash cement (PFC), Portland pozzolanic cement (PPC), and composite Portland cement (CPC). The latter mainly consists of 7 types based on their performance and application, which belong to 6 systems according to the chemical and mineral compositions of clinkers, such as silicate or Portland cement (PC), aluminate cement (AC), fluroaluminate cement (FlAC), sulphoaluminate cement (SAC), ferroaluminate cement (FAC), and miscellaneous types as shown in Table 1.

Table 1. Classification of Special Cements in China

System Type	Silicate	Aluminate	Fluroaluminate	Sulphoaluminate	Ferroaluminate	Miscellaneous
High early strength cement	High early strength PC Modified PC	High early strength AC Set-regulated cement	Quick setting and rapid hardening FlAC	High early strength SAC	High early strength FAC	—
Expansive and self-stressing cement	Expansive PC Self-stressing PC	Expansive AC Self-stressing AC	—	Expansive SAC Self-stressing SAC	Expansive FAC Self-stressing FAC	CaO expansive agent Composite expansive agent
Cement for Hydraulic construction	Moderate heat PC Low heat PSC & PPC High belite cement Sulfate resistance cement	—	—	—	—	Low heat and mini-expansion cement
Oil well cement	Classes A, B, C, D, E, F, G, H well cement	Special well cement	—	Special well cement	Special well cement	Oil well cement without clinker
High temperature resistance cement	—	High alumina cement				Phosphate cement Water glass binder
Cement for decoration	White PC Colored PC	—	—	Colored SAC	—	Colored PC without clinker
Miscellaneous	Cement for road Masonry cement Barium PC Strontium PC	Barium AC	Cement for sand molding Cement for anchoring	Low alkalinity cement	—	Acid resistance cement Mg oxychloride cement Alkali silicate cement Supersulfated cement Alinite cement

3. R & D OF SPECIAL CEMENTS

The development of special cements in China has been carried out in 3 stages since the 1950s, i.e. the stage of imitation, development through self-reliance and renovation[1], and more than 60 types of special cements have been developed, of which around 20 types are manufactured in large scale or batch production. The annual output of special cements in China in recent years is about 8 million tons. Most of the cements have corresponding National or Ministry standards to guide their production and application. Some typical low energy special cements are briefly introduced as follows.

3.1 Modified Portland Cement (MPC)

The main mineral compositions of MPC clinker are the same as general purpose PC except for C_3A being substituted by $C_4A_3\overline{S}$, i.e.,

C_3S 40-55%, C_2S 20-30%, $C_4A_3\overline{S}$ 5-20%, C_4AF 5-10%[2]

The raw mix is burnt at 1350°C with the addition of a certain amount of mineralizer which results in the coexistence of C_3S and $C_4A_3\overline{S}$ and the MPC clinker is therefore formed. Compared with general purpose PC, the MPC exerts expansive properties and higher early strength. The expansion rate and expansion ratio can be adjusted through the amount and the type of calcium sulfate blended in the cement, which can be used to produce high early strength concrete with shrinkage compensation. The strength development of MPC and PC are given in Figure 1.

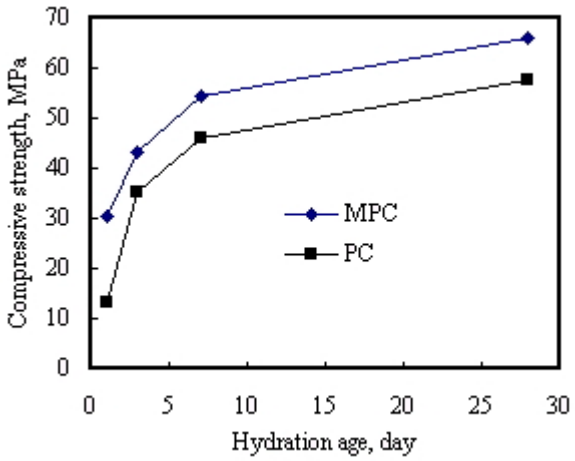

Figure 1. Comparison of strength development of MPC and PC

3.2 Fluroaluminate Cement (FlAC)

FlAC is also a kind of low energy cement due to the inclusion of $C_{11}A_7$ CaF_2 in the clinker phase[3]. Cement sets fast and its early strength gain becomes greater with the increase in the quantity of $C_{11}A_7$ CaF_2. Table 2 gives some properties of this cement. Because of the quick setting and rapid hardening performance of this cement, FlAC is usually used for urgent repairs where 6-hr strength is needed or as a molding sand binder where 1-hr strength is required.

Table 2. Some properties of fluroaluminate cement

System	Main Composition, %			Setting, min		1:2.5 Mortar Compressive Strength, MPa		
	C_3S	C_2S	$C_{11}A_7$ CaF_2	Initial	Final	4h	1d	28d
C_3S-$C_{11}A_7$ CaF_2	48-58	6-12	20-30	<30	<45	20-23	28-32	45-53
C_2S-$C_{11}A_7$ CaF_2	—	12-20	68-76	<15	<20	28-32	37-42	50-60

3.3 Sulfoaluminate Cement and Ferroaluminate Cement (SAC, FAC)

SAC and FAC belong to the CaO-Al_2O_3-SiO_2-SO_3 and CaO-Al_2O_3-SiO_2-Fe_2O_3-SO_3 systems respectively[4,5]. Both cements contain more than 45% of calcium sulfoaluminate, which therefore possess the characteristics of high early strength. The burning temperature of SAC and FAC clinkers is 1300-1350º . By controlling the expansion ratio, several new cements such as set-regulated cement, expansive cement, and self-stressing cement can be made, which are usually used in construction at low temperatures and for preparation of shrinkage compensating concrete, self-stressing concrete pipes and other concrete products. Some typical properties of these cements are listed in Table 3.

Table 3. Typical properties of SAC and FAC cement mortar (1:2.5)

System	Cement Type	Compressive Strength, MPa				*Linear Expansion ratio, %	28d Self stress, MPa
		12h	1d	3d	28d		
SAC	High early strength cement	35-50	40-55	45-68	52-76	<0.5	—
	Expansive cement	—	28-40	—	45-60	<1.0	—
	Self-stressing cement	—	28-40	—	45-60	0.8-1.5	4.0-7.0
FAC	High early strength cement	30-45	40-52	43-56	46-68	0.15-0.26	—
	Expansive cement	—	28-40	—	45-60	0.26-0.65	—
	Self-stressing cement	—	28-40	—	45-60	0.8-1.5	4.0-7.0

*Mortar specimen without constraint tested at 28d hydration age

3.4 High Belite Cement (HBC)

HBC is a kind of newly developed low energy cement in the CaO-SiO_2-Al_2O_3-Fe_2O_3 system[6-7]. Typical mineral composition of HBC clinker is as follows:

C_3S 20-30%, C_2S 45-60%, C_3A 3-7%, C_4AF 10-15%

A current study[8] demonstrates that HBC can be considered as a promising cement with characteristics of energy-saving, natural resources conservation and low CO_2 emission, which is the result of low calcium design in the raw mix. The burning temperature of HBC clinker is 1350°C.

Compared with general purpose PC, HBC exhibits better performances in workability, strength and durability. It therefore has potential in the preparation of high performance concrete, massive concrete and hydraulic engineering concrete, etc. Figure 2 shows the strength development of PC and HBC cement mortar (1:2.5) and concrete.

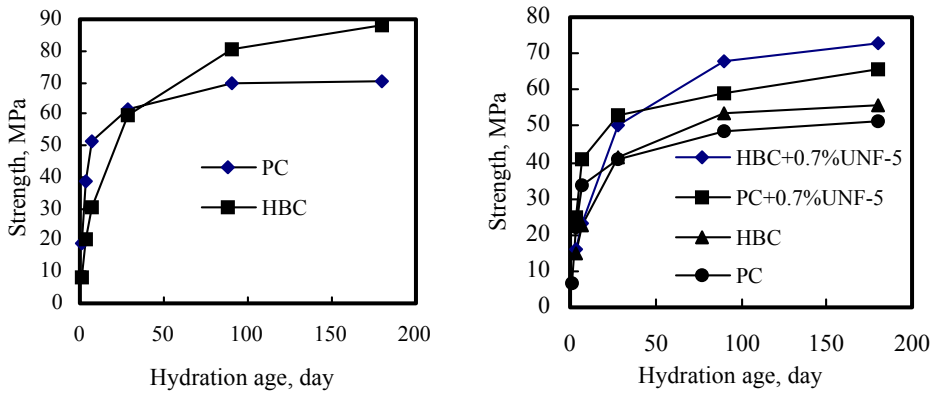

Figure 2. Strength development of cement mortar (left) and concrete (right)
(UNF-5 is naphthalene-based superplasticizer)

Although the early compressive strength (1d-7d) of HBC is relatively low in comparison with PC, its later age strength gain is rapid. The 28d strength of HBC is more than 55MPa, which is equivalent to that of PC. The strength of HBC at 90d-180d is 15-20MPa higher than that of PC. The performance of low heat evolution and high strength gain is therefore achieved for HBC. The durability-oriented property of HBC was introduced elsewhere[6]

4. FUTURE DEVELOPMENT TREND

Great progress has been achieved in China in the research and development of special cements. Yet there still exist two major works to be done. One is the percentage of special cements among the total cement production is less than 2%, which is much lower than in many developed countries. The other is that the basic research on special cements needs to be enhanced so as to further promote the application of special cements. The future development of China's special cements will follow the strategy of sustainable development and concentrate on reducing the environmental impact, utilizing industrial wastes and improving the properties of these cements.

REFERENCES

[1] Wang Youyun, "On the development of China's cement industry", 2nd Beijing International Symposium on Cement and Concrete, Beijing, China, Vol.1, Oct., 1989

[2] Technical report of China Building Materials Academy, 1992. (in Chinese)

[3] Chen Wenhao, Tong Xueli and Xu Jizhi, Journal of China Building Materials Academy, 42 (3), 1980 (in Chinese).

[4] Deng Junan, Ge Wenmi, SuMuzhen and Li Xiuying, "Sulfoaluminate cement series", Proc. of 7th ICCC, Paris, 1980, Vol..4, 381-386

[5] Wang Yanmou, Su Muzhen, Deng Junan and Li Dedong, "A Study of the Mineral Composition of Cement in the Quinary System $CaO-SiO_2-Al_2O_3-Fe_2O_3-SO_3$", J. Chin. Ceram. Soc., 10 (4), 1982, 369-376 (in Chinese)

[6] Sui Tongbo, Liu Kezhong, Guo Suihua, et al, "Research on high belite cement." Part I and Part II, 4th Beijing International Symposium on Cement and Concrete, Beijing, China, Vol. 2, Oct. 27-30, 1998

[7] Tongbo SUI, Kezhong LIU, et al, "Study on the Properties of High Belite Cement", Journal of Chinese Ceramic Society, No.4, 1999 (in Chinese)

[8] Tongbo SUI, "Study on the Low Calcium Portland Cement with High Performance & Low Environmental Impact", Ph D Dissertation, April, 2001(in Chinese)

RESTORATION WITH MORTARS BASED ON OPTIMISED SUPERSULPHATED CEMENT (SGP) – EXAMPLES ON HISTORICAL BUILDINGS IN GERMANY

K. G. Böttger[1] and D. Knöfel[2]

Institute for Building and Material Chemistry, University of Siegen, Siegen, Germany.
E-mail: [1]boettger@chemie.uni-siegen.de and [2]knoefel@chemie.uni-siegen.de

ABSTRACT

The possibilities of restoring historical buildings by applying optimised supersulphated cement (SGP) with low Al_2O_3 content are demonstrated on various examples (Zeitz cathederal, Stralsund "Kampischer Hof", Magdeburg cathedral etc.). It is also recommended that optimised supersulphated cement be used to repair aged dams built with supersulphated cement concrete.

SGP is a binder based on blast-furnace slag, gypsum and Portland cement. The hydraulic stimulation of the slag with a content of approx. 80-90 M.-% is done by sulphatical or/and basic stimulation, preferably making use of gypsum as the sulphatical stimulus, but also anhydrite, whereas Portland cement serves as the basic stimulus. The strength is developed in dependence of the ettringite formation. Beside a high sulphate resistance, mortars and concretes made of SGP show - compared to Portland cement - a lower shrinkage at similar strengths. The use of blast-furnace slag - with lower Al_2O_3-contents (<14-15%) than recommended by Kühl et al. - to produce supersulphated cement, is possible. However, it is necessary to optimise the amount of sulphatic activator (gypsum or anhydrite) and Portland cement to guarantee high strength. SGP cement shows an extremely high sulphate resistance.

Examples for production and use of various mortars with a high sulphate resistance show potential fields of application for SGP, as there are injection mortars for masonry, mortars for joint repair, and mortars for repair of sandstone buildings. In all cases of application the low shrinkage, the high sulphate resistance and the high salt resistance of these mortars offers many advantages. With the addition of an expansive compound (a mixture of aluminous cement and gypsum, ratio 1:1, 15-25% referred to binder) a shrinkage compensated SGP cement can be produced.

1. INTRODUCTION

The restoration of historical buildings or the repair of modern buildings whose materials show high sulphate concentrations - either due to environmental influences or to previously used building materials – may lead to the situation that common binders such as high sulphate resisting Portland cements cannot be used. The need for hydraulic binders under such unfavourable conditions has led to the development of a binder with very high resistance against sulphate attack.

Supersulphated cement with a very high resistance against sulphate attack was produced in Germany till 1970. The production of this cement goes back to a 1908 patent by Kühl [1]. Since 1920 French and Belgian cement plants have produced supersulphated cement under the brand names Cilor and Supercilor [2]. In Germany, supersulphated cement was first produced for commercial use in 1937 [3], and standardised in 1959 in the standard DIN 4210 which is no longer in existence.

Proceedings of the 11th International Congress on the Chemistry of Cement (ICCC)
'Cement's Contribution to the Development in the 21st Century'
Hosted by: The Cement and Concrete Institute of South Africa
CD-ROM produced by: Document Transformation Technologies
11 - 16 May 2003, Durban, South Africa
ISBN Number: 0-9584085-8-0
Editors: Dr G. Grieve and G. Owens
Congress Organised by: Event Dynamics

Nowadays, the sulphate blast-furnace slag cements are still standardised in Belgium [4], France [5], Great Britain [6], Korea [7], and Spain [8]. These cements should contain at least 13 % Al_2O_3, Kühl [9] recommended 14-15 % Al_2O_3 as necessary. Due to the modifications in the steel production process, the Al_2O_3 content consequently dropped below the limits required by DIN 4210. Due to this, supersulphated cement production had to be stopped in 1970, in spite of strong demand.

The purpose of this investigation was to optimise a supersulphated cement with slag sands containing low Al_2O_3 content, and to develop mortars for the applications for masonry injections for backfill mortars, for the jointing of brickwork and for stone substitute mortars. During the development of the slag/gypsum/Portland cement (SGP), the aim was to maintain - even using slag sands with lower contents of Al_2O_3 - the favourable characteristics of the supersulphated cements, as described in reference [9]. As raw materials for the binder, various slag sands and sulphate activators as well as a Portland cement were used.

2. RAW MATERIALS

The used SGP cement was made of slag sand (BS), a sulphate mineral (ST), and a Portland cement (PC). The chemical analyses are shown in table 1. For the production of this binder, the following materials with the given specific surfaces were used:

Slag sand: R: Ruhrgebiet Slag sand (Germany), 4000 cm²/g, Al_2O_3-content 11% (BS-R)
I: Ijmuiden Slag sand (Netherlands), 4000, 5000 and 10000 cm²/g, Al_2O_3-content 16% (BS-I)
Sulphate mineral: - natural gypsum, 6000 cm²/g (Blaine), Osterode am Harz, Germany (G)
- natural anhydrite, 6000 cm²/g (Blaine) Osterode am Harz, Germany (A)
Portland cement: - ordinary Portland cement, ca. 3000 cm²/g (Blaine) (PC)

Table 1. Chemical analyses of the basic materials in weight percent (%)

Binders	BS-R	BS-I	G	A	PC
CaO	38,77	34,19	41,03	41,20	60,02
MgO	7,70	10,42	1,34	1,22	0,77
Al_2O_3	11,36	15,86	0,05	0,19	3,14
SiO_2	37,17	31,92	0,64	0,58	22,95
Fe_2O_3	0,58	0,51	0,05	0,01	6,94
TiO_2	0,31	0,89	0,01	0,01	0,18
MnO	0,29	0,51	0,01	0,01	0,14
Na_2O	0,19	0,01	0,01	0,01	0,12
K_2O	0,86	0,08	0,01	0,01	0,40
P_2O_5	0,26	0,11	0,01	0,01	0,10
SO_3	2,50	0,14	56,86	55,80	3,62
GV	0,00	1,70	14,86	1,72	1,63

Slag sand produced by quick cooling and composed essentially of glass is a latent hydraulic material which must be activated in order to show a sufficiently quick rate of hardening. This can be achieved by sulphate and alkaline activators or by a combination of both. Daimon [10] described the chemistry of the hydration of slag sand (glass) in the presence of portlandite (1) and gypsum (2) by the following equations:

$$C_5S_3A + 2CH + 14\,H \rightarrow C_4AH_{13} + 3\,CSH^* \quad (1)$$

$$3\,C_5S_3A + 6\,Cs + 76\,H \rightarrow 2\,(C_3A{\cdot}3Cs{\cdot}32H) + 9\,CSH + AH_3 \quad (2)$$

The hardening mechanism of sulphate activation cannot be easily compared with that of alkaline activation. When activating with portlandite [$Ca(OH)_2$] or Portland cement, an alkaline environment is only created to activate the acid aluminate-silicate members of the glassy slag particles, whereas a reaction to form ettringite takes place under the sulphate activation. The ettringite phase creates strength and does not endanger the structure by expansive reaction as it mostly begins to form when the cement paste is still in plastic state. Moreover, it is a through-solution reaction because of the fact that the Al_2O_3 is homogeneously distributed in the slag sand [11]. In addition, the content of $Ca(OH)_2$ is low which, according to Mehta [12], leads to the formation of well crystallised ettringite that causes minor expansion only. It is also becoming evident that the contents and the availability of Al_2O_3, important for the slag sand's reactivity, depending on its fineness.

3. PRODUCTION AND COMPOSITION OF THE BINDERS

The composition of the cements was designed such that as much sulphate as possible is provided for hydration of slag sand. The gypsum or the anhydrite are expected to completely react with the slag sand at the latest by 28 days. Portland cement was used as an alkaline activator. Five different binder compositions were made as listed in Table 2.

Table 2. Composition of the SGP cements

	1	2	3	4	5
S	80	80	83	85	87
G / A	17	15	10	10	8
PC	3	5	7	5	5

S - blast-furnace slag A - anhydrite
G - gypsum PC - Portland cement

3.1 Investigative Methods For Binder Optimisation

The evaluation of the binders produced was done by examining standard prisms made in accordance to DIN EN 196 (part 1). Water content was different from the standard requirements, it was based on a standard consistency of mortar (slump of 17±0,5 cm). The following tests on fresh mortar and hardened mortar were performed:

- Slump 17±0,5 cm according to DIN 18555 (part 2)
- Water requirement according to DIN 18555 (part 2)
- Compressive strength according to DIN EN 196 (part 1)
- Flexural strength according to DIN EN 196 (part 1)
- Expansion and Shrinkage according to Knöfel [13] Method A4M
- Leachability
- Liability to efflorescence according to Knöfel [13] Method B6

3.2 Results Of Binder Optimisation

The results of these investigations are briefly summarised below. More detailed results are described in [14]. The water/binder ratio varied between 0,50 (BS-I) and 0,52 (BS-R). The water requirement of the slag sand of the Ruhrgebiet was higher than the one of the Dutch slag sands. The sulphate types, i. e. gypsum and anhydrite, had no influence on the water/binder ratio.

As expected, the compressive strengths of the mortars increased with curing time and with higher fineness. Compared with slag sand from the Ruhrgebiet, the SGP with Dutch slag sand achieved higher strengths at similar grinding fineness (Figure 1). However, compared to Portland cement, the compressive strengths are lower. The flexural strengths developed in parallel to the compressive strengths, and 28-day data for SGP varied between 1,2 and 8 MPa. The ratio between compressive strength/flexural strength, 6,0-11,1 is more favourable when compared to Portland cements. Similar

results were reported earlier with supersulphated cements [15, 16]. With Dutch slag best results were obtained with a cement containing 85 % slag sand (S), 10 % gypsum (G), and 5 % Portland cement (P). The slag from the Ruhrgebiet achieved highest strengths with a composition of 83 % (S), 10 % (G) and 7 % (P). Its Portland cement content is higher and the slag content is lower. Reducing the Portland cement content in the favour of the slag sand contents (Ruhrgebiet) led to lower strength values.

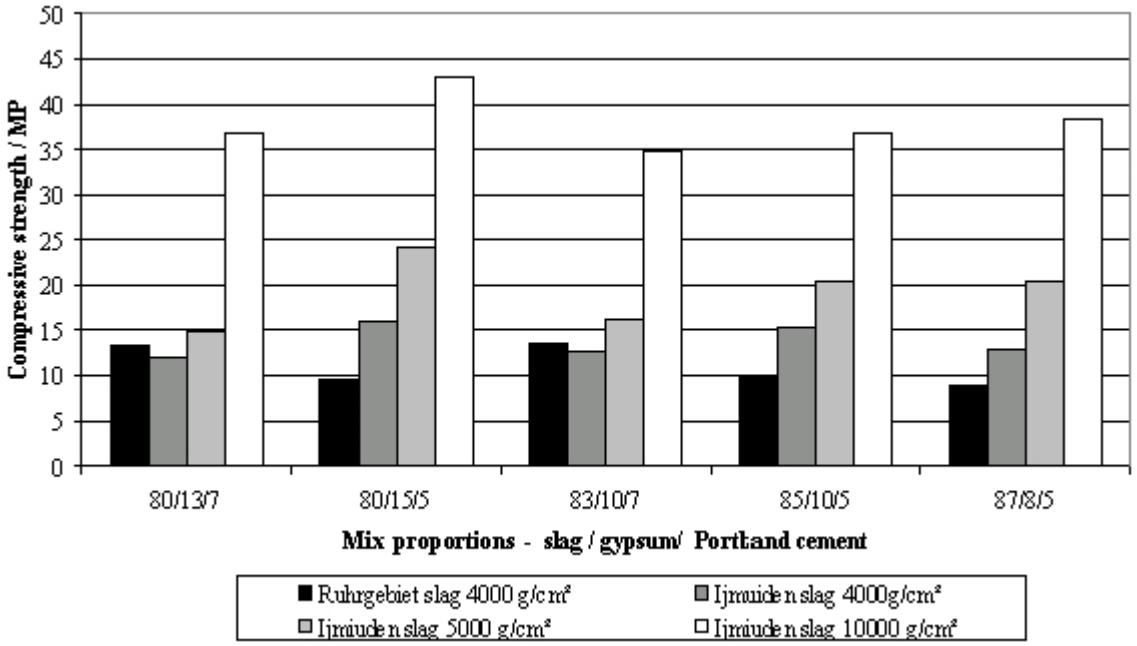

Figure 1. Compressive strengths of the SGP and various slag sands at the age of 28 days

The shrinkage of the SGP mortars made with Dutch slag was lower than those made from the Ruhrgebiet slag. The relatively low shrinkage compared to Portland cement is consistent with the results of other authors [17]. Expansion tests on mortar specimens after 28 days of storage under water showed low values on the order of <0,3 mm/m.

The leachability test for sulphate ions was performed on mortars at the age of 28 days in order to determine the conversion of sulphate minerals. The prisms were crushed to a grain size of 2-4 mm, and shaken with distilled water for 24 h. Thereafter, SO_4^{2-} was determined by means of ionic chromatography. The mortars were made with binders having different gypsum or anhydrite contents. The leachability was lower with the Dutch slag as compared to the Ruhrgebiet slag. The investigation of liability to efflorescence was carried out for over 20 cycles during which the head sides of the prisms were put in distilled water (depth 1 cm) for 24 h and thereafter dried for 48 h at a temperature of 23°C and 50% relative humidity. Very little efflorescence was observed. The results can only be differentiated in so far as the liability to efflorescence increased with lower gypsum contents. The salts formed could be identified as epsomite and gypsum, by x-ray analysis.

In recent times, the composition of supersulphated cement with suitable Dutch slags was optimised for the repair of storage dams. Stark [18] found an optimised composition of 85 % slag sand, 13,5 % anhydrite, and 1,5 % Portland cement with a specific surface of 4500 cm²/g (Blaine) [19]. In this case, compressive strengths of 51,6 MPa of concrete could be achieved.

4. EXAMPLES OF APPLICATION OF SGP

Below, examples of application of SGP are given in the preservation of historical buildings. In these applications high sulphate resistance is a necessary precondition for the successful restoration

of buildings. In Figure 2, the expansion behaviour of various common cements and SGP is demonstrated in the sulphate resistance test according to Henkel [20]. This investigation was made by producing a mortar with a binder/aggregate ratio of 1:3, a gypsum addition of 15 % referred to the binder, and with a slump of 17±0,5 cm. The test samples were stored for one day at 20°C and 95% relative humidity, after that 6 days at 23°C and 50% relative humidity. Afterwards they were stored under water at a temperature of 5 - 8°C to favour an expansion caused by formation of ettringite. In Figure 2, expansion data are shown for Portland cement, Portland cement with high sulphate resistance, blast-furnace slag cement with high sulphate resistance, and SGP cement. As can be seen in Figure 2 all binders, except SGP, showed expansion and were destroyed. This proves the high sulphate resistance of SGP cements and their suitability for the restoration of historical buildings. Similar investigations have been made by Stürmer [21], who also mixed the mortars with old materials containing sulphates instead of gypsum.

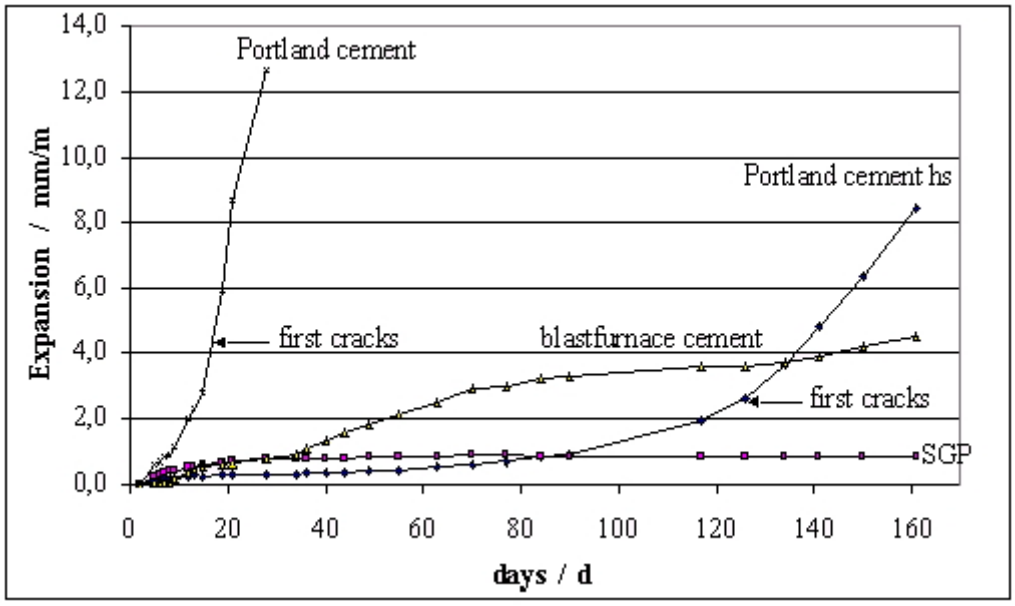

Figure 2. Expansion of mortar prisms made with sereval binders after storage in 8°C water

4.1 SGP mortars for masonry injection

For grouting of multi-shell masonry, an injection mortar with high sulphate resistance was developed on the basis of the above-mentioned investigations (14, Part II). Beside standard sand, various lightweight cellular aggregates were used, such as glass globes, fly ash and foamed glass. Their proportion was between 3 and 15 % referred to the binder. The binder/aggregate ratio was 1:4. Additives such as plasticizers, stabilisers, and, if necessary, air entrainers were also used. For the laboratory investigations, the mortars were produced with a slump of 17±0,5 cm. The mortar consistency for the pressing was increased so that the mortars had good flowing properties. The composition of the mortars and the properties of the fresh and hardened mortars are given in table 3. They show the suitability for the purpose intended.

Compared with an injection mortar made of blast-furnace slag cement, the SGP cement injection mortars showed strengths which are approx. 20 % lower. As expected, distinctly higher strengths are achieved when using plasticizers. Most of the time, the various additives do not have a strong effect, only the use of foamed glass compared to solid glass globules showed some effect. Foamed glass reduced the strengths by half, while solid glass globules increased the strength by approx. 10%. The injection mortars showed slight expansion and shrinkage, air voids had a positive effect and foamed glass had a negative effect on volume changes.

Table 3. Composition and properties of the injection mortars for masonry grouting

	HOZ	N	NF15	NF10V	NF10LP	NgG	NG8
Binder	HOZ	SGP	SGP	SGP	SGP	SGP	SGP
Aggregate						**	
Standard sand %	100	100	85	90	90	25	92
Fly ash %	0	0	15	10	10	0	0
Foamed glass %	0	0	0	0	0	75	0
Solid glass globules %	0	0	0	0	0	0	8
Fly ash %	0	0	0	0	0	0	0
Admixtures*							
Plasticizer %	0	0	0	5	0	0	0
Air entrainer %	0	0	0	0	0,3	0	0
Properties							
w/b-value	0,60	0,60	0,62	0,43	0,60	0,62	0,56
WRC %	71,1	78,0	82,8	91,1	81,3	89,1	81,1
Air Voids %	2,5	3,4	3,5	1,5	6,0	11,0	3,1
Bulk density g/cm³	2,26	2,24	2,15	2,32	2,13	1,22	2,25
Expansion mm/m	0,09	0,04	0,10	0,14	0,07	0,05	0,06
Shrinkage mm/m	-1,02	-1,01	-1,03	-0,77	-0,95	-1,24	-1,08
dyn. E-Modulus MPa	40900	32000	31500	44000	31000	9000	35100
Compr. Strength MPa	42,6	35,0	35,6	59,5	34,7	17,4	38,1

* - referred to the binder ** in V.-%

Recently, other researchers have also developed injection mortars for masonry using SGP cement or SAP cement (anhydrite instead of gypsum as a source of sulphate ions). Stürmer [23] composed a binder with foam instead of aggregate, and grouted masonry successfully with this injection mortar.

4.2 SGP Backfill mortars to conserve lime plasters

The restoration projects of the Heydau monastery, Altmorschen, Germany and the Magdeburg cathederal, Germany, have involved the development and testing of backfill mortars. They have been developed in order to conserve a permanent connection between highly sulphated historical lime plasters and the underground, so as to preserve them for future generations.

All tested injection mortars fulfilled the requirements regarding the flowing and penetration behaviour. The SGP-backfill mortars showed compressive strengths and dynamic modulus of elasticity nearly close to historical lime plasters. The additives (PUR, polymer dispersion) reduce the elastic modulus, increasingly when more are added; methylhydroxyethylcellulose (MC) even reduces compressive, bending, and bond strengths.

Two injection mortars SGP and SGP without MC were applied on test surfaces and 12 months later the bonding properties, see Figure 3, and the bonding strength were checked. The bonding properties were undisturbed, newly formed noxious salts could not be detected, and the bonding strength was within the range of the laboratory results. More information in [24].

Figure 3. Core (∅ 5 cm) of restaurated plaster - bond between gypsum backfill mortar and loam

4.3 SGP mortar for brickwork jointing

For the production of jointing mortars, one should take advantage of the high resistance of SGP cement against sulphate and salt attack [20, 21, 25]. The carbonation of SGP may have a disadvantageous effect on these mortars leading to granular disintegration. The carbonation of ettringite leads to a considerable volume reduction, the consequence of which is the granular disintegration. This damaging process was described by D´Ans and Eick [26]. Due to this reason, SGP mortars were seldom used on the external surfaces of buildings. This negative property of the SGP cement could be improved by using, among others, redispersible polymer powders [27]. When re-jointing ancient masonry, a special situation must be considered. Jointing mortars have to provide a safe external cover of the masonry to guarantee protection against weather influences. Due to this reason, they should guarantee a perfect crack-free adhesion to the brickwork. The shrinkage of the mortars, however, causes the contrary effect. The use of expansion compounds, in turn, offers the possibility to reduce the shrinkage of the mortar. The ideal case would be a shrinkage-compensated mortar which, instead of shrinking, expands slightly until the mortar is hardened. Successful investigations in this direction were made by Knöfel, Degenkolb and Winnefeld [28, 29, 30]. Mixtures of aluminous cement and gypsum (ratio 1:1), with 15-25 % addition to the binder have proved effective in this case.

Various additives and aggregates were used to develop a pointing mortar based on SGP and SAP. The binder/aggregate ratio was 1:5. The exact compositions of the jointing mortars are given in table 4. Aggregates such as standard sand, and mixtures of standard sand and light weight aggregates such as perlite and expanded slate, were applied. The use of an expansive compound composed of aluminous cement and gypsum in a ratio of 1:1, should reduce the shrinkage and thus improve the adhesion to the brickwork. In order to improve the adhesive strength and to reduce granular disintegration, polymers were used. Methyl cellulose was used to increase the water retention capacity (WRC) and this provided the conditions for good hydration. The thickener's task is to improve the workability of the mortar but it causes higher water demand. A plasticizer was added in order to reduce the demand for water. Retarder was used to reduce the rate of workability loss.

The mechanical properties of the jointing mortars are improved by polymers (KD) and methyl cellulose (MC). The same is valid for the tendency to granular disintegration. In the same way, the use of plasticizers (FM), thickeners (Vd) as well as of retarders leads to further improvements. The expansive agent reduces the mechanical properties in the same way as the use of light-weight

aggregates. A high impermeability is usually associated with superior mechanical properties. As a consequence of this, the water absorption coefficients are reduced by the additives and the resistance to water vapour diffusion are increased. The use of expansive compound leads to a higher permeability. The expansion on moisture exposure are in general quite low. Shrinkage of unmodified jointing mortars is in the range of–0,66 mm/m. It is lowered by the use of KD and MC. The use of expansive compounds results in an improvement on the shrinkage to values of–0,11 to –0,12 mm/m.

Table 4. Composition and properties of jointing mortars on the basis of SGP/SAP

	HF1	HF3	HF4	HF5	HV1	HV1+	HV3	HV3+
Binder	SGP	SGP	SAP	SAP	SAP	SAP	SAP	SAP
Aggregate	SA	SA	SA	SA	SA	SABP	NS	SABP
b/a	1:5	1:5	1:5	1:5	1:5	1:5	1:5	1:5
QK	0	0	0	0	0	0	15	15
KD	0	5,00	0	5,00	5,00	5,00	5,00	5,00
MC2	0	0,10	0	0,10	0	0	0	0
MC3	0	0	0	0	0,15	0,15	0,15	0,15
FM	0	0	0	0	1,00	1,00	1,00	1,00
Vd	0	0	0	0	1,10	1,10	1,10	1,10
VZ	0	0	0	0	0,11	0,11	0,26	0,26
w/b / -	0,68	0,58	0,68	0,58	0,54	0,69	0,54	0,69
ρ_f / g/cm³	2,24	2,06	2,22	2,08	2,05	1,95	2,05	1,96
AV / Vol.-%	4,5	11,0	4,8	11,5	8,4	8,4	8,0	8,8
WRC / %	73,2	95,7	73,7	95,4	99,0	97,6	98,6	98,2
E_{dyn} / MPa	13200	13500	10900	12200	28800	20900	12700	10300
$ß_{BZ}$ / MPa	2,1	4,7	1,3	3,8	7,0	5,0	3,0	2,6
$ß_D$ / MPa	13,2	15,7	9,2	11,0	36,8	25,0	10,0	8,1
$ß_{HZ}$ / MPa	0,14	0,42	0,28	0,68	1,18	1,12	0,78	0,80
ω / kg/m²√h	2,5	0,6	3,7	0,6	0,3	0,5	3,0	4,3
μ / -	24	25	n. i.	n. i.	121	58	17	15
EB / mg	434	55	159	35	0	7	49	67
ε_s / mm/m	-0,60	-0,52	-0,66	-0,53	-0,80	-0,67	-0,11	-0,12
ε_q / mm/m	+0,27	+0,16	+0,24	+0,10	+0,29	+0,36	+0,13	+0,33
ε_{s2} / mm/m	-0,26	-0,37	-0,19	-0,28	-0,52	-0,71	-0,17	-0,62

SGP and SAP: Supersulphated Cement, mixtures of blastfurnace slag, gypsum (SGP) or anhyrite (SAP) and Portland Cement

n. i. not investigated

SA standard aggregate

SABP Mixture of standard sand:Perlite:expanded slate 3:0,5:0,5 (related to bulk factor)

b/a binder/aggregate value

* Added quantity related to binder

QK Expansive compound – 15% of cement is substituted by a mixture of aluminous cement:gypsum 1:1

KD redispersible polymer powder, basis vinylacetate-versatate-copolymer

MC2 Methyl cellulose, Viscosity 15000 mPas

MC3 Methyl cellulose, Viscosity 25000 mPas

FM Superplasticizer on melaminous basis

Vd Thickener on sepiolithic basis

VZ Retarder on the basis of potassium-sodium-tartrate

w/b Water/Binder value

ρ_f Fresh mortar's bulk density

AV Air voids

WRC Water retention capacity

E_{dyn} Dynamic Modulus of elasticity

$ß_{BZ}$ Flexural strength

$ß_D$ Compressive strength

$ß_{HZ}$ Bond strength

ω Water absorption coefficient

μ Resistance to water vapour diffusion

EB Efflorescence behaviour

ε_s Shrinkage

ε_q Swelling

ε_{s2} 2. Shrinkage

After having used the mortars HF5 and HV3+ at the Kampischer Hof in Stralsund, no negative effects on of the sample surfaces including granular disintegration have been observed to date.

4.4 Artificial stone mortar for reprofiling damaged natural stone

For the repair of damaged natural stone at Zeitz cathedral, Germany, aritical stone mortar was developed: for composition and properties see table 5 and Figure 4. The natural stone used at Zeitz cathedral was a sandstone with dolomite binder. Atmospheric influences lead to the formation of epsomite and gypsum which leads to decay, see Figure 5. The salt content was up to 13 %. This high concentration of sulphates leads to the use of SGP-binder, but also of blast furnace cement with a high content of blast furnace slag. The aggregate of the artificial stone mortar was as fine and of the same colour as the particles of the sandstone.

To achieve the durability of the mortars several additives were used - redispersible polymer powder which improved the bond strength and entrained air voids and air entrainer. The amount of air voids was higher than 20% to allow space for the formation of salts permeating off the natural stone into the artificial stone mortar, see Figure 7. The properties of the artificial stone mortars used at the Zeitz cathedral are: compressive strength 8-10 MPa, bond strength 0,3-0,4 MPa, water absorption coefficient <1,0 kg/m²√h and resistance to water vapour diffusion <30 as well as a high durability to freeze-thaw-cycling test. The artificial stone mortar has a high resistance against efflorescence. Special tests, were undertaken in accordance with existing tests in Germany and are reported more fully in [31]. The restoration of Zeitz cathedral took place with mortar H5OM0 in 1997, see Figure 6, no damage has been found to date.

Table 5. Composition and properties of artificial stone mortars

	H5OM0	H5OM2	H5OG0	H4SM2	H4SM2	H4SG0	H5SM0	H5SM2	H5SG0	H2LM0	H2LM2	H2LG0
w/b-ratio	0,57	0,59	0,48	0,48	0,51	0,44	0,54	0,56	0,48	0,35	0,35	0,34
Air voids / V.-%	21	15	11	25	26	24	25	24	22	26	17	19
E_{dyn} 90 d / MPa	8150	12200	18700	12000	10600	10200	12600	16600	18000	6900	8450	6400
$ß_{BZ}$ 90 d / MPa	3,01	5,27	6,84	4,67	4,14	3,18	6,03	5,35	5,16	2,48	3,04	1,32
$ß_D$ 90 d / MPa	7,4	14,0	18,5	14,5	12,1	10,5	16,6	19,1	19,0	8,1	9,8	5,9
ω / kg/m²√h	0,52	0,46	0,35	0,62	0,37	0,67	0,46	0,29	0,81	1,01	0,77	0,92
μ / -	29	52	86	32	41	34	35	28	23	17	11	17

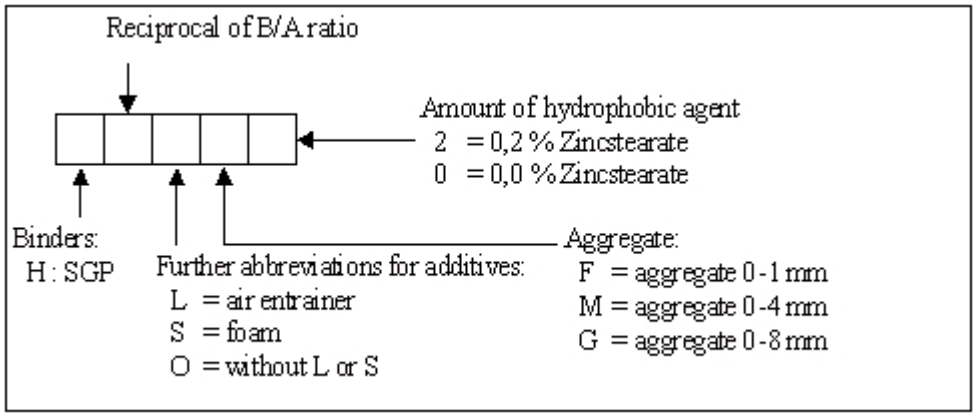

Figure 4. Zeitz cathedral damaged stone

Figure 5. Zeitz cathedral damaged stone

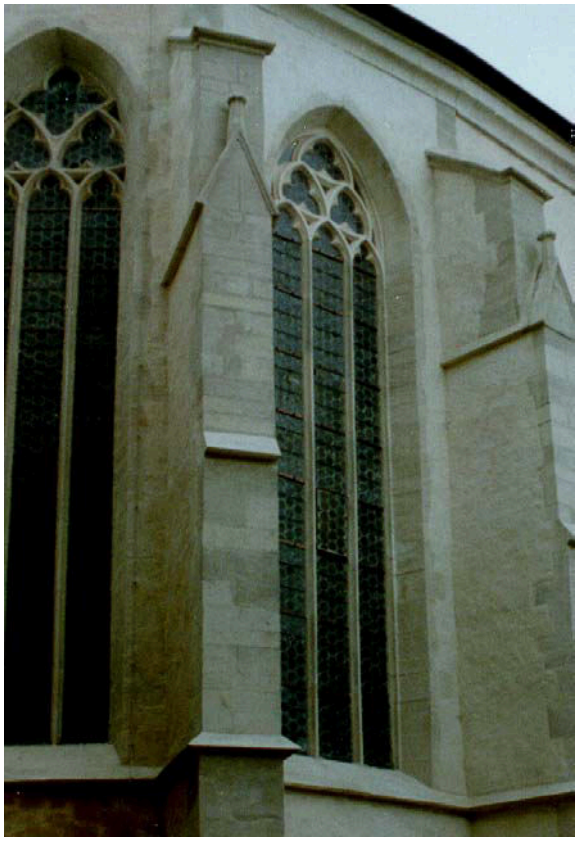

Figure 6. Zeitz cathedral after restoration

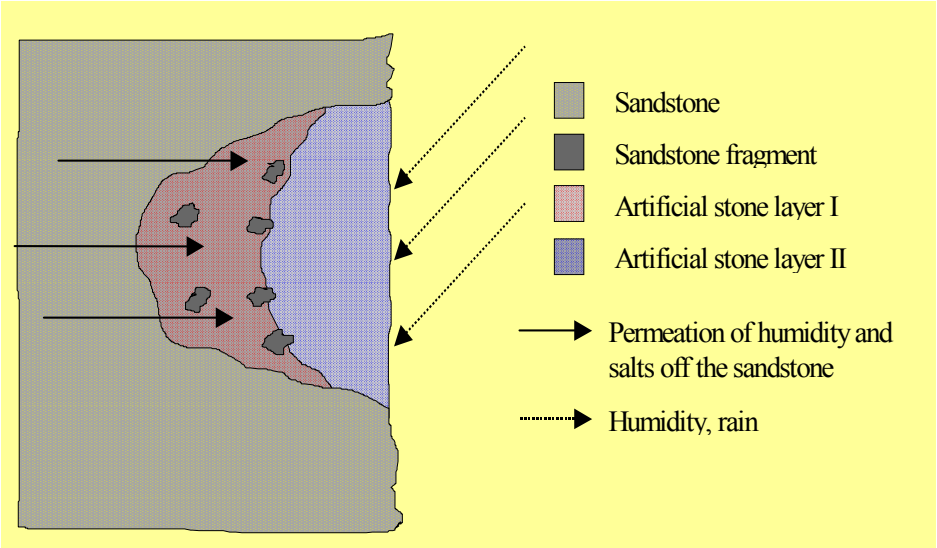

Figure 7. Restoration of damaged sandstone with artificial sand stone

5. CONCLUSIONS

The use of blast-furnace slag - with lower Al_2O_3-contents (<14-15%) than recommended by Kühl et al. - to produce supersulphated cement, is possible. However, it is necessary to optimise the amount of sulphatic activator (gypsum or anhydrite) and Portland cement to guarantee high strength. This cement is called SGP cement (S – slag, G – gypsum, P – Portland cement). SGP cement shows an extremely high sulphate resistance and a low shrinkage compared to Portland cement.

Examples for production and use of various mortars with a high sulphate resistance show potential fields of application for SGP, as there are injection mortars for masonary, mortars for the repair of damaged historical plasters, mortars for joint repair, and mortars for repair mortars for sandstone buildings. In all cases of application the low shrinkage, the high sulphate resistance and the high salt resistance of these mortars offer many advantages.

The addition of an expansive compound (a mixture of aluminous cement and gypsum, ratio 1:1, 15-25% referred to binder) a shrinkage compensated SGP cement can be produced. The high volume stability is caused by the low portlandite content in this binder system. This leads to a coarse morphology of ettringite that causes minor expansion only.

The mechanical properties of the jointing mortars are improved by polymers (KD) and methyl cellulose (MC). The same is valid for the liability to granular disintegration.

REFERENCES

[1] Kühl, H. Verfahren zur Herstellung von Zement aus Hochofenschlacke; Deutsche Reichspatent 237777, patentiert im Deutschen Reich vom 23.12.1908.

[2] Trautmann, I. Entwicklung eines Mörtels aus Hüttensand, Gips und Portlandzement (H-G-Z) zur Injektion in mehrschaliges Mauerwerk; Dissertation, Philipps-Universität Marburg, Marburg, 1992.

[3] Zulassung von Sulfathüttenzement; Reichsblatt Nr. 2/38 part I, p. 11, 31.12.1937.

[4] Standard NBN 132159, Belgien.

[5] Standard NFP 15-313 (1. Change 1967), Frankreich, 1964.

[6] Standard BS 4248 Supersulphatecement, Großbritannien, 1974.

[7] Standard KUK-JU 1606 Sulphate cement, Korea, 1960.

[8] Standard UNE 41159 Supersulphated Cement, Spanien, 1966.

[9] Kühl, H. Schleicher, E. Gipsschlackenzement; 2. edition, Fachbuch GmbH Leipzig, Leipzig, 1953.

[10] Daimon, M.: Mechanism and kinetics of slag cement hydration. Proc. of the 7th International Congress on the Chemistry of Cement (ICCC)Paris, vol. I, III-2/1-2/9, 1980.

[11] Cohen, M. D. and Richards, C. W.: Effects of the particle size of expansive clinker on strength expansion characteristics. Cement and Concrete Research, vol.12, 1984, p. 717-725.

[12] Mehta, P. K.: Mechanism of expansion associated with ettringite formation. Cement and Concrete Research, vol.3, 1973, S. 1-6.

[13] Knöfel, D. und Schubert, P.: Mörtel und Steinergänzungsstoffe in der Denkmalpflege. Herausgeber: Knöfel, D. und Schubert, P., Verlag Ernst und Sohn, Berlin, 1993.

[14] Trautmann, I. and Knöfel, D.: Entwicklung eines Hüttensand-Gips-Portlandzement-Mörtels zur Injektion in mehrschaligem Mauerwerk. Zement-Kalk-Gips, vol.46, 1993, p. 95-101 – Part. I and: Optimierung des Mörtels. Zement-Kalk-Gips, vol.47, 1994, p. 219-224 - Part II.

[15] Kramer, W.: Eigenschaften und Anwendungsmöglichkeiten des Sulfat-Hüttenzementes. Betonstein-Zeitung, 1952, No. 11.

[16] Blondiau, L.: Les ciments metallurgiques sursulfatés et applications dans les travaux exposés aux agents agressifs. La revue des matériaux de construction et de travaux publics, No. 351 (1938), p. 246-277.

[17] Mußgnug, G.: Einige charakteristische Eigenschaften des Gipsschlackenzementes. Zement-Kalk-Gips vol.8, 1951, S. 208-213.

[18] Stark, J. and Diming A.: SHZ-Mörtel/Beton-Modifizierung und Beschichtung. Wissenschaftliche Zeitschrift der Bauhaus-Universität Weimar, vol.42, 1996, p. 47-54.

[19] Müller, R.: Nachstellung eines Sulfathüttenzementes (SHZ). Diplomarbeit, Hochschule für Architektur und Bauwesen Weimar, Weimar, 1995

[20] Henkel, S. and Knöfel, D.: Zur Verträglichkeit von Mörteln für die Betoninstandsetzung. 12. Internationale Baustofftagung - ibausil, Tagungsbericht Band 2, Hochschule für Architektur und Bauwesen, Weimar, 1994; p. 58 – 66.

[21] Stürmer, S. and Mielke, I.: Verträglichkeitsuntersuchungen Teil 1: Verträglichkeitsuntersuchungen mit verschiedenen Bindemitteln und Altmaterial. Wissenschaftliche Zeitschrift der Hochschule für Architektur und Bauwesen Weimar-Universität, vol.39, 1993, p. 99-105.

[22] Böttger, K. G.; Knöfel, D.: SGP - a binder with high sulphate resistance for mortars and concrete. Proceedings of the 6th Canmet/ACI International Conference on Fly Ash, Silica Fume, Slag, and Natural Pozzolans in Concrete, Juni 1998, Bangkok, Supplementary Papers, S. 307-322

[23] Stürmer, S.; Mielke, I.; Stark, J.: Injektionsschaummörtel für die Bauwerkssanierung. Wissenschaftliche Zeitschrift der Hochschule für Architektur und Bauwesen Weimar-Universität, vol.40, 1994, p. 15-22.
[24] Böttger, K. G.: Mörtel für die Erhaltung historischer Kalkputze: Haftmörtel, Hinterfüllmörtel und Kalkmörtel. Dissertation, Bauhaus-Universität Weimar, Weimar 1997, Logos Verlag Berlin, 1997.
[25] Stürmer, S. and Herbach, D.: Verträglichkeitsuntersuchungen Teil 2: Verträglichkeitsuntersuchungen mit Natursteinen und Salzen. Wissenschaftliche Zeitschrift der Hochschule für Architektur und Bauwesen Weimar-Universität, vol.41, 1995, p. 125-127.
[26] D´Ans, J. and Eick, H.: Untersuchungen über das Abbinden hydraulischer Hochofenschlacken. Zement-Kalk-Gips, vol.12, 1954, p. 449-459.
[27] Stephan, D.; Böttger, K. G.; Knöfel, D.: Entwicklung von hochsulfatwiderstandsfähigen, schwindarmen Schlämmen mit an Terrakotten angepaßten Eigenschaften. 4th International Colloquium: Werkstoffwissenschaften und Bausanierung, vom 17.-19.12.1996, vol. I, p. 481-495.
[28] Knöfel, D.; Degenkolb, M.; Winnefeld, F.: Modifizierung von Mörteln auf der Basis sulfatisch aktivierter Hüttensand-Bindemittel. In: Advances in Building Materials Science, Festschrift Wittmann, Hrsg. A. Gerdes, Aedificatio Publishers, Freiburg, Unterengstringen, 1996, p. 229-242.
[29] Degenkolb, M. and Knöfel, D.: Investigations on shrinkage compensated and expansive repair mortars and general behaviour to typical influences. Proc. of the 10th International Congress on the Chemistry of Cement (ICCC), Gotheburg, 1997, vol. 2, paper 2ii074, 8pp.
[30] Winnefeld, F. and Knöfel, D.: Mauermörtel für Ziegelmauerwerk. Proceedings of the 13th ibausil, Weimar, 1997, vol 2, p. 2-0815 - 2-0826.
[31] Stephan, D.; Böttger, K.G. und Knöfel, D.: Entwicklung von Rezepturen zur Restaurierung von Sandsteinen mit Steinergänzungsmassen. Proceedings of the 13th ibausil, Weimar, Sept. 1997, lecture-Nr. 2.203, vol. 2, p. 777-789.

ORGANIC HYDROPHOBIC ADMIXTURES AND HYDROPHOBIC PORTLAND CEMENTS. LITERATURE REVIEW AND MARKET SEARCH

John Bensted*, **Michael Schieber****and Mihai Nadu*****

* School of Crystallography, Birkbeck College, University of London, Malet Street, London WC1E 7HX, U.K.; E-mail: bensted.j@btinternet.com
** The Fredy and Nadine Herrmann School of Applied Sciences, Hebrew University of Jerusalem, Jerusalem 91904, Israel; E-mail: schieber@vms.huji.ac.il
*** Corresponding author. Affiliation as in **. Postal address: PO Box 10587, Jerusalem 91103, Israel; E-mail: mihai_nadu@hotmail.com

ABSTRACT
The paper reviews the present state of knowledge about the entitled subject. The HPC finds application in high humidity climate conditions (building sites with poor storage conditions, The paper reviews the present state of knowledge about *Organic Hydrophobic Admixtures and especially about the Hydrophobic Portland Cement*. Such a cement finds application in high humidity climate conditions (building sites with poor storage conditions, long distance shipping of the cement etc..) and can replace the Ordinary or the Rapid Hardening Portland Cements which would deteriorate prior to use. By including in the cement a certain hydrophobic admixture, it is possible to obtain a high quality concrete, even if the cement is kept prior to use in humid air conditions or in moderate rain.

1. INTRODUCTION

Hydrophobic Portland Cement (HPC), a cement for use in high humidity climate, is not widely known. It is often confused with the waterproofing cements used to obtain impermeable concrete or other building structures. The literature is relatively limited. The present report will address these issues and it is composed of two parts, as follows:

- **Part I** represents a literature search [1-26]. It represents an extension of a report submitted by the Hebrew University of Jerusalem to the Israel Cement Foundation in April 1997, entitled "*Literature and Market Search on Organic Hydrophobic Admixtures and Hydrophobic Portland Cements*"[1], containing further quotations from other sources [especially, 17a]. The quotation of certain newer publications (1993-2002) may not be pertinent, due to the frequent terminological confusions between hydrophobic and waterproofing admixtures or between hydrophobic and waterproofing cements [24-26];

- **Part II** represents a scientific and an industrial market search on the same items. In order to perform it, we sent inquiries to many specialists in the field (scientists, producers of chemicals to improve the qualities of building materials etc.). We have obtained in answer different personal communications [17b,27-32] , clarifying (at least partially) questions concerning:

[1] Report written in 1997 by Prof. M. Schieber, Dr. M. Nadu, Dr. J. Nissenbaum and Mr. M. Braiman at the Hebrew University of Jerusalem. The report was corrected following the kind suggestions given by Prof. John Bensted [17b] (corrections of the English of the draft report and a correct interpretation of what was quoted in his name [17a]).

- Why we could not find “hydrophobic admixtures” or “hydrophobic cements” in different commercial catalogues. Is there any intention of producing hydrophobic admixtures in the future? If there are not, why? Are there better alternatives?
- Data concerning the technical characteristics of these products or an existing standard that defines quality requirements and testing methods.
- Data concerning prices and other information available on the subject.

PART I: LITERATURE SEARCH

2. HISTORIC AND SCIENTIFIC BACKGROUND

A major problem which exists in humid climates the whole year, and particularly in the rainy or snowy seasons, is the storage of portland cement. On many building sites there are poor storage conditions. Therefore, these poor storage conditions problems are solved or can be solved using *hydrophobic Portland cement*, in many places, such as Russia[1-8], Romania[9-11], South Korea[12], India[13,17,23], England[15-17], Austria[18], Germany[19,20], USA[21] and Canada[22]. For instance, hydrophobic portland cement shipped from England (manufactured by Blue Circle Cement) was employed in the Falkland Islands in 1982, at the end of the war, to build an extended infrastructure, including a new airport concrete runway and to erect the exterior walls of a military cemetery[17] .

Standard requirements for hydrophobic portland cement are available in some countries like the CIS (ex USSR) [8] and India[13]. There are no standards for hydrophobic cements in the countries of Western Europe or North America. In these countries hydrophobic Portland cement is produced to comply with the performance requirements of ordinary portland cement, such as BS12 in England[17] and DIN 1164 in Germany[20].

Admixtures in small amounts (up to 5% by the weight of the cement) of various organic and inorganic materials in pastes, mortars or concrete are known to interact with the hydrating cementitious system and to modify different properties in the fresh, setting, hardening or hardened state. Smaller amounts of various organic surfactant materials (<0.5%) are in current use as water-reducer/retarding admixtures and in even smaller amounts (0.02-0.1%) as air-entrainers[13,22]. However, certain organic surfactant materials added in amount of 0.06-0.3%, can act as a hydrophobic agent which, if added to dry cement, repel water from the cement grains, until mixed with aggregates and water[1-11, 15-22].

It is known that solid surfaces either can or cannot be wetted by liquids. If they can, the wetted surfaces are lyophiles (hydrophile in the case of the water). If not, the surfaces are lyophobes (hydrophobes respectively). The cement grains are hydrophylic, but for the hydrophobic cement this property is temporarily canceled because adsorption of the hydrophobic admixture by the cement grains implies the appearance of mono-molecular hydrophobic layers on their surface and a drastic reduction of the capillary absorption of water. Mixing of the concrete or of the mortar, destroys the layer, the admixture loses its hydrophobic properties and instead becomes a plasticizer, a water reducing agent and/or an air entraining agent[11,21]. Hydrophobic cements should not be confused with waterproofing cements, which are claimed to make a more impermeable concrete than ordinary portland cement. There is a controversy about the effectiveness of these waterproofing cements[11,16].

Hydrophobic Portland cements, firstly suggested by Prof. Khigerovich, came into general use in Russia after 1949. One of the authors of this report (Dr. Nadu, a former student of Khigerovich) received, some 35 years ago, favorable laboratory results: (a) Testing a sample of hydrophobic Portland cement sent to him by his former professor; (b) Preparing and testing of hydrophobic

Portland cement samples, each sample being obtained by simultaneous laboratory grinding of clinker with ~ 6% gypsum and 0.1-0.3% organic hydrophobic admixture. It was proven that *the temperature of the grinding material* and/or *the possibility of preliminary dissolving of the admixture in organic solvents* are significant parameters of the technology required to obtain homogeneous and high quality products. Similar experimental results were later reported[9,11,17]

For Khigerovich's theory of hydrophobic cement, a noteworthy abstract was given by Wolfgang Eitel in the 1957 Chem. Abs.[1b] : *"Surfactants added in the amounts of 0.1-0.25% to clinker during grinding give to the resulting cement a hydrophobic characteristic. Particularly efficient are admixtures of oleic acid, naphthenic acids, or higher fatty acids, their H_2O-soluble salts, oxidized petroleum , paraffin etc. The calcium stearate does not react with the cement but is included in the grain, therefore is not suitable...The naphthenic acid salts decrease the surface tension at the boundary air/water in the cement mortar and thus bring about an air emulsion in the mix....The surfactants intensify the efficiency of clinker grinding and make cement more stable in storing, even in moist air, without a loss in hydraulicity (even by "self activation") an increase in aged cements was observed). Chemisorption on the surface of the cement grain and the plastifying effect of surfactants which brings about a desirable reduction of the water/cement ratio (in concrete by 9-12%, in lean mortars even by 15-25%). This plasticity increase is not caused by the air-entraining action (which is a desirable associated effect). The polar-active groups of the hydrophobic agents are strongly adsorbed on the cement grains, in contrast with the aliphatic chains at the ends of their molecules. The latter bring about a gliding or lubricating effect by their mobility in the oriented adsorption layer on the cement grain. The adsorption systems therefore are thixotropic. Technological properties important for hydrophobic cements are their increased frost resistance and reduced capillary suction in the mortar structure, the suppression of salt efflorescence in concrete and a reduction of the water permeability by an improved homogeneity of the mortar."* The hydrophobicity of the cement depends on the hydrophobicity of each clinker mineral that decreases as follows : Tricalcium silicate > Dicalcium silicate >> Tetracalcium aluminoferrite ≥ Tricalcium aluminate[4].

3. SOURCES OF HYDROPHOBIC ADMIXTURES

Hydrophobic admixtures consist of different waste materials from the petroleum or from other industries. Examples: **(a)** Oil soaps, an oleos material, sodium salts of different organic water insoluble acids, obtained as waste from the alkaline purification process of some petroleum distillates; **(b)** "Asidol" - a viscous liquid, a mixture of similar organic acids; **(c)** Methyl and/or ethyl sodium siliconates or polyethyl hydrosiloxane, representing waste materials of the organo-silicon compounds industry [5] and other waste products; **(d)** Sodium abietate.

In order to find the best, commercially available organic additive in Israel, either solid or liquid, we have performed a literature and a commercial market search. Different technical requirements available in the literature and in different standards have been compared and optimized to the conditions in Israel. Commercial catalogues published by industry specializing in chemical products for building materials improvements that we have access to at present, do not mention hydrophobic admixtures. We have studied this aspect in detail in our market search**.**

4. STANDARD REQUIREMENTS CONCERNING THE HYDROPHOBIC ADMIXTURES

The Russian standard specifications for hydrophobic portland cement do not specify the type of hydrophobic agents used in its manufacture[8]. The former editions of the same standard specified the following additions, well known also as grinding aids in cement manufacture, as air entraining and as water-reducing agents: 0.08-0.10% oleic acid, 0.10-0.12% naphthenic acids derived from certain crude oils ($C_nH_{2n-1}COOH$ where n=8-13) or 0.20-0.25% soap naphtha derived from the

alkali treatment of the oils and containing 50% water. In the CIS (Community of Independent States, former USSR), such cements are employed mainly as a protection against deterioration during storage but also as masonry cements due to their plasticity, water retentivity and ease of pumping. In addition, in the CIS, oilwell cements can be rendered hydrophobic by being treated with up to 0.3% (dry weight) triethanolamine or other hydrophobic agents in order to extend the stipulated shelf life from the normally stipulated 30 days maximum, to a new maximum of 60 days [17a, 17c].

The Indian standard specifications for hydrophobic portland cement specify that "some of the agents used in the manufacture...are oleic acid, naphthenic acid, stearic acid, pentachlorophenol etc." The inclusion of 0.1-0.5% by weight "of approved hydrophobic agent" is specified [13].

5. METHODS OF TESTING FOR HYDROPHOBIC PORTLAND CEMENT

Hydrophobic admixtures are added to the clinker (at the cement factory or at the building site), or to the cement (only at the building site). Optimum amounts (%) of each hydrophobic admixture for each clinker exist and need to be found by individual laboratory research. An underdose does not lead to the obtaining of a hydrophobic cement; an overdose may lead to an uncontrolled air entraining, to weakening strength effects etc.

- *Khigerovich's didactic demonstration of the hydrophobicity*: Sprinkle a small quantity of hydrophobic cement on water in a container. An ordinary match may be struck after its submerging through the molecular layer formed at the surface of the water[9].
- *Indian standard qualitative test (flotation):* Sprinkle a small quantity of hydrophobic cement on water in a container. The cement shall float on the water for a period of not less than 24 hours[13].
- *Russian standard qualitative test*: the normal cement absorbs a drop of water from its surface in 1-2 sec, the hydrophobic cement may absorb the drop in a period of not less than 5 minutes[8].
- *Indian standard quantitative test*: Take 5 g each of fresh and free flowing portland cement and the hydrophobic cement under test and spread each of the samples evenly in a thin layer in 15 cm (dia) petri dish. Expose it to a relative humidity of not less than 99.9 percent at 27±2^{o}C for 24 hours. Determine the mass loss at 550^{o}C for the two samples. Hydrophobic cement shall not show loss on ignition more than 30% of the value for the ordinary portland cement[13].

All the above methods are preliminary tests to determine if the cement sample is or is not hydrophobic. The cement sample which will be found hydrophobic, will be further tested according, for example, to the requirements of the Israeli Standard #1 (Specifications for Portland Cement) and/or #466 (Concrete Code) and, in case of need, according to the requirements of some European and/or ASTM standards for portland cement.

6. STANDARD SPECIFICATIONS FOR HYDROPHOBIC PORTLAND CEMENT

What is "Hydrophobic Cement"?: a) "A cement obtained by grinding ordinary portland cement clinker with an additive which will impart to ground cement a water repelling property which shall be destroyed only by wet attrition, such as in a concrete mixer. The hydrophobic quality of cement would facilitate its storage for longer periods in extremely wet climatic conditions"[13]; b) "A cement that absorbs a drop of water placed on its surface in a period of not less than 5 minutes" [8]. *Do not use* hydrophobic cement together with superplasticizers [8].

Chemical, physical and mechanical requirements: as for ordinary portland cement [8,13].

7. MANUFACTURE OF HYDROPHOBIC PORTLAND CEMENT IN COUNTRIES WHERE STANDARDS ARE NOT AVAILABLE

In the countries of Western Europe and North America the hydrophobic portland cement (HPC) is produced so as to comply with the performance requirements of ordinary portland cement, like CEM I now in Europe. Bensted[17a] has reported an example of the English experience in this field. Hydrophobic Portland cement was obtained by grinding ordinary portland cement clinker with 0.34% fat (stearic acid) and gypsum with the following laboratory performances: *The chemical analysis*: 20.6% SiO_2; 0.48% insoluble residue; 6.1% Al_2O_3; 3.3% Fe_2O_3; 63.8% CaO; 0.91% MgO; 2.1% SO_3; 0.34% fat; 1.4% loss on ignition; 0.58% K_2O; 0.36% Na_2O. *The modular composition:* Lime saturation factor (LSF) = 92.8; Lime combination factor, (LCF)=88.8; Silica ratio (S/[A+F]) = 2.2; Alumina ratio (A/F) =1.9.; *The potential composition %* : C_3S =40.4; C_2S=30.5; C_3A=10.6; C_4AF=10.3. *The compressive strength* (MPa): 21.6 at 3 days, 31.5 at 7 days and 41.3 at 28 days. *The HPC sample* met the BS-12 requirements for ordinary portland cement at the time.

7.1 Examples of uses

Hostile climates and humid environments offer scope to the applications of hydrophobic portland cements in mortars and concretes. It was used in the Falkland Islands in 1982, at the end of the war, to supply major construction works. There were initially either no or inadequate storage facilities for cement in the cold, damp climatic conditions experienced in this part of the South Atlantic. Also, for repair or extension works to the changing rooms of sport clubs that are in regular use and when humidity levels are often very high, hydrophobic cements have been successfully used.

7.2 Some more on the properties

Hydrophobic portland cement is made by grinding portland clinker with gypsum and a film making compound like oleic acid to form the cement, which can be ground to ordinary portland cement fineness, but is more commonly ground to rapid-hardening portland cement fineness. The water repellent film formed around and adsorbed onto each cement grain provides a great degree of protection against premature hydration by air moisture and offers the following:

- Reduction of the rate of deterioration of cement during storage or transport under unfavorable conditions, like those where deliveries can only be made at infrequent intervals. For example, Portland clinker ground with 0.3% oleic acid gave a cement that withstood 6 months air exposure without loss of strength, whilst untreated portland cement lost over three-quarters of its strength after a month of aeration [15]. Hence this cement is of value in damp equatorial climates, dressing rooms of sport club in use etc.
- The good workability of this cement is caused by its being more jelly-like in consistency than most other cements. Concretes made with HPC normally have compressive strengths similar to those of comparable untreated portland cements. Any retarding influence of the hydrophobic additive is usually offset by the lower water : cement ratios normally used in practice.

PART II: SCIENTIFIC AND MARKET SEARCH

8. ENUMERATION OF THE RECEIVED INFORMATION

- Prof. Bensted writes: “In my opinion, why you could not find hydrophobic admixtures in different commercial catalogues of chemicals for improving cements and concretes in given situations is because of the endless confusion that exists in many users’ minds between waterproofing and hydrophobicity. Some consider all such admixtures to be waterproofers or hydrophobic agents, whilst others do appreciate the need for two separate categories. It is thus not surprising that commercial catalogues may not specifically name hydrophobic agents” [17b].

- Handy Chemicals has a long overall experience in the manufacture and in the use of organic admixtures (superplasticizers and others) to obtain high performance concrete. Their experience would dictate caution with the simultaneous presence in the concrete of two organic chemicals: the first to manufacture a high performance concrete, the second to use in the manufacture of a hydrophobic portland cement. Nevertheless, Handy Chemicals, having a joint research program on cement grindings aids with the University of Sherbrooke, have included in this program the use of some hydrophobic admixtures and plan to expand more specifically in the direction of producing hydrophobic cements [27].

- Handy Chemicals' specialists and their colleagues from the University of Sherbrooke, are fully aware that there are no specific standards in North America involving the testing of the admixtures used to produce hydrophobic cements. They intended to search such standards [27].

- Hydrophobic portland cement (HPC) is produced in India on the basis of specific orders according to IS:8043-1978, which is the current version. There is no continuous production and no precise data on the quantity being produced, but, in any case, it will be a very small proportion of the total cement production, which was about 70 million tonnes in 1996 [28].

- There is no separate class of users of HPC in India. HPC is used equally with ordinary portland cement (OPC), except when the user anticipates prolonged moist storing of the cement. In view of the above it was not possible to obtain from an Indian commercial source a sample of hydrophobic cement for testing. It is recommended to prepare test samples by laboratory inter-grinding of ordinary portland cement (OPC) with 0.2-0.5% oleic or stearic acids, obtained from leading chemical manufacturers' suppliers such as Merck, BDH etc. Such products as asidol and siliconates are formulated wastes from primary industries and should be evaluated only if locally available. Dr. Mullick kindly offers to supply on request an HPC laboratory sample [28].

- Merck does not offer compounds that might be used for the preparation of HPC in industrial quantities, their compounds are designed only for chemical laboratory and small scale production plant. It was recommended to contact: a) Henkel from Dusseldorf to supply oleic or stearic acids; b) Peter Greven from Bad-Munstereifel to supply sodium salts of oleic or stearic acids; c) International companies like Texaco to supply naphtha soaps [31].

- We did not receive any answer from Henkel and Texaco. Peter Greven Fett-Chemie informed: (i) on its competence in building protection with hydrophobic agents to obtain "water repellent high quality plasters"; (ii) on supplies of sodium oleate under the name "LIGA Natriumoleate 90%" ; that is a sodium soap of a technical oily acid, which is a "raw material for the production of cleansers" or may be used as "reactive water-repellent for the constructional proofing", or as admixture for the rubber industry. No information was given on the use of Peter Greven products to obtain hydrophobic cements [29].

- Mr. Michael Langdon informs that Sealocrete does not manufacture admixtures specifically for producing hydrophobic cements. "This is mainly because there is not a significant market in Western Europe. Most cement is transported and used fresh and recent changes have been made to bag packaging for cement to include a waterproof membrane". As suggested, we contacted Blue Circle Cements, the producers of the HPC shipped from England in the Falklands Islands in 1982 but we did not receive any answer at the time.[17a,30]

- Mr Carlos Cacon from the Spanish Branch of Sika informs that there are no hydrophobic cements in Spain and that only the Research and Development Department in Sika central offices in Zurich Switzerland can give information if Sika intend to commercialize in the future hydrophobic admixtures. We did not receive any reply from Sika-Zurich. [32].

- Some seven years ago we had a talk with leading researchers of the Romanian National Cement Institute (CEPROCIM S.A. Bucharest): There were in Romania numerous old small and middle size cement lines, now replaced by the existence of more than 12 giant dry, low fuel consumption production lines (3000 T/day). Why did the comprehensive and successfully performed studies on hydrophobic cements not end with an industrial manufacture? The answers are: 1) The manufacture of hydrophobic cement, on the basis of specific orders, is no longer a problem after the performed studies; 2) A continuous production is not justifiable because there is not and there will not be a continuous market for this cement [11].

- Some 50 years ago, a similar point of view and the alternative of the building site blending to avoid manufacturing complications, was presented to his students by Prof. Khigerovich, (Chair of Chemistry at the Moscow Civil Engineering University). At the same times, at the "Voskresensk Cement Plant" (near Moscow) a manufacture of hydrophobic Portland cement was first built.

9. CONCLUSIONS AND FUTURE PLANS

- *We have produced a sufficiently exhaustive literature and market survey (1950-1997)* on hydrophobic admixtures and on hydrophobic portland cements including considerations on the composition, technology, work mechanism, properties and applications. There have been no major advances in this area since 1997.
- *The specialized chemical products industry to improve the quality of cement and concrete* often ignores the hydrophobic admixtures partially due to terminological confusion between waterproofing and hydrophobicity and also because there is not a continuous manufacture and market for hydrophobic cement. Another reason may be due to a certain incompatibility between superplasticizers and hydrophobic admixtures and also due to recent changes made to bag packaging of cement to include a waterproof membrane.
- *Standards concerning the quality requirements and the testing methods for the hydrophobic admixtures and for the hydrophobic portland cement* exist in Russia and in India. In other countries (U.K., Germany, Romania) there are no specific standards but, if necessary, manufacturing would be not a difficult problem.
- *In many countries*, including Israel, a practical experience on the manufacture and on the use of hydrophobic admixtures and on hydrophobic portland cements, does not exist. If needed in the future, to avoid manufacturing complications in cement plants, there are two alternatives: building small scale site manufacture or/and import. We think that for both alternatives preliminary small scale laboratory experience is a necessity.

ACKNOWLEDGMENTS

The authors wish to thank the individuals and companies who responded to the market survey, which was undertaken on a neutral perspective and not an endorsement of the trade products mentioned.

REFERENCES

[1] Khigerovich M. I.: (a)*Hydrophobic cement and hydrophobic plastifying admixtures*, (in Russian), Moscow, Promstroiizdat, 1957 , pp 208; Chem Abs. 52:8499b/1957; (b) *Theory of hydrophobic cement*, (in German), Silikattechnik, vol 8, p. 534-6, 1957; Chem Abs.52:4950/1957 ; (c) *Synthetic acids obtained from naphtha hydrocarbons, as hydrophobic agents for cements*, (in Russian), Nauch . Doklady Visshey Shkoly, Stroitel'stvo 1959 ,No 1 , p.187-93; Chem. Abs. 54:8025/1960 .

[2] Khigerovich M.I., Skramtaev B.G., Velikovskii D.S., Leibovich Kh.M.: *Hydrophobic Cement* ,USSR Patent 124.862, Dec. 12, 1959; Chem. Abs. 54:10269/1960

[3] Khigerovich M.I., Zuikov G.G.: *Hydrophobisation of cement by addition of synthetic fatty acids* , Russian, Tzement, vol. 31,March,p.12 1965; Chem. Abs. 63:6705/1965

[4] Kosina J. : *The influence of hydrophobic cements on concrete properties*, German , Wiss. Z. ,Hochsch., Bauwesen, Leipzig , 1959, No.4., p 105; Chem. Abs. 54:8026/1960
[5] Butt I.M., Okorokov S.D., Sycev M.M.,Timashev V.V. : *The Technology of Binder Materials, (in* Russian}, p.497, Ed. "Vishaya Shkola", Moscow 1965
[6] Voljensky A. V. : *Mineral Binder Materials* , (in Russian) , Stroyizdat, Moscow , 1986
[7] Koknaev N. F.:*Hydrophobisation of minerals in Portland cement* ,(in Russian), Neorg. Mater., 1993, vol.29 ,3, p.426-427
[8] Standard of the former SU, GOST 10178-85 (revised edition from 1988, corresponding to the standard of the former COMEC, SEV 5683-86): *Portland cement and Portland blastfurnace cement. Specifications.*
[9] Nadu M: (a) *Plastifier, air entraining and hydrophobic agents for cement and for concrete, (in* Romanian), Seminar for Ph.D. in Engineering Students . Chair of Chemistry and Building Materials. Institute for Civil Engineering, Bucharest , January ,1968; (b) *Special cements for hydrotechnic & hydroelectric construction building,* Romanian, Symposium ICH, September 1978
[10] Moldovan V. : *Admixtures in Concrete,* (in Romanian), Technical Editions, Bucharest 1978.
[11] Brezeanu L., Ilas V., Ghiu C. : *Obtaining of hydrophobic cements and properties of the concrete manufactured by using these cements.* (in Romanian), Materiale de Constructii (Bucharest), 1992, vol. 22, 1, p 23-26, wrongly entitled in Chemical Abstract 96204c, vol.117,1992 *(Manufacture and characteristics of concrete made of waterproof cement)*
[12] Pyo H.W., Ouk J. S., Man C.: *A study on the development of waterproofing Portland cement* , published in a South-Korean journal in 1977, Chemical Abstract-126380a,vol. 90, 1979
[13] Indian Standard IS 8043-90 : *Specifications for Hydrophobic Portland Cement.*
[14] Paillere A.M., Ben Bassat M., Akman S.: *Guide for use of admixtures in concrete*. Materials and Structures,1992, 25,49-56. The guide was drafted within the framework of RILEM Technical Committee 84.AAC: Applications of Admixtures for Concrete.
[15] Lea F. M. : *The chemistry of cement and concrete*, 3rd Ed., Arnold Publishers Ltd., p. 13-14 and p. 536 ("Hydrophobic cement") London 1970.
[16] Neville A. M. *Properties of Concrete,* Pitman Ed., (p.71-72), London 1965.
[17] Bensted J.*:* a) *Hydrophobic Portland cement*, World Cement, 1992, vol. 23,7,p.30-31 & 1993, vol. 24, 5, p.54-55; .b) *Personal Communications* (letters to the Hebrew University of Jerusalem dated 15.11.1996 , 14.01.1997 and 26.01.1997) c) *Oilwell cement standards-an update.* World Cement, March 1992, pp 38-42; d) *The hydration of Portland Cement.* World Cement, August 1991, pp27-32; e) *Special Cements,* in *"Lea's Chemistry of Cements and Concrete",* 4th Edition, (Ed. Hewlett, P.C.), p828, Arnold Publishers, London 1998
[18] Czernin W.: *Cement Chemistry and Physics for Civil Engineers,* 2nd Engl.Ed. , p 181,Bauverlag Berlin 1980
[19] Kuhl H.:*Zement-Chemie*, Verlag Technik 3rd Ed.,(Vol. III p.449-450), Berlin 1961
[20] Handbook (edited by Josef Eibl): *"Beton- Kalender",* 84th Ed., Part I, p.10, Ernst & Sohn Verlag, Berlin 1995
[21] Powers T.C. : *The Properties of Fresh Concrete,* John Wiley & Sons, Inc., p.325-357 (Air Entrainment in Cement Paste and in Concrete) and p.434-436 (Remarks on Terminology) New-York 1968
[22] Ramachandran V. S. (Ed), *Concrete admixtures Handbook.. Properties, Science and Technology,* Noyes Publications,p.116-210 (Water-Reducers/Retarders),p.269-302(Air-Entrainers) and p.518-524 ("Dampproofing and Waterproofing Admixtures") Park Ridge,New Jersey, USA 1984
[23] Jackson P.J., Lawton J.M. : *The Development of Standards for Cements*. Proc. of the 9th International Congress on the Chemistry of Cements, Vol.5 p.157-166, New Delhi, India 1992.
[24] Darwin D. C., Jeknavorian A., Koyata H.: *Chemical Admixtures, section 9.2, Water proofing admixtures,* Chapter 7 of "Cement Research Progress 1993" Copyright © 1995 by the American Ceramic Society, p. 127
[25] Jeknavorian A., Jardine L., Darwin D. C., Kerkar Av: *Chemical Admixtures, section 9.3, Water proofing admixtures,* Chapter 6 of "Cement Research Progress 1994" Copyright © 1996 by the American Ceramic Society, p.131
[26] Chemical Abstracts. General Subject Index. Vol.124,1996: *Cement waterproofing membranes for adhering to freshly poured concrete / of buildings by coating cement-epoxy resin undercoat....*
[27] Page M., (Handy Chemicals Ltd., La Prairie, Quebec, Canada): *Personal Communication* (letter to the Hebrew University of Jerusalem dated 29.08..1996).
[28] Mullick A. K., (National Council for Cement and Building Materials, New Delhi, India): *Personal Communication* (letter to the Hebrew University of Jerusalem dated 28.10. 1996).
[29] Peter Greven Fett-Chemie GmbH & Co. KG (Bad-Munstereifel, Germany): *Personal Communications (*letters to the Hebrew University of Jerusalem dated 12. 11. 1996 and 21.01. 1997).
[30] Langdom M., (Sealocrete PLA LTD, Greenfield Lane, Rochdale Lancs, UK): *Personal Communication* (letter to the Hebrew University of Jerusalem dated 27.08..1996).
[31] Merck KGaA., (Darmstadt, Geremany): *Personal Communication* (letter to the Hebrew University of Jerusalem dated 04.12..1996)
[32] Chacon C., (Sika, S.A. Espana, Alcobendas, Madrid, Spain): *Personal Communication* (letter to the Hebrew University of Jerusalem dated 20.08..1996).

ORGANIC HYDROPHOBIC ADMIXTURES AND HYDROPHOBIC PORTLAND CEMENTS. LITERATURE REVIEW AND MARKET SEARCH

John Bensted*, **Michael Schieber****and Mihai Nadu*****

* School of Crystallography, Birkbeck College, University of London, Malet Street, London WC1E 7HX, U.K.; E-mail: bensted.j@btinternet.com
** The Fredy and Nadine Herrmann School of Applied Sciences, Hebrew University of Jerusalem, Jerusalem 91904, Israel; E-mail: schieber@vms.huji.ac.il
*** Corresponding author. Affiliation as in **. Postal address: PO Box 10587, Jerusalem 91103, Israel; E-mail: mihai_nadu@hotmail.com

CURRICULUM VITAE

John Bensted

John Bensted studied for his BSc in chemistry and for his PhD in the area of transition metal chemistry at the University of London. In 1967 he joined the Research Division of the Blue Circle Cement Group as a research scientist, eventually becoming a Priccipal scientist. John was not only involved in research and development over the entire range of cement types for Blue Circle worldwide, but was also heavily involved in technical service and troubleshooting as well as numerous aspects of quality control. In recognition of his research efforts, he was awarded the AITEC Medallion by thetechnico-economic organisation of the Italian cement industry in 1978 and the DSc degree of the University of London in for his published work in cement chemistry in 1981.

In 1985 John joined British Petroleum as a Senior Drilling Engineer at their Sunbury-on-Thames Research Centre, becoming Research Associate in Cement Technology. He directed research programmes on oilwell cements and functioned as an internal consultant on all aspects of cement technology (both oilfield and construction) for the different BP businesses worldwide.

Since 1992 John has become more involved with academic research in cement and concrete technology, primarily as a Visiting Professor in Cement Science at the Universities of London (Birkbeck College) and Greenwich. He is an International Consultant in Cement Technology for the oil, construction and chemical industries, involved in research, development, technical advising and troubleshooting matters in the cement and concrete arena. Also, he acts as an expert witness in legal cases connected with cement and concrete.

In 2000 John was a co-inventor of a new MDF type cement at Keele University (where he was a Visiting Professor 1996-2000) called MicroPaste, which has improved ductility and is manufactured under licence by Castle Cement (UK). This cement has been used to line pipes that convey drinking water.

In 2002 John was given a Distinguished Services Award by the Society of Chemical Industry for his work with their Construction Materials Group, where he has served as Secretary and later as Chairman, and with their London Section. John is also active in national (UK), European and international standardisation work. Since 1995 he has been leader of the UK delegation to the ISO sub-committee on drilling and completion fluids, and well cements.

ALKALI-AGGREGATE REACTION (AAR) IN CONCRETE IN ISRAEL

Mihai Nadu[1], Michael Schieber[2] and Elmar Tschegg[3]

[1]Hebrew University of Jerusalem, PO Box 10587, Jerusalem 91103, Israel. Corresponding author.
E-mail: mihai_nadu@hotmail.com
[2]Hebrew University of Jerusalem, Jerusalem 91904, Israel. E-mail: schieber@vms.huji.ac.il
[3]Labor fur Materialwissenschaften, TU Wien, Wiedner Hauptstrsse 8-10, 1040 Wien.
E-mail: tschegg@ifp.tuwien.ac.at

ABSTRACT

Israel is one of the last of the world's developed countries were the building engineers generally ignore a very timely subject: the alkali-aggregate reaction (AAR) in concrete and the involvement of AAR in the different durability and security problems for the building structures. Our team performed the first and only Israeli laboratory investigations on AAR. We succeeded in proving that two of the seven investigated Israeli concrete aggregate quarries are very reactive and may be dangerous in an uncontrolled use. The two highly-reactive investigated aggregates are: a siliceous limestone from "Ein Harod", and a mixture of stones from the "Zeelim" river basin. Both aggregates correspond to the requirements for the Israeli "concrete code" and to the Israeli standard specifications for mineral aggregates etc. Ensuring the durability and the security of Israeli building structures is conditional upon the continuation of AAR studies.

1. GENERALITIES ON THE AAR

AAR is a reaction, occurring between alkali hydroxide present in the pore solution of concrete, and certain aggregates containing reactive components in catalyzing environmental conditions. The reaction, having a very complex mechanism, produces expansive gels (hydrated alkali-silica, magnesium hydroxide etc.) which can cause expansion and cracking of concrete structures, with the consequent damage ranging from superficial in mild cases to loss of structural integrity in severe cases. The cracking of structures due to AAR enhances other concrete deterioration processes due to exposure of the interior of the concrete or of the reinforcement to aggressive agents in the environment. Depending on the AAR type, the time after construction for evident cracking of concrete can be up to 5, 10 or 20 years [1-4]. The global destructive effect on the concrete durability is generally a function of the combination of different possible deleterious environmental, physical, technological and chemical under-effects. If it exists, eventual AAR harmful effects may be amplified by many other factors such as the earthquakes, the defective design or construction, the effects of the hot and dry climate, drying and wetting cycles, the effects of the "classical" types of concrete corrosion (by sea water, by chloride penetration, by sulfates, by acids, by magnesium or by ammonium salts etc.)

2. AAR IS A PROBLEM THROUGHOUT THE WORLD, INCLUDING ISRAEL

The misconception until twenty years ago, that AAR is limited to certain regions of the world (e.g. USA, Canada and Denmark) and that others are free of it, starts to be more and more confuted [4]. The assertion that "Israeli aggregates do not have dangerous species attacked by AAR" [5] are

Proceedings of the 11th International Congress on the Chemistry of Cement (ICCC)
'Cement's Contribution to the Development in the 21st Century'
Hosted by: The Cement and Concrete Institute of South Africa
CD-ROM produced by: Document Transformation Technologies
11 - 16 May 2003, Durban, South Africa
ISBN Number: 0-9584085-8-0
Editors: Dr G. Grieve and G. Owens
Congress Organised by: Event Dynamics

refuted by our AAR studies on Israeli aggregates [6-11]. However, in the 1980s many countries (most European countries, Japan, China [as in 12-18]) discovered concrete structures suffering from AAR, which proved that AAR occurs in many geographical locations. In a recent paper dealing with new chemical admixtures (lithium compounds) which "calms reactive aggregates", is said that "pavement engineers now have a potent new weapon against ASR which increasingly is being recognized as a major threat to Portland cement concrete pavements and structures", that the reactivity "is something of a ticking time bomb in pavements" or "the AIDS" of concrete...[19]. The interest in the AAR engineering problems arose significantly in recent years in Germany (especially in Niedersachsen) and in Switzerland, [20,21]. An AAR Swiss standard, based on French test methods [22] was also adopted by the European and world standards organization [23].

3. THE AAR IS RELATIVELY NEWS

The questions concerning the AAR and its most well-known types, i.e. the alkali-silica reaction (ASR) and the alkali-carbonate reaction (ACR), as there are pointed in different standards [3, 22-27], represent a relatively new chapter in the cement & concrete science and in the field of the engineering concerns with assuring the durability of concrete structures: the first reports concerning the destructive effects of AAR were published in 1940, that is 115-150 years after the "invention" of the Portland Cement and after the report of Vicat explaining the concrete destruction mechanism of the of the harbor of Alger[1]. The interest in AAR problems arose more and more in the last 25 years. Since the mid-1970s, 11international conferences on AAR were held throughout the world, the 10th being held in Melbourne, in August 1996 (where a paper was published on the first Israeli AAR investigations [9]). The last 11th conference on AAR was held in Quebec City (Canada) in June 2000.

4. ISRAELI SPECIFIC AAR PROBLEMS

- According to ASTM and to other specifications (Canadian, European, Japan), from a geochemical point of view, an important part of the available Israeli natural aggregates are suspected to be alkali reactive, until the contrary will be proven experimentally.
- The presence of alkalis in the concrete can be due to their presence in the clinker, in the mineral admixtures, in the water (mixing or/and environmental) or in the aggregates themselves.
- The Israeli standard specifications for aggregates (IS-3) for Portland-cement (IS-1), the Concrete Code (IS-466) or other standards do not dwell on AAR problems, the possibility of there being deleterious alkali-reactive aggregates nor do they limit the maximum amount of alkalis in the cement or in the concrete.
- The cement users are generally unaware of AAR and its possible effects on the durability of the concrete structures, as was the case in the last 15 years in Belgium [16], in the United Kingdom [14] in Japan [24] and in other countries where awareness on AAR arose. The authors of this report contend that AAR research is important in Israel since various concrete aggregates may be suspected of different types of potential reactivity (alkali-silica, alkali-carbonate etc.).
- Excepting our studies, Israel is one of the last of the world's developed countries were the building engineers ignore generally the AAR in concrete problem and the associated structural durability problems. They are applying ostrich politics, i.e., they are putting their head in the sand to not see eventual dangers.
- There are an abundance of published examples of destroyed structures due to the AAR, examples coming from an array of the world's developed countries [18]. However, there are no published examples from Israel; even the published pathology studies on destroyed structures, performed generally by the National Building Research Institute (Technion-Haifa), do not take into account the possible harmful effect of AAR. To the best of our knowledge the authors of this report consider then, until the contrary is proved experimentally [28-30], that AAR effects could explain the degradation processes in important Israeli concrete structures, for example

structures in contact with the Mediterranean Sea (harbors, retaining walls, supporting pillars for the coal supply bridge in Hedera power-stations) or drainage tubs under the highway Bersheva-Dimona.

- The most significant result of our first experimental studies on AAR in Israel [6-11, 27]: two of the seven Israeli concrete aggregate quarries investigated to date (the siliceous limestone from Ein Harod and the mixture of stones of the Zeelim river basin) are very reactive and may be dangerous in uncontrolled use.

5. THE AAR INVESTIGATIONS ON SEVEN ISRAELI AGGREGATE QUARRIES

The AAR investigations were performed on the following seven Israeli concrete aggregate quarries: 1) & 2) Sheffar-Am and Hanaton, both placed at some 40 km. NW of Nazareth; 3) Ein-Harod, placed at some 40 km SE of Nazareth; 4) Modiin, placed at some 60 km SE of Tel-Aviv; 5) Har-Deragot, placed at some 50 Km SE of Beersheba; 6) Zeelim, placed at some 40 Km SW of Beersheba; 7) Ashdod harbor placed at some 60 km SW of Tel-Aviv. Table 1 gives a synopsis of the investigations.

Table 1. Synopsis of the AAR investigations

No	Name	Grading	Description	AAR results	References
1	Sheffar-Am	3 coarse and 1 fine aggregate fractions	Calcite-dolomite	Non-reactive	6, 7, 9, 10
2	Hanaton	As in 1/1	As in 1/1	Non-reactive	27
3	Ein-Harod	As in 1/1	Limestone with some 4% amorphous silica	Highly-reactive	6-11, 27
4	Modiin	As in 1/1	10-20% limestone, 80-90% dolomite	Non-reactive[1]	27
5	Har-Deragot	As in 1/1	14-22% limestone 76-86% dolomite	Non-reactive	57
6	Zeelim	As in 1/1	Stones mixture from Zeelim river basin[2]	Highly-reactive	6-11, 27
7	Ashdod	Sea-sand	Quartzes	Non-reactive[3]	7, 27

The following should be noted:

- The tested calcite dolomites (1, 2, 4, 5) and the quartz sea sands (7) did not show alkali-aggregate reactivity.
- For the complex mixture of stones, from a south Israeli river basin quarry (No 6, Zeelim) containing various types and proportions of amorphous SiO_2 and carbonates, the alkali reactivity reactivity was expected according to its composition and when tested in accordance with some different classical methods [6-11].
- An experimental surprise represents a limestone containing ~4% SiO_2, supplied from a quarry situated in the north of Israel (Ein Harod). The expansion kinetics of the concrete prisms showed "a late expanding alkali-silicate/silica reaction" and the same aggregate did not show reactivity according its chemical composition and when tested according to different former classical methods [6-11].

[1] It is necessary to repeat the performed tests due to the heterogeneity of the quarry, to its importance (the largest Israeli rock quarry) and to the unusual stoichiometry of the aggregate

[2] Containing a) amorphous SiO2 minerals and rocks (tzor), with or without chalk or limestone inclusions;
b) Carbonate minerals and rocks (chalk, limestone, dolomite, dolomite limestone) with or without SiO2 inclusions etc.

[3] Water washing before use may be necessary to avoid the enrichment of alkalis in the concrete

All seven aggregates meet the requirements of the Israeli "concrete code" and the Israeli standard specifications for mineral aggregates etc. Further discussions relate to the two aggregates, which might be dangerous in an uncontrolled use (Ein Harod and Zeelim).

6. EXPERIMENTAL PROCEDURES

6.1 The 24-hour ASTM C289 chemical test with an altered graph (examples in [2, 9, 10, 26d])

The immersion of a graded aggregate sample in 1N NaOH solution for 24 hours at 80°C is followed by chemical analysis of the filtered solution for dissolved silica (Sc) and for reduction of alkalinity (Rc). The results are plotted on a graph showing four regions of aggregates: (A) "innocuous"; (B) "generally non-reactive", but in this field the interference of carbonates in the reaction between SiO_2 and NaOH lead to inconclusive results requiring long-term mortar bar or concrete prism expansion testing; (C) "highly reactive, potentially deleterious", but if the pessimum (worst) percentage of reactive silica is exceeded, the mortar bars might display insignificant expansions; (D) "deleterious reactive". The original ASTM C-289 graph comprises only three regions the (A+B) region being considered innocuous. The ASTM chemical test was excluded from the last CAN/CSA. An alternative method consists of performing the ASTM procedure on the insoluble residue obtained by dissolution of the carbonates in concentrated hydrochloric acid [31, 32] and by a new French chemical method [22 f].

6.2 The 2-3 week NBRI[4] mortar bar test [3e, 26g]

Mortar bars, 25x25x285-mm [26c] are maintained at 80°C, one day in water up to the zero reading (after 24 hours) and afterward in 1N NaOH solution. The following mortar bar expansion limits are suggested [32]: at 14 days <0.10% for innocuous aggregates and ≥ 0.15% for deleterious aggregates. Shayan et al [35] suggested that: (i) mortar bar expansion of 0.10% in 10 days and 0.10% in 22 days to be taken as indicating reactive aggregate of short induction period and long induction period, respectively.

6.3 The long-term mortar bar test. [3a, 26d]

The reactivity limits are 0.05% at 3 months or 0.1% at 6 months or more, for mortar bars with high alkali content (1.25% Na_2O equivalent relative to the cement weight or 7.5 kg Na_2O equivalent per $1m^3$ of mortar) maintained at 38°C, in wet air. According to [3b, 33] the absorbent material used in the containers might cause diminished expansions due to the alkali- leaching of the mortar bars. The test is not included in the 1994 edition of CSA Standard. It is to consider an alternative method, which would replace the bars with mortar prisms 40 by 40 by 160 mm according to the European and to the Japanese experience [4, 12, 24, 22c].

6.4 The long term concrete prism expansion methods

Two versions (ACR and AS/SR) of the CSA A23.2-14A-M90 and the French Standard NF P18-587 were applied [3c, 22d]. Each 1990 version of the CSA was intended to test concrete aggregate suspected to suffer from alkali carbonate reaction (ACR) or Alkali Silicate/Silica Reaction (AS/SR). The main difference between the two 1990 versions is the storage temperature of the specimens in moist air, being 23°C for ACR and 38°C for AS/SR. The1990 CSA was replaced in June 1994 with a new CSA A23.2-14A-M94 [3a, 3b, 3c, 3d]. The main modifications are: (i) the cement content increased from 310 to 420 kg/m^3 and an alkali content of 1.25 %Na_2O equivalent (eq.) by mass of cement, resulting in an increase of the alkali content in concrete from 3.90 to 5.25 kg. Na_2O eq./m^3; (i, i) a 38°C storage temperature in moist air is required for all the specimens, independent of the AAR type. The French standard looks like the 1994 CSA, with cement content of 410 kg/m^3, corresponding to 5.13 kg Na_2O eq./m^3 of concrete. *ACR expansions are considered deleterious*: depending on the micro-climate to which the structure is to be exposed, if the length change

[4] South-African National Building Research Institute

exceeds 0.010% after 3 months or 0.025-0.040% after 12 months (former CSA); independent of the micro-climate, if the length change exceeds 0.015% after 3 months or 0.025% after 6 months or 0.030% after 12 months (ASTM C1105 [26f]). AS/SR expansions were considered deleterious by the 1990 CSA, depending on the microclimate to which the structure is to be exposed, if the length change exceeds 0.040-0.075% after 12 months. The 1994 CSA considers that expansions are deleterious, independent of the AAR type, if the length change exceeds 0.040% after 12 months, noting that "in critical structures such as those used for nuclear containment or large dams, a lower expansion limit may be required" (CAN/CSA A23.1-94. Appendix B, [3b]). The French test conditions [22d] are stricter than the Canadian. To the best of our knowledge there are no French standard limits for critical AAR expansions, a 0.040% limit at 8 months seems to be accepted by scientists to indicate reactivity but it is still being discussed [12]. However it seems that the interpretation of the French test results is covered by the Canadian standard limits. Significant AAR compositions for mortar and concrete test prisms are to be prepared taking into account the experimentally found worst ("pessimum") content of the reactive particles [12, 22 f].

6.5 Measuring the fracture energy of AAR affected concrete [11]

The influence of AAR on the fracture mechanical behavior deterioration of the concrete was determined using the wedge splitting method, elaborated and patented by K.K.Tschegg [34]. Cubic shaped concrete specimens used for the wedge splitting tests were obtained by cutting from a long time processed experimental product: a lot of two years and more old AAR concrete prisms, coming from a former laboratory study investigating the alkali reactivity of different concrete aggregate by different standard methods including a long-term concrete prism expansion method. The influence of different concrete mixes and storage conditions on AAR-induced fracture energy loss is studied on six experimental variants (concrete mix vs. storage temperature), including four concrete mixes. Each concrete mix is characterized by the aggregate, by the cement content and by the alkali content. [10-11]). The used wedge-splitting method is explained in detail in [34]**.**

6.6 The quick 2-3 day mortar bar autoclave method [26b, 32]

The AAR process could be accelerated by an ASTM 151 treatment of mortar bars enriched in alkalis by addition of NaOH in the mixing water up to 3.5% Na2O equivalent relative to the cement weight. The expansion is measured after 5 hours of steam curing at 1.72 Mpa (130ºC). An expansion limit to define a deleterious reactivity is still in discussion.

7. AAR ANALOGOUS RESULTS ON BOTH EIN HAROD AND ZEELIM AGGREGATES

For both aggregates, the AAR studies by the 24 hour chemical method are not conclusive. On the graph the range of the tested samples is plotted on the doubtful zone B, due probably to the presence of carbonates interfering with the reaction between NaOH and the dissolved silica. In order to clarify if the tested aggregate is reactive, ASTM C33 [26a] requires long time tests. The mortar bar tests ASTM C 227 [26c] do not show reactivity. After two years the average expansion is small (up to 0.013%), less then the reactivity limits. The chemical composition and/or the petrography of the aggregate are only partially conclusive. The high reactivity of the aggregates is shown by: a) the 2-3 week NBRI mortar bar method; b) the 2-3 days mortar bar autoclave method; c) the long term concrete prism expansion method; d) the wedge splitting method to test the specific fracture energy of AAR affected concrete [11].

8. AAR RESULTS ON THE EIN HAROD CONCRETE AGGREGATES

This aggregate was known as a "pure limestone" and we considered it as a comparative blank (non alkali - reactive) sample. Considerations based on the chemical analysis corroborate the assumption of non-reactivity. The different grain sizes of the aggregate were analyzed by induction-coupled plasma. The chemical analysis corroborates the assumption of non alkali-silica reactivity since it

contains less than 5% SiO_2 insoluble residue in HCl [32]. The analysis also corroborates the assumption of non alkali-carbonate reactivity (ACR) according to a new CSA test [3f], consisting of plotting on a graph, the CaO/MgO ratio as function of the Al_2O_3 content. For a CaO/MgO ratio ≥ 24 and for a content of ≤ 0.19% Al_2O_3, the sample is placed on the non-ACR zone of the graph.

The limestone sample was studied by several AAR methods which led to inconclusive results but the non-reactivity assumption was finally refuted when our investigations comprised simultaneously: (1) high alkali containing concrete specimens, stored in warm and humid air; (2) late ages (11 months and more) measurements; (3) testing by the AS/SR version of the 1990 Canadian or French concrete prism expansion method [3c, 22d].

8.1 The long term testing on concrete prisms (expansion and fracture mechanical parameters)
The results are given in Table 2. For the last variant (F), Figure 1 represents the expansion kinetics for each of the three F type studied specimens (noted #151, #152, #153 [9-11]). Figure 2(b) represents the load-displacement curves for the same specimens [11]. Figure 2(a) represents the load-displacement curves for AAR affected (F) and unaffected (A) specimens.

Table 2. Long term expansion and fracture mechanical testing on concrete prisms

Experimental variant	A	E	C	F
Cement content in concrete, kg/m^3	310	310	410	410
Water-cement ratio (W/C) [5]	0.63	0.62	0.52	0.52
Additions of NaOH in the mixing water	No	Yes	Yes	Yes
Alkalis relative to the cement, % [6]	0.47	1.25	1.25	1.25
Alkalis relative to the concrete kg/m^3	1.46	3.90	5.13	5.13
Storage temperature in air of 100% R.C, ^oC	22	38	22	38
Average 2 years length change **ε, %** [7]	-0.005	0.011	0.002	0.188
Specific fracture energy, G_F **(N/m)**	152	98	125	114
Coefficient of variation **C_V (%)**	10	7	11	6
Horizontal force component causing the fracture **F_{Hmax} (N)**	2010	1470	1790	1460
Nominal notch tensile strength **σ (N/mm^2)**	4.56	3.54	4.00	3.28
Coefficient of variation **C_V (%)**	8	7	8	11

8.2 AAR studies by the 2-3 weeks accelerated mortar bar test
In a first test, after 14 days of storage at 80°C in 1N NaOH solution, an average expansion of 0.08% was recorded, showing no alkali reactivity for the tested aggregate. In a second, more accurate and longer test, with the Australian improvements, the recorded expansions (Table 3) characterize the Ein Harod quarry as giving aggregates of long AAR induction period [10].

8.3 Studies by the quick, 2-3 day mortar bar autoclave method
Conclusive and reproducible results were recorded (Table 3, [8,10]).

[5] The amount of water (with optional addition of NaOH) should correspond to an 80 mm fresh concrete "slump" however the fresh concrete with 310 kg cement/m^3 (mix 1 & 2) was "no slump" since a small increase of the water/cement ratio causes the fall of the concrete cone, immediately after the mold removal. For a cement content of 410 kg/m^3, (mix 3 & 4) the desired slump was easily obtained
[6] The total alkali content, as Na_2O_{eqv}, from cement and from mixing water
[7] Negative (-) values represent shrinkage

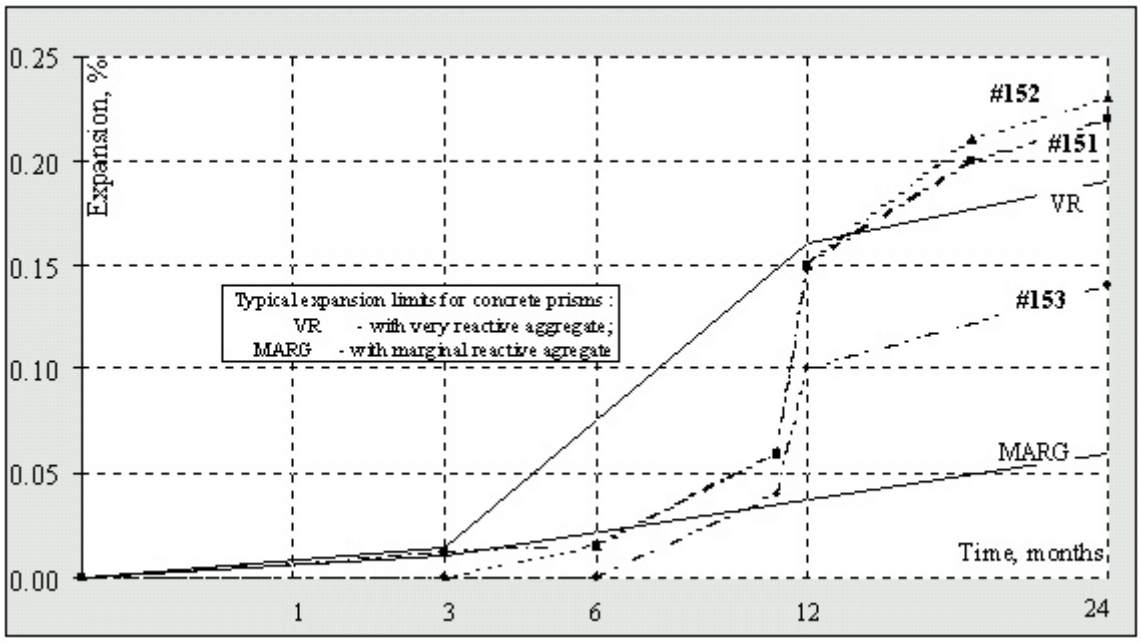

Figure 1. Expansion kinetics for each of the three F type studied specimens (noted #151, #152, #153) are shown as dotted lines and are compared with solid lines "VR" and "MARG" representing the Canadian "characteristic expansion curves for concrete prisms made with the greywacke-slow/late-expanding alkali-silicate/silica reactive aggregates" compiled from page 100 of the former CSA A23.1. App B-90. The time is plotted on a square cubic root. [3a, 10].

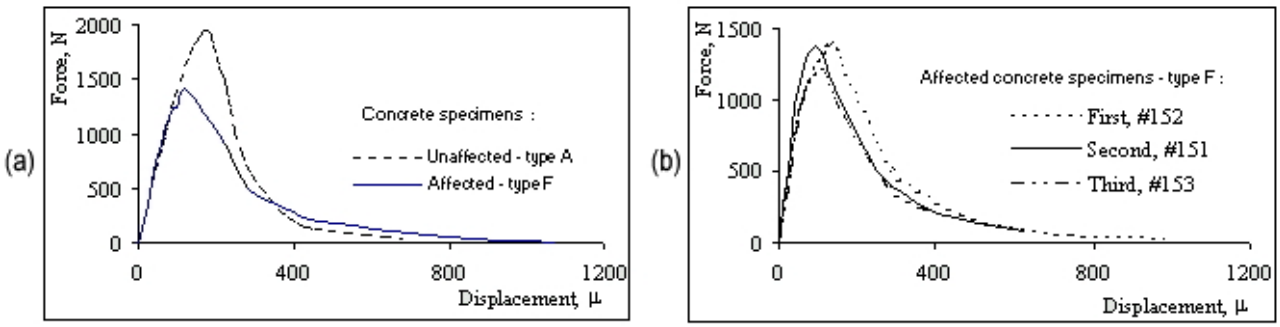

Figure 2. Load-displacement curves for AAR affected and unaffected concrete specimens and for three F type AAR affected specimens [11, 34].

Table 3. a) Results by the accelerated (2-3 week) improved "NBRI" method;
b) Results by the quick (2-3 day) autoclave method

Name of the required parameter	Number of specimen	Mean expansion	Standard deviation	Coeff. of variation
a) Preliminary (physical) expansion (%) after 1 day immersion in water at 80°C	6	0.047	0.0056	12
a) Expansion in %, after immersion in NaOH, - 1 day - 5 days - 7 days -10 days -14 days -21 days	 5 5 5 5 5 6	 0.004 0.013 0.034 0.100 0.151 0.180	 0.0017 0.0078 0.0149 0.0190 0.0240 0.0300	 56 60 44 19 16 17
b) Expansion in % after 5 hours of steam curing in the autoclave at 1,72 MPa (130°C),	6 5	0.059 0.063	0.008 0.005	14 8

9. AAR RESULTS ON THE AGGREGATES FROM THE ZEELIM RIVER BASIN

The petrography is described in footnote 2, page 3. The high content of amorphous silica particles corroborates the assumption of alkali-silica reactivity. The results on the long term testing on concrete prisms (expansion and fracture energy parameters) are given in Table 4.

AAR studies by the 2-3 week NBRI accelerated mortar bar test with Australian improvements. The results (Table 5) show that the mixture of stones from the Zeelim river basin is an aggregate of an AAR short induction period. Studies by the quick, 2-3 day mortar bar autoclave method**.** Good reproducible results are given in Table 5.

Table 4. Long term expansion and fracture mechanical testing on concrete prisms

Experimental variant	I	J
Cement content in concrete (kg/m^3)	410	410
Water-cement ratio (W/C) [8]	0.49	0.49
Presence of NaOH in the mixing water	Yes	Yes
Alkalis relative to the cement (%), [9]	1.25	1.25
Alkalis relative to the concrete, kg/m^3	5.13	5.13
Storage temperature in 100% R.H. air (^{o}C)	20	38
Average 2 years length change **ε(%)** [10]	-0.002	0.037
Specific fracture energy, G_F **(N/m)** Coefficient of variation **C_V (%)**	149 8	130 10
Horizontal force component causing the fracture **F_{Hmax} (N)** Nominal notch tensile strength **σ (N/mm^2)** Coefficient of variation **C_V (%)**	2200 5.03 9	1390 3.28 12

Table 5. a) Accelerated (2-3 weeks) improved"NBRI" method;
b) Quick (2-3 days) autoclave method

Name of the required parameter	Number of specimens	Mean expansion	Standard deviation	Coef. of variation
a) Preliminary (physical) expansion (%)after 1 day immersion in pure water at 80^{o}C	6	0.044	0.0042	10
a) Expansion in %, after immersion in NaOH, - 1 day - 5 days - 7 days -10 days -14 days -21 days	 6 6 6 6 6 6	 0.003 0.041 0.076 0.128 0.177 0.226	 - 0.0038 0.0026 0.0024 0.0029 0.0099	 - 9 3 2 1 4
b) Expansion in % after 5 hours of steam curing in the autoclave at 1,72 Mpa (130^{o}C),	6	0.104	0.0043	4

[8] See footnote 5, page 6
[9] See footnote 6, page 6
[10] See footnote 7, page 6

The studies performed lead to the following conclusions:

- There is a good correlation between the results based on rapid methods and between the results based on long term (2 years and more) concrete prism expansion method [6-11].
- The expansion measurements are less significant than the mechanical parameters (G_F, F_{Hmax} and σ) to quantify the AAR damage: only the specimens F and J expand significantly, for the variants A, C, E and I the length changes are insignificant and within the error of measurement [11].
- As in the case of the concrete corrosion involved by the sulfate expansion, it is never possible to find a biunivocity relation between the apparent expansion and the reduction of the strength parameters [11,36].
- We succeeded in assimilating the following rapid methods to predict the AAR behavior of slow reacting and of carbonate containing aggregates, by specifying after a few days or weeks if an aggregate is or is not potentially reactive: a) the 2-3 weeks NBRI mortar bar expansion method with Australian improvements by immersion of mortar bars in 1N NaOH solutions at 80°C; b) *the 2-3 day mortar bar autoclave methods* based on an autoclave treatment, according to ASTM C151 of mortar bars enriched in alkalis by addition of NaOH in the mixing water by up to 3.5% Na_2O equivalent, relative to the cement weight.
- The Australian improvements to the NBRI method [35] lead to a better interpretation of the results. The limestone containing ~4% SiO_2 from Ein-Harod is a "reactive aggregate of long induction period"; the aggregate from the Zeelim river basin, containing SiO_2 and carbonates is a "reactive aggregate of short induction period". It is a good opportunity to promote an Israeli standard for the accelerated 2-3 week AAR mortar bar test ("the NBRI method"). In comparison with other classical AAR methods, the laboratory model of the NBRI method represents a better simulation of the AAR relative to marine harbor specific conditions.
- A further carrying on of the AAR studies is very timely: a) in view of the l destruction of the Wedding Hall "Versaille", built a short time ago, using the "PAL-KAL method", it is necessary to consider other possible failures of structures such as AAR; b**)** to reduce the risk of seismic actions on structures suffering from earlier AAR processes.
- It is strongly necessary to draft a first Israeli standard on AAR in concrete, in order to avoid its possible harmful effects on the durability of concrete structures.

ACKNOWLEDGEMENTS

The authors acknowledge with thanks the kind technical and scientific support received from Dr. Gershon Coster and from his Nesher - Israel Cement Enterprises LTD. colleagues

REFERENCES

[1] Bogue R.H., The Chemistry of Portland Cement, Reinhold Publ Corp New-York 1947.
[2] Bredsdorff P., Idorn G. M, Kjaer A., Plum N. M. & Poulsen E, Chemical Reactions Involving Aggregate, Proc. 4th Int. Symp. Chem. of Cem.Washington, 1960.
[3] Canadian Standards: a) & b) CSA A23.1-1990 &1994, Appendix B, Alkali- aggregate reaction; c) & d) CSA A23.2. -14 A-1990 & 1994, Potential Expansivity of Cement- Aggregate Combinations, Concrete Prism Expansion Method; e) CSA A23.2-25A-1994 Test Method for Accelerated Measure of Expansion of Mortar Bars due to the ASR (NBRI Method); f) CSA A23.2. -26A-1994, Test of Potential Alkali-Carbonate Reactivity of Quarried Carbonate Rocks by Chemical Composition.
[4] Idorn G. M.: Concrete Progress from Antiquity to the Third Millennium, Thomas Telford Publishing,London, 1997.
[5] Corin U.: Aggregates in Building Industry, Chemistry and Chemical Engineering, No9, 1992 (Hebrew)
[6] Schieber M., Nadu M., Nissenbaum J., Schlam.R, Boyko.S & Shtackelberg D.: Possibilities of Concrete Durability Loss Due to the AAR under Specific Conditions in Israel, First annual report, Submitted to the Cement Foundation of Israel, April 1993.
[7] Schieber M., Nadu M., Nissenbaum J., Braiman M., Boyko S., Shtackelberg D., The title as in 6. Second annual report, January 1995.

[8] Schieber M., Nadu M., Nissenbaum J., Lukach M., Boyko S., Shtackelberg D., New rapid tests to identify potentially alkali-reactive aggregates in Israel, Annual report, Submitted to the Cement Foundation of Israel, September 1997.
[9] Nadu M., Schieber M., Nissenbaum J., Braiman M., Boyko S., Shtakelberg D.: AAR Experiments in Israel, Proc. 10th Int. Conf. On AAR in Concrete, Melbourne, Australia August 1996.
[10] Nadu M., Schieber M., Nissenbaum J., Braiman M., Lukach M., Boyko S., Shtakelberg D.: Limitations of Standard Test Methods to Predict Delayed damaging AAR in Concrete, Proc. 10th Int. Symp. Chem. of Cem. paper 3v022, Gothenburg, June 1997.
[11] Rotter H.M., Tschegg E. K., Nadu M., Schieber M.: Testing the Specific Fracture Energy of AAR Affected Concrete Using the Wedge Splitting Method. Magazine of Concrete Research.50, 1998.
[12] CorneilleA. & Bollotte.B. , French recommendations for AAR concrete damage prevention, Proc Int. Conf. "Durability of Concrete", Nice, France, 725 1994.
[13] Baileul P.: Sika Information , 1990 p.22.
[14] Hobbs D. W.: Cracking and Expansion Due to ASR in the UK, Proc. 8th Int. Conf. On AAR in Concrete, Kioto, Japan 1989.
[15] Okada K.: Preface, ibid [14], 1989.
[16] Van Gemert D.: AAR in Belgium, ibid. [14] , 1989.
[17] St John D.A., Poole A.B., Sims I.: Concrete Petrography. A Handbook of Investigative Techniques. Arnold Editions, London, Sidney, Auckland. 1998.
[18] X x x The Alkali-Silica Reactions in Concrete. Edited by R.M.Swamy. Blackie and Son LTD, (Described national experience: &5, in the UK; &8, in Canada; &9, in New Zealand; &10, in Japan) Glasgow and London 1992.
[19] Kuennen Tom: Lithium Calms Reactive Aggregates, Concrete products, April 1996 p.30
[20] Zement Taschenbuch 2000, edited by Verlag Bau + Technik, GmbH Dusseldorf 2000, pp 409-423.
[21] X x x Alkali Aggregate Reaction, in Cement Bulletin, May and September 2000, edited by TFB (Technische Forschung und Beratung für Zement und Beton), Wildegg, Swiss.
[22] French Standards (AFNOR): a) NF-P18-011, Concrete, Classification of Aggressive Environments; b) NF-P18-584, Aggregates, Potential Alkali-Silica-Reactivity. Chemical Test; c) NF-P18-585, Aggregates, Dimensional Stability in Alkali Medium-Mortar Test; d) NF-P18-587, as c). Concrete Test; e) NF-P18-588, as c) Microbar-Test; f) NF-P18-589, Alkali-Silica or/& Alkali- Silicate Reactivities Chemical Test; g) NF-P18-590, Potential reactivity, Autoclave test.
[23] Swiss Standard SN EN ISO 8402, Management of the Quality.
[24] Japan Industrial Standard, JIS A 5308, Ready Mixed Concrete, Detection of Alkali Reactivity of Concrete Aggregates, p. 19, Appendix 1, Table 4, 1993.
[25] Romanian Standard, STAS 5440, Test Methods for AAR, 1984.
[26] ASTM Standards (from vol. 04/01 Cements & 04/02-2000. Concrete and Aggregates: a) C-33 Specifications for Concrete Aggregates; b) C-151 Test Method for Autoclave Expansion of Portland Cement; c) C-227 Test for Potential Reactivity of Cement-Aggregate Combinations d) C-289 Test Method for Potential Reactivity of Aggregates. Chemical Method; e) C-586 Test Method for Potential AC Reactivity (Rock Cylinder Method); f) C-1105 Length Change of Concrete Due to ACR; g) C-1260 Accelerated Detection of Deleterious Expansion of Mortar Bars Due to ASR; h) C-1293 Length Change of Concrete Due to ASR
[27] X x x Report to the Israeli Building Ministry on the AAR Investigations Performed in 1999-2000
[28] Natesayer K., Stark D., and Hover C.: Gel Fluorescence Reveals Reaction Product Traces. Journal of ACI, January 1991, p.25.
[29] Nikiski S. Satake M.: Gohke M., Quick Detection of AAR by AE Monitoring Progress in Acoustic Emission V, The Japanese Society for NDI 1990.
[30] New Mexico State Highway and Transportation Department, 1995: New strategies for improving the nation's highway by the SHRP research (treating concrete with uranyl acetate solution and then examining concrete under ultraviolet light), Joe Barella information by fax 505-827-5649.
[31] Dron R.: Personnel Communication, LCPC, Paris, France 1992.
[32] Fournier B., Berube M.A.: Canadian Experience with Testing Methods for AAR in Concrete, Cement & Concrete Composites, 15, 27.1993.
[33] Rogers C.A., Hooton R.D.: Leaching of Alkalis in Alkali-Aggregate Reaction, in [2], p.327, 1989
[34] Tschegg E.K.: Equipment for Fracture Test of Concrete. Materials testing, 1991, p287
[35] Shayan A., Diggins R.G., Ivanusec I. and Westgate P.L.: Acc. Testing of some Australian and Overseas Aggregates for AAR, Cem. & Concr. Res. 18, 843-851'1988.
[36] Nadu M., On the Validity of Appreciation, Using Different Usual Methods, of the Sulfate Resistance of Cements. (French) Proc. of the RILEM Symp. On the durability of concrete, Prague, 1969 & Revue des Materiaux de Construction, Paris No 654, 1970.

ORGANIC HYDROPHOBIC ADMIXTURES AND HYDROPHOBIC PORTLAND CEMENTS. LITERATURE REVIEW AND MARKET SEARCH

Mihai Nadu**,** Dr Eng, PhD & MSc, Scientific Researcher

Graduate School of Applied Science, The Hebrew University of Jerusalem
Mail: POBox 10587, Jerusalem 91103; Phone & voice box: 972-2-6731339;
E-mail: mihai_nadu@hotmail.com

CURRICULUM VITAE

DATE/PLACE OF BIRTH: 20/12/1929, (Galatz City, Romania)

MARITAL STATUS: Married, with a son and a daughter

EDUCATION:

1972	Ph.D in engineering ("Doctor-inginer"), Chair of Chemistry and Building Materials, Institute for Civil Engineering, Bucharest, Romania.
1953	MSc in Technological Engineering for Applied Material Science, Diploma with distinction, Institute for Civil Engineering,("MISI") Moscow, USSR.
1948	Theoretical baccalaureate diploma at the National College "Mihai Viteazul", Bucharest, Romania. Classified the 6th among 94 candidates passing the baccalaureate.

LANGUAGES: Very good: Romanian, French and Russian.
Good: Hebrew, English, German

EXPERIENCE

From 1989 'til now[1]	Hebrew University of Jerusalem, Israel. Staff member of the University and Senior Research Engineer in a team headed by Prof. Michael Schieber. Project items: (1) High Temperature Crystal Growth from Solution (1989-1994); (2) Hydrophobic Admixtures and Hydrophobic Portland Cements (from 1995) (3) Alkali-Aggregate Reaction (AAR) in Concrete, under specific Israeli conditions (from 1992).
1988	Nesher Cement Enterprises, Ramla, Israel: Quality tests of cement and concrete.
1953-1986	In Romania: **(**1) Management in different cement or concrete plants; (2) Design of new plants or improvement of different working cement plants (3) Founder and head of a research team, dealing with the choosing and testing, especially for large dams, of materials concrete is made of, that is cements, aggregates and admixtures. (4) Investigation of the impact of environmental conditions on different structures with different technical requirements. Specific potential

[1] Part-time work since 1995

corrosion processes were tested and recommendations for measures to assure the durability of complex concrete structures were issued. There are in view large gravity (on Bicaz and Bistritza rivers) high and sophisticated arched dams (On Arges and on Dragan Rivers), locks, galleries, power stations like the ones on the Romanian inner rivers and on the Danube. (5) Drawing up of Romanian Standards (STAS) concerning: a) requirements and testing methods for different types of cement and concrete; b) evaluation of water and environmental aggressiveness against concrete; c)evaluation and improvement of the concrete structure durability against thermal stresses, sulfate corrosion, alkali-aggregate reaction in concrete etc;. d) Test methods to evaluate the sulfate resistance of cements, the alkali reactivity of the concrete aggregates etc (6) Laboratory, pilot and industrial investigations to optimise the manufacture of special Portland cements in different plants.

PUBLICATIONS ITEMS[2]

- *Manufacture, use and properties of cements*: A didactic book and 5 papers
- *Concrete durability, corrosion processes and water aggressiveness*: 5 papers
- *On the Alkali-Aggregate Reaction (ACR) in Concrete*: 6 papers
- *Sulfate corrosion and resristance of cement and of concrete*: A Ph.D thesis and 6 papers

TAKING PART IN FORMER ICCC
6th ICCC (Moscow 1974), 7th ICCC (Paris 1980), 10th ICCC (Goteborg 1997)

[2] A reference list is available upon request

THE PERFORMANCES OF BLENDED CEMENTS BASED ON SULFOALUMINATE BELITE AND PORTLAND CEMENTS

M. Palou[1], J. Majling[2] and I. Janotka[3]

[1]Faculty of Chemical and Food Technology, Slovak University of Technology, Bratislava, Slovak Republic; E-mail: palou@chtf.stuba.sk
[2] Institute of Construction and Architecture, Slovak Republic

ABSTRACT

A series of blended cements based on Low-Energy Cements (two sulfoaluminate belite cements, SAB, synthesised in laboratory and high belite Portland cement fired in industrial conditions) and ordinary Portland cements were investigated. Although the hydration of both cement types leads to the same hydrated products, the kinetics of hydration as well as the mechanical and physical properties fundamentally differ due to differences in mineralogical and chemical composition. While SAB are fast setting cements (set point within 30 min.) their hydration courses have been retarded by blending with OPC giving setting times of 60-80 minutes. Hydration kinetics were modified by adding Portland cement with high content of C_2S. The blending of OPC with SAB was optimised in order to get normalised setting time and to fulfil the condition of passivation of steel in mortar. The mechanical strength of cements, pore-structure, absorption capacity and dynamic modulus of elasticity are described.

1. INTRODUCTION

Sulfoaluminate belite cements (shorthand, SAB) form a group of cements belonging to the class of Low-Energy Cements (LEC) [1]. The production of SAB cements not only requires lower clinkerisation temperatures 1 200 - 1 300°C in comparison to OPC, but can be made from raw meals containing natural minerals and industrial by-products such as fly ash, red mud and blast - furnace slag [2,3].

The cement industry is an industry with a high demand for energy, thermal as well as electrical. Many investigations have been carried out to decrease this demand and consequently reduce CO_2 emission. One of the primary ideas in a development of LEC [4-6] was to reduce the $CaCO_3$ content of the raw meal, thereby decreasing part of the energy necessary for the decomposition of calcite. The decrease in $CaCO_3$ leads further to decreases in the content of the "high energy" mineral - C_3S^+; - ultimately to its complete absence. Cements based on $C_4A_3\bar{S}$ are developed and studied [7]. The hydration reaction of $C_4A_3\bar{S}$ with $C\bar{S}$ leads to the formation of ettringite in the earlier period, while dicalcium silicate, hydrates in the last period to form calcium silicate hydrates as with OPC [10].

In spite of the excellent experimental results obtained throughout laboratories and the numerous manifest advantages of large scale production [2,8,9], with the exception of Chinese and some UK plants, is not until now widely used and some doubts remain regarding its use as a masonry material in civil engineering[8].

$^+$/ C = CaO, S = SiO_2, A = Al_2O_3, F=Fe_2O_3, $\bar{S}$ = SO3;

2. EXPERIMENTAL

Three kinds of Low-Energy Cements were prepared

1. Two SAB cements which are C_3S- free, but have about 20% by wt $C_4A_3\bar{S}$; other phases are C_2S, C_4AF and $C\bar{S}$.
2. High belite Portland cement which is free from $C_4A_3\bar{S}$, but contains active belite clinker with a reduced content of C_3S.

The high belite Portland cement (HBC) has been burnt from natural raw materials (limestone, burnt clay, pyrite, sand) by the dry process at 1260°C. The reduction of clinkering temperature and the total amount of calcite have led to the energy saving of 400 kJ/kg compared with production of OPC (also used in this experiment, CEM I 42,5) in the same plant. The clinkers thus obtained were ground in an industrial closed mill circuit with 3% gypsum.

2.1 Materials, mixing and curing

Ordinary Portland cement (CEM I 42.5), two samples of SAB cements, HBC and standard sand were used [11]. Then two mixes were prepared from OPC and SAB cements in weight proportion of 15 and 85 % (B1 and B2). Two mixes from HBC and SAB cements were also prepared in ratios of 30 : 70 % by weight (B3 and B4). Chemical and mineralogical composition of cements and blended cements B1 (85 % OPC + 15 % SAB1), B2(85 % OPC + 15 % SAB1), B3(70 % HBC + 30 % SAB1) and B4(70 % HBC + 30 % SAB2) are listed in Table 2 and their physical properties in Table 3. Mechanical properties at 28- and 90-days are reported in Table 4. Phase composition of the B1, B2, B3, B4 blended cements are derived by the linear interpolation to achieve mixing ratios /15 % OPC + 85 % SAB and 70 % HBC + 30 % SAB/.

Mortars with cement to sand ratio of 1 : 3 by weight and w/c = 0.5 were prepared as prism specimens 40 x 40 x 160 mm made in steel moulds on a vibration table (50 Hz, 0.35 mm) with a maximum vibration time of 30 seconds. The specimens were stored at 20°C and 100 % R.H. for 28 and 90 days.

The rate of hydration was measured by using conduction calorimeter. The equipment is coupled to a computer for continuous monitoring of the rate of heat generation.

Table 1. Formulation of samples

	OPC	HBC	SAB1	SAB2
	100	100	100	100
B1	15		85	
B2	15			85
B3		30	70	
B4		30		70

Table 2. Chemical and mineralogical composition of tested cements and blends

	OPC	HBC	SAB1	SAB2	B1	B2	B3	B4
SiO_2	20.82	20.20	19.69	18.00	19.86	18.42	19.84	18.66
CaO	62.30	58.20	52.58	53.53	54.03	54.84	54.26	54.93
Al_2O_3	6.00	6.50	15.45	8.14	14.03	7.82	12.76	7.64
Fe_2O_3	4.39	7.70	2.60	4.94	2.86	4.85	4.13	5.76
SO_3	1.84	2.70	6.12	10.77	5.47	9.43	5.09	8.35
MgO	2.18	1.50	1.50	1.35	1.60	1.47	1.47	1.40
C_3S	44.5	30.30	-	-	6.67	6.7	9.00	9.09
C_2S	25.8	37.80	56.5	58.50	51.7	53.6	50.90	52.30
C_3A	8.50	24.70	-	-	1.3	1.3	7.41	7.41
C_4AF	13,40	3.30	7.90	10.80	8.7	11.20	5.73	8.55
$C_4A_3\bar{S}$	-	-	10.00	12.30	8.50	10.46	7	8.61
$C\bar{S}$	4,70	3.90	16.10	5.70	14.40	5.60	12.44	5.16
C_{free}	0.10	0.27	0.00	0.18	0.01	0.17	0.08	0.08

2.2 Test methods

Mortar specimens were tested on flexural and compressive strength, dynamic modulus of elasticity (DME.

Ultrasonic pulse velocities were measured on ultrasonic apparatus UNIPAN type 543 . The DME values were calculated by equation (1):

$$E_{bu} = \rho . v_L^2 . \frac{1}{k^2} . 10^{-6} \qquad (1)$$

where E_{bu} = dynamic modulus of elasticity, MPa
ρ = volume density of mortar specimens, kg . m^{-3}
v_L = impulse speed of longitudinal ultrasonic waves, m . s^{-1}
k = dimensional coefficient for 40 x 40 x 160 mm prisms

For the DME calculations, three - dimensional environment in mortar specimens and Poisson coefficient γ_{bu} = 0.20 were considered according to STN-EU [12] and k = 1.0541 was determined.

3. RESULTS AND DISCUSSION

Blending ratios of OPC / HBC and SAB1/SAB2 had previously been optimised to the value of 15 to 85, or 70 to 30, in wt. Proportions. These were used in a series of many combinations with regard to the initial setting time as well as to maximum quantity of SAB1 and SAB2 to retain passivation of steel in mortar.

The hydration kinetics of HBC, OPC and blends (B1, B2, B3, B4) are summarised in Figures 1a-g. The evolution curves of HBC and OPC are shown in Figure 1-a. Apart from the quite initial period of hydration, little difference is observed between samples.

After a small initial peak, observed when water first comes into contact with the cement, HBC shows a slow rate of heat evolution. SAB1 does not show a second peak and is characterised by the absence of an induction period, while SAB2 shows the higher initial and second peaks with a small induction period in between.

The blended samples show important changes in the heat-evolution curves. The second peak appears (Figure 1-d and Figure 1-e) and in the case of B3 (Figure 1-f) also a little third one. The initial setting time values, in Table 3, clearly prove the change in hydration process. It is not easy to determine the initial and final setting time from calorimetric curves, although no doubt exists on the influence of the rate of the heat-evolution (as determined by the calorimeter) upon the whole process of setting and hardening. While in OPC, this process is governed by C_3S hydration, in SAB cements, it is driven by hydration reaction of $C_4A_3\bar{S}$ and $C\bar{S}$ leading to the formation of ettringite. It is why the SAB cements are often fast-setting. Indeed, cement mortar is a multi-phase assemblage composed of sand, unreacted minerals, hydrated products and voids filled by water and air. If we consider that after setting time, cement grains are enclosed by primary products formed during the initial period of hydration, and that the hydration reaction without induction period characterises fast setting process, it is expected that after long period of curing the coarse pores will remain in cement matrices, and thus, will influence their mechanical and physical properties.

Table 3. Physical properties of cements

	Specific surface [m^2/kg]	Normal consistency [%]	Setting time, Pastes	
			Initial [min.]	Final [min.]
OPC	345	29	190	305
HBPC	320	26	220	360
SAB1	340	34	20	37
SAB2	330	33	25	28
B1	330	31	70	90
B2	320	30	65	105
B3	325	28	80	110
B4	310	28	80	110

Water demand is related to the mineralogical composition of given samples. Sulfoaluminate belite cement with $C_4A_3\bar{S}$ as one of mineral clinker uses more in the formation of ettringite in initial period of hydration. SAB cements are fast-setting cements within 30 minutes. By blending with OPC or HBC hydration, reactions are retarded to ensure workability of concrete.

Table 4. Mechanical properties of cements and blends in concrete

	DME [Gpa]		Flexural strength [MPa]		Compressive strength [MPa]	
	28 days	90 days	28 days	90 days	28 days	90 days
OPC	41.7	43.00	8.7	10.30	42.80	48.30
HBC	38.80	45.70	9.4	10.6	41.5	53.9
SAB1	26.4	31.40	5.60	7.30	17.4	30.10
SAB2	28.40	33.60	6.70	9.37	20.40	38.70
B1	31.90	36.20	6.90	8.40	24.60	41.30
B2	30.50	40.20	8.00	9.20	32.60	44.80
B3	32.00	37.40	6.30	8.10	28.60	48.20
B4	33.20	42.40	10.4	11.3	46.5	58.1

Both SAB cements were clinkered of 1 250°C, which is markedly lower than those reported for Chinese and British cements which are manufactured at 1 300 - 1 350°C and 1 400°C respectively. Perhaps for this reason the strength characteristics and utility properties of SAB-1 and SAB-2 cements are lower than those of the Chinese and British products. Energy saving and reduction in

CO_2 emissions of SAB-1 and SAB-2 cement production are expected to be significantly improved relative to cements fired at temperatures between 1 300 -1 400°C.

The flexural and compressive strengths of mortars are considerably influenced by curing conditions and type of cement (Table 4).

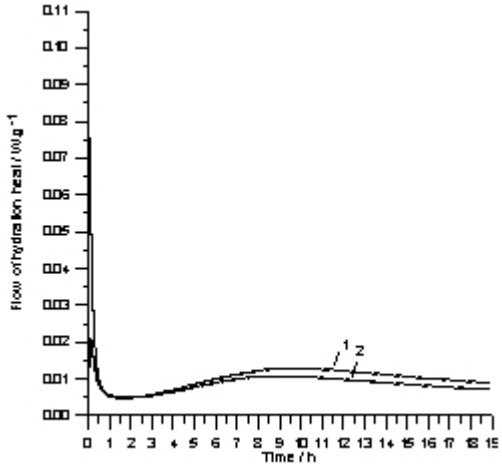

Figure 1(a). Calorimetric curves 1-OPC 2-HBC

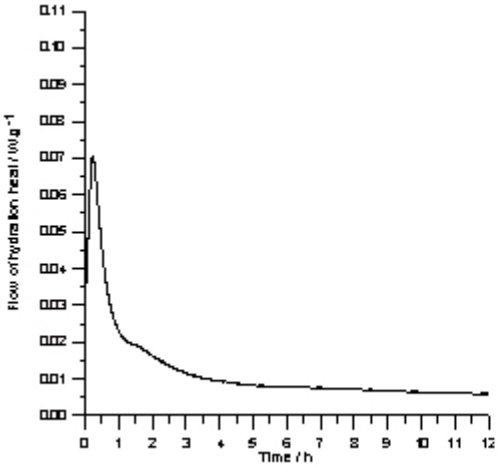

Figure 1(b). Calorimetric curves of SAB1

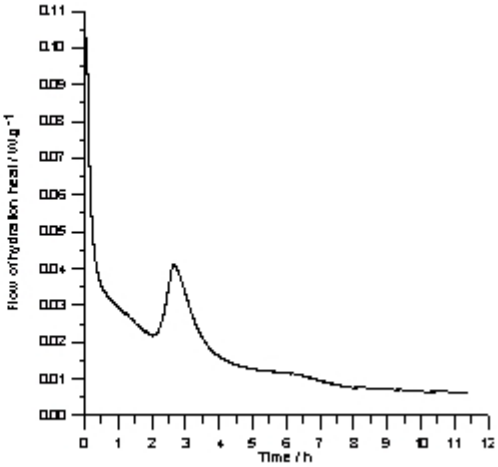

Figure 1(c). Calorimetric curves of SAB2

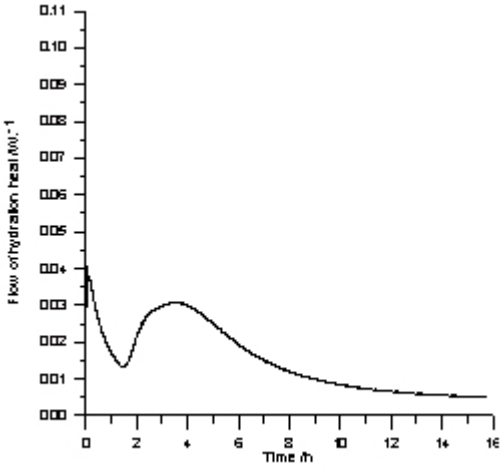

Figure 1(d). Calorimetric curves of B1

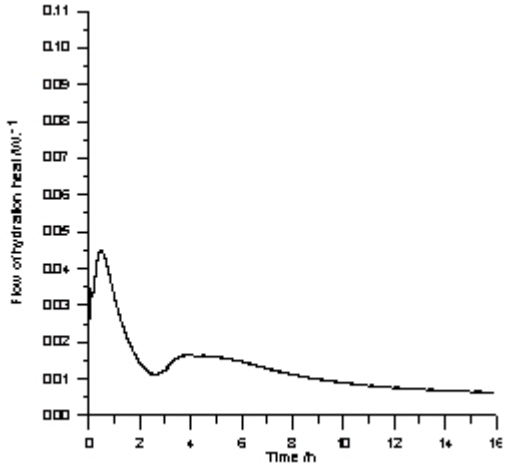

Figure 1(e). Calorimetric curves of B2

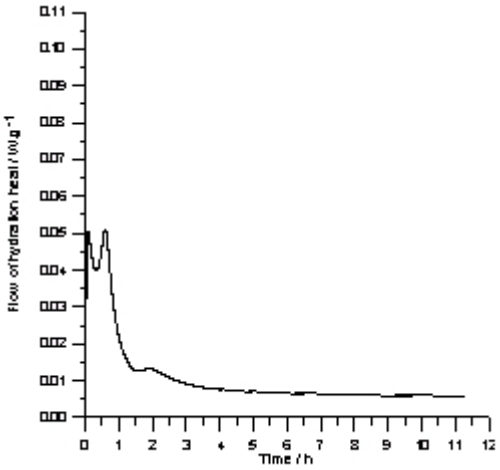

Figure 1(f). Calorimetric curves of B3

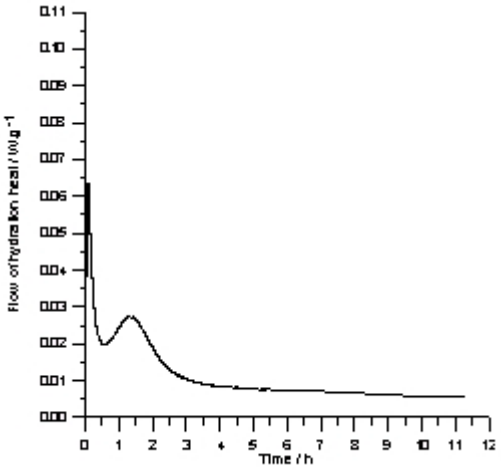

Figure 1(g). Calorimetric curves of B4

4. CONCLUSIONS

An attempt has been undertaken to investigate the possibilities of use of sulfoaluminate belite cements:

1. It is possible by blending SAB cement with Portland cement to upgrade SAB cement properties.
2. Initial set times are at least 60 minutes. This is sufficient time for mortar-making procedures.
3. The mortars made with the above blend indicate increased strength as well as dynamic modulus of elasticity compared to SAB cement mortar.
4. Mechanical and physical properties depend on the type of SAB added to HBC. The results thus obtained show that such type of cement or its blended forms can be used successfully in the replacement of OPC.

ACKNOWLEDGEMENTS

The authors wish to thank the European Commission for its support of a COPERNICUS project - and the Slovak Grant Agency VEGA No. 1/9140/02.

REFERENCES

[1] Mehta, P. K. Energy resources and the environment, World Cement Technology, July/August, 1978, pp.144 - 160.

[2] Palou, M.T. and Majling, J. Preparation of the high iron sulfoaluminate belite cement from raw mixtures incorporating industrial wastes, Ceramics-silikát, vol.2, 1995, pp. 63-.67.

[3] Sahu, S. and Majling, J. Preparation of sulphoaluminate belite cement from fly ash, Cement and Concrete Research, 1994, vol. 24, pp.1065 - 1072.

[4] Sahu, S. and Majling, J. Phase compatibility in the system CaO-SiO_2-Al_2O_3-Fe_2O_3-SO_3 referred to sulphoaluminate belite cement clinker, Cement and Concrete Research,1993, vol.23, pp.1331 - 1339.

[5] Moir, G. K. and GLasser, F. P. Mineralisers, modifiers and activators in the clinkering process, Proceedings of the 9th International Congress on the Chemistry of Cements, New Delhi, 1992, vol.1, pp.125 - 152.

[6] Ludwig, U. and Pohlmann, R. Investigation on the production of low lime Portland cements. Proceedings of the 8th ICCC, Rio de Janeiro, 1986, vol. 2, pp. 363 - 371.

[7] Lawrence, C. D. Notes on low-energy cements based on belite. Notes on energy requirements in the production of cements for construction, Copernicus Program Report CIPA-CT 94-0105, 1995.

[8] Viles, R. F. Some commercial uses of calcium sulphoaluminate cements in the construction and mining industries. Proceedings of the Conference, Cements for the Future Calciumsulfoaluminates, London, 1998, Session 4, Book of Abstracts.

[9] Johnson, D. Specialist uses of calcium Sulfoaluminate cement in the construction industry. Proceedings of the Conference, Cements for the Future - Calciumsulfoaluminates, London, 1998, Book of Abstracts.

[10] Sherman, N., Beretka, I., Santoro, L. and Valenti, G. L. Long-term behaviour of hydraulic binders based on calcium Sulfoaluminate and calcium sulfosilicate, Cement and Concrete Research, 1995, vol. 25, pp.113 - 126.
[11] Havlica, J., Roztocká, D. and Sahu, S. Hydration kinetics of calcium-aluminate phases in the presence of various ratios of Ca^{2+} and SO_4 ions in liquid phase, Cement and Concrete Research,1993, vol.23, pp. 294 - 300.
[12] Slovak Technical Standard: STN 72 1208 - Testing sands (in Slovak).
[13] Slovak Technical Standard : STN 73 1371 - Method of ultrasonic pulse testing of mortar (in Slovak).
[14] Zhang L., SU M. and Wang Y. New development of use of sulfo-and ferro-aluminate cements in China. Proceedings of the Conference, Cements for the Future -Calciumsulphoaluminates, London, 1998, Book of Abstracts.
[15] Brown A. D. R. Commercial production, composition and properties of calcium sulfoaluminate cement. Proceedings of the Conference, Cements for the Future - Calciumsulfosaluminates, London, 1998, Book of Abstracts.

THERMOANALYSIS STUDY OF HARDENING PROCEDURE OF CLAY-HARDENING GROUT (CHG)*

Wang, Xinghua

Institute of Tunnel and Underground Engineering, Central South University at Tiedao Campus, Changsha, Hunan, P.R.China, 410075.

ABSTRACT

As a new cheap grouting material, Clay-hardening grout (CHG) is getting close attention. But it is necessary to carefully study what hardening reaction is taking place and what compounds are produced during the hardening procedure of CHG. In this paper thermoanalysis (differential thermal analysis, DTA) has been used to study the chemical composition of resulting compounds of CHG during the hardening process. In accordance with the study results, a new model of hardening mechanism of CHG has been put forward.

Keywords: Clay-hardening Grout (CHG), Hardening Model, Hardening Mechanism, DTA.

1. INTRODUCTION

When adding cement and solidifying agent into clay-hardening grout, chemical reactions commence within the grout. As time passes, these chemical reactions continue to enable the grout getting hard till it has eventually hardened into stone. But what hardening reactions are taking place? What compounds should be produced during the hardening process of CHG? What is the hardening mechanism? All these questions puzzle us and require further careful study.

Various methods are used to study mineral components. Among them, chemical analysis, gas chromatography, mass spectrographic analysis, thermoanalysis and electron micro-identification are in common use. Since it is very difficult to purify materials like clay and silicate because of their complicated compositions, thermoanalysis and electron microidentification are usually used to analyze and identify the composition and microstructure of clay and silicate minerals. In this paper, thermoanalysis (differential thermal analysis, DTA) has been used to study the chemical composition of compounds of CHG during the hardening procedure. In accordance with the study results, a new model of the hardening mechanism of CHG has been put forward.

2. TEST MATERIALS AND PREPARATION OF CHG[1,2]

2.1 Test materials

The clay used in this work is the clay block produced by Sichuan Minshan Mineral. With rather small clay particle size (average size of 10.1um of the particle weighted 50%) and specific surface area of 6103.9cm^2/g, the clay consists mainly of kaolin, smectite, oligosite, halloysite, illite, etc. The cement used is the standard silicate cement 425# produced by Sichuan Ermei Cement Plant. The self-prepared CHG Solidify B (Chinese Patent No.96117823.X) consists of some inorganic salts with main composition of 30-50%aluminate, 5-20% sulphate, 5-15% silicate, 1-10% silicon oxide, 1-10% calcium oxide, etc.

2.2 Preparation of CHG sample

The preparation procedure of CHG is as follows: first add cement into clay mud, then add Solidify B and finally solidify A (water glass). Stir the clay hardening grout with different mix proportion and make standard CHG sample and then start the thermoanalysis tests at different ages while maintain test specimens in water. Before the thermoanalysis test, the hydration of CHG samples was terminated by and heating and then grinded till it fully passed through the 4900 sieve. Japan-made Rigaku PTC-10A multi-parameter thermoanalysis instrument is the instrument used.

3. HARDENING MECHANISM STUDY OF CHG

As clay hardening grout consists of clay, cement, sodium silicate (Solidify A), Solidify B and water, the chemical reactions taking place inside the CHG should be associated with the basic reactions inside CHG, such as the hydration of cement, the reaction of cement with sodium silicate, the reaction of cement with clay and the reaction of sodium silicate with clay. But, since Solidify A is also, so the chemical reactions taking place inside CHG are not totally the same as those reactions described above.

3.1 Hydration process of CHG

The hydration taking place inside CHG includes the hydration of cement as well as the effects of Solidify B and Solidify A on the hydration process.

3.1.1 The hydration process of cement[3,4]

Tricalcium silicate, dicalcium silicate, tricalcium aluminate and tetracalcium ferrate aluminate in the cement added into CHG first undergo hydration with water.

Among them, tricalcium silicate undergoes hydration and hydrolysis with water as below:

$$2(3CaO\bullet SiO_2)+6H_2O\rightarrow 3CaO\bullet 2SiO_2\bullet 3H_2O+3Ca(OH)_2 \quad (1)$$

When tricalcium silicate mixes with water, hydration is fast. At the beginning, the compounds of lime and silica enters the solution in stoichiometric ratio, i.e. the same mole ratio 3:1 as they exist in the anhydrous compound. The quick decrease of the concentration of silica caused by the continuous increase of the concentration of lime soon yields the appearance of crystal of hydrated lime and the formation of gelatinous or near amorphous hydrated calcium silicate as well. The hydrated calcium silicate formed on the surface of tricalcium silicate produces a thin film to make it very difficult for water to enter into it, and thus to slow down the ongoing hydration.

Equation (1) is the chemical reaction equation of tricalcium silicate when it totally hydrated. But his simple equation can not reflect the complex nature of the reaction. At the beginning of hydration, the immediately yielded resultants $CaO:SiO_2$ with a ratio near 3 form a thin film covering the surface of tricalcium silicate and thus retard its hydration. Several hours later, the film of this initial compound dissolves or breaks to accelerate the hydration of tricalcium silicate and produce C-S-H second gelatinous compounds with relatively lower mole ratio (1.5 or less) which instantly turn into the stable third resultants.

Dicalcium silicate undergoes hydration with the equation as below:

$$2(2CaO\bullet SiO_2)+4H_2O\rightarrow 3CaO\bullet 2SiO_2\bullet 3H_2O+Ca(OH)_2 \quad (2)$$

When the solution is saturated with hydrated lime, the hydration of dicalcium silicate does not stop, but keeps on going. Furthermore, the reaction incessantly liberates calcium lime in the form of hydrated lime crystals and forms hydrated silicate that remains stable when contacting the saturated lime solution. Although the reaction processes are different, the hydrates of dicalcium silicate and

tricalcium silicate are in the same form. The ratio of the initial resultants CaO/SiO_2 covered on the surface of dicalcium silicate particle is near 2. About 12 hours later, it converts into lime and the ratio of CaO/SiO_2 drops to the minimum 1.1-1.2. Finally, a stable compound is produced.

Tricalcium aluminate undergoes hydration with the equation as below:

$$3CaO•Al_2O_3 + 6H_2O \rightarrow 3CaOAl_2O_3•6H_2O \quad (3)$$

$$3CaO•Al_2O_3 + Ca(OH)_2 + nH_2O \rightarrow 4CaaO•Al_2O_3•nH_2O \quad (3^*)$$

Although tricalcium aluminate reacts with water very quickly, it reacts slowly with water in the saturated lime solution. Part of the lime in tricalcium aluminate can be replaced and yields in $Na_2O•8CaO•3Al_2O_3$. At the same time, the hydration could be accelerated because of the existence of alkalis.

The hydration of tetracalcium ferrate aluminate is shown as below:

$$4CaO•Al_2O_3•Fe_2O_3+2Ca(OH)_2+10H_2O \rightarrow 3CaO•Al_2O_3•6H_2O+3CaO•Fe_2O_3•6H_2O \quad (4)$$

The rate of the reaction of ferric aluminate with water is in proportion to the content of aluminum oxide in ferric aluminate. The hydration of tetracalcium ferrate aluminate will not produce hydrated lime. But the hydration process in excess water [5,6,7] is similar to the hydration of anhydrous CA with $C_{12}A_7$. Both produce saturated Calcium Aluminate solution except that the mole ratio of CaO : Al_2O_3 varies between 2:1 and 3:1.

3.1.2 The catalysis process of Solidify B

When adding Solidify B into clay cement grout, the inorganic salt in solidify B first dissolves in the water, producing a great number of aluminate ions, sulfate ions and silicate ions. Calcium also undergoes hydration and produces hydrated lime which provides adequate conditions for equation (4) and accelerates the hydration of tetracalcium ferrate aluminate. Meanwhile, hydrated lime is soluble in water with a relatively lower solubility. The dissolution of hydrated lime produces Ca^{+2} and OH^{-1} which make saturated solution soon, reacts with aluminate ion, sulfate ion and silicate ion to produce crystal compounds of hydrated tricalcium aluminate, calcium sulfate and hydrated $CaSiO_2$, and dissolves part of the silica to produce $Na_2O•SiO_2$:

$$OH^{-1} + nSiO_2 \rightarrow Na_2O•nSiO_2 + H_2O \quad (5)$$

Where $Na_2O•nSiO_2$ reacts with hydrated lime in the solution (equation 6) to produce hydrated calcium silicate, a gel with certain strength.

$$Ca(OH)_2+Na_2O•nSiO_2+mH_2O \rightarrow CaO•nSiO_2•mH_2O+NaOH \quad (6)$$

Where calcium sulfate in water solution decreases the solubility of hydrated lime, thus enabling the accelerations of the formation of hydrated lime crystals and accelerating the development of equation 1, 2 and 3* to right side. And also, calcium sulfate undergoes hydration with tricalcium aluminate and water as below:

$$3CaSO_4+3CaO•Al_2O_3+32H_2O \rightarrow 3CaO•Al_2O_3•3CaSO_4•32H_2O \quad (7)$$

This quick reaction consolidates great deal of free water in the form of crystals. The amount of free water decreased in the solution is 46% of that of cement increased.

But the content of calcium in the Solidify is low and cement has been added prior to the adding of the Solidify which resulted in the hydration of grog minerals in cement with water and the production of hydrated lime. The product of Ca^{+2} after hydrated lime has been dissolved combines with the aluminate ion, sulfate ion and silicate ion in the Solidify and yields hydrated tricalcium

aluminate, calcium sulfate and hydrated $CaO•SiO_2$, thus decreasing the concentration of Ca^{+2} in the solution and accelerating the hydration of grog minerals in cement.

$$Al_2O_2^{-2} + Ca^{+2} + H_2O \rightarrow 3CaO•Al_2O_3•6H_2O \quad (8)$$
$$SO_4^{-2} + Ca^{+2} + H_2O \rightarrow CaSO_4•2H_2O \quad (9)$$
$$SiO_2^{-4} + Ca^{+2} + H_2O \rightarrow 2CaO•SiO_2•nH_2O \quad (10)$$

3.1.3 The catalysis process of solidify A (water glass)

$$NaO•nSiO_2 + H_2O \rightarrow 2NaOH + nSiO_2 \quad (11)$$

When finally adding water glass, it hydrolyzes immediately as shown in equation 11 which is a reversible one. The amorphous silica in Solidify B accelerates this reaction to the left side to produce more $NaO•SiO_2$ which reacts with hydrated lime in the solution (equation 6) to produce hydrated calcium silicate, a gel with certain strength. Now, the amorphous silica limits the hydrolysis of water glass and accelerates its reaction in the direction of producing hydrated $CaO•SiO_2$, thus speeding up the reaction rate.

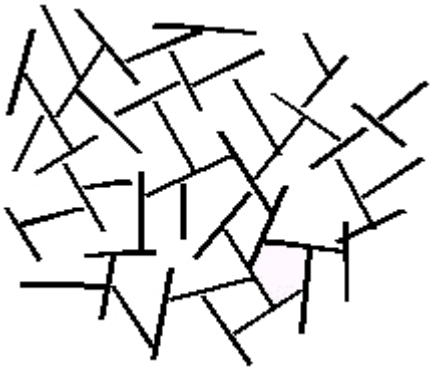

Figure 1. Sketch of Ladder

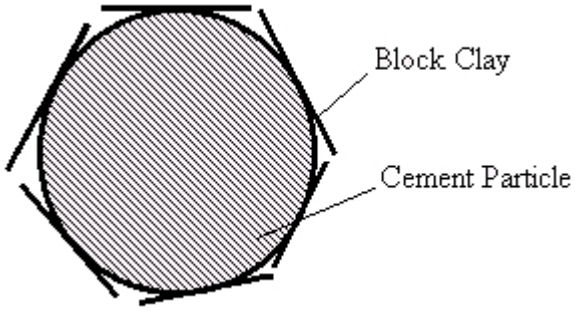

Figure 2. Sketch of clay cement ball

At the same time, the amorphous silica plays a role of crystal nuclei on the surface of cement particles and accelerates the formation of hydrate crystals. The crystals of hydrated tricalcium aluminate, calcium sulfate and hydrated $CaO•SiO_2$ produced by the aluminate ion, sulfate ion and silicate ion in Solidify B constitute the crystal nuclei for the crystal growth of successive reactants, thus accelerating the growth of various hydrate crystals, the increase of crystal's strength and the hardening of grout and shortens the initial set time.

3.2 The Reaction of Clay Particle with Cement and Hydrates

At the same time when various hydrates of cement are produced, part of these hydrates keep on hardening to form the skeleton of cement hydrates while the other part reacts with the nearby clay particle with certain activity because the hydration and hydrolysis of cement in CHG is completely surrounded by the medium of mud with certain activity. The main ways of reaction are ion exchange, nodularization (granulation) and hardening reaction which constitute a complicated physical chemistry reaction process.

When the clay particles in CHG are dispersed into block clay in water, the surface and edge of these block clays have different charges. In a relatively larger PH range, the edge always has positive charge and the surface has opposite charge, the number of which is far more than that of positive on the edge [8]. So, the edge and surface attract each other and form a ladder structure (Figure 1)[9,10]. The added cement particle with positive charge on the surface is thicker than clay particles. When it meets the surface of block clay with opposite charge, electrostatic attraction between them occurs and part of the ladder structure is broken. The surface of block clay is attracted towards cement

particles and forms clay-cement ball centered with cement particle (Figure 2). Ladder and clay-cement ball structure exist together because the amount of cement added is small and it is impossible to break the ladder completely. The hydration compounds of cement particles in clay-cement ball start to form at the surface of the cement particle and then diffuse outwards and fill the vacancy of clay particle to grow strength.

Except for absorbing with cement particles with positive charge, the surface of clay particles also undergo equivalent absorption with Ca^{+2} in hydrated lime, resulting from cement hydration, and enables the dispersed clay particle to form bigger clusters to increase the strength of CHG. Because its surface area is far larger than the surface area of cement particles, the gel produced by the hydration of cement has very big surface energy and strong absorption activity. It can further combine with bigger mud cumularspharolith to form cluster structures and blockade the vacancy of each mud cumularspharolith to form a unity combination.

3.3 Thermoanalysis study of CHG reaction mechanism

When adding Solidify agents into CHG, hydration takes places quickly and solidifies very soon. At present, we can not study the hydrates in 1-2 hours after the hydration but can only study the hydrates 3 days after the hydration because of the limitation of experimental conditions.

From the previous analysis, we know that the main compounds of hydration of CHG are $Ca(OH)_2$, hydrated $CaO•SiO_2$ and $CaO•Al_2O_3•Fe_2O_3$, etc. Figure 3 is the typical differential thermal curve of clay-hardening grout which clearly shows the characteristic heat liberation peak of $Ca(OH)_2$ (518°C), hydrated $CaO•Al_2O_3$ 580°C and hydrated $CaO•SiO_2$ (730°C).

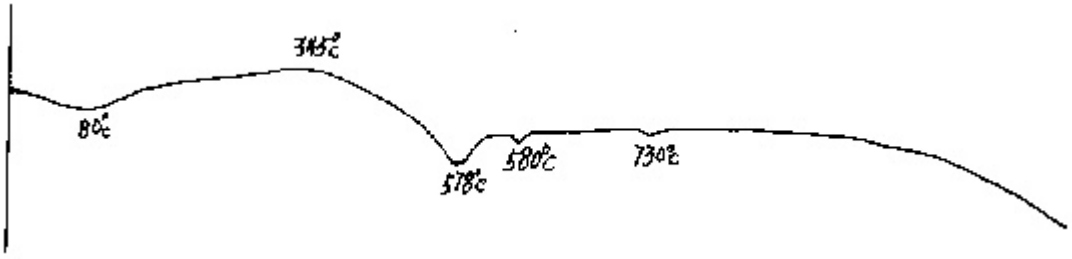

Figure 3. Typical differential thermal curve of clay-hardening grout (CHG)
(Rate of increasing temperature 20°C /min, age 14days)
Mud viscosity 67.8", Cement 10%, Solidify A (SA)3%, Solidify B (SB) 5%

As hydration further undergoes, more and more hydrates are produced and the curves of differential age (Figure 4) proves that even more hydrated $CaO•SiO_2$ and $Ca(OH)_2$, which are the main hydrates playing the role of strength in CHG, are increased. Figure 4 shows that the contents of these two type of hydrates increase with the increase in age and the curves also reflects that the area of characteristic peak of these hydrates increase with the increase of time of hydration. Even at the later period of hydration, the characteristic peak (218-225°C) of hydrated ettringite ($CaO•Al_2O_3•CaSO_4$) occurs.

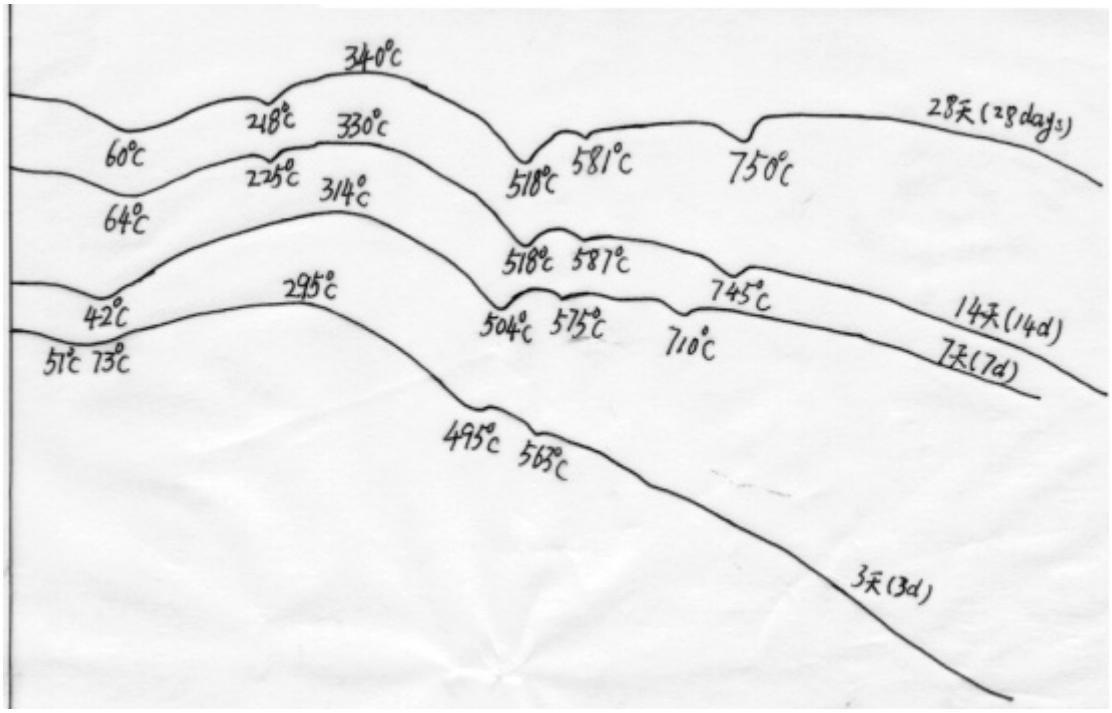

Figure 4. Curves of differential age (Rate of increasing temperature 20°C /min)
Mud viscosity 67.8", Cement 10%, SA 7%, SB 5%

With the increase of Solidify A (water glass), the content of hydrated $CaO•SiO_2$ in hydrates decreases while the content of $Ca(OH)_2$ increases. This can be reflected by the decrease of the characteristic peak area (about 710-757°C) of hydrated $CaO•SiO_2$ and the increase of the characteristic peak area (about 495-525°C) of $Ca(OH)_2$ in differential thermal curves (see Figure 5).

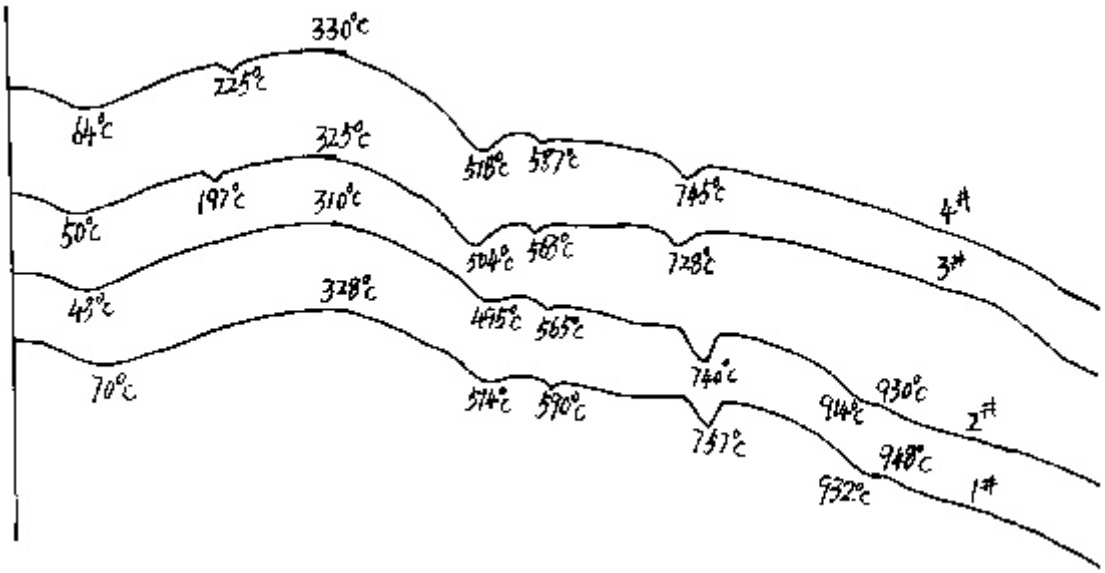

Figure 5. Affecting curves of SA on hydrate
(Rate of increasing temperature 20°C /min, age 14days)
1#: Mud viscosity 67.8", Cement 10%, SA 1%, SB 5%;
2#: Mud viscosity 67.8", Cement 10%, SA 3%, SB 5%
3#: Mud viscosity 67.8", Cement 10%, SA 5%, SB 5%
4#: Mud viscosity 67.8", Cement 10%, SA 7%, SB 5%

An increase in cement will definitely increase the content of cement hydrates. The differential thermal curves shows that with increase of cement, the output of hydrated $CaO•SiO_2$ increases and its characteristic peak area (about 710-778°C) also increases while the output of $Ca(OH)_2$ decreases and its characteristic peak area (about 485-520°C) decreases as well till it almost disappears when cement increases to 15% (see Figure 6).

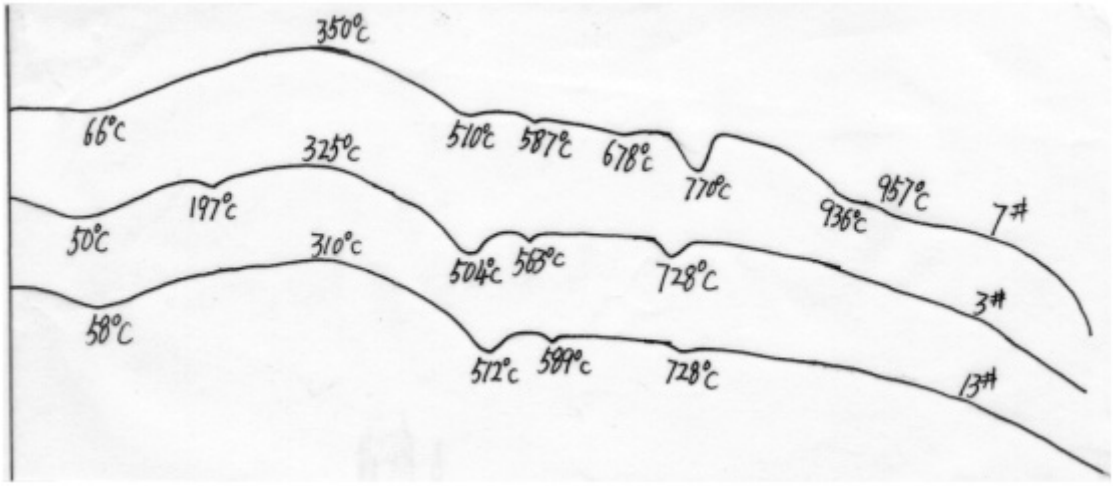

Figure 6. Affecting curves of cement on hydrate
(Rate of increasing temperature 20°C /min, age 14days)
3#: Mud viscosity 67.8", Cement 10%, SA 5%, SB 5%
7#: Mud viscosity 67.8", Cement 15%, SA 5%, SB 15%
13#: Mud viscosity 67.8", Cement 5%, SA 5%, SB 10%

Solidify B is added into CHG as catalyst of the hydration of cement. Reference 11 tells us that there is a optimal value for the increase of solidify B (less than 5%). This can be proved by the differential thermal analysis: with the increase of solidify B, the hydrates in CHG change by decreasing the content of hydrated $CaO•SiO_2$ and $Ca(OH)_2$ (their characteristic peak areas decrease) and appearing a small amount of hydrated $CaO•Al_2O_3$ (heat liberation peak with characteristic peak 910-958°C) appears (see Figure 7).

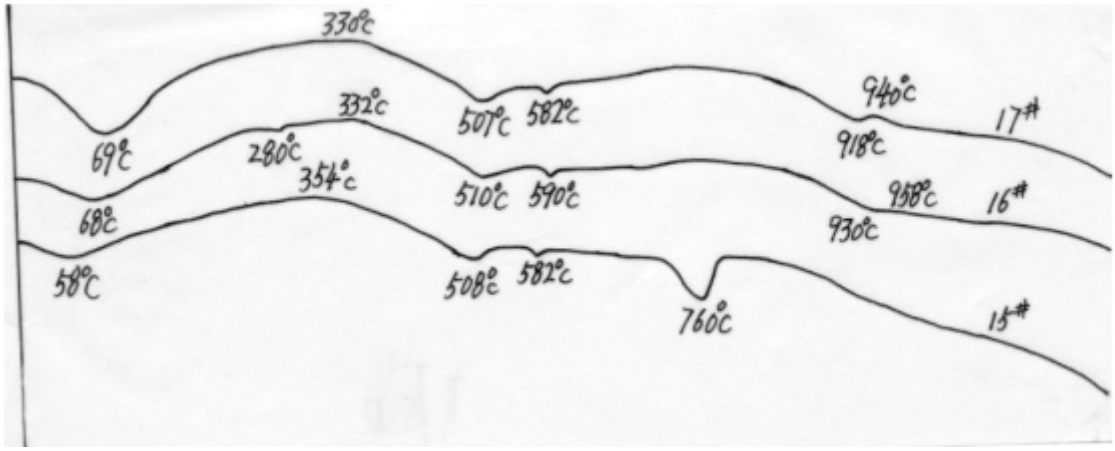

Figure 7. Affecting curves of SB on hydrate
(Rate of increasing temperature 20°C /min, age 14days)
15#: Mud viscosity 67.8", Cement 10%, SA 3%, SB 5%
16#: Mud viscosity 67.8", Cement 10%, SA 3%, SB 15%
17#: Mud viscosity 67.8", Cement 10%, SA 3%, SB 10%

4. THE HARDENING MODEL OF CHG

Based on the previous analysis, we can draw the hardening model sketch of clay hardening grout (see Figure 8) and conclude that the reaction process of the two stages of CHG hardening process and the role of Solidify A and B have played are both directly associated with the hydration of cement.

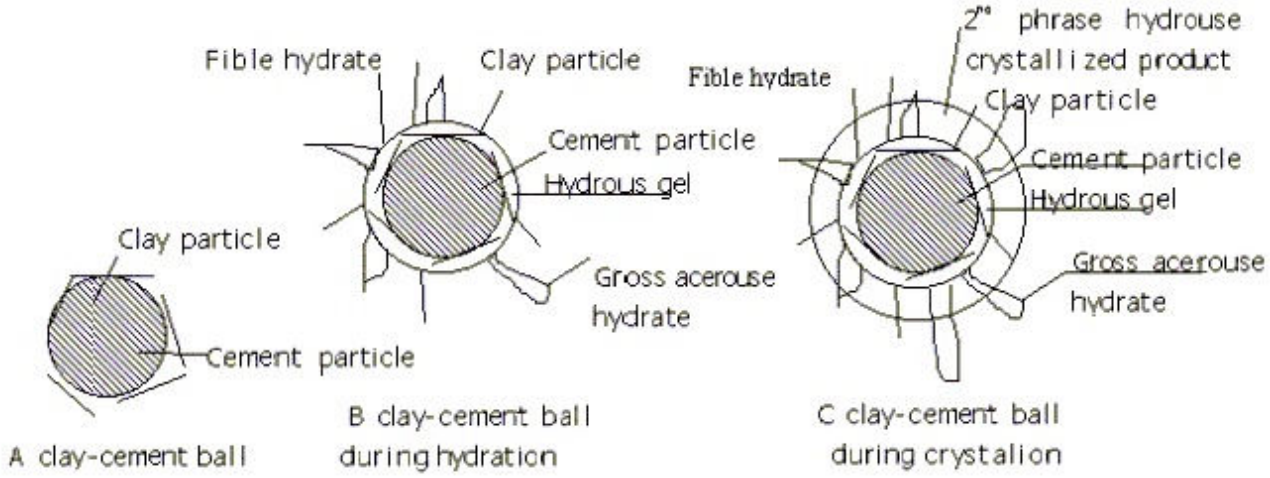

Figure 8. Hardening modeling sketch of clay hardening grout

In the first stage, the adding of cement into CHG breaks the original ladder structure of CHG and liberates part of free water which immediately undergoes hydration with cement particle surface with the compounds dispersing in the water in the state of very little solids. Meanwhile, some part of the solid dissolves in the water and produces a great deal of ions (like Ca^{+2}) to enable clay particles to be consolidated and thickened and the grout to be viscous. Then the new surface of cement particle is again exposed and continues to react with water till the liquid around the cement particle becomes saturated. The added Solidify A and B accelerate the dissolution of cement particle surface and the crystallization of hydrates. After the solution is saturated, the compounds of the reaction of cement and water will not dissolve any more, but disperse in the solution to form amorphous colloids. Among them, part of microscopic solids is absorbed by the surface of SiO_2 and grows, part of amorphous colloid is sedimentated on the surface of the accumulated clay particle and glues them together to form certain strength. The ongoing hydration continuously adds new gels and decreases free water. The grout begins to develop strength.

In the second stage, the colloid hydration is not stable, the gels of $Ca(OH)_2$, hydrated $CaO{\bullet}Al_2O_3$ and hydrated $CaO{\bullet}Al_2O_3{\bullet}Fe_2O_3$ are gradually crystallized with the action of SiO_2 particle and closely combines with colloids to fill the voids between clay particles and form cement stone. With the prolonging of the hydration, the inner part of cement particle not yet hydrated continues to be hydrated. Crystals continue to grow and penetrate each other to fill the voids between clay particles. As a result, the strength and gelatibility of the grout keeps on increasing.

5. CONCLUSIONS

The following conclusions are made based on the previous analysis:

- The hydration hardening process of CHG are basically similar with the hydration of cement. But since CHG is added with a large amount of clay and Solidify A and B, there are some differences mainly caused by the nucleation and catalysis of the inorganic salts in Solidify B which accelerates the hydration rate of cement and the increase of strength.
- The main hydrates of CHG in hardening process are $Ca(OH)_2$, hydrated $CaO{\bullet}SiO_2$ and $CaO{\bullet}Al_2O_3{\bullet}Fe_2O_3$, etc.

- With the increase of age, the content of $Ca(OH)_2$ and hydrated $CaO•SiO_2$ increase quickly. Thus the strength of grout increases quickly.
- With the increase of solidify A, the content of hydrated $CaO•SiO_2$ in hydrates decreases while the content of $Ca(OH)_2$ increases.
- With the increase of cement, the content of hydrated $CaO•SiO_2$ in hydrates increases while the content of $Ca(OH)_2$ decreases.

REFERENCES

[1] Wang, Xinghua, Study of rheology properties and grouting technology of clay-cement (solidifying) grout [Ph.D. Degree Thesis] Changsha, Central-South University of Technology, 1995; in Chinese

[2] Wang, Xinghu. The study of hardening mechanism of clay hardening grouts(CHG)----application of grouting, sealing, solidifying, digging of CHG in the inter-tunnel (Yangqicun~Tiyuxilu) of Guangzhou subway. [Post-doctoral researching report]Chengdu South-West Jiaotong University 1997.6 in Chinese

[3] F. M. Lee, [Tang, Mingshu et. al. Translation], Chemistry of Cement and Concrete (3rd edition), Beijing, China Press of Building Materials, 1984 in Chinese

[4] Wang, Youzhi et. al Translation, New Cement and Concrete, Beijing, China Press of Building Materials, 1982 in Chinese

[5] E. P. Flint; H. F. McMurdie and L. S. Wells, J. Res. Natn, Bur. Stand, 26(13)(1941)

[6] M. J. Brocard, Annls. Inst. Batiment, New Series No. 12(1948)

[7] E. J. Carlon, J. Res. Natn. Bur. Stand, 68A(453)(1964)

[8] Li, Shizhong, Drilling Technology (2nd edition),Beijing, China Geology Press, 1987; in Chinese

[9] Wang, Xinghua, Zeng, Xiangxi,Shear thinning and rheopoxy of clay-cement grouts, Mining and Metallurgical Engineering, 15(Suppl.1)(1995):23~25 in Chinese

[10] Wang, Qihong; Rheology of Materials, China Press of Construction Industry, Beijing, 1985; in Chinese

[11] Wang, Xinghua Li, Wei, Study of growing rule and affecting factors of unconfined compressive strength of Clay-Hardening Grouting, The Chinese Journal of Nonferrous Metals, 9(1):180-184, 1999; in Chinese

THE LONG-TIME CREEP AND DURABILITY OF THE CONCRETE AND REINFORCED CONCRETE

A.N. Plugin[1], X. Wang [2], A.A. Plugin[3], O.A. Kalinin[1] and S.V. Miroshnichenko[1]

[1]Department of Building Materials, Constructions and Buildings, Ukraine State Academy of Railway Transport, Kharkov, Ukraine. E-mail: plugin@lincom.kharkov.ua
[2] College of Civil Engineering, Changsha Railway University, Changsha, P R China. E-mail: xhwang@csru.edu.cn
[3]Department of Building Materials and Products, Kharkov State Technical University of Construction and Architecture, Kharkov, Ukraine. E-mail: plugin@lincom.kharkov.ua

ABSTRACT

The long-time creep of concrete is a phenomenon underlying the durability of bulky reinforced concrete constructions. The mechanism of this phenomenon is evaluated from a study of the physical-chemical mechanics of dispersed systems. The theoretical and experimental fundamental of an assessment and prognosis are proposed.

Mankind strives for beautiful and stately reinforced load-bearing concrete structures. However increases of overall dimensions and length of these constructions has aggravated the problem of their trouble-free and durable exploitation.. For example, in bridges with long spans of 100 to 200 m, the building of which commenced after 1950s, there were unexpected major deflections of bridge spans developed over a rather long term time frame and these have not stabilized even after 20 to 30 years (Figure 1) [1].

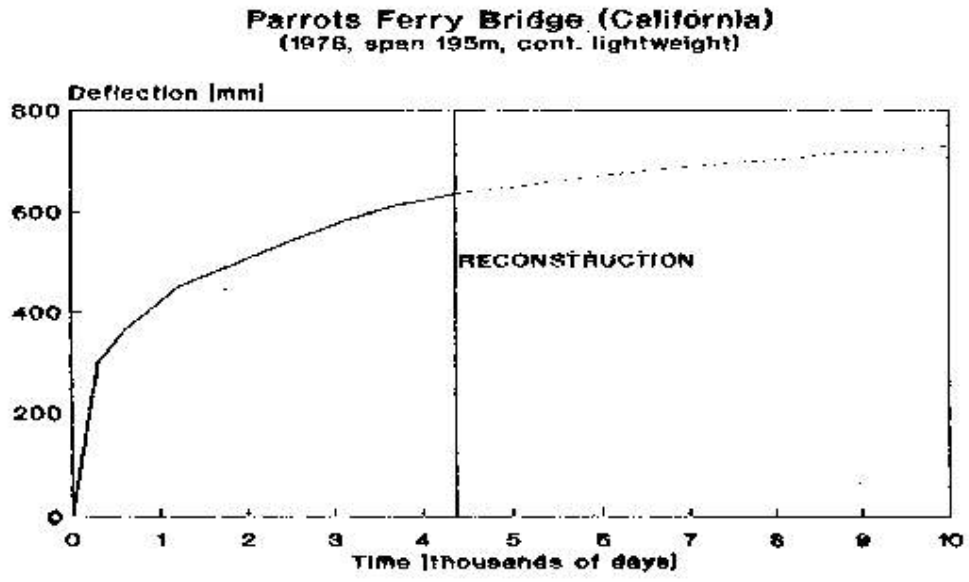

Figure 1. The chart of a sag accumulation of bridge span [1]

Problems have also been reported with major reinforced-concrete bridges and tunnels. The conclusions of an international commission on the cause of higher than permitted deflections of bridge spans was ascribed to the unexplored early creep of concrete of the construction in its

compressed zone as well as long-term creep. In this case this creep was not stopped even after the addition stress of new reinforcement during renovation.

At the same time in many countries the designs of concrete structures of ancient times continue to perform, ages reaching 5 to 7 thousand years. There are pyramids and other buildings of Egypt, Cyprus, Syria and Italy etc. One of the features of such ancient structures is the absence of reinforcement and shapes which eliminate tension zones. We do not know of any case of similar durability of large dimensional and thin-wall mass concrete or reinforced concrete structures, which carry bending or tension. Therefore the opinion about durable reinforced concrete structures can only be attribute to concretes in the compression zone.

The cause of low-level durability of modern concrete or reinforced concrete structures, according to our opinion, is the inadequate knowledge of the performance of concrete at its structures subject to bending, that is in turn connected to the lack of knowledge about properties and behavior of concrete in structures which carry bending, on pre-stressed constructions, under loaded deformations, and also in conditions of an ingress of water. The methods of proportioning concretes is also imperfect and cannot supply the necessary homogeneity of reinforced concrete structures to provide durability. Different normative documents on the maintenance of engineering constructions are also incapable of forecasting durability.

1. THE REASON FOR AN ABOVE NORMAL CREEP OF CONCRETE. THE STRUCTURAL CHARACTERISTICS OF CONCRETE DETERMINING ITS CREEP AND THEIR OPTIMIZATION

As a result of this research, we established that above normal creep is explained by the non-uniformity of concrete under the structural characteristics - coefficients of expansion of coarse aggregate grains α (the relation of a volume of mortar to the void volume in coarse aggregate) and sand, the relation of a cement paste volume to the void volume in sand). These characteristics essentially influence the creep of concrete under long-term compression. With deviation α and μ from optimum values the creep of concrete is sharply increased. Creep depends also on the consumption of water and cement in a concrete mix. Thus the increase of creep is affected both by the increase of cement volume paste in the concrete, and by the increase of the true value of water-cement ratio *W/C* over the optimum value (≈0.23). Taking into account all the above, the creep of concrete and mortar can be reduced to a minimum by optimum composition with normalized α, μ and *W/C*. The method of determination of such structure is presented here. The concretes and mortars with normalized composition are recommended for applying both for manufacturing new structures and for repair and renewal works.

The theoretical basis for obtaining mortars and concretes with an optimum structure ensuring maximum cracking resistance and water tightness, have been developed at the sub-faculty on the basis of a colloid chemistry and physio-chemical mechanics of disperse cement systems [2]. In accordance with these ideas the structure of concrete is poly-disperse, in which different levels of strucure – macro, mezzo, micro and sub-micro (Figure 2) are combined. A dispersing medium is physio-chemically bound by water. The structure-forming elements form the structure of concrete at each level (in proportion to their size and quantitative ratio).

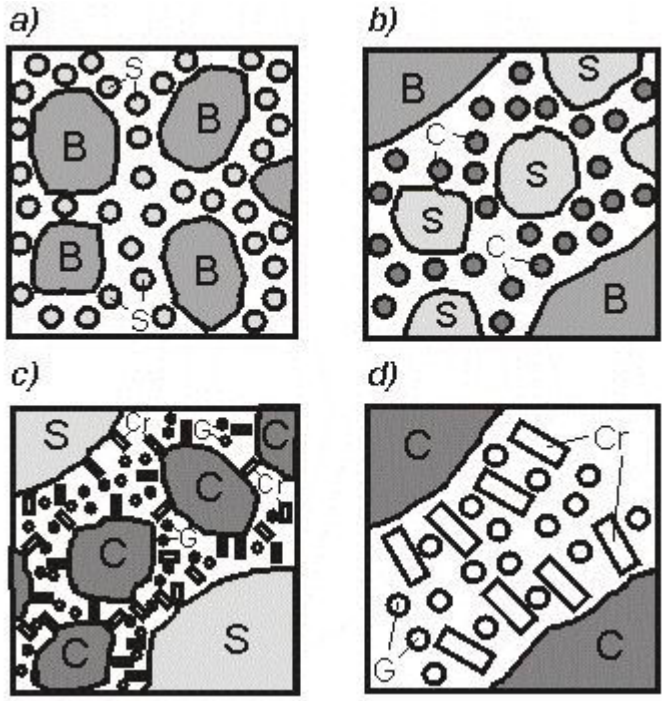

Figure 2. Schematic of concrete structure at levels: *a* – macro, *b* – mezzo, *c* – micro, *d* – sub-micro; *B* – grain of large aggregate – broken stone (10 to 15 mm), *S* – grain of small-sized aggregate– sand (0.2 to 0.5 mm), *C* – cement particles (10 to 50 μm), *Cr*, *G* – accordingly, crystalline-hydrated (100 to 500 nm) and gel (≤100 nm) products of a hydration

The formation of the properties of concrete and mortar is influenced by the arrangement of small-sized fragments in an interlayer between a number of contacts arising between larger fragments (Figure 3). The structure on a micro-level is determined by water-cement ratio *W/C*. In Figure 4 the experimental dependence of cement paste strength *R* on *W/C* is shown. As we can see from Figure 4, the greatest strength corresponds to a value of $W/C \approx 0{,}23$. It is determined by the quantity of chemically bound water, – about 23 % by weight of cement. Increasing *W/C* results in the increase of the quantity of free water and, accordingly, porosity of the paste, and a reduction leads to the decrease of the degree of cement hydration.

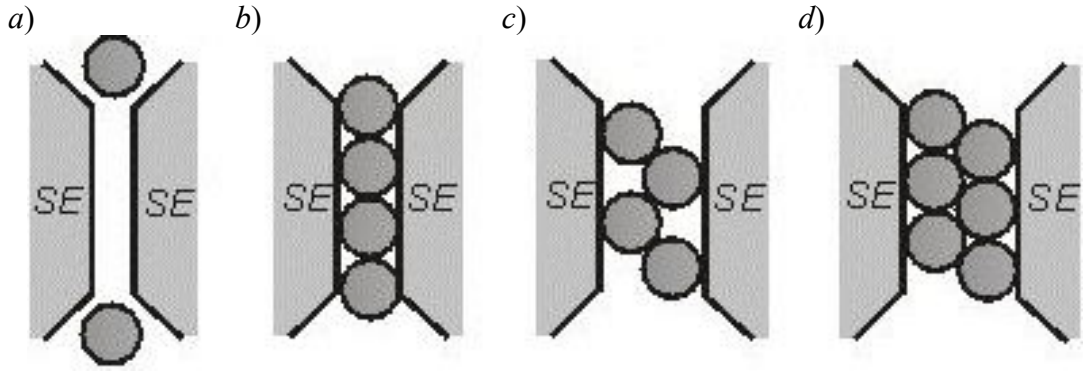

Figure 3. Schematic of inter-layer formation between structure-forming elements *SE*: *B*–*S*–*B* – on macro-level, *S*–*C*–*S* – on mezzo-level, *C*–(*Cr*,*G*)–*C* – on micro-level; *a*, *c* – non-optimum; *b*, *d* – optimum

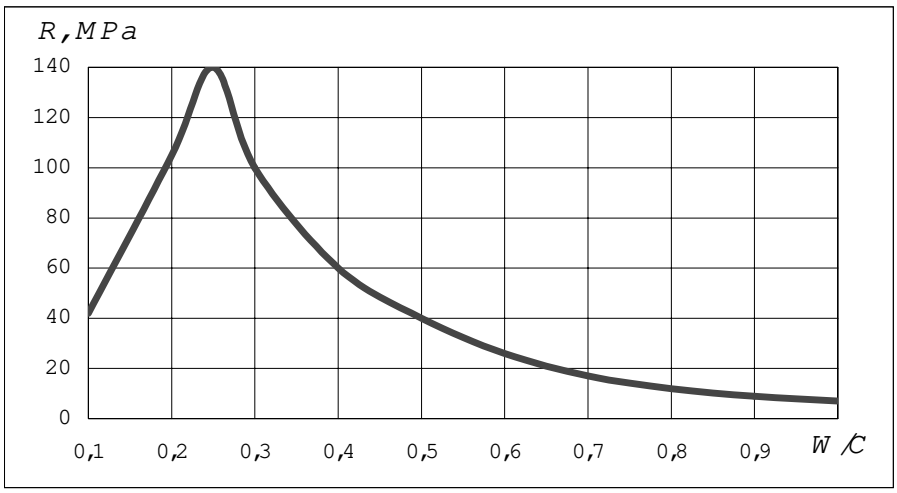

Figure 4. The dependence of cement paste strength R on the 28 day Hardeness vs water-cement ratio *W/C*

For mortar and concrete compositions with maximum strength and impermeability it is necessary to achieve true values of *W/C* (taking into account for water requirements of aggregate), close to 0.23. The mobility of such mixes is provided for the application of the super-plasticizer. At such *W/C* the creep of a cement paste, mortar and concrete is minimised according to our opinion, by the optimum structure of new-formations (crystalline-hydrated and gel) between incompletely reacted cement grains (Figure 3).

The nature of structure on mezzo-level is determined by a ratio of the quantity of both sizes of cement particle and grains of sand and on macro-level – by the ratio of quantity both aggregate size of sand and coarse aggregate. Maximum strength, impermeability and minimum creep of concrete and mortar are reached in that case when inter-layers between grains of stone sand are filled with one full series of grains of sand particles of cement. (Figure 3, *b*). When the quantity of finer grains (particles) is less than optimum, (Figure 3, *a*) is formed and when their quantity exceeds optimum, (Figure 3, *c*) is formed. In these cases, as we can see from Figures 3, *a*, *c*, the quantity of contacts between elements and packing density of more small-sized particles decreases, that results in decreasing of strength and density. It is necessary to draw attention particularly to the fact that indicated regularity has a statistical property and the packaging shown in a Figure 3, are average values of the sizes of elements and the thickness of inter-layers, i.e. ensuring maximum packing density of all the elements and the quantity of contacts between them.

The stated ideas about the structure of concrete (and of in inter-layers between the grains filling and about the mechanism of the structure-formation of these inter-layers allows us to deduce mathematical expressions for best values of coefficients of expansion α_{opt} and μ_{opt}:

$$\alpha_{opt} = 2{,}1 \cdot \left(1 + \frac{d_s}{d_b}\right)^3 - 1{,}1\,, \qquad \mu_{opt} = 2{,}1 \cdot \left(1 + \frac{d_c}{d_s}\right)^3 - 1{,}1\,, \tag{1}$$

where d_s, d_b, d_c – mean sizes, accordingly of grains of sand, coarse aggregate and particles of cement.

The stated ideas have also allowed us to work out methods of determination of concrete and mortar structure with maximum strength, waterproofness, crack resistance and minimum creep of both mortar and concrete [3] as follows:

$$B = \frac{1}{\frac{\alpha_{opt}}{\rho_b^w} \cdot V_b + \frac{1}{\rho_b}}, \quad S = \frac{1 - \frac{B}{\rho_b}}{\frac{\mu_{opt}}{\rho_s^w} \cdot V_s + \frac{1}{\rho_s}}, \quad C = \rho_c \cdot \left(1 - \frac{B}{\rho_b} - \frac{S}{\rho_s} - \frac{W}{\rho_w}\right), \text{ kg/m}^3 \quad (2)$$

where W – minimum according to the required workable (with super-plasticizer).

To decrease long-time creep and increase of waterproofness of concrete it is expedient to use super-plasticizing admixture in a concrete mix. In this case there will be an increase of the consumption of cement at the expense of the reduction of water quantity. In this case fine fillers – substitutes of cement can be used. However it should be accompanied by the necessary research. Alongside a long-time creep of concrete the considerable influence on the operational properties brought about by creep of concrete showing itself in particular, during tests of pre-stressed concrete sleepers and beams, and also during transit of rolling stock above them. As tests have shown, it also strongly depends on the above mentioned characteristics α and μ and the consumption of water W.

2. THE COLLOIDAL-CHEMICAL NATURE OF CREEP OF HARDENED CEMENT PASTE

In accordance with [2, 4 etc.] the main cause of a creep is the deformation of cement gel, paste gel or migration of water under pressure. Electron microscopic and colloidal - chemical research of cement paste structure and its components executed by us on the basis of existing and our own experiments, allow us to consider-cement paste as a colloidal-chemical system consisting of micro-structural blocks – of incompletely reacted cement particles, bound by elastic-plastic crystalline-hydrated skeleton consisting of submicroscopic particles of portlandite and hydro-sulfoaluminate of calcium, filled with saturated highly disperse hydro-silicate gel. The indicated elastic deformations and micro-cracking as carriers of plastic deformations take place in a crystalline-hydrated skeleton (larger fragments in Figure 5 [5]), and creep deformations – in hydro-silicate gel (more small-sized fragments of the spherical shape in Figure 5).

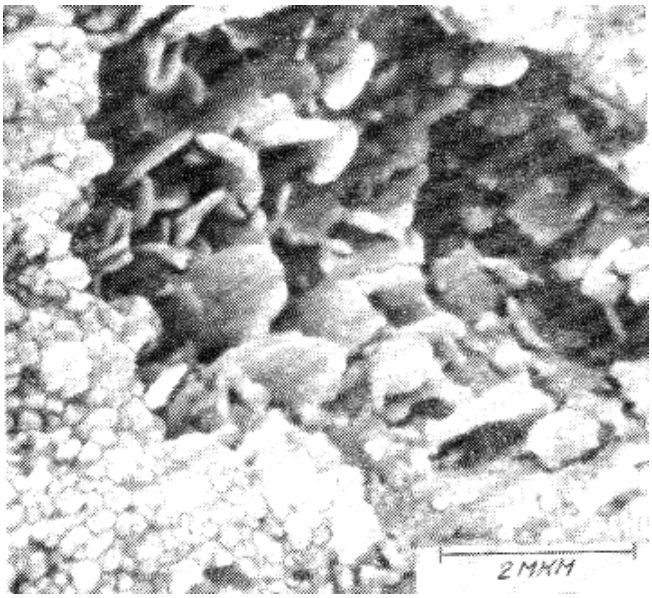

Figure 5. The cement paste, hydrated within 6 hours at 70 °C [5]

In the connection with a prevailing volume of hydro-silicate gel (75 % among all hydrated new-formations [4]), the compressive stress is not immediately carried by the crystalline-hydrated skeleton and its contacts, and is transmitted at the beginning to gel components and the water in it.

In the process of extrusion of water from the gel the elastic skeleton accepts the increasing pressure, and the amount of gel and water in it becomes less and the contribution of water to pressure decreases. Under pressure, increasing plastic deformations of a crystalline-hydrated skeleton, is influenced by micro-fractures. On achieving the stresses, which are equal to the strength of the crystalline skeleton, cement paste and concrete are being destroyed.

Thus, the sub-microstructure of cement paste consisting of a crystalline-hydrated skeleton, filled with water-bearing hydro-silicate gel, stipulates the development (of elastic-plasticity and flowability) by concrete simultaneously with the properties of solid-shaped and aqua-shaped bodies, accordingly,

Thus the elastic and plastic properties are affected by the process of squeezing water from gel and transfering pressure to the crystalline-hydrated skeleton and, consequently are limited by properties of flowability. It gives the basis to consider the deformation properties of concrete as rheological. The typical rheological properties thus are relaxation and creep.

3. FULL RELAXATION AND KINETICS OF CONCRETE CREEP

Creep deformations affected by squeezing of definite quantity of water from hydro-silicate gel of cement paste (gel water,) to be subordinate to the law of a filtration of a Dharcy. Thus time and volume of squeezed water are in relation, flowing out from this law

$$t = \frac{\Delta W_g h}{SK_f P}, \tag{3}$$

where ΔW_g – water volume squeezed from the gel during t, m^3; h – path of a filtration (size of a sample or considered piece of a construction), m; S – cross-sectional area of a filtration flow (cross section of a sample or piece of a construction), m^2; P – hydrostatic head (delivery head) of waters at a filtration, m, which is equal to the pressure in gel water at compression of concrete; K_f – coefficient of filtration of concrete, m/s.

The value of the coefficient of filtration k_f determines the kinetic regularity, i.e. the speed of deforming of concrete under compression, and value ΔW_g the amplitude of volumetric deformation during t. In the case corresponding to an ultimate deformation, the value t corresponds to a maximum relaxation time t_r^{max}, and value ΔW_g to the limiting (maximum) volume of squeezed gel water for this period of time. Unlike the conventional concept of a relaxation time t_r a maximum relaxation time t_r^{max}, means time, at which the pressure in gel water disappears and its compression stops.

For a cross-sectional area of a sample S the value ΔW_g is determined by its limiting deformation Δh during time t_r^{max}:

$$\Delta W_g = \Delta h^{lim} S = \varepsilon^{lim} h S, \tag{4}$$

Hydrostatic head P we shall express through the equivalent to him pressure in concrete:

$$P = \frac{\sigma}{\rho_w g}, \tag{5}$$

where σ – pressure load in a concrete; ρ_w – density of water; g – acceleration of gravity.

The value of ultimate deformation of concrete corresponds to its compressive strength R, and can be determined approximately from the expression

$$\varepsilon^{lim} = R / G, \tag{6}$$

where G – module of deformation of concrete under compression.
Let's substitute expressions (4), (5) and (6) in (3):

$$t_r^{max} = \frac{Rh^2\rho_w g}{GK_f\sigma} = \frac{h^2\rho_w g}{GK_f y}, \quad (7)$$

where $y = \sigma/R$ – the level of loading of concrete under compression.

Let's enter parameter, having called its as time factor

$$T_t = \frac{t}{t_r^{max}} = \frac{t}{h^2}\frac{R\rho_w g}{GK_f\sigma} = \frac{t}{h^2}\cdot\frac{GK_f y}{\rho_w g}. \quad (8)$$

Corresponding to a known expression in a colloid chemistry, the relative creep deformation of cement paste in concrete at compression ε_t in an instant t will follow the form of:

$$\varepsilon_t = \varepsilon^{lim}\cdot[1-exp(-T_t)]. \quad (9)$$

According to (7) and (9) the kinetics of creep deformation of concrete are determined mainly by the magnitude of a design h, by the coefficient of filtration of concrete k_f and by the level of loading y. Accordingly, the bigger the size of a structure, the less the coefficient of filtration of concrete and the less the level of loading, the slower creep deformations of concrete under compression (Figure 6).

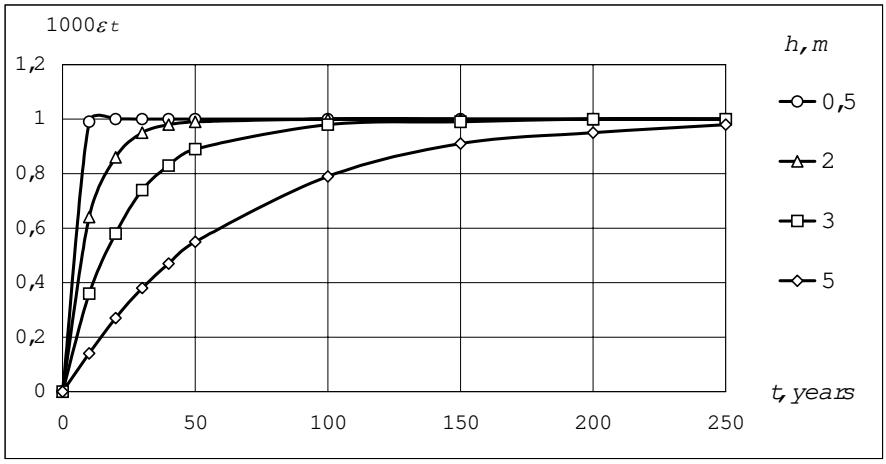

Figure 6. Development of calculated deformations ε_t in time t

Figure 6 was obtained from (9) with allowance for (8). The limiting values of deformations $1000\varepsilon^{lim}$ are adopted for unit. As we can see in Figure 6, the limiting deformation does not depend on h and is identical to concrete. At the same time h renders strong influence on speed of development and general duration of deformation. For h = 0,5 m the speed of deforming is higher, and its ultimate value can be reached in 2÷3 years. For h = 5 m the ultimate deformation is reached only in several hundreds of years.

After the above explanation, the experimental research of the mechanism of a customary and long-time cement paste creep was investigated with the purpose of prediction in structures. The experimental studies of deformations were undertaken on a prismatic sample of the dimensions 10×10×40 cm from cement paste obtained at W/C = 0.4, hardening under normal conditions. The aging base of deformations compounded (made) 30 see. The experimentally obtained curve mirrors the instantaneous elastic deformation (Graph 1), then an exponential field of elastic-plastic deformation, or customary creep (stage 2), reducing flow (streaming) 10 to 20 days, then long-lived

linear (stage 3) reducing over more than 150 days, and at last, horizontal field observing within 1 month, testifying about the termination of further deformation.

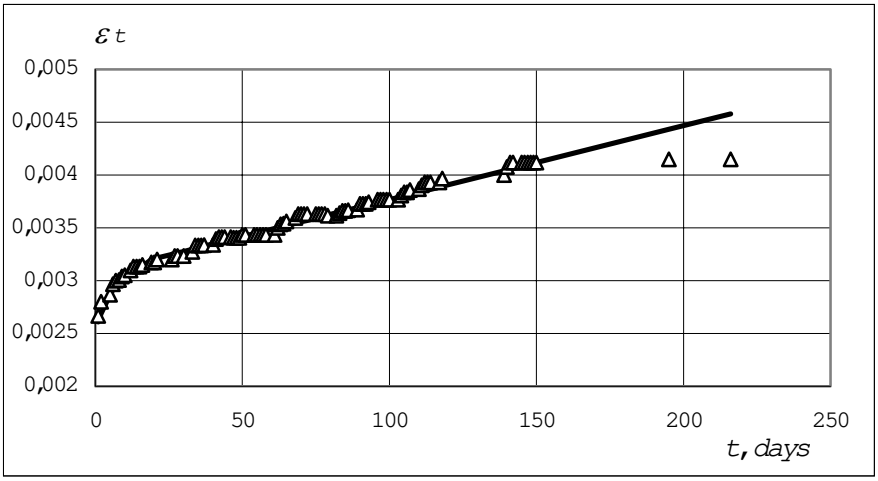

Figure 7. Kinetics of relative deformations of creep cement of a rock at pressure load 14 MPa (W/C = 0.4, normal conditions of concreting). dots – experimental data, full line – on the equations 9 & 8

The linear relation of most extended 3-rd stage mirrors plastic deformation and confirms to the reality of long-lived creep of the cement paste [1] and testifies to the filtration mechanism.

Usage of elastic-plastic deformation [2] and Dharcy law of filtering with reference to the cement-aqueous system, has permitted the introduction physical and mathematical models for complete deformation cement paste under compression to an instant t at a long-lived loading

$$\varepsilon_t = \varepsilon_{el}^{\lim} + \varepsilon_{cr}^{\lim} \cdot \left[1 - \exp\left(-T_t\right)\right] + \frac{tK_f \sigma}{h^2 \rho_w g}, \tag{10}$$

where ε_{el}^{lim} – limiting elastic deformation; ε_{cr}^{lim} – limiting deformation of creep of the cement paste; T_t – time by the equation (8); K_f - coefficient of the cement paste filtration.

Defining the role of hydro-silicate gel and water in the creep of concrete allows us to determine strain amplitude of creep of cement paste, on volume basis wrung out from hydro-silicate gel, V_{cav}^{g}.

$$\varepsilon = \frac{C\left(W/C - \alpha_h W_{cb}/C\right) - V_{cav}^{g}}{3C\left(1/\rho_c + W/C\right)} \cdot K^c K^{nf}, \tag{11}$$

where C – expenditure of cement on 1m^3 cement paste; W_{cb}/C = 0.23 – water-cement ratio conforming chemically to bound water; K^c, K^{nf} – quotients which are taking into account influencing of frame cement paste.

The permeability and deformation properties of concrete are determined already at the stage of making the concrete and is confirmed by the data of Figure 8. As is visible, at $\mu < \mu_{opt}^{exp}$ experimental sizes of density ρ_{exp} is much lower than design ρ_{des}, particular from the principle of absolute volumes which have been used in traditional methods of calculation of concrete proportioning. It allows us not only to forecast long-term creep and durability of reinforced-concrete structures, but also substantially to control durability of concrete and structures by designing the proportioning of concrete with the optimum structural performances α_{opt} and μ_{opt}.

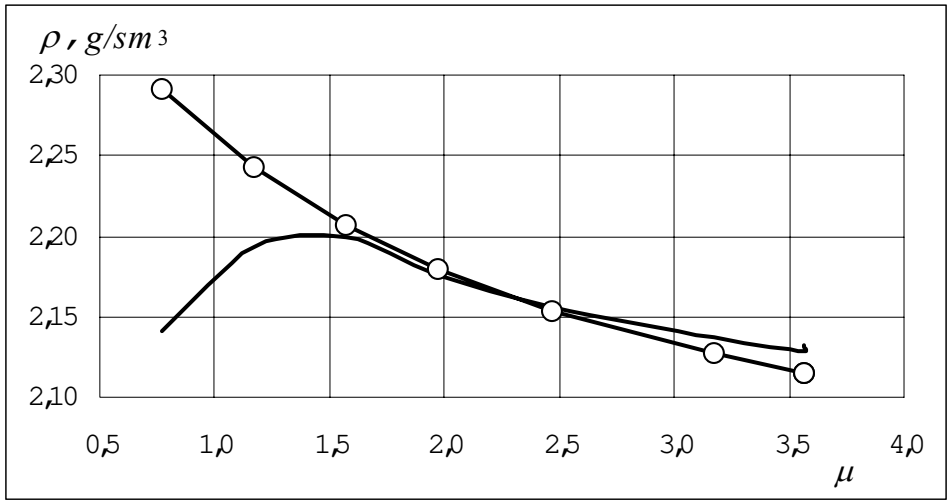

—o— design data ρ_{des}, ——— experimental data ρ_{exp}

Figure 8. Dependences of density of cement-sandy solution ρ from coefficients of expansion of grains of sand μ (sand with modulus of grain size *Mgs* = 2.5).

The closeness of fit above confirms all design and experimental data.

REFERENCES

[1] Vitek, J.L. Behaviour and modelling in serviceability limit states including repeated and sustained loads, Section 7, Long-term deflections of large pre stressed concrete bridges, Contribution to the State of the Art Report, Prague: Czech Technical University, 1996, p. 34.

[2] Plugin, A.N., Prokopova, I.G., Wild, S. and Plugin, A.A. The Mechanism of Water and Ionic Permeability of Concrete, Proceedings of the 10th International Congress of the Chemistry of Cement, Gothenburg: Inform Trycket AB, 1997, Vol.4, 4iv075, p. 8.

[3] Plugin, A.N., Kalinin, O.A., Birukov, A.I. et al. The method of definition of a composition of a concrete admixture, Patent №1787972 USSR, Announced 26.06.90, Published 15.01.93, Bul.№2, (in Russian).

[4] Sheikin, A.Ye., Chechovsky, Yu.V. and Brusser, M.I. The structure and properties of cement concretes, Moscow: Stroyizdat, 1979, p. 344, (in Russian).

[5] Lakh, V. and Buresh, Ya. The phase composition and microstructure of the cement paste, hydrated at heightened temperatures, Proceedings of 7th ICCC, Moscow: Stroyizdat, 1976, Vol. II, Book 2, pp. 129-135, (in Russian).

THE LONG-TIME CREEP AND DURABILITY OF THE CONCRETE AND REINFORCED CONCRETE

A. N. Plugin[1], X. Wang [2], A. A. Plugin[3],O. A. Kalinin[1] and S. V. Miroshnichenko[1]

[1]Department of Building Materials, Constructions and Buildings, Ukraine State Academy of Railway Transport, Kharkov, Ukraine. E-mail: plugin@lincom.kharkov.ua
[2] College of Civil Engineering, Changsha Railway University, Changsha, P R China. E-mail: xhwang@csru.edu.cn
[3]Department of Building Materials and Products, Kharkov State Technical University of Construction and Architecture, Kharkov, Ukraine. E-mail: plugin@lincom.kharkov.ua

Prof. PLUGIN, Arkady N.

Eng (1963), PhD (1970), DSc (Chem,1989)
Active member of Transport Academy of Ukraine (TAU, 1998) and New York Academy of Sciences (NYAS, 1998)
Head of the Department of Building Materials, Constructions and Buildings
Ukraine State Academy of Railway Transport

Feyerbakhs' sq., Kharkov 61050, Ukraine
Tel./Fax (038 057) 7156914
E-mail: plugin@lincom.kharkov.ua

Was born in 1941 in Mary, Turkmenistan
1958-63, Kharkov Institute of Engineers of Railway Transport (Kharkov, Ukraine) – Student
1963-70, Plant of Reinforced Concrete and Building Details of South Railway (Kharkov): Master, Head of the Laboratory, Chief Engineer
1970-74, Ukraine State Project Institute of the Local Industry (Kharkov) – Chief Engineer
1974-till now, Ukraine State Academy of Railway Transport
(before 1994 Kharkov Institute of Engineers of Railway Transport):
Senior Research Associate (1974),
Head of the Branch Research Laboratory of Reinforced Concrete Sleep (1976),
Associate Professor (1985), Professor (1989),
Head of the Department of Building Materials, Constructions and Buildings (1992)

Scientific concerns: physic-chemical mechanics building materials and constructions, durability of buildings of a railway transport
Student of Prof. Mchedlov-Petrosian Otar P.
Is married, has a son.

Prof. WANG, Xinghua

PhD
Director of International Cooperation and Exchange Office
Institute of Tunnel and Underground Engineering
Central South University at Tiedao Campus University
22 South Shaoshan Road, Changsha, Hunan , 410075, P R China
Tel. (86731)2655421, Fax (86731)5656182
E-mail: xhwang@csru.edu.cn

Dr. PLUGIN, Andrei A.

Eng (1985), PhD (1994)
Associate Professor of the Building Materials and Products Department
Kharkov State Technical University of Construction and Architecture

Sumskaya Str., Kharkov 61002, Ukraine
Tel. (038 0572) 402999
E-mail: plugin@lincom.kharkov.ua

Was born in 1963 in Kharkov, Ukraine
1980-85, Kharkov Institute of Engineers of Railway Transport (Kharkov, Ukraine) – Student
1985, 87-90, Plant of Building Details of Transport Constructions (Kharkov):
Head of Department of Technical Control, Chief Technologist, Chief Engineer
1985-87 – on military service
1990-till now – Kharkov State Technical University of Construction and Architecture
(before 1994 Kharkov Engineering Constructions Institute):
Postgraduate (1990), Assistant (1993), Associate Professor (1995)

Student of Prof. Babushkin Vladimir I.
Is married, has two sons.

Dr. KALININ Oleg A.

Eng (1985), PhD (1996)
Head of the Branch Research Laboratory of Reinforced Concrete Sleep and Special Reinforced Concrete
Ukraine State Academy of Railway Transport

Feyerbakhs' sq., Kharkov 61050, Ukraine
Tel./Fax (038 057) 7156914

Was born in 1963 in Kalush, Ukraine
1980-85, Kharkov Institute of Engineers of Railway Transport (Kharkov, Ukraine) – Student
1985-87 – on a military service
1987-89, Plant of Building Details of Transport Constructions (Kharkov) –
Head of Department of Technical Control
1989- till now, Ukraine State Academy of Railway Transport
(before 1994 Kharkov Institute of Engineers of Railway Transport):
Postgraduate (1989), Research Associate (1992),
Head of the Branch Research Laboratory of Reinforced Concrete Sleep
and Special Reinforced Concrete(1994)

Scientific concerns: physic-chemical mechanics building materials and constructions,durability of buildings of a railway transport
Student of Prof. Plugin Arkady N.
Is married, has a daughter.

Dr. MIROSHNICHENKO Sergei V.

Eng (1993), PhD (1999)
Head of the Branch Research Laboratory of Corrosion
and Protection from Corrosion
Ukraine State Academy of Railway Transport

Feyerbakhs' sq., Kharkov 61050, Ukraine
Tel./Fax (038 057) 7156914

Was born in 1972 in Kharkov, Ukraine
1988-89, 90-92, Kharkov Institute of Engineers of Railway Transport (Kharkov, Ukraine) – Student
1989-90 – on a military service
1992-till now, Ukraine State Academy of Railway Transport
(before 1994 Kharkov Institute of Engineers of Railway Transport):
Postgraduate (1992), Research Associate (1995), Head of the Branch Research Laboratory of Corrosion and Protection from Corrosion (2000)

Scientific concerns: physic-chemical mechanics building materials and constructions, durability of buildings of a railway transport
Student of Prof. Plugin Arkady N.
Is married, has a son.

STUDY ON THE PHASE COMPOSITIONS AND POZZOLANIC ACTIVITY OF HEAT-TREATED FLY ASH

Wensheng Zhang, Xingyang He, Hongtao Zhang, Yongxin Li and Yimin Chen

China Building Materials Academy, Guanzhuang Beijing, 100024, P. R. of China.
Email: bjzhangwensheng@sohu.com

ABSTRACT

Fly ash can be treated at high temperature and the pozzolanic activity index of heat-treated fly ash is improved. Heat-treated fly ash may be more suitable as a cementing material than the original fly ash. The phase compositions and pozzolanic activity of the fly ash, which was treated at the temperature 950°C with the chemical reagent CaO, CaF_2 and Na_2CO_3, was studied with XRD, TGA etc. in this paper. The physical properties of partially heat-treated fly ash were also tested. The results illustrate that the reagent added in the fly ash could change the phase compositions during the heat-treatment process. For example, the new phases of $NaAlSiO_4$ or $(Na,Ca)(SiAl)_4O_8$ exist in the heat-treated fly ash. Moreover, the chemically bonded water content of heat-treated fly ash, which hydrated for different ages, increased according to the TGA result. The $Ca(OH)_2$ content in the hydrated heat-treated fly ash with CaF_2 is less than that of the fly ash without CaF_2. The compressive strength of the heat-treated fly ash with 3.0wt% gypsum is more than the control s. For example, the compressive strength of heat-treated fly ash hydrated for 21 days may reach 1.67 MPa and the control's is 1.13 MPa.

Keywords: Fly Ash; Heat-treated; CaF_2; Pozzolanic Activity

1. INTRODUCTION

Pozzolanic activity of fly ash is well known for a long time.[1] However, the development rate of the pozzolanic activity is very low. There are many methods, such as ultra-grinding and alkali activation, to improve the pozzolanic activity index of fly ash. In this paper, fly ash was heated at the temperature 950°C for 30 min with the chemical reagent CaO, CaF_2 and Na_2CO_3. The phase compositions and pozzolanic activity of heat-treated fly ash were researched.

2. EXPERIMENT

2.1 Raw Materials

The chemical composition of fly ash is shown in Table 1. Figure 1 is the XRD pattern of the fly ash. The chemical reagent includes CaO, CaF_2 and Na_2CO_3 (class Analytical Reagent).

Table 1. The chemical composition of the original fly ash

Component	Loss	SiO_2	Al_2O_3	CaO	Fe_2O_3	MgO	Σ
Content (%)	3.17	47.22	38.94	2.92	4.34	1.09	97.68

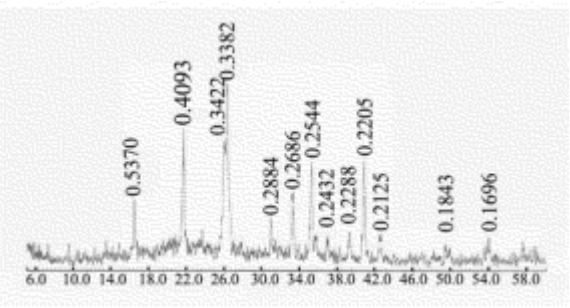

Figure 1. XRD pattern of the original fly ash (d: nm)

There is a characteristic that the Al_2O_3 content in the fly ash is very high. According to the ASTM classification, it is considered as class F fly ash. The mineral mullite is the main mineral phase according to the XRD test result. (see Figure 1).

2.2 Heat-treated Method and Strength Test

Fly ash mixed with the different chemical reagents is heated at the temperature 950°C for 30min. The phase composition of the heat-treated sample is tested with the method of XRD. The heat-treated fly ash hydrated for different ages is tested with XRD and TGA. Specimen size of the fly ash paste is 2 cm × 2 cm × 2 cm for the strength test. The ratio of water to fly ash is 0.48.

3. RESULTS AND DISCUSSION

3.1 Effect of Na_2CO_3 on the Composition of Fly Ash

The mass ratio of fly ash to Na_2CO_3 is shown in Table 2. The XRD patterns of part of the heat-treated fly ash with Na_2CO_3 are shown in the Figure 2.

Table 2. The mass ratio of fly ash (abbr. FA) to Na_2CO_3 (abbr. N)

No.	P-1	P-2	P-3	P-4	P-5	P-6	P-7	P-8
FA:N	1.0:1.0	1.0:0.75	1.0:0.5	1.0:0.25	1.0:0.15	1.0:0.1	1.0:0.05	1.0:0.0

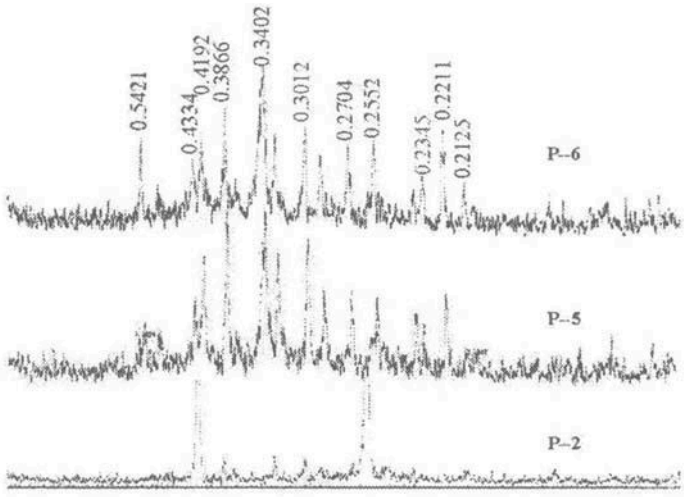

Figure 2. XRD patterns of part of the heat-treated fly ash with Na_2CO_3

The phases of fly ash were changed because of the addition of Na_2CO_3. $NaAlSiO_4$ is the only mineral existing in the heat-treated fly ash when the ratio of fly ash to Na_2CO_3 is equal to 1.0 (No.

P-1). The mullite and quartz disappeared. The quantity of the mineral type in the heat-treated fly ash increases as the addition amount of Na_2CO_3 decreases. For example, there are the minerals $NaSiAlO_4$ and $CaO\text{-}Al_2O_3\text{-}SiO_2$ in the sample No. P-3. However, the mineral mullite and quartz have completely reacted with Na_2CO_3 and the characteristic peak of mullite and quartz in the XRD pattern could not be found. Although the new phases $NaSiAlO_4$ and $CaO\text{-}Al_2O_3\text{-}SiO_2$ have been formed in the No. P-4, the mineral mullite also exists. The phase composition of Nos. P-5, P-6 and P-7 are similar to that of the No. P-4.

3.2 Effect of Na_2CO_3 and CaF_2 on the Composition of Fly Ash

The addition of Na_2CO_3 and CaF_2 in the fly ash, which contains 20wt% CaO, is listed in the table 3 and the XRD patterns of some heat-treated fly ashes are shown in Figure 3.

Table 3. The addition of the Na_2CO_3 and CaF_2 (%)

No.	PF-1	PF-2	PF-3	PF-4	PF-5
CaF_2	0.4	0.4	0.4	0.2	0.6
Na_2CO_3	0.0	5.0	3.0	3.0	3.0

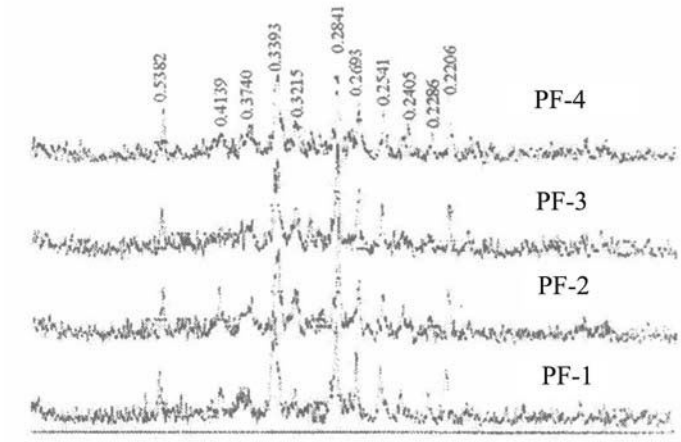

Figure 3. XRD patterns the heat-treated fly ash No. PF-1, 2, 3 and PF-4

The results of the XRD test illustrate that the reaction of Na_2CO_3 with the CaO, SiO_2, Al_2O_3 has taken place and the new crystalline phase $(Na,Ca)(SiAl)_4O_8$ has formed. It is deduced according to the chemical characteristic of CaF_2 that the melting temperature of fly ash is decreased and the phase $11CaO\text{-}7Al_2O_3\text{-}CaF_2$ will form because of the reaction CaF_2 with CaO and Al_2O_3. It is apparent that the glass structure of the fly ash will be changed because of the addition of CaF_2.

3.3 The Hydration of Fly Ash with CaF_2 and Na_2CO_3

The heat-treated fly ash (No. PF-1, 2, 3, 4 and 5 in the table 3) was ground to the specific surface fineness 500 m^2/kg (Blaine). The paste of the heat-treated fly ash (water/ash=0.5) cured for 2 months and the hydrated fly ash is tested with the method of TGA (testing temperature range: from ambient to 350°C; rate of temperature increase:20°C/min). The test results of TGA are shown in the table 4.

Table 4. The TGA results of the hydrated fly ash (ambient ~350°C)

No.	PF-1	PF-2	PF-3	PF-4	PF-5
Weight loss (%)	2.032	1.487	1.831	1.284	1.687

From the table 4, it is shown that the content of the chemically bonded water in No. PF-1 is 2.032%. It is illustrated that the hydration degree of No. PF-1 is highest among all of the samples. That is to

say, there is the most appreciable addition 0.4% for the CaF_2 when the addition of Na_2CO_3 in the fly ash is 3.0%. For the heat-treated fly ash with the same addition of CaF_2, the content of the chemically bonded water in the hydrated fly ash decreases as the addition of Na_2CO_3 increases.

3.4 Compressive Strength and Hydration of the Heat-treated Fly Ash

3.4.1 Compressive strength of the heat-treated fly ash

In order to research the effect of CaF_2 and Na_2CO_3 on the strength of fly ash, the addition of CaF_2 is respectively 0.5wt%, 1.0wt% and 1.5 wt% (based on the weight of fly ash which contains 20wt% CaO) and the addition of Na_2CO_3 in the sample is 3.0wt%. Table 5 is the addition of CaF_2 and Na_2CO_3 in the fly ash.

Table 5. The addition of CaF_2 and Na_2CO_3 in the fly ash (%)

No.	SP-1	SP-2	SP-3	SP-4	SP-5	SP-6	SP-7
Na_2CO_3	0.0	0.0	0.0	0.0	3.0	3.0	3.0
CaF_2	0.0	0.5	1.0	1.5	0.5	1.0	1.5

The above-mentioned samples were heated at the temperature 950°C for 30 minutes and the specific surface fineness of the heat-treated fly ash with 3.0wt% gypsum was 500 m^2/kg. The compressive strength of the heat-treated fly ash with 3.0wt% gypsum is listed in the table 6.

Table 6. The compressive strength of the heat-treated fly ash with gypsum (MPa)

No.	SP-1	SP-2	SP-3	SP-4	SP-5	SP-6	SP-7
21 days	1.13	1.67	1.41	1.25	<0.5	<0.5	<0.5
42days	3.96	4.55	4.60	4.07	/	/	/

From the table 6, it is deduced that the compressive strength of the heat-treated fly ash decreased with the increase of CaF_2 content. For example, the paste strength of heat-treated fly ash with the 0.5wt% CaF_2 hydrated for 21 days may be attain to 1.67MPa. However, the paste strength of the sample with 1.5wt% is only 1.25 MPa at the same hydration age. The compressive strength results of the heat-treated fly ash certified the above-mentioned TGA results.

According to the test results of sample Nos. SP-5, SP-6 and SP-7, Na_2CO_3 has a negative effect on the strength of the heat-treated fly ash although it could apparently change the phase composition and the structure of the original fly ash.

3.4.2 Hydration of the heat-treated fly ash

(a) XRD analysis

Figure 4 is the XRD patterns of sample Nos. SP-1, SP-2, SP-3 and SP-4 hydrated for 21 days. Figure 5 is the XRD patterns of sample Nos. SP-5, SP-6 and SP-7 hydrated for 42 days.

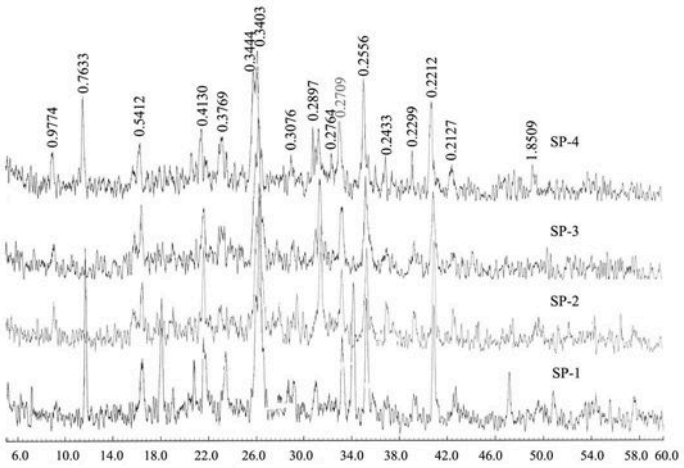

Figure 4. XRD patterns of the sample No. SP-1, SP-2, SP-3 and SP–4 hydrated for 21 days

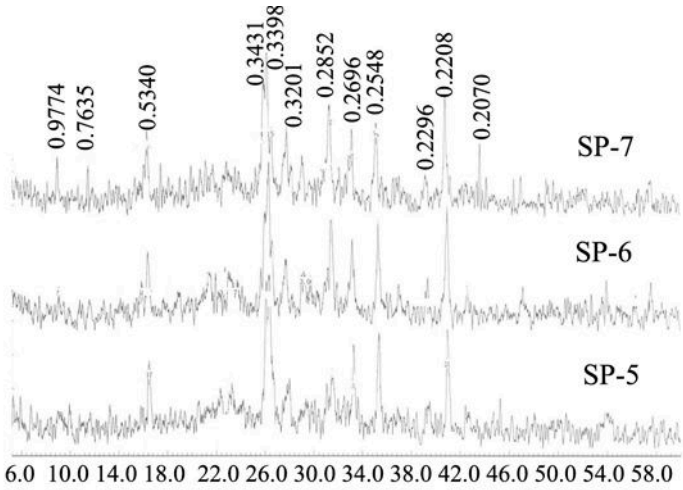

Figure 5. XRD patterns of the sample No. SP-5, SP-6 and SP–7 hydrated for 42 days

For the fly ash without CaF_2, the calcium hydroxide and gypsum exist in the hydrated paste. However, the calcium hydroxide content in the hydrated sample with CaF_2 is less than that of the fly ash without CaF_2. It could be certified from the change of the characteristic peak strength of the mineral calcium hydroxide in the hydrated sample.

There are two assumptions about the change of the gypsum content in the hydrated sample. One is that gypsum reacted with the compositions of the heat-treated fly ash in a large degree and its characteristic peak could be detected in the XRD patterns when the CaF_2 addition in the fly ash is less than 1.0wt%. Another assumption is that the reaction content of gypsum with the compositions of fly ash is small when the CaF_2 addition in the fly ash is 1.5wt%.

Ettringite exists in all of the hydrated samples with CaF_2 and its peak strength in the sample No.SP-5, SP-6 and SP-7 is less than that of sample No.SP-2, SP-3 and SP-4.

(b) TGA analysis

The TGA results of the hydrated fly ash cured for 21 days and 42 days were shown in the table 7.

Table 7. The TGA results of the hydrated fly ash cured for different ages (weight loss %)

No.	**SP-1**	**SP-2**	**SP-3**	**SP-4**	**SP-5**	**SP-6**	**SP-7**

Chemical-bonded water	2.46	4.65	5.36	4.93	4.88	4.07	4.27
$Ca(OH)_2$	1.51	0.0	0.0	0.30	0.0	0.0	0.0
$CaCO_3$	1.39	0.54	0.48	0.74	1.48	0.79	0.60

Note: No. SP-1, SP-2, SP-3 and SP-4 hydrated for 21 days; No. SP-5, SP-6, SP-7 hydrated for 42 days.

The weight loss of calcium hydroxide of the sample SP-1is 1.51wt% and the weight loss of $CaCO_3$ is 1.39wt%. However, at the same hydration age the weight loss of calcium hydroxide of sample SP-2, SP-3, SP-4 is zero and the weight loss of $CaCO_3$ is very low.

The chemically bonded water of the sample containing Na_2CO_3, which hydrated for 42 days, is lower than that of the sample without Na_2CO_3 which hydrated for 21 days.

4. CONCLUSIONS

The effect of Na_2CO_3, CaF_2 and CaO on the composition and strength of fly ash was studied in this paper. The following conclusions were drawn:

(1) Na_2CO_3 could react with the compositions of fly ash at the temperature 950°C and the crystal phases $NaSiAlO_4$ and $CaO\text{-}Al_2O_3\text{-}SiO_2$ have been formed. But Na_2CO_3 is not beneficial to the strength improvement of the heat-treated fly ash.
(2) CaF_2 could change the structure of fly ash at the temperature 950°C and the pozzalanic property of the fly ash is improved. CaF_2 additions in appreciable quantities to the fly ash could increase the strength of the heat-treated fly ash. The optimum addition of CaF_2 based on the fly ash containing 20wt% CaO is 0.4wt%.
(3) The hydration degree of the heat-treated fly ash with CaF_2 is increased and the content of $Ca(OH)_2$ in the paste of heat-treated fly ash with CaF_2 is less than that of the paste of the original fly ash at the same hydration ages. The hydration product for all of the heat-treated fly ash is similar.

REFERENCES

[1] Peter C. Hewlett. Lea'S Chemistry of Cement and Concrete (Fourth Edition), London: Arnold, 1998, p. 480.

STUDY ON THE PHASE COMPOSITIONS AND POZZOLANIC ACTIVITY OF HEAT-TREATED FLY ASH

Wensheng Zhang, Xingyang He, Hongtao Zhang, Yongxin Li and Yimin Chen

China Building Materials Academy, Guanzhuang Beijing, 100024, P. R. of China.
Email: bjzhangwensheng@sohu.com

WENSHENG ZHANG

Name: Wensheng Zhang

Affiliation: The Key Laboratory of Cement-based Materials Science of China Building Materials Academy

Email: bjzhangwensheng@sohu.com

Mail: Key Laboratory of Cement-based Materials Science of China Building Materials Academy Guangzhuang, Beijing, 100024, P. R. of China

ISOTHERMAL CONDUCTION CALORIMETRY STUDY OF CLASS G OILWELL CEMENT HYDRATED WITH ADDITIONS OF CALCIUM CHLORIDE, CALCIUM FORMATE AND SODIUM ALUMINATE AT LOW AND AMBIENT TEMPERATURES

J. S. Lota[1], J. Bensted[2] and P. L. Pratt[3]

[1]Ashmole School, Southgate, London N14 5RJ UK. E-mail jasbir_lota@hotmail.com
[2]Birkbeck College, University of London, London WC1E 7HX, UK.
E-mail bensted.j@btinternet.com
[3]Emeritus Professor of Crystal Physics, Department of Materials, Imperial College of Science, Technology and Medicine, University of London, London SW7 2BP, UK.

ABSTRACT

Oilwell cements are used in the oil industry both in exploration and in the production of oil and gas. Their primary use is to seal the annular space between the walls of a borehole and the steel casing that lines the well. The hydration characteristics of Class G oilwell (OWG) at 20°C and 5°C with the addition of calcium chloride, calcium formate and sodium aluminate as accelerating admixtures have been investigated. There is no universal mechanism of acceleration of cement hydration. The actual mechanism depends upon the particular accelerating admixture, its concentration, the time of acceleration and the temperature. The rate-of-heat evolution of the OWG with the different admixtures at 20°C and 5°C is discussed.

1. INTRODUCTION

Normally, in gas- and oil-well cementing, the temperatures are mostly above ambient and pressures above atmospheric, often considerably so, which necessitate the use of retarders in the cement slurries to produce workable thickening or setting times. However, during the casing cementing of well sections at or near the surface under cold conditions, where the temperatures may be as low as around 0-5°C the cement hydration reactions are slowed down and chemicals, like 'accelerating' admixtures, are used to promote hydration. These admixtures adequately accelerate the cement hydration reactions so that the cement performs its intended function, whether this is chemical, physical or both, and consequently aids the extraction of oil or gas.

The original aim was to investigate the hydration of OWG at 20°C and 5°C and to characterise and understand how its microstructure develops with time in the presence of accelerating admixtures using a variety of experimental techniques and methods *viz*; isothermal conduction calorimetry, thermal analysis, X-ray powder diffractometry, infrared spectroscopy, scanning electron microscopy and development of compressive strength [1]. At low temperatures the cement hydration reactions are kinetically slowed down and it is not practicable both logistically and economically to accelerate the hydration of the cement simply by heating the cement and mix water prior to pumping the resulting slurry down the borehole. Thus other cheaper and more efficient means of accelerating the cement hydration processes are required.

Calcium chloride, calcium formate and sodium aluminate were employed in this study. Here we report the comparison of these admixtures with respect to conduction calorimetry. Other aspects of

Proceedings of the 11th International Congress on the Chemistry of Cement (ICCC)
'Cement's Contribution to the Development in the 21st Century'
Hosted by: The Cement and Concrete Institute of South Africa
CD-ROM produced by: Document Transformation Technologies
11 - 16 May 2003, Durban, South Africa
ISBN Number: 0-9584085-8-0
Editors: Dr G. Grieve and G. Owens
Congress Organised by: Event Dynamics

hydration can be found elsewhere [1,2,3,4]. At present the manner in which these admixtures are thought to function upon the cement hydration process is far from completely understood, despite their extensive employment in practice. The findings of this research work apply equally to hydraulic Portland cements used in the oil and construction industries.

2. EXPERIMENTAL METHODS AND TECHNIQUES

The OWG cement was obtained from Blue Circle Industries. This cement was a coarsely ground high sulphate-resisting cement with the potential phase composition (Bogue weight %) of tricalcium silicate ~53.3, dicalcium silicate ~21.9, and tricalcium aluminate ~1.5 and tetracalcium aluminoferrite ~ 15.9.

The calcium chloride, calcium formate and sodium aluminate of analytical grade were obtained from British Drug Houses Chemicals Limited, Dorset, UK. The rate-of-heat evolution was measured using the JAF Wexham Isothermal Conduction Calorimeter [7] and the development of cement microstructure was examined using a JEOL JSM-35CF scanning electron microscope.

The cement was mixed with distilled water to give a cement paste having a water to cement ratio of 0.44. The admixtures were dissolved in the mix water prior to mixing. This is the recommended ratio used for testing [8]. Further experimental details are given elsewhere [1]. The concentrations of the admixtures in the mix water are given in Table 1 below and are referred throughout this paper as Molar concentrations.

Table 1. Concentration of Admixtures in the Mix Water

Molar (mol/l)	Concentration of Admixtures in the Mix Water As Weight Percentage of Cement [Weight Percentage of the Mix Water]		
	Calcium Chloride $CaCl_2$	Calcium Formate $Ca(HCO_2)_2$	Sodium Aluminate $NaAlO_2$
Control	0	0	0
0.1	0.5 [1.1]	0.6 [1.4]	0.4 [0.9]
0.3	1.5 [3.4]	1.7 [3.9]	1.1 [2.5]
0.5	2.4 [5.5]	2.9 [6.6]	1.8 [4.1]
1.0	4.9 [11.1]	5.7 [13.0]	3.6 [8.2]
1.3	6.3 [14.3]	7.4 [16.8]	4.7 [10.7]

3. HYDRATION OF OWG

The effect of temperature upon the rate-of-heat evolution of the paste hydrating at 20°C and 5°C is shown in Figure 1.

The first heat peak, Peak 1, could not be measured since, in the type of calorimeter that was used, the samples were externally hand mixed for three minutes outside the calorimeter before data could be recorded.

At 20°C the second heat peak, Peak 2, which is primarily due to the hydration of the alite phase, occurs earlier and has a greater rate-of heat evolution than that at 5°C. In addition the length of the induction period is smaller.

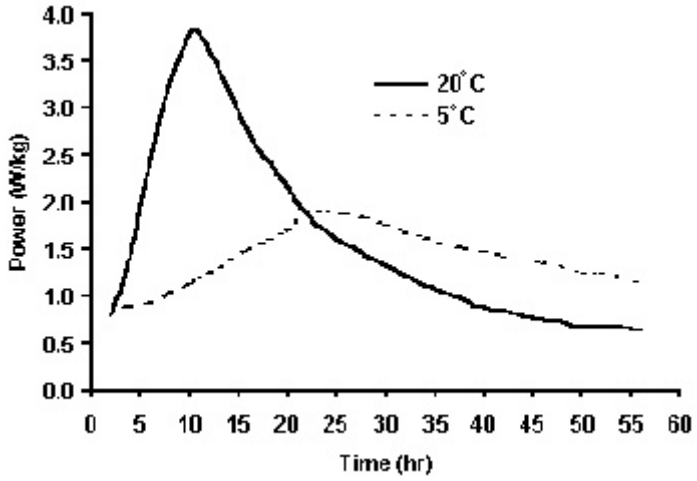

Figure 1. Rate-of-Heat Evolution Curves of OWG Hydrated at 20°C and 5°C

At 5°C, the heat evolution is spread out over a greater length of time than at 20°C. At later times, greater than 24 hours, the amount of heat that is evolved at 5°C is higher than at corresponding times at 20°C. This is to be expected since at the lower temperature the hydration reactions will be kinetically slowed down and consequently take a longer time to complete.

3.1 Hydration Of OWG With Calcium Chloride

The rate-of-heat evolution of the paste with or without the addition of calcium chloride at 20°C and 5°C is shown in Figures 2 and 3 respectively.

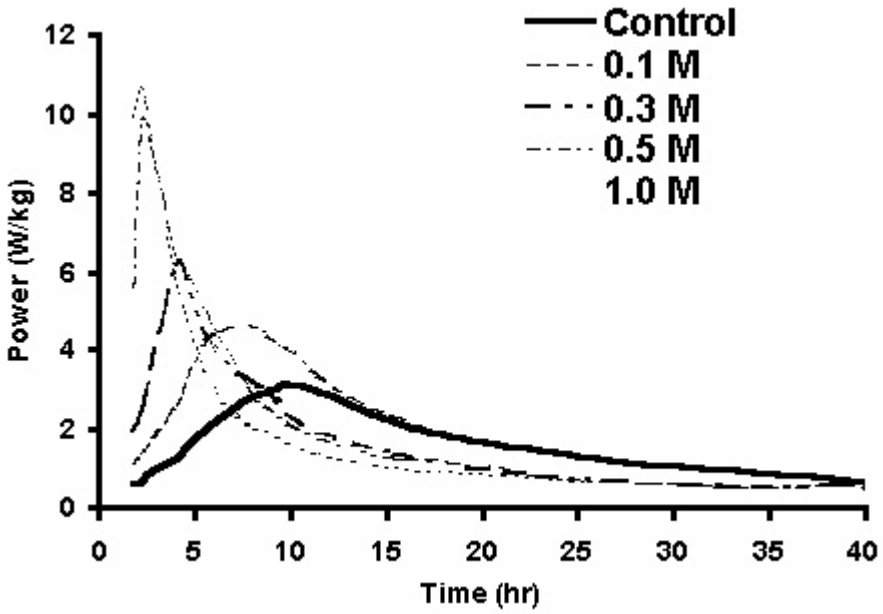

Figure 2. Rate-of-Heat Evolution Curves of OWG Hydrated with Various Additions of Calcium Chloride at 20°C

As the dosage of calcium chloride is increased, the acceleratory effect is shown by Peak 2 occurring at earlier times and becoming more intense. In addition the length of the induction period decreases. Similar results have been reported elsewhere [8,9]. The positions of the various parts of the rate-of-heat evolution curves could indicate acceleration or retardation [10]. The shoulder on the left of Peak 2, visible in the control sample, becomes less obvious with the addition of calcium chloride. This shoulder is thought to be from hydration of the ferrite phase.

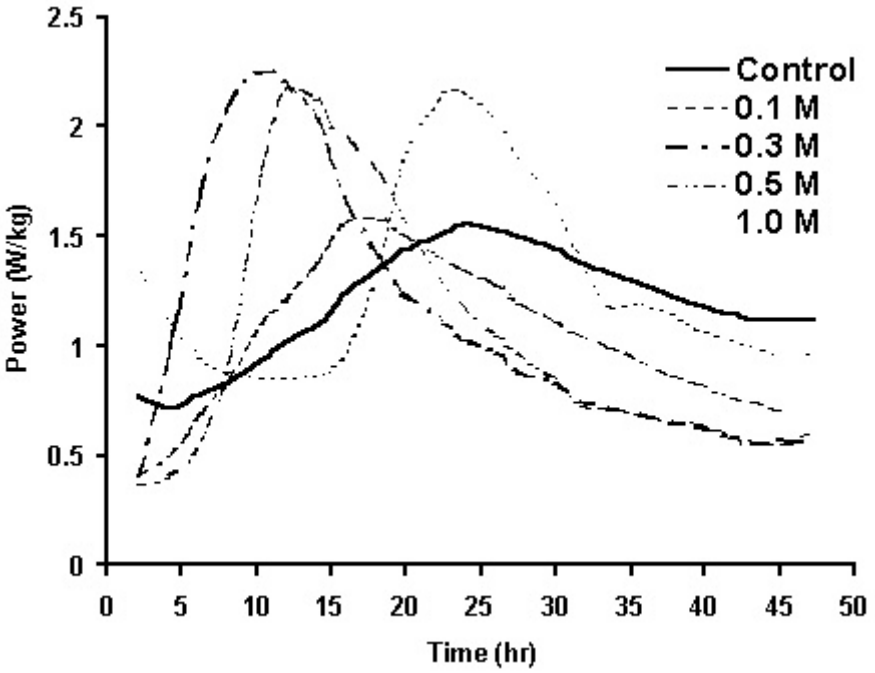

Figure 3. Rate-of-Heat Evolution Curves of OWG Hydrated with Various Additions of Calcium Chloride at 5°C

At 5°C, there is surprisingly no longer a sequential response to the increased addition of calcium chloride in contrast to the pattern observed at 20°C. The greatest acceleration is shown with the 0.3M and 0.5M additions. With the 0.5M addition the shoulder on the left of Peak 2 is almost evident. The 1.0M addition causes a long induction period suggesting a retardation effect, but contradicting this, the height of the induction period is increased and Peak 2 is enhanced relative to the control sample suggesting an acceleratory effect. In addition on the right of Peak 2 there are two shouldering peaks.

As the dosage of calcium chloride is increased, the acceleratory effect is shown by Peak 2 occurring at earlier times and becoming more intense. In addition the length of the induction period decreases. Similar results have been reported elsewhere [9,10]. The positions of the various parts of the rate-of-heat evolution curves could indicate acceleration or retardation [11]. The shoulder on the left of Peak 2, visible in the control sample, becomes less obvious with the addition of calcium chloride. This shoulder is thought to be from hydration of the ferrite phase.

The rate-of-heat evolution curves of the paste with additions of calcium chloride (0.1-0.5M) are higher than that of the control. After 24 hours, however, the control paste evolves considerably more heat than that of the accelerated paste. This suggests that some different hydration processes are occurring with the addition of calcium chloride to the paste.

3.2 Hydration Of OWG With Calcium Formate

The rate-of-heat evolution curves of the OWG hydrated with various additions of calcium formate at 20°C and 5°C are shown in Figures 4 and 5 respectively.

The 0.1M and 0.3M additions to the paste show an acceleration, as indicated by the advancement of Peak 2 relative to the control paste. Maximum acceleration is indicated with the 0.3M addition. An adaptation of the JAF calorimeter so that the cement paste could be mixed internally and hence allow the measurement of the first heat Peak on first contact with the mix water was made [1]. The height of the first heat peak with the 0.3M addition is nearly twice as high as that of the control paste. The 0.5M addition shows Peak 2 occurring slightly later with the induction period lengthened in comparison to the control paste. With 1.0M, addition Peak 2 occurs earlier than that of the

control paste, but has a lower heat output at all times. This can be interpreted in two ways; first, as an acceleratory effect since Peak 2 occurs at an earlier time as compared to the control and second, as a retardation effect as the hydrating cement evolves heat at a lower rate than the control sample due to lowered cement hydration.

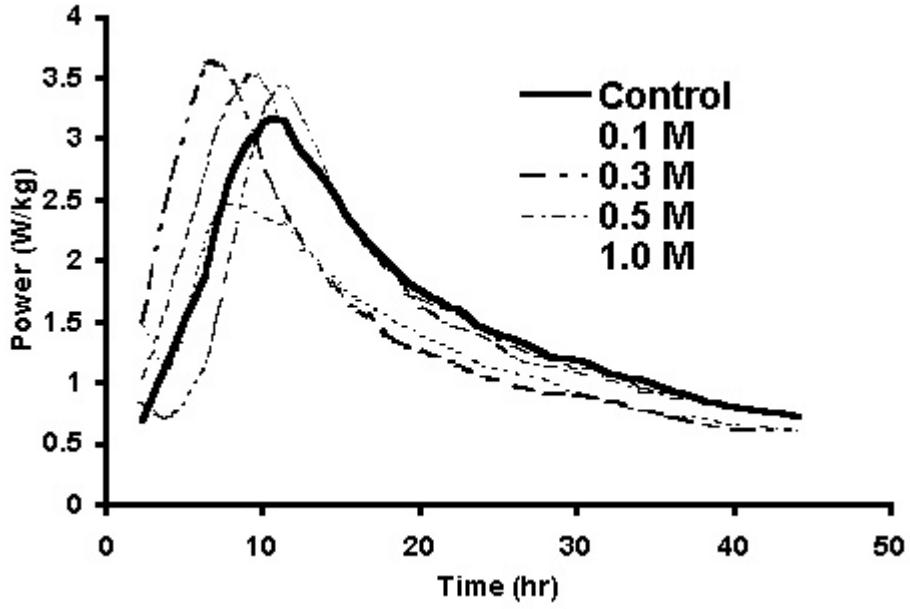

Figure 4. Rate-of-Heat Evolution Curves of OWG Hydrated with Various Additions of Calcium Formate at 20°C

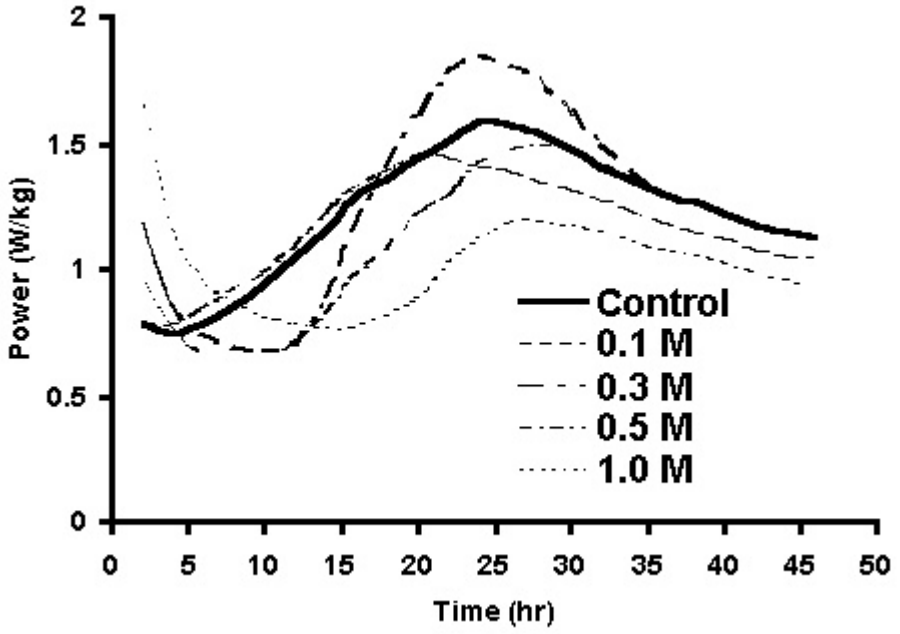

Figure 5. Rate-of-Heat Evolution Curves of OWG Hydrated with Various Additions of Calcium Formate at 5°C

The addition of calcium formate to the paste results in complex rate-of-heat evolution curves at 5°C. The 0.1M addition shows an acceleratory effect *i.e.* Peak 2 occurs at an earlier time than observed for the control paste. With 0.3M addition both acceleratory and retardation effects are shown; Peak 2 is enhanced relative to the control sample but the induction period is lengthened. The

0.5M and 1.0M additions appear to retard the hydration as shown by lengthening of the induction period with the result that Peak 2 occurs at later times than observed for the control paste.

3.3 Hydration Of OWG With Sodium Aluminate

The rate-of-heat evolution curves of the paste with additions of sodium aluminate at 20°C and 5°C are shown in Figures 6 and 7.

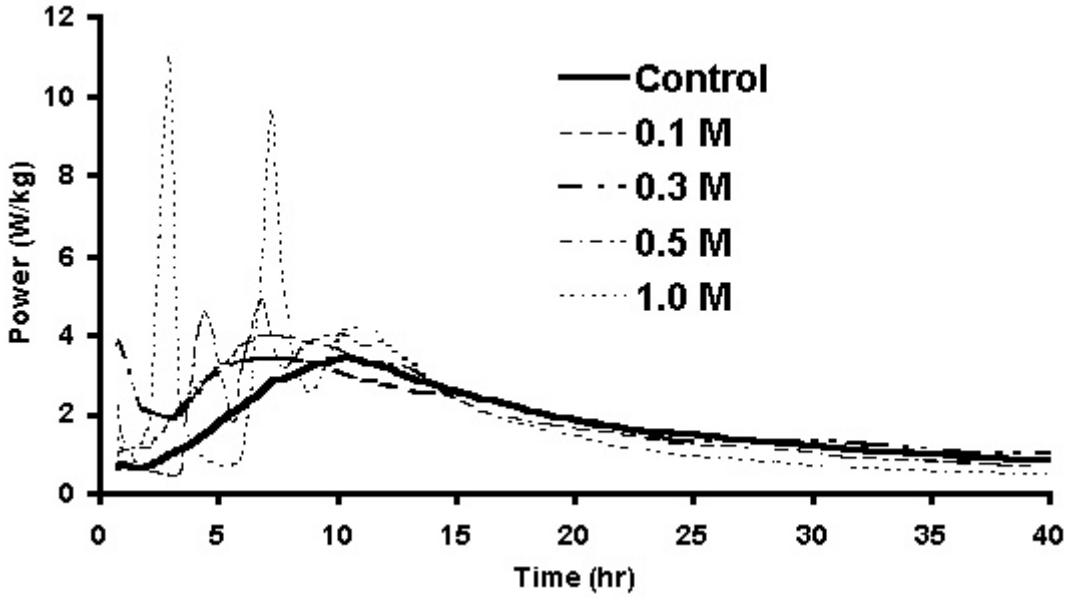

Figure 6. Rate-of-Heat Evolution Curves of OWG Hydrated with Various Additions of Sodium Aluminate at 20°C

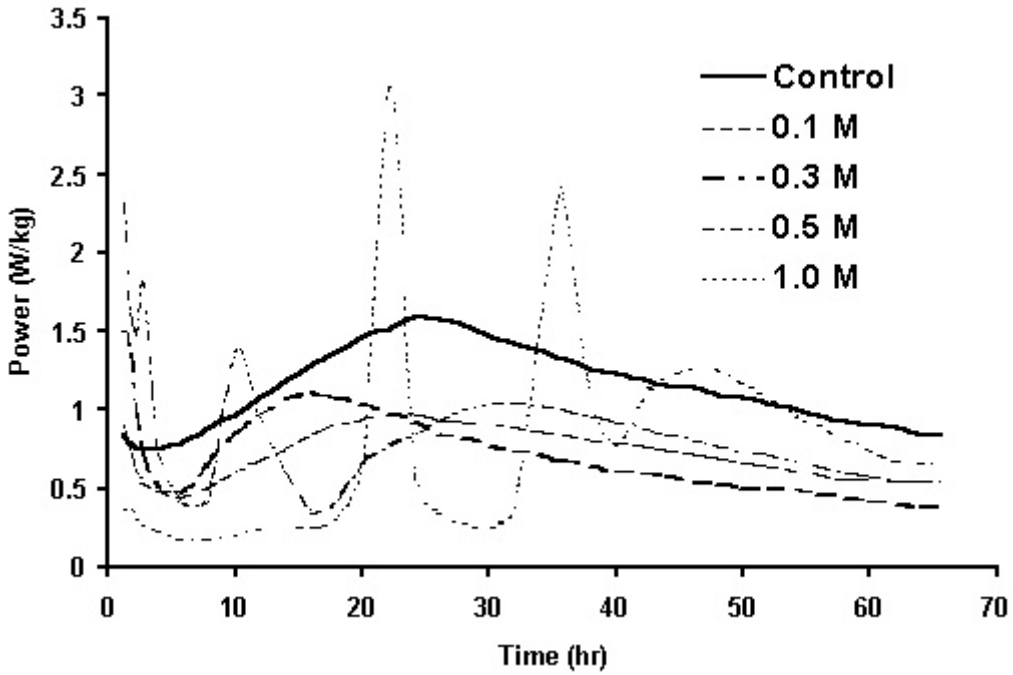

Figure 7. Rate-of-Heat Evolution Curves of OWG Hydrated with Various Additions of Sodium Aluminate at 5°C

At 20°C, the 0.1M addition of sodium aluminate produces a heat evolution curve more typical of a Portland cement or alite phase. The 0.1M and 0.3M additions show an acceleratory effect in terms

of Peak 2 occurring at shorter times than the control paste. The first heat peak, measured by the adapted JAF calorimeter with 0.3M addition is much higher than observed for the control paste [1]. The 0.5M addition shows an enhancement of Peak 2, whereas with 1.0M addition Peak 2 occurs at a later time suggesting a retardation effect.

The heat evolution curves are further complicated, however, by the presence of supplementary peaks, which lie between Peak 1 and the beginning of Peak 2. These supplementary peaks increase in magnitude and change position as the amount of sodium aluminate in the paste is increased. With 0.1M addition no supplementary peaks were observed. With 0.3M addition, there is a single peak which occurs in the descending portion of Peak1. With 0.5M addition, two supplementary peaks occur between the end of the induction period and the maximum of Peak 2. With 1.0M addition, however, the first supplementary peak occurs during the normal induction period whilst the second is as the start of Peak 2.

At 5°C, the 0.1M and 0.3M addition to the paste both show an acceleratory effect, as revealed by the advancement of Peak 2 relative to the control paste, of which the 0.3M addition is the most effective. With higher additions (0.5M and 1.0M), Peak 2 occurs after that of the control paste, implying a retardation effect. Although the 0.1M and 0.3M additions show an acceleratory effect, the height of the Peak 2 in both cases is significantly lower than that of the control paste. This is also observed with 0.5M and 1.0M addition.

As at 20°C there are supplementary peaks on the heat evolution curves. With 0.3M addition, a peak appears on the descending part of Peak 1. With 0.5M addition, two peaks appear, the first on the downside of Peak 1 before the induction period, and the second during the induction period. In contract, the 1.0M addition to the paste causes a long induction period to develop, with one peak before its end and another on the rising part of Peak 2. The lengthening of the induction period with 1.0M addition suggests that paste hydration is not accelerated, but retarded.

The two supplementary peaks can be tentatively be assigned as '$C_3A_{(aq)}$ sodium aluminate' and '$C_3A_{(aq)}$ ferrite phase. The order of releasing aluminate ions into solution is:

Sodium aluminate >> tricalcium aluminate >> tetracalcium aluminoferrite

The supplementary peaks are likely to be from the sodium aluminate and tetracalcium aluminoferrite phase since the cement contains about 1.5% and 15.9% tricalcium aluminate and tetracalcium aluminoferrite phase respectively.

The variation in the rate-of-heat evolution curves of the OWG with the various admixtures strongly suggests that the hydration of the ferrite phase plays an important part in the sequence of hydration products that are subsequently produced during the course of hydration [1, 2, 12]. Clearly, the definition of what is an accelerator needs careful thought. In this paper we have demonstrated how an accelerating admixture can behave as a retarder as a function of the type of admixture, the dosage level used and the temperature of hydration.

4. CONCLUSIONS

- Acceleration of cement hydration by accelerating admixtures depends upon which property is being measured on the rate-of-heat evolution curves.
- The accelerating admixtures in some instances cause a retardation effect.
- Supplementary peaks occur before the main heat Peak 2 with sodium aluminate.

- There is no universal mechanism of acceleration of cement hydration. The actual mechanism depends upon the particular accelerating admixture, its concentration, the time of hydration and the temperature.

REFERENCES

[1] Lota, J.S. The hydration of Class G oilwell cement**,** PhD Thesis, Imperial College of Science Technology and Medicine, University of London (1994)

[2] Lota, J.S., Bensted,J. and Pratt, P.L. Hydration of Class G oilwell cement at 20°C and 5°C with calcium formate, Proceedings of the 21st International Cement Microscopy Conference, International Cement Microscopy Association, Ed. Nisperos, A., Las Vegas, U.S.A. April 1999, pp 160-179.

[3] Lota J.S., Bensted J., Pratt P.L. Effect of sodium aluminate on Class G oilwell cement hydration at low and ambient temperatures. Proceedings of the 10th International Congress on the Chemistry of Cement, Gothenburg, Sweden, vol. 3, June 2-6 1997, paper iii014.

[4] Lota, J.S., Bensted,J. and Pratt, P.L. Hydration of Class G oilwell cement with additions of calcium chloride at 20°C and 5°C. Proceedings of the International Conference Creating With Concrete, Modern Concrete Materials: Binders, Additions and Admixtures, Eds. Dhir, R.K. and Dyer, T.D., University of Dundee, Scotland, UK. 8-10 September 1999, pp 411-418.

[5] Lota J.S., Bensted J., Munn J., and Pratt P. L**.** Hydration of Class G oilwell cement at 20^{o}C and 5^{o}C, Industria Italiana del Cemento, N° 725, Ottobre di 1997, pág. 776 - 798.

[6] Lota J.S., Pratt P.L., Scrivener K.L., Bensted J., The hydration of Class G oilwell cement at low and ambient temperatures with additions of sodium aluminate, 9th International Congress on the Chemistry of Cement**,** New Delhi, 1992, vol. IV, Communication papers, Theme 3, 1992, pp 10 - 16.

[7] Forrester, J.A**.** A conduction calorimeter for the study of cement hydration. Cement Technology, vol. 1, 1970, pp 95-99.

[8] International Organisation for Standardisation. Cements and materials for well cementing, Part 1; Specification, ISO 10426-1, ISO, Geneva 2000.

[9] Lerch, W. The influence of gypsum in the hydration and properties of Portland cement paste. Proceedings of the American Society for Testing and Materials, vol. 46, 1946, pp 1252-1292.

[10] Tenoutasse, N. The hydration mechanism of C_3S and C_3A in the presence of calcium chloride and calcium sulphate. Proceedings of the 5th International Symposium on the Chemistry of Cement, vol. 2, Supplementry paper II-118, Cement Association of Japan, Tokyo,1968, pp 372-378.

[11] Lota, J.S., Scrivener, K.L., Pratt, P.L. and Bensted, J. Accelerated hydration of Class G oilwell cement, Proceedings of Ceramic Transactions,Advances in cementitious materials**,** vol. 16, Ed. S. Mindess, American Ceramic Society Incorporated, Westerville, Ohio, USA, 1991, pp 251-270.

[12] Lota J.S., Bensted J. and Pratt P. L**.** Characterisation of an unhydrated Class G oilwell cement Industria Italiana del Cemento, N° 729, Febbraio di 1998, pág. 172 - 183.

ISOTHERMAL CONDUCTION CALORIMETRY STUDY OF CLASS G OILWELL CEMENT HYDRATED WITH ADDITIONS OF CALCIUM CHLORIDE, CALCIUM FORMATE AND SODIUM ALUMINATE AT LOW AND AMBIENT TEMPERATURES

Jasbir S. Lota[1], John Bensted[2] and Peter L. Pratt[3]

BIOGRAPHY

Dr Jasbir Singh Lota has gained 15 years experience in cement science and technology (Imperial College, Building Research Establishment, Concrete Technology Unit - Dundee University and Birchall Centre - Keele University) covering its chemistry, materials science and engineering aspects relating to chemical admixtures, mineral additions, mechanisms of hydration and instrumental techniques. Other interests include processing, properties and application of cementitious materials employed in the oil and construction industries. Following a year at the Institute of Education (University of London), he is teaching science at secondary level and actively encouraging schoolchildren to develop interests in science and engineering.

Professor John Bensted has worked for 25 years in the cement and oil industries (Blue Circle Industries and British Petroleum) in cement technology and is a visiting Professor of Cement Science at the Universities of London (Birkbeck College) and Greenwich. In addition, he is an international consultant in cement technology to the construction, chemical and oil industries. He has been at the cutting-edge of cement science and trouble-shooting, covering construction Portland, oilwell, high alumina, blended, decorative and other cements. Also he is an expert witness in legal matters concerning cement and concrete.

CONTACT DETAILS

Dr Jasbir S. Lota
Ashmole School
Cecil Road
Southgate
London
N14 5RJ UK.

Tel: +44(0) 20 8361 2703
Fax: +44 (0) 20 8368 0315

E-mail: jasbir_lota@hotmail.com

Professor John Bensted
23 Callander Road
Catford
London
SE6 2QA

Tel: +44(0) 20 698 9831
Fax: +44 (0) 20 698 9831

E-mail: bensted.j@btinternet.com

INTEGRATED MODEL OF STRUCTURE FORMATION IN POLYMER MODIFIED CONCRETE

A. Beeldens[1], D. Van Gemert[2] and Y. Ohama[3]

[1] Belgian Road Research Centre, Brussels. E-mail: Anne.Beeldens@bwk.kuleuven.ac.be
[2] Department of Civil Engineering, Katholieke Universiteit Leuven, Belgium.
E-mail: Dionys.Vangemert@bwk.kuleuven.ac.be
[3]Department of Architecture, College of Engineering, Nihon University, Koriyama, Japan.
E-mail: ohama@arch.ce.nihon-u.ac.jp

ABSTRACT

An integrated model is proposed to understand and to predict the properties of polymer modified cementitious materials. The reciprocal influences between the polymer particles and the cement hydrates are discussed and implemented in the model.

The influence of a lower drying rate on the film formation process as well as the retardive effect of the polymer particles and polymer film the cement hydration are discussed. The results demonstrate the coincidence of the polymer film formation process and cement hydration in the case of dry curing conditions.

1. INTRODUCTION

The properties of polymer modified cementitious materials (PCC) are determined by the components, i.e. cement particles and cement hydrates and polymer particles and polymer film. However, the properties of the individual components are as important as the synergetic action between these components. The influence of the presence of the cement particles on the polymer film and polymer film formation is investigated, as well as the influence of the polymer particles on the cement hydration.

To understand and to predict the properties of polymer modified cementitious material, an integrated model of structure formation is proposed in which these mutual influences are incorporated. Based on the three-step model presented by Ohama [1], an integrated model of structure formation is proposed in which the interaction between the cement hydrates and the polymer particles in relation to a time-scale is presented. Modifications and remarks on the Ohama-model, proposed by different authors [2, 3, 4] are also taken into account.

Drying of the polymer dispersion in the hardening PCC environment causes three important alterations of the drying conditions of the polymer dispersion compared to the pure air drying of the polymer particles. A high relative humidity is present in the case of water and moist cure, accompanied by a large dilution of the polymer dispersion in combination with the mixing water. The water phase almost immediately changes into an alkaline solution due to the start of the cement hydration. Finally a change in drying rate is noticed, which influences the minimum film formation temperature of the polymer dispersion. The influence of these alterations on the film formation process of different types of polymer dispersions is presented.

Proceedings of the 11th International Congress on the Chemistry of Cement (ICCC)
'Cement's Contribution to the Development in the 21st Century'
Hosted by: The Cement and Concrete Institute of South Africa
CD-ROM produced by: Document Transformation Technologies
11 - 16 May 2003, Durban, South Africa
ISBN Number: 0-9584085-8-0
Editors: Dr G. Grieve and G. Owens
Congress Organised by: Event Dynamics

Also the influence of the presence of the polymer particles and polymer film on the hydration and the properties of the cement particles is examined. Through strength measurements, the retardive influence of polymer modification is observed. On the other hand, the increase of the flexural strength, measured at a young age on mortar prisms, indicates the coincidence of the polymer film formation process and the cement hydration in the case of dry curing conditions. More detailed information is presented in [5].

2. POLYMER FILM FORMATION IN THE PRESENCE OF CEMENTITIOUS MATERIAL

The influence of the altered conditions on the minimum film forming temperature (MFT) [6] of the polymer dispersion is important for the film formation process in the presence of cementitious material. The variation of the MFT determines if a continuous film is formed throughout the cement matrix, even at temperatures lower than the MFT, or if the polymer particles will act separately on the cement particles and cement hydrates.

2.1. Influence of Relative Humidity on Film Formation and Drying Rate

Film formation, and especially the drying rate are influenced by relative humidity (RH). At high relative humidity, the equilibrium between the atmosphere and the pore solution is reached almost immediately and only a few water molecules escape to the atmosphere. Therefore, the water molecules that are present at the outer surface of the polymer particles due to the presence of surfactants, are only released very slowly. Rearrangements of the molecules may take place. At low relative humidity, a large amount of water molecules escapes to the atmosphere to obtain equilibrium between the atmosphere and the liquid. The water molecules surrounding the polymer particles are released very quickly and no further rearrangement can take place. In that case, a continuous film will only be formed if the polymer particles have sufficient thermal energy to coalesce together, i.e. when the curing temperature is higher than the MFT. However, due to the different drying rate at high R.H. and at low R.H., the MFT is altered and will be higher at lower R.H. than at higher R.H. This is illustrated with an example.

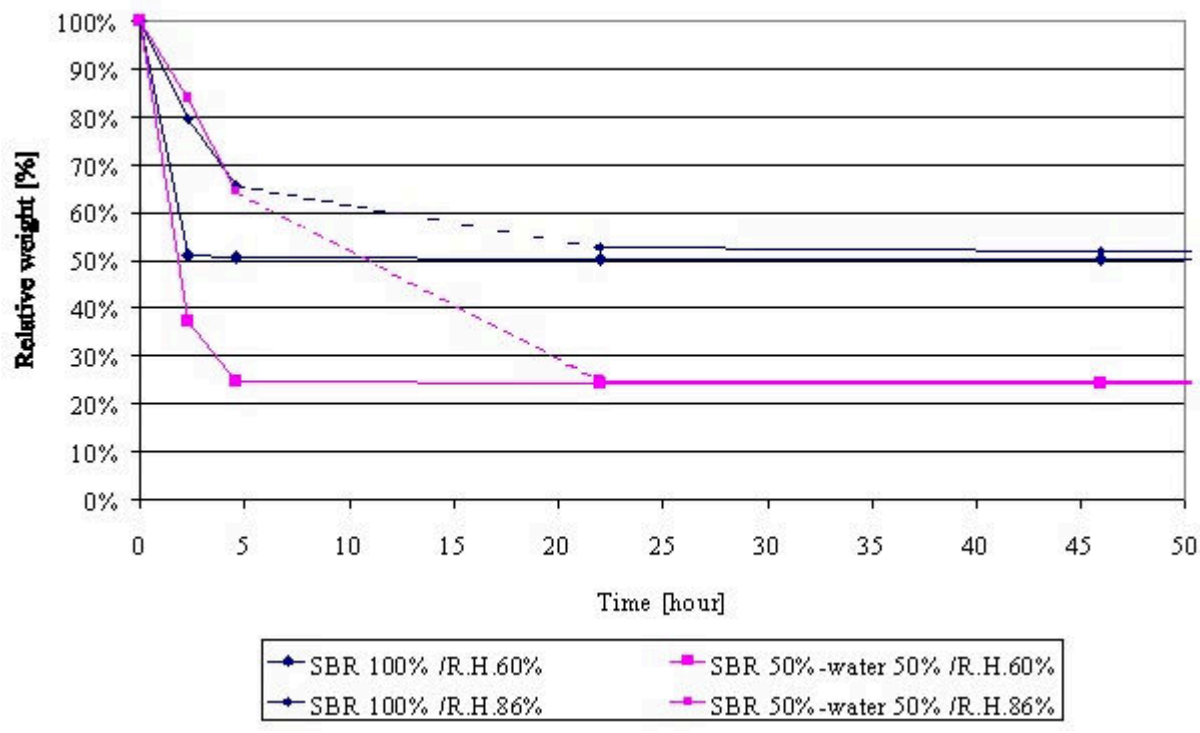

Figure 1. Weight variation of polymer dispersion after curing at 60% R.H. and 86% R.H.

To investigate the influence of the relative humidity on the film forming capacity of the polymer dispersion, three different curing conditions were taken: curing at R.H. higher than 98%, at R.H. of 86% and at R.H. of 60%. An atmosphere with R.H. of 86% was obtained in a sealed desiccator partly filled with a saturated KCl-solution. Temperature was equal to 20°C±3°C for the three conditions. The influence of the R.H. was investigated for the 8 different types of polymer dispersion, with MFT ranging between 0°C and 32°C. Samples were prepared pouring a thin layer of the polymer dispersion on a glass plate. The amount of solids poured on the glass plate was kept constant to obtain an equal thickness for all samples. The results indicated a delayed film formation in the case of 86% R.H. for all specimens with MFT < 20°C, compared to film formation at 60% R.H. At higher relative humidity, the film was formed only after 6 hours in the case of the pure polymer emulsion, where it needed less than 2 hours at a R.H. of 60%.

Figure 1 presents the results for a SBR polymer dispersion, with MFT of 5°C, cured at 60% R.H. and at 86% R.H. The pure polymer dispersion was tested as well as a diluted solution, containing 50% polymer dispersion, i.e. 25% solids, 25% emulsion water and 50% tap water. The results indicated a rapid linear decrease in weight, due to the evaporation of the water until only the solid part of the dispersion was left. The results of the different dispersions reflected a constant drying rate. In the case of the SBR1 samples dried at 86% R.H., this was not clear due to the lack of measuring points between 5 hours and 24 hours after the start of the test, as indicated by a dashed line between both points. A constant drying rate may be presumed until the 50%, respectively 25% relative weight is reached. From the results a simple calculation of the drying rate is possible extrapolating the drying rate between 0 and 2 hours. Only in the case of the pure dispersion, dried at 60% R.H., the drying rate could not be calculated since the 2 hours interval time was too long. The drying rate in this case was smaller than 0.21 g/h. The results are given in Table 1.

Table 1. Drying rate to obtain a pure polymer film

Composition	Curing at 60% R.H.	Curing at 86% R.H.
100% SBR1	<0.21g/h	0.08g/h
50% SBR1, 50% tap water	0.27g/h	0.08g/h

The results indicated very little alteration of the drying rate due to the dilution of the polymer dispersion, especially for drying at high R.H. The increased relative humidity on the other hand reduced to a large extent the drying rate of the polymer dispersion.

Although a small drying rate decreases the MFT, no continuous film was formed in the case of SAE dispersion, MFT of 32°C, even not at a R.H. of 86%. Curing at a R.H. higher than 98% resulted in a white-transparent material. This points at a slight reduction of the MFT. Also in the case of the other dispersions, with a MFT lower than 20°C, no continuous film could be seen after 7 days storage for the samples stored at 98% R.H., although some alterations were noticed. Some of the polymer dispersions changed into a slimy white paste and in some cases into a fragile film. After storage during 7 days at the high R.H., the specimens were stored at R.H. of 60% and 20°C, without stirring the formed paste or fragile film. This resulted in coalescence into a continuous film if the MFT of the dispersion was lower than 20°C. Extending the curing time at higher R.H. resulted in a continuous film, even for the polymer dispersions with higher R.H.

2.2 Influence of the Alkalinity

Due to cement hydration and release of CaO, the alkalinity of the pore solution becomes very high. This could cause interaction with the surfactants and result in a delayed or even completely stopped

film formation. To test the influence of the alkalinity of the pore solution, a simulation has been done with pure dispersion. The test was carried out on the SBR dispersion. The polymer dispersion was mixed with a NaOH-solution with pH equal to 13. The solution contained 50% of polymer dispersion which corresponds to 25% parts of solid, and 50% of the NaOH solution and had a pH value of 12.70. after stirring the solution, it was then poured on a glass plate and stored at laboratory conditions, R.H. 60% and at a R.H. of 86%.

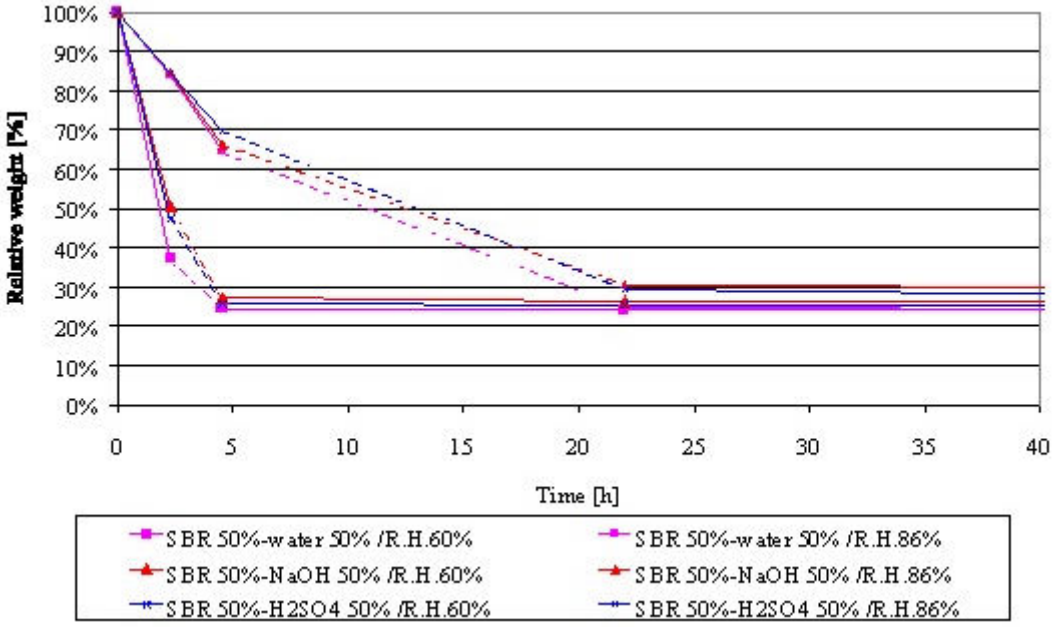

Figure 2. Weight variation of the SBR1 dispersion after dilution with distilled water, a NaOH-solution and a H_2SO_4-solution repectively

Figure 2 gives the results in comparison to the diluted dispersion with 50% tap water. At the same time, a 50% dilution with an H_2SO_4-solution, with pH of 1, was made to see the influence of an acidic environment. Obviously, this is not the case in the fresh concrete. The pH of the solution with H_2SO_4 measured 1.39. The results are also presented in Figure 2. Analogous to Table 1, the drying rate was calculated. The results are presented in Table 2.

Table 2. Drying rate to obtain a polymer film

Composition	Drying at 60% R.H.	Drying at 86% R.H.
50% SBR1, 50% tap water	0.27g/h	0.08g/h
50% SBR1, 50% NaOH	0.21g/h	0.07g/h
50% SBR1, 50% H_2SO_4	0.23g/h	0.07g/h

The results indicate a small reduction in drying rate for the dispersions diluted with the NaOH solution as well as for the dispersion diluted with the H_2SO_4-solution, possibly due to the interaction between the surfactants and the ions in the solution. However, the effect was limited. In all cases, a continuous film was formed. The influence of the relative humidity is much more important than the pH value of the solution.

2.3. Polymer Film Formation in the Pore Solution of Cementitious Material

The film formation process and especially the MFT is mainly influenced by the drying rate. Therefore, the variations of the film forming process in the pore solution of cementitious material can be reduced

to the influence of the altered conditions on the drying rate of the polymer dispersion.

Only limited variation of the drying rate was observed in an alkaline and acidic environment. Film formation of the tested dispersions was not hindered in these environments. The relative humidity on the other hand altered the drying rate to a large extent. A reduced drying rate was measured at higher relative humidity. This resulted in a decreased film forming temperature for the pure polymer dispersion at higher relative humidity. This explains partly why, even after curing at temperatures lower than the MFT of the pure polymer dispersion, as was the case for the mortar and concrete specimens modified with SAE, a continuous polymer film was noticed throughout the cement matrix

In addition, due to cement hydration supplementary forces may be exerted on the water of the polymer particles. Extra water-withdrawal results in more closely packed polymer particles and coalescence can take place at even lower temperatures [7]. As is shown in the following section, this was the case for the SAE dispersion. A clear continuous polymer film was formed even at curing temperatures of 20°C, which is lower than the MFT of 32°C. Measurement of the temperature at the inner part of the specimens showed only a limited increase of the temperature due to the release of heat caused by hydration.

3. CEMENT HYDRATION IN POLYMER MODIFIED MATERIAL

Cement hydration in polymer modified material is influenced by the presence of the polymer particles and polymer film in the fresh state, during hydration as well as in the hardened state. The properties of the fresh mixture are influenced to a large extent by the surfactants, present at the surface of the polymer particles. The cement particles are better dispersed in the mixture and a more homogeneous material is formed. Since hydration is closely related to the strength development of the material, the influence of polymer hydration is investigated through the influence on the strength development at early ages.

3.1. Strength Evolution at Early Age

The strength evolution at early ages is closely related to the hydration of the cementitious material and the film formation. The influence of the polymer modification is twofold. Due to the polymer and the surfactants, a retardation of the cement hydration can be noticed. This is especially visible in the compressive strength of the mortar beams. On the other hand, due to the film formation or due to the interaction between the cement hydrates and the polymer particles, the tensile strength of the binder matrix as well as the adhesion strength between the aggregate and the binder increase. This is especially seen in the flexural strength of the mortar beams. To illustrate and to clarify these statements, the compressive and flexural strength of mortar beams are presented in relation to time and to polymer-cement ratio. Polymer modification was done with the SAE emulsion. The curing conditions applied for the test were standard curing, wet curing and dry curing.

The flexural strength and the compressive strength of the mortar are given in Figures 3 and 4. Due to the small amount of sand in the mortar, sand-cement ratio of 0.16, the samples were subjected to large shrinkage. In the case for wet or standard cured samples, where a long moist or water curing condition was followed by a dry period, micro-cracks appeared due to the shrinkage which resulted in a loss of strength. Therefore, only the results of the dry cured specimens are discussed.

In general the flexural strength increased with increasing p/c ratio with a maximum around 15% p/c ratio. The addition of polymer emulsion acted as a retarder for the hydration of cement. The retardive effect was more pronounced with increasing p/c ratio. In Table 3, the relative increase (>0) or decrease (<0) of the flexural and compressive strength with varying p/c ratio are given in relation to the strength of the non-modified mixture.

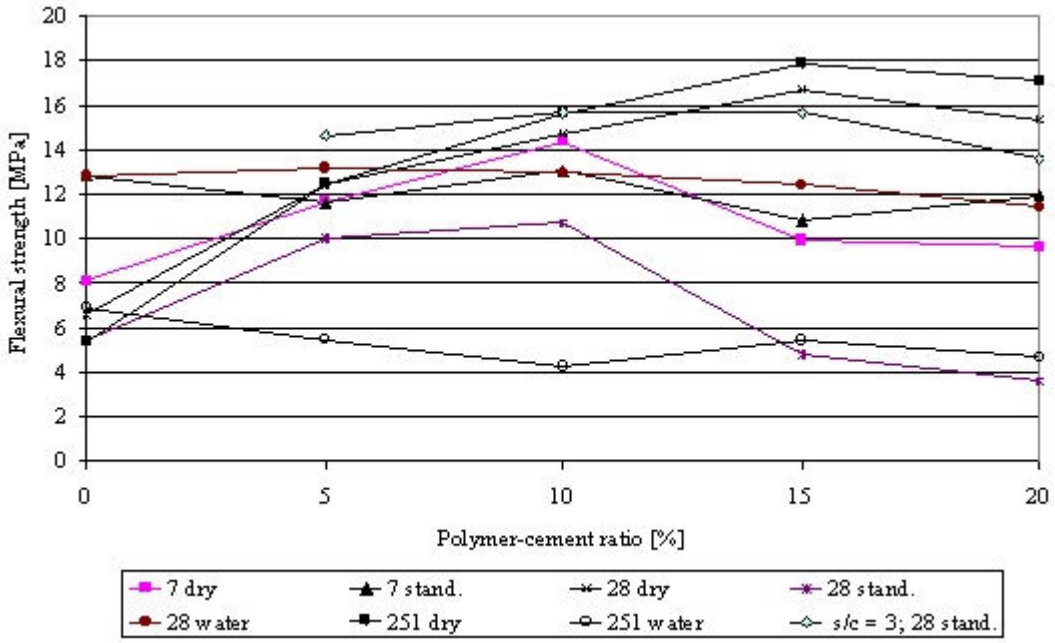

Figure 3. Flexural strength, constant w/c ration, porous concrete mortar composition

Table 3. Relative increase and decrease of the compressive and flexural strength for the dry-cured samples

p/c-ratio	7 days curing		28 days curing		251 days curing	
	compr. strength	flex. strength	compr. strength	flex. strength	compr. strength	flex. strength
0% 5% 10% 15% 20%	60 N/mm² - 1.8 % - 10.5 % - 22.5 % - 24 %	8.1N/mm² + 44 % + 77 % + 23 % + 19 %	72 N/mm² + 8.7 % + 8.5 % - 6.4 % - 11.1 %	5.7N/mm² + 88 % + 123 % + 153 % + 132 %	73 N/mm² + 11 % + 1.3 % + 0.6 % - 3.4 %	6.4N/mm² + 133 % + 192 % + 234 % + 220 %

The results indicate a decrease of compressive strength during the first days of curing. This points at a delayed cement hydration, since after longer curing periods, the modified as well as the unmodified specimens reach equal compressive strength. The negative influence of the polymer modification on the compressive strength is therefore minimized if a long curing period is considered, at least in the case of modification with the SAE dispersion. A maximum compressive strength is reached with a polymer-cement ratio equal to 5%. However, higher compressive strength would be obtained in the case where a longer wet curing period was introduced, followed by a dry curing period, if shrinkage is limited.

Two different, but related mechanisms are at the base of the retardive effect on cement hydration. First, the presence of surfactants is important. When the mortar is modified with a polymer emulsion, part of the water has to come from this emulsion. This water is partly bound to the hydrophilic part of the surfactants present at the surface of the micelles by hydrogen bonds. The release of this water takes time, so hydration is retarded.

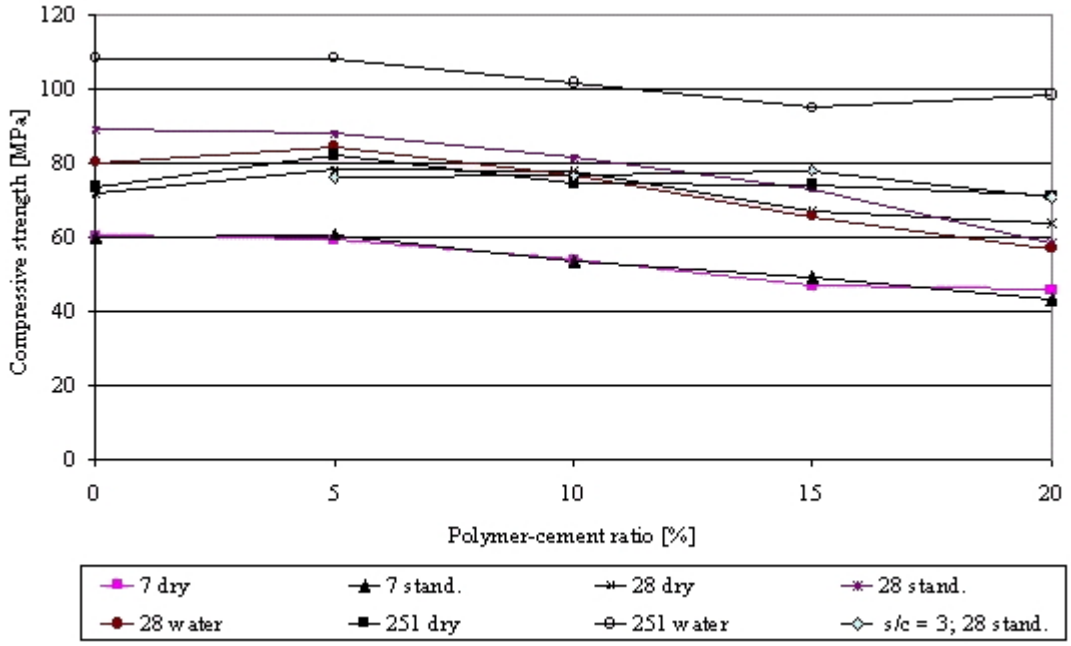

Figure 4. Compressive strength, constant w/c ration, porous concrete mixture composition

On the other hand it is also possible that by mixing the unhydrated cement particles and the polymer emulsion, some of the micelles clings to the surface of the unhydrated cement particles and form there a continuous film, due to the water extraction by the first hydration of the cement particle, i.e. the formation of the outer C-S-H phase. This results in a partly or fully covered cement particle. The hydration of this particle will be much slower since the water first has to migrate through the layer of polymer film or closely packed polymer particles.

From the results of the mechanical tests, conclusions regarding the film formation mechanism and especially the time at which film formation takes place may be drawn. When the compressive and flexural strength after 7 days dry curing are looked at (Figures 3 and 4) together with the reduction, respectively increase of the strength in relation to the strength of the unmodified mortar (Table 3), an increase in flexural strength is noticed, although the cement hydration is retarded when the polymer-cement ratio is increased (lower compressive strength). This points at the existence, already at an early stage of curing, of a polymer film or at least at the interaction between polymer particles and cement particles. However, the incapacity of the modified “porous” mortar specimens to overcome the large shrinkage stresses after 7 days or 28 days moist curing, indicates that the continuous polymer film is not yet formed in the case of water saturated conditions. No influence of the polymer modification on the flexural strength is noticed in the case of standard cured and water cured samples as long as no dry curing period is applied.

So, one may conclude that at high relative humidity, the influence of polymer modification on the flexural strength at short term is limited. From the moment a dry curing period is introduced, a polymer film starts to build up through the binder phase and an increase in flexural strength is measured with increasing polymer-cement ratio. The influence on the flexural strength of the retardation of the cement hydration is compensated by the presence of the polymer film. When long term behaviour is considered, a maximum of flexural strength is established around 15% polymer-cement ratio.

4. INTEGRATED MODEL OF STRUCTURE FORMATION

The mutual influences between the cement hydrates and the polymer particles and film are incorporated in an integrated model of structure formation. The model is based on the three-step model as proposed

by Ohama, but stresses the positioning of the mechanisms on the time scale and the interaction between the different components.

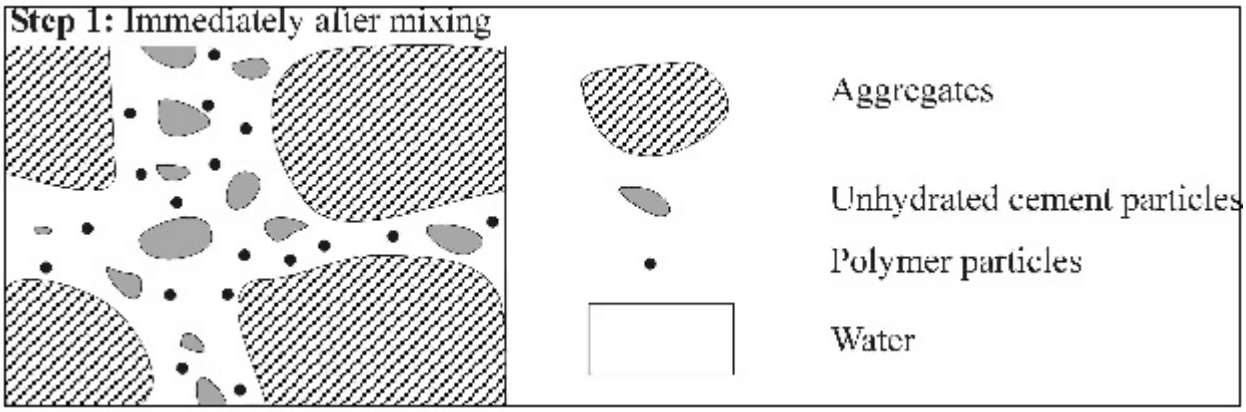

Figure 5. Step 1, immediately after mixing

The formation of the polymer film can take place from the moment two polymer droplets have sufficient energy to overcome the repulsion forces originating from the surfactants. In other words, if the temperature is high enough to cause sufficient Brownian motion, or if additional forces are working on the liquid layer around the polymer droplets, such as capillary forces or water withdrawal by further cement hydration, two droplets can come close to each other and can coalesce into each other and a polymer film is formed. This process simultaneously can take place with the cement hydration mechanism, especially in the case of dry curing conditions. Therefore, partial or full encapsulation of the cement hydrates is possible, which retards the hydration process. The different steps of the conclusive model are presented in Figures 5 to 8.

Immediately after mixing, the cement particles and polymer particles are dispersed in the water. The first hydration of the cement takes place, which results in an alkaline pore solution. This is indicated as step 1, Figure 5.

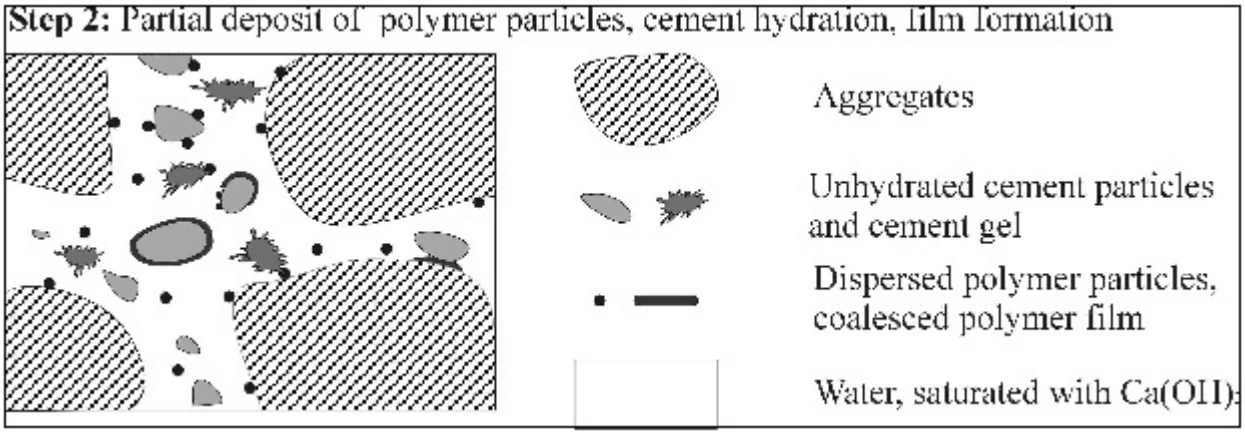

Figure 6. Step 2, after mixing. The polymer particles interact with the cement particles and the aggregates. In the case a dry curing period is introduced. A continuous film may be formed locally.

The second step is presented in Figure 6. A portion of the polymer particles is deposed on the surface of the cement grain and the aggregate. The polymer-cement ratio determines the amount of polymers present in the pore solution and present at the aggregate surface. Part of the polymer particles may coalesce into a continuous film. This preferably takes place at the surface of the cement hydrates where extra forces are exerted on the polymer particles due to the extraction of water for cement hydration. The polymer film can partly or completely envelop a cement grain which results in a retardation or even a complete stop of the hydration of the cement grain.

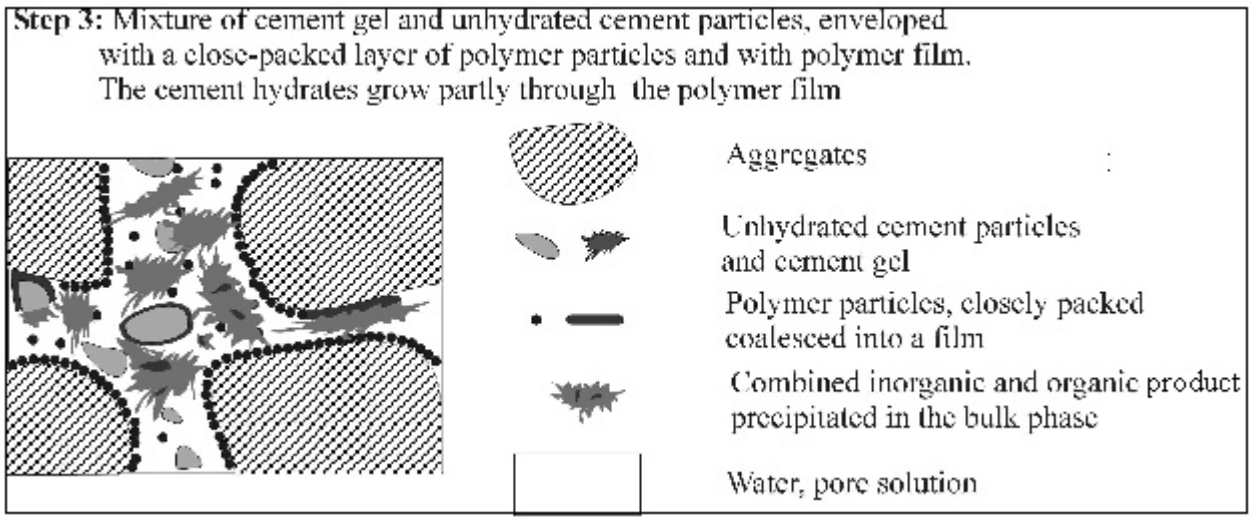

Figure 7. Step 3, cement hydration proceeds, a polymer film formation starts on specific spots.

The following step, Figure 7, consists of cement hydration, polymer flocculation and possibly polymer coalescence into a film. The processes that take place depend on the curing conditions. If no dry curing period, i.e. curing at a lower R.H., is included, the overall film formation is retarded and the influence on the properties of the fresh mixture is limited at this stage. If a dry curing period is included, polymer film formation takes place during this step, which influences the cement hydration process as well as the strength development at early ages. In the bulk liquid phase, hydrate precipitations are present, which form a combined inorganic and organic product. The fractions of the different types of product formed depend on the polymer/cement ratio used. The polymer fractions included in these hydration products do not contribute to the strength development of the specimen [7].

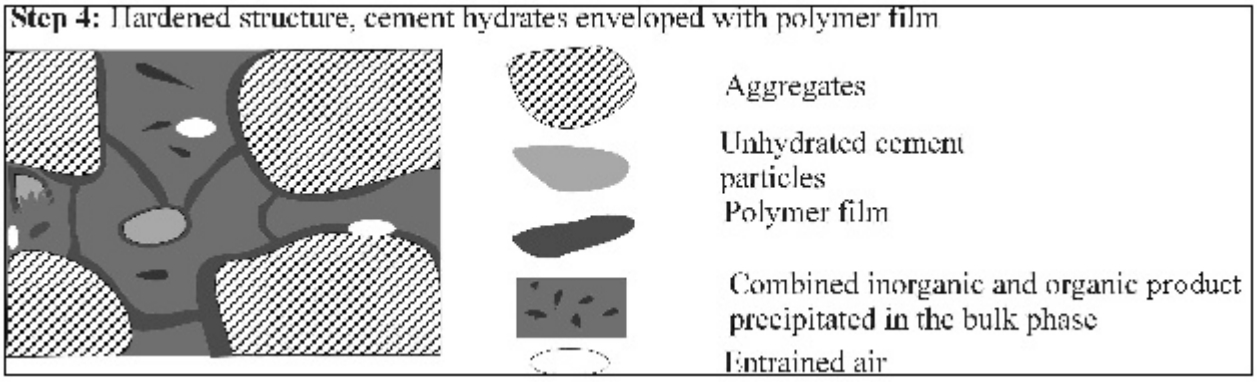

Figure 8. Final step 4, cement hydration continues, the polymer particles coalesce into a continuous film

The final step, Figure 8, includes further hydration and final film formation. Through the cement hydrates, a continuous polymer film forms as water is further removed from the pore solution. The part of the polymer particles, that is still present in the dispersion, is restricted to the capillary pores and at the interface of the aggregates and the bulk polymer-cement phase. It is this part which contributes the most to the elastic and final strength properties. The continuity of the polymer phase through the binder matrix is more pronounced in the case of a higher polymer-cement ratio. In the case the MFT of the polymer dispersion is much more elevated than the curing temperature, the polymer particles may not coalesce into a continuous film, but remain as closely packed polymer particles.

The use of the model can be illustrated with the different curing conditions. From the results it is concluded that optimal conditions towards the strength development are a wet curing period followed by a dry curing period. The longer the moist and water curing period is, the higher the final flexural strength will be if shrinkage is prevented and if a curing period at lower R.H. is introduced. This means that first cement hydration takes place and only limited film formation. Therefore, the polymer particles remain in the pore solution and a larger amount of polymer particles will be incorporated into the continuous film that is formed in the final stage. If the drying period is introduced earlier in the process, the film formation will start sooner, i.e. before and simultaneously with the cement hydration, resulting in enlarged encapsulation of the cement hydrates as well as incorporation of the polymer phase in the hydration product precipitated from the pore solution.

5. CONCLUSIONS

The influence of polymer modification on the cement hydration process as well as the influence of the presence of the cement particles on the polymer film formation process was investigated. The results were incorporated in a descriptive model for the structure formation of polymer modified material, based on the model of Ohama and taking into account the modifications and developments proposed by different researchers.

The polymer film formation process is influenced by the presence of the cement hydrates in different ways. First there is the large dilution of the dispersion by the mixing water which quickly changes into an alkaline solution. Test results on a diluted polymer emulsion showed little or no influence on the film formation process due to the alkalinity for the investigated types of polymer dispersion. The relative humidity of the surrounding atmosphere had a large influence on the film formation and especially on the drying rate. The higher the relative humidity of the surrounding atmosphere, the lower the drying rate became. This influences to a large extent the film forming temperature of the dispersion. The lower the drying rate, the lower the amount of energy needed for the polymer particles to coalesce into a continuous film. Therefore, the MFT is reduced with a reduced drying rate. Tests indicated that even at laboratory circumstances, i.e. 20°C, the SAE dispersion with a MFT of 32°C, could form a continuous film, as long as the drying rate was low enough.

This is also revealed in the microstructure of the SAE-modified specimens. Through the cement matrix, a continuous polymer film is visible. At a p/c-ratio lower than 5%, the continuity is only present through small tiny bridges at a limited amount of spots. At higher p/c-ratio's, the film is more dense. The film connects the different aggregates and is homogeneously present over the material. However, in the case of small p/c ratio's, a preferred positioning close to the aggregate is noticed.

The cement hydration is retarded due to polymer modification. From the moment a dry curing period is introduced, polymer film formation and cement hydration coincide. This results in a partly or completely encapsulation of the cement particles which reduces the hydration rate. Encapsulation also occurs due to the extra water withdrawal from the polymer particles situated at the surface of the cement grains. The cement hydration is also influenced by the fact that water is longer retained due to the presence of the surfactants at the surface of the polymer particles. This results in a better dispersion of the polymer particles and the cement hydrates, but also retards the cement hydration. The influence increases with increasing p/c-ratio.

The presence of the polymer particles also influences the hydration products and especially the portlandite crystals. In the case of polymer modification, the portlandite crystals will be less distorted in the presence of the polymer dispersion. This increases interlaminar bonding forces, which increase the resistance of the portlandite towards aggressive solutions to some extent. Besides the presence of the polymer film throughout the cement hydrates in the bulk binder phase, the transition zone is also influenced by the polymer modification. Clear connections between the aggregate and the bulk binder

matrix exist and become more continuous and dense at higher polymer-cement ratios. Study of the microstructure of the polymer modified material points out that the p/c-ratio should be higher than 5% to obtain a sufficiently continuous polymer film throughout the material. This is confirmed by the results of the mechanical tests.

The previous findings are incorporated in a model of structure formation. This model accentuates two important changes towards the original model of Ohama. First of all, a relation to the time scale of the different processes is made. In the case a dry curing period is included, cement hydration and polymer film formation coincide and the encapsulation of cement particles is possible. Further, the formation of an interstitial phase, consisting of inorganic and organic precipitates in the bulk phase is pointed out. This is important towards an optimal benefit of polymer modification since the polymers present in this phase are contributing less to the final properties of the material. The optimum conditions are evident from these findings, i.e. a long period of water or moist curing (up to 28 days) during which the cement hydrates develop followed by a period of curing at lower relative humidity during which the polymer film formation is promoted.

REFERENCES

[1] Ohama, Y. Handbook of Polymer-Modified Concrete and Mortars, Properties and Process Technology, Noyes Publications,1995, p. 236.

[2] Bijen, J. M. and Su, Z. Polymer Cement Concrete: a Contribution to Modelling of the Microstructure, Technical Committee TC-113, Symposium on properties and test methods for concrete-polymer composites, Oostende, pp. 19-27.

[3] Puterman, M. and Malorny, W.Some Doubts and Ideas on the Microstructure Formation of PCC, IXth International Congress on polymers in concrete ICPIC'98, Bologna, 1998, pp. 165-178.

[4] Schorn, H. and Schiekel, M. Shape and Distribution of Polymer Particles in PCC - Investigated by Environmental Scanning Electron Microscope (ESEM), Tenth International Congress on Polymers in Concrete, Hawaii, 2001, CD-Rom.

[5] Beeldens, A. Influence of polymer modification on the behaviour of concrete under severe conditions, PhD dissertation, Faculty of Engineering, Katholieke Universiteit Leuven, 2002, p. 248.

[6] Beeldens, A. Monteny, J. Vincke, E. De Belie, N. Van Gemert, D. Taerwe, L. and Verstraete, W. Resistance to Biogenic Sulphuric Acid Corrosion of Polymer-Modified Mortars, Cement and Concrete Composites, volume 23/1, 2001, pp. 47-56.

[7] Tabor, L. J. Dispersed Polymers, Revision of Concrete Society Technical Report No.9 - Polymer Concrete, chapter 7, Contribution to the Fifth International Congress on Polymers in Concrete at Brighton, UK, 1987, pp. 83-94.

[8] Su, Z. Larbi, J. A. and Bijen, J. M. The Interface Between Polymer-Modified Cement Paste and Aggregate, Cement and Concrete Research, volume 21, no. 6, 1991, pp. 983-990.

IMPROVED PERFORMANCE OF BLAST FURNACE SLAG CEMENT MADE WITH HIGH ALKALI CLINKER

B. Mus

Denizli Cement Plant, P.Box 29, 20100 Denizli, Turkey.

ABSTRACT

A series of laboratory tests are described with ISDEMiR blast furnace slag (BFS) and four different cement plant clinkers.

Materials are ground up to 4.500- 4.000 cm^2/gr (Blaine, specific surface) for OPC and BFS respectively. Mixture samples prepared with 40, 50, and 60 % BFS contents were tested for compressive strengths both in the Denizli & Iskenderun cement plant and the Turkish Cement Manufacturers' Association Laboratories.

It is concluded that:

- In the light of 2, 7, 28 and 80 days compressive strength figures, under normal and sulfated water conditions, clinkers containing around 1.1 % total alkali are best suited for BFS cement production.
- % total alkali content is sufficient to activate BFS activity index grade 80.
- Clinker C increases BSF content up to 60.28% additive ratio in BFS cement production (the approach is done with the aid of 2-day compressive strengths, an exponential approach)

1. INTRODUCTION

Different characteristic behaviors are observed in the tests done with Isdemir BFS and four different character clinkers. The most significant result is observed by clinker C; although its compressive strength is 17% lower than A,B and D clinkers (3.000 cm^2/gr in finess), it is a better activator for BFS at higher additive contents. The behavior of OPC and blast furnace slag cement (BFSC) in sulfated water is described.

1.1 As a summary

- Chemical and mortar tests are applied for 40%, 50%, 60% BFS content mixtures prepared in laboratory. BFS activity indexes are determined according to ASTM 989 (TS 24 and TS 687).
- Mortar tests were done according to EN 196-1.W/C ratio was 0,50.Concrete prisms's dimensions were 40*40*160 mm. Four prisms have been used at each age.Two day compressive strengths were the limiting parameter for adding BSFslag due to the validity of two day compressive strength limits in Turkish Standards. (the early strength figures are decreasing with increasing BFSlag content).Exponential regression was applied in derivation of the mathematical function of two days compressive strengths.
- Behavior of different BFS content cements are observed in sulfated water as specified by ASTM 1012 (5% Na2S04)
- Hydration followed in 7 and 28 day mortars kept under sulfated and normal water are analyzed by XRD and electron microscope.
- Setting time of cement is analyzed while clinker characteristics and BFS content changing.

2. METHODS

2.1 Analysis Plan

Material: BSF ; 10 Kg of Iskenderun Iron Plant blast furnace slag ground by Denizli &Iskenderun Cement Plant's closed circuit ball mill (3.920 cm^2/gr in fineness) CLINKER; 10 Kg of Denizli and 3 different Plants' clinkers each.

2.2 Analysis Conditions

Each plant's clinkers will be tested separately.

- OPC SAMPLE:
  Prepared in a test mill with 4% gypsum ground up to 3100 ± 100 cm^2/gr in fineness
- BFS SAMPLE:
  Ground (3920 cm^2/gr)
- HIGH GYPSUM CONTENT CEMENT: (HGC)
  Prepared in test mill with 8% gypsum ground to 4.450 ± 100 cm^2/gr fineness
- BLAST FURNACE SLAG CEMENT SAMPLE:
  %40 BFS; %60HGC
  %50 BFS; %50 HGC
  %60 BFS; %40 HGC

2.3 Analysis standards to be applied

Chemical analysis	: EN 196-2
Mortar analysis	: EN 196-1
BFS activity index	: ASTM 989

Behaviors in sulfated water are analyzed only in compressive strength basis according to ASTM 1012 and pH trend of sulfated water is additionally observed

3. RESULTS

- Chemical and mortar analysis results of clinker and slag samples (Four different type of clinkers were tested as a function of time.
- After mixing ground BFSlag & high gypsum content cement; Chemical and mortar analysis results of prepared samples of 40%, 50%, and 60 % BFS content mixtures (three different type clinkers were tested for different periods).
- Slope and mathematical function of max. BFS addition capability.
- Compressive strength profiles of 7, 28, 80 days prisms (40*40*160 mm, dimension) under normal and sulfated water condition.4 samples were tested.
- Setting times changed as a function of BFS content and clinker type.
- XRD and electron microscope results in 7 and 28 days prisms under normal and sulfated water.

Summary 1:

1-Clinker & Blastfurnace slag results

Results table-1:
a-chemical analysis & compressive strength of clinker
b-chemical analysis & compressive strength of Blastfurnace slag
Table 1-a:

Sample name		Compressive strength & Physical analysis Strength N/mm² 2day	7day	28day	80day	Setting time;hr	water req;%	Chemical analysis (with volumetric method on EN196-2) Total SIO2 %	Al2O3 %	Fe2O3 %	Cao %	Mg0 %	SO3 %	*total alkalis %	LSF %	C3S %
Clinker A	1)	25,4	39,7	51,2	-	2:15	26	20,6	5,3	3,8	65,3	2,0	1,1	0,52	98,2	60,8
	2)	28,4	39,4	48,4	-	1:45	25	20,9	5,2	3,8	64,9	2,0	1,0		96,7	58,1
	3)	29,9	42,1	48,8	53,2	2:05	27	21,0	5,5	3,8	63,3	2,0	1,0	0,63	93,6	49,2
Clinker B	1)	26,3	36,9	50,7	-	2:45	26	20,7	5,2	3,9	65,2	2,0	1,0	0,63	97,7	60,2
	2)	25,1	38,5	48,5	-	2:45	25:0	20,8	5,2	3,8	64,8	2,0	1,1		96,9	58,2
	3)	26,1	39,0	48,7	-	2:15	25	19,9	7,6	3,8	61,5	2,3	0,9	0,72	91,8	36,5
Clinker C	1)	24,6	32,7	37,2	-	3:45	28	21,5	5,2	3,7	62,8	2,0	1,3	1,22	91,4	44,2
	2)	29,3	33,0	38,6	-	3:35	29	21,3	5,3	3,6	62,8	6,0	1,2		92,1	45,5
	3)	29,3	37,8	41,7	43,6	4:00	28	21,4	5,2	3,7	64,5	2,1	1,2	1,11	94,4	52,4
Clinker D	1)	25,4						21,1	4,5	4,6	64,5	1,9	0,8	0,66	95,7	58,9
	2)															
	3)	27,8						20,4	4,4	4,3	65,6	1,9	0,7	0,65	100,6	69,9

Table 1-a:

	**activity index,N/mm²													
ISDEMİR BFSlag	-	79	-				39,91	13,05	0,28	35,44	8,04		1,01	-	-

* total alkalis=Na2O+0,658*K2O
** according to ASTM 989 activity index grade is 80 and for the test clinker-A was used as the reference cement.

Summary 2:

2- Blastfurnace slag cement results containing %40,50,60 BFS

Results table-2-b:
b-chemical analysis & compressive strength of clinker-B

Sample name		Compressive strength & Physical analysis,EN 196-1 Strength N/mm² 2day	7day	28day	80day	Setting time;hr	water req;%	Chemical analysis with volumetric method ,EN196-2 Cao %	Mg0 %	SO3 %	Cl %	*total alkalis %
%40 BFS in cement	1)	15,7	25,9	43,8		3:15	27,7	53,2	4,4	2,4	0,051	0,52
	2)	16,4	25,6	43,3		3:00	27,3	51,5	4,4	2,3	0,053	0,74
	3)	16,9	27,5	42,8		2:55	28,7	51,1	4,8	1,9	0,054	0,93
%50 BFS in cement	1)	13,0	21,9	42,0		3:35	28,0	50,3	4,7	2,3	0,063	0,64
	2)	12,5	21,4	41,7		3:45	28,7	48,6	4,2	2,1	0,065	0,68
	3)	13,6	24,6	42,2		3:05	29,3	48,5	5,0	2,0	0,065	0,76
%60 BFS in cement	1)	9,0	19,1	37,7		3:40	28,3	47,3	5,0	2,3	0,08	0,93
	2)	8,6	17,5	37,6		3:50	29,7	45,7	5,7	2,0	0,078	0,91
	3)	10,2	19,9	36,9		3:25	30,0	45,9	5,2	1,8	0,074	0,84

* total alkalis=Na2O+0,658*K2O

2- Blastfurnace slag cement results containing 40,50,60 %

Results table-2-c:
c-chemical analysis & compressive strength of clinker-C

Sample name		Compressive strength & Physical Strength N/mm2 2day	7day	28day	80day	Setting time;hr	water req;%	Chemical analysis with volumetric method ,EN196-2 Cao %	Mg0 %	SO3 %	Cl %	*total alkalis %
%40 BFS in cement	1)	19,3	30,8	45,1		04:00	30,3	51,8	3,74	1,88	0,054	1,14
	2)	19,4	30,0	45,2		03:50	28,7	51,05	4,36	2,44	0,056	1,11
	3)	18,4	31,2	45,4	52,7	03:30	29,3	51,82	4,95	2,28	0,052	1,08
%50 BFS in cement	1)	14,1	24,9	42,3		03:45	29,7	49,07	4,75	1,81	0,060	1,17
	2)	14,6	24,4	41,0		04:05	29,0	48,46	5,01	2,08	0,068	0,93
	3)	14,1	26,0	40,7	49,6	03:30	29,7	49,18	5,09	2,08	0,065	0,98
%60 BFS in cement	1)	10,0	20,1	38,9		03:55	29,7	46,33	5	1,78	0,083	1,17
	2)	10,1	18,9	37,5		04:00	29,3	45,87	5,78	1,89	0,080	1,14
	3)	10,3	21,0	37,4	46,3	03:25	30,0	46,43	5,56	1,98	0,075	1,13

* total alkalis=Na2O+0,658*K2O

There is no numerical finding of about solubility of K_2S0_4 of clinker C in water. An assumption could be made as 28 days compressive strength loss of clinker C prisms in comparison with clinker A & B may be caused because of + 1 % more soluble K_2S0_4 content.

2- Blastfurnace slag cement results containing 40,50,60% BFS

Results table-2-d:
d-chemical analysis & compressive strength of clinker-D

Sample name		Compressive strength & Physical analysis, TS24 Strength N/mm^2 2day	7day	28day	80day	Setting time;hr	water req;%	Chemical analysis with volumetric method, TS 687 Cao %	Mg0 %	SO3 %	Cl %	*total alkalis %
%40 BFS in cement	1)	18,1	28,2	44,2	55,5			49,14	5,06	2,66	0,0154	0,80
	2)											
	3)	18,5	30,0	45,5	55,2			49,97	5,24	2,36	0,0197	0,81
%50 BFS in cement	1)	14,5	31,8	45,0	53,6			46,74	5,72	2,63	0,0159	0,84
	2)											
	3)	13,9	24,6	42,1	54,2			47,74	5,6	2,18	0,0161	0,85
%60 BFS in cement	1)	9,7	20,6	36,6	48,0			43,59	6,61	2,04	0,0115	0,92
	2)											
	3)	9,2	21,3	37,1	51,4			42,85	7,56	1,79	0,0119	0,94

* total alkalis=Na2O+0,658*K2O

Summary 3: Slope and mathematical function of maximum BFS addition capability
It is observed that the limiting parameter for maximum BFS addition capability is the 2-day compressive strength limit (as 10,0 Mpa). In other words the BFS addition capability of 59 -60 % could be increased up to 62 -63 % if there would be no validation of 2 days compressive strength limit in TS 20, EN 197-1 standards.

Clinker	Max. BFS Addition Capability	2 Days Compressive Strength Exponential Function	R^2
A	60,58	23.604exp(-0.2883x)	0,9987
B	55,70	23.037exp(-0.3228x)	0,9917
C	60,28	26.945exp(-0.3288x)	0,9993
D	58,90	70,442exp(-0.0331x)	0,9769

Summary 4: Compressive strength profiles of 7, 28, 80 day prisms under normal and sulfated water conditions.

Behaviours of cements under sulfated water of 5,0 % Na2S04 content could be summarized as,
If figure 2-a &2-a/s and figure 3-a &3-a/s are visualized it could be observed that cement prisms prepared by clinker A are absolutely defected by sulfated water and loose compressive strength in 28 and 80 days period.

Results table-4-a:
a- 7,28,80 day compressive strengths of clinker-A after normal water & sulphated water treatment.

Sample name	Clinker -A case:					
	7days, N/mm²		28days, N/mm²		80days, N/mm²	
	normal water,7	sulphated water,7	normal water,28	sulphated water,28	normal water,80	sulphated water,80
Portland cement	42,1	40,4	48,8	48,2	53,2	51,6
40%BFS	30,0	30,0	47,1	47,5	60,2	53,9
50%BFS	25,6	25,3	44,6	45,8	57,0	54,3
60%BFS	21,0	21,7	40,5	44,4	53,4	52,3

Results table-4-c:
c- 7,28,80 day compressive strengths of clinker-C after normal water & sulphated water treatment.

Sample name	Clinker -C case:					
	7days, N/mm²		28days, N/mm²		80days, N/mm²	
	normal water,7	sulphated water,7	normal water,28	sulphated water,28	normal water,80	sulphated water,80
Portland cement	37,8	38,0	41,7	43,5	43,6	47,0
40%BFS	31,2	31,8	45,4	45,8	52,7	54,2
50%BFS	26,0	26,9	40,7	43,6	49,6	51,0
60%BFS	21,0	21,3	37,4	39,8	46,3	48,4

Results table-4-d:
c- 7,28,80 days compressive strengths of clinker-C after normal water & sulphated water treatment.

Sample	Clinker -D case:(Low KST case)					
name	7days, N/mm²		28days, N/mm²		80days, N/mm²	
	normal water,7	sulphated water,7	normal water,28	sulphated water,28	normal water,80	sulphated water,80
Portland cement	40,2		44,5			
40%BFS	30,0	31,3	45,5	44,9	55,2	53,1
50%BFS	24,6	27,8	42,1	43,4	54,2	53,8
60%BFS	21,3	21,7	37,1	39,3	51,4	48,4

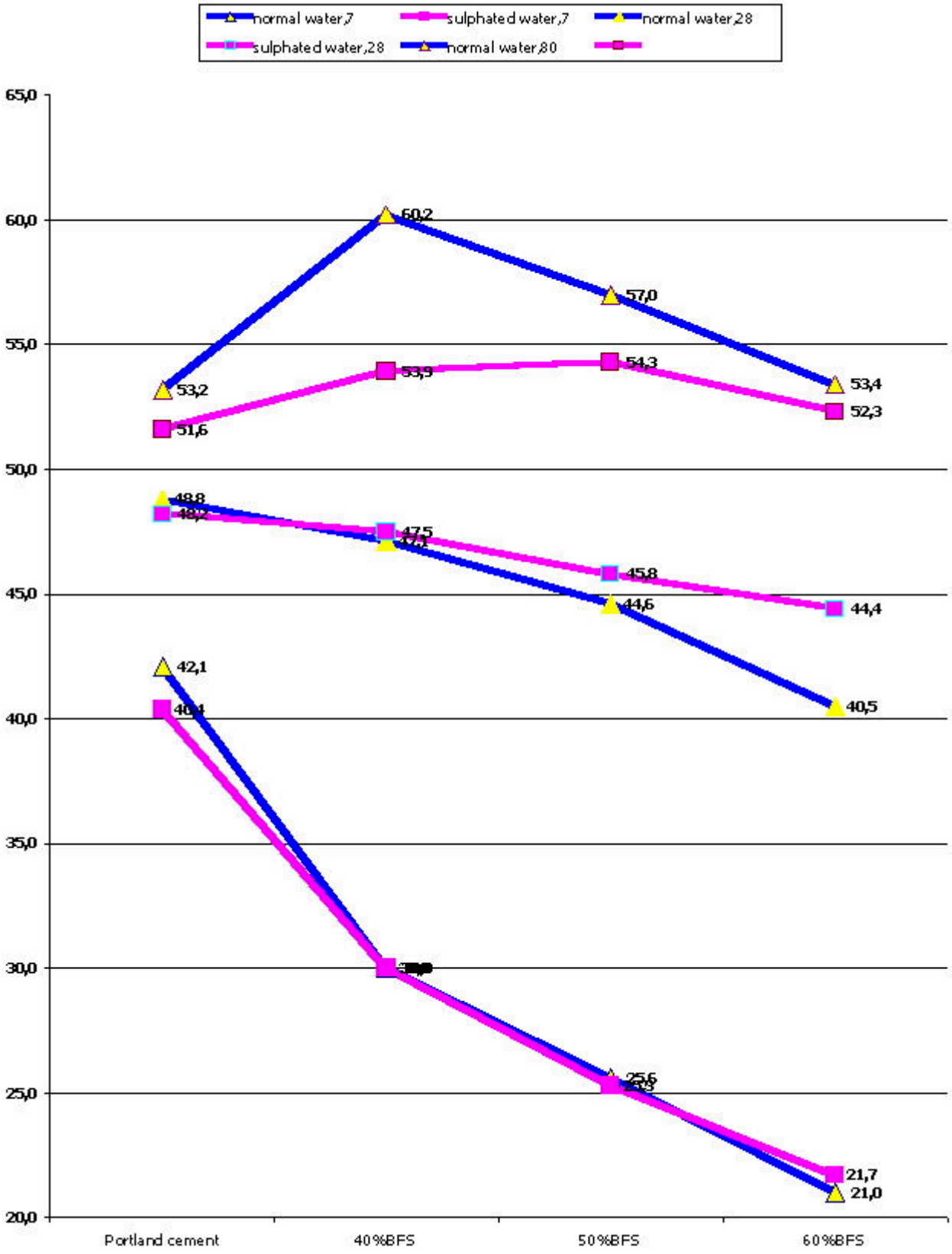

Figure 1. Graph for clinker-A: 7, 28, 80 day strength in normal/sulphated water condition

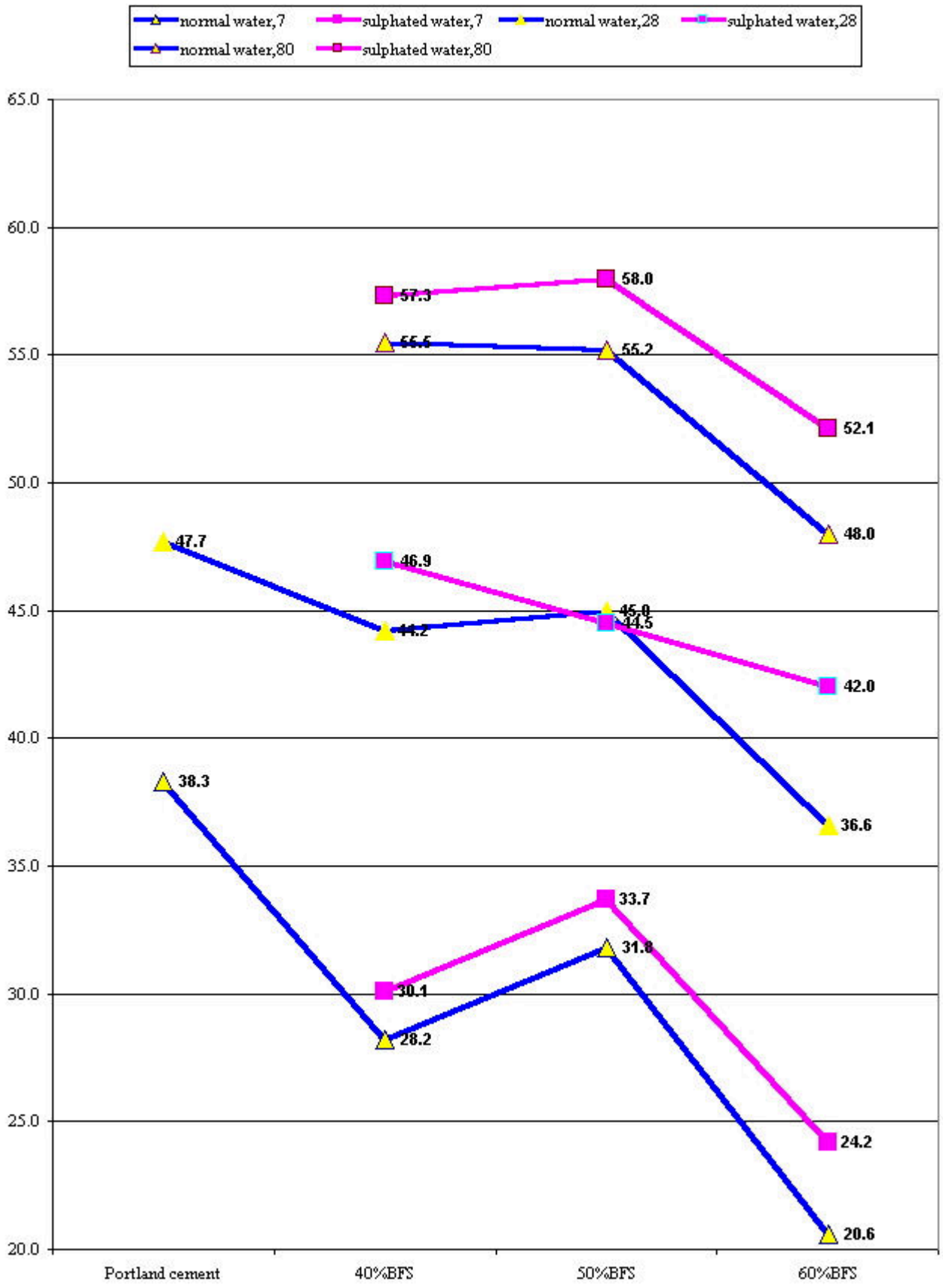

Figure 2. Graph for clinker-C: 7, 28, 80 day strength in normal/sulphated water condition

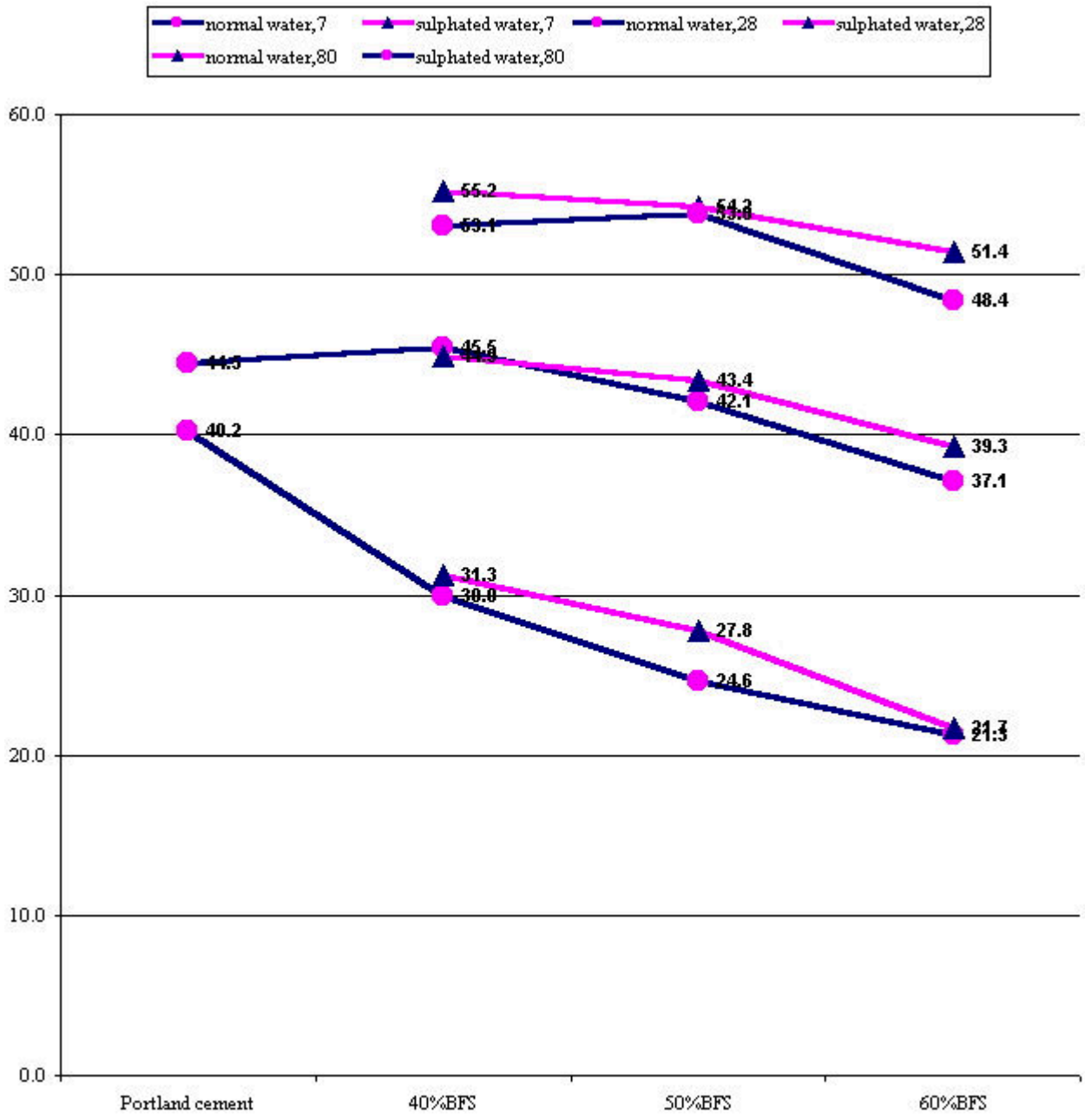

Figure 3. graph for clinker-D: 7, 28, 80 day compressive strength in normal/sulphated water condition

Figures 1, 2 and 3 show that cement prisms prepared by clinker C are positively affected by sulfated water in 28 and 80 day periods.

- No significiant effect evidence in the 2 and 7 day periods.
- At the end of 28 days period

For clinker-A:

- Mortars prepared with OPC are negatively affected by 28 days strengths decrease from 48.8 to 48.2 N/mm^2
- The positive effect of BFS is apparent at 40% content and increases at BFS contents of 50% and 60 %. The mortar compressive strength increases from 40.5 to 44.4N/mm^2 in sulfated water.

For clinker-C:

- Mortars prepared with OPC undergo a decrease in compressive strength from 41.7 to 43.5 N/mm^2 at 28 days, a drop of 4.3%.
- In BFS containing cements the positive effect is observed in sulfated water with increasing BFS content at 60% BFS content, a 6% compressive strength increase occurs from 37.4 to 39.9 N/mm^2 by 28 days.
- At the end of 80 days period (figures 1 and 3)

For clinker-A:

- Negative effect of sulfated conditions have increased on mortars prepared by OPC to decrease compressive strengths from 53.2 to 51.2 N/mm^2 (fig 1)
- The tests show that in 80 days, even the addition of BFS has not stopped the negative effect of the sulfated condition on mortars prepared with the clinker.

For clinker-C:

- Mortars prepared with OPC continued to be affected positively by sulfated water and their compressive strengths increased by 7.3% from 43.6 to 46,8 N/mm^2.

An absolute positive effect of sulfated water on OPC prepared using clinker C and BFS is obtained.
In OPC from 43.6 to 46.8 N/mm^2, => %7,3 ↑
%40BFS from 52,7 to 54,2N/mm^2 => %5,3 ↑
%50BFS from 49,6 to 51,0N/mm^2 => %3,0 ↑
%60BFS from 46,3 to 48,4N/mm^2 => %4,8 ↑

As it will be seen fig.3 the positive effect of sulfated water on compressive strengths with respect to normal water are observed after 80 days. The effects of sulfated water at longer ages will also be followed.

Summary 5:

Table 5. Setting time data in accordance with clinker type and BFS content

Beginning of setting ,hr			
	Clinker-A	Clinker-B	Clinker-C
PC	2:02	2:35	3:48
%40BFSlag	2:43	3:03	3:47
%50BFSlag	3:13	3:28	3:47
%60BFSlag	3:38	3:38	3:47

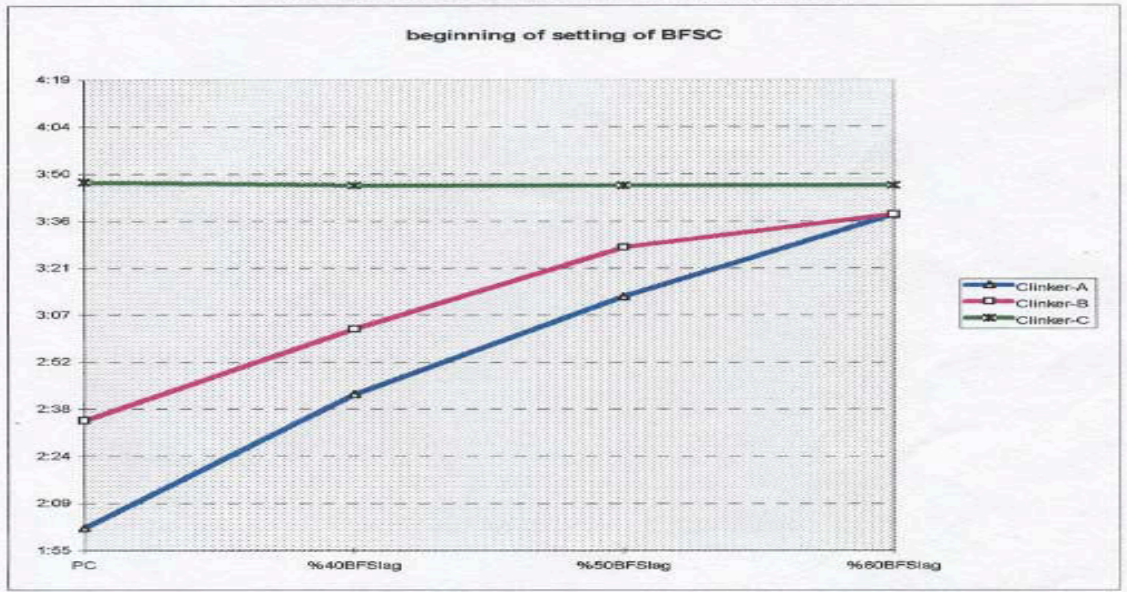

BFS cements prepared with clinker A & B exhibit longer set times with increasing BFS contents. The cement prepared with clinker C is affected because of activation by its high alkali content.

3.1 Results of XRD and electron microscopes

1 cm particles broken from mortar prisms were covered with gold by POLARON PS 100 and their microstructure analyzed in the secondary electron mode using a LEITZ AMR 1000 scanning electron microscope but no figures are included.

Mineralogical structure of mortar prisms of OPC and BFS cements of 40%, 50%, 60 % contents were analyzed by XRD after hydration in normal water conditions .The results are given below.

3.1.1 Clinker-C in 28 days period .under normal /sulphated water;

- More Portlandite forms in Portland cement mortars in comparison with BFS cements. Additionally hydrogarnet formation is observed.
- Portlandite formation is more significant in sulfated water.
- In BFS cements there is less portlandite formation in comparison with sulfated waters. Formatted portlandite quantity is not affected by BFS content of cement.

3.1.2 Clinker-A at 28 days. Normal /sulphated water;

- More Portlandite forms in Portland cement mortars in comparison with BFS cements. Additionally hydrogarnet formation is observed.
- When sulfated water conditions are analyzed there is no significant difference among the BFS cement mortars. Portlandite formation is not observed in 60% BFS-containing cement mortars.

In the 2, 7, 28 day study of industrial slag significant hydration was only observed after 28 days. The Ca (OH) 2 content decreases in samples containing 20 and 50 % slag and disappears in cements with an 80 % Slag content. The slag hydrate is richer in MgO and Al_20_3 than that Al_20_3 from OPC.

To avoid any harmful alkali-aggregate reaction, it is recommended that low alkali cement (not more than 0.6 % Na_20 equivalent) be used. Alternatives for avoiding alkali-aggregate reactions are adding pozzolans to the concrete mix. They combine rather rapidly with the alkalis. Blastfurnace slag has a similar effect. This takes place at a time when the concrete is still deformable without deterioration.

3.2 The role of alkalis in concrete

The soluble alkali compounds (present mainly as alkali sulphate) influence the composition of the solution in the fresh cement paste. Alkalis reduce the solubility of lime and increases that of alumina and silica, thus increasing rate of hydration of the main constituents of cement.

The presence of water soluble alkalis accelerates the hydration of cement and thus increases the early strength whereas the 28-day strength is reduced.

Alkalis in hardened concrete may react with some reactive types of aggregate forming a voluminous gel. Reactive aggregate can be: Opal, chert, flint, chalcedony, cryptocrystalline or amorphous silica, shaly dolomite, or badly crystallized volcanic rock.

The volume increase linked with the formation of alkali silicate hydrate gel or the dedolomitization induces expansion and severe deterioration of concrete. Whether the reactions of alkalis are beneficial or detrimental depends on their timing. If they occur when the concrete is still deformable, they are beneficial.

Similarities and differences between the hydration of Portland cement and Portland-BFS cement mixtures are important in explaining their properties.

For slag hydration, Portland cement and the alkalis, gypsum and $CaOH_2$ (all of which derive from the cement) act as activators and reactants. NaOH has a greater effect than $CaOH_2$ with increasing addition. Alkali activators accelerate the dissolution of ions containing Si and Al by breaking the Si-O and Al-O bonds in the slag glass structure which is followed by precipitation of low-solubility calcium silicate and calcium aluminate hydrates due to increased ionic concentrations in the liquid phase. At high pH values dissolution of Al is accelerated which initiates slag hydration when the pH of the liquid phase reaches approximately 12, at which condition ettringite is formed stably. The hydration is most accelerated $CaOH_2$ after hydration of cement causes the carbonation reactions its rate depending on cement content, w/c ratio, compaction of concrete and climatic conditions in order to avoid from the carbonation reactions pozzolanic reactions contribute to strength formation.

4. CONCLUSIONS

It is better to produce Blastfurnace slag cement with high total alkali contents (around 1,1 and higher) in clinker, especially for service in the sulphated water.

Total alkalinity of clinker C is 0.60 % higher than clinkers A,B and D. It can be accepted that this excess alkali is enough to activate BFS as illustrated by the setting time figures.

It is possible to add 60% BFS to clinkers A & C. Although clinker A has 10 N/mm^2 more compressive strength than OPC, both clinkers A and C reach the same point in the case of added BFS. At this point this can be claimed that total alkali content of more than 1.1% is sufficient to activate BFS of activity index of 80. High Na_2S0_4 content water cure results in positive strength gains in 28 - 80 days. Tests on prisms using clinker containing more than 1.1% total alkali and Iskenderun iron plant BFS. Compressive strength reductions are observed in the 80 day period when clinkers with only 0,60 % alkali content are used.

REFERENCES

[1] Structure and Performance of Cements;edited by J.Bensted and P.Barnes
[2] Sub- Theme 111-2 Structure and behavior of slag, Portland Cement hydrates M.REGOURD/ Microstructure Department C.E.RI.L.H. Paris, FRANCE
[3] Cement and Concrete Research.Vol.21.pp.101-108.
[4] CANMET -properties and durability of alkali activated slag concrete-Nov 1990
[5] Cement and Concrete Research.Vol.20.pp.961-974/early activation and properties of slag cement.
[6] Cüruflar ve Cüruflu Çimentolar-Doç.Dr.Mustafa TOKY AY&Korhan Erdoğdu.
[7] Cement Seminar, materials technology-Cement, sect 16
[8] Progress in cement and concrete-Hydration of slag cement-AMalekpp.85-112
[9] Progress in cement and concrete-Durability of blended cement-pp. 449-465
[10] The properties and behavior of bentonite/cement slurries by A Güner, 1978 London
[11] The chemistry of cements by H.F. W. Taylor vol-2.
[12] ACI Manual of concrete practice 1996 - part 1
[13] Endüstriyel ve tarimsal artiklarin çimento üretiminde degerlendirilmesi by H.Ölmez, Samsun 1988

IMPROVED PERFORMANCE OF BLAST FURNACE SLAG CEMENT MADE WITH HIGH ALKALI CLINKER

B. Mus

Denizli Cement Plant, P.Box 29, 20100 Denizli, Turkey.

Personal Details: **Date: Dec, 3rd 2002**

Name	**Birgül**
Surname	MUS
Birth Place	**Istanbul**
Birth Date	**8.5.1960**
Status	**Married**
Sex	**Female**
Driving License	**B class**
Language	**English**

Address:
Denizli Çimento Fabrikasi Denizli / TURKEY
Tel no : 00 90 258 762 12 60
Fax no : 00 90 258 762 12 80
E- Mail: bmus@denizlicimento.com.tr

Academic &Professional Details:

1-Academic Details

From:	To:	University/city	Certificate	Title
1978	1985	Middle East Technical University / Ankara-TURKEY	BS diploma	Chemical Engineer
	1978	Yenimahalle Lisesi/Ankara-TURKEY	High School diploma	

2-Professonal details

From:	To:	Company / City	Title/Reporting to:	Major/Subject
Dec-2001	now	**DENIZLI** Cement Plant	Quality Assurance Manager	Responsible from, ISO9001 Quality Assurance System together with Quality Control and Researching.
July-98	Dec-2001	**EMD** Proses ve Kalite Rehabilitasyon Ltd Sti.	Monetary &Quality Manager	Turnkey rehabilitation projects for the existing cement plants to improve their capacities; ISO9002 systems adaptation

Apr-96	July-98	**OYSA** Iskenderun Çimento San. ve Tic. A.S. Iskenderun	Quality Assurance and Research Chief / General Manager	Responsible from, ISO9002 Quality Assurance System together with Quality Control and researching. (as a Management Responsible)
Jan-96	Apr-96	**Yibitas LAFARGE** Sivas Çimento San. ve Tic.A.S/SIVAS	Quality Development Manager / General Manager	Responsible from Process Control and Improvement.
Mar-93	Jan-96	**Yibitas LAFARGE** Sivas Çimento San. ve Tic.A.S/SIVAS	Quality Control Chief / General Manager	Responsible of Quality and Process Control
Mar-93	Sep-91	Yibitas Çimento San. ve Tic.A.S/YOZGAT	Quality Control Chief Assistant /Quality Control Chief	Responsible of Quality Controlling
Feb-87	May-91	Adana Çimento San. ve Tic.A.Ş/ADANA	XRF engineer / Quality Control Chief	Establishment of ARL spectrometer lab.
Sep-86	Feb-87	Turkish Electricity Association /ANKARA	Chemical Engineer	in a technical team dealing with Afsin-Elbistan Power Plant

3-Professional courses given:

From	To	Organized Company -City	To Company	Major/Subject
Jun-95	Oct-95	Çitosan /ANKARA	SET Group Cement Holding	"Quality Control of Cement"

4-List of main Publications, papers:

Date	Notation	Organized by Institute/Company	Major/Subject
Nov-97		1.National Cement Additives Congress Organized by **TÇMB**	**The Effect of Total Alkaline content of Clinker in the production of Blastfurnace Slag Cement.**
Oct-95	55.18	**LAFARGE/CKHC**, Cement Know-how Center-Paris	"**Improvement of Clinker Quality**" (in Sivas Plant)
Oct-95	55.17	**LAFARGE/CKHC**, Cement Know-how Center-Paris	"**Clinker Optimization formulas**" (empirical derivation)
Oct-95	pg 9-12	MÜSTAHSILLER BIRLIGI-Ankara	**"Alkaline-Sulfur balance and build-ups in the kiln"**

5-Computer skills

- Windows 3.11 workgroups, word, excel
- Oxford XRF MDX1000 software- Expertise in Windows 3.11 workgroups
- ARL XRF 8680 software-DPS/T

HIGH STRENGTH CEMENT-MELAMINE FORMALDEHYDE RESIN PRODUCTS

V.K. Singh, S.D. Khatri and R.K.Singh

Department of Ceramic Engineering, Institute of Technology,
Banaras Hindu University, Varanasi - 221 005, India.
Tel: 0091 542 307042 Fax: 0091 542 368174
E-mail: vksingh_cer@yahoo.com, vksingh@banaras.ernet.in

ABSTRACT

The effect of melamine formaldehyde resin addition to ordinary cement on its properties like heat of hydration, setting time, compressive and tensile strength has been studied by adding 0.5 to 5.0% additive by weight of cement. Hardness has been tested using the Vickers indentation method. Fracture toughness of cementitious bond and bending strength have been determined by using three point bending system. Corrosion resistance of resulting products has been tested against 0.1 and 1.0 N HCI and H_2SO_4 and seawater respectively. Water absorption/open porosity and microstructure have also been determined. It was observed that strength, hardness, toughness and corrosion resistance increase up to 5.0% addition of melamine formaldehyde resin in ordinary Portland cement. The polymeric phase is interspersed in cement causing a decrease in water absorption/open porosity. Its interaction with hydrating cement caused additional bond formation leading to the increase in strength.

1. INTRODUCTION

Building materials such as cements based on calcium silicates, calcium aluminate and calcium sulfate which exhibit low flexural strength with their differing chemical compositions, varying degrees of hydration and setting mechanism are never used in flexure or tension without reinforcement. Flexural as well as the compressive strengths of cement are increased with polymer addition. Polymer cement mortars and concrete have potential applications in the engineering aspects of the new class of high strength materials. Organic polymer used in cement mortar and concrete can be divided in to three groups namely latex, liquid resin and water-soluble polymer. In the process of modification with liquid resins, considerable amounts of polymerizable low molecular weight polymers are added in a liquid form to cement mortar and concrete during mixing.

In this modification, polymerization is initiated in the presence of water to form a polymer phase, and simultaneously the cement hydration occurs. As a result, a co-matrix phase is formed with a network structure of interpenetrating polymer and cement hydrate phases which binds aggregate strongly. Consequently, the strength and other properties of modified mortar and concrete are improved. Preparation of polymer admixtures requires special attention for modifying cements to get changes in their microstructure, physico-chemical and physico-mechanical properties. The effect of different quantities of such additions on kinetics of hydration of cement and the characteristics of hydration products are of considerable importance [1-7]. The present work, undertaken in view of these considerations, reports the effects of melamine formaldehyde resin on the properties of ordinary cement. The properties studied include setting time of cement, compressive and tensile strength and corrosion resistance of cement mortar and microstructure, flexural strength, fracture toughness and hardness of neat cement products.

2. EXPERIMENTAL

Ordinary Portland cements taken from the local market, sands from the Sone river and reagent grade melamine formaldehyde resin were chosen for the present work. The effect of melamine formaldehyde resin has been studied by mixing 0.5 to 5.0 percent additive by weight of cement. 1:3 cement/sand mortar was used for the determination [2] of strength. For determination of heat of hydration, different percentages of additive were dispersed in water required for standard consistency of cement paste. Dispersed additive was then mixed with cement and the paste so obtained was filled in specimen tubes (20 × 20 mm) corked and then sealed with wax. They were stored in vertical position at 25 ± 2°C in 90% relative humidity. The heat of hydration was obtained from the difference of the heat of solution of unhydrated and hydrated cement samples.

The calorimeter consisted of assembly of units as per Bureau of Indian Standards [2], which was calibrated with analytical reagent grade zinc oxide. Infra-red spectra [5] of neat cement and also with additive (cured for 90 days) was recorded on JASCO, JAPAN, FT/IR-5300 with KBr. X-ray diffraction patterns of neat hydrated cement and modified cement containing additive were taken on x-ray diffractometer (RICH SEIFERT CO. GmbH & COKGD-2076, Germany, Model No. ID 3000) using CuK_α radiation with Ni filter. Intensity and d-values of observed peaks were compared with the values given in JCPDS cards [3] for different phases. The initial and final setting time of cement with and without additive were determined as per Bureau of Indian Standards [2]. Cube samples of 50-cm^2 cross-section were prepared on a vibrating machine (AIMIL 416) for the determination of compressive strength and standard briquettes were prepared for the tensile strength. Samples for both the tests were kept in 90% relative humidity at 25 ± 2°C for 24 hours and then demoulded and cured at the same humidity and temperature for 7, 28 and 90 days.

Hardness of neat cement samples with and without additive was determined using the Vickers Indentation method at 5, 10, 50 and 100N loads on 90 days cured polished samples. Flexural strength and fracture toughness were determined on rectangular (1 × 1 × 5 cm^3) bar samples under three point bending flexure using a Universal testing machine (Shimadzu, Japan). Toughness was determined using single-edge notched beam (SENB) at 20 mm span length and cross head speed of 0.5 mm/min. Water absorption was determined using cube samples with 25 cm^2 cross-section area. Resistance to corrosion in five aggressive media (0.1 and 1.0N H_2SO_4, 0.1N and 1.0N HCl and seawater) was determined on cube mortar specimens (25 × 25 ×25 cm^3) containing 0.5 to 5.0 percent additive.

3. RESULTS AND DISCUSSION

Ordinary cement constituents e.g. C_3A and $C_{12}A_7$ (C = CaO and A = Al_2O_3) react with water to produce hydrates like CAH_{10}, C_2AH_8 and C_3AH_6 (H = H_2O) and calcium silicates e.g. C_3S and C_2S (S = SiO_2) to produce C-S-H_I, C-S-H_{II} and $C_5S_6H_5$ etc. In the presence of the polymer additive, some new phases are also formed. Infrared spectra of the 90 days hydrated cement and mix with 5% melamine formaldehyde are shown in Fig.1.

It shows that the bands between 972 and 3645 cm^{-1} are because of hydrated calcium aluminates and between 3437 and 3645 cm^{-1} are predominantly due to water molecule [5] or OH group vibration from Ca $(OH)_2$ and other hydrates present in the systems. The bands between 453 and 873 cm^{-1} are quite broad and not properly resolved. They may be due to the Si-O and Al-O stretching vibration of silicate and aluminate groups. The bands between 800 and 972 cm^{-1} are strong and broad indicating polymeric silicate (SiO_4) and aluminate group vibrations. The band observed at 972 cm^{-1} is due to the higher shifting of absorption band of C_2SH_2 and C-S-H phases present in cement.

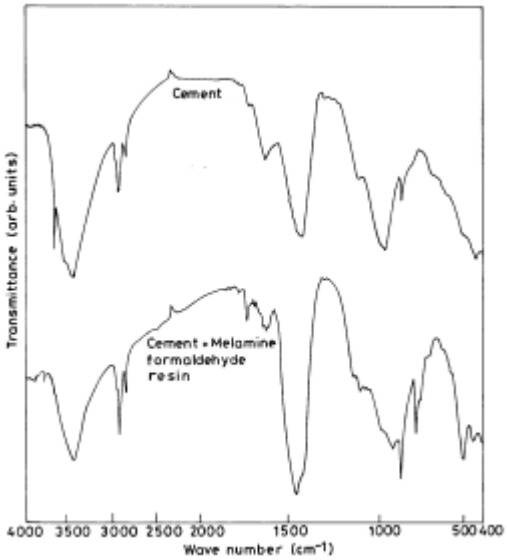

Figure 1. IR of 90 days hydrated cement and cement containing 5.0% melamine formaldehyde resin

The bands between 1500 and 2000 cm^{-1} are not very well resolved. The bands at 1637 cm^{-1} may be because of monosulfate group [5] which indicate the heterogeneous character of the materials involving cement components and the gypsum which are hydrated and their infrared bands overlap. As compared to the infrared absorption band of hydrated cement, some new bands were detected in the sample hydrated with melamine formaldehyde resin.

The new band at 3645 cm^{-1} of OH group vibration was found to be absent in the cement-melamine formaldehyde resin mix cured under similar conditions. Fig. 1 shows that two new bands were observed at 2926 and 2854 cm^{-1} in the mix which may be because of –CH stretching vibration from $-CH_2$ group. A new band at 1743 cm^{-1} may be because of -NH bending group present in the melamine formaldehyde resin. The bands at 3423 and 1629 cm-1 may be because of O-H stretching and monosulfate group at 875 and 520 cm^{-1} may be because of polymeric silicates and aluminates and C_3AH_6 group respectively. The shift in positions as compared to neat cement may be because of the interaction between melamine formaldehyde resin and hydration products of cement.

X-ray diffraction patterns of 7, 28 and 90 days cured hydrated cement show the important peaks of cementitious phases formed during hydration (Fig.2A, B & C). Cement on hydration produces hydrated calcium silicate namely $Ca_2SiO_5H_2$ which has intense peak at 2θ=26.60° (d=3.34Å), 18.05° (4.90Å), 34.40° (2.62Å), 47.17° (1.92Å) and CaO_2H_2 at 2θ=50.84° (d=1.79Å) in 7 days hydrated cement samples.

Their intensities decrease as the hydration time increases from 7 to 90 days. The peak intensity of tobermorite phase ($C_5S_6H_5$) at 2θ=29.39° (d=3.03Å) increases from 26 to 93 with increase in hydration time from 7 to 90 days. The peaks of trisulfate phase ($C_3A.3CaSO_4.32H_2O$) were detected at 2θ=15.73° (d=5.62Å), 24.29° (3.66Å), 25.13° (3.53Å), 26.60° (3.34Å), 37.81° (2.37Å) and 38.57° (2.33Å) in 7 days hydrated cement sample while the peaks of monosulfate ($CA.CaSO_4.11H_2O$) appeared at 2θ=19.90° (d=4.45Å), 31.34° (2.85Å) and 34.84° (2.48Å) in 28 days cured samples and 2θ=32.99° (d=3.86Å), 25.05° (3.55Å), 32.27° (2.77Å), 36.95° (2.43Å) and 56.56° (1.62Å) in 90 days hydrated cement sample. The other important phases detected in hydrated cement were C-S-H_I at 2θ=41.25° (d=2.18Å) and 60.10° (1.53Å) at 7 days and CSH_{II} at 2θ=42.32° (d=2.18Å), 59.92° (1.54Å) and 2θ=36.95° (d=2.43Å) and 60.01° (1.54Å) in 28 and 90 cured samples respectively. Important phases detected in 90 days cured cement samples were $Ca_2SiO_5H_2$ at 2θ=11.10° (d=7.59Å), 15.81° (5.59Å), 25.05° (3.55Å), 26.67° (3.33Å), 34.12° (2.62Å), 50.82°

(1.79Å) and 2θ=62.57º (d=1.48 Å), Ca3Al2O12H12 at 2θ=26.67° (d=3.33 Å), 32.27° (2.77 Å), 38.66° (2.32 Å) and 2θ=50.82° (d=1.79 A), $Ca_5Si_6O_{22}H_{10}$ at 2θ=29.38° (d=3.03Å) and $Ca_3Fe_2O_{12}H_{12}$ at 2θ=51.88° (d=1.76Å) and 2θ=62.57° (d=1.48Å). The organic additive to cement influences the hydration of cement and is also influenced by the hydration of cement because of chemical interaction. The ions or molecules formed during the hydration of cement control the formation of cement-melamine resin products. On the addition of melamine formaldehyde resin in cement the relative intensities of the peaks corresponding to hydrated cement phases were altered and a few new peaks were detected along with the disappearance of some of the peaks shown in 90 days hydrated neat cement samples. In the 5% melamine resin-cement mix, XRD pattern (Fig.2D) has shown that new peaks appear at 2θ=23.53° (d=3.77Å), 26.17° (3.40Å) and 2θ=28.20° (3.16Å).

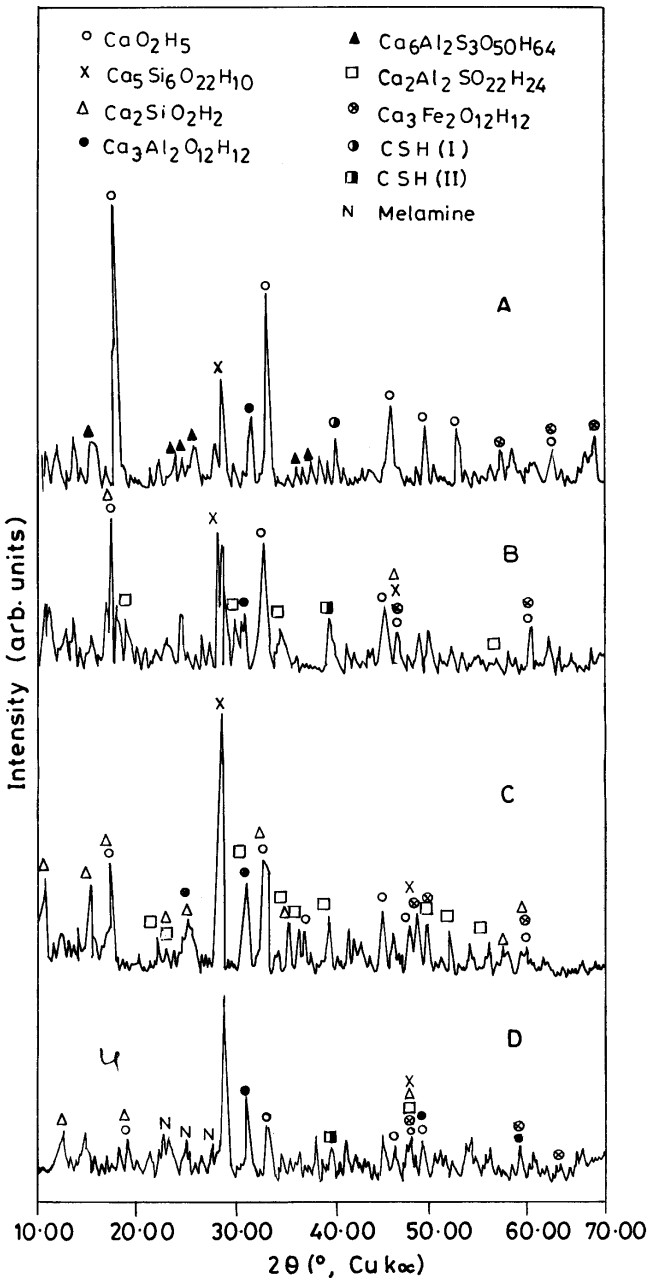

Figure 2. X-ray diffraction pattern of cement hydrated for(A) 7 days, (B) 28 days, (C) 90 days and (D) 90 days hydrated cement containing 5.0% melamine formaldehyde resin

The peaks of monosulfate at 2θ=22.92° (d=3.87Å) and 2θ=25.56° (d=3.48Å) and C-S-H_{II} at 2θ=58.82° (d=1.56Å) have increased intensities as compared to their intensities in 90 days hydrated neat cement. Some of the peaks of 90 days hydrated cement were adversely affected by the

melamine formaldehyde resin addition and their intensities were considerably reduced e.g. peak intensities of free lime at 2θ=18.87° (d=4.90Å), the intensity of which was reduced from 46 to 12 and of $Ca_2SiO_5H_2$ at 2θ =11.70° (d=7.96Å), 34.26° (d=2.62 Å) and 2θ=47.07 ° (d=1.92 Å) from 33 to 16, 43 to 18 and from 25 to 11 respectively. A new peak formed at 2θ=23.53° (d=3.77Å) due to melamine [3] compound, indicates the formation a distinct new phase in the melamine formaldehyde resin-cement mix during interaction which may be causing the increase in strength.

3.1 Heat of Hydration

When cement reacts with water, the process is accompanied by the evolution of heat and leads to the decrease in the energy of the system [4]. The hydration process of cement can be assessed by the measurement of the heat evolved during hydration. Several of the properties important to the user of Portland cement and other hydraulic materials are direct results of the hydration reaction taking place between the components of the cement and water.

3.2 Kinetics of Dissolution

If T_e is the maximum temperature rise (°C) after complete dissolution and T, the temperature at any time, t (min), the following relation can express [22] the dissolution kinetics of cement:

$$\log T_e - \log (T_e - T) = Kt \qquad (1)$$

where K is a constant. It is the equation of a straight line and represents a first order kinetics. Cement dissolves in the mixture of nitric acid and hydrofluoric acid and thereby the temperature of the reaction mixture rises. It increases rapidly in the beginning and, thereafter, slows down. Fig. 3 shows the plot of temperature-rise against the time of dissolution for the dry cement as well as the cement hydrated for 3, 7, 28 and 90 days. As the time of hydration increases from 3 to 90 days, the final temperature rise decreases from 5.19 to 3.91°C. Dry cement gave a value of 5.29°C, while the same was 5.19, 4.85, 4.56 and 3.91°C for cement samples hydrated for 3, 7, 28 and 90 days respectively. The curves were found to be parabolic where rapid temperature rise takes place in the beginning and, thereafter, it slows down. Knowing the rise in temperature, one can assess the quantity of cement dissolved in the acid mix at a particular time. The data show that it is higher for dry cement as compared to the same for hydrated samples dissolved at a particular time. The maximum temperature rise obtained after the complete dissolution of a known weight of cement is a constant value (T_e). Thus log T_e may be assumed to be a constant in the equation (1) and (T_e-T) varies with time, t. A plot of log (T_e-T) Vs t was found to be a straight-line relationship. The values of slopes (Table 1) of straight lines were 0.70, 0.67, 0.64 and 0.58 for 3, 7, 28 and 90 days hydrated cement respectively. The dry cement gave a straight line of slope 0.73. As the hydration time increases, the slope values decrease.

Table 1. K values for dissolution process

Hydration time (days)	K values (min^{-1})	
	Cement	Cement-5% melamine formaldehyde resin mix
3	0.70	0.66
7	0.67	0.59
28	0.64	0.54
90	0.58	0.50

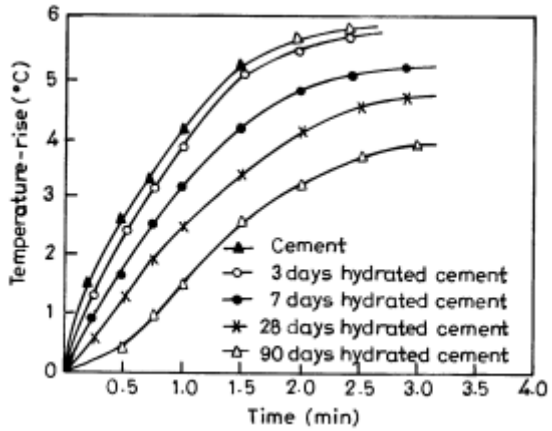

Figure 3. Temperature-rise during the dissolution of cement and hydrated cement in HF + HNO_3 mixture.

The plot of temperature rise against the time of dissolution for the cement-5% melamine resin mix hydrated for 3, 7, 28 and 90 days was also parabolic. In this system, as the time of hydration increases from 3 to 90 days, the final temperature rise decreases from 5.09 to 3.91°C. The maximum temperature rise (T_e) is a constant value of each sample. Plots of log (T_e-T) Vs t (Fig. 4) for cement–melamine resin system were also found to be a straight-line relationship. The values of slope were 0.66, 0.59, 0.54 and 0.50 for 3, 7, 28 and 90 days hydrated samples respectively. The average K value obtained was lower with melamine resin additive compared to the values for neat hydrated cement. The dissolution of cement with and without additive was found to be of first order reaction kinetics.

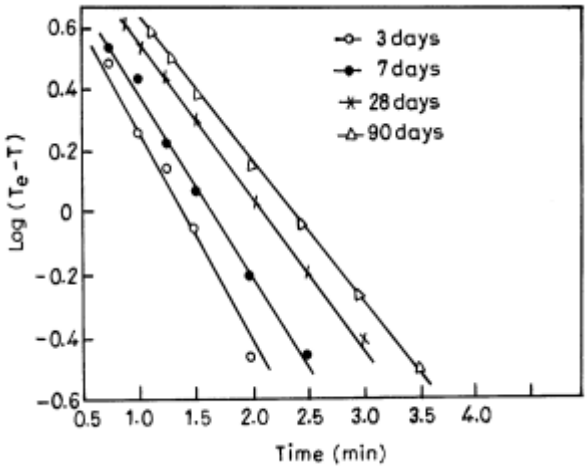

Figure 4. Plot of log (T_e - T) vs. time of dissolution for cement hydrated with 5.0% melamine formaldehyde resin

Table 2 shows the heat of hydration of cement-melamine resin mixes as calculated by the difference in the heat of solution of unhydrated and hydrated samples. The values of heat of hydration of cement were 259.57, 326.41, 364.11 and 439.95 J/g for samples hydrated for 3, 7, 28 and 90 days respectively. The values for cement-melamine resin mixes were 264.09, 328.67, 368.04 and 440.99 J/g with 0.25%, 268.69, 330.93, 371.89 and 442.41 with 0.50%, 277.80, 335.40, 379.92 and 446.80 with 1.0%, 286.03, 344.34, 395.05 and 451.81 with 2% and 303.80, 348.48, 399.81 and 452.19 with 3.0% and 304.50, 349.43, 402.81 and 456.46 J/g with 5.0% melamine formaldehyde resin addition in cement hydrated for 3, 7, 28 and 90 days respectively. The values of heat of hydration (Table 2) increase with increasing concentration of melamine formaldehyde resin in cement up to 5.0%.

Table 2. Values of heat of hydration of cement with different quantities of melamine formaldehyde resin

% Additive	Heat of Hydration (J/g)			
	3 days	7 days	28 days	90 days
0.00	259.57	326.41	364.11	439.95
0.25	264.13	329.76	366.41	439.96
0.50	269.23	332.39	368.75	440.53
1.00	278.93	339.87	373.44	441.53
2.00	296.06	352.83	382.84	444.04
3.00	310.78	354.09	392.25	446.38
5.00	318.22	358.63	396.91	448.78

3.3 Setting Time

The hydration of cement constituents gives a variety of hydrates (Fig. 5 &6). The calcium silicates have been shown to have tetrahedral $[SiO_2 (OH)_2]^{2-}$ structure having accessible sites for the interlocking of hydrates. The gel structure of the tobermorite phases and the interlocking of hydrated aluminates and silicates bring about the stiffening of the paste and are responsible for setting of the cement paste [2]. The setting times of cements containing 0.1 to 5.0% melamine formaldehyde resin are given in Table 3. The value of initial setting time and final setting time of cement used was found to be 130 and 230 minutes respectively. Melamine formaldehyde resin mixed in cement has brought changes in its setting time as shown in Table 3. It was found to act as a retarder and has increased the initial setting time from 132 to 169 minutes with 0.1 to 5.0% addition in cement. Final setting time was also increased from 232 to 273 minutes for similar percentages of melamine formaldehyde resin added in cement.

Table 3. Setting time of cement with different quantities of melamine formaldehyde resin

% additive	Setting time (min)	
	Initial	Final
0.0	130	230
0.1	132	232
0.3	135	237
0.5	141	242
1.0	149	250
3.0	157	259
5.0	169	273

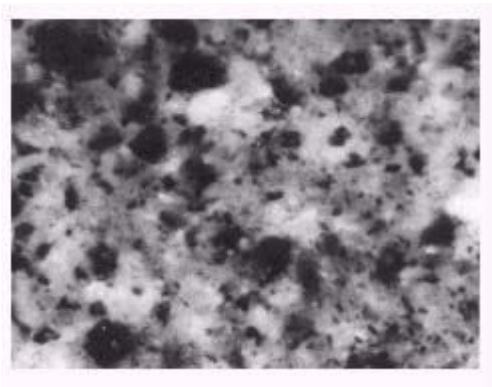

Figure 5. Microstructure of 90 days Hydrated Cement [x20]

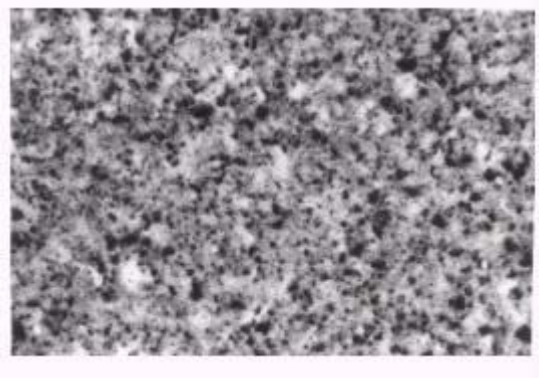

Figure 6. Cement mixed with 5.0% melamine Formaldehyde resin [x20]

3.4 Compressive and Tensile Strength

The strength is caused by the intergrowth and welding together of the splines of calcium silicate hydrate and other phases in set Portland cement. Fig. 7 shows the compressive strength of cement mortars cured for 7, 28 and 90 days. The values are 31.60, 43.32 and 58.10 MPa respectively. The variations in the strength of cement with 0.5 to 5.0% melamine formaldehyde resin are also shown in Fig. 7. The values are 32.67, 32.79, 33.45 and 34.62 MPa at 7 days cured cement mortar, 45.10, 47.24, 49.79 and 52.76 MPa at 28 days and 59.48, 60.70, 63.96 and 66.10 MPa at 90 days with 0.5, 1.0, 3.0 and 5.0% melamine formaldehyde resin mixed in cement respectively. The values of compressive strength increase with increasing concentration of melamine formaldehyde resin up to 5.0% in cement. Cement is weak when tested under tension and organic additives have been found to increase the tensile strength. Fig. 8 shows the tensile strength of cement mortar cured for 7, 28 and 90 days. The values are 3.10. 4.43 and 5.75 MPa respectively. When melamine resin was mixed in the cement mortar, the values of tensile strength (Fig. 8) were 3.59, 3.80, 4.04 and 4.30 MPa at 7 days, 4.79, 5.03, 5.28 and 5.47 MPa at 28 days and 6.13, 6.41, 6.56 and 6.94 MPa at 90 days respectively with 0.5, 1.0, 3.0 and 5.0% melamine resin mixed in cement. The values of tensile strength increased up to 5.0% melamine resin addition in cement.

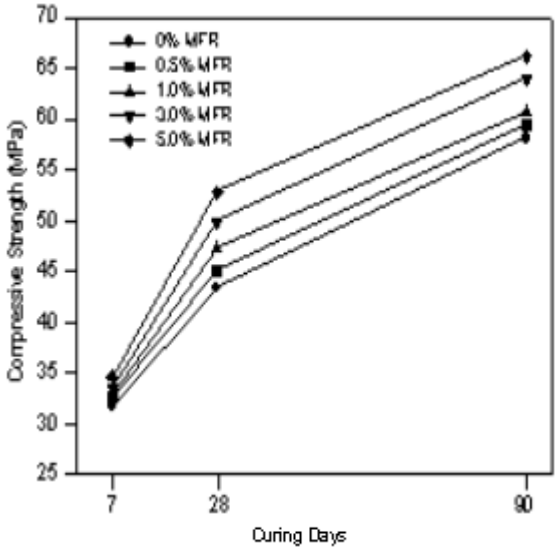

Figure 7. Compressive strength of cement with different percentages of melamine formaldehyde resin

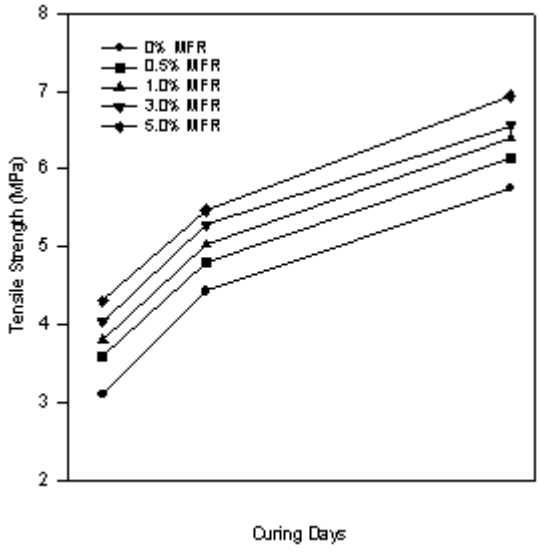

Figure 8. Tensile strength of cement with different percentages of melamine formaldehyde resin

3.5 Indentation Hardness

With progress in setting reactions, new bonds are formed in cement products and their strength as well as hardness increase. Polymer present in the products contributes additional bonds, which causes further increase in the hardness values. Hardness (H) values were calculated by the equation: $H = 1.854\ P/d^2$ in which the values of diagonal length (d) and the applied indentation load (P) were substituted. Fig. 9 shows hardness values of 90 days cured samples of neat cement as well as melamine formaldehyde resin modified cement. The hardness values of neat cement were 6.26, 6.38, 6.64 and 6.13 MPa when tested at 5, 10, 50 and 100N load respectively. In melamine resin modified cement system, the hardness (Fig. 9) value increased with the melamine resin content in cement up to 5.0%. The values were 6.62, 6.79, 6.94 and 6.98 MPa with 0.5%, 7.04, 7.39, 8.29 and 8.72 MPa with 1.0% and 8.67, 8.90, 9.27 and 9.52 MPa with 3.0% and 9.00, 9.50, 10.50 and 11.00 MPa with 5.0% melamine resin in cement tested at 5, 10, 50 and 100N loads respectively. Hardness increased at the indentation loads with increase in concentration of melamine resin.

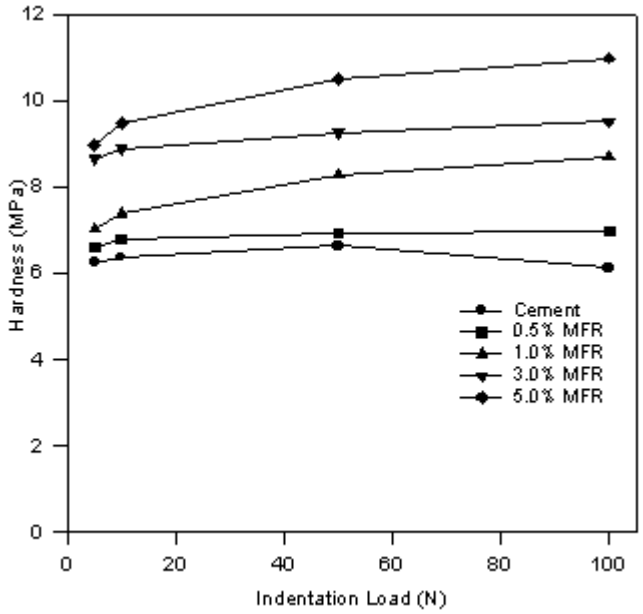

Figure 9. Hardness of cement with different percentages of melamine formaldehyde resin

3.6 Flexural Strength and Fracture Toughness

The flexural strength (FS) of neat cement samples, as calculated by equation $FS = 3WL/2bd^2$ (Where W = Fracture load, L = Span of the bar between the two supporting edges, b = Width of the sample and d = depth of the sample at the fracture plane) was 8.82 MPa after curing for 90 days. The flexural strengths of melamine formaldehyde resin modified cement systems containing 0.5 to 5.0% additive is shown in Fig. 10. The flexural strength values obtained were 9.17, 11.63,14.77 and 16.14 MPa with 0.5, 1.0, 3.0 and 5.0% melamine formaldehyde resin respectively after curing for 90 days. It increases with increasing concentration of melamine resin up to 5.0% in cement. The fracture toughness (K_{1c}) of 28 and 90 days hydrated neat cement samples were 0.62 and 1.06 MPa $m^{1/2}$ respectively as calculated by equation $K_{1c} = P_Q S/BW^{3/2} f(a/w)$ (where PQ = Fracture load in Newton, S = Span length, B = Width of the sample, W = Depth of the sample and a = Notch depth).

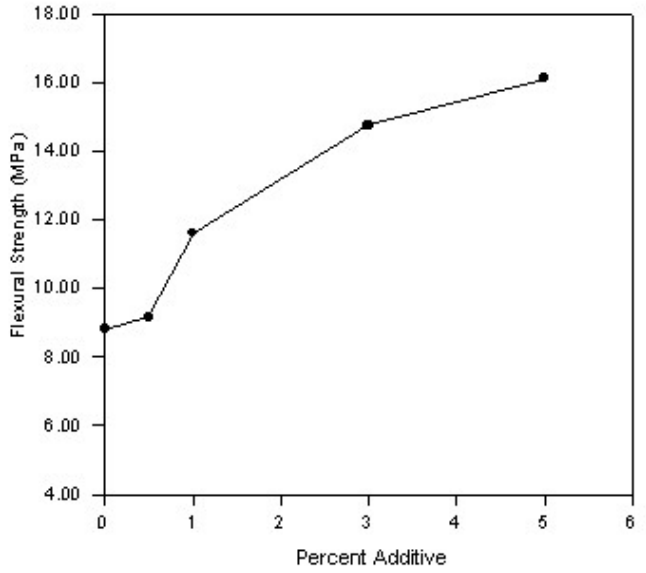

Figure 10. Flexural strength of cement with different percentages of melamine formaldehyde resin

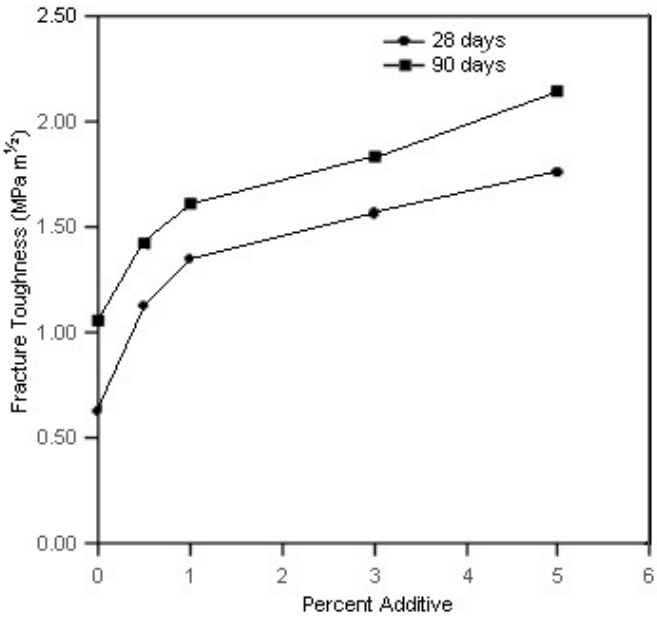

Figure 11. Fracture toughness of cement with different percentages of melamine formaldehyde resin

The average fracture toughness of cement containing 0.5 to 5.0 percent of melamine formaldehyde resin is shown in Fig. 11. The values were 1.12 and 1.42 MPa $m^{1/2}$ with 0.5%, 1.34 and 1.61 with 1.0%, 1.56 and 1.83 with 3.0% and 1.75 and 2.14 MPa $m^{1/2}$ with 5.0% melamine resin in cement respectively. In this system the values of fracture toughness increases with increasing concentration of additive up to 5.0% at both the ages. 5.0% additive has given good resistance to crack propagation against the applied load as evidenced by a value of toughness equal to 2.14 Mla.$m^{1/2}$ as compared to 1.06 MPa $m^{1/2}$ of cement under the experimental conditions.

3.7 Water Absorption

Cement mortar and concrete absorb water because of their porosity when they are brought in contact with water. The water absorption in 90 days-cured cement mortar was 9.91% by weight. Fig. 12 shows the water absorption of cement melamine formaldehyde resin mortars containing 0.5 to 5.0-wt. % additive. The values were 9.79, 9.56, 8.51 and 8.15 percent with 0.5, 1.0, 3.0 and 5.0% melamine resin addition in cement respectively (Fig. 12). The values of water absorption decreased with increasing concentration of melamine formaldehyde resin up to 5.0% as compared to unmodified cement mortar.

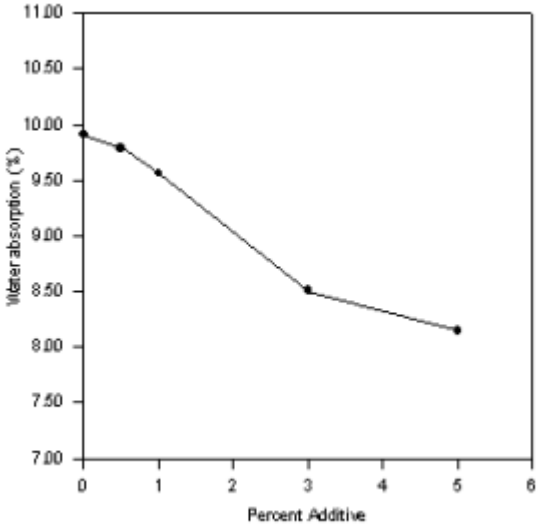

Figure 12. Water absorption of cement mortar with different percentages of melamine formaldehyde resin

3.8 Corrosion Resistance

The corrosion resistances of the cement- melamine resin composites were measured by the weight loss in the mortar samples after 4 days (2 renewals each day) immersion in 0.1 and 1.0N H_2SO_4 and HCl respectively. The weight loss is much less in the composites as compared to the blank cement mortar. It shows that the polymer is able to impart corrosion resistance to cement. These findings are similar to earlier results reported on corrosion resistance of polymer composites. The weight loss in 90 days cured ordinary cement mortar after 4 days immersion in 0.1 and 1.0N H_2SO_4 were 1.15 and 6.24% respectively. The percent weight loss in samples made with different quantities of melamine formaldehyde resin mixed in cement is shown in Fig. 13. It can be seen that the percent weight loss decreases with increasing concentration of melamine resin in cement up to 5.0%. The values were 0.69 and 6.14% with 0.5%, 0.46 and 5.35 with 1.0%, 0.02 and 3.50% with 3.0% and 0.01 and 1.90% with 5.0% additive in cement after immersion in 0.1 and 1.0N H_2SO_4 respectively for 4 days.

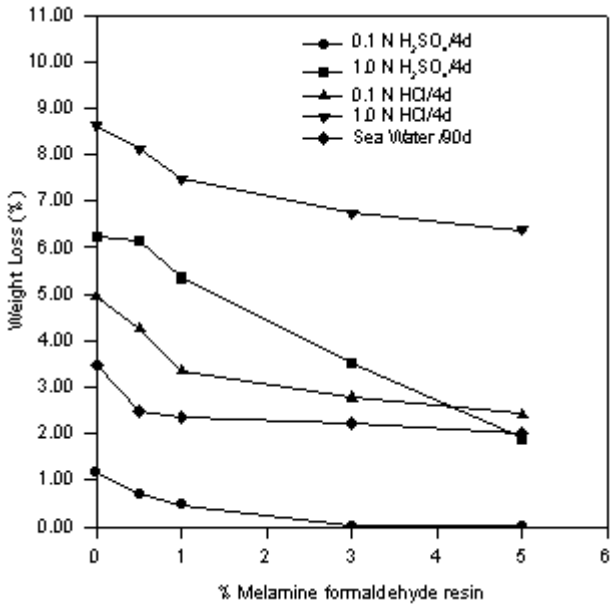

Figure 13. Corrosion resistant cement with different percentages of melamine formaldehyde resin in different aggressive media

The weight loss values were less as compared to the values for neat cement mortar with different percentages of additive. The value of weight losses in ordinary cement mortar after 4 days immersion in 0.1 and 1.0N HCl were 4.95 and 8.61% respectively (Fig. 13). The weight losses were 4.28 and 8.11 percent with 0.5%, 3.36 and 7.48 with 1.0%, 2.77 and 6.74 with 3.0% and 2.42 and 6.38 percent with 5.0% melamine formaldehyde resin in cement and immersed in 0.1 and 1.0N HCl respectively.

The 5.0% melamine resin additive to cement was found to be more resistant than other proportions. The weight loss of ordinary cement-mortar after one-month immersion in seawater was 3.48 percent. The weight losses were also determined with 0.5 to 5.0 percent melamine formaldehyde resin in cement-mortar after one-month immersion in seawater. The values were 2.48, 2.34, 2.23 and 2.00 percent with 0.5, 1.0, 3.0 and 5.0 percent additives (Fig. 13) respectively. The percent weight loss decreases with increasing concentration of melamine formaldehyde resin in cement up to 5.0%.

3.9 Microstructure

Microscopic examination of the composite revealed the presence of polymer in the capillary canals, pores and micropores of the hydrated cement gel. The microscopic photographs have shown a difference between the modified and ordinary cement samples (Fig. 5&6). The microphotograph of the melamine resin modified cement paste shows a glassier surface than the cement gel, probably due to the presence of melamine resin within the high-surface area structure of the hydrated cement.

There is mutual influence of both organic polymer and cement on the hydration and polymerization process under the preparation and curing conditions. In mixes, cement and melamine resin are interspersed and react with each other at room temperature to create a material with high flexural strength, which is free from major defects. The microstructure of these composites consists of close packed, cement particles, embedded in a continuous matrix.

4. CONCLUSIONS

1. The studies indicate that modified cement possess higher strength compared to ordinary neat cements.
2. This increase has been related to the decrease in porosity. The decreased porosity may be due to high water solubility and presence of organic material in pores.
3. The melamine resin modified cements are also more resistant to corrosion.
4. Melamine formaldehyde resin interacts with neat cement through the NH_2 reactive/functional group.

REFERENCES

[1] Ohama, Y. Concrete Admixture Handbook : Properties, Science and Technology, Noyes Publication, New Jersey, 1984, p.347.

[2] IS:4032, Indian Standard Methods of Physical Tests for Hydraulic Cement, Indian Standards Institution, New Delhi, 1968.

[3] Powder Diffraction File: Cards Nos. 10-373, 3-649, 4-733, 1-0038 etc. Joint Committee on Powder Diffraction Standards, P.A.

[4] Puri, B.R. and Sharma, L.R. Principles of Physical Chemistry, 9th edition, S. Nagain & Co., Jallaunder city-1, 1974, p. 436.

[5] Benstel, J. and Verma, S.P. Some application of infrared and Raman spectroscopy in cement chemistry, Part I : examination of dicalcium silicate, Cement Technology, Vol.5, 1974, pp.1256-61.

[6] Brezny, R. and Green, D.J. Fracture behaviour of open cell ceramics, Journal of American Ceramic Society, Vol.72, 1989, pp.1145-52.

[7] Brezny, R. and Green, D.J. Effect of cellrize on mechanical behaviour of cellular ceramics, Acta Metallurgica, Vol.38, 1990, pp.2517-26.

HIGH STRENGTH CEMENT- MELAMINE FORMALDEHYDE RESIN PRODUCTS

V.K. Singh

Department of Ceramic Engineering, Institute of Technology,
Banaras Hindu University, Varanasi - 221 005, India
Tel: 0091 542 307042 Fax: 0091 542 368174
E-mail: vksingh_cer@yahoo.com, vksingh@banaras.ernet.in

BIOGRAPHY

Author presenting the paper, Dr. V.K.Singh was born on June 10, 1944. Married to Dr. Sushila Devi, has three sons. He obtained his B.Sc. Silicate Technology in 1968, M.Sc. Ceramic Engineering in 1970 and Ph.D. Ceramic Engineering in 1976. He joined as Faculty member of the Banaras Hindu University in 1971 and since then he is continuing his services and at present he is a Professor and Head, Dept. of Ceramic Engineering, Institute of Technology, Banaras Hindu University. He has about 65 published papers in Journals like American Ceramic Society, British Ceramic Transactions and Journal, Journal of Material Science, Journal of Material Science Letter, Ceramic International, Cement and Concrete and National Journals of repute.

He was awarded International Scientific Exchange Fellowships to work in U.K., South Korea and Slovak Republic. He has attended and presented papers in U.S.A., Sweden and Slovak Republic. He is a fellow of Indian Institute of Ceramics and also a member of the Award Committee of the Indian Ceramic Society. At present he is also the In-charge of the Library and Museum of Indian Ceramic Society at Banaras Hindu University. An Ex-Officio Council Member of Indian Ceramic Society and a member of Center for Development of Glass Industries, Govt. of India, he is also an Expert Member of Bureau of Indian Standards.

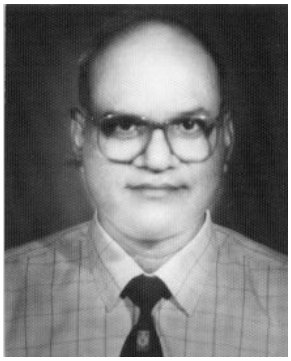

GHG, OTHER GASES AND POLLUTANT EMISSION TRENDS AND PROJECTIONS FOR THE CEMENT INDUSTRY IN INDIA

Sumana Bhattacharya[1], S P Ghosh[2] and A. V Srinivasan[3]

Winrock International-India , Cement Manufacturers'Association of India.

ABSTRACT

Global warming and the consequent climate change is likely to pose a serious threat to the present habitat and many life-forms on the planet. This has raised concern amongst all nations. The UN Framework Convention on Climate Change (UNFCC) binds all countries which are party to this Convention to take up a common but differentiated responsibility in addressing the issues of Climate Change. The concentration of CO_2 has increased by 31% since pre-industrial times and is earmarked for priority abatement through the mechanism of "carbon trading" between developed and developing countries. The cement industry consumes 5% of the total global industrial energy and contributes to 5% of GHG emission. The present article is a summing up of inferences for the Indian cement industry from several on-going studies in India on estimation of GHG emission during the last two decades in different sectors of the national economy. Among GHGs Carbon dioxide (CO_2), and Nitrous oxides (NO_x) and, in addition, Sulphur oxides (SO_x) are emitted by cement manufacturing process. In general, about 1 ton of CO_2, is released from 1 ton of cement manufactured. (NO_x) and (SO_x) emissions are relatively insignificant in comparison and are in the 10 to 20 kg per ton of cement produced. The emission of these last two can also be brought to negligible levels through the adoption of modifications in process parameters and operations. The approximate contributions of each of the 3 main sources of CO_2 emissions are: Calcination = 50 – 55% Fuel Combustion = 40 - 50% and Electricity including captive power generation = 0 - 10%. Thus for the 1990s, the Indian Cement industry emitted CO_2 on an average annually about 50 million tons due to the process of calcination, 40 million tons from coal combustion, and 7.4 million tons from electricity consumption, using grid or captive power.

The Indian cement industry being the second largest in the world in installed capacity and annual production, has a major role to play in CO_2 emissions reduction. A review of the Indian cement industry over the last two decades shows that although state-of-art plants are comparable to the best in the world in energy consumption and CO_2 emission, the industry average of 1.102 tons of CO_2 emissions per ton of cement is much higher than the world average of 0.746 tons. The calculated CO_2 emissions for the Indian cement industry on annual basis for the period 1980 to 2000 shows that technological upgrading has curbed the annual growth rate of CO_2 emissions. Thus, although India emitted a total of about 778 million tons of CO_2 from all activities in 1995 and about 1000 million tons in 2000, the share of the cement industry to the total CO_2 emission has increased marginally from 4 to about 5% during these years. The present annual growth rate of the industry (8 to 10%) and its pattern portend this trend of CO_2 emissions to continue. However, the expected massive upsurge in the long-sought infrastructure development in the coming years may lead to a quantum leap in growth of cement capacity and production.

[1] Expert Consultant, Winrock International India
[2] Advisor (Technical), Cement Manufacturers' Association of India
[3] Secretary General, Cement Manufacturers' Association of India

This will call for Clean Development Mechanisms and other devices to be adopted on a large scale to minimise CO_2 emissions.

1. INTRODUCTION

There is overwhelming evidence that rapid industrialization since the last century has led to a rise in greenhouse gas (GHG) emissions such as CO_2, CH_4 and N_2O in the atmosphere leading to an additional warming of the Earth's atmosphere. Over the 20th century the increase in the earth's surface temperature has been 0.6 ± 0.2°C and under the combined influence of Green House Gases and sulfate aerosols, climate may warm globally by 1.4 to 5.8°C by the year 2100 [1]. As a result the global sea level will rise between 0.09 to 0.88 m in the period 1990 to 2100 and extreme events like excessive rain, flash floods, droughts, cyclones and forest fires are likely to increase, threatening major climate change and impact on the entire earth system in an unprecedented manner [1]. Global leaders have by and large accepted the fact that climate change is the most pressing and dangerous threat to life on earth today.

Among the responses to counter this major threat, the most significant response formulated is the United Nations Framework Convention on Climate Change (UNFCCC) of May 1992 ratified so far by 182 countries. The three important provisions in the Convention required developed countries to (a) bring down their Green House Gas (GHG) emissions by 2000 to the level at which it was in 1990; (b) prepare national communications with information on policies and measures undertaken for reducing GHG emissions, and, (c) provide financial resources to meet the agreed full costs incurred by developing country parties in complying with their commitments relating to national communications. The annual Conference of Parties (COP) is the consequence of this framework. In 1997, the third such meeeting (COP-3) at Kyoto adopted a Protocol, which sought to reduce emissions even more. The Kyoto Protocol required Annex 1 countries (Annex 1 listed 41 countries: industrialised and developed nations as well as Economies in transition like the former Soviet Union countries and Eastern European nations) to collectively reduce GHG emissions by 5.2% below 1990 levels in the course of the implementation period of 2008 to 2012.

So far, countries contributing 37% of Annex 1 countries' total emission had ratified the Kyoto Protocol. Now, Russia contributing 17% and Canada contributing 2% of global GHG emissions have indicated the likelihood of their ratifying the Kyoto Protocol at COP-8 to be held at New Delhi.

1.1 Significance of the Present Study

In addition to the aforestated, the Annex-1 Parties in the Kyoto Protocol, individually or jointly, agreed to reduce their overall emissions of the six GHGs to at least 5 percent below 1990 levels in the first Quantified Emission Reduction commitment period 2008-2012. Cuts in the three most important GHG gases viz, Carbon dioxide (CO_2), Methane (CH_4) and Nitrous oxide (N_2O) will be measured against the baseline year 1990 while the cuts in other 3 gases viz, Hydrofluorocarbons (HFC), Perfluorocarbons (PFC) and Sulphur Hexafluoride (SF_6) can be measured against baseline year 1990 or 1995. 180 Signatory countries to the Kyoto Protocol are therefore putting their acts together for a reliably accurate assessment of emission of the stated gases over the past decades and are formulating action plans for emission reduction in the coming years.

India is a Party to UNFCCC but, being a developing country, it does not have any emission reduction commitments under the Kyoto Protocol. India has taken many steps to achieve energy efficiency, fuel switching, afforestation, and use of renewable energy technology (RET) as a part of the national planning process. These deliberate actions have aligned economic development to a more climate friendly path. In order to achieve sustained economic growth, India cannot stop growth in energy consumption. The energy consumption in India is rising due to growing

industrialisation, rising incomes, expanding urbanisation, and modernisation of agriculture. Carbon emissions, the major GHG emitted, has almost grown parallel to energy use. Local pollutant emissions show a slower rate of growth. Biomass emissions which contribute significantly to total emissions, have grown below 2% per year.

The present article is a summing up of inferences for the Indian cement industry from several on-going studies in India on estimation of GHG emission during the last two decades in different sectors of the national economy.

2. MAJOR SOURCES OF EMISSION

The activities that are believed to be responsible for climate change induced by GHG emission are the levels of anthropogenic activities. Fossil fuel (coal, oil, natural gas) burning in the energy and transportation sector, industrial processes, agriculture activity, land use, land use change and forestry, and waste generation due to industrial activities since 1750s has led to the increase in CO_2, CH_4 and NO_X concentrations in the atmosphere by 31%, 151% and 17% respectively [1]. In the urban and industrial centres, energy intensive activities in various industrial processes such as power generation, chemical (fertilisers, pesticides, pharmaceuticals, textile fabric etc) and metallurgical processes (iron and steel and various metals production), mining and construction and related activities (cement, brick and other construction materials), consumer goods, heating and cooling systems (airconditioners, refrigerators, heaters) have contributed to significant emission of the 7 major GHGs like Carbon dioxide, Methane, sulphur oxides, nitrous oxide, Hydrofluorocarbons (HFC), Perfluorocarbons (PFC) and Sulphur Hexafluoride (SF_6). The major sources of these emissions are:

Carbon dioxide: It is the biggest villain. The sources for its emission include human exhalations, industrial and economic activities, limestone dissociation in industrial processes like lime, cement, fertilisers, chemicals and pesticide manufacturing etc., biomass burning, incomplete combustion of vehicular fuel and land use and land use change.

Methane: The sources include emissions from agriculture such as rice cultivation, enteric fermentation, collection and storage of organic matter like animal manure, extraction and transport of fossil fuel.

Nitrous oxide: The sources of this gas are supply and use of fossil fuel, fertiliser, high temperature processes leading to combination of atmospheric nitrogen and oxygen.

Sulphur Hexafluoride: Is used as an electric insulator, heat conductor and freezing agent.

Hydro Fluoro Carbons/Per Fluoro Carbons: Used as ozone safe replacements.

In 1995-1996, the greenhouse gases emitted in India were about 1259 million tons in terms of CO_2 equivalent which is only about 3% of the total global GHG emissions. Out of the total Indian GHG emissions, CO_2, CH_4 and N_2O emissions were at 778, 18 million and 0.225 million tons respectively. Additionally, about 5.3 million tons of SO_2 and 3.4 million tons of NOx , which are local pollutants, were also emitted. Table 1 gives the GHG and pollutant emissions from various sectors in India for the year 1995-1996.

Table 1. GHG emissions from India in 1995

CO_2 emissions	***Million tons***	***% of the total***
Electric power generation	348	44.6
Transport sector	113.4	14.6
Cement	59.2	7.6
Steel	94	12.1
Fertiliser	24.3	3.1
Other industries	96.5	12.4
Other sectors	43.5	5.6
TOTAL CO_2	778	100
CH_4 emissions	***Million tons***	***% of the total***
Agriculture reside	0.10	0.6
Biomass	2.88	15.9
Coal production	0.38	2.1
Oil and Natural Gas	0.79	4.4
Livestock	7.26	40.2
Manure Management	0.40	2.2
Paddy cultivation	4.0	22.2
Waste	2.24	12.4
TOTAL CH_4	18.05	100
N_2O emissions	***Million tons***	***% of the total***
fertiliser	0.164	65.3
Burning of crop residue	0.030	12.0
Indirect soil emissions	0.024	9.5
Biological nitrogen fixation	0.005	2.0
Livestock excretion	0.011	4.4
Coal consumption	0.008	3.2
Nitric acid consumption	0.007	2.8
Oil consumption	0.002	0.8
Natural gas consumption	negligible	-
TOTAL N_2O	0.251	100
SO_2 emissions	***Million tons***	***% of the total***
Electric power	2.14	40.68
Steel industry	0.43	8.17
Fertiliser industry	0.18	3.42
Cement industry	0.15	2.85
Other industries	0.86	16.34
transport	0.36	6.84
Food processing	0.03	0.57
Biomass combustion	0.22	4.18
Sulfuric acid production	0.05	0.95
Lead, zinc, copper smelting	0.66	12.54
Other sectors	0.18	3.422
TOTAL SO_2	5.26	99.962
NOx emissions	***Million tons***	***% of the total***
Coal	1.36	40.0
Oil	1.37	40.29
Natural gas	0.0001	0.0029
Biomass	0.66	19.41
Industrial processes	0.013	0.38
TOTAL NOx	3.403	100

Source: [4], [5].

As can be seen from Table 1, within the industrial processes, CO_2 emissions from steel production exceed those from cement production contributes CO_2 only next to the emissions from steel production. Since the cement production in the country in the year 2000 has increased by about 35% since 1995, the GHG and pollutant emissions from this sector will also have grown. The cement industry involves mainly the emission of the following GHGs:

2.1 Carbon dioxide

(a) Dissociation of limestone in the raw mill
(b) Burning of fossil fuels
(c) Captive power generation either from diesel generating sets or from thermal power plants
(d) Fuel and power use respectively for mining of limestone and other raw materials and packing and handling of cement

The average quantity of CO_2 emitted is in the range of about 1 ton per ton of cement produced.

2.2 Nitrogen dioxide

Nitrogen oxides are generated in the process of burning of fuel at high temperatures of about 1500^oC where atmospheric nitrogen and oxygen combine to form Nitrogen oxides. The quantity generated however, is insignificant and ranges between 1.7 to 2.1 gms per kg of clinker. The quantity released is thus relatively small.

2.3 Sulphur Oxides

These are released in the process of combustion of fossil fuel and also from oxidation of sulphur contained in the raw materials in the process of clinker formation. Almost 70 to 90% of sulphur oxide released during the burning process is absorbed by the nascent clinker. The balance, released as stack emission, varies from 2 to 5 gms per kg of clinker. The quantity released is also relatively small.

The other components of GHGs are not emitted during the process of cement manufacturing.

It is clear from the aforesaid that CO_2 constitutes the lion's share amongst all the GHG emission from the cement manufacturing process, and almost equals the quantity of cement produced. In this paper, we therefore present the account of GHGs and pollutants emitted from the cement sector with specific focus on CO_2 emission and try to link this emission with the change in technology over the years.

3. THE INDIAN CEMENT INDUSTRY

The cement industry in India has been growing at a fast pace during the last 20 years - both in terms of its capacity and improved technology, particularly after 1982, when the Government adopted the policy of partial decontrol. The progress has been possible through modernisation of cement production technology, development of infrastructure, energy-efficiency, and the R&D work carried out by the research institutions. In 1999 and 2000 India produced about 7% of the total global production and is second only to China (see Table 2).

Table 2. Major cement-producing countries

Country	Production (million tons)	
	1999	2000
China	573.0	597.7
India	99.1	101.8
USA	85.0	84.7
Japan	83.47	85.95
South Korea	49.5	52.2
Other countries	711.22	742.34
TOTAL GLOBAL	1601.29	1664.69

Source: CEMBUREAU [6]

Cement industry is a core sector industry and forms the backbone of infrastructure development of the country. The Industry has shown steady and consistent growth in the last three decades. The industry grew 4 times both in terms of capacity and production in the last two decades. The capacity and production, which were nearly 29 MT and 21 MT in 1981, shot up to 133.55 MT and 98.35 MT respectively in 2001, with the capacity utilization in the industry being 70%-80% over this decade. The industry is presently growing at the rate of 8% - 10% per annum (Table 3).

Table 3. Production, capacity and capacity utilization of Major cement plants in India (Excluding Mini and white cement plants)

Year	Cement production (million tons)	Capacity at the end of year (million tons)	Production Growth(%)
1981	20.77	28.87	
1982	22.54	31.78	8.5
1983	25.14	35.86	12.7
1984	29.14	39.10	14.7
1985	31.11	41.85	6.8
1986	33.65	49.10	8.2
1987	36.97	55.51	9.9
1988	40.72	55.04	10.1
1989	42.07	56.36	3.3
1990	44.87	58.12	6.7
1991	49.47	60.61	10.3
1992	50.87	62.46	2.8
1993	52.78	66.90	3.8
1994	57.57	73.19	9.1
1995	62.08	82.06	7.8
1996	68.86	90.17	10.9
1997	74.75	99.92	8.6
1998	79.42	108.41	6.2
1999	91.72	109.44	15.5
2000	95.94	116.82	4.6
2001	98.35	133.55	2.5

Source: Basic Data, Indian Cement Industry, 2001, 2002

Cement manufacturing in India is location-specific. Most cement plants (65%) have been built in clusters in areas which have limestone deposits. The regional distribution of plants, specifically for large plants, leads to long haul of cement to consumption areas by rail and road transport. Distances being large in India, the transport of cement assumes an important aspect of cement business. Road transport which is less eco-friendly due to its entire dependence on fossil fuels than the railways and waterways, carries nearly 68% of the cement produced. A reduction in road-share of cement transport will lead to a reduction in CO_2 emissions – a potential contribution of cement business.

In the year 2001, the entire Indian cement industry, comprised 123 large cement plants and 365 mini plants, with a total installed capacity of about 144.65 million tons and a production of 102.35 million tons, comprising ordinary Portland cement (57.3%), blended cements (40.5%) and others [Basic data, Indian Cement Industry, 2001-2002]. However, as indicated in Table 3, the production of cement from large plants only was about 98.35 million tons out of the capacity of 133.55 million tons. In an industry which is in its ninth decade of existence, there is naturally a spread in the age, technology and capacities of the plants but this has steadily been sought to be narrowed down by renewal, modernisation and expansion. The energy performance of Indian cement plants is comparable to the best in the world (Table 4).

Nearly 94% of the plants are based on the modern dry process technology with suspension pre-heaters and precalciners, and 63 out of 123 large plants have annual capacity of 1 million tons and over, many of them approaching international benchmarks in specific thermal and electrical energy consumption. Semi dry and wet process are used by 2% and 4% respectively of the Indian cement manufacturing capacity. Dry process is the most energy efficient of all the technologies in use. Figure 1 shows how the plants have shifted to use dry technology from wet technology from 1980 onwards.

Table 4. Best Energy Performance by State-of-art Indian Plants and the Best in the World.

Energy Performance (2001)	**Best in India**	**Best in the World**
Thermal (Kcal/kg of clinker)	665	650
Electrical (kwh/tons of cement)	69	65

Source: Forecasting Technologies for the Indian Cement Industry, Department of Science and Technology, Government of India, 2002.

For the production of cement, three types of clinkers are distinguished from energy consumption and gaseous emission viewpoint: rotary kilns (large), rotary kilns(small) and shaft kilns. Out of a total 144.65 million tons installed capacity in 2001, large rotary kilns constituted 133.56 million tons, mini rotary (including white cement) and shaft kilns constituted 11.10 million tons capacity. Out of the latter category, rotary mini plants constituted about 4 million tons and shaft kilns about 7 million tons. Out of a total 102.35 million tons cement production in 2001, 98.35 million tons was contributed by large plants and only 4 million tons by the others. Out of a total 125.30 million tons installed capacity in 2000, large rotary kilns constituted 116.3 million tons, mini rotary (including white cement) and shaft kilns constituted 9.0 million tons. Out of the latter category, rotary mini plants constituted about 4 million tons and shaft kilns about 5 million tons. Out of the total 102.35 million tons production in 2001, 95.94 million tons was contributed by large plants and only 6.24 million tons was contributed by the others [**7**]. These figures substantiate the relatively insignificant role of small rotary and shaft kilns in cement manufacture.

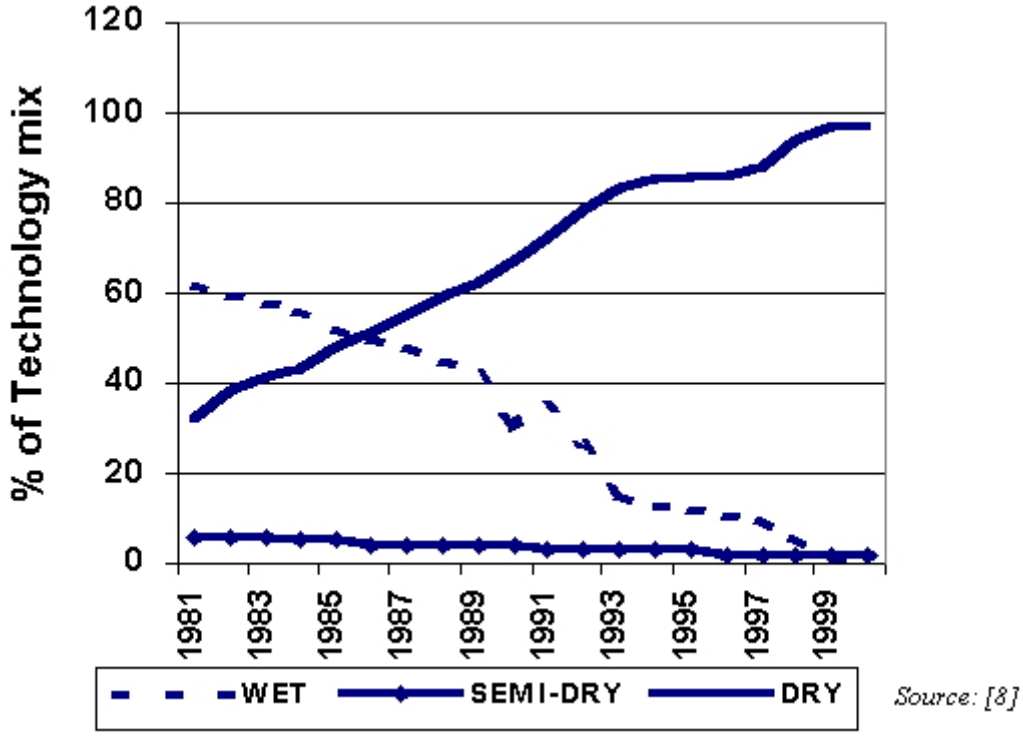

Figure 1. The changing face of technology mix in the Indian cement sector since 1980s

4. PROCESS PARAMETERS

Presently most of the cement produced in large cement plants is through the dry process. In the year 1997 approximately 88% of the country's total production was from dry process (source: CMA Basic Data, 1998). Dry process is the most energy efficient of all the technologies in use. In contrast, in the year 1947 almost 100% of country's production was from the wet process and only Ordinary Portland Cement was produced.

Each unit operation in cement making involves either thermal (fuel) or electrical energy and related GHG emission. These are designated as (f) for fuel related emission and (e) for electrical energy related emission (thermal power plants and captive power generation).

5. ENERGY CONSUMPTION PATTERN

As mentioned earlier, cement manufacturing is a very energy-intensive process. The most energy-intensive stage of the process is clinker production, which accounts for up to 90 percent of the total energy used. The grinding of raw materials and of the cement are both electricity-intensive steps and account for much of the remaining energy used in cement production.

Coal (as a thermal energy source) and electricity are the two major energy sources for Cement production in India. Besides these, some petroleum (HSD & Furnace Oil) is used in the manufacturing process.

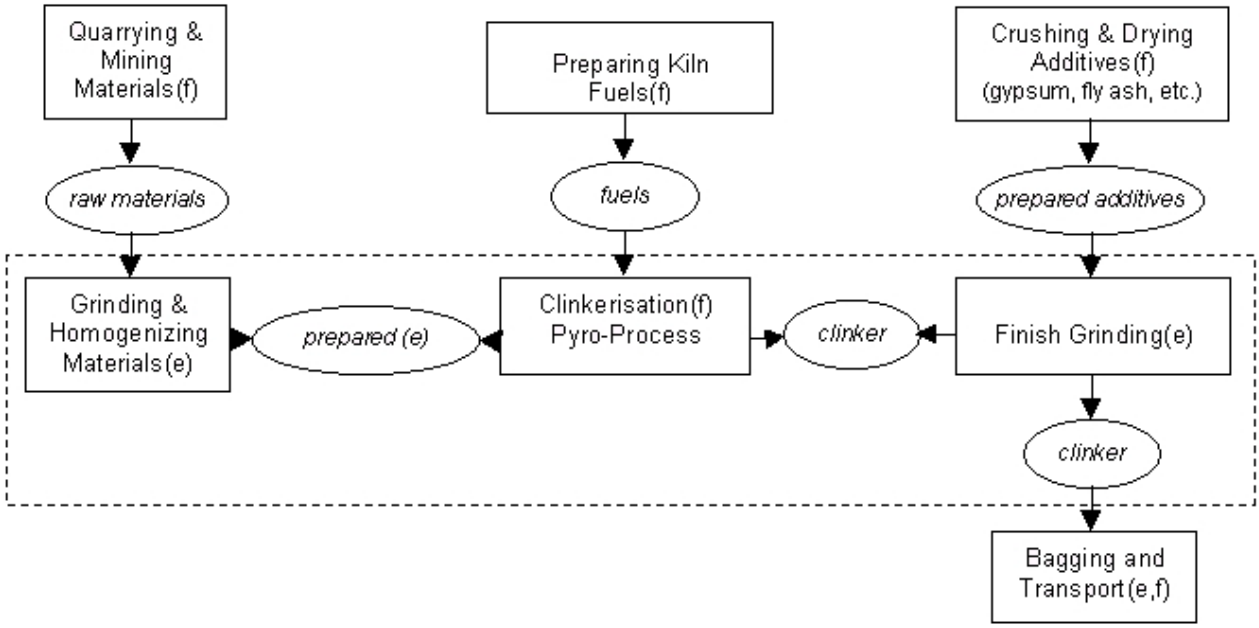

Figure 2. The Cement Production Process

Figure 3 shows the trend of coal consumed in the country for cement production. This data includes use of coal, lignite, and petroleum products for captive power plants.

Energy requirements for cement grinding are roughly double those for raw material preparation because the cement is harder and needs to be ground more finely than the raw materials. An important issue when considering "best practice" energy requirements for grinding is that energy use is related to the hardness of the raw materials and the additives included before cement grinding as well as the desired fineness of the finished product. These features can vary, so it is important to specify the fineness and composition of the product when discussing energy use.

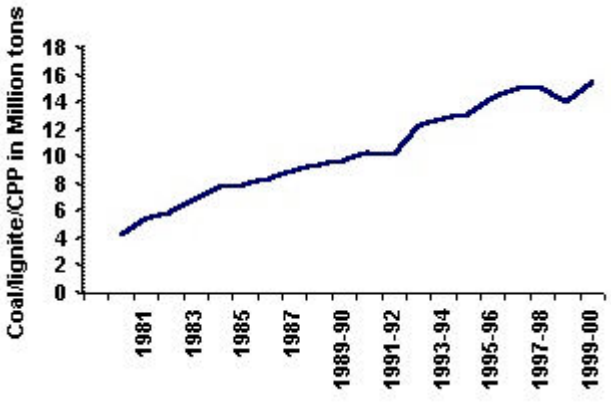

Figure 3. Fuel consumption in the cement sector

The Specific energy consumption of a cement plant is reckoned in two forms: –

- kilo calories/kg. of clinker for the thermal energy and
- kWh/t of cement produced for the electrical energy

The average values for these two on an overall Indian cement industry basis are 840 kcal/kg and 114 kw/t respectively. There are also some cement plants, which have very low specific energy consumption and are comparable with the best in the world.

Specific energy consumption values of the Indian cement industry have been coming down over the past several years with the changes taking place from wet to semi-dry and then to dry process and also with the adoption of energy efficient technologies and improvement in the energy management systems.

Various studies carried out by the Confederation of Indian Industries (CII), NCB and Cement Manufacturing Association (CMA) show that thermal and specific energy consumption levels in different technologies vary between 800-1600 Kcal/Kg clinker and 98-135 Kwh/t cement produced respectively for different processes (Table 5).

Table 5. Energy consumption levels of different technologies in Indian Cement Sector

Technology	Specific Fuel Consumption (Kcal / Kg of Clinker Formation)	Specific Power Consumption (Kwh/t of Cement Production)
Dry Process	800 -1060	98 - 114
Semi Dry / Semi Wet Process	950 -1140	112 - 145
Wet Process	1 300-1600	114 - 135

The total consumption of fuel and electricity in the cement industry has grown significantly. However, the specific fuel consumption has reduced over the years. Also, electricity consumption per ton of cement has been significantly reduced due to the compensating effects of the closure of old energy-inefficient wet process plants and setting up of modern dry process plants with progressively more and more energy-efficient machinery for grinding and clinkerisation. Some of the recent studies carried out by the Confederation of Indian Industry (CII) & National Council for Cement & Building Materials (NCB) for cement plants indicate that the average specific thermal energy consumption is around 815 Kcal/kg for dry process and 1340 kcal/kg of clinker for wet process. Also, the average specific energy consumption for dry process is pegged at 112 kWh/T and for wet process it is 101 KWh / T (see Tables 6 and 7). Almost all cement plants have installed captive power plants to meet the essential power supply as the power supply from the grid system is unreliable and has wide fluctuations. The captive power plant capacity in megawatts of the cement industry is given in Table 8 both for Diesel Generating (DG) Sets and for thermal generation.

Table 6. Data on Energy Consumption for 33 Dry and 3 Wet Process Cement Plants

Energy Consumption	Dry Process		Wet Process	
	Range	Weighted	Range	Weighted
Specific Thermal Energy Consumption (Kcal / Kg)	671 - 1017	815	1279 - 1406	1340
Specific Electrical Energy Consumption (Kwh / T)	86 - 152	112	90 - 111	101

Source: [14]

Table 7. Data on Energy Consumption for 54 Dry & 10 Wet Process Cement Plants

Energy Consumption	Dry Process		Wet Process	
	Range	Weighted	Range	Weighted
Specific Thermal Energy Consumption (Kcal / Kg)	720 - 990	819	1279 - 1406	1340
Specific Electrical Energy Consumption (Kwh / T)	74 - 125	111.5	90 - 180	122

Source: [12]

Table 8. Installed Captive Power (MW)

As on	D.G. Sets*	Thermal	Wind Farms	Total
31.12.1998	845.20	311.25	80.25	1236.70
31.12.2000	1088.96	432.85	80.25	1602.06

Source: [7]

6. GREENHOUSE GAS, OTHER TRACE GASES AND POLLUTANT EMISSIONS FROM THE CEMENT INDUSTRY

Cement manufacture is based on consumption of major quantities of non-renewable natural resources like limestone, coal, gypsum etc.; the clinkerisation process involves generation of CO_2- a greenhouse gas. In the year 2000, 1.66 billion tons of cement was produced throughout the world and 1.4 billion tons of CO_2, CO and NOx were released into the atmosphere, contributing thereby to a major share of global warming. The effect of greenhouse gas to global warming is now widely accepted and efforts are being made to limit these emissions. This has given a boost to efforts for energy efficiency as stated above.

Alternative energy-economic routes of cement manufacture (eg., microwave clinkerisation) or large value-addition to the main down-stream product (eg. concrete) through high performance (high durability) binders (eg., Macro Defect Free, Densified System of Phases) with lesser cement consumption are new areas of technology evolution. The other area of environmental concern is the emission of Suspended Particulate Matter (SPM) that causes dust pollution.

The cement industry has looked upon this problem positively, as efforts to reduce SPM could increase output of cement and therefore thermal efficiency. It is with these efforts that cement industry, which was considered as a highly polluting industry in the early days, is now accepted as one of the modern industries which is far less polluting than many others. This has been achieved by fitment of efficient ESPs, use of bag filters, etc. These modifications have resulted in bringing down SPM levels to 70 mg/Nm^3 and even up to 50 mg/ Nm^3 in some cases.

Cement production is also one of the most energy intensive processes. This industry consumes about 2% of the global total of primary energy consumption or almost 5%. Due to the dominant use of carbon intensive fuels, e.g. coal, in clinker making, cement manufacture is a major emitter of CO_2. Besides energy consumption the clinker making process also emits CO_2 due to calcining process of limestone involving the release of CO_2 from dissociation of calcium carbonate in limestone. About 5% of the total global emissions of CO_2 are attributed to the cement sector.

Emissions in the cement industry comprise five gases considered as GHG viz. carbon dioxide, carbon monoxide, NOx, sulphur oxides (SO_x), and hydrogen sulphide. In developed countries, limits have already been prescribed for NOx and SO_x in the kiln stack. However, in India only two states, namely Meghalaya and Gujarat have adopted such norms. The Central Pollution Control Board (CPCB) is reported to be contemplating fixing the emission limits for SO_x, and NOx. The role of each of these gases as emission, and the role and impact of heavy metals in cement manufacture have been excellently explained in [3] and are summarised below.

6.1 Oxides of Nitrogen

The clinker burning process causes the formation of nitrogen oxides (NO_x) in the sintering zone as also in the low temperature calcining zone. In the sintering zone there is predominant formation of thermal NO_x from atmospheric nitrogen, partially overlaid by the formation of nitrogen oxides from the nitrogen in the fuel. In the calcining zone the NO_x is formed from nitrogen in fuel. The source

for NO_x emission has been compounded in the cement industry due to the compulsive use of lower grades of solid fuels as well as industrial wastes containing combustibles.
The statistical calculation of NO_x emission measurements at a large number of cement plants equipped with / preheater rotary kilns showed a mean value of 2.1 g N per kg of clinker, which corresponds to 1050 mg/Nm^3 in the exhaust gases related to 10% oxygen. While $N0_x$. emissions are not spiky and highly variable in specific plants there would be short or long term changes.

The ways of reducing the NO_x emission are classified broadly as primary and secondary. The primary methods are designed to act on the following influencing factors to minimise the generation of NO_x during the combustion process:
(a) Flame shape and temperature
(b) Combustion chamber temperature
(a) Combustion air temperature
(b) Excess air in the combustible gases
(c) Residence time of fuel
(d) Nitrogen content of fuel

The most important measure is to ensure an optimum and stable kiln operation with homogenised raw mix, uniformly dosed fuel, effective cooler operation, etc. It is claimed that certain low-NO_x burners also help in achieving lower emission. Designs of low-NO_x burners vary in detail but essentially the coal and air are injected into the kiln through 3 or 4 concentric tubes with only 6-10% of primary air. The general effectiveness of a low-NO_x burner reportedly is limited.

On the other hand, the secondary reduction measures reconvert the already formed NO_x back into elementary nitrogen by any of the following processes:
(a) Selective non-catalytic reduction (SNCR)
(b) Selective catalytic reduction (SCR)
(c) Multistage burning (MSC)

For the SNCR process the basic principle is to reduce NO_2 with the help of ammonia injection through special nozzles into the kiln inlet zone. Ammonia disperses freely in the gas stream and the reduction reaction occurs in the temperature range of 900°-1100°C. The reaction obviously is dependent on the molar ratio of NH_3 to NO_2. The SNCR technique has undergone year-long trials in a 2000 tpd cement ki1n, in which the above molar ratio was maintained at about unity with NO_2 reduction rate of up to 80% without any escape of NH_3. Data collected for 2 months from a good number of plants showed the efficacy of the SNCR technique of keeping the stack NO_x emission always below the limit despite wide fluctuations in the NO_x generation inside the kilns.

In the SCR technique the NO_x reduction process is carried out on a noble-metal loaded catalyst surface with NH_3 injection at a lower temperature of 350°C without any adverse effect on sulphur-bearing gases. The process is extensively used in the power sector but seems to be too expensive to be adopted in the cement industry.

The concept of MSC is also borrowed from the power industry and involves installation of burners at different stages of the pyroprocessing line to reduce NO_2. In the Prepol MSC the kiln gases encounter a burner at the kiln inlet which produces a reducing atmosphere and decomposes a part of the nitrogen oxides generated in the sintering zone. Further in the precalcining stage the fuel is burnt with a quantity of tertiary air, producing a reducing atmosphere there. In the last combustion stage the remaining tertiary air is fed into the system as ‘top air’ for residual combustion. Thus, in this specific design there were four stages of combustion starting from the burning zone.

Based on similar concepts, a few other denitrating designs of precalciners have been developed and used, one being in India being DD-furnace of erstwhile Nihon Cements of Japan.

With all these developments in place, the statutory emission limit either in force or awaiting introduction in many countries is now 800 or 500 mg/Nm^3 (10% O_2) which would correspond to 1.7 or 1.19 NO_2 per kg of clinker, although the World Bank Environmental Requirements demand a limit of 400 mg/Nm^3 for stack emission and 100 µg. m^3 of NO_2 as annual arithmetic mean for ambient air quality.

6.2 Sulphur Dioxide

It is well known that the source of SO_2 in the gaseous emissions is sulphur and its compounds appearing in fuel and raw materials. Unlike other industries such as steel and power, the cement industry has a unique inbuilt desulphurisation mechanism, by virtue of which the lime and alkali from the raw materials react with sulphur compounds and trap it in the clinker. Generally, it is observed that 70-90% of sulphur gets trapped this way and 10-30% would only appear in the stack gases.

The roller mills turns out to be the most effective machine for combined drying and grinding and consequently to utilise large quantities of kiln gases to treat raw materials containing up to 20% moisture. This mode of operation obviously allows maximum absorption of SO_2 from the kiln gases in the raw mill.

So far as the kiln systems are concerned the pattern of emission is influenced by the content and form of sulphur in raw materials and fuels and the sulphur cycle that develops in the kiln-preheater system. The precalciner kilns with high levels of free lime in the precalcined material behave as better absorbents of SO_2 into the kiln feed and consequently into the clinker.

On the whole the SO_2 emissions are highly variable in cement plants. Even from a particular kiln the emissions may fluctuate widely (10: l or greater).

The abatement of SO_2 emission is generally effected through the following approaches:

(a) Process and plant modifications
(b) On-line techniques
(c) Off-line techniques

In the first approach the possibilities of minimizing the input of sulphur into the system are explored. The maintenance of oxidising conditions (O_2 > 2%) at the back end of the kiln and in the lower stages of the preheater is important to facilitate the faster reaction between CaO and SO_2 . For the same reason reducing conditions are avoided at the gas outlet of the precalciners. In the raw mix design stage the stoichiometric balance between alkali and sulphate is attempted to ensure entrapment of sulphur in the clinker phases.

For on-line abatement plant-scale trials have been carried out with injection of hydrated lime into the riser duct between the two top preheater stages. This injection system consists of a storage silo for the hydrated lime, proportioning and conveying equipment and a pneumatic injection unit The success depends on the uniform distribution of the hydrated lime in the gas stream for effective gas-so1id reaction. Operating results have indicated that the SO_2 emission can be reduced by up to 70%, when the in input of hydrated lime is highly over-stoichiometric. It may be relevant to mention here that these kinds of desulphurisation process (wet or dry) are expensive to install and mostly produce a waste product that may be difficult to recycle directly into the clinkering process. To overcome some of these problems one of the plant suppliers has attempted to install a pilot plant with a

travelling bed reactor which can absorb high SO_2 emissions into a medium that would serve to provide secondary gypsum for cement grinding.

So far as the off-line facilities are concerned, they relate to processes like wet-scrubbing or dry absorption of SO_2 and are required only when major reduction of SO_2 is called for. In wet scrubbing the gases are first passed through a heat exchanger and then reacted with limestone slurry in an absorber. The clean gas, after reheating, is released into the atmosphere. There are alternate routes like injection of slaked lime into a spray drying chamber or into an existing conditioning tower of the cement plant

A dry plant to absorb SO_2 has also been developed which uses a circulating fluidised bed of calcium hydroxide mixed with raw meal. This system has been operating in a Swiss plant. Another dry scrubber is based on activated coke as a filtering medium for the dirty gas and has been installed at another Swiss plant. This type of dry scrubber is capable of reducing not only the SO_2 emission but also other pollutants like NO_x and heavy metals.

The main problems of these offline systems are high capital and operating costs as well as recycling of effluents. So far as environmental regulations for SO_2 emissions are concerned, the norms vary from country to country in the range of 200 to 1000 mg/Nm^3, the preferred range being 400-600 mg/Nm^3 for normal raw materials. Many countries have kept special regulatory provisions up to 1800 mg/Nm^3, if especially high-sulphur raw materials are used The environmental requirements of World Bank for the cement plants have the following limits for SO_2:

Stack emission	400 mg/Nm^3
Ambient air quality	100 µg/m^3

However, the norms provide for some relaxation in the ambient air quality by permitting maximum 24-h peak value to touch 500 µg/m^3 outside the plant fence and 1000 µg/m^3 inside the plant.

6.3 Trace Elements and Metals

Since trace elements including alkaline, transition and heavy metals occur to some extent in all raw materials and fuels, their appearance in the cement manufacturing process is almost inevitable. Some trace elements tend to volatilise and move on with the kiln gases to form volatile cycles. On condensation on the dust stream these metals are principally incorporated in the clinker, although a small portion is carried out in the form of SPM. Generally the heavy metals are classified in 3 groups:

I. Hg, Cd, TI
II As, Co, No, Se, Te
III. Sb, Pb, Cr, Cu, Mn, V, Sn Plus Zn

Generally the emissions of the first two groups of metals do not exceed 0.1 mg/Nm^3 while the third group emission maintains at less than 0.3 mg/Nm^3, unless the initial concentration of the trace elements in the raw materials and fuel is abnormally high. Hence in common practice these emissions do not pose any serious threats.

6.4 Carbon dioxide emissions

Carbon dioxide generated from the cement industry is the major contributor of GHG. For example, in producing a ton of Portland cement clinker, 0.87 to 1.00 ton of CO_2 gas is discharged from the calcination of limestone and combustion of fuel. Taking into account the global production of different varieties of Portland cement it is estimated that about 500 million tons of CO_2 emission per year is broadly attributable to the cement industry, which works out to be 2% of gross emissions of all industries.

The two processes from which CO_2 is emitted from cement manufacturing are (i) calcination and (ii) emission from fuel use. CO_2 is released from calcining the limestone in the raw mix. The quantity of CO_2 released is proportional to the calcium carbonate content of the limestone. Compilation of individual plant-wise quantity and quality limestone consumed for the studied years provides accurate assessment of the total CO_2 released:

$$CaCO_3 + \text{heat} \rightarrow CaO + CO_2$$
$$1\text{ kg} + \text{heat} \rightarrow 0.56\text{ kg} + 0.44\text{ kg}$$

The share of CaO in clinker usually amounts to 64-67%. The remaining part consists of silica, iron oxides and aluminum oxides in decreasing order. CaO content of clinker is a fairly accurate measure of CO_2 emission from limestone dissociation, unless the source of Ca0 is other than limestone. Such exceptions, e.g., plants using lime-sludge or partly (insignificantly) calcium silicate in crystalline limestone are known and are accounted for in the assessment. The specific process of calculating CO_2 emission from cement production depends on the ratio of clinker to cement. The ratio varies from 0.5 to 0.95, depending upon the type of cement produced.

The fuel in pyroprocessing for clinker making is primarily coal. Lignite has been marginally used by the industry, and only in a few regions in the proximity of lignite sources. The amount of CO_2 released during this process depends on the type of coal used and its ultimate analysis (coal, fuel oil, natural gas, petroleum coke, alternative fuels). The total CO_2 released depends on:

- Types of production process (efficiency of the process or sub-process)
- Fuel used – coal, lignite, natural gas
- Clinker/cement ratio

For the Indian cement industry, quality and quantity of coal supplied to plants under the linkage agreement between cement industry and Coal India Ltd. (the sole coal mining and supply authority since 1972) is well documented. CO_2 emission owing to coal burning in each year is therefore calculated on the basis of proximate analysis (fixed carbon and volatile matter content) and cross checked from the ultimate analysis.

As a common yardstick, total CO_2 emissions per ton of cement range between 0.85 to 1.15 tons, assuming clinker to cement ratio to be 0.95 [IPCC, 1996]. The approximate contributions of each of the 3 main sources of CO_2 emissions are:

Calcination	=	50 – 55%
Fuel Combustion	=	40 - 50%
Electricity	=	0 - 10%

Thus, for the year 2001, the average level of CO_2 Emission worked out for the Indian cement industry is found to be 50 million tons due to the process of calcination, 40 million tons from coal combustion, and 7.4 million tons from electricity consumption, using grid or captive power. Table 9A provides an estimate of CO_2 emission in million tons in different regions of the globe including India from process and energy related activities in cement manufacturing for the year 1994-95. For Indian cement industry, only major plants constituting more than 94% of capacity and production are considered (as most of world production of cement, except China is from large plants only). Table 9B shows the level of GHG emission from total cement manufacturing in India in the year 1994-95 in comparison to the world average. It is evident that the CO_2 emission level in India estimated at 1.102 tons per ton of cement is significantly higher than the world average of 0.746 tons. This situation at that time called for adopting measures for reduction of GHG emission by the Indian cement industry.

Table 9A. CO_2 Emissions in million tons

1994-95	Due to		Total
	Process	Energy	
Total Global	587	830	1126
China	175	197	372
Europe	73	56	129
OECD pacific	65	41	105
Middle east	51	44	95
North America	39	40	79
Latin America	41	30	71
India*	28	30	58
Other Asia	56	179	105

Source: [12]

** Large plants (data for mini and white cement plants not included)*

Table 9B. CO_2 Emissions per ton of Cement

1994-95	Due to		Total (tons)
	Process	Energy	
World Average	0.746	0.277	1.023
India*	1.102	0.626	1.728

Source: [14]

** Includes both large as well as white and mini cement plants*

The contemporary dry process plants in India has been continuously adopting modernisation and technology upgradation measures for the obvious benefits of increasing productivity, lowering cost of production mainly through reduction of energy consumption. This has been providing the direct benefit of gradually reducing GHG emissions. Table 10A provides an estimate of energy consumption of dry process plants in course of the last decade, which clearly shows a decreasing trend. Table 10B gives some of the typical data on specific heat consumption, specific power consumption and corresponding CO_2 emission from some of the modern dry process plants in the country in the year 1999.

Table 10A. Reducing Energy Consumption by Dry Process Plants in the Last Decade

Year	Thermal (Kcal/kg of clinker)	Power (kwh/t of cement)
1989	876	120
1998	763	97
1999	750	91
2000	734	89

Table 10B. CO_2 Emission values of some energy efficient Indian cement plants 1999

Plant No.	Location	Capacity MTPA (TPD)	Production MTPA	Specific heat consump-tion kcal/kg	Specific power consumption kWh / clinker cement	CO_2 Emission during the year MT	CO_2 Emission /ton of cement
1	Rajasthan	0.825 (2500)	0.884	720.5	105.6	0.728	0.82
2	Gujarat	1.06 (3200)	0.651	735	105.8	0.504	0.77
3	Madhya Pradesh	2.05 (6225)	1.64	780	92.5	1.412	0.86
4	Madhya Pradesh	2.33 (7050)	1.93	706	105.5	1.352	0.70
5	Rajas-than	1.95 (5900)	1.29	728.5	80.0	1.054	0.81
6	Tamil-Nadu	0.89 (2700)	0.76	832	110.6	0.587	0.77

Source: [15]

CO_2 emission from the Indian cement industry for each calendar year for the period 1980 to 2000 has been estimated with relatively fair accuracy based on the following parameters:

(a) CO_2 emission in each year due to decarbonation of limestone measured from annual clinker production and cross-checked by annual plant-wise consumption of limestone (and its total carbonate content)

(b) CO_2 emission in each year from plant-wise coal and other substitute fuel consumption in clinkerisation process based on plant-wise annual fuel consumption and its total carbon content (in terms of fixed carbon and volatile matter).

(c) CO_2 emission in each year from plant-wise diesel consumption by Diesel generating (DG) sets and coal consumption by captive thermal power plants.

(d) CO_2 emission in each year from plant-wise limestone raising and cement packing related fuel and power consumption

For estimation purpose, parameters (b) and (c) have been combined to give the total CO_2 emission due to fossil fuel burning in the cement production process. Parameter (d) has not been dealt with in this paper as this is not directly involved with the cement manufacturing process. Besides, in the national GHG estimates, the limestone raising process is taken care of under the Head limestone mining.

Based on these assumptions the CO_2 emission from the cement industry for the years 1996 to 2001for the process, fuel burning and other indirect sources is shown in Table 11 and Figure 4 indicates the trend of total emission of CO_2 from the Cement sector for the last two decades. As can be seen the emissions are increasing continuously. Figure 4 gives the total CO_2 emitted from the cement sector. The dashed line gives the production of cement and the bold line describes the CO_2 emission from this source.

Table 11. Computation of year-wise CO_2 emission by the Indian Cement Industry for the last five years

Year	Production (in Mn. T)		Emission of Carbon Dioxide (in Mn. T)						Grand Total (a+b)
	Cement	Clinker	Direct Source			Indirect Source			
			Calci-nation	Fuel Combus-tion	Total (a)	Power Consu-mption	Trans-port Activities	Total (b)	
2001 (83 plants)	93.52	83.82	42.70 (46.38)	38.06 (41.34)	80.76 (87.73)	8.97 (9.55)	2.33 (2.53)	11.30 (12.27)	92.06 (100)
2000 (83 plants)	94.21	85.18	43.39 (47.26)	37.54 (40.88)	80.93 (88.14)	8.54 (9.30)	2.35 (2.56)	10.89 (11.86)	91.82 (100)
1999 (81 plants)	81.76	72.23	36.79 (45.30)	34.72 (42.77)	71.51 (88.07)	7.65 9.42)	2.04 (2.51)	9.69 (11.93)	81.20 (100)
1998 (89 plants)	76.74	71.91	37.12 (44.00)	37.81 (44.81)	74.93 (88.81)	7.52 (8.91)	1.92 (2.27)	9.44 (11.19)	84.37 (100)
1997 (94 plants)	69.98	64.42	32.78 (39.52)	41.33 (49.83)	74.11 (89.35)	7.08 (8.54)	1.75 (2.11)	8.83 (10.65)	82.94 (100)
1996 (88 plants)	64.54	58.63	29.88 (38.80)	39.19 (50.88)	69.07 (89.68)	6.34 (8.23)	1.61 (2.09)	7.95 (10.32)	77.02 (100)

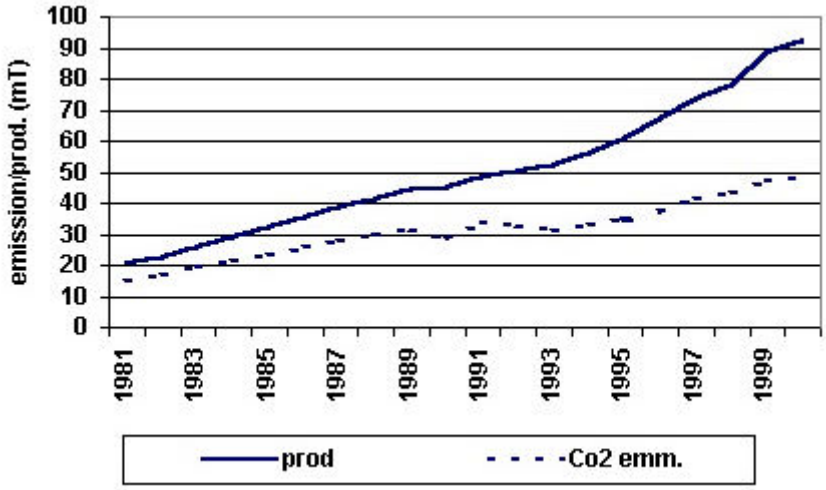

Figure 4. Annual CO_2 emission from the Indian Cement sector

The graph shows that CO_2 emission from the cement industry has increased progressively over the stated years, but the growth rate is much lower than the growth rate of production of cement in the country. This indicates that the cement industry has been continuously adopting energy conservation measures, as explained in Tables 10A and 10B. The various technological interventions over the years for improving efficiency has lead to an almost constant CO_2 emission from the year 2000 onwards.

Thus, although India emitted a total of about 778 million tons of CO_2 from all activities in 1995 and about 1000 million tons in 2000, the share of the cement industry to the total CO_2 emission has increased marginally from 4 to about 5% during these years.

7. GHG EMISSION PROJECTIONS

It is projected from the contemporary trend that CO_2 emission from the year 2002 onwards will remain almost static or will increase marginally during the next few years, despite 8 to 10% annual growth in production, if the technological interventions are continued at the present rate. This is because increase in production and capacity at present are based primarily on debottlenecking measures (95%) involving major energy conservation and insignificant greenfield capacity addition (5%), the last mentioned too is based on modern highly energy efficient technology. Thus if production increases with relatively much lower energy consumption, the overall impact will be that the average energy consumption will remain nearly the same. Correspondingly, CO_2 emission from cement manufacture will remain the same or will increase marginally for a few years.

However, in the long term projections the cement industry in India has to grow at a faster rate to match the increasing demand of the infrastructure development programmes. With growth in the infrastructure sector namely, roads, housing, power generation installations etc. the demand of cement will increase and more of Greenfield projects are bound to come up to bridge the gap. This will also compensate to some extent the very low per capita consumption of cement which is at present 96 kg in comparison to the world average of 269 kg [Cement in Japan, Japan Cement Association, 2002]. Such a quantum jump in growth of cement capacity much beyond the present 8-10% through Greenfield projects is bound to increase energy consumption by leaps and bounds, and therefore, its natural fallout will be increased GHG emission. One can therefore logically presume an increased GHG emission from the cement industry in the later part of the present decade and next decade. This will also open up the opportunity for carbon trading by the Indian Industry through adoption of CDM related technologies. A preliminary analysis of CO_2 reduction from the Indian Cement Industry by the year 2015 is shown in Table 12. The measures that are

likely to be used include energy efficiency with higher electrical energy efficiency and use of supplementary fuel, conversion of technologies using wet process to dry process; conservation of thermal energy by insulating brick lining and using of mineralisers; recycling industrial waste as fuel; raw mix optimization and use of co-generation power.

Table 12. Potential reduction of CO_2 from Indian Cement Industry by the year 2015

Areas for Improvement	**Future Use (2015) (%)**	**Likely CO_2 Reduction (%)**
Production blended Cement (PPC-50%; PSC-15%)	75	22 - 24
Use of CNG as Fuel	20	8 - 9
Use of Waste Derived fuels	10	8 - 9
Use of Non-Conventional Energy Sources (Wind, Hydro)	8	2 - 3
Energy Efficiency Improvement	10	8 - 10
Total CO_2 Reduction		48 - 55

8. THE FUTURE OUTLOOK

Quantitative assessment of GHG and pollutant emissions from the cement industry is the theme of this paper. Amongst all the emissions discussed in the above section, CO_2 is the major gas constituting more than 95% of total GHG emission from this source. Also, the change in technology over the years though has moved towards an efficient energy use, but the total emission from this source, both process based and due to fossil fuel consumption is still increasing (refer to Table11 and 12 and Figure 4.) rising because of greater demand. The increasing demand for cement as a construction material means that in as little as a decade, world cement CO_2 emissions could equal 3,500 million tons including the share of the growing Indian cement industry. The effect of these CO_2 emissions on the world's fragile climate and global warming could be catastrophic. Therefore steps should be taken to reduce this emission.

There are various methods by which CO_2 can be reduced, one of the practical avenues being reduction of fuel consumption itself. Over the last two decades, the fuel consumption has been reduced to a level below 700 kcal/kg clinker as against the theoretical requirement of 425-450 kcal/kg clinker. Within the present state of technology it seems that there is not much scope for further significant reduction of fuel consumption for clinker making unless a break -through kind of technology comes to the forefront in the industry. It is also well known that an effective avenue for reduction of CO_2 emission is the production of blended cements by using cementitious and pozzolanic mineral admixtures at the time of grinding. It is obviously possible to bring down the clinker consumption in cement grinding through such routes, thus reducing the CO_2 emission in totality.

For many years the cement industry has been making a significant contribution to environmental case by burning a wide range of secondary fuels. The benefits include reduction in atmospheric emissions including CO_2, apart from energy recovery from waste materials and conservation of

nonrenewable fossil fuels. Another possibility that exists but still continues to be in the realm of research and development is to dovetail a facility to stabilise CO_2 through production of chemicals as an appurtenant to an existing cement plant (4).

For an energy intensive and energy efficient industry like cement, proposals are being considered in the industrialized countries to apply certain fiscal instruments for stabilization of CO_2 emission. There is also a parallel approach in countries like The Netherlands to adopt a voluntary measure to improve energy efficiency or to reduce or stabilise CO_2 emission. The German and French industries have recently developed the elements of an agreement on energy efficiency and CO_2 reduction. It appears that in near future the strategy of eco-trading may help in stabilising the CO_2 emission.

REFERENCES

[1] IPCC –TAR –WKGI, 2001

[2] IPCC –Policy Makers Report, 2001

[3] Chatterjee A K. How Clean and Environmentally Benign the Cement Plants can be? World Cement, October, 2001 and Proceedings of the International Seminar on Energy and Environment in the Cement Industry, New Delhi, January 2002

[4] Greenhouse Gas Emissions in India, Atmospheric Environment, Garg Amit, Bhattacharya Sumana, Shukla P.R.and Dadhwal, V. K., 2001a.

[5] Sub-region (district) and sectoral level SO2 and NOx emissions from India: Assessment of Inventories and Mitigation flexibility, Amit Garg, P. R. Shukla, Sumana Bhattacharya and V. K. Dadhwal, Atmospheric Environment, Vol 35, issue 4, pages 703-713,2001

[6] CEMBUREAU, World Cement Report, 2001-2002.Basic Data-Indian Cement Industry, Publn of Cement Manufacturers'. Association (CMA) of India-2001 and 2002

[7] Report of the Working Group on Cement Industry, Xth Five Year Plan –2002 to 2007, Planning Commission, Government of India, 2002

[8] Cement Statistics-2001 and 2002, Publication of CMA of India, 2001 & 2002

[9] Unpublished Periodical/Annual Reports of CMA and Coal India Ltd. on Coal Linkage for Cement Industry, 1980 to 2001.

[10] Energy Performance Achievements in Indian Cement Industry – 2000 and 2001, Publication of the National Council for Cement and Building Materials (NCCBM), 2002

[11] Energy Audit Manual, Confederation of Indian Industries (CII) , 2001

[12] Hendick, C. A., Wrrel, E., D. de Jager, Blok, K., and Riemer, P. Emission. Reduction of Greenhouse Gases from the Cement Industry, 2000[www.ieagreen.org.uk/prghgt42.htm]

[13] Ghosh S P, Afsah S, Srivastava S and Partha Sarathy R. Energy Efficiency and Productivity Improvements through Performance Monitoring and Benchmarking. 7th NCCBM International Seminar on Cement and Building Materials, New Delhi, 2000

[14] Global Warming and Cement, CMA Publication, New Delhi, October 2001 and 2001

[15] Environment Friendly Indian Cement Industry –CMA Publications, October 2001

[16] CO_2 Emission from fuel combustion, International Energy Agency Document, 1997).

CEMENT CONFERENCES PRIOR TO THE "FIRST"

Ferenc D. Tamás (University of Veszprém, Hungary)

The "Historical Preface" of the Proceedings of the 3rd International Symposium on the Chemistry of Cements (London, 1952) mentions that the First Symposium, to deal solely with the chemistry of cement, was held during the first World War, on 14th January 1918, when the Faraday Society arranged a meeting in London to discuss "The setting of cements and plasters". This preface mentions that there had been former symposia too, organised by the International Association for Testing Materials (IATM) dealing, however, not only with cement, but also with other building materials. The first of them, as far as can be traced, was held in Stockholm, Sweden in 1897 and the next in Budapest, Hungary in 1901.

By searching libraries and archives, I was able to find out some data of the Stockholm and Budapest conferences, 106 and 102 years ago, respectively.

The Stockholm conference [1] was held on 23-25 August 1897. More than 250 experts attended, among them 93 from Germany, 51 from Sweden and 38 from France, and discussed problems in three categories: A./ Steel structures, B./ Natural and artificial stones (mostly cementitious materials) and C./ Other materials. The conference was opened by the mayor of Stockholm, and was followed by plenary papers and their discussion. The list of plenary papers in Section B./was:

1. Wahlberg, A. (Stockholm, Sweden): Testing of building materials in Sweden
2. Osmond (Paris, France): Methods of metal microscopy used for the investigation of clinker
3. Buess (Hamburg, Germany): Durability of natural stones
4. Gary (Berlin, Germany): Investigation of concrete tubes
5. Michaelis, W.: Hardening of calcium containing binding materials
6. Meyer, M. (Mallstatt, Germany): Quality testing of hydraulic binders
7. Eurich (Carlstadt, Germany): Setting disturbances of cements
8. Greil (Vienna, Austria) – Tetmayer (Zürich, Switzerland): Workability of cement paste when testing strength and density
9. DeShärengard (Louma, Sweden): Törnebohm's investigations on the petrography of clinkers

During this congress the President and the Steering Committee of the IATM were elected. L. Tetmajer (of ETH, Zürich) was re-elected as president, and 8 vice-presidents were also elected (one-each from Switzerland, Germany, France, Russia, Austria, Great Britain, Sweden and U.S.A.).

The Budapest conference, organised by IATM, was held on 9-14 September 1901, discussed problems in two sections: A. Steel structures, B. Cementitious materials. The venue of the conference was the Technical University (official name at this time: Royal Hungarian "József" Technical University); 380 participants, coming from 17 countries attended. (152/Hungary, 70/Germany, 41/Austria, 36/France, 26/Russia, 12/Italy, 10/Switzerland, 9/Denmark, 8/Netherlands, 5/Sweden, 4/UK, 3/Norway, 3/Belgium, 3/USA, 3/Spain,1/Romania, 1/Serbia).

Proceedings of the 11th International Congress on the Chemistry of Cement (ICCC) 11 - 16 May 2003, Durban, South Africa
'Cement's Contribution to the Development in the 21st Century' ISBN Number: 0-9584085-8-0
Hosted by: The Cement and Concrete Institute of South Africa Editors: Dr G. Grieve and G. Owens
CD-ROM produced by: Document Transformation Technologies Congress Organised by: Event Dynamics

The opening ceremony was held in the Aula of the (at this time newly built) TU. The first speaker was the president of the IATM, professor L. Tetmayer (Zürich, Swiss Federal Polytechnic, the famous ETH), followed by addresses by the Hungarian government (Minister of Trade and Industry, Mr. S. Hegedüs) and several national and international celebrities. The Rector of TU Budapest (professor L. Ilosvay) gave a short speech, followed by one from the chairman of the Hungarian organising committee, professor G. Czigler.

The work of the Organising Committee deserves great praise; they accomplished a great deal, even by today's standards. All printed material: information, agendas of the conference, preprints of the plenary papers, abstracts of others, etc. were given to attendees in four languages (English, German, French and Hungarian). Besides that a "Technical Guide-book of Budapest" was distributed too (again in four languages), which described showpieces of Budapest from an engineering point of view, with photos and technical sketches; many of which are nowadays an obvious part of tourists' itineraries, but were brand new a century ago: the cog-railway to Svab-hill, the underground railway under the Andrássy street (actually, this was the first on the European continent, its only predecessor was the first underground line of London), the Elisabeth bridge over the Danube (not finished at this time), etc.

Ten plenary lectures were held in Section A., while 17 were given in Section B. (Cementitious Materials) of the conference.

The full list of plenary papers of Section B follows:

1. Considère (Paris, France): Studies on reinforced concrete
2. Feret (Boulogne, France): Adhesion of mortar and concrete
3. Feret (Boulogne, France): Calculation of reinforced concrete slabs
4. H. LeChatelier (Paris, France): Rapid methods for cement soundness testing
5. H. LeChatelier (Paris, France): Decomposition of cement in seawater
6. Deval (Paris, France): The role of calcium sulfates on cement
7. Deval (Paris, France): Composition of sulfo-aluminates in hydraulic lime
8. Foss (Copenhagen, Denmark): Determination of the breaking strength of cements by Feret's method
9. L. Tetmajer (Zürich, Switzerland): Effect of inorganic salts on the setting and hardening of cementitious materials
10. L. Tetmajer (Zürich, Switzerland): The swelling of cement
11. Leduc (Boulogne, France): Carbonation and decomposition of hydraulic binders
12. Zielinski and Zhuk (Budapest, Hungary): Investigation of Roman cements
13. Mercier (Paris, France): Flexural strength of cements
14. Maynard (Paris, France): Corrosion of cements in seawater
15. P. Siméon (Paris, France): Comparison of strength values of cylinders vs. cubes
16. M. Gary (Charlottenburg, Germany): Actual problems of cement testing in Germany
17. Cajo (Ancona, Italy): Corrosion of concrete by alkali sulfates

All this shows that important, almost "evergreen" topics of cement chemistry were discussed a century ago; at times when practically wet chemical analysis and optical microscopy were the only tools to study the chemistry of cements – when X-ray diffraction, electron microscopy, thermal analysis, EDX, etc., etc. had not yet been discovered. Abstracts of papers and details of discussions can be found in references 2 and 3.

Some names of expert notabilities of the time who attended: Wilhelm Michaelis (Berlin, Germany), Prince Gagarin (St. Petersburg, Russia), Sir William Bayley (Manchester, U.K.), Bertram Blount (London), Emil Svartz (Novorossiisk) and others.

Some technical excursions were included in the agenda of the congress. A specal train was ordered for attendees to visit two factories: the Resica Steel Works (now in Romania) for participants of Section A., and the Cement Factory of Beocsin (now in Yugoslavia) for participants of Section B. Some factory visits in Budapest had been organised too, as well as one to the building site where the Elisabeth bridge was being erected.

The extracurricular activities were interesting too: a boat trip was made to see the Water and Sewage Works, with an on-board buffet. A committee organised several activities for the ladies, where the programme included visits to museums, galleries and also a fashion show.

The Conference Reception was held in the most luxurious hotel in Budapest at this time, the Hotel Royal. Here, obviously after a pledge to King Henry, LeChatelier gave the first toast, praising the international community of scientists and engineers. Dr. Wedding, a quarry consultant of Prussia complimented the work of the Ladies Committee, ending his German toast with the words "Three cheers for the ladies!", in Hungarian.

REFERENCES

[1] M. Gary: Wanderversammlung des Internationalen Verbandes für die Materialprüfungen der Technik. (Meeting of the International Association for Testing Materials). Thonindustrie-Zeitung Vol. 21, (1897). No. 89, p. 980-03

[2] M. Gary: Dritte Wanderversammlung des Internationalen Verbandes für die Materialprüfungen der Technik. (3rd Meeting of the International Association for Testing Materials). Thonindustrie-Zeitung Vol. 25, (1901). 1st part: No. 127, p. 1905-07. 2nd part: No. 130, 1942-47

[3] D. Goslich: Bericht über die Dritte Wanderversammlung des Internationalen Verbandes für die Materialprüfungen der Technik. (A report on the 3rd Meeting of the International Association for Testing Materials). Thonindustrie-Zeitung Vol. 26, (1902). No. 76, p. 1919-23

THE CHEMISTRY, REINFORCEMENT AND FRACTURE IN GEOPOLYMERIC CEMENT COMPOSITES

F.J. Silva and C. Thaumaturgo*

Departamento de Engenharia Mecânica e de Materiais
Instituto Militar de Engenharia - IME.
Pç. General Tibúrcio, 80, Praia Vermelha, 22290-270 Rio de Janeiro, RJ, Brasil.
E-mail: imes4cle@epq.ime.eb.br

ABSTRACT

Pozzolanic and alkali-silica reactions open new opportunities for the future (1, 2). The inorganic polymeric materials called geopolymers are a result of this technology. This work presents a comparative study of fracture toughness of mortar composites, using a polysialate-siloxo (PSS) geopolymeric cement (3) with Si/Al =3 ratio and a reference Portland cement (PC) as binders and natural wollastonite micro-fibers (Ca[SiO3]) as reinforcement and stabilization elements. The values of K_{Ic}^{s} and $CTOD_c$ were determined and the G_I^s and R-curves were calculated. The results show that with 2% of fiber volume, there is an increase in maximum toughness. With high fiber volumes (3% and 5%), there is a decrease of fracture parameter values, probably caused by porosity elevation. The microstructural results show the occurrence of toughening mechanism such as debonding and fiber pullout, have been more common in PSS cement composites. The toughness difference between both PSS and PC cement pure matrices (0% of fibers) is of order of 100%, showing the high performance of these geopolymeric materials.

Keywords: Fracture toughness, geopolymer, reinforcement, wollastonite.

1. INTRODUCTION

The alkali-activation of granulated blast-furnace slags and pozzolanic materials opens new opportunities for development of high-performance structural materials [1-3]. Inorganic polymers based on aluminosilicates, obtained by alkali-silica reactions, called geopolymers [1-4], are a new generation of high-performance products that are classified within the domain of "advanced materials". In the fresh state, its viscosity is like thatof organic resins. After polymerization, it develops ceramic properties, and in this way can create competition with the Portland cement and with other traditional materials, for various applications.

The geopolymer with Si/Al ratio between 2 and 3, is called poly(sialate-siloxo) or PSS and presents functional units composed by SiQ4(2Al) tetrahedrons, with aluminum atoms in four-fold coordination numbers, generating cross-link polymeric chains. This three-dimensional arrangement forms an irregular structure of low mobility. The polycondensation reaction is not uniform in bulk material and mineral fillers are necessary for mechanical stabilization. In this case, the polycondensation reactional subproduct is water [1,4,5].

The addition of fibers as a reinforcement element is an efficient form for improvement of toughness in brittle and quasi-brittle materials. The fracture toughness is the relevant material property and shows the energy absorption capacity until rupture. The geopolymer studied presents quasi-brittle

material properties. Therefore, the concepts of Non-linear Fracture Mechanics (NLFM), developed to evaluate stones and concretes were applied. [6]. NLFM considers the inelastic response of structures caused by the presence of a fracture process zone (FPZ), an inelastic zone formed in the region of a crack tip around by stress concentration [7].

The RILEM Technical Committee 89 – Fracture Mechanics of Concrete – Test Methods[8], recommends the employment of the two-parameter fracture model (TPFM) based on the studies of Jenq and Shah [9] for determination of the fracture toughness of mortars and concretes. The model considers that elasto-plastic deformations occurred ahead of the tip of a macrocrack induced by a notch. The unloading compliance (C_u) measured from the unloading at 95% of the maximum load (post-peak load) in diagrams load versus CMOD (crack mouth opening displacement), allows the determination of the fracture properties of the material. Those properties are indicated by the critical stress intensity factor (K_{Ic}^s), the critical crack tip opening displacement ($CTOD_c$) and the critical crack effective extension ($\Delta a_c = a_c - a_0$). The compliance in the initial loading (C_i) gives the modulus of elasticity (E) of the composite. The parameters K_{Ic}^s and $CTOD_c$ were used to calculate the G_I^s and *R*-curves.

This work presents a study of the fracture toughness of a mortar composite of PSS cement matrix with ratio Si/Al = 3, reinforced with natural wollastonite ($Ca[SiO_3]$) micro-fibers, a natural mineral of high modulus of elasticity (120 GPa) and aspect ratio (10-20), employed in the ceramic industry as reinforcement and stabilization elements. The volumes of fibers studied were of V_f = 0% (pure matrix) to V_f = 5%. The fracture parameters were measured and compared with the results obtained with the Portland cement mortar composites.

2. MATERIALS AND METHODS

For achieving the calcium, potassium and sodium poly(sialate-siloxo), Na,K,Ca-PSS requirements, the main source of aluminum and silicon was metakaolin, obtained by burning of kaolin originating from Rio Grande do Norte (RN), Northeast of Brazil. The time and temperature of burning were the subject of another study, because they depend on the purity and the degree of the kaolin crystallinity. Burning for 12 hours at 700 ^oC promotes the desidroxylation of the kaolinite and the conversion of aluminum coordination number from VI to IV, disordering the lattice [5]. Since the ratio between the silicon and the aluminum in the metakaolin is lower than 3, an extra source of silicon, a commercial alkaline polysilicate was used. In order to obtain a pH of 14, necessary to begin the polymerization, potassium hydroxide (Vetec P.A.) was also used as a complementary alkali source. The source of calcium was granulated blast furnace slag (GBFS) supplied by Belgo Mineira S.A.

The reference Portland cement was CPIIE-32 (type II of ASTM C 150), of Campeão/Mauá S.A. and the fine aggregate was river sand supplied by IPT S.A. (Normalized Brazilian sand). The proportion between binder and aggregate was 1:3, by weight for all the composites and the water/binder dry ratio was 0.48 for the Portland cement composites and 0.38 for the PSS composites. The consistency index (flow table - ASTM C 230) for both composites systems was of 165 $\pm$ 5 mm, with V_f = 0%.

The wollastonite used was NYAD-G® grade (Figure 1) of Nyco Minerals Inc. (New York - USA). Table I shows the main characteristics of the raw materials used in this study.

The mixture of the basic constituents and the moldings of the specimens followed the procedures described in the NBR 7215 Brazilian standard. The wollastonite micro-fibers were dispersed in the water before mixture with others materials. In order to determine the fracture toughness, the procedures established by TC-89 FMT Draft Recommendations of RILEM were adopted as already

mentioned. The dimensions of the toughness test specimens and the experimental configuration are shown in the Figure 2. The Na,K,Ca-PSS cement (PSS) composites were cured in air at 25 ± 2 °C, and the Portland cement (PC) composites were cured immersed in water at 22 ± 2 °C until the test date.

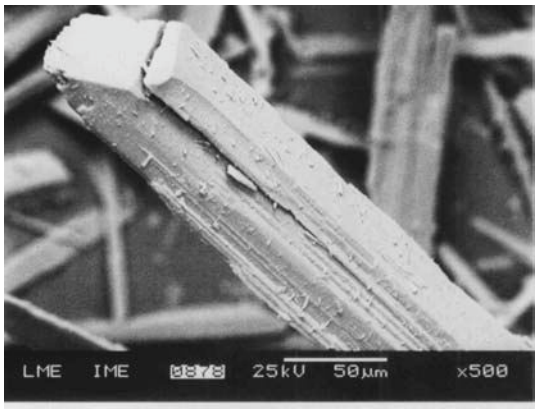

Figure 1. Micrograph (SEM) of wollastonite micro-fibers used (500 X).

Table 1. Chemical composition and physical properties.

Materials	Chemical Composition (%)									L.O.I. (%)	Specific Area Blaine ($m^2.Kg^{-1}$)	Specific Weight ($g.cm^{-3}$)
	CaO	MgO	Na_2O	K_2O	Fe_2O_3	SO_3	Al_2O_3	TiO_2	SiO_2			
Metakaolin	< 0.01	0.01	0.04	0.33	0.30	-	39.8	0.11	44.4	14.4	**1060.76**	2.56
Na-Silicate	-	-	17,3	-	-	-	-	-	35.6	44.3	-	1.75
GBFS	47.8	0.63	0.21	0.26	0.72	0.47	13.0	0.38	39.7	0.14	**345.43**	2.98
Wollastonite	46.55	0.15	0.01	0.05	0.75	-	0.28	0.04	51.37	0.34	-	2.90
CPIIE-32	60.4	1.4	0.15	0.34	1.6	3.9	5.0	-	20.0	6.30	**349.92**	3.04

Strength Activity Index (ASTM C 618) of metakaolin ∅ < 0.074 mm = 107.88%.
% Retained in the sieve # 325 Tyler-Mesh = 12.35%.
Aspect ratio of wollastonite: 10 to 20.
CPIIE-32 – Bogue composition (ASTM C 150): 46,60% C_3S; 22,18% βC_2S; 10,54% C_3A; 4,87 C_4AF.

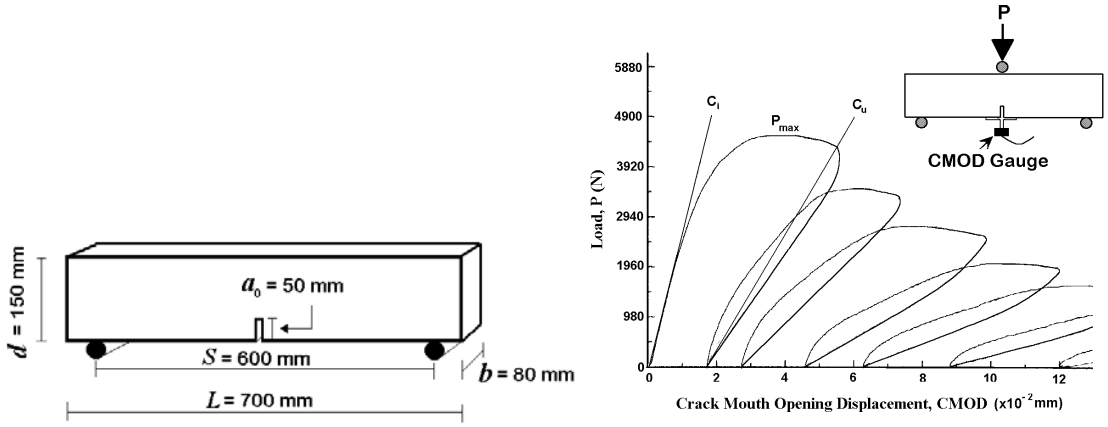

Figure 2. Dimensions of specimens and tests configuration. The maximum load (P_{max}), initial compliance (C_i) and unloading compliance (C_u) are obtained from the diagram and used as input for the TPFM.

The strain energy release rate, G_I^s, was calculated from relationship $G_{Ic}^s = (K_{Ic}^s)^2/E$ and the crack propagation resistance, *R*, was obtained using the model proposed by Ouyang and Shah [10]. The R-curve was obtained by solving of a linear differential equation with constant coefficients, written as

$$R = \sum_{n=1}^{\infty} \beta_n c^{d_n} \qquad (1)$$

where the β_n are constants to be determined and the d_n are roots of the differential equation. If only terms up to $n = 2$ are considered, which indicates that G_I^s is approximated by a quadratic expression of crack length, the solution of Eq. (1) is:

$$R = \beta\psi(\Delta a)^{d2} \tag{2}$$

where

$$\psi = 1 - \frac{d2\alpha - \alpha + 1}{d1\alpha - \alpha + 1}\left(\frac{\alpha a_0 - a_0}{\Delta a}\right)^{d2-d1} \tag{3}$$

and

$$d1, d2 = \frac{1}{2} + \frac{\alpha - 1}{\alpha} \pm \left[\frac{1}{4} + \frac{\alpha - 1}{\alpha} - \left(\frac{\alpha - 1}{\alpha}\right)^2\right]^{\frac{1}{2}} \tag{4}$$

The roots $d1$ and $d2$ represented in Eq. (4) are calculated taking the signal (+) to root $d1$ and (-) to root $d2$.
Using the critical conditions $R = G_{Ic}^s$, the parameters **a** and **b** can be determined as

$$\alpha = \mu + \sqrt{\mu^2 + 1} \tag{5}$$

and

$$\beta = \frac{\left(K_{I_c}^s\right)^2 (d1\alpha - \alpha + 1)}{E\alpha(d1 - d2)\left(\alpha a_0 - a_0\right)^{d2}} \tag{6}$$

where

$$\mu = \frac{\pi E^2 CTOD_c}{0.0195 a_0 \left(K_{Ic}^s\right)^2} \tag{7}$$

After determination of the fracture properties, samples were selected for scanning electron microscopy (SEM – Jeol 5800 LV) to determine the damage mechanisms. The fracture surfaces were observed by secondary electron imaging. Since the samples are not conducting, a gold deposition sputter coating was utilized.

3. RESULTS AND DISCUSSIONS

Figure 3 shows the values of K_{Ic}^s and $CTOD_c$ for PSS cement composites and PC composites. For PC composites, the $CTOD_c$ values decreased to fiber volumes up to 2%. The influence of fibers is governed by closing pressure on cracked surfaces that tends to close the crack tip. The presence of fibers provides a bridging effect and prevents the opening of the crack. This phenomenon causes an additional toughening on PC composites indicated by increase of K_{Ic}^s.

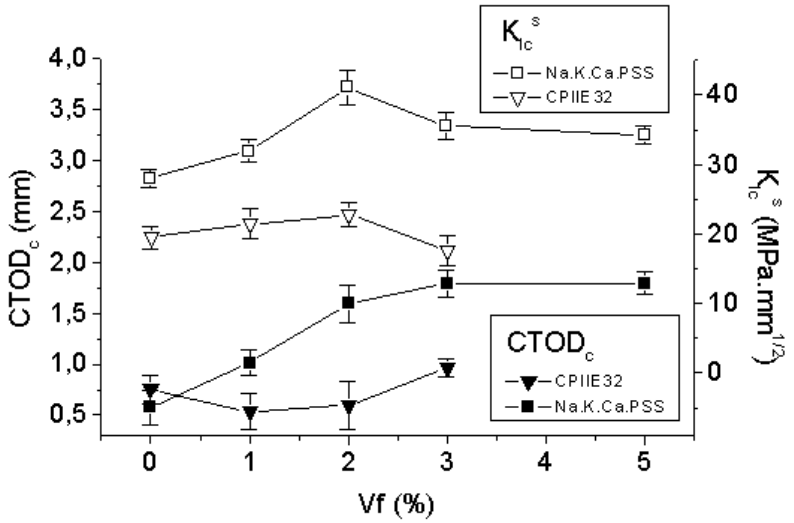

Figure 3. Variation of $CTOD_c$ and K_{Ic}^{s} as function of fiber volume.

The PSS cement composites showed $CTOD_c$ values always peak, independent of wollastonite fiber volume. It is noted that in PSS composites, the fiber-matrix bond is more denser than in the PC composites. The toughness gain obtained without $CTOD_c$ decrease in PSS composites was caused by more active debonding and pullout fiber mechanisms (Figure 4). However, in the PC composites, the rupture of fiber in the crack plane is the principal mechanism in action (Figure 5). This indicates that because of the high porosity of PC matrix, the embedded length of wollastonite is smaller than the critical debonded length. Both composite matrices showed K_{Ic}^{s} increase up to 2% of fiber volume. On other hand, for fiber volumes higher than 2%, a K_{Ic}^{s} decrease occurs. Since the stress intensity factor is the driving force to open a crack, it can be supposed that the porosity increase has occurred due to the excess of fiber addition.

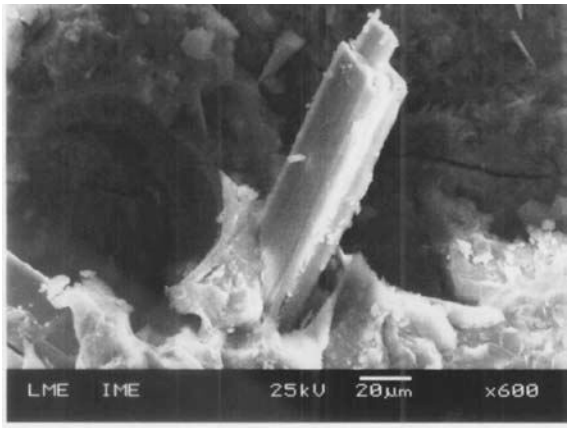

Figure 4. Micrograph (SEM) of PSS cement composite showing the pullout of wollastonite micro-fiber. (600 X)

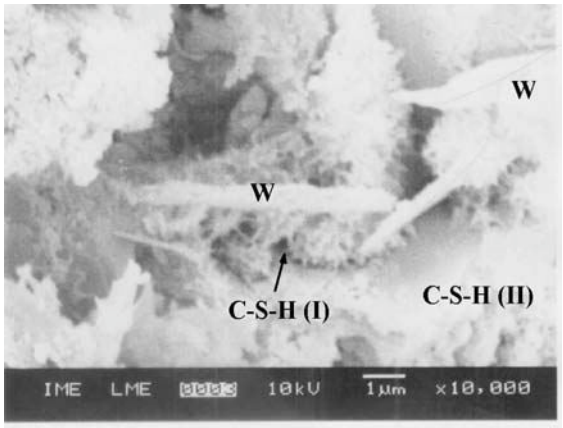

Figure 5. Micrograph (SEM) of Portland cement composite showing details of wollastonite micro-fibers embedded in porous outer C-S-H products. (10000 X)

The strain energy release rate, G_I^s, calculate by relationship $G_{Ic}^{s} = (K_{Ic}^{s})^2/E$, was plotted as Δa function, to both composites systems, as shown in Figures 6 to 8. The negative values of Δa are due to the interpolation form $a = a_0$ up to $a = 0$.

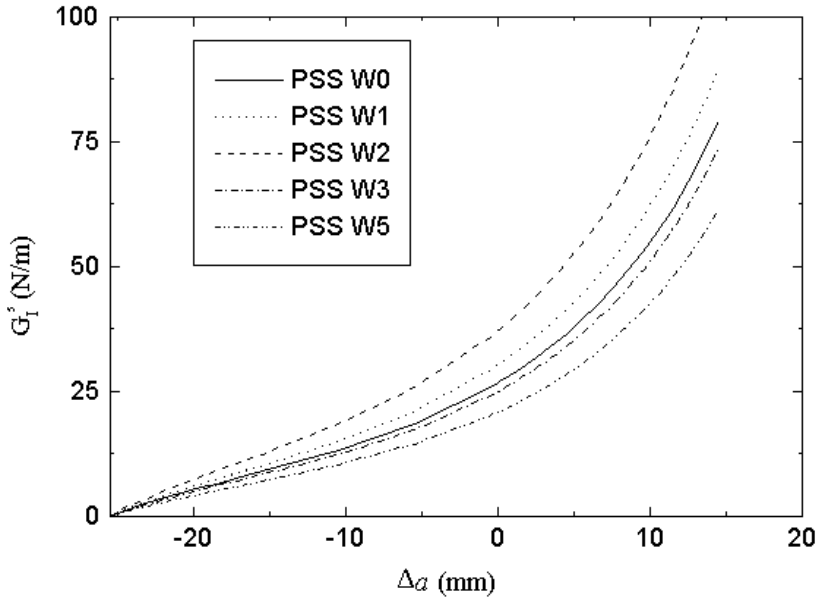

Figure 6. Variation of strain energy release rate, G_I^s, as function of effective crack extension, Da, for the PSS cement composites with V_f = 0 to 5%.

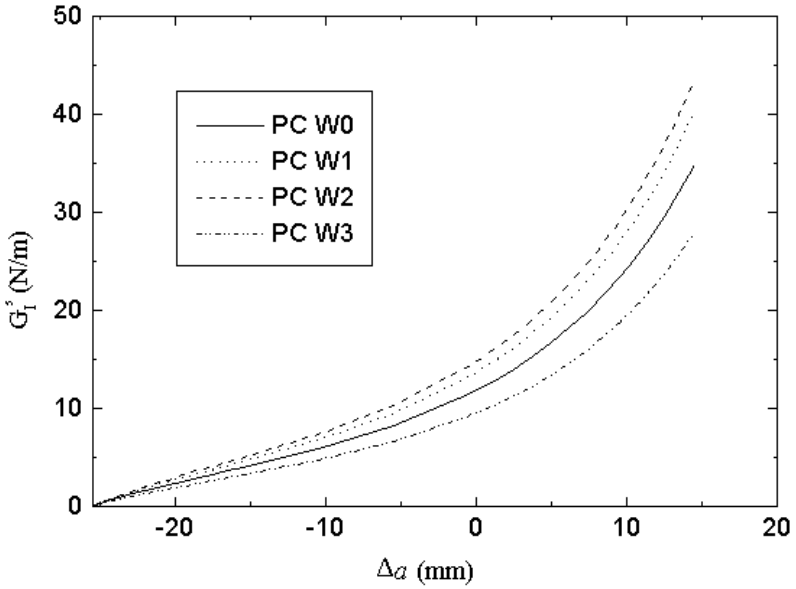

Figure 7. Variation of strain energy release rate, G_I^s, as function of effective crack extension, Da, for the Portland cement composites with V_f = 0 to 3%.

The performance of reinforcement was evaluated by G_I^s-Δa responses. It was noted that for certain Δa value, there was increase of G_I^s for volumes of fibers up to 2%. An identical behavior was presented by PC composites, however the PSS composites presented G_I^s values 100% higher than PC composites, showing the more efficiency of fiber reinforcement (Figure 8).

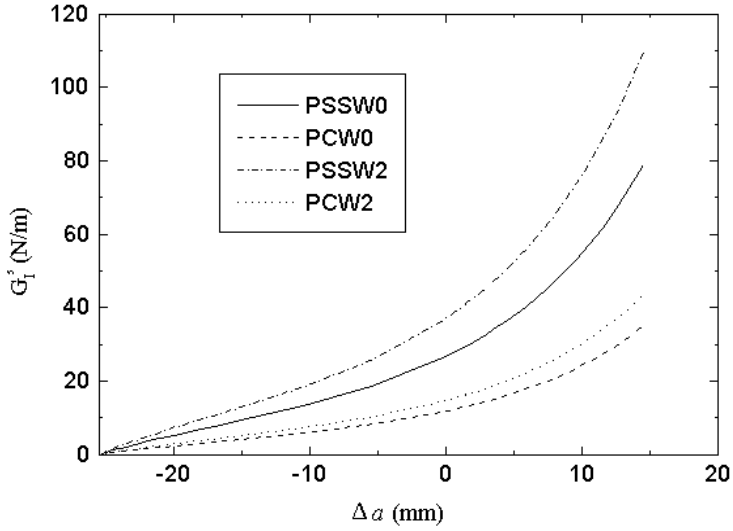

Figure 8. Comparison of G_I^s values between the both composites matrices, with $V_f = 2\%$.

The *R*-curves obtained show more clearly the toughness increase that occurred in each composite system. Again it is seen the positive contribution of fibers to fracture response (Figure 9 and 10). As $R = 0$ for $a < a_0$, the *R*-curves were ploted for positive values of Δa. An increase in *R*-value to unstable crack propagation (its maximum value) was observed of order of 34% to PSS composite and 20% to PC composite with 2% of fibers in relation to its pure matrices (0% of fibers).
The results confirm the efficiency and compatibility of wollastonite micro-fibers as stabilizer and as the reinforcement element to the composites systems studied. The fracture toughness measurements indicate that the PSS cement is tougher than PC, and totally adequate for structural applications.

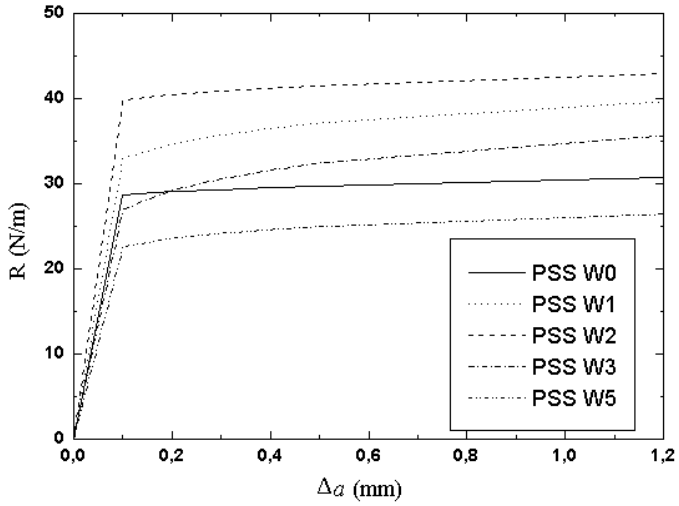

Figure 9. *R*-curves to PSS cement composites with different fiber volumes. $V_f = 0$ to 5%.

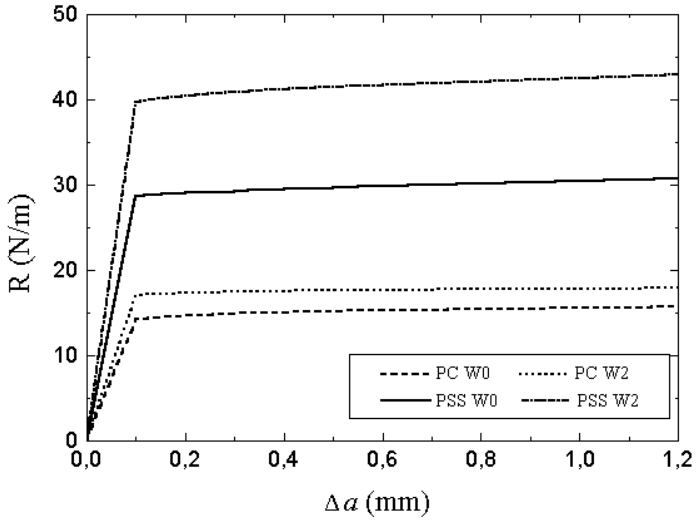

Figure 10. Comparison of *R*-curves between both composite matrices with $V_f = 2\%$.

4. CONCLUSIONS

The necessity of stabilization of a PSS matrix and the opportunity to improve its fracture toughness were successfully achieved by use of the wollastonite micro-fibers. The two-parameter fracture model permitted an evaluation of the influence of fiber addition in the fracture behavior of composites. Better values of K_{Ic}^{s} and $CTOD_c$ were obtained with 2% of fiber volume, to both composite systems. The microstructural analyses showed that the fiber-matrix bonds in PSS cement composites are more efficient and this provides the actuation of debonding and pullout mechanisms. The G and *R*-curves showed a maximum relative toughness increase of the order of 34% to PSS cement composites and of 20% to PC cement composites. The comparison between PSS cement and PC pure matrices, shows the high performance of PSS cement matrix. The difference in toughness is about 100% higher than the PC matrix. These results indicate that the PSS cement is perfectly viable for structural applications.

ACKNOWLEDGEMENTS

The authors thank to CETEM for the chemical analyses and to Belgo Mineira S.A. for the GBFS supply. F. J. Silva should like thanks to CAPES for the financial support.

REFERENCES

[1] Silva, F. J. Reforço e Fratura em Compósitos de Matriz Álcali-ativada,. PhD Thesis, Rio de Janeiro, IME, 2000.
[2] Roy, D. M.. Alkali-Activated Cements Opportunities and Challenges, Cement and Concrete Research, vol. 29, 1999, pp. 249-254.
[3] Bakharev, T.; Sanjayan, J. G., Cheng, Yi-B.. Alkali Activation of Australian Slag Cements, Cement and Concrete Research, vol. 29, 1999, pp. 113-120.
[4] Davidovits, J. Geopolymers of the First Generation:SILIFACE-Process, Proceedings of I Geopolymer International Conference, Université de Tecnologie, Compiège, France , 1988, pp. 49-67.
[5] Babosa, V. F. F.. Síntese e Caracterização de Polissialatos.,. PhD Thesis, Rio de Janeiro, IME, 1999.
[6] Shah, Surendra P.. An Overview of the Fracture Mechanics of Concrete, Cement Concrete and Aggregates, vol. 19, 1997, p.p.79-86.
[7] Prokopski, G.; Halbiniak, J. Interfacial transition zone in cementitious materials, Cement and Concrete Research. vol. 30,2000, pp. 579-583.
[8] RILEM Committee on Fracture Mechanics of Concrete – Test Methods, Determination of The Fracture Parameters (K_{IC}^{S} e $CTOD_C$) of Plain Concrete by Three-Point Bend Tests, Materials and Structures, vol. 23, 1990, pp. 457-460.

[9] Jenq, Y. S.; Shah, S. P. A Two-Parameter Fracture Model for Concrete,. Journal of Engineering Mechanics, vol. 111, 1985, pp. 1227-1241.
[10] Ouyang, C. Mobasher, B.; Shah, S. P. An R-Curve Approach for Fracture of Quasi-Brittle Materials, Cement and Concrete Research, vol. 20, 1990, pp. 901-916.

THE INFLUENCE OF THE NEW GENERATION SUPERPLASTICIZERS ON THE RHEOLOGICAL PROPERTIES OF CEMENT PASTES

Stefania Grzeszczyk[1] and Marek Sudol[2]

[1] Technical University of Opole, Faculty of Civil Engineering,
ul. Katowicka 48, 45-061 Opole, Poland, E-mail: stf@po.opole.pl
[2] Opole University, Institute of Chemistry,
ul. Oleska 48, 45-052 Opole, Poland, E-mail: grzymek@uni.opole.pl

ABSTRACT

The influence of acrylate superplasticizers on the rheological properties of cement pastes has been studied. It is shown that the copolymers belonging to the same group influence the rheological properties of cement pastes in a different way, depending on qualitative and quantitative composition of mer segments in a macromolecule. In the case of the superplasticizers examined, the increase in content of oxyethylene groups in the copolymer as well as the decrease in the content of hydrophobic methyl acrylate segments result in a significant increase in yield value and plastic viscosity of the cement paste.

1. INTRODUCTION

The technology of state-of the-art composite materials, including composites based on reactive powders and self-compacting concrete, requires addition of more efficient plasticizers compared with those used in the 80's. In those days, the plasticizers based on water-soluble polymers containing sulfo groups (SMF, SNF) were mostly used [1].

In the last decade a new kind of more efficient superplasticizer based on acrylic copolymers (AP) has been introduced [2, 3]. The mechanism of their action, consisting in dispersion of cement grains, is related to the effect of steric hindrance caused by the presence of long branched chains. It differs significantly from the mechanism of action of the SMF and SNF-type superplasticizers. Acrylic copolymers include various compounds that differ in the structure of particular blocks and their sequence. Therefore their influence on the degree of fluidization of suspensions based on cement may be different.

Modern superplasticizers belong to the class of multifunctional copolymers of a regular and/or block sequence of mers in the macromolecules. The state-of-the-art superplasticizers are most frequently tri-block and tetra-block copolymers of different properties depending on the kind of mer blocks and their contents in macromolecules [4, 5]. Identical blocks of mers form the so-called segments showing similar properties, thus reacting on particular external stimuli such as temperature, acidity (pH) or ionic strength (salt content). Non-polar segments of copolymers, such as aliphatic hydrocarbon chains or aromatic rings increase hydrophobicity of superplasticizers and decrease their solubility in water. Polar segments, including mainly hydroxyl and carboxyl groups as well as ionic salts cause hydrophilic character. The increased content of hydrophilic segments in a copolymer results in better water solubility [6, 7]. Oxyethylene or trialkylamine segments make the superplasticizers sensitive to temperature and the changes in ionic strength of the solution. All superplasticizers contain both hydrophilic and hydrophobic groups; hence they are amphiphilic. The

ratio of hydrophilic segments to the hydrophobic ones determines the water solubility of the superplasticizers. If this ratio increases, the water solubility rises and *vice versa*. The properties of superplasticizers may be controlled through the careful selection of the kind and amount of comonomers in the process of polymerization. The study of the influence of the kind and amount of segments of mers in the chemical structure of superplasticizers on the rheological properties of cement pastes was found to be interesting.

The influence of two commercially used superplasticizers based on acrylates on the rheological properties of cement pastes has been studied. Since the composition and chemical structure of the superplasticizers studied was not known, the qualitative and quantitative analysis of these compounds was carried out by means of Fourier-Transform Infrared Spectroscopy (FTIR).

2. EXPERIMENTAL

2.1. Materials

The tests were performed using cement pastes obtained from cement prepared in the laboratory by milling commercial clinker with the addition of 5 wt. % of gypsum dihydrate. Chemical and phase composition of clinker is shown in Table 1.

Table 1. Chemical and phase composition of clinker

Component	% by wt.
Loss on ignition	0,57
Insoluble residue	0,19
SiO_2	20,23
Fe_2O_3	3,53
Al_2O_3	6,64
CaO	66,05
MgO	1,42
SO_3	0,53
Na_2O	0,19
K_2O	0,85
CaO free	1,46
C_3S	58,75
C_2S	13,40
C_3A	11,60
C_4AF	10,74

Blaine specific surface of the cement was 318.6 m^2/kg.

Rheological studies were carried out using two acrylate superplasticizers, denoted as A and B, used as 20 % water solutions. Superplasticizers were introduced into batch water in the amount of 1 wt. % of solution, keeping the water cement ratio at 0.25 and 0.3.

2.2. Methods

2.2.1. Infrared studies

Qualitative analysis

The qualitative analysis of A and B superplasticizers was carried out by means of absorption spectrometry in the region of middle infrared. The samples in the form of pellets contained 1–2 mg of the superplasticizer and 600 mg of potassium bromide.

The absorption spectra of the samples were recorded using Philips Analytical PU 9804 FTIR spectrometer with the constant spectral resolution of 2 cm^{-1}. Ten scans for each pellet were recorded in the full region of 4000–400 cm^{-1} using EAGLE v.4.31 computer program. The characteristic frequencies of absorption bands were assigned to the appropriate functional groups of copolymers which were present in plasticizers. The interpretation is partially shown in the appropriate spectra. Full interpretation is presented in the tables. The structural segments of copolymers were determined on the grounds of functional groups detected.

Quantitative analysis

On the grounds of FTIR spectra the relative absorption of the following bands was determined:

– ester band at 1724 cm^{-1} (A), 1735 cm^{-1} (B), $_{STR}C{=}O_{ES}$ of hydrophobic segments,

– carboxylic salt band at 585 cm^{-1}, $_{STR}COO^-$ of hydrophilic as well as pH-sensitive segments, and

– ether band at 1108 cm^{-1}, $_{STR}C–O–C$ of oxyethylene chains as hydrophilic segments which are sensitive to temperature and presence of salts in the solution. The absorption at 2873 cm^{-1} $_{STR}CH_2$ (A) and 2874 cm^{-1} $_{STR}CH_2$ (B) was chosen as an internal reference. The contribution of absorption bands of ester, carboxylic and oxyethylene segments for both A and B superplasticizers was determined on the grounds of relative absorption of appropriate bands. This was the measure of content of particular segments in the copolymers.

2.2.2. Rheological tests

The rheological measurements were carried out using the rotative viscosimeter type Rheotest RV-2.1, with the modified surfaces of both cylinders. The tests were performed at a constant temperature 21°C. Measurements started 10 minutes after mixing with water. The rheological properties of cement pastes were determined from the flow curves, at growing and reduced rates of shearing in the range from 0 to 146 s^{-1} and the course of stress changes in time at constant shear rate ($\dot{\gamma}$ = 46 s^{-1} for 60 minutes). The yield value and plastic viscosity were determined from the descending part of flow curve, according to Bingham's model.

3. RESULTS AND DISCUSSION

3.1. Quantitative and qualitative spectral analysis of the A and B superplasticizers

The FTIR spectra of the A and B superplasticizers are shown in Figures 1 and 2, respectively.

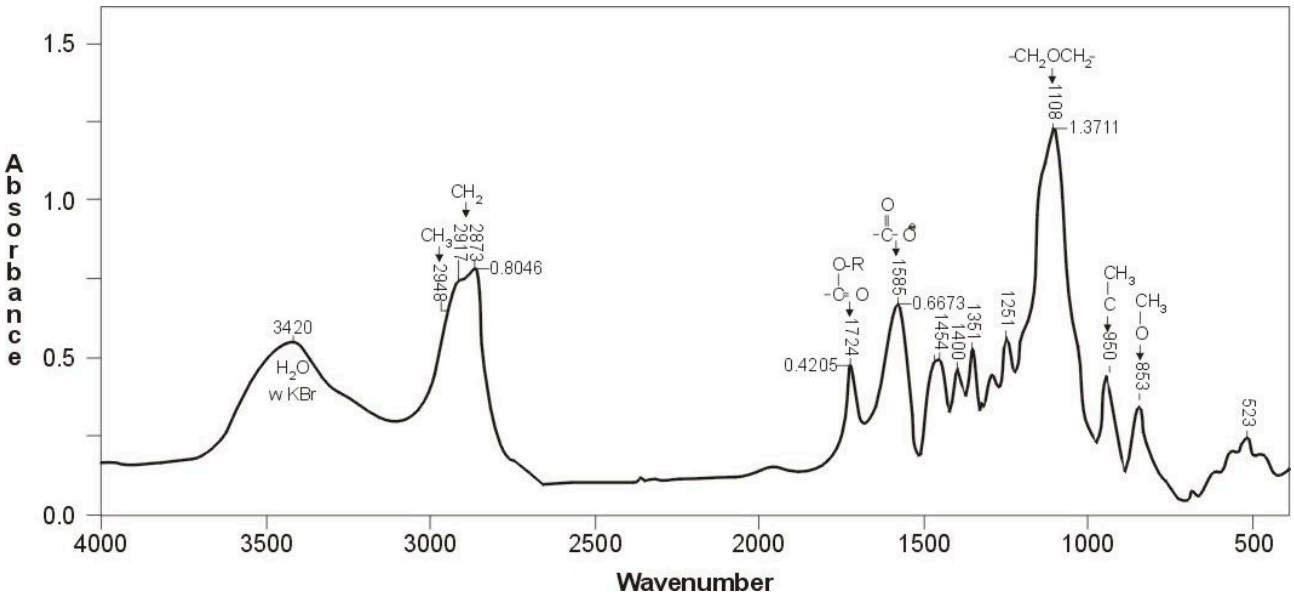

Figure 1. FTIR spectrum of the A superplasticizer

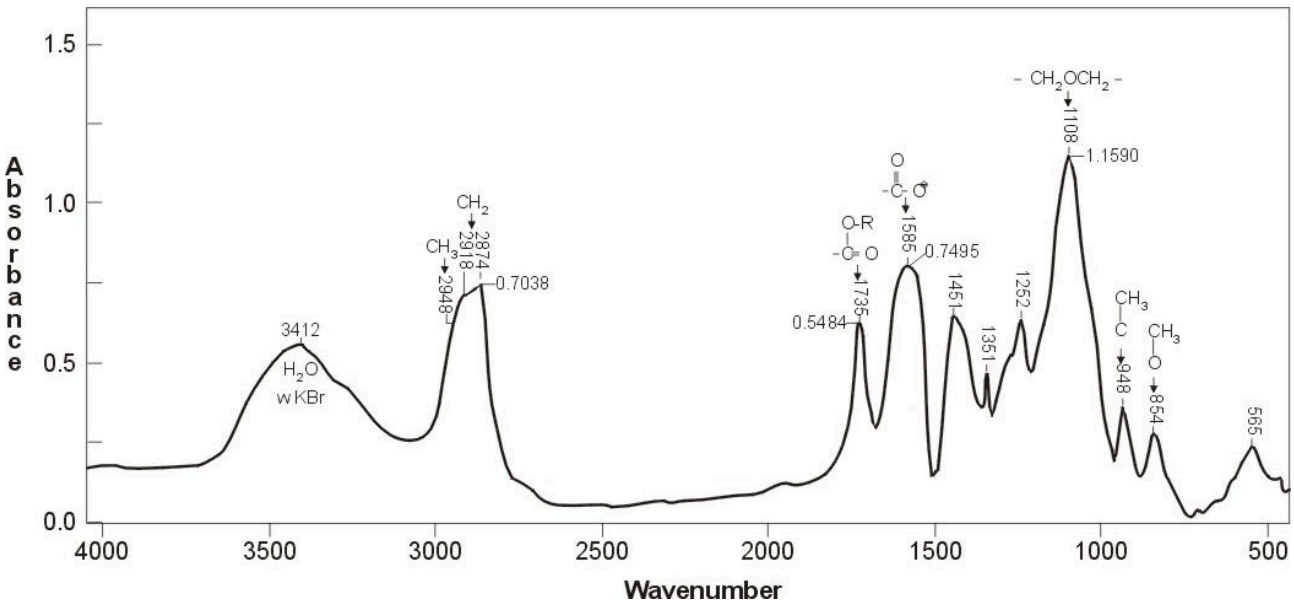

Figure 2. FTIR spectrum of the B superplasticizer

The wavenumbers corresponding to the characteristic absorption minima were determined using the EAGLE v.5.31 computer program. The appropriate types of vibrations were determined and the functional groups present in the macromolecules of superplasticizers were assigned. Full specification of characteristic frequencies together with the corresponding types of vibrations and kinds of functional groups is shown in Table 1 (for the A superplasticizer) and Table 2 (for the B superplasticizer).

Table 2. Characteristic FTIR frequencies for the sample of the A superplasticizer.

Wavenumber, cm^{-1}	Type of vibrations	Structural fragments
2948	$_{STR/A}$ CH_3	Methyl group on the chain R
2917	$_{STR/A}$ CH_2	Methyl group in the chain
2873	$_{STR/S}$ CH_3	Methylene group in the chain
1724	$_{STR}$ C=O $_{ES.\ KET}$	Ester or ketone carbonyl group
1585	$_{STR/A}$ COO^- $_{SALT}$	Carboxyl group of the metal salt
1468	$_{DEF}$ CH_2	Methylene group in the chain R
1454	$_{DEF}$ CH_2	Methylene group adjacent to a heteroatom (O, N)
1400	$_{STR/S}$ COO $_{SALT}$	Carboxylic group of the metal salt
1351	$_{SCI}$ CH_2	Methylene group adjacent to the O atom
1251	$_{STR/A}$ C–C–O $_{ES}$	C–C–O ester group
1108	$_{STR/A}$ COC $_{ET}$	Aliphatic ether group R–O–R
950	$_{RK}$ CH_3 (C)	Methyl group adjacent to the C atom
853	$_{RK}$ CH_3 (O)	Methyl group adjacent to the O atom

Table 3. Characteristic FTIR frequencies for the sample of the B superplasticizer.

Wavenumber, cm^{-1}	Type of vibrations	Structural fragments
2948	$_{STR/A}$ CH_3	Methyl group on the chain R
2918	$_{STR/A}$ CH_2	Methyl group in the chain
2874	$_{STR/S}$ CH_3	Methylene group in the chain
1735	$_{STR}$ C=O $_{ES.}$	Ester carbonyl group
1585	$_{STR/A}$ COO^- $_{SALT}$	Carboxyl group of the metal salt
1451	$_{DEF}$ CH_2	Methylene group adjacent to a heteroatom (O, N)
~1400	$_{STR/S}$ COO $_{SALT}$	Carboxylic group of the metal salt
1351	$_{SCI}$ CH_2	Methylene group adjacent to the O atom
1252	$_{STR/A}$ C–C–O $_{ES}$	C–C–O ester group
1108	$_{STR/A}$ C–O–C $_{ET}$	Aliphatic ether group R–O–R
948	$_{RK}$ CH_3 (C)	Methyl group adjacent to the C atom
853	$_{RK}$ CH_3 (O)	Methyl group adjacent to the O atom

The descriptions of FTIR spectra contain the following abbreviations:

$_{STR...}$ – stretching vibrations
$_{STR/A...}$ – asymmetric stretching vibrations
$_{STR/S...}$ – symmetric stretching vibrations
$_{DEF...}$ – deformation vibrations
$_{SCI...}$ – scissoring in-plane vibrations
$_{RK...}$ – rocking in-plane vibrations
$_{WAG...}$ – wagging in-plane vibrations
$_{TWI...}$ – twisting out-of-plane vibrations
$_{ADJ...}$ – vibrations of adjacent atoms
$_{...AL.}$ – aliphatic hydrocarbon chain
$_{...AR}$ – aromatic ring
$_{...ALC}$ – alcohol, hydroxyl functional group
$_{...AC}$ – acid; carboxyl functional group
$_{...SALT}$ – salt; carboxyl functional group
$_{...ES}$ – ester, ester functional group
$_{...ET}$ – ether; ether functional group
$_{...KET}$ – ketone; ketone carbonyl group

The conclusion based on the data presented in Tables 2 and 3 is that the A and B superplasticizers do not contain aromatic rings because the FTIR spectra do not show characteristic bands corresponding to the following vibrations: $_{STR}CH_{AR}$, $_{STR}CC_{AR}$, $_{WAG}CCC_{AR}$, $_{DEF}CH$ and $_{ADJ}H_{AR}$.

The A superplasticizer (table 2) contains the following functional groups:
- aliphatic groups: methyl CH_3, methylene CH_2, methine CH,
- aliphatic ester groups O=C–O–R,
- carboxyl groups of sodium salt $O=C–O^-Na^+$
- n-oxyethylene groups $(–CH_2–CH_2–O–)_n$.

The logical reasoning indicates that the A superplasticizer is a regular or block copolymer (probably block copolymer, taking into account the costs of synthesis), containing segments of alkyl, sodium and oxyethylene acrylates and/or methacrylates and/or maleates of the following structure (according to the methacrylate blocks):

alkyl (meth)acrylate

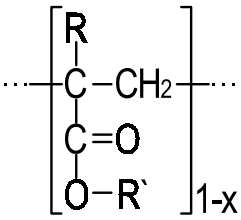

where: R = H, CH_3
R' = CH_3, C_2H_5
hydrophobic segment
decreasing solubility

sodium (meth)acrylate

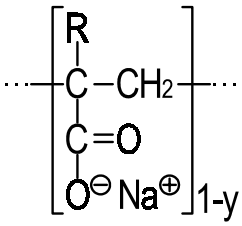

where: R = H, CH_3
hydrophilic segment
ion and pH-sensitive

n-oxyethylene (meth)acrylate

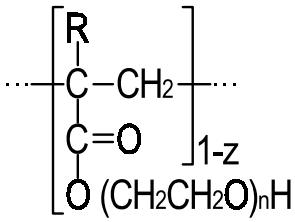

where: R = H, CH_3
hydrophilic segment
ion and temperature-sensitive

Therefore, the A superplasticizer contains the following fragments:

– ester fragments which make the superplasticizer more hydrophobic and lower its solubility in water,
– carboxylic salts which make the superplasticizer more hydrophilic and increase its solubility in water as well as sensitivity to presence of ionic salts and pH of solution,
– oxyethylene fragments which increase hydrophilicity of the superplasticizer and its sensitivity to ambient temperature as well as presence of salts in solution.

Unfortunately, it is impossible to determine the sequence of particular segments in the macromolecule and to decide whether the segments are alternating regularly or irregularly by means of FTIR. It is also impossible to determine the average molecular mass and molecular mass distribution, i.e. the parameters which also influence water solubility of the superplasticizer as well as its properties in solution.

Comparison of both FTIR spectra and spectral data of the A and B superplasticizers leads to a conclusion that both superplasticizers contain identical functional groups, structural elements and segments. Therefore both superplasticizers are qualitatively identical. The only quantitative difference relates to the size of ester, carboxyl and oxyethylene segments in the copolymer. It is possible that the sequence of segments might also be different, but this cannot be solved using FTIR spectroscopy.

The results of quantitative analysis of the A and B superplasticizers, including determination of absolute and relative absorption of the ester band at 1724 cm^{-1} (A), 1735 cm^{-1} (B), carboxylic salt band at 1585 cm^{-1} and ether band of oxyethylene groups at 1108 cm^{-1} together with their contribution to the total absorption are shown in Table 4.

Table 4. The results of quantitative analysis of A and B superplasticizers.

Superplasticizer	Absolute absorption of a band				Relative absorption of a band			Absorption fraction		
	standard A^{2874}	ester A^{1730}	salts A^{1585}	ethers A^{1108}	esters A^{1730}/A^{2874}	salts A^{1585}/A^{2874}	ethers A^{1108}/A^{2874}	esters %	salts %	ethers %
A	0.8046	0.4205	0.6673	1.3711	0.5226	0.8293	1.7041	17.1	27.1	55.8
B	0.7038	0.5484	0.7495	1.1590	0.7794	1.0649	1.6467	22.3	30.5	47.2

The data presented above indicate that the absorption of the A superplasticizer, which is related to the ether groups deriving from n-oxyethylene acrylate, is 8.6 % greater comparing with the B superplasticizer. It corresponds to the content of oxyethylene groups, which is greater by 18 wt. %.

On the other hand, the absorption of ester groups deriving from methyl (or ethyl) acrylate in the B plasticizer is 5.2 % greater and the absorption of carboxyl groups deriving from sodium acrylate is 3.4 % greater. It corresponds to the content of ester groups which is 30 wt. % greater and content of carboxyl groups which is 12 wt. % greater in the B superplasticizer comparing with the A superplasticizer. Therefore, the A superplasticizer shows better solubility in water and higher sensitivity to temperature compared with the B superplasticizer. The B superplasticizer shows lower water solubility (greater content of hydrophobic ester segments) and higher sensitivity to pH of solutions comparing with the A superplasticizer.

The differences in IR absorption of functionally different elements of the structure of both copolymers indicate different content of particular mers in the macromolecule as well as different size of segments (blocks) in microchains. It is obvious that the structural differences result in different physicochemical properties, including rheological properties of cement pastes.

3.2. Rheological study

The influence of the A and B superplasticizers on the rheological properties of cement pastes was determined on the grounds of rheological measurements carried out for pastes with the addition of these superplasticizers. The results of the rheological study are shown in Figures 3, 4 and Table 5.

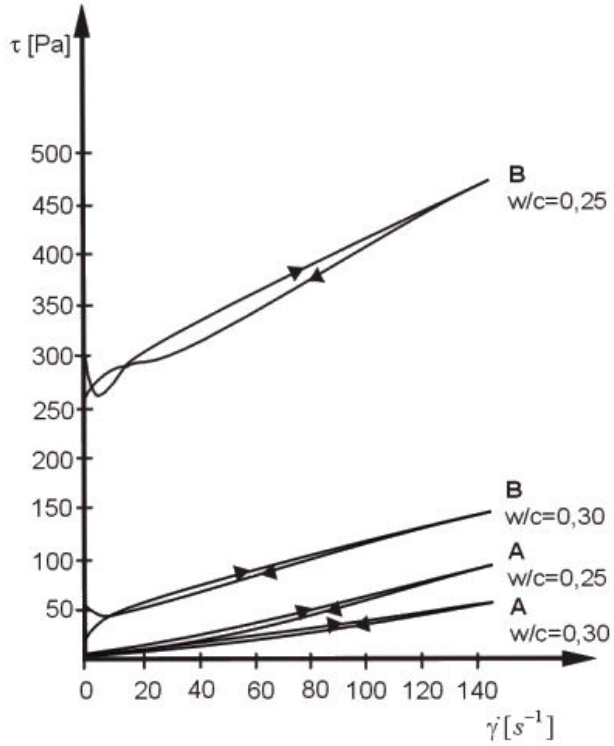

Figure 3. Flow curves of cement paste containing A or B superplasticizer

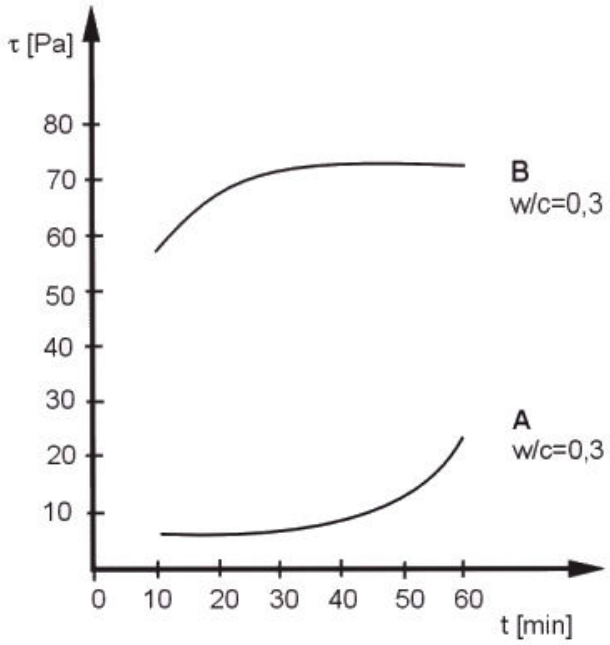

Figure 4. Stress growth for cement paste containing A or B superplasticizer

Table 5. Yield value and plastic viscosity of cement paste containing A or B superplasticizer

superplasticizer	w/c	yield value τ_o [Pa]	plastic viscosity η_{pl} [Pa · s]
A	0,25	lack	0,25
	0,30	lack	0,18
B	0,25	250	0,79
	0,30	44	0,36

It can be stated that the cement pastes containing equal amounts of the A or B superplasticizers, which belong to the same group of acrylate plasticizers and are built of qualitatively identical structural segments and differ only in the size (and possibly the sequence) of these segments, show different rheological properties.

The A superplasticizer, which contains 20 wt. % more n-oxyethylene acrylate segments, or the same amount of acrylate segments $(–CH_2CH_2O–)_n$ but containing oxyethylene chains longer by 20 % and also less hydrophobic methyl acrylate segments by ca. 20 wt. % compared with the structure of the B superplasticizer, shows significantly better efficiency. Cement pastes with the addition of the A superplasticizer show the properties of Newtonian liquid at the w/c ratio of both 0.3 and 0.25. With the presence of the B superplasticizer, analogous pastes show the properties of viscoplastic liquid. At the w/c equal 0.25 the yield value of paste reaches a huge value of 250 Pa at the plastic viscosity of 0.79 Pa·s. The dependence of shear stress on time (Figure 4) indicates better efficiency of the A superplasticizer as well. The paste with the addition of the A superplasticizer shows very low values of shear stress and its negligible increase within one hour compared to the paste containing the B superplasticizer.

4. CONCLUSIONS

On the grounds of the rheological study carried out, it has been shown that the superplasticizers which belong to the same group of copolymers may influence the rheological properties of cement pastes in a different way, depending on the qualitative and quantitative composition of mers in the copolymer macromolecules.

The FTIR analysis of the A and B superplasticizers carried out indicates that both superplasticizers belong to the same group of acrylate copolymers, probably of a block microstructure. They are composed of qualitatively identical segments of three kinds of acrylate mers of different properties. These segments play different parts in water solutions of plasticizers.

On the grounds of the detailed FTIR analysis it has been established that both superplasticizers consist of the following segments of acrylate and/or methacrylate mers: methyl/ethyl (co)acrylate, sodium (co)acrylate and n-oxyethylene (co)acrylate.

The efficiency of superplasticizers which belong to the same group of copolymers and show identical qualitative composition of mer segments depends to a great extent on the quantitative composition of particular segments as well as their size in the macromolecules. For the acrylate superplasticizers examined, the increase in content of oxyethylene groups as well as the decrease in the content of hydrophobic methyl acrylate segments lead to the increase in water solubility of the superplasticizer, as well as increased values of rheological parameters (yield value and plastic viscosity) of the cement suspension.

The results of the study lead to the conclusion that the controlled synthesis of acrylate superplasticizers of particular properties may be carried out through the appropriate selection of comonomers and their amount in the process of polymerization.

REFERENCES

[1] V.S. Ramachadran, V.M. Malhotra, Concrete Admixtures Handbook. Properties, Science and Technology, Ed.: V.S. Ramachadran, Chapter 7, 1995.

[2] H.M. Ludwig, F. Weise, W. Hemrich, N. Ehrlich, BFT, no 6, 2001, pp.58.

[3] D. Hamada, T. Sato, F. Yamoto, T. Mizunuma, Development of New Superplasticizer and Its Application to Self-Compacting Concrete, Sixth CANMET/ACI Int. Conf. on Superplasticizers and Other Chemical Admixtures in Concrete, Ed.: V.M. Malhotra, ACI SP 195-17, 2000.

[4] M. Kinoshita, T. Suzuki, T. Yonezawa, K. Mitsui, Properties of an Acrylic Graft Copolymer-based new Superplasticizer for Ultra High-strength Concrete, Fourth CANMET/ACI Int. Conf. on Superplasticizers and Other Chemical Admixtures in Concrete, Ed.: V.M. Malhorta, ACI SP 148-16, 1994.

[5] M. Kinoshita, T. Nawa, M. Iida, M. Ichiboji, Effect of Chemical Structure on Fluidizing Mechanism of Concrete Superplasticizer Containing Polyethylene Oxide Graft Chains, Sixth CANMET/ACI Int. Conf. on Superplasticizers and Other Chemical Admixtures in Concrete, Ed.: V.M. Malhorta, ACI SP 195-11, 2000.

[6] A. Borsoi, S. Collepardi, L. Copolla, R. Troli, M. Collepardi, Il Cemento, vol. 96 (3), 1999, pp.741.

[7] A. Ohta, T. Sugiyama, T. Uomoto, Study on Dispersing Effects on Polycarboxylate Based Dispersant on Fine Particles, Sixth CANMET/ACI Int. Conf. on Superplasticizers and Other Chemical Admixtures in Concrete, Ed.: V.M. Malhorta, ACI SP 195-14, 2000.

SUPERCLASSIFIED PFA FOR SELF-COMPACTING CONCRETE

S.D. Fossey, E.A. Byars and H.Y. Zhu

Centre for Cement and Concrete, University of Sheffield, UK. E-mail: DrByars@aol.com

ABSTRACT

In recent years the demand for Self-Compacting Concrete (SCC) has grown significantly due to the tightening health and safety regulations and good concrete practice. However, the high cement contents and volumes of expensive admixtures necessary for satisfactory SCC make it largely uneconomical. This paper reports on the use of ultra fine super-classified PFA (SPFA) to achieve the required workability and cohesion for SCC with low cement contents and no need for specialist admixtures. Initial tests show self-compacting SPFA concrete displays both high workability and stability with w/c ratio as low as 0.2 and that SPFA SCC is significantly more economical than other forms of SCC.

Keywords: Self-Compacting Concrete, Super-classified PFA, Admixtures, Strength, Absorption

1. INTRODUCTION

In the 1980's a chronic skills shortage in the Japanese construction industry was partially solved by using high-workability mixes that could be consolidated without vibration [1]. This type of concrete became known as Self-Compacting Concrete (SCC). An additional advantage of SCC was found to be the ability of the concrete to flow into complex formwork, but with increasing variety and usage of SCC, some problems with excessive bleeding and segregation have emerged requiring additional expensive admixtures[2].

A major driving force encouraging the use of SCC is the impending European Health and Safety Directive covering hand-arm vibration [3]. However, SCC also has implications for traditional large concrete pours and post-tensioning placement where its uniform strength development may benefit the stressing procedure and reduce cracking. In addition, with SCC the associated reduction in labour and plant reduces cost and improves QA procedures as the sample test cubes are more representative of in-situ concrete than vibrated normal workability concrete cubes [2].

2. AIMS AND OBJECTIVES

The aims of this project were to optimise SPFA concrete mixes to maximise workability and cohesion and achieve self-compaction at low water cement ratios. Several objectives were defined as follows:

1. To assess the effects of SPFA on water demand of concrete.
2. To optimise the aggregate gradings used in combination with flowing cement paste to create cohesive flowing SPFA concrete.
3. To minimise the cement content used in very high performance self-compacting SPFA mixes.

4. To measure the compressive and tensile strength development, absorption and UPV of the self-compacting SPFA concrete mixes.
5. To compare the economy and performance of SPFA self-compacting concrete mixes with concrete made with other materials of equal mix proportions.

3. MATERIALS

3.1 Materials properties

Selected physical and chemical properties of all cementitious materials used are given in Table 1.

Table 1. Typical physical and chemical properties of the materials used in this project

PARAMETER	OPC	PFA	GGBS	MS	SPFA
Surface Area (m^2/kg)	350	350	400	20000	13000
Specific Gravity	3.2	2.1	2.9	2.2	2.3
Particle Range (µm)	5–100	1-150	3-100	0.01–0.5	0.25–25
SiO_2 (%)	20.8	48.0	35.8	92.9	53.5
Al_2O_3 (%)	5.0	28.0	14.0	0.6	34.3
Fe_2O_3 (%)	3.2	9.0	0.5	0.9	3.6
CaO (%)	63.7	3.0	39.7	0.4	4.4
MgO (%)	2.6	2.5	8.6	1.58	1.0

3.2 Cements

Blue Circle OPC to BS12 [4] was used throughout the experimental program.

3.3 SPFA

The SPFA used throughout the research was a Class F PFA to ASTM 311[5] with a mean particle size of 6µm [6], compared to 1-200µm for Class 1 PFA[7]. The water requirement of the SPFA is shown plotted in Figure 1[6].

3.4 Pulverized-Fuel Ash (PFA)

The PFA used for this research conformed to BS3892: Part 1[8].

3.5 Ground Granulated Blast furnace Slag (GGBS)

The GGBS used complied with BS6699 [9].

3.6 Micro-Silica (MS)

The MS used was in a 50/50 ($\pm 2\%$) aqueous slurry form and complied with ASTM C 1240[10].

3.7 Superplasticizer

A single polycarboxylate polymer water-reducing admixture to ASTM C494 [11] and BS5075[12] was used.

3.8 Aggregates

The grading of the aggregates used is described in Table 2. The coarse aggregate was a continuously-graded well-rounded aggregate with a nominal particle size of 5-10mm. The fine aggregate used was well graded concrete sand to BS812 [13].

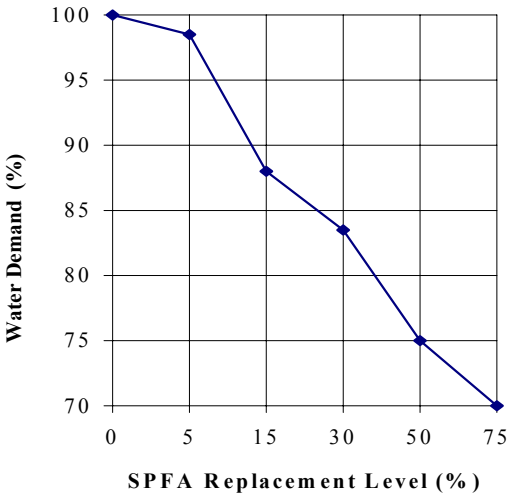

Figure 1. Water requirement of SPFA

Table 2. Aggregate Sieve Analysis

SIEVE SIZE (mm)	% PASSING BY MASS	
	10-5mm	Sand
28	100	100
20	100	100
14	100	100
10	99.4	100
6.3	42.6	100
5	15.2	98.6
2.36	6.2	85.5
1.18	-	76
0.6	-	62.1
0.3	-	17
0.15	-	3.7
0.075	-	0.1

Table 3. Final Mix Proportions

MIX CODE	FINAL MIX PROPORTIONS (kg/m^3)											
	OPC	SPFA (30%)	GGBS (45%)	MS (10%)	PFA (30%)	Water	W/B	Aggregate			SP (%Cem)	Total
								10mm	Fines	Total		
SPFA1	249	107	0.0	0.0	0.0	160	0.45	1029	842	1871	0.3	2387
GGBS	196	0.0	160	0.0	0.0	160	0.45	1036	848	1884	0.3	2400
MS	320	0.0	0.0	36	0.0	160	0.45	1069	874	1943	0.3	2399
PFA	249	0.0	0.0	0.0	107	160	0.45	1029	842	1871	0.3	2387
SPFA2	420	180	0.0	0.0	0.0	120	0.20	962	787	1749	1.0	2469

4. TEST METHODS

4.1 Rheology

Three methods were employed to test the fresh concrete rheology.

4.1.1 Slump Test

The slump test [14] was used on stiffer mixes.

4.1.2 Slump Flow Test

Where the concrete displayed a significant fluidity it was tested using the slump flow test [15]. A 600mm spread was taken to be the lower boundary for SCC. Mixes displaying excessive segregation or bleeding at this stage were rejected.

4.1.3 SSCI Test

The third test method, the 'Sheffield Self-Compactability Index (SSCI) test, Figure 2, was developed as part of the project. The top funnel section of the apparatus is filled with concrete then a gate removed, which allows the concrete to flow down a shallow slope through a throat which is heavily congested with rebar. A comparison of the results obtained using the slump flow test and

the SCCI test led to the conclusion that Self-Compactability (600mm flow) corresponded to the concrete flowing to touch all four corners of the lower reservoir when the SSCI apparatus was inclined at 15º to the horizontal. However, the SSCI was found to be more sensitive to lack of cohesion in SCC mixes than slump flow. Visual observation showed aggregates "balling" in the SSCI throat in some instances, and therefore a further restriction on SCC acceptability was imposed: zero segregation in the SCCI test.

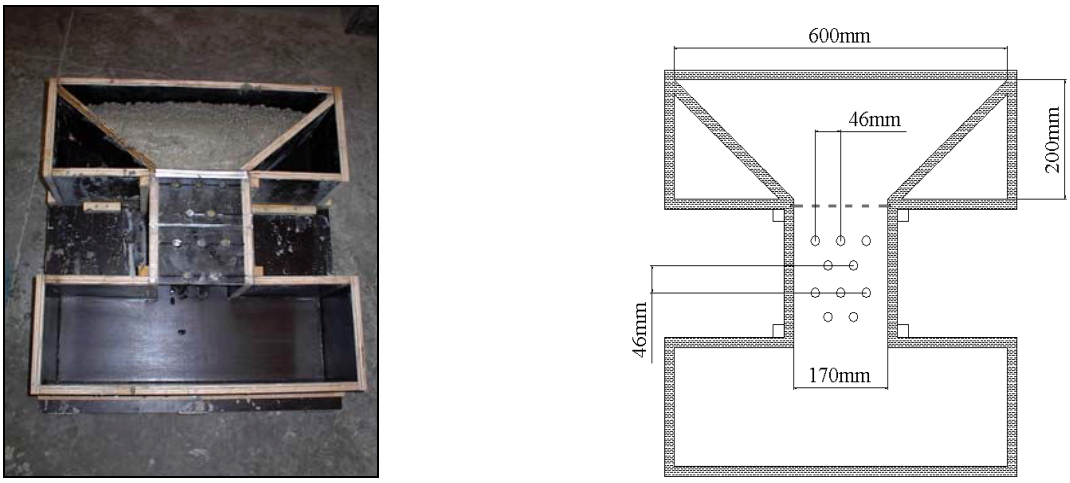

Figure 2. The SSCI test apparatus

4.2 Hardened Properties of Concrete

For each of the final mixes described in Table 3, the appropriate numbers of 100mm cube samples were made [16]. Where the concrete was self-compacting, no vibration was used. Half of the cubes were cured in water at 20ºC to BS1881 [17] and half in air at 20ºC and 65% RH. Further tests were carried out at appropriate ages as shown in Figure 3.

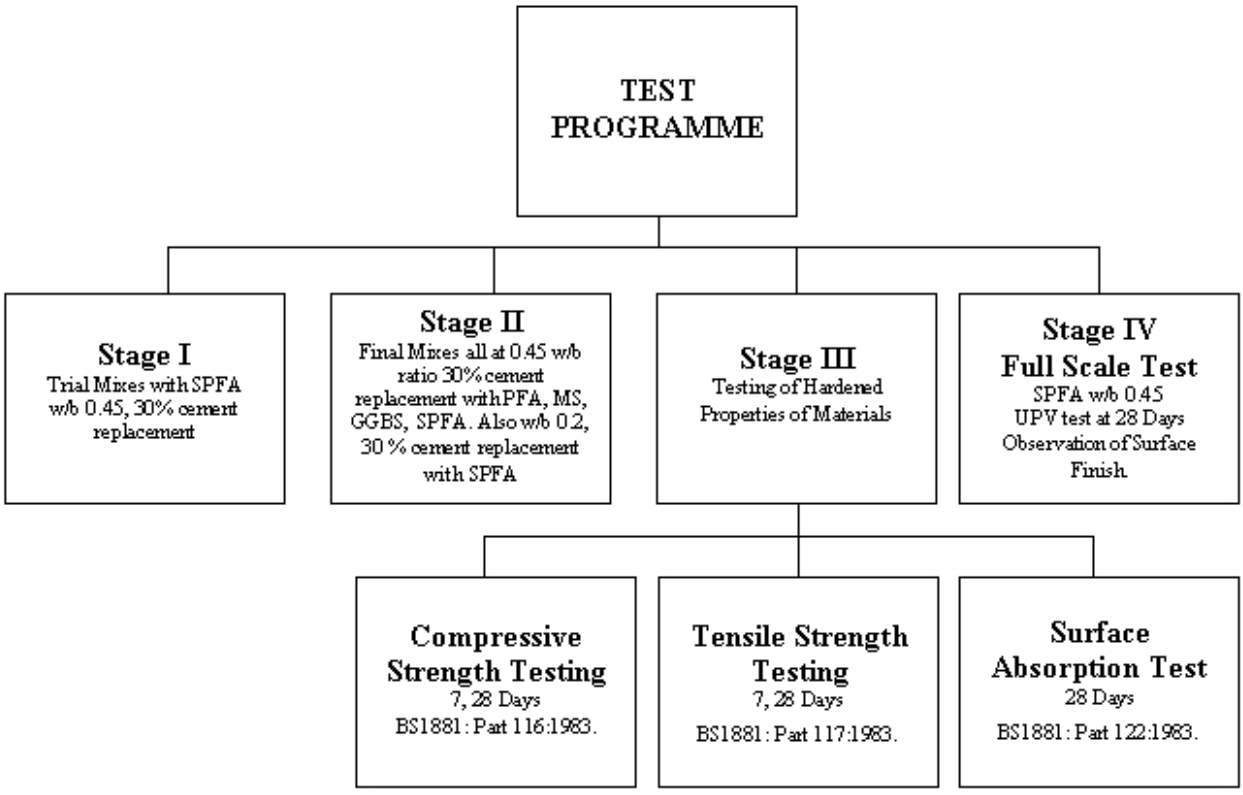

Figure 3. Testing Flow Chart

4.2.1 Compressive Strength
Cubes were tested for compressive strength at 7 and 28 days to BS1881 [18]. The air-cured cubes were saturated prior to test by immersion in a water tank for 24 hours (7 day test) or 48 hours (28 day test).

4.2.2 Tensile Strength
The indirect tensile strength of the cylinders was tested [19] at 7 and 28 days, with the air-cured cylinders being saturated as per the compression test samples.

4.2.3 Surface Absorption
Absorption tests were carried out on both the water and air cured samples after 28 days [20]. Cubes were preconditioned by oven drying for 72 hours, or until the % mass change in 24 hours was ≥0.2%.

4.2.4 Ultrasonic Pulse Velocity (UPV)
The UPV test was carried out on a full size element (a column measuring *1.5x0.2x0.2m* cast from SCC1) and tested to BS1881: Part 203 [21].

4.3 Mix Development

From previous studies carried out at the CCC [6], it was decided to use SPFA at a 30% replacement for cement and a w/b ratio of 0.45 for the initial trials. The influence of fine aggregate content on the concrete stability and the ratio of coarse to fine aggregate was carefully monitored duringa series of trials and particular attention was given to cementitious material and superplasticizer minimisation, as shown in Table 4. Mixes were proportioned on a trial and error basis to assess the influence of changes and the rheology assessed using the slump flow test, Table 4. If the flow equalled or exceeded 600mm, the mixes were also tested using the SSCI test to assess cohesiveness.

Table 4. Summary of the Mix Proportions used during the development of SCC with SPFA

MIX CODE	MIX PROPORTIONS (Kg/m³)									Flow (mm)	SSCI TEST
	OPC	SPFA	WATER	W/B	AGGREGATE			SP (%Cem)	TOTAL		
					10mm	Fines	Total				
TRIAL 1	218	93	140	0.45	1179	786	1965	1	2416	510	×
TRIAL 2	218	93	140	0.45	1179	786	1965	0.5	2416	600	×
TRIAL 3	218	93	140	0.45	1179	786	1965	0.25	2416	350	×
TRIAL 4	218	93	140	0.45	1297	668	1965	0.5	2416	-	×
TRIAL 5	218	93	140	0.45	1139	825	1964	0.6	2415	520	×
TRIAL 6	218	93	140	0.45	1139	825	1964	0.65	2415	540	×
TRIAL 7	218	93	140	0.45	1120	845	1965	0.65	2416	540	×
TRIAL 8	218	93	140	0.45	1100	864	1964	0.6	2415	520	×
TRIAL 9	218	93	140	0.45	1100	864	1964	0.5	2415	560	×
TRIAL 10	187	80	120	0.45	1173	885	2058	0.6	2445	400	×
TRIAL 11	187	80	120	0.45	1173	885	2058	1	2445	450	×
TRIAL 12	187	80	120	0.45	1173	885	2058	2	2445	450	×
TRIAL 13	233	100	150	0.45	1055	863	1918	0.25	2401	580	×
TRIAL 14	249	107	160	0.45	1029	842	1871	0.3	2387	640	✓
SPFA1	249	107	160	0.45	1029	842	1871	0.3	2387	650	✓

Instability and segregation were found to be the greatest hurdles during trial mixing and required significant manipulation of the fines content of the concrete mixes.

The SPFA concrete mix that was adopted as self-compacting had a Coarse: Fines (C: F) ratio of 55:45, Table 4. Trial 13 was almost self-compacting (580mm slump flow) and had an excellent aggregate distribution with no sign of segregation, Figure 4, suggesting that the mix had excellent cohesivity.

4.4 Full Scale Trial

A full-scale sample column was cast in the lab to study self-compactability at full scale. The element, measuring 1.5m x 0.2m x 0.2m, was cast in one pour using mix SPFA1, then cured overnight in a humid environment in accordance with BS1881 [17]. At 28 days the sample was tested with UPV [21] to establish any variation of density with depth.

Extending from the data of the 0.45w/b trials, a 0.2w/b ratio mix (SPFA2) was developed as shown in Table 5.

Table 5. Summary of the mix proportions used to develop mix SPFA2

MIX CODE	MIX PROPORTIONS (kg/m3)									FLOW (mm)	SSCI TEST
	OPC	SPFA	WATER	W/B	Aggregate			SP (%Cem)	Total		
					10mm	Fines	Total				
TRIAL 15	420	180	120	0.2	962	787	1749	2.00	2481	720	✕
TRIAL 16	420	180	120	0.2	962	787	1749	1.50	2478	710	✕
SPFA2	420	180	120	0.2	962	787	1749	1.00	2475	710	✓

Figure 4. Section through a cylinder of Trial 13

5. RESULTS

5.1 Rheology

Table 6 summarises the rheology test results measured on the five final mixes. It can be seen that the workability of the two mixes containing SPFA is far superior to the other mixes despite the mix proportions being identical.

Table 6. Rheology results

TEST	SPFA1	GGBS	MS	PFA	SPFA2
SSCI	PASS	FAIL	FAIL	FAIL	PASS
Slump Flow (mm)	650	-	-	-	710
Slump (mm)	-	220	50	210	-

Observations were made with reference to the stability of the mix throughout the testing procedure and it was noted during rheology testing that SPFA displayed an excellent degree of cohesion as shown in Figure 5. Cutting through a cylinder of SPFA1 confirmed the cohesivity of the mix, which showed excellent aggregate distribution throughout the sample and no bleeding or laitance.

Figure 5. Mix SPFA1 following a slump flow test and the aggregate distribution in a hardened sample

5.2 Effect of alternative replacement materials

It was found that only SPFA produced fluid, cohesive, self-compacting concrete mixes using the minimum cementitious materials and low water content of SPFA1. To produce a high fluidity concrete using other cement replacement materials requires greater volumes of water, cementitious materials and admixtures. The implications on cost mean that whilst generally the use of SCC can be expensive, the inclusion of SPFA can reduce costs to a competitive level, (see Figure 7).

5.3 Hardened Properties

5.3.1 Compressive Strength

The compressive strength results of the water and air cured samples are shown plotted in ure 6. It is clear from these that the SPFA1 concrete, whilst in this set of tests having slightly lower compressive strength than other comparable mixes, develops greater strength with time in both water and air-curing environments.

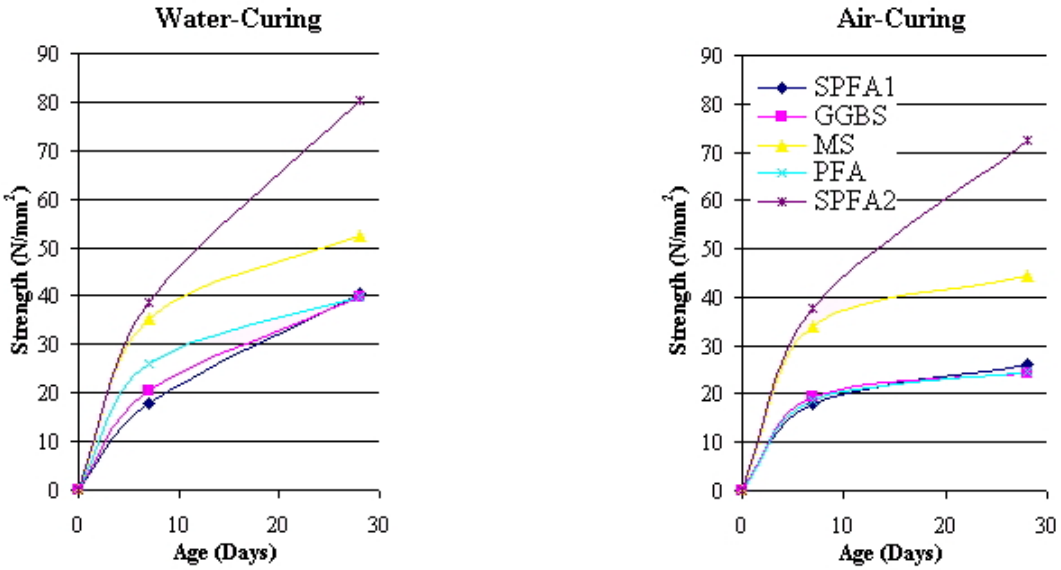

Figure 6. Compressive strength development for air and water cured samples

5.3.2 Tensile Strength

The tensile strength trends, Table 7, are similar to those observed for compressive strength development. The SPFA1 mix initially has a slightly lower tensile strength than other mixes, but this increases relatively with time.

Table 7. Tensile strength results

MIX CODE	Water Cured (N/mm^2)		Air Cured (N/mm^2)	
	Age (Days)		Age (Days)	
	7	28	7	28
SPFA1	3.7	5.6	2.5	4.6
GGBS	4.2	5.7	3.1	4.3
MS	4.9	6.4	4.0	5.1
PFA	3.9	5.4	2.9	4.4
SPFA2	4.9	7.1	4.2	6.4

5.3.3 Water Absorption

The results from the water absorption test, Table 8, show that the SPFA mixes have significantly lower absorption than other mixes. All air-cured samples showed greater absorption than water-cured ones, yet it is clear from these results that the SPFA mixes are significantly less affected by air curing than similar mixes made at the same w/b ratio with other materials. This is of particular note when one compares the strength results of the SPFA1 and MS concrete mixes, the latter developing considerably higher strength at the age of 28 days, when the absorption tests were conducted. The differences between the SPFA and the PFA concrete absorption is also very well defined with air-curing, which suggests an unexpectedly high level of pore refinement with SPFA.

Table 8. Water Absorption Results

MIX CODE	PRECONDITIONING MASS (kg) Age (hours)				SATURATED MASS (kg)	WATER ABSORPTION (%)
	0	24	48	72		
Water Curing						
SPFA1	2.356	2.341	2.326	2.322	2.341	0.80
GGBS	2.275	2.261	2.252	2.249	2.277	1.27
MS	2.359	2.350	2.346	2.343	2.362	0.83
PFA	2.392	2.381	2.373	2.370	2.392	0.93
SPFA2	2.386	2.385	2.383	2.382	2.397	0.63
Air Curing						
SPFA1	2.286	2.284	2.282	2.282	2.324	1.84
GGBS	2.194	2.194	2.192	2.191	2.294	4.70
MS	2.247	2.245	2.244	2.242	2.310	3.01
PFA	2.306	2.305	2.304	2.302	2.405	4.45
SPFA2	2.365	2.365	2.364	2.364	2.407	1.40

5.3.4 Full Scale Trial

A 1.5×0.3×0.3m column of SPFA1 concrete was cast and tested using UPV at 28 days to establish if there was any variation in density with depth, which could identify segregation. Readings were taken over the full height of the column and are shown in Table 9.

Table 9. UPV Test Results

Height Above Ground (m)	Time Reading (μs)
1.5	46.0
1.2	45.3
0.9	45.0
0.6	45.3
0.3	44.3
0.0	45.4

The minimal difference in the readings suggests that the concrete is of constant density and that no significant degree of segregation has taken place, which implies that the SPFA1 concrete mix developed in this study has the potential to be used for full-scale works.

6. DISCUSSION

The SPFA used in this study has proved to be extremely effective for making self-compacting concrete. Indeed, when the total binder contents used in this study to make 0.45 w/b ratio SCC are compared with those from other studies, it can be seen that the use of SPFA results in SCC with a binder content of 105-270 kg/m^3 lower than used in comparable studies around the world [22], Figure 7.

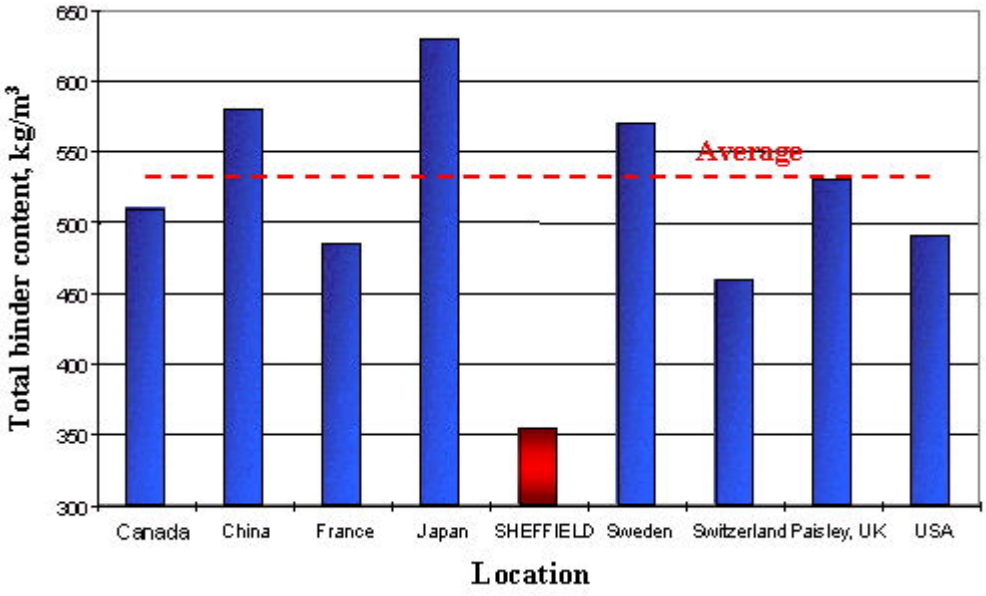

Figure 7. Comparison between total binder contents used in this research and leading projects worldwide.

The explanation for this lies with the nature and properties of the SPFA particles. As a Bingham fluid, in order to maximise the ability of concrete to deform under its own self-weight, the internal yield stress must be minimised. This can be achieved by preventing the formation of Van der Waals bonds between adjacent cement particles as they flocculate in the cement paste. Generally, this is achieved via the addition of expensive admixtures, which adhere to the cement particles and impart a charge, causing repulsion. This deflocculation improves the dispersion of free water throughout the mix thereby increasing the workability of the concrete. PFA can work in the same

way, coating the surface of the cement particles and giving them a charge[23]. SPFA will similarly adsorb to the surface of cement particles however due to the smaller particle size, SPFA does this more effectively. Further, in common with PFA, SPFA is hydrophilic in nature and introduces additional water entrainment into the mix thereby giving more consistent dispersion of free water and in turn reducing the tendency for bleeding and segregation and increasing cohesion due to the higher number of interparticular contact points associated with the smaller SPFA particles.

The research on this new area of concrete and ash technology is continuing at the CCC to develop a complete range of SCC mixes using SPFA at various levels and at staged water-binder ratios, in addition to ultra-high strength, compactable concrete for flexible architectural solutions.

7. CONCLUSIONS

1. Superclassified PFA (SPFA) has been shown to suitable for making low cementitious content, extremely cohesive, self-compacting concrete at water-binder ratios between 0.2 and 0.45.
2. A 30% replacement of SPFA for cement has been found to be the optimum replacement level.
3. When SPFA is used to make SCC, the cementitious content is markedly lower (up to 280kg/m^3) than other SCC concretes made with conventional materials.
4. Virtually zero segregation or bleeding and extremely high cohesiveness and flow characteristics are observed in SCC made with SPFA.
5. The SSCI test has been shown to be more sensitive to the tendency for SCC mixes to segregate than the slump-flow test and has been adopted as a second check on SCC developed at Sheffield University.
6. Self-compacting SPFA concrete mixes may be considerably more durable than similarly-proportioned concrete mixes made with other alternative cement replacement materials, as shown by their significantly lower absorption, which indicates a better resistance to physical penetration of aggressive ionic species.
7. In a large-scale trial, the SPFA SCC cast as a column exhibited no signs that segregation of any description had taken place over it's height.

ACKNOWLEDGEMENT

The authors are grateful for the support and materials received from Sphere-Fill (Pty) Ltd that allowed the research work leading to this paper to be carried out.

REFERENCES

[1] Ouchi M and Okamura H, Self-compacting Concrete Development, Present use and future. Proc. 1st Int. Symposium on Self-Compacting Concrete, RILEM, Sweden, 1999.
[2] Bartos, PJM, Going with the Flow, Concrete Engineering, November, P27, 1998.
[3] Internet source, www.britishsafetycouncil.co.uk/safetymanagement/news/vibration.htm, accessed 29/04/2002.
[4] British Standards Institution. Specification for Portland Cement. BS12, BSI, London, 1991.
[5] American Society for Testing and Materials. Standard Test Methods for Sampling and Testing Fly Ash or Natural Pozzolans for Use as a Mineral Admixture in Portland-Cement Concrete. ASTM, Pennsylvania, ASTM C 311-00. 2000.
[6] Tsartsari and Byars. Ultra-high-strength concrete using conventional casting. Concrete, Vol. 36, No. 1, January. 2002, pp. 16-17.
[7] British Standards Institution. Pulverised-fuel ash-cementitious component in concrete. BS 3892 : PART 1, BSI, London, 1997.
[8] Internet source, personal.cityu.edu.hk/~bshxwen/ 1912Index/Pozzolan/Pozzo6.doc, accessed 29/04/2002.
[9] British Standards Institution. Specification for ground granulated blastfurnace slag for use with Portland cement, BS6699, BSI, London, 1992.
[10] American Society for Testing and Materials. Standard Specification for Silica Fume for Use as a Mineral Admixture in Hydraulic-Cement Concrete, Mortar, and Grout. ASTM, Pennsylvania, ASTM C 1240-99. 1999.
[11] American Society for Testing and Materials. Standard Specification for Chemical Admixtures for Concrete. ASTM, Pennsylvania, ASTM C 494 M-99, 1999.

[12] British Standards Institution. Concrete admixtures. Specification for superplasticizing admixtures, BS 5075, BSI, London, 1985.
[13] British Standards Institution. Testing Aggregates, BS812, BSI, London, 1985.
[14] British Standards Institution. Testing concrete : Part 102, Method for determination of slump, BS1881,BSI, London, 1983.
[15] British Standards Institution. Testing concrete :Part 105, Method for determination of flow, BS1881, BSI, London, 1984.
[16] British Standards Institution. Testing concrete : Part 116, Method for making test cubes from fresh concrete, BS1881, BSI, London, 1983.
[17] British Standards Institution. Testing concrete : Part 111, Method of normal curing of test specimens (20°C method), BS1881, BSI, London, 1983.
[18] British Standards Institution. Testing concrete : Part 116, Method for determination of compressive strength of concrete cubes, BS1881, BSI, London, 1983.
[19] British Standards Institution. Testing concrete : Part 117, Method for determination of tensile splitting strength, BS1881, BSI, London, 1983.
[20] British Standards Institution. Testing concrete : Part 122, Method for determination of water absorption, BS1881, BSI, London, 1983.
[21] British Standards Institution. Testing concrete : Part 203, Recommendations for measurement of velocity of ultrasonic pulses in concrete, BS1881, BSI, London, 1986.
[22] Petersson O and Skarendahl. Ed. Proc. 1st Int. Symposium on Self-Compacting Concrete, RILEM, Sweden, 1999.
[23] Yuan R.Z, Jin, S.X & Qian, J.C. Effects of fly ash on the rheology of fresh cement. p182-191 in Skalney, J.P. Ed. Effect of Surface and colloid phenomena on properties of fresh concrete. Proceedings, Symposium M, Materials Research society, Annual Meeting, November, 1982.

IMPORTANCE OF MINOR PHASE INCLUSION IN THE RIETVELD ANALYSIS OF CEMENT CLINKER

V. K. Peterson[1], A. Ray[1] and B. A. Hunter[2]

[1]Department of Chemistry, Materials and Forensic Science, University of Technology, Sydney, Australia. E-mail: vkp@ansto.gov.au
[2]Neutron Scattering, Australian Nuclear Science and Technology Organisation, Menai, Australia. E-mail: bah@ansto.gov.au

ABSTRACT

The effect of minor phases on the quantitative phase analysis of cement clinker by the Rietveld method was investigated. Simulated laboratory x-ray data-sets were constructed from set quantities of cement clinker components that approximated a known clinker, with differing counting statistics. These simulated data-sets were then refined with and without prior knowledge of the phases present. In half of the refinements the smallest weight percentage phase, the rhombohedral tricalcium silicate phase, was not included in the refinement. Comparison of the phase quantification results obtained from these different strategies showed that in the refinements from the high count data-set, the phase quantities were not significantly disturbed by not including the minor phase, whereas the refinements using the low count data-set showed a large variation in phase quantification results. This has implications for the interpretation of quantitative phase analysis results from low count data such as obtained from on-line cement analysis.

1. INTRODUCTION

There has been an increase in the use of Rietveld refinement of powder diffraction data for the quantitative phase analysis of cement and analysis of cement components in recent years [1]. The complex nature of cement clinker components and structural modifications of each phase makes phase quantification of cement clinker difficult. Although Rietveld provides the most consistent results for even the interstitial phases, overlapping phase peaks from the multiphase system in diffraction patterns further complicated phase analysis by this method.

Major phases present in clinker are tricalcium silicate (Ca_3SiO_5), dicalcium silicate (Ca_2SiO_4), tricalcium aluminate ($Ca_3Al_2O_3$), and tetracalcium aluminoferrite ($Ca_2(Al_2O_3)_x(Fe_2O_3)_{1-x}$). Clinker composition is complicated by the crystal modification of some of these phases. The solid solution of tricalcium silicate in cement is called alite. Three structural models are commonly used in the Rietveld analysis of cement clinkers, including a triclinic, a monoclinic and a rhombohedral model. Only one of the dicalcium silicate polymorphs has been shown likely to be present in cement clinkers, the monoclinic ß-type. Tricalcium aluminate exists in three modifications, a monoclinic, an orthorhombic, and a cubic type, through ion substitution. The cubic and orthorhombic modifications of this phase are likely to be present in clinker. Tetracalcium aluminoferrite appears in one form, with a varying Al:Fe ratio.

Rietveld analysis techniques are currently applied to on-line powder diffraction data from cement clinker directly from the kiln. A common practise is to refine until a good figure of merit is achieved. One of the problems with the Rietveld analysis of cement clinkers is the existence of

multiple small weight percentage phases. Often these smaller phases can exist below the detectable limit for Rietveld methods, which is dependent on the size and complexity of the unit cell being modelled. The compounded effect of multiple missing phases in the Rietveld model means that if the fit of the model to the data is still good despite multiple missing phases, then the model is compensating for these missing phases which could generate incorrect results. If the Rietveld analysis model is being used for phase quantification purposes, the effect of missing phases could result in incorrect quantitative phase analysis of the clinker material.

2. EXPERIMENTAL

Simulated data was used as a tool for investigating the effect of minor phases on Rietveld analysis of data with differing counting statistics. Cement clinker powder diffraction data-sets were simulated using the Rietveld program Rietica [2]. Typical counting intensities were modelled from real data collected using Cu Kα radiation on the Scintag x-ray diffractometer at the Australian Nuclear Science and Technology Organisation (Scintag X1, Scintag Instruments, U.S.A.). Data were simulated over the range $2\theta = 2.00 – 90.00°$ with a stepping of 0.02°. A single-term 5^{th} order polynomial function was used to model the background, and peak shape parameters were based on real cement clinker sample data taken from the instrument that was simulated. Rietveld scale factors were calculated from weight percentages based on real clinker compositions using the ZMV relationship [3], where Z is the number of formula units per unit cell, M is the mass of the formula unit and V is the unit cell volume. Instrumental noise was simulated using a random number generator with a normal distribution. Two data-sets were generated, one known as the high count data-set, where counting statistics resulted in the most intense peak from the pattern having an intensity of around 3000 counts, the other known as the low count data-set, where this peak had an intensity of around 600 counts. The background term used in the low count data-set was $1/5^{th}$ of that used in the high count data-set. Modelled phase compositions were based on a real ordinary Portland cement clinker composition. The model constitution is outlined in Table 1.

Table 1. Component structures and composition used in data simulation

Phase	Structural reference	Wt. % from ZMV
Alite	-	61.14
Tricalcium silicate triclinic	T_1 [4]	19.84
Tricalcium silicate monoclinic	M_3 [5]	38.86
Tricalcium silicate rhombohedral	R [6]	2.44
Dicalcium silicate	β [7]	17.07
Tricalcium aluminate	Orthorhombic [8]	9.21
Tetracalcium aluminoferrite	Orthorhombic [9]	12.58

Each data-set was at first refined with a new refinement data file, and approached with prior knowledge of all phases present, but without knowledge of peak shapes, scale factors, or any refinable parameters. This was known as refinement strategy number 1. The next refinement was performed in the same manner as the first, but approached as a blind data-set refinement, without prior knowledge of the phases present. This was known as refinement strategy number 2. Refinements were deemed finished when no further significant improvement in fit could be made.

3. RESULTS AND DISCUSSION

Table 2 shows the ZMV calculated or “ideal” phase quantities, as well as the phase quantification results for the two refinements made for each data-set. The Rietveld figures of merit R_p and Goodness Of Fit (GOF) are listed in Table 3. In the first column of Table 3, the figures of merit are based on fits of the ideal input to the simulated data without refinement of any parameter. In the case of refinement strategy 2 of both data-sets, the fits of the model to the data were deemed good

enough to not to continue searching for any further phases. The approach to Rietveld refinement of a cement clinker data-set often involves the search for one polymorph of tricalcium silicate at a time. As the rhombohedral modification of tricalcium silicate is usually present in much lower quantities than all other polymorphs, if at all, it is usual to include this as a final step of phase identification. Hence refinements using strategy number 2 did not include the search for this phase. Inspection of the difference line did not yield visual clues to the possibility of a missing phase. The intensity of the largest reflection from this phase was observed as approximately 135 counts in the low count data-set, and 675 counts in the high count data-set.

In Figures 1-4, crosses represent the observed data, and the solid line through the observed data is the result of the Rietveld fit. The line below the markers represents the residual or difference line.

Figures 1 and 2 represent refinements of the high count data-set, and Figures 3 and 4 represent refinements of the low count data-set. The short vertical bars mark the positions of the Bragg reflections of each phase. Figures 1 and 3 represent refinements with all phases present, and peak markers from top to bottom represent the phases triclinic tricalcium silicate, rhombohedral tricalcium silicate, dicalcium silicate, monoclinic tricalcium silicate, tricalcium aluminate and tetracalcium aluminoferrite respectively. Figures 2 and 4 represent refinements without the rhombohedral tricalcium silicate phase present, and peak markers from top to bottom represent the phases triclinic tricalcium silicate, dicalcium silicate, monoclinic tricalcium silicate, tricalcium aluminate and tetracalcium aluminoferrite respectively.

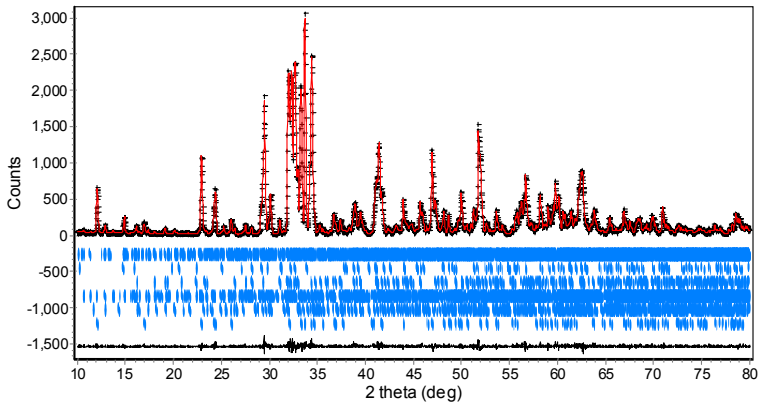

Figure 1. High count data-set refinement with all phases.

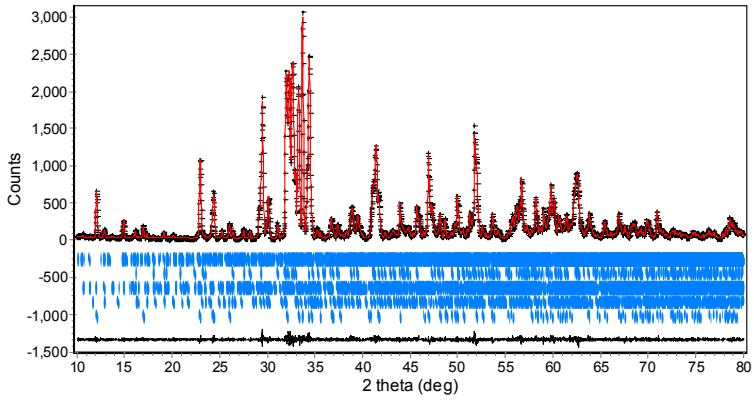

Figure 2. High count data-set refinement not including rhombohedral tricalcium silicate

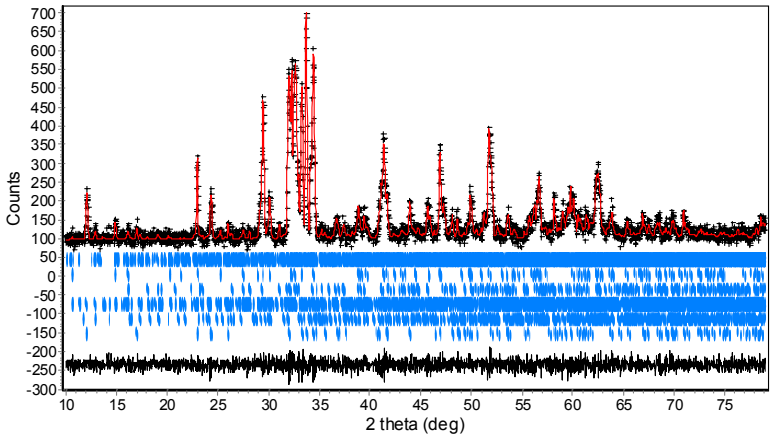

Figure 3. Low count data-set refinement with all phases

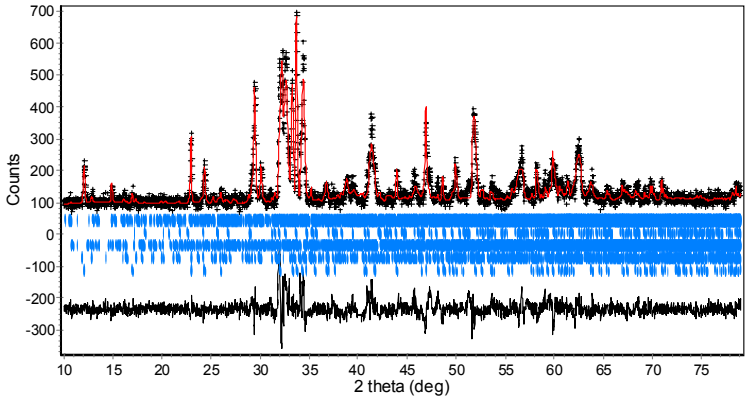

Figure 4. Low count data-set refinement not including rhombohedral tricalcium silicate

Table 2. Phase quantification results from refinements of the low and high count data-sets

	Wt. % "Ideal"	Wt. % 6 phases	Wt. % 5 phases	Wt. % 6 phases	Wt. % 5 phases
Phase/Refinement		1 (High count)	2 (High count)	1 (Low count)	2 (Low count)
Alite	61.1	61.4(5)	61.5(3)	62.4(9)	72.1(7)
Ca_3SiO_5 T_1	19.8	20.0(3)	20.1(2)	20.0(6)	69(1)
Ca_3SiO_5 M_3	38.9	39.1(5)	41.9(3)	41(1)	2.8(4)
Ca_3SiO_5 R	2.4	2.4(3)	Not inc.	1.71(6)	Not inc.
Ca_2SiO_4	17.1	16.8(2)	16.9(2)	16.0(5)	4.9(5)
$Ca_3Al_2O_3$	9.2	9.2(1)	9.1(1)	9.0(3)	9.8(4)
Ca_2FeAlO_5	12.58	12.63(9)	12.56(7)	12.6(2)	13.3(2)

Table 3. Figures of merit for refinements of the low and high count data-sets

Figures of merit/Refinement	"Ideal"	Refinement 1 6 phases	Refinement 2 5 phases
GOF (High count)	1.031	1.030	1.051
Rp (High count)	3.002	2.993	3.027
GOF (Low count)	1.036	1.022	2.266
Rp (Low count)	6.653	6.662	9.913

As expected, Rietveld figures of merit were generally better for the refinements of the high count data-set than for those of the low count data-set, although refinement strategy number 1 of the low count data-set resulted in an unusually good GOF, even when compared to the “ideal” GOF. This result was not reflected in the R_p value. In both data-sets, refinement with all phases (refinement

strategy number 1) resulted in better Rietveld figures of merit than were obtained from using refinement strategy number 2, where a phase was missing from each model.

Refinement using strategy number 1 of both data-sets, where all phases were used, yielded phase quantification results near to the "ideal" amounts. Refinement strategy number 2, where the rhombohedral modification of tricalcium silicate was not modelled, yielded similar results to the "ideal" amounts from the high count data-set, but the low count data-set exhibited some large phase quantification variations. The most significant differences in results between the two data-sets using the refinement strategy number 2 was the weight percentages of tricalcium silicate and dicalcium silicate phases. Using refinement strategy number 2 and the high count data-set, an amount of dicalcium silicate and tricalcium silicate polymorphs (both the triclinic and monoclinic forms) similar to the ideal quantity was found. The corresponding refinement of the low count data-set however, resulted in approximately 71wt. % less dicalcium silicate, 245 wt. % more triclinic tricalcium silicate, 93 wt. % less monoclinic tricalcium silicate, and 18 wt. % more total alite than was found using refinement strategy number 1. This result is alarming, as the incorrect result is not reflected in the figure of merit, which is still reasonably good. The amounts of tricalcium aluminate and tetracalcium aluminoferrite phases found using refinement strategies 1 and 2 were not notably different.

Rietveld packages specifically designed to give phase quantification results of cement clinker are being increasingly used in industry, and although they represent the best routine analysis methods available, they are limited by the statistics available from the data count rates. The tricalcium and dicalcium silicate phase in cement powder diffraction patterns are heavily overlapped and the effect of this can be detrimental to phase quantification results from Rietveld analysis, especially at lower count rates when resolution becomes an issue. As the powder patterns for the polymorphs of tricalcium silicate are similar, it is difficult to locate which polymorphs are present in clinker, although it is important that care be taken to look for all polymorphs. Low count data appears to be more prone to false refinement minima during Rietveld analysis that the high count data.

ACKNOWLEDGEMENTS

This work forms part of a PhD thesis to be submitted by V. Peterson. The research project is funded by an Australian PhD and an Australian Institute of Nuclear Science and Engineering post-graduate award.

REFERENCES

[1] Peterson, V.K., Ray, A. and Hunter, B.A. Rietveld phase quantification of cement clinker using powder diffraction data, Journal of the American Ceramics Society, submitted for publication.
[2] Hunter, B. Rietica – A visual Rietveld program, Powder Diffraction Newsletter, vol.20, 1999, pp. 21.
[3] Hill, R.J. and Howard, C.J. Quantitative phase analysis from neutron powder diffraction data using the Rietveld method, Journal of Applied Crystallography, vol.20, 1987, pp. 467-474.
[4] Golovastikov, N.I., Matveera, R.G. and Belov, N.V. Crystal structure of the tricalcium silicate 3CaO.SiO2 = C3S, Sov. Phys. Crystallogr. Vol.20, 1975, pp. 721-729.
[5] Nishi, F., Takèuchi, Y. and Maki, I. Tricalcium silicate Ca3O[SiO4]: The monoclinic superstructure, Zeitschrift fur Krystallographie, vol.72 1985, pp. 297-314.
[6] Ilinets, A.M., Malinovskii, Y. and Nevskii, N.N. Crystal structure of the rhombohedral modification of tricalcium silicate Ca3SiO5, Dokl. Akad. Nauk SSSR, vol. 281, 1985, pp. 191-193.
[7] Mumme, W.G., Hill, R.J., Bushnell-Wye G. and Segnit, E.R. Rietveld crystal structure refinements, crystal chemistry and calculated powder diffraction data for the polymorphs of dicalcium silicate, Neues Jahrb. Mineral., Abh., vol. 169, 1995, pp. 35-68.
[8] Nishi, F. and Takèuchi, Y. The Al6O18 rings of tetrahedra in the structure of Ca8.5NaAl6O18, Acta Cryst., vol. B31, 1975, pp. 1169-1173.
[9] Colville, A.A. and Geller, S. Crystal structures of Ca2Fe1.43Al0.57O5 and Ca2Fe1.28Al0.72O5, Acta Cryst**.,** vol. B28, 1972, pp. 3196-3200.

THE DEVELOPMENT OF AN AFFORDABLE KGALAGADI SAND BUILDING BLOCK (KSBB) – A POSITION PAPER

Esau U. Masuku[1] and Botshelo H. Maedza[2]

[1] Member of Zimbabwe Institution of Engineers (MZIE), E-mail: masuku@botec.bw
[2] Member of Botswana Institution of Engineers (MBIE), E-mail: har709@botec.bw

ABSTRACT

About three-quarters of Botswana is covered by Kgalagadi Sands (KS). KS are invariably closely graded, consist of medium to fine sub-rounded particles and contain insignificant amounts of silty and clayey fractions. As a result of these physical and chemical properties, KS lack packing and therefore compactibility, have very high voids ratios and are cohesionless. Consequently, the wet and dry strengths (compressive, shear and flexural), dimensional stability, durability and aesthetics of building blocks moulded with KS alone, in the very rare cases where they occur with silts and clays of the right quantities and quality, are well below acceptable values.

This position paper describes the extensive experimental work currently underway at Botswana's major multi-disciplinary Research and Development (R&D) Centre – Botswana Technology Centre. The work seeks to render this immensely abundant and widely available, but hitherto unusable resource, utilizable in construction. The affordability of the resultant KSBB shall derive from the local availability of KS as a raw material, usage of locally manufactured equipment and exploitation of local, largely unskilled labour force under supervision by semi-skilled artisans.

Keywords: Acceptable values (of KSBB properties), medium to fine particles (of KS), packing (of KS)

1. INTRODUCTION

Utilisation of a given soil as a building material implies a fundamental choice between three options. The first case involves using the soil available on site as it is. Under such circumstances the properties of the soil have to be accommodated in the project design process. In other words, the project has to be adapted as much as possible to the quality of the soil. The second option is to import soil with the desirable properties. Such a soil would be one with properties more suited to the requirements of the project. Finally, the soil may be improved by imparting to it the desirable properties. The locally available soil is modified so that it is better suited to the requirements of the project.

Kgalagadi sands are invariably characterised by a narrow medium to fine particle size distribution and insignificant silt and clay contents. They thus lack packing and therefore compactibility. They also lack cohesiveness. Compactibility and cohesiveness of the soil are the two major factors that account for the strength, durability and finish of a soil block. It is thus quite apparent that soil-block making cannot be adapted to Kgalagadi sands as they naturally occur. About ¾ of Botswana is covered by Kgalagadi sands. Therefore, the option of importing soils more suited to the requirements of soil-block making is quite clearly not cost-effective. That leaves open only the third option. The abundantly available Kgalagadi sands must be modified so that they are suited to the

requirement of building block making. Improving a given soil by imparting to it purpose-specific properties is generally termed soil stabilisation.

This paper presents a methodology for stabilising Kgalagadi sands. The methodology is based on improving both the compactibility and cohesiveness of the Kgalagadi sands. The compactibility of a given Kgalagadi sand is enhanced by "widening" its particle size distribution. Cohesiveness is imparted to the given Kgalagadi sand through the introduction of a three dimensional matrix that binds Kgalagadi sand particles together. Cement is the key determinant of the strength and durability of the matrix. Therefore, the chemistry of cement is of pivotal importance in developing the methodology for stabilizing Kgalagadi sands. In adherence to the subject of the Conference, this paper will focus on the chemistry of cement as a stabiliser for Kgalagadi sands.

2. CEMENT AS A STABILISER FOR KGALAGADI SANDS

Soil stabilisation is not necessarily cost-effective, at least immediately. Experience shows that it can involve considerable extra costs ranging from 30 to 50% of the final cost of the building materials [1]. On that account, the cost implications of soil stabilization have a direct bearing on the development of the methodology for imparting the desirable properties to a given soil.

Being narrowly graded and consisting of medium ($0.20<\phi\leq0.60$mm)[1] to fine ($0.06<\phi\leq0.2$mm)[1] subrounded grains, Kgalagadi sands are characterized by very high voids ratios ranging from 48 to 72 % by volume [2]. A combination of such high voids ratios and cohesionlessness of Kgalagadi sands significantly increases cement paste demand in the KSBB. Consumption of cement, by far the most energy-intensive and therefore most expensive component in the KSBB, increases correspondingly. It thus makes economic sense to use a pozzolan – a much less expensive substance to substitute in part the cement content in the KSBB. In Botswana, the only readily available pozzolan is fly ash produced by the Morupule Thermal Power Station. Therefore, the strength and durability of the three-dimensional matrix binding Kgalagadi sand particles together is determined by three major factors. They are the type of cement used, the type of pozzolan used and the cement + fly ash : Kgalagadi sand : water, ratio by mass.

2.1 Choice of cement for stabilising Kgalagadi sands

The selection of a cement for stabilising Kgalagadi sands is dependent on the set of indicators identified and analysed below.

2.1.1 Lime content of Morupule flyash

Given that only Morupule flyash is readily available as the potential cement extender, the choice of cement for stabilising Kgalagadi sands depends on the lime (CaO) content of this artificial pozzolan. Table 1 below shows that Morupule flyash is a low lime flyash. Since the CaO content in Morupule flyash is less than 10%, the latter is classified as a Class F flyash.

[1] Jackson, N.Ravindra, K.D. (Editors). Civil Engineering Materials 4th Edition

Table 1. Content of oxides in Morupule flyash

No.	Oxide	Content, % by mass				Range
		B.K. Sahu[2]	BPC	SIRDC[3]	T. Kudo	
1	SiO_2	41.20	40.80	43.00	53.70	40.80 – 53.70
2	Al_2O_3	33.60	34.70	33.50	23.20	23.20 – 34.70
3	Fe_2O_3	5.08	8.80	5.20	2.80	2.80 – 8.80
4	MgO	3.00	3.50	3.30	2.90	2.90 – 3.50
5	CaO	6.45	8.70	8.10	9.70	6.45 – 9.70
6	Na_2O	0.10	0.10	-	0.05	0.05 – 0.10
7	K_2O	0.44	0.40	-	0.03	0.03 – 0.44
8	SO_3	-	-	-	0.90	-
9	TiO_3	2.31	2.10	-	0.17	0.17 – 2.31
10	P_2O_5	< 0.05	0.90	-	0.20	0.20 – 0.90
11	MnO	-	-	-	0.07	-

* While the % oxide content in the first three columns were sources from B.K. Sahu, BPC & SIRDC, they in fact were all determined from SACAA laboratories. T. Kudo's results were obtained in Japan on our request. Therefore, the sharp differences in values could be ascribed to the methods of testing used at the two facilities. To a lesser extent, that could be due to the variability of flyash properties – a normal phenomenon. A re-run of the analysis has been requested.

The hardened cement paste (hcp) based on cement + Morupule flyash as the cementitious component has very low early age strength. This is because the production of tricalcium disilicate hydrate ($C_3S_2H_3$) by the pozzolanic reaction (1) is secondary to the production of the same chemical compound by hydration of cement, represented by reactions (2) and (3).

$$2S + 3CH \longrightarrow C_3S_2H_3 \quad (1)$$

$$2C_3S + 6H \longrightarrow C_3S_2H_3 + CH \quad (2)$$

$$2C_2S + 4H \longrightarrow C_3S_2H_3 + CH \quad (3)$$

where: S – SiO_2, CH – $Ca(OH)_2$, $C_3S_2H_3$ - $3CaO.2SiO_2.3H_2O$, C_3S – $3CaO.SiO_2$,
H – H_2O, C_2S – $2CaO.SiO_2$.

The calcium hydroxide (CH) that takes part in the pozzolanic reaction would have been produced by reactions (2) and (3) in the process of hydration of cement. The tricalcium disilicate hydrate produced by the pozzolanic reaction starts to appear at about the time of initial set, when the ettringite [$Ca_6Al_2(SO_4)_3(OH)_{12}.26H_2O$] from adjacent cement particles starts to develop.

On the basis of the above characterisation of Morupule flyash, cement for stabilising Kgalagadi sands must be of high early strength class.

2.1.2 Water content of KSBB mix.

There are three major determinants of KSBB strength. In order of significance, they are : the strength of the transition zone between the hcp and the aggregate (Kgalagadi sand particles), the

[2] Unconfined Compressive Strength of Fly ash stabilised Sandy Soil (Proceedings of the Kgalagadi Sand Building Block Workshop, 18-19 March, 1999, Gaborone Botswana)

[3] History and properties of South African Flyash and Portland flyash cements. The South African Coal Ash Association (SACAA).

strength of the hcp and the strength of the aggregate. The first two factors are inversely proportional to the water/cementitious ratio. In the case of the hcp, the relationship to the W/C ratio is through porosity. Porosity is directly proportional to the W/C ratio. In a nutshell, the lower the W/C ratio (the "drier" the mix), the stronger the KSBB, provided that the mix is adequately compacted.

It follows from the above analysis of the influence of the W/C ratio on KSBB strength that the binder for stabilising Kgalagadi sands must have a of minimal water demand. Figure 1 below illustrates the influence of the W/C ratio on strength development of OPC + pozzolan concrete.

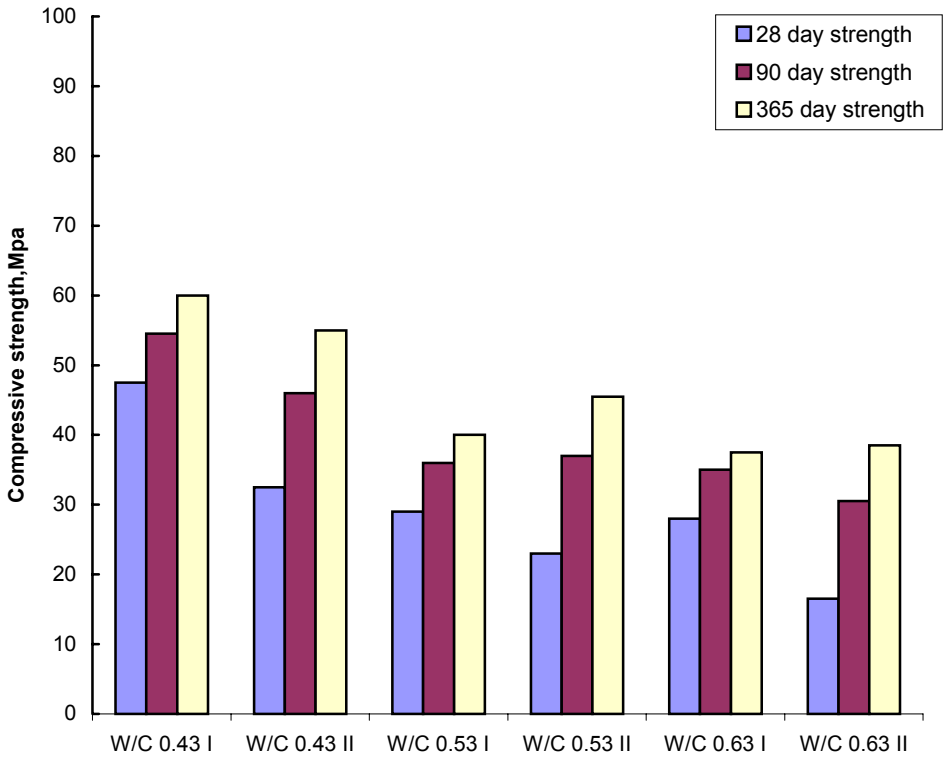

I – OPC:FA = 100:0, by mass II – OPC:FA = 100:30, by mass

Figure1. Influence of W/C ratio on strength development of OPC + pozzolan concrete (after Blanks and Kennedy, 1955).

2.1.3 Rate of hydration

Ordinary Portland cement (OPC) generates considerable heat of hydration in its early age. The resultant heating/cooling cycle aggravates thermal shrinkage and therefore cracking of the cement product. Partial replacement of OPC with flyash can significantly reduce or even completely eliminate cracking due to early age heat of hydration-induced alternate heating and cooling.

Therefore, cement for stabilising Kgalagadi sands does not have to be of low early age heat of hydration.

2.1.4 Alkalinity

OPC exhibits significant levels of alkalinity. Alkalinity may lead to the disruptive alkali-silica reaction (ASR). Experiment shows that although a flyash may contain high total alkali (K_2O + Na_2O) levels, the extent to which this contributes to the total alkalinity of the total pore water appears to be insignificant when the flyash is combined with high alkalinity cement. The effective total alkalinity is reduced. Substitution of OPC by at least 25% of flyash has been observed to limit

the total alkali content of concrete, to less than 3.0kg/m^3. That is less than the threshold of 3.5 – 4.0 kg/m^3, below which no disruption will occur, even with reactive aggregates.

As a consequence of the effect fly ash has on high alkalinity cements, cement for stabilising Kgalagadi sands need not be of low alkalinity.

The analysis given above shows that a cement for stabilising Kgalagadi sands must preferably be of high early strength and of low water demand. Furthermore, that cement does not have to satisfy the requirements of low heat of hydration or low alkalinity. In other words, it is of no consequence that the cement is of high heat of hydration and/or high alkalinity. The significance of this analysis is that the choice of cements for stabilising Kgalagadi sands is widened. Table 2 below gives preferred cements, selected on the basis of the four indicators outlined above.

Table 2. Selected cements for stabilising Kgalagadi sands

No.	Standard	Class/Type	Description
1	SABS ENV 197 – 1:1992	32.5 R	High early – strength
2	"	42.5 R	"
3	"	52.5 R	"
4	ASTM C150	I	Normal, general purpose
5	"	IA	Normal, air - entraining
6	"	III	High early – strength
7	"	IIIA	High early – strength, air - entraining

3. SUITABILITY OF MORUPULE FLYASH FOR USE AS CEMENT EXTENDER

According to Sersale (1980), flyash suitable for use as a cement extender must have a chemical composition such that the following conditions are satisfied:

$$SiO_2 + Al_2O_3 + Fe_2O_3 \geq 70\%, \text{ by mass} \quad (4)$$

$$2.5\ \% < SO_3 < 5\%, \text{ by mass} \quad (5)$$

$$MgO \leq 5\%, \text{ by mass} \quad (6)$$

$$(K_2O + Na_2O) \leq 1.5\%, \text{ by mass} \quad (7)$$

$$LOI \leq 12\%, \text{ by mass} \quad (8)$$

The total alkali content ($K_2O + Na_2O$) generally exceeds the 1.5% by mass limit. This will not pose a problem as long as the alkali available for reaction is below the stipulated limit of ($K_2O + Na_2O$) ≤ 1.5%, by mass.

The Loss on ignition (LOI) is related to the carbon content of the ash. The presence of carbon does not, as such, influence the pozzolanic reaction. Its limitation has to do with discoloration of the KSBB. Table 3 below shows that Morupule flyash satisfies all but one requirements stipulated by Sersale.

Table 3. Suitability of Morupule flyash for use as a cement extender according to the Sersale criteria

No.	Property	% content, by mass			
		B.K. Sahu	BPC	SIRDC	T. Kudo
1	Si + Al + Fe	79.88>70	84.30>70	81.70>70	79.70>70
2	SO_3	-	-	-	0.90<5
3	MgO	3.00<5	3.50<5	3.30<5	2.90<5
4	$K_2O + Na_2O$	0.54<1.5	0.50<1.5	-	0.03<1.5
5	LOI	-	-	-	3.50<12

The requirement that sulphur tri-oxide (SO_3) must be greater than 2.5%, by mass is unacceptable. It actually contradicts the requirement that utilisation of flyash as a cement extender should not result in creating an acidic medium in the cement paste. In this case the acidic medium would be a result of the formation of either the unstable weak sulphurous acid (H_2SO_3) or the stable highly corrosive sulphuric acid (H_2SO_4).

It is noteworthy that the chemical composition of a pozzolan is not a reliable criterion for its reactivity. Furthermore, chemical tests to evaluate reactivity may indicate the presence of a pozzolanic reaction. However, that would not indicate the strength characteristics of the OPC + pozzolan hcp. The only safe way to determine the suitability of a given pozzolan for use as a cement extender is to test it in product mixes. It is generally accepted that strength tests are the most suitable method of evaluating the activity of a pozzolan. Compressive strength is normally used as a measure of strength and cube specimens are preferable to cylinders because the latter require some form of capping to ensure that the ends are plane and parallel.

4. OPC + MORUPULE FLYASH : KGALAGADI SAND : WATER, RATIO

Determination of the above ratio is the ultimate goal of the methodology for stabilising Kgalagadi sands. Figure 2 shows that cost-effectiveness of the final product (KSBB) serves as the measure for optimal mix design.

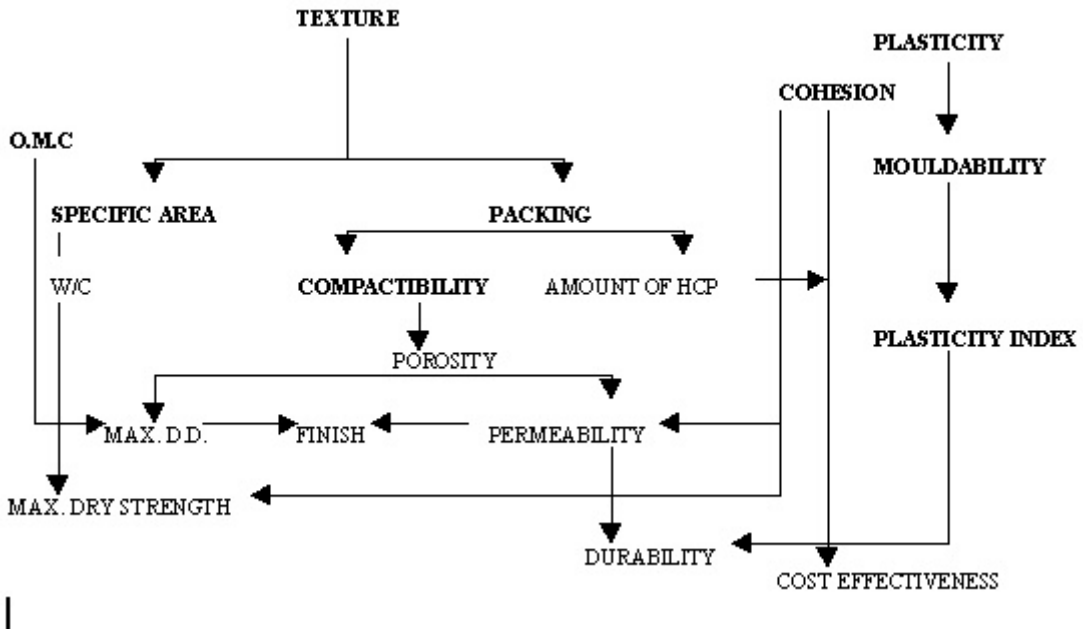

Figure 2. Connectivity between soil and KSBB properties

As pointed out in 2.0, the cement component is by far the most expensive ingredient of the KSBB. Therefore, the cost-effectiveness of the final product will be greatly enhanced by a significant reduction in the cement content of the KSBB. In other words aggregate packing must be improved. This can be achieved by widening the very narrow grading of Kgalagadi sands (see Figure 3 below) through mixing them with coarser aggregates from readily available calcretes.

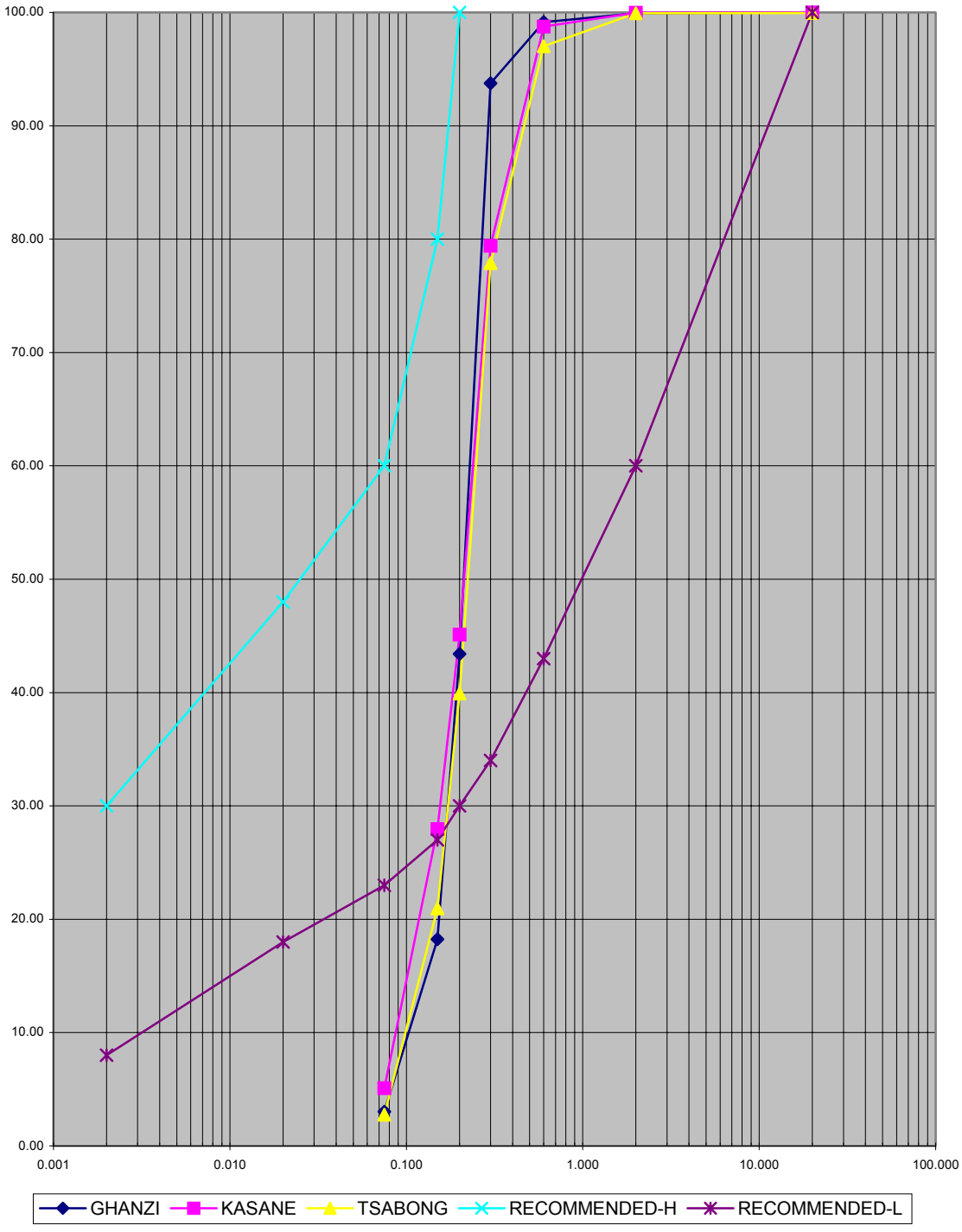

Figure 3. Particle size distribution of Kgalagadi sands

Figure 4 condenses the methodology for stabilising Kgalagadi sands:

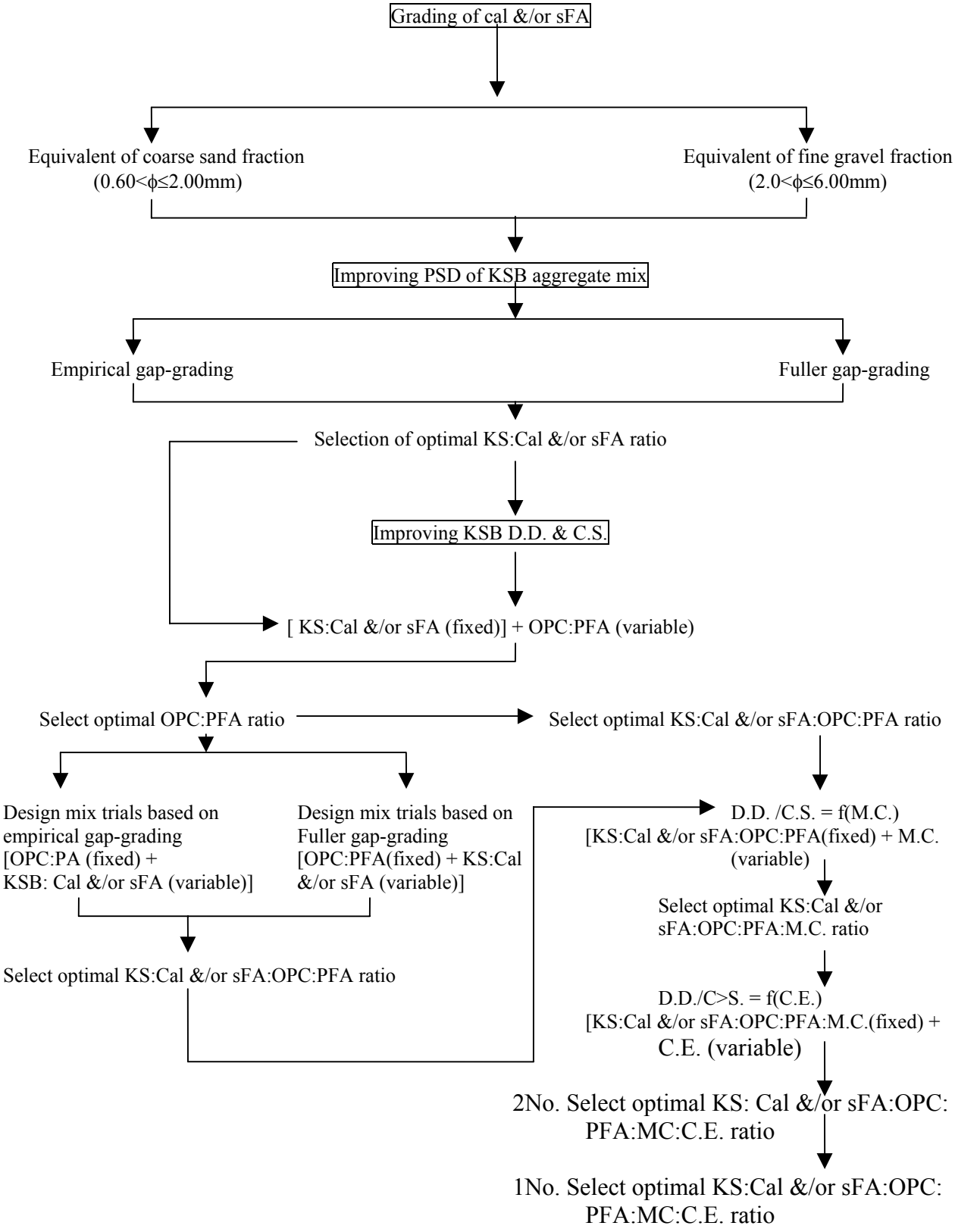

Figure 4. Flowchart of purpose-specific experiments

N.B. For brevity, the expression “calcrete &/or sintered FA” is abbreviated to “cal &/or sFA”; “Dry Density” to “D.D.”; “Compressive Strength” to C.S.”; Moisture Content” to M.C. & “Compacting Effort” to “C.E.”.

5. CONCLUSIONS

Cement holds the key to the exploitation of the abundant Kgalagadi sands as a viable raw material for building block production. The built-environment needs of such a developing country like Botswana can be catered for by the use of cement as a stabiliser for Kgalagadi sands provided that it is cost-effective. Therefore, cement, an expensive product, must be extended through blending it with a readily available pozzolan – Morupule flyash. The chemistry of the interaction of cement with, among other constituents of the KSBB, flyash, must be focused upon. This will provide for the development of a strong, durable, aesthetically acceptable and affordable KSBB with predictable chemical, physical and mechanical properties.

REFERENCES

[1] Houben, H.; Guilland, H.; Earth construction. A comprehensive guide. Intermediate technology Publications, London, UK, 1994. p. 74.

[2] Mockett, L.D.; Barton M.E. (Southampton University); Woodbridge, M.E. & Newill, D. (Transport Research Laboratory). Collapsing sand from the Kalahari region of Botswana, Transport Research Laboratory, 1992, p. 16.

THE DEVELOPMENT OF AN AFFORDABLE KGALAGADI SAND BUILDING BLOCK (KSBB) – A POSITION PAPER

Esau U. Masuku[1] and Botshelo H. Maedza[2]

[1] Member of Zimbabwe Institution of Engineers (MZIE), E-mail: masuku@botec.bw
[2] Member of Botswana Institution of Engineers (MBIE), E-mail: har709@botec.bw

Dr Esau U. Masuku

Senior Civil Engineer (Materials)
Botswana Technology Centre
Private Bag 0082
Plot No. 50654, Machel Drive
Gaborone Botswana
Tel: +267 3914161
Fax: +267 3974677
Email: masuku@botec.bw

Obtained his :
- Masters Degree in Industrial and Civil Construction at Patrice Lumumba Peoples' Friendship University (PLPFU), Moscow, Russia in 1985
- PhD in Structural Engineering at the Moscow State University of Civil Engineering (MSCEU) and the Moscow Central Research Institute for Light Metallic Structures in 1994

He worked as:

- Assistant Lecturer in Town Planning at the PLPFU for one year
- Assistant Consultant in Physical Planning at the Yugo – Zapadny District, Moscow City, Russia for two years
- Research Scientist in Building Materials and Structural Design at the MSCEU for three years
- Senior Research Scientist at the Scientific and Industrial Research and Development Centre (SIRDC) Harare, Zimbabwe.
- A consultant for Civil Engineering Consultancies and Contractors.

The Presenter has also published a number of S&T papers, policy papers on R&D and Client-specific reports

THE LONG-TERM PERFORMANCE OF CEMENTITIOUS MATERIALS IN UNDEGROUND REPOSITORIES FOR NUCLEAR WASTE

Thorsten Meyer and Horst-Jürgen Herbert

Gesellschaft für Anlagen- und Reaktorsicherheit (GRS) mbH, Braunschweig. E-mail: met@grs.de

ABSTRACT

The long-term behavior of cemented fly ashes in high saline brines has been investigated by means of a time accelerating leaching experiment and by the geochemical modeling of the observed reactions. The investigated materials, cemented hard coal fly ash (SFA) and brown coal fly ash (BFA), were mixtures of fly ashes, blast furnace cement, halite and saturated NaCl solution. The leaching fluids were a saturated NaCl-$CaSO_4$ solution and an IP21 solution, likely to occur in salt and potash mines, used in Germany as repositories for radioactive and hazardous chemical wastes. The employed leaching experiment was developed at GRS specifically for the boundary conditions of underground repositories. The experimentally observed reaction path was modeled using the computer code EQ3/6. In a second step the laboratory-scale and modeled results were compared with results of a full-scale experiment in the Asse salt mine.

The results of a 10-year leaching experiment with cemented fly ashes are in good agreement with the reaction path obtained by the time accelerating cascade experiment and geochemical modeling. Thus we can demonstrate that the experimental and modeling tools employed have proved suitable for the evaluation of the long-term behavior of cementitious materials in repositories in salt formations. It can be concluded that the investigated cementitious materials in Mg-rich brine will be less stable than in NaCl-$CaSO_4$ solution.

1. INTRODUCTION

In the German concept cements and cement based systems are proposed as technical barriers like dams and backfill materials for the final disposal of radioactive and hazardous wastes in salt formations. Cemented waste forms can represent a significant part of the inventory material, based on cements and fly ashes. Additionally, fly ashes can also be used as backfill material in the final disposal of radioactive and hazardous wastes. The long history of cementitious materials in this area is founded on the durability and persistence under environmental conditions. They have chemical and physical retention potential for nuclear waste and are resistant to many solutions and materials.

In contact with high saline solutions cementitious materials can show a significant change in their structure. Therefore the safety assessment of the repository system implies detailed knowledge of the geochemical behavior of cement and concrete systems in the salt environment. In case of a brine intrusion in the repository, significant changes of the structure, the chemical and themineralogical composition can be expected. Dissolution and precipitation processes will result in changes of the brine composition and pH. All these changes have a high impact on the long-term performance of the technical barriers but also on the solubilities of radionuclides and toxic heavy metals in the repository.

Proceedings of the 11th International Congress on the Chemistry of Cement (ICCC)
'Cement's Contribution to the Development in the 21st Century'
Hosted by: The Cement and Concrete Institute of South Africa
CD-ROM produced by: Document Transformation Technologies
11 - 16 May 2003, Durban, South Africa
ISBN Number: 0-9584085-8-0
Editors: Dr G. Grieve and G. Owens
Congress Organised by: Event Dynamics

2. CASCADE EXPERIMENTS

In order to understand the complex interactions in the leaching and corrosion processes, a special laboratory scale experiment was developed, which leads in several steps (cascades) towards the thermodynamic equilibrium. It is a fast experimental method for the investigation of the reaction path of the fluid-solid interactions.

In a cascade experiment a weighed mass of the ground material is reacted with a certain mass of solution (first cascade). After 2-3 days of equilibration under continuous rotation of the reaction vessel at 25°C, the solution is extruded through a pressure filter onto unreacted material (second cascade). While these steps are repeated, the effective solid-solution ratio increases. The number of steps in the experiment ranges from 10 to 20. The number of steps is limited by the continuously decreasing volume of leachate. For each cascade the solution as well as the solid material are analyzed by ICP-MS and ICP-OES, in addition the mineral phases of the solids are analyzed by XRD. Further experimental details are given in [1].

The results of this laboratory experiment are compared with the results of geochemical modeling and with results of a full-scale in-situ experiment in the Asse salt mine.

3. GEOCHEMICAL MODELING

The Gibbs enthalpy for the formation of a solid phase from an aqueous solution consisting of species *i* is given by the following expression:

$$\Delta G = \Delta G^0 + RT \ln \prod_i a_i^{\nu_i} \tag{1}$$

At equilibrium, $\Delta G = 0$ and the product of activities becomes K, the equilibrium constant:

$$\Delta G^0 = -RT \ln K \tag{2}$$

The activities are a product of the molalities m_i and the activity coefficient γ_i of the species:

$$K = \prod_i a_i^{\nu_i} = \prod_i m_i^{\nu_i} \gamma_i^{\nu_i} \tag{3}$$

The theory of Debye and Hückel is based on the assumption that strong electrolytes are completely dissociated in solution. Following the theoretical considerations of Debye and Hückel the activity coefficient of a strong electrolyte is a function of the solution's ionic strength. For Debye-Hückel the activity coefficient can be expressed:

$$\ln \gamma_i = -A z_i^2 \sqrt{I}\,; \qquad I = \frac{1}{2} \sum_i m_i z_i^2 \tag{4}$$

A: Debye-Hückel coefficient; z_i: ion charge; m_i: molalities of the species

The Debye-Hückel-Theory is valid only for ionic strength less than 10^{-2} - 10^{-3} M. Several extended equations has been established (Güntelberg, Davies). Pitzer and Co-workers developed a model which extends the Debye-Hückel expression for the calculation of ion activity coefficients in terms of the specific interactions between two or three ions.

The Pitzer formalism extends the Debye-Hückel expression with a virial expansion to account for binary and ternary ionic interactions between ions of like and opposite charge:

$$\ln \gamma_i = f(I) + \sum_I \lambda_{i,j}(I) m_j + \sum_j \sum_k \mu_{i,j,k} m_j m_k \quad (5)$$

f(I): Debye-Hückel expression; $m_{j,k}$: molalities of the species; λ, μ: interaction coefficients

The Pitzer expression includes specific parameters which have to be determined for each individual ionic interaction.

The experimentally observed reaction path was modeled using the computer code EQ3/6 [2-3], release 7.2a, and the thermodynamic database for the seawater system of Harvie, Møller and Weare [4], extended by Pitzer coefficients for Al and Si estimated by Reardon [5]. The solubility data used for cement phases (Table 1) were those published by Revertegat et al. [6], Berner [7] and NEA data listed by Glasser et al. [8].

Table 1. Solubility data of cement and mineral phases.

Phase	Formula	log K_{sp}	Phase	Formula	log K_{sp}
Brucite	MH	17.11	Friedel's salt	C_3ACcH_{10}	70.72
Chrysotile	$M_3S_2H_2$	31.13	Quartz	S	-4.00
CSH (0.8)	$C_{0.8}SH$	11.07	SiO_2 (am)	S	-2.71
CSH (1.1)	$C_{1.1}SH$	16.71	Hydrogarnet	C_3AH_6	80.80
CSH (1.8)	$C_{1.8}SH$	32.54	Si-Hydrogarnet	C_3ASH_4	69.35
Gibbsite	A	7.74	Portlandite	CH	22.80
Gypsum	CsH_2	- 4.58	Talc	M_3S_4H	22.41
Ettringite	C_3A3CsH_{32}	57.00	Tobermorite	$C_5S_6H_9$	64.35

A = Al_2O_3, C = CaO, Cs=$CaSO_4$, Cc=$CaCl_2$, H=H_2O, M = MgO, S = SiO_2

The chemical composition of the cemented materials for the main components to be modeled are listed in Table 2. The cemented BFA contains 54 wt-% of rock salt (94 wt-% of halite and 6% of anhydrite). The water cement ratio of cemented SFA is w/c =0.4, that of cemented BFA w/c=1.8.

The initial composition of the IP21 and NaCl-$CaSO_4$ solutions are given in Table 3. The solutions were first computed via an EQNR3 run. The reaction path of the material interaction with the different solutions were modeled in an EQ6 run using the titration model. The steps of the EQ3/6 run (z_i) correspond to the reaction i.e. the corrosion progress.

Table 2. Main components of the investigated materials.

Element	BFA	Cemented BFA	Cemented SFA
	[mg/kg]	[mg/kg]	[mg/kg]
Al	103330	16710	81012
Ca	154750	36610	151214
Cl	2920	506800	40340
K	8750	11160	22553
Mg	13340	5760	9473
Na	1980	299130	77690
S	17570	2330	9700
Si	178800	35060	126750

In order to simulate the corrosion of cementitious materials, the dissolution of portlandite, a main component in cement systems, can be used in a first attempt to predict the solution composition [9-11]. For the prediction of the reaction of complex systems like cementitious materials in contact to saline solutions special reactants were defined by using the chemical composition of the material.

Table 3. Composition of the IP21 and NaCl-$CaSO_4$ solution.

Element	IP21	NaCl-$CaSO_4$
	mol/kg H_2O	mol/kg H_2O
Ca	0.001	0.044
Cl	8.873	6.077
K	0.547	0.000
Mg	4.241	0.000
Na	0.462	6.077
S	0.309	0.044
Density [g/cm^3]	1.292	1.200

4. RESULTS AND DISCUSSION

The comparison of the experimental results of the dissolution of the cemented hard coal fly ash with the modeled dissolution of the special reactant shows a good agreement for the ions Mg^{2+}, Na^{+}, Cl^{-} and SO_4^{2-} in solution. Figure 1 shows the experimental and calculated development of the elements in solution during the leaching process of cemented coal fly ash (SFA). The strong decrease of Mg^{2+} in solution is very similar to that of portlandite dissolution [11]. This decrease is due to the precipitation of the mineral phase brucite ($Mg(OH)_2$). Parallel to this process an increase of Ca^{2+} was found up to 2.1 mol/kg H_2O in the third cascade. After the third cascade a reduction of Ca^{2+} in solution could be observed accompanied by the precipitation of newly formed CSH and CSAH phases.

The modeling with the special reactant reflects the decrease of Ca^{2+} in solution according to the experimental results after the third cascade. K^{+} stays nearly constant in the experiment, in the modeling K^{+} increases. Due to the high concentration of NaCl in the cemented SFA Na^{+} increased, whereas Cl^{-} slightly decreased. These results were observed in the experiment as well as in the modeling. During the first cascade SO_4^{2-} decreased to an amount of $< 10^{-4}$ mol/kg H_2O in solution (Figure 4). The sulfate ions were fixed in the newly formed phase gypsum, which could be identified in the XRD spectrum of the solid material after the first cascade. The pH rose stepwise from 5.8 to 12.4.

Brucite is formed during the first four cascades in rather large quantities. The formation of this phase is controlled by the amount of Mg^{2+} in solution. Brucite precipitates as a gel-like phase. This gel was observed macroscopically but it could not be detected by XRD as it is not in a crystalline state immediately after precipitation. It controls the pH during the first four cascades. After the consumption of all Mg^{2+} brucite precipitation ceases and the pH increases stepwise up to 12.4. The minerals detected in the cascade experiment partially correspond to those found in the geochemical modeling. In addition the modeling indicates that further minerals like chrysotile may be involved in the reaction. Talc occurs as an intermediate phase which becomes stable at a certain step of the reaction path and disappears later. Halite is also present in the system in large quantities and therefore not shown in Figure 1.

The reaction of BFA (Figure 2) and cemented BFA in contact to IP21 solution resulted in very similar solution compositions and precipitated mineral phases. These reactions will be discussed together and compared with the reaction of SFA in contact with IP21 solution. Similar to the reaction of cemented SFA, an increase of Ca^{2+} in solution was found as well as a decrease of Mg^{2+}. The decrease of the leaching fluid terminated the cascade experiment at an early step of the reaction path. The calculated reaction path indicates that Mg^{2+} will be precipitated in the phase talc. In the further progress of the reaction the Ca^{2+} will, similar to the reaction of SFA, decrease. The experimentally observed and the calculated Na^{+} concentration keeps constant for the different solid/solution ratios. The K^{+} and Cl^{-} increases slightly in the cascade experiment as well as in the modeling of the considered reaction. In addition, the SO_4^{2-} decreases during the first three cascades. The pH stayed at about 8.5. Similar to the SFA reaction, the precipitation of anhydrite/gypsum was observed and brucite was responsible for the Mg^{2+} decrease in solution. The modeled phases are given in Figure 2. According to the modeling of SFA in contact with IP21 solution, gibbsite was calculated. Si was computed as SiO_2.

The modeled results and the experimentally obtained data for the reaction of cemented BFA in contact with NaCl-$CaSO_4$ solution are displayed in Figure 3. The comparison of the experimental results of the dissolution of the cemented BFA with the modeled dissolution of the special reactant shows a good correspondence for the ions Na^{+}, K^{+}, Ca^{2+}, Cl^{-} and SO_4^{2-} in solution. There was a slight decrease of Cl^{-} and increase of Na^{+} observed in the cascade experiments as well as in the

chemical modeling. Ca^{2+} slightly decreases during the first cascades, limited by precipitation of anhydrite in the modeling.

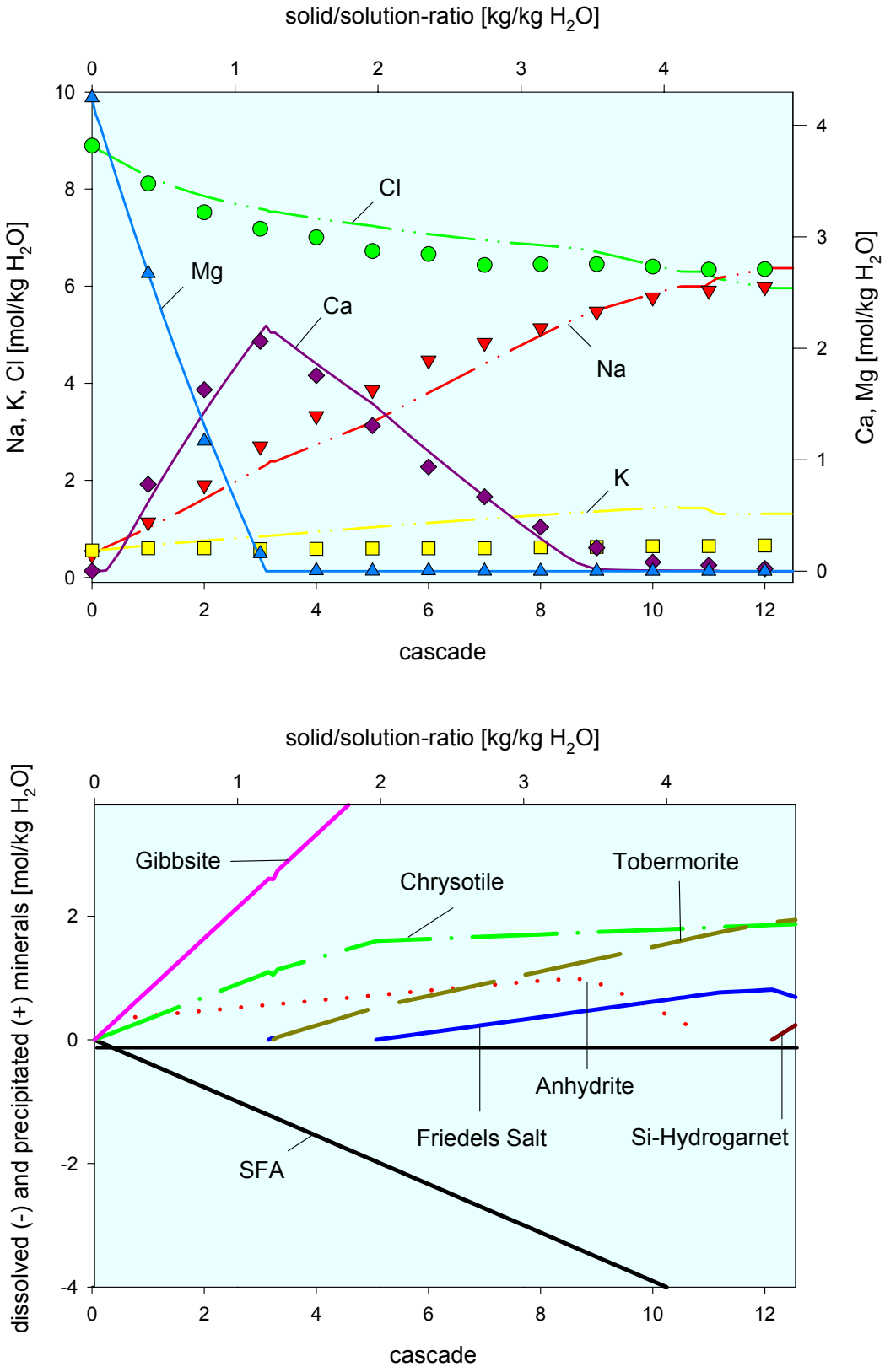

Figure 1. Reaction path of the dissolution of cemented hard coal fly ash (SFA) in a Mg-rich high saline solution (IP21); upper part: evolution of the solution composition, symbols mark the experimental data and lines the calculated results; lower part: calculated dissolved and newly formed phases.

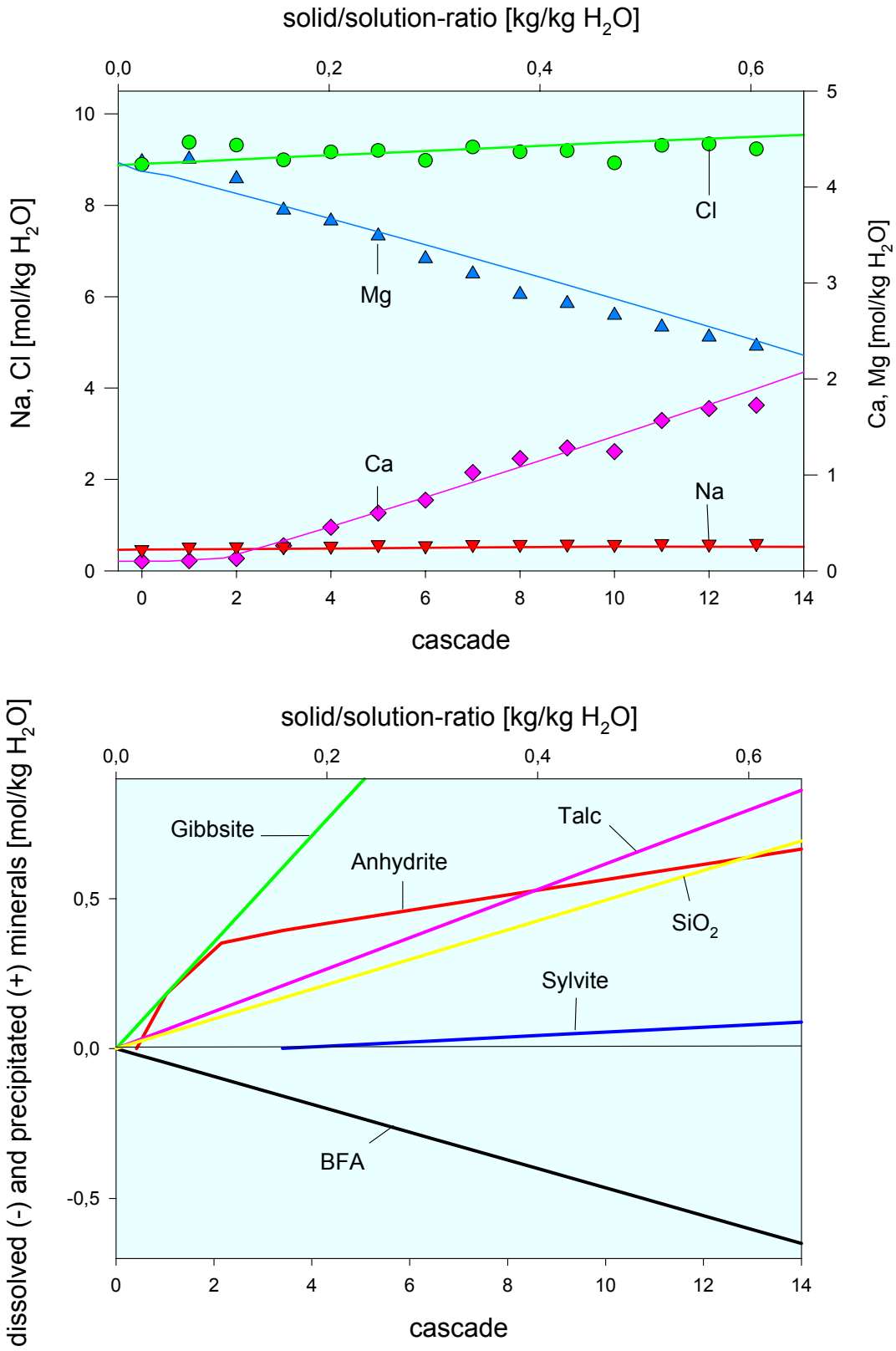

Figure 2. Reaction path of the dissolution of brown coal fly ash (BFA) in a Mg-rich high saline solution (IP21); upper part: evolution of the solution composition, symbols mark the experimental data and lines the calculated results; lower part: calculated dissolved and newly formed phases.

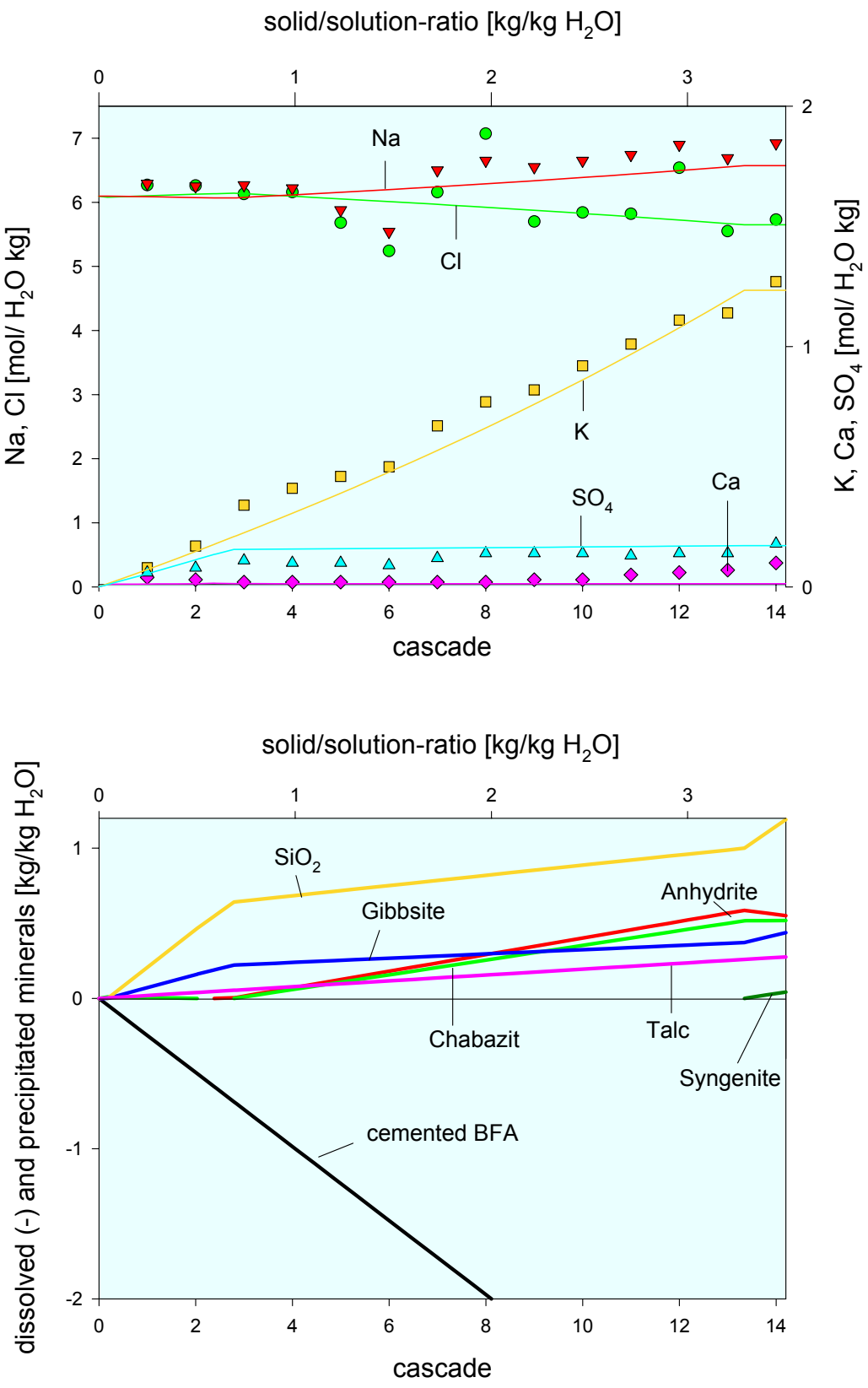

Figure 3. Reaction path of the dissolution of cemented brown coal fly ash (SFA) in a high saline solution (NaCl-$CaSO_4$); upper part: evolution of the solution composition, symbols mark the experimental data and lines the calculated results; lower part: calculated dissolved and newly formed phases.

Besides halite the phases SiO_2, chabazit and syngenite were computed by EQ3/6. Equal to the reaction with IP21 solution the phases anhydrite, talc and gibbsite were calculated. The reaction of

cemented BFA in contact to saturated NaCl-$CaSO_4$ solution is similar to that of pure BFA with the exception of SO_4^{2-} in solution. During the reaction of BFA in contact with NaCl-$CaSO_4$ solution SO_4^{2-} increases to an amount of 0.8 mol/kg H_2O.

A good agreement between the prediction of the modeled and the calculated solution composition for all five systems was obtained. Further attempts to improve the database for the cement phases will advance the prediction ability. The cascade experiment is a time accelerating experiment. Under in-situ conditions these reactions take several hundred years. Comparing the full scale with the laboratory scale experiments a rough estimate of the reaction time under in-situ conditions until the thermodynamic equilibrium suggests that the investigated materials could have long-term stabilities of several hundred years.

5. COMPARISON OF THE LABORATORY EXPERIMENT WITH FULL-SCALE IN-SITU EXPERIMENT IN THE ASSE SALT MINE

In the Asse salt mine 200 liter forms of cemented waste were leached in IP21 solution over a period of about 10 years [12]. The inactive simulated waste samples for intermediate-level waste (ILW) were fabricated by filling the unhydrated product into drums. After complete hydration of the product, the samples were removed out of the drums and stored at the Asse salt mine exposed to the ambient temperature of 28 ± 1°C at the 490-m level. Sampling was done periodically at a higher frequency during the initial period and only once a year after a few years of reaction.

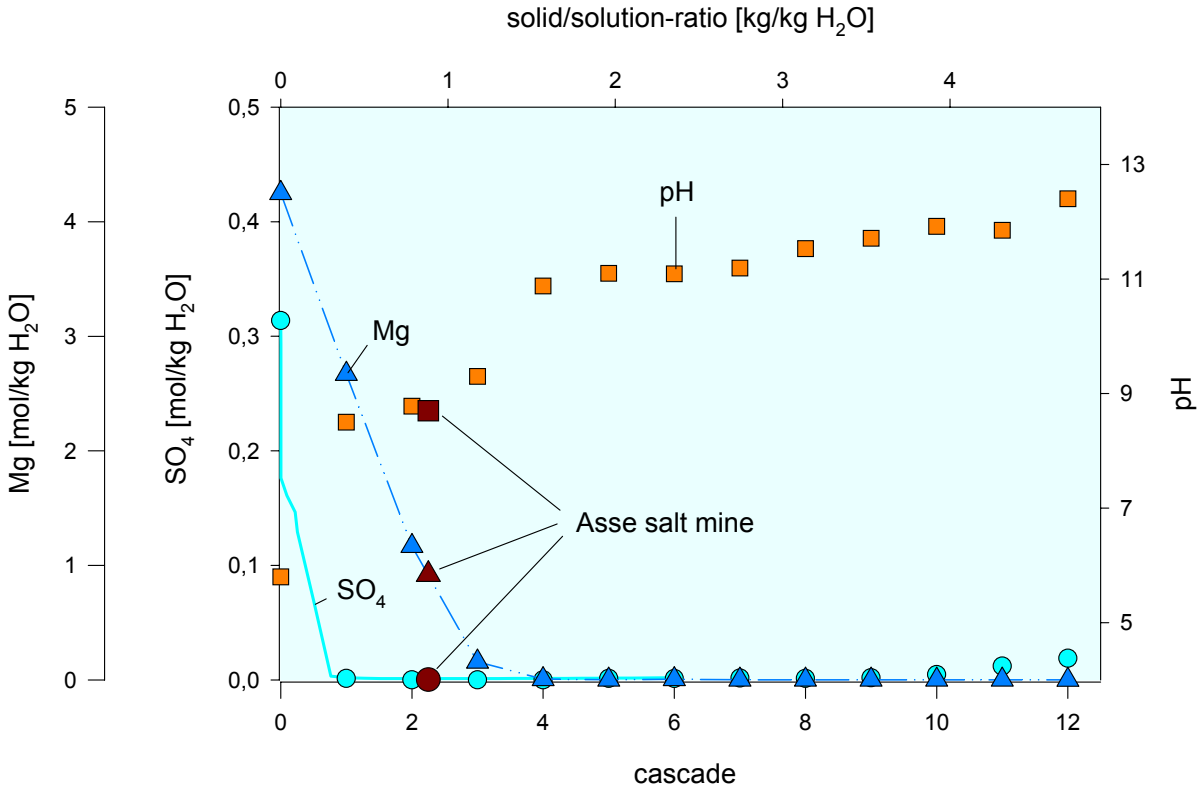

Figure 4. Comparison of the Mg^{2+}, SO_4^{2-} and the pH in solution in the corrosion experiments in the Asse salt mine and the laboratory GRS cascade experiment; symbols mark the experimental data (cascade and dark red the Asse experiment) and lines the calculated results.

A comparison of the results of the laboratory-scale cascade experiment with the full-scale in-situ experiment in the Asse salt mine shows a good agreement. The concentrations observed in the

leaching solution after 10 years in the Asse experiment correspond to the concentrations between the second and third cascade of the laboratory scale leaching experiment (Figure 4).

6. CONCLUSIONS

Considering the good agreement between the long lasting full-scale in-situ experiment and the time accelerating laboratory-scale cascade experiments, we conclude that it is possible to predict the chemical behavior of cementitious materials in salt solutions. The cascade experiment is a fast method that enables the prediction of the chemical changes in solution during the cement corrosion processes. For the investigated materials in contact with brines, a good agreement between the experimental data and the modeling results was obtained.

The existing thermodynamic database for the geochemical modeling however is still incomplete. Solubility data and dissolution models for CSH phases are incomplete or missing. The Pitzer coefficients of Si and Al still need to be determined more accurately. However the present state of the geochemical modeling with the existing database allows a valuable insight into the processes taking place along the reaction path in the extremely complex system. The experimental and modeling tools employed have proved to be suitable for a prediction of the long-term chemical behavior of cementitious materials.

7. REFERENCES

[1] Herbert, H.-J. und Mönig, J. (1996): Exemplarische Untersuchungen von Wechselwirkungsreaktionen UTD-relevanter chemisch-toxischer Abfälle mit hochsalinaren Lösungen, GRS-Bericht 126.

[2] Wolery T. (1992) : EQ3NR: A Computer Program for Geochemical Aqueous Speciation – Solubility Calculations. Theoretical manual, User's guide, and related documentation (Vers. 7.0), Lawrence Livermore National Laboratory, Livermore, California.

[3] Wolery T. (1992) : EQ6: A Computer Code for Reaction-Path Modeling of Aqueous Geochemical systems. Theoretical manual, User's guide, and related documentation (Vers. 7.0), Lawrence Livermore National Laboratory, Livermore, California.

[4] Harvie, C. E., Møller, N. and Weare, J. H. (1984): The prediction of mineral solubilities in natural waters: the Na-K-Mg-Ca-H-Cl-SO_4-OH-HCO_3-CO_3-CO_2-H_2O system to high ionic strengths at 25°C. - Geochimica et Cosmochimica Acta, v. 48, 723 - 751

[5] Reardon, E.J. (1990): An ion interaction model for the determination of chemical equilibria in cement/water systems, Cement and Concrete Research, 20, 175-192.

[6] Revertegat, E.; Adenot, F.; Richet, C.; Wu, L.; Glasser, F.P.; Damidot, D.; Stronach, S.A. (1997): Theoretical and experimental study of degradation mechanisms of cement in the repository environment, Report EUR 17642 EN.

[7] Berner U. (1990): A thermodynamic description of the evolution of pore water chemistry and uranium speciation during the degradation of cement, PSI report No. 62..

[8] Glasser, F.P., Paul M., Dickinson C.L., Reed D. (2001): Barrier performance of cements and concretes in nuclear waste repositories, Report EUR 19780 EN.

[9] Herbert, H.-J. und Meyer, Th. (1998): Untersuchung und Modellierung des Lösungsverhaltens von tragendem Versatz im ERAM. – GRS report for BfS, AG-Nr. 1512, 71.

[10] Meyer, Th. und Herbert, H.-J. (1999): The long-term behaviour of cemented materials in highly saline solutions, 2nd Geochemistry Workshop FZK Karlsruhe, Speyer, March 25.-26th 1999.

[11] Meyer, Th. und Herbert, H.-J. (1999): Geochemische Modellierung der Betonkorrosion - International Symposium Environment 2000, Halle, Sept. 22.-25th. 1999.

[12] Kienzler, B., Vejmelka, P., Herbert, H.-J. Meyer, H. and Altenhein-Haese, C. (2000): Long-term leaching experiments of full-scale cemented waste forms: Experimental and modelling results.- Nuclear Technology, vol. 129, 18p.

THE LONG-TERM PERFORMANCE OF CEMENTITIOUS MATERIALS IN UNDEGROUND REPOSITORIES FOR NUCLEAR WASTE

Thorsten Meyer and Horst-Jürgen Herbert

Gesellschaft für Anlagen- und Reaktorsicherheit (GRS) mbH, Braunschweig. E-mail: met@grs.de

Dr. T. Meyer

Born 1-20-1968 in Kassel, nationality German, studies of chemistry at university of Brunswick from 1987 to 1994, 1994-1997, Doctor dignity to Dr. rer. nat. at university of Brunswick. Professional experience: 1994 to 1997 scientific assistant in the institute of physical chemistry of this university. Since 1997 employee of the department of geochemistry in the division of final repository safety research at the society of plant and reactor safety "Gesellschaft für Anlagen- und Reaktorsicherheit (GRS) mbH".

Qualifications:

Experimental investigations and geochemical modelling on the interaction of solutions in salt formations in contact with cementitious materials and chemical toxic waste. Estimation of the corrosion properties of sealing and backfill materials for the prediction of the long-term stability of multi-barrier systems in underground repositories. Project manager in the EC project ECOCLAY II for the investigations of effects of cements on clay material.

CROSSLINKING OF POLYMER CHAINS IN HIGH-ALUMINA AND PORTLAND MACRO-DEFECT-FREE MATERIALS

Aldo Bonapasta[1 (*)], Francesco Filippone[1], Pierre Colombet[2] and Gian Guerrini[2]

[1]Consiglio Nazionale delle Ricerche, Istituto di Chimica dei Materiali (ICMAT), Via Salaria km 29,5, CP 10, 00016 Monterotondo Scalo, Italy. E-mail: aldo.amore@mlib.cnr.it
[2]CTG-Italcementi Group, Laboratories Department, Via G. Camozzi 124, 24121 Bergamo, Italy. E-mail: g.guerrini@itcgr.net

ABSTRACT

Although several experimental studies have related the peculiar mechanical properties of macro-defect-free (MDF) polymer-cement composites to the existence of a crosslinking of the polymer chains by Al or Ca ions coming from the hydration reactions of the cement, the importance of the crosslinking effects on the MDF properties is still debated. In the present study, the results of previous and present theoretical investigations on the existence and the strength of crosslinking in four different MDF materials are analysed. The combination of two different polymers, polyvinyl alcohol (PVA) and polyacrilic acid (PAA), and two different cements, high-alumina and Portland cements have been considered, that correspond to the Al-PVA, Al-PAA, Ca-PVA, and Ca-PAA ion-polymer systems. The results suggest the following relative strengths of the polymer-chain crosslinking: Al-PVA > Al-PAA > Ca-PAA > Ca-PVA. This scale of relative strength is consistent with the different mechanical properties observed in the case of high-alumina cement and Portland cement MDFs, thus suggesting that crosslinking can significantly affect the MDFs properties.

1. INTRODUCTION

The flexural strength of high-alumina and Portland cement-based materials can be increased dramatically by incorporating a polymer component (e.g., polyvinyl alcohol - PVA) in the cement paste under high shear and subsequent molding under pressure at 80°C [1-4]. The polymer acts as a rheological aid facilitating particle packing as well as a filling agent reducing the material porosity [2]. These modified cements were called Macro-Defect-Free (MDF) cements, referring to the absence of the relatively large voids or defects which are usually present in cement pastes [1, 3].

Several experimental studies have then clarified that a "new" composite material is produced by the incorporation of the polymer in the cement paste, the microstructure of which is characterized by grains of partially hydrated cement particles embedded in a matrix of polymer [5, 6]. Interphase regions coat the individual cement grains. In the case of high-alumina cement (HAC) MDFs, these regions consist of an amorphous phase of $Al(OH)_3$ and PVA inside of which are dispersed fine crystallites of hydration products. The peculiar mechanical properties of the HAC-MDF materials were initially related to the reduced density of defects in the final cement paste [2, 3]. Further studies have shown that the mechanical behavior of the interphase regions play an important role during the fracture of the MDF materials. Thus, it has been suggested that the mechanical strength of the MDFs can be related to chemical reactions occurring between the polymer and the inorganic ions produced by the cement constituents dissolved in water. More specifically, the existence of a crosslinking of the PVA chains by Al ions has been suggested, i.e., the formation of O-Al-O bonds

where an Al atom is bonded to the O atoms of two different PVA chains [7, 8]. The crosslinking of the polymer chains may have significant effects on the mechanical properties of the MDF materials. Metallic ions may link polymer chains together as well as polymer chains to O atoms of the inorganic matrix, thus strengthening both the network of the polymer chains around the cement grains and the organic-inorganic interfaces. Moreover, crosslinking may favor an intimate mixing of the cement and the polymer as well as the formation of the interphase regions. On the other hand, an excessive networking of the polymer chains induced by crosslinking may damage the interphase regions and hinder the achievement of a workable paste during the material processing. Thus, crosslinking may influence the peculiar strength attained by the MDF materials in two different ways: it may strengthen the organic-inorganic interfaces as well as affect the development of the cement-polymer paste, which in turn affects the final microstructure and the mechanical properties of the MDF materials. Only indirect evidence of a linkage of the polymer chains by ions released by the cement has been found by experiments [5, 6, 9].

Experimental investigations of crosslinking are difficult due to the complex structure of the MDF materials, to the fact that crosslinking is likely localized at the organic-inorganic interfaces, and to a possible interplay between crosslinking effects and material processing. For what concerns the last point, in the case of the HAC-PVA material, it has been suggested that crosslinking reactions are induced by the mechanical work performed during the mixing process [10]. On the other hand, in the case of Portland cements and PVA, it results difficult to obtain a workable paste, possibly because of crosslinking effects given by the Ca ions released by calcium silicates (the main components of Portland cements). The final microstructure and the mechanical properties of the MDFs can also be affected by a post-processing curing of the MDF materials [11].

In conclusion, the mechanical properties attained by an MDF material are likely affected by a complex interplay between crosslinking, processing effects and post-processing treatments. In this scenario, a systematic, theoretical investigation has been started on the existence and the strength of the crosslinking of different polymer chains by different metallic ions. In detail, the crosslinking of two different polymers, i.e., PVA and PAA (polyacrilic acid in anionic form), has been investigated in two different cements: HAC, where Al ions come from the hydration of the cement costituents, and Portland cements, where Ca ions come from the hydration of calcium silicates. Objectives of that investigation were: i) to estimate the potential effects of crosslinking on the material properties by separating them from the processing or post-processing effects; ii) to evaluate the relative strength of crosslinking in different MDF materials. This strength can be directly related to the flexural strength of the MDFs if the processing or post-processing conditions can be arranged to obtain materials with a similar microstructure, i.e., with similar density and type of defects. Further, the results of a theoretical investigation of crosslinking can give suggestions on possible effects of crosslinking on the material processing.

Previous theoretical studies have investigated the ion-polymer interaction in the Al-PVA, [12] Ca-PAA, [13] and Ca-PVA[14] systems. In the present study, some preliminary results achieved in the case of the Al-PAA system are reported. This system completes the possible combinations between the ions coming from the HAC and Portland cements and the PVA and PAA polymers. Present and previous theoretical results are then analysed together to clarify the effects of crosslinking on the properties of the HAC-PVA, HAC-PAA, Portland-PAA and Portland-PVA MDF materials. These results support the existence of crosslinking in all the above MDFs and show that the characteristics of crosslinking in the systems investigated can explain why the mechanical properties of Al-PVA MDFs are better than those of the Al-PAA MDFs and why the properties of the Portland-cement MDFs improve when the PVA polymer is replaced by the PAA polymer [15-17]. Furthermore, they give suggestions about the effects of crosslinking on the material processing.

Previous and present theoretical results have been obtained by performing ab initio calculations using the Car-Parrinello approach [18]. This method has been employed to investigate the equilibrium geometries, the total energy and the dissociation energy of model systems where an Al or a Ca ion is bonded with the O atoms of polymer chains.

2. COMPUTATIONAL METHODS

In the Car-Parrinello (CP) method, the interatomic forces are computed from the instantaneous quantum-mechanical electronic ground state in the Born-Oppenheimer approximation. The electronic ground state corresponding to a given atomic geometry is obtained within the density-functional theory. The exchange-correlation function used in the calculations includes gradient corrections to the local density approximation in the form proposed by Becke and Perdew. Only the valence electrons are taken into account in a pseudopotential approach. The single-particle Kohn-Sham wavefunctions are expanded on a plane-wave basis-set, thus implying the use of periodic boundary conditions (PBC). In the present calculations, the PBC have been applied to a supercell (i.e., the simulation box) containing fragments of a PVA or a PAA chain aligned with one side of the cell. As an example, in the calculations, the fragments of the PVA chains shown in Figure 1(a) are repeated along the chain axis in order to simulate chains of infinite length. This approach allows us to describe a PVA chain as a system with full translational periodicity in one dimension. CP calculations have been successfully performed in the investigation of structural and electronic properties of complex organic molecules. Further tests have been performed here in order to verify the convergence of the calculations with respect to the kinetic energy cutoff (which controls the number of planewaves used in the calculations) as well as to check the methods in the case of simple molecules. As far as the kinetic energy cutoff is concerned, convergence has been achieved by using a value of 22 Ry. Details on the methods and further references are given in Ref. 14.

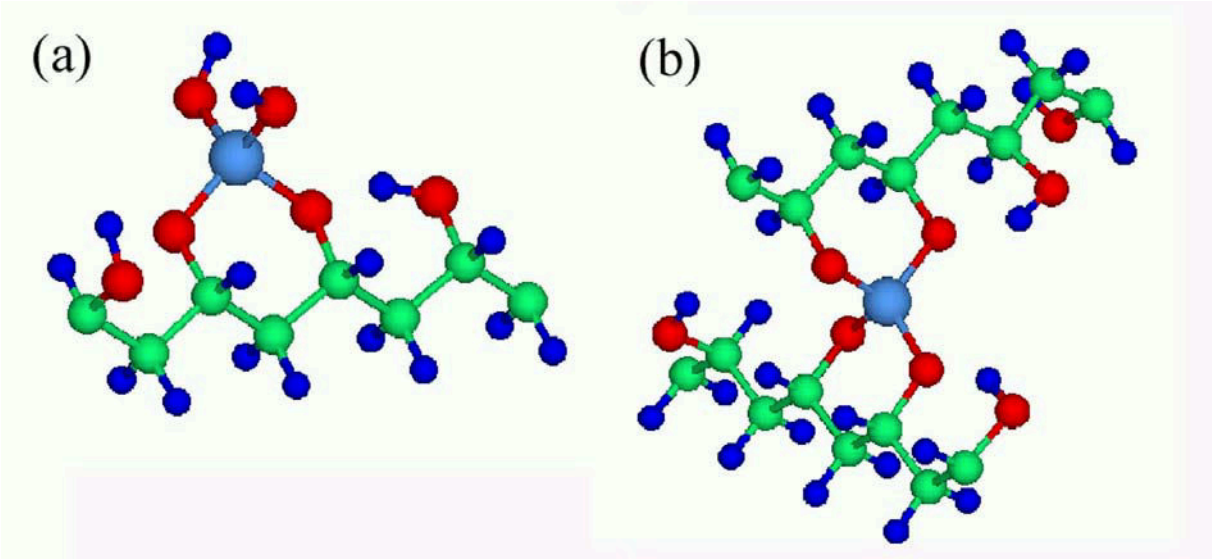

Figure 1. Al-PVA model systems: (a) structure of the $[PVA](O)_2Al(OH)_2^-$, model, (b) structure of the $(2[PVA](O)_2)Al^-$ model. The Al, C, O, and H atoms are identified by the colours cyan, green, red, and blue, respectively

3. RESULTS AND DISCUSSION

A number of model systems have been considered in order to investigate four different cases of crosslinking: i) linkage of PVA chains by Al ions, ii) linkage of PAA chains by Al ions, iii) linkage of PVA chains by Ca ions, and iv) linkage of PAA chains by Ca ions. These cases correspond to crosslinking of polymer chains in the MDF materials formed by: i) PVA and HAC, ii) PAA and HAC, iii) PVA and Portland cements, and iv) PAA and Portland cements, respectively. The model

systems corresponding to the linkage of PVA chains by Al ions are shown in Figure 1. These systems may be produced by polycondensation reactions occurring between the PVA polymer and the $Al(OH)_4^-$ complex coming from the hydrated cement. In the Al-PVA systems of Figure 1, the Al^{3+} ions form two different tetrahedral AlO_4 complexes. In the former complex, two oxygen atoms belong to a PVA chain and two further O atoms belong to hydroxyl groups, thus giving rise to an intrachain linkage, see Figure 1(a). In the latter complex, the O atoms belong to two PVA chains, thus giving rise to an interchain linkage (i.e., a crosslinking of the polymer chains), see Figure 1(b). The polymer fragment with two O atoms interacting with the Al ion will be designated as $[PVA](O)_2^{2-}$ to stress the number of $-O^{-1}$ groups of the fragment involved in the ion-polymer bonding (the $-O^{-1}$ groups come from ionized –OH groups of the chain). Within this convention, the systems of Figure 1 and a fragment of the PVA chain will be designated as $[PVA](O)_2\ Al(OH)_2^-$, $(2[PVA](O)_2)Al^-$ and $[PVA](OH)_2$, respectively. The geometries of the above systems and of the $Al(OH)_4^-$ complex have been optimized by following the atomic forces and by minimizing the total energies. A stable configuration has been found for each system. The strength of the Al-O bonds in the AlO_4 complexes has been then investigated by considering hypothetical reactions of dissociation where the Al-O bonds are broken by producing Al^{3+} and negative ions, e.g.:

$$Al(OH)_4^- \longrightarrow Al^{3+} + 4OH^- \quad (1)$$

The corresponding dissociation energies (D) have been evaluated by differences of total energies (E) of the involved species, e.g.:

$$D = E[Al^{3+}] + 4E[OH^-] - E[Al(OH)_4^-] \quad (2)$$

There are no experimental counterparts for the above reactions of dissociation. Notwithstanding, these reactions have been considered here because they lead to the formation of similar ionic species, thus permitting a comparison of the strength of the Al-O bonds formed in different systems, see Table 1. In the table, negative values of the dissociation energy D indicate endothermic reactions. The dissociation energy per Al-O bond is referred to as D_b.

Table 1. Dissociation energy values, D, calculated for reactions involving molecules and Al-PVA model systems investigated in the present work. D_b is the dissociation energy per Al-O bond. An endothermic reaction is identified by negative values of D and D_b. All values are given in eV

Reaction of dissociation	D	D_b
$Al(OH)_4^- \longrightarrow Al^{3+} + 4OH^-$	-61.0	-15.4
$[PVA](O)_2Al(OH)_2^- \longrightarrow Al^{3+} + [PVA](O)_2^{2-} + 2OH^-$	-60.0	-15.0
$(2[PVA](O)_2)Al^- \longrightarrow Al^{3+} + 2[PVA](O)_2^{2-}$	-60.4	-15.1

The results obtained show that the AlO_4 fragments have quite similar geometries in the $Al(OH)_4^-$ complex and in the Al-PVA systems. The D and D_b values of Table 1 show that the strength of the Al-O bonds in the Al-PVA systems is comparable to that of the corresponding bonds in the stable $Al(OH)_4^-$ complex. In particular, the D and D_b values indicate that Al-O bonds of comparable strength are formed in the cases of intrachain and interchain linkages.

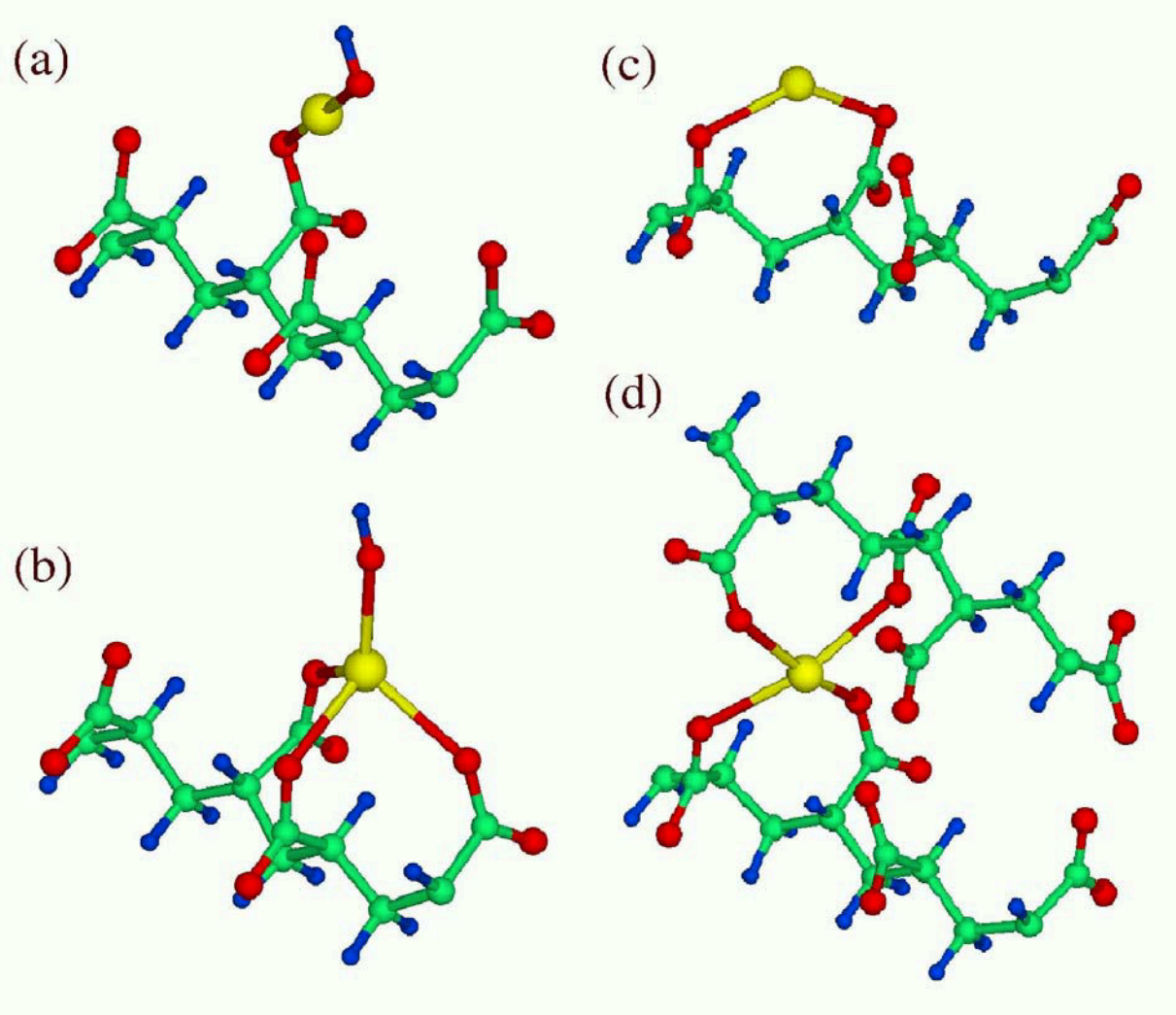

Figure 2. Ca-PAA model systems: (a) and (b) show the structure of the $[PAA](COO)Ca\text{-}OH^{3-}$ system at the beginning and at the end of a geometry-optimization procedure, respectively (see text); (c) intrachain linking in the $[PAA](COO)_2CA^{2-}$ (two Ox.) system; (d) interchain crosslinking in the $(2[PAA](COO)_2)CA^{6-}$ system (a Ca ion is bonded to four O atoms of two PAA chains). The Ca, C, O, and H atoms are identified by the colours yellow, green, red, and blue, respectively

The formation of the above Al-PVA systems has also been investigated by evaluating the energy released in polycondensation reactions involving the $Al(OH)_4^-$ complex and one or two PVA chains. These energies are given by:

$$\Delta E_1 = E\{[PVA](O)_2Al(OH)_2^-\} + 2E\{H_2O\} - E\{[PVA](OH)_2\} - E\{Al(OH)_4^-\} \quad (3)$$

and

$$\Delta E_2 = E\{(2[PVA](O)_2)Al^-\} + 4E\{H_2O\} - 2E\{[PVA](OH)_2\} - E\{Al(OH)_4^-\} \quad (4)$$

The values calculated for ΔE_1 and ΔE_2, -0.28 eV and -1.16 eV, respectively, clearly indicate that an interchain linkage is favored. Thus, the above results strongly support the existence of a crosslinking of the PVA chains by the Al ions.

A similar investigation has been performed in Al-PAA model systems. In this case, a fragment of the polymer chain of the poly(acrylic acid) in anionic form is represented by $[PAA](COO)_2^{-4}$ to stress the number of $-COO^{-1}$ groups of the fragment involved in the ion-polymer bonding (actually, the fragment carries four $-COO^{-1}$ groups). PAA fragments in Ca-PAA model systems are shown in

Figure 2. In the case of the Al-PAA systems, the intrachain and interchain linkages have been simulated by considering the $[PAA](COO)_2Al(OH)_2^{3-}$ and the $(2[PAA](COO)2)Al^{5-}$ systems, respectively. In the former system, the Al^{3+} ion is bonded to two O atoms of a $[PAA]^{4-}$ fragment and to two hydroxyl groups in an atomic arrangement similar to that of Figure 1(a). In the latter system, the Al^{3+} ion is tetrahedrally bonded to the four O atoms of two PAA chains, thus giving rise to an atomic arrangement similar to that of Figure 1(b). The dissociation energies evaluated for these two Al-PAA systems are given in Table 2. In both systems, the D and D_b values are smaller than those found for the Al-PVA systems. Furthermore, they slightly favor an intrachain linkage with respect to the interchain one. These results indicate that a linking of the PAA chains should be produced by the Al ions. However, this crosslinking is expected to be less strong than that produced in the case of the Al-PVA systems.

The interaction of Ca ions with PVA or PAA polymer chains may give rise to more complex atomic arrangements with respect to those found in the Al-PVA and Al-PAA systems. This is related to the tendency of Ca and O atoms to give rise to complexes where a Ca ion coordinates a different number of O atoms also in excess of six. Thus, different configurations of the Ca-PVA and Ca-PAA systems have been investigated, where the number of the coordinated O atoms has been varied by locating several hydroxyl groups close to the Ca ion. For example, D values are reported in Table 3 for the $Ca(OH)_2$ molecule and two $Ca(OH)_4^{2-}$ complexes. In the case of the Ca-PVA systems, the intrachain linkage has been investigated by considering three different models. In the first model, the Ca ion is simply bonded to an O atom of a PVA chain and to an hydroxyl group. The geometry of this system is similar to that shown in Figure 2(a) for the corresponding Ca-PAA system. In the second model, the Ca ion is tetrahedrally bonded to two O atoms of a PVA chain and to two hydroxyl groups. Within the convention used for the Al-PVA systems, the above Ca-PVA systems are designated by $[PVA](O)Ca\text{-}OH$ and $[PVA](O)_2Ca(OH)_2^{2-}$, respectively. Two further hydroxyl groups have been located close to the Ca ion of the $[PVA](O)_2Ca(OH)_2^{2-}$ system in order to reach a sixfold coordination for this ion. However, this last model is unstable.

Table 2. Dissociation energy values, D, calculated for reactions involving the Al-PAA model systems investigated in the present work. D_b is the dissociation energy per Al-O bond. An endothermic reaction is identified by negative values of D and D_b. All values are given in eV

Reaction of dissociation	D	D_b
$[PAA](COO)_2Al\text{-}(OH)_2^{3-} \longrightarrow Al^{3+} + [PAA](COO)_2^{4-} + 2OH^-$	-58.3	-14.6
$(2[PAA](COO)_2)Al^{5-} \longrightarrow Al^{3+} + 2[PAA](COO)_2^{4-}$	-55.8	-13.9

An intrachain linkage can also be recognized in a third model, the $[PVA](O)_2Ca$ model, where the Ca ion is bonded to two O of the same PVA chain, as shown in Figure 2(c) for a similar Ca-PAA model. The interchain linkage has been investigated by considering a $(2[PVA](O))Ca$ model, where two Ca-O bonds are formed by involving two PVA chains, and a $(2[PVA](O))Ca(OH)_2^-$ model which involves two PVA chains and two hydroxyl groups bonded to the Ca ion. In detail, the geometry of the $(2[PVA](O))Ca(OH)_2^-$ system is characterized by an almost planar CaO_4 fragment where two O atoms are provided by the PVA chains and two further O atoms belong to hydroxyl groups. Even in the case of interchain linkages, model systems where the Ca ion is coordinated, sixfold are unstable.

The dissociation energies of the above model systems are reported in Table 3. The D values reported in the table show a general tendency of the Ca ion to bind four O atoms. The D value corresponding to the intrachain linkage recognized in the $[PVA](O)_2Ca(OH)_2^{2-}$ model is close to the D values of the $Ca(OH)_4^{2-}$ complexes and larger than the values estimated for the interchain systems, i.e., the $(2[PVA](O))Ca$ and $(2[PVA](O))Ca(OH)_2^{2-}$ systems. Furthermore, the D_b values

indicate that the more stable Ca-O bonds are formed when the Ca ion is bonded to only two O atoms. In that case, the D_b values of the Ca-PVA systems approach the value estimated for the bonds in the $Ca(OH)_2$ molecule. All the above results indicate that the models realizing a crosslinking of the PVA chains must compete with a more stable intrachain Ca-PVA system and the $Ca(OH)_4^{2-}$ complexes. It is expected, therefore, that the crosslinking of PVA chains by Ca ions is less efficient than that realized by Al^{3+} ions.

Finally, the results achieved for the Ca-PAA model systems are reported in Table 4. In the first system investigated, $[PAA](COO)Ca\text{-}OH^{3-}$, a Ca^{2+} ion is bonded to an O atom of the $[PAA](COO)_4^{2-}$ fragment and to an OH^- group. Figure 2(a) and 2(b) show the geometry of this system at the beginning and at the end of the geometry-optimization calculation, respectively. These figures show, once more, a tendency of the Ca ion to bind four O atoms. In a second system, $[PAA](COO)_2Ca^{2-}$ (two Ox.), the Ca ion is bonded to two O atoms belonging to the carboxylate anions of a same PAA chain, thus realizing an intrachain O-Ca-O linking, see Figure 2(c). In the third model system, $(2[PAA](COO)_2)Ca^{6-}$, the Ca atom is bonded to four O atoms of two PAA chains, thus realizing an interchain O_2-Ca-O_2 linkage, see Figure 2(d). In this system, the relative positions of the two polymer chains have been chosen to permit the interaction of the Ca ions with more than two O atoms. At the beginning of the geometry-optimization procedure the Ca atom is bonded to two O atoms only, which belong to different PAA chains. As the geometry of the system is fully relaxed by following the atomic forces, two further O atoms move toward the Ca atom, thus leading to the formation of a CaO_4 fragment. Further model systems have been investigated to analyze the effects of OH^- ions and higher coordination numbers of the Ca atom on the stability of the intrachain and interchain linking. In the case of intrachain linking, the $[PAA](COO)_2Ca(OH)_2^{4-}$ system has been considered, which can be derived from the $[PAA](COO)_2Ca^{2-}$ (two Ox.) system of Figure 2(c) when two OH^- ions are bonded to the Ca ion. In the case of the interchain linking, a $(2[PAA](COO)_2)Ca(OH)_2^{8-}$ system has been also investigated which derives from the $(2[PAA](COO)_2)Ca^{6-}$ system of Figure 2(d) when two OH^- ions are bonded to the Ca ion. The optimized geometry of this system presents a distorted octahedral configuration for a CaO_6 complex where the four O atoms of the PAA chains form the square basis of the octahedron and the O atoms of the OH^- ions occupy the two remaining vertexes of the octahedron. It is worth noting that the $(2[PAA](COO)_2)Ca(OH)_2^{8-}$ system is metastable with respect to the $(2[PAA](COO)_2)Ca^{6-}$ system, as shown by the reaction of dissociation

$$(2[PAA](COO)_2)Ca(OH)_2^{8-} \longrightarrow (2[PAA](COO)_2)Ca^{6-} + 2OH^- \quad (5)$$

which results to be exothermic with a D value of +1.4 eV.

Table 3. Dissociation energy values, D, calculated for reactions involving molecules and Ca-PVA model systems investigated in the present work. D_b is the dissociation energy per Ca-O bond. An endothermic reaction is identified by negative values of D and D_b. All values are given in eV

Reaction of dissociation	D	D_b
$Ca(OH)_2 \longrightarrow Ca^{2+} + 2OH^-$	-16.7	-8.4
$Ca(OH)_4^{2-}$ (planar) $\longrightarrow Ca^{2+} + 4OH^-$	-20.4	-5.1
$Ca(OH)_4^{2-}$ (tetr.) $\longrightarrow Ca^{2+} + 4OH^-$	-20.4	-5.1
$[PVA](O)Ca\text{-}OH \longrightarrow Ca^{2+} + [PVA](O)^{1-} + OH^-$	-15.4	-7.7
$[PVA](O)_2[PVA](OH)_2^{2-} \longrightarrow Ca^{2+} + [PVA](O)_2^{2-} + 2OH^-$	-20.1	-5.0
$[PVA](O)_2Ca \longrightarrow Ca^{2+} + [PVA](O)_2^{2-}$	-14.5	-7.3
$(2[PVA](O))Ca \longrightarrow Ca^{2+} + 2[PVA](O)^-$	-13.9	-6.9
$(2([PVA](O))Ca(OH)_2^{2-} \longrightarrow Ca^{2+} + 2[PVA](O)^- + 2OH^-$	-18.8	-4.7

For what concerns the stability of the above Ca-PAA systems, in the case of intrachain linking the tendency of the Ca ion to coordinate more than two O atoms, already shown by the evolution of the $[PAA](COO)Ca\text{-}OH^{3-}$ geometry, is confirmed by the large negative D value of the $[PAA](COO)_2Ca(OH)_2^{4-}$ system. On the other hand, an analysis of the D_b values corresponding to the above systems shows that the the $[PAA](COO)_2Ca^{2-}$ (two Ox.) system of Figure 2(c) has the most stable Ca-O bonds, that is, this system is quite stable once it is formed. For what concerns the interchain linking, the $(2[PAA](COO)_2)Ca^{6-}$ system has the larger negative D and D_b values with respect to the $(2[PAA](COO)_2)Ca(OH)_2^{8-}$ system. An overall analysis of the results given in Table 4 shows that the D value corresponding to the $(2[PAA](COO)_2)Ca^{6-}$ system is the largest negative value, thus indicating that the formation of this system is favored with respect to the other systems involving PAA chains and the molecular complexes formed by Ca and hydroxyl ions (see Table 3). In particular, the interchain O-Ca-O linking results to be more stable than the intrachain linking. The above results support therefore the existence of a crosslinking of PAA chains by Ca ions. Further support comes from a detailed analysis of the D_b values of Table 4. Although these values indicate that each Ca-O bond formed in the $(2[PAA](COO)_2)Ca^{6-}$ system (D_b = -5.6 eV) is weaker than a single Ca-O bond formed in the $Ca(OH)_2$ molecule (D_b = -8.4 eV) or in the $[PAA](COO)_2Ca^{2-}$ (two Ox.) system (D_b = -7.3 eV), the breaking of the crosslink between two polymer chains implies (at least) the breaking of two Ca-O bonds because the Ca ion is anchored to four points of two PAA chains (two points for each chain), see Figure 2(d). This process requires an energy of -11.2 eV, thus stabilizing the crosslinking of the PAA chains.

Table 4. Dissociation energy values, D, calculated for reactions involving different Ca-PAA model systems investigated in the present work. D_b is the dissociation energy per Ca-O bond. An endothermic reaction is identified by negative values of D and D_b. All values are given in eV

Reaction of dissociation	D	D_b
$[PAA](COO)Ca\text{-}OH^{3-} \longrightarrow Ca^{2+} + [PAA](COO)_2^{4-} + OH^-$	-18.6	-4.6
$[PAA](COO)_2Ca^{2-}$ (two ox.) $\longrightarrow Ca^{2+} + [PAA](COO)_2^{4-} + 2OH^-$	-14.7	-7.3
$[PAA](COO)_2Ca(OH)_2^{4-} \longrightarrow Ca^{2+} + [PAA](COO)_2^{4-} + 2OH^-$	-19.2	-4.8
$(2[PAA](COO)_2)Ca^{6-} \longrightarrow Ca^{2+} + 2[PAA](COO)_2^{4-}$	-22.4	-5.6
$(2[PAA](COO)_2)Ca(OH)_2^{8-} \longrightarrow Ca^{2+} + 2[PAA](COO)_2^{4-} + 2OH^-$	-21.0	-3.5

4. CONCLUSIONS

An analysis of the D and D_b values calculated for all the model systems investigated in the present study indicates that the Al ions realize stronger crosslinking than the Ca ions with both PVA and PAA chains. This result agrees with the general properties of the Al and Ca elements. It reflects indeed the different strength of the Al-O and Ca-O bonds as shown, e.g., by the different D values estimated in the case of the $Al(OH)_4^-$ and $Ca(OH)_2$ molecules. Moreover, present results show that the potential capability of the Ca ion to reach higher coordination numbers with respect to the Al ion does not affect the relative strength of the bonds formed by the two ions with the O atoms, in the systems investigated. The Al-PVA crosslinking is also stronger than the Al-PAA one. In the case of Ca-polymer systems, the PAA crosslinking results are stronger than the PVA crosslinking. The above results suggest the following relative strengths of the polymer-chain crosslinking: Al-PVA > Al-PAA > Ca-PAA > Ca-PVA. This theoretical estimate of the strength of polymer-chain crosslinking is consistent with the different mechanical properties observed in the cases of high-alumina cement and Portland cement MDFs formed with PVA and PAA polymers, thus suggesting that crosslinking plays a significant role in the realization of MDFs materials with peculiar mechanical properties. Furthermore, the different strength of the Al-O and Ca-O bonds may account for the differences observed in the material processing of HAC-PVA and Portland-PAA

MDFs. In the former case, high activation energy is expected for the crosslinking reactions. This agrees with the fact that crosslinking is realized only in presence of the mechanical work performed during the mixing process. In the latter case, lower activation energies should be required for the crosslinking reactions, thus inducing a fast crosslinking of the polymer chains. This can explain the difficulties experienced in obtaining a workable paste during material processing.

REFERENCES

[1] Birchall, J.D., Howard, A.J. and Kendall, K. Flexural strength and porosity of cements, Nature, Vol. 289, 1981, pp. 388-389.

[2] Kendall K. and Birchall, J. D. Porosity and its relationship to the strength of hydraulic cement pastes, Mater. Res. Soc. Symp. Proc., Vol. 42, 1985, pp. 143-150.

[3] Della Roy, M. Advanced cement systems, including CBC, DSP, MDF, 9th Int. Congress on the Chemistry of Cement, New Delhi, 1992, Vol. 1, pp. 357.

[4] Lewis, A.J. and Kriven, M.W. Microstructure-property relationships in Macro-Defect-Free cement, MRS Bulletin, March 1993, p. 72.

[5] Popoola, O.O., Kriven, W.M. and Young, J.F. Microstructural and microchemical characterization of a Calcium Aluminate-Polymer composite (MDF cement), J. Am. Ceram. Soc., Vol. 74, 1991, p. 1928.

[6] Popoola, O.O. and Kriven, W.M. Interfacial structure and chemistry in a ceramic/polymer composite material, J. Mater. Res., Vol. 7, 1992, p. 1545.

[7] Rodger, S.A., Sinclair, W., Groves, G.W., Brooks, S.A. and Double, D.D. High strength cement pastes: Part 2 Reactions during setting, J. Mat. Sci., Vol. 20, 1985, p. 2853.

[8] Rodger, S.A., Sinclair, W., Groves, G.W., Brooks, S.A. and Double, D.D. Reactions in the setting of high strength cement pastes, Mater. Res. Sym. Proc., Vol. 42, 1985, p. 45.

[9] Harsh, S., Naidu, Y.C. and Ghosh, S.N. Chemical interaction between PVA and hydrating HAC: infrared spectroscopy and thermoanalytical investigations, 9th Int. Congress on the Chemistry of Cement, New Delhi, 1992, Vol. 3, p. 406.

[10] Tan, L.S., McHugh, A.J., Gulgun, M.A. and Kriven, W.M. Evolution of mechano-chemistry and microstructure of a calcium aluminate-polymer composite: Part II. Mixing rate effects, J. Mater. Res., Vol. 11, 1996, p. 1739.

[11] Ohama, Y., Demura, K. and Kobayashi, T. A few techniques for improvement in water resistence of macro-defect-free cements, Proceedings of Maeta Workshop on High Flexural polymer-Cement Composite, Sakata (Japan), 1996, pp. 69-77.

[12] Amore Bonapasta, A., Buda, F. and Colombet, P. Cross-linking of Poly(vinyl alcohol) chains by Al ions in Macro-Defect-Free cements: a theoretical study, Chemical Materials, Vol. 12, 2000, p. 738.

[13] Amore Bonapasta, A., Buda, F. and Colombet, P. Interaction between Ca ions and Poly(acrylic acid) chains in Macro-Defect-Free cements: a theoretical study, Chem. Mater., Vol. 13, 2001, p. 64.

[14] Amore Bonapasta, A., Buda, F., Colombet, P. and Guerrini, G.L. Cross-linking of Poly(vinyl alcohol) chains by Ca ions in Macro-Defect-Free cements, Chem. Mater., Vol. 14, 2002, p. 1016.

[15] Guerrini, G.L. private communication.

[16] Shuguang, H. The increasing strength mechanism of the role of the interfacial bond in MDF cement, 9th Int. Congress on the Chemistry of Cement, New Delhi, 1992, Vol. 3, p. 393.

[17] Shuguang, H. XPS nondestructive depth analysis method and its application in cement based composite materials, Cem. Concr. Res., Vol. 24, 1994, p. 1509.

[18] Car, R. and Parrinello, M. Unified approach for Molecular Dynamics and Density-Functional Theory, Phys. Rev. Lett., Vol. 55, 1985, p. 2471.

(*) To whom correspondance should be addressed

MINERALOGICAL COMPOSITION OF CLINKER BY BOGUE AND RIETVELD METHOD: THE EFFECT OF MINOR ELEMENTS

Umberto Costa[1]* and Maurizio Marchi[1]

[1]CTG – Italcementi Group, Via G. Camozzi, 124, 24121 Bergamo, Italy. E-mail: u.costa@itcgr.net

ABSTRACT

Quantitative phase analysis by means of X-ray powder diffraction performed using the Rietveld method (hereinafter QXPA) has been applied to a large number of industrial clinkers produced at different plants. The results have been compared with those obtained by calculation methods based on chemical analysis, such as the Bogue method. QXPA usually gives higher C_3S and lower C_2S values than those derived by Bogue. Regarding the composition of the aluminate phases, when only cubic C_3A is present, QXPA values are lower than Bogue values; the opposite is observed when also C_3A orthorhombic polymorph is found. In those samples having a high C_3A content, the C_4AF content is lower than the one calculated by Bogue. Differences between the mineralogical composition obtained by QXPA and by the calculation methods seem to be strongly dependent on the alkali and sulfate contents in the clinker. Moreover, a good correlation has been found between the sulfate module and the C_3S/C_2S and C_3A/C_4AF content ratios obtained by QXPA.

1. INTRODUCTION

Knowledge of the mineralogical composition of clinker is necessary to predict and justify clinker performances. In the cement industry, the most currently used method to estimate the mineralogical composition of clinker is the Bogue calculation [1] based on chemical analysis. It has been stated that the Bogue calculation gives approximate results because equilibrium is not reached during clinker cooling. In addition, the four major phases contain foreign ions, and in such a way, the compositions assumed for the phases are inaccurate [2,3]. Optical microscopy, either by visual linear analysis [4] or by point counting, is the most widely adopted experimental method for the quantitative determination of the mineralogical composition of clinker. This method has however some disadvantages. It is time-consuming (at least a thousand points need to be considered) and operator-dependent, and some difficulties may arise when determining the aluminate phases (C_3A, C_4AF). Actually, since their micro-crystallinity may sometimes make them insufficiently resolved, the aluminate phases are usually quantified as a group and reported as "interstitial phase".

In recent years the alternative use of X-ray powder diffraction associated with the Rietveld method has gained ground.

The Rietveld method [5] is a full-profile fitting method, basically consisting of calculating a theoretical diffraction pattern starting from the crystallographic information gained from the existing phases (space groups, cell parameters, atomic co-ordinates, thermal parameters) and from instrumental information. The calculated pattern is then optimized through an iterative calculation procedure in order to obtain the best possible fit to the experimental diffraction pattern.

Originally conceived for structural analysis, the method has been applied by Bish and Howard [6] to the quantitative phase analysis by means of X-ray powder diffraction (QXPA).

Proceedings of the 11th International Congress on the Chemistry of Cement (ICCC) 11 - 16 May 2003, Durban, South Africa
'Cement's Contribution to the Development in the 21st Century' ISBN Number: 0-9584085-8-0
Hosted by: The Cement and Concrete Institute of South Africa Editors: Dr G. Grieve and G. Owens
CD-ROM produced by: Document Transformation Technologies Congress Organised by: Event Dynamics

Compared to traditional methods, this technique presents a host of advantages: internal standards or calibration curves are not required and the severe peak overlapping and preferred orientation problem don't affect the results.

Moreover, additional information – cell parameters for example - are available, which can provide useful indications of possible atomic substitutions in the crystalline phases caused by the formation of solid solutions.

The Commission on Powder Diffraction of IUCr [7] has recently promoted a round robin test for the purpose of comparing various methods known as "full profile fitting" and obtaining analytical uncertainty data.

Several examples of QXPA application to determine the mineralogical composition of cements [8,9,10,11,12] are available in the literature. Differences between the composition obtained by QXPA and that calculated according to Bogue have always been found.

The present study was carried out on a large number of clinkers and provided important information on aluminate phase composition of industrial clinkers produced in different plants with a large variability of raw materials and fuels.

2. EXPERIMENTAL

Diffraction patterns have been collected using a SIEMENS D-5000 diffractometer with the instrumental Bragg-Brentano geometry equipped with a Cu-tube (λ 1.5456 Å) and a graphite monochromator on the diffracted beam.

The experimental conditions were: tube power of 40KV, 40mA, fixed divergence and anti-scattering slits equal to 1°, receiving slit aperture of 0.1 mm, sample holder spinning of 30 rpm.
Diffraction patterns were collected from 10 to 70° 2θ, at a scanning step of 0.02° 2θ and counting time of 12 s/step.

Clinker samples were finely ground to pass the 45-μm sieve and loaded on an aluminum sample holder, devised for side loading, for the purpose of minimizing preferred orientation effects.
Rietveld refinements were carried out using TOPAS software from Bruker AXS [13]. The phase structural models used to perform the refinements are summarized in table 1.

Table 1. Crystallographic data of the main clinker phases used in refining operations

Name	Space Group	References
C_3S M1/M3	Monoclinic, C m	[14]
C3S M3	Monoclinic, C m	[15]
β-C_2S	Monoclinic, P $2_1/n$	[16]
C_4AF	Orthorhombic, I bm2	[17]
C_3A	Cubic, P a3	[18]
Na-C_3A	Orthorhombic, P bca	[19]

The background was modeled by a Chebyshev polynomial with six refinable coefficients; the 2θ zero shift and the unit cell parameters, crystallite size and scale factors for all phases were simultaneously refined. The preferred orientation of alite in all samples was also considered by using spherical harmonic correction [20]. For the ferrite phase, also the aluminum and iron phase

fractions in the octahedral and tetrahedral sites were refined in the final step, using soft constraints to maintain the sum in each site equal to one.

3. RESULTS

To better recognize the ranges within which the chemical composition of the clinkers is found to vary, table 2 indicates average, maximum, and minimum values of some of the main compositional parameters.

Table 2. Variability of chemical parameters of clinkers

SR			AR			LSF			Msulf		
MIN	MAX	Mean	MIN	MAX	Mean	MIN	MAX	Mean	MIN	MAX	Mean
2.0	4.1	2.6	0.9	2.7	1.6	88.3	100.5	96.4	0.1	2.9	1.2

SR= silica ratio; AR= alumina ratio; LSF= lime saturation factor; M_{sulf}= sulfate modulus

Tables 3 and 4 summarize the silicate and aluminate contents as derived from Bogue and Newkirk calculations [21] and by QXPA. Compared to Bogue, the Newkirk method is an attempt to refine the calculation of the aluminate phase composition, by distinguishing the cubic and orthorhombic polymorphs of C_3A, the latter designated by the NC_8A_3 formula.

Table 3 Silicate contents obtained by different methods

	C3S				C2S			
IDENTIF.	Bogue	Newkirk	QXPA	Δ*	Bogue	Newkirk	QXPA	Δ*
Sample1	54.2	53.7	52.5	*-1.7*	21.7	21.8	27.4	*5.7*
Sample2	56.0	53.3	51.3	*-4.8*	19.7	21.5	30.8	*11.1*
Sample3	58.9	60.3	65.1	*6.2*	18.0	24.6	11.2	*-6.8*
Sample4	52.1	53.0	58.6	*6.6*	24.5	27.3	19.5	*-5.0*
Sample5	58.8	59.3	65.8	*7.0*	17.7	17.9	14.5	*-3.2*
Sample6	67.2	66.6	69.6	*2.4*	6.5	6.7	7.8	*1.3*
Sample7	66.6	65.9	70.4	*3.8*	11.4	11.7	11.4	*0.0*
Sample8	68.7	69.5	71.0	*2.3*	11.3	15.8	9.2	*-2.1*
Sample9	63.0	62.9	70.6	*7.6*	15.7	15.4	13.3	*-2.4*
Sample10	55.4	56.0	59.7	*4.3*	19.7	14.6	16.7	*-3.1*
Sample11	59.7	59.1	64.5	*4.8*	18.9	19.0	18.1	*-0.7*
Sample12	67.0	66.3	69.1	*2.1*	11.9	12.1	12.3	*0.4*
Sample13	61.9	61.3	65.1	*3.2*	19.4	19.5	21.3	*1.8*
Sample14	60.6	60.1	65.7	*5.1*	16.8	16.8	18.4	*1.6*
Sample15	45.6	45.8	49.6	*4.0*	31.9	34.3	31.6	*-0.3*
Sample16	63.1	64.4	69.3	*6.1*	14.3	26.0	7.5	*-6.7*
Sample17	45.4	42.9	47.1	*1.7*	27.5	29.1	32.8	*5.4*
Sample18	72.0	72.2	71.8	*-0.2*	5.3	15.0	6.0	*0.7*
Sample19	70.5	71.3	72.5	*2.0*	6.9	14.5	4.2	*-2.6*
Sample20	63.1	63.7	66.7	*3.6*	18.3	28.5	16.8	*-1.5*
Sample21	60.8	61.0	69.0	*8.2*	15.1	16.6	9.3	*-5.8*
Sample22	54.0	55.2	58.0	*4.0*	22.1	25.6	18.4	*-3.8*
Sample23	61.6	59.8	62.1	*0.4*	13.0	14.1	16.9	*3.9*
Sample24	70.2	68.4	67.9	*-2.3*	7.6	8.6	14.5	*6.9*
Sample25	58.0	58.9	62.6	*4.5*	16.9	21.7	12.5	*-4.3*
Sample26	63.9	62.0	67.5	*3.7*	12.1	13.1	14.0	*1.9*
Sample27	61.0	59.1	66.0	*5.1*	14.9	16.0	15.3	*0.4*
Sample28	60.5	62.1	52.0	*-8.5*	18.1	22.7	29.3	*11.1*
Sample29	65.9	64.7	69.7	*3.8*	10.2	10.8	10.3	*0.1*
Sample30	62.4	64.2	70.5	*8.1*	15.1	7.0	8.9	*-6.3*
Sample31	68.3	68.4	73.4	*5.1*	11.9	21.9	10.2	*-1.7*
Sample32	69.7	69.8	69.5	*-0.2*	7.4	14.0	6.9	*-0.5*
Sample33	61.9	61.1	61.1	*-0.8*	15.5	15.8	20.3	*4.7*
Sample34	63.2	62.4	62.8	*-0.4*	11.9	12.2	16.7	*4.8*
Sample35	69.8	67.2	77.8	*8.0*	8.7	10.3	8.6	*-0.1*
Sample36	50.0	53.9	60.8	*10.8*	21.5	18.5	19.4	*-2.1*
Sample37	59.0	62.6	62.1	*3.1*	16.1	7.7	17.7	*1.6*
Sample38	63.3	66.3	72.7	*9.3*	9.8	7.6	5.9	*-4.0*
Sample39	60.2	62.7	66.3	*6.1*	12.8	10.9	12.3	*-0.5*
Sample40	59.1	59.5	71.0	*11.9*	17.0	9.5	11.1	*-5.9*
Sample41	60.0	62.1	66.3	*6.3*	16.8	22.7	9.6	*-7.2*
Sample42	60.0	59.2	64.0	*4.0*	16.9	24.5	10.8	*-6.1*
Sample43	57.1	60.7	64.4	*7.3*	17.7	18.0	11.9	*-5.8*
Sample44	57.1	57.7	63.6	*6.5*	17.7	12.3	14.1	*-3.6*
Sample45	66.6	63.4	64.2	*-2.4*	10.7	12.8	18.3	*7.6*
Sample46	58.6	58.8	63.4	*4.7*	17.3	29.1	15.1	*-2.3*
Sample47	55.9	54.9	59.8	*4.0*	21.9	22.3	22.4	*0.5*

* Difference between QXPA and Bogue values

Table 4. Aluminate contents obtained by different methods

	BOGUE	NEWKIRK		QXPA		C4AF		
IDENTIF.	C3A	C3A	NC8A3	C3A cub	C3A ortho	Bogue	Newkirk	QXPA
Sample1	11.2	11.2	0.0	11.9	0.0	7.3	7.3	6.4
Sample2	11.5	11.5	0.0	10.3	0.0	8.0	8.0	6.1
Sample3	10.0	8.9	1.0	1.1	13.8	9.4	9.4	7.7
Sample4	9.4	8.9	0.4	4.8	8.3	9.7	9.7	8.1
Sample5	9.0	7.3	1.6	7.7	2.2	9.5	9.5	9.0
Sample6	11.2	11.2	0.0	7.6	0.0	8.9	8.9	11.7
Sample7	6.6	6.6	0.0	3.1	0.0	9.7	9.7	12.3
Sample8	7.9	7.8	0.0	2.6	6.9	7.8	7.8	9.0
Sample9	9.0	9.0	0.0	2.6	0.0	7.3	7.3	10.6
Sample10	11.8	11.8	1.5	11.0	4.7	6.7	6.7	4.2
Sample11	8.9	8.9	0.0	8.5	0.0	6.0	6.0	6.3
Sample12	7.0	7.0	0.0	2.0	0.0	8.5	8.5	13.0
Sample13	3.6	3.6	0.0	1.9	0.0	10.5	10.5	10.3
Sample14	6.5	6.5	0.0	3.7	0.0	10.1	10.1	11.6
Sample15	6.4	6.4	0.6	3.0	3.0	10.9	10.9	11.6
Sample16	11.3	9.4	1.8	3.1	12.9	7.3	7.3	5.8
Sample17	10.9	10.9	0.0	9.0	0.0	8.1	8.1	8.3
Sample18	7.1	6.9	0.0	2.4	3.8	12.5	12.5	16.0
Sample19	7.1	6.7	0.3	4.1	5.1	12.3	12.3	14.1
Sample20	4.2	2.7	1.4	0.2	4.5	7.4	7.4	6.9
Sample21	10.5	10.4	0.0	9.0	2.7	7.9	7.9	8.0
Sample22	5.4	4.4	0.9	0.0	7.7	12.9	12.9	13.7
Sample23	9.4	9.4	0.0	10.6	0.0	7.1	7.1	6.2
Sample24	5.0	5.0	0.0	2.1	0.0	11.1	11.1	13.2
Sample25	10.1	9.9	0.1	9.3	5.2	9.6	9.6	9.9
Sample26	8.1	8.1	0.0	2.6	0.0	10.4	10.4	13.8
Sample27	8.5	8.5	0.0	2.8	0.0	9.4	9.4	14.1
Sample28	6.4	6.4	0.0	5.8	0.0	12.7	12.7	12.9
Sample29	8.3	8.3	0.0	6.4	0.0	8.9	8.9	10.5
Sample30	10.2	10.1	0.0	4.8	8.6	7.9	7.9	6.5
Sample31	2.2	2.2	0.0	1.6	0.0	12.2	12.2	13.2
Sample32	5.9	5.8	0.0	3.4	1.9	13.4	13.4	17.1
Sample33	6.7	6.7	0.0	3.7	0.0	10.4	10.4	12.7
Sample34	9.3	9.3	0.0	6.7	0.0	9.1	9.1	11.5
Sample35	7.6	7.6	0.0	3.4	0.0	7.5	7.5	8.8
Sample36	8.4	8.4	0.1	6.1	0.0	9.8	9.8	10.1
Sample37	8.6	8.2	0.3	5.0	3.1	9.9	9.9	9.5
Sample38	8.0	8.0	0.0	4.7	0.0	10.8	10.8	14.2
Sample39	9.8	9.8	0.0	9.8	0.0	9.8	9.8	11.2
Sample40	7.3	7.1	0.0	2.9	2.4	10.0	10.0	11.6
Sample41	8.6	4.4	4.1	1.8	13.7	9.2	12.7	5.9
Sample42	9.8	8.1	1.2	3.9	9.0	9.3	9.2	10.8
Sample43	8.8	9.7	0.0	6.8	7.7	11.3	9.3	8.4
Sample44	8.8	8.2	0.5	4.4	2.5	11.3	11.3	14.6
Sample45	6.4	6.4	0.0	2.6	0.0	10.0	10.7	12.2
Sample46	9.2	9.1	0.0	3.3	5.4	10.0	10.0	11.6
Sample47	7.8	7.8	0.0	5.7	0.0	10.8	10.8	11.0

By taking the results obtained by Rietveld method as a reference, the following statements can be made in comparison to Bogue calculations:

a) The C_3S content obtained by QXPA is on average 5% greater, with 14 cases for which the deviation is greater than the average (as high as 12%). Only 5 samples evidenced C_3S-Bogue values overestimated with respect to QXPA.
b) The C_2S content, as is logical, is correspondingly on average 3% lower than Bogue.
c) The C_3A content is generally underestimated by around 2-3% except if orthorhombic C_3A occurs, in which case the Rietveld method identifies C_3A contents greater than 3%.
d) The C_4AF content is more or less in good agreement with the calculated one, except in those samples having a high C_3A content, where lower values were found.

As a whole, the contents in C_3S and C_2S calculated after Newkirk reproduce the same results as those obtained with Bogue. Concerning C_3A, no better agreement with the QXPA results was observed.

4. CORRELATION STUDY

A correlation analysis between minor element contents (mainly alkalis and sulfur) and mineralogical composition obtained by QXPA has been tried.

For this investigation, the parameter considered was the sulfate module (M_{sulf}), calculated according to the formula:

$$M_{sulf} = SO_3/(1.29Na_2O+0.85K_2O) \quad (1)$$

$M_{sulf} \geq 1$ immediately indicates the potential combination of the alkalis occurring in the clinker as sulfates. On the other hand, values smaller than one would indicate stoichiometric alkali excess with respect to SO_3 becoming available for the formation of solid solutions in the clinker phases.

The replacement of calcium ions by alkalis in the crystalline lattice of C_3A may be very wide and lead to structural modifications [19]. Beyond a certain replacement limit, the cubic structure of C_3A becomes orthorhombic. This transition is easily detected by X-Ray diffraction, which is also capable of distinguishing between the two forms when they coexist.

The formation of orthorhombic C_3A, whenever availability of alkalis occurs, is confirmed by the results of the quantitative analysis performed on the clinkers. Figure 1 gives the contents in orthorhombic C_3A as determined by QXPA on clinkers, whose sulfate module varies within a wide range (0.2-2.9). As can be observed, the presence of orthorhombic C_3A is efficaciously detected when the sulfate module is smaller than one. It is also apparent how this C_3A polymorph progressively increases as the sulfate module decreases.

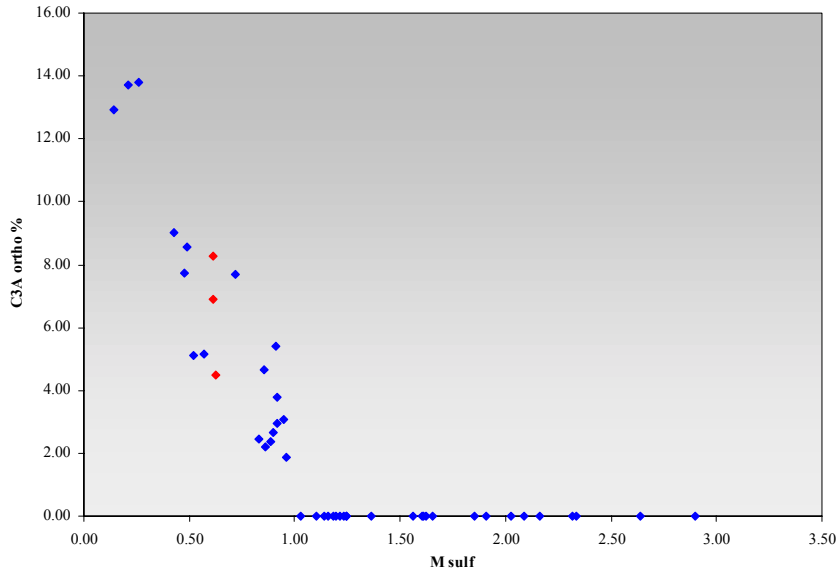

Figure 1. Trend of orthorhombic C_3A content as a function of the sulfate module

The relatively wide range within which the C_3A content is found to vary at equal sulfate module may be due to the influence exerted by AR, which is not constant across the different samples.
In fact, considering the three clinkers marked in red on the chart, and having a M_{sulf} equal to 0.6, it can be observed how the orthorhombic C_3A content may vary from 4.5 to 8.3 and AR from 1.29 to 1.76.

With a view to thoroughly understand how the sulfate module affects the mineralogical composition of the clinker, we should more opportunely consider clinkers characterized by compositions falling

within narrow ranges; for this purpose in the correlation study, we have considered only clinkers showing an AR of 1.7-1.8 and a LSF of 95-96.

The charts given in figures 2 and 3 illustrate the phase composition as identified by QXPA and expressed as weight ratios of C_3A/C_4AF and C_3S/C_2S respectively versus the sulfate module. The same charts show a horizontal line, which corresponds to the theoretical ratios according to Bogue calculation for clinkers having AR and LSF falling in the selected range.

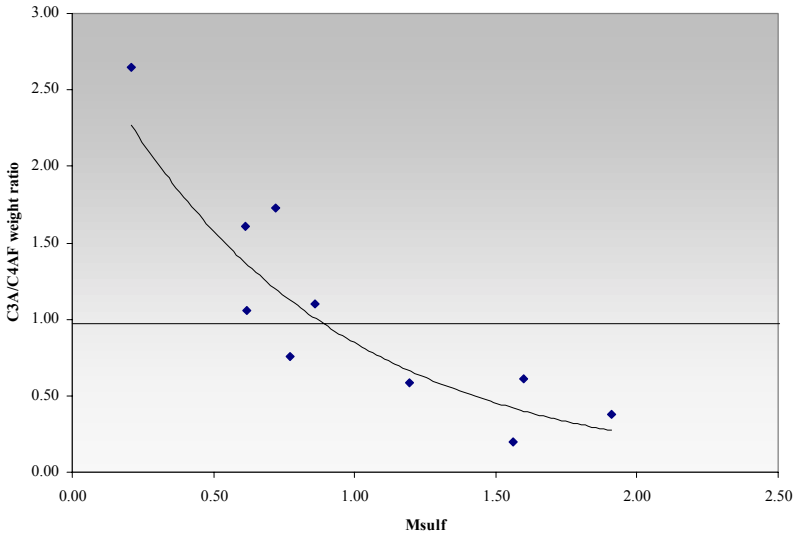

Figure 2. Trend of the C_3A/C_4AF weight ratio obtained by QXPA as a function of the sulfate module

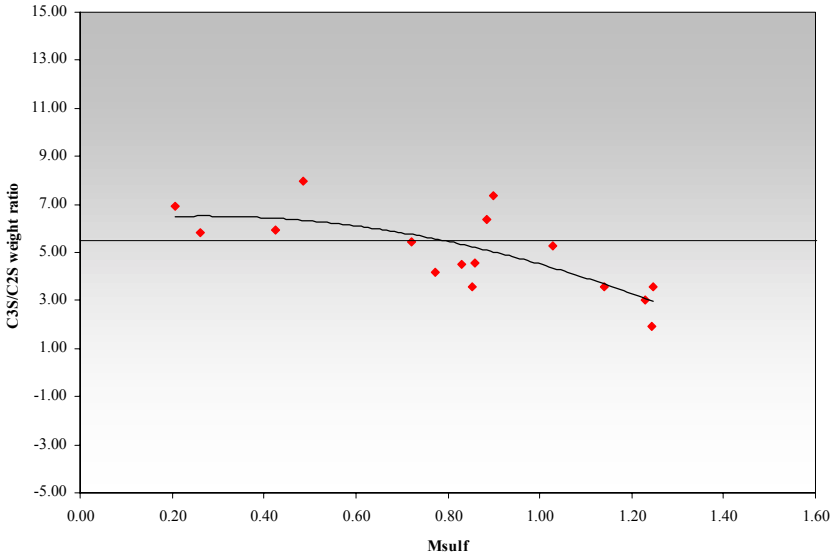

Figure 3. Trend of the C_3S/C_2S weight ratio obtained by QXPA as a function of the sulfate module

Figure 2 shows that, compared to a theoretical C_3A/C_4AF weight ratio of 0.97 that corresponds to an AR of 1.75, the experimental ratios tend to increase as the sulfate module decreases. If M_{sulf} is greater than one, then the C_3A/C_4AF ratio is lower than the theoretical ratio. If M_{sulf} is smaller than one, the C_3A/C_4AF ratio increases progressively until it becomes 2.5 times greater than the theoretical one. The curve that interpolates the experimental data intersects the reference line when M_{sulf} is about one.

The increase in the aluminate/ferrite ratio is linked to the formation of orthorhombic C_3A, which is probably promoted by thermodynamic effect.

The increase in C_3A content also affects the Al/Fe molar ratio of the ferritic phase. Figure 4 shows that for clinkers with a sulfate module smaller than 1, Al in the ferritic phase is less than in the C_4AF composition normally assumed in the Bogue calculation. This may be explained by the Al input that is needed for the formation of a larger amount of orthorhombic C_3A.

The opposite occurs when the sulfate module is greater than one, that is – as previously seen – when the amount of C_3A formed is less than expected.

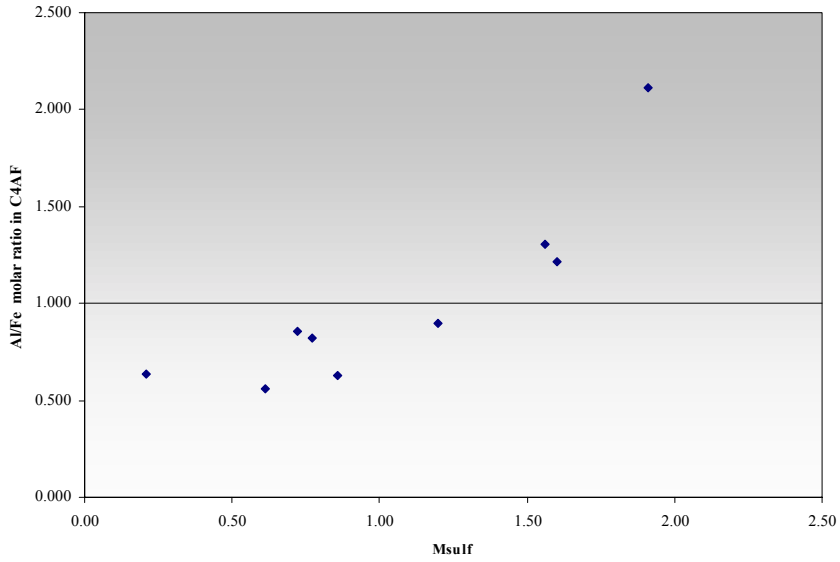

Figure 4. Trend of Al/Fe molar ratio as determined by Rietveld refinement in C4AF as a function of the sulfate module

The C_3S/C_2S ratio seems to be possibly affected by the sulfate module, too (figure 3). In clinkers characterized by a sulfate module smaller than 1, the C_3S/C_2S ratio takes on values being approximately equal to or greater than the theoretical one, i.e. 5.6. The C_3S/C_2S ratio is definitely lower (between 2 and 3) in clinkers with a sulfate module greater than 1.

In this case, experimental data turn out to be more scattered around the correlation curve compared to what was observed for C_3A. This might be because alite and belite contents as determined by QXPA are affected by a greater error than those found in the aluminate phases. However, the downward trend of the C_3S/C_2S ratio is rather clear when the sulfate module is greater than one. This statement is in agreement with Strunge's observation [22] according to which an increase in the SO_3 content in the clinker corresponds to a decrease in alite and an increase in belite content. This statement is also in agreement with Uda et al. [23]: when investigating the influence of SO_3 on the $CaO\text{-}SiO_2\text{-}Al_2O_3\text{-}Fe_2O_3$ equilibrium diagram, they found that an increase in SO_3 causes the stability field of alite to narrow.

5. CONCLUSIONS

Differences found between mineralogical composition of clinkers obtained by QXPA and Bogue are consistent with the findings of other authors, who applied this type of analysis on a smaller series of clinker samples.

The application of the Rietveld method to a wide series of industrial clinkers provided very interesting information about the influence exerted by alkali and SO_3 contents on the mineralogical composition of clinkers with particular regard to the aluminate phases.

It has been found that when alkalis are balanced by sulfates (sulfate module = 1), the contents in C_3A (in the cubic form) and ferrite are in good agreement with those calculated by traditional methods.

When alkalis exceed sulfates (sulfate module <1), orthorhombic C_3A is formed. In this case, the total C_3A content turns out to be greater than the one derived from calculations. Consequently, also a lower Al/Fe ratio in the ferritic phase has been found.

In clinkers where SO_3 is in excess with respect to alkalis, the C_3A/C_4AF and C_3S/C_2S weight ratios tend to be lower than the values as calculated. These results are in good agreement with the assumptions put forward in those studies concerned with the influence of SO_3 on the phase equilibria of a quaternary system.

The above observations let us assume that alkalis in excess with respect to SO_3 modify the phase equilibria in the system $CaO\text{-}SiO_2\text{-}Al_2O_3\text{-}Fe_2O_3$ on which the Bogue calculations are based.

For the time being, there are no recent theoretical investigations regarding the influence of alkalis on the phase equilibria within the quaternary system supporting the above assumption.

REFERENCES

[1] Bogue, R.H., Industrial Engineering Chemistry (Analytical Edition), , Vol 1, 1929, pp. 192

[2] Taylor, H.F.W., "Modification of the Bogue Calculation", Adv. Cem. Res., Vol. 2 (6),1989, pp. 73-77

[3] Barry T. I. and Glasser, F. P., Calculations of Portland cement clinkering reactions, Adv. Cem. Res., Vol. 12 (1), 2000, pp. 19-28

[4] Scheubel, B., Exact characterization of Portland cement clinker using visual linear analysis, Proceedings of the VI International Conference on Cement Microscopy, 1984, pp. 427-437

[5] Rietveld H. M., A profile refinement method for nuclear and magnetic structures, J. Appl. Cryst., Vol. 2, 1969, pp. 65-71

[6] Bish D.L. and Howard, S.A., Quantitative phase analysis using the Rietveld method, J. Appl. Cryst., Vol. 1, 1988, pp. 86-91

[7] Madsen I.C., Scarlett N.V.Y. and Cranswick L.M.D., Thaung Lwin, Outcomes of the International Union of Crystallography Commission on powder diffraction round robin on quantitative phase analysis: sample 1a to 1h, J. Appl. Cryst., Vol. 34, 2001, pp. 409-426

[8] Moller H., Automatic profile investigation by the Rietveld method for standardless quantitative phase analysis, Zement Kalk Gips, Vol. 1, 1998, pp. 40-50

[9] Taylor J.C., Hinczack I. and Matulis C.E., Rietveld full-profile quantification of Portland cement clinker: The importance of including a full crystallography of the major phase polymorphs, Powder Diffraction, Vol. 15 (1), 2000, pp. 7-18

[10] Motzet H., Poellmann H., Koenig U. and Neubauer J., Phase quantification and microstructure of a clinker series with lime saturation factor in the range of 100, Proceedings of the 10th International Congress on the Chemistry of Cement, Vol. 1, Göteborg 1997, 1i039

[11] Neubauer J., Pollmann H. and Meyer H.W., Quantitative X-ray analysis of OPC clinker by Rietveld refinement,Proceedings of the 10th International Congress on the Chemistry of Cement, Vol. 3, Göteborg 1997, 3v007

[12] Plotze M., Quantitative determination of Clinker Minerals by the Rietveld Method, CETIC, June 2000

[13] Bruker AXS, TOPAS V2.0: General profile and structure analysis software for powder diffraction data. - User manual, Bruker AXS, Karlsruhe, Germany, 2000Bellotto M. and Signes-Frehel, M., Contribution à la détermination de la structure de l'alite par diffraction des rayons X sur poudres, J. Phys. IV France, (8), 1998, pp. 511-518

[15] Nishi F., Takeuchi, Y. and Maki, I., Tricalcium silicate, $Ca_3O(SiO_4)$: the monoclinic superstructure, Zeit. Kristallogr., Vol. 172, 1985, pp. 297-314

[16] Jost, K.H., Ziemer, B. and Seydel, R., Redetermination of the structure of □-Dicalcium silicate, Acta Cryst., B33, 1977, pp. 1696-1700

[17] Coville A.A. and Geller, S., The crystal structure of Brownmillerite, Ca_2FeAlO_5, Acta. Cryst., B27, 1971, pp. 2311-2315
[18] Mondal P. and Jeffery J.W., The crystal structure of tricalcium aluminate, $Ca_3Al_2O_6$, Acta Cryst., B31, 1975, pp. 689-697
[19] Takeuchi Y., Nishi, F and Maki I., Structural aspect of the C_3A-Na_2O solid solution, Proceedings of the 7th International Congress on the Chemistry of Cement, Vol. 4, Paris 1980, pp. 426-431
[20] Von Dreele, Quantitative texture analysis by Rietveld refinement, J. Appl. Cryst., Vol. 30, 1997, pp. 517-525
[21] Newkirk T.F., The alkali phases in Portland cement clinker, *3rd* ISCC, 1954, pp. 151-168
[22] Strunge J., Knöfel D. and Driezler I., Influence of alkalies and sulphur on the properties of cement, Zement-Kalk-Gips, Vol. 38, 1985, pp. 150-158
[23] Uda S., Asakura E. and Nagashima M., Influence of SO_3 on the Phase Relationship in the System CaO-SiO_2-Al_2O_3-Fe_2O_3, J.Am.Ceram.Soc., Vol. 81 (3), 1998, pp. 725-729

TRAPPING MECHANISMS OF TRACE METALS (CR, CU, NI, PB, V, ZN) IN THE LEACHED LAYER OF PURE CEMENT PASTES: EVIDENCES FROM IN SITU STUDIES (SEM-EDS, LOCAL XRD, ICP-MS WITH LASER ABLATION)

[1]Moudilou, E., [2]Defosse, C., [1]Bollotte, B., [3]Scardi, P. and [4]Touray, J.C.

[1]CTG Italcementi Group.
[2]Ciments Calcia Italcementi Group, Route des Technodes, B.P.01, 78931 Guerville Cedex, France.
[3]Dipartimento di Ingegneria dei Materiali, Università di Trento, 38050 Mesiano (TN), Italy.
[4]Ecole Superieure de l'Energie et des Materiaux, Rue Leonard de Vinci, 45072 Orleans Cedex 2, France.

ABSTRACT

In the European Union, national regulations regarding the quality of drinkable water are based on numerous EEC directives, synthesized by the council directive 98/83/EC (1998) [1] on the quality of water intended for human consumption. With respect to the low tolerable concentration levels of toxic metals, each possible source of pollution has to be identified. Cementitious materials may be of concern, especially cement pipes used for water transport, because this man-made material may contain toxic metals. Industrial clinker contains amounts of heavy metals usually in the 20 to 100 mg/kg range and sometimes higher (up to 300 mg/kg) [2]. Metals in industrial clinker could come from: i) raw materials and fossil fuels and ii) co-incinerated wastes such as used tyres, tars, heavy oils etc. During the industrial process, some metals (e.g.: Cr, Cu, Ni, V, Zn and a fraction of Pb) are mainly incorporated in the clinker itself [2, 5, 7]. Other metals (e.g.: Hg, Cd, Tl) are mostly carried out by the gas flows and fixed in the kiln-dust collected in bag filters [2-4, 6].

Recently, using "environmental-like" experimental conditions for studying the long-term leaching of toxic trace metals from Portland cement concrete, Hillier and al. [8] concluded that "well cured Portland cement concrete released no detectable concentrations of the toxic metals outlined in directive 80/778/EEC water fit for human consumption". They only noticed detectable concentrations of vanadium released from poorly cured samples.

Different conclusions were obtained from former studies detecting trace toxic metals in the leachates so that clearly, the "soft" experimental conditions used by Hillier and al. (semi-dynamic leaching test method , no agitation throughout the test, no artificially aggressive leachants) represent at best usual interactions between water and cementitious materials, but are difficult to extrapolate to model long-term leaching, because of the purely empirical character of their study.

In order to address metal behavior during water-cement interaction, two experimental methods have been followed: i) the investigation of the composition of leachates, fitted on a kinetic law [9] and ii) the characterization of the distribution of toxic metals within the "leached layer" of a cement paste. Only, this last approach is presented in this article.

1. MATERIALS

A way to understand metal behavior during the leaching of cement pastes is to use a special clinker, enhanced by the addition of extra heavy metals well beyond usual contents in industrial products

[10, 16]. However, at elevated concentrations, the phase repartition of metals may differ from what occurs in industrial clinkers. Accordingly, non-doped cements were studied.

The Portland cement sample (n° 4440A) presented here, was made of pure clinker with gypsum addition of about 5wt% (CEM I 52.5N type following the EN 197-1 European norm of cements). Its chemical composition and trace metals content are given in tables 1 and 2

Table 1. Chemical composition of OPC samples.

Sample	Ig. Loss	SiO_2	Al_2O_3	Fe_2O_3	CaO	MgO	SO_3	Na_2O	K_2O
N°4440A (%)	0.93	20.62	4.61	2.85	63.77	3.38	2.66	0.15	0.78

Table 2. Trace metals content of OPC sample.

Sample	Cr	Cu	Ni	Pb	V	Zn
n°4440A (mg/kg)	74	23	60	18	215	69

2. SPECIMEN PREPARATION AND CHARACTERIZATION

The paste specimens used during leaching runs were cylinders of 90 mm in diameter and 100 mm in height whose upper and lower 25 mm had been cut off with a diamond saw for characterization. The water to cement ratio was 0.5; specimens were cured for 28 days, under a relative humidity of 100%. Samples have portlandite contents of 19.5% (determined by TGA). Mercury Intrusion Porosimetry indicates a total porosity of 27%, with 11.5% micropores (diameter lower than 25 nm) and 15.5% capillary pores

3. DYNAMIC LEACHING DEVICE PRINCIPLE

The CTG-LEACHCRETE (Figure 1) [11] device used for leaching runs is based on a modified version of the Soxhlet extractor.

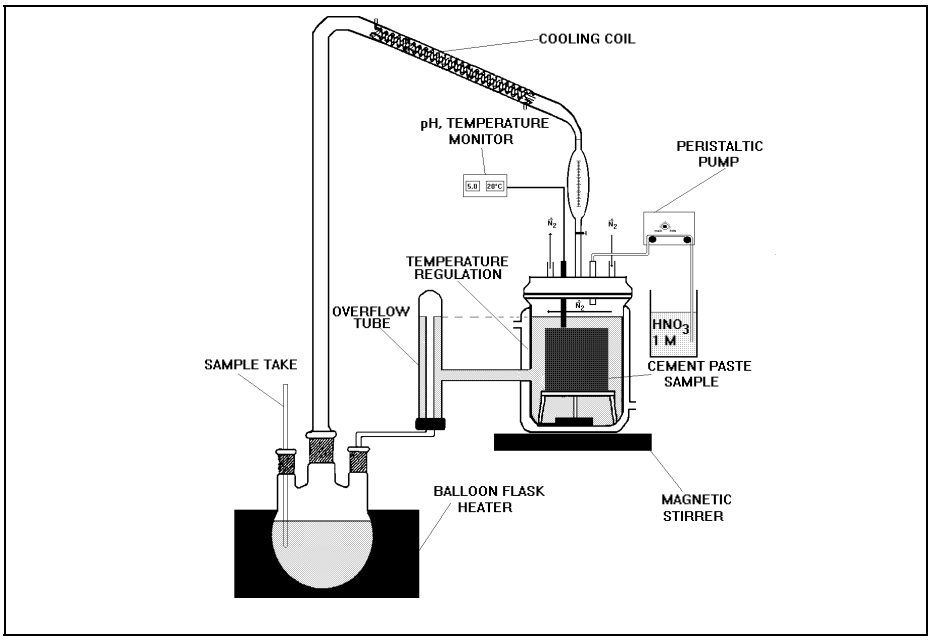

Figure 1. CTG-LEACHCRETE device principle

It is mainly composed of a reactor (leaching cell) containing the cylinder of cement paste and of a boiler concentrating the leachates and producing recycled water vapor. In this device, the sample

cell is temperature and pH controlled, CO_2 free and separated from the boiler cell which produces the distilled water. In fact, the escaped vapor from the boiler cell is condensed by a cooling coil and the sample cell is continuously refilled by a constant water flow. At the output of the reactor, an overflow tube maintains a constant volume of water in contact with the cement paste sample. Then the overflow tube refills the boiler. Periodically, aliquots of solution are sampled in the boiler for analyses, an equivalent volume of water being added.

The reactor temperature may be regulated between 20°C and 40°C with a thermostatic bath. Pure N_2 is flowing through the leaching cell to limit the carbonation of the sample surface layer. Acidity in the reactor is regulated to pH = 5 +/- 0.2, using progressive additions of diluted HNO_3 (1 M). Nitric acid has been used because nitrate ions do not disturb cement hydration [19]. Literature shows that nitrate ions do not have an oxidizing [20, 21] or a complexing [22, 23] action on metals present in the interstitial solution ions (Cr(+VI), Cu(+II), Ni(+II), Pb(+II), V(+V) and Zn(+II)). Finally, using nitric acid accelerates the leaching process only by increasing the pH gradient between leachate and interstitial solution.

As an example of kinetic results, the Cumulate Fractions Leached (C.F.L) of Chromium have been plotted vs time on graphic 1 for three different runs at 20°C of about 1000 hours using specimens of cement n°4440 A. Although C.F.L are lower than 0.5%, the reproducibility is very good.

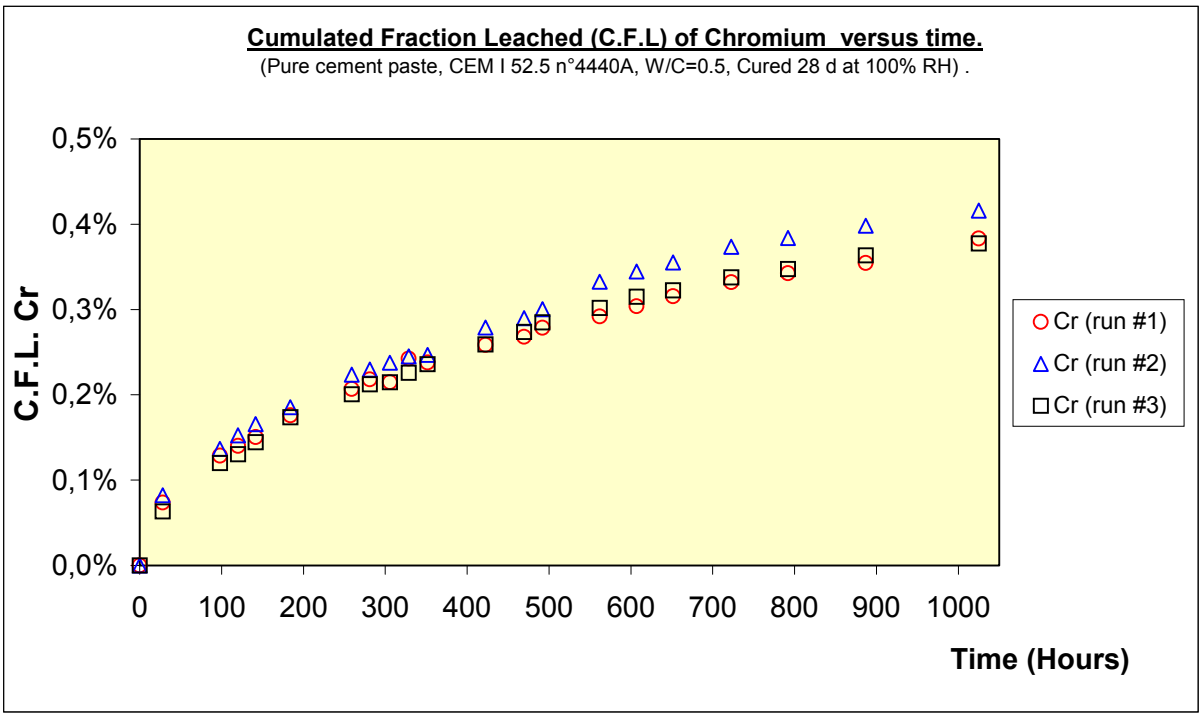

Graphic 1. Reproducibility of the Chromium release kinetic measurements for three different runs (O.P.C n°4440A) of dynamic leaching experiments with the CTG-LEACHCRETE device at 20°C and pH=5.

4. RESULTS AND DISCUSSION

4.1 Evidencs of a Fe-Rich surface after leaching

After about 2 weeks of leaching, an irregular brown-ochre layer appears at the surface of paste specimens. From SEM-EDS studies, this layer is Fe-enriched and Ca-depleted with respect to the original paste [9]. No toxic metal has been detected, however EDS sensitivity is poor (about 0.5%). After sampling by delicate brushing, this brown-ochre layer has been analyzed by XRD. Quartz,

calcite, vaterite and, more surprisingly, anhydrous C_4AF (brownmillerite) have been detected. A large diffusion halo is indicative of the presence of an amorphous material.

The study of this layer has been complemented by GIXD (Grazing Incidence X-ray Diffraction) at 0.5 and 1° incidences, but directly on the surface of a leached cement paste sample. The same phases with additionnal hydrotalcite have been detected; the diffusion halo has disappeared and an extra-peak at 2θ =17.96° attributed to oriented feroxyhyte [9] was found. Following the above data and the hydration equation of brownmillerite given by Fortune and Coey [12], the brown-ochre colour could result from the presence of iron oxyhydroxydes (feroxyhyte and poorly crystallized ferrihydrite) and of ferric hydrogarnets.

4.2 Characterization of the Ca-depleted layer

After about 1000 hour runs, sections of the leached specimens sawn perpendicularly to cylinder axis, have been enclosed in a resin and then diamond-polished. EDS profiles of Ca (Graphic 2) reveal that in the unleached core the CaO concentration fluctuates around the mean value of the anhydrous cement composition; On the other hand, near the surface a significant decrease appears.

For example, a thickness of 1350 µm of a Ca-depleted layer is determined on a specimen of cement n°4440 A, after 1025 hours of leaching at 20°C and pH=5.

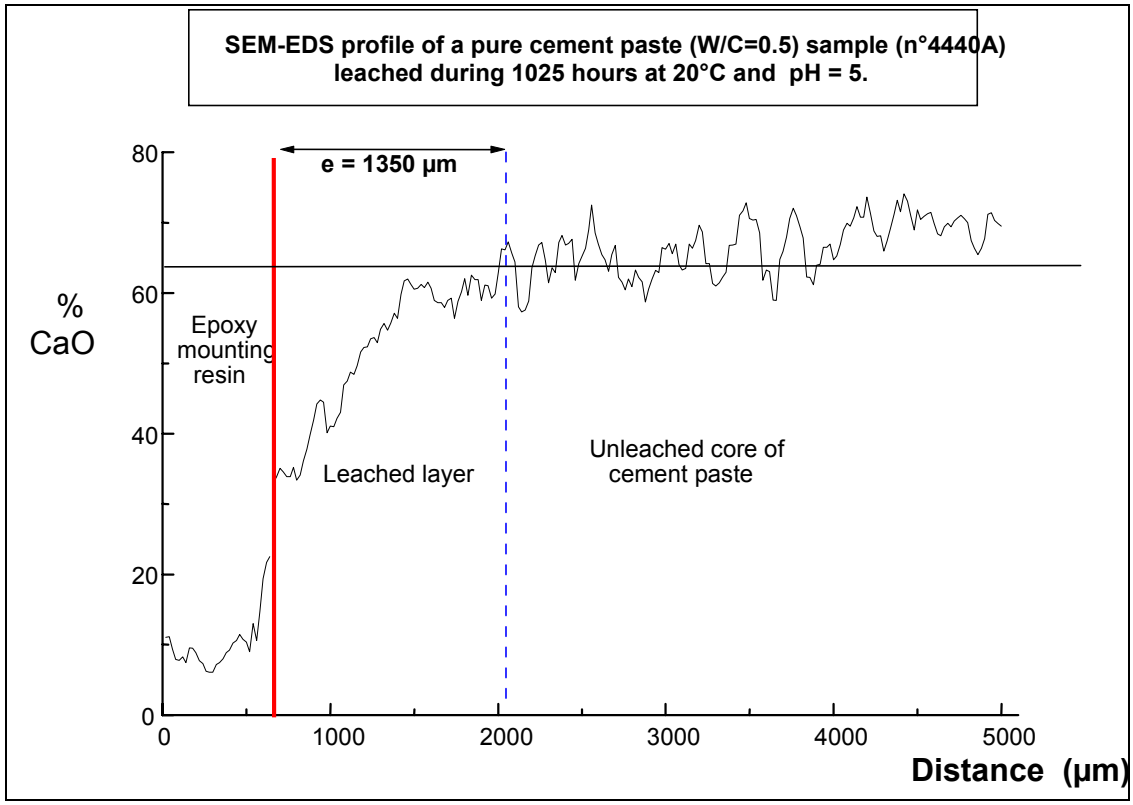

Graphic 2. SEM-EDS profile of CaO content in the cement paste sample after 1025 hours of dynamic leaching at 20°C and pH=5 in the CTG-LEACHCRETE device.

On the same sample, EDS "chemical cartographies" of Ca, Al, Si, Fe, Mg and S were made. The most interesting distributions (Photographs 1-3) are relative to:
-Ca, with a steep concentration decrease towards the surface;
-Si with a enrichment increase towards the surface,
-S which is presented a clear front in the degraded layer very close to the unleached paste from the core.

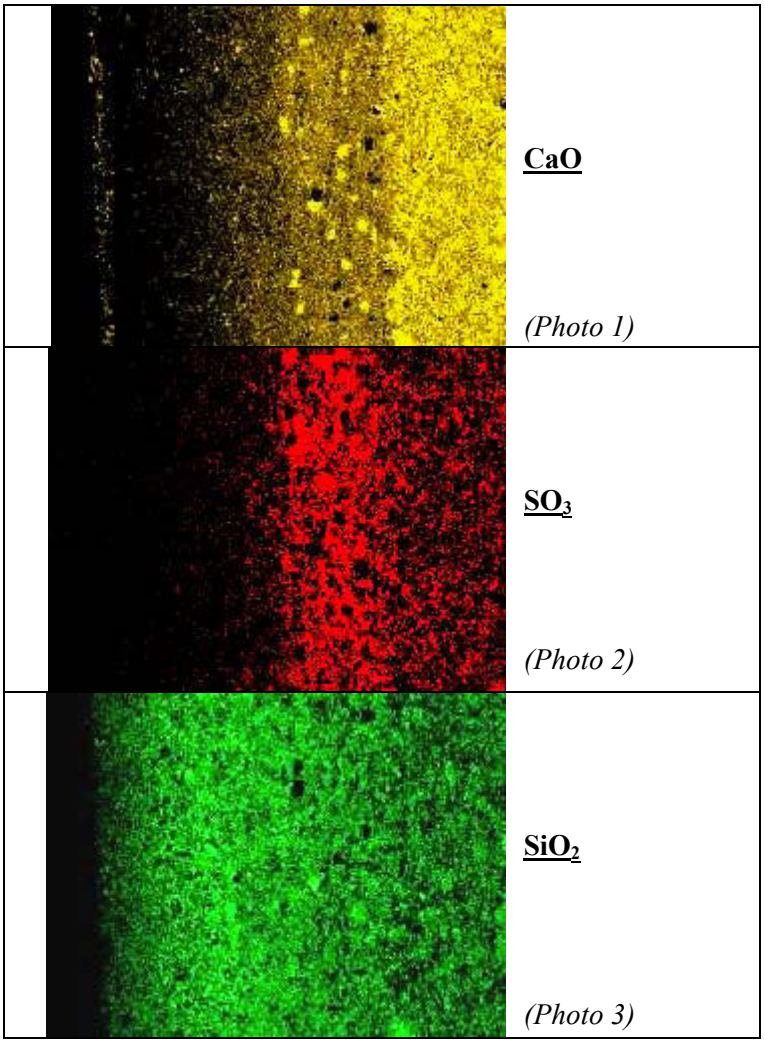

Photographs 1, 2, and 3.

From chemical distribution of Ca, Si and S, one may conclude that cement paste/leachant interaction resulted in portlandite dissolution, formation of a surface silica rich zone and precipitation of secondary ettringite. These conclusions are supported by an XRD investigation on a local scale.

Local XRD leads to identification of the distribution of mineral phases within a solid. Experiments were performed in Trento University (Italy), in the Department of Material Engineering. Analytical conditions are given elsewhere [9,15]. A total of 12 diffractograms have been made, from 2.75 mm beneath the surface to the surface itself, by successive steps of 0.25 mm. Areas of selected peaks, respectively representative of portlandite, calcite and ettringite, and of the diffusion halo corresponding to amorphous phases, have been measured. The relative variation from step to step of these areas is a quantitative indication of the spatial distribution of the different phases (Figure 2).

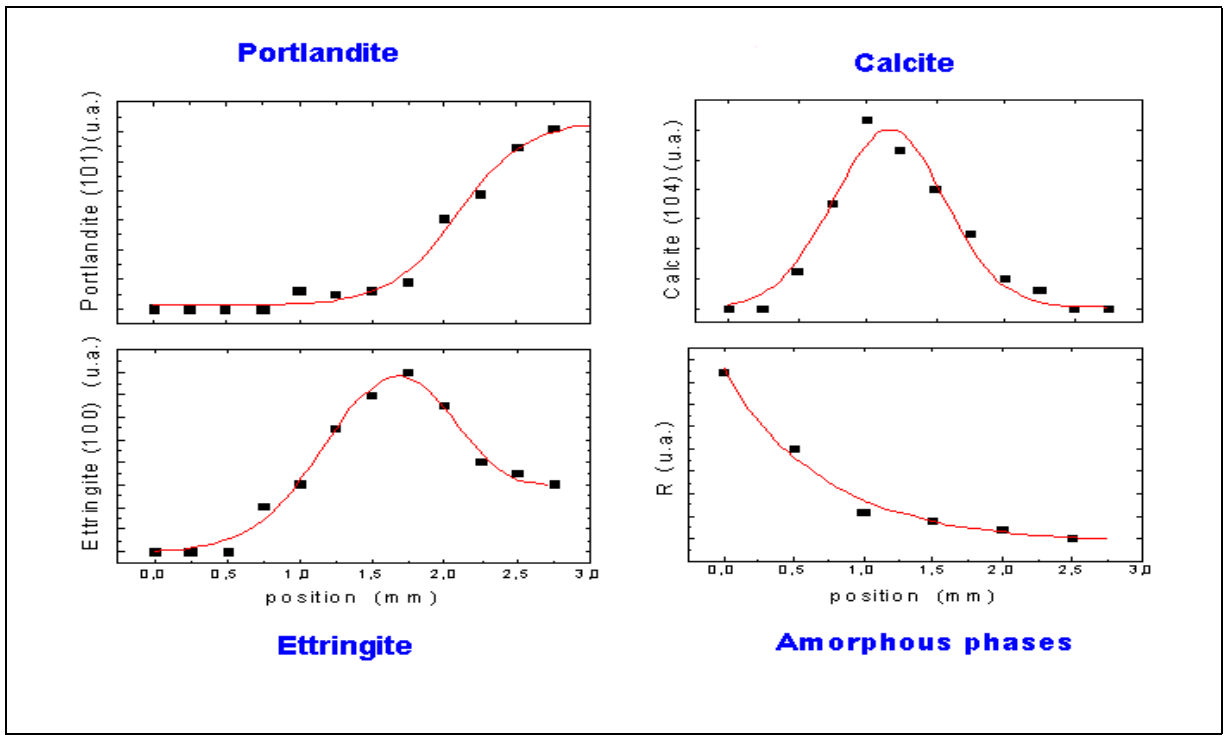

Figure 2. Evolution of the concentrations of portlandite, ettringite, calcite and amorphous phases in the leached layer, from the unleached core (2.5 mm) to the surface of the sample (0.0 mm)

This approach permitted the identification of:

- -The solubility front of portlandite, i.e. the beginning of the leached zone
- -The precipitation of secondary ettringite at the bottom of the leached zone
- -The precipitation of calcite within the leached zone which indicates a residual CO_2 presence in the device despite the N_2 flow
- -The formation of an amorphous silica gel at surface related to the CSH incongruent dissolution

The "spatial" characterization data of hydrates is relevant for an interpretation of the localization of trace metals in leached cement paste, especially the distribution of secondary ettringite and the presence of a calcite front.

4.3 Localization of trace heavy metals within the leached layer using ICP-MS analysis with laser ablation

Inductively Coupled Plasma Mass Spectrometry is a sensitive technique for trace element analysis. Applications to in situ solid analyses result from the "pulverization-vaporization" of the solid at the impact of a powerful laser ray (about 10^{10} watts/cm^2) with the creation of a local microplasma [13] taken off to the ICP-MS system by an argon flow and finally analyzed. Usually, samples are moved while the laser ray remains fixed; this results in the formation of a crater, whose width result depends on laser power and solid properties (e.g.: hardness); typical values scatter in the 20 to 100 micrometer range. As determined by SEM examination, craters are about 20 micrometers large in the present investigation (Photograph 4).

Studied samples were polished sections cut perpendicularly to the axis of cylinder-shaped paste specimens. Analyses have been performed in the "Laboratoire d'analyses Radiochimiques et Chimiques" of the French Atomic Energy Commission (CEA) at Cadarache (Southern France). An ICP-MS spectrometer P.O.E.M.S (Thermo-Jarrell-Ash) and a laser ablation system LSX-100 (CETAC Technologies) have been used. Analyzed elements were 6 trace metals (Cr, Cu, Ni, Pb, V and Zn) and Si. Analytical conditions have been given elsewhere [9].

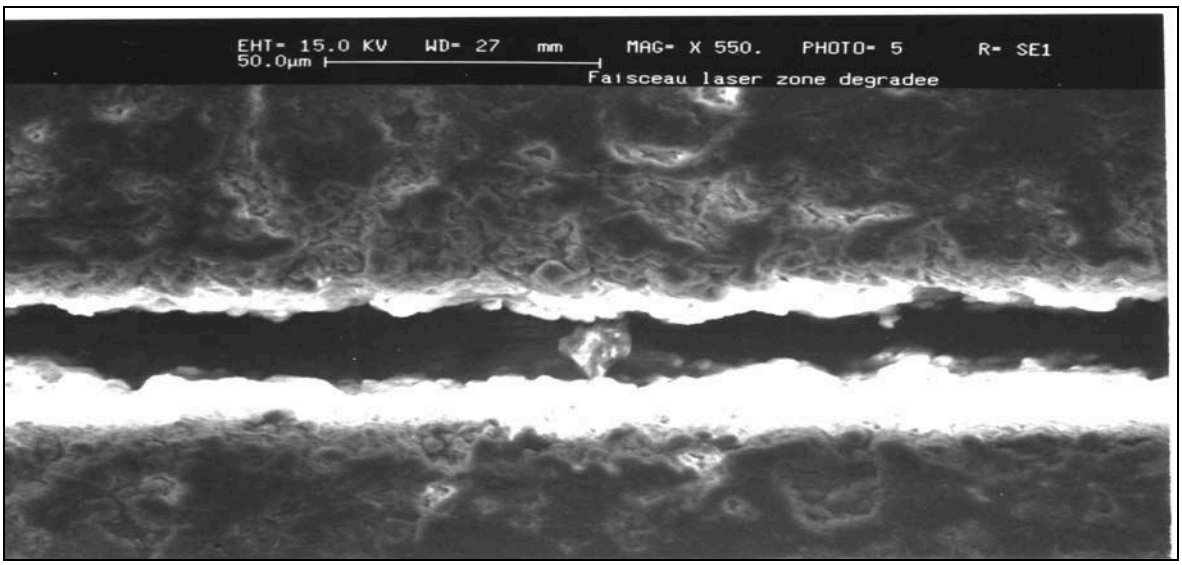

Photograph 4. Laser-Ablation crater on a pure cement paste sample (n°4440A) studied after a leaching run.

Only intensity profiles of characteristic mass/charge ratios (e.g. 29 for Si) are presented and discussed below, even if in the constant non altered zone, intensity profiles directly reflect concentration gradients. Indeed, the microstructural heterogeneity of the leached layer, precludes any quantitative determinations of trace metal concentration profiles. Accordingly, we choose to compare the different profiles of the various metals with the silicon profile, bearing in mind mineralogical variations with depth observed by local XRD within the leached layer.

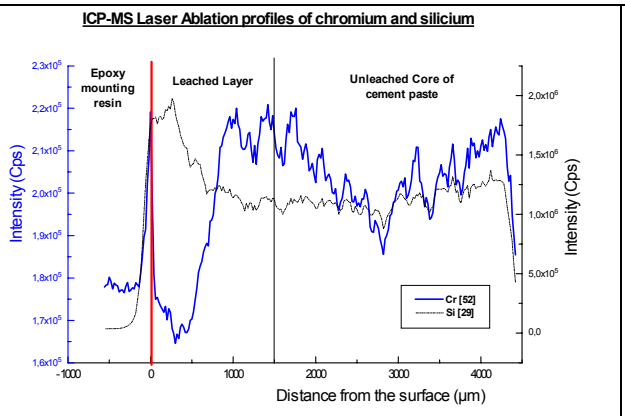

Graphic 3- Cr

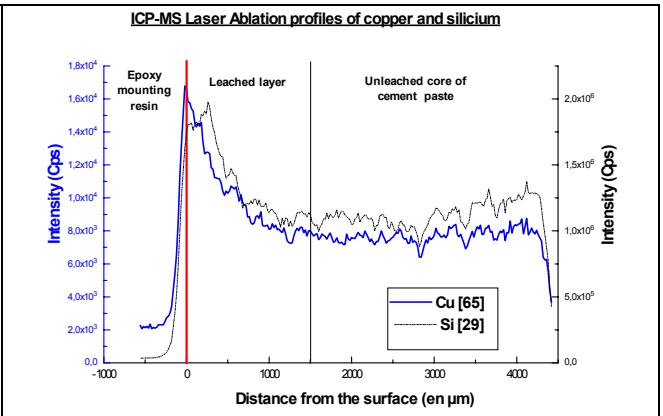

Graphic 4 – Cu

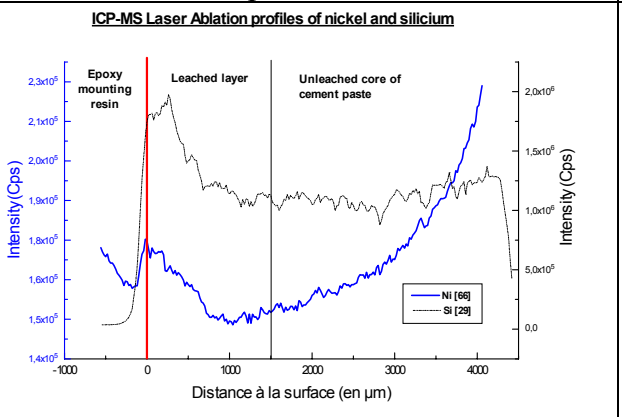

Graphic 5 - Ni

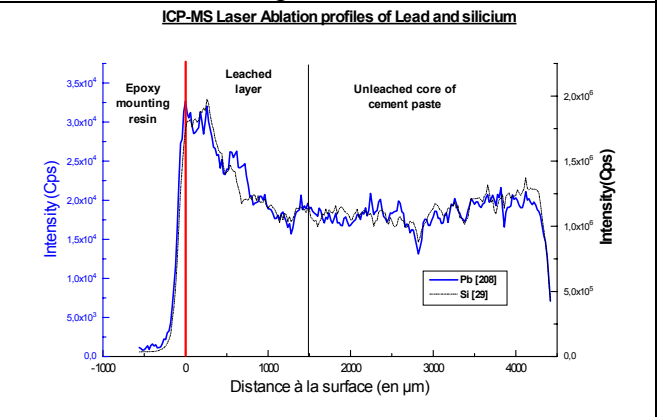

Graphic 6 – Pb

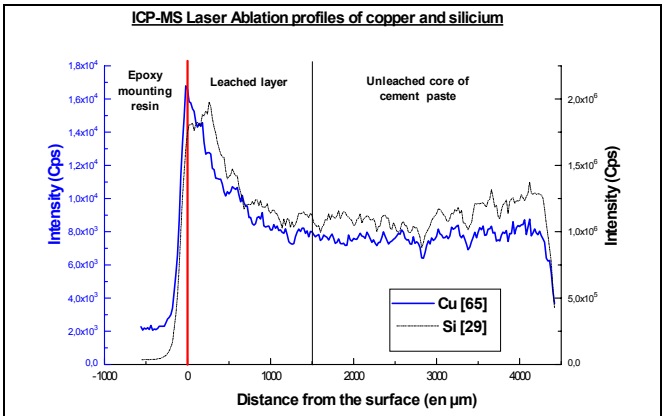

Graphic 7 - V

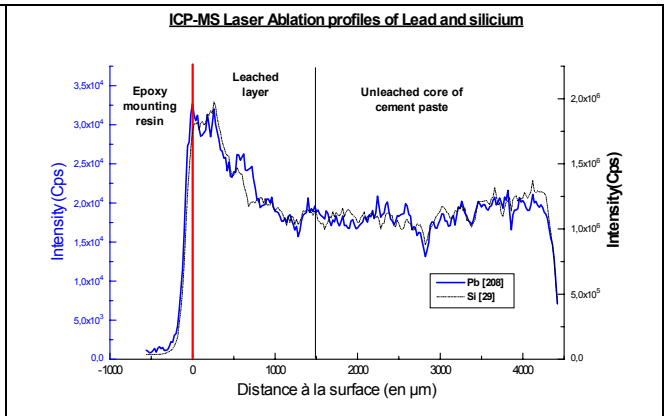

Graphic 8 – Zn

Graphic 3-8 – ICP-MS Laser Ablation profiles of trace heavy metals in the leached layer

From an inspection of the graphics 3 to 8, the following comments can be made:

- In the pristine zone, the Si profile is roughly constant, with expected variations reflecting size and composition of the components of the cement paste.
- In the pristine zone, profiles of the different metals are either parallel or discordant with silicium. Good fits, including simultaneous fluctuations of metal and Si, are observed in the case of Cu, Pb, V and Zn. This correlation strongly suggests metal localization within a range of silicate phases. Misfits are noticed with Cr and mostly with Ni whose concentration is disturbed by an isobaric interference.
- In the altered zone, a decreasing fit between metal and silicium is observed, ranging from an excellent concordance for Pb to good parallelism for Cu, Ni and V. These data suggest a unique trapping of Pb in CSH phases and a major control of Cu, Ni and V by these phases. In contrast, misfits are noticed with Zn and mostly Cr.
- In the altered zone, the succession of mineralogical zones may be expected to be similar to that deduced on theoretical bases [14], complemented by data from figure 2. With respect to this distribution and graphics 3 and 8, one may suggest that secondary ettringite is the major hosting phase for Cr under CrO_4^{2-} substituting to SO_4^{2-} and suggest a significant trapping of Zn by calcite.

5. CONCLUSIONS

By comparing the particular hydrates' distribution and the trace metals' profiles within the leached layer, we can propose the following trace metals trapping mechanisms:

-Vanadium and chromium are present under their oxy-anionic forms in our experimental conditions. However, they are not hosted by the same major phase in the leached layer: Local XRD, SEM-EDS and local ICP-MS data are compatible with the hypothesis of CrO_4^{2-} substituting to SO_4^{2-} in the structure of secondary ettringite, while VO_4^- localization is clearly distinct.

- Secondary calcite probably plays a part for Zn trapping, because calcite and Zn display their maximum values in the median zone of the leached layer

- CSH of the altered zone appear to be significant host phase for Cu, Ni, Pb, and V. Adsorption and ionic substitutions to Ca^{2+} of these divalent cations Cu^{2+}, Ni^{2+}, Pb^{2+}may be advocated [16], [17], [18]. Concerning VO_4^-, the adsorption on the CSH surface seems to be the major mechanism.

Thus, these results obtained from measurements on hardened cement pastes are closely correlated with the kinetics of trace metal releases measured in the liquid phase [9] using the CTG-LEACHCRETE dynamic leaching device.

REFERENCES

[1] Council Directive 98/83/EC on the quality of water intended for human consumption; OJL 330, p 32-54, 1998
[2] Portland Cement Association, publication SP110, Skokie, IL, USA, 1992
[3] Ming-Yen W., Jeng-Long S. And Jyh-Cherng C., Journal of Air & Waste Management association, Vol.49, pp. 444-453, 1999
[4] Kamm K., Zement-Kalk-Gips, Vol. 38, n°9, pp. 324-329, 1989
[5] Sprung S., Kirchner G. And Rechenberg W., Zement-Kalk-Gips, Vol. 37, n°10, pp. 513-518, 1984
[6] Kirchner G., Zement-Kalk-Gips, Vol. , n°10, 555-562, 1986
[7] Francois D., Ciment-Beton-Plâtre et Chaux, n°790, pp. 161-164, 1991
[8] Hillier S.R., Sangha, C.M., Plunkett B.A., Walden P.J., Cement and Concrete Research, Vol. 29, pp. 515-521, 1999
[9] Moudilou E., PhD Thesis, University of Orleans, France, 2000
[10] Serclerat I. PhD Thesis, University of Lyon, France, 1996
[11] Moudilou E., Waste Management, Vol. 22, n°2, pp. 153-157, 2002
[12] Fortune J.M., Coey J.M.D, Cement and Concrete Research , Vol. 13, pp. 696-702, 1983
[13] ARJAN J.G. And MASON P.R.D., Journal of Analytical Atomic Spectrometry, Vol. 14, pp. 1143-1153, 1999
[14] Adenot F., Richet C., Faucon P., International Conference on Engineering Materials Proceedings, Ottawa, Canada, 1997
[15] Scardi P., Setti S., Bellotto M., Moudilou E., Proceedings Acts of 5th "AIMAT" Congress, Spoleto, Italy, 2000
[16] Moulin I., PhD Thesis, University of Aix-Marseille, France
[17] Ziegler F., Johnson A., And Giere R., "Waste Stabilization & Environment Conference" Proceedings Actes, Lyon, France, pp. 36-40, 1999
[18] Rigo E. and al., Zement Kalk Gips International, Vol. 53, n°7, pp. 414-423, 2000
[19] Dumm J.Q., Brown P.W., "Phase assemblages in the system $Ca(OH)_2$-Al_2O_3-$Ca(NO_3)_2$-H_2O", Advances in Cement Research, Vol. 8, n°32, pp. 143-153, 1996
[20] Macphee D.E., Glasser F.P., "Immobilization Science of Cement Systems", Materials Research Society Bulletin, Vol. 18, n°3, pp. 66-71, 1993
[21] Pourbaix M., "Atlas d'equilibres Electrochimiques à 25°C", Ed. Gauthier Villars, 1963
[22] Ringbom A., "Complexation in Analytical Chemistry", 395 p., Interscience Publishers, New-York, USA, 1963
[23] Kotrly S., Sucha L., " Handbook of chemical equilibria in analytical chemistry", 414 p., Ellis Horwood Lt, 1985

A NEW FAST METHOD FOR ASSESSING FROST SUSCEPTIBILITY OF CEMENTITIOUS MATERIALS

Stefano Cangiano[1], Roberto Cucitore[1], Giovanni Plizzari.[2], Antonio Principallo[1] and Luigi Sorelli[3]

[1] C.T.G. – Italcementi Group, Via G. Camozzi, 124, 24121 Bergamo, Italy.
E-mail: s.cangiano@itcgr.net
[2] Università degli studi di Bergamo, E-mail: plizzari@unibg.it
[3]Università degli studi di Brescia, E-mail: sorelli@ing.unibs.it

ABSTRACT

In the present work, the dimensional changes of several water-saturated concrete specimens during freeze/thaw cycles were continuously monitored using dilatometric equipment. Many concrete mixes were characterised by the presence or absence of air entraining agents, by different types and classes of cement and by various w/c ratios. Moreover, for most of the aforementioned concretes, the correlation between the results obtained with a standardized test method and the method presented herein is shown.

The main aims of the work were the study of the phenomena associated with water freezing in concrete specimens and the setting up of a differential dilatometer able to continuously monitor the length changes of specimens.

The results have shown that after a few freeze/thaw cycles it is possible to evaluate the frost susceptibility of concretes. Moreover, the results obtained are in good agreement with the results obtained by means of UNI 7087 which has been proven to furnish results comparable with those given by ASTM C 666.

1. INTRODUCTION

The frost deterioration of concrete, whether with or without de-icing salts, results from different coupled phenomena such as mass transport (water and/or vapour transport, ion diffusion, etc.) [1-4], ice formation in the porous structure of concrete [5], and osmotic pressure arising from different ionic concentrations [6]. When the water content in the porous structure of concrete is greater than a critical value [7], the deterioration of concrete may in some cases result from cumulative damage phenomena due to freeze/thaw cycles.

In order to prevent frost from damaging the concrete structures, the design of concrete mixes and the checking of their conformity to freeze resistance requirements should be carried out before the scheduled casting operations.

In this context, a test method able to quickly evaluate the frost sensitivity of concrete may be a useful tool for verifying the performance of the designed concrete mixes.
The main objective of this work is to develop an instrument able to provide frost judgement about concrete frost susceptibility.

Proceedings of the 11th International Congress on the Chemistry of Cement (ICCC)
'Cement's Contribution to the Development in the 21st Century'
Hosted by: The Cement and Concrete Institute of South Africa
CD-ROM produced by: Document Transformation Technologies
11 - 16 May 2003, Durban, South Africa
ISBN Number: 0-9584085-8-0
Editors: Dr G. Grieve and G. Owens
Congress Organised by: Event Dynamics

2. EXISTING STANDARD TEST METHODS

Current test methods concern the evaluation of the internal damage of concrete (e.g. in absence of de-icing salts) and the assessment of surface damage due to de-icing salts and freeze/thaw cycles.

Despite the common aim of all the standard test methods, the procedures differ with respect to:
a) size and shape of the specimens;
b) freeze/thaw cycle (temperature limits, cooling and heating rate);
c) cooling and heating fluid (water, air, kerosene, etc.);
d) measurement technique to evaluate internal damage.

Accepting that it is not easy and not advisable to compare results obtained according to different standards, due to the differences related to the items a), b) and c), some comments can be made on the prescribed measurement techniques (item d).

An in-depth analysis of the standard test methods [8] allows observing that:
- the test duration can range from some weeks to some months;
- discontinuous measurements are time-consuming because there is the necessity to stop the test and to condition the specimens; moreover the conditioning period can lead to losing some information related to specimen damage;
- manual measurements may be more subject to error than automatic measurements;

3. EXPERIMENTAL

3.1 Equipment

The testing apparatus consists of an INVAR frame, in which the specimen and a reference INVAR rod are located (Figure 1). Two INVAR pins are constrained to the top and base of the specimen and the invar rod; in such a way the length changes can be transmitted to the outside of the frame. Two external gauges are mounted on INVAR rods, which are constrained to the measuring frame as well (see details on Figure 1). This testing arrangement was specifically designed in order to minimise errors due to spurious length changes introduced by thermal displacements of the equipment [9].

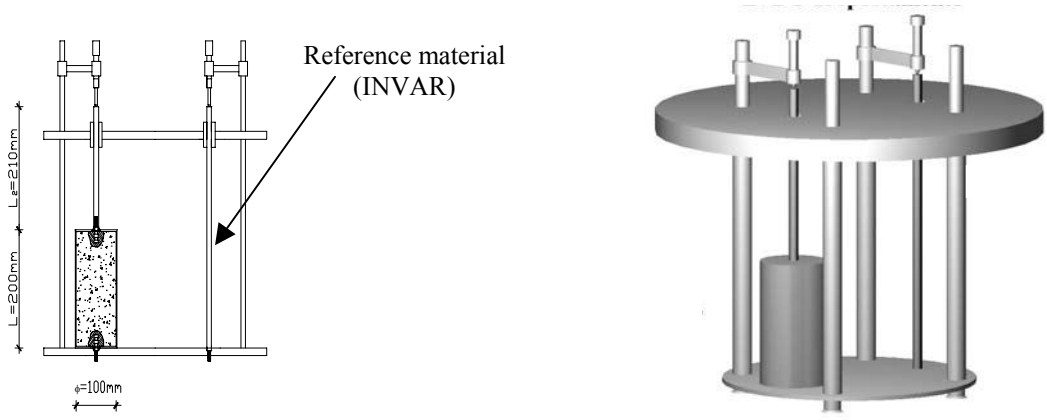

Figure 1. INVAR frame for differential measurements

Moreover, to reduce spurious displacements further, the length change values detected on the concrete specimens during a freeze/thaw cycle are referred to the dimensional variations measured on the reference INVAR rod. In this way, the actual length changes of specimens are provided by the following relationship:

$$\Delta L_{cls} = L_1 - L_2 + \alpha_{INVAR}\,\Delta T\,L_0 \quad (1)$$

where:
L_1 = displacement measured by LVDT on the concrete specimen;
L_2 = displacement measured by LVDT on the INVAR reference specimen;
α_{INVAR} = thermal dilation coefficient of INVAR by [10];
ΔT = temperature variation;
L_0 = reference length of INVAR rod at laboratory temperature (20 ± 2°C).

The testing frame is submerged into a diathermal oil bath contained in a cylindrical stainless steel vessel where freeze/thaw cycles are performed by circulating a primary diathermal oil coming from a heat/freeze source into a copper coil. The freeze/thaw cycle is realised by controlling the flow rate of primary diathermal oil with a proportional valve operated by a command signal coming from a programmable controller. The control loop is closed by the feed-back signal coming from a temperature gauge (Pt 100) immersed in the secondary diathermal oil up to mid-plane of the bath.
A pneumatic rotating mixer stirs the secondary diathermal oil.

The displacements are detected by a measuring chain composed of two LVDT (Linear Variable Differential Transformers) that are connected to two amplifiers/conditioners of the signal.
The temperature data are detected with different gauges as indicated in Table 1.

Table 1. Placement and technical data of the adopted temperature gauges

Gauge type	Placement	Uncertainty
Pt100	Secondary oil bath	0.3 °C
Surface thermoresistance	On specimen surface	0.4 °C
Thermocouple	Inside the specimens	0.4 °C

3.2 Freeze/thaw cycles

In order to evaluate the sensitivity of the test method to the cooling/heating rate, the nominal thermal cycles described in Table 2 were applied. For temperature values and time intervals, a tolerance of ±2 °C and ±15' respectively has been considered acceptable.

Table 2. Thermal cycles adopted.

	Cooling/heating rate		
	Slow [1.5°C/h]	Medium [5°C/h]	Fast [10°C/h]
Phase	**Duration [h]**		
Storing at +5 °C	4	3	3
Cooling from 5 °C to –25 °C	20	6	3
Storing at –25 °C	4	3	2
Heating from -25 °C to +5 °C	20	6	3
Total time	**48**	**18**	**11**

3.3 Equipment calibration

All the measuring gauges were in calibration at the time of testing; the calibration of the equipment was carried out by fast cycles.

The performance of the dilatometer was verified in terms of:
1) deviation of bath temperature from the reference value of the set temperature cycle;
2) agreement between the measured temperature displacement relationship and the corresponding reference relationship provided by [10] for the reference specimens;
3) repeatability.

Commercially available rods (∅=12 mm; h= 200 mm) made of aluminium (97% Al) and electrolytic copper were used as reference specimens. Figure 2 shows the temperature profile (fast cycle) imposed to the oil bath compared with the measured temperature (feed-back quantity).

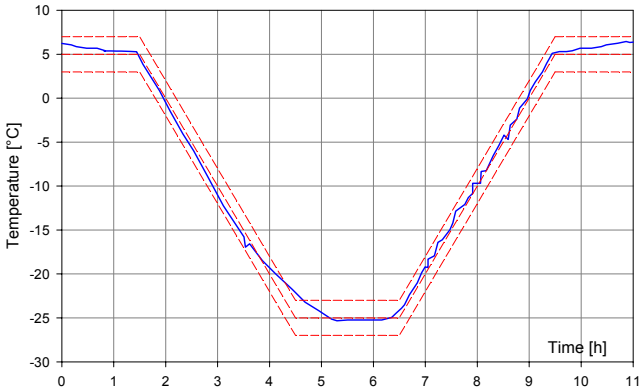

Figure 2. Comparison between the thermal cycle imposed to the oil bath and the measured temperature in the oil bath.

In Figure 3a and 3b the temperature/strain relationships for reference materials are compared. For both copper and aluminium specimens, a good agreement with the relationships given by [10] and shown in Table 3 was found.

Table 3. Temperature/strain relationships for aluminium and copper (reference materials)

$Strain = \alpha \cdot T + \beta \cdot (T)^2$ [T=Temperature]		
Material	α	β
Aluminium	2.2×10^{-5}	0.09×10^{-7}
Copper	1.61×10^{-5}	0.040×10^{-7}

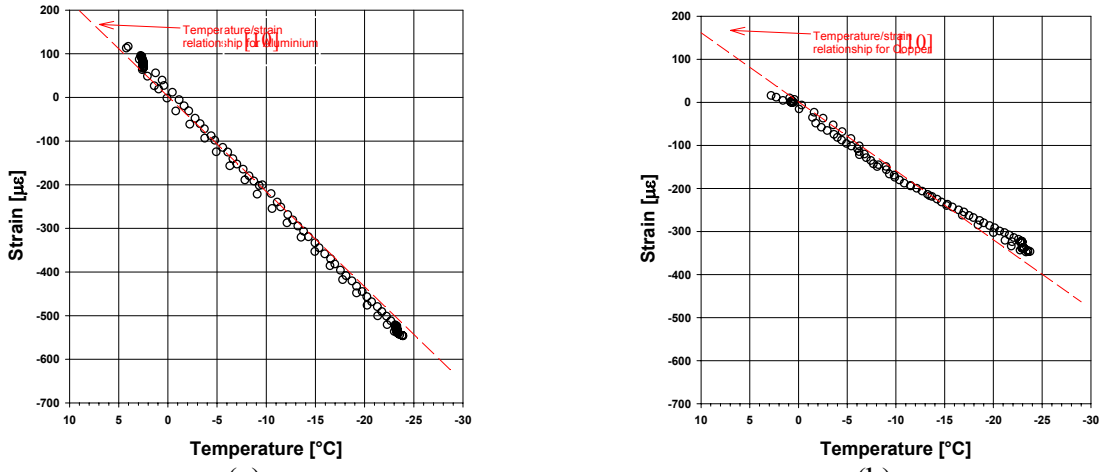

(a) (b)

Figure 3. Comparison between the measured temperature/strain relationships and those given by [10]

The mean deviation of the measured thermal strain from the reference values is less than 25 με for both the reference materials.

As regards aluminium reference specimens, repeatability tests were carried out by detecting six times the temperature/displacement relationship. The slope of the best fitting straight line of the temperature/displacement relationship has been calculated and the results are shown in Table 4; the

same table shows the mean value, the standard deviation and the variation coefficient of the slope (α) of the best fitting straight line. The good repeatability performance was highlighted by the low value of the coefficient of variation

Table 4. Repeatability tests for aluminium rod

Slope (α) of the best fitting straight line									
Test No.	1	2	3	4	5	6	Mean	σ	**CV [%]**
α [ε °C^{-1}]	2.35E-5	2.34E-5	2.36E-5	2.34E-5	2.35E-5	2.34E-5	2.35E-5	5.67E-8	**0.24**

Moreover, the thermal gradient in the mass of a cylindrical specimen (∅=100 mm; h=200 mm) was detected in order to evaluate the distribution of temperature in its middle plane. The results, shown in Figure 4, highlighted that the temperature was in the range whose upper and lower limits are defined in § 3.2.

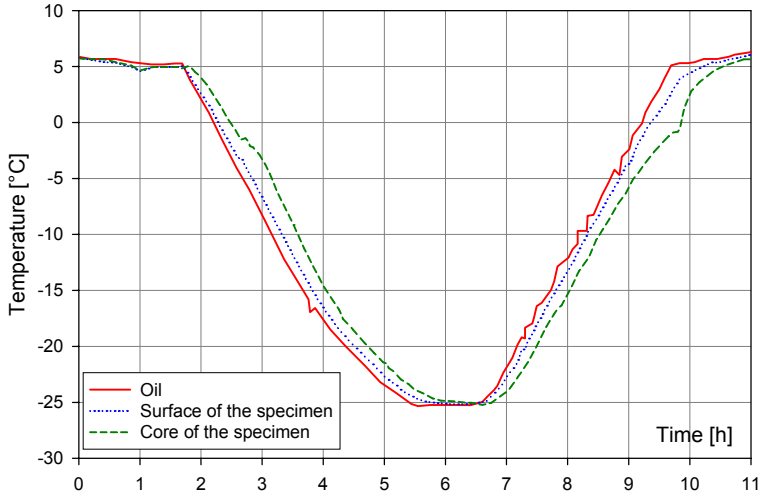

Figure 4. Temperature distribution in a concrete specimen during a freeze/thaw cycle

3.4 Concrete mixes

The experimental program has been set up to evaluate the frost behaviour of concrete with respect to the type, class and content of cement, the w/c ratio, and the type and content of admixture. The cement content was 350 kg/m^3 for all the mixes. Table 5 shows the concrete composition and the compressive strength values at 28 days.

Table 5. Composition of adopted concrete mixes

Material	**CEM type**	**w/c**	**Admixture [%CEM]**	**Density [kg/m^3]**	**Slump [mm]**	**Air [%]**	**Rc$_{28d}$ [MPa]**
32S40	32.5R II/A-L	0.40	1.5% Superflux	2477	60	-	48.4
32N50	32.5R II/A-L	0.50	-	2394	20	1,7	37.8
42N50	42.5R II/A-L	0,50	-	2409	10	1.8	44.6
42P52	42.5 IV/A	0,52	-	2456	40	-	41.3
32N58	32.5R II/A-L	0,58	-	2355	100	1.9	29.5
32A58	32.5R II/A-L	0,58	0.5 %Aermix	2228	100	4.8	23.3
42N58	42.5R II/A-L	0,58	-	2390	150	-	36.1
42A58	42.5R II/A-L	0,58	0.5 %Aermix	2278	170	5.1	31.2

4. RESULTS

4.1 Detected quantities

Figure 6 shows the typical results from two freeze/thaw cycles in terms of longitudinal strain versus concrete temperature; the same figure shows the quantities adopted to evaluate the frost sensitivity of the test specimens.

In particular the following quantities were detected (Figure 6):

- residual strain ($\varepsilon_{res,cum}$) exhibited by the specimen at the end of each freeze/thaw cycle;
- net thermal strain (ε_T) computed at the bottom limit of the cycle. To evaluate this quantity, a linear extrapolation (up to the minimum temperature of the cycle; Figure 5) of the strain-temperature curve measured for positive values of temperature must be considered;
- maximum strain ($\varepsilon_{max,cum}$) recorded during each cycle and referred to the net thermal strain;
- cumulative area (A_{cum}) computed as the sum of the areas included by the strain-temperature curves.

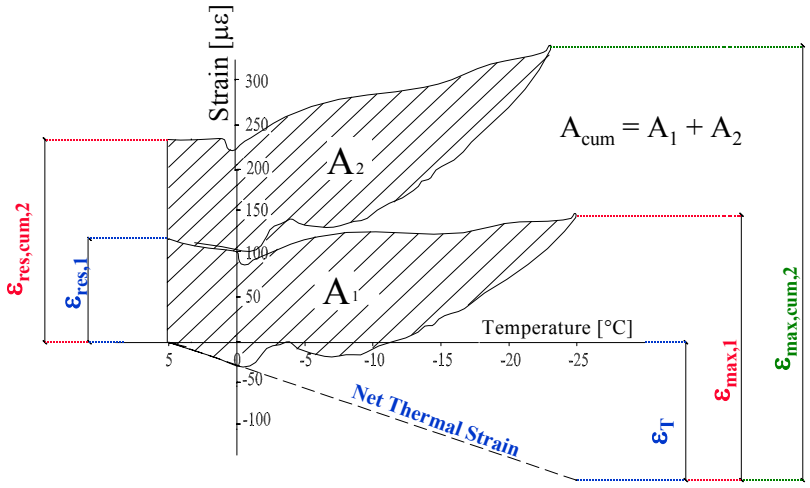

Figure 5. Detected quantities

Taking into account that hysteresis and residual strain are typical display of occurrence of internal frost damage of concrete [1-4], all the above quantities, with the only exception of the net thermal strain, may be considered as useful tools to evaluate the frost sensitivity of concrete.

4.2. Experimental data

4.2.1 Sensitivity of the method to concrete composition and to testing parameters

A typical result of a complete freeze/thaw test is reported in Figure 7 that shows the (longitudinal) concrete strain versus the temperature for the concrete specimen 42N58. It can be observed that the increase in the residual strain at the end of each cycle is quite constant, thus determining a quasi-linear increase in cumulative residual strains. The hysteresis area shows a slight increase at each cycle; therefore, also the cumulative hysteresis area increases continuously. A similar behaviour can be observed also for the maximum strain. These results point out the growth of a cumulative (and non-reversible) internal damage that is already evident after the first cycle. Furthermore, it can be observed that, in this case, a very small number of cycles (not more than 3-5 cycles) is sufficient to confirm the presence of concrete damage.

Figure 7 shows the curves related to an air entrained concrete specimen (42A58) subjected to 5 cycles. It can be observed that both residual and maximum strain is significantly reduced with respect to that exhibited by the corresponding non-aerated concrete (42N58). In addition, the hysteresis area is appreciably reduced and, after the first cycle, it no longer increases. For comparative purposes, the same figure gives the strain-temperature relationship related to an oven dried specimen (32N58). The comparison clearly indicates how the behaviour of the air entrained specimen, even if less susceptible to frost damage than the non-aerated specimen, nevertheless exhibits evidence of the frost action.

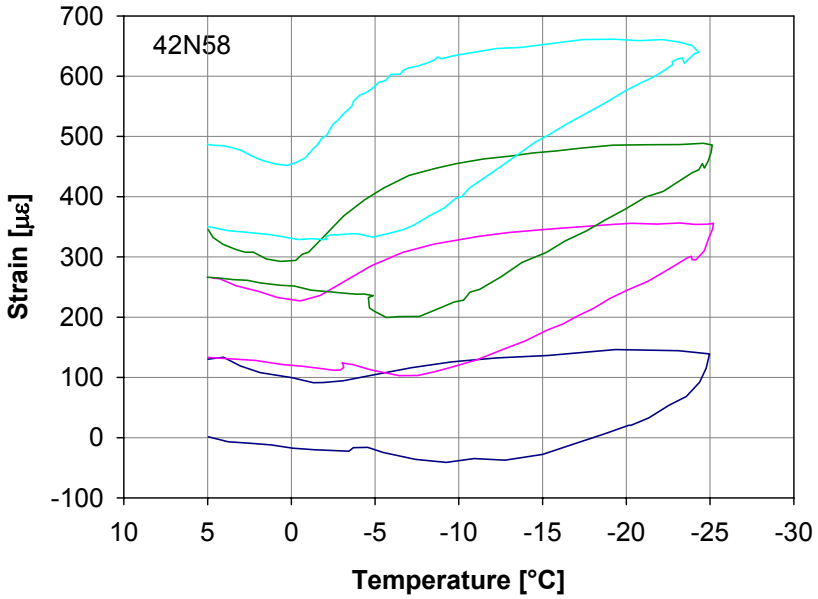

Figure 6. Result of the freeze/thaw test by the dilatometric method for concrete 42N58

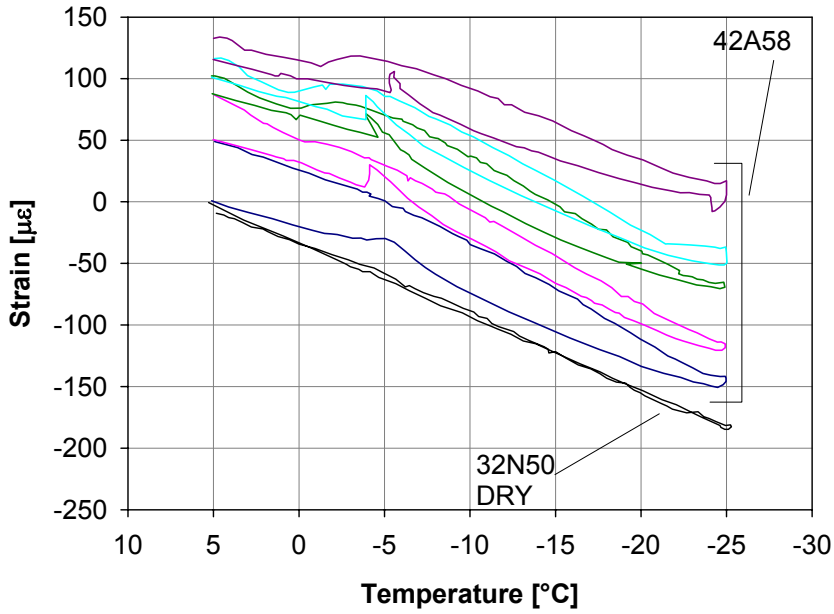

Figure 7. Result of the freeze/thaw test by the dilatometric method for concrete 42N58 compared with the measured strain for a dry specimen made with concrete mix 32N50.

In Figure 8 the sensitivity of the test method to w/c ratio, other parameters being constant, is shown. By passing from w/c=0.4 to w/c=0.58 all the damage indexes (maximum strain, residual strain, hysteresis area) are appreciably increased just after the fourth cycle.

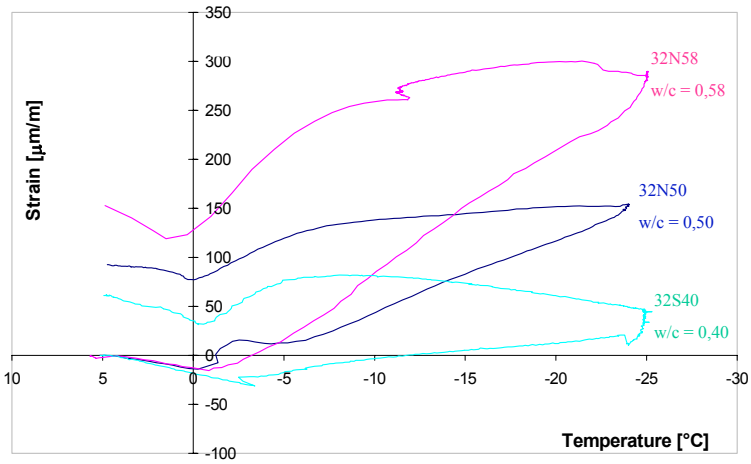

Figure 8. Diagram of the strain versus the temperature as obtained from specimen 32S40, 32N50 and 32N58

Figure 9 shows the dilatometric curves obtained for three specimens subjected to freeze/thaw cycles, and characterised respectively by three different cooling thermal gradients: 1.5, 5 and 10 °C/h. A clear dependency of concrete behaviour on the imposed cooling gradient can be noted. In fact, all the above-defined parameters, chosen to evaluate the frost sensitivity, increase markedly with the cooling gradient.

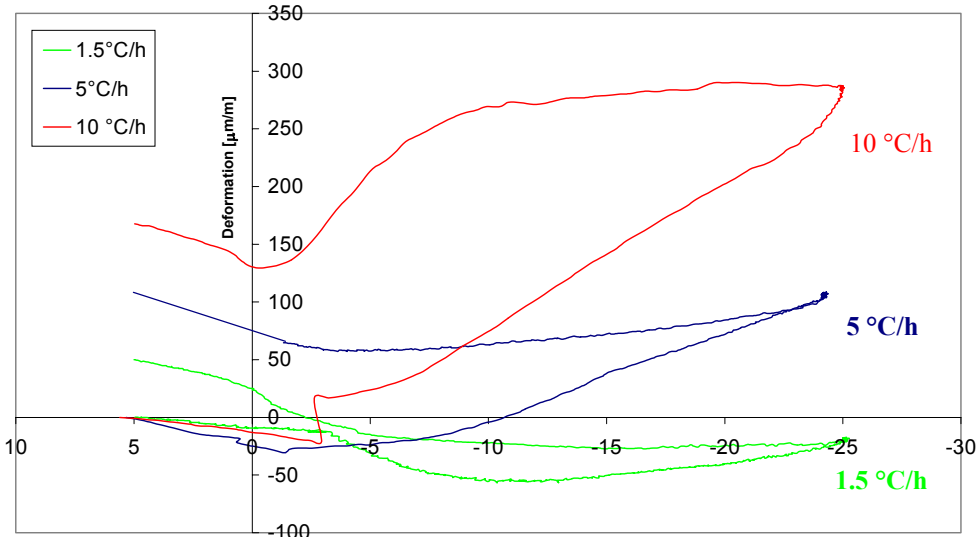

Figure 9. Diagram of the strain versus the temperature as obtained from specimen 32N50 for three different cooling rates

4.2.2 Comparison with Italian standard test method

In order to verify the relationship between the results obtained with the proposed freeze/thaw test and the standard methods according to UNI 7087 [11], tests on specimens prepared with the mixes listed in Table 2 were carried out. The results obtained after five cycles according to the dilatometric method have been compared to those obtained after 50 cycles carried out according to UNI 7087. The relationship between the UNI degradation factor and the detected quantities according to the dilatometric method has been investigated. In Figures 10a, 10b and 10c, the damage indexes detected after five cycles are plotted versus the degradation factor measured after 50 cycles according to UNI 7087. The correlation coefficient is generally good; in particular, the relationships between the maximum strain and the degradation factor, with $r^2 = 0.92$, confirm that the early response given by the dilatometric method provides a reliable assessment.

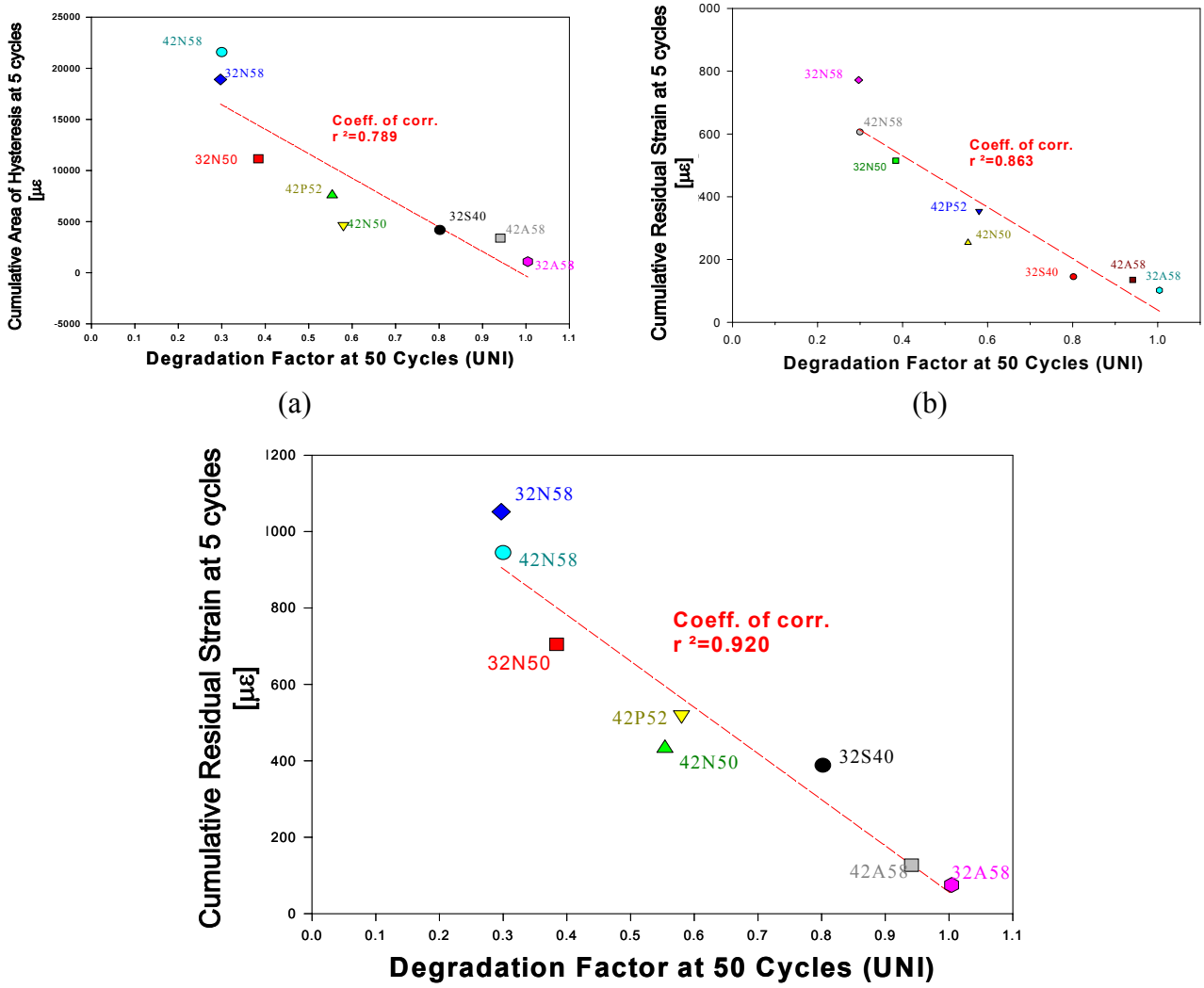

Figure 10. Correlation between results obtained with the proposed method and with UNI 7087

5. CONCLUSIONS

All the current standard test methods aimed at evaluating the evolution of internal damage due to freeze-thaw cycles are very time-consuming. In the present work, a fast test method able to provide an assessment of frost resistance after few days is presented.
A testing apparatus has been set up and its reliability has been verified by calibration and repeatability tests.

The equipment allows continuous monitoring of axial displacement during freeze/thaw cycles. In this way the test can be stopped whenever evidence of degradation is apparent, and it is therefore no longer necessary to wait until completion of the scheduled number of cycles. This equipment has shown that the dilatometric method is very sensitive to the composition parameters of concrete and to the cooling rate of the cycles.

The experimental data obtained after five cycles are in very good agreement with the results after 50 cycles carried out by the UNI standard method, which has been proven to furnish test results comparable with ASTM C666 [12].

REFERENCES

[1] Powers, T.C. and Helmuth, R.A. Theory of volume changes in hardened Portland cement pastes during freezing, Proceedings of the Highway Research Board, Vol.32, 1953, pp.285-297.

[2] Powers, T.C. and Brownyard, T.L. Studies of the physical properties of hardened Portland cement pastes, Portland Cement Association Bulletin, Bulletin 22, 1948.

[3] Litvan, G.G. Phase transitions of adsorbates: IV, Mechanism of frost action in hardened cement paste, Journal of American Ceramic Society, Vol. 55 (1), 1972, pp.38-42.

[4] Wittmann, F.H. Interaction of hardened cement paste and water, Journal of the American Ceramic Society, Vol.56 (8), 1973, pp.409-412.

[5] Powers, T.C. A working hypothesis for further studies of frost resistance, Journal of the American Concrete Institute, Vol. 16 (4), 1945, pp.245-272.

[6] Powers, T.C. Freezing effects in concrete, ACI special Publication SP-47, Vol. 50, 1975, pp.741-760.

[7] Fagerlund, G. Degré critique de saturation. Un outil pour l'estimation del la résistance au gel des matériaux de construction, Matériaux et constructions, Vol. 4, 1971, pp.271-285

[8] Cangiano, S., Cucitore, R., Plizzari, G. and Sorelli, L. Rapid evaluation of freeze-thaw resistance of cement-based materials by a dilatometric method L., 7th European Conference on Advanced Materials and Processes, Rimini, 2001

[9] Sorelli, L. (Relator Plizzari, G.; Co-relator Cangiano, S.), Studio del Comportamento Deformativo di Calcestruzzi Soggetti a Cicli di Gelo e Disgelo (Study of deformation behaviour of concretes subjected to freeze-thaw cycles), Degree thesis, University of Brescia, 1998.

[10] Perry, R. H. and Chilton, C.H. Chemical Engineers' Handbook, 5th Edition: McGraw-Hill, 1973, p.3-99-101

[11] UNI 7087: 2002, Determination of the resistance to the degradation due to freeze-thaw cycles, Milano: Ente Nazionale Italiano di Unificazione.

[12] ASTM C 666: 1994, Resistance of concrete to rapid freezing and thawing, Philadelphia: American Society for Testing and Materials, 1994

WHITE CEMENT FOR ARCHITECTURAL CONCRETE, POSSESSING PHOTOCATALYTIC PROPERTIES

Luigi Cassar[1], Carmine Pepe[1], Giampietro Tognon[2], Gian Luca Guerrini[1] and Rossano Amadelli[3]

[1] CTG-Italcementi Group, Via G. Camozzi, 124, 24121 Bergamo, Italy. E-mail: l.cassar@itcgr.net
[2] Consultant
[3] Department of Chemistry, University of Ferrara, Italy

ABSTRACT

White cement is a key ingredient in architectural and decorative concrete. By using it, in particular, the resulting concrete not only becomes an expressive material that having an infinite range of colour tones, intensifying one of its aesthetic qualities, but can also be used to produce high-strength in concrete for structural applications.

This paper is intended to provide technical information to both designers, architects, and contractors in order to obtain a high performance concrete that is similar to natural materials like marble and which possesses relevant properties in terms of durability, performance and added environmental benefits. Indeed, the new type of white cement proposed here contains TiO_2 and possesses photocatalytic properties, which allow the maintenance of the aesthetic characteristics of concrete over time. It also contributes to eliminating dangerous pollutants from the urban environment.

A remarkable application is also described, concerning the innovative construction of a church in Rome, named "Dives in Misericordia" whose sails were built using white High Performance Concrete, based on this new cement. The main physical and mechanical properties of this HPC are described.

1. WHITE CEMENT

Thanks to the continuous laboratory research efforts aimed at obtaining outstanding properties in addition to an excellent degree of whiteness, white cement has been rendered increasingly and noticeably a high performance binder. White clinker is produced by taking care that the content of ferrous composites and other heavy metal composites (not exceeding 0.15%), whose presence give common Portland cement its distinctive grey colour. For this purpose, it is first of all necessary to carefully select the raw materials: only mineralogically pure kaolins and white limestone are used.

1.1 Colorimetric properties

Chromatic control (especially in the case of white cement) takes the form of reflected light colorimetry using highly reflective materials such as magnesium oxide or titanium.

Briefly, the "white" quality of the cement is measured using three parameters:
- purity, i.e. the intensity of the shade. Purity is measured by colour percentage;
- dominant wave length, i.e. the tonality of the shade that accompanies and characterises each white (for this reason, not all white bodies are equal). The length of the dominant wave lies between yellow and blue;

Proceedings of the 11th International Congress on the Chemistry of Cement (ICCC)
'Cement's Contribution to the Development in the 21st Century'
Hosted by: The Cement and Concrete Institute of South Africa
CD-ROM produced by: Document Transformation Technologies
11 - 16 May 2003, Durban, South Africa
ISBN Number: 0-9584085-8-0
Editors: Dr G. Grieve and G. Owens
Congress Organised by: Event Dynamics

- brilliance, i.e. the power to reflect incident light (the most distinctive characteristic of white bodies), expressed as the difference in percentage between the light reflected by a surface of white cement and that reflected by a similar surface of magnesium oxide, traditionally considered as the ideal white body.

As far as cements are concerned the colorimetric characteristic can only be represented by two parameters: brilliance and purity, as the third parameter (i.e. the basic wave length), which is normally requested for the various powders in the cements, remains roughly the same (for ordinary cements, $\lambda = 577 \pm 2$ nm; for white cements, $\lambda = 567 \pm 2$ nm).

Figure 1 shows the brilliance/purity curve with the colorimetric data for different types of hydraulic binders: ordinary cements, clear binders and white binders [1].

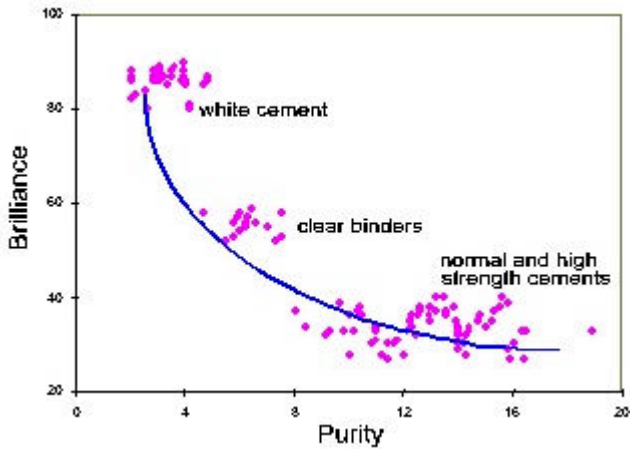

Figure 1. Brilliance/purity for the various types of cement

Reading from the left to right, the chromatic component increases: this is between 8 and 17% for grey cements; 5-7% for light cements and 4-5% for white cements: The brilliance also increases from 25 to 40, from 50 to 60 and from 80 to 90 respectively.

This graph allows us to compare the variability in purity with that of the brilliance. It is worth noting that the inaccuracy of visual evaluation of the brilliance (at least in the case of white cements) is about 2 points.

1.2 Photocatalitic properties

Scientific studies on photocatalysis were started about three decades ago [2-9]. Since then research has taken several turns, but it is in the last 10 years only that the most exciting potential of this technology has emerged: the application of photocatalysis to environmental clean-up [10].
This also gave impetus to industrial and institutional applications research. A huge increase in worldwide patent applications was observed and in 1999 more than 400 international applications were filed [11].

The strict environmental regulations imposed by the authorities have stimulated academic and industrial research groups to develop new strategies for the abatement of dangerous aqueous and gaseous pollutants. As regards the latter, much attention has been focused on the removal of NOx, hydrocarbons and organic chlorides, since these pollutants are an issue of high social impact in everyday life.

In particular, it should be noted that reactions in the atmosphere between NO_x and several hydrocarbons, under solar irradiation (Photochemical Smog), increase health hazards especially within heavy-traffic urban areas.

1.2.1 Cement containing photocatalysts

Within the framework of a strategy aimed at remedying environmental pollution through the use of construction materials containing photocatalysts, a system comprising Titanium dioxide (TiO_2) and white cement was investigated.

A first technology including the photocatalytic degradation of organic pollutants was utilised for maintaining the aesthaetic characteristics of concrete structures [12-15]. The introduction of suitable amounts of TiO_2 into cement mixes made the surface of cementitious structures photocatalitically active. In fact, concrete products are expected to maintain their aesthetic characteristics unchanged over time (particularly colour), even in the presence of aggressive urban environments.

The maintenance of the aesthetic appearance of cementitious materials, in particular those based on white cement, is specially desired. Indeed, the main reason that brings about a colour change in cementitious materials is the presence of coloured organic compounds that remain on their surfaces.

The inorganic powders adhere to the surface of the cementitious material in the presence of an organic interface or of macroporosities. The technology of heterogeneous photocatalysis is based on the irradiation of a semiconductor photocatalyst. Semiconductors are characterized by a narrow band gap between their valence and the conduction bands.

The absorption of a quantity of luminous energy being greater than or the same as the band gap (E_{BG}) of the semiconductor results in an abrupt transfer of electrons from the valence to the conduction band and the consequent creation of holes (h^+) in the valence band.
Such charge transfer introduces some unbalanced conditions which in turn lead to the reduction or oxidation of the species adsorbed onto the surface of the semiconductor.

In order to verify the efficacy of the photocatalytic activity on a cement matrix containing TiO_2, many experiments focusing on the oxidation of several kinds of aromatic organic compounds were carried out.
Figure 2 shows the surface restoration by irradiation of cementitious mortar samples containing TiO_2 and phenanthroquinone. TiO_2 can form two different cristallographic forms: rutile and anatase. The photocatalyitic activity is much higher when TiO_2 is mainly in the anatase form.

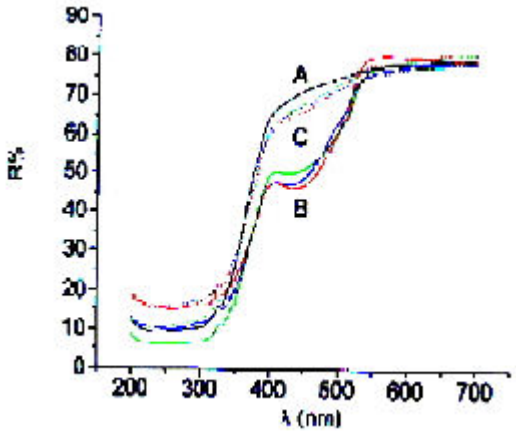

Figure 2. Reflectance spectra versus wavelength for a white cement sample

Samples of white cement having a thickness of 2 mm were placed on supports having a discoid form with a diameter of 3.2 cm and a thickness of 7 mm, containing 5% of TiO_2 (P-25 Degussa type).

In order to obtain reproducible organic substances on the sample, a phenanthroquinone solution in methanol was deposited by means of an aerograph thereby giving to the surface an amount of phenanthroquinone equal to 0.1 mg/cm^2. At the end of the treatment, the sample showed a homogenous surface having a yellow colour.

Both before and after the deposition of phenanthroquinone, reflectance spectrophotometric analyses were carried out with a Perkin Elmer lambda type spectrophotometer. The instrument was fitted with an integrating sphere to eliminate any scattered light responsible for anisotropy and surface irregularities. The samples were irradiated by means of a solar flow simulator, emitting radiation with a wavelength greater than 290 nm. The device used for irradiating purposes consisted of four 400 Watt lamps placed at the vertices of a square having at its center a carrying sample roundabout rotating on its own axis. By means of that device, simultaneous irradiation of more samples with the same amount of photons per time unit was possible.

The irradiation device SOLAR SIMULATOR SET-UP12/24 allowed accelerated ageing tests to be carried out, whereby approximately 100 irradiation hours correspond to 1 year of sunlight. For samples at different times and various percentages reflectance values (R%) as a function of wavelength (nm) were obtained. The percentage of reflectance of the samples was reported in Figure 2 at different times as a function of the wavelength (nm). With particular regard to Figure 2, curve A represents the spectrum before depositing the organic substance, curve B represents the situation after deposition of the substance, curve C represents the situation after 8 hours of irradiation.

As can be seen, after 8 hours of irradiation the situation is almost the same as before the treatment with the pollutant.

1.2.2 Photocatalysis and the removal of NO_X

Two main practical directions of NO_X elimination can be cited:

i) Reduction by hydrocarbons or ammonia
ii) A two-step adsorption-reduction or thermal destruction process

Photocatalysis has recently gained considerable recognition as a reliable method of NO_X abatement under mild experimental conditions, employing sunlight as a low cost renewable energy source. It is interesting that, in this field too, recent developments suggest the use of mixed catalysts in which a photoactive component such as TiO_2 is mixed with adsorbents, e.g. zeolites [16]. As reported, this improves the overall efficiency of NO_X elimination since the high absorbing capacity of zeolites compensates for or complements the low adsorbing power of TiO_2.

The use of mixed catalysts therefore seems a promising research direction in photocatalysis, too. Realising that a composite system consisting of TiO_2 dispersed into a cementitious matrix is one of such photocatalysts holds important practical implications. Research under way at our laboratories and at other research institutions [17] shows that concrete containing TiO_2 has very good potential application as a resolving technology in pollution control.

The mechanism of nitrogen oxide removal by photocatalysis is not simple. It is assumed that NO in the air is oxidised when the catalyst is exposed to light. Through the intermediate step of nitrogen dioxide (NO_2), it is then converted to nitrate. When NO_2 is formed, part of the gas may escape from

the photocatalytic surface but, in the presence of the cement matrix, the gas may be effectively entrapped together with the nitrate salt formed.

Laboratory tests of photoconversion of NO_X were carried out on films of:

- TiO_2 mixed with cement (5% by cement weight)
- Cement matrix without photocatalyst

Figure 3 summarises the tests carried out in the dark. NO_X is considered as a residual amount; a percentage is referred to an initial concentration of 100%. In this case, the observed concentration decrease is only due to adsorption. It is probable that such absorption is attributed to the ability of alkaline oxides forming the cement matrix to adsorb NO_X.

Photochemical tests after 7 hours of light of the samples, still considered as a percentage referred to an initial concentration of 100% are reported in Figure 4 below
It can be noted the removal of NO_X by action of the photocatalyst plus the cementitious matrix which is higher than the photocatalyst alone.

The reason is that on the surface NO is oxidised to NO_2 by reaction with OH radicals:

$$NO + OH^{\cdot} \longrightarrow NO_2 + H^{+} \qquad (1)$$

NO_2 is oxidised and, like nitrate, remains adsorbed :

$$NO_2 + OH^{\cdot} \longrightarrow (NO_3)^{-}_{ads} + H^{+} \qquad (2)$$

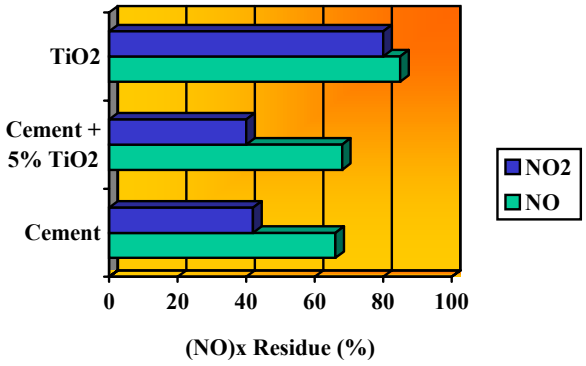

Figure 3. NO_x treatment in the dark

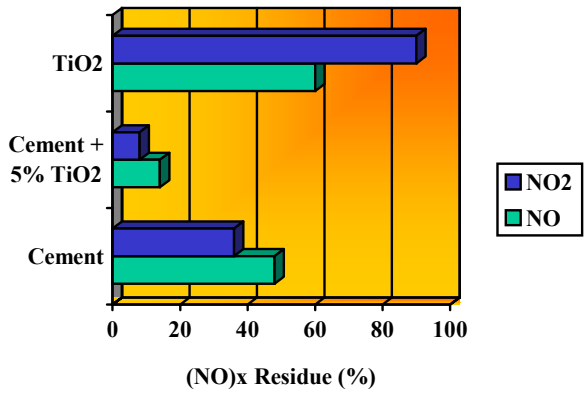

Figure 4. NO_x treatment under UV light

Furthermore, the examination of the data of Figure 4 shows that the cementitious matrix without TiO_2 also holds a certain catalytic effect, as is often observed in the case of organic substrates, probably due to the presence of photocatalytic oxides in the matrix itself.

A white cement containing TiO_2 (TX Millennium) has already been used for the construction of the Church for the Jubilee "Dives in Misericordia" in Rome [18], for the construction of the "City of Music" in Chambérie (France) and for the construction of a school in Mortara (Italy). Cementitious paints containing photocatalysts were also developed. [19].

2. WHITE CEMENT CONCRETE: MIX DESIGN

The mix design for a concrete made with white cement needs to be developed taking into consideration two fundamental aspects:

- the aesthetics or surface finish (including final photocatalytic properties);
- the strength or structural suitability

In other words, the right materials need to be chosen to create a delicate balance between the mix components and to guarantee the rheological behaviour of the resulting mix.

In the particular case of High Performance Concrete (HPC), the raw materials are: water, cement and aggregates (the same as in the ordinary cement mix), to which mineral and superplasticizer admixtures may be added as required. As a result, HPC has a microstructure significantly different from that of ordinary concrete: high density, low porosity and improved interfacial binding between cement paste and aggregates thus leading to different macroproperties in terms of strength and durability [20].

2.1 Aggregates

In the case of white cement concrete, an adequate choice of aggregates is absolutely necessary, in order to achieve the white colour in the concrete.

All aggregates must be clean, free from clay, mineral dusts and impurities. Contamination with other materials must be avoided.

Coarse aggregates. Their colour is of utmost importance for those surfaces to be treated to reveal the aggregate (e.g. bush-hammered, sand-blasted and washed). They should be reasonably uniform in colour.

Fine sands. Their use is decisive for the colouring of the open surfaces without further treatment after the removal of the formworks (extremely light coloured sand is needed if we specifically want a perfectly white surface, while a coloured sand may be adequate if the whiteness is less critical).

In both cases, the use of white cement in the “open” concrete allows to obtain a far more brilliant mortar in contrast to the colour of the aggregate, thus enhancing this if the surfaces are “worked” and making casts brighter if the surfaces are left “as they are”. The surface of a mortar obtained with white cement:

- acquires more brilliance, the less brilliant the sand
- assumes an increasingly less pinkish and more bluish tone than that of the sands. In fact, the wavelength of the loose materials is longer than that of the hardened surfaces.
- loses colour percentage (the colour is weaker) and thus the use of coloured sands is not enough on its own to get a concrete with distinctly coloured surfaces.

The results of the sand/mortar colour experiments show that it is not necessary to use particularly white sands, which are often hard to find, to create a white cement concrete: we can quite easily use normal sands.

The “colour loss” or rather the shades obtained by passing from sand to mortar can have a very pleasing chromatic effect, often preferable to pure white.

However, when the designer wants to achieve a brilliant and definite colour, he changes the colour of the surface by adding a mortar of the relevant colour capable of accentuating the colouring and giving the required dominant wave length.

In this way, it is possible to get a virtually infinite spectrum of colour tones.

2.2 Mineral additions

For the improvement of strength, chemical and physical durability, mineral additions can be included in the mix design.

In the case of white cement concrete, it is clear that fine pozzolanic materials (such as silica fume, blastfurnace slag, fly ash, rice husk ash and metakaolin) must be white and among all the materials currently available only the latter can be considered [21-23]. Indeed, particular types of white silica fume or precipitated silica are too expensive.

Metakaolin is by nature white and is highly reactive, sometimes used as a valid alternative to silica fume. It is an aluminium silicate obtained through calcination of pure kaolin within a set temperature range. The average size of the particles is 1.5 microns (ten times finer than Portland cement CEM I 52.5 R). Metakaolin works in different ways:

- as a filler, with immediate action
- by accelerating the hydration at greater intensity within the first 24 hours
- by means of a pozzolanic reaction with the C-H between the 7th and 28th days

In addition, other advantages can be obtained:

- reducing water permeability
- limiting efflorescence problems - presence of $(CaOH)_2$
- controlling the hygrometric shrinkage
- improving the paste/aggregate bond
- controlling bleeding.

2.3 Water-reducing admixtures

Since water demand levels in HPC correspond to a water/binder ratio of 0.20-0.35, the use of acrylic superplasticizers is preferable, rather than melamine-formaldehyde or naphthalene-formaldehyde sulphonate condensates. In the particular case of white concrete, the choice of admixtures is also strictly connected with their colour.

Besides, if there are possibilities of cement-admixture incompatibility, the use of a compatibility agent is absolutely necessary. Recently, this problem was solved by using a system of admixtures supported by the metakaolin used as the pozzolanic addition [24].

3. WHITE SAILS FOR THE CHURCH "DIVES IN MISERICORDIA", IN ROME

The Church "Dives in Misericordia", a project of Richard Meier, a master of contemporary architecture, is the first example in which Italcementi participated using photocatalytic innovative materials. The simple yet severe design which manages to combine the sacredness of the inside of the building with the liveability of large external spaces, is characterised by three large white concrete sails which swell as though driven by a wind from the East.

In the church there are two distinct architectural bodies: the sacred building, approximately 2,500 sq.m, which occupies the southern part; the community centre, approximately 4,300 m^2 situated in the northern part. The churchyard connects the Church to the centre of the residential area. The church roof is a glass skylight which runs along the entire length and impressive glazed windows characterise the lateral facades. Four large shells in reinforced white concrete measuring 16 and 28 metres in height embrace the central body of the nave occupying more than 700 m^2; the main hall, the weekday chapel and the baptistery separate the spaces inside the building. There is a 26 m high pillar-bell-tower near the central body. The impressiveness of the work and the specifications of the project: 20,000 m^3, 22 metres high, the tall bell-tower and the three immense curved shells, required Italcementi's contribution for the bold technical-structural solutions. Italcementi, technical sponsor

of the project, is participating in the construction of the Church, by supplying know-how, technical assistance and structural calculations, in addition to the highly technological and innovative products amongst which is the new white cement "TX Millennium", whose formulation (patented) guarantees unparalleled whiteness which remains constant over time.

The three sails are made of 346 white, reinforced, precast concrete blocks (mean dimensions: 3x2x0.8 m), Figures 5 and 6. They are spherical, curving horizontally and vertically. A single stainless-steel form, adjustable on the ends only, was used for every block.

All the rows are post-tensioned vertically and horizontally with steel rods and cables so that the entire shell is in continuous compression.

3.1 Mix design of white HPC for the sails

For this application, Italcementi's R&D Department developed the white HPC for the project, including photocatalytic particles in the mixture which oxidize organic and inorganic atmospheric pollutants, so that the brightness and the colour will not degrade over time [18].

Figure 5. Construction of the Church (sails)

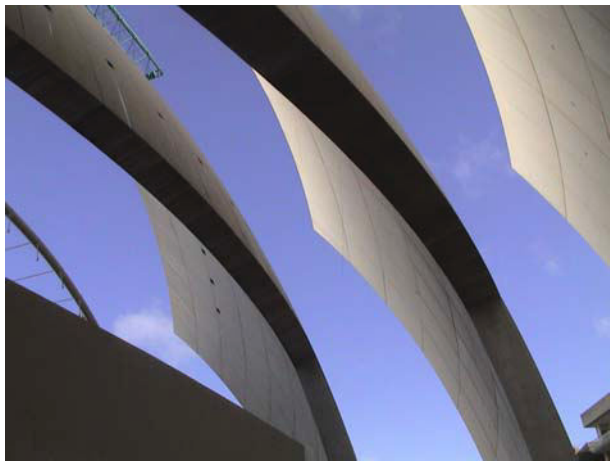

Figure 6. Church in Rome – Internal view

Thanks to the possibility of staying close to a w/b ratio of roughly 0.38 and to the double-admixture technique (compatibility agent + acrylic superplasticizer), the actual amount of white TX Millennium cement needed was quite low (380 kg/m^3) and the workability of the concrete was high. The compatibility agent increases substantially the action of the acrylic superplasticizer in order to maintain the workability of the fresh white concrete till about 60 minutes. As this structure had to be entirely white, a white Apuan marble aggregate was selected (from the Carrara area), consisting of a crushed metamorphic limestone with a fine grain, compact and uniform saccharoid structure. The maximum particle size was limited to 20 mm to ensure that the concrete would flow through the reinforcement and covers (40 mm) and at the same time to contain or at least greatly reduce surface defects (bug holes, gravel clusters, etc.) also linked to the elevated bulk of the aggregate due to the wall effect. A white metakaolin and an acrylic superplasticizer were also used. Table 1 shows the typical composition of the white HPC utilized [18].

Table 1. Mixture proportions

White cement TX Millenium	380 kg/m^3
White metakaolin (with special compatibility agent)	38.7 kg/m
Aggregates: Crushed marble d_{max} = 20 mm	1850 kg/m^3
Acrylic superplasticizer (solution, 30% dry extract)	10.5 kg/m^3
Water	160 l/m^3

3.2 Physical and mechanical properties

The consistency class was S5, the mean volumic mass weight was 2430 kg/m^3.

Table 2 below shows the varying compressive strength of the concrete at different stages in the curing process. Other mechanical properties are shown in Table 3.

Table 2. Compressive strength, MPa

24 hours	35.0
30 hours	41.0
2 days	47.7
3 days	58.2
7 days	69.8
9 days	72.5
28 days	86.2
90 days	89.8

Table 3. Other mechanical properties

Flexural strength, 7 days	7.0 MPa
Flexural strength, 28 days	10.4 MPa
Indirect tensile strength, 28 days	7.0 MPa
Dynamic elastic modulus, 28 days	44.6 GPa
Static elastic modulus, 28 days	41.0 GPa

Further information concerning hygrometric deformation (shrinkage), creep values, freeze-thaw behaviour and thermal behaviour are reported in [18, 25].

4. CONCLUSIONS

Cementitious materials containing TiO_2 mainly in the form of anatase, when irradiated with adequate light, enhance the oxidation efficiency on organic substances with which they come into contact.
Building elements containing white cements to which TiO_2 has been added are capable of maintaining their aesthetic appearance unaltered with time.

With respect to the improvement in our living standards, we believe that a massive and continuous use of photocatalysts in construction materials can be a new way of contributing to minimizing the contaminants attacking the urban environment.

Many applications are possible, using white cement: dry pre-mix mortar for aesthetic and structural rehabilitation of deteriorated surfaces, cement-based paints, cladding and flooring, urban settings, art restoration and mortars for plasters and spray coatings.

REFERENCES

[1] Tognon, G. Fair-faced concretes. Mixtures and skin, BIBM 75 - 8th Int. Concress, Stresa, Italy, 1975, pp. 19.
[2] Serpone, N. and Pellizzetti, E. Photocatalysis. Fundamentals and applications, J. Wiley & Sons Ed., 1989.
[3] Linsebigler, L., Lu, G. and Yates, J.T. Chem. Rev., vol. 95, 1995, p. 735.
[4] Herrmann, J.M. Lectures from the summer school at the Plataforma Solar de Almeria, Applications of Solar Chemistry, 1998.
[5] Litter, M. Appl. Catalysis B: Environmental, vol. 23, 1999, p. 89.
[6] Amadelli, R., Maldotti, A., Sostero, S. and Carassiti, V.J. Chem. Soc. Faraday Trans., vol 85, 1991, p.3267.
[7] Hoffmann, M.R., Martin, S.T., Choi, W. and Bahnemann, D.W. Chem. Rev., vol. 95, 1995, p. 69.
[8] Honda, K. and Fujishima, A. Nature, vol. 238, 1972, p. 37.
[9] Kawai, T. and Sakata T. Nature, vol. 286, 1980, p.474.
[10] Fujishima, A., Hashimoto, K. and Watanabe, T. TiO_2 Photocatalysis: Fundamentals and its Applications, BKC Inc., 1999.
[11] Ehses, M., Frenzer, G., Müller, P. and Schmidt, H. Workshop on Utilization of Photocatalytic Coatings for Clean Surfaces, Saarbruecken, Germany, 2001.
[12] EP Patent Nr. 946450, Italcementi SpA, 1999.
[13] Cassar, L., Pepe, C., Pimpinelli, N., Amadelli, R. and Bonato, T. Seminario FAST – Materiali: Ricerca e Prospettive Tecnologiche alle Soglie del 2000, Milano, Italy, 1997, p. 591.
[14] Cassar, L., Pepe, C., Pimpinelli, N., Amadelli, R. and Bonato, T. Gordon Conference, Il Ciocco, Lucca, Italy, 1999.
[15] Cassar, L., Pepe, C., Pimpinelli, N., Amadelli, R. and Antolini, L. Rebuilding the City of Tomorrow, 3rd European Conference REBUILD, Barcelona, Spain, 1999.
[16] Hashimoto, K., Wasada, K., Osaki, M., Shono, E., Adachi, K., Toukai, N., Kominami, H. and Kera, Y. Appl. Catal. B: Environmental 30, 2001, p. 429.
[17] Murata, Y. et Al. J. Dv. Oxid. Technol., Nr. 4, 1999, p. 227.
[18] Cassar, L., Pepe, C., Tognon, G., Guerrini, G.L., Cangiano, S. and Goisis, M. L'Industria Italiana del Cemento, Nr. 751, 2000, p. 160.
[19] US Patent Nr. 6,117,229, Italcementi SpA, 2000.
[20] FIP/CEB, High Strength Concrete, Bull. Inf. Nr. 197, August 1990, pp. 61.
[21] Sokkar, S.L. and Aimuxu Why use mineral admixtures in high performance concrete, L'Industria Italiana del Cemento, 1996, pp. 714-726.
[22] Caldarone, M., Gruber, B. and Burg, R. High-reactivity metakaolin: a new generation mineral admixture, Concr. Int., vol. 16, 1994, pp. 37-40.
[23] Wild, S., Khatib, J.M. and Jones, A. relative strength, pozzolanic activity and cement hydration in superplasticized metakaolin concrete, Cement and Concrete Research, vol. 26, 1996, pp. 1537-1544.
[24] Goisis, M., De Marco, T., Pepe, C. and Cassar, L., PCT Application WO 99/55634, Italcementi SpA, 04/11/1999.
[25] Guerrini, G.L. and Rosati, G.P. Residual strength of white cement concrete exposed to high temperature, Paper accepted for Presentation and Publication at 6th CANMET/ACI International Conference on Durability of Concrete, Thessaloniki, Greece, June 2003.

DIFFERENT ASPECTS FOR THE HYDRATION OF C_3A AT ROOM TEMPERATURE

H.Y. Ghorab

Faculty of Science, Helwan University, Cairo, Egypt. E-mail: h_ghorab@hotmail.com
G & W Science and Engineering Company, Cairo, Egypt.

ABSTRACT

The mechanism of hydration of C_3A in water, alkali hydroxide and alkali sulfate solutions, also in the presence of gypsum, lime and alite is interpreted in terms of the change in the concentrations of the dissolved sulfate, aluminate and calcium ions, with time, in correlation with the stability of the solids. In the absence and the presence of gypsum, the dissolved lime enhances the gel-like character of the hydrate coat around the C_3A and retards its hydration. The composition of the gel varies between that of the calcium aluminate- carbo-and sulfoaluminate hydrates. C_3A is directly consumed by excess lime, but its hydration is strongly retarded by a mixture of gypsum and excess lime. Excess lime in strong alkali hydroxide solution causes a direct consumption of both C_3A and gypsum. Alkali hydroxide depresses the solubility of lime and favors the formation of the monophases.

The dissolved lime is responsible for the decomposition of the monophases to ettringite in the absence of an external sulfate supply, for the precipitation of syngenite and hydroglauberite in $\geq$0.5M alkali sulfate solutions and for the transformation of hydroglauberite to ettringite with time. The ettringite forms as a result of different types of interactions and with various morphology depending on the solution composition and the hydration time.

1. INTRODUCTION

The hydration of C_3A is quite a complicated process and depends on the types of the reactants and the respective solution composition. It was the subject of work by many researchers starting a few decades ago [1-5]. Because of its importance in phenomena occurring in cement and concrete such as delayed ettringite formation [6-10] and the function of superplasticizer [11-12], its chemistry needs further understanding. The present work presents a contribution to this field of research.

2. EXPERIMENTAL

The C_3A and alite samples were prepared through burning stoichiometric mixes of calcite with alumina at 1350 ^oC and calcite with quartz with minor additions of alumina and magnesia at 1450^oC. Gypsum, lime, alkali hydroxides and alkali sulfates were reagent grade. The system no I studied included mixtures of C_3A with different gypsum additions of SO_3/Al_2O_3 ratio of 0.6, 0.8, 1 and 1.5 [13,14]. The mixture with a ratio of 1.5 was taken as reference to study the effect of lime and alite. In system II, the reaction was carried out in an unsaturated lime solution of 0.6 g CaO/l as well as in the presence of an excess amount of lime (6g/ l) [13,15]. In system III and IV, three concentrations of alite were added to the reference mixture and to that containing lime [16,17]. ~ 0.3g of the C_3A was used in each system, and the weights of the reactants corresponding to the

ratios taken were applied. In system V, 0.3g of alite was hydrated with different gypsum additions in the absence of C_3A [16,17].

The mixture of C_3A and gypsum chosen as the reference mixture, with a mole ratio of SO_3/Al_2O_3 equal to 1.5, also in the presence of lime and alite were used to study the hydration reaction in 0.1, 0.5 and 1M alkali sulfate solutions [18,21] and in 0.01, 0.1 and 1M alkali hydroxide solutions at room temperature [22,23]. 1M potassium sulfate solution could not be prepared because it formed a supersaturated solution. The systems studied are cited in table [1].

The reactants were stirred in 100ml of redistilled water in tightly closed glass flasks at room temperature for time intervals 2, 15, 30 minutes, 1, 3, 6, 24 hours and 3, 5, 7 days. At the definite interval, the solutions were filtered off, and in the filtrate, the sulfate ions were determined turbidimitrecally [24] and the aluminium colourimetrically using aluminon indicator [25]; the pH-values were also determined. The solids obtained after filtration were dried for 24 hours at 50°C then analyzed by means of X-ray diffraction. A few samples were examined by the scanning electron microscope and analyzed by EDAX.

Table1. The systems studied on the reaction of C_3A and gypsum in water at room temperature.

Sys.	Mixture	Mole ratio and reaction media
I	C_3A-G*	a) 1:0.6 b) 1: 0.8 c) 1:1 d) 1:1.5 in water 1:1.5 in 0.01,0.1,1M sodium hydroxide solutions 1:1.5 in 0.1, 0.5, 1M alkali sulfate solutions
II	C_3A-G-C	a) 1:1.5:1 b) 1:1.5:10 in water and 0.01, 0.1 1and 1M sodium hydroxide solutions 1:1.5:1 in 0.1 and 1M alkali sulfate solutions
III	C_3A-G-A	a) 1:1.5:0.1 b) 1:1.5:1 c) 1:1. 5:10 in water
IV	C_3A-G-A-C	a) 1:1.5:0.1:1 b) 1:1.5:1.0:1 c) 1:1.5 :10 :1 in water 1:1.5:1:1 in 0.5 and 1M alkali sulfate solutions
V	G-A	a) 0.1:1 b) 1:1 c) 10:1 in water

*G= Gypsum C=CaO A=Alite

3. RESULTS

The reaction mechanism of the C_3A in water is well known to occur in three steps: The instantaneous reaction, the dormant period and the acceleration period. These stages can be described on the basis of the solution composition of the different systems studied as follows:

3.1 The instantaneous reaction

3.1.1 The aluminate of the solution

The absolute solubility values of the C_3A depends on the reactivity of the prepared crystals, the solution composition and the W/S ratio; the one cited may be considered as a guide.

The reaction of the C_3A with water leads to a quick release of hydroxyl ions to reach a pH- value of around 11 with the solubilization of 70ppm aluminium. Close values are found in the presence of a low gypsum addition (mole ratio G:C_3A = 0.6) as well as in 0.1M Na_2SO_4 solution. The solubility of C_3A increases to 160 ppm Al in 1M Na_2SO_4. By increasing the gypsum addition to a mole ratio of 0.8 to 1.5, also in 1M NaOH and 0.1M K_2SO_4 solutions, the solubility of C_3A is depressed to a range of 13-19 ppm Al. In 0.6g CaO/l the aluminium concentration is depleted to 4ppm in the absence of gypsum, and to a zero value in its presence.

3.1.2 The sulfate of the solution

As soon as water is added to a mixture of C_3A with gypsum (mole ratio G:C_3A=0.6-1.5), 21 to 33% of gypsum dissolves releasing calcium and sulfate ions to the solution, and around 55% are left in the solid. The concentration of the dissolved ions increases, the higher the gypsum content. Meanwhile a thin coat of hydration products forms around the C_3A grains and the coated crystals remains in an intimate adherence to the gypsum left.

The calcium sulfate concentration of the solution measured after 2 minutes from the reaction start is less than the solubility value of gypsum at room temperature in spite of having enough solid to attain this value. This indicates that the hydrate coat formed around the C_3A results from the uptake of the calcium sulfate of the solution and should therefore incorporate the respective calcium sulfate concentration in its structure, a process which must have occurred within the first few seconds of the reaction. The amount of calcium sulfate consumed from the liquid phase was found to be in the range of 33 to 22% of the gypsum added. In the presence of alite there is an additional uptake of the dissolved calcium sulfate by the calcium silicate hydrate coat of the C_3S grains with a further depression of the calcium sulfate from the solution.

The initial solubility of gypsum is not influenced by lime which, however, affects the morphology and the type of the hydrate coat. Alkali hydroxide solutions tend to retain the sulfate of gypsum as sodium sulfate and to precipitate portlandite. Gypsum dissolves in 0.1M NaOH. In a solution of $\geq$0.1M alkali sulfate, the gypsum phase, does release no more of its sulfate because of the common ion effect.

3.1.3 The calcium ions of the solution.

The calcium ion concentration in the water solution of C_3A and gypsum is expected to be parallel to that of the sulfate with a minor contribution of the calcium aluminate phase. It decreases with alkali hydroxide content because of the precipitation of the less basic portlandite. Alkali sulfate solutions may accommodate calcium ions up to the solubility value of lime at room temperature. This is reached by the addition lime and/or alite. Because of the common ion effect, the amount of calcium released from gypsum in alkali sulfate solutions is slightly depressed.

3.1.4 The hydrate coats around the C_3A grains:

It is to be remembered that the carbonation effect plays an important role in the hydration of the C_3A especially in the absence of gypsum. The tetracalcium aluminate hydrate is very susceptible to atmospheric CO_2, and forms a series of solid solutions including different concentrations of hydrated lime and carbonate ions which are called the sulfate-free monophases (Mo). A complete carbonation of the tetracalcium aluminate hydrate results in the formation of the monocarboaluminate hydrate (Mc). Hydrated lime and sodium hydroxide are also subjected to carbonation. The process seems to proceed at a rate slower than that of the carbonation of the tetracalcium aluminate hydrate.The tetracalcium aluminate hydrate and its carbonated forms may form a solid solution with the monosulfate hydrate (Ms) which may be called the sulfate bearing monophases..

The crystalline tetracalcium aluminate hydrate or some of its carbonated solid solution, forms a coat around the C_3A grains as soon as the reaction begins in water or sodium hydroxide solution. This occurs in a solution of a calcium ion concentration < 0.6g CaO/l, and 10 to 70 ppm aluminium. At a CaO solution $\geq$ 0.6g/l with no dissolved aluminium, hydrogarnet forms. The hydrate coat may incorporate calcium sulfate with a concentration equal to the amount taken from that instantaneously released from gypsum to the solution. The low and high sulfate forms of the calcium sulfoaluminate hydrate are formed instantaneously in a solution with 240-940 ppm $SO4^{--}$ and 70 to13 ppm Al. At a calcium ion concentration equal to 0.6g CaO/l, and less than the solubility

value of lime, the reaction occurs with no contribution of C_3A to the liquid phase because the aluminium is totally depleted from the solution. Under these conditions a gel-like ettringite forms. In the presence of gypsum and excess lime a gel-like monophase forms. In the presence of gypsum, excess lime and 1M NaOH C_3A and gypsum are consumed and only portlandite remains. In alkali sulfate solution of 0.1M, a more crystallized ettringite forms which increases its gel–like properties by lime addition. At 0.5M K_2SO_4 and in the presence of lime, syngenite precipitates beside the ettringite, but in 1M Na_2SO_4 solution rich in lime, the sodium sulfate salt precipitates and not hydroglauberite because of the supersaturation effect.

Tables (2) and (3) give a short summary on some of the phases composing the instantaneous coat of the C_3A grain as soon as its reaction begins with the aqueous medium, in the absence and presence of gypsum.

Table 2. The phases formed instantaneously around the C_3A grains during its hydration in the absence of gypsum and the respective solution composition.

Phases formed	CaO (g/l)	Al (ppm)	Reaction medium	Remarks
Sulfate –free Mo/Mc*)	<0.6	10-70	H_2O/0.01-1M NaOH	
Mc-Hg*	0.6	4	H_2O	
CH*	1.13	Zero	H_2O/1M NaOH	Excess lime. Quick consumption of C_3A

Table 3. The phases formed instantaneously around the C_3A grains during its hydration in the presence of gypsum and the respective solution composition.

Phases formed	CaO (g/l)	Al (ppm)	$SO4^{--}$ (ppm)	Reaction medium	Remarks
Ms+E*	<0.6	13-70	240-940	H_2O	
E	<0.6	160	~8000	0.1M Alkali sulfate	
Gel-like E	$\geq$0.6-<1.13	Zero-4	$\leq$8000 $\geq$940	H_2O/0.1M Alkali sulfate	
Gel-like Mo	1.13	Zero	940	H_20	Excess lime
Sulfate-bearing Mo*	<0.6	Zero-38	~1400	0.01 to 1M NaOH	
CH	1.13	20	~1400	1M NaOH	Excess Lime. Quick dissolution of C_3A and gypsum
E+Syngenite	$\geq$0.6	Zero	$\geq$48000	$\geq$ 0.5M K_2SO_4	

*Sulfate-free Mo: Solid solution between tetracalcium aluminate hydrate and its carbonated forms Mc: Monocarboaluminate hydrate
Hg : Hydrogarnet
CH : Hydrated lime (portlandite
Sulfate-bearing Mo: Solid solution between tetracalcium aluminate hydrate, its carbonated forms and monosulfate hydrate
Ms : Monosulfate hydrate
E : Ettringite

3.2 The dormant period and the acceleration reaction

The reaction of C_3A with water decelerates after the instantaneous formation of the hydrate coat around the surface of its grains. This stage lasts until the hydrates precipitate as a result of

increasing the crystallization pressure, and new surfaces of C_3A are exposed to further reactions. The behavior of the ions in the liquid phase are mostly indicative of the dormant period and the acceleration reaction. The duration times of the reactions described below are a useful guide for the different interactions but their absolute values may vary with the reactivity of the phases and the W/S ratio.

In the absence of gypsum, the crystallized calcium aluminate hydrates coat first formed during the hydration of C_3A in water, continues to form over 15 minutes while the aluminium increases in the solution from 70 to 90 ppm, then remains constant The C_3A is consumed at 3 hours with the precipitation of a well crystallized hydrate. The hydration of C_3A in 1M NaOH solution leads to a steady increase of the aluminium concentration in the solution from 19 to 80 ppm with an accompanying formation of amorphous calcium aluminate hydrates which crystallize as monocarboaluminate hydrate at a later time. In 1M NaOH, the C_3A consumption is delayed to 1 day. 0.6 g CaO/l depresses the initial solubility of C_3A to 4 ppm and leads to the formation of hydrogarnet. The dissolved aluminium rises to 7 ppm within few minutes then becomes constant. In this unsaturated lime solution, the C_3A is consumed at 1 day. In the presence of excess lime, the aluminium ion is totally depressed from the solution but the C_3A is consumed within the first two minutes as a result of a solid-solid reaction. Under these conditions, mainly portlandite precipitates beside weakly crystallized carbonated tetracalcium aluminate hydrate which then transforms to hydrogarnet with time.

In the presence of gypsum, the hydration of C_3A decelerates as a result of the formation of a coat of calcium sulfoaluminate hydrates around its surface. In a solution of CaO concentration <0.6g/l. the dormant period is indicated by a constant sulfate ion concentration of the liquid phase, and lasts 15 minutes. The gypsum left in the solid then reacts with the dissolved aluminium which decreases in the solution from a highest value of 70 ppm to a minimum of 8 ppm Al in the different mixtures studied. The solubility curves of aluminium are lower, the higher the gypsum content. During this duration, both types of the calcium sulfoaluminate hydrates continue to form while the initial sulfate concentration of the solutions is constant. In this system, the dormant period is controlled by the consumption of gypsum and ends with the crystallization of the hydrate coat from around its grains. The new C_3A surface reacts then with the dissolved calcium sulfate with the precipitation of ettringite crystals. When all the dissolved calcium sulfate is used up, the excess C_3A reacts with the ettringite to form the monosulfate hydrate with the evolution of aluminium to the solution.

In solution with 0.6g CaO/l, the initial solubility of C_3A is totally depressed and results of an instantaneous formation of a gel-like ettringite coat. This hydrate continues to form with the progress of the reaction as a result of the diffusion of the gypsum left in the solid through its layer. Under these conditions, gypsum is consumed in 5 hours with a marked prolongation of the dormant period compared to that in the absence of lime. The dissolved calcium sulfate does not take part in this reaction and is seen to even increase slightly to approach the solubility of gypsum at room temperature. After the dormant period, the fresh C_3A surface reacts with the dissolved calcium sulfate to form ettringite and in a calcium sulfate- free solution the ettringite reacts with the excess C_3A to form the monosulfate hydrate. This in turns decomposes partially to ettringite because of the availability of calcium ion in solution.

In the presence of excess lime, the coat is composed of gel-like monophase, rich in calcium hydroxide. This further retards the gypsum diffusion and its consequent consumption to 1 day, the calcium sulfate of the solution remaining constant. At the end of the dormant period the fresh C_3A surfaces reacts with the dissolved calcium sulfate precipitating the ettringite. After the depletion of the dissolved sulfate, however, the ettringite phase does not convert to the monophase. This is attributed to the increased usage of the C_3A by lime over the progress of the reaction and little is available for the stage of the ettringite-monophase conversion.

In a solution <0.6g CaO/l, the alite phase contributes to the reaction of C_3A with gypsum by releasing part of the incorporated calcium sulfate taken up from the solution at the first moment of the reaction, while gypsum is reacting with the dissolved aluminate in a way similar to that of C_3A with gypsum; and with a similar duration of 15 minutes. The increased alite addition leads to the rise of lime concentration of the solution which process does not take place directly but needs an appreciable duration of time. When the lime concentration of the solution reaches a value $\geq$ 0.6 CaO/l, the aluminium is depleted, and a long lasting diffusion control mechanism occurs.

In an alkali sulfate solution and in the absence of gypsum, the C_3A releases more aluminium to the solution, the higher the concentration of the alkali sulfate The instantaneous value of aluminium is as high as 160 ppm in 1M Na_2SO_4 at a lime concentration of 0.1g CaO/l and a sulfate concentration of 96g SO_4^{--}/l This sulfate-rich solution precipitates both ettringite and the sodium sulfate salt all over the reaction period. An ettringite coat around the C_3A grains must have occurred because the C_3A consumption takes place after 3 hours during which constant values of the dissolved aluminium and calcium are maintained. After the dormant period, the fresh C_3A reacts with some of the existing sulfate of the solution with a further precipitation of ettringite, the calcium ion of the solution decreases and aluminium is released. When gypsum is added to the C_3A, it reacts with the dissolved aluminium in a way similar to that occurring in water while the calcium ion is kept constant in solution. In $\geq$0.5M Na_2SO_4 solution, lime enhances the precipitation of sodium sulfate hydrate crystals which takes up the dissolved calcium and sulfate ions with time to form hydroglauberite. This in turns transforms to the more stable ettringite with a further uptake of calcium from the solution. Syngenite is more basic than hydroglauberite and precipitates more readily from 0.5M K_2SO_4 solution of C_3A, gypsum in the presence of enough lime. It should be noted that, in 1M alkali sulfate solution, the C_3A reaction is quite fast because of the precipitation of the salts and double salts, but if the solution becomes saturated with lime and alite, it is slightly retarded. The retardation effect is, however, more clear in a solution of a lower alkali sulfate concentration of 0.1M (9.6g SO_4^{--}/l) and a lime concentration >0.6 CaO/l, which sulfate concentration is lower than that needed for the precipitation of the double salts or the saturation value of the salts. A mixture of C_3A, gypsum, lime and alite with a mole ratio of 1:1.5:1:1 may cause a dormant period of C_3A of 7 days long as indicated by a constant calcium ion concentration in an aluminium-free solution. At the acceleration period, the calcium ion decreases with a slight decrease of the sulfate from the solution.

Alkali hydroxide tends to retain the sulfate of gypsum as sodium sulfate as well as some of the aluminate and to precipitate portlandite. The hydrate coat becomes rich in calcium hydroxide and poor in sulfate and causes the retardation of C_3A hydration. In the acceleration period the fresh C_3A surface reacts with the dissolved calcium sulfate left in solution rather than taking up the sulfate dissolved as sodium salt. In an extreme case for the reaction of C_3A in 1M NaOH and in the presence of excess lime, both gypsum and C_3A are consumed instantaneously, the completion of the precipitation of portlandite is the rate determining step for the reaction while the dissolved sulfate remains constant in solution. The portlandite then reacts with some alumina with the formation of monophases.

3.3 Summary of the mechanism of the C_3A hydration

The above described reactions of the C_3A hydration are seen to be strongly dependent on the concentrations of the solid reactants as well as the respective ions in the solutions. The hydration kinetics of the C_3A is mainly governed by the behavior of the calcium oxide in the solution, rather than that of the calcium sulfates. The dissolved calcium oxide controls the solubility of C_3A with respect to the release of aluminium to the solution. The aluminium is evolved to the solution at a lime concentration less than 0.6g CaO/l and leads to the formation of a sulfate-free or sulfate-bearing hydrate coat of a crystalline character, in water, alkali hydroxide solution, in the absence or

the presence of a sulfate supply . At a limited supply of calcium sulfate as in the presence of gypsum (mole ratio to $C_3A \leq 1.5$) the monosulfate hydrate appears beside the ettringite as long as the calcium aluminate is available in the solution. At an excess supply of sulfate as in alkali sulfate, only ettringite forms. The hydration of C_3A is thus quite rapid if the calcium aluminate in the solution contributes to the reaction. If the aluminate is, however, in the form of sodium aluminate with no calcium ions in solution the reaction may be retarded because of the interaction of C_3A with the precipitated portlandite.

The depletion of the aluminium concentration of the solution by a lime concentration $\geq$ 0.6g CaO/l and <~1.13g CaO/l leads to a gel-like hydrates around the surface of the C_3A grains and the hydration of C_3A is retarded. This occurs when the reaction of C_3A proceeds in water, alkali hydroxide solution also in the presence of gypsum and in alkali sulfate solutions. The successive reaction of C_3A is then governed by a diffusion reaction either of more hydroxyl ions or of gypsum and is a slow process. This occurs in the presence of alite which releases few lime to the solution at the beginning of the reaction with a slight delay of the precipitation of portlandite.

The C_3A hydration may be accelerated in an aluminium-free solution in the presence of excess lime because of a quick solid-solid reaction but is, however, strongly retarded by gypsum addition which has to diffuse through the thick hydrate coat of the monophases This occurs in water, in <0.1M alkali sulfate solution but in strong alkali hydroxide solution of 1M, gypsum dissolves and the C_3A hydration is again accelerated.

The double salts syngenite and hydroglauberite precipitate from alkali sulfate solutions $\geq$ 0.5M and a CaO concentration $\geq$ O.6 g/l. Because of the strong basic character of potassium the syngenite precipitates directly but the hydroglauberite precipitation is delayed.

3.4 Interpretation of some results of the literature

Stark et al [26] used two types of cement with low and high alkali content (soluble potassium oxide of 0.33% and 1.09%). The ettringite formed directly in paste with a W/S of 0.3 in the low alkali cement and together syngenite in that of the high alkali. The syngenite appears at later stages of the alkali-poor cement but transforms to ettringite with time. According to the present results, the syngenite must have precipitated from a potassium sulfate solution $\geq$ 0.5M and a lime concentration $\geq$0.6 CaO/l. The transformation of syngenite to ettringite must take place in a way similar to that of hydroglauberite, i.e. through the uptake of more lime available in the solution, the expected consequence is the release of the potassium ion to the solution either as potassium hydroxide or in the presence of enough sulfate as potassium sulfate.

The present work shows that, at the stage following the acceleration period, the monosulfate hydrate remains as the only calcium sulfoaluminate hydrate if the solution of C_3A and gypsum with a mole ratio of 1:1.5, has a CaO concentration < 0.6 g/l which allows the release of the aluminium to the solution. At a lime concentration equal to 0.6g CaO/l part of the monosulfate hydrate decomposes to ettringite and both phases remain in the solid. The sulfate content in both the ettringite and the monophase are of actual discussion [27] and is suggested to be lower than the stoichiometric value. This explains the existence of both ettringite and the tetracalcium-sulfoaluminate hydrate as final product in the work of Stark et al [26] The uptake of sulfate ions from alkali sulfate solution by sulfate deficient calcium sulfoaluminate hydrate is not favored if the solution is poor in calcium.

Sakai et al [28] reported that the production of gel containing SO_4^{--}on the C_3A surface is important for the retardation of C_3A with various types of calcium sulfates. The present work shows that, the gel coat forms at a lime concentration of the solution $\geq$0.6 g CaO/l because of the depression of the aluminium which process occurs in the presence or absence of gypsum. Gypsum leads to the formation of an X-ray amorphous ettringite coat instead of the an X-ray amorphous calcium

aluminate or carboaluminate hydrate formed in its absence. The concentration of the sulfate in the gel increases with the increase of gypsum content and the decrease of the lime concentration in the solid. Hemihydrate contributes to the reaction by supplying more calcium sulfate to the solution compared to gypsum and the amount of the gypsum left in the solid to control the diffusion mechanism with C_3A decreases. The presence of lime with hemihydrate contribute to the reaction by increasing the monophases coat around the C_3A grains and causing a further retardation.

The crystalline character of the hydrate coat is gained at a lime concentration of the solution below <0.6g CaO/l which allows the release of aluminium . In the presence of gypsum, an uptake of the calcium sulfate from the solution occurs with the formation of both types of the calcium sulfoaluminate hydrate and the hydration reaction of C_3A is not retarded.

REFERENCES

[1] Schwiete, H.E., Ludwig,U. and Jaeger,P.L. Symposium on structure of Portland cement pastes and Concrete (Spec.report 90), Highway Research Board, Washington,1966,pp.353

[2] Locher, H.F.W.: Hydration of pure Portland cements. 7th International Congress on the Chemistry of Cement, Paris, vol 4, 1980, pp. 49-55.

[3] Stein,H.N.: Silicates Industrials,.vol. 28, 1963, pp.141.

[4] Collepardi,M.,Baldini,G.,,Pauri,M.,and Corradi, M.: Cement and Concrete Research, vol. 8, 1978, pp.571.

[5] Seligmann,P. and Greening,N.R. HighwayResearch Board., 62, 1964, pp.89.

[6] Taylor,H.F.W., Famy,C. and Scriviner,K.L. : Delayed ettringite formation . Cement and Concrete Research vol.31, 2001, 683-693.

[7] Scriviner, K., Famy,C., Michaud,V.: Under what conditions can the formation of ettringite cause damage in concrete.14th International Baustofftagung, Weimar, vol.1,2000,pp.1-1173.

[8] Diamond,S. Delayed ettringite formation- processes and problems. Cement Concrete Composite. Vol,18 (3), 1996, 205-215.

[9] Johanson, V., Thaulow, N. J. Skalny,J. Simultaneous presence of alkali- silica gel and ettringite in concrete. Advanced Cement Research, vol. 5 (17), 1993,pp. 23-29.

[10] Stark,J.,Bollmann, K,. Seyfarth,K.1998. Ettringite-cause of damage, damage intensifier or uninvolved third party? Zement Kalk Gips International. Vol. 51 (5), 998, pp.280-292.

[11] Ramachadran,V.S., Malhotra,V.M., Jolicoeur,C. and Spiratos,N.. Superplasticizers: Properties and application in concrete. CANMET, Canada, 1998.

[12] Masazza, F., Costa,U. and Corbella,E.. Influence of beta naphthalene sulfonate formaldehyde condensate superplasticizing admixture on C_3A hydration in the reaction of aluminates during setting of cements. CEMBUREAU Rept.,3, 1977.

[13] Abou El Fetouh,S.H..: Studies on the hydration of the tricalcium aluminate. Ph.D. Thesis, Ain Shams University, 1985.

[14] Ghorab, H.Y, Abou El Fetouh, S.H. :Effect of gypsum additions on the hydration of tricalcium aluminate at 30°C. Egyptian Journal of Chemistry, vol. 29, 1986, pp. 265-273.

[15] Ghorab, H.Y, Abou El Fetouh A new approach to the hydration reaction of the tricalcium aluminate with gypsum Part 1: Effect of lime. Zement Kalk Gips, vol. 38, 1986,pp. 267-270.

[16] Ahmed, H.M. Studies on some factors affecting the hydration reaction of tricalcium aluminate. M.Sc. Thesis, Ain Shams University, 1989.

[17] Ghorab,H.Y. and Ahmed,H.M. The liquid-solid interaction in pure systems of Portland cement Part I: The alite-gypsum-water system Zement Kalk Gips,vol. 11, 1989, 581-583. Part II: The effect of alite on the hydration reaction of C_3A with gypsum also in the presence of lime Zement Kalk Gips,vol. 1, 1990, 34-37.

[18] Nour ElDin,.M.A. Effect of sulfate and chlorides on the hydration reaction of the cement compounds. M..Sc.Thesis, Ain Shams University, 2000.

[19] Ghorab,H.Y,.Anter,A. and Nour El Din,M.A.The hydration of C_3A in water and sodium sulfate solution: A comparative study. The 4th International symposium on cement and concrete, Beijing, 1998,269-273.

[20] Ghorab,H.Y., Ahmed,S.T. and Ahmed,H.M. :The alkali-cement system. Advances in Cement Research,vol.1(4), 1991/1992,.39-46

[21] Ghorab,H.Y, Salem,T. Anter,A,. Nour El Din, M.A. : The $C_3A$and gypsum in alkali metal sulfate solutions. In preparation.

[22] Ghorab,H.Y., Abou El Fetouh, S.H. and. Marusin, L.S.: Effect of lime and alkali on the hydration reaction of C_3A in presence of gypsum.7th International Conference on Cement Microscopy, Texas,.1985,p.232-241.

[23] Ghorab, H.Y,and Abou El Fetouh,S.H. :The role of sodium hydroxide in the system C_3A-$CaSO_4$.H2O at 30°. Material Research Society,vol.85, 1987,pp. 255-260.

[24] APHA-AWWA-WPCF: Standard methods for the examination of water and waster water American Public Health Association 15th Edition, 1980, 439.
[25] Vogel,A.I. Quantitative inorganic analysis. Longmans Green &Co Ltd, 1961,p. 792.
[26] Stark.J., .Moeser.B., Bellman,F. New approaches to ordinary Portland cement hydration in the early hardening stages. The 5th International Symposium on Cement and Concrete. Shanghai, 2002, vol.1, pp.56-70.
[27] Ghorab,H.Y. :Causes of the delayed ettringite formation. Internationa.Symposium on Non-Traditional Cement & Concrete. Brno, Czech Republic. June (2002),472-481.On the chemistry of the delayed ettringite formation. Report on the delayed ettringite formation.Lausanne 2002. To be published RILEM.The stability of the calcium sulfoaluminate hydrates. The 5th International Symposium on Cement and Concrete. Shanghai,2002,vol.1,pp.202
[28] Sakai, E, Kang J-K, Diamon M. Control methods for the early hydration in $Ca_3Al_2O_6$-gypsum system with superplasticizers. The 5th International Symposium on Cement and Concrete,. Shanghai, 2002, vol.1, pp.195-201.

DIFFERENT ASPECTS FOR THE HYDRATION OF C_3A AT ROOM TEMPERATURE

Hanaa Y. Ghorab

Faculty of Science, Helwan University, Cairo, Egypt. E-mail: h_ghorab@hotmail.com
G & W Science and Engineering Company, Cairo, Egypt.

Biography

Prof.Dr.rer.nat.Hanaa Youssef Ghorab (Mrs.). B.Sc.Chemistry, Honor Degree, Faculty of Science Ain Shams University (1966), Cairo Egypt. Master in Solid State Science, American University, Cairo (1968). Master Physical Chemistry, Ain Shams University, Cairo (1974). Doctor rer.nat Aachen, Germany (1979). Lecturer to Professor, Director of Cement Chemistry Laboratory, Ain Shams University (1980-1992).Professor Helwan University, Cairo, since 1995, Vice Dean for Environment (1995-1998),(2002).

ON LINE QUALITY CONTROL INSTRUMENTATION FOR THE COMPLETE CEMENT MANUFACTURING PROCESS

A. Haider

Iteca, France.

ABSTRACT

New instrumentation is now available on the market that provides an effective way of controlling the complete cement manufacturing process.

Traditionally these controls were carried out by taking samples from the process, and analyzing them in a central laboratory, either manually or in some cases automatically.

This approach is being challenged in modern cement plants, by the installation of an 'On Line measurement systems', that present a number of advantages over the traditional methods, notably in terms of higher frequency and more timely controls, resulting in energy savings and better and more stable product quality.

These instruments also have the advantage of being cheaper, and simpler to operate then central automatic laboratories.

The object of this article is to give a brief description of each of these instruments and the main cost justifications.

1. RAW MIX CONTROL

A stable raw mix with the right concentration of each of the 4 major oxides (Ca, Si, Al, Fe) is essential for the stability of the kiln operation, and the quality of the finished product. Fluctuations in the composition result in a harder to burn raw mix, resulting in energy loss and a poor quality clinker, with lower strengths that needs to be ground finer (more energy loss) to achieve the required strengths.

Traditionally a sample is brought back to the laboratory to be analyzed every 1 to 2 hours, and the results of the analysis are used to correct the component mix.

With the online instrument the analysis is carried out on site every 5 minutes, and the corrections to the mix can be done automatically.

1.1 Components of the system

1.1.1 Sampling system

The material is sampled in a chute after the separator using a screw sampler. A volumetric sampler grabs the sample to be analyzed at the discharge of this sampler, and the sampled material drops by gravity into the analyzer. The excess material is returned into the material flow. The whole system is airtight and is not affected by pressure fluctuations in the chute.

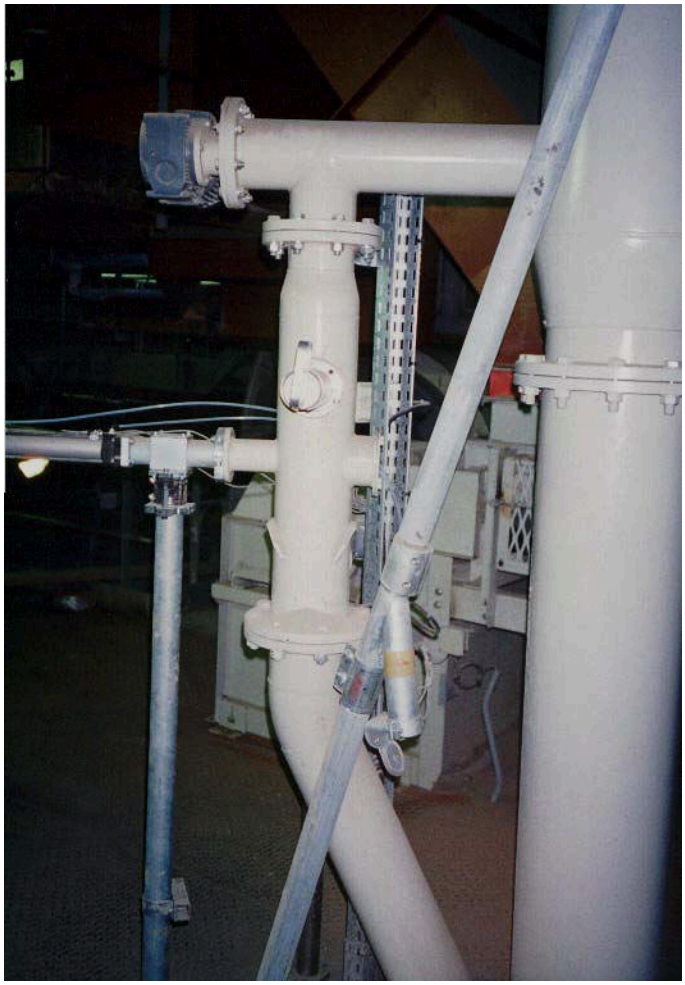

1.1.2 The raw mix analyzer

A 25 gram sample of raw mix is ground using a high efficiency patented grinder. The average particle size of the ground powder is less than 4 microns, ensuring an accurate analysis.

The sample is then prepared and automatically analyzed using an Oxford Labx3000, and the results of the main oxides are sent to the plant control system.

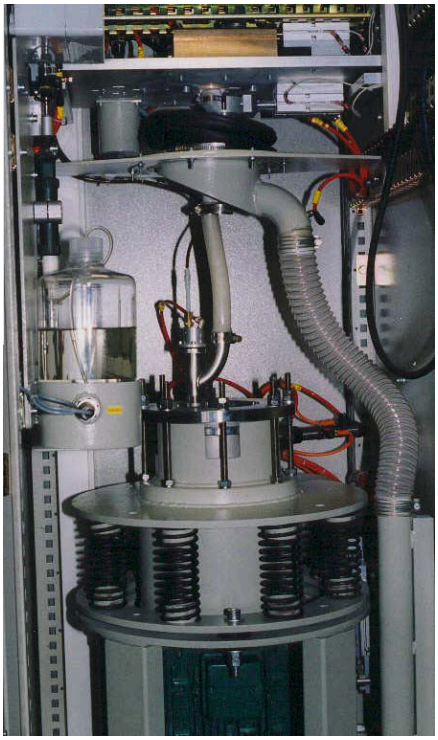

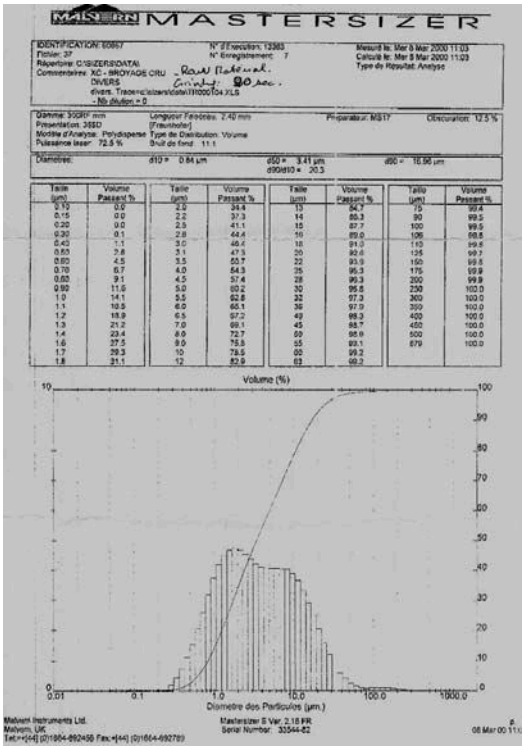

2. PRECALCINER CONTROL

The knowledge of the calcination level of the material at the kiln inlet, is essential to control the firing conditions in the precalciner, and thus to optimize the fuel consumption.

Traditionally a grab sample is collected manually at a considerable risk to the operator, and brought back to the laboratory to be analyzed every 8 to 24 hours.

With the online instrument the analysis is carried out on site every 30 minutes.

2.1 The components of the system

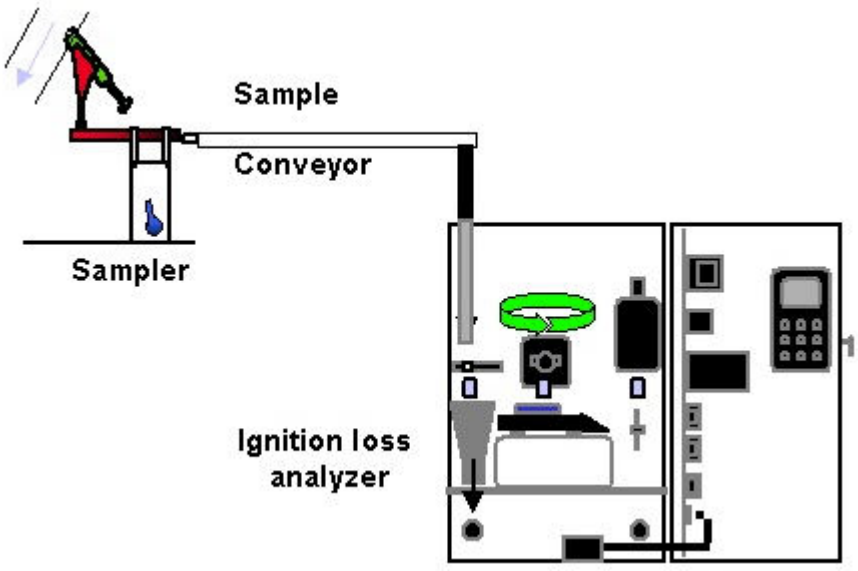

A sample is collected automatically from the kiln inlet chute. It is air cooled to freeze the calcination reaction and is then conveyed to the analyzer located near the sampling point.

2.2 The sampler

2.3 The ignition loss analyzer

The sample is introduced into a special stainless steel alloy crucible, it is weighed, heated to 975°C for 25 minutes and weighed again. The loss in weight gives the calcination level of the material.

3. CLINKER CONTROL

Free lime determination is an essential element to determine the quality of Portland cement. A high free lime (CaO) in cement causes the finished concrete to expand as the free lime hydrates to form hydrated lime (Ca(OH)2), resulting in cracks and flakes in the concrete structure.

High free lime rates in correctly prepared raw material are generally the result of an underburnt clinker. The percentage of free lime in clinker decreases as the burning zone temperature in the kiln is increased.

Traditionally, so as to avoid excessive free lime, kiln operators are instructed to operate the kiln so as to have, on average, a free lime value that is significantly lower than the authorized level. The free lime is commonly determined by a laboratory technician, on a frequency of once an hour to once a shift. The clinker sample in such cases is taken manually on the pan conveyor after the cooler discharge and analyzed in the laboratory using a titration after a glycol extraction.

With the online instrument the analysis is carried out on site every 10 minutes, and the corrections to the firing conditions in the kiln can be done automatically. It is therefore possible to operate the kiln in the optimum range of free lime, saving costs on the burning process as well as on the grinding process, as hard burnt clinker is also harder to grind.

3.1 Components of the system

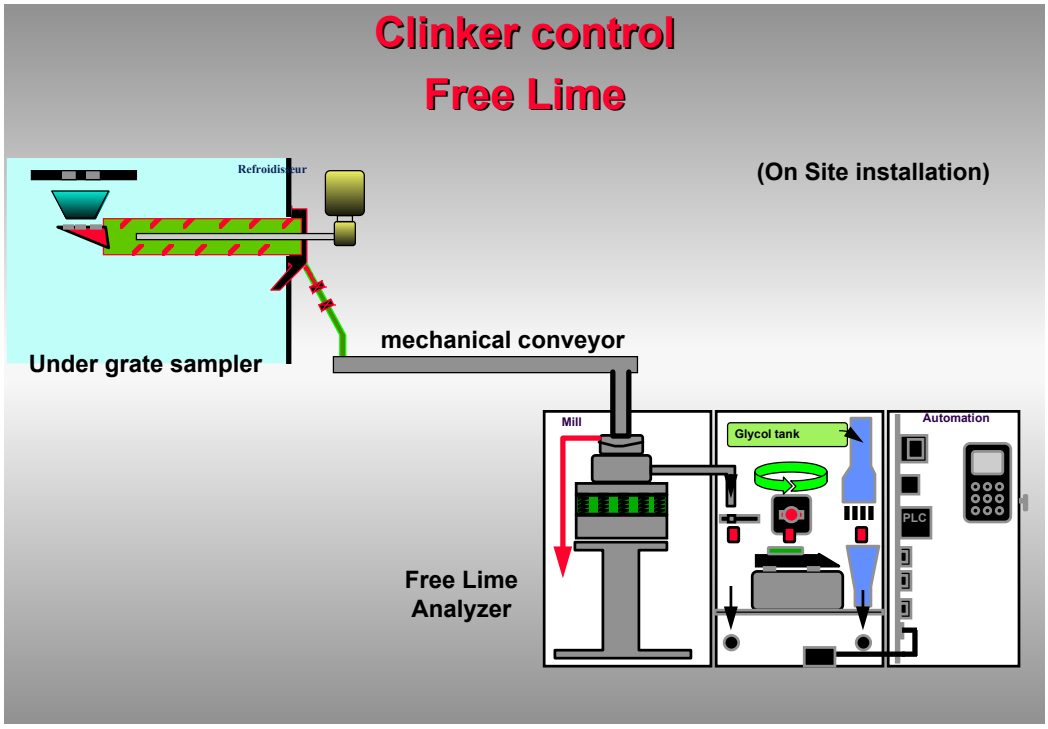

The clinker can be sampled in various locations in the cooler, either at the fall of the kiln before the cooler, underneath the grate plates in the 2nd or 3rd chamber of the cooler, or after the crusher at the cooler outlet.

The clinker sample is then transported to the analyzer located near the sampling point.

3.2 Sampling equipment

3.2.1 Sampling at the kiln outlet

The sampling system is installed in the throat of the cooler.

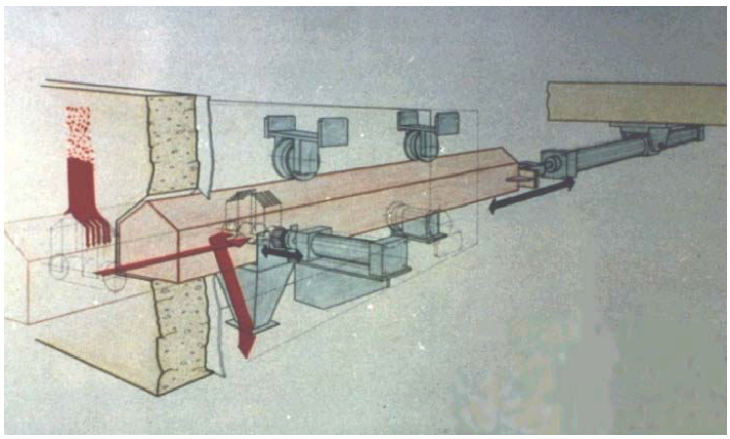

Clinker is collected directly at the fall of the kiln, using an air-cooled refractory steel beam. The beam is pushed into the material stream using a pneumatic actuator. About 300 grams of material is collected. The beam is retracted, and the sample is removed from inside the beam.

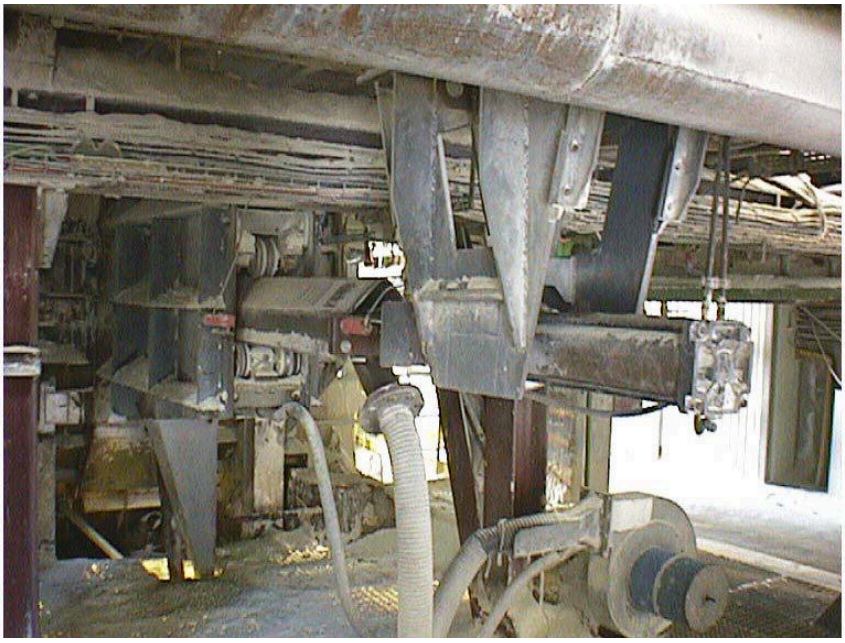

3.2.2 Sampling under the grate plates

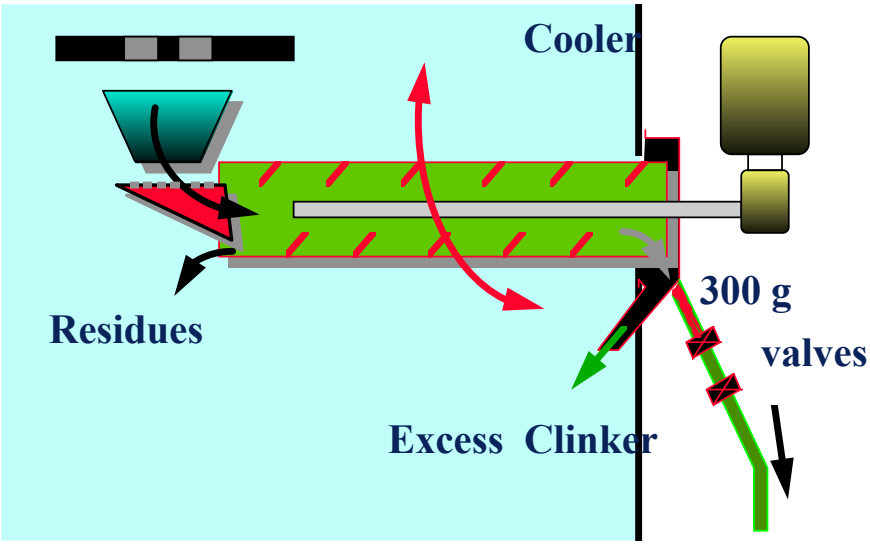

The sampling system is installed in the 2nd or 3rd chamber of the grate cooler (depending on the clinker temperature - maximum temperature 500°C).

The clinker continuously falls through 2 to 4 fixed grate plates in which 30 to 50 mm holes have been drilled.
When a sample is required, the screw sampler is operated and about 300 g of material is extracted from the side of the cooler. Excess clinker falls into the under grate drag chain.

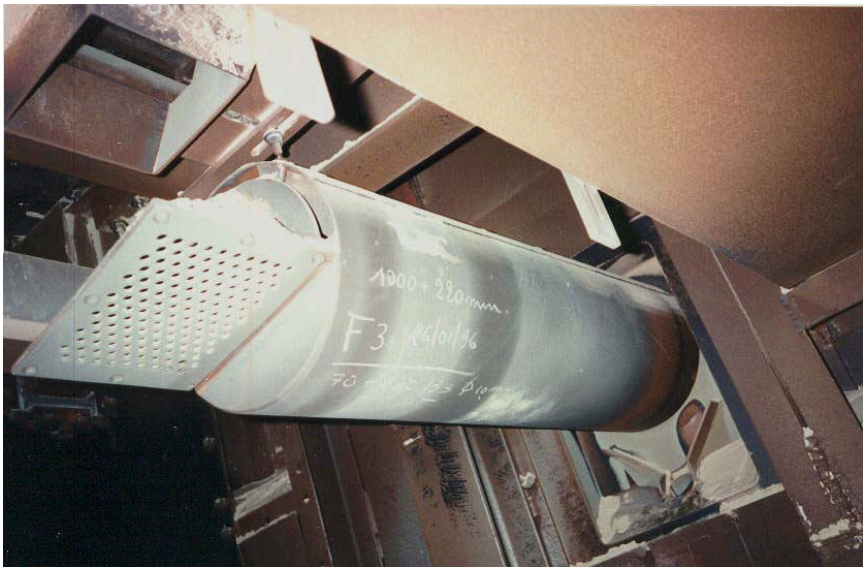

3.3 The free lime analyzer

Clinker is ground using a disk mill. The ground clinker and the glycol are weighed using an electronic scale, and are then fed into a reaction beaker. The solution is heated and stirred. Once the free lime is dissolved, the electroconductivity of the solution is measured and the result is converted into the FCaO value that is shown on the front display panel, and sent electronically to the central control room.

3.4 Kiln Control strategies using an On Line Free Lime Analyzer

3.4.1 On line measurement values and kiln operation data

The following graph shows the data obtained by Tokuyama Soda (Japan) a few months after having installed a free lime analyzer system.

The data shows the correlation between free lime values and kiln operation data that was measured by changing the feed volume of coal (energy) intentionally while the kiln was operating in a stable condition.

It can be seen that as the coal feed is decreased the free lime values increase and the burning zone temperature decreases, and as the coal feed is increased the free lime values decrease and the burning zone temperature increases.

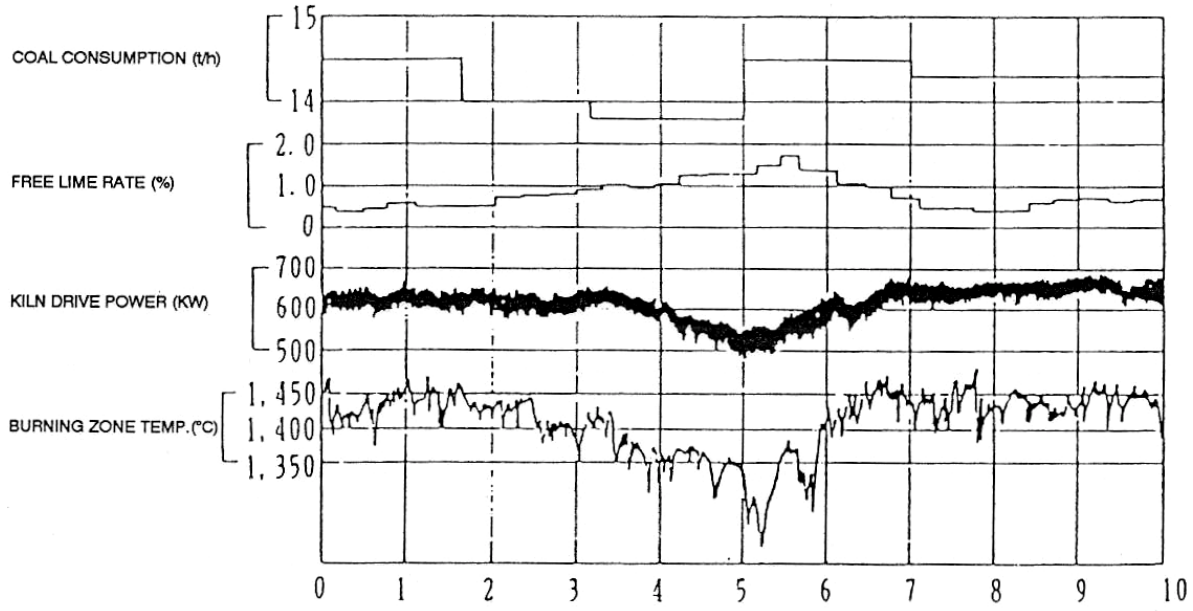

From this data we can see the following facts:

- a change in fuel feed results in a noticeable change in free lime prior to a change in kiln amps, and about the same time as a change in burning zone temperature.
- burning zone temperature is an unstable measurement for higher values of free lime, as the kiln tends to be dustier, and therefore the clinkering zone more difficult to see.
- the kiln amps only show significant signs of change for large fluctuations in free lime.
- kiln amps are not a stable indicator of the burning zone conditions. It can be seen on the graph that the kiln amps for the second half of the graph are higher than in the first part, for a free lime value that is about the same.
- free lime peaks can last less than 1 hour on precalciner kilns, as can be seen between hours 5 and 6

3.4.2 Possible kiln control strategies

Free lime as measured by the on line analyzer is an absolute number that is not dependent on factors that may otherwise affect the other control parameters normally used for kiln control purposes :

- Kiln Amps, the most widely used parameter for kiln control, is typically affected by buildup in the kiln.
- Burning zone temperature measurement may be influenced by a change of concentration of dust or a buildup between the pyrometer and the clinkering zone being measured.

- NOx, can be influenced by several factors including quality of the fuel, or the accuracy of the gas sampling system at the back end of the kiln.

Based on these facts some of the strategies currently being used, use the following logic :

- Incremental instantaneous control is based on either NOx, BZT, or Kiln Amps, or a weighted combination of these factors, around given set points.
- Free Lime is measured automatically at a high frequency (typically every 10 to 20 minutes so as to see the trends developing). The clinker is sampled as close as possible to the clinkering zone, so as to reduce the lag time between the free lime result, and the kiln operational data. The free lime result is then used to update/correct the set points for each of the factors.

3.4.3 Application at the Blue Circle Ravena Plant USA

A system was installed in June 98 at the Ravena plant on 2 wet kilns. The graph below shows the average monthly values of free lime.

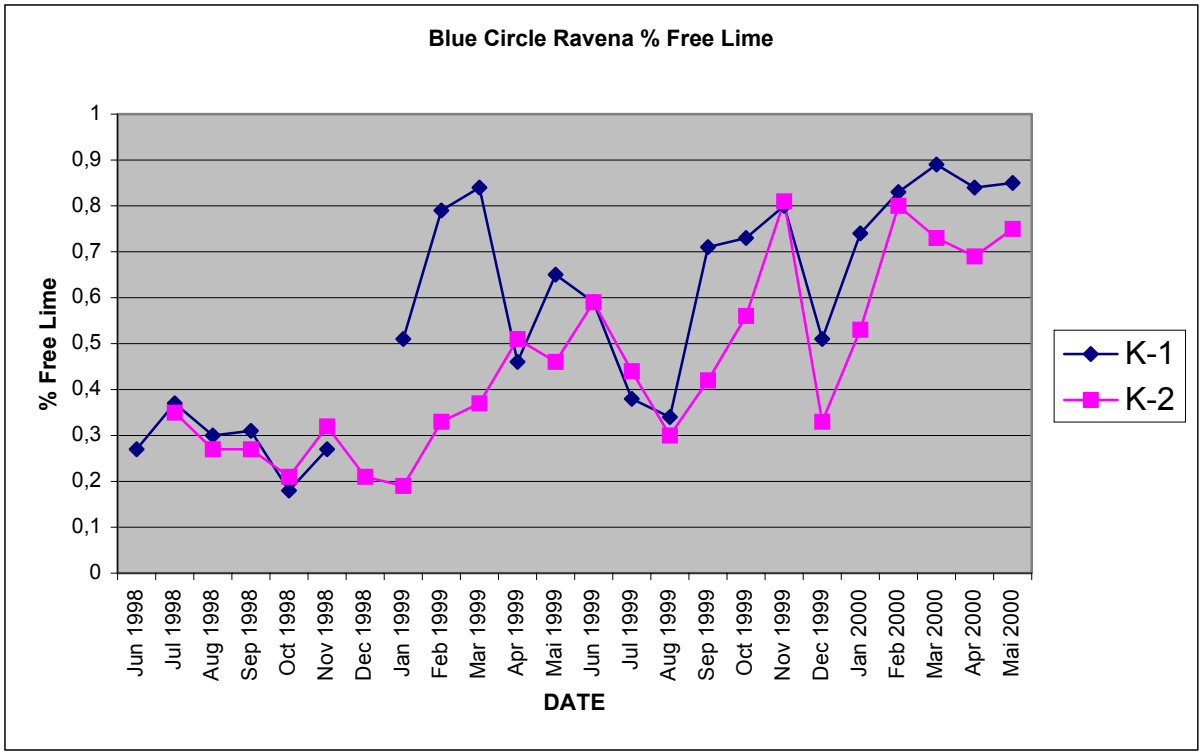

From June 1998 to January 1999, the free lime data was collected but was not used to control the kiln. From January 1999 to December 1999, the kiln expert control system was shut down for modification, and the kiln was controlled manually by the kiln operator, using the free lime data as the main control factor. As it can be seen the average free lime values were higher, but with some variances.

From January 2000 and onwards, the kiln expert control system was reconnected using free lime as the main control factor. The kiln is now running at stable values around 0.5% to 0,6% higher than they were at the start of the project.

This resulted in fuel savings of about 15 Kcal/KgKK as well as about 1 Kwh/tonKK of savings on the cost of grinding as the clinker was easier to grind (not over burnt). The high frequency control also had the advantage of producing better clinker, as it was possible to catch and deal with off specification clinker faster.

Given the savings and the 2 million ton per annum capacity of the plant, the system paid for itself in much less than a year.

4. CEMENT CONTROL

The main controls that are normally carried out to determine the quality of cement are :

- Gypsum addition : by measuring the SO3 content of the finished cement.
- Limestone addition : by measuring the carbon content in the finished cement
- Blaine analysis : traditional method that uses air permeability to characterize the fineness of the cement.
- PSD analysis : this newer technology gives the complete grain size distribution of the finished cement, and has now replaced Blaine measurement as the de facto control method in all the modern plants

Traditionally a sample is brought back to the laboratory to be analyzed every 1 to 2 hours, and the results of the analysis are used to correct the process.

4.1 Cement additions control

It is essential to control gypsum additions as this has a direct impact on the setting time of the finished cement. With the same instrument it is also possible to determine the limestone additions.
The close monitoring of limestone additions can lead to substantial savings as it is possible to replace expensive clinker with cheap limestone without exceeding the maximum regulatory limits.

4.1.2 The CO2/SO3 analyzer

A cement sample is dosed into a ceramic crucible. The cement sample is weighed. Tungsten and iron are added to the crucible. The crucible is then introduced into an inductive furnace, and the cement sample is heated up to 1400°C under a constant flow of oxygen. The Carbon and Sulfur present in the cement combine with the oxygen to form CO^2 and SO_3. These gases are then measured using Infrared detectors. Knowing the concentration of CO^2 and SO_3 as well as the mass of the cement sample it is possible to determine the C and S present in the cement, and therefore the gypsum and limestone content.

4.2 Fineness control

Using an On Line PSD analyzer, giving a real time continuous measurement, it is possible to dynamically control the speed of the separator, and therefore optimize the fineness, and hence save on the cost of the energy required for grinding.

4.2.1 The particle size analyser

The photograph is of the optical head and real-time sampling interface of the EPCS system. Particles pass through an air purged flow cell, which supports a fixed alignment laser transmitter and solid state detector based on the classical ensemble laser diffraction technique. As particles pass through the laser beam, light scattered in the forward direction is collected by the receiver lens and focused onto a log-scaled annular ring detector. The detector is scanned at high speed, recorded, digitized for continuous real-time analysis.

Material is sampled using a screw sampler in a chute at the discharge of the separator. A bypass/dilution system is used to extract a portion of the flow, pass it through the instrument, and then back into the primary flow line. This system incorporates a near iso-kinetic tap that is driven by a venturi eductor.

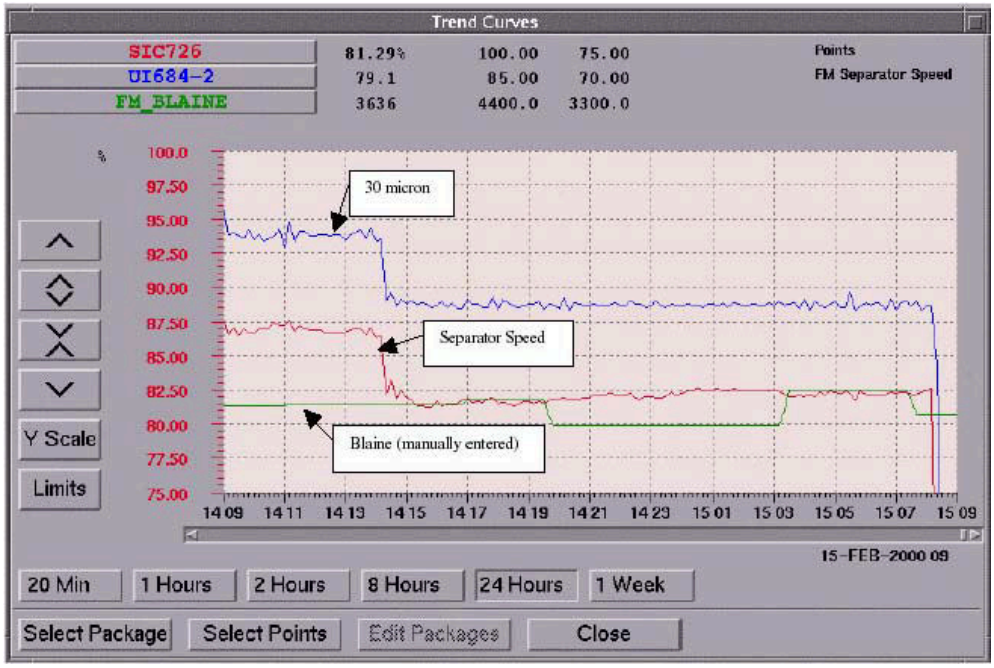

This system provides real time information on the particle size distribution of the cement, and the data can be tied in directly to control the separator speed as shown below (data provided by the Ashgrove Lemington plant USA).

It can be seen in this case that the 30 micron residue and the change in the separator speed match very closely, whereas the manual Blaine value does not.

DISPERSING MECHANISM OF PNS SUPERPLASTICIZER IN HIGH-PERFORMANCE CONCRETE

Byung-Gi Kim[1] and Pierre-Claude Aïtcin[2]

[1] Kyunggi Chemicals Ltd. San 103, Okkil-dong, Sosa-gu, Bucheon-shi, Kyunggi-do, Korea, 422-080. E-mail: byunggikim1965@hanmail.net
[2] Department of Civil Engineering, University of Sherbrooke, Sherbrooke, QC, Canada, J1K 2R1
E-mail: pca@sca.gci.usherb.ca

ABSTRACT

The interaction between superplasticizer and cement has not been well understood up to now due to its complexity. This study examines the effect of alkali content in cement on the properties of cement pastes containing different alkali contents. In addition, superplasticizer/cement interactions are discussed with respect to the adsorption of polynaphthalene sulfonate (PNS) on cement and its hydration. Moreover, quantitative relationships have been established between the fluidity of cement pastes, the amount of adsorbed superplasticizer, the concentration of sulfate ions, and the pH of the interstitial solution. Results show that the fluidity at a specific time is strongly controlled by the amount of PNS remaining in the interstitial solution in the fresh cement paste, which in turn depends on the sulfate ion concentration, as well as the pH. The dispersing mechanism of PNS based superplasticizer is explained, and, the role of alkalis in the dispersing mechanism is discussed.

1. INTRODUCTION

It is generally acknowledged that when a PNS superplasticizer is adsorbed onto cement particles, this adsorption conveys a net negative electrical charge (electrostatic repulsive force) to the surface of cement particles and short-range steric repulsive forces between cement particles [1-6]. These repulsive forces induced by the superplasticizer adsorption can be established by measuring the zeta-potential of cement particles [1-2], or measuring the thickness of the layer of superplasticizer adsorbed [5]. On the other hand, a depletion effect of superplasticizer remaining ("free superplasticizer") in the interstitial solution on dispersing cement particles was proposed by Napper *et al*[7]. Moreover, other effects, such as Tom's and tribology effects, of the available free superplasticizer on the dispersing mechanism were put forward by Tanaka *et al* [8].

The interaction between a PNS superplasticizer and C_3A phases has been investigated [9-10]. Fernon *et al* [9] showed that when a PNS superplasticizer is added to a cement paste where there are not enough SO^{-2}_4 ions, some PNS molecules are trapped within C_4AH_x. As a result, these superplasticizer molecules are no longer available to neutralize the electrical charges present on the cement particles. On the contrary, when there are enough SO^{-2}_4 ions in solution, ettringite is formed around C_3A. This ettringite temporarily prevents further hydration of C_3A, so that cement setting can be controlled. Baussant [10] has shown that PNS molecules influenced the morphology of the ettringite crystals that are formed. He pointed out that the usual long ettringite needles appearing on the C_3A surface when C_3A hydrates in the presence of calcium sulfate are no longer visible. When a PNS is introduced in the system, the ettringite needles are replaced by small spheroidal particles. He also found that the higher the molecular weight of the PNS molecules, the smaller the spheroidal

Proceedings of the 11th International Congress on the Chemistry of Cement (ICCC)
'Cement's Contribution to the Development in the 21st Century'
Hosted by: The Cement and Concrete Institute of South Africa
CD-ROM produced by: Document Transformation Technologies
11 - 16 May 2003, Durban, South Africa
ISBN Number: 0-9584085-8-0
Editors: Dr G. Grieve and G. Owens
Congress Organised by: Event Dynamics

particles. According to his work, PNS molecules can be trapped in ettringite crystals.

The interaction between calcium sulfate and a PNS superplasticizer has been studied in the literature[11-15]. Their results showed some disagreement on the effect of the PNS on the dissolution rate of calcium sulfate. Some [11-13] explain that the early stiffening as a result of cement–PNS incompatibility may occur because the presence of PNS leads to an insufficient supply of dissolved calcium sulfate to form ettringite. Others [14-15] showed that the presence of PNS increases the solubility of calcium sulfate.

Although several studies have investigated the dispersing mechanism of superplasticizer in cement pastes and the interaction between superplasticizer and C_3A or calcium sulfate, they provide only partial information to understand the dispersing mechanism of the superplasticizer, or they did not fully consider that the repulsive and attractive forces derived from superplasticizers vary with hydration time. There is no single model which can fully explain the dispersing mechanism of PNS superplasticizer and all the interactions between cement (mostly C_3A) and PNS superplasticizer. Therefore, an integral model is needed in order to explain the dispersing mechanism of superplasticizer from an overall perspective. When proposing an integral model, it should be considered that the repulsive forces induced by superplasticizers are modified with hydration time because cement particles continuously react with available water.

The purpose of this paper is to study the influence of the alkali content of a cement on the rheological properties of a cement paste and concrete. In addition, the dispersing mechanism of PNS superplasticizer is explained more integrally considering the amounts of PNS adsorbed or remaining in solution and the chemical composition of the interstitial solution, and cement hydration during hydration time.

2. MATERIALS AND EXPERIMENTAL METHODS

The phase composition of the six cements tested and their alkali contents is presented in Table 1. The cements display a wide range in C_3A and total Na_2O eq. contents. A liquid sodium salt of PNS, having an average molecular weight of 14 000 g/mol measured by Gel Permeation Chromatography, was used [16].

Table 1. Phase composition and alkali content of the six cements used

Phase composition (%)	C1	C2	C3	C4	C5	C6
C_3S	73	66	53	51	69	56
C_2S	6	12	18	20	5	17
C_3A	3	2	10	6	7	11
C_4AF	12	13	7	9	10	6
Na_2O eq.	0.31	0.52	0.92	0.74	0.35	0.31
Soluble alkalies*	0.19	0.41	0.57	0.72	0.07	0.06

* Jiang et. al. [17]

The cement pastes were prepared at a water/cement ratio (W/C) of 0.35. The superplasticizer dosage in the mix is expressed on a dry mass basis. The fluidity of cement pastes was evaluated by the mini-slump test [17}. The adsorption of PNS superplasticizer was evaluated by measuring the amount of PNS remaining in the interstitial solution extracted from the fresh cement pastes using a UV spectrometer. This concentration was determined at the peak absorbance wavelength between 293 nm and 276 nm bands. The amount of adsorbed PNS was calculated by subtracting the

measured concentration in the extracted solution from the initial concentration (initial dosage of PNS). The sulfate content dissolved from the cement was calculated by subtracting the sulfur content originating from the PNS superplasticizer from the total sulfur content of the filtrate measured by the ICP. The pH of the filtrate was also measured using an Orion pH-meter.

Figure 1 shows that the cement pastes made with cements C2, C3 and C4 keep a high mini-slump value over 90 minutes. In contrast, the pastes made with cements C1 and C5 present a high initial mini-slump, followed by a rapid slump loss. The paste made with cement C6 has a relatively low initial mini-slump at 5 minutes. It can be said that cements C1, C5, and C6 containing relatively low-alkali contents are not compatible with the PNS, while cements C2, C3, and C4 containing high-alkali content are compatible. Therefore, these results clearly indicate that the alkali content, especially the soluble alkali content, is an important parameter affecting the compatibility of cement and PNS superplasticizer.

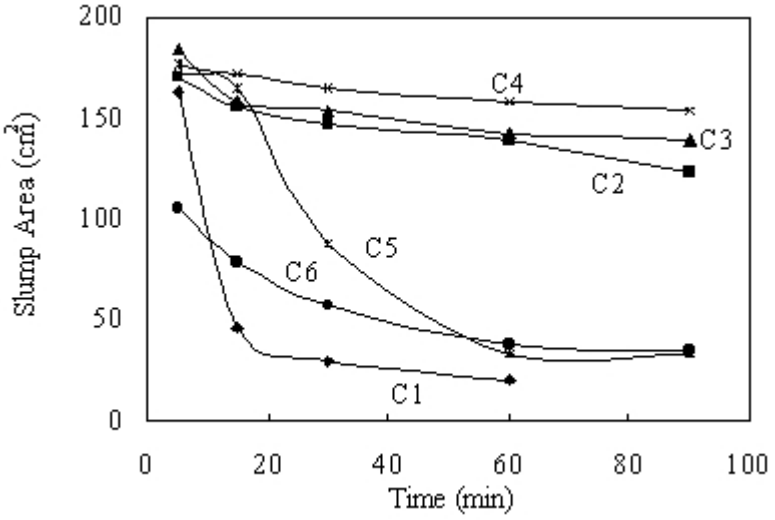

Figure 1. Slump area as a function of hydration time

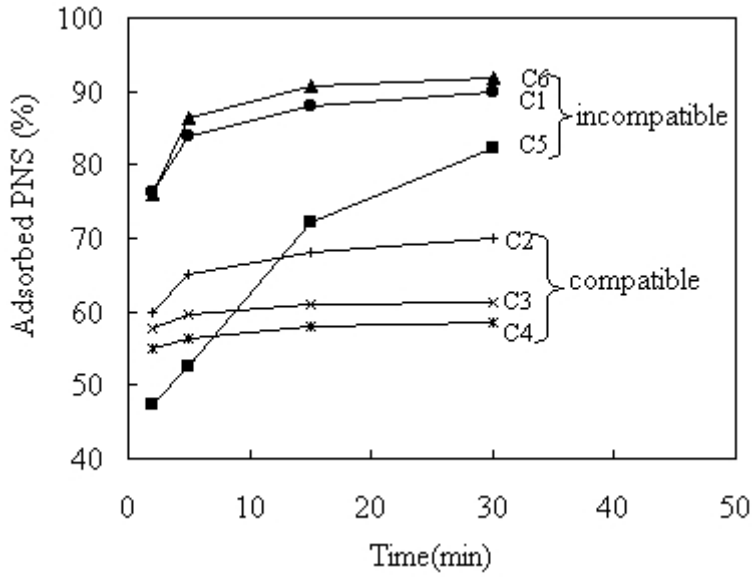

Figure 2. Amount of PNS adsorbed as a function of hydration time

The amount of PNS adsorbed by the six cements as a function of time is presented in Figure 2. This figure shows that the incompatible cements have a tendency to rapidly adsorb a large amount of

PNS superplasticizer (C1 and C6) or to continuously adsorb the PNS superplasticizer with time (C5), while the compatible cements do not, leaving a substantial amount of PNS superplasticizer in solution. The addition of Na_2SO_4 can significantly reduce the amount of PNS adsorbed on the cement pastes made with the three incompatible cements C1, C5, and C6. It can be clearly seen in Fig. 3 that the percentage of adsorbed PNS decreases as the amount of Na_2SO_4 increases.

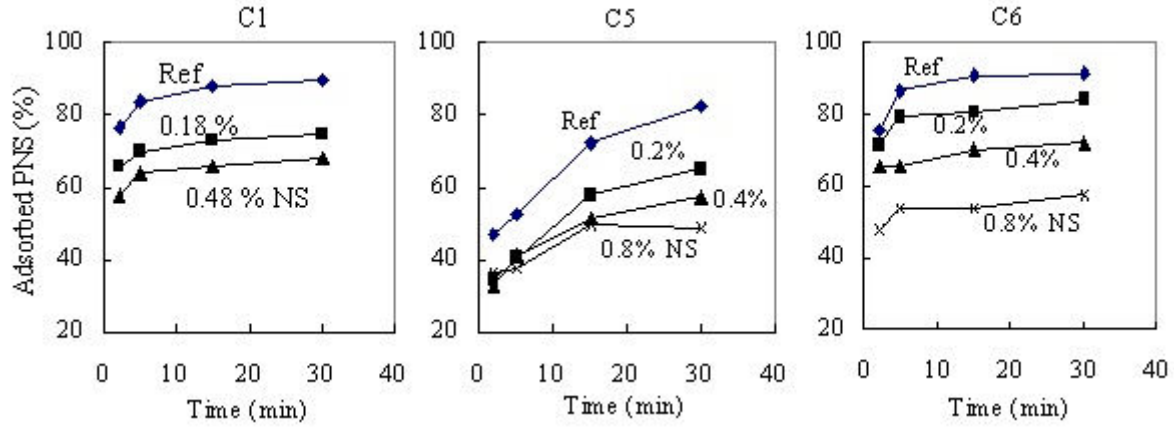

Figure 3. Effect of Na_2SO_4 addition on the amount of PNS adsorbed

As shown in Figure 4, a direct relationship between the amount of PNS remaining in the interstitial solution at 60 minutes and the mini-slump value at 60 minutes was found. That is, the higher the amount of PNS remaining in the interstitial solution, the higher the fluidity of cement pastes. This result can be understood when the role of PNS remaining ("free PNS") in the dispersing mechanism is considered. The PNS molecules, which are initially adsorbed on cement particles, become ineffective as hydration proceeds because of their incorporation into newly formed hydration products. The PNS remaining in solution is then progressively adsorbed on the newly hydrated surfaces; the continuous supply of PNS molecules maintains the electrostatic and steric repulsive forces which conserve paste fluidity. In the case of incompatible cements, the excessive early PNS adsorption leaves little free PNS molecules for replacing the PNS consumed into the hydration product. In such a case, the fluidity of cement pastes decreases with hydration time.

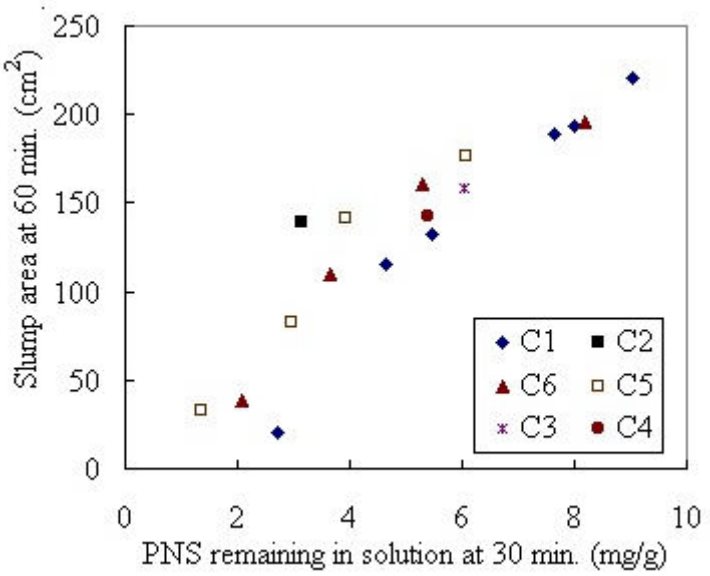

Figure 4. Relationship between mini-slump area and PNS remaining in solution

The relationship between the adsorption of PNS and sulfate concentration/pH in the solution of the cement pastes was established as shown in Figure 5 where the dependence of the amount of adsorbed PNS on the sulfate concentration and pH in the interstitial solution is shown. The decrease of PNS adsorption due to the addition of an alkali sulfate can be explained by the increase in both sulfate ions concentration and the pH of the interstitial solution. Both SO_4^{2-} ions and OH^- ions in the initial solution inhibit the adsorption of PNS on C_3A and C_4AF, thus reducing the amount of PNS adsorption on cement. Based on our results, and those from other investigators [18-19], a plausible mechanism of rapid slump loss in a superplasticized, low W/C ratio concrete can be proposed. In a superplasticized concrete having a low w/c ratio, the workability is related to the dispersing effect of the superplasticizer, which is related to the adsorption rate of the superplasticizer and to the hydration rate of the cement pastes in presence of a superplasticizer. In order to maintain the dispersing effect of a superplasticizer, the adsorption rate of the superplasticizer and the hydration rate of the cement have to be reduced, so that a certain amount of superplasticizer remains in the solution. When the residual concentration of the superplasticizer becomes so low that the residual superplasticizer is primarily composed of monomer or low molecular weight PNS because of their lower adsorption affinity [16, 20], the dispersion effect of the superplasticizer disappears: concrete stiffens and exhibits a significant slump loss. Hence, maintaining a certain concentration of a superplasticizer in solution is necessary to maintain a fluidized state within the concrete. Therefore, the concentration of the superplasticizer remaining in solution could be considered as a good indicator of the workability of concrete. According to this mechanism, any action which reduces the rate of superplasticizer consumption may be explored to maintain concrete workability. Some actions, such as a delayed addition of superplasticizer, the addition of Na_2SO_4, and the addition of a retarder can be explained by this mechanism. It was found that the most effective way to lower the slump loss was to adjust the amount of soluble alkalis or soluble sulfate content in the cement [17, 21]. The presence of enough alkali sulfate in the interstitial solution maintains enough PNS in solution, which effectively disperses the cement particles. Therefore, the presence of enough alkali sulfate in the interstitial solution is crucial to prevent premature slump loss of concrete.

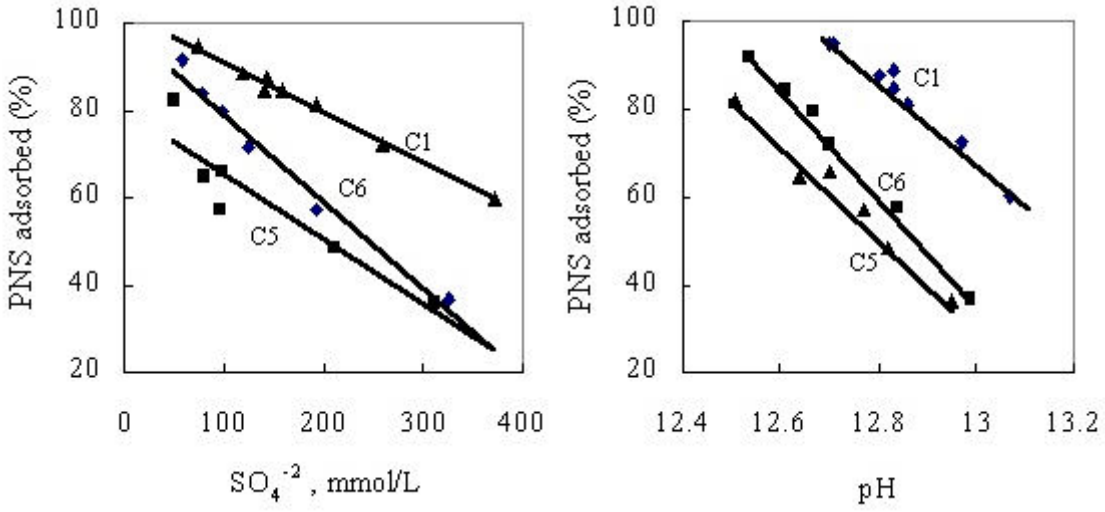

Figure 5. Relationship between amount of PNS adsorbed and sulfate/pH in solution by the addition of sodium sulfate

3. DISCUSSION

The results obtained in this study of the adsorption of the PNS molecules clearly show the different adsorption behavior in high- and low-alkali cements. The different adsorption behaviors of PNS superplasticizer in high- and low-alkali cement with hydration time are schematically presented in Figure 6. These figures indicate which superplasticizer molecules contribute to dispersing cement particles, and which superplasticizers do not, as a function of hydration time.

As found in Fig. 2, low-alkali cements (C1, C5, and C6) adsorb large amounts of PNS superplasticizer, while high-alkali cements adsorb smaller amounts. Therefore, the multi-layers of PNS adsorbed are much thicker in low-alkali cements than in high-alkali cements at initial state, as shown in Figure 6.

In low-alkali cements, large amounts of PNS adsorbed in the multi-layers are rapidly consumed to form an organomineral compound as proposed by Fernon *et al* [9] and/or hydration products [10, 22] in the intermediate state and shown in Figure 6. In addition, larger PNS molecules are consumed because they are more likely to adsorb on cement particles, leaving PNS molecules in the interstitial solution which consist of monomers, dimers, and smaller PNS molecules [20, 23]. Consequently, a much thinner layer of PNS adsorbed generates weakly repulsive forces between cement particles because of insufficiency of PNS remaining ("free" PNS) and large PNS molecules in solution. In such a case, some slump loss is likely to occur. Finally, the thin layer is also gradually incorporated by the newly formed hydration products, so that there are little repulsive forces in this system (Final state).

In contrast, in the case of high-alkali cements (C2, C3, and C4), a smaller amount of PNS is adsorbed and large amounts of PNS remain in the interstitial solution, which contains many larger PNS molecules. Consequently, a smaller amount of PNS is consumed by the organomineral compounds [9] and/or the hydration products [10, 22], as shown in the previous intermediate state in Figure 6. Moreover, the multi-layers of the PNS structure adsorbed on cement particles maintain their thickness because there are many free and large PNS molecules in solution, which adsorb continuously on the cement particles. Therefore, the multi-layers of PNS adsorbed generate strong repulsive forces between cement particles, as shown in Figure 7.1 (Intermediate I state).

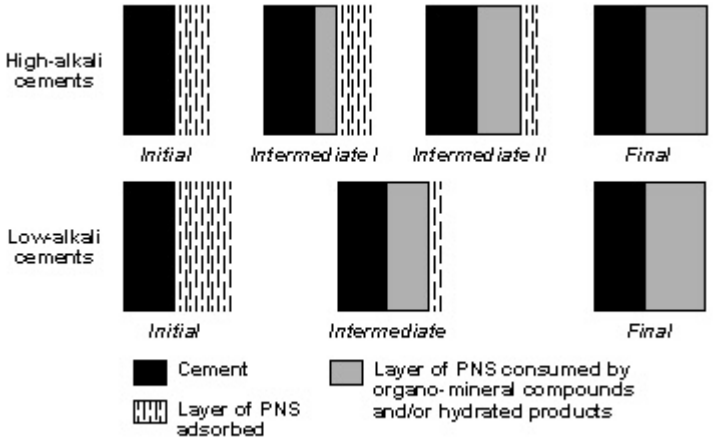

Figure 6. Schematic representation of PNS adsorption on high- and low-alkali cements

In such a case, the cement paste can maintain its initial slump much longer. As the cement hydration proceeds, the multi-layers of PNS adsorbed are gradually consumed by the organomineral compounds and/or the newly hydration products (Intermediate II state). Consequently, some slump loss occurs. Finally, when all the layers of PNS are adsorbed or incorporated, there are few repulsive forces in this system (Final state).

As seen in Figure 6, the time from initial to final state is longer for high-alkali cements than for low-alkali cements. Therefore the cement pastes made with a high-alkali cement can maintain their initial fluidity much longer than those made with a low-alkali cement.

As found earlier in our study, the alkalis of a cement play an important role in improving the fluidity of cement pastes and concrete when a PNS superplasticizer is used because the alkalies

influence significantly the amount of PNS adsorbed. The role of the alkali was explained by Nawa *et al* [24] and Vernet *et al* [25], proposing the competition mechanism between PNS and sulfate ions. However, in our study, it was found that the addition of alkalies increased not only the amount of sulfate ions, but also the amount of hydroxyl ions in the interstitial solution. Moreover, it decreased the concentration of calcium ions. Consequently the addition of alkalis reduced the amount of PNS adsorbed on cement particles. From the results obtained from our study, it was clearly seen that although the difference in pH between high- and low-alkali cements is in the range of 0.3 – 0.8, this difference near the zero-point of zeta potential of C_3A significantly influences the amount of PNS adsorbed on C_3A [26]. Therefore, the competition mechanism between PNS and sulfate ions proposed needs to be modified to the competition between PNS and hydroxyl as well as sulfate ions, as schematized in Figure 7. This mechanism of action results in a reduction of the amount of PNS consumed by the formation of organomineral compounds and/or the hydrated products incorporating PNS, leaving greater amount of PNS and large PNS molecules in solution that could be adsorbed on the silicate phases as well.

In our study, it was also shown how alkalies significantly reduce the amount of PNS removed from the interstitial solution. The results obtained from the measurement of the amount of ettringite formed showed that this amount does not significantly increase when the amount of sodium sulfate increases. Therefore, it can be said that alkali sulfates neutralize the active sites on cement particles without increasing significantly the amount of ettringite formed. Therefore they inhibit the adsorption of the PNS molecules by effectively reducing the positive zeta potential of C_3A and C_4AF [27] and leave more PNS molecules in solution.

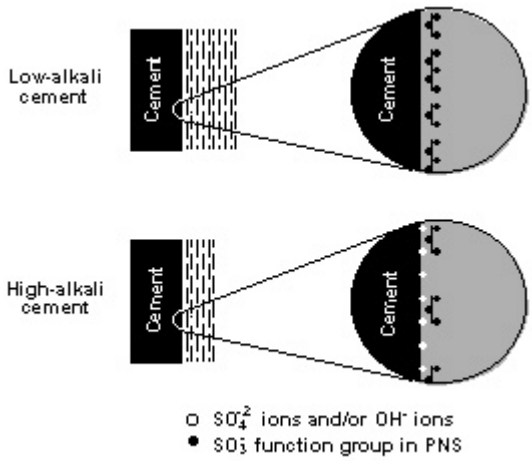

Figure 7. Schematic representation of the competition mechanism between PNS and sulfate/hydroxyl ions derived from the alkalies

The free PNS molecules remaining in solution may act as an additional repulsive barrier between cement particles, and play an important role in the fluidification of the paste. The additional forces induced by the free superplasticizer molecules were reviewed by Tanaka *et al* [8]. They reported that these additional forces are generated from the depletion effect, depletion coagulation effect, Tom's effect, and the tribology effect of the free superplasticizer polymers that remain in solution. Moreover, Uchikawa [28] considered these additional forces in representing the acting forces between cement and superplasticizer as follows:

$$F = F_A + F_{RE} + F_{RS} + R \quad (1)$$

Where, F_A is the van der Waal's forces (F_A),
F_{RE} is the electrostatic repulsive forces (F_{RE})

F_{RS} is the steric repulsive forces (F_{RS})
R is the acting forces of the free superplasticizer induced by the surface tenstion effect, the depletion effect, and tribology effect etc.

When it is considered that the size of PNS molecules is much smaller than the cement particles, the R, as shown in equation (1) could probably be considered as just the repulsive forces because there are no attractive forces from the free PNS molecules induced by the depletion coagulation effect mentioned by Tanaka *et al* [8]. Therefore, when considering the additional forces from the free PNS molecules, the repulsive forces between the free PNS/adsorbed PNS and cement particles can be illustrated in Figure 8.

These figures show that cement particles are well dispersed when the free PNS is present. As hydration proceeds, the PNS adsorbed on the solid surface becomes ineffective as a dispersant because it is incorporated into the organomineral compounds [9] and/or the hydration products [10, 22]. The free PNS in solution is then progressively adsorbed onto the newly hydrated surfaces. The continuous supply of PNS molecules maintains the fluidity of the paste because the additional repulsive forces (R) from the free PNS are gradually converted to the electrostatic (F_{RE}) and steric repulsive forces (F_{RS}) generated after being adsorbed on cement particles. In conclusion, in order to increase the efficiency of a PNS superplasticizer to disperse cement particles at equal PNS dosages, it is necessary to reduce the amount of PNS consumed (or removed) by cement particles.

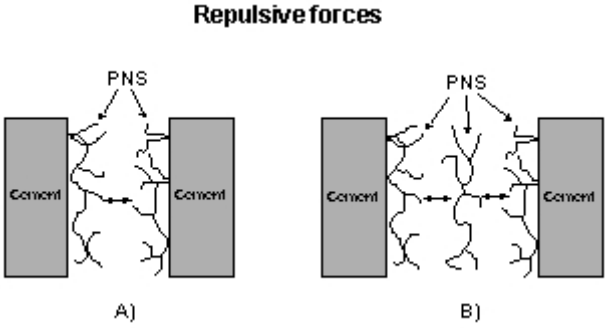

Figure 8. Schematic representation of the repulsive forces from the PNS adsorbed and the free PNS, a) without, b) with the free PNS

4. CONCLUSION

Quantitative relationships between the fluidity of cement pastes, the amount of the superplasticizer adsorbed, the sulfate concentration, and the pH in the interstitial solution have been established. These relationships clearly indicate that the fluidity at a specific time is strongly controlled by the amount of PNS remaining in the interstitial solution at that time. Moreover, the amount of adsorbed PNS decreases when the sulfate concentration or pH in the interstitial solution increases. A plausible mechanism of rapid slump loss in a superplasticized concrete having low W/C ratio is presented. Maintaining a certain amount of superplasticizer in the solution is of primary importance to control concrete workability. In addition, the dispersing mechanism of PNS superplasticizer is integrally discussed considering the soluble alkali content. In addition, the role of the soluble alkali in the dispersing mechanism of PNS superplasticizer is explained.

REFERENCES

[1] Daimon, M., Roy, D. M. (1978), Rheological properties of cement mixes: I. Methods Preliminary Experiments and Adsorption Studies, Cement and Concrete Research, vol. 8, pp. 753-764.
[2] Daimon, M., Roy, D. M. (1979) Rheological properties of cement mixes: II. Zeta potential and preliminary viscosity studies, Cement and Concrete Research, vol. 9, pp. 103-110.

[3] Banfill, P. F. G. (1979), A discussion of the papers "Rheological properties of cement mixes" by Daimon and Roy, Cement and Concrete Research, vol. 9, pp. 795-796.
[4] Anderson, P. J., Roy, D. M. and Gaidis, J. M. (1987), The effect of Adsorption of Superplasticizers on the Surface of Cement, Cement and Concrete Research, vol. 17, pp. 805-813.
[5] Uchikawa, H., Hanehara, S., Sawaki, D. (1997), The role of steric repulsive force in the dispersion of cement particles in fresh paste prepared with organic admixture, Cement and Concrete Research, vol. 27(1), pp. 37-50.
[6] Yamada, K., Hanehara, S., and Honma, K. (1998), The effect of naphthalene sulfonate type and polycarboxylate type superplasticizers on the fluidity of belite-rich cement concrete, in Self compacting Concrete Workshop, Kochi, August.
[7] Napper, D. H. (1983), Polymeric Stabilization of Colloidal Dispersion, Academic Press, New York.
[8] Tanaka, Y., Otis, A., and Sugiyama, T. (1999), Polycarbonate-based advanced superplasticizers, Proceedings of the Intern. RILEM Symposium on "The role of Admixtures in High-Performance Concrete", Monterrey, Mexico, pp. 135-142
[9] Fernon, V. (1994), Etude de nouveau solides lamellaires obtenus par coprécipitation d'hydrate aluminocalcique et de sulfonate aromatique, Ph.D. Thesis (in French), Université d'Orléans.
[10] Baussant, J .B. (1990), Nouvelles Methodes d'etude de la formation d'hydrates des Ciments-Applications a l'analyse de l'effect d'adjuvants organique. Ph.D. dissertation, Univertité de Franche-Comté.
[11] Dodson, V.H., Hayden, T. D. (1989), Another Look at the Portland cement/chemical Admixture incompatibility Problem, Cement, Concrete and Aggregates, vol. 11 (1), pp. 52-56.
[12] Tagnit-Hamou, A., Aitcin, P.C. (1993), Cement and Superplasticizer Compatibility, World Cement, pp. 38-42, August.
[13] Ranc, R. (1990), Interactions entre les reducteur d'eau-plastifiants et les ciments, Ciments, étons, Ptatres, Chaux, vol. 782, pp. 19-21, Janv.
[14] Jolicoeur, C, Nkinamubanzi, P. C., Simard, M. A., and Piotte, M. (1994), Progress in understanding the functional properties of superplasticizers in fresh concrete, Proceedings of 4th CANMET/ACI Intl. Conf. On Superplasticizers and Others Chemical Admixtures in Concrete, Montreal, ACI SP 148-4, pp.63-88.
[15] Fernon, V., Vichot, a., Le Goanvic, N.,, Colombet, P., Corazza, F., and Costa, U. (1997), Interaction between Portland cement hydrates and polynaphthalene sulfonates, Proceeding of the Fifth CANMET/ACI Intern. Conf. on Superplasticizer and Other chemical admixtures in concrete, Rome, Italy, Ed.V. M. Malhotra, ACI SP-173, pp. 225- 248.
[16] Kim, B.-G., Jiang, S.P., and Aïtcin, P.-C., (1999), "Influence of molecular weight of polynaphthalene sulfonate superplasticizers on the properties of cement pastes containing different alkali content", Proc. Int'l. Sympo. on the Role of Admixtures in High Performance Concrete, Monterrey, pp. 97-111.
[17] Jiang, S.P., Kim, B.-G. and Aïtcin, P.-C., (1999), "Importance of adequate soluble alkali content to ensure cement/superplasticizer compatibility", Cement and Concrete Research 29 (1) pp. 71-78.
[18] Nawa, T. and Eguchi, H., (1992), "Effect of cement characteristics on the fluidity of cement paste containing an organic admixture", Proc. 9th Intl. Congress on the Chemistry of Cement, Vol. 4, pp. 597-603.
[19] Matsukawa, K., (1991), "Quantitative analysis of interactions between Portland cements and superplasticizers", Ph.D. Thesis, Purdue University.
[20] Ferrari, G., Cerulli, T., Clemente, P., and Dragoni, M., (1997), "Adsorption of Naphthalene Sulfonate Superplasticizers by cement particles through Gel Permeation Chromatography", Proc. 5th CANMET/ACI Int'l. Conf. on Superplasticizer and Other chemical admixtures in concrete, Rome, ACI SP-173, pp. 869-892.
[21] Jiang, S.P., Kim, B.-G. and Aïtcin, P.-C., (1998), "Some practical solutions dealing with cement and superplasticizer compatibility", Proceedings of the 4th Beijing Intl. Symposium on Cement and Concrete, Vol. 1, pp.724-729.
[22] Nawa, T., Eguchi, H., and Fukaya, Y. (1989b), Effect of alkali sulfate on the rheological behavior of cement paste containing a superplasticizer, in Proceedings of the 3rd CANMET/ACI Intl. Conf. on Superplasticizers and Other Chemical Admixtures in Concrete, ACI SP -119, pp. 405-424.
[23] Nkinamubanzi, P.-C. (1993), Effet des dispersants polymériques (superplastifiants sur les propriétes des suspensions concentrées et des pâtes de ciment, Ph.D dissertation, Université de Sherbrooke (in French).
[24] Nawa, T. and Eguchi, H. (1989a), Effect of sulfate on adsorption behavior of superplasticizer, 43th CAJ Proceedings of Cement and Concrete, pp. 90-95.
[25] Vernet, C., Noworyta, G. (1992), Interaction des adjuvants avec l'hydration du C3A: points de vue chimique et rheologique, Journee Technique << Les couples ciment/adjuvants>>, Technodes S.A., Guerville, september
[26] Tadros, M. E., Jackson, W. Y., and Skalny, J. (1976), Study of the dissolution and electrokinetic behavior of tricalcium aluminate, in Colloid and Interface Science, ed. Kevker M.
[27] Bonen, D. and SARKAR, S. L. (1995), The superplasticizer adsorption capacity of cement pastes, pore solution composition, and parameters affecting flow loss, Cement and Concrete Research, vol. 25 (7), pp. 1423-1434.
[28] Uchikawa, H. (1999), Function of organic admixture supporting high performance concrete, Proceedings of the Intern. RILEM Symposium on "The role of Admixtures in High-Performance Concrete", Monterrey, Mexico, pp. 69-96.

PROCESS EFFICIENCY AND OPERATIONAL IMPROVEMENT THROUGH THE CEMSTAR^{SM} TECHNOLOGY

[1]D. Perkins and [2]M. Wortley

[1]TXI/CemStar, Dallas, Texas, USA.
[2]Hatch Africa, Johannesburg, South Africa.

ABSTRACT

CemStar has helped to increase production at several cement plants in the U.S., including TXI's Midlothian Plant expansion project, which was completed in May 2001. A significant lowering of both NO_X and CO_2 emissions has also been demonstrated while using this technology. This paper provides an overview, discusses how the technology was developed and provides a more detailed process description. Operational experiences are discussed with respect to production and emissions benefits, with a discussion on CemStar's integration with TXI's new Midlothian kiln line.

1. INTRODUCTION

Despite the slowing worldwide economy, with U.S. recession and terrorism impacts stemming from the events of September 11, the U.S. cement industry has continued to face relatively resilient demand. Consumption has remained steady because of such factors as low mortgage rates and federal paving projects. Moreover, 2001 import levels hovered at approximately 25 million metric tons - comparable to quantities of immediate past years. To help meet this excess demand, numerous expansion projects across the country have been undertaken – between 1998 and 2004 U.S. production capacity is projected to grow by nearly 25% (Queen, 2002). However, it is not likely that this strong pace will continue, given the increasing stringency that environmental regulations are placing on the permitting process. Unless such expansion can be achieved without significantly increasing emissions – typically through extensive air pollution control equipment and more efficient process technologies – governmental permitting of additional greenfield or brownfield expansion projects is likely to continue to become prohibitively restrictive.

Specifically, there has been an increasing focus on emissions from cement production facilities during the past decade, primarily resulting from regulatory requirements to address ground-level ozone levels and NO_X emissions along with heightened awareness of the potential impact that greenhouse gas can have on the environment. These factors have together presented cement producers with the challenge of raising production levels in a cost-effective manner that maintains process efficiency but also has minimal impact on the environment.

While exploring ways to improve production and reduce the quantity of byproducts that were produced from its operations, Texas Industries, Inc. (TXI), discovered one such process that achieves production increase in an environmentally-beneficial manner. TXI is a U.S.-based producer of cement, steel, lightweight and heavy aggregates, brick, and ready-mixed concrete, and has developed an innovative technology that enables cement producers to address these vital issues concerning production and emissions. The CemStar^{SM} process was first developed in 1994, as the company began to explore potential synergies between its Midlothian, Texas cement and steel

Proceedings of the 11th International Congress on the Chemistry of Cement (ICCC) 11 - 16 May 2003, Durban, South Africa
'Cement's Contribution to the Development in the 21st Century' ISBN Number: 0-9584085-8-0
Hosted by: The Cement and Concrete Institute of South Africa Editors: Dr G. Grieve and G. Owens
CD-ROM produced by: Document Transformation Technologies Congress Organised by: Event Dynamics

facilities. Two U.S. patents were granted for this process: the first being in June of 1995 and the second issued in February of 1996, along with multiple foreign patents.

2. HISTORY OF DEVELOPMENT

During the early 1990's, TXI began to inspect its operations for ways to improve production efficiency, minimize or eliminate waste and ultimately to achieve a more sustainable approach to manufacturing in its energy- and raw material-intensive businesses. To identify solutions and potential synergies, a task force was formed, which was termed STAR - Systems and Technologies for Advanced Recycling. The task force focused on identifying waste and byproduct materials generated from the Midlothian, Texas cement and steel operations and examining production processes to determine whether any synergies existed that could minimize or eliminate any of the byproducts. Slag from TXI Chaparral's Midlothian steel mill, an electric arc furnace line capable of producing greater than 1.6 million metric tons of steel, was evaluated during this process. One of the electric arc furnaces at the Chaparral plant is shown in Figure 1. After an extensive laboratory testing and evaluation project overseen by Rom Young, TXI's Director for Research and Development, the process was tested in a full-scale demonstration in one of the four wet process cement kilns at the Midlothian plant.

Figure 1. Midlothian Kiln Line #5 Commissioned in 2001

After sufficient operational knowledge was gained through testing and analysis and as familiarity with the process increased, the technology was fully implemented. CemStar was subsequently employed at TXI's Hunter, Texas cement plant, a 2,500 mtpd preheater/precalciner facility, as well as TXI's Oro Grande, California cement plant, a 3,000 mtpd long dry facility, thereby demonstrating the flexibility of this process across all cement kiln technologies. In addition, the process was incorporated into the design of the Midlothian expansion project, undertaken in 1999 to expand production at the plant from 1.1 million metric tons per year to just over 2.5 million metric tons per year. This four-stage preheater/precalciner line was completed in May of 2001, with the process being employed from day one. Figure 2 shows the new kiln line at Midlothian.

TXI has also begun a licensing and support program to other U.S. cement companies, which include Holcim, Inc., North Texas Cement Company, RMC Pacific Materials, Inc., and Rio Grande Portland Cement Co. In addition to domestic licensing, TXI has initiated an effort in certain

markets outside the U.S. to promote the technology. These countries include Brazil, Australia and South Africa.

Figure 2. TXI Chaparral Midlothian Electric Arc Furnace Steel Making Operation

3. CEMSTAR TECHNOLOGY OVERVIEW

In the CemStar process, slag – a byproduct of steel production, is added to the cement clinker manufacturing process. This slag comes from three primary sources: 1) Electric Arc Furnace slag – referred to as the "mini-mill" process which uses scrap as the raw material; 2) Basic Oxygen Furnace slag – from integrated operations that use pig iron produced from ore; and 3) Blast Furnace slag – from integrated operations smelting the raw ore material. The result is an increase in clinker production of as much as 15% with no net increase in emissions. More specifically, the process involves the addition of slag into the back or feed end of the kiln through a relatively uncomplicated and inexpensive delivery and metering system. Due to the chemical composition of the slag and the energy-intensive nature of the steel production process, the material requires little or no additional fuel to convert it into cement clinker. In other words, the great majority of the thermal work has already been done in the steel mill and significant amounts of energy can be saved when the process is added to a cement clinker line.

The result is improved fuel efficiency - lower total fuel consumption per ton of clinker is a direct result of CemStar. This translates into a net reduction in of carbon dioxide (CO_2) and oxides of nitrogen (NO_X) emissions per ton of clinker produced. In fact, process testing, as described in more detail below, has shown a direct and statistically significant correlation between use of the technology and lowered NO_X emissions, and the U.S. Environmental Protection Agency has recognized this process as alternative control technology for NO_X in cement kilns (U.S. EPA, 2000).

Additionally, the flexibility of this technology has allowed it to be implemented at preheater/precalciner plants, wet process plants and long dry process plants – both in existing lines and designed as an integral component of a new line. The overall result is a process that can easily be designed into a new production line or integrated into virtually any existing cement plant at low capital cost which will provide a significant increase in production. Additional major benefits are lowered emissions and reduced fuel consumption with the potential of eliminating or reducing the need for traditional raw material components such as shale, clay or mill scale.

4. SPECIFIC PROCESS DESCRIPTION

During the steel manufacturing process, lime - calcium oxide - (CaO) is added to the molten steel as a flux to remove impurities. This process, which takes place at around 1,650 degrees Celsius, results in the lime combining chemically with silica, magnesium, aluminum and other oxides present in the steel. These oxides, which are considered to be undesirable in the steelmaking process, produce compounds that are also found in cement clinker – namely calcium silicates, aluminates and aluminoferrites. The slag material floats to the top of the molten steel and is ultimately poured off as the byproduct known as slag. This process, which occurs at temperatures equivalent to those in a cement kiln, converts the CaO to silicates that are similar to those in cement clinker. In addition, the slag incorporates mineralizers that promote clinker formation.

During the CemStar process, slag is crushed and screened to approximately 18 to 22 millimeter diameter, and added as a component of the raw material mix into the back or feed end of the kiln. Because of the amount of heat the slag has been subjected to during the steel making process, it has a relatively low melting temperature and does not require significant pre-processing before being placed into the kiln.

CemStar generally has the potential to increase clinker production by as much as 15%, but the specific amount at a particular clinker producing line is controlled by mix design that takes into account such factors as the chemical composition of the slag, the type or types of clinker being produced, as well as the traditional raw material inputs which are used at a specific plant. Feed chemistry is adjusted to compensate for the iron, aluminum, silica and calcium in the steel slag that is being added to the kiln.

During the kiln pyro process, the slag mixes with the raw materials and a number of chemical reactions take place. Because the melting point of slag is typically between 1,260 and 1,315 degrees Celsius, it begins to react with the other raw feed components before the clinkering temperature zone. In the liquid phase, the slag becomes extremely reactive and will seek other material with which to combine, i.e., the raw feed being supplied to the kiln. As the process moves through the kiln, mineralizers present in the slag, such as manganese, help to catalyze clinker formation reactions. In addition, dicalcium silicate, which is also present in varying amounts in slag, is converted into tricalcium silicate by combining with the calcined limestone (CaO) from the raw feed. This exothermic reaction results in slag being an energy efficient and highly effective addition to the cement manufacturing process.

5. CEMSTAR AND KILN OPERATIONS – PRODUCTION IMPACTS

Reflecting on 7+ years of operational experience in utilizing the process, significant production and operational advantages are derived from implementation of the technology. These include improved production rates of clinker, minimal capital investment required, little or no additional fuel consumption, and more stable kiln operations.

Testing has been performed to evaluate the specific impact that CemStar has on production and operations as well as emissions, which is described in more detail in the following section. In addition, long-term review of production levels at TXI facilities employing the process has confirmed what the relatively short-term testing has shown. Production is directly increased by the addition of slag into the kiln.

5.1 Testing

More specifically, testing performed in 1999 on a single wet process kiln line at TXI's Midlothian plant showed an increase in production of greater than 9% - with the amount of increase directly

coming from the mass of slag being added to the kiln. The test closely monitored all inputs to the kiln and maintained constant all inputs but the slag feed rate variable. The testing involved analysis of two basic conditions: Mode 1 - without CemStar; and, Mode 2 with CemStar. Figure 3 more closely illustrates the production results. In addition to the production increase measured during this test, heat input was reduced on a mass basis by almost 6%, translating to a greater than 13% reduction on a kilocalorie per kilogram of clinker basis. This demonstrated the ability of the slag to act as a flux that enables fusion of the calcined materials into clinker with less heat demand (En-Tellect, 1999).

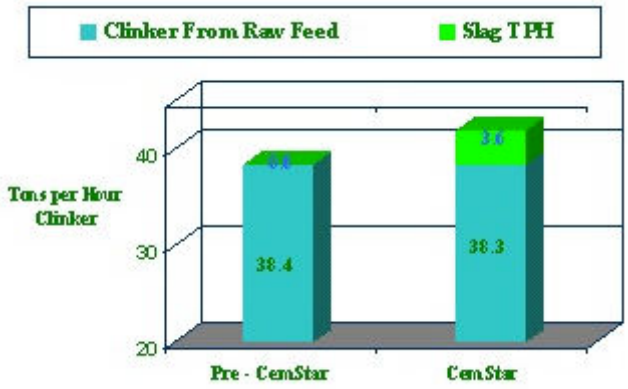

Figure 3. 1999 CemStar Testing Data from TXI Midlothian Wet Kiln

5.2 Long-Term Data

In addition, the long-term benefits of the CemStar technology from a production perspective are illustrated by a review of production data at TXI's Hunter, Texas plant. While more difficult to evaluate because of factors exogenous to usage of the technology (i.e., roller mill up time, fuel sulfur, raw material alkali levels, fuel quality, etc.), a review of twelve years of production shows a nearly 6 percent increase in production on average with CemStar in place. Using 1988 as a baseline year at 100, Figure 4 makes an indexed representation of the relative changes on a year-on-year basis in production level of the kiln on a tons-per-hour basis.

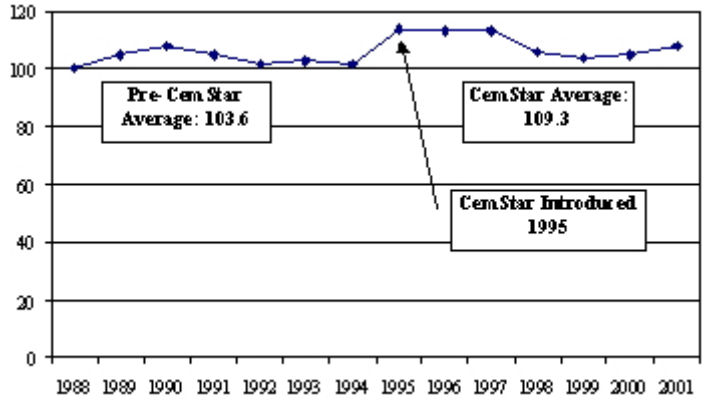

Figure 4. TXI Hunter Plant - Indexed Changes in Kiln Production TPH 1988 through 2001

5.3 Integration and Impact Upon Kiln Operations

Merging the technology into kiln operations requires analysis of a plant's existing raw material composition and developing a mix design that will accommodate the chemistry of the slag material. These mix design considerations determine the optimum slag addition rates. Additionally, based on raw material compositions at individual plants, incorporation of the CemStar process has allowed a significant reduction or elimination altogether of traditional raw materials such as shale, clay or iron

additive such as mill scale. This, in turn results in lower sulfur and alkali input into the system and can potentially increase raw mill production rates.

As discussed, lower kiln temperatures result from implementation of the process, and pyro-processing adjustments must be made to accommodate the mix. As kiln operation is modified accordingly, control operators will see improved kiln stability and will find it easier to recover from kiln upsets and slow downs. In addition, an overall improvement of refractory life has been noted, based on increased annual clinker production rates with no additional downtime for kiln brick jobs. Finally, steadier clinker control has been achieved, which also reflects improved overall process balance and efficiency.

Traditional methods of expanding clinker production capacity are typically very costly and time consuming, require a large quantity of resources and can disrupt continuous facility operations. Conversely, installation of a CemStar process system at a facility can be accomplished in a relatively short period of time, with minimal disruption in continuous kiln operations, all at a significantly lower cost than required for more traditional process capacity upgrades. Moreover, the process can be implemented in as little as three to four months upon the final decision of the facility to use the technology.

5.4 Clinker Chemistry Changes

Due to the individual nature of cement plants as well as the varied chemistry of slags that are produced, the chemical impact of the process is understandably diverse. There are some general chemical impacts that are associated with using slag in the clinker manufacturing process however, due to the conditions under which the slags are formed in the steelmaking process. A typical chemical analysis range for slag produced from an electric arc furnace or basic oxygen furnace, commonly referred to as “steel slags,” is represented as follows:

SiO_2	10 – 15%
Al_2O_3	5 – 10
Fe_2O_3	25 – 35
CaO	30 – 40
MgO	5 – 12
SO_3	0 – 0.5
Cr_2O_3	0.5 – 2.0
Mn_2O_3	4 – 8
Na_2O	0 – 0.3
K_2O	0 – 0.1
ZnO	0 – 0.1
SrO	0 – 0.1

Based on these ranges of constituents in slag chemistry, general chemical impacts on the clinker can include a lowering of tricalcium aluminate (C_3A), due to the higher Fe content in the mix. This impact is mitigated somewhat if the general chemical mix of the raw materials is deficient in Fe, and it must be added through incorporation of iron ore, mill scale, or some other high-Fe material. The Fe can be added through use of slag, and the overall chemistry can be maintained fairly close to the original proportions.

Also, addition of slag can contribute to a higher liquid phase in the mix along with a lower silica ratio, which indicates improved burnability. These two impacts must be managed, however, to prevent excessive liquid phase, which can lead to kiln condition problems and reduced clinker quality. Overall, the slag chemistry can be incorporated into the mix design the same as any other

raw material, with impacts on the final clinker chemistry varying based on the nature of the slag, of the raw materials, and finally of the desired clinker chemistry outcome.

6. MIDLOTHIAN, TEXAS EXPANSION PROJECT

Drawing on the amount of operational experience derived from using the CemStar process since 1995, TXI made the decision to incorporate a slag handling and feeding system into the design of its new kiln line for the Midlothian, Texas plant. The facility, designed to produce 1,800,000 metric tons per year, was designed and supplied by F.L. Smidth, Inc. and more than doubled the annual capacity at the Midlothian plant. In order to meet stringent air permitting requirements, the facility incorporated a number of innovative technologies, including a sulfur scrubber for SO_2 emissions, a regenerative thermal oxidizer system for carbon monoxide (CO) emissions, and a low NO_X ILC calciner. Along with these technologies, the CemStar process was incorporated to the new line to assist in meeting strict regulatory permit requirements as well as to enhance the clinker production levels.

Ground was broken on the new facility in 1999 and the line began commissioning in May of 2001. When the first feed was added to the preheater tower, the system was tied in and slag was fed to the kiln: the plant has used slag as a production component the entire period of commissioning. The CemStar handling and feeding system for the new line is shown in Figure 5.

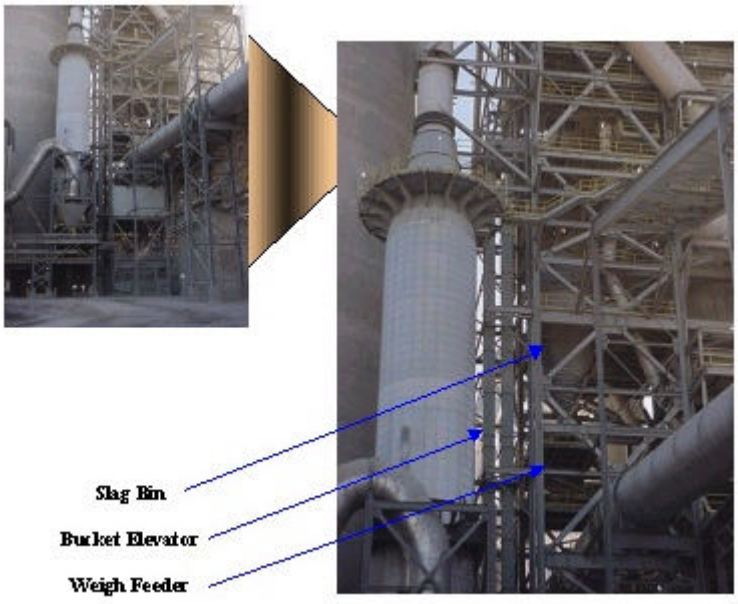

Figure 5. CemStar Handling and Feeding System, TXI Midlothian Kiln Line Expansion

Since startup, slag usage has hovered between 6 and 7% of clinker production, with an annual consumption at approximately 90,000 metric tons. As all components of the facility begin to consistently run at full capacity, the usage of the process is projected to rise by another 50%. In summary, the decision to incorporate CemStar into the new clinker production line which was a major capital investment for TXI, and utilize it at the outset of commissioning of this facility, was based on the extensive operational experience and success that TXI has had with the process at its facilities.

7. ENVIRONMENTAL BENEFITS

Because of the characteristics of slag, implementation of the process has been shown to have a beneficial net effect on emissions from the cement manufacturing process. The primary benefits

derived from this process are an overall reduction of greenhouse gas emissions (CO_2) as well as a decrease in NO_X emissions. Tied in with these is the overall reduction in fuel consumption per unit of clinker produced as well as an overall increase in process efficiency. Finally, employing a byproduct material that has been traditionally underutilized by converting it into high value clinker is a significant benefit.

7.1 Emissions Reductions and Testing

Extensive testing has been conducted to quantify the emissions reductions gained from implementation of the CemStar technology. These tests were conducted at the two Texas facilities operated by TXI – one wet process kiln at the Midlothian facility and the preheater/precalciner line at the Hunter facility. In addition, the testing employed certified continuous emissions monitors and independent consultants to quantify the changes in stack emissions of a number of common gaseous compounds. During these tests, implementation of the process showed significant decreases of NO_X and CO_2 emissions when compared to baseline data.

7.1.1 Short-Term Testing

The first round of testing was conducted at the Hunter, Texas plant and yielded an average reduction in NO_X of 35% (kg NO_X/metric ton clinker) from baseline conditions. The second round of testing was conducted at the Midlothian, Texas plant, where an average reduction in NO_X of about 45% from baseline conditions was observed. In both sets of testing, CO_2 reductions between 5 and 10% were also observed (measured per metric ton of clinker produced). The reductions of CO_2 were observed primarily as a result of the chemical composition of slag, which requires no additional calcining and emits no additional CO_2, unlike limestone, which liberates significant quantities of CO_2 from the cement production process.

7.1.2 Long-Term Testing

Long-term testing was subsequently conducted at the Midlothian facility over a number of weeks, and reductions in emissions of NO_X of about 25% were observed as a result of the analysis, measured on a kg/metric ton clinker basis. Moreover, burning zone temperatures were lower by an average of 200 degrees Fahrenheit when compared to baseline conditions. Correspondingly, thermal NOx, which is temperature dependent and exponentially sensitive to changes in this parameter, was significantly reduced when the CemStar process was in place.

7.2 EPA Awards and Recognition

TXI received two awards from the U.S. Environmental Protection Agency (U.S. EPA) in 1999 recognizing the environmental benefits of the CemStar process. TXI was awarded the Climate Protection Award to recognize the potential of the technology to reduce CO_2 emissions as well as its positive effects on NO_X emissions. TXI was also honored by the U.S. EPA with a special recognition award through the Climate Wise program, again for the contribution of the process in reducing emissions of CO_2 and NO_X.

TXI has also worked with the U.S. EPA in their development of a report outlining NO_X control technologies for the cement industry. This report, which was issued at the end of 2000, outlines available technologies for the U.S. cement industry to reduce NO_X emissions, and includes the CemStar technology as a recognized control method.

Furthermore, as tighter rules are developed in industrialized countries around the world, achieving emission reductions will become an ever-growing priority. NO_X emissions allowance trading programs, such as the Ozone Transport Region in the northeastern 22 states of the U.S., are one method that is utilized to help areas meet ozone reduction goals. The market value of reductions in emissions provides a significant incentive to implement the most cost-effective method of NO_X control. Considering a conservative range of $3,000 to $5,000 U.S. market price per ton of NO_X in

different regions of the U.S., the technology may provide facilities with an economically beneficial method to meet these requirements.

8. CONCLUSIONS

CemStar has been shown to be a cost-effective method to help in meeting additional demand requirements while requiring minimal time for implementation and has positive environmental benefits. Overall, the process offers producers simultaneous means to produce more clinker, improve operational efficiency and stability while providing significant net emission reductions.

REFERENCES

[1] Queen, Douglas M., 2002. The U.S. Cement Industry in a Global Context, 1982 – 2001. Presentation, 2002 Intercem Americas Conference, January 28-29, 2002, Miami, Florida, USA.

[2] En-Tellect Environmental Services, 1999. The Effects of the CemStar Process on a Wet Process Cement Kiln. Independent Consultant Stack Test Report. p. 17.

[3] United States Environmental Protection Agency, 2000. NO_X Control Technologies for the Cement Industry – Final Report. Office of Air Quality and Planning Standards, Research Triangle Park, NC.

IN–AND ON-LINE APPLICATION OF AUTOMATIC PARTICLE SIZE ANALYSIS IN CEMENT PRODUCTION

Pankewitz, A.[1] and Behrens, C.[1]

[1]Sympatec GmbH, System-Partikel-Technik, Clausthal-Zellerfeld, Germany.
E-mail: apankewitz@sympatec.com and cbehrens@sympatec.com

ABSTRACT

Particle size is more and more recognized as a major quality criterion for dry powders and a decisive parameter for production processes. Therefore real time particle analysis is needed to optimize processes, especially regarding energy efficiency and can be applied to close the control loop. Demanding challenges can be found in many industrial applications.

Most industrial processes use pipes as the connection between different process stages. Without sampling it is quite often not possible to measure correctly in the process. Measurements in the particle production stream extend the capabilities of laser diffraction instruments for particle size analysis. The sampling must be representative in order to obtain meaningful results.

The sample preparation should be adaptable to the properties of the product to be analyzed. The dispersion of the sample must be complete but breaking or milling of particles has to be avoided in order to achieve the correct information about the particles in the product and the process.

Many successful installations in the cement industry as well as in other fields of application prove the suitability of in-line measurements under process conditions.

The paper will present the MYTOS family, rugged instruments for -in-on- and at-line particle size analysis that meet the abovementioned demands and cover a variety of applications where real time particle size analysis is crucial for the product, energy efficiency and process quality.

1. INTRODUCTION

In production of cement, the particle size distribution of the final product is one of the important parameters for quality and is decisive for the final strength of the concrete. The required particle size distribution is normally achieved by milling and classifying. Since milling of cement is extremely energy consuming, on-line particle size control of the milled product can improve not only the quality but increase the energy efficiency and the throughput since the recirculated coarse fraction can be reduced.

Today particle size analysis by laser diffraction is an increasingly standard procedure for quality control of cement. The first generation of laser diffraction instruments was presented in the early 1970's. At this time all products, even cement, had to be analysed exclusively in wet suspension since no suitable dry dispersers were available. For cement analysis the liquid had to be isopropanol which required additional challenges for proper treatment after being used.

In 1984 a new generation of laser diffraction instruments was introduced. It is based on the simple idea that the instrument used for the characterisation of quality parameters has to adapt to the demands of the products and the process and not vice versa, i.e. that the products have to be adaptable to the instrument. Dry powders should be dispersed dry, wet products and suspensions should be dispersed in the wet state. This is the practical and logical conclusion, and the new idea led to the development of a range of laser diffraction analysers and dispersing systems that are of modular design thus being easily adaptable to a wide variety of products and process.

Sympatec GmbH from Germany has developed an unrivalled disperser for dry powders in the particle size range from 0.1 micron to nearly 10mm. The patented disperser RODOS allows for a smooth, complete and product-adaptable dispersion of all kinds of powders. In combination with the well established laser diffraction instrument HELOS, a powerful and proven system for industrial particle size analysis of dry powders is available.

The HELOS & RODOS combination has been successfully installed in nearly 150 cement plants all around the world and is on its way to becoming the standard laboratory equipment for dry particle size analysis of cement. This also applies for automated labs where the unit is fed continuously by a robot to perform up to several hundred measurements per day. Of course this only became possible by using a fast dry dispersion module, since wet dispersion does not allow this analysis frequency by nature. Besides this aspect, fast on-line analysis of dry cement powder using a wet dispersion method would lead to an enormous amount of liquid waste even if pressure filtration for the required isopropanol is applied. Therefore dry dispersion is the only sustainable approach for on-line particle size analysis of dry powders.

Today the HELOS & RODOS core technology is combined in the compact MYTOS system which is especially designed for in- and on-line particle size analysis under process conditions.

2. MYTOS LASER DIFFRACTION AND DISPERSING

The principle of laser diffraction requires three main components to be integrated into an analytical instrument as presented in Figure 1.

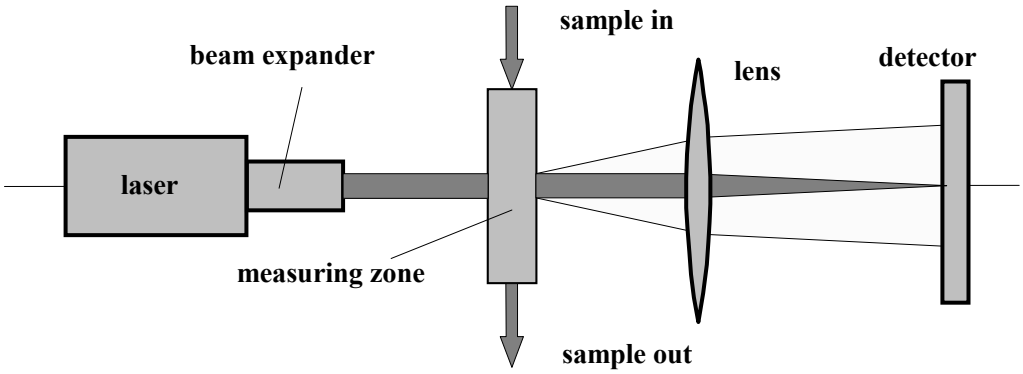

Figure 1. Optical setup of a Sympatec laser diffraction instrument in general

1. At first a laser light source is required. Even today the performance of laser diodes is quite poor from the analytical point of view, so a helium neon laser is preferred. To perfectly adapt the laser beam diameter to the demands of the product and the optical setup, a beam expander is used.
2. A Fourier transformation lens of a distinctive focal distance projects the laser diffraction pattern generated by the interaction between laser light and particles passing the measuring zone to the detector. Depending on the required focal distances, optical modules are available

today that allow virtual focal distance up to 5m on a real distance of less than 50cm which leads to more compact and rugged instruments.

3. The core part of a laser diffraction analyser is the detector. Built up from 31 semicircular elements it detects the diffraction pattern which is converted by a mathematical algorithm into a particle size distribution. From the physical point of view a detector equipped with a semicircular allocation of the detector elements is crucial for highest sensitivity and optimum results, especially for non-spherical particles like cement. Since only a perfect alignment of the complete optical setup guarantees best results, a 3-D auto focus system is a must.

The powder dispersing unit is a fully integrated part of the MYTOS system. Originating from the well established RODOS dry disperser applied for laboratory and automated systems, it disperses even the finest powder successfully. Dispersing is of extremely high importance since a milling process is not characterised by agglomerates, but the produced primary particles. Since laser diffraction instruments analyse all particles presented to the laser beam it becomes clear that full dispersion of agglomerates is required.

In the cement industry very often the Blaine value is still used to characterise the final product. The specific surface area (equivalent to the Blaine value) measured by laser diffraction and calculated from the complete particle size distribution can only be derived from perfectly dispersed powder.

Figure 2 presents MYTOS integrated into a process pipe and shows the details of the laser diffraction and dispersion unit.

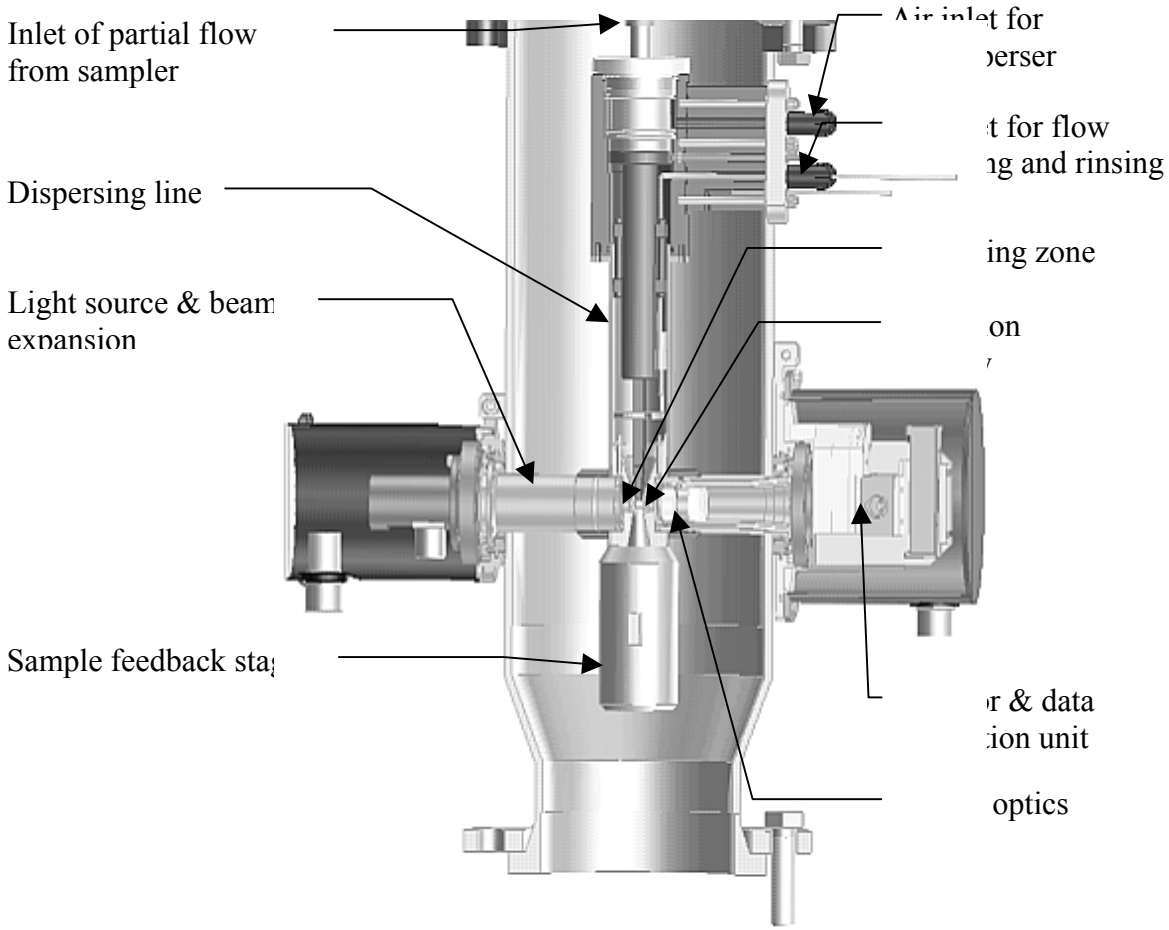

Figure 2. Cutaway view of MYTOS, the unique combination of core parts of HELOS & RODOS, integrated in a production pipe

In the above figure, MYTOS is integrated into a pipe as an in-line measuring device as one possible example of an installation. The required sampling procedure and possibilities of adaptation to existing samplers will be presented in chapter 4.

The sampled particles enter the instrument at the sample inlet. Using compressed air the dispersing takes place in the dispersing line. The dispersed particles are introduced to the measuring zone. Additional rinsing air is applied to focus the particles in the centre of the measuring zone in order to keep the protection windows clean. The analysed particles leave the instrument by the sample feedback stage. Since MYTOS is designed for fully automatic operation, cleaning of the optical components is minimized. No need for cleaning of the windows for periods of several months is documented. If cleaning should be required it is a matter of less than 3 minutes and can be performed without the need to shut down the process.

3. MYTOS FAMILY

Since process and product requirements vary, MYTOS comes as a complete family of instruments introduced in this chapter. Besides the presented in-line solution of MYTOS (Figure 2), on- and at-line versions are available. Figure 3 presents an on-line version to be mounted outside of the process pipe and directly connected to a sampler. Figure 4 shows an at-line solution equipped with the vibration feeder VIBRI mounted on top of the sampler which can be either fed manually or fully automatically.

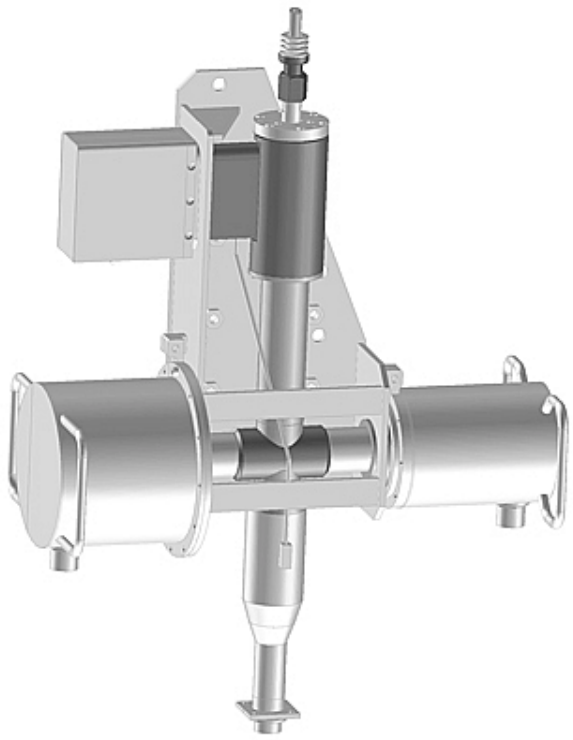

Figure 3. On-line MYTOS

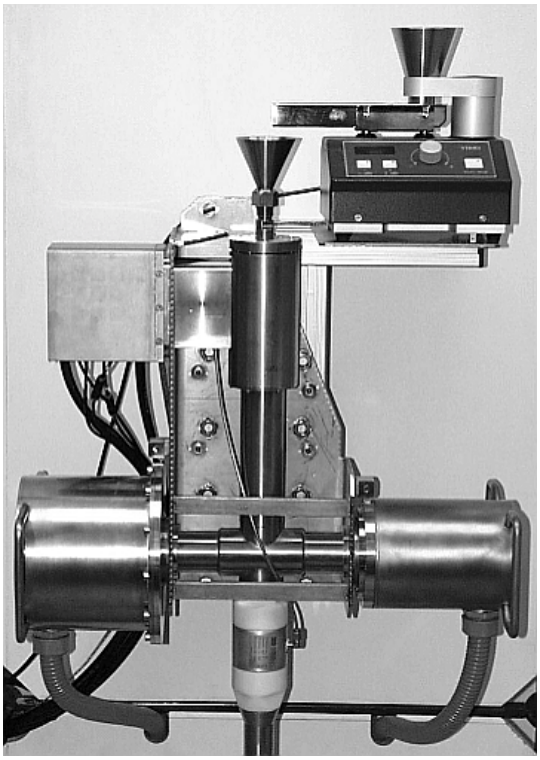

Figure 4. At-line MYTOS

MYTOS & VIBRI are also available as a module solution shown in Figure 5. The module was developed for the German company Krupp Polysius and is used in their AMT (**A**dvanced **M**odular **T**echnology) modules as the standard solution for particle size analysis of cement.

Supplied with wheels the rollable module can be used in automated laboratories or directly in the process environment. All required parts are integrated into this compact solution. The evaluation computer is connected to the module by fibre optical cables up to several hundred meters long. As an alternative a laptop computer can be used for full mobility.

As with all other MYTOS family members, the MYTOS & VIBRI module is adaptable to a variety of samplers and extendable to a full on-line solution for automatic particle size analysis of dry powders.

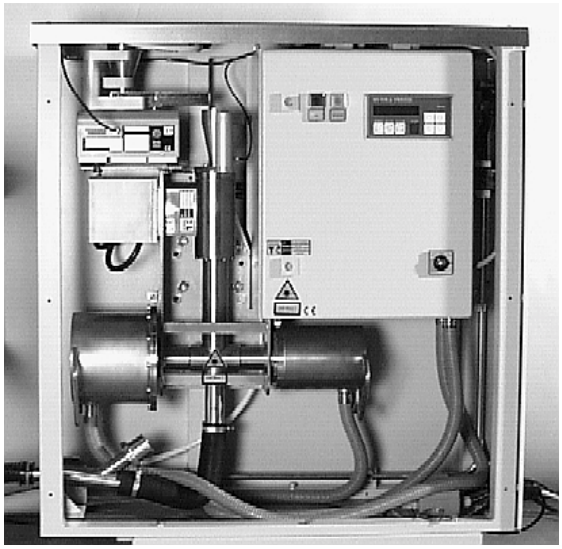

Figure 5. Opened MYTOS & VIBRI module

4. SAMPLING

The principle of laser diffraction requires representative sampling since the product concentration in the production pipe typically exceeds the possibilities of the sensors. In the cement industry additional challenges can be found since the product is very abrasive and large throughputs and high product velocity are normal. Figure 6 shows the in-line sampler TWISTER which is designed to be combined with the previously discussed MYTOS system. TWISTER is proven in the main stream of many industrial applications like chemistry, pharma, iron-powder or silica, to name just a few. Nevertheless the typical process conditions of a cement plant require a pre-sampling stage and a by-pass to avoid extraordinary wear of the sampler. A screw feeder sampling into a by-pass line will be sufficient as a pre-sampling stage, for example.

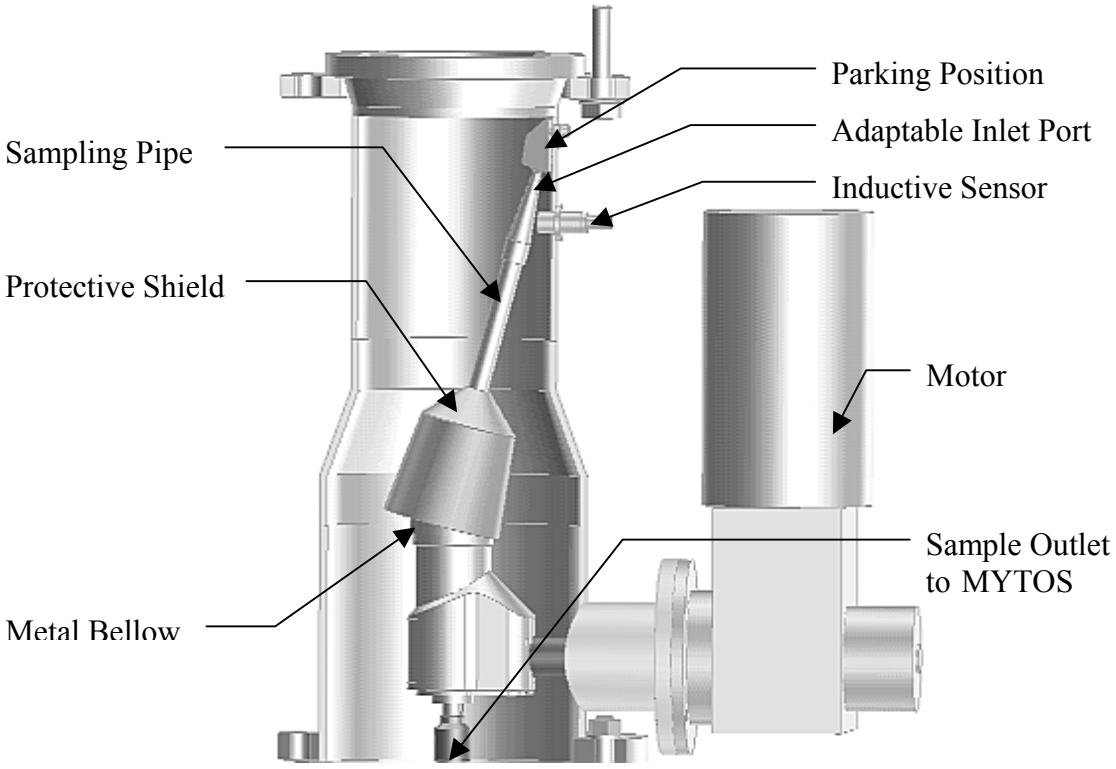

Figure 6. Representative in-line sampler TWISTER in parking position

Starting from a shielded parking position, TWISTER scans the complete cross-section of the pipe in a spiral path so that all areas of the pipe contribute equally weighted to the result. This leads to truly representative sampling. The unit is adaptable to a very wide concentration range by variation of the inlet port.

If a by-pass installation of TWISTER is not possible for whatever reason, then use of a stationary and easy to access sampling tube in the main pipe is recommended. The stationary probe is connected directly to the inlet of MYTOS. A valve between the probe and MYTOS shuts off the powder flow through MYTOS for regular background measurements. Back blowing through the probe ensures that the stationary sampler is not filled with material if no measurements are performed. Since a stationary sampling point is used in this case, the location of the probe should be considered carefully.

In the case of an existing automatic sampler MYTOS & VIBRI are adaptable to it as well. As soon as the funnel of the vibration feeder is filled with product, the analysis starts automatically by a level sensor signal. A solution including an additional sample splitter also acting as a dosing device for VIBRI is designed especially for cement applications. In this case a screw feeder transports a certain amount of cement into a bypass-line where the dosing device is mounted. The doser feeds a partial sample into the VIBRI funnel. After the particle size analysis by MYTOS the cement is re-introduced into the main line.

5. RESULTS

Figure 7 presents typical results for very fine cement and standard PZ35 as an example of comparison of the cumulative and frequency distribution.

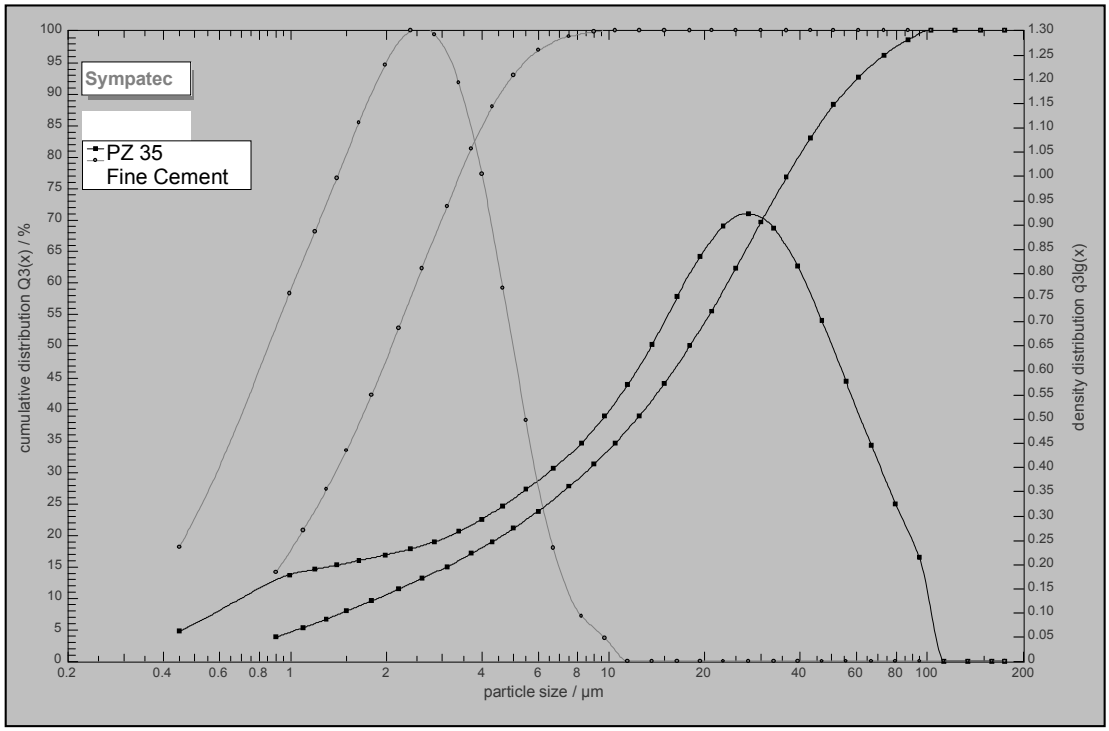

Figure 7. Comparison of measured particle size distributions of fine cement and PZ35

It becomes obvious that the significant difference in the product behaviour of both kinds of cement are resulting from completely different particle size distribution. For on-line control every characteristic value of the measured particle size distribution, or calculated parameters like the

specific surface area, will be displayed as a trend over time to monitor the milling process and to close the control loop.

6. CONCLUSION

The MYTOS & TWISTER concept for real-time particle size analysis combines representative sampling, powerful dispersion and well-known particle size analysis of dry powder by laserdiffraction. The various members of the MYTOS family allow the adaptation to all kind of dry processes. Using real time particle size analysis for closing the control loop of milling process, i.e. in cement, faster response times to process changes guarantees a better efficiency, higher throughput, optimum use of energy-input and finally a better product quality.

IN–AND ON-LINE APPLICATION OF AUTOMATIC PARTICLE SIZE ANALYSIS IN CEMENT PRODUCTION

Pankewitz, A.[1] and Behrens, C.[1]

[1]Sympatec GmbH, System-Partikel-Technik, Clausthal-Zellerfeld, Germany,
E-mail: apankewitz@sympatec.com and cbehrens@sympatec.com

Christian Behrens

Born on 25.09.1971 in Bad Kissingen / Germany
Sales engineer for in-line technology
Married, 1 child

Technical University

1991 – 1999	Process engineering with focus on Mechanical and Thermal process engineering at theTechnische Universität Clausthal / Germany Several works in the field of powder technology and particle size analysis including USA internship Final examination on particles size analysis with Ultrasonic Extinction in cooperation with SYMPATEC GMBH / Clausthal-Zellerfeld / Germany
Degree	Diplom Ingenieur (Dipl.-Ing.)

Sales Engineer

Since 1999	with SYMPATEC GMBH / Clausthal-Zellerfeld with responsibility for complex applications in the fields of in-line particle size analysis based on Laser Diffraction and Ultrasonic Extinction including representative sampling and process adaptations

---

Papers

2002	"Qualitätsmanagment durch in-line Partikel-größenanalyse mittels Laserbeugungsspektormetrie" Bauverlag Germany, ZKG-International (Cement-Lime-Gypsum), 8/2002
2002	"In-line Crystal size analysis with a highly adaptable and Industrially approved sensor based on Ultrasonic Extinction". 15 th Intern. Symposium on Industrial Crystallization (ISIC15th), Sorrent, Italy
2003	"In- And On-Line Particle Size Analysis With A Highly Adaptabel And Industrally Approved Sensor Based On Ultrasonic Extinction" IFPAC's 17th International Forum Process Analytical Chemistry, 21.-24.January 2003, Phoenix, AZ USA

RESEARCH ON THE ACTIVITY OF GRANITE AGGREGATE USED IN THE THREE-GORGE PROJECT

Huaquan Yang, Yingchun Wang, Jiazheng Li, Pengju Cao and Jianhua Lu

The Material Structure Institute of Yangtze Academy of Science Wuhan China 430010

ABSTRACT

The gravel made of diorite-plagioclase granite will be used as coarse aggregate, and the sand made of flecky granite will be used as fine aggregate for the dam concrete of the Three-Gorges project. Because of the strained quartz in the granite, undulance extinction appears in the granite, furthermore, in the the stress concentration area, quartz will form different kinds of dislocation, so the alkali activity reaction will be very slow and will last a long time. In this paper we study the geomorphology, the petrographic, physical and chemical aspects, and also used several methods for comparison. The experimental results show that the granite is mainly composed of feldspar, quartz, biotite and some hornblende or chlorite, etc. The granite aggregate is assessed as non-active aggregate by means of the petrography method, chemical method, mortar bar length method, small bar ultra-accelerated method, mortar bar ultra-accelerated method and the concrete prism experiment. Where there is a low content alkali, there will be no harmful expansion, but if the content of alkali is high, the expansion rate of concrete will still increase even after several years. In order to ensure the safety of the dam, it is very important to control the alkali content of the cement strictly.

Keywords: Three-Gorges project, alkali-aggregate reaction, granite aggregate, concrete

1. INTRODUCTION

The Three-Gorges project is a key project for both governing and developing the Yangze river. It has the functions of flood control, generating electricity, shipping, water supply, etc. The concrete used for the second phase of the project will use the gravel made of diorite-plagioclase granite from footing excavation as coarse aggregate, and a sand made of flecky granite from the basin at Xiaanxi of the dam will be used as the fine aggregate. Because the granite distributes at folded zones of different eras and also shields areas of pre-Cambrian, it bears the stress from strong geologic structure. The rocky mineral will have strongly plastic deformation, and the crystal will have many kinds of dislocation, the defect includes dislocation bow crook, dislocation net and dislocation tangle, thus the energy is stored at the lattice of crystal. So the granite sometimes will have the character of slowly-reacting type alkali activity, the time for the dam to crack because of expansion can last several decades[1]. Once the concrete dam and construction is damaged by alkali aggregate reaction, it is very difficult to fix it, and the economic loss is also very large.

As for the reason of alkali activity of granite, one deduces that it may be related to the strained quartz. B.S.Gogte[2] pointed out: in cases where the content of strained quartz is greater than 20%, and the average undulance extinction angle of the strained quartz is geater than 15 degrees, then the aggregate has potential activity. On the other hand, A.K.Mullick[3] suggested when the undulance extinction angle of strained quartz is greater than 25 degree, and the content is greater than 25%, then the aggregate has potential activity. And there are also some others who don't think there is relationship between the alkali activity and the strained quartz. The defects will be formed in the

crystal because of the stress, and then the crystals characterize undulance extinction. P.E.Grattan-Bellew[4] studied three kinds of granite, and found that the undulance extinction angle of quartz is approximately proportional to the alkali activity expansion rate, that means, the larger the undulance extinction angle of quartz, the larger alkali activity expansion rate.

The granite used at the Three-Gorges project contains strained quartz which generates the undulance extinction. Furthermore, in the stress concentration area, quartz will form different kinds of dislocation, such as dislocation bow crook, dislocation net and dislocation tangle, and they are the main sources of alkali activity of the granite used ont the Three-Gorges project. Because of the complexity of the alkali aggregate reaction, the alkali activity reaction of granite will be very slow and will last a long time. To ensure the safety of the project, the granite aggregate used at the project was studied from geomorphology, petrographic, physical and chemical aspects, and also many methods are used for comparing and testing in order to evaluate the alkali activity of the granite.

2. ALKALI-AGGREGATE REACTION AND THE EXPERIMENT METHODS

2.1 Alkali-Aggregate Reaction

Alkali-Aggregate Reaction (briefly named “AAR”), is where the alkali in cement reacts with some active aggregate, which may cause uneven expansion in concrete, and finally result in damage. Since T.E.Stanton found this problem in 1940, there are many examples of engineering damage because of AAR in US, France, India and other countries. The Moxot Power Dam in brazil used biotite granite as concrete aggregate, and it suffered harmful AAR eight years later. The Shambon Dam in France used gneiss and isinglass granite as aggregate; the vertical expansion of the dam is over 10cm, and the top of the dam inclined about 15cm towards upstream. So careful attention is paid to AAR all over the world.

AAR can be divided to two types: Alkali-Silica Reaction(briefly named “ASR”) and Alkali-Carbonate Reaction(briefly named “ACR”). ASR is where the alkali in cement reacts with the active SiO_2, such as micro-crystaline SiO_2 , cryptocrystalline SiO_2, glassy SiO_2 , strained quartz and flint, and alkali silicate gel will be produced. The gel will absorb water and expand, which will result in the expansion and even cracking of concrete. Opal, flint, quartzite, sandstone and scoriae all contain active SiO_2.

ACR is where the alkali in cement reacts with some carbonate aggregate, such as dolomite reacts with the alkali and results in the concrete cracking. Dolomite contains clay, the alkali ions can penetrate the clay wrapped on the dolomite particles and then diffuse to the dolomite particles. The reactant can not diffuse to the outside passing by the clay particles, this will lead to the aggregate expansion, and crack of the concrete.

The following are conditions necessary for AAR; and thus the alkali content in cement should be over the safe quantity, there is a significant amount of active aggregate, and sufficient water. If there is no water, the reaction will be reduced or completely stopped.

Many factors can affect AAR, such as alkali content in cement, humidity, temperature, additive, dopant material, the cement content in concrete or mortar, the quantity of active aggregate, etc.

Where the non-active aggregate is used in concrete, AAR will not happen. But if there is a moist environment, the alkali content in concrete is high and there is active aggregate, then AAR can take place and result in the expansion and even cracking of concrete. So it is very necessary to appraise whether there are active components or not for the aggregate used in project, and also the alkali content in cement should be measured. Preventative actions should be taken if it is necessary.

2.2 Experiment method of AAR

There is not an international consensus on the method to determinethe activity of aggregates. The petrographic method has important instruction for selecting the suitable measurement method. It is always considered as the preferential method to determine alkali activity of aggregate. It judges whether the aggregate has activity or not using microscopic means of evaluating the type and composition of aggregate, especially to identify those known mineral compositions. The disadvantage is that the quantitative relationship between the active aggregate quantity and the expansion rate is unknown The chemical method is the common international traditional method. This method cannot show the slowly expanding aggregate caused by the micro-crystal quartz or strained quartz. The other disadvantage is there are always some disturbances from carbonate, gypsum and clay, which can result in errors. The sand slurry length method is a classical method, which is similar to ASTM227, but it is only suitable for highly active and rapid expanding rocks and minerals, and is not suitable for slowly expanding aggregate. The sand slurry bar ultra-accelerated method is a standard method adopted by America(ASTM 1260) and Canada(CSA A23.2-14A) in 1994. The result of comparing the research to application records indicates that this method has a good validity for silicious aggregates, especially for slow expanding aggregate. This method is considered as a relatively accurate one. The problem is that it is too strict. Sometimes, the aggregate proved to be harmless will be considered as harmful. The concrete prism method can be greatly affected by the cement fineness, water/cement ratio, curing condition (temperature, humidity) and the component ratio, and the experiment duration of time is also very long.

3. EXPERIMENT

3.1 The granite petrographic identification

The granite minerals from both basement excavation and the the bottom of the dam at Xiaanxi was identified, the result is shown in Table 1. From Table 1, you can see that main component is plagioclase, quartz, biotite and some hornblende and chlorite.

Table 1. The lithofacies identification result of granite from footing groove

Sample number	Main mineral component	Granite name	Quartz undulance extinction angle
96—52	plagioclase61%，quartz16%，biotite10%，hornblende5%，sericite7%	Biotite-plagioclase gneiss	1 ~ 3
96—56	plagioclase60%，quartz23%，biotite9%，hornblende8%	Diorite-plagioclase granite	3 ~ 6
96—61	plagioclase59%，quartz25%，biotite10%，hornblende5%	Diorite-plagioclase granite	2 ~ 5
96—70	plagioclase60%，quartz28%，biotite8%，hornblende3%	Diorite-plagioclase granite	2 ~ 6
96—71	feldspar55%，quartz30%，ammochrysos10%	plagioclase granite	4 ~ 8
96—72	plagioclase87%，chlorite12%，hematite3%	Chloritization dolerite	
96—73	quartz80%，kalifeldspath10%，plagioclase5%，quartzite crumb3%	quartzite	3 ~ 9
96—74	plagioclase65%，chlorite31%	Chloritization dolerite	

Table 1 continued…

Sample number	Main mineral component	Granite name	Quartz undulance extinction angle
96─77	plagioclase45%，potash feldspar26%，quartz25%，chlorite2%	Porphyritic monzonitic granite	3 ~ 5
96─78	plagioclase35%，potash feldspar28%，quartz33%，chlorite3%	Porphyritic monzonitic granite	3 ~ 8
96─86	plagioclase31%，potash feldspar34%，quartz31%，chlorite12%	Porphyritic monzonitic granite	2 ~ 7
96─87	plagioclase65%，chlorite17%，epidote 10%，leucoxene5%	Chloritization dolerite	
96─88	plagioclase70%，chlorite14%，epidote 5%，hematite5%	Chloritization dolerite	
96─90	plagioclase53%，potash feldspar14%，quartz31%	Granite diorite	2 ~ 9
96─99	plagioclase43%，potash feldspar30%，quartz24%，chlorite2%	Porphyritic monzonitic granite	2 ~ 7

The granite of Three-Gorges Dam foundation and Xiaanxi basin is about 8 hundred million years old. The stratum came into being before sinian of superior proterozoic. The stratum is comparatively stable, but orogenic movement has had some influence on the granite of this area. The quartz is characterized by undulance extinction because of the stress effect, but the angle is not big, the biggest angle is only about 9º. Meanwhile there are different kinds of dislocation forms in the stress concentration area, including bow crook, dislocation net and dislocation tangle. The particle size of quartz is about 0.3~2 mm, and no micro particles were found.

The main minerals of the granite were determined by means of electron probe microanalysis. Plagioclase is in adamellite, and acidity of plagioclase is higher. The Ab concentration varies between 96.04 and 97.70. The category is albite. The acidity of plagioclase is low in diorite, the Ab concentration varies between 79.37 and 81.25, the category is potash feldspar. The category of diorite-plagioclase granite is andesine. Potash feldspar mainly belongs to kalifeldspath, and only the big phanerocrysl belongs to barbierite.

3.2 The full chemical analysis of rock

The chemical composition of the sample is measured according to *the method of cement chemical analysis* (GB/T176-1996). The results which can be seen in Table 2, show that the main components of the rock are SiO_2, Al_2O_3, and also a few Fe_2O_3 FeO, MgO and CaO. The concentration of K_2O is about 0.54%~2.89%, and the average value is 1.54%, the concentration of Na_2O is about 1.40%~7.73%, and the average value is 4.91%, the equivalent weight of alkali (Na_2Oe) is about 2.47~8.20%, and the average value is 5.92%.

3.3 Granite measurement by means of the chemical method

The granite measurement by means of the chemical method is carried out according to the *experiment regulations of water power engineering concrete* (SD105-82). The appraising standard of active aggregate is as follows; if the experiment result meets with either of following conditions, Rc >70 and Sc>Rc or Rc >70 and Sc>35+Rc/2, then this aggregate is considered to be potential active aggregate. The measurement results of the sample by means of the chemical method are shown in Table 3. The results show that all sample are non-active aggregates.

Table 2. The experiment result of granite chemical composition anlysis

Sample number	Granite name	Chemical composition (%)							
		SiO_2	Al_2O	Fe_2O_3	FeO	MgO	CaO	K_2O	Na_2O
96—52	Biotite-plagioclase gneiss	61.79	17.00	1.45	4.00	2.74	5.06	1.50	4.21
96—56	Diorite-plagioclase granite	63.15	16.76	1.20	3.78	2.19	5.23	1.44	4.03
96—61	Diorite-plagioclase granite	64.53	16.23	1.56	2.74	2.03	3.25	1.76	5.45
96—66	Plagio-diorite lamprophyre	49.03	12.30	1.85	6.45	12.36	7.12	0.57	2.44
96—67	Broken plagioclase granite	63.62	15.59	1.20	2.48	1.70	3.46	0.69	6.84
96—70	Diorite-plagioclase granite	65.30	15.64	1.47	2.97	2.03	4.24	1.75	4.02
96—31	Diorite-plagioclase granite	64.88	15.99	1.41	3.06	1.98	4.57	1.60	4.05
96—71	plagioclase granite	74.53	14.50	0.34	1.03	0.23	0.77	2.55	4.64
96—72	Chloritization dolerite	55.47	16.69	6.73	1.78	2.66	3.44	1.72	7.07
96—73	quartzite	85.89	6.53	2.15	0.55	0.32	0.16	1.62	1.40
96—74	Chloritization dolerite	51.62	17.04	2.93	4.78	7.14	2.95	1.54	5.32
96—75	Porphyritic monzonitic granite	74.13	13.88	0.52	0.96	0.38	1.40	2.89	4.41
96—78	Porphyritic monzonitic granite	73.15	14.18	0.50	1.14	0.50	1.85	2.71	4.52
96—86	Porphyritic monzonitic granite	73.46	14.42	1.08	0.57	0.44	1.18	2.64	4.62
96—87	Chloritization dolerite	52.61	16.72	5.58	2.94	3.66	7.31	0.98	4.83
96—88	Chloritization dolerite	54.80	16.67	6.74	1.74	2.61	4.40	0.54	7.73
96—99	Porphyritic monzonitic granite	70.62	15.21	0.51	0.88	0.34	1.40	5.10	4.04

3.4 The mortar bar length method

The mortar bar length method is carried out according to *the experiment regulations of water power engineering concrete* (SD105-82). The appraising standard of this experiment is as follows; if the expansion rate is over 0.1% within half year, then the aggregate is considered to be potentially active. The cement used for this experiment is moderate heat Portland cement 525#, except for the alkali contained in the cement itself. Extra alkali was added to the cement, and the equivalent weight of alkali reached 0.8%,1.2%. The experiment result in table 4 shows that the expansion rate

of the sample is related to the equivalent weight of alkali of cement, and also related to the age. The greater the equivalent weight of alkali in the cement, then the greater the expansion rate, and the expansion rate will increase as the age increases. The expansion rate of all samples with 180 day age are lower than 0.1%, which indicates that the aggregate is non-active when appraising it by means of *mortar bar length method*.

Table 3. The granite measurement by means of chemical method

Sample number	Granite name	The decreased value of alkalinity Rc(mmol/L)	soluble SiO_2 Sc((mmol/L))	Appraising result
96─52	Biotite-plagioclase gneiss	223.1	15.4	Non-active
96─56	Diorite-plagioclase granite	81.54	17.1	Non-active
96─61	Diorite-plagioclase granite	58.3	13.73	Non-active
96─66	Plagio-diorite lamprophyre	135.9	18.31	Non-active
96─67	Broken plagioclase granite	99.0	9.98	Non-active
96─70	Diorite-plagioclase granite	54.36	20.39	Non-active
96─71	plagioclase granite	108.72	21.64	Non-active
96─72	Chloritization dolerite	178.94	27.47	Non-active
96─73	quartzite	202.5	106.34	Non-active
96─74	Chloritization dolerite	247.5	75.75	Non-active
96─75	Porphyritic monzonitic granite	114.75	90.73	Non-active
96─78	Porphyritic monzonitic granite	36.0	17.48	Non-active
96─86	Porphyritic monzonitic granite	189.0	50.36	Non-active
96─87	Chloritization dolerite	49.5	21.64	Non-active
96─88	Chloritization dolerite	90.0	14.57	Non-active
96─90	Granite diorite	58.89	28.72	
96─99	Porphyritic monzonitic granite	41.9	19.98	Non-active

Table 4. The experiment result of mortar bar length method

Sample number	Granite name	equivalent weight of alkali (%)	Sample expansion rate (%)			
			30d	60d	90d	180d
96—52	Biotite-plagioclase gneiss	0.54	0.006	0.006	0.007	0.007
		0.80	0.007	0.007	0.009	0.009
		1.20	0.013	0.015	0.016	0.018
96—61	Diorite-plagioclase granite	0.54	0.002	0.002	0.005	0.005
		0.80	0.005	0.006	0.012	0.012
		1.20	0.016	0.021	0.023	0.026
96—66	Plagio-diorite lamprophyre	0.54	0.002	0.004	0.005	0.005
		0.80	0.008	0.011	0.013	0.015
		1.20	0.011	0.016	0.018	0.020
96—71	plagioclase granite	0.54	0.013	0.019	0.020	0.020
		0.80	0.014	0.019	0.020	0.020
		1.20	0.017	0.022	0.024	0.024
96—72	Chloritization dolerite	0.54	0.008	0.009	0.009	0.009
		0.80	0.008	0.009	0.009	0.009
		1.20	0.012	0.014	0.014	0.014
96—73	quartzite	0.54	0.004	0.005	0.008	0.010
		0.80	0.005	0.005	0.008	0.013
		1.20	0.012	0.013	0.019	0.034
96—75	Porphyritic monzonitic granite	0.54	0.005	0.007	0.007	0.011
		0.80	0.005	0.007	0.007	0.012
		1.20	0.008	0.011	0.012	0.017
96—87	Chloritization dolerite	0.54	0.001	0.005	0.005	0.005
		0.80	0.001	0.005	0.005	0.006
		1.20	0.004	0.009	0.009	0.012

The diorite-plagioclase granite of Three-Gorges Dam base was observed over a long period by means of the mortar bar length method. The cement used is 600# dam cement(now is moderate heat Portland cement 525#). The alkali concentration is 0.78%, except for the alkali contained in the cement itself, extra alkali is added to the cement till the equivalent weight concentration of alkali reaches 0.8%,1.2%, 1.5%, 2.0%. The result is shown in Figure 1. We can see that the mortar sample expansion rate of diorite-plagioclase granite increases with age, and it reaches the greatest value when the age is 13 years. After 13 years, the expansion rate has the tendency of decreasing, and it seems that the reaction stagnates. The expansion rate also has relationship to the equivalent weight concentration of alkali in cement, it increases as the equivalent weight concentration of alkali in cement increases. When the alkali concentration reaches 1%, the expansion rate of the sample aged 14 years is still less than 0.1%, the threshold harmful value of expansion rate.

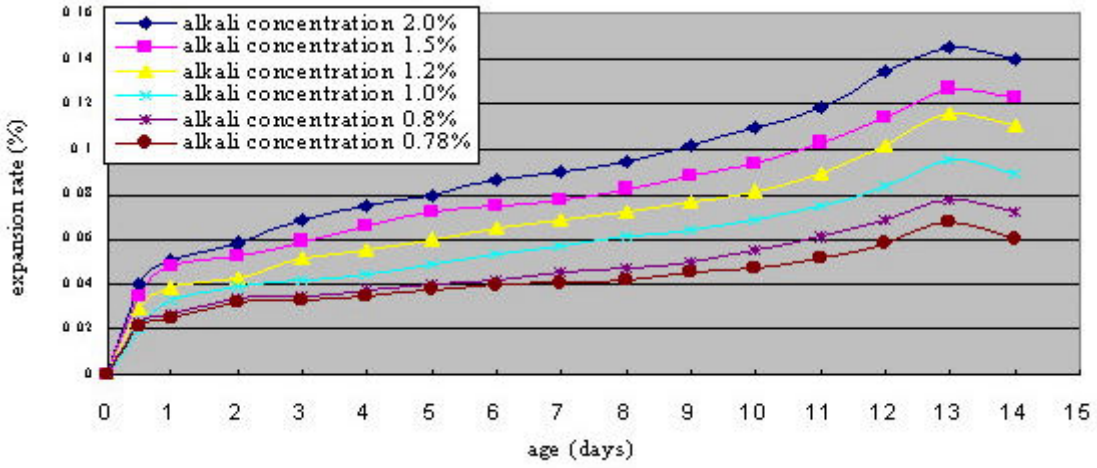

Figure 1. The relation curve of expansion rate vs. age time of Biotite-plagioclase gneiss by means of mortar bar length method

Table 5. The granite experiment result by means of small bar ultra-accelerated method

Sample number	Granite name	Expansion rate (%)	Appraising result
96—52	Biotite-plagioclase gneiss	0.037	Non-active
96—61	Diorite-plagioclase granite	0.030	Non-active
96—66	Plagio-diorite lamprophyre	0.041	Non-active
96—67	Broken plagioclase granite	0.064	Non-active
96—68	Broken granite	0.060	Non-active
96—71	plagioclase granite	0.034	Non-active
96—72	Chloritization dolerite	0.036	Non-active
96—73	quartzite	0.039	Non-active
96—74	Chloritization dolerite	0.039	Non-active
96—75	Porphyritic monzonitic granite	0.030	Non-active
96—80	Granite diorite	0.056	Non-active
96—87	Chloritization dolerite	0.066	Non-active

3.5 Small bar ultra-accelerated method

Small bar ultra-accelerated method is carried out according to the method CECS48:93. The testing of the sample is as follows; one of the three samples which have the greatest expansion rate is used to appraise the alkali activity of aggregate. If the expansion rate is over or equal to 0.1%, then the aggregate is considered to be active, if the expansion rate is lower than 0.1%, then the aggregate is considered to be non-active. This method is only suitable for evaluating the alkali activity of

silicious aggregate. The experimental results of the aggregate by means of small bar ultra-accelerated method are shown in Table 5. From the results it can be seen that the biggest expansion rate of the sample is 0.064%, which is lower than 0.1%, and this indicates that the aggregate is non-active according to the small bar ultra-accelerated method.

3.6 Mortar bar ultra-accelerated method

Mortar bar ultra-accelerated method is carried out according to the method ASTM C1260-94. The testing standard of the experiment is as follows: if the sample expansion rate at the age of 14 days is lower than 0.1%, then the aggregate is harmless, if the expansion rate is over 0.2%, then the aggregate has potential alkali reactivity. If the expansion rate is within 0.1%~0.2%, then the other auxiliary experiments should be carried out, and it is also allowed to assess it when the age reaches 28 days. The result of the mortar bar ultra-accelerated method of the granite from two basins is shown in Table 6. From table 6 it can be seen that the expansion rate of the sample with the age of 14 days is lower than 0.1%, which indicates that the aggregate is non-active according to the mortar bar ultra-accelerated method.

Table 6. The sample experiment result by means of mortar bar ultra-accelerated method

Sample number	Granite name	Expansion rate (%)		
		3d	7d	14d
96─52	Biotite-plagioclase gneiss	0.005	0.008	0.015
96─56	Diorite-plagioclase granite	0.003	0.007	0.018
96─61	Diorite-plagioclase granite	0.008	0.018	0.044
96─66	Plagio-diorite lamprophyre	0.009	0.024	0.074
96─67	Broken plagioclase granite	0.005	0.012	0.033
96─70	Diorite-plagioclase granite	0.005	0.011	0.014
96─71	plagioclase granite	0.008	0.010	0.019
96─72	Chloritization dolerite	0.005	0.008	0.012
96─73	quartzite	0.013	0.025	0.061
96─74	Chloritization dolerite	0.005	0.008	0.008
96─87	Chloritization dolerite	0.014	0.022	0.035
96─99	Porphyritic monzonitic granite	0.017	0.023	0.035

3.7 The prism experiment of concrete

The common prism experiment of concrete is Canadian method, is CSA A23.2-14A. The alkali concentration of cement is set at 1.0%± 0.2%, and by means of adding NaOH, it can make the alkali concentration of cement reach 1.25%. The expansion rate of the sample aged one year is used to assess the alkali activity of aggregate. If the expansion rate of sample aged one year is equal to or over 0.04%, then the aggregate is considered to be potentially harmfully active. If the expansion rate is lower than 0.04%, then the aggregate is considered to be non-active. The experiment result of *the prism experiment of concrete* of coarse and fine aggregate from the same granite is shown at table 7. From table 7 it can be seen that the expansion rate of the concrete with the age time of 364 days is lower than 0.04%, which indicates that the aggregate is non-active according to *the prism method*.

Table 7. The sample experiment result by means of *the prism experiment of concrete.*

Sample number	Granite name	Expansion rate (%)				
		14d	28d	91d	182d	364d
96─130	Biotite-plagioclase gneiss	– 0.0004	0.0011	0.0061	0.0117	0.0175
96─131	Diorite-plagioclase granite	– 0.0073	– 0.0029	0.0018	0.0062	0.0081
96─132	Broken plagioclase granite	– 0.0015	0.0040	0.0040	0.0061	0.0043
96─134	Chloritization dolerite	0.0008	0.0052	0.0069	0.0084	0.0061
96─135	Porphyritic monzonitic granite	– 0.0017	– 0.0005	0.0040	0.0052	0.0033
96─138	Granite plagioclase	– 0.0021	– 0.0010	0.0028	0.0065	0.0084

4. CONCLUSION

The mineral composition of the granite in the foundation excavation of Three-Gorge Dam is mainly plagioclase, quartz, biotite, and some hornblende, the rock has granitoid and massive structure. The mineral composition of the granite from the basin at Xiaanxi is mainly plagioclase, potash feldspar, quartz, and some chlorite, the rock has granitoid, porphyritic structure and massive structure, the undulance extinction angle is small, and there is no micro-crystaline-quartz.

The diorite-plagioclase granite in the foundation excavation of Three-Gorge project and the porphyritic granite in the basin at Xiaanxi show to be non-active after being tested by means of the method of petrographic, chemical analysis method, mortar bar length method, small bar ultra-accelerated method, mortar bar ultra-accelerated method and the prism experiment of concrete.

Because of the complexity of AAR, there is no international common method for appraising the activity of aggregate. When considering the endurance of concrete and the safety of construction, it is important to strictly control the alkali concentration of cement.

REFERENCES

[1] Congxi Liu, Shenyun Wen, Zaiqin Wang, Lizhen. The property of concrete aggregate and the manufacturing process ,Guangzhou:the publishing company of Huanan university of science and technology,1999.8, pp 233.

[2] B.S.Gonte, An Evaluation of Some Common Indian Rocks with Special Reference to Alkali-Aggregate Reaction. Engineering Geology, Vol.7, pp 135-153,1973.

[3] A.K.Mullick,R.C.Wason,S.K.Sinha and L.H.Rao, Evaluation of Quartzite and Granite Aggregates Containing Strained Quartz. Proceeding of the 7th International Conference on Alkali-Aggregate Reaction in Concrete. 1986,VII, pp428-433.

[4] Grattan-Bellew,P.E,Is High Undulatory Extinction in Quartz Indicative of Alkali-Expansivity of Granitic Aggregates? Proceeding of the 7th International Conference on Alkali-Aggregate Reaction in Concrete.1986.

[5] A.J.C.T.Cavalcanti,Alkali-Aggregate Reaction at Moxoto Dam,Brazil,Proc 7th Int Conf.Ottawa,pp168-172,1986.

[6] Masel Anord (France), the latest study on AAR of the siliceous aggregate in France, the construction of Chinese Three-Gorge, 1998.5.

NEW GENERATION OF ADMIXTURE POLYMERS AND ITS ROLE IN CONCRETE TECHNOLOGY

M.W. Danzinger[1], K. Saitoh[1], P. Jost[2] and U. Maeder[3]

[1]Sika Japan, [2]Sika USA, [3]Sika Technology Ag

1. INTRODUCTION

Polycarboxylicacid-Polyether-Polymers were first considered as an admixture 20 years ago in Japan. Since this time various polymers based on different mechanisms became available.

Compared to traditional admixtures based on lignosulfonate, naphthalene-sulfonate, melaminesulfonate or gluconate, the polycarboxylic based polymers show significant performance advantages: higher water reduction rate, extreme extended slump life, very low and stable concrete viscosity and finally, fast setting times. The key factor for Self Compacting High Strength Concrete (SCC) is very low concrete viscosity even at W/C ratios far below 20%.

Due to the threat of seismic activities and high land prices, the demand of Ultra High Strength Concrete in Japan is rapidly growing. The advantages for construction work are first a smaller number of columns and second an increased lettable area.

Concretes with a compressive strength of 100 N/mm^2 are currently produced. These concretes are applied only as SCC.

This presentation gives an overview of the potential of the Sika polycarboxylic based admixtures and their impact on concrete technology. Concrete mix designs and special binder systems are described, The focus lies on concretes with a W/C ratio of 15 - 35%.

A new construction system CFT (Concrete Filled Steel Tubes) is also briefly introduced. It is one of the application methods for SCC High Strength. Currently most of the high rise buildings under construction in Japan are based on CFT.

2. ULTRA HIGH STRENGTH CONCRETE: 60 – 150 N/mm^2

As schematically illustrated, below a W/C ratio of 35% conventional construction methods can no longer be applied. To achieve strengths up to 150 N/mm^2 very high binder contents and very low W/C ratios are necessary.

This results in highly viscous concretes and makes it impossible to compact the concrete correctly. Dense reinforcement and complex structures also prevent a proper filling of the formwork

The newly developed polymers extend the W/C ratios far below 20%, the concrete viscosity is low and stable for up to 120 minutes.

Proceedings of the 11th International Congress on the Chemistry of Cement (ICCC)
'Cement's Contribution to the Development in the 21st Century'
Hosted by: The Cement and Concrete Institute of South Africa
CD-ROM produced by: Document Transformation Technologies
11 - 16 May 2003, Durban, South Africa
ISBN Number: 0-9584085-8-0
Editors: Dr G. Grieve and G. Owens
Congress Organised by: Event Dynamics

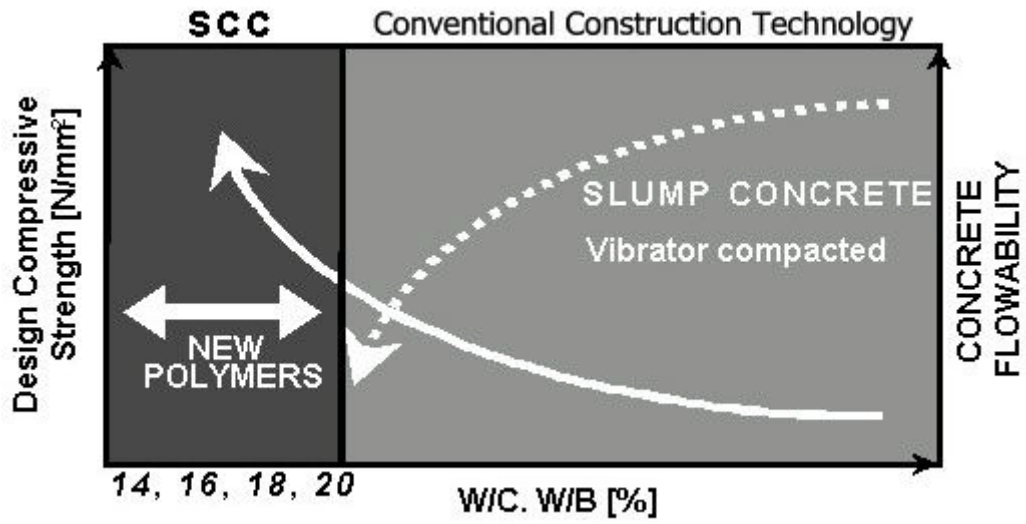

3. CONCRETE MIX DESIGNS AND BINDER SYSTEMS

In the past years new cements and binder systems were released. The application field and the composition of the cements are shown below. Low Heat Cement is currently widely used as well as a premix of low heat cement with silicafume. VKC 100 is a blend of cement with special slag and silicafume. Moderate Heat Cement is the newest among these cements and is used at W/C above 30%.

Low Heat Cement hydrates more slowly than Normal Portland Cement due to the high amount of belite clinker phase. The heat generated during the hydration process is less resulting in reduced thermal cracking. The final strength is also significantly higher than for normal portland cement.

Moderate Heat Cement is at the moment used for concrete with W/C between 30 – 45%.

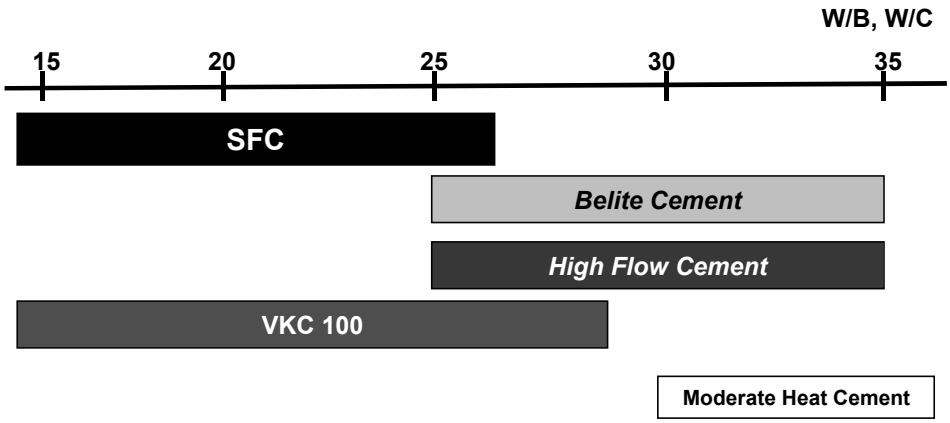

The mix design of concretes with a design strength between 24 and 120 N/mm^2 is shown below, as they are actually used.

The aggregate factor (= vol% aggregate per m^3 concrete) for 80, 100 and 120 N/mm^2 is kept constant as is the amount of water. Silicafume is used as an additive to improve workability and final strength.

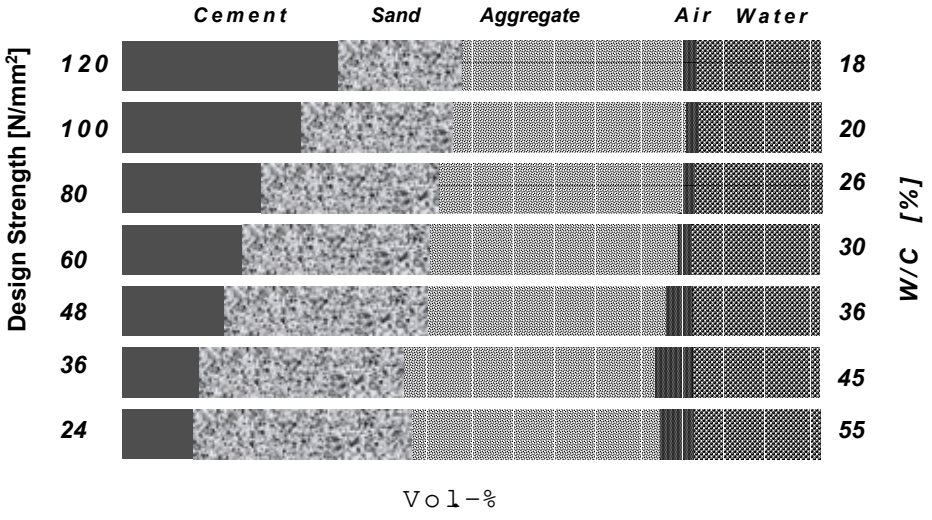

24 – 48: Normal Portland Cement
60 – 80: Low Heat Cement
100 –120: Low Heat Cement + Silicafume

Different special cements and binder systems are used as a base for the SCC High Strength, as is shown in the table below.

Company	Notation	Density	Specific Surface	Chemical Composition			Clinker Component			
		[g/cm³]	[cm²/g]	MgO	SO_3	Na_20 eq	C_3S	C_2S	C_3A	C_4AF
Taiheiyo	L	3.22	3450	0.7	2.2	0.46	29	54	3	8
Sumitomo Osaka	L	3.23	3300	0.8	2.4	0.5	25	56	2	10
Ube-Mitsubishi	L	3.24	3430	1.05	2.52	0.51	23	57	3	
Ube-Mitsubishi	L 5	3.22	3780	0.86	2.5	0.51	32	50	3	
Taiheiyo	HF	3.2	4100	0.7	2.7	0.5	34	47	3	8
Taiheiyo	M	3.21	3150	1.3	2.0	0.54	43	36	4	12
Sumitomo Osaka	M	3.21	3100	1.2	1.9	0.58	44	33	4	12
Taiheiyo	N	3.16	3310	1.4	2.0	0.62	52	24	9	9
Ube-Mitsubishi	N	3.15	3280	1.6	1.9	0.65	53	22	9	9

L: Low Heat- or Belite Cement. HF: High Flow Cement. M: Moderate Heat Cement
N: Normal Portland Cement

4. CONCERTE TEST RESULTS

The sand and aggregate used for these mix design is also used for concretes with a design strength of 24 – 48 N/mm². Special aggregate is available but was not used.

Mixing of the concrete: 1) cement + sand + water + admixture
2) + aggregate

The mixing times for the concretes described below were in the range of 2.5 to 4.5 min.

The ***SIKA polymers*** used for these mix designs showed excellent slump retention properties and the viscosity only slightly increased after 120 min.

Design Strength 100 - 150 N/mm², Binder: VKC 100

W/B	Water	VKC 100	Sand	Aggregate	Admixture	**Slump Flow**	Temperature
	[kg/m^3]				[%]	**[cm]**	[^{0}C]
15	150	1000	567	802	2.1	**75 x 75**	25
18	150	834	647	802	1.6	**70 x 69**	25
21	150	715	749	802	1.5	**68 x 67**	25

W/B	Compressive Strength [N/mm2]			
[%]	7 days	28	56	91
15	120	134	145	150
18	116	129	139	142
21	104	112	121	130

Design Strength 50 - 80 N/mm^2, Binder: Low Heat Cement
These mix designs currently have the biggest market share in Japan.

W/B	Water	L-Cement	Sand	Aggregate	Admixture	**Slump Flow**	Temperature
	[kg/m^3]				[%]	**[cm]**	[^{0}C]
25	165	660	684	899	1.3	**67 x 69**	25
30	165	550	772	802	1.2	**70 x 69**	25
35	165	471	837	802	1.05	**68 x 67**	25

W/B	Compressive Strength [N/mm2]			
[%]	7 days	28	56	91
25	36	70	82	87
30	45	79	90	97
35	61	95	107	113

Design Strength 100 - 150 N/mm^2, Binder: Silicafume Cement (10% silicafume)
The highest compressive strength was achieved with the premix low heat cement and silicafume. Compressive strength will also be tested after one year; data will be available soon.

W/B	Water	SFC	Sand	Aggregate	Admixture	**Slump Flow**	Temperature
	[kg/m^3]				[%]	**[cm]**	[^{0}C]
15	155	1034	442	855	2.8	**72 x 71**	25
18	155	862	588	855	2.1	**69 x 69**	25

W/B	Compressive Strength [N/mm2]			
[%]	7 days	28	56	91
14	98	138	151	162
18	92	130	139	148

5. NEW CONSTRUCTION METHOD: CFT

CFT, ***C***oncrete ***F***illed Steel ***T***ubes, is a new method used for the construction of high rise buildings.

The basic principle is very simple: the framework of the building consists of steel pillars connected with steel beams. SCC High Strength is filled into the steel pillars which up to now do not contain reinforcement. The slump flow is in the range of 60 – 70 cm, the slump flow must be constant for up to 120 min, the concrete viscosity soft and stable. The concrete is either filled into the pillars by pumping from the bottom of the pillar by connecting the pump hose or is pumped to the top of the pillar and dropped in. The pillar diameter reaches up to 2 m, the height of filling is in the range of 100 – 180 m.

The concrete must be easy to pump even to heights of up to 300 m, segregation of the concrete must be prevented as it would be reflected in the compressive strength. This construction method allows for extremely fast construction.

6. SUMMARY

The new generation of polymers is extending the application range of concrete as a construction material.

Extremely high compressive strengths can be achieved due to the water reduction rate of the Sika polycarboxylic polymers. The slump is stable for 120 minutes and the excellent workability of the concrete makes it easy to use on site even with W/C ratios far below 20 %.

As different polymers (water reduction – and slump retaining polymers) are used to formulate the admixture product, technical requirements like water reduction or slump life can easily be adjusted.

The usage of the new polymer based admixtures will not be limited to SCC applications, and is likely to make further inroads into conventional concrete supplied for site use.

These new polymers are the basis for the development of new construction methods.

CHEMICAL AND PHASE ANALYSIS IN CEMENT PROCESS AND QUALITY CONTROL: ROLE OF XRF AND XRD INSTRUMENTS AND THEIR INTEGRATION

Yellepeddi, R.[1], Bonvin, D.[1] and Bateman, S.[2]

[1]Thermo Electron Corporation, Thermo ARL En Vallaire, CH 1024 Ecublens, Switzerland.
[2]Thermo Electron Corporation, Thermo ARLabs Kempton Park, South Africa.

ABSTRACT

The analytical needs of cement are constantly evolving from basic oxides analysis to comprehensive phase analysis of clinkers, additives and associated materials. Advances in X-ray instrumentation have shown that it is possible to integrate both XRF and XRD in one instrument as a total solution to the process and quality control. In addition, low or medium power WDXRF instruments are becoming cost effective with adequate analytical performance in small to medium size cement plants. Advances in the development of "standard-less" XRF and XRD analysis programs are providing powerful means of analysing non-routine samples in addition to monitoring the clinker phases. Various possible solutions will be presented: A combination of a stand-alone XRF and a stand-alone XRD is a more appropriate solution for a central service laboratory involved in method development and investigative work requiring flexibility and expertise with a view to analyse varying sample types. A fully integrated XRF-XRD platform is more suitable to a process or quality control laboratory requiring on-line, continuous analysis using dedicated, easy-to-use quantitative programs for a more comprehensive chemical and phase analysis. Results from different case studies will be presented and discussed.

1. INTRODUCTION

Analytical requirements in the cement industry are continuously evolving and different solutions are available for different situations. In particular, chemical analysis by X-ray fluorescence is being extended to cover materials and elements other than the usual oxides in raw materials through to the final products. This has become possible thanks to the development of more flexible XRF instruments and analytical programs referred to as "standard-less". Moreover, analysis of phases in clinker including free lime by X-ray diffraction is being increasingly solicited. This latter application has become routine and on-line thanks to the development of integrated X-ray instruments. However, apart from these analytical criteria, there are other operational issues that need to be addressed in deciding on a suitable X-ray instrument. For example,

- Capital investment, running and maintenance costs for the lifetime of the instrument (sometimes referred to as total cost of ownership)
- Production capacity of the plant (small to large) with corresponding justification for investment
- Grinding station versus a production site
- Types of cement produced and additives used (limestone, slags, fly ash, silica dust, gypsum)
- Number of samples to be analyzed per hour or per day
- Typical response time for complete analysis (chemical and phase)
- Sample preparation methods available

Proceedings of the 11th International Congress on the Chemistry of Cement (ICCC) 11 - 16 May 2003, Durban, South Africa
'Cement's Contribution to the Development in the 21st Century' ISBN Number: 0-9584085-8-0
Hosted by: The Cement and Concrete Institute of South Africa Editors: Dr G. Grieve and G. Owens
CD-ROM produced by: Document Transformation Technologies Congress Organised by: Event Dynamics

- Need for automation or integration in process control

The type of X-ray instruments to be used in a cement industry can be broadly classified in three different scenarios, each with their own conditions or constraints.

2. PROCESS AND QUALITY CONTROL LABORATORIES IN MEDIUM TO LARGE CEMENT PLANTS

These laboratories are generally looking for:

- Routine quantitative analysis of all the oxides with high degree of accuracy and reliability
- Dedicated calibration programs for each major matrix involved
- Reliable on-line analysis of free lime in clinkers as one of the most important kiln control parameters
- Continuous monitoring of clinker phases if possible as quality indicators
- Quantification of additives such as limestone and slags in cement
- Occasional non-routine analysis

Instruments integrating XRF for chemical analysis and XRD for specific phase analysis are ideally suited for process and quality control (QC/QA laboratory) in medium to large capacity cement plants. In such applications, higher throughput, integration in the process and some degree of analytical flexibility are required. Complete and uncompromising chemical analysis is obtained through XRF and XRD is used for specific phase analysis such as Free Lime in clinkers, limestone additions in cement and other related phases.

Complete analysis is obtained using one instrument, one sample and one analytical program in about 3 to 5 minutes depending on the configuration. Quantitative analysis of routine oxides, free lime in clinkers and limestone additions in cement with such systems is well established.

When all sorts of various oxidic raw materials need to be controlled a single calibration program based on fusion beads technique covering elements from sodium to iron as given in Table 1 can be used. But in most instances pressed pellets preparation is used in the cement industry for specific material types.

Table 1. Elements/oxides and their corresponding concentration range and Standard Error of Estimate covered using a general program for oxides.

Element	**Range [%]** (on ignited samples)	**Typical SEE [%]**
CaO	0.02 - 94.4	0.26
SiO_2	0.35 - 99.7	0.25
Fe_2O_3	0.025 - 94	0.32
MgO	0.01 - 97.3	0.22
Al_2O_3	0.16 - 89.2	0.19
K_2O	0.006 - 15.4	0.05
MnO	0.005 - 8	0.04
Cr_2O_3	0.002 - 17.4	0.1
TiO_2	0.011 - 3.8	0.03
P_2O_5	0.014 - 40.0	0.04
SO_3	0.015 - 3.7	0.05
Na_2O	0.045 - 10.4	0.15

Analysis of clinker phases - C_3S, C_2S, C_3A and C_4AF - is being increasingly considered for implementation in process and quality control laboratories. It is certainly advantageous to be able to accomplish this analysis alongside the usual XRF analysis with the same clinker sample and in a quantitative manner. There are different approaches to the analysis of clinker phases starting from the very approximate and empirical estimations from Bogue equations through microscopy to Rietveld based programs. There are debatable strengths and weaknesses in each of these methods in terms of their implementation in on-line process control. What is perhaps useful in a process control environment is a continuous monitoring of the clinker phases for their variations in conjunction with the corresponding free lime and related oxides. In this sense, an integrated analysis incorporating clinker phases by XRD and the oxides by XRF is likely to be more easily acceptable in a routine method.

Figure 1 shows the scan obtained using the integrated XRD system of a combined XRF-XRD instrument on different clinker samples. Apart from an intense free lime peak, the major clinker phases can be identified with their individual peaks. Other intense peaks are due to combination of several phases and cannot be used for quantification.

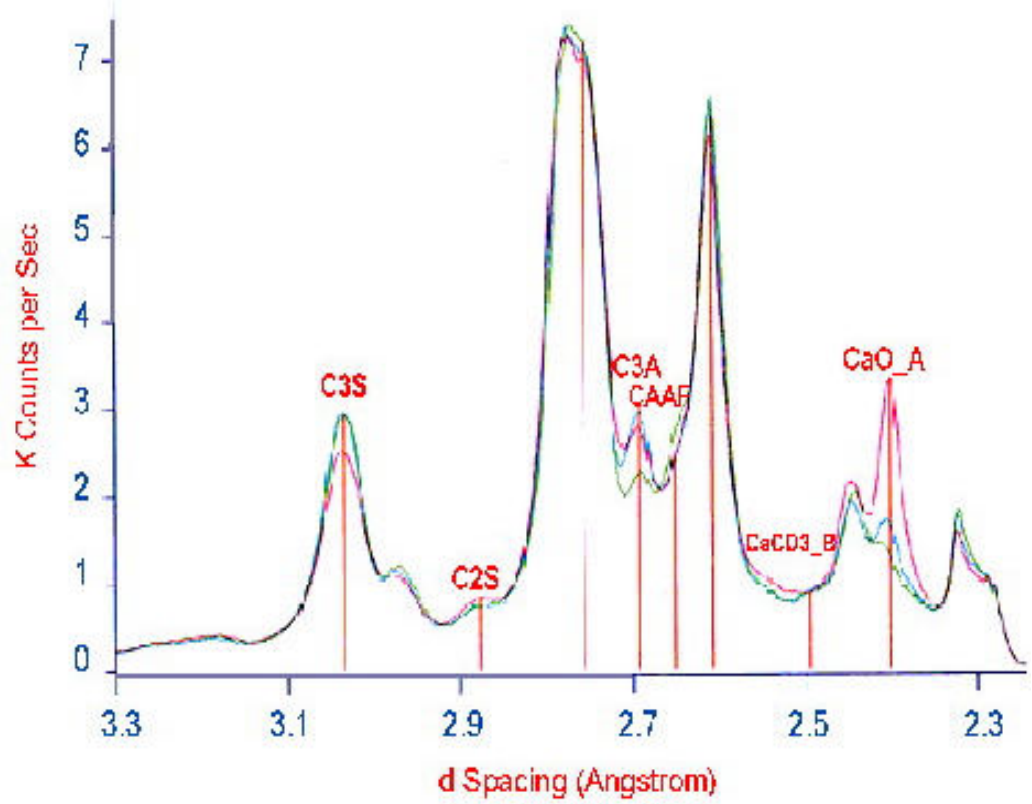

Figure 1. XRD scans obtained on different clinker samples using ARL Total Cement Analyzer showing clearly free lime and the four clinker phases.

A study has been performed in order to determine if the clinker phases of real world clinker can be estimated through XRD. As a first step a correlation has been established between the clinker concentration calculated through the Bogue equation.

Figure 2 shows a calibration curve obtained for C_3S using its XRD peak intensity and the estimated C_3S concentration from Bogue.

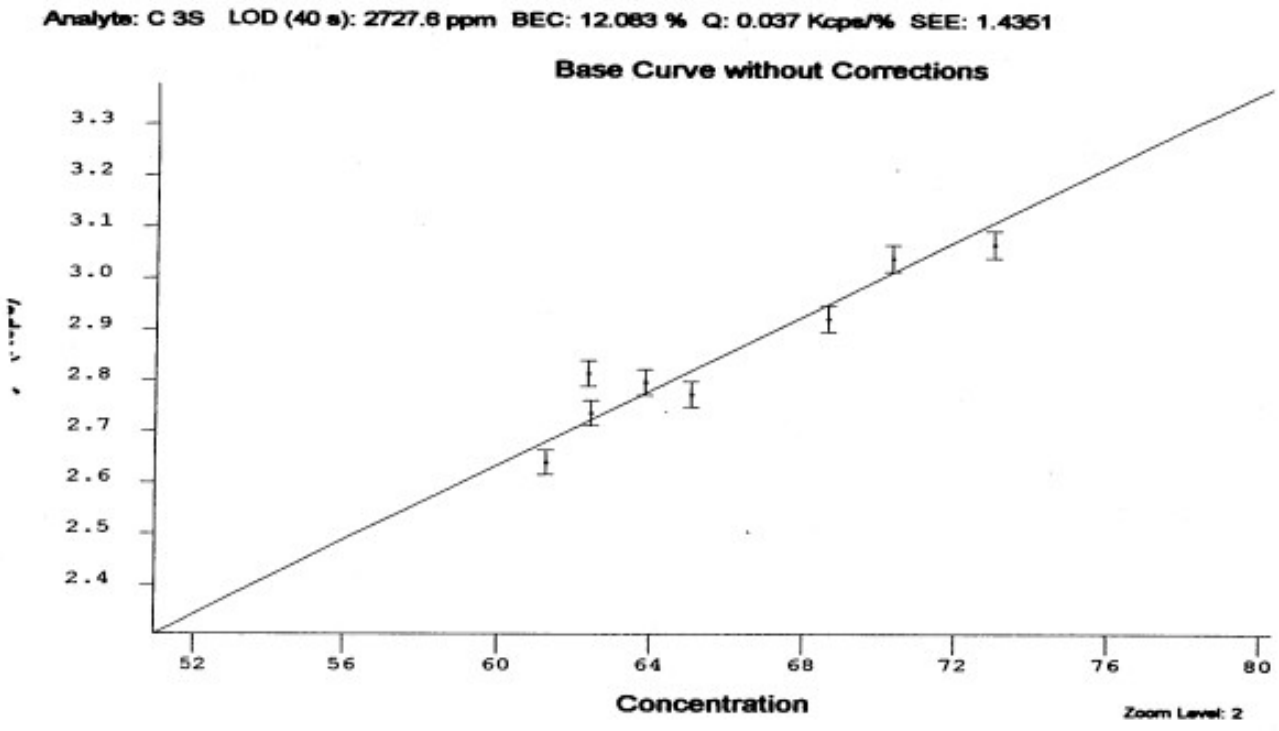

Figure 2. XRD calibration curve obtained for C_3S in a series of real clinker samples using levels calculated through Bogue equation. Analysis time 100 seconds.

Figure 3 shows a calibration curve obtained for C_3S using its XRD peak intensities of a series of clinker samples and C_3S concentrations estimated through microscopy counting . Similar curves were obtained for the three other clinker phases-C_2S, C_3A and C_4AF. The standard error of estimate or the accuracy depends, of course, on the relative accuracy of the reference technique used. It is therefore possible to implement calibration curves for the four clinker phases and to perform quantitative analysis of these phases using an integrated XRD system. The analysis of the clinker phases will be finished in 2 to 3 minutes.

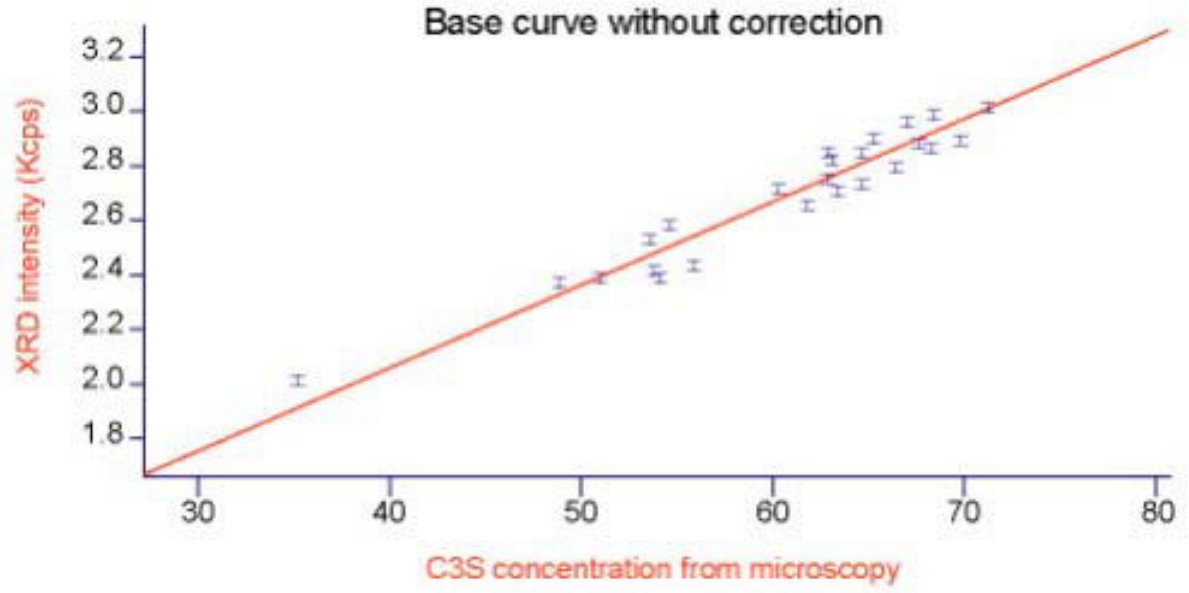

Figure 3. XRD calibration curve obtained for C_3S in a series of real clinker samples characterized by optical microscopy. Analysis time 100 seconds.

3. CENTRAL LABORATORIES FOR INVESTIGATIVE WORK AND METHODS DEVELOPMENT

The principal activities of central laboratories

- Analysis of various types of samples (solids, liquids, loose powders) with known or totally unknown matrix
- Quantitative XRF analysis using both specific calibrations and general purpose "standard-less" analysis programs
- Qualitative and quantitative investigations of phases or minerals in raw materials, clinkers and cements using XRD in conjunction with Rietveld based programs
- Analytical support and development of methods in the context of new processes or materials manufacturing.

It is clear that full power of XRF and XRD techniques can be exploited in a central laboratory where there is expertise and the need for investigative work. Other complimentary analytical techniques are usually available in the central labs making the data correlation and verification process more easily achievable.

Given this profile and the nature of samples received in such laboratories, it is legitimate to think of two independent instruments of XRF and XRD with full flexibility and their corresponding analytical programs more open for investigation than needed for a routine analytical laboratory.

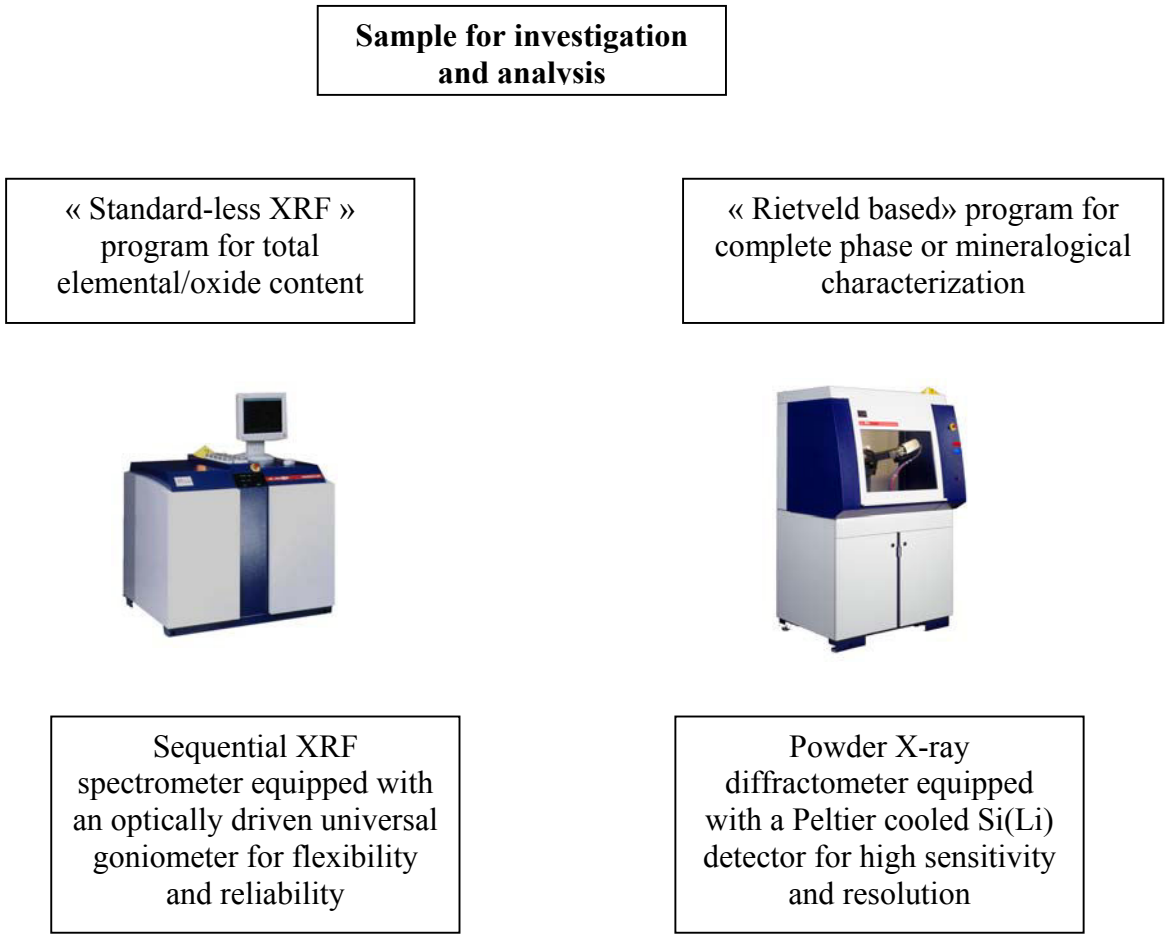

Figure 4. Combination of a sequential XRF and a powder XRD in a central laboratory

A summary of typical analytical tasks that can be handled (both routine and non-routine) using a conventional sequential XRF instrument (X-ray tube below the sample) as shown in Figure 4.

Analytical functions of a sequential XRF instrument using Universal Goniometer:

Quantitative analysis of known materials

- **CaO, SiO_2, Al_2O_3, Fe_2O_3, MgO, Na_2O, S, Cl, K_2O, etc. in raw materials, raw meal, clinker and cement.**
- **Analysis time < 2 min**
- **Analysis of sulphide versus sulphate in slags (as additive in cement)**

Standard-less analysis programs for samples from

- **Quarry**
- **Coal ash**
- **Additives**
- **By-pass (Na, Cl, S, ...)**
- **Gypsum (minors & traces)**
- **Oils & Waste Liquid Products used as alternate fuels**
- **Filters and other environmental control systems**

On the other hand, a powder XRD instrument is a powerful tool to study various cement related materials for their mineralogy and can be exploited for more advanced investigation related to the structures. A typical XRD scan on a clinker sample is shown in Figure 5.

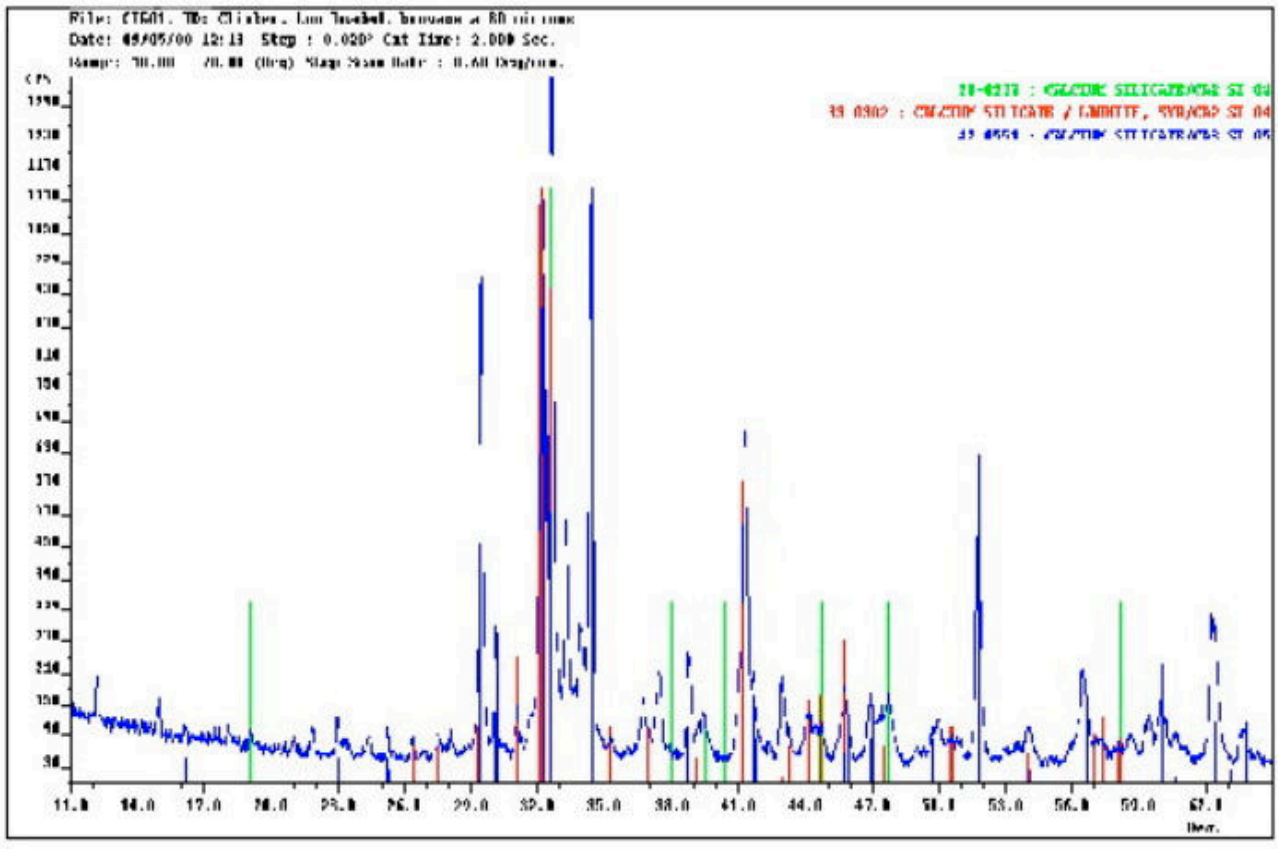

Figure 5. XRD scan on a clinker sample obtained using a diffractometer equipped with a Peltier cooled Si(Li) detector. Thanks to the high sensitivity and resolution of this type of detector, faster acquisition of data is possible. Typical scan time - 3 minutes.

Results from Rietveld analysis using the SiroQuant™ program on cement samples are shown in Table 2.

Table 2. Rietveld analysis of cement compared with grain counting method

Cement Standard	Analysis Method	C3S	ß-C2S	C3A		C4AF
				Ortho	Cubic	
E1	Siroquant	69.0 (1.0)	14.2 (0.7)	2.0 (0.7)	4.4 (0.7)	7.2 (0.6)
	Grain Counting	71.1 (3.4)	12.8 (7.6)	6.7 (1.3) (sum)		9.5 (2.4)
E2	Siroquant	79.2 (0.9)	7.2 (0.6)	0.3 (1.3)	8.3 (0.4)	3.3 (0.6)
	Grain Counting	80.7 (3.4)	7.7 (2.6)	6.3 (1.3) (sum)		4.9 (2.4)

4. SMALL CEMENT PLANTS, GRINDING STATIONS AND/OR BACK-UP IN CENTRAL LABORATORY

In this third and final situation, the analytical requirements are generally less demanding and they can be summarized as follows:

- Limited to the essential oxides for process control (small cement plants) and/or quality control in the final product (grinding stations)
- Lower sample throughput
- Much lower capital investment
- Easy to use, easy to maintain instrument with significantly lower running costs

Bench top energy dispersive XRF (ED-XRF) or non-dispersive XRF systems were used in the past in such situations because most wavelength dispersive XRF (WD-XRF) systems were either too expensive or too complicated for the performance required. With the development of entry-level WD-XRF instruments, small size cement plants and grinding stations can now benefit from high quality analysis even for sodium. Indeed, the new generation of XRF instruments does not require water cooling (neither external nor internal) and can be configured for simple, stand-alone operation with no peripheral dependence. Such units can be configured as sequential-simultaneous instruments fitted with compact goniometer for flexibility and/or a few fixed channels for simultaneous analysis of elements from sodium onwards.

WD-XRF brings a much better spectral resolution than conventional ED-XRF instrument as well as superior precision, short and long-term stability. Light elements like Na and Mg can be analysed without problem. Figure 6 shows a typical calibration curve obtained for Na, one of the critical elements to be determined in the cement industry with precision and reliability. These results were obtained with samples prepared as fusion beads and show quality data even when the sample is diluted with Lithium tetraborate in order to fuse it in the form of a glass bead.

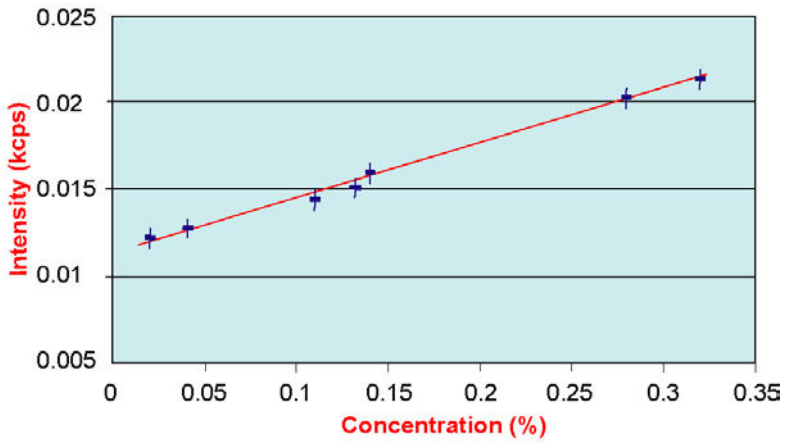

Figure 6. Entry level WD-XRF instrument: calibration curve for Na in cement prepared as fusion bead. Standard error of estimate is 0.011% in a range from 0.02% to 0.32%

Table 3 shows precision data on various oxides obtained for such entry level WD-XRF instrument on a pressed pellet of cement. Precision usually demanded for the analysis of cement is given in this table in comparison with that obtained using this new instrument. This data was obtained by analyzing the pellet for three days continuously and *without drift correction* of the instrument. The precision for all the oxides including Na_2O is much better than what is generally required. The total analysis time can be reduced to about 3 minutes in order to meet the precision demanded for all the oxides.

Table 3. Excellent repeatability (precision) data obtained with ARL OPTIM'X on a cement pellet. Total analysis time: 3 minutes. Test done over three days of measurements without drift correction.

Elements	**Concentration Range (%)**	**Precision demanded**	**Precision found**
CaO	*58 – 66*	*0.03-0.035*	*0.028*
SiO2	*18 –23*	*0.02*	*0.018*
Al2O3	*3 – 5*	*0.02*	*0.013*
Fe2O3	*1.5 – 5*	*0.01-0.02*	*0.008*
MgO	*0.5 – 4*	*0.02*	*0.015*
SO3	*2 – 5*	*0.01-0.015*	*0.009*
K2O	*0.1 – 0.6*	*0.02*	*0.005*
Na2O	*0.1 – 0.7*	*0.015*	*0.007*
P2O5	*0.05 – 0.3*	*0.01-0.015*	*0.009*
MnO	*0.05 – 0.3*	*0.015*	*0.003*
TiO2	*0.1 – 0.4*	*0.015*	*0.005*

In addition to the analysis of cement and related materials in small size cement plants or in grinding stations, WD-XRF entry level instruments can also be a cost effective back up instrument for a main laboratory instrument. Further, analysis of liquids or loose powders can also be accomplished under a helium atmosphere using such instruments. This feature is particularly useful when alternate fuels or other waste products need to be monitored.

5. CONCLUSIONS

Continuous innovations in X-ray instrumentation and analytical techniques are providing the cement industry with a wider choice of solutions suitable for process and quality control or investigative laboratories with integrated platforms or stand-alone instruments respectively. Small cement plants or grinding stations can also obtain high-quality analysis thanks to the development of entry level WD-XRF instruments requiring significantly lower capital investment and running costs.

CEMENT STANDARDS
"THEIR ROLE IN REGULATING AND PROMOTING TRADE"

Julies, E.L.

South African Bureau Of Standards (SABS). Private Bag X191, Pretoria, 0001
Tel: +27 12 428-6002/6025. Fax: +27 12 428-6751. Cell: 083 632 4994

ABSTRACT

"If you control an industry's standard, you control that industry lock, stock & ledger" [1]
W Edwards Deming

In today's modern environment trade barriers are of concern. Standards can be used either to overcome these barriers or to establish them - the essence then is to know and understand how to effectively use the advantage standards provide.

Another issue is that trade barriers occur predominantly in the regulatory domain where countries are sometimes inadequately equipped to manage the process. A suggested form that such a regulatory regime should encompass is discussed; together with the benefits a well-defined and transparent regulatory domain can bring to any industry.

A brief comparison is made between activities of SABS and those, which any National Standards Body should undertake; with specific reference to the South African Cement Standards.

The conclusion is then reached that instead of seeing standards as a hindrance, it is in fact the basis for all trade, it acts as a means to transfer technology, and should be seen as a useful adjunct to any country's trade policies

1. USING INTERNATIONAL STANDARDS TO LEVERAGE WORLD MARKETS

The Greek mathematician and scientist Archimedes once boasted that given a spot to stand and place a lever, he could move the world. Today's Archimedeans are still interested in leverage, but of the entrepreneurial type – gaining access to world markets and increasing trade. One of the levers used by the modern Archimedeans is international standards.[2]

For many companies this is a challenging time - whilst it is a good time to "go global", it is also a time for great caution as others seek the same opportunities. Whilst we have seen a decrease in certain trade barriers, they have become more subtle, both in nature and form. Tariff Trade Barriers are those, which have fallen most rapidly, to be replaced by sometimes-quantitative restrictions, import licensing or local content requirements as very effective barriers to trade. Conformance assessment can also create a trade problem. And sometimes, standards are the barrier.

2. INTERNATIONAL STANDARDS ARE STRATEGIC TRADE LEVERS

There are many ways in which companies can use international standards as strategic levers to avoid or evade trade barriers, or to create new trade opportunities. In the first instance, international

standards may provide companies (and their governments) with the means to challenge national standards as being restrictive trade barriers. This is especially true where national standards have no basis in fact or practice. It could be construed as having been implemented because of unique local conditions, which necessitate their use. An example of this could be the standard for iodised salt. Secondly, international standards can provide business opportunities since they may act as a unifying agent for technical requirements, thereby unifying markets. Thirdly, there is a strong link between global trade and global production. International standards allow companies to produce a product in one country, to the same performance and quality expectations as in any other country and then allow the marketing of the product globally. Finally, the rapidly changing political, social and economic landscape has opened many new markets around the world. But companies in less developed or emerging markets are new to the world of trading partners and thus find themselves in need of standards. In this case there are no (or very few) national standards, and so international standards are helpful for such companies to achieve market entry.

3. PROMOTE GLOBAL PRODUCTION

We are living in a world where we have globally spread suppliers, unlike in the past where production took place in a single country, by a single manufacturer, using local suppliers. Today the major manufacturers (so-called multinationals) in many instances have been reduced to assemblers of components manufactured by their many, geographically spread contract suppliers.

In this world the lines between competitors, suppliers, and contractors have become blurred. Mergers and acquisitions are the order of the day. Strategic alliances abound, where former competitors are now partners. One of the easiest ways to get access to markets is for a firm to acquire interests in foreign companies.

We find as well that products are becoming increasingly designed, manufactured and supported on a worldwide basis, taking advantage of the different talents around the world, while at the same time reducing the cost of labour, materials and transportation. This is the so-called “think global, act local” approach finding favour with most firms today. In the new era that we are entering no single company or even a single country, can hope to successfully compete in the global game by itself.

Under these trying circumstances the sole dependable feature is that if an international standard is used as the basis for specifying the performance, composition, quality requirements, manufacturing characteristics or even shape, of a product, then that product will, anywhere in the world, be exactly the same, no matter who manufactures it. (We are of course assuming here that manufacturing standards are equivalent and that skills, expertise etc. are similar). This is in a nutshell the key role that international standardisation plays.

4. STANDARDIZATION & REGULATION

We see that in order to regulate trade, it is to offer a level playing field to the competing firms, and to offer a measure of consumer protection, business and citizens need a regulatory environment, which is clear, effective and workable. Some organisations have postulated that in the rapidly changing global market place, formal regulation is not always the answer, and are pushing for alternative approaches.

The claim they make is that these alternative approaches are more effective, however the jury is still out on this issue.

The challenge here is to ensure high levels of protection while avoiding over-regulation. This is not possible in the absence of strict liability laws where the onus is placed on the individual, in the

context of representing the firm, to ensure that a product they supply conforms in all possible aspects with the legal (and sometimes, dare we say, moral) requirements.

It is the sad and unfortunate reality that those countries most in need of a regulatory regime (or strict liability laws) are often those without any, or where few exist. This makes them an easy target for companies whose sole objective is to make money for their shareholders.

It is therefore unlikely that governments will in the foreseeable future agree to, or buckle under the sometimes severe pressure being brought to bear upon them by large corporations (whose turnover often exceeds by far the total GDP of the country) to change either the standards by which they judge, or the manner in which they regulate products, which may negatively impact upon their citizen's health and/or safety.

Under these circumstances the voluntary use of standards in regulation requires a clear definition of each party's roles, responsibilities and competencies.

A Technical Regulation Best Practice Model was developed in South Africa to comply with WTO/TBT requirements; i.e. to protect the consumer through technical regulations without creating a technical trade barrier:

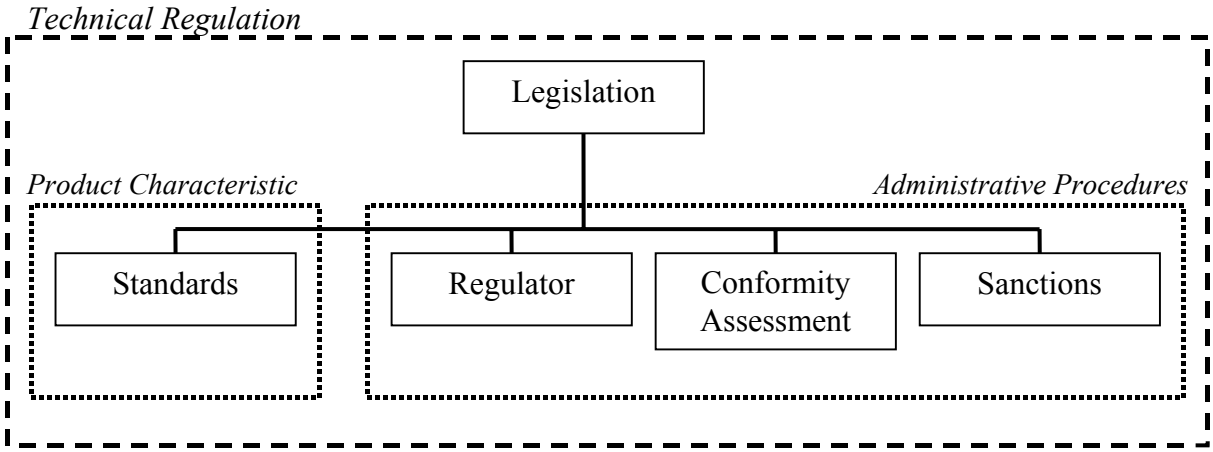

Above is a schematic representation of this model, which clearly shows the roles various sectors play in implementing the regulations.

5. STANDARDIZATION AND TRADE

A cursory glance at trade figures shows that global trade continues to increase year by year. We have earlier said that the use of international standards can enhance market access and facilitate trade. But standards may also give rise to "trade frictions", in particular if there are no international standards with global recognition capable of being employed by a player in the market. International standardization via one of the recognised institutions such as ISO/IEC or ITU to name but three, offers globally applicable solutions to the parties concerned.

It is moot that internationally traded goods need international standards wherever possible so as to make buyers and sellers "ad idem" as to what it is they are exchanging, to provide a sound basis for contracts, and to ensure inter-changeability and inter-operability across national boundaries. Standardization and the use of standards are also an important part of any community's external trade policy, and that community must comply with international agreements concerning standards, amongst which is the WTO Agreement on Technical Barriers to Trade (TBT Agreement).

6. ADVANCING STANDARDIZATION AND CONFORMITY ASSESSMENT TO FOSTER TRADE [3]

To recap what we said before:

6.1 Standards are an important aspect of daily life, but play an even more important role in the economic development of a country, since they deal with issues as diverse as*:*

- Protection of the environment
- Promotion of health and safety
- Enhancing the quality of life
- Opening up of trade, both regional and international
- Facilitating delivery of quality
- Raising the overall levels of quality across industries in a nation
- Acting as consumer protection

6.2 Standards are many and varied in their actions*:*

- They facilitate trade by providing a basis for comparison and measurement.
- Act as a mechanism to transfer technology.
- Improve communication and mutual understanding of technical issues.
- Act as protection of health, safety and the environment.
- They are positive stimulus for innovation.

With this in mind, we can then come to the crux of our discussion, specifically what is the role of a national standards body (NSB) in this, and with particular reference to South Africa, both as a developing country and as a global player (we would like to think leader) in the field of international standardisation, what is SABS' role.

7. THE INVOLVEMENT OF A NATIONAL STANDARDS BODY (NSB) WITH SPECIFIC REFERENCE TO SABS INVOLVEMENT

It is becoming more and more clear these days that the role, which an NSB plays, is much more complex than was at first understood. If we are correct that standards are the basis for international trade and that a country should recognise that the basis for all of its trade in a large measure is supported by standards, then the role of the NSB is clear.

That is, it acts as a source of information, not only on standards, but also on the application of such standards to its business, and to trade specifically. It adopts, adapts or develops, international standards for local conditions and use. NSB's should form a part of all trade negotiation missions where they can provide technical support and input at the early stages of discussions.

Since standards form the basis for technical specifications they also form the basis for the conformity assessment regimes that measure compliance with such specifications, as well as form the basis for the measures of competency, not only of individuals, but also of organisations engaged in conformity assessment practices.

7.1 The following cement standards were adopted

7.1.1 EN/ENV 413 Series (adopted in 1996):

Generic Title: Masonry Cement

Part 1: Specification (ENV)

Part 2: Test methods (EN)

7.1.2 EN 196 Series (adopted in 1996):

Generic Title: Methods of testing Cement

Part 1: Determination of strength
Part 2: Chemical analysis of cement
Part 3: Determination of setting time and soundness
Part 4: Quantitive determination of constituents
Part 5: Pozzolanicity test for pozzolanic cement
Part 6: Determination of fineness
Part 7: Methods of taking and preparing samples of cement

7.1.3 EN 197 Series (adopted in 2002): [previously formed the ENV 197 series]

Generic Title: Cement

Part 1: Composition, specifications and conformity criteria for common cements
Part 2: Conformity evaluation

This has brought it in line with most of its major trading partners, and makes SA a leading country amongst developing economies adopting such modern standards.

By request of several stakeholders in the Southern Africa cement industry, and in order to prevent the fraudulent practices rife during the late 80's up until today, it was decided to regulate the sale of cement as a commodity having a serious impact on human safety.

In order to regulate the distribution and sale of cement, it was decided to turn the applicable voluntary specifications into compulsory specifications, and coupled this with a requirement that it would be illegal to sell cement in South Africa without a distinctive mark. The mark chosen, in the absence of any alternative at the time, was the SABS proprietary mark.

To obtain the SABS mark, a company needs to apply for a permit issued by an accredited holder of the SABS licence. Currently the licence holder is Global Conformity Services (GCS) and only they may issue the permit, valid for three years, which will enable firms to participate in the Product Certification Scheme run by GCS. Participation is open to all firms (national and international) that meet the strict requirements of the EN standards.

Over many years of successful construction activity in Southern Africa, the construction industry realized the importance of specifying and using only approved cement and cementitious products. These products are specified for use and tested according to the strict guidelines laid out in the standard and are thus the only ones approved for use in construction and building operations.

The certification of cement entails proper control of manufacturing - from raw material to the final product. The principle is that only a well defined, well known, stable and capable process can qualify for certification under any mark scheme, be it local or international. Under such a certification scheme, the service provider ensures that the process is monitored at various stages and that regular independent testing of the product is carried out.

Note that as an adjunct to this certification process, valuable assistance and advice on the proper utilization and use of cement is given by the Cement & Concrete Institute (C&CI) which does constant research in this regard and offers training to industry.

8. CONCLUSION

In conclusion it is clear that standardisation has come a long way from simply being a nuisance to those who wish to "get on and do it", to where today it is an indispensable part of trade, both policy and implementation.

"ALL THAT GLITTERS IS NOT GOLD"

"King Hiero II of Syracuse knew that all that glitters is not gold" – which is precisely why he tasked Archimedes to devise a standard test method to determine the gold content in his crown.

REFERENCES

[1] Dr. W Edwards Deming, Out of the Crisis, Massachusetts Institute of Technology (1986)
[2] Stephen C. Lowell, 1st Place, World Standards Day Paper Competition, "The Modern Day Archimedes: Using International Standards to leverage World Markets", (1997)
[3] EL Julies, "Regional Market Integration – Africa, SADC Countries", (2000)
[4] EL Julies, PASC XXV Paper, "Advancing standardization & conformity assessment to foster trade", (2002)
[5] SABS Civil & Building Department
[6] SABS Regulatory Regime, Overview, (2001)
[7] EL Julies, "The importance of Standards to an Economy", (2002)
[8] EL Julies, SAIMAS Keynote Address, "Streamlining for Effectiveness" (2002)
[9] Mechanical, Automotive & Civil Standards Department

CEMENT STANDARDS
"THEIR ROLE IN REGULATING AND PROMOTING TRADE"

Julies, E.L.

South African Bureau Of Standards (SABS). Private Bag X191, Pretoria, 0001
Tel: +27 12 428-6002/6025. Fax: +27 12 428-6751. Cell: 083 632 4994

EXPERIENCE

01/03/1998 to present:	**President (CEO), SABS**
02-1996 - 02-1998:	Corporate Quality Assurance Manager, Eskom
1996:	Consultant to Aviation Industry (Simera Aviation)
1995:	Head of Industrial Engineering, Process Manager
1984-1990:	Mainstream Engineering (Assistant Engineer), Melbourne (Rockledge) Florida, USA
1980-1984:	Quality Assurance Manager, GUD Filters, Atlantis
1977-1980:	Navigating Cadet and 3rd Navigating Officer, Unicorn Shipping Line, Durban

SUMMARY OF QUALIFICATIONS

1977-1980:	Government Certificate of Competency, Second Navigating Officer, RSA/Radar Observer, Restricted radio telephone operator
1982-1983:	Certificate in Quality Assurance and Quality Control (with distinction), City and Guilds of London Institute
1982-1983:	Executive Education, Cape Town (Diploma Business Management, first class) / Diploma Management and Cost Accounting)
1991-1997:	The following short courses and certificates were obtained: Cert. Loss Control (NOSA/ILC), Cert. Total Quality (EMSA), Self-Directed teams (UCAR) - Problem Solving Techniques (Kepner Tregoe), Systems Auditing (Eskom), Marketing (Aubrey Wilson Inc), Industrial Relations (Andrew Levy & Ass)

EDUCATION

- 2000: UNISA, MBL
- 1988-1990: University of Florida, Gainesville, USA: MSc (Mech Eng) (with high honour)

ACHIEVEMENTS

- Business Times Newsmaker of the Week *(2001)*
- Patron - SAIMAS
- COHORT representative on NACI Panel
- Board Member on THRIP
- Appointed by Dr Ben Ngubane to sit on NEPAD Committee
- Reviewer of Integrated Manufacturing Strategy
- Member of ASSAF
- Received SASQ Award for contribution to Quality

DIRECTORSHIP

- SABS Council
- SABS Holdings
- SA Excellence Foundation (SAEF)

INTERESTS & OTHER

- Reading
- Travel
- Community Activities:
  - Elected member Meyerton Primary School Gov Body *(1995-1997)*
  - Vereeniging Technical College Council member *(1993 to present)*
- Volunteer Experience:
  - Henley Neighbourhood Watch Office Bearer *(5 years)*
  - Pinellas County Schools, youth co-ordinator *(2 years)*
  - Brevard County Schools, student tutor *(4 years)*
  - High school student tutor (maths, science) *(2 years)*

SUSTAINABLE DEVELOPMENT IN THE CEMENT INDUSTRY: THE SOUTH AFRICAN RECORD

de Rougemont, F.

Association of Cementitious Material Producers (ACMP)

ABSTRACT

The process of manufacturing cement results in the generation of emissions and wastes. With increasing international awareness of environmental issues and concern for the impacts of industrial operations on the environment, the international cement industry has taken a leading role to evaluate its responsibilities and a group of major producers has agreed on future actions to ensure sustainability of the industry.

The cement manufacturers in South Africa participated in the above evaluation process and have assessed the emissions being made in South Africa. While the record demonstrates a downward trend, the South African manufacturers have committed to an Action Plan in the interests of meeting future stakeholder needs in a sustainable manner.

1. INTRODUCTION

Cement is an essential material in today's society because, as a major constituent of concrete, it forms a fundamental element of any housing, commercial or infrastructure development. Measured on a kilogram per capita basis, concrete is the second most widely "consumed" material in the world, second only to water.

The cement manufacturing process, as is the case with any heavy industrial process, has significant impacts on the environment as it is very energy intensive. Cement manufacture includes long-term quarry management and is a major industrial operation at the scale of a local community. The typical impacts are:

- Local impacts
  - Landscape disturbance and modification
  - Dust emissions
- Global impacts
  - CO_2, SO_X, NO_X emissions

Because of these impacts sustainable development has recently become a major strategic issue for cement manufacturers around the world. For cement manufacturers, sustainable development is about positioning ourselves to ensure the long-term life of our industry, an industry which is so important for the wellbeing and comfort the world's people.

Our industry is giving very specific and serious attention to the managing of CO_2 emissions. The cement manufacturing process produces CO_2 emissions through the consumption of energy. In addition, the process involves the calcination of limestone by driving off the bound carbon dioxide. We know that CO_2 is one of the greenhouse gasses which are believed to be contributing to global warming.

The Kyoto protocol requires Annex B developed countries to make commitments to reducing national CO_2 emission levels to a level below that determined by national inventories in 1990.

Despite the failure of some major countries to sign the Kyoto protocol, many governments have, or are likely to, adopt carbon management policies. This may include taxes on carbon dioxide emissions and this is likely to remain as one of the main drivers for change in the cement industry.

In 2000, a group of ten major international cement companies collaborated as the "Working Group Cement" (WGC) to sponsor a study under the auspices of the World Business Council for Sustainable Development (WBCSD) into the sustainability of the cement industry. The WBCSD commissioned the independent organisation, the Batelle Memorial Institute to undertake the study. The study culminated in a report published in March 2002[1] entitled "Towards A Sustainable Cement Industry".

To reinforce the independence of the Batelle study, an external Assurance Group was set up to review the research and make certain that the work fairly represented the multiple viewpoints and the range of issues that needed to be included.

Facts which emerge from the report indicate that the cement industry:

- Provides the construction industry with a key ingredient in the most commonly used material for the world's infrastructure – concrete
- Produces about 1.5 billion tonnes of cement per year
- Has grown at a rate of nearly 4 percent per year over the past decade
- Operates manufacturing or processing facilities in 150 countries
- Has an estimated annual turnover of $97 billion (US)
- Directly employs an estimated 850,000 workers worldwide

It suggested that Sustainable Development (SD) represents a vision of industrial progress that respects both human needs and global ecosystems, preserving the foundations upon which human quality of life depends. Three dimensions of a sustainable business are defined as the triple bottom line, i.e.

- Economic prosperity
- Environmental stewardship
- Social responsibility

While clearly all three dimensions are important, this paper mainly focuses on the issue of environmental stewardship i.e. the steps that cement manufacturers can take to reduce the environmental impact of their operations.

2. ENVIRONMENTAL ISSUES ASSOCIATED WITH CEMENT INDUSTRY OPERATIONS

The environmental issues confronting the global cement industry were reported to include:

- Impacts of resource extraction (fossil fuel, limestone, and other minerals) upon environmental quality, biodiversity, and landscape aesthetics
- Depletion of non-renewable or slowly renewable resources (fossil fuels or groundwater)
- Dust emissions (from quarrying, cement production, and transport)
- Other emissions that can affect air quality: nitrogen oxides (NO_x), sulfur dioxide (SO_2), carbon monoxide (CO), volatile organic compounds (VOC), dioxins, metals, etc.
- Emissions of carbon dioxide (CO_2) involved in global climate change
- Solid wastes, including cement kiln dust (in some countries where standards restrict recycling back into the production process).

None of these issues are insurmountable and all are amenable to mitigation through careful management. The Batelle report suggests that the cement industry can ensure its continuity and prosperity by focussing on win-win opportunities to create value for society, and working with its stakeholder towards a long-term vision of sustainability.

Batelle offered the following vision: "By 2020 cement companies have integrated sustainable development into their global operations, are known as innovators in industrial ecology and carbon dioxide management, are regarded as attractive employers, and have established relationships of trust with the communities in which they operate."

The actions leading to this integrated sustainable development were suggested to be:

1) **Resource productivity -** The industry makes productive use of specific materials that otherwise would be discarded as waste, and applies state-of-the-art technologies and operating practices to cost-effectively improve its efficiency in energy and material consumption.
2) **Climate protection** – The industry has implemented practical, technological, operational, and market-based strategies to significantly reduce emissions of CO_2 and is technologically positioned for even greater reductions in the future.
3) **Emission reduction** – The industry has continuously improved its environmental practices and controls to achieve a minimal release of wastes or emissions that could adversely affect human health, ecosystems, and aesthetics.
4) **Ecological stewardship** – The industry develops, operates, and retires its plants and quarries in a manner that minimises adverse impacts on the environment, including biodiversity and aesthetics, and protects and restores potentially impacted ecosystems. In doing so, it has earned support and recognition in the eyes of the community and regulators.
5) **Employee well-being** – The industry builds and operates its facilities in a way that fosters employee satisfaction and productivity, provides fair wages and benefits, and is a safe, clean, healthy and desirable place to work.
6) **Community well-being** – The industry is well understood and respected by the communities in which it operates because companies and plants make efforts to understand community needs and to help find ways to meet those needs. The industry has implemented measures to address nuisance disturbances associated with quarrying, transportation, and plant operations.
7) **Regional development** – The industry and its associated value chain are viewed as positive contributors to local and regional economies and countries welcome the growth and prosperity of the industry because it is considered a critical component of infrastructure development and maintenance.
8) **Shareholder value creation** – The industry provides competitive returns to investors and is able to readily secure capital resources. Cement companies that have adopted SD practices are desirable investments for sustainable development index funds, and have increased their profitability and market share.

The Batelle report went further to recommend sustainable development goals and key performance indicators for cement manufacturers using the same list of actions given above.

Their suggestions were:

Recommended SD Goals and Key Performance Indicators		
Issues	**Goal**	**KPIs**
Resource productivity	Conserve resources by using less energy and recycling wastes	Energy efficiency: Tonnes of cement per megajoule (quarry and plant) Fuel material substitution rate (%) Raw material substitution rate (%)
Climate protection	Reduce greenhouse gas emissions	Net CO_2 (kg) emissions per tonne of cement
Emission reduction	Reduce environmental waste streams	Waste (non-product output) produced (kg) per tonne of cement (can include airborne emissions waterborne effluents, fugitive dust, and solid wastes)
Ecological stewardship	Reduce adverse impacts of quarrying	*Potential KPIs: investments in quarry restoration, overburden waste reduction, water use efficiency, biodiversity action plans etc*
Employee well-being	Assure worker health and safety	Incident rate (injury, work-related illness) per 200,000 hours (can include both employees and contractors)
Community well-being	Respect the needs of local communities	*Potential KPIs: frequency of community meetings, hours of volunteer community service, public health initiatives, community opinion surveys, etc*
Regional development	Support host region economies	Potential KPIs; job creation, local investment, technology transfer, contribution to GDP, etc
Shareholder value creation	Create superior value for shareholders	*Potential KPIs: return on investment (ROI), return on assets (ROA), return on net assets (RONA), return on capital employed (ROCE), economic value added (EVA), etc.*

2.1 The Working Group Cement's response

After publication of the Batelle report, the WGC developed their "Cement sustainability Initiative - Agenda for Action" in a document published in July 2002 [2].

The WGC identified the purpose of the initiative as:

- Explore what sustainable development means for these ten companies and the cement industry
- Identify and facilitate actions that companies can take as a group and individually to accelerate the move toward sustainable development.
- Provide a framework through which other cement companies can become involved.
- Provide a framework for engaging external stakeholders

The Agenda sets out a programme of work for the next 5 years for both joint project and individual company action, focusing on the main work areas listed below:

- **Climate protection** – Implement an industry protocol, developed as part of the research program, for monitoring and reporting CO_2 emissions from the cement manufacturing process. Each company will set individual CO_2 emissions targets.
- **Fuels and raw materials** – Develop guidelines for responsible use of all fuels and raw materials in cement kilns.

- **Employee health and safety** – A Health and Safety Task Force will ensure delivery of effective systems of measuring, monitoring and reporting on health and safety performance. Companies will share their experiences to identify causes of accidents and to reduce injuries.
- **Emissions reduction** – Develop an industry protocol for measuring, monitoring and reporting emissions, and individual companies will publicly report emissions targets.
- **Local impacts** – create guidelines for Economic and Social Impact Assessment by cement companies.
- **Internal business processes** – Integrate sustainable development as a set of principles into management systems, relationships with business partners and relationships with civil society.
- **An invitation to join** – Other cement companies are invited to join these activities, and third party stakeholder groups are encouraged to engage with the initiative.
- **Reporting progress** – There will be an interim progress report on all of this work in 3 years' time, with a full report to be published in 2007. Individual companies will continue to report their progress on their own activities.

The following summary lists the actions the WGC participants have committed to:

Joint projects	**Individual company actions**
The Cement Sustainability Initiative intends to create joint projects to:	*As part of our ongoing commitment to good practice and innovation in sustainable development, companies agree to:*
Climate projection	
▪ Develop a Carbon Dioxide (CO_2) Protocol for the cement industry. (Project already delivered.) ▪ Work with WBCSD/World Resources Institute (WRI) and other organisations to investigate public policy and market mechanisms for reducing CO_2 emissions.	▪ Use the tools set out in the CO_2 protocol to define and make public their baseline emissions. ▪ Develop a climate change mitigation strategy, and publish targets and progress by 2006. ▪ Report annually on CO_2 emissions in line with the protocol.
Fuels and raw materials	
▪ Develop a set of guidelines for the responsible use of conventional and alternative fuels and raw materials in cement kilns.	▪ Apply the guidelines developed for fuel and raw material use.
Employee health and safety	
▪ Set up a Health and Safety Task Force. (Project already delivered.) ▪ Establish a Health and Safety information exchange.	▪ Respond to the recommendations of the Health and Safety Task Force on systems, measurement and public reporting.
Emissions reduction	
▪ Develop an industry protocol for measurement, monitoring and reporting of emissions, and find solutions to more readily assess emissions of substances such as dioxins and volatile organic compounds.	▪ Apply the protocol for measurement, monitoring and reporting of emissions. ▪ Make emissions data publicly available and accessible to stakeholders by 2006. ▪ Set emissions targets on relevant materials and report publicly on progress

Local impacts	
▪ Develop guidelines for an Environmental and Social Impact Assessment (ESIA) process which can be used at all cement plant sites and associated quarries.	▪ Apply the ESIA guidelines, and develop tools to integrate them into decision making processes. ▪ Draw up rehabilitation plans for their operating quarries and plant sites, and communicate them to local stakeholders by 2006.
Internal business processes	
▪ Investigate methods to track the performance of the cement industry, including development and use of key performance indicators. ▪ Product a full progress report after 5 years, and an interim report after 3 years.	▪ Integrate sustainable development programs into existing management, monitoring and reporting systems. ▪ Publish a statement of business ethics by 2006. ▪ Establish a systematic dialogue process with stakeholders to understand and address their expectations. ▪ Report progress on developing stakeholder engagement programs. ▪ Develop documented and auditable environmental management systems at all plants.

3. MITIGATORY MEASURES UNDERTAKEN IN SOUTH AFRICA

Three of the four clinker producing cement manufacturing companies active in South Africa are members of the WGC, and have therefore committed themselves to the above-mentioned joint projects and individual company actions. The 4th company present in South Africa has a demonstrated track record of similar commitment to sustainable development initiatives.

The locations of the various cement industry facilities are shown in Figure 1 below.

A common commitment in the individual South African clinker manufacturing company's environmental policies is a policy of continuous environmental performance improvement and legal compliance.

All South African clinker manufacturers contributed information to the WBCSD cement sectoral report undertaken by Batelle.

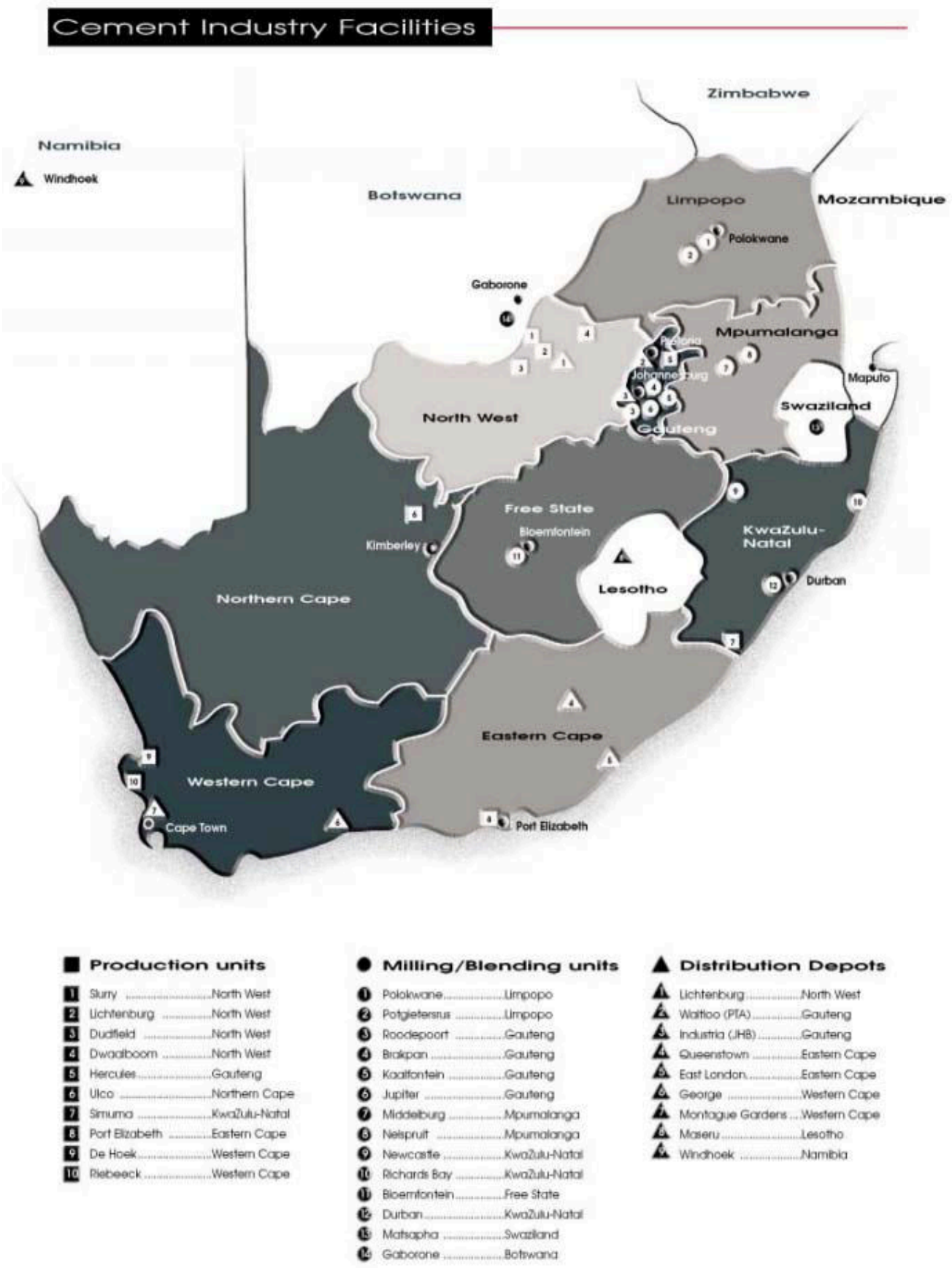

Figure 1. The locations of the various cement industry facilities

In addition, the following are examples of specific achievement by the South African clinker manufacturers:

- **Climate protection** – All South African clinker producers have already commenced with the production of blended cements which use less clinker per ton of cementitious material. This is illustrated in the trend of reducing specific CO_2 emissions shown in the graph given in Figure 2. This graph was compiled from a consolidation of data supplied on a confidential basis by each of the 4 clinker producing companies to the Association of Cementitious Material Producers, ACMP. While there have been improvements in operational energy efficiency through investment in modern manufacturing plant, the impact on CO_2 emissions has been relatively modest. The effect of reducing the clinker content of the product range produced has been more significant. Some South African clinker producers also have interests in the processing and direct sale of cement extenders to end-users. Figure 2 shows the impact of the inclusion of this additional consumption of cement extenders on the specific CO_2 emissions. (Specific CO_2 emission is the quantity (tons) of CO_2 emitted per ton of cementitious material produced).

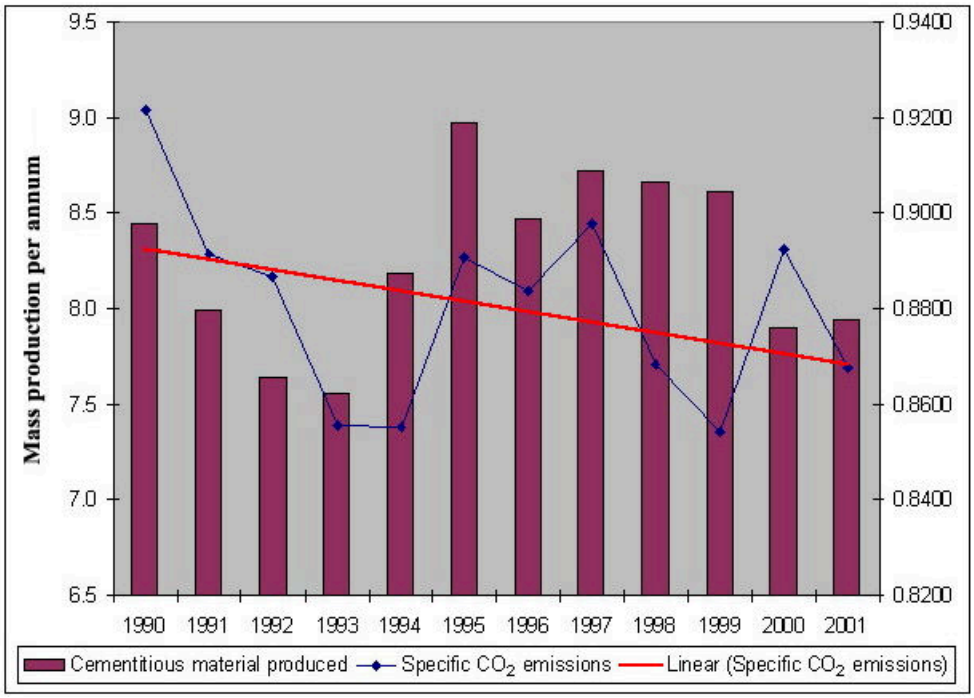

Figure 2. Cementitious material produced and specific CO_2 emitted in South Africa

Table 1 provides additional evidence of this trend. It shows how the downward trend of CEM I sales accelerated in 2002.

Table 1.

Sales History (t/a) by Product Type						
Product Type	**1998**	**1999**	**2000**	**2001**	**2002**	**% change 2002/2001**
CEM I	3 670 166	3 289 051	3 155 490	2 977 067	2 146 527	-27.9
CEM IIA	2 821 896	2 523 738	2 522 163	2 714 994	3 605 823	32.8
CEM IIB	664 181	1 596 884	1 759 790	1 839 139	2 278 044	23.9
CEM III	619 770	506 991	483 261	488 212	494 416	1.3
Masonry MC 12.5	74 866	64 102	49 211	16 418	456	-97.2
Masonry MC 22.5X	887 501	86 926	1 401	0	0	0.0
GGBS Slag	308 774	343 763	372 652	495 645	501 777	1.2
Fly Ash	129 452	134 269	130 604	105 541	118 808	12.6
Other	404 877	461 875	516 857	528 170	478 419	-9.4
Totals	9 581 483	9 007 599	8 991 429	9 165 186	9 624 270	5.0

- **Fuels and raw materials** – All South African clinker producers have undertaken feasibility studies to evaluate the use of alternative fuels in their kilns. The clinker producers are members of the SA Tyre Recycling Process Company, a concern dedicated to the fight against pollution resulting from used tyres. All manufacturers are evaluating the use of power station wastes as alternative raw materials in their processes. Advantage is being taken of by-products of other industries to supply the gypsum needs of South African manufacturers.
  While South African cement producers will be competing for alternative fuels, they are jointly developing guidelines for the safe and responsible use of such fuels while interacting with government to determine the role of the cement industry in achieving the National Waste Management Strategy and the commitments covered by the Polokwane Waste Declaration.
- **Emissions reduction** – Manufacturers have dust-capturing equipment in place at their manufacturing facilities and comply with South African legislation with regard to particulate emission. The South African manufacturers will develop an industry protocol for measuring, monitoring and reporting emissions.
- **Local impacts** – South African manufacturers have met all local legislation in rehabilitating quarries.
- **Social responsibility** – There is a clear commitment to safety management as well as actions on AIDS prevalence reduction.

4. ACTION PLAN AGREED BY SA CLINKER PRODUCERS

Action plan agreed by Association of Cementitious Material Producers

- ACMP members have committed to reducing CO_2 emissions per ton of cementitious material.
- ACMP members will submit safety statistics to ACMP for consolidation and subsequent analysis for trends that require corrective action.
- Members will undertake Employee Health Management Programmes with particular attention given to HIV/AIDS programmes for workers.
- Starting in 2005, individual companies will publicly report on emissions and emissions targets.
- ACMP will commence with reporting on the sustainability of member company operations starting in 2005.

REFERENCES

[1] World Business Council for Sustainable Development, Towards a sustainable cement industry, Geneva: WBCSD, 2002.

[2] World Business Council for Sustainable Development, Towards a sustainable cement industry - Summary report, Geneva: WBCSD, 2002

[3] World Business Council for Sustainable Development, The cement sustainability initiative: our agenda for action, Geneva: WBCSD, 2002.

SUSTAINABLE DEVELOPMENT IN THE CEMENT INDUSTRY: THE SOUTH AFRICAN RECORD

de Rougemont, F.

Association of Cementitious Material Producers (ACMP)

Frederic de Rougemont

Born : 18 Oct 1958
Married, 3 children

EDUCATION

Ecole Polytechnique, France, graduated 1982

PhD Atomic and Molecular Physics (Universite d'Orsay), 1987

CAREER

Fundamental Research : 1983 - 1989

1983–1987: Charge de recherche (CNRS) : Laboratoire d'Optique Quantique (Ecole Polytechnique)
1988 – 1989 : Visiting Scientist : IBM Research Center, Yorktown Heights, USA

Lafarge: 1990 – to date

1990 - 1993 : Development Engineer, Cormeilles Cement Plant (France).
1993 - 1995 : Cement Institute Director, Lyon
1995 - 1997 : Senior VP Internationalisation HR , Paris
1997 - 2001 : Senior VP Corporate R&D
2001 – to date: CEO Lafarge South Africa

ACMP:
The Association of Cementitious Material Producers (ACMP) is a relatively new association founded in May 2002, to represent clinker and cementitious material producers, on industry related producer issues. The intention of ACMP is to target a broader membership base, and not only the traditional cement producers.

The main objectives of the association are as follows:
- To lobby with various bodies in order to further the common interests of members.
- To promote the broader interests of it's members relating to legislation impacting on the cementitious industry.
- To co-ordinate the activities of standing, sub and ad hoc committees established by the association and to monitor and report on matters relevant to the industry.

The Executive Director of ACMP is Naude Klopper.
The chairmanship of ACMP rotates on a two yearly period, Lafarge are currently tasked with the chairmanship.

SOME ASPECTS OF RHEOLOGY OF CEMENT BASED PARTICLE SUSPENSIONS SUCH AS FRESH CONCRETE

O.H. Wallevik

The Icelandic Building Research Institute, 112 Keldnaholt. E-mail: wallevik.o@rabygg.is

ABSTRACT

The application and benefits of rheology as a tool in evaluating the properties of fresh concrete are briefly discussed. A coaxial cylinder viscometer can be used to evaluate the rheological properties of fresh concrete. Several examples are shown using parameters such as increased water content, air content, silica fume content and different dispersing admixtures.

Increased use of high performance concretes such as High Strength Concrete and Self Compacting Concrete demands better knowledge of properties such as viscosity for their successful application.

Keywords: Fresh concrete, rheology, viscometer, application.

1. INTRODUCTION

Rheology is the science of flow and deformation of matter and should therefore be the appropriate tool to describe the workability and mobility of fresh cement-based materials like cement paste, mortar or concrete. The theory is already used by many concrete technologists in the evaluation of hardened concrete i.e. creep. The theory is also used for fresh cement-based materials, though most of the research has been concentrated on basic theoretical aspects. In some cases there have been difficulties applying rheological test results, as measurement techniques used were somewhat questionable.

The application of rheology to understanding the properties of fresh concrete is definitely relevant. However, without a tool to confirm the theory, it will always be questionable and it will be difficult to know if it is realistic and applicable for concrete.

During the past three years a research program has been ongoing at the Icelandic Building Research Institute (IBRI) named “Rheology of fresh cement-based coarse particle suspension such as cement paste, mortar and concrete”. The scope of this work is to obtain a better basic understanding of the mechanism and the influencing factors as well as the effect of each constituent of the composite material.

2. VISCOMETER

The ConTec BML [1-2] Viscometer and the ConTec Viscometer 4U [3] are coaxial cylinder viscometers for coarse particle suspension. They have proven to be good tools to evaluate the rheological properties of cement suspensions. The BML Viscometer can be used to measure dilute suspensions such as cement paste as well as relatively stiff concrete mixes.

Ideally the viscometer is applicable for concrete with plastic to flowing consistency. When designed, it was made for concrete with a slump value of about 120 mm and higher. However, depending on the mix design, it is possible to get sufficiently good measurements when the slump is as low as 50 mm.

a) b)

Figure 1. The viscometers: a) The BML viscometer. b) The ConTec viscometer 4.

The viscometers are ideal instruments to measure the rheological behaviour of special concretes such as High Performance Concrete (HPC), Underwater Concrete (UWC) and Self-Compacting Concrete (SCC). They are also suitable to evaluate different variables such as; various admixtures, cement types, different deliveries of cement etc. The more fluid the testing material is or the higher the plastic viscosity is relative to the yield value, the more accurate are the test results.

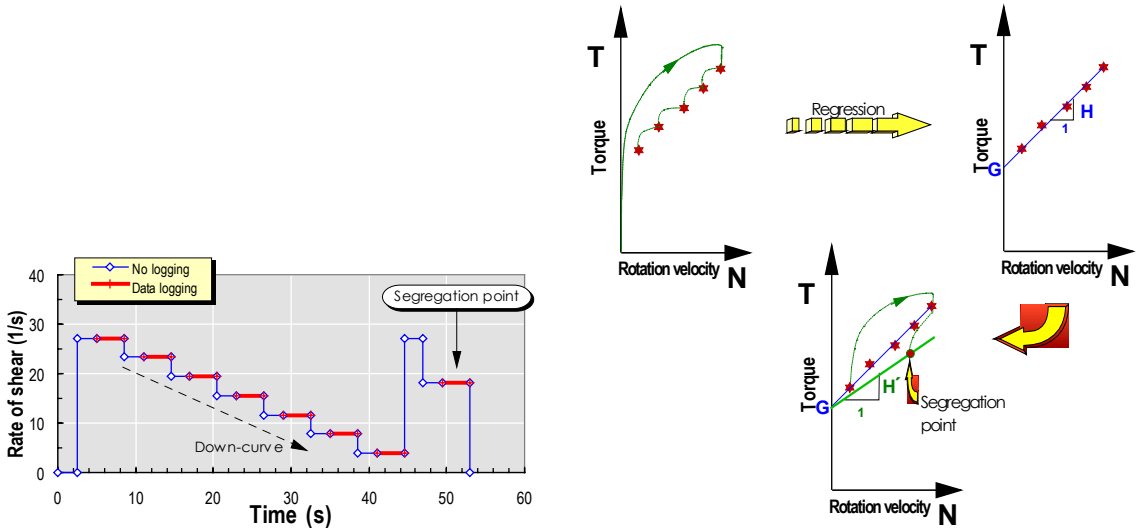

Figure 2. Rate of shear as a function of time and torque-velocity (T-N) diagrams of a standard test in the BML Viscometer (including the segregation measurement).

The viscometer measures the resistance (torque) of the fresh concrete at various (rotation) speeds. From these measurements so-called G- and H-values are calculated. The G-value ("flow resistance") is a measure of the force necessary to start a movement of the concrete. The H-value ("viscosity factor") is a measure of the resistance of the concrete against an increased speed of movement. In most cases the Bingham parameters, the yield value and the plastic viscosity can be calculated from the G- and H-value, respectively. Notwithstanding, the G- and H-values should be

used if there occurs a significant plug during testing (even though there exist advanced mathematics to calculate the Bingham parameters when plug occurs).

Figure 2 illustrates testing as a function of time. In standard tests one always starts at the highest speed, thereafter stepwise reducing the velocity until the lowest speed is applied. Thereafter the segregation point is measured.

3. SOME EXAMPLES

A principal illustration of the effect on the yield value and the plastic viscosity when increasing the content of water, silica fume, "air" and superplasticizer in the concrete mix is given in Figure 3. The figure also shows the influence on the shear stress as a function of the rate of shear.

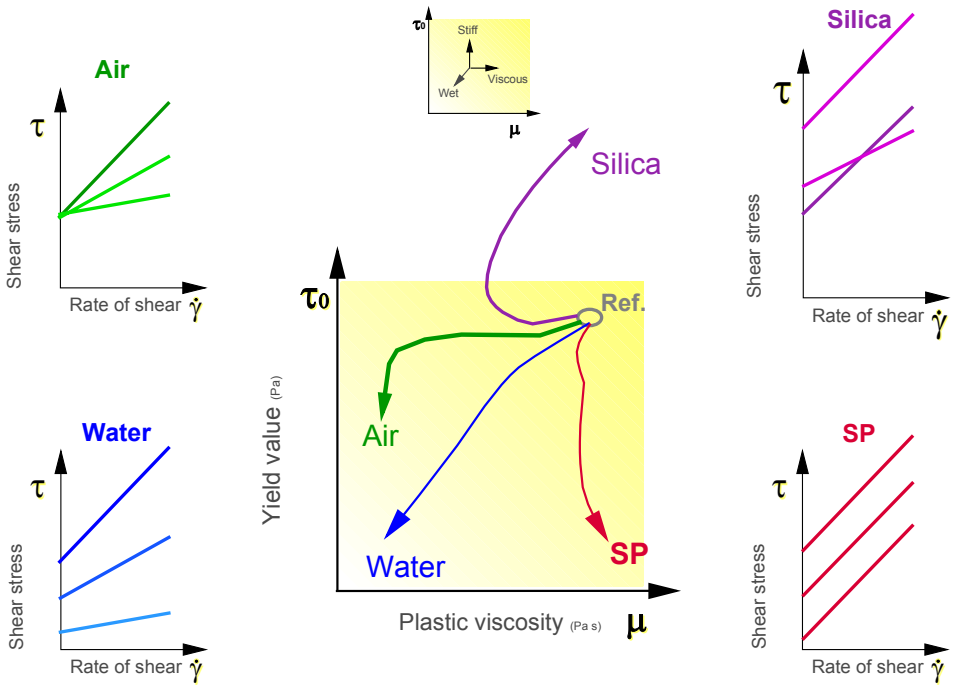

Figure 3. Illustration of the effects of water, air, SP and silica fume on the flow behavior of the fresh concrete.

In Figure 4 measurement values from testing 22 mortar mixes are shown. The sand:cement ratio in the mixes was 2:1. The plastisicer used was melamine based and the dosages used are shown as dry polymer per unit weight of cement.

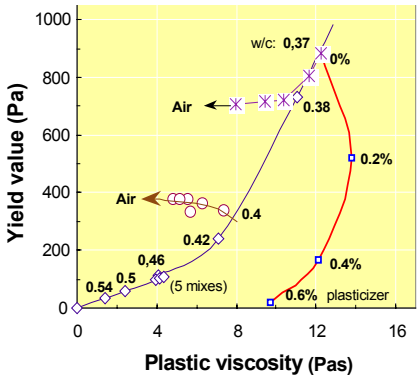

Figure 4. Effect of water, air and plasticizer on the yield value and the plastic viscosity.

Figure 5 shows test results of four concrete mixes from a ready mix concrete plant where the water content of the mixes is variable. One result is from HSC in the strength category C100. The results in the figure with yield values below 100 Pa represents SCC (also from different countries).

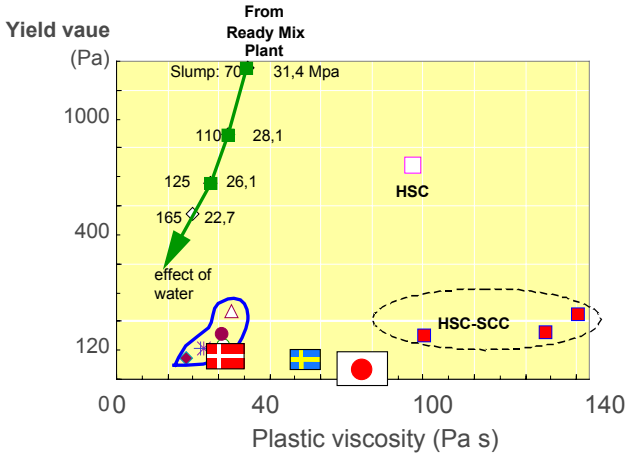

Figure 5. Test results from SCC/HSC compared to test results of concrete from a ready mix concrete plant [4].

In Figure 6 are indicated the desired yield and plastic viscosity values of a concrete mix for different applications. For instance, the goal is to reduce the plastic viscosity of the high performance concrete (HSC) as the viscosity normally causes problems. Problems with the viscosity limit the strength potential of the concrete if it should remain workable.

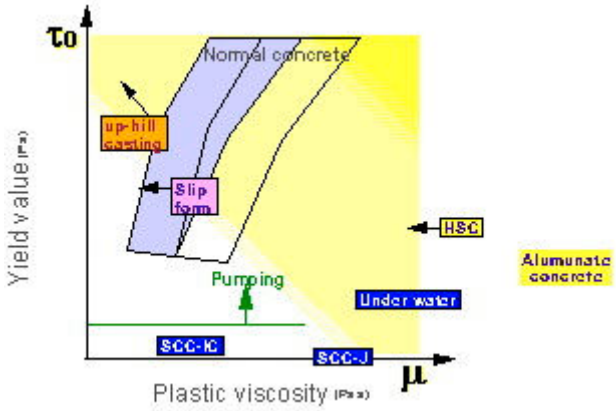

Figure 6. Desired rheological values for different applications of concrete.

Figure 7 shows the workability loss over a period of 1.5 hours where some of the new generation dispersing admixtures were tested and compared to conventional melamine based super-plasticizers.

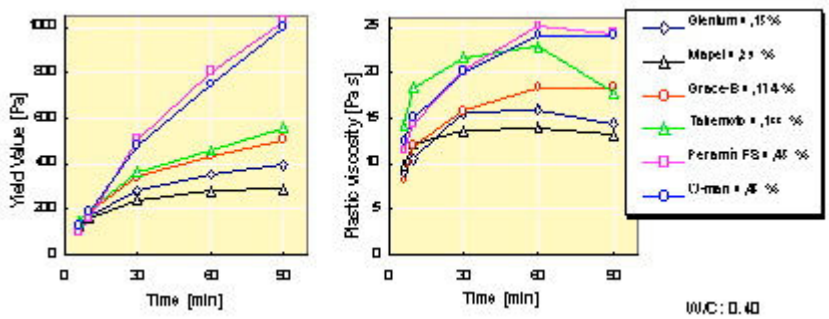

Figure 7. Workability loss of mortar mixes containing various dispersing admixtures.

4. FINAL REMARKS

Results of the current research project are promising and the research aims have been met. The research project also includes advanced theoretical aspects such as the coagulation rate theory (Hattori-Izumi theory).

Use of viscosimetry in concrete technology is not common for the time being as concrete is a very complex material. However, this will change with increased use of high performance concrete such as HSC and SCC. Knowledge of viscosity is essential for successful application of these concrete types. Hence further research in this field is valuable for further development of concrete.

ACKNOWLEDGEMENT

The author would like to thank the Icelandic Research Fund (Rannis) for their financial support of the project. The colleagues at IBRI are also thanked for their assistance.

REFERENCES

[1] Wallevik, O. H., Gjørv, O. E., "Development of a Coaxial Cylinder Viscometer for Fresh Concrete", Properties of Fresh Concrete proceedings of the Rilem Colloquium. Chapman & Hall. Hanover, October, 1990, pp. 213-224.

[2] Nehdi, M., Wallevik, O.H., Saasen, A., Gjorv, O.E., "Effect of filler materials on the rheological properties of fresh concrete" ACI Materials Journal 93 (4), JUL-AUG, 1996, pp. 396-398.

[3] Wallevik, J.E., Wallevik, O.H., Effect of eccentricity and tilting in coaxial cylinder viscometer when testing cement pastel, Nordic Concrete Research, (www.itn.is/NCR), Oslo, August, 1998. pp. 144-152.

[4] Wallevik. O., Nielsson, I., "Self Compacting Concrete – A Rheological approach", International Workshop on SCC, Kochi, Japan {JSCE Concrete Engineering Series no. 30}, August, 1998, pp. 136-159.